

Göteborg 1997

PROCEEDINGS OF THE 10TH INTERNATIONAL CONGRESS ON THE CHEMISTRY OF CEMENT

Gothenburg, Sweden, June 2-6, 1997

PROCEEDINGS OF THE 10TH INTERNATIONAL CONGRESS ON THE CHEMISTRY OF CEMENT
Gothenburg, Sweden, June 2-6, 1997

VOLUME 1

PLENARY LECTURES

~~~~~~~

CLINKER AND CEMENT PRODUCTION

10th ICCC
Göteborg 1997

Edited by

Dr. Harald Justnes
SINTEF Civil and Environmental Engineering, Cement and Concrete
Trondheim, Norway
~~~~~~~

Published by Amarkai AB and Congrex Göteborg AB in 1997

Copyright © Amarkai AB and Congrex Göteborg AB

All rights reserved. No part of this publication may be reproduced, stored in a retrieval system, or transmitted in any form or by any means, electronic, mechanical, photocopying, recording or otherwise without prior permission of the publishers.

Inform Trycket AB, Göteborg 1997
ISBN 91-630-5495-7

HONORARY COMMITTEE

Governor Göran Bengtsson,
Provincial Government Göteborg o Bohuslän, Göteborg, Sweden

Professor Per Ahlberg,
The University of Göteborg, Sweden

Director General Gösta Blücher
National Board of Housing, Building and Planning, Karlskrona, Sweden

Director General Jan Brandborn,
Swedish National Road Administration, Borlänge, Sweden

Director Ulf Dinkelspiel,
Swedish Trade Council, Stockholm, Sweden

Lord Mayor Jörgen Linder,
City Council, Göteborg, Sweden

Director General Bertil Petterson,
Swedish Council for Building Research, Stockholm, Sweden

President Anders Sjöberg
Chalmers University of Technology, Göteborg, Sweden

Consul General of Austria Martin Thomas,
Chief Executive Officer, AB Färdig Betong, Göteborg, Sweden

Senior Industrial Development Officer Halime Şeniz Yalçindağ
Chief, Building Materials Unit, UNIDO, Vienna, Austria

Industrial Development Officer Kojo O. Hagan.
Chemical Industries Branch (Cement, Lime & Binders), UNIDO, Vienna, Austria

~~~~~~~~~~~~~~~

ORGANISATION COMMITTEE

PRESIDENT & SECRETARY GENERAL

CEO Wilgodt Andersson, 10th ICCC, Sweden

MEMBERS

Proj. Mgr. Anita Ericsson, CONGREX, Sweden

Prof. Fred P. Glasser, University of Aberdeen, United Kingdom

Dr. Harald Justnes, SINTEF Civil and Environmental Engineering, Norway

Dir. Bengt Wolffram, Swedish National Road Administration, Sweden
~~~~~~~~~~~~~~~

SCIENTIFIC COMMITTEE

PRESIDENT

Fred P. Glasser, University of Aberdeen, United Kingdom

VICE PRESIDENT & SECRETARY

Harald Justnes, SINTEF Civil and Environmental Engineering, Norway

MEMBERS

A.I. Boikova, Russian Academy of Sciences, Russia
J.G. Cabrera, University of Leeds, United Kingdom
A. Capmas, Lafarge L.C.R., France
L. Czarnecki, Warsaw University of Technology, Poland
M. Daimon, Tokyo Institute of Technology, Japan
A.E. Fiorato, Portland Cement Association, USA
T.C. Hansen, DTU, Denmark
H. Kukko, VTT Building Technology, Finland
V.M. Malhotra, CANMET, Canada
A.K. Mullick, NCB, India
S. Nagataki, Tokyo Institute of Technology, Japan
Y. Ohama, Nihon University, Japan
H. Olafsson, Islandic Building Research Institute, Iceland
V. Penttala, Helsinki University of Technology, Finland
V.S. Ramachandran, NRC, Canada
D.M. Roy, Pennsylvania State University, USA
S.L. Sarkar, Sarkar & Associates Inc., USA
P. Schießl, IBAC, Germany
E.J. Sellevold, NTNU Structural Engineering, Norway
R.N. Swamy, University of Sheffield, United Kingdom
B. Talling, Renotech Oy, Finland
F.D. Tamás, University of Veszprém, Hungary
H. Uchikawa, Chichibu Onoda Cement Corp., Japan
D. van Gemert, Katholieke Universiteit Leuven, Belgium
W. Wieker, TU Berlin, Germany
J.F. Young, Center for Cement Composite Materials, USA

FOREWORD TO THE PROCEEDINGS

I extend a most cordial and fraternal welcome to all delegates to the X Congress.

In this, the Jubilee Congress, it is appropriate to note some special features of the X Congress relating to the proceedings. Many Congresses publish a written transcript of their proceedings which is ephemeral, but those on the Chemistry of Cement are rightfully regarded as landmark publications. They are virtually unique in terms of their frequency of citation by the relevant scientific Community. Most workers in the field regard the published proceedings as affording an unique insight of current awareness and of progress in all aspects of cement science.

The Scientific Committee have taken steps to assure that the Conference proceedings retain this position of eminence. Amongst the steps which have been taken are the following;

- to ensure high but fair standards of refereeing,
- promote uniformity of format and good legibility of the individual contributions,
- reduce the time between final receipt of manuscripts and publication, to ensure that the Congress reflects the state of art up to 1997,
- provide subject indices for the Proceedings to assist rapid retrieval of information and, to facilitate library cataloguing, by providing an ISBN number.

We hope this measures meet with the approval of readers.

I would like to express my thanks to the many individuals and organisations who have facilitated publication of the Proceedings.

First and foremost to Dr. Harald Justnes who has had the major task of receiving manuscripts, and ensuring their orderly progress through refereeing, collation and, finally, despatch to the printer. Many individuals have contributed to the refereeing and it is a tribute to the Scientific Community that so many individuals have contributed generously of their time and energy. Their efforts have immeasurably improved the free communication of ideas and results, and the clarity of the written discussions.

Ultimately the success of the Congress is decided by those who attend as well as by those who use these Proceedings. It is not for me to decide whether future Congresses will be held or, if held, what form they will take. But, if there is a next Congress, it will be held in a new millennium. Never has the pace of change in communication been so rapid: I speculate that this might be the last paper proceedings which will ever be published! But whatever form future Congresses may take, and however its proceedings are disseminated, the fraternity of science and the principle of peer review will, I am confident, continue to be a hallmark of future proceedings.

F.P. Glasser
President of Scientific Committee
23 March 1997

EDITORIAL REMARKS

The papers of the five main themes and sub-topics of the Congress has been distributed between the 4 volumes of the Proceedings in a manner to compromise between two conflicting interests; to make it easy for the reader to find the wanted paper and to have volumes about equal in size. This resulted in proceedings comprising about 2,200 pages distributed in 4 volumes ranging from about 400 to 700 pages each. Volume 1 contains Plenary lectures and Theme I, the content of Volume 2 is Theme II (except additives) and Volume 4 includes Theme IV. The only mixed volume is Volume 3, encompassing Additives from Theme II, Theme III and Theme V.

The volumes are not paginated, but the first page of each paper is marked with a code and number of pages in the upper right corner. If the number of pages are uneven, a blank page is inserted in order to ensure that every paper starts on a right hand page. Since the papers are relatively short (usually 4 or 8 pages) it should be easy to go from one code to the next to find the required paper. The code consists of three parts; volume (arabic numerals), theme (roman numerals) and 3 digits giving the paper number within the corresponding theme. For instance, 3ii091 means paper no. 91 within Theme II found in Volume 3.

Every volume starts with a list of contents for that volume only where authors, titles, code and number of pages are listed in the order they appear. At the end of every volume there is an author index as well as a key-word index giving the corresponding paper codes for the total proceedings. Volume 4 also includes a few colour figures with reference to the corresponding papers after the author and key-word indices.

Finally, I would like to express my sincere thanks to the individuals who in addition to myself have taken active part in the reviewing process of abstracts and/or draft papers:

A.I. Boikova, Russian Academy of Sciences, Russia
A. Capmas, Lafarge L.C.R., France
S. Chandra, Gothenburg, Sweden
F.P. Glasser, University of Aberdeen, United Kingdom
V.M. Malhotra, CANMET, Canada
A.K. Mullick, NCB, India
V. Penttala, Helsinki University of Technology, Finland
V.S. Ramachandran, NRC, Canada
E.J. Sellevold, NTNU Structural Engineering, Norway
D. Sorrentino, Lafarge L.C.R., France
R.N. Swamy, University of Sheffield, United Kingdom
F.D. Tamás, University of Veszprém, Hungary
H. Uchikawa, Chichibu Onoda Cement Corp., Japan
D. van Gemert, Katholieke Universiteit Leuven, Belgium
W. Wieker, TU Berlin, Germany
J.F. Young, Center for Cement Composite Materials, USA

Harald Justnes (Editor)
15 April 1997

List of contents for Volume 1

PLENARY LECTURES

A.K. Mullick: "Why Concrete is not Always Durable", Plen1, 31 pp

W. Wieker, C. Hübert, D. Heidemann: "Recent Results of Solid State NMR Investigations and it's possibilities of Use in Cement Chemistry", Plen2, 24 pp

I CLINKER AND CEMENT PRODUCTION

I.A Process technology

T.V. Kouznetsova: "Development of Special Cements", 1i001, 4 pp

K. Raina, B. Nedumaran, S.N. Mehrotra: "Utilization of Kiln Dust for Clinker Production Using Cri-modern Vertical Shaft Kiln Technology", 1i002, 4 pp

A. D. Agnihotri, S. George, S.M. Shingote, S. B. Yadav ,K. V. Kalyani: "Environmental Impact Assessment of a Spesific Cement Plant/New Project Cluster in India", 1i003, 4 pp

V. Klassen, V. Belyaeva: "Cement Clinker Burning Process Optimization", 1i004, 4 pp

J. Stark, A.P. Osokin, E.N. Potapova: "Technology and Properties of Low-Aluminate Clinkers and Cements", 1i005, 4 pp

A.P. Osokin, V.G. Akimov, E.N. Potapova: "The Thermochemical Activation of Clinker Formation", 1i006, 5 pp

L.M. Sulimenko, B.S. Albats: "Clinkering of Pre-formed Mixes", 1i007, 4 pp

S.A. Khadilkar, P.G. Lele, D. Ghosh, A.K. Chatterjee: "Melting Process for Clinkerisation - A Technical Reexamination", 1i008, 8 pp

L. Opoczky, M. Hilger: "Grinding Technology and Quality of Composite Cements", 1i009, 4 pp

Y. Fang, D.M. Roy, Y. Chen, M.R. Silsbee, R. Roy: "Cement Clinker Formation from Fly Ash by Microwave Processing", 1i010, 4 pp

V.D. Barbanyagre: "Clinker Formation in High-Silicate Low-Temperature Melt", 1i011, 4 pp

H. Shi, C. Lu: "Research on the Mechanism of Forming Coating and Clinker Mass in Precalciner Kiln System", 1i012, 4 pp

L. Ya. Goldstein: "Energy-Saving Technology of Cement Production by means of Combined Grinding of Clinkers of Variable Compositions", 1i013, 6 pp

I.B Low energy clinker formation

A.P. Osokin, Y.R. Krivoborodov, S.V. Samchenko: "Melt Structure and Properties of Clinkers Containing Calcium Sulphoferrites and Sulphoalumoferrites", 1i014, 8 pp

B.S. Albats, A.L. Shein: "High Quality Portland Cement Produced from Low-Base Raw Mix with Low Energy Consumption", 1i015, 4 pp

Vipin K. Singh, R. Pyare, Vinaya K. Singh: "Formation Kinetics of Beta Dicalcium Silicate", 1i016, 4 pp

M.M. Komljenović, B.M. Živanović, A. Rosić: "β-Dicalcium Silicate Synthesis by Liquid State Reaction", 1i017, 4 pp

A. Garbacik: "Properties of Low-temperature Portland Clinkers", 1i018, 8 pp

I.C Utilization of industrial by-products and wastes

S.C. Ahluwalia, V.K. Arora, Y.P. Sehti: "Agricultural/Industrial Combustible Wastes as Fuel in Indian Cement Industry", 1i019, 4 pp

Z.B. Entine, B.E. Ioudovitch: "The Multicomponent Cements (MCs)", 1i020, 4 pp

Y. Pan: "Effects of Using Iron Mud as Raw Material in Cement Manufacture", 1i021, 4 pp

Z. Konik, A. Stok, J. Iwanciw: "The Possibilities of Utilisation of Waste and Raw Materials Containing Al_2O_3, Fe_2O_3 and TiO_2 for Obtaining Ferrates", 1i022, 4 pp

G. Hu: "The Application of High Magnesium Oxide Content Limestone in Cement Industry", 1i023, 7 pp

R.I.A. Malek: "Synthesis and Characterization of New Alkali-Activate Cements", 1i024, 8 pp

K. Ikeda, K. Fukuda, H. Shima: "Calcium Sulphoaluminate Cements Prepared from Low-Alumina Waterworks Slime", 1i025, 8 pp

I. Odler and H. Zhang: "Possibilities of Utilizing High SO_3 Fluidized Bed Ash in the Production of Portland Clinker and Cement", 1i026, 8 pp

L. Cassar, G.L. Guerrini, C. Gilioli: "Thermal Disposal of Asbestos-Cement and Re-Utilization in Cement Industry", 1i027, 6 pp

I.D Application of mineralizers, modifiers and activators

P. Li, C. Liu, H. Zhuo: "Practice Application of Composite Mineralizer Technology in Precalcining Cement Kiln", 1i028, 8 pp

I.G. Luginina: "Surface Microphases and Chemical Activity of the Admixtures-Catalysts Action", 1i029, 5 pp

S.P. Ghosh, K. Mohan: "Use of Waste Low Grade Fluorspar as a Mineralizer for the Manufacture of Clinker/Cement", 1i030, 5 pp

A.K. Mullick, S.C. Ahluwalia, R. Bhargawa: "Use of Fluorspar and Barite for Improved Burnability and Clinkerisation of Cement Raw Mixes", 1031, 7 pp

L.I. Sychova, M.V. Anufriev: "Clinkerisation of Anhydrite with Phosphogypsum and Calcium Fluoride", 1i032, 4 pp

S.P. Gandhe, D. Ghosh, A.K. Chatterjee: "Synthesis of Mineralisers for Clinker Making", 1i033, 8 pp

F. Puertas, M.T. Blanco-Varela, A. Palomo, T. Vázquez, J.G. Palomo: "Burnability of Mineralized White Cement: Optimization of Raw Meals", 1i034, 8 pp

S. Lagzdina, U. Sedmalis: "Kinetics of $2CaO \cdot SiO_2$ and $3CaO \cdot SiO_2$ Formation in the Presence of Sodium and Potassium Compounds", 1i035, 5 pp

W.-H. Chae, G.-C. Yum, H.-K. Oh, S.-H. Choi: "The Effects of Additives on Formation of C_2S, $C_4A_3\bar{S}$ and C_4AF", 1i036, 5 pp

R. Sanjaasuren, P.F. Rymyantsev: "Synthesis of Low-Temperature Portland Cement Clinker by Using Composite Mineralizer", 1i037, 10 pp

I.E Correlating process parameters with clinker properties

K. Svinning, H. Justnes: "Application of Partial Least Square Regression Analysis in Examination of Correlations between Production Conditions, Microstructure in Clinker and Cement and Cement Properties", 1i038, 8 pp

H. Motzet, H Pöllmann, U. König, J. Neubauer: "Phase Quantification and Microstructure of a Clinker Series with Lime Saturation Factors in the Range of 100", 1i039, 8 pp

L.M. Sulimenko, Y.R. Krivoborodov: "Influence of Physical-Chemical Hydrodynamics Processing of Raw Mix on Clinker Quality", 1i040, 4 pp

G.K. Moir: "Influence of Raw Mix Heterogeneity on Ease of Combination and Clinker Strength Potential", 1i041, 8 pp

O.P. Mchedlov-Petrossyan: "Solid State Reactions in the Chemistry of Cement", 1i042, 4 pp

M.V. Kougiya: "Heavy Metals Content of Raw Materials, Clinker and Dust of Cement Plants", 1i043, 3 pp

S.C. Ahluwalia, R.K. Goswami, S. Harsh: "Modelling the Kinetics of Clinkerisation", 1i044, 3 pp

S.C. Ahluwali, R.K. Goswami, S. Harsh: "Burnability of Cement Raw Mixes at 1400°C", 1i045, 4 pp

Z.B. Entine, B.E. Ioudovitch: "The Liquid Phase Alite Generation Model in Sintering Portland Cement Clinker", 1i046, 4 pp

V.K. Gore, S.A. Khadilkar, P.G. Lele, D. Ghosh: "Interrelationship of Clinker Properties with Process Parameters in Coal Fired Kilns", 1i047, 8 pp

L. Sas: "Effect of Coarse Quartz and Limestone Grains on the Properties of Raw Meal, Clinker and Cement", 1i048, 8 pp

H. M. Cheong, S. H. Choi, K. S. Han: "Effect of Alkalies and SO_3 on the Tricalcium Silicate Formation and Microstructure", 1i049, 8 pp

I.F Clinker structure and mineralogy

Ö. Andaç, F.P. Glasser: "Influence of Sodium and Fluorine on the Stability and Polymorphism of Alite", 1i050, 7 pp

A. Saini, N. Giuliani: "Crystal Size and Content of the Aluminate Phase in Portland Cement Clinker", 1i051, 8 pp

K. Fukuda, I. Maki, S. Ito: "Transformation-Induced Microtextures of Belite Crystals", 1i052, 8 pp

V.K. Mathur, K.M. Sharma, R.S. Gupta, S.C. Ahluwalia: "Effect of Al_2O_3 and Fe_2O_3 in the Formation of Dicalcium Silicate Phase", 1i053, 4 pp

Y. Pan, Y. Chi, X. Fu: "The Influence of Molybdenic Compound on Formation of Cement Clinker", 1i054, 4 pp

Y. Pan, Y. Chi, X. Fu: "The Distribution of MoO_3 in Clinker Mineral Phases", 1i055, 4 pp

F. Goetz-Neunhoeffer, J. Neubauer: "Crystal Structure Refinement of Na-substituted C_3A by Rietveld Analysis and Quantification in OPC", 1i056, 8 pp

A.I. Boikova, O.I. Fomicheva, I.G. Luginina: "Phases in High-Magnesium Clinkers", 1i057, 5 pp

A.I. Boikova, O.I. Fomicheva, L.V. Grishchenko: "Barium-Containing Clinker Phases", 1i058, 4 pp

V.D. Barbanyagre: "Monomineral Binders in the CaO-Al_2O_3-ZnO System", 1i059, 8 pp

A. Emanuelson, S. Hansen, E. Henderson, A. Landa-Cánovas, E. Sjöstedt: "Ferrite-Microstructure in Clinker and Hydration of Synthetic Phases and Sulphate Resisting Cements", 1i060, 8 pp

PLENARY LECTURES

WHY CONCRETE IS NOT ALWAYS DURABLE

Ajoy K Mullick
National Council for Cement and Building Materials, New Delhi, India

INTRODUCTION

Scientists and engineers who trust cement and concrete to be noble building materials can draw little comfort in the fact that only a minor proportion of concrete constructions face durability problems. The somewhat provocative title of this presentation is to activate the search for a 'zero-defect' situtation. Concrete systems are dynamic in nature, and responsive to the characteristics of the service environment. Apart from mechanical properties which govern strength and deformation of concrete, physico-chemical aspects of durability in service are also important manifestations of performance of cements. Durability of concrete has been a subject of discussion in the previous Congresses on the Chemistry of Cement, as indeed in many Engineering Conferences organised from time to time.

Because of its multi-disciplinary nature, it is necessary to take a holistic view of the problem. A grudge among some members of civil engineering fraternity is that the subject of durability of concrete does not receive the attention of scientists (mainly chemists) in the academic institutions that it deserves (Hime, 1993). On the other hand, in a forum devoted to the chemistry of cements, it is unlikely that the aspects of structural design, detailing of sections and reinforcements, and workmanship under situations prevailing in a construction site, all of which also influence the response of a concrete structure to the service environment, can be and will be discussed to any great length. What is possible, however, is to discuss certain chemical aspects of durability of concrete, without being oblivious to the fact that there are other factors in the background, which complete the cause-effect scenario. In other words, it is necessary to view durability of concrete as a 'System' (Mullick and Chandra, 1992).

A common criticism has been that inspite of voluminous research on various aspects of durability of concrete throughout the world for nearly six decades, there seem to be more difficulty in making concrete of adequate durability now, than in the past (Neville, 1987, Gerwick, 1989). Such a situation has been thought to have arisen due to changing properties of cement as presently manufactured in modern cement plants, diversity of usage of cement concrete in various types of construction, inadequate level of workmanship and quality assurance in many construction sites and limitations of specifications of structural concrete (Mehta et al 1992, Mullick and Chandra, 1992). Large incrase in the volume of constructions with resultant increase in number of structures showing signs of distress has also contributed to such a perception. Increased atmospheric pollution in metropolitan cities and industrial townships also add to the problem.

Durability research, in general, follow three distinct streams. The first group deals with identification of processes of concrete deterioration and the basic mechanisms at work. Closely related to this is the second group of investigations on the effects of various factors and parameters on the deterioration processes, leading to steps for improving the durability of concrete. The third group deals with laboratory test methods and site investigations of concrete structures under service environment and recording the performance of concrete.

Examples of the first group of research projects, which have been in the forefront since the Ninth Congress in New Delhi,. are related to delayed ettringite formation (DEF), and deterioration due to climatic and biological causes. In the second group, research dealing with effect of supplementary cementing materials like fly ash, granulated blast furnace slag and silica fume on pore structure, diffusivity, electrical resistance of concrete and improvements in paste-aggregate interface as well as chloride-binding capacity received major attention.

Compared to the first two groups, reports on deterioration of concrete structures in service as well as diagnostic techniques and test methods under field conditions comprised major portion of the published literature. Among the various causes, corrosion of reinforcement in concrete, and alkali-aggregate reaction commanded greater attention.

In such a situation, our capability of building durable concrete structures can not have a one-to-one relationship with the number of research papers published. On the other hand, the relatively large number of papers dealing with deterioration of concrete structures in service indicate that there must be reasons because of which concrete is not always durable.

In this presentation, we will seek possible answers to this question. The present state of knowledge on chemical aspects of durability of concrete will be gone through to identify any gaps in knowledge and, therefore, the approaches required to improve the situation. No attempt will be made to present a comprehensive state-of-art review, or even to cover all aspects of concrete durability. In particular, the subjects of freeze-thaw resistance or resistance to de-icing salts and salt scaling etc. will not be covered, primarily because of the author's lack of familiarity with such field problems.

At the time of preparation of this presentation, it was not possible to take into account the papers in the Proceedings of this Congress. No doubt, there will be many contributions devoted to the issues raised in this paper, which will form a complementary knowledge-base.

BASIC CHEMICAL REACTIONS OF DETERIORATION OF HYDRATED CEMENT PASTE

In so far as cement systems are concerned, the response of the hydration products of portland cement comprising CaO - SiO_2 - H_2O and CaO - Al_2O_3 - H_2O in presence of $CaSO_4$, to the principal deteriorating agencies like sulphate (SO_3^{--}), chlorides (Cl^-) and carbon-di-oxide (CO_2) are well documented (Mullick and Chandra, 1992). The basic

chemical reactions, which are widely reported in the literature are depicted in **Fig. 1**. The products of hydration of cement are mainly C-S-H, C-H and C-A-H. While calcium hydroxide and calcium aluminate hydrates are the fast reacting components of the cement pate, C-S-H is also subject to attack by all the three aggressive ions in differnt degrees. In many cases, the type and extent of reaction depends upon the cations.

Sulphate attack on concrete follows two principal reactions; formation of gypsum ($C\bar{S}$) in reaction with CH and reaction of $C\bar{S}$ and C-A-H to form ettringite, Magnesium sulphate reacts, in addition, with the C-S-H phase leading to its decalcification i.e. substitution of Mg^{+} for Ca^{+}, and formation of M-S-H and other expansive salts identified above. Foramation of MH (brucite) in sea-water has also been reported (Van Derwegen et al, 1993). When alkali sulphate concentration is high and conditions are favourable, formation of mirabilite ($N\bar{S}H$) takes place (Mehta, 1993).

Besides being the principal cause of reinforcement corrosion, chloride salts react with hydrate phases also. Reaction of chlorides with hydrates of C_3A and C_4AF, forming Friedel's salt and its ferrite analogue is the primary reason of 'chloride-binding', which will be discussed later on. Magnesium chloride leads to ion exchange between calcium and magnesium. Calcium chloride reacts with cement hydrates to form expansive compound calcium oxychloride ($3CaO, CaCl_2, 15H_2O$) (Collepardi et al, 1994).

CO_2 in air or dissolved in water reacts with calcium hydroxide forming calcium carbonate. It also can react with other products of cement hydration, leading to formation of calcium carbonate and hydrated silica, alumina and ferric oxide. For example, total carbonation of C-S-H can lead to formation of calcite and amorphous silica (Kobayashi et al, 1994). Formation of thaumasite has also been reported. In all such reactions, OH^{-} is consumed, thus lowering down the pH of pore solution.

One may hasten to add that the above description of the mechanism of action by individual ions on individual phases of hydration of cement is rather simplistic. In reality, considerable synergistic interaction takes place. This is discussed further in subsequent sections.

Delayed Ettringite Formation

Once hydrated cement paste in concrete has set and hardened, any appreciable expansion at a later stage can give rise to disruption under conditions of restraint. In recent years, a number of cases of premature cracking and failure of concrete structural elements, which were steam cured, have been reported. The distress has been identified to be caused by formation and reformation of ettringite (Day, 1992, Taylor, 1994, Diamond, 1996). In cement, hydration of C_3A takes place in the presence of gypsum in C_3A - $CaSO_4.2H_2O$ - H_2O system. Ettringite begins to form after 15 minutes. It may later on get converted to monosulphoaluminate hydrate in reaction with uncombined C_3A. Kalousek and Adams (1951) had pointed out that such hydrated sulphoaluminate phases rapidly become undetectable, when the cement paste is cured at a temperature of $70^{o}C$ or above. On dissociation of ettringite, the released sulphate ions enter the pore solution, remain in

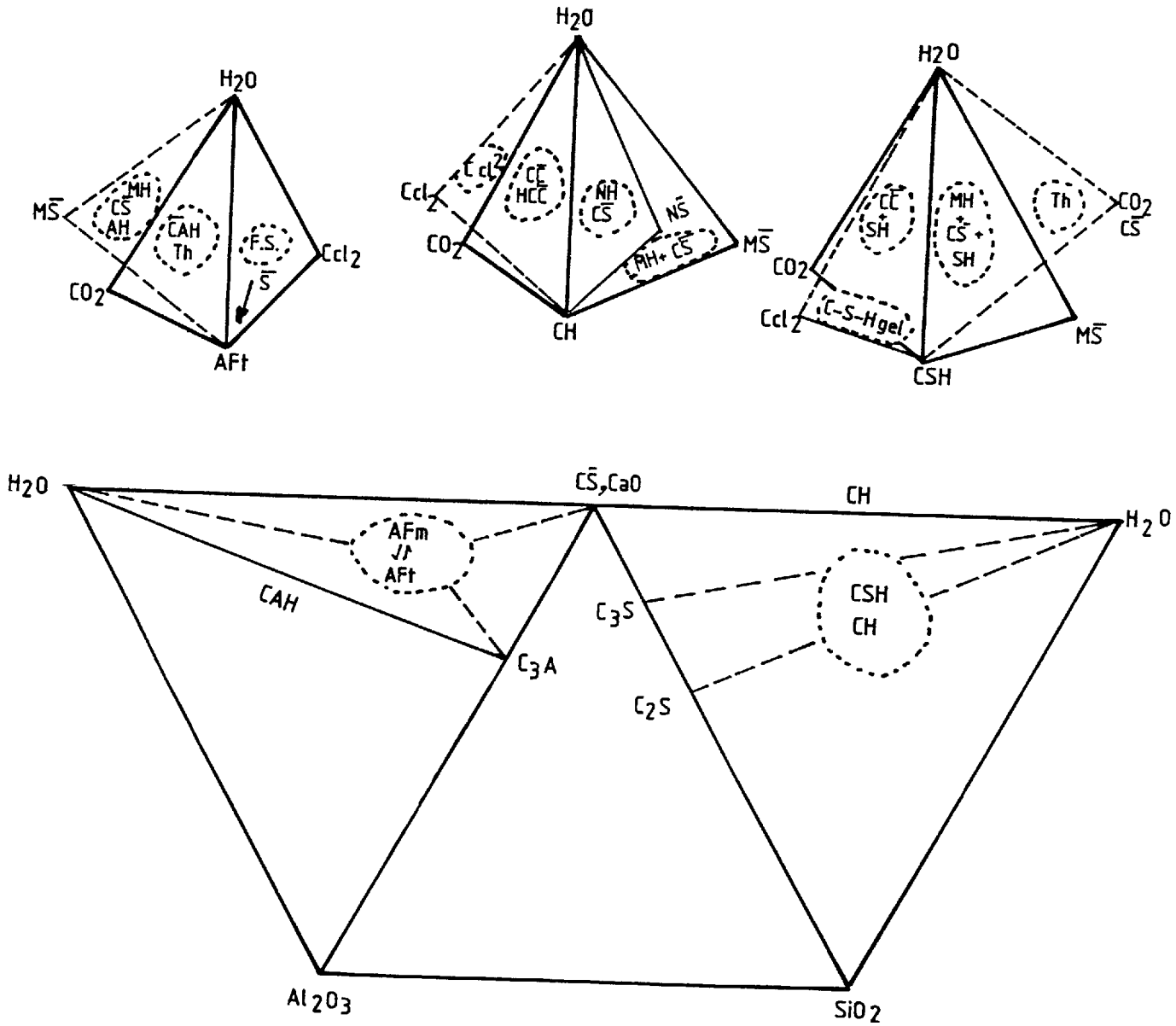

LEGEND

CSH – CALCIUM SILICATE HYDRATES

$C\bar{S}$ – $CaSO_4, 2H_2O$

AFt – ETTRINGITE

AEm – MONOSULPHO ALUMUNATE HYDRATE

$\bar{C}AH$ – MONO CARBOALUMUNATE HYDRATE C_3A, $CaCO_3, nH_2O$

$C\bar{C}$ – $CaCO_3$

$M\bar{S}$ – $MgSO_4 .5H_2O$

MH – $Mg(OH)_2$

NH – NaOH

CH – $Ca(OH)_2$

AH – $Al(OH)_3$

SH – $SiO_2 \times H_2O$

Th – $\left\{ \begin{matrix} Ca\ Si(OH)_6\ 12H_2O \\ SO_4\ CO_3 \end{matrix} \right\}$

F.S. – $C_3A\ Cacl_2\ 10\ H_2O$

$HC\bar{C}$ – $Ca(HCO_3)_2$

Fig. 1 : Basic Chemical Reaction of Aggressive Ions on Hydrate Phases

monosulphoaluminate form or get adsored in the C-S-H phases. When the hydrated cement, after heat treatment, is stored in water or in saturated condition at ordinary temperature, ettringite is again formed (Taylor 1994). This phenomenon is called 'delayed ettringite formation' (DEF).

Precast concrete products, which are steam-cured for early demoulding, have been reported to have suffered distress due to delayed ettringite formation, typically along with occurence of alkali-silica reaction (ASR) (Shayan and Ivanusec, 1996, Mielenz et al 1995). In such cases, recrystallised ettringite is noticed as bands around aggregate (Taylor 1994), or filling up voids and cracks in the mortar phase or mortar-aggregate boundaries (Shayan and Ivanusec, 1996).

Taylor (1994) has pointed out that expansion due to DEF per se is a relatively weak effect. According to him, expansion and cracking due to DEF can be either very slow or non-existent, unless some other process like ASR, freezing and thawing, microcracking caused by the applied loading or the thermal curing etc. has initiated the damage. On the other hand, Yang et al (1996) have reported that cement pastes cured at $100^{o}C$ and then stored in room temperature, showed expansions after relatively longer storage under water. According to them, DEF expansions in cement pastes did not depend upon presence of aggregate particles or presence of extreneous cracking due to ASR or freezing and thawing etc., although such factors can reduce the induction period for expansion. They postulated that secondary ettringite crystallising in such cases cannot intermix with the outer product C-S-H gel and are forced to occupy voids and the inner zones or form crystalline ettringite bands, which causes expansion of cement pastes.

Diamond (1996) has stated that delayed formation of ettringite in heat cured concrete followed by moist storage under normal temperature is not different from secondary ettringite formed due to excess sulphate or other factors in concretes cured under normal temperature all through, and both show similar pattern of cracking and ettringite deposition. According to Diamond, the observed crack pattern is that of a network with component crack segments running partly along boundaries of aggregates and connecting crack segments through cement paste. The pattern appears to reflect local and inhomogeneous crack propagation rather than general and homogeneous expansion of cement paste. Diamond (1996) emphasised that stress concentration effect associated with ettringite crystallising in cracks or precipitating near crack trips make association of DEF with prior cracking caused by ASR, freezing and thawing or load effects fundamental to the DEF process.

Unsoundness due to Free Lime and MgO

Another source of delayed expansion in concrete is due to hydration of free (uncombined) lime, MgO and calcium sulphate phases in cement, which is commonly known as 'unsoundness' of cement. All national Specifications prescribe accelerated test for unsoundness. Le Chatelier test involves expansion of neat cement paste under boiling water which measures unsoundness due to presence of free lime. Autoclave test involving high temperature and pressure conditions is indicative of expansion due to crystalline MgO phase as well as due to free lime. Because of strict enforcement of Specification requirements, no unsound cement is likely to have been used in constructions. Thus, actual performance of unsound cements under service conditions is

difficult to obtain. Criticisms of soundness tests, mostly autoclave test, arise due to the differences in the hydration products formed under high pressure steam curing, which are different from those formed under normal temperature, and lack of correlation between laboratory test and field perforamance (Mehta, 1977).

Dead burnt CaO and MgO, if present in cement, exist as intercrystallised with the silicate phases. Their hydration reactions are, therefore, delayed and remain localised, and the Ca^{2+} or Mg^{2+} hydroxides formed cannot be dispersed. The surrounding cement paste is partly or fully saturated with alkaline solution, which allows diffusion of Ca^{2+} or Mg^{2+} and OH^- ions out of the supersaturated solution surrounding the hydrated $Ca(OH)_2$ or $Mg(OH)_2$ phases. The slower the rate of hydration of CaO and MgO, as under normal service conditions, the more will be the diffusion and lower will be the effective supersaturation, the crystal growth pressure and hence the expansion.

Chatterjee (1995) has explained that during the autoclaving of the neat cement bars, both the hydration of free oxide and the elongated growth of hydroxide occur simultaneously and quickly. There is no time for diffusion of ions and the lowering of supersaturation. This causes the sharp rise in expansion in the autoclave tests. In the case of water storage, the free oxide particles hydrate slowely and there is the time for the diffusion of ions away from the hydrating oxide particles. This diffusion of materials not only reduces the supersaturation but also removes Ca^{2+}, Mg^{2+} and OH^- ions from the neighbourhood of the hydrating oxide particles, thereby reducing the material source for elongated growth.

The limit of MgO content in OPC is set at 6% in cement Specifications in India and some other countries. This is because of presence of somewhat higher amount of MgO in limestone in some deposits. Together with this, free lime content in Indian cements tend to be somewhat higher, due to marginal quality of raw materials and fuels, that have to be used in some situations. Thus, soundness test by both Le Chatelier and Autoclave are prescribed in IS-Specifications. In order to offset the unsoundness in autoclave test due to presence of free lime, in case a sample fails in autocalve test, aeration of the sample is now permitted before retest. Such aeration is permitted in Le Chatelier test in many countries. The permissible expansion in the aerated sample is lowered to 0.6% i.e. 75% of 0.8% in unaerated samples. Typical results obtained in India shown in **Fig. 2** indicate that in many cases, the samples satisfied the specification requirement of expansion after aeration, even if the expansion were greater than the permissible limit the first time i.e on unaerated samples.

In an on-going investigation on the effect of unsoundness of cement, long-term expansion behaviour of concrete under moist storage conditions, made with two cements which showed unsoundness in Autoclave test, are monitored (NCB, 1997). One cement, prepared in the laboratory, contained 6.1 percent MgO; the other, commercially produced, contained 5.2 percent. Expansions upto three years are shown in **Fig. 3**, which indicate linear expansion upto 0.085 percent in concrete. In absence of any established limiting value, the magnitude of expansion can be compared with those prescribed for other deleterious reactions. For ASR, limiting expansion in concrete prism test as per

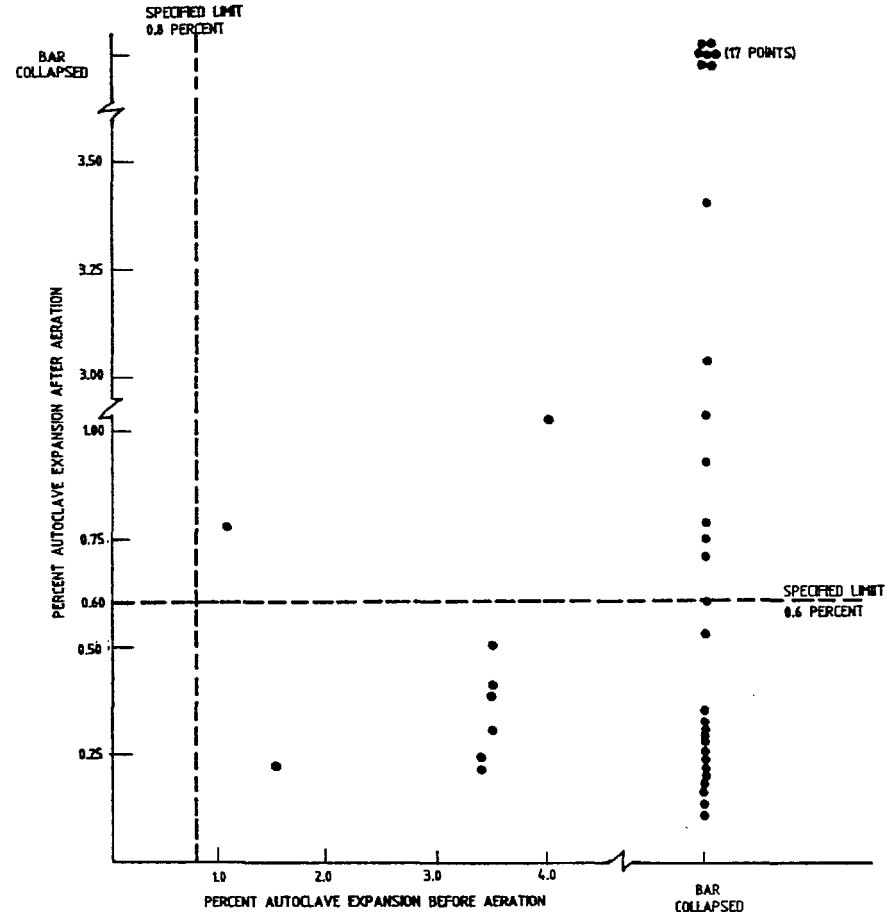

Fig.2 Effect of Aeration on Autoclave Expansion of Unsound Cements

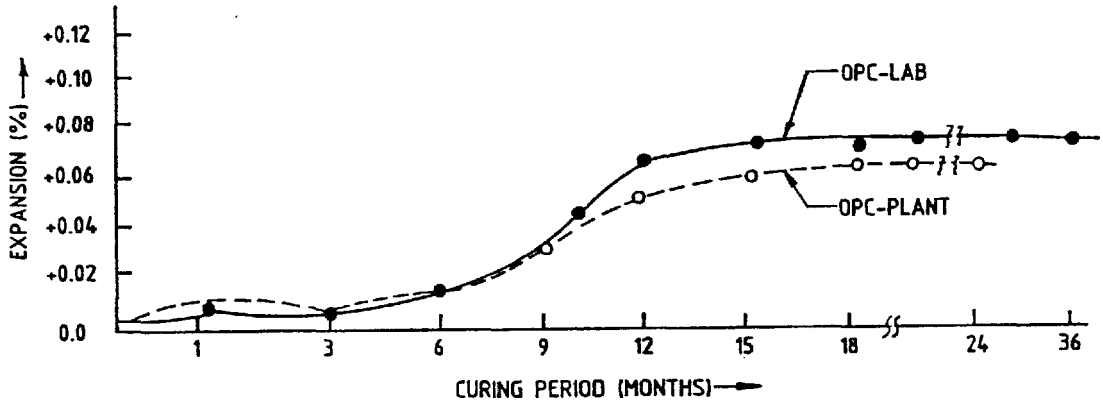

Fig.3 Expansion in Concrete made with High MgO Content under Water Storage

ASTM 1293-95 is held at 0.04 percent, which is lower than what has been obtained with unsound cements. However, no signs of cracking or external distress, neither any retrogression in compressive strength are noticed. Products of hydration of cement

containing 6.1% MgO in normal water storage indicate the presence of C-S-H,CH, ettringite and Brucite (**Fig. 4**). Remains of unreacted MgO after three years of hydration are also detected on XRD, (NCB 1997), which is not shown here. These results are presented with the hope that the significance of accelerated laboratory tests on unsoundness of cement and implications of using such unsound cements in constructions are assessed to a greater extent than done so far.

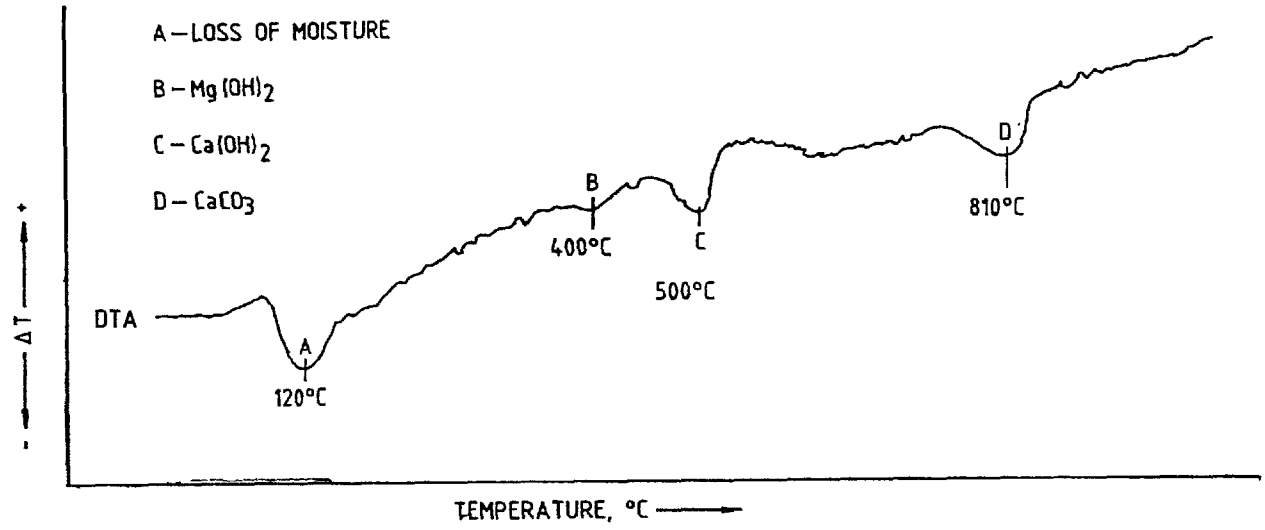

Fig.4 DTA of Hydrated High MgO Cement

Biodeterioration and Environmental Pollutants

Degradation of concrete is caused by biological components including bacteria, spores or fungi, as well as pollutants in the environment (Mullick and Chandra, 1992). The gaseous pollution include SO_2 and NO_2, whereas particulates include SO_4^{2-}, NO_3^-, Cl^- and NH_4^+ besides inorganic matters. Measurements indicate concentrations to be greater during winter months and in open exposures, than in dry months in covered areas (Rendehl et al, 1996). The pH of the leaching solution from the particulates was in the neutral interval (8.37 - 6.13), but during rain periods in open exposure, pH was found to be in the acid interval (7.33 - 3.82).

Both the acidic nature of the environment and ions like sulphates, chlorides and ammonia are known to be aggressive to concrete. NO_2, in association with SO_2, can produce H_2SO_4 in presence of H_2O. Energies like heat and light activate pollutant gases, aerosols and liquids, which can become detrimental to concrete (Chandra, 1990). Samples of concrete from a damaged bridge has shown the presence of reaction products like calcium monosulphoaluminate, carbo-aluminate, chloro-aluminate hydrates, calcium oxy-chloride etc., which were reported to be indicative of attack by atmospheric sulphurous oxides, chlorides and carbon dioxide (Chandra, 1996).

Microscopic examination by SEM of concrete samples from deteriorated structure, 7 to 30 years old, have shown signs of biological deterioration by micro-organisms, which

were yet to be fully identified (Rivas Silva, 1996). The envrionmental humidity varied from dry (12% RH) to moist, and temperature moderate (20°C) to cold (0°C). Microsocpy of concrete samples allowed observation of many morphologies, some of which were identified as micro-organisms. These were in the form of cells, strings and empty tubes etc. In addition, bacteria like Thiobacillus which oxidises iron, and Notrobacteriae, which dissolve Ca-bearing compounds, were observed. Although the identity of the micro-organisms were not established, the metabolism responsible for different kinds of deterioration of concrete observed were postulated (Ribas Silva, 1996).

The extent of deterioration due to atmospheric gases and particulates is location - specific and found to depend upon the level of industrial pollution. Comparing the extent of deterioration of C-steel, zinc, copper and sandstone in old structures located in Stockholm, and in Prague, the corrosion rates were found to be greater in the city, which was more polluted (Rendahl et al, 1996). Risk of distress due to corrosion of reinforcement in concrete has been estimated to be greater in the principal cities of Japan where the pollution is heavy than in some locations where the degree of air pollution is extremely low (Morinaga, 1996).

AGGREGATES AND REINFORCEMENTS IN CONCRETE

Apart from deterioration of the hydrated cement paste itself, considerable attention is paid to the role of hydrated cement paste or the mortar to protect the reinforcement or the aggregates in concrete. The results are distress to concrete structures due to the corrosion of reinforcement and chemical reaction with aggregates respectively. These are briefly discussed below.

Corrosion of Reinforcement

The basic mechanism of corrosion of steel as an electro-chemical phenomenon can be summarised in terms of an anode process and a cathode process (**Fig. 5**) (Mullick and Chandra, 1992).

Anode : Fe (metallic iron) $\longrightarrow 2e^- + Fe^{2+}$ ... (1)

Cathode : $1/2O_2 + H_2O + 2e^- \longrightarrow 2(OH)^-$ ... (2)

and the corrosion undergone by steel is due to combination of iron and (OH^-) ions;

$Fe + 1/2O_2 + H_2O \rightarrow Fe^{2+} + 2(OH) \rightarrow$ iron hydroxide (rust) ... (3)

The oxygen dissolved in water enhances corrosion when the pH is in between 4 and 10. For pH more than 10, reaction (3) takes the form :

$2Fe^{2+} + 3H_2O \longrightarrow Fe_2O_3 + 6H^+ + 2e^-$ ... (4)

$3Fe^{2+} + 4H_2O \longrightarrow Fe_3O_4 + 8H^+ + 2e^-$ ... (5)

For transformation of metallic iron to rust, iron must be available in a metallic (Fe) state at the surface of the reinforcing steel; oxygen and moisture must be available for the

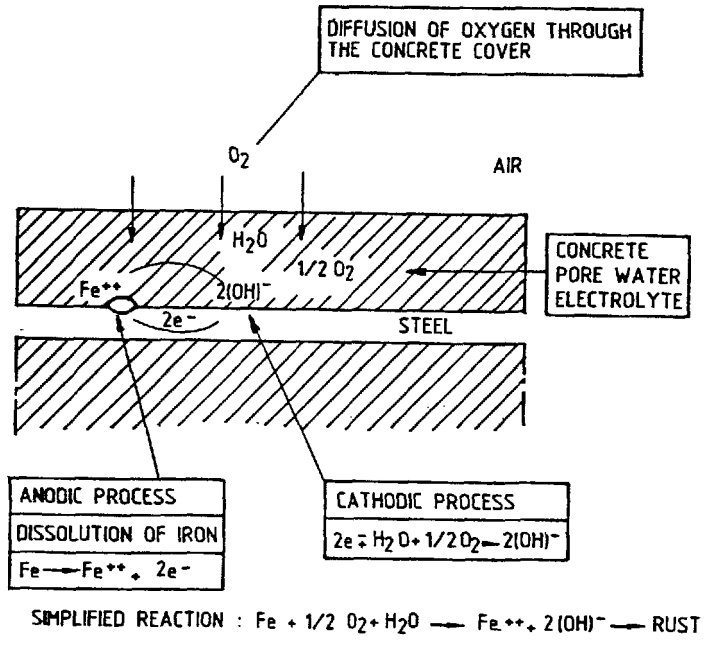

Fig.5 A Simplified Model of Corrosin of Steel in Concrete

cathode process; and the electrical resistivity of concrete must be low to facilitate the electron flow in the metal from anodic to cathodic areas.

From engineering stand point, two types of situations are necessary to be considered. The steel reinforcement, being well protected in the alkaline medium in concrete, would take a certain amount of chloride ion to be present in order that corrosion can take place. On the other hand, if the passivity is destroyed because of one reason or the other, and the pH of concrete is lowered below a certain threshold value, all that is needed for corrosion to take place is oxygen and water, and presence of chlorides is not necessary. Concrete constructions, in order to be durable, have to ensure that the limiting amount of chloride ions is not exceeded in concrete and neither the pH value of concrete is lowered below the threshold value. Practical limits of tolerable chloride ion concentration and limiting pH value are best arrived at by in-service record of concretes.

Chloride ion concentration present in the pore water in an equilibrium situation depends on the other ions present in the pore water; for example, at a given total chloride ion content, the higher the hydroxyl (OH^-) concentration the more free chloride ions are present (Neville, 1995). For this reason, the Cl^-/OH^- ratio is considered to affect the progress of corrosion. The significance of this parameter is discussed later.

Alkali-Aggregate Reaction

In so far as chemical reactions involving aggregate are concerned, expansive reactions entitled alkali-aggregate reaction (AAR) have commanded major attention, although othere reactions involving oxidation of ferrous iron, pyrites or marcasite in aggregate have been reported (Mullick and Chandra, 1992). Chemical reactions between

aggregate containing certain reactive constituents and alkalies and hydroxyl ions released by the hydration of cement can have deleterious effects on concrete. Alkali-silica reaction (ASR) involves rocks and minerals containing reactive forms of silica. Expansion and cracking, leading to loss of strength, elasticity, and durability are among the physical manifestations of ASR. Mehta et al (1992) have identified amorphous silica (e.g. opal), microcrystalline and poorly crystalline silica (e.g. chalcedony), fractured or strained quartz and glassy silica (e.g. andesitic and rhyolitic glasses) as among the commonly known alkali-reactive forms of silica. Depending on the alkali content of cement and the water-to-cement ratio, the pH of the liquid phase in a hydrated portland cement may be 13 and above. Mehta et al (1992) point out that minerals containing silica with a disordered structure would not remain stable in such a strongly alkaline solution. According to them, depending on the degree of disorder, porosity, particle size, and temperature, the deploymerization of silica structure (i.e. dissolution of O-Si-O bonds) will gradually occur, followed by adsorption of the alkali-metal cations on newly created surface of the reaction product. When in contact with water, the alkali-silicate gels swell by sorpotion of water through osmosis. The hydraulic pressure so developed is believed to cause expansion and cracking of the affected aggregate particle, and subsequently the cement paste matrix surrounding it.

Effects of Pozzolana and Slags

Beneficial effects of incorporation of pozzolanic materials like flyash, silica fume or latent hydraulic materials like slag on corrosion of reinfocement and alkali-aggregate reaction have been intensively researched in the recent times. Such beneficial effect in improving the durability of concrete results from formation of dense CSH microstructure, modifications of the pore structure and pore size distribution, lowering the conductivity of concrete and aiding chloride binding etc. The alleviation of alkali silica reaction due to addition of flyash or silica fume is considered to be due to the arrest of alkali ions in the CSH product formed by pozzolanic reaction, which is of lower C/S ratio, in which alkalies from cement can be incorporated. Pozzolona and slag themselves contain alkali; however, these are not supposed to participate in promoting alkali silica reaction and only a fraction of the alkali from pozzolona and slag are supposed to be at par with the alkali derived from ordinary portland cement in causing alkali silica reaction.

Although flyash, slag and silica fume are being used in concrete constructuions for a long time, reports of performance of such structures in service are rather limited. Performance of concrete structures like dams, raod bridges, foundation blocks and concrete tank walls in the United Kingdom, incorporating flyash have been reported by Thomas and Mathews (1993). Results of tests on field samples indicated that while the 28-day concrete strength of concrete incorporating flyash was lower than OPC concrete, strengths at later ages were higher. OPC concrete was more permeable than flyash concrete, sometimes upto 20 times. Flyash concrete showed greater resistance to penetration of chloride ions. There were no signs of ASR in concrete dam using flyash, where the aggregate was reactive and which have resulted in ASR in an OPC concrete dam. It has been a practice in Iceland since last two decades to intergrind silica fume in cement, to mitigate the effects of severe ASR taking place in that country. On the basis of periodic condition surveys, it has been reported that no cases of ASR damage have been found in Icelandic structures built since such a practice began (Gudmundsson and Olafsson, 1996).

Chloride Binding

Chloride ions reside within the concrete system with different amounts of fixicity. Part of the chloride ions remain free in the pore water solution, whereas the remaining part is bound to the products of hydration of cement by adsorption and chemical reaction (Tang and Nilsson, 1993). The phenomena of thus fixing a part of the chloride ions is called 'chloride-binding' capacity of concrete. As a very general rule, bound chloride in ordinary portland cement paste may vary from 40 to 60 percent of the total chloride ions present. Chloride binding by sorpotion is reversible and can be desorbed following drying. Fixation of chlorides in the hydration products follows the progress of hydration of cement. It is thus a function of time.

Such chloride ions which are chemically combined, react with products of hydration of C_3A, forming calcium chloroaluminate hydrate, and its ferrite analogue with C_4AF - phase. In addition, these are physically adsorbed to the pore surface. Chloride ions also get absorbed to the surfaces of pozzolonic additons like flyash etc and enter into chemical reaction with its aluminate phase. As a result, the chloride binding capacity of concrete increases with the C_3A content in the cement, as well as by addition of flyash, slag and silica fumes etc. (Nagataki et al 1993, Dhir et al 1994). Increase in alkali content in cement was found to decrease chloride-binding (Al-Gahtani et al, 1994).

The actual proportion of bound chloride depends upon a number of factors and can change with temperature or humidity. Stability of calcium chloro-aluminate hydrate in the presence of sulphate ions is not fully established and there are stipulations that ultimately such bound chloride ions end up with the formation of calcium sulphoaluminate hydrate in case of simultaneous presence of SO_3^{--} ions, thereby once again increasing the proportion of free chloride available for corrosion process (Neville, 1995). Atmorpheric carbonation leads to increased solubility of Friedel's salt, thereby incrasing the amount of free chloride (Suryavanshi and Swamy, 1996). Talib et al (1994) reported lower chloride binding with increase in temperature.

POSSIBLE REASONS OF INADEQAUTE PERFORMANCE

According to Mather (1994), the procedure for obtaining concrete that will result in desired performance is simply to include the relevant requirements in the contract document and ensure through proper owner quality assurance and contractor quality control that the requirements of the specifications are followed. In other words, **order the concrete that you need and make sure that you get it**. The basic approach to work out appropriate specifications for durable concrete were summarised (Mullick and Chandra, 1992) as;

* characterise the service environment in totality,
* determine severity of environment,
* make concrete impermeable,
* ensure appropraite workmanship, design and detailing

With such a basic approach in view, any instance of insufficient durability of concrete can lead to two possible questions;

* **Was the specification of concrete appropriate to ensure durability under the given service environment?**

* **Were the requirements of the specification adhered to in practice?**

While the first question relates to the overall perception of the issues governing the durability of concrete; the second question is perhaps somewhat easier to answer. It has to be admitted that distress to concrete structure is quite often due to non-adherence to the requirements of specifications. The areas of non-compliance not only relate to use of appropriateness of ingredients of concrete and adequacy of mix proportions, but also to workmanship, notably placing, compaction and curing of concrete.

One major requirement for durability is to make concrete as impermeable and as water-tight as possible. Since presence of moisture is required for most of the chemical reactions, use of as low a water-cement ratio as possible, is helpful. The water permeability of concrete has been tested on laboratory specimens and related to porosity and pore size distribution in the microstructure of the hydrated cement paste. Influences of addition of flyash, slag, silica fume etc and incorporation of chemical admixtures have also been studied. However, in absence of adequate campaction and moist curing, the amount of voids that can be left in the concrete at a macro-scale are much more serious. Poor workmanship, poor quality of concrete, and inusfficient concrete cover to steel reinforcement are quite often reported to be the main causes of deterioration in most cases. Poor placing and compaction techniques result in variable cement content in hardened concrete, variations in ultrasonic pulse velocity and thickness of cover to reinforcement at different locations in the structure. Such locational differences in the quality parameters can themselves set up electro-chemical corrosion cells (Mullick and Rajkumar, 1993).

Depth of carbonation is a good indicator of the health and quality of structural concrete. In sound concrete, the depth of carbonation under normal situations can range from 1 to 6 mm per $(\text{year})^{1/2}$. For a 25 years old concrete, 5 to 30 mm carbonation depth can thus be expected, depending upon the service condition and quality of concrete. Measurements of depth of carbonation ranging from 10 to 65 mm in concrete structures in India, as obtained in our laboratory, or 11 to 66 mm as reported for structures in Singapore and Malaysia (Wong et al. 1993) have been reported. Even allowing for uncertainty in the estimation of carbonation depth using phenolphthalein (Chandra, 1996) under field conditions, these values are much in excess of what is normally expected and thus point to serious deficiency in field practices. Concrete under such a situation cannot be expected to be durable. We will leave it at that.

SPECIFICATION FOR AN INTERACTIVE SYSTEM

In search of possible reasons of non-performance, it is necessary to recognise the interactive nature of various factors and the extent, to which the specifications for concrete cater to these. A System's approach to durability of concrete has been advocated (Mullick and Chandra, 1992). In such a system, deterioration of concrete is seen to be due to a number of causative factors, aided by a host of promoting and accelerating factors. A simple example is of sea-water containing both sulphates and chlorides of various cations; or the soil or ground water in many situations entrain more

than one type of salt, In reality, the micro-environment in an element in concrete is subject to interaction between various chemical and environmental factors and the system is more complex. In many cases, the interaction is synergistic.

Interaction between Aggressive Ions

The products of hydration of cements and attack on these by various aggressive ions, which were discussed before, are such that their stability can be altered by ionic substitution, complexing or forming solid solution. In addition, the kintics of reaction and equilibrium are governed by the hygrothermal conditions. Some examples below will illustrate the point.

* Sulphate attack in concrete due to SO_3^{--} ions, can be significantly mitigated by concommitant presence of high concentration of chlorides (Al-Amoudi, 1995).

* Simultaneous presence of SO_3^{--} ions enhance the risk of corrosion of reinforcement due to Cl^- ions. This takes place due to the competing reactions on C_3A phase of cement both by Cl^- and SO_3^-, thereby reducing the formation of Friedel's salt (which bind chloride ions) and leading to formation of ettringite. This increases the concentration of free chloride ions in pore solution (Saleem et al, 1996).

* Electrical resistivity of concrete, for a given moisture content, was found to be lower in presence of NaCl plus Na_2SO_4 than in presence of NaCl or Na_2SO_4 alone (Saleem et al, 1996).

* Atmospheric carbonation reduces the stability of Friedel's salt and ettringite (Suryavanshi and Swamy, 1996). Ettringite is even less stable in sea water, which contain more than normal CO_2 (Mehta, 1993).

* Simultaneous presence of SO_3^- as Na_2SO_4 increases the alkalinity of the pore solution, which inhibits chloride-binding (Al-Amoudi et al, 1994).

* Synergistic effect of SO_3^- ion on chloride ingress in portland cement concrete is to decrease chloride penetration and diffusivity. Presence of CO_2 at the same time, decreases chloride diffusivity. However, in case of portland cement-slag blend, the effects of SO_3^- and CO_2 on chloride penetration were just the opposite (Tumidajski and Chan, 1996).

* Addition of alkali (KOH) resulted in increase in carbonation of concrete, the rate of carbonation increasing with increase in KOH content (Xu, Rodhe and Chandra, 1996). A catalytic effect of the alkali on carbonation was suggested.

* Extent of carbonation in cement mortar was found to be greater when exposed to a mixture of CO_2 and SO_2 gases, than when exposed to CO_2 alone (Chandra, 1996).

Interaction of Temperature and Humidity

Laboratory research on durability is generally carried out using concrete and mortar specimens under controlled hygrothermal conditions. The temperature is maintained within narrow ranges as per the national norms e.g. 18°C in Europe, 21°C in North America and 27°C in India. The specimens are maintained under moist storage conditions. In order to assess the performance of concrete under site conditions, the effects of temperature and relative humidity (RH), both ambient as well as in pore solutions, have to be taken into account. With increase in the operative temperature, all deleterious chemical reactions can be thermally activated and, therefore, the extent of reaction increases.

Chloride diffusivity of concrete is reported to increase with curing temperature (Detwiler et al, 1994). Increase in electrical conductivity of concrete and depth of carbonation with increase in curing temperature has also been reported (Moriwake et al, 1994). Increase in temperature can cause evaporation of free water from the concrete and lower the internal RH. Coarsening of pore structure takes place.

These bring out the improtance of appropriate moist curing under field condition. Moist curing of concrete beyond 7 days is seldom carried out. There are instances, when the actual curing was much more inadequate. Arafah et al, (1996) has reported that in Middle East countries with high temperature upto 45°C and low relative humidities of about 4 percent during summer, all that goes in the name of curing is actually sprinkling of water without burlap cover for one or two times a day. The effect of such curing practices are usually noted in terms of development of compressive strength. However, the effect of inadequate curing on parameters affecting durability are much more pronounced. Ramezanianpour and Malhotra (1995) have shown that continous moist curing was essential to achieve the highest strength, lowest porosity and the highest resistance to penetration of chloride ions. When concrete, after demoulding, was left to cure under ambient conditions of 38°C and 65 percent relative humidity, the poorest results were obtained.

The interactive effects of temperature and humidty are also manifest on the hydration of the portland cement paste and of mineral additions. Hydration of cement can take place only when the capillary pores are filled with water - either the mix water or curing water imbibed from outside. Hydration reactions cease when the relative humidity within concrete falls below 80% (Spears, 1983). In pozzolana having limited (lime) - reactivities, not much pozzolanic reaction take place even upto 28-days under moist curing (Mullick et al, 1986). When the reactivity of pozzolana is higher e.g. with silica fume, reactions are somewhat faster and even then, there will be an initial period for first few days when no pozzolanic reaction take place. Some contribution to the strength development can take place by the physical action i.e. filler effect.

Continuation of pozzolanic reactions is dependent upon the relative humidity. In Thomas' (1989) experiments, OPC and OPC/PFA pastes after curing for 1,3 or 7 days in $Ca(OH)_2$ solution, were kept at RH from 9 to 93% until the test age of 28 or 180 days and analysed for $Ca(OH)_2$ content and pore structure. It was found that in case of OPC, at RH below 81% the hydration of cement was severly retarded and appeared to cease

below 66% RH. In case of OPC/PFA pastes, at relative humidities of 81% and below, there was little evidence of any pozzolanic reaction at 28 days. However, at the age of 180 days, evidence for some pozzolanic reaction at the RH of 81% was found by a small reduction in the $Ca(OH)_2$ content of the paste. However, little on no $Ca(OH)_2$ depletion was detected in PFA pastes stored for upto 180 days at relative humidities of 66% even after initial curing period of 7 days.

From the foregoing it is clear that in relatively dry environments and after initial moist curing limited to less than 7 days or so, subsequent reaction with pozzolana, flyash or slag can not be realised to the fullest extent. Therefore, all the beneficial effects claimed to be obtained by such mineral additions will not be forthcoming. In particular, the limiting relative humidity can be such, which will lower the pore water pressure to a value of 0.8 or so, in which case, continued hydration reactions of OPC will also be hindered.

Since most of the deleterious chemical reactions like corrosion of reinforcement, sulphate attack and alkali-silica reaction can take place only in the presence of sufficient moisture, the relative humidity of concrete is also important from the deterioration process. Mather (1994) has said that any concrete will be durable regardless of other considerations, if it is allowed to get dry and stay dry. He said that 'dry' in this context means that the evaporable water is allowed to and does escape, and the internal realtive humidity drops below 80 percent, under which conditions there are no longer any chemical reactions that can take place and there is no water that can freeze.

There is wide occurance of corrosion of reinforcement in concrete reported in the Indian subcontinent (Mullick and Rajkumar 1993) as well as from the Middle East (Rasheeduzzafar et al, 1992) where the environments are dry. The question is, is it not dry enough to stay the process of corrosion of reinforcement or sulphate attack ? The same holds for alkali-silica reaction, which have traditionally been associated with hydraulic structures like dams where the concrete is either in contact with water or exposed to moist conditions and high relative humidities. Stark (1991) have shown that internal relative humidity of concrete inside concrete pavements built in arid desert regions of California was of the order of 80 percent and alkali-silica reaction did take place. Similar experiences have also been noted in massive tubro-generator foundation blocks in India, where alkali silica reaction of concrete was noticed, when reactive aggregates were used and the cement content was relatively high (Mullick 1994). In other words, there is an area of uncertainty in relation to relative humidity condition inside concrete which may be low for the beneficial pozzolanic raction to take place, but may not be low enough to stop the deleterious chemical ractions.

Carbonation does not take place either in saturated concrete or in dry condition - it is greatest in intermediate values of relative humidity of the order of 65% (Ewertson and Petersson, 1993). Widespread carbonation of concrete and corrosion of reinforcement are notied to go hand in hand (Mullick and Rajkumar, 1993). Clearly, corrosion of reinforcement do take place in such intermediate RH values, which also support carbonation of concrete. Enevoldsen et al (1994) reported that active corrosion did not

take place below a threshold internal humidity, which was estimated to be 80% from laboratory data and about 70% ambient in the field.

Browne (1982) has stated that concrete resistivity must fall below 5000 to 10000 Ohm-cm in order to support reinforcement corrosion. Increasing moisture content of concrete, as indeed presence of chloride, or sulphate ions have been found to decrase the resistivity of concrete (Saleem et al, 1996). In addition, there is considerable interaction due to simulateneous presence of chloride and sulphate ions. For a given moisture content of concrete, the electrical resistivity was the lowest when both Cl^- and SO_4^- ions were present together than when present singly. Typical results are reproduced in **Fig. 6** and **Fig. 7**. The results showed that in presence of excess chloride ions, even in nearly dry concrete, there is chance of corrosion because of low resistivity. Decrease in electrical resistivity of concrete due to sulphate contamination was also a matter of concern, as the reinforcement corrosion in such situtations will be sustained due to carbonation (Saleem et al, 1996).

The highest corrosion risk is usually associated with concrete which is subjected to cyclic wetting and drying, not only at the concrete surface but also at the reinforcement. The reinforcement will under such conditions experience large local potential variations, since the potential is strongly affected by the oxygen concentration at the steel surface, which in turn is controlled by the moisture state. Large local potential variations are suspected to promote galvanic types of corrosion.

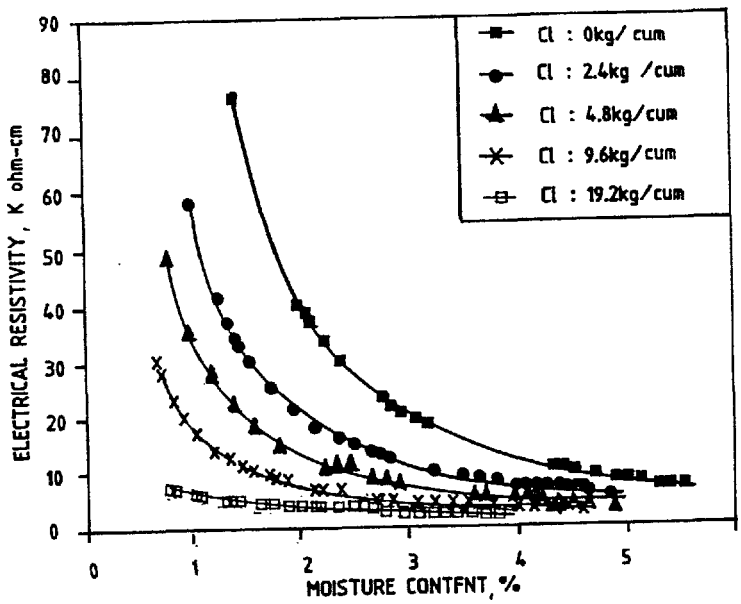

Fig.6 Relationship between Moisture Content and Electrical Resistivity in Chloride-contaminated Concrete (Saleem et al, 1996)

Prolonged drying in combination with saline wetting and drying causes salts to be transported into concrete by means of suction and diffusion (Sandberg, 1996). If the concrete dries at the reinforcement, the concentration of chlorides and other ions in the

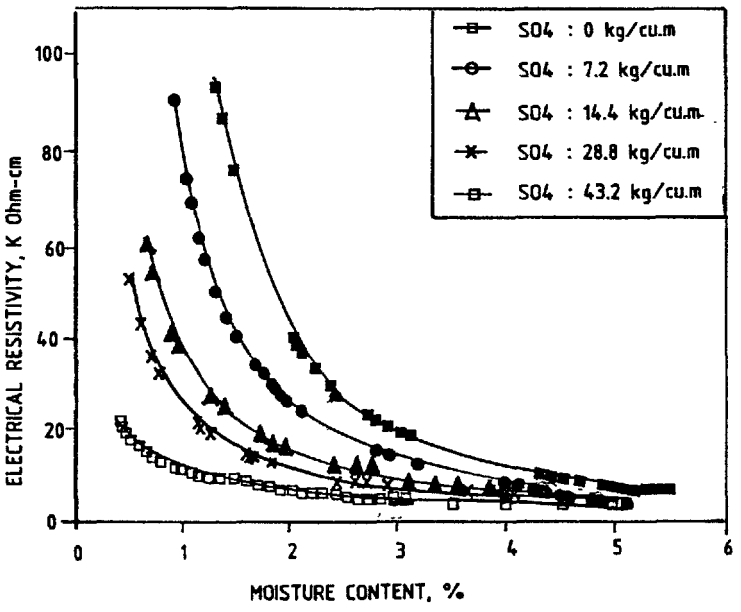

Fig. 7 Relationship between Moisture Content and Electrical Resistivity in Sulphate-contaminated Concrete (Saleem et al, 1996)

pore solution may thus increase. Besides the concentrating effect of solvent removal upon drying, the chloride adsorbing capacity of the cement gel has been found to decrase upon drying. Sandberg (1996) has stated that it remains to be investigated if it is the difference in passive steel potential (e.g. oxygen availability), or any shrinkage cracking at the interface between the reinforcement and the binder matrix, or the more concentrated pore solution, which is the main reason for the increased corrosion activity in concrete subjected to wetting and drying. From practical experience it is known that the moisture state and the thickness of the cover are of vital importance.

Cl - OH - CO_2 Interaction

For corrosion to take place in mild steel stored in the open, presence of only water and oxygen are required. Portland cement concrete provides protection to reinforcing steel by the highly alkaline nature of the pore solution. At high pH around 13, steel is passivated in the presence of oxygen by formation of γ- Fe_2O_3 film as well as the lime-rich layer at steel-concrete interface. Depassivation of steel can take place by the reduction of pore solution pH, which, in turn, is caused by carbonation as well as ingress of chloride ions. Clearly, there is an interaction between Cl^- - OH^- - CO_2, which is critical for corrosion of reinforcement in concrete to take place.

The relationship between chloride content and corrosion of steel depends upon the pH value. **Fig. 8** obtained from data on a large number of concrete structures in India damaged due to corrosion of reinforcement show that the amount of chloride ions that can be tolerated is higher, the greater the pH value and vice versa. In particular, Figure 8 indicates that depassivation was reached at a pH of about 10.

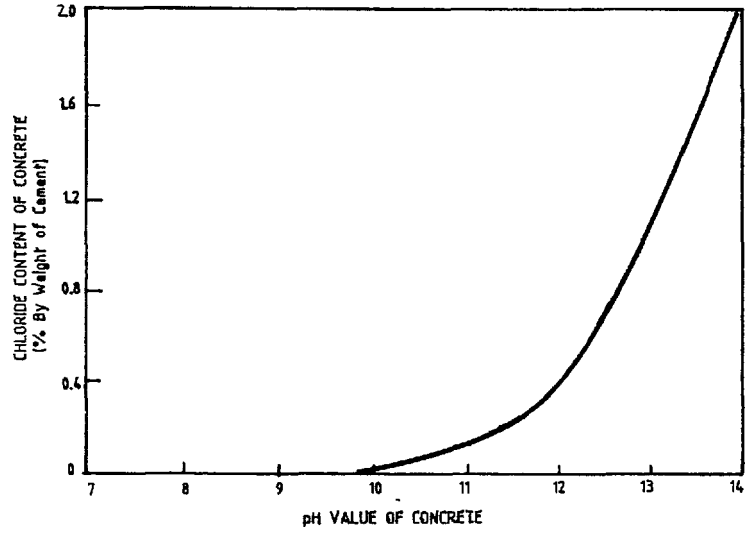

Fig.8 Interaction Diagram of pH Value and Chloride Content in Corrosion-damaged Concrete Structures in India

From corrosion point of view OH^- ion concentration is more important, the latter being related to, but not the same as pH value. The alkalinity in the pore solution in concrete is due to $Ca(OH)_2$ as well as C-S-H phases, the alkali and alumina etc. For pH value of 12.5 corresponding to calcium hydroxide solution, a threshold depassivation Cl^-/OH^- ratio of 0.60 was proposed (Hauzmann, 1968). For higher pH values obtaining in hydrated cement systems, the threshold ratio of Cl^-/OH^- will be lower than 0.60, and for lower pH values the ratio higher (Rasheeduzzafar et al, 1992).

Depending upon the chloride-binding capacity of the cement hydrates, the amount of free chloride ions available for corrosion to take place will influence the relevant Cl^-/OH^- ratio. The pH value of the pore solution itself is dependant on the amount of chloride ions; in general, presence of chloride ions which are acidic in nature lowers the pH value. On the other hand, fixation of chloride ions in the C_3A and C_4AF phases forming Friedel's salt and its ferrite analogue, will increase the OH^- ion concentration in the pore solution (Suryavanshi et al, 1996). Thus the net effect on alkalinity of the pore solution will depend upon the amount of chloride-ions and how much of it is fixed - i.e the same parameters governing the risk of corrosion of steel in concrete.

Carbonation is the primary cause of lowering of alkalinity. The pH value of concrete can be as low as 8.5 due to carbonation. Greater carbonation will lead to greater risk of corrosion. Suryavansi and Swamy (1996) have examined the effect of carbnonation on stablity of Friedel's salt. Typical results reproduced in **Fig. 9** and **Fig. 10** show that due to carbonation in the outer surface of the slab specimens (0-5 mm), both Friedel's salt and ettringite were absent. However, at depths 45-65 mm, where no carbonation had taken place, peaks corresponding to portlandite, ettringite and Friedel's salt were present. These results indicate that in presence of CO_2, the risk of corrosion is also increased due to dissolution of calcium chloro-aluminate and consequent release of chloride ions to pore solution.

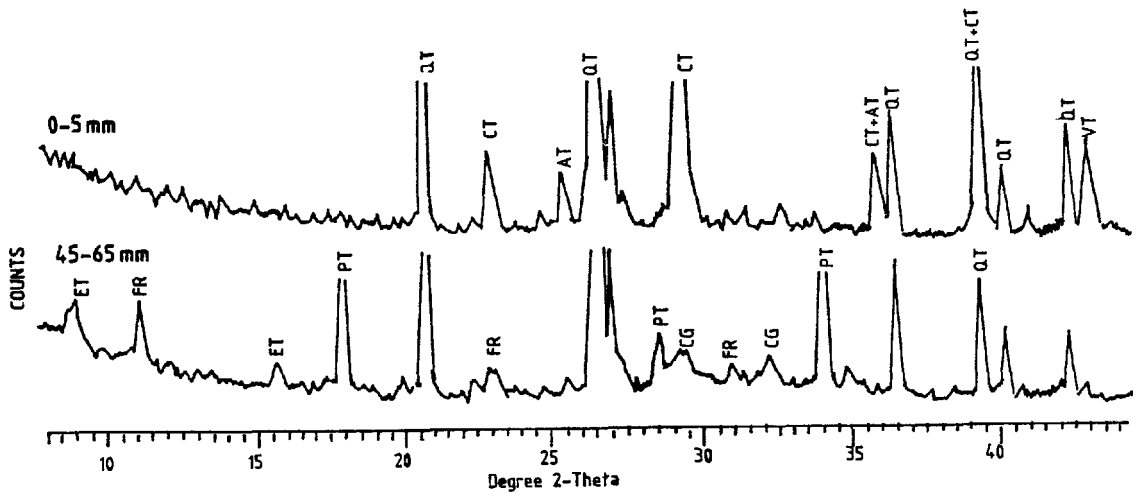

Fig. 9 XRD Diffractogram for Slab exposed to Carbonation
(Key: ET:Ettringite, FR:Friedel's salt. PT:Portlandite, QT: -Quartz, AT:Aragonite, CT:Calcite, CG:C-S-H gel and VT:Vaterite. The keys in bold letters indicate the 100% intensity peaks)
(Suryavanshi and Swamy, 1996)

Interactive effects of addition of flyash, slag and silica fume etc on chloride binding and pore solution chemistry are equally complex. Such mineral additions help in chloride binding due to physical adsorption. Because of reaction with $Ca(OH)_2$ liberated by hydration of cement, lowering of pH value is sometimes apprehended. However, presence of enough calcium ions in cement, in excess of what is required to combine with silica in cement and pozzolana, can ensure that a saturated solution of calcium

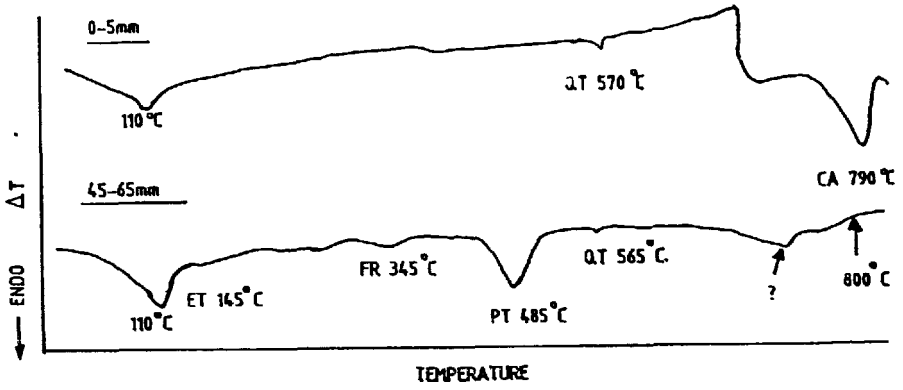

Fig. 10 DTA Thermograms for Slab shown in Figure 9
(Suryavanshi and Swamy, 1996)

hydroxide will always result (Mather, 1994). The alumina and alkalies in the pozzolana and slag also help in maintaining the required pH. Glasser (1989) has pointed out that, because of contribution of alkali content of slags and pH-buffer effect of residual

$Ca(OH)_2$ and C-S-H, the internal pH of slag-cement blends is well above the minimum likely to be required to provide passivation for steel reinforcements.

Rasheeduzzafar et al (1992), found that incorporation of 10 and 20 percent silica fume in cement pastes containing 0.6 percent Cl^- ions by weight of cement resulted in pore solution being 5 and 77 times more aggressive than in plain cement, and Cl^-/OH^- ion ratio much higher than the safe threshold value. A corrolary of higher Cl^-/OH^- ratio in the pore solution of flyash concrete compared with OPC concrete of the same total chloride content was that increasing flyash content was found to decrease the threshold chloride level for corrosion (Thomas, 1996). The threshold levels obtained were 0.70 percent acid - soluble chloride by mass of cement for plain concrete, which gradually decreased to 0.65% for 15% flyash, 0.50% for 30% flyash and 0.20% for 50% flyash added in the concrete mix. In both cases, incrasing the Cl^-/OH^- ratio of the pore solution did not necessarily result in greater ingress of chloride ions or greater corrosion taking place, due to improvements in the pore structure, dense microstructure and increased resistance to chloride ion penetration. Typical results obtained by Rasheeduzzafar et al (1992) and Thomas (1996) are reproduced in **Fig. 11** and **Fig. 12** respectively.

Thus, the actual result will depend upon the extent pozzolanic reaction take place, and the fixicity of chloride ions.

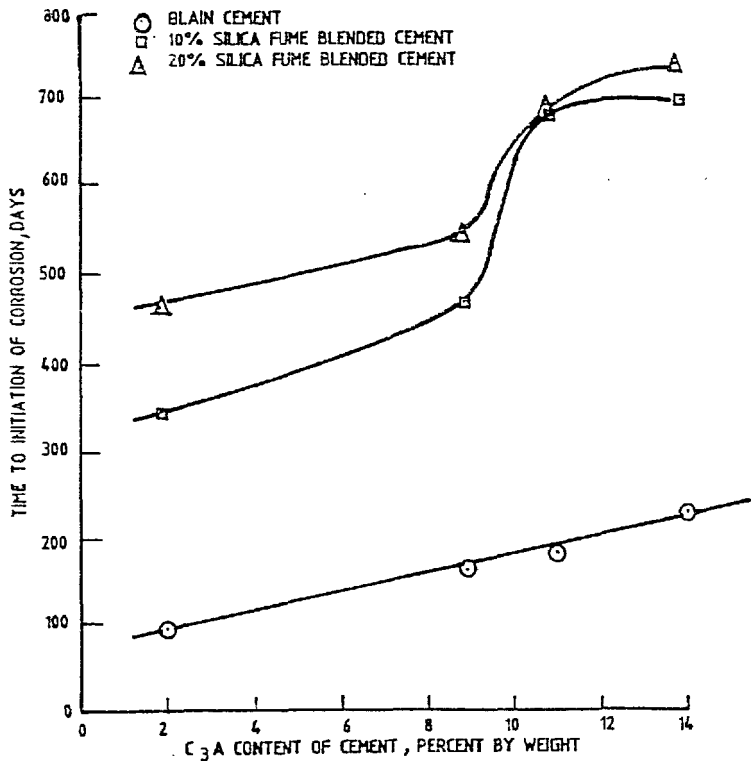

Fig. 11 Effect of C_3A Content of Cement and the Increasing Replacement of Cement by Silica Fume on Corrosion of Reinforcing Steel in Concrete (Rasheduzzafar et al, 1992).

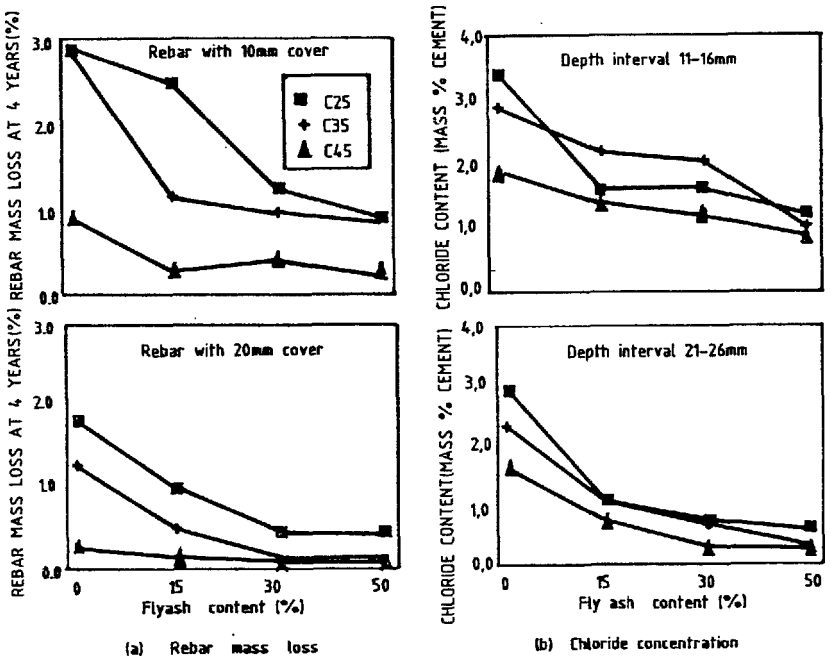

Fig. 12 Effect of Flyash on Concrete Performance after 4 years Exposure (Thomas, 1996)

Interface with Reinforcement

Interfacial regions in concrete, either in contact with aggregate or with reinforcement, are in general quite different from the 'bulk' cement paste in terms of morphology, composition and density. The interficial regions are more porous than the bulk phase, leading to lower density (Mindess, 1989). It consists of a thin rim of massive C-H crystals, in contact with the reinforcement, backed up by a porous layer consisting of needle-like C-S-H and ettringite. The thickness varies from 40 to 50 μm. The passivating film formed at the surface of the reinforcement is a mixture of iron products, like FeO-OH, $Fe(OH)_2$ or $Fe(OH)_3$, and calcium hydroxide. However, when fresh concrete surrounds a steel, rusted due to exposure prior to use, mixing water flows into rust pores, cement hydration products forming in such pores react with the iron products. Oriented platy spinel crystals in the inner layer and mixture of fine-grained spinel and α-FeOOH, with C-H being present in both the layers have been identified (Sagoe-Crentsil and Glasser, 1989).

In spite of the porous nature of the transition zone, passivation is due to the presence of lime-rich layer. The solubility of portlandite maintains an alkaline pH and the presence of portlandite continues to provide adequate pH-buffering to keep the interface region highly alkaline with pH greater than 12 (Sagoe-Crentsil and Glasser, 1989).

Sandberg (1996) has stated that effect of physical adhesion between cement hydrates and iron oxides formed at the steel interface is very important. Formation of voids at the steel-mortar interface is a necessary condition for active corrosion to start in concrete with moderate chloride content. Such voids can form due to inadequate compaction as

well as segregation and bleeding in fresh concrete. Effects of inadequate workmanship on the voidage, strcuture and chemical composition of the interfacial transition zone has not been adequately modelled, and not much is known even on a semi-quantitative order.

THE 'CRITICAL' SYSTEM

Taking into account the very many interactive factors enumerated above, it is possible to identify a situation in practice, which may pose to be critical to the system of durability. Risk of corrosion of reinforcement in concrete is chosen as an example. Presence of aggressive ions like sulphates and chlorides etc., atmospheric carbonation, relatively dry environment and high ambient temperature comprise essential components of such a scenario. Ambient temperature of the order of 35 to 40°C and dry conditions with realtive humidity around 60 percent, coupled with inadeqaute moist curing will not allow hydration of cement and pozzolanic reactions to progress very far. Carbonation will be accelerated, lowering the pH value. Much of the chloride ions will be free in the pore solution and resistivity of concrete will remain below the desired level of about 5000 to 10000 Ohm-cm (Browne, 1982). Cl^{-}/OH^{-} ratio in the pore solution will be higher than the threshold value, leading to corrosion of reinforcement.

It is presumed that the prescriptions of quality of cement, pozzolana, aggregate, admixtures and mix water as required for the anticipated environment and laid down in numerous publications are adhered to. If not, it will add further to the vulnerability of the system. Inadequate workmanship and inappropriate quality assurance will be very detrimental. This aspect is not elaborated here.

Such a critical system can not be simulated in the laboratory, in all aspects. On the other hand, there are many instances of distress of such concrete 'systems' in service. It is essential that condition surveys and case histories report all the durability indicators as obtaining in the structure. These will include, inter alia;

i) Ambient temperature and relative humidty
ii) Moisture content and internal relative humidity
iii) Status of hydration reactions and hydration phases present
iv) Cover thickness, quality of concrete, cement content, w/c ratio
v) Extent of carbonation, by phenolphthalein test and presence of portlandite and/or calcite at various depths by XRD
vi) pH value of pore solution extract and of concrete cover
vii) Ingress of chloride and sulphate ions at different locations
viii) Measure of free (water-soluble) and total (acid-soluble) chloride in concrete
ix) In-situ permeability of concrete, pore size distribution in the hydrated cement
x) Electrical resistivity of concrete; etc.

It is not suggested that the above list be taken as exhaustive. What is being emphasised, is the need of measuring as many relevant durability parameters as possible, which have a bearing on the performance of the system. Careful analysis of data and correlation with

various durability indicators will lead to a better understanding of the causes of distress under field conditions.

DURABILITY WITH NEWER CEMENT SYSTEMS

The discussions so far are based on concrete made with ordinary portland cements, with appropriate addition of flyash, slag or silica fume, wherever so decided. In addition, newer cement systems have been explored with a view to result in conservation of raw materials and energy resources. The status of industrial exploitation of such concepts was reviewed (Mullick, 1992). In view of limited commercial production of these, durability of concrete structures made with such cements have not been adequately investigated and/or reported. Limited laboratory data available, however, indicate interesting possibilities, as discussed below.

Cements in oxide system $CaO - Al_2O_3 - SiO_2 - SO_3$, having assemblages of phases $C_4A_3\bar{S}$, β-C_2S, CA and $C\bar{S}$ etc were postulated and explored by Mehta (1980), and many others. Typical hydration products include ettringite, C_3AH_6, C_4AH_{13} and $C_3A\bar{C}H_{12}$ (Mudbhatkal et al, 1986). A common feature of these systems is the absence of $Ca(OH)_2$ as a product of hydration. Similar trends have been reported in systems with incorporation of MgO, i.e. $CaO - Al_2O_3 - Fe_2O_3 - SiO_2 - SO_3 - MgO$ (Ali et al, 1997). The products of hydration include ettringite, CSH and unreacted β-C_2S and $Ca_3Mg(SiO_4)_2$, the latter phase in the clinker bring essentially inert (**Fig. 13**). Limited durability studies in both the systems indicated improved sulphate resistance and adequate resistance against corrosion of steel reinforcement in accelerated tests (Mudbhatkal et al, 1986, Ali et al, 1997). Results of corrosion tests reported by them are shown in **Fig. 14**.

Interest on these systems arise due to absence of $Ca(OH)_2$ phase as a hydration product, which is one of the fast reacting components of hydrated cement paste in OPC systems. Similar situation exists in alkali activation of slags. The hydration products are poorly crystalline, often of geletinous nature; C-S-H (I), and $[(C,M)_4AH_{13}]$ belonging to the solid solution series with end members C_4AH_{13} and M_4AH_{13} have been identified (Schilling, et al 1994). Ali et al (1996) have also reported similar results, and no $Ca(OH)_2$ was present.

In view of importance of $Ca(OH)_2$ - phase in deleterious alkali-silica reaction of expansion-causing type, the author had speculated that a cement system, which did not contain $Ca(OH)_2$ as a hydration product may be beneficial to alleviate ASR (Visvesvaraya et al 1986). Preliminary investigations on accelerated mortar bar tests with known reactive aggregates and laboratory prepared supersulphated alumino-belite cements ($C_4A_3\bar{S}$ - β-C_2S system) had shown encouraging results which have not been published. Ali et al (1996) have reported that expansion in mortar bar tests with alkali-slag cements and known reactive aggregates was much lower than with high alkali OPC. Changgao and Raihua (1996) have also reported lower ASR activity in accelerated tests of concrete samples made with alkali activated slag-flyash system. In such systems, the alkali ions react with the Al_2O_3, SiO_2 and CaO in ground slag (and ground flyash), hence there is no free soluble alkali available. However, due to the presence of alkali salts in the activators as well as those present in the slags, adequate alkalinity in the pore solution above 13, is maintained, even in absence of $Ca(OH)_2$ phase. Typical results are

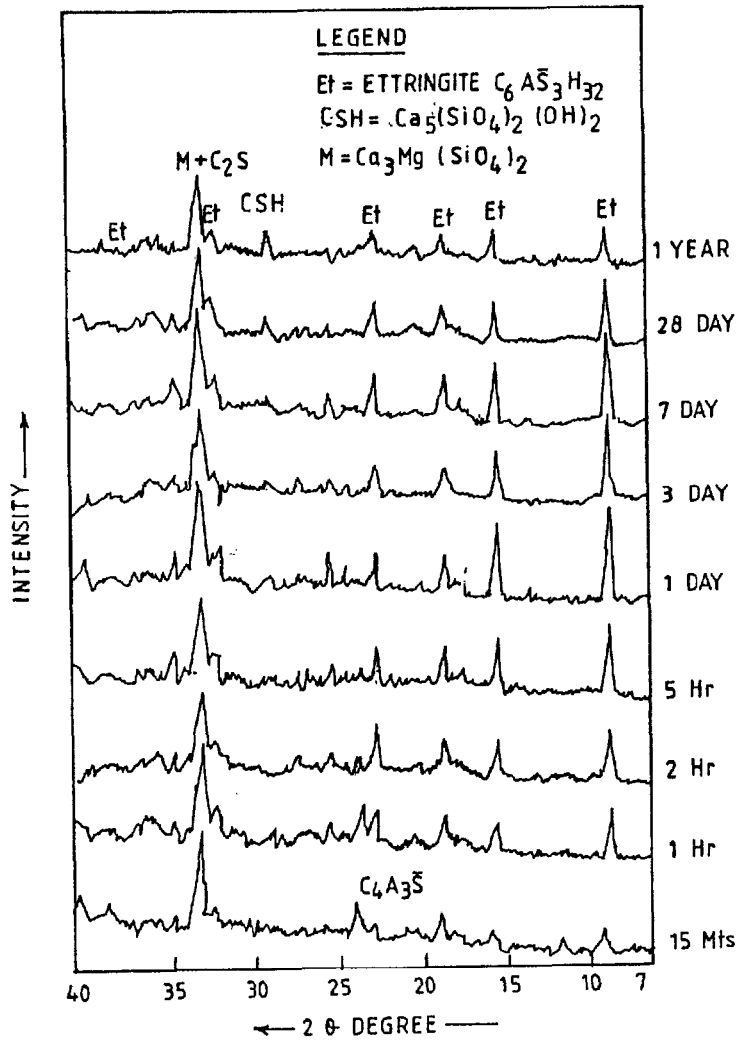

Fig. 13 XRD of Hydrated Sulphoaluminate Belite Cement Containing MgO (Ali et al, 1997)

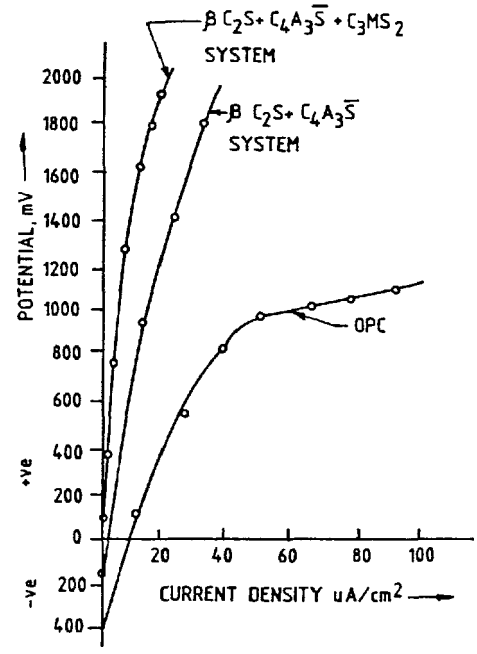

Fig. 14 Accelerated Corrosin Test on Concretes made with Sulpho-aluminate based Cements (Mudbhatkal et al 1986, Ali et al 1997)

shown in **Fig. 15** (Byfors et al, 1989). The rate of chloride ion diffusion was lower than in OPC.

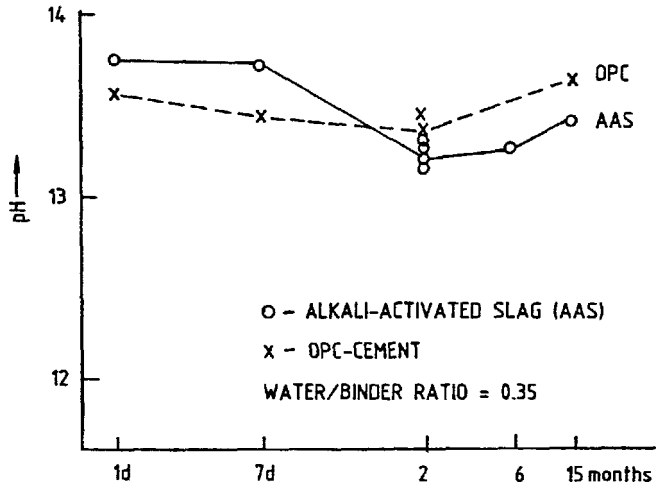

Fig. 15 pH of Pore Solution (Byfors et al, 1989)

Use of lithium-salts in concrete has been known since longtime to alleviate alkali-silica reaction or reducing the expansive and cracking effects associated with ASR (McCoy and Caldwell, 1951). Feasibility studies of intergrinding lithium compounds with portland cement to produce a high alkali ASR-resistant cement has been reported (Gajda, 1996). Lithium hydroxide monohydrate (LiOH) upto 1.2 percent by mass of cement clinker containing about 1.06 percent alkali (Na_2O - equivalent), were interground along with gypsum. Accelerated mortar bar tests showed the level of LiOH to control expansive ASR was at a level slightly in excess of equivalent alkali content of the cement.

CONCLUDING REMARKS

Durability of concrete has been discussed in two aspects. The first is the durability of the products of hydration of cements -- the calcium silicate hydrates (C-S-H), calcium aluminate hydrates (C-A-H) and calcium hydroxide (C-H), against chemical agents like SO_3^{--}, Cl^- and CO_2 etc. The second is the durability of inclusions like aggregate and embedments like mild steel reinforcement in the matrix of hydrated cement paste. Between these two, the situation in the former is somewhat more reassuring. Hydrated cement paste in concrete, by and large, can be made to withstand aggressive chemical environments. In cases of very aggressive environments e.g. in chemical and fertiliser industries, additional external protection to concrete, like coatings, paints and barriers may be required (Mullick, Rajkumar and Jain, 1991). Such applciations have not been discussed in this paper.

Problems do arise in the other aspect, which involves the protective and compatible roles of hydrated cement paste in the composite, in the sense that majority of reports and case studies on distress to concrete structures in service pertain to corrosion of reinforcement or alkali-aggregate reaction. Desperate measures are sometimes recommended to combat

the situation. If the aggregate within economical lead are likely to be reactive, the safest course recommended is to avoid them. Additional protection to mild steel reinforcement like galvanising, epoxy coating, cathodic protection, corrosion inhibitors, removal of chloride ions by realkalisation or ion exchange, use of stainless steel or non-metallic reinforcement like glass-reinforced plastic, are some measures which have sometimes been adopted to avoid distress due to corrosion of reinforcement. Life-cycle cost analyses indicate such desperate measures to be economical in many situations, which goes to show how desperate the situation can be !

Laboratory reseach has helped in great measures in understanding of the problem. Research has also led to understand, why common specifications do not address to the interactive effects of various hygrothermal, environmental and service parameters, which can not be fully simulated in laboratory tests. Reports of investigations on concrete structures in service and case studies should be addressed and carefully analysed to lead to greater understanding of the interactive material - environment system. This will enable to speficy 'concrete that is needed', with greater assurance.

Adequate performance of ordinary portland cements have been demonstrated in majority of concrete structures in service. There is need of more data and reports on performance of concrete incorporating pozzolana and slags, in different types of service environments. Improvement in durability should be the focus of development of newer types of cements, in addition to material and energy conservation.

In conclusion, it must be noted that large majority of concrete structures are indeed durable., With some more insight gained by laboratory research and field investigations and continuous improvements in specifications and construction practices, it should be possible to make concrete a material for all seasons (and all situations).

ACKNOWLEDGEMENT

The author has freely used unpublished results and data on on-going research projects at the National Council for Cement and Building Materials (NCB), New Delhi. Thanks are due to M M Ali, Shri Harsh, K Mohan and S Laxmi, colleagues at NCB, for suggestions and help in preparation of the paper. M S Uppal and K B Puri helped in the preparation of the manuscript. The paper is presented with permission of Director General, NCB.

REFERECNES

Al-Amoudi, O.S.B., Durability of Reinforced Concrete in Aggressive Sabkha Environments, ACI Materials Journal 92(3), May-June 1995, pp 236-245.

Al-Amoudi, O.S.B., et al, Influence of Sulphate Ions on Chloride - Induced Reinforcement Corrosion in Portland and Blended Cement Concretes, Cement, Concrete and Aggregate, 16(1), June 1994, pp 3-11.

Al-Gahtani, A.S., Rasheeduzzafar and Hussain, S.E., Effect of Alkali Content of Cement on Chloride Binding and Corrosion of Reinforcing Steel, Proc. Int. Conference on Corrosion and Corrosion Protection of Steel in Concrete, Ed. Swamy, R.N., 1994, Vol. I, pp 472-481.

Ali. M.M., Agarwal, S.K. and Handoo, S.K., High Performance Alkali-Slag Cements, Proc. 5th NCB Int. Seminar on Cement and Building Materials, Nov. 26-29, 1996, New Delhi, Vol. 3, pp XXIII-45-50.

Ali, M.M., Bhargava, R. and Ahluwalia, S.C., Hydration Characteristics of Magnesia Assimilated Sulphoaluminate - Belite Cement, 10th Int. Congress on Chemistry of Cement, June 2-7, 1997, Goteborg (Accepted for Publication).
Arafah, A., Al-Zaid, R. and Al-Haddad, M., Influence of Non-Standard Curing on the Strength of Concrete in Arid Areas, Cement and Concrete Research, 26(9), Sept 1996, pp 1341-1350.
Browne, R.D., Design Prediction of the Life for Reinforced Concrete in Marine and other Chloride Environments, Durability of Building Materials, 1, 1982, pp 113-125.
Byfors, K., Klingstedt, G., Lehtonen, V., Pyy, H. and Romben, L., Durability of Concrete Made with Alkali-Activated Slag, Proc. 3rd CANMET/ACI Int. Conference on Flyash, Silica Fume, Slag and Natural Pozzolans in Concrete, Ed. Malhotra, V.M., Trondheim, 1989, ACI SP-114, Vol. 2, pp 1429-1466.
Chandra, S., Influence of Pollution on Mortar and Concrete, Doc. D6: 1990, Swedish Council for Building Research, 83 p.
Chandra, S., Deterioration of Mortar and Concrete by Pollutant Gases, Proc. 7th Int. Conference on Durability of Building Materials and Components, Stockholm, 19-23 May 1996, Ed. Sjostrom, C., Vol. 1, pp 586-595.
Changgao, L. and Raihua, L., The Reserach of Control the Alkali-Aggregate Reaction for the High Performance FKJ Concrete, Proc. 5th NCB Int. Seminar on Cement and Building Materials, New Delhi, 26-29 Nov 1996, Vol. 4, pp XV-81-84.
Chatterjee, S., Mechanism of Expansion of Concrete Due to Presence of Dead Burnt CaO and MgO, Cement and Concrete Research, 25(1), 1995, pp 51-56.
Collepardi, Mario, Coppola, L. and Pistolesi, C., Durability of Concrete Structures Exposed to $CaCl_2$ Based De-icing Salts, Proc. 3rd ACI/CANMET Int. Conference on Durability of Concrete, 1994, Ed. Malhotra, V.M., ACI SP-145, pp 107-120.
Day, R.L., The Effect of Secondary Ettringite Formation on the Durability of Concrete: A Literature Review. Research and Development Bulletin RD108T, Portland Cement Association, Skokie, 1992.
Detwiler, R.J., Fapohunda, C.A. and Natale, J., Use of Supplementary Cementing Materials to Increase the Resistance ot Chloride Ion Penetration of Concrete Cured at Elevated Temperatures, ACI Material Journal 91(1), 1994, pp 63-66.
Dhir, R.K., Jones, M.R. and McCarthy, M.J., PFA Concrete : Chloride-Induced Reinforcement Corrosion, Magazine of Concrete Research, 46 (169), Dec 1994, pp 269-277.
Diamond, S., Delayed Ettringite Formation - Processes and Problems, Cement and Concrete Composites, 18, 1996, pp 205-215.
Enevoldsen, J.N., Hansson, C.M. and Hope, B.B., The Influence of Internal Relative Humidity on the Rate of Corrosion of Steel Embedded in Concrete and Mortar, Cement and Concrete Research, 24(7), July 1994, pp 1373-1382.
Ewertson, C., and Petersson, P.E., The Influence of Curing Conditions on the Permeability and Durability of Concrete. Results from a Field Exposure Test, Cement and Concrete Rsearch, 23(3), March 1993, pp 683-692.
Gajda, J., Development of a Lithium Bearing Cement to Inhibit Alkali Silica Reactivity in Hardened Concrete, World Cement, Research and Development, Aug. 1996, pp 58-62.
Gerwick, B.C., Pressing Needs and Future Opportunities in Durability of Concrete in Marine Environment, Proc. Ben Gerwick Symposium on International Experience with Durability of Concrete in Marine Environment, Berkeley, 1989, Ed. Mehta, P.K., pp 1-5.

Glasser, F.P., Chemical, Mineralogical and Microstructural Changes Occuring in Hydrated Slag Cement Blends, Materials Science of Concrete, Vol. II, Ed. Skalny, J., American Ceramic Society, 1989, pp 41-81.
Gudmundsson, G. and Olafsson, H., Silica Fume in Concrete - 16 years of Experience in Iceland, Proc. 10th Int. Conference on Alkali-Aggregate Reaction in Concrete, Aug 18-23, 1996, Melbourne, Ed. Shayan, A., pp 562-569.
Hauzmann, D.A., Steel Corrosion in Concrete, Materials Protection 6(19), Nov. 1968, pp 19-23.
Hime, W.G., The Corrosion of Steel - Random Thoughts and Wishful Thinking, Concrete International, ACI, Oct. 1993, pp 54-57.
Kalousek, G.L. and Adams, M., Hydration Products Formed in Cement Pastes at 25 to 175 C, Journal ACI, 48(1), 1951, pp 77-90.
Kobayashi, K., Suzuki, K. and Uno, Y., Carbonation of Concrete Structures and Decomposition of C-S-H, Cement and Concrete Research, 24(1), Jan 1994, pp 55-61.
Mather, Bryant, Durable Concrete, Advances in Cement and Concrete, Eds. Grutzeck, M.W. and Sarkar, S.L., ASCE, 1994, pp 52-63.
McCoy, W.J. and Caldwell, A.G., New Approach to Inhibiting Alkali-Aggregate Reaction, Journal ACI, 22(9), 1951, pp 693-706.
Mehta, P.K., History and Status of Performance Tests for Evaluation of Soundness of Cements, Proc. Symposium on Cement Standards - Evaluation and Trends, 7 Dec. 1977, St. Louis, Ed. Mehta, P.K., ASTM, STP 663, pp 35-60.
Mehta, P.K., Investigations on Energy - Saving Cements, World Cement Technology, Nov. 1980, pp 166-177.
Mehta, P.K., Schiessl, P. and Raupach, M., Performance and Durability of Concrete Systems, Proc. 9th Int. Congress on Chemistry of Cement, New Delhi, Nov 1992, Vol. I, pp 571-659.
Mehta, P.K., Sulphate Attack on Concrete : A Critical Review, Durabilidad del Concreto (Durability of Concrete), 1993, Ed. Villarreal, R.R., pp 107-132.
Mielenz, R.C., Marusin, S.L., Hime, W.G. and Jugovic, Z.T., Investigation of Prestressed Concrete Railway Tie Distress, Concrete International, ACI, Dec 1995, pp 62-68.
Mindess, S., Interfaces in Concrete, Materials Science of Concrete, Vol. I, Ed. Skalny, J., American Ceramic Society, 1989, pp 163-180.
Morinaga, S., Remaining Life of Reinforced Concrete Structures After Corrosion Cracking, Proc. 7th Int. Conference on Durability of Building Materials and Components, Stockholm, 19-23 May 1996, Vol. I, Ed. Sjostrom, C., pp 127-136.
Moriwake, A., Fukute, T. and Suzuki, Y., Influence of Curing Temperature on Degradation of Concrete in Terms of Corrosion of Reinforcing Steel, Proc. Int. Conference on Corrosion and Corrosion Protection of Steel in Concrete, 1994, Ed. Swamy, R.N., Vol. I, pp 581-590.
Mudbhatkal, G.A., Parmeshwaran, P.S., Heble, A.S., Pai, B.V.B. and Chatterjee, A.K., Non-Alitic Cement from Calcium-Sulphoaluminate Clinker - Optimisation for High Strength and Low Temperature Application, Proc. 8th Int. Congress on the Chemistry of Cement, Sept. 1986, Rio-de-Janeiro, pp 364-370.
Mullick, A.K., Babu, K.H. and Rao, P.B., Evaluation of Pozzolanic Activity and its Impact on Specification of Bleneded Cements, Ibid, Vol VI, pp 308-311

Mullick, A.K., Rajkumar, C., and Jain, N.K., Performance of Concrete Structures in Industrial Environment, Proc. 2nd Int. Conference on Durability of Concrete, Montreal, 4-9 Aug 1991, Ed. Malhotra, V.M., ACI SP 126, Vol. I, pp 577-597.
Mullick, A.K., Advances in Portland Cements and Utilisation of Industrial Wastes - Towards Sustainable Development, Special Lecture, Proc. 9th Int. Congress on Chemistry of Cement, New Delhi, Nov. 1992, Vol VII, pp 58-79.
Mullick, A.K. and Chandra, S., Physico-Chemical, Biological and Thermal Degradation including Environmental Effects, Ibid, Vol. I, pp 695-734
Mullick, A.K. and Rajkumar, C., Multi-Disciplinary Investigation of Distress to Concrete Constructions, Proc. 3rd Int. Conference on Concrete Technology for Developing Countries, Tripoli, Oct 1993, pp 168-181.
Mullick, A.K., Alkali-Silica Raction due to Slowly Reactive Aggregates, Proc. P K Mehta Symposium on Durability of Concrete, Nice, May 1994, pp 175-206.
Nagataki, S., Otsuki, N., Wee, T-H. and Nakashita, K., Condensation of Chloride Ion in Hardened Cement Matrix Materials and on Embedded Steel Bars, ACI Mater. Journal, 90(4), 1993, pp 323-332.
National Council for Cement and Building Materials (NCB), Long Term Performance Evaluation of High Magnesia Cement, Unpublished Progress Report, March 1997.
Neville, A.M., Why We Have Concrete Durability Problems, Proc. Concrete Durability Katherine and Bryant Mather Int. Conference, 1987, ACI SP-100, Vol 1, pp 21-30.
Neville, A.M., Chloride Attack of Reinforced Concrete : an Overview, Materials and Structures, 1995, 28, RILEM, pp 63-70.
Ramezanianpour, A.A. and Malhotra, V.M., Effect of Curing on the Compressive Strength, Resistance of Chloride-Ion Penentration and Porosity of Concrete Incorporating Slag, Flyash and Silica Fume, Cement and Concrete Composites, 17, 1995, pp 125-133.
Rasheeduzzafar, Al-Saadoun, S.S. and Al-Gahtani, A.S., Reinforcement Corrosion - Resisting Characteristics of Silia Fume Blended - Cement Concrete, ACI Materials Journal, 89(4), July-August 1992, pp 337-344.
Rendahl, B., Kuccra, V., Vlckova, J., Knotkova, D., Norberg, P. and Sjostrom, C., The Microenvironment and Corrosivity in Different Positions on the Royal Palace in Stockholm and on Prague Castle, Proc. 7th Int. Conference on Durability of Building Materials and Components, Stockholm, 19-23 May 1996, Vol. 1, Ed. Sjostrom, C., pp 191-200.
Rivas Silva, M., Climates and Biodeterioration of Concrete, Ibid, pp 191-200.
Sagoe-Crentsil, K.K. and Glasser, F.P., Steel in Concrete, Part I - A Review of the Electrochemical and Thermodynamic Aspects, Magazine of Concrete Research, 41(149), 1989, pp 205-212.
Saleem, M., Shameem, M., Hussain, S.E. and Maslehuddin, M., Effect of Moisture, Chloride and Sulphate Contamination on the Electrical Resistivity of Portland Cement Concrete, Construction and Building Materials, 10(3), 1996, pp 209-214.
Sandberg, P., Cost-effective Service Life Design of Concrete Structurues in Saline Environment, Proc. 7th Int. Conference on Durability of Building Materials and Components, Stockholm, 19-23 May 1996, Ed. Sjostrom, C., Vol. 2, pp 1195-1204.
Schilling, P.J., Roy, A., Eaton, H.C., Malone, P.G. and Brabston, W.N., Microstructure, Strength and Reaction Products of Ground Granulated Blast Furnace Slag Activated by Highly Concentrated NaOH Solution, Jour. Material Research, 9(1), Jan 1994, Materials Research Society, pp 188-197.

Shayan, A., and Ivanusec, I., An Experimental Clarification of the Association of Delayed Ettringite Formation with Alkali-Aggregate Reaction, Cement and Concrete Composites, 18, 1996, pp 161-170.
Spears, R.E., The 80 Percent Solution to Inadequate Curing Problems, Concrete International, ACI, April 1983, p 15-18.
Stark, D., The Moisture Condition of Field Concrete Exhibiting Alkali-Silica Reactivity, Proc. 2nd CANMET/ACI Int. Conference on Durability of Concrete, Aug 4-9, 1991, Montreal, Ed. Malhotra, V.M., ACI SP-126, Vol. II, pp 973-987.
Suryavanshi, A.K. and Swamy, R.N., Stability of Friedel's Salt in Carbonated Concrete Structural Elements, Cement and Concrete Research, 26(5), May 1996, pp 729-741.
Suryavanshi, A.K., Scantlebury, J.D. and Lyon, S.B., Mechanism of Friedel's Salt Formation in Cements Rich in Tri-Calcium Aluminate, Ibid, pp 717-727.
Talib, A.Y., Rasheeduzzafar and Al-Gahtani, A.S., Effect of Temperature on Chloride-Binding Capacity of Silica Fume Blended Cement, Proc. Int. Conference on Corrosion and Corrosion Protection of Steel in Concrete, 1994, Ed. Swamy, R.N., Vol. 2, pp 806-816.
Tang, L., and Nilsson, L-O.,Chloride Binding Capacity and Binding Isotherms of OPC Pastes and Mortars, Cement and Concrete Research, 23(2), March 1993, pp 247-253.
Taylor, H.F.W., Delayed Ettringite Formation, Advances in Cement and Concrete, Eds. Grutzeck, M.W. and Sarkar, S.L., ASCE, 1994, pp 122-131.
Thomas, M., Chloride Thresholds in Marine Concrete, Cement and Concrete Research, 26(4), April 1996, pp 513-519.
Thomas, M.D.A., The Effect of Curing on the Hydration and Pore Structure of Hardened Cement Paste Containing Pulverised Fuel Ash, Advances in Cement Research, 2(8), Oct 1989, pp 181-188.
Thomas, M.D.A. and Mathews, J.D., Performance of Fly Ash Concrete in U.K. Structures, ACI Materials Journal, 90(6), Nov-Dec 1993, pp 586-593.
Tumidajski, P.J. and Chan, G.W., Effect of Sulphate and Carbon Dioxide on Chloride Diffusivity, Cement and Concrete Rsearch, 26(4), April 1996, pp 551-556.
Van Derwegen, G., Bijen, J. and Van Delst, R., Behaviour of Concrete Affected by Sea Water under High Pressure, Materials and Structures 26(163), 1993, pp 549-556.
Visvesvaraya, H.C., Mullick, A.K., Samuel, G., Sinha, S.K., and Wason, R.C.,Alkali-Reactivity of Granitic Rock Aggregates, Proc. 8th Int. Congress on Chemistry of Cement, Sept 1986, Rio-de-Janeiro, Theme 4, Vol V, pp 208-213.
Wong, W.F., Chiew, S.P. and Ho, N.Y., Evaluation of In-situ Test Data from Existing Concrete Structures, Concrete 2000, Eds. Dhir, R.K. and Jones, M.R., 1993, Vol. 2, pp 1147-1159.
Xu, A. Rodhe, M. and Chandra, S., Influences of Alkali on Carbonation of Concrete, Proc. 7th Int. Conference on Durability of Building Materials and Components, Stockholm, 19-23 May 1996, Ed. Sjostrom, C., Vol. I, pp 596-604.
Yang, R., Lawrence, C.D. and Sharp, J.H., Delayed Ettringite Formation in 4-year Old Cement Pastes, Cement and Concrete Research, 26(11), Nov 1996, pp 1649-1659.

Recent Results of Solid-State NMR Investigations and their Possibilities of Use in Cement Chemistry

WOLFGANG WIEKER, CORNELIA HÜBERT and DETLEF HEIDEMANN

Technische Universität Berlin, Institut für Bauingenieurwesen, AG Baustoffchemie

1 Introduction

Nuclear magnetic resonance (NMR) spectroscopy and its application to the study of solid substances is a method which can look back now for about 50 years of its successful use. Therefore it shall not be the aim of this paper to give an introduction into the theoretical fundaments of the solid state NMR spectroscopy because there are several books in that field [e.g. 1-4]. In the meantime this method, which is applicable to all substances containing atomic nuclei with a magnetic moment, has been developed to a very powerful tool in the investigation of structural problems of solid state materials.

Because in silicate and cement chemistry a relative big number of elements with a magnetic moment like ^{29}Si, ^{1}H, ^{17}O, ^{27}Al, ^{23}Na, ^{43}Ca, ^{25}Mg and ^{19}F plays a dominant role the NMR technique has got an increasing importance in the material science of building materials.

Already at the VI. International Congress of Cement Chemistry in Moscow in 1974 the first ^{1}H solid-state NMR investigation of 14 Å Tobermorite and $CaNaHSiO_4$ have been presented [5]. At the beginning of the 80th of this century ^{29}Si and ^{27}Al solid-state NMR measurements came more and more in use and it became possible to investigate the chemical structure of silicates, alumosilicates, including zeolites, and aluminates in solid samples without dissolving them (see [6] and references cited therein). Since that time it is possible to decide between four- or sixfold oxygen-coordinated silicon atoms and to determine the number of Si-O-Si bonds of fourfold coordinated silicons (Q^n, n=1,2,3,4, where n denotes the number of bridging oxygens) by means of the measured isotropic ^{29}Si shift values. At the same time similar correlations have been established for the aluminum. The measurement of the isotropic ^{27}Al shifts allow to distinguish between Al atoms in tetrahedral or octahedral coordination with respect to oxygen atoms. Furthermore, NMR experiments can be used to detect possible Si-O-Al bonds in Al_2O_3-containing silicates.

---

present address: WITEGA GmbH, Rudower Chaussee 5, Haus 4.1, D-12484 Berlin

In the last decade solid-state NMR investigations have been performed using ^{23}Na, ^{17}O, ^{25}Mg and even ^{43}Ca nuclei as probe for structural investigations in silicates and CSH phases.

Parallel to the number of nuclei which can be investigated by the NMR technique the sensitivity of the spectrometers has been enormously increased. By developing of sophisticated mechanical (e.g. MAS, DOR) and electronic procedures (e.g. multiple pulse programs, two-dimensional NMR techniques) it also became possible to minimize the line broadening due to the anisotropy of the chemical shift and dipole-dipole- or quadrupolar interactions of the nuclei in order to get a higher resolution of the spectra.

But for the application of solid-state NMR to cement-based materials by our opinion there are still some problems which are e.g.

- the presence of para- and ferromagnetic components in the samples since these can mask the chemical shift effects by large line broadening effects,
- the precision of quantitative determination of structural units from the intensities of NMR spectra due to the widely unknown relaxation time behaviour of the nuclei (especially that of the ^{29}Si nuclei) in different binding states which can lead to saturation effects during the NMR experiments .

In spite of these and many other problems the application of the solid-state NMR to solve questions in the field of silicate- and cement science arising from basic research in scientific laboratories of universities and from the practice of the building material industry has been developed very fast in the recent years. This is demonstrated by an increasing number of publications in that field and that a series of special meetings devoted to the "Application of NMR Spectroscopy to Cement Science" has been created in Guerville (France) in 1992 [7]. The last one of this series was arranged in Bergamo (Italy) last year and a book containing the full papers given on that meeting will appear till to the end of this year [8].

Because it can't be the task of our paper to present on this conference a complete summary of all contributions made since the last congress in Delhi in 1992 to the science of building materials by using NMR spectroscopy the following chapters shall give a short survey on some individually selected results of solid-state NMR investigations in the wide field of cement chemistry, as there are:

- structure of CSH- and CAH-phases,
- influence of alkali-ions on reactive silica and CSH-phases with respect to the alkali-silica-reaction (ASR) in concretes,
- application of NMR to problems of the building material industry.

These examples can be treated only very briefly to show, those who are not very familiar with the solid-state NMR, what is possible to do with this method today and how far this method can be applied in cement and concrete science to solve the problems of preparation and use of building materials.

It is an aim of our contribution to give an encouragement for further studies in this field of science by the presented examples and the cited literature.

2 NMR Studies of the Structure of CSH

The application of the ^{29}Si MAS NMR spectroscopy to the study of the structure of CSH, the poorly crystalline hydration product of C_2S and β-C_2S or alite and belite in portland cement has already a long tradition. Exactly fifteen years ago the first ^{29}Si MAS NMR study of the hydration of C_3S was published [9]. Already this first study has shown that the final hydration product of C_3S, a CSH with a C/S ratio ~1.8, consists only of Q^1 and Q^2 units, higher condensed units do not occur. This result indicates that the silicate part of CSH contains only chains and dimers and that no two- or three-dimensional silicate structures are present in these early hydration products.

In the meantime this has been confirmed by many other groups and it has been established that the intensities of the Q^1 and Q^2 signals vary in dependence on the C/S ratio of the CSH-phase investigated (see e.g. [10] and references cited therein).

Very recently Cong and Kirkpatrick presented a detailed systematic investigation of the structure of CSH with C/S ratios in a range from 0.4 up to 1.8 using ^{29}Si- [11,12] and ^{17}O- [13] MAS NMR spectroscopy.
Some of their ^{29}Si MAS NMR spectra are collected in figure 2.1.

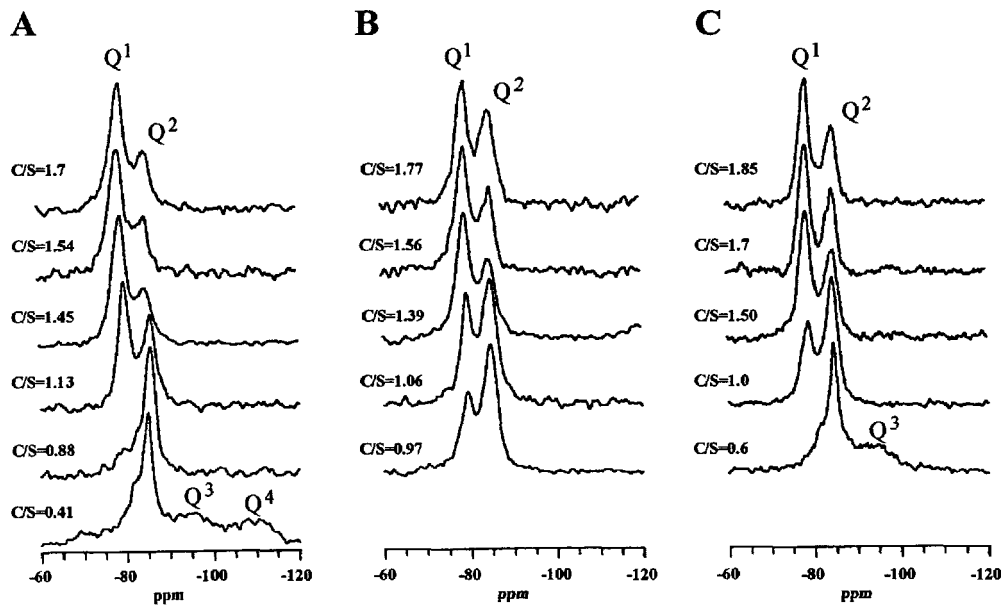

Fig. 2.1. ^{29}Si MAS NMR spectra of different CSH phases with varying C/S ratios formed **A:** by an aqueous reaction of CaO with silica fume; **B:** by hydration of highly reactive ß-C_2S and **C:** by hydration of silica fume with highly reactive β-C_2S (adapted with some changes from [12])

These spectra show again that CSH consist of Q^1 and Q^2 units and that with decreasing C/S ratio the amount of Q^2 units increases. Similar results were obtained by Okada et al. [14] investigating hydrothermally formed CSH.

In the spectra of that CSH phases which were prepared by using fumed silica (fig. 2.1A and 2.1C) a signal for Q^3 units appears at low C/S ratio (silica-rich samples) probably as a result of a "pozzolanic reaction" (see chapter 4). The Q^4 signal of the bottom in fig. 2.1A is due to unreacted silica used in the preparation of this sample.

While the ^{29}Si NMR allows only the characterization of the silicate part of the CSH structure further information can be received from the ^{17}O NMR which probe all parts of the CSH phases, the silicate portion, the calcium-oxygen layers and the water molecules, because oxygen atoms are present in all of them.

Typical ^{17}O MAS NMR spectra from the reaction of CaO and silica fume in a water suspension [13] are presented in figure 2.2A.

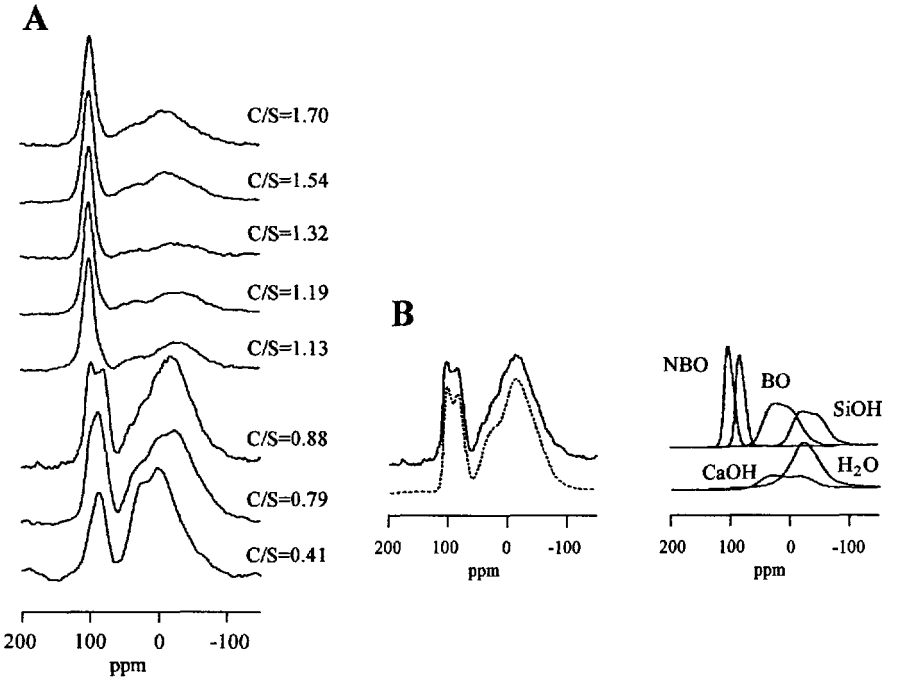

Fig. 2.2. Typical ^{17}O MAS NMR spectra of CSH with different C/S ratio prepared by the reaction of CaO and silica fume with water. **A:** experimental spectra; **B:** result of the line-shape simulation for the sample with C/S ratio of 0.88 (spectra adapted from [13]).

These spectra are much more complicated due to the interaction of the ^{17}O quadrupole moment with the electric field gradients of the different O-sides. The interpretation of these spectra requires a deconvolution of the line-shape by using spectra simulations as presented in fig. 2.2B. By this way it is possible to identify at least six O-sides in the CSH structure, two nonbridging oxygens (NBO) which link a silicon with two or three Ca^{2+}, a bridging oxygen (BO) which links two silicons by Si-O-Si bonds and one oxygen for each of CaOH, SiOH and H_2O.

From both the ^{29}Si- and ^{17}O MAS NMR results a model has been derived for the CSH structure, called "defect-tobermorite structural model" the principle of which is demonstrated in figure 2.3.

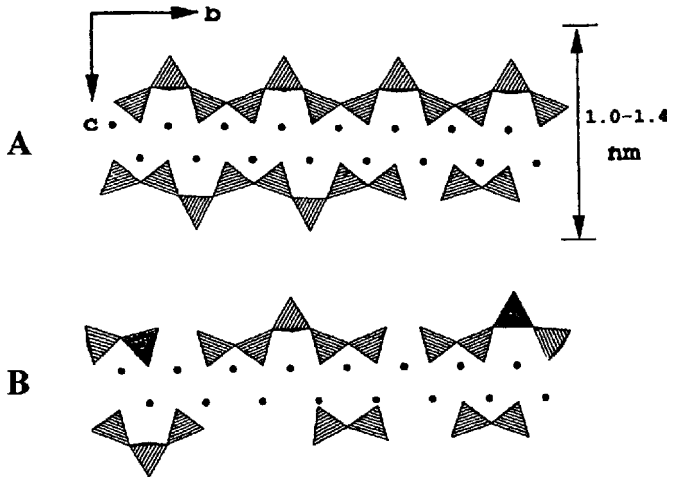

Fig. 2.3. Proposed defect-tobermorite structural model for CSH, showing dreierketten and central CaO layers (filled circles). The interlayer Ca^{2+}, OH^- groups and the H_2O molecules are omitted (adapted from [12]).

The layer A represents a relatively perfect 14 Å tobermorite layer in which only a small portion of the bridging tetrahedra is missing. This picture describes the structure of CSH with a small C/S ratio, in which the Q^2 units from polysilicates with long chainlike structures dominate.

The layer B represents a distorted layer in which individual SiO_4 tetrahedra and silicates with short chains may tilt, rotate or be displaced along the b axis. Most bridging tetrahedra are missing, resulting in many dimeric silicates. This picture describes the structure of CSH with a high C/S ratio.

It is well known from a great number of publications that the C/S ratio of CSH phases can vary in a relatively wide range from C/S ~ 0.4 to ~2.5. This fact leads to the question, what are the counter anions to balance the negative charges at the polymeric silicate anions. Especially, are there H^+ in form of SiOH groups or OH^- in form of $CaOH^+$ cations involved in the formation of the CSH structures?

Charge balance calculations on basis of the NMR results [12] showed that both SiOH and CaOH bonds occur in CSH. The SiOH groups should occur with decreasing C/S ratio while the $CaOH^+$ cations should be expected with an increase of this ratio.

This behaviour is in good agreement with the results of the mentioned ^{17}O investigations [13] and our experimental results of ^1H MAS NMR studies on CSH [15,16].

We found that the CSH phases formed during the hydration of C_3S and C_2S contain mainly protons in H_2O and CaOH but no (or only a very small amount of protons) in SiOH groups.

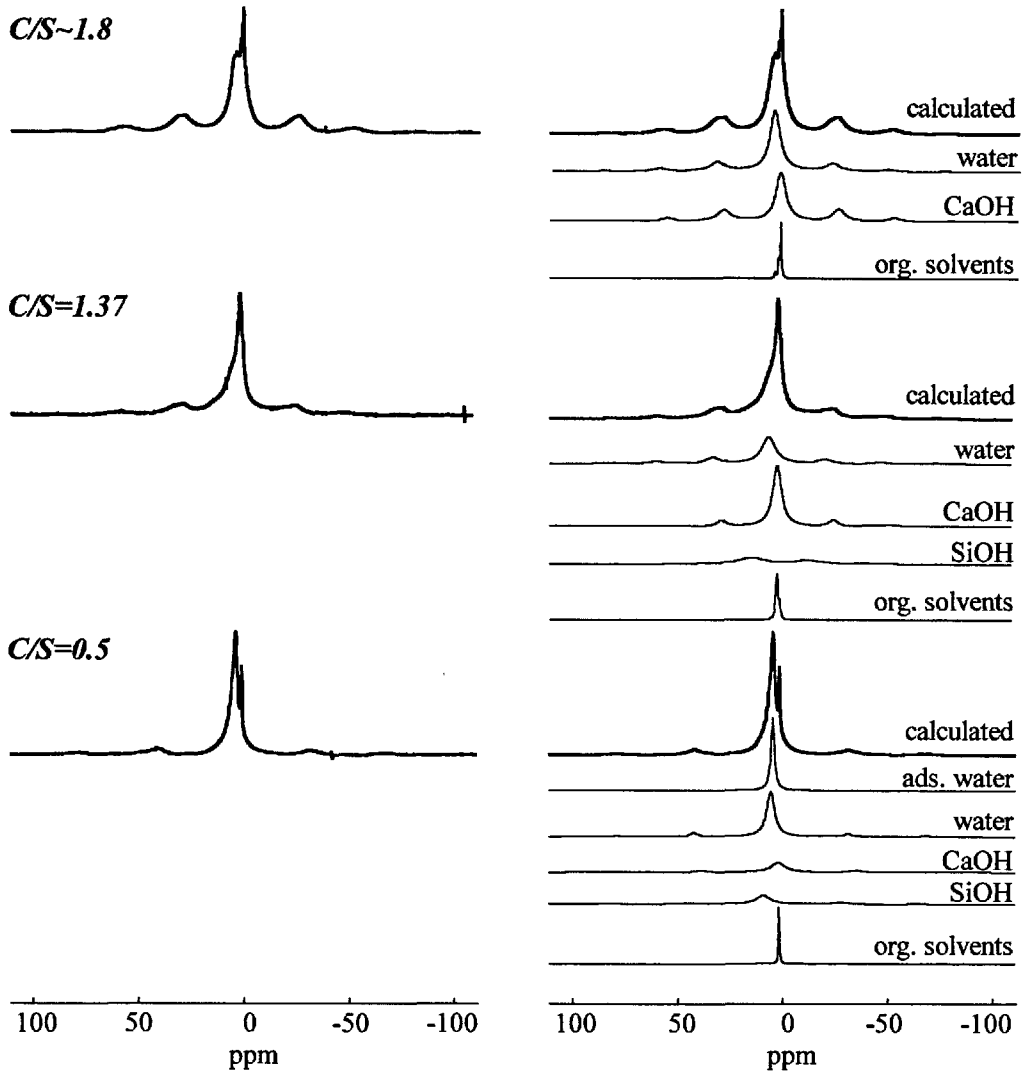

Fig. 2.4. Selected ^1H MAS NMR spectra of CSH with different C/S ratios, on the left the experimental spectra, on the right the results of a deconvolution procedure.

On the other hand, in hydrothermally formed or precipitated CSH phases with C/S ratios between 0.5 and 1.3 we detected besides the protons bonded in H_2O and CaOH also protons bonded in SiOH groups. The corresponding ^1H MAS NMR spectra are presented in fig. 2.4.

In all spectra appeared small signals attributed to mobile protons of traces of organic solvents which we used to stop the hydration reaction [15].

Because the water content of the CSH phases strongly depends on the preparation and the drying procedure used it makes no sense to discuss the relative intensities of the different proton sites. Therefore, we calculated only the ratio of CaOH/SiOH from the deconvolution of the spectra which is not influenced by the amount of proton bonded in water molecules. The calculated CaOH/SiOH ratios are summarized in table 2.1.

These data reflect exactly the prediction of [12] that with increasing C/S ratio the abundance of SiOH decreases and that of CaOH increases.

Tab. 2.1. CaOH/SiOH ratio of the studied CSH

C/S of the sample	CaOH	SiOH
~1.8	1	0
1.37	1	0.45
0.5	1	0.95

As a result of the NMR investigations in this field the chemical structure of CSH phases must be formulated as

Acidic salts of Calcium-hydroxi-polysilicate-hydrates

in which

the amount of acidic and basic groups

and

the condensation degree of the polysilicates

depend on the C/S ratio.

3 NMR Studies of the Structure of CAH

While in the hydration process of calcium silicates poorly crystalline CSH-phases appear, the hydration of calcium aluminates, which are the main components of high-alumina cements and partly present at low concentrations even in ordinary portland cements, leads to well ordered calcium aluminate hydrates and aluminium hydroxide (gibbsite).

Because the hydration of Ca-aluminates involves a conversion of tetrahedrally coordinated aluminum (Al(4) with respect to oxygen) in the anhydrous phases to octahedrally coordinated aluminum (Al(6)) in the hydrates the ^{27}Al MAS NMR is well suited to follow the hydration reaction. The first study in this field was reported by Müller et al. [17] in 1984 following the hydration of CA by use of ^{27}Al MAS NMR. The spectra of that paper (fig. 3.1A) is compared with the spectra of a paper published by Müller et al. [18] on the same subject in 1994 (fig.3.1B) to demonstrate the progress in the ^{27}Al MAS NMR spectroscopy for monitoring the hydration of calcium aluminate cements.

The spectra collected at higher resonance frequency (higher magnetic field) by using higher MAS spinning rates and ^{1}H decoupling (fig 3.1B) show a much higher resolution which allows to follow the formation of C_3AH_6 separately.

Further ^{27}Al MAS NMR investigations were applied to study the hydration of calcium aluminates in white portland cement [19] and different types of high alumina cements [20,21].

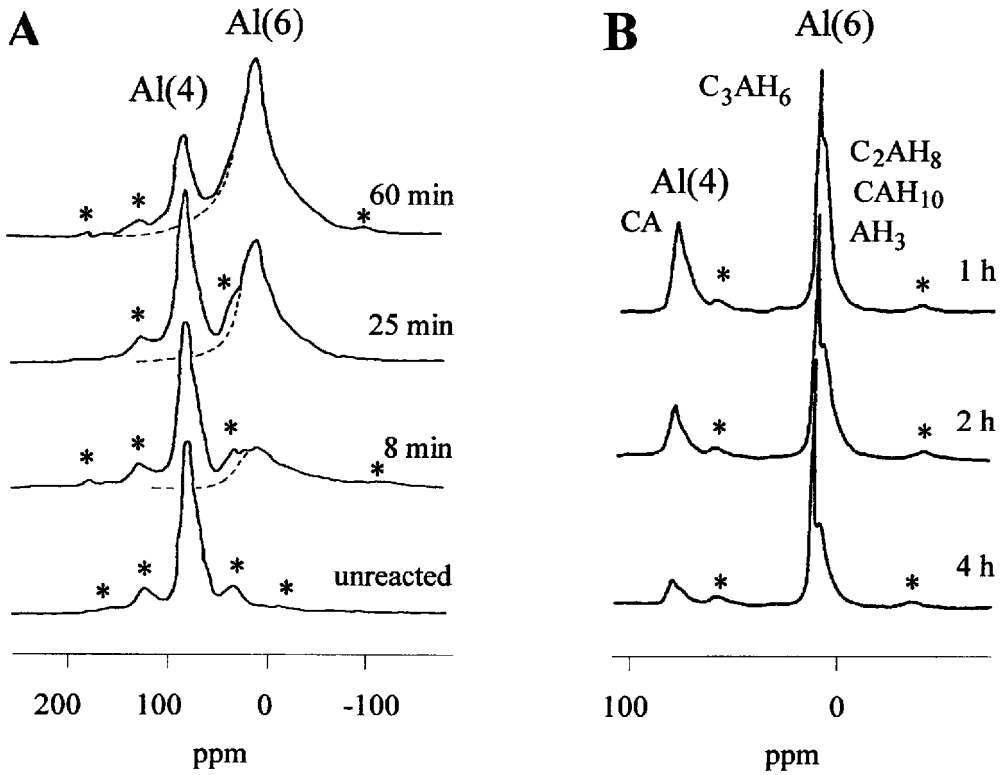

Fig. 3.1. ^{27}Al MAS NMR spectra of hydrated CA cured at 70° C, **A:** 70.4 MHz spectra measured by using MAS spinning rates of 3.3 kHz (adapted from [17]); **B:** 104.2 MHz spectra measured by using MAS spinning rates of about 6 kHz and ^{1}H decoupling (adapted from [18]). * denotes spinning sidebands.

Recently a very detailed ^{27}Al MAS NMR study on the characterization of calcium aluminate phases in cements was published by Skibsted et al. [22]. Besides the analysis of the center part spectra arose from the central transition (m=1/2 m=-1/2) of the Al nuclei even a careful analysis of the spinning sideband manifolds due to the satellite transitions (m=1/2 m=3/2 and m=3/2 m=5/2) was performed. Fig. 3.2A shows the ^{27}Al MAS NMR spectrum of monosulfate ($C_4A\bar{S}H_{12}$), fig. 3.2B the corresponding spectrum of C_4AH_{13} having nearly identical center parts of the spectra (b) but different spinning sideband pattern (c) indicating different quadrupole coupling parameters.

This procedure used in [22] resulted in quadrupole coupling parameters and chemical shift values of high accuracy for the most important calcium aluminates and their hydration products. Based on these data the hydration products of calcium aluminates in high alumina cements and portland cements have been characterized.

It has been established that in the hydrated high alumina cement the CAH-phases C_3AH_6 and AH_3 were the dominating hydration products but also minor amounts of unhydrated CA and CA_2 were observed.

In an ordinary portland cement hydrated for 28 days ettringite and monosulfate were found to be the hydration products of the calcium aluminate phases.

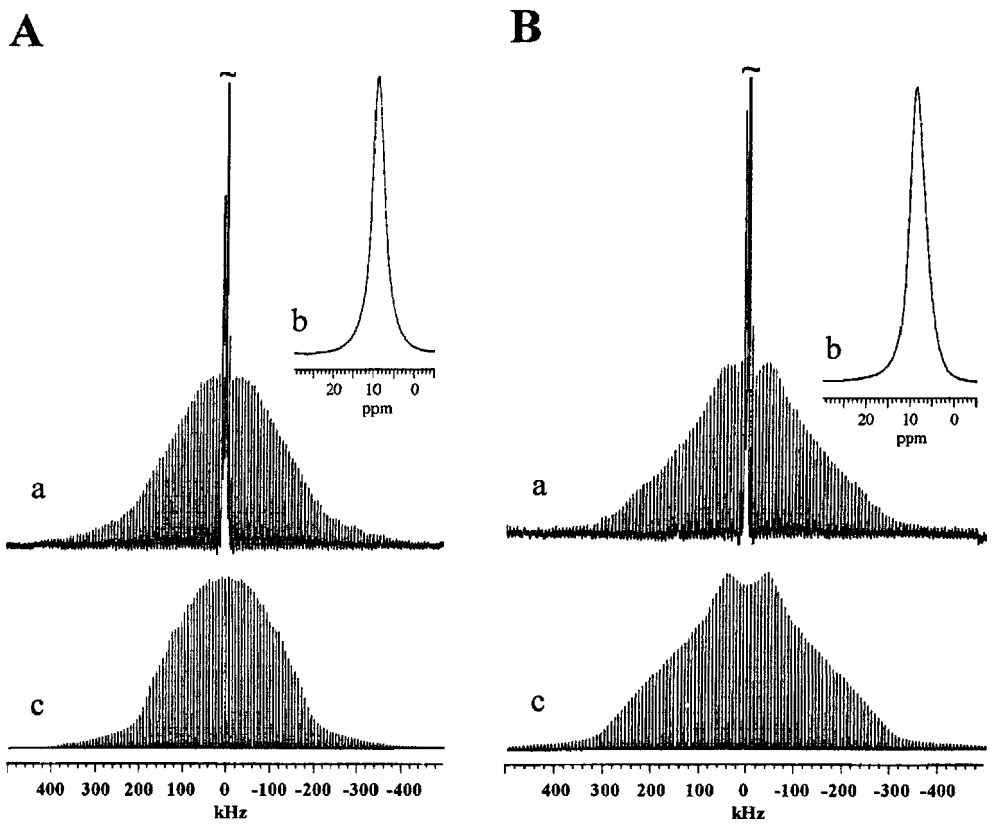

Fig. 3.2. ^{27}Al MAS NMR spectra of $C_4A\overline{S}H_{12}$ (**A**) and C_4AH_{13} (**B**), **a:** experimental spectra, **b:** center bands, **c:** simulated spinning sideband manifolds (adapted from [22]).

4 NMR Studies on the Influence of Alkali-Ions on Reactive Silica and CSH-Phases with Respect to the Alkali-Silica-Reaction (ASR) in Concretes

Since Stanton observed in 1940 the destructive effect of the formation of an alkali containing silica gel in concretes [23] several efforts were made to get a deeper insight into the mechanism of this concrete damaging process.

In the meantime it is well established that the source of this crack formation in concrete is a result of a reaction of alkali hydroxides like NaOH and KOH with reactive silica by which an amorphous alkali silicate gel of unknown constitution is formed (see e.g. [24]). This gel adsorbs water and swells by which stresses are generated in the concrete leading to crack formation and an expansion of concrete constructions. The chemical composition of such gel varies very much with respect to their Me/Ca- and the (Me + Ca)/SiO_2 ratio, where Me=Na, K.

The main problem for a better understanding of the chemical mechanism of the ASR with respect to counteract this destructive effect on a well founded scientific base is that we have a lack of knowledge about the structural types of the silicates in these ASR gels.

Especially in this field during the last two years some new results appeared encouraged by NMR investigations, which shall be presented in this chapter.

In the 80ies Young [25] and Grutzeck et al. [26] investigated ASR gel samples from different concrete constructions by ^{29}Si MAS NMR experiments and found that these gels consist of Q^2, Q^3 and Q^4 groups where the Q^3 groups are the dominating building units. This means that the gels should contain predominantly alkali silicate layer structures.

Some years later in 1993 Cong et al. [27] published ^{29}Si MAS NMR investigations on the reaction of different highly-condensed silica sources (Nevada opal, Beltane opal, cristobalite) with KOH solution in the presence and absence of $Ca(OH)_2$ by which they tried to produce a gel similar to that from real ASR damaged concrete constructions. In the reaction of Beltane opal with mixtures of KOH solution and $Ca(OH)_2$ they found (see fig. 4.1A) that the Q^4 groups of the threedimentional SiO_2 network (signal at -112 ppm) are converted with increasing reaction time to Q^1 (signal in the range of -79 ppm), Q^2 (signals between -82 ppm and -85 ppm) and Q^3 groups (signals in the range from -92 ppm up to -97 ppm).

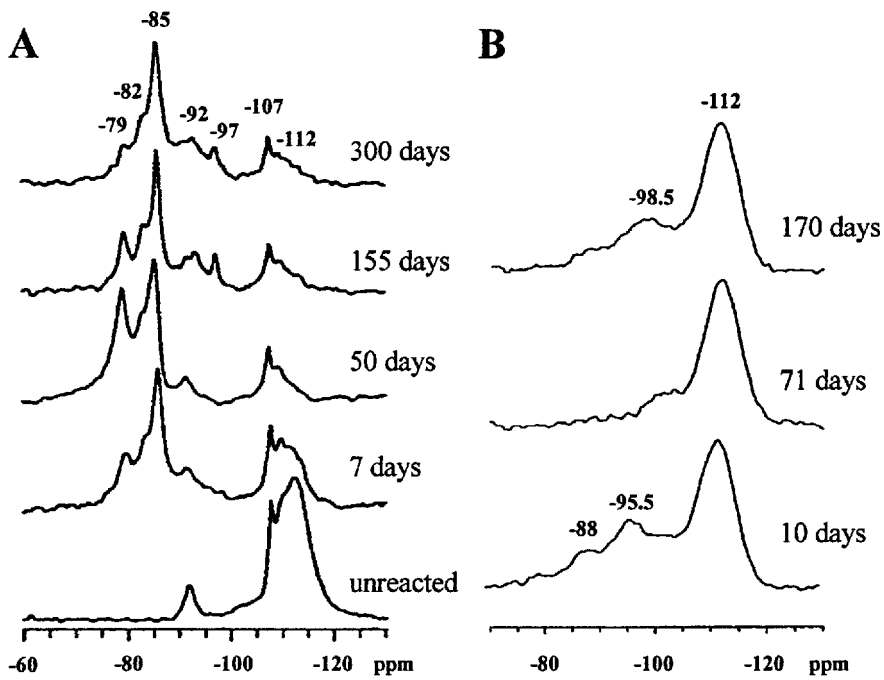

Fig. 4.1. ^{29}Si MAS NMR spectra of the reaction products of Beltane opal with KOH solution. **A:** reaction in the presence of $Ca(OH)_2$, **B:** reaction in the absence of $Ca(OH)_2$ (adapted with some changes from [27]).

The intensities of the NMR signals of the Q^3 groups (δ=-92 till -97 ppm) from the layer silicates are relatively low. But it is surprising that there is one signal with a relatively small line width at -97 ppm which is an indication that a crystalline layersilicate of unknown structure is formed.

A total different set of spectra they obtained when they studied the reaction of Beltane opal only with a KOH solution. The corresponding spectra are presented in fig. 4.1B. The spectra collected till to a reaction time of 170 days show that mainly Q^3 groups (NMR signals between -95.5 and -98.5 ppm) are formed attributed to branching SiO_4 tetrahetra of layersilicates. Q^1 and Q^2 groups are present only in very small amounts.

These differences between the reaction products formed in the reaction of Beltane opal and KOH solution in the presence of $Ca(OH)_2$ and that of opal and KOH solution in the absence of $Ca(OH)_2$ seems to us of great importance with respect to the mechanism of the ASR. But the authors of that paper did not discuss these differences to characterize the chemical process in this reaction.

We will come back to these results later on in this chapter.

To follow the reaction of silica and $Ca(OH)_2$ with water also at the early states of this process Brough et al. [28] used for their ^{29}Si MAS NMR studies ^{29}Si enriched silica which allowed them to collect spectra with a good signal-to-noise ratio in a relatively short time. To exclude the influence of alkali hydroxide they omitted in one of the reactions studied the addition of KOH. In this way they tried to study a "poor" puzzolanic reaction. The resulting spectra of this ^{29}Si MAS NMR investigation which was performed using samples with a solution/solid ratio of 0.7 are presented in fig. 4.2.

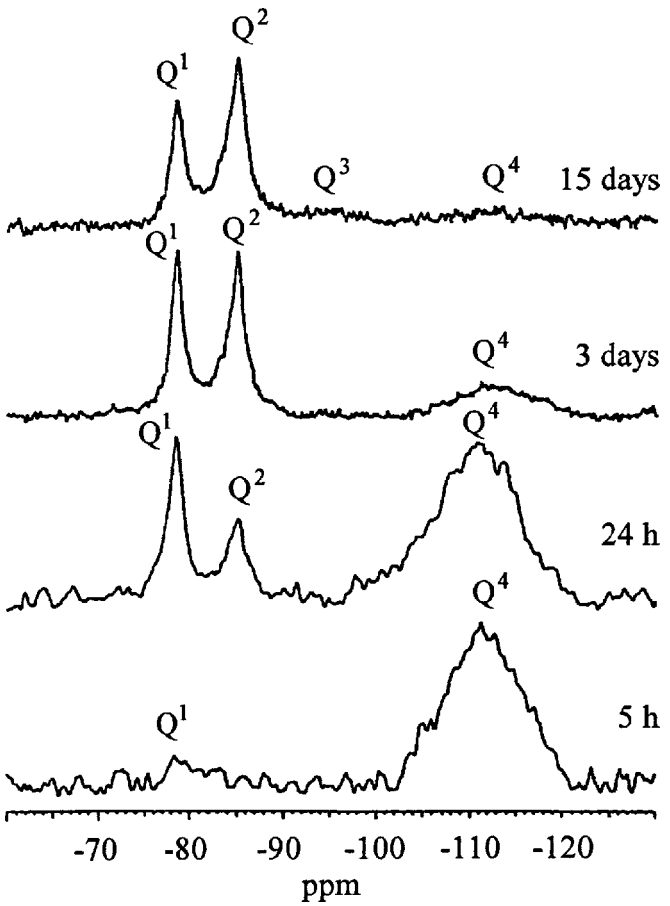

Fig. 4.2. Selected ^{29}Si MAS NMR spectra showing the reaction of calcium oxide with water and silica (adapted from [28]).

From these spectra it can be seen that the Q^4 groups of silica are transferred to Q^1 (end groups) and Q^2 (middle groups) indicating relatively low molecular chainlike anions. Only a very small amount of Q^3 groups can be recognized the nature of which is still unknown. These results are very similar to those of Cong et al. [27] with only one exception that in the paper of Cong et al., possibly as a consequence of the presence of KOH, the Q^3 signal is more intensive. To this difference we will also refer later on in this chapter.

To investigate a reaction which is more similar to the cement hydration Brough et al. studied in the already mentioned paper [28] also the reaction of C_3S with silica and water in the presence of KOH using samples with a solution/solid ratio of 0.5. In the reaction referred here a C_3S containing ^{29}Si in natural abundance and a silica labeled with enriched ^{29}Si were used. Such an experiment is profitable in so far, as one can see in the NMR spectrum only the signals of those silicate species which result from the reaction of the ^{29}Si enriched silica with $Ca(OH)_2$ and KOH solutions while the corresponding reaction products of the C_3S hydration are not detectable because of its low ^{29}Si content. The results of this ^{29}Si MAS NMR investigation are presented in fig. 4.3.

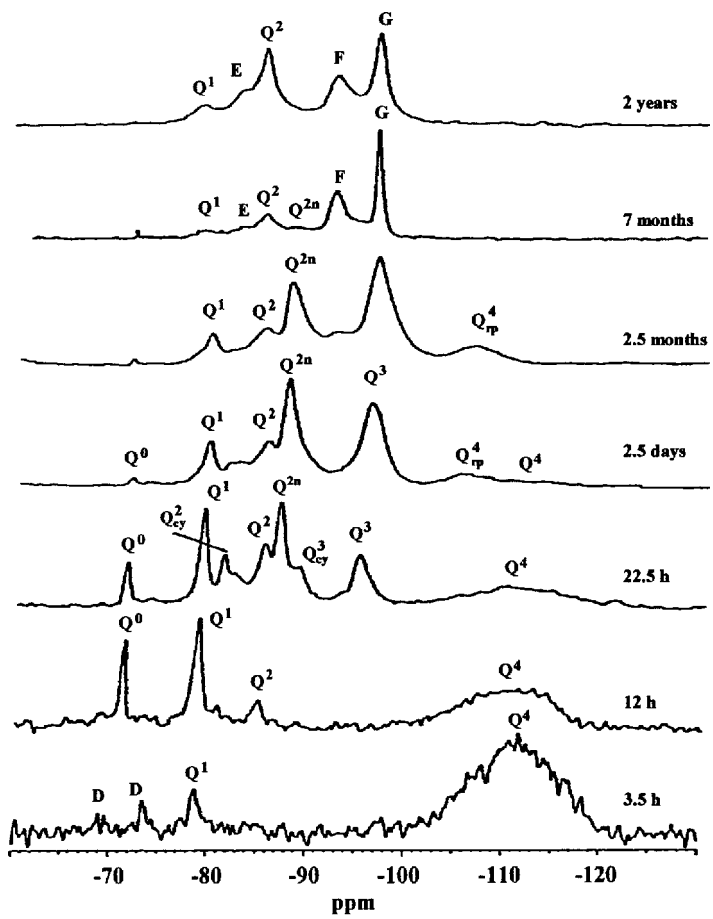

Fig. 4.3. ^{29}Si MAS NMR spectra showing the reaction of KOH solution with a blend of C_3S containing ^{29}Si in natural abundance and silica enriched in ^{29}Si in dependence of time (adapted from [28]).

Already after 12 h of hydration monomeric Q^0, end groups (Q^1) and middle groups (Q^2) groups are formed by the alkaline attack of $Ca(OH)_2$, resulting from the hydration of C_3S, and KOH. In addition to these reaction products after 22.5 h Q^2 groups of cyclic silicates and a second sort of Q^2 groups are formed. But already at this stage of the reaction NMR signals of Q^3 groups (G) appear at -97 ppm with a relatively strong intensity. This signal and a further one (F) in the Q^3 region increases with increasing reaction time. Compared to this the intensity of the NMR signals of the Q^0 groups decreases to zero, so that after 2 years only signals of Q^1, Q^2 and two different Q^3 groups can be detected.

With exception of a higher resolution of the ^{29}Si MAS NMR spectra these results are totally comparable with those obtained by Cong et al. [27] using Beltane opal instead of silica.

The NMR investigations mentioned above clearly show that during the hydration in the system SiO_2 — $Ca(OH)_2$ which is very similar to the C_3S hydration and the puzzolanic reaction only Q^1 (end groups) and Q^2 (middle groups) forming low molecular chainlike polysilicates as in CSH phases are formed.

In contrast to this in the system C_3S — $Ca(OH)_2$ — SiO_2 — alkali hydroxide in addition to the Q^1 and Q^2 groups Q^3 groups can be detected. On the basis of these results we assume that the expansion of concrete in the alkali-silica-reaction is a consequence of the layersilicate formation [29].

But because it was not possible at that time to assign the chemical shift values of the observed Q^3 groups to special type of layersilicate structures and to decide if there are alkali layersilicates which are able to swell, we performed systematic investigations of different alkali silicate minerals consisting of layer structures by means of solid-state NMR studies and tested their ability to give an expansion.

Analyzing the literature we found the following alkali silicate minerals summarized in table 4.1.

Table 4.1. Alkali silicate minerals

mineral	*idealized composition*
Natrosilite	$Na_2[Si_2O_5]$
Silinaite	$NaLi[Si_2O_5] \cdot 2\ H_2O$
Kanemite	$Na[HSi_2O_5] \cdot 2\ H_2O$
Makatite	$Na_2[H_2Si_4O_{10}] \cdot 4\ H_2O$
Magadiite	$Na_2[H_2Si_{14}O_{30}] \cdot x\ H_2O$
Kenyaite	$Na_2[H_2Si_{20}O_{42}] \cdot x\ H_2O$

From these silicates we were most interested in the mineral Kanemite because in 1994 Tapper et al. [30] showed that a synthesis of this compound is possible by the conversion

of the δ-modification of $Na_2[Si_2O_5]$ with SiO_2 in the presence of water in a "solid-state like" reaction, according to the following reaction equation,

$$\delta\text{-}(Na_2Si_2O_5)_x + 2SiO_2 + 7\,H_2O \longrightarrow 2[NaHSi_2O_5 \cdot 3\,H_2O]_x$$

which seems to be very similar to the alkali-silica-reaction.

A detailed investigation of Kanemite by multinuclear solid-state NMR spectroscopy has shown, that the silicate layers of this compound consist of identical SiO_4 terahedra (Q^3 groups) which are characterized in the ^{29}Si MAS NMR spectrum by one sharp signal at -97.7 ppm [31,32].

To follow *in situ* the formation of Kanemite according to the reaction described by Tapper et al. we used in our ^{29}Si MAS NMR experiments silica samples which were enriched in ^{29}Si [33,34].

Selected ^{29}Si MAS NMR spectra of these investigations are presented in fig. 4.4 showing the reaction of two different silica after increasing reaction times.

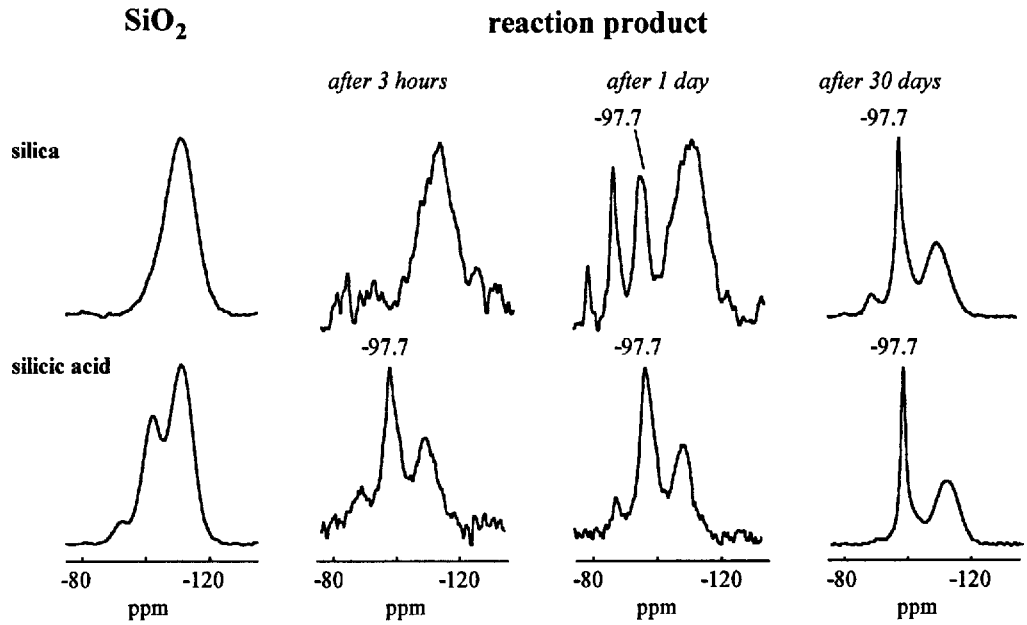

Fig. 4.4. ^{29}Si-MAS-NMR spectra of *in situ* studies of the formation of Kanemite starting from different ^{29}Si-enriched SiO_2 sources at increasing reaction times.

It is clearly to be seen that the Q^4 groups of the starting silica (signals at about -112 ppm) are not directly converted to Q^3 groups of Kanemite (signal at -97.7 ppm). After short reaction times also Q^1 and Q^2 groups can be observed. That means that the degradation of the silica structure goes via the splitting off low molecular silicate species as we demonstrated by degradation experiments of silica gels in alkaline solutions [35]. With increasing concentration of the silicates in the aqueous phase at least high molecular layerslicates are formed as it is a general rule in silicate chemistry.

Even though these experiments are performed with sodium silicates we found the same ^{29}Si NMR signal at -97 ppm for the Q^3 groups as Brough et al. [28] found investigating

the reaction with potassium hydroxide. This means that in both cases the same Kanemite-like silicate layer structures are formed.

To test if the Kanemite formation is connected with an expansion we pressed samples from mixtures of δ-$Na_2Si_2O_5$ and a reactive silica in the mole ratio 1:2 according to the above mentioned equation. The samples were stored in an exsiccator with a relative humidity of 100 %. From fig. 4.5 one can see that this reaction is indeed connected with a relatively high expansion.

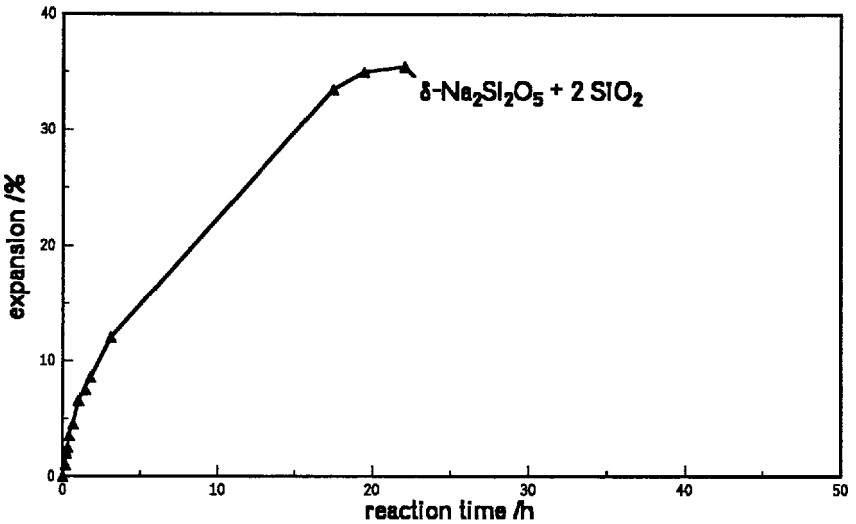

Fig. 4.5. The expansion of Kanemite formed in the reaction of δ-$(Na_2Si_2O_5)_x$ and SiO_2 in the presence of water in dependence on the reaction time.

To demonstrate that this is a real model reaction for the ASR we used instead of reactive silica also minerals i.e. opal or siliceous chalk in the reaction with δ-$Na_2Si_2O_5$. As fig. 4.6 shows we got the same expansion reactions.

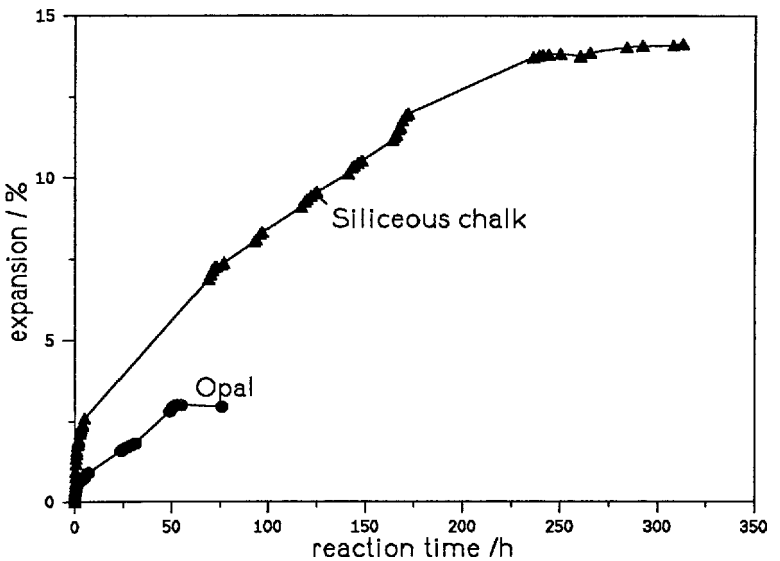

Fig. 4.6. The expansion of the reaction products of δ-$(Na_2Si_2O_5)_x$ and opal and of δ-$(Na_2Si_2O_5)_x$ and siliceous chalk in the presence of water in dependence on the reaction time.

XRD investigations of the reaction products of these experiments show that also in these cases Kanemite as the swelling component is formed.

A further question coming from the above mentioned experiments of Cong et al. and Brough et al. was, in what way $Ca(OH)_2$ will influence this reaction between δ-$Na_2Si_2O_5$ and SiO_2.

Therefore we performed expansion measurements of pressed samples of mixtures from δ-$Na_2Si_2O_5$ and SiO_2 to which $Ca(OH)_2$ was added. These experiments show (see fig. 4.7) that $Ca(OH)_2$ diminishes the expansion but not the total reaction.

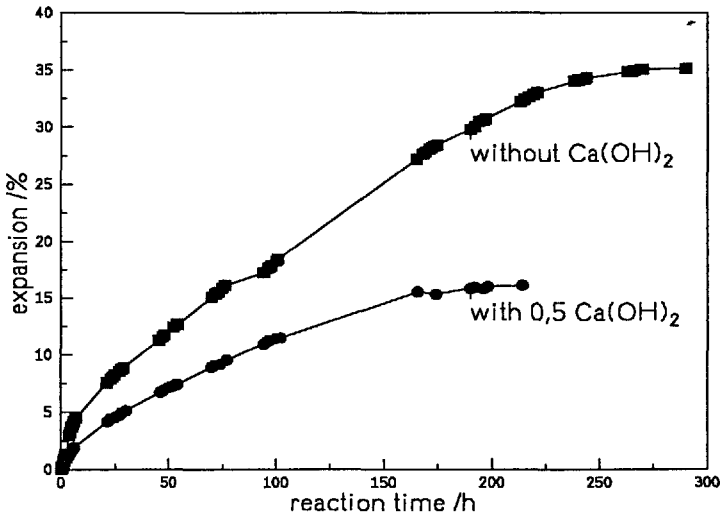

Fig. 4.7. The expansion of the reaction products of δ-$(Na_2Si_2O_5)_x$, SiO_2 and water in the presence and in the absence of $Ca(OH)_2$ in dependence on the reaction time.

Further XRD investigations showed that Kanemite is formed also under these conditions and that the Kanemite structure is not generally changed by a possible incorporation of Ca^{2+} ions by ion exchange into the lattice of Kanemite. The Ca^{2+} containing Kanemite is able to swell like clay minerals with silicate layer structures, too. This would mean that at first alkali silicate layer structures were formed which incorporate Ca^{2+} ions in a secondary reaction step.

On the other hand, in the system SiO_2 — $Ca(OH)_2$ — H_2O or the C_3S — H_2O system without the presence of alkali hydroxides the solubility of Ca-silicates is so low that only very small silicate concentrations can be obtained in the aqueous phases. We know that in very dilute silicate solutions only low molecular silicate species exist which at all the time are precipitated by Ca^{2+} ions. This fact results at least in the formation of the usual CSH phases which are formed in the C_3S- and C_2S hydration as well as in the pozzolanic reaction containing Q^1- and Q^2 groups.

In those cases in which alkali hydroxides are present in the poor aqueous systems of SiO_2 — $Ca(OH)_2$ or C_3S and C_2S , both reaction mechanisms discussed above

- the formation of alkali layersilicate and the following incorporation of Ca^{2+} ions into the layer structures

- the formation of Q^1 and Q^2 groups due to precipitation of low molecular silicate species from the solution by Ca^{2+} ions

are involved in the formation of the hydration products as the ^{29}Si MAS NMR studies referred in this chapter clearly have shown.

Together with the discussions on the mechanism of the alkali-silica-reaction and the structure of the silicates in the ASR gels arose the question if CSH phases itself are able to effect as a SiO_2 source in the alkali-silica-reaction. To answer this question we performed ^{29}Si MAS NMR experiments on samples prepared by hydration of mixtures of δ-$Na_2Si_2O_5$ and different CSH phases [36]. As an example in fig. 4.8 the ^{29}Si MAS NMR spectra of an unreacted CSH phase with a C/S ratio of 1.36 prepared by a hydrothermal reaction of SiO_2 and $Ca(OH)_2$ according to [37] (fig 4.8A) and of the product of the reaction of this CSH with δ-$Na_2Si_2O_5$ in the presence of water vapour after 12 days (fig. 4.8B).

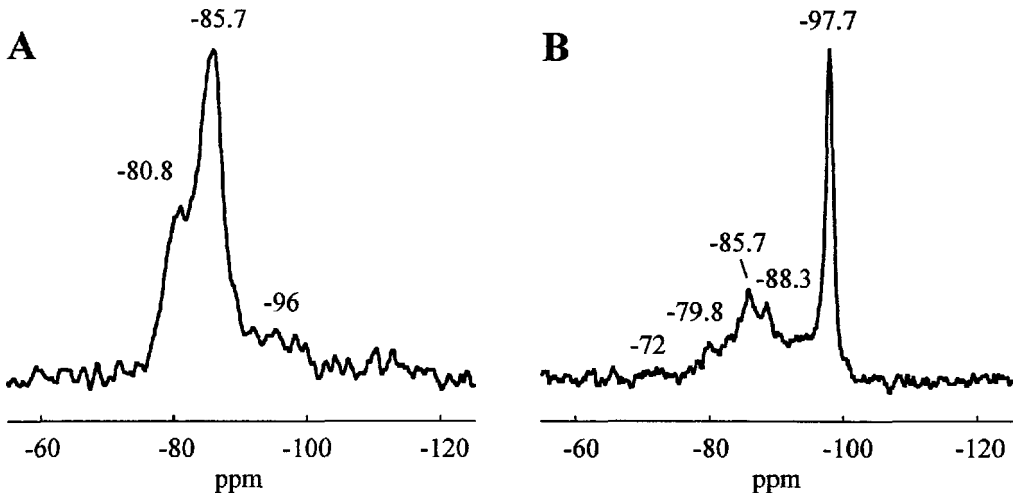

Fig. 4.8. ^{29}Si-MAS-NMR spectra of **A:** CSH, C/S=1.36 and **B:** the product of the reaction of this CSH with δ-$(Na_2Si_2O_5)_x$ in the presence of water vapour after 12 days.

The comparison of both spectra shows at first that also in this reaction Kanemite is formed as demonstrated by the appearance of the small NMR signal at -97.7 ppm. The Kanemite formation goes via a consumption of the original CSH phase visible by the drastic decrease of the intensities of the NMR signals of the CSH in fig. 4.8B. In addition to the signals of Kanemite (-97.7 ppm) and of the residual CSH phase (-80.8, -85.7, -96 ppm) new signals appear at -72 and -88 ppm indicate that during this reaction also low concentrations of monomeric and dimeric silicate species as possible intermediate products are formed.

Expansion measurements on mixes of a CSH phase with C/S=1.3 and δ-$Na_2Si_2O_5$ in the presence of water also show strong expansion (see fig 4.9). ^{29}Si MAS NMR experiments on this sample (not shown here) demonstrate the formation of Kanemite in this case, too.

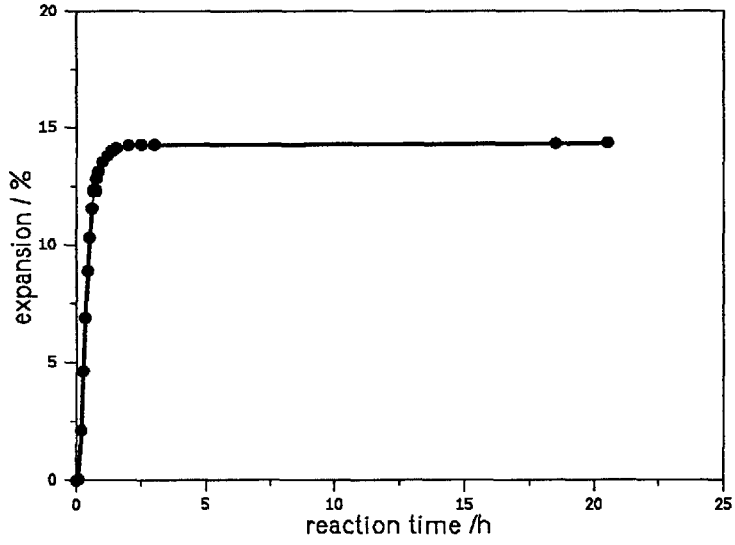

Fig. 4.9. The expansion of the reaction products of a CSH (C/S=1.3) with δ-$(Na_2Si_2O_5)_x$ and water in dependence on the reaction time.

The results indicate that at high alkali hydroxide concentrations CSH phases can be converted to alkali silicates and calcium hydroxide according to the equation

$$Ca_xSi_yO_z + 2x\,NaOH \longrightarrow Na_{2x}Si_yO_z + x\,Ca(OH)_2.$$

These very recent results presented in this chapter showed a few new insights in the understanding of the alkali-silica-reaction but at the same time new question and problems arose from them. In our opinion the further application of the solid-state NMR spectroscopy accompanied with chemical methods should be able to solve also these problems with the aim to reduce or to avoid the corrosion of concrete constructions by ASR in the future.

5 Production Near Application of Solid State NMR

The chemical and engineering properties of portland cements are determined largely by their mineral composition the main constituents of which are alite and belite. In praxis the content of these cement minerals is estimated using the Bogue calculation [38] based on the elemental composition obtained from analytical methods. An improved Bogue calculation has been proposed by Taylor [39].

Already in 1988 Hjorth et al. [19] showed by using ^{29}Si MAS NMR experiments to analyze the alite and belite content of an Aalborg white cement that their results were in significant contrast to the results obtained by the Bogue calculations.

Recently a deep and extensive ^{29}Si MAS NMR investigation of the determination of alite and belite in a large number of different portland cements with variable bulk Fe_2O_3 contents up to 6.7 wt.% was presented by Skibsted et al. [40].

While the ^{29}Si MAS NMR spectra of the crystalline calcium silicates C_3S and β-C_2S are characterized by small well resolved signals (see fig. 5.1A and 5.1B) the spectra of the clinker minerals alite and belite in cements are more complicated. Especially those of the alite modifications consist of much more broader overlapping signals resulting in an unresolved lineshape due to the incorporation of impurities (see fig. 5.1C). The corresponding spectrum of belite is more similar to that of β-C_2S as it is shown in fig. 5.1D.

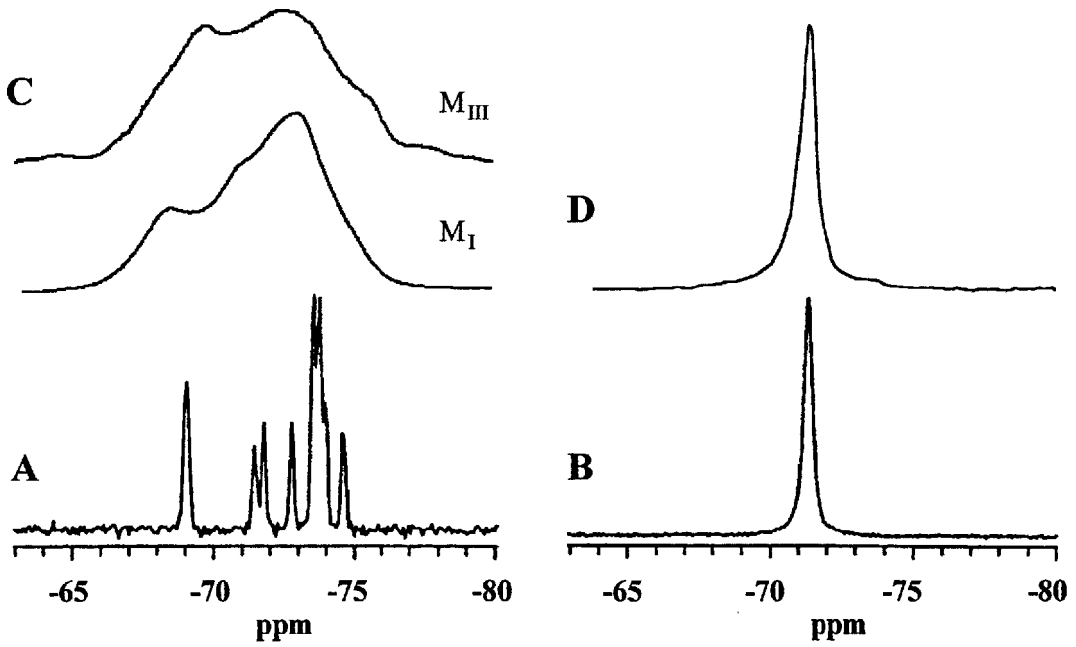

Fig. 5.1. ^{29}Si-MAS-NMR spectra of C_3S.(A), β-C_2S (B), belite (D) and of the M_I and the M_{III} modifications of alite (C). (Spectra A and B were adapted from [41], spectra C and D from [40]).

On basis of the known spectra of alite and belite an improved method for deconvolution of the measured ^{29}Si MAS NMR spectra was developed to decide between the corresponding subspectra of alite and belite and to determine the relative amounts of these minerals. The technique used in [40] is demonstrated in fig. 5.2 for a ^{29}Si MAS NMR spectrum of an oilwell cement.

The results obtained by applying the above illustrated method show that the different cements contain between 5 and 28 wt.% of belite and between 50 and 78 wt.% of alite.

The basis for the high accuracy of these results was that the authors excluded the possibillity of partial saturation effects in their ^{29}Si MAS NMR maesurements by determining the ^{29}Si spin-lattice relaxation times (T_1) for alite and belite in two cements and optimizing the experimental conditions on basis of the T_1 values. The large differences in the T_1 values for alite and belite allowed them to quantify the relative quantities of the two minerals in an independent way. The resulting quantities were in

good agreement with those obtained from the deconvolution of the corresponding ^{29}Si MAS NMR spectra.

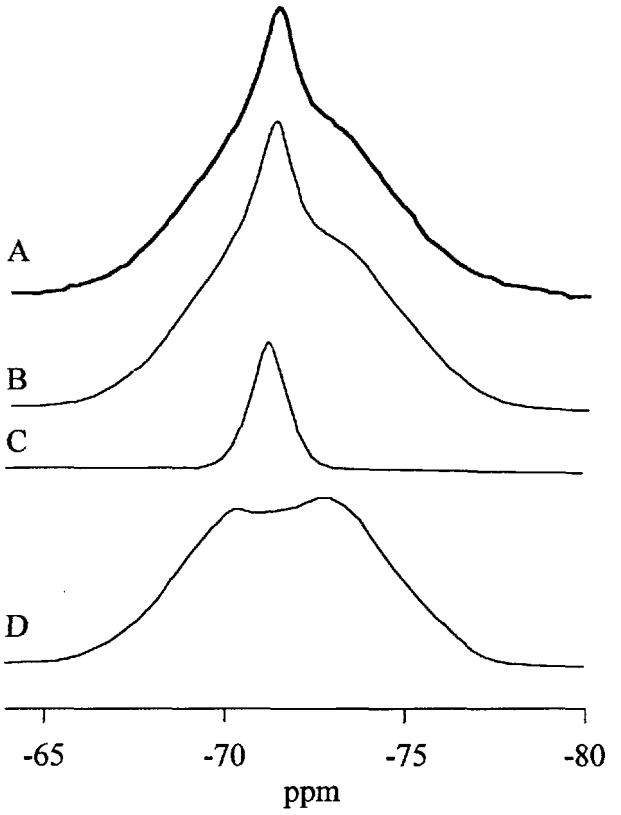

Fig. 5.2. Experimental (A) and simulated (B) ^{29}Si-MAS-NMR spectra of an oilwell cement. The simulated spectrum corresponds to a superimposed subspectrum of belite (C) on a subspectrum of the M_{III} form of alite (D). (adapted from [40]).

These data were compared with those of corresponding Bogue calculations. For the referred example of the oilwell cement the following values were presented (see Table 5.1).

Table 5.1. Results of the determination of calcium silicate phases in an oilwell cement from ^{29}Si MAS NMR, Bogue and Taylor-Bogue calculations (adapted from [40])

^{29}Si MAS NMR		**Bogue calculation**		**Taylor-Bogue calculation**	
alite (wt.%)	belite (wt.%)	alite (wt.%)	belite (wt.%)	alite (wt.%)	belite (wt.%)
72.0	11.2	59.0	17.4	67.4	13.2

This comparison shows that the Bogue calculation strongly overestimates the belite content and underestimates the quantity of alite. In contrast to this the data estimated using the Taylor-Bogue calculation show not such large deviations from the NMR results.

These results suggest that we will have in the future a new and powerful method for the determination of alite and belite in cements.

6 Conclusion

As shown by the selected investigations on some problems of the cement chemistry the solid-state MAS NMR spectroscopy is a powerful method to solve structural problems of amorphous and crystalline compounds in building materials. This method has the advantage that it is possible to investigate the samples directly without chemical conversions.

In this paper we focused our discussions predominantly on the results of NMR measurements. But it has to emphasize that in these investigations it is necessary to have a close collaboration of NMR spectroscopists and chemists beginning from the preparation and the reliable characterization of the samples and ending with the discussion of the yielded NMR spectra.

Such a close collaboration becomes much more important in the future because new and more complicated problems will arise from research on cement based materials and, on the other hand, new and more sophisticated NMR techniques we have not discussed till now will be applied to study solid state problems in this field.

Such techniques are e. g. the two-dimensional NMR spectroscopy which can determine bindings between different SiO_4 tetrahedra ("connectivities") [42] and between SiO_4 tetrahedra and protons [43]. Further new developments in NMR spectroscopy, which can be applicated to research on building materials, are NMR-tomography ("NMRI - nuclear magnetic resonance imaging") allowing e.g. to study the water diffusion in hardened cement pastes [44] or the water distribution in pore systems of building materials [45]. For higher resolution in NMR spectra of quadrupolar nuclei like ^{27}Al, ^{23}Na or ^{17}O the DOR technique (double orientated rotation) comes more and more in use to study scientific problems of the cement chemistry [46]. New developments also appeared in the field of high temperature NMR spectroscopy allowing *in situ* studies up to 2400 K [47].

We are sure that further contributions at this congress on cement chemistry will additional underline the usefulness of NMR investigations in research of building materials.

Acknowledgement

For the part of our own investigations we would like to thank the Deutsche Forschungsgemeinschaft for financial support.

References

[1] A. Abragam, Principles of Nuclear Magnetism, Oxford Press, Oxford 1960

[2] U. Haeberlen, High resolution NMR in solids, Academic Press, New York 1976

[3] M. Mehring, Principles of High Resolution NMR in Solids, 2nd ed., Springer Verlag, Berlin 1983

[4] R. Ernst, G. Bodenhausen, A. Wokaun, Principles of Nuclear Magnetic Resonance in One and Two Dimensions, Oxford Clarendon Press, Oxford 1987

[5] W. Wieker, VI. Internat. Congress of the Chemistry of Cement, a principal paper, Moscow 1974

[6] G. Engelhardt, D. Michel, High resolution Solid State NMR of Silicates and Zeolites, Wiley, New York 1987

[7] P. Colombet, A.-R. Grimmer (eds), Application of NMR Spectroscopy to Cement Science, Gordon and Breach, London 1994

[8] P. Colombet, A.-R. Grimmer (eds), Nuclear Magnetic Resonance Spectroscopy of Cement-based Materials, Springer Verlag, Berlin 1997, in press

[9] E. Lippmaa, M. Mägi, M. Tarmak, W. Wieker, A.-R. Grimmer, Cem. Concr. Res. **12** (1982) 597

[10] A.-R. Grimmer, In: P. Colombet, A.-R. Grimmer (eds) Application of NMR Spectroscopy to Cement Science, Gordon and Breach, London 1994, p. 77

[11] X.-D. Cong, R. J. Kirkpatrick, Adv. Cem. Res. **7** (1995) 103

[12] X.-D.Cong, R. J. Kirkpatrick, Advn. Cem. Bas. Mat. **3** (1996) 144

[13] X.-D. Cong, R. J. Kirkpatrick, J. Am. Ceram. Soc. **79** (1996) 1585

[14] Y. Okada, H. Ishida, T. Mitsuda, J. Am. Ceram. Soc. **77** (1994) 765

[15] D. Heidemann, W. Wieker, In: P. Colombet, A.-R. Grimmer (eds) Nuclear Magnetic Resonance Spectroscopy of Cement-based Materials, Springer Verlag, Berlin 1997, in press

[16] D. Heidemann, W. Wieker, submitted to Cem. Concr. Res.

[17] D. Müller, A. Rettel, W. Gessner, G. Scheler, J. Magn. Reson. **57** (1984) 152

[18] D. Müller, A. Rettel, W. Gessner, J. P. Bayoux, A. Capmas, In: P. Colombet, A.-R. Grimmer (eds), Application of NMR Spectroscopy to Cement Science, Gordon and Breach, London 1994, p 259

[19] J. Hjorth, J. Skibsted, H. J. Jakobsen, Cem. Concr. Res. **18** (1988) 789

[20] T. Luong, H. Mayer, H. Eckert, J. Am. Ceram. Soc. **72** (1989) 2136

[21] X.-D. Cong, R. J. Kirkpatrick, J. Am. Ceram. Soc. **76** (1993) 409

[22] J. Skibsted, E. Henderson, H. J. Jakobsen, Inorg. Chem. **32** (1993) 1013

[23] T. E. Stanton, Proc. Am. Soc. Civil Engineers **66** (1940) 1781

[24] H. E. Vivian, Bull. No **256** Studies in Cement-Aggregate Reaction, CSIRO, Melbourne 1950

[25] J. F. Young, J. Amer. Ceram. Soc. **71** (1988) C-118

[26] M. Grutzeck, A. Benesi, B. Fanning, J. Amer. Ceram. Soc. **72** (1989) 665

[27] X.-D. Cong, R. J. Kirkpatrick, S. Diamond, Cem. Concr. Res. **23** (1993) 811

[28] A. R. Brough, C. M. Dobson, I. G. Richardson, G. W. Groves, J. Mater. Sci. **31** (1996) 3365

[29] W. Wieker, C. Hübert, R. Ebert, 10th Internat. Conf. on Alkali-Aggregate Reaction in Concrete, Melbourne 1996, proc. p. 919

[30] A. Tapper, R. Adrian, G. Schimmel, EP 0627 383 A1 v. 30.04.1994

[31] W. Wieker, D. Heidemann, R. Ebert, A. Tapper, Z. anorg. allg. Chem. **621** (1995) 1779

[32] D. Heidemann, R. Ebert, W. Wieker, 17th Conference and Workshop on Magnetic Resonance and the Structure of Matter, Gosen 1995, proc. p. 158

[33] D. Heidemann, R. Ebert, W. Wieker, 9. Deutsche Zeolith-Tagung, Halle 1997, Tagungsband Po 87

[34] W. Wieker, C. Hübert, D. Heidemann, R. Ebert, 3rd Conf. on Solid State Chem., Bratislava 1996, proc. p. 88

[35] C. Hübert, Ph. D. Thesis, Akademie der Wissenschaften der DDR, Berlin 1988

[36] W. Wieker, D. Heidemann, to be published in Cem. Concr. Res.

[37] H. Stade, Z. anorg. allg. Chem. **470** (1980) 69

[38] H. F. W. Taylor, Cement Chemistry, Academic Press, London 1990

[39] H. F. W. Taylor, Adv. Cem. Res. **2** (1989) 73

[40] J. Skibsted, H. J. Jakobsen, C. Hall, J. Chem. Soc. Faraday Trans. **91** (1995) 4423

[41] R. J. Kirkpatrick, X.-D. Cong, In: P. Colombet, A.-R. Grimmer (eds), Application of NMR Spectroscopy to Cement Science, Gordon and Breach, London 1994, p. 55

[42] A. R. Brough, G. W. Groves, I. G. Richardson, S: A. Rodger, C. M. Dobson, In: P. Colombet, A.-R. Grimmer (eds), Application of NMR Spectroscopy to Cement Science, Gordon and Breach, London 1994, p. 201

[43] I. Klur, J. Virlet, In: P. Colombet, A.-R. Grimmer (eds) Nuclear Magnetic Resonance Spectroscopy of Cement-based Materials, Springer Verlag, Berlin 1997, in press

[44] G. Papavassiliou, F. Milia; M. Fardis, R. Rumm, E. Laganas, O. Jarh, A. Sepe, R. Blinc, M. M. Pintar, J. Am. Ceram. Soc. **76** (1993) 2109

[45] G. Guillot, A. Dupas; In: P. Colombet, A.-R. Grimmer (eds), Application of NMR Spectroscopy to Cement Science, Gordon and Breach, London 1994, p. 313

[46] D. Massiot, D. Müller, P. Florian, J. P. Coutures, EENC, Oulu (Finland) 1994, proc.

[47] B. Cote, D. Massiot, J. P. Coutures, B. Poe, P. McMillan, In: P. Colombet, A.-R. Grimmer (eds), Application of NMR Spectroscopy to Cement Science, Gordon and Breach, London 1994, p. 171

THEME I

CLINKER AND CEMENT PRODUCTION

TOPIC I.A

Process technology

DEVELOPMENT OF SPECIAL CEMENTS

Tamara V. KOUZNETSOVA
Mendeleev University of Chemical Technology of Russia,
Moscow, Russia

ABSTRACT As the production of any kind of cement is based on theoretical and social demands the main trends in the development of special cements are reported. Generally the developments of aluminate, sulphoaluminate, expansive and oil-well cements are discussed.

KEY-WORDS Sulphoaluminate,aluminate cement,expansive cement.

INTRODUCTION

Progress in new technology and engineering,improvement of the existing technological processes in the different field of the production require the creation of special cements whose characteristics were outside the properties of Portland cements and which may replace Portland Cement in special application. More than thirty kind of special cements are manufactured in the world (Chatterji, 1992, Muzhen et al, 1992, Kouznetsova, 1986, Roy, 1986). In this paper the author rewiews some of them.

PHYSICAL-CHEMICAL BASE OF TECHNOLOGY OF SPECIAL CEMENTS

The study of clinker formation.

Fundamental investigations in clinker chemistry were carried out (Butt and Timashev, 1967, Taylor, 1990). The main clinker minerals, their solid phases and polimorphic transformation were studied. At present the great attention is paid to mineral modifies and their influence on the liquid phase of clinkers.

Depending on the nature and the concentration of modifiers, oxide and oxide-salt liquid phases are formed. Their properties depend on the element correlation in local volume of clinker granule. When the salts are disolved at the oxide liquid phase the melt zones appear, where significant ammounts of CaO are disolved, the process of alite formation is enhenced (Osokin et al, 1993).

It was established that mineralogical composition as well as the character of alite and belite crystallization play an important role in the formation of cement properties (Kouznetsova, 1980)

Clinkers with the different degres of crystallization of the constituent minerals provide cements with different comprehensive strengths (Maki, 1980).

It was establised that alite and belite crystals of the industrial clinkers have inhomogeneous compositions. In crystal

cores the relation of CaO/SiO_2 is bigger than in the periphery parts. Inregular distribution of the minor ions are obvious. This leads to the formation of defect crystal structure of minerals, and to changes in their hydraulic activity.

Accumulated knowledge permitted development of high strength cements (Kravchenko et al, 1971). Later this study was transformed to obtain cement with low water requirements (LWR) and high-Performance Concrete (Carino and Clifton, 1991).

Hydration and hardening of cement paste.

Today most of the crystal hydrates composing set cement have been determined, regularities of intergrowth of various crystal hydrates with each other and strength of aggregation of various crystal types have been studied. Models of cement as a composition material have been worked out. The role of crystalline and gellike phases in the formation of hardened cement paste structure has been established. With the help of detailed electron microexaminations, the interrelations between microstructures of the main phases in subject to external load o have been analyzed. It has been shown that the appearance of interphase microcracks, joining together in main cracks of failure is caused by difference between the crystal symmetry of crystals and aggregations.

Microcracks arise at the boundaries microregions with lower symmetry near the zones of portlandite and calcium hydroaluminates. Silicate and aluminate hydrogels resist the development of these microcracks thanks to microstress relaxations and to reinforcement of gels by crystalline aggregations of needle-shaped fibres of calcium hydrosilicates and ettringite.

It is established that dimensions of some fibres and geometric characteristics of aggregations can be changed, affecting the cement composition and its grinding conditions. A mathematical theory of strength of fibre-gellike structures is needed which is able to indicate the best dimensions of fibres and the best arrangement in the aggregates in oder to approximate the optimum characteristics using technological methods.

Thus, theoretical study and experimental data became the base of special cement development.

High Alumina Cement. This cement is characterized by high strength, refractoriness and resistance to corrosive media and molten metal. Concrete strength is known to depend on the mineralogical and granulometric composition.

To optimize the conditions of calcination of alumina cement containing generally monocalcium aluminate the phase condition diagrams of the $CaO-Al_2O_3$ mineralizer system were investigated. The mineralizer was one of the following compounds: calcium chlorides, fluorides, borates and chromates. The mechaniam of interaction of Al_2O_3 and CaO in the presence of these

mineralizers was described and the possibilty of changing of mineralogical composition of high alumina cement was reported.

Modification of hihg alumina cement is carried out by producing barium and strontium aluminates whose application range is limited to 1800°C. For higher temperatures zirconium-bearing cements must be used. These cements include barium zirconium aluminate, calcium zirconium aluminate and strontium zirconium aluminate types. The basic components are barium zirconates and calcium aluminates as well as strontium aluminates and zirconates. These cements exhibit a high heat resistance up to 2400°C, compressive strength up to 65 MPa, and low shrinkage (about 1%).

Spinel-bearing cements include spinel and alkali aluminates. Depending on the spinel composition, these cements relate to two types: aluminomagnesia spanel, $MgO{\cdot}Al_2O_3$, and chromia-magnesia spinel, $MgO{\cdot}Cr_2O_3$. These cements relate to high resistant, early setting, and high strength materials because they contain calcium aluminates in addition to spinels.

Expansive cements. Development of these cements proceed in two ways:
- production of clinker containing C_3S and C_4A_3S simultaneously, used for manufacture of expansive and self-stressing cements (Kravchenko, 1978). The clinker produced contained 50-60% of C_3S and considerable amount of C_4A_3S. The cement made of the such clinker had the initial setting time of 12 to 48 min and the final setting time of 17 to 145 min. The strength at 3 days was 20-40 MPa. A great deal of attention is devoted to the problem of durability of these cements. It was reveled that the samples of concrete made of expansive cement after 10 years had the same durability as those of portland cement.
Thus the cements with composition of $3CaO{\cdot}3Al_2O_3{\cdot}CaSO_4$ as well as its mixture with portland cement represent type of cement resistant to attack by aqveous sulphate and magnesium .

- mix of expansive cement with polymer. Current studies at RCTU and Minskmetrostroj showed the polymer-cement system to have significantly higher mechanical properties. Expansive cement with polymer addition is used for quality chemical basins.
Using fine milled slag or portland cement polymer-slag composite allowed production of doors, window frames and wear-resistant bench tops as a replacement for plastics, asbesto-cement units or aluminum.

Oil-well cements. In order to be an effective seal, the cement must possess the following properties:
-have a low permeability,
-form a good bond with the rock and the casing
-maintain these properties under downhole temperature and pressure conditions, and also whilst the casing undergoes vibration caused by continued drilling.

In addition to providing zonal isolation, the cement also

performs two other important functions:
-protecting the casing against aggressive wellbore fluids,
-protecting the casing against collapse by rock creeping in on the wellbore.

It is known more than 30 types of these cements (Benstead, 1983, Klusov at al, 1987).

Oil-well cements differ in a number of important aspects from construction cements. They need to be of higher reactivity than construction cements and simultaneously to allow sufficient time for pumping the slurries into position in the annulus before hardening.

CONCLUSION

The brief summary of special cement development will be caused by theoretical researches, development of chemistry cement. The high properties of special cements are used for the production of various types of concrete and construction.

REFERENCES

Bensted, J "Oilwell cements". Chemistry and Industry, 1983, No10, p.776-778

Butt, Y.M., Timashev, V.V. "Portland cement clinker", Moscow, Stroijzdat, 1967, 303 p.

Carino, N.Y., Clifton, Y.R. "High-Performance Concrete: Research Needs to Enhance its Use", Authorized reprint from: September, 1991 issue of ACI Concrete International, p. 70-76.

Chatterji, A.K. "Special and New Cements" Procudings of 9th International Congress on Cement Chemistry, 1992, v.1, p.177-213

Kravchenko, I.V., Kouznetsova, T.V., Chlusov, V.B. "Alitesulpho-aluminate clinker and cements on its base"., Cement, 1978, No 8, p. 7-9.

Klusov, A.A., Shalapin, M.M., Kouznetsova, T.V. "Fast-setting oilwell cements for low temperature", Moscow, Gase Industry, 1987, 32 p.

Kouznetsova, T.V. "Aluminate and sulphoaluminate cements", Moscow, Stroijzdat, 1986, 206 p.

Kravchenko, I.V., Vlasova M.M., Yudovich, B.E. "Fast hardening and high strength cements", Moscow, Stroijzdat, 1971, 231 p.

Maki, I. "Relationship of processing parameters to clinker properties", Proceedings of 8th International Congress on Cement Chemistry, 1986, v.1, p. 34-51

Muzhen, S., Kurdowski, W., Sorrentino, F. "Development in non-portland cements", 9th International Congress on Cement Chemistry, 1992, p. 317-357

Roy, D.M. "Advanced Cement Systems, including CBC, DSP, MDF", 9th International Congress on Cement Chemistry, 1992, v.1, p. 357-383

Taylor, H.F.W. "Cement Chemistry", London, Academic Press, 1990, 475 p.

Kn o. 26. OKT. 2000 d o k 31002

1i002
4 pp

UTILISATION OF KILN DUST FOR CLINKER PRODUCTION USING CRI - MODERN VERTICAL SHAFT KILN TECHNOLOGY

Dr (Ms) K RAINA, B NEDUMARAN and S N MEHROTRA
National Council For Cement and Building Materials, New Delhi, India

ABSTRACT Dust collected from the waste gases of cement rotary kiln contain higher concentration of alkalies and chloride. Accumulated dust within the area of the plant, represents permanent source of pollution. The present work establish the utilisation of kiln dust as a useful raw material for clinker manufacture through CRI-Modern Vertical Shaft Kiln (CRI-MVSK) Technology. Analysis of resultant clinker produced indicate low alkali and chloride content, hence making it a low alkali cement.

Key Words: Alkali, Chloride, Microscopy, SEM, XRD

INTRODUCTION

Large quantities of dust are collected from the waste gases of all cement kilns during burning process. Kiln dust represents a material which has already been quarried, ground, blended and partially calcined having fineness of 5000-6000 blaine. The undesirable materials such as potash, sodium, chloride and sulphur from raw materials and fuel concentrate are present in the dust (Malroum, 1994). Large quantity of kiln dust can not be returned to the kiln because of coating and clogging problems especially in wet process kilns. Dust generated from wet process kilns are approximately 8-12%. Indian cement industry generates about 0.4 - 0.6 million tonnes of kiln dust from its 25 wet process cement plants. In many countries including India the disposal of kiln dust is an increasing problem and accumulation of this waste within the area of the plant represents permanent source of pollution as it is a harmfull waste due to its high alkali and chloride content.

Many uses of kiln dust has been surveyed by Bhatty (1984). However National Council for Cement and Building Materials, India has developed an economically viable technology for making cement in a Verical Shaft Kiln using black meal process (Jain et al , 1982). The objective of this investigation is to highlight the feasibility of using kiln dust as raw material ingradient in the black meal process for the manufacture of alkali free cement.

EXPERIMENTAL

Kiln dust was collected from the wet process rotary kiln and other raw materials from a runing VSK plant. The composition of raw materials are shown in Table 1. The raw mix designs were prepared one with maximum kiln dust utilisation (Raw Mix I) second with minimum utilisation of kiln dust (Raw Mix II) and a control raw mix (Raw Mix III) without kiln dust. All these raw meals were nodulised and dried in an oven at 105°C for 2 hours. These dried nodules were fired in an electric furnace at 1450°C with the retention period of 20 minutes. Clinkers obtained were air cooled at ambient temperatures and subjected for elemental analysis to study the volatilisation of alkalies and chlorides from the raw mix. To determine the crystal size, shape and stabilisation of mineral phases following methods were used.

a) Microscopic studies were carried out on polished sections by fixing the clinker in araldite under vaccum. These sections were examined under reflected light using Carlzite, Amplivol

b) SEM studies were carried out on a fractured clinker samples using philips model (ST) M01G Scaning Electron Microscope.
c) X - ray diffraction studies were conducted on ordered samples using DHMax, Rrigaku, Japan diffractometer.

Table 1
Chemical Composition of Raw Materials

Material	CaO	SiO_2	Fe_2O_3	Al_2O_3	MgO	LOI	K_2O	Na_2O	Cl-
Kiln Dust	43.18	14.89	1.59	4.84	1.74	26.44	4.36	0.46	2.18
Lime stone	53.06	0.97	0.03	0.31	0.98	43.09	-	-	-
Clay	1.64	76.53	4.21	9.42	1.21	4.72	-	-	-
Laterite	0.74	16.28	54.96	14.16	0.37	11.47	-	-	-
Coke Breeze	2.55	11.16	2.29	5.11	1.68	75.74	-	-	-

After the bulk firing clinker obtained was ground in a ball mill to a fineness of 30 +/- M^2/Kg with gypsum to maintain a level of 1.75% SO_3. The resultant cement was evaluated for performance characterisation.

RESULTS and DISCUSSIONS

The elemental analysis of raw meals and the resultant clinker is presented in Table 2. Most of the alkalies and chlorides in the raw mixes are due to the presence of kiln dust. It is known that alkalies and chlorides volatalise at 800- 1000°C and the get condenced on cooler parts in the rotary kiln and generate alkali and chloride cycles (Lee,1970). It is also well known that since in the vertical shaft kiln the burning zone is very much on the top and hence all alkalies/ chlorides present in the system get volotalised and escape with exhaust gases through the chimney (Raina, 1995). Hence no alkali/ chloride cycles are generated and do not take part in the solid state reactions. This is clear from the data of Table 2 where alkali contents have gone down from 2.70% to 0.39% and chloride content from 1.12 % to 0.07 % in RM I which is having highest percentage of kiln dust. The values of alkali and chloride contents in RM I and RM II are very close to the value obtained in RM III (Control) which is made without addition of kiln dust.

Optical microscopic studies conducted on clinker I and II samples and mineral phases determine as shown in Table 3 compare favourably with the mineral composition as obtained by Bogues equations. The granulometric results indicates the average crystal size as well as grain size more or less the same. The scaning electron micrographs of clinker I, II and III are shown in plate I, II and III respectively.

The distribution of phases is uniform. Clusters of belite is present in the pores which is expected in the black meal process clinker (Ahluwalia et al, 1992). Alite graines are well formed with sharp edges indicating that no effect of high chloride and alkali content on the morphology of clinker produces by using kiln dust. X - ray diffraction studies on clinker I, II and III reveal the presence of all major phases that is C_3S, C_2S, C_3A and C_4AF as indicated in Fig 1. The percentage of

Table 2
Elemental Analysis of raw meal and Clinker

Sample	LSF	SM	AM	CaO	SiO_2	Fe_2O_3	Al_2O_3	MgO	LOI	K_2O	Na_2O	Cl-	CaO_f
RM I	0.96	1.70	1.57	38.62	11.93	2.73	4.29	1.56	34.14	2.42	0.28	1.12	-
RM II	0.93	1.67	0.92	37.64	12.11	3.78	3.47	1.26	38.03	1.00	0.30	0.53	-
RM III (Control)	0.90	1.88	0.73	37.19	12.58	3.87	2.81	1.07	40.80	0.23	0.29	0.07	-
Clinker I				68.63	18.12	4.15	6.54	2.37	-	0.13	0.26	0.07	Traces
Clinker II				60.69	19.54	6.11	5.60	2.04	-	0.04	0.30	0.07	"
Clinker III				62.80	21.25	6.53	4.75	1.80	-	0.10	0.27	0.03	"

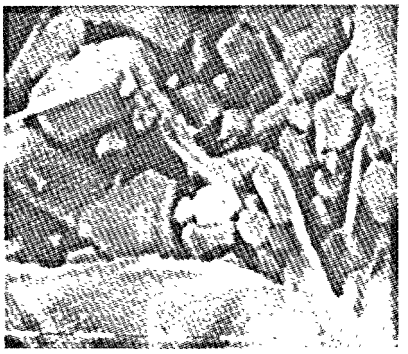

PLATE 1 : Clinker I



PLATE 2 : Clinker II



PLATE 3 : Clinker III

SEM OF CLINKERS

of alite phase is comparable in all the three clinkers and is in abandance. Physical performance of cement obtained by grinding clinker I, II and III with gypsum is shown in Table 4. The quality of cement is good in terms of early as well as 28 days strength. All the cements pass the soundness tests.

ECONOMIC ASPECTS

Non returnable kiln dust is a by product and free to a cement plant. When it is mixed upto 60 % (say) with the raw materials for production of clinker in VSK, it will correspondingly reduce the cost of raw materials. In India both the cost of installation and production for VSK are lower than those for rotary plant. It is therfore economically attractive also to utilise kiln dust and produce clinker from it in VSK.

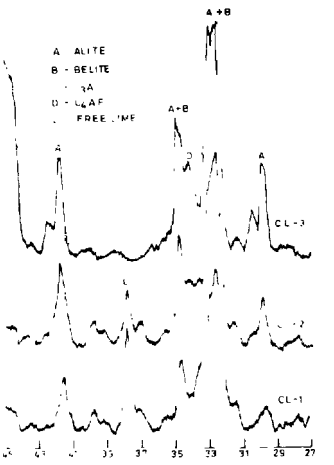

Fig 1. XRD of Clinkers

Table 3
Mineral Analysis of clinker samples by Bogue's and Optical Microscopy.

Sample	Phases present	Quantity (%) Bogue's	OM	Granulometry, u Max	Min	Avg
Clinker I	C_3S	51.20	50.00	5	20	15
	C_2S	13.60	14.00	5	20	18
	C_3A	10.30 }	36.00			
	C_4AF	12.60}				
Clinker I	C_3S	52.10	50.00	8	30	39
	C_2S	17.00	19.00	6	40	25
	C_3A	4.50 }	39.00			
	C_4AF	18.60}				
Clinker I	C_3S	52.90	49.00	5	35	25
	C_2S	21.30	19.00	5	35	21
	C_3A	1.50 }	32.00			
	C_4AF	19.90}				

Table 4
Physical Data of Cement prepared

Properties	Cement I	Cement II	Cement III
Fineness, M^2/Kg	31.90	31.70	31.95
Compressive strength, Mpa			
3 Days	33.0	33.1	32.8
7 Days	40.5	40.0	40.0
28 Days	51.5	50.0	50.1
Soundness			
Le Chat., mm	7.0	6.0	7.0
Auto Clave, %	0.5	0.5	0.3

CONCLUSION

Kiln dust, a waste from rotary cement plants, inspite of its higher concentration of alkalies and chloride can be used for the manufacture of cement by black meal process of cement manufacture in VSK using as raw material ingredient producing low alkali cement.

ACKNOWLEDGEMENT

The authors have freely drawn upon data available as an outcome of project of National Council for Cement and Building Materials. This paper is being published with the permission of Director General, National Council for Cement and Building Materials, New Delhi, India.

REFERENCES

Ahluwalia S.C and Raina K, "Morphology and microstructure features of clinker from Vertical Shaft Kiln", 9th International Congree on the Chemistry of cement, New Delhi, India, 146-152, 1992

Bhatty M. S, "Use of cement kiln dust in blended cement", World Cement, May 1984.

Jain V.K, Rao D.B.N, Gupta S.K and Singh D.K, "Technology for mini cement plants", NCB proceedings of National Seminar on mini cement plants, 41-53, 1982

Lee F.M, "The chemistry of cement and concrete", 3rd ed, Edward Arnold Publishers Ltd, London, 1970, p154

Malcroum H A, "Disposal of bypass dust", World Cement, 17 - 21, Oct 1994.

Raina K, Cement manufacture by Vertical Shaft Kiln technology, Kugi Enterprises, New Delhi, India

ENVIRONMENTAL IMPACT ASSESSMENT OF A SPECIFIC CEMENT PLANT/NEW PROJECT CLUSTER IN INDIA

A D AGNIHOTRI, S GEORGE S M SHINGOTE, S B YADAV AND K V KALYANI
National Council for Cement and Building Materials, New Delhi, INDIA

ABSTRACT In India, cluster of cement plants is fast emerging in limestone rich belts. Environmental Impact Assessment was conducted for Bilaspur-Raipur cluster. Data was analysed, interpreted and environmental load predicted considering overlapping effect of cement plants, to ascertain if expansion or green field cement project can be established.

Key-words: cluster,environmental load,impact prediction, impact evaluation

INTRODUCTION

The cement industry is location specific. It has resulted in the formation of seven clusters near limestone reserves in different states of India. The Bilaspur-Raipur belt in Madhya Pradesh, rich in limestone reserves stretches over 100 km in length. This cluster has nine cement plants with an installed capacity of 11.35 million tonnes per annum. Though the individual cement plants of cluster zone are well equipped with state-of-the-art technology for pollution control and meet the stipulated regulations, the collective environmental impact due to operation of all the plants and other industries in the area, requires monitoring of environmental parameters, assessment, evaluation and management. Thus, what is required is an integrated and comprehensive EIA/EMP study of the cluster zone considering futuristic trend of likely expansions of existing cement plants or coming up of new green field cement projects.

DESCRIPTION OF THE CLUSTER

The cement plants in the cluster are located in Madhya Pradesh (Fig 1).

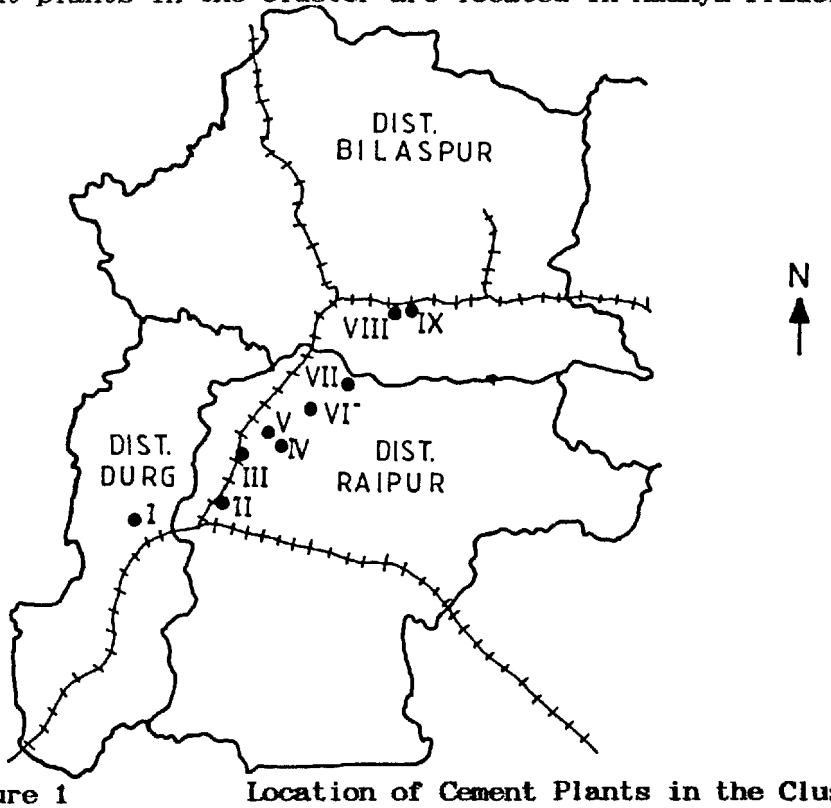

Figure 1 Location of Cement Plants in the Cluster

The distance between plant I & plant No IX is 125 Km by rail. The area lies between 21°18' & 22° 0'-north latitude and 81°30' & 82°27' east longitude at an altitude of 260 m above MSL.

Eight cement plants are based on dry process technology and only one is based on wet process technology. Some plants started production as early as 1964 while some as recent as 1995. The capacities of the kilns vary from 500 tpd to 4500 tpd. The plants have installed modern pollution control equipment like Electrostatic Precipitators (ESP) and Fabric Filters (FF). In addition, water spray system, unit filters etc. are also installed to prevent fugitive emissions.

PRESENT ENVIRONMENTAL STATUS

Measurements were carried out in summer season, 1995 for Stack emission, Noise levels, Ambient Air Quality (SPM, SO2, NOx & CO), Water and Soil quality. Data has been collected/generated on Demographic details, Flora and Fauna, Socio-economic aspects and Meteorology.

The stack emission levels in the plants range from 35 to 149 mg/Nm^3 which meet prescribed standard of 150 mg/Nm^3.

The ambient air quality levels are as follows :-

Parameters	Measured Value (ug/m^3)	Prescribed Std.(ug/m^3)
SPM	90 - 183	200
SO2	6 - 21	80
NOx	10 - 28	80
CO	87 - 203	2000

The average ambient noise levels are 39-54 dBA during day time and 31-42 dBA during night time which meet the prescribed standards of 55 & 45 dBA respectively.

Measurements were carried out for wind velocity & direction, temperature, humidity and rainfall. Wind rose diagrams have been drawn. The average wind speed is 5 Km/hr and predominant wind direction is West. The area is generally dry and arid. Humidity ranges from 6-66% and mean temperature from 18.6 - 45.9°C.

The land use pattern indicates that 68% of area is cultivated, 11% is cultivable waste, 1.5% forest land and 19.5% not available for cultivation. The demographic details such as population, literacy rate, occupational pattern, educational, medical and other amenities available indicate that the population density is 160 persons/sq km and literacy rate is 14.5%. The data on basic amenities suggest that availability of durables, educational, medical, transport and marketing facilities need further development.

ENVIRONMENTAL IMPACT ASSESSMENT (EIA)

The environmental impact assessment/prediction of impact has two distinct dimensions : (i) Assessment of impact of existing projects, and (ii) Prediction of impact for new project.

Assessment of Impact of Existing Projects

EIA was carried out by the individual cement plants, prior to commissioning. This provided the pre-project environmental scenario. It is found that there is a marginal degradation in the ambient air quality by an increase of 10-15 ug/m^3 in SPM. However, there is a tremendous improvement in the socio-economic environment of the habitats which includes educational, medical, transportation, communication, market facilities, drinking water, electricity supply and employment opportunities.

Prediction of Impact for New Projects

Environmental impact for a new one million tonne per annum green field cement project has been predicted using mathematical modelling. The emission rate is estimated as 45 Kg/hr at a stack emission level of 50 mg/Nm^3. The maximum ground level concentration (GLC) in the downwind direction is predicted at 6.8 ug/m^3 and would occur at a distance of 2000 m from project site. The resultant maximum GLC in the area would be within the prescribed standard of 200 ug/m^3. Development of green belt (trees & shrubs) in the downwind direction would considerably arrest the pollutants and the net impact on the inhabitants, flora & fauna beyond the project site would be minimal.

EVALUATION OF IMPACTS

Evaluation of impact has been carried out using Battelle Environmental Evaluation System (BEES). Environmental quality assessment is undertaken by evaluating 21 parameters which are likely to be affected positively or otherwise due to the new cement plant. These parameters are broadly classified under five major categories such as air, water, land, biological and socio-economic environment. The environmental impacts are estimated by calculating an index in terms of Environmental Impact Units (EIU) for each parameter. Relative weight has been assigned to each parameter expressed in Parameter Importance Unit (PIU). The evaluation is based on a total of 1000 PIU. The parameters identified and the relative weights assigned are given in Table 1.

Table 1 **Battelle Environmental Evaluation System (1000) Classification of Parameters**

Air Env. (240)		Water Env. (150)		Land Env (110)		Biological Env. (120)		Socio-Economic Env.(380)	
SPM	90	BOD	60	Landuse	80	Vegetation/ Green belt	50	Employment Potential	100
SO2	30	Turbidity	30	Soil quality	30	Agricultural Crops	30	Communication & Transport	50
NOx	30	Suspended Solids	35			Forestry	20	Educational Facilities	50
CO	30	Dissolved Solids	25			Habitat	20	Std.of living	70
Noise	60							Human Settlement	60
								Health, Safety	50

Impact evaluation has been accomplished through the use of functional relationship of each parameter with the environmental quality. Environmental Quality Index (EQ) varies from 0 to 1.0, where 1.0 stands for excellent and 0 stands for poor Environmental Quality.

EIU is given by EQ multiplied by PIU. The positive value (+33) in Table 2 indicates that the overall impact on the environment is beneficial.

Table 2 **Environmental Evaluation (Battelle Technique)**

Parameters	Imp. Value	Impact Units (EIU)		
		Existing	Predicted	Difference
Air Env.	240	174	165	-9
Water Env.	150	119	119	0
Land Env.	110	95	88	-7
Biological Env.	120	96	91	-5
Socio-Eco. Env.	380	239	293	54
	1000	723	756	33

CONCLUSION

The study reveals that the overall impact on the environment in the cluster area, due to a new green field cement plant, is positive. The area can accommodate additional environmental load towards sustainable development, beneficial to habitat, flora and fauna of the Bilaspur-Raipur cluster. The study provides a model for conducting Environmental Impact Assessment (EIA) studies, for national level institutions, scientific and engineering personnel, regulatory authorities and policy makers concerned with environmental quality management.

ACKNOWLEDGEMENT

The authors have freely drawn upon published literature/ completed R&D work/status reports of NCB. The paper is being published with the permission of Director General, NCB.

REFERENCES

Harrison and Perry, "Handbook of Air Pollution Analysis."

Herbert E Lund, "Handbook of Pollution Control Management."

Mahoney J R, "Meterological aspects of Air Pollution", Industrial Pollution, edited by Irving Sax, 1974.

Pasquill F, "Atmospheric Diffusion", 1974.

Sharma D K, Nijhawan S C and Roychoudhary D, "Environmental Impact Assessment studies of Cement Plants", Indian Jl. of Env. Protection, Vol. 15, No. 3, March 1995, pp. 210-212.

CEMENT CLINKER BURNING PROCESS OPTIMIZATION

Victor KLASSEN, Doc.Tech.Sc., Prof., Belgorod, Russia
Valentina BELYAEVA, Cand.Tech.Sc., Senior Researcher, Belgorod, Russia

ABSTRACT The paper provides the results of clinker forming processes investigation in the kilns with clinker dusting and clinker optimum granulation. The ways of clinker burning optimization are shown in order to reduce heat rate and improve cement quality.

Key-words: Clinker formation, Aluminoferrite, Qualitative

INTRODUCTION

Cement clinker burning process optimization provides for heat rate reduction and cement quality improvement. When solving the problem of heat rate reduction one should proceed from the theoretical relationships established by H.Eigen (1953) the essence of which consists in that the closer is heat losses reduction to the kiln hot end the greater are the kiln total heat savings. In operating industrial plants the kiln hot end heat savings are reduced to the heat losses decrease with clinker across the kiln body, and with gas flow by means of heat transfer improvement.

As a rule, fuel saving and quality improvement problems are interconnected and interdependent. The ways shown for heat savings in the kiln hot end favour clinker grading improvement and cement strength properties.

Many of cement mills with non-optimum burning conditions feature large content of fine fraction in clinker - the so called clinker dusting. Clinker dusting impedes clinker cooling, lowers cooler efficiency, impairs heat transfer conditions in the kiln and increases heat losses through the kiln body leading to increase of fuel specific flow. Clinker dust fraction is enriched with alite and depleted of flux minerals. Strength of cement produced of the dust fraction is somewhat higher than of granulated fraction, but generally cement strength properties are higher by 25-35% with clinker dusting than with clinker optimum granulation. More than 0.95 DS (degree of saturation) increasing, $Al_2O_3 \leq 3.2\%$ content in the raw material, re-entry of precipitated dust enriched with R_2SO_4 and KCl, use of high-sulphur fuel

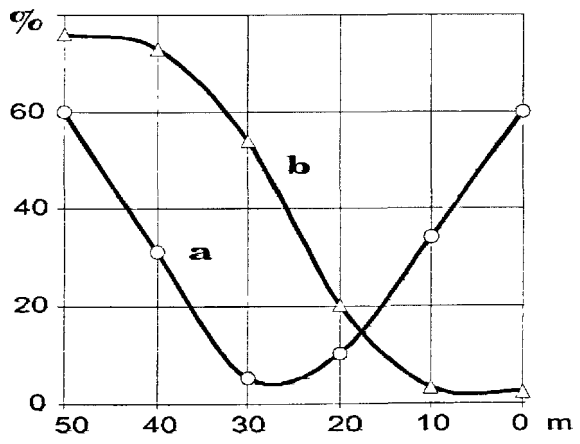

Fig. 1. Changes in the material granulometric composition along the kiln length with clinker dusting (a)

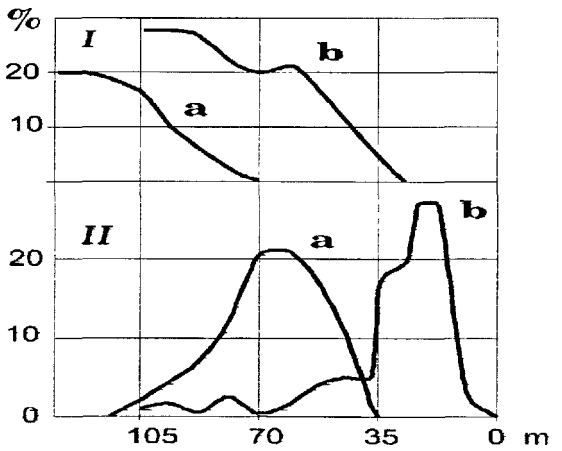

Fig. 2. Changes in material CO_2 (I) and CaOfree (II) amounts along the kiln length with clinker

oil and reducing medium in the kiln promote clinker dust formation. As it has been established, burning condition optimization makes it possible to produce high-quality granulated clinker.

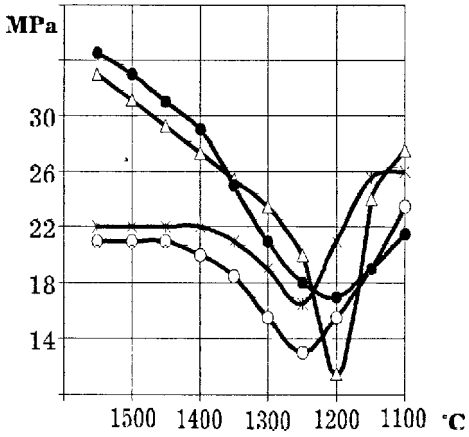

Fig. 3. Effect of additional holding in the kiln upon the strength of the clinker granules

RESULTS AND DISCUSSION

Analysis of the material granulometric composition along the length of kilns of wet and dry production methods shown (Fig.1) that granulated clinker is observed at clinker dusting at a distance of 20-30m from the kiln hot edge, with the granules subsequent destruction. As a result (see Fig. 2) CaO assimilation completes at a distance of 30-35 m from the kiln hot edge, whereas at optimum granulation it competes at a distance of 5-15 m.

Hence clinker dusting occurs as a result of process zones displacement to the kiln cold edge, and burned clinker additional holding at high temperatures. This was confirmed by the laboratory experiments, when additional 30 minutes holding of clinker granules in the kiln in the melt crystallization temperature zone led to 2-2.5 times strength reduction and encouraged granules destruction (Fig. 3).

Alkali and salt containing impurities reduce strength additionally by 1.5-2 times, a 10-fold strength reduction and complete granule destruction occur at burning reducing conditions and at slow cooling in reducing medium, respectively. As a result of the system approaching the equilibrium conditions at slow cooling partial alite decomposition and crystallization of aluminoferrite phases enriched with Al_2O_3.

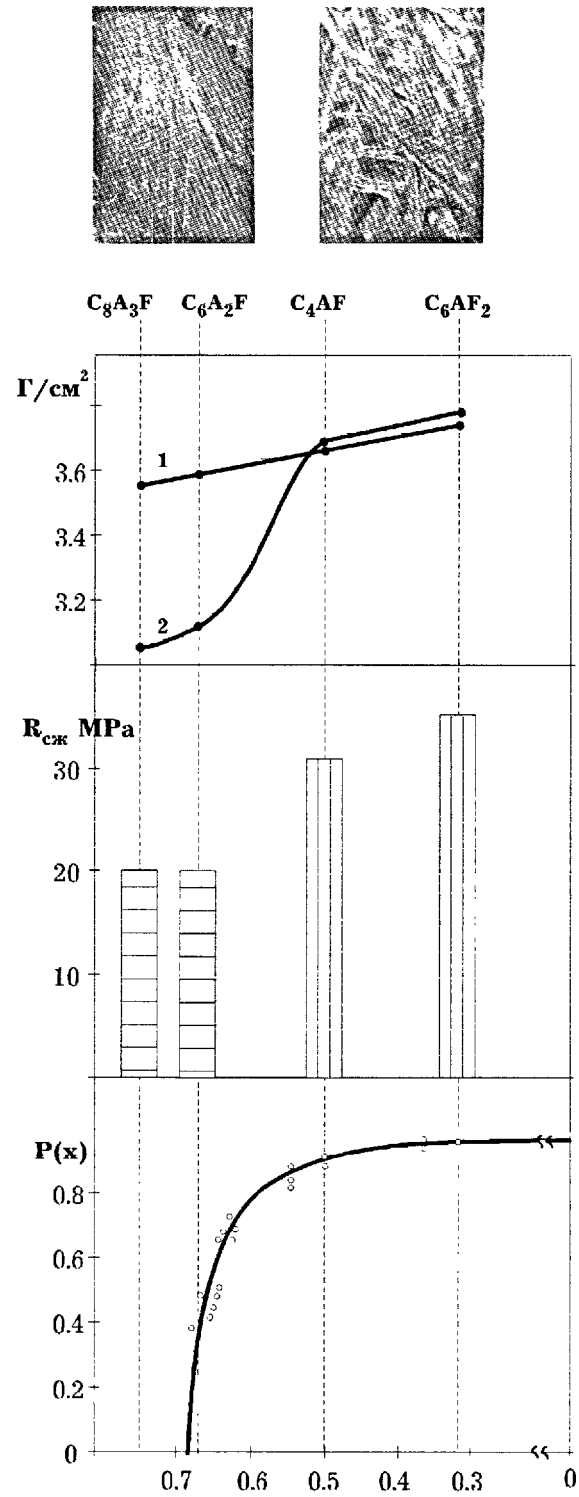

Fig. 4. Macrostructure, density, calculated by X-ray phase analysis (1) and determined by pycnometer (2), calcium aluminoferrite cakes strength and probability of flow in Fe-O-Fe links.

Investigation of series C_8A_3F-C_6AF_2 aluminoferrite phase transformations using Mцss-bauer spectroscopy, X-ray phase and differential thermal analyses made it possible to establish macrostructure discrete change and cake density and strength within the interval of C_4AF-C_6A_2F (Fig. 4).

This phenomenon can be explained when considering effect of diamagnetic dilution upon C2F ferromagnet magnetic properties. $C_2A_xF_{(1-x)}$ orthorhombic structure can be stable only in the presence of exchange interaction between Fe^{3+} ions. While replacing Fe^{3+} with diamagnetic Al^{3+} magnetic interaction between Fe ions, and hence crystalline structure stability and probability of flow in Fe-O-Fe links are reduced. With $Al^{3+}<0.5$ concentration practically all Fe^{3+} ions form a fixed system with $P(x)>0.9$ flow probability. Sudden P(x) reduction starts for $x>0.6$, which corresponds to discrete change of aluminoferrite series properties. P(x) reaches its zero value at $x=0.68\pm0.02$ being critical for magnetic concentration transition, which corresponds to $C_{6.67}A_{2.33}F$ composition. That is why clinker crystallization with Al oxide enriched aluminoferritic phases having lesser cake density and strength, being held in the kiln for a long time, causes formation of the less dense and strong clinker granules showing greater tendency to destruction. Besides, this clinker produces cement of reduced strength.

As it was mentioned above sulphur oxide and sulphur-containing compounds influence greately cement strength. According to the data of V.I.Korneev (1973), C.D.Okorokov (1960) sulphur anhydride is introduced mainly in belite increasing simultaneously its strength when adding gypsum to the initial charge. With high-sulphur fuel oil being used considerable portion of sulphur anhydride is added to the material in the kiln high-temperature portion, including alite formation stage, with introducing into the structure of the latter. According to the data of V.Gatt (1976) up to 2.9% of SO_3 reducing alite astringent properties can be put into C_3S.

It is esdtablished that cement strength is reduced considerably with calcium silico-sulphate being formed in the kiln intermediate zones, or sulphur anhydride being added in high-temperature zones. In this connection clinker quality depends greatly on high-sulphur fuel oil burning conditions. Large excess of combustion air displaying O_2 content in flue gases increases the extent of sulphur oxidation to SO_3 and SO_3 addition in the kiln high-temperature portion resulting in formation of $2C_2S{\cdot}CaSO_4$, which forms alite of reduced activity. It is possible to reduce considerably sulphur addition degree to the material and increase cement strength by 5-15 MPa by changing burning conditions (Fig. 5).

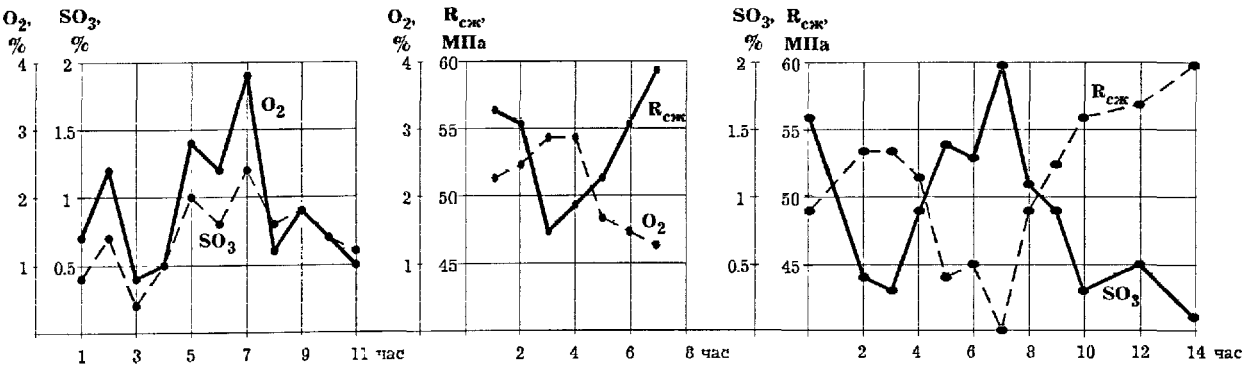

Fig. 5. Effect of O_2 in flue gases upon SO_3 content in clinker and cement strength.

With high SO_3 concentration in clinker reduction of cement strength properties is possible also due to insufficient gypsum introduction during grinding, because some portion of clinker sulphur anhydride is being titrated and, hence, quantity of introduced gypsum is being overstated obviously against its actual content when determining gypsum content in cement by cation method.

CONCLUSION

An important dependence of clinker quality upon burning conditions and fuel burning ones has been established:
- the optimization of a fractional composition and an activity increase are achieved by the decrease in clinker holding time in a cooling zone when aluminoferrite phases enriched with an iron oxide are crystallized out;
- the oxyden content reduction in a flame space favours a quality improvement, particularly using high-sulfur fuel types;
- the decrease in heat losses with clinker coming out of the kiln, through a kiln body and with a gas flow result in the decrease in specific fuel consumption and clinker quality improvement.

REFERENCES

Gatt,V., Ners, R., "Portland Cement Phase Composition. VI International Congress On Cement Chemistry", Moscow, Stroyizdat, V.1, 1976, pp.78-88.

Eigen, H., "Untersuchung der beiden Warmesysteme des Drehofens fur Portlandzement//Tonindustrie-Zeitung", 77, No.1/2, 1953, S. 2-8.

Klassen, V.K., "Cement Clinker Burning", Moscow, Stroyizdat, 1994, 320 p.

Korneev, V.I., Sychyov, M.M., Myule, F., Kasyanova, G.N., "Phase Relationships in Alite-Belite Sulphur-Containing Clinkers.Collected Papers, Lensoviet LTI, Leningrad, 1973, pp.22-26.

Okorokov, S.D., Golynko-Volfson, S.L., "Mineralizing Effect of Sulphates on Synthesis of Clinker Separate Minerals", Lensoviet LTI, Leningrad, No.56, 1960, pp.84-92.

TECHNOLOGY AND PROPERTIES OF LOW-ALUMINATE CLINKERS AND CEMENTS

Johann STARK, Building Materials Institute n.a. F.A. Finger, Weimar Construction and Architecture University (Germany)
Aleksandr P.OSOKIN, Ekaterina N.POTAPOVA, Russian University for Chemical Technology n.a. D.I. Mendeleev, Research Technical Centre "Alpha-Cement".

ABSTRACT. A technology has been elaborated and properties investigated of special clinkers and cements containing less than 1 % of Al_2O_3. Optimal compositions and conditions of synthesis of such clinkers from raw materials of various nature and properties have been determined. Kinetics and sequence of synthesis of clinker minerals as well as phase compositions, microstructure and properties of synthesized clinkers have been considered.

KEY-WORDS: aluminoferrite, kinetics, sintering, structure, temperature

Introduction

In order to enhance life durability of concrete which is subject to corrosion attack, frequent changes of temperature, freezing and thawing, moistening and drying, cements are to be used which contain no three-calcium aluminate. Along with it, the concentration of Al_2O_3 in clinker has not to exeed 1 %. To obtain such clinkers, low-aluminate limestone, ferrous and siliceous components are to be used. A raw mix based on these materials is characterized by bad clinkering ability due to low content of the liquid phase during clinkering. The arising melt differs substantially in its composition and properties from melts obtained with the use of traditional Portland cement raw mixes.

Clinkering of low-aluminate mixes

Since no C_3A should arise in the low-aluminate clinker to be developed, changed formulas were used to calculate raw mixes proceeding from obtaining of C_3S, C_2S, C_2F and high-ferrous aluminoferrite phase C_6AF_2 during clinkering. Both pure reagents and natural materials (dolomites and chalks from various deposits, sand, pyrite cinders and various ferrum-containing wastes) were used as raw materials.

Raw mixes with lime saturation factor (LSF) = 0.75 - 0.90 and n (silica modulus) = 2.3 - 3.0 were subject for clinkering for 20 minutes at the temperature of 1450°C. The content of C_3S > 50%, Al_2O_3 < 1% and free CaO < 1% was used as criterion for quality appraisal of synthesized clinker. The raw mix with LSF = 0.85; n = 3.0 and p (alumina modulus) = 0.07 met these conditions most closely. All further investigations were conducted using this raw mix.

In order to explore kinetics of mineral formation the raw mix was subject to burning for 10 to 60 min. at temperatures 1360 - 1465°C. The formation of alite started at the temperature of 1330°C but, at low temperatures, the degree of combining of calcium oxide to form C_3S remained within 0.34 - 0.71 limits when burning duration changed from 10 to 60 minutes (Fig. 1). At temperatures of 1400 - 1425°C, α (degree of combination of CaO with C_2S in C_3S) grows up to 0.8 - 1.0 during the same period. The share of alite increases at temperatures of 1350 - 1450°C (burning time τ = 20 min.) from 25 to 51%. The further increase of the temperature up to 1465°C results in decrease of C_3S content to 41%, may be due to alite decomposition. This is accompanied by the increase of belite content from 32% to 39% with no free calcium oxide.

The obtained results enable one to suggest that the emerging active lime dissolves in the intermediate aluminoferrite phase causing the saturation or supersaturation of the latter. The following reaction takes place:

$$C_3S + C_2F(A) \rightarrow C_2S + C_3F(A)$$

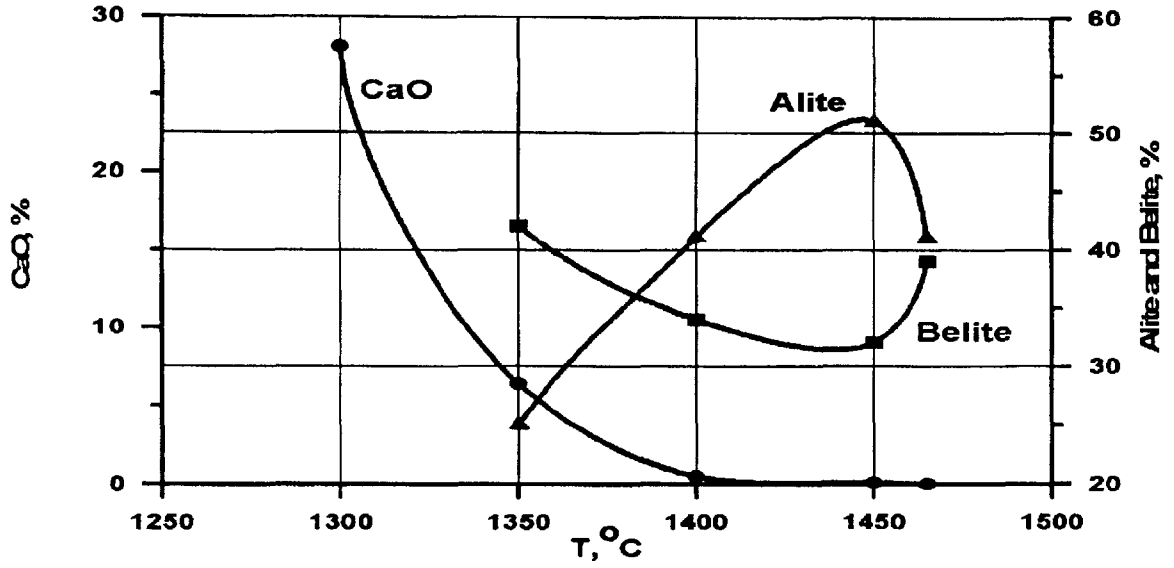

Fig. 1. Impact of clinkering temperature on content of free CaO, alite and belite in clinker (τ =20 min).

In order to describe kinetics of alite formation process 12 kinetic equations were choosen (Osokin, 1993). The nearest convergence of experimental and estimated results took place for R. Kondo and Erofeev-Kolmogorov equations. It was found using the "n" constant of the Erofeev-Kolmogorov equation that at 1350°C the formation of alite occurs in the transition area (n = 0.87); the rate of reaction prevails (n = 1.10) within 1400 - 1425°C and when the temperature increases up to 1450°C, reaction and diffusion rates become commensurable (n = 0.84). The activation energy of alite formation decreases from 75.4 kJ/mol (at 1350°C) to 34.9 kJ/mol (at clinkering temperature of 1450°C).

The analysis of the differential-thermal curve of the raw mix and x-ray phase analysis of cakes syntesized at various temperatures allowed to reveal the sequence of clinker minerals formation. The carbonaceous component becomes decomposed at 760 - 1000°C (max. 950°C), then solid-phase reactions of dicalcium silicate take place (at temperatures above 1060°C), the melt emerges at 1290°C and the formation of three-calcium silicate starts at 1330°C. At temperature of 1350°C there are CaO (d = 2.76; 2.39; 1.69 Å), C_2S in its β- and γ-forms, C_3A (d = 2.699; 1.908; 1.558 Å) and C_4AF (d = 2.770; 2.762; 2.630 Å) present in the low-aluminate clinker cakes (Fig. 2). The increase of burning temperature up to 1400°C causes solution of C_3A in C_4AF; diffraction maximums 2.699 Å (C_3A) and 2.672 Å (C_4AF) vanish and a distinct analytical line 2.678 Å appears relating to C_2F. At 1350°C cakes get often crumbled what confirms the presence of γ-C_2S (see Fig. 2f) but when temperature increases up to 1400°C and 1450°C, dense cakes develop. Analytical line d = 1.752 characteristic for C_3S occurs instead of CaO (d = 1.688 Å) and γ-C_2S (d = 1.754 Å) lines.

Phase composition, structure and properties of clinkers

According to results of the x-ray phase analysis the low-aluminate clinker with LSF = 0.85 and n = 3.0 consisits of 51% C_3S, 32% C_2S, 4% C_2F and 12% of aluminoferrite phase.

The structure of low-aluminate clinker is analogous to Portland's one (Fig.3). Along with distinctly crystallized alite and belite irregularly shaped crystals occur. The intermediate phase is well crystallized as rounded C_2F grains and acicular or prismatic crystals of calcium aluminoferrite.

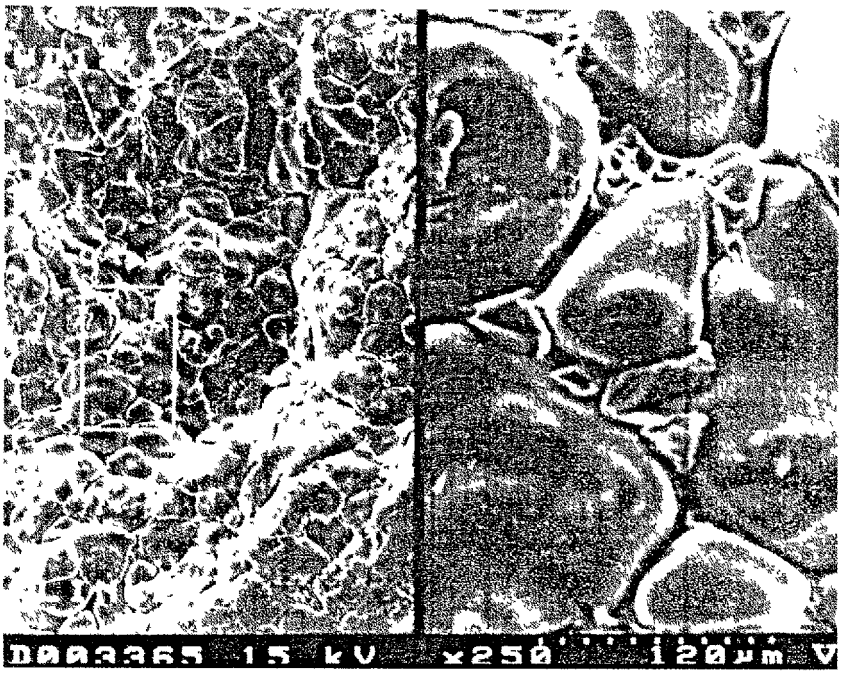

Figure 3. Microstructure of the low-aluminate clinker.

The enhanced content of belite and presence of calcium ferrites provide for reduced grindability of the low-aluminate clinker. The grinding for 10 minutes in a laboratory ball mill ensure the specific surface of 150m^2/kg (grinding of Portland cement clinker under the same conditions ensures S_{spec} of 350m^2/kg). After grinding for 60 min. the specific surface increases to 430m^2/kg. But it should be noted that the hard-to-grind C_2S and C_2F provide for more uniform grinding of clinker since they play the role of additional grinding agents. A study of particle size distribution with the use of a "Fritsch" (Germany) granulometr showed that particles of 7 to 30 mkm (50.6%) prevail in the cement, the residue on a 008 screen is 1.2%. For the Portland cement respective values are 39.9% and 11.4%.

Due to the lack of three-calcium aluminate in the clinker, gypsum added during grinding has no effect on normal thickness and setting time of the cement paste, but changes strength values of the cement. A study of effect of gypsum content (within 0.5 to7%), conditions of hardening and the dispercity of cement (S_{spec} = 260 to 460m^2/kg) showed that the best strength values show cements with specific surface of 320 to 350 m^2/kg, containing 2% of gypsum which were subject to hardening in water: at the age of 28 days their compressive strength was 46 MPa and flexural strength - 6.5 MPa. Unlike the Portland cement, the low-aluminate cement hardens slowly during early periods. The intensive gain of strength begins after 7 days.

With the use of a complex of physico-chemical methods products of hydration of the low-aluminate cement were determined, which at the age of 28 days were presented by the following phases: CSH(II), $Ca(OH)_2$, $C_4A(F)H_{19}$, $C_3A(F)\cdot 3CaSO_4\cdot H_{32}$ and $C_3A(F)\cdot H_6$. The hydration degree was 55 to 68%.

At clinkering temperatures up to 1450°C the diffraction maximum d = 2.678 remains the same while analytical lines d = 2.685 and d = 2.680 appear which can be referred to solid solutions of calcium aluminoferrites. The distinct analytical line d = 1.9395 Å enables one to determine composition of emerging aluminoferrites (Midgley, 1958) as $C_2F_{0.9}A_{0.1}$ or $C_{2.22}FA_{0.11}$. These results coincide with results of x-ray micro spectral analysis of clinkers having various saturation factors (Table 1.)

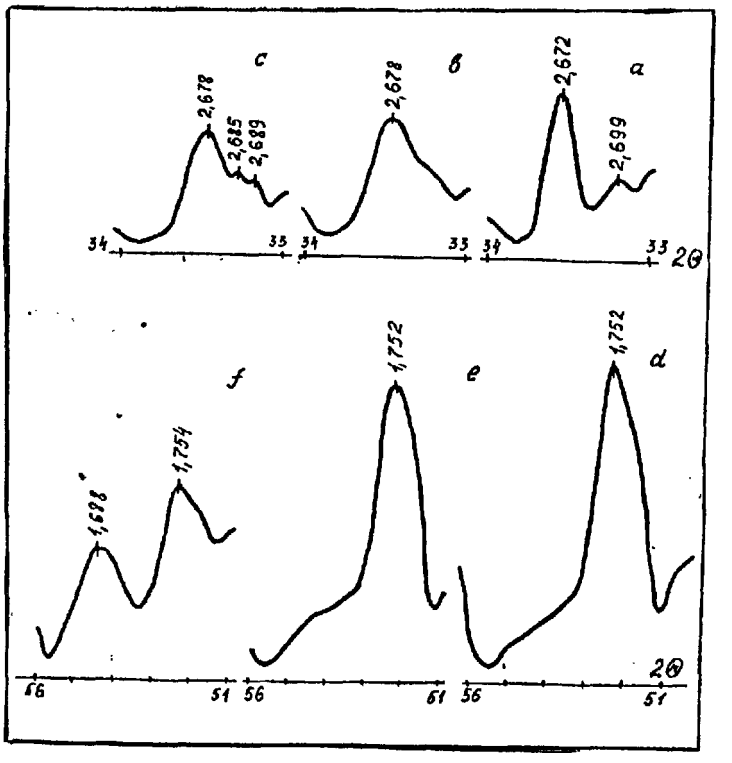

Fig. 2 Fragments of x-ray patterns of clinkers fired at the following temperatures, °C: 1450°C - a,d; 1400°C - b,e; 1350°C - c,f.

Table 1.

LSF of clinker	Composition of calcium aluminoferrites	CaO/SiO_2 ratio of	
		alite	belite
0.75	$3.70CaO \cdot Fe_2O_3 \cdot 0.17Al_2O_3$	2.80	2.18
0.85	$2.85CaO \cdot Fe_2O_3 \cdot 0.11Al_2O_3$	2.85	2.07
0.90	$2.65CaO \cdot Fe_2O_3 \cdot 0.035Al_2O_3$	2.94	2.09

In clinkers with LSF = 0.85 in aluminoferrite phase there are 0.11 moles of Al_2O_3 per 1 mole of Fe_2O_3 (A/F = 0.11). The decrease of the basicity of clinkers (to LSF = 0.75) results in the growth of Al_2O_3/Fe_2O_3 ratio but, for high-base clinkers (with LSF > 0.90) the Al_2O_3/Fe_2O_3 ratio deminishes.

The above study enabled one to develop a set of technical and technological documents and to produce an experimental lot of special low-aluminate clinker and a cement based on it under industrial conditions.

REFERENCES

Midgley, G., "Ferrite Phase. Discussion", The 3rd International Congress on the Chemistry of Cement, Moscow, Stroyizdat, 1958, pp. 98-100.

Osokin, A.P., Krivoborodov, Yu.R., Potapova E.N., "Modified Portland Cement", Moscow, Stroyizdat, 1993, p. 328.

THE THERMOCHEMICAL ACTIVATION OF CLINKER FORMATION

Aleksandr P. OSOKIN, Valerij G. AKIMOV, Ekaterina N. POTAPOVA, Russian University for Chemical Technology, Research-Technical Centre Alpha-Cement, Russian Federation.

ABSTRACT. The thermochemical activation of clinker formation affects positively the mineralogical composition and microstructure of clinker. Areas develop in crystals of minerals with non-ideal ratio ($CaO/SiO_2 \neq 3$ or 2, $CaO/Al_2O_3 \neq 3$) which ensure an increase of clinker hydraulicity including that of belite clinker. The reduction of fuel consumption for the synthesis of such clinker is not less than 7 to 12%.

KEY-WORDS: activation, alite, belite, clinker formation

INTRODUCTION. Significant increase in the cost of fuel and energy necessitates the search for scientific and technical solutions to reduce heat consumption for production of Portland cement with high hydraulicity, including firing of clinker. The process of alite formation in clinker is characterised by the presence of low basicity areas and zones which contain excessive quantities of calcium oxide. The degree of completeness of alite formation depends on the rate of reaction of these micro volumes, which in its turn, depends on the reactivity of CaO and C_2S and the properties of the liquid phase of clinker. Two basic methods can be used to accelerate alite formation depending on the activity of interacting phases: increase the reactivity of solid phases (CaO and C_2S) and modify the liquid phase by adding elements which change its properties. One solution is to synthesise low-basicity clinkers under non-equilibrium conditions ensuring a deviation of the actual phase composition of the clinker from the estimated one (towards increase of alite concentration) with formation of basic minerals with defective structure characterised by increased ability to react with water. This can be achieved using any of following ways: by feeding one of raw materials to the area of clinkering (Osokin, 1993) or by high-speed heating-up of a raw mix with low-basicity LSF = 0.85 to 0.87 (Albats, 1992) as well as by the use of carbonaceous additives from coal mining and benefication wastes (Kouznetsova, 1992). Theoretical considerations and industrial tests evidence that the specific consumption of fuel for clinker production can be reduced by not less than 10 - 25 kg.

EXPERIMENT RESULTS AND DISCUSSION

For comparison, clinkers were chosen (including low-basicity compositions with LSF = 0.85) synthesised from natural raw materials (chalk, clay, shales). The following firing conditions were used (t - sintering temperature; υ_1 - rate of heating-up of the raw mix; υ_2 - rate of clinker cooling; τ - soaking at the maximum temperature):

1. Test mixes

Specimen No.1 (LSF = 0.92; n = 2.00, p = 1.20): t = 1450°C, υ_1 = 6°C/min; υ_2 = 200 °C/min; τ = 30 min;

Specimen No.2 (LSF = 0.85; n = 2.56, p = 2.00): t = 1400°C, υ_1 = 6°C/min; υ_2 = 200 °C/min; τ = 30 min;

2. Experimental mixes

Specimen No.3 (LSF = 0.85; n = 2.56, p = 2.00): t = 1400°C, υ_1 = 20°C/min; υ_2 = 200 °C/min; τ = 30 min;

Specimen No.4 (LSF = 0.85; n = 2.56, p = 2.00): t = 1400°C, υ_1 = 6°C/min; υ_2 = 200 °C/min; τ = 30 min. An additive based on brown coal mining wastes amounting to 1% and containing 9.5 % C was introduced into the raw mix.
Specimen No.5 (LSF = 0.85; n = 2.56, p = 2.00): t = 1450°C, υ_1 = 6°C/min; υ_2 = 200 °C/min; τ = 30 min. A portion of thermally activated carbonaceous component was introduced into the raw mix.
Specimen No.6 (LSF = 0.90; n = 2.58, p = 2.00): t = 1450°C, υ_1 = 6°C/min; υ_2 = 200 °C/min; τ = 30 min. A portion of thermally activated carbonaceous component was introduced into the raw mix.

All raw mixes contained 3% of particles having sizes above 200 mkm, but specimen No.3 featured increased dispercivity (R_{200} = 1%).

The study of chemical and mineralogical composition, microstructures, particuliarity of structure of minerals and synthesised clinkers and their hydraulicity was conducted with the use of x-ray qualitative and quantitative phase analysis, electronic microscopy, x-ray spectral and chemical analysis. It was found that synthesis of all clinkers was complete; mineralogical composition of the clinkers is displayed in Table 1.

Table 1. Mineralogical composition of clinkers.

No.	Modular characteristics			Concentration, %							
				estimated				experimental			
	LSF	n	p	C_3S	C_2S	C_3A	C_4AF	C_3S	C_2S	C_3A	C_4AF
1	0.92	2.00	1.20	57	15	7	15	57	22	7	12
2	0.85	2.56	2.00	48	30	11	9	48	28	11	11
3	0.85	2.56	2.00	48	30	11	9	55	25	13	7
4	0.85	2.56	2.00	48	30	11	9	56	25	11	8
5	0.85	2.56	2.00	48	30	11	9	56	23	11	10
6	0.90	2.58	2.00	60	19	10	9	64	17	11	8

It should be noted that estimated values of mineralogical composition deviate from experimental ones. This is due, first of all, to the presence in raw materials of large amount of various impurities (Ti, Na, K, Mn etc.), involved into the formation of solid solutions in clinker minerals. Moreover, the thermochemical activation of mineral formation affects the clinker composition, too. The amount of alite in less basic thermoactivated clinkers No. 3-5 exceeds reference values (clinker No. 2) by 7-8% and amounts to 55-56%, while the share of belite decreases by 3-5% to 23-25%. A similar phenomenon is observed for high-alite clinkers. In clinkers Nos. 3 - 5, β- and α- modifications of belite are stabilised, however, concentration of the α- modifications of belite is 2 - 4 %. During thermal activation of the suspended carbonaceous component its particles are subject to grinding as result of the thermal shock, but the crystal lattice of arising calcium oxide has no time to assume the stable, cubic structure. As result, products of impulse firing obtain well-developed specific surface (430 m^2/kg), low density (2930 kg/m^3), and increased values of crystal lattice parameter of CaO (4.82 Å) (Osokin, 1993). Under the usual heating-up conditions these parameters, correspondingly, are – 210 m^2/kg; 3180 kg/m^3 and 4.79Å. When passing from the regular firing with slow heating-up to

pulse high-temperature treatment of carbonaceous components, the size of CaO crystals decreases from 1-2 to 0.5 mkm and the number of microscopic distortion of crystalline lattice increases by 4 -10 times. Crystals of the metastable modification are formed, which intensively dissolve in the clinker melt. Its becomes over-saturated with Ca^{2+} ions 2 - 3 times over the equilibrium level. As a result, one can observe an acceleration of alite formation, change of microstructure of clinker grains, formation of a more active triclinic modification of alite with defect structure. According to results of the x-ray micro spectral analysis of alite crystals formed at high degree of melt over-saturated with respect to calcium ion during the initial interaction period, their central area, as compared to the periphery, had an increased content of silicon but decreased calcium and aluminium (zonal structure, with the CaO/SiO_2 ratio increasing from the centre to periphery). This is due to the fact that alite synthesis occurs close to dissolving belite grains in melt areas which are over-saturated with silicate anions. The resulting crystals display a high unit cell volume (2147 $Å^3$ as against 2140 $Å^3$) and increased hydraulicity. Heat of hydration of CaO obtained when heating-up limestone at the rate of 10 degrees/min to 1300°C was 70.8 J/g, but after abrupt firing (τ=1 c at 1650°C) it increased to 108.1 J/g (after 6 hours hydration). An increase of chemical activity of material due to the intensification of decarbonation and decrease in the period of collective recrystallization of CaO and C_2S ensures acceleration of the liquid phase clinkering in industrial rotary kilns. This is confirmed both by the relatively regular size distribution of clinker grains and more uniform crystalline structure of clinkers. The morphology of alite crystallisation becomes more distinct, with prevailing hexagonal grains having sizes from 20 to 40 mkm. The most significant changes in microstructure were observed during the interaction of less-basic clinkers with the thermally activated carbonaceous component.

The difference between structures of reference clinkers and test ones consists in developing greater quantities of zoned calcium silicate crystals with higher lattice defect contents.

To determine the influence of mineralogical composition and peculiarities of the structures of clinker minerals on heat consumption, heat content values of clinkers and main minerals were calculated. The study was based on the measurement of heat effect at dissolving of the material in concentrated hydrofluoric acid HNO_3 mixtures at the standard temperature of 298°C (Osokin, 1989). The solid : liquid ratio was 1:200. Dissolution heat was measured with an adiabatic calorimeter with thermostatic cell. The value of thermal effect at clinker formation depends on the composition of Portland cement. For ordinary alite clinker it is 1900 - 1910 kJ/kg, and for belite one with LSF 0.8-0.85 it is 1580 - 1690 kJ/kg, respectively, i.e. 13 - 17 % less.

A deviation from the ideal ratio CaO/SiO_2= 3.0 and 2.0 of minerals caused by non-uniform distribution of the main and impurity elements in the crystalline lattices is especially significant for thermochemical activation of clinker formation and brings about a change of heat content of materials. For the formation of calcium silicates with the CaO/SiO_2 ratio of 2.8 and 3.2, 665 and 710 kJ/kg, respectively, are required (Table 2). This is 13 and 6 % less, than for the mineral with CaO/SiO_2 ratio of 3.0 (764 kJ/kg). According to results of heat content measurements, the formation of highly active belite is also more energy effective, although values of enthalpy of their formation do not differ significantly (720-726 kJ/kg).

Table 2 Thermal effect of reaction of dissolution of mineral powders ($S_{spec.}$= 3000 g/cm^2) in HF (S:L=1:200) at 298°C and enthalpy of their formation.

No.	CaO/SiO_2	CaO/Al_2O_3	Q, kJ/kg	ΔH_f, kJ/kg
1	2.8	89.3	5.13	665
2	3.0	106.4	3.44	764
3	3.2	121.0	4.25	710
4	1.8	40.0	3.42	726
5	2.0	40.2	3.65	728
6	2.2	44.2	3.55	720
7	14.9	2.8	2.02	781
8	13.1	3.0	2.16	784
9	29.9	3.2	1.89	732

The hydraulicity of cements (2.5% SO_3) at w/c = 0.32 has been assessed by alite hydration degree and by increase strength of hardening cement paste after different periods of curing (Table 3).

Table 3. Hydraulicity of cements

No.	Alite hydration, %			Strength, MPa		
	3 days	7 days	28 days	3 days	7 days	28 days
1	63	68	78	21,3	28,6	40,3
2	60	65	76	16,5	24,3	35,3
3	69	74	87	22,0	27,1	42,3
4	69	76	87	22,7	28,5	42,6
5	68	77	84	21,4	31,0	41,9
6	69	75	85	25,5	34,5	52,1

The hydraulicity of test cements exceeds that of reference ones after any age of curing. The 28 days strength of less basic cements is 35.3 - 42.6 MPa (cements No. 2-5). With the use of thermochemical activation during clinker formation the strength of hardened cement paste can be increased by 6.6 - 7.3 MPa. This exceeds reference values (cement No. 1 with LSF = 0,92) by 1.6 - 2.3 MPa. Similar regularities can be observed in hydration of the basic cement No. 6. No significant differences of phase compositions of cement paste hydration products were found by means of X-ray- and electron-microscopic study. An increase in less basic calcium hydrosilicates, by 7-10%, occurs upon hydration of cements No. 3 - 6. Analysis of alite hydration values has shown that its reactivity in the thermally activated clinkers, regardless of their basicity, was 6-12% higher than in reference specimens, both at early and late hydration periods. This relates to an increase by several orders (1-4) of magnitude in the concentrations of dislocations as detected by electron microscopy (Fig.1) and free charge carriers, concentration of which was calculated for alite crystals areas having $CaO/SiO_3 \neq 3$ with regard to the Hall effect.

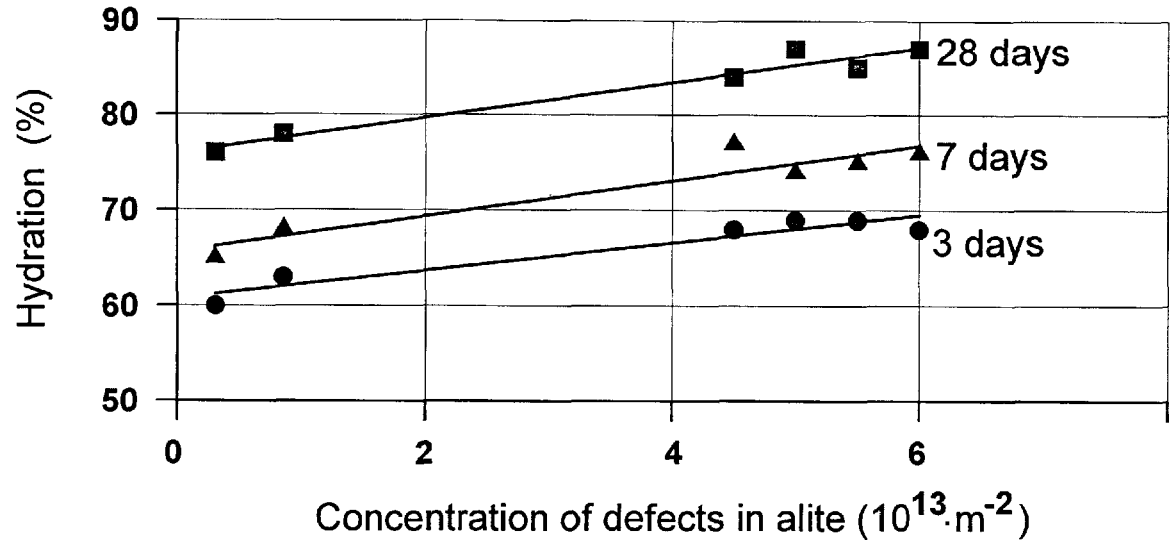

Fig. 1. Dependence of hydration degree on concentration of dislocations in alite crystals.

Thus, in spite of the smaller amount of alite in less basic clinkers, increas in reactivity results both from the chemical thermoactivation of clinker formation by any of the methods considered above and stabilisation of high-temperature belite modifications. Economy of fuel at the syntheses of such thermoactivated clinker will be not less than 7-12 %.

REFERENCES

Albats, B.S., Shein, A.L. "Kinetics of Alite Formation at Sintering of Industrial Raw Mixes". Cement. No. 2, 1992. p.89-94.

Kouznetsova, T.V., Osokin, A.P., Akimov, V.G., Paniouchkin, V.N., "Structure and Properties of Low CaO Contained Clinker", 9-th Int. Congr. on the Chemistry of Cement, Vol. 2, 1992, pp. 88 - 93.

Osokin, A.P., Akimov, V.G., Potapova, E.N., "Peculiarities of Structure and Properties of Modified Cements", Cement. No. 5, 1993. pp. 43-47.

Osokin, A.P., Akimov, V.G., Paniouchkin, V.N.,. "Structure and Reactivity of Clinker Minerals", Proceed. of the RUCT n.a. D.I. Mendeleev, No. 157. 1989, pp.43-47.

CLINKERING OF PRE-FORMED MIXES

Lev M.SULIMENKO, Boris S.ALBATS, Russian University for Chemical Technology n.a. D.I. Mendeleev, Research-Technical Centre Alpha-Cement, Moscow, Russia.

ABSTRACT. Agglomeration of particles of a material in rotary kilns occurs mainly in the clinkering zone. It is mainly spontaneous and causes instability of the technological process as well as non-uniformity of composition and properties of clinker. The forced agglomeration in the stage of batch preparation or its thermal treatment ensures a higher efficiency of the process and better clinker quality.

KEY-WORDS: nodulization in clinker formation, fineness, rotary kiln, sintering, temperature.

INTRODUCTION. In preheating and clinkering zones of kilns material occurs in the form of polydisperse powder-like mass. Its particles tend towards agglomeration due to excessive surface energy emerging in the course of fine grinding of raw materials.

In most kilns, agglomeration is of spontaneous character and introduces elements of instability to the clinker formation process negatively affecting process efficiency and product quality (Butt and Timashev, 1967; Klassen, 1994). Replacement of powder-like raw mixture with pre-formed pellets or briquettes enables a substantial increase of technical and economical production characteristics (Sulimenko, Albats, 1994).

Results are presented on the investigation of clinkering of pre-formed mixes.

Experimental data and results

Agglomeration of slimes can occur through removal of the liquid phase either by means of mechanical methods (filtration) or thermal ones (spray drying). Both methods are widely known and will not be analyzed in this paper.

In kilns utilizing dry process, the forced agglomeration can be regarded as an effective technological solution. The most widely known one is the pelletizing with binder before feeding into the kiln. Pellets obtained in disk pelletizers are, as a rule, characterized by inhomogeneous laminated structure with ring pores. This provides for reduction of heat resistance of pellets which are partially destroyed in the course of subsequent heating. The more reliable method appears to be the briquetting of raw mixes at 5 Mpa pressure to obtain agglomerates with section of 10 to 15 mm which are able to preserve their form during clinkering.
A promising method is agglomeration of a powder-like raw mix in the process of thermal treatment, for example, while transporting it from a heat exchange cyclone where the temperature of 750-800°C is maintained to a rotary kiln. It is favoured by an increase of the degree of self-adhesion of particles as the temperature increases (Table 1.) as well as by the emerging of pyroplastic properties of the material.

Table 1. Effect of temperature on the stability of inter-particle contacts of chalky marl ($d_{particles}$ = 10 mkm)

Temperature, °C	20	460	700	900
Relative dencity, %	0.51	0.45	0.41	0.36
Rupture strength, Pa	$2.1 \cdot 10^2$	$4.5 \cdot 10^2$	$8.6 \cdot 10^2$	$9.2 \cdot 10^2$
Number of contacts $1/m^2$	$9 \cdot 10^9$	$7 \cdot 10^9$	$5 \cdot 10^9$	$4 \cdot 10^9$
Average stability of contacts, kN	2.3	6.4	12.3	23

An experiment carried out in industrial 7/6.4 x 95 m kiln utilizing dry process gave the following results. The introduction of lignosulfonate water solution at the spout where material is fed to the kiln from the lower cyclone, the prevailing size of particles at the distance of 3 m from the feed end of the kiln increased from 0.19 to 3.1 mm and at the distance of 20 m - from 0.21 to 1.1 mm. The homogeneity of grain size of material increased by 3 to 4 times as well. The size of clinker grains increased from 10.7 to 15.5 mm.

A study of the nature of the material flow along the kiln with and without addition of lignosulfonate with the use of radioactive tracer technique showed that the agglomerated material flows more slowly (by 2 times), especially in the initial stage. On the contrary, in the clinkering zone the velocity increases to a certain extent. The LOI value of the material for 20 m of kiln length decreases in the case of agglomeration from 22 to 19 %. The finished clinker on the basis of agglomerated raw material is characterized by growth of alite content by 5 % and a certain increase of hydraulicity (by 2.5 Mpa).

A relatively low agglomeration degree which, in this case, is accompanied by inevitable attrition of particles in the kiln, will hardly be useful.

In this respect, the most promising method is the hot compaction of powder-like meal (Butt, Timashev et all, 1968; Sekava at all, 1992; Kupper and Rother, 1993; Ivanov et all, 1994). Here, the pressure applied is added to surface tension force ensuring a speed-up of clinkering based on diffusive transfer of material.

According to data obtained by the authors, the recovery of free CaO in the course of solid- and liqiud-phase reactions becomes more intense (Table 2).

Table 2. Assimilation of free CaO during firing of powder and hot-compacted (p = 50 MPa) raw mix.

Firing temperature, °C	Soaking, min.	Content of free CaO, %	
		powder raw mix	raw mix after hot compaction
1250	5	17.51	13.86
	10	15.19	10.04
	15	17.35	11.06
1450	5	7.19	6.07
	10	6.54	4.66
	15	5.82	2.51
	30	4.87	0.56

The shown results suggest that clinker can be obtained at lower, than usual, temperatures.

Specimens compacted under the pressure of 10 MPa at temperatures 800-1000°C show 6 to 8 times greater strength as compared to both cold-compacted specimens and pellets produced in drying zone of the rotary kiln. The dencity of hot-pressed specimens grows approximately by 1.5 times and porosity and specific surface decreases correspondingly evidencing the growth of the contact surface of the material (Table 3).

Table 3. Effect of conditions of specimens forming on their properties

Method of forming	Clinkering temperature, °C	Density, kg/m^3	Total porosity, %	Compression strength, MPa	Specific surface, m^2/kg
Cubical specimens of dried slime	800	1270	55.5	1.6	222
	900	990	69.2	1.3	281
	1000	970	70.5	2.0	285
Cold-pressed briquettes, p=15 MPa	800	1380	53.1	1.7	233
	900	1090	66.2	1.5	206
	1000	1080	67.3	2.2	280
Hot-pressed briquettes (at firing temperatures, p=10 MPa)	800	1690	40.9	8.2	210
	900	1410	55.8	12.5	199
	1000	1390	57.0	12.0	150

Though dencity of specimens grows generally within compaction pressures of 2 to 25 MPa, this process runs most intensely up to 10 to 15 MPa. This is associated with transfer and more compact arrangement of particles. Along with this, partial destruction of small particles and of contacts between them is possible. Large pores (above 10^4 Å) are filled with the material and their volume decreases by 50 times. The further increase of pressure results in reduced intencity of compaction. With pressure growing, the strength of hot-pressed specimens increases according to the power law.

Thus, the forced agglomeration of Portland cement raw mixes is an efficient method of intensification of technogical processes requiring modern technical solutions.

REFERENCES

Butt, Yu.M., Timashev, V.V., "Portlandcement clinker", Strojizdat, Moscow, 1967, p.302.

Butt, Yu.M., Timashev, V.V., Sulimenko, L.M., Albats, B.S., "A Method of Portlandcement Clinker Production", USSR, Inventor's certificate No. 234197, dated October 11, 1968.

Ivanov, N.I., Gavrilov, A.P., Sedov, M.S., Fyodorov, N.F., "A Method of Ceramic and Cement Clinker Production", Russian Patent No. 2010779, 1994.

Klassen, V.K., "Firing of Cement Clinker", Strojizdat, Krasnoyarsk, 1994, p.320.

Kupper, D., Rother, W., "Verfahren zur Herstellung von Zementklinker", Krupp Polisius AG, No. 4219697.3., FRG, 1993

Sulimenko, L.M., Albats, B.S., "Agglomeration Processes in Building Materials Production", All-Russian Research Institute for Economics of Building Materials, Moskow, 1994, p.247

Sekava, T., Mukan, K., Tatakhayasi, K., "A Cement Clinker Firing Plant", Japan, No. 2229745, 1990.

MELTING PROCESS FOR CLINKERISATION - A TECHNICAL REEXAMINATION

S. A. KHADILKAR, P. G. LELE, D. GHOSH, A. K. CHATTERJEE
Research & Consultancy Directorate
The Associated Cement Companies Ltd,
Thane - 400604, INDIA

ABSTRACT In continuation of our studies on clinkerisation through the melting process as reported at the 9th International Congress on Chemistry of Cement, further progress has been achieved on lab and pilot scale. Clinkers were manufactured through melting process at temperatures of 1350 ° C - 1450 ° C. The effect of concentration of fluxes and mineralisers on melting temperature and chemico-mineralogical properties of clinker were studied. The process of progressive liquefaction of raw mixes, changes in melt properties, effect of cooling rate on nature of solidification were some of the aspects studied in some detail. A comparison of microstructural and hydraulic properties of clinker obtained through the melting process and the conventional liquid - phase sintering is presented in the paper, which also highlights the technical feasibility of clinkerisation through melting illustrating the potential advantages and likely disadvantages.

KEY-WORDS Clinker Formation, Melt, Temperature, Ferrite Phase, Characterisation.

INTRODUCTION

In its search for avenues of reducing investment and energy costs in cement manufacture ,the Research and Development Division of the Associated Cement Companies have been investigating a number of alternative approaches at R&D level. Melting process for clinkerisation is one such project which has shown some likely possibilities. Preliminary investigations were reported by the authors at the 9th International Congress on Chemistry of Cement (Khadilkar et al 1992). Since then considerable progress has been made on establishing the feasibility of melting process of clinkerisation at the lab and pilot scale level.This paper summarises the findings on optimisation of compositional parameters to achieve lower fusion temperature of the portland cement raw mix.The paper also discusses the chemico-mineralogical , physico-mechanical and hydraulic potential of the pilot-scale clinkers produced by the melting process,comparing the properties with the clinkers produced by conventional sintering process.

The paper also compares the heat of clinkerisation of melting process to that of conventional sintering route and attempts to draw out a comparative energy requirements of the two processes.

EXPERIMENTAL WORK

Laboratory studies were carried out to assess the influence of compositional parameters on fusion temperature of the ordinary cement raw mixes and to study the effect of different fluxes and mineralisers on phase formation.

Optimisation of compositional parameters

About 30 different raw mixes were prepared with different modulii values (LSF,SM,AM) and Fe_2O_3 contents. The fusion temperature of the raw mixes was determined by Leitz

Heating Microscope.The data base was used for multilinear regression analysis to understand the influence of different parameters on fusion temperature of the cement raw mixes.
The statistical analysis confirmed that LSF and Fe_2O_3 content of clinker have strong relationship with the fusion temperature of the cement raw mixes, as indicated by the correlation coefficients of 0.96.
The multilinear regression is of the first order in nature,the empirical equation relating the burnt raw mixes clinker LSF ,Fe_2O_3 and the fusion temperature is illustrated below:

Fusion temperature (^{0}C) = 2545.6 LSF - 32.77 Fe_2O_3 - 596.05

The theoretically predicted values of fusion temperature and the experimentally determined fusion temperature of different raw mixes are graphically represented in Fig.1which indicates the reliability of the regression equation. The equation is valid when no mineralisers or fluxes other than iron ore ,bauxite, laterite are used.

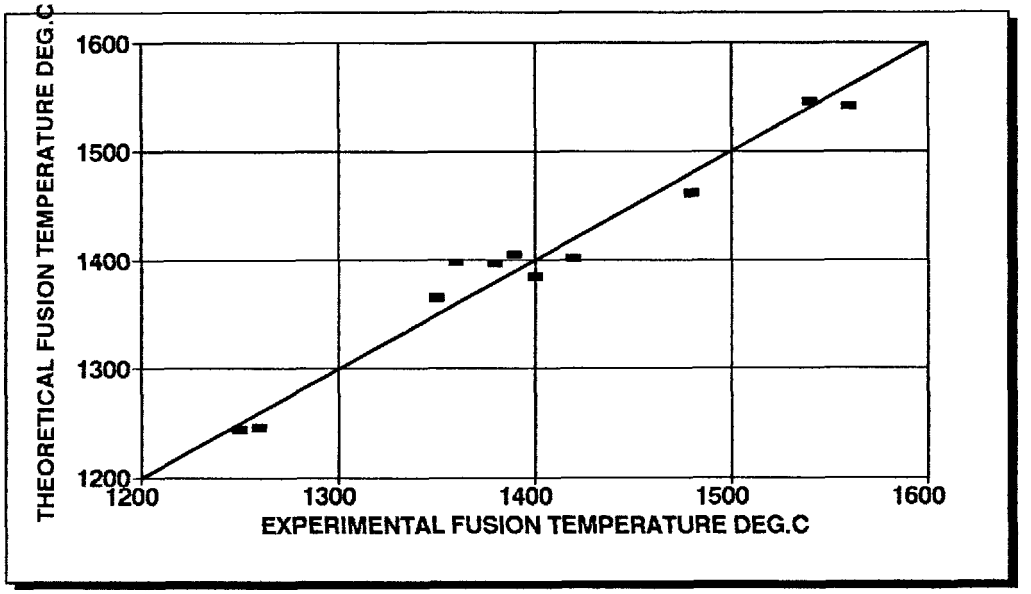

FIG.-1 : RELATION BETWEEN THEORETICAL & EXPERIMENTAL FUSION TEMPERATURE

Effect of fluxes and mineralisers

The effect of fluxes like Borax, K_2CO_3,CaF_2, Blast furnace slag and Basalt (volcanic rock) on the fusion temperature and clinker phase formation was studied.Several raw mixes were designed (RawMixes -A, B, C, D & E) , targeting LSFand Fe_2O_3 in clinkers within a very close range.The details of the raw mixes is given in Table-1.The fusion temperatures of these raw mixes was determined by Heating Microscope.

The raw mixes were also melted in an electrical furnace and the melting process clinkers produced were analysed by X-ray Diffraction Analysis to assess the clinker phase formations. X-ray Diffractograms of the clinkers are shown in Fig.2.

Table 1 **Raw material composition and proportion in raw mixes along with their fusion temperature**

RAW MATERIALS	CHEMICAL COMPOSITION					RAW MATERIAL PROPORTIONS OF RAW MIXES				
	SiO_2	Al_2O_3	Fe_2O_3	CaO	LOI	A	B	C	D	E
LIMESTONE -A	32.5	2.7	1.3	34.2	27.6	28.0	28.0	28.0	21.4	22.5
LIMESTONE -B	7.4	1.1	1.1	48.0	38.5	66.3	66.3	66.3	71.3	68.3
LATERITE	25.8	12.9	49.0	0.4	10.8	3.1	3.1	3.1	1.8	4.2
BAUXITE	10.0	45.0	25.0	2.0	7.0	1.6	1.6	1.6	0.5	–
BASALT	48.5	16.0	16.0	8.5	3.4	–	–	–	5.0	–
B.F.SLAG	33.2	23.0	1.0	38.0	0.5	–	–	–	–	5.0
K_2CO_3	–	–	–	–	–	1.0	–	–	–	–
$B(OH)_3$	–	–	–	–	–	–	1.0	–	–	–
CaF_2 (PURITY 80%)	–	–	–	–	–	–	–	1.0	–	–
L.S.F						0.88	0.88	0.88	0.88	0.88
Fe_2O_3						4.5	4.5	4.5	4.3	4.5
FUSION TEMPERATURE (^{0}C)										
THEORETICAL						1496	1496	1496	1500	1490
EXPERIMENTAL						1480	1480	1400	1420	1450

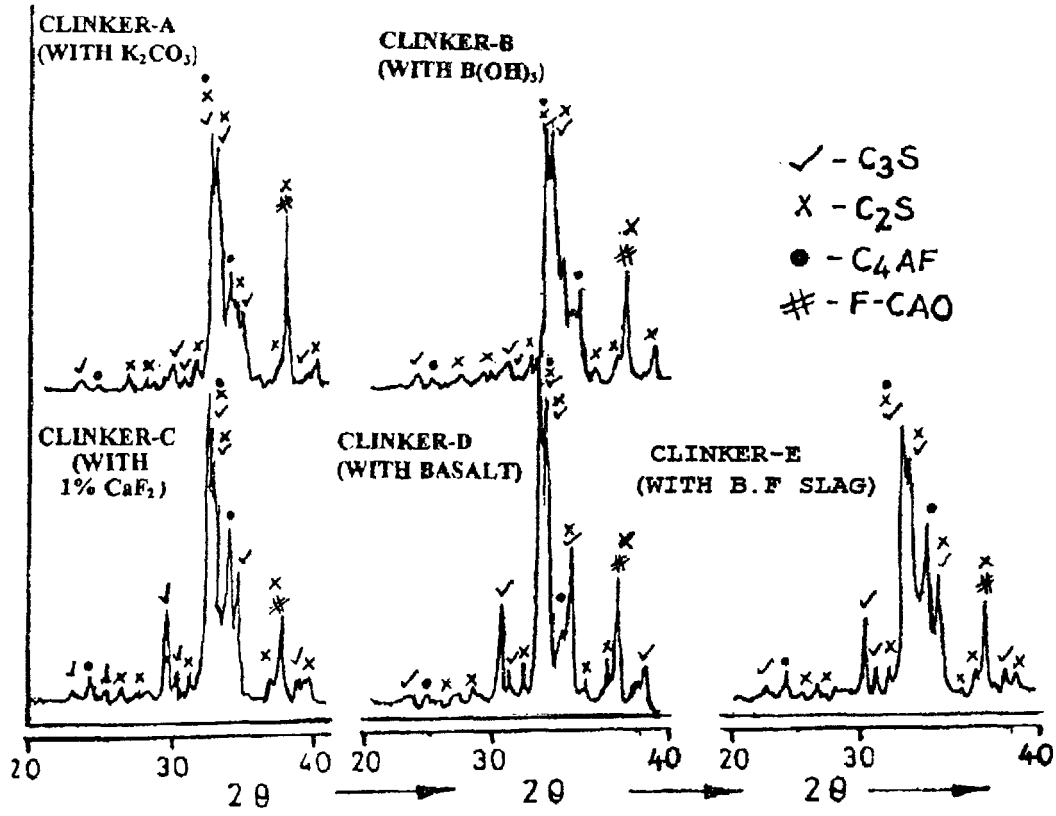

FIG. 2 : XRD SCANS OF CLINKERS WITH FLUXES AND MINERALISERS

The results illustrate that :

- $B(OH)_3$ and K_2CO_3 do not have influence on fusion temperature as well as on clinker phase formation.
- Use of 1% CaF_2 (80 % purity) reduces the fusion temperature by 50 ° C.
- With the use of B.F Slag and Basalt as corrective, the fusion temperature of the raw mixes is lower than expected at the respective LSF and Fe_2O_3 contents,this can be attributed to the lower fusion temperatures of these correctives themselves (1240^0-1260^0 C).
- Clinker phase formation in raw mixes C,D,E i .e . with Basalt, B.F Slag and 1% CaF_2 respectively is better than Raw mixes A and B (with $B(OH)_3$ and K_2CO_3)

Heat Of Clinkerisation Of Melting Process Raw Mixes

The heat of clinkerisation of the pilot scale raw mixes was determined by Thermal Analysis method standardised at the authors' laboratory .The values of heat of clinkerisation for the pilot scale raw mixes were observed to be in the range of 350-380 cal/g as compared to the conventional raw mix values of 390-430 cal/g, which indicates that the Enthalpy values of the melting process mixes were lower than conventional cement raw mixes.

Effect of aqueous quenching

To assess the effect of aqueous quenching on the mineralogy and microstructure of the melting process clinkers were quenched in water. No significant difference was observed in the XRD-pattern,however, the water-quenched clinkers exhibited fine grained alite.Similar observations were reported by the authors in their earlier publication.(Khadilkar et al 1992)

PILOT SCALE CLINKERISATION

Several raw mixes were prepared for pilotscale clinkerisation using limestone of three different sources broadly covering a range of LSF from 0.81 to 0.91 with Fe_2O_3 contents at appropriate levels (according to regression equations) targeting fusion temperatures in the range of 1350° C - 1450 ° C. Some Raw Mixes were also prepared with 0.5% CaF_2 (80 % purity) as mineralisers. The generated data on some of the raw mixes is discussed in this paper viz: PS-1(LSF 0.81), PS-2 (LSF 0.84), PS-3 (LSF 0.87) PS-4 (LSF 0.91) PS-5(LSF 0.91with 0.5% CaF_2) .The chemical composition of raw materials and raw material proportions of the raw mixes is given in Table-2.

Pilot Scale melting process

The secondary crushed raw materials of size 4 - 6 mm were mixed in appropriate proportions and melted in a magchrome refractory lined melting furnace(capacity:25Kg) at temperatures of 1450°C.The fused clinkerised mass was maintained under molten condition for 1 hr; after which it was air quenched using compressed air to produce the clinker.

The pilot scale clinkers so produced were evaluated for chemical composition (Table-3), grindability index (Table-3),mineralogical composition by XRD, microstructural features by Optical Microscopy, and Hydraulic characteristics were assessed by testing the lab-ground cement prepared from the pilot scale clinkers (Table-4).

Table-2 Raw material composition and raw material proportions of pilot scale raw mixes

RAW MATERIALS	CHEMICAL COMPOSITION					RAW MATERIAL PROPORTIONS OF RAW MIXES				
	SiO_2	Al_2O_3	Fe_2O_3	CaO	LOI	PS-1	PS-2	PS-3	PS-4	PS-5
LIMESTONE-1	12.2	2.0	1.0	46.1	37.5	80.0	23.8	79.0	79.2	78.5
LIMESTONE-2	17.4	6.0	1.0	42.4	35.7	17.0	73.0	15.2	–	–
LIMESTONE-3	25.9	3.9	1.3	35.3	31.4	–	–	–	14.8	15.0
IRON ORE	6.4	4.4	86.4	0.1	2.6	3.0	3.2	3.3	3.2	3.2
BAUXITE	4.3	42.2	28.0	0.1	23.6	–	–	2.5	2.8	2.8
CaF_2 (PURITY 80 %)	–	–	–	–	–	–	–	–	–	0.5

Table-3 Chemical composition of pilot scale clinkers

OXIDES	PS-1	PS-2	PS-3	PS-4	PS-5 *	CONVENTIONAL CLINKER
SiO_2	24.7	24.35	19.6	21.3	21.2	21.5-23.0
Al_2O_3	4.23	3.87	4.9	5.4	5.3	4.5-5.5
Fe_2O_3	6.07	5.75	7.0	7.0	7.0	3.6-4.0
CaO	63.6	64.6	56.7	64.3	64.3	63.4-66.0
free CaO	3.5	4.0	3.8	4.0	2.8	<2.0
LSF	0.81	0.84	0.87	0.91	0.91	0.87-0.92
SM	2.40	2.53	1.64	1.72	1.72	2.2-2.5
AM	0.70	0.67	0.71	0.77	0.77	1.3-1.6
C_3S	20.0	27.3	23.4	37.2	43.5	40-55
C_2S	55.8	49.3	38.6	33.1	28.0	30-40
C_3A	1.0	0.5	1.3	2.5	2.2	7-10
C_4AF	18.5	17.5	21.3	21.3	21.3	10-15
Fusion Temp. ^{O} C	1260	1350	1390	1480	1420	–
Bond grindability Index (Kwh/sh.ton)	24.8	23.5	20.8	22.0	22.5	16-20

* WITH F=0.22%

Table-4 Physical tests results of lab ground cements prepared from pilot scale clinkers (Indian Standard Test Method)

Test	PS-1	PS-2	PS-3	PS-4	PS-5 *
Fineness (cm^2/g)	3000	3000	3000	3000	3000
Setting Time (minutes)					
Initial	90	65	100	100	100
Final	100	135	135	150	180
Compressive strengths (MPa)					
1-day	8.0	10.0	12.0	15.0	16.5
3days	16.0	19.0	22.0	24.0	34.0
7-days	22.0	28.0	32.0	33.5	41.5
28-days	33.0	39.0	43.0	48.0	55.0

***with 'F' as mineraliser**

RESULTS AND DISCUSSIONS

1) Chemical composition of the pilot scale clinkers is given in Table-3. The analysis of the clinkers indicated high free lime content in the range of 3 - 4%,which may be due to limitations of the melting furnace in which the melt could not be made to flow and mix, causing localised inhomogenity.The fusion temperatures observed at pilot scale level were

similar to that predicted by the empirical equation except for P.S-5 in which case it was observed to be lower due to mineralising effect of the CaF_2.

2) Bond Grindability index (Kwh/Sh.Ton) of the pilot scale clinkers found in the range of 22.0 to 24.8 indicating that the melting process clinkers are difficult to grind compared to conventional clinkers which are normally in range of 14.0 to 20.0 kwh/sh.ton.

3) The XRD patterns of the clinkers indicate differences in the peak positions of Belite and Alite as compared to clinkers produced by conventional sintering process. Similar observations have been reported earlier by the Authors(Khadilkar et al 1992) on melting process clinkers.

4) The microstructural features for all the melt process clinkers irrespective of their compositions are more or less similar and somewhat different compared to the clinkers produced by liquid phase sintering. In the melting process clinkers, the alites are mostly prismatic, elongated to rod shaped (Plate-I) or large, stout crystals with wavy margins (Plate-II). The matrix is generally highly differentiated with coarse and small grains. The distribution of the alite, belite and liquid phase is inhomogenous, sometimes large nests of either belite, alite or liquid phase seen. (Plate-III). The belites are mostly β or α' variety. The inhomogeneity and occurrence of coarse crystals are due to insufficient mixing and diffusion of the constituent oxides released from the coarse grains, which in this case were released from coarse particles that were not finely ground. Probably, this could be avoided if the molten material in the furnace is allowed to mix before it is cooled.

5) The lab-ground cements were prepared from the pilot scale clinkers by cogrinding with gypsum. maintaining SO_3 content of 2.2% and fineness of 3000cm^2/g. The physical test results (Table - 4) indicates that the compressive strength of cements increases with increasing LSF (PS-1 to PS-4) and as expected, addition of mineralisers (PS-5) helps in the gain of compressive strengths as well. The cement quality data also indicates (a) possibility of manufacturing Ordinary and Rapid Hardening cements ; (b) the melting process clinker shows the same relationship of increasing compressive strength with LSF like conventional clinkers and (c) unlike the conventional clinkers the melting process clinkers show much higher rate of strength development at later ages than at the early ages.

Process Considerations

Based on the investigations, a schematic flowsheet (Fig.3) for clinker manufacture by melting process and conventional sintering is shown diagramatically to illustrate unit stages of manufacturing in melting process route. It can be seen that in the conventional sintering process, the raw mill grinding and homogenisation can be totally eliminated in the melting process route.

A tentative comparison of energy consumption for clinkerisation using the melting process and the conventional sintering process has been attempted (Table 5) which indicates that the total energy consumption for melting process, quite contrary to the normal expectation may turn out to be lower than the conventional sintering process.



Plate I Elongated to rod shaped Alite (Mag X 200)



Plate II Large stout alite crystals with wavy margin (Mag X 200)

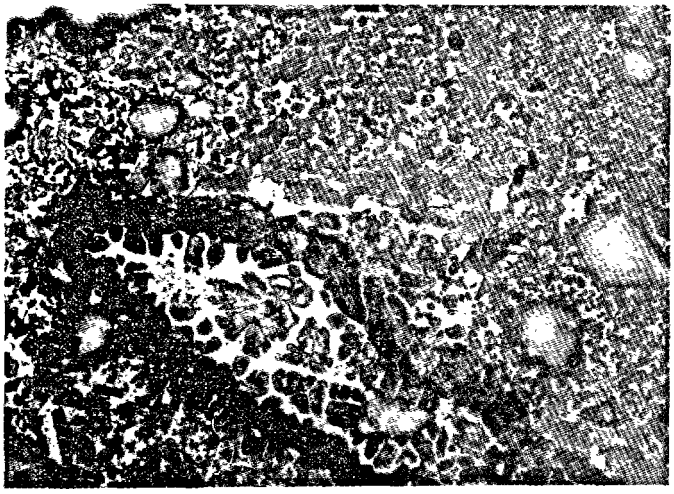

Plate III Large nests observed in melting process clinker (Mag X 160)

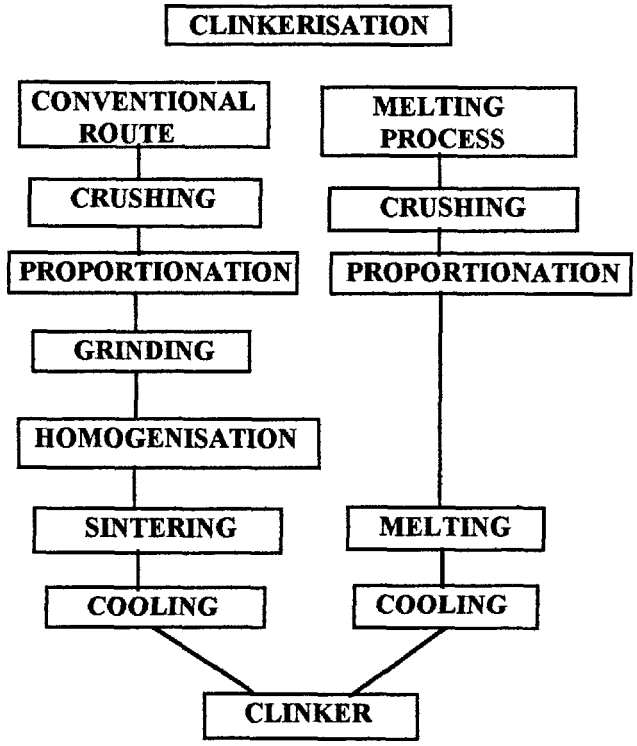

Fig 3 Schematic Representation of Conventional & Melting Process

Table-5 Approximate comparison of energy consumption between Melting and Conventional sintering process of clinkerisation (Basis : kcal/kg clinker)

PARAMETERS	CONVENTIONAL	MELTING PROCESS
CLINKERING TEMPERATURE (^{0}C)	1450	1500
COMMUNITION **		
CRUSHING	0.6	0.6
GRINDING & BLENDING	23.0	–
SP.HEAT CONSUMPTION		
HEAT OF CLINKERISATION	410	400
S.H.KILN EXIT	185	60
COOLER EXIT	50	50
CLINKER EXIT	19	100
RADIATION		
KILN }		
COOLER }	70.0	20.0
PREHEATER }		
KILN DUST }		
COOLER DUST }	7.0	2.0
CALCINATION DUST }		
MOISTURE }		
-	764.6	652.6

* BASIS OF CONVERSION : 1 Kwh = 860 Kcal

CONCLUSIONS

1) The experimental work defined an empirical equation for predicting fusion temperature of raw material mixes which can be used as a parameter while designing mixes for the melting process of clinker manufacture .Amongst the fluxes and mineraliser as expected, fluorine was found to be effective in lowering the melting temperature.

2) The laboratory investigation has been scaled up to pilot scale levels and clinkers could be manufactured successfully in 25 kg batches.

3) The cements prepared from the melting process clinkers exhibited strength properties, where gain in cement strengths were observed at all ages(1 Day to 28 Days) and the rate of strength development at later ages were higher as compared to the early ages.

4) It is envisaged that melting process route for clinker manufacturing can eliminate the raw material grinding and homogenisation of the conventional route. Tentative calculations on energy consumption for melting process of clinkerisation appears to be attractive.

REFERENCES

S.A.Khadilkar, P.G.Lele, C.H.Page and A.K.Chatterjee " Clinkerisation through Melting - A New Approach" 9th International Congress on Chemistry of Cement, New Delhi 1992, Vol. II, pp 190-195.

GRINDING TECHNOLOGY AND QUALITY OF COMPOSITE CEMENTS

Ludmilla OPOCZKY and Miklós HILGER,
Cement Research & Development Ltd.,
Budapest, HUNGARY

ABSTRACT
It is proved that particle size distribution highly affects the water demand of cement. Cements of "wide range" particle size distribution are of least water demand. There is a definite relationship between grindability and particle size distribution, i.e. the easily grindable materials provide grinding products of "wider range" particle size distribution. With the aid of suitable combination of materials of different grindability composite cements of advantageous peculiarities can be produced.

Key-words: Composite cements, additives, particle size distribution, grinding technology

INTRODUCTION
The production of composite cements containing different additives is reasoned by economic and environmental aspects. As regards the composition of composite cements, the European standard suggestions provide a lot of possibilities but do not provide unambiguous bases to select the reasonable composition. The application technical features of multicomponent cements are highly influenced by their grinding technological features (grindability, particle size distribution), in addition to the clinker of given quality and additives. Knowing these features it is possible to produce composite cements of rational composition through the suitable combination of additives. In the following the investigation results representing the grinding technological and quality relationships (composition - grindability - particle size distribution - specific surface - water demand - strength) will be presented.

INVESTIGATION RESULTS
To perform the investigations, clinker (C_3S = 54.7 %; C_2S = 23.1 %; C_3A = 7.1 %; C_4AF = 11.1 %) and hydraulically active (granulated blast furnace slag, fly ash, trass) and inert (limestone) additives were used. In Fig.1. the "specific grindability" (W_t) of the starting materials (except the fly ash) is shown. The specific surface of fly ash was ~300 m^2/kg in its original state. Grindability was determined with the Zeisel-instrument. Fig.2. illustrates the relationship between grindability and particle size distribution. In the figure the particle size distribution curves and characteristic fineness parameters of the milling products produced from the experimental materials in laboratory ball mill under the same grinding time, are shown. Particle composition of the milling products was determined by a CILAS 715 type laser granulometer (3-200 μm). To describe the particle size distribution the RRSB equation and its two constants, i.e. the n factor of uniformity and $\bar{x}$ fineness number were used, respectively. It is to be noted that the factor of uniformity (n) is the number of the "range" of dispersion, the smaller is n the "wider" is the particle size distribution; the fineness number $\bar{x}$ refers to the fineness of the milling product, the smaller is $\bar{x}$, the finer is the product.

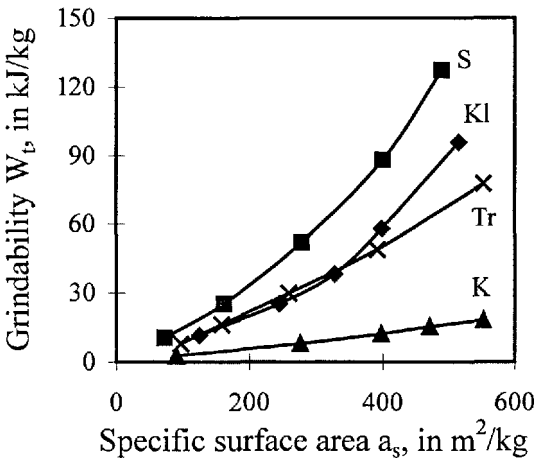

Kl:Klinker; S:Blast furnace slag;
Tr:Trass; K:Limestone

Fig.1
Grindabilities of the starting materials

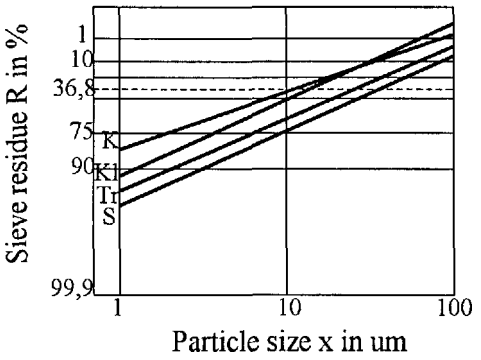

Material	Grinding time	Specific surface	RRSB	
			n	$\bar{x}$
	h	m^2/kg		μm
Blast Furnace (S)	1	200	0,9572	36
Klinker (Kl)	1	350	0,923	18
Trass (Tr)	1	300	1,0628	22
Limestone (K)	1	700	0,6477	15

Fig.2
Grindability and particle size distribution

It can be stated that clinker, blast furnace slag and trass can be more heavily ground ($W_t \sim 35$ - 21 kWh/t), while the limestone can be assigned to the materials of easy grinding ($W_t \sim 5$ kWh/t). It can be seen in Fig.2. that from the easily grindable limestone products of smaller factor of uniformity, i.e. of "wider range" of particle size distribution, from the heavily grindable blast furnace slag and trass products of greater factor of uniformity, i.e. of "narrower range" of particle size distribution can be produced. It is to be noted that fly ashes separated on the elctrofilters and used as additive are of characteristic "narrow range" of particle size distribution ($n \geq 1$) even in their original state and this the result of separation and not that of grinding. Based on the results presented the conclusion can be drawn that the addition of different additives to the cement will affect its particle size distribution in different manner, i.e. it will be "widened" or "narrowed down". As an example, in Fig.3. the formation of particle size distribution and of the factor of uniformity of cements of different trass (a) and limestone (b) contents is presented.

The water demand of cements can be also seen. (Water demand means the water quantity needed to the preparation of cement mash of standard deliquescence.) The addition of trass while "narrowing down" the particel size distribution (the n factor of uniformity increases) increases the water demand of the cement. This effect increases with increasing trass quantity. Similar effect can be experienced in case of fly ash and blast furnace slag, in case of fly ash this is greater than in that of trass and blast furnace slag, in case of trass is greater than in case of blast furnace skag addition. On the contrary, the addition of limestone "widens" the particle size distribution of the cement (the n factor of uniformity decreases), and simultaneously this reduces the water demand of it. This effect can be observed already in case of addition of 2-10 $^{m}/_{m}$ % limestone.

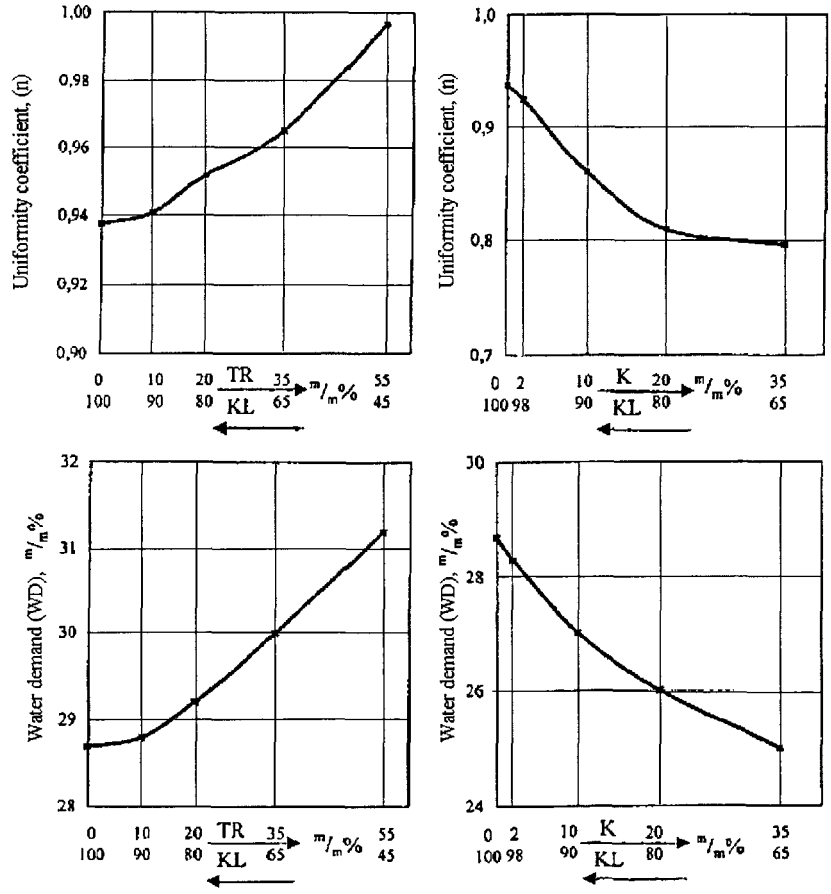

a, b,

Fig.3

Change of uniformity coefficient (n) and water demand (WD) of cement depending on trass-content (a); on limestone-content (b)

In the course of previous investigations it was demonstrated (Opoczky, 1992) that in case of joint grinding of clinker and limestone, the easily grindable limestone accumulates in the finest (< 5 μm), the clinker in the relatively coarser fraction. The fine particels of limestone are located in the holes and interspaces among the clinker particles providing thus a "complete" space filling". Limestone particles are highly suitable to this due to their morphology. Consequently, with the addition of limestone the particle size distribution and thus the water demand of the cement can be favourably affected. In addition to this positive effect, the addition of the practically inert limestone reduces the strength of the cement. This strength reduction can be compensated by increasing the grinding fineness of the cement only to certain extent, all the more so the limestone inclines to adhesion and agglomeration.When adding hydraulically active additives, besides the grinding fineness that can be reached in practice, as well, cements of required strength can be produced. Nevertheless, most of the hydraulically active additives increase the cement's water demand that becomes obvious in case of cements with high amount of additives. The great water demand of these cements can be reduced by adding suitable limestone.

Our experiments prove that using hydraulically active and inert additives (e.g. trass + limestone) together, clinker-saving composite cements of favourable particle size distribution and water demand can be produced. In Fig.4. the compression strength of 28 days (a), factor of uniformity and water demand (b) of composite cements of ~ 400 m^2/kg specific surface produced by joint

grinding containing trass and limestone and trass plus limestone are seen, that turned to favourable in case of composite cements of trass plus limestone content.

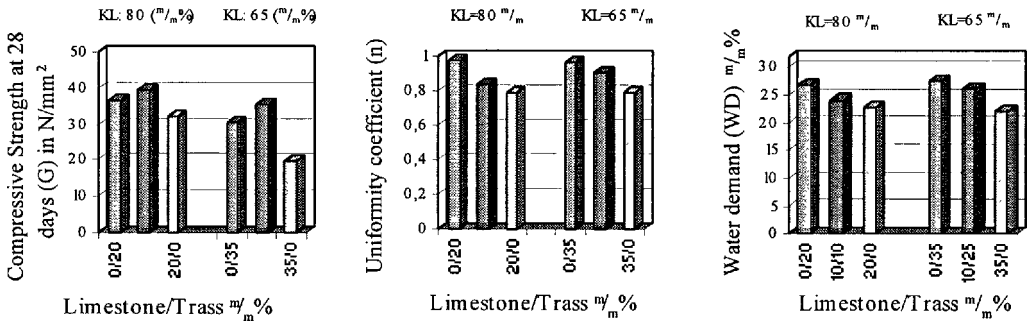

a, b,

Fig.4

Compressive strength (a), uniformity coefficient and water demand (b) of composite cements

MAIN CONCLUSIONS

The water demand of cement is considerably influenced by the particle size distribution. Cements of "wider range" particle size distribution are of less water demand. Additives studied in this work differ not only in the hydraulic activity but in the effect they exert on the particle size distribution and water demand of the cements: the limestone "widens" the particle size distribution and reduces the water demand of the cement; fly ash, trass, granulated blast furnace slag "narrow down" the particle size distribution range and increase the water demand. Additives keep their characteristic particle size distribution even during grinding together with clinker. When preparing cement mash water is added more than theoretically required. This water surplus is used to fill the holes and interspaces among clinker particles and to wet the surface of clinker grains in order that these be moveable beside each other. In a milling product the smaller is volumetric proportion of the solid state matter and the greater is the volume of the holes to be filled, the "narrower" is the particle size distribution. The water demand reducing effect of limestone is related to its "wider range" particle size distribution and to its "space filling" effect. There is a concrete relationship between grindability and particle size distribution, i.e. easily grindable substances produce milling products of "wider range" particle size distribution. By means of the suitable combination of substances of different grindability clinker-saving composite cements of favourable grinding technological and quality features can be produced.

The support of OTKA (National Scientific Research Fund) No. T 14872 is gratefully acknowledged.

REFERENCE

Opoczky, L.: „Progress of the particle size distribution during the intergrinding of a clinker-limestone mixture." Zement-Kalk-Gips, **46**, (No.2.) pp.54-57, 1993. (E)

CEMENT CLINKER FORMATION FROM FLYASH BY MICROWAVE PROCESSING

Y. FANG, D.M. ROY, Y. CHEN, and M.R. SILSBEE
Materials Research Laboratory
The Pennsylvania State University, University Park, Pennsylvania 16802, U.S.A.

ABSTRACT Cement clinkers based on class F flyash have been prepared by microwave processing at temperatures up to 1350°C. For appropriate chemical compositions, CaO or $CaCO_3$ was the main additional component phase added to the raw material mixture. CaF_2 and $CaSO_4 \cdot 2H_2O$ were used as fluxes or mineralizers to lower processing temperature. The clinkers thereby obtained show compositions with similar phases present in commercial portland cement. Microwave processing is generally characterized by volumetric heating, high heating rate, and a short processing time; combined with considerably energy efficiency.

Keywords: clinker formation; waste material utilization; X-ray powder diffraction

INTRODUCTION

Flyash is a waste product of coal-burning power plants and is being produced in huge amounts. In the United States, for example, more than 70 million tons of flyash is produced each year. The accumulation of flyash not only consumes valuable landfill space, but also results in soil contamination. Because of this, proper disposal of flyash is of great concern, and making use of such a waste material is even more valuable for both environment protection and resource saving.

Flyash can be added to cement as an admixture to produce flyash cement. However, since flyash is mainly composed of hollow or solid glass spheres which generally only hydrate to a limited degree, the strength development of low calcium flyash cement is slow and the mechanical strength is lower than portland cement.

Flyash is mainly composed of SiO_2, Al_2O_3, Fe_2O_3, CaO, etc., similar to portland cements in composition, but different in proportion. By using appropriate correcting materials, it is possible to produce cement clinker based on flyash. Indeed, fly ash is commonly used as feedstock in many cement kilns. In this study, we prepared cement clinker using flyash as a basic material and microwave heating as the processing technique. Microwave processing is emerging as a new technique in ceramic fabrication and is generally characterized by volumetric heating, high heating rates, and short processing time, with a possibility of improvement in product properties. (Sutton, 1989) Among the various microwave processed ceramic materials is the portland cement clinker prepared by Quemeneur et al. (1983) and Fang et al. (1996). Roy et al. (1985) have shown that silica and alumina gels can be easily heated to high temperatures by microwave irradiation. This has been confirmed by Fang et al. (1996) in the study on microwave processing of diphasic aluminosilicate gels. Since glassy silica is the major constituent of flyash, it is expected that flyash can absorb microwaves fairly well and thus be easily heated by microwaves.

EXPERIMENTAL

Starting materials

Class F flyash (supplied by the American Fly Ash Co., Des Plaines, IL) as defined in ASTM C 618 was used as the main starting material. The chemical composition of the flyash is shown in Table 1, along with that of a typical Type III portland cement for comparison.

From Table 1, it is seen that the flyash was rich in SiO_2 but poor in CaO. To produce compositions suitable for cement clinker, CaO was added. Small amounts of CaF_2 and gypsum

($CaSO_4 \cdot 2H_2O$) were used as flux. Coal was added (5%) to the mixture for two reasons: (a) it is present in most commercial raw meals as fuel and, (b) it absorbs microwaves well and favors microwave heating.

Table 1 Chemical composition of the flyash (wt. %) and Type III cement

	SiO_2	Al_2O_3	Fe_2O_3	CaO	MgO	Na_2O	K_2O	SO_3	L.O.I
Flyash	53.0	18.6	15.6	6.37	1.26	0.94	2.08	2.02	1.68
Cement*	20.6	4.52	3.02	62.3	2.09	0.24	0.82	3.80	1.12

* Typical Type III, Lafarge Corp., Montreal, Canada.

The weight proportion of the raw mixture was flyash/CaO = 36/60. The amount of flux was CaF_2 = 1.93%, gypsum = 1.45%. Correspondingly, the factors (Tailor, 1990) used in cement industries for proportioning of raw meals, namely, lime saturation factor (LSF), alumina modulus (AM), and silica modulus (SM), are calculated as the following.

$$LSF = CaO / (1.2\ Al_2O_3 + 0.65\ Fe_2O_3 + 2.8\ SiO_2) = 0.97 \quad (1)$$

$$AM = Al_2O_3 / Fe_2O_3 = 1.19 \quad (2)$$

$$SM = SiO_2 / (Al_2O_3 + Fe_2O_3) = 1.55 \quad (3)$$

where each chemical formula represents the weight percentage of the corresponding composition in the mixture. Typical values of LSF, SM, and AM for commercial clinkers are 0.92-0.98, 2.0-3.0, and 1.0-4.0, respectively, depending on the desired properties of the product.

Flyash, CaO, fluxes and deionized water were mixed according to ASTM C 305, with a water/solid ratio of 0.15. The mixture was uniaxially pressed into pellets of 12.7 mm diameter and 5 mm thick. A small amount of water not only promotes development of appropriate green strength, but also favors microwave heating at low temperature since water absorbs microwaves very well.

Processing

The microwave processing was carried out in a 500 W, 2.45 GHz microwave oven (JE43, General Electric Co.). The details of the sintering setup and temperature measurement are described elsewhere.(Fang et al., 1994; Fang et al. 1996) The samples were heated in the microwave oven up to 1350°C and cooled down after a 10 min. soaking.

Characterization

Dilatometry was carried out with a computer-driven system (Innovative Thermal Systems, NY) at a heating rate of 5°C per min. on pure flyash as well as the flyash-based raw mixture in order to characterize the stages of reaction. Powder X-ray diffraction (XRD) was carried out on the clinkers using CuKα radiation on a Scintag x-ray diffractometer (Scintag Inc., Sunnyvale, CA). Calorimetry was conducted at 25°C to measure the heat evolution of the microwave processed clinker and the conventional sample (Type III portland cement) during the first 40 h of hydration. The microwave clinkers were ground with 3% gypsum before being investigated by isothermal hydration calorimetry.

RESULTS AND DISCUSSION

Figure 1 shows the dilatometry curves of (a) pure class F flyash and (b) the flyash-based clinker mixture. Shrinkage took place gradually in pure flyash from 700°C to 1194°C. The smooth and gradual shrinking curve indicates a process of reduction of inter-sphere pores due to necking between the flyash spheres. Above 1194°C, a sharp peak appears in the curve, corresponding to a volume increase and then decrease. This is believed to be a dilation process of the softened flyash spheres followed by collapse of the spheres, releasing the entrapped air. The linear shrinkage at 1200°C was

corresponding to the necking between flyash particles. There was no shrinkage between 950°C and 1120°C. Instead, a plateau appears in this range. This is believed to correspond to the occurrence of clinkering reactions. Above 1120°C. gradual shrinkage continued. There was no dilation near 1200°C as in the case of pure flyash. The total linear shrinkage till 1250°C was 17.5%.

Figure 2 shows the XRD patterns of the clinkers microwave processed for 10 min. at 1150, 1250, and 1350°C, respectively, compared with that of Type III portland cement (PC). The main phase compositions of the microwave processed clinkers were basically the same as PC, composed of alite ($3CaO{\cdot}SiO_2$, or C_3S) brownmillertite ($4CaO{\cdot}Al_2O_3{\cdot}Fe_2O_3$, or C_4AF) tricalcium aluminate ($3CaO{\cdot}Al_2O_3$, or C_3A), etc. The relative proportions of the components were different because of the differences in starting material as well as the processing conditions. In the microwave processed clinkers, the content of alite increased as processing temperature increased (C_3S is considered not to be formed stably below 1250°C, but here is observed as low as 1150°C. However, Gutt (1968) has observed that C_3S is formed at a lower temperature in the presence of fluoride, consistent with the current findings). The sample processed at 1350°C contained more alite than those processed at 1150 and 1250°C. The clinker processed at 1350°C shows very strong diffraction at 32.1° 2θ (d = 2.789Å), indicating that a preferential crystal growth of alite took place during microwave processing.

The hydration kinetics of microwave processed clinker showed that microwave clinker had a slower hydration rate and lower cumulative heat evolution than the commercial Type III PC sample. This was possibly due to the lower content of the main hydraulic minerals achieved in the short period of microwave processing. Additional studies should optimize the clinker and cement composition.

SUMMARY

Microwave processing of cement clinkers based on flyash has been carried out, and appears very promising. The preliminary results show that the phase compositions of the microwave processed clinkers are similar to that of industrial portland cement. Due to insufficient clinkering time, the current microwave processed flyash cement shows slower hydration rate and lower heat evolution which could be improved by optimizing the processing conditions and cement composition.

ACKNOWLEDGMENT

This work was financially supported by the US Environmental Protection Agency.

REFERENCES

Fang, Y., D.K. Agrawal, D.M. Roy, and R. Roy, "Microwave Sintering of Hydroxyapatite Ceramics", J. Mater. Res., 9[1], 180 (1994).

Fang, Y., Y. Chen, M.R. Silsbee, D.M. Roy, Mater. Letters, "Microwave Sintering of Flyash", 27[6], 155-159 (1996).

Fang, Y., D.M. Roy, R. Roy, Cem. Concr. Res., "Microwave Clinkering of Ordinary and Colored Portland Cements", 26[1] 41-47 (1996).

Fang, Y., J. Cheng, D.K. Agrawal, D.M. Roy, and R. Roy, "Microwave Processing of Diphasic Aluminosilicate Gel", to be published (1996).

Gutt, W., "Manufacture of Portland Cement from Phosphastic Raw Materials", 5th Intl. Congr. Chem. Cem., I, 93-105 (1968).

Quemeneur, L., J. Choisnet, B. Raveau, J.M. Thiebaut and G. Roussy, "Microwave Clinkering with a Grooved Resonant Applicator", J. Am. Ceram.Soc., 66[12], 855 (1983).

Roy, R., S. Komarneni, L.J. Yang, J. Am. Ceram. Soc., "Controlled Microwave Heating and Melting of Gels", 68[7], 392 (1985).

Sutton, W.H., "Microwave Processing of Ceramic Materials", Am. Ceram. Soc. Bull., 68[2], 376 (1989).

Taylor, H. F.W., Cement Chemistry, Academic Press Ltd. London, p. 60 (1990).

about 16.5%. When CaO, CaF_2, and $CaSO_4 \cdot 2H_2O$ were added to flyash, the dilatometry curve is different (Fig. 1-b) because of the reactions during heating. Three shrinkage steps are obvious. The first took place between 392 to about 500°C, with a shrinkage of about 2%, probably corresponding to the dehydration of gypsum ($CaSO_4 \cdot 2H_2O$). The second took place between 700°C and 950°C,

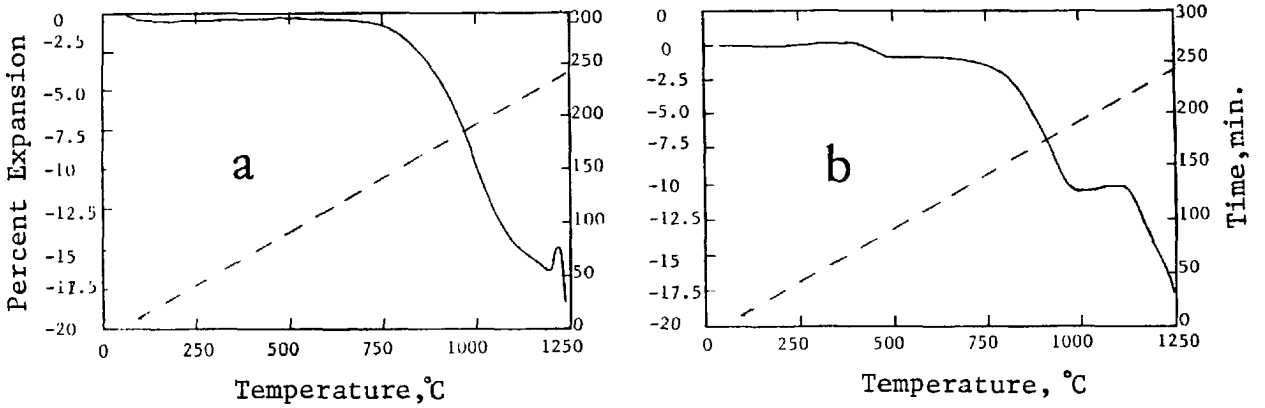

Figure 1. The results of dilatometry on (a) pure type F flyash and (b) flyash-based raw mixture for cement clinker.

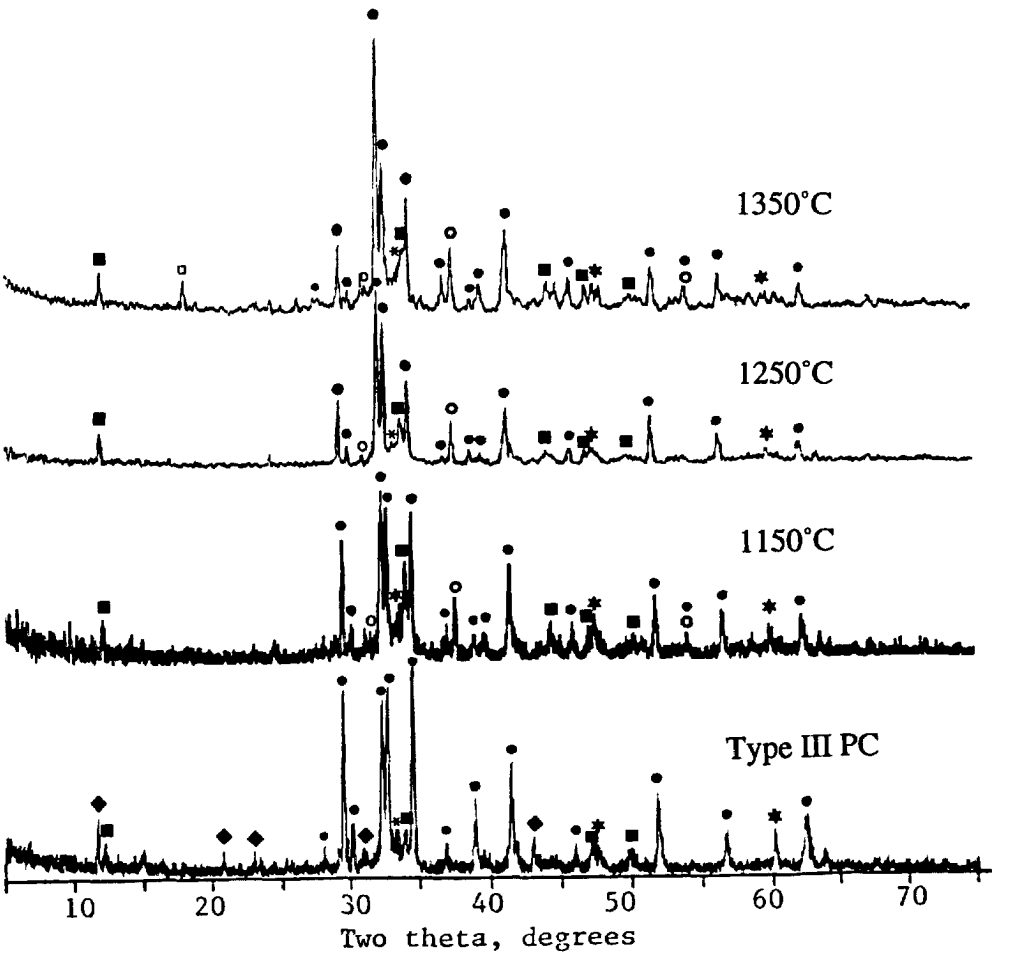

Figure 2. XRD patterns of the flyash cement clinkers microwave processed at various temperatures, compared with a typical commercial PC (Type III). The main peaks are identified as (•) alite, (*) tricalium aluminate, (°) lime, (♦) gypsum. (▪) brownmillertite, and (□) $Ca(OH)_2$.

CLINKER FORMATION IN HIGH-SILICATE LOW-TEMPERATURE MELT

Vladimir D. BARBANYAGRE, The Belgorod Technological Academy of Building Materials, Belgorod, Russia

ABSTRACT Exclusively technological methods have been studied and offered. Due to the involvement of a larger quantity of silica into clinker melt, these methods allow to reduce considerably melt formation temperature and clinker sintering temperature without using catalytic admixtures and low-melting fluxes.
CLINKER FORMATION, MELT, NONEQUILIBRIUM BURNING

INTRODUCTION

The main chemical and physical processes occurring during portland cement clinker sintering are determined by the constitutional diagram of CaO-SiO_2-Al_2O_3-Fe_2O_3 (C-S-A-F) system, as well as ternary and binary constitutional diagrams. However, in view of the fact that the diagrams describe an equilibrium state of the system, and the clinker sintering process is known to be nonequilibrium, the phase composition of clinker may differ considerably from the state of equilibrium described more completely for cooling process. Depending upon cooling rate the phase composition of clinker may be represented either by glass, or by crystalline phases or by mixtures crystalline and glass-like phases.

Unlike clinker cooling processes, nonequilibrium processes related to the heating of a raw mix are not studied properly. Meanwhile, as will be shown in the present paper, under heating very great changes in the quantity of clinker melt, its composition, viscosity and other properties upon which clinker sintering depends may take place. The main result of these changes is a degree of deviation of the mix from a state of equilibrium. Three methods of creating a state of nonequilibrium in the process of cement raw mix heating are considered.

Fast Heating of a Raw Mix

It has been established that the heating rate of the materials may exceed the rate of chemical reaction under fast burning when the raw mix enters a high-temperature zone. As a result original compounds, in the form of low-basicity calcium silicates, aluminate and ferrites, form a high-silicate melt having the composition given in Table 1. Pseudowollastonite and iron bearing melilite are a specific feature of the above melt. Then clinker minerals are formed by means of this melt. Thus, the well-known intensification of clinker sintering processes under the fast burning results partially from time-simultaneous dissociation processes of original compounds and synthesis processes of minerals (Chebukov, 1950). The main reason for the said intensification is the formation of a high-silicate, low-basicity melt.

Cement raw mix with a coarse ground carbonate component

High-silicate, low-temperature melt with the composition similar to that given in Table 1 is formed during the burning of the raw mix with a coarse ground calcium carbonate. Because of the large size of calcium oxide grains, a part of the material (30-35%) concentrated in the centre of coarse grains is temporary withdrawn from the reaction and, as a result, the synthesized compounds have

low basicity and at appropriate temperature (1130 - 1200 °C) they form a high-silicate melt.

The quantity of the melt depends upon a grain composition of the carbonate component and can reach 40 - 50 % of clinker weight. The X-ray phase analysis and the density measurements of granules burnt at different temperatures confirm this. Melt formation at low temperatures increases the effective length of the sintering zone of a rotary kiln. The appropriate increase in the kiln productivity is achieved when a grain composition of a carbonate component is optimal; positive results of using coarse grinding of raw mixes were obtained at cement plants of Russia and CIS countries. These results, according to the present paper, are substantiated theoretically. It should be pointed out that a positive effect obtained due to coarse grinding was explained earlier by exclusively thermotechnical factors, and, in particular, as though thermal power were in excess in the combustion zone of a rotary kiln.

Method of two-batch technology

The main point of this method is that an original raw mix is prepared from two batches which are heated seperately up to a definite temperature, then both the batches in a hot state are mixed and burnt till they sinter at 1300 - 1350 °C (Barbanyagre et al., 1981). The most simple method of calculation of both batch compositions is done by partial withdrawal of a carbonate component from the cement raw mix in the form of an independent batch. Thus, the remaining part of the batch acquires the composition which promotes the production of low-temperature melt with the required composition and properties (Table 1).

Table 1. Low-temperature melt used in two-batch technology.

Sl. No.	Composition of oxides, weight %				Moduli			Melting temperature, °C
	SiO_2	Al_2O_3	Fe_2O_3	CaO	KH*	$\frac{S}{A+F}$	$\frac{A}{F}$	
1	41.53	13.51	9.71	35.25	0.082	1.79	1.39	1135
2	40.21	13.07	9.47	37.25	0.11	1.78	1.38	1170
3	46.28	9.66	5.49	38.57	0.16	3.05	1.76	1205
4	44.74	9.34	5.20	40.72	0.19	3.08	1.80	1220
5	40.68	8.55	6.96	43.81	0.24	2.62	1.23	1235
6	47.83	9.97	9.06	33.14	0.10	2.51	1.10	1200

* $KH = \frac{CaO - 1.65Al_2O_3 - 0.35Fe_2O_3}{2.8SiO_2}$

Thus, the preparation of the mix from two batches makes it possible to obtain a batch with low basicity and minimum melting temperature (1130 - 1220 °C). Due to the use of the whole amount of silica and additional quantity of calcium oxide in the melt, the amount of such melt increases to 50 - 60 % of the whole batch. Unlike the common clinker melt, the melt produced by the two-batch technology contains 5 - 6 times more silica and but only half as much calcium oxide. Its melting temperature is 150 - 200 °C less. All these features characterize it as high-silicate, low-basicity and low-temperature melt. The compound composition of crystallized high-silicate melt includes generally iron-

containing solid solutions of melilite and pseudowollastonite. The advantage of such melt can be shown by way of an example of the burning of a cement raw mix, the initial composition of which is characterized by the following data: Fe_2O_3 = 2,75%; A/F = 1.30; S/(A+F) = 2.20; KH = 0.92; CO_2 = 35,1% (Table 2).

Table 2. The free lime content (%) in a raw mix burnt at a temperature (^{0}C):

A mehtod of burning	1200	1250	1300	1350
Existing technology	41.27	30.34	67.84	1.55
Two-batch technology	17.00	16.69	3.87	0.38

At cement plants the two-batch technology is implemented, for example, by the method of two-side feeding of a rotary kiln. A carbonate batch is fed to the cold end of the kiln and a fusible batch is blown by compressed air into the combustion zone of the kiln through the pipe above the torch. So the whole reaction does not proceed in the solid state, as it occurs as in ordinary technology, but the melt takes part in these reactions and, therefore, synthesis of clinker minerals finishes at 1300 °C, that is 100 - 150 °C lower in comparison with the conventional method of burning. Clinkers produced by the two-batch technology are distinguished by having fine crystals and have a higher hydraulic activity (more than 12 - 15%) because of their less recrystallization.

The use of a two-batch technology saves 7 -8 % of fuel relative to dry process clinker burning and 20 % relative to a wet process kiln (Barbanyagre et al., 1988). However, the feeding of larger amounts of material into the hot end of a rotary kiln requires additional design concepts.

PROSPECTS

A four-component constitutional diagram of C-S-A-F system is of great importance for theory and practice of cement production. But this diagram is studied only partially. Some $C_{12}A_7$-C_2S-C_4AF and C-C_2S-C_4AF sections in the inner part of triangular pyramid as well as in the limited volume of a part of the elementary C_3S-C_3A-C_4AF-C_2S tetrahedra were studied by Lea and Parker. In addition, C_3S-C_3A-C_2S sections were studied at different values of C_4AF (Lea and Parker, 1934).

However, the results of the research show that due to non-stationary conditions and the use of two-batch technology fusible melts are formed, the compositions of which are not studied in the system mentioned above. So it is necessary to examine these areas of C-S-A-F diagram that are not properly studied in chemistry and technology of cement, namely:

- areas with the increased (25% SiO_2) content of silica (high-silica compositions);
- areas with the increased (10% Fe_2O_3) content of iron oxide;
- areas with the increased (15% Al_2O_3) content of aluminium oxide (high-aluminate compositions).

Papers (Barbanyagre, 1981, 1984, 1988, 1991, 1992, 1993) begin researches in this trend. The detailed examination of the above compositions allows development of physico-chemical principles and new techniques and the selection of the compositions of special cements.

CONCLUSIONS

1. Non-stationary technological methods were developed. They allow production of low-temperature melts while burning a cement raw mix with a common composition:
   - a two-batch technology method;
   - a special grading composition of a cement raw mix;
   - the rapid burning of a raw mix.

Low-temperature, high-silicate melts of the above composition accelerate considerably the synthesis of clinker minerals and decrease the temperature of portland cement clinker sintering up to 1300 °C with certain fuel saving because of the reduction in heat losses.

REFERENCES

Chebukov, M. F., Proceedings of the USSR Academy of Science, Vol. 71, Nos. 4, 7, 25; 1950.

Barbanyagre, V. D. et al., "Portland Cement Clinker Sintering by the Two-Mixture Technology." In the book: "Developments in Building Materials Chemistry and Technology", MISI, Moscow, 1984, pp. 91-98.

Barbanyagre, V. D. et al., "The Method of Portland Cement Clinker Production." The USSR Inventor's Certificate No. 833681 C O4 B 7/36. BI, No. 20, 1981, p.66.

Lea, F. M., Parker, T. W.," Phil. Trans.," 1934, **A234,1**.

Barbanyagre, V. D., Shamshurov V. M. "Transformations of Aluminoferrite Phases and Clinker Properties." Proceedings of the 7th All-Union Conference on Chemistry and Technology of Cement, Part 1, TSNIICHermet, Moscow, 1988, pp. 62-67.

Barbanyagre, V. D. et al, The 8th All-Union Meeting on Chemistry and Technology of Cement / Sections I and II/, Moscow, 1991, pp. 110-113, 114-116, 98-101.

Barbanyagre, V. D., Shamshurov V. M., Timoshenko T. I., "Specific Features of Cement Mix Sintering Process." Cement Journal, No. 2, 1993, pp. 21-24.

Barbanyagre, V. D., Shamshurov V. M., Timoshenko T. I., " Peculiarities of the Process of Cement Clinker Formation by Changing the Interaction Sequence of Reacting Components." / National Council for Cement and Building Materials. New Delhi, M-10, Part II, New Delhi, 110049, India, 1992, pp. pp. 196-200.

RESEARCH ON THE MECHANISM OF FORMING COATING AND CLINKER MASS IN PRECALCINER KILN SYSTEM

SHI Huisheng, Mater. Sci. & Eng. Dept., Tongji Uni., Shanghai 200092, P. R. China
LU Chunxuan, China Building Materials Academy, Beijing 100024, P. R. China

ABSTRACT The authors have made a study on two kinds of uncommon coatings in suspension preheater and large clinker lumps in the precalciner kiln. The mechanism of forming these coatings and clinker mass in precalciner kiln system has been discussed, and the precautionary measures have been proposed in this paper.

Key-words: Alkali, Chloride, Calcium sulfate, Melt, Temperature

INTRODUCTION

In the manufacture of portland cement clinker the kiln feed and fuel generally contain some minor constituents that are volatile in nature. These are essentially compounds of potassium, sodium, sulfur and chlorine. Unlike the nonvolatile oxides, these constituents occur in the vapour phase as well as in the condensed phases. Because of this dual role, these constituents may cycle and enrich in precalciner kiln system, which can affact kiln operation and product quality. In this paper, effects of these constituents on the formation of uncommon coatings and clinker mass in the precalciner kiln system of XJ cement works have been studied.

ANALYSIS AND DISCUSSION

Formation of coating

Coating is often formed in preheating system of preheater kilns and precalciner kilns. The characteristic minerals such as $2CaSO_4 \cdot K_2SO_4$, $2C_2S \cdot CaCO_3$, $2C_2S \cdot CaSO_4$, $Ca_{10}[(SiO_4)_2(SO_4)_2](OH^-, Cl^-, F^-)$, quadratic $CaSO_4$, KCl and $3CA \cdot CaSO_4$ are likely to form and act as solid and/or liquid bonds binding raw minerals ($CaCO_3$ and SiO_2) and clinker minerals (CaO, C_2S, $C_2(A,F)$, etc.), which results in the formation of coating. Thus, coating is formed together with these characteristic minerals and disappears after they have decomposed. Surely alkali and sulfur constitute them directly. Chlorine promotes their formation and enters into them also (Lu et al., 1993).

In addition to the coatings generally formed in many precalciner kilns, a coating formed in the surface of refractory at the passage from 1-stage preheater to precalciner is discovered in the kiln of XJ cement works. The coating consists of almost pure KCl and NaCl, which is yellow crystals like salt. Severe alkali attacks have occured in the refractory there. Besides, there is another coating in the horizontal air pipe connecting the upper two preheaters. The coating is a hardened cementing mix which consists of quadratic calcium sulfate and raw feed such as $CaCO_3$, SiO_2 and etc.. Its formation and growth cause air resistance to increase greatly, so that the pipe has to be renewed after only

used for a few months.

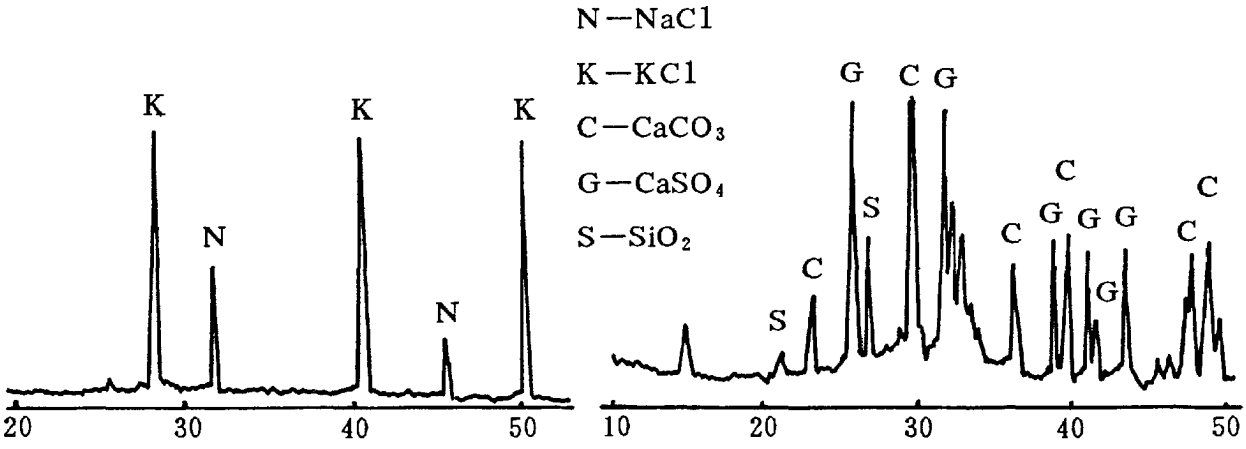

(a) in passage (b) in air pipe

Figure 1 XRD of uncommon coatings in precalciner kiln system

Table 1 Contents of R_2O, SO_3 and Cl^- in kiln charge (%)

Sample	K_2O	Na_2O	SO_3	Cl^-
Raw feed	0.81	0.47	0.57	0.011
4-stage preheater charge	1.04	0.42	0.54	0.163
3-stage preheater charge	0.79	0.31	0.58	0.236
2-stage preheater charge	1.48	0.60	1.06	0.437
1-stage preheater charge	2.13	0.58	1.38	0.573

From Table 1, it can be seen that all the volatile constituents enriched in kiln charges at various parts to some extent, especially the content of Cl^- in 1-stage preheater charge is much more than that in raw feed. Once the surface temperature of kiln charge and/or refractory are lower than the melting point of alkali chlorides, which can condense there. As a result of unstable thermal conditions the temperature often goes up and down, which cause the alkali chlorides in coating to melt or crystallize over and over again, leading to the formation of pure crystal.

If alkalies are present together with SO_3, alkali sulfates are first formed. Any excess SO_3 may react with CaO to form $CaSO_4$. So the molar ratio of SO_3 to total alkali oxides generally is controlled lower than unity in works. However, even though the molar ratio is lower than unity in raw feed and fuel, because of the enrichment of volatile constituents in kiln system and alkali first reacting with chlorine, the corrected molar ratio is much more than unity in the upper preheater charges, so that the quadratic $CaSO_4$ can be formed. The frequent shut-down of kiln facilitates the formation of this coating in the air pipe.

Formation of clinker mass

In order to avoid forming coating in preheater, XJ cement works intentionally controls

the temperature of kiln gas at kiln inlet below 980℃. As a result, the apparent decomposition rate of hot charge entering the kiln is only 80% and decomposition continues in the back end part of kiln. The partial pressures of CO_2, SO_3, R_2O and Cl^- in the kiln gas increase considerablly and some characteristic minerals mentioned above are formed continuously, so that kiln charge can coagulate into lump there. Sometimes the clinker lump has a diameter over one meter, which makes the kiln has to be shut-down. Large clinker lumps left the kiln contain R_2O and SO_3, especially Cl^- higher than the normal sized clinker does.

Table 2 Composition of charges in precalciner kiln of XJ cement works

From kiln inlet (m)	Sample feature	Contents (%)				Characteristic minerals				Clinker mineral	Raw minerals	
		K_2O	Na_2O	SO_3	Cl^-	KCl	$2C_2S \cdot caCO_3$	$2C_2S \cdot CaSO_4$	$2CaSO_4 \cdot K_2SO_4$	C_2S	$CaCO_3$	SiO_2
8.7	lump	4.10	0.74	9.35	3.96	###	###	###	###	###	+	-
	powder	2.39	0.54	2.20	0.84	##	##	-	-	###	###	###
11.6	lump	3.58	0.72	7.16	3.04	###	###	###	###	###	+	-
	powder	2.29	0.46	2.19	0.84	##	##	-	-	###	###	###
23.2	lump	3.12	0.61	2.99	2.41	###	###	###	###	###	+	-
	powder	2.48	0.50	2.76	0.77	##	##	-	-	####	###	-

Note: + very few, ## few, ### medium, #### much

Table 3 Contents of R_2O, SO_3 and Cl^- in different sized clinkers (%)

Sample	K_2O	Na_2O	SO_3	Cl^-
Center of clinker lump	1.26	0.55	0.79	0.130
Surface of clinker lump	1.20	0.48	0.72	0.087
Normal sized clinker	0.74	0.35	0.65	0.006

Obviously, the mechanism of formation of clinker mass is same as that of coating, i.e., the contents of volatile constituents in local part of kiln charge at certain time are too much, which leads to forming large amounts of characteristic minerals and then causing the formation of coating or clinker mass. The only difference is the position formed, in preheating system or in rotary kiln.

Precautionary measures

Therefore, the fundamental way to restrain and eliminate coating and lump formation is to control the amount of volatile constituents of any local part of kiln charge at any condition not to be excessive. Moreover, the kiln dust must be homogeneously blended into raw meal before it is returned back into the kiln. The times of shut-down of the precalciner kiln must be cut down as low as possible in order to reduce the amount of volatile constituents condensed onto the kiln charge and wall of kiln system. As for the specific conditions in the precalciner kiln of XJ cement works, coating-resistant and alkali-refractory lining accompanied by airblast device should be used to restrain coating formation. The temperature of flue gas at the inlet end of rotary kiln should be increased to more than 1000℃, so that the apparent decomposition rate of hot charge en-

tering the rotary kiln will be raised to 90-95%. Thus the possibility of lump formation will be eliminated. If necessary, the bypass device can be used.

CONCLUSION

The mechanism of formation of clinker mass is same as that of coating in precalciner kiln system. The contents of volatile constituents in local part of kiln charge at certain time are too much, which leads to forming large amounts of characteristic minerals and then causing the formation of coating or clinker mass.

Whether the quadratic calcium sulfate and alkali chlorides are formed relates to the contents of sulfur, alkalies and chlorine, not only in raw feed and fuel, but also in local part of kiln charge.

Designing technological processes correctly and making thermal conditions stable are the key to preventing the formation of coating and clinker mass in precalciner kiln system.

REFERENCE

Lu, C. et al., "How to Make better Use of Cement Raw Materials of Higher Alkali Content", Journal of the Chinese Ceramic Society, Vol. 21, No. 6, November-December, 1993, pp. 554-563.

ENERGY-SAVING TECHNOLOGY OF CEMENT PRODUCTION BY MEANS OF COMBINED GRINDING OF CLINKERS OF VARIABLE COMPOSITIONS

Leonid Ya. GOLDSTEIN, AOOT "Giprocement", St. Petersburg, Russia

ABSTRACT The energy saving problem has always been and retains urgent for the cement technology. One of directions of tackling this problem important both in the scientific and practical respects is production and use of clinkers with lower lime content (lower basicity) which are burnt at a comparatively low specific fuel consumption. However, in this case it turns out to be very difficult to maintain the strength characteristics of cement at the wanted level.

The findings of the research and pilot-production works conducted at AO "Giprocement" allow one to suggest an optimal process at which using the energy-saving technology it is possible not only to maintain, but to increase the strength characteristics of cement. First of all at the early hardening ages.

Key-words: interground cement, fuels for clinker making, economy

INTRODUCTION

The data on the fact that clinkers of variable mineral compositions, in particular, of alite and belite one, differ greatly in their grindability are a matter of common knowledge. Many authors were engaged in these problems, among them Koryakin et al in Russia, or more exactly, in the former Soviet Union.

Clearly such clinkers when ground to closely related finenesses are characterized by a variable grain-size distribution (considerably differing grain composition). This property as demonstrated by investigations made, for example, at the institute of NIITsement (Kravchenko et al, 1967) can be used to improve the strength characteristics of cement. So, the authors mentioned above have suggested a method of manufacture of an early-strength cement by means of mixing 30-40% cement containing more than 60% C_3S and more than 5% C_3A with 70-60% cement containing no more than 50% C_3S and no more than 8% C_3A.

Of great interest from the point of view of increase in the strength characteristics of cement is the use of the other method - of the combined grinding of clinkers of a variable composition. Such attempts have been also taken as evidenced, for example, by patents of Austria. But in this case the clinker of the ordinary (normal) portland cement composition was ground together with the other clinker (sinter) characterized by a very low, uncommon value of the lime saturation factor, KH, according to V.A. Kind. So, the patents of Austria mentioned protected the method of production of cement through combined grinding of clinker of the ordinary composition (KST according to H. Kuehl is more than 90*, KH according to V.A. Kind is more than 0.85*) and of another clinker obtained

---

* It should be pointed out that the values of KST (lime standard) were calculated by the formula:

in sintering at a temperature of 700-1100^{0}C characterized by KH in the range from 0.77 to 0.35 (KST = 85 ÷ 50). It was even recommended to use a sinter with KST = 10-15 which corresponds to negative KH values (so, this sinter represented not a clinker, but is essentially a high-lime (high-basic) slag). The grave disadvantage of the method suggested was the reduction of the strength characteristics of cement at all hardening ages as compared with the ordinary initial cement of the portland cement composition.

Another way has been suggested at AO "Giprocement": a combined grinding of two portland cement clinkers - one of the normal composition (manufactured usually at cement plants) and another one characterized by a well-defined belite composition. We started therewith from the real possibilty of obtaining low-lime (low-basic) clinkers with the use of the equipment available at cement plants considering that production of clinkers (sinters) with very low KH values (of high-lime (high-basic) slag type) in present-day burning units may turn out to be difficult and in some cases even impossible. Here it is worth noting that even preliminary studies showed that at combined grinding of clinkers of a variable composition (first of all, differing in KH values)higher strength characteristics of cement can be obtained as against the corresponding characteristics of cements produced through mixing of the same clinkers preground. The latter cement production process is unlikely to be considered as promising, even though the problem of difficulty of the thorough mixing of cement powders under production conditions is not touched on which is solved easy at the combined grinding of clinkers of a variable composition.

On the basis of the above reasoning, the main object of the experimental works was to determine a possibility and conditions of increase in the strength characteristics of cement by means of the combined grinding of clinkers of a variable composition. It seemed that of the greatest interest was to study the influence of KH value (alite-to-belite ratio) on the process of grinding clinkers ground together and strength characteristics of cements because of variations in their grain-size distribution (grain composition).

RESULTS OF THE EXPERIMENTAL WORKS

The programme of the first experiments carried out at the pilot-production plant of the institute of "Giprocement" provided for obtaining several clinkers of a variable composition (Table 1) with the use of traditional raw materials (limestone, clay, correction additives). The pelletized raw mixes were burnt by the dry process in a small rotary kiln measuring 0.5 x 7.0 m. The clinkers with KH values varying within wide limits were ground in different

---

$$KST = \frac{100 \times \%CaO}{2.8 \times \%SiO_2 + 1.65 \times \%Al_2O_3 + 0.35 \times \%Fe_2O_3}$$

and the KH values - with the formula of V.A. Kind

$$KH = \frac{\%\ CaO_{total} - \%CaO_{free} - 1.65\ \%Al_2O_3 - 0.35\ \%Fe_2O_3 - 0.7\ \%SO_3}{2.8\ (\ \%SiO_{2\ total} - \%SiO_{2\ free}\ )}$$

as is customary in the cement industry of Russia.

ratios in a laboratory mill in two stages: at first - by balls up to a residue of 33-35% on the No. 008 sieve and then - by cylpebs up to the specific surface of 300 m^2/kg.

Table 1 Results of study of cements obtained under pilot conditions (at the pilot-production plant of the institute of "Giprocement")

Proporiton of clinkers with KH, %				Mineral composition, %		Ultimate strength, MPa				Specific power consumption for grinding, kWh /t cement
						bending		compression		
						age, days				
0.78	0.85	0.88	0.95	C_3S	C_2S	3	28	3	28	
100				25	45	2.4	5.8	15.8	49.4	69.0
	100			38	31	4.0	5.9	19.6	52.4	49.0
		100		45	23	4.3	6.3	24.1	52.5	46.5
			100	56	13	4.5	6.5	27.3	53.3	45.0
10			90			5.0	7.5	32.8	61.0	-
25			75	48	21	4.7	6.9	28.5	57.7	43.5
50			50	40	29	4.8	7.0	27.5	57.6	46.0
	10	90	-	-	-	4.7	6.4	24.7	54.6	-
	25	75		43	25	4.1	6.7	23.7	54.3	59.0
	50	50		42	27	4.3	6.4	23.3	53.8	60.0

The results of the standard physical-and-mechanical tests and grindability characteristics (Table 1) showed that it is expedient to be oriented towards the combined grinding of clinkers with the most differing KH values by two reasons. In the first place, this results in a possibility to improve the strength characteristics of cement to the greatest extent, and second, to avoid a marked increase in the specific power consumption for grinding of clinkers. Moreover, it is obvious that production of one clinker with the KH value as low as possible will lead to the maximum reduction of the specific heat consumption (fuel saving) for clinker burning as well as to increase in the kiln unit output (on account of the reduction of the carbonaceous component content of the raw mix).

The first short-run production experiment has been carried out at one cement plant of the Russian Federation using as a carbonaceous component the marble-like limestone with a higher magnesium oxide content (the MgO content of clinkers was 5.1 - 5.4%). The clinkers were burnt in a ø 4.0 x 3.5 x 4.0 x 150 m rotary kiln. When burning the low-lime (low-basic) clinker the process fuel consumption was reduced by about 10 - 12%. The results of the standard physical-and-mechanical tests of cements (Table 2) obtained at combined grinding of the low-lime and ordinary clinkers were not in contraduction with those obtained when conducting pilot-production experiments (Table 1). It should be pointed out that the maximum gain in the cement strength at the combined grinding of clinkers was obtained here (with the low-lime clinker content of the mix under 50%). It may be suggested that the chemical-and-mineral features

of raw materials (probable influence of admixtures, e.g. MgO, on viscosity characteristics of the clinker melt and hence on the clinker misrostructure) have a pronounced effect on the cement strength gain value.

Table 2 Results of tests of cements from clinkers obtained under production conditions

Proportion of clinkers with KH, %		Grinding fineness, R_{008}, %	Paste normal consistency, %	Mortar water-cement ratio	Cone flow, mm	Ultimate strength, MPa			
						bending		compression	
						age, days			
0.92	0.83					2	28	2	28
100	-	9.4	25.75	0.40	107	4.3	5.7	26.8	46.3
-	100	11.6	25.00	0.40	110	4.0	5.5	21.5	26.9
75	25	9.0	25.75	0.40	110	5.3	6.3	30.4	52.1
50	50	9.6	25.25	0.40	112	5.0	6.1	30.9	50.0
25	75	9.4	25.60	0.40	106	4.1	5.6	24.5	42.1

The longer and thorough experimental works under production conditions have been performed at one of the cement plants of the Russian Federation using as one of the basic raw material components the alumina production waste - the nepheline (belite) slurry consisting of β-C_2S for 70-75% on the average. It is well known that such cement plants while operate by the wet production process are characterized by a very low specific fuel consumption for the clinker burning. In spite of it, when burning the low-lime raw slurry with KH = 0.77-0.79 the reduction of the specific fuel consumption of more than 9% was fixed and the kiln cutput increase of 2.5% as well. The burning was executed in a ø 3.6 x 60 m rotary kiln with a slurry thickener for 2 days. The combined grinding of clinkers was also performed during 2 days in a cement mill measuring 2.4 x 13 m. The cement samples were taken at the same time from a cement mill of the same type where only the ordinary clinker was ground. The results of the standard physical-and-mechanical tests given in Tables 3-4 supported the data obtained earlier and further indicated that the greatest gain in the cement strength could be expected at the very early hardening times, e.g. at the age of 1 day. As is generally known, this is particularly important for the construction.

Table 3 Results of tests of physical properties of cements obtained under production conditions

Proportion of clinkers with KH, %		Grinding fineness, specific surface, m^2/kg	Paste normal consistency, %	Mortar water-cement ratio	Cone flow, mm	Soundness	Setting times hours-minutes	
							Initial	Final
0.77	0.90							
25	75	217	23.50	0.38	113	sound	2-00	6-55
-	100	334	24.00	0.29	115	sound	2-15	4-00

Table 4 Results of tests of mechanical characteristics of cements obtained under production conditions

Proportion of clinkers with KH, %		Ultimate strength, MPa							
		age, days						after steam treatment	
		1	3	28	1	3	28		
0.77	0.90	bending			compression			bending	compression
25	75	3.8	5.3	7.5	14.9	29.0	45.9	5.0	34.0
-	100	3.0	4.7	7.0	12.6	25.0	42.9	4.9	30.0

Attempts have been undertaken of comparison studies of the grain-size distribution of the representative samples of cement taken both when grinding under production conditions of the clinker mix and of the ordinary portland cement clinker used for preparation of the clinker mix. The studies were conducted with the help of the "Granulometer - 715" device produced by a French company. The operation principle of this device is based on the dispersion of the light beam leaving the low-power helium-neon laser and crossing the sample of the material to be analyzed suspended in a fluid. As the working fluid use was made of the ethyl alcohol.

The results of the determinations presented in Fig 1 allow to make a conclusion that there are noticeable differences between the grain-size distributions of cements obtained under the combined grinding of clinkers with variable KH values and cement produced when grinding clinker of the ordinary composition. First and foremost, attention is drawn to the fact that cements obtained at the combined grinding of clinkers are characterized by a rather higher content of the finest fractions of the grain composition (from 0 to 6 μm - almost twice - thrice as much). So, the higher strength characteristics of such cements in comparison with the ordinary portland cement become clear and quite explicable. Noteworthy also is the more uniform, relatively smoothly varying by fractions, grain composition of cement obtained through the combined grinding of clinkers.

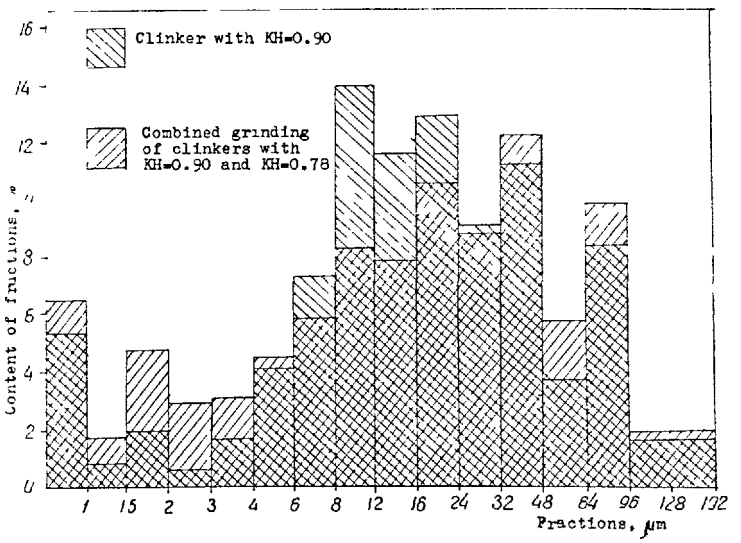

Figure 1 The grain-size distribution of cements

Thus, the data presented convincingly lead to the conclusion that at the combined grinding of materials characterized by variable grindability degrees favourable conditions are set up for both grinding process itself and for properties of the product obtained. The author shares the opinion of some researchers (e.g. Osokin et al, 1983) on a possible influence of the mechanoactivation process of materials ground simultaneously. It is well known that the effect of this process can show itself not only in the increase of their dispersity, but also in the structural variations of the surface layer making for increase in the reactivity of the disperse systems.

CONCLUSIONS

The data presented point, in the author's opinion, to the greatest promise of the suggested process making it possible to improve the most important characteristics of cement in addition to the energy saving. It should be noted that the properties of cements produced through the combined grinding of clinkers of a variable composition can be influenced by many factors which are to be refined to fit the particular conditions. These factors may include the production process (wet or dry) and the associated features of the clinker structure, particularly, of their pore content) as well as the presence in the raw materials of minor components, e.g. MgO, and trace elements and so on. It is also worthy to note that to achieve the best results consideration must be given to not only silicate but also to aluminate and alumoferrite phases ratio. Such data have been obtained at AO "Giprocement" recently.

REFERENCES

Goldstein, L.Ya., "Combined Cement Production Processes", Stroiizdat, Leningrad, 1985, p. 10

Duda, W.H., "Cement-Data-Book" (Translated from German), Stroiizdat, Moscow, 1981, pp. 23-24

Kind, V.A. and Okorokov, S.D., "Construction Materials", Gosstroiizdat, Moscow - Leningrad, 1934, pp 146 - 147

Koryakin, S.F., "Grindability and Physical-and-Chemical Properties of Commercial Portland Cement Clinkers", Proceedings of VNIITS, No. 23, Leningrad, 1938, pp. 16 - 24

Kravchenko, I.V., Vlasova, M.T., Yudovich, B.E., Trusov, V.V., Denisenko, Ye.I., and Singirtsev, I.A., "Process of Early-Strength Cement Manufacture", USSR Certificate of Authorship No. 237667, Oct. 09, 1967

Kwech, L. and Jung, F., "Zement und Verfahren zu seiner Herstellung", OE Patentschrift Nr. 353156, Juli 22, 1975

Kwech, L. and Jung, F., "Verfahren zur Herstellung eines Zementes", CE Patentschrift Nr. 370061, August 27, 1957

Osokin, A.P., Arzamastsev, G.I. and Pirotsky, V.Z., "Mechanoactivation of Portland Cement Clinker at Combined Grinding with Solid Mineral Additives", Proceedings of NIITsement, No. 73, Stroiizdat, Moscow, 1983, pp. 17 - 29

TOPIC I.B

Low energy clinker formation

MELT STRUCTURE AND PROPERTIES CLINKERS CONTAINING CALCIUM SULPHOFERRITES AND SULPHOALUMOFERRITES

OSOKIN A.P., KRIVOBORODOV Y.R., SAMCHENKO S.V.,
Research Technical Centre of JSC "Alfa Cement",
Mendeleev Chemical Technology University
of Russia, Moscow, Russia

ABSTRACT Calcium aluminoferrites of compositions C_6AF_2, C_4AF, C_6A_2F, pure or contained calcium sulfate, were synthesized by sintering and melting. Melt properties (viscosity and surface tension) of sulphoferrite and sulphoalumoferrite clinkers were studied. The connection between melt properties and their structure was shown. A new type of clinker was obtained consisting of calcium ferrite phases with minor amounts of a sulfate and silica phase.

KEY-WORDS: Solid solution, sulphoaluminoferrite, structure, melt, viscosity.

INTRODUCTION

At present aluminate and sulphoaluminate cements have wide application due to their rapid hardening and high strength. The use of these cements provide the high tightness, low water permeability and crack resistance concrete (Kouznetsova, 1986). Besides special cements based on calcium sulphoferrite are very useful thanks their chemical corrosion resistance (Osokin et al, 1992).

Much interest exists concerning alite-containing sulphoaluminoferrite clinkers, which consist of calcium silicates, which are responsible for strength, and sulphoaluminoferrites, as an expansive agent (Krivoborodov, Samchenko, 1992). This paper deals with the properties of sulphoaluminoferrite cements.

Upon burning raw mixes containing high quantities of gypsum, calcium sulphoferrite and sulphoaluminoferrite formation proceeds in the presence of the sulphate ferrosilicate and alumoferrosilicate melts. Regulation of the properties of these melts allows reduction in energy consumption.

EXPERIMENTAL

Sample preparation

Using chemical reagents, calcium sulfoaluminoferrites were prepared by sintering and melting. Raw mixes were calculated so as to produce aluminoferrites with calcium sulfate. Samples were

prepared by pressure molding (50 MPa) blended mixes with a sintering temperature of 1300 °C and a melt temperature of 1700 °C.

Aluminoferrite and sulphoaluminoferrite clinkers were produced in an experimental rotary kiln using natural raw materials (limestone, bauxite, clay, and gypsum) and a burning temperature of 1350 °C ±50 °C. The raw mixes were calculated to obtain calcium alumoferrite, sulphoferrite, and belite.

The melt region of sulphoferrite and sulphoalumoferrite clinkers is found in the phase diagrams of the systems $CaO-Fe_2O_3-SiO_2$ and $CaO-Al_2O_3-Fe_2O_3-SiO_2$ in its high iron content part as differentiated from sulphoferrite clinkers in which Al_2O_3 is limited to 4-5%; in sulphoaluminoferrite clinkers, it plays the role of a mineral formating oxide.

Calcium sulphate was used as mineralizer and it formed solid solutions with the ferrite phase. The crystallization path of the choosen clinker compositions passes through the invariant points corresponding to the compositions forming in actual practice from melts. In the high iron content part of diagram $CaO-Al_2O_3-Fe_2O_3-SiO_2$, melt is formed at 1623 K; according to (Berezhnoy, 1970) it has the composition 49.6% CaO; 6.5% SiO_2; 17.1% Al_2O_3; 26.8% Fe_2O_3 (melt 1). In the system $CaO-Fe_2O_3-SiO_2$, melt composition is characterized by follow oxide contents: 29% CaO; 5% SiO_2; 66% Fe_2O_3 (melt 2) the liquidus temperature of which is 1463 K (Levin et al, 1964).

Analytical methods

Chemical analysis, infrared spectroscopy (IR), optical microscopy (OM), X-ray powder diffraction (XRD), and scanning electron microscopy (SEM)of polished sections were used to characterize the samples. Each clinker was vacuum-impregnated with an ultra-low viscosity resin, cut to expose a fresh surface, and polished with a series of diamond pastes to 0.25 μm. About 10 nm of carbon was evaporated on the polished surface providing a conductive layer necessary for SEM examination. Samples were examined using an accelerating voltage of 15 kV and a probe current of about 2nA.

The persistence of silicate melts to temperature below that of the solidus and their ability to form glass phase at fast cooling allows us to study melt structures by IRS.

Melt viscosity was determined by rotary viscosimetry, surface tension was studied by method of maximum pressure in gas bubble. Raw mixes according to the compositions of melts 1 and 2 were melted at above liquidus temperature. Minor compounds were added into to melt just prior to measuring the melt properties. After determination, melt samples were fast cooling and the glass state was determined controlled by microscopic analysis.

RESULTS AND DISCUSSION

According to IRS, cooled melts consist of silicon-oxygen SiO_4^{4-} (absorption spectral band 800-980 cm^{-1}) and more polymerized silicon tetrahedra (absorption waves are in the region of 1050-1080 cm^{-1}).

Aluminium and iron ions (Fig.1, 2) are both in IV and VI coordination forms (absorption waves are 400 cm^{-1}, and 500-600 cm^{-1}, respectively).

At clinker burning all minor components enter into the melt composition and change the structure and properties of the melt. The impact of some components on melt structure and properties is collectively more complicated than of individual components. Melt saturated by aluminium and iron oxides has an alumina ratio, AR=0.64. Addition of 6% Al_2O_3 to melts 1 and 2 leads to the change of melt structure and to the displacement of IR - spectrum absorptions from 1050 cm^{-1} to 1070 cm^{-1}. It means that aluminium ions enter into silicon-oxygen parts of the melt and partly into alumino-silicate compounds. In this case, the alumina ratio (AR) of melt 1 increases to 0.9. This small change of melt structure leads to insignificant changes in viscosity, from 0.05 Pa·s to 0.02 Pa·s for melt 2. The viscosity change as a function of Al_2O_3 is a linear function (Fig.3). As AR of the melt decreases from 1 to 0.4 viscosity decreases to 0.01 Pa·s. Such rate of the viscosity decrease is explained by melt structure change. The reduction of the absorption band intensity 1080 cm^{-1} shows that aluminium and iron ions are significantly in VI coordination, as AlO_6^{9-} and FeO_6^{9-}, which are more mobile and promote the intensive viscous flow of melt.

In the melt, calcium sulphate is decomposed to Ca^{2+} and SO_4^{2-} ions and depolymerize silicon-oxygen complexes. Ca^{2+} ions form silicate structures although polymerized silicate and aluminoferrosilicate complexes also occur in the melt. SO_4^{2-} ions displace the dynamic equilibrium between the different coordination forms of amphoteric oxides to the formation of FeO_6^{9-} and AlO_6^{9-}. This is confirmed by IRS data; absorption wave intensity increases in the region of 500-600 cm^{-1}. Melt 1 and 2 viscosities are 0.015 Pa·s and 0.012 Pa·s, respectively.

5% calcium sulphate addition to the melts appreciably reduces melt viscosity but further increases do not change melt properties.

MgO reduces melt viscosity most of all (Fig.3). By analogy with Ca^{2+}, Mg^{2+} ions depolymerizes melt,entering between tetrahedrons SiO_4^{4-}, although at the same time there are polymerized alumoferro-silicate complexes.

The joint action of minor components and calcium sulphate in melt 2 influences acid-base equilibrium in the melt. The increase of the absorption wave intensity in the region of 580-

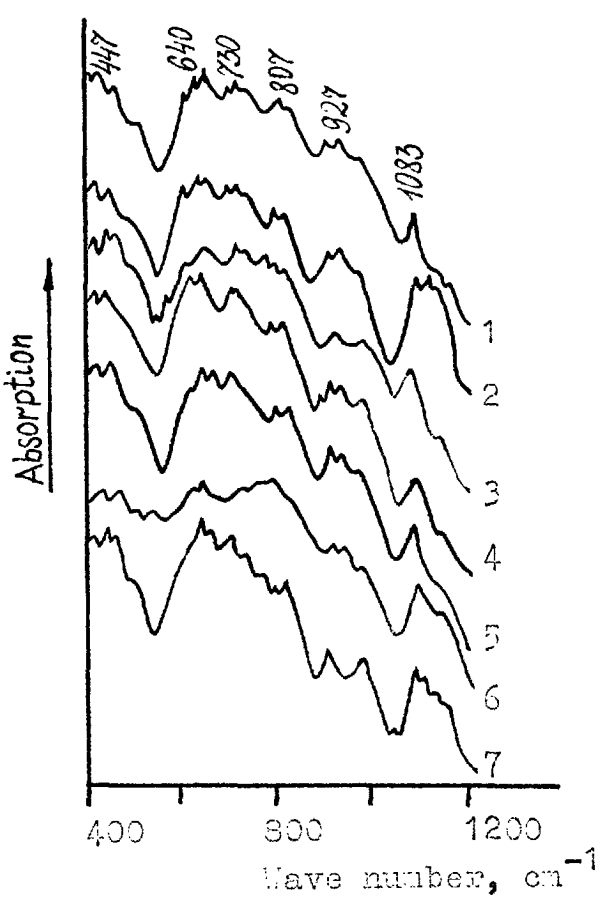

Fig.1 IRS of fast cooled alumoferrite melt 1
1- initial melt with AR=0.64; 2- melt with AR>0.64; 3- melt with AR<0.64; 4- $CaSO_4$; 5- MgO; 6- MgO and $CaSO_4$, AR>0.64; 7- MgO and $CaSO_4$, AR<0.64

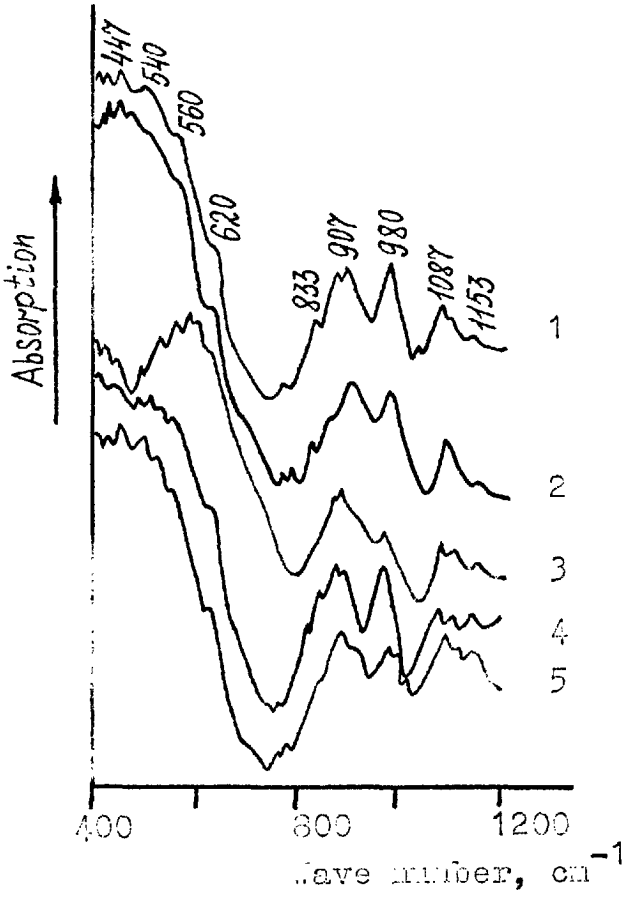

Fig.2 IRS of fast cooled ferrosilicate melt 2
1- initial melt; 2- with Al_2O_3 addition; 3- MgO; 4- $CaSO_4$ addition; 5- Al_2O_3, MgO and $CaSO_4$ additions

600 cm^{-1}, the absence of the absorption wave 1070 cm^{-1}, typical for Si-O bond in ferrosilicates shows that aluminium oxide affects acid-base equilibrium. The increase Ca-O bonds with silicon-oxygen tetrahedra in melt compensates the depolymerisation action of MgO on melt structure.

The joint action of calcium sulphate and MgO on the structure and properties of melt 1 is complicated and can be explained by two types of action. Firstly, it influence the depolymerization of aluminoferrite complexes, secondly, the acid-base equilibrium $[MeO_4]^{5-} \rightleftarrows [MeO_6]^{9-}$, where Me - Al^{3+} and Fe^{3+}-ions, is displaced to $[MeO_6]^{9-}$, which are more mobile and promote the decrease of the viscosity.

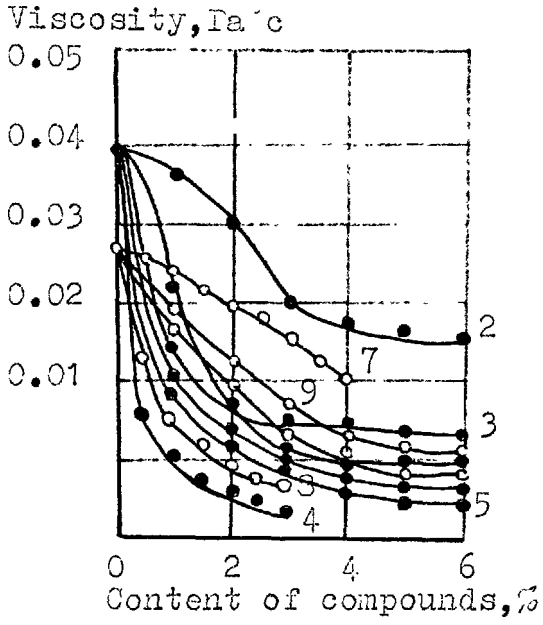

Fig.3 Isothermic lines of viscosity of melt 1 (T=1623 K) and melt 2 (T=1493 K). Some compounds are dissolved in the melts: 1-6 — melt 1, AR=0.64; $CaSO_4$; MgO; $CaSO_4$ and MgO.
7-10 — melt 2 with Al_2O_3; MgO; $CaSO_4$, Al_2O_3+MgO+$CaSO_4$

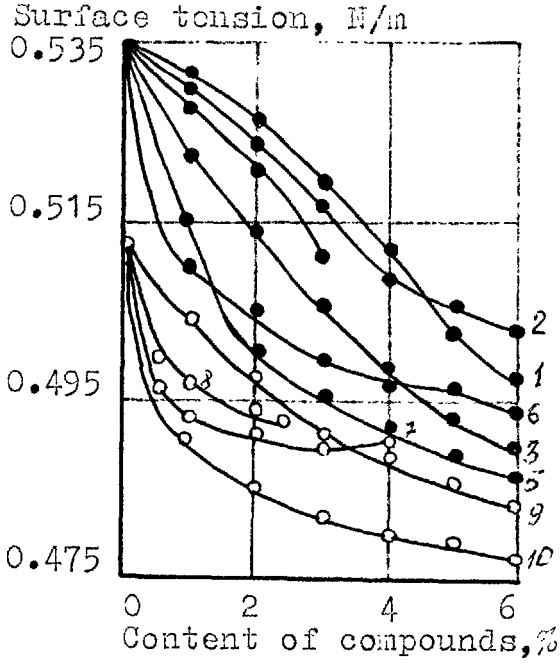

Fig.4 Isothermic lines of surface tension of melt 1 (T=1623 K) and melt 2 (T=1193 K), in which some compounds are dissolved:
1-6 for melt 1: AR>0.64; AR<0.64; $CaSO_4$, MgO; $CaSO_4$ and MgO (AR>0.64); $CaSO_4$ and MgO (AR<0.64);
7-10 for melt 2: Al_2O_3; MgO; $CaSO_4$; Al_2O_3+MgO+$CaSO_4$

When AR<0.64 these effects are absent and melt has lower viscosity. Depending on additive type and AR value, liquidus temperatures are reduced by 30-60 °C. It intensifies mineral formation, and crystallization ability of melt and the synthesis of crystals is improved, because surface tension of the melt is reduced (Fig.4).

Most of all, calcium sulphate reduces the surface tension of the melt because SO_4^{2-} ions have high surface activity and Ca^{2+} ion depolymerizes silicon-oxygen complexes which are in the surface layer of the melt.

Magnesium, alumina and iron ions are characterized by low surface activity which is why they have less influence on the melt surface tension.

It was found that the addition of MgO, Al_2O_3 and $CaSO_4$ into melts of sulphoferrite and sulphoaluminoferrite clinkers reduced melt viscosity and surface tension changed moderately. These factors

are favourable to the compaction in the sintering zone of the rotary kiln and to the dust reduction.

By changing the composition and structure of sulphoferrite and sulphoaluminoferrite clinker melts, through incorporation of the different minor components, it is possible to regulate the formation of calcium sulphoferrite and sulphoaluminoferrite and to modificate these phases.

Using these data, three clinkers were produced on an experimental cement plant with capasity of 1 t/h. The chemical composition of these clinkers is given in Table 1.

Table 1. Chemical composition of clinkers, in weight percent.

Clinker Index	SiO_2	Al_2O_3	Fe_2O_3	CaO	MgO	SO_3	R_2O	Σ
AF-8	17.50	7.61	9.93	58.50	1.71	3.67	0.22	99.2
AF-12	20.97	5.60	4.62	62.84	1.95	3.32	0.34	99.6
SFC-6	11.14	3.93	32.64	41.70	2.08	7.53	0.13	99.2

Backscattered electron (BE) imaging and X-ray microanalysis are very useful in examining the microstructure of polished clinker sections. Since the BE signal is proportional to the average atomic number of the material, high-Z phases will appear brighter than lower-Z phases. For cement clinker, free lime will appear brightest, followed by ferrite, alite, belite, aluminate, periclase, and finally the resin-filled voids. X-ray microanalysis can assist in phase identification when clinker phases of similar average Z compositions exhibit similar brightness in the BE image. Clinker phase identification from SEM images is made on the basis of phase brightness, grain morphology, and grain association via the BE image, and chemical composition by qualitative and quantitative EDS analysis.

Clinker AF-8 is a medium- to coarse-grained clinker with euhedral to subhedral alite, well-rounded belite, a dense, blocky ferrite matrix, with lessor amounts of aluminate and alkali sulfates. Brightness of the ferrite phase varies within this clinker and the bright ferrite will be referred to as ferrite-1, and the darker designated sulphoaluminoferrite (ferrite-2). Spot EDS analyses of the ferrites showing ferrite-1 to be higher in iron and ferrite-2 higher in aluminum are consistent with their relative brightness in the BE image.

Clinker AF-12 is similar to the previous clinker being medium to coarsely crystalline with euhedral to subhedral alite, rounded belite, minor aluminate, and a dense, blocky ferrite matrix. Belite and ferrite inclusions in alite are common and alkali sulfates partially fill some of the voids. Spot EDS analyses indicates that variations in ferrite BE intensity reflect

changes in ferrite composition in a similar manner to clinker AF-8.

Clinker SFC, in contrast with the previous clinkers, exhibits a fine-grained microstructure composed of calcium silicosulfate (C_5S_2S), dicalcium silicate (C_2S), and a matrix of calcium ferrites. Two calcium ferrite phases appear in the BE images, the first is bright and massive, much like the ferrites in clinkers AF-8 and AF-12 and the second ferrite occurs as darker, rounded grains enveloped by the bright ferrite. The second ferrite is calcium, iron and SO_3-rich and Al-poor. The dark, blocky belite (C_5S_2S) grains are composed of Ca,Si,S,and Mg.

The degree of hydration (Fig.5) of clinker SFC is 20 to 30 percent greater after three days and 15 to 20 percent greater after twenty-eight days than clinker AF-12 under identical curing condition. Clinker AF-8 is intermediate, between AF-12 and SFC-6.

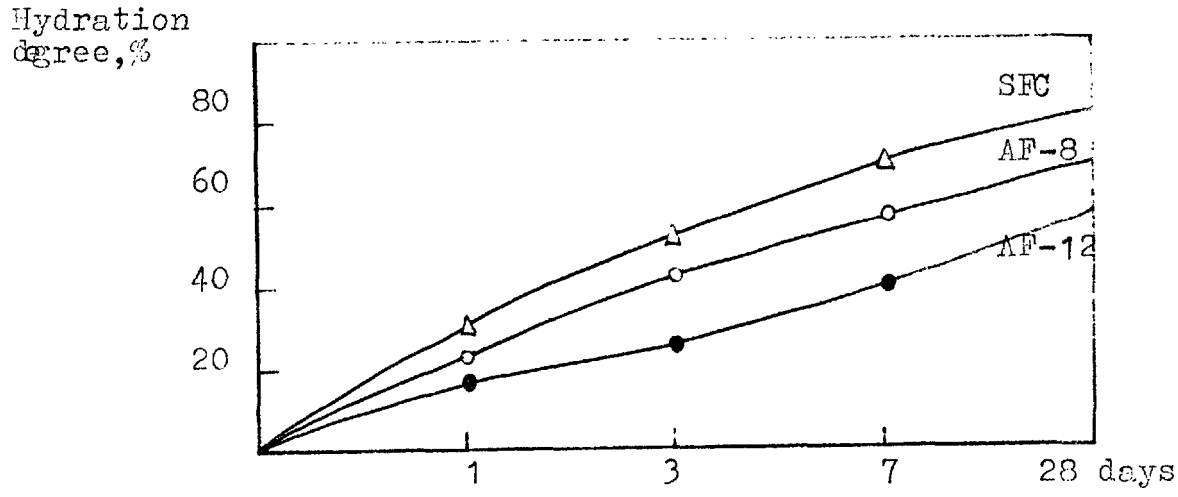

Fig.5 Degree of hydration of clinkers.

Clinker SFC-6 was used as an addition to portland cement clinker. The blend of portland cement clinker (83%), sulfoferrite clinker SFC-6 (10%), and gypsum (7%) was ground to a fineness of 4000 cm^2/g. The resulting cement, whose properties are given in Table 2, is classified as expansive with an expansion of 0.1 percent and a strength of 42 MPa after 28 days of curing.

Table 2. Strength and expansion of cement paste.

Cement	Strength, MPa				Expansion, %			
	1d	3d	7d	28d	1d	3d	7d	28d
PC + SFC	8	20	35	42	0.01	0.02	0.08	0.09

CONCLUSIONS

Melting of calcium aluminoferrites with calcium sulfate leads to sulfoaluminoferrite phases. SO_4 ions replace both tetrahedral AlO_4 and FeO_4 groups. By changing the composition and structure of sulphoferrite and sulphoaluminoferrite clinker melts it is possible to regulate the formation of calcium sulphoferrite and sulphoalumoferrite phases.

A new type of clinker was obtained consisting of calcium ferrite phases with minor amounts of a sulfate and silica phase. This clinker contains 7 percent sulfate and is used for expansive cements.

Acknowledgements

The authors wish to thank G.Fronhsdorff, Y.Clifton and P.Stutzman of NIST, Gaithersburg, USA, who kindly helped in BE-imaging study the part of clinker samples.

REFERENCES

Berezhnoi, A.S. "Multicomponent Systems of Oxides", Kiev, Naukova Dumka, 1970, 545 p.

Kouznetsova, T.V."Alumina and sulfoalumina cements", Moscow, Stroijzdat, 1986, 206 p.

Krivoborodov, J.R.,Samchenko, S.V. Phase formation in alumoferrite systems in presense of calcium sulfate. 2nd International symposium on cement and concrete. Beijing, China. 1989, v.4 p. 78-81.

Krivoborodov, Yu.R., Samchenko, S.V. "Sulfate-bearing solid solution of calcium aluminates and ferrites", 9th International Congress on the Chemistry of Cement. New Delhi, 1992, volume 3, p. 201-215.

Levin, E.M., Robbins, C.R. "Memurdie H.F. Phase Diagrams for Ceramists", The Amer.Cer.Sos., 1964, p. 413

Osokin, A.P., Krivoborodov, Yu.R., Dyukova, N.F."Sulfoferrite cements", 9th International Congress on the Chemistry of Cement. New Delhi, 1992, volume 3, p. 256-261.

HIGH-QUALITY PORTLAND CEMENT PRODUCED FROM LOW-BASE RAW MIX WITH LOW ENERGY CONSUMPTION

Boris S. ALBATS, Aleksandr L. SHEIN, Russian University for Chemical Technology n.a. D.I. Mendeleev, Research-Technical Centre Alpha-Cement, Moscow, Russia.

ABSTRACT. An efficient method of reducing energy consumption has been considered which consists in production of clinker with reduced energy consumption from a low-base raw mix similar by its grindability, hardening rate and strength characteristics to ordinary clinker suitable for production of 42.5 class Portland cement.

KEY-WORDS: alite, belite, ferrite phase, mineral phase, synthesis.

INTRODUCTION. It is theoretically shown that the lowering of heat consumption for reduction of raw mix LSF* by 0.1 is close to 3.5% of the total heat consumption for dry process or approximately 2% for the wet one (Merik, 1988). Since this calculation is based on the change of heat consumption for clinker firing only, one can expect a more substantial saving through lowering temperature level of the process and, consequently, reduction of heat losses to environment with waste gases and clinker.

The most widely used way of producing belite clinkers is the thermochemical stabilization of the more active high-temperature modification, α-C_2S, which can be obtained by means of rapid clinker cooling (above 1000°/min within the 1300...900°C range) and addition of barium oxides, alkalies, manganese and $R_2O + Al_2O_3 + Fe_2O_3$; $MgO + Mn_2O_3 + Al_2O_3 + Fe_2O_3$ etc. complexes (Uchikawa et al, 1994., Milke et all, 1994, Moranville-Regourd and Boikova, 1994).
In active belite clinkers, sulfoaluminate, sulfoferrite and sulfoalumoferrite also occur giving reduced saturation factors (Osokin et al, 1993).

Sudakas (1989) and Myasnikova (1992) formulated a concept of reasonability to establish maximal non-equilibrium conditions of belite phase synthesis enabling one to exclude its re-crystallization which affects the further clinker formation in a negative way.

Experimental study

The study was undertaken with the use of raw mixes with LSF = 0.77 to 0.87; n = 1.9 to 2.2 and p = 0.9 to 2.1 based either on pure reagents or on natural components with various mineral compositions. Mixes with LSF = 0.90 to 0.94; n = 2.0 to 2.2 and p = 0.9 to 1.2 were used for reference purposes. These characteristics were calculated proceeding from chemical compositions of raw mixes determined, for CaO, by complexometry (accurate to ±0.3% with fixed concentrations as assessed with regard to the recurrence error); for SiO_2, Al_2O_3, Fe_2O_3, MgO, by photocolorimetry (accurate to ±0.15%); for SO_3, by gravimetry (accurate to ±0.04%).

Conditions of clinker synthsis were as follows: in experimental mixes, the silica component was subject to additional grinding and the rate of heating was increased within the practically accessible limits. Identical rapid air cooling was used for all mixes. Characteristics of some of mixes, conditions of sintering and phase compositions of resulting clinkers are shown in Table 1. The actual phase composition was determined by the quantitative X-ray phase analysis;

* LSF - Lime Saturation Factor

designed compositions were calculated using the Kind method which is customary in Russia. The content of silica phases as calculated by the Kind method can differ by 3-4% from results obtained using the Bogue method (for alite, results calculated by Kind method exceed those obtained by Boggue method). As to C_3A and C_4AF, content of these is practically the same whichever method is used.

According to results of x-ray micro spectral analysis (performed with the use of a Jeol electron microscope equipped with a Link energy dispersion analyser), along with heating rate increasing from 5 to 20 degrees/min and alumina module increasing from 1.2 to 2.0 the CaO/SiO_2 ratio in alite crystals of clinkers produced from low-base carbonate-clay mixes decreases from 3.07 to 2.84 approaching to CaO/SiO_2 ratio of 2.85 characteristic for alite of the ordinary (reference) clinker. On the contrary, the A/F ratio in the alumoferrite phase increases from 0.99 to 2.29 also approaching value characteristic for the ordinary clinker which is 2.04. Here, average molar concentrations of oxides are presented as calculated from results of numerous measurements made on surfaces of crystalline phases with spacing between them being 4 μm.

Mechanism of the process

The mechanism of "alitization" when actual alite content exceeds the estimated one, is achieved as follows. A portion of CaO dissolves in the melt, which is not combined in solid solution with silicate phases (evidenced by CaO/SiO_2 reduction in alite) and reacts with belite leading to formation of additional quantities of alite. Furthermore, a part of C_3A which is unstable at high temperatures is subject to partial decomposition according to the following scheme: $7C_3A \rightarrow C_{12}A_7 + 9C$. Released lime also reacts with belite. $C_{12}A_7$ dissolves in the alumoferrite phase shifting to the aluminate-rich range according to the scheme $C_{12}A_7 + 2C + 7C_4AF \rightarrow 7C_6A_2F$. The schema presented should not be considered as a sequence of solid phase reactions. The precesses occur in the melt by acid-base interaction of Ca^{2+}, $[AlO_4]^{5-}$, $[FeO_4]^{5-}$, $[AlO_6]^{9-}$, $[FeO_6]^{9-}$ ions.

Results

Clinker properties change according to change of phase composition of clinkers and chemical composition of individual phases, particularly when the less dense C_6A_2F prevails. Their grindability and compressive strength as well as hardening rates of obtained cements come close to values characteristic for alite (reference) compositions (Tables 2, 3).

Table 2
Grindability of clinkers obtained from various raw mixes

Composition			Grinding time (min) of clinker to S=300 m^2/kg
LSF	n	p	
0.77	1.9	1.8	40
0.81	2.1	0.9	43
0.87	1.9	1.9	32
0.90	2.1	1.2	30

Table 1.

Raw mix characteristics			Dispersity** values	Temperature of clinkering, °C	Rate of heating-up of the mix, deg/min.	Phase composition (quantitative x-ray phase analysis), mass %				
LSF	n	P				C_3S***	C_2S	C_3A	C_4AF****	C_6A_2F****
Limestone + clay										
0.81	2.0	1.2	1100	1400	20	42.5 37.5	42.0	-	13.6	-
0.82	2.0	2.0	1100	1400	20	49.0 40.0	32.0	8.3	-	8.0
0.92	2.0	1.2*	550	1450	5	51.0 56.0	29.0	2.0	-	14.0
Marl										
0.82	2.0	1.9	0.60	1400	20	45.5 42.4	31.0	11.5	-	12.0
0.86	2.0	2.0	0.52	1400	20	58.5 49.2	20.7	10.6	-	10.2
0.94	2.0	1.2*	3.20	1450	5	63.5 63.7	18.5	3.8	-	14.2

* Reference (production) mixes

** For the limestone-clay mix, specific surface values of the silicieous component are shown, m^2/kg; for the marl mix - quantities of residue of raw mix on the 02 screen, %.

*** Numerator - actual composition, denominator - estimated composition

**** The composition of the AF phase was determined with the use of micro x-ray spectral analysis.

Table 3
Strength of cements based of clinkers obtained from various raw mixes

Composition			Compressive strength, MPa (acc. to SU State Standard GOST 310-81) after	
LSF	n	p	3 days	28 days
Limestone + clay				
0.81	2.0	1.2	23.0	50.1
0.82	2.0	2.0	41.2	56.0
0.92	2.0	1.2	33.2	50.0
Marl				
0.82	2.0	1.9	15.4	43.8
0.86	2.0	2.0	20.4	47.8
0.94	2.0	1.2	27.2	41.2

REFERENCES

Merik, Zh.P., "Clinker formation with low heat consumption", Proceedings of the 8th International Congress on Cement Chemistry, Rio-de-Janeiro, 21-27 of September 1988, Theme 1 "Formation and Properties of Clinker", Moscow, All-Russian Research Institute for Economics of Building Materials, 1988, pp.80-89.

Milke, I., Muller, A., Stark, I., "Active Belite Cement" ", Proceedings of the 9th International Congress on Cement Chemistry, New-Deli, 1992, Theme 1 "Formation and Properties of Clinker", Moscow, Institute for Cement Research, 1994, pp.11-20.

Moranvil-Regur, M., Boikova, A.I., "Chemistry, Structure, Properties and Quality of Clinker", Proceedings of the 9th International Congress on Cement Chemistry, New-Delhi, 1992, Theme 1 "Chemistry, Structure and Properties of Clinker", Moscow, Institute for Cement Research, 1994, pp.11-66.

Myasnikova, E.A., "Clinker Formation in Basalt-containing Raw Mixes with Reduced Saturation Factor", Cement, 1992, No.2, pp. 31-37.

Osokin, A.P., Krivoborodov, Yu.R., Potapova, E.N., "Modified Portlandcement", Moscow, Strojizdat, 1993, p.297.

Sudakas, L.G., Kraplya, A.F., Fedik, A.A., "Scientific Principles of Production of Active Low-base Clinkers", Cement, 1989, No.3, pp. 16-17.

Uchikawa, Kh., Khanekhara, Sh., Shirosaka, T., "Relationship between Belite Zone Structure and Technology of Production, Composition and Crystalline Structure of it.", Proceedings of the 9th International Congress on Cement Chemistry, New-Delhi, 1992, Theme 1 "Formation and Properties of Clinker", Moscow, Institute for Cement Research, 1994, pp.11-20.

Kn o. 2 6. OKT. 2000 d o k 31016

1i016
4 pp

FORMATION KINETICS OF BETA DICALCIUM SILICATE

Vipin K. SINGH, R. PYARE and Vinay K. SINGH, Department of Ceramic Engineering Institute of Technology, Banaras Hindu University, Varanasi - 221 005, India

ABSTRACT A single phase polycrystalline beta-dicalcium silicate has been prepared using chemical processing followed by pyrolysis. Formation kinetics of ß-C_2S in the temperature range 600-1000°C has been studied using X-ray diffraction analysis. The quantity of unreacted lime was determined by glycerol- ethenol estimation method. It was observed that the rate of formation of ß-C_2S increased with rise in temperature as well as with increase in reaction time. The kinetics of its formation has been studied using Arrhenius plot. The activation energy for the formation of ß-C_2S was found to be 7.3 kcal/mol.

Key-words reactivity, free lime, X-ray diffraction analysis, stabilization

INTRODUCTION

Dicalcium silicate (C_2S) is of considerable importance to cement and ceramic technologies. There are five polymorphs of C_2S which can exist at atmospheric pressure: namely α, α'_H, α'_L, ß and γ (Schwieté et al, 1968, Midfley et al, 1974 and Hanic et al, 1987). The ß-C_2S is at normal pressure and room temperature a metastable modification which is probably responsible for its important hydraulic properties. The transformation ß-γ, accompanied by a large volume increase (~12%) takes place (Chan et al, 1992) provided the grain sizes exceed the critical dimensions. The phase does not hydrate and hence the more reactive ß phase has been stabilized at room temperature.

Various strategies have been employed (Roy et al, 1977, Struillon et al, 1980 and Kralj et al, 1986) to produce ß-C_2S without stabilizers and at low temperature : by heating γ-C_2S at 1000°C for several hours and cooling rapidly, by repeated firing of CaO and SiO_2 at 1100°C or from calcium nitrate/oxalate and colloidal/amorphous silica at temperatures ranging between 750 and 1050°C. In the present study a single phase polycrystalline beta dicalcium silicate has been prepared up to 1000°C which is useful to study the stress induced ß-γ transformation toughening of ceramics or as an alternative to cement (as belite cement). The aim of the work was to study the kinetics of formation of beta dicalcium silicate at low temperature.

EXPERIMENTAL PROCEDURE

Analytical reagent grade calcium nitrate and high purity silica gel were chosen for the preparation of ß-C_2S. Dried silica gel was disintegrated in a centrifugal ball mill and sieved through a 90 µm sieve. It was amorphous and no trace of any crystalline phase was found by X-ray diffraction. Calcium nitrate and dried silica gel powder were separately weighed in 2:1 molar proportions to give the C_2S composition. $Ca(NO_3)_2.4H_2O$ was completely dessolved in distilled water and kept on a hot magnetic stirrer. Dried silica gel powder was slowly added into this solution. The slurry was continuously stirred on the hot magnetic stirrer where its temperature was maintained at 80°C. When the slurry was too viscous to stir, the viscous material was baked at 150°C until dryness. The dried powder was fired at temperatures in the range 600-1000°C with holding time from 10 to 300 minutes. Powders were characterized by XRD (ID-3000, SEIFERT) for the determination of different phases present. Unreacted CaO in the fired samples was estimated by the glycerol-ethenol method,

RESULTS AND DISCUSSION

Samples fired in the temperature range 600 - 1000°C in reaction time from 10 to 300 minutes have shown the presence of CS, C_3S, CaO along with ß-C_2S. Fig 1 is the XRD of samples fired at 700-1000°C for 2 hours which shows that appreciable quantity of ß-C_2S is formed in the reaction mixes and the highest peak at $2\theta = 32.4$ seems to be present because of ß-C_2S. For further analysis, peaks due to individual phases were chosen as for ß-C_2S at $2\theta = -41.3$, $d = 2.189$, for C_3S $2\theta = 41.0$ $d = 1.926$, for CS $2\theta = 54.6$, $d = 1.670$ and for CaO at $2\theta = 54.0$, $d = 1.701$. Fig 2 shows the intensity of various phases formed at 600°C up to 5 hours. Monocalcium silicate and tricalcium silicate are formed along with beta dicalcium silicate. Appreciable quantity of unreacted Cao was present at 600°C in the chosen reaction time. The intensity of ß-C_2S increased with time while the intensities of C_3S, CS and free CaO decreased. No free SiO_2 was found which may be because of its rapid utilization for the formation of various silicates or because of its poor crystallinity and the gel form.

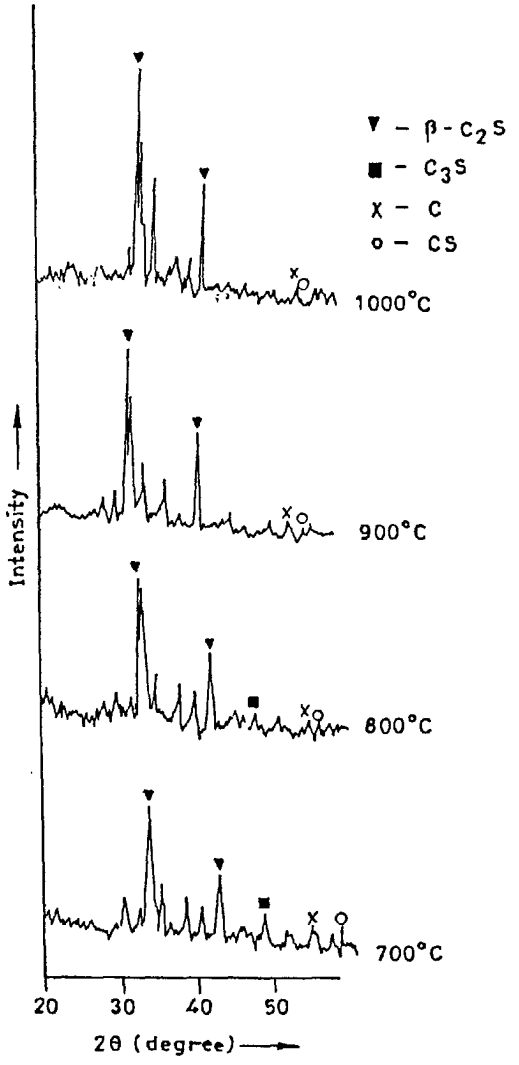

Fig. 1. Intensity of various phases formed at different temperatures in 2 hours

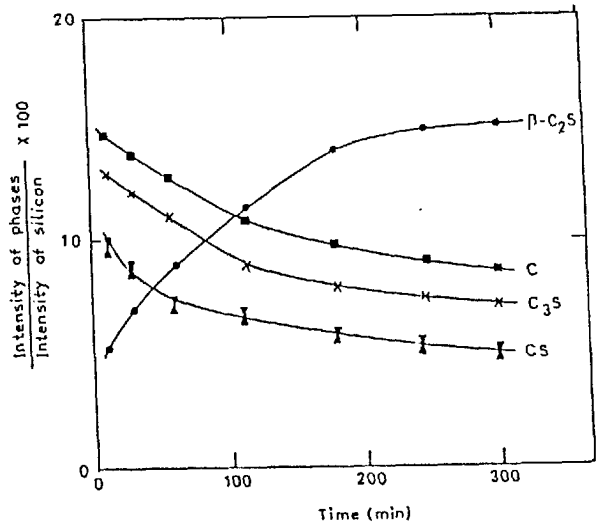

Fig. 2. Intensity ratio of different phases vs reaction time at 600°C

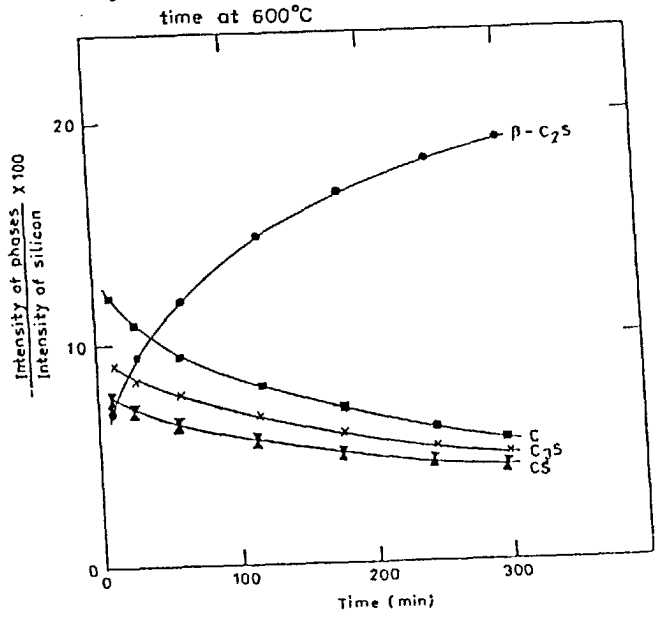

Fig. 3. Intensity ratio of different phases vs reaction time at 700°C

At 700°C the intensity of ß-C_2S was more than that formed at 600°C (Fig 3) which shows that the quantity of ß-C_2S formed at 700°C was more than that at 600°C in similar time. Quantities of CS, C_3S and CaO decreased at faster rate under similar conditions. The amount of these phases decreased at much faster rate at 800°C with increase in the reaction time along with increase in the quantity of ß-C_2S as compared to its formation at 600 and 700°C (Fig 4). No C_3S was detected at 900 and 1000°C. Small quantities of CS and unreacted CaO were observed and their quantities decreased with reaction time at higher rate. Highest rate was observed at 1000°C for the formation of ß-C_2S (Fig 5) where CS and CaO disappeared by about 3 hours and only ß-C_2S phase is left after which is free from reactant and reaction intermediates.

As the temperature increases from 600 to 1000°C, the quantity of ß-C_2S formed increases. It also increases with increase in reaction time at all the temperatures. The curves for the formation of ß-C_2S at different temperatures were found to be parabolic, the log - log plot for which was found to linear. Fig 6 shows the log - log plot of fraction of ß-C_2S formed vs reaction time in minute at 600, 700, 800, 900 and 1000°C. The slope of straight lines obtained was found to increase with increase in firing temperature and hence their slopes were taken as a measure of rate constant 'K'. Fig 7 shows the plot of log k against reciprocal absolute temperature ($1/T^{\circ}K$) which is again a straight line relationship. The slope of the straight line is equal to Q/R where Q is the activation energy and R the universal gas constant. The activation energy calculated from the slope of the plot was found to be 7321.7 Cal/mol.

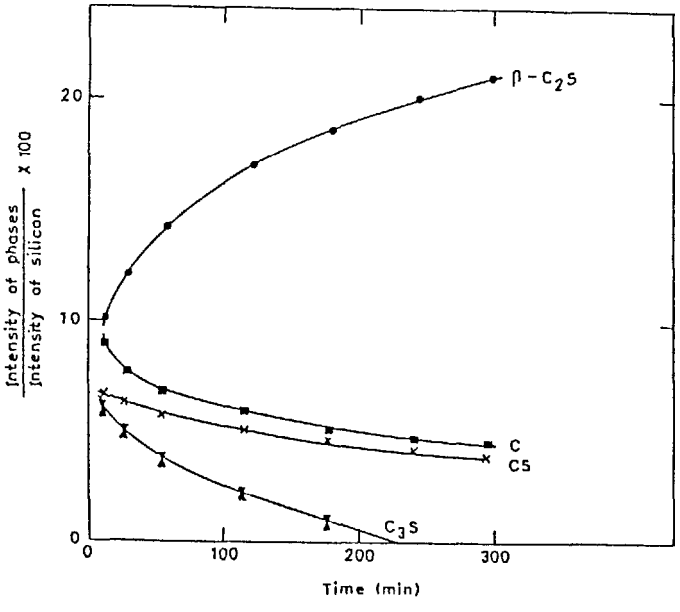

Fig.4. Intensity ratio of different phases vs reaction time at 800°C

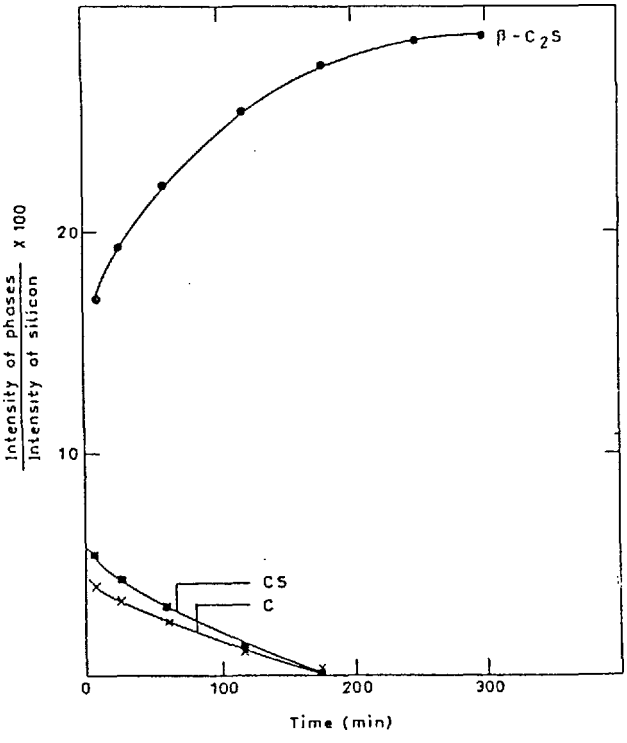

Fig.5. Intensity ratio of different phases vs reaction time at 1000°C

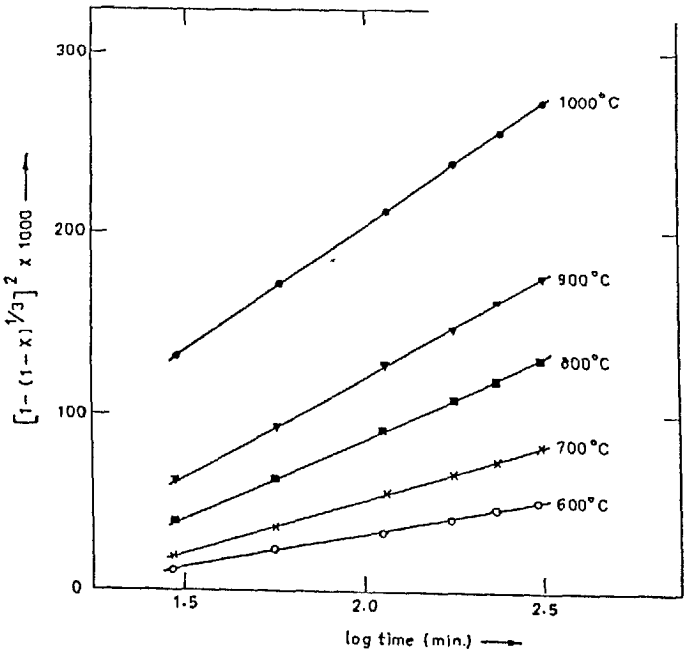

Fig. 6. Formation of β-C_2S

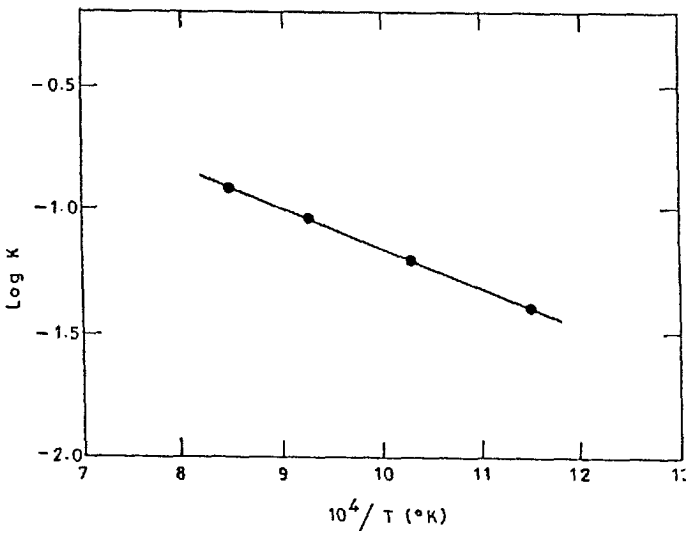

Fig. 7 . Temperature dependence of reaction rate

The key to the quantitative synthesis of β-C_2S at low temperature is the formation of a highly reactive reaction mix of CaO and SiO_2. The synthesis of β-C_2S at low temperature depends on the ability of reactants to combine in order that the kinetics of formation are reasonably fast. SiO_2 is highly reactive because of its presence as gel, poor crystallinity and high surface area. When CaO is formed by the decomposition reaction, it is initially in a highly reactive state due to high surface area and poor crystallinity. However, when annealed at elevated temperature, the oxide rapidly develops a more crystalline structure with lower specific surface and lower reactivity. β-C_2S is retained because of rapid cooling and annealing at 550°C i.e. above the β- inversion temperature for dicalcium silicate.

REFERENCES

Chan, C.J., Kriven, W.M. and Young, J.F., "Physical Stabilization of the β- to γ Transformation in Dicalcium Silicate", J. Am. Ceram. Soc., Vol. 75, No. 6, 1992, pp. 962 - 67.

Hanic, F., Kamarad, J., Stracelsky, J., and Kapralic, I., "The p - T Diagram of Ca_2SiO_4", Br. Ceram. Trans. J., Vol. 86, 1987, pp. 194 - 98.

Kralj, D., Matkovic, B. and Trokjo, R., "Preparation of Dicalcium Silicate at 950°C", J. Am. Ceram. Soc., Vol. 69, No. 8, 1986, pp. C-170 - C-172.

Midfley, H.,"The Polymorphism of Dicalcium - Orthosilicate", Proceedings of 6th International Congress on the Chemistry of Cement, Supplement Paper I, Moscow, 1974, pp. 1 - 16.

Roy, D.M. and Oyefesobi, S.O., "Preparation of very Reactive Ca_2SiO_4 Powder", J. Am. Ceram. Soc., Vol. 60, No. 3-4, 1977, pp. 178 - 80.

Schwiete, H.E., Kronert, W. and Deckert, K., "Existance Range and Stabilization of High - Temperature Modification of Dicalcium Silicate", Zem - Kalk - Gips, Vol. 9, 1968, pp. 359 - 66.

Struillon, R. and Armould, M., "Synthesis at About 750°C and Properties of a Sulphated β-C_2S", Proceedings of the 7th International Congress on the Chemistry of Cement, Paris, 1980, Vol. 3, pp. V/75 - V/79.

β-DICALCIUM SILICATE SYNTHESIS BY LIQUID-STATE REACTION

Miroslav M. KOMLJENOVIĆ, Center for Multidisciplinary Studies, University of Belgrade,YUGOSLAVIA
Branislav M. ŽIVANOVIĆ, Center for Multidisciplinary Studies, University of Belgrade, YUGOSLAVIA
Aleksandra ROSIĆ, Faculty of Mining and Geology, University of Belgrade, YUGOSLAVIA

ABSTRACT It is possible to synthesize β-dicalcium silicate by liquid-state reaction (hydrothermal method), via the synthesis of intermediary dicalcium silicate hydrate, using finely ground quartz (<20μm) as a siliceous material. Upon heating, dicalcium silicate hydrate is completely decomposed below 600°C and well crystallized β-dicalcium silicate is synthesized. β-dicalcium silicate produced is stable at room temperature and has a very large specific surface area.

KEY WORDS: β-dicalcium silicate, hydrothermal synthesis,

INTRODUCTION

β-dicalcium silicate is an important constituent of portland cement and is usually synthesized through solid-state reaction between lime and silica, stabilized by the presence of impurities. Also, it can be synthesized by liquid-state (hydrothermal) reaction between lime and silicic acid, via the synthesis of intermediary dicalcium silicate hydrate and without presence of stabilizing impurities, as reported by Ishida et al (1992, 1993). β-dicalcium silicate synthesized by liquid-state is exhibiting considerably higher hydraulic activity.

EXPERIMENTAL PROCEDURE

The starting materials were technical grade lime (70,94%CaO) and finely ground quartz (98,48% SiO_2; 95%<20μm). Experimental procedure (hydrothermal synthesis conditions) is given in Table 1.

β-DICALCIUM SILICATE SYNTHESIS

β-dicalcium silicate samples were synthesized according to following procedure: starting components (molar ratio C/S is given in Table 1) were thoroughly mixed with destilled water, so the water/solid ratio was 10. The suspension was subjected to hydrothermal conditions in an autoclave with constant stirring (200rpm). Intermediary calcium silicate hydrates synthesized were dried to constant mass at 105°C and analyzed for phase identification by XRD and for phase transformation by TGA-DTA up to 1000°C. Samples synthesized were heated up to 1000°C for dehydration and then also analyzed by XRD. Dominant crystal phases of both reaction products are given in Table 1.

Table 1 Experimental procedure and reaction products dominant crystal phases

	Hydrothermal synthesis conditions				dominant crystal phases*	
Sample	Molar ratio CaO/SiO_2	Tempe-rature (°C)	Pressure (atm)	Time (h)	Samples dried at 105°C	Samples heated 2^h at 1000°C
1	1.5	225	25.5	6	α-C_2SH, C_5S_5H	β-C_2S, CS, (C_3S_2)
2	1.5	250	40.0	6	α-C_2SH, C_5S_5H	β-C_2S, CS, (C_3S_2)
3	1.5	275	60.0	6	α-C_2SH, C_5S_5H, C_3SH_2	β-C_2S, CS, (C_3S_2)
4	1.8	225	25.5	6	α-C_2SH, CH, S,	β-C_2S, C, S
5	1.8	250	40.0	6	α-C_2SH, CH, S C_3SH_2	β-C_2S, C, S
6	1.8	275	60.0	6	α-C_2SH, CH, S C_3SH_2	β-C_2S, C, S
7	2.0	200	15.5	3	α-C_2SH, CH, S	β-C_2S, C, S
8	2.0	200	15.5	6	α-C_2SH, CH, S	β-C_2S, C, S
9	2.0	225	25.5	3	α-C_2SH, CH, S	β-C_2S, S, C
10	2.0	225	25.5	6	α-C_2SH, CH, S, C_3SH_2	β-C_2S, S, C
11	2.0	250	40.0	3	α-C_2SH, CH, S, C_3SH_2	β-C_2S, S, C
12	2.0	250	40.0	6	α-C_2SH, CH, S, C_3SH_2	β-C_2S, C, S
13	2.0	275	60.0	3	α-C_2SH, CH, S, C_3SH_2	β-C_2S, C, S
14	2.0	275	60.0	6	α-C_2SH, CH, S, C_3SH_2	β-C_2S, C, S
15	2.2	225	22.5	6	CH, α-C_2SH, S, C_3SH_2	-
16	2.2	250	40.0	6	CH, α-C_2SH, S, C_3SH_2	C, β-C_2S, S
17	2.2	275	60.0	6	CH, α-C_2SH, S, C_3SH_2	-
18	2.5	225	22.5	6	CH, α-C_2SH, S, C_3SH_2	-
19	2.5	250	40.0	6	CH, α-C_2SH, S, C_3SH_2	C, β-C_2S, S
20	2.5	275	60.0	6	CH, α-C_2SH, S, C_3SH_2	-

* Standard abbreviations in cement chemistry: C=CaO, S=SiO_2, H=H_2O.

RESULTS AND DISCUSSION

Results given in Table 1 indicate that in all experiments α-dicalcium silicate hydrate (α-C_2SH) was synthesized. Depending on the hydrothermal synthesis conditions this predominant phase was accompanied by some other crystal phases, most often lime (CH), which is more present when molar ratio C/S is higher. When molar ratio is constant, lime is more present when temperature is higher (especially above 225°C). In some cases unreacted quartz was also present. Tricalcium silicate hydrate (C_3SH_2), beside α-dicalcium silicate hydrate, was often synthesized. It could be noted that at lower molar ratio higher temperature is needed for the appearance of C_3SH_2 (C/S≥2.0, 225°C; C/S=1.8, 250°C and C/S=1.5, 275°C) and also at higher temperatures higher quantity of C_3SH_2 is present. This dependence could be the dominant factor for reaction controlling.

TGA-DTA studies gave basis for conclusion that α-C_2SH dehydration process is completed under 600°C. After heating up to 1000°C (above the $\beta \rightarrow \alpha'_L$ transition temperature) and on cooling, well crystallized β-C_2S was synthesized. When C/S=1.5 β-C_2S as most predominant phase is accompanied by β-wollastonite (CS), whereas when C/S>2.0 by significant amount of unreacted calcium oxide (C). Unreacted calcium oxide was also more present when temperature is too low (insufficient time for completing reaction) or too high (favouring C_3SH_2 appearance, which is thermally decomposed to β-C_2S and C). Therefore, optimal conditions for β-C_2S synthesis are: molar ratio C/S from 1.8 to 2.0 and temperature from 225 to 250°C.

Specific surface area (BET, N_2) of both hydrated and dehydrated samples as a function of processing temperature was analyzed. The results are given in Table 2, showing that both α-C_2SH (samples 10 and 11) and β-C_2S have a very large specific surface area, although the later was smaller than the former. At 700°C, after the dehydration process has completed, tested samples showed a significant increase of specific surface area (20-70%), but it is not yet clear which phase it can be attributed to, probably some kind of crystalline dicalcium silicate.

Table 2. Specific surface area (m^2/g) as a function of processing temperature

Sample	Temperature (°C)		
	25	700	1000
10	7,60	9,11	4,16
11	6,43	11,16	4,87

CONCLUSION

It is possible to synthesize β-dicalcium silicate by liquid-state reaction (hydrothermal method), via the synthesis of intermediary dicalcium silicate hydrate, using finely ground quartz (<20μm) as a siliceous and lime as calcareous material. Upon heating to 1000°C, dicalcium silicate hydrate is completely decomposed below 600°C and on cooling well crystallized β-dicalcium silicate is synthesized. β-dicalcium silicate produced is stable at room temperature and has a very large specific surface area.

REFERENCES

Ishida,H., Sasaki, K. and Mitsuda,T."Highly Reactive β-Dicalcium Silicate: I, Hydration Behavior at Room Temperature", J.Am.Ceram.Soc., **75**, 2, 353-58, (1992).

Ishida,H., Mabuchi,K., Sasaki,K. and Mitsuda,T., "Low-Temperature Synthesis of β-Ca_2SiO_4 from Hillebrandite", J.Am.Ceram.Soc., **75**, 9, 2427-32, (1992).

Ishida,H., Yamazaki,S., Sasaki,K., Okada,Y. and Mitsuda,T., "α-Dicalcium Silicate Hydrate: Preparation, Decomposed Phase and its Hydration", J.Am.Ceram.Soc., **76**, 7, 1707-12, (1993).

PROPERTIES OF LOW-TEMPERATURE PORTLAND CLINKERS

Albin GARBACIK, Institute of Mineral Building Materials (IMMB), Cracow, Poland

ABSTRACT In the paper properties of energy-saving low-lime clinkers of high hydraulic reactivity have been discussed. Using special raw materials it was possible to reduce the clinkerization temperature down to 1250-1300°C. Clinkers produced on laboratory, semi-commercial and plant scale from marly-chalky raw-mix and marly complete raw material have been investigated. Very high hydraulic reactivity and mechanical properties of the low-temperature belite clinker comparable with OPC clinker was stated.

Key-words: burning conditions of clinker, low temperature, belite, reactivity

INTRODUCTION

The most important problem in the energy-saving low-lime clinker technology is how to obtain binding material with hydraulic properties approximating to those of OPC. In belite cements with a high content of dicalcium silicate (Ca_2SiO_4) problems are caused by the very poor hydraulic activity of this phase. In view of the advantages to be gained from the modification of OPC to higher content of dicalcium silicate, methods are being developed which would increase the hydraulic activity of belite. The aim of these works is to determine the factors which bear an effect on the acceleration of dicalcium silicate hydration and to define the technological conditions for active belite clinker production.

The production technology of active belite clinkers has been confirmed on macro-industrial scale by employment of extremely rapid quenching of belite clinker from clinkerization temperature (Bei and Ludwig, 1990, Stark and Müller, 1988). In Poland however the low-temperature belite clinkers production conditions are being developed (Kurdowski and Garbacik, 1985, Garbacik and Peukert, 1992). Very active belite clinker is produced from raw-mix containing chalky and marly raw materials with high silica modulus and very good burnability. This makes it possible to achieve a considerable lowering the clinker temperature. Low burning temperature and high silica modulus of clinker determine formation of very fine - crystalline very active forms of silicate. Low-temperature belite clinker may be additionally activated by increasing the fineness of cement. The energy consumption for the grinding process is low, owing to the very good grindability of soft-burnt poorly sintered belite clinker.

The article presents selected questions concerning of the technology and properties of low-temperature clinkers, including those produced from marly complete raw material. Complete raw material provides an excellent natural geo-chemical homogenisation of the reaction components and hence ensures specific conditions for synthesis and properties of the clinker.

CLINKER SYNTHESIS

Laboratory and semi-commercial experiments

The synthesis conditions were determined for clinkers sintered from a marly complete raw material. Samples for investigations were taken from an organogenic deposit of chalky raw materials mining by a cement plant. This raw material is used to production ordinary and belite clinkers from marly and chalky raw-mix which, as mentioned above, have excellent burnability. Some parts of this deposit contain marl with a chemical composition similar to the raw-mixes composition for belite and OPC clinker production. The chemical composition of the samples

selected for testing is shown in **Table 1**. The samples of marl, in its natural state, were sintered in a laboratory electric furnace. The sintering temperature was ranged from 1000 to 1400°C at interval of 25°C. The sintering time was fixed at 30 min. The phase composition and free calcium oxide (CaO_{free}) content in the sintered material were inspected by means of X-ray diffractometer and the glycol method respectively. It was stated that depending on basicity of marly complete raw material full clinkerization was achieved at 1200-1350°C. Ca_2SiO_4 was present in the clinkers as β-C_2S form. Despite of the very high silicate module in the raw material and the small concentration of MgO and alkalis, the beginning of the alite synthesis was observed already at temperature of 1225°C.

Table 1 Chemical composition of marly complete raw materials.

Component	Marl 1	Marl V	Marl VI
	Component concentration [% by mass]		
LOI	34.28	34.74	35.40
SiO_2	18.55	17.13	15.75
Al_2O_3	2.21	2.41	2.17
Fe_2O_3	0.74	0.77	0.75
CaO	43.20	43.61	44.55
MgO	0.15	0.15	0.15
SO_3	0.05	0.09	0.17
Na_2O	0.09	0.15	0.10
K_2O	0.48	0.50	0.48
Total	99.75	99.57	99.52
LSF	0.76	0.82	0.93
SM	6.29	5.39	5.39
AM	2.99	3.06	2.90

The laboratory experiments carried out for the sintering of the complete raw material was checked on a semi-commercial scale. A rotary mazout kiln of dimensions 0.57×7 m was used. The complete raw material portions of chemical composition as described in Table 1 were burnt. The furnace was fed with material from the quarry ground down to the grain size of 10-20 mm. The sintering process was monitored by determining the phase composition and content of CaO_{free} in the clinker. The experiments carried out on the semi- commercial scale confirmed the excellent burnability of the complete raw material. The clinkerization process for the tested samples of complete raw material was conducted in temperatures similar to those quoted above for the laboratory tests. The chemical and phase composition of the clinkers burnt in the semi-commercial conditions are given in **Table 2**. The phase composition of the clinkers calculated from Bogue's equations was confirmed by diffractometry. The products of clinkerization were - in order of increasing basicity of the complete raw material - belite clinker containing up to 80% C_2S, belite-alite clinker and alite-belite clinker. In all the samples Ca_2SiO_4 was identified chiefly as β-C_2S form. The lowest-lime clinkers very strong sintered at temperature over 1400°C, was found to give polymorphic transformations β-C_2S to γ-C_2S form.

Table 2 Chemical composition of clinker from marly complete raw materials.

Component	Clinker		
	Marl I	Marl V	Marl VI
	Component concentration [% by mass]		
LOI	0.32	0.60	0.48
SiO_2	29.80	25.64	24.30
Al_2O_3	3.82	3.60	3.45
Fe_2O_3	1.22	1.13	1.11
CaO	64.10	68.00	69.80
MgO	0.30	0.45	0.45
SO_3	0.02	0.06	0.02
CaO_{free}	0.12	0.80	1.50
LSF	0.69	0.85	0.92
SM	5.91	5.42	5.32
AM	3.13	3.19	3.11
C_3S	6	53	69
C_2S	81	34	18
C_3A	8	7.5	7.5
C_4AF	4	3.5	3.5

Plant production

Clinker was produced in a long wet-process rotary kiln with planetary coolers. Two types of clinker were produced: belite clinkers from the complete raw material and belite clinkers from the chalky-marly raw mix. The temperature of synthesis was varied. The temperature in the burning zone and sintering degree were regulated by the amount of the coaldust fed into the kiln. The sintering degree was estimated by measurements of free lime content and litre weight of the clinker. The characteristics of the clinkers produced are shown in **Table 3**. In the process of clinker production from complete raw material the kiln was fed with broken material from the quarry ground down to a grain size between 20-40 mm. The $CaCO_3$ concentration in complete raw material was about of 75 %. The material was sintered at temperature about 1250°C with the litre weight kept within the limits of 1200-1300 g. Belite clinker containing up to of 60 % C_2S was produced. In the clinker C_2S was present as β-C_2S form. Substantial quantities of γ-C_2S form were identified only in harder sintered clinker samples.

Belite clinkers from slurry raw-mix were burnt at a different temperature. The litre weight of the low-temperature clinker was 1150-1250 g. The hard sintered clinker litre weight was about of 1450 g. Belite clinker with LSF 0.80 and containing about of 45 % C_2S was produced (Table 3). No sign of β-C_2S to γ-C_2S transformation was remarked.

Table 3 Properties of belite clinkers.

Component	Clinkers from raw mix			Clinker from marly complete raw material
	1 - 1150 *)	2 - 1250 *)	3 - 1450 *)	I - 1250 *)
LOI	0.72	0.50	0.50	0.42
SiO_2	25.00	24.70	24.70	26.70
Al_2O_3	5.60	5.70	5.60	4.29
Fe_2O_3	2.20	2.20	2.30	2.11
CaO	66.00	65.80	65.70	64.78
MgO	0.40	0.40	0.40	0.30
SO_3	0.30	0.20	0.15	1.02
Na_2O	0.21	0.18	0.14	0.18
K_2O	0.81	0.69	0.35	0.86
CaO_{free}	0.84	0.39	0.34	0.32
LSF	0.79	0.80	0.79	0.75
SM	3.20	3.13	3.12	4.17
AM	2.54	2.60	2.50	2.03
C_3S	35	36	35	24
C_2S	46	44	44	58
C_3A	11	11	11	8
C_4AF	7	7	7	6
Phase composition - X-ray measurements	β - C_2S, C_2S, C_3A, C_4AF, CaO_{free}			
*) 1150 / 1250 / 1450 / 1250 - litre weight [g]				

CLINKER PROPERTIES

Testing samples

Tests were conducted on samples of the clinkers produced on the semi-commercial and industrial scale. Clinkers displaying the characteristics presented in Tables 2 and 3 produced from the marly complete raw material and from slurry raw-mix were submitted to the tests.

Phase composition and physical properties

The phase composition for the tested samples, as calculated using Bogue's equations and as determined by means of X-ray diffractometer is presented in the already mentioned Tables 2 and 3. The compressive strength of cements obtained by grinding of the clinkers samples to a specific surface of 3500 cm^2/g with 5 % gypsum addition were investigated in compliance with European Standard EN 196-1. The results are given in **Tables 4 and 5** and shown on **Figs 1 and 2**.

Table 4 Mechanical properties of belite clinkers from marly complete raw material.

Clinker				Compressive strength [MPa], after days			
Production scale	No. of clinker	LSF	Belite content [%]	3	7	28	90
Semi-plant test (table 2)	Marl I	0.69	81	8.9	12.3	23.5	40.3
	Marl V	0.85	34	20.4	27.3	46.4	58.4
	Marl VI	0.92	18	25.8	36.4	54.4	60.3
Field scale (table 3)	I - 1250	0.75	58	14.3	20.5	40.1	53.2

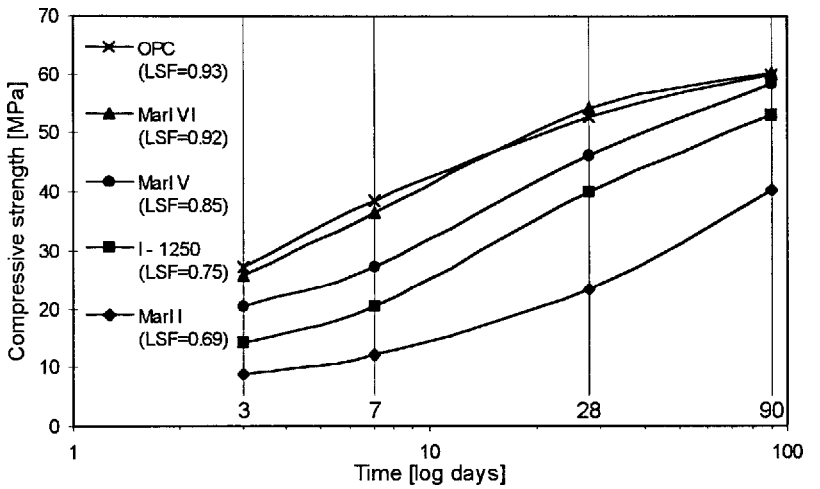

Figure 1 Compressive strength of cement from clinkers in Table 4.

Table 5 Mechanical properties of belite clinkers from marly - chalky raw mix.

Clinker in Table 3			Compressive strength [MPa], after days			
No. of clinker	Litre weight [g]	LSF	3	7	28	90
1.	1150	0.79	26.2	33.4	45.2	54.8
2.	1250	0.80	25.0	33.6	44.3	54.7
3.	1450	0.79	19.4	27.4	38.7	51.1
OPC CEM I 42.5	1480	0.93	27.4	38.7	52.8	59.8

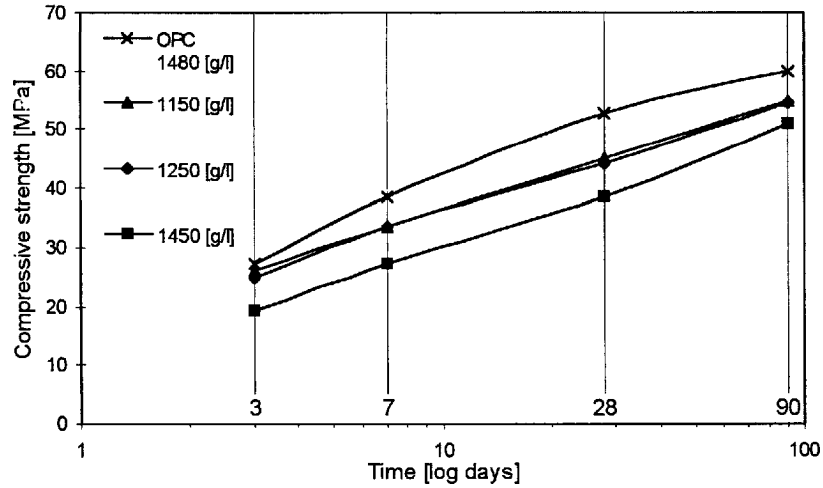

Figure 2 Compressive strength of cement from clinkers in Table 5.

It can be stated that mechanical properties of low-temperature belite clinkers show a clear enhancement in the hydraulic activity. A note worthy feature is the strength development rate of clinkers. This relation may be observed in the comparison of OPC and belite clinker, especially produced from complete raw material (Figs 1 and 2). Low-temperature belite clinkers are marked by high early strength, a poor rate of increase in strength between the third and seventh day of hardening, and another very high rate of strength development after 7 and 28 days of hardening. From the point of view of the production technology for active belite cements this change in the kinetics of hardening is extremely advantageous. The strength development of belite clinker is thereby similar to that for OPC. At a moderate cement fineness, the low-temperature belite clinkers give cements which meet the requirements for CEM I 32.5 and CEM I 42.5.

Heat of hydration

Measurements of the heat of hydration were conducted using a semi-adiabatic calorimeter. The cements obtained from the belite clinkers at various levels of sintering (Table 3) were subjected to these tests. The graphs for the rate of heat for selected cements are shown in **Fig 3**.

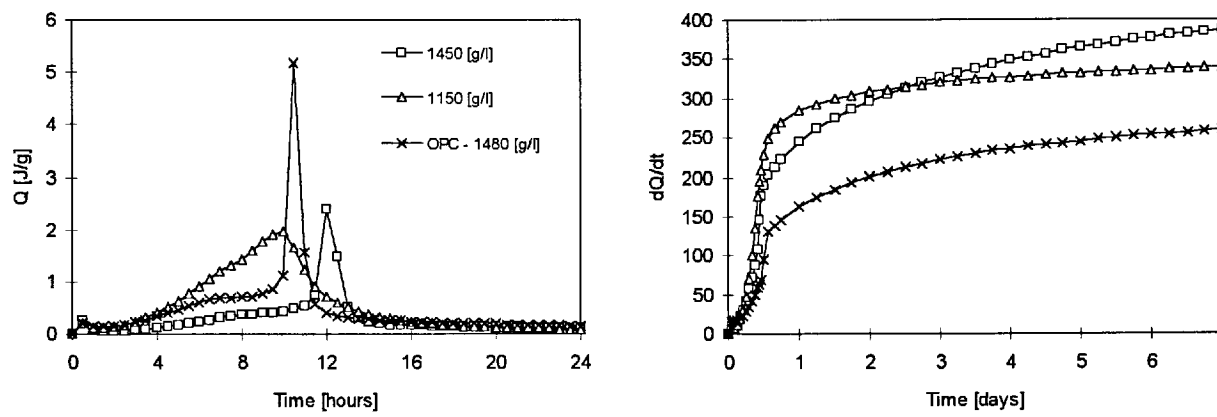

Figure 3 Heat of hydration of cement from clinkers in Table 5.

It may be observed that the curves for the rate of heat emitted by the belite cements are very similar to those characteristic of OPC. The fundamental heat effect shows two maxima typical for the hydration of OPC with the gypsum addition. Thus the hydration mechanism for this active belite clinker must be similar to the hydration process for OPC clinker. The heat of hydration

value of belite clinker varies with the sintering degree. Heat of hydration value of active sofr burnt belite clinker is comporable with OPC clinker (Fig 3). For the low-temperature clinker there is very good correlation between very high heat of hydration and high hydraulic activity and mechanical strength.

Porosity of the clinkers

The porosity of the clinkers was estimated by means of a mercury porosimeter. The results are shown in **Table 6**. The data collected for the porosity tests show significant differences between the porosity of the low-temperature belite clinkers and OPC clinker. In the former case the low-temperature clinkers obtained were found to be characterised by a high degree of porosity, which should explain the enhanced process of hydration and strength development. The highly porous structure of these clinkers also contribute their excellent grindability.

Table 6 Porosity of belite clinkers.

Clinker in Table 4		Porosity [cm^3/g]	
No. of sample	Litre weight [g]	58000 - 5 nm	7500 - 5 nm
1.	1150	0.1876	0.1357
2.	1250	0.1243	0.1098
3.	1450	0.0624	0.0486
I	1250	0.1602	0.1291
OPC clinker		0.0948	0.0468

The microstructure of the clinkers

The crystal habit and dimensions of the mineral phases is a very important aspect of the microstructure of the low-temperature clinkers. These relations were observed with the use of a Zeiss-Jena metallurgical microscope. The changes observed in reflected light for the microstructure of the silicate phases in the tested clinkers are described in **Table 7**.

Table 7 Microstructure of belite clinkers.

Clinker in Table 3		Grain size [μm]		Silicate phase microstructure - microscope tests
Sample No.	Litre weight [g]	Alite	Belite	
1	1150	5-20	5-10	Fundamental mass consists of irregular alite and belite grains. Some part of alite crystals has very fine characteristic pseudo-hexagonal habit. Also small characteristic isometric belite crystals have been observed sporadically.
2	1250	5-20	5-20	Alite and belite microstructure very similar to that of sample No. 1.
3	1450	10-40	20-80	Belite in form of isometric grains with very characteristic set of striations. Type I grains predominant, often with numerous inclusions. Smooth grains without any striations were observed, probably as γ-C_2S.
I	1250	5-20	5-20	Alite and belite microstructure very similar to that of samples 1 and 2.

The described changes in the microstructure of the silicate minerals in the low-temperature belite clinkers provide an explanation for their enhanced hydraulic activity. The very fine crystalline and almost amorphous alite and belite structure in soft sintered clinkers will tend to high hydraulic activity of these phases in the hardening process of cement.

The lowering of the sintering degree exerts a particularly large influence on the microstructure of the dicalcium silicate. The dimensions of the belite range from 80 mm in the strongly sintered clinker to 5-10 mm in the low-temperature clinker. The dominant alite structure in the highly sintered clinkers are crystals with a characteristic pseudo-hexagonal habit. Contrary, alite in the low-temperature clinkers forms fine-grain, xenomorphous structure. The microstructure of clinkers derived from the complete raw material is very similar to that of the low-temperature belite clinkers from raw-mix. However, the microstructure of the clinker obtained from the complete raw material is more tight and with higher density of pores.

CONCLUSION

Belite and alite-belite clinkers produced from the marly complete raw material are marked by specific properties of their microstructure and exhibit favourable mechanical properties caused by the conditions of sintering. Depending on the level of clinker basicity the clinkerization of complete raw material may be achieved at temperatures ranging from 1250-1350°C.

The extremely small dimensions of the Ca_2SiO_4 crystals, which occur in the low-temperature belite clinkers, appear to be stabilizing factor of β-C_2S phase in clinker containing up to 80% belite.

The very good mechanical properties exhibited by the low-temperature belite clinkers are brought about by the enhanced hydraulic activity of the alite and belite as compared with the properties of OPC clinker. The decisive factor is the very fine crystalline structure of these minerals. The quite small amounts of very active alite in the low-temperature belite clinkers has a significant effect on the early strength of these clinkers.

REFERENCES

Bei, R., Ludwig, U., "Hydraulic Reactivity of Belite-rich Portland Cements", Zement-Kalk-Gips, No, 10, 1990, pp. 506-510.

Garbacik, A., Peukert, S., "Energy-saving Belite-pozzolanic Cement", Proceedings of the 9-th Inter Congress on the Chemistry of Cement, Vol. VII, 1992, pp. 83-87.

Kurdowski, W., Garbacik, A., "Energy-saving Belite Cements", Beijing Inter Symp on Cement and Concrete, China Academic Publishers, No. 4, 1985.

Stark, J., Müller, A., "International Development Trends in Low Energy Cements", Zement-Kalk-Gips, No. 4, 1988, pp. 162-165.

TOPIC I.C

Utilization of industrial by-products and wastes

AGRICULTURAL / INDUSTRIAL COMBUSTIBLE WASTES AS FUEL IN INDIAN CEMENT INDUSTRY

S C AHLUWALIA, V K ARORA, Y P SETHI,
National Council for Cement and Building Materials

ABSTRACT Various combustible wastes such as rice husk, bamboo dust, bagassee, carbon slurry have been studied with reference to their availability, technology of use, logistics, costs etc. The paper gives impact of their use on the quality of product, process related problems, system design for storage, handling, and feeding. Experience of use of these have been reported and technology options suggested.

Key-words: Fuels for cement making, Rotary kiln, Waste material utilisation, Rice husk, Bamboo dust.

INTRODUCTION

India is an agricultural country and the agrobased industries generate nearly 250 million tonnes combustible wastes of which rice husk, bagassee account for nearly 10%. The wastes are widely spread over the country and depending upon logistics, these are considered to be potential cost effective alternate/substitute fuel to coal. The present paper deals with the potential of their use, impact on product quality, appropriate technology and cost effectiveness.

EVALUATION OF COMBUSTIBLE WASTES

The following factors need to be considered in evaluation of the wastes for their suitability in cement manufacturing process.

i/ Availability
ii/ Proximate and ultimate analysis, ash composition
iii/ Ignition and combustion aspects
iv/ Storage, handling, feeding and firing system
v/ Impact on pyroprocessing and clinker quality
vi/ Environmental considerations

INTERNATIONAL STATUS OF USE OF COMBUSTIBLE WASTES

The technological solutions have been evolved for ue of large varieties of agricultural and industrial combustible wastes. The cement rotary kilns have been reported to be one of the most efficient systems of combusting waste fuels and immobilising toxic having matters and other pollutants. Despite this, the actual use of waste fuel is not encouraging. The scrap rubber tyres are being used by the cement plants in Japan and Germany. A few cement plants in Japan are reported to substitute 25% of their main fuel by scrap motor tyres. The use of oil shale in one of the cement plants in Germany replaced fuel oil consumption by about 40%. The use of rice husk, bamboo/raw dust, waste oil etc have been reported to be used in the precalcinator in some of the cement plants in Germany replacing coal upto 30%. Most of the cement plants in North America are using petroleum coke along with coal. In Sweden, the sewage sludge after mechanical dewatering is successfully burnt in cement kilns

POTENTIAL COMBUSTIBLE WASTES IN INDIA

Out of various combustible wastes as outlined earlier, rice husk, bamboo dust, bagassee and carbon slurry seem to have good potential of use as fuel in India.

Rice Husk

The availability of rick husk is about 30 million tonnes per year mainly during harvest time spread over 4 months. Rice husk is very light in weight having bulk density of 100 kg/m^3 and has excellent fluidising property. It contains low moisture content varying from 6-8% whereas volatile matter is found to be high (60-65%). The calorific value is 3000 kcal/kg and hence it can be used as a supplementary fuel to coal. The most appropriate use has been established as a secondary fuel in the precalcinator and fed without further processing.

Bamboo Dust

Bamboo dust, a waste from paper industry is a fibrous material and hygroscopic in nature. The quantity available at present is about 0.5 million tonne per year. It is having a bulk density of 300 kg/m^3. The moisture content in the bamboo dust is initially found to be around 30% which comes down to 2-3% on sun-drying. The calorific value of bamboo dust is 3700 kcal/kg. The typical proximate and ultimate analysis of bamboo dust and its comparison with rice husk & coal is shown in Table 1.

Table 1 : Comparative Analysis of Coal, Bamboo Dust and Rice Husk

Particulars	Coal	Bamboo Dust	Rice Husk
PROXIMATE ANALYSIS, %			
Ash	38.51	13.70	16.21
Volatile Matter	26.14	68.02	64.24
Moisture Content	2.72	2.79	7.13
Fixed Carbon	32.63	15.49	12.42
ULTIMATE ANALYSIS, %			
Carbon	44.27	39.49	34.66
Hydrogen	3.10	3.85	4.37
Nitrogen	0.51	0.42	0.36
Sulphur	0.75	0.08	0.09
Oxygen	12.86	42.46	44.31
Calorific value, kcal/kg	4040	3710	3000

Carbon Slurry

The availability of this waste in the country is limited and projected at only 50 thousand tonnes per year. Carbon slurry is initially stripped off in the absorption column in the form of slurry containing 70-90% moisture and dumped in the lagoons for sun-drying to 50-60% On dried basis, it contains about 95% carbon with less than 1% ash content having calorific value around 7000 kcal/kg. The material has fine grains passing through 40 micron sieve.

Bagassee

About 2 million tonnes of bagassee is available per year in India. The bagassee contains 40-45% moisture with ash content of 2-3%. The calorific value on dried basis is 4200-4300 kcal/kg and can therefore be effectively burnt in the precalcinator as substitute fuel to coal.

IMPACT ON PYROPROCESSING AND CLINKER QUALITY

Since most of the combustible wastes have low ash content as compared to coal, the resultant ash content in the mixed fuel goes down. The use of these wastes in kiln system will have no adverse effect from ash view point. The firing of combustible wastes in the kiln is not favoured as these tend to lower the flame temperature and affect the flame shape for which burner design is required to be modified. These wastes can be burnt effectively in the precalcinator as supplementary fuel.

The potential clinker quality has been worked out with a typical raw mix at 10 and 20% of coal substitution by rice husk or bamboo dust (Table 2). The results indicate that there is an increase in CaO content with corresponding decrease in SiO_2 content which is an indication to the improvement in clinker quality.

Table 2 : Impact of Rice Husk/Bamboo Dust on Clinker Quality

Item	Potential Clinker Quality				
	Coal Substitution				
		By Rice Husk		By Bamboo Dust	
	0	10	20	10	20
SiO_2	20.48	20.41	20.33	20.36	20.24
Al_2O_3	6.33	6.22	6.11	6.23	6.14
Fe_2O_3	4.52	4.52	4.52	4.52	4.52
CaO	64.36	64.51	64.66	64.57	64.77
C_3S	57.34	59.25	61.16	59.77	62.10
C_2S	15.46	13.81	12.15	13.28	11.18
C_3A	9.13	8.85	8.56	8.86	8.62
C_4AF	13.75	13.74	13.73	13.75	13.75

STORAGE, FEEDING AND FIRING SYSTEM

The storage capacity and the quantity of these agricultural/industrial wastes will vary from plant to plant depending upon daily requirement of fuel as well as extent of fuel substitution. However, it is advised to store these wastes calculated to a minimum of 3 days requirement.

Mixing combustible waste with coal in the gantry and then feeding to coal mill leads to a number of operational and handling problems such as reduction in coal mill output rate, entrainment of combustible wastes to the dust collectors and catching fire thereafter and damaging the filters, fire in the coal mill circuit etc. The smooth flow of combustible wastes alongwith fine coal, segregation in the coal feeding bin are some of the problems encountered when combustible wastes are mixed with fine coal and fed to kiln/precalcinator. It is advised to feed combustible wastes only in the precalcinator just at the tertiary air entry in the precalcinator or in the riser duct of the kiln.

UTILISATION OF RICE HUSK/BAMBOO DUST

A Study had been carried out to use rice husk and bamboo dust in Indian cement plants. Based on the investigations a maximum of 20% coal substitution by bamboo dust was envisaged. The high volatile and low

calorific value of rick husk/bamboo dust restricted its use in the kiln firing owing to change in flame shape and its temperature however it did not have adverse effects in the temperature profile of preheater system after firing in the precalcinator. Various options were considered such feeding of rice husk/bamboo dust alongwith coal to grinding mill, mixing with pulverised coal after the mill and directly feeding to precalcinator without grinding. Keeping in view the merits and demerits of various options, it was inferred that rice husk and bamboo dust must be directly fed to the precalcinator without any processing.

STATUS OF COMBUSTIBLE WASTES UTILISATION IN INDIA

The combustible wastes are sporadingly being used by cement plants in the country. Due to their irrational utilisation, the results of coal substitution are not encouraging. Rice husk is reported to have replaced 5-10% coal by five cement plants in the country. These plants reported the problems of storage and handling particularly during rainy reason. No environmental problems were faced by these plants. The plants experienced quick burning of this waste in precalcinator. Two cement plants reported using bamboo dust replacing 5% coal with similar experiences of burning. Two more cement plants are reported to have used the carbon slurry with some problems encountered during feeding. One cement plant replaced about 15% of coal by bagassee.

COST ECONOMICS

The partial substitution of coal by any combustible waste must be evaluated for cost economics after technical evaluation to arrive at the final utilisation of combustible wastes in cement industry. Cost economics has been worked out at varying cost of coal from Rs 1000 to Rs 1600 per tonne and combustible waste from Rs 500 to Rs 600 per tonne depending upon the lead distance and mode of transportation. The savings to the plants on account of coal substitution from 5 to 20% vary from Rs 3 to 35 per tonne clinker.

CONCLUSION

The extent of substitution of coal by the agricultural and industrial wastes depends upon their availability, calorific value and economics of use. Systematic set up for controlled feeding needs to be adopted by the cement industry to achieve lowering of cost of energy input and finally the cost of cement manufacture. Besides this will help in solving the problems of waste disposal and treatment.

ACKNOWLEDGEMENT

The authors have freely drawn upon completed R&D work/status reports of NCB and some of the unpublished work in NCB. This paper is being published with the permission of Director General, NCB.

REFERENCES

Use of Agricultural and Industrial Combustible Wastes as Fuel in Indian Cement Industry - NCB's Report

Sethi Y P et al, Cost Effective Utilisation of Combustible Wastes in Indian Cement Industry, 4th NCB International Seminar on Cement and Building Materials, New Delhi, 12-15 Dec. 1994, Volume 1, pp 63-71

Report on Technical Feasibility of Using Bamboo Dust as a Partial Substitute of Coal, CPE-SP-589

Huhta R S, Waste as Fuel: A Survey Report, Rock Products, May 1990, pp 92-100

THE MULTICOMPONENT CEMENTS (MCs)

Zinovii B. ENTINE, Boris E. IOUDOVITCH
NIICement, Moscow, Russia

ABSTRACT Some new data in the domain of MCs are presented concerning: 1) active mineral additions (AMAs) and fillers; 2) Portland cement clinkers for MCs; 3) grinding aids with non-Rehbinder mechanism of action for MCs and ordinary Portland cement (OPC) production.

Key-words: Additives. Blended cements. Filler. Slag. Pozzolana. Zeolites.

INTRODUCTION

In Russia the terms ``MCs`` or ``MCs of high fineness` degree`` are used (Schubin, Entine, 1992) for denomination of improved varieties of blended cements which are practically equivalent by properties to OPC. From the thirties it had been known that such MCs decrease the energetic consumption and air pollutions in cement production and the cost of concrete. The peculiarities of chemistry and technology of MCs are the objective of this report.

EXTENDED ASSORTMENT OF ACTIVE MINERAL ADDITIONS (AMAs)

Expensive transportation obliges the usage of local AMAs. Some of them had not broadly been used earlier. For MCs producing in Russia it has began application next AMAs (Table 1). AMAs and fillers included firstly in the project of new Russian standard are underlined.

Table 1. New active mineral additions and fillers in Russian MCs

Hydraulic or pozzolanic	Pozzolanic	Fillers
Slags of non-ferrous metallurgy (in connection with its chemical composition)	Zeolitic rocks	Limestones
	Basalts (with amorphised intercrystalline matter)	Dolomites[1]
	Lyparite (rhyolite) types ♦ dense: obsidian pechstein ♦ porous: pumice ♦ crystallise: porphyry ♦ weathered: porphiroides ♦ artificial: glass breakage	Sands ♦ quartz[2] ♦ feldspar ♦ carbonatizated
	Volcanic origin weathered/ /metamorphised shales ♦ with 12 - 25% Al_2O_3 - ordinary; ♦ > 25% Al_2O_3 - extensible; ♦ pyrofillites	Sand stones[2]

Notes: [1] ≤3 weight % as calculated on dolomite in MC. [2] ≤ 10 weight % of pure quartz in MC

Among new AMAs are mainly of interested:

♦ *zeolitic rocks;* in Russia clinopthylolite is the main mineral of; the peculiarity of MC is temporary (by 1-2 months) reduction of strength by 5-15% during 3-12 months of hardening; to avoid reductions Kuznetzova et al. (1989) used mixes of zeolitic and slag or pozzolanic additions; the most probable reason for reduction the periodic way out of the alkalies in hardening MC paste from zeolitic particles to liquid phase and the absorbtion said alkalies from the last by slag/pozzolanic particles; rational selection of zeolitic MC fineness level is also enough for preventing reduction;

♦ *slags of non-ferrous metallurgy* consist up to 60% ferrous oxides (Entine et al.,1983); the greater FeO content in the slag the higher must be oxidizing potential (o.p.) of clinker particles in hardening MC (Entine, Ioudovitch,1996a); one can indirectly evaluate this o.p. by ferrous sulphate introducing upto 3 weight % to plain OPC by joint grinding; if then OPC class of strength has been diminished the clinker o.p. is low (Ioudovitch et al, 1996); methods of o.p. increasing is mentioned below; this MC is recommended for using with the water/cement ratio range up to 0.4 and for hardening without steam curing to prevent the oxidation of unhydrous slag particles; those have been lost an activity after Fe(II) ⇒ Fe(III) transition.

♦ *basalts* are suitable when contain amorphised intercrystalline matter (Nguen, Entine, 1994, Entine et al.,1995); on the contrary *porphyroides* must have some crystals in glass matrix;

♦ *shales* with good pozzolanic activity had been found in Russia recently (Bazoev et al, 1992); the MC based on is the first known expansive cement without burned components having the expansion at the air hardening (at relative humidity level down to 30%).

In Russia fillers are the comparatively new components of MC. The consumers used such MC reluctantly and had some arguments for. New specified conditions for limestone using as filler, for clinker in conjunction with and for MC as a whole (Table 2) are based on the results of industrial experiments (Entine, Ioudovitch, 1996a) and liberate MCs with limestone from defects.

Table 2. The specified conditions for limestone filler, PC clinker and MC based on

Demands to limestone filler			*Demands to PC clinker and MC as a whole*		
			Clinker characteristics		
Compressive strenght	$N.mm^{-2}$	≥400	C_3A content	weight%	≥5
Microhardness	- `` -	≥3000	C_3S content	- `` -	≥50
Calcite content	weight%	≥80	MgO content	- `` -	≤2.5
Clay impurities	- `` -	≤2	P_2O_5 content	- `` -	≤0.15
Dolomite impurities[1]	- `` -	≤10	Free lime	- `` -	≤1.0
			Loss of ignition (L.O.I.)	- `` -	≤0.3
			MC characteristics		
			L.O.I. up to 700°C	- `` -	≤1.0
			Specific surface,	m^2/kg	≥300
			- the better level	- `` -	≥400

Note: [1]Usage of filler with dolomite content higher than 10% is admitted only after experimental checking

In the hardening of MC paste the limestone filler takes part in hydroaluminates' formation in the case of clinker particles prehydration during of MC grinding process especially in situation with non-predried and soft filler used in large quantities. Moreover for MC strength the hydrosilicates semicontact carbonation by filler is worse than that of hydroaluminates particularly in the time of steam curing of concrete and it can cause the cracking of cured reinforced concrete articles

(Dolbilova,1995). Such are the reasons for demands to components and to MC listed in Table 2.

SPECIAL PORTLAND CEMENT CLINKERS FOR MCs

Activation of clinker with high alkali level is realised by using of additives - ``cement promoters`` (Ioudovitch, Zubekhine, 1996) to cement raw mix to increase alite generation rate and clinker o.p. at burning, decrease insoluble residue and R_2O content, exclude the presence of marginal phases - $C_{12}A_7$, R_2O-containing C_3A (the former RC_8A_3), C_2F, CF etc. (Entine, Ioudovitch, 1996b), ensure the better phase composition (Table 3) and reduce the resistance to grinding.

Table 3. Phase composition of high alkaline clinkers for MC in comparison with OPC

Clinkers for OPC (R_2O > 1 weight %) without SO_3 / R_2O balance		Clinkers for MC (R_2O > 1 weight %) with balance SO_3=(0.7–1.0)R_2O in weight %	
Main phases	Marginal phases	Main phases	Weight %
C_3S	R_2O-contained C_3A	C_3S	65 - 75
C_2S	(= RC_8A_3)	C_2S	< 10
C_3A	$C_{12}A_7$	C_3A	8 - 12
$C_2(A,F)$	R_2O-contained $C_2(A,F)$	$C_2(A,F)$	8 - 13
		Minor components and impurities	
	Alkaline ferrites[1] (e.g.$Na_2O.Fe_2O_3$)	Free CaO[2]	≤ 0.5
		Free MgO[2]	≤ 2.5
Minor components and impurities		SO_3	≥ 0.7
Free CaO[3]	Free MgO[3]	Calcium-alkaline sulphates	≥ 1.6
Alkaline sulphates (R_2SO_4)		Insoluble residue	≤ 0.5

Notes: [1]Estimated as an impurity in $C_2(A,F)$ by microchemical reaction with methylenblue (Skl`arenko, Zoubekhine, 1995). [2)] as a rule less than [3)] by the weight.

This is essential mostly for MC because marginal phases not only create obstacles to alite hydration by forming passive glass pellicles around alite crystals in clinker but also form gelious hydrates, firstly AH_3 from $C_{12}A_7$ which the stronger delied reaction C_3A with gypsum in hardened cement paste the more AMA content in MC. Elimination of obstacles raises the MC quality.
Activation of MC based on sedimentary pozzolanas reaches by using the modified Ferrari type clinker with extremely high LSF (upto 1.5), including ``hyperalite`` $C_{3,3-3,8}S$ (65-80%) and free lime (5-15%) in form of $(C - C_2F)_{ss}$ which allows to finish the pozzolan reaction during 1-2 months versus 20-30 years in hardening MC based on OP clinker (Zoubekhine, Ioudovitch, 1996).The low resistance to grinding of the first clinker type (time of grinding the portion of 5 kg in laboratory mill chamber with dimensions .5 m in diameter, .28 m in longitude, milling load 53 kg and angle velocity .7 of critical level upto Blaine number 420–450 m^2/kg is 40–50 min. versus 1.5–4.5 hours for OP clinker) determined by its specific crystal structure guarantees *both* the increasing value of clinker content in the fine MC fraction (≤ 5 μm in effective diameter) that is the principal condition of MC high quality in connection with intensifying action upon the pozzolanic reaction (Entine, 1993) and upon the rate of middle clinker fraction (5–30 μm in diameters) hydration (Ioudovitch, 1972) *and* the best size distribution of alite particles for uniform dissolution in water. For the second type of mentioned clinker time of grinding in same laboratory conditions is shortening to 25–35 min. In compositions with sedimentary pozzolanas such clinker determines extremely low energy consumption by cement mill. Besides in MC it is useful the presence of two mineral additions - the first with larger hardness than of clinker and

the second with lesser hardness for intensification the grinding of clinker part of MC and for disaggregation the last on finish grinding stage accordingly (Entine,1993). Such MC composition brings into concord the low energy consumption in producing and high quality of.

NEW CEMENT GRINDING INTENSIFIERS

In Russia new grinding intensifiers` group had been worked out in eighties. They can increase the mill output by 30 - 100%. The mechanism of action is non-Rehbinder (Rehbinder, 1931, had shown that liquid surface active intensifier acts by decreasing of surface energy of ground particles what can increase the mill output by 15-20% only) and connects with decreasing of dry friction angles (grinding matter by steel and steel by steel). Usually new grinding aid is dry matter which forms chemical bonds with active centers on said particle surfaces permitting the jumping diffusion of the matter from-one-to-another surface dislocation zones to activate them during contact motions. This matter must be able to be added to cement without any harm on technical properties of. For MC it can be liquid too but easy soaked in porous AMA particles. The Russian intensifier based on dry S-3 had increased the output of tube mill with dimensions 3.4 x 10.6 m in MC grinding (with 20–30% of slag upto Blaine number 400–450 m^2/kg) from 37 t/h without aid to 70-75 t/h with it while with Blaine number 300 – 320 such data were 47 and 80 - 85 t/h accordingly (tests had been carried out by Ioudovitch, Babaev, 1992). In Russia for MC grinding mill 2.6 x 13 m (both said mills worked in open cirquit) another Russian intensifier based on lignosulphonates LSTM-2 in the presence of AMA (15%) gave growth of the output from 12–15 to 28–32 t/h (for the first of mentioned Blaine number, Ioudovitch,1982). Because MC must have higher fineness degree than OPC such grinding aids are useful for MC producing.

REFERENCES

Bazoev, O.K., Kesaev, E.Z., Titova, L.N., Zvezdov,A.I., Beilina, M.I. Russian Patents No. 2049079 - 2049081, Dec. 30, 1992.

Dolbilova, I.E., NIICement, Private Communication, Nov.1995.

Entine, Z.B. Doct. Tech. Sci. Thesis. Mendeleev`s Chemistry-and-Technology University, Moscow, 1993, 49 pp.

Entine, Z.B., Albaz, B.S., et al. Author`s Sertificate of USSR, No. 1131854, Aug.15,1983.

Entine, Z.B., et al., Tsement (Leningrad), 1995, No. 4, p. 13.

Entine, Z.B., Ioudovitch, B.E., Tsement (Leningrad), Spec. Publ., May 1996, pp. 27-34 (all ref. before - in Russian)

Entine, Z.B., Ioudovitch, B.E. ``The liquid phase alite generation model in sintering Portland cement clinker``. Report presented to this Congress, 1996.

Ioudovitch, B.E. Cand. Tech. Sci. Thesis. NIIcement, Moscow, 1972, 24 pp. (in Russian)

Ioudovitch, B.E. Unpublisned Report. NIICement, Moscow, 1982, 65 pp.

Ioudovitch, B.E., Babaev Sh.T. Unpublished Rep. of Proc. in Spain, La Robla, 1992, 3 pp.

Ioudovitch, B.E., et al. Proc. I Int. Conf. on the Chemistry of Cements, Moscow, 1996, pp.114 - 116 (in Russian)

Ioudovitch, B.E., Zoubekhine, S. A. Ibidem, 1996, p. 110 (in Russian).

Kuznetzova, T.V., Potapova, E.N. et al., Tsement(Leningrad),1989,No.7,pp.22-23 (in Russian).

Nguen,Than Tung, Entine Z.B. Tsement (Leningrad), 1994, No. 4, p. 38 (in Russian).

Rehbinder, P.A. Zeitschrift für Physik, 1931, B. 72, H. 2, s. 191.

Schubin, W.I., Entine Z.B. Zement-Kalk-Gips, 1992, B. 45, H. 12, ss. 653-656.

Skl`arenko, I.E., Zoubekhine, S.A. NIICement. Private Communication, Aug.1995.

Zoubekhine, S.A., Ioudovitch B.E.``Nonshrinking Sulphate Resisting Cement for Conventional and Fine Grained Concretes``, VNIIESM Rew., Moscow, 1996, ser.1, No.3,pp.8-35 (in Russian)

EFFECTS OF USING IRON MUD AS RAW MATERIAL IN CEMENT MANUFACTURE

Yizhou PAN
Zhejiang Building Materials Scientific Research Institute, Hangzhou, P. R. CHINA

ABSTRACT The effect of iron mud on producing portland cement and the mechanism of influence of five trace component on clinker formation in particular have been studied by XRD , chemical analysis . The results indicated that iron mud was very good and lower priced composite raw materials because it is iron , aluminium oxide raw materials as well as complex trace component mineralizer in cement production .

Key-words: Iron mud Burnability Five trace components

INTRODUCTION

The mineral balance in the nature is disturbed with depletion of natural minerals on one hand and the rapid growth of by products and solid wastes from increased industrial activities creating handing disposal and environmental problems on the other. Industrial wastes containing useful minerals having intrinsic mineralizer potential offer ready to use solution (Kumar 1981 , Mori 1992 , Moranville-Regourd 1992) . Iron mud is a kind of natural material which looked like clay and caused from low level iron ore oxidized in air . There are widespread and great reserves of it in our province in China , It hasn't been exploited due to its poor quality for a long time past . For the purpose of wide application of the solid wastes , we have carried out many studies on it .

EXPERIMENT

Materials and Methods

The chemical and spectral analysis results (table1) indicated the iron mud consist mainly of silicon , iron , calcium and aluminium oxid and five trace components (Mn , Cu , Zn , Ba , Pb, the amount of them is 0.2-1.0%, 0.1-0.3%, 0.2-0.8%, 0.3-0.5% and 0.1-0.3%). In order to study the effect of five trace composition and avoid other impurities interference on clinker formation , the experimental work were divided into two groups . In one group, raw mixes were made by chemical pure reagents with the appropriate amount of five trace components, that was mixed by MnO_2 , CuO , ZnO , Pb_3O_4 and $BaSO_4$ in the same weight proportion . The other group was composed of natural materials and iron mud instead of iron power , same of clay and mineralizer . The samples were preheated at the chosen temperature in electric furnace and cooled in air .

Table 1. Chemical Composition and Price of Materials(%)

Sample	Loss	SiO_2	Al_2O_3	Fe_2O_3	CaO	MgO	Total	Price
Iron Mud 1	9.21	41.50	11.51	30.70	1.36	1.66	95.94	$2.5/t
Iron Mud 2	16.61	24.16	7.28	43.50	2.09	2.45	96.18	
Iron powder	2.60	20.57	4.28	60.12	7.99	2.75	97.81	$ 10/t
Copper slag	-2.70	28.26	3.71	58.23	3.76	3.07	97.03	$ 10/t
Clinker	/	20.90	6.00	4.80	68.30	/	100.00	/

The project is supported by the Zhejiang Natural Scientific Foundation , P. R. China

RESULTS AND DISCUSSION

1. Effect of five trace components on burnability of raw mixes

Results of burnability of raw mixes by adding five trace components is illustrated in Figure 1 . At the temperature of 1200℃ , the free lime content of the sinter containing 1% five trace components and 1% fluorite (F-5) is 15.8% , but is 30.5% and 24.6% for contrast sample (0-0) and adding 1% fluorite alone sample (F-0) respectively. At 1300℃, the free lime of samples F-5 , F-0 , 0-0 is 1.7% , 5.7% , 12.1% ; and is 0.3% , 1.0% and 3.0% separately at 1350℃ . The free lime of sintered samples at the burning temperature is in the following order : 0-0>F-0>F-5 . The difference in the free lime indicated that addition of five trace components was obtained quite effectively because it could lower the free lime and improve the burnability of the raw meals during the clinkering process .

2. Effect of five trace components on absorption of free lime

Figure 2 show XRD pattern of the samples . The intensity of peaks of free lime (at 2θ=54 , I=1.699) at the burning temperature of 1200℃ are 0-0>F-0>F-5 . When temperature reached to 1300℃ , the peaks of free lime decrease obviously for sample F-0 and disappear for F-5 . The peaks vanish for F-0 and still can been found for 0-0 at the temperature of 1350℃ . This results are in accordance with that of former experiments and testify that five trace components could improve the absorption of free lime efficiently in clinkeration process. The variation of peaks compared alite with belite at the different temperature illustrate the decrease of free lime to sintered samples with the development of belite crystal and formation of alite below 1300℃ , as well as with the disappearance of belite and growth of alite at 1350℃ . The changes of XRD patterns of silicate minerals have directly relation to the kind of addition .

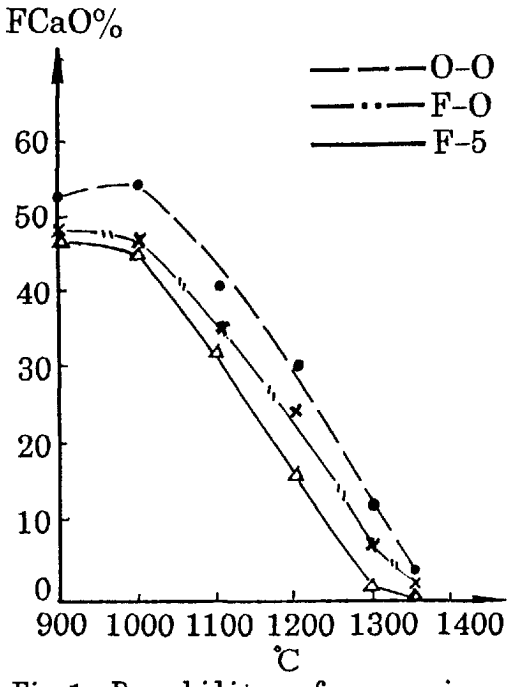

Fig. 1 Burnability of raw mixes
0-0: contrast sample; F-0: 1% CaF_2; F-5: 1% CaF_2+1% five trace components

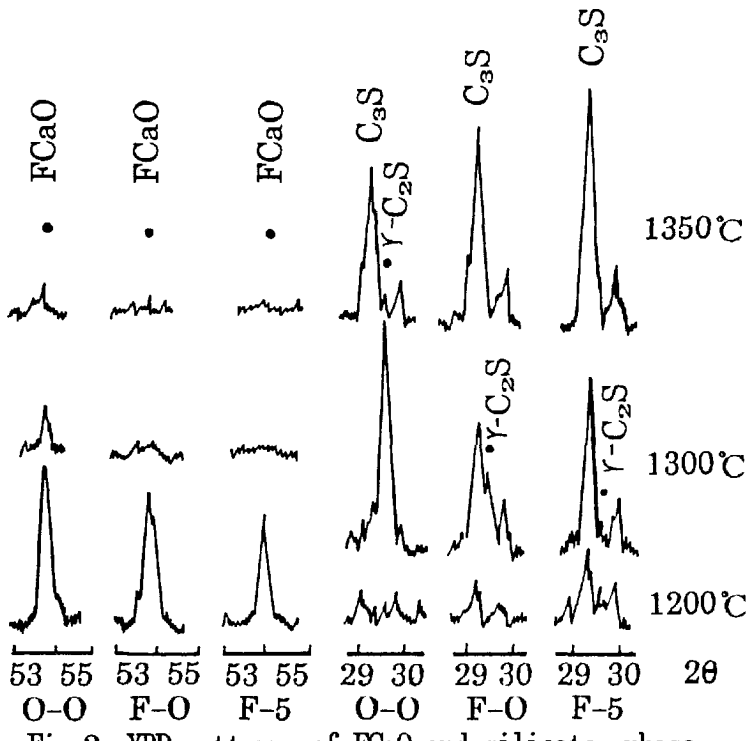

Fig. 2 XRD patterns of FCaO and silicate phase

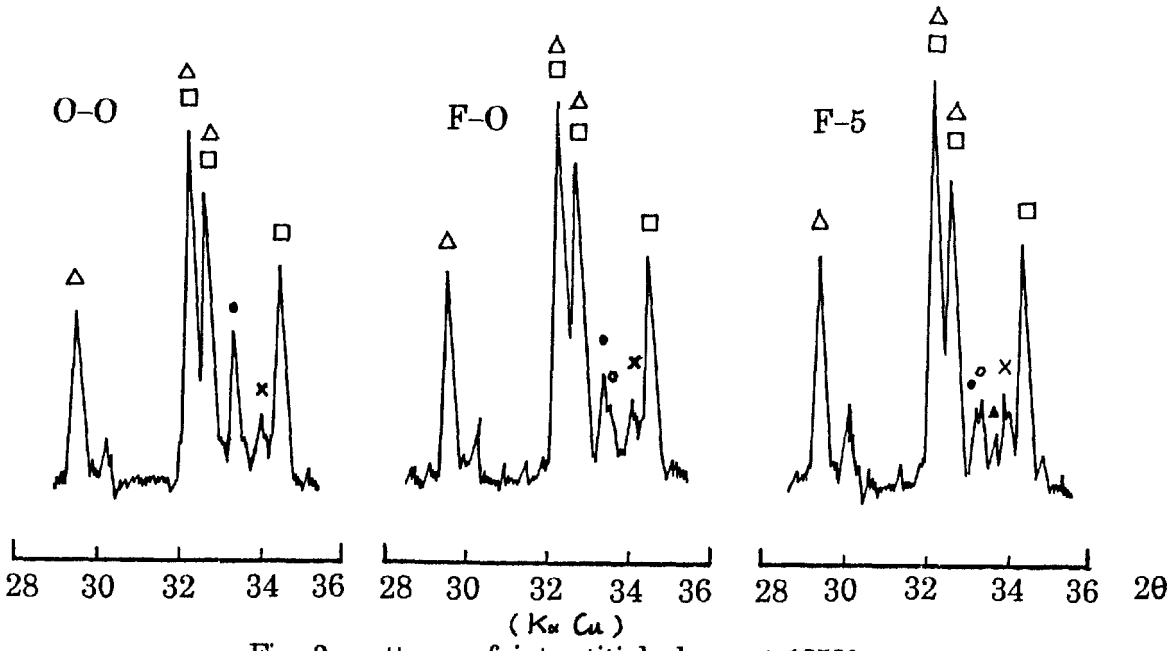

Fig. 3 patterns of interstitial phase at 1350℃
△C_3S, □C_2S, •C_3A, ×C_4AF, ○$C_{11}A_7CaF_2$, ▲C_6A_2C

3. Effect of five trace components on silicate minerals

Figure 2 shows that a number of alite are formed to F-5 sample and only a few to F-0 and no any sign of it is found to 0-0 at 1200℃. At the temperature of 1300℃, The peaks of alite are F-5>F-0>0-0. On the contrary, peaks of belite show opposite results. At 1350℃, the changes of alite are similar to those at 1300℃, moreover, peaks of belite disappear to F-5, F-0 and still can been found to the control sample 0-0. The above results indicated that addition of five trace component was found quite effectively on properties of the liquid phase. The alite micro-crystals formed from solid phases reaction and decomposition of $C_{19}S_7CaF_2$ can continually grow at 1200℃, and get into rapidly develop at 1300℃ and in addition quite a few of alite are formed. The improvement of alite formation at low temperature is obvious compared with CaF_2 doped sample F-0 and pure clinker sample 0-0, which can only be attributed to addition of five trace components, decrease the viscosity and surface tension of the liquid phase and proportionally increase the diffusion velocity of liquid phase, as a result accelerating the reaction of $C_2S+CaO=C_3S$, and providing favorable conditions to form alite quickly.

4. Effect of five trace components on interstitial phase

The C_3A and C_4AF phases are satisfactory crystallized in XRD patterns to 0-0 sample at 1350℃ (Fig. 3). There are some differences to samples F-5, F-0 with 0-0. The presence of fluorite lower and widen peak of C_3A, which indicate $C_{11}A_7CaF_2$ and C_3A phases existed together in clinker, no difference of C_4AF phase has been found to F-0 and 0-0. Peaks of C_3A phase to F-5 are similar to F-0, but the peaks of aluminoferrite phase rise and turn to the direction of C_6A_2F, which are related to five trace components selected into the phase.

5. Effect of iron mud

Addition of iron mud together with fluorite mineralizer provide significantly improves

the burnability and clinker quality. Burnability experiments of raw mixes performed in presence of iron mud compared with other ferrous materials prove the effect of them on clinkering of cement raw mixes to be in following order : iron mud > copper slag > iron powder . Fluorite and iron mud in combination acts as a complex mineralizing agent , producing better results due to combination of CaF_2 with trace components . This composite mineralizer is formed which lowers the temperature of phase transition of solid-liquid phase and reduces the viscosity and surface tension of the liquid phase during the clinkering process and accelerates the rate of ions mobility in liquid and significantly increases the rate of C_3S formation . Based on the results of our laboratory experiments , an industrial production was carried out in six shaft kilns of two plants , for one year and excellent results were obtained . It is found to markedly increase kiln output and quality of clinker as manpower requirement has decreased by improved working of kiln . An increase in kiln output of mean 16.2% corresponded to the coal and electricity saving at mean 4.7% and 13.4% respectively and free lime content also decreased. Beside , raw mixes with iron mud are not only considered as a substitute for all ferrous materials and parts of natural mineral of clay , but also acts as trace composition mineralizer and it has showed significant effect on the output, quality and cost of cement manufacture .

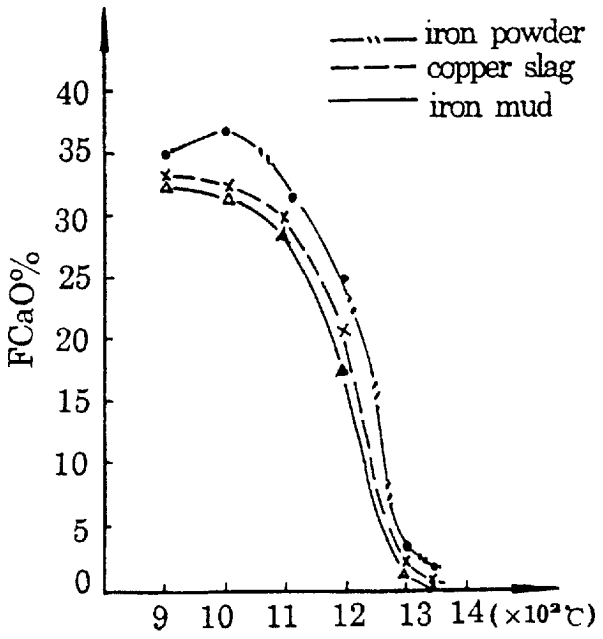

Fig. 4 Influence of iron mud on burnability of raw mix

CONCLUSIONS

1. Five trace components in iron mud increase the combination of cement clinker and this may be attributed to the change of the melt properties through reduction of viscosity and surface tension of melt , and increasing absorption of free lime and accelerating rate of C_3S formation .
2. The results of industrial production experiments indicated that the use of iron mud to produce portland cement can not only promote burnability of raw mixes and achieve fuel saving , but also improve the formation of clinker and the quality of cement .

REFERENCES

Kumar,S.S et al, "Oplimization of burning characteristics of raw meal for fuel economy by special mineraliser", World Cement Technology , Vol. 12 , No. 4 , 1981 . pp 279-285 .

Moir G.K. and Glasser F. P. , "Mineralisers , modifiers and activators in the clinkering process", 9th ICCC . New Delhi , Vol. 1 , 1992 . pp 125-154 .

Moranville-Regourd M. and Boikova A. I., "Chemistry , Structure , properties and quality of clinker", 9th ICCC . New Delhi , Vol. 1 , 1992 . pp 3-48 .

THE POSSIBILITIES OF UTILIZATION OF WASTE AND RAW MATERIALS CONTAINING Al_2O_3, Fe_2O_3, AND TiO_2 FOR OBTAINING FERRATES.

Zofia KONIK, Andrzej STOK and Janusz IWANCIW, University of Mining and Metallurgy, Cracow, Poland

ABSTRACT The waste materials from the alumina production can be succesfully used in the synthesis of low energy cement clinkers.These clinkers are composed mainly of the C_4AF and $C_4A_3\bar{S}$ phases. In this work the low energy clinker from the red mud and other by-product of high Al_2O_3 content corrected with lime was produced. The phase composition studies of sinters to elucidate the conditions of sintering and the studies of hydratation products were carried out.

Waste material utilization, Sintering, Brownmillerite, Aluminate phase, Hydration.

INTRODUCTION

The cements containing C_2S, $C_4A_3\bar{S}$ and C_4AF are produced at lower energy consumption than the normal portland cements, These cements can be manufactured from the waste materials and usually reveal fairly adequate strength.
The waste materials of high Fe_2O_3 and Al_2O_3 contents , for example so-called red muds, can be used in the C_4AF synthesis. On the other hand, the by-products from alumina industry, having significant Al_2O_3 content can be processed to the sulphate-aluminate $C_4A_3\bar{S}$ containing clinker. These two raw materials, mixed at proper proportion and ground, can be used in the production of sulphate-aluminate cement.

EXPERIMENTAL

The C_4AF phase was produced from the red mud, a by-product in the Bayer alumina production method. The chemical composition of this red mud was as follows:

Table 1 Chemical composition of red mud

Compound	Composition [wt. %]
	red mud
LOI	12.4
CaO	2.1
SiO_2	7.4
Al_2O_3	24.4
Fe_2O_3	40.8
SO_3	0.2
MgO	0.4
TiO_2	7.2
Na_2O	4.5

This red mud was enriched with the lime-bearing raw material of 54,8% CaO content. The mixture of the following composition was prepared: red mud -43 %, lime-bearing component -57%. The raw material thus produced was heated at temperatures:1000, 1100, 1200, 1300 and 1350°C respectively, with subsequent rapid cooling. The products burned at 1000 and 1100°C were poorly sintered, while those burned at 1300 and 1350°C were partially or totally molten. This sinters thus obtained were subsequently ground and subjected to the phase composition analysis by XRD. On the XRD patterns of samples produced at 1000 and 1100°C a considerable amount of unreacted CaO was observed, together with the products, such as C_4AF and C_4T_2F. In the sinter heated at 1200 °C free CaO was not detected and the C_4AF phase was found as a main component together with C_4T_2F and some ß C_2S. At higher temperatures , the C_4AF content decrease. In Figure 1 the XRD pattern of the sinter produced at 1200°C is presented.

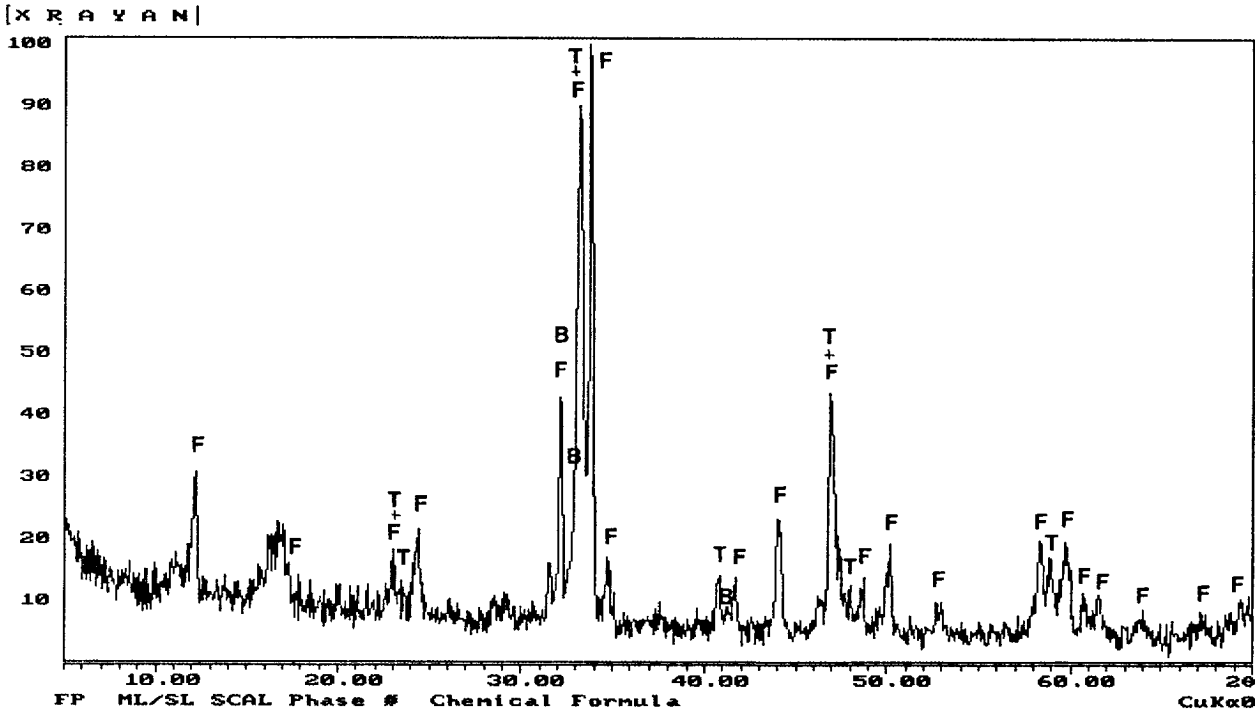

Fig. 1 The XRD pattern of the sinter heated at 1200° C.
F- C_4AF, T- C_4T_2F, B- ß C_2S.

The results of XRD studies have been confirmed by SEM observation.
The C_4A_3S phase was synthesized from the 68% Al_2O_3 containing by-product mixed with lime-bearing component and anhydrite. The raw material thus prepared was subsequently heated at 1250° C. The amount of the C_4A_3S phase in the sintered product has been evaluated for over 70%. The XRD pattern of this sample is shown in Figure 2.
The ground C_4AF and C_4A_3S containing sinters were mixed at 1:1 ratio (without $CaSO_4$ and CaO admixtures), homogenized and hydrated at w/c = 0,33. The rapid setting of cement thus produced occurring within 10 min., was observed (initial setting - 5', final setting - 15').
The samples cured in standart conditions were subjected to the compressive strength tests. The following results have been obtained: 1 day - 11,5 MPa, 3 day - 17,5 MPa, 7 day - 40,8 MPa, 28 day - 48,9 MPa. The standart procedures did not show any undeserable volume changes.
The phase composition determination after 7 days hydration was characterized by XRD.The results are presented in Figure 3.

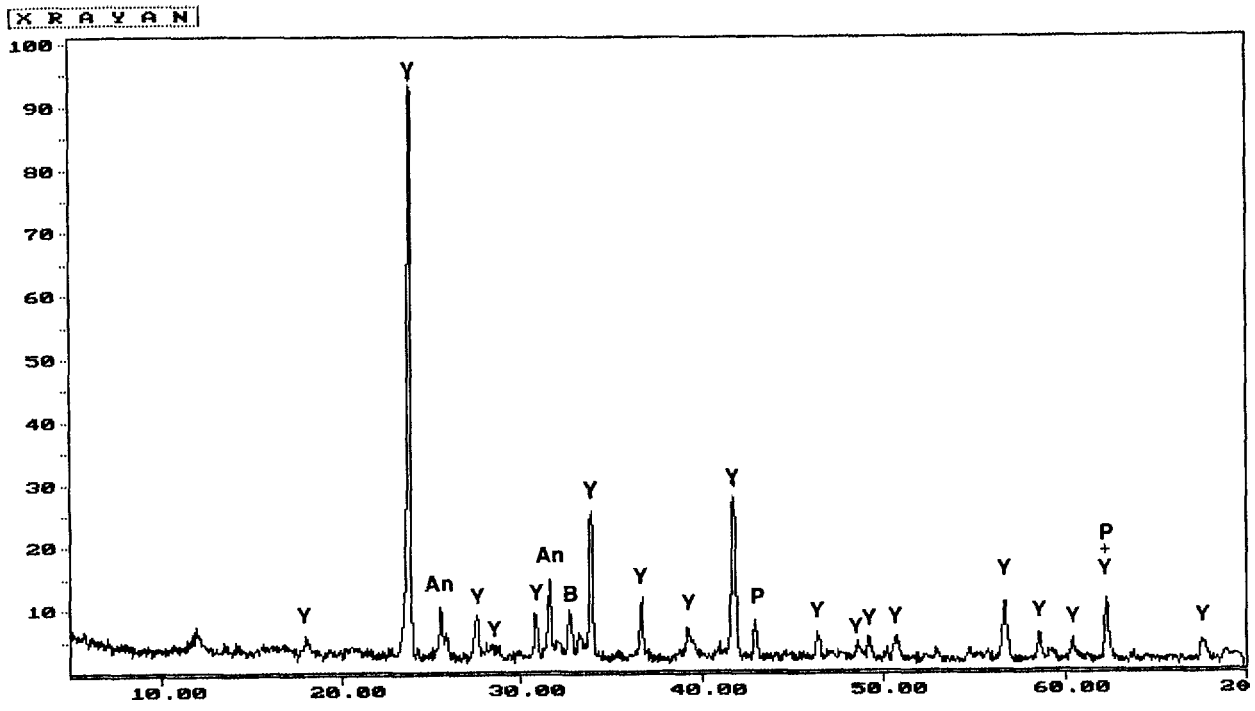

Fig. 2 XRD pattern of $C_4A_3\bar{S}$ containing sinter.
Y - $C_4A_3\bar{S}$ P - MgO B - ß C_2S An - Anhydrite

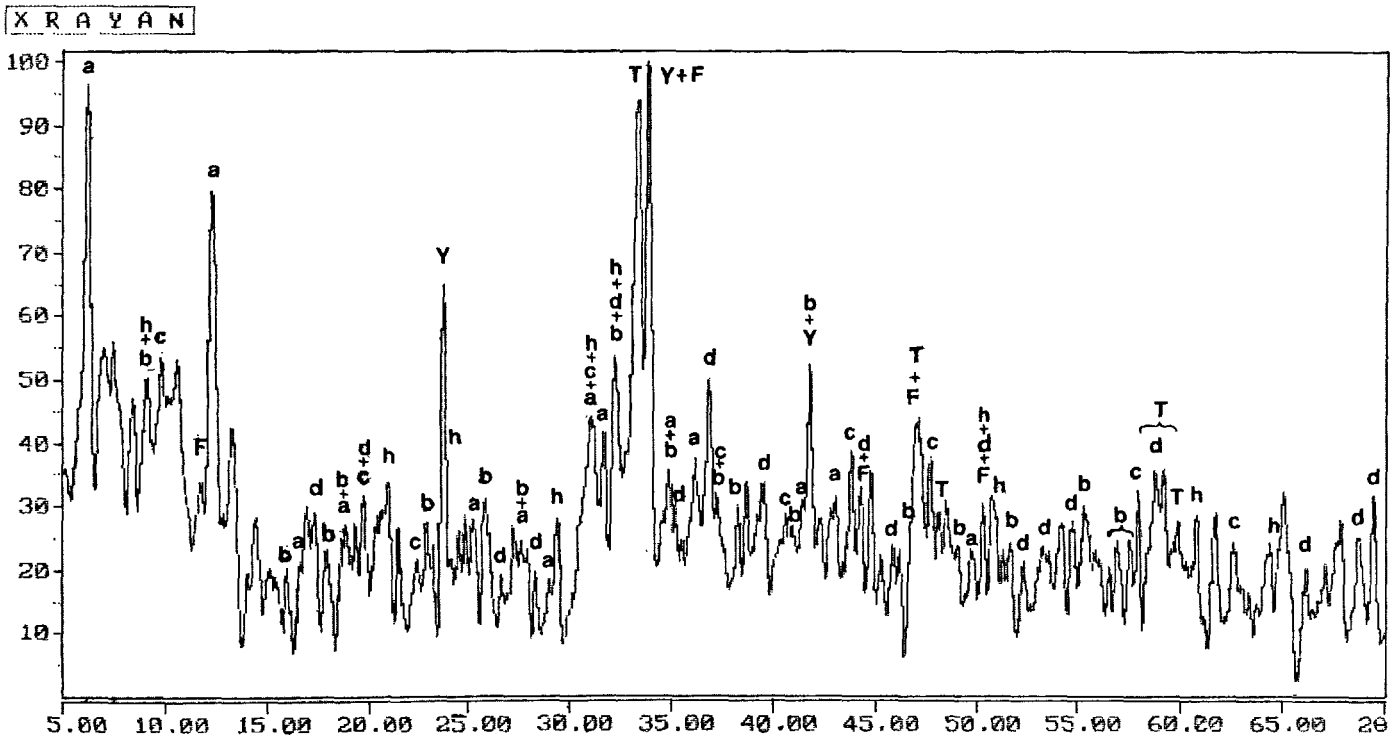

Fig. 3 XRD pattern of 7 days hydrated $C_4AF + C_4A_3\bar{S}$ mixture.
a - CAH_{10} b - $C_3A.(CS)_3.H_{32}$ c - $C_3A.CS.H_{12}$ d - C_3AH_6 h - CSH
F - C_4AF T - C_4T_2F Y - $C_4A_3\bar{S}$

The following hydration products have been found: CAH_{10} , $C_3A.(CS)_3.H_{32}$, $C_3A.CS.H_{12}$, C_3AH_6 and CSH , apart from the residual, unhydrated C_4AF, C_4T_2F and $C_4A_3\bar{S}$ components. The background increase results from the presence of amorphous and poorly crystalline hydration products.

CONCLUSIONS

1. The temperature of reaction between the by-product red mud and lime bearing component to produce the sinter of optimum phase composition was determined for 1200°C. In this temperature C_4AF is formed as a main phase and TiO_2 is bound in the C_4T_2F phase.
2. The mixture of C_4AF and $C_4A_3\bar{S}$ reacts with water to form a significant amount of amorphous and poorly crystalline material. The other, cristalline hydration products are: CAH_{10} , $C_3A.(CS)_3.H_{32}$, $C_3A.CS.H_{12}$, C_3AH_6 and CSH.

REFERENCES

Kurdowski , W. "Chemistry of Cement", ed. Wydawnictwo Naukowe PAN, Warszawa, 1991, pp. 436-439 (in Polish).

Kuzniecowa ,T.W. "Aluminate and Sulpho-Aluminate cements", ed. Stroizdat, Moskwa, 1986. pp. 112-125.

Massazza , F., Daimon M. "Chemistry of Hydration of Cements and Cementitious Systems", 9th International Congress on the Chemistry of Cement, New Delhi, India, 1992, Vol. I, pp. 383-446.

Mubhatkal , G.A., Chatterjee, A.K.. at al, "Non Alite cement from Calcium Sulfoaluminate Clinker, Optimization for High Strength and Low Temperature Application ", Intern. Conference on Chemistry of Cement, Rio, Brasil, 1986, 4, pp 364-370.

Muzhen , S., Kurdowski ,W., Sorrentino, F., "Development in Non-Portland Cements", 9th International Congress on the Chemistry of Cement, New Delhi, India, 1992, Vol. I, pp. 317-352.

Scrivener , K.L., Wieker, W., "Advances in Hydration at Low, Ambient and Elevated Temperatures", 9th International Congress on the Chemistry of Cement, New Delhi ,India,1992, Vol. I, pp. 463-464.

THE APPLICATION OF HIGH MAGNESIUM OXIDE CONTENT LIMESTONE IN CEMENT INDUSTRY

Guojun HU, Department of Materials Science & Engineering, Zhejiang University, Hangzhou 310027, P.R.China

ABSTRACT The burning mechanisms of the clinker and autoclave expansion of cement using the high MgO content limestone have been investigated in this paper. Experimental results show that MgO in clinker mainly occur in alite and belite phases. The amount of MgO solid solution in clinker fluxing mineral increases with the increase in the content of fluxing mineral. During the clinker burning process, the amount of periclase in clinker would be reduced to a minimum under the proper proportion and burning conditions. When the mineral additions are added in cement, the autoclave expansion of the high MgO content cement decreases.

Key-words: MgO, Solid Solution, Burning Conditions of Clinker, Autoclave Soundness

INTRODUCTION

As early as the 19th century, there was great attention on the phenomenon that many concrete buildings broke down, because the free MgO (periclase) in cement hydrates and causes the volume expansion. Periclase hydrates very slowly at room temperature, for example, up to years or longer (Kasselouris et al., 1985). When periclase reacts with water and produces $Mg(OH)_2$, the volume of hardened cement paste expands about 117%. As a result, the hardened cement paste cracks or breaks down. Therefore, the MgO content in cement is limited at the range 2.5~6.0 wt% in many countries (Ramachandran et al., 1981 and Rosa, 1965).

MgO in ordinary portland cement comes from MgO containing minerals that are used in cement clinker production. These minerals decompose into magnesium oxide during calcination. Some of MgO dissolves in a liquid phase and clinker minerals. When the clinker cools, the free MgO forms, which is periclase. But, MgO in the solid solution does not hydrate (Reshi, 1983). The amount of limestone producing portland cement clinker is about 80% of the all raw materials, therefore, MgO mainly comes from carbonated limestone. In order to decrease the MgO content in cement, many companies use the high quality limestone. Most of limestone with high MgO content is rarely used in China, for this reason, it is necessary to consider the problem about the application of high MgO content limestone in cement industry(Hu, 1987).

A great amount of research work has been done on the MgO in cement clinker burning, such as the distribution of MgO in clinker, the effects of burning temperature, cooling condition and the periclase hydrate expansion (Dreizler and Knofel, 1982). The aim of this work is to study the burning mechanisms of the clinker using high MgO content limestone, investigate the producing parameter, and test the autoclave soundness of high MgO content cements.

EXPERIMENTAL

Raw materials

The raw materials used for the preparation of clinker were limestone, clay and iron ore, all of which were of industrial origin. Their chemical composition is shown in Table 1. In accordance with research work, the high MgO content limestone was used in experiments. X-ray analysis

results showed that the mineral composition of high MgO limestone was mainly dolomite [$CaMg(CO_3)_2$] (Hu, 1992).

Table 1 Chemical composition of raw materials (wt%)

	CaO	MgO	Fe_2O_3	Al_2O_3	SiO_2	Loss	Total
Limestone(I)	31.91	17.15	0.37	1.25	4.72	43.05	94.62
Limestone(II)	51.94	0.86	0.14	0.76	2.47	42.20	98.37
Clay	0.27	0.81	8.40	19.24	63.13	6.66	98.51
Iron ore	3.14	1.95	44.24	7.55	34.38	3.04	94.08

Note: Limestone(I) is high MgO content limestone

Raw mix proportioning and burning

In this experiment, two essential components were adopted, which were a) different MgO content and b) different KH value(lime saturation coefficient). The samples were burned in electric furnace at the fixed condition(discused as follow) and cooled quickly in air. Table 2 is the chemical composition of clinkers.

Table 2 Chemical composition and modulus of clinkers

	Chemical composition(wt%)						Modulus		
	CaO	MgO	Fe_2O_3	Al_2O_3	SiO_2	Total	KH	SM	IM
Clinker A	65.18	1.52	4.62	5.96	20.80	98.08	0.921	1.97	1.29
Clinker B	62.88	5.05	4.54	5.40	20.38	98.25	0.921	2.04	1.19
Clinker C	61.78	6.01	4.30	5.25	20.50	97.84	0.899	2.14	1.22
Clinker D	60.57	8.00	4.40	4.93	20.21	98.11	0.899	2.17	1.12
Clinker E	58.42	11.00	4.44	4.44	19.71	98.01	0.898	2.22	1.00
Clinker K86	61.29	4.98	5.17	6.09	20.57	98.10	0.859	1.83	1.18
Clinker K88	61.64	4.99	5.06	6.02	20.27	97.98	0.881	1.83	1.19
Clinker K90	62.03	4.98	4.95	5.94	20.05	97.95	0.899	1.84	1.20
Clinker K92	62.40	5.00	4.99	5.89	19.78	98.06	0.919	1.82	1.18
Clinker K94	62.77	4.98	4.88	5.81	19.56	98.00	0.940	1.83	1.19

Method of clinker analysis

The chemical compositions of clinker and the contents of F-CaO in clinkers were determined by chemical analysis according to Chinese Standard (GB176-87). The contents of MgO in mineral solid solution and F-MgO (periclase) in clinkers were measured by chemical analysis (Building Materials Academy of China, 1989).

Cements

The cement specimens were prepared by intergrinding above clinkers with gypsum (SO_3=1.80 wt% in cement) and different mineral additions--blastfurnace slag or fly ash. The surface area of cements was about 300 cm^2/Kg.

Testing of autoclave soundness of cement

The autoclave soundness of cement neat paste specimens was tested at 2.0 MPa (216 °C) for 3 hours after cured in 100 °C water for 4 hours, according to Chinese standard (GB750-65) (Building Materials Academy of China, 1985).

RESULTS AND DISCUSSION

Study of clinker burning with high MgO content limestone

The clinker containing different MgO content burned

The MgO contents of specimens (clinker A, B, C, D and E) are 1.52 wt%, 5.05 wt%, 6.01 wt%, 8.00 wt% and 11.00 wt% respectively. Samples are burned at 1380 °C for 50 minutes. The MgO contents in different phases of clinker are shown in Table 3.

Table 3 Distribution of MgO in Clinker (wt%)

	Total MgO	F-MgO	MgO in alite and belite	MgO in ferrite phase	MgO in other phases	F-CaO
Clinker A	1.52	0.00	0.86	0.23	0.43	0.26
Clinker B	5.05	2.53	0.92	0.87	0.73	0.74
Clinker C	6.01	3.14	0.74	1.27	0.86	0.32
Clinker D	8.00	4.14	0.73	1.54	1.59	2.15
Clinker E	11.00	6.90	0.74	1.77	1.59	1.96

Note: F-MgO is periclase.

From the X-ray analysis results (Hu, 1992), these five specimens were burned completely and the minerals of clinker were mainly C_3S, C_2S, C_3A and C_4AF. The results of chemical analysis show that the periclase content in clinkers increases with the increasing of MgO content. Besides periclase, remain part of MgO resides in each mineral of clinker. MgO prefer to dissolve in alite and belite phase, and the amount of MgO solid solution is about 1.1 wt% of the total amount of alite and belite phase in clinker.

The clinker burned at different burning temperature

In cement producing process, the clinker would be burned at the range of burning temperature. At the different burning temperature, the minerals of clinker form differently. The distribution of MgO and the formation of periclase also change. Sample C burned at different temperature are studied, the results are shown in table 4.

Table 4 The distribution of MgO of sample C burned at different temperature (wt%) (Burning time is all 50 minutes)

	EXPERIMENTAL Total MgO	F-MgO	MgO in alite and belite	MgO in ferrite phase	MgO in other phases	F-CaO
1200 °C	6.01	5.82	0.12	0.07	0.00	11.50
1250 °C	6.01	5.10	0.12	0.65	0.14	3.30
1300 °C	6.01	3.54	0.48	1.50	0.49	0.26
1350 °C	6.01	3.36	0.74	1.19	0.73	0.14
1375 °C	6.01	3.18	0.72	1.25	0.86	0.14
1380 °C	6.01	3.14	0.74	1.27	0.86	0.32
1400 °C	6.01	2.61	0.72	1.45	1.23	0.16
1420 °C	6.01	1.99	0.74	1.60	1.72	0.12

Below 1300 °C, the mix materials do not burn well, the amount of F-CaO is high and the amount of periclase in clinker is also high. The samples are burned good only when the burning temperature above 1300 °C. In the case, the amount of solid solution of MgO in alite and belite is about 1.1 wt% of the total amount of alite and belite phases. But the amount of solid solution of MgO in ferrite phase and other phases increases with the burning temperature increasing, therefore, the periclase content in clinker greatly reduces. The reason is that MgO can be dissolved in minerals more and more with the burning temperature increasing.

Effect of the different mineral components

During the burning of clinker, due to the different raw materials and burning conditions or the type of clinker, the mineral compositions of clinker change in a certain range. Of course, the amount of MgO solid solution in clinker minerals also changes. When the lime saturation coefficient (KH) increases (modulus SM and IM keeping constant), the amount of fluxing minerals decreases, and the amount of solid solution of MgO in ferrite phase and other phases reduces, therefore, the content of F-MgO in clinker increases(Table 5).

Table 5 Distribution of MgO in clinker with different KH value (wt%)

	KH	Total MgO	F-MgO	MgO in alite and belite	MgO in ferrite phase	MgO in other phases	F-CaO
Clinker K86	0.891	4.98	1.94	0.79	1.21	1.06	0.27
Clinker K88	0.881	4.99	2.43	0.92	0.70	0.90	0.31
Clinker K90	0.899	4.98	2.44	0.94	0.77	0.85	0.67
Clinker K92	0.919	5.00	2.69	0.75	0.71	0.85	2.66
Clinker K94	0.940	4.98	2.96	0.89	0.43	0.72	3.01

The soundness of autoclave of cements containing high MgO content

The soundness of autoclave of cements made by different MgO content clinker

Cements were synthesized by intergrinding different MgO content clinker with gypsum (SO=1.80% in cement). The cement pastes were prepared with a water-cement (w/c) of 0.25 and cured 24 hours at 20±2 °C wet air, then tested the soundness of autoclave(in 100 °C water for 4 hours and at 2.0 Mpa for 3 hours). The test results are shown in Table 6.

Table 6 The expansive rate of autoclave of cements with different MgO content

	Amount in clinker(wt%)		Expansive rate(%)	
	Total MgO	F-MgO	After 4 hours in 100 °C water	After 3 hours at 2.0 MPa
Cement A	1.52	0.00	0.063	0.074
Cement B	5.05	2.53	0.048	0.199
Cement C	6.01	3.14	0.068	0.333
Cement D	8.00	4.14	0.131	broken down
Cement E	11.00	6.90	0.119	broken down

Note: Expansive rate is cement neat paste free expansive value.

It is clear, when the MgO content in clinker is less than 6.0 wt%, the volume expansion causing by periclase hydrated is little. But, when the MgO content in clinker is greater than 6.0 wt%, the cement specimens can not pass the autoclave test. This is the reason why the maximum of MgO content in cement is 6.0 wt% in many country's standards.

The soundness of autoclave of cements with different KH values

From the above experimental results, when the lime saturation coefficient (KH) of clinker increases, F-MgO in clinker increases, then, the autoclave expansive rate of cements produced by these clinkers also increases (Table 7). Because the total amount of MgO in clinker is only 5.0 wt%, these cements can pass the test of soundness of autoclave.

Table 7 The properties of cements with different KH value around autoclave

	Amount in clinker (wt%)		Expansion rate (%)		Compressive strength (MPa)	
	Total MgO	F-MgO	After 4 hours in 100 °C water	After 3 hours at 2.0 MPa	After 4 hours in 100 °C water	After 3 hours at 2.0 MPa
Cement K86	4.98	1.94	0.048	0.154	58.5	52.4
Cement K88	4.99	2.43	0.063	0.168	70.0	45.6
Cement K90	4.98	2.44	0.052	0.198	67.2	51.9
Cement K92	5.00	2.69	0.140	0.310	63.8	36.5
Cement K94	4.98	2.93	0.190	0.376	71.0	39.0

Note: Compressive strength is that of the hardened cement paste ($20x20x20cm^3$)

Because the periclase hydrates and causes expansion, the structure of the hardened cement paste is disturbed to a certain degree. The strength of the hardened cement paste after autoclave reduces. When the periclase content increases, the expansive rate also increases and the strength of the hardened cement paste decreases.

Effect of the mineral additions

Much research work has indicated that, when the mineral additions are added in the high MgO content cement, the expansive rate of autoclave of periclase reduces. There are both physical and chemical effects on above results. The content of F-MgO in cement becomes less because of the adding of the mineral additions. On other hand, these mineral additions absorb the $Mg(OH)_2$, which is the product of periclase hydrating, change the structure of the hardened cement paste, and lessen the expansive rate. Of course, there are different effects with adding of the different mineral additions. The results of Table 8 show that the autoclave expansion of high MgO content cement, which is added blastfurance slag or fly ash, can be restrained effectively. The effect on controlling the autoclave expansion is more obvious with the increasing of the adding amount. For example, the cement D1 containing 8.00 wt% MgO is destroyed after 3 hours autoclave, but the cement D3, D4 and D6, which are added 25 wt% and 40 wt% blastfurnace slag and 30 wt% fly ash respectively, can pass the test of autoclave. The cement E6 with 30 wt% fly ash decreases the autoclave expansion, which is made by the clinker containing 11.00 wt% MgO. The test results also indicate that the fly ash has more obvious effect on controlling the autoclave expansion of high MgO content cement than the blastfurnace slag.

Table 8 The expansive rate of autoclave of cements with adding amount of mineral addition

	Adding amount of mineral addition (wt%)		F-MgO in cement(wt%) (result of account)	Expansive rate (%)	
	Blastfurnace slag	Fly ash		After 4 hours in 100 °C water	After 3 hours at 2.0 MPa
Cement A1	0	0	0	0.063	0.074
Cement A2	13	0	0	0.069	0.080
Cement A3	25	0	0	0.050	0.037
Cement A4	40	0	0	0.060	0.010
Cement A5	0	13	0	0.064	0.027
Cement A6	0	30	0	0.007	-0.028
Cement B1	0	0	2.43	0.048	0.199
Cement B2	13	0	2.10	0.037	0.132
Cement B3	25	0	1.80	0.030	0.096
Cement B4	40	0	1.42	0.067	0.075
Cement B5	0	13	2.10	0.031	0.052
Cement B6	0	30	1.67	0.023	0.007
Cement C1	0	0	3.04	0.068	0.333
Cement C2	13	0	2.61	0.048	0.264
Cement C3	25	0	2.23	0.055	0.124
Cement C4	40	0	1.76	0.055	0.091
Cement C5	0	13	2.61	0.050	0.087
Cement C6	0	30	2.07	0.045	0.021
Cement D1	0	0	3.97	0.131	broken down
Cement D2	13	0	3.35	0.064	broken down
Cement D3	25	0	2.94	0.080	0.361
Cement D4	40	0	2.32	0.066	0.236
Cement D5	0	13	3.35	0.070	broken down
Cement D6	0	30	2.73	0.039	0.206
Cement E1	0	0	6.62	0.119	broken down
Cement E2	13	0	5.73	0.110	broken down
Cement E3	25	0	4.90	0.084	broken down
Cement E4	40	0	3.86	0.064	broken down
Cement E5	0	13	5.73	0.087	broken down
Cement E6	0	30	4.55	0.044	0.718

CONCLUSIONS

In order to use the high MgO content limestone in cement industry, the rational producing parameters should be considered. Experimental results show that MgO in clinker mainly solves in alite and belite phases, and the amount of solid solution is about 1.1 wt% of the total amount of alite and belite phases in clinker. The amount of MgO solid solution in clinker fluxing mineral increases with the increasing of the content of fluxing mineral. During the clinker burning process, the periclase in clinker would be minimum under the proper proportion and burning conditions. Experimental results also show that the specimens of normal portland cement containing less than 6 wt% MgO can pass the autoclave test. When the mineral additions are added in cement, the autoclave expansion of the high MgO content cement becomes less. The previous unsound high MgO content cement can pass the test of soundness.

REFERENCES

Building Materials Academy of China, Physical Test of Cement(in Chinese), Building Industry Publish, Beijing, 1985, p.111.

Building Materials Academy of China, Chemical Analysis of Cement(in Chinese), Building Industry Publish, Beijing, 1989, pp475-496.

Dreizler, I. and **Knofel**, D., Zement-Kalp-Gips, No.10, 1982, pp537-550.

Hu, Guojun, Master Thesis(in Chinese), Zhejiang University, Hangzhou, China, 1987.

Hu, Guojun, Zhejiang Cement(in Chinese), No.4, 1992, pp.5-10.

Kasselouris, V. et al., Cement and concrete Research, Vol.15, No.5, 1985, pp.758-764.

Ramachandran, V.S. et al., Concrete Science--Treatise on Current Research, Heyden & Son Ltd., 1981, pp.401-415.

Reshi, S. S., in Advances in Cement Technology (Edited by S. N. Ghosh), Pergamon Press, London, 1983, pp467-481.

Rosa, J., Zement-Kalk-Gips, Vol.18, 1965, pp.460-471.

SYNTHESIS AND CHARACTERIZATION OF NEW ALKALI-ACTIVATE CEMENTS

R.I.A. MALEK, and D.M. ROY, Materials Research Laboratory, The Pennsylvania State University, University Park, PA. 16802, USA.

ABSTRACT A novel approach to synthesize aluminosilicate cementitious materials has been developed. The new cement utilizes large volumes of waste materials and industrial by-products and can reduce CO_2 emission resulting from decarbonation of limestone and use of fossil fuel in the kiln. Isothermal calorimetry experiments indicated an acceleration of hydration and the strength is nearly equivalent to that of neat cement pastes. The pore structure of the new systems is finer than normal cement and the reactivities towards alkali-silica reaction are minimal. The magic angle NMR studies indicate that Si/Al ratio is 1-1.3.

Key-words: Aluminosilicate, carbon dioxide, Nuclear Magnetic Resonance, synthesis, zeolites.

INTRODUCTION

There is no longer any doubt that we are entering a period in which the CO_2 emission to the environment must be regulated. The cement industry constitutes the largest volume among manufactured materials in the world and is one of the major contributors to carbon dioxide in the atmosphere. This is the result of decomposition of calcite and use of fossil fuel in the kiln during cement manufacture. In the last two decades, there has been an increasing interest in the use of alkali activated materials as substitutes of Portland cement. Originally, it was limited to the activation of granulated slags using alkali metal hydroxides (Purdon, 1940), but recently the alkali activated cements have been extended to include several industrial by-products and wastes. Therefore, developing means to utilize large volumes of waste materials in blended cements for the construction of infrastructure and other building projects should provide significant economic and environmental benefits (Malek and Roy et al, 1986, 1987a, 1987b and 1993). The use of alkali-activated slags as a binder has significantly increased in recent years. Various national and international standards allow different contents of ground granulated slag in the blends with cement: up to 65% in Great Britain and USA; 70% in Japan; and 80% in Germany, Russian republics, and Czechoslovakia (Roy and Malek, 1993). The chemical activation of slag by different metal salts such as calcium or sodium sulfates or chlorides is sometimes used. Very interesting are the rapid hardening mixtures of slag + fly ash + gypsum + cement or lime (Davidovits, 1983) the purpose of which is to economize the building materials costs and the energy. Thermal activation of slag without chemical activators is another possibility. Roy et al., 1992, summarized studies of Portland cement alkali-activated blends.

A new class of binders is formed by mixing some form of alkaline activator with a wide variety of silicate and/or aluminum rich minerals and glasses to form aluminosilicate frameworks. Therefore different fine-grained alumino-silicates (clay, ground rock, ash, slag) can be used as raw materials. The possible mechanism involves the chemical reaction of aluminosilicate with alkalis and alkali polysilicate yielding polymeric or crystalline Si--O--Al bonds. The new class of aluminosilicate cementitious materials can reduce CO_2 emission resulting from manufacture of Portland cement. It has an advantage over the traditional pozzolanic cementitious materials by being potentially zeolitic in nature which makes it particularly useful in trapping hazardous ions as in the case of radioactive waste disposal and in fixation of the alkali metal ions responsible for alkali-silica (aggregate) reaction. The new cement utilizes large volumes of waste materials and industrial by products such as slags and fly ash and should provide significant economic and environmental benefits.

The durability of aluminosilicate structures arises from the fact that they may form three dimensional networks that encompass the entire structure through chemical bonding. This structure is potentially more durable than the hydrated Portland cement in which the strength is mostly mechanical through foiled sheets of calcium silicate hydrate. Because of the difference in charge between Si and Al, a balancing positive charge must be present for each aluminum in the structure. The existence of positively charged ions in their structure offers an advantage to fix alkali metal cations such including radioactive ions.

The purpose of this paper is to report on the preliminary results on the nature of phases formed and their durability. The effect of these phases on the long-term engineering properties is discussed. In the present investigation, two systems were studied, namely, a low-calcium and a high-calcium systems. A new approach to formulate these systems was followed by adjusting the Si/Al ratio to be nearly equivalent to natural aluminosilicate materials. Additional blends were made with Portland cement.

EXPERIMENTAL

A broad range of alkali-activated aluminosilicate frameworks was prepared with target composition of variable n and m in the formula:

$$\frac{n}{x} M^{x+} [(SiO_2)_m (AlO_2)_n] \cdot yH_2O \qquad [1]$$

where M is an alkali or alkaline earth metal cation. Two systems were studied, namely, low-calcium and high-calcium systems. The low-calcium system is composed of metakaolinite, Class-F fly ash, potassium silicate and potassium hydroxide. The high-calcium system is composed of metakaolinite, Class-C fly ash, ground granulated blast-furnace slag, potassium silicate and potassium hydroxide. Two and three dimensional composition diagrams were used to design the target compositions. Figs. 1 and 2 represent the composition diagrams for aluminosilicate mixtures presented in the present paper, where x = 1, n = 1, and m = 4, for both low-calcium and high-calcium formulations. Blends with cement were prepared as follows:

a. Portland Cement 80% + high-calcium cement 20%
b. Portland Cement 50% + high-calcium cement 50%
c. Portland Cement 80% + low-calcium cement 20%
d. Portland Cement 50% + low-calcium cement 50%

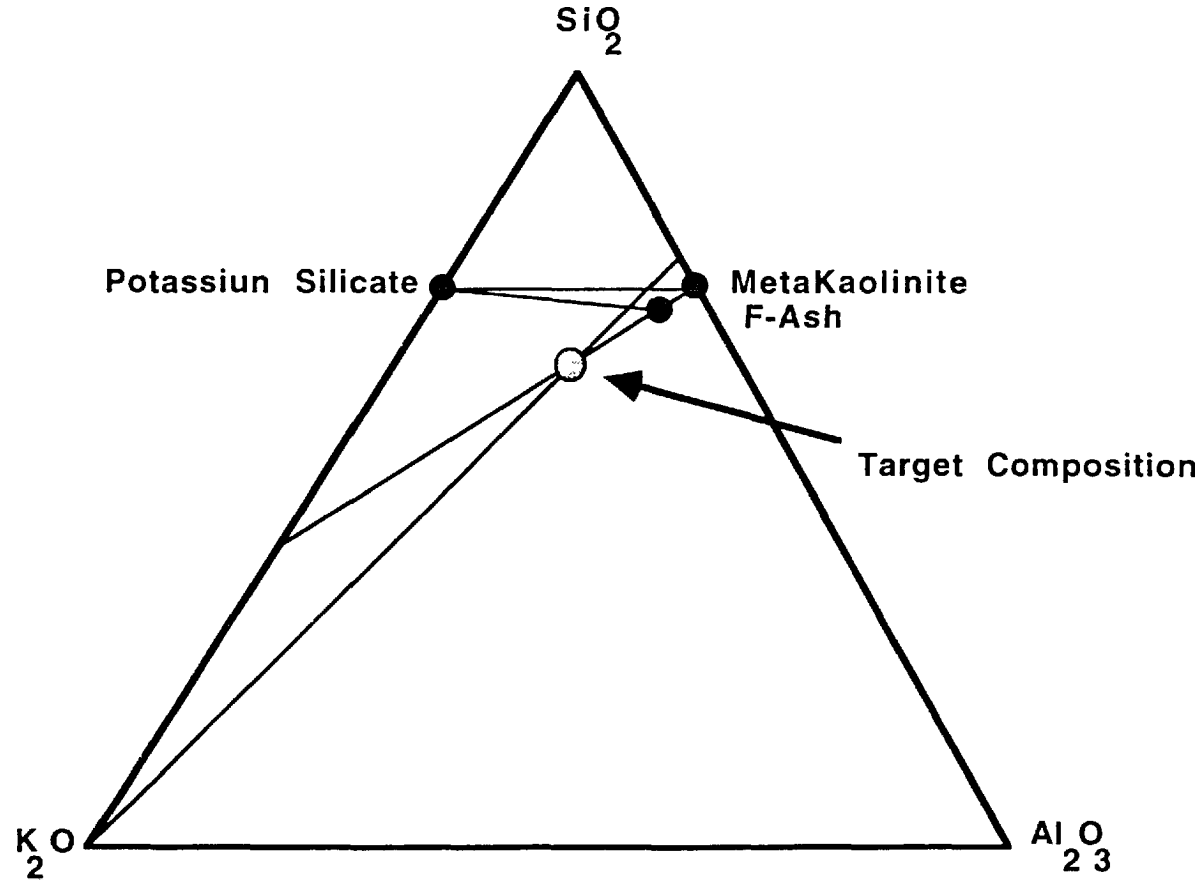

Figure 1. K_2O-SiO_2-Al_2O_3 diagram showing target composition (x=1, n=1, m=4) and components used in formulating the low-calcium aluminosilicate cementitious materials.

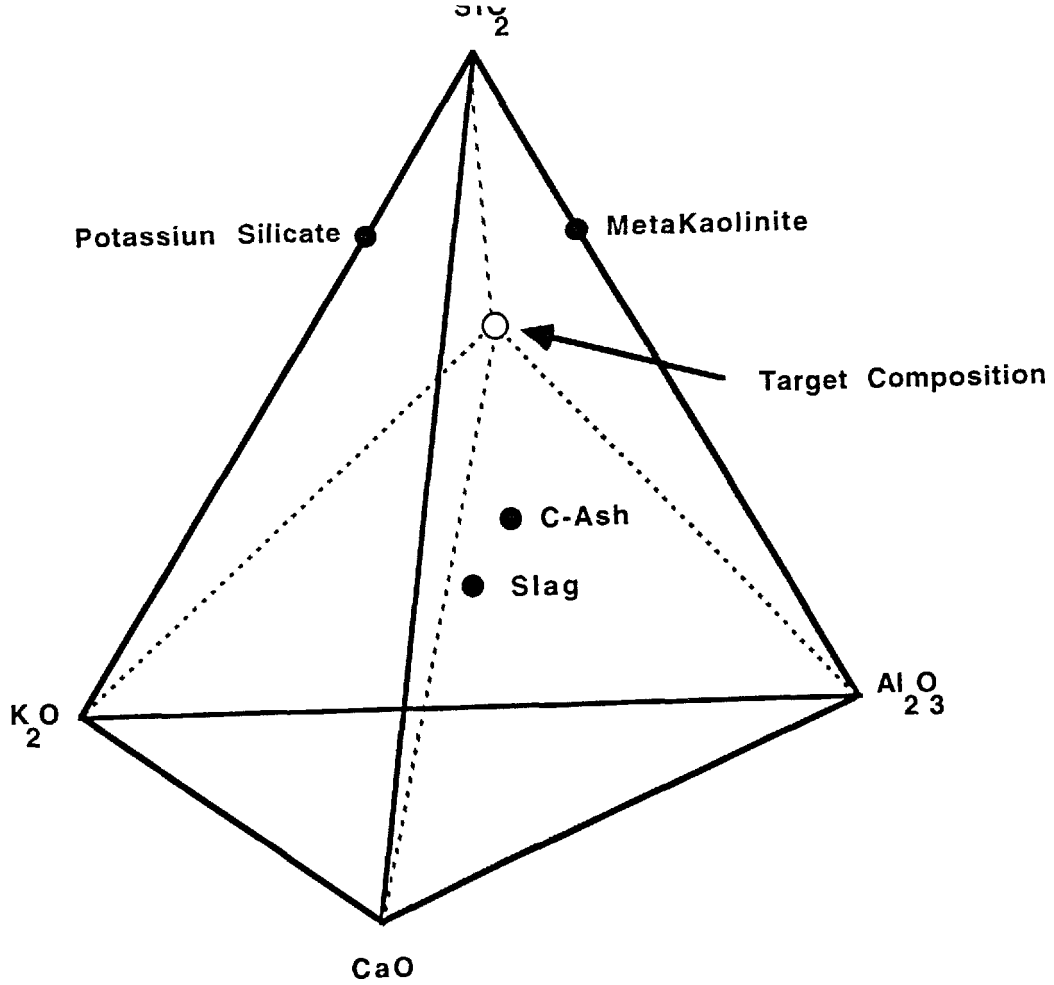

Figure 2. K_2O-CaO-SiO_2-Al_2O_3 diagram showing target composition (x=1, n=1, m=4) and components used in formulating the high-calcium aluminosilicate cementitious materials.

The water content was adjusted to obtain workable pastes (0.35 in the samples presented in this paper). Samples were cured at 38° and 100% saturated humidity. Properties of the samples were monitored, and characterized by various methods. These methods include investigation of mechanical and physical properties. The evolution of the pore system in comparison with plain Portland cement was also made. Mortar bar expansion tests were made according to ASTM C227 standard for alkali-aggregate reactivity using Beltane Opal as a reactive aggregate.

Although naturally occurring aluminosilicate structures are highly crystalline, their formation into cementitious materials is expected to be almost always in a micro crystalline form with crystal dimensions of the order of microns, or at low temperatures, amorphous structures with only short-range order. In addition, the lack of Si, Al ordering means that only average structures will be obtained from diffraction measurements. The solid-state, high-resolution NMR spectroscopy has emerged as a powerful technique for structural investigations of these materials. Solid-state ^{29}Si and ^{27}Al magic angle NMR spectroscopy was used to characterize the products. The spectra were obtained at 7.04T using a Chemagnetics CMX-300 spectrometer. The ^{29}Si spectra were obtained at 59.08 MHz with a 90° pulse and a recycle delay time of 30s. The ^{29}Si shifts were referenced to tetramethylsilane (TMS). The ^{27}Al spectra were collected at 77.48 MHz with a 90° pulse of 5 ms and a recycle time of 2 s. The ^{27}Al chemical shifts were measured with reference to a 1M aqueous solution of $[Al(H_2O)_6]^{3+}$. The ^{29}Si magic angle spinning (MAS) NMR spectra of these systems are expected to show one or a combination of five resonances corresponding to the five local silicon environments: Q^4(4 Al), Q^4(3 Al), Q^4(2 Al), Q^4(1 Al), and Q^4. Al atoms in the framework are always in tetrahedral sites and the ^{27}Al MAS NMR spectra should show single resonances characteristically at 40-60 ppm. Octahedrally coordinated aluminum gives rise to signals at ~0 ppm.

RESULTS AND DISCUSSION

Isothermal calorimetry data of the cement pastes containing 50% of low-calcium and high-calcium blends at 38°C are presented in Figs 3 together with those of neat Portland cement paste for comparison. This figure shows the gradual increase in reactivity as the extent of potassium increases.

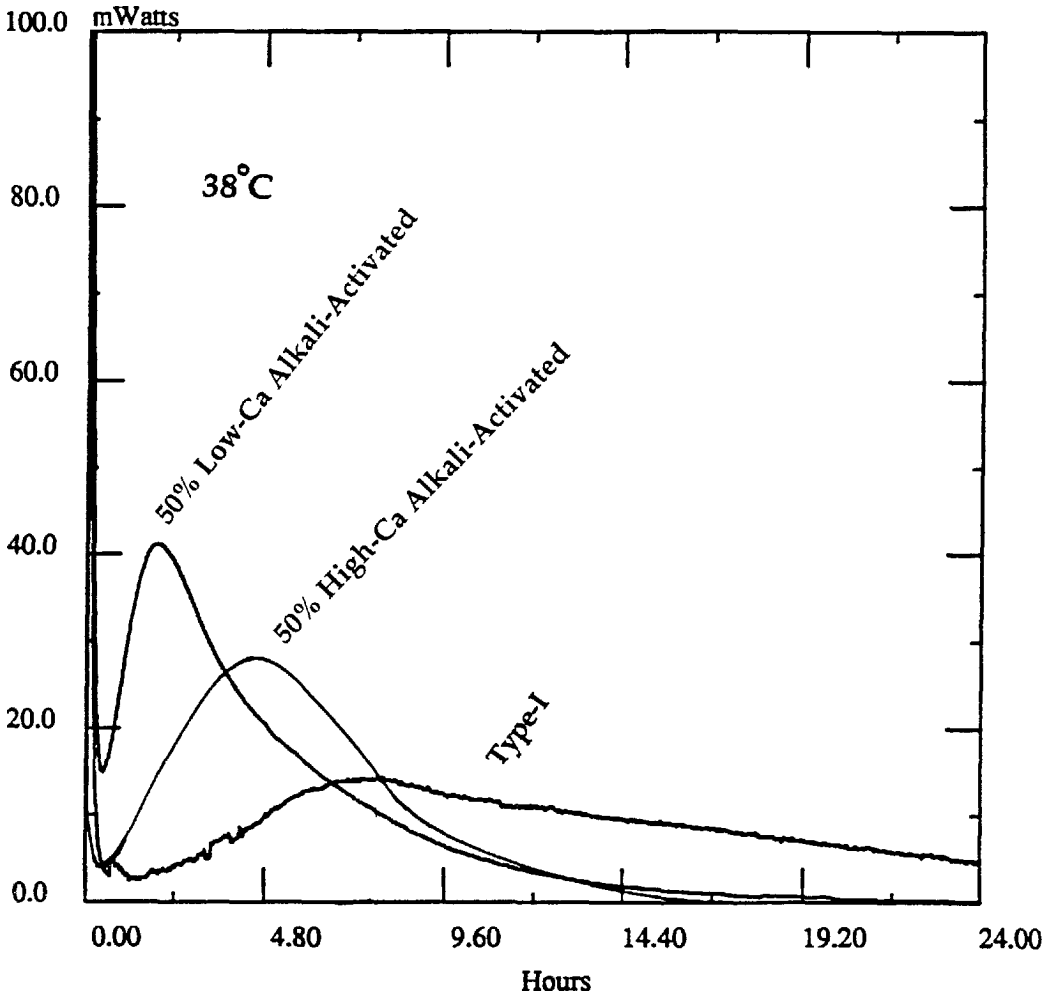

Figure 3. Isothermal calorimetry data of 50% low-calcium and 50% high-calcium materials together with that of neat cement.

Compressive strength data at 7 and 14 days for samples cured at 38°C are presented in Figs 4 and 5, respectively. In these figures, the compressive strength data on neat Portland cement pastes and a commercially available aluminosilicate binder (Pyrament) at the same age and temperature are included for comparison. It is evident that the compressive strength values of cement pastes containing 20% and 50% of high-calcium materials are equivalent to those of neat cement pastes and slightly exceed those of the Pyrament. The corresponding blends made with low-calcium materials are lower in strength but their strength seems to increase with time. The pore structure evolution has been studied by mercury intrusion porosimetry. Results of pore size distributions at 14 days of the blends containing 50% alkali activated materials cured at 38°C are presented in Fig 6. In the same figure, the pore size distribution of the neat cement paste at the same age and curing temperature is shown. It is evident that the alkali activated systems develop a finer pore structure compared to neat cement pastes. In addition, the blends with high-calcium materials seems developing the finest pore structure, possibly because they are more fully reacted. The 28-day mortar bar expansion using ASTM C-227 to test potential alkali-silica reaction are presented in Fig 7. Results of high alkali cement (1.2% Na_2O equivalent), Type-I Portland cement with potassium hydroxide (3% by weight) and Pyrament are included for comparison. It is clear that the alkali activated aluminosilicate materials gave the lowest reaction with silica.

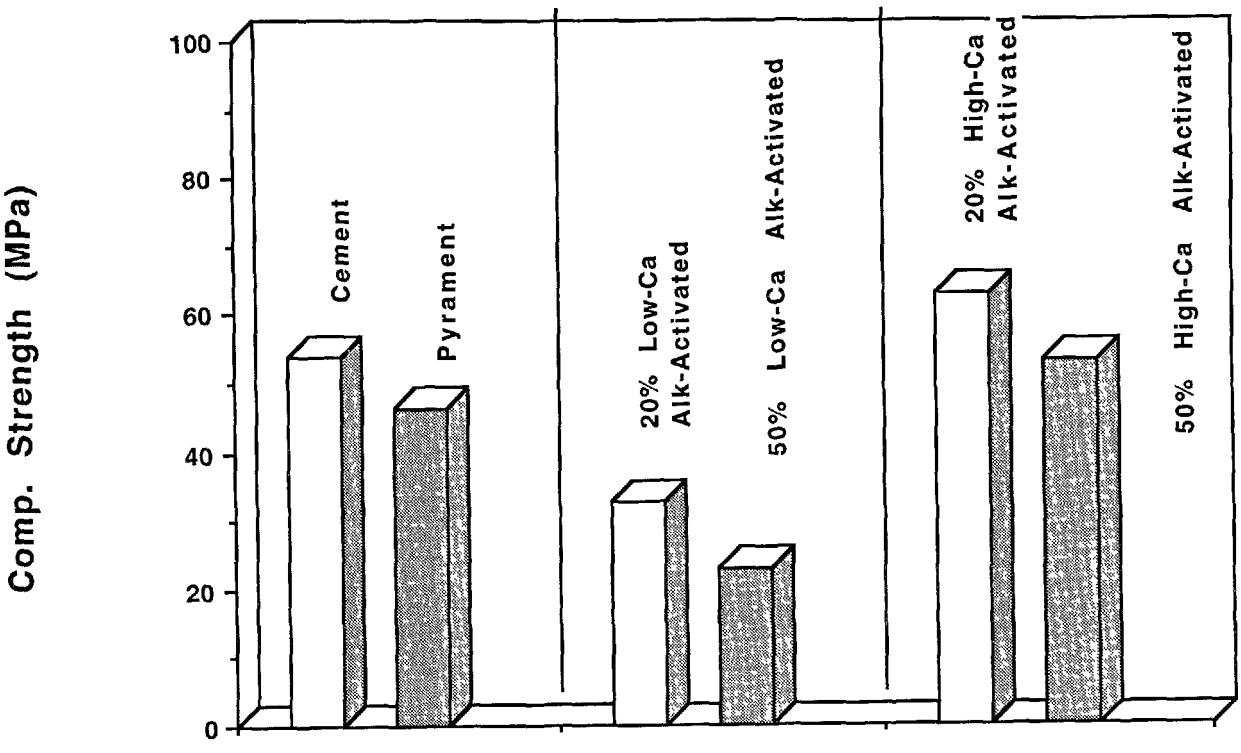

Figure 4. Compressive strength of low-calcium, high-calcium blends, Portland cement, and Pyrament at 7 days, 38°C.

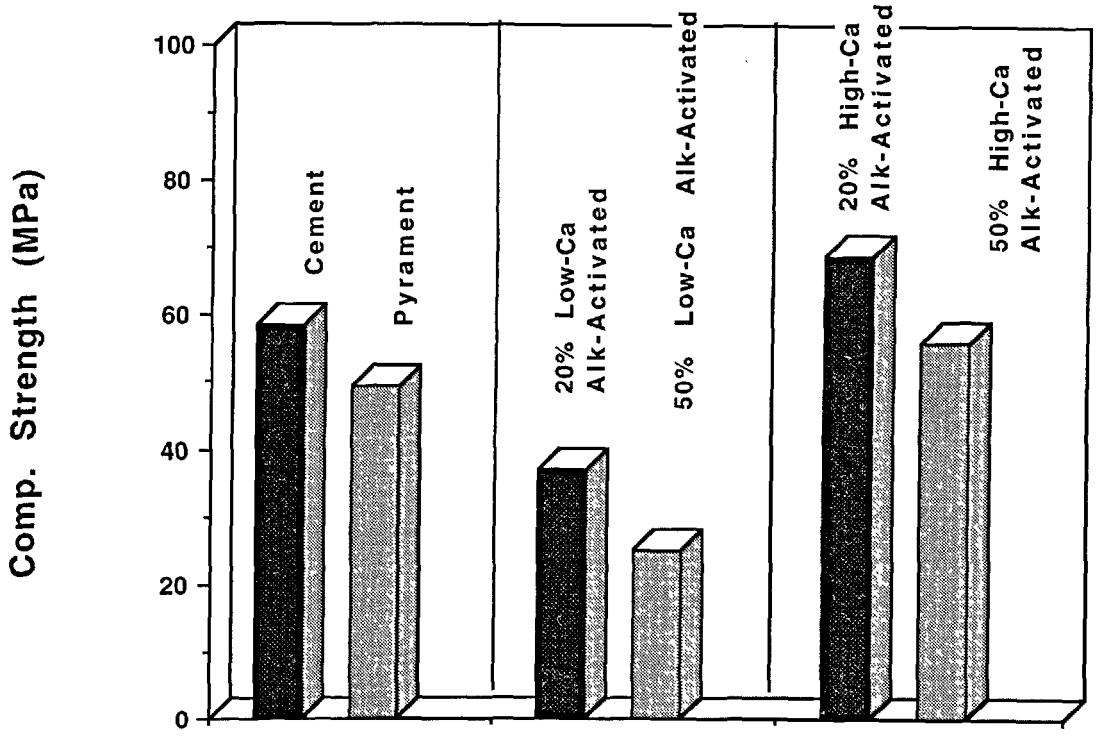

Figure 5. Compressive strength of the low-calcium, high-calcium blends, neat Portland cement, and Pyrament at 14 days, 38°C.

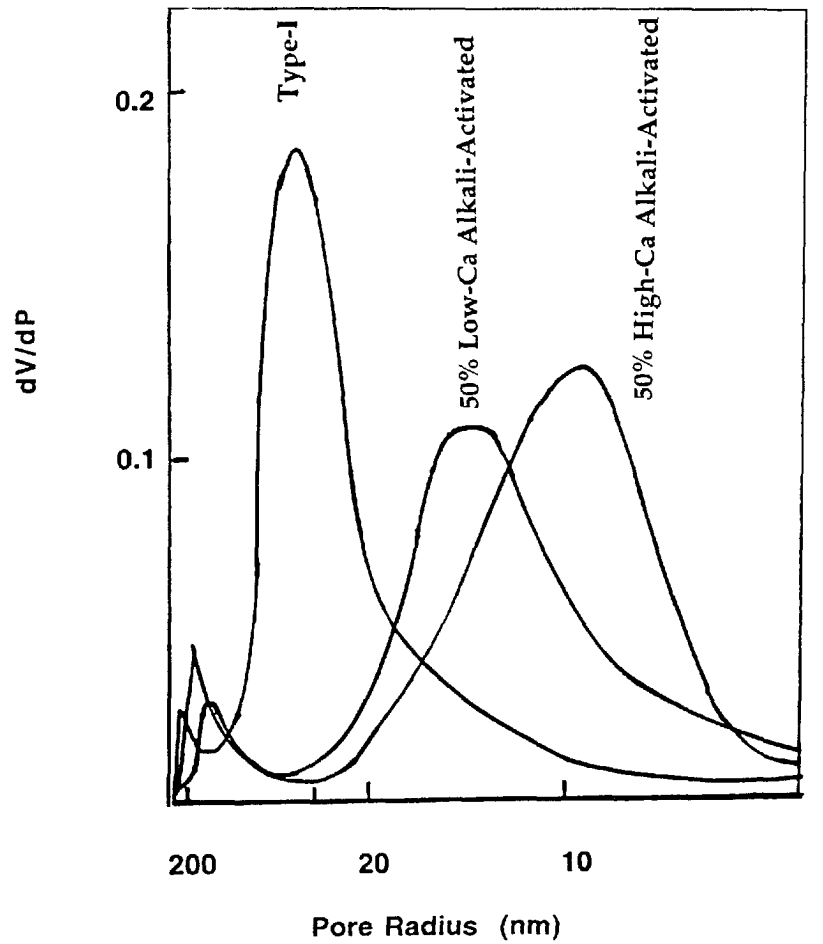

Figure 6. Pore size distribution of low-calcium and high-calcium blends together with those of neat Portland cement paste cured for 14 days at 38°C.

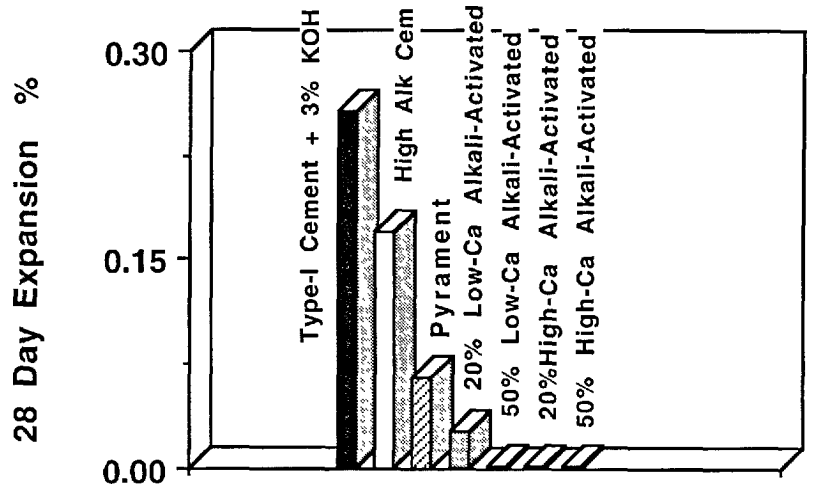

Figure 7. 28-days mortar bar expansions (ASTM C-227) for testing alkali-silica reaction.

The ^{29}Si magic angle NMR spectroscopy of the low-calcium materials cured for 14 days at 38°C is shown in Fig 8. The same figure contains a simulation of the zeolitic peaks Q^n (nAl). The spectrum shows two major features: a broad peak centered at about - 83 ppm arises from the silicoaluminate species Q^4 (4 Al). The broad nature of this peak is an indication of the disordered micro crystalline structure (x-ray amorphous). The other feature is the presence of a series of minor resonances ranging from - 92 ppm to -102 ppm arising from other aluminosilicate species. The peak locations and assignments were estimated and are given in Table I.

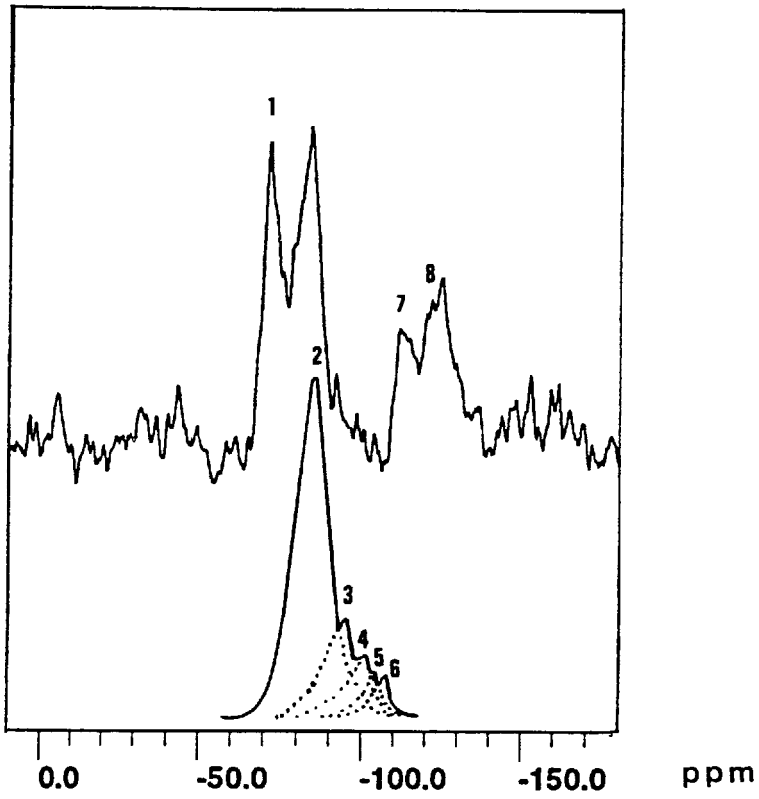

Figure 8. Observed and simulated ^{29}Si magic angle NMR spectroscopy of the low-calcium materials cured for 14 days at 38°C. Peak assignments are given in Table I.

Table I. Calculated parameters of ^{29}Si magic angle NMR spectrum of the low-calcium material cured for 14 days at 38°C.

Peak number	Peak location, ppm	Peak assignment	% Area*
1	- 72	Monomeric SiO_2	
2	- 83	Q^4 (4 Al)	81.4
3	- 92	Q^4 (3 Al)	11.0
4	- 98	Q^4 (2 Al)	3.3
5	- 100	Q^4 (1 Al)	3.2
6	- 102	Q^4	1.1
7	- 110	Unreacted SiO_2	
8	- 1 20	Unreacted SiO_2	

* Peak areas are calculated for the zeolitic peaks only Q^n (n Al).

The relative zeolitic peak areas as calculated from a deconvolution procedure and their relative areas are also given in Table I. The Si/Al ratios were calculated using the relation:

$$Si/Al = \sum_{n=0}^{4} I_{Si}(n\,Al) \Big/ \sum_{n=0}^{4} \frac{n}{4} I_{Si}(n\,Al) \qquad [2]$$

It was found that the Si/Al ratio of K-activated structures is 1.3. In an attempt to find the structure that corresponds to this Si/Al ratio, a comparison was made to known structures that have closest Si/Al ratio. It has been found that the structure of low-Ca materials lies between or a mixture of $KAlSi_2O_6.nH_2O$ (Si/Al = 2) and $KAlSiO_4.nH_2O$ (Si/Al = 1). The spectrum of high-Ca shows a broad peak centered at about -84 ppm. Curve fitting procedures indicate that this peak is a

characteristic of aluminosilicate frameworks with Si/Al ratio of 1 (Fyfe et al, 1991). Comparing this with aluminosilicate structures of the same Si/Al, it was found that the high-Ca structures could be assigned to the formula (K,Ca) $Al_3(SiO_4).nH_2O$. It should be noted that the NMR results reflects the local environments of the Si atoms averaged throughout the structure and do not necessarily imply any simple long-range ordering. Therefore, the low Si/Al ratios predicted from NMR results [m/n ratio = 4 in formula 1] are due to the short-range ordering of these structures. The ^{27}Al magic angle NMR spectroscopy indicates that Al exists in both octahedral and tetrahedral positions in both structures.

The durability of aluminosilicate structures arises from the fact that they exist in three dimensional networks that encompass the entire structure through chemical bonding. This structure is more durable than the hydrated cement in which the strength is mostly mechanical through foiled sheets of calcium silicate hydrate. Because of the difference in charge between Si and Al, a balancing positive charge must be present for each aluminum in the structure. The existence of positively charged ions in their structure explains the ability of these materials to minimize the extent of alkali-silica reaction through tie-in of the alkali metal cations (Malek and Roy, 1983).

CONCLUSIONS

Aluminosilicate materials were developed as an attempt to provide an option to Portland cement with building materials of equivalent or better properties. The synthesized aluminosilicate materials provide significant economic and environmental benefits through reducing the CO_2 emission and utilizing industrial wastes for the construction. The aluminosilicate materials are three dimensional durable frameworks formed by chemical bonding. They fix alkali metal ions in their structure offering an advantage to minimize the extent of alkali-silica reaction.

ACKNOWLEDGMENT

This research has been supported by the US Environmental Protection Agency, Grant # 819482.

REFERENCES

Davidovits, J., "Geopolymers II, processing and applications of ultra high temperature, inorganic matrix resin for cast composite structures, molds and tools for RP/C and metal industries," Proceedings of the Society of Plastic Engineering, "PACTEC '83", Anaheim, CA, 1983, pp. 222-230.

Davidovits, J.,"Geopolymers," University of Tech., Compiegne France,V.2,1989, pp. 149-168

Fyfe, C.A., Feng, Y., Grondy, H., Kototailo, G. and Gies, H.,"One- and Two-Dimensional High-Resolution Solid-State NMR Studies of Zeolite Lattice Structures," Chem. Rev.,No. 91,1991,pp.1525-43.

Malek, R.I.A. and Roy, D.M., "Effect of slag cements and aggregate type on alkali-aggregate reaction and its mechanisms," Proceedings of the International Conference "Alkalis in Concrete, Research and Practice", Eds. G.M. Idorn and S. Rostam, Danish Concrete Association, Kopenhaven, Denmark, 1983,pp. 223-230.

Malek, R.I.A., Roy, D.M., Licastro, P.H. and Langton, C. "Slag cement-low level radioactive waste forms at Savannah River plant," Ceramic Bulletin, No. 65, 1986, pp. 1578-1583.

Malek, R.I.A. and Roy, D.M., "Electrochemical stability of embedded steel and toxic elements in fly ash/cement beds," Proceedings of the Materials Research Society Symposia, No. 86, "Fly Ash and Coal Conversion By-products: Characterization, Utilization, and Disposal III," Eds. G.J. McCarthy, F.P. Glasser, D.M. Roy and S. Diamond, Materials Research Society, Pittsburgh, PA, 1987a, pp. 59-65.

Malek, R.I.A., Roy, D.M. and Licastro, P.H. "Diffusion of chloride ions in fly ash/cement pastes and mortars", Proceedings of the Materials Research Society Symposia, No. 8 "Microstructural Development During the Hydration of Cement," Eds. L. Struble and P. Brown, Materials Research Society, Pittsburgh, PA, 1987b, pp. 223-231.

Purdon, A."The Action of Alkalis on Blast-Furnace Slag," J. Soc. Cem. Ind., 59,1940,191-202.

Roy, D.M., et al., "Alkali-Activated Materials: An Overview," Materials Research Society, Symp. Proc., Vol. 245, 1992, pp 153-164.

Roy, D.M. and Malek, R.I.A., "Hydration of Slag Cement," Progress in Cement and Concrete Series, No. 4, Chapter 2, ABI 1993, pp. 84-117.

CALCIUM SULPHOALUMINATE CEMENTS PREPARED FROM LOW-ALUMINA WATERWORKS SLIME

Ko IKEDA, Kunio FUKUDA and Hiromi SHIMA
Department of Advanced Materials Science and Engineering,
Yamaguchi University, Ube 755, Japan.

ABSTRACT Calcium sulphoaluminate cements have been prepared from waterworks slime comprising low-alumina by firing clinkers at 1100℃and 1200℃ with subsequent dosage of much gypsum to the cements. Although compressive strength up to 34.2MPa was reached at 28 d age by paste hydration at W/S 0.40, instability of strength was encountered for some specimens probably due to morphological changes of ettringite during hydration.

Key-words: Sulphoaluminate, Waste material utilization, Ettringite.

INTRODUCTION

Calcium sulphoaluminate cements, henceforth called CSAC's, were originally studied by Viswanathan et al.(1978) and have been practically applied in some countries where bauxite is available to use for alumina source. Much attention has been paid on CSAC's firstly because of low firing temperature and secondly because of less requirement of limestone than for Portland cements in manufacture (Takuma et al.,1994). These properties are all favorable to the environmental conservation in view of saving energy and less emission of carbon dioxide. Mineral compositions of CSAC's are generally characterized by C_4A_3S(Al-hauyne) and belite with minor association of calcium aluminates such as CA and $C_{12}A_7$ and calcium ferrite, although there is a variety enriched in iron to form much amount of C_4AF (Mehta, 1980). So many types of CSAC's can be produced with variable amount of Al-hauyne. When the content of this mineral is high, cements show high early strength. On the contrary, when it is low, the early strength becomes low (Mehta, 1980, Ikeda, 1980). CSAC's are sulphate resistant (Viswanathan et al., 1978) and show good affinity with Portland cement constructions to be repaired so urgently (Chatterjee, oral commun.). Furthermore, CSAC's can be increased in quantity by second dosage of calcium sulphates such as gypsum in quite large amounts after pulverizing the clinkers(Ikeda, 1981, Ikeda et al., 1993, 1994).

In waterworks generally source water is treated with aqueous aluminum polychloride to supply clear water. By this treatment suspending clayey fines are coagulated to sink as slimes and discarded to damping yards after some dewatering processes. The slimes are enriched with alumina-component more or less, generally in the form of gibbsite gel due to hydrolysis of the added polychloride and are considered to be unsuitable to vegetation due to inharmonious chemical compositions with surroundings, when discarded.

CSAC's have superior characters as mentioned, but the most serious problem may be the bauxite whose occurrence is restricted to small number of countries. To cope with

Table 1 Typical chemical compositions for waterworks slimes as dry, in %.

Slime	SiO_2	TiO_2	Al_2O_3	Fe_2O_3	MnO	CaO	MgO	Na_2O	K_2O	P_2O_5	SO_3	LOI	TOTAL
NA-1	38.12	0.51	25.94	5.28	0.19	24.84	1.22	0.65	1.53	1.38	0.28	0.20	100.14
HI-1	40.85	0.34	45.68	5.00	0.79	1.25	0.80	0.51	1.03	0.64	0.23	2.84	99.96
AS-2	25.64	0.21	55.97	3.64	3.87	0.90	0.57	0.29	0.90	3.13	0.63	4.26	100.01

this problem substitutes for bauxite such as anorthosite rocks (Viswanathan et al., 1978), fly ashes (Ikeda, 1984, Sahu and Majling, 1994), multicombination of wastes (Beretka, 1992), dusts of aluminum sash productions and high-alumina blast furnace slags have been studied and above all, the latter two are practically applied in real manufacture. Recently we studied CSAC's prepared from alumina-rich waterworks slimes as the substitutes and successful results were obtained (Ikeda et al., 1993, 1994). In this paper CSAC's will be studied by using alumina-poor waterworks slime with special emphasis to the second dosage of gypsum to the cements.

EXPERIMENTAL

Chemical compositions typical to waterworks slimes are represented in Table 1. In this study NA-1 was used by mixing with appropriate amounts of gypsum and portlandite according to the computer program developed in our laboratory to minimize the amount of free lime based on the chemical compositions of the slime analyzed by the ICP technique as seen in Table 2. The raw meal as mixed was kept for 3 d to dryness at ambient temperature for easy handling which was attainable by forming ettringite, since the slime was wet. After this treatment clinkers were burnt at 1100℃ and 1200℃ for 1 h, each designated as clinkers A and B or cements A and B. Then, the clinkers were pulverized by a pot mill to obtain cements. Finally 2 series and 8 kinds of cements were prepared by blending gypsum as listed in Table 3.

Pastes were prepared by using small scale molds having 1 x 1 x 4 cm dimension. Water to solid ratio, W/S was 0.40 for all specimens. Curings of specimens were performed in 20℃ air having 100 % R.H. for the first day encased with the molds and then, in 20℃ water after demolding at 1 d age. Strength tests were performed at 1 d, 3 d, 7 d and 28 d ages, respectively, for both flexural and compressive strengths, using the 3 prismatic specimens to obtain average values. The span length was 2.5 cm for the 3-point flexural tests. The fractured pieces were collected to store in acetone and then, examined by the XRD and SEM techniques at need as well as the source materials and the raw meal. The amounts of free lime and anhydrite remaining in the clinkers were determined by conventional techniques, ammonium acetate titration and qualitative XRD, respectively.

RESULTS AND DISCUSSION

Waterworks slime and subsidiary sources

Chemical compositions of the waterworks slime, NA-1 are characterized by relatively small amount of alumina and high content of silica vice versa (Table 1). The alumina to silica weight ratio, A/S, considered to be a measure of possible application is 0.68, which may be nearly the lower limit for practical use (Ikeda, 1980). In addition, this slime contains high amount of lime originating from the

Table 2 Physicochemical characteristics of source materials and raw meal.

	Specific surface area, Blaine, cm^2/g	Bulk density, g/cm^3	Mixing proportion of raw meal, %
Slime, NA-1	25000	2.06	78.09
Gypsum	4200	2.32	4.23
Portlandite	15400	2.20	17.68

Chemical composition of raw meal, % dry base.

SiO_2	30.95	MnO	0.16	K_2O	1.24
TiO_2	0.42	CaO	35.53	P_2O_5	1.12
Al_2O_3	21.07	MgO	0.99	SO_3	3.71
Fe_2O_3	4.28	Na_2O	0.53		

* As dry base and water content of the wet slime is 73.8 %.
Al_2O_3/SiO_2 weight ratio, A/S = 0.68
JIS 1st grade chemicals were used for gypsum and portlandite.

dewatering process in waterworks. Kaolinite, illite and quartz were identified in the slime by XRD, all originating from the geology of river system in the basin concerned. In addition, presence of tetracalcium hydrate, C_4AH_{13} was observed. This may be attributed to the in situ reaction between gibbsite gel derived from the hydrolysis of aluminum polychloride and slaked lime added to. Therefore, we consider no free gibbsite gel remains in this slime, different from usual slimes. Values of water content and specific surface area are very high as seen in Table 2 where physical characteristics of other sources are also tabulated.

Pretreatment of raw meal

The mixing proportion of source materials is shown in Table 2. Formation of ettringite takes place with consumption of added gypsum and portlandite. The reaction terminated in 3 d and the raw meal became completely dry. On this stage no trace of gypsum was detected, while considerably large amount of remaining portlandite was noted after the reaction at ambient temperature.

Clinker minerals

Formations of Al-hauyne and belite in β -form are obviously seen with minor association of calcium aluminate, CA and sulphospurrite irrespective of firing temperatures as seen in Fig 1. Slight free lime and anhydrite were detected to remain as indicated in Table 3. Potential clinker minerals are tabulated in Table 3 on the basis of computer calculation.

Grindability of clinkers

Present clinkers were very easy to grind. This property is reflected to the fineness of cements represented in Table 3, especially for clinker A due to low temperature firing and also due to very fine character of the waterworks slime itself. We could not prepare cements having standard specific surface area around 3000 g/cm^2 on account of these reasons. Furthermore, we could not prepare pastes for A-0, probably caused by the ultrafine character of cement A. This was improved by second dosage of gypsum. Therefore, we consider the reason of hard kneading is attributed to the free lime included as much as 3.41 percent in clinker A. If remaining anhydrite was much

Table 3 Physical characteristics and mineral compositions of present cements.

	Specific surface area, cm^2/g	Bulk density, g/cm^3	Free lime and anhydrite Percent	
Cement A	8900	3.08	3.41	0.74
Cement B	4300	3.01	2.93	0.35
Potential clinker minerals common to cements A and B, in percent.				
C_4A_3S	C_2S-C_3P	CA	C_2F	
24.51	65.93	4.33	5.23	
C_2S-C_3P: solid solution (C_3P=3CaO.P_2O_5), belite in β -form.				
Derivative cements with gypsum dosage represented by numerals in %.				
A-series (A-0, A-50, A-80, A-100)		B-series (B-0, B-50, B-80, B-100)		

more in the clinker, A-0 pastes could be prepared.

Strength of pastes

Results of strength tests are summarized in Fig 2. Pastes could not be prepared for A-O due to hard kneading caused by very fast setting as mentioned above. Generally, the strength was higher for A-series than for B-series. A-50 showed high early strength and 35.4MPa was reached at 7 d age. However, slight instability of strength was observed between 7 and 28 d ages, especially to flexural strength. Too much dosage of gypsum makes the strength low as seen for A-80 and A-100.

B-0 showed moderately high early strength, but marked depression of strength was observed in both flexural and compressive strengths. This defect was improved by the second dosage of gypsum as seen in B-80 and B-100, showing smooth development of strength against age. However, the strength was not so high, around 15MPa in compressive strength even at 28 d age. Free lime up to 9 percent is permitted in CSAC clinkers, if clinkers contain sufficient amount of anhydrite (Sudoh et al., 1980). Therefore, more enrichment of anhydrite as well as free lime in clinkers may promote the strength as achieved by Sahu et al., 1994.

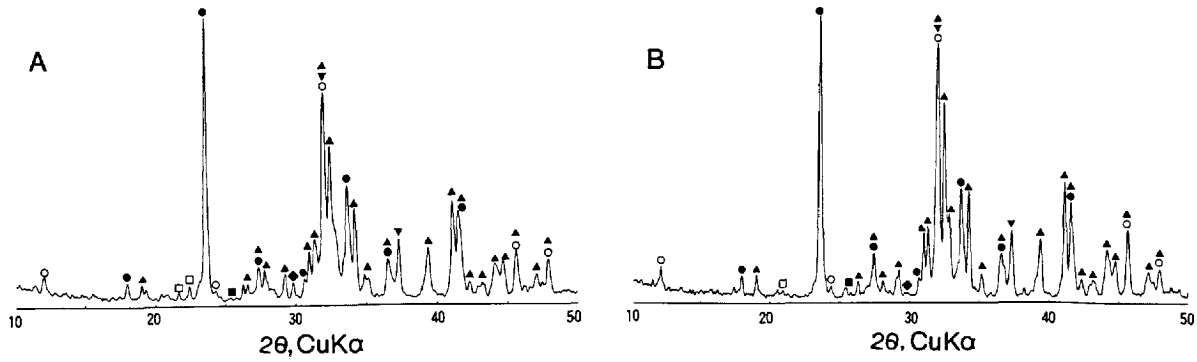

Figure 1 XRD diagrams for clinkers A and B.
● C_4A_3S, ▲ β - C_2S, ◆CA, ○ C_2F, □ C_5S_2S, ■ CS

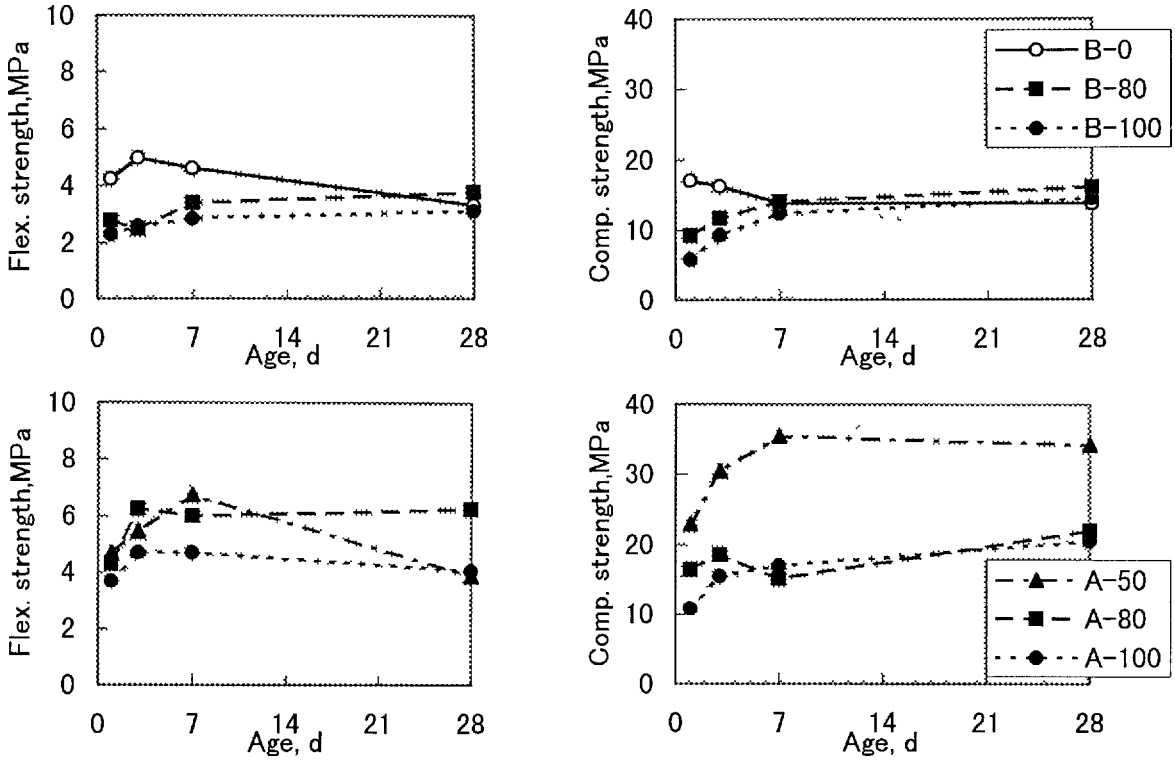

Figure 2 Flexural and compressive strengths for cements A and B.

Hydrates

Basically as tabulated in Table 4, enhanced formation of ettringite associated with minor formations of calcium monosulphate hydrate and/or CAH_{10} was observed throughout all specimens except B-0 where formation of stratringite was detected instead of ettringite. Formation of C-S-H was uncertain by XRD due to the ill-crystalline nature of this mineral, but it was detected in some pictures by SEM. Gypsum remained in abundance even in advanced age. Al-hauyne was not detected in entire range of age due to the rapid hydration nature of this mineral, while abundant C_2S was detected to remain in entire range of age.

Morphological changes of ettringite

This phenomenon is noteworthy in relation to the instability of strength. Ettringites appeared in acicular shapes in the first 1 d humid air-curings with no exceptions. After the 1 d curings, hardened bodies were demolded and saoked in water for subsequent water-curings. On this stage, cracks were suddenly generated

Table 4 Hydrates identified by XRD for 28 d age specimens.

	A-0	A-50	A-80	A-100	B-0	B-50	B-80	B-100
$C_6A\overline{S}_3H_{32}$	*	+++	++	++	-	++	++	++
$C_4A\overline{S}H_{12}$	*	+	+	+	-	+	-	+
CAH_{10}	*	+	-	+	-	+	-	+
C_2ASH_8	*	-	-	-	+	-	-	-

+++ enhanced, ++ moderate, + small, - nil in relative XRD intensities.
C-S-H was not clearly detected by XRD. * No data due to hard kneading.

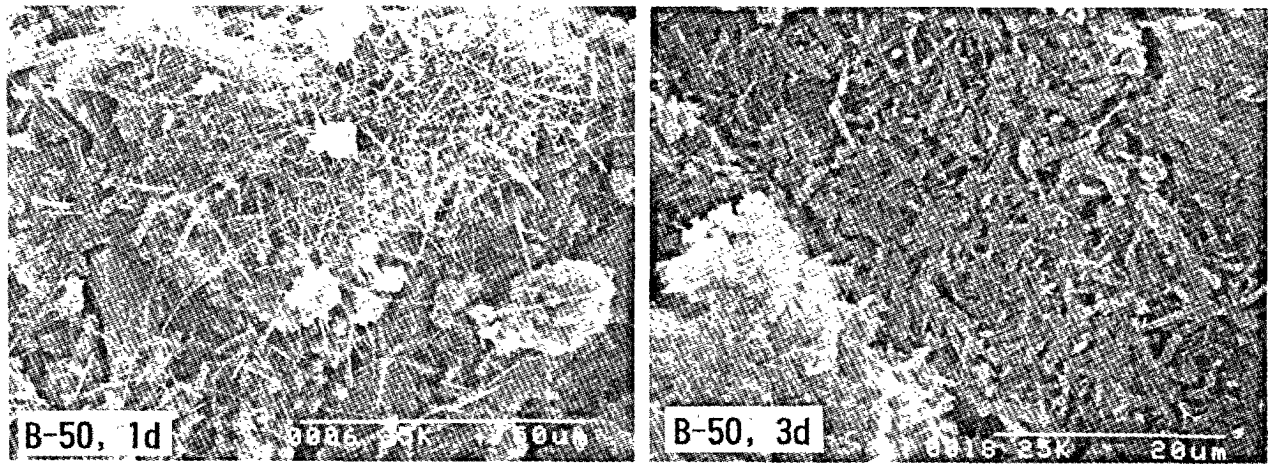

Figure 3 SEM photomicrographs showing morphological change of ettringite.

for specimens B-50 due to well-known expansion caused by ettringites. No cracks were observed in specimens other than specimens B-50. At the moment just after 3 d age, we found drastic changes of morphology of ettringites from acicular to prismatic or acicular to fibre-like for A-series specimens, and from acicular to fibre-like or from acicular to lath-like for B-series specimens. Namely, all specimens were subjected to the morphological changes continuously during water curings. However, the transformations from acicular to lath-like were concentrated at 3 d age and only limited to B-series specimens. The ettringites exhibiting the lath-like shapes were always seen around gypsums in foot print textures as indicated in Fig 3. Therefore, We consider that these morphological changes took place by the through-solution mechanism.

Namely, the original acicular ettringites precipitated from Al-hauyne and gypsum via solution became unstable due to supplying Ca^{2+} ions from belite and precipitated around gypsums in lath-like shapes. Thereby, some volume expansion of ettringite may take place. If the specimens concerned have not sufficient resistance against the expansion on this stage, they will brake. In this respect, B-series specimens all may have a fate of disintegration, but some compensation of voids may take place in B-80 and B-100 specimens due to including much more gypsum. This situation may be the same to A-series specimens. However, cement A has very high specific surface area so that initial hydration may take place under the strong influence of belite hydration from the beginning, releasing more Ca^{2+} ions into the solution. We consider that the differences of transformation schemes of ettringites originate from the differences of initial Ca^{2+} concentrations in solutions. The strength depressions occurring in some gypsum containing specimens may also be related to these transformation phenomena.

Stratlingite

In B-0 hydration, which was not added with second gypsum, stratlingites were found instead of ettringites as encountered in previous study (Ikeda et al., 1994), (Table 4). Initial hydration strength of B-0 was moderately high, but the strength decreased in later age. This may be attributed to crystal size growth of stratlingites as seen in Fig 4, resulting more pore volumes. We did not detected marked presence

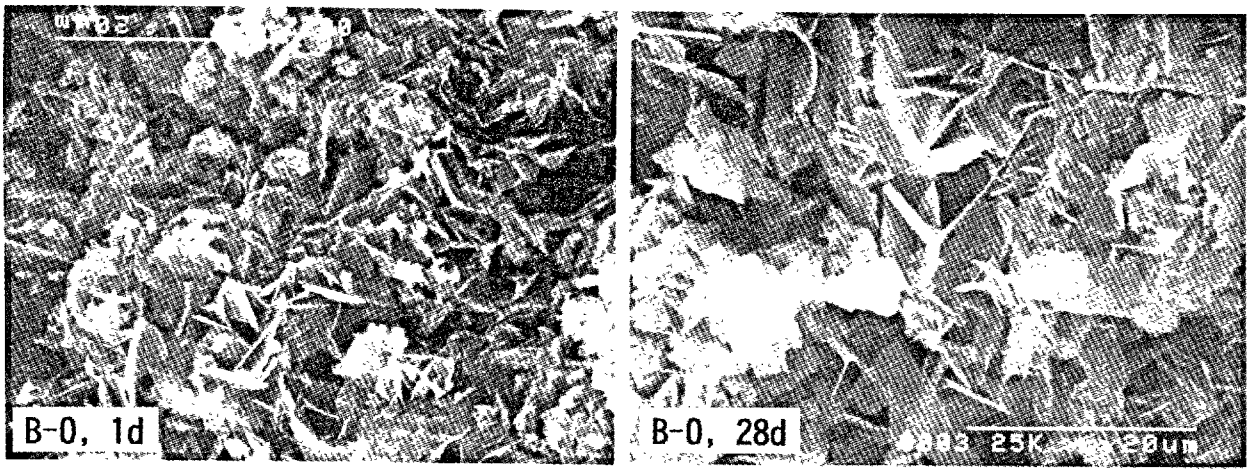

Figure 4 SEM photomicrographs showing development of stratringite.

of monosulphates. Therefore, we believe sulphate ions are incorpotated into the stratlingites.

CONCLUSION

Following conclusions have been drawn in this study.

(1) CSAC's can be prepared from low-alumina waterworks slimes by firing at 1100℃.

(2) Clinkers fired at 1100℃ show high grindability and high specific surface areas of cements around 9000 cm^2/g were reached with ease.

(3) Such finely pulverized cements show hard kneading, which can be improved by second dosage of gypsum as much as 50% to the cements, resulting high early strength, 22.9 MPa at 1 d age by paste hydration at 0.40 W/S.

(4) Clinkers fired at 1200℃ show not so high grindability as 1100℃ ones due to more sintering, resulting less strength and sometimes with cracks, which was discussed in relation to the morphological changes of ettringites from acicular to lath-like.

(5) Some depressions of strength encountered in advanced age may also be caused by the morphological changes of ettringites from acicular to prismatic or from acicular to fibrous, which have more room to be investigated precisely.

REFERENCES

Beretka, J.,Santoro,L.,Sherman,N.and Valenti,G.L.,"Synthesis and Properties of Low Energy Cements Based on $C_4A_3\overline{S}$",Proc. 9th Inter.Cong.Chem.Cem.,New Delhi,Vol.3,1992,pp.195-200.

Ikeda,K.,"Cements along the Join $C_4A_3\overline{S}$-C_2S",Proc. 7th Inter.Cong.Chem.Cem., Paris,Vol.2,1980,pp Ⅲ.31-Ⅲ.36.

Ikeda,K.,"Improvement of the Strength of Hauyne-Belite Cement by the Addition of

Calcium Sulphates",Yogyo-Kyokai-Shi,Vol.89,No.1,1981,pp.54-55.
Ikeda,K.,"Hauyne-Belite Cements Utilizing Fly Ash",Yogyo-Kyokai-Shi, Vol.92,No.10,1984,pp.592-599.
Ikeda,K.,Matsui,H.and Tashiro,C.,"High Performance Novel Cements Prepared fromWaterworks Slime Enriched in Alumina",APCChE & CHEMECA 93 Official Proc., Melbourne,Vol.2,1993,pp.531.2-535.2.
Ikeda,K.,Matsui,H.and Tashiro,C.,"Calcium Sulfoaluminate Cements Prepared from Waterworks Slime",Ceramic Trans.,vol.40,1994,pp.289-296.
Mehta,P.K.,"Investigations on Energy-Saving Cements",World Cement Technology, Vol.11,No.5.,May,1980,pp.166-177.
Sahu,S. and Majling,J.,"Preparation of Sulphoaluminate Belite Cement from Fly Ash",Cem.Con.Res.,Vol.24,No.6,1994,pp.1065-1072.
Sudoh,G.,Ohta,T.and Harada,H.,"High Strength Cement in the CaO-Al_2O_3-SiO_2-SO_3 System and its Application", Proc.7th Inter.Cong.Chem.Cem.,Paris,Vol.3,1980,pp. V.152-V.157.
Takuma,Y.,Shirasaka,T.,Kanaya,M.,Kobayashi,K.and Uchida,S.,"Effect of Reducing the Emission of CO_2 and the Characters of Clinker in the System C_2S-$C_4A_3\overline{S}$-C_4AF-CS", J.Ceram.Soc.Japan,Vol.102,No.12,1994,pp.1115-1121.
Viswanathan,V.N.,Raina,S.J.and Chatterjee,A.K.,"An Exploratory Investigation on Porsal Cement",World Cement Technology,Vol.9,No.3,May-June,1978,pp.109-118.

POSSIBILITIES OF UTILIZING HIGH SO_3 FLUIDIZED BED ASH IN THE PRODUCTION OF PORTLAND CLINKER AND CEMENT

Ivan ODLER and Hua ZHANG, Technical University Clausthal, Clausthal-Zellerfeld, Germany

ABSTRACT A Portland cement clinker may be produced by burning a raw meal made from a high SO_3 fluidized bed ash and limestone, with added fluorspar, at temperatures lower than those common in the production of conventional clinkers. Such clinker contains most of the present SO_3 in form of the phase C_4A_3s, which is formed at the expense of C_3A. Cements made from such clinker exhibit a strength development and expansion similar to those of conventional Portland cements, whereas the setting time tends to be shortened and the initial hydration heat liberation enhanced.

INTRODUCTION

In the burning of coal in conventional power plants fly ash is produced as the main solid residue. The amount of sulfur in conventional fly ashes is usually low, as most of the sulfur that had been present in the coal is converted to SO_2 and escapes into the environment with the flue gas. The produced fly ash may be used either as a raw meal constituent in the production of Portland clinker, or as a pozzolanic constituent in the production of blended cements, or it may be added directly to concrete mixes to replace a part of cement and fine aggregate.

In recent years a variety of "clean" burning technologies has been developed, in which the SO_2 is either absorbed from the flue gas, or is prevented from being formed by binding the sulfur of the coal within the produced ash. Among the latter technologies those based on fluidized bed combustion found greatest acceptance and are being already widely used. Here, pulverized coal is burnt, after being blended with adequate amounts of limestone, at temperatures of about 850°C. Under these conditions the sulfur present in the fuel is converted to calcium sulfate (anhydrite II) and remains in this form in the formed ash.

Fluidized bed ashes differ distinctly from conventional fly ashes. In addition to calcium sulfate, whose amount depends on the sulfur content of the used fuel, they contain also distinct amounts of free calcium oxide, as limestone must be introduced in over-stoichiometric amounts, to assure a sufficient reduction of SO_2 emission. Due to the reduced burning temperature, a glass phase, normally present in conventional fly ashes, is absent in fluidized bed ashes. Instead, the clay minerals, originally present in the coal, remain preserved, though in partially decomposed form. Other constituents typically present in fluidized bed ashes include quartz, iron oxides, some residual calcium carbonate and residual carbon.

Even though fluidized bed ashes exhibit a distinct hydraulicity/pozzolanicity, they can be used as constituents of blended cements or added to concrete mixes only in limited amounts, due to their high SO_3 content. They are also not suitable to be used as constituents of raw meals in the production of conventional Portland cement clinkers, as elevated SO_3 contents in the raw meal are known to impede or even prevent the formation of the C_3S phase and along with it to increase the free lime content in clinker. In addition, a noticeable thermal dissociation of the anhydrite present in the ash, associated with an escape of sulfur oxide, takes place at temperatures common in clinker burning. Thus, alternative solutions for their use must be sought, to avoid costs associated with their disposal.

In our previous work (Odler and Zhang, 1996), performed with pure chemicals, we found that well burnt clinkers may be produced from raw mixes with high calcium sulfate contents if small amounts of calcium fluoride are added to the mix and the burning temperature is reduced to about 1250-1300°C. Such clinkers contain side by side the phases C_3S and C_4A_3s and may contain, in addition, also the phases C_2S, C_4AF and even C_3A. At the same time the free lime content may be reduced to acceptable levels. Based on these results, within the present work we studied the possibility of using high SO_3 fluidized bed ash in the production of Portland cement. To adjust the oxidic composition of the raw mix the used ash was blended with calcium carbonate. The properties of the resultant cement were conpared with those of a standard Portland cement of a well defined composition.

CLINKER PREPARATION

As starting materials an ash from a fluidized bed combustion unit, installed in a German power plant, was employed. The composition of the ash is given in Table I. The ash was blended with powdered calcium carbonate in a ratio ash : carbonate = 1 : 1.62 . 1.0 per cent of CaF_2 was added to the resultant mix. Te raw mix was burnt in batches of 300g. It was placed into a Pt-dish and burnt in an electric furnace (heating rate: 10°C/min.; max. temperature: 1230°C; burning at max. temperature: 30 min.; cooling in air). In a similar way a reference clinker with a potential phase composition of 70% C_3S and 10% of each C_2S, C_3A and C_4AF was burnt at 1450°C.

By X-ray diffraction the phases C_3S, C_2S, C_3A and C_4AF were identified in the reference clinker and C_3S, C_4AF and C_4A_3s in the experimental high SO_3 clinker. To determine quantitatively the phase composition of the produced experimental clinker, the free CaO was analyzed by the Franke extraction method, the C_3S phase, together with free lime, was dissolved in a methanolic salicylic acid solution, and the mutual ratio of C_4AF and C_4A_33 in the extraction residue was estimated by X-ray diffraction. Table I. shows the phase composition of the clinker found this way, as well as the oxidic composition of the whole clinker and the two fractions separated by salicylic acid extraction.

The texture of the produced experimental clinker was studied by back scatter electron imaging, after impregnating the sample with a low viscosity epoxy resin. As may be seen from Figure 1, the clinker exhibited a significant porosity, unlike conventional Portland clinkers produced at higher burning temperatures.

The grindability of the produced clinkers was assessed by grinding 50 g of the material, precrushed to a size 1-2 mm, in a laboratory swing mill and plotting the Blaine specific surface area of the product as function of grinding time. From Figure 2 it is apparent that the grindability of the experimental high SO_3 clinker was significantly better than that of the reference, apparently due to its great porosity.

CEMENT PROPERTIES

To determine the "optimum gypsum" value, a series of cements was prepared by grinding the experimental clinker with variable gypsum additions to a specific surface area of 300 m^2/Kg. Figure 3 shows the compressive strength of pastes made from these cements (w/c=0.30) after different hydration times. It appears, that after 1 and 3 days the highest strengths were obtained in the cement ground without added gypsum, whereas the 28 day strength was highest in the cement with amounts of gypsum corresponding to 2 % SO_3. An acceptable rheology and normal setting of the pastes was observed both with and without gypsum interground with the cement.

For further studies a cement integround with 2 per cent of SO_3 (as gypsum) was employed. Its setting time was determined with the Vicat method. The strength development was studied on 10x10x10 mm^3 test specimens made out of ISO mortar (cement : sand = 1:3; w/c = 0.5). The

Table I. Composition of fluidized bed ash, clinkers and high SO_3 clinker fractions.

	ash	reference clinker	high SO_3 clinker	SASF	SAER
Al_2O_3	17.9	5.84	10.01		25.96
CaO	2	68.92	61.68	1.97	39.73
Fe_2O_3	28.9	3.33	3.08	71.7	
K_2O	0	-	0.37	1	8.44
MgO		-	0.86		
Na_2O	6.20	-	0.42	0.40	2.72
SO_3		-	6.10	-	
SiO_2	1.86	21.91	16.22		0.84
TiO_2		-	0.21	0.86	
	1.25				0.60
CaF_2		-	0.97	0.33	19.37
	0.38			-	
	12.2			23.4	1.09
	0			9	
	30.3				0.56
	6			0.02	
	0.66				0.47
	-			1.21	
CaOFr. :				0.6	
C3S				66.1	
					15.5
C4AF					17.8
C4A3S					

SASF: salicylic acid soluble fraction
SAER: salicylic acid extraction residue

Table II. Properties of reference and high SO_3 Portlant cements.

	Reference Cement	High SO_3 cement
Gypsum (%SO_3)	3.0	2.0
Specific surface area (m^2/Kg)	300	300
Setting time		
beg:	265	140
end:	355	205
Compr. Strength Mpa		
1 d:	11.1	8.3
3 d:	24.8	22.7
28 d:	51.8	48.5
Expansion 28d (mm/m)		
air:	5	6
water:	5	7

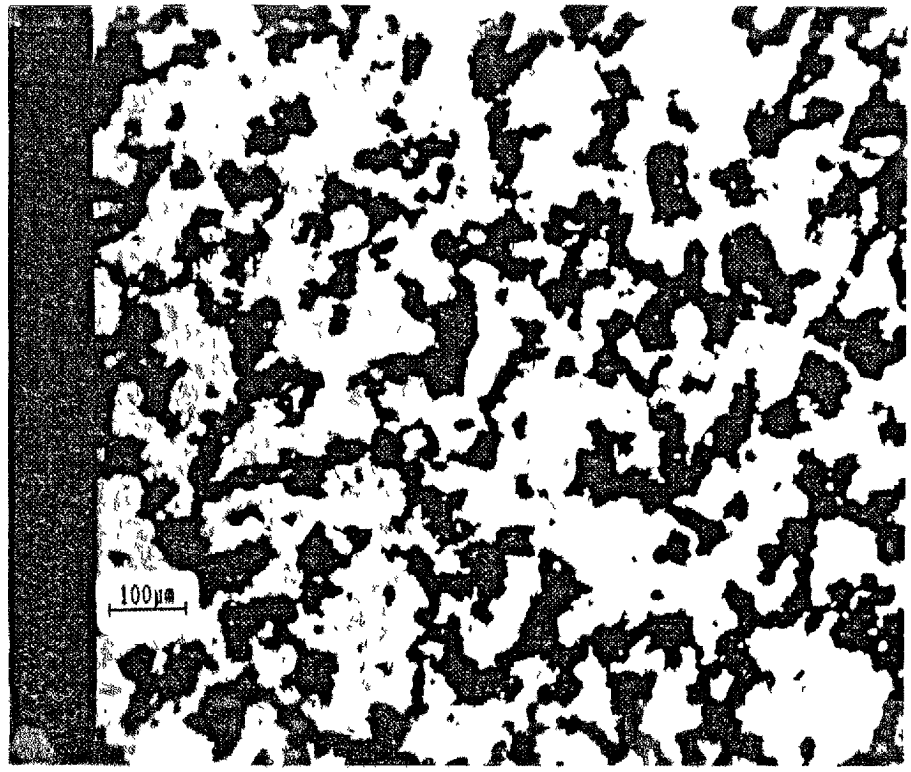

Figure 1. BSE image of clinker produced from high SO3 fluidized bed ash

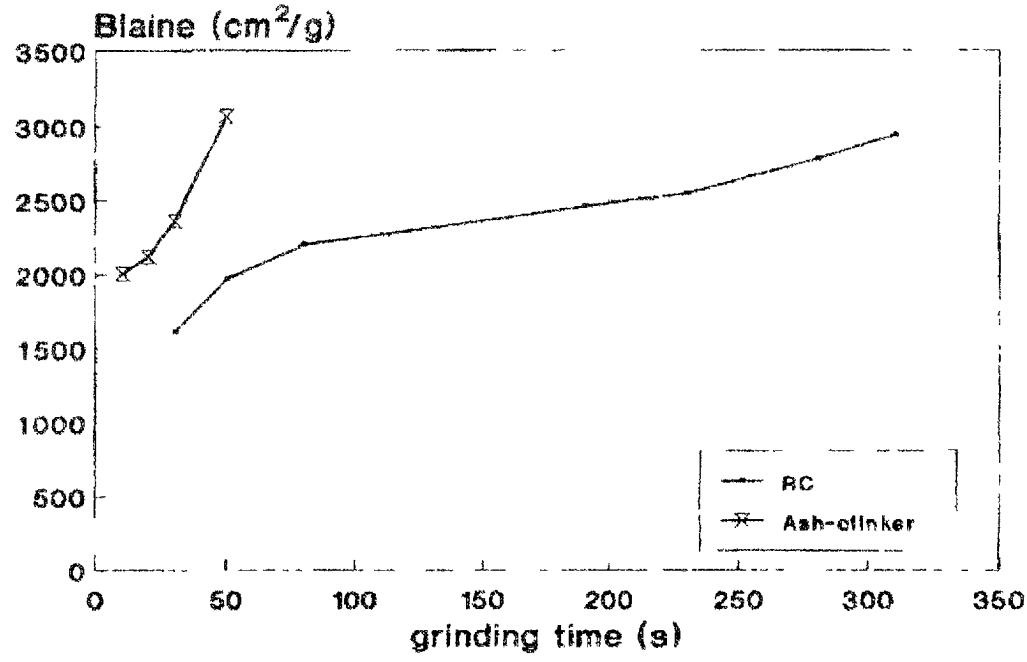

Figure 2 Grindability of conventional Portland cement clinker [RC] and clinker made from high SO3 fluidized bed ash [Ash-clinker]

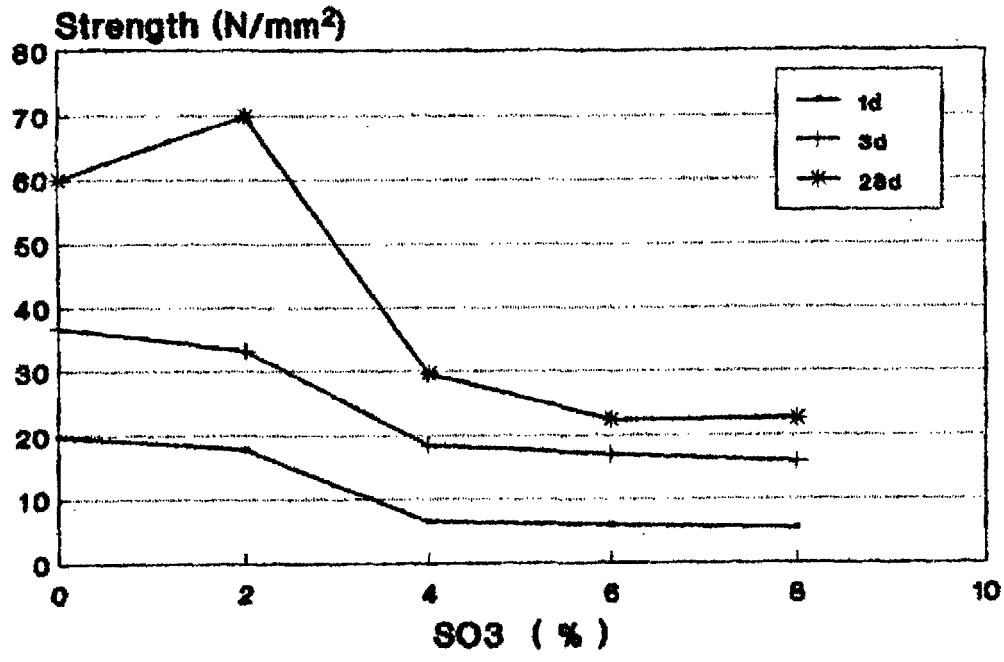

Figure 3 Compressive strengths of pastes made from cements ground with variable amounts of gypsum (clinker made fom high SO3 fluidized bed ash)

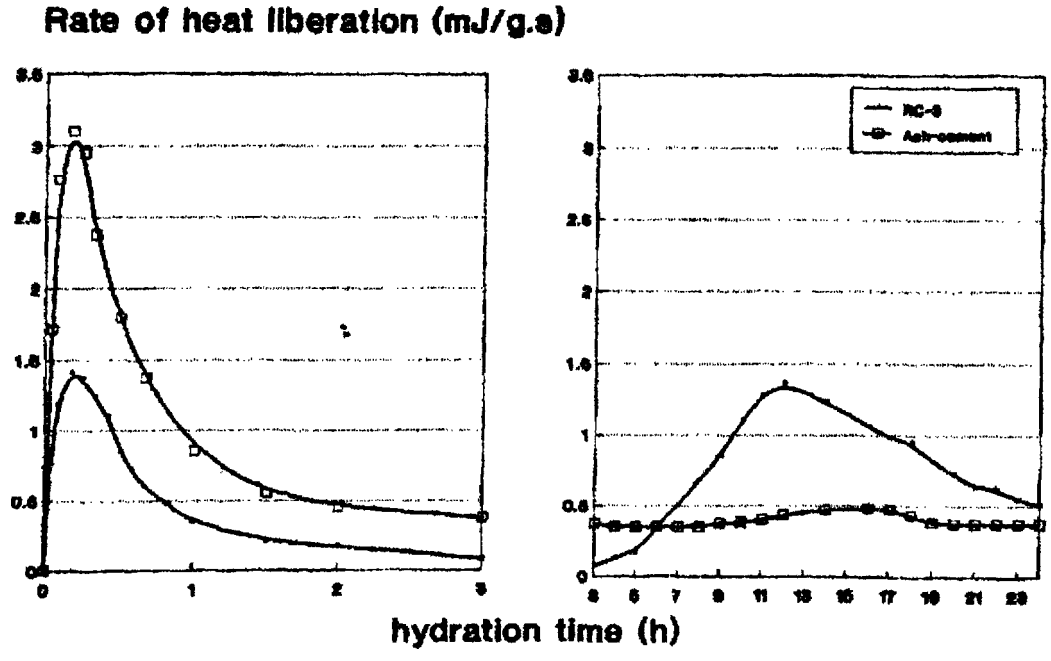

Figure 4. Hydration heat evolution of conventional portland cement and cement produced from high SO3 fluidized bed ash

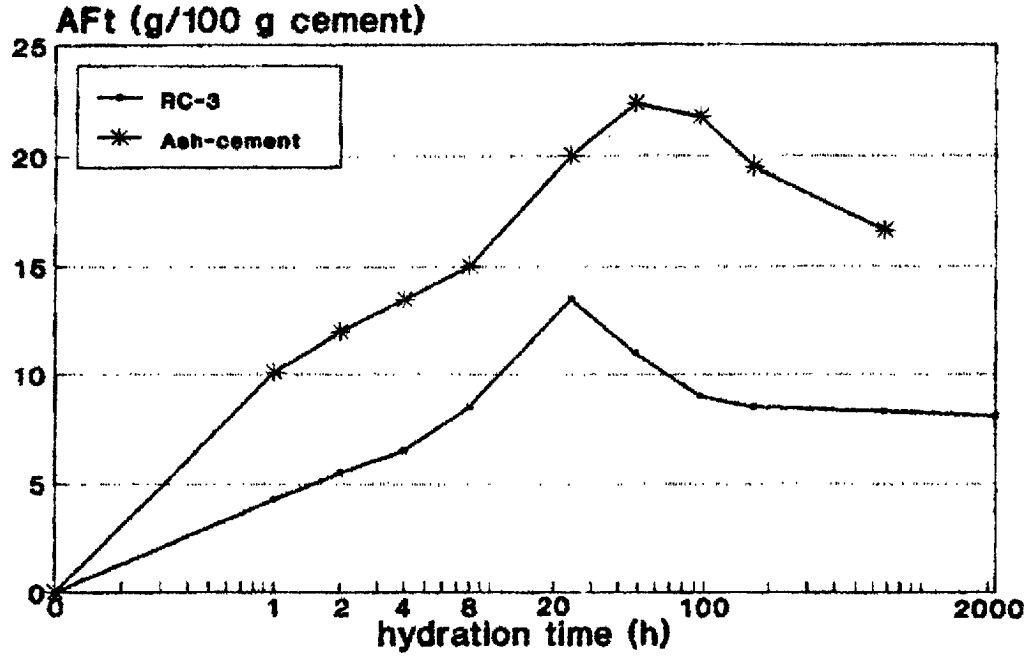

Figure 5. Amount of ettringite in conventional and high SO3 cement pastes as function of hydration time

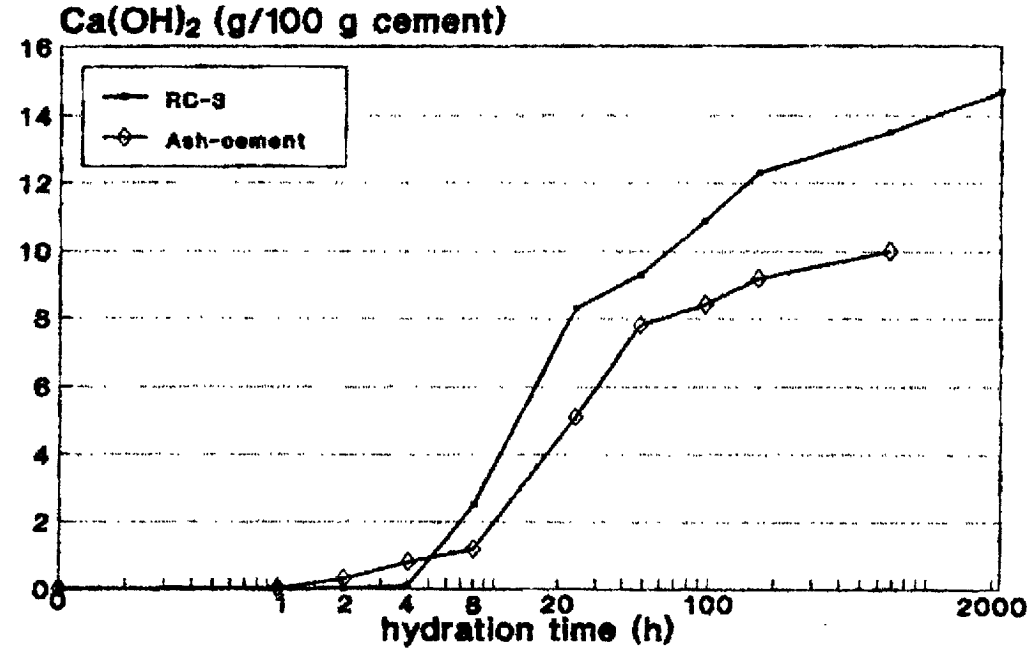

Figure 6. Amount of calcium hydroxide in conventional and high SO3 cements as function of hydration time

expansion was measured on cement paste test specimens (w/c = 0.30) cured either in humid air or placed under water after three days of humid air curing. Under both conditions any expansion was completed wihin the first 10 days of curing and no further length/volume changes were observed later on. The obtained results are summarized in Table II. If compared to the reference cement, the experimental cement produced from the high SO_3 fluidized bed ash exhibited a distinctly shorter setting time and a roughly equal strength development and expansion.

The hydration heat liberation of both cements, as studied by isothermic calorimetry, is shown in Figure 4. If compared to the reference cement, the experimental high SO_3 cement exhibited a significantly increased hydration heat liberation within the first 5 hours and a reduced one later on.

The hydration process was studied on paste samples in which the hydration was stopped and the non-reacted water was removed by extraction with acetone and ethyl ether. On this material the combined water was determined as the loss on ignition; the free calcium hydroxide, gypsum and ettringite was determined by differential thermal analysis. The interground gypsum became completely consumed within 24 hours in both cements. The ettringite content in the experimental cement paste was consistently above that of the reference paste; in both pastes the amount of ettringite started to decline after the present gypsum had been consumed (Fig. 5). A distinct formation of calcium hydroxide, indicating the end of the induction period in the hydration of C_3S, got under way sooner in the paste of the experimental cement, indicating an increasing reactivity of the present C_3S phase. After 5 hours, however, the amount of calcium hydroxide in the reference cement became higher, apparently due to a higher C_3S+ C_2S content in this cement and due to the formation of ettringite in the hydration of C_4A_3s in the experimental cement paste (Fig. 6). The amount of combined water was higher in the experimental cement at any hydration time, mainly due to the formation if increased amount of ettringite, a phase with an exeptionally high combined water content.

DISCUSSION AND CONCLUSIONS

Our experiments confirmed the possibility of using fluidized bed ashes in the production of Portland cement clinker. A cement produced from clinkers made this way will differ from conventional Portland cements in several respects:

It will contain the phase C_4A_3s among its constituents, whereas the amount of C_3A will be reduced, or this phase will be absent completely.

Due to the presence of C_4A_3s, the cement will exhibit a shorter setting time and a more intensive hydration heat liberation at the beginninng of hydration.

The hydrated paste will contain increased amounts of the AFt phase and reduced amounts of portlandite, however, also here, just as in ordinary Portland cement pastes, the C-S-H phase will remain the main hydration product.

There appear to be several advantages resulting from the use of high SO_3 fluidized bed ashes as raw meal constituents in the production of Portland cement:

Fluidized bed ash, a burdensome end-product od fluidized bed combustion of coal, may be meaningfully utilized and the amount of raw materials from natural sources reduced correspondingly.

The energy consumption in the burning process will be reduced due to the fact that a significant fraction of CaO in the raw meal will be present in decarbonated form, rather than as $CaCO_3$. An additional reduction of energy consumption will be due to the reduced burning temperature employed. Moreover, the residual carbon, consistently found in fluidized bed ashes in variable amounts, may supply a part of the needed energy.

The emission of CO_2 will be reduced due both to a reduced fuel consumption and and a reduced $CaCO_3$ content in the raw meal. At the same time the emission of NOx will be also reduced, due to a lower maximum burning temperature.

The power consumption in the grinding process, and along with it the wear of the grinding

equipment, will be reduced, due to the improved grindability of the produced clinker.

On the other hand, the following facts have to be taken into consideration if using a fluidized bed ash as raw meal constituent:

The necessity to add fluorspar to the raw meal will eliminate a part of savings brought about by the reduced fuel and power consumption.

Some uncertainties may exist about the long term durability of the formed hardened cement paste, mainly due to higher amounts of ettringite in the hydrated material and the possible consequences of a reaction of this phase with the CO_2 of the air.

Concrete mixes made with this kind of cement may not be suitable for steam curing at high temperatures, due to a possible expansion associated with delayed ettringite formation.

The produced cement wil not comply with existing specifications for "Portland cement", mainly due to an SO_3 content higher than admitted.

In related studies S. Gimenez et al. (1991)produced a "white" low iron cement by burning the raw meal with added $CaSO_4$ and CaF_2 and found fluorellastidite ($3C_2S.3CaSO_4.CaF_2$) as the main SO_3 bearing phase. Borgholm et al. (1995) produced a blended cement based on a clinker made from an SO_3 and F containing raw meal and found most of the SO_3 present in clinker in form of $C_2K_2s_3$.

REFERENCES

Borgholm, H.E., Herfort, D. and Rasmussen, S., "A New Blended Cement Based on Mineralised Clinker", World Cement, Vol. 25, No. 8, 1995, pp. 27-32.

Gimenez, S., Blanco, M.T., Palomo, A. and Puertas, F., "Production of Cement Requiring Low Energy Expenditure - An Industrial Test", Zement-Kalk-Gips, Vol. 44, No. 1, 1991, pp. 12-15.

Odler,I. and Zhang, H., "Investigations on High SO_3 Portland Clinkers and Cements I. Clinker Synthesis and Cement Preparation, II. Properties of Cements", Cem. Concr. Res., Vol. 26, No. 9, 1996, pp. 1307-1313, 1315-1324.

THERMAL DISPOSAL OF ASBESTOS-CEMENT AND RE-UTILISATION IN CEMENT INDUSTRY.

Luigi CASSAR, Gian Luca GUERRINI and Cesare GILIOLI, CTG Italcementi Group, Bergamo, Italy

ABSTRACT This paper describes an environmentally friendly overall process for the disposal of asbestos-cement products by high temperature treatment. The end product could be reuse (a) as ingredient for the production of portland cement, according to present standards (ENV 197/1), or as raw material in cement production cycle (clinkerisation kiln feed).

Key-words: Asbestos-cement, Disposal, Thermal treatment, Waste material utilization

INTRODUCTION

Since the early decades of the century, asbestos fibers were been used in large numbers of different products (fiber-cement products, sprayed insulation, fabrics, etc.) but as is well-known, they (and related manufacts) now are classified as hazardous substances and their use is forbidden in majority of European countries.

The largest quantity of asbestos fibers (about 75%), especially chrysotile, were used to produce asbestos cement products (flat and corrugated sheets, roofing panels, pipes, chimneys, etc.). Reliable estimations about 16-20 millions ton asbestos cement corrugated sheets are installed only in Italy and most of them will be probably removed and substituted with asbestos-free sheets. Generally, these wastes are disposed of in a few specially designed landfills destined to be filled in a short time.

Asbestos-cement products, which consist of about 85% hardened cement paste and about 15% asbestos fibers could, however, be reutilized after appropriate thermal treatment. Several methods for thermal treatment of asbestos wastes have been proposed in literature (see for instance Sakai et al., 1991, Tamas et al., 1991, Clausen et al., 1994, Ambrosius S. et al., 1996), some already in the industrial scale, others only in pilot-plant or laboratory scale: ceramics production, plasma flame or electric furnace, vitrification (using melt accelerators), rock wool production (using mineralizing agents) and various thermo-chemical treatments. In these processes, the processing temperature is normally over the melting temperature of asbestos (T_m = ca. 1350°C). In some cases (for ex. plasma flame treatment), the end product has a chemical composition similar to the process feed material, in other cases the method allows to obtain a completely different material (glass, ceramics, rock wool).

THE PROCESS

The above mentioned processes show several limits because of high costs - due to the high energy consumptions and/or to the additives utilised - and industrial scale-up difficulties. This paper is concerned with an Italian-patented process (Cassar, 1992) which includes the destruction of the asbestos fibers contained in asbestos-cement products by 800°C-900°C temperature treatment in furnaces heated by methane, L.P.G. or in electric furnaces, without production of polluting fumes (no-containing fibers); it is also possible to use other fuels (for ex. combustible oils), but it is necessary to have recourse to adequate filtration systems aimed to prevent fiber emission.

For this reason, a great care was given to obtain an environmentally friendly destruction of asbestos fibers, setting up processing conditions both on laboratory and pilot-plant scale. The process engineering and safety findings obtained in this way form the basis for a possible trial under production conditions on industrial plants.

The process for asbestos-cement sheets consists of several steps, (Fig 1):

◊ in-place incapsulation of asbestos-cement sheets, using polymeric products;
◊ removal, palletization and transportation of manufacts to the oven;
◊ thermal treatment in an oven
◊ grinding of product treated

The process shown includes two possible reutilisation of the final product after the thermal treatment:

⇒ re-use of end product as ingredient for the preparation of Portland cement, according the present standards (ENV 197/1, section 4.8).
⇒ recycling as raw material in cement production cycle (clinkerisation kiln).

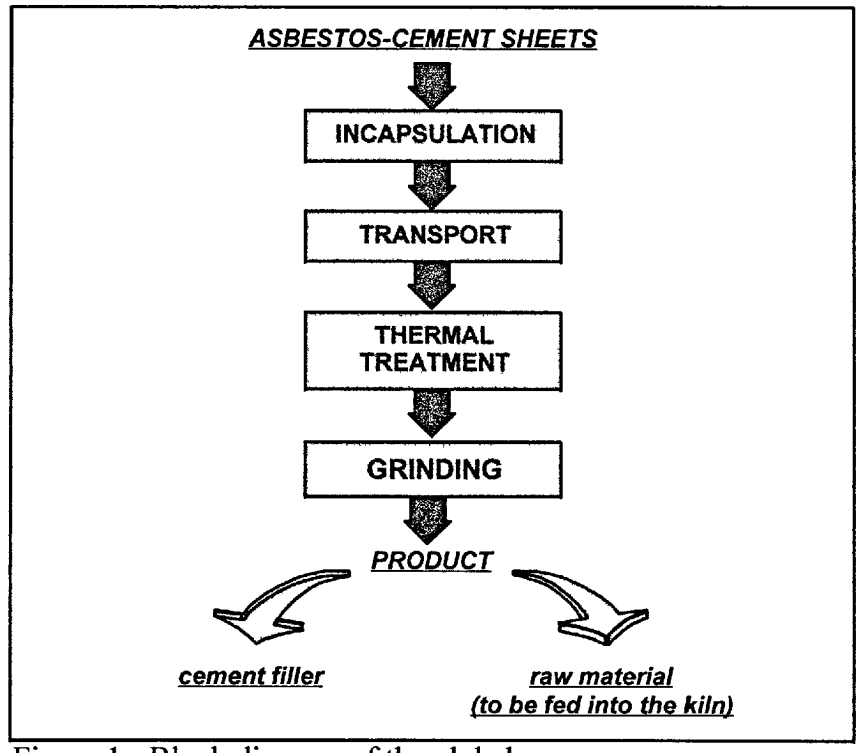

Figure 1 - Block diagram of the global process

The result is a residue-free process which makes it possible to recycle asbestos-cement product at costs comparable with the prices of acceptance in landfills and decisely lower than the costs of other thermal treatments above mentioned.

RESULTS

The inactivation process consists of a pyrolytic asbestos attacking action - by heating the samples to a temperature no lower than 580°C - which allows to eliminate the water present in the molecule, converting the fibrous crysotile into another non-fibrous and inert Mg-silicate (forsterite). Forsterite is an inert refractory mineral which is found in nature as a constituent of olivine. The reaction is:

$$Mg_6(OH)_8Si_4O_{10} = 3Mg_2SiO_4 + 4H_2O + SiO_2$$

Other than forsterite, it can be observed the presence of quartz (SiO_2), diopside ($CaO.MgO.2SiO_2$) and periclase (MgO).

From the morphological point of view, asbestos fibers begin to agglomerate themselves, giving fibrous agglomerates which never have the initial aspect ratio (length/diameter), typical of asbestos fibers, but clearly lower (Le Bouffant, 1983).

Samples were analysed before and after each treatment condition, by using a quantitative method developed in CTG laboratories: (1) material grinding up to 90 mm particle diameter (2) chemical attack using chloride-salicilic acid solution (as provided in ENV 196/4) (3) X-Rays diffraction (XRD) analysis of samples. This method allows to detect asbestos residual contents up to the lower limit of 0.1% weight, the one tenth of corresponding classic XRD analysis. The XRD analysis was completed with Scanning Electron Microscopy (SEM) morphological analysis.

Actually, this adopted sequence - combination of both analytical and microscopical methods - seems to be one of the most accurate methodologies to determine the smallest quantity of asbestos contained in cement products.

Basic study was the optimisation of thermal treatment experimental parameters (temperature, time) of asbestos (chrysotile)-cement samples in a laboratory furnace. Table 1 shows the experimental results referred to different process conditions (temperature = 700-1000°C, time 10-40 min).

Table 1 Asbestos residual contents in samples thermal treated at different process conditions (temperature, time).

	treatment time, min			
	10	20	30	40
temperature, °C				
700	45.8	2.9	0.6	0.2
800	0.2	0	0	0
900	0	0	0	0
1000	0	0	0	0

Quantities expressed as the ratio of main peaks obtained from XRD on chloride-salicilic residuals as regards the samples untreated.

After the thermal treatment, XRD (Fig 2) and SEM analysis (Fig 3) proved that the material doesn't contain any residual asbestos fiber or fibrous structures referable to the same fibers.

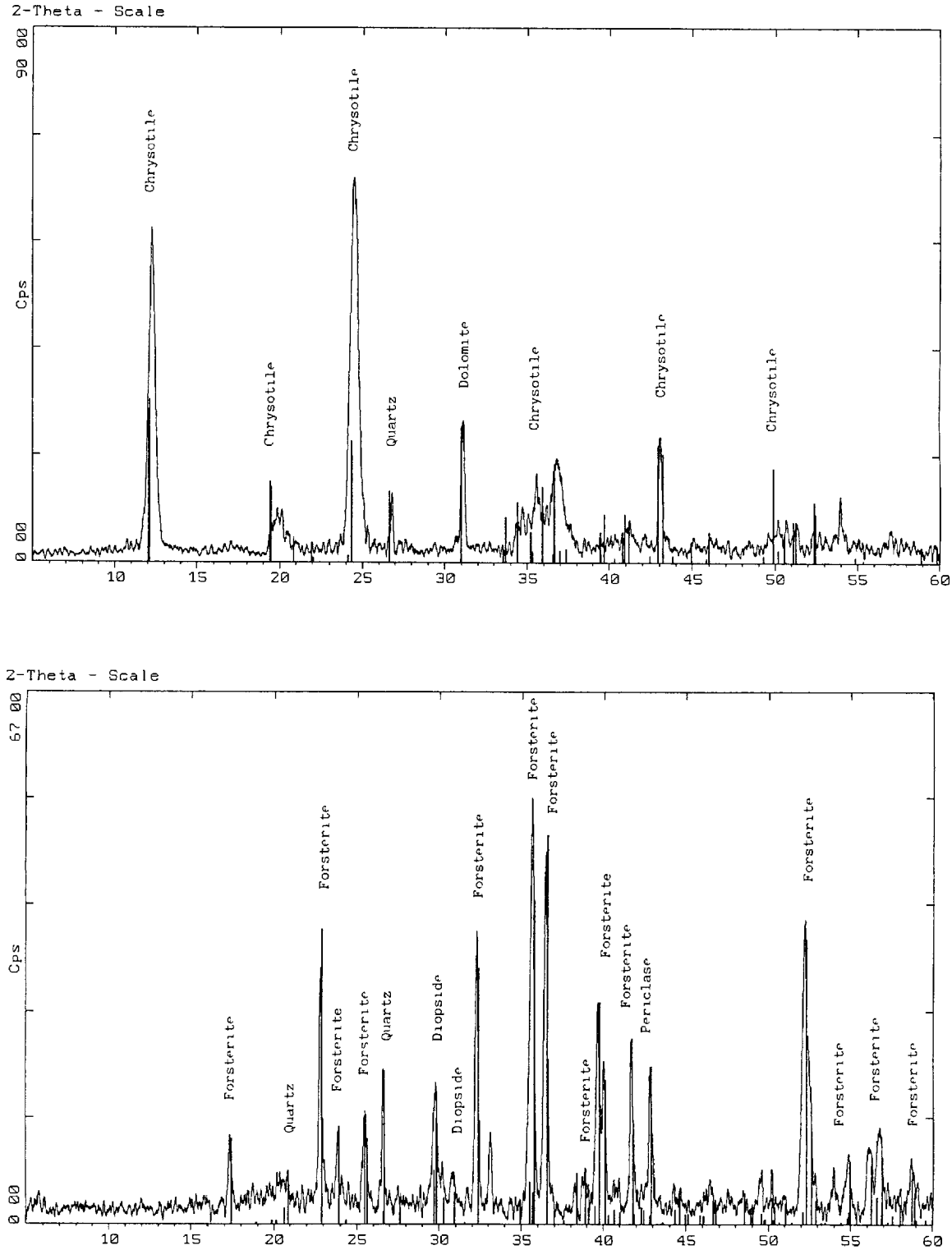

Figure 2 Asbestos-cement samples: XRD on chloride-salicilic acid residue before (up) and after (down) the high temperature thermal treatment

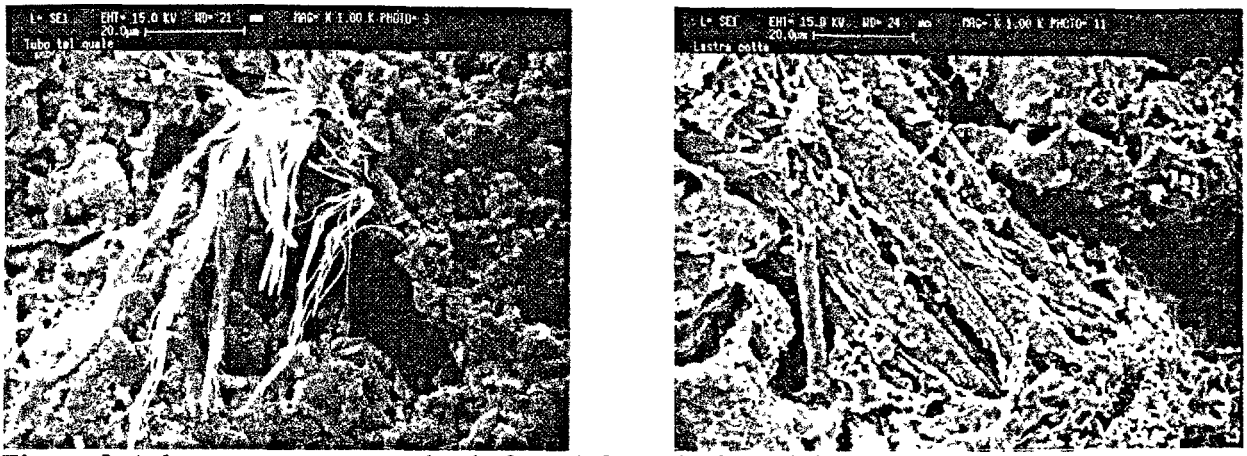

Figure 3 Asbestos-cement samples before (left) and after (right) the high temperature thermal treatment

Elementary microanalysis, executed on samples of material treated, confirmed the presence of pieces containing Mg, derived from the melting of asbestos fibers, having an aspect ratio completely different from original asbestos fibers, Fig. 4. The same powder morphology was observed in the samples first thermal treated and then grinded, so as to obtain a granulometry similar to the cement powder one.

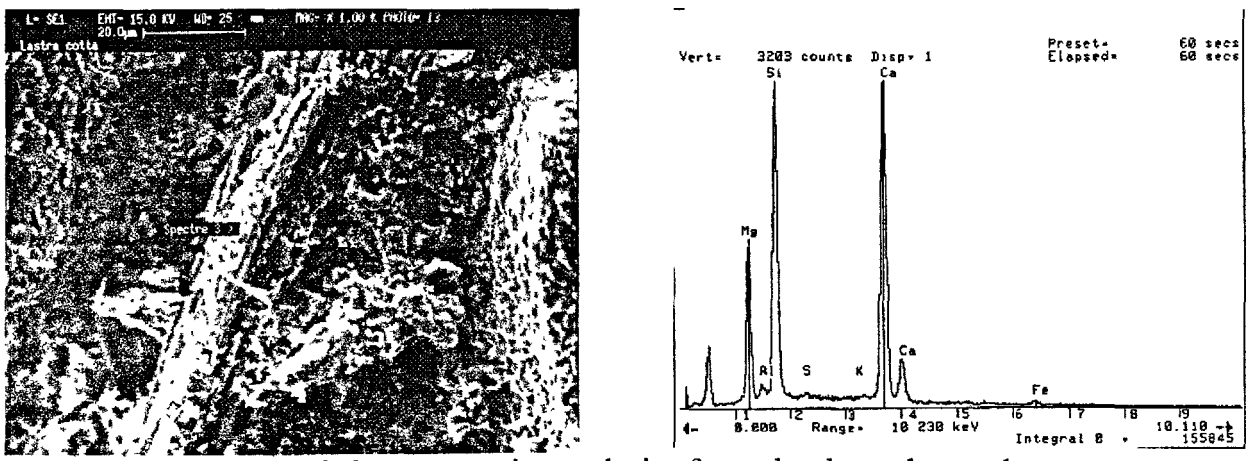

Figure 4 SEM image and elementary microanalysis of samples thermal treated

The material obtained from this process can be used in cement production cycle, since its chemical composition is similar to the cement one:

- as a partial substitute of raw meal feed
- as a mineral filler in cement preparation, as provided by the ENV 197/1 standard, section 4.8.

In both cases, it is necessary to be sure that the standard limit for MgO is not to be exceeded. Further experimental work was done to evaluate the above mentioned applications and to assess the maximum quantity could be re-used for each of them.

In the former case, a high content of MgO in raw meal could provoke undesired reactions: for this reason it was estimated a maximum feed of 5-10%. In the latter case the maximum limit content is provided by the ENV 197/1 standard, that is 5% weight.

No expansion phenomena were observed in standard pastes prepared with cement containing asbestos-cement thermal treated (Le Chatelier test). Besides, evaluation tests in concrete and mortar compositions showed good rheological and mechanical properties in comparison with a cement of similar chemical composition, Table 2.

Table 2 - Workability and mechanical properties of concretes

			reference cement	**cement prepared with 5% material filler**
slump		cm	5	6
VE-BE, sec		sec	3	3
compressive	1 day	MPa	15.6	13.8
strength	7 days	"	33.9	35.8
	28 days	"	37.9	39.0
flexural strength	7 days	"	5.0	5.1
	28 days	"	5.6	6.0

W/C = 0.56, SP = 1.2%, aggregates max. diameter = 20 mm

CONCLUDING REMARKS

After these considerations we can conclude that this suggested process could permit to recycle asbestos-cement wastes completely, as well as all the other asbestos products, which represent a small percentage of the total asbestos wastes.

In a few years the cement industry could be able to recycle the asbestos wastes without applying to landfill disposal.

The process is indeed environmentally friendly and cost effective, in comparison with other proposed methods. Analytical measurements demonstrated the completely disappearance of asbestos fibers.

REFERENCES

Ambrosius S., Gundlach H. and kieser J., "Thermische Verwertung von zementgebundenen Asbestprodukten in Zementöfen", ZKG Intern. (49 Jahrgang) Nr. 8/1996, pp. 444-453

Cassar L. and Gilioli C., "Processo per il riciclo di manufatti di cemento-amianto", Italian Patent n. MI92A001803, July, 24, 1992

Clausen A., Christensen V.R. and Jensen S.L., "Method of Converting Asbestos Cement into a Harmless Product", PCT Patent No. 94/23801, Oct. 27 1994

Le Bouffant L., Bruyère S., Daniel H. and Martin J.C.; "Influence d'un traitement thermique des fibres de Crysothile sur leur comportement dans le poumon", VDI - Berichte n. 475 (1983), pp. 253-259

Sakai S., Takatsumi H., Hraoka M. and Tsumeni T., Water Sci. Techn., 23, 2029 (1991)

Tamas F.D. and Amrich L., "Disposal of Asbestos Waste in the Cement Industry", Int. Cem. Review, Aug. 1991, pp. 52-56

TOPIC I.D

Application of mineralizers, modifiers and activators

PRACTICE APPLICATION OF COMPOSITE MINERALIZER TECHNOLOGY INPRECALCINING CEMENT KILN

LI peiquan and LIU changfa, China Building Materials Academy, Beijing, China

Zhuo hongmi, Linguang Cement Plant, China

ABSTRACT Composite mineralizer was adopted in pre-calciner and good results were obtained: 1) the compressive strength of high alkali clinker (R_2O 1.45-1.80%) is remarkably increased, 2) the quality of kiln coating is good, 3) clinker outputs increase by 5-15%, 4) coal consumption decrease by 5-15% and 5) the running period of the kiln is prolonged and the fast speed rotary running rate is raised.

Keywords: Composite Mineralizer, High Alkali Clinker, Pre-calciners.

摘要： 复合矿化剂在窑外分解窑上的生产实践效果良好。

1. 大大提高了高碱熟料(R_2O 1.45～1.80%)的强度，熟料抗压强度，3天43.4MPa，7天50.3MPa，28天由53MPa提高到60.2MPa，稳定地生产了525(R)硅酸盐水泥。
2. 窑皮质量好。熟料易烧性好。
3. 熟料增产5～15%。
4. 节煤5～15%。
5. 窑运转周期延长，快转率高。

叙述了熟料的矿物组成和熟料及水泥的物理力学性能。

阐明了高碱熟料强度大大提高的机理，消除窑外分解窑予热器系统结皮和窑内结球的机理。

关键词： 复合矿化剂，高碱熟料，窑外分解窑。

INTRODUCTION

At present, the most pressing problem which a precalciner kiln faces is the low running rate, frequent kiln stoppage and lower clinker grade (generally 56MPa). In a precalciner, circulation and amassment of sulphur and alkalis are apt to lead to coating, blocking in the preheater system and globing in the kiln that would lower the clinker qualities and output. The temperature of clinkers emerging from the kiln is high, that causes more breakdown of coolers which influence the running rate of the kiln.

The serious problems which the precalciner is facing can be solved by using composite mineralizer leading to low-temperature burning in portland cement clinker formation.

The technology is the project in "National Science and Technology Achievements highly popularized programme". Its number is I1-5-1-9 and certificate number is 0896. The practice application of "composite mineralizer technology in precalcining cement kiln" has achieved good results:

1. The compressive strength of high alkali clinker (R_2O 1.45-1.80%) was remarkably increased. e.g. the 3-day-strength reached 43.4MPa and 28-day-strength increased from 53MPa to 60.2MPa. So the high-mark(R) portland cement can be consistently produced.
2. The quality of kiln coating is good.
3. Clinker output increased by 5-15%.
4. Coat consumption reduced by 5-15%.
5. The running period of a kiln is prolonged and the fast speed rotary running rate is raised.
6. Composite mineralizer accelerates the decarbonation of $CaCO_3$ and the clinker burning.
7. Composite mineralizer is contributed to eliminate the coating in the preheater system and the globe in the kiln of precalciner.
8. Kiln feed's burnability is good, the operation of burning is convenient and easy to control.

Up to now, in abroad, "The technology of composite mineralizer in low-temperature-burning portland cement clinker" has used in precalcining kiln. "Composite mineralizer technology" and "precalcining technology" are closely intergrated and supplement each other that results in increasing outputs and reducing energy consumption remarkably, as well as improving the quality of clinkers. The new technology is really a effective way deserved to devote major efforts to spread to develop the building material industry.

"The technology of composite mineralizer in low-temperature-burning portland cement clinker" is advancing in the world.

LABORATORY SECTION

High Alkali Clinker

Chemical composition of clinkers

The chemical composition of the projected clinkers are list in Table 1. The chemical analysis results of the clinkers are basically consistent with the projected composition. Samples group A have been burned for 45 minutes at 1450℃ and samples group B burned for 45 minutes at 1370℃, they were all cooled in the air.

Table 1 Chemical composition of clinkers

Sample No.	Chemica Com position (wt%)								
	SiO_2	Al_2O_3	Fe_2O_3	CaO	MgO	K_2O	Na_2O	SO_3	F^-
A-0	20.59	6.31	4.62	64.51	1.76	0.81	0.20		
A-1	20.42	6.26	4.60	64.00	1.75	1.58	0.20		
A-2	20.31	6.22	4.56	63.63	1.74	2.15	0.20		
A-3	20.17	6.19	4.45	63.23	1.73	2.77	0.20		
A-4	20.04	6.14	4.50	62.85	1.72	3.39	0.20		
B-0	19.86	6.00	4.40	63.06	1.72	0.78	0.20	1.54	0.63
B-1	19.65	5.95	4.38	62.56	1.70	1.60	0.20	1.54	0.62
B-2	19.65	5.91	4.43	62.17	1.69	2.17	0.20	1.54	0.62
B-3	19.44	5.89	4.33	61.78	1.68	2.73	0.20	1.54	0.62
B-4	19.31	5.84	4.29	61.41	1.67	3.34	0.20	1.54	0.62

The influence of alkalis in the formation of clinkers

Fig.1 shows the correclation between the f-CaO and alkali content of the samples group A and B.

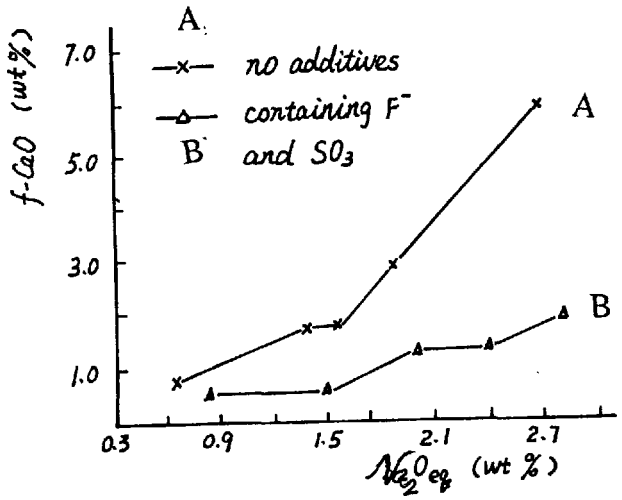

Fig.1 Corrlation between f-CaO and alkali content in the clinker at the burning temperature.

Fig.1 shows:1. With no additive in samples group A, the f-CaO content raise with increasing alkali content. Especially when Na_2O eq exceeds 1.60%, the f-CaO content is extremly high and the clinkers are hard to form. The reasons are:

(1) Large amount of K_2O entering high-temperature melt leads to increasing the liquid phase viscosity and decreasing the diffusion rate of the ion that makes the clinker minerals difficult to form. Furthermore, that the alkalis entering liquid phase increases the alkality, reduces CaO solubility in liquid phase and enlarges CaO initial phase region. These are the reasons why f-CaO raises with increasing alkali content.

(2) Alkalis entering belite phase makes belite constructure more steady and decreasing the absorbing capacity of free CaO that prevents forming alite.

2. Although the burning temperature of samples group B with fluorite and gypsum decreases by 80℃, the f-CaO is still low in clinkers. f-CaOcontent of sample B-3 is only 1.33 when K_2O content is as high as 2.20% (Na_2O eq: 2.43%). It's obviously that the mechanism of the alkalis affecting the clinker formation has been changed by introducing fluorite and gypsum. The reasons are as followed.

(1) Fluroite and gypsum are good flux which can lower the temperature at which liquid phase emerges, and their contribution of lowering the liquid phase viscosity are indicated in many meterials. В У Т Т [1] Pointed out that the liquid phase viscosity increases wih alkalis but decreases with both alkalis and sulphur. It's therefore that fluorite and sulphur together can compensate the negative effect of alkalis in melt viscosity.

(2) Fluorite and sulphur are effective mineralizers and the composite mineralization can make C_3S form at the temperature below the temperature range of its steadiness.

Production in a cement plant

The composite mineralizer technology got great achievements in the production in L plant (precalcining kiln $\phi 3 \times 48M$), solved the importand problem that high alkali clinker can not be produced to high mark (R) portland cement because of the low strength, and resulted in significant social economic interests.

Clinker

1) Minerals in the clinkers

The minerals in the clinkers were determined with XRD and the patterns are shown in Fig.2.

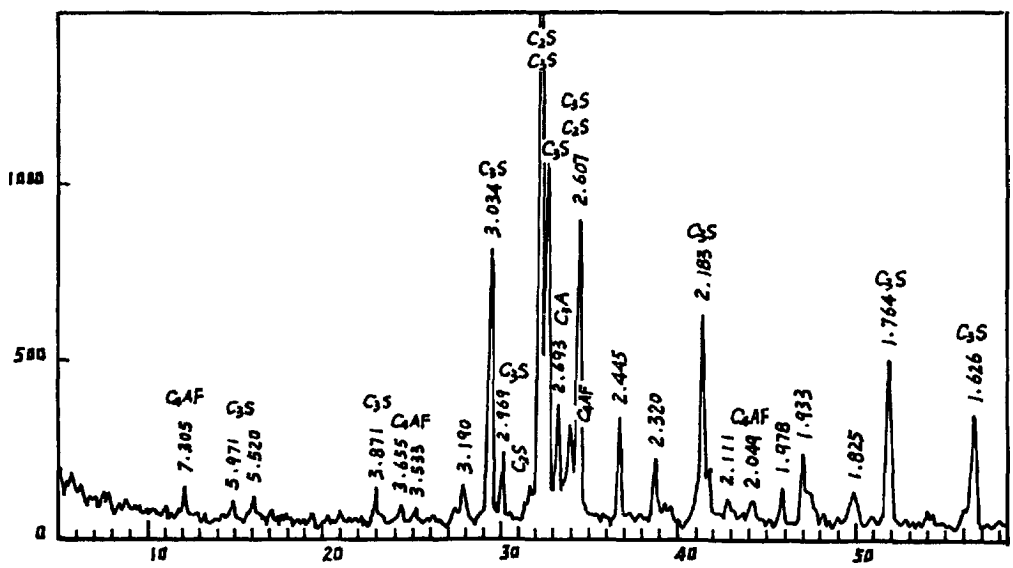

Fig.2 XRD patterns of clinker

Fig.2 shows that the main minerals are C_3S, C_2S, C_3A and C_4AF. The R_2O content in the clinker is as high as 1.45-1.80, so the clinker is high alkali clinker.

2) Physical properties of the clinkers

The physical properties of the clinkers are listed in Table 2.

TABLE 2 Physical properties of the clinkers

Sample No	Standard consisteny %	Sound-ness	Setting time Initial h:m	Final h:m	Compressive streength MPa 3	7	day 28	Bending strength MPa 3	7	days 28
LGC-1	25.00	passed	1:34	4:25	45.8	54.3	63.7	6.6	7.5	9.2
LGC-2	24.50	passed	2:27	4:52	47.0	52.8	61.5	6.5	8.1	9.0
LGC-3	24.50	passed	3:37	5:07	44.8	53.5	64.7	7.3	7.9	8.7
LGC-4	26.00	passed	1:53	4:10	43.4	50.3	60.2	7.2	7.7	8.8
LGC-5	24.75	passed	2:12	4:07	46.2	50.5	61.0	7.0	7.6	8.6

Table 2 indicates that the clinkers compressive strength are above 43.4 MPa for 3-day, above 50 MPa for 7-day and above 60 MPa for 28-day. It's obviously that the clinkers 3-day compressive strength are high.

Cement

The physical properties of porltand cement are given in Table 3.

TABLE 3 Physical properties of portland cement

Sample No	Standard consisteny %	Sound-ness	Setting time Initial h:m	Final h:m	Compressive streength MPa 3	day 28	Bending strength MPa 3	days 28
LGC-1	26.50	passed	3:45	5:20	41.0	64.0	6.3	8.7
LGC-2	26.00	passed	3:31	5:18	42.2	61.9	6.2	8.6
LGC-3	26.00	passed	2:55	4:45	44.2	63.6	6.3	8.9
LGC-4	26.00	passed	3:18	4:46	44.4	62.0	7.0	8.7
LGC-5	26.00	passed	3:39	4:39	41.4	61.5	7.1	8.5

Table 3 shows that the physical properties of portland cement conform with National standard (GB175-92) for 525(R) portland cement perfectly.

DISCUSSION

Why can this technology increase the strength of rich alkali clinkers remar-kably?

The reason is that using composite mineralizer can introduce suitable gypsum and fluorite additives to raw meal. When there is a suitable proportion of SO_3 and R_2O in rich alkali clinkers, R_2O can form R_2SO_4 instead of detrimental minerals $KC_{23}S_{12}$ etc.

emerges with characteristic minerals formation and disappears with minerals decomposition.

Characteristic minerals generally are $2CaSO_4 \cdot K_2SO_4$, $2C_2S \cdot CaCO_3$, $2C_2S \cdot CaSO_4$, $CaSO_4$, $3CA \cdot CaSO_4$, $Ca_{10}[(SiO_2)_2(SO_4)_2](OH,Cl,F)$.

Coating increases the circulation dust contents between the I and V cyclon of the preheater and reduces the thermal efficiency of rotary kiln ramarkably. The raw meal will be difficult to transport because of large quanlity of low melting point alkalis. By-pass and "composite mineralizer low temperature burning portland cement clinker technology" can be used in order to avoid coating, blocking and increase the quality of the clinker.

To control the effect of sulphur and alkalis effectively,sulphur saturation(SG) is often used in Westen Europe industry.

It's necessary to control SG properly when using high alkali raw materials, that contributes to make full use of the energy and fully develop the properties of the clinkers and cements. Generally the SG is controlled in the range from 60% to 100%.

It's better to use "composite mineralizer technology" than control SG single. "Composite mineralizer technology" can not only reduce coating and blocking of the preheater system but also increase the strength of the high alkali clinkers significantly. The burning temperature of the raw meal can be lowered about 100° K and the volatilizing alkali content decreased by adding composite mineralizer. On the other hand, it's necessary to control the atomersphere in the kiln and restrain the volitilization of $CaSO_4$, thus $CaSO_4$ would form complex salts with alkalis that reducing the volitile content of alkalis. That the clinkers emerging with sulphate from the kiln leads to reduce the circulation and amassment of the detrimental compositions and coating, blocking in the preheater system. Furthermore, the composite mineralizing and fluxing effects of gypsum and fluorite increase the decomposing rate of calcium carbonate in kiln feed, lower the burning temperature, decrease the volatility of alkalis and reduced coating and blocking. Therefore, the running rate of the kiln is improved.

Why can "composite mineralizer" prevent globing in the kiln?

There are globes in the kiln because of some detrimental components in the raw meal and fuels such as K_2O, Na_2O, Cl^- and SO_3. That adding right amount of gypsum and controlling the ratio of sulphur to alkalis is contributed to the combination of sulphur and alkalis to form sulphate and fix in the clinkers. So the circulation of alkalis in the kiln and alkali volatility can be reduced and the globe would be difficult to form in the kiln. And also the composite mineralizing and fluxing effects of gypsum and fluorite can increase the decomposing rate of calcium carbonate in kiln feed, lower

that is benificial to late strength. On the other hand, it is predicated that different alkalinity existing in clinkers also influences the process of hydration and hardening of the clinkers and finally rasults in different strength. Because of the high solubility, R_2SO_4 transforms to liquid phase very quickly in case meeting water. So, when the alkalinity of liquid phase increases quickly that impedes the diffussion of Ca^{2+} and decreases the hydrating speed of clinkers in early hydration period. When the alkalis exist as R_2O in clinkers, because R_2O transforms to liquid phase more slowly with minerals hydrating that the diffusion resistance of Ca^{2+} is weaker as well as the hydrating rate is higher. The differences between the two hydrating speeds in early hydration period are bound to result in the difference of crystalizing rate and influence the crystalization and growth of hydration products. As the crystalizing is slow when R_2SO_4 formed in clinkers, the structures and crystalization of hydration products can become perfect. This is a positive factor to later strength development of clinkers.

It is generally believed that CaF_2 is positive to the volatility of R_2O but $CaSO_4$ is negative regarding from the volatility of the alkalis. What is the situation when CaF_2 and $CaSO_4$ coexists? According to our experiments, using low temperature burning technique with fluorite and gypsum would reduce both flying loss of R_2O and possibility of foaming solid solution because gypsum combines R_2O first. At the same time, the severe fluxing effect of fluorite leads to reduce the clinkering temperature and prevent gypsum from decomposing to a certain extent at high temperature. So the combined mineralizing effect of both gypsum and fluorite is fully developed and improve the clinker strength. On the other hand, the alite content of clinkers using this technique are usually above 60% that enhances clinker strength greatly. So the technique is the main factor in improving clinker strength.

Why can the coating and blocking of the preheater system be reduced and the running rate of the kiln be increased by adding composite mineralizer to kiln feeds?

When the kiln feed burn at 1400℃ in the rotaly kiln, some components of the meal and fuel especially the alkalis, sulphur and fluorite will volatilize at burning zone and enter the preheater with waste gas, then condense and return to burning zone with the raw meal. They will partly volatilise again and the refeated vaporization and condensation of the votitile result in the internal circulation. So, the alkali content of the kiln feed increase continuously and cause the remaining alkali content in the clinkers increasing. This is the assemble process of alkalis. When alkali circulation reaches a certain extent, the liquid salts emerge and adhere to the preheater wall becoming coating, that will block the preheater and decrease the utilization of the kiln when seriously coating. The quality of the clinkers will be lowered if the volitile left in the clinkers.

The coating in the preheater system are caused by coherence of the coating characteristic minerals and unreacted raw meal compenents such as $CaCO_3$, SiO_2 and clinker minerals CaO, β-C_2S, C_4AF, $C_{12}A_7$, C_3A etc. Generally speaking, coating

the burning temperature and reduce the alkali volatility that effectively prevent globing in the kiln, better burning conditions and improve the running rate of the kiln.

CONCLUSION

1. The practice application of "composite mineralizer technology" in precalcin-ing kiln leads to good results and remarkable social economic effects.
1) The compressive strength of high alkali clinkers (R_2O 1.45-1.80%) are remarkably increased. e.g. the 3-day-strength reach 43.4MPa, 7-day-strength reach 50.3MPa and 28-day-strength reach 60.2MPa. The 525(R) portland cement have been steadily produced.
2) Both the quality of kiln coating and burnability of the clinkers are good.
3) Clinker outputs increase by 5-15%.
4) Coat consumption reduce by 5-15%.
5) The fast speed rotary running rate is raised and the running period of a kiln is prolonged.

2. The coating in the preheater system of precalcining kiln and globing in the kiln are effectively eliminated by "composite mineralizer technology".

REFERENCES

[1] Ю. м. Б У Т Т Ч с м с ю т No. 9 (1974)
[2] R. BLLCCHI 7thICCC V.I.P.I (1980)

SURFACE MICROPHASES AND CHEMICAL ACTIVITY OF THE ADMIXTURES-CATALYSTS ACTION.

Iya G. LUGININA, Doctor of Science, professor, The Belgorod Technological Academy of Building Materials, Belgorod, Russia.

ABSTRACT *The visual examination of calcite with catalysts in the heating chamber of* the microscope revealed surface microphases before the beginning of dissociation. A positive influence of the aimed addition of catalysts during the production of some cement grades was established. The best effect was obtained in the initial period of the tests conducted for cement strength.

KEY-WORDS. Microscopy, Melt, Low temperature, Strength Development

INTRODUCTION

The wide use of catalysts - mineralizers in the cement technology ensures fuel and power saving and achieves results which often exceed the cost of the additional equipment or the modernization. Zhuravlev (1950) was the first to pay attention to the chemical interaction of NaF with raw mix silica. In subsequent works, researchers addressed to the selection of admixture concentration and raw mix proportioning. In the 1970 - 1980s Russian plants used fluorides, silicofluorides, phosphogypsum and calcium chloride during the production of ordinary and white cement (Volkonsky, 1964). However, studies revealing the essence of proceeding interactions, essential to making efficient use of admixtures, were not made.

OBSERVATION OF DECARBONIZATION WITH A HEATING MICROSCOPE

Numerous measurements of the carbon dioxide quantity during the period of calcite dissociation in the Berg gas burette were taken (Berg, 1952). Having compared kinetics of gas emission of various calcite fractions (Fig 1), it was revealed that while adding an

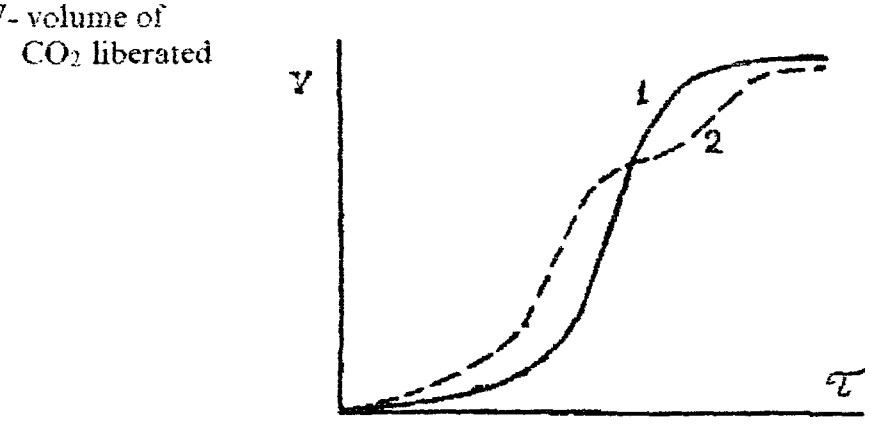

Figure 1 The influence of a catalyst upon the kinetics of carbon dioxide emission.
1 - calcium without a catalyst;
2 - calcium with a catalyst.

admixture the quantity of carbon dioxide may decrease and emission slowed. When the temperature increased, gas emission resumed. It was necessary to establish in which types of compounds carbon dioxide was preserved during a temporary stoppage of dissociation. The observation of dissociation with a polarizing microscope in the heating chamber (Rumyantsev, 1963), supplemented with the X-ray phase analysis of cakes, allowed the causes of the changes to be established. In the heating chamber transparent calcite crystals were fixed in the platinum heater. A drop of NaF, NaCl and Na_2CO_3 aqueous solutions (1 - 5 %) was applied with a needle on the surface of a calcite crystal (2.5 x 1.5 x 0.5 mm) facing the objective lens. A drop diameter was approx. 0.1 mm, a few drops of different solutions were applied on large crystals. Up to 250 - 300 °C the solution dried up, drop boundaries expanded and admixture migration started on the crystal. When applying NaF solution new products concentrating near microcracks were formed round the contour as the drop dried. At 500 °C secondary recrystallization proceeded and a new phase melting at 550 °C separated. Being very mobile, crystals emerged on the melt surface at 620 - 640 °C, which was an indication of gas emission from the melt. Solid products melting at 785 - 795 °C covered calcite at 700 - 780 °C. A thin film of the melt spread rapidly in different directions. The initial melt movement rate was up to 100 μm/sec, but decreased depending upon temperature and the concentration of the admixture. The melt was characterized by the limited temperature of the stability and low viscosity; melt saturated with gas was able to cover a large area. The sequence of the phenomena could change visually, as it reflected the influence of such factors as the condition of a chipped calcite surface, heating-up rate and admixture concentration. The observations showed that the admixture action was multistage and it began before calcite dissociation. The microscope allowed observation of catalyst impurity interacting with a matrix-calcite and new products being formed on its surface. These products caused crystal microheterogeneity in some areas. The limited power of the platinum heater compelled the development of a new attachment to the microscope (Luginina, 1994). A new chamber allowed observations to be made in an atmosphere of carbon dioxide, steam or dry air. A crystal was fixed between flat and point platinum contacts in the ceramic body of the microfurnace which provided for the uniform heating: the platinum contacts conveyed electric current and held the crystal. When conducting the electric current through the crystal at the 6 - 10-th minute of heating NaF melt was observed to move in the direction of the negative terminal. When applying NaCl solution melt was not formed, but the brown colouring was seen, which was an indication that admixture diffusion occurred in the direction of the negative contact. The change in the sign of the contact shifted accordingly the contour of the colouring or the melt (Fig 2). Therefore, surface diffusion of positive ions caused the brown colouring. The chamber was completed with a connecting pipe for the supply of steam or carbon dioxide and the installation of an electromagnet, thus allowing the influence of the magnetic field upon the behaviour of microphases to be observed. The heating of the crystal with the admixture without applyng electric or magnetic fields caused a symmetrical spread of the melt or of colour (Fig 2a). The electric field shifted the melt to the negative terminal (Fig 2b and 2d). The peculiar shifting of the melt along cleavage cracks took place under the influence of a magnetic field (Fig 2c). The observation of the separation of surface compound ions is possible in an electric field of high voltage up to 1.25 kW/cm. Magnetic field strength was 0.445 Tl. In later works (Klassen, 1987) it was established that the admixture decreased the initial temperature of dissociation but at the final stage, carbon dioxide emission proceeded at a higher temperature. The composition of new surface products of the calcite mix, sintered with sodium fluoride, was CaF_2 and $Na_2Ca(CO_3)_2$. Leonov (1988) studied surface microphases in oxides and he is of the opinion that grain surfaces are the main constituent of the structure. Chemical interactions with surface atoms are accompanied by bigger changes in

free energy than the same in the volume; a mass transfer proceeds faster at the boundaries of crystals which are richer in vacancies.

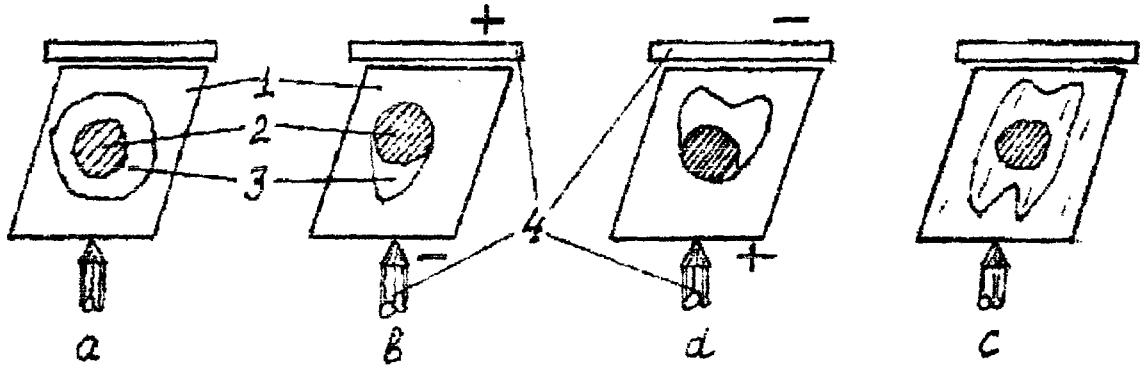

Figure 2 The shifting of the melt (colouring) on calcite crystals under the influence of electric and magnetic fields:
1- crystal;
2- drop of solution contour;
3- contour of the colouring (melt);
4- contacts.

Therefore, unsaturated surface ions are more active on the "fresh" chipped surface of calcite than those located in the volume. The reaction:

$2CaCO_3 + 2NaF = Na_2Ca(CO_3)_2 + CaF_2$

proceeds on the calcite surface under the influence of the admixture when the temperature increases slightly. The double salt is stable within the limited temperature range; a surface microphase melts, and decomposing, it saturates the melt with carbon dioxide; the melt obtains low viscosity and spreads on the crystal surface. The double carbonate melts at 770 °C and decomposes (815 - 820 °C) with formation of CaO and CO_2 according to the reaction:

$Na_2Ca(CO_3)_2 = Na_2CO_3 + CaO + CO_2$.

High efficiency of NaF is conditioned by the emergence of the melt and salts which form low-melting eutectics with $CaCO_3$. The tendency of calcite group minerals to the formation of double salts is well known. Double carbonates including calcium carbonate are known to chemists. However, the connection between the above complexes and the manifestation of a catalyst effect during the production of binders was not observed previously.

RECOMMENDATIONS.

Raw materials in the cement technology are ground finely. The systems with the developed surface have unsaturated valence links of surface ions, a strained crystal lattice, a lot of dislocations and vacancies; surface amorphism is feasible. These factors contribute to the emergence of surface microphases when a catalyst is added. When solving a technological problem the decision was taken to create the most favourable conditions for the interaction of calcite and a catalyst by means of primary contacts. The catalyst addition turned out to be most effective when added during limestone grinding (Luginina, 1994). Similar conditions were created in order to neutralize unwanted impurities in raw materials. Irrespective of the clinker phase composition (alite, fast-hardening, sulphate-resistant and

decorative cements were compared), after the aimed addition of the catalyst the cement strength was 9 - 12 % higher after 3 days' water hardening and it was 6 - 8 % higher after a month's water hardening. The less the age of samples under test is, the higher effect of the initial mixing is. The conditions of the catalyst addition reflected on the phase composition: the content of alite and tricalcium aluminate decreased. The alite phase accepted the minimum quantity of impurities in the form of a solid solution. The production tests of the said method were conducted at two cement plants. According to the technological scheme of one of the production processes the catalyst was added into iron slurry. After changing the grinding conditions the raw mix was better sintered, clinker hardness decreased, clinker dusting stopped and the cement strength increased under hydration (Table 1).

The strength of standard samples which were prepared from the mortar 1:3 and grew hard in water at 20 °C is given in the Table.

Table 1 The influence of mixing conditions upon cement strength.

Age of samples, days	Compressive strength of standard samples, MPa	
	Offered method	Plant method
3	33.3	25.5
7	40.6	33.2
28	50.8	42.9

The plant method consisted in the addition of a catalyst to a raw mix without premixing an additive with one of the components of the raw mix. The proposed method provided for the grinding of the additive with limestone followed by mixing with the rest of the raw mix components.

The catalyst is calcium fluoride with admixtures of sedimentary rocks. The fluoride content in the raw mix was fractions of a percent.

The mixing of a mineralizer with individual components of raw mixes produced a stronger effect upon the increase in the strength during the first days of tests (in 3 and 7 days).

All the plants located near the one applying the above technology used the favourable influence of the mixing conditions. Using sodium silicofluoride as a catalyst, similar results were obtained.

REFERENCES

Berg, L.G., "Fast Quantitative Phase Analysis", USSR Academy of Sciences , Moscow, 1952, 52 pp.

Klassen, V.K., Luginina I.G., "Phase Transformations in Open Carbonate - Sulphate - Silicate Systems" // "Physicochemical Fundamentals of Oxide and Silicate Materials Synthesis", Proceedings of the Moscow Mendeleyev Chemical Engineering Institute, Moscow, 1987. pp. 137 - 143.

Leonov, A.I., Kostikov, Yu.P., Strykanov, V.S., "The Influence of Surface Microphases on Physicochemical Properties of Oxides", Successes in Chemistry Journal, 1988, pp. 1233 - 1251.

Luginina, I.G., Konovalov, V.M., "Cement from Substandard Raw Materials", Novocherkassk, 1994, 230 pp.
Rumyantsev, P.F., "The Use of a High-Temperature Microscope for Silicates" // "Silicates and Oxides in High-Temperature Chemistry", Mendeleyev All - Union Chemical Society, 1963, pp. 41 - 51.
Volkonsky, B.V., Konovalov, P.F., Makashev, S.D., " Mineralizers in Cement Industry", Gostroiizdat Publishers, Moscow, 1964, 197 pp.
Zhuravlev, V.F., Golynko-Volfson, S.L., Sychev, M.M.. "Mechanism of Mineralizer Action", Cement Journal, No. 3, 1950, pp. 3 - 7.

USE OF WASTE LOW GRADE FLUORSPAR AS A MINERALIZER FOR THE MANUFACTURE OF CLINKER/CEMENT

S. P. GHOSH, National Council for Cement and Building Materials, New Delhi, India
K. MOHAN, National Council for Cement and Building Materials, New Delhi, India

ABSTRACT Investigations have been conducted for utilization of low grade fluorspar, a waste from non-ferrous metallurgy as well as from mining, as a mineralizer for the manufacture of clinker/cement from relatively difficultly burnable plant raw mixes. Burnability and microscopic studies have been carried out with different raw mixes prepared in the laboratory and kiln feed from plants with and without different doses of low grade fluorspar as mineralizer. The impact of granulometry of raw mix on burnability vis-a-vis mineralizer addition has also been studied. The cements prepared from clinkers with and without mineralizer have also been evaluated for their physical performance.

KEY-WORDS : Burnability of raw mixes, Mineralisers in clinker making, Microscopy

INTRODUCTION

Various studies have been carried out in different countries on the use of mineralizers for accelerating the clinkering reactions, lowering the burning zone temperature and energy savings. A comprehensive review on the use of mineralizers in clinkering process has been presented by Klemm and Skalny (1976) and Moir and Glasser (1972). Among most of the mineralizers, fluorides have been most experimented mineralizer.

In the present study, investigations have been conducted (a) for utilisation of low grade fluorspar, a waste from non-ferrous metallurgy as well as from mining, as a mineralizer for the manufacture of clinker/cement from relatively difficultly burnable plant raw mixes, and (b) on the impact of granulometry of raw mix on burnability vis-a-vis mineralizer addition.

EXPERIMENTAL

Materials

Two samples of limestone, one sample each of laterite, bauxite, iron ore, and coal and three samples of kiln feeds (plant raw mixes) from different cement plants were used in this study. Waste low grade fluorspar was used as a mineralizer.

Chemical compositions of limestones, laterite, bauxite, iron ore, coal ash and low grade fluorspar are given in Tables 1 and 2.

Table 1 - Chemical Compositions of raw materials, additives and coal ash

Sample Reference	LOI	SiO2	Al2O3	Fe2O3	CaO	MgO
Limestone 1	35.12	12.95	2.90	1.47	45.10	0.80
Limestone 2	36.20	12.37	3.07	1.41	45.33	0.60
Laterite	14.20	15.20	13.10	53.00	1.50	1.00
Bauxite	21.03	6.70	40.27	28.90	1.50	0.70
Iron Ore	-	-	-	90.13	-	-
Coal Ash	-	62.20	27.00	5.00	4.80	0.50

Table 2 - Chemical Composition of Waste low grade fluorspar

SiO2	Al2O3	Fe2O3	CaF2
49.35	2.10	1.50	40.00

Chemical compositions of plant raw mixes (kiln feeds) are given in Table 3.

Table 3 - Chemical compositions of plant raw mixes (kiln feeds)

Sample Reference	LOI	SiO2	Al2O3	Fe2O3	CaO	MgO	LSF	SM	AM
KF-1	35.96	12.19	3.13	2.57	44.63	0.73	1.13	2.14	1.22
KF-2	36.81	11.53	2.71	2.62	45.17	0.42	1.21	2.16	1.03
KF-3	35.66	13.11	2.98	2.4	44.55	0.68	1.06	2.44	1.24

Chemical compositions of two laboratory prepared raw mixes, one designed with limestone-1 and laterite and another designed with limestone-2, bauxite and iron ore are given in Table 4. The plant raw mixes (kiln feeds) and laboratory prepared raw mixes were so chosen as to represent variation with respect to their compositions.

Table 4 - Chemical Compositions of laboratory prepared raw mixes

Sample Reference	LOI	SiO2	Al2O3	Fe2O3	CaO	MgO	LSF	SM	AM
RM-1	35.40	13.00	3.10	2.50	44.20	0.79	1.06	2.32	1.24
RM-2	36.60	12.13	3.03	2.50	44.86	0.60	1.14	2.19	1.21

Method

Raw Mix Preparation and Burnability Studies

Laboratory prepared raw mixes were prepared by weighing raw materials as per the designs of RM-1 and RM-2. The fineness of raw mix RM-1 was kept at (a) 15% residue on 170 mesh and 1% residue on 72 mesh, and (b) 20% residue on 170 mesh and 3% residue on 72 mesh, whereas the fineness of RM-2 was kept at 15% residue on 170 mesh and 1% residue on 72 mesh. The fineness of the plant raw mixes (kiln feeds) KF-1, KF-2 and KF-3 were determined and these were in the range of 15-16% residue on 170 mesh and 1-1.5% residue on 72 mesh. The fineness of fine coal was kept at 15% residue on 170 mesh and 1% residue on 72 mesh.

About 100 gms of raw meal was prepared, for each of the plant and laboratory prepared raw mixes. Proportionate quantity of coal ash (7%), with and wihout different doses (0.5%, 1.0% and 1.5%) of low grade fluorspar was added to the raw meal and homogenized thoroughly. About 10 to 12 mm size nodules were then made manually using tap water. The nodules were then oven dried at 105°C for two hours and the dried nodules were fired at laboratory furnace at 1350°C, 1400°C and 1450°C separately with 30 minutes retention time in each firing. The clinkers so prepared were quenched in water and they were analysed for their free lime contents. Selected clinkers were subjected to optical microscopic examination also.

Burnability studies on the following raw mixes were carried out :

(i) KF-1, KF-2, KF-3, RM-1 (havinig 15% residue on 170 mesh and 1% residue on 72 mesh) and RM-2 with and without 0.5%, 1.0% and 1.5% low grade fluorspar.

(ii) RM-1 (having 20% residue on 170 mesh and 3% residue on 72 mesh) with and without 0.5% and 1.0% low grade fluorspar.

Performance Studies of Cements

The possible effects of low grade fluorspar on the performance of cement was also studied by preparing cements from clinkers with and without low grade fluorspar and comparing their setting times and compressive strengths.

Cement-1 was prepared by intergrinding clinker, prepared at 1450°C from KF-2 without low grade fluorspar, with 5% gypsum and cement-2 was prepared by intergrinding clinker, prepared at 1400°C from KF-2 with 1% low grade fluorspar, with 5% gypsum. The fineness of both cements were kept at around 2700 cm^2/gm.

RESULTS AND DISCUSSION

The effect of addition of low grade fluorspar on the burnability of raw mixes

The results of the burnability studies of the plant and laboratory prepared raw mixes with and without low grade fluorspar at different temperatures are summarized in Tables 5 and 6.

Table 5 - Burnability Studies of Plant Raw Mixes

Sl No	Sample Reference	Dosage of Fluorspar (%)	Free Lime (%)		
			1350oC	1400oC	1450oC
1	KF-1	0.0	1.7	0.9	0.6
2	KF-1	0.5	1.3	0.6	0.3
3	KF-1	1.0	0.6	0.4	0.3
4	KF-1	1.5	0.5	0.4	0.2
5	KF-2	0.0	2.7	1.4	0.9
6	KF-2	0.5	1.8	1.1	0.9
7	KF-2	1.0	1.4	0.9	0.7
8	KF-2	1.5	1.1	0.9	0.5
9	KF-3	0.0	3.3	2.0	1.3
10	KF-3	0.5	3.0	1.9	1.3
11	KF-3	1.0	2.6	1.4	1.3
12	KF-3	1.5	2.0	1.2	1.0

Table 6 - Burnability Studies of Laboratory Prepared Raw Mixes

Sl No	Sample Reference	Dosage of Fluorspar (%)	Free Lime (%)		
			1350oC	1400oC	1450oC
1	RM-1	0.0	1.8	1.3	0.9
2	RM-1	0.5	1.6	0.9	0.8
3	RM-1	1.0	1.3	0.8	0.6
4	RM-1	1.5	1.1	0.7	0.5
5	RM-2	0.0	1.5	0.8	0.5
6	RM-2	0.5	0.8	0.5	0.4
7	RM-2	1.0	0.5	0.4	0.3
8	RM-2	1.5	0.4	0.2	0.2

The results indicate that for both the plant and laboratory prepared raw mixes the free lime contents of clinkers decrease with an increased dosage of low grade fluorspar from 0 to 1.5% at each temperature 1350°C, 1400°C and 1450°C.

The free lime contents of clinkers prepared at 1350°C from KF-1 and RM-2 with 1.0% low grade fluorspar are more or less the same as those of clinkers prepared at 1450°C without low grade fluorspar.

The free lime contents of clinkers prepared at 1400°C from KF-2 and KF-3 with 1.0% low grade fluorspar are more or less the same as those of clinkers prepared at 1450°C without low grade fluorspar.

The free lime content of clinker prepared at 1400°C from RM-1 with 0.5% low grade fluorspar is more or less the same as that of clinker prepared at 1450°C without low grade fluorspar.

The above results indicate that low grade fluorspar acts as a mineralizer and not more than 1% of low grade fluorspar (0.4% CaF_2) is required for obtaining improved burnability. However, the amount of mineralizer and the degree of lowering of burning temperature vary from raw mix to raw mix with minimum lowering of clinkerisation temperature by 50°C and maximum by 100°C.

The above findings are in agreement with the results obtained by Klemm and Skalny (1976), Klemm and Jawed (1980) and Blanco et al (1984).

Optical Microscopic Studies

The clinkers prepared at 1450°C from KF-1 and RM-1 without low grade fluorspar, clinker prepared at 1350°C from KF-1 with 1% low grade fluorspar and clinker prepared at 1400°C from RM-1 with 0.5% low grade fluorspar were subjected to optical microscopic studies.

The clinker prepared at 1450°C from KF-1 without low grade fluorspar shows microhomogeneity with alite and belite occurring mostly in separate clusters. Both these phases are mostly subhedral to anhedral in form without indistinct grain boundaries. Alite and belite grains are mostly regular in shape. The clinker prepared at 1350°C from KF-1 with 1% low grade fluorspar shows better morphology and much less microinhomogeneity. Alite and belite are evenly distributed with the interstitial phases. Alite grains are well formed with distinct boundaries.

The clinker prepared at 1450°C from RM-1 without low grade fluorspar shows predominant microinhomogeneity with alite and belite occurring mostly in separate clusters. Both these phases are mostly anhedral in form with indistinct grain boundaries. Alite grains are mostly irregular in shape. The clinker prepared at 1400°C from RM-1 with 0.5% low grade fluorspar shows better morphology and much less microinhomogeneity. Alite grains are subhedral, tabular to prismatic. Belite grains are anhedral to subhedral, round in form.

The mineral composition by optical microscopy shows that the clinkers prepared with low grade fluorspar have higher alite and lower free lime contents than those prepared without low grade fluorspar.

The above results indicate that clinkers with mineralizer show better burnability and morphology of clinker phases.

The effect of granulometry of raw mix on the burnability of raw mixes vis-a-vis mineralizer addition

The results of the effect of granulometry of raw mix on the burnability of laboratory prepared raw mix vis-a-vis mineralizer additon are given in Table 7.

Table 7 Burnability Studies of Laboratory Prepared Raw Mix with different fineness

	Sample	Dosage of	Residue of Raw Mix (%)		Free Lime (%)		
Sl No	Reference	Fluorspar(%)	+ 170	+ 72	1350oC	1400oC	1450oC
1	RM-1	0	15	1	1.8	1.3	0.9
2	RM-1	0	20	3	2.1	1.6	1.1
3	RM-1	0.5	15	1	1.6	0.9	0.8
4	RM-1	0.5	20	3	1.7	0.9	0.9
5	RM-1	1	15	1	1.3	0.8	0.6
6	RM-1	1	20	3	1.5	0.9	0.6

The results indicate that the free lime contents of clinkers decrease at both the fineness levels with increase in the dosage of low grade fluorspar from 0 to 1.0% at each temperatures 1350°C, 1400°C and 1450°C.

The free lime content of clinker prepared at 1450°C from finer ground raw mix (15% residue on + 170 and 1% residue on + 72) without low grade fluorspar is more or less the same as those of clinkers prepared at 1400°C from coarser ground raw mix (20% residue on + 170 and 3% residue on + 72) with 0.5% and 1.0% low grade fluorspar. The results indicate that even with coarser ground raw mix but by addition of 0.5% to 1.0% low grade fluorspar, the burnabillity of raw mix improves alongwith lowering of burning temperature by 50°C.

The effect of mineralizer on the properties of cement

The results of the effects of low grade fluorspar on the properties of cement are presented in Table 8.

Table 8 - Effect of mineralizer on the properties of cement

Sl No	Sample Reference	Dosage of Fluorspar(%)	Setting Time (Min)		Compressive Strength (kg/cm2)		
			Int.	Final	3-days	7-days	28-days
1	Cement-1	0.0	125	195	200	280	410
2	Cement-2	1.0	135	200	220	310	440

The results indicate that cement prepared from mineralized clinker has slightly higher compressive strengths. This may be due to better quality and morphology of mineralized clinker.

CONCLUSION

Waste low grade fluorspar can be used as a mineralizer for the manufacture of Clinker/Cement from relatively difficultly burnable plant raw mixes. The optimum dosage of the mineralizer coupled with control of the granulometry of the kiln feed can provide the desired results.

REFERENCES

Blanco, M.T., Palomo, A. and Vazques, T., "Effect of fluorspar on the formation of clinker phases", Cement and Concrete Research, Vol. 14, 1984, pp. 397-406.

Klemm, W.A. and Skalny, J. "Mineralizers and fluxes in the clinkering process", Cement Research Progress, 1976, pp. 256-291.

Klemm, W.A. and Jawed, I., "Mineralizers and fluxes in the clinkering process III Burnability of synthetic and Industrial raw mixes", 7th International Congress on the Chemistry of Cement, Paris, Vol.II, 1980, pp. I-150-I-155.

Moir, G.K. and Glasser, F.P., "Mineralizers, modifiers, and activators in the clinkering process", 9th International Congress on the Chemistry of Cement, New Delhi, Vol. I, 1992, pp. 125-152.

Tong, D. and Tin, Z., "The role of CaF_2 and $CaSO_4$ in cement clinkering", 8th International Congress on the Chemistry of Cement, Rio de Janeiro, Vol.II, 1986, pp. 117-121.

USE OF FLUORSPAR AND BARITE FOR IMPROVED BURNABILITY AND CLINKERISATION OF CEMENT RAW MIXES

Ajoy K MULLICK, Subhash C AHLUWALIA, Rakesh BHARGAWA
National Council for Cement and Building Materials, New Delhi, India

ABSTRACT Investigations on the use of barite to improve the lime assimilation of the cement raw mix have indicated improved burnability and lowering of burning temperature by 55°C. Use of fluorspar (0.1-0.25 percent F) significantly lowered the first liquid formation temperature but rendered the raw mix sensitive to temperature change in the range 1355-1400°C with the raw mix fusing at ~1375°C.

Keywords: Burnability of raw mixes, Clinker formation, Mineralizers in clinker making.

INTRODUCTION

The role of minor components in portland cement clinkers used as mineralisers have been discussed and reviewed adequately (Timashev, 1980, Bucchi, 1980, Moir and Glasser, 1992), Some mineralisers provide fluxing action to reduce the temperature of first liquid formation, modifying viscosity and surface tension of the liquid and morphology of crystals. In addition, clinker phase relations and the hydraulic activity are modified by solid solution effects. This paper presents the results of an investigation on the use of naturally occurring fluorspar and barite to mineralise cement raw mixes in a dry process cement plant.

ROLE OF FLUORINE AND BARIUM

Among the various minor components studied, the role of fluorides (F) and barium (Ba) additions are of particular relevance to the present investigation. Performance of a mineraliser depends upon the components and proportions of the raw meal as well as other minor components present. In general, fluoride-bearing mineralisers have been reported to lower the temperature of first liquid formation and reduce the viscosity and surface tension of the clinker liquid (Timashev, 1980). In addition, mineralising action of enhancing the thermodynamic stability of C_3S phase relative to C_2S, enabling the former to be formed at temperature below 1250°C, has also been reported (Welch and Gutt, 1960). On the other hand, barium containing additives are reported to activate C_2S phase by formation of solid solution of Ba in C_2S and modifying interstitial aluminate phases linking belite grains (Rajczyk and Nocum-Wezelik, 1992). The clinkerisation temperature was lowered and hydraulic activity increased. In another investigation, the use of barite was found to be particularly useful in cement clinker with lower LSF and higher C_2S content and although addition of barite increased free lime content, the compressive strength of cement increased due to activation of C_2S phase by Ba (Xianyu, Liqun and Jian, 1992). Combined addition of barite and fluorspar had the additional effect of lowering free lime content and increasing C_3S content and much higher compressive strength were obtained in commercial clinkers.

In appreciating the role of barite as mineraliser, the effect of sulphate have to be taken into account, in addition to Ba. In the oxidising environment of the cement rotary kiln all sulphur compounds are oxidised to SO_3 which is absorbed in the basic cement mix.

Small quantities (0.1-0.5%) of SO_3 have a catalysing effect on fixing CaO and increases the alite content (Butt and Timashev, 1974). SO_3 upto 3 percent is also reported to reduce the melt viscosity significantly. SO_3 when present as R_2SO_4 acts as mineraliser and promotes formation of C_3S from its component oxides and some of the adverse affects of SO_3 are modified (Gutt and Smith, 1971). Presence of SO_3 also improves the clinker grindability.

EXPERIMENTAL

The investigations were aimed at optimising the raw mix including use of mineralisers for a 3700 tpd dry process cement plant with five-stage preheater and a separate line precalcinator of FLS design. The main raw material - limestone was obtained from three different mines and blended at the plant site in a stacker reclaimer. There was considerable variation in the CaO content of limestone from different mines as well as in samples from a single source obtained at different intervals. Typical composition of composite limestone is shown in **Table 1**. Chemical composition of other constituents of the three component raw mix - laterite and bauxite as well as barite and fluorspar to be used as mineralisers are also given in Table 1. Limestone contained about 13.2% SiO_2. Laterite and bauxite, used as corrective materials to supplement Al and Fe in the raw mix, also contained 14 to 15 percent SiO_2.

Table 1 Chemical Analysis of Raw Materials and Mineralisers

Sl No	Raw Materials	LOI	SiO_2	Fe_2O_3	Al_2O_3	CaO	MgO	Na_2O	K_2O	$SiO_{2(f)}$	TiO_2	$BaSO_4$	F
1	Limestone (Composite)	35.96	13.20	0.90	2.17	45.60	0.60	0.30	0.42	9.28	--	--	--
2	Laterite	12.98	14.31	58.93	11.45	1.39	0.29	0.14	0.08	--	0.63	--	--
3	Bauxite	11.05	15.12	30.17	34.97	0.92	0.66	0.09	0.02	--	7.09	--	--
4	Barite	0.36	--	--	--	--	--	0.07	0.10	--	--	97.25	--
5	Fluorspar	3.30	18.33	0.78	2.06	45.13	0.30	0.55	0.73	--	--	--	29.85

Coal from different sources obtained commercially, used with lignite (5-10 percent) were blended at the plant site to result in ash content of 30-31 percent and calorific value of 4250-4350 kcal/kg in the blended coal. The raw mix made with such raw materials was difficult to burn. Because of presence of free SiO_2 in raw materials and absorption of coal ash, the mixes had to be lime-rich and free lime in commercial clinkers was of the order of 1.5 percent or more.

The investigations were taken up in two stages. In the first stage, the raw mix was optimised to reduce the free lime in the resultant clinker without lowering cement strength properties. This comprised not only altering the raw mix composition, but also optimising the grinding of raw mixes and fuel as well as control on the entire pyroprocessing. Complete details are given in the Project Report (NCB 1996); as such only salient details will be reported here. The second stage was the use of mineralisers to further improve the burnability of the optimised raw mix, and improve the quality of clinker produced from it.

OPTIMISATION OF RAW MIX

On evaluation of operating and design parameters, the raw mix was aimed to be optimised so as to have LSF 0.88, SM 2.45 and AM 1.5 in the clinker. After repeated trials, three raw mixes RM-A, RM-B and RM-C were chosen for further evaluation. The details of the three mixes along with the mix adopted by the plant so far are given in **Table 2**. The trial raw mixes were prepared with coal ash absorption of 5.5 percent which corresponded to the prevailing level of fuel ash absorption. Fineness of the ground mix had 17 percent residue on 90 μ sieve. Burnability studies were carried out on pressed pellets fired in a laboratory furnace at temperatures of 1350°, 1400° and $1450^{o}C$; the retention time being 20 minutes in each case. The clinkers prepared from the raw mixes after firing were analysed for free lime content. Mineralogy, morphology and microstructure of clinkers were also determined.

Table 2 Comparison of Design Parameters of Raw Mixes

Sl No	Raw Mix	Raw Materials				Moduli Values			Potential Phase Composition				
		Limestone	Bauxite	Laterite	Coal ash	LSF	SM	AM	C_3S	C_2S	C_3A	C_4AF	Liquid content
1	Plant Raw Mix - P	96.0	2.0	2.0	--	0.91	2.74	1.31	49.84	28.46	6.47	11.11	--
2	RM - A	99.75	0.02	2.23	5.5	0.89	2.73	1.35	55.31	23.76	6.73	10.83	24.10
3	RM - B	97.22	0.77	2.01	5.5	0.88	2.60	1.39	50.64	27.43	7.36	11.16	25.38
4	RM - C	96.42	1.67	1.91	5.5	0.87	2.39	1.39	45.39	31.08	7.95	12.04	27.29

The results are presented in **Fig.1**. All the three trial mixes gave free lime content less than 0.5 percent at $1450^{o}C$. Raw mix B was chosen for preparation of bulk clinker which was studied for chemical, mineralogical and physical properties. The potential Bogue composition indicated C_3S and C_2S contents of 49 and 29 percent respectively, which were estimated to be 48 and 32 percent by XRD. Optical microscopic analysis showed fairly well developed and homogeneously distributed phases (NCB, 1996).

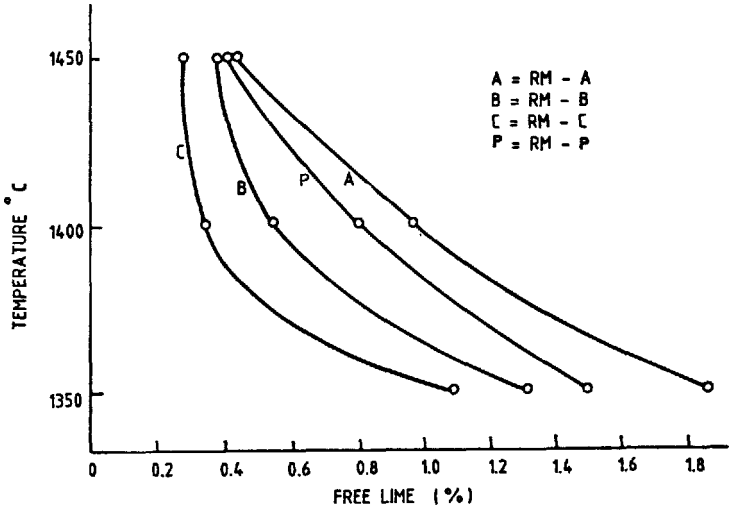

Figure 1 Burnability of Designed Raw Mixes and Plant Raw Mix

EVALUATION OF MINERALISERS

Locally available fluorspar and barite sample were used in the trials. Barite with 97.25 percent $BaSO_4$ contained very little impurities. Fluorspar sample had CaF_2 content of the order of 61.27 percent (F 29.85 percent) and SiO_2 as impurity of 18.33% (Table 1).

Fluorspar

Investigations were carried out using 0.15, 0.25 and 1.0 percent F on all the three raw mixes RM-A, RM-B and RM-C. Full details are available in the Project Report (NCB, 1996), as such results with optimised raw mix RM-B will only be presented. Burnability studies were carried out at 1300, 1350 and 1400°C with retention time of 20 minutes. Heating microscopic studies were also carried out to study the effect of the mineraliser on the first liquid formation temperature.

Burnability isotherms are given in **Fig. 2**. At 1 percent level of F there was softening in temperature range of 1300-1350°C, which was not desirable. At 0.15 percent level F, the burnability temperature (corresponding to 0.5 percent free lime) was 1325°C and for 0.25 percent F, it was 1300°C, compared to 1425°C for raw mix RM-B without mineraliser. Similar trends were obtained with raw mixes RM-A and RM-C also. Thus fluorspar at levels of 0.15 and 0.25 percent F has considerable mineralising effect. Hot stage microscope studies indicated that the raw mixes had a tendency to fuse at 1375°C and were considerably sensitive to temperature, especially with 0.25 percent F : Thus 0.15 percent level F (0.5 percent fluorspar) was chosen for further evaluation.

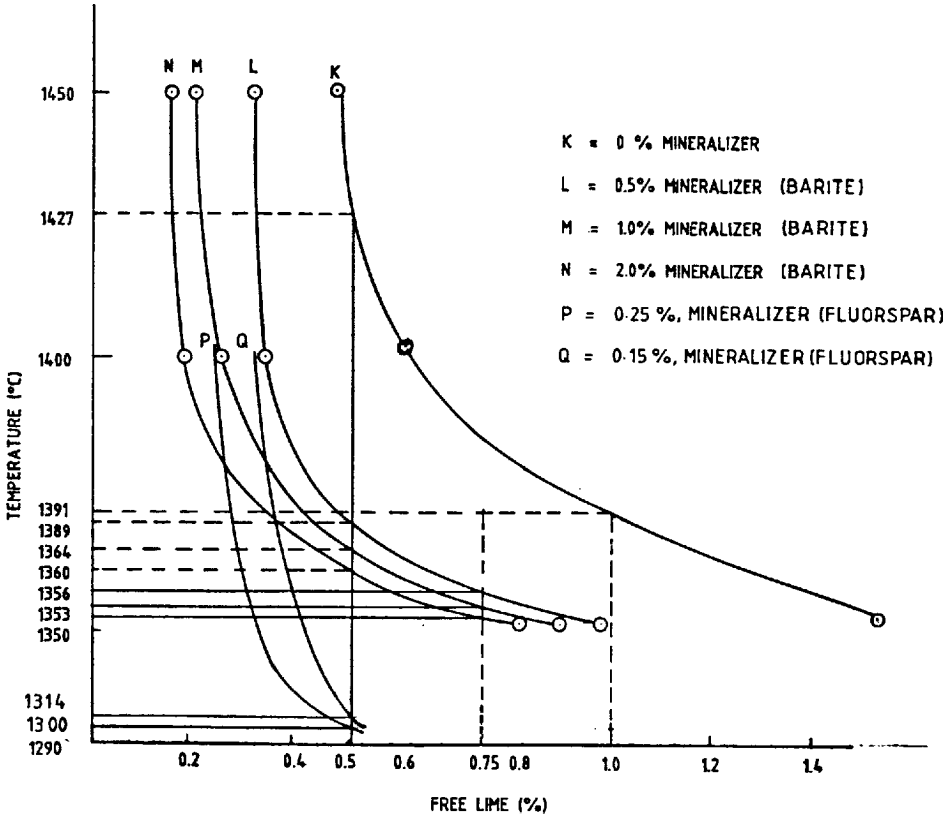

Figure 2 Effect of Barite and Fluorspar Mineralizer on Burnability of Raw Mix RM-B

Barite

Similar burnability studies were carried out on the three raw mixes RM-A, RM-B and RM-C using 0.6, 1.0 and 2 percent BaO. Unlike with fluorspar, no softening upto 1450°C was noticed in hot stage microscopy, when using barites. Burnability studies were, therefore, carried out upto 1450°C. Results of raw mix RM-B as burnability isotherms are shown in Fig. 2 along with those for fluorspar. Barium (Ba) was found to impart mineralising effect in improving burnability by reducing free lime content, although to a lower degree than fluorspar. A dose of 0.5 percent BaO was chosen for evaluation in bulk clinker, as there was no marked advantage of using higher dosages.

Evaluation of Clinker and Cements

Bulk clinkers prepared from raw mix B with 0.15 percent F (with fluorspar) and 0.50 percent BaO (with barite) were compared for physical, chemical and mineralogical characteristics. On the basis of burnability studies, the pelletised mixes were fired at 1450°C when plain raw mix was used and at 1350°C and 1400°C with fluorspar and barite respectively. Ordinary portland cement was prepared in each case by grinding with gypsum (purity 85.57 percent) so as to maintain SO_3 content 1.75 percent, at a fineness of 300 m^3/kg Blaine's. Free lime content in mineralised mixes were less than 0.5 percent (**Table 3**) even when fired at lower temperatures than the parent raw mix XRD studies (**Fig. 3**) revealed increase in C_3S contents with use of mineralisers and use of barite resulted in 53 percent C_3S compared to 49 percent in case of fluorspar (Table 3). Optical microscopy indicated improvement in crystal morphology and microstructure of clinkers containing fluorspar (**Plate 1**) and barite (**Plate 2**) mineralisers. The mineral compositions obtained from optical microsocpy and XRD were in close agreement.

Table 3 Characteristics of Clinkers and Cements from Raw Mix B

Details of Raw Mix and Clinker	Free Lime (%)	Phase Comp. by XRD, %				Properties of Cement						
		C_3S	C_2S	C_3A	C_4AF	IST (mts)	FST (mts)	Comp. St. (N/mm^2) 3d	7d	28d	Soundness Auto. (%)	Lechat. (mm)
Plain, 1450°C	0.35	48	29	6	12	110	160	27.5	39.6	53.0	0.02	1.0
With Barite, 1450°C	0.33	53	28	6	12	100	152	33.1	44.4	57.5	0.02	1.0
With Fluorspar, 1350°C	0.41	49	28	7	13	90	145	28.6	40.5	54.2	0.02	1.0

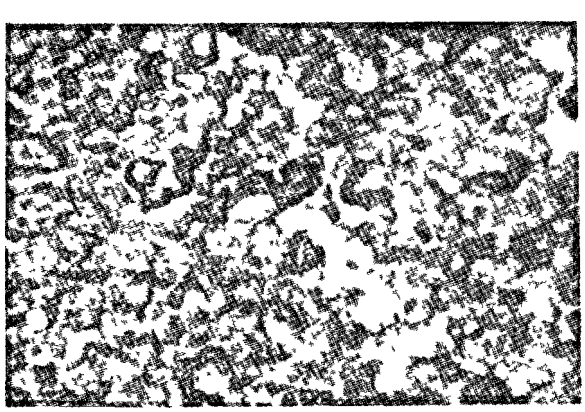

Plate 1

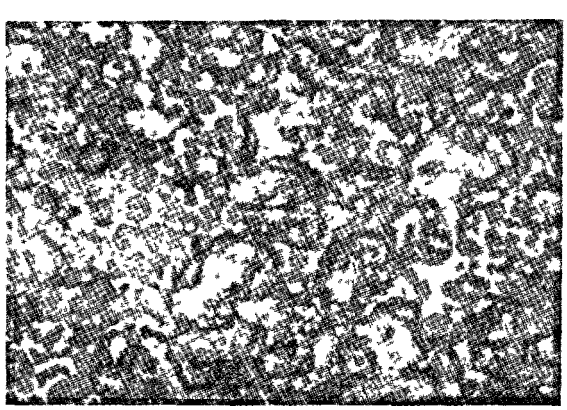

Plate 2

Evaluation of cements prepared from bulk clinkers indicated no change in setting times and increase in compressive strength, especially with barite (Table 3).

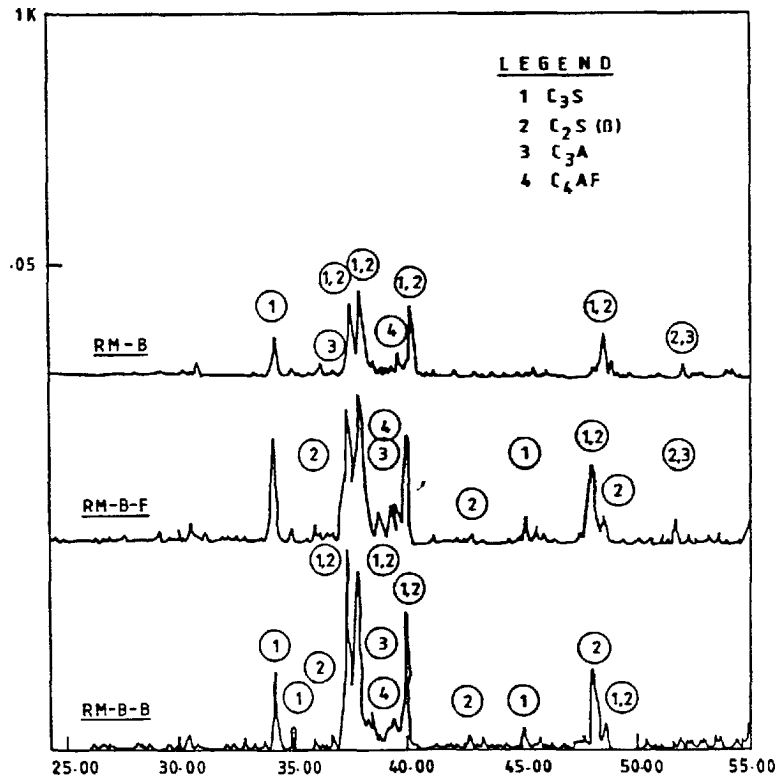

Figure 3 X-Ray Diffractogram of Clinkers Prepared with/without Mineralizers

DISCUSSION

The results of the investigations have clearly indicated that although fluorspar, in the concentrations studied, has considerably higher mineralising effect compared to combined effect of BaO and SO_3 derived from barite as mineraliser, it has severe limitation in application due to high temperature sensitivity of the commercial raw mix mineralised with fluorspar. It could make the pyroprocessing operations difficult, particularly the granulometry, cooling characteristics, morphology and microstructure of the clinker. Literature record conflicting results with use of Ba as mineraliser. The study indicated perceptible advantages, both in terms of lime assimilation as well as clinker quality with use of Barite.

CONCLUSION

For difficult-to-burn raw mixes prepared with crystalline limestone having 14 percent silica, optimisation resulted in lowering of free lime content. Further improvements in burnability were achieved with the use of fluorspars as well as barites as mineralisers. Between the two, barite was preferred, as mixes with fluorspars were sensitive to temperature rise and therefore, likely to be difficult to control. The cost of mineraliser was more than offset by lowering the fuel cost, which resulted due to lowering of clinkerisation temperature by 55°C. Decrease in air required for coal combustion could allow increase in clinker production.

ACKNOWLEDGEMENT

This paper is published with the permission of Director General, National Council for Cement and Building Materials, New Delhi, India.

REFERENCES

Bucchi, R., "Influence of the Nature and Preparation of the Raw Materials on the Reactivity of the Raw Mix", Principal Reports, I-1/3-1/43, Vol. 1, 7th International Congress on Chemistry of Cement, Paris, 1980.

Butt, Y.M., Timashev, V.V., and Osokin, A.P. (1974) "The Mechanism of Clinker Formation-Processes and the Modification of its Structure", 6th International Congress on Chemistry of Cement, Moscow.

Gutt, W., Smith, M.A., (1971), "Studies of Sulphates in Portland Cement Clinker", Cement Technology, 2, 143.

Moir, G.K. and Glasser, F.P., "Mineralisers, Modifiers and Activators in the Clinkering Process", Generic and Specific Theme Reports, 125-152, Vol. 1, 9th International Congress on Chemistry of Cement, New Delhi, 1992.

NCB Report, "Optimisation of Raw Mix Design" for M/s JK Cement Works, Nimbahera, Distt: Chittorgarh, Rajasthan, India (1966).

Rajczyk, K. and Nocun - Wczelik, W., "Studies of Belite Cement from Barium Containing Byproducts", Theme I, 250-254, Vol. II, 9th International Congress on Chemistry of Cement, New Delhi, 1992.

Timashev, V.V., "The Kinetics of Clinker Formation - The Structure and Composition of Clinker and its Phases", Proc. 7th International Congress on Chemistry of Cement, Paris, Vol. 1, I-3/1-3/20, 1980.

Welch, J.H. and Gutt, W., "The Effect of Minor Components on the Hydraulicity of the Calcium Silicates", Proc. 4th International Symposium on Chemistry of Cement, Washington, 1, 59, 1960.

Xianyu, Xu, Liqun, Jang and Jian, Chen, "Burning Cement Clinker from the Raw Meal using Barite and Fluorspar as a Combined Admixture", Them I, 427-433, Vol. II, 9th International Congress on Chemistry of Cement, New Delhi, 1992.

CLINKERISATION OF ANHYDRITE WITH PHOSPHOGYPSUM AND CALCIUM FLUORIDE

Ludmila I. SYCHOVA, Mikhail V. ANUFRIEV., Russian University for Chemical Technology n.a. D.I. Mendeleev

ABSTRACT. Problems related to liquid phase sintering in systems based on calcium sulfate, calcium fluoride and phosphogypsum have been considered. Methods of optimisation of a process of liquid phase sintering of gypsum raw mixes have been proposed.

KEY-WORDS: anhydrite, calcium fluoride, sintering, shrinkage, viscosity.

INTRODUCTION. Over the recent years, great attention has been paid to the use of wastes in production of various types of clinkers due, first of all to the necessity of environment protection, as well as to high costs and shortage of natural raw materials. Anhydrite cement, produced from industrial wastes, is a highly efficient construction and finishing material due to a number of remarkable characteristics, namely quick setting and hardening, high strength, water resistance and whiteness. The technology of anhydrite cement consists of firing at 900 - 1000°C a raw mix based on a gypsum-containing component (phosphogypsum) and mineralising additives, introduced to enhance the hydraulicity of the anhydrite. Since phosphogypsum contains technological admixtures which reduce firing temperatures, the study of clinkering mechanism of such raw mixtures is of scientific and practical interest.

RESULTS

The aim of the present study was to investigate processes of clinker formation occurring both in the model system $CaSO_4$-CaF_2, and on the basis of industrial raw components: phosphogypsum and wastes containing calcium fluoride.

The synthesis of anhydrite clinker is accompanied by a number of physico-chemical processes consecutively occuring during firing of gypsum-containing raw mixes, namely dehydration of phosphogypsum, inversion of crystalline structure of anhydrite and its sintering. The formation of clinker pellets at temperatures of 500 - 700°C is determined by processes of re-crystallizations and compaction of anhydrite structure and the local appearance of a small quantity of low-temperature eutectic melt, formed by admixtures (first of all phosphates) of phosphogypsum and calcium sulfate. As the temperature increases, a sulphate-fluorine salt melt appears, the presence of which has a major influence on the structure, composition and properties of clinker. The melt occurs in clinker in the form of drops and interlayers of different sizes.

Shrinkage is the measure of intensity of sintering. The linear sizes of specimens during heating-up were measured by dilatometry. Fig. 1 shows the relation between linear sizes of specimens and the temperature (speed of heating was constant). Data obtained show that the shrinkage of specimens in the model system starts in the temperature range of 450 - 550 °C. The extent of shrinkage is connected to the $CaSO_4/CaF_2$ ratio (mixes were investigated which have molar ratio of components from 8/1 to 0,5/1).The shrinkage grows insignificantly (by 2 - 4%) with increasing proportions of calcium fluoride. However, with the growth of temperature this difference vanishes. Sintering of samples based on phosphogypsum increases, and the temperature at which shrinkage begins decreases.

Due to the process of sintering of systems based on calcium sulphate being complex and poorly studied, equations of chemical kinetics were used for the calculation of shrinkage parameters,

which allow us to describe this process with sufficient accuracy. In this instance the sintering process has been considered as a chemical reaction (Ivensen, 1976).

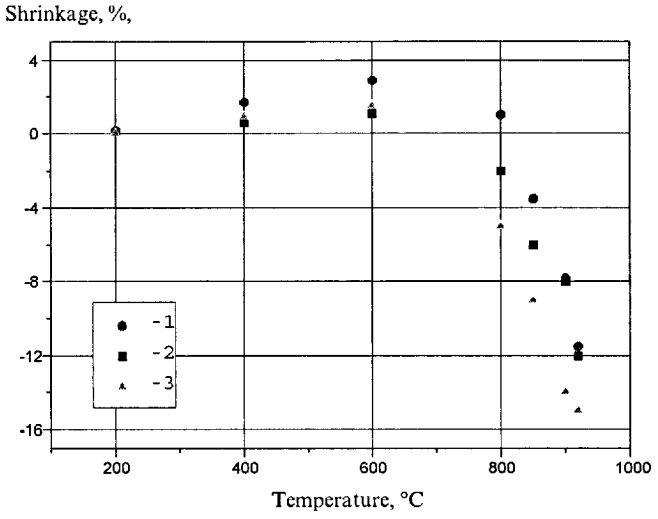

Fig.1 Change of specimens shrinkage in the $CaSO_4$-CaF_2 system during heating-up. Molar ratio $CaSO_4/CaF_2$: 1- 1; 2- 4; 3- 8.

The most accurate description of kinetics of isothermal sintering process can be obtained by means of Kolmogorov's equations (Young, 1969) [1];

$$\varphi = 1 - \exp(-k\tau^n) \quad [1]$$

where φ is the amount of material which has entered into reaction; k, reaction rate constant , s^{-1}; τ, time, s; n, a factor depending on the mechanism of sintering and temperature.

Since the shrinkage is isotropic the value of φ can be determined from changes in specimen length [2];

$$\varphi = (l_1 - l_2)/(l_2 - l_3) \quad [2]$$

where l_1 is the initial length of the specimen; l_2, the length of the specimen at a fixed temperature; l_3, length of the specimen held at the given temperature.

From equations [1] and [2] a dependency can be obtained allowing us to calculate the constants of the process [3]; an energy of activation (E_a) was determined using the Arrenius equation:

$$\ln k + n \ln\tau = \ln\{-\ln(1 - \varphi)\}. \quad [3]$$

Some parameters of the sintering process are shown in the Table 1.

The eutectic melt in the system $CaSO_4$-CaF_2 appears at 951°C. The melt composition is as follows - 63.45 % of $CaSO_4$, 36.55 mass % of CaF_2 (Posypajko, 1980). Its density is 2.528 g/cm^3, viscosity 0.029 Pa·s. This is significantly lower than viscosity of oxide-salt melts which appears during firing of a Portland cement clinker (the viscosity of the salt melt was determined by the vibration method, which consists in the determining relationship between amplitude and frequencies of vibrations of probe immersed into the melt and viscosity of the melt).

Practically, 8 to 12% of melt develops at the production of anhydrite clinker production; it is significantly less, compared to firing of a Portland cement clinker. However, physico-chemical characteristics of the melt (mainly, low density and viscosity) promote synthesis of a high-quality clinker with relatively small amount of liquid phase.

Table 1 Parameters of sintering process in systems $CaSO_4$-CaF_2 and phosphogypsum - CaF_2

Parameter	Molar ratio $CaSO_4/CaF_2$			Molar ratio phosphogypsum/CaF_2
	8 / 1	4/1	1/1	30 / 1
$K*10^2$ at 700°C	0.33	0.10	0.09	0.01
$K*10^2$ at 800 °C	2.04	1.93	1.56	2.90
$K*10^2$ at 900 °C	5.61	4.23	10.2	13.0
n at 700 °C	0.27	0.46	0.41	0.74
n at 800 °C	0.15	0.15	0.20	0.18
n at 900 °C	0.12	0.12	0.07	0.04
A (constant of the Arrenius equation)	$6.46*10^{-4}$	$5.72*10^{-6}$	$9.18*10^{-8}$	$2.79*10^{-17}$
E_a kJ/mol	135218	179224	222680	403400

The amount of melt forming during clinker firing, as well as its properties, can be optimised by introduction of different additives into the melt. Since the viscosity of salt melts is controlled by the mobility of the largest elements of their structure, the introduction of additives containing large anions or anion complexes results in increasing the viscosity of the melt up to 0.014 - 0.020 Pa s. Such components are, for example, glass, $Ca_3(PO_4)_2$, and excessive amounts of $CaSO_4$. On the other hand, excessive amounts of CaF_2 and introduction of the K_2SO_4 additive reduces this factor to 0.007 Pa s (Fig.2). Along with this, in the presence of the potassium sulphate the temperature at which melt starts to develop diminishes by 50°C.
Dependency of viscosity of the salt melt upon the temperature (in logarithmic form) is described by the following equation (Delimarskiy, 1985, Abe, 1982) [4]:

$$\ln \eta = B + E_a / RT \qquad [4]$$

where η, melt viscosity, Pa s; B, a constant; E_a, energy of activation of the viscous flowing, kJ/mol; T, temperature, K.
Results of the study show that dependency between ln η and 1/T is linear, thus, the heating up causes no structure changes in the melt.

The phase composition of the cooled clinker melt includes anhydrite, calcium fluoride and vitreous phase. Crystallisation of phases during cooling of the melt occurs with a deviation from the stoichiometry; the vitreous phase is saturated by the component, which is deficient compared with the eutectic relationship. The microstructure of the cooled sulphate-fluorine melt is formed by tabular and prismatic anhydrite crystals of 10-20 μm (Fig.3). Increasing cooling time brings about a change of morphology of the crystals: they increase in size and assume a distinct crystallographic form. Admixtures present in the phosphogypsum, especially calcium phosphates, develop accicular anhydrite crystals in the crystallised melt.

The insoluble anhydrite is a main phase of clinker. As result it was found that crystalline structure of anhydrite is modified by calcium phosphates present in initial phosphogypsum and additives, introduced into the raw mix. For example, in the presence of calcium phosphates the volume of elementary cell of anhydrite increases from 3.038*10-1 nm^3 to 3.057*10-1 nm^3. Thus, the anhydrite present in the clinker has a distorted, defective crystalline structure. This provides for its increased solubility and, consequently, increased hydration activity.

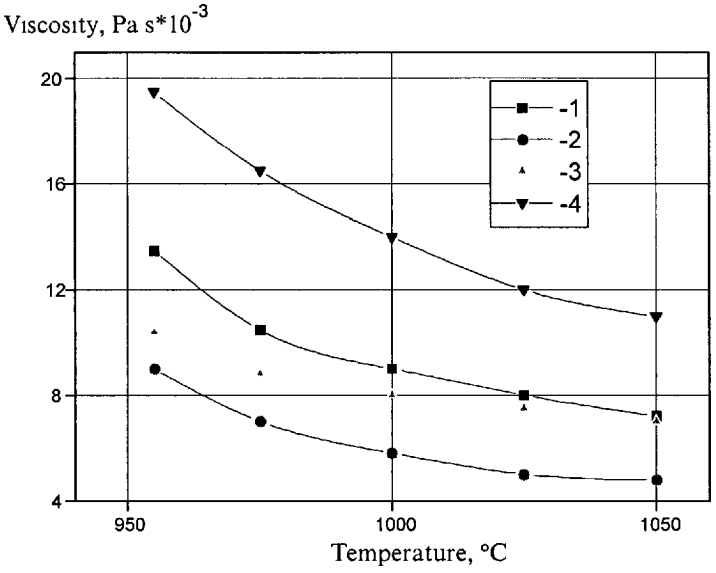

Fig. 2 Dependency of viscosity of the eutectic salt melt in the system $CaSO_4$ - CaF_2 upon the temperature. Content of additives (%):
1. no additives; 2. 4% of CaF_2; 3. 2% of K_2SO_4; 4. 9% of glass.

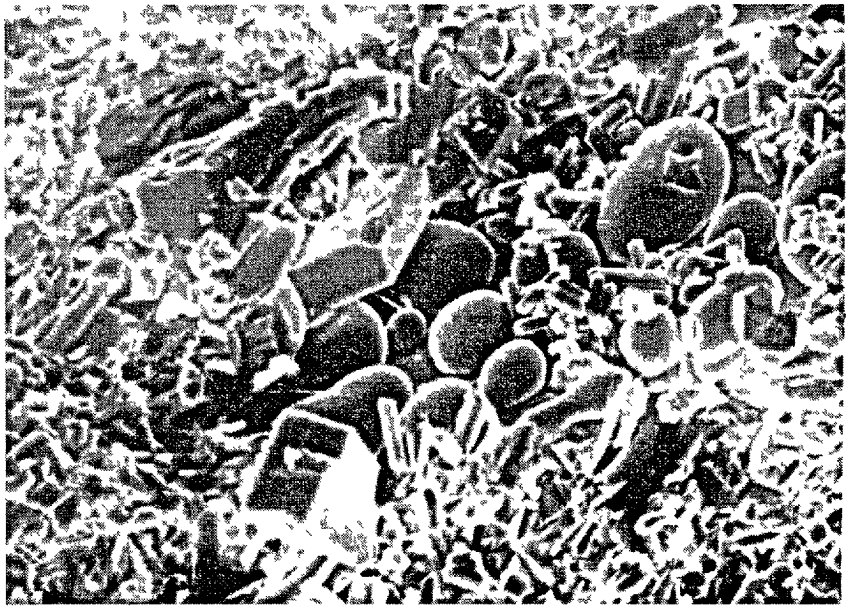

Fig.3. Micro structure of the slowly cooled melt at magnification of 900^x.

REFERENCES

Abe Y. et al., "Viscosity measurements on molten fluoride at elevated temperatures", Proc. 8-th Sump. Theorphys. Prop. New-York, vol. 2, 1982, pp. 282-286.

Delimarskiy, Yu.K., "Chemistry of ionic melts", Naukova Dumka Publishers, Kiev, 1985, 328pp.

Ivensen, V.A.. "Kinetics of compaction of metallic powders", Metallurgiya Publishers, Moscow, 1976, 269pp.

Posypaiko V.I., Alekseeva V.A., Vasina, N.A. "Diagrams of meltability of salt systems", Chimiya Publishers, Moscow, 1980, Vol 3, 204pp.

Young, D., "Kinetics of decomposition of solid materials, Mir Publishers, Moscow, 1969, 263pp.

SYNTHESIS OF MINERALISERS FOR CLINKER MAKING

S.P. GANDHE, D. GHOSH, A.K. CHATTERJEE
Research & Consultancy Directorate
The Associated Cement Companies Ltd.,
Thane - 400 604, INDIA

ABSTRACT The mineralisers used in cement manufacturing are either natural raw materials such as gypsum, fluorspar or industrial by-products like sodium silicofluorides. To achieve process economy and to overcome the problems of usage of high ash fuel , there has been proliferation of usage of mineralisers,however, the main constraint being the effective economic viability. In this context, an attempt has been made to synthesise fluorine based compounds like calcium silicofluoride, iron silicofluoride and sodium silicofluoride using low cost materials like low grade limestone, scrap iron, etc. The efficacy of these synthesised mineralisers was evaluated based on rate of lime combination with temperature. The comparative scenario of these synthetic mineralisers has been depicted vis-a-vis the mineralisers of natural and industrial by product categories in the process of clinkerisation.

KEY- WORDS Synthesis, Mineralisers in clinker making, Waste material utilization.

INTRODUCTION

The Industrial application of mineraliser as a means of energy conservation as well as an avenue to improve quality or to overcome various process problems in clinker burning is well established in India. The Associated Cement Companies Ltd.(ACC) with 12 million tones of installed capacity has been using commercially available mineraliser under diverse process condition at few of its plants. A variety of mineralisers have been used for different objectives, however, the selection is governed by compatibility with a given kilnfeed & process, physical form of mineralisers and source with respect to location of cement plant and cost of transportation. In view of the above considerations together with the rising demand and competitiveness in quality of cement and also the increasing demand of mineralisers in areas other than cement has compelled R&D Division of ACC to undertake studies for synthesis of certain mineralisers.

A range of fluorine based mineraliser using low cost materials were synthesised. The efficacy of these synthesised mineraliser was compared with one another and also with commercially available mineraliser by studying the lime combining behaviour of raw mixes as a function of burning temperature, time and added amount of mineraliser.

UTILISATION OF MINERALISERS / MINERALISER USAGE PATTERN

The selection and use of mineraliser on an industrial scale is primarily to improve quality of clinker or process which depends on its compatibility with the given kilnfeed.

The variety of mineraliser used in ACC's cement plants for various objectives are shown in Table 1

Table 1 Usage Of Mineralisers And Benefits Obtained At ACC Plants

SR. NO.	TYPE OF PLANTS	PROBLEM OF PLANT	MINERALISERS USED	RESULTS OBTAINED	OTHER BENEFITS i.e. SAVING IN KCal/Kg OF CLINKER
1	Semidry Process	Hard burning resulting in high free CaO & low kiln output	Na_2SiF_6	Free CaO reduced. increased kiln output	94
2	Wet Process	Higher consumption of floated limestone due to high loss of lime rich dust.	CaF_2	Reduction in floated limestone by 10%	170
3	Wet Process	Low cement strength 420-525 Kg/cm^2 in 28 days	Gypsum and blue dust combination	Cement strength improved to 540-650 Kg/cm^2 in 28 days	112
4	Wet Process	Unsoundness in clinker	Gypsum and iron ore	Autoclave exp. brought down in freshly ground OPC to less than 0.2%	No data
5	Precalciner Kilns	High generation of dust	Magnesite	Improvement in clinker granulometry	--
6	Wet Process	Unstable coating on refractory lining	Rock Phosphate	Coating stability	--

SYNTHESIS OF MINERALISERS

The experience gained over the years of using mineraliser on a plant scale and also available literature on mineraliser,(Chatterjee et al -1985,Kleem et al -1980,Moir et al -1992) reveals that fluoride either alone or in combination in certain dosages is an effective mineralising compound. Based on this, Fluorine based compounds were chosen for synthesis. In the synthesis the basic objective was to select compounds which are normally found in cement systems and the process of synthesis should yield economically viable product. Therefore the raw materials for the synthesis were chosen to be either waste or reject materials / Chemicals (Subba Rao et al -1984) from process industries. The process involves reaction of commercially available H_2SiF_6 (15%) with limestone (~ 80% purity), scrap iron and soda ash to form Calcium silicofluoride ,Ferrous silicofluoride and Sodium silicofluoride.The details of chemical composition, fineness of the raw material used for synthesising these mineralisers are given in Table 2 and mixed as per stiochiometric proportions. The synthesised products were then examined with respect to their purity, yield and phases formed.

Table 2 Chemical composition of Raw materials used for synthesising mineralisers

	FLUOSILICIC ACID	LOW GRADE LIMESTONE	SODA ASH	IRON SCRAP
% SiO_2	8.3	16.9	--	1.0
% Al_2O_3	--	2.5	--	
% Fe_2O_3	--	0.80	< 0.01	94.0
% CaO	--	43.2	--	0.005
% MgO	--	0.50	--	0.03
% LOI	--	35.7	--	
% P_2O_5	0.50	--	--	< 0.1
% Na_2O	--	--	--	0.003
% K_2O	--	--	--	0.004
% F^-	12.2	--	--	--
% Purity (on F^- basis)	15.4	--	--	--
% Total Carbonates	--	78.4	--	--
% Na_2CO_3	--	--	98.9	--
% NaCl	--	--	0.50	--
%Na_2SO_4	--	--	< 0.01	--
Availability	Commercially available in liquid form	Lump form from limestone quarry	Commercially available in powder form	Available as Sheet form from Scrap
Required Size	As in available form	powder form preferably -200 μ	powder form	To be made in small pieces

The following methods were employed for studying Physico-chemical characteristics of synthesised Silicofluoride powders of Calcium, Iron and Sodium.

- Percentage purity of each powder was determined by using Orion's Fluoride ion analyser model-407. The same was reconfirmed by determining other ions other than fluoride by IL - Atomic Absorption model 951.
- X-ray diffraction (XRD) using Siemens model D 500 for determining phase purity.
- IR spectrum of individual powders were taken using Perkin Elmer IR Model-577. The analysis results of lab synthesised Silicofluorides of Calcium, Iron and Sodium are given in Table 3.

Table 3 Analysis of lab scale synthesised Silicofluoride of Calcium, Iron and Sodium

	$CaSiF_6$	$FeSiF_6$	Na_2SiF_6
APPEARANCE	WHITE	BROWNISH GREEN	WHITE
% PURITY F^-	41.8	26.1	45.5
% PURITY	80.0	70.0	75.0
% YIELD	90.0	94.0	97.0
XRD PHASES MAJOR MINOR ABSENT	 $CaSiF_6.2H_2O$ $CaSiF_6$ CaF_2 & CALCITE	 $FeSiF_6.6H_2O$ $FeSiF_6$ --	 Na_2SiF_6 -- NaF
IR SPECTRA - PRESENCE	-- SiF_6	-- SiF_6	-- SiF_6

Percentage purity of $CaSiF_6.2H_2O$, $FeSiF_6.6H_2O$ and Na_2SiF_6 on % F basis is of the order of 80%, 70% and 75% respectively (Table 3) at an yield of over 90%.

XRD Patterns of Calcium Silicofluoride indicates presence of well crystallised phases of $CaSiF_6.2H_2O$ as well as $CaSiF_6$, and phases of CaF_2 & calcite are absent. XRD patterns of Ferrous Silico fluorides and Sodium Silicofluoride indicate well crystallised phases of the respective compounds (Fig. 1). Infrared analysis of all the mineralisers confirm presence of SiF_6 (Fig. 2).

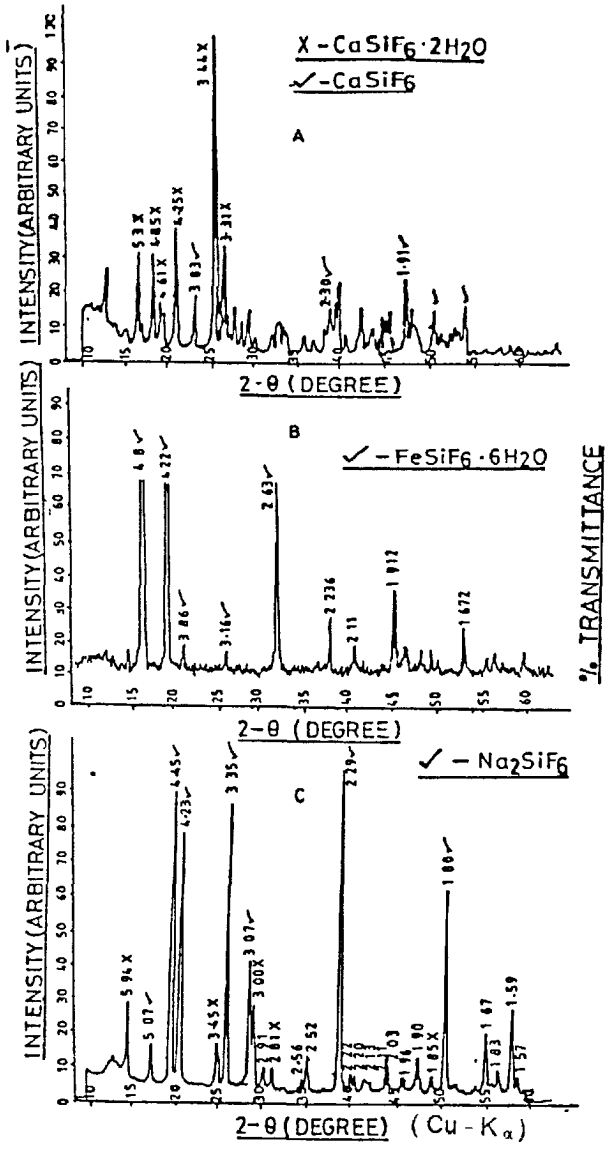

Figure 1 X-Ray Diffracto Grams of Synthesised Silicofluorides
A) Calcium Silicofluoride
B) Ferrous Silicofluoride
C) Sodium Silicofluoride

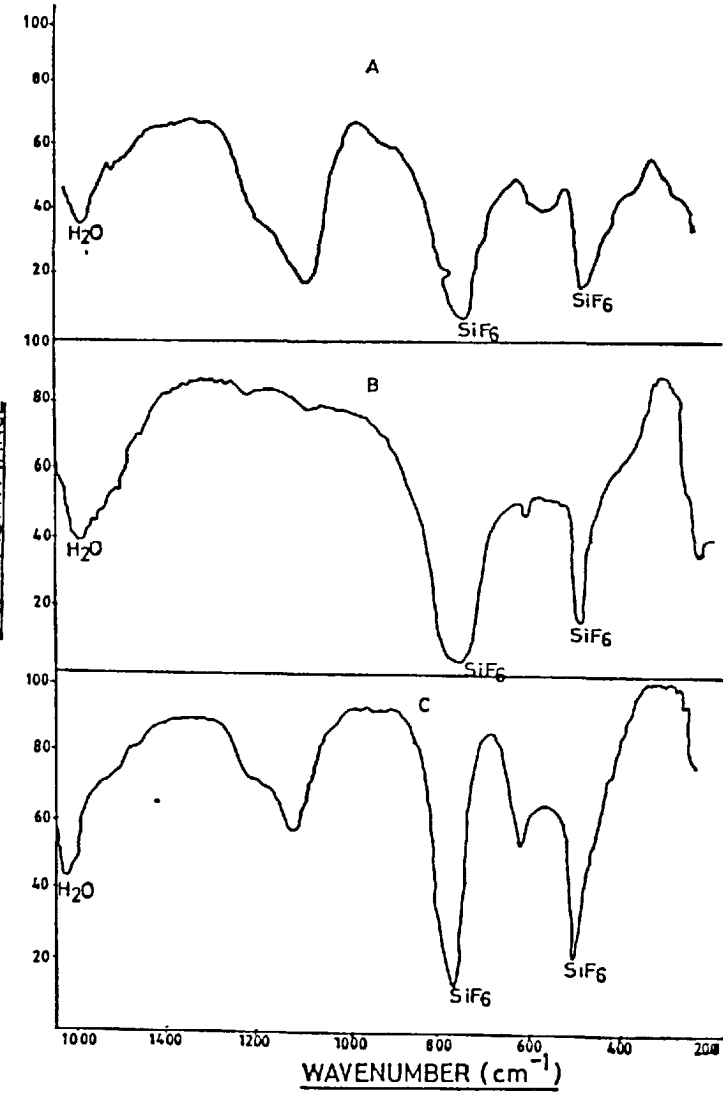

Figure 2 Infrared Sprectra of Synthesised Silicofluorides
A) Calcium Silicofluoride
B) Ferrous Silicofluoride
C) Sodium Silicofluoride

EVALUATION OF SYNTHESISED MINERALISER

For the purpose of evaluating all the synthesised mineralisers, kilnfeed (Table 4) was prepared using pure compounds of Quartz, Technical Alumina, Iron Oxide & Calcite of 99.5% purity.

The effectiveness of the synthesised mineralisers were initially evaluated based on burnability studies at the author's laboratory .In this study synthesised Calcium silico fluoride, Ferrous silicofluoride and Sodium silicofluoride were added to the kiln feed making 0.2 % Fluoride on kiln feed basis and heated in the laboratory furnace at temperatures of 1300 ^{0}C , 1350 ^{0}C,1400 ^{0}C with retention time of 20 minutes in each case. The free CaO at all temperatures and Total CaO at 1400 ^{0}C were determined (Table 5).

Table 4 Composition of kilnfeed prepared from pure compounds & clinker

	% SiO_2	% Al_2O_3	% Fe_2O_3	% CaO	SM	AM	LSF
KILNFEED	14.8	4.1	2.6	44.0	2.2	1.58	0.92
CLINKER	22.4	6.25	3.95	67.1	2.2	1.58	0.92

Table 5 Free CaO in synthetic kilnfeed with synthesised mineralisers

DOSAGES : 0.2 % F^- , KILN FEED BASIS

	% FREE CaO AT			AT 1400 ^{0}C	
	1300 ^{0}C	1350^{0}C	1400 ^{0}C	% F^-	% TOTAL CaO
SYNTHETIC K.F	16.0	4.0	2.0	–	66.4
SYNTHETIC K.F + $CaSiF6.2H_2O$	14.0	2.2	0.8	0.20	66.5
SYNTHETIC K.F + $FeSiF_6.6H_2O$	10.1	2.2	0.7	0.19	66.5
SYNTHETIC K.F + Na_2SiF_6	8.0	1.5	0.6	0.21	66.5

It can be seen from data in Table-5 that all the three synthesised mineralisers were effective in reducing Free CaO content with increase in temperature or at the same temperature, the Free CaO is lower than the feed without mineraliser. Comparatively the Sodium silicofluoride was found to be more effective in kiln feed with pure compound situation followed by Ferrous silicofluoride & Calcium silicofluoride.

In order to understand the effectiveness with respect to kilnfeed prepared from natural materials, a plant kilnfeed was selected for further experiments with Modulli values as LSF : 0.99 SM : 2.27 & AM : 1.24. Expansion shrinkage and burnability (with respect to free CaO)of lab synthesised $CaSiF_6.2H_2O$, $FeSiF_6.6H_2O$ & Na_2SiF_6 as mineralisers with 0.2% F dosage on kilnfeed basis were conducted separately.The technique of shrinkage/expansion & lime combinability was developed in the author's laboratory & the details were published earlier (Chatterjee et al -1985, Page et al -1986). According to this technique the components of appropriately designed raw mix are ground,blended, homogenised and compacted to 33 X 15 mm cylindrical pellets under a pressure of about 500 Kg / cm ^{2}. The pellets are fired at the desired range of temperature following the heating and cooling schedule as necessary.The pellets are drawn out at selected temperatures and the volume,shrinkage/expansion is measured and plotted. The total lime, free lime ,loss on ignition and residual mineraliser contents are also determined in the

fired pellets. As indicated in Fig. 3, the addition of each of these mineralisers enhanced the expansion characteristic indicating a higher extent of solid-solid reactions at temperature range of 900-1100^0 C.The shrinkage indicates the appearance of liquid formation at that temperature and formation of eutectic is indicated by the shrinkage pattern. Steeper the slope of the shrinkage plot, higher is the rate of C_3S formation. The same phenomena is observed as the percent shrinkage is maximum with $CaSiF_6$ (11.4%) than with $FeSiF_6.6H_2O$ & Na_2SiF_6 for which the shrinkage are almost similar viz. 10% & 10.2%.

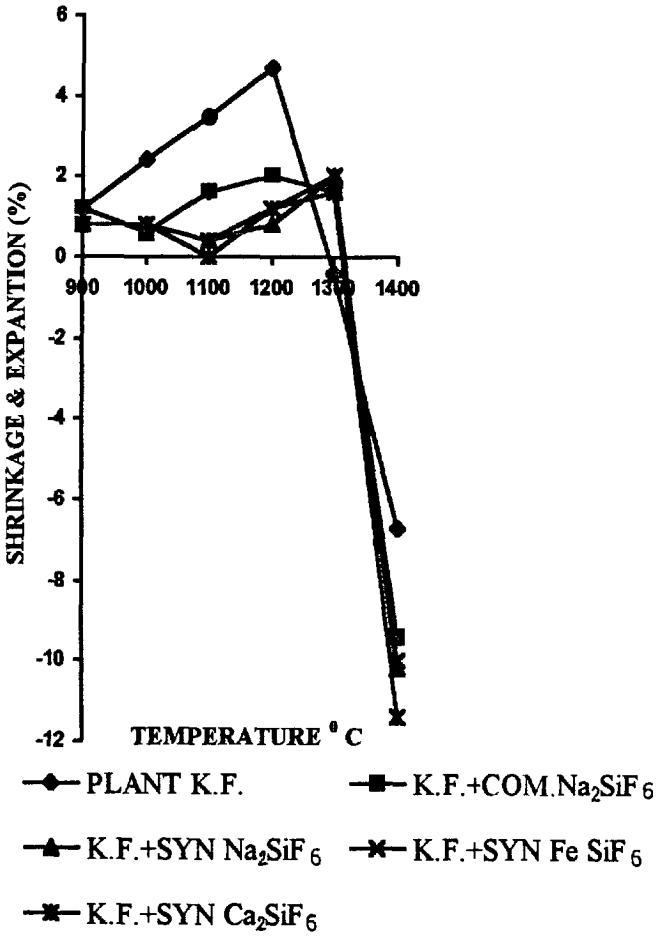

FIGURE 3 EFFECT OF MINERALISERS ON EXPANSION-SHRINKAGE WITH TEMPERATURE

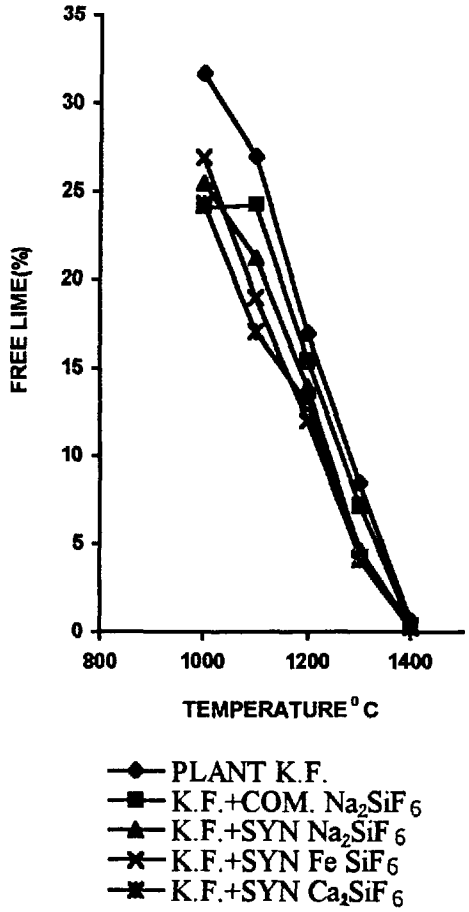

FIGURE 4 EFFECT OF MINERALISERS ON FREE LIME WITH TEMPERATURE

Further in order to understand the effectiveness of the synthesised Sodium silicofluoride, a commercial grade Na_2SiF_6 was also studied on similar lines.The shrinkage observed with commercial grade Na_2SiF_6 is, however, less (9.4%) as compared to that of all the three synthetic Silicofluorides, thus indicating improved sintering performances of the synthetic Silicofluorides over commercial Na_2SiF_6 (Fig 3). The percent free CaO against temperature (Fig. 4) in kilnfeed with and without synthetic mineraliser indicates that at high temperature (1400°C) the free lime is almost same in clinkers from kilnfeed with and without mineralisers but at lower temperature 1000°C to 1300°C the free CaO in fired

material with mineraliser is lower than without mineraliser and is least in the case of Calcium silicofluoride. The data in Fig. 4 also indicates that all the synthetic mineralisers are more effective in reducing free lime than commercial grade mineraliser i.e. Sodium silicofluoride.

In order to understand effectiveness of mineralising compounds at lower temperature reactions (Chatterjee et al -1985, Page et al -1986). ternary plots were prepared based on " free", "unliberated" and "combined" lime at temperatures upto 1000°C using same kiln feed with each of these mineralisers. The ternary plot pattern (Fig.5) shows better combinability of lime and less amount of unliberated lime and free lime with the three synthesised Silicofluorides of Calcium,Iron and Sodium as shown by curves moving more towards the lower right half of the triangle, indicating influence of these mineraliser on liberation and combining of lime due to the improved overall reactivity at the corresponding temperatures.

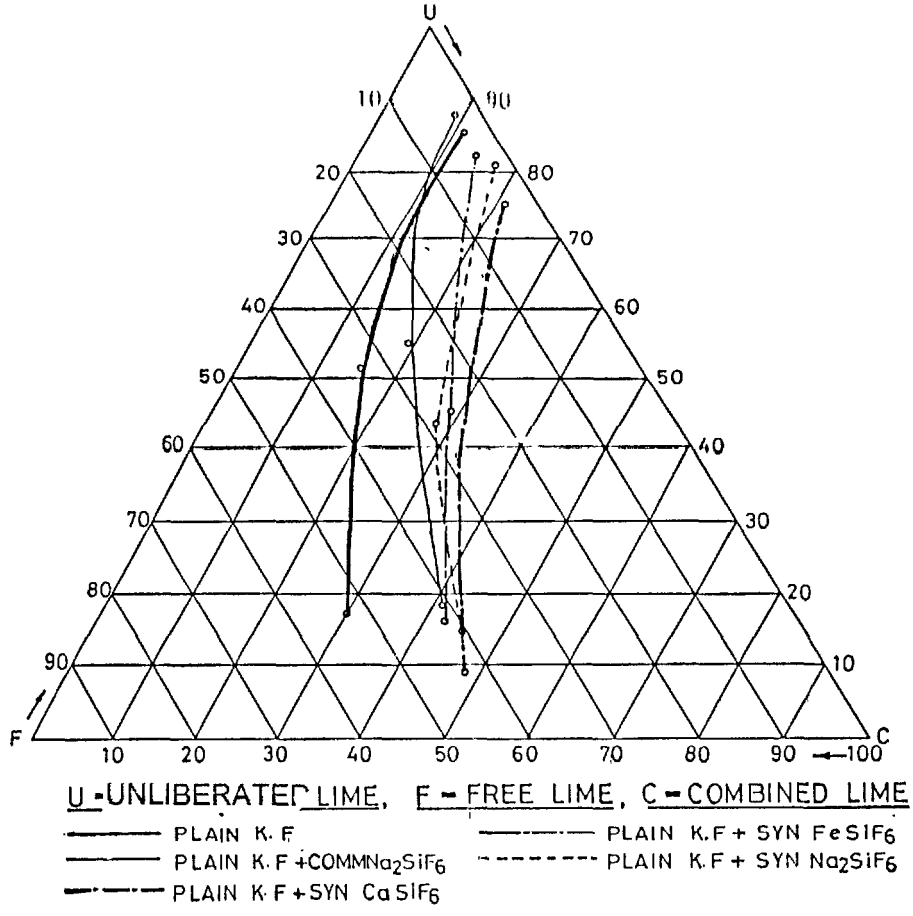

FIG.5. TERNARY PLOT U, F, C AT 800°C, 900°C & 1000°C

CONCLUSIONS

- The technical feasibility of manufacturing three Silicofluorides viz. Calcium Silicofluoride, Ferrous Silicofluoride is established on lab scale.
- All the three Silicofluorides have been found to be effective mineralisers and slightly better compared to commercially available mineralisers.

- Calcium silicofluoride appears to be the most effective mineraliser amongst others.
- The synthesis route of mineraliser opens up the possibility of making mineraliser near to the consumption center or at a central location with obvious advantages in reducing cost of transportation.
- Attempts have ben made to make preliminary estimate of cost for synthesising mineralisers. In this exercise the cost inputs of commercial grade fluosilicic acid, low grade limestone, scrap iron, soda ash and brine solutions were considered alongwith the yield of these mineralisers. The cost of synthesis for Calcium, Iron and Sodium silicofluorides works out to be 0.6, 0.5 and 1.1 times respectively against the cost of commercially available Sodium silicofluoride.
- Although $FeSiF_6.6H_2O$ appears to be cheapest among all the mineralisers, but it has certain limitations such as chemical reactivity, physical size of iron scrap etc.

ACKNOWLEDGEMENTS

Participation in this study by Mr. D.N. Thanawala and Mr. N.A. Krishnan is gratefully acknowledged.

REFERENCES

Chatterjee, A.K., C.H. Page and D. Ghosh "Industrial experience of using mineralisers." International Seminar on Energy conservation, Beijing. (1985), pp. 174-190

Kleem, W..A.,I.Jawed, "Mineralisers and Fluxes in the Clinkering Process III .Burnability of Synthetic and Industrial raw mixes". 7 th International Congress on the Chemistry of Cement, Paris (1980) Vol-II, pp.I-150-154.

Moir, G.K., Glasser, F. P. " Mineraliser, Modifiers, Activators in the Clinkering process ." 9 th International Congress on the Chemistry of Cement,NCBM (1992), pp. 125-154 .

Page,C.H., D. Ghosh and A.K. Chatterjee "Influence of Mineralizes on the constitution & properties of Industrial clinkers",8th ICC, 1986 Vol. II, pp. 152 - 157.

Subba Rao,U.V., " Utilisation of inferior grade raw materials and industrial waste in cement manufacture". All India Seminar on Cement and Allied Building Materials, New Delhi,(1984)) I , pp. 136-152.

BURNABILITY OF MINERALIZED WHITE CEMENT: OPTIMIZATION OF RAW MEALS

Francisca PUERTAS, Instituto Eduardo Torroja (CSIC), Spain
M. Teresa BLANCO-VARELA, Instituto Eduardo Torroja (CSIC), Spain
Angel PALOMO, Instituto Eduardo Torroja (CSIC), Spain
Tomás VÁZQUEZ, Instituto Eduardo Torroja (CSIC), Spain
José G. PALOMO, E. U. Arquitectura Técnica (UPM), Spain

ABSTRACT A methodology for optimizing cement raw mixes dosages is presented. The methodology is based on a statistical tool generally named Experimental Design. It has been applied to a real case: the manufacture in a Spanish factory of a mineralized cement obtained by using the fluxing and mineralizing pair CaF_2 and $CaSO_4 \cdot 2H_2O$ among the raw materials.

Key-words: Burnability of raw mixes, mineralizers in clinker making, low energy.

INTRODUCTION

Mineralizers and/or fluxes are often added to cement raw meals to accelerate reactions and enhance burnability. In such cases the traditional methods (Ludwig and Ruckensteiner, 1974), (Fundal, 1979), (Christensen, 1979), (Johansen, 1979), for evaluating burnability of raw mixes are inapplicable, rendering evaluation quite difficult.

Burnability can be substantially improved by adding the mineralizing pair CaF_2 and $CaSO_4$ to the raw mixes, especially at temperatures between 1300 and 1400° C. The rate of alite formation in this case is even higher than that found for mixes mineralized with CaF_2 only (Johansen and Kouznestsova, 1992). This higher rate is due essentially to the thermodynamic effect of the widened stability range and primary phase field of crystallization of C_3S induced by CaF_2, together with enhanced ion mobility in the melt due to $CaSO_4$ and CaF_2 and the appearance of a new liquid phase at temperatures under 1200°C (Blanco-Varela et al, 1986) (Giménez and Blanco-Varela, 1995). Fluorellestadite ($3C_2S.3CaSO_4.CaF_2$) is the main compound of such a liquid whose approximate composition by weight is: CaO - 54, Al_2O_3 - 4, Fe_2O_3 - 3, SiO_2 - 11, CaF_2 - 4, $CaSO_4$ - 24.

CaF_2 and $CaSO_4$ can be used to partially replace the traditional fluxes Al_2O_3 y Fe_2O_3, to produce clinkers with low aluminate contents at temperatures between 1300 and 1400° C (Giménez and Blanco-Varela, 1995) (Blanco-Varela et al, 1985, 1990). In this type of material the essentially fluorsulfatic liquid phase is composed mainly of molten fluorellestadite (60 -75% by weight), ferrites and aluminates. The low clinkering temperature of these raw mixes reduces the loss of F_2 and SO_3.

The use of this mineralizing pair to partially replace aluminates is particularly useful in the manufacture of white clinker, because of the potential for energy conservation and because seawater- or sulfate-resistant white cements can be produced when such additives are used (Giménez et al, 1991). A Spanish factory interested in the new process and material proposed to achieve an industrial test. For that, the main objective of this paper is to propose a mathematical model to predict the burnability of raw mixes made using CaF_2 and $CaSO_4$ as fluxes and mineralizers for fabrication white clinker for its implementation in a cement factory.

EXPERIMENTAL

The chemical analyses of the raw materials supplied by the cement factory are shown in Table 1.

Table 1 Chemical Analysis of Raw Materials

	LIMESTONE	KAOLIN	SAND II	SAND I	GYPSUM	FLUORITE
I.O.	43.21	11.50	2.13	3.25	--	10.54
SiO_2	0.68	53.56	91.78	87.90	1.41	18.80
R.I.	0.12	0.12	--	--	--	--
Al_2O_3	0.05	32.78	4.16	5.91	0.09	--
Fe_2O_3	0.19	0.57	0.14	0.19	--	--
CaO	56.78	1.21	1.40	2.54	32.94	13.43
MgO	--	--	0.03	0.06	0.70	--
SO_3	--	--	--	--	43.86	--
Na_2O	0.02	0.06	0.03	0.02	--	--
K_2O	0.01	0.76	0.04	0.10	--	--
CO_2	--	--	--	--	2.12	--
H_2O Comb.	--	--	--	--	19.30	--
F_2Ca	--	--	--	--	--	51.4

A two-level factorial experimental design was used for modelling (Box et al, 1989). The parameters given in Table 2 were considered to be the most relevant for raw mix burnability assessment. That table also shows the two levels (+ and -) defined for each factor.

Lime saturation factor (LSF) selected levels (93 and 98) are in the range usually used in industrial practice. In a previous paper (Blanco-Varela et al, 1996) was demonstrated through the same methodology the little influence of the silica modulus (Ms) (11 o 14) on the final free lime of clinkers. From these results only one level was decided to be used, particularly, the value of Ms=11. These values of Ms are very much higher than those employed in traditional grey and white clinker production. These values are necessary to produce sulfate resistant cement. Clinkerization is possible due to the mineralizing and fluxing effects of CaF_2 and $CaSO_4$. The AR (alumina iron ratio) values in these raw mixes are in the range between 7.3 and 7.6.

Sizes of limestone and sands were selected by sieving, kaolinite is very fine having an average size of 6 μm.

Table 2 Relevant Factors and Corresponding Levels

Factors	Factors Identification	Levels (-)	(+)
LSF	A	93	98
CaF_2 (%wt)	B	0.65	1.30
$CaSO_4$ (%wt)	C	2.6	3.9
Size Particle of Sand (%wt)	D	100% <45 μm	80% <45 μm 20% <45 μm
Size Particle of Limestone (%wt)	E	100% <125 μm	80% <125μm 20% >125μm
Temperature	F	1350°C	1400°C

LSF = Lime Saturation Factor

In the present work the influence of the nature of sand (Sand I and Sand II) on the raw meals burnability has been studied. Sand II was obtained from Sand I by water washing, removing most of the clayey material, resulting in quartz grains which were mineralogically identical.

Sand I mixes were prepared. A 2^{6-1} design was done; this means 32 different experiments or different clinkerizations. These experiments correspond to the 8 different dosages obtained through the combination of three compositional parameters (LSF, % CaF_2 and % $CaSO_4$) at two levels (2^3). Also Sand II mixes were prepared. In this case the design corresponded to a 2^6 one.

The raw mixes were prepared from the corresponding amounts of limestone, sand, kaolin, fluorite and gypsum (the two former with previously selected sizes). The mixes were hand homogenized, taking great care to avoid any modifications of particle size and then dried. The dispersive medium used was ethanol. With each of the raw mixes, cylindrical pellets of 2.5 cm diameter and 1.5-2cm length were prepared.

Temperature treatment of these pellets was done in laboratory kilns at selected temperatures. Heating time was always constant and equal to 30 minutes. The measured variable was free CaO in clinkers through the ethylene-glycol method (UNE Standard, 1986).

RESULTS AND DISCUSSION

The statistical analysis of free CaO values of the all clinkers obtained has been done using the variance analysis method (V.A.), neglecting interactions higher than second order. This V.A. method is based on decomposing observations as a sum of terms, each one depending on a factor or an interaction of factors.

The burnability model of white cement raw mixes prepared using Sand I as raw material, follow the equation [1]:

$$\%\ CaO_{Free} = 3.36 + 0.37\ X_A - 1.05\ X_B - 0.60\ X_C + 0.003\ X_D + 1.57\ X_E + 0.11\ X_F + 0.34\ X_B\ X_C - 0.49\ X_B\ X_E - 0.28\ X_C\ X_E + \Sigma \quad [1]$$

Where $\Sigma \approx N(0, \sigma)$, $\sigma = 0.41$ by Variance Method (V.A.) neglecting interactions greater than second order. The coefficient of determination (R^2) is 98.87%.

The burnability model of those raw mixes prepared with Sand II as raw material, follow the equation [2]:

$$\%\ CaO_{Free} = 4.64 + 0.62\ X_A - 1.62\ X_B - 0.89\ X_C + 0.28\ X_D + 1.70\ X_E - 0.24\ X_F - 0.21\ X_A\ X_B + 0.24\ X_A\ X_D - 0.36\ X_B\ X_E + \Sigma \quad [2]$$

Where $\Sigma \approx N(0, \sigma)$, σ estimation is of 0.51, neglecting interactions higher than third order. The coefficient of determination (R^2) is 97.72%.

Those interactions with coefficients lower than 0.2 have not been considered as significant. In equation [1] and in order to analyze their importance, main factors X_D, and X_F have been considered in spite of having coefficients lower than 0.2.

3.36 or 4.46 %wt are the mean free lime contents found in clinkers obtained by burning raw mixes for 30 minutes at pre-established temperatures. X_A, X_B, X_C, X_D, X_E, and X_F are assigned a value of -1 or +1 depending upon the level, - or +, that each of these factors have in the raw mixes. The coefficient applied to factors $X_A....X_G$, is a measure of each one's contribution to raw mix burnability.

The value of coefficients will depend on the range selected for each parameter. It means that the obtained model can be only applied (in the most strict sense) to explain the burnability of raw mixes having their characteristics parameters within the selected ranges. In this study the chosen range of each parameter were the most adequate for producing fluor-sulfate white clinker.
The statistical analysis of experimental data shows that, the considered factors as well as their interactions, explain 98% of the burnability results of those raw mixes. So, it can be considered that the proposed model explains well the behaviour of the raw mixes studied.

From the analysis of both models the following two aspects can be distinguished:

a) The particular contribution of each of selected factors, as well as their level on the final free lime on clinkers, and

b) Comparison of the models for determining the influence of sand nature on the contribution of the other factors on the burnability of the raw materials.

In relation to the first aspect, it has been verified that, in both models, the factors E (limestone particle size), B (fluorite percentage) and C (gypsum percentage) are the most important factors with respect to clinkers final free CaO contribution. These main factors not only contribute to the free lime content of samples at individudal level but they are involved in the main significative binary interactions. In fact the coefficient of the BE binary interaction is higher than the one´s of some individual factors as sand particle size (D) or clinkering temperature (F).

Then, for example, the effect of limestone particle size (E) on burnability depends not only on its own level but also on CaF_2 and $CaSO_4$ levels.

The great significance of B and C factors (the greater CaF_2 and $CaSO_4.2H_2O$ amount in the raw mix, the lesser is free CaO proportion in the clinker) confirms the important flux-mineralizer role of the fluorite-gypsum pair.

Fourth factor in significance in both models is lime saturation factor (LSF).

The factors D (sand particle size) and F (clinkering temperature) are the parameters which have less influence on the final free lime content of the clinker. But their influence is different in the studied models. Thus, whereas in the Sand II raw mixes the value of the coefficients of these factors are very similar, in the Sand I raw mixes the coefficient of D factor is much less than that of the temperature.

Those raw meals, at which parameters D and E take the maximum level value (see Table II), have about 15% wt of limestone particles higher than 125 μm, while the proportion of sand particles coarser than 45 μm is 3% wt; that is, the ratio between coarse limestone and sand particles is 5:1 in weight. Supposing that in the variation range studied, there is a linear relation between limestone or sand particles percentage higher than 125 μm and 45 μm respectively, and the free CaO percentage produced, the contribution of 1% in weight of coarse limestone and sand particles to the clinker free CaO can be calculated. This contribution would be from Sand I raw mixes:

1 % sand particles > 45 μm = 0.03 % wt CaO
1 % limestone particles > 125 μm = 0.20 % wt CaO

So, the specific contribution of coarse limestone particles to free CaO is more than six times superior to the coarse sand particles contribution. These results have a great technological importance, because of the expensive process to obtain sand particles finer than 45μm; and grinding processes require an important energy cost. The correlation coefficient for the coarse sand fraction obtained in this work is different from that established by others authors (4). However, the experimental conditions in the studies are quite different, and a direct comparation is not possible.

That contribution from Sand II mixes are:

1% wt sand particles > 45 μm= 0.111% wt in CaO
1% wt limestone particles > 125 μm= 0.113% wt in CaO

Thus, the specific contribution of coarse limestone and sand particles to the free CaO, is practically the same.

In Sand I model the sign preceeding temperature coefficient is positive. Then, free CaO content in clinkers, from raw mixes treated at 1350°C is higher that from meals treated at 1400°C. Analysis carried out in ten different clinkers have shown that clinkers obtained at 1350°C have a SO_3 loss lower than 10% .In those obtained at the highest temperature the loss of SO_3 is around 25-40 %wt. This loss of SO_3 and the consequent increase in effective LSF could explain the increase in final free lime content of clinkers obtained at 1400°C.

Although the loss of SO_3 observed in laboratory clinkering tests is very important, the industrial experience shows that the loss of SO_3 is very much lower. This is because of the high partial pressure of SO_2 in the kiln atmosphere from the fuel combustion and SO_2 capture by the incoming feed. Hence the range at adequate clinkering temperature for these raw mixes can be established as being 1350-1400°C.

Comparing equations [1] and [2], some relevant conclusions can be extracted about sand nature influence on the burnability of these white cement raw mixes. In fig. 1 the coefficients of main factors in the two models obtained are shown. In burnability equation [1], almost all coefficients and the independent term are inferior, in absolute value, to those in equation [2], and all except temperature retain the same sign. In any case, the absolute value of temperature coefficient in both models is small, confirming its scarce influence on clinkers free CaO.

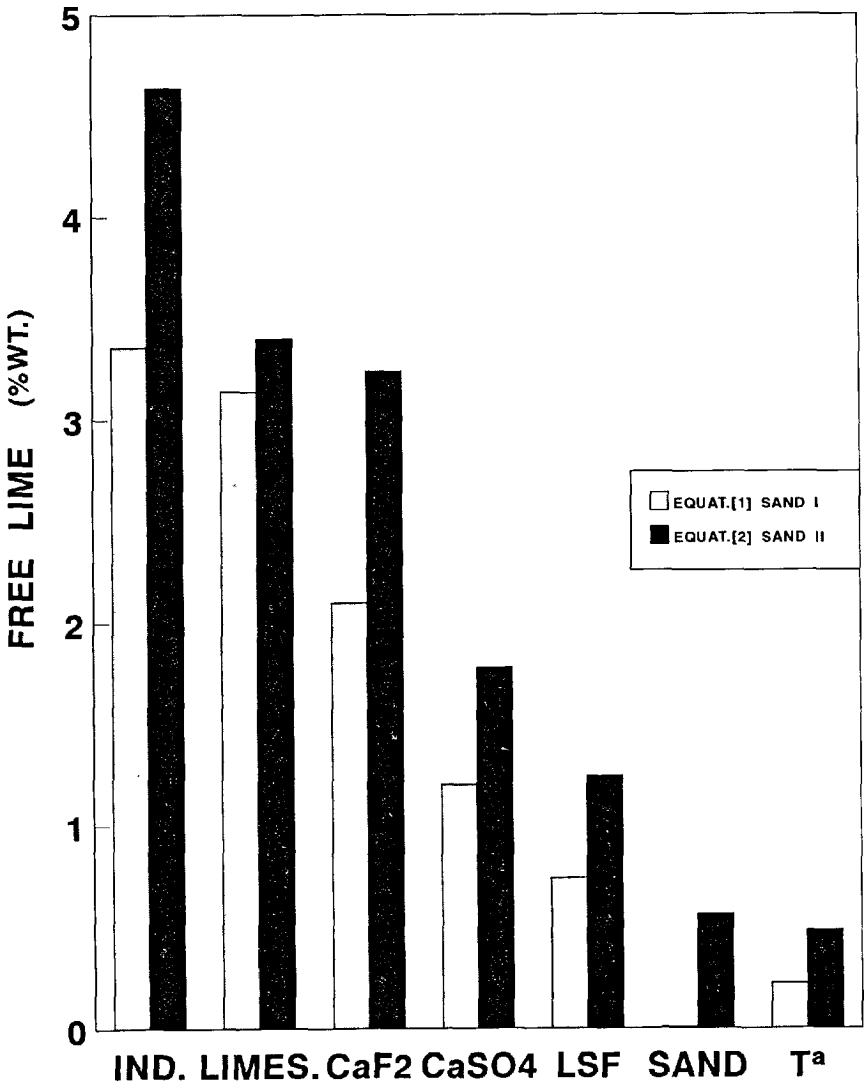

Fig. 1 Contribution of Factors Considered in Eq 1 and 2 on Free CaO Contents in Clinkers.

From these results it can be deduced the better burnability of Sand I raw mixes with respect to Sand II raw mixes. D factor, corresponding to sand particle size, is the greater difference, confirming the positive effect of Sand I on raw mixes burnability.

The enhanced burnability for Sand I raw mixes is due to the presence in their composition of a small proportion of clay (mainly aluminous in contact with quartz grains) acting as a flux. This produces, at adequate temperatures, a certain quantity of melt phase around quartz particles enabling reactions to occur at a higher rate. This clayey material can be very advantageous to enhance formation and stabilization of raw mixes nodules before their kiln entrance, confirming that the industry practice of sand washing allows to have a better control of some parameters (dosage, cromophore elements,etc.) but may make calcination and burnability difficult.

CONCLUSIONS

From the proposed methodology and applying it to industrial raw materials, it is possible to determine the optimal dosage of raw mix for fabrication in the industrial kiln of a white mineralized cement resistant to sulfates and sea water. The dosage is defined from the following parameters:

LSF = 98
Ms = 11
% wt F_2Ca = 1.3
% wt $CaSO_4$ = 3.9
Sand with the characteristics of Sand I.

The industrial test was carried out and a white mineralized clinker with a high quality was obtained. The manufacture of this clinker has an estimated energy consumption of 10% lesser than that of the traditional process.

REFERENCES

Blanco-Varela, M.T., Vazquez, T., Palomo, A., "A study of a new liquid phase to obtained low-energy cements". Cem. Concr. Res. Vol 16, 1986, pp. 97-104.

Blanco-Varela, M.T., Vazquez, T., Palomo, A., Spanish Patent nº 542691, 1985.

Blanco-Varela, M.T., Vazquez, T., Palomo, A., Puertas, F., Giménez, S. Spanish Patent nº 9001906, 1990.

Blanco-Varela, M.T., Puertas, F., Vazquez, T., Palomo, A., "Modelling of the burnability of white cement raw mixes made with CaF_2 and $CaSO_4$". Cem. Concr. Res., Vol 26, Nº 3, 1996, pp. 457-464.

Box, G.E.P., Hunter, W.G., Hunter, J.S., "Statistic for Experimenters. An Introduction to Design, Data Analysis and model Building". Ed. John wiley & Sons, 1989.

Christensen, N.H., "Burnability of cement raw mixes at 1400°C. I The effect of the chemical composition. II The effect of the fineness". Cem. Concr. Res. Vol 9, 1979, pp. 219-228. Cem. Concr. Res. Vol 9, 1979, pp. 285-294

Fundal, E., "The burnability of cement raw mixes". World Cement Technology. 10, Nº6, 1979, pp. 195-204.

Giménez, S., Blanco-Varela, M.T., "Solid state phases relationship in the $CaO-SiO_2-Al_2O_3-CaF_2-CaSO_4$ system". Cem. Concr. Res. Vol 25, nº 4, 1995, pp. 870-882.

Giménez, S., Blanco-Varela, M.T., Palomo, A., Puertas, F., "Production of cement requiring low energy expenditure-An industrial test". Zement-Kalk-Gips., nº1, Vol 44, 1991, pp. 12-15.

Johansen, V.V., "Anwendung des gleichgewichtsdiagramms beim klinkerbildungsvorgang industriell hergestellter klinker". Zement-Kalk-Gips, 32 Nº 4, 1979, pp. 176-181.

Johansen, V.V., Kouznetsova, T.V., "Clinker formation and new processes" 9th Intern. Cong. Chem. Cem., Vol 1, (New Delhi), 1992, pp. 49-79.

Ludwig, U., Ruckensteiner, G., "Uber die brennbarkeit von zememtromehlen". Cem. Concr. Res. Vol 4, 1974, pp. 239-246.
UNE Standard 80-243-86. "Métodos de ensayo de cementos. Determinación del óxido de calcio libre; método del etilenglicol", 1986.

KINETICS OF $2CaO \bullet SiO_2$ AND $3CaO \bullet SiO_2$ FORMATION IN THE PRESENCE OF SODIUM AND POTASSIUM COMPOUNDS

Silvija LAGZDINA, Uldis SEDMALIS, Riga Technical University, Institute of Silicate Materials, Riga, Latvia

ABSTRACT The formation kinetics of principal portlandcement clinker compounds tricalcium silicate (C_3S) and dicalcium silicate (C_2S) in model systems in presence of sodium and potassium salts (PO_4^{3-}, SO_4^{2-}, CO_3^{2-}, F^-, Cl^-) was investigated. The rate constants and activation energy of reactions in the temperature range 900-1450°C were calculated. Rather all salts used promoted calcium silicates formation. This finding was confirmed in practice. Using alkali rich (4-6% R_2O) starting materials for producing clinker high quality cement was obtained when simultaneously the silica modulus of the batch was increased to 2,5-3,0.

Key-words: additives, alkali, calcium silicate, kinetics, silica modulus.

INTRODUCTION

The long-time experience of producing portlandcement in Latvia has shown (Glasenapp, 1910) that the quality of cement decreases when high alkali content raw materials are used. To explain this fact the investigation of principal portlandcement clinker minerals formation kinetics in model systems with additive of various sodium and potassium salts (4% in terms of R_2O) was carried out. It was established that the R_2O content in the raw materials batch is in a range 0,5-4% which increases in a case of recycling rotary kiln dust catched by electrofilters.

EXPERIMENTAL

Starting materials used were chemically pure $CaCO_3$ and SiO_2 - silica fume with specific area 175 m^2/g and sodium and potassium salts with anions: PO_4^{3-}, CO_3^{2-}, SO_4^{2-}, Cl^-, F^-, the batches were prepared in stoichiometric relations for synthesis C_3S and C_2S, additives were introduced into the batches 4% of R_2O over 100%. Specimens $\varnothing 18 \times 3$ mm were prepared by pressing under 80 MPa. Isothermal treatment was carried out in the temperature range 900-1450°C for 3-120 min. For the C_2S, C_3S formation kinetics study free CaO was determined by the alcohol glycerine method. DTA, X-ray diffractometry and microscopy in the research also were used.

EXPERIMENTAL RESULTS AND DISCUSSION

The conversation degree (α) was calculated from the results of free CaO detection

$$\alpha = \left(\frac{CaO_{total} - CaO_{free}}{CaO_{total}} \right) \cdot 100,\% \qquad [1]$$

With the increase of temperature the degree of conversation CaO changes more sufficiently as with time. In the presence of additive, character of the curves does not change considerably (Fig 1). Initially the process proceeds rapidly but consequently slows down. The curves of C_2S synthesis were similar.

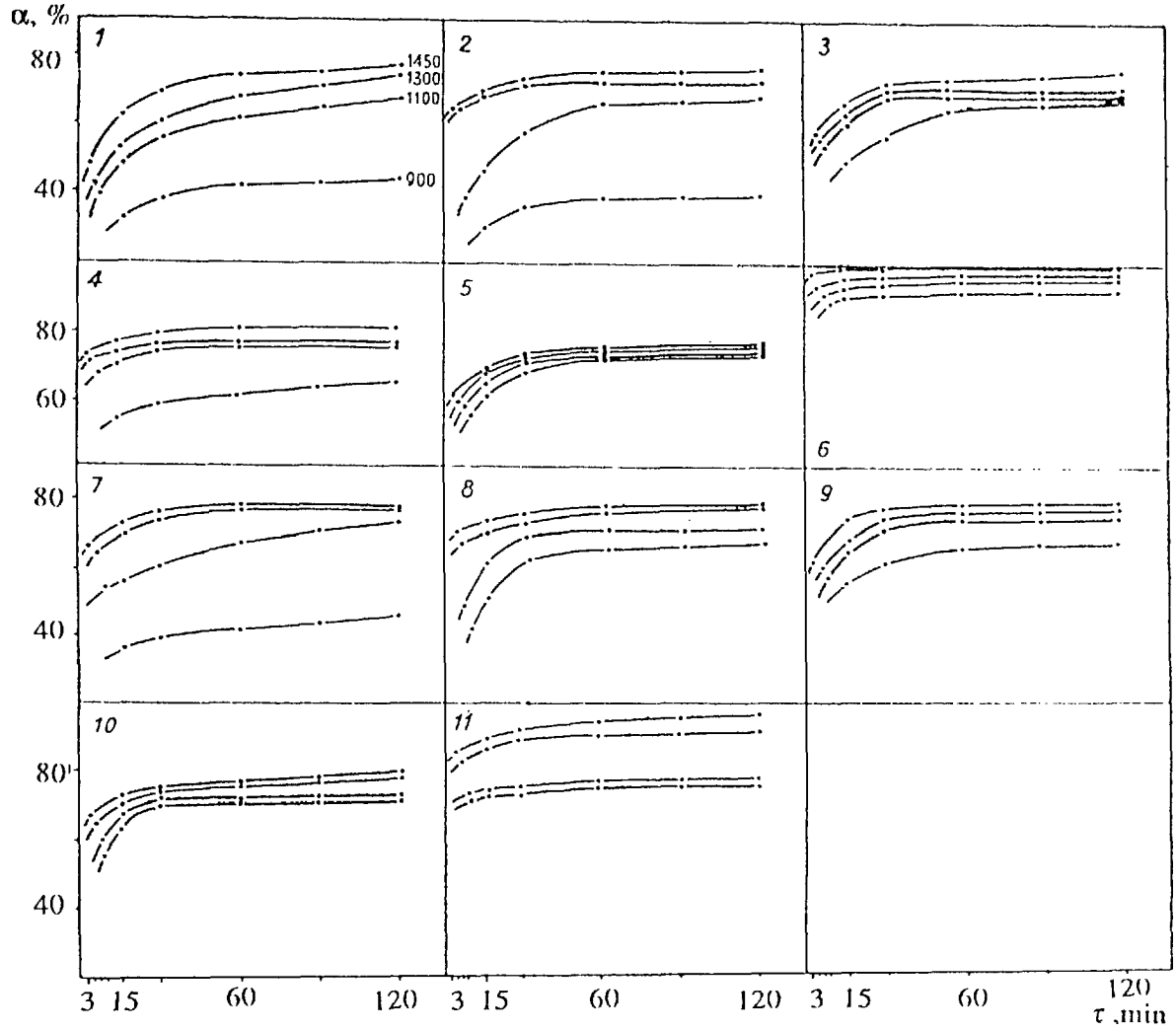

Figure 1 Degree of CaO conversation (α) of synthesis C_3S in dependence on temperature, (τ) time and additive: 1-without additive; 2-Na_3PO_4; 3-Na_2CO_3; 4-Na_2SO_4; 5-NaCl; 6-NaF; 7-K_3PO_4; 8-K_2CO_3; 9-K_2SO_4; 10-KCl; 11-KF.

The rate of C_3S and C_2S synthesis (Table 1) is described by the Kolmogorows equation (Belkevich, 1952)

$$\alpha = 1 - e^{-k\tau^n}, \qquad [2]$$

were α - degree of CaO conversion, k - rate constant, τ - time, n - kinetic parameter.

Kinetic parameter (n) was obtained from the expression [lg-lg(1-α)] versus lgτ (as the tg of the slope of the lines) (Lagzdina, 1969). It was in the range 0,2-0,39. The activation energy (E) of reactions was calculated by Arrenius equation

$$k = k_0^{-E/RT} \qquad [3]$$

Table 1 Values of the constant (k) and the activation energy (E) of C_3S and C_2S synthesis depending on temperature and additives

Additive	C_3S					C_2S				
	$K \cdot 10^2$, min^{-1}, at°C				$E_{900\text{-}1450°C}$	$K \cdot 10^2$, min^{-1}, at°C				$E_{900\text{-}1150°C}$
	900	1100	1300	1450	kJ	900	1100	1300	1450	kJ
without additive	7,9	13,2	16,6	20,9	36,4	5,6	9,3	18,2	25,1	53,5
Na_3PO_4	13,8	22,4	38,0	40,7	46,0	5,3	9,1	19,2	26,1	53,5
Na_2CO_3	18,6	23,4	26,9	31,6	15,5	14,8	19,0	24,0	26,9	19,2
Na_2SO_4	18,2	38,9	44,7	51,3	15,5	11,7	18,6	21,3	27,5	23,0
NaCl	22,4	25,1	27,5	30,2	11,3	15,8	25,1	27,5	31,6	24,7
NaF	69,2	81,3	91,1	-	9,6	50,1	56,2	63,1	-	9,6
K_3PO_4	31,6	23,4	35,5	40,7	34,3	9,1	19,9	37,1	47,9	30,5
K_2CO_3	13,2	40,7	46,8	49,0	34,3	23,4	33,1	44,7	47,9	19,2
K_2SO_4	21,4	28,8	33,1	38,0	24,3	23,4	30,2	38,0	45,7	19,2
KCl	19,0	26,9	39,8	42,7	26,8	33,9	38,9	41,7	47,8	23,0
KF	47,9	52,5	67,6	74,1	15,5	32,3	41,7	50,1	55,0	15,5

Small values of n<1 as well as E allowed to conclude that the limiting stage of C_3S and C_2S formation is diffusion.

The results of investigation demonstrated that rather all salts used promote C_3S and C_2S formation in model systems.

Figure 2 shows that in synthesis of C_3S the temperature of $CaCO_3$ decarbonation from 900°C in batch without additive decreases to 860-880°C with additive of sodium and potassium carbonates, chlorides and fluorides. Possible it is connected with duble salts formation and decomposition of them at temperatures which are lower than that one of $CaCO_3$ decomposition. Solid state reactions also proceeds more rapidly in presence of additives. C_3S formation could be noticed already at 900-950°C. In the presence of potassium salts at 1100°C the phase $KC_{23}S_{12}$ (d/n = 2,75; 2,63; 2,29; 2,24; 1,95; 1,59 Å) was recognized, which dissapeared with elevating the temperature. At the 1300-1450°C the amount of R_2O decreased to 0,3-1,2% nevertheless

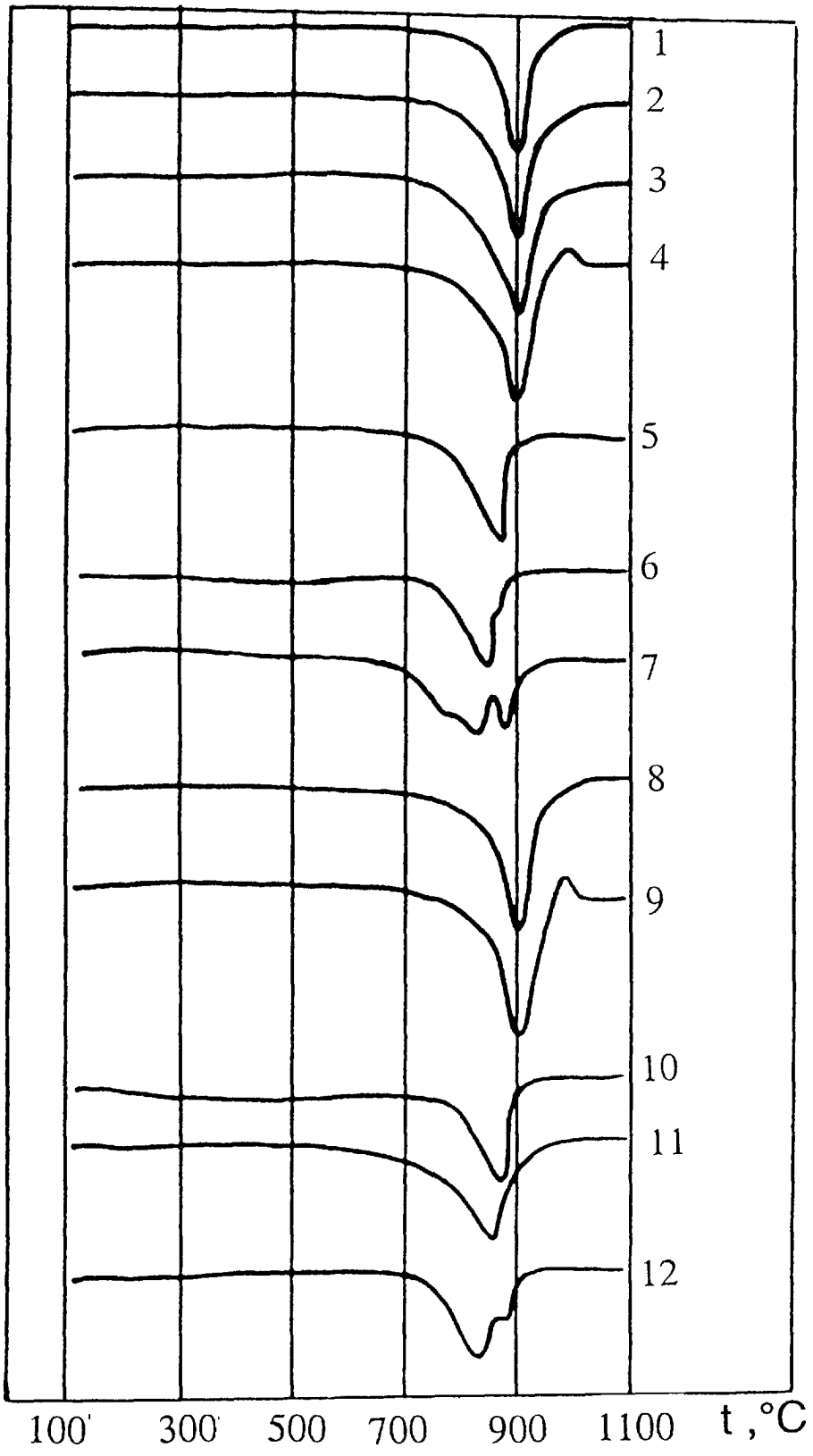

Figure 2 The DTA heating curves of $CaCO_3$ (1) and batches: $3CaCO_3 + SiO_2$ (2); 2 + Na_3PO_4 (3); 2 + Na_2SO_4 (4); 2 + Na_2CO_3 (5); 2 + NaCl (6); 2 + NaF (7); 2 + K_3PO_4 (8); 2 + K_2SO_4 (9); 2 + K_2CO_3 (10); 2 + KCl (11); 2 + KF (12).

there was the consequence of alkali action. The microscopic investigation showed that the size of C_3S crystalls with alkali additive was 20-40μm instead of 2-18μm without additives. Investigations have been carried out also using natural raw materials (Table 2,3).

Table 2 Chemical composition of raw materials, mass %

Raw materials	SiO_2	Al_2O_3	Fe_2O_3	CaO	MgO	SO_3	K_2O	Na_2O	Ign. loss	Total
Limestone	5,54	1,57	1,21	49,55	2,03	0,48	0,60	0,10	38,92	100,00
Clay	58,68	14,00	6,33	7,71	2,00	0,07	2,20	0,20	8,79	99,98
Sand	83,24	5,51	2,01	4,41	1,16	0,17	1,65	0,25	1,60	100,00
Fe_2O_3 rich material	15,38	0,50	72,29	2,08	0,70	2,61	0,65	0,85	4,89	99,95
Kiln dust	16,57	5,37	4,05	36,50	1,48	3,64	4,57	1,29	26,54	100,01

Batches containing 1,2-5,1 % of R_2O and with silica modulus n = 2,1-3,0 were prepared. Examples of chemical composition of clinker produced at the factory as well as the compressive strength of cement obtained are given in the Table 3.

Table 3 Chemical composition of clinker and compressive strength of cement (MPa)

Clinker	Chemical composition, mass %						k	n	Specific area	Compressive strength, MPa		
	SiO_2	Al_2O_3	Fe_2O_3	CaO	Na_2O+K_2O	CaO free			cm^2/g	3 days	7 days	28 days
1	20,85	5,85	4,08	64,71	1,40	1,20	0,920	2,10	5103	39,3	42,7	46,9
2	23,07	4,47	4,55	64,65	0,68	0,80	0,854	2,56	5115	47,8	54,2	62,9
3	22,18	4,67	3,77	66,14	0,62	0,84	0,919	2,63	4757	42,4	49,5	61,4
4	23,52	4,54	3,45	64,65	0,64	0,70	0,853	2,94	5469	43,9	51,6	70,6
5	22,96	3,52	3,52	65,63	0,46	0,70	0,920	3,04	5660	38,9	50,9	68,7

$$k = \frac{CaO - (1{,}65 \cdot Al_2O_3 + 0{,}35 Fe_2O_3)}{2{,}8 \cdot SiO_2} \qquad [4]$$

$$n = \frac{SiO_2}{Al_2O_3 + Fe_2O_3} \qquad [5]$$

Taking into account the results obtained it is concluded that if for the producing the cement clinker alkali rich starting materials (kiln dust containing up to 6% of R_2O) are used high quality cement can be obtained when the silica modulus of the batch is increased to 2,5-3,0 instead of 2,1-2,3.

REFERENCES

Belkevich P.J. "New interpretation of Kolmogorows-Jerofejews equation", Translated from News Academy of Sciences of Byelorussia N° 4, 1952, pp. 121-126.

Glasenapp M. "Die Anfänge der Zementfabrikation in Riga", Rigashe Industrie Zeitung, N° 21, 1910, pp. 321-323.

Lagzdina S.J. "Influence of sodium and potassium salts on to the clinker minerals formation", Translated-Dissert. thesis Riga, 1969, pp.19.

THE EFFECTS OF ADDITIVES ON FORMATION OF C_2S, $C_4A_3\bar{S}$ AND C_4AF

Woo-Hyeong CHAE, Geun-Chang YUM, Hee-Kap OH, Ssangyong Research Center, Taejon, Korea
Sang-Heul CHOI, Hanyang Univ., Seoul, Korea

ABSTRACT Formation of C_2S, $C_4A_3\bar{S}$ and C_4AF were investigated by adding borax, calcium phosphate and barite. It has been found that borax stabilizes β, α'-C_2S, and helps C_4AF formation. Calcium phosphate stabilizes β-C_2S, but has negative effects on C_4AF formation. Barite lowers the forming temperature of C_2S and helps C_4AF formation. The additives hinder $C_4A_3\bar{S}$ formation.
Key-words Modified Belite Cement, borax, calcium-phosphate, barite

INTRODUCTION

Modified Belite Cement (MBC) which is composed of β-C_2S, $C_4A_3\bar{S}$ and C_4AF as major clinker minerals is generally synthesized around 1300℃. At this relatively low firing temperature as compared with that of Ordinary Portland Cement (OPC), small amount of impurity can significantly influence on the clinkerization reaction and physical properties of MBC. There has been many studies showing the effects of additives on the stabilization of high temperature polymorphs of C_2S. Gies (1986) observed the stabilized α' and α type C_2S by the effect of alkali solid solution showing excellent hydration properties of their belite rich cement. Using B_2O_3 as a stabilizer, Jenic (1978) observed the different hydration behaviour between α' and β-C_2S having different structural imperfectness. Matkovic (1986) studied the belite stabilizing effect of P_2O_5 and the relation between microstructure and strength development of hydrates. Zimer (1984) and Nettleship (1993) reported the effect of BaO and SO_3 on C_2S formation. Temperature, viscosity and surface tension of melt can be changed by these additives. In this study, borax comprising of Na_2O and B_2O_3, calcium phosphate comprising of CaO and P_2O_5, and barite comprising of BaO and SO_3, were used for stabilizing C_2S at room temperature in MBC. The effects of these not only on the C_2S stabilization but also on the $C_4A_3\bar{S}$ and C_4AF formation were investigated.

EXPERIMENTAL PROCEDURE

Raw mixtures of C_2S, $C_4A_3\bar{S}$ and C_4AF were prepared using reagent such as $CaCO_3$, SiO_2, Al_2O_3, Fe_2O_3 and $CaSO_4$, and adding 3% of borax, calcium phosphate and barite. They were sintered at temperatures from 1050℃ to 1350℃ for 1 hour and quenched in the air. Free CaO (amount of uncombined CaO) analysis was carried out on the sintered samples. Relative XRD peak intensities of β-C_2S (d=2.794), $C_4A_3\bar{S}$ (d=3.757) and C_4AF (d=2.635) were compared with internal standard material (Al_2O_3 ,d=2.085). With the established MBC clinker composition (60% C_2S, 20% $C_4A_3\bar{S}$ and 20% C_4AF), 3 types of raw mix were prepared by adding 3% of each additive. The raw mixes were sintered at temperatures from 1050℃ to 1350℃ for 1 hour and quenched in the air. Free CaO, XRD, SEM/EPMA were carried out on the sintered samples to identify their clinkerization.

RESULT AND DISCUSSION

Remark) Plain : additives-free raw mix or clinker
NB3 : 3% Borax-bearing raw mix or clinker
CP3 : 3% Calcium Phosphate-bearing raw mix or clinker
BS3 : 3% Barrite-bearing raw mix or clinker

Formation of C_2S, $C_4A_3\bar{S}$, C_4AF

As a result of XRD analysis, γ-C_2S was identified in all additive-free sample fired at 1050~1350℃, while not in additive-bearing samples fired at higher than 1100℃. Fig. 1 and 2 are the results of free CaO analysis and the relative intensity of β-C_2S peak. All the additives had effects on reducing free CaO. In NB3, free CaO was decreased from 1200℃, and α' and β-C_2S peak were observed. These effects can be explained by the fact that formation of melt at low temperature by fluxing effect of borax of which melting point is around 750℃. The melt can physically inhibit $\beta \rightarrow \gamma$ expanding transition through surrounding C_2S grains. And also the result can be explained by the retaining influence of solid solution with Na^{2+} and B^{3+} ions which can easily dissolve into belite phase. (1980) In the form of solid solution containing a few % of Na_2O, Greene (1955) succeeded in bringing the α form to room temperature without inversion by means of rapid quenching. Bates (1955) prepared β-C_2S with boric acid in amounts of less than 1 per cent.

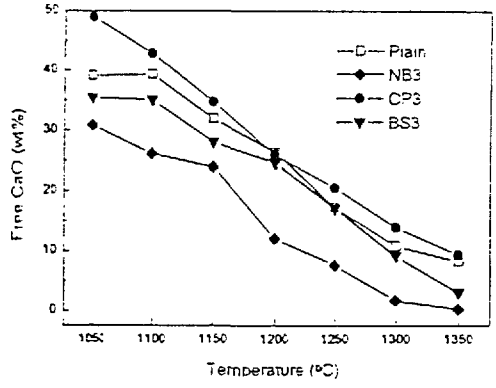

Fig. 1 Changes in free CaO amount with burning temperature in the raw mixtures of C_2S with or without additives.

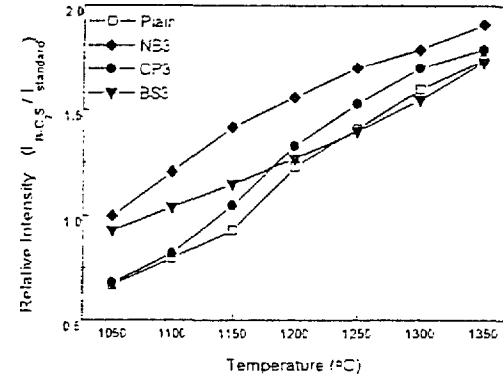

Fig. 2 Changes in XRD peak intensity of β-C_2S with burning temperature in the raw mixtures of C_2S with or without additives

In CP3, larger C_2S peaks than those in Plain were observed. This result also can be explained by the subsititution of P_2O_5 into C_2S. In BS3, large β-C_2S peaks were observed at 1050℃. In this, it seems that by the solution of BaO and SO_3 in C_2S, the $\beta \rightarrow \gamma$ transition temperature can be lowered, thereby β-C_2S can be easily stabilized in the room temperature.

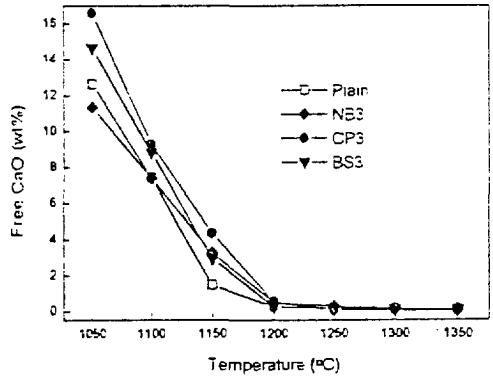

Fig. 3 Changes in free CaO amount with burning temperature in the raw mixtures of $C_4A_3\bar{S}$ with or without additives.

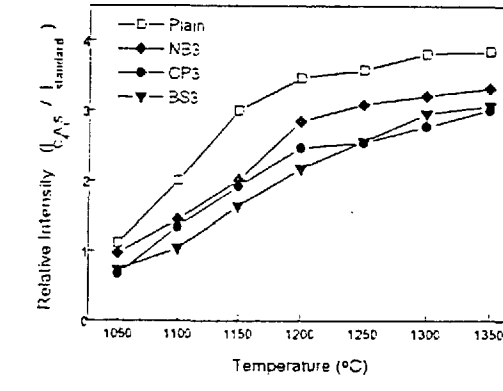

Fig. 4 Changes in XRD peak intensity of $C_4A_3\bar{S}$ with burning temperature in the raw mixtures of $C_4A_3\bar{S}$ with or without additives

Fig. 3 and 4 are the results of free CaO analysis and the relative intensity of $C_4A_3\bar{S}$ peak. In the additive-bearing samples, the results of free CaO analysis were similar to those of Plain, but weaker $C_4A_3\bar{S}$ peaks and peaks of calcium aluminate, which is not found in Plain, were identified in the samples fired between 1200℃ and 1300 ℃.(Fig. 5) From these results, it seems that $C_4A_3\bar{S}$ can be formed directly from the raw materials, CaO, Al_2O_3, $CaSO_4$ in additive-free sample, while as occuring stabilization of calcium aluminate, $C_4A_3\bar{S}$ is formed by the reaction ($3CA+CaSO_4 \rightarrow C_4A_3\bar{S}$), thereby formation of $C_4A_3\bar{S}$ is delayed in additive-bearing samples.
In NB3, free CaO was decreased and the C_4AF peak was increased from 1050℃. (Fig. 6, 7) These results could be related to the melt formation by the fluxing effect of Na_2O and B_2O_3 in borax. An amount of melt helps the aluminium ions moving into crystal lattice of C_2F and speeds up the C_4AF formation. It seems that most of C_4AF is formed at 1250℃, while more viscous melt by the effects of Na_2O and B_2O_3 were formed at higher than 1250℃ and stabilized as glassy state in the room temperature by quenching.

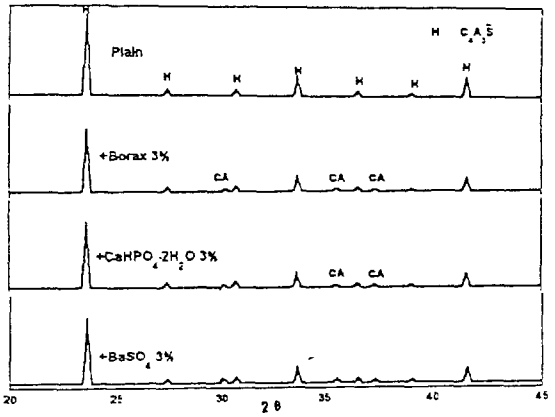

Fig. 5 XRD patterns of each clinkers fired at 1250℃ for 1 hour in the raw mixtures of $C_4A_3\bar{S}$ with or without additives

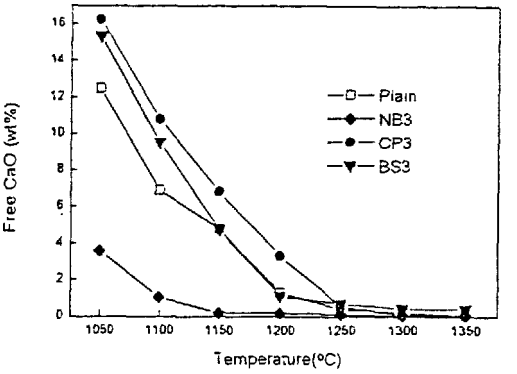

Fig. 6 Changes in free CaO amount with burning temperature of the raw mixtures of C_4AF with or without additives.

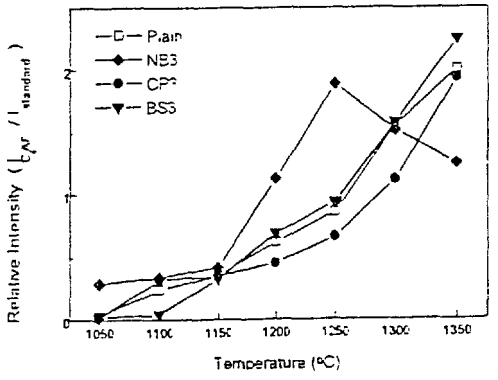

Fig. 7 Changes in XRD peak intensity of C_4AF with burning temperature in the raw mixtures of C_4AF with or without additives

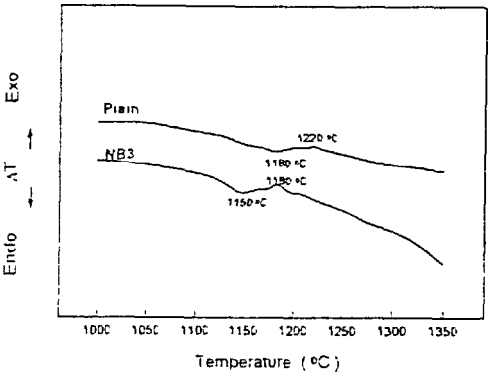

Fig. 8 DTA curves of C_4AF raw mixtures with or without additives

The trend of liquid and C_4AF phase formation is consistent with the result of DTA. (Fig. 8) It seems that the beginning of melt formation is indicated by the endothermic peak at 1150℃ in NB3 and 1180℃ in Plain, and the formation of C_4AF is indicated by the following exothermic peak at 1180℃ in NB3 and 1220℃ in Plain.

In addition to continuous increase of the melt is indicated by the endothermic peak beginning around 1200℃ in NB3. Comparing to Plain, worse-formation of C_4AF was shown at higher than 1150℃ in CP3. This seems because P_2O_5 prefer to form structurally stable $AlPO_4$ with Al^{3+} ions diffused through liquid phase at higher temperature, thereby it doesn't have fluxing effect on C_4AF formation. In BS3, better-formation of C_4AF was shown at higher than 1200℃. It may be related with $BaSO_4$ decomposition at this temperature.

Clinkerization in C_2S-$C_4A_3\bar{S}$-C_4AF system

On each MBC clinker, free CaO (Fig. 9) was less than 1% from 1050℃ in NB3, while from 1250℃ and from 1300℃ in the other samples. XRD analysis of the clinkers fired at 1300℃ (Fig. 10) shows major clinker minerals are β-C_2S, $C_4A_3\bar{S}$ and C_4AF. Considering γ-C_2S still exist in additive-free sample, it seems that each additive stabilze β or α'-C_2S in the other samples.

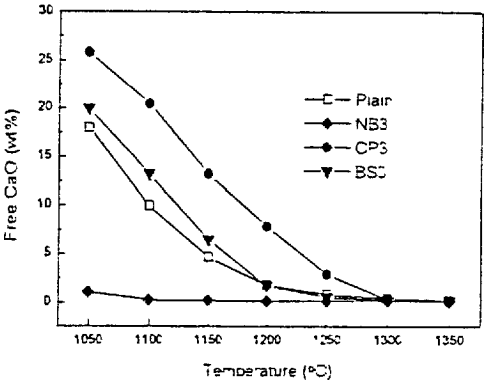

Fig. 9 Changes in free CaO amount with burning temperature in the raw mixtures of MBC clinker with or without additives.

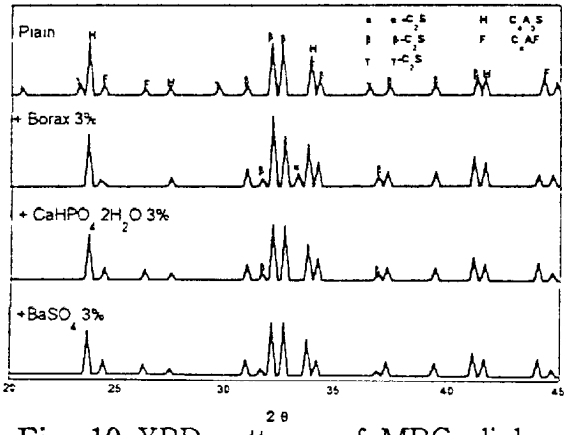

Fig. 10 XRD patterns of MBC clinker with or without additives

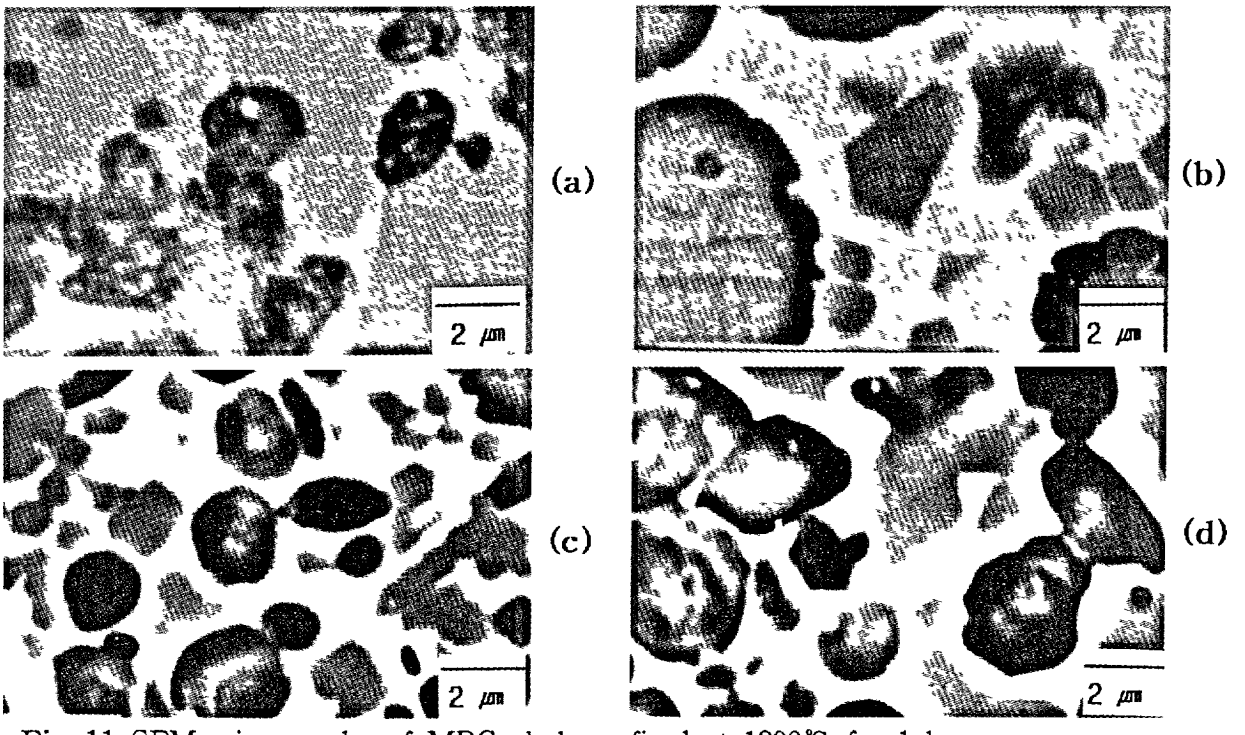

Fig 11 SEM micrographs of MBC clinkers fired at 1300℃ for 1 hr.
: (a)Plain, (b)NB3, (c)CP3, (d)BS3

SEM micrographs of Plain clinker (Fig. 11-a) shows 2~3μm C_2S and 7~8μm $C_4A_3\bar{S}$ crystals. In NB3, (Fig. 11-b) larger C_2S, and smaller $C_4A_3\bar{S}$ than those in Plain were shown. In CP3, (Fig. 11-c) similar size of C_2S and smaller $C_4A_3\bar{S}$ were shown. Larger C_2S and smaller $C_4A_3\bar{S}$ were shown in BS3 (Fig.11-d). In additive-bearing samples, large C_2S crystals might be formed from the result that diffusion of Ca^{2+} ion was hindered by more viscous melt influenced by the additives.

Table 1 Chemical Compositions of C_2S Crystals According to EPMA

	CaO	SiO_2	Al_2O_3	SO_3	Fe_2O_3	Na_2O	B_2O_3	P_2O_5	BaO
Ideal	65.11	34.89	-	-	-	-	-	-	-
Plain	59.96	35.52	2.49	0.62	1.41	-	-	-	-
NB3	63.54	32.76	0.59	0.43	0.63	0.50	1.55		
CP3	63.26	30.72	1.30	0.60	0.98	-	-	3.14	-
BS3	61.12	33.42	1.21	1.52	1.01	-	-	-	1.69

Table 2 Chemical Compositions of $C_4A_3\bar{S}$ Crystals According to EPMA

	CaO	Al_2O_3	SO_3	Fe_2O_3	SiO_2	Na_2O	B_2O_3	P_2O_5	BaO
Ideal	36.76	50.12	13.12	-	-	-	-	-	-
Plain	36.87	47.86	13.13	1.96	0.20	-	-	-	-
NB3	37.14	45.87	13.01	1.77	0.84	0.23	1.14	-	-
CP3	37.09	47.46	12.69	2.00	0.56	-	-	0.20	-
BS3	34.47	46.50	12.69	1.95	0.71	-	-	-	3.68

The incorporation of additive was determined by means of EPMA. Table 1 shows the oxides amount in C_2S crystals. It seems that the less amount of Al_2O_3 and Fe_2O_3 in additive-bearing samples is resulted from better-incorporation of additives in C_2S crystal. Less amount of SiO_2 in NB3 and CP3 is resulted from substitution between SiO_2 and B_2O_3 or P_2O_5 which have tetragonal structures. Table 2 shows the oxides amount analyzed in $C_4A_3\bar{S}$. Na_2O, B_2O_3 and P_2O_5 were less than in case of C_2S. In BS3, more BaO, but less CaO were analyzed. This trend seems to be related with the substitution between Ba^{2+} and Ca^{2+} ions.

CONCLUSION

Borax, calcium phosphate and barite stabilized β-C_2S. Especially, borax stabilized α'-C_2S. No effect or negative effect was observed on $C_4A_3\bar{S}$ formation. Borax and barite accellerated C_4AF formation. In additive-bearing MBC clinker, larger C_2S crystals and smaller $C_4A_3\bar{S}$ crystals were observed than in additive-free clinker. Na_2O, B_2O_3 in borax, P_2O_5 in calcium phosphate and SO_3 in barite well-incorporated in C_2S, and BaO in barite was well-incorporated in $C_4A_3\bar{S}$.

REFERENCES

Bucchi, R., "Influence of the Nature and Preparation of Raw Materials on the Reactivity of Raw Mix," Proc. 7th Inter. Cong. Chem. Cem.,Vol. 1, 1-1, Paris (1980)

Gies, A., Knofel, D., Bujan, M.," Influence of Alkalies on the Composition of Belite-rich Cement Clinkers and the Technological Properties of the Resulting Cement", *Cem. Conc. Res.*, **16**(3), pp411-422 (1986)

Jenic, I., Bezjak, A., Bujan, M., "Hydration of B_2O_3 stabilized α' and β Modifications of Dicalcium Silicate", *Cem. Conc. Res.*, 8(2), pp173-180 (1978)

Matkovic, B., Carin, V., Halle, R., Young, J. F. , "Dicalcium Silicates Doped with Phosphates," Proc. 8th Int. Symp. Chem. Cem., Vol. 2, pp276-281, Rio de Janeiro (1986)

Nettleship, I., Slavick, K. G., Kim, Y. J., Kriven, W. M., "Phase Transformation in Dicalcium Silicate: Ⅲ, Effects of Barium on the Stability of Fine-grained α_L' and β Phases," *J. Am. Ceram. Soc.*, **76**(10), pp2628-34 (1993)

Ziemer, B., Altrichter, B., "Effect of SO_3 on Formation and Hydraulic Reactivity of Belite", *Cem. Conc. Res.*, **14**(4), 686-692 (1984)

Kn o. 14. DEZ. 2000 d o k 31467

1i037
10 pp

SYNTHESIS OF LOW TEMPERATURE PORTLAND CEMENT CLINKER BY USING COMPOSITE MINERALIZER

R.SANJAASUREN , Centre of Chemistry and Technology of New Materials ,
The National University of Mongolia ,
Ulaanbaatar , Mongolia

P.F.Rymyantsev , Ins. of Silicate Chemistry of Russian Academy of Sciences ,
St. Petersburg , Russia

ABSTRACT In this paper presented the results of physico-chemical studies for synthesis of Portland cement clinker at lower temperature conditions by using basaltoid containing raw mixes in combination with composite mineralizers . It is fixed that in the presence composite mineralizers clinker formation was completed at the temperature of 1250-1280°C .

I. INTRODUCTION

For the last 20-30 years thank to the efforts of many researchers number aspects of mineralizers which were very important and less studied particularly regularity and sequence of intermediate flouride containing silicate compound formation allowing synthesis alite phase at the lower temperature than in the traditional conditions without using mineralizers [1-7].

In the paper presented new experimental data on regularity of influence of modifying substances on physico-chemical characteristics (viscosity , surface tension , mobility of ions etc.) of clinker liquid phase and also on the crystallochemical features of cement clinker minerals structure [8-14].

For the last 10-20 years an interest to searching for new types of aluminosilicate raw materials able to replace (fully or partially) clay rocks in composition of raw mixes for making the Portland cement clinker , and in this sense such magmatic rocks as perlite , basalt , volcanic tufas and slags have a perspective significance.

In this paper were considered questions about possibilities to use the volcanic rock from the group of alkaline basaltoids for the synthesis of the Portland cement clinker. Alkaline basaltoids defer from basalts by the alkaline characters expressed in the mineral composition as well as in chemical composition. Basalts and basaltoids belong to the different groups.

Alkaline amount in basaltoids reaches 5-8 mass percent. One of ways reducing alkaline amount in the clinker is a considerable increasing of thier volatility by the mean of adding mineralizers assisting alkaline volatility during the firing raw mixes.

Goals of this Paper is:

*Experimental basing possibilities of using of alkaline basaltoids in the capacity of the aluminosilicate component for the synthesis of the Portland cement clinker in the presence of composite mineralizers in the low temperature conditions.

EXPERIMENTAL PROCEDURE

Objects of this study were two-and three component mixes consisting of calcium carbonate (or limestone) , basaltoid and iron additions characterized by concrete digital parametres (KM , SM , AM) for making the Portland cement clinker.

Chemical composition of the initial materilas used for making mixes is shown in table 1.

Table 1.

Chemical composition of used initial materials

%	Materials		
	limestone	Basaltoid	Iron ore
SiO_2	5.36	54.16	9.55
TiO_2	-	2.22	-
Al_2O_3	1.27	14.54	1.59
Fe_2O_3	0.22	4.00	64.38
FeO	-	4.35	15.75
MgO	0.32	4.65	2.78
CaO	51.30	6.90	0.71
Na_2O	0.10	4.94	0.10
K_2O	0.10	2.65	0.23
LOI	40.26	1.13	4.20

Component ratio and module characteristics of studied mixes are shown in table 2.

Table 2.

Composition of studied mixes and thier module characteristics

N of mix	Content of components (%)				KH	Modulus	
	$CaCO_3$	Limestone	Basaltoid	Fe_2O_3		n	p
1.	74.62		25.38		0.93	2.12	1.90
2.	73.98		24.82	1.20	0.93	1.78	1.23
3.		82.42	17.58		0.93	2.43	2.31
4.		82.00	17.23	0.77*	0.93	2.20	1.69
5.		81.62	18.38		0.89	2.42	2.29
6.		77.37	22.63		0.71	2.36	2.20

*-iron-ore was used

Powdered fine initial components , taken in proper dozes (as shown in table 2) , homogemsed by liquid methods (in acetone) in the ball mill during 1-2 hours, and then mixes dryed and prepared briquettes under the pressure in the shape of cylinders with size of 1.5×1.5cm firing had been done in the laboratory silicon carbide furnace with speed of 400°C an hour in the platinium caps and keeping in the certain temperature within 45min and the cooling of samples was on air and slow.

X-rayDiffraction Analysis (XRD) had been done by Diffractometry DRON-1.0 , derivatographic analysis was made by Derivatograph (1500D).

To define starting point of melting temperature of basaltoid rocks and mixes was used the method of electroconductivity of the samples with continuis heating (heating speed is 7° min) on the electric device made in the Institute of silicate chemistry of St.Petersburg, Russia.

RESULTS AND DISCUSSION

1.The thermal behaviour of raw mix composition of "Limestone + Basaltoid"

In the Fig.1 shown Derivatogramma of the mix composition 3, where could been seen that the process of decomposition of carbonate component starts at the temperature of 630°C and ends at the temperature of 950°C. The deep Endothermic peak at the temperature of 915°C on the DTA curve identifies with the decomposition of the basic mass of carbonate component in the studied mix.

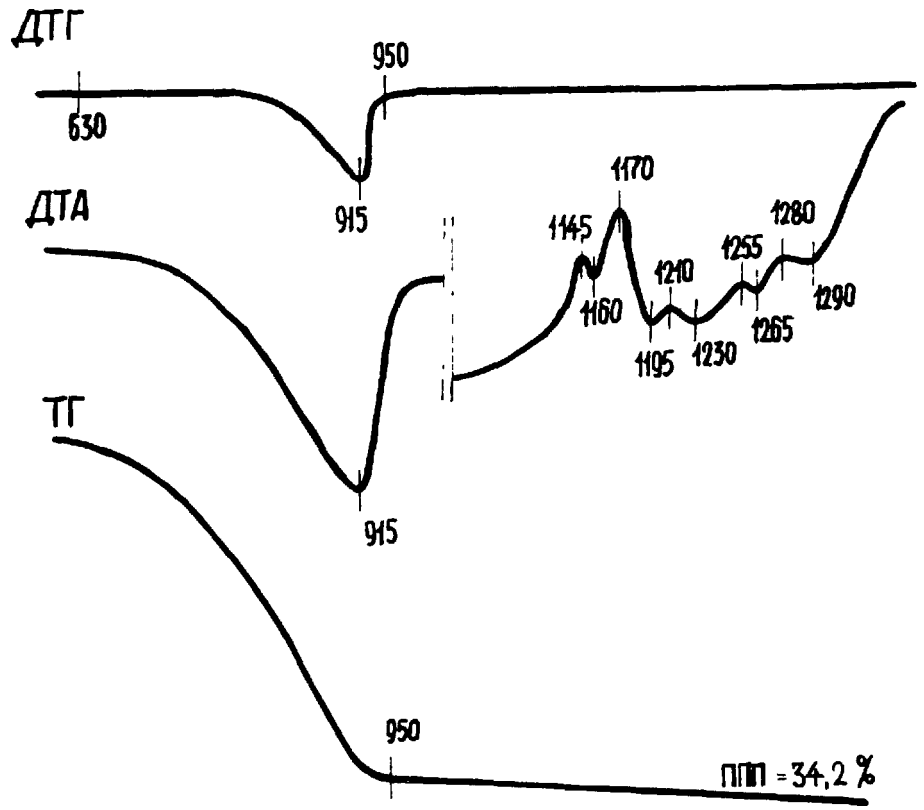

Figure 1. Derivatogramma of the mix composition 3,

In order to define reasons of appearing of series of Endothermic and Exothermic peaks within high temperature section (higher than 1000 °C) of the DTA curve was used the XRD method. Results of XRD studies are shown in Fig.2.

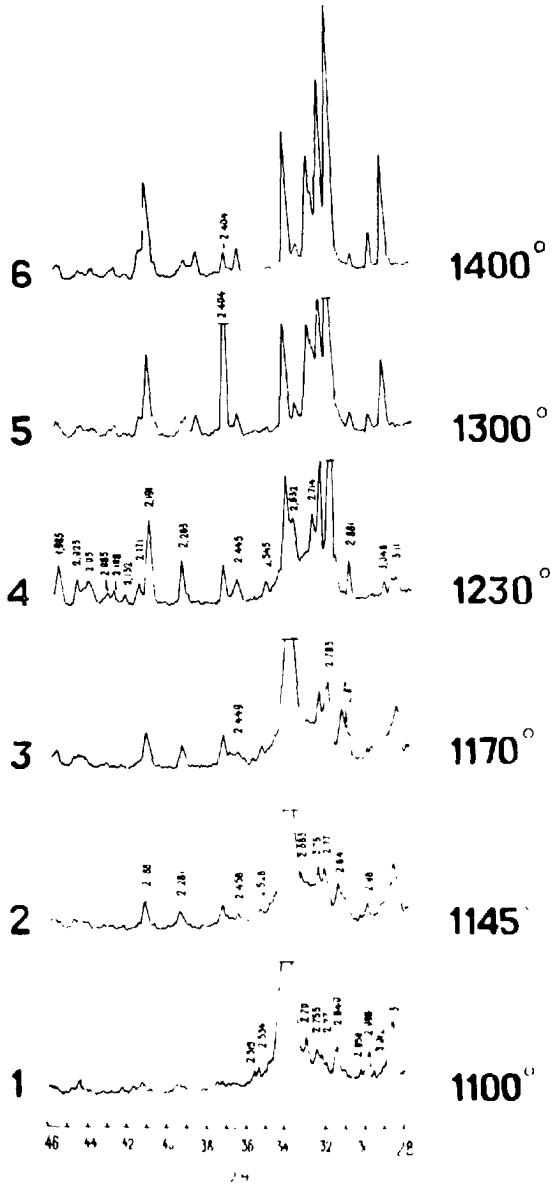

Figure 2. Phragments of the XRD of samples heated till the temperature where thermic effects could be seen on the DTA curve of mix 3.

The XRD analysis have shown that the exothermic peak at the temperature of 1145 °C on the DTA curve caused by $C_{17}A_7$ and gehlenite, the exothermic peak at the temperature of 1175 °C identified with β-C_2S formation, and the small exothermic peak in the range of 1210 °C caused by alite crystallization. Endothermic peaks in the range of 1230 °C and 1265 °C caused by nonequilbrium liquid phases and dissolution of belite phase in them.

In order to define the beginning of the liqiud phase formation temperature in twocomponent mix (Limestone + Basaltoid, with KM=0.93, n=2.43) during the heating process there were made measures of Electroconductivity depending on the heating temperature. These studies have shown that the liquid phase in studied twocomponent mix starts at the temperature of 1015°C [16].

2.The thermal behaviour of raw mix composition of "Limestone + Basaltoid" with addition of composite mineralizers consisting of Fe_2O_3 and CaF_2

In the Fig.3. shown DTG and DTA curves of mixes compositions 3 and 4 (KH=0.93) with addition of 1.0 mass.% CaF_2.

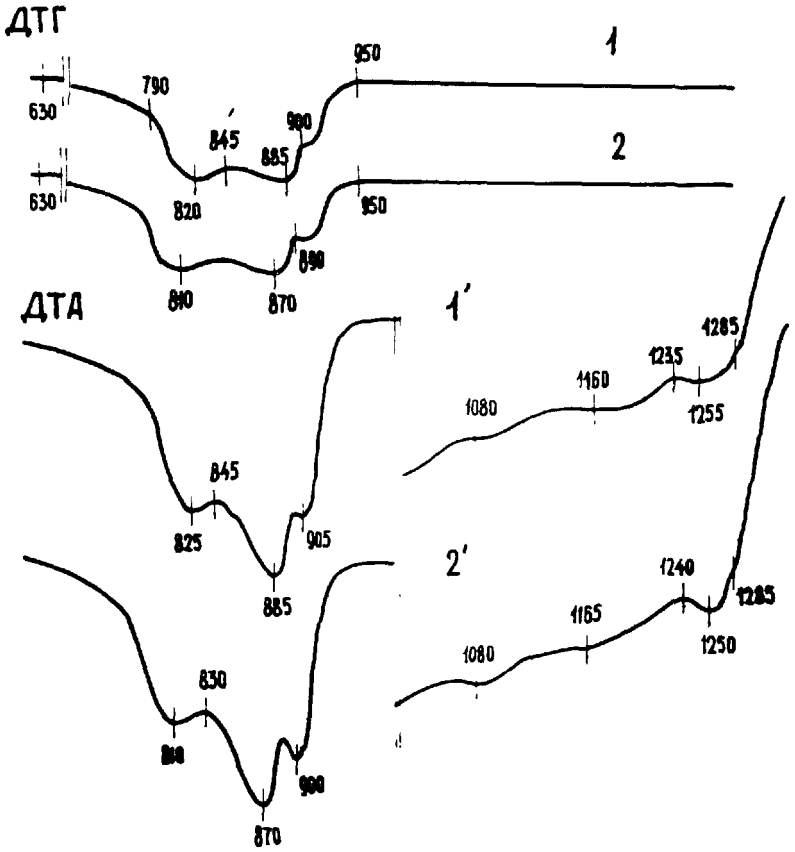

Figure 3. DTG and DTA curves of mixes containing 1.0% CaF_2, 1,1'-raw mix 3, 2,2'-raw mix.

Comparing DTG and DTA curves shown in Fig.1. and Fig.3. it is possible to say that with addition of composite mineralizers Fe_2O_3 + CaF_2 into mixes , phase formation processes during the heating are changing considerably.

Experiments on electroconductivity measures of the mix composition 3 containing the addition of CaF_2 have shown that the liquid phase during the heating of the mix starts at the temperature of 980 °C otherwise with addition 1.0 % mass. CaF_2 into the mix the starting point of the temperature of the liquid phase formation lowered for 35-40 °C [16]. As shown our studies early formation of the liquid phase assists speeding up C_3S , C_3A , C_4AF formation , and also considerable decreasing clinker sintering temperature.

In Fig.4 shown the XRD patterns of clinker samples getting from mixes consisting of natural materials (compositions 3, 4, 5 and 6) with addition 1.0 mass.% each of flouride calcium.

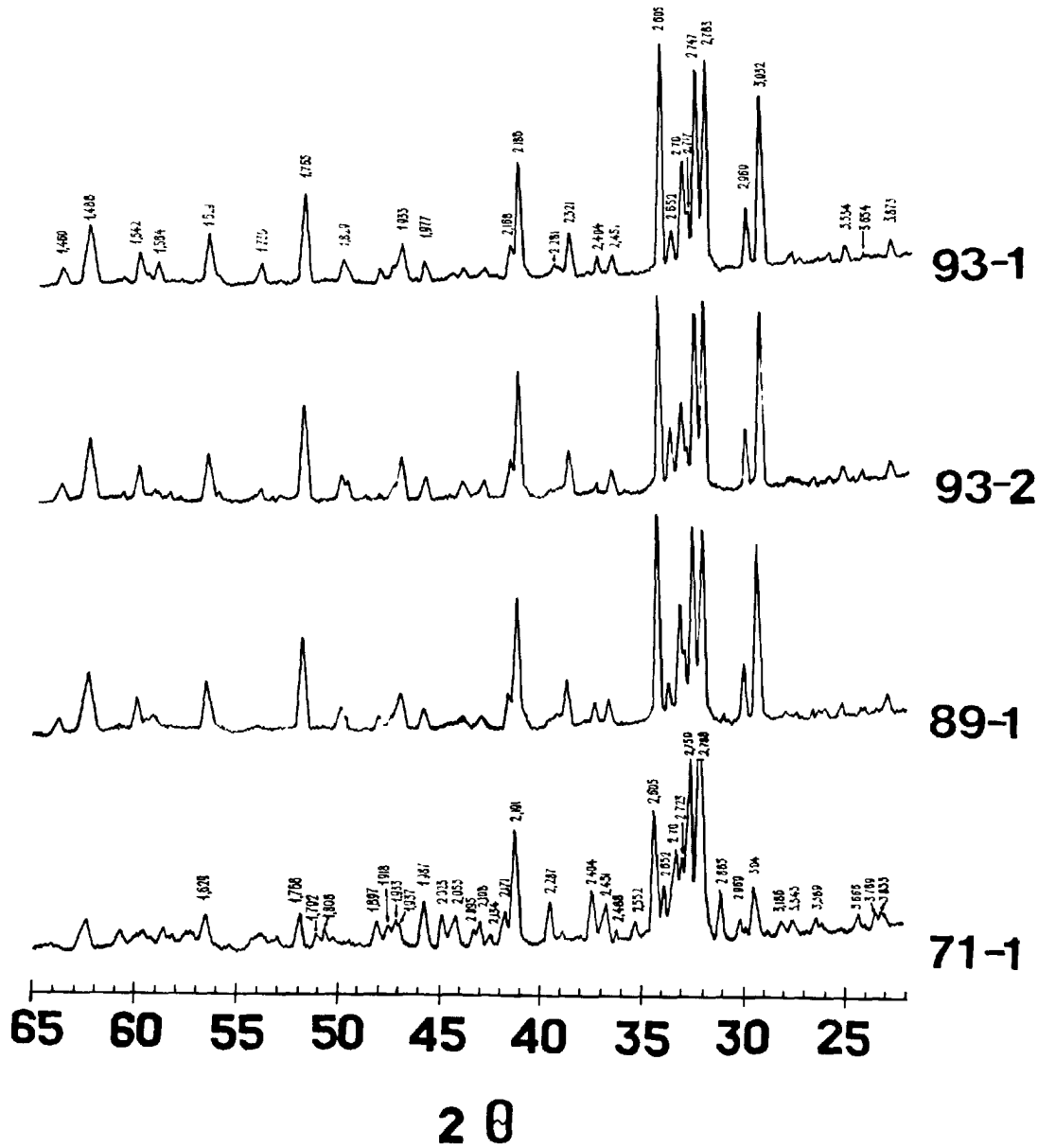

Figure 4. XRD patterns of clinkers made of mixes with addition of 1.0% CaF_2 each
1- composition 3, 1300°C 2- composition 4, 1300°C
3- composition 5, 1280°C 4- composition 6, 1200°C

Analysis of the XRD patterns has shown that on the XRD patterns of simples got from mixes with KH=0.93 and KH=0.89 there are many lines identifying with alite (d=3.534 ; 3.032 ; 2.969; 2.605; 2.321; 2.168; 1.932; 1.829; 1.765; 1.629A° etc.) which indicate considerable alite phase content in these clinkers. Peaks with d=3.873 and 2.717 A° could be identified with α'-C_2S and peak with d=2.747 and 2.81 A° -to α-C_2S phases; peaks with d=2.697 and 1.564 A° indicate the presence of C_3A phase , and peaks with d=2.697 and 2.451 A° could be identified with flouride aluminate calcuim composition-$C_{11}A_7CaF_2$ which has a small quantity. Line with

d=2.652 and 1.730 A^{o} indicative of the presence of aluminoferrite phase, and the line with d=2.651 A^{o} is typical to aluminoferrite phase with composition C_6A_2F.

Because of high content of alite an identification of β-C_2S becomes much more difficult but peaks with d=2.783 (very strong) and 2.451 A^{o} could be identified with C_2S β-forms however these peaks levy on peaks of alite and $C_{11}A_7CaF_2$.

Addition of composite mineralizer Fe_2O_3+CaF_2 promotes acceleration speed of decomposition process of basic components of the raw mixes , and the combining of free oxide CaO depending on the temperature of the firing the mix composition 2 (KH=0.93; n=1.78) containing composite mineralizer Fe_2O_3 and CaF_2 is shown in Fig.5.

The curve in Fig.5 reflects kinetics of the combining of free CaO in the mix composition 1, containing neither Fe_2O_3 nor CaF_2 , and the curve 2 belongs to threecomponent mix containing Fe_2O_3=1.20% without addition of CaF_2 (composition 2) , so course of these curves shows that addition of Fe_2O_3 noticebly accelerate processes of the combining of free oxide calcuim however both mixes can not ensure finishing of clinker formation processes in the low temperature conditions.

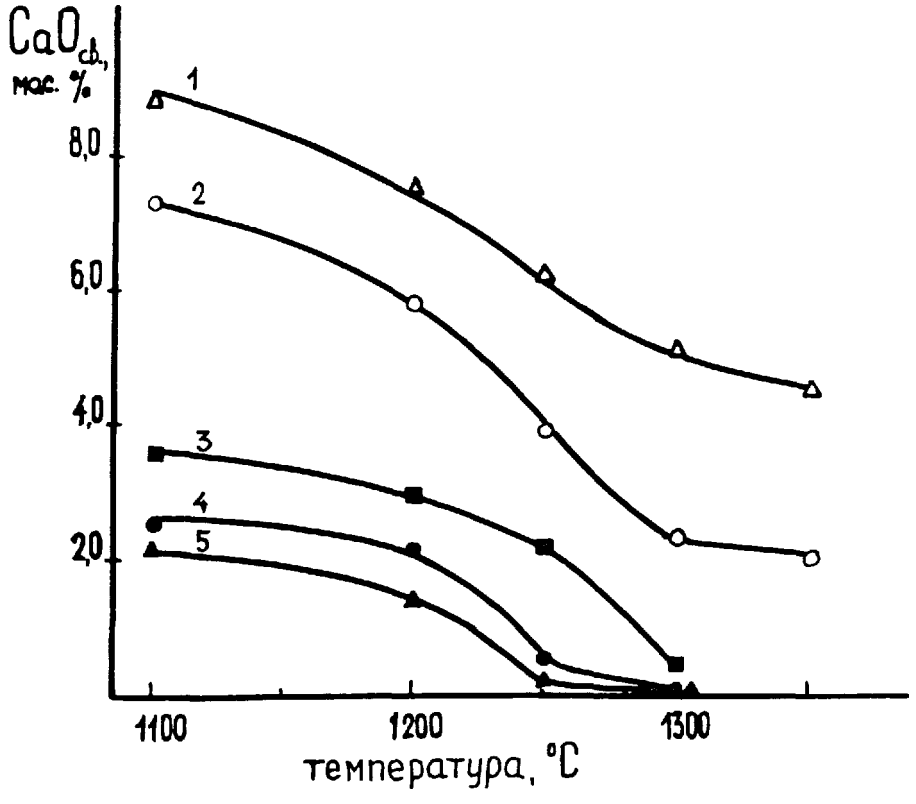

Figure 5. Relationship between free oxide calcuim content in simples and the temperature of the firing of the mix with CaF_2

1- content 1 without CaF_2,
2- content 2 without CaF_2,
3- content 2+0.25% CaF_2,
4- content +0.5% CaF_2,
5- content +1.0% CaF_2

Curves 3,4 and 5 in Fig.5 show kinetics of combining of free CaO in mixes composition 2 containing at the same time either Fe_2O_3 and CaF_2 with different quantities of CaF_2 addition. The course of these curves testifies that together added Fe_2O_3 and CaF_2 into the studied mix strongly accelerate speed of combining of free oxide calcuim and with addition of 0.25 mass.% CaF_2 clinker formation finishes almost at the temperature of 1300°C , and with addition of CaF_2 in the quantity of 0.5 and 1.0 mass.% clinker formation finishes at the temperature of 1250 °C i.e. addition of composite mineralizers containing of Fe_2O_3 and CaF_2 quite strongly intensified physico-chemical processes of clinker formation and allowed to finish clinker sintering at the considerably low temperature.

Microscopis studies have shown that with increasing of CaF_2 dose there is observed sharp increasing of alite phase content and decreasing of belite quantity. Influence of CaF_2 dose in initial mix on the ratio of forming minerals in the clinker could be presented by the following experimental data got by microscopic method analysis:

Quantity of addition CaF_2 (mass.%)	Alite	Belite	Intermediate phase
0.0	30	50.0	15
0.5	65-67	10-12	22-23
1.0	67-69	7-8	21-24
2.0	70	4-5	22-24

Thus composite mineralizer Fe_2O_3+ CaF_2 added in small quantity into basaltoid containing mix has considerable influence not only on the speed of physico-chemical processes of mineral formation during the heating of studied mixes but also on processes of microstructure formation and phase composition of synthesised clinkers.

3.The thermal behaviour of raw mix composition of "$CaCO_3$+ Basaltoid+CuO(ZnO)+ $CaSO_4$+CaF_2"

Last few years we have been conducting researches on influence of following composite mineralizers on the behaviour of raw mixes during thier thermal treatment:

(a) CuO+ $CaSO_4$+CaF_2

(b) ZnO+ $CaSO_4$+CaF_2

Conducted researches' results had shown that the above mentioned composite mineralizers speed up physico-chemical processes of clinker phases formation , and lower the temperature of cement clinker sintering till 1250 °C -1280°C.

Thus addition to the cement raw mix of copper or zinc containing minerilizers together with sulfate and flouride containing mineralizers does not bring to considerable lowering of the temperature of clinker formation process finishing in comparision with composite mineralizer consisting of Fe_2O_3 and CaF_2.

Researches on optimisation of compositions of chemical substances' types as well as of quantity ratio of component included in composite mineralizers composition are continuing in Laboratories of our Centre.

CONCLUSION

1.It is fixed that during the firing of basaltoid containing raw mix with addition of composite mineralizers (Fe_2O_3+ CaF_2) in the range of decomposition (630 °C -950°C) of carbonate component has been observed formation of metastable carbonate spurrite.Spurrite formation starts at 750 °C -770 °C , and the composes completely in the range of 860 °C -885 °C temperature.

2. In the presence of composite mineralizer "Fe_2O_3+ CaF_2" in basaltoid containing mixes starting from 800 °C have formed flouridealuminates and flouridesilicates calcium which assist basic clinker phases in more lower temperature conditions rather than in traditional clay mixes.

3.Flouride calcium (0.5-2.0%) addition to basaltoid containing raw mixes lowers the temperature of liquid phase till 980 °C temperature i.e. approximetely 280 °C lower than in usual clay containing raw mixes.

4.Under the influence of CaF_2 addition alkalis are loosing the properties as inhibitors in consequence of which in basaltoid containing mixes in the presence of CaF_2 alite formation starts from 1000 °C -1100 °C , which is lower 150 °C -170 °C than in clay containing mixes.

5. It is fixed that addition of composite mineralizer consisting of Fe_2O_3+ CaF_2 into the basaltoid containing mix assists more speed clinker minerals formation in consequence of which clinker formation finishes at the temperature of 1250 °C -1280 °C.

REFERENCES

1.**Волконский Е.Ф., Коновалов П.Ф., Макашев С.Д.,** Минерализаторы в цементной промышленности,-М.Стройиздат,1964.-199с.

2.**Лугинина,И.Г.**, Влияние режима обжига и минерализаторов на декарбонизацию и клинкеробразование: Автореферат . ... д-ра техн.наук. - Новочеркасск, 1968.-31ё.

3.Gutt, W., Osborne, G.J. The system CaO-2CaO-CaF_2 , Trans.Brit.Ceram.Soc.-1970-Vol.69,N3.125-129pp.

4.**Christensen N.H., Johansen V.,** Mineralizers and fluxes inthe clinkering process, II.Kinetics effects on alite formation, 7th Int.Congr.Chem.Cement.-Paris.1980.,Vol.II.1-5pp.

5.**Moir G.K., Glasser E.P**., Mineralizers, modifiers and activators in clinkering process , 9th Int.Congr.Chem.Cement.-New Delhi,India,1992,vol.1,125-152pp.

6.**Lu Zhongyuan, Huang Wenxi and Xu Guangliang**: The effect of composite mineralizers of CaF_2, $CaSO_4$, ZnO on the formation of Portland Cement Clinker in a rapid heating-up burning, 9th Int.Congr.Chem.Cement.- Int.Congr.Chem.Cement.- -New Delhi,India,1992,vol.2, 396-389pp

7.**W.A.Klemm, I.Jamed** (USA) Mineralizers and fluxes in the clinkering process.III.Burnabelity of synthetic and industrial raw mixes.in 7th Int.Congr.Chem.Cement.-Paris.1980.,.1-150pp

8.**Timashev V.V**., The kinetics of clinker formation, The structure and composition of clinker and its phases, 7th Int.Congr.Chem.Cement.-Paris.1980.,Vol.I,1-3/1-1-3/17

9.**Кузнецова Т.В., Осокин А.П.,** и др. Строение и свойства оксидносолевых клинкерных расплавов, Расплавы 1987,-т.1.Вып.1,с.74-79.

10.**Осокин А.П., Кривобородов Ю.Р., Потапов Е.Н.,** Модифицированный портландцемент ,М., Стройиздат,1993,с.328.

11.**Regourd M.M., Boikova A.I.**,Chemistry, structure, properties and quality of clinker, 9th Int.Congr.Chem.Cement.- New Delhi, India,1992,vol.1, 3-45pp

12.**Sychev M.M.,** Problem of admixtures, Proc.5th Int. Symp.Chem.Cement, Tokyo, 1968, I, 157pp.

13.**Tanaka M.,Sudon G.,Akaiwa Sh**., New compound Ca12 Si4O19F2 in the system CaO-SiO2-CaF2 and the role of CaF2 in the burning of cement clinker, 5th ISCC, Suppl. paper, Paper N1-78,28p.

14.**Maki I.,** Relationship of processing parameters to clinker properties: Influence of minor components , 8th ICCC, Rio de Janeiro , 1986,vol.1,34-47pp.

15.**Sanjaasuren R.**, Formation of low temperature Portland cement clinker by using non-traditional aluminosilicate rock and mineralizer, 9th Int.Congr.Chem.Cement.- New Delhi, India,1992,vol.2, 315-321pp.

16.**Sanjaasuren R.**, Physico-chemical basis for synthesis of low temperature Portland cement clinkers by using alkalic basaltoids, Thesis Dr. Science,1987,371p.

TOPIC I.E

Correlating process parameters with clinker properties

1i038
8 pp

APPLICATION OF PARTIAL LEAST SQUARE REGRESSION ANALYSIS IN EXAMINATION OF CORRELATIONS BETWEEN PRODUCTION CONDITIONS, MICROSTRUCTURES IN CLINKER AND CEMENT AND CEMENT PROPERTIES.

Ketil SVINNING, Norcem R & D, NORCEM A.S, Brevik, Norway

Harald JUSTNES, SINTEF Structures and Concrete, Trondheim, Norway

ABSTRACT Statistical models by application of partial least square regression for prediction of cement properties have been evaluated. The model contains variables describing the XRD profile in the range of 2θ equal to (32.9, 34.1)°, free lime, superficial microstructure of clinker and gypsum, detected by TGA, and fineness. Amount of free lime and the XRD profile was found to be a sufficient description of relevant mineralogical structure in clinker for predictions with accepted accuracy of setting time and compressive strength development until 28 days. Predictions of changes in properties by changes in the XRD profile due to changes in the production of clinker have been demonstrated.

Key-words: Modelling, microstructure, setting, strength development.

INTRODUCTION

A general investigation of the microstructure in clinker and cement has been carried out for several years as a project with the main goal of correlating cement characteristics with cement and concrete performance. The two main activities of the project are statistical investigations of : 1) The influence of the microstructure in clinker and cement on cement properties and 2) The influences of productions conditions on the microstructure. Results from 1) and 2) are presented in the two papers Svinning and Bremseth /1/ and Svinning, Bremseth and Justnes /2/, respectively. The objective of the research is to enable design of clinker quality and cement properties by controlling the production conditions in the kiln. This paper will present models for describing correlations between microstructure and cement properties. The paper will also present predictions, in two steps, of influence of production condition in kiln on cement properties. In the first step the influence of the production condition on profiles of selected XRD peaks are predicted, and in the second step the influence of the same profiles on cement properties are predicted.

The part of the microstructure in clinker being investigated is represented as the X-ray diffraction (XRD) profile including dominating aluminate and ferrite peaks in the range $2\theta \in (32.9, 34.1)°$, using CuK_α radiation. The statistical method applied for modelling was partial least square regression (PLSR). To achieve maximal explanation of variance in the properties, the following additional variables are included in the modelling: 1) Amounts of di- and hemihydrate of $CaSO_4$, 2) Mass losses which indicate different kinds of moist exposure and carbonation of clinker minerals during production and storage, 3) Amount of Fe^{2+}, 4) Amount of unhydrated free lime and 5) Fineness of the cement. The values of the two first categories of variables are determined by thermogravimetric analysis (TGA). Cement properties examined

in this work are setting time and compressive strength development until 28 days.

The production conditions whose influence on the properties are to be predicted, are those experienced in the kiln no. 6 at Dalen Plant, Brevik, Norway. The modelling of influence on the microstructure of the production condition is already performed by Svinning et. al. /2/.

METHODS

X-ray diffractograms were recorded at Norsk Hydro a.s, Research Center, Porsgrunn, Norway. The XRD profile was obtained by an X-ray diffractometer in steps of 2θ equal to 0.02 °. The scaling of the intensities and correction of the 2θ - positions of the peaks were based on equalising the areas and adjusting the positions of the diffraction peaks at d = 3.52 Å of anatas (TiO_2), which was added in an amount of 10 wt% to the total samples.

The methods for determination of the values of the other variables included in the modelling of cement properties are described in /1/.

In case of a great number of variables relative to number of observations or objects, data compression by expressing the original x - variables by fewer latent variables or factors could be necessary. Partial least square regression (PLSR) does calculation and optimization of number of factors for maximum explanation of variance, for prediction, in y. In addition, model parameters are calculated for prediction of y for new values of x. PLSR of several y-variables together or a vector of y-variables as well as of one y-variable can be performed. Before the start of the regressions the variables are centered and scaled by putting a weight on each variable. The weight is equal to the inverse of the standard deviation of the respective variable. The iterative algorithms for calibration, validation and prediction are described in detail by Martens and Næs /3/. The software applied for PLSR was UNSCRAMBLER ®. Applications of PLSR in examination of microstructure and clinker quality are presented in /1/ and /2/.

RESULTS

Modelling.

The observation **X** - matrix included in the investigation on influences of the microstructure in clinker and cement on the cement properties, contains 31 variables and 34 observations. The cement samples included in the examinations in this work is the same as in /1/ but in addition 4 more samples are included. The XRD profile is described by intensities at every 0.06° (2θ). A complete list of x-variables is given in table 2. The cement properties to be modelled and defined as y - variables are setting time [min] and compressive strengths [MPa] at 1, 2, 7 and 28 days. Results from the PLSRs are given in table 1.

Table 1: Results from the PLSRs.

Model no.	Variable(s)	Explained variance of total variance for prediction [%]	Number of factors no. for max. explained variance
1	Setting time	76	5
	Compressive strengths:		
2	1 day	86	5
3	2 days	76	5
4	7 "	53	4
5	28 "	60	4
6	Compressive strength development until 28 days (y-vector containing the four latter variables)	67	5

Table 2 contains the model coefficients, b_w, for predicting setting time and compressive strength at 1 and 28 days with weighted data. b_w indicate an influence of a variable relative to the others' on the property. The indication is possible because of the equalisation of the mean values (= 0) of and the variance in the variables in the observation **X** - matrix before the regressions on the variables.

Prediction.

Prediction of changes in properties due to changes in XRD profile in the range $2\theta \in (32.9, 34.1)^\circ$ again due to two chosen cases of changes in the production in kiln no. 6, Dalen Plant, Brevik, Norway will be demonstrated. The first case is from production of standard clinker to production of sulphate resistent clinker, as shown in figure 1 a), and the second from production of standard to high strength clinker, figure 1 b). The changes are simulated to take place in two steps. In the first step only the chemical composition in clinker is changed. In the second step the process parameters are also changed as much as what is necessary to maintain a stable process and an optimal production capacity with respect to satisfying the quality requirements. Some of the changes in the process which influence the XRD profile during step 2 to production of sulphate resistent clinker is as follows: 1) Simultaneous increases in the collinear variables secondary air temperature and amount of NO_x(g) and 2) An increase in volume flow of tertiary air. Similar changes for the change to production of high strength clinker are as follows: 1) An increase in volume flow of tertiary air and 2) An increase in the pressure in the kiln hood.

Table 2. Model coefficient for predicting setting time and compressive strength with weighted data (no. in brackets are referring to what models are applied in table 1).

Variables		Model coefficients, b_w, for prediction of:		
		Setting time (no.1)	Compressive strength at: 1 day (no. 2)	28 days (no.6)
Free lime, unhydrated	[wt%]	-0.1829	-0.0788	0.0485
$CaSO_4 \cdot 2H_2O$	"	-0.0704	0.0760	0.2014
$CaSO_4 \cdot ½H_2O$	"	-0.0228	-0.0390	-0.1652
TGA onset temperature for dehydration of gypsum	[°C]	0.1265	0.1365	-0.0255
Mass losses from TGA due to:				
Dehydration of aluminatehydrate and syngenite	[wt%]	-0.0230	0.0617	-0.0199
Dehydration of $Ca(OH)_2$	[wt%]	-0.2083	0.1117	-0.0657
Dehydration of CS-hydrates	[wt%]	0.2729	-0.1561	0.0449
Decarbonation of $CaCO_3$	[wt%]	0.0126	-0.0080	0.1486
Fe^{2+} soluble in buffer solution with pH = 5	[wt%]	0.0414	0.1944	-0.0117
Fineness	[m^2/kg]	-0.5119	0.3600	0.0868
XRD intensities [counts] at the following 2θ angles [°]:				
32.90		-0.0373	-0.0955	0.1702
32.96		-0.0386	-0.1557	0.0854
33.02		0.0555	-0.1961	0.0386
33.08		-0.0055	0.0774	-0.0326
33.14		0.0387	0.0922	-0.0737
33.20		-0.1180	0.2348	-0.0737
33.26		-0.0382	0.1885	-0.1290
33.32		-0.0573	0.1585	-0.0966
33.38		-0.1110	0.0513	-0.1193
33.44		-0.0651	0.0287	-0.0913
33.50		0.0501	0.0243	-0.0478
33.56		-0.0355	0.0759	-0.0510
33.62		0.0374	-0.0243	-0.0109
33.68		-0.0212	-0.0062	-0.0234
33.74		0.0653	-0.0724	-0.0030
33.80		-0.0629	0.0609	-0.0005
33.86		-0.1367	0.1739	-0.0234
33.92		-0.0899	0.2034	-0.0380
33.98		-0.1085	0.2131	0.0429
34.04		0.0427	0.0751	0.0891
34.10		0.0654	-0.0489	0.1373

a)

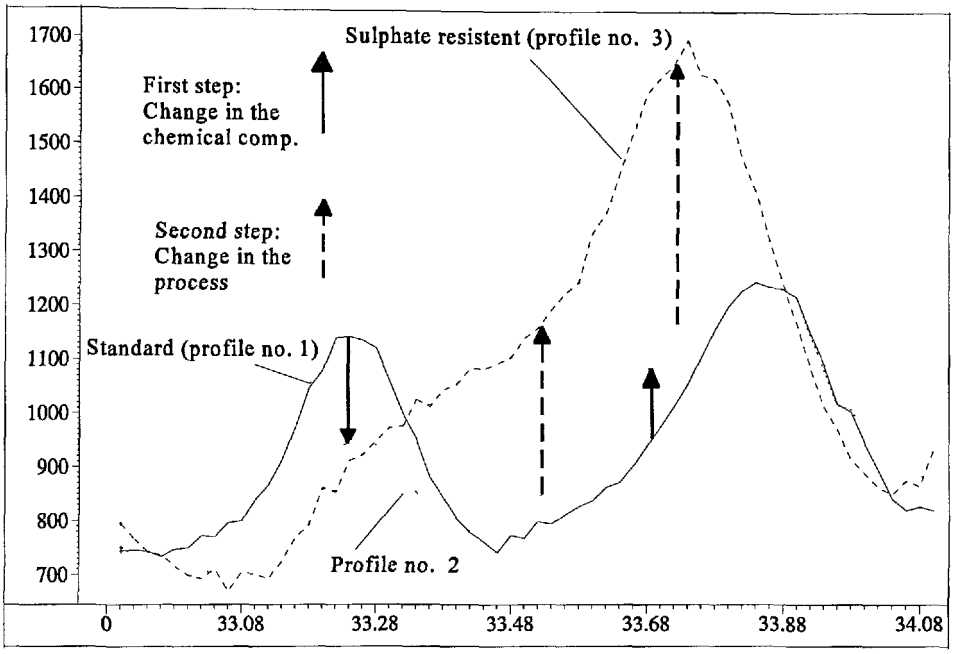

b)

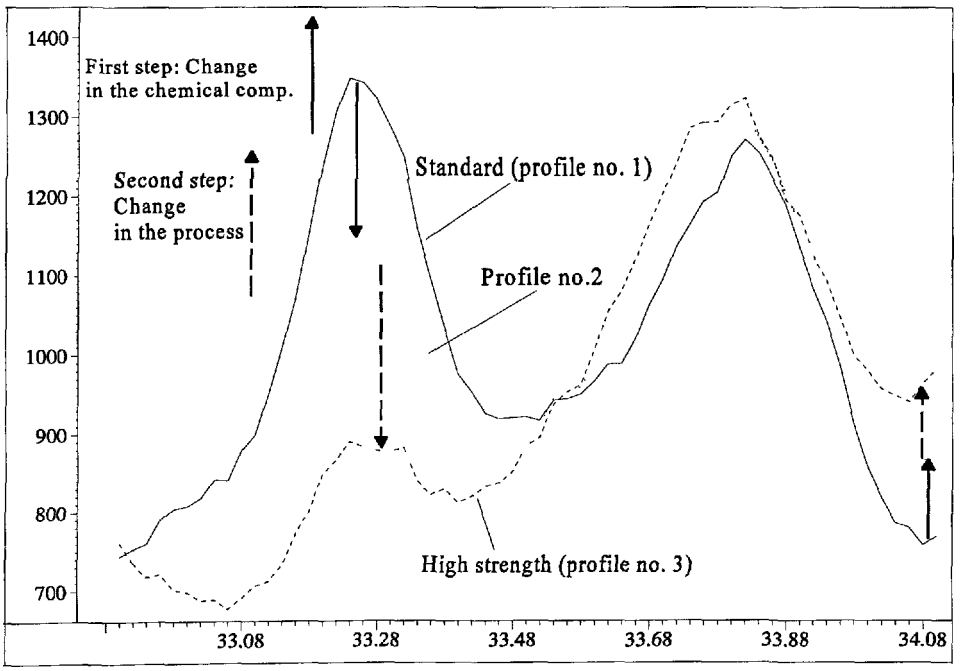

Figure 1. Two cases of predicted changes in the XRD profile [counts] in the range of $2\theta \in (32.9, 34.1)°$ by changing in two steps from the production of one type of clinker to production of another . The types included in the two cases are as follows:

a) From standard, LSF: 95.3, SM: 2.52 , AM: 1.41, to sulphate resistent, LSF: 93.5, SM: 2.61, AM: 0.71.

b) From standard, LSF: 96.1, SM: 2.48, AM: 1.54, to high strength, LSF: 96.1, SM: 3.04, AM: 1.33.

Table 3 gives the predicted values of the setting time and the strength development until 28 days for the XRD profiles described in figures 1 a) and b). In figure 2 the total changes in compressive strength at one day explained by change in the XRD profile are compared with contributions to these totale changes in strength from the changes of each of the 21 intensities included as variables in the models. The changes in strength shown in the figure, are due to changes in the process (second step) to produce sulphate resistent and high strength clinker, respectively.

Table 3: Predicted setting time and strength development until 28 days inclusive standard deviation for the XRD profile described in figures 1 a) and b).

XRD profile no.	Setting time [min]	Compressive strength [MPa] at 1 day	2 days	7 days	28 days
Change from production of standard clinker to production of sulphate resistent clinker:					
1	149±17	17.5±1.8	29.7±2.9	43.8±3.6	59.1±3.9
2	154±16	15.6±1.9	28.5±3.0	45.0±3.7	61.5±4.0
3	141±9	16.2±0.9	27.2±1.3	41.5±1.6	56.4±1.5
Change from production of standard clinker to production of high strength clinker:					
1	139±12	19.9±1.1	30.5±1.6	42.0±2.0	53.0±2.0
2	146±11	17.8±1.2	29.4±1.6	43.0±2.2	57.4±2.3
3	156±14	14.9±1.7	27.9±2.3	44.0±3.2	62.1±3.4

DISCUSSION

Modelling

SiO_2, Al_2O_3, Fe_2O_3, CaO, MgO and K_2O are shown by Svinning et. al. /2/ to influence the XRD profile in the range of 2θ equal to (32.9, 34.1)°. In this work the chemical composition included as variables in the model in /1/ for predicting the properties is therefore tried replaced by variables describing the XRD profile. In addition, XRD intensities at d ≈ 2.78 and 2.74 Å are excluded from the model. Comparing of the results from this work with previous /1/, approximately the same or even a higher explained variances as the result of the replacement.

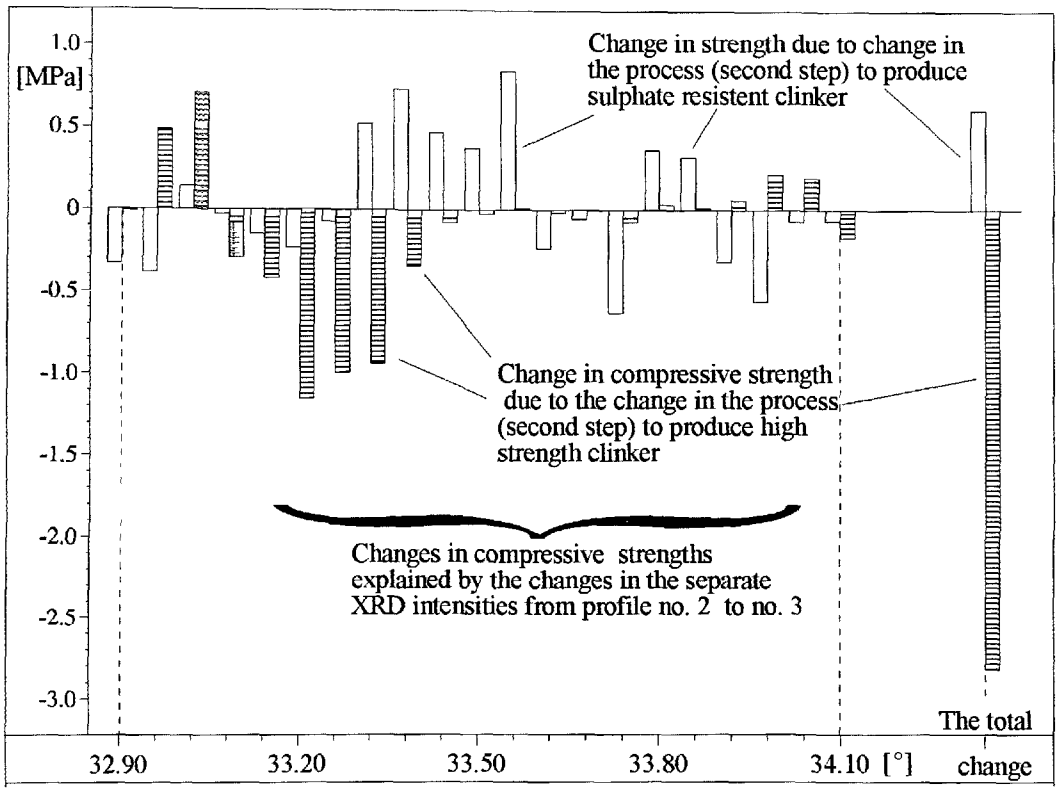

Figure 2.

Contributions to total predicted changes in compressive strength at one day from changes in each of the XRD intensities at $2\theta \in (32.9, 34.1)°$. The changes in strength are due to changes in the process (second step) to produce sulphate resistent (blank bars) and high resistent clinker (shaded bars), respectively.

The XRD profile indicates mainly amounts and structure of aluminate and ferrite, but relative changes in these will of course affect the C_3S/C_2S ratio. There is a general experience that aluminate has a major influence on the properties of cement at early ages than most of the other clinker minerals have. As expected, the explained variance in compressive strength at 1 day is therefore higher than for 28 days.

Studying the model coefficients in table 2 gives the impression that a change in the XRD profile generally results in less relative change in the setting time than in the compressive strength development.

Prediction

In the evaluations of the results from the predictions a predicted change is defined in this work to be significant if there is no overlap of confidance intervals equal to the mean value $\pm$ 1 standard deviation. According to the results in table 3 the only predicted significant changes in the properties are the those in compressive strength at 1 and 28 days for change of

production from standard to high strength clinker. The compressive strength at 1 day is predicted to decrease significantly both with the change in the chemical composition and with the changes in the process. The compressive strength at 28 days is predicted to increase significantly in the both cases.

The change in the XRD profile by changing the process to produce sulphate resistent clinker is pronounced. According to figur 2 relatively high increases in compressive strength at one day explained by changes in a few XRD intensities are predicted. They are, however, almost quite counterbalanced by many more but smaller decreases. The predicted total increase in compressive strength is therefore small and not significant.

CONCLUSIONS

Statistical models for prediction of cement properties have been evaluated. The model contains variables describing the XRD profile in the range of 2θ equal to (32.9, 34.1)°, superficial microstructure of clinker and gypsum, detected by TGA, and fineness. Amount of free lime and the XRD profile was found to be a sufficiant description of relevant mineralogical structure in clinker for predictions with accepted accuracy of setting time and compressive strength development until 28 days. The modelling gave explained variances in setting time and strength development equal, for prediction, to 76 and 67 %, respectively. The explained variance in compressive strength at 1 day was 86 %.

Prediction of changes in properties by changes in the XRD profile due to changes in the production of clinker have been demonstrated. Changing from production of standard clinker to high strength clinker was simulated to take place by first changing the chemical composition and then changing the process. Both changes were predicted to have signifcant influences on the compressive strengths at 1 day and 28 days.

REFERENCES

/1/ **Svinning, K.,** Bremseth, S.K.: "The Influence of Microstructure in Clinker and Cement on Setting Time and Strength Development until 28 days", Proceedings of the 18th. International Conference on Cement Microscopy, Houston 1996, pp 514-513.

/2/ **Svinning, K.,** Bremseth, S. K., Justnes, H.: "X-Ray Diffraction Studies on Variations in Microstructure in Portland Clinker Correlated to Variations in Production Conditions in the Kiln", Proceedings of the 18th. International Conference on Cement Microscopy, Houston 1996, pp 233-249.

/3/ **Martens, H.,** Næs, T.: "Multivariate Calibration", Wiley & Sons, Chichester 1989.

PHASE QUANTIFICATION AND MICROSTRUCTURE OF A CLINKER SERIES WITH LIME SATURATION FACTORS IN THE RANGE OF 100

Hubert MOTZET, Herbert POELLMANN, Uwe KOENIG, Institute for Geological Sciences, Dept. of Mineralogy and Geochemistry, University Halle, Germany
Juergen NEUBAUER, Mineralogical Institute, University Erlangen-Nuremberg, Germany

ABSTRACT
Clinker samples with a Lime Saturation Factor (LSF) in the range of 93 - 103 were investigated by XRF, XRD, SEM-fluorescence and microscopy. A LSF of greater 100 is possible without an exceeded free lime content. Bogue calculation of these clinkers gives negative values for the Belite content and is therefore not useful. The quantification of phases by Rietveld analysis is confirmed by reflected light microscopy. Optical microscopy and SEM-fluorescence give more detailed information on the microstructure of the clinker samples.

Key-words: Quantitative, Microstructure, Bogue calculation, Microscopy, Rietveld analysis

INTRODUCTION
The production of cements with high early compressive strength, like CEM I 52,5 R, is usually done by grinding the clinker to a high specific surface area of more than 450 m^2/kg (BLAINE). In comparison to CEM I 32,5 R the energy consumption of this grinding process is very high. A modification of the clinker phase composition to higher Alite contents causes also higher strength values. Thus part of the expensive electrical energy for running the ball mills can be replaced by the cheaper burning process with less energy consumption, although a higher temperature level in the rotary kiln is needed with increased Alite formation.

To produce a clinker rich in Alite the raw meal has to be designed with a higher lime content. The maximum acceptable content of CaO in a Portland cement clinker was determined by Lea and Parker (1935). If equilibrium is established during burning and cooling, the phase composition can be calculated from the ratio of the four main oxides. The Lime Saturation Factor (LSF) gives the ratio by weight of CaO to SiO_2, Al_2O_3, and Fe_2O_3 with respect to the molar proportions.

The LSF calculation can only be an approximation because of the formation of solid solutions and of neglected minor components. A clinker with a LSF greater than 100 should have free lime. LSF values below 100 can give an approximation at the C_3S/C_2S ratio. Typical clinkers are in the range of 92 - 98 (Taylor, 1990).

This work shows that a LSF of greater 100 does not inevitably lead to an elevated free lime content.

For investigation of the phase composition and the microstructure of the clinkers different quantification methods were used. Besides the BOGUE calculation, that implements the same problems with solid solutions like the calculation of the LSF, Rietveld analysis based on XRD measurement, and reflected light microscopy completed the investigation methods. Additionally the SEM-fluorescence technique was carried out, to investigate the capability of this method in examining the microstructure and for possible application of this method for automatic phase quantification.

EXPERIMENTAL

Sample Preparation

A clinker series of 11 samples was taken from a production plant after the clinker cooler. The production process should be running with a LSF of 100. It should be demonstrated that under this burning conditions no free lime will appear. 1 kg of each sample has been crushed to a particle size of < 4 mm. The fraction 2 - 4 mm was homogenized and separated for the subsequent examinations.

Chemical Analysis: Bogue Calculation and LSF

The chemical analysis has been done by XRF from glass pellets. Volatile elements like alkalies were analysed classically. The free lime content was determined according to the method of Schläpfer and Bukowski (1933). Based on these results, the BOGUE (Bogue, 1929 in Taylor, 1990) and the LSF (Lea and Parker, 1935 in Taylor, 1990) calculation was done as follows:

$$
\begin{aligned}
\text{BOGUE: } c(C_3S) &= 4.071CaO - 7.602SiO_2 - 6.719Al_2O_2 - 1.430\ Fe_2O_3 \\
c(C_2S) &= -3.071CaO + 8.602SiO_2 + 5.068Al_2O_3 + 1.079\ Fe_2O_3 \\
c(C_3A) &= 2.650Al_2O_3 - 1.692\ Fe_2O_3 \\
c(C_4AF) &= 3.043\ Fe_2O_3
\end{aligned}
$$

$$LSF = [CaO/(2.80SiO_2 + 1.18Al_2O_3 + 0.65Fe_2O_3)] * 100$$

The BOGUE calculation results were normalized to 100 %.

Rietveld Analysis

The phase quantification based on the Rietveld refinement is a quite new technique. Its application in OPC quantification is described in detail by Taylor (1993), Möller (1995) and Neubauer (1996, 1997). The basic principle of this method is the comparison and refinement of observed X-ray pattern with pattern calculated from the structure data of all included phases.

For the clinker analysis the crushed samples were ground for 2 minutes in a disc mill to get efficient fineness. All measurements were carried out with a Siemens D5000 X-ray diffractometer. Besides the four main phases periclase and free lime were evaluated. For comparison with the microscopy results and the Bogue results the content of the main phases was normalized to a total of 100 %.

Reflected Light Microscopy

6 to 8 grains of each clinker were embedded in epoxy resin and polished. The surface of this polished section specimen was treated for 30 s with a solution of 1 g salizylic acid in 125 ml deion. water + 125 ml ethyl alcohol. This etching technique colours the clinker minerals and makes a differentiation of alite, belite and the interstitial phase (tricalcium aluminate plus ferrate) possible (Campbell 1986). Small amounts of periclase and free lime were added up and marked as additionals.

The quantitative analysis was done by point counting with a 100x air lens and a step width of 0.4 * 0.05 mm. On each specimen more than 10 000 points were counted. The mass contents of the clinker phases were calculated from the resulting volume-% by the average specific weights (Alite: 3.20 g/cm³, Belite 3.28 g/cm³, Interstitial phase 3.60 g/cm³).The portion of „additionals“ amounts to 1- 2 mass-% in the clinker and was neglected. The values of the three main phases were normalized to 100 %.

SEM-fluorescence

Some of the polished sections that were used for reflected light microscopy were prepared for the SEM-fluorescence. The polished sections were sputter coated with a carbon layer and investigated in the SEM with a OXFORD Mono Cathodoluminescence (CL) system. CL is the process by which electron bombardment of materials results in a characteristic emission of light. Used as a technique within a SEM, detection of CL allows the imaging and mapping of the sample texture (Heard 1996, Wright et al. 1991).

The clinkers were observed with an accelerating voltage of 15 kV. The fluorescence effect of the different phases depends on the stimulation by the beam current. The stimulation of the fluorescing resin at a quite low beam current of 10 µA makes the pore structure visible (Fig. 7). The study of the clinker phases is possible at a beam current of > 50 µA (Fig. 8, 9).

Quantification has been carried out with an image analysis system using fixed grey levels for the three main phases Alite, Belite and Interstitial phase. Clearly differentiated grey values enable an automatic quantification with an image analysis system.

RESULTS

Phase Quantification

The LSF of the 11 investigated samples are given in Table 1. The samples were arranged in order of increasing LSF values. Main attention is put to the samples no. 9 - 11 with a LSF greater than 100.

Tab. 1: Lime Saturation Factor (LSF) of the clinker samples

Sample No.	1	2	3	4	5	6	7	8	9	10	11
LSF	93.4	95.3	96.5	97.6	97.9	99.1	99.2	99.2	101.0	101.9	102.9
C_3S/C_2S ratio *)	5.9	8.5	8.3	10.3	12.0	12.8	12.7	17.5	35.1	35.4	19.2
free lime (m.-%)	0.36	0.08	0.09	0.12	0.45	0.08	0.62	0.64	0.14	0.28	0.31

*) Rietveld results

It could be shown that a LSF of greater 100 does not inevitably cause an elevated free lime content. The free lime content is statistically distributed in the range of 0.1 - 0.6 mass-% with no significant correlation to the LSF. Thus the clinker did not reach the equilibrium, or solid solutions of the clinker minerals falsify the LSF calculation.

The following Figures 1 - 3 show graphically the results of the phase quantification obtained from the three methods Bogue calculation, Rietveld analysis and microscopical point counting.

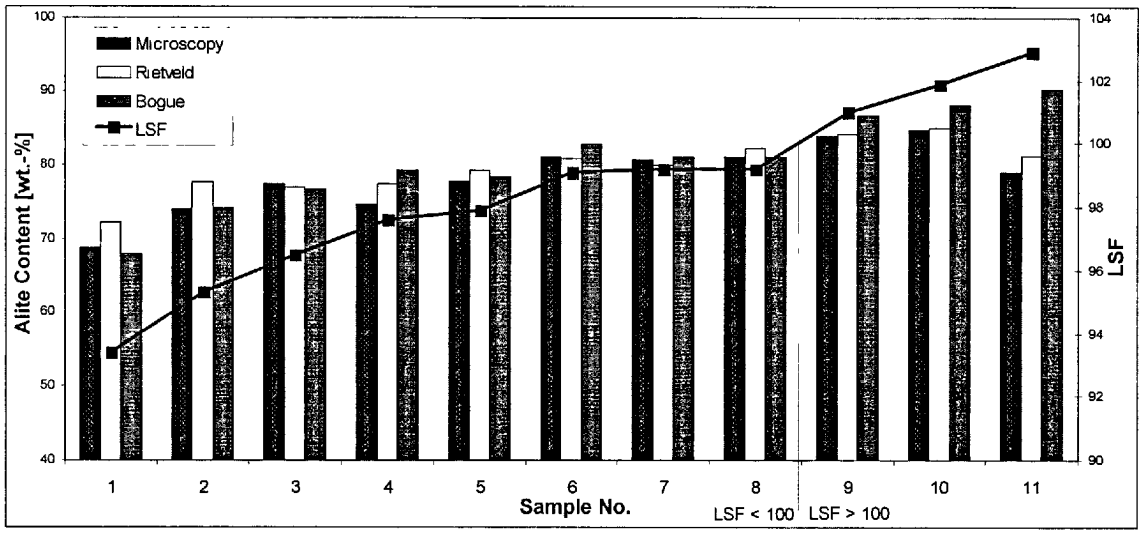

Fig. 1: Alite content in the clinker samples

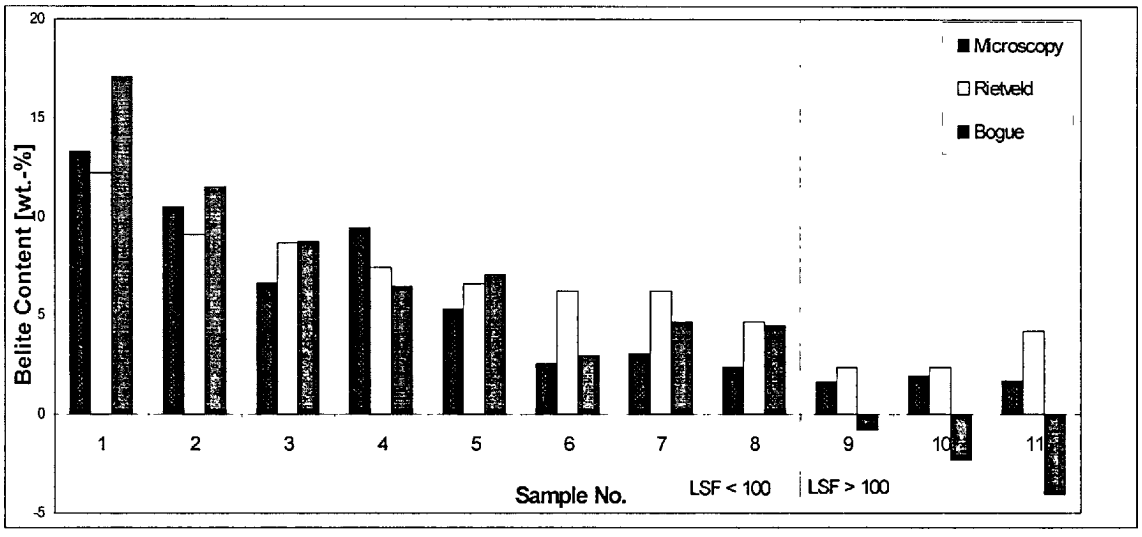

Fig. 2: Belite content in the clinker samples

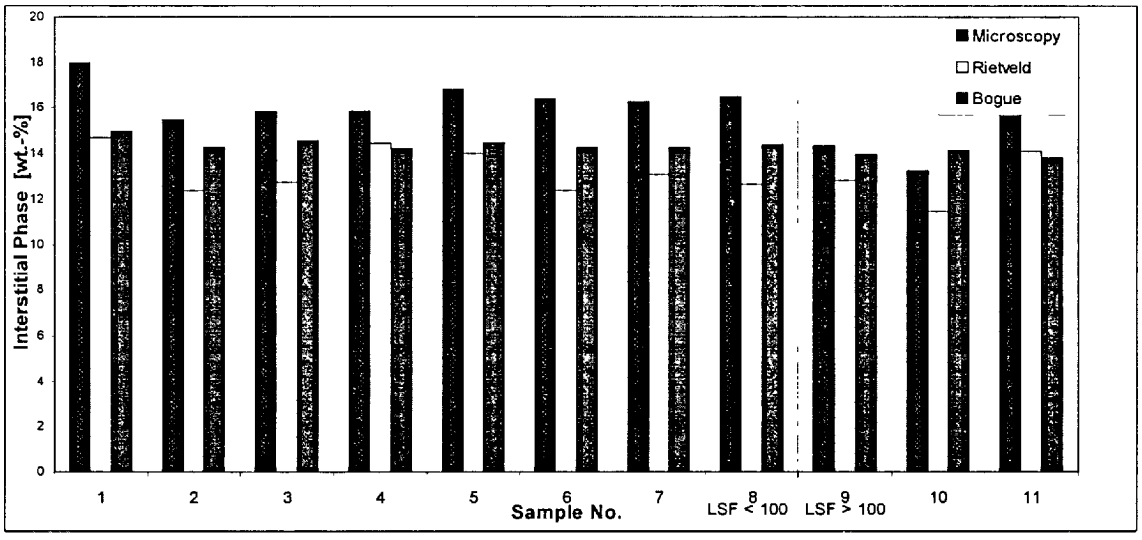

Fig. 3: Interstitial phase content in the clinker samples

Alite content
The three quantification methods give comparable values in the Alite content (except the Bogue calculation of sample no 11). The content of alite in the clinker increases with higher LSF values from approx. 70 m.-% up to 80 m.-%.

Belite content
Common belite contents of about 10 m.-% can be comparable calculated with the three used methods. The microscopic point counting of minor contents below 5 m.-% is difficult because of the clustering of the belites. At LSF values of greater 100 the Bogue calculation gives a negative belite content, although it can be clearly shown by microscopy, that belite exists in clusters in these clinkers (Fig. 5).

Interstitial phase content
The content of interstitial phase is independent from the LSF and more or less constant at about 14 m.%.

Microstructure
The microstructure of the 11 clinker samples has been studied by reflected light microscopy. The mainly idiomorphic alite crystals are in a size of 20 - 30 µm. They are embedded in a grey ground mass of aluminate and ferrate (Fig. 4). The 10 - 20 µm sized Belite can be observed in clusters (Fig. 5) and indicate an inhomogenity of the raw meal respectively coarse quartz grains, which are not disperse grounded by the raw mill.

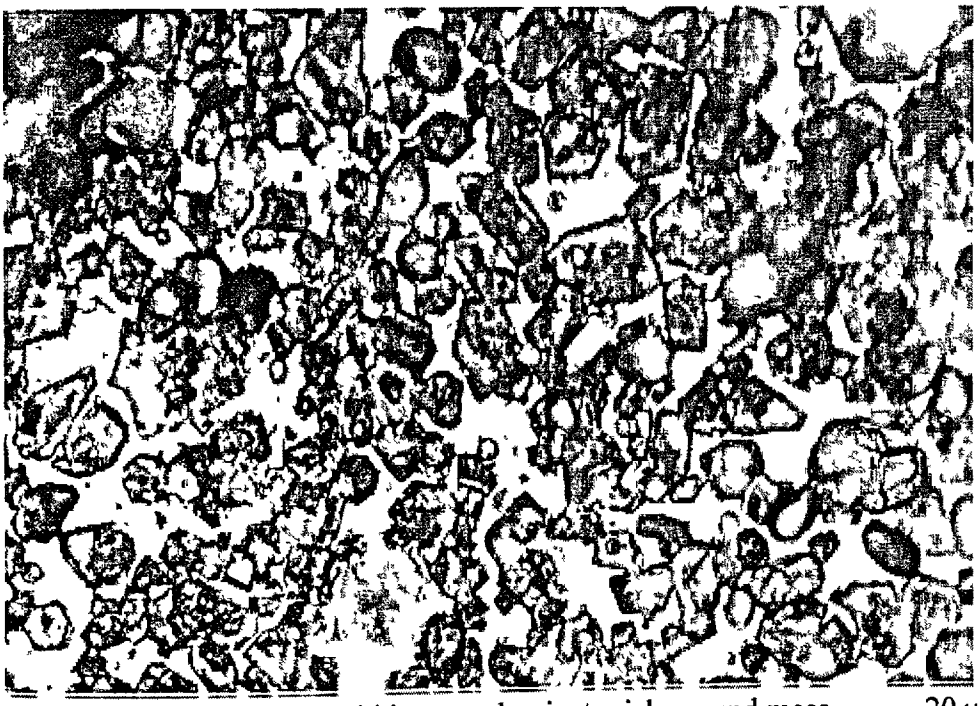

Fig. 4: Idiomorphic Alite within grey aluminate rich ground mass ------ 20 µm
(Sample 11, LSF=102.9)

Colour versions of Figs 4, 5 and 6 are given in
the special colour photo section of the proceedings.

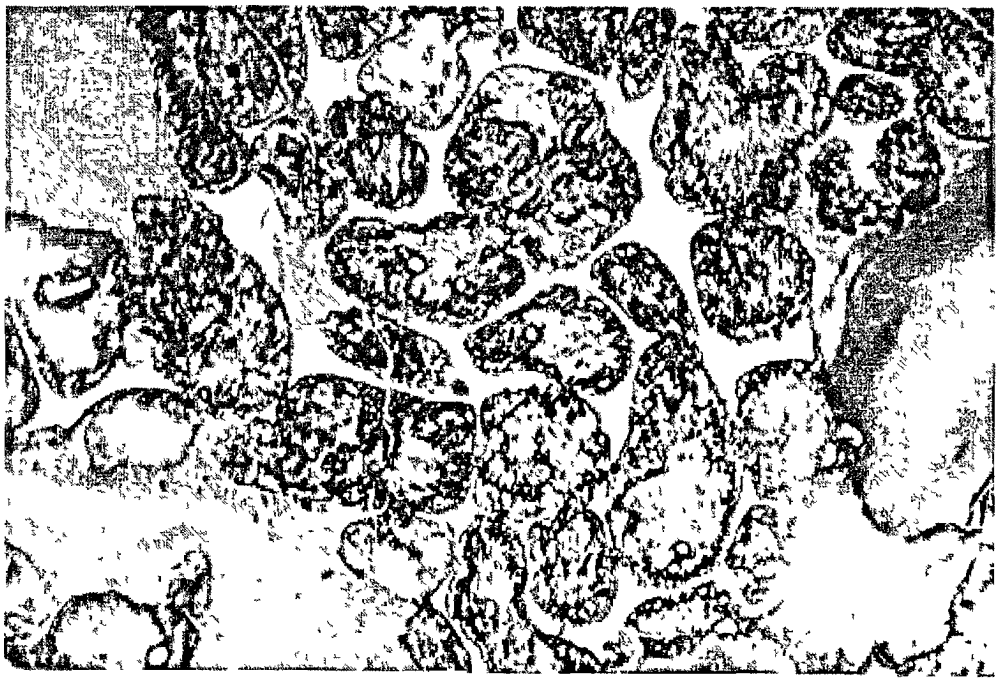

Fig. 5: Rounded Belite in cluster (Sample 11, LSF=102.9) ------- 10 μm



Fig 6: Belite cluster (right part) and Alite (left part) (Sample 10, LSF 101.9) ------ 20 μm

SEM-fluorescence

SEM-fluorescence allows an examination of the microstructure as well as a quantification of the three main phases Alite, Belite and Interstitial phase. When using a fluorescing resin, the pore structure can be studied and quantified at low beam currents (Fig. 7). Increasing the beam current up to 50 μA the characteristic structure of Alite, Belite and Interstitial phase can be observed because of their different fluorescing behaviour. Figure 8 shows the typical idiomorphic Alites (grey) besides rounded Belites (bright) in a dark aluminous ground mass. Even the typical cross lamellaes of the Belite (exsolution effect) and resorbed Belite relicts within the Alite crystals can be seen (Fig. 8, 9).

Quantification results are given only for this particular photographs and not representative for the whole clinker sample. An automatic quantification procedure seems possible by calculating the average of a large number of images obtained by PC controlled sample stage.

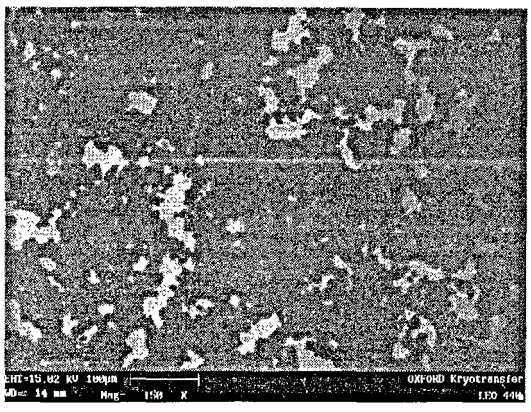

grey: pores (14.2 vol.-%)
dark: clinker minerals (85.8 vol.-%)

prep.: carbon sputtered polished section
high voltage: 15 kV
beam current: 10 µA

Fig. 7: SEM-fluorescence picture of a clinker: overview of pore structure

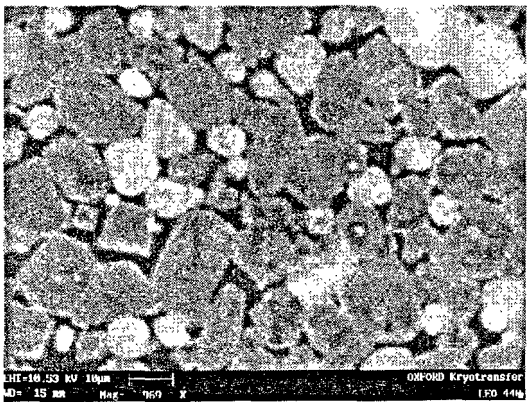

bright: Belite, see relicts in Alite (23.8 vol.-%)
grey: Idiomorphic Alite (66.4 vol.-%)
dark: Interstitial phase (9.8 vol.-%)

prep.: carbon sputtered polished section
high voltage: 10 kV
beam current: 50 µA

Fig. 8: SEM-fluorescence picture of a clinker: overview of clinker minerals

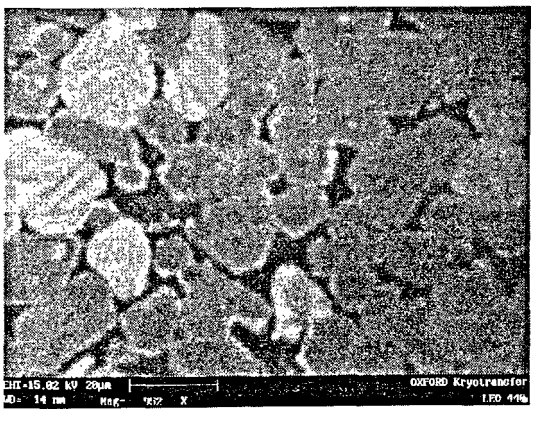

bright: Belite with cross lamellae (12.9 vol.-%)
grey: Idiomorphic Alite (77.3 vol.-%)
dark: Interstitial phase (9.7 vol.-%)

prep.: carbon sputtered polished section
high voltage: 15 kV
beam current: 50 µA

Fig. 9: SEM-fluorescence picture of a clinker: details of clinker minerals

DISCUSSION AND CONCLUSION

Increasing LSF values cause higher contents in Alite and decreasing content in Belite. The content of Interstitial phase does not correlate with the LSF. Even clinkers with a LSF greater 100 do not show elevated free lime contents. The calculation of the LSF does not take into account solid solutions of the main clinker minerals and also inhomogenities in the raw meal are not considered.

The Bogue calculation is only a practical technique when the clinker production process is running on a constant level. Under extreme burning conditions or extreme clinker composition the Bogue calculation is not useful for the quality control. The Rietveld analysis represents a new technique with the capability for online quality control. The Rietveld calculation takes into

account the real composition of clinker minerals and of minor phases. The free lime content can be detected simultaneously. Expense for the equipment for the use of Rietveld analysis in automatic clinker quality control is comparable to the expense of chemical analysis and subsequent Bogue calculation.

For special investigations, like pore structure or crystal distribution and size, microscopic techniques are indispensable and vindicate the higher time and personnel expense, which is especially needed for point counting. It could clearly be shown that belite exists in clinkers with a LSF greater 100 in clusters. This indicates that inhomogenities in the raw meal or coarse grained quartz particles occur in the raw meal. Automatic quantification by image analysis is not possible because of the varying colours of the etched clinker minerals, depending on their reactivity with the etching agent and on polishing effects.

The SEM-fluorescence allows a combined examination of the microstructure as well as a quantification of the pore volume and of the clinker minerals. The information on the microstructure is similar to that from reflected light microscopy (crystal distribution, crystal size, resorption and exsolution effects) but the quantification seems to be more comfortable with an image analysis system. Depending on the SEM-beam current the three main phases of the clinkers clearly show different grey levels. The capability of this technique for automatic phase quantification will be investigated in further studies.

ACKNOWLEDGEMENT
The authors wish to thank Dr. Pankau from the Scientific Research Division of OXFORD Instruments for carrying out the SEM-fluorescence studies.

REFERENCES
Campbell D. H. „Microscopical Examination and Interpretation of Portland Cement and Clinker" Construction Technology Laboratories, Portland Cement Association, Skokie, Illinois, 1986
Heard, P. „Cathodoluminescence - Interesting Phenomenon or Useful Technique" Reprint from Microscopy and Analysis, January 1996
Lea, F. M. and Parker, T. W. „The Quaternary System CaO-Al_2O_3-SiO_2-Fe_2O_3 in Relation to Cement Technology" Building Res. Techn. Paper 19, 52 pp., HMSO, London, 1935
Möller, H. „Quantitative Phasenanalyse mit Rietveld-Methoden in der Zementindustrie" 6th Philips Symposium Röntgenbeugung, Bad Hersfeld, S. 221- 237, 1995
Neubauer, J., Kuzel, H.-J. and Sieber, R. „Rietveld Quantitative XRD Analysis of Portland Cement: Part II Quantification of Synthetic and Technical Portland Cement Clinkers" Proc. of the 18th Int. Con. On Cement Microscopy, Houston, Texas, pp. 100 - 111, 1996
Neubauer, J., Poellmann, H. and Meyer, H. „Quantitative X-ray Analysis of OPC Clinker by Rietveld Refinement" Proc. of the 10th Int. Congr. On Cement Chemistry, Goteborg, Sweden, 1997
Schläpfer and Bukowski; Ber. Eidgen. MPA, Nr. 63, S. 1 - 39, Zürich, 1933
Taylor, H. F. W. „Cement Chemistry" Academic Press, 475 pp., ISBN 0-12-683900, London, 1990
Taylor, J. C. and Aldridge, L. P. „Full-Profile Rietveld Quantitative XRD Analysis of Portland Cement: Standard XRD Profiles for the Main Phase Tricalciumsilicate" Powder Diff. 8 (3), pp. 138 - 144, 1993
Wright, P. J. and Kearsley, A. „Recent Advances in the Use of Cathodoluminescence for the Study of Geological Materials" Proc. of the 49th annual meeting of the Electron Mic. Soc. Am. 1991

INFLUENCE OF PHYSICAL-CHEMICAL HYDRODYNAMICS PROCESSING OF RAW MIX ON CLINKER QUALITY

Lev M.SULIMENKO, Yuri R.KRIVOBORODOV, Research Technical Centre of JSC "Alfa Cement", Mendeleev Chemical Technology University of Russia, Moscow, Russia

ABSTRACT Using the equipment (RPA) where the raw materials are exposed to the high hydraulic impact and cavitation (HC) it is possible to obtain very-fine grained raw mixture. Its homogenic composition and fineness improved the clinker burnability. Morphology of clinker mineral crystals and C_3S/C_2S ratio in clinker are changed. The most positive results are noticed when fly-ash was used as a raw component instead of clay.

KEY-WORDS: Burnability of raw mixes, grinding technology.

INTRODUCTION

The reactivity of cement raw mixtures, at equal conditions, is a function of the particle size distribution (Goswami, et al, 1990, Johansen and Kouznetsova, 1992, Krivoborodov, et al,1988, Locher, 1975, Sulimenko, 1985). Experiments have shown the burning temperature may be decreased by 50°C for finely ground raw mixes (Sulmenko, 1991). Particle size distribution of the raw mixtures ground in the different mills is different from each other. The researchers showed that the type of equipment influence on the reactivity of raw mixture (Bucchi, 1980, Osbaek and Johansen, 1989). The mechano-chemical activation of raw mixes is effective when the raw mixes are exposed to the frequency of hydraulic impact and cavitation.

EXPERIMENTAL

Materials

Chemical composition of the raw materials used in the experiments is given in Table 1.

Using these components, two groups of raw mixtures were prepared. One of the group of mixture (No 1, 1.1, 1.2) consisted of the traditional components: clay, iron, limestone. In the other group (2, 2.1, 2.2) fly-ash was used instead of clay. The mixtures 1.1 and 2.1 were exposed to hydraulic impact using the equipment RPA. Rotor-pulsative apparatus (RPA) consists of two disks having the coaxical position each to other. All disks have trapezoidal teeth and slots. During rotation of one disk relatively other one the fast alternation of the coincidence and

noncoincidence of the slots, which causes the change of the moving speed of materials through the slots. Pulsation of the liquid flow appears. In the result the materials are exposed to high shear stress, hydraulic impacts, hedrodynamic cavitation and pulsation in the wide range. These factors in association with the intensive mechanical exposure increase the milling processes and improve the size distribution of materials. At the preparation of the mixtures 1.2 and 2.2 only limestone was exposed to hydraulic impact.

Table 1. Chemical composition of raw materials

No	Raw component	Oxides, % by wt.					
		SiO_2	Al_2O_3	Fe_2O_3	CaO	MgO	SO_3
1	Limestone	4.82	1.69	0.82	50.68	1.16	0.03
2	Clay	66.14	14.16	5.39	4.29	1.62	0.15
3	Iron	1.42	4.52	75.13	2.59	1.05	4.19
4	Fly-ash	56.10	11.42	5.80	15.88	2.20	2.65

Analytical methods

The fineness and particle size distribution were determined by granulometer and sieve analysis. Composition of the different fractions was studied by chemical analysis and XR-diffraction. Besides that DTA was used for study of all the raw mixes. Phase composition of clinker was studied by XRD, optical microscopy. Cement samples were made and tested by Standard methods.

RESULTS AND DISCUSSION

The experimental data showed that the equipment (RPA) promotes the fine structure of materials change: the crystal parameters, crystal defects, phase transformation. Thus, by RPA-grinding calcite transfers into aragonite. Grinding clay, the layer with the AlO_6 is fractured. As a result, material reactivity increases by up to 30% for clay and by 50-60% for limestone.

The change of the fineness and particle structure of raw materials gives the temperature change of mineral formation at clinker burning. According to DTA (Table 2) the temperature of carbonization of raw mixtures decreases by 25-30°C, belite formation decreases by 10-15°C. Clinker melt appears at 1300°C.

The results reveal that grinding of raw mixes by RPA gives a change of mineral composition in clinker (Table 3).

Table 2. Results of DTA

Processes	Temperature, °C mixture numbers					
	1	1.1	ΔT	2	2.1	ΔT
Decarbonization - beginning	670	655	25	680	650	30
Belite formation	1270	1250	20	1270	1255	15
Melt appearance	1330	1300	30	1315	1300	15

Table 3. Mineral composition of clinkers,%

Clinker number	C_3S	C_2S	C_3A	C_4AF
1	62	21	12	6
1.1	68	16	9	5
1.2	67	16	10	6
2	65	22	3	12
2.1	69	17	1	12
2.2	68	18	1	12

Optical microscopy of clinkers 1.1, 1,2, 2.1 and 2.2 represent very good crystallization of alite and belite in comparison with the initial clinker (1 and 2). The mentioned change in clinker gives the different hydraulic activities of cement. In Table 4 rhe test results of cements are given.

Table 4.Strength of cements

No cement	Strength, MPa							
	bending				compressive			
	3d	7d	14d	28d	3d	7d	14d	28d
1	4.2	8.0	11.8	17.8	13.8	37.0	56.0	68.0
1.1	6.9	16.1	18.3	20.0	23.0	60.0	73.0	76.0
1.2	4.9	14.2	18.0	21.1	18.6	51.5	66.0	70.6
2	2.5	5.8	8.8	13.2	11.0	27.0	39.0	51.0
2.1	5.7	15.0	18.8	20.5	19.5	46.4	68.0	82.0
2.2	4.0	12.3	16.0	18.0	13.6	39.0	64.5	81.0

Cements based on activated clinker hardened more rapidly than initial cement and had strength increased by 5-10 MPa at 3 days and 8-30 MPa after 28 days hardening. The most high strength of cement was noticed for clincer burned the activated fly-ash contained raw mixture (2.1, 2.2).

CONCLUSION

Mechano-chemical activation of raw mixes using RPA is effective method to increase the reactivity and burnability of clinker. Cement on base of such clinker riched the higher strength in comparision with cement based on ordinary clinker.

REFERENCES

Bucchi,R. "Influence of nature and preparation of raw materials on the reactivity of raw mix", 7th International Congress on The Cement Chemistry, 1980, v.1, p.1/3 - 1/43.

Goswami,A., Panda, J.D.,Chatterji,S. "A study of Homogeneity of Cement Raw mixes Processed in Two Types of Mills", World Cement, November 1990, p.489-492.

Johansen,V., Kouznetsova, T.V. "Clinker formation and new processes", 9th Interational Congress on Chemistry of Cement, 1992, p. 49-83.

Krivoborodov,Y.R, Plotnikov,V.V, Martens,K. "Mineral formation in the burning of the activative raw mixes", 10 International Baustoff und Silikattagung, Weimar, 1988, v.1, p.

Locher,F.M."Einfluss der Klinkerherstellung auf die Zementeigenschaften", Zement-Kalk-Gips, 1975, v.28, No 7, p. 16-20

Osbaek,B, Johansen,V." Particle size distribution and Rate of Strength Development of Portland cement", J.Am.Ceram.Soc., 1989, 72(2), p. 197-201.

Sulimenko,L.M., Kouznetsova,T.V., Meisner,S. "Mechanische Aktivierung carbonatischer Materialien", Tonindustrie-Zeitung, 1985, v. 109. n6, p. 23-25

Sulimenko,L.M. "Mechano-chemical and mechano-activative effects in thechnology of raw materials", The Conference on Cement Chemistry and Technology, Moscow, 1991, p. 45-48.

INFLUENCE OF RAW MIX HETEROGENEITY ON EASE OF COMBINATION AND CLINKER STRENGTH POTENTIAL

Graeme MOIR, Blue Circle Industries, Technical Centre, Greenhithe, Kent.

ABSTRACT The range of firing temperatures required to combine raw mixes from 15 cement plants have been related to raw mix heterogeneity and in particular the level of acid insoluble material present in the 90 micron residue. It is also shown that the extent and nature of raw mix heterogeneity has an influence on cement strength development. Mixes with calcareous residues tend to yield higher 28 day strengths than those with siliceous residues.

Key-words: Burnability of raw mixes, Strength development, alite, belite.

INTRODUCTION

The optimum raw meal fineness for optimum kiln operation and clinker quality is mainly determined by raw material mineralogy and the clinker chemistry parameters of LSF, SR and AR‡. Insufficient grinding, perhaps arising from an undersized raw mill, will necessitate hard burning with consequent penalties to fuel consumption, refractory life, clinker grindability and cement quality. Kiln operation may also be adversely affected by kiln and preheater blockages associated with the evaporation and condensation of volatiles. Conversely, excessively fine grinding, whilst permitting lower kiln temperatures, may restrict kiln output as a result of the increased dust loss or recycle within the kiln system.

The influence of raw mix mineralogy, and in particular the relative influences of coarse calcite and silica rich particles on the level of free lime remaining after firing at 1400 C, has been quantified by Christensen (1978) and Fundal (1979). Quartz particles coarser than 44 microns have a marked influence on the ease of combination, whilst for calcite, the significantly sized fraction is that coarser than 125 microns. More recently Fundal (1996) has further refined the predictive model by introducing the influence of the proportion of heterogeneous coarse particles on the chemical composition of the fine fraction. The concept of quantifying raw mix heterogeneity by means of the chemical analysis of different size fractions and relating this to sintering behaviour was examined by Dreizler and Schafer (1990).

The prediction of cement strengths from cement characteristics has been investigated by several workers, eg. Osbaeck (1979), Relis et al (1988) and Tsivilis and Parissakis (1995). In recent years the introduction of computerised databases for cement production quality control has greatly facilitated the interpretation of strength variations and the prediction of cement 28 day strength from quality control data. In-house models have been developed which satisfactorily predict day to day variations in 28 day strength at any one cement plant, but significant differences exist between the predicted strength levels at different cement plants if a common expression is used. This is attributed to differences in clinker microstructure but the factors responsible, kiln feed mineralogy, burning conditions etc., are poorly understood. An investigation was initiated using materials from 15 cement plants to determine whether factors

‡ *In this paper*

$$LSF \quad \frac{CaO}{2.8\ SiO_2 \quad 1.2\ Al_2O_3 \quad 0.65\ Fe_2O_3} \qquad SR \quad \frac{SiO_2}{Al_2O_3 \quad Fe_2O_3} \qquad AR \quad \frac{Al_2O_3}{Fe_2O_3}$$

such as kiln feed heterogeneity and estimated kiln burning temperature might provide an explanation for the differences in clinker strength potential.

COMBINABILITY INVESTIGATION

Experimental Details

Average samples of kiln feed from the 15 plants were split into minus 90 micron, plus 90 micron and plus 150 micron fractions and chemically analysed. The 90 micron and 150 micron residues were also treated with hot 1.0 N HCl to determine the proportion of silica rich material present in the coarse fractions.

The raw mixes were proportioned with fine coal ash to adjust the LSF to the plant's normal value and a sub-sample of the homogenised mixes was formed by hand into nodules of approximate diameter 12 mm. The pellets were fired in a programmable horizontal tube furnace following the heating regimes outlined in Figure 1, and the temperature required to achieve a free lime level of 1% estimated from curves of the type shown in Figure 2.

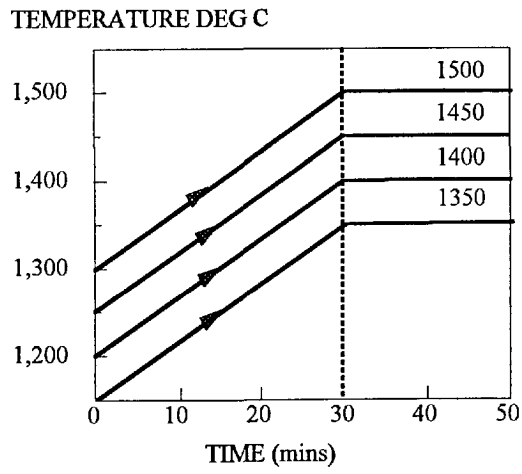

Figure 1 Combinability test heating regime

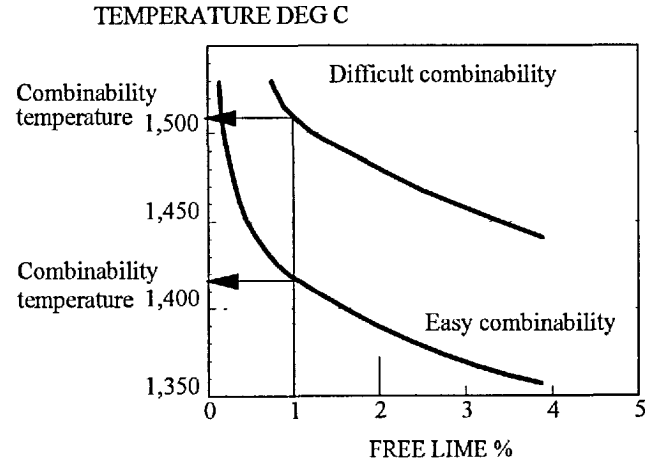

Figure 2 Typical combinability curves

Sub-samples of the ground clinkers were chemically analysed to confirm that chemical parameters similar to those of current clinker production had been achieved.

Results

The chemical analysis data and the combinability results are summarised in Table 1.

Figure 3 illustrates that, as might be expected on account of the relative hardeness of quartz and silica rich minerals, most plants had siliceous (low LSF) residues. Three works had calcareous residues. In the case of plant J, this is attributable to the method of kiln feed preparation in which sand and iron oxide are ground separately from the main raw mix constituents of chalk and clay.

Figure 4 illustrates that there was no clear relationship between combinability temperature and the main clinker chemical parameters of LSF and SR.

The data were analysed using multiple linear regression analysis (MLRA) to relate raw mix fineness and heterogeneity to combinability temperature. Figure 5 illustrates that the range of

Table 1 Characterisation of kiln feed samples and combinability test results

Plant Process Type‡	A SP	B PC	C SD	D PC	E SP	F W	G SW	H SP	I SD	J W	K LD	L SP	M W	N LD	O LP
Kiln Feed															
LSF	97.3	97.1	96.1	98.9	98.7	99.1	99.6	98.1	98.9	103.1	100.2	105.7	92.4	98.8	97.2
SR	3.20	2.46	2.59	2.49	2.65	2.49	2.71	2.92	2.83	2.32	2.71	2.43	2.61	2.62	2.98
AR	1.71	2.11	2.18	1.52	2.47	1.39	1.83	2.69	1.67	1.95	1.43	1.08	1.57	1.36	1.94
+ 150 microns															
%	0.7	3.7	1.9	4.4	6.3	0.8	2.4	2.1	1.7	4.0	9.4	9.8	26.4	7.3	5.4
LSF	90.2	83.6	99.6	49.2	72.1	8.9	60.0	46.1	98.6	169.5	90.2	82.6	122.7	90.0	137.0
SR	3.40	6.03	3.34	6.97	3.52	12.27	6.39	5.31	3.67	2.13	6.60	6.36	3.81	31.13	2.97
AR	1.94	1.42	2.14	1.00	2.71	0.53	0.24	3.08	1.60	1.22	2.13	1.00	1.07	1.40	1.77
Acid Insoluble %	0.19	0.59	0.19	0.95	1.45	0.62	0.69	0.51	0.21	0.21	1.56	1.37	2.61	1.03	0.32
LSF	-7.1	-13.5	3.5	-49.7	-26.6	-90.2	-39.6	-52.0	0.3	66.4	-10.0	-23.1	30.3	-8.8	39.9
+ 90 microns															
%	4.9	12.6	8.1	13.4	16.3	4.2	5.5	11.6	8.8	13.1	23.5	29.8	39.3	16.7	15.3
LSF	79.9	102.5	83.8	53.8	72.8	24.8	54.0	47.3	81.5	249.1	93.2	83.2	119.2	80.2	127.8
SR	3.25	4.22	3.96	61.4	3.50	7.89	8.98	5.52	4.06	2.38	4.61	4.92	3.46	3.06	2.85
AR	2.09	1.67	2.03	0.97	2.71	0.41	0.41	2.63	1.62	1.22	1.33	0.65	1.00	1.22	1.56
Acid Insoluble %	0.78	0.95	1.01	2.68	2.82	1.84	1.51	2.86	0.86	0.35	3.81	4.44	3.95	2.66	1.15
LSF	-17.3	5.4	-12.3	-45.1	-26.0	-74.3	-45.6	-50.8	-17.4	145.9	-7.0	-22.4	26.8	-18.6	30.6
-90 microns															
LSF	98.4	96.4	97.4	111.5	105.6	108.6	104.2	110.9	101.0	93.5	102.6	118.9	79.7	103.3	92.8
SR	3.19	2.32	2.50	2.10	2.49	2.27	2.51	2.59	2.73	2.32	2.35	1.82	2.33	2.52	3.00
AR	1.69	2.15	2.19	1.60	2.42	1.46	1.93	2.70	1.67	2.01	1.45	1.21	1.84	1.40	2.00
LSF	1.1	-0.8	1.3	12.6	6.8	9.5	4.6	12.8	2.0	-9.6	2.4	13.2	-12.7	4.5	-4.3
Combinability Clinker															
LSF	95.8	95.3	93.9	95.7	95.9	92.0	95.7	97.6	99.2	95.2	93.6	94.9	94.2	92.7	92.3
SR	3.07	2.51	2.50	2.49	2.64	2.5	2.59	3.0	2.76	2.20	2.58	2.28	2.69	2.48	2.84
AR	1.81	2.22	2.14	1.53	2.77	1.43	1.93	2.52	1.69	2.03 4	1.49	1.23	1.53	1.47	2.04
Combinability Temperature for 1% free lime	1420	1480	1460	1470	1520	1430	1470	1560	1510	1440	1530	1510	1570	1470	1460
Mean annual average free lime %	1.4	1.5	1.7	1.5	1.4	0.43	0.8	1.4	2.0	0.45	0.69	1.0	0.25	0.23	0.37
Eq kiln temperature for average free limes	1400	1460	1420	1440	1480	1530	1480	1550	1460	1520	1560	1510	1600	1540	1510

‡
Key to process types:- SP - suspension preheater; PC - precalciner; LD -long dry; SD - semi-dry (Lepol); SW- semi-wet (filter press); W - wet.

LSF = LSF fraction - LSF kiln feed

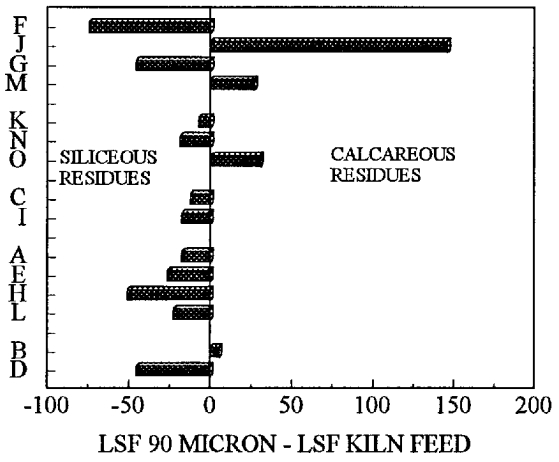

Figure 3 LSF difference between 90 micron residue and kiln feed

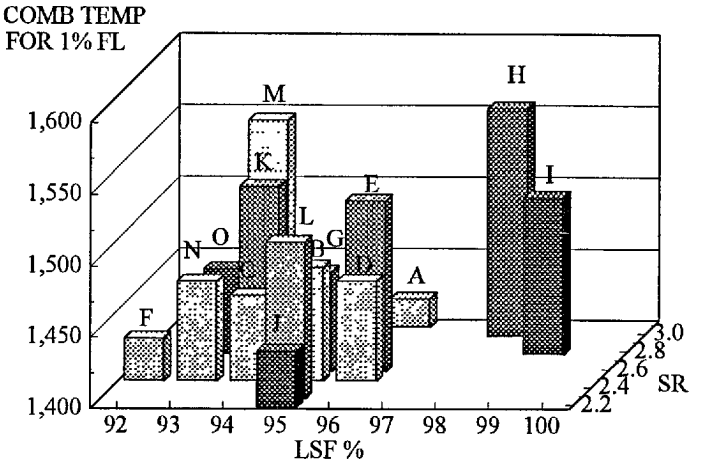

Figure 4 Relationship between combinability temperature and clinker LSF and SR

combinability temperatures could be satisfactorily explained using the relationship

combinability temperature for 1% free lime = 414 + 21 x acid insoluble 90 micron residue
+ 10 x clinker LSF
+ 3 x 150 micron residue
+ 32 x clinker AR.

The multiple correlation coefficient was 0.923.

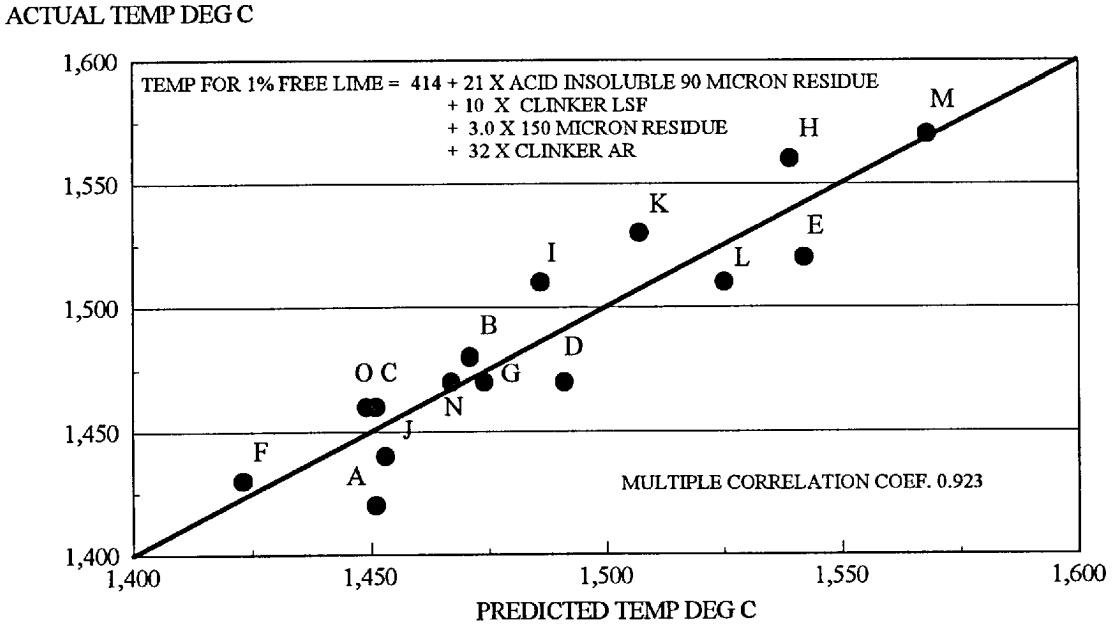

Figure 5 Actual v predicted combinability temperature for 1% free lime

The single most significant parameter was the level of acid insoluble 90 micron residue. If this parameter was excluded from the data analysis then the following relationship was derived:-

combinability temperature 1% free lime = 535 + 4.4 x raw feed 90 micron residue
+ 9.0 x clinker LSF
- 0.33 x LSF of 90 micron residue
+ 34 x clinker AR.

The multiple correlation coefficient was almost unchanged at 0.920.

Discussion

Both of the relationships derived are 'sensible'. It is stressed that they are only likely to be generally applicable within the range of chemistries of the current clinkers, viz. LSF 92 to 99, SR 2.2 to 3.1 and AR 1.2 to 2.5. It was perhaps surprising that with this set of data, increasing AR had a greater negative influence on the combinability temperature than increasing SR. The AR primarily influences the nature of the clinker liquid, viscosity etc., whilst the SR determines the quantity of liquid formed.

The similar correlation coefficient obtained when the terms 'acid insoluble 90 micron residue' and '150 micron residue' were replaced by '90 micron residue' and 'LSF of 90 micron residue' confirm the importance of raw mix heterogeneity on combinability, and in particular the negative influence of a concentration of silica in the coarse fractions.

INFLUENCE OF RAW MIX HETEROGENEITY ON CLINKER STRENGTH POTENTIAL

Analysis of data

Table 2 summarises the chemical and physical characteristics of Type I (pure Portland) cement produced by cement plants A to O.

Table 2 Chemical and physical characteristics of cements.

	Chemical Parameters									Fineness		Comp-ressive Strength EN 196-1	
Plant	LSF %	SR	AR	Free Lime %	SO_3 %	eq Na_2O %	LOI %	C_3S %	C_3A %	SSA m^2/kg	45 microns	2d	28d N/mm^2
A	95.0	3.20	2.02	1.2	2.8	0.55	3.0	52.9	7.7	342	7.7	29.1	57.7
B	95.7	2.45	1.92	1.6	3.2	0.63	0.8	52.1	9.5	358	10.7	29.3	57.6
C	92.9	2.38	2.15	2.0	3.1	0.66	1.5	42.0	10.8	349	8.6	26.3	57.4
D	94.7	2.46	1.50	1.5	3.1	0.41	0.8	51.8	7.6	391	13.8	24.9	58.7
E	96.3	2.63	2.49	1.8	3.2	0.59	1.0	52.3	10.9	345	17.0	28.0	57.1
F	93.0	2.62	1.54	0.6	3.0	0.59	2.8	48.0	7.2	352	10.5	24.8	56.3
G	96.3	2.68	1.83	0.9	2.9	0.56	1.4	58.9	8.5	380	12.6	28.3	57.8
H	96.4	2.82	2.40	1.3	2.9	0.75	1.0	56.2	10.0	374	8.0	31.2	57.0
I	97.1	2.71	1.68	2.4	2.9	0.57	0.9	53.7	7.4	390	10.6	27.4	56.2
J	92.5	2.40	1.89	0.5	3.2	0.59	2.5	47.0	9.4	361	17.6	25.3	58.5
K	94.4	2.69	1.44	0.9	3.2	0.45	0.7	56.4	6.8	355	7.7	31.1	61.1
L	97.4	2.47	1.13	1.1	2.5	0.24	1.4	63.2	5.1	375	3.0	29.1	66.3
M	91.3	2.70	1.70	0.7	3.1	0.64	1.1	47.5	7.8	382	6.8	25.4	64.9
N	92.8	2.56	1.36	0.5	2.5	0.48	0.5	54.1	6.7	322	4.8	25.3	63.4
O	94.0	2.90	1.98	0.8	3.2	0.85	1.4	53.5	8.5	313	8.5	31.9	59.6

Data for plants A to J are the means of 9 random samples.
Data for plants K to O obtained with single accumulated average sample.

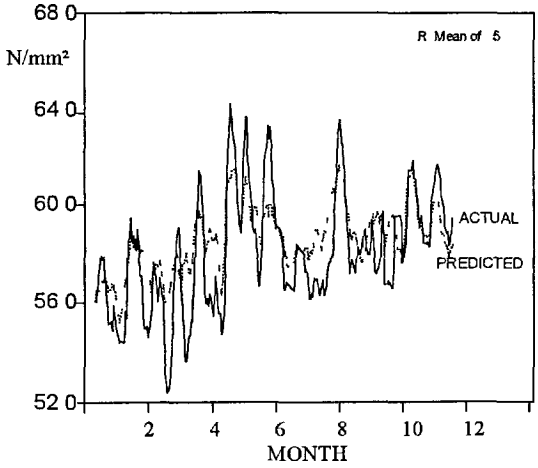

Figure 6 Predicted and actual 28 day strengths - Plant F

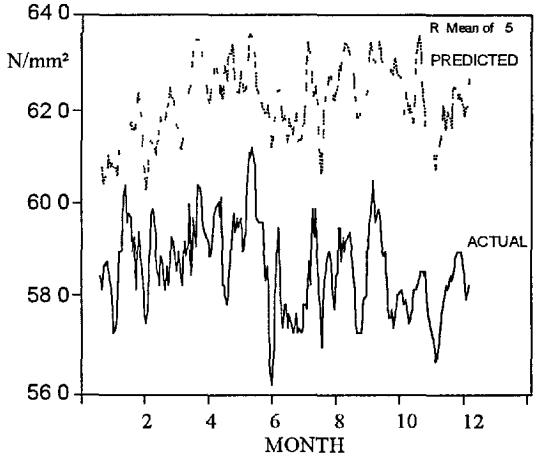

Figure 7 Predicted and actual 28 day strengths - Plant G

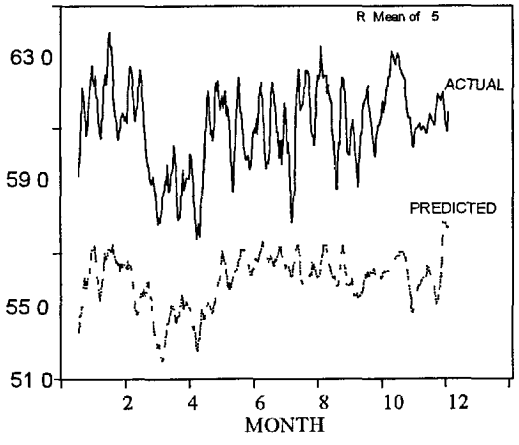

Figure 8 Predicted and actual 28 day strengths - Plant J

Table 3 Predicted strengths calculated using global equation

WORKS	ACTUAL	PREDICTED	DIFFERENCE
A	57 7	58 3	-0 6
B	57 6	60 3	-2 7
C	57 4	57 3	0 1
D	58 7	61 9	-3 2
E	57 1	57 9	0 8
F	56 3	56 1	0 2
G	57 8	60 6	2 8
H	57 0	60 2	-3 2
I	56 2	61 2	5 0
J	58 4	53 6	4 8
K	61 1	64 9	-3 8
L	66 3	69 5	-3 2
M	64 9	60 2	4 7
N	63 4	65 6	-2 2
O	59 6	57 4	2 2

Predicted strength = 64 - 0 4 residue +0 2 C3S - 13 eq Na2O 2 LOI

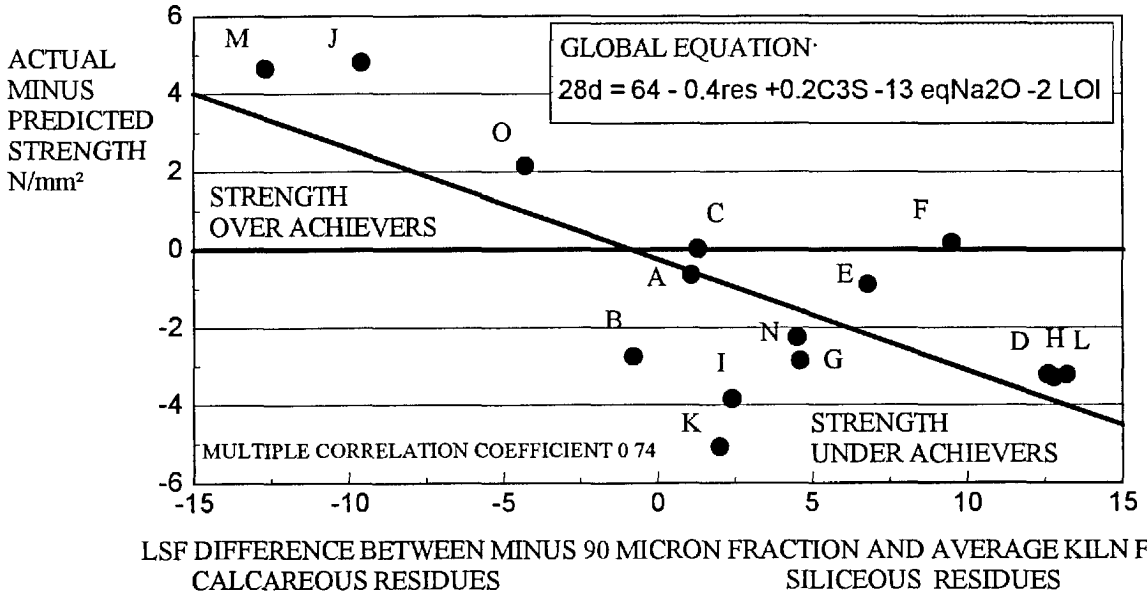

Figure 9 Relationship between predicted and actual strength and raw mix heterogeneity

Cement plant quality control data have been analysed satisfactorily within Blue Circle using MLRA since the mid-1980s. In general it is possible to predict day to day variations at individual plants with reference to 5 key chemical and physical parameters

- 45 micron residue
- C_3S
- eq Na_2O
- SSA
- LOI

When predicting early strength it is the level of soluble alkali, present as alkali sulfates, which is important rather than the total alkali. Early strengths are strongly influenced by surface area but, at least in the EN 196-1 mortar test when using vibration compaction, the influence of this parameter on 28 day strength is relatively small, in comparison with the influence of the proportion of coarse clinker particles, as indicated by the 45 micron residue.

Whilst individual plants must develop their own relationships to achieve the best strength predictions, a so-called "global equation" of the form

28d = 64 - 0.4 residue plus 45 microns + 0.2 C_3S - 13 eq Na_2O - 2.0 LOI

will predict strength fluctuations at most cement plants.

The coefficients used agree closely with those determined in experiments when, as far as practicable, only one parameter was changed at a time. Note that the coefficient for LOI (loss on ignition) is influenced by the source of the loss and should be higher if the contribution is predominantly from prehydrated clinker rather than from $CaCO_3$ introduced as a minor additional constituent.

Figure 6 illustrates that most of the strength variation at plant F over a 12 month period can be satisfactorily explained using the global equation. Similarly, the same equation indicates the trends in strength at plant G (Figure 7) but significantly overestimates the mean strength level. Conversely at plant J (Figure 8) the same equation underpredicts the mean strength level. Table 3 indicates the differences between predicted and actual strength for cements produced by the 15 cement plants.

There is clearly another factor at play in addition to those indicated in the prediction equation. It is believed that this factor is related to clinker microstructure. Although microstructure can be studied using optical microscopy it is rather difficult and time consuming to characterise objectively. In order to determine whether factors such as raw mix fineness, heterogeneity, estimated equivalent kiln burning temperature etc. might provide an explanation for these strength differences the entire data block of raw mix and cement data was analysed using MLRA.

Figure 9 illustrates the main finding. Cement produced from raw mixes with calcareous residues (J, M and O) tend to give higher strengths than those produced from feeds with siliceous residues. There is no significant correlation between strength difference and the estimated equivalent kiln burning temperature.

Discussion

It is suspected that the lower strength potential of clinkers with siliceous raw mix residues may be associated with the presence of belite clusters, formed from relatively coarse quartz or silica rich particles. Belite makes a significant contribution to strength development between 7 and 28 days under standard curing conditions at 20 C (Kelham and Moir 1992).

Maki et al (1995) have studied microscopically the formation of belite clusters from quartz grains and found differences in impurity level which correspond to differences in etching behaviour. It is expected that these differences in etching behaviour may also relate to differences in hydraulic activity.

Campbell (1994) has suggested that "belite nests may have a major control on late strength gain" and proposed a correlation factor to take into account the percentage and type of belite nests when predicting 28 day strengths using the Ono method.

It should be recognised that raw mix heterogeneity is only one source of clinker heterogeneity, and that the poor assimilation of high ash coals can make a major contribution. However, at plants which have coarse siliceous raw mix residues the cement 28 day strength is likely to benefit from finer grinding of the raw mix, or separate grinding of the silica rich component, if this is practicable. The influence of increased raw mix fineness on kiln operation aspects such as the internal dust cycle must also be taken in account.

REFERENCES

Campbell, D.H., "A summary of Ono's method for cement quality control with emphasis on belite color", Petrography of Cementitious Materials, ASTM STP 1215, Editors DeHayes, S. M. and Stark, D. 1994, pp 13-25.

Christensen, N.H., "Burnability of cement raw mixes at 1400 C. Part II. The effect of the fineness", Cement and Concrete Research, Vol 9, 1979, pp 285-294.

Dreizler, I. and Schafer, H.-U., "Fraction analysis for evaluating the heterogeneity of raw meals", Zement Kalk Gips, No 9, 1990, pp 445-451.

Fundal, E., "The burnability of cement raw mixes", World Cement Technology, July/August 1979, pp 195-204.

Fundal, E., "Burnability of cement raw meal with matrix correction", World Cement Research and Development, April 1996, pp 63-68.

Kelham, S. and Moir, G.K., "The effect of cement C_3S level on concrete properties", Ninth International Congress on Chemistry of Cement, New Delhi, 1992, Vol V, pp 3-8.

Maki, I., et al., "Formation of belite clusters from quartz grains in Portland cement clinker", Cement and Concrete Research, Vol 25, 1995, pp 835-840.

Osbæck, B., "The influence of alkalis on the strength properties of Portland cement", Zement Kalk Gips, No 2, 1979, pp 72-77.

Relis, M., Ledbetter, W.B. and Harris, P., "Prediction of mortar-cube strength from cement characteristics", Cement and Concrete Research, Vol 18, 1988, pp 674-686.

Tsivilis, S. and Parissakis, G., "A mathematical model for the prediction of cement strength", Cement and Concrete Research, Vol 25, 1995, pp 9-14.

To the Memory of Arvid Hedvall

SOLID STATE REACTIONS IN THE CHEMISTRY OF CEMENT

Otar P. MCHEDLOV-PETROSSYAN, State Technical University of Building and Architecture, Kharkov, Ukraine

ABSTRACT Solid state reactions occur in the initial stages of clinker mineral formation but the appearance of melt obscures the role of the mentioned initial processes. The works of the outstanding Swedish scientist Arvid Hedvall had already showed that various external impacts on the stages in solid state reactions can essentially affect the completeness of interactions in solid state. In this paper the role of activation of solid state reactions is studied.

Key-words: aragonite, calcium carbonate, thermodynamics, solid state reactions

INTRODUCTION

At the level of modern technological development different variants of impacts on the reactions in solid state are examined. The analysis of different methods of activation of the solid state reactions are discussed.

SOLID STATE REACTIONS

Selection of raw mixture components of higher activity

Portland cement is usually made from a raw mixture of calcium carbonate and clay. By calcium carbonate we mean calcite, and by clay - kaolinite. Meanwhile with the development of the building materials industry and the availability of increasing number of technogenic products we can often see the replacement of the components by the latter (Zhavoronkov et al., 1979) and on the other hand more detailed study of the mineral composition of the raw mix components can be observed (Mchedlov-Petrossyan et al., 1980). As mentioned above it is very important to look at the impact of the "Hedvall effect" (Hedvall, 1938, 1943, 1966) on the process of solid state reactions in the raw mix. For instance, sometimes (though seldom) calcium carbonate can be replaced partly by aragonite, and clay - by various silicate minerals - montmorillonite, pyrophillite and others.

If we examine the results of the thermal analysis of these raw materials we can see that for the most compounds taking part in this reactions, on reaching the interval characteristic of interaction temperature, effects characterizing modifying transformations or dissociation can be observed. So, for aragonite, the effect of slow transformation into calcite takes place at 410-450 ^{o}C, for kaolinite in the region of 500 ^{o}C (and on grinding even lower), for

pyrophillite and for monothermite at 400-600 °C. Earlier (Ramachandran and Sereda, 1971) the possibility of using the "Hedvall effect" for the study of clinker minerals activity was shown. Therefore in choosing the raw mix components and planning a technological process it is necessary to take into account the possibility of activation of solid state processes in a wider aspect.

Especially interesting is the fact that by prolonged grinding, calcite transforms into aragonite at room temperature (Burns and Bredig, 1956).

Thermodynamic calculation (Nikolayev et al., 1984b) shows that for aragonite $T_{\Delta G=0}$ is approximately 150 °C lower than for calcite which results in the intensity of solid phase reactions. In high degree it depends on admixture of silicate components in the carbonate part. The study of the influence of the physico-chemical properties of calcium carbonate on the clinkerization (Nikolayev et al., 1984a) showed that the presence of clay impurities allows C_2S to be obtained in the temperature interval 780-830 °C.

Preliminary thermo-mechano-chemical impacts on the initial components

Partial decarbonatation of the raw mix leads to entering of active calcium oxide into the kiln while the dehydrated clay intensifies the solid state reactions. A deep grinding of preliminary dehydrated clay component leads to the same result. The Hedvall effect plays a specific part in fine grinding, chemical influences, and modification of phase transformations.

The measure of activity of the solid phase is the difference:

$$\Delta G_{exc} = \Delta G_{act} - \Delta G_{norm},$$

where ΔG_{exc} is excess energy, ΔG_{act} and ΔG_{norm} are Gibbs energies for activated and normal state, respectively. ΔG_{exc} is increased by structural defects (free surface, lattice distortion, dislocations etc.). Therefore this problem belongs to mechanochemistry (Heinicke, 1984).

Of great interest is the use of jet mills (Yudovich and Akunov, 1989). It was found that the addition of CaF_2 accelerates the formation of C_2S (Ayed et al, 1992) and that different compounds of calcium, for example $Ca(NO_3)_2$, or the addition of NaF promotes the C_2S forming (Singh et al, 1992). As to aragonite, though it needs prolonged grinding it can appear as a result of microadmixtures (PbO, MgO) or microadditives (water vapour, alkali) in raw mixtures. Sometimes raw mix includes a considerable (more than usual) quantity of quartz and some amount of alkali. In this case, water vapour results in intensifying the interaction. It should be noted that more and more interest is given to mechano-chemical activation of solid phase reactions through selecting grinding conditions (Boldyrev et al., 1987) and

consideration of shear deformations (Enikolopian, 1989) which can lead to substantial acceleration of processes.

External physico-technical impacts on the reaction mixture

The velocity of solid state reactions can also be accelerated by the influence of electrical (Kröger, 1964) or magnetic (Budnikov et al., 1950) fields, as well as by ultrasonic fields (Pines et al., 1969). All this is to be taken into account while working out improved methods of clinker production.

REFERENCES

Ayed, F., Costanet, R. and Sorrentino, F.P. "Thermal Behaviour of Mineralized Portland Cement Row Meal" IX ICCC, Theme I-C, New Delhi, India, 1992.

Boldyrev, V.V. et al., "Collective Effect of Grinding", Dokl. Akad.Nauk SSSR, Vol.293, No.1, 1987, pp.123-125.

Budnikov, P.P. et al., "The Influence of Magnetic Fields on the Solid State Reaction in the System Calcium Oxide - Silica", Dokl. Akad.Nauk SSSR, Vol.70, No.2, 1950, pp.285-286.

Burns, J.H. and Bredig, M.A., "Transformation of Calcite to Aragonite by Grinding", J.Chem. Phys., Vol.25, No.6, 1956, pp.1281.

Enikolopian, N.S., "Superspeed Reactions in Solid Bodies", Zh.Fiz.Khim., Vol.89, No.9, 1989, pp.2289-2297.

Hedvall, J.A., "Reaktionsfähigkeit fester Stoffe", Ambrosius Barth, Leipzig, 1938, S.67.

Hedvall, J.A., "Einführung in die Festkörperchemie", Vieweg, Braunschweig, 1943, S.169-172.

Hedvall, J.A., "Solid State Chemistry", Elsevier Publish. Comp., Amsterdam, 1966, pp.26-28.

Heinicke, G., "Tribochemistry", Akademieverlag, Berlin, 1984.

Kröger, F.A., "The Chemistry of Imperfect Crystals", North Holland Publ., Amsterdam, 1964.

Mchedlov-Petrossyan, O.P. et al., "The Influence of the Mineral Composition of the Raw Mix on the Clinker Building Process", Zement, No.1, 1980, pp.7-9.

Nikolayev, A.P. et al., "Physico-Chemical Peculiarities of the Burnability of Mixtures based on Carbonate Raw Material with Clay Impurities", Zement, No.10, 1984, pp.18-19.

Nikolayev, A.P. et al., "The Use of the Parameters of the Thermal Dissociation of Chalk for the Characteristic of its Reactivity", Zement, No.11, 1984, pp.13-14.

Pines, B.Ya. et al., "Poroshkovaya Metallurgiya", No.9, 1969, pp.19-23.

Ramachandran, V.S. and Sereda, P.G., "Hedvall Effect on Cement Chemistry", Nature Physical Science, Vol.233, 1971, pp.134-135.

Singh, N.B., Singh, S.P. and Shukla, A.K. "Formation and Solid State Properties of β-Dicalcium Silicate" IX ICCC, Theme I-A, New Delhi, India, 1992.

Yudovich, B.E. and Akunov, V.I., "Activation of Cement during jet Grinding", Zement, No.5, 1989, pp.13-18.

Zhavoronkov, N.M. et al., "Theoretical Fundamentals of the Use of New Raw Materials Types in the Cement Industry", Dokl. Akad.Nauk SSSR, Vol.245, No.3, 1979, pp.666-669.

This work was supported in part by the International Soros Education Program through grant No.SPU063038.

HEAVY METALS CONTENT OF RAW MATERIALS, CLINKER AND DUST OF CEMENT PLANTS

Marina V. KOUGIYA, Giprocement, Phys.-Chem. Studies, St. Petersburg, Russia

ABSTRACT Data on contents of 10 heavy metals of raw materials, raw mixes, dust and clinker from five cement plants of Russia are presented. The results obtained are compared with the findings of investigations in Germany, USA, England and India.

KEY-WORDS: ecology, heavy metals, clinker formation.

INTRODUCTION

In view of environmental controls and improved potentialities of analytical equipment, Sprung and Rechenberg (1978) determined Pb and Zn contents of limestones and clays used at cement plants, as well as of clinker. Kræmar, Linner, Weisweiler (1994) carried out determinations of more than 23 trace elements in cement materials of Germany. Tulles (1992) presented averaged data for 89 North American cement plants on contents of 12 heavy metals of dust and cement. Moir and Glasser (1992) gathered information on contents of 10 heavy metals in clinkers of cement plants of England. Krishnan, Gore et al (1992) determined concentrations of 12 trace elements in raw materials, mixes and dust of cement plants of India.

EXPERIMENTAL

For investigations use was made of raw materials, slurries, electrostatic precipitator dust and clinker of five wet process cement plants located in various regions of Russia. The contents of Mn, Mo, Pb, Cr, Tl, Co, Ni, Zn, Cu and V were monitored. The analysis was performed with the help of atomic absorption as well as of X-ray spectrum analysis procedure developed with the participation of the author. The data obtained are presented in Table 1 and 2. Maximum permissible concentrations in soil were presented by Bespamyatnov (1985). Concentrations of trace elements in samples taken from three fields of electrostatic precipitators were also determined: the results are presented in Table 3.

Table 1 Heavy metals content of raw materials and fuel

Element	Contents, g / t							
	Carbonaceous component		Aluminosilicate component		Pyrite cinders		Coal	
	min	max	min	max	min	max	min	max
Mn	20	50	300	600	120	2000	150	250
Mo	1	4	1	4	10	25	1	2
Pb	6	15	15	25	600	1500	8	10
Cr(total)	10	50	50	150	100	200	10	60
Tl	-	-	-	-	5	8	-	-
Co	1	10	5	20	25	130	10	80
Ni	5	60	25	100	100	170	5	40
Zn	15	40	60	100	9000	10000	13	60
Cu	3	15	15	25	4000	5000	15	35
V	5	25	40	150	10	20	8	12

Table 2 Heavy metals content of slurry, clinker and electrostatic precipitator dust

Element	Contents, g / t						
	Raw slurry		Clinker		Electrostatic precipitator dust		Maximum permissible concentration in soil
	min	max	min	max	min	max	
Mn	-	-	600	1200	300	800	1500
Mo	1	1	1	4	1	2	-
Pb	40	100	50	70	150	400	20
Cr(total)	60	80	60	150	40	80	-
Tl	-	-	-	-	2	3	-
Co	40	50	5	50	40	80	-
Ni	80	140	40	150	100	120	35
Zn	80	150	300	700	180	250	110
Cu	10	15	400	1000	15	45	23
V	20	30	50	100	10	40	150

Table 3 Chemical composition and heavy metals content of electrostatic precipitator dusts

Oxide, element	Units	Sample		
		1	2	3
LOI	%	20,16	21,79	22,08
SiO_2	%	14,97	14,72	14,57
Al_2O_3	%	6,44	6,58	6,65
CaO	%	49,36	47,44	46,33
K_2O	%	3,51	3,90	4,78
Mn	g/t	600	800	800
Mo	g/t	1,5	2,0	2,5
Pl	g/t	250	350	400
Cr(total)	g/t	80	70	80
Tl	g/t	2	3	3
Co	g/t	70	75	75
Ni	g/t	110	125	125
Zn	g/t	210	220	220
Cu	g/t	20	18	18
V	g/t	30	40	40

DISCUSSION OF RESULTS

The least quantity of heavy metals was found in carbonaceous rocks; clays are more enriched in trace elements. Variations in contents of heavy metals and their qualitative composition are associated with the geologic age and origin of natural rocks of regions where the plants are located. This correlates with geochemical data (Shcherbina, 1972) and the findings of Sprung and Rechenberg. Concentrations of trace elements for all rocks did not exceed the regional background contents and maximum permissible concentrations in soils (Bespamjatnov, 1985).

Similar data were obtained for coals. For these technogeneous materials, heavy metals concentrations were much higher. For example, contents of Cu, Pb and Zn are hundreds to thousands times greater then those of natural rocks. Besides, thallium, in amounts of 5-8 g/t, In occurs in amounts of 3-6 g/t and Ge - 6-10 g/t in pyrite cinders. High concentrations of As (3000 g/t) and Sb (250-300 g/t) were also noted. In this connection it is desirable to keep the pyrite cinders content of the mix as low as possible.

The trace elements concentrations of raw slurries were in line with their content of initial raw materials and in accordance with raw material components ratios of the total mix mass. Cu, Zn, Pb, Cr, Ni, Mn were revealed as the main bound elements in clinker. This correlates with the data obtained by Sprung, Weisweiler, Moir. The higher contents of about the same set of heavy metals were encountered in the electrostatic precipitator dust, this is in agreement with findings of Krishnan. The Mn, Mo, Cr, Zn, Cu, V contents were lower than those of clinker, but Co and Pb concentrations were higher. Attention is drawn to the increase in the thallium content for all dust samples studied. It was found that finer particles were precipitated in electrostatic precipitators: the lower were the CaO and SiO_2 contents, the higher were the contents of K_2O and certain heavy metals. This suggests the probability of trace elements carrying out together with fine particles of dust and gases.

CONCLUSIONS

The studies conducted have shown a good correlation between the data on the heavy metals content of natural cement raw materials and fuel used and valid control values for soils, i.e. the environmental compatibility of these materials has been demonstrated. The situation with technogenous materials in the form of clinker, cinders and dusts is more complicated. As to clinker it should be pointed out that this is a product where concentrations of heavy metals are within the limits valid for air-dry soils. The permissible total contents are almost not exceeded, but for Cu, Zn, Ni the environmental impact of which is assessed to be far less. The studies are to be continued for drawing up heavy metal balances as applied to wet process kilns for determination of atmosphere emission composition and elaboration of environmental control measures.

REFERENCES

Bespamyatnov, G.P. and Krotov, Yu.A., "Maximum Permissible Concentrations of Chemical Substances in the Environment", Khimia, Leningrad, 1985, 528 pp.

Kræmar, W., Linner, B., Weisweiler, W., "Investigations into the behaviour of trace elements during clinker burning in a rotary kiln system with grate preheater", Zement - Kalk - Gips, 1994, 12, pp 335-340.

Krishnan, N.A., Gore, V.K., et al. Proc. 9 Intern. Congress on the Chemistry of Cement. , New Delhi, India, 1992, b. 2, pp 67-73.

Moir, G.K., Glasser, F.P.,"Mineralisers, modifiers and activators in the clinkering process ", Proc. 9 Intern. Congress on the Chemistry of Cement. , New Delhi, India, 1992, b. 1, pp 125-152.

Scherbina, V.V., "Fundamentals of Geochemistry", Nedra, Moscow, 1972, 295 pp.

Sprung, S. and Rechenberg, W., "Die Reaktionen von Blei und Zink beim Brennen von Zementklinker", Zement - Kalk - Gips, 1978, 7, pp 321-329.

Tulles, G., "Rare Metals in Cement and Dust", International Cement Review, 1992, pp. 69-73.

MODELLING THE KINETICS OF CLINKERISATION

S C AHLUWALIA*, R K GOSWAMI AND S HARSH

National Council for Cement and Building Materials,
New Delhi, India

ABSTRACT An attempt has been made to evolve a general model for the kinetics of clinkerisation in the temperature range of 1300-1450°C. Experimental studies were conducted on industrial raw mixes and a Jander type polynomial function was made to fit on the data. It is found that reaction velocities for most of the materials can be related by values of N as 12 and 14 in the temperature range of 1300-1375°C and 1375-1400°C respectively.

Key-words: Rate equations; Kinetics; Clinker formation; Modelling

INTRODUCTION

The alite formation reaction has a low rate and occurs in the temperature range of 1300-1500°C. Formation of alite, though possible in the solid state, is preceeded or accompanied by melt formation in practice. The melt phase is formed at around 1300°C and plays a vital role in the kinetics of alite formation. It is very fluid and strongly wets the solid phases. Further it has good transport properties, is capable of dissolving substantial amounts of all major and minor components and is present in sufficient amount not only to bridge adjacent grains but also to facilitate materials transport over longer distances.

The solid reactants CaO and C_2S get dissolved in the melt and counter diffuse. The dissolved CaO and C_2S react to form C_3S

$$CaO + C_2S \longrightarrow C_3S \qquad \ldots\ldots\ldots [1]$$

Initially the C_3S remains dissolved in the melt. However, when the melt gets super saturated with C_3S, the C_3S crystallizes out from melt. For such reaction Jander [1931] proposed following equation

$$(1-\sqrt[3]{1-\alpha})^2 = Kt \qquad \ldots\ldots\ldots [2]$$

Where, α is reaction ratio, t the time of reaction and K is a constant. The reaction ratio for clinkerisation reaction can be defined as

$$\alpha = \frac{CaO_T - CaO_f}{CaO_T} \qquad \ldots\ldots\ldots [3]$$

Where CaO_T is total calcium oxide content of clinker and CaO_f is free calcium oxide at any time t.

The logarithmic form of Jander's equation

$$\log (1 - \sqrt[3]{1-\alpha}) = 1/2 \log K + 1/2 \log t \qquad \ldots\ldots\ldots [4]$$

indicates that the plot of $\log (1 - \sqrt[3]{1-\alpha})$ and log t should be a straight line having a slope of 0.5 on log t axis.

* Presently with OCL (India) Ltd., New Delhi

Several studies [Kondo, 1960] have indicated that slope of lines obtained for clinkerisation reaction varies over a large range and changes with the temperature of reaction. Therefore, a more general form of Jander's equation is considered to represent the clinkerisation reaction as :

$$(1 - \sqrt[3]{1-\alpha})^N = K\,t \qquad \ldots\ldots\ldots [5]$$

or

$$\log (1-\sqrt[3]{1-\alpha}) = (1/N)\ \log K + (1/N)\ \log t \qquad \ldots\ldots\ldots [6]$$

The results of present study indicate, the value of N can be as high as 10-18.

EXPERIMENTAL

Well characterised raw mixes (Table-1) were fired in pellet form in laboratory muffle furnace at temperatures of 1300°, 1350°, 1400° and 1450°C for soaking periods of 5, 10, 15, 20, 25, 30 and 35 minutes. The free lime in the resulting clinker was estimated by ethylene glycol method.

Table 1 : Chemical Analysis of Raw Mixes (Clinker Basis)

Sl No	CaO%	SiO_2%	Al_2O_3%	Fe_2O_3%	MgO%	K_2O%	Na_2O%	SO_3%
CL-1	65.76	20.23	4.94	3.27	3.80	0.57	0.32	Nil
CL-2	63.20	20.73	4.75	4.58	4.05	0.87	0.33	0.69
CL-3	64.99	21.03	6.44	4.96	1.00	0.93	0.13	0.16
CL-4	64.15	23.44	5.62	3.75	2.00	0.31	0.24	ND

RESULTS AND DISCUSSIONS

Values of the function $\log (1- \sqrt[3]{1-\alpha})$ were computed from the experimentally determined values of CaO_f for various time intervals at different temperatures. These values were plotted soaking period against log t (t=in minutes). Data was found to be linearly correlated and the characteristic parameter of best fit lines are summarised in table 2.

Above data shows that the value of slope varies in narrow range i.e. 0.0562 (θ=3.22°) and 0.0978 (θ=5.59°). However, when converted to N(=1/slope), the variation extends from 10.22 to 17.79. The value of N remains confined to a smaller range of 10 to 13 for the observation recorded at 1300°C and 1350°C, and have a tendency to centre around 12. In the higher temperature range (1400-1450°C), the value of N is scattered from 10 to 18. Leaving aside two extreme cases on either side, the range comes down to 12 to 16. Also, it has a tendency to centralise around 14. This implies that the slopes of the lines tend to become gentler as the reaction temperature is increased.

An earlier study on the subject [Kondo, 1960] has reported the value of N as low as 0.6 and as high as 11.9. It is further reported that average value of N in higher temperature (1375-1450°C) range was 5. In contrast, the present study establishes

Table 2 : Results of linear regression analysis

Temperature		CL - 1	CL - 2	CL - 3	CL - 4
1300°C	Slope	0.0797	0.0801	0.0825	-
	Intercept	-0.4479	-0.3637	-0.3286	-
	N(=1/Slope)	12.54	12.48	12.12	-
1350°C	Slope	0.0894	0.0820	0.0771	0.0979
	Intercept	-0.3967	-0.3378	-0.2903	-0.2401
	N(=1/Slope)	11.19	12.19	12.97	10.25
1400°C	Slope	0.0693	0.0715	0.0978	0.0640
	Intercept	-0.3230	-0.2743	-0.2881	-0.1790
	N(=1/Slope)	14.43	13.98	10.22	15.62
1450°C	Slope	0.0811	0.0741	0.0689	0.0562
	Intercept	-0.2986	-0.2504	-0.2391	-0.1605
	N(=1/Slope)	12.33	13.49	14.51	17.79

the value of N at 12 for lower temperature range (1300-1375°C) and at 14 for higher temperature range (1375-1450°C). The cause of marked deviation from the theoretically established value of 2 (Eq. 2) probably lies in the fact that cement raw mixes have a wide particle size distribution and their shapes also differ from ideally considered spherical particles on account of mineralogy and size reduction unit operations. A comparatively narrower distribution of values of N in 1300-1350°C range indicates that rate of reaction is more or less same for all types of materials at the time of appearance of liquid phase. As the temperature of reaction goes up, the properties of liquid phase, like viscosity and surface tension, are affected to a great extent. Therefore, the rate of reaction shows larger variations and becomes material dependent in this temperature range.

CONCLUSION

It is not found possible to propose a unified model for the reaction velocity of clinkerisation, mainly on account of variations in chemical composition, mineralogy and particle size distribution of raw mixes. However, the values of N taken as 12 and 14 for the temperature ranges of 1300-1375°C and 1375°C-1450°C respectively shows good agreement with experimentally observed values.

ACKNOWLEDGEMENT

The authors have freely drawn upon published and unpublished R&D work of National Council for Cement and Building Materials. The paper is being published by permission of Director General, NCB.

REFERENCES

Jander W : Die grandlagender reaktionen in festen zustande and ihre bedeutung fiir die erzengungdes zements, Zement, Vol. 20, (1931), pp. 936-39; 951-53.

Kondo R : Reaction velocity in portland cement clinker formation, paper II-S6 Proceedings of 4th Int. Symposium Chemistry of Cement. Washington 1960. pp. 107-112.

BURNABILITY OF CEMENT RAW MIXES AT 1400°C

S C AHLUWALIA*, R K GOSWAMI AND S HARSH

National Council for Cement and Building Materials,
New Delhi, India

ABSTRACT A mathematical model for determining the amount of free lime in clinker, obtained by firing raw mixes at 1400°C for 30 min. has been proposed. The model is based on chemical composition of clinker and fineness of raw mix. The model is valid over a wide range of compositional and fineness variations and statistical confidence level of 95%.

Key-words: Burnability of raw mixes; Free-lime; Modelling

INTRODCUTION

Burnability of cement raw mixes is assessed by a number of empirical burnability indices and burnability factors, which qualitatively give the relative ease of burning a raw mix. Need had always been felt of a model to assess burnability quantitatively as the amount of free lime in clinker after burning the raw mix under some standard conditions. Kock (1974) presented a statistical model based on a large number of chemico-mineralogical parameters as well as fineness of the raw mix. To improve the reliability, the model was based on at least one reference testing and chemico mineralogical parameters of the reference sample are used for computation. As the model requires a large number of inputs including a reference testing, it becomes quite cumbersome to work and the convenience offered by earlier indices and factors is lost. Further, a fresh reference testing will be required for a different set of raw materials. Christensen (1981) has treated the matter in a different way and proposed that the occurence of free lime in clinker, with LSF less than 100, is due to microinhomogeneities and macroinhomogeneities and both should be considered separately. They proposed a statistical model based on LSF and SM only for computation of free lime due to microinhomogeneities and suggested an empirical approach for the other part. The model required estimation of certain minerals like calcite, quartz and acid insoluble residue in various sieve fractions of raw mix. The model proposed is as under:

$$CaO_f = 0.33\,[LSF + 5.1\,SM - 107] + 0.93\,SiO_2^{+44} + 0.56\,CaCO_3^{+125} + 0.2\,Aq^{+44} \quad \ldots\ldots\ldots [1]$$

Where CaO_f=Free lime in clinker after firing at 1400°C for 30 min

SiO_2^{+44} = Weight percent of quartz coarser than 44 μm.

$CaCO_3^{+125}$= Weight percent of Calcite Coarser than 125 μm.

Aq^{+44} = Weight percent of acid insoluble residue, other than quartz, coarser than 44 μm.

* Presently with OCL (India) Ltd., New Delhi

The last three terms in Eq. 1 are designed to predict the free lime content coming from coarse minerals or macroinhomogeneities while the first term gives statistical estimate of free lime coming due to microinhomogeneites.

This paper reports the development of a statistical model based on modulii values of raw mix and its fineness, with a view to minimize the experimental work.

EXPERIMENTAL

Well characterized raw mixes covering a wide range of oxide composition, modulii values and fineness were chosen for this study. The raw mixes were intermixed with coal ash (5-6%) to consider the influence of coal ash absorption. Chemical analysis of corresponding clinkers is given in table 1. The mixes were pelletised and fired at 1400°C for a period of 30 minutes in electrical muffle furnace. Free lime of resulting clinker was estimated by ethylene glycol method.

TABLE 1 CHEMICAL ANALYSIS OF CLINKER

Sample No	CaO	SiO_2	Al_2O_3	Fe_2O_3	MgO	K_2O	Na_2O	SO_3	TiO_2	P_2O_5	Mn_2O_3
CL-1	63.33	20.33	6.33	4.66	4.44	0.36	0.27	0.32	0.08	0.167	0.04
CL-2	63.32	21.87	6.07	3.84	1.90	0.79	0.97	0.34	0.09	0.17	0.02
CL-3	64.28	21.21	5.91	3.80	1.86	0.76	0.94	0.33	0.08	0.16	0.02
CL-4	66.23	20.84	5.81	2.43	1.85	0.73	0.91	0.33	0.10	0.17	0.03
CL-5	65.25	21.50	5.97	2.48	1.89	0.76	0.95	0.32	0.09	0.16	0.02
CL-6	61.43	21.75	5.57	3.52	5.11	1.13	0.48	0.31	0.09	0.17	0.04
CL-7	62.04	20.61	5.00	3.67	5.15	1.12	0.50	0.32	0.08	0.17	0.045
CL-8	63.63	21.54	4.62	2.38	5.28	1.14	0.48	0.33	0.10	0.17	0.04
CL-9	65.78	23.22	4.42	3.70	1.74	1.14	0.43	0.35	0.09	0.15	0.04
CL-10	67.23	21.96	4.59	3.37	1.74	1.15	0.44	0.33	0.08	0.15	0.04
CL-11	65.44	19.97	4.76	3.15	4.67	0.95	0.33	0.40	0.29	0.30	0.05
CL-12	63.20	20.73	4.75	4.58	4.05	0.87	0.33	0.69	0.35	0.23	0.10
CL-13	65.76	20.23	4.94	3.27	3.80	0.57	0.32	Nil	0.32	0.15	0.02
CL-14	64.15	23.44	5.62	3.75	2.00	0.31	0.24	ND	ND	ND	ND
CL-15	64.99	21.03	6.44	4.96	1.00	0.93	0.10	0.16	0.67	0.18	0.33
Overall Range	61-68	20-23.5	4.4-6.4	2.4-5	1.00-5.3	0.3-1.15	0.1-1.0	0.16-0.7	0.08-0.67	0.15-0.30	0.02-0.33

RESULTS AND DISCUSSIONS

Experimentally measured values of free lime in clinker after firing at 1400°C for 30 min. are listed as CaO(1) in table 2. As the aim of present work was to develop a purely statistical model, it was decided to retain the first term of Eq 1 as such and replace the last three terms by a single term as under:

$$CaO_f = 0.33\ [LSF + 5.1\ SM - 107] + A \quad \ldots\ldots\ [2]$$

The difference between experimentally measured free lime and free lime given by first term of Eq 2 is listed as CaO(2) in table 2. In fact, these are the values for which a model is required to be developed. As the term A reflects the free lime contribution by coarse mineral particles, attempts were therefore made to correlate the CaO(2) values with various powers and roots of

TABLE 2

Sl No	LSF	SM	R_{90}	CaO(1)	CaO(2)	$\sqrt{R_{90}}$	CaO(3)	Diff.
CL-1	94.00	1.85	4.10	0.25	1.43	2.02	0.22	0.03
CL-2	89.18	2.21	4.37	0.25	2.42	2.09	0.0	0.25
CL-3	93.20	2.18	4.17	0.46	1.35	2.04	0.52	-0.06
CL-4	99.01	2.53	4.52	3.50	1.89	2.10	3.06	0.44
CL-5	93.63	2.55	4.77	1.23	1.36	2.18	1.37	-0.14
CL-6	87.92	2.39	7.26	0.38	2.66	2.69	0.0	0.38
CL-7	92.37	2.15	6.28	0.30	1.52	2.51	0.48	-0.18
CL-8	94.41	3.08	6.83	1.45	0.43	2.61	2.77	-1.32
CL-9	90.45	2.86	1.83	0.15	0.81	1.35	0.35	-0.20
CL-10	92.20	2.76	1.56	0.19	0.44	1.25	0.70	-0.51
CL-11	100.20	2.52	17.37	3.62	1.63	4.17	4.66	-1.04
CL-12	93.65	2.22	18.52	2.06	2.74	4.30	2.07	-0.01
CL-13	99.73	2.46	12.92	5.03	3.30	3.59	4.06	0.97
CL-14	84.16	2.56	31.49	1.48	4.72	5.61	0.29	1.19
CL-15	91.22	1.84	30.64	0.19	2.31	5.54	1.36	-1.17

CaO(1) = Free lime after firing the raw mix at 1400°C for 30 min. (Experimentally Measured)
CaO(2) = CaO(1) - 0.33 [LSF + 5.1 SM - 107]
CaO(3) = Calculated free lime (according to Eq 4)

residue on various sieves. Best results were obtained with square root of residue at 90 um sieve. The linear regression equation

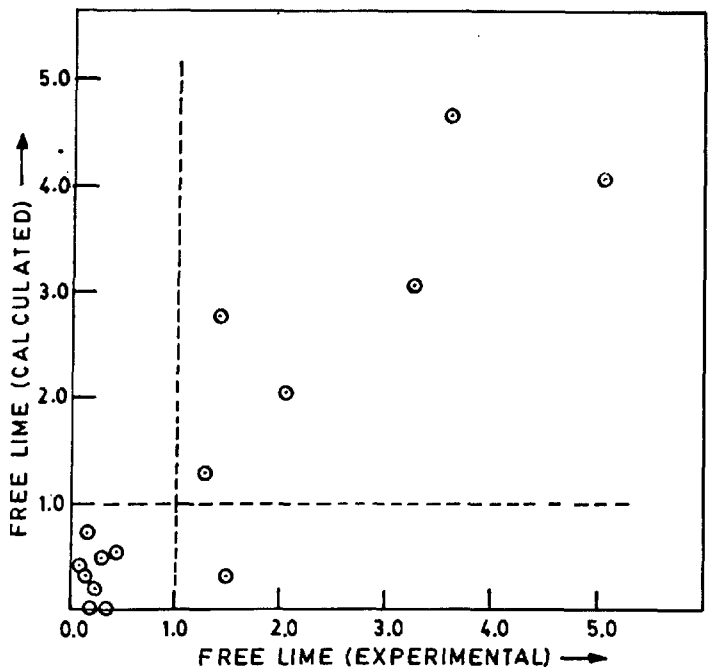

FIG 1 SCATTER DIAGRAM OF CALCULATED vs. EXPERIMENTALLY MEASURED FREE LIME

obtained is as under :

$$A = 0.21 + 0.59\sqrt{R_{90}} \quad \ldots\ldots\ldots [3]$$

The relationship has a correlation coefficient of 0.606 as against the listed values of 0.497 and 0.623 at 95 and 99 percent confidence levels respectively for relevant degrees of freedom. The model was further subjected to analysis of variance and F test. All these tests show that the model is significant statistically to a level of 95% or more. When combined with Eq 2, a complete relationship can be given as:

$$CaO_f = 0.33\ LSF + 1.68\ SM + 0.59\sqrt{R_{90}} - 35.1 \quad \ldots\ldots\ldots [4]$$

Free lime values calculated using this relationship are tabluted under CaO(3) in table 2. The differences between experimentally determined and calculated free lime values for various samples are listed in the last column of table 2. Scatter diagram of calculated free lime values [CaO(3)] verses experimentally measured free lime [CaO(1)] content is shown in Fig. 1. Taking a critical value of 1.0%, it is observed that the predictions in most of the cases are in line with experimental observations.

CONCLUSION

A statistically significant model, valid over a wide range of compositional and fineness variations for calculation of free lime in clinker has been developed. The model does not explicitly take into account the influence of minor constituents but implies their influence over normal range of their occurence in clinker. The residue of raw mix on 90 um sieve is found to be a significant parameter for calculation of free lime. The relationship has been developed for a firing temperature of $1400^{o}C$ and 30 min. duration, but free lime content at other durations can be calculated using mathematical formulations of kinetics of clinkerisation.

ACKNOWLEDGEMENT

The authors have freely drawn upon published and unpublished R&D work of National Council for Cement and Building Materials. The authors are grateful to Director General, NCB, for granting permission to publish the work presented in this paper.

REFERENCES

Christensen N H, "Modelling the Clinker reaction". World Cement Technology Vol. 12, No 5, 1981 pp. 238-247.

Kock, H et.al "A statistical model for determining the burnability of cemet raw mix". VI International Congress on Chemistry of Cement, Moscow, 1974, paper No. 59.

THE LIQUID PHASE ALITE GENERATION MODEL IN SINTERING PORTLAND CEMENT CLINKER

Zinovii B. ENTINE, Boris E. IOUDOVITCH,
NIICement, Moscow, Russia

ABSTRACT From XRDA, IRS and ferromagnetography of the sintered and quickly cooled raw mix samples, an alite generation model in the presence of liquid phase has been worked out.

Key-words: Clinker formation. Mechanism. Melt. Glass. Mineralogy.

INTRODUCTION

Some facts in the genesis of clinker phases are impossible to explain by taking into account only one reaction for alite formation: $C_2S + C = C_3S$. Among them these are the decrease of C_3A content to nothing and consequent rise up to its potential level in the presence of clinker melt (Entine et al.,1978), the appearance of $C_{12}A_7$ and its disappearance (Sapozhnikova, 1983) and the analogous behavior of calcium ferrites (Nikolaev, 1985). The objective of this investigation was to develop an alite generation model originally to explain these facts.

EXPERIMENTAL AND METHODS

For clinker burning a vertical tube electric kiln was used with Pt-heating winding of variable steps. This kiln had a stable vertical temperature distribution in the interval from 1100 to 1450$\pm$ 0.5°C on the height levels range about 250 mm with each level fixed within 0.1 mm by means of microcathetometer. It had a Pt crucible to contain the cement raw mix sample (upto 3 g / space) hung by a Pt-thread along the kiln axis. Rupture of said thread guaranteed quick cooling of the crucible in a cup of Hg under the kiln. The higher burning temperature demands a shorter thread length. The slowest cooling (2 - 3 h.) was achieved by switching off the heating element with the crucible in the kiln. Cement raw mix samples with silicate components - clays, coal ash and its mix, limestone and pyrite ore, were burned in the said kiln for 15 and 30 minutes at constant temperature in the interval of 1100 - 1400°C with the gradation of 25°C. The majority of samples were quickly cooled. With pregraduated scales for X-ray diffraction analysis (XRDA), infra-red spectrometry (IRS) and ferromagnetography instruments for clinker mineralogy composition calculations, the actual content of clinker phases was found. Optical, transmission and scanning electron microscopy and electron microprobe analysis were used for structure studies.

RESULTS

Raw mixes chemical compositions were characterized with lime saturation factor (LSF) by V.A.Kind [= (C - 1,65A - 0,35F)/2,8S] (Duda, 1977) 0.92 $\pm$ 0.005, silicate and aluminate moduli [n = S/(A+F) and p = A/F] are equal to 2.2 $\pm$ 0.1 and 1.3 $\pm$ 0.1 respectively, with average clinker potential composition, %: C_3S 61.5, C_2S 14.7, C_3A 7.4, C_4AF 13. The schematic graphs of content data (weight %) based on XRDA analitical reflections of C_3S, C_3A, C_4AF and free lime, on IRS absorbtion line for $C_{12}A_7$ (Sapozhnikova, 1983) and on ferromagnetography , utilising the much higher permeance of C_2F and CF relative to C_4AF and to a clinker as a whole (Nikolaev,1985), for raw mix with ash and for clinker burned and quickly cooled samples are given in Fig.1.

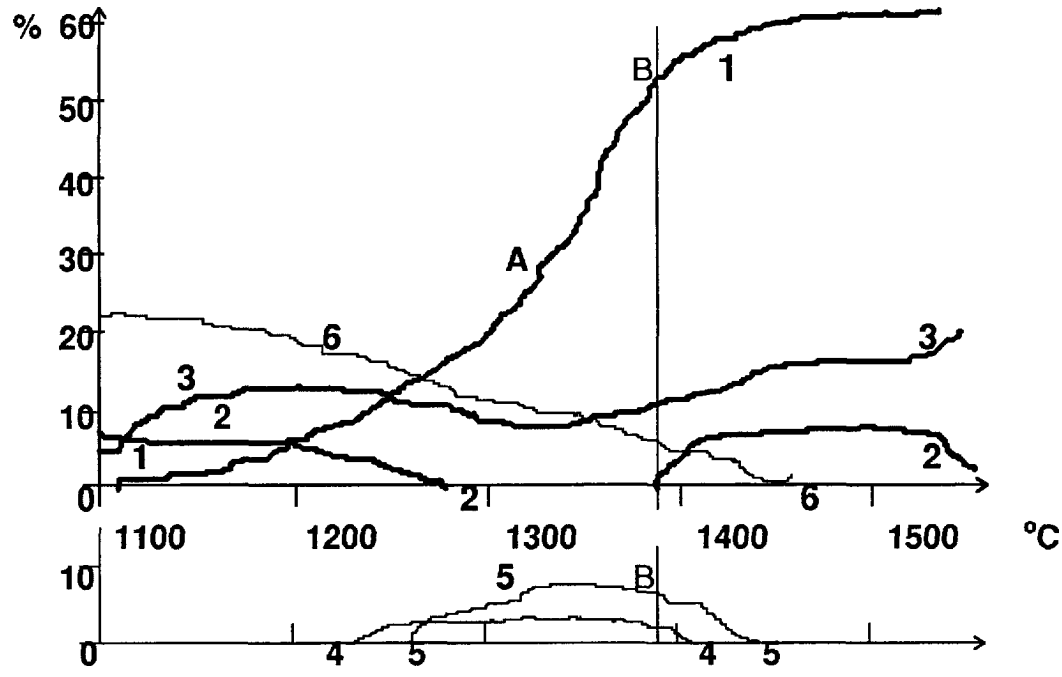

Figure 1 The phase formation in burned and quickly cooled raw mix based of ash
Designations: 1- C_3S, 2 - C_3A, 3 - $C_2(A,F)$, 4 - $C_{12}A_7$, 5-C_2F+CF, 6 - C.

These data show that with quick cooling the C_3A content really decreases from initial extremum (which is almost equal to its potential level) to nought with following increase up to the potential level and so for $C_2(A,F)$ content but with non-zero-minimum as free lime is completely assimilated. In cases of clay or clay + ash based raw mixes, one can see a single difference: the initial extremae of C_3A and C_4AF content are much less than potential levels. In all raw mixes the lower cooling rate accords to the higher minimum values of C_3A and C_4AF contents in samples burned in the temperature interval of 1250 - 1325°C and in this condition the minimum C_3A content is above zero. Simultaneously in this temperature interval the maximum rate of alite generation is obtained (this maximum accords to maximum value of the inclination angle of tangent line on the rising alite content graph - point A on Fig.1). When C_3A and C_4AF contents decrease are termed the initial extremae the secondary $C_{12}A_7$, C_2F and CF rise; that is evident from ISR and magnetography data. The last phases, which marginal (below) have no visible XRDA reflections that testifies to their noncrystalline form. After the burning temperature increases to 1350 - 1400°C the marginal phases content in quick cooled samples decreases gradually to zero. Simultaneously the lower cooling rate corresponds to lower contents of the marginal phases and to the higher alite content.

DISCUSSION

All data obtained are in accord with the next two pairs of equations, defining a the cyclic conjugate reversible reaction model:

$$9\ C_2S + 7\ C_3A \Leftrightarrow 9\ C_3S + C_{12}A_7, \quad [1]$$

$$C_{12}A_7 + 9\ C \Leftrightarrow 7\ C_3A. \quad [2]$$

$$6\ C_2S + 7\ C_4AF \Leftrightarrow 6\ C_3S + C_{12}A_7 + 3\ C_2F + 4\ CF, \quad [3]$$

$$C_{12}A_7 + 3\ C_2F + 4\ CF + 3\ C \Leftrightarrow 7\ C_4AF. \quad [4]$$

The conjugation of reactions within said pairs and among them is determined by the condition that one or more reaction products are the reagents for next and previous reactions. This model also takes into account: 1) the marginal phases appearing in the course of alite generation by the reason of the lower rate of reactions in Eqs 2 and 4 compared with reactions in Eqs 1 and 3 accordingly, especially in the initial part of temperature interval (1100°C - point A); 2) their disappearance when the degree of reactions in Eqs 1 and 3 is more than 70-75% in consequence of decreasing the rate of last reactions compared with reactions in Eqs 2 and 4; 3) the coincidence the minimae of C_3A and C_4AF content with point.A - maximum rate of alite generation; 4) the greater rate of reactions in Eqs 1 and 2 versus reactions in Eqs 3 and 4 and, as a consequence, - shift in the position of point A and an aluminate character of clinker melts in the range of 1100 - 1225°C, has been reported (Konovalov et al.,1962) and in our case is obtained from observing the refractive index of cooled melt particles in immersion probes by optical microscope; 5) sumultaneous formation of secondary $C_{12}A_7$ in the reaction pairs, beginning in the first of them, and secondary C_2F and CF in the second pair. It can be noted that this point has been known long ago (Bogue, 1955): in ferrous systems, C_2F + CF are analogs for $C_{12}A_7$+C_5A_3 in alumina systems. Moreover, the $C_{12}A_7$ is evolved from the melt with excess of oxygen content compared to its stoichiometrical composition (Taylor, 1990), just as the C_2F and CF have the oxygen deficiency in the same sense. That may be one of reasons for the simultaneousness of these marginal phase formations; the redox conditions in the kiln, namely in the clinker melt, must play a decisive part; 6) reactions in Eqs 1 - 4 are reversible: in Eqs 1 and 3 - with slower cooling than 1 hours from 1300 to 1175°C, in Eqs 2 and 4 - with slower heating of the kiln than 1-2 hours at 1350 - 1450°C and shorter - at the higher temperature range. These are the reasons why alite dissociation occurs without free lime crystallisation in slowly cooled clinkers and clinker glass pellicles (with thickness of 1 ÷ 3 μm) formation around crystals in overheated and quickly cooled clinkers which one can see by means of electron microscopy; 7) by electron microprobe analysis of clinker ferrous phase in the layer with thickness of about 1 μm around the part of alite crystals one cannot fix some iron; it would be concluded that these alite crystals are formed by reactions in Eqs 1 and 2 and the rest are alite crystals formed by reactions in Eqs 3 and 4; 8) the complex of such phenomena is impossible without dissociation of all reagents in the melt to ionic groups which are well preserved as anionic fragments particularly of the annular frameworks of crystal lattices (Taylor, 1990); 9) Impurities influence these reactions and cause some accessory reaction` schemes:

$$3\ C_{12}A_7H \Rightarrow 7\ C_5A_3 + 3H\uparrow + C, \qquad [5]$$

where $H = H_2O$, with excess of oxygen in the melt, and then

$$7C_5A_3 + 28\ C \Rightarrow 21C_3A, \qquad [6]$$

$$C_5A_3 + 3\ C_2F + 15\ C \Rightarrow 18\ C_3A + 3\ C_4AF. \qquad [7]$$

Reactions in Eqs 6 and 7 may be the direct reason for said alite dissociation because of the large lime demand; and so the reaction which had found by Boikova et al (1976) at the presence of much alkalies without sulphate equivalent ($R=Na_2O_e = Na_2O+0{,}66K_2O$):

$$3\ C_{12}A_7 + 20\ C + 7\ R \Rightarrow 7\ RC_8A_3. \qquad [8]$$

Now we use `` $RC_8A_3$`` as a designation of alkalies contained forms of tricalcium aluminate.
The binding of C by the last reaction is the reason why the free lime cannot be used as a measure of clinker burning degree in such cases.

This model is used to explain how plant kiln condition variations affect clinker (cement) characteristics, e. g.: 1) the presence of marginal phases in underburned clinkers (see, for example the line B, Fig. 1), sometimes with small amount of free lime but the result is bad cement quality; 2) the presence of two alite forms (e.g. polymorph modifications) with different sets of impurities; 3) simultaneousness of FeO and C_2F+CF formation in sintering underburned or overburned clinkers (in the last case, as a consequence of the inverse course of Eq 4 etc.) with generation of C_2F+CF especially in the cases of p = A/F < 0,8 in raw mix that provokes the clinker dusting in rotary kilns by decreasing the melt viscosity which decreases the hydration rate of cement because of deficiency of electron vacancies in the crystal lattices of the clinker phases (Chatterjee et al.,1964); 4) cases of cement false set, created by presence of $C_{12}A_7$ or RC_8A_3 in clinkers; 5) low frost and chemical resistance of concrete in the presence of marginal phases in cement at the level higher than 1-2% because of direct and undirect negative influence of them upon the cement hydration rate and degree and the structure of hardened cement pastes, mortars and concretes.

CONCLUSION

This model is fully coordinated with phase relations in system CaO - Al_2O_3 - SiO_2 etc. Moreover, Toropov (1956) had written an equation close to Eq 1 only on the base of deep analysis of the Rankin -Wright phase diagram of the relevant system. But at that time he was not supported by colleagues. The present model had been firstly suggested as a working hypothesis about eighteen years ago for explaining such sets of data as given in Fig. 1 and used by us for improving clinker burning process and cement quality - practically without publications but as well as without any contradictions with practice in cement plant and cement customer works. After Zhmoidin - Chatterjee reported (1986) pseudomolecular annular structures in some slag melts it becomes possible to conclude that this phenomenon can exist in clinker melts. The experimental arguments for this point of view have been obtained (Zubekhine, Ioudovitch, 1996). All that rather improves the scientific base of the present model but a better understanding of the role of redox and of the role of impurities in clinker melts is needed for the development of these models.

REFERENCES

Bogue, R.H.,``The Chemistry of Portland Cement``, Reinhold, N.Y., 1955, pp. 379-383.
Boikova, A.I., et al., Tsement (Leningrad), 1976, N 8, pp. 20 - 22 (in Russian).
Chatterjee, A.K., et al., Nature (London), 1964, v. 203, N 494, p. 138.
Duda, W.H., ``Cement Data Book.`` Bauverlag, Wiesbaden - Berlin, 1977, Chapter 1.
Entine, Z.B., et al., Proc.Vth All-Union Scientific and Technical Conference on the Chemistry and Technology of Cement. Moscow, 1980, pp. 67-68 (in Russian).
Konovalov, P.F., et al.,``Atlas of microstructures of cement clinkers, refractories and slags``, Gosstrojizdat, L.-M., 1962, p. 208 (in Russian).
Nikolaev, A.P.Cand.Tech.Sci.(CTS)Thesis.NIIcement, Moscov, 1985,pp.24(in Russian)
Sapozhnikova, N.I., CTS Thesis, Yuzhgiprocem., Charkov, 1982, pp.16 etc.(in Russian)
Taylor, H.F.W., ``Cement Chemistry``, Academ.Press, London et al.,1990, pp.36 - 37.
Toropov, N.A., ``The Chemistry of Cement``, Gosstrojizdat, Moscow, 1956, p. 98 (in Russian)
Zhmoidin, G.I., Chatterjee, A.K. ``Slags for refining of metal. The Dynamics of System CaO-$Al_2O_3$-CaO Properties``, Metallurgy Publ., Moscow, 1986, p.286 (in Russian)
Zubekhine, S.A., Ioudovitch B.E.``Nonshrinking Sulphate Resisting Cement for Conventional and Fine Grained Concretes``,VNIIESM Rew., Moscow,1996,ser.1, No. 3, pp. 9-10 (in Russian)

1i047
8 pp

INTERRELATIONSHIP OF CLINKER PROPERTIES WITH PROCESS PARAMETERS IN COAL FIRED KILNS

V.K. GORE, S.A. KHADILKAR, P.G. LELE, D. GHOSH
Research & Consultancy Directorate
The Associated Cement Companies Ltd.
Thane - 400 604, INDIA

ABSTRACT The Indian Cement Industry is characterised by the use of limestones of widely differing geological age and consequently vastly differing mineralogical and microstructural characteristics on one side and use of coal of different geological age and characteristics on the other that include the variation in the ash content from 15 to 40% and volatiles from 20 to 40%. These input variations, when coupled with different processes operating in plants, create situations where the interrelationship of clinker properties with process parameters turns out to be a complex phenomenology. In this complexity, an attempt has been made, based on a large number of operational data of industrial kiln systems to isolate the variations in some of the critical coal characteristics and limestone mineralogy on the clinker mineralogy and microstructure. A few case studies have been discussed where the interrelationship between clinker properties and process parameters were used for process optimisation.

KEY-WORDS Limestone, Coal, Process parameters, Microstructure, Reactivity.

INTRODUCTION

The Cement manufacturing in the present hardware systems and with use of diverse fuels and raw materials is a complex process. Only parametric interrelations, however emperical, can only ensure stable operation. Based on this concept the operational data base of the company has been used to study the parametric interrelations.

The input variations of coal and limestone characteristics due to their source, coupled with different processes of cement manufacture lead to certain implications in terms of raw mix design and processing conditions, imprints of which are revealed by the microstructural characteristics of clinker. In this complexity the authors have made an attempt to identify certain practical interrelationships that might be of direct use in material selection, process optimisation and trouble shooting.

CATEGORISATION OF LIMESTONE AND COALS

Categorisation Of Limestone

Attempts have been made to categorise the limestones through use of a chemical index; termed as the hydraulic modulus (C+M)/(S+A+F). The limestones were observed to get categorised into three clusters each representing the geological ages of the limestone deposits

Cluster-A : Tertiary deposits HM in the range of 4.0 to 6.8
Cluster-B : Vindhyan deposits HM in the range of 2.2 to 4.7
Cluster-C : Archaean deposits HM in the range 1.8 to 2.4

Table1 CHEMICO-MINERALOGICAL CHARACTERISTICS OF LIMESTONES

(RANGE)	CLUSTER- A TERTIARY		CLUSTER- B VINDHYAN		CLUSTER- C ARCHAEN	
	MIN.	MAX	MIN.	MAX	MIN.	MAX
SiO_2	4 0	7 0	9 0	15 0	13 0	20 0
Al_2O_3	1.3	1 8	1 5	3 5	1 8	3 8
Fe_2O_3	1 0	1 05	1 0	2 4	0 9	1 2
CaO	40 0	51 0	42 0	48 0	43 1	47 1
MgO	0 6	1 0	1 0	3 0	0 6	1 0
LOI	39 0	41 0	35 0	38 0	34 0	36 0
Trace Elements(PPM)						
Ba	50	60	50	90	600	1300
Sr	15	20	100	400	80	100
Mn	110	140	100	300	300	450
Cr	5	6	9	20	18	20
Co	8	10	12	14	11	14
Ni	12	15	16	20	20	22
Zn	8	10	17	20	30	40
Bi	40	50	70	80	50	90
Cd	3	4	10	16	10	12
Sb	20	25	60	90	30	50
Pb	12	14	8	16	4	18
Cu	4	5	4	8	7	9
As	-	-	-	-	-	-
T.C	88 0	92 0	75 0	85 0	85 0	80 0
CHEMICAL INDICES						
HM	4 0	6 8	2 2	4 7	1 8	2 4
(C+M)/S	5 7	11 4	3 0	4 7	2 1	2 8
(C+M)/(A+F)	11 3	23 1	7 4	19 6	11 3	13 9
S / (A+F)	1 5	3 4	2 2	9 5	4 6	9 1
Avg. Calcite Size	60	90	15	150	600	1100
Avg. Quartz Size	170	190	15	300	280	480
Bond Index	7	10	11	14	12	16
Metal Wear Index	200	300	200	300	400	600
MINERALS PRESENT (MINOR)						
	Oolite,		Muscovite		Muscovite	
	Aragonite		Illite		Hornblende	
	Shaley Minerals		Mica		Pyrites	
	Microfossils		Dolomite		Labradonite	

HM =(C+M)/(S+A+F)

Table 2 CHARACTERISTICS OF COALS

(RANGE)	GROUP - I TERTIARY		GROUP - II UPPER GONDWANA		GROUP - III LOWER GONDWANA	
(%)	MIN.	MAX	MIN.	MAX	MIN.	MAX
VM	29 7	47 2	25 3	35 6	24 4	27 8
ASH	3 7	21 6	22 6	32 9	34 5	43 3
F.C	36 4	58 5	41 0	46 5	32 5	37 7
C.V (Cal/g)	5345	6950	4925	5800	3850	4710
C	54 6	72 4	50 4	60 2	40 0	48 7
H	5 1	5 8	3 9	4 9	3 4	4 5
S	0 9	3 1	0 5	0 8	0 8	1 2
N	0 3	0 6	0 3	0 7	0 3	0 4
O	6 2	14 9	6 6	8 1	5 6	7 5
ASH ANALYSIS (%)						
SiO_2	32 4	57 5	31 7	65 5	59 3	68 4
Al_2O_3	11 1	30 0	22 0	26 8	20 5	23 4
Fe_2O_3	5 1	11 8	5 2	9 0	6 2	6 7
CaO + MgO	11 2	39 7	4 7	7 7	2 2	5 2
Na_2O	0 14	1 06	0 17	0 32	0 10	0 30
K_2O	0 29	1 24	0 91	1 83	0 57	0 78
SO_3	3 1	11 8	1 7	3 4	1 4	2 6
Trace Elements(PPM)						
Ba	150	750	50	500	50	150
Sr	1	2	0 5	4	4	6
Mn	150	550	100	250	100	150
Cr	100	1600	70	20	40	60
Co	10	150	1	13	11	14
Ni	30	150	20	40	20	30
Zn	71	90	30	90	20	40
Bi	-	-	-	-	-	-
Cd	1	2	2	8	4	10
Sb	1	2	20	30	30	40
Pb	20	120	15	30	15	30
Cu	80	100	20	150	20	30
As	1	2	1	4	1	4
A.F.T °C	1240	1510	1470	1610	1570	1670
C.T.V °C	330	467	330	360	318	350
C.C.T °C	445	620	465	505	455	480

A.F.T °C : ASH FUSION TEMPERATURE
C.T.V °C : COMBUSTION TEMPERATURE OF VOLATILES
C.C.T °C : COMPLETE COMBUSTION TEMPERATURE

Other chemical indices viz (C+M)/S, (C+M)/(A+F) and silica modulus have also been used to indicate the nature and type of correctives that would be required for use of these limestones for cement manufacture (Fig. 1) The chemical, mineralogical, microstructural and physico-mechanical characteristics of the three clusters is summarised in Table 1 The following inferences can be drawn from the illustrated features.

The quality of limestone shows a deterioration from Tertiary to the Archaean formations The tertiary deposits with (C+M)/S ratio of 5.7 to 11.4 and a lime to flux ratio (C+M)/(A+F) of 11.3 to 23.1, would require high siliceous and ferrugenous correctives while in the Archaean formations with (C+M)/S ratio of 2.1 to 2 8 and lime to flux ratio of 11.3 - 13 9 use of high grade limestone and aluminous/ferrugenous correctives would be a necessity. Lower HM values for the Archaean formations illustrate that these deposits would invariably require beneficiation

The decrease in HM values from Vindhyan to the Archaean deposits is indicative of an increased metamorphism and higher extent of basic and acidic intrusions

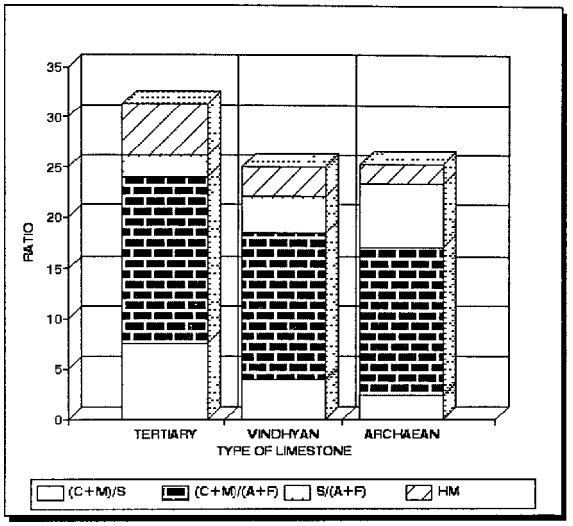

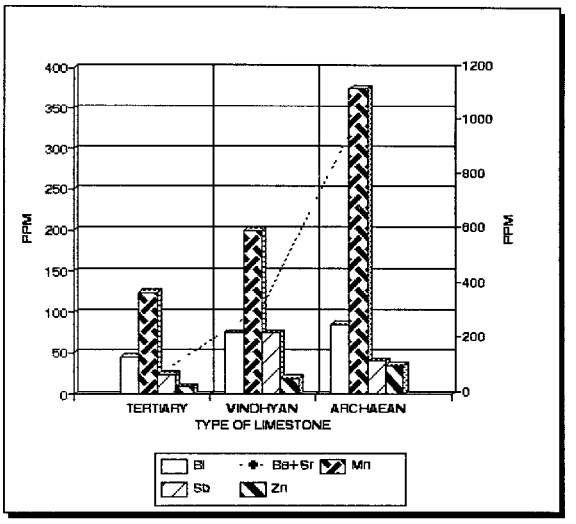

Fig. 1 : Compositional Characteristics of Limestones.

Fig. 2 : Distribution of Trace Elements in Limestone

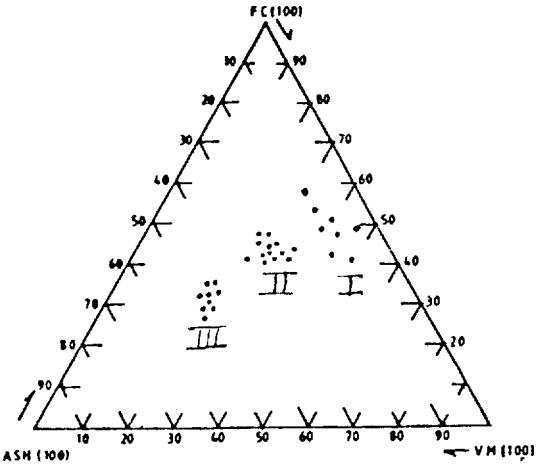

Fig . 3 Ternary Diagram of Coals

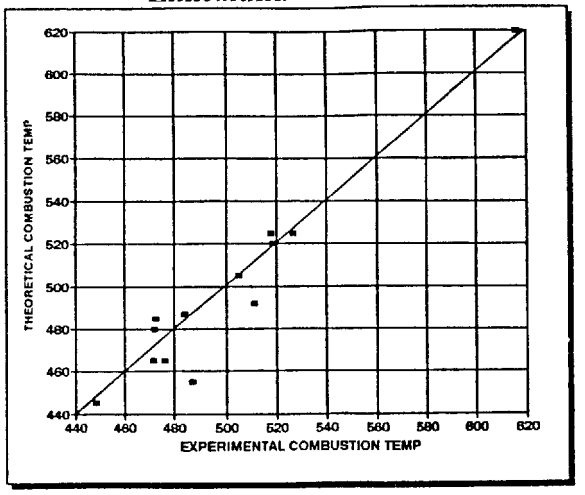

Fig . 4 Relation between Theoretical and Experimental C.C.T

This is also indicated by the increase in crystal size of Calcite and Quartz, increase in Bond grindability index and Wear index of the limestones of these deposits. The trend of metamorphism from Tertiary to the Archaean deposits is also exemplified by the relative increase in levels of the trace elements viz. Ba, Sr, Mn, Bi and Zn. (Fig. 2) from Tertiary to the Archaean deposits.

Categorisation Of Coal : The Indian coal formations are called the Gondwana coals named after the hypothetical supercontinent Gondwana. The coals are of drift origin with high mineral matter contents, thoroughly disseminated. Some mesozoic and tertiary coals are also found in the country. Using a ternary plot of VM, FC & Ash content of coals (Fig.3),attempt have been made to classify the coals into three groups.

Group I : Tertiary
Group II : Upper Gondwana
Group III : Lower Gondwana

Ultimate, proximate composition of coals, Hardgrove index, Ash fusion temperature, volatile combustion temperature and complete combustion temperatures are summarised in Table 2. The volatile combustion temperature and complete combustion temperatures were determined by DTA analysis. The **Complete Combustion Temperature** being the temperature at which the entire carbonaceous content of coal gets burnt.

It is evident form the data that :

- Group I (Tertiary) coals have higher VM, fixed Carbon, Calorific Value with lower ash content. As Hydrogen content of these coals is higher, there is a decrease of H/C ratio which is related to increase in aromaticity of the coals. Such characteristics are associated with High volatile bituminous coals, i.e. higher rank coals tending towards the anthracitic ranks. Expectedly such coals would possess higher complete combustion temperature.
- Group II & Group III are coals representative of the general coals of Upper & Lower Gondwana in which the coal seams are invariably interbedded with sandstone and shales of sedimentary origin. Such coals have highly fluctuating VM, not necessarily related to the calorific value.
- The Ash fusion temperature(AFT) of all the coals illustrate a high relation to the oxide composition of coal ash. Statistical analysis of the data reveals that the correlation could be exemplified by an empirical relation given below :

$$\mathbf{AFT(deg\ C) = 21.92\,SiO_2 - 2.92Al_2O_3 + 31.56Fe_2O_3 - 399.15Na_2O + 32.877SO_3 + 11.865CaO + MgO + 101.61K_2O} \quad [1]$$

- The data base on coal was also used for multilinear regression analysis to understand the factors influencing the complete combustion temperature of coal. The statistical analysis indicate that VM, Carbon content, % free carbon. (Fixed Carbon - Elemental Carbon/Fixed carbon), Hydrogen content, Sulphur content and combustion temperature of volatiles(C.T.V), have a strong relationship with complete combustion temperature, as indicated by correlation coefficient of 0.975. The correlation can be represented by an empirical equation which would be applicable to any rank of coals.

$$\mathbf{Complete\ Combustion\ Temp\ (^{\circ}C) = 1.7117\,C + 1.5367VM + 5.3276\ Free\ C + 11.013H_2 + 11.3045S + 0.8284C.T.V - 418.46} \quad [2]$$

The theoretically predicted values and experimentally determined values of Complete Combustion Temperature are graphically shown in Fig. 4

- Trace element distribution (Table 2) indicates that the distribution of these elements is more a function of the type of mineral deposits in the vicinity of the colliery rather than the age or rank of coals.

INTERRELATIONSHIP OF COAL AND LIMESTONE CHARACTERISTICS

The type of limestone and coal use by plant would substantially influence the raw mix design, selection of communition hardware and process parameters of cement manufacture. These influences would get eventually reflected in the mineralogical, microstructural characteristics of the clinker. In earlier publications from the authors laboratory (Hargave et al 1983,1985) attempts were made to evolve microstructural indices of clinker to assess the effect of different processes of

cement manufacture and also to relate these indices to the hydraulic potential of the clinker(Venkateswarn. et al 1991). Some of these microstructural indices are also influenced by the mineralogy and microstructural characteristics of limestones and quality of coal. In these case studies discussed below an attempt has been made to isolate the variations of coal and limestones characteristics to assess the influence on clinker mineralogy and microstructure.

CASE -1: This case study relates to Plant-A with limestone of the tertiary deposits (Chemical composition in Table-3) using Group II Coal (Upper Gondwana) having average ash content 25.9% and Ash fusion temperature of around 1420 deg C. The plant is a dry process plant of capacity 3000 TPD with suspension preheater and pre calciner. The clinker composition and microstructural features are given in Table-3. The microstructural studies reveal the following:

- Phase index of 1.38 is indicative of higher content of C_3S formation and also reflects on higher reactivity of the limestones.
- The morphological index(MOI) of Alite and Belite are 4.4 and 0.9 respectively which is indicative of good crystallinity of the silicate phases.
- The chord length index value is 6.0 which is indicative of easy grinding characteristics of the clinker.
- Cluster size of 0.23 mm is indicative of lower crystal size of quartz in limestone and homogeneous distribution of coal ash. This is also further substantiated by lower cluster frequency observed.

CASE-2 : This case study relates to Plant B having limestone similar to Plant A but using Group III coal with ash content in the range of 35 - 38%. The plant is also a dry process plant with suspension preheater and precalciner of comparable capacity. Thus primarily the plant differs from Plant A in terms of quality of coal used. The microstructural indices are summarised in Table-3. Trials carried out at the plant using Group-I Coal (C-1) with ash content of 11.8%, VM of 29.7 %, CV 6422 cal/g indicated a change in the microstructural indices of the clinker which reflect on suitability of microstructural indices for assessing the effect of coal characteristics.

- The phase index of the Plant B clinker (2A) with Group III coal was 1.00 with morphological index of alite and belite being 3.0 and 0.5 respectively with Cluster frequency of 0.25 mm and cluster index of 0.2. The chord length index was observed to be 1.77.

With use of Group-I coal the microstructural indices of the clinker (2B) were MOI of alite and belite 4.2 and 0.8 respectively with cluster size of 0.25 and cluster frequency of 0.2. The chord length index was 8.8.

It could be noted here that use of Group-I coal have resulted in clinker microstructural indices similar to Plant-A, thus modification in clinker quality characteristics could be achieved by the change in quality of coal.

CASE-3: This case study is of a semi wet process plant with suspension preheater and precalciner of capacity 2500 TPD(Plant C) .The Plant uses limestone of Archaean deposits having higher extent of free silica content and coarser sizes of Calcite and Quartz. However, the plant also uses floated limestone, the extent of requirement of the floated

Table - 3 Diagnostic data of case studies

LIMESTONE							COAL ASH					CLINKER					
PLANT	A	B	C-1	C*	D- 1	D-2	A	B	BC 1	C	D	1	2A	2B	3	4A	4B
SiO2	7.4	11.7	19.1	10.7	10.0	13.4	61.6	59.3	51.9	58.5	58.0	21.9	22.4	22.4	23.2	20.9	21.8
Al2O3	2.6	1.7	1.2	1.6	4.0	3.9	22.0	23.4	28.9	24.3	26.8	5.7	5.3	5.1	4.3	6.9	6.7
Fe2O3	1.0	0.9	0.9	1.0	1.4	2.1	6..2	6.2	6.9	5.2	9.0	4.0	4.1	3.9	3.6	2.9	3.4
CaO	48.0	46.7	43.4	47.7	44.9	42.3	3.9	4.5	2.9	5.1	2.0	65.6	65.2	65.6	65.5	63.9	64.4
MgO	1.0	0.6	0.7	0.5	1.9	2.0	0.8	0.7	2.0	1.1	0.8	1.5	1.1	1.0	0.9	2.5	2.6
LOI	39.2	37.0	34.2	37.8	37.0	35.0	0.5	1.1	1.1	0.5	0.5	0.5	1.0	1.0	1.4	0.4	0.4
Ba	80	87	695	385	40	40	80	80	417	112	80	60	80	78	595	63	62
Zn	10	17	39	28	22	20	30	32	230	46	45	32	32	31	71	55	100
Cu	5	8	9	7	6	4	24	25	96	23	26	22	19	18	23	15	22
Pb	18	18	14	11	10	10	18	17	0.4	15	30	18	55	58	56	53	58
Sr	17	82	89	79	83	94	8	8	0.4	8	8	52	179	185	237	135	132
As							4	1	0.1	1	4.2	1.1	2.6	2..4	0.8	1	1.1

COAL CHARACTERISTICS (Gross On Dry)

PLANT	VM(%)	FIX. C(%)	ASH(%)	CV(Cal/g)	C (%)	H(%)	S(%)	AFT	CTV	CCT
A	29.8	41.0	29.2	5352	53.6	4.9	5	1410	355	487
B	27.8	37.7	34.5	4710	48.7	4.5	0.9	1570	350	480
B C -1	29.7	58.5	11.8	6422	72.4	4.7	0.6	1450	331	520
C	25.3	46.5	28.2	5269	56.8	3.9	0.8	1430	360	492
C - C1	29.5	58.0	12.5	6355	72.4	4.7	0.6	1460	331	520
C- C2	38.6	51.2	10.2	6630	67.5	5.6	0.9	1410	467	620
D	26.1	44.5	29.4	5169	52.4	5.1	0.7	1470	329	505

CLINKER PARAMETERS

MODULII VALUES				MICROSTRUCTURAL FEATURES									
PLANT	LSF	MS	MA	% C3S	% C2S	% C3A	% C4AF	PHASE INDEX	MORPHOLOGY INDEX		CLUSTER NDEX		CHORD LENGTH INDEX
									Alite	Belite	Size	Freq.	
1	0.93	2.26	1.42	58	22	7	13	1.38	4.4	0.9	0.23	0.05	6.0
2A	0.91	2.38	1.30	50	31	7	12	1.00	3.0	0.5	0.25	0.20	1.8
2B	0.91	2.48	1.30	58	24	6	12	1.38	4.2	0.8	0.15	0.08	8.8
3	0.9	2.90	1.20	56	26	7	12	1.27	3.6	0.5	0.50	0.40	1.8
4A	0.93	2.13	2.4	47	28	12	13	0.89	2.4	0.3	0.40	0.50	3.5
4B	0.90	2.16	2.0	50	26	12	12	1.0	3.9	0.8	0.21	0.25	4.5

limestone depending on quality of coal. The plant presently uses coal of Group-II and trials were conducted with two coals of Group-I variety (C-1 & C-2), C-2 coal was of higher rank with higher complete combustion temperature. While the other coal C-1, was similar to the one used in the trials at plant Group-I coal used at Plant-B.With use of coal with higher combustion temperature (C-2) the plant reported number of processing problems:

- The coal mill outputs were decreased substantially.
- Fine coal residues on 90 microns were higher.
- Reducing condition were observed at the Kiln inlet which accelerated the formation of coatings/build-ups at the kiln inlet and preheater cyclones which affected the pyroprocessing operations

These processing problems were subsequently diagnosed to be due to (a) Poor grindability of the coal (Hard Grove Index 45).(b) Lower ash fusion temperature (1370-1400 ^{0}C). (c) Higher complete combustion temperature of coal (620 ^{0} C)

While use of the other variety of Group-I coal the clinker indices showed drastic changes (Table-3) and inspite of the use of limestone of Archaean deposits the clinker quality was compared to Plant A/B clinkers. Use of this quality coal not only improved the kiln performance but also resulted in substantial decrease in floated limestone consumption.

CASE-4: This case study relates to a cement plant (Plant D) using the same limestone (Vindhyan) in semi dry process (Lepol grate) and dry process with suspension preheater and precalciner using Group-II quality of coal. The microstructural indices of the clinkers exemplifies the effect of process of cement manufacture (Table-3).

- The semi dry process clinker exhibit lower values of morphological indices of alite and belite and although the ash absorption is lower in the semi dry process and Quartz size is not coarse in limestone, the cluster size and frequency observed is 0.4 mm and 0.4% respectively, which is indicative of localised ash absorption. On the contrary, the dry process clinker exhibits higher phase index, lower cluster size and frequency and higher values of morphological indices of alite and belite indicative of better crystallinity of silicate phases.

BEHAVIOUR OF TRACE ELEMENTS IN DIFFERENT PROCESSES OF CEMENT MANUFACTURE

In the different case studies presented in this paper, the trace element concentrations in the clinker if compared with that of the raw materials and fuel (ash). The following observations can be made on trace element behaviour :

- Concentration of Ba, Sr in the clinker do not exhibit any enrichment in clinkerisation process
- Concentration of Cu, Zn, Sb and Pb were observed to be higher in clinker as compared to the limestone and coal ash. The order of the degree of enrichment of these elements being Pb > Sb > Cu > Zn. The trend is indicative of volatile cycle of these elements in the kiln system. The enrichment is relatively more in dry process and semi wet process (Plant A, B & C) than in semi dry process (Plant D - 4A clinker) where kiln dust was not circulated.The authors have presented in detail the behaviour of trace elements in different processes in earlier publications(Khadilkar et al 1993)

CONCLUSIONS

- The Indian limestones categorised on the basis of Hydraulic Modulus tend to get clustered as per the geological ages. The other chemical indices can be resorted to for choice of correctives.
- The trace elements distribution in limestone has been observed to be related to the metamorphism of the limestone deposit.
- The Indian coals of Gondwana origin can be clustered based on Ternary plots of VM,FC and ash content, this clustering have been observed to be also related to ranking of coals.
- Empirical equations have been derived for prediction of Ash fusion temperature of coal ash, and Complete combustion temperature of coal. These parametric interrelations could be used for optimising pyroprocessing conditions and quality of clinker produced.
- Microstructural Indices of clinker have been used to exemplify the influence of limestone and coal characteristics coupled with cement manufacturing processes.
- The trace elements Ba and Sr do not exhibit tendency of forming volatile cycles, while Cu,Zn, Bi and Pb have been observed to show such a tendency. The extent of enrichment of these elements in clinker depend up on the type of process and volatility of other volatiles like Na_2O,K_2O and SO_3.

ACKNOWLEDGMENTS

The authors are grateful to Dr. A.K. Chatterjee, Director for his suggestions during the course of this evaluation work.

REFERENCES

1. **Hargave, R.V.,** Venkateswaran, D., Chatterjee, A.K., and Rangnekar, B.S., "Assessment of process effects on clinker microstructure through its Quantification" Proc. Of the 5th International conference on Cement Microscopy, 1983 Nashville USA, pp. 99 - 120.
2. **Hargave, R.V.,** Venkateswaran, D., Deshmukh, V.V., and Chatterjee, A.K., "Quantification on varying effects of a set of clinker microstructural parameters on cement strength at various ages." (March1985) Proceedings of The 7th International Conference On Cement Micrroscopy Ft Worth Texas,USA, pp 407 - 418.
3. **Venkateswaran, D.,** and Gore, V.K., "Application of microstructural parameters to the grindability prediction of Industrial clinkers Proc. of 13th International Conference on Cement Microscopy". April 8-11 1991. Tampa. Florida pp. 60 - 70.
4. **Khadilkar, S.A.**, Krishnan, N.A., Ghosh, D., Page C.H.,Chatterjee,A.K.,"Kiln dust characteristics from High Ash coal fired kilns of Different processes : VDZ KONGRESS 1993, Process Technology of Cement Manufacturing, Bauverlog GMBH WIESBADEN UND BERLIN pp. 561 - 569.

EFFECT OF COARSE QUARTZ AND LIMESTONE GRAINS ON THE PROPERTIES OF RAW MEAL, CLINKER AND CEMENT

László SAS,
CEMKUT Kft - Cement Research & Development Ltd.
Budapest, HUNGARY

ABSTRACT
In the course of laboratory and plant experiments and starting from different raw materials the effect of coarse (45, 80, 150, 300 μm) quartz and limestone grains on the burnability of raw meal, on the textures of clinkers and on the strength of cements was investigated. It was stated that the quality deteriorating effect of coarse quartz grains is much stringer than that of the limestone grains. The presence of coarse quartz grains deteriorates directly the burnability of raw meal and the texture of clinkers, and indirectly the strength of cements.

Key-words: Burnability of raw mixes, Clinker, Texture, Strength, Limestone, Quartz

INTRODUCTION
The research aimed at the investigation of the relationships between grinding fineness, grain size distribution, lime saturation, reactivity and burnability of raw meal produced from raw materials of different origin and the clinker microstucture with special regard to the effect of quartz and limestone grains of supercritical size.

LABORATORY EXPERIMENTS
The chemical, mineral and microstructural peculiarities of two raw materials deriving from two cement factories (limestone, clay) were studied since the differences among these peculiarities may affect the features of raw meal produced from them (grain size distribution, reactivity etc.). Raw meals of different lime saturation and grinding fineness were produced from these raw materials and the features of burnability of the raw meals were studied. Subsequently, the effect of raw material particles of supercritical size (quartz > 45 μm; limestone > 150 μm) on the burnability of raw meals and on the clinker microstucture was investigated. Limestones and clays deriving from two different cement factories were marked by I. and II.

Investigation of the raw materials
The chemical composition of limestones, clays and of the auxiliarily used pyrite cinder was analyzed (Table 1), the petrographic characteristics of limestones were studied under optical microscope in thin sections (Figs. 1 and 2), while the mineral composition of clays was studied by X-ray diffraction (Table 2).

Table 1.
Chemical composition of limestone, clay and pyrite cinder

Components, %	Limestone I	Limestone II	Clay I	Clay II	Pyrite cinder
Ignition loss	43.05	41.36	10.27	9.65	2.08
SiO_2	1.48	5.62	58.17	62.27	3.14
Al_2O_3	0.61	1.16	13.01	12.34	0.76
Fe_2O_3	0.28	0.46	5.03	4.60	84.76
CaO	54.36	50.71	6.69	5.07	7.19

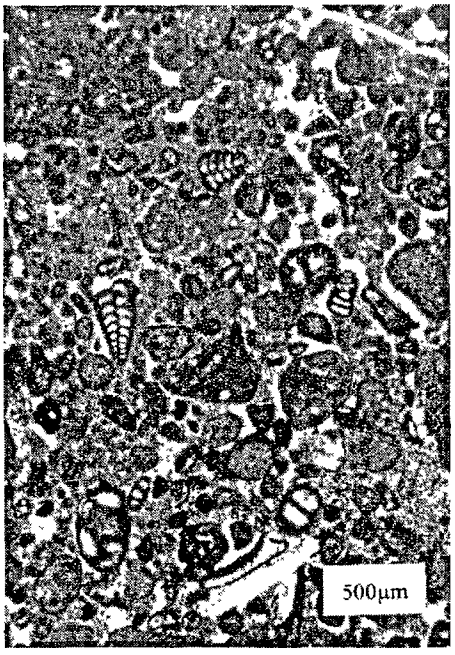

Fig.1
Texture of the limestone I

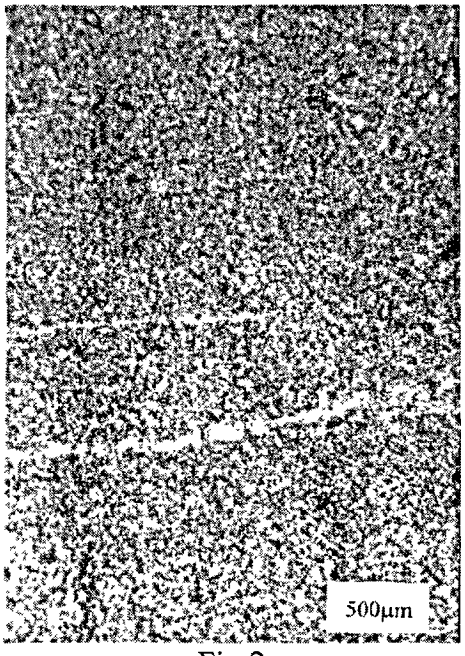

Fig.2
Texture of the limestone II

Table 2.
Mineral composition of the clays

Component, %	Clay I	Clay II
quartz	33	38
calcite	9	10
dolomite	6	2
feldspar	8	6
illite	14	12
montmorillonite	5	8
kaolinite	7	11
amorphous	18	13

It can be stated that limestones are pure and of high calcite content. Sample I is a compact Lower Cretaceous limestone containing intra- and bioclasts while Sample II is a compact Triassic limestone of recrystallized texture. As a result of mechanical effects the limestone I disintegrates to greater grains (~ 0.2 mm). As regards the chemical and mineral compositions of clays, these are rather similar, the quartz content of sample II is somewhat higher.

Effect of grinding fineness and lime saturation on the burnability of raw meals

Raw meal mixtures of different lime saturation (LSF = 90, 94, 98) but of the same silicate modulus (SM = 2.45) were produced and ground in laboratory mills to different specific surface (Blaine number: 4000, 5000, 6000 cm^2/g), respectively. The grain size distribution and burnability features of these raw meals were studied. To characterize the grain size distribution the parameters of the RRSB equation were used ($\bar{x}$ - fineness number; n - factor of uniformity). As an example, in Table 3. the results of raw meals of LSF = 94 and Bl = 5000 cm^2/g are shown, the values being characteristic of other samples, as well. Results of burnability analyses are shown in Fig.3.

Table 3.
Grinding fineness and grain size distribution of raw meal milling products
(in case of LSF = 94, Bl = 5000 cm2/g)

Raw materials	Moduli	Parameters of the RRSB equation		Specific surface
		n factor of uniformity (-)	$\bar{x}$ fineness number (μm)	(cm^2/g)
I.	LSF=94 SM = 2.45 AM = 1.40	0.7068	26	5000
II.	LSF=94 SM = 2.45 AM = 0.97	0.8250	21	5000

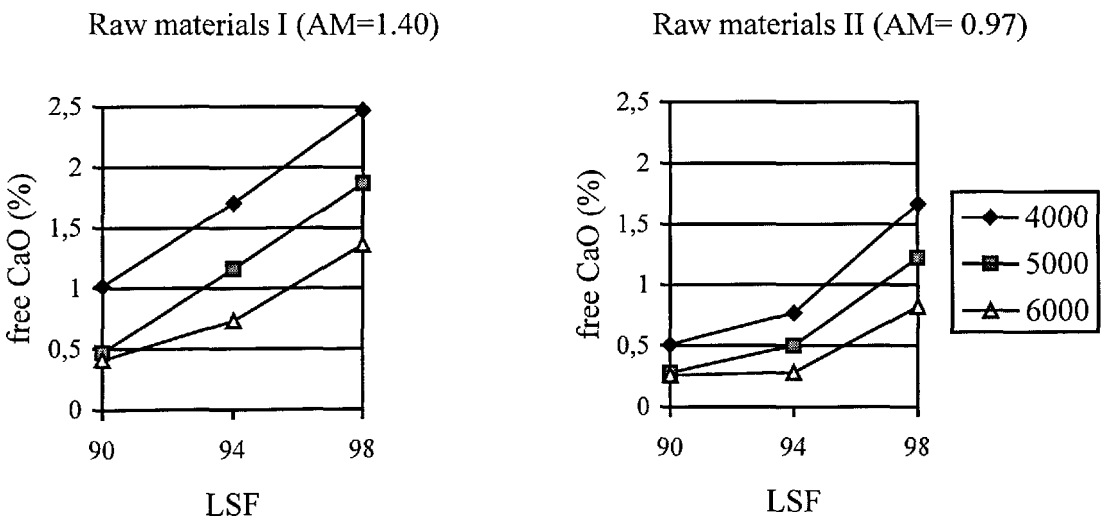

Fig.3.
Results of burnability tests of raw meals produced from the raw materials I and II
(Blaine number: 4000, 5000, 6000 cm^2/g)

It can be stated that in case of limestone II of recrystallized texture a raw meal milling product of "narrower" grain size distribution (n) and finer state ($\bar{x}$) can be produced in case of raw meal of all sorts of grinding fineness.
Further, it can be stated that those raw meals produced from raw materials II are of more favourable burnability features. The free CaO content of raw meals I increases nearly linearly with lime saturation, while in case of raw meals II this hardly changes up to LSF = 94, then it begins suddenly to increase.

Effect of quartz grains of supercritical size (> 45 μm)

Having used the raw materials I and II mixtures were produced for experiments from which when adding 1 % quartz the raw meals of lime saturation and silicate modulus studied above can be produced. Mixtures were ground to 5000 cm^2/g specific surface and 1 % quartz was added.

Quartz fractions were produced by grinding and fractionation of "normal sand". Quartz fractions of four different grain size were added: ~ 45 μm; ~ 80 μm;~150 μm and ~300 μm. The effect of 1 % quartz fractions on the burnability can be seen in Fig.4.

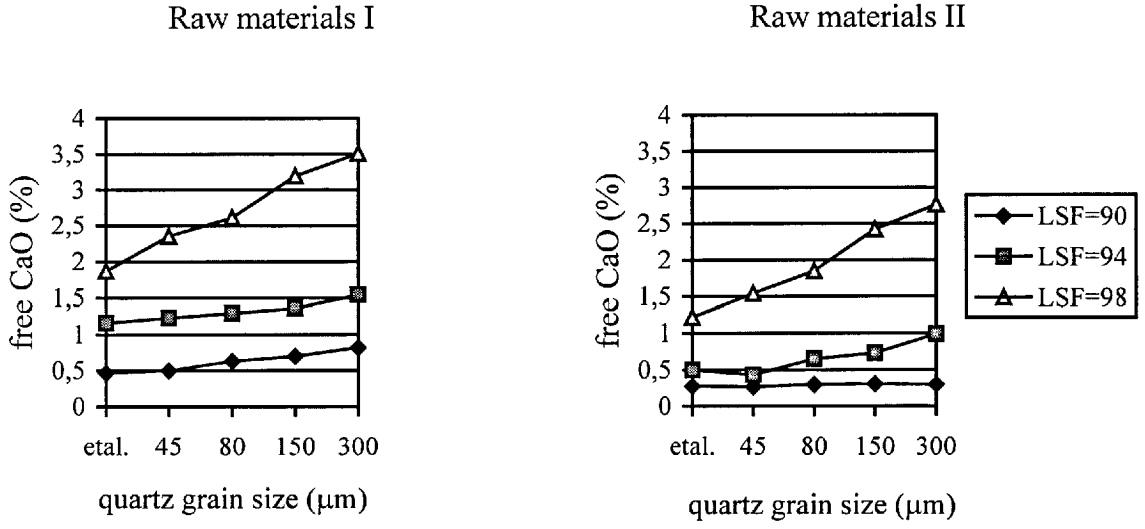

Fig.4.
Effect of quartz grains of different size on the burnability of raw meal

It can be stated that the quality deteriorating effect of quartz grains of supercritical size increases parallel with the increase of lime saturation, in case of raw meals of high lime saturation the presence of coarse quartz can be considered to be harmful. Quartz grains of different size have had nearly the same effect in case of different raw materials.

Investigations under optical microscope (Champbell, 1986) and literature data (Dorn, 1978, 1980) proved that quartz grains of 45 μm grain size do not result in observable changes. Grains greater than 45 μm generate nearly the same changes in case of different raw materials. Parallel with the the increase of quartz grain size the dimension of the developing belite clusters also increases.Quartz grains of 80 μm generate 150-250 μm belite clusters, those of 150 μm 200-300 μm ones while from the 300 μm quartz grain a belite cluster of 400-900 μm is generated. Parallel with the increase of belite clusters the appearance of "nests" becomes characteristic, i.e. in the centre of the belite cluster a hole is developed that was the locality of the reacted and absorbed quartz grain. Belite clusters are often interconnected forming continuous belite regions. Belite clusters can be considered as phases poor in lime since the CaO needed to the formation of alite cannot enter the belite clusters and react within them. Thus, in the phases abundant in lime the quantity of free CaO increases.

In Figs. 5 and 6 belite clusters of ~600 μm developed from quartz grains of 300 μm can be seen. In Fig.5 an unreacted quartz is seen in the centre of the belite cluster that is surrounded by closely pressed belite crystals of ~100 μm (there is practically no "intermediate phases"). In Fig.6 three types of belite clusters can be observed: 1 - belite "nest" in the centre of which a pore is seen; 2 - belite cluster with unreacted quartz in the middle; 3 - belite cluster consisting of closely pressed crystals.

It can be stated that a belite cluster is formed from the quartz grain of supercritical size the diameter of which is twice and half times greater than that of the quartz grain (>45 μm) and this means a volume of increase of 8-15 times.



Fig. 5.
Belite cluster forned from quartz particle of 300 μm (LSF=94)



Fig. 6.
Belite clusters of different type from quartz particles of 300 μm (LSF=94)

Effect of calcite grains of supercritical size(>150 μm)

The experiment was performed similarly as described above the only difference was that 1 % calcite of different size was added to the suitably composed and ground raw meals. The different calcite fractions were produced from the limestone II. The effect of 1 % calcite fractions on the burnability can be seen in Fig.7.

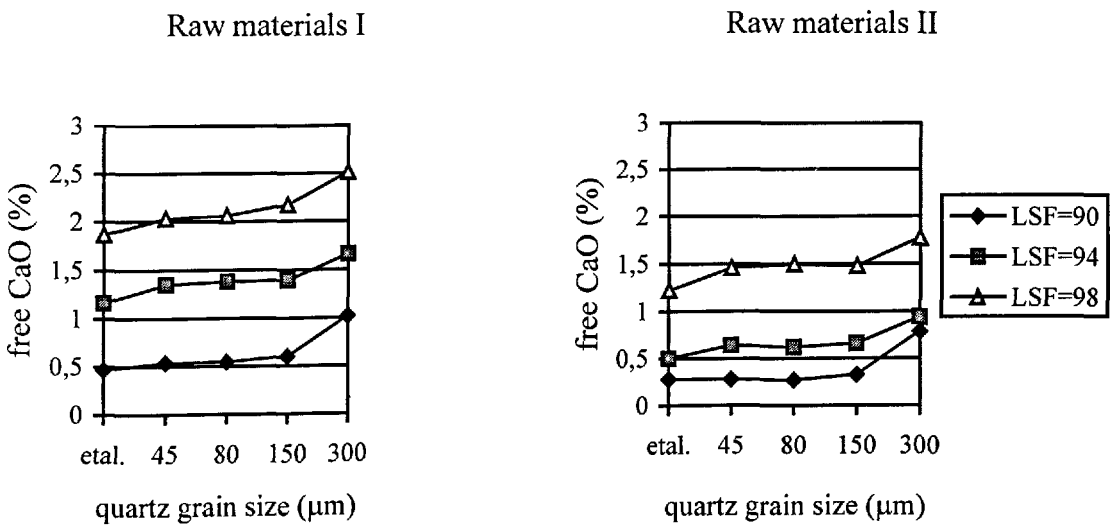

Fig. 7
Effect of calcite grains of different size on the burnability features

It can be stated that calcite fractions of 45, 80, 150 μm size do not affect remarkably the burnability features. The calcite fraction of 300 μm size slightly deteriorated the burnability in all cases.
The effect on burnability and clinker microstructure is rather similar in case of different raw materials.
Investigations under the optical microscope proved the grains of 45 and 80 μm size do not alter the textural peculiarities. When adding limestone grains of 150 and 300 μm size the quantity of free CaO increases parallel with the increase of saturation factor. In samples of low lime saturation the free CaO can be observed as free CaO clusters of 150 and 300 μm size developed from the coarse limestone. Parallel with the increase of lime saturation the quantities of "racemose" and individual free CaO clusters are also increasing, in addition to that of the "clusters". Consequently, free CaO clusters of nearly the same size develop from the limestone grains of supercritical size (Fig. 8).

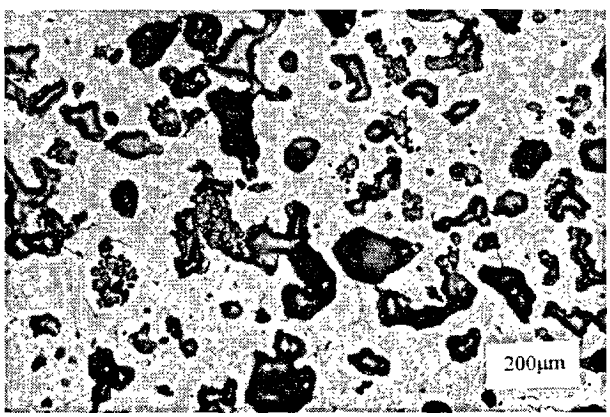

Fig.8
Free CaO cluster and "racemose" free CaO formed from limestone grain of 150 μm (LSF=98)

PLANT EXPERIMENTS

In the course of experiment furnace meal of different silicate modulus but of the same lime saturation was produced under plant conditions (DCM Ltd/Vác/Hungary - 2700 t clinker/day), from which clinker was burnt and cement was ground. The peculiarities of furnace meals, clinkers and cements were studied.

Furnace meals

The chemical composition, grinding fineness, the quartz content of coarse fractions as well as the burnability features were studied. Results are seen in Table 4. The Zeisel grindability of clinkers burnt from furnace meals can be seen in Fig.8.
Cement was ground from clinkers under plant conditions, in the same cement mill, under the same wind separation conditions and of the same specific surface (Blaine number: 3200 cm^2/g). Results of compression strength tests of these cements are seen in Fig.9.

Table 4.
Main characteristics of furnace meals

		Sample sign		
		L I	L II	L III
Moduli	AM	1.55	1.63	1.73
	SM	2.51	2.20	2.08
	LSF	100.6	100.6	100.3
Grinding fineness Blaine number	cm^2/g	5300	5400	5000
Screen residue > 200 μm	%	1.2	0.8	0.8
Screen residue > 90 μm	%	22.0	18.3	18.7
Quartz content				
in fraction of > 200 μm	%	16.0	18.0	15.0
in fraction of > 90 μm	%	15.0	14.0	12.5
Quartz grains of > 90 μm in the raw meal	%	3.40	2.70	2.46
Burnability test				
free CaO	%	5.28	4.38	3.89

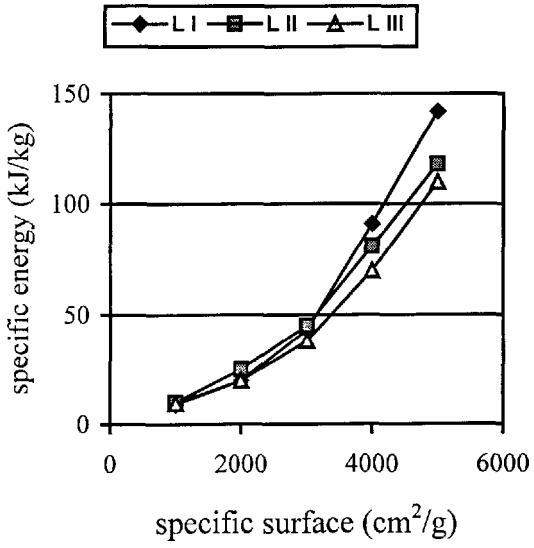

Fig.9
Grindability test by the Zeisel method

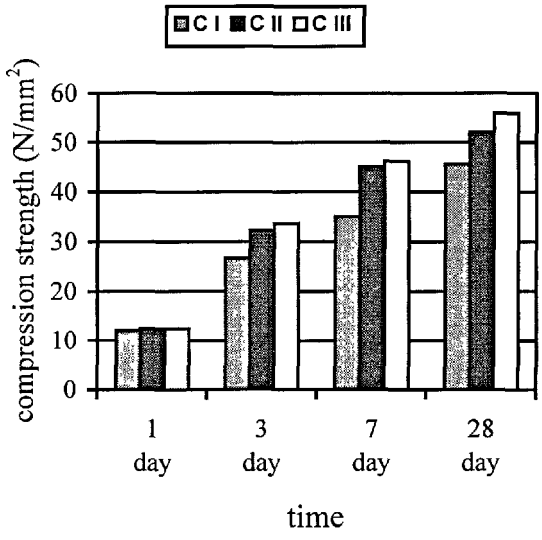

Fig.10
Results of compression strength tests of cements

It can be stated that the quartz content unfavourably affects directly the burnability of furnace meals and the grindability of clinkers, while indirectly the strength of the cements.
In the course of clinker burning the degree of completion of clinker formation processes is controlled by the analysis of free CaO content. In the course of burning furnace meals with large-sized and high quantity quartz this may be misleading. The lime saturation of belite clusters forming from the quartz crystals proceeds slowly and in a complicated way. When the quartz quantity increases in the furnace meal and it is desired to keep the free CaO contents prescribed to the furnace meal of low quartz content, the furnace meal has to be considerably overburnt. This overburning deteriorates the heat consumption of burning and reduces the

lifetime of fire resistant material on the one hand, and reduces the hydraulic activity of alite and belite, increases the danger of swelling due to delayed hydratation of CaO, on the other.
Since among the cement industrial raw materials quartz bears the highest hardness, quartz is responsible for the wearing phenomen occurring in the raw material grinding and transporting equipments.

STATEMENTS AND CONCLUSIONS

Based on the investigations performed the following can be stated:

- Limestones of nearly the same chemical and mineral composition considerably differ from each other and this affects the grain size of raw meals produced from, them and in this way affects their burnability features;
- Parallel with the increasing specific surface and decreasing lime saturation burnability becomes easier, the measure of these changes, however, depends on the starting raw materials;
- Quartz grains of supercritical size unambiguously deteriorate the burnability of raw meals, the grade of which is increased when grain size is growing. In case of high lime saturation the presence of large-sized quartz is harmful;
- Belite clusters of different types and of a diameter twice as large as that of the quartz grains are formed from the coarse quartz grains that form belite regions. Parallel with this phenomenon the quantity of free CaO that cannot enter the belite clusters, also increases;
- Limestone grains of supercritical size less deteriorate the burnability of raw meal than the quartz grains do. Free CaO cluster of nearly the same size is formed from the coarse limestone.

In case of all studied raw materials the addition of 1 % quartz and limestone particles of different size resulted in changes of nearly the same measure and character in the burnability and in the microstructure.
Plant experiments proved that the increase of quartz content of supercritical size in furnace meals unambiguously reduces the burnability of raw meals, the grindability of clinkers and the strength of cements.

REFERENCES

Champbell,D.H.,"Microscopical Examination and Interpretation of Portland Cement Clinker"Skokie,Illinois,60077-4321, 1986
Dorn,J.,"Microscopic Methods for Burnability Improvement",Cement and Concrete Research,Vol.8, pp.635-646, 1978
Dorn,J.,"Effect of Belite Clusters on Clinker Grindability",Second Annual Conference on Cement & Clinker Microscopy,Dallas,Texas,1980

ACKNOWLEDGEMENT: Author is highly indebted to the managers and workers of the DCM Ltd/Vác/Hungary for their professional work and aid during plant experiments.

Key-words: Quartz, Limestone, Burnability of raw mixes, Microstructure, Strength development

EFFECT OF ALKALIS AND SO_3 ON TRICALCIUM SILICATE FORMATION AND MICROSTRUCTURE

Hai Moon CHEONG, Ssangyong Cement Industrial Co. Ltd., Taejon, KOREA
Sang Heul CHOI, Hanyang University, Seoul, KOREA
Ki Sung HAN, Inha University, Inchon, KOREA

ABSTRACT K_2SO_4 was immiscible with oxide clinker melt and could not affect C_3S formation as well as microstructure. The optimal K_2O and SO_3 content was 1.43 of SO_3/K_2O mole ratio. Whereas C_3S crystals with exceeding K_2O were grown round and in a much larger size. C_3S was hindered severely by Na_2SO_4. Since C_2S was stabilized by Na^+ and SO_4^{2-}, it could not react to give C_3S formation. C_3S crystal with Na_2SO_4 had very irregular surfaces and much inclusions.

Key-words : alkali, SO_3, C_3S, clinker formation, microstructure

INTRODUCTION

There have been growing interest in the minor components of clinker because of changes in burning technology, the concern for energy conservation, and strict environmental regulations Minor components derived from raw materials, fuel, refractories and other plant materials can affect not only the reactions of clinker formation but also the hydraulic properties of the resulting cements(Taylor, 1990). Until now, many researchers have been studying the effects of minor components (Moranville-Regourd et al, 1992 ; Moir et al , 1992).

Alkali-and-SO_3-bearing compounds can be found in whole processes of cement manufacturing, preheater, kiln lining, kiln dust, flue gas and storage silo as well as in clinker(Jawed et al, 1977 ; Glasser, 1980). Alkali elements such as K and Na lead to harmful effects on clinkering and hydration properties such as higher clinkering temperature, rapid setting and the strength decrease at later ages. If SO_3 could coexist, alkalis used to react with SO_3 preferentially to form alkali sulfate. SO_3 has been considered as an effective mineralizer which makes the clinker melt at lower temperature, decreases the viscosity and surface tension of the melt and increases the mobility of the ions(Butt, 1974 ; Bucchi, 1980). However, SO_3 has harmful effects on the formation of C_3S at higher SO_3 concentration(Strunge et al, 1985, 1986 and 1990 ; Maki, 1986). The authors reported that the critical amount of SO_3 in C_3S formation was 1.4 wt.% in absence of alkalis(Cheong et al, 1993). Up to the present time, many results for alkalis and SO_3 on the clinker formation and cement hydration do not coincide and especially the relationship between alkali and SO_3 has not become clear yet In this study, the effect of alkali and SO_3 on C_3S formation and microstructure was investigated, using K_2SO_4, Na_2SO_4, K_2CO_3, Na_2CO_3 and $(NH_4)_2SO_4$.

EXPERIMENTAL PROCEDURE

Materials

It was well known that the mechanism of C_3S formation was diffusion - precipitation in which C_2S and CaO were dissolved into the clinker melt(Kondo et al, 1968). In this study, C_3S formation from the reaction of C_2S and CaO in presence of clinker melt was chosen. Synthesis of C_2S and cliker melt were prepared prior to the addition of alkalis and SO_3. C_2S was synthesized by firing the mixture of 2 moles of $CaCO_3$ and 1 mole

of SiO_2 at 1400 ℃ for 3 hours. The clinker melt was prepared by firing the mixture(CaO 54.8, Al_2O_3 22.7, SiO_2 6.0 and Fe_2O_3 16.5 wt%) at 1450 ℃ for 3 hours. The composition and structure of this clinker melt is similar to the interstitial phase of the commercial ordinary Portland cement. As alkalis and SO_3 sources, reagent grades of K_2SO_4, Na_2SO_4, K_2CO_3, Na_2CO_3 and $(NH_4)_2SO_4$ were used. $(NH_4)_2SO_4$ is decomposed to ammonia and SO_3 gas in firing process, so it is regarded as gaseous SO_3.

Synthesis of the clinkers with alkali and SO_3

For the batch mixtures of C_3S, molar ratio of C_2S and $CaCO_3$ was 1 : 1, and 25 wt.% of crushed clinker melt was added. And various alkalis and SO_3 sources were mixed. These batch mixtures were calcined at 1000 ℃ for 1 hour and sintered at 1450 ℃ for 30 minutes, and then cooled rapidly in ambient air.

Characterization of the clinkers

For the characterization of the resulting clinkers, chemical analysis, quantitative X-ray diffractometry, optical microscopy and SEM/EDS were carried out.

RESULTS AND DISCUSSION

Effect of K_2SO_4 and Na_2SO_4 on C_3S formation.

First, effect of K_2SO_4 and Na_2SO_4 on C_3S formation was studied, because alkalis reacted preferentially with SO_3 to form alkali sulfate. The desired content was varied to 6 wt%(SO_3 base). Fig. 1 and 2 are the results of free lime and C_3S formation content of the clinkers sintered at 1450 ℃ for 30 minutes with the various amount of K_2SO_4 and Na_2SO_4. When Na_2SO_4 was added by only 1 wt.%, free lime content increased remarkably. However increasing K_2SO_4 content did not make free lime content increase. With increasing free lime, C_3S content decreases. In case of K_2SO_4, C_3S formation was almost constant. Results of the determination of clinker products by quantitative XRD showed that C_3S was the major phase when free lime was small in quantity.

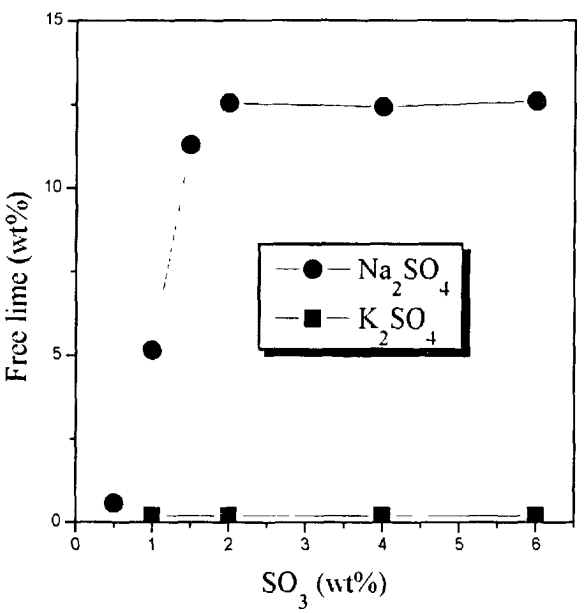

Fig. 1 Free lime content of the clinkers with various dosages of K_2SO_4 and Na_2SO_4

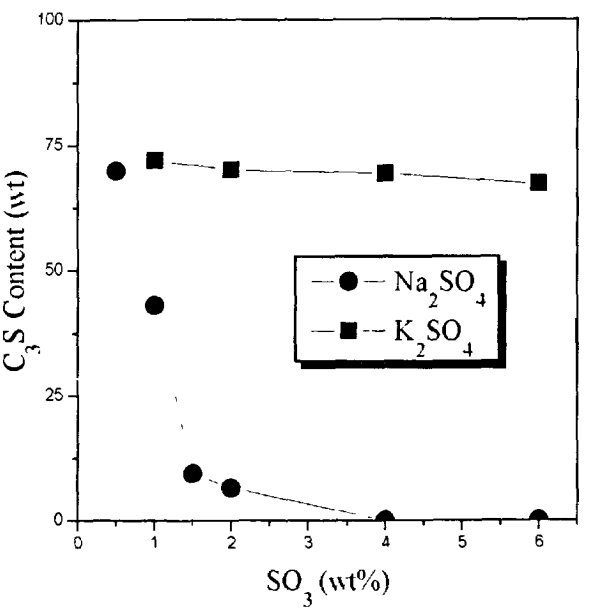

Fig 2 C_3S content of the clinkers with various dosages of $K_2SO_4$and Na_2SO_4.

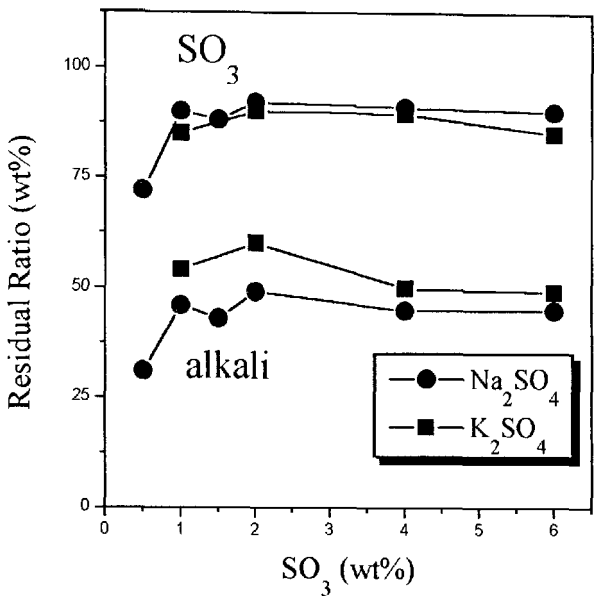

Fig. 3 Alkalis and SO_3 content of the clinkers with various amounts of K_2SO_4 and and Na_2SO_4.

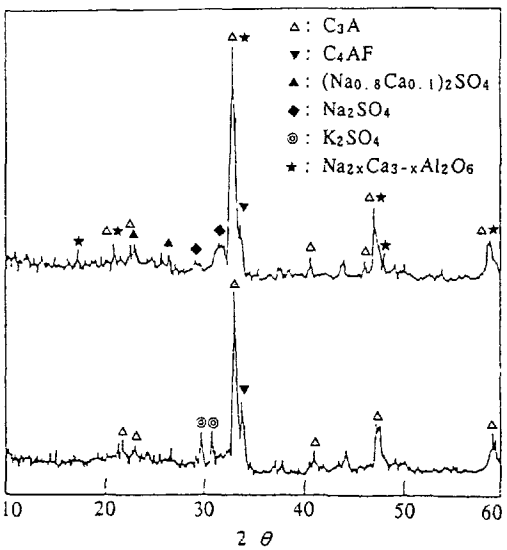

Fig. 4 XRD patterns of the residue after salicylic-methanol. solution method.

However with larger amount of free lime, C_3S phase diminished and C_2S and CaO became major phases. In Na_2SO_4 addition, it was considered that C_2S and unbounded CaO did not react to form C_3S.

Fig. 3 indicates alkali and SO_3 content of the clinkers. 70 - 95 percent of SO_3 and 40 - 60 percent of alkalis resided. Potassium resided in the clinker more than sodium.

In order to check on alkali and SO_3-containing compounds, the clinkers were treated by salicylic-methanol method(Gutteridge, 1979), and the residue characterized by XRD(Fig. 4). While Na_2SO_4 addition resulted in compounds such as $(Na_{0.8}Ca_{0.1})_2SO_4$ and NC_8A_3, K_2SO_4 did not react with other components.

Fig. 5 shows the distribution of alkalis and SO_3 in the clinkers. More K, Na and S were detected in interstitial phase than in calcium silicate. Especially a large amount of Na and S were also incorporated in C_2S crystal. It was considered that $2Na^+$ ions were substituted for Ca^{2+} and $2SO_4^{2-}$ for SiO_4^{4-} (Ghose, 1980).

In case of Na_2SO_4, it was found that amount of C_3S decreased remarkably. K_2SO_4 did not hinder C_3S formation. For examination into this phenomena, the process of clinker formation during burning was investigated. The sample with 6.0 wt.% of Na_2SO_4 was heated up to 1450 ℃, and then analyzed at each temperature from 1000 ℃ to 1450 ℃. The sample with 6.0 wt.% of K_2SO_4 also was analyzed for the comparison with Na_2SO_4, although formation of C_3S was not prevented at high concentration. Fig. 6 shows XRD patterns of the clinkers with 6wt% of K_2SO_4 and Na_2SO_4 sintered at various temperature. In case of Na_2SO_4, C_2S and unreacted CaO were present at 1450 ℃, so C_3S formation did not occur. On the other hand, K_2SO_4 did not form any intermediate products, and C_3S formation was not hindered .

Fig. 7 indicates SEM/EDS result of the clinker with 6 wt.% of Na_2SO_4 at 1350 ℃. A large amount of Na and S were also incorporated in C_2S crystals.

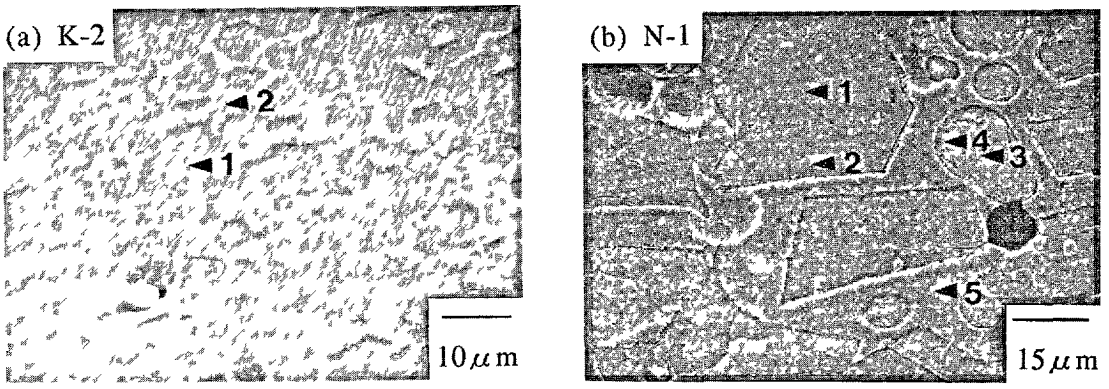

	Sample	Point	CaO	SiO_2	Al_2O_3	Fe_2O_3	SO_3	K_2O	Na_2O
(a)	K_2SO_4	1 (C_3S)	71 45	22 14	1 45	2 19	1 64	1 14	
	2wt%	2 (Interstitial)	54 64	4 60	23 25	14 99	1 70	0 84	
		1 (C_3S)	67 75	21 50	5 30	3 87	0 46		1 11
		2 (C_3S)	72 20	22 67	2 16	1 38	0 55		1 03
(b)	Na_2SO_4	3 (C_2S)	64 35	25 86	3 25	2 21	2 13		2 20
	1wt%	4 (C_2S)	63 42	25 94	3 75	2 42	2 76		1 72
		5 (Interstitial)	51 89	3 99	24 44	16 76	0 57		2 34

Fig 5 SEM micrographs and EDS analysis of the clinkers with K_2SO_4 and Na_2SO_4

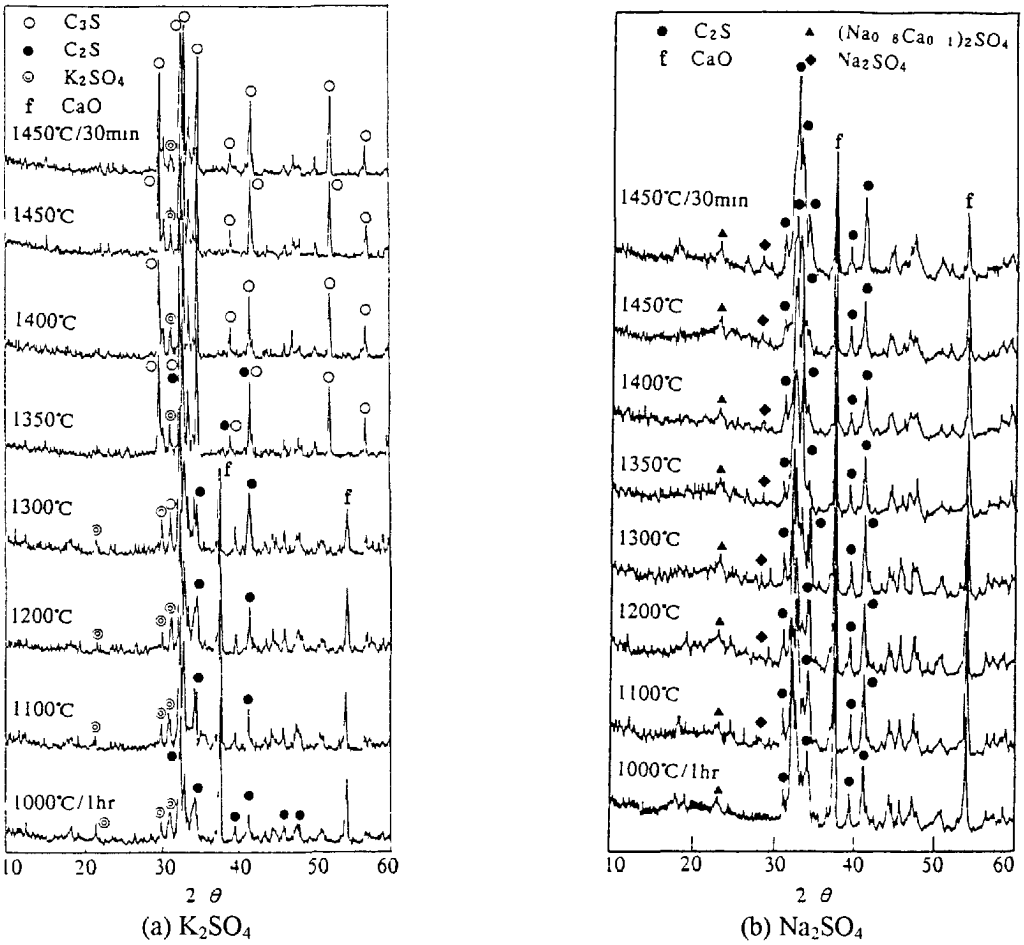

Fig 6 XRD patterns of the clinkers with 6wt% (a) K_2SO_4 and (b) Na_2SO_4 sintered at various temperature

It was considered that C_2S stabilized by Na^+ and SO_4^{2-} could not react to form C_3S. As mentioned above, K_2SO_4 appeared to be immiscible with other components, so it could not influence the dissolution of C_2S and CaO into clinker melt.

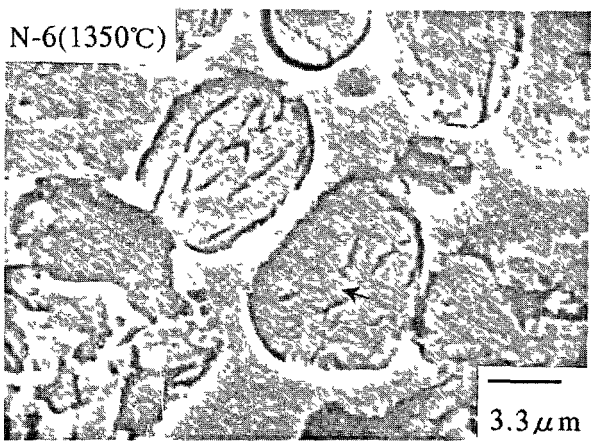

CaO	56.38
SiO_2	26.60
Al_2O_3	4.89
Fe_2O_3	5.80
SO_3	5.80
Na_2O	3.77

Fig 7 SEM micrograph and EDS analysis of the clinker with 6wt% Na_2SO_4 sintered at 1350 ℃

Relationship between alkali and SO_3 for C_3S formation

Effect and optimal content of alkali and SO_3 were investigated using K_2CO_3, Na_2CO_3 and $(NH_4)_2SO_4$ as alkali s and SO_3 sources. $(NH_4)_2SO_4$ which was decomposed into ammonia and SO_3 gas could be regarded as gaseous SO_3 condition. The clinkers were prepared by sintering at 1450 ℃ for 30 minutes. Alkalis and SO_3 content were varied upto 6 wt% respectively.

Fig. 8 illustrates the response surface plot for the free lime content of the clinkers. The optimal K_2O and SO_3 content was 1.43 of SO_3/K_2O mole ratio. Exceeding K_2O and SO_3 led to abrupt increase of free lime. However only 1 wt% of Na_2O and SO_3 promoted C_3S formation. Exceeding Na_2O and SO_3 hindered C_3S formation strongly. Exceeding alkalis had more negative effect on C_3S formation than exceeding SO_3. When SO_3/Na_2O was also 1.43, a little C_3S was formed. A small amount of Na_2SO_4 was formed in this mole ratio and these phases were immiscible with clinker melt, thus C_3S crystals were formed locally. Although K and Na were the same alkali group, their influences on C_3S formation revealed to be very different. It was considered that the degree of sulfatization for K_2O was much higher than in case of Na_2O.

Fig. 9 and 10 shows the optical micrographs of the clinkers. C_3S crystals with 1.43 of SO_3/K_2O mole ratio were never changed in size and morphology(Fig. 9(c)). C_3S crystals with exceeding K_2O were grown round and in a much larger size(Fig. 9(b)), whereas C_3S crystals with exceeding Na_2O had very irregular and rough surfaces and contained more inclusions than those grown with K_2O(Fig. 10(a)(b)(c)). However exceeding SO_3 had facet surfaces and also grew largely(Fig. 9(a)). It was the reason why the growth rate of C_3S crystals with exceeding Na_2O was more rapid and unstable. C_2S with alkalis had better developed-lamellae structure than SO_3(Fig. 9(d), Fig. 10(c)(d)). Prismatic C_3A crystals resulted from alkalis substitution were shown(Fig. 9(d)).

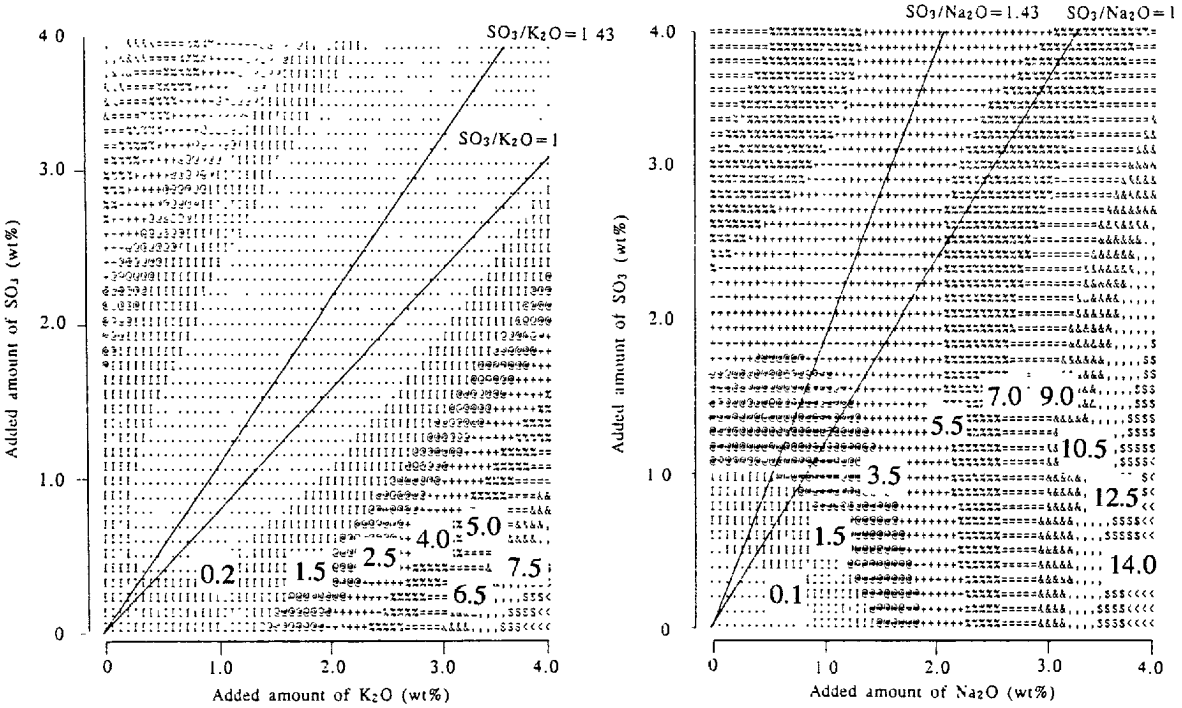

Fig. 8 Response surface plotting of free lime content of the clinkers with various alkali and SO_3 content

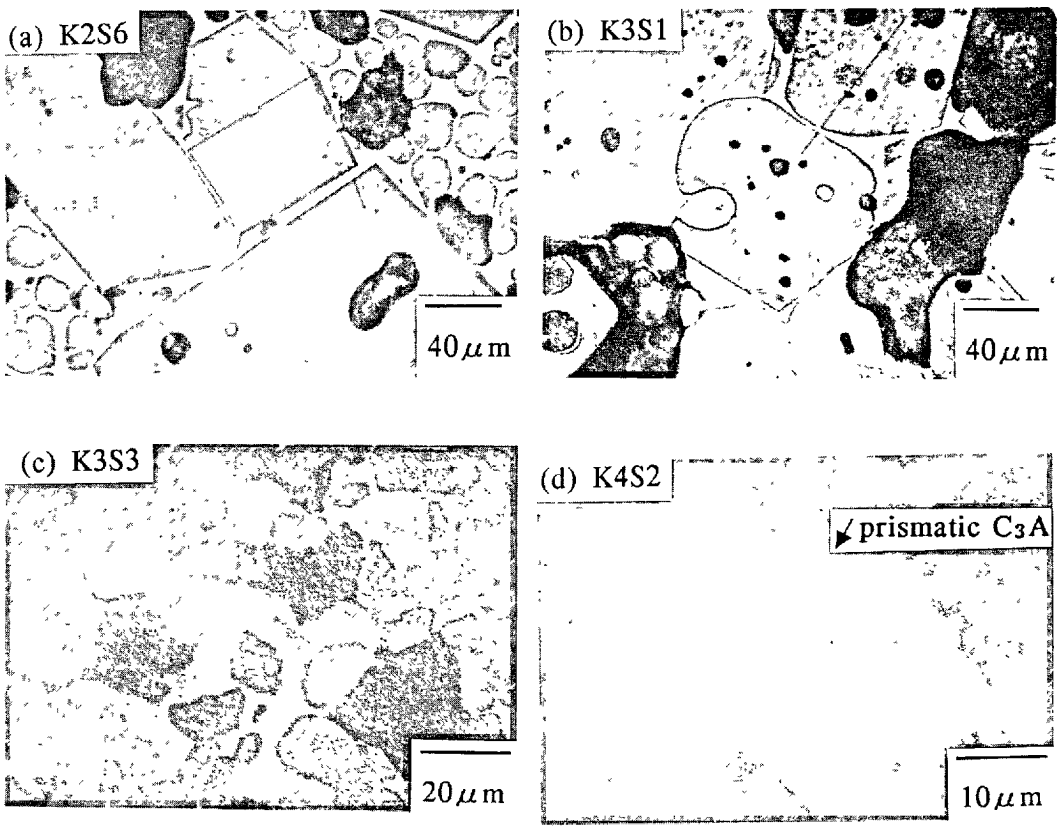

Fig. 9 Optical micrographs of the clinkers with various K_2O and SO_3 content
(K : K_2O S : SO_3 number : Added amount)

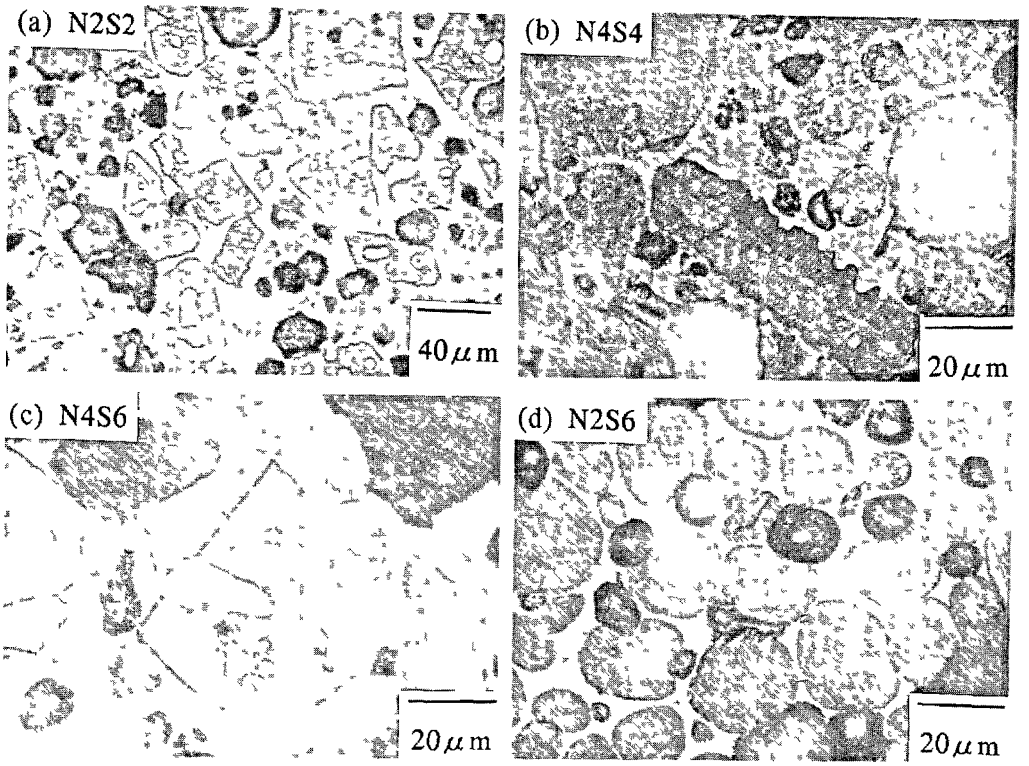

Fig 10 Optical micrographs of the clinkers with various Na_2O and SO_3 content
(N Na_2O S SO_3 number Added amount)

CONCLUSIONS

Effect of alkalis and SO_3 on C_3S formation and microstructure was studied, using K_2SO_4, Na_2SO_4, K_2CO_3, Na_2CO_3 and $(NH_4)_2SO_4$ The conclusions are as follows

1 When Na_2SO_4 was added by only 1 wt %, free lime content was more than 5 wt % However much K_2SO_4 did not make free lime content increase It was considered that C_2S stabilized by Na^+ and SO_4^{2-} could not react to form C_3S On the other hand, K_2SO_4 did not form any other intermediate products

2 The optimal K_2O and SO_3 content was 1 43 of SO_3/K_2O mole ratio Exceeding K_2O and SO_3 led to rapid increase of free lime However only 1 wt% of Na_2O and SO_3 promoted C_3S formation Exceeding Na_2O and SO_3 hindered C_3S formation strongly

3 C_3S crystals with 1 43 of SO_3/K_2O mole ratio were never changed in size and morphology C_3S crystals formed with exceeding K_2O were grown round and in a much larger size, whereas C_3S crystals with exceeding Na_2O had very irregular and rough surfaces and contained more inclusions than those grown with K_2O However exceeding SO_3 had facet surfaces and also grew largely It was the reason why the growth rate of C_3S crystals with exceeding Na_2O was more rapid and unstable

REFERENCES

Bucchi,R., "Influence of the Nature and Preparation of Raw Materials on the Reactivity of Raw Mix," 7th Inter.Cong.Chem.Cem , Paris, France, 1980, Vol.I, Sub-Theme 1-1.

Butt,Y.M. and Timashev,V.V., "The Mechanism of Clinker Formation Process and Ways of Modification," 6th Inter.Cong.Chem.Cem., Moscow, USSR, 1974, Principal Paper-3.

Cheong,H.M., Choi,S.H. Han,K.S. and Jaung, J.D., "Effect of SO_3 on the Reaction of C_3S Formation," 9th Inter.Cong.Chem.Cem., New Delhi, India, 1992, Vol.2, pp.335-341.

Ghose,A. and Barnes,P., "Distribution of Minor Elements in Cement Clinker-Macroscopic and Microscopic Variation," Wor. Cem. Tech., Nov, 1980, pp.441-443.

Glasser,F.P., "The Sulfur Cycle in Cement Kilns," Review of the 34th General Meeting-Technical Session Held in Tokyo, The Cement Association of Japan, 1980, pp.20-24.

Gutteridge,W.A., "On the Dissolution of the Interstitial Phases in Portland Cement," Cem. Concr. Res., 9, 1979, pp 319-324.

Jawed,I. and Scalny,J., "Alkalis in Cement : A Review I, Forms of Alkalies and Their Effect on Clinker Formation," Cem. Concr. Res., 7, 1977, pp.719-730.

Kondo.R. and Choi,S.H., "Mechanisms and Kinetics of Portland Cement Clinker Formation for an Example of the Solid State Reaction in the Presence of Liquid Phase," 5th Inter.Symp.Chem.Cem , Tokyo, 1968, Vol.1, pp.163-171.

Maki,I., "Relationship of Processing Parameters to Clinker Properties ; Influence of Minor Components," 8th Inter.Cong.Chem.Cem., Rio de Janeiro, Brazil, 1986, Vol.1, Sub -Theme 1-2.

Moir,K.M. and Glasser,F P., "Mineralizers, Modifiers and Activators in the Clinkering Process," 9th Inter.Cong.Chem.Cem., New Delhi, India, 1992, Vol.1, pp.125-152.

Moranville-Regourd, M and Boikova,A.I., "Chemistry, Structure, Properties and Quality of Clinker," 9th Inter.Cong.Chem.Cem., New Delhi, India, 1992, Vol.1, pp.3-45.

Strunge,J. and Knofel,D., "Influence of Alkalis and Sulphur on the Properties of Cement ; Part-I," Zem.Kal.Gip., 38, 1985, pp.150-158 ,"Part-II," ibid., 38, 1985, pp.441-450 ; "Part-III," ibid., 39, 1986, pp.380-386 ;"Part-IV," ibid., 43, 1990, pp.199-208.

Taylor, H.F.W., "Cement Chemistry," Academic Press Limited, 1990, pp.92-95.

TOPIC I.F

Clinker structure and mineralogy

INFLUENCE OF SODIUM AND FLUORINE ON THE STABILITY AND POLYMORPHISM OF ALITE

Ömer ANDAÇ, University of Aberdeen, Scotland.*
Fredrik Paul GLASSER, University of Aberdeen, Scotland.

ABSTRACT Phase relations have been studied in part of the NaF-CaO-SiO_2 system by isothermal annealing at 800°-1300°C followed by examination of quenched charges at ambient using microscopy, X-ray and electron diffraction and wavelength dispersive microprobe. Extensive solid solution occurs between Ca_3SiO_5 and $NaCa_2SiO_4F$. The crystallography and constitution of ordered alite-like phases containing Na and F are described. General theories of the reactivity of activated alite are discussed.

Alite, Mineralised clinker, Phase diagram: Ca_3SiO_5 - $NaCa_2SiO_4F$

INTRODUCTION

The application of fluxes and mineralisers to cement production has been discussed at every preceding International Congress on the Chemistry of Cement. Mineral additives to cement systems may act as fluxes, to assist in the development of a liquid phase and improve its transport properties, or may act as mineralisers, to enhance the stability of a particular phase - normally alite - with respect to others. Some substances act as both flux and mineraliser.

Fluorine is prominent as a fluxing and mineralising additive. It is known to stabilise aluminates, notably the fluorinated form of "$C_{12}A_7$", i.e., $C_{11}A_7 \cdot CaF_2$, but the extent of fluorine substitution in silicates, if any, is less well established. Shame and Glasser (1987) showed that coupled substitution of Al and F for Si and O led to formation of extensive alite-type solid solutions. The lower stability limit of alite, with respect to its disproportionation to mixtures of CaO and Ca_2SiO_4, decreased from ~1250°C for pure alite, to as low as ~1050°C.

Other fluorine-containing silicates are known: notably the phase whose formula is now established as $Ca_{11}Si_4O_{18}F_2$; also, $Ca_5Si_2O_8F_2$. Moreover, Perez-Mendez et al (1984) reported solid solutions based on alite having the type formula $Ca_{6-0.5x}Si_2O_{10-x}F_x$: values of x ranged up to 1.0. However, these phases have melting points well below those normally used in clinkering and are unlikely to persist at normal clinkering temperatures; moreover, they have relatively high fluorine contents. Thus they are unlikely ever to be important constituents of commercial clinkers. Attention has therefore returned to coupled substitutions based on alite and we report on part of the system NaF-CaO-SiO_2.

RESULTS

Experimental

Samples were prepared from analytical reagent grades of $CaCO_3$,CaF_2 and a silica source, either crushed optical-grade quartz, ~0.08 wt % non-volatile with HF, or pre-reacted Ca_3SiO_5 made from $CaCO_3$ and SiO_2. Approximately 32 compositions were prepared on join Ca_3SiO_5 - $NaCa_2SiO_4F$, mostly in the range 0-60 mol % $NaCa_2SiO_4F$. These were annealed in air in electric furnaces controlled to ±2°C for vertical tube quench furnaces or ±10°C for muffle furnaces. Charges were examined primarily by powder X-ray diffraction and backscattered electron microscopy; point analyses used a wavelength dispersive analytical system. In this way, selected

crystals could be analysed directly for both F and O as well as for Ca, Si and Na. Fluorine loss was monitored by weight change, supplemented by wet chemical bulk analysis of representative charges for fluorine using a F-sensitive electrode. Where appropriate, DTA, electron diffraction and high temperature X-ray diffraction were used to provide additional characterisation data.

Data Analysis

Single crystals of $NaCa_2SiO_4F$ were grown from the melt and the crystal structure determined by classical X-ray single crystal analysis. The structure is closely related to that of alite: oxygen not attached to Si in alite is wholly and preferentially replaced by fluorine in $NaCa_2SiO_4F$ (Andaç et al, 1997).

The system Ca_3SiO_5 - $NaCa_2SiO_4F$ is not binary at low temperatures, below which Ca_3SiO_5 decomposes, nor above the solidus where extensive incongruent melting occurs. Nevertheless, the system is binary at some temperatures and a phase diagram, depicted as a binary system, Fig. 1, is helpful to depict the complex relationships amongst the alite-like phases. Data used in its construction are given in a Thesis (Andaç, 1996)

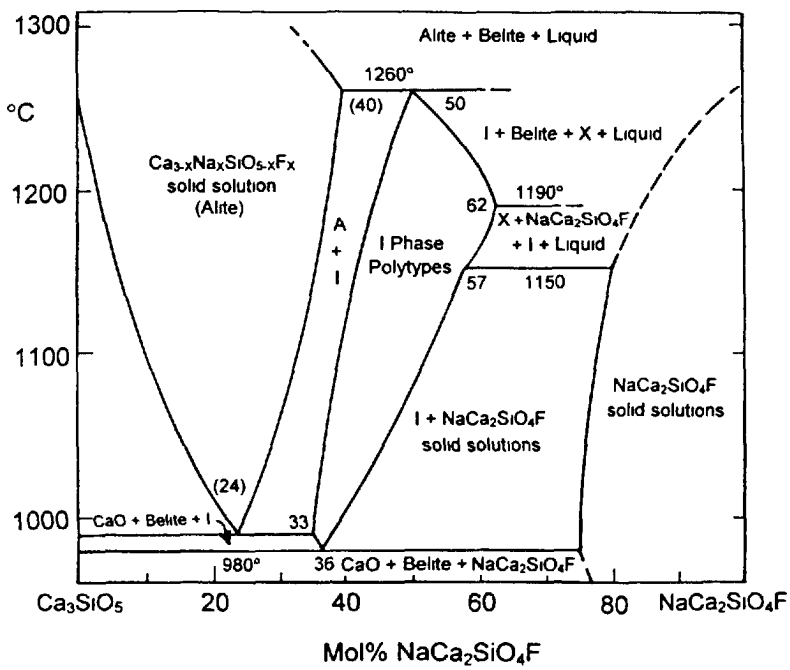

Figure 1. Phase diagram of the Ca_3SiO_3 - $NaCa_2SiO_4F$ system. Detail has been omitted except in those portions which behave as a binary system.

Fig. 1 shows the main features of the phase diagram at temperatures above 850°C. Alite structured solid solutions having the general formula $Na_xCa_{3-x}SiO_4(O_{1-x}F_x)$ extend to a maximum of x = 0.36 at ~1270°C. Perhaps of more interest is the extension of the stability field of homogeneous alite type solid solutions to lower temperatures, reaching a thermal minimum of ~990°C at x ~0.24. Formation and decomposition reactions at the lower limit of stability of Ca_3SiO_5 are extremely sluggish (x = 0), but become more rapid at intermediate x values, in the range 0.05, to 0.15, despite the decrease in temperature. However reaction again becomes

sluggish towards the thermal minimum. Thus reversibility has been demonstrated along part of this curve, but the 990°C limit is based only on the forward reaction, i.e., formation of alite solid solutions from reactants.

The solid solutions obtained at ambient appear by powder X-ray diffraction to be triclinic at x = 0, but monoclinic in the range x = 0.08 to 0.18 and rhombohedral in the range x = 0.27 and 0.36. Nevertheless, the rhombohedral cell could not be indexed commencing with the cell dimensions reported by Jeffrey (1952), despite lack of significant shifts in the positions of symmetry-related reflections. Given the near constancy of ionic radii of the species, Na~Ca and F~O, this near constancy of the main reflections is not surprising. Table 1 shows the apparent unit cell obtained by indexing the reflections on a triclinic cell. There is no doubt from backscattered electron imaging that chemical homogeneity is maintained over the limits cited, but the exact symmetry of the quenched solid solutions is unknown. Table 1 is therefore mainly useful to show how, when indexed on a self consistent basis, unit cell parameters remain essentially unchanged. The high temperature X-ray data were more diffuse than at ~25°C but no difficulty was encountered in indexing 1100°C powder patterns between x = 0 and 0.36 on a rhombohedral cell with $\underline{a}$ ~ 7.15 and $\underline{c}$ ~ 25.57Å. Thus the high-F alites are rhombohedral at ~ 1100°C but, while remaining at least pseudo-rhombohedral at ~ 20°C, have a true symmetry and cell size which remains to be defined.

Table 1. Self-consistent unit cell parameters of $Na_xCa_{3-x}SiO_{5-x}F_x$ solid solutions: italic values are esd's.

X	a(Å)	b(Å)	c(Å)	β(°)	Volume (Å^3)
x=0.04	33.073(0.007)	7.064(0.003)	18.556(0.006)	93.891(0.029)	4325.08 (1.79)
x=0.08	33.096(0.005)	7.061(0.002)	18.578(0.003)	94.050(0.019)	4330.67(1.08)
x=0.18	33.080(0.013)	7.059(0.003)	18.573(0.007	94.023(0.041	4326.98(2.61)
x=0.27	33.038(0.015)	7.063(0.004)	18.565(0.007)	94.035(0.038)	4320.36(2.05)
x=0.36	33.045(0.017)	7.064(0.003)	18.561(0.007)	94.074(0.033)	4321.40(2.15)

Samples quenched in the range 33-62 mol % $NaCa_2SiO_4F$, depending on quench temperature, often appeared homogeneous yet gave a distinctive X-ray powder pattern. Fig. 2 shows tracings from two regions of the diffraction patterns which are generally considered to be diagnostic for alite modifications. As might be expected from its high symmetry, $NaCa_2SiO_4F$ has a relatively simple pattern while the slightly substituted alite, pattern c, exhibits the line splitting characteristic of a low symmetry alite. The pattern b of the phase designated as I, (I = intermediate) has similarities to, but is distinctively different from that of a more highly substituted rhombohedral alite, pattern d.

Moreover, the differences characteristic of the I phase persist to high temperatures as shown by high temperature X-ray powder patterns. Mixtures of two phases, I phase + alite, were frequently encountered in a consistent manner, indicating the existence of a two-phase region. Fig. 3 shows a portion of a pattern obtained at 1100°C. Some evaporation of Na and F occurs in the course of stabilising the temperature and in the time taken to record the pattern, so the initial value of x, from experience, will have decreased from its target value of 0.40 to about 0.36. The association of specific reflections with either alite or I phase allows for thermally-induced shifts in reflection positions.

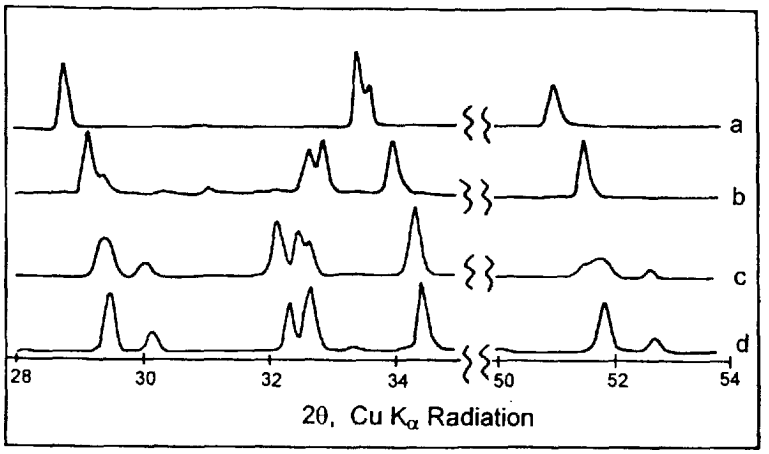

Figure 2. X-ray powder patterns, showing regions diagnostic of alite phases Trace (a) is of $Na_2Ca_2SiO_4F$, trace (b) is of the I phase, at x = 0.42, trace (c) is of a partially-stabilised alite at x = 0.04 and trace (d) is of a pseudo rhombohedral or rhombohedral alite at x = 0.36. All traces were obtained at ~ 20°C.

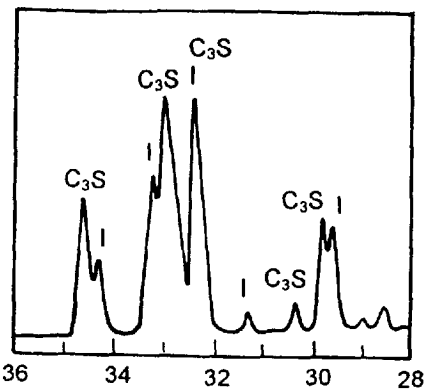

Figure 3. High temperature X-ray powder pattern obtained at 1100°C, CuKα radiation, nominally at x = 0.46, showing the assignment of reflections to a mixture of alite and I phase solid solutions. Slight loss of F during heating occurs, so the effective x value is probably ~ 0.36.

A corresponding larger batch, at x = 0.36, was heated in a muffle furnace at 1070°C. Fluorine loss from the larger batch was negligible. Twenty one crystals were analysed by EMPA; the results are shown as a histogram in Fig. 4. The postulated mechanism of solid solution demands that Na = F, and this condition is well met by all the analytical data. However the results form a bimodal distribution: the left-hand population group is associated with an alite- type solid solution and the right-hand group, with I phase These bimodal distributions were observed in numerous other appropriate temperature-composition experiments and these results from EPMA of compositions which, from X-ray powder diffraction, were believed to lie in the two-phase gap, help to confirm the validity of this conclusion and to define its extent on each isotherm.

Crystallography of the I phase and its relation to alite

The crystal structure of Ca_3SiO_5 may be viewed as a stacking sequence of elementary layers, each having the composition $M_3(TO_4)x$. In this view, $NaCa_2SiO_4F$ consists of a regular two-layer repeat sequence while Ca_3SiO_5 is built of more complex stacking sequences. Different investigators have reported different sequences for alite and it is probable that all those reported sequences occur, although conditions for their formation are not well defined. However, electron diffraction revealed that the I phase is comprised of two hitherto unreported stacking sequences. The *c* (or pseudo *c*) axis periodicities of these stackings correspond to 15 and 24 layer repeats. Fig. 5 shows the elementary layer unit and sufficient of the proposed stackings, together with translation motions, necessary to visualise the structure of the 15 and 24 layer variants. All I phase preparations examined consisted of mixtures of these two variants although not always in the same proportions. No firm and consistent evidence was obtained showing that significant differences in Na:Ca or F:O ratios occurred between the two variants.

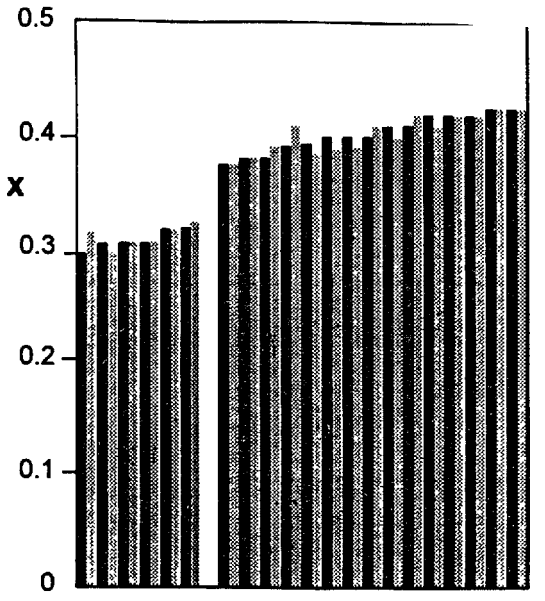

Figure 4. Analysis cluster of a quenched charge at x ≃ 0.36 heated at 1070°C consisting, by XRD of a mixture of C_3S and I phases. Analyses were made by EMPA of selected single crystals. 21 out of 24 analyses were accepted: 3 were rejected because Na + Ca ≠ 3 and or O + F ≠ 5. The x values are paired: dark for Na, shaded for F. A division into two populations is suggested, one on the left of C_3S (alite) type and the other, rather Na + F richer, of I phase.

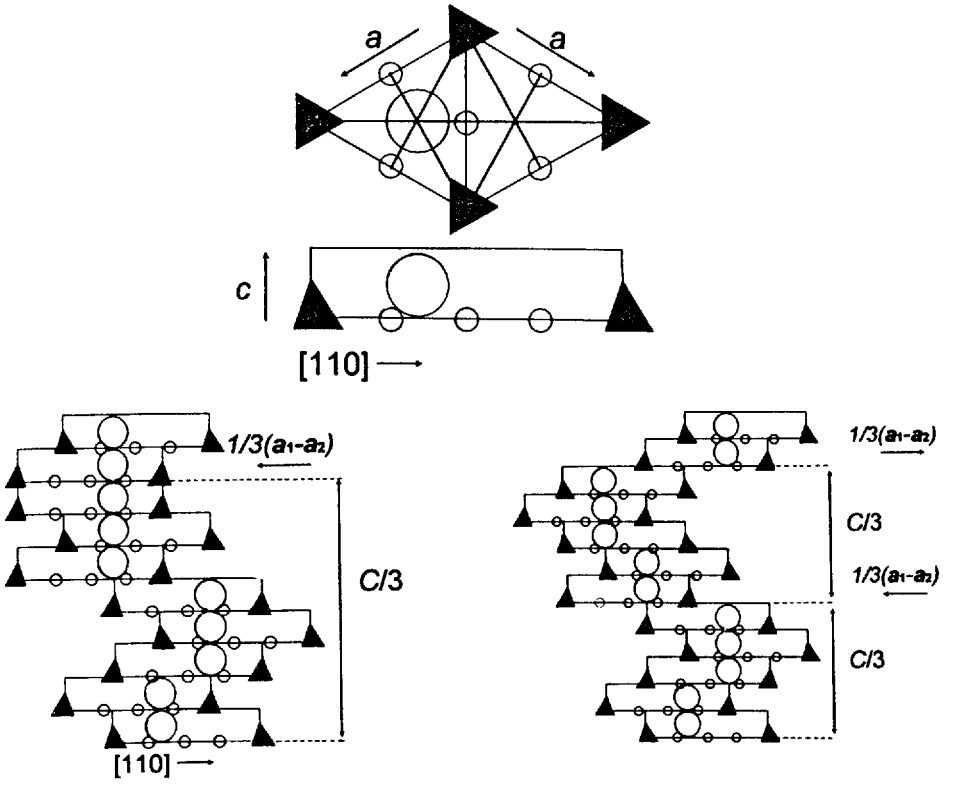

Figure 5. Structure of phase I. At the top is a drawing in two projections of the elementary layer unit common to alite type structure. Silicate tetrahedra are shown: large open circles are oxygen, small open circles are calcium. These are partly replaced by fluorine and oxygen respectively. The sketch at lower left shows stacking and translations necessary to form the 24 layer sequences (3 x 8 layer blocks) and at the lower right, the 15 layer sequence (3 x 5 blocks)., Both 24 and 15 layer sequences are characteristic of the I phase.

Reactivity towards water

No systematic studies of reactivity have been made in the course of the present study, but both Na and F substituted alites and I phase are very reactive towards water. Na_2CaSiO_4F, on the other hand, is only feebly reactive.

DISCUSSION

The present study raises a number of questions. Firstly, is the I phase best regarded as a new polymorph or as a polytype of Ca_3SiO_5, albeit with substantial chemical doping? Given that some compositions can be transformed reversibly from I phase to C_3S type, or vice versa, by changing temperature, but always with an intervening two phase gap, I behaves operationally, as though it were a polymorph. However, in this view, the polymorph must have two polytypic variants: the 15 and 24 layer stackings. Transformation between 15 and 24 layer stackings is not readily accomplished: the mechanisms involved suggest that the transformation must be at least semi-reconstructive. Indeed, it is characteristic of many polytypic mixtures that, once formed, the polytypic distribution is difficult to alter.

How many variants of the alite structure occur? At present we do not know the answer: probably, quite a few. The structural stabilities of the variants are envisaged as being controlled partly by chemistry, and partly by availability, without undue penalty in terms of increasing the free energy, of the translational mechanisms necessary to create the new structures. These translations result in the introduction of shear planes, which behave like an extended defect. Thus alite type structures gain additional entropy stabilisation and characteristically become stable at temperatures in the range >900-1200°C, i.e. at substantially lower temperatures than pure Ca_3SiO_5.

The reactivity of the alite structure towards water has been the subject of much debate. It is suggested that the reactivity arises from three factors. Firstly, absolute thermodynamic instability at typical (0-60°C) cement hydration temperatures, is a primary requirement for rapid reaction. This is a characteristic shared with other silicates, notably α, α', β and β' Ca_2SiO_4, all of which are reactive at ambient. Secondly, the presence of extended defects throughout the structure enhances reaction rate. Translation motions, occurring every five or eight elementary layers in the I phase, are postulated to be the principal source of defect-conditioned reactivity, although the contribution of other types of defect to reactivity is not excluded. Finally, at least some of the chemical constituents must be soluble and, moreover, soluble so as to condition a high pH. This high pH is favourable for breaking M-O bonds which are, in any event, unstable in aqueous solutions. Both Ca_3SiO_5 and the I phase meet all three criteria and are reactive: $NaCa_2SiO_4F$, on the other hand, is thermodynamically stable at ambient so it fails one of the criteria.

ACKNOWLEDGEMENT

Ömer Andaç would like to thank the Turkish Government for a scholarship which allowed him to pursue PhD studies at the University of Aberdeen. The financial support of the Engineering and Physical Sciences Research Council for the electron microprobe and to Alison Coates, for her assistance with probe calibration and techniques, is also gratefully acknowledged. Dr Eric Lachowski contributed greatly to the taking and interpretation of the electron diffractions.

REFERENCES

Andaç, Ö. "Calcium Sulfoaluminate Based Cements" PhD Thesis, University of Aberdeen, March 1996.

Andaç, Ö., Glasser, F.P. and Howie, R.A., "Sodium Dicalcium Silicate Fluoride" Acta Cryst **C** (in press, 1997)

Jeffrey, J. W., "The Tricalcium Silicate Phase". Proc. 3rd International Symposium on the Chemistry of Cement (London) 30-48 (1952)

Perez-Mendez, M., Howie, R.A., and Glasser, F.P. "Ca_3SiO_5 and its Fluorine and Stabilised Aristotype: Synthesis, Stability and Postulated Structure of $Ca_{6-0.5x}Si_2O_{10-x}F_x$". Cement and Concrete Research, 14, 57-63 (1984)

Shame, F.G. and Glasser, F.P. "Synthesis and Properties of Stable Ca_3SiO_5 Solid Solutions Made Between 1050°C and 1250°C. Brit. Ceram. Trans. and Jour. 86 13-17 (1987)

*
Ömer Andaç (current address)
Egitim Fakultesi,
Kimya Bolumu,
55200 Atakum-Samsun
Turkey

CRYSTAL SIZE AND CONTENT OF THE ALUMINATE PHASE IN PORTLAND CEMENT CLINKER

Alberto SAINI, Centro Ricerche UNICEM, Guidonia, Italia
Nicoletta GIULIANI, Centro Ricerche UNICEM, Guidonia, Italia

ABSTRACT As the aluminate phase decreases, its crystal degree evolves from well developed crystals to a crystal size tending to diminish till to give aluminate a microcrystal appearance. In accordance to microscopy examination, the main aluminate phase XRD reflex (2θ = 33.2) also tends gradually to decrease till to vanish by forming a glassy state. Beyond a C_3A value calculated by Bogue equation, formation of a C_3A glassy state occurs. This is of interest for a sulphate resistant cement formulation because a glassy C_3A is less susceptible by sulphate attack.

Key-words: aluminate phase, crystal size, glass, microscopy, x-ray diffraction analysis.

INTRODUCTION

Through an investigation about clinkerization conditions with the aim to improve the raw meals burnability, the effectiveness of an iron ore addition to make burning easier, through a silica modulus decrease, has been industrially tested.
To get a comprehensive and exhaustive characterization, chemical analysis of industrial clinkers has been supported by an XRD and Optical microscopy (OM) examination with the purpose to point out possible phase variations in the interstitial material. The XRD-OM combined use allows to detect a simultaneous decrease of content and crystal size of the aluminate phase, as the addition increases.

The microscopy examination has been conventionally performed on a suitable grain size fraction of the as-received clinker. This fraction has been encapsulated, polished and etched, while the XRD pattern has concerned clinker residues resulting from two selective extractions to remove the interfering phases such as the silicate and sulphate phases ones. The procedures to prepare the samples for the XRD and OM analyses are reported in the following experimental part.

EXPERIMENTAL PART

The procedures to prepare the samples of analysis and the modalities to remove the interfering phases by selective extractions have been previously reported (Saini, 1994; Tabikh, 1971; Burkes, 1983) and are now briefly mentioned.

A) Sampling and preliminary quartering

To obtain a representative sample to analyze by XRD (D 500, Siemens) and optical microscopy (Leitz, Laborlux 12 Pol S), any as-received clinker sample has been preliminary quartered so to obtain enough material for both the techniques. One half has been crushed to obtain the fraction for the microscopical test, while the other has been finely grounded for XRD analysis, as following reported.

B) Sample preparation for XRD analysis

Crushed clinker is finely wet grounded and then dried by evaporation. Silicon powder, previously grounded, is used as internal standard for quantitative analysis according to Chung's Method (Chung, 1974). It is mixed in known proportions with the finely grounded material and subsequently it is wet milled. After the liquid evaporation, the resulting material is selectively extracted to remove the silicate and sulphate phases by treatment with an alcoholic maleic acid solution and then with an aqueous NH_4Cl solution.

C) Preparation of samples for microscopical reflected light examination

The crushed clinker fraction is encapsulated and the sample located in a vacuum bell to remove the air bubbles. After an oven curing, the sample is polished and then its surface etched with KOH water solution. C_3A stains blue while C_4AF remains brightly white (Campbell, 1986; Hoffmänner, 1973).

CHEMICAL, MINERAL, MICROSCOPICAL AND BY SELECTIVE EXTRACTION ANALYSIS

Chemical and mineralogical analysis of three series of clinkers (A, B and C) coming from different plants are reported in the Tables 1 and 2.

Table 1 Chemical analysis

	Serie A			Serie B			Serie C		
	A1	**A2**	**A3**	**B1**	**B2**	**B3**	**C1**	**C2**	**C3**
% LOI	0,24	0,65	0,89	0,21	1,25	1,20	0,60	0,22	0,12
% SiO_2	21,91	21,99	21,60	22,06	21,54	21,56	21,65	20,87	20,30
% Al_2O_3	4,67	4,53	4,30	4,97	4,53	4,30	4,87	4,80	4,24
% Fe_2O_3	2,70	4,22	4,71	2,63	4,00	4,50	3,28	3,93	4,81
% CaO	67,48	65,04	64,42	66,86	64,81	64,91	64,05	65,47	65,63
% MgO	1,47	1,42	1,42	1,17	1,49	1,35	3,56	1,71	1,60
% SO_3	0,49	0,97	0,79	0,65	0,93	0,82	0,59	1,56	2,04
% K_2O	0,79	0,76	0,79	0,80	0,75	0,74	0,62	1,00	0,85
% Na_2O	0,18	0,18	0,19	0,30	0,14	0,17	0,17	0,21	0,18
% Mn_2O_3	0,074	0,100	0,100	---	0,100	0,100	0,079	0,050	0,050
% Free lime	2,24	1,29	1,68	3,36	2,07	2,69	1,79	1,23	1,30
SM	2,97	2,51	2,40	2,90	2,53	2,45	2,66	2,39	2,24
AM	1,73	1,07	0,91	1,89	1,13	0,96	1,48	1,22	0,88
LSF	98,35	93,18	94,88	96,42	94,76	94,94	93,51	97,64	99,73
SD	58	110	86	61	114	97	79	139	214
LF 1450°C	22,46	25,45	25,90	23,10	24,97	25,29	26,34	26,16	26,17

Mineral composition has been calculated by Bogue and Newkirk modified (MgO > 1%) formulas (Gailland et al., 1973) and according to Holderbank equations (Eqs. 1, 2, 3 and 4) (Holderbank, 1977).

$$C_3S = C_3S_{Bogue} + 4.0\,MgO + 5.5\,K_2O \quad [1]$$

$$C_2S = C_2S_{Bogue} - 1.5\,MgO - 2.2\,K_2O \quad [2]$$

$$C_3A = C_3A_{Bogue} + 7.8\,Na_2O + 1.5\,AM - 2.1\,SO_3 - 5 \quad [3]$$

$$C_4AF = C_4AF_{Bogue} - 6.5\,Na_2O - 1.7\,AM + 5.0\,Mn_2O_3 + 3 \quad [4]$$

Additionally, phase contents have been experimentally evaluated by optical microscopy through the known point counting technique (Hoffmänner, 1973; Cetic, 1978). The C_3A content has been evaluated by XRD on the clinker residue from selective extractions (Table 3). Phase composition

by selective extraction is reported in Table 3. It shows, respectively, the values of silicate amounts (corrected by the free CaO chemical one), those of sulphate and then of interstitial phases ones, including aluminate and aluminoferrite.

Table 2 Mineral composition: by Bogue (1), by Newkirk (2), by Holderbank (3)

		Serie A			Serie B			Serie C		
		A1	**A2**	**A3**	**B1**	**B2**	**B3**	**C1**	**C2**	**C3**
1	% C_3S	67,22	55,66	57,49	55,68	52,55	51,01	63,03	67,42	72,80
	% C_2S	16,39	25,31	22,82	25,38	26,41	27,56	19,78	13,37	7,63
	% C_3A	7,81	4,87	3,44	8,73	5,24	3,79	7,36	6,08	3,11
	% C_4AF	8,21	12,83	14,32	8,00	12,16	13,68	9,97	11,95	14,62
2	% C_3S	67,48	56,01	57,87	56,40	52,82	51,44	61,68	67,55	72,95
	% C_2S	8,69	23,87	19,30	18,73	25,01	25,70	17,10	12,04	6,30
	% $KC_{23}S_{12}$	6,43	0,00	2,08	5,06	0,00	0,37	2,22	0,00	0,00
	% C_3A	6,70	4,87	2,94	6,45	5,24	3,64	6,63	6,07	3,10
	% NC_8A_3	1,12	0,00	0,49	2,29	0,00	0,15	0,73	0,00	0,00
	% C_4AF	8,22	12,84	14,33	8,00	12,17	13,69	9,98	11,96	14,64
	% $CaSO_4$	0,00	0,16	0,00	0,00	0,19	0,00	0,00	0,75	1,85
	% Na_2SO_4	0,22	0,41	0,35	0,29	0,32	0,36	0,26	0,48	0,41
	% K_2SO_4	0,80	1,41	1,29	1,06	1,39	1,34	0,96	1,85	1,57
3	% C_3S	72,36	62,36	63,74	61,62	59,10	57,30	65,98	76,17	82,63
	% C_2S	11,88	19,66	17,56	20,11	20,92	22,10	18,93	6,94	0,00
	% C_3A	5,78	0,85	0,00	7,54	1,08	0,00	4,68	1,27	0,00
	% C_4AF	7,47	13,33	15,03	5,83	12,82	14,45	9,74	11,76	15,20

Table 3 Phase composition by selective extractions (1) and XRD (2)

		A1	**A2**	**A3**	**B1**	**B2**	**B3**	**C1**	**C2**	**C3**
1	% Silicates	84,5	81,5	80,9	82,9	82,2	81,3	80,9	80,3	79,4
	% Sulfates	1,8	1,7	2,6	1,5	2,3	2,9	2,0	3,8	4,7
	% Interstitial phase	13,8	16,8	16,5	15,2	15,5	15,8	17,1	15,9	15,9
2	% C_3A	5,2	1,1	0,8	6,0	1,4	0,6	5,3	1,8	0,0

XRD ANALYSIS

After the silicates and sulfates removal, residues have been XRD examined. A few patterns of clinker samples before (ruled area) and after (blank area) the selective removal are as an example reported in Fig 1. To overcome the remarkable overlapping peak phenomena and then to allow the measure of the aluminate phase through the evaluation of its integrated peak areas, the Diffrac AT FIT by Siemens program application is suggested. It involves the angular region (33-35 2θ) including the main aluminate reflection at 33.3 2θ, the 33.1 2θ peak of noncubic forms (if there are any), then the aluminoferrite peak at 33.9 2θ and its doublet at 33.5 2θ.

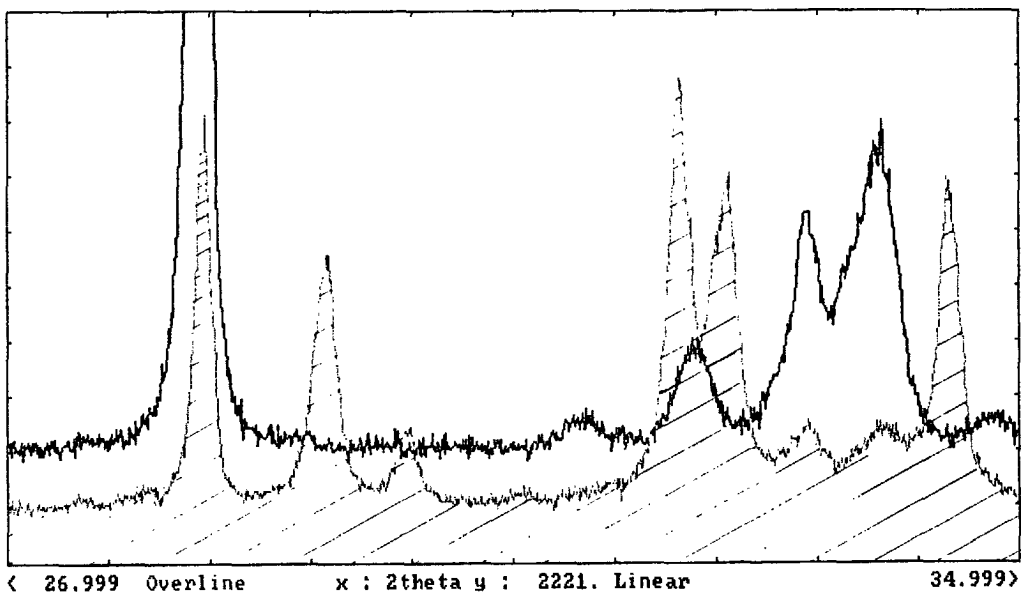

Figure 1 Overlapping of clinker XRD patterns before and after selective extractions.

In Figs 2, 3 and 4 a zoomed pattern's portion, that is the angular region from about 32.8 2θ to about 34.4 2θ, including the experimental profile (black trace) and the fitted ones by deconvolution (differently marked), is reported.

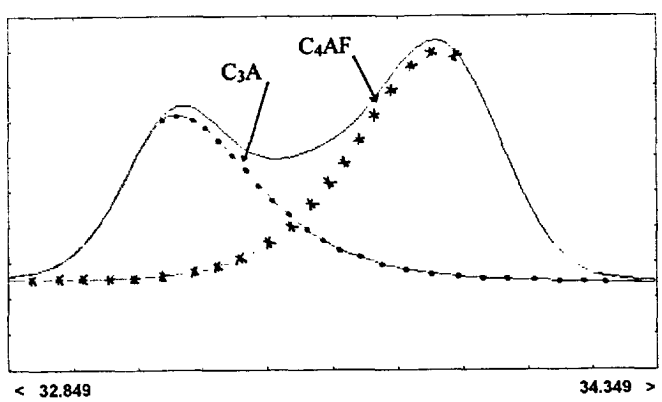

Figure 2 Trends of experimental profile and deconvoluted ones (sample C1).

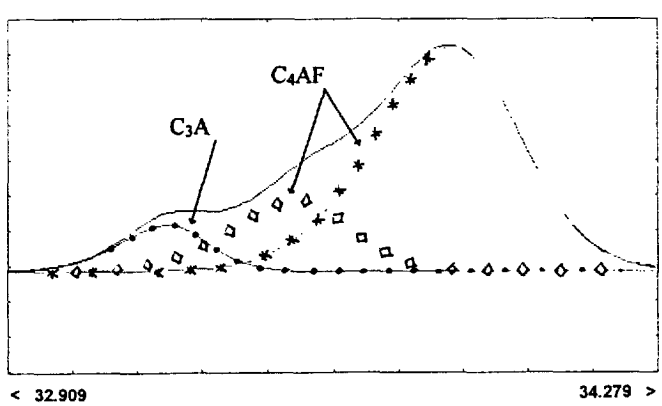

Figure 3 Trends of experimental profile and deconvoluted ones (sample C2).

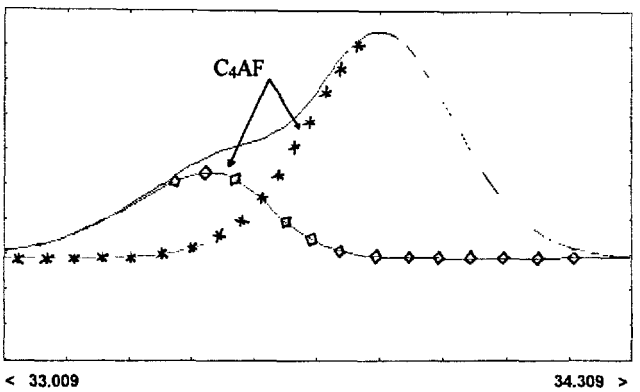

Figure 4 Trends of experimental profile and deconvoluted ones (sample C3).

The other figures include two graphics to immediately control the accuracy of the fitting program application; they show, respectively, the overlapping degree of the experimental profile and that obtained by the sum of the lines and the background (Fig 5) and the residual pattern that is the algebraic sum between the values of the deconvoluted profile and the experimental one (Fig 6).

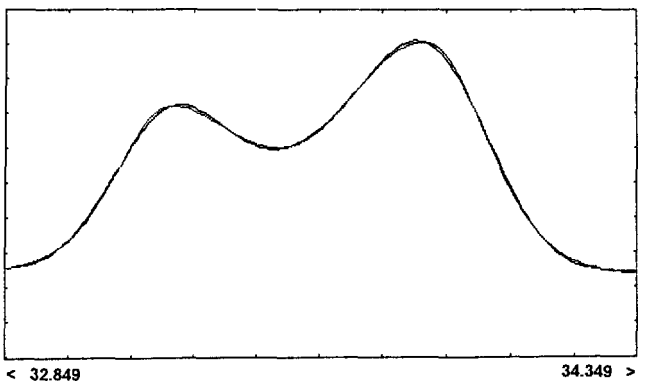

Figure 5 The overlapping between the experimental profile and the deconvoluted one

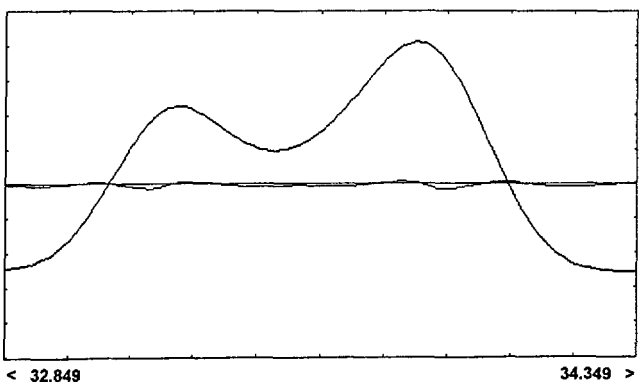

Figure 6 The residual pattern

The comparison between calculated values by Bogue-Newkirk formulas or Holderbank equations and experimental ones by XRD confirms (Table 4) the XRD technique trend to generally underestimate aluminate phase (Regourd, 1986). This trend could be explained by taking in account the situation, detected by optical microscopy, in terms of shapes and crystal sizes. Really, combined use of microscopy and XRD allows to notice a progressive size reduction of the C_3A crystals as its content, calculated or experimentally measured, changes. More particularly, in the

clinkers having a middle C_3A content (samples A1, B1 and C1), aluminate phase forms large and well developed (15-30 microns) prismatic crystal (Fig 7).

Table 4 % Aluminate phase: comparison between calculated and XRD data

	A1	A2	A3	B1	B2	B3	C1	C2	C3
Bogue - Newkirk	7,8	4,9	3,4	8,7	5,2	3,8	7,4	6,1	3,1
Holderbank	5,8	0,9	0,0	7,5	1,1	0,0	4,7	1,3	0,0
XRD	5,2	1,1	0,8	6,0	1,4	0,6	5,3	1,8	0,0

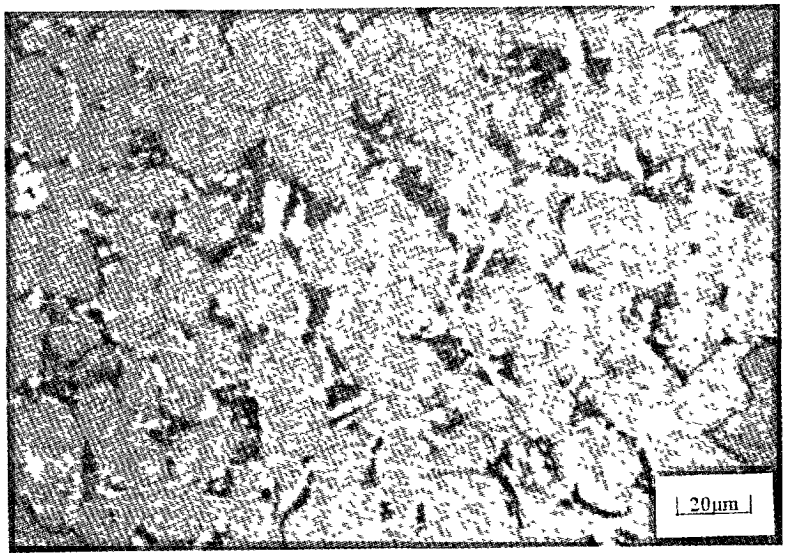

Figure 7 Sample C1. Well formed C_3A cubic crystals.

As the C_3A content decreases (samples A2, B2 and C2), an amount of microcrystalline crystals starts to occur, next to crystals still well formed but smaller than the previous ones (Fig 8).

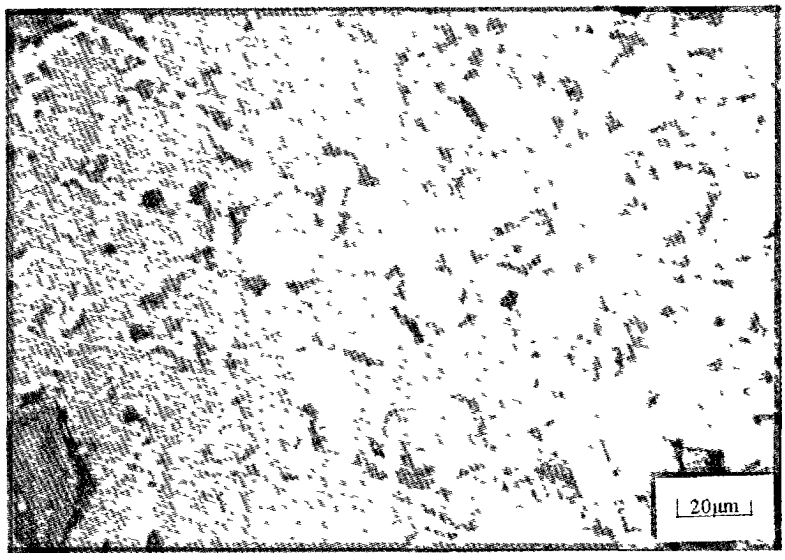

Figure 8 Sample C2. Middle size C_3A crystals.

This amount gradually increases till to prevail when the C_3A content values become very low (samples A3, B3 and C3) (Fig 9). Clinkers of this group have only very small C_3A crystals so to be almost reflexes-free and then XRD undetectable (i.e., Fig 4).

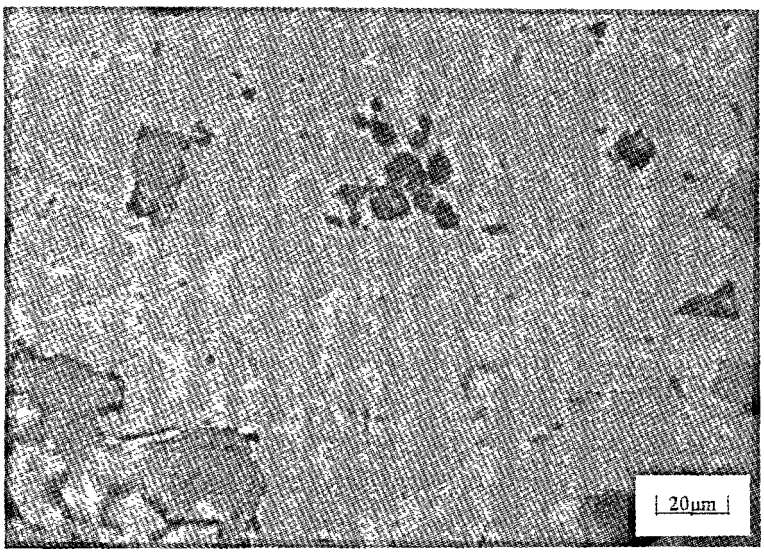

Figure 9 Sample C3. Very small size C_3A crystals.

According to this, difference between measured and calculated values could be explained. Data in Table 4, as well as those reported in a previous paper of the same Authors (Saini and Giuliani, 1994), confirm that Holderbank equations give values closer to XRD data.

CONCLUSIONS

The point that aluminate phase, below a calculated C_3A value differing from clinker to clinker, assumes a crystal size such as to be transparent to X-ray and to have amorphous behavior is of interest from an application point of view. In the light of what literature reports about the low reactivity of a glassy aluminate phase (Han, 1982; Locher, 1975,1980,1982; Regourd, 1978; Sylla, 1975; Lea, 1970; Zgambo, 1987; Carin, 1991; Tsuyuki, 1986), the occurrence of this X-ray amorphous phase when C_3A content decreases below a certain value could be of interest in terms of sulphate resistant cement formulation. Also Alunno Rossetti (1995) recently confirms Parker's observations. Parker (1939) observed that cements cooled rapidly showed greater resistance in sulphate solutions than specimens of the same composition and curing, but cooled more slowly. In his study Alunno Rossetti examined synthetic cements prepared using different concentrations of C_3A with vitreous or crystalline structure and he considered also the influence of various curing conditions. The results obtained show that cements with vitreous C_3A are less expansive than those with crystalline C_3A (At room temperature (20°C) the sulphate expansion is 50 percent reduced and more than four-five times with low (90°C) and high (190°C) pressure steam curing). Sulphate expansion is further reduced when glassy C_3A concentrations increased (expansion is four times reduced at 20°C and about five and twelve times at 90°C and 190°C, respectively). Really, in the presence of a hard sulphate attack, cements having an XRD measured C_3A content not above 1% have frequently required. The fulfilment of this severe condition involves the manufacturing of a very low C_3A clinker consistently with some main actual sulphate resistant cement regulations (ASTM C150, UNI 9156 and its revision FA262, ENV 197-X, BS 4027). The combination of a very low C_3A content with the lower reactivity of a glassy aluminate clinker phase is consistent with a formulation of high-sulphate resistant cement. In this connection, the paper, on one hand, points out the similar trends of C_3A content and its crystal

size, on the other hand suggests an XRD procedure to evaluate the crystalline C_3A content. This procedure, based on an analysis by a profile fitting program performed on a residue from two selective extractions for the removal of interfering phases, could be useful, in authors's opinion, for the cement standardization and its control.

REFERENCES

Alunno Rossetti V., Medici F., "The influence of C_3A crystallinity and curing temperature on the sulphate expansion of synthetic cements", Il Cemento vol. 95, n°4, 1995, 215-224

Burkes J.P., Bruck A.D., "Use of selective dissolution and X-ray diffraction to determine form of tricalcium aluminate in portland cement", Proc. 5th Int. Conf. Cem. Micr. 1983, 247-251

Campbell D.H., Microscopical Examination and Interpretation of Portland Cement and Clinker, Construction Technologies Laboratories, pp. 128, 1986

Carin, Halle, "Effect of matrix form on setting time of belite cement which contains tricalcium aluminate", Ceramic Bullettin n°2, 1991; 251-253

CETIC, "Determination de la composition mineralogique du clinker par analyse microscopique et dissolution selective des phases", Revue des Mat. des Constr., vol. 4, 1978, 205-211

Chung F.H., "Quantitative interpretation of x-ray diffraction patterns of mixtures. I. Matrix-Flushing Method for quantitative multicomponent analysis", J. Appl. Cryst. 7, 519, (1974)

Gailland L, Magnan R., Vibert C., "Les compositions mineralogiques potentielles et reelles des clinkers de Portland', Rev. des Mat., n° 680, 24-30, (1973)

Han K.S., Choi M., Seo I.Y., "Effect of potassium oxide on the early hydration of C_3A" Yo Op Hoe Chi, 19(2) 133-138 (1982); Chem. Abstr. 98, 21347 (1982)

Hoffmänner F., Microstructure of Portland Cement Clinker, Holderbank Management & Consulting Ltd, Holderbank, Switzerland, 1973, pp. 48

Holderbank Management & Consulting, "Cement Handbook" - Mat. Tech, vol. 1, 1977

Lea F.M., "The Chemistry of Cement and Concrete" (1970) 149-150

Locher F.W., "Einfluß der klinkerherstellung auf die Eigenschaften des Zements", ZKG 7, 265-272 (1975)

Locher F.W., "Influence of burning conditions on clinker characteristics", World Cement Tech. 3, 67-73 (1980)

Locher F., Richartz W., Sprung S., Sylla H.M., "Setting of cement, Part III. Influence of clinker manufacture", ZKG 35 (12) 669-676 (1982)

Parker T.W., " Influence of the heat-treatment of Portland Cement clinker on the properties of the cement", Jour. Soc. Chem. Ind., London 58, 203 (1939)

Regourd M., "Cristallization et reactivite de l'aluminate tricalcique dans les ciments portland", Il Cemento, 3, 323-336 (1978)

Regourd M., "Application of X-ray diffraction to some problems of the cement industry", Chem. Script, vol 26A, 1986, 37-45

Saini A, Giuliani N., "XRD Analysis of C_3A and C_4AF phases on the selective extraction clinker residue by using a profile fitting program. Comparison between experimental and calculation data in the light of optical microscopy examination", Proc. 16th Int. Conf. Cem. Micr.,1994, 24-43

Sylla H.M., "Einfluß der klinkerkühlung auf Erstarren und Fesigkeit von Zement", ZKG 9, 357-362 (1975)

Tabikh A, Weht R.J., "An X-ray diffraction analysis of Portland Cement", Cem. Concr. Res., vol. 1, n°3, 1971, 317-328

Tsuyuki N., Otake H., Miyokawa T., Kasai J., "Physical properties and hydration of tricalcium aluminate ($3Ca.Al_2O_3$) quenched after fusion", Yogyo Kyokaishi 94(7), 636-643 (1986); Chem. Abstr. 105, 65287e (1986)

Zgambo T.P., Griffin J.G., Daugherty K.E. and Cohen M.D., "Calorimetry of the hydration of calcium aluminates with varoius glass contents", Thermochim. Acta 113, 331-90 (1987)

TRANSFORMATION-INDUCED MICROTEXTURES IN BELITES

Koichiro FUKUDA, Iwao MAKI and Suketoshi ITO
Department of Materials Science and Engineering, Nagoya Institute of Technology,
Nagoya, Japan

ABSTRACT Upon polymorphic phase transition of $\alpha \rightarrow \alpha'$, the α'-phase nucleates within the parent α-phase so that there is a good lattice matching across the interface. The coherent interfaces occur in parallel with $<210>_{\alpha}$ and form an angle of 27° with $(001)_{\alpha}$. The transition is a nucleation and growth process, of which the start and finish are shown on a time-temperature-transformation diagram. As a function of the cooling rate, the phase constitution and microtexture after the transition can be predicted from the diagram. Within the completely inverted α'-phase grains, a remelting reaction successively occurs; a liquid phase nucleates and grows heterogeneously on the lamella boundaries leading to a decrease in impurity concentration in the host α'-phase. The resulting microtexture depends on the cooling history as well as on the wettability of the belite lamellae by the exsolved liquid. The progress of the α'-to-β martensitic transformation during cooling is detected by the growth of the plate-like reliefs on the parent crystal surface. Upon heating, the reverse transformation occurs with the shrinkage of the reliefs. The growth and shrinkage behavior and negative thermal hysteresis are in conformity with the thermoelasticity.

Key-words: Belite, Microstructure, Microscopy, Kinetics, Phase diagram.

INTRODUCTION

Microtextures of belites (broadly defined as Ca_2SiO_4 solid solutions in the present paper) carry a wealth of information on the thermal history of portland cement clinkers especially during cooling. When the belites are cooled from elevated temperatures, phase transformations occur successively, leading to the formation of complex microstructures within the crystals. These microtextures mainly depend on temperatures of belite formation and on cooling rates. Accordingly, we can deduce the detailed cooling history of the clinkers from quantitative information (e.g., chemical composition and phase constitution) on the reaction products.

The microtextures induced by phase transformations during cooling have been classified into four types: I, Ia, II and III (Insley, 1936; Insley *et al.*, 1938). The texture denoted by Type I is characterized by "two or more sets of intersecting lamellae". The texture of Type Ia is distinguished from that of I by "the presence of discrete particles along what are apparently traces of twinning planes". The texture of Type II is described as "a single set of parallel twinning lamellae". The Type III, "often containing irregular cracks or veinlets but without distinctive twinning lamellae, occurs sometimes as overgrowths on crystals of type I and Ia and sometimes as individual crystals." The present study deals with the relationship of the phase transformations in belites to these intracrystalline microtextures. The transformations concerning the above are the polymorphic transition of $\alpha \rightarrow \alpha'$, the remelting reaction of $\alpha \rightarrow \alpha' +$ liquid, and the martensitic transformation of $\alpha' \rightarrow \beta$. The remelting reaction requires atomic diffusion, while the rest involve no diffusion process. Because the α'_H-to-α'_L transition does not affect the relevant microtextures, both phases were simply represented by α' in the present paper.

POLYMORPHIC PHASE TRANSITION OF $\alpha \rightarrow \alpha'$

Stereographic Analysis of Lamella Structure

The lamella structure of the Type I belite is formed by the α-to-α' transition. During further cooling, the α'-phase is often inverted to the β-phase, leading to the formation of polysynthetic twinning at the submicroscopic level within each lamella (Groves, 1982; Fukuda and Maki, 1989a; and Kim *et al.*, 1992).

The orientation of the lamellae in the host α-phase was found by observation of three kinds of orientation defined polished sections, of which the polished surfaces were perpendicular to the *c*-axis, the *a*-axis and <210> of the former α-phase (Fukuda and Maki, 1989a). Because the striations appear as intersections of the lamellae and the polished surfaces, the overall lamella structure was determined by the stereographic analysis of the striation directions. The result showed that there were six sets of crystallographically equivalent lamellae, each of which is parallel to $<210>_\alpha$ and intersects $(001)_\alpha$ at an angle of 27° (Fig 1).

Orientation of Perfectly Coherent Interface Boundaries Between α- and α'-phases

In homogeneous nucleation and growth transformations, the structural relationship between the new phase and the matrix will determine the nature of the interface between them (Putnis and McConnell, 1980). When both phases have a similar structure, the new phase may be oriented in the form of lamellae within the matrix so that there is a good lattice matching across the interface (Robinson *et al.*, 1977).

In the nucleation of the α'-phase lamellae within the host α-phase, the interphase boundaries were expected to be perfectly coherent (Fukuda and Maki, 1993a). The orientation of such coherent interfaces was determined by the matrix algebra analysis as used in martensitic transformations (Wayman, 1964). Because of the trigonal symmetry for the parent α-phase, there were six sym-

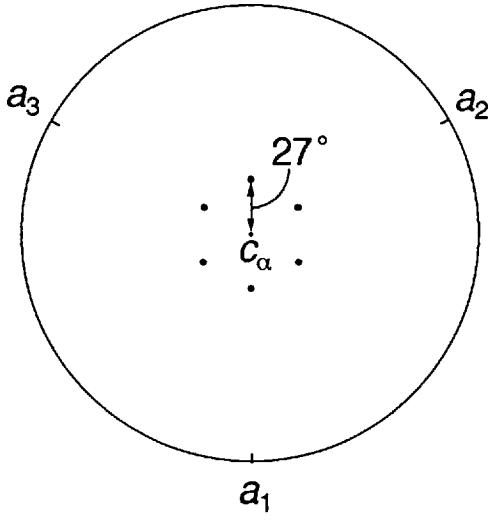

Figure 1 Stereographic plotting of six symmetrically related lamellae. The lamellae are in parallel with $<210>_\alpha$ and form an angle of 27° with $(001)_\alpha$.

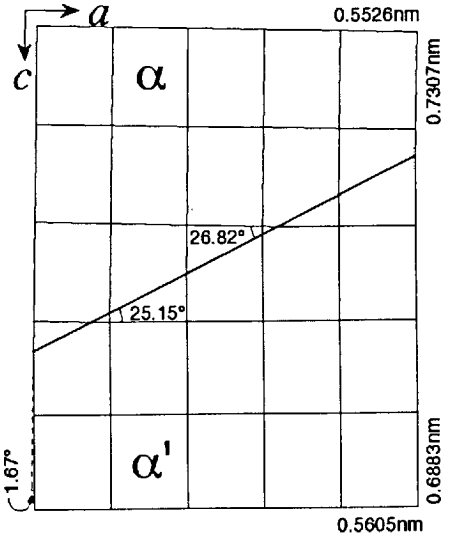

Figure 2 Lattices of the α- and α'-phases, fitted together at the coherent interface. The interface intersects $(001)_\alpha$ at 26.82°.

metrically related sets of interfaces in all, which intersected $(001)_\alpha$ at 26.82° (Fig 2). This is in fair agreement with 27° obtained experimentally. In a similar manner, the intersection angle of 27.64° was obtained as the most probable one at the transition temperature (1425°C) by Fukuda (1994c), taking into consideration the temperature dependence of cell parameters for the α- and α'- phases (Yamaguchi *et al.*, 1963; Regourd *et al.*, 1968; and Saalfeld, 1975).

Determination of Crystallographic Orientation from Striation Directions

The stereogaphic understanding of the overall lamella structure (Fig 2) enables us to produce every kind of geometrical features of the striations on any orientational polished surface. By comparing the striation directions found from calculation with those by observation, we can reconstitute the crystallographic orientation of the parent α-phase. Figure 3B shows schematically the striations observed in Fig 3A, together with the angles between them. The orientation of the parent α-phase axes was superimposed on the figure, indicating that the inclination of the c_α-axis from the surface normal was about 9°.

Kinetics

The α-to-α' transition is a nucleation and growth process. Thus, the transition process was shown on the time-temperature-transformation (TTT) diagram (Fukuda *et al.*, 1993b). In Fig 4, the left C-shaped curve represents the time and temperature at which the product α'-phase is first detectable, and the right curve the time at which the reaction is complete. In the region between the two curves, the belite is composed of both the α- and α'-phases, and the fraction of the α'-phase increases with time for a given temperature. The broken lines in the figure give the thermodynamic transition temperature between α and α'; the α'-phase exists in equilibrium with the parent α-phase at 1280°C. The temperature

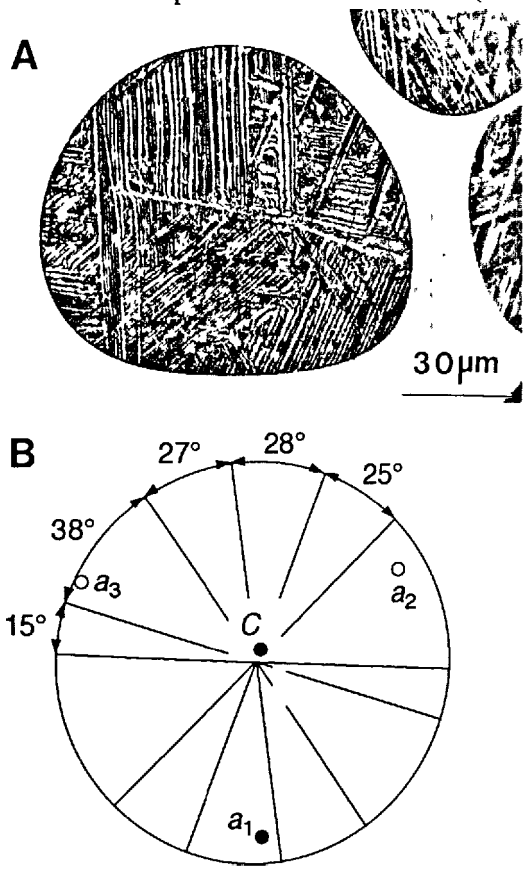

Figure 3 (A) Lamella structure in belite. Polished section. Reflected light. (B) Probable orientation of crystallographic axes of the parent α-phase. Stereographic plotting. Heavy lines represent the six orientational striations observed in A.

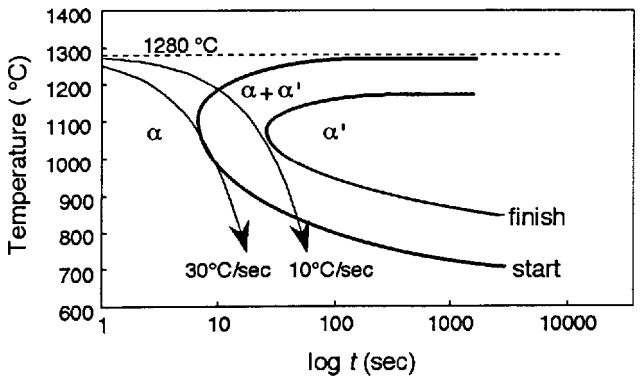

Figure 4 Time-Temperature-Transformation diagram for the α-to-α' transition in belite with the chemical formula: $(Ca_{1.87}Na_{0.13})_{\Sigma 2}(Si_{0.90}Al_{0.04}Fe_{0.03})_{\Sigma 0.97}O_{3.83}$. The cooling curves in the figure are for the linear cooling from 1280°C.

at which the transition occurs at a maximum rate was about 1100°C. With decreasing concentration of foreign oxides (Na_2O, Al_2O_3 and Fe_2O_3) in solid solution, the time at which the reaction is first detectable decreased steadily.

Two cooling curves for the linear rate of 30°C/sec and 10°C/sec have been superimposed on the TTT diagram (Fig 4). The fastest cooling curve does not cross the starting C-shaped curve, and hence the α-phase will be quenched without the α-to-α' transition being initiated. For a cooling rate between 30°C/sec and 10°C/sec, the transition will start at around 1150°C, though it will not be complete. Thus, the crystal grains must show the α'-phase lamellae in the host α-phase. During subsequent cooling, the transition of α' → β will occur within the lamellae, and the resulting crystal will be made up of the β-phase lamellae and the α-phase host at ambient temperature. For a cooling rate lower than 10°C/sec, the α-phase will be entirely inverted to the α'-phase. After that, the remelting reaction, as mentioned below, will immediately occur within the crystal.

REMELTING REACTION*

Phase Stability

On the CaO-SiO_2-Fe_2O_3 ternary phase diagram, the liquidus field of Ca_2SiO_4 extends toward the $CaFe_4O_7$ component (Levin *et al.*, 1964); the liquid coexisting with Ca_2SiO_4 varies in composition along the line Ca_2SiO_4-$CaFe_4O_7$. Fukuda *et al.* (1995a) established the phase diagram of this pseudobinary system as given in Fig 5. The diagram shows that, when the α-phase crystal coexisting with liquid is cooled below 1290°C, the remelting reaction occurs.

To illustrate an ideal sequence of the cooling process in the system, we will consider the changes which take place in the mixture of the α-phase crystal (composition S1) and the liquid (L1) at 1600°C (Fig 5). When the mixture is cooled to 1200°C, the α-phase crystal (S1) will decompose into the liquid (L2) and the α'-phase crystal (S2), which is lower in impurity concentration than the former α-phase. At the same time, from the liquid (L1) coexisting with the α-phase (S1), the α'-phase crystal of composition S2 will be newly nucleated.

The direct transformation of α → liquid + α' shown in the diagram (Fig 5), however, seems to require a large activation energy. Accordingly, the α-to-α' polymorphic transition first occurs upon cooling without a change in chemical composition. After the transition, the liquid exsolves heterogeneously on the lamella boundaries because of the favorable activation energy for nucleation (Fukuda *et al.*, 1992a).

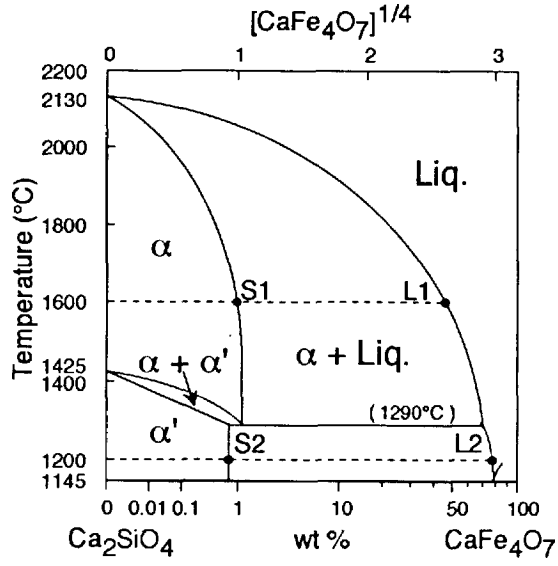

Figure 5 Phase diagram of the P_2O_5-bearing pseudobinary Ca_2SiO_4-$CaFe_4O_7$ system. For convenience, $[CaFe_4O_7]^{1/4}$ was used as the concentration scale.

*A reaction in which a solid decomposes into another solid and a liquid during cooling. The first report on the remelting reaction in belite given by Fukuda *et al.* (1992a).

Wettability of Belite Lamellae by Exsolved Liquid

The rate of the remelting reaction depends on the wettability of the α'-phase lamellae by the exsolved liquid as well as on the temperature (Fukuda *et al.*, 1993c and 1994a). The difference in wettability should come from the chemical composition of the exsolved liquid, which depends on the kinds of impurities and their relative concentration (Al/Fe ratio) in the parent α-phase belite.

When the wettability is low, the liquid forms droplets on the lamella boundaries (Fukuda *et al.*, 1992a). The belite with Al/Fe < 1 exsolved such liquids (Fig 6). The liquid with minimum interfacial area would immediately reach a local equilibrium with the belite matrix. Inside the lamellae, the remelting reaction was hardly expected to occur because of the large activation energy for homogeneous nucleation of the liquid. Under these conditions, the rate-determining step was the volume diffusion of foreign ions from the bulk to the liquid droplets on the lamella surfaces, and thus the reaction was very sluggish. The reaction rate after the formation of droplets was so low that, despite slow cooling, the outline of the belite grains and the intracrystalline lamella structure tended to remain for a long time. This microtexture showing liquid droplets disposed in lines on the lamella boundaries has been denoted as Type Ia.

On the contrary, the liquid exsolved from the belite with Al/Fe > 1, due to the high wettability, spread over the lamellae and disintegrated the lamella structure (Fukuda *et al.*, 1993c). Because of the large interfacial area between the lamellae and the liquid, the reaction proceeded until the parent crystals were completely replaced by the new α'-phase crystals (Fig 7). During the decomposition process, the impurity concentration continued to decrease, and various microtextures (e.g., "fingers extending into the matrix material" by Insley, 1936, and "serrated edges" by Insley *et al.*, 1938) resulted. From the liquid coexisting with the α-phase crystals, the α'-phase crystals (labeled "P" in Fig 7) were newly precipitated and usually overgrew the former α-phase crystals. This texture has been denoted as Type III. During further cooling, the transition of $\alpha' \rightarrow \beta$ should

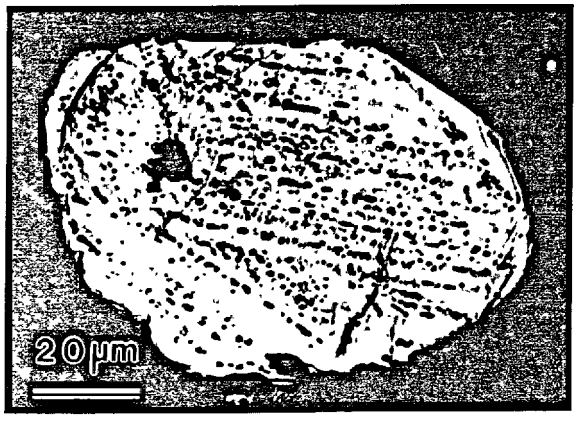

Figure 6 Optical micrograph using transmitted light under crossed polars. The small liquid droplets (now glass at ambient temperature) disposed in lines on the lamella boundaries indicate that the remelting reaction occurs after the α-to-α' polymorphic transition. The chemical formula of the parent crystals is: $(Ca_{1.931}K_{0.030}Al_{0.004}Fe_{0.006}\square_{0.029})_{\Sigma 2.000}$-$(Si_{0.936}P_{0.067})_{\Sigma 1.003}O_4$ (Al/Fe = 0.7 < 1).

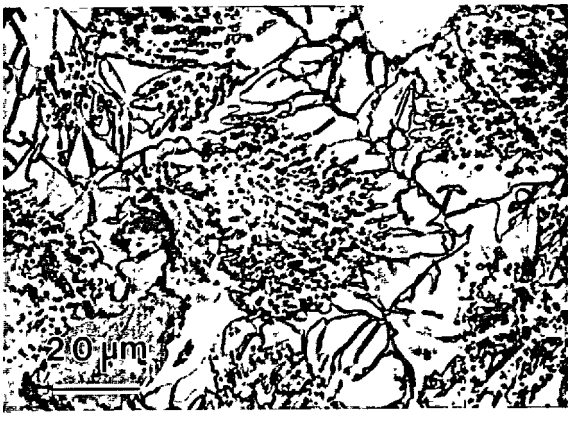

Figure 7 Optical micrograph using reflected light. Etched with nital. Cooled from 1600°C at 36°C/min and quenched at 1200°C. The chemical formula of the parent crystals is: $(Ca_{1.960}Mg_{0.015}Na_{0.017}K_{0.005}Ti_{0.004})_{\Sigma 2}$-$(Si_{0.917}Al_{0.048}Fe_{0.021}S_{0.008})_{\Sigma 0.994}O_{3.954}$ (Al/Fe = 2.3 > 1). The inner part (labeled "I") shows many inclusions of the exsolved liquid.

occur within the overgrown crystals, leading to the formation of the polysynthetic twinning frequently on $(100)_\beta$ and rarely on $(001)_\beta$ (Kim *et al.*, 1992). When the twin planes were almost perpendicular to the polished surface and the specimen was properly etched, the single orientational lamella structure, which has been denoted as Type II, would be observed under the reflected light.

Kinetics

The quantitative relationship between the fraction remelted and the cooling rate was determined for the belites doped with Na_2O, Al_2O_3 and Fe_2O_3 (Fukuda *et al.*, 1995b). Because the Al/Fe ratio was larger than 1, the remelting reaction proceeded to its final stage with prolonged heat treatment. The β-angle varied most sensitively with the Na/(Na+Ca) ratio (= x) according to $\beta\ (°) = 94.55 - 8.86x$ ($0 \le x \le 0.03$). The decrease in x caused by the remelting reaction was therefore detected by the increase in β. When the belite was cooled at a constant rate r (°C/sec) over the temperature range in which the remelting reaction occurred, the fraction remelted (ζ) was expressed by $\zeta = 1\text{-}\exp(-1.33r^{-0.25})$.

THERMOELASTIC MARTENSITIC TRANSFORMATION

The α'-to-β phase transformation has been considered to be martensitic (Groves, 1981, 1982 and 1983; Barnes and Ghose, 1983; Kim *et al.*, 1992). Recently, Fukuda *et al.* (1996a, 1996b) have reported that the transformation was thermoelastic. They confirmed the relief effect, which is characteristic of martensitic transformations, on the parent crystal surface. The growth and shrinkage behavior of the plate-like reliefs (martensite plates) during cooling and heating was observed in situ under a high-temperature optical microscope to determine the transformation temperatures. The thermal hysteresis (A_s - M_s) was negative in accord with the thermoelasticity (Delaey, 1991), where A_s and M_s are the start temperatures of the reverse and forward transformations, respectively.

Because of the transformation being athermal, the transformed fraction remained unchanged when the temperature was kept constant. As the temperature was decreased from M_s, the fraction increased up to M_f, at which the reaction was complete. Accordingly, the phase constitution at any temperature (T) during cooling was determined as α' ($M_s < T$), α' and β ($M_f \le T \le M_s$) and β ($T < M_f$). Upon heating, the reverse transformation occurred, which was also athermal between A_s and A_f (the finish temperature).

INCOMMENSURATE PHASE TRANSFORMATION

A one-dimensional incommensurate phase has been reported to occur in the belites doped with P_2O_5 (Saalfeld, 1971; Saalfeld and Klasla, 1981; Fukuda and Maki, 1989b; Fukuda *et al.*, 1994b) or other oxides (Jelenic and Bezjak, 1982; Fukuda *et al.*, 1992b). The crystal grains consisted of orthorhombic domains related by 120° rotation around the c-axis of the former α-phase. The domains were at the submicroscopic level and the boundaries were irregular. Thus, the crystal grains showed mottled extinction under crossed polars. From the electron diffraction pattern, all the reflections were expressed by $Q = h\mathbf{a}^* + k\mathbf{b}^* + l\mathbf{c}^* + n\mathbf{k}$ using four indices (h, k, l, and n) with $\mathbf{k}$ as the

wave vector (Fukuda *et al.*, 1994b). This vector was redefined using N and the unit vectors **a*** and **c*** as $(1/N)\mathbf{a}^*+\mathbf{c}^*$, where N is the modulation wavelength. A good correlation was observed between N and P/(Si+P) ratio. From the relationship, a commensurate phase with $N = 4$ is expected at P/(Si+P) = 0.148. The crystal structure may be close to that determined by Saalfeld and Klaska (1981), who refined the structure of $6Ca_2SiO_4 \cdot 1Ca_3(PO_4)_2$ (P/(Si+P) = 0.250 and $N = 3.75$) assuming $N = 4$.

TRANSFORMATIONS OF BELITE IN NORMAL CEMENT CLINKERS

The belite in cement clinkers is mostly formed in the stable temperature region of the α-phase. Upon cooling, the α-to-α' transition usually occurs. Because of its isothermal process, the fraction transformed increases with decreasing cooling rate. With rapid cooling, the belite can be composed of both the α- and α'-phases. The product α'-phase will be completely inverted to the β-phase as long as M_f is higher than the ambient temperature, which is often the case with the belite in normal clinkers. When the α-phase belite is cooled more slowly, it can be inverted to the α'-phase completely. After that, the remelting reaction will immediately occur. The resulting microtexture depends on the cooling rate as well as on the Al/Fe ratio of the parent α-phase.

REFERENCES

Barnes, P. and Ghose, A. (Barnes, P. (Ed)): "The Microscopy of Unhydrated Portland Cement", Structure and Performance of Cements. Applied Science Publishers, U.K., 1983, pp. 139-203.

Delaey, L. (Hassen, P. (Ed)): "Diffusionless Transformations", Phase Transformations in Materials, VCH, Weinheim, 1991, pp. 339-404.

Fukuda, K. and Maki, I., "Orientation of β-Ca_2SiO_4 Solid Solution Lamellae Formed in the Host α-Phase", Cem. Concr. Res., Vol. 19, 1989a, pp. 913-918.

Fukuda, K. and Maki, I., "Transitional Phase of Ca_2SiO_4 Solid Solution with Incommensurate Superstructure", J. Am. Ceram. Soc., Vol. 72, 1989b, pp. 2204-2207.

Fukuda, K., Maki, I. and Ito, S., "Remelting Reaction within Belite Crystals During Cooling", J. Am. Ceram. Soc., Vol. 75, 1992a, pp. 2896-2898.

Fukuda, K., Maki, I. and Adachi, K., "Structure Change of Ca_2SiO_4 Solid Solutions with Ba Concentration," J. Am. Ceram. Soc., Nol. 75, 1992b, pp. 884-888.

Fukuda, K. and Maki, I., "Orientation of Coherent Interphase Boundaries Formed by the α to α'_H Phase Transition in Belite Crystals", Cem. Concr. Res., Vol. 23, 1993a, pp. 599-602.

Fukuda, K., Maki, I., Toyoda, K. and Ito, S., "Kinetics of the α-to-α'_H Polymorphic Phase Transition of Ca_2SiO_4 Solid Solutions", J. Am. Ceram. Soc., Vol. 76, 1993b, pp. 1821-1824.

Fukuda, K., Maki, I., Ikeda, S. and Ito, S., "Microtextures Formed by the Remelting Reaction in Belite Crystals", J. Am. Ceram. Soc., Vol. 76, 1993c, pp. 2942-2944.

Fukuda, K., Maki, I., Ito, S., Yoshida, H. and Kato, C., "Effect of Al/Fe Ratio in Belite on the Microtexture Induced by the Remelting Reaction", J. Am. Ceram. Soc., Vol. 77, 1994a, pp. 3027-3029.

Fukuda, K., Maki, I., Ito, S., Yoshida, H. and Aoki, K., "Structure and Microtexture Changes in Phosphorous-Bearing Ca_2SiO_4 Solid Solutions," J. Am. Ceram. Soc., Vol. 77, 1994b, pp. 2615-2619.

Fukuda, K., "Microtextures Formed by the Polymorphic Transition and Remelting Reaction in

Belite", J. Mineral. Soc. Jpn., Vol. 23, 1994c, pp. 179-188 (in Japanese).
Fukuda, K., Maki, I., Ito S. and Yoshida, H., "Phase Stability Study on the Remelting Reaction in Ca_2SiO_4 Solid Solutions", J. Am. Ceram. Soc., Vol. 78, 1995a, pp. 3387-3389.
Fukuda, K., Maki, I., Ito, S. and Toyoda, K., "Kinetics of Remelting Reaction in Ca_2SiO_4 Solid Solutions", J. Ceram. Soc. Jpn., Vol. 103, 1995b, pp. 444-448.
Fukuda, K., Maki, I. and Ito, S., "Thermoelastic Behavior in Ca_2SiO_4 Solid Solutions", J. Am. Ceram. Soc., Vol. 79, 1996a, pp. 2925-2928.
Fukuda, K., Maki, I. and Ito, S., "Thermal Hysteresis for the $\alpha'_L \leftrightarrow \beta$ Transformations in Strontium Oxide-Doped Dicalcium Silicates ", J. Am. Ceram. Soc., Vol. 79, 1996b, pp. 2969-2970.
Groves G. W., "Portland Cement Clinker Viewed by Transmission Electron Microscopy," J. Mat. Sci., Vol. 16, 1981, pp. 1063-1070.
Groves G. W., "Twinning in β-Dicalcium Silicate", Cem. Concr. Res., Vol. 12, 1982, pp. 619-624.
Groves G. W., "Phase Transformation in Dicalcium Silicate," J. Mat. Sci., Vol. 18, 1983, pp. 1615-1624.
Insley, H., "Structural Characteristics of Some Constituents of Portland Cement Clinker", J. Res. Natl. Bur. Stand., Vol. 17, 1936, pp. 353-361.
Insley, H., Flint, E. P., Newman, E. S. and Swenson, J. A., "Relation of Compositions and Heats of Solution of Portland Cement Clinker", J. Res. Natl. Bur. Stand., Vol. 21, 1938, pp. 355-365.
Jelenic, I. and Bezjak, A., "Electron Diffraction Evidence for Superstructures in α'-Modification of Dicalcium Silicate," Cem. Concr. Res., Vol. 12, 1982, pp. 785-788.
Kim, Y. J., Nettleship, I. and Kriven, W. M., "Phase Transformations in Dicalcium Silicate: II, TEM Studies of Crystallography, Microstructure, and Mechanisms", J. Am. Ceram. Soc., Vol. 75, 1992, pp. 2407-2419.
Levin, E. M., Robbins, C. R. and McMurdie, H. F. (Reser, M. K. (Ed)): Fig. 656 in Phase Diagrams for Ceramists. American Ceramic Society, Columbus, OH, 1964.
Putnis, A. and McConnell, J. D. C.: Principles of Mineral Behaviour. Backwell Scientific Publications, Oxford, 1980.
Regourd, M., Bigaré M., Forest, J. and Guinier, A., "Synthesis and Crystallographic Investigation of Some Belites", Proc. 5th Int. Symp. Chem. Cement, Tokyo, Vol. 1, 1968, pp. 44-48.
Robinson, P., Ross, M., Nord, G. L. Jr., Smyth, J. R., Jaffe, H. W., "Exsolution Lamellae in Augite and Pigeonite: Fossil Indicators of Lattice Parameters at High Temperature and Pressure", Am. Mineral., Vol. 62, 1977, pp. 857-873.
Saalfeld, H., "Kristallchemische Untersuchungen im System Ca_2SiO_4-$Ca_3(PO_4)_2$. Beitrag zur Frage der Diadochie des Siliciums und Phosphors", Z. Kristallogr., Vol. 133, 1971, pp. 396-404.
Saalfeld, H., "X-Ray Investigation of Single Crystals of β-Ca_2SiO_4 (Larnite) at High Temperatures", Am. Mineral., Vol. 60, 1975, pp. 824-827.
Saalfeld, H. and Klaska, K. H., "The Crystal Structure of $6Ca_2SiO_4 \cdot 1Ca_3(PO_4)_2$," Z. Kristallogr., Vol. 155, 1981, pp. 65-73.
Wayman, C. M.: Introduction to the Crystallography of Martensitic Transformations. The Macmillan Company, New York, 1964.
Yamaguchi, G., Ono, Y., Kawamura, S. and Soda, Y., "Differential Thermal Analysis and High Temperature Powder X-ray Diffraction of $2CaO \cdot SiO_2$", J. Ceram. Assoc. Jpn., Vol. 71, 1963, pp. 105-108.

EFFECT OF Al_2O_3 AND Fe_2O_3 IN THE FORMATION OF DICALCIUM SILICATE PHASE

V K MATHUR, K M SHARMA AND R S GUPTA
National Council for Cement and Building Materials,
New Delhi, India

S C AHLUWALIA, OCL India Ltd., New Delhi, India

ABSTRACT Infrared and XRD studies of the Fe_2O_3 and Al_2O_3 doped dicalcium silicate phase indicate that Al_2O_3 in the system $CaCO_3$ and SiO_2 (2:1) stabilizes β-C_2S phase while Fe_2O_3 leads to the formation of β- and γ-C_2S. The activation energies (Ea) of C_2S formation decreases upto addition of 0.5 wt. percent with both the dopents and then rises with increasing concentration of dopants.

Key-words: Activation energy,Dicalcium silicate,Dopant,Polymorphs

INTRODUCTION

Cationic and anionic dopants have been reported to have a significant effect on the formation and stabilization of various polymorphs of dicalcium silicate mineral and some of the investigators (Lai, et al 1992) have reported results at variance, which could be due to difference in experimental conditions. A systematic study of the effect of number of dopants on the kinetics of formation and stabilization of various polymorphs of dicalcium silicate have been reported earlier (Ahluwalia and Mathur, 1986,1988 and Mathur, Gupta and Ahluwalia, 1992). The present paper is a part of these investigations and deals with the effect of Al_2O_3 and Fe_2O_3 as dopants.

EXPERIMENTAL

Different mixtures of calcium carbonate and quartz powder (purity > 99.5 %) were prepared in 2:1 molar ratios without and with varying concentrations of Al_2O_3 and Fe_2O_3 as dopant. Nodules were prepared from these mixtures. These nodules after drying at $100^{\circ}C \pm 5^{\circ}C$ were stored for experimental work.

DTA studies of the above samples were conducted on Mettler thermal analyser (TA-1) and formation temperature of C_2S phase and other minor compounds were recorded (Table 1). For identification of the products formed, the starting materials were again fired to the temperature where the thermal peaks obtained. These fired samples were then quenched in liquid nitrogen and stored in air tight containers. The quenched products were then identified by IR (Perkin Elmer model IR - 621) in 1800 - 400 cm^{-1} region and XRD (Philips model PW 1120 diffractometer with Ni-filtered Cu radiation). The Ginstling - Brownshtein diffusion equation (Feng and Shangren, 1986 and Mathur et al 1992) was used to calculate the rate constant Kr and the activation energy (Ea) was calculated by the Arrhenius equation.

RESULTS AND DISCUSSION

IR and XRD studies of the quenched products without and with varying concentrations of Al_2O_3 as dopant revealed that β-C_2S

phase is formed in all these samples alongwith some minor compounds of calcium aluminates (Table 1, Fig. 1). Al_2O_3 as dopant in concentration range of 0.1 - 0.5 wt. percent forms small quantities of $CaAl_2O_3$, 1.0 wt. percent $Ca_2Al_2SiO_7$ and 5.0 wt. percent of Al_2O_3 as dopant forms $Ca_3Al_2O_6$ $Ca_2Al_2SiO_7$, $CaAl_2O_4$ (Ahluwalia and Mathur, 1988). A drop in intensity of absorption band was observed at 890 cm^{-1} (Bensted and Varma, 1974) which could possibly be due to substitution of Al^{3+} in SiO_4 tetrahedra. Strong IR bands at 520, 540 and 840 cm^{-1} correspond to β -C_2S while at 898 cm^{-1} to C_3A with 5.0 wt. percent of Al_2O_3 dopant (Fig. 1).

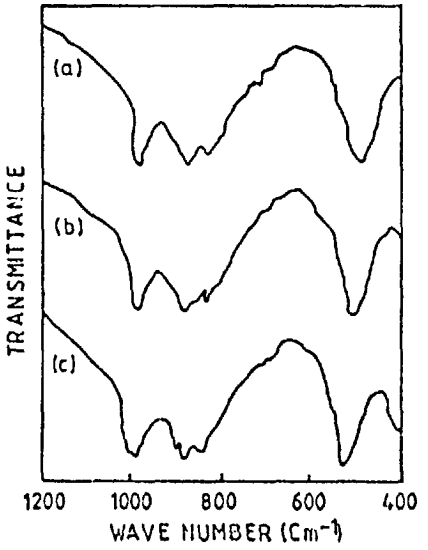

FIG 1 IR SPECTRA OF Al_2O_3 DOPED DICALCIUM SILICATE PHASE

(a) 0.1 % (b) 1.0 % (c) 5.0 %

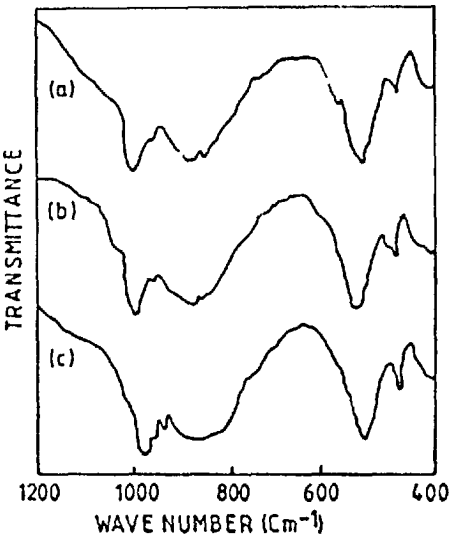

FIG 2 IR SPECTRA OF Fe_2O_3 DOPED DICALCIUM SILICATE PHASE

(a) 0.1 % (b) 1.0 % (c) 5.0 %

IR and XRD studies of the Fe_2O_3 doped C_2S revealed that by increasing the concentration of Fe_2O_3, stabilization of γ-C_2S phase is more intense while occurrance of β -C_2S phase decreases (Table 1, Fig. 2). The IR bands appearing at 440, 445 and 565 cm^{-1} correspond to γ-C_2S while at 520 and 845 cm^{-1} to β -C_2S phase. The most predominant peak of γ -C_2S phase appears at 855 cm^{-1}. With 1.0 wt. percent Fe_2O_3 . α -Fe_2O_3 is formed in small quantity while with 5.0 wt. percent of Fe_2O_3 small quantities of Fe_3O_4, $CaFe_3O_5$ and FeO are also formed. It is inferred that some Fe_2O_3 may be reduced to Fe_3O_4 and FeO due to limited supply of air and high temperature. This FeO is said to be responsible to stabilise γ-C_2S phase (Ahluwalia and Mathur, 1988). The strong band corresponding to β -C_2S phase at 890 cm^{-1} was found missing. The shifting of the band indicates that iron is partially substituted for silicon.

The activation energy (Ea) of the reaction process of C_2S phase formation in pure system was reported to be 180 KJ mol^{-1}, (Mathur, et al, 1992) which decreases to 154 KJ mol^{-1} with 0.5 wt. percent Al_2O_3 and to 148 KJ mol^{-1} with 0.5 wt. percent Fe_2O_3 (Table 1). By further addition of these dopants Ea again starts rising (Table 1) which may be attributed to the formation of the other minor compounds alongwith dicalcium silicate phase.

Both Al3+ and Fe3+ substitute Si4+ in its tetrahedral yielding a compound of chemical composition $Ca_2 [M_x SiO_{4-x/2}]$ where M is Al^{3+} or Fe^{3+} as also reported by forest (1967).

Table 1 KINETICS & POLYMORPHISM OF 2 $CaCO_3$: SiO_2 SYSTEM WITH VARYING CONCENTRATIONS OF DOPANTS

Dopant's Name	Concentration of Dopant in $2CaCO_3 : SiO_2$ System (% wt.)	DTA Peak after $CaCO_3$ Decomp. (^oC)	Activation Energy of Reaction Process of C_2S Formation ($KJ\ mol^{-1}$)	Constituents Formed as Discerned by IR and XRD of Liquid Nitrogen Quenched Samples
Al_2O_3	0.0	1425	180	β-C_2S, γ-C_2S
	0.1	1445	163	β-C_2S, $CaAl_2O_4$
	0.5	1445	154	β-C_2S, $CaAl_2O_4$
	1.0	1445	158	β-C_2S, $Ca_2Al_2SiO_7$
	5.0	1420	165	β-C_2S, $Ca_2Al_2SiO_7$ $CaAl_2O_4$, $Ca_3Al_2O_6$
Fe_2O_3	0.1	1440	160	γ-C_2S, β-C_2S ($\beta > \gamma$)
	0.5	1430	148	γ-C_2S, β-C_2S ($\gamma > \beta$)
	1.0	1430	152	γ-C_2S, β-C_2S ($\gamma > \beta$) α-Fe_2O_3
	5.0	1400	158	γ-C_2S (Most intense), β-C_2S (small qty) FeO Fe_3O_4, $CaFe_3O_5$

CONCLUSION

Al_2O_3 with different concentration stablizes β-C_2S alongwith other phases e.g. $CaAl_2O_4$ C_2AS (Gehlenite) and $Ca_3Al_2O_6$. Fe_2O_3 with all concentration studied helps the formation of a mixture of and C_2S phase with other iron bearing phases like α-Fe_2O_3, Fe_3O_4, $CaFe_3O_5$ etc. Activation energy (Ea) of reaction process of C_2S phase formation decreases upto 0.5 wt. percent with both the dopants and then rises by further addition of any of these dopants, which could be attributed to the formation of other minor phases.

ACKNOWLEDGEMENT

The authors have freely drawn upon completed R&D work/status reports of National Council for Cement and Building Materials. The paper is being published with the permission of Director General, NCB, New Delhi, India.

REFERENCES

Ahluwalia, S C and Mathur, V K, "Thermal Studies on the Effect of Some Transitional Metal Oxides on the Kinetics of Formation and Stabilization of β-Dicalcium Silicate", 8th Intl. Cong. on the Chem. Cem., Brazil, Vol. II, 1986, pp. 40-45.

Ahluwalia, S C and Mathur, V K,"Influence of Al_2O_3 and Fe_2O_3 Dopants on the Thermal Decomposition of $CaCO_3$: SiO_2 (2:1) System",NCB Quest, Volume 2, No. 2, 1988, pp. 34-44.

Bensted, J and Varma, S P, "Some Applications of Infared and Raman Spectrocopy, Part I, Examination of Dicalcium Silicate", Cem. Tech. Volume 5, No. 5, pp. 256.

Feng, Qihuang, shangren, Yu., "A Study on the Kinetics of the Burning of Portland Cement clinker in Different Processes", 8th Intl. long on the Chem. Cem., Brazil, Vol. 2, 1.1,1986,pp. 16-20.

Forest, J, "Study of Local Incrustation in Cement rotary kilns and Belite, Silicate Industriels, Vol. 32, No. 11, 1967, pp. 373.

Lai, Gao-Chao et al, "Studies of the stability of β-Ca_2SiO_4 Doped by Minor Ions," Cem. Concr. Res., Vol. 22, No. 5, 1992, pp. 743-754.

Mathur, V K, Gupta, R S and Ahluwalia, S C, "Lithium As Intensifier in the Formation of Dicalcium Silicate Phase", 9th Intl. Cong. on the chem. Cem., India, Vol. II, 1-C, 1992 pp. 406-412.

THE INFLUENCE OF MOLYBDIC COMPOUND ON FORMATION OF CEMENT CLINKER

Yizhou PAN Yuechong CHI Xingfu FU
Zhejiang Building Materials Scientific Research Institute, Hangzhou, P. R. CHINA

ABSTRACT In this paper , the effect of different form of molybdic compounds on clinker formation is studied , and the formation rate for clinker with composite mineralizer has the following order: [MoS_2+CaF_2] > [MoO_3+CaF_2] > [$CaSO_4$+CaF_2] > no mineralizer .

Key-words: Molybdic compounds Burnability of raw mixes Clinker formation

INTRODUCTION

Reducing energy consumption and improving clinker quality are two of the main purpose in the development of cement technology . In order to raise output and quality as well as to save energy , great attention has been paid worldwide to low burning temperature in clinker process with the mineralizer .

It is found that molybdic compounds acting as mineraliers would produce different effect on clinker formation due to the difference form of them during the studies on producing portland cement with trace components in tailings of molybdenum-iron ore (Pan 1992) . A lot of reports about the mineralizers have been published , but few of them deal with the research field of tailings of molybdenum-iron ore as mineralizer (Timashev 1980 , Xu 1993 , Chen 1993 , Li 1993). In this paper , the effect of separate addition of MoO_3 , MoS_2 , $CaSO_4$ and the complex effect of them combined respectively with fluorite was studied vis-a-vis gypsum-fluorite mineralizer . The results show that the composite mineralizer MoS_2+CaF_2 exhibit better effect on absorption of free lime than others in clinkerization process .

EXPERIMENT

Materials and Methods

Raw mixes for experiments were proportioned by chemical pure agents according to the parameter : $KH=(CaO-1.65AL_2O_3-0.35Fe_2O_3)/2.8SiO_2=0.917$, $SM=1.96$, $AM=1.25$, and mixed in a ceramic mill for 30 min , then were made into cylinder 15 mm in diameter and 20 mm in height . The samples were placed in electric furnace and preheated at the chosen temperature for a certain time interval and cooled in air . Free lime in the sintered samples was determined by using glycerin-alcohol solution .

RESULTS AND DISCUSSION

Effect of separate mineralizer

When the content of separate compounds doped in mixtures is 1% (Fig. 1) , the

This project is supported by the Zhejiang Natural Scientific Foundation, P. R. China

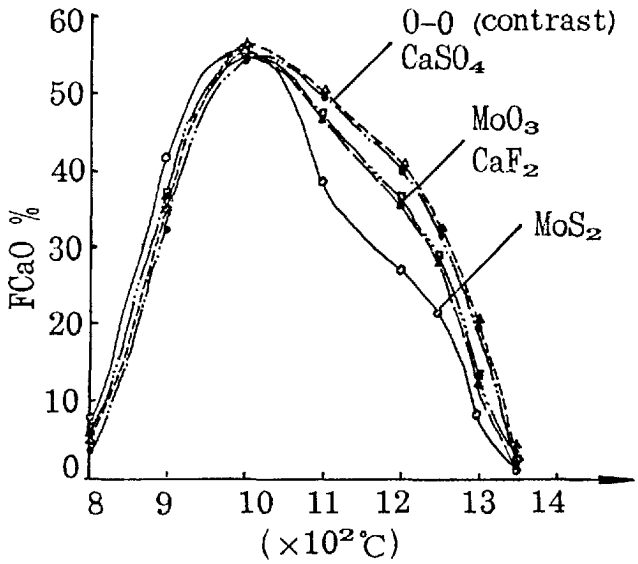

Fig. 1 Effect of mineralizer in 1% addition on burnability of raw mixes

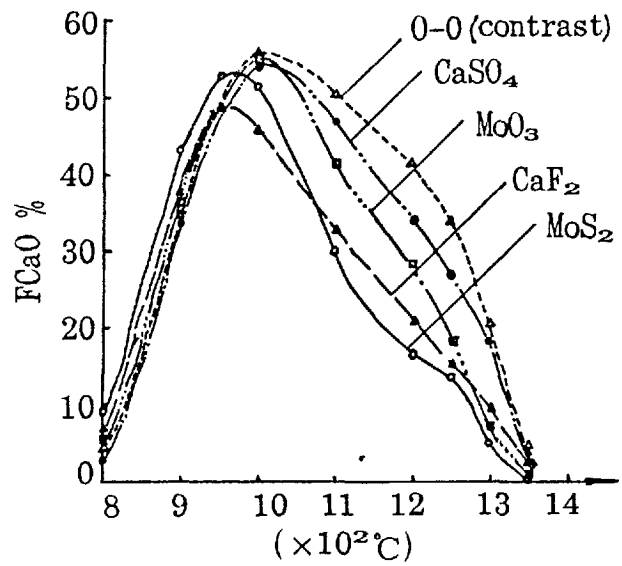

Fig. 2 Effect of mineralizer in 2% addition on burnability of raw mixes

free lime of mixture with MoS_2 contained was significantly lower free lime than others at 1000-1300℃ , and mixture with MoO_3 or CaF_2 was second low and mixture with $CaSO_4$ appears close to contrast sample . At 2% addition of compounds alone (Fig. 2), the maximum point of free lime to mixtures with CaF_2 or MoS_2 is early 50℃. The difference of free lime at 1100-1300℃ is obvious and the quantity of it is in the following order : 0-0 > $CaSO_4$ > MoO_3 > CaF_2 > MoS_2 . It is worth to mention that the region of this temperature is important stage of appearance of early liquid and the formation and the decomposition of intermediate transition phases as well as nucleation and crystal growth of alite . During the clinkering process , the remarkable reduction of free lime create advantage condition to form alite quickly and improve the clinkeration of raw mixes at lower temperature . The experimental results prove that MoS_2 mineralizer exhibit better effects on free lime absorption , especially in low temperature in clinkering process .

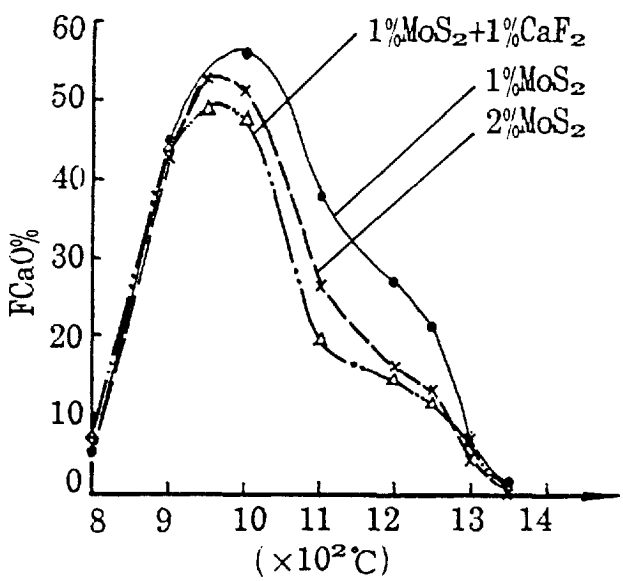

Fig. 3 Effect of MoS_2 on burnability

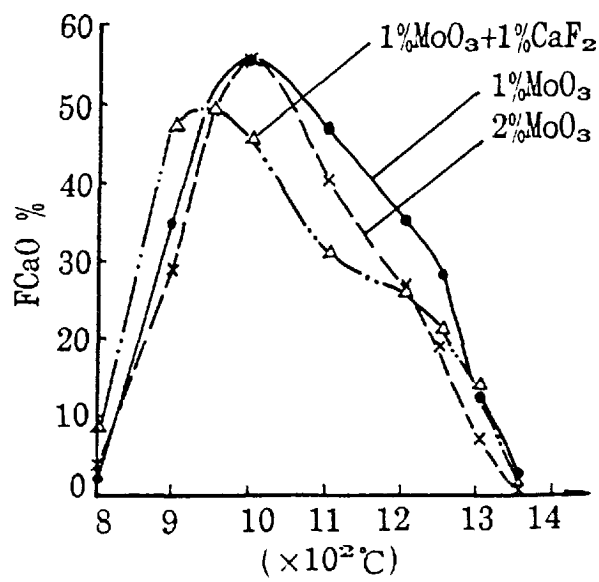

Fig. 4 Effect of MoO_3 on burnability

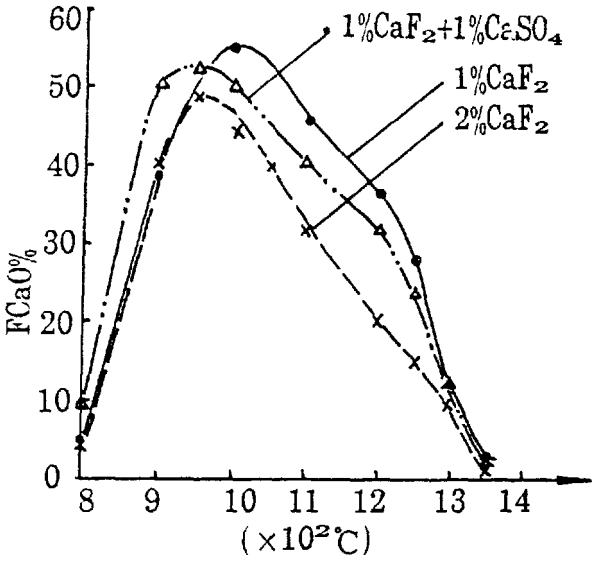

Fig. 5 Effect of CaF_2 on burnability

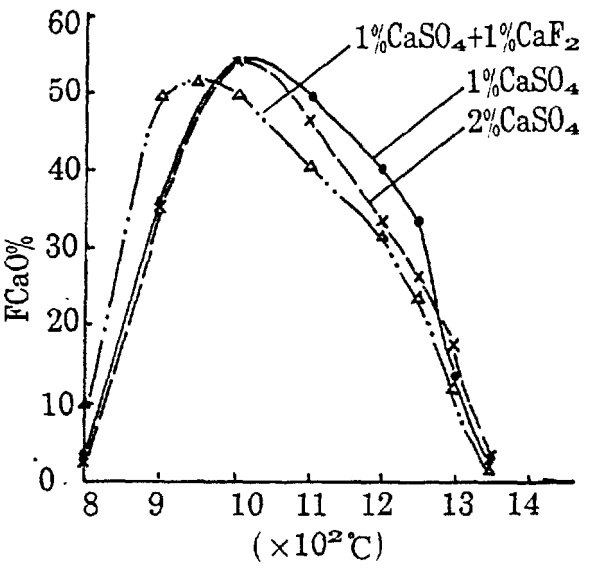

Fig. 6 Effect of $CaSO_4$ on burnability

Effect of complex mineralizer

The maximum point of free lime appears 50℃ early to mixture with MoS_2+CaF_2 and the free lime quickly decrease at 1000-1100℃ which may be attributed to formation of early liquid and intermediate transition compounds (Fig 3) . The mixture has lower free lime vis-a-vis mixture with MoS_2 alone .

MoO_3 and CaF_2 in combination (Fig 4) can improve the decomposition of $CaCO_3$ and make the maximum point of free lime 50℃ early and exert a considerable effect on reducing free lime within the temperature region of 950-1200℃ , moreover , this action is not obvious at 1250-1350℃ in comparison with that of MoO_3 alone .

The complex effect of $CaSO_4$ and CaF_2 on accelerating the decomposition of $CaCO_3$ and lower the free lime of clinker is evident compared to the effect of $CaSO_4$

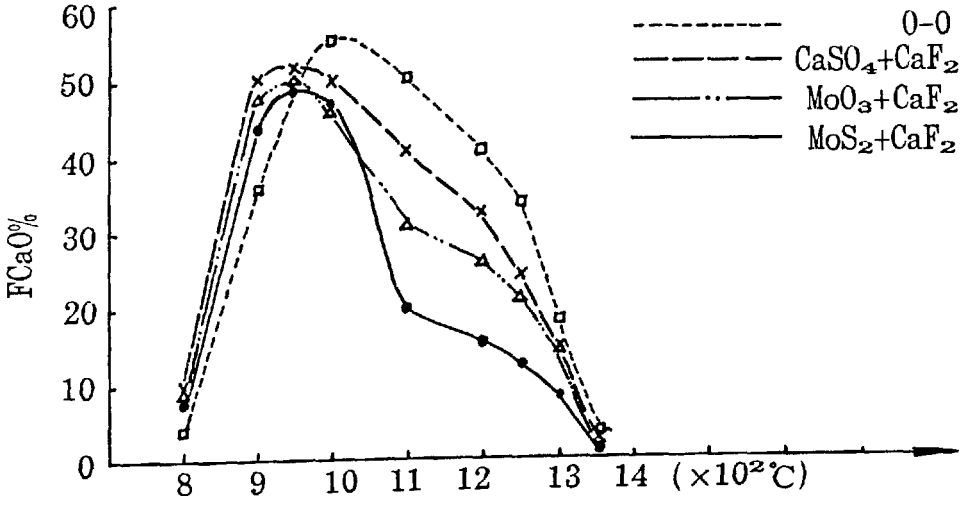

Fig . 7 Effect of complex mineralizers on burnability of raw mixes

alone (Fig. 5, 6) , but is smaller than that of 2% CaF_2 addition and higher than that of 1% CaF_2 addition .

Comparison of the complex mineralizer

The common behaviors of MoS_2 , MoO_3 , and $CaSO_4$ combined with CaF_2 respectively would improve decomposition of $CaCO_3$ and let the maximum point of free lime of mixtures ahead of 50℃ (Fig 7) . The decrease rate of free lime in mixtures at 1000 -1300℃ is MoS_2+CaF_2 > MoO_3+CaF_2 > $CaSO_4$+CaF_2 > 0-0 , and indicated difference among them is 10% separately at 1100℃ as well as the difference of free lime decrease when the temperature rise . The effect of complex mineralizer on reducing free lime is MoS_2+CaF_2 in first place , MoO_3+CaF_2 in second , and $CaSO_4$+CaF_2 in third . The different form of molybdic compounds produce the different influence on burnability of raw mixes and formation of clinker . The obvious effect of complex mineralizers on reducing free lime is owing to the decrease of liquid viscosity and the lower temperature of the liquid appearance which led to accelerate formation of alite and improve the burnability of raw mixes .

CONCLUSIONS

1. The formation rate to mixtures with separate mineralizer sintered at given temperature has the following order: MoS_2 > MoO_3 = CaF_2 > $CaSO_4$ > pure clinker at 1% addition ; and MoS_2 > CaF_2 > MoO_3 > $CaSO_4$ > pure clinker at 2% addition .
2. The common effect of MoS_2 , MoO_3 and $CaSO_4$ combined with CaF_2 respectively would improve the decomposition of $CaCO_3$ and make the maximum point of free lime earlier 50℃ .
3. The difference from of molybdic compound appears the difference behaviors on absorption of free lime and the effect of complex mineralizers on clinker formation is in the order of [MoS_2+CaF_2] > [MoO_3+ CaF_2] > [$CaSO_4$+CaF_2] > control sample .

REFERENCES

Chen,Y.M., et al. "C_3S formation at low temperature and its mechanism in fluoride high ferrite system .." THe 3rd Beijing International Symposium on cement and concrete, China , 1993 . Vol 1 , pp 223-228

Li,P.Q., et al. "Research and application of composite mineralizer in rotary kiln", 9th ICCC , New Delhi , 1992 . Vol 2 , pp 393-340 .

Pan, Y.Z., "Studies on producing Portland cement with tailing of molybdenum-iron ore" , 9th ICCC , New Delhi , 1992 . Vol 2 , pp 271-277 .

Timashev, V.V., "The kinetic of clinker formation . The structure and composition of clinker and its phases" 7th ICCC , Paris. , 1980 . Vol 1 , pp 1-17.

Xu, X.Y., Yan L.Q. , and Xiong Q.X. , "Study on effect of ZnO , BaO , CaF_2 , $CaSO_4$ on formation rate of clinker . "The 3rd Beijing International Symposium on cement and concrete , China , 1993 . Vol. 1 , pp 209-214

THE DISTRIBUTION OF MoO_3 IN CLINKER MINERAL PHASE

Yizhou PAN Yuechong CHI Xingfu FU
Zhejiang Building Materials Scientific Research Institute, Hangzhou, P. R. CHINA

ABSTRACT In this paper the influence of Mo ionic geometry size , electric structure and charge on silicate and aluminoferrite phases and selective distribution in minerals are studied on base of some concepts of solid physics and structural chemistry., and the effect of Mo ion on chemical activation of ferrite phase is also investigated .

Key-words: MoO_3 Calcium silicate Aluminoferrite Crystal structure

INTRODUCTION

The scope for utilizing tailing of minerals and industrial wastes to produce cement has recently widened owing to the necessity to utilize wastes and exploit new raw material resources . It is verified that the use of tailings of molybdenum iron produce cement clinker is not only considered as a substitute for all ferrous materials and parts of natural minerals of limestone and clay , but also acts as mineralizers instead of mineral gypsum and results in improving quality and output and decrease cost of cement manufacture (Pan 1992) . The mechanism of trace elements Mo on clinker formation has been discussed in published papers , but the solid solubility and distribution of Mo in various phases of clinker and the effect of it on structure of clinker are not clear from published date (Timashev 1980 , Kakali 1989 , Kakali 1990) . These problems need further studying . In this paper the influence of Mo ionic geometry size , electric structure and charges on silicate and aluminoferrite phases and selective distribution in minerals are studied on base of concepts of solid physics and structural chemistry .

EXPERIMENT

Materials and Methods

Raw mixes for the experimental work were proportioned by natural limestone , clay and iron power with the appropriate amount of chemical pure reagent MoS_2 according to the designed ingredients and mixed in a homogenizer . All raw mixes were thermally treated in an electrical furnace and cooled rapidly in air . Clinkers were fired at 1350℃ for one hour and gypsum (3% w/w) were respectively ground in a ceramic mill for 40 min, keeping w/c= 0.3 in all the cases , the mortar compressive strengths were measured on 20×20×20 mm specimens .

RESULTS AND DISSCUSION

Distribution of molybdenum in various phases of clinker

A previous study showed that the Mo is mainly dissolved in the interstitial phase and least in the silicate phase (Pan 1992) . It is further supported by the point energy spectrum analysis in clinker mineral phase (Fig. 1) , that Mo exists in a relatively minor amount and is similar contents of solid solution in dicalcium silicate and

This project is supported by the Zhejiang Natural Scientific Foundation, P. R. China

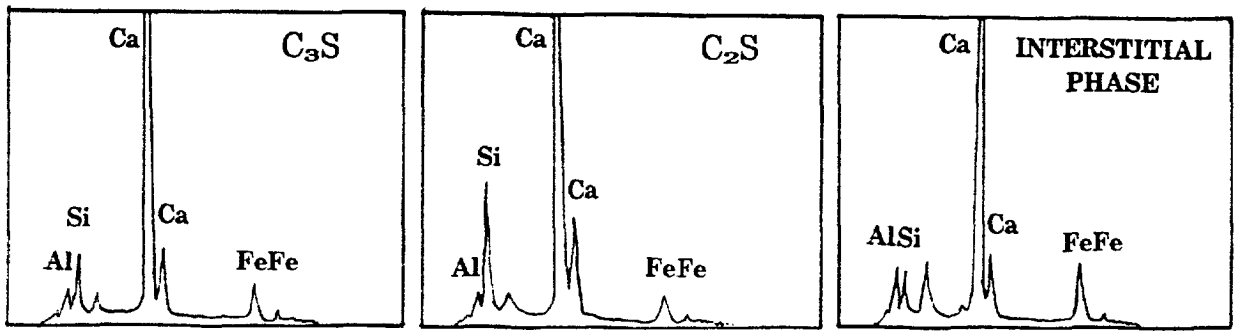

Fig. 1 The point energy spectrum curve of clinker with Mo

tricalcium silicate . Figure 2 shows the X-RD patterns of clinkers with and without Molybdenum . As it can be seen , the principal phases of clinker are satisfactory crystallized . The peaks of aluminate in two samples are similar but aluminoferrite of clinker containing Mo rise obviously . This indicates that molybdenum in interstitial phase mainly dissolved in the aluminoferrite phase .

Effect of molybdenum on silicate phase

As is known that silicate phase in clinker (C_3S , C_2S) is built up of the skeleton structure of silicon-oxygen radicals . Amphoteric Al^{3+} and Fe^{3+}ions with Si^{4+} ions can form partial dissolved solid solution due to radius difference between Al^{3+} , Fe^{3+} ions with Si^{4+} ions is >38%(table 1), as well as they exhibit a lower polarizability than do the silicon ions . Therefore , there is only minor replacement of Si^{4+} by Al^{3+} or Fe^{3+} . The different ratio of radius between Mo^{6+} ions with Si^{4+} ions is 47% , but the radius of Mo^{6+}ions is close to Fe^{3+} and Al^{3+}ions . The Mo ions in clinker may replay part of Fe^{3+} and Al^{3+} ions dissolved in alite and belite . Moreover , Mo^{6+} ions have high polarization ability and substitution potential of MoO_4^{2-} for SiO_4^{4-} forming solid solution . The amounts of substitution was limited by the difference of ion radius and charges . Therefore , the total amount of Mo dissolved in silicate phase is minor , which is in agreement with experimental results , the effect of adding Mo ions on internal structure of silicate phase is limited .

Table 1 Characteristic of Ions

Ions	Ionic Radius (R) A		Difference of Radius (%) $(R_i-R_{Si})/R_{Si}$	Polarizability C^2 / R	
	IV	VI		IV	VI
Si^{4+}	0.34	—	0	47.0	—
Ca^{2+}	—	1.08	—	—	3.7
Fe^{3+}	0.57	0.73	68	15.8	12.3
Al^{3+}	0.47	0.61	38	19.1	14.8
Mo^{6+}	0.50	0.68	47	72.0	52.9

Aluminoferrite solid solution with molybdenum

The XRD analysis indicate that Mo in clinker interstitial phase mainly existed in aluminoferrite phase . It is worth to discuss effect of Mo^{6+} ions on Fe^{3+} ions in the phase . Amophoteric Fe present in the mineral in the form of tetrahedral $[FeO_4]^{5-}$ and octahedral $[FeO_6]^{9-}$ groupings . For the radius difference of Mo^{6+}ion with Fe^{3+} is 12% , smaller than 15% , and the type of crystal structure of both ions is same , so they can form complete dissolved solid solution for each other. When Mo ions get into lattice of aluminoferrite phase , the formation of substitution type solid solution make the crystal structure strongly distorted and violate charges balance of original crystal as result improving the activity of ferrite phase .

Effect of molybdenum on the strength of clinker

Figure 3 shows the results of clinker mortar strength tests . Compared with the clinker samples without Mo, samples mixed with Mo exhibit better strength increase at early ages (3 days) at 0.5%-3% MoO_3 addition . The strength of clinker mixed with 2% MoO_3 reaches the maximum one and 0.5% MoO_3 addition in clinker is considered as optimum with high compressive strength which was measured at 28 days . the strength change of clinker containing Mo ions may be connected with Mo ions concentrated in the aluminoferrite phase according to the distribution of Mo in various phase .

Formation of solid solution of the substitution type

The radius of Mo ions is close to Fe ions and Mo can form complete dissolved solid solution with Fe ions in ferrite as well as cause the Fe coordination changes . When Mo ions replacing Fe ions and forming substitution type solid solution , Mo ions having smaller radius and higher valence and polarizability than that of Fe ions may occupy tetrahedral vacancies and make Fe^{3+} ions position from low coordination to higher one. The distance between iron and oxygen at octahedral is higher than that at tetrahedral. Therefore these results decrease the strength of Fe-O bands which were readily broken down in hydration process and increase the hydration of ferrite .

Effect of electrovalence

The replacement of Fe^{3+} by Mo^{6+} in aluminoferrite phase belongs to heterovalent replacement and creates cation vacancies to compensate unbalancing electric valences . The reaction of vacancies may be expressed by the following equation .

$$MoO_3 \xrightarrow{Fe_2O_3} Mo_{(Fe)}^{+++} + V_{(Fe)}''' + 3O_O^{\times}$$

The increase of vacancies amounts in ferrite phase lattice bring about the strong

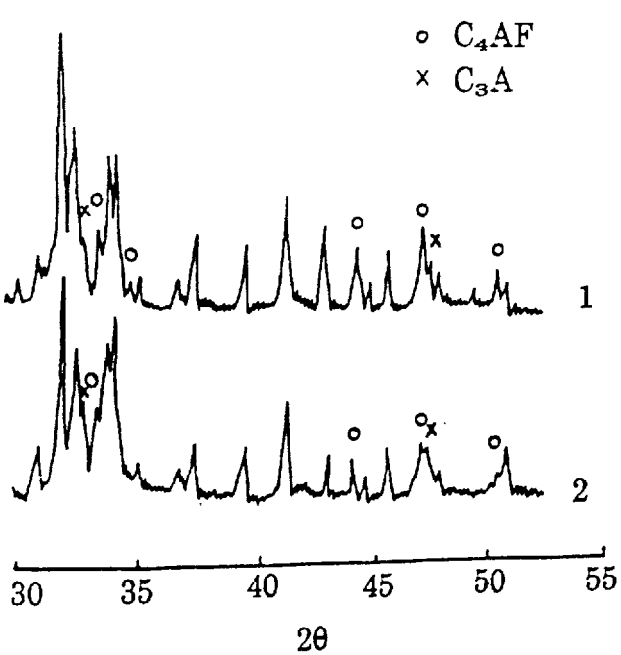

Fig. 2 XRD patterns of clinker
1. Clinker with Mo 2. Pure clinker

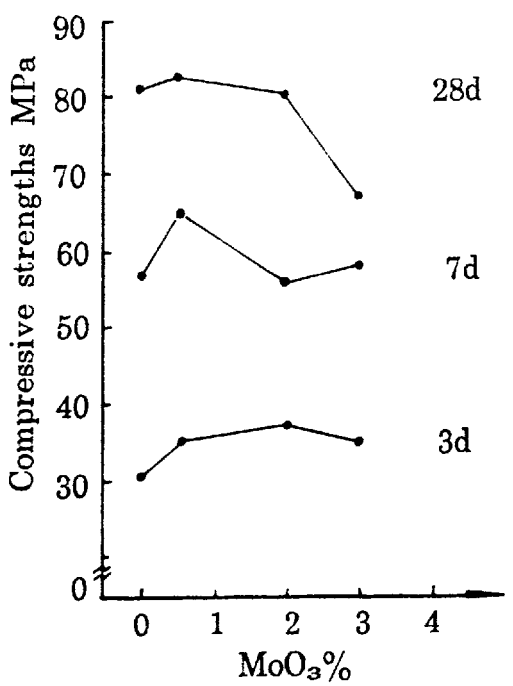

Fig. 3 Compressive strength of clinkers with different amounts of MoO_3

lattice distortion of the crystal structure and raising the internal energy . This results in all system get into thermodynamic instability , the vacancies of Fe^{3+} and composition defects in aluminoferrite produced in hetrovalent replacement destroy original regular arrange and increase the crystal imperfection and structure distortion as well as become the starting place of hydration when H^+ and OH^- ions of water enter the lattice of the crystal during the hydration process .

Polarizability of ions

The combination of ions in aluminoferrite crystal may be looked as mutual stacking of iron oxygen radius, Fe enters vacancies of tetrahedral and octahedral stacked by oxygen . Mo^{6+} ions having higher positive charges and smaller radius than that of Fe^{3+} ion , the polarizability of it is more than 4 times and 15 times of Fe^{3+} and Ca^{2+} ions respectively (table 1) , and that is able to affect the distortion of O^{2-} ions electric clouds and make them close to Mo^{6+}ions, which leads not only to increase the distance of Fe , Ca with O ions , reduce the strength of Fe–O and Ca–O bonds as well as create crystal structure distortion of ferrite with Mo , but also to raise the internal energy and instability of all structure and improve the chemical activity of the minerals .

Therefore one of the reasons of high early strength to clinker containing Mo is closely related to Mo^{6+} ions replacing Fe^{3+}ions to form solid solution of substitution type and produce a series of changes in aluminoferrite internal structure and increase the activity of hydration .

CONCLUSIONS

1 . Because of the characteristic of Mo ions , such as ionic radius , electrovalence and the polarizability . It is difficulty to form part dissolved solid solution with Si ions in silicate minerals , The proportion of Mo ions in silicate solid solution is finite .
2 . The radiuses of Mo and Fe ions are relatively close , Mo ions can form complete dissolved solid solution with Fe ions in aluminoferrite phase . This is the reason for molybdenum mostly dissolved in interstitial phase .
3 . In the clinker with Mo, the electric valence of Mo ion is different with Fe and solid solution of substitution type is formed when heterovalent replacement of Fe^{3+} ions by Mo^{6+}ions in aluminoferrite phase . This will modify the coordination number of iron ions, increase crystal imperfection and structure distortion , violate the regular range of atoms and result in higher internal energy and promoting aluminoferrite hydration .

REFERENCES

Kakali ,G., et al., "hydration and strength development of cements produced from raw mixes containing MoO_3 , Nb_2O_5 , WO_3 , ZnO_2", Cem Concr. Res., 1989, Vol19 , pp 968–972 .
Kakali ,G., et al., "Investigation of the effect of Mo , Nb , W and Zn oxides on the formation of portland cement clinker", Cem . Concr. Res., 1990 , Vol. 20 , pp 131–138 .
Timashev ,V.V. , "The kinetic of clinker formation . The structure and composition of clinker and its phases" 7th ICCC, Paris., 1980. Vol. 1 , pp 1–17.
Pan ,Y.Z., "Studies on producing Portland cement with tailing of molybdenum–iron ore", 9th ICCC , New Delhi , 1992. Vol. 2 , pp 271–277 .

CRYSTAL STRUCTURE REFINEMENT OF NA-SUBSTITUTED C_3A BY RIETVELD ANALYSIS AND QUANTIFICATION IN OPC

F. GOETZ-NEUNHOEFFER and J. NEUBAUER
Department of Mineralogy, University of Erlangen, Germany

ABSTRACT

In some OPC clinker non-cubic C_3A occurs alone or together with cubic C_3A. The presented study deals with full profile Rietveld quantification of C_3A in OPC clinker. Calculated and synthesized cubic and Na-substituted C_3A were refined as single phases, mixtures and synthetic blends of OPC.

Key-Words: Aluminate phase; quantitative; Rietveld analysis; structure; X-ray Powder Diffraction.

INTRODUCTION

During production process of Portland cement the clinker has to be controlled on-line to ensure a constant quality. The properties of the clinker are strongly depending on quantity and composition of the clinker phases. Phase quantification is commonly performed by Bogue calculation, microscopic methods or XRD-methods. An innovative and very reliable method to quantify multicomponent mixtures is the Rietveld analysis of XRD-data. Because the Rietveld method uses a pattern-fitting algorithm, all reflection lines for each phase are considered and overlapping reflections are not problematic. Phases with variable chemical composition can be formed during production process due to varying raw mixture composition and burning conditions. The possibility of structure refinement of this phases in the same step as phase quantification shows the advantage of the Rietveld analysis.

The aluminate phase C_3A is a main constituent of OPC clinker besides alite, belite and C_4AF. Normally C_3A crystallizes in the cubic space group Pa3 (Mondal & Jeffrey, 1975). C_3A forms solid solutions with some minor components such as Na_2O, MgO, K_2O, Fe_2O_3 etc., present in OPC clinker (Taylor, 1990). Substitution of Ca^{2+} by Na^+ leads to symmetry changes from cubic to orthorhombic and monoclinic (Takéuchi et al., 1980). In some OPC clinker non-cubic C_3A can be determined alone or together with cubic C_3A. For this study only the structures of cubic and orthorhombic C_3A were chosen for comparing the results of their quantification in OPC by Rietveld analysis. It was to clarify whether it is advisable to quantify C_3A phase in OPC with the cubic structure even when orthorhombic C_3A is found together with cubic C_3A.

EXPERIMENTAL

Cubic C_3A was prepared starting from a mixture of finely ground CaO and Al_2O_3. For synthesis of orthorhombic C_3A mixture of CaO, Al_2O_3 and the desired amount of Na_2CO_3 was used. In the case of orthorhombic C_3A certain excess of Na_2CO_3 was added to counteract the evaporation of Na_2O. The mixtures were sintered for 1h at 1350°C and after cooling finely powdered in a disc mill. Sintering and grinding process was performed ten times to get cubic and orthorhombic C_3A free of mayenite ($C_{12}A_7$). These by solid-state reaction synthesized samples and different blends of pure alite, belite, brownmillerite, cubic and orthorhombic C_3A were characterized by using X-ray powder diffraction method. All diffraction data were recorded with a SIEMENS D5000 X-ray diffractometer. For Rietveld analysis a modified program of S. A. Howard [a)] was employed.

[a)] A program for Rietveld analysis of X-ray and Neutron powder diffraction data: H 2.0

DESCRIPTION OF STRUCTURES

Cubic C_3A

The unit cell of cubic C_3A contains 72 Ca, 48 Al and 144 O atoms and the asymmetric unit consists of six Ca, two Al and six O atoms. The structure of cubic C_3A is built of sixfold rings of two types of distorted AlO_4 tetrahedra centered on threefold axes. (Mondal & Jeffrey, 1975). The rings of $(Al_6O_{18})^{18-}$ are highly puckered, such that the aluminum atoms lie near to six of the corners of a cube (Figure 1). The real cell (SG= Pa3, a_o=15,263Å, Z=24) is composed of 64 pseudo-cells. Eight of these subcells are occupied by $(Al_6O_{18})^{18-}$-rings. The Ca atoms occupy 56 body-centering positions of the subcells leaving eight of them vacant. The corners of the subcells are occupied by all of the 48 Al atoms and the remaining 16 Ca atoms. Depending on their position in the structure, two types of Calcium coordination can be distinguished (Moranville-Regourd & Boikova, 1992):

a) The Ca(1), Ca(2), and Ca(3) atoms at the corners of the subcells are octahedrally coordinated to the oxygen atoms
b) The Ca(4), Ca(5), and Ca(6) atoms in centered positions are irregularly coordinated

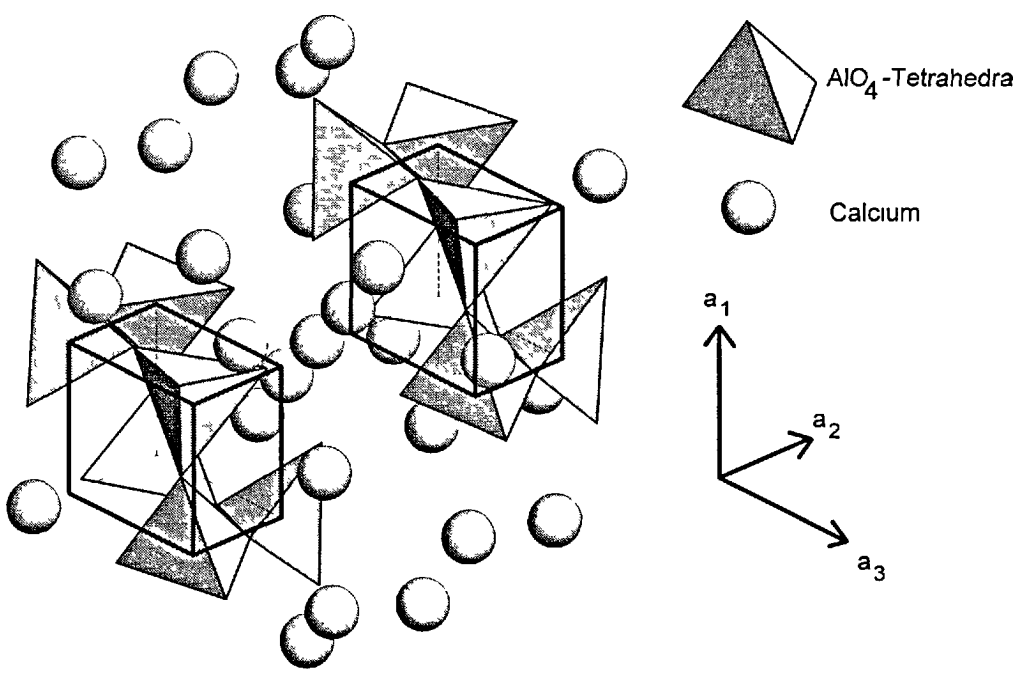

Figure 1: Part of the structure of cubic C_3A (Plotted with ATOMS[b)] according to structure data of Mondal & Jeffery, 1982)

Orthorhombic Na-substituted C_3A

The unit cell is now half the cubic cell volume with c_o-parameter remaining almost unchanged and with a_o different from b_o (SG=Pbca, a_o=1.0875Å, b_o=10.859Å, c_o=15,105Å, Z=12) (Nishi & Takéuchi, 1975). The Ca and Al atoms are distributed in the structure at positions very near to the corners and body centers of the pseudocubic subcells. Six tetrahedra are joined to form a distorted $(Al_6O_{18})^{18-}$-ring with a pseudo-threefold axis through the origin and the point 0,1/2,1/4.

---

b) ATOMS for Windows, V3.2, 1995, Eric Dowty

With regard to the pseudo-threefold axis, the apices of the tetrahedra are alternately pointing in one direction and the other Figure 2). There are 36 available locations for the 34 Ca atoms in the unit cell. The excess locations are preferably distributed in the set of Ca(5) positions to accommodate one half of the Na atoms. The remaining Na atoms are located at the centers of the tetrahedral rings, the origin of the cell.

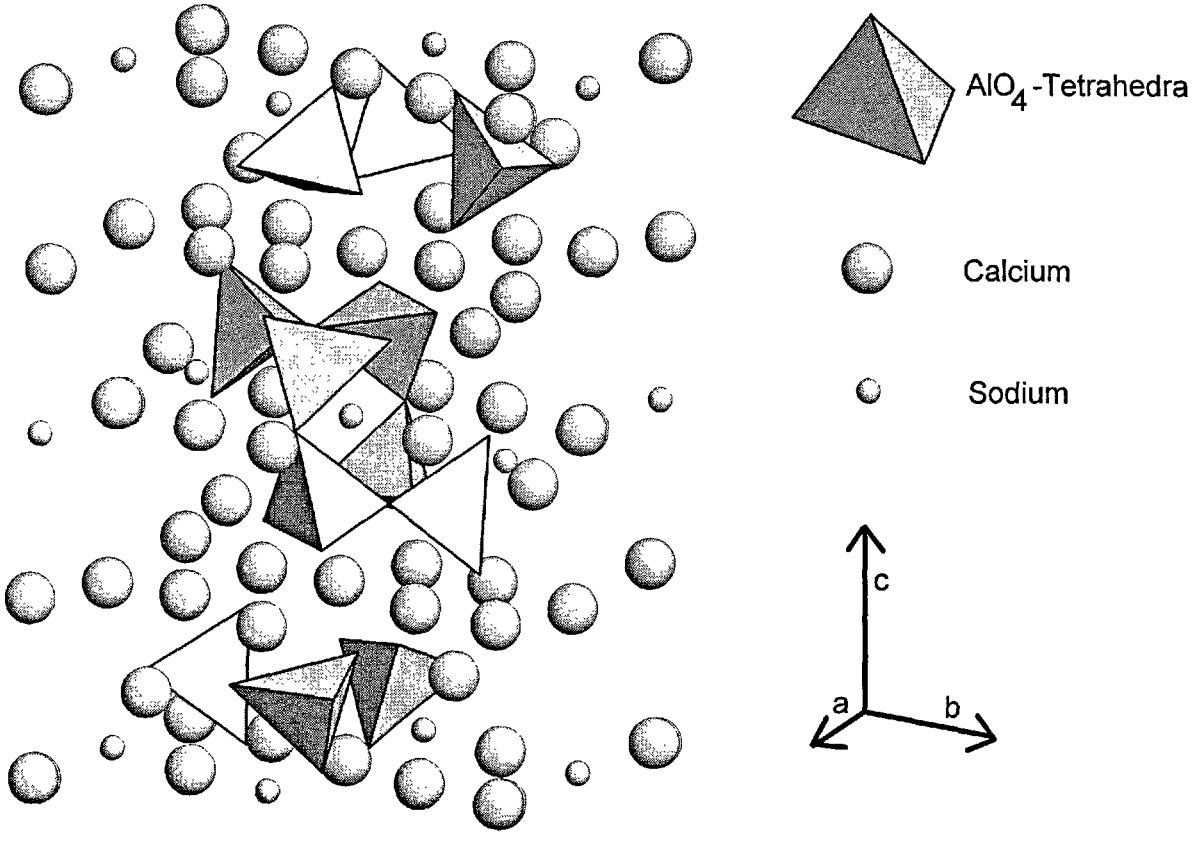

Figure 2: Part of the structure of orthorhombic Na-substituted C_3A (Plotted with ATOMS according to modified structure data of Nishi & Takéuchi, 1975)

RIETVELD REFINEMENT OF CALCULATED PLOTS

Theoretical XRD-diagrams of cubic C_3A on basis of structural data of Mondal & Jeffery (1982) and orthorhombic Na-substituted C_3A according to structural data of Nishi & Takéuchi (1975) were calculated with the Rietveld program. In Figure 3 two important ranges of the diagrams are plotted with the indices of the reflections (32,7-33,5°2Theta and 47,2-48,3°2Theta). The main reflection (044) of the cubic C_3A splits into the (224) and (400) reflections for the orthorhombic Na-substituted C_3A. In the second range it is shown that the (008) reflection of the cubic phase splits into (440) and (008) reflections for the orthorhombic phase.

Refinement of orthorhombic Na-substituted C_3A with the structure of cubic C_3A

Refinement of a calculated pattern of orthorhombic C_3A with the cubic structure shows best the main problem of accurate quantification of orthorhombic C_3A. Intensities of the difference plot are much higher than intensities of the refined phase. The symmetry change leads to split reflections for the orthorhombic phase with the consequence that neither intensities nor peak position can be refined correctly with the structure of the cubic phase.

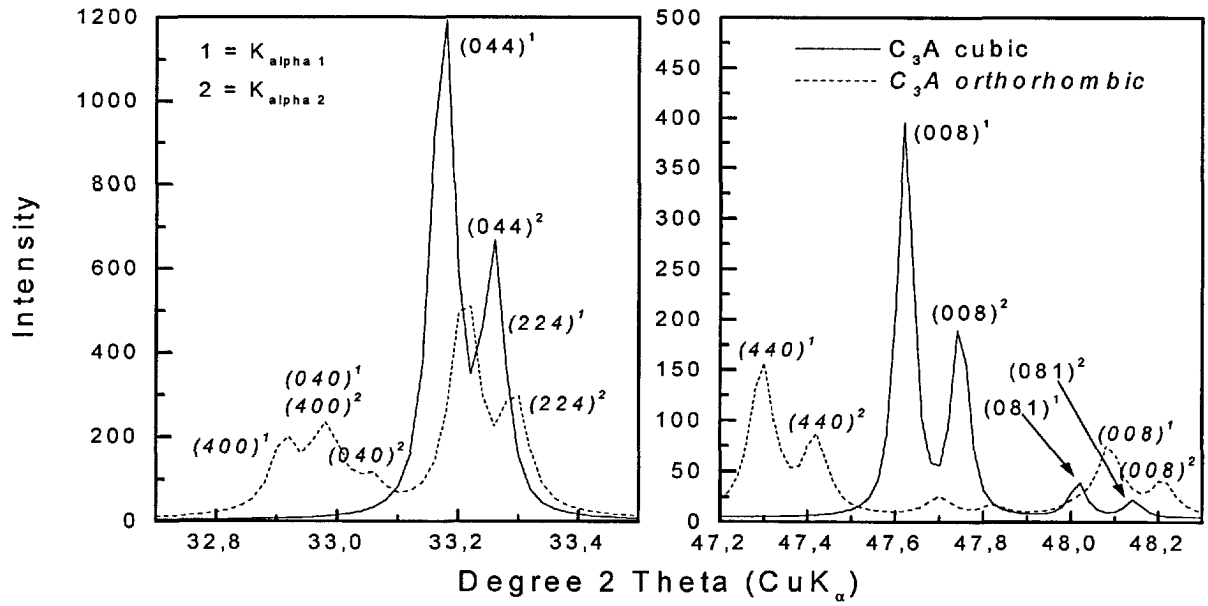

Figure 3: Calculated XRD-diagrams of the cubic C_3A and the orthorhombic Na-substituted C_3A

RIETVELD REFINEMENT OF SYNTHESIZED C_3A

In the next step full profile refinement of the synthesized C_3A phases was performed in order to control purity of the syntheses and to find a refinement procedure which gives the best fit of calculated with the observed pattern. In case of orthorhombic Na-substituted C_3A additionally occupancy factors were included in the refining procedure.

Refinement of pure cubic C_3A

For the refinement of cubic C_3A structural data of Mondal & Jeffrey (1982) were applied. The observed data were recorded with 0.02 °2 theta step size and 8s counting time. The refinement procedure included zero shift, background parameter, scale factor, Pearson coefficient, FWHM parameter, and lattice parameter. The remaining differences of calculated and observed pattern of cubic C_3A are due to intensity differences between refined and observed pattern. This fluctuations in intensity which are explained by statistical deviations can be reduced by increasing counting time. Table 1 shows the refined a_0-lattice parameter and residual errors.

Table 1: Refined a_0-lattice parameter and residual errors of cubic C_3A

	a_0-lattice parameter [Å]	*R [%]*	*R_{Bragg} [%]*
cubic C_3A	15.263±0.001	8.2	9.6

Refinement of pure orthorhombic Na-substituted C_3A

Synthesized orthorhombic Na-substituted C_3A, with a formula close to $Ca_{8.5}NaAl_6O_{18}$, was refined with the modified structural data of Nishi & Takéuchi (1975). One part of the Na atoms occupy positions at the centers of the tetrahedral rings and the other Na atoms are preferably accommodated in the set of Ca(5) positions.

The observed data were recorded with 0.02 °2 theta step size and 8s counting time. The refinement procedure included zero shift, background parameter, scale factor, Pearson coefficient, FWHM parameter, lattice parameter, and the occupancy factors. Table 2 shows the refined lattice parameter and residual errors.

Table 2: Refined lattice parameter and residual errors of orthorhombic Na-substituted C_3A

	a_o [Å]	b_o [Å]	c_o [Å]	R [%]	R_{Bragg} [%]
orthorhombic C_3A	10.866±0.001	10.846±0.001	15.115±0.001	8.2	8.8

RIETVELD REFINEMENT OF MIXTURES OF CUBIC AND ORTHORHOMBIC C_3A

Three mixtures of cubic and orthorhombic Na-substituted C_3A were investigated to proof the accuracy of quantification by the Rietveld method. The observed data were recorded with 0.02 °2 theta step size and 4s counting time. The refining procedure included zero shift, background parameter, scale factor, FWHM parameter, and lattice parameter. The results of quantification are listed in Table 3. From five independent experiments a maximum standard deviation of 0.7 wt. % was determined for both modifications of C_3A.

Table 3: Quantification of different mixtures of cubic C_3A and orthorhombic Na-substituted C_3A

Theoret. comp. [wt. %]		*Calc. Comp. [wt. %]*		*R [%]*	*R_{Bragg} [%]*	
Cubic	*Orthorh.*	*Cubic*	*Orthorh.*		*Cubic*	*Orthorh.*
50.0	***50.0***	50.7	49.3	9.8	7.6	8.8
75.0	***25.0***	73.7	26.3	10.4	6.9	12.0
25.0	***75.0***	26.7	73.3	8.0	7.4	12.3

Refinement of a mixture of 50% cubic C_3A and 50% orthorhombic Na-substituted C_3A

Figure 4 shows parts of the observed and refined plots of a mixture 50% cubic C_3A and 50% orthorhombic Na-substituted C_3A. In the range between 32.7 and 33.5° 2Theta the difference plots shows divergence at the positions where the $K_{\alpha 1}$ and $K_{\alpha 2}(044)$ reflection of the cubic phase and the $K_{\alpha 1}$ and $K_{\alpha 2}(224)$ reflection of the orthorhombic phase are overlapping.

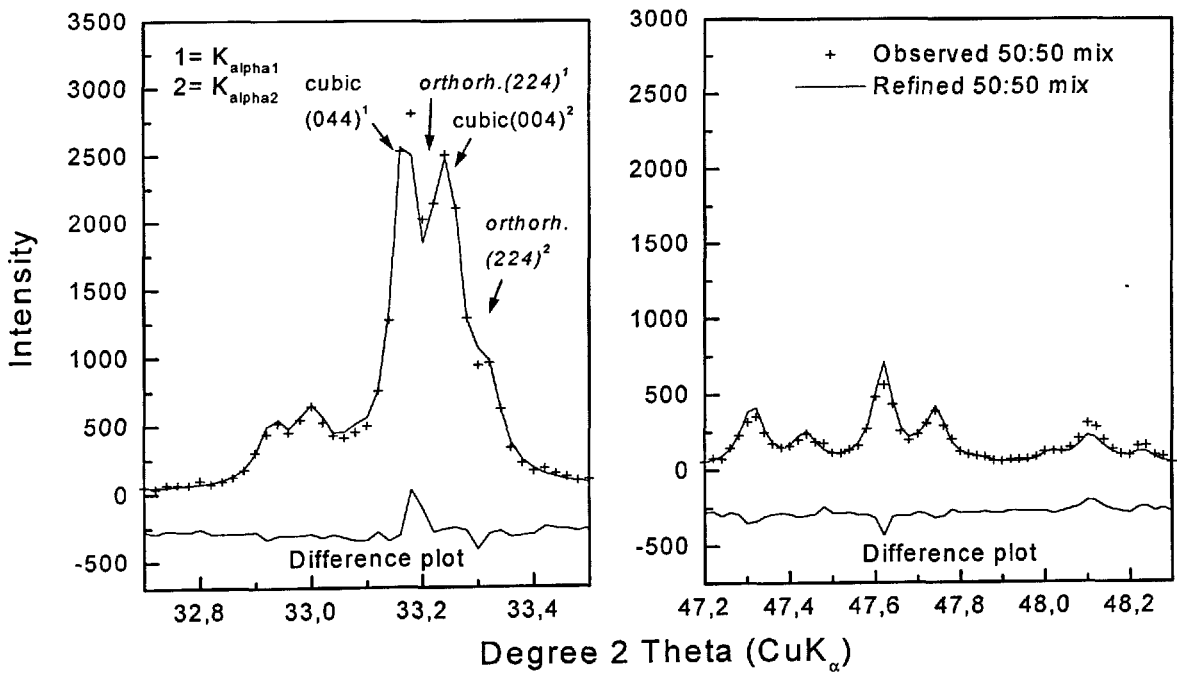

Figure 4: Parts of the observed and refined plots of a mixture 50% cubic and 50% orthorhombic C_3A

This divergence is due to statistical causes and can be diminished by reduction of step size or by increasing counting time. This does not influence the goodness of quantification. It could be shown that the optimized refining procedure which includes cubic and orthorhombic phase leads to very precise quantification results of a synthetic mixture of both phases.

RIETVELD REFINEMENT OF DIFFERENT SYNTHETIC BLENDS OF OPC WITH CUBIC AND ORTHORHOMBIC C_3A

Three synthetic blends of OPC clinker with cubic and orthorhombic Na-substituted C_3A were investigated and quantified by the Rietveld method. The observed data were recorded with 0.02 °2 theta step size and 4s counting time. The refining procedure included zero shift, background parameter, scale factor, FWHM parameter, and lattice parameter. The results of quantification are listed in Table 4 (Appendix A). From several independent experiments a maximum error of ±1.5 wt. % was determined for alite and belite and a maximum error of 0.8 wt. % for C_4AF and both modifications of C_3A.

In the last step of the presented investigation three synthetic clinker were quantified by the Rietveld method. Based on the results of the refinements of the mixtures of cubic C_3A and/or orthorhombic Na-substituted C_3A three quantification routines were created for evaluation of synthetic blends of OPC clinker:

Only C = refinement of the total C_3A in the blend with cubic structure
Only O = refinement of the total C_3A in the blend with orthorhombic structure
C&O = refinement of the total C_3A in the blend with both cubic and orthorhombic structure

The compositions of clinker A, B and C are listed in Table 4 (Appendix A). Total content of C_3A in synthetic clinker A - a mixture of cubic C_3A and orthorhombic Na-substituted C_3A with pure synthetic alite, belite and brownmillerite - is 15 wt. %. For synthetic clinker B only orthorhombic Na-substituted C_3A (15 wt. %) and for synthetic clinker C only cubic C_3A (10 wt. %) was added to pure synthetic alite, belite, and brownmillerite.

Figure 5 shows the results of quantification of cubic and orthorhombic Na-substituted C_3A in three mixtures of synthetic OPC clinker with different quantification routines.

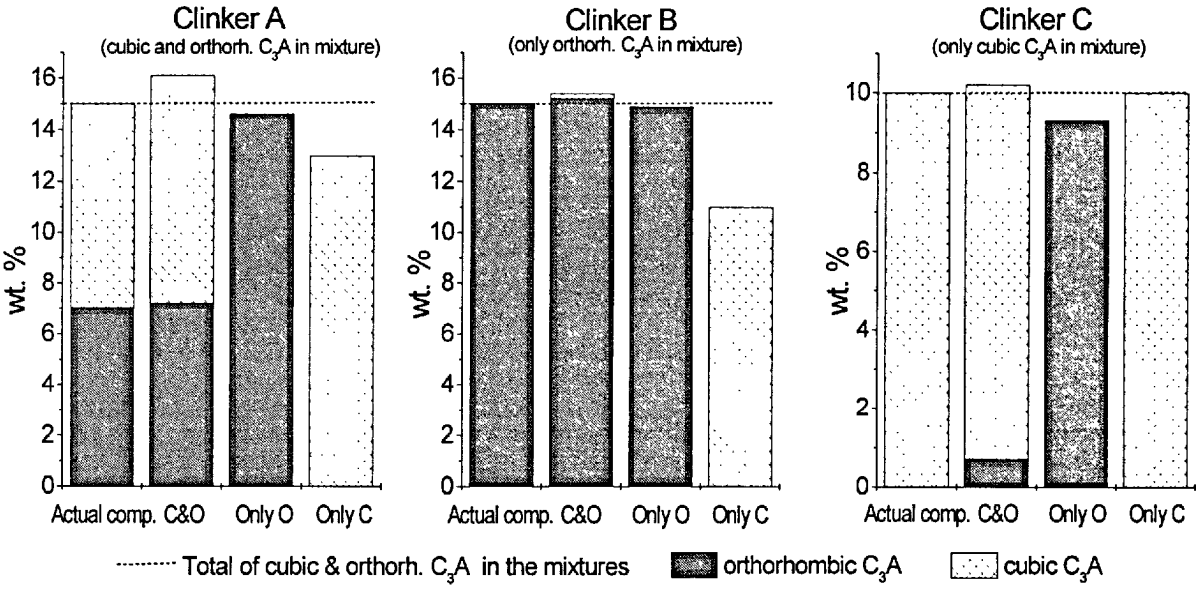

Figure 5: Results of C_3A quantification of three mixtures of synthetic OPC clinker with different quantification routines

For synthetic clinker A which contains cubic and orthorhombic C_3A the quantification routine ***O*** (both modifications were refined together with orthorhombic structure) and ***C&O*** (refinement with cubic and orthorhombic structure of C_3A) are leading to the best results for C_3A. In case of synthetic clinker B, which contains only orthorhombic C_3A, quantification results of both routines ***O*** and ***O&C*** are matching the actual content of C_3A in the blend. The best quantification of C_3A in clinker C (only cubic C_3A was added to the mixture) can be achieved with routine ***C***, but quantification with routine ***C&O*** is also reproducing the overall composition of the blend satisfactory. For quantification with routine ***O*** the error is still below 1 wt. %.

Results show best agreement of calculated and actual content of C_3A using refinement routines with only ***O*** or ***C&O***. Pure orthorhombic C_3A (clinker B) calculated with cubic structure (only ***C***) leads to deviations up to 4 wt. % from the given content. The main disadvantage of routine ***C&O*** is that more parameters have to be refined compared with routine ***C***. In case of very low contents of C_3A routine ***C&O*** is running not enough stable. After evaluating the results of all tested refinement procedures we found that routine ***O*** is best representing the overall content of C_3A in the synthetic clinker. This routine gives very precise results either for clinker A (cubic C_3A and orthorhombic Na-substituted C_3A in the mixture) or clinker B (only orthorhombic Na-substituted C_3A in the mixture) or clinker C (only cubic C_3A in the mixture).

CONCLUSION

For the refinement of cubic C_3A structural data of Mondal & Jeffrey (1982) were applied. Synthesized orthorhombic Na-substituted C_3A, with a formula close to $Ca_{8.5}NaAl_6O_{18}$, was refined with the modified structural data of Nishi & Takéuchi (1975). The best refinement of orthorhombic Na-substituted C_3A was achieved by using in addition to the structure data of Nishi & Takéuchi (1975) a position for the Na atoms in the set of Ca(5) which were refined together in one step.

A refinement procedure for different mixtures of cubic C_3A and orthorhombic Na-substituted C_3A which led to optimized quantification results was developed. It could be shown that the optimized refining procedure which includes both cubic and orthorhombic phase leads to very precise quantification results of a synthetic mixture. Remaining differences are due to statistical causes and can be diminished by reduction of step size or by increasing counting time.

For adjustment the results of Rietveld quantification of C_3A phase to quality control of OPC clinker we have tested the method with different blends of synthetic clinker with compositions of ordinary Portland cement clinker products. We found that routine ***O*** is best representing the overall content of cubic and orthorhombic C_3A in the synthetic clinker and is leading to very precise quantification results.

Nevertheless it has to be taken in account that the results of quantification of pure cubic and orthorhombic Na-substituted C_3A of very good crystallinity in the different mixtures can not be compared directly with the results in a multiphase system like OPC with 5-15 wt. % of C_3A phase and much lower crystallinity. For this reason the results need the adaption to an ordinary produced Portland cement clinker in a final step.

ACKNOWLEDGMENT

We thank P.O.G. Gaeberlein for performing the experimental part - syntheses and XRD - of the investigation.

REFERENCES

Mondal, P. & Jeffrey, W.J., "The crystal structure of tricalcium aluminate $Ca_3Al_2O_6$" Acta Cryst., 36, 1975, pp. 689-697.

Moranville-Regourd, M. & Boikova, A. I., "Chemistry, structure, properties and quality of clinker", 9th ICCC, New Delhi, Vol. 1, 1992, pp. 3-45.

Takéuchi, Y., Nishi, F. & Maki, I., "Structural aspect of the C_3A-Na_2O solid solutions", 7th ICCC, Paris, Vol, 4, 1980, pp. 426-431.

Taylor, H.F.W., "Cement Chemistry", Academic Press, London, 1990, p 475.

APPENDIX A:

Table 4. Results of quantification of three blends of synthetic OPC clinker with different quantification routines

Synthetic clinker A		*Quantification routine*		
Phase	*Actual comp.*	*Only C* [1)]	*Only O* [2)]	*C & O* [3)]
Alite [wt. %]	65	64.3	64.4	64.2
Belite [wt. %]	15	16.2	14.9	13.6
C_3A(orthorh.) [wt. %]	7	--	14.6	7.2
C_3A(cubic) [wt. %]	8	13.0	--	8.9
C_4AF [wt. %]	5	6.5	6.1	6.1

Synthetic clinker B		*Quantification routine*		
Phase	*Actual comp.*	*Only C* [1)]	*Only O* [2)]	*C & O* [3)]
Alite [wt. %]	65	66.0	64.9	64.5
Belite [wt. %]	15	18.2	15.2	15.1
C_3A(orthorh.) [wt. %]	15	--	14.9	15.2
C_3A(cubic) [wt. %]	--	11.0	--	0.2
C_4AF [wt. %]	5	4.8	5.0	5.0

Synthetic clinker C		*Quantification routine*		
Phase	*Actual comp.*	*Only C* [1)]	*Only O* [2)]	*C & O* [3)]
Alite [wt. %]	65	64.6	66.0	64.4
Belite [wt. %]	20	21.0	20.3	20.9
C_3A(orthorh.) [wt. %]	--	--	9.3	0.7
C_3A(cubic) [wt. %]	10	10.0	--	9.5
C_4AF [wt. %]	5	4.4	4.4	4.5

[1]) **Only C** = refinement procedure with cubic structure of C_3A
[2]) **Only O** = refinement procedure with orthorhombic structure of C_3A
[3]) **C&O** = refinement procedure with both cubic and orthorhombic structure of C_3A

PHASES IN HIGH-MAGNESIUM CLINKERS

BOIKOVA A.I., FOMICHEVA O.I. and LUGININA I.G.
Institute of Silicate Chemistry Russian Academy of Sciences, St.-Petersburg, Russia

ABSTRACT Phase composition and chemical compositions of phases in commercial clinkers containing up to 7 wt% MgO were studied by means of X-ray diffraction method and electron probe microanalysis. For comparison the phases in clinkers with a small amount of MgO (less than 1 wt%) were also considered. As usual all commercial clinkers studied contained a certain amount of other minor components (Na_2O, K_2O, MgO, TiO_2, SO_3). The hydration reactivity (degree of hydration) of MgO directly in clinkers was investigated by means of X-ray diffraction method.

Key-words: magnesium phases, solid solutions, hydration

INTRODUCTION

At the present time the problem of utilization of clinkers and cements with more than 5 wt% MgO is widely discussed, particularly with MgO content about 7 wt%. It is known that only about 2 wt% MgO can be incorporated into the lattices of four main clinker phases as a component of solid solutions. However, there are clinkers which contain less than 1 wt% MgO. Thus the amount of MgO in clinkers may be within sufficiently wide limits. One may suppose that phases in all such clinkers will differ concerning MgO content in solid solutions. Therefore the properties of magnesium containing clinkers and cements will depend not only on uncombined MgO (Periclas) but also on MgO content in phases as a component of solid solutions. The main task of our investigation consisted in elucidating the role of MgO in the formation of phases in clinkers with different amounts of this oxide. For all this it is necessary to pay attention to the presence of other minor components in solid solutions too.

EXPERIMENTS AND RESULTS

Chemical composition of phases of magnesium containing clinkers was studied by EPMA. Clinkers with MgO content both less than 1 wt% and about 7 wt% of this oxide were chosen. The results of chemical analysis of some clinkers studied are shown in Table 1. Two of them (N 1 and N 2) contain less than 1 wt% MgO while three clinkers (N 3, N 4 and N 5) contain about 6.5-7.0 wt% MgO.

Table 1 Chemical compositions of clinkers studied (wt %)

N clinkers	Oxides										Loss of ign.
	CaO	Al_2O_3	Fe_2O_3	SiO_2	Na_2O	K_2O	MgO	TiO_2	P_2O_5	SO_3	
1	65.16	4.31	4.06	23.13	0.36	0.80	0.66	0.43	0.03	0.20	0.78
2	66.62	5.56	3.77	21.34	0.17	0.86	0.65	0.18	0.09	0.34	0.45
3	61.20	5.14	4.34	20.13	0.12	0.78	6.41	0.00	0.05	0.33	0.91
4	60.62	5.27	4.84	19.82	0.11	1.16	6.37	0.00	0.11	1.16	0.44
5	60.17	5.01	4.17	20.28	0.21	1.51	6.92	0.22	0.15	0.89	1.00

Phase composition of clinkers studied depended both on MgO content and on the presence and the amount of the other minor components. X-ray diffraction analysis showed that clinkers with less than 1 wt% of MgO did not contain any Periclas (uncombined MgO) while in clinkers with about 7 wt% MgO there was about 6 wt% of Periclas. K_2SO_4 was detected in clinkers with potassium and sulphur. Almost all clinkers with these components contained belite in β- and α'- modifications. As usual alite was in a monoclinic form. Depending on the amount of Al_2O_3 and Fe_2O_3 aluminoferrite phase is a polycomponent solid solutions on the basis of 6:2:1 ($6CaO\ 2Al_2O_3\ Fe_2O_3$) or of 4:1:1 (clinker 5). X-ray and microscopical examination also showed that the presence of a considerable amount of magnesium in the clinker provides for the alite stable formation and existence conditions because magnesium suppresses the destructive influence of sodium, potassium, titanium, phosphorus and sulphur on the alite (Boikova, Fomicheva and Galafutnik, 1994; Moranville-Regourd and Boikova, 1992). The quantity of alite formed becomes maximal in clinkers with a high magnesium content. Thus, the X-ray examination of phase composition of clinkers with different amounts of alkali oxides showed that the material with 5-7 wt% MgO contained a higher quantity of alite (20% as high) than the clinker with less than 1 wt% MgO.
Chemical composition of phases in clinkers containing less than 1 wt% MgO and in those with about 7 wt% MgO were examined by means of EPMA. Table 2 contains the results of EPMA. The averaged data are given.

When analyzing the chemical composition of phases in magnesium containing clinkers attention should be drawn to the following points.
Firstly, the amount of MgO in the solid solutions of all phases increases with increasing amount of this oxide in clinkers. It is evident from the EPMA results. For example the amount of MgO in alite (clinker N 1 and N 2) is about 0.5 wt% while in alite of clinkers N 3, N 4 and N 5 it is about 1.7-1.8 wt%. The same is true for belite, calcium aluminoferrite and aluminate phases (see Table 2). It is useful to mention that among all clinker phases magnesium prefers to be situated into the lattice of calcium aluminoferrites due to Mg favourable tetrahedral and octahedral sites. Therefore the amount of MgO in the calcium aluminoferrite solid solutions is much greater than in any other phases. However the aluminoferrite phase in clinkers with a small amount of MgO (clinkers N 1 and N 2) contains smaller quantities of this oxide than that in clinkers with about 7 wt% MgO (clinker N 3, N 4 and N 5).

Secondly, attention should be drawn to the role of MgO in the formation of clinker silicate phases. It was found that the amount of minor components in the alite and belite solid solutions increases with the increase of MgO in the clinker (see Table 2). For example, the amount of minor components (in oxides) in alite solid solutions (clinkers N 1 and N 2) is about 2 wt% while that in clinkers N 3, N 4 and N 5 is about 4 wt%. This is approximately that maxima amount of minor components which can be incorporated into the alite lattice. This is also the case with belite phase. The amount of impurities in the belite lattice in clinkers with ≈ 0.5 wt% MgO is about 4.85 wt% while that in clinkers with 6.5-7.0 wt% MgO is about 6.5 wt%. The explanation for this fact comes probably from the decrease of viscosity of clinker liquid phase with increasing MgO amount which facilitates the process of complex composition phases formation. Earlier on the basis of investigation of commercial clinkers it was shown that the greatest amount of minor components are concentrated in the aluminate (≈ 12-13 wt% in oxides) and aluminoferrite (≈ 10-11 wt%) clinker phases owing to the peculiarities of their crystal structures. Belite and alite (especially the latter) are less capable of adopting minor component into the lattices than two other phases. Thus the maximum amount of minor components in the lattice of C_2S (belite) is about 6 wt% and that in C_3S (alite) is about 4 wt% (Boikova, Esayan and Lazukin, 1980; Boikova, 1986). Indeed the amount of impurities in the

lattices of alite and β-belite was found to be the maximal possible for these phases in high-magnesium clinkers.

Table 2. Chemical composition of phases in magnesium containing clinkers (wt %)

N[x]	Phases	Components of solid solutions									Σ impur. in phases
		Na_2O	K_2O	MgO	CaO	Al_2O_3	Fe_2O_3	SiO_2	TiO_2	SO_3	
1	a	0.14	0.10	0.46	73.72	0.82	0.96	23.50	0.08	0.04	2.60
	b	0.48	1.02	0.18	65.44	1.30	1.22	29.60	0.28	0.34	4.82
	af	0.38	0.62	2.20	50.94	2.32	20.32	3.38	0.96	0.08	7.62
	al	1.70	1.80	1.20	55.45	30.90	4.55	3.80	0.10	0.20	13.35
2	a	0.06	0.10	0.56	73.08	0.82	0.56	24.52	0.0	0.0	2.10
	b	0.36	1.20	0.38	62.64	1.62	1.20	32.24	0.12	0.20	5.08
	af	0.12	0.16	1.70	52.58	21.24	20.80	2.54	0.60	0.06	5.18
	al	0.95	0.90	0.40	55.90	34.30	3.65	3.55	0.0	0.15	9.60
3	a	0.16	0.12	1.84	70.60	0.98	0.86	24.78	0.0	0.24	4.20
	b	0.54	1.28	0.58	62.20	1.40	1.24	31.78	0.0	0.90	5.90
	af	0.15	0.18	2.63	48.03	23.40	22.73	2.45	0.0	0.45	5.90
	al	1.75	1.20	0.60	57.30	32.10	3.55	3.15	0.0	0.30	10.55
4	a	0.14	0.16	1.66	71.64	1.20	1.14	24.84	0.0	0.16	4.46
	b	0.50	1.15	0.60	61.20	1.80	1.48	32.45	0.0	0.77	6.30
	af	0.12	0.10	2.60	47.45	19.90	26.0	3,37	0.0	0.32	6.50
	al	2.00	2.35	0.50	57.00	30.80	3.50	3.45	0.0	0.30	12.10
5	a	0.08	0.32	1.70	71.00	1.38	1.55	23.00	0.0	0.37	5.40
	b	0.15	1.40	1.00	62.42	1.96	1.78	30.08	0.0	0.45	6.74
	af	0.10	0.20	2.85	43.92	23.00	28.42	1.46	0.0	0.30	4.91

[x] Clinker numbers are the same as in Table 1.
Abbreviations: a -alite, b - belite, af - aluminoferrite and al - aluminate phases.

EPMA showed that some high-magnesium clinkers contained individual crystals of unusual belite whose chemical composition differed from that of ordinary belite (β-belite). These unusual belite was identified as α'- and α-phases. These modifications contained somewhat more minor components in the lattices than β-belite and were similar to Bredigite and Nagelschmidtite. Clinker Periclas contain minor components in the lattice as well namely about 0.8 wt% CaO. 1.5 wt% Fe_2O_3 and 0.2 wt% SO_3.

Hydration behaviour (degree of hydration) of Periclas was examined by means of X-ray diffraction analysis according to the change of relative intensity of maxima. The experiment was unusual in that the hydration of this phase was studied directly in the clinker in the presence of other phases. For analysis the maximum at 20 43^0 in the pattern

was chosen which was overlapped neither by the maxima of other phases nor by those of hydration products. Samples were prepared in the paste form with a w/c ratio of 0.4 and placed into special cuvettes covered with a transparent amorphous and inert film. The sample of unhydrated clinker was also covered with such kind of film for identical conditions of X-ray patterns production. The experiment temperature was 20-22°C. When analyzing the results of hydration process of clinker phases on the basis of X-ray patterns attention should be paid to the fact that after a month of hydration under the conditions above Periclas was not found to have reacted with water in detectable amounts while the other phases did. Fig. 1 demonstrate quite clearly these results.

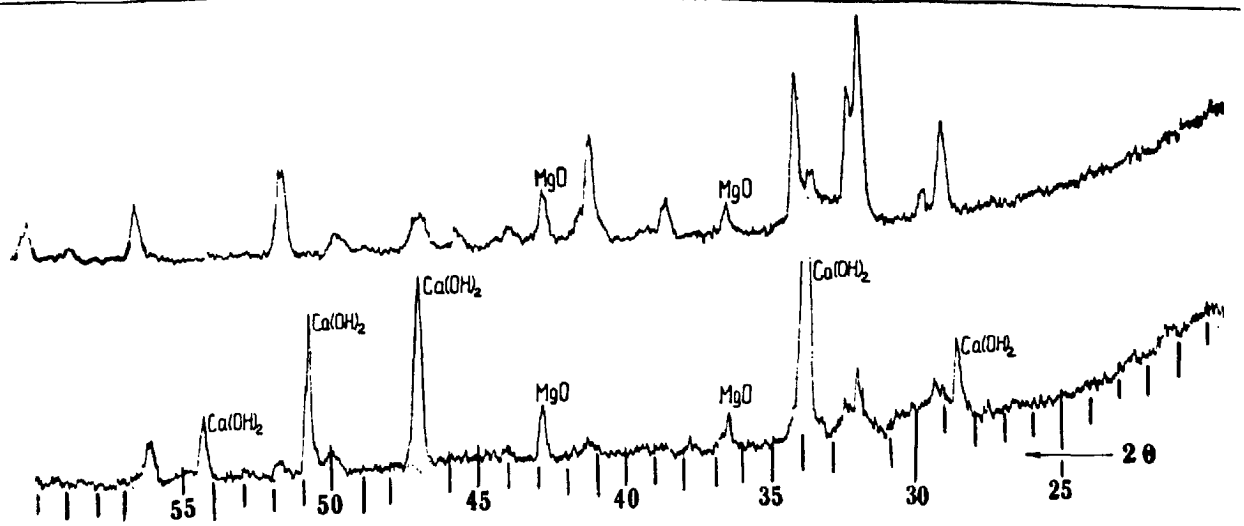

Figure 1 X-ray diffraction patterns of unhydrated (the upper pattern) and hydrated (the lower pattern) clinker N 3

The upper pattern in Fig.1 is one of clinker N 3 which shows the maxima of all main clinker phases including Periclas. The lower pattern is the pattern of the same but hydrated clinker N 3. One can observe in this figure unchanged MgO maxima, $Ca(OH)_2$ maxima as a result of hydration first of all of silicate phases and weakly intensive maxima of unreacted part of the main phases (alite, belite, calcium aluminoferrite and aluminate phases). Only after three month of hydration about 10-15 % of Periclas was found to have reacted.

CONCLUSION

When analyzing the data of the EPMA of phases for chemical composition of high-magnesium clinker, attention must be drawn to the following facts. All phases in high-magnesium clinkers contain the greatest possible amount of MgO as a solid solutions component. The MgO amount in phases of complex chemical composition is increased with the increase of the amount of this oxide in clinkers. The properties of high-magnesium clinkers and cements depend not only the amount of uncombined MgO (Periclas) but also on the amount of MgO in phases of complex composition. With increasing of MgO content in clinkers the amount of minor components in the solid solutions of silicate phases (alite and belite) is increased.

The quantity of alite formed becomes maximal in clinkers with high-magnesium content since magnesium oxide suppresses the destructive influence of sodium, potassium, titanium, phosphorus and sulphur on the alite structure. Due to EPMA we succeeded in detecting uncombined MgO (Periclas) even in clinkers containing less than 2 wt% MgO which we failed to achieve by X-ray diffraction method.

Investigation of periclas hydration (by X-ray method) in clinkers in the presence of other phases shows extremely passive behaviour of this phase during interaction with water under ordinary conditions.
So periclas was not found to have hydrated in detectable amount after a whole month of interaction with water.
Probably periclas begins to hydrate while other clinker phases have already interacted with water to a great exstent.
Periclas hydration inside the material during a long period of time has a negative effect on the properties of this material due to destructive character of the process.

REFERENCES

Boikova A.I., Fomicheva O.I. and Galafutnik L.G. "Role of MgO in the formation of clinker phases", Proc. 12 Int. Conf. Construction Materials, Weimar, Germany 22-24 September 1994, Vol. 3, pp. 324-329.
Moranville-Regourd M and Boikova A.I. "Chemistry, Structure, Properties and Quality of Clinkers", Proc. 9th Int. Congr. Chemistry of Cement, New Delhi, India, 1992, Vol 1, pp. 3-45.
Boikova A., Esayan A. and Lazukin V. "On the composition of cement minerals", Proc. 7th Int. Congr. Chemistry of Cement, Paris, France, 1980, Vol. 1Y, pp. 183-185.
Boikova A.I. "Chemical composition of raw materials as the main factor responsible for the composition, structure and properties of clinker phases", Proc. 8th Int. Congr. Chemistry of Cement, Rio de Janeiro, Brazil, 22-27 September, 1986, Vol 1, pp. 19-31.

ACKNOWLEDGEMENT

The authors are deeply grateful to Miss Tatiana Ignatova for her help in preparation of the manuscript.

BARIUM CONTAINING CLINKER PHASES

BOIKOVA Alexandra I., FOMICHEVA Olga I. and GRISHCHENKO Lubov V.
Institute of Silicate Chemistry of the Russian Academy of Sciences; St.-Petersburg, Russia

ABSTRACT Special role of barium is connected with protective properties against radiation of cements containing this element. This paper contains the results of the investigation of the distribution of barium between phases in commercial barium containing portland clinker by means of electron probe micro analysis. Besides barium containing clinker phases of complex chemical composition (polycomponent solid solutions) were synthesized and studied. Hydration properties of barium containing phases were also studied. Compressive strength of phases synthesized was determined.

Key-words: clinker barium phases, compressive strength

INTRODUCTION

It is known that barium containing wastes and components are used for clinker production. However there are no accurate data about interaction of barium with clinker phases. Such kind of investigation is primarily connected with the definition of the role of barium in the distribution of this element between the four main clinker phases in commercial clinkers. It is also important in this respect to possess information about the possibility of solid solution formation between $3CaO\ SiO_2$ and $3BaO\ SiO_2$ as well as between $2CaO\ SiO_2$ and $2BaO\ SiO_2$. It is known that there is wide field of solid solution between C_2S and Ba_2S on the basis of C_2S. However the information about the solid solutions of Ba_3S in C_3S is rather contradictory. There is also no common opinion about the existence of the compound $3BaO\ SiO_2$. Besides there are contradictory data about the influence of barium on the hydration properties of clinker phases as well as clinkers and cements.

EXPERIMENTS AND RESULTS

Barium containing commercial clinker was examined with respect to the distribution of barium between alite, belite and calcium aluminoferrite by means of electron probe microanalysis (EPMA). Attempts to find the aluminate phase suitable for EPMA failed.

All crystals looked like a fine intergrowth within the aluminoferrite phase.
Phase composition of clinker studied was determined by X-ray diffraction method and microscopic examination. According to these findings clinker contained alite, belite in the β- and α'-modifications, calcium aluminoferrite on the basis of 4:1:1 and not too much aluminate phase. Chemical composition of clinker studied is given in Table 1.

Table 1 Chemical composition of clinker (wt %).

SiO_2	Al_2O_3	Fe_2O_3	TiO_2	CaO	MgO	BaO	Na_2O	K_2O	SO_3	L.of Ign.	Σ
20.90	4.90	5.46	0.30.	62.73	0.95	0.65	0.35	0.95	0.36	2.90	100.45

The chemical composition of alite, belite and calcium aluminoferrite is presented in Table 2, according to EPMA results. Only some data are given here.
The results obtained show that barium tends to be incorporated into the belite lattice. So, barium becomes a component of polycomponent belite solid solutions together with other components (Na, K, Mg, Al, Fe, S). Polycomponent solid solutions of clinker phases may

be presented both in atomic and in oxide forms. In $2CaO\ SiO_2$ lattice Ba^{2+} can occupy the positions of Ca^{2+}.

Table 2 EPMA results of the chemical composition of phases.

Oxides wt% / Phases	Na_2O	K_2O	MgO	CaO	BaO	Al_2O_3	Fe_2O_3	SiO_2	SO_3
alite	0.2	0.2	1.2	70.0	0.1	1.1	1.7	25.5	0.0
	0.2	0.2	1.2	71.5	0.1	1.2	1.6	23.9	0.0
belite	1.1	2.6	0.5	59.2	1.0	1.4	2.0	32.8	0.2
	1.4	2.0	0.5	60.0	0.6	1.2	1.7	33.0	0.2
calcium alumino-ferrite	0.0	0.2	1.7	44.1	0.3	21.7	32.3	0.0	0.0
	0.1	0.2	2.1	41.3	0.4	22.4	32.9	1.0	0.0

EPMA showed the aluminoferrite phase to contain a smaller amount of barium then did belite. Less suitable for barium incorporation seems to be the crystal lattice of alite (see Table 2).

Another task of this study consisted in the synthesis of phases of complex composition having analogy with real clinker phases and in the investigation of their hydration properties (the compressive strength). Phase batches composition was chosen according to EPMA data of commercial clinker. The preparation of each of the phases appeared to be possible choosing an appropriate heat treatment schedule. Heat treatment of batches of each phase depends on their characters. The samples in the form of tablets were burnt under the following conditions: all samples were heated up to 1000°C and exposed at this temperature during 30 min; then the burning temperature of alite samples was raised up to 1450°C, the exposure was from 40 min up to 1 hour 20 min; the burning temperature of belite was 1350°C, the exposure was 40 min; the burning temperature of calcium aluminoferrite was 1300°C and the exposure 40 min. However after this burning schedule alite still contained some amount of uncombined CaO. Therefore alite was burnt a second time at 1450°C with 40 min exposure. The chemical composition of phases obtained was examined by chemical analysis. The identification of phases was made by means of X-ray diffraction. Table 3 gives the chemical composition of phases synthesized.

Table 3 Chemical compositions of phases obtained.

Oxides wt% / Phases	Na_2O	K_2O	MgO	CaO	BaO	Al_2O_3	Fe_2O_3	SiO_2	SO_3
alite 1	0.12	0.10	1.45	69.99	0.69	1.54	1.64	24.28	0.0
2	0.10	0.10	1.47	70.62	0.56	1.03	1.51	24.37	0.0
3	0.10	0.10	1.24	70.74	0.82	1.25	1.25	24.84	0.0
belite 1	1.10	2.46	0.61	57.25	2.08	1.54	1.44	32.45	0.25
2	1.15	2.08	0.62	58.14	1.52	1.33	1.62	32.83	0.30
3	0.82	2.46	0.43	57.69	1.07	1.40	2.04	33.20	0.29
4	1.16	1.87	0.40	58.78	0.71	1.25	1.63	33.13	0.39
calcium alumino-ferrite	0.22	0.30	1.38	41.79	0.93	21.78	31.63	1.48	0.0
	0.18	0.37	1.86	40.77	0.64	21.43	32.48	1.43	0.0

As an example we give the formula of each of the phase in atomic and in the generally accepted oxide form.

Alite (sample 1 according to the Table 3):
$3.09CaO\ SiO_2\ 0.005Na_2O\ 0.002K_2O\ 0.089MgO\ 0.01BaO\ 0.037Al_2O_3\ 0.025Fe_2O_3$;
$Ca_{3.09}\ Si_{1.00}\ Na_{0.01}\ K_{0.004}\ Mg_{0.09}\ Ba_{0.01}\ Al_{0.07}\ Fe_{0.05}\ O_{5.38}$.

Belite (sample 1):
$1.89CaO\ SiO_2\ 0.033Na_2O\ 0.048K_2O\ 0.028MgO\ 0.026BaO\ 0.028Al_2O_3\ 0.017Fe_2O_3$
$0.006SO_3$;
$Ca_{1.89}\ Si_{1.0}\ Na_{0.066}\ K_{0.096}\ Mg_{0.028}\ Ba_{0.026}\ Al_{0.056}\ Fe_{0.034}\ S_{0.006}\ O_{4.18}$;

Calcium aluminoferrite (sample 1):
$3.76CaO\ 1.08Al_2O_3\ 1.0Fe_2O_3\ 0.02Na_2O\ 0.015K_2O\ 0.17MgO\ 0.03BaO\ 0.13SiO_2$
$Ca_{3.76}\ Al_{1.08}\ Fe_{1.0}\ Na_{0.04}\ K_{0.03}\ Mg_{0.17}\ Ba_{0.03}\ S_{0.13}\ O_{10.50}$.

Fig.1 shows the X-ray diffraction patterns of the barium containing alite, belite as well as calcium aluminoferrite.

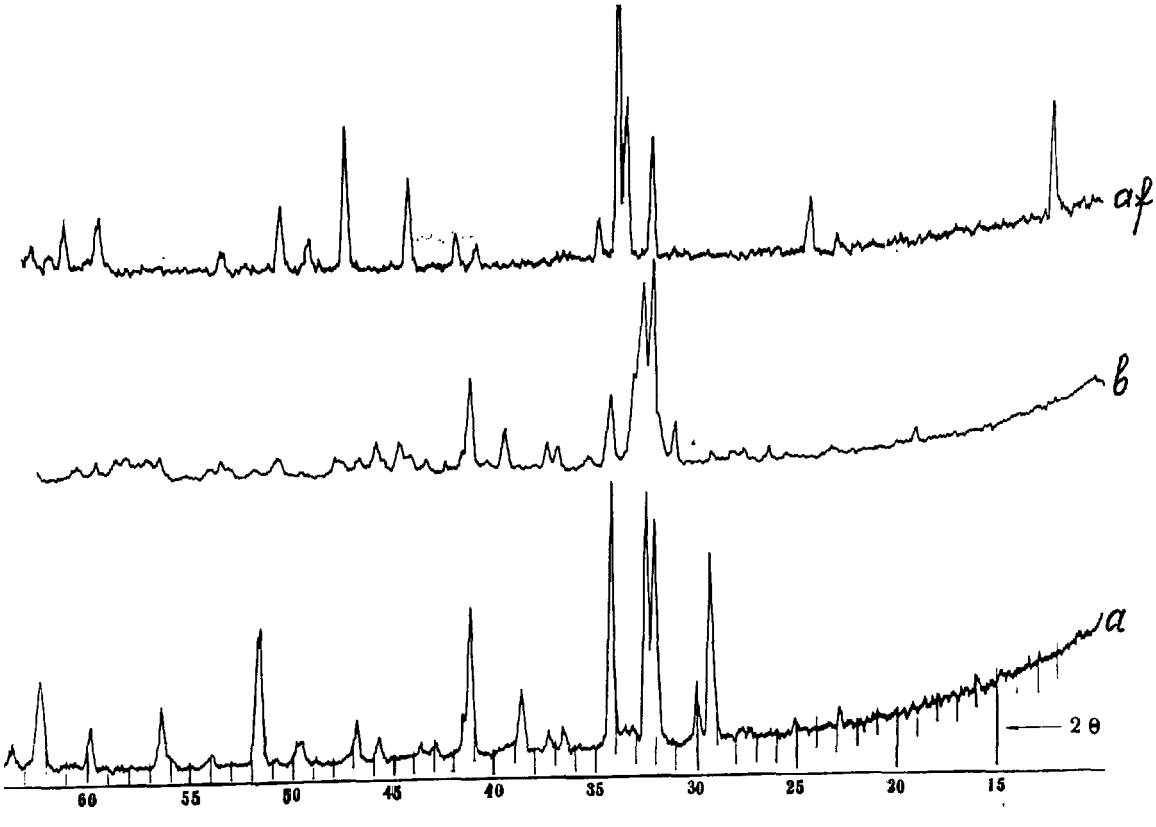

Figure 1 Bariumcontaining clinker phases synthesized: a - alite, b - belite, af - calcium aluminoferrite.

The broadening of many reflections in belite X-ray pattern is an evidence of imperfect crystallization of this phase.
X-ray examination permitted to reveal that samples of belites contain β-, α'- and α-modifications. Alite with Ba in its lattice is characterized by monoclinic symmetry.
Investigation tending towards obtaining the solid solutions of $3CaO\ SiO_2$ with $3BaO\ SiO_2$ have been taken up. Batches calculated on s.s. containing from 1.0 up to 5.0 wt% Ba_3S were burnt at 1500°C. It was revealed that samples with 1 wt% Ba_3S and more

contained C_2S and uncombined CaO. The more barium in the solid solutions batches the more C_2S and free CaO in the products. Barium appears to prevent the formation of C_3S. Solid solutions apparently can contain less than 1 wt% Ba_3S. As for Ba_3S, we would like to stress that the fact of existence of this compound is debatable. It is useful to mention, that there is a wide field of solid solutions between C_2S and Ba_2S on the basis of C_2S.
Due to the instability of C_3S or alite in the presence of barium it is better to use bariumcontaining wastes for clinkers with low Lime Saturation Factor (LSF).

The compressive strength of barium containing phases synthesized were examined. The value of compressive strength was obtained as the average sum of four measurements. The measurements were made on 10x10x10 mm cubes; w/c = 0.3; the granulometric composition was controlled by sieve N 0071; the temperature of experiment was 20-22^{0}C. The 28-day compressive strength of barium containing alites and calcium aluminoferrites were for alite: N 1 - 57 MPa; N 2 - 36 MPa; N 3 - 57 MPa and aluminoferrite: N 1 - 40 MPa; N 2 - 43 MPa. The sample number is the same as in Table 3.

Barium containing belite phases hardened very slowly. Their 28-day compressive strength was practically neglegible. The value of 3-month compressive strength was in the range of 12.5 - 17.5 MPa. It is important to mention that when estimating phase compressive strength value and considering the influence of barium it is necessary to take into account the presence of both barium and other minor components in solid solution structure.

CONCLUSION

The results of electron probe microanalysis (EPMA) of barium containing clinker shows thet barium tends to be incorporated first of all into the belite lattice. The aluminoferrite phase contained a smaller amount of barium. Less suitable for barium incorporation seems to be the crystal lattice of alite.

The complex phases analogous to phases of commercial clinkers were synthesized in laboratory conditions. The polycomponent solid solutions of belite contained the greatest amount of barium but not exceeding 2 wt% (as BaO). It was found that barium promoted stabilization of α' - and α - modifications of belite of complex composition. The synthesized Ca-aluminoferrite phase was obtained with smaller amount of BaO in polycomponent solid solutions. The smallest barium content was found in synthesized alite. It is important to stress that in the presence of barium alite is decomposed into belite and uncombined CaO.

Important conclusion could be drawn from the behaviour of alite in the presence of barium i.e. from its decomposition. It is resonable to use the barium containing wastes for clinkers with low Lime Saturation Factor.
The examination of hydration properties of barium containing phases permit to observe that barium containing belites seem to gain compressive strength quite slowly while barium containing alite is characterized by high value of compressive strength (up to 57 MPa). The value of compressive strength in calcium aluminoferrite is also high.

ACKNOWLEDGEMENT

The authors are deeply grateful to Miss Tatiana Ignatova for her help in preparation of the manuscript.

1i059
8 pp

Kn o. 18. JAN. 2001 d o k 31639

MONOMINERAL BINDERS IN $CaO-Al_2O_3-ZnO$ SYSTEM

Vladimir D. BARBANYAGRE, The Belgorod Technological Academy of Building Materials, Belgorod, Russia

ABSTRACT Two new ternary compounds having the composition of $3CaO{\cdot}2Al_2O_3{\cdot}ZnO$ and $14CaO{\cdot}5Al_2O_3{\cdot}6ZnO$ were synthesized in the $CaO-Al_2O_3-ZnO$ system. Their atomic structure, roentgenometric characteristics and some physicochemical properties were determined. Synthesized calcium aluminozincates are hydraulic binders and can be used as high-temperature putty under the conditions of a higher sulphuric anhydrite concentration.
CALCIUM ALUMINOZINCATES, BINDER, ISOMORPHISM, HYDRATION

INTRODUCTION

Zinc compounds are active catalysts in the processes of cement clinker sintering, only yielding to fluorides a little bit in this respect (Odler, Schmidt, 1980). The decrease in the quantity of an aluminate phase in clinker is observed with increasing ZnO concentration above 1%. It indirectly testifies to the fact that, first of all, zinc reacts with calcium aluminate and probably forms a more complex, ternary compound. This circumstance prompted an independent study of high-temperature interactions in the $CaO-Al_2O_3-ZnO$ system.

Ternary compounds of calcium aluminate with alkali oxides having the composition of $Na_2O{\cdot}8CaO{\cdot}3Al_2O_3$ and $K_2O{\cdot}8CaO{\cdot}3Al_2O_3$ (Susukawa, 1956), with barium oxides: $BaO{\cdot}2CaO{\cdot}4Al_2O_3$ (Brisi, 1962), strontium oxides: $Sr{\cdot}2CaO{\cdot}3Al_2O_3$ (Massazza, 1959) and magnesium oxides: $MgO{\cdot}3CaO{\cdot}2Al_2O_3$ (Majumdar, 1964), are known. However, judging from the literature available to us, the $CaO-Al_2O_3-ZnO$ system had not been studied.

HIGH-TEMPERATURE INTERACTIONS IN $CaO-Al_2O_3-ZnO$ SYSTEM

Fifty mixes having different molar ratios of components were prepared from original calcium, aluminium and zinc oxides of a chemically pure type. The components, as tablets, were heated up to 1450 °C in a furnace with silicon carbide electric heaters and were subjected to isothermal holding for 30 minutes (Barbanyagre, et al., 1990, 1991, 1992, 1994). Burning products were studied by X-ray phase, chemical, crystal optic, thermal and petrographic analyses. Diffraction peaks were revealed in diffractograms of a number of compositions which did not belong to original oxides and the known two-component compounds; they testified to the formation of a new unknown phase or phases. Varying the composition of mixes and burning conditions, we managed to produce a sinter in which diffraction peaks of original oxides and the known two-component compounds were practically absent. Crystal optic and petrographic analyses showed that the cake consisted of, at least, two phases with different refractive indices, crystal morphology and colour.

Using the different solubilities of these two phases in 1N hydrochloric acid, we managed to isolate one of the phases in a rather pure state and determine its preliminary bulk composition and roentgenometric characteristic. After that similar data were obtained for the second phase, too. The first phase occurring in the form of prismatic, colourless and white crystals was called a high-temperature phase (a HT phase). The second phase, represented by crystals of

an orange colour, was called tentatively a low-temperature phase (a LT phase). The ratio of oxides in moles, as follows:

a HT phase: $CaO : Al_2O_3 : ZnO = 3 : 2 : 1$

a LT phase: $CaO : Al_2O_3 : ZnO = 2.31 : 2 : 1.09$.

THE SYNTHESIS OF CALCIUM ALUMINOZINCATES

For the synthesis of the LT phase in the form of a hard polycrystalline cake it is sufficient to heat up a mix of original oxides to 1350° with 30 minutes' isothermal holding and subsequent fast cooling in air. The sequence of LT phase synthesis reactions has the following form:

$$CaO+Al_2O_3+ZnO \xrightarrow{850\text{-}1000^\circ C} CaO \cdot Al_2O_3 \xrightarrow{1000\text{-}1100^\circ C} CaO \cdot Al_2O_3+ZnO \cdot Al_2O_3$$

$$\xrightarrow{1100\text{-}1200^\circ C} CaO \cdot Al_2O_3 + ZnO \cdot Al_2O_3 + \text{LT phase} + \text{HT phase} \xrightarrow{1250\text{-}1300^\circ C}$$

$$ZnO \cdot Al_2O_3 + \text{LT phase} + \text{HT phase} \xrightarrow{1300\text{-}1350^\circ C} \text{LT phase}$$

The interaction of oxides in the mix having predetermined composition starts at 850 °C with $CaO \cdot Al_2O_3$ formation. Subsequently $ZnO \cdot Al_2O_3$ is formed within a range of 1000 - 1100 °C. The synthesis of calcium aluminozincates starts at 1100 °C and is complete at 1350 °C.

The synthesis of the second HT phase requires a slightly higher temperature and proceeds in the following sequence:

$$CaO+Al_2O_3+ZnO \xrightarrow{850\text{-}1000^\circ C} CaO \cdot Al_2O_3 \xrightarrow{1000\text{-}1050^\circ C} CaO \cdot Al_2O_3+ZnO \cdot Al_2O_3+\text{HT phase}$$

$$\xrightarrow{1100\text{-}1200^\circ C} CaO \cdot Al_2O_3 + ZnO \cdot Al_2O_3 + \text{LT phase} + \text{HT phase} \xrightarrow{1250\text{-}1300^\circ C}$$

$$ZnO \cdot Al_2O_3 + \text{LT phase} + \text{HT phase} \xrightarrow{1300\text{-}1400^\circ C} \text{HT phase}$$

The sequence of phase transformations under the synthesis of calcium aluminozincates has a multistage character with the formation of a number of intermediate compounds. It should be pointed out that both calcium zincates coexist within a certain range of temperatures and original oxide compounds. This fact created considerable difficulties at the initial stage of the synthesis of new phases and the interpretation of their roentgenograms.

THE SYNTHESIS OF CALCIUM ALUMINOZINCATE MONOCRYSTALS

The synthesis of calcium aluminozincate monocrystals was made to determine an atomic structure and specify a composition and physicochemical properties of new compounds (Table 1). The conditions of monocrystal synthesis were selected on the basis of the thermal analysis data and accomplished by a very slow crystallization of original melts.

The X-ray analysis of monocrystals (Ilyinets, Barbanyagre, 1990) allowed us to determine an atomic structure and a chemical formula of synthesized phases:

a LT phase: $Ca_{14}Al_{10}Zn_6O_{35}$ or $14CaO \cdot 5Al_2O_3 \cdot 6ZnO$ ($C_{14}A_5Z_6$)

a HT phase: $Ca_3Al_4ZnO_{10}$ or $3CaO \cdot 2Al_2O_3 \cdot ZnO$ (C_3A_2Z).

Table 1. Characteristics of synthesized zinc-containing compounds

Index	$Ca_{14}Al_{10}Zn_6O_{35}$	$Ca_3Al_4Zn_6O_{10}$
Molecular formula	$14CaO \cdot 5Al_2O_3 \cdot 6ZnO$	$3CaO \cdot 2Al_2O_3 \cdot ZnO$
Chemical composition, weight %	CaO = 44.04 Al_2O_3 = 28.65 ZnO = 27.30	CaO = 37.09 Al_2O_3 = 45.03 ZnO = 17.88
Cell parameters, Å	a = 14.868	a = 5.142 b = 16.756 c = 10.710
Space group	F23	Pbc2i, Z=4
Single crystals habit	Cubooctahedral	Hexagonal prismatic
IR-absortion bands (cm^{-1})	910; 850; 760; 700; 660; 560; 520; 485; 440	910; 800; 760; 680; 660; 585; 510; 440
Index of refraction	n = 1.750	n_1 = 1.702 n_2 = 1.706
Density, gr/cm^3	3.6	3.09
Microhardness	5.5	6.7
Single crystals melting point, °C	1425	1455
Single crystal colour	Orange	Colourless
Solubility: alcohol, acetone HCl, NaOH water	 non-soluble soluble hydrates	 non-soluble soluble hydrates
Hydrate phases	$CaO \cdot 2ZnO \cdot 5H_2O$; $n\,Zn(OH)_2 \cdot y\,Al(OH)_3 \cdot aq$; $2CaO \cdot Al_2O_3 \cdot 8H_2O$; Phase of non-established composition (d=7.98; 8.1 Å)	$2CaO \cdot Al_2O_3 \cdot 8H_2O$; $n\,Zn(OH)_2 \cdot y\,Al(OH)_3 \cdot aq$; Phase of non-established composition (d=7.98; 8.1 Å)

ROENTGENOMETRIC CHARACTERISTIC OF CALCIUM ALUMINOZINCATES

Roentgenometric characteristics of $Ca_3Al_4ZnO_{10}$ and $Ca_{14}Al_{10}Zn_6O_{35}$ monocrystals determined according to the powder method within a range of 2Θ = 5-164° are given in Tables 2 and 3. The diffractogram measurements of polycrystalline products of a solid-phase synthesis of the LT phase and the HT phase turned out to be identical accordingly. The diffractograms of both the compounds are characterized by the availability of the considerable number of intensive diffraction peaks which are not overlapped by reflections of calcium aluminates, aluminoferrites and silicates, what allows their certain identification in compositions of cements and other complex ceramic materials.

HYDRATION OF CALCIUM ALUMINOZINCATES

The interactions of calcium aluminozincates with water were studied in the diluted suspension at a liquid-to-solid ratio of 100 : 1 and in the paste at a liquid-to-solid ratio of 0.25 - 0.50 (Barbanyagre, Timoshenko, 1994).

C_3A_2Z Hydration

According to the data of the X-ray phase analysis a hydration product in the suspension has the following composition: $2CaO{\cdot}Al_2O_3{\cdot}H_2O$ (C_2AH_8); $n\,Zn(OH)_2{\cdot}y\,Al_2(OH)_3{\cdot}aq$ and an X-ray amorphous gel phase forming a diffusion halo within a range of 2Θ = 15 - 26° and 30 - 42° in the diffractogram. Hydrate phases are carbonized comparatively easily with $C_3A\,CaCO_3{\cdot}12H_2O$ formation.

$C_{11}A_5Z_6$ Hydration

$C_{14}A_5Z_6$ hydration in the suspension produces the following hydrate phases: $CaO{\cdot}2ZnO{\cdot}5H_2O$ (CZ_2H_5); $n\,Zn(OH)_2{\cdot}y\,Al(OH)_3{\cdot}aq$; C_2AH_8; gel formation is not observed.

HYDRAULIC PROPERTIES OF CALCIUM ALUMINOZINCATES

Hydraulic properties of calcium aluminozincates were studied in the form of pastes at a liquid-to-solid ratio of 0.25 - 0.50. Due to the limited quantity of the synthesized material, setting time and strength were determined using samples with reduced sizes under nonstandard conditions. For C_3A_2Z, initial set occurs in 45 minutes and the completion of the set in 55 minutes. For $C_{14}A_5Z_6$, set is completed in 30 seconds and retarders are required for practical applications.

It was established that saccharose, boric acid, citric acid and glycerine considerably retarded the setting. Sodium salts, acetic acid, hydrochloric acid and triethanolamine accelerated the setting. In that case gypsum additions up to 10 % did not exert a considerable effect.

The strength of cube-samples having 1.4 cm edge size and 20 ± 2 °C is given in Table 4.

Table 2. X-ray (Cu, K_α) powder diffraction pattern of $Ca_{14}Al_{10}Zn_6O_{35}$ (d,Å; I, %)

d_{calc}	d_{obs}	I	h	k	l	d_{calc}	d_{obs}	I	h	k	l
8.5840	8.585	5	1	1	1	1.3142	1.1342	6	8	8	0
5.2566	5.257	1	2	2	0	1.2990	1.2992	4	9	7	1
4.4829	4.483	13	3	1	1	1.2941	1.2943	4	8	8	2
4.2920	4.292	4	2	2	2	1.2566	1.2567	3	10	6	2
3.7170	3.717	2	4	0	0	1.2390	1.2392	1	12	0	0
3.4110	3.411	7	3	3	1	1.2263	1.2263	2	11	5	1
3.3246	3.325	13	4	2	0	1.2221	1.2221	2	12	2	0
3.0349	3.035	18	4	2	2	1.2060	1.2061	4	12	2	2
2.8613	2.861	63	5	1	1	1.1942	1.1941	2	11	5	3
2.6283	2.628	100	4	4	0	1.1754	1.1755	3	12	4	0
2.5132	2.513	41	5	3	1	1.1610	1.1611	2	10	8	0
2.4780	2.479	17	6	0	0	1.1370	1.1370	5	11	7	1
2.3508	2.351	8	6	2	0	1.1113	1.1114	3	13	3	1
2.2673	2.267	19	5	3	3	1.0961	1.0962	2	12	6	2
2.2414	2.242	6	6	2	2	1.0873	1.0872	5	13	3	3
2.1460	2.1460	6	4	4	4	1.0647	1.0648	3	13	5	1
2.0819	2.0823	7	5	5	1	1.0513	1.0513	2	14	2	0
2.0618	2.0620	5	6	4	0	1.0435	1.0436	2	11	9	1
1.9869	1.9869	7	6	4	2	1.0410	1.0409	2	10	10	2
1.9356	1.9363	26	7	3	1	1.0211	1.0211	3	14	4	0
1.8585	1.8588	13	8	0	0	1.0047	1.0049	5	13	7	1
1.8030	1.8030	5	8	2	0	0.9934	0.9934	3	12	8	4
1.7522	1.7527	15	6	6	0	0.9868	0.9868	2	15	1	1
1.7168	1.7172	17	7	5	1	0.9847	0.9847	2	14	4	4
1.7055	1.7054	2	6	6	2	0.9678	0.9678	2	14	6	2
1.6623	1.6625	3	8	4	0	0.9538	0.9538	1	15	3	3
1.6320	1.6321	7	9	1	1	0.9518	0.9518	2	12	10	0
1.6222	1.6226	6	8	4	2	0.9385	0.9385	3	15	5	1
1.5849	1.5852	7	6	6	4	0.9239	0.9239	1	15	5	3
1.5586	1.5589	9	9	3	1	0.9151	0.9151	2	14	8	2
1.5175	1.5176	33	8	4	4	0.8949	0.8949	2	16	4	2
1.4943	1.4942	3	7	7	1	0.8838	0.8838	1	15	7	3
1.4579	1.4580	4	10	2	0	0.8761	0.8761	3	12	12	0
1.4373	1,4375	21	7	7	3	0.8701	0.8701	2	16	6	0
1.3864	1.3864	2	9	5	3	0.8642	0.8642	4	14	10	0
1.3573	1.3573	4	10	4	2	0.8584	0.8584	2	14	10	2
1.3406	1.3406	2	11	1	1	0.8486	0.8486	1	17	3	3
						0.8472	0.8472	1	16	6	4

Table 3. X-ray (Cu, K_α) powder diffraction pattern of $Ca_3Al_4Zn_6O_{16}$ (d, Å; I, %)

d_{calc}	d_{obs}	I	h	k	l	d_{calc}	d_{obs}	I	h	k	l
8.3780	8.378	3	0	2	0	1.4892	1.4894	6	3	3	3
6.5988	6.599	2	0	2	1	1.4772	1.4775	4	2	5	5
4.4676	4.468	5	1	1	1	1.4609	1.4609	11	1	1	7
4.1890	4.189	8	0	4	0	1.4497	1.4500	7	3	4	3
4.0560	4.056	13	1	2	1	1.4371	1.4375	23	0	4	7
3.9012	3.901	19	0	4	1	1.4178	1.4177	8	2	6	5
3.7090	3.709	24	1	0	2	1.3586	1.3582	5	0	8	6
3.6213	3.621	7	1	1	2	1.3418	1.3422	9	0	6	7
3.2843	3.284	8	0	2	3	1.3135	1.3135	5	1	8	6
3.0898	3.090	25	1	3	2	1.3064	1.3064	3	2	10	3
2.8886	2.888	100	1	1	3	1.2917	1.2918	3	1	1	8
2.7927	2.793	15	0	6	0	1.2817	1.2814	3	4	1	0
2.7679	2.768	26	1	2	3	1.2748	1.2749	3	3	4	5
2.7158	2.716	44	1	5	1	1.2607	1.2607	4	1	12	3
2.6775	2.678	6	0	0	4	1.2418	1.2422	3	1	13	1
2.5964	2.597	5	1	3	3	1.2355	1.2357	3	0	8	7
2.5413	2.541	8	2	1	0	1.2289	1.2290	2	4	4	0
2.4865	2.487	29	1	5	2	1.2063	1.2060	2	4	1	3
2.4762	2.476	27	0	6	2	1.1874	1.1874	2	2	0	8
2.4579	2.458	14	2	2	0	1.1753	1.1757	2	1	6	8
2.4024	2.402	11	1	4	3	1.1561	1.1563	4	4	1	4
2.3355	2.336	20	2	3	0	1.1424	1.1420	5	2	4	8
2.2848	2.285	6	1	2	4	1.1377	1.1380	7	4	5	3
2.2560	2.256	7	0	4	4	1.1347	1.1343	3	4	3	4
2.2310	2.231	5	1	6	2	1.1298	1.1298	3	0	10	7
2.2069	2.2070	7	1	5	3	1.0948	1.0950	2	0	6	9
2.1855	2.1856	3	1	3	4	1.0814	1.0816	1	4	3	5
2.1407	2.1408	5	2	3	2	1.0624	1.0628	2	0	2	10
2.0223	2.0225	11	1	6	3	1.0344	1.0344	2	2	10	7
2.0038	2.0039	4	2	5	1	1.0249	1.0250	2	1	10	8
1.9506	1.9505	6	0	8	2	1.0108	1.0110	3	1	15	4
1.9327	1.9330	15	0	6	4	1.0019	1.0019	3	4	10	2
1.9087	1.9088	5	1	8	1	1.0000	1.0000	9	0	6	10
1.8627	1.8628	7	2	6	1	0.9862	0.9862	2	1	16	3
1.8545	1.8546	8	2	0	4	0.9841	0.9841	2	1	9	9
1.8065	1.8065	8	0	8	3	0.9813	0.9813	2	3	14	0
1.7835	1.7840	26	2	6	2	0.9699	0.9699	3	2	16	0
1.7600	1.7600	14	2	3	4	0.9671	0.9671	3	0	2	11
1.7290	1.7290	3	2	7	1	0.9326	0.9330	3	1	4	11
1.7140	1.7144	5	3	0	0	0.9305	0.9305	3	5	7	2
1.6996	1.6998	9	0	6	5	0.9199	0.9201	3	1	5	11
1.6792	1.6793	5	3	2	0	0.9134	0.9134	3	3	11	7
1.6639	1.6639	4	1	9	2	0.8456	0.8457	2	2	17	5
1.6421	1.6425	8	0	4	6	0.8423	0.8425	2	3	2	11
1.6148	1.6150	5	2	2	5	0.8320	0.8320	2	2	18	4
1.5931	1.5931	2	1	10	0	0.8271	0.8271	2	5	5	7
1.5669	1.5669	7	3	3	2	0.8249	0.8251	1	0	16	8
1.5195	1.5197	25	3	2	3	0.8212	0.8110	2	5	10	5

Table 4. Hydraulic activity of monomineral binders

se. No.	Binder	Specific surface, m^2/kg	H_3BO_3, %	Liquid-to-solid ratio	Compressive strength, MPa, at the age		
					3 days	7 days	28 days
1	C_3A_2Z	270	-	0.25	-	47.3	47.9
2	-"-	-"-	-	0.30	-	38.0	45.6
3	-"-	-"-	-	0.40	-	35.7	43.2
3	-"-	-"-	-	0.50	-	25.9	38.8
5	-"-	-"-	1	0.25	27.9	25.3	58.9
6	$C_{14}A_5Z_6$	265	-	0.25	-	45.3	54.9
7	-"-	-"-	-	0.30	-	40.2	49.6
8	-"-	-"-	-	0.40	-	36.7	43.1
9	-"-	-"-	-	0.50	-	23.7	34.8
10	-"-	300	1	0.25	34.0	38.4	57.3
11	CA	-	-	-	-	21.2	24.8
12	CA_2	-	-	-	-	8.6	7.0
13	C_5A_3	-	-	-	-	35.7	36.7
14	C_3A	-	-	-	-	7.7	7.2
15	$C_{12}A_7$	-	-	-	-	36.0	38.0

* 11-15 according to the literature data

The data given in Table 4 show that calcium aluminozincates can be used as special-purpose hydraulic binders as they surpass many well-known calcium aluminates in strength. In this case the hydration degree of $C_{14}A_5Z_6$ samples reached 30 % in a day, 38 % in 3 days, 42 % in 7 days and 50 % in 28 days. Although its degree of hydration was 1.5 times higher, as compared with C_3A_2Z, the strengths of both the binders were roughly similar.

$C_{14}A_5Z_6$ hydration products are distinctly more crystalline relative to C_3A_2Z where gel predominates. Unlike calcium aluminates, the recrystallization of hexagonal hydroaluminates into cubic C_3AH_6 is not observed even after 6 months' water hardening under the hydration of calcium aluminozincates.

Calcium aluminozincate having the $C_{14}A_5Z_6$ composition was identified by us in the composition of white clinker, when adding zinc oxide into the original raw mix. A new phase is synthesized within a temperature range of 1000 - 1200 °C, and at 1280 °C it forms a melt having low viscosity, which accelerates considerably the formation of all clinker minerals. $C_{14}A_5Z_6$ is crystallized out only under slow cooling, occurring in the form of glass during fast clinker cooling. Calcium aluminozincate having the $C_{14}A_5Z_6$ composition decreases the sintering temperature of white clinker by 100 - 150 °C and increases its hydraulic activity by 15 - 20 % and whiteness by 7 - 8%.

CONCLUSIONS

1. A rare variant of heterovalent isomorphism is observed in the process of a high-temperature interaction in the CaO - Al_2O_3 - ZnO system. According to

it zinc statistically substitutes aluminium in alumino-oxygen tetrahedra with the formation of hitherto unknown ternary phases.

- $Ca_3Al_4ZnO_{10}$ or $3CaO{\cdot}2Al_2O_3{\cdot}ZnO$ (C_3A_2Z);
- $Ca_{14}Al_{10}Zn_6O_{35}$ or $14CaO{\cdot}5Al_2O_3{\cdot}6ZnO$ ($C_{14}A_5Z_6$).

New compounds are synthesized from an oxide mix having an appropriate composition at 1300 - 1400 °C and can be produced in the form of monocrystals under appropriate slow cooling of melts.

2. The determined roentgenometric characteristics, atomic structure and some physicochemical properties of synthesized calcium aluminozincates allow their certain identification in the composition of more complex materials and map out the areas of practical application. Both the compounds are hydraulic binders surpassing many calcium aluminates in their strength.

3. The regularities established under study of the CaO - Al_2O_3 - ZnO system are of more general character and continue being studied on the basis of similar systems involving tin, zirconium, titanium and other elements. Although the results obtained are tentative, they predict the formation of new binders and certain correlation in the theory of binding properties manifestation.

REFERENCES

Odler, I., Schmidt, O., "Structure and Properties of Portland Cement Clinker Doped with Zinc Oxide." Journal of the American Ceramic Society, 01.63, Nos. 1-2, 1980, pp. 13-16.

Susukawa, I., Zement-Kalk-Gips, vol. 9, No. 8, 1956, p. 345, No. 9, 1956, p. 390.

Brisi, C. A., Appendino-Montorsi, Ann. Chim. (Roma), Vol. 52, Nos. 9-10, 1962, p. 785.

Massazza, F., M Cannas, Ann. Chim. (Roma), Vol. 49, Nos. 7-8, 1959, pp. 1342-1352.

Majumdar, A. I., Trans. Brit. Ceram. Soc., Vol. 63, No. 7, 1964, p. 347.

Barbanyagre, V. D., Timoshenko, T. I., Ilyinets, A. M., Shamshurov, V. M., "High-Temperature Interaction in CaO-Al_2O_3-ZnO System." // Proceedings of the 12th Meeting on X-radiography of Mineral Raw Materials. Sochi, March 1992, Moscow, GINRAN, 1992, p. 148.

Barbanyagre, V. D. et al., "Calcium Zinc Aluminate of $Ca_3Al_4Zn\ O_{10}$ Compositions as Monomineral Binder." USSR Inventories Certificate No. 1699970, dtd 23.12.91, BI No. 47.

Barbanyagre, V. D., Timoshenko, T. I., Ilyinets, A. M., Shamshurov, V. M. "New Ternary Compounds in CaO-Al_2O_3-ZnO System, Their Properties as Particular Binders in the Composition of White Cement." // Proceedings of the 8th All-Union Scientific Technological Meeting on Chemistry and Cement Technology. Moscow. Souzstroimaterialy, 1991, pp. 128-134.

Ilyinets, A. M., Barbanyagre, V. D., "Characteristic Properties of Atomic Structure of Solid Solutions in CaO-Al_2O_3-ZnO System. Crystalline Structure of $Ca_3Zn\ Al_4O_{35}$." In the Proceedings: Modern Methods of Studies in Building Materials Technology. Gosstroi SSSR, Moscow, 1990, pp. 21-34.

Barbanyagre, V. D. et al., "The Composition of the Structure of New Monomineral Binders in CaO-Al_2O_3-ZnO System." Building Materials Journal (Stroitelnye Materialy), No. 8, 1994, pp. 20-21.

FERRITE - MICROSTRUCTURE IN CLINKER AND HYDRATION OF SYNTHETIC PHASES AND SULPHATE RESISTING CEMENTS

Anna EMANUELSON*, Staffan HANSEN*, Eric HENDERSON#,
Angel LANDA-CÁNOVAS§, Elisabeth SJÖSTEDT□

*National Center for HREM, Inorganic Chemistry 2, Chemical Center, Lund University, P.O. Box 124, S-221 00 Lund, Sweden
#Cementa AB, Ideon Lund, Sölvegatan 41, S-223 70 Lund, Sweden
§Centro de Microscopia Electronica, Universidad Complutense, E-28040 Madrid, Spain
□Scancem Research AB, Ideon Lund, Sölvegatan 41, S-223 70 Lund, Sweden

ABSTRACT The composition, distribution and defect structure of ferrite in sulphate resisting portland cement clinker was studied by electron microscopy. The hydration kinetics of synthetic ferrite solid solutions and model cements has been investigated by differential scanning calorimetry. The hydration products were characterised in the scanning electron microscope. Comparisons of early hydration rates were made with sulphate resisting production cements. Internal and external factors affecting the reactivity of ferrite are discussed.

Key-words: Ferrite phase, solid solution, electron microscopy, reactivity, AFt phase

INTRODUCTION

The rheological properties of concrete and mortars made using sulphate resisting industrial cements have been found to be somewhat variable. Many of these changes have been related to the extent of dehydration of the added gypsum. However, hydration studies and other results indicate that some of these variations are probably related to the reactivity of the clinkers and at these early times, particularly the changes in the characteristics of the ferrite phase. Ferrite is the major oxide interstitial phase in sulphate resisting portland cement (SRPC), while aluminate occurs in such small amounts that it is usually hard to detect by X-ray powder diffraction or X-ray elemental mapping (Bäckström & Hansen; 1996 and 1997), cf. Fig. 1. The hydration reactions of ferrite have been reviewed by Brown et al. (1986) and Sjöstedt (1996). Our approach has been to perform electron microscopy studies of SRPC clinker ferrites, followed by hydration investigations of synthetic ferrites mimicing those in the clinker and finally comparisons with hydrating SRPC.

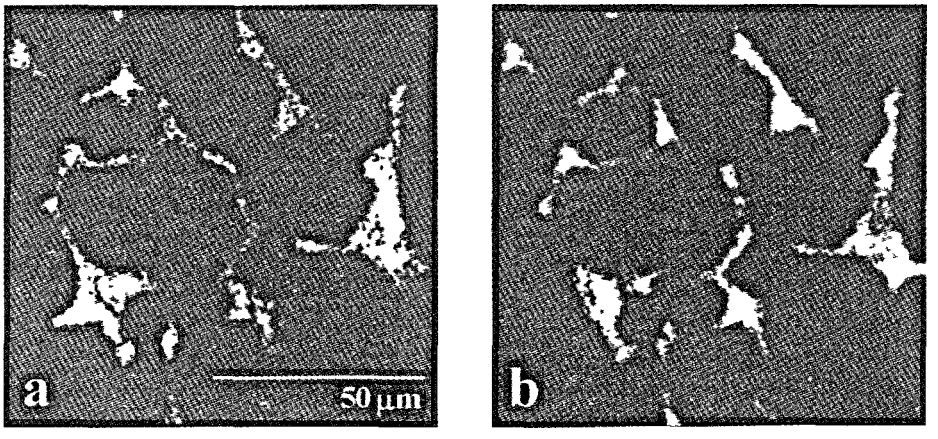

Fig. 1. Elemental maps of polished SRPC clinker; (a) Al and (b) Fe. Areas with both Al and Fe contain ferrite, while areas with Al alone indicates aluminate, e.g. in the lower left corner.

EXPERIMENTAL

Preparation of samples Swedish production clinker was ground to an average particle size of 5 μm. The powder was then stirred with salicylic acid dissolved in methanol for 24 h, vacuum filtered and washed with acetone. Polished clinker was obtained according to a standard procedure used for preparing specimens for clinker microscopy (reflecting light), but excluding the final acid etching. Two powder mixtures, no 1 and 2 in Table 1, were prepared using ferrite, Ca_2AlFeO_5 prepared at 1350°C, and the following chemicals; $CaSO_4 \cdot 2H_2O$ (Merck, p.a.), Ca_3SiO_5 (prepared from $CaCO_3$ and SiO_2 at 1450 °C) and ground quartz (SiO_2). Two synthetic solid solution series of composition $Ca_2(Al_xFe_{1-x})_2O_5$ (x= 0 to 0.67) were prepared by firing the appropriate proportions of the constituent oxides at 1450°C and at 100°C below the respective melting point, until the free lime content was 0.5 wt% or below. In the instance of the lower temperature preparations, a maximum of three firings with intermediate grinding was required. All were then ground to a Blaine surface of 300 m^2kg^{-1} and the BET surface, and particle size distribution to 0.1 μm determined. Two types of mixture (no 3 and 4, Table 1), were prepared from ferrite solid solutions to simulate the nominal phase composition of Swedish SRPC. The alite in these samples was purchased from CTL, Skokie, Illinois, USA. This had to be shaken with water (H_2O/solid = 2 by weight) for 5 min, then rapidly filtered and acetone dried, before final drying for 30 min at 800°C, because preliminary mixtures using the original alite were found to be extremely unreactive, as compared to earlier studies using pure C_3S of the same Blaine surface. K_2SO_4 (Merck, puriss) was used in mix 4. 0.5 g of no 1-3 were mixed with 0.5 ml of distilled water for 30 s, using a spatula. 0.5 g of no 4 was mixed with 0.5 ml 0.05 M KOH (Merck). The hydration was stopped by mixing with acetone (99.5%) for 30 s, followed by vacuum filtering, and washing with acetone 4 times with final drying by vacuum filtering for 8 min.

Table 1. Composition (wt%) of mixtures in hydration experiments.

No	ferrite	gypsum	C_3S	alite	K_2SO_4	quartz
1	60.0	20.0	-	-	-	20.0
2	60.0	20.0	10.0	-	-	10.0
3	15.0	5.0	-	50.0	-	30.0
4	15.0	3.7	-	50.0	1.3	30.0

X-ray powder diffraction The X-ray diffraction spectra of the ferrite solid solutions were recorded in reflection mode on a Siemens D500 diffractometer (CuKα1 radiation) and were inspected for phase purity. The hydrated samples (no 1-2); pure Ca_2AlFeO_5; and extracted interstitial materials were mixed with Si and mounted on Scotch tape. X-ray powder diffraction films were recorded using a Guinier-Hägg camera (CuKα1 radiation). The phases were identified and the unit cell parameters determined using the least squares method.

Electron microscopy A JSM-840A scanning electron microscope, interfaced with a Link AN10000 energy dipersive X-ray microanalysis system, was used in these studies. Elemental analysis was performed on polished clinker, extracted interstitial material and the hydrated samples 1 and 2. Small amounts of extracted clinker and hydrated samples were mounted on copper stubs covered with a conducting polymer. A thin layer of carbon was then evaporated onto the samples. Secondary electron images were taken of the hydrates formed in samples 1 and 2, after small amounts of the samples had been mounted on copper stubs using adhesive tape and then covered by sputtering with a thin layer of gold. The extracted interstitial phases were dispersed on copper grids with a holey

carbon film, and then investigated using a transmission electron microscope JEM-2000FX (200 kV) equipped with a Link AN10000 X-ray microanalysis system, or a JEM-4000EX (400 kV).

Differential scanning calorimetry The hydrated samples were sealed in pans, with a 50 μm laser pierced hole in the lid to control the dehydration process. Aluminium oxide was utilised as an inert reference material in the measurements. The temperature range covered was 25 °C to a maximum of 400 °C and the samples were heated at a rate of 20 °C min^{-1}. A Perkin Elmer-DSC7 differential scanning calorimeter was used. The enthalpy of dehydration of the AFt was calculated from analysis of the area of the main DSC peak, in relation to the consumption of gypsum, in reactive mixtures containing 30% C_4AF, 15 % gypsum and ground silica. The enthalpy was estimated to be 540±40 Jg^{-1}; the value used to calculate the AFt content in all the pastes, as compared with the value of 590 Jg^{-1} for pure ettringite quoted by Struble (1986), although values as high as 790 Jg^{-1} have been found (Eber, private communication).

RESULTS AND DISCUSSION

Clinker ferrite

Extended defects. The structure of synthetic $Ca_2(Al_{0.5}Fe_{0.5})_2O_5$ contains chains of tetrahedra along the c direction, all pointing in the same direction as shown in Fig. 2. In the corresponding iron compound $Ca_2Fe_2O_5$, the chains in the bottom layer point forward, while those in the top layer point backward. A phase transition takes place close to the composition $Ca_2(Al_{0.3}Fe_{0.7})_2O_5$. Electron diffraction studies of extracted clinker ferrite (Landa-Cánovas & Hansen, 1996 and in prep.) show that the structure is essentially that of $Ca_2(Al_{0.5}Fe_{0.5})_2O_5$. But electron diffraction has in addition revealed sheets of diffuse scattering, which indicate the presence of disordered line-defects along the c direction in clinker ferrite. We propose that the disordered line-defects consist of single chains of tetrahedra pointing in the opposite direction compared to the basic structure in Fig. 2. The number of defects in a crystal increases with annealing temperature and defects are known to increase the subsequent reactivity of a material. It has for example been shown that planar defects in the structurally related compound $YBa_2Cu_3O_7$ serve as points of attack, when the crystal surface is exposed to water (Rupeng et al. 1992).

Substitutions. The unit cell parameters of ferrite from Swedish SRPC and ordinary Portland cement (OPC) are similar to those determined for synthetic Ca_2AlFeO_5, see Table 2.

Table 2. Lattice parameters

sample	a/Å	b/Å	c/Å
ferrite - SRPC	5.550(1)	14.526(4)	5.347(2)
ferrite - OPC	5.541(2)	14.516(5)	5.328(2)
Ca_2AlFeO_5	5.560(1)	14.511(2)	5.343(1)
AFt - sample 1	11.213(6)	-	21.51(2)
AFt - sample 2	11.163(3)	-	21.959(4)

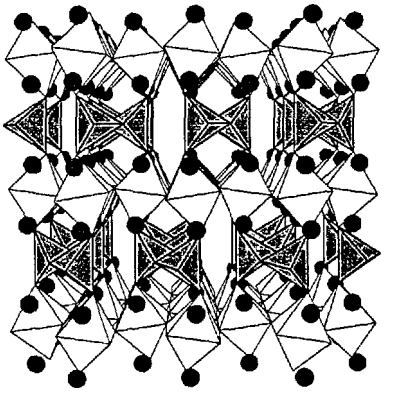

Fig. 2. Crystal structure of $Ca_2(Al_{0.5}Fe_{0.5})_2O_5$ (C_4AF) seen along the c direction. Octahedra are preferentially centred by Fe atoms, the tetrahedra by Al, while spheres represent Ca atoms. Oxygens (omitted for clarity) are situated at corners shared by two polyhedra.

Nevertheless, X-ray microanalysis of extracted clinker ferrite performed in a transmission electron microscope (TEM) shows that trivalent ions in the crystals are subject to substantial substitution according to the scheme: 2 M(3+) ↔ M(2+) + M(4+); M(3+) = Al, Fe; M(2+) = Mg, Mn; M(4+) = Si, Ti). Many of the analyses exhibit an atomic ratio Al/Fe in the range 0.7-0.9, with an average composition of $Ca_{2.03}Al_{0.72}Fe_{0.87}Mg_{0.11}Mn_{0.05}Si_{0.17}Ti_{0.03}O_5$, which is very similar to values obtained on the same sample using a scanning electron microscope (Bäckström & Hansen, 1997). The higher spatial resolution of the analyses in the TEM reveals the presence of more Al-rich areas, see Fig. 3. The ratio Al/Fe can thus change rapidly on the micrometer scale. The most Al-rich analysis observed (Al/Fe = 1.90) gave the composition $Ca_{1.96}Al_{1.20}Fe_{0.63}Mg_{0.06}Mn_{0.03}Si_{0.09}Ti_{0.01}O_5$. Similar short-range variations in ferrite composition has been observed in oil-well cement clinker by Richardson et al. (1993). The influence of dopant ions on the reactivity of ferrite is hard to predict and has to be studied experimentally.

Synthetic ferrite

Hydration and additives. The hydration studies, on mixture 1 and 2 using DSC, showed that in presence of sulphates, the hydration starts with the formation of sulphate-AFt (ettringite), while gypsum is being consumed. When the calcium sulphate has been depleted, unreacted ferrite remains and AFm phase (monosulphate) starts to form, whilst AFt disappears. When the hydration is carried out in the presence of tricalcium silicate and added gypsum, the formation of AFt is delayed, due to the introduction of a pronounced dormant period during AFt formation, see Fig. 4. It appears that a high concentration of hydroxide is necessary for the creation of this extended induction period, since it also occurs when C_3S is replaced by $Ca(OH)_2$ or KOH (Emanuelson, 1995; Emanuelson, Henderson & Hansen, 1996). There seems to be general agreement that this type of behaviour is due to the formation of a protective layer of products on the hydrating grains (Brown et al. 1986).

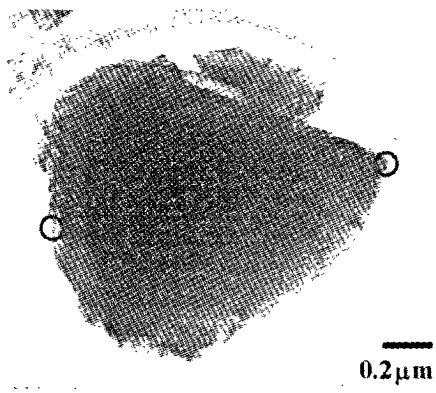

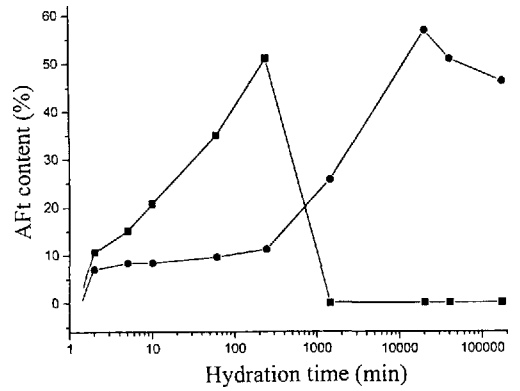

Fig. 3. Transmission electron micrograph of a ferrite grain extracted from SRPC clinker. Elemental analysis of the circled areas gave Al/Fe ratios of 0.7 (left) and 1.4 (right).

Fig. 4. Formation of AFt phase from $Ca_2(Al_{0.5}Fe_{0.5})_2O_5$ (C_4AF) and gypsum (squares) or gypsum + C_3S (circles) as a function of time.

Protective product layer. The morphology of the AFt formed in the presence of gypsum (no 1) and also added C_3S (no 2) are compared in Figs 5a-b and c-d. This shows that the initial crystals of AFt are much smaller when formed in the presence of a base. The observation is consistent with the notion of microcrystalline ettringite forming a protective layer, which causes retardation of the hydration reaction as shown in Fig. 4. Elemental analysis indicates that the AFt crystals formed with a base present tend to be more iron-rich (Al/Al+Fe ≈ 1/2) than those produced without base (Al/Al+Fe ≈ 3/4); compare the c axis expansion in Table 2 (Emanuelson & Hansen, manuscript).

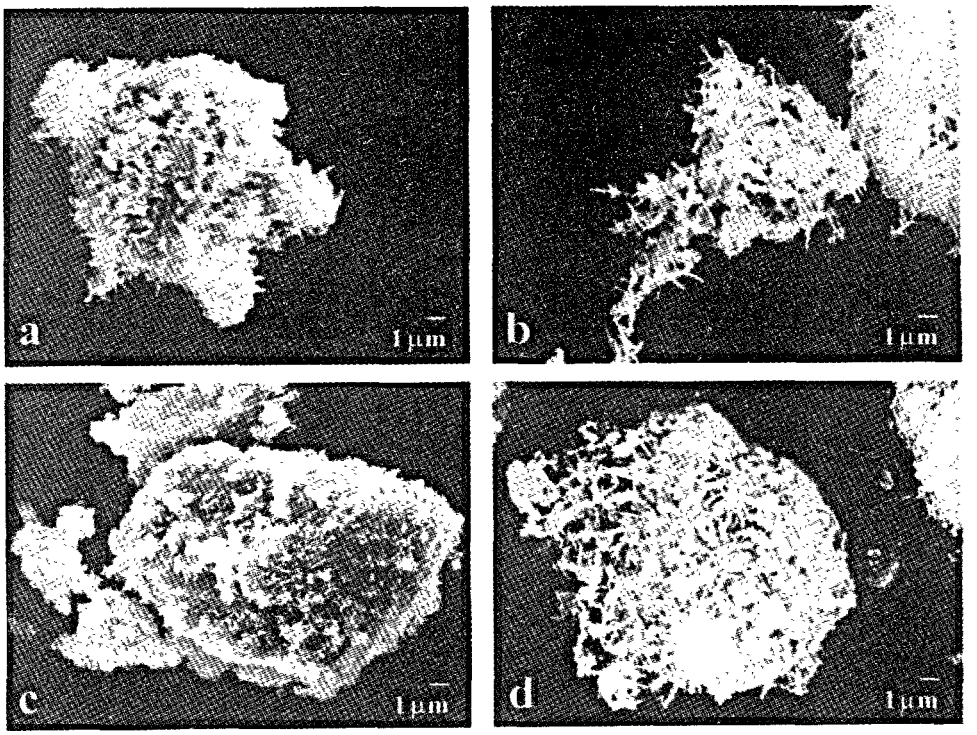

Fig. 5. Scanning electron micrographs of AFt crystals formed from synthetic C_4AF; (a) water with gypsum, 5 min; (b) water with gypsum, 2 h; (c) water with gypsum and C_3S, 5 min; and (d) water with gypsum and C_3S, 28 days.

It has been suggested that an amorphous iron-rich compound forms when ferrite is hydrated. This gel should also contain some calcium according to Brown (1987) and Liang & Nanru (1994). In both of our samples, dark particles can be seen in the light microscope, which we interpret as pseudomorphs after ferrite grains, see Fig. 6. These pseudomorphs have been observed earlier by Fukuhara et al. (1980). Our investigations reveal that the dark phase is X-ray amorphous, but its chemical composition is fairly constant and corresponds to $CaFe_4O_7 \cdot xH_2O$ (CF_2H_x), if the iron is assumed to be trivalent and a minor content of Al is neglected. This phase is another candidate for the formation of the protective layer.

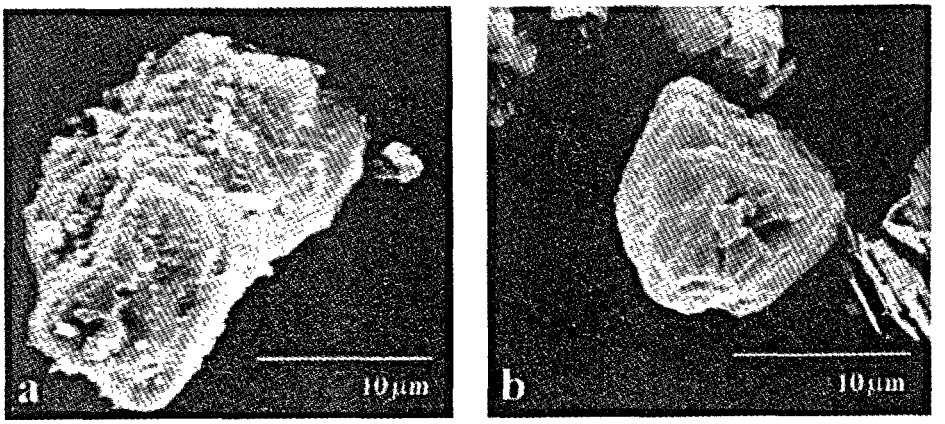

Fig. 6. (a) Grain of synthetic C_4AF with a terraced morphology. (b) Ferrite pseudomorph consisting of $CaFe_4O_7 \cdot xH_2O$ (CF_2H_x).

Model cements and SRPC

Early hydration of ferrite solid solutions. The influence of increasing the aluminium content in the solid solution series $Ca_2(Al_xFe_{1-x})_2O_5$ on the early hydration behaviour has been studied. This has been monitored by measuring the rate of formation of the ettringite-like AFt phase using DSC. Mixes (no 3) simulating the typical phase composition of a Swedish SRPC were used, as they were considered appropriate for comparison with the early reactivity of production cements. The results obtained for the two series produced in melt condition and in the solid state are presented in Fig. 7. The similar reactivity of the solid solution formed from the melt and that prepared in the solid state could be due to insufficient cooling rates, leading to similar defect concentrations in both series. The results show a near continuous, relatively small, increase in the rate of formation of AFt with increasing Al content, with the significant increase occurring between x = 0.5 and 0.67. The greatest overall differences were, however, only observed after 100 min hydration. These results are consistent with those obtained by Negro & Stafferi (1979). Although their hydration times, like many others Boikova (1986), or Carlson (1964), tend to be on the days time scale. Smith (1962) found a structural change close to x = 0.3 in the solid solution series and interestingly there is a small jump in the rate in just this region, see Fig. 7.

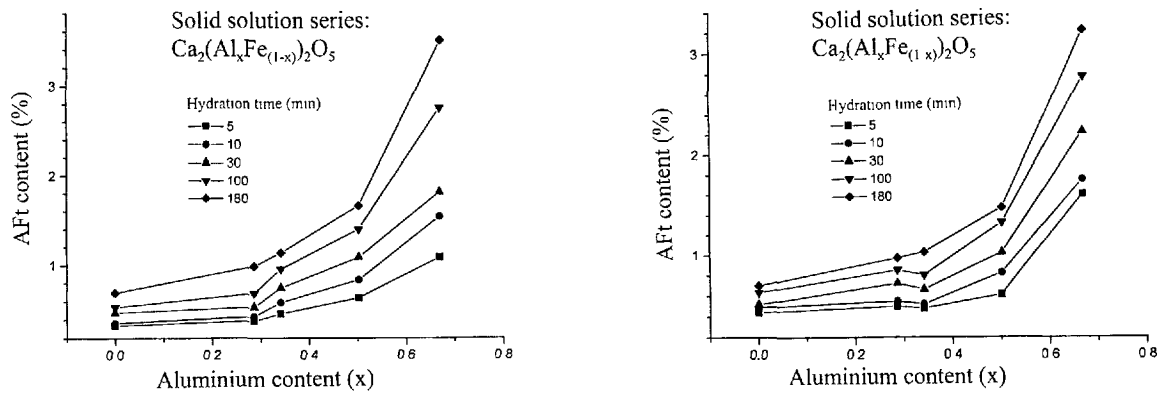

Fig. 7. Influence of the Al content on the formation of AFt (wt%). The ferrite solid solution prepared at 1450 °C (left) and the series prepared at 100 °C below the respective melting points (right).

Early hydration of SRPC. The hydration behaviour of sulphate resisting cements produced during 1995 has been studied and the results summarised in Fig. 8. These have been separated into three reactivity (wt% AFt) bands according to results obtained from 20 cements; two, did, in fact, have somewhat lower reactivity, but these have not been included. In addition, the diagram includes the hydration results obtained for $Ca_2(Al_{0.5}Fe_{0.5})_2O_5$ (C_4AF); the solid solution member, with the Al/Fe molar ratio close to that of the interstitial phase in production cements. There is a large difference in the rate of formation of the AFt phase between the cements and the apparently equivalent synthetic blend (no 3) of similar particle size distribution and BET surface. This is especially true of the paste hydrations containing alkalies (mix no 4); simulating the initial pore solution concentration of Swedish SRPC (Henderson, unpublished results), when an even lower rate of AFt formation is observed; see Fig. 8. However, without further analysis of the surface microstructure of the complex multiphased clinker particles (Scrivener, 1984), in the ground cements, it is difficult to compare the available surface of the interstitial phase, with that of the ground synthetic ferrites. Clearly the cement ferrite phase reacts far more rapidly from the very intial stage during mixing itself, as shown by the differences after only 2 min hydration, see Fig. 8. Simply, increasing the Al content to the solid solution limit does not appear to increase the initial reactivity enough (see Figure 7), to explain the

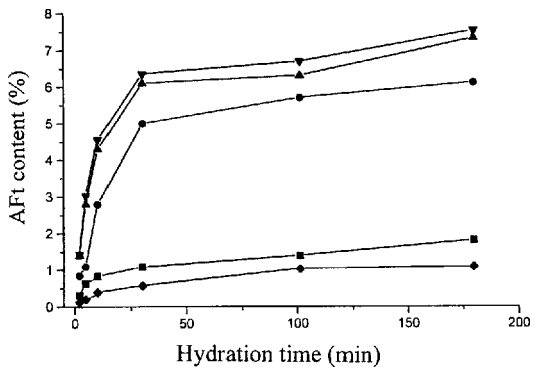

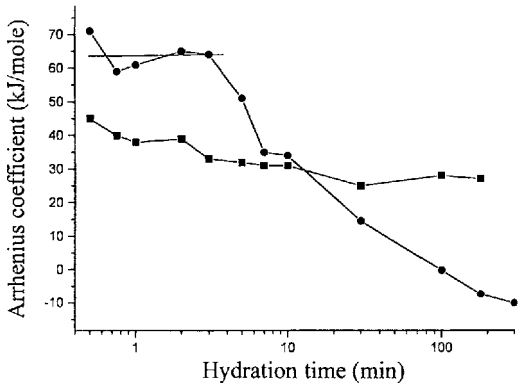

Fig. 8. Comparison between the reactivity of production SRPCs (triangles, dots) with that of synthetic ferrite (C_4AF) mixes in water (squares) and potassium hydroxide (diamonds).

Fig. 9. Comparison between the Arrhenius temperature coefficient, for the formation of AFt from a production SRPC (dots) and a model cement containing synthetic ferrite, C_4AF (squares).

very large differences observed, even though equivalent compositional variations are present in the interstitial phase of high ferrite clinkers (Richardson et al. 1993). However, the increased relative reactivity of the end member (x = 0.67) compared to that of the earlier members could be important.

Temperature effects. Further indications of the difference between the hydration behaviour of the cement ferrite phase and the apparently equivalent synthetic phase was found from the results of hydration studies undertaken at two different temperatures, i.e. 1.9 and 23.3 °C. The results obtained were analysed assuming the Arrhenius equation, $k(\%AFt) = Ae^{-E/RT}$, where the rate constant k is substituted by the AFt content at a given time, at temperature T and E is the nominal activation energy. The temperature coefficient of the rate of formation of AFt as a function of the hydration time is shown in Fig. 9. The differences in the Arrhenius "activation energy" observed, would clearly indicate a change in the mechanism of the complex heterogeneous reaction, leading to the development of the AFt phase, between that for the synthetic phase in mix 3 compared to that for the apparently similar ferrite phase in SRPC. In the instance of the synthetic ferrite, there appears to be small continuous decrease throughout the period studied. In contrast, only during the first 3 min hydration of SRPC is there a consistent value of 64 ± 5 $kJmol^{-1}$, but thereafter there is a continuous rapid fall to negative values after 100 min, indicative of the reaction becoming increasingly dependent on the nature of the product layer. Only during the first 3 min is there any similarity between the two materials. Thereafter they rapidly diverge, with more reactive cement phase hydration becoming increasingly dependent on the product layer, whilst the synthetic phase never appears to reach this stage, due probably to the small amount of product formed. Although, in the instance of the cements, the mechanism apparently becomes increasingly dependent on the amount of product (AFt), after only few minutes hydration; nevertheless, the absolute rate of formation remains initially far higher, than that of the synthetic phase. It is therefore, possible to compare the solid state reactivity of different ferrites, with that of the cements, only during the very initial stages, when the more primary solid surface mechanism is predominant and not when the product layer controls the rate. In the instance of the present cement hydration results, this begins to occur after only 3 minutes hydration. The reasons for such large differences in the rate of formation of AFt remain uncertain.

Conclusions

Clinker ferrite. Ferrite in industrial SRPC clinker exhibits a disordered array of one-dimensional crystal structure defects. Normally, about 20% of the trivalent ions in clinker ferrite are substituted by a mixture of divalent and tetravalent ions, as compared to Ca_2AlFeO_5. However, the aluminium content in ferrite crystals can sometimes vary considerably on the micrometer scale.

Synthetic $Ca_2(Al_{0.5}Fe_{0.5})_2O_5$. The presence of a base is necessary in order for gypsum to retard the formation of AFt during hydration. When a base is present, the early AFt crystals are much smaller and the AFt is richer in iron, compared to hydration with gypsum alone. Iron-rich pseudomorphs after ferrite grains have a fairly constant composition, i.e. $CaFe_4O_7 \cdot xH_2O$, and are X-ray amorphous.

Model cements with $Ca_2(Al_xFe_{1-x})_2O_5$. Hydration of mixtures simulating SRPC indicates that the ferrite becomes more reactive with increasing Al content. No difference in reactivity could be detected between a ferrite solid solution prepared in the solid state and one prepared from the melt.

Model cement and SRPC. Comparison between the AFt formation in hydrating production SRPCs and model cements with Ca_2AlFeO_5 shows that the initial reactivity of SRPC is higher than that of the model cements. Only part of the difference in reactivity can be attributed to (i) the presence of about 2 wt% $Ca_3Al_2O_6$ in the SRPC, (ii) possible enrichment of Al close to the surface of clinker ferrite grains, (iii) excess relative surface area of clinker ferrite.

Temperature effects. If the temperature is lowered to 1.9 °C, the hydration mechanism of SRPC is strongly affected. No such change is observed in the case of a model cement.

Acknowledgement

This project has been supported financially by the Euroc Fund, Cementa AB and Euroc Research AB. The authors would like to thank Euroc Research AB, Slite, for preparation of specimens and Sven-Erik Johansson, Jan Lind, Claes-Göran Nilsson and Paul Sandberg for helpful discussions.

REFERENCES

Boikova, A. I., 8th ICCC, Rio de Janeiro, Vol. 1, 1986, pp. 19-33.

Brown, P.W. et al., Matér. Constr., Vol. 19, 1986, pp. 137-147.

Brown, P.W., J. Am. Ceram. Soc., Vol. 70, 1987, pp. 493-496.

Bäckström, E. and Hansen, S., Proceedings, 48th Annual Meeting, The Scandinavian Society for Electron Microscopy (A.B. Maunsbach, ed.) pp 156-157, Aarhus 1996: SCANDEM-96.

Bäckström, E. and Hansen, S., Adv. Cem. Res., Vol. 9, 1997, pp. 17-23.

Carlson, E.T., J. Res. Natl Bur. Stand., Vol. 68A, 1964, pp. 453-63.

Emanuelson, A., Masters Thesis, Lund University, LUTKDH/TKOO-5023/1-44/1995 (in Swedish).

Emanuelson, A., Henderson, E. and Hansen, S., Cem. Concr. Res., Vol. 26, 1996, pp. 1689-1694.

Fukuhara, M., Goto, S., Asaga, K., Daimon, M., Kondo, R. and Ono, Y., Yogyo Kyokaishi, Vol. 88, 1980, pp. 435-440; Chem. Abstr. 94:70318.

Landa-Cánovas, A.R. and Hansen, S., Proceedings, XI European Congress on Microscopy, poster M13-3, 2 pp., Dublin 1996: EUREM'96.

Liang, T. and Nanru, Y., Cem. Concr. Res., Vol. 24, 1994, pp. 150-158.

Negro, A. and Stafferi, L., Zem.-Kalk-Gips, Vol. 32, 1979, pp. 83-88.

Richardson, I.G., Hall, C. and Groves, G.W., Adv. Cem. Res., Vol. 5, 1993, pp. 15-21.

Rupeng, Z., Goringe, M. J., Myhra, S. and Turner, P. S., Phil. Mag. A, Vol. 66, 1992, pp. 491-506.

Scrivener, K.L., Ph.D. Thesis, University of London, 1984.

Sjöstedt, E., Licentiate Thesis, Lund University, LUTKDH/TKOO-2006/1-28/1996 (in Swedish).

Smith, D.K., Acta. Crystallogr., Vol. 15, 1962, pp. 1146-1152.

Struble, L.J., 8th ICCC, Rio de Janeiro, Vol. 6, 1986, pp. 82-86.

AUTHOR INDEX

A
M.S. Abdel-Aziz; 3v012
A.A. Abdel-Kader; 2ii027
A. H. Abedel-Reheem; 3ii124
A. Achmetov; 2ii013
F. Adenot; 3v003
A. D. Agnihotri; 1i003
S.C. Ahluwalia; 1i019, 1i031, 1i044, 1i045, 1i053, 2ii006, 3ii094, 4iv013, 4iv067
H. Ai; 3iii018
V.G. Akimov; 1i006
I. G. Al-Alm Rashed; 3ii124
B.S. Albats; 1i015, 1i007
A.H. Ali; 4iv014
M.M. Ali; 2ii006
M^{a}C. Alonso; 4iv004, 4iv082, 4iv083
V. Alunno Rossetti; 3v026
Ö. Andaç; 1i050
T. Ando; 2ii017
C. Andrade; 4iv004, 4iv082, 4iv083
M.V. Anufriev; 1i032
H. Anzai; 3v013
N. Arano; 4iv051
S. Argarwal; 4iv067
S.K. Argarwal; 4iv067
P. Arjunan; 3v020
V.K. Arora; 1i019
K. Asaga; 3ii107, 3iii022
E. Asakura; 2ii005
M.A. Aviles; 3v019

B
O. Baumanis; 3v025
Sh.T. Babaev; 3iii021
V. Babkov; 2ii048
V.I. Babushkin; 4iv039
P. Baccini; 4iv076
S. Bagosi; 4iv045
G. Balázs; 2ii060, 4iv002
K.D. Baltzopoulou; 4iv052
J.R. Baragaño; 3iii004
V.D. Barbanyagre; 1i011, 1i059
P. Barret; 2ii024
N.F. Bashlykov; 3iii021
A.F. Battagin; 3ii102, 3ii103
Y. Bazhenov; 4iv058
A. Beeldens; 4iv007
V. Belyaeva; 1i004
M. Benkaddour; 2ii041
J. Bensted; 3iii014
D.P. Bentz; 2ii078
J. Berekta; 2ii029
H. Bergqvist; 3ii106
A.F. Bernatsky; 4iv079
C. Bessada; 3v002
R. Bhargava; 1i031, 2ii006
K.N. Bhattacharjee; 3ii115
Y. Biryukovich; 4iv056
M^{a}T. Blanco-Varela; 1i034, 3ii096, 3ii113, 3iii004, 3iii015
A.I. Boikova; 1i057, 1i058
K. Bollmann; 4iv062
L. Bonafous; 3v002
D. Bonen; 4iv022
S. Bonnet; 4iv078
M. Boros; 2ii060
S. Bouraoui; 2ii012
P. Bowen; 3iii002
S. Boyko; 3v004, 3v022
M. Braiman; 3v022
K.D. Breneman; 2ii057, 2ii058
F. Brivot; 4iv074
A.R. Brough; 3v001
H.J.H. Brouwers; 2ii052
L. Brower; 3iii031
W. Brylicki; 3ii095
N. R. Buenfeld; 4iv070
T.A. Bürge; 3iii002

C
R. Cabrillac; 3v003
C. Caestecker; 4iv007
R. Caldwell; 4iv042
G. Camarini; 3ii102, 4iv063
L. Cassar; 1i027
P. Cassat; 3v014
M. Castellote; 4iv082
S.L. Centurione; 2ii079
W.-H. Chae; 1i036
J. Champa; 3iii027
S. Chanda; 3ii092
S. Chandra; 3ii106
P.K. Chang; 3v006
I. Chartschenko; 2ii010
A.K. Chatterjee; 1i008, 1i033, 2ii039

S. Chaturvedi; 4iv057
T. Chaussadent; 4iv074
M. Chen; 3iii016
Y. Chen; 1i010, 2ii031
H. M. Cheong; 1i049, 2ii037
V.L. Chernyavski; 4iv071
Y. Chi; 1i054, 1i055
V. Chistyakov; 2ii019, 2ii023
D.W. Cho; 2ii037
H. Choi; 3iii009
S.H. Choi; 1i036, 1i049, 4iv054
B.J. Christensen; 2ii057
M.A. Cincotto; 3ii102, 4iv063
R. Cioffi; 4iv017
P. Colombet; 3iii003, 3v002, 3v014
D. Constantiner; 3iii013
A.G. Constantinou; 4iv084
F. Corazza; 3iii003
U. Costa; 3iii003
J.-P. Coutures; 3v002, 3v005
T. Coverdale; 3iii027
N.J. Crammond; 4iv026
E. Csányi; 4iv002
L.J. Csetenyi; 4iv045
F. Curcio; 3v026, 4iv006
L. Cussino; 4iv006

D
M. Daimon; 2ii002, 2ii017, 2ii022, 3ii088, 3ii107, 3iii022
D. Damidot; 2ii024, 2ii025, 2ii026, 3iii007, 4iv066
T. Dashkova; 4iv056
B. De Blaere; 4iv007
B. De Vito; 4iv017
E. De Winne; 4iv007
M. Degenkolb; 2ii074
A.E. Degtyaryev; 2ii019
J. Deja; 4iv015
K. Demura; 3iii033
M. Deng; 4iv029
S.P. Dennington; 3iii008
R.K. Dhir; 4iv012
G. Diaz; 3v023
S. Dietz; 3ii087
J.M. Diez; 4iv040
S. Dimitrova; 3ii101
A.M. Dmitriev; 3iii021
C.M. Dobson; 3v001
A. Douy; 3v005
A. Dozono; 2ii001
M. Drabik; 3iii011
R. Dron; 4iv074
G.Ya. Drozd; 4iv039
V.Y. Dubnitsky; 4iv071
G. Dumitru; 3iii015
A.M. Dunster; 4iv026
S. Duszak; 4iv027

E
C.M. Economou; 4iv052
M. Ecker; 2ii032, 4iv044
L. Eckert; 3iii027
A.N. El-Afify; 3ii124
E.B. El Aouni; 2ii041
B.A. El-Sabbagh; 4iv014
H.A. El-Sayed; 4iv014
A. Emanuelson; 1i060
Z.B. Entine; 1i020, 1i046, 3v024
H. Ezirim; 3ii112

F
D. Fairhurst; 4iv008, 4iv009
V.R. Falikman; 3iii021
Y. Fang; 1i010
S.A. Farrington; 3iii013
P. Faucon; 3v003
X. Feng; 2ii043
A. Fernandez-Jimenez; 3ii098
V. Fernon; 3iii003
R. Ferrari; 4iv006
R.C. First; 2ii075
R. Flatt; 3iii002
O.I. Fomicheva; 1i057, 1i058
E. Forssberg; 3ii104
L.S. Fraiman; 3ii081
R. François; 4iv078
O. Francy; 4iv078
G. Frigione; 4iv017, 4iv050
X. Fu; 1i054, 1i055
H. Fujisawa; 2ii005
H. Fujiwara; 2ii001
K. Fukuda; 1i025, 1i052

G
L. Galikova; 3iii011
S.P. Gandhe; 1i033
A. Garbacik; 1i018

M.C. Garci; 2ii058
L. A. M. Garcia; 4iv037
S. Gauffinet; 2ii055
M. Gawlicki; 3ii089
Mª T. Gaztañaga; 4iv003
J. Geiseler; 4iv001
S. George; 1i003
W. Gessner; 3iii007, 3v018
D. Ghosh; 1i008, 1i033, 1i047
S.N. Ghosh; 3ii092
S.P. Ghosh; 1i030, 2ii018
G. M. Giaccio; 2ii036
Z. Giergiczny; 4iv019
C. Gilioli; 1i027
P. Gill; 3iii024
N. Giuliani; 1i051
G.K. Glass; 4iv070
F.P. Glasser; 1i050, 3ii091, 4iv066
V. Glukhovskiy; 4iv056
F. Goetz-Neunhoeffer; 1i056
L. Ya. Goldstein; 1i013
E. Gomez; 3v019
S. Goñi; 4iv003, 4iv004, 4iv024, 4iv040, *4iv083*
J.W. Goodwin; 3iii008
V.K. Gore; 1i047
G. Goswami; 3v008
R.K. Goswami; 1i044, 1i045
S. Goto; 2ii070
A.M. Grabiec; 3iii019
M.L. Granizo; 3ii113
L.V. Grishchenko; 1i058
I. Grosvalds; 2ii009
G.W. Groves; 3v001
M. Grutzeck; 2ii067
G. Gu; 3iii016
A. Mª Guerrero; 4iv003, 4iv024
G.L. Guerrini; 1i027
R.S. Gupta; 1i053

H
H. Hagiwara; 3iii017
J. Han; 3ii122
K. S. Han; 1i049
M. Handa; 2ii017
S.K. Handoo; 3v019, 4iv013, 4iv067
S. Hanehara; 2ii014, 3iii001
F. Hanic; 3iii011
S. Hansen; 1i060
N. Hara; 2ii065
S. Harsh; 1i044, 1i045, 4iv013
M. Hasegawa; 3iii010
N.M. Hassanein; 4iv070
M. Hatano; 3iii009
A.S. Heble; 2ii039
H. Hedlund; 2ii077
D. Heidemann; Plen2
E. Henderson; 1i060
Mª S. Hernandez; 4iv003, 4iv024
A. Hidalgo; 4iv004, 4iv083
T. Higaki; 3iii022
M. Hilger; 1i009
H. Hirao; 2ii014
S. Hirose; 3iii022
F.J. Hofmann; 4iv038
H. Hofmann; 3iii002
S.-Y. Hong; 4iv068
K. Hormann; 4iv038
S. Hoshino; 2ii002
J. Houghton; 4iv025
Y.F. Houst; 3iii002
G. Hu; 1i023
S. *Huang; 4iv032*
Z. Huang; 4iv073
F.H. Hubbard; 4iv012
C.L. Hwang; 2ii035; 3ii108, 3v006, 3v021
C. Hübert; Plen2
C. Hyeon; 4iv072
R. Härdtl; 3ii082

I
M. Ichikawa; 3iii005
K.A. Idriss; 3v012
S.-i. Igarashi; 4iv051
T. Iisaka; 2ii003
T. Ikabata; 2ii007
K. Ikeda; 1i025
M.R. Ilić; 4iv023
N. Inoue; 2ii065
Y. Inoue, 2ii040
B.E. Ioudovitch; 1i020, 1i046, 3iii021, 4iv036
G. C. Isaia; 3ii110
A. Ishida; 3iii017
Y. Ishikawa; 2ii003
Y. Isojima; 3ii109, 3ii119
S. Ito; 1i052, 3ii121
J. Iwanciw; 1i022

H. Iwasaki; 3iii033

J
J.F. Jacquinot; 3v003
H.J. Jakobsen; 2ii056
S. Jalali; 3ii084
I. Y. Jann; 3v021
I. Jedda; 2ii020
H.M. Jennings; 2ii057, 2ii058
O.M. Jensen; 2ii056
M.-Y. Jeong; 4iv055
L. Ji; 2ii030
S.P. Jiang; 2ii053
W. Jiang; 3ii100, 3iii030
A.C. Johnson; 4iv076
J.-E. Jonasson; 2ii077
M. Jorda; 3v003
D.M. Joshi; 3ii092
H. Justnes; 1i038, 2ii069, 3iii012, 4iv064, 4iv081

K
K. V. Kalyani; 1i003
M. Kanaya; 3iii005
I. Karimov; 2ii048
A. Katz; 3ii083
S. Kawaguchi; 4iv051
M. Kawamura; 4iv051
T. Kawano; 3iii010
S. Kelham; 4iv060
M. Kersten; 2ii059
S.A. Khadilkar; 1i008, 1i047
Y. Kihara; 3ii085, 4iv048
H. Kikukawa; 2ii003
B.-K. Kim; 4iv068
N.-H. Kim; 2ii044
A. Kindness; 3ii091
P. Kittl; 3v023
V. Klassen; 1i004
J. Kļaviņš; 3v025
W.A. Klemm; 4iv041, 4iv059
A. Klusov; 2ii013
D. Knöfel; 2ii074
T. Kobayashi; 3iii010
M.M. Komljenović; 1i017
P.G. Komokhov; 2ii016
J. Komonen; 3iii029
N. Kondo; 2ii017
V.I. Kondrashchenko; 2ii066
Z. Konik; 1i022
G. Koprowski; 4iv018
H. R. Kota; 3ii104
M.V. Kougiya; 1i043, 3ii081
T.V. Kouznetsova; 1i001, 2ii027, 2ii028
J. Krištín; 3v009
É. Kristóf-Makó; 3v010
P.V. Krivenko; 2ii033, 4iv046
A.R. Krivoborodov; 4iv053
Y.R. Krivoborodov; 1i014, 1i040, 2ii013
D. Križan; 3ii085, 4iv020
R. Krzywobłocka-Laurów; 3iii019
A.B. Kudryavtsev; 2ii028
H. Kuga; 3ii107
W. Kurdowski; 4iv027
S. Kwan; 2ii067
L. J. Kyu; 2ii022
B. Ködderitzsch; 3v018
U. König; 1i039

L
E. E. Lachowski; 3ii091
A. Łagosz; 3ii089
S. Lagzdina; 1i035, 2ii009
A. Landa-Cánovas; 1i060
E. Lang; 4iv001
J. LaRosa-Thompson; 2ii067, 3iii024
C.K. Larsen; 4iv069
X. Lecoq; 2ii055
H.-S. Lee; 2ii044
I.S. Lee; 2ii044
S. H. Lee; 3ii088
Y.-J. Lee; 2ii044
P.G. Lele; 1i008, 1i047
M. Lewis; 4iv025, 4iv061
D. Li; 4iv029
P. Li; 1i028
R. Li; 4iv028
S. Li; 4iv030
V. Lilkov; 3ii116
J.R. Lim, 2ii037
L.K. Lin; 3ii108
J. Lindgård; 4iv064
C. Liu; 1i028
J.N. Liu; 3ii114
J.S. Lota; 3iii014, 4iv012
C. Lu; 1i012, 4iv028
H.M. Ludwig; 4iv034, 4iv035
I.G. Luginina; 1i029, 1i057

M. Lukach; 3v022
K. Luke; 3ii091
T. Lyashenko; 3v004

M
A. Macias; 4iv040
J. Madrid; 4iv040
N. Maeda; 3iii010
Y. Maejima; 2ii005
S. C. Maiti; 3iii020
J. Majling; 3v009
I. Maki; 1i052
R.I.A. Malek; 1i024
J. Małolepszy; 2ii064, 3ii089, 4iv043
S. Manjit; 3ii093
B. Marchese; 4iv050
E. Marciano Jr.; 2ii079, 3ii103
V. Maringolo; 2ii079
M. Marroccoli; 2ii029
V. Martinez; 3v023
D. Massiot; 3v002, 3v005
S. Matala; 3v017, 4iv005
V.K. Mathur; 1i053
V.A. Matviyenko; 2ii076
W.J. McCarter; 3ii112, 4iv011
O.P. Mchedlov-Petrossyan; 1i042, 2ii021
S.N. Mehrotra; 1i002
I. Meland; 4iv064
V.S. Melentyeva; 3ii117
E. Menendez; 4iv004
B. Meng; 3ii105
H.W. Meyer; 3v007
V. Michaud; 2ii011, 4iv049, 4iv065
A. Miezis; 3v025
T. Mihara; 3iii017
N. Mikhailishina; 4iv056
S.R. Miletić; 4iv023
F.M. Miller; 4iv041, 4iv059
K. Miskiewicz; 3ii087
S. Miyazawa; 2ii071
K. Mohan; 1i030, 2ii018
B.N. Mohapatra; 3v008
G.K. Moir; 1i041
G. Morales; 3ii123
M. Morioka; 3iii017
H. Motzet; 1i039
J.F. Muller; 3v014
A.K. Mullick; Plen1, 1i031, 3v019, 4iv047
D. V. Mundshtukov; 2ii020
J.C. Mutin; 2ii053
D. Müller; 3iii007
U. Mäder; 3iii002
S. Möhmel; 3v018

N
M. Nadu; 3v022
S. Nagataki; 2ii001
A. Nakamura; 2ii022
H. Nakata; 2ii070
S. Nakaya; 2ii017
D. Nazarsky; 4iv021
B. Nedumaran; 1i002
L.S. Nefyodova; 3v024
H. Nemoto; 3v013
C. M. Neubauer; 2ii057, 2ii058
J. Neubauer; 1i039, 1i056, 3v007
Y. Nikaido; 2ii017
T. Nishikawa; 3ii121
J. Nissenbaum; 3v022
W. Nocuń-Wczelik; 4iv043
T. Noguchi; 4iv072
H. Noma; 2ii065
A. Nonat; 2ii053, 2ii055, 4iv049, 4iv065
E.C. Nygaard; 3iii012

O
I. Odler; 1i026, 2ii063
H. Ogata; 2ii005
H.-K. Oh; 1i036, 4iv054, 4iv068
Y. Ohama; 3iii033
Y. Ohba; 2ii002, 2ii022
A. Ohno; 3v015
A. Olginsky; 2ii015
G.B. Olson; 2ii058
L. Opoczky; 1i009, 2ii004
A.P. Osokin; 1i005, 1i006, 1i014
Z. Owsiak; 4iv018

P
S. Pagliolico; 4iv006
A. Palomo; 1i034, 3ii096, 3ii113, 3iii004
J.G. Palomo; 1i034
M. T. Palou; 3v009
Y. Pan; 1i021, 1i054, 1i055
J.D. Panda; 3v008
P.K. Panigrahy; 3v008
I. Papayianni; 3ii086
A. Papo; 2ii004

C.-K. Park; 4iv068
P. Parmentier,; 3ii120
M. Pátkai-Horváth; 3v010
P. Paulini; 2ii072
S. Pavlenko; 3ii080, 4iv058
V. Penttala; 3iii029, 4iv033
J.L. Perez-Rodriguez; 3v019
B. Perrin; 4iv078
B. Persson; 2ii073
O.E. Petrov; 3ii116
S. Peukert; 2ii034, 3iii023
W.G. Piasta; 4iv018
A.K. Platten; 4iv008, 4iv009, 4iv073
A.A. Plugin; 4iv039, 4iv075
A.N. Plugin; 2ii054, 4iv075
A. Poltavtsev; 2ii019
A. Pompo; 2ii029
E.N. Potapova; 1i005, 1i006
J.H. Potgieter; 2ii049, 3v011
P.L. Pratt; 3iii014
I.G. Prokopova; 4iv075
J.R. Prusinski; 3ii090
F. Puertas; 1i034, 3ii096, 3ii098, 3ii113, 3iii004, 3iii015
E.K. Pushkaryeva; 2ii033
G.K.D. Pushpalal; 3iii010
R. Pyare; 1i016
Z. Pytel; 2ii064
H. Pöllmann; 1i039, 2ii032, 3iii032, 3v007, 4iv044

Q
V.A. Quarcioni; 3ii085

R
M. Radenkova-Yaneva; 2ii047, 3ii101
K. Raina; 1i002
K. Rajczyk; 2ii045
Sh. M. Rakhimbaev; 2ii046
X. Ren; 2ii030
A. Rettel; 2ii026, 3iii007
M. Ribas Silva; 4iv037
I.G. Richardson; 2ii068, 3v001
A. Risch; 4iv044
J. Roberts; 4iv073
E. Rodum; 4iv081
M^{a}.L. Romero; 3ii096
V. Ronin; 3ii104, 2ii077
G. Rosenthal; 3iii031
A. Rosić; 1i017
W. Roszczynialski; 3ii097
D.M. Roy; 1i010, 3ii100, 3ii114, 3iii030, 3v020
R. Roy; 1i010
R.F. Runova; 2ii054, 3ii117
O.V. Rybakova; 4iv053
P.F. Rymyantsev; 1i037

S
S. Sahu; 3v009
A. Saini; 1i051
E. Sakai; 2ii002, 2ii017, 2ii022, 3ii088, 3ii107
S.V. Samchenko; 1i014
G. Samuel, 4iv047
M.A. Sanitsky; 3iii025
R. Sanjaasuren; 1i037
S. Sano; 3iii005
S.L. Sarkar; 3ii090
L. Sas; 1i048
A.E. Savva; 4iv052
D. Sawaki; 3iii001
Z. Sawicz; 4iv018
B.E. Scheetz; 3ii111, 3iii024
M. Schieber; 3v022
P. Schiessl; 3ii105, 4iv016
M. Schmidt; 3ii087, 4iv038
C. R. Schweizer; 4iv076
K.L. Scrivener; 2ii026, 4iv025, 4iv061, 4iv084
H. Sedaira; 3v012
U. Sedmalis; 1i035, 2ii009
Y.P. Sehti; 1i019
K. Seki; 3iii009
Ž. Sekulić; 3iii028
M.M. Seleim; 3v012
E.J. Sellevold; 2ii069
V. Serbin; 2ii023
V.N. Serdyuk; 3iii021
R. Sersale; 4iv017
N.N. Shangina; 2ii016
S.V. Shapet'ko; 2ii033
K.M. Sharma; 1i053, 3ii094
P.S. Sharma; 3ii094
S.C. Sharma; 4iv057
M.A. Shater; 3ii124
Y.N. Sheen; 2ii035
A.L. Shein; 1i015

N. Sherman; 2ii029
V. Shevchenko; 2ii019
C. Shi; 3ii099, 4iv042
H. Shi; 1i012
L. Shi; 2ii031
Y. Shigetomi; 2ii040
H. Shima; 1i025
G.-Y. Shin; 4iv068
S.M. Shingote; 1i003
M. Shmelkov; 3ii080
M. Shoya; 3ii109, 3ii119
D. Shtakelberg; 3v004, 3v022
A.K. Shukla; 3ii115
K. Sideris; 2ii061, 4iv052
K.K. Sideris; 2ii061, 4iv052
M.R. Silsbee; 1i010, 3ii100, 3ii114, 3iii024, 3v020
N.B. Singh; 3ii115
Vinaya K. Singh; 1i016
Vipin K. Singh; 1i016
S.K. Sinha; 4iv047
A.G. Sinyakin; 2ii021
S.P. Sivkov; 2ii020
E. Sjöstedt; 1i060
J. Skibsted; 2ii056
R.C.T. Slade; 3iii011
S. Smeplass; 4iv064
K.A. Snyder; 2ii078
J.-T. Song; 4iv055
V.P. Sopov; 2ii066
D. Sorrentino; 4iv049, 4iv065
F. Sorrentino; 2ii025
J. D. Sota; 2ii036
J. Stark; 1i005, 2ii010, 4iv031, 4iv034, 4iv035, 4iv062
M. Stefanović; 3iii028
J. Stegemann; 4iv042
E.T. Stepkowska; 3v019
A. Stok; 1i022
J. Strigáč; 3v009
C.A. Strydom; 2ii049
P.E. Stutzman; 2ii078
S. Stürmer; 4iv031
St. Stöber; 3iii032
M. Su; 2ii030, 3iii026, 4iv029, 4iv030
L.G. Sudakas; 2ii008
R. Suderman; 2ii011
S. Sugita; 2ii043, 3ii109, 3ii119
L.M. Sulimenko; 1i007, 1i040
U. Sulser; 3iii002
T. Suzuki; 2ii005
L.B. Svatovskaya; 2ii062
K. Svinning; 1i038
R.N. Swamy; 4iv080
L.I. Sychova; 1i032
J. Szczerba; 3iii023

T

A. Tagnit-Hamou; 2ii012
S. Takahashi; 3ii107, 3v013
T. Takahashi; 2ii070
H. Takemura; 2ii007
Y. Takuma; 3ii118
F. Tamás; 2ii060, 3v010, 4iv002
C.E.S. Tango; 3ii085
E. Tazawa; 2ii071
J.J. Thomas; 2ii058
D.W. Thompson; 3iii008
F. Tomosawa; 2ii051, 4iv072
E.E. Toumbakari; 4iv010
B. Touzo; 3v005
R. Trettin; 2ii050
J. Tritthart; 3v010, 4iv069
D. Trumeau; 3v005
B. Trybalska; 4iv027
Y. Tsuchida; 3ii118
Y. Tsukinaga; 3ii109, 3ii119
N. Tsuyuki; 3iii009

U

S. Uchida; 3ii118
H. Uchikawa; 2ii014, 3iii001
T.S. Um; 4iv054
W.S. Um,; 2ii044
H.P. Unsworth; 4iv012
A. V. Usherov-Marshak; 2ii021, 2ii066, 3v016
H. Ushiyama; 2ii040
J.I. Ustimenko; 3ii117

V

H. Vaishnav; 3ii092
G.L. Valenti; 2ii029
K. Van Balen; 4iv010
C. Van Den Brande; 4iv010
R.J. van Eijk; 2ii052
A. Van Gemert; 2ii069
D. Van Gemert; 2ii069, 3ii120, 4iv007,

4iv010
M. Van Messem; 4iv007
F. Van Rickstal; 3ii120
K. Vanbelle; 3ii120
P. Vanis; 2ii063
L.B. Vasiliyeva; 2ii008
T. Vázquez; 1i034, 3ii096, 3iii004, 3iii015
F. Verboven; 2ii069
A. Vichet; 3iii003, 3v014
J. Virlet; 3v003
K. Viswanathan; 2ii039
V. Voznesensky; 3v004

W
A. Walliser; 2ii075
J.F. Wang; 2ii038
P. Wang; 3iii006, 3iii016
X. Wang: 3iii016
Y. Wang; 4iv029, 4iv030
R.C. Wason; 4iv047
D. Watson; 4iv011
J. Widmer; 3iii002
W. Wieker; Plen2
U. Wiens; 4iv016
S. Wild, 4iv075
J. Wu; 3iii006
K. Wu; 3ii122
X. Wu; 4iv032

X
Y. Xi; 3ii111
A. Xu; 4iv077
J. Xu; 4iv030

Y
D. Yadav; 3ii094
S. B. Yadav; 1i003
T. Yamamoto; 3v015
Q. Yang; 4iv032
Q. Ye; 2ii042
K. Yoshida; 2ii070
J.F. Young; 3iii018
Q. Yu; 2ii043, 3ii109, 3ii119
G.-C. Yum; 1i036

Z
N.M. Zaitchenko; 2ii076
M. Zdaniewicz; 3iii023
D.Yu. Zelensky; 4iv039
F. Zenone; 4iv017
R. L. Zerbino; 2ii036
F. Zhang; 4iv030
H. Zhang; 1i026
L. Zhang; 3iii026, 4iv029
X. Zhang; 3ii122
H. Zhuo; 1i028
B. Živanović; 3iii028, 4iv020
B.M. Živanović; 1i017
S.A. Zoubekhine; 3iii021, 4iv036

KEY-WORD INDEX

A

Accelerated test; 3iii033
Accelerators; 3ii103, 3iii005, 3iii012, 3iii014, 3iii022, 3iii027, 3iii032,
Acid attack; 3ii109, 4iv002, 4iv021, 4iv038, 4iv039, 4iv040
Activation; 1i006, 2ii016, 2ii045, 2ii062, 2ii076, 3ii083, 3ii092, 3ii094, 3ii098, 3ii099, 3ii100, 3ii103, 3ii104, 3ii113, 3ii114, 3iii028, 4iv047
Activation energy; 1i053
Activity coefficient; 4iv083
Additives; 1i009, 1i020, 1i035, 2ii003, 2ii009, 2ii045, 2ii074, 3ii116, 3iii017, 3iii032
Adiabatic temperature rise; 4iv072
Admixtures; 2ii012, 2ii034, 2ii036, 2ii047, 3ii087, 3ii095, 3ii097, 3iii001, 3iii002, 3iii004, 3iii009, 3iii018, 3iii019, 3iii023, 3iii024, 3iii025, 3iii026, 3iii029, 3iii030, 3iii031, 3v015, 4iv004
Adsorption; 2ii001, 3iii002, 4iv077
AFm phase; 2ii032, 3iii032, 3ii089, 4iv034, 4iv061
AFt phase; 1i060, 4iv034, 4iv041, 4iv059
Aggregate; 2ii015, 3v024, 4iv053, 4iv057
Air entraining; 4iv031, 4iv057
Air pollution; 4iv002
Alinite; 2ii030, 3ii118
Alite; 1i006, 1i015, 1i041, 1i050, 2ii040, 2ii042, 2ii056, 3ii107, 3ii117, 3iii005, 3iii031
Alkali; 1i002, 1i012, 1i028, 1i035, 1i049, 2ii012, 2ii065, 3ii083, 3ii098, 3ii100, 3ii103, 3ii113, 3ii114, 3ii117, 3iii025, 4iv003, 4iv028, 4iv055, 4iv066
Alkali aggregate reaction; 3iii033, 3v022, 4iv048
Alkali silica reaction; 4iv047, 4iv049, 4iv065, 4iv074
Alkali silicate solutions; 4iv049, 4iv065
Alkaline cement; 4iv046
Alumina; 2ii027, 2ii026, 3iii010
Aluminate phase; 1i001, 1i022, 1i051, 1i056, 2ii041, 2ii060, 3iii010, 3iii015, 4iv027, 4iv034, 4iv066
Aluminoferrite; 1i004, 1i005, 1i055, 2ii031
Aluminosilicate; 1i024, 4iv046
Anhydrite; 1i032, 2ii011, 2ii022, 2ii029, 3ii092, 4iv059
Aragonite; 1i042
Arc furnace dust; 4iv042
Asbestos; 1i027
Ash; 3ii080
Autoclavation; 3ii120, 4iv054
Autoclave soundness; 1i023
Autogeneous shrinkage; 2ii069, 2ii070, 2ii071, 2ii073

B

Backscattered electron image; 2ii014, 4iv061
Bacterial attack; 4iv038, 4iv039
Bamboo dust; 1i019

Barite; 1i036
Barium phases; 1i058
Belite; 1i006, 1i015, 1i018, 1i041, 1i052, 2ii007, 2ii040, 2ii045, 2ii056, 3v009
Belite cement; 1i036
Binder; 1i059, 2ii047, 2ii054, 3ii080, 3ii101, 3iii021, 4iv057
Blastfurnace slag; 2ii068, 2ii074, 3ii082, 3ii093, 3ii095, 3ii096, 3ii098, 3ii099, 3ii101, 3ii102, 3ii103, 3ii104, 3ii115, 3ii122, 3iii009, 3iii017, 4iv001, 4iv005, 4iv009, 4iv015, 4iv035, 4iv040, 4iv063
Blended cement; 1i020, 3ii089, 3ii091, 3ii111, 3ii114, 3ii115, 3ii121, 3v026, 4iv004, 4iv017, 4iv020, 4iv052,
Bogue calculation; 1i039, 3v007, 3v009
Borax; 1i036
Bottom ash; 3ii090
Bound water; 2ii072, 3iii019, 3v019
Brick; 3ii080
Brownmillerite; 1i022, 2ii029, 2ii032,
Burnability of raw mixes; 1i021, 1i030, 1i031, 1i034, 1i040, 1i041, 1i045, 1i048, 1i054
Burning conditions of clinker; 1i018, 1i023

C

Calcium carbonate; 1i042
Calcium aluminate; 2ii022, 2ii025, 2ii050, 3iii022, 3v005
Calcium aluminate cement; 2ii024, 2ii026, 2ii027, 2ii028, 3iii007, 3v018, 4iv003, 4iv025, 4iv026
Calcium aluminate sulphate; 2ii010, 4iv068
Calcium aluminozincates, 1i059
Calcium hydroxide; 2ii049, 2ii059, 3ii082, 3ii106, 3ii107, 3ii108, 3ii112, 3iii031, 3v019, 4iv067
Calcium fluoride; 1i032, 2ii042
Calcium langbeinite; 2ii011
Calcium nitrate; 3iii012
Calcium phosphate; 1i036
Calcium phosphate cement; 2ii063
Calcium silicate; 1i035, 1i055, 2ii055, 2ii050, 2ii062, 4iv054
Calcium sulphate; 1i012
Calorimetry; 2ii021, 2ii025, 2ii041, 2ii066, 3iii032, 3v016, 3v017, 4iv042
Capillary; 2ii048
Carbon dioxide; 1i024, 2ii032, 4iv010
Carbonation; 2ii073, 4iv003, 4iv004, 4iv005, 4iv006, 4iv010, 4iv017, 4iv026, 4iv035, 4iv048, 4iv070, 4iv084
Case studies; 4iv002
Cement; 3ii092
Cement hydration equation; 2ii061, 4iv052
Characterization; 1i008, 2ii062, 3ii088, 3v011, 3v020 3v023, 3v026, 4iv019
Chemical analyis; 3v012
Chemical attack; 4iv015, 4iv026, 4iv028, 4iv031
Chemical prestressing; 3iii016

Chemical shrinkage; 2ii069, 2ii070, 2ii072
Chloride; 1i002, 1i012, 2ii030, 3ii118, 4iv006, 4iv015, 4iv027, 4iv078, 4iv080, 4iv081, 4iv082, 4iv083
Chloride Binding; 4iv016, 4iv069, 4iv070, 4iv078
Classification; 4iv046
Clay; 2ii020
Clinker; 1i048, 1i058
Clinker composition; 1i028, 4iv036
Clinker formation; 1i004, 1i006, 1i008, 1i010, 1i011, 1i026, 1i031, 1i037, 1i043, 1i044, 1i046, 1i049, 1i054, 2ii006, 3ii118
Cluster; 1i003
Coal; 1i047, 3ii090
Composite cements; 1i009, 2ii016, 2ii034, 3ii122
Composition; 2ii007, 2ii071, 3v004, 3v011, 3v026, 4iv007, 4iv023, 4iv060
Concrete; 2ii035, 3ii108, 3iii024, 3iii029, 3v021, 3v022, 4iv025, 4iv035, 4iv073
Cooling of clinker; 3v005
Corrosion; 2ii006, 4iv014, 4iv020, 4iv023, 4iv027, 4iv028, 4iv030, 4iv038, 4iv039, 4iv071, 4iv082, 4iv084
Creep; 4iv018
Cross-linking; 3iii011
Crystal; 2ii015
Crystal size; 1i051, 3iii031
Crystal structure; 1i055, 2ii048
Crystallisation pressure; 4iv049
Crystallography; 2ii054
CSH; 2ii044, 2ii047, 2ii053, 2ii055, 2ii059, 2ii064, 2ii067, 2ii068, 3ii082, 3ii093, 3ii121, 3v001, 3v003, 4iv016, 4iv041, 4iv043, 4iv061, 4iv074, 4iv076
Curing; 2ii037, 2ii078, 3ii091, 4iv055, 4iv059, 4iv067

D

Deformation; 4iv021, 4iv058
Degree of hydration; 2ii051, 2ii053, 2ii062, 2ii077, 3v019, 4iv016
De-icing salts; 4iv006, 4iv035
Delayed ettringite formation; 4iv059, 4iv061, 4iv062, 4iv063, 4iv064
Delayed expansion; 3iii016
Design life; 4iv071
Dicalcium silicate; 1i017, 1i053
Differential thermal analysis; 2ii041, 4iv031
Diffusion; 2ii046, 3ii084, 3ii098, 4iv010, 4iv015, 4iv016, 4iv056, 4iv080, 4iv081
Diffusivity; 4iv008, 4iv009
Dilation; 4iv033
Dispersion; 2ii005
Disposal; 1i027
Dopant; 1i053
Drying; 3iii018, 3v018, 4iv011, 4iv077, 4iv079
Durability; 2ii011, 3ii095, 3iii024, 3v022, 4iv004, 4iv007, 4iv022, 4iv023, 4iv026, 4iv029, 4iv030, 4iv037, 4iv040, 4iv046, 4iv048, 4iv062, 4iv065, 4iv070, 4iv075, 4iv082

E
Economy; 1i036, 3ii114
Ecology; 1i043
Electron microscopy; 1i060
Electron spectroscopy for chemical analyses (ESCA); 2ii044
Electrical conductivity; 4iv011
Electrical impedance; 3ii112
Electrical properties; 4iv079
Electrical resistivity; 3v021
Energy; 2ii046
Environment; 1i003, 3ii093
Equilibria; 2ii057, 2ii058
Ettringite; 1i025, 2ii006, 2ii010, 2ii017, 2ii029, 2ii031 2ii056, 2ii070, 2ii074, 3iii022, 4iv012, 4iv018, 4iv031, 4iv060, 4iv062, 4iv065
Evaporable water; 3v019
Expansion; 2ii006, 2ii074, 3iii017, 3v022, 4iv057, 4iv060, 4iv062, 4iv064
Expansive cement; 1i001, 2ii010
Extraction methods; 3v020

F
False set; 3iii013
Ferrite phase; 1i008, 1i015, 1i060, 3iii005, 3v003
Ferroaluminate; 4iv029
Filler; 1i020, 2ii002, 2ii020, 3ii081, 4iv056
Fineness; 1i007, 2ii001, 2ii002, 2ii018, 2ii043, 2ii060, 3ii088, 3v008, 4iv060
Fingerprinting; 3v010, 3v011
Fire; 4iv073
Fire damage; 4iv067
Flow; 2ii017, 3v024
Flue gas desuphurisation product; 3ii090
Fluidity; 2ii001, 2ii002, 2ii012
Fluoride phases; 2ii043, 3v002
Fly ash; 3ii081, 3ii082, 3ii083, 3ii084, 3ii085, 3ii086, 3ii087, 3ii088, 3ii089, 3ii090, 3ii110, 3ii115, 3ii116, 3ii122, 3v006, 3v020, 3v021, 4iv004, 4iv009, 4iv012, 4iv019, 4iv020, 4iv023, 4iv058, 4iv077
Fracture mechanics; 2ii075
Free lime; 1i016, 1i045, 2ii049, 4iv036
Freeze-thaw damage; 2ii016, 3iii019, 4iv034, 4iv035
Freezing; 4iv033
Friedel's salt; 4iv027, 4iv080
Fuels for clinker making; 1i013, 1i019

G
Gel; 3ii105, 3iii007, 3iii022, 4iv074
Glass; 1i046, 1i051, 3ii088, 3ii119, 4iv030, 4iv055
Grinding aids; 2ii020, 3v014
Grinding technology; 1i009, 1i040

Ground silica; 3ii120
Grout; 2ii005
Gypsum; 2ii040, 2ii044, 2ii060, 3ii093, 3ii115, 3iii025, 3v008, 3v023, 4iv017

H
Hardening; 2ii008, 2ii034, 2ii039, 2ii047, 2ii052, 2ii054, 2ii076, 3ii112, 3v016, 4iv071
Heat capacity; 4iv033
Heat evolution; 2ii021, 2ii035, 2ii051, 2ii076, 2ii077, 3ii102, 3ii105, 3iii029, 3v016, 4iv042, 4iv072
Heavy metals; 1i043, 2ii014, 3v010, 3v013, 4iv041, 4iv043
High alumina cement; 2ii023, 2ii033, 3iii010, 3ii096, 4iv013, 4iv027, 4iv038
High performance; 2ii035, 2ii038, 3ii108, 3v006, 3v021
High strength; 2ii037, 3ii120
High sulphate clinker; 2ii011
High temperature; 3ii111, 3iii020, 4iv067
Humidity; 4iv011, 4iv079
Hydration; 1i022, 1i057, 1i059, 2ii004, 2ii006, 2ii008, 2ii007, 2ii012, 2ii013, 2ii015, 2ii019, 2ii021, 2ii022, 2ii023, 2ii024, 2ii025, 2ii026, 2ii028, 2ii029, 2ii030, 2ii031, 2ii033, 2ii035, 2ii036, 2ii039, 2ii040, 2ii041, 2ii042, 2ii043, 2ii044, 2ii046, 2ii047, 2ii050, 2ii052, 2ii055, 2ii057, 2ii058, 2ii061, 2ii067, 2ii069, 2ii070, 2ii078, 3ii089, 3ii094, 3ii097, 3ii099, 3ii100, 3ii101, 3ii102, 3ii107, 3ii116, 3ii118, 3ii119, 3iii008, 3iii014, 3iii015, 3iii019, 3iii025, 3v006, 3v016, 3v018, 4iv072, 4iv071
Hydrothermal synthesis; 1i017

I
Identification; 3v010
Image analysis; 4iv084
Immobilization; 2ii014, 2ii016, 2ii052, 4iv043, 4iv045
impact prediction; 1i003
Impact evaluation; 1i003
Induction period; 2ii019, 2ii055
Infra red absorption spectra; 3ii104
Inhibitor; 3iii033
Interfacial zone; 4iv050, 4iv051, 4iv053, 4iv056, 4iv084
Interground cements; 1i013, 3v026
Interstitials; 2ii007
Ion exchange resin; 4iv045
Ionic assocoiation, 4iv083
Ions; 2ii036, 2ii046, 2ii065, 3iii012, 3iii013, 4iv075, 4iv079
Iron mud; 1i021
Isomorphism; 1i059

K
Kinetics; 1i005, 1i035, 1i044, 1i052, 2ii019, 2ii023, 2ii028, 2ii043, 2ii055, 3ii098, 3iii008, 4iv076

L
Latex; 3iii008
Leaching; 2ii014, 4iv012, 4iv041, 4iv043, 4iv045
Light microscopy; 3iii031, 3v007
Lignosulphonates; 2ii004, 3iii013, 3iii021
Lime; 2ii049, 2ii074, 3ii084, 3iii005, 4iv010
Limestone; 1i047, 1i048, 2ii022, 4iv018
Long age; 2ii016, 4iv050
Low energy; 1i034, 2ii045
Low temperature; 1i018, 1i029, 1i037, 2ii009, 2ii013, 2ii038, 3iii014, 3v017
Lumos; 2ii079

M
Magnesium chloride; 4iv022
Magnesium sulphate; 4iv022
Magnesium oxide; 1i023, 2ii064, 3v012
Magnesium phases; 1i057
Mass spectroscopy; 3v014
Maturity; 3ii111
Macro Defect Free; 3iii010, 3iii011, 4iv013
Mechanical properties; 3v025
Mechanism; 1i046, 2ii025, 2ii026, 2ii035, 2ii050, 2ii057, 2ii058, 3ii100, 3iii003, 3iii006, 3iii012, 3iii025,, 3v014, 4iv074
Melt; 1i008, 1i011, 1i012, 1i014, 1i029, 1i046, 3v005
Mercury Intrusion Porosimetry; 3ii104
Metakaolin; 3ii113, 3ii114, 4iv011
Method; 2ii021, 3v011, 3v013, 3v016, 3v018, 3v022, 3v023, 4iv081
Microcrack; 4iv021
Microgravity; 2ii075
Microscopy; 1i029, 1i030, 1i039, 1i051, 1i052
Microstructure 1i038, 1i039, 1i047, 1i049, 1i052, 2ii008, 2ii014, 2ii018, 2ii037, 2ii064, 2ii075, 3ii091, 3ii095, 3ii096, 3ii099, 3iii014, 4iv005, 4iv015, 4iv025, 4iv037, 4iv047, 4iv050, 4iv051, 4iv053, 4iv055, 4iv068, 4iv084
Mineralisers in clinker making; 1i028, 1i030, 1i031, 1i033, 1i034, 1i037, 1i050, 3v002
Mineralogy; 1i046, 3ii087, 3ii105
Mineral phase; 1i015, 2ii009, 2ii015, 4iv028
Mixing procedure; 3ii120
Mobility; 2ii065, 4iv083
Modelling; 1i038, 1i044, 1i045, 2ii048, 2ii052, 2ii078, 3ii085, 3ii084, 3iii013, 3v004, 4iv005, 4iv070, 4iv071, 4iv073, 4iv078
Modified cement; 2ii004, 2ii020, 3ii085, 3ii097, 3ii104, 3iii021, 3iii023
Moisture; 2ii079, 3iii011,3v004, 4iv010, 4iv013, 4iv062
Molybdic compounds; 1i054, 1i055
Monosulphate; 2ii056
Mortar; 4iv033

N
Naphtalene Formaldehyde Sulphonate; 3iii003, 3iii009, 3iii030
Nitrate attack; 4iv002
Nodulization in clinker formation; 1i007
Non-equilibrium burning; 1i011
Nuclear Magnetic Resonance; 1i024, 2ii028, 2ii056, 2ii067, 2ii068, 3iii007, 3v001, 3v002, 3v003, 3v004, 3v005, 3v006

O
Oilwell cement; 2ii013, 3iii014
Organic; 3v015
Osmotic pressure; 4iv049

P
Packsetting; 2ii079
Particle size distribution; 1i009, 2ii018, 2ii053, 3ii110, 3v024
Pattern recognitin; 3v010
Penetration; 2ii005, 2ii038, 3ii109, 4iv080
Performance; 4iv073
Permeability; 4iv008, 4iv075
Petroleum coke; 3ii090
pH; 4iv065
Phase composition; 3ii091
Phase diagram; 1i050, 1i052, 2ii024, 2ii057, 2ii058, 4iv066, 4iv074,
Phase transition; 4iv033
Phase transformation; 4iv034
Phosphate; 4iv057
Physical properties; 3v025
Plasticizers; 2ii020
Polymer; 3iii008, 3iii009, 3iii010, 3iii027, 4iv013
Polymorphs; 1i053
Pore size distribution; 4iv077
Pore solution; 2ii036, 3iii003, 3iii013, 3iii022, 3ii091, 4iv040, 4iv069
Pore structure; 2ii037, 2ii066, 3ii111, 3iii009, 3iii018, 3v017, 4iv001, 4iv005, 4iv080
Porosity; 2ii036, 2ii048, 2ii066, 2ii072, 3ii085, 3ii119, 3iii023, 3v017, 4iv006, 4iv007, 4iv008, 4iv013, 4iv017, 4iv024, 4iv040, 4iv048, 4iv054, 4iv078
Portland cement; 3ii107, 3iii006, 3v025, 4iv012
Potentiometry; 4iv083
Powder; 2ii002
Pozzolana; 1i020, 2ii073, 2ii077, 3ii106, 3ii107, 3ii108, 3ii112, 3ii115, 3ii117, 3ii123, 3ii124, 3v001
Pozzolanic cement; 4iv036
Pozzolanic reaction; 3v006
Pozzolanic reactivity; 3ii088
Pre-calciners for clinker making; 1i028
Prehydration; 2ii079
Process parametres; 1i047

Q
Qualitative; 1i004, 3v010, 3v011, 3v015
Quantitative; 1i039, 1i056, 3v007, 3v012, 3v013, 3v015, 3v020
Quartz; 1i048

R
Rapid hardening cement; 2ii017
Rate equations; 1i044
Reaction products; 4iv049
Reactivity; 1i016, 1i018, 1i047, 1i060, 2ii049, 2ii050, 3ii082, 3ii109, 3ii110, 3v020, 4iv016, 4iv050
Refractory; 2ii027, 4iv053, 4iv057
Relative humidity; 2ii073
Residual silica; 4iv049
Retarders; 3iii007, 3iii020, 3iii032
Rheology; 2ii003, 2ii004, 2ii011, 3iii003, 3iii027
Rice husk; 1i019
Rice Husk Ash; 3ii108, 3ii109, 3ii110
Rietveld analysis; 1i039, 1i056, 3v007
Roller compaction; 3ii086
Rotary kiln; 1i007, 1i019

S
Salt scaling; 4iv001
Scanning Electron Microscopy; 1i002, 2ii078, 3ii083, 3ii120, 3iii008, 3v019, 4iv037, 4iv064
Sea water; 4iv025
Secondary ettringite formation; 4iv065
Self deccication; 2ii073
Setting; *1i038, 2ii019, 2ii039, 2ii053, 2ii063, 3ii101, 3ii112, 3iii006, 3iii012, 3iii023, 3iii026,* 3v008
Sewage; 3ii123, 3ii124, 4iv038, 4iv039
Shotcreting; 3iii027
Shrinkage; 1i032, 3iii018, 4iv036, 4iv056
Silica; 3ii080
Silica colloid; 3ii106
Silica fume; 2ii037, 3ii105, 3ii106, 3ii110, 3ii116, 3ii120, 3v001, 4iv014, 4iv069
Silica modulus; 1i035
Silicate; 2ii060, 3iii027, 4iv065
Simulation; 2ii078, 3iii001
Sintering; 1i005, 1i007, 1i022, 1i032
Slag; 1i020, 3ii080, 3ii092, 3ii094, 3ii097, 3ii100, 4iv050, 4iv051, 4iv058
Slump loss; 3iii003, 3iii020
Sodium chloride; 4iv022
Solid solution; 1i014, 1i023, 1i057, 2ii059, 1i060, 3v009
Solid state reactions; 1i042
Solidification; 4iv042
soluble glass; 2ii033

Sorption isotherms; 4iv077
Specific surface; 3iii028
Spectrophotometry; 3v012
Stability; 4iv065
Stabilization; 1i016, 2ii045, 4iv041
Standards; 3v025
Steam curing; 3ii102, 4iv036, 4iv063
Steel; 4iv014, 4iv082
Steric repulsive force; 3iii001
Strain softening; 2ii075
Strength; 1i048, 1i058, 3ii109, 4iv057
Strength development; 1i029, 1i038, 1i041, 2ii007, 2ii017, 2ii018, 2ii033, 2ii051, 2ii053, 2ii054, 2ii060, 2ii063, 2ii072, 2ii076, 2ii077, 3ii085, 3ii089, 3ii097, 3ii111, 3ii117, 3ii119, 3ii121, 3iii004, 3iii026, 3iii028, 3iii029, 3v024, 4iv024, 4iv052, 4iv054, 4iv055, 4iv056, 4iv058, 4iv063
Strength retrogression; 4iv019
Stress; 4iv049
Structure; 1i005, 1i014, 1i056, 2ii054, 2ii066, 2ii067, 2ii068, 2ii069, 2ii076, 4iv007, 4iv025, 4iv042, 4iv043, 4iv075
Sucrose; 3iii006
Sulphate; 1i049, 2ii012
Sulphate attack; 4iv002, 4iv018, 4iv020, 4iv021, 4iv024, 4iv057, 4iv059
Sulphate resistance; 3iii004, 3iii015, 4iv017, 4iv019, 4iv023
Sulphoaluminate; 1i001, 1i025, 2ii029, 3iii026, 3v009, 4iv029, 4iv030, 4iv068
Sulphoaluminoferrite; 1i014
Superplasticizers; 2ii002, 2ii004, 3iii001, 3iii002, 3iii019, 3iii020, 3iii021, 3iii030, 4iv001
Support; 2ii015
Synthesis; 1i015, 1i024, 1i033, 2ii064, 3ii113

T

Temperature; 1i005, 1i007, 1i008, 1i012, 2ii021, 2ii023, 2ii026, 2ii043, 2ii066, 3iii002, 3iii029, 3v001, 4iv047, 4iv060, 4iv068, 4iv069
Terminology; 4iv046
Texture; 1i048
Thawing; 4iv033
Thermal stress; 4iv072
Thermal treatment; 1i027
Thermodynamics; 1i042, 2ii024, 2ii057, 2ii058, 2ii059, 2ii062, 2ii066, 4iv039, 4iv066
Thermogravimetry; 2ii049, 3ii105, 3iii011 4iv003, 4iv037
Thermoporosimetry; 3v017
Tobermorite; 2ii064, 2ii065, 3v003
Trace components; 1i021
Transmission Electron Microscopy; 2ii068
Tricalcium silicate; 1i049 2ii041, 2ii044

U

Unreacted core model; 2ii051

V
Vibration; 2ii017
Viscosity; 1i014, 1i032, 2ii001, 2ii003, 2ii005
Void spacing factor; 3v024
Volume change; 2ii009, 2ii039, 2ii071, 2ii072, 4iv031

W
Waste disposal; 4iv012
Waste material utilization; 1i010, 1i019, 1i022, 1i025, 1i026, 1i027, 1i033, 2ii052, 3ii081, 3ii093, 3ii101, 3ii116, 3ii118, 3ii119, 3ii121, 3ii123, 3ii124, 3v003, 3v013, 4iv014, 4iv024
Water; 4iv075
Water sorption; 4iv008
Water suction; 4iv008, 4iv011, 4iv078
Water-to-cement ratio; 2ii071
Waterglass; 3ii092
Wedge splitting; 2ii075
White Portland Cement; 3iii004
Workability; 2ii011, 3iii029

X
X-ray Diffraction Analysis; 1i051, 1i016, 2ii041, 3iii028, 3ii087, 3ii114, 3v008, 4iv003
X-ray Fluorescense Analysis; 3v011
X-ray Powder Diffraction; 1i002, 1i010, 1i056, 2ii065, 4iv018

Z
Zeolites; 1i020, 1i024, 4iv028, 4iv045, 4iv046
Zeta potential; 3iii001, 3iii002

PROCEEDINGS OF THE 10TH INTERNATIONAL CONGRESS ON THE CHEMISTRY OF CEMENT

Gothenburg, Sweden, June 2-6, 1997

VOLUME 2

CEMENT HYDRATION

10th



ICCC

Göteborg 1997

Edited by

Dr. Harald Justnes
SINTEF Civil and Environmental Engineering, Cement and Concrete
Trondheim, Norway

PROCEEDINGS OF THE 10TH INTERNATIONAL CONGRESS ON THE CHEMISTRY OF CEMENT
Gothenburg, Sweden, June 2-6, 1997

VOLUME 2

CEMENT HYDRATION

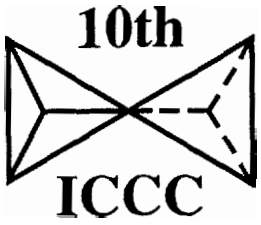

Göteborg 1997

Edited by

Dr. Harald Justnes
SINTEF Civil and Environmental Engineering, Cement and Concrete
Trondheim, Norway

Published by Amarkai AB and Congrex Göteborg AB in 1997

Copyright © Amarkai AB and Congrex Göteborg AB

All rights reserved. No part of this publication may be reproduced, stored in a retrieval system, or transmitted in any form or by any means, electronic, mechanical, photocopying, recording or otherwise without prior permission of the publishers.

Inform Trycket AB, Göteborg 1997
ISBN 91-630-5496-5

List of contents for Volume 2

II PORTLAND, BLENDED AND SPECIAL CEMENTS

II.A Rheology

H. Fujiwara, S. Nagataki, A. Dozono: "Effect of Size Distribution of Powders on Yield Value and Viscosity of Mortar", 2ii001, 7 pp

E. Sakai, S. Hoshino, Y. Ohba, M. Daimon: "The Fluidity of Cement Paste with Various Types of Inorganic Powders", 2ii002, 8 pp

H. Kikukawa, T. Iisaka, Y. Ishikawa: "A Study on the Method of Estimating Rheological Constants of Cement Paste Containing Chemical Admixtures", 2ii003, 8 pp

L. Opoczky, A. Papo: "Reological and Hydration Properties of a High Strength Gypsum-Free Cement", 2ii004, 8 pp

E. Asakura, T. Suzuki, H. Ogata, Y. Maejima, H. Fujisawa: "Penetrability of Suspension Grout Influenced by Dispersion Characteristics of Ultrafine Cement in the Grout", 2ii005, 4 pp

II.B Hydration kinetics and microstructure development

M.M. Ali, R. Bhargava, S.C. Ahluwalia: "Hydration Characteristics of Magnesia Assimilated Sulpho Aluminate - Belite Cement", 2ii006, 6 pp

T. Ikabata, H. Takemura: "Influence of the Composition of Interstitial Phases on the Hydration Properties of Belite Cements", 2ii007, 4 pp

L.G. Sudakas, L.B. Vasiliyeva: "Distinguishing Features of Hardening of Portland Cement Systems on a Basis of Clinker of Various Microstructure", 2ii008, 4pp

I. Grosvalds, S. Lagzdina, U. Sedmalis: "Dolomitic Roman Cement - Low Temperature Hydraulic Binder", 2ii009, 4 pp

J. Stark, I. Chartschenko: "Theoretical Fundamentals of the Application of Expansive Cement Concretes", 2ii010, 6pp

V. Michaud, R. Suderman: "Sulphate Solubility in High SO_3 Clinkers", 2ii011, 10 pp

A. Tagnit-Hamou, S. Bouraoui: "Effect of Alkali Sulfates on Cement Hydration at Low and High Water-to-cement Ratios", 2ii012, 8pp

A. Klusov, Y.R. Krivoborodov, A. Achmetov: "The Change of the Liquid Phase Composition and Properties of Hardened Cement Paste at Low Temperature", 2ii013, 4 pp

H. Uchikawa, S. Hanehara, H. Hirao: "Behavior of Heavy Metal Elements in the Hardening of Cement Paste", 2ii014, 7 pp

A. Olginsky: "Formation of Hydration on Mineral Support", 2ii015, 4 pp

P.G. Komokhov, N.N. Shangina: "Controlling the Hydration of Portland Cement and Concrete's Physical and Chemical Properties by the Surface of Mineral Aggegates", 2ii016, 4 pp

N. Kondo, Y. Nikaido, S. Nakaya, M. Handa, T. Ando, E. Sakai, M. Daimon: "Relationship between Ettringite Formation and the Development of Strength for Rapid Hardening Cement", 2ii017, 8 pp

S.P. Ghosh, K. Mohan: "Interrelationship among Lime Content of Clinker, its Microstructure, Fineness of OPC Grinding and Strength Development of Hydrated Cement at Different Ages", 2ii018, 4 pp

V. Chistyakov, V. Shevchenko, A.E. Degtyaryev, A. Poltavtsev: "Kinetic Peculiarities of Hydrate and Structure Formation in Portland Cement at Initial Stages of Hardening", 2ii019, 4 pp

S.P. Sivkov, D. V. Mundshtukov, I. Jedda: "Organo-Mineral Fillers for Cements", 2ii020, 4 pp

A.V. Usherov-Marshak, O.P. Mchedlov-Petrossyan, A.G. Sinyakin: "The Thermokinetic Factor in Cement Hardening", 2ii021, 4 pp

Y. Ohba, A. Nakamura, L. J. Kyu, E. Sakai, M. Daimon: "Influence of $CaCO_3$ on the Hydration of Various Types of Calcium Aluminates with Anhydrite", 2ii022, 8 pp

V. Chistyakov, V. Serbin: "Sequence of Hydration Process During Hardening of High Alumina Cement", 2ii023, 4 pp

D. Damidot, P. Barret: "Calculation of the Maximum Supersaturation Curve of C_2AH_8 in the CaO-Al_2O_3-H_2O system at 20°C", 2ii024, 8 pp

D. Damidot, F. Sorrentino: "Modification of the Hydration Process from $C_{12}A_7$ to C_3A at 20°C", 2ii025, 8 pp

A. Rettel, D. Damidot, K. Scrivener: "Study of the Hydration of Mixtures of CA and α-Al_2O_3 at Different Temperatures", 2ii026, 8 pp

T.V. Kousnetsova, A.A. Abdel-Kader: "Influence Solid Solution of Calcium Aluminate on Alumina Cement Properties", 2ii027, 3 pp

A.B. Kudryavtsev, T.V. Kouznetsova: "On the Possibilities of the *in situ* Studies of Hydration of Aluminate Cements Using ^{27}Al NMR and Proton Relaxation Rate Measurements", 2ii028, 8 pp

J. Berekta, N. Sherman, M. Marroccoli, A. Pompo, G.L. Valenti: "Effect of Composition on the Hydration Properties of Rapid-Hardening Sulfoaluminate Cements", 2ii029, 8 pp

L. Ji, X. Ren, M. Su: "Effect of Chloride on Hydration Properties of Alinite Cements", 2ii030, 4 pp

Y. Chen, L. Shi: "Rate of Ettringite Formation from Calcium Aluminoferrite Hydration", 2ii031, 8 pp

M. Ecker, H. Pöllmann: "Synthesis and Charcterization of CO_3-containing Ca-Al-Fe Hydrates", 2ii032, 4 pp

P.V. Krivenko, E.K. Pushkaryeva, S.V. Shapet'ko: "Alkaline Aluminate Binders", 2ii033, 4 pp

S. Peukert: "Cement for High Performance Cement Concretes", 2ii034, 4 pp

Y.N. Sheen, C.L. Hwang: "Hydration Mechanism of High Performance Concrete", 2ii035, 4 pp

J. D. Sota, G. M. Giaccio, R. L. Zerbino: "High Perfomance Concrete: Study of Mortar Pore Solution", 2ii036, 5 pp

H.M. Cheong, J.R. Lim, D.W. Cho: "Properties and Microstructure of Ultra High Strength Cement Composites", 2ii037, 5 pp

J.F. Wang: "High Performance Cementous Binder", 2ii038, 4 pp

A.S. Heble, K. Viswanathan, A.K. Chatterjee: "Blends of Basic Cements of Different Phase Compositions - Hydraulic Behaviour Studies", 2ii039, 8 pp

H. Ushiyama, Y. Shigetomi, Y. Inoue: "Effect of Gypsum on the Hydration of Alite and Belite", 2ii040, 4 pp

E.B. El Aouni, M. Benkaddour: "The Effect of C_3S on the Hydration of C_3A", 2ii041, 4 pp

Q. Ye: "A Study on the Hydration Activity of Alite Containing F^- and SO_3", 2ii042, 8 pp

Q. Yu, X. Feng, S. Sugita: "Hydration Characteristics of $11CaO{\cdot}7Al_2O_3{\cdot}CaF_2$", 2ii043, 8 pp

N.-H. Kim, Y.-J. Lee, W.S. Um, H.-S. Lee, I.S. Lee: "Study on the Interaction between Gypsum and the C-S-H Phases in C_3S Hydration Using ESCA", 2ii044, 8 pp

K. Rajczyk: "Hydraulic Activity of Low Temperature Dicalcium Orthosilicate Modified by BaO Addition", 2ii045, 4 pp

Sh. M. Rakhimbaev: "Thermodynamical and Crystal-Chemical Aspects of Inorganic Binders Hydration", 2ii046, 4 pp

M. Radenkova-Yaneva: "Hydration and Structure Formation of Inorganic Binders", 2ii047, 4 pp

V. Babkov, I. Karimov: "The Strength of the Hydrate Phases in the Portland Cement Pastes", 2ii048, 4 pp

C.A. Strydom, J.H. Potgieter: "An Investigation into the Chemical Nature of the Reactivity of Lime", 2ii049, 6 pp

R. Trettin: "Reactivity and Mechanism of Hydration of Cement Phases", 2ii050, 8 pp

F. Tomosawa: "Development of a Kinetic Model for Hydration of Cement", 2ii051, 8 pp

R.J. van Eijk, H.J.H. Brouwers: "Simulation of Cement Hardening in the Presence of Carbon using Hydra2d", 2ii052, 7 pp

A. Nonat, J.C. Mutin, S.P. Jiang: "Physico-chemical Parameters Determining Hydration and Particle Interactions during Setting of Silicate Cements", 2ii053, 8 pp

R.F. Runova, A.N. Plugin: "Colloid-Chemical Principles of the Strength Theory of Contact Hardening Cements", 2ii054, 4 pp

A. Nonat, X. Lecoq, S. Gauffinet: "Calcium Hydroxide Concentration in Solution: Parameter Determining the Kinetics of the Early Hydration of Tricalcium Silicate and the Characterics of the Products", 2ii055, 8 pp

J. Skibsted, O.M. Jensen, H.J. Jakobsen: "Hydration Kinetics for the Alite, Belite, and Calcium Aluminate Phase in Portland Cements from ^{27}Al and ^{29}Si MAS NMR Spectroscopy", 2ii056, 8 pp

H.M. Jennings, C. M. Neubauer, K.D. Breneman, B.J. Christensen: "Phase Diagrams Relevant to Hydration of C_3S. Part 1: A Case for Metastable Equilibrium", 2ii057, 9 pp

C.M. Neubauer, J.J. Thomas, M.C. Garci, K.D. Breneman, G.B. Olson, H.M. Jennings: "Phase Diagrams Relevant to Hydration of C_3S. Part II: A Phase Diagram for the CaO-SiO_2-H_2O System", 2ii058, 15 pp

M. Kersten: "Thermodynamic Aqueous Solubility Diagram for the Binary Solid-Solution System C-S-H - H_2O", 2ii059, 8 pp

G. Balázs, M. Boros, F. Tamás: "Factors Affecting Cement Strength Studied by Model Cements Made of Clinker Minerals", 2ii060, 8 pp

K. Sideris, K.K. Sideris: "The Cement Hydration Equation and its Application to several Hydration Criteria according to the Literature", 2ii061, 11 pp

L.B. Svatovskaya: "Energy and Electronic Transformations in the Process of Binders Solidification", 2ii062, 6 pp

P. Vanis, I. Odler: "Investigations on Calcium Phosphate Cements", 2ii063, 8 pp

II.C Structural models for hydrated cementitious pastes

Z. Pytel, J. Małolepszy: "The Role of MgO in the synthesis of C-S-H and Tobermorite", 2ii064, 7 pp

N. Hara, N. Inoue, H. Noma: "Thermal Behaviour of Tobermorite Intercalated with Alkalie Ions", 2ii065, 5 pp

A.V. Usherov-Marshak, V.P. Sopov, V.I. Kondrashchenko: "The Regularities of Forming and Modelling the Microstructure at the Early Stages of Cement Stone Hardening", 2ii066, 4 pp

M. Grutzeck, J. LaRosa-Thompson, S. Kwan: "Characteristics of C-S-H gels", 2ii067, 10 pp

Ian G. Richardson: "The Structure of C-S-H in Hardened Slag Cement Pastes", 2ii068, 8 pp

II.D Chemical and physical shrinkage

H. Justnes, A. Van Gemert, F. Verboven, E.J. Sellevold, D. Van Gemert: "Influence of Measuring Method on Bleeding and Chemical Shrinkage Values of Cement Pastes", 2ii069, 8 pp

T. Takahashi, H. Nakata, K. Yoshida, S. Goto: "Autogeneous Shrinkage of Cement Paste During Hydration", 2ii070, 8 pp

E. Tazawa, S. Miyazawa: "Influence of Cement Composition on Autogeneous Shrinkage of Concrete", 2ii071, 8 pp

P. Paulini: "Chemical Shrinkage as Indicator for Hydraulic Bond Strength", 2ii072, 8 pp

B. Persson: "Long-term Shrinkage of High-Performance Concrete (HPC)", 2ii073, 9 pp

M. Degenkolb, D. Knöfel: "Investigations on Shrinkage Compensated and Expansive Repair and General Behaviour to Typical Influences", 2ii074, 8 pp

II.E Influence of mixing techniques and curing conditions

R.C. First, A. Walliser: "Mechanical Property/Microstructure Relationships in a Mortar Fabricated in Microgravity Environment", 2ii075, 9 pp

V.A. Matviyenko, N.M. Zaitchenko: "Hardening of Cements, Polarized in Electric Field", 2ii076, 4 pp

V. Ronin, J.-E. Jonasson, H. Hedlund: "Advanced Modification Technologies of the Portland Cement-based Binders for Different High Performance Applications", 2ii077, 8 pp

D.P. Bentz, K.A. Snyder, P.E. Stutzman: "Hydration of Portland Cement: The Effects of Curing Conditions", 2ii078, 8 pp

E. Marciano Jr., S.L. Centurione, V. Maringolo: "Identification of Causes of Lumps Formation in Industrial Cements", 2ii079, 4 pp

Topic II.A

Rheology

Kn o. 25. JAN. 2001 d o k 31763

2ii001
7 pp

EFFECT OF SIZE DISTRIBUTION OF POWDERS ON YIELD VALUE AND VISCOSITY OF MORTAR

Hiromi FUJIWARA, Nihon Cement Co., Ltd., Tokyo Japan
Shigeyoshi NAGATAKI, Tokyo Institute of Technology, Tokyo, Japan
Akito DOZONO, Nihon Cement Co., Ltd., Tokyo Japan

ABSTRACT: This paper clarifies the relationship between size distribution of powders and rheological properties (yield value and viscosity) of mortar, which directly affect the properties of high fluidity concrete. The results of this study show that yield value of mortar is influenced by the n-value of the Rosin-Rammler equation, which is the main factor of excess water volume in mortar, and that viscosity of mortar is influenced by the Blaine surface area, which results from the effect obtained by combining absorption of superplasticizer and thickness of water film.

Key-words: adsorption, fineness, fluidity, viscosity

INTRODUCTION

In recent years, high fluidity concrete, which demonstrates the properties of high fluidity and resistance to segregation, has been receiving particular attention. In order to achieve resistance to segregation, a viscosity controlling admixture is added or the amount of powder is increased. Another method of achieving effective resistance to segregation is adjustment of powder grading. Therefore, it is necessary to clarify the relationship between grading and the rheological properties of concrete or mortar. For this paper, the relationship between powder grading and viscosity and yield value of mortar were studied.

RELATIONSHIP BETWEEN POWDER GRADING AND RHEOLOGICAL PROPERTIES OF MORTAR

Outline of experiment

The two principal factors affecting grading distribution conditions, Blaine fineness (BF) and the n-value (NV), or distribution constant of the Rosin-Rammler equation, were varied and mortar was mixed using these powders; the yield value and viscosity, which are the rheological properties of these mortars, were measured and their relationship with BF and with NV was investigated.

Materials used

Normal Portland cement (NPC: BF=3,210 cm^2/g, specific gravity=3.15, NV=1.06) and limestone powder (LS: specific gravity=2.70) were used. Chemical composition of NPC is

shown in Table 1. Limestone was ground to BF in the range of 2,200~10,000 cm^2/g using a ball mill and mixed with cement in the proportions of 1 : 1 by volume. The results, as shown in Fig 1, were 51 types of powders within the range BF=3,500~7,500 cm^2/g, NV=0.7~1.1. ß-Naphthalene sulfonic acid (NS) was used as the superplasticizer and crushed sand (specific gravity=2.61, FM=2.91, percentage of solid volume=66.2%) was used as the fine aggregate. Fig 2 shows the grading curve for fine aggregate.

Table 1 Chemical composition of normal Portland cement (NPC) and moderate-heat Portland cement (MPC)

Cement	Ig. loss	Insol	CaO	SiO_2	Al_2O_3	Fe_2O_3	MgO	SO_3	Na_2O	K_2O	TiO_2	P_2O_5	MnO	f-CaO	Total
NPC	1.6	0.3	61.6	20.1	5.0	3.0	1.1	2.0	0.38	0.43	0.26	0.06	0.17	0.6	96.00
MPC	0.7	0.1	64.2	23.1	3.8	4.0	0.8	2.1	0.32	0.39	0.19	0.05	0.08	0.4	99.83

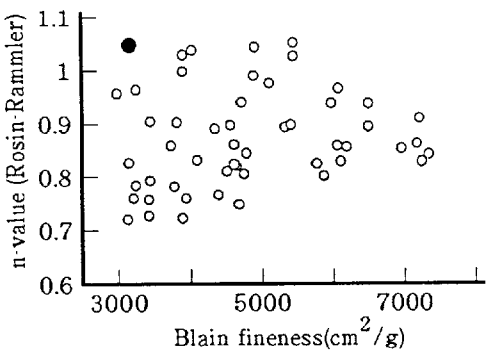

Fig 1 Blaine fineness and n-value

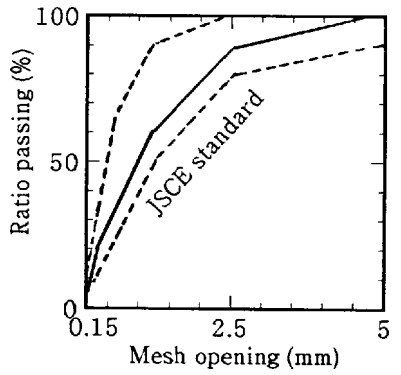

Fig 2 Grading curve for fine aggregate

Conditions of experiment

Mortar, composed of powder, water and fine aggregate in the proportions 22.7 : 22.9 : 54.5 (% by vol.) was mixed in a two-liter paddle mixer for two minutes. This composition is equivalent to the mortar component used in standard high fluidity concrete.

Test items

The yield value and viscosity of the mortar were measured immediately after mixing using a rotation viscosimeter.

Results of experiment

Yield value of mortar

The contour line of the yield value of mortar is shown in Fig 3. From these results it is clearly seen that the yield value of mortar is strongly influenced by the NV; the smaller the NV, the lower the yield value. Further, as the BF decreases, the yield value decreases slightly.

However, for NV lower than 0.8, it was confirmed that the yield value tends to increase as the NV decreases. This is thought to result from changes in the fineness distribution caused by early hydration.

Viscosity of mortar

Fig 4 shows the contour line of the viscosity of mortar, which differs greatly from that of the yield value. Thus, the NV exerts a strong influence when the BF is in the range below 4,000 cm^2/g, and the viscosity decreases as the NV becomes smaller. However, when BF is in the range above 4,000 cm^2/g, the influence of the BF exceeds that of the NV and as the BF increases, viscosity increases. In general, the yield value and viscosity are strongly interrelative and as the yield value increases, viscosity also increases. Therefore, when BF is in the range below 4,000 cm^2/g, it is thought that the influence of the yield value is stronger. However, when the BF exceeds 4,000 cm^2/g, it is thought that other factors are at work. Further, as for the yield value, when the NV is in the range below 0.8, it was confirmed that viscosity increases as the NV decreases. As for yield value, this is thought to result from changes in the fineness distribution caused by early hydration.

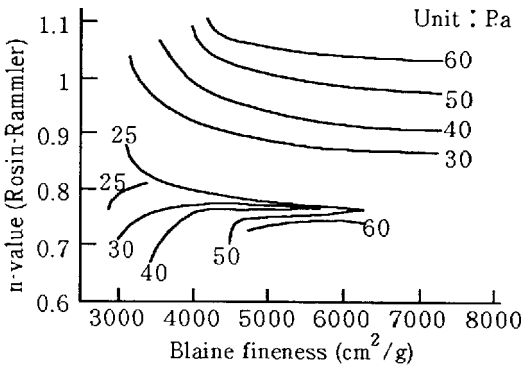

Fig 3 Relationship of contour line of yield value with Blaine fineness and n-value

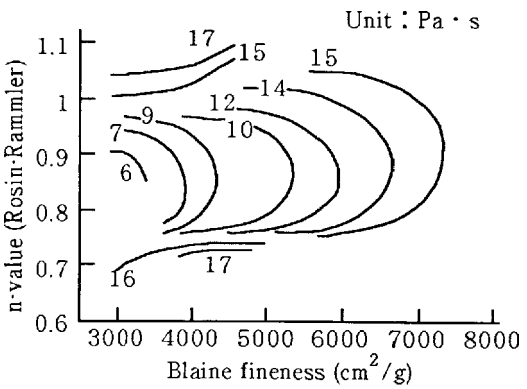

Fig 4 Relationship of contour line of viscosity with Blaine fineness and n-value

FACTORS INFLUENCING YIELD VALUE AND VISCOSITY OF MORTAR

Packing ratio

Outline of experiment

Using the powders in Fig.1, packing tests were carried out by tapping and the packing ratio was measured. Material was heaped in a cylindrical vessel and the vessel was dropped 500 times from same level by using a powder tester to provide a constant packing ratio.

Results and discussion

The contour line for packing ratio is shown in Fig 5. NV exerts a strong influence on packing ratio and packing ratio increases as NV decreases. The influence of BF is small, but it was confirmed that packing ratio increases slightly as BF decreases. This is in accordance with prior information that as the fineness distribution becomes wider and the particle size increases, the packing ratio increases (Powder Technology, 1986). Further, Fig 5 shows a trend similar to that shown for yield value (Fig 3). In general, packing ratio is an indicator of the volume of water required to fill the voids in the powder and shows that, as the packing ratio increases, the volume of excessive water increases. The results of this experiment show that there is a close relationship between yield value and volume of excessive water.

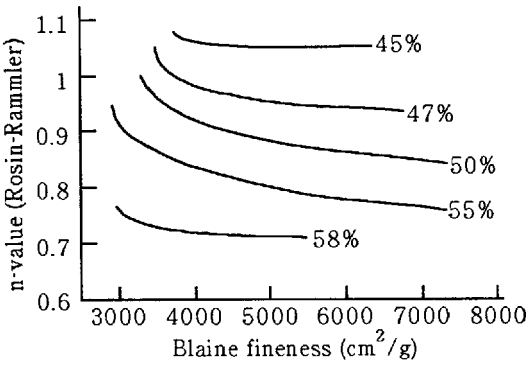

Fig 5 Relationship of contour line of packing ratio with Blaine fineness and n-value

Changes in grading due to early hydration

Outline of experiment

NPC having a constant BF of 4,720 cm^2/g and NV in the range of 0.70~0.94 was controlled at 4 levels; each was mixed to form a paste having W/C=40% and 2% addition of NS. Five minutes after water was poured, hydration was stopped by adding acetone and changes in fineness were measured.

Results and discussion

Table 2 shows the NV, BF and fine particles with particles of 1μ or smaller before pouring water and fine particles and NV five minutes after pouring of water. From these results, it can be seen that fine particles content increases as NV decreases before water is poured, but the ratio of fine particles decreases sharply when water is poured, resulting in a great increase in the NV. In particular, for powder with NV of 0.8 or less before pouring water, the relationship between large NV and small NV is reversed after pouring water. This is thought to be a result of the great amount of bridging by fine particles which occurs during hydration. This phenomenon, where the trend of the NV is reversed after pouring of water for NV of 0.8 or lower, is also assumed to be the cause of the reversal in yield value and viscosity of mortar.

Table 2 Powder grading distribution characteristics before and after pouring water

Grade	Before pouring water				After pouring water	
No.	Fine particles (%)	BF (cm^2/g)	NV	Packing ratio (%)	Fine particles (%)	NV
1	6.5	4,720	0.94	47.6	6.1	0.97
2	7.9	4,710	0.86	54.2	6.6	0.90
3	9.0	4,720	0.76	56.8	6.5	0.85
4	9.8	4,720	0.70	58.4	6.8	0.87

Excessive thickness of water film

In the studies by Yoshino et. al (1993), when the yield value and type of additive in the paste were the same, the viscosity of the paste formed a linear relationship with the thickness of the water film (Yoshino, 1993). Further, it is known from studies by Uchida, that the effects of cement fineness which influences fluidity of mortar do not change the effect of the trend or basic properties of the fluidity of the paste (Uchida, 1990). The excessive thickness of the water film on the mortar paste was calculated by the following equation and the relationship with grading was studied.

Excessive thickness of the water film $(\mu)=(1-Vc/Gc)/(Vc\cdot\rho\cdot F)\times 10{,}000$ [1]

Vc: volumetric ratio of powder in paste
Gc: tapping packing ratio
ρ: specific gravity of powder (g/cm^3)
F: Blaine fineness (cm^2/g)

Fig 6 shows the contour line of excessive water film thickness based on these calculations. From the figure, it can be seen that the thickness of the water film decreases as the NV or the BF increases. If Fig 6 is compared with Fig 4, it seems that the thickness of the water film affects the viscosity of mortar, but the trend is not completely the same. Therefore, in order to explain the trend of viscosity of mortar, it is necessary to consider other factors as well as the thickness of the water film.

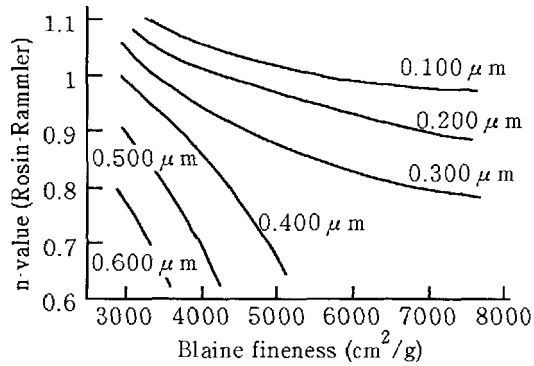

Fig 6 Relationship of contour line of excessive water film thickness with Blaine fineness and n-value

Absorption of superplasticizer

Outline of experiment

Moderate heat Portland cement (MPC: specific gravity=3.22; chemical composition as shown in Table 1) within the range of BF=3, 160~6,240 cm^2/g, NV=0.75~1.05 was graded into 11 finenesses and mixed with water and fine aggregate in the proportions 18.4 : 29.6 : 52.0% by volume; superplasticizer in the amount of 3.0% by weight of cement was added and the mortar mixed. Five minutes after pouring water, the liquid phase was extracted by suction filtering and diluted to 1/1,250 and 1/2,500; absorption of the superplasticizer was calculated by absorptimetry.

Results of experiment and observations

The contour line of superplasticizer absorption was drawn based on the results of measurement and is summarized in Fig 7. From these results, it was found that as the NV decreases and the BF increases, the amount of superplasticizer absorption increases. For the purpose of investigating the relationship between absorption and viscosity, superplasticizer absorption, and yield value and viscosity of mortar were measured for four points (No. 1~4) on the excessive water film thickness 0.200μ line in Fig 7; the results are shown in Fig 8. From this figure, it can be seen that, even when excessive water film thickness is constant, the increase in superplasticizer absorption causes an increase in viscosity. From this, it was learned that: 1) as BF increases, excessive water film thickness decrease is accompanied by increases in superplasticizer absorption and viscosity; and 2) as the NV decreases, excessive water film thickness increases but the increase in superplasticizer absorption offsets the effect on viscosity. These results are assumed to indicate the trend of viscosity as shown in Fig 4.

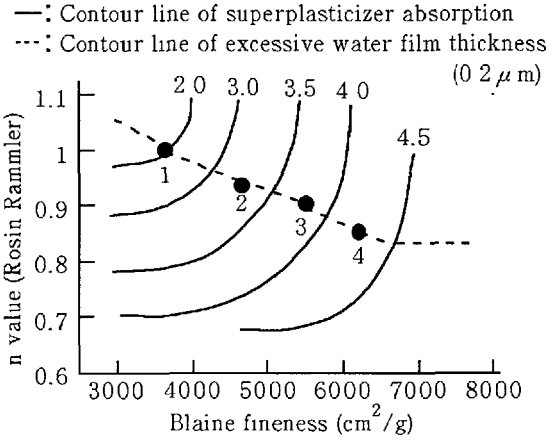

Fig 7 Relationship of contour line of superplasticizer absorption with Blaine fineness and n-value

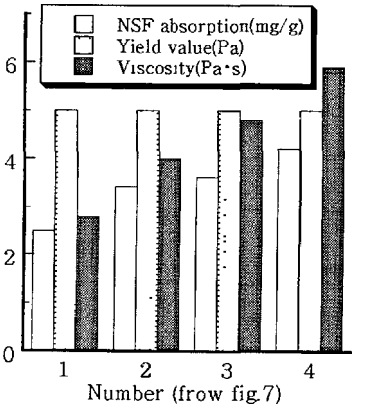

Fig 8 Relationship of superplasticizer (NSF)absorption with yield value and viscosity

CONCLUSION

In this study, the viscosity and yield value of the mortar component which have a great effect on the properties of high fluidity concrete and their relationship with the Blaine fineness and NV as calculated by the Rosin-Rammler equation were studied. As a result, the following three points were learned.

1) The influence of the NV of the powder which controls the volume of excessive water is the factor controlling yield value of mortar.
2) For NV 0.8 or lower, the yield value and viscosity increase as the NV decreases. This is the result of changes in fineness distribution due to early hydration.
3) In the Blaine fineness range of 4,000 cm^2/g or lower, viscosity is influenced in the same way as yield value; however, above that range the effect of Blaine fineness becomes a controlling factor and viscosity increases as Blaine fineness increases. This is thought to result from the complex effects of excessive water film thickness and amount of absorption of superplasticizer.

REFERENCES

The Society of Powder Technology, Japan, "Powder technology observations", Nikkan Kogyo Shinbun-sha Co. Ltd., 1986, pp. 105-108.

Uchida, S., Okamura, R., Take, H., Uchikawa, H., "Influence of characters of cement on fluidity of fresh cement paste and mortar with organic additives", Japan Cement Association Proceedings of Cement and Concrete, No. 44, 1990, pp. 86-91

Yoshino, A., Nishibayashi, S., Kono, S., "Effect of characteristics of admixtures and cementitious materials on viscosity of paste", Proceeding of the 48th Annual Conference of the Japan Society of Civil Engineers, Vol. 5, 1993, pp. 938-939.

2ii002
8 pp

Kno. 25. JAN. 2001 dok 31764

THE FLUIDITY OF CEMENT PASTE WITH VARIOUS TYPES OF INORGANIC POWDERS

Etsuo SAKAI, Seiichi HOSHINO*, Yoko OHBA and Masaki DAIMON
Department of Inorganic Materials, Tokyo Institute of Technology, Tokyo, Japan
*Central Research Laboratory, Nihon Cement Co., Ltd., Tokyo, Japan

ABSTRACT Lime-stone powder are under development in order to enable production of flowing concrete without need for vibration during their placement. Influence of various types of inorganic powders having the same particle size distribution of ordinary cement on the fluidity of cement paste with polycarboxylate type AE high range water reducing agent has been investigated. It is clear that the shape and the packing of powders are influencing the fluidity of cement paste with superplasticizer.

Key-words: Fluidity, Filler, Fineness, Powder, Superplasticizers

INTRODUCTION

In Japan, many investigators have been studied the properties of flowing concrete with various types of inorganic powders and polycarboxylate types of AE high range water reducing agents (Okamura and Ozawa,1994). And the flowing concrete with lime stone powder or granulated blast furnace slag were practically applied to National projects such as Honshu-Shikoku Bridges (Yasuda et al,1993) or ordinary concrete products. By using of inorganic powders, the fluidity and segregation of flowing concrete is improved and the dosage of AE high range water reducing agent is reduced compared with the case of same fluidity of concrete without inorganic powders. On the other hand, lime stone powder was very useful for the saving of energy and the production amounts of CO_2 gas for cement production and portland limestone cement was used in Europe (ECS,1992). Many investigators have been suggested that monocarbonate and hemicarbonate were produced by the reaction of C_3A and limestone powder (Grandet and Olliver,1980,Kuzel and Pollman,1991). The more detail studies of it's reaction mechanism and mechanisms of improvement for fluidity of cement with limestone powder are necessary. We have reported the reaction mechanisms of limestone powders and various types of calcium aluminate such as C_3A,amorphous $C_{12}A_7$ and $C_{11}A_7 \cdot CaF_2$ by quantitative measurements of anhydrates or hydrates (Hosokawa et al,1995, Nakamura et al,1996a).

In this report, we discuss the fluidity of cement with various type of inorganic powders such as lime stone powder, granulated blast furnace slag, fly ash and fused silica with various fineness including the particle size distribution similar to ordinary portland cement, from view points of their shape and packing properties. In addition, new (polycarboxylate) types of AE high range water reducing agent having polyethylene oxide graft chains are need for the development of flowing concrete. Therefore the dispersion mechanisms of these agents are introduced by the calculation of interparticle potential using measured the segment density and the thickness of adsorbed polymers (Sakai and Daimon,1996b).

POLYCARBOXYLATE TYPE AE HIGH RANGE WATER REDUCING AGENT

AE high range water reducing agent has a higher water reducing ratio, small change of slump with the passage time and less set retarding properties. It is now being used

extensively in flowing concrete. These are not the group such as naphthalene sulfonate formaldehyde high condensate or melamine resin sulfonate which have been used hitherto for the production of high strength and flowing concretes with a great slump loss, but the one named action mechanism generically as polycarboxylate group. Polycarboxylate group fundamentally comprise macromolecules having polyethylene oxide graft chains.

As for the factors related to the stabilization of the dispersive system by the macromolecule, it is thinkable that the steric hindrance due to the action of adsorbed macromolecule and the depletion stabilization due to the action of non-adsorbed macromolecule have important. This functions as repulsion. Using the interparticles potential curve obtained from the sum total of repulsion and van der Waals interaction, argument concerning the stabilization of disperse system is started.

$$V_{\text{interparticle potential}} = V_{\text{steric hindrance}} + V_{\text{depletion stabilization}} + V_{\text{van der waals interraction}}$$

We have been calculated interparticle potential of alite in alite-water system with macromolecule which are shown in Fig 1 and have degree of polyethylene oxide graft chain having the polymerization(n) from 7 to 90 (Sakai and Daimon,1996b). Steric hindrance effect was calculated by the thickness of actual adsorbed polymer and the segment density of adsorbed polymer, while depletion stabilization was calculated by the volume fraction of polymer. Calculation is made paying attention to only polyethylene oxide chain and the volume fraction was obtained by using of Rotational Isometric State-Monte Carlo Method. Magnitude of van der Waals interaction can be obtained by the use of Hamarker constant. According to Lifshitz theory, Hamarker constant of C_3S and C-S-H can be

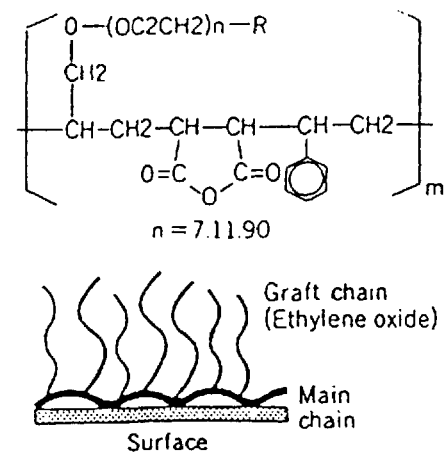

Figure 1 Molecular structure

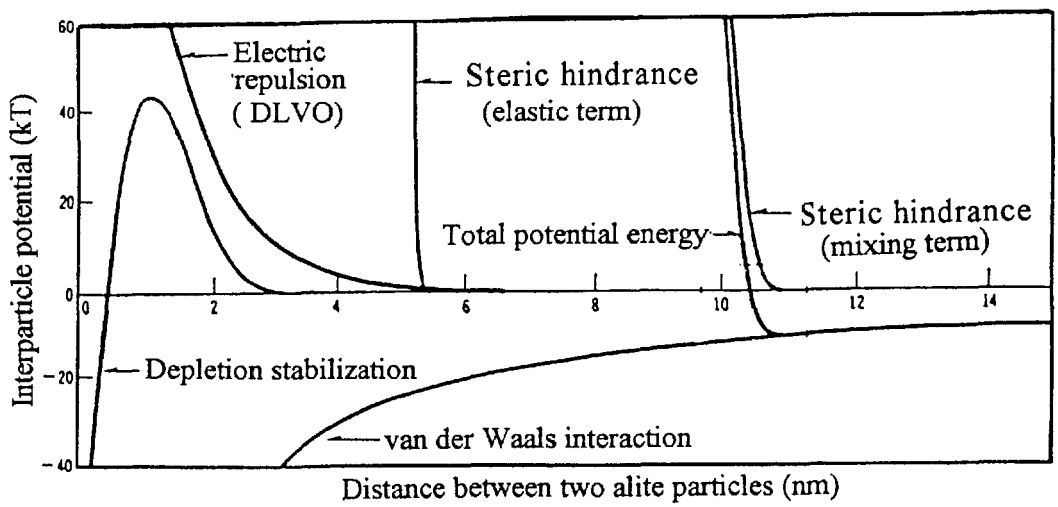

Figure 2 Interparticle potential of alite with AE high range water reducing agent

calculated. Fig 2 shows the inter-particle potential in the case of n=11 is adsorbed to alite particles with a radius of 1 μ m. In addition, electric repulsion effect calculated by DLVO theory was also shown. Van der Waals force exerts attraction from long distance and the mixing effect of steric hindrance effect puts out a strong repulsive power from some distance to prevent aggregation. On the other hand,depletion stabilization and the electric repulsion effect works just at short distance and does not exert a strong repulsive power. Therefore,an important factor to play a role for the dispersion of cement particles may be van der Waals force and steric hindrance effect of adsorbed AE high range water reducing agent having polyethylene oxide graft chains.

SHAPE EFFECT OF PARTICLES

Influence of shape of powders were investigated on the fluidity of cement paste. The fluidity of paste is indicated to $1/\eta$. The apparent viscosity(η) of paste was measured by rotating cylinder viscometer at 20℃. Prepared fused silica have about same particle size distribution of ordinary portland cement as shown in Fig 3. Particle size distribution of powders was measured by laser type of light scattering method. Various types of fused silica were separated by precision air separator Samples having the class range of below 7,7-12,12-20 and 22-33 μ m were respectively obtained. Prepared crushed fused silica (PCS) and prepared spherical fused silica (PSS) were produced by the combination of their samples. SEM photographs of these powders are shown in Fig 4. The spherical shape of PSS can be observed. SiO_2 contents of their fused silica are over 99.9% and their specific gravity are 2 22

The replacement ratio of these powders to cement were changed from 10 to 40%. Water to powder ratio was 0 9vol% and the dosage of polycarboxylate type of AE high range water reducing agent having polyethylene oxide graft chains was1 6% of powder by weight. If the dosage of this agent is added over this value,the fluidity of paste in not changed and indicated the constant fluidity. Fig 5 shows the fluidity of paste with PCS and PSS. The fluidity of paste is

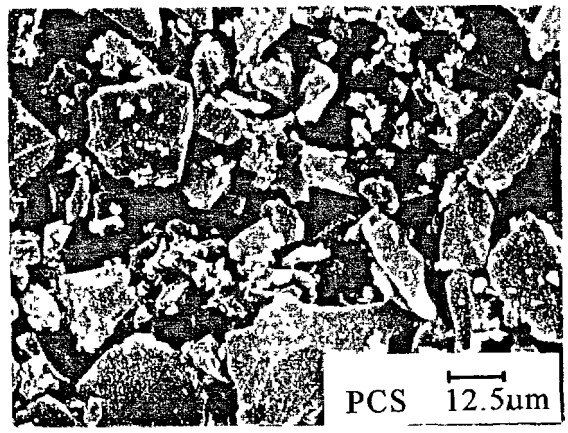

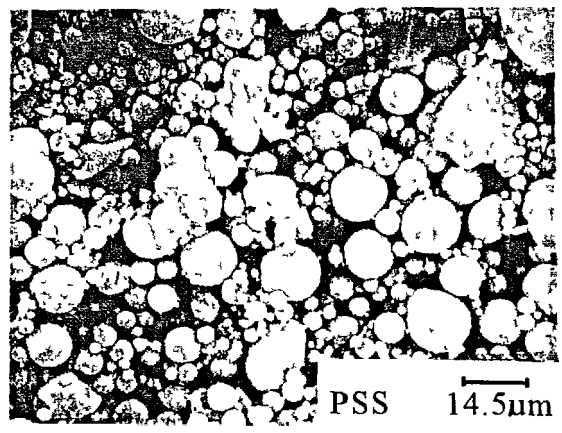

Figure 4 SEM photographs of PCS and PSS

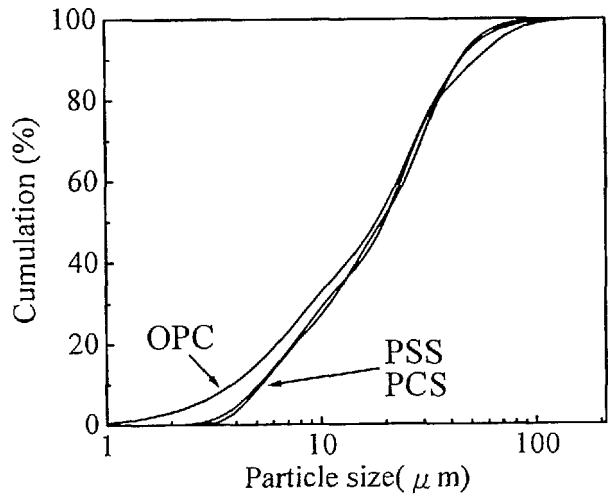

Figure 3 Particle size distribution.

increasing with the increasing of replacement ratio of prepared fused silica. And the fluidity of paste with PSS is larger than that of paste with PCS. Fig 6 shows the relation between to the fluidity of paste with fused silica and the replacement ratio of PSS to PCS. The replacement ratio of fused silica to cement is 40%. When the replacement ratio of spherical powders is increased, the fluidity of paste is improved. A plot of the fluidity of paste and the replacement ratio is found to be approximately linear. Particle size distributions of PSS and PCS are indicated the same results. Therefore, it is clear that the shape of powder is influenced on the fluidity of paste.

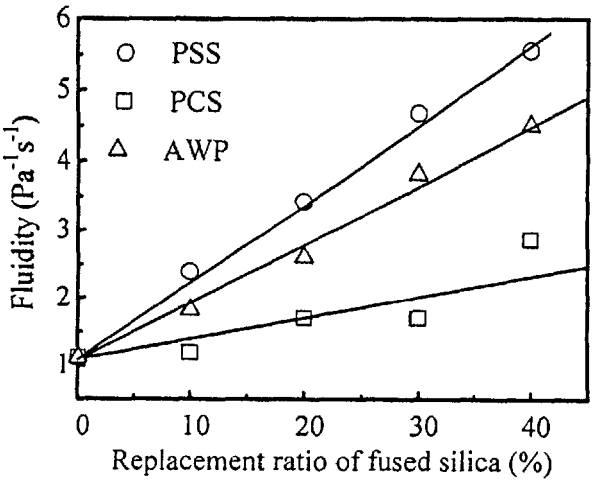

Figure 5 The fluidity of pastes with PSC or PSS

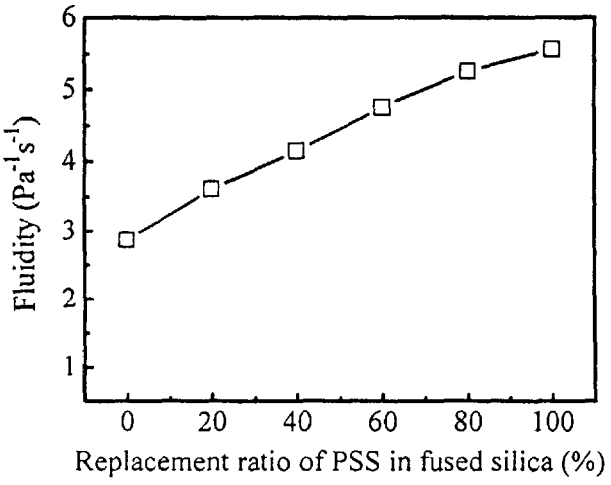

Figure 6 Influence of PSS contents on the fluidity of paste

Fig 7 shows the packing density of cement paste with PCS or PSS. Packing density was measured by next method. In pastes with PCS or PSS, powder cakes containing water and supernatant water were separated by centrifuge (6000rpm,10min). Ratio of powder to powder cake is the packing density of paste. The tendency of packing density is indicated the same results for the fluidity of pastes. The higher the packing density of paste,the higher the fluidity of paste. The packing density of paste is related to the amounts of retention water in cluster of powder. The difference in amounts between total water and retention water of paste (called free water) is effected on the fluidity of paste. The smaller the amounts of retention water, the higher the fluidity of paste. The amounts of retention water of paste with PSS is smaller than that of the paste with PCS. Fig 8 shows the flow model of pastes with PSS or PCS.

By the addition of water, the amounts of free water of paste with PCS are prepared the same values of the case of paste with PSS. The fluidity of these pastes (AWP) is increased as shown in Fig 5. But the fluidity of paste with PSS is smaller than that of AWP paste. The difference in fluidity between the AWP paste and the

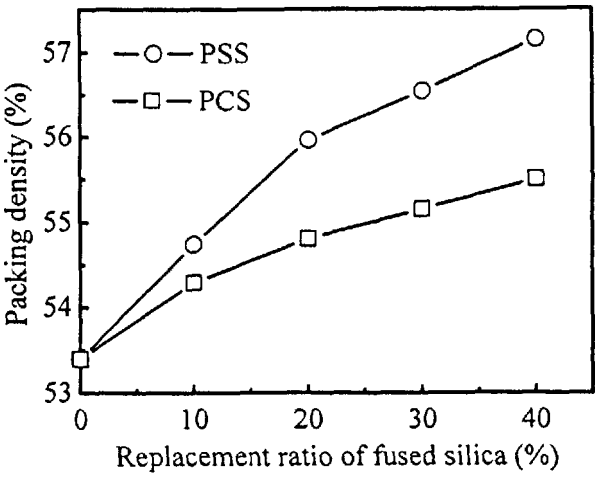

Figure 7 Packing density of paste with PCS or PSS.

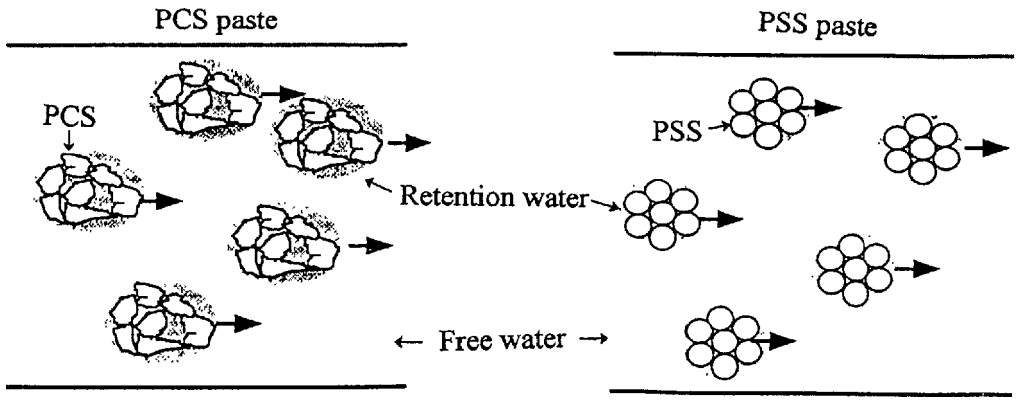

Figure 8 Schematic illustrations of flow model of PCS and PSS pastes

paste with PCS is related to the effect of packing effect. And the difference of the fluidity of paste with PSS and AWP paste may be contributed to ball bearing effect. Therefore, the shape effect of inorganic powders on the fluidity of paste consists of the packing effect and the ball bearing effect of powders.

INFLUENCE OF VARIOUS TYPES OF INORGANIC POWDERS

Table 1 shows the chemical compositions of various types of inorganic powders. Prepared inorganic powders having the particle size distribution similar to ordinary cement are made by air separation and mixing as mentioned above. Experiments carried on used prepared granulated blast furnace slag (PBFS), prepared limestone (PLS), prepared fly ash (PFA), PCS and PSS. When prepared powders are used, the effect of particle size distribution of powders on the fluidity of paste can be neglected.

Table 1 Chemical composition of inorganic powders

Samples	Ig.loss	SiO_2	Al_2O_3	Fe_2O_3	CaO	MgO	Na_2O	K_2O	Total C
PBSF	0.2	34.5	14.0	0.5	41.0	6.8	0.22	0.29	-
PLS	43.2	0.7	0.2	0.1	55.2	0.4	0	0	-
PFA	1.1	63.4	17.4	4.8	4.3	1.5	0.71	0.8	0.54

Table 2 shows the packing bulk density and the sphericity factor (packing bulk density/specific gravity) of inorganic powders and the fluidity of cement paste with prepared inorganic powders. In measurement of fluidity of paste, the replacement ratio of prepared inorganic powders is 40% and the water to powder ratio is 0.9vol%. The dosage of AE high range water reducing agent is 1.6%. By using of powders having higher sphericity factor, the fluidity of paste can be improved. Sphericity factor of PSS is higher than that of PCS. Sphericity factor of particles is related to shape of particles as shown in Fig 4. The higher the sphericity factor of powders, the higher the contents of spherical particles. Sphericity factor of PFA is smaller than that of PLS or PCS. This is contributed to the contents of carbon. It was reported that the contents of carbon having a irregular shape in PFA is determined the fluidity of cement paste with PFA (Lee et al,1996c). Sphericity factor of powders is one of the main factor in order to improve the fluidity of cement paste with inorganic powders.

Table2 The fluidity of cement paste with various types of inorganic powders and their shape factor(Sphericity factor = Packing bulk density/Specific gravity)

Samples	Specific gravity	Packing bulk density	Sphericity factor	Fluidity($Pa^{-1}s^{-1}$)
OPC	3.17	1.639	0.520	1.1
PBSF	2.70	1.563	0.539	2.1
PLS	2.71	1.604	0.592	3.5
PFA	2.32	1.282	0.553	2.6
PCS	2.22	1.282	0.578	2.8
PSS	2.22	1.465	0.660	5.2

OPC: Ordinary portland cement

INFLUENCE OF PARTICLE SIZE DISTRIBUTION

Fig 9 shows the particle size distributions of classified limestone (LS) powders. Classified limestone powders were prepared by hydraulic elutriation of limestone powder (Blaine's specific surface area:440m^2/kg, Specific gravity;2.71). Relation between to the fluidity of cement pastes with classified limestone powders and their average particle size are shown in Fig 10. The replacement ratio of classified limestone to cement is 20% by weight. Water to powder (cement+classified limestone powder) ratio is 0.9vol% and the dosage of polycarboxylate AE high range water reducing agent is 1.6% by weight of powders. The average particle size of ordinary portland cement is18 μ m. The fluidity of cement paste with samples B,C and D having average particle size similar to ordinary cement are lower than that of cement paste with coarse or fine classified limestone powders (samples A and E).

Fig 11 shows the packing density of paste with classified limestone powders. These

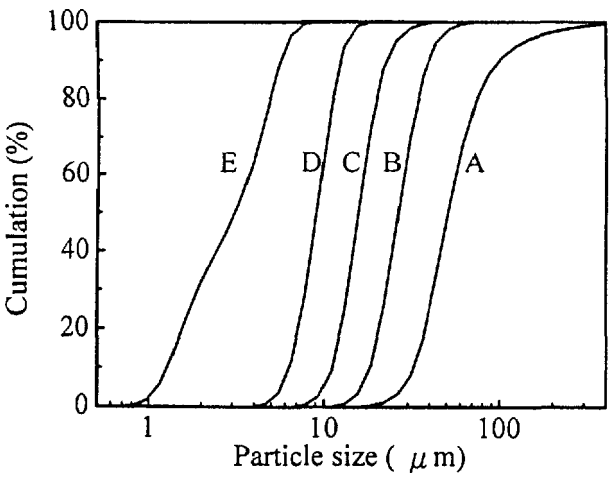

Figure 9 Particle size distribution of classified LS.

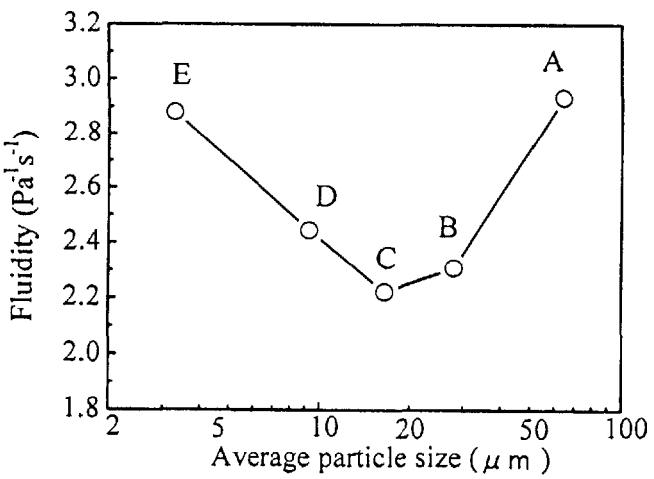

Figure 10 The fluidity of cement pastes with classified LS.

values are measured by above-mentioned method. The packing density of pastes with coarse or fine classified limestone powder (samples A or B) is larger than that of the others. Packing density of paste is related to the amounts of retention water or free water as shown in Fig 8. The higher the packing density of paste, the larger the amounts of free water. By using A or B, the amounts of retention water is reduced and the amounts of

free water is increased. Therefore, the fluidity of cement paste with A or E is superior to the others.

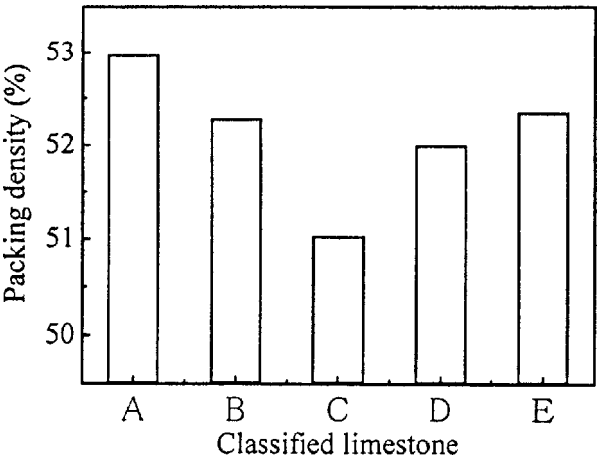

Figure 11 Packing density of pastes with classified LS.

Fig 12 shows the fluidity of cement paste with the mixtures of two kinds of classified limestone powders compared with the case of ordinary portland cement with or without prepared limestone powder. Replacement ratio of mixtures to cement is 20%. Symbol AB and BA mean the blended ratio of A and B are respectively 2:1 and 1:2. By using of the mixtures, the fluidity of paste is improvement compared to the case of using of prepared limestone powder. The fluidity of cement paste with sample AE (mixture of coarse and fine samples) is largest than that of the others. These phenomena may be caused on the amounts of free water in pastes. Generally, the packing density of powders is increased by mixing of two kinds of particles having the different particle size (Dallavalle,1948). The higher the packing density of powders, the larger the amounts of free water in paste. The packing density of the mixture of cement and limestone is determined by their particle size distribution. In order to development of suitable particle size distribution of powders for flowing cement concrete, more detail investigations are necessary.

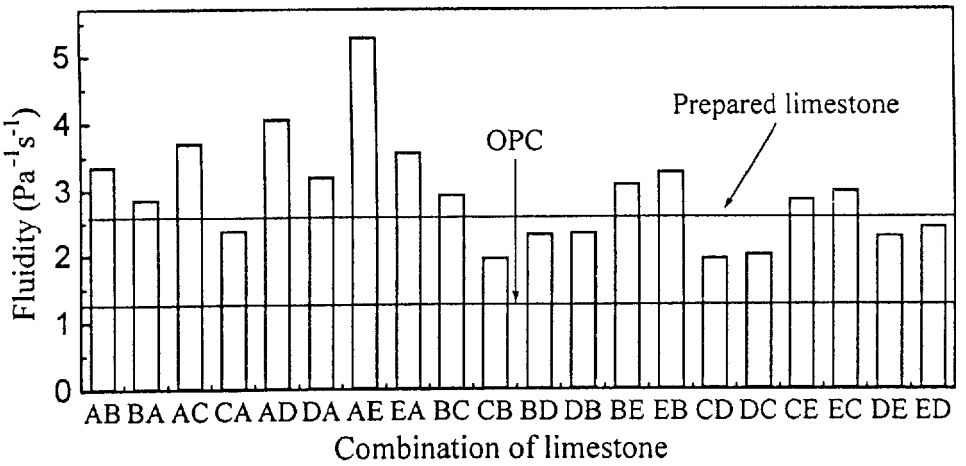

Figure 12 Influence of the mixtures of classified LS on the fluidity of pastes.

CONCLUSION

In order to clarify the mechanisms of inorganic powder for the fluidity of flowing cement concrete, we investigated the fluidity of cement pastes with polycarboxylate type of AE high range water reducing agent and classified or prepared powders. In addition,the dispersion mechanisms of polycarboxylate type AE high range water reducing agent based on the calculation of interparticle potential were introduced. An important factor to play a role for the dispersion cement particles may be van der Waals force of particles and steric hindrance effect of these agents. The shape and particle size distribution of inorganic powders are influenced on the fluidity of cement with these powders. The

larger the sphericity factor of inorganic powders, the higher the fluidity of cement paste with these powders. And the fluidity of cement paste with fine or coarse or these mixtures larger than that of cement paste with the others. These were related to the packing density of cement paste with inorganic powders. The higher the packing density of paste, the higher the fluidity of paste. The shape effect of inorganic powders on the fluidity of paste consists of the packing effect and ball bearing effect of powders.

ACKNOWLEDGEMENTS

The authors would like to thank Mr.S.Takahashi and Mr.T.Nagata of Japan Cement Association, for their help during the air separation of inorganic powders.

REFERENCES

Dallavalle,J.M.:"Micromeritics",Pitman Publishing Corporation,1948,135 pp.

ECS(European Committee for Standardization):"European Prestandard ENV 197-1",1992.

Grandet ,J. and Olliver,J.P.,"Etude de la Formation du Monocarboaluminate de Calcium Hydrate au Contact d'um Granulat Caraire dans une Pate de Ciement Portland",Cem. Concr.Res.,Vol 10,No 6,1980,pp.759-770.

Hosokawa,T., Ohba,Y. Sakai,E and Daimo,M.,"Hydration of C_3A,amor-$C_{12}A_7$ and $C_{11}A_7 \cdot CaF_2$ in the presence of Calcium Carbonate(in Japanese)",Annual meeting of Ceram.Soc.Japan,1995,488 pp.

Kuzel,H. and Pollman,H., "Hydration of C_3A in the presence of $Ca(OH)_2$,$CaSO_4 \cdot 2H_2O$ and $CaCO_3$",Cem.Concre.Res.,Vol 21,No.5,1991,pp.885-895.

Lee,S.H.,Hoshino,Sakai,E. and Daimon,M.,"Characteristics of Coal Ash Collected from Electrostatic Precipitator(in Japanese), Proc.of the Japan Concrete Institute, Vol 18, No 1,1996b,pp.327-332.

Nakamura,A., Ohba,Y. Sakai,E and Daimo,M.,"Hydration of C_3A,amor-$C_{12}A_7$ and $C_{11}A_7 \cdot CaF_2$-$CaSO_4$-$CaCO_3$ Systems (in Japanese)",Annual meeting of Ceram. Soc.Japan,1996a,446 pp.

Okamura,H. and Ozawa,K.,"State of the art for Self-Compactable Concrete(in Japanese)",J.Japan Soc.Civil Eng.,No 496,V-24,1994,pp1-8.

Sakai, E and Daimon,M.,"Dispersion Mechanisms of AE High Range Water Reducing Agent-Calculation of Interparticle Potential(in Japanese)",Cement & Concrete in Japan, No.595, 1996b,pp1-10.

Yasuda,M.,Furuya,N.,Itohidani,T. and Arima,I.,"Construction of Anchorage with Highly Workable Concrete Capable of Casting 1900 Cubic Meter per Day(in Japanese)",Cement & Concrete in Japan,No.558,1993,pp.60-64.

K n o. 2 5. JAN. 2001 d o k 31766

2ii003
8 pp

A STUDY ON THE METHOD OF ESTIMATING RHEOLOGICAL CONSTANTS OF CEMENT PASTE CONTAINING CHEMICAL ADMIXTURES

Hiroji KIKUKAWA, Dept. of Civil Engineering, Meijo University, Japan
Takeo IISAKA, Dept. of Civil Engineering, Meijo University, Japan
Yasuaki ISHIKAWA, Dept. of Civil Engineering, Meijo University, Japan

ABSTRACT Research into viscous behavior of cement pastes containing chemical admixtures led to a viscosity equation of cement pastes. The authors propose a method of estimating their plastic viscosity using this equation. Estimation of yield values was also made possible by determining the relationship between the plastic viscosity and the yield value.

Key-words: Additives, Rheology, Viscosity

INTRODUCTION

Qualities of cement paste, which forms the matrix of mortar, directly affect qualities of concrete. After a series of investigations on the rheology of mortar and concrete, the authors began the present study by exploring a method of estimating the rheological constants of cement paste. A number of reports have been published on the methods of estimating the plastic viscosity and yield value of cement paste containing no chemical admixtures (Petrie, 1976, Kakuta and Akashi, 1978, and Murata and Kikukawa, 1985). However, the use of chemical admixtures, such as an air-entraining agent and water-reducing agent has become general practice in recent years. With the aim of eventually proposing a viscosity equation for concrete containing chemical admixtures, the authors conducted basic research to derive a viscosity equation mainly from the viscous behavior of cement paste containing chemical admixtures. This paper proposes a method of estimating the plastic viscosity of such cement pastes. Simultaneously, the estimation of the yield value of cement paste was also made possible by experimentally determining the relationship between the plastic viscosity and the yield value. Attempts were also made to formulate a method of estimating rheological constants whereby the changes in temperature and elapsed time are incorporated, as rheological constants depend on these factors.

MATERIALS AND MIX PROPORTIONS

Ordinary, high-early-strength, ultrahigh-early-strength, and moderate heat portland cements were used for the experiments. Their physical properties are given in Table 1.

Table 1 Physical properties of portland cements

	O P	H P	U H P	M P
Specific gravity	3.15	3.14	3.11	3.20
Specific surface area (cm^2/g)	3240	4450	6290	3000

Note) OP : Ordinary portland cement.
HP : High early strength portland cement.
UHP : Ultra high early strength portland cement.
MP : Moderate heat portland cement.

The chemical admixtures used are a proprietary water-reducing agent and superplasticizer, whose main components are polyol complexes and highly condensed triazine compounds, respectively. They contain no chlorides and are not air-entraining. Their dosage is expressed in solid equivalents to be consistent with other admixtures. The water-cement ratio ranges from 40 to 80% with a regular increment of 5 percentage points. The dosage of the water-reducing agent and superplasticizer ranged from 0.01% to 0.12% in terms of solid percentage by mass of cement.

EXPERIMENTS

Cement pastes were mixed using a Hobart type mortar mixer as follows: Add all ingredients in the mixer and mix for 1 min at a low speed of 157 rpm. Rest for 30 sec, during which time scrape off any material adhering to the paddle and wall of the mixing bowl. Mix finally for 2 min at a high speed of 396 rpm. The mixtures were tested immediately after mixing. The temperature of the freshly mixed samples was adjusted to 10, 20, and 30°C. Subsequent tests were conducted at 30 min intervals up to 150 min following the initial test. At each test time, the J funnel efflux time, flow spread, and rheological constants were determined. An inner cylinder rotating type viscometer was used for measuring the rheological constants.

VISCOSITY EQUATION

Plain cement paste

Roscoe's viscosity equation (1952), which is an application of Einstein's viscosity equation to high concentration suspensions, was used as the basis, on the assumption that cement paste is a suspension in which cement particles are suspended in water:

$$\eta_{re} = \left(1 - \frac{1}{C} \bullet V\right)^{-K} \tag{1}$$

where

η_{re} = relative viscosity
C = coefficient for percentage of absolute volume of solute
K = shape factor for agglomerates of solute
V = volume concentration of solute

Roscoe's equation assumes that solute particles behave collectively, and therefore is applicable to a suspension with a significantly high concentration. However, it assumes that suspended particles are uniform and spherical, and therefore is not applicable to particles with complicated shapes. For this reason, the authors arranged the experiment results with respect to the shape factor, K, of the agglomerates, and found that K can be expressed as a linear function of the specific surface area of cement by Blaine. Accordingly, the viscosity equation incorporating the specific surface area of cement particles is written as:

$$\eta_{re} = \left(1 - \frac{1}{C} \bullet V\right)^{-(K_1\phi + K_2)} \tag{2}$$

where

ϕ = specific surface area of cement by Blaine (cm^2/g)
K_1 = -15.6 (experimental constant)
K_2 = 11.2 (experimental constant)

The plastic viscosity of plain portland cement paste can be estimated from Eq. (2) by assuming that the viscosity of the suspending medium (viscosity of water) η_0 is 1×10^{-3} Pa·s (20°C). It is known that the plastic viscosity of cement paste with different temperatures immediately after mixing can be calculated by the following equation (Kikukawa, 1987):

$$\Delta\eta_{t1} = a_1(W/C)^2 + b_1(W/C) + c_1 \tag{3}$$

where

$\Delta\eta_{t1}$ = change in plastic viscosity (Pa·s/°C) per degree C of temperature change
W/C = water-cement ratio
a_1, b_1, and c_1 = 1.50, -1.84, and 0.576, respectively (experimental constants)

The following is the method of correcting plastic viscosity values for a different temperature of cement paste:

(1) Determine the plastic viscosity of cement paste at 20°C using Eq. (2).
(2) Determine the changes in the plastic viscosity per degree C of cement temperature using Eq. (3) for each water-cement ratio, and calculate the plastic viscosity of cement paste at a desired temperature.

The following has been found regarding the effect of elapsed time after mixing:

There is a time span in which the plastic viscosity increases linearly from immediately after mixing. Such a time span length depends on the temperature of freshly mixed paste: about 120, 90, and 60 min when the temperature is 10-15°C, 20-25°C, and 30°C, respectively, in a cement paste with a water-cement ratio of 0.40 to 0.60. The increment of plastic viscosity per unit time is approximated by a quadratic curve of paste temperature.

$$\Delta\eta_{ct1} = \alpha_1 t^2 + \beta_1 t + \gamma_1 \tag{4}$$

where

$\Delta\eta_{ct1}$ = increment in plastic viscosity of cement paste per unit time after mixing (Pa·s/h)
t = paste temperature (°C)
α_1, β_1, γ_1 = experimental constants as given in Table 2

Table 2 Coefficients in eq 4

W / C	0.40	0.45	0.50	0.55	0.60
α_1	0.0016	0.00033	0.00017	0.00017	0.00012
β_1	-0.029	-0.0019	-0.0015	-0.0031	-0.0033
γ_1	0.340	0.139	0.099	0.066	0.050

The ratios of the values thus estimated to measured values have been proven to approach the expected value, 1 (Kikukawa, 1987).

Cement paste containing chemical admixtures

The viscosity equation of cement paste containing chemical admixtures is also assumed to be basically similar to Roscoe's equation. Test results were arranged with respect to the shape factor of agglomerates, K, as shown in Fig. 1. As seen from the figure, K is expressed as linear functions of the fineness modulus (specific surface area by Blaine) of cement: $K = K_3\phi + K_4$. Also, K_4 varies depending on the water-cement ratio (W/C) and is expressed as an exponential function of the volume concentration of cement paste as shown in Fig. 2: $K_4 = K_5 V^b$. The authors attempted the formulation by assuming that the effect of the addition of water-reducing agents on the viscosity loss of cement paste is equivalent to the effect of reducing the water-cement ratio (W/C). In this case, the shape factor and absolute volume percentage of agglomerates are the same as the case with no water-reducing agents. As a result of the experiment, the relationship between the coefficient for the dosage of the water-reducing agents, A, and the dosage of the water-reducing agents, P (solid percentage by mass of cement) is as shown in Fig. 3 and expressed as $A = \xi P^n$. Consequently, the following can be presented as the viscosity equation for cement paste containing water-reducing agents:

$$\eta_{re} = \left[1 - \frac{1}{C} \cdot V\left(1 - \xi P^n\right)\right]^{-\left(K_3\phi + K_5 V^b\right)} \tag{5}$$

where
P = dosage of water-reducing agents (solid percentage by mass of cement)
ξ = 0.152 (experimental constant)
n = 0.680 (experimental constant)
$K_3 = 3.107 \times 10^{-5}$ (experimental constant)
K_5 = 1.422 (experimental constant)
b = -1.345 (experimental constant)

The ratios of plastic viscosity values of cement paste estimated using Eq. (5) to measured values approach the expected value, 1, as given in Table 3. The plastic viscosity of cement paste containing water-reducing agents can therefore be estimated satisfactorily using Eq. (5).

The correction equation of the plastic viscosity for a different temperature of cement paste was obtained as follows:

The plastic viscosity and yield value of cement pastes made with one brand of ordinary portland cement (see Table 1) were measured using a rotational viscometer. The water-cement ratios of the cement pastes were 0.45, 0.50, 0.55, and 0.60 and the temperatures of freshly mixed pastes were 10, 20, and 30°C. The measurements are shown in Fig. 4. The figure reveals that, even when water-reducing agents are contained, the plastic viscosity of cement paste increases as the paste temperature rises, suggesting that the viscosity increase due to solvation with the suspending medium surpasses the viscosity loss of the suspending medium due to temperature rise. A linear relationship is observed between the temperature and the plastic viscosity of pastes in the paste temperature range of 10 to 30°C. The average increments in plastic viscosity per degree C rise in the temperature of cement pastes were 0.085, 0.021, 0.014, and 0.0099 Pa·s for water-cement ratios of 0.45, 0.50, 0.55, and 0.60, respectively.

The relationship between the water-cement ratio and the plastic viscosity increment is approximated by an exponential curve as shown in Fig. 5. The same tendency was observed with dif-

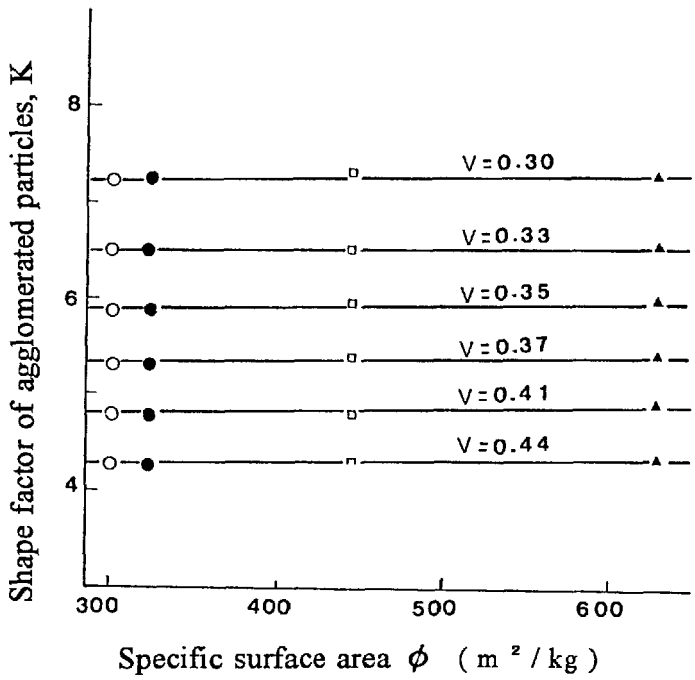

Figure 1 Relationship between shape factor of agglomerated particles in cement paste and specific surface area of cement

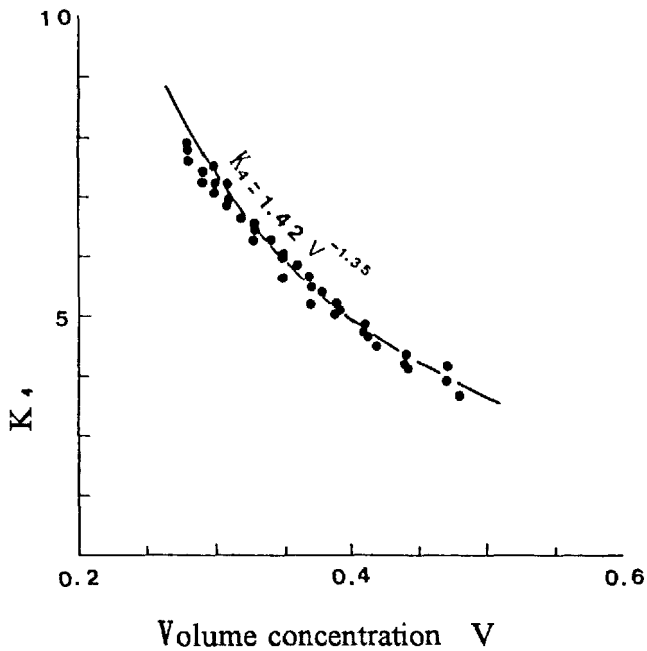

Figure 2 Relationship between experimental constant K_4 and volume concentration of cement

ferent dosages of admixtures. Accordingly, the relationship between the water-cement ratio and the plastic viscosity increment is expressed as:

$$\Delta\eta_{t2} = a_2 \cdot W/C^{b_2} \qquad (6)$$

where

$\Delta\eta_{t2}$ = change in plastic viscosity per degree of temperature change of cement paste containing water-reducing agents (Pa·s/°C)
W/C = water-cement ratio
a_2 = 0.0002 (experimental constant)
b_2 = -7.245 (experimental constant)

The effects of elapsed time after mixing on the plastic viscosity of cement pastes containing admixtures were incorporated as follows:

The increments in the plastic viscosity of cement pastes made of one brand of cement paste (see Table 1) were measured at 30, 60, 90, 120, and 150 min after mixing. The water-cement ratios of the pastes were 0.45, 0.50, 0.55, and 0.60, and their temperatures immediately after mixing were 10, 20, and 30°C. The measured increments are shown in Fig. 6.

The increment in plastic viscosity with time increased as the water-cement ratio decreased and as the paste temperature increased. The increment in plastic viscosity per unit time is expressed as a linear function of the paste temperature as follows:

$$\Delta\eta_{ct2} = a_3 t + b_3 \qquad (7)$$

where

$\Delta\eta_{ct2}$ = increment in plastic viscosity of cement paste containing water-reducing agents per unit time (Pa·s/h)
t = temperature of sample (°C)
$a_3 = \alpha_2 (W/C)^2 + \beta_2 (W/C) + \gamma_2$ (experimental constant)
$b_3 = a_4 (W/C) + b_4$ (experimental constant)
W/C = water-cement ratio
α_2 = 0.400, β_2 = 0.508
γ_2 = -0.162, a_4 = -0.942, b_4 = 0.608

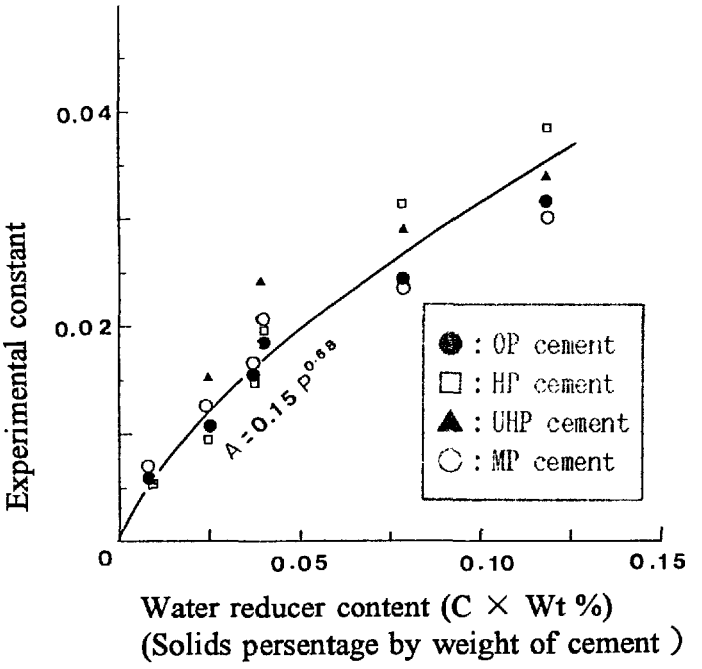

Figure 3 Relationship between experimental constant and water reducer content

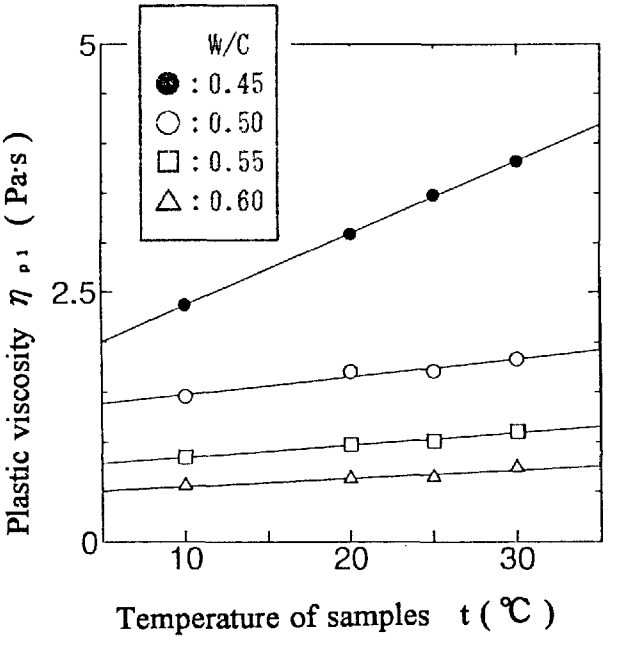

Figure 4 Relationship between plastic viscosity and temperature of samples

Table 3 Ratios of calculated values to measured values of plastic viscosity of cement paste

w／c	Cement content C (kg/m³)	Volume concentration V	Water * reducer (c× wt%)	Plastic viscosity		A／B
				Calculated A	Measured B	
0.60	1223	0.39	0.026	0.44	0.51	0.86
			0.081	0.37	0.41	0.90
			0.121	0.34	0.40	0.85
0.70	983	0.31	0.028	0.35	0.35	1.00
			0.045	0.33	0.33	1.00
			0.090	0.30	0.31	0.97

Note) * : Solid percentage by weight of cement.

Table 4 Ratios of calculated plastic viscosity values to measured values of cement paste containing a water reducer incorporating changes in time and temperature

Time elapsed (min.)	Temperature of cement paste (°C)						A／B		
	20		25		30				
	Calculated value A	Measured value B	Calculated value A	Measured value B	Calculated value A	Measured value B	20°C	25°C	30°C
30	0.500	0.532	0.593	0.578	0.686	0.707	0.94	1.03	0.97
60	0.564	0.582	0.664	0.678	0.765	0.768	0.97	0.98	1.00
90	0.628	0.638	0.736	0.743	0.844	0.838	0.98	0.99	1.01
120	0.692	0.738	0.807	0.825	0.923	0.855	0.94	0.98	1.08
150	0.756	0.828	0.879	0.861	1.001	1.028	0.91	1.02	0.97

Note 1) Ordinary portland cement is used.

2) Water cement ratio is 0.55.

3) Water reducer content is 880 (g/m^3).

The ratios of the plastic viscosity values of cement paste estimated as mentioned above to the measured values nearly approached the expected value of 1 as given in Table 4.

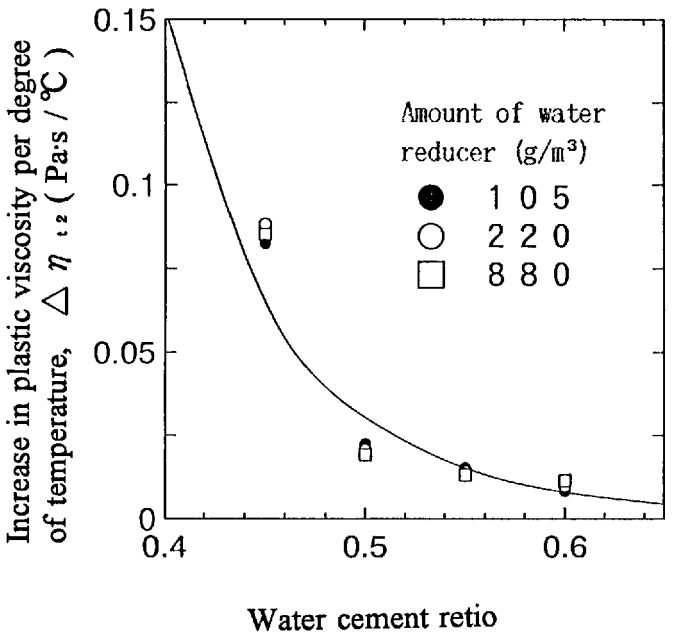

Figure 5 Increase in plastic viscosity versus W/C

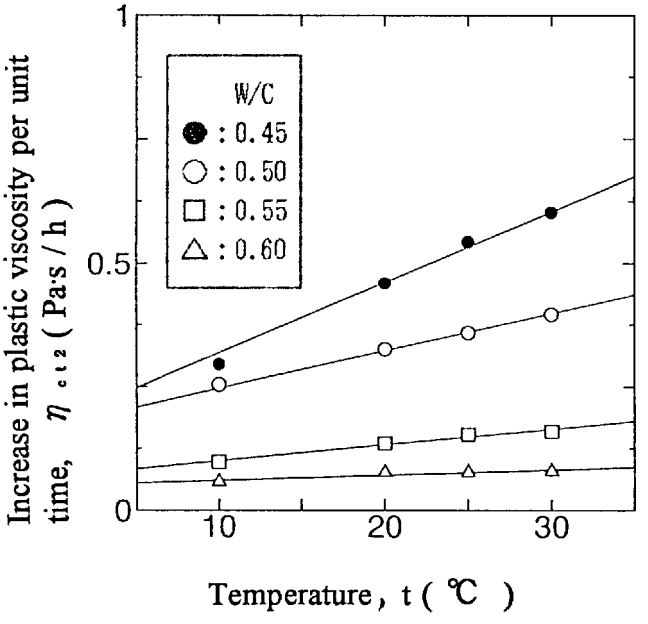

Figure 6 Increase in plastic viscosity per unit length of time after mixing of portland cement paste

RELATIONSHIP BETWEEN YIELD VALUE AND PLASTIC VISCOSITY

Where high concentration suspension is concerned, as the concentration of the suspended material increases, the plastic viscosity increases and the yield value is considered to increase due to reduced distances between suspended particles. When no chemical admixture is contained, the plastic viscosity is linearly proportional to the yield value. It has been confirmed that the yield value can be estimated using this relationship (Murata and Kikukawa, 1985).

The use of admixtures is found to bring about subtle changes in the plastic viscosity and yield value, leading to an exponential relationship between them as shown in Fig. 7.

$$\tau_f = n_1 \eta_{Pl}^{\ n_2} \qquad (8)$$

where
n_1 = 13.16 (experimental constant)
n_2 = 2.17 (experimental constant)

The ratios of the yield values estimated by Eq. (8) to the measured values are nearly the expected value, 1. When the cement paste contains water-reducing agents, its yield value can be estimated by Eq. (8).

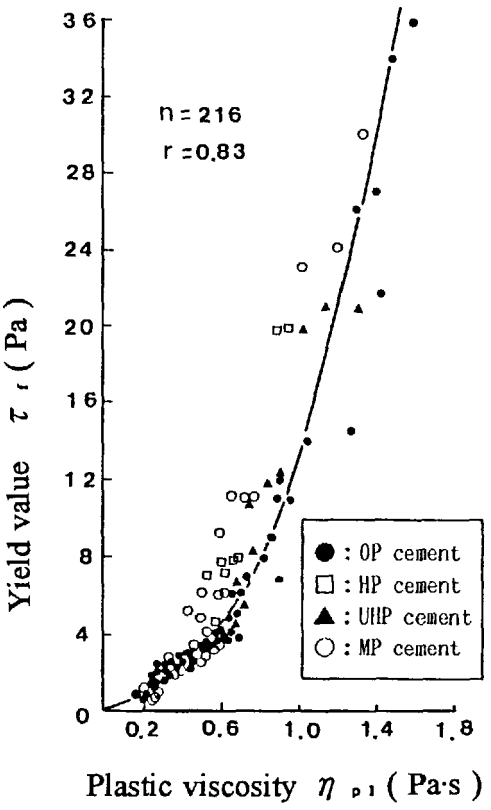

Figure 7 Relationship between yield value and plastic viscosity of cement paste

CONCLUSION

The rheological constants of cement pastes containing various water-reducing agents at different times and temperatures can be satisfactorily estimated by using a viscosity equation and temperature correction equation.

ACKNOWLEDGMENT

The authors express their appreciation for the grant from the Meijo University Fund for Academic Research.

REFERENCES

Kakuta, S. and Akashi, T., "Viscosity Equation of Cement Paste," Review of the 32nd General Meeting - Technical Session, Cement Association of Japan, pp. 88-91, 1978 (in Japanese).

Kikukawa, H., "A Study on Formulation and Application of Viscosity Equations of Fresh Concrete," Dissertations at Tokyo Metropolitan University, pp. 73-74, 1987 (in Japanese).

Petrie, E.M., "Effect of Surfactant on the Viscosity of Portland Cement-Water Dispersions," Ind. Eng. Chem. Prod. Res. Dev. Vol. 15, No. 4, 1976.

Roscoe, R., "The Viscosity of Suspension of Rigid Spheres," British J. of Applied Physics, Vol. 3, pp. 267-269, 1952.

Murata, J. and Kikukawa, H., "A Study on Viscosity Equations of Portland Cement Paste," Proceedings of JSCE (Tokyo), No. 354, pp. 109-118, 1985 (in Japanese).

Kn o. 25. JAN. 2001 d o k 31767

211004
8 pp

RHEOLOGICAL AND HYDRATION PROPERTIES OF A HIGH STRENGTH GYPSUM-FREE CEMENT

Ludmilla OPOCZKY, Cement Research & Development Ltd. Budapest, Hungary
Adriano PAPO, The University, Inst. of Chemistry, Udine, Italy

ABSTRACT
The very high strength, good workability, increased frost resistance etc. of gypsum-free cement are assured by the homogeneous and compact microstructure of the cement as well as by the presence of calcium-silicate hydrates (C-S-H-phase) of higher polycondensation degree. Flow curves of such cement pastes are of pseudoplastic type, and the shear-dependent behaviour pastes can be described by the Bingham-model.

Key-words: rheology, hydration, lignosulphonates, superplasticizers, modified cement.

INTRODUCTION
In the course of research work the production technology of gypsum-free high strength cement (in the following MNC) was developed and its pilot plant production was realized. The basis of MNC is an ultrafine clinker of suitable mineral composition and of uniform particle size distribution, to which the mixture (in the following LSN) of Ca-lignosulfonate (in the following LS) and Na-carbonate (in the following N) is added in 1-1.5 $^{m}/_{m}$ % quantity in order to control the binding and hardening. The MNC-cement is workable even at low w/c (0.2-0.35), and it is characterized by rapid increase of strength and high final strength (70-80 MPa). The research aimed at the investigation of the rheological and hydration features of MNC pastes as well as that of the microstructure of the hardened pastes.

RHEOLOGICAL INVESTIGATIONS
Rheological measurements were carried out with a ROTOVISKO RV 20 type coaxial cylindrical rotation viscosimeter. As starting material a clinker milling product made from plant clinker (C_3S = 63.6 %, C_2S = 12.9 %, C_3A = 8.6 %, C_4AF = 10.5 %), ground in laboratory ball mill was used, of which the specific surface was ~ 550 m^2/kg. LSN additive was added to the clinker milling product in different quantities (1.1-1.8 $^{m}/_{m}$ %). Comparative analyses were also made with a clinker milling product containing 6 $^{m}/_{m}$ % gypsum. Pastes were produced from the cements, changing the water-cement factor between 0.36 and 0.42 in case of MNC and between 0.38 and 0.54 in case gypsum-containing cement. Measurements were performed under constant shearing velocity ($\dot{\gamma}$) as well as under the gradual decrease and increase of the shearing velocity and the hysteresis curves were determined (PAPO et al. 1994). In the following some important results will be presented.

Shear-dependent behaviour of MNC cement pastes
In the course of measurement, subsequently to mixing, the cement paste was studied under constant shearing velocity. The initial shearing stress (τ_i) belonging to each shearing velocity was determined that corresponds to the structural state just after mixing, and the minimal shearing stress (τ_e) corresponding to the shearing record and function of time was also determined. In this way information was gained on the time dependence of the shearing process and on the initial section of hardening process of the cement.

The final as well as the starting and equilibrium flow curves can be determined for each shearing velocity. The area between the two curves is characteristic of the thixotropy. The shearing stress (τ_i) and shearing velocity (τ_e) data determined experimentally were inscribed into rheological models of different $\tau = f(\dot{\gamma})$ type (Bingham, Casson, Wiliamson, Herschel-Bulkley etc.). In case of all models most suitable parameters can be produced by minimization of variance of the experimental and calculated values.

The equilibrium flow curves of MNC pastes prepared with different w/c factors (besides adding 1.1 $^{m}/_{m}$ % LSN), and of the MNC pastes of different LSN content under a given w/c = 0.38 are shown in Figs. 1 and 2, while the flow curves of the clinker + gypsum mixture are seen in Fig.3.

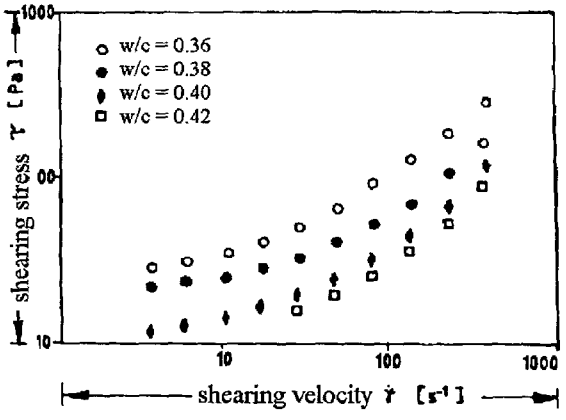

Fig. 1.
. Flow curves of MNC pastes at different w/c factors (LSN = 1.1 $^{m}/_{m}$ %)

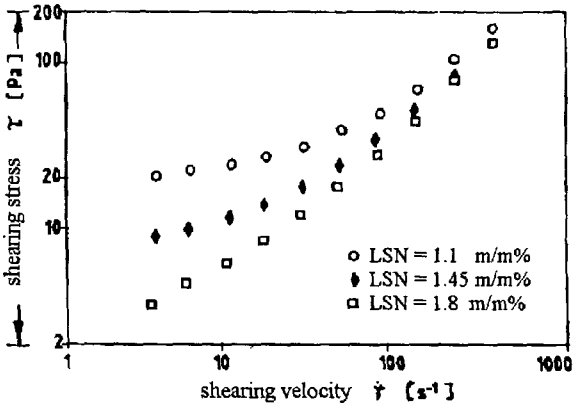

Fig. 2.
Flow curves of MNC pastes under constant w/c factor and under addition of of different LSN

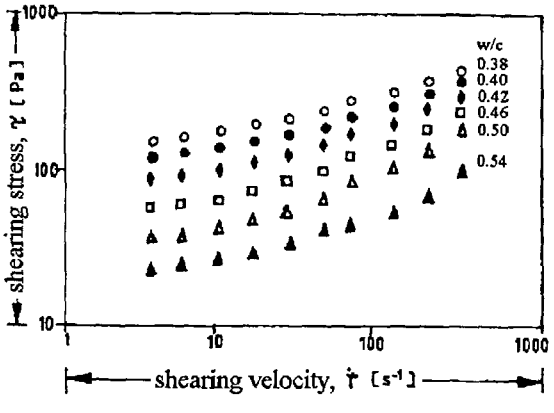

Fig. 3.
Flow curves of pastes made of the mixture of clinker milling product + 6 $^{m}/_{m}$ % gypsum under different w/c factors

All the flow curves are of pseudoplastic type and all substances studied possess flow limit, respectively. The shear-dependent behaviour of MNC pastes can be described by the Bingham model (Fig.4), that of the gypsum-bearing cement pastes by the Casson and Herschel-Bulkley models (Fig.5). Cement pastes with gypsum content are of higher viscosity and flow limit than the MNC pastes.

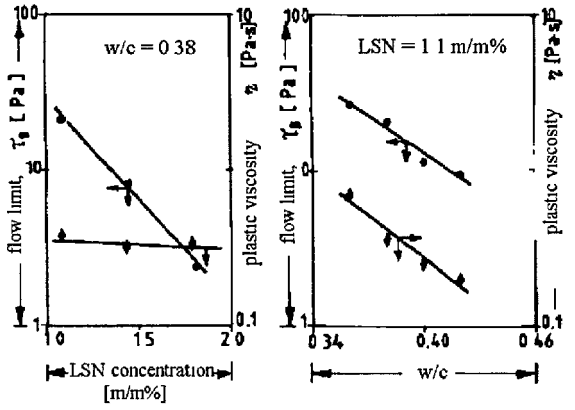

Fig. 4.
The Bingham flow limit (τ_B) and the plastic viscosity (η_B) in case of MNC pastes.
a) as a function of the LSN concentration;
b) as a function of the w/c factor.

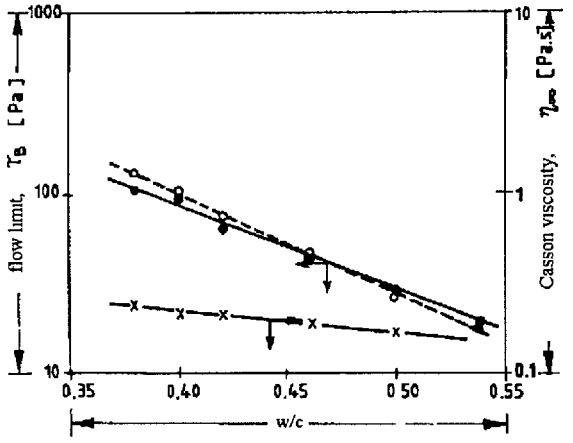

Fig. 5.
Relationship between the Herschel-Bulkley flow limit and Casson-parameter and the w/c factor in case of pastes made of clinker milling product and gypsum.
x: Herschel-Bulkley flow limit; o: Casson flow limit; * : Casson viscosity (η_∞).

When MNC pastes are exposed to shearing, their structure undergoes a decomposition process: the shearing stress - time relationships displays a shearing stress peak (τ_P) that can be related to the reconstruction of the structure immediately after mixing. Shearing reduces this value to a minimum (τ_e), that can be related primarily to the thixotropic decomposition, then the shearing stress begins gradually to grow as a function of time, when the structure begins to develop (Fig.6).

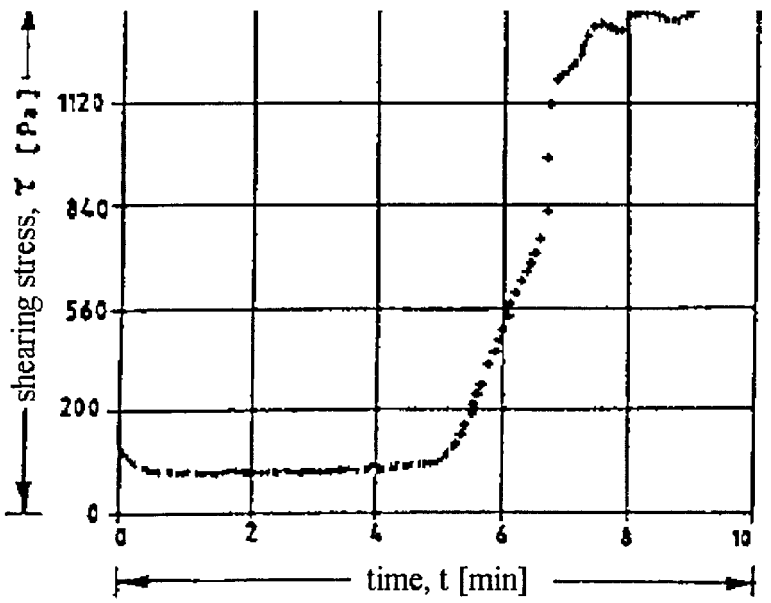

Fig. 6.
Shearing stress - time relationship of the MNC paste
(w/c = 0.38; LSN = 1.1 $^{m}/_{m}$ %;
$\dot{\gamma}$ = 234 s^{-1}).

Let us study in detail the growing section of shearing stress. The temporal growth of shearing stress proceeds in three steps: the initial development proceeds with reduced velocity, then a transitional section follows and finally the ultimate development takes place with increasing velocity. This behaviour is illustrated in Fig.7. where ln (τ - τ_e) is plotted as a function of ln t. The transitional section lies usually within the induction or lower period of the hydration process of the cement. Here a delay time can be presumed that indicates the end of the "sleeping" period and the start of the main phase of hydration.

In Fig.7 the shearing stress - time curves of a given MNC paste recorded at different shearing velocities are shown. The relationship of t_d and $\dot{\gamma}$ can be seen in Fig.8. The relationship is approximately of force law type:

$$t_d = 41.8\ \dot{\gamma}^{0.344} \qquad [1]$$

As it is shown in Figs. 9. and 10, t_d is linearly proportional to the LSN concentration. The function of the t_d-LSN concentration can be described with the linear relationship below:

$$t_d = -51.9 + 51.9\ LSN \qquad [2]$$

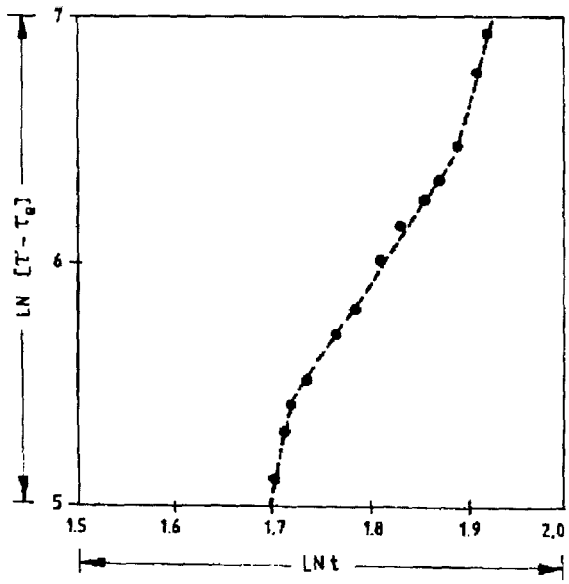

Fig.7.
The ln(τ - τ_e) vs ln t diagram of the MNC paste

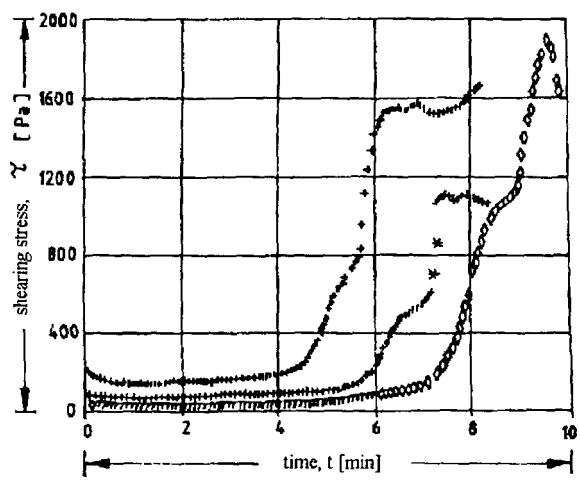

Fig.8.
Shearing stress - time relationships of MNC pastes at different shearing velocities (w/c = 0.38; LSN = 1.1 $^{m}/_{m}$ %; shearing velocities (s^{-1}); + 390; * 140; ◊ 17.9).

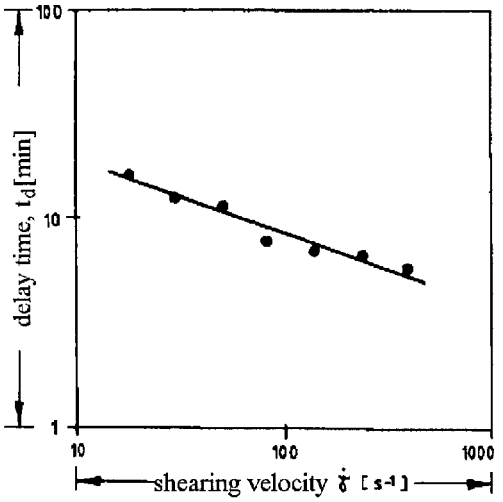

Fig.9.
Change of delay time (t_d) as a function of shearing velocity ($\dot{\gamma}$) in case of MNC paste
(w/c = 0.38; LSN = 1.1 $^{m}/_{m}$ %).

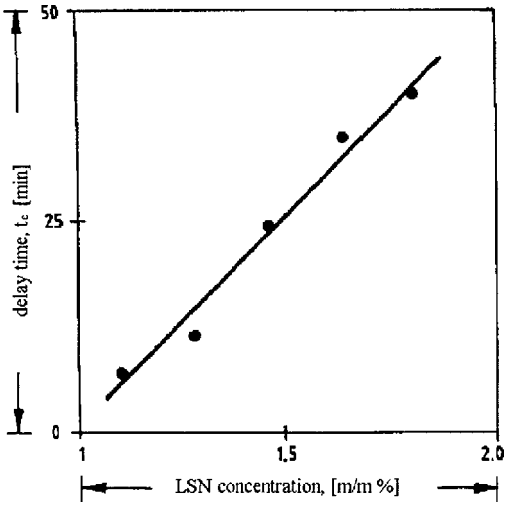

Fig.10.
Change of delay time (t_d) as a function of the LSN concentration in case of MNC pastes.
(w/c = 0.38; $\dot{\gamma}$ = 234 s^{-1}).

Hydration of the MNC cement

The experimental sample was prepared in laboratory ball mill, produced from the clinker of a mineral composition presented earlier, its specific surface was ~ 550 m^2/kg (n factor of uniformity 0.913, $\bar{x}$ fineness number 8 μm), to which 1.25 $^{m}/_{m}$ % LSN was added. With w/c = 0.25 cement paste was made from the MNC cement. For comparison, a cement paste was prepared (in the following OPC) from the same clinker containing 6 $^{m}/_{m}$ % gypsum, with a specific surface of ~ 300 m^2/kg (n = 0.899, $\bar{x}$ = 21 μm), with w/c = 0.31. Experiments were also carried out with gypsum-free cement pastes containing only Ca-lignosulfonate in 0.4 $^{m}/_{m}$ % and only Na-carbonate in 0.8 $^{m}/_{m}$ %, with w/c = 0.25. Fig.11. shows the strength of the MNC and OPC cements (a), the $Ca(OH)_2$ content determined from thermogravimetric curves (b), the chemically bound water quantity (c) as a function of hardening time. In Figs. 11b and 11c the characteristic curves of pastes containing only LS and only N are also seen.

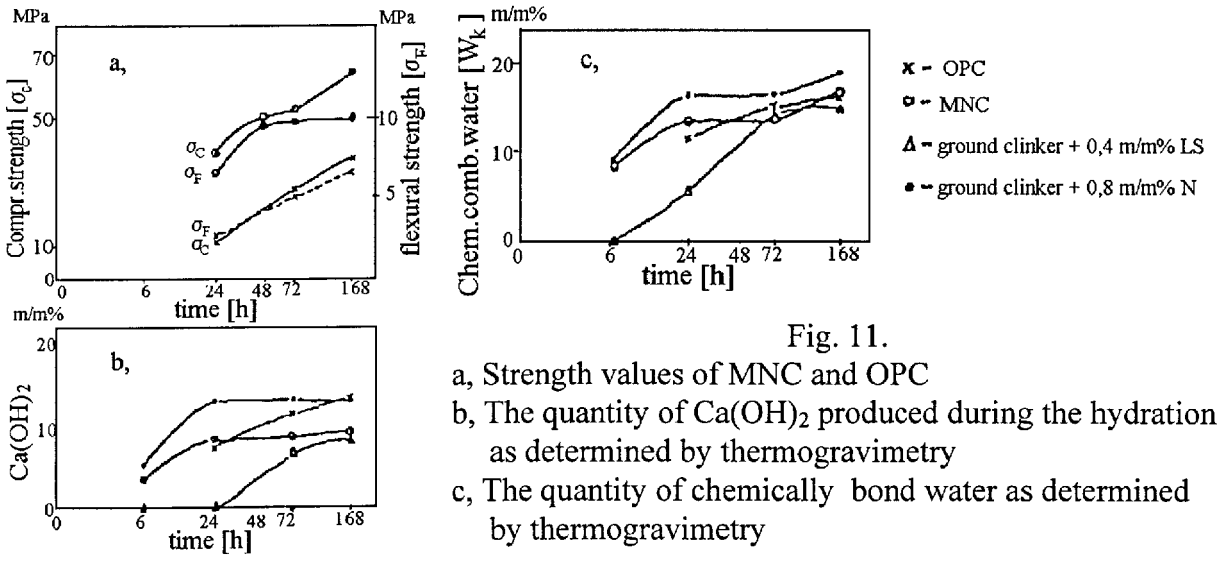

Fig. 11.
a, Strength values of MNC and OPC
b, The quantity of $Ca(OH)_2$ produced during the hydration as determined by thermogravimetry
c, The quantity of chemically bond water as determined by thermogravimetry

MNC is characterized by the rapid increase of strength (after 24 hours ~ 40 MPa) and by the high final strength (after 28 days ~ 28 MPa). In case of MNC the quantity of $Ca(OH)_2$ increases up to 24 hours, then hardly changes. The chemically bound water shows similar changes, the only difference is that between 72 and 168 hours further increase can be experienced. The quantity of $Ca(OH)_2$ is nearly the same in MNC, in later times it is always lower than that of OPC. The endothermal peak characteristic of the decomposition of $Ca(OH)_2$ occurs by 15-20 °C lower in the MNC, than in the OPC. In case of cement paste containing only LS the peak characteristic of the decomposition of the $Ca(OH)_2$ occurs only at 72 hours, the quantity of chemically bound water is also minimal in the early periods. The most intense hydration can be observed in the cement paste containing only N, the quantities of $Ca(OH)_2$ and of the chemically bound water are highest. The hydration heat values determined on the basis of dissolution heat measurements are seen in Table 1.

Table 1.

Time	Hydratation heat J/g MNC	OPC
6 hours	75.3	-
1 days	215.8	216.6
3 days	257.6	290.9
7 days	290.2	429.2

It can be seen that at 24 hours the hydration heats of MNC and OPC are practically the same but parallel with the hardening time the difference increases. So, at 7 days (168 hours) the hydration heat of MNC is lower by 33 % than that of OPC. It can be stated that in case of MNC cement the high compression and flexural strengths are accompanied by relatively low hydration degree. As to the derivatographic and X-ray diffractometric analyses, in case of MNC in addition to the hexagonal calcium-aluminium hydrates (C-A-H) C-S-H phases are also formed at the beginning of hydration. Later (between 24 and 48 hours) the increase of the quantity of C-S-H phase slows down but in spite of this phenomenon the strength of the cement considerably increases. The strength of the C-S-H phase highly depends on the degree of polycondensation of the SiO_4^{4-} anions. Analytical results concerning the anion structure of potassium silicates developed during the hydratation of MNC are shown in Table 2. Analyses were performed by means of trimethysilylation.

Table 2.
Trimethylsilylation data of hydrated cement pastes

	Age: 24 hours					Age: 168 hours					
	QM_4	Q_2M_6	Q_3M_6	Q_3M_8	O/M	QM_4	Q_2M_6	Q_3M_6	Q_3M_8	Q_4M_8	O/M
MNC	55.98	39.43	1.39	3.20	0.7861	49.73	44.82	-	5.75	-	1.0168
Ground clinker +LS	70.26	25.74	-	4.00	0.4232	46.39	46.23	2.06	5.33	-	1.1550
Ground clinker +N	49.24	44.05	-	6.72	1.0310	39.19	49.25	0.90	7.69	3.00	1.5530

QM_4	- monosilicate	$[SiO_4]^{4-}$	Q_4M_8	- cyclotetrasilicate	$[Si_4O_{12}]^{8-}$
Q_2M_6	- disilicate	$[Si_2C_7]^{6-}$	Q	- SiO_4^{4-}	
Q_3M_6	- cyclotrisilicate	$[Si_3O_9]^{6-}$	M	- trimethyl-silyl group	$[CH_3]_3$-Si-
Q_3M_8	- linear trisilicate	$[Si_3O_{10}]^{8-}$	OM	- [dimer+oligomers]/monomer	

It is shown that in MNC, in addition to the disilicate hydrates of remarkable quantity trisilicates are also formed at 24 hours, their quantities increase as a function of time. The addition of LS hampers the initial hydration of Ca-silicates (24-48 hours), thus less hydration product is formed but the polycondensation processes of anion are accelerated, this is why the product of 24 hours contains trisilicate hydrate of considerable quantity. The presence of N

considerably accelerates both the hydration of calcium silicates and the polycondensation processes of anions. The main constituent of the solidified MNC paste is the C-S-H phase, in its compact, homogeneous microstructure the columnar crystals of portlandite characteristic of the traditional portland cement cannot be detected. The pore structure of hardened MNC paste is extraordinarily dense and uniform (Fig.12/a), while this relatively stable pore structure is formed at an early stage of hydration (Fig.12/b). Total porosity of the hardened MNC paste does not exceed 13-15 % with pore sizes and pore size distribution markedly differing from those of OPC. In MNC paste at the age of 24 hours the 45 nm sized and at 7 days the 25 nm sized pores are predominating. Close relationships between strength, frost resistance and porosity are shown in Fig.12 and 13. For example, Fig.13 illustrates, on one hand, that MNC paste incorporates only a minimal quantity of pores in which water can freeze at -15 to -20 C, and the very-very slight expansion of the paste upon freezing, on the other.

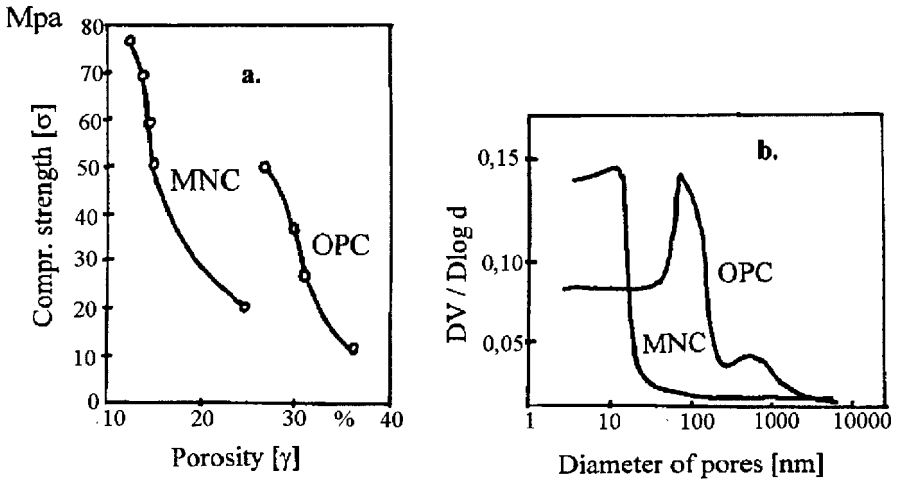

Fig. 12.

a, Correlation between total porosity and compressive strength

b, Pore size distribution of hydrated MNC and OPC pastes. Age: 7 days

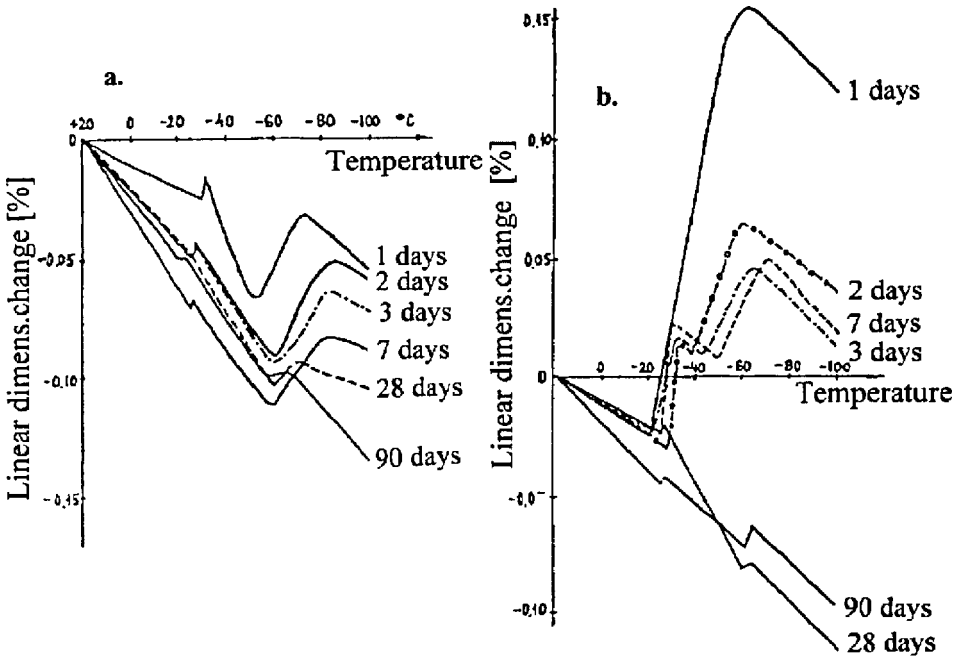

Fig. 13.

Low temperature dilatation curves of hydrated cement pastes

a, MNC b, OPC

CONCLUSIONS

The MNC cement is characterized by the rapid increase of strength and the high final strength. MNC cement is fairly well workable at small w/c factors (0.2-0.35).

The flow curves of MNC pastes are of pseudoplastic type, its shear-dependent behavious can be best described by the Bingham model.The structure of MNC pastes decomposed at shearing is redeveloped immediately after mixing. The development of the structure proceeds in three steps: the initial formation proceeds with reduced velocity, then a transitional section follows and the final formation proceeds with increasing velocity. The transitional section lies within the induction and "sleeping" periods of the hydration process of the cement and the so-called delay time (t_d) indicates the beginning of the main hydration phase of the cement. t_d is linearly proportional with the LSN additive concentration.

The high strength of the hardened MNC cement is assured by the homogeneous and compact microstructure of the cement and by the presence of calcium silicate hydrates (C-S-H phase) of greater degree of polycondensation. The addition of the mixture of Ca-lignosulfonate and Na-carbonate (LSN) increases the rate of hydration, promotes the early formation of the stable pore structure and accelerates the polycondensation process of calcium silicate hydrates. In the development of the strength of the MNC cement the following facts play decisive role: the ultrafine state and uniform particle size distribution of the clinker milling product; the phenomenon that already in the age of 24 hours an extremely compact and stable pore structure is developed in which - due to the small pore size - there is no space for the formation of novel hydration product and for crystal growth. This is favourable to the formation of calcium silicate hydrate oligomers of higher degree of polycondensation, of higher strength and of less space demand.

The support of OTKA (National Scientific Research Fund) No. T 14872 is gratefully acknowledged.

REFERENCE

Papo, A.-Opoczky,L.-Horváth,I.: Rheological properties of gypsum-free cements of modified set. Építőanyag, 46, (No.6), pp.152-158, 1994 (in Hungarian)

K n o. 2 5. JAN. 2001 d o k 31768

2ii005
4 pp

PENETRABILITY OF SUSPENSION GROUT INFLUENCED BY DISPERSION CHARACTERISTICS OF ULTRAFINE CEMENT IN THE GROUT

Etsuro ASAKURA*, Tetsuya SUZUKI**, Yasunari MAEJIMA* and Hiroyuki FUJISAWA*
* Mitsubishi Materials Corporation, Japan
** Civil Engineering Research Institute, Hokkaido Development Bureau, Japan

ABSTRACT Ultrafine cement particles agglomerate easily in suspension grout and form many particles larger than the maximum cement size of 12 μm. This would be the main reason why the grout tends to be injected unsatisfactorily into the ground composed of fine sand. Therein, the simultaneous application, namely addition of chemical admixture and short time use of ultrasonic vibrator is helpful to prevent particles from agglomerating in the grout for a long time, and facilitates the grout penetration even into fine sand.

Key–words: Grout, Penetration, Dispersion, Viscosity

INTRODUCTION

It is said that the suspension grout is difficult to be injected into the ground composed of comparatively fine grains (e.g., Mori et al. 1991). However, in recent years, strengthening of such ground has been increasingly required in Japan owing to high demand of civil constructions even upon such ground. In this paper, the authors investigate the main cause of the difficulty of the grout penetration into fine sand and propose the countermeasure for ensuring the satisfactory injection thereof.

EXPERIMENTAL

Materials

Two kinds of ultrafine cement were used in this work. One is the ultrafine cement named for FINE HARD (cement A) produced by Mitsubishi Materials Corporation. The other is the half–and–half mixture (cement B) composed of above cement A and kaolin clay collected at Itaya district, Japan. The size distribution of these two materials measured by a model CILAS 715 laser granulometer is shown in Table 1. The materials to be studied were mixed with distilled water in a container by means of a mechanical stirrer and an ultrasonic vibrator. The chemical composition of ultrafine cement A is shown in Table 2. The ultrafine cement A consisting of Portland cement and blast furnace slag has Blaine surface area of 1,260 m^2/kg, maximum grain size of about 12 μm and the 50 % grain size of about 3.0 μm. While, kaolin clay has maximum grain size of about 8 μm and the

Table 1 Particle size distribution of ultrafine cement A and kaolin clay

	Cement A	Kaolin
> 6 μm	17.6%	9.9%
>12 μm	0.3%	0.0%
>32 μm	0.0%	0.0%
50% grain size	3.0 μm	3.1 μm

Table 2 Chemical composition of ultrafine cement A

SiO_2	31.6%
Al_2O_3	13.6%
Fe_2O_3	0.7%
CaO	46.4%
MgO	6.1%
SO_3	1.6%

50 % grain size of about 3.1 μm. As might be seen, such kinds of clay are occasionally mixed with ultrafine cement in order to improve the penetrability of grout. β-naphthalene sulfonate formaldehyde high condensate (NSF) was used as chemical admixture.

Specimen preparation

Grouts were synthesized through mixing of each ultrafine cement and distilled water under the water/cement ratio of 6.0 by means of an electrical mixer for one minute at 25℃. Therein, say in the comparison test of several specimen, NSF and/or ultrasonic vibration were used for some samples to facilitate uniform dispersion of the ultrafine cement in the grout. NSF with the amount of 0.5 % or 1.0 % against the total weight of cement which is dissolved in water was prepared prior to mixing with the ultrafine cement. At the same time, the ultrasonic vibration could be undertaken to the grout contained in a 300 ml beaker for one minute by using a ultrasonic cleaner whose vibration frequency was set to be 40 kHz.

Size distribution of ultrafine cement in grout

The measurements were performed by aforesaid laser granulometer in which an ultrasonic generator is equipped as a standard accessory. However, as a matter of course, such ultrasonic generator was not operated during this measurement procedure in order to avoid further dispersion of the agglomerated cement particles in grout. A very small amount of the grout sample was taken at every 0, 30 and 60 minutes after mixing, then let them disperse in an excessive amount of distilled water and the size distribution was measured as to respective samples.

Viscosity of grout

The viscosity of the grouts was obtained by using a coaxial rotational viscometer (Shibaura system "Digital Vismetron VDA").

Penetrability of grout into fine sand

As shown in Fig.1, the testing apparatus consisting of a cylindrical separating funnel of 200 ml in which Japanese standard sand (106 – 300 μm in diameter, and normally used for the cement mortar test) with 20 cm thickness was filled was adopted to measure the penetrability of the grouts into dense as well as fine sand bed. The grout of 300 ml was poured into the funnel, and the penetrating depth into the fine sand was measured from outside of the funnel as the index of its penetrability.

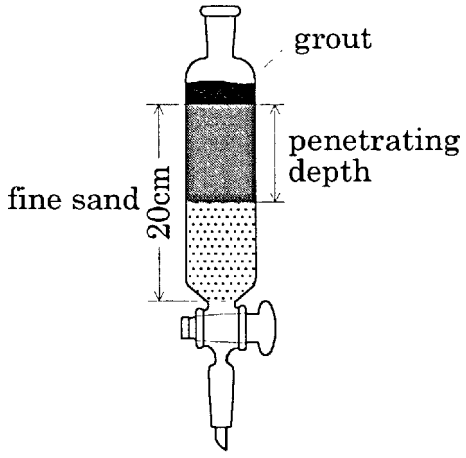

Fig.1 Setup for penetrability test of grout

RESULTS AND DISCUSSION

Ultrafine cement A

Table 3 shows the influence of different dosage of NSF together with or without ultrasonic vibration against the properties of grouts composed of ultrafine cement A. The grout sample taken immediately after mixing with neither NSF addition nor ultrasonic vibration

Table 3 Properties of grouts with ultrafine cement A

NSF (%)	Ultrasonic Vibration (sec.)	Time (min.)	Particle size distribution of ultrafine cement in grout (%)				Viscosity ($\times 10^{-3}$ Pa·s)	Penetrability (cm)
			> 6 μm	>12 μm	>32 μm	>96 μm		
0	0	0	86.1	36.3	0.6	0.0	8.4	4.0
		30	90.3	52.2	0.3	0.0	13.6	1.5
		60	94.1	70.3	1.8	0.0	22.2	0.2
0	60	0	75.2	5.6	0.0	0.0	8.9	8.0
		30	88.2	45.5	0.0	0.0	14.8	2.0
		60	93.0	65.7	0.2	0.0	25.9	0.5
0.5	0	0	21.9	0.9	0.0	0.0	3.8	15.0
		30	46.5	5.1	0.0	0.0	9.2	2.0
		60	82.4	33.8	0.0	0.0	24.3	0.5
0.5	60	0	18.4	0.3	0.0	0.0	4.3	18.0
		30	59.9	9.0	0.0	0.0	12.7	6.0
		60	86.0	33.9	0.0	0.0	31.4	2.0
1.0	0	0	21.0	1.8	1.2	1.2	3.1	>20.0
		30	18.5	0.5	0.0	0.0	3.0	>20.0
		60	17.0	0.3	0.0	0.0	3.1	>20.0
1.0	60	0	16.9	0.5	0.0	0.0	3.0	>20.0
		30	16.9	0.7	0.0	0.0	3.0	>20.0
		60	16.7	0.2	0.0	0.0	3.1	>20.0

contained 36.3 % particles which was larger than 12 μm, and its penetration depth was only 4.0 cm. This large particles might be caused by agglomeration of ultrafine cement whose maximum size is about 12 μm. While, the addition of 0.5 % NSF to the above mentioned grout reduced the rate of large particles as well as the viscosity of the grout. Furthermore, when ultrasonic vibration was undertaken to this sample, such tendency became clear more or less. This phenomenon is deemed to be the reflection of the dispersion effect by ultrasonic vibration on the agglomerated particles in same effect as the case of NSF. However, in this case, the amount of larger particles and the viscosity of the grout increased gradually as time goes by, which conducted its penetrability to be lower consequently. On the other hands, the addition of 1.0 % NSF made the particle size and the viscosity maintained almost constant for 60 minutes, and then the penetration was remarkably improved, exceeding 20 cm, regardless of whether ultrasonic vibration was applied or not.

Ultrafine cement B

In a same manner as above mentioned test for cement A, Table 4 shows the influence when cement B was used. Comparing to the case of cement A, the grout of cement B tended to contain many larger particles over 32 and 96 μm and became more viscous when ultrasonic vibration was not undertaken. This might be due to agglomeration between cement and kaolin promoted by mixing of kaolin clay, and its penetrability into fine sand became worse accordingly. When only ultrasonic vibration was undertaken without NSF addition, the viscosity increased abnormally, presumably owing to the

Table 4 Properties of grouts with ultrafine cement B

NSF (%)	Ultrasonic Vibration (sec.)	Time (min.)	Particle size distribution of ultrafine cement in grout (%)				Viscosity ($\times 10^{-3}$ Pa·s)	Penetrability (cm)
			> 6 μm	>12 μm	>32 μm	>96 μm		
0	0	0	67.1	33.1	19.2	3.0	24.9	0.0
		30	73.0	36.8	19.0	3.1	33.2	0.0
		60	76.3	40.5	19.5	4.0	51.1	0.0
0	60	0	34.0	2.4	0.0	0.0	188	0.0
		30	45.1	6.8	0.0	0.0	435	0.0
		60	54.7	13.5	0.0	0.0	534	0.0
0.5	0	0	53.5	38.1	25.7	6.6	4.0	0.2
		30	61.6	35.1	22.4	5.1	15.4	0.0
		60	68.5	36.9	22.0	5.2	25.9	0.0
0.5	60	0	19.1	0.5	0.0	0.0	12.4	8.0
		30	33.9	2.8	0.0	0.0	42.4	2.0
		60	44.3	6.5	0.0	0.0	73.2	0.5
1.0	0	0	47.8	31.8	20.0	0.0	3.4	2.0
		30	45.1	29.4	18.5	2.5	3.4	0.2
		60	42.1	25.2	14.2	0.0	4.9	0.0
1.0	60	0	13.6	0.0	0.0	0.0	3.6	>20.0
		30	13.0	0.0	0.0	0.0	3.9	>20.0
		60	13.9	0.0	0.0	0.0	5.9	>20.0

increase of fine clay particles. It was revealed that the case that the penetration depth of the grout exceeded over 20 cm was the only case of the addition of 1.0 % NSF together with ultrasonic vibration In this case, ultrasonic vibration gave a pronounced effect towards dispersion of the agglomerated particles for a long time, and consequently larger particles over 12 μm had disappeared and the viscosity became low.

CONCLUSION

The purpose of this study is to clarify the main cause that makes the penetration of suspension grout difficult into fine sand, and then conduct countermeasures thereof. The conclusion can be summarized as follows :

1) Ultrafine cement particles agglomerate easily in suspension grout and form many particles larger than the maximum size of cement, which tends to be remarkable with the lapse of time after grout mixing. This phenomenon is deemed to cause the condition of the viscosity increase as well as unsatisfactory injection of grout.

2) Regarding the countermeasure, the combination of addition of chemical admixture and short time use of ultrasonic vibrator is helpful to prevent particles from agglomerating in the grout for a long time and to decrease its viscosity, and finally facilitates the grout penetration even into fine sand.

REFERENCE

Mori, A., Tamura, M., and Aoki, K., "Permeation Limit of Grouts with Ultra-fine Granular Materials (in Japanese)" , Proc. of JSCE, Vol.426/V-14, 1991, pp. 237-240.

Topic II.B

Hydration kinetics and microstructure development

Kn o. 2 5. JAN. 2001 d o k 31769

2ii006
6 pp

HYDRATION CHARACTERISTICS OF MAGNESIA ASSIMILATED SULPHOALUMINATE - BELITE CEMENT

M M ALI, R BHARGAVA* AND S C AHLUWALIA**

National Council for Cement and Building Materials, New Delhi, India

ABSTRACT Clinker composition containing mineral phases $C_4A_3\bar{S}$, C_2S, C_3MS_2, C_4AF, $C\bar{S}$ and upto 10 percent MgO showed rapid hardening with almost complete hydration of $C_4A_3\bar{S}$ in one day. C_3MS_2 remained inert upto one year studied. Autoclave and potential sulphate expansions were 0.15 and 0.04 percent respectively. The cement showed much resistance to corrosion of reinforcement steel in sea water.

Key-words: Clinker Formation, Corrosion, Ettringite, Expansion,Hydration

INTRODUCTION

In oxide system $CaO-Al_2O_3-Fe_2O_3-SiO_2-SO_3-MgO$, several phase assemblages of phases such as $C_4A_3\bar{S}$, C_2S, C_2AS, C_3MS_2, C_4AF, $C\bar{S}$ etc. have been reported which have cementitious properties (Ali et al, 1992, Beratka et al, 1992, Ikada, 1990, and Mehta, 1980). In presence of MgO formation of C_3MS2 phase occurs which is stable upto 1381°C (Schlandt, 1966). The temperature of clinkerization is generally lower and there is a potential of making cement using low grade high MgO limestone and by product waste materials (Ali, 1992, Mehta, 1980).

In the present investigation sulphoaluminate belite cement containing upto 10% MgO has been prepared and studied for the hydration products, performance characteristics, sulphate resistance and corrosion of steel embedded in concrete. A comparative evaluation of corrosion in ordinary and sea water curing over a period of 1 year using OPC and high magnesia sulphoaluminate belite cement has been presented.

EXPERIMENTATION

High magnesia sulpho aluminate - belite cement was prepared by preparing raw mix using limestone, clay, bauxite, gypsum and MgO powder. Raw materials were ground and raw mix with fineness of about 12 percent residue on 170 mesh was nodulized and fired for one hour at 1325°C by keeping in an electric furnace and air quenching the resultant clinker. The clinker was evaluated for mineral phases using x-ray diffractometer and scanning electron microscope for morphology of clinker. Clinker sample was ground in a ball mill to achieve a fineness of about 26 M^2/Kg Blaines's. The cement was analysed for constituent oxides and physical performance characteristics determined as per IS : 4031 - 1988. The hydration study was carried out by preparing cement paste at w/c ratio of 1.0 in plastic bottles by keeping for 15 minutes, 1, 2, 5 hours, 1, 3, 7, 28 and 360 days and arresting hydration through acetone treatment. Mineralogy was determined using x-ray diffraction. The hydrated specimen in lump form and having smooth and shining surface along the base of containg bottles were also studied under reflected light in optical microscope alongwith the SEM of fractured surface. The cement was evaluated for potential sulphate expansion as per ASTM-C 452-1989.

---

* Shree Cement, Beawar, Rajasthan, India
** OCL India Ltd., New Delhi, India

The cement was also tested for corrosion activity in steel embedded in concrete along with OPC by curing the two in ordinary and sea water composition for one year and then measuring potentials generated in steel (Gouda, 1975).

RESULTS AND DISCUSSION

The potential phase composition of the clinker without addition of MgO is shown in Table 1.

Table 1 Potential Mineral Phases of the Clinker

Phases	$C_4A_3\bar{S}$	C_2S	C_4AF	$C\bar{S}$
Proportion (%)	32	40	20	8

Two clinkers with 10 and 11 percent MgO replacing CaO were fired. Mineral phases developed are shown in Fig. 1.

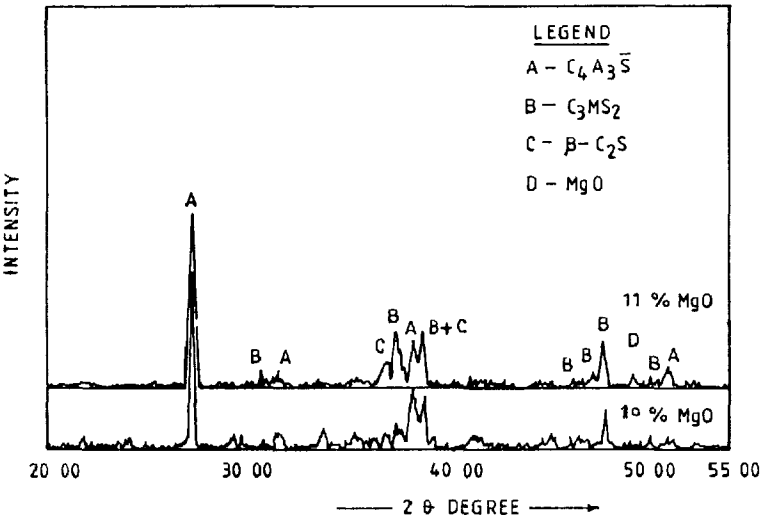

Figure 1 XRD of Clinker Samples

Clinkers fired at 1325°C were found well burnt and XRD studies showed formation of $C_4A_3\bar{S}$, C_3MS_2 and C_2S. Mix with 11 percent MgO indicated appearence of periclase in small amount.

The fracture surface morphology of clinker is shown in SEM (Fig 2).

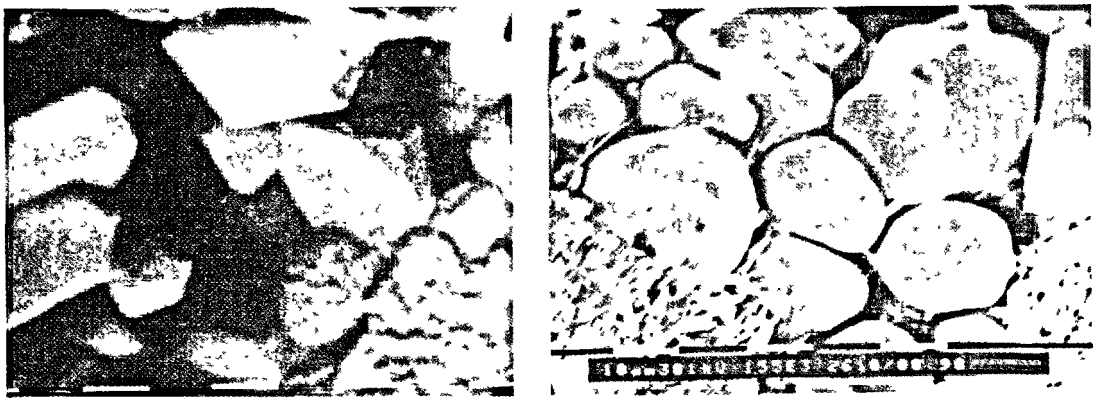

Figure 2 SEM of Clinker Sample

The crystals of $C_4A_3\bar{S}$ are well developed hexagonal tabular shaped along with coarse grained two grained rounded particles of silicate phases which are evenly distributed.

The chemical analysis of clinker is given in Table 2.

Table 2 : Constituent Oxides in Sulphoaluminate Belite Cement

Constituents	LOI	SiO_2	Fe_2O_3	Al_2O_3	CaO	MgO	SO_3	Na_2O	K_2O	TiO_2	FCaO
Weight (%)	0.63	14.06	6.45	18.68	40.41	9.93	7.8	0.24	0.14	0.40	0.2

The physical performance characteristics of sulphoaluminate - belite cement is given in Table 3.

Table 3 : Performance Characteristics of Cement

	Property	Values
1.	Fineness, Blaines (M^2/Kg)	26.0
2.	Setting Time (Minutes)	
	Initial	35
	Final	80
3.	Autoclave Expansion (%)	0.15
4.	Compressive Strength (N/mm^2)	
	1 Day	18.0
	3 Day	21.0
	7 Day	25.0
	28 Day	34.5

It is clear from Table 3 that the cement shows rapid hardening and substantial strength gain at one day of hydration. Autoclave expansion is only 0.15 percent which indicates that even with 10 percent MgO the cement is volume stable which is expected in view of the near absence of periclase and presence of non hydraulic MgO bearing phase. The XRD of autoclaved sample showed presence of C_3MS_2(Fig 3)as non-hydraulic phase.

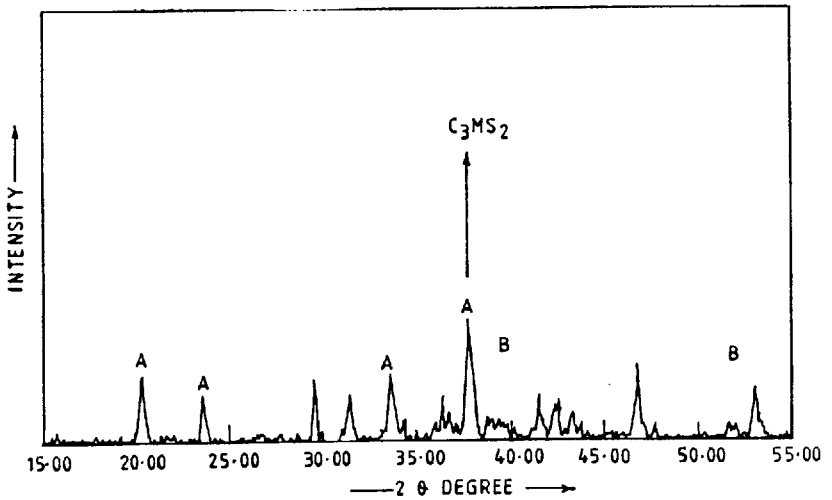

Figure 3 XRD of Autoclaved Cement Sample

The hydration phases developed under ambient water curing are shown in figure 4.

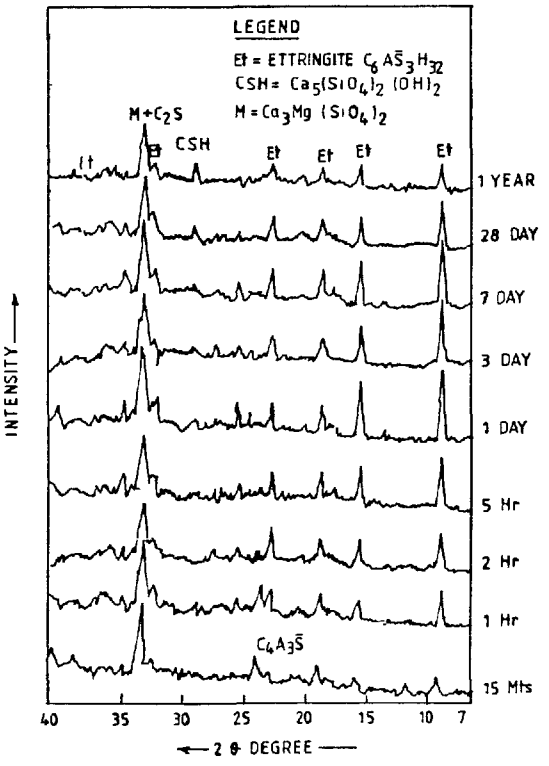

Figure 4 XRD of Hydrated Cement Samples

Figure 4 shows that the hydration of $C_4A_3\bar{S}$ occurs rapidly and at one day as is evident from the disapperance of pak at 2O=23.92 and apperance of ettringite peak at 2O=9.08. Its hydration led to a considerable formation of ettringite in 15 minutes. The hydration of C_2S is slower (Ono, 1989) and the XRD patterns do not clearly show the rate of hydration as the C_2S peaks are masked by C_3MS_2. However formation of crystalline CSH appears in XRD at one year of hydration.

The rapid hardening and higher strength characteristics at early ages are owing to rapid hydration of $C_4A_3\bar{S}$ and C_2S phases (Hanayawa, 1975, Kasselouri et al, 1995).

The optical micrographs of hydrated samples (Fig 5) showed crystalline needle shaped hydrates of ettringite.

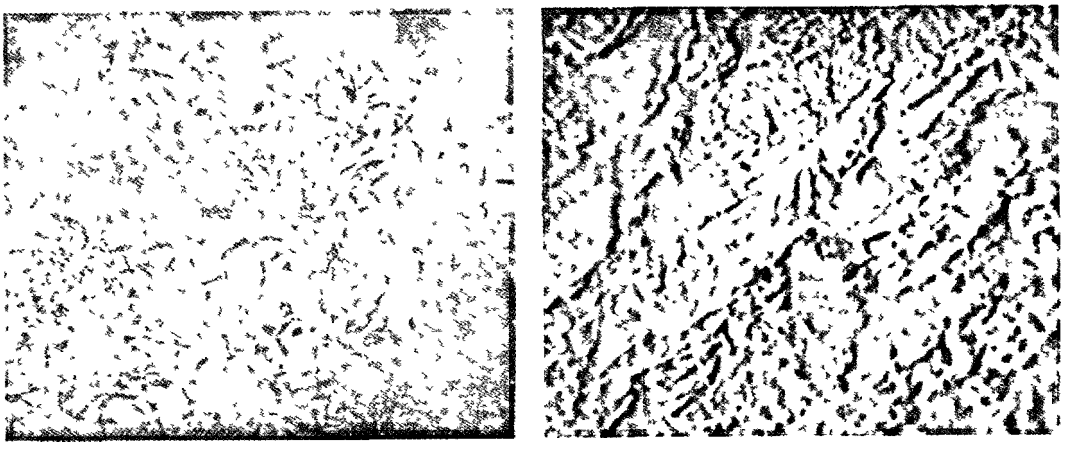

Figure 5 OM & SEM of hydrated Samples

The ettringite crystals fill the void spaces in the paste and form dense mass. SEM of hydrated specimens show that at later ages, the needles get converted into rounded prismatic forms.

The potential sulphate expansion determined was found to be 0.04 percent which is comparable to the limit prescribed for ASTM V type cement. Therefore sulphoaluminate-belite cement could be used for constructions in sulphate bearing environment.

Measurement of corrosion in reinforcing steel embedded in sulpho aluminate cement and OPC is shown in Fig 6.

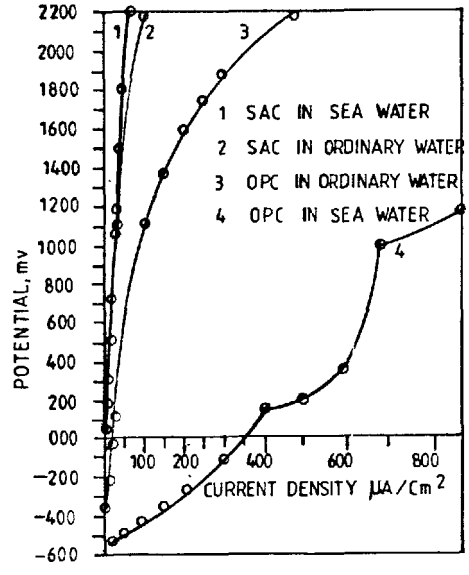

Figure 6 Corrosion test of Steel reinforced Sulphoaluminate (SAC)and Ordinary Portland Cement (OPC)

It is clear that sulphoaluminate-belite cement is highly resistant to corrosion of reinforced steel compared to OPC upto a period of one year studied.

CONCLUSIONS

1. Sulphoaluminate belite cement is a low temperature, energy saving cement and can exploit low grade, dolomitic limestone in its manufacture.
2. The high magnesia sulphoaluminate belite cement containing 10 percent MgO fixed mostly as C_3MS_2 was found to be volume stable.
3. The C_2S phase hydrates at slower rate due to presence of coarse grain size.
4. The cement is resistant to sulphate attack and shows resistance to corrosion of reinforcing steel compared to OPC in sea water conditions.

Acknowledgement
The authors are thankful to Director General-NCB, New Delhi for giving permission to publish the work.

REFERENCES

Ali M M, Sharma P S and Bhargava R, "Potentials of using Dolomitic limestone in making sulfoaluminate - silicate cements", Proc. 9th Int. Conf. Chem. of cement New Delhi, India, 1992. Vol. III pp. 227-232.

Beretka J, et al, "Synthesis and Properties of Low Energy Cements Based on $C_4A_3\bar{S}$," Proc., 9th Int. Cong. Chem of Cement, New Delhi, India Vol. III, 1992, pp. 195-200.

Francis Hanayawa, "Technical note on Calcium sulphoaluminate, cement 1975. CBI 2:75.

Gouda V.K., Shater, M A and Mikhail, R, Hardened Portland blast furnace slag cement pastes II. The corrosion behaviour of steel reinforcement Cem. & Conc. Res. 1975, 5(1), 1-13.

Ikada K, "Cements along the join $C_4A_3\bar{S}$-C_2S", Paris sysmposium on chemistry of cement, 1990, Vol. III-31.

Kasselouri, V. Tsakiridis, P. "A study on the hydration product of a non expansive sulphoaluminate cement", Cem. & Conc. Res. Vol. 25, No. 8 1995, P 1726-1736.

Mehta P K, "Investigation on low energy cements," World Cement Technology, 1980, May 166-177.

Ono, Y., "Proc. Holderbank Microscopy, Workshop, Ch. 16, 1989.

Schlandt C M and Roy D M, "The join Ca_2SiO_4-$CaMgSiO_4$", J. Am Ceram. Soc. 1966, 49(8), PP 430 - 432.

Kn o. 2 5. JAN. 2001 d o k 31770

2ii007
4 pp

INFLUENCE OF THE COMPOSITION OF INTERSTITIAL PHASES ON THE HYDRATION PROPERTIES OF BELITE CEMENTS

Tatsuo IKABATA and Hideki TAKEMURA, Cement/Concrete Research Lab.,
Sumitomo Osaka Cement CO. LTD., Japan

ABSTRACT The hydration properties of belite cement were investigated by varying the composition of the interstitial phases. Results indicated that the heat of hydration / compressive strength of mortar ratio was at a minimum when the composition of the interstitial phase was near to C_6AF_2. Additionally, concrete tests were conducted using belite cement having a minimum ratio of heat of hydration / compressive strength of mortar.

Key-words: Belite, Composition, Hydration, Interstitials, Strength development

INTRODUCTION

Following recent advances in concrete technology, there has been an increase in the rapid construction of concrete buildings and structures composed of large-sized units or modules. When such massive concrete structures are built, effective methods to reduce thermal stress, caused by hydration during the course of concrete hardening, are important to avoid cracking of the structures and improve their durability. To resolve this problem, low-heat Portland cement has recently come into use. This type of cement is now often used also when high strength and flexibility are required of concrete. To date, several types of low-heat Portland cement, including belite rich cement (named belite cement) with a C_2S content ranging from 50 to 75%, have been studied. (Ikabata et al, 1990and 1991; Yoshida and Igarashi, 1991; Nawa et al, 1993) Most of these types of low-heat Portland cement used C_3A-C_4AF for the interstitial phase. However, few studies have examined the influence of the composition of the interstitial phase in this type of cement.

The present study was undertaken to examine the effects of interstitial phase composition on the hydration properties of belite cements, i.e., the effects on the hydration heat and mortar strength. In addition, concrete pieces made of selected belite cements were tested.

SAMPLE PREPARATION

Synthesis of clinker

The raw mixes were prepared by grinding a mixture of SiO_2, Al_2O_3, Fe_2O_3, $CaCO_3$, $Mg(OH)_2 \cdot MgCO_3$, Na_2SO_4, K_2SO_4, Na_2CO_3 and K_2CO_3, which were chemical reagent grade materials. The raw mixes were molded under pressure, then heated in a furnace for 1 hour at 1,450° C. After that, all clinkers were quenched in the air.

The clinkers were characterized by chemical analysis, X-ray diffraction and observation by reflective microscopy. The chemical composition and calculated mineral composition of the clinkers are shown in Table 1.

Preparation of cement

The clinkers were mixed with gypsum and ground using a ball mill to a Blaine fineness of 290 to 300 m^2/kg (Experiment 1) or 440 to 460 m^2/kg (Experiment 2). The amount of SO_3 was 2% (Experiment 1) or 1.0, 1.5 and 2.0 (Experiment 2).

EXPERIMENTAL PROCEDURE

Standard tests (Experiments 1 and 2)

The heat of hydration of the cement and the compressive strength of mortar were measured according to the method proposed by Japanese Industrial Standards (JIS R5203, 1987 and JIS R5201, 1992). In Experiment 1, both samples were tested at 1 week , 4 weeks, 13 weeks and 1 year. On the other hand, 1, 4 and 13 weeks samples were tested in Experiment 2.

Table 1 Chemical and mineral composition of clinker

Experiment	Sample	clinker									SO_3 of Cement (%)
		SiO_2 (%)	Al_2O_3 (%)	Fe_2O_3 (%)	CaO (%)	Na_2O eq.(%)	C_3S (%)	C_2S (%)	IM	interstitial phases	
1	A	28.0	4.0	3.5	62.9	0.34	11	72	1.14	C_3A-C_4AF	2.0
	B	27.1	3.7	3.5	63.8	0.37	24	60	1.06	C_3A-C_4AF	2.0
	C	28.0	4.2	2.4	63.5	0.38	14	70	1.75	C_3A-C_4AF	2.0
	D	28.0	2.9	4.7	62.7	0.40	16	68	0.62	C_4AF	2.0
	E	27.9	1.3	6.8	62.3	0.38	16	68	0.19	C_6AF_2	2.0
	F	27.8	0.1	8.3	61.7	0.52	16	68	0.01	C_2F	2.0
2	G-1	26.6	1.6	6.0	60.0	0.47	18	63	0.27	C_6AF_2	1.0
	G-1.5										1.5
	G-2										2.0

Concrete tests (Experiment 2)

Table 2 Mix proportion of concrete

Water-cement ratio (%)	Sand-aggregate ratio (%)	Unit content (kg / m^3)				Chemical admixture (l / m^3)
		Cement	Water	Sand fine aggregate	Coarse aggregate	
50	39	300	150	710	1160	0.75

Concrete tests were conducted using sample (G -2) and commercial low-heat Portland cement. The concrete samples were mixed in the proportions listed in Table 2 using a double shaft pugmill mixer. After mixing the concrete samples, slump, compressive strength and adiabatic temperature rise of each concrete were measured.

RESULTS AND DISCUSSION

Characterization of clinker

Our analysis of mineral composition by X-ray diffraction revealed that the C_2S contained in the test samples was of β-phase. The interstitial phases of samples A through C were found to be composed of C_3A and ferrite phases, while those of samples D through G were composed of ferrite alone. These findings are consistent with the mineral composition shown in Table 1. The features of the interstitial phases as observed under a reflective microscope also agreed with the findings shown in Table 1. Type I belite formation was seen in all clinkers. As the ratio of the amount of Al_2O_3 to the amount of Fe_2O_3 contained in the clinker (the Al_2O_3/Fe_2O_3 ratio) became smaller, the crystal size of the belite phase formed became greater. Fig. 1 shows representative results obtained by reflective microscopy. The increase in the crystal size of the belite appeared to be related to changes in the viscosity of the liquid clinker following a decrease in the Al_2O_3/Fe_2O_3 ratio.

Experiment 1

Figures 2 shows the relationship between the mineral composition and the heat of hydration in Experiment 1, while Figures 3 shows the relationship between the Al_2O_3/Fe_2O_3 ratio of the clinker (IM) and the compressive strength of the mortar in the same experiment. When the C_3S content

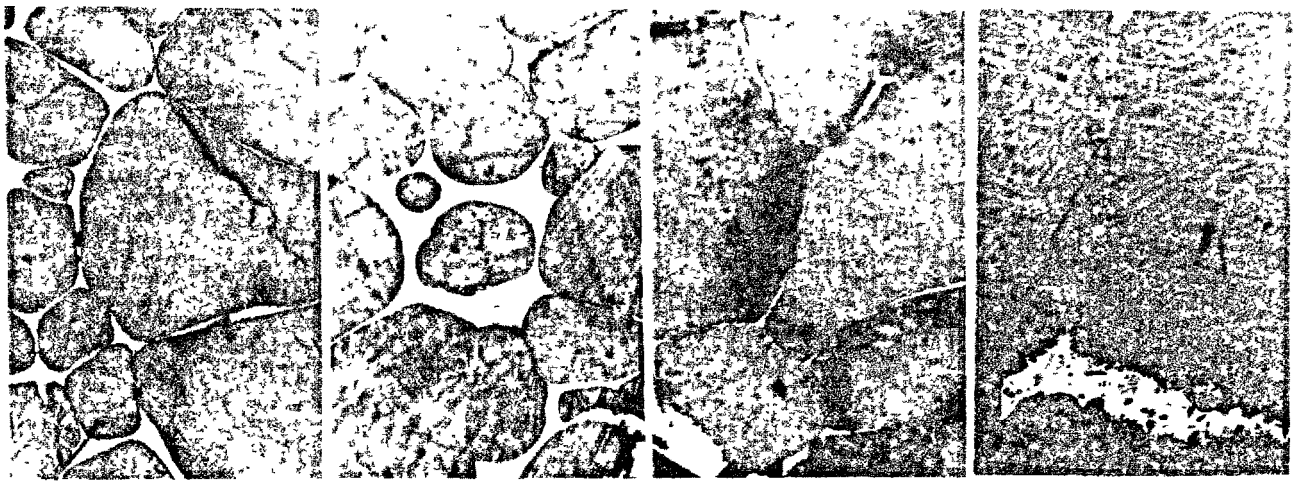

Fig 1 Polished and etched surface of the belite clinker.

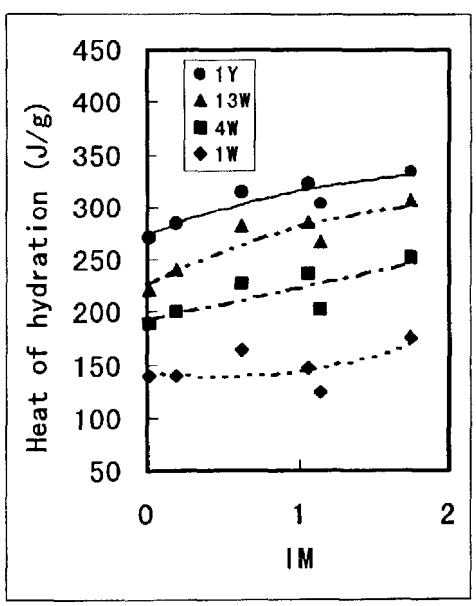

Fig 2 Relationship between IM and heat of hydration.

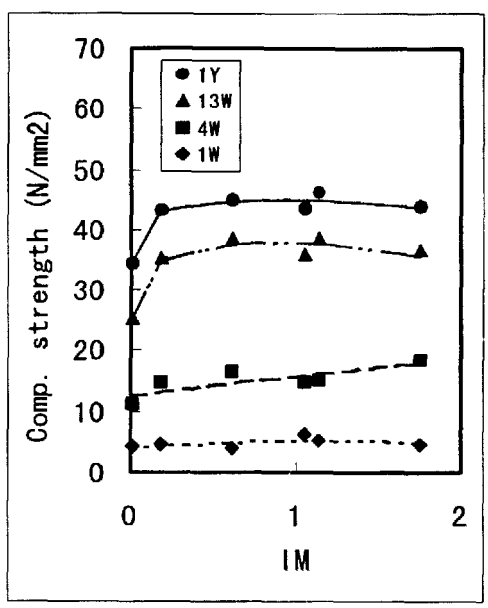

Fig3 Relationship between IM and compressive strength

was the same, an increase in the Al_2O_3/Fe_2O_3 ratio resulted in an increase in heat of hydration. This increase in heat of hydration was greater in samples of lower age. A characteristic relationship was observed between the compressive strength of the mortar and the interstitial phase composition. That is, in samples of relatively low ages (less than 4 weeks), an increase in the Al_2O_3/Fe_2O_3 ratio tended to increase the compressive strength of the mortar, while in samples more than 13 weeks old, the compressive strength reached a peak when the Al_2O_3/Fe_2O_3 ratio was about 0.6 (corresponding to type C_4AF). When the ratio of heat of hydration to the compressive strength of the mortar was analyzed in relation to the interstitial phase composition, as shown in Fig 4, it was found to be lowest when the Al_2O_3/Fe_2O_3 ratio was about 2 (corresponding to type C_6AF_2). The interstitial phase types C_4AF through C_6AF_2 therefore seem to be most suitable for belite cement.

Experiment 2

Following the findings obtained in Experiment 1, clinker (G) was synthesized and used for producing belite cement with an interstitial phase composition close to type C_6AF_2. Using this clinker, the optimum amount of gypsum that should be added to the belite cement was examined. Before beginning this experiment, we had expected that the amount of SO_3 needed would be smaller than that used for ordinary low-heat cement on the grounds that the Al_2O_3/Fe_2O_3 ratio of this belite cement is low. However, the ratio of heat of hydration to the compressive strength of the mortar was low when the SO_3 content in younger samples was small, and this ratio showed no difference associated with the SO_3 content in 13 week old samples. Therefore, contrary to our expectation, 2% seems to be the optimum SO_3 concentration.

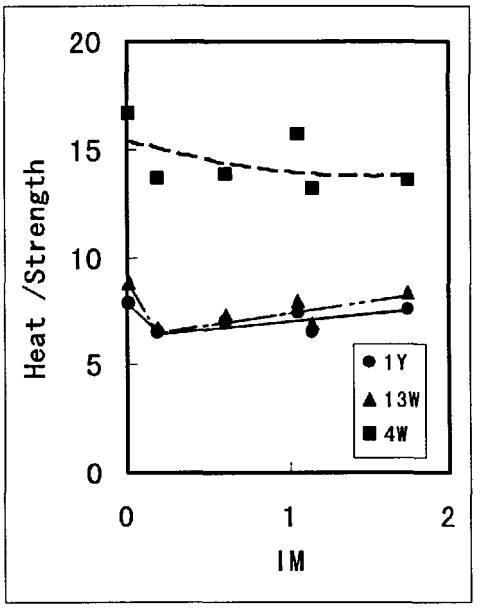

Fig 4 Relationship between IM and the ratio of heat of hydration / compressive strength

Table 3 shows the results of concrete tests using belite cement with the above-mentioned optimum SO_3 concentration and a commercial low-heat cement. Although the initial strength of the belite cement was not satisfactory, this cement was found to have two favorable features: (1) the concrete had a high strength when measured 28 days or more after it was made from this cement; and (2) the adiabatic temperature rise was low.

Table 3 Results of concrete tests

Sample	slump (cm)	Air (%)	Compressive strength (N/mm^2)			Adiabatic T.R. (℃)
			1W	4W	13W	
G-2	8.5	4.7	4.6	35.1	50.5	35.9
L.H.	6.0	4.9	15.6	33.4	44.7	40.1

CONCLUSIONS

1. Judging from the compressive strength of the mortar and the heat of hydration, the optimum interstitial phase composition of belite cement is C_4AF through C_6AF_2.
2. A test of concrete made of belite cement with a C_6AF_2 type composition of the interstitial phase revealed that this belite cement has two favorable features (an excellent long-term strength and a low adiabatic temperature rise).

REFERENCES

Ikabata, T., Yoshida, H., Matsuoka, Y. and Uchida, K., "Effect of curing temperature on the microstructure of cement pastes", CAJ Proceedings of cement and concrete, No.44, 1990, pp.46-51

Ikabata, T., Takemura, H. and Uchida, K., "Heat / strength characteristics and microstructure of low heat cement", CAJ Proceedings of cement and concrete, No.45, 1991, pp. 134-139

Yoshida, K., and Igarashi, H. "Effect of some factors on strength and heat of hydration of low heat cements", CAJ Proceedings of cement and concrete, No.45, 1991, pp. 140-145

Nawa, T., Fukaya, Y., Suzuki, K. and Yanagida, K., Concrete research and technology, Vol.15, No.1, 1993, pp.143-148

Kno. 25. JAN. 2001 dok 31771 21100
4 pp

DISTINGUISHING FEATURES OF HARDENING OF PORTLAND CEMENT SYSTEMS ON A BASIS OF CLINKERS OF VARIOUS MICROSTRUCTURE

Lev G.SUDAKAS, Giprocement, Phys.-and Chem.Studies, St.Petersburg, Russia
Lyudmila B.VASILIYEVA, Giprocement, Phys.-and Chem.Studies, St.Petersburg, Russia

ABSTRACT The diffirent in the microstructure of commercial portland cement clinkers at their completely identical origin and chemical-and-mineral composition tells upon the dynamics of formation at hardening of crystalline phases-portlandite and ettringite. This dynamics determines to a large extent the strength of systems at control ages and is controllable with the help of chemical additives.

Key-words: Hardening, Hydration, Misrostructure

INTRODUCTION

The description of portland cement clinkers through their misrostructure dates back to the end of the XIXth century (Le Chatelier, 1887). In the modern times investigation (Sheikin, 1960), (Kuznetsova, 1968), (Sudakas, Kraplya et al, 1975) a link was established between the clinker microstructure and the strength of the associated cement systems. It was shown in one of the recent works (Kraplya and Sudakas, 1986) that the hardening systems on a basis of commercial clinkers differ in dynamics of variations in their content of portlandite, $Ca(OH)_2$, and proposal was made that the varying strength of such systems can be attributable to these differences.

EXPERIMENTAL

5 clinkers of the Ulyanovsky plant sampled under the petrographic control were taken for the investigations. All the clinkers were burned from one type of slurry within 3 days. The clinkers differed in their microstructure in the range from 2 to 6 on the Giprocement scale. The clinkers did not differ in their chemical-and-mineral composition as demonstrated by the chemical analysis data: KH=0.92; n=2.06÷2.1; p=1.3÷1.4; $\%SO_3$=0.97÷1.17; %MgO=1.12÷1.14; $\%R_2O$=0.73÷ 0.86.

The clinkers were ground with 4.5% gypsum stone to the specific surface of 300±10 m^2/kg. The tests were conducted in accordance with the Russian standard GOST 310.4 (Table 1).

Table 1 Compressive strengths of cements on a basis of clinkers of various microstructure

Misrostructure, Giprocement scale number	Compressive strength, MPa			
	1 days	3 days	7 days	28 days
2	16.4	24.6	28.7	36.6
3	17.4	32.6	34.8	38.0
4	14.3	30.4	36.9	42.6
5	16.2	34.0	38.6	45.7
6	12.7	25.4	45.0	50.0

Concurrently investigation was made into dynamics of changes in the content of the main crystalline new formations - portlandite and ettringite. Their content was assessed by the intensity of the X-ray diffraction peaks of 4.90 A for portlandite and 9.8 A for ettringite. Fig 1-1 through 1-5 show the dynamics at different basis of clinkers of various microstructure.

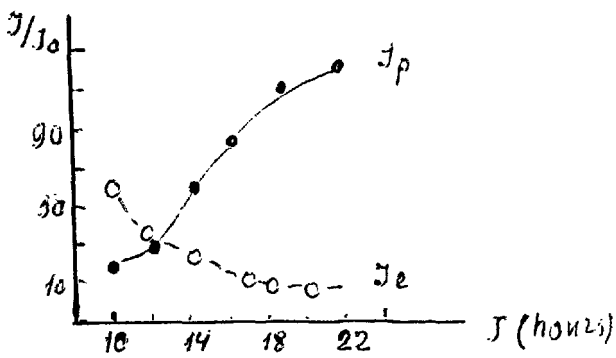

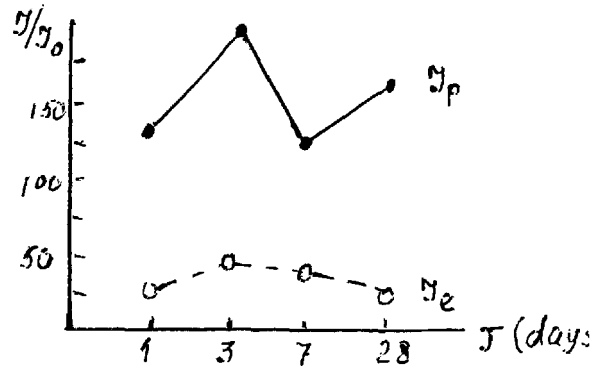

Fig 1-1 Clinker, 2 numbers

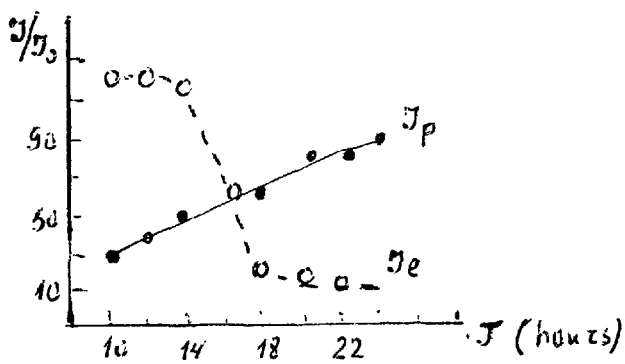

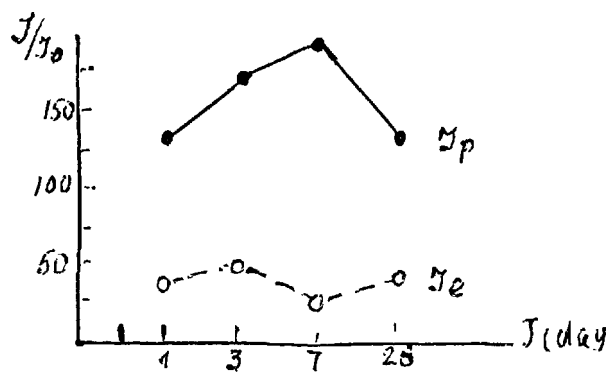

Fig 1-2 Clinker. 3 numbers

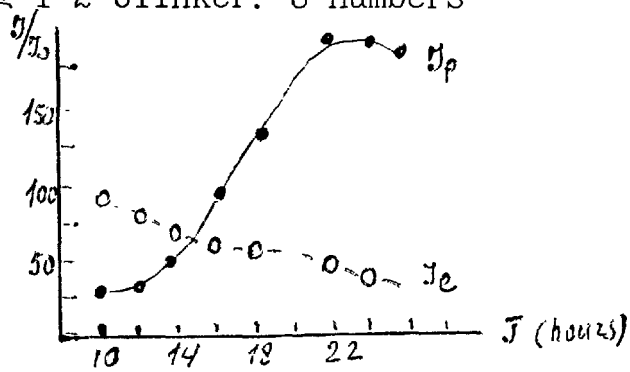

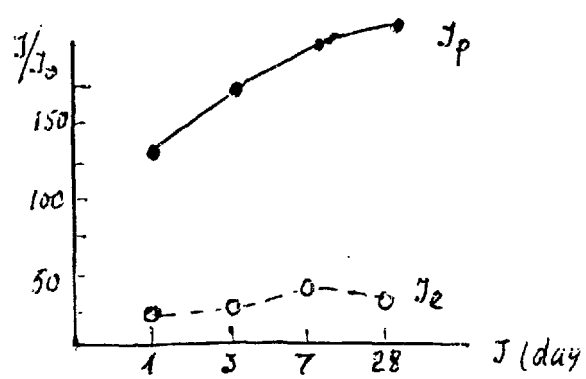

Fig 1-3 Clinker, 4 numbers

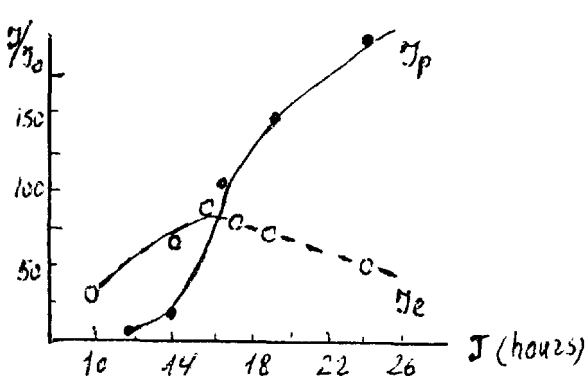

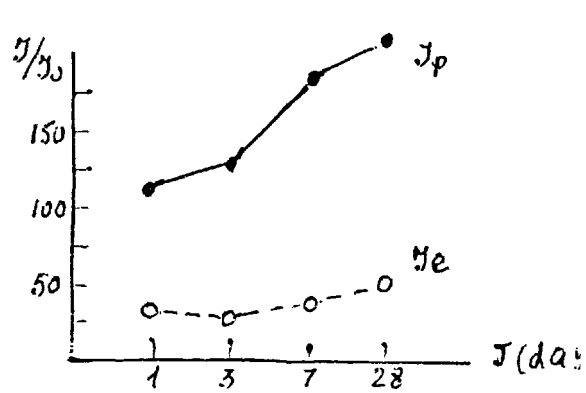

Fig 1-4 Clinker, 5 numbers

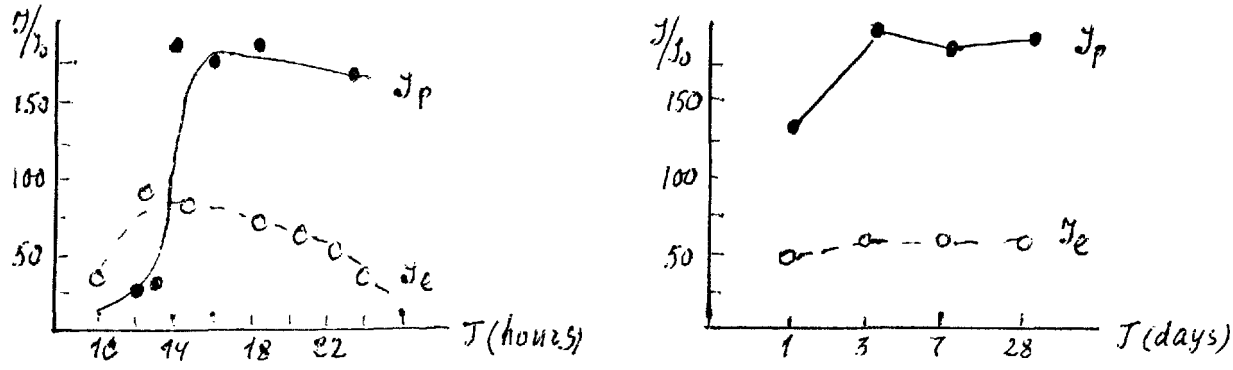

Fig 1-5 Clinker, 6 numbers
Figure 1 Dynamics of changes in the content of portlandite (p) - and ettringite (e) - in hardening cement systems on a basis of clinkers of varying microstructure

A possibility to change the dynamics of the crystalline phases formation with the help of chemical additives was examined at a time. Fig 2 shows such a change at introduction of 0.1% monosubstituted ammonium citrate into the system on a basis of clinker with the microstructure of 2 numbers. The compressive strengths of such systems were as follows: at the age of 3 days - 20.8; at the age of 7 days - 27.8; at the age of 28 days - 47.4 MPa.

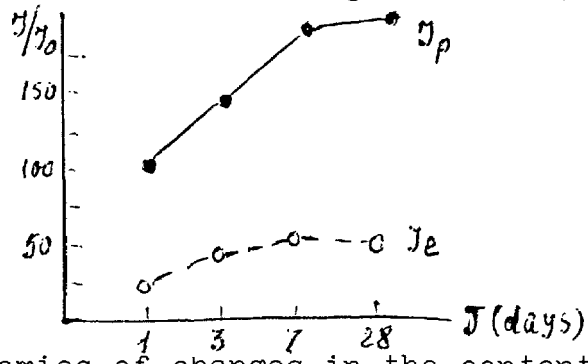

Figure 2 Dynamics of changes in the content of portlandite (p) - and ettringite (e) - in hardening cement systems on a basis of clinker with microstructure of number 2 with addition of 0.1% monosubstituted ammonium citrate

DISCUSSION OF RESULTS AND CONCLUSIONS

The difference in the clinker microstructure tells upon the strength synthesis unambiguously: the more perfect is the clinker microstructure, the higher is the 28-days strength systems. at the early ages, particularly at 1 day, the dependence therewith can be inverse. The clinkers with disordered structures (2,3 numbers) at the age of 1 day can give higher strengths than the ones with ordered structures (6 numbers). This correlates with the change in the content of crystalline phases. The less crystallochemically ordered clinkers because of their rather high chemical activity in the first (up to 10) hours form systems with a higher than usual initial content of ettringite and portlandite (the latter is formed after 6-7 hours of hardening). Later on the clinker structural order leads to a monotone increase in the crystalline phases conent of the hardening system, while in system based on clinkers of the inferior microstructure the formation of the crystalline phases is retarded and on frequent occasions takes on an alternating character. This points to the destruction of crystalline structures formed initially in the hardening systems.

Thus, such a change in dynamics of the crystalline phase formation is one of the causes of the lower strength of the cement stone.

This is supported also by the experiense of introduction of the ammonium citrate additive into the system of disordered clinker microstructure (number 2). The dynamics of the crystalline phase formation takes on the character inherent in systems based on clinkers of a perfect microstructure, and this results in the strength increase at the control ages.

REFERENCES

Kraplya, A.F. and Sudakas, L.G. "Influence of Clinker Features on the Cement Stone Formation", Inorganic Materials, vol.22, N°.6, 1986, p.p 1025-1029

Kuznetsova, T.F. "Investigation into Factors Influencing the Microstructure and Engineering Properties of Clinkers", Dissertation, Moscow, 1968

Le Chatelier "Recherhes experimentales" Ann de Mines, Mai 1987

Sheikin, A.Ye. "Influence of Clinker Microstructure on Physical-and- Mechanical Properties of Portland Cement", Proceedings of NIItsement, 14, M., 1960

Sudakas, L.G., Kraplya, A.F. et al. "Influence of Structural Features of Clinkers on their Quality", Cement, N° 2, 1975

Kno. 25. JAN. 2001 dok 31772 2ll009 4 pp

DOLOMITIC ROMANCEMENT - LOW TEMPERATURE HYDRAULIC BINDER

Ilgars GROSVALDS, Silvija LAGZDINA, Uldis SEDMALIS, Riga Technical University, Institute of Silicate Materials, Riga, Latvia

ABSTRACT Dolomitic romancement although has advantages of low manufacturing cost because of low embodied energy and convenient use in building industry, has some essential limitations also- quick setting (begin 5-10 min, end 10-25 min) and uneven volume change during hardening of cement. These shortages were overcame by wetting and keeping in a storage in moist atmosphere for about 2 weeks dolomitic material obtained by firing domerite (dolomite containing 18-25% of clay) before milling as well as using additive.

Key-words: additives, mineral phase, low temperature,volume change.

INTRODUCTION

In Latvia dolomitic romancement was known long ago. It was produced as far back as in 1865 using as raw material domerite i.e. clayey dolomite by firing at the temperature 800-900°C and fine milling. The fired product can be considered as clinker only conventionally, because it is not sintered and dense. Dolomitic romancement like portlandcement is a hydraulic binder, however the mechanical strength of romancement is about one fourth as that of portlandcement. At the same time the mechanical strength of romancement after some days of hardening is greater as that of lime after 28 days of hardening. Essential limitations of dolomitic romancement are it quick setting, uneven volume change during hardening and small mechanical strength (5-10 MPa). The purpose of present investigation was to overcome quick setting, uneven volume change as well as to improve the mechanical strength of dolomitic romancement.

RESULTS AND DISCUSSION

Raw material used was Sloka-Kudra domerite. The chemical and mineralogical composition of Sloka-Kudra domerite and Sloka-Slocene domerite, the latter for comparision, are given in Table 1.

Table 1 Chemical and mineralogical composition of domerite , mass %

Ingredients	Sloka-Kudra deposit	Sloka-Slocene deposit
loss on ignition	37,68	39,70
SiO_2	12,06	13,88
Al_2O_3	3,64	1,91
Fe_2O_3	2,38	1,27
CaO	26,65	25,40
MgO	16,99	17,51
	Σ=99,40	Σ=99,67
dolomite+calcite	77,7+5,4	81,06
clay	16,3	18,61

Domerite was crushed by laboratory jaw crusher, screened into the sizes 3-7 mm and fired in the muffle kiln at temperatures 800, 850, 900°C. The rate of raising the temperature was 10°C/min, the entire time at the maxima temperature - 4h. The firing temperature was chosen on the basis of DTA results (Fig 1).

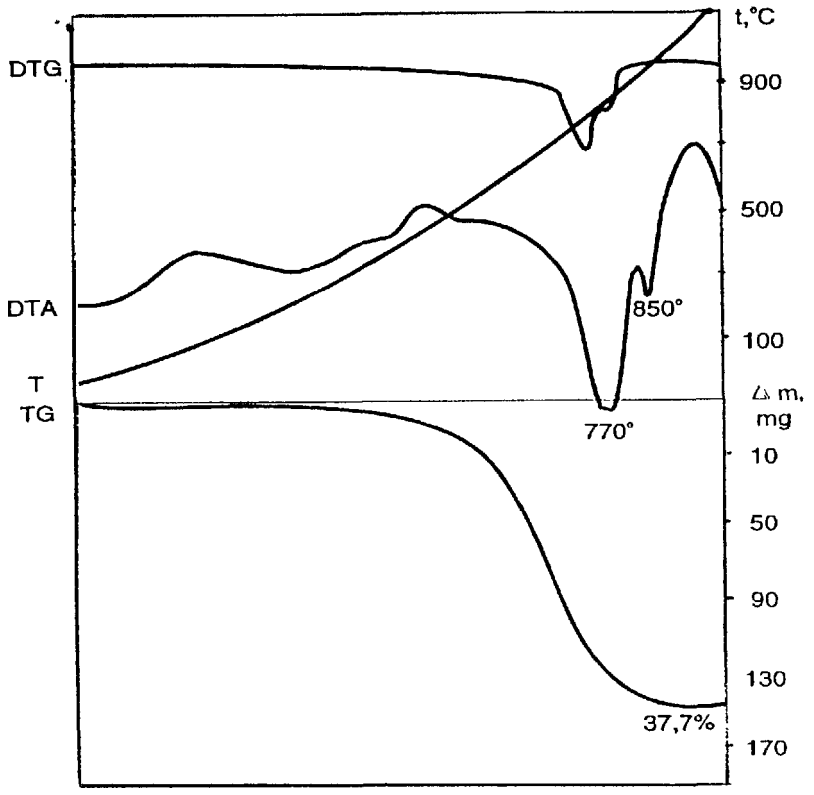

Figure 1 Derivatogram of Sloka-Kudra domerite;
curves: DTG - differential mass losses;
DTG - differential thermal analysis;
T - temperature;
TG - mass losses.

In the DTA curve the first endotherm at 770°C is due to the decarbonation of $MgCO_3$, the second - at 850°C relates to the decarbonation of $CaCO_3$. 850°C have been established to be the optima firing temperature of Sloka-Kudra domerite for obtaining dolomitic romancement. The main phases in material identified by powder X-ray diffraction (XRD) patterns are: β-$2CaO{\cdot}SiO_2$ (d/n=2,98; 2,51; 2,41Å), $2CaO{\cdot}Fe_2O_3$(d/n=2,80; 2,68; 3,70 Å); MgO(d/n=2,108; 2,43; 1,49Å); $CaO{\cdot}Al_2O_3$(d/n=2,98; 2,51; 2,41Å); $CaCO_3$(d/n=3,03; 1,87; 2,09Å). Free CaO is determined by saccharate method. The quantitative phase composition of material calculated from the results of chemical analysis is listed in Table 2.

Table 2 The quantitative phase composition of dolomitic romancement in dependence on the firing temperature of domerite

Phase	% of phase at the temperature	
	800°C	900°C
free CaO	2,00	4,35
$CaCO_3$	13,70	2,29
$CaO{\cdot}Al_2O_3$	8,09	9,58
$2CaO{\cdot}Fe_2O_3$	2,83	2,83
$2CaO{\cdot}SiO_2$	41,19	50,04
free MgO	13,21	21,61
total MgO	27,48	28,97
insoluble residue	3,74	1,23
total	99,03	99,34

Formation of various calcium containing phases is in agreement with DTA data-it is confirmed that simultaneously with decomposition processes of carbonates solid state reactions of formation of new phases take place. In Table 3 characteristic properties of dolomitic romancement obtained at 850°C and containing various additives are shown. Using special additive the setting time of dolomitic romancement is prolonged - with 1% - 2,5 times, with 2% - 4,7 times. Uneven of volume change is avoided and the mechanical strength is increased combining 2% of special additive with other additives such as; superphosphate; $CaSO_4 \cdot 2H_2O$ etc. (Table 3).

Table 3 Characteristic properties of dolomitic romancement containing 2% of special and other additives.

Additive	Water demand, %	Setting time		Change in volume	Compressive strength, MPa		Strength, %
		begin	end		7 days	28 days	
-	35	22min	1h40min	uneven	4,9	15,7	100
1% apatite	35,1	35 min	1h15min	"	5,8	12,0	
3% "	34,4	30min	1h	"	5,7	18,2	
5% "	35	20min	40min	"	7,3	20,4	130
1% supher-phosphate	35,6	20min	1h30min	even	5,3	22,9	
3% "	36	30min	1h35min	even	6,0	22,6	143
0,1% ligno-sulphonate	37	35min	1h	uneven	8,0	17,2	111
0,3% "	30,6	20min	30min	"	6,3	7,6	
5% $CaSO_4 \cdot 2H_2O$	35	35min	1h20min	even	11,2	20,2	
8% "	35	1h40min	3h40min	even	10,3	22,9	143
10% "	38	2h	3h10min	even	12,2	22,0	
12% "	32	2h	3h	even	7,3	15,1	
1% $CaSO_4 \cdot 0,5H_2O$	35	15min	25min	uneven	12,6	25,1	167
2% "	34	20min	45min	even	12,6	23,3	
3% "	35,8	1h25min	2h20min	even	7,6	21,3	
5% $CaSO_4$	34	40min	2h	uneven	14,9	27,1	172
8% "	34	1h30min	2h35min	even	12,1	20,2	
10% "	32	1h35min	3h15min	even	6,1	14,4	

It is stated that the fast hydration of the calcium aluminate ($CaO \cdot Al_2O_3$) is the factor which causes the quick setting of dolomitic romancement. The free lime activates this process. The way to avoid the influence of calcium aluminate and free lime is wetting and storage of fired dolomitic material in moist atmosphere before milling as well as using special additive. These procedures avoid also uneven volume change caused by overburned MgO, but simultaneously reduces the mechanical strength of dolomitic romancement. To improve the mechanical strength various additives are used. The most suitable additives and optima concentration of them are established. However the mechanism of interaction between additives and main phases of dolomitic romancement is not clear. It is proposed that up to optima concentration of

additives the chemical interaction between additives and active phases of romancement take place. But above the optima concentration additives are as aggregates and in some extant even hinder the chemical processes. It results in reducing the bonded water and mechanical strength of dolomitic romancement.

REFERENCES

Grosvalds, I., Lagzdiņa, S., Sedmalis, U., "Dolomitic romancement with improved properties", Proceedings of the 4th International Conference "Modern Building Materials Structure and Properties", May 14-17 1995, Vilnius, Lithuania, Ed. Technic, pp. 13-17.

Kn o. 25. JAN. 2001 d o k 51773 2ii010 6 pp

THEORETICAL FUNDAMENTALS OF THE APPLICATION OF EXPANSIVE CEMENT CONCRETES

Jochen Stark, Institute of Building Materials at the University Weimar, Germany
Igor Chartschenko, Institute of Building Materials at the University Weimar,Germany

ABSTRACT. The greatest stability of properties is found in expansive cements made on the basis of calcium aluminate sulphate and/or the formation of ettringite. The factors influencing the properties of ettringite-forming expansive cements are represented in a phenomenological model. The factors influencing the properties and the process of expansion are analysed.

Key-words: Expansive cement, ettringite, calcium aluminate sulphate

INTRODUCTION

Nowadays all the types of expansive cement that are suitable for industrial use cocsist of a matrix-forming binder and swelling components. Most of the expansive cements used in the building trade are based on ettringite, i.e. in addition to various types of Portland cement they also include additives containing calcium aluminosulphates as swelling components. The volume change which can be achieved when an expansive cement hardens depends to a great extent on the kinetic harmonization of these two processes which actualy operate in opposite directions. The swelling process depends on the quantity of the etrimgite, ist morphologiy, and the nature of ist formation, i.e. whether it crystallizes in the solution or on the surface of particles. The swelling potential can also be altered by changes in the ratio between the Portland cement matrix and the swelling component, as well as by the addition of various additives which have a specific effect on the ionoc content of the reaction solution.

Phenomenological model of expansive cements

Practical experience shows that the greatest stability of properties is found in expansive cements made on the basis of calcium aluminate sulphate and/or the formation of ettringite. The properties, i.e. first of all the process of expansion, which may be represented in the form of a tree ("expansive cement tree") (Fig. 1), depend on "external" and "internal" factors of influence. By the influence of these factors on the mechanism of ettringite formation, on the morphology of ettringite phase, on the amount of ettringite phase formed, on the kinetics of ettringite formation and on the properties of the portland cement matrix, which is called the fifth root of the expansive cement tree, the process of the formation of microstructure during the hardening of expansive cement can be controlled. The "external" factors of influence are temperature (sun), moisture (rain or drying-out) and the extent of impediment to the expansion process.

The "internal" factors of influence are, first of all, the hydraulic activity of the Portland cement portion, the expansive components and the additives which determine the content of ions in the reaction solution in the process of hydration. In addition, there are, of course, the water-cement ratio and the additives which enable the desired coordination between the hardening of the Portland cement matrix and the formation of ettringite to be achieved. The desired properties of expansive cements and a control of the expansion process in time and space can only be achieved if the processes which all five "roots" have to go through under the "external" and "internal" factors of influence are under control. As in nature, it is difficult to decide which root is the most important for the life of the tree and the quality of the fruit (in this case the properties of expansive cements). All of them make a different but equally important contribution.

Hydration and formation of the microstructure in expansive cements under the influence of "internal" factors

The physical-mechanical characteristics of expansive cements and expansive cement concretes are closely correlated with the relationship between the speed of hardening of the expansive cement matrix (= Portland cement portion) and the speed of ettringite formation in the first 3 to 5days of hardening and/or with the active formation of the microstructure of the hydrated cement. This may, for instance, be achieved by deliberately changing the fineness of both components of the expansive cement, i.e. the expansive cement matrix and the expansive component (Cohen and Richardts, 1982).

According to several authors (Cohen and Richardts, 1982; Kusnezova, 1986; Clastres et al, 1984; Deng and Tang, 1994; Ludvig; 1991) and our own test results (Chartschenko et al, 1994; Chartschenko and Stark, 1993a and 1993b; Chartschenko, 1994) there is no universally valid relationship between the amount of ettringite formed and the amount of expansion. An interdependence does only exist if the quality of all components of expansive cement is constant and the external conditions do not change (Kusnezova, 1986).

By changing the concentration of ions and particularly the OH-content in the reaction solution it is possible to exert an active and deliberate influence on the crystallization of ettringite and the formation of a certain type of crystal (Cohen and Richardts, 1982). Practically, by means of the properly adjusted pH-value during the initial hardening of expansive cements the morphological formation of ettringite and thus the formation of the microstructure of the hydrated cement may be controlled.

Our investigations have shown that different mineral additives to high-alumina/gypsum expansive cement (TG-QZ) can influence the ion-content and particularly the content of OH-ions in the reaction solution and in this way also the kinetics of ettringite formation, the morphology of ettringite and finally the properties of expansive cement. The expansive cement was produced by homogenizing a mixture of high alumina cement and ground gypsum in the stoichiometric relationship of the ettringite for 60 minutes. Mineral additives were silica powder (SF), ground opal (O) as natural puzzolanic component, siliceous chalk (K) burnt at 1000°C and ground, pure calcium hydroxide (CH) and ground silica sand.

Our investigations have shown that depending on the type of mineral additives the pH-value of the pore solution of high alumina/gypsum expansive cement (TG-QZ) differed greatly in the first 24 hours after mixing had begun (addition of mixing water) (Fig. 2).

Particularly interesting are the properties of TG-QZ with calcium hydroxide (CH) and siliceous chalk (K). These additives showed an very great difference between amount of expansion and compressive strength (Fig. 3 and 4). Although just after mixing the pH-value was nearly the same, it decreased from 12.5 to 9.7 within the first six minutes when burnt siliceous chalk was used and then remained constant for up to 72 hours. The analysis of the products of hydration showed that ettringite was formed at the same speed and after three days amounted to about 85%. In TG-QZ with calcium hydroxide the pH-value remained practically constant for the first ten minutes and decreased to 9.6 in the following 10 minutes. After a period of stabilisation on this level in the following 7 hours the pH-value increased to 12.3 and remained constant for 28 days. The formation of ettringite amounted to 70% after 24 hours and after 48 hours had achieved 90% of the final value.

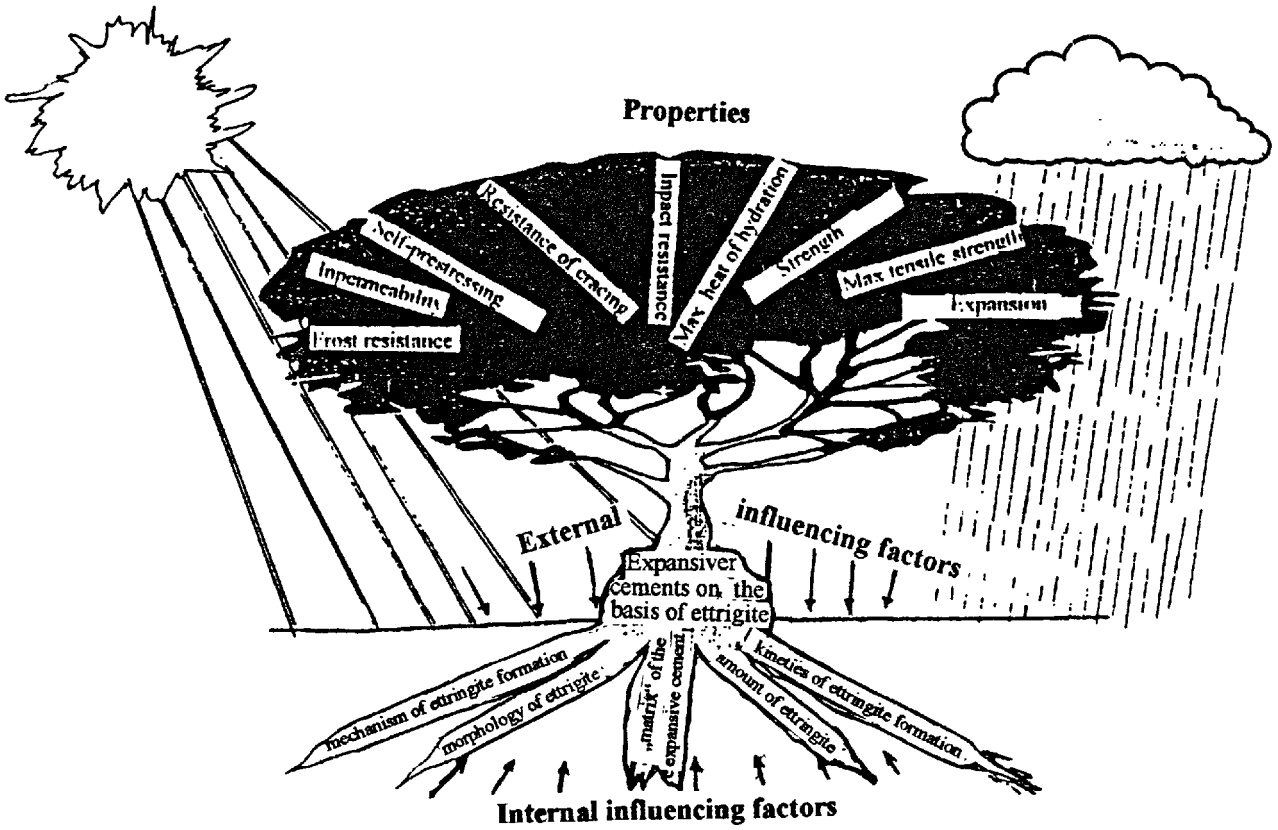

Figure 1: Expansive cement „tree"

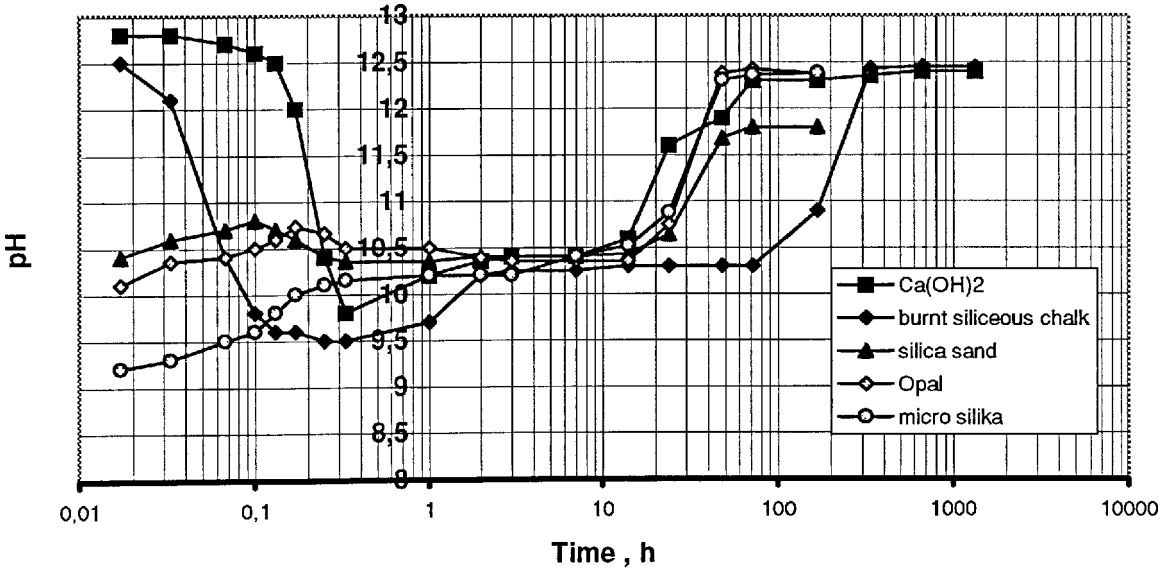

Figure 2: Changes in pH-value during the hydratation of high alumina/gypsum expansive cement with different mineral additives

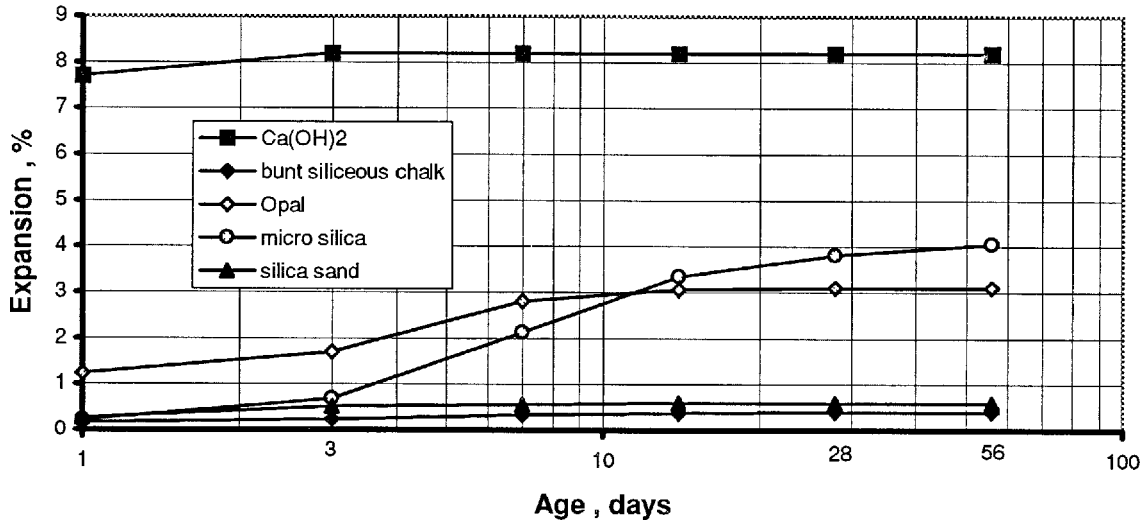

Figure 3: Amount of expansion of high alumina/gypsum expansive cement with different mineral additives

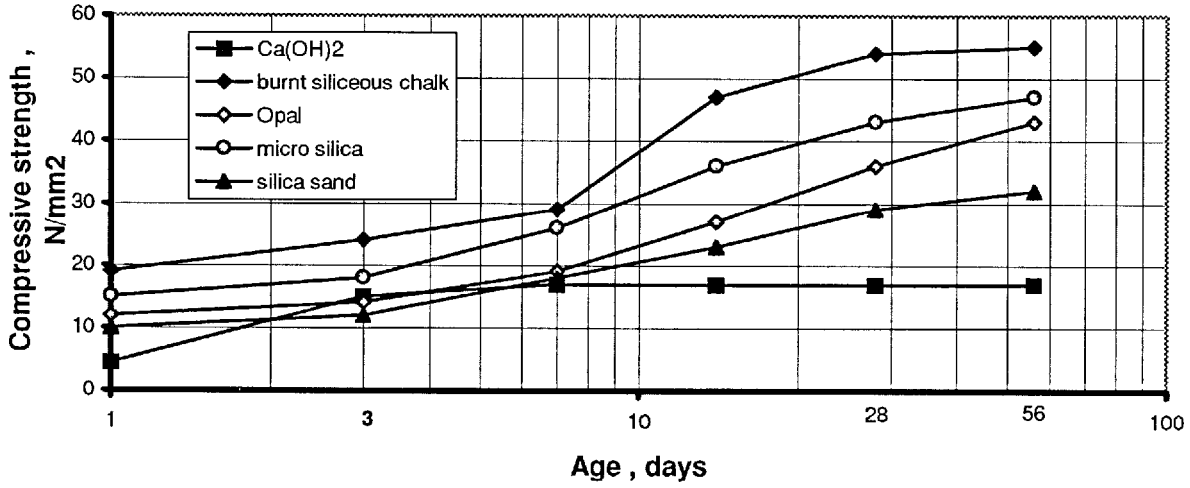

Figure 4: Compressive strength of high alumina/gypsum expansive cement with different mineral additives

The interspace between the separating layer and the unhydrated clinker minerals becomes too small and the ettringite shell is destroyed. After the destruction of the ettringite shell around the clinker mineral particles the process of hydration is continued as can be seen from the strong increase of the pH-value (Fig. 2). After this period a highly active expansion process with an increase in volume by more than 8% can be observed (Fig. 4).

The hydration process of TG-QZ with burnt siliceous chalk (K) as an additive, its kinetics of ettringite formation, process of expansion, and other properties of the hydrated cement differ greatly from the preceding descriptions, although the pH-value in the first minute was nearly the same. The phase analysis of siliceous chalk after burning at 1000°C showed that this additive contained calcium oxide as well as calcium silicate of a low basicity. Each component had a specific influence on the kinetics of the ettringite crystallization, its morphology and finally on the properties of the expansive cement. In the first two minutes the hydration process of TG-QZ is similar to that of the above mentioned expansive cement with calcium hydroxide. The higher pH-value of 12.3 is due to the calcium oxide content in the burnt siliceous chalk. It may be considered to be the cause of the increased solubility of the calcium aluminates just after mixing and of the formation of the separating layer of fine crystalline ettringite on the surface of unhydrated cement clinker particles. Burnt siliceous chalk contains only a relatively small amount of calcium oxide or calcium hydroxide after mixing with water and these amounts are quickly neutralised by calcium aluminate. Therefore, only a rather thin layer of ettringite crystals is developed whose strength and density are lower than in the case of pure calcium hydroxide. After a reaction time of about 60 minutes the pH-value increases from 9.4 to 10.3 which may be considered a consequence of the destruction of the ettringite layers. The phase analysis in this period showed an increase in ettringite content and proportionally a decrease in gypsum content in the hydrated cement. Due to the difference in concentration of hydration products below the separating layer and beyond it ettringite nuclei "dart" at a high speed deeply into the capillary pore space near the cement particles where they crystallize. First studies into the formation of ettringite under an environmental scanning electron microscope confirm that in the presence of reacting agents ettringite forms suddenly and not as previously assumed by slow growth of the crystals.

The ettringite nuclei play the role of a crystallization centre, i.e. as the nucleus of the crystallization of the primary ettringite. Microscopic examinations showed that in the further course of hydration single clusters of ettringite developed independently and without any connection to each other. It may be concluded that in this case the crystallization pressure of the hair-shaped ettringite does not contribute to the increase in volume of the cement paste and rather plays the role of a fibre reinforcement for the gel-like hydrates.

The consequence of these stresses is an increase in volume of up to 0.25% during the hardening of the expansive cements in the first three days, the formation of fine crystalline hair-shaped ettringite which crystallises under the influence of the low pH-value of 10.2, and at the same time the development of pressure. These results confirm that the amount of expansion is not only determined by the amount of ettringite formed but that the morphology of ettringite, which depends on the pH-value, also plays an important role.

ACKNOWLEDGEMENTS
The autors gratefully acknowledge the help and financial support by the Alexander von Humboldt Foundation.

REFERENCES

Cohen, M.D. and Richartds, C.W. : „Effects of the Particle Size of Expansive Clinker on Strength expansion characteristics of Type K Expansive Cement", Cem. Concr. Res., V.12,1982, pp. 717-725

Kusnezova, T.V.: „Physikalisch-chemische Grundlagen zur Technologie von Quellzementen", Moscow, NIIZement, V.38, 1986, pp.77-84

Clastres, P.; Murat, M.; Bachiorini, A.: „Hydratation of expansive cement correlation between expansion and formation of hydrates", Cem.Concr.Res., V.14, 1984, pp. 199-206

Deng Min & Tang Migshu : „Formation and Expansion of Ettringite Crystals", Cem. Concr. Res., V.24,1994, pp.119 - 126

Ludvig, U. : „Probleme der Ettringitrückbildung bei wärmebehandelten Mörteln und Betonen", 11. Intern. Baustoff- und Silikattagung, Weimar, 1991, pp. 164 - 175

Chartschenko, I.; Gathemann, B.; Stark, J.: „Injektionsmörtel mit Quelleffekt zur Sanierung von historischen Bauwerken", 12. Intern. Baustofftagung, ibausil , Weimar, 22-24. Sept. 1994, 1, pp. 12 - 17

Chartschenko, I. & Stark, J.: „Steuerung des Strukturbildungsprozesses bei Quellzementen sowie Betonen auf deren Basis", Wiss. Zeitschr. Hochsch. Arch. Bauwesen Weimar, 39/3, 1993, pp. 163-171

Chartschenko , I. & Stark, J. :"Untersuchungen über den Einfluß des pH-Wertes auf die Ettringitbildung", Wiss. Z. Hochsch. Arch. Bauwes., 39, 1993, pp. 171 - 177

Chartschenko , I.: „Theoretische Grundlagen zur Anwendung von Quellzementen in der Baupraxis", Habilitation, Weimar, Deutschland, 1995, pp. 201

Kn o. 2 5. JAN. 2001 d o k 31774

2ii01
10 p

SULFATE SOLUBILITY IN HIGH SO_3 CLINKERS

V. MICHAUD & R. SUDERMAN,
LAFARGE CANADA INC., Corporate Technical Services, Montreal, Quebec, Canada

ABSTRACT Changes in the cement manufacturing process such as the use of higher sulfur fuels have tended to raise clinker sulfate levels and SO_3/alkali ratios. As a consequence, interground gypsum additions to cement have dropped because more sulfate is available from the clinker. Also, these clinker sulfates tend to be available as double sulfate salts; calcium langbeinite instead of potassium sulfate.
What is the impact of clinkers with high SO_3 level on concrete performance; mainly on its workability and durability ? The aim of this study is to provide some answers to this question.
Calcium langbeinite is rapidly dissolved. Because of its dissolution rate and ability to form "blocking ettringite", high calcium langbeinite clinkers should provide improved rheological properties. Moreover, cements made with clinkers containing significant quantities of calcium langbeinite should have a similar workability and durability to a cement made with a low sulfate clinker to which larger quantities of gypsum have been added.
The dissolution rate of anhydrite potentially existing in very high SO_3/alkali clinker has also been simulated. Experiments indicate that it dissolves and reacts quite quickly so that it should not provide any durability problem if present in cement and concrete.

KEY-WORDS : high SO_3 clinker, clinker anhydrite, calcium langbeinite, workability, rheology, durability.

INTRODUCTION

Changes in the cement manufacturing process such as the use of higher sulfur fuels, reduced dust wasting and lower SO_x emissions have tended to raise clinker sulfate levels and SO_3/alkali ratios. As two of the direct consequences :

- interground gypsum additions to cement have dropped because more sulfate is available from the clinker,
- calcium langbeinite ($Ca_2K_2(SO_4)_3$) is present as the predominant clinker sulfate phase, instead of arcanite (K_2SO_4) and aphthitalite ($K_3Na(SO_4)_2$) for low SO_3/alkali clinker.

Very few studies have been done on the impact of high SO_3 level clinkers on concrete performance. The aim of this study is to shed some light; mainly on its workability and durability.

Sulfate ions play an important role on concrete performance at short term ; namely its workability. According to the nature of the sulfate phases, they will have different dissolution rates and solubilities. If they provide sufficient quantities of calcium and sulfate ions to the solution, they contribute to the formation of the hydrated calcium sulphoaluminate layer at the surface of the C_3A and, for a period of time, "block" further aluminate hydration. If the sulfate and calcium ions are less readily soluble,

C_3A hydration is not slowed, and hydrated calcium aluminate phases and ettringite are formed in the solution away from the surface of the C_3A particle. Because of their morphologies, if these phases are present in sufficient quantities, they adversely affect concrete rheology.
When cement is prepared from clinker with a low SO_3/alkali ratio, the sulfate phases; alkali sulfate, gypsum and hemihydrate, have a good efficiency in slowing C_3A hydration. The hemihydrate, by providing a much higher quantity of calcium and sulfate ions into solution than the gypsum, contributes the most to blocking C_3A hydration.
It is known that calcium langbeinite dissolves quite rapidly but its rate has not been determined in relation to the early hydration reactions. Because calcium langbeinite is present in clinkers with high SO_3/alkali ratios, which could require little or no interground gypsum addition, it will be determined if this phase can be dissolved rapidly enough to slow C_3A hydration.

It has recently been suggested that high SO_3 clinker could contain anhydrite (Mielenz et al., 1995) and that it would dissolve particularly slowly because of the high temperature of clinkerization. They alleged that it would continue liberating sulfate ions into the solution for a long period, forming ettringite, and therefore would have a negative effect on concrete durability.
Clinker anhydrite is certainly not common. Up to now it has never been detected even in modern industrial clinkers with a relatively high SO_3 level (Miller, 1996). Therefore, it might only be present in clinkers with extremely high sulfate amounts.
This study will examine the dissolution rate of anhydrite potentially existing in clinker as it could impact on concrete durability.

DISSOLUTION RATE OF CALCIUM LANGBEINITE AND DETERMINATION OF ITS EFFICIENCY TO BLOCK C_3A HYDRATION.

High SO_3 clinker containing calcium langbeinite has been simulated by pure phase materials and hydrated without any addition of calcium sulfate up to one hour. Solid and liquid phase evolution with time have been followed.
The pure clinker phase materials used are the ones implicated in early hydration; calcium langbeinite, C_3A and $Ca(OH)_2$. The calcium hydroxide represents clinker free lime which provides a source of calcium and hydroxide ions for short term hydration, soon after water is added.

Two different initial quantities of calcium langbeinite were used. The amount of water added was calculated to be equivalent to clinkers containing :

- 0.74% K_2O and 2.1% SO_3,
- or 1.18 % K_2O and 3.36 % SO_3, respectively

hydrated at a water/cement ratio of 0.35.

Experimental conditions

Calcium langbeinite (either 0.223 or 0.357 mole per liter) , C_3A (0.185 moles per liter) and $Ca(OH)_2$ (0.675 moles per liter) were stirred at 23°C with water for various times between 5 seconds to 1 hour.
At selected time intervals after water addition, the liquid and solid phases were separated by filtering. The solid phases, after being washed with acetone and ether,

were analyzed by X.R.D. The solution concentrations were measured by atomic absorption spectroscopy for calcium and potassium, by turbidimetry for sulfate and by titration with a 0.05 N HCl solution in the presence of helianthine indicator for the hydroxide ions.

The calcium langbeinite was synthesized by heating an inter-ground mixture of arcanite and gypsum in the stoechiometric proportions of calcium langbeinite in a closed container at 800°C for 48 hours.

Dissolution rate of calcium langbeinite

For the two initial quantities of calcium langbeinite, the changes in the solution concentration with time are shown in Fig 1 (Fig 1(a) is an enlargement of Fig 1(b)).

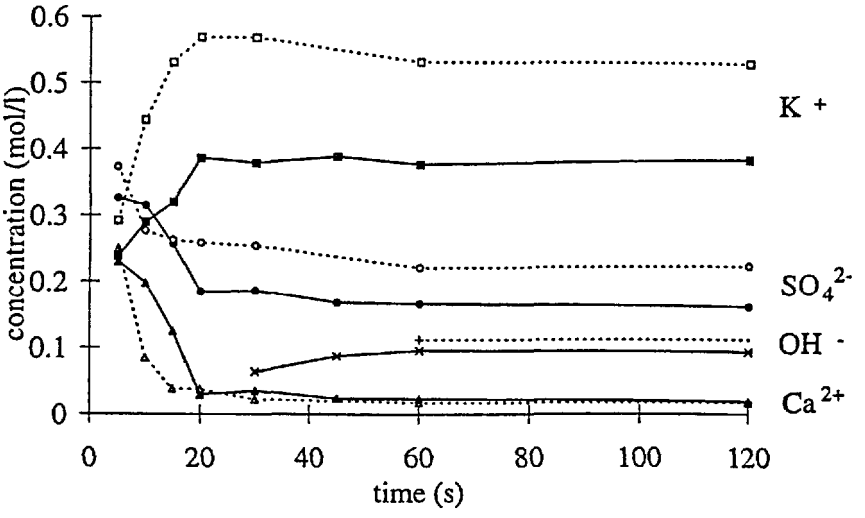

Figure 1a

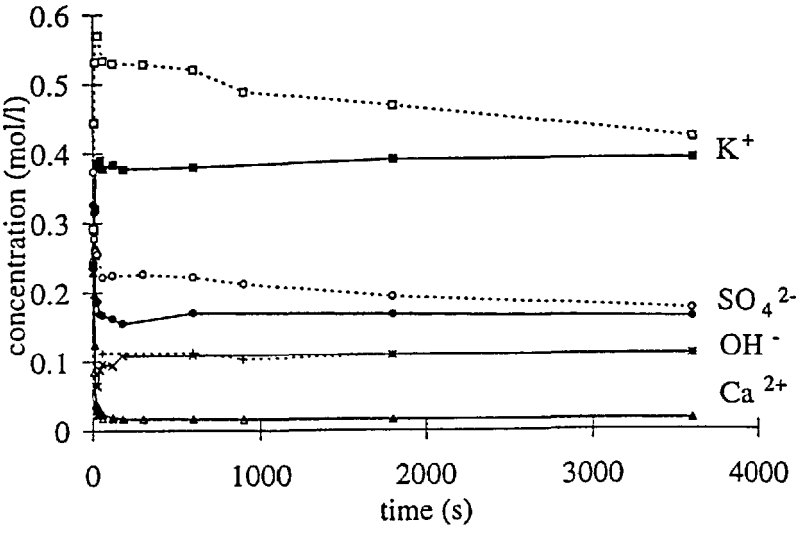

Figure 1b

Figure 1 Evolution of the ions in solution for mixtures of calcium langbeinite, C_3A and $Ca(OH)_2$. The dotted lines represent an equivalent clinker SO_3 of 2.1% and the solid lines a clinker SO_3 of 3.36% hydrated at a water/solids ratio of 0.35.

From these results and the XRD analysis of the residual solid phases, the calcium langbeinite reacts very rapidly. It is mostly dissolved after 5 seconds and totally after 20 seconds. Its dissolution initially liberates a very high quantity of calcium, sulfate and potassium ions into the solution.

How does the system evolve once the solution is very concentrated in calcium, sulfate and potassium ions ? The solution is supersaturated with respect to gypsum for the two amounts of calcium langbeinite and to syngenite only for the higher initial amount of calcium langbeinite. These phases precipitate consuming calcium, sulfate and potassium ions. Whatever the initial quantity of calcium langbeinite, gypsum begins to precipitate as soon as 10 seconds of hydration, and its quantity increases up to 30 seconds of hydration. With the higher initial quantity of calcium langbeinite, syngenite is also precipitated after 30 seconds and its quantity increases up to 1 hour.
The calcium and sulfate ions also react with aluminate ions provided by C_3A to form ettringite. This latter phase can be detected by X.R.D. after 3 minutes of hydration.
However, after one hour, only a very minor quantity of C_3A has reacted.

As shown on Fig 1(a), the solutions for the two initial quantities of calcium langbeinite tends towards the same composition ($[K^+]$=0.385 mol/kg, $[Ca^{2+}]$= 0.0153 mol/kg, $[SO_4^{2-}]$= 0.155 mol/kg, $[OH^-]$=0.11 mol/kg), determined by the phases in thermodynamic equilibrium with the solution; ettringite, gypsum, syngenite and portlandite.

The almost instantaneously dissolution of the calcium langbeinite liberates a very high quantity of calcium and sulfate ions into the solution. This condition, in conjunction w-ith the small amount of C_3A that had reacted after 1 hour indicates that calcium langbeinite can form a "blocking" ettringite layer around the C_3A.

Is the calcium langbeinite as efficient as the sulfate phases in a cement composed of low SO_3 clinker, arcanite, gypsum, and hemihydrate in blocking C_3A hydration ?

To compare the ability of calcium langbeinite in blocking C_3A hydration with either potassium sulfate and gypsum or hemihydrate, the same experiments were performed using blends of potassium sulfate and gypsum, or potassium sulfate and hemihydrate, instead of calcium langbeinite. Relative quantities of K_2O, SO_3, C_3A, calcium hydroxide and water have been maintained identical to the ones for the simulated clinker with an equivalent SO_3 of 2.1%.
The gypsum used was an industrial grade product with 97 % purity. The hemihydrate was prepared by heating the gypsum at 100°C for 14 hours.

The changes in solution with time for the mixture containing potassium sulfate and gypsum are compared with the ones containing calcium langbeinite and are shown in Fig 2.

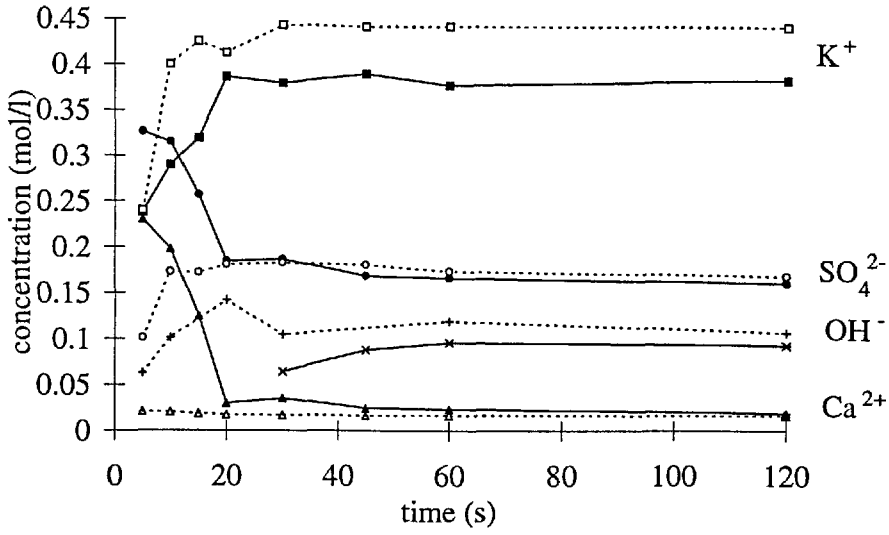

Figure 2 Comparison of the evolution of the ions in solution for mixtures containing either calcium langbeinite or potassium sulfate and gypsum. C_3A and $Ca(OH)_2$ are also present. The dotted lines represent potassium sulfate and gypsum. The solid lines represent calcium langbeinite. The initial sulfate quantity in both cases is equivalent to a clinker with 2.1% SO_3.

From these results and the XRD analysis of the residual solid phases, the mixtures initially composed of either calcium langbeinite, or arcanite and gypsum :

- have a different behaviour for the first 20 seconds of the hydration. At 5 seconds, the sulfate and calcium ions concentrations of the calcium langbeinite mixture is much higher than of the potassium sulfate and gypsum mixture; 0.32 mol/l versus 0.10 mol/l for the sulfate and 0.23 mol/l versus 0.021 mol/l for the calcium ions.
- have a similar behaviour after 20 seconds of hydration. They contain the same solid phases; gypsum, portlandite and also ettringite detected after 3 minutes of hydration. The ionic concentrations are virtually identical and governed by the solid phases in equilibrium with the solution.
  Syngenite is also present in a very minor amount after one hour for the mixture initially conposed of arcanite and gypsum.
  The only difference is the lower potassium concentration for the mixture initially composed of calcium langbeinite; a consequence of the stoichiometry of the calcium langbeinite used here. Its $K_2SO_4/CaSO_4$ ratio is slightly less than 0.5.

Therefore, the calcium langbeinite is at least as efficient as potassium sulfate and gypsum in slowing C_3A hydration.

The changes in the solution concentrations with time for the mixture containing potassium sulfate and hemihydrate are compared with the ones containing calcium langbeinite and are shown in Fig 3. (Fig 3(b) is an enlargement of Fig 3(a)).

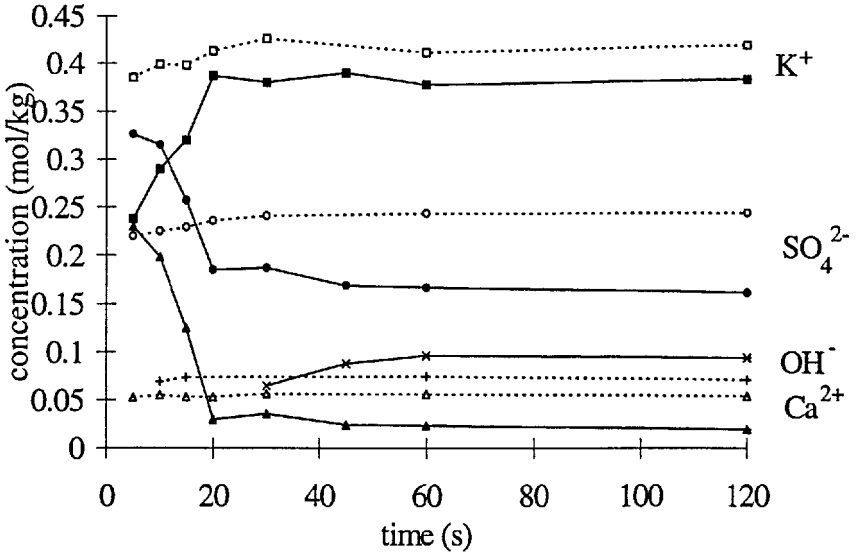

Figure 3a

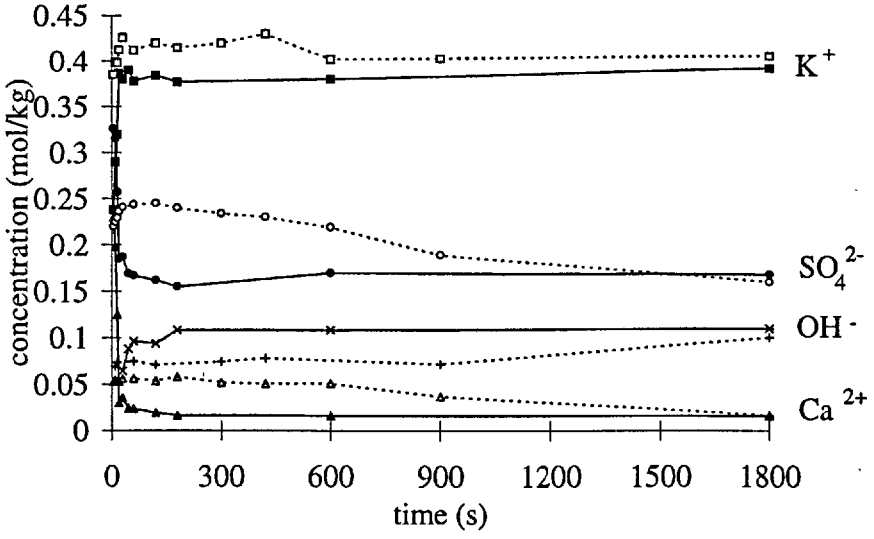

Figure 3b

Figure 3 Comparison of the evolution of the ions in solution for mixtures containing either calcium langbeinite or potassium sulfate and hemihydrate. C_3A and $Ca(OH)_2$ are also present. The dotted lines represent potassium sulfate and hemihydrate. The solid lines represent calcium langbeinite. The initial sulfate quantity in both cases is equivalent to a clinker with 2.1% SO_3.

For the first 15 minutes, the concentrations of calcium, sulfate and hydroxide ions in solution are different for the two mixtures. For the first seconds, due to the instantaneous dissolution of calcium langbeinite, the mixture initially containing this

phase exhibits higher calcium and sulfate ion concentrations than the hemihydrate and potassium sulfate mixture. After 15-20 seconds, the reverse is true and the hemihydrate mixture provides higher calcium and sulfate ion concentrations. This results from the presence of residual hemihydrate in this mixture for the first 5 minutes. The calcium and sulfate concentrations in solution are at that time determined by its solubility. Then the quantity of hemihydrate decreases until it is not detectable after 10 minutes. At the same time, after 5 minutes, gypsum begins to precipitate and its quantity increases up to 30 minutes. This is accompanied by a decreasing of the sulfate and calcium concentrations and an increasing of the hydroxide ion concentration. The concentrations tend towards those of the mixture of calcium langbeinite. Ettringite begins to be detected by XRD after 3 minutes of hydration.
After 30 minutes of hydration, the mixtures initially containing either calcium langbeinite or arcanite and hemihydrate, have identical behaviors. The ion concentrations and the solid phases are nearly similar; gypsum, portlandite and ettringite. At that time, the solution is virtually in equilibrium with the solid phases. A small amount of syngenite is also detected after one hour in the arcanite and hemihydrate mixture.

From these results, it is difficult to determine if the calcium langbeinite is as effective in slowing C_3A hydration as potassium sulfate and hemihydrate. For the first few seconds calcium langbeinite provides the solution with more calcium and sulfate ions however after 20 seconds the situation reverses.

THE DISSOLUTION RATE OF ANHYDRITE.

In this part of the study, the dissolution rate of anhydrite potentially existing in very high SO_3/alkali clinker was studied by hydrating model systems simulating clinker containing anhydrite.
For comparison and to predict the influence of clinker anhydrite on concrete durability, a mixture with a similar chemical composition but containing gypsum instead of clinker anhydrite has also been examined.

Clinker and cement have been simulated using pure phase materials; C_3A, $Ca(OH)_2$, calcium langbeinite and anhydrite or gypsum. Since anhydrite may only be found in clinker with a very high SO_3 / alkali ratio in conjunction with calcium langbeinite, the mixtures used here contain both.
Clinkerisation temperatures of 1400°C are typical and the burning zone residence time is 10 - 20 minutes. Thus in order to synthesize anhydrite similar to that which could be present in clinker, it was produced from gypsum burned at 1400°C for 2 hours. For comparison, dissolution rates of natural anhydrite and anhydrite synthesized from gypsum burned at 500°C have also been determined.

Experimental conditions

Mixtures containing C_3A (0.875 moles per liter), portlandite (1.0135 moles per liter), calcium langbeinite (0.223 mole per liter) and either anhydrite or gypsum for comparison (0.335 moles per liter), were stirred at 23°C for various times between 2 hours and 16 days. These amounts correspond to a clinker or cement which contains 0.74% K_2O, 2.81% SO_3 and 3.12% Al_2O_3, hydrated at a water / solids ratio of 0.35.

The solid phases were examined by XRD. The ionic concentrations were measured for the first 5 days.

Results and interpretation

Fig 4 indicates that the 1400°C anhydrite dissolves at the same rate as natural anhydrite. It has totally reacted at 4 days. The 500°C anhydrite dissolves much faster.

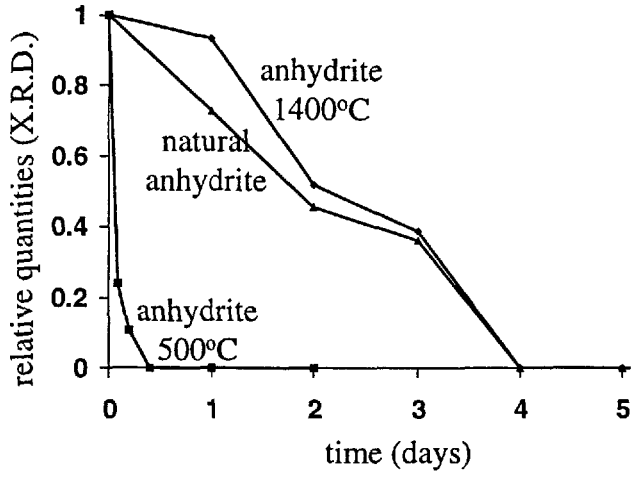

Figure 4 Evolution of the anhydrite amount for mixtures containing either 1400°C, 500°C or natural anhydrite. Calcium langbeinite, C_3A and $Ca(OH)_2$ are also present.

The changes with time of the amounts of the various solid phases present in the hydrating mixtures containing calcium langbeinite and gypsum are shown in Fig 5. They have been determined from XRD analysis.

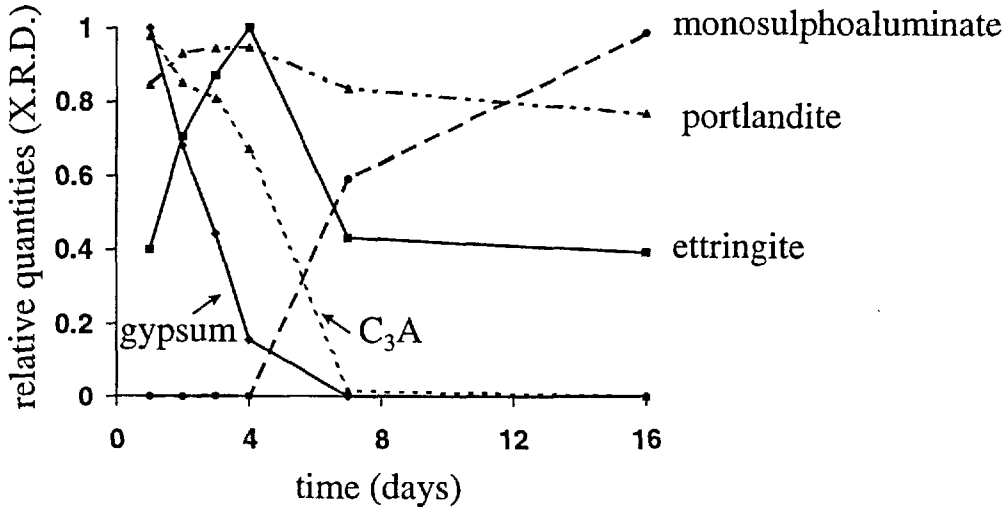

Figure 5 Evolution of the various solid phases quantities with time for the mixture of gypsum, calcium langbeinite, C_3A and $Ca(OH)_2$.

Secondary gypsum is precipitated from calcium langbeinite within a few minutes of the start of hydration. The solid residue at that time is composed of gypsum, ettringite, portlandite, a very little quantity of syngenite and residual C_3A. C_3A is converted to ettringite while significant quantities of gypsum are present. For this period, the solution concentrations remain constant regulated by the solid phases in

equilibrium with the solution; $[K^+]$=0.385 mol/kg, $[Ca^{2+}]$= 0.0153 mol/kg, $[SO_4^{2-}]$= 0.155 mol/kg, $[OH^-]$=0.11 mol/kg.
After 5-6 days, when the gypsum amount is negligible, the amount of ettringite begins to deplete as the remaining calcium and aluminate reacts with ettringite to form monosulfoaluminate.

This study has been carried out without calcium silicates. However, even if C-S-H were present, the equilibria should not be appreciably different. A thermodynamic calculation from ionic activities, by using the method by Pitzer and Mayorga (1973) has shown that the C-S-H phase is in equilibrium with the hydrated phases present in the first 5 days; ettringite, gypsum, syngenite and portlandite and its presence does not affect the concentrations in solution.

The evolution with time of the amounts of the various solid phases present in the hydrating mixtures containing calcium langbeinite and either 1400°C anhydrite or gypsum are compared in Fig 6. They have also been determined from XRD analysis.

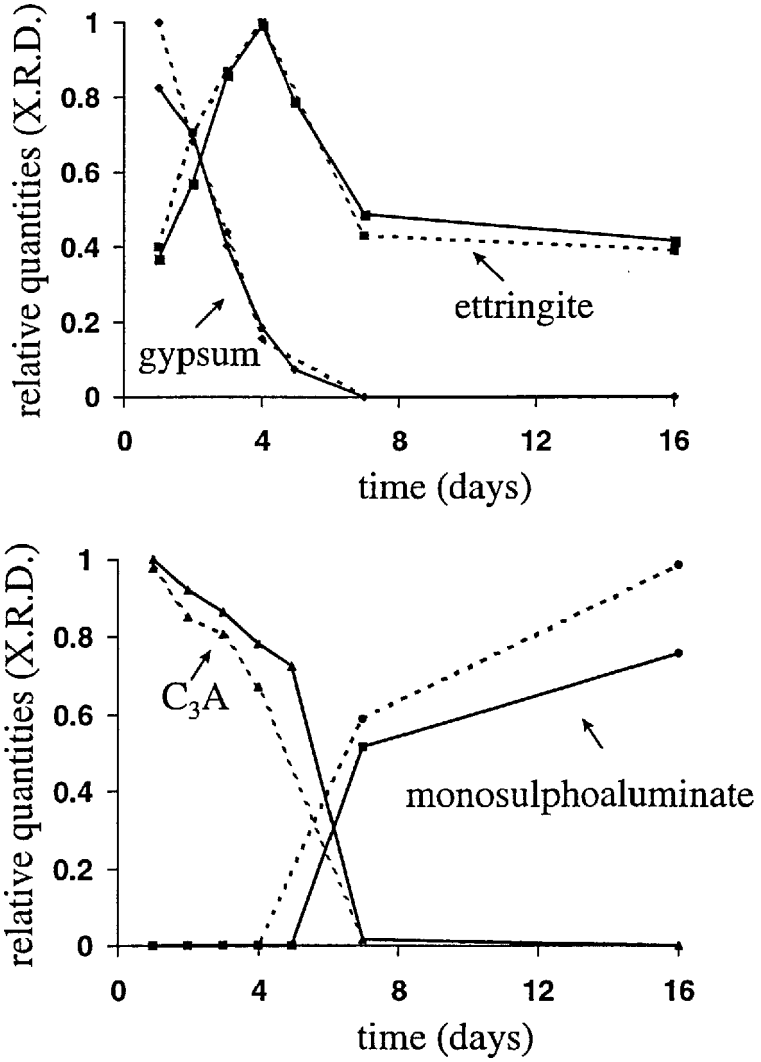

Figure 6 Comparison of the evolution of the various solid phases quantities with time for the mixture containing calcium langbeinite and either gypsum or 1400°C anhydrite. C_3A and $Ca(OH)_2$ are also present. The dotted lines represent gypsum. The solid lines represent 1400°C anhydrite.

Fig 6 shows that the two mixtures have a similar evolution of the hydrated phase amounts with time. It is also true for the portlandite, not shown here. Also, the anhydrite is gone before the remaining C_3A reacts with ettringite to form monosulfoaluminate. Therefore, the presence of anhydrite in the clinker should not affect the durability of the cement paste.

CONCLUSIONS

The present study shows that calcium langbeinite, one of the sulfate forms found in clinkers with high SO_3 level and SO_3/alkali ratio, is rapidly soluble. Cements made with clinkers containing significant quantities of calcium langbeinite even without addition of any calcium sulfate, should have similar performances at short and long term to a cement made of a low sulfate clinker to which large quantities of gypsum have been added.

As for anhydrite, the study indicates that even if it is burned at 1400°C for 2 hours, it has a relatively high dissolution rate. If present in clinker, it should not adversely affect the durability of concrete.

This study also provides indications of the maximum content of potassium in cement to avoid syngenite precipitation and associated false set. For a cement containing only potassium as alkalis, this phase will precipitate if the concentration of potassium in the pore solution is higher than 0.39 mole per liter. In a hydrating cement system with a w/c ratio of 0.5, this corresponds to an available K_2O content of 0.93%.

REFERENCES

Mielenz, R.C., Marusin, S.L., Hime, W.G., Jugovic, Z.T., "Investigation of Prestressed Concrete Railway Tie Distress", Concrete International, pp. 62-68 (dec. 95)

Miller, F.M. and Tang, F.J., "The Distribution of Sulfur in Present-Day Clinkers of Variable Sulfur Content", Cement and Concrete Research, 26, 12, pp. 1821-1829 (1996)

Pitzer, K.S. and Mayorga, G., "Thermodynamics of electrolytes. II. Activity and osmotic coefficients for strong electrolytes with one or both ions univalent ". The Journal of Physical Chemistry, 77, pp. 2300-2308 (1973)

Kn o. 2 5. JAN. 2001 d o k 31775

2ii012
8 pp

EFFECT OF ALKALI SULFATES ON CEMENT HYDRATION AT LOW AND HIGH WATER - CEMENT RATIOS

Arezki TAGNIT-HAMOU and Salaheddine BOURAOUI

Faculty of Applied Sciences, Université de Sherbrooke, Sherbrooke (Québec) CANADA

ABSTRACT The optimum SO_3 content in cement is determined by the required setting time and compressive strength, as well as rheological properties and expansion of the paste. Part of the SO_3 found in cement is provided by alkali sulfates. In this study, three differents clinkers having high and low C_3A contents were investigated with different forms of alkali sulfates and/or calcium sulfates. Test results indicate that the sulfate form has an important effect on the slump of cement paste. This slump is negatively affected by the presence of arcanite or aphthitalite but improved by calcium langbeinite . Mortars made with gypsum addition give the best compressive strength at 28 days. The action of the superplasticizer is affected by alkalis from alkali sulfate.

Key-words: Admixtures, alkali, fluidity, hydration, sulfate.

INTRODUCTION

Cement hydration is a complex phenomenon. The effect of the major phases of portland cement have been reviewed extensively by various researchers. The effect of minor elements has however been less studied and can lead to different interpretations. The addition of different forms of calcium sulfates (gypsum, hemihydrate or anhydrite) to the clinker controls the hydration of C_3A. This hydration is controlled by providing SO_4^{2-} and Ca^{2+} ions to the solution to precipitate ettringite ($C_3A.3CaSO_432H_2O$). The influence of calcium sulfate on rheological characteristics of cement paste is not only dependant on the calcium sulfate content, but also on its solubility (Tang and Tresouthick, 1992). The faster the SO_4^{2-} ions go into the solution, the better the workability and its retention can be.

Sulfate ions in paste solution are not provided only by adding calcium sulfates, but also by the alkali sulfates of the clinker . These alkali sulfates are very soluble (more than any added calcium sulfate) (Bensted, 1983). Depending on its form, the alkali sulfate provides different alkalis (K^+, Na^+) or calcium ions (Ca^{2+}) to the solution. The alkalis are known as activating agents for the cement hydration.

In low W/C ratio concretes, the control of rheological properties is critical because of the low water content and the need to use superplasticizer. The interaction between C_3A, sulfates and alkalis is complicated by superplasticizer addition (Tagnit-Hamou and Aïtcin, 1993).

In this paper, results on the effect of different alkali sulfates on fluidity and compressive strengths of three different cement pastes and mortars are presented.

ORIGINS AND FORMS OF ALKALI SULFATES IN CEMENT

Portland cement clinker is produced by heating a raw mix of calcium carbonate (limestone), aluminosilicates (clay) and iron to a temperature of about 1450° C. In the raw mix and near the main constituents (silicon, aluminium, calcium and iron) there are some minor constituents: magnesium, potassium, sodium, sulfur and others. Nowadays, extensive energy-saving attempts have resulted in a change in pyroprocessing technology, the decreasing in low alkali raw materials and of course, the severe environmental restrictions lead to an increase in alkali and sulfate concentrations in clinker. Clinker contains four main mineralogical phases, i.e. tricalcium silicate (C_3S), dicalcium silicate (C_2S), tricalcium aluminate (C_3A) and tetracalcium aluminoferrites (C_4AF). Alkalis and sulfur give rise to alkali sulfates because sulfur makes prior demands on the alkalis. The remainder can be introduced in the crystal structure of the phases.

Potassium sulfate (K_2SO_4) is likely to occur either alone or in one of two double sulfate forms, aphthitalite ($Na_2SO_4.3K_2SO_4$) or calcium langbeinite ($2CaSO_4.K_2SO_4$). Sodium sulfate may occur in double sulfate form (aphthitalite) only. Calcium sulfate occurs either alone or as calcium langbeinite, subject to the prior formation of double alkali sulfate (Jawed and Skalny, 1977; Pollit and Brown, 1968; Tagnit-Hamou and Sarkar, 1990). The ratio of total clinker sulfur to total alkali, determines the quantity of alkali sulfate. This ratio is known as sulfatization degree ($SD\% = SO_3 \times 100 / 1.292\ Na_2O + 0.85K_2O$). Kiln environments have some effect on double salt formations. Calcium langbeinite is formed in oxydating conditions, but aphthitalite is better formed in reducing conditions (Mander and Skalny, 1977). After the formation of alkali sulfates, the remaining alkali and sulfur are combined in silicate, aluminate and aluminoferrite phases. Sodium is mainly incorporated in C_3A lattice and gives rise to orthorombic C_3A . These phases are known as less reactive than the cubic form. Potassium and sulfur are substituted mainly in C_2S (Regourd, 1983).

OBJECTIVE

This research is divided into two parts. The first part investigates the effect of addition of different alkali sulfate and calcium sulfate forms on cement hydration, at constant SO_3 content. The second part deals with the effect of addition of different alkali sulfate forms combined with mixtures of gypsum and hemihydrate on cement hydration, at constant alkali contents.

EFFECT OF DIFFERENT CALCIUM SULFATE AND ALKALI SULFATE FORMS ON CEMENT HYDRATION, AT CONSTANT SO_3 CONTENT

Three clinkers are mixed and ground in laboratory ball mill with different additions of calcium sulfates (gypsum or hemihydrate) or alkali sulfates (arcanite, aphthitalite or calcium langbeinite). The clinkers used have different phase compositions (Table 1). The K01 and K02 clinkers have the same C_3A content (6%); however, the K01 clinker has a mixture of cubic and orthorombic, while the K02 clinker had a cubic C_3A. Clinker K03 has 9% of C_3A in cubic form (Figure 1). Alkali sulfates are synthesized in laboratory ovens and controlled by X-ray diffraction.

Table 1 Chemical and Bogue compostions of tested clinkers

Chemical composition (%)				Phases composition (%)			
Clinker	K01	K02	K03		K01	K02	K03
SiO_2	21.3	21.99	22.22	C_3S	65	70	69
Al_2O_3	4.6	4.05	4.35	C_2S	12	11	11
Fe_2O_3	4.0	3.02	1.75	C_3A	6	6	9
CaO	65.3	65.9	66.33	C_4AF	12	9	5
MgO	2.2	2.82	2.92	CaOf	0.6	1.4	0.3
SO_3	0.8	0.6	0.78	L.O.I.	0.5	0.4	0.5
Na_2O	0.25	0.34	0.30	SD*	72	91	100
K_2O	0.92	0.26	0.46				
Na_2O eq.	0.80	0.51	0.61				

* $SD = SO_3 . 100 / 1.292\ Na_2O + 0.85\ K_2O$

Sulfates are added in order to ensure 3% of SO_3 for the K01 and K02 clinkers and 4.5% for the K03 clinker which has a higher C_3A content. The cement Blaine fineness was kept constant at 360 m^2/kg. Table 2 summarizes the characteristics of the cements.

Table 2 Cements SO_3 and alkalies (as Na_2O) composition

Cement	SO_3 (%)	Na_2Oeq (%)	Cement	SO_3 (%)	Na_2Oeq (%)	Cement	SO_3 (%)	Na_2Oeq (%)
C01G	3.0	0.8	C02G	3.0	0.51	C03G	4.5	0.61
C01H	3.0	0.8	C02H	3.0	0.51	C03H	4.5	0.61
C01CL	3.0	1.38	C02CL	3.0	1.13	C03CL	4.5	1.57
C01Arc	3.0	2.54	C02Arc	3.0	2.37	C03Arc	4.5	3.48
C01Aph	3.0	2.51	C02Aph	3.0	2.37	C03Aph	4.5	3.48

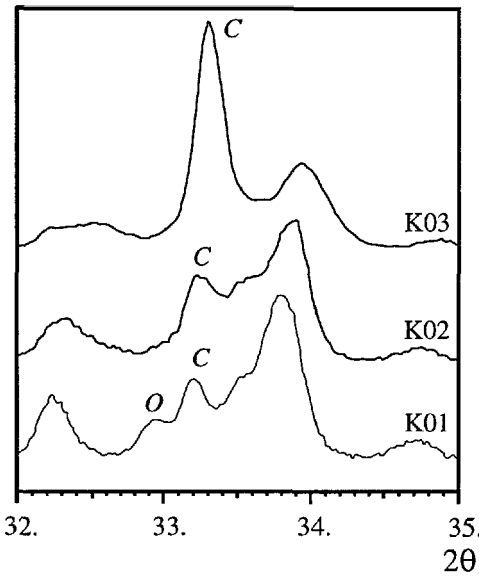

Figure 1 X-ray diffraction spectrum of three clinkers (C= cubic C_3A, O= Orthorombic C_3A)

All cements grouts were mixed with water at two different W/C ratios, 0.50 and 0.30. A naphtalene-sulfonate superplasticizer (SP) was used with the lower W/C grout. The optimum superplasticizer content was selected for each cement using the flow time test measured by the Marsh Cone (Baalbaki, 1990). The hydration was followed by X-ray diffraction, calorimetry and extracted pore solution analysis by atomic absorption for Ca^{2+} and K^+ and by colorimetry for SO_4^{2-}. Cement grouts and mortars were also tested for rheological and compressive strength behavior.

Results

Figure 2 shows the mini-slump results of the three cement pastes at W/C ratios of 0.50 and 0.30.

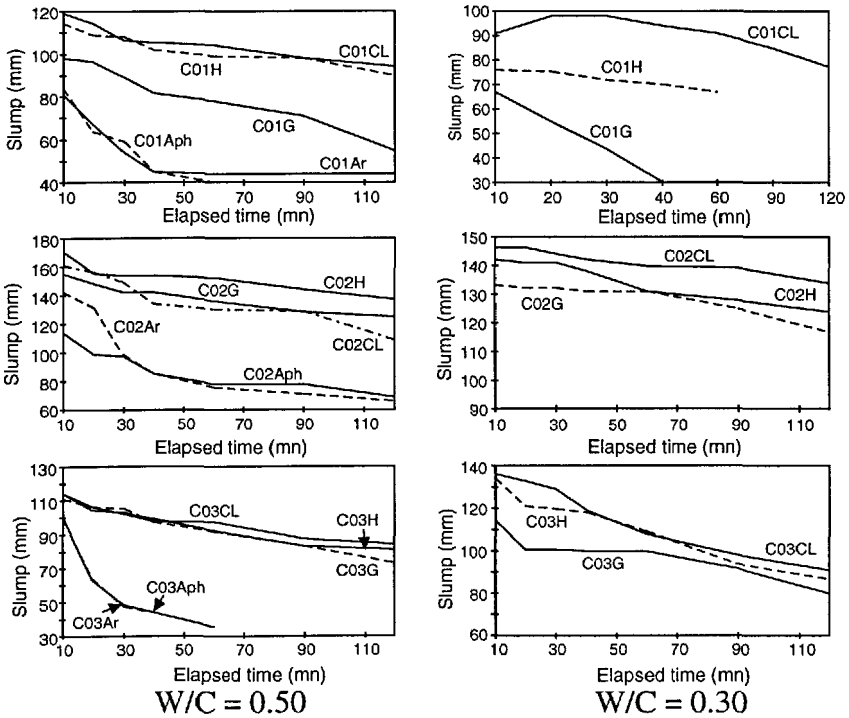

Figure 2 Mini-slump versus hydration time of the three cement pastes at W/C 0.50 or 0.30.

Despite these clinkers' identical major phase contents, with the C01 series cements, in all the cases, lower slumps and faster slump loss were obtained than with the C02 series. This is because of the reactivity of C_3A. Because of its orthrombic C_3A content, the K01 clinker is less reactive than the K02 clinker. This leads to a faster ettringite formation in the C02 cements, which exhibits better slump retention. According to Sorrentino (Sorrentino, 1996), the ettringite formed with reactive C_3A is an effective hydration controler which is not the case with needle-like crystallized ettringite formed with less reactive C_3A . The reactivity of those cements is also shown in the calorimetric analysis (Figure 3).

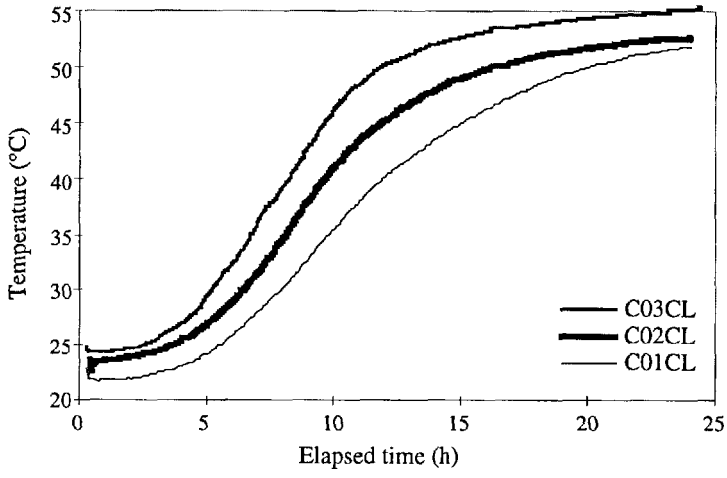

Figure 3 Calorimetric analysis of C01CL, C02CL and C03CL cements

Because of the lower C_3A content, the cements of the C02 series show higher slump than those of C03 series despite a higher SO_3 content (4.5%) in the latter series. Due to high alkali content, the cements of all three series with arcanite or aphthitalite show very poor slump at 0.50 W/C and do not flow at all at a W/C of 0.30, even with 0.8% superplasticizer content.

Calcium langbeinite cement shows very good slump, which was equal or better than the hemihydrate or gypsum cements, despite its high alkali content. This good slump of calcium langbeinite cement is enhanced at the low W/C of 0.30. This is due to very fast release of SO_4^{2-} and also Ca^{2+} ions into the solution.

In order to follow the effect of high alkali content on SP content, the mini slump of different pastes prepared with cements from C01, C02 and C03 series incorporating aphthitalite (C01 Aph, C02 Aph and C03 Aph) was measured. The pastes had a W/C of 0.50 and varying SP contents. Figure 4 summarizes the results.

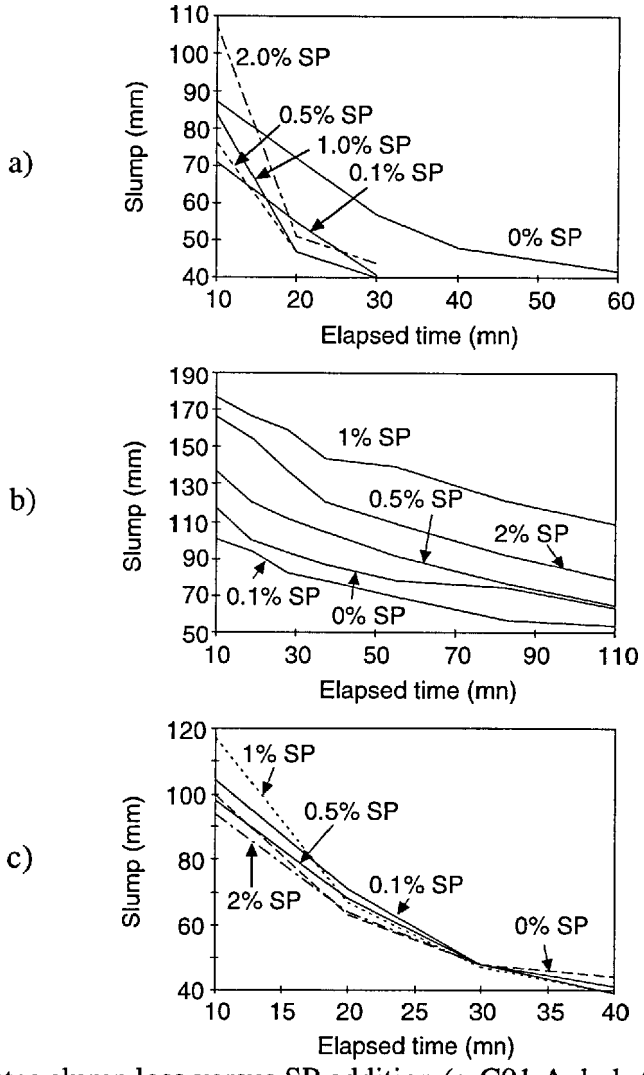

Figure 4 Cement pastes slump loss versus SP addition (a-C01 Aph, b-C02 Aph, c-C03 Aph) at 0.50 W/C

This figure shows that even at 0.50 W/C, the C03 cements need at least 1% of SP to reach the same slump as the lower alkali content cements. Such pastes exhibit sharp loss in fluidity. The less reactive C_3A (C01) and the high C_3A content cements (C03) show very fast slump loss, and the effect of SP dosage disappears after 30 minutes. At a 2% SP dosage, the slump loss is more critical than the case of 1% SP content. It is clear here that with this amount of alkalies (2.5% for C01 Aph, 2.37% for C02 Aph and 3.48% for C03 Aph), it is impossible to improve the flow of the paste, especially when the C_3A content is high (C03) or when it is less reactive (C01). According to Nawa et al. (Nawa et al., 1989) the low alkali sulfate content in the clinker decreases the SP adsorption on C_3A and C_4AF and increases the paste fluidity by a better effect on silicate phases. An excessive alkali sulfate content, however, increases the viscosity by compressing the electric double layer of the silicate phases and the strong floculation of cement particles.

From extracted pore fluid analysis of C02 and C03 cements after 10 and 60 minutes of hydration for pastes with 0.50 W/C, it is clear that because of their high solubility, arcanite and aphthitalite are providing more SO_4^{2-} ions to the solution at given time than the other sulfates followed by calcium langbeinite (Figure 5). Among the various calcium sulfate types, the hemihydrates give more SO_4^{2-} ions to the solution than that of the gypsum. The difference in SO_4^{2-} provided by arcanite or aphthitalite and calcium langbeinite is that the former is converted to gypsum or syngenite but arcanite or aphthitalite stays in the solution, as confirmed by XRD. This is also shown by the low Ca^{2+} content in the pore solution in the case of calcium langbeinite. This shows that the SO_4^{2-} ions alone are not sufficient to

control the paste fluidity; the concentration of Ca^{2+} ions are also very important. For that reason, calcium langbeinite shows good ability to control cement paste fluidity. This effectiveness is also shown at a W/C of 0.30 with SP which is even better than calcium sulfates because of its slow conversion to gypsum or syngenite.

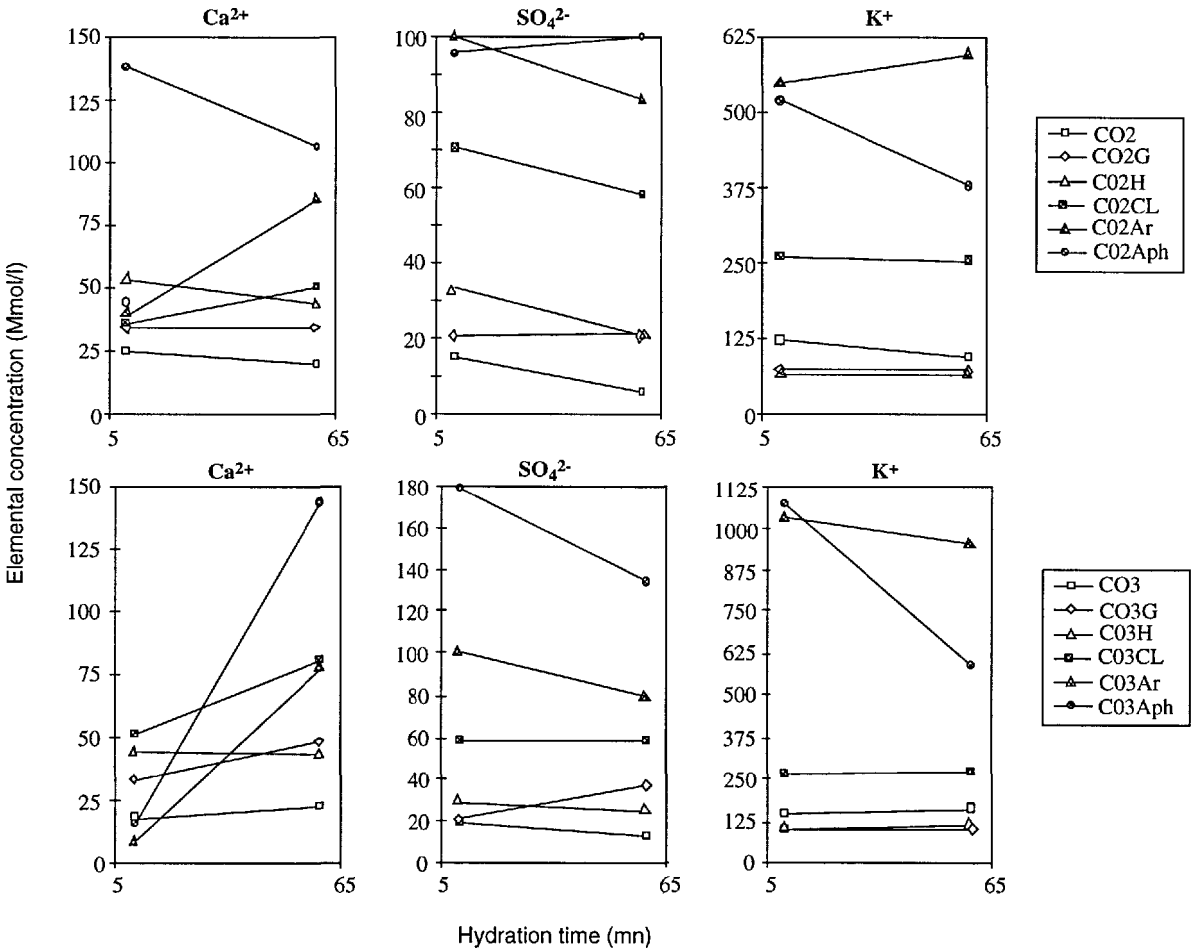

Figure 5 Extracted pore fluid analysis of C02 and C03 cement pastes at 0.50 W/C ratio

EFFECT OF DIFFERENT ALKALI SULFATES COMBINED WITH THE MIXTURE OF HEMIHYDRATE AND GYPSUM ON CEMENT HYDRATION, AT CONSTANT ALKALI CONTENT

The two clinkers K02 and K03 were all ground with different additions of alkali sulfates to ensure 1.2% Na_2O eq. in each cement. A mixture of gypsum and hemihydrate was also added to ensure a content of 3% SO_3 in the K02 clinker and 4.5% in the K03 clinker. One can note that to reach this goal with the K02 clinker, there was no need for gypsum or hemihydrate in the case of calcium langbeinite. The cements' Blaine fineness was kept constant (around 370 m^2/kg).

Results

Figure 6 shows the mini-slump results of cements pastes prepared at 0.50 and 0.30 W/C ratio.

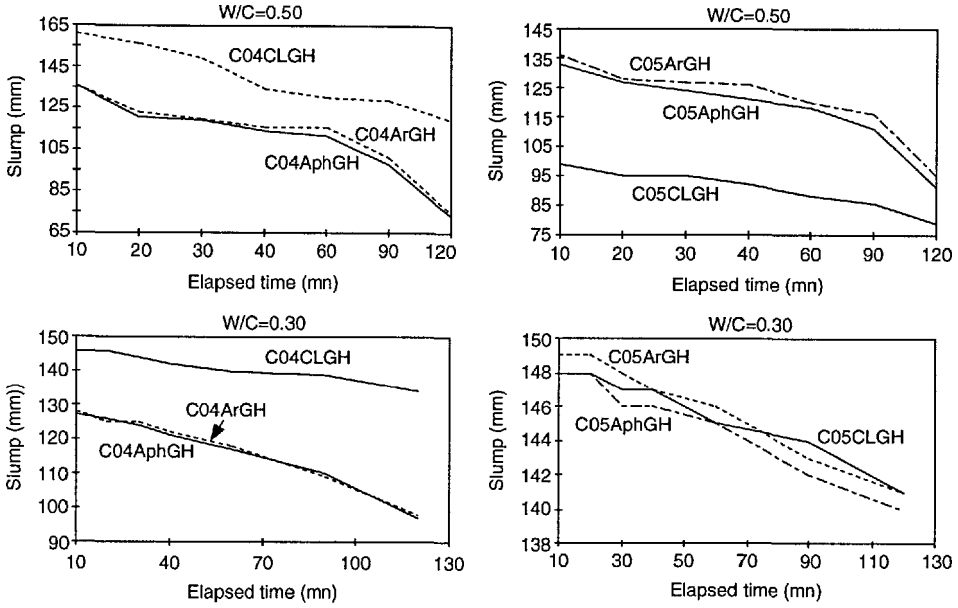

Figure 6 Mini-slump versus hydration time of the C04 and C05 cements at 0.50 and 0.30 W/C ratio

Again, the effectiveness of calcium langbeinite is shown to improve the paste fluidity. Even at the same alkali content (1.2% Na_2O eq.), calcium langbeinite cements exhibited the best flow with the K02 clinker. This confirms again that with the same alkali and SO_3 contents, the type of alkali sulfate is important, and Ca^{2+} ions from calcium langbeinite can control the alkali effects on fluidity. When the alkali sulfates, are mixed with gypsum and hemihydrate, they give rise to bad fluidity by syngenite and gypsum crystalization. This is the case for arcanite and aphthitalite cements but also for calcium langbeinite cement produced with the K03 clinker. At the low W/C ratio, the fluidity was well improved.

Compressive strength

The compressive strength results of all cement grouts are presented in Table 3. The well-known positive effect of alkalis on compressive strength at early age and negative effect at 28 days is noted here.

Table 3 Compressive strength of mortars

Cement	Compressive strength (MPa)						Cement	Compressive strength (MPa)					
	W/C = 0.50			W/C = 0.30				W/C = 0.50			W/C = 0.30		
	1d	7d	28d	1d	7d	28d		1d	7d	28d	1d	7d	28d
C02G	15	36	43	39	65	80	C04CLGH	25	34	38	44	56	68
C02H	14	28	32	34	59	73	C04ArGH	28	33	39	44	49	58
C02CL	15	28	33	35	43	57	C04AphGH	25	32	39	44	49	57
C02Ar	17	24	28	--	--	--	C05CLGH	24	33	39	54	60	68
C02Aph	17	24	29	--	--	--	C05ArGH	28	37	43	49	55	62
C03G	18	43	50	50	78	91	C05AphGH	25	37	42	48	55	61
C03H	15	31	34	37	67	80							
C03CL	16	30	35	39	55	69							
C03Ar	20	29	30	--	--	--							
C03Aph	20	29	31	--	--	--							

Cements with gypsum alone exhibited very good strength at all ages, especially at 28 days. This is more pronounced at a W/C of 0.30. Calcium langbeinite gives good results at early and late ages. In mixed calcium and alkalis sulfate cements, calcium langbeinite shows the best results mainly at 0.30 W/C .

CONCLUSION

The form of C_3A has a profound effect on the fluidity of cement paste. The effect of addition of alkali sulfates on such fluidity can be positive by providing sulfate (SO_4^{2-}) and calcium (Ca^{2+}) ions to the pore solution, or negative by the activating effect of alkali ions (Na^+, K^+), or by crystallization of syngenite. At high content in cement aphthitalite or arcanite present mainly the negative effect and require large amounts of calcium sulfate to control this effect which is worst at a low W/C ratio and with superplasticizer. Calcium langbeinite shows very good ability to control the very early cement hydration by providing Ca^{2+} and SO_4^{2-} ions to the pore solution. This ability is better at a low W/C ratio system containing SP. The best 28-day compressive strength is obtained when gypsum is incorporated in the cement.

ACKNOWLEDGEMENT

The financial support of NSERC is gratefully acknowledged.

REFERENCE

Baalbaki, M., "Façon pratique d'évaluer le dosage en superplastifiant: La détermination du point de saturation", Séminaire sur les superplastifiants, Centre de recherche interuniversitaire sur le béton, Université de Sherbrooke, Sherbrooke, 1990, pp. 69-79.

Bensted, J., "Hydration of Portland Cement", Advances in Cement Technology, Ed. S.N. Ghosh, Pergamon Press, Exeter, 1983, pp. 307-347.

Jawed, I. and **Skalny**, J., "Alkalies in Cement: A review, Part I Forms of Alkalies and Their Effect on Clinker Formation", Cement and Concrete Research, 1977, Vol. 7, pp. 719-730.

Mander, J.E. and **Skalny**, J., "Calcium Alkali Sulfates in Clinker", Ceramic Bulletin, Vol.. 56, No. 1, p. 987, 1977.

Nawa, T., **Eguchi**, H. amd **Fukaya**, Y., "Effect of Alkali Sulfate on the Rheological Behevior of Cement Paste Containing a Superplasticizer", Proceedings of the 3rd CANMET/ACI International Conference on Superplasticizers and Other Chemical Admixtures in Concrete, Ottawa, SP-119, pp. 405-424, 1989.

Pollit, H.W. and **Brown**, A., "The Distribution of Alkalies in Portland Cement Clinker", Proceedings of the 5th International Congress of the Chemistry of Cement, Tokyo, Vol. I, p. 322, 1968.

Regourd, M., "Crystal Chemistry of Portland Cement Phases", Structures and Performances of Cements, Ed. Barnes, Applied Sciences Publishers Ltd., London, 106 pp., 1983.

Sorrentino, D., "La mesure de la cinétique d'hydratation des liants hydrauliques: Un outil essentiel pour la maîtrise des propriétés à court terme", Proceedings of the International RILEM Symposium "Béton - Du matériau à la structure", Arles, September 11-12, 1996.

Tagnit-Hamou, A. and **Aïtcin**, P.-C., "Cement and Superplasticizer Compatibility", World Cement, Vol. 24, No. 8, pp. 38-42, 1993.

Tagnit-Hamou, A. **Baalbaki**, M., and **Aïtcin**, P.-C., "Calcium Sulphate Optimization in Low Water/Cement Ratio Concretes", Proceedings of the 9th International Congress of the Chemistry of Cement, New Delhi, Vol. V, pp. 21-25, 1992.

Tagnit-Hamou, A. and **Sarkar**, S.L., "Influence of varying Sulfate Content on the Microstructure of Commercial Clinkers and Properties of Cements", World Cement, Vol. 21, No. 9, pp. 389-393, 1990.

Tang, F.J. and **Tresouthick**, S.W., "Hydration and Performance of Cements with Various Amounts and Forms of Added Sulfate", Proceedings of the 9th International Congress of the Chemistry of Cement, New Delhi, Vol. IV, pp. 317-323, 1992.

2ii013
4 pp

Kno. 25. JAN. 2001 dok 31776

THE CHANGE OF THE LIQUID PHASE COMPOSITION AND PROPERTIES OF HARDENED CEMENT PASTE AT LOW TEMPERATURE

Anatolij KLUSOV, RAO "GAZPROM", Moscow, Russia
Yuri KRIVOBORODOV, RCTU, Moscow, Russia
Asat ACHMETOV, Tumengazprom, Tumen, Russia

ABSTRACT Liquid phase composition, pH, density, electric conduction and freezing temperature during hardening of cement paste at +20 and -5°C with NaCl and $CaCl_2$ were studied. Oil-well cement of G-type was used. It was established that $CaCl_2$ reacted with calcium aluminate and ferrite earlier than ettringite. This fact excludes corrosion of the drill pipe.

KEY-WORDS: Hydration, low temperature, oilwell cement.

INTRODUCTION

There are many problems connected with the gas and oil deposit exploitation in the Arctic. In the first place is complicated geological conditions requiring special cements to isolate the pressured or week zones encountered whilst drilling of a well. On the other hand the rock temperature varies between -10 and 0°C. Therefore it is necessary that the cement should set at low temperatures, that the surrounding ground should not be disturbed by erosion during drilling or cementing or in the subsequent life of the well. Mixture based on Portland cement and $CaCl_2$ or NaCl could be used. But in spite on data of many researchers (Bensted, 1983, Butt and Kolbasov, 1976, Mironov and Lagoida, 1975, Skalny and Young, 1980, Taylor, 1990, etc.) on cement hydration at low temperature, using such accelerators as calcium chloride, they were not applied. Technical barriers appearing due to scepticism connected with the posibilities of cement paste destruction and well corrosion have been discussed. At the same time it impeded the study of hydration and structure formation of cement paste with high quantity of calcium and sodium chlorides.

EXPERIMENTAL

Materials and techniques

For study oil-well cement including C_3S=63.4%, C_2S=11.7%, C_3A=8.4%, C_4AF=12.2% was used. Using this cement and its mixture with 8% $CaCl_2$ or 8% NaCl standard samples were prepared. They cured at +20°C and -5°C in water. Hydrated products were examinated by XR-diffraction, differential thermal analysis (DTA), IR-spectroscopy (IRS) and electron microscopy (EM).

RESULTS AND DISCUSSION

At 20°C the main hydrate products are ettringite (endotherm at 140°C in DTA curves, absorption wave is in region 1120 cm^{-1}), CSH(I), which is observed by endotherm at 135°C, absorption wave of 980 cm^{-1} at IRS-curves, the fibrous material distinquished by EM) and $Ca(OH)_2$ crystallized in hexagonal crystals. NaCl-additive promotes the formation of $3CaO{\cdot}Al_2O_3{\cdot}3CaCl_2{\cdot}30H_2O$ (endotherm at 352°C and d=0.314 nm at XRD powder diffraction pattern).

At $CaCl_2$ presence the transoformation of CSH(I) into CSH(II) increases and besides them $3CaO{\cdot}CaCl_2{\cdot}16H_2O$ is formed, which observed by endotherm at 580°C on DTA-curves.

The hydration temperature decrease up to -5°C leads to the delay of ettringite formation. Addition of NaCl leads to C_4AH_{13}, $3CaO{\cdot}CaCl_2{\cdot}16H_2O$ formation. $CaCl_2$ accelerates the crystallization of $3CaO{\cdot}CaCl_2{\cdot}16H_2O$, CSH(II) and $3CaO{\cdot}Al_2O_3{\cdot}3CaCl_2{\cdot}30H_2O$.

Hydration of cement paste proceeds at the continuous change of ion composition of liquid phase, which influence on structure formation of cement paste. At same time liquid phase composition depends on the cement type, clinker structure, the presence of minor components in it, the addition of chemical compounds, and temperature conditions of hardening.

Liquid phase of cement paste hardened at 20°C is characterized by supersaturated $Ca(OH)_2$.Concentration of SO_4^{2-}ions is the result of two factors: in the first is the dissolution of $CaSO_4$, on the other hand ettringite is formed with the increase supersaturation of $Ca(OH)_2$.

NaCl addition into cement paste leads to high increase of Ca^{2+} ion concentration in liquid phase as well as the concentration of SO_4^{2-}ions, which showed that ettringite formation rate is reduced(Fig.1).

$CaCl_2$ addition of more than 10 times increases the supersaturation of liquied phase by Ca^{2+}. Nevertheless chlorine-ion decreases due to its adsorption by calcium hydrosilicates and formation of hydroxideclhoride compounds. The fast formation of ettringite was obvious.

At the presence of NaCl, the temperature increase does not influence on kinetics of liquied phase composition change: concentration maximum of Ca^{2+}, Na^{+}, SO_4^{2-} and pH reached up to 4 hours of hydration at 20°C. During 8 hours, concentration Cl^{-} ions decreased due to calcium hydroxide formation.

At -5°C concentration of Ca^{2+} ions increase during 1 hours, after that it is stabilized. At the presence of $CaCl_2$ and NaCl in this conditions (-5°C) the fast and large quantity of calcium hydroaluminachloride formation was obvious.

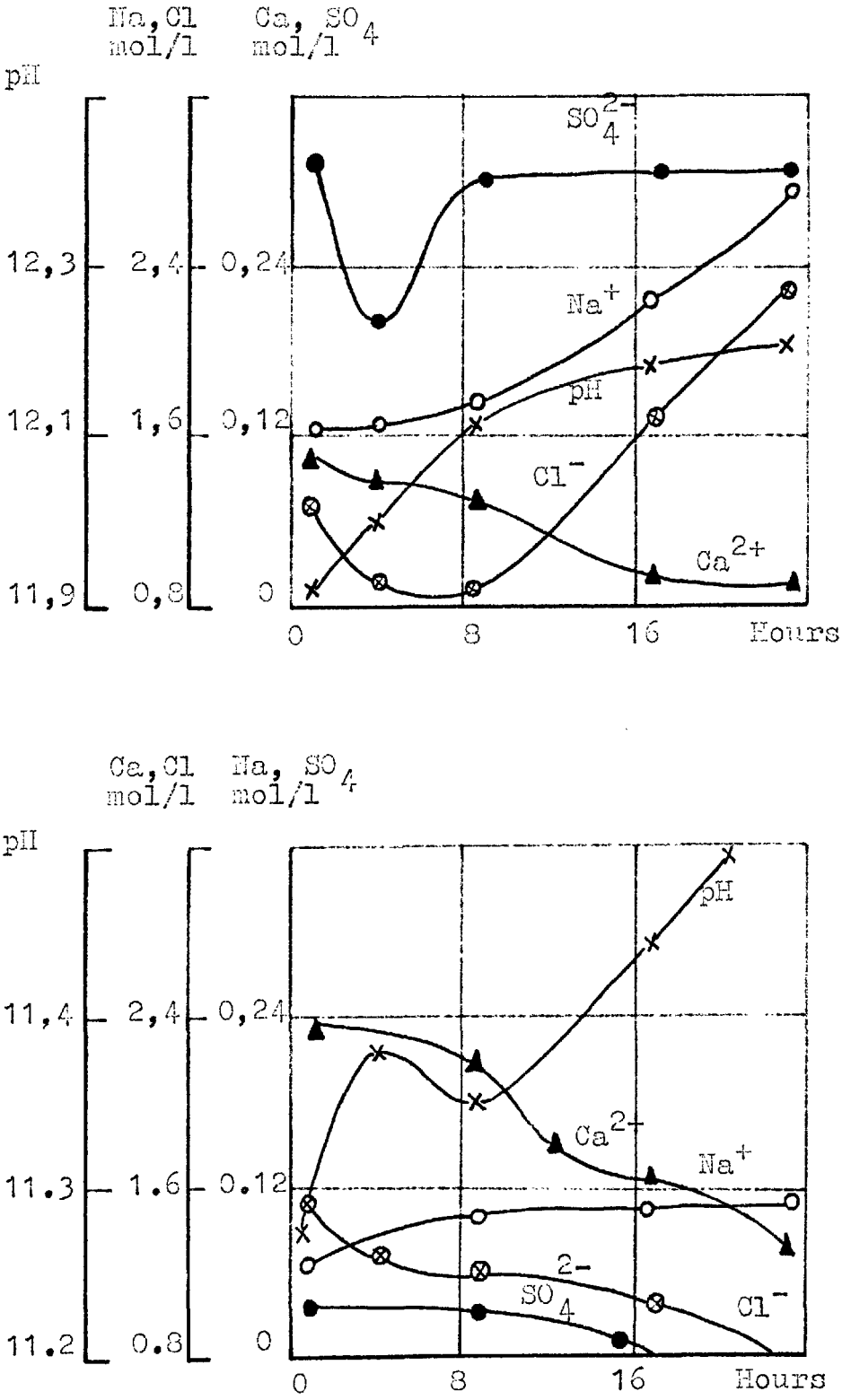

Fig.1 The change of ion concentration and pH of liquid phase in cement paste (temperature -5°C).

Comparing analysis of experimental data shows as follows:
- at 20°C ettringite formation proceedes not only through the solution but topochemically on the surface of gypsum grains because their solubility are less than C_3A crystals,
- at $CaCl_2$ presence the formation of calcium aluminochloride compounds proceeds simultaneously with ettringite formation,
- at -5°C cement hydration is stopped and only the addition of NaCl and $CaCl_2$ decreases the freezing temperature of liquid phase. In this case cement hydration takes place and hydrated products are formed. It was established that $CaCl_2$ and NaCl reacted with calcium aluminate therefore calcium aluminochloride is formed rapidly. Ettringite is crystallized after $3CaO \cdot Al_2O_3 \cdot 3CaCl_2 \cdot 30H_2O$ formation. At this time pH of liquid phase as well as Na^+ concentration increases. This excludes the corrosion of drill pipe string.

CONCLUSION

In presence of high concentration of $CaCl_2$ and NaCl in cement paste, calcium aluminochloride compound is formed.
The high pH of liquid phase of cement paste, and the absence of oxygen medium in air-tight grouting hole, exclude the corrosion of steel.

REFERENCES

Benstead, Y. "Oilwell cement", Chemistry and Industry, 1983, No 17, p. 776-780
Butt, Y.M. and Kolbasov, V.M. "Influence of cement composition and hardened conditions on the structure formation of cement paste". 6th International Congress on Chemistry of Cement, Moscow, 1976, v.2, p. 281-283
Mironov, C.A. and Lagoida, A.V. "Concrete hardening in the freezing condition", Moscow, Stroijzdat, 1975, 263 p.
Skalny, Y.P. and Young, Y.F. "Mechanisms of Portland cement hydration", 7th International Congress on the Cement Chemistry, 1980, v.2, p. 1-30
Taylor, H.F.W. "Cement Chemistry", London, Academic Press, 1990, 476 p.

2ii014
Kno. 25. JAN. 2001 doi31777
7 pp

BEHAVIOR OF HEAVY METAL ELEMENTS IN THE HARDENING OF CEMENT PASTE

Hiroshi UCHIKAWA, Shunsuke HANEHARA and Hiroshi HIRAO,
Chichibu Onoda Cement Corporation, Japan

ABSTRACT The rate of hydration, morphology and composition of hydrates, distribution and dissolution of minor and trace element in and from, respectively, the hardened cement paste prepared by adding small amounts of various elements including heavy metals were investigated using normal portland cement and blastfurnace slag cement containing 50% of slag in order to clarify the effects of them from waste recently often used as alternative raw material and fuel on the properties and performance of concrete.

Key-words:Microstructure,Backscattered electron image,Heavy metals,Immobilization,Leaching

INTRODUCTION

With the spread of the utilization of waste as alternatives to the raw materials and fuel for manufacturing cement, it is feared that the elements of heavy metals, halogens and others remaining in cement detrimentally affect the performances of concrete (Uchikawa, 1992; Uchikawa, 1994; Uchikawa et al, 1997).

In this paper, the distributions of minor and trace elements of heavy metals, halogens and others in hardened cement paste and the quantities of them dissolved from the hardened specimens are determined and the effects of those elements on the hydration of cement and the formation of hardened structure are investigated.

EXPERIMENTS

Sample and preparation of cement paste

Normal portland cement and blastfurnace slag cement containing 50% of slag shown in Table 1 are used. The elements of heavy metals, halogens and others are added to the mixing water at the preparation of cement paste. The added amounts of them are fixed as shown in Table 2 considering the quantities of them previously contained in the waste (Shirasaka et al, 1996). The elements of heavy metals, halogens and others are added as their nitrates, chlorides, alkaline salts or ammonium salts. The W/C of cement paste is 0.5. It is weighed out into a 200ml-hermetically sealed vessel made of polyvinyl chloride to age at 20°C for 14 days. After aging, hardened cement paste is cut into pieces 5mm square with a diamond cutter and these pieces are immersed in acetone to terminate the hydration and dried in RH of 11% or D-drying to submit to various tests.

Table 1 Composition and fineness of cement used

	Chemical composition (%)								Bl'
	SiO_2	Al_2O_3	Fe_2O_3	CaO	MgO	SO_3	Na_2O	K_2O	(m^2/kg)
Normal portland cement	21.6	5.3	3.3	64.9	1.1	2.3	0.45	0.35	331
50% Blastfurnace slag cement	25.9	8.6	1.8	55.9	4.1	2.2	0.27	0.36	371

Bl': Blaine specific surface area

Analyses of hydration of cement and hardened cement paste

The rate of hydration of cement is estimated by the determination of combined water using the ignition loss at 1000°C and of amount of Ca(OH)2 produced by Thermogravimetry - Differential Scanning Calorimetry (TG-DSC). The hydrates are observed by powder X-ray diffractometry.

The distribution of the elements of heavy metals, halogens and others is determined and the content of them are determined by the point analysis at twenty points by computer aided electron probe microanalysis (CMA/EPMA). The structure of hardened cement paste is observed by secondary electron image and back scattered electron image with a scanning electron microscope (SEM). The pore structure is determined by mercury-intrusion porosimetry.

Measurement of quantities of elements of heavy metals, halogens and others dissolved from hardened cement paste

The dissolved amounts of elements are measured according to Notification No.13 of Environment Agency of Japan as follows : the hardened cement paste at the age of 14 days is crushed into particles 0.5 to 2.5mm in diameter; the particles are immersed to pure water ten times as much as them; the mixture is shaken at 20°C for 6 hours; the particles are separated by filtration; and the contents of various elements in the filtrate are measured by high-frequency inductively coupled plasma analysis (ICP) or ion chromatography.

Table 2 Amount of minor and trace element added to cement for preparing cement paste

Element	added mount of element (%)	Type of salt
F	0.5	ammonium salt
P	0.5	ammonium salt
Cl	2.0	chloride
Ti	0.2	nitrate
V	0.1	ammonium salt
Cr	0.1	potassium salt
Cr^{6+}	0.1	ammonium salt
Mn	0.1	nitrate
Cu	0.1	nitrate
Zn	0.2	nitrate
As	0.1	sodium salt
Sr	2.0	nitrate
Cd	0.1	nitrate
Sb	0.1	chloride
Ba	0.2	nitrate
Hg	0.1	nitrate
Pb	0.1	nitrate

RESULTS

Effects of elements on hydration of cement

As mentioned above, the elements of heavy metals, halogens and others were added to cement as the form of salts. The effects of anions bound to the elements concerned will be reported separately.

The measured values of the combined water and the amount of Ca(OH)2 produced in normal portland cement and blastfurnace slag cement are illustrated in Fig 1. C-S-H, monosulfate hydrate (AFm) and Ca(OH)2 are identified in the hardened cement paste, while no ettringite (AFt) is identified.

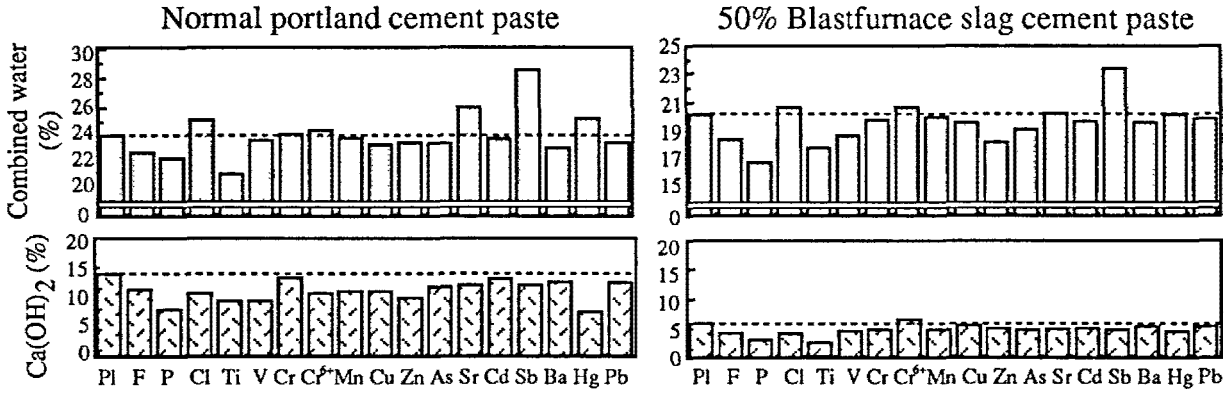

Figure 1 Amount of combined water and Ca(OH)2 in hardened normal portland cement paste and 50% blastfurnace slag cement paste prepared by adding various elements

Normal portland cement and blastfurnace slag cement contained 24.0 and 20.2% of the combined water, respectively. The content of combined water in normal portland cement paste adding Cl, Cr(III, VI), Sr, Sb, Ba and Hg was higher and that in blastfurnace slag cement paste adding Cl, Mn, Sr and Sb was higher than that without addition of them. Meanwhile, the amount of Ca(OH)2 produced in normal portland cement paste and blastfurnace slag cement paste adding those elements were less than that without addition of them. Maybe this is mainly because C-S-H with high Ca/Si ratio was produced.

The hydration of cement in normal portland cement and blastfurnace slag cement is remarkably depressed by adding P and Ti but accelerated by adding Cl, Sr, and Sb.

Effects of elements on morphology of hydrates and hardened structure

The secondary electron image of the fracture surface and the back scattered electron image of the polished surface of normal portland cement paste adding the elements of heavy metals, halogens and others are illustrated in Fig 2 together with those of the cement paste without adding any of

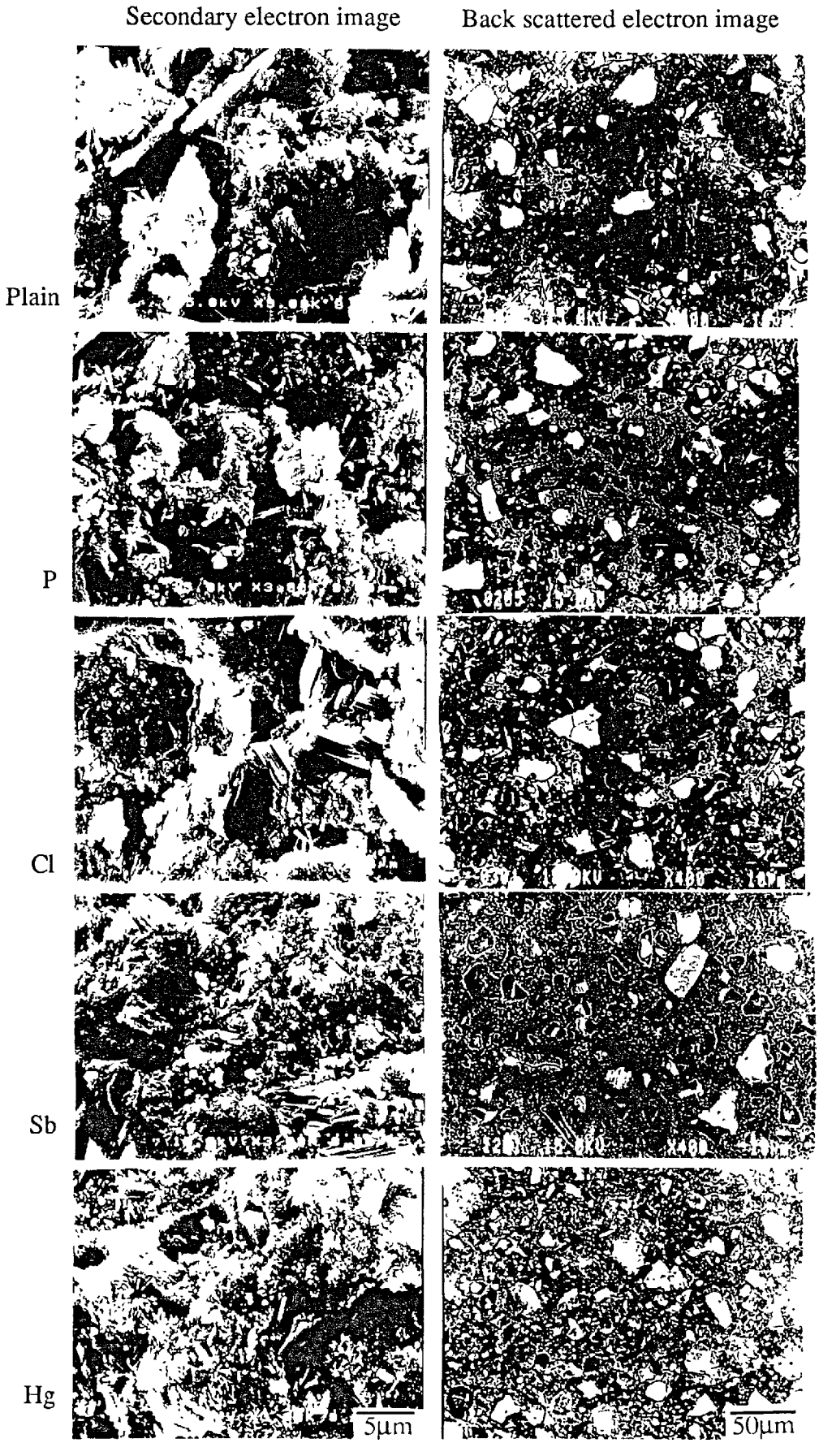

Figure 2

Secondary electron image and back scattered electron image of hardened cement paste prepared by adding various elements (W/C=0.5, 20°C, 14days)

those elements. The figure reveals that large crystals of $Ca(OH)_2$ were deposited in layers between the deposit of type I columnar C-S-H 1μm long and 0.1μm in diameter and that of type III equi-dimensional C-S-H and the platy AFm are scattered. The back scattered electron image reveals that type IV C-S-H(inner-hydrate) 5 to 10μm thick existed on the surface of unhydrated alite particles, and that the hydration of belite hardly proceeds and some of it were surrounded by the crystals of $Ca(OH)_2$.

The thickness of type IV C-S-H (inner-hydrate) on the surface of alite was reduced by half that in normal portland cement paste without containing the elements by adding P to it, which suggests the hydration of alite particles was depressed. The size of the crystal of $Ca(OH)_2$ is approximately 30 μm which is larger than that in the cement paste without adding the elements. It is inferred from the dark color tone of the back scattered electron image of the deposit of C-S-H that it is porous. The deposit of C-S-H in its own shape was 2μm long and 0.2μm in diameter, which was larger than that in the cement paste without adding the elements.

The thickness of type IV C-S-H (inner-hydrate) on the surface of alite in the cement paste adding Cl was 1.5 times as large as that in the cement paste without adding the elements. This suggests that the hydration of alite was accelerated. C-S-H without having its own shape predominated. $Ca(OH)_2$ was deposited in layers connecting the cement particles.

C-S-H deposited in the cement paste adding Sb was as fine as 0.1μm and most of it did not have its own shape. $Ca(OH)_2$ was deposited in layers between the C-S-H crystals. The back scattered electron image reveals that the unhydrated alite particles are extremely fewer than those in the cement paste without adding the elements. This suggests that the hydration of alite remarkably proceeded. Meanwhile, a relatively large quantity of the interstitial phase unhydrated was observed in hardened specimens.

The texture of the hydrated cement paste adding Ti was similar to that in the cement paste adding P. The fine columnar crystals of C-S-H was tend to grow radiately in the cement paste adding Cd or Hg. Although the texture of hardened cement paste adding the other elements were similar to that in the cement paste without adding the elements, the morphology of C-S-H, $Ca(OH)_2$ and Afm were changed.

Effects of elements on pore structure

The capillary pore size distribution of the hardened normal portland cement paste and blastfurnace slag cement paste is illustrated in Fig 3. Volume of gel pore of 6nm or under corresponding to the distance between the C-S-H crystal intra-layers increases with the increase of the production of C-S-H (Uchikawa et al, 1990). The content of gel pore was increased by adding Cl, Sr and Sb though it was slightly increased by adding Cr, Ba and Hg. The

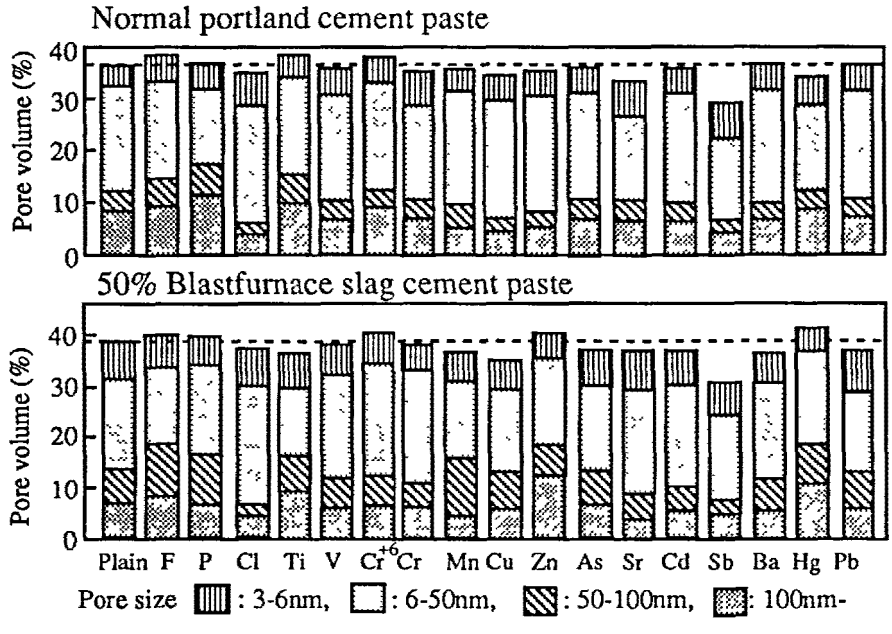

Figure 3 Structure of capillary pore of hardened cement paste prepared various elements measured by mercury porosimeter

capillary pore volume as small as 50 nm or less had the same trend as the gel pore. The total pore volume was generally decreased, but the volume of pore as small as 50 nm or under was increased by adding the elements having an effect increasing the content of combined water to the hardened paste. This suggests that the hydration reaction proceeds in it. The same tendency was observed in case of blastfurnace slag cement paste.

Distribution of element to hydrates in hardened cement pastes

The distribution of each element contained in C-S-H, $Ca(OH)_2$ and AFm of the hardened cement paste prepared by adding minor and trace elements was determined from the analytical result of by the point analysis and imaging with EPMA. The result of point analysis is listed in Table 3. Since any standard samples of V, As, Cd, Sb and Hg were unavailable, the data concerning these elements were omitted. The two-dimensional distributions of the elements added at the mixing cement with water are illustrated in Fig 4 together with the back scattered electron images of the fields of view corresponding to them.

Table 3 Concentration of element in each hydrate of hardened paste determined by point analysis using EPMA

Element	Concentration of element in each hydrate determined by EPMA (%)			
	C-S-H	AFm	$Ca(OH)_2$	
F	0.54 - 0.82	0.05 - 0.24	0.00 - 0.04	
P	2.26 - 6.10	0.32 - 0.80	0.20 - 0.35	(as P_2O_5)
Cl	0.16 - 0.38	1.31 - 2.88	0.01 - 0.10	
Ti	0.14 - 0.32	0.22 - 0.35	0.05 - 0.09	(as TiO_2)
Cr	0.04 - 0.10	0.08 - 0.11	0.00 - 0.04	(as Cr_2O_3)
Mn	0.07 - 0.11	0.03 - 0.05	0.00 - 0.03	(as MnO)
Cu	0.06 - 0.11	0.06 - 0.10	0.00 - 0.02	(as CuO)
Zn	0.08 - 0.14	0.07 - 0.11	0.00 - 0.02	(as ZnO)
Sr	2.03 - 3.10	0.81 - 1.03	0.10 - 0.32	(as SrO)
Ba	0.09 - 0.14	0.09 - 0.12	0.00 - 0.01	(as BaO)
Pb	0.15 - 0.21	0.04 - 0.07	0.00 - 0.04	(as PbO)

A large quantity of P was contained in C-S-H, while a relatively small quantity of it was contained in monosulfate hydrate (AFm) and $Ca(OH)_2$. P also seems to be deposited as fine crystals of calcium phosphate.

F was mainly contained in C-S-H, while it was less contained in AFm and hardly contained in $Ca(OH)_2$. Maybe this is because F was converted to CaF_2 which was deposited in C-S-H. F^- is easily substituted for OH^-. The hardened paste contained some portions with high concentration of F. This suggests the existence of the congregate texture of fine CaF_2 crystals.

Cl were mainly contained in AFm and the content of it in C-S-H was 1/10 or under as much as the content in AFm. Cl was hardly contained in $Ca(OH)_2$. It is estimated that Cl in AFm partially forms a Friedel's salt and that the bonds of Cl is loose and Cl is partly adsorbed onto the surface of the crystal. Cl contained in the hardened cement paste was relatively easily dissolved in it as mentioned later.

V is distributed to the position corresponding to AFm and C-S-H.

Although Cr^{3+} was less unevenly distributed to each hydrate, it was tend to be more distributed to AFm than to C-S-H. It was hardly contained in $Ca(OH)_2$. Some places with high content of Cr observed by EPMA may be formed by the deposition of Cr as $Cr(OH)_3$. Cr^{3+} in AFm is easily substituted for Al^{3+}. It is considered that Cr^{3+} in C-S-H is adsorbed onto the surface of crystal and between the layers (Ivey et al, 1990). It is considered that Cr^{6+} is either substituted for SO_4^{2-} in AFm or AFt as a solid solution of CrO_4^{2-} or taken up between the intra-crystal layers in C-S-H.

Although Mn was also less unevenly distributed to each hydrate, it was tend to be more distributed in C-S-H than in AFm. It is also hardly contained in $Ca(OH)_2$. It is considered that Mn^{2+} and Mn^{3+} are substituted for Ca^{2+}, and Al^{3+} or Fe^{3+}, respectively, and these ions exist in C-S-H and AFm. EPMA reveal that most of those ions existed in type IV C-S-H (inner-hydrate) on the surface of alite particles.

Fig 4 is given in the colour photo section at the end of the proceedings.

Cu was distributed equally to C-S-H and AFm but hardly distributed to $Ca(OH)_2$. And it was relatively evenly distributed to hardened paste.

Zn was mainly distributed to C-S-H and AFm. It is considered that Zn is substituted for Ca in C-S-H or bonds Ca on the surface of it into calcium containing zinc oxide compound and that Zn^{2+} and ZnO_4^{6-} are substituted for Al^{3+} and SO_4^{2-}, respectively, as solid solutions. Zn was relatively evenly distributed to hardened paste.

As was hardly unevenly distributed to each hydrate. Sr was largely distributed to C-S-H and relatively largely to AFm. It is hardly distributed to $Ca(OH)_2$. It is considered that Sr^{2+} is substituted for Ca^{2+} in these hydrates as solid solutions. Cd and Sb are hardly unevenly distributed to each hydrate.

Ba is mainly distributed to C-S-H as same as Sr. Although a small quantity of it was contained in AFm, it was not contained in $Ca(OH)_2$. EPMA reveals that some portions had high concentration of Ba. It is considered that the rest of Ba as a solid solution of hydrate is deposited as a $Ba(OH)_2$. EPMA results reveals that Hg was mainly adsorbed to C-S-H. Pb was relatively largely fixed to C-S-H and hardly contained in AFm and $Ca(OH)_2$.

Dissolution of minor and trace elements from hardened cement paste

The quantities of minor and trace elements dissolved from hardened cement pastes of normal portland cement and blastfurnace slag cement are illustrated in Fig 5.

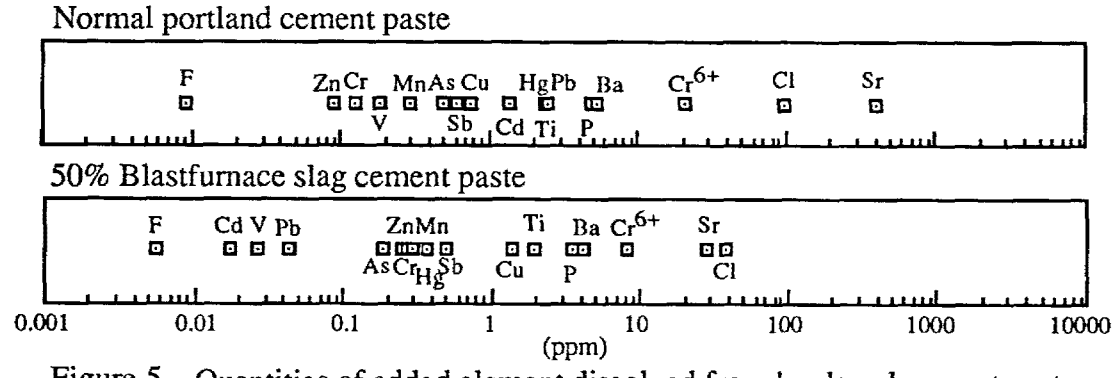

Figure 5 Quantities of added element dissolved from hardened cement paste

More than 1ppm of the elements dissolved from the hardened normal portland cement paste included Cl, Sr, P, Cr^{6+}, Ti, Cd, Ba and Hg. The quantity of Cr^{6+} dissolved from it among them exceeded the general emission criteria. More than 1 ppm of the elements dissolved from the hardened blastfurnace slag cement paste included seven components of Cl, Sr, Cr^{6+}, P, Ba, Pb, Ti and Cu. The quantities of the elements of heavy metals, halogens and others dissolved from the hardened blastfurnace slag cement paste were generally less than those dissolved from the hardened normal portland cement paste. For example, those of Cd and Pb were reduced to approximately one-hundredth, that of Cr^{6+} was reduced by half and those of Cl, Sr, V and others were remarkably reduced. The elements dissolved as much as 1 ppm or less from the hardened normal portland cement paste including Zn, Cr, Mn and Cu showed the increased quantities of dissolution from the blastfurnace slag cement paste.

Cl has relatively high solubility that most of it exists in the pore water and accordingly it is easily dissolved in the outside. Even the elements fixed as Friedel's salt are also unstable. It is considered that Sr and Ba once fixed in hydrates by substituting for Ca are leached out. Although the elements of heavy metals, halogens and others are more easily dissolved from the hardened paste than those contained in clinker because in this study these elements are added to cement paste together with the mixing water, most of the added amounts of elements except the elements of Cl, Cr^{6+}, Sr and Ba were fixed in the hardened cement paste within a range from 0.1 to 2%.

As mentioned above, the quantities of the elements of heavy metals, halogens and others dissolved from the hardened paste of blastfurnace slag cement were generally less than from that of normal portland cement. Maybe this is because the amount of deposited Ca(OH)2 forming a porous texture for passing those ionized elements (Uchikawa et al, 1989) were small and a large quantity of C-S-H with low Ca/Si easily adsorbing co-existing elements were produced.

CONCLUSIONS

The rate of hydration, morphology and composition of hydrates, distribution and dissolution of minor and trace element in and from, respectively, the hardened cement paste prepared by adding small amounts of various elements including heavy metals were investigated using normal portland cement and blastfurnace slag cement containing 50% of slag. The results obtained are summarized as follows:

1) Although the amounts of combined water in normal portland cement paste and blastfurnace slag cement paste containing Cl, Cr, Sr, Sb, Ba and Hg were higher than those without adding any elements, amount of Ca(OH)2 produced was reduced by adding any of those elements. The change of the volumes of gel pore and the total pore were coincide with that of the amount of combined water.
2) The C-S-H produced by adding P and Ti were as large as 2 μm long and 0.2 μm in diameter and were idiomorphic. Non-idiomorphic were increased and the layer structure of Ca(OH)2 between cement particles was formed by adding Cl. The C-S-H was non-idiomorphic and the size of it were reduced as fine as 0.1 μm by adding Sb. The back scattered electron images revealed that the C-S-H layers formed by adding Cl, P and Ti were thick and the rate of hydration were high in this order. This suggests that the higher the rate of hydration, the smaller the C-S-H crystal was and the poorer the development of its own shape was.
3) The elements of heavy metals, halogens and others added to cement paste distributed more in C-S-H and AFm than in Ca(OH)2 in such a manner that P, F, Sr and Pb congregated in C-S-H, Cl did in AFm, but Ti, Cr, Mn, Zn, Ba, As, Cd and V distributed equally in both hydrates. When large quantities of P, F, Cr, Cl, Zn and Ba were added, the compounds composed of respective elements were deposited.
4) The quantities of the elements of Cl, Sr, Cr^{6+}, Ba and Ti dissolved from the hardened pastes of normal portland cement and blastfurnace slag cement were more than 1 ppm, especially that of Cr^{6+} exceeded the general emission criteria. The quantity of an element dissolved from the hardened blastfurnace slag cement paste was less than that of ordinary portland cement. For example, those of Cd and Pb were as small as approximately one-hundredth and that of Cr^{6+} was as small as a half. Since Cl has high solubility, it is easily dissolved out. Although Sr and Ba are substituted for Ca and once fixed as hydrates which are easily leached out. Most of the Added amounts of elements, except Cl, Cr^{6+}, Sr and Ba were fixed to the hardened cement paste when the addition of elements were within a range from 0.1 to 2% . Less quantities of the elements dissolved from the hardened blastfurnace slag cement paste may be caused by few cluster of Ca(OH)2 forming a porous texture for passing those ionized elements and by a large production of C–S–H with low Ca/Si easily adsorbing the co-existing elements.

REFERENCE

Uchikawa, H., " Present Problem in Cement Manufacturing" Proceeding of 9th International Congress, Vol.7, 1992, pp.23-57.

Uchikawa, H., "Management Strategy in Cement Technology for the Next Century", Proceeding of an Engineering Foundation Conference 'Advances in Cement and Concrete', pp.524-561, 1994

Uchikawa, H. and Hanehara, S., "Recycling of Waste as Alternative Raw Materials and Fuels in Cement Manufacturing", chapter of 6 of the book entitled 'Waste Materials and Industrial By-product in Concrete Manufacturing", Noyer publications under printing.

Shirasaka, T., Hanehara, S. and Uchikawa, H., "Influence of Six Minor and Trace Element in Raw Material on the Composition and Structure of Clinker", World Cement, March, 1996, pp.102-115.

Uchikawa, H., Uchida S. and Hanehara, S., "Measuring Method of Pore Structure in Hardened Cement Paste, Mortar and Concrete", Il Cemento, Vol.88, 1990, pp.67-90.

Ivey, D.G., Heiman, R.B., Neuwirth, M., Shumborski, S., Conard, D., Milula, R.J and Lam, W.W., "Electron Microscopy of Heavy Metal Waste in Cement Matrices", Journal of Materials Science, Vol.25, 1990, pp.5055-5062.

Uchikawa, H. Uchida S. and Hanehara, S.,"Relationship between Structure and Penetrability of Na ion in Hardened Blended Cement Paste, Mortar and Concrete", Proceeding of the 8the International Conference on Alkali-agregate Reaction, Vol.1, 1989, pp.121-128.

Kn o. 2 5. JAN. 2001 d o k 31778

2ii015
4 pp

FORMATION OF HYDRATION ON MINERAL SUPPORT

Alexander OLGINSKY, D. Sc. (Eng.) Kharkov State Automobile
and Highway Technical University, Kharkov, Ukraine

ABSTRACT The degree of joining of hydrates with mineral support by "criterion of mating" is suggested to be determined. Forecast of the compactness of contact zone is carried out by special programme, based on the account of parameters of crystallic lattice of mating mineral phase. Main cement hydrates (and the products of their corrosion) are divided into five classes.

KEY-WORDS: Aggregate, Crystal, Hydration, Mineral phase, Support.

INTRODUCTION

Many works were dedicated to the problems of hydration of cement minerals and formation of hydrates. It is well known that, regularity of formation of hydrates are influenced by chemical additives, temperature, pressure and also under the influence of mineral support. However, problem of establishment of the regularity
of formation of compact contact of hydrates with the minerals of cement materials is not sufficienly studied. This problem includes the questions about the formation of hydrates on mineral support, particularly, oriented increase of hydrates on the surface of aggregate. As a result forms the compact zone of contact in composite materials and rises their operational resistance.

The oriented crystallization of different substances on metallic support is studied in detail (Palatnik, 1964; 1971). There exsist experimental data about the possibility of regular joining of different cement hydrates between themselves (Butt et al, 1972;
Timashev and Kolbasov, 1981) and also with calcite and quartz (Butt et al, 1970; 1971). These studies coinfirm the formula of (Royer, 1928).

$$\Delta=(a_1 - a_2) / a_1, \qquad [1]$$

a_1 and a_2 of crystallic lattice of mating mineral phases.

According to this formula, the possibility of intergrowing the crystalline phase is evaluated on the base of parameters "a", "b" and "c" of crystallic lattice of mating mineral phases. Incorrect are the statements that, the same type of connection, the principle of geometrical similarity of contacting crystals of mineral phases and closeness of parameters of crystallic lattice is the obligatory condition. At chemical interaction among contacting substances, the epitaxical growth is possible for the substances with Δ not more than few percent. From solutions, crystals grow at $\Delta < 15\%$. It is established that perfection of mating increases with the decrease of value.

At significant similarity between crystal-chemical properties and the parameters of lattice of increasing crystals and support, the formation of nucleus in the field of spiral dislocation can be mainly relied upon. If the growing crystals are distributed extremely
dissimilarly, then this is an evidence for the influence of deformed fields of surface upon forming the nuclei.

FORMATION OF NUCLEI ON THE CRYSTALLIC SUPPORT

Introduction

Formation of nuclei on the crystalline support may take place as the form of continuous growth and spontaneous crystallization. In the first case an atom, which reached the support, migrates on its surface toward an active center. These centers are the different defects of crystallic lattice, dislocation, steps of spalling or unfinished atomic planes. Migration of atom takes place until it does not occupy the position with minimum energy. These surface defects are the "atomic traps", which contribute to accumulate depositable particles. Different distortions of surface offer the place of "flow" for migrating atoms.

Theory

Unlike the first way of nucleus formation (Palatnik, 1964; 1971) spontaneous crystallization is not unacceptable for cement systems, since spontaneous formation of nuclei happens when oversaturation of liquid phase exceeds the critical value. In our case this is not realistic.

Hydrolysis of cement minerals is less active process than the formation of true solutions. Additionally, in the zone of contact with mineral support the processes of adsorption and ion exchange are developed. At insignificant oversaturation, which may take place in liquid phase of cement paste, the nuclei will join along the bulges on the surface of the support. On crystal surface of an aggregate with significant contents of impurities in solution, the formation of "parallel growths of solid solution" (mating) will take place. Formation of growths of four types may be possible: one crystal is the direct continuation of another; crystallic growths are formed along the common surface (cristallographic plane); in one line (axis); in the common point (at the center of growth).

Oriented growing of new formations on crystal support received the name "epitaxy". It may take place by two similar mechanisms, which display the successive stages of epitaxic crystallization. By one mechanism atoms or molecules of new formations in accordance with the requirements of minimum inter-phase surface energy, continue crystallic lattice of the support preserving its symmetry. The value of the periods of lattice of support in the plane of mating (at the same symmetry) may be preserved . The second mechanism is realized, if there is big discrepancy between the periods of plane cells on the boundary of mating between the new formation and the support.

Analysis of Laue-patterns and microdiffractogramms of contact zones of mated crystals showed (Butt et al, 1972; Timashev and Kolbasov, 1981), that intergrowth may take place after the diagram of Royer-Fridel. It is realized along plane nets, identical in form and approximately equal in dimensions through superposition of crystallic lattices of contacting mineral phases without formation of "contact seam" (Butt et al 1970; 1971) . In such way, the formula of Royer (Royer, 1928) is applicable for the evaluation of possible mating of hydrate phases between themselves and with minerals of the support. And on the base of value of Δ up to 15%, the perfection of structure of contact zone "hydrate (the product of corrosion) - mineral of support" may be evaluated . This determines the ability of crystallic lattices of contacting elements to form epitaxic structures of intergrowth.

Minerals in the surface zone of aggregate, as well as the hydrates originated on their surface, may have an infinite number of different orientiations in relation to each other. That is why it is reasonable to establish the value of potential interaction of their crystallic lattices by the summary and medium intensity of the interaction between hydrates and minerals an aggregate (Dubnytchky et al, 1993) . Such system is realized in the programming language "C ++" in IBM compatable computer.

Results

For cement hydrates and the products of their chemical corrosion was found the sum of potential interactions in the scale of - S, with each of main rock forming minerals of aggregate within certain quantity of interaction - n.

Widespread cement hydrates : portlandite; hydroaluminates of calcium containg 3, 6, 8, 13 and 19 molecules of water; gel of tobermorite and its 0,9; 1,1; 1,4 nm varieties; low-basic hydrosilicates of CSH type; double-basic hydrosilicates; C_2SH_2; xonotlite, okenite, girolite, hillebrandite; complex compounds of calcium carboaluminates, hydrosulfoaluminates, chloroaluminates of calcium; and also the products of corrosion - gypsum, calcite were evaluated. As mineral supports were considered natural and artificial minerals represented by unhydrated and hydrated silicates; aluminosilicates, carbonates, oxides and hydroxides (42 minerals).

The level of mating of hydrates (or products of corrosion) with the minerals of aggregete was suggested to be determined by the value of relation S/n, so called the "criterion of mating" .

We succeeded to reveal the tendency of cement hydrates to grouping (Fig.1) by the ability to form epitaxic intergrowths with support. The five classes of cement hydrates with the different level of intergrowing with the minerals of aggregate were selected:
I class - most active; II - highly active; III - active; IV - medium active; V - low active.

Reliability of selection of classes is confirmed by the compactness of grouping of different mineral phases, caused by the closeness of criterions of mating, and also by the neighbourhood of compounds close in crystallochemical aspect.

Classification of hydrate phases follows the closeness of the values of criterions of mating combined in certain groups. For example, in the first class there are hydrates with close crystallochemical parameters - different double basic hydrosilicates and secondary calcite (product of corrosion). The possibility of mating of hydro-silicates of type 1.1 nm tobermorite with the surface of clay mineral beydelite was shown. According to the value of Δ =0.4% the most possible mating may take place between "b" axes - of beydelite and "c" - of tobermorite.

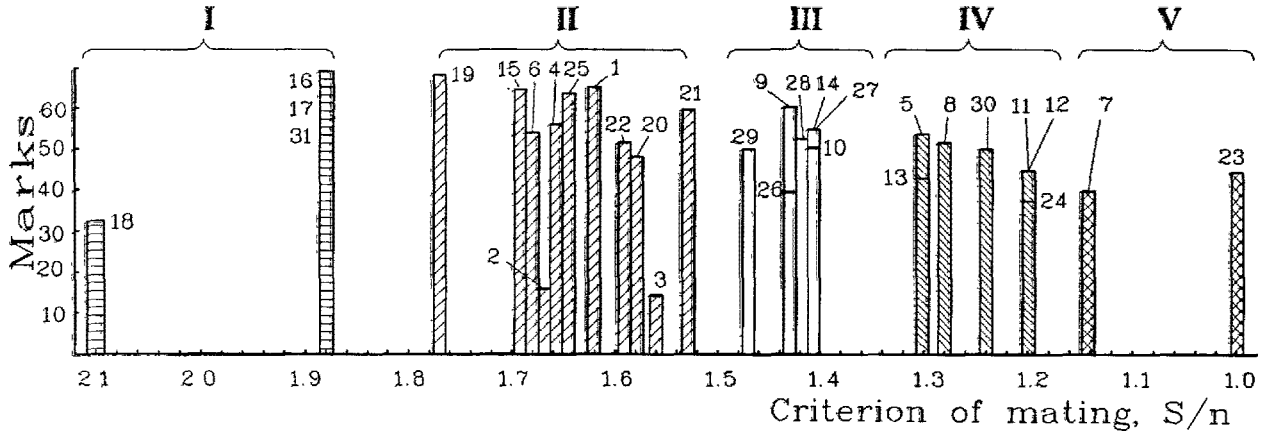

Figure 1. Classification of hydrates by the criterion of their mating with the minerals of aggregates:

1 - portlandite; 2 - CAH_3; 3 - C_3AH_6; 4 - b C_2AH_8; 5 - C_4AH_{13}; 6 - C_4AH_{19}; 7 - alumosilicate; 8 - $C_3A{\cdot}CaCO_3{\cdot}13H_2O$: 9 - gel of tobermorite; 10 - 0.9 nm tobermorite; 11 - 1.1 nm tobermorite: 12 - 1.4 nm tobermorite; 13 - CSH I; 14 - CSH II; 15 - low-basic hydrosilicate ; 16 - double-basic hydrosilicate 1; 17 - double-basic hydrosilicate 2; 18 - C_2SH_2 1; 19 - C_2SH_2 2; 20 - xonotlite; 21 - okenite; 22 - girolite; 23 - afwillite; 24 - hillebrandite; 25- $C_3A{\cdot}CaSO_4{\cdot}12H_2O$; 26 - $C_3A{\cdot}CaSO_4{\cdot}32H_2O$; 27 - carboaluminate; 28 - chlorinealuminate 1; 29 - chlorinealuminate 2; 30 - gypsum; 31 - calcite.

The suggested classification of cement hydrates by the criterion of mating, allows to evaluate their potential possibility, while forming strong epitaxical aggregation with mineral filler. This will ensure predicting the possibility of obtaining the compact and strong structure of contact zone in cement materials.

REFERENCE

Butt Y.M. et al. The regularities of formation of crystalls and crystal intergrowths of HSC in hardening cement rock. - Cement, N 9, 1970. - p. 14-16;

Butt Y.M. et al. Crystals and crystal intergrowths of hydrosilicates of calcium and their complex compounds in hardening cement rock. - Cement, N 7, 1971. - p. 7-9.

Butt Y.M. et al. Aggregation of hydroxide of calcium with quartz and calcite.- Cement, N 5, 1972. - p. 13-14;

Dubnytchky V.Y., et al. - Experimental - Statistical models in comruterized study of materials / Abstract of International Seminar. - Odessa, May 1993. - p. 3-4.

Palatnik L.S., Papirov I.I. Oriented crystallisation. - Moscow, 1964 - 408 pp.

Palatnik L.S., Papirov I.I. Epitaxical films. - Moscow., 1971. - 480 pp.

Royer L. Bull. Soc. franc. mineral, 51, 7, 1928. - p. 42-46.

Timashev V.V. and Kolbasov V.M. Properties of cement with carbonate admixtures. - Cement, N 3, 1981. - p. 10-12.

Kn o. 25. JAN. 2001 d o k 31779

2ii016
4 pp

CONTROLLING THE HYDRATION OF PORTLAND CEMENT AND CONCRETE'S PHYSICAL AND CHEMICAL PROPERTIES BY THE SURFACE OF MINERAL AGGREGATES

P.G.KOMOKHOV, University of Means of Communication, St.Petersburg, Russia
N.N.SHANGINA, University of Means of Communication, St.Petersburg, Russia

ABSTRACT The process of hydration of portland cement may have a different degree and composition of formed products, depending on the acid-base properties of aggregates' surfaces. Fine-ground mineral additives with the predicted properties of the surface can be used for I) improving concrete's mechanical properties; 2) obtaining concrete protecting from ionizing radiation.
Activation, composite cements, freeze-thaw damage, immobilization, long age

INTRODUCTION

The existence of different types of active centres of three-calcium and β-two-calcium silicates and their influence on the process of cement's hydration has been proved by a number of methods (Decamp, 1976; Chatterji, 1983 and Boikova, 1984). Besides, there are conceptions about the possibility to control the hydration and the properties of a cement stone by introducing substances, including almost insoluble ones, which are able of influencing the active centres of clinker minerals or the electronic sub-structure of the surface (Svatovskaya and Sychyov, 1983).

When using a fine aggregate as a constituent of concrete one should take into consideration its properties such mineralogical composition, specific area and pozzolanic activity. Normally, the presence of active centres on the aggregate's surface and its influence on the hydration of cements is not estimated. In this research the acid- base properties of surfaces of aggregates used in cements were investigated with the indicator method.

ACID-BASE PROPERTIES OF MINERAL AGGREGATES

The differences in the acid-base properties of mineral aggregates' surfaces can be seen when the adsorption centres distribution (ACD) curves, built for such widespread natural mineral aggregates as fine-ground basalt and natural purely quartz sand, are compared (Fig. 1).

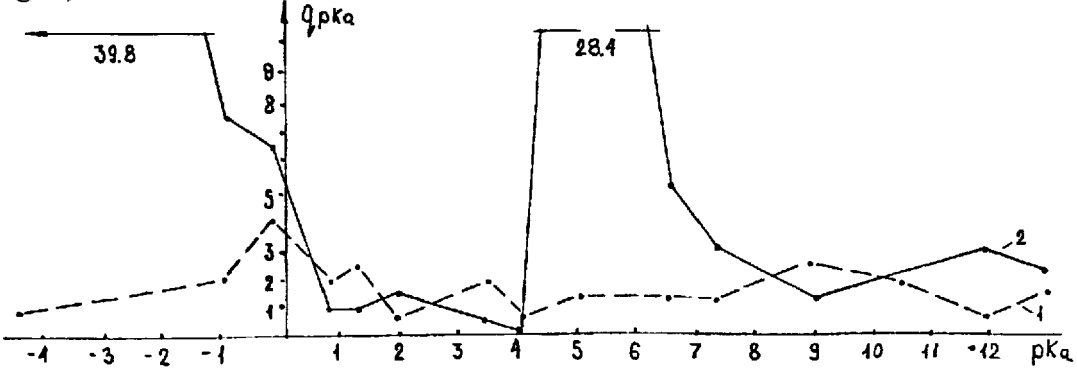

Figure 1 Distribution of acid-base centres on the surface of 1. - natural sand and 2. - basalt

The specific area of the studied samples is equal (0.9 - 1.16 m^2/g). The curves are built on the coordinates $q_{pKa}x = S(_{pKa}x)$, where $q_{pKa}x$ is the content of active centres equivalent to the amount of the adsorbed indicator of such acidic force ($_{pKa}x$).

Table 1 gives the generalized data, which allow to estimate the acid-base properties of substances' surfaces by the area of stripes on ACD spectra.

Table 1 Distribution of acid-base centres on the surface of mineral substances

Mineral substance	Area of stripes on ACD spectra		
	pKa^x from 5 to 0	pKa^x from 0 to 7	pKa^x from 7 to 14
Limestone	17,30	9,76	10,97
Marble	4,62	9,45	4,04
Natural gypsum	6,65	8,14	15,05
Shungite	46,54	22,93	45,59
Shungisite	40,75	22,11	16,39
Zeolite (Clinoptilolite)	47,10	22,58	13,18
Basalt	95,78	41,71	15,55
Clay (Kaolinite)	26,26	44,63	42,95
Ceramsite	12,94	15,38	11,51
Slag 1	27,80	58,22	22,59
Slag 2	19,07	10,17	4,86
Pure quartz	3,41	20,43	6,18
Quartz sand	7,45	8,70	10,32
Sea sand	28,87	26,67	30,97

INFLUENCE OF ACID-BASE PROPERTIES OF AGGREGATES SURFACES ON THE STRENGTH OF THE CEMENT STONE

The results of testing of samples made of portland cement with aggregate admixtures, as well as the investigation of cement's hydration products allow us to make the following conclusions:

1) The replacement of a part of cement by substances, which have intensive stripes on the ACD spectrum in the sphere of acidity indication pKa =0-7, does not reduce, and in some cases even increases the cement's strength. The typical example is the equal strength of a cement stone and a mixed binding cement containing 50% basalt. During the investigation of the hygration products of cement with basalt additives with the x-ray phase analysis method, an increase in the degree of hydration was established. Such influence of the aggregate is explained by the accepting properties of atoms of the surface's metal, capable of activating the surface of clinker minerals.

2) The presence on the aggregate's surface of strong Lewis's base centres (pKa = 5-0) can increase the ionic content OH^- in the contact zone between the aggregate and cement, locally increasing pH and favouring the transfer of calcium ions in the mortar for the compensation of the negative charge

3) The intensification of the donor properties of the aggregate's surface atoms (pKa>7) is accompanied by the lowering of the degree of clinker minerals' hydration and a

decrease in the material's strength, which is explained by the capacity of substances-donors of electrones to suppress the activity of clinker minerals surface

Table 2 Changing of acid-base properties of the aggregate's surface and the strength of the cement stone sample.

Aggregate	Area of stripes on ACD spectra			Changing of strength in compression, % of the control samples	
	pKa = -5-0	pKa = 0-7	pKa = 7-14	7 days	28 days
Natural sand	28,87	26,67	30,97	93	88
Natural sand after a heat treatment at t = 600°C	13,07	39,27	21,75	126	117
The same at t = 900°C	28,31	9,12	22,08	74	91
Modified natural sand $NiCl_2$**	7,62	48,12	10,0	162	147

* The strength of the cement stone without an aggregate is taken for 100%; the aggregate content is 20% of the cement's weight; w/c = 0.29

** The modification is done by the injection of $NiCl_2$ from the water solution.

OBTAINING CONCRETE OF HIGHER FROST-RESISTANCE

The changing of the acid-base properties of the aggregate's surface in the case of modification, as the data of x-ray phase and differential thermal analyses show, increases the degree of cement's hydration and changes the composition of the formed calcium hydro-silicates. The content of low base C-S-H rises, with which an increase of concrete's frost-resistance is connected (Fig.2).

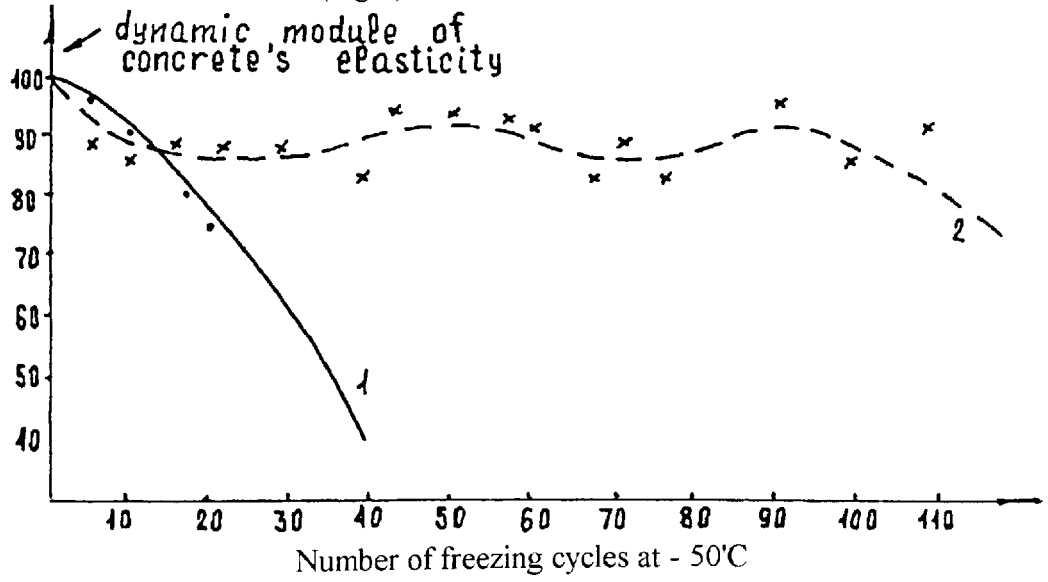

Figure 2 Changing of the dynamic module of concrete's elasticity during frost resistance tests 1 - control composition; 2 - with the aggregate (modified sand $NiCl_2$).

OBTAINING CONCRETE FOR PROTECTION FROM IONIZING RADIATION

The choice of the carbon-containing aggregate for concrete was based on the data of Table 1. Natural shungite has peaks of high intensity on the ACD spectrum in the sphere of acidity indication pKa from 7 to 4, which has a negative effect on cement hydration. The heat treatment of, with the purpose of obtaining the artificial material shungisite, changes the properties of the surface. The area of stripes on the ACD spectra in the sphere pKa = 7-14 is reduced by three times, the activity in the sphere pKa = 5-7 being invariably high. Figure 3 shows the kinetics of changing of concrete's strength with normal hardening and γ-radiation.

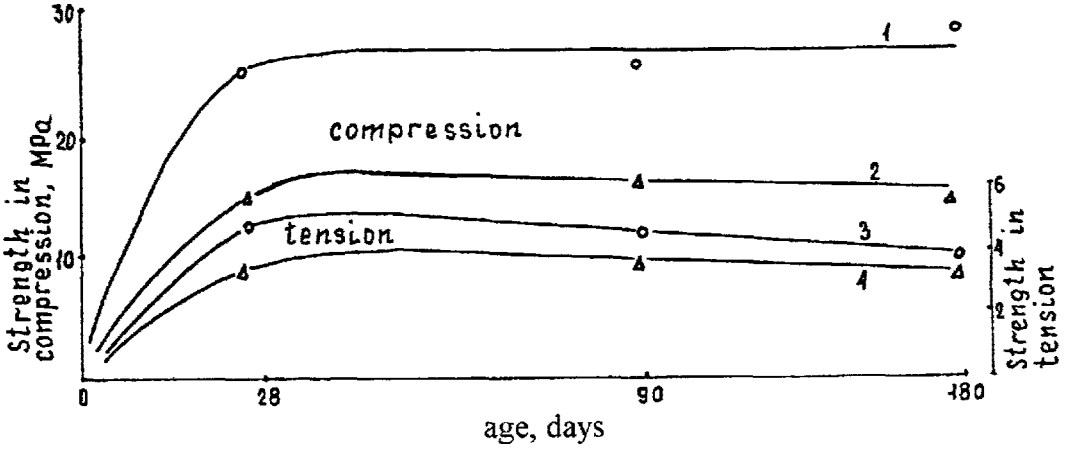

Figure 3 Kinetics of changing of concrete's strength (the aggregate is shungisite) with γ-radiation. 1 and 3 - concrete's strength when radiated. 2 and 4 - concrete's strength of control samples of normal hardening .

REFERENCES

Boikova, A.I., "Physical and Chemical Properties and Crystal Chemical Peculiarities of Phases of Portland Cement Clinker", Dissertation Report for the Degree of Doctor of Chemical Sciences, Leningrad, 1984, p. 38.

Chatterji, A.K., Phatak, T.S., "Semiconduction and Cement Hardening", Nature, 1983, No 16.

Decamp, G., Feran, P., Verhagen, D.P., "Chemical Defects and Hydration of Activated C,S", Works of 6th International Cement Chemistry Congress, Moscow, Stroiizdat, 1976, Part. 2, Vol. 1.

Svatovskaya, L.B., Sychyov, M.M., "Activated Hardening of Cements", Leningrad, Stroiizdat, 1983, p.159.

Tanabe, K., "Solid Acids and Bases", Translation from English by A.A.K.ubasova and B.V.Romanovsky, Moscow, Mir, 1974

Kno. 25. JAN. 2001 dok 31180

2ii017
8 pp

RELATIONSHIP BETWEEN ETTRINGITE FORMATION AND THE DEVELOPMENT OF STRENGTH FOR RAPID HARDENING CEMENT

Naotaka KONDO*, Yasuyuki NIKAIDO*,Seiiti NAKAYA*, Minoru HANDA*,
Tetsuya ANDO*, Etsuo SAKAI** and Masaki DAIMON**
* Cement & Special Additive Laboratory, Denki Kagaku Kogyo Co.,Ltd., NIIGATA, JAPAN
**Dep. of Inorganic Materials, Tokyo Institute of Technology, TOKYO, JAPAN

ABSTRACT The greatest factors for the bond strength development of rapid hardening cements are the vibration and the flowability. In the case of cement which produces ettringite form water pouring, the flowability lowers with time, and it should be given a stronger vibration in order to provide a high bond strength. In the case of cement which forms a little ettringite for several minutes from water pouring, the flowability is maintained until the termination of handling time and high bond strength is developed easily by the vibration.

Key-words : rapid hardening cement, strength development, ettringite, vibration, flowability

INTRODUCTION

In Japan, sudden increase in traffic density has caused remarkable damage to the floor slab of the bridge by the old design standard. It can't be coped with by local repairing when the damage spreads a extensive area. On this account, "superstructure reinforcing method with overlaid reinforced concrete" is adopted for reinforced construction to extend the whole floor slab.

The outline of the superstructure reinforcing method with overlaid reinforced concrete is as follows. First, the weak portion on the surface of the existing floor slab to be reinforced is removed, next the concrete which is used rapid hardening cement and mixed with steel fiber by 1.27vol% ($100kg/m^3$) is placed. Then the floor slab is made to have greater thickness than before, and further rapid hardening concrete is vibrated and finished the surface by a concrete finisher. An example of the superstructure reinforcing method with overlaid reinforced concrete was showed by a cross section in **Figure 1**. The characteristics against shearing and bending stress of the floor slab are increased by this reinforcing method (Express highway research foundation of Japan, 1995).

The main properties required for the rapid hardening concrete the reinforced the steel fiber are prescribed that slump is 50±15mm and handling time is more than 40min, compressive strength at three hours is $24N/mm^2$ more and bond strength is $1N/mm^2$ or more. Particularly the bond strength is a important property. The reinforcement effect by this method is reduced to half, if the old and new concrete isn't unified. When a kind of rapid hardening cement varies, bond strength is different in the present situation. The influence of the vibration for the bond strength of a rapid hardening concrete has been reported already (Express highway research foundation of Japan, 1995). The bond strength development varied the rapid hardening cement. However there are few reports about it (Momiyama et al,1996).

This report intends to clarify the relationship between ettringite formation and bond strength clear by grasping the factors affecting the bond strength and by analyzing of the initial stage of hydration of the rapid hardening cements.

THE RAPID HARDENING CEMENTS

In the superstructure reinforcing method with overlaid reinforced concrete, the rapid hardening cement is used in order to satisfy a prescribed property which the compressive strength at 3 hours is24N/mm^2. In this report, two kinds of rapid hardening cement was examined. The one was a cement Type-A that was burned and crystalline calcium fluoro aluminate ($11CaO \cdot 7Al_2O_3 \cdot CaF_2$). The other was a cement Type-B that was admixed high early strength portland cement with amorphous calcium aluminate ($12CaO \cdot 7Al_2O_3$). Both $11CaO \cdot 7Al_2O_3 \cdot CaF_2$ and $12CaO \cdot 7Al_2O_3$ are materials that have the property of quick setting. **Table 1** showed the chemical composition of two types of rapid hardening cement.

[cross section]

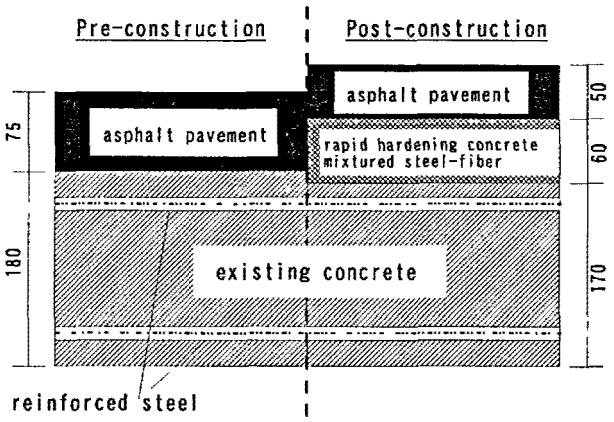

Fig.-1 Example of superstructure reinforcing method with overlaid reinforced concrete

EXPERIMENTAL

Materials

Table 2 shows materials used for experiments.

Table 1 Chemical composition of Rapid hardening cement (%)

Cement	Igloss	Insol	SiO_2	Al_2O_3	Fe_2O_3	CaO	MgO	SO_3	Na_2Oeq	main component
Type-A	0.6	0.1	13.8	11.4	1.5	59.1	0.9	10.2	0.8	crystalline $11CaO \cdot 7Al_2O_3 \cdot CaF_2$
Type-B	2.0	0.2	15.7	9.7	2.0	58.2	0.8	9.7	0.7	amorphous $12CaO \cdot 7Al_2O_3$

Table 2 Materials used for experiments

Mark	Materials		Specifi gravity	Note
C	Rapid hardening cement	Type-A	3.04	Specific surface area : 5300 cm^2/g
		Type-B	3.02	Specific surface area : 4700 cm^2/g
(HPC)	High-early-strength cement		3.12	Specific surface area : 4250 cm^2/g
S	Sand		2.61	Producing district in Gifu, Japan Coefficient of water absorption : 1.95% Fineness modulus (FM) : 2.94
G	Gravel		2.66	Crushed stone, Producing district in Gifu Coefficient of water absorption : 1.10% Solid volume percentage : 61.1% Fineness modulus (FM) : 6.60
HWRA	High-range Water-Reducing Admixture	for Type-A	1.21	Sodium salts of naphthalene sulfonates formaldehyde high condensates
		for Type-B	1.14	Mixture of Sodium salts of naphthalene sulfonates formaldehyde high condensates and Sodiumsalts of refined lignosufonates
S F	Steel Fiber		7.85	ϕ 0.6 × 30mm

Test conditions of concretes and mortars

The mixing of concretes and mortars were carried out in a 50 liter capacity vertical pan mixer. The mixing time was fixed 3 minutes. Then a retarder was added by 0.2% to the cement Type-A in order to be equal with Type-B at the handling time. It was dissolved in mixing water to be used.

The bond strength was measured about rapid hardening concretes reinforced with steel fiber and mortars of C/S=1/2. In the bond test using concrete, the relationships between the bond strength and the slump loss, the slump value and vibration time were examined. In the mortar test, relationship between the bond strength and water-cement ratio (W/C) was investigated.

Table 3 showed the mix proportion and the test conditions.

Method of bond strength

Table 4 showed the mix proportion and the physical properties of the base concrete used for the bond strength test. The method of the bond strength test was as follows :

i) The surface of the base concrete was roughed. The surface was dry same as the actual construction.

ii) The rapid hardening concrete or mortar was placed on the base concrete.

iii) The jointing concrete or mortar was given vibration by a vibrator.

iv) The cores were bored by a drill with 10mm diameter after 2 hours or more from the mixing.

v) The bond strength was measured by tension tester at 1day.

Table 3 Mix Proportion of Concrete and Mortar

TEST No.		Cement -type	Gmax (mm)	Slump (mm)	Air (%)	W/C	s/a (C/S) (%)	Unit (kg/m³) W	C	S	G	SF	HWRA	Vibration Time (sec)	SL or Flow (mm)	Handling Time (sec)	Compressive strength (N/mm²) 3hr	1day
I	1	A	20	50	2.0 ± 1.0	0.39	55.0	179	460	916	764	100	9.20	20	50	42	23.7	48.8
	2	B		50		0.36	52.0	167	468	877	825		9.36		50	33	35.8	49.0
II	1	B		20		0.36	52.0	159	445	899	845		8.90	20	20	35	35.6	50.9
	2			20										20				
	3			80		0.36	52.0	175	490	857	806		9.80	20	75	32	32.3	50.4
	4			80										20				
III	1	B		50		0.36	52.0	167	468	877	825		9.36	5	55	36	34.0	52.8
	2			50										10				
	3			50										15				
	4			50										30				
	5	A		50		0.39	55.0	179	460	916	764		9.20	10	45	40	24.1	51.8
	6			50										15				
	7			50										30				
IV	1	A			2.0 ± 1.0	0.35	1/2	237	678	1356	non	non	non	20	128	30	31.8	66.6
	2					0.45		286	634	1268	non	non	non		207	36	20.8	46.7
	3					0.55		328	596	1192	non	non	non		235	38	12.4	34.1
	4	B				0.35		237	677	1354	non	non	non		206	36	35.6	57.5
	5					0.45		285	633	1266	non	non	non	non	269	46	13.0	31.6
	6					0.55		327	595	1190	non	non	non		317	56	7.9	21.2

Table 4 Mix proportion and Physical properties of Base-concrete for Bond-test

Mix Proportion of Base-concrete										
Cement	Gmax (mm)	Slump (mm)	Air content (%)	Water-Cement ratio	Sand-Aggregate ratio (%)	Unit (kg/m ^{3})				
						W	C	S	G	HWRA (A)
HPC	20	80	4.0	0.34	39.5	162	477	666	1040	4.77

Properties of Fresh concrete			Strength of Hardened concrete (N/mm ^{2})	
Slump	Air cont.	Concrete temp.	Compressive(age:7d)	Tensile (age:7d)
85 mm	3.0 %	21.0 ℃	54.4	4.43

Table 5 Testing items and methods

Items	Methods and others
a)Slump	Follow JIS A 1101 : Method of test for slump of concrete
b)Handling Time	Time maintained the workability from mixing up to rise to 1 ℃ in a temparature
c)Compressive Strength	Follow JIS A 1108 : Method of test for compressive strength
d)Bond Strength	Dimension of mould : W 550 × D 400 × H 180 (mm) Base-Concrete Age : 7 days Physical properties : Table-3 Thickness : 80 mm Rapid hardening concrete Slump : 20,50,80 mm Steel fiber in concrete : 1.27 vol.% (100kg/m ^{3}) Rapid hardening mortar W/C : 0.35,0.45,0.55% Steel fiber in mortar : non Thickness : 80 mm Vibrator Frequency : 158 Hz Ampitude : 0.6 mm Vibration Time : 5,10,15,20,30 sec Core diameter : ϕ 10mm (7850mm ^{2}) Equipment : Tention tester
e)Table Flow	Follow JIS R 5201 : Physical testing methods for concrete

The concrete or the mortar was were placed at immediately after mixing unless the time was specified. **Table 5** showed items of the evaluation and the method. All experiments were conducted in a constant-temperature chamber at 20±2℃.

Method of analysis of initial hydration for cement pastes

Two cement paste were mixed at a water-cement ratio (W/C) of 0.5. In the same way as in the concrete test, the retarder was added by 0.2% to the cement Type-A, and was dissolved in mixing water to be used. Mixed paste was put in a styrene bottle, and was stored in an experimental chamber at 20±2℃. Hydration was stopped after a predetermined time, and sampling was made. The hydration stop method was as follows : A large quantity of acetone was added to grind the material using an alumina mortar. (Nikaido et al, 1995) Thereafter, it was dried in a constant temperature bath at 50℃ for 16 hours. Sampling time was 5, 30, 60, 90, 120,180, and 300 minutes.

Specimens sampled were analyzed in term of X-ray diffraction added with α-alumina by 10% as the internal standard. Ettringite determination was conducted by applying the method of least squares to the ettringite peak (d=0.973nm) to calculate the area.

RESULTS AND DISCUSSION

The bond strength of the rapid hardening concretes

a) The relationship between the time from mixing and the slump loss

Concerning rapid hardening concrete Type-A and Type-B, the relationship between the time from mixing and the slump was investigated. The result was shown in **Figure 2**. The handling time for the rapid hardening concrete was 40 minutes for Type-A, and 33 minutes for Type-B. The concrete used cement Type-A decreased the slump with passed time from mixing. However the concrete with cement Type-B changed little slump with time.

b) The relationship between the time of concrete placing and the bond strength

The bond strength at 1 day of concretes were measured with various time of concrete placing from mixing. These concretes were vibrated for 20 seconds. The result was shown in **Figure 3**. The time in Figure 3 corresponded to the slump loss as shown in Figure 2. In the case of cement Type-A, the bond strength reduced in proportion to the time of concrete placing. In the case of cement Type-B, the bond strength decreased with time likewise. However, the bond strength of the concrete Type-B had a lower rate of reduction than that of concrete Type-A. The fractured section was a boundary between base concrete and joined concrete.

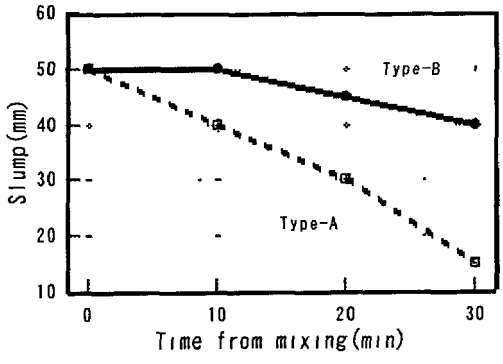

Fig 2 Relationship between Time from mixing and Slump of rapid hardening concrete

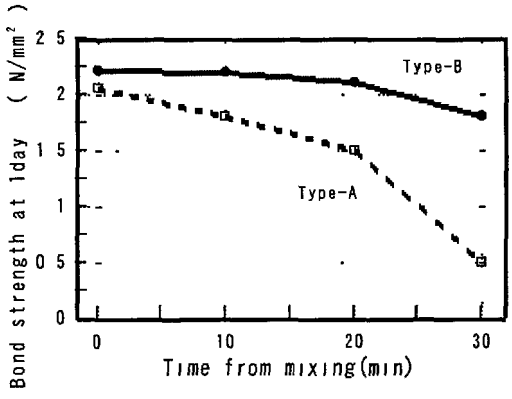

Fig 3 The relationship between Time of concrete depositing from mixing and Bond strength

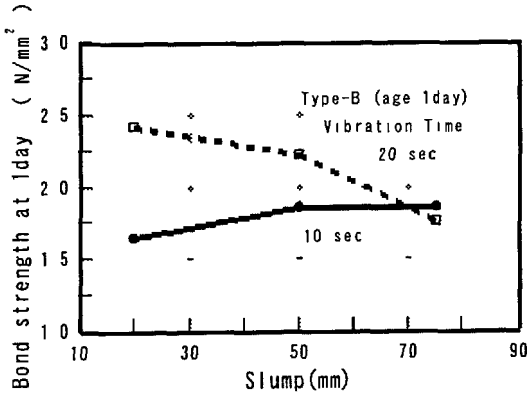

Fig 4 The relationship between Various slump and Bond strength of concrete used cement Type-B

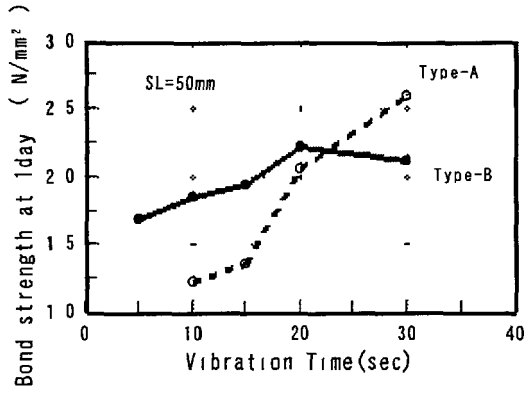

Fig.5 The relationship between Vibration time and Bond strength at 1day

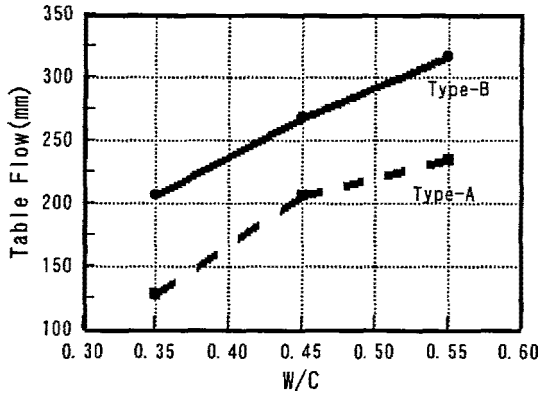

Fig.6 The relationshoip betweem Mortar Flow and Water-cement ratio,W/C

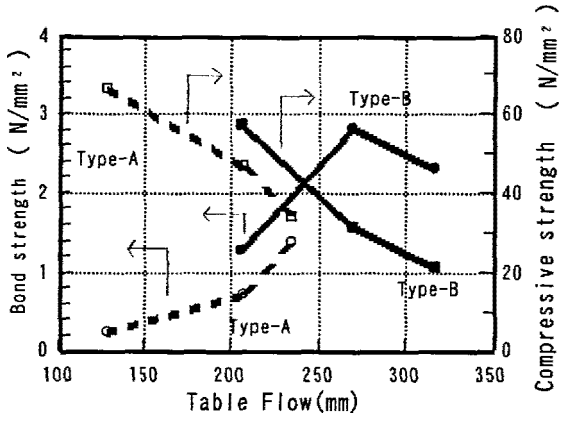

Fig.7 The Relationship between Mortar flow and Bond strength and Compressive strength at 1day

c) The relationship between various slump and the bond strength

The relationship between the slump and the bond strength for concrete Type-B was tested with the vibration time varied. **Figure 4** showed the result. When the vibration time was 10 seconds, the bond strength wasn't affected by the slump, and was almost fixed. However, in the case of the vibration time with 20seconds, the bond strength became higher with lower slump.

d) The relationship between the vibration time and the bond strength

Concerning concrete Type-A and type-B whose slump was 50mm, the change in the relationship between the vibration time and the bond strength was investigated, and its result was shown in **Figure 5**. The bond strength of Type-A was higher with the longer vibration time. The difference of the bond strength between Type-A and Type-B was shortened, when the vibration was longer. The bond strength of Type-B decreased at vibration time 30 seconds and was lower than that of Type-A. Therefore it is considered that the most suitable condition of the vibrating compaction is different between Type-A and Type-B.

The bond strength of the rapid hardening mortars

Table flow, compressive strength and bond strength of mortars were examined, when water-cement ratio (W/C) was varied 0.35 , 0.45 and 0.55 for cement Type-A and Type-B. The vibration time was set to 20 seconds for Type-A mortars. In the case of Type-B, the mortar of W/C = 0.35 was vibrated for 20 seconds, and the others were given no vibration. At the same W/C, Type-B took higher flow than Type-A (**Figure 6**). **Figure 7** showed compressive strength and bond strength ranged by the flow table spread. Type-A showed higher than Type-B about the compressive strength, however Type-B had higher the bond strength than Type-A. Mortar having high flowability develops strong bond strength with no vibration. The flow table spread of Type-B mortar mixed with W/C = 0.55 was 317mm. This mortar was broken itself when measured the bond strength. The destruction of mortar happened to cause that the tensile strength was weaker than the bond strength. In Figure 7, the bond strength and the compressive strength were in inverse proportion. Therefore it's thought that the bond strength is affected by flow table spread, that is, the flowability, and that the compressive strength does not become a great factor for the bond property.

As results of various bond strength test, it's found that two types of rapid hardening cement

having different flowability take different bond strength development by the vibration. A mechanical mechanism of the vibration compacting of a concrete is explain by the next process. When a vibration is given to a concrete, a force of inertia acts to particles in the concrete whereby the shearing resistance between the particles is lost. Then the concrete become to move. Afterwards the concrete particles are subsided or moved by gravity, and arranged again (MURATA, 1996). On this account, to give the vibration energy to the concrete is to move it, and then high bond strength is obtained. It's considered that the concrete having high flowability is easy to be moved by vibration. Therefore, it's thought that the concrete used with Type-A can't be promoted a movement by a vibration, unless a stronger vibration energy is given in it. And it's considered that it may be possible to prevent the bond strength from lowering if even concrete with slump-loss is given strong vibration.

In the case of Type-B, it is similar as Type-A that the bond strength increases in proportion to magnitude of given vibration energy. Its bond strength become higher than that of Type-A since Type-B has higher flowability and is liable to be moved. However the bond strength of Type-B lowers when the vibration time is too long. It's supposed that this trend appears with a concrete having higher flowability conspicuously. In the case of mortar as a grout material, it is considered that strong bond strength is developed with no vibration. It's necessary to study in detail measurement of the vibration energy by the response value of the concrete in the future.

Initial stage of hydration of the rapid hardening cement pastes

In previous sections, it is found that the fresh concrete or mortar which is not setting is important for the bond strength development. The rapid hardening cement develops the strength early by means of ettringite formed by hydration of calcium aluminate (Uchikawa,1972). **Figure 8** showed the result obtained by determining ettringite with XRD. It has been found the rapid hardening cement Type-A and Type-B differ in amount of formation of ettringite during initial hydration process from water pouring to terminated handling time. In the case of cement Type-A, formed ettringite was seen immediately after water was poured. The handling time of Type-A finished when the formation of ettringite has progressed to some degree.

It's considered about the concrete of Type-A that the rate of slump loss is fast since the ettringite is formed more by degrees from water pouring. However the correlation between a quantity of the ettringite formation and termination of the handling time is a subject in the future.

In the case of cement Type-B, a little ettringite was found for several minutes from water pouring. The handling time was over when the ettringite started to form suddenly. Therefore it's thought that the flowability is maintained until the termination of handling time. The following can be considered about the bond strength development for the vibration, the flowability and the initial hydration process.

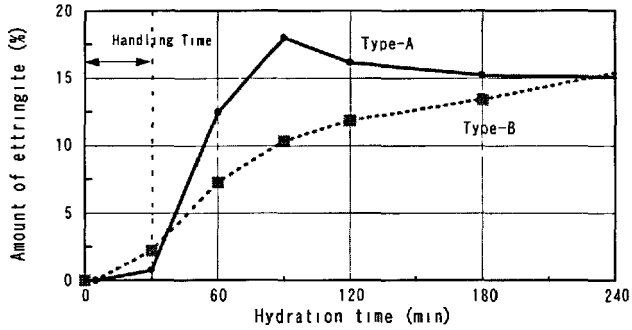

Fig.8 The relationship between the hydration time and amount of ettringite by XRD

The flowability is maintained during handling time. Then the concrete or mortar is liable to be moved by vibration. In the case of cement Type-A, ettringite is produced continuously from the early stage. The concrete or mortar of Type-A should be moved by given a stronger vibration in order to obtain a high bond strength. On the other hand, the bond strength of the concrete or mortar of cement Type-B is higher than one of Type-A if the vibration is given it. Its reason is considered that Type-B is liquefied easier than Type-A since Type-B forms less ettringite than Type-A during handling time. However, when too strong vibration is given it, the reason which the bond strength is lowered is considered that a thin layer having a plenty of segregation water and low strength is formed at the jointing surface between the base concrete and the rapid hardening concrete because cement Type-B is moved easily.

CONCLUSION

In our study, the followings were made clear about the relationship between the ettringite formation and the development of bond strength for two kinds rapid hardening cement.

i) The development of bond strength is affecting the vibration energy given to the concrete and the flowability of the concrete or the mortar, and the compressive strength isn't a strong factor for the bond property.

ii) It is considered that to give the vibration energy to the concrete and mortar is to move it, and then high bond strength is obtained.

iii) The most suitable condition of the vibrating compaction is different between cement Type-A and Type-B.

iv) The flowability is different since the ettringite formation is different at initial stage of the hydration between Type-A and Type-B.

v) In the case of Type-A, the flowability lowers with time, and the concrete or mortar should be given a stronger vibration in order to provide a high bond strength, since ettringite is produced continuously form water pouring.

vi) In the case of cement Type-B, the flowability is maintained until the termination of handling time and high bond strength is developed easily, since a little ettringite is formed for several minutes from water pouring by the vibration. However, the bond strength is decreased when too strong vibration energy is given to it.

The correlation between a quantity of the ettringite formation and the termination of handling time, and a measurement of magnitude of the vibration energy given to the concrete are subjects in the future.

REFERENCE

Express highway research foundation of Japan, Superstructure reinforcing method with overlaid reinforced concrete manual, 97-99 (1995)

Murata,J., "Some knowledge of Concrete vibrators," Proceedings of Japan Concrete Institute, Vol.33, No.8, 1995

Nikaido,Y. Itoh,T. Sakai,E. and Daimon,M., Proceedings of the Japan Concrete Institute, Vol. 17, No.1 (1995)

Sakai,E. Nikaido,Y. Itoh,T. and Daimon,M., "Ettringite formation and microstructure of rapid hardening cement," to be presented (1996)

Uchikawa,H. and Uchida,S.,"The hydration of $11CaO \cdot 7Al_2O_3 \cdot CaF_2$ at 20℃ " Cement & Concrete Res., Vol.2 , 681-695 (1972)

K n o. 2 5. JAN. 2001 d o k 31781

2ii018
4 pp

INTERRELATIONSHIP AMONG LIME CONTENT OF CLINKER, ITS MICRO-STRUCTURE, FINENESS OF OPC GRINDING AND STRENGTH DEVELOPMENT OF HYDRATED CEMENT AT DIFFERENT AGES

S. P. GHOSH, National Council for Cement and Building Materials, New Delhi, India
K. MOHAN, National Council for Cement and Building Materials, New Delhi, India

ABSTRACT A rational correlation among lime content of clinker, its microstructure, fineness of OPC grinding and strength development of hydrated cement at different ages has been established. The study shows that the two most important factors affecting strength development of hydrated cement are : (i) mineral phase composition and microstructure of clinker, and (ii) particle size distribution of ground cement. The granulometry of clinker affects its grindability, measurable in terms of specific surface, whereas the mineral phase composition and microstructure of clinker affects the variations in (a) particle size distribution of ground cement, and (b) strength development of hydrated cement at different ages.

KEY-WORDS: Microstructure, Fineness, Strength development, Particle size distribution

INTRODUCTION

Microscopical observation is the most handy method to check the quality of cement. The microscopical method has been successfully used on the quality control in Japan, the USA and Canada. The relations between the burning conditions and the microscopical characters of clinker minerals are rather simple. The relations between the hydraulic activity and the microscopical characters are complicated. There are many factors which are closely related with activity, but cannot be detected by microscope. Howevere, the principal parts of the factors can be derived from the burning conditions, which can be detected by microscope. And so, the 28 days strength can be predicted by microscopical observation. The early strength at 1, 3 and 7 days is strongly influenced by the particle size distribution of cement, the contents of alkali and sulphates, C_3A solid solution and probably many other unknown factors. Therefore, the early strength cannot be predicted by microscopical observation (Ono, 1980).

In distinction to methodologies (Ono et al, 1965 and Ono, 1980), evolved for prediction of 28 days strength of cement from formulae based on morphology and microstructure of the corresponding clinker, the present investigation aims at establishing a rational correlation among lime content of clinker, its microstructure, fineness of OPC grinding and strength development of hydrated cement at different ages.

CASE STUDIES

Studies on day-to-day variation in cement strength for two dry process plants - plant A and plant B - have been carried out. The data reported in the present study has been collected from two plants over a considerable period of time (3-4 months). From operational view point, since the particle size distribution of ground cement is dependent upon the cement mill type and design, number of compartments, grinding media type and compartment-wise loading, the studies have been done under the aforesaid process and operational parameters remaining nearly constant. The details of cement mill of both the plants are given in Table 1.

Table 1 Details of Cement Mill of Plants A and B

	Parameters	Plant A	Plant B
(i)	Capacity	80 TPH	80 TPH
(ii)	No of Compartments and length	2;4.85m x 8.15m	2;4.5m x 8.15m
(iii)	Horse Power of main drive	Twin, 2000 HP	Twin, 2000 HP
(iv)	Grinding media used	Hi-Chrome	Hi-Chrome
(v)	Grinding Media charge (Tonne)	I Compt 65.6	I Compt 64
		II Compt 129.7	II Compt 129

Table 1 - continued

	Parameters	Plant A	Plant B
(vi)	Mill Inlet draft (mm WG)	15-20	20-25
(vii)	Mill Outlet draft (mm WG)	150-160	160-170

Effect of lime content of clinker and fineness of cement on strength development of OPC

In general, compressive strength development in hydrated OPC is conventionally attributed to lime content of the base clinker and fineness (specific surface) of ground cement. The results of the effect of lime content of clinker and fineness (specific surface) of cement on strength development of OPC for both plants A and B are shown in Table 2.

Table 2 Clinker CaO, Cement fineness and Compressive Strength

Sl No	Sample Reference	Clinker CaO (%)	Specific Surface m2/kg	Compressive Strength (MPa)		
				3-days	7-days	28-days
	Plant A					
1	OPC-1	62.5	260.0	18.0	26.0	40.0
2	OPC-2	63.5	265.0	20.0	29.0	40.0
3	OPC-3	64.5	260.0	23.0	32.0	41.5
4	OPC-4	62.5	275.0	20.0	27.5	41.5
5	OPC-5	63.5	277.5	21.0	31.0	42.5
6	OPC-6	64.5	277.5	24.0	34.5	43.0
7	OPC-7	62.5	292.5	23.0	32.0	46.0
8	OPC-8	63.5	292.5	27.0	36.3	47.0
9	OPC-9	64.5	290.0	28.5	40.0	49.0
	Plant B					
10	OPC-10	63.5	252.5	21.0	29.0	42.0
11	OPC-11	64.5	255.0	26.5	35.0	43.0
12	OPC-12	65.5	252.5	27.5	37.0	45.0
13	OPC-13	63.5	272.5	24.0	36.0	47.0
14	OPC-14	64.5	270.0	27.5	39.0	48.0
15	OPC-15	65.5	270.0	29.5	41.0	47.0
16	OPC-16	63.5	285.0	29.5	39.0	49.0
17	OPC-17	64.5	285.0	31.5	43.0	50.0
18	OPC-18	65.5	282.5	33.0	44.0	50.0

In order to make a proper analysis and to arrive at a correct conclusion, only those clinkers have been included in the Table 2 which have more or less the same free lime and litre weight.

The results indicate that for plant A the compressive strengths at 3 and 7 days increase by about 20-30% and 20-25% respectively with increase in lime (CaO) content of clinker from 62.5% to 64.5% but with more or less the same fineness of cement. However, the compressive stsrength at 28 days is not affected much with increase in lime content of clinker. Similarly, for plant B the compressive strengths at 3 and 7 days increase by about 15-30% and 15-25% respectively with increase in lime content of clinker from 63.5% to 65.5% but with more or less the same fineness of cement. However, the compressive strength at 28 days remains unaffected with increase in lime content of clinker.

The results also indicate that for Plant A the compressive strengths at 3, 7 and 28 days increase by about 20-25%, 20% and 15-20% respectively with increase in fineness of cement from 260.0

m^2/kg to 290.0 m^2/kg but with same lime content of clinker. However, for plant B the compressive strength at 3, 7 and 28 days increase by about 20-40%, 20-35% and 10-20% respectively with increse in fineness of cement from 252.5 m^2/kg to 285.0 m^2/kg, but with same lime content of clinker.

The overall results show that for any particular plant, although higher lime content of clinker and finer grinding (higher specific surface) of cement is generally found to give a higher strength, the relationship is found to be mostly non-linear in majority of cases.

Effect of mineral phase composition and microstructure of clinker on strength development of OPC

The results of the effect of mineral phase composition and microstructure of clinker on strength development of OPC for both plants A and B are shown in Table 3.

Table 3 Mineral Phase Composition and microstructure of Clinker and Cement Compressive Strength

		Mineral Phase Composition %					Compressive Strength MPa		
Sl No	Sample Reference	C3S	C2S	C3A	C4AF	Microstructure	3-days	7-days	28-days
1	Clinker-1 (Plant A)	25-40	30-35	11-13	10-12	Alite with irregular outline and inclusion of belite. Belite better developed with twinning. More microhomogeneity in its normal phase distribution.	18.0-28.5	26.0-40.0	40.0-49.0
2	Clinker-2 (Plant B)	30-45	25-40	10-12	11-13	Well developed alite and belite. No twinning of belite. Rims of belite around alite and inclusion of belite within alite rare. More homogeneous microstructure.	21.0-33.0	29.0-44.0	42.0-50.0

The results indicate that the compressive strengths at 3 and 7 days of clinker-2 (from plant B) are higher than those of clinker-1 (from plant A), but the compressive strength at 28 days is more or less the same. This is because of higher C_3S content and better microstructure of clinker-2. Clinker-1 has 25-40% C_3S, whereas clinker-2 has 30-45% C_3S. Clinker-1 has alite with irregular outline and inclusion of belite. Belite is better developed with twinning. There is more microinhomogeneity in its normal phase distribution. Whereas, clinker-2 has well developed alite and belite and there is no twinning of belite. Rims of belite around alite and inclusions of belite within alite are rare. This clinker has more homogeneous microstructure.

Effect of particle size distribution on strength development of OPC

The results of the effect of particle size distribution of cement on strength develoipment of OPC for both plants A and B are shown in Table 4.

Table 4 Particle size distribution and compressive strength of cement

Sl No	Sample Reference	Particle Size Distribution (%)		Compressive Strength MPa		
		+90/u	+45/u	3-days	7-days	28-days
1	Cement-1 (Plant A)	8-12	35-40	18.0-28.5	26.0-40.0	40.0-49.0
2	Cement-2 (Plant B)	6-10	30-35	21.0-33.0	29.0-44.0	42.0-50.0

The result indicate that the compressive strengths at 3 and 7 days of cement-2 (from plant B) are higher than those of cement-1 (from plant A), but the compressive strength at 28 days is more or less the same. This is because of better particle size distribution of cement-2 as compared to cement-1. Cement-2 has 6-10% residue on 90/u and 30-35% residue on 45/u, whereas cement-1 has 80-12% residue on 90/u, and 35-40% residue on 45/u. The better particle size distribution of cement-2 is due to higher C_3S content and better microstructure of clinker-2.

The above findings are in agreement with the results obtained by Frigione and Mara (1976).

Effect of granulometry of clinker on grindability

The results of the effect of granulometry of clinker on grindability, measurable in terms of specific surface of ground cement, for both plants A and B are shown in Table 5.

Table 5 Clinker granulometry and grindability

Sl No	Sample Reference	Clinker Granulometry (%)			Specific Surface (m2/kg)
		+ 25mm	+ 12.5mm	+ 6.5mm	
1	Clinker-1 (Plant A)	10-15	10-25	15-20	240-290
2	Clinker-2 (Plant B)	8-12	15-20	20-2520-25	250-310

The results indicate that clinker-2 (from plant B) is easier to grind as compared to clinker-1 (from plant A). This is because of smaller size nodules of clinker-2. Clinker-2 has 8-12% residue on +25mm, 15-20% residue on +12.5mm and 20-25% residue on +6.5mm, whereas clinker-1 has 10–15% residue on +25mm, 10-25% residue on +12.5mm and 15-20% residue on +6.5mm.

CONCLUSION

The two most important factors affecting strength development of hydrated cement are : (i) mineral phase composition and microstructure of clinker, and (ii) particle size distribution of ground cement. The granulometry of clinker affects its grindability, measurable in terms of specific surface, whereas the mineral phase composition and microstructure of clinker affects the variations in (a) particle size distribution of ground cement, and (b) strength development of hydrated cement at different ages.

REFERENCES

Frigione, G. and Mara, S., "Relationship between particle size distribution and compressive strength in Portland Cement", Cement and Concrete Research, Vol.6, 1976, pp. 113-116.

Ono, Y. and Soda, Y., "Effect of the crystallographic properties of alite and belite on the strength of cement", Semento Gijutsu Nenpo, Vol.17, 1965, pp. 93-103.

Ono, Y., "Microscopical estimation of burning condition and quality of clinker", 7th International Congress on the Chemistry of Cement, Paris, Vol.II, 1980, pp. I-206-I-211.

Kn o. 2 5. JAN. 2001 d o k 31782

2ii019
4 pp

KINETIC PECULIARITIES OF HYDRATE- AND STRUCTURE FORMATION IN PORTLAND CEMENT AT INITIAL STAGES OF HARDENING

Valeriy CHISTYAKOV, Kiev State Technical University of Construction and Architecture, Ukraine
Valentin SHEVCHENKO, Metastrom Ltd., Kiev, Ukraine
Anatoliy DEGTYARYEV, Stock Society "Podylskiy Tsement", Kamenetsk-Podolskiy, Ukraine
Alexandr POLTAVTSEV, Kiev State Technical University of Construction and Architecture, Ukraine

ABSTRACT The regulations under which the processes of hydroxylation, polarization and condensation of new formations in the hardening Portland cement system have been experimentally revealed and discussed. The obtained results demonstrate that the initial stages of hardening, which cover the period from the moment when water was added to a cement, affect essentially the processes of nucleation and formation of a primary matrix based on how a condensation - crystallization structure (a bearer of strength of a cement paste) develops.

Key-words: Hydration, Kinetics, Induction period, Setting.

INTRODUCTION AND EXPERIMENTAL

The study is based on a phenomenon of resonance of elastic vibrations of a disperse structure of cement paste within a range of sound frequencies varying from 500 to 1500 Hz (Grankovskiy, 1984). A resonance frequency reflects variations in elastic characteristics of the hardening system (Khaikin, 1971). The works (Chistyakov et al, 1986) demonstrate that, along with determination of elastic properties, the above method allows to observe change in dispersion degree of the hardening system. It was proved theoretically and experimentally that the increase in resonance amplitude ($A_{res.}$) of hardening cement paste indicates the increase in degree of dispersing of the particles, whereas the decline of $A_{res.}$ may be attributed to the processes of aggregation and condensation of new formations.

Using a specially designed device "IG-IR"(Grankovskiy, 1984) at a value of input energy some orders lower than that resulting in destruction of the system, the quantitative dependencies reflecting variations in in elastic properties ($\omega_{res.}$) and dispersivity ($A_{res.}$) of the particles of the hardening cement pastes were produced. The patterns of the hydrating cement (points 1-12, Fig 1) were taken along with determination of amplitude- frequency characteristics. The hydration of the samples was stopped by washing out the water by 96 % ethanol. Solid residue was dried at 40^0C. The identification of the samples was done using X-ray Diffraction(XRD), Differential Thermal Analysis (DTA), and Infrared spectroscopy (IR).

RESULTS AND DISCUSSIONS

Considering the processes of hydrate formation in dependence with variations in elastic properties ($\omega_{res.}$) and degree of dispersing of the hardening system ($A_{res.}$) (Fig 1) allowed to reveal some regularities of strength development in portland cement paste. After mixing with water, the initial stage of hydration of portland cement is characteristic of the following general features:
a). high velocity of interaction of cement with water and intensive dispersing of the primary cement particles (Fig 1, curve Δm and $A_{res.}$, interval 0-1);
b). increase in interfacial surface and degree of its hydroxylation (Fig 1, curve I_1/I_o; Fig 2, data of IR spectroscopy).

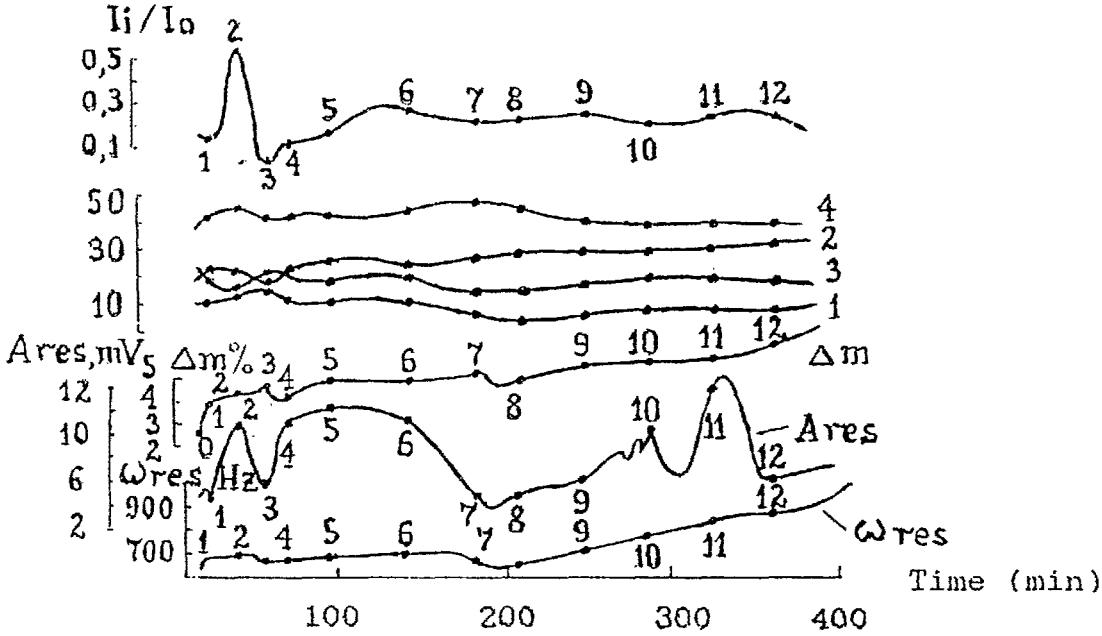

Figure 1 Kinetic curves of structure formation of the cement paste (w/c=0.28): $\omega_{res.}$- resonance frequency, Hz; $A_{res.}$- resonance amplitude, mV; Δm- degree of hydration (loss in mass of the specimens when heating up to 1000°C,%), 1-4- relative losses of mass within intervals of characteristic temperatures $\Delta m_i/\Delta m$, %: 1- 20- 140°C; 2- 140- 180°C; 3- 180-480°C; 4- 480-790°C; I_i/I_0- change of rate of hydroxylation of the particles of cement- water dispersion; 1- 12- points of selection of patterns of hardening cements for DTA, IR, and XRD.

Num.	Δm %	DTA curves	$lg \frac{I_i^*}{I_0}$	IRspectra	$\frac{I_i^{**}}{I_0}$
0	2,6	140 170 480 785	0,149	3412 cm^{-1}	1,0
1	4,0	179 482 787	0,127	3427	0,93
2	4,1	144 175 482 792	0,386	3393	0,85
3	4,3	115 158 465 780	0,114	3400	0,93
4	3,7	170 460 784	0,146	3433	1,06
5 6	4,6	168 480 788	0,267	3407	0,92
7	4,9	135 160 473 790	0,217	3417	0,83
8	4,4	137 158 480 785	0,230	3407	1,14

Figure 2 Data of DTA, IR scectroscopy and XRD: lg I^*_i/I_0- optical density of IR spectroscopy within a field 3400 cm^{-1}; I^{**}_i/I_0- the ratio between XRD lines (d=0.259 nm).

c). gain of critical (at a given stage of hardening) degree of water content in the new formations (Fig 1, curve Δm, point 3; Fig 2, data of DTA). The increased content of the OH^- groups which are centers of physical adsorption of water (Kiselev and Lygin, 1972) is a cause of immobilization and structurization of a liquid phase in the surrounding of dispersion particles;
d). accumulation in the hardening system of excess energy. A characteristic total exothermal convexity of the DTA curves-patterns 2 and 3 proves, according to (Berg, 1962), the presence of finely dispersed hydrate new formations that are known to possess the excess energy (Fig 2);
e) retardation of the hydrate formation processes (Fig 1, curve Δm, interval 1-2);
f) gain by the cementitious system of critical metastable state (Fig 1, point 2) and initiating of the processes of inner structural condensation in the dispersion particles (curve $A_{res.}$, interval 2-3) with lowering the degree of their hydroxylation (curve I_1/I_0) and release within the interval 3-4 of some portion (10-30%) of the earlier bound water (curve Δm), strength of the hydrating system not increasing, but some loss of strength is observed (decline of $\omega_{res.}$).

During rearrangement of the initially formed hydrates their flaking from the cement grains takes place and new not hydrated surfaces occur. This correlates well with the increase in intensity of the lines appropriate for clinker minerals in the XRD. This effect is clearly seen in variations of intensity of the line d= 0.259 nm appropriate for C_3S and β-C_2S. Some increase in chemical activity of the liquid phase promoting intensification of the hydrate formation processes is fixed within the interval 4-5. After rearrangement of the primary structure upon achievement of critical concentration of new formations and setting an interstructural condensation causing strength gain is fixed. The processes of condensation of the new formations of a cement- water dispersion are found to be regulated by a value of excess energy and degree of hydroxylation of the surface of hydrates.

Within the interval 4-8 the above processes repeat, meanwhile a cause for this turned out to be phase transformations of the primary new formations and they occur in the conditions already formed periodic colloid structure.

Induction period

In the curve Δm reflecting a rate with which new formations attract water are fixed two sections (1-2 and 5-6) in which the rate of hydration does not change in practice (Fig 1). A wide band of continuous absorption within a field 1500- 4000 cm^{-1} is seen on the IR spectrums of the patterns selected within these time intervals giving proofs to the formation in the system of symmetrical hydrogen bonds characteristic of high rate of polarization (Tsundel, 1972). The occurrence of such bonds may exist in cases when, as a result of dispersing the solid phase particles, the distance between tetrahedrons $(SiO_4)^{4-}$ does not exceed 0.3 nm.The interaction of proton with ion O^{2-} in a crystalline lattice of the clinker mineral is a cause of initial elementary act of cement hydration. By strengthening the polarization of hydrogen bonds detected by the IR spectroscopy, the process of transfer of the proton by the hydroxyl oxygen ions or moleculars of water to ion of oxygen in the structures of clinker minerals. The amount of water bound per time unit in the section 1-2 lowers by 15-20 times as compared with the initial stage (interval 0-1). Thus, the polarization effects regulating the intensity of cement protonization is found to be one of the reasons initiating induction period.

Setting of cement

Some researchers consider ettringite as the main factor of setting. However, the latest experimental data does not prove this point of view. So, Bensted (1983) showed that during the

setting a share of ettringite in practice did not rise. While setting (Fig 1,curve Δm, interval 8-11), the degree of cement hydration increased insignificantly- from 5.6 to 6.2 %. The initial setting (point 8) corresponds to increase in dispersion degree (curve $A_{res.}$) and interface surface of the hardening system. With the use of dispersive analysis of the patterns of hardening cement selected as guided by the kinetic curves of structure formation a multiply as compared with the initial cement increase in quantity of the particles with size up to 4 μm (10-fold) and within a range from 4 to 10 μm (two-fold) within the interval 8-11 is fixed. This results in immobilization of the earlier bound water. Thus, the setting of cement is caused, predominantly, by immobilization of water by cement particles and primary hydrosilicate phases dispersing during this stage.

After the setting of cement paste a stable increase in intensity of the XRD lines appropriating for $Ca(OH)_2$ is fixed. An intensive increase in elastic properties and strength of the system after point 11 is caused by the formation of a space framework of portlandite as well as predominance of condensation processes over dispersing and destructive ones.

CONCLUSIONS

The experimental study allowed to demonstrate that a chemical potential and physical state of liquid phase, degree of hydroxylation of new formations which determine the intensity of hydrate formation, degree of interaction of associates, elastic properties of the hardening system and collective directivity of energy and concentration fluctuations vary cyclically at a stage of formation and colloid structure development.

The characteristic transition periods of structure formation corresponding to a predominant flow of dispersing or aggregation (condensation) processes in a cement-water dispersion were revealed. The intensity of flow and degree of completeness of these processes determine the conditions for formation of the matrix on a base of which the cement stone structure develops. The optimal actions and periods corresponding to rearrangement of the hardening system intensify and modify naturally occurring periods of transition of quantitative changes in the system into its qualitatively new state. Taking into account the revealed regularities allows to appoint optimal time of applying and technological regimes (moulding, repeated vibration, curing, etc.) (Grankovskiy, 1984 and Chistyakov, 1994).

REFERENCES

Bensted, J., Further Aspects of the Setting of Portland Cement, Silikat.Ind.Journal, 48, No.9, 1983, pp.167-170.

Chistyakov, V.V., Grankovskiy, I.I. and Gotz, V.I., "Formation of Structure of Hardening Slag Alkaline Cement", Prikladnaya Himia Journal, Vol.59, No.3, 1986, pp.590-595.

Chistyakov, V.V.,"Physico-chemical Aspects of the Intensification of Hydrate- and Structure Formation Processes in Mineral Cementitious Systems",DrSc Thesis, Kiev, 1994, 34 pp.

Grankovskiy,I.G., Structure Formation in Mineral Cementitios Systems, Naukova Dumka.Publish., Kiev, 1984, 299 pp.

Khaikin, S.E., Physical Bases of Mechanics, Nauka Publish., Moscow, 1971, 751 pp.

Kiselev, A.V. and Lygin,V.P., "Infrared Spectrums of Surface Compounds of Adsorped Substances, Nauka Publish., Moscow, 1972, 459 pp.

Berg,L.G., Introduction into Thermography, Nauka Publish., Moscow, 1969, pp.78-79.

Tsundel, G., Hydration and Intermolecular Interaction, Mir Publish., Moscow, 1972, 404 pp.

Kn o. 2 5. JAN. 2001 d o k 31783

2ii020
4 pp

ORGANO-MINERAL FILLERS FOR CEMENTS

Serge P. SIVKOV, Dmitry V. MUNDSHTUKOV, Imed JEDDA, D. Mendeleev University of Chemical Technology of Russia, Moscow, Russia

ABSTRACT The smectite and kaolinite clays modified by SNF plasticizer were used as filler additives to portland cement. It has been established, that the modified clays facilitate a grinding procedure, improve a granularity of cements, reduce their w/c ratio. The compressive strength and density of cements thus is increased considerably.
Key-words: filler, clay, grinding aids, plasticizers, modified cement.

INTRODUCTION

The properties of a hardened cement paste such as compressive strength, porosity, impermeability, dimensional stability, etc. are improved proportionaly with the reduction in the water/cement (w/c) ratio of a fresh mix. Plasticized cements containing so called superplasticizers as additives water-reducers have the w/c ratio by 25-50 % less than ordinary cements. Their compressive strength reaches 75-80 MPa. Such cements enable to create high-performance cement composites (Babaev et al., 1990, Durekovic, 1992, Batrakov et al., 1988).

The technology of production of plasticized cements consists in simultaneous pulverisation of clinker portland, gypsum, puzzolanic admixtures with a dry powder of a superplasticizer. But there's too great a superplasticizer consumption in this process (up to 2-5 % mass.) becaus of its chemiosorption and destruction that are intensified by high temperature in a cement mill (Nanazashvili and Babaev, 1990).

This article deals with scope for an application of organo-mineral nanocomposites to production of plasticized cements. In the organo-mineral nanocomposite the molecules of an organic substance (polymers or monomers) are intercalated within interplanar spaces, channels and cavities of a molecular dimension in the crystal structure of an inorganic material (Theng, 1982, Tunney and Detellier, 1993, Messersmith and Giannelis, 1993). The resulting hybrides possess unique mechanical, electrical, optical and thermal properties. Thus, the intercalated polymer exhibits higher thermal and chemical stability not observed in a bulk polymerized macromolecules and can be liberated by dissolution or by decomposition of the host (Wang and Pinnavaia, 1994, Wu and Lerner, 1993).

EXPERIMENTAL

The high-plastic smectite (montmorillonite ≈ 88 %) and kaolin (kaolinite ≈ 94 %) clays and the industrial sulphonated naphthalene formaldehyde superplasticizer (**SNF**) were used for the synthesis of organo-mineral plasticizers (**OMP**). The clays and the superplasticizers were mixed in 1:1, 2.5:1 and 5:1 ratios. The mixture was wetted by adding the necessary amount of water, than homogenized during 12 hours and dried at 80 °C.

Ordinary portland clinker (C_3A = 9 %, C_3S = 58 %) was taken for experiments. Gypsum (5 %) and **OMP** (1 and 3 %) were applied as additives to cement. The pure clays and pure dry **SNF** plasticizer were used for grinding of control cements. The grinding procedure was carried out in the laboratory mill "Pulverisette-7" closely under steady conditions.

RESULTS AND DISCUSSION

Table 1 gives the Blaine specific surface of the pulverized cements.

Table 1 Blaine specific surface and w/c ratio of cements

	Blaine specific surface, $m^2 \cdot kg^{-1}$		W/C ratio for constant fluidity,	
Cement	OMP smectite	OMP kaolin	OMP smectite	OMP kaolin
Control	383.0		30	
+ 1 % SNF	411.3		23	
+ 1 % pure clay	403.6	418.7	29	27
+ 1 % OMP 1:1	409.3	429.0	23	23.5
+ 1 % OMP 2.5:1	416.1	436.2	24	24
+ 1 % OMP 5:1	418.0	438.9	26	25.5
+ 3 % pure clay	409.2	429.6	32	31
+ 3 % OMP 1:1	426.0	445,7	21	20
+ 3 % OMP 2.5:1	437.5	452,9	22	20.5
+ 3 % OMP 5:1	438.3	477,7	23	23

A significant increase in the specific surface area of the cements with **OMP** can not be explained only by the clay's influence because, on the one hand, the addition of pure clays changes the specific surface area slightly and, on the other hand, the BET surface specific of the clays modified by **SNF** is 1.4-1.5 times lower than the one of the starting clays (54.82 *v.* 39.18 $m^2 \cdot g^{-1}$ for smectite and 21.87 *v.* 15.11 $m^2 \cdot g^{-1}$ for kaolin respectively).

The particle size analysis of cements performing with laser-diffraction particle size distribution analyser "Analysette-22" shows (Fig. 1 and Table 2) that in cements with **OMP** the content of fine particles is increased. The granularity of cement with 1 % **SNF** differs slightly from the one of the control cement.

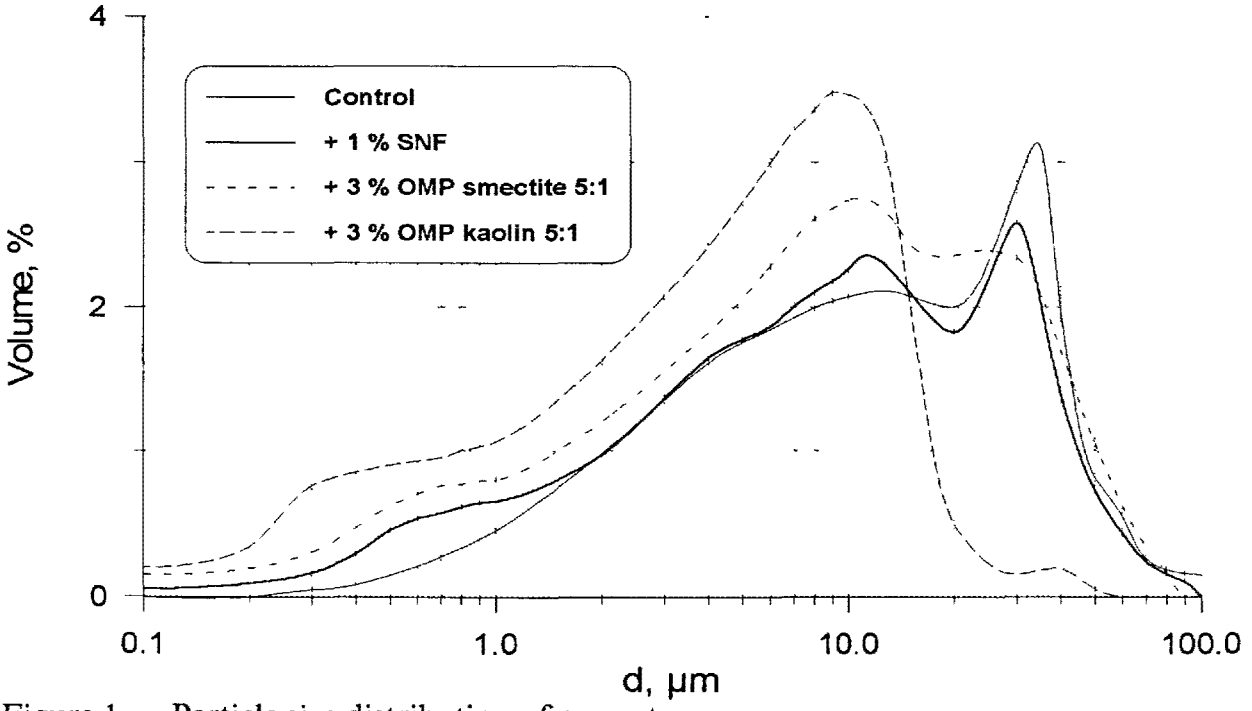

Figure 1. Particle size distribution of cements

According to the classical Rebinder's theory adsorption of molecules of a tensioactive substance on a surface of solids decreases the surface energy, promotes microfissures sprawl and inhibits particle agglomeration (Fig.2a).

Table 2. Particle size characteristics of cements

Cement	Arithmetic mean diameter, μm	Geometric mean diameter, μm	Spec. surface area (calc), $m^2 \cdot ml^{-1}$	Spec. surface area (BET), $m^2 \cdot g^{-1}$
Control	15.45	8.29	1.89	1.10
+ 1 % SNF	14.75	8.01	1.92	2.14
+ 3 % OMP smectite 5:1	13.30	7.29	2.05	2.24
+ 3 % OMP kaolin 5:1	8.66	5.21	2.85	2.32

Nevertheless when cements are ground with a dry superplasticizer in a dry atmosphere of a cement mill it is difficult to presume the separation of a superplasticizer into individual molecules, its diffusion and the uniform spread over the cement particle surface. On the other hand the **OMPs** have the slight hardness and are ground quikly to particles < 1 μm. Penetration of fine **OMP** particles with molecules of the tensioactive substance adsorbed on their surfaces within microfissures of clinker portland (Fig. 2b) facilitates and expedites the grinding of cements, hinders the aggregation of cement grains.

The w/c ratio of the cements containing **OMPs** is less than w/c of the cements with 1 % **SNF**, though with 3 % **OMP** of the 5:1 composition the content of superplasticizer in cement is no greater than 0.5 % (Table 1).

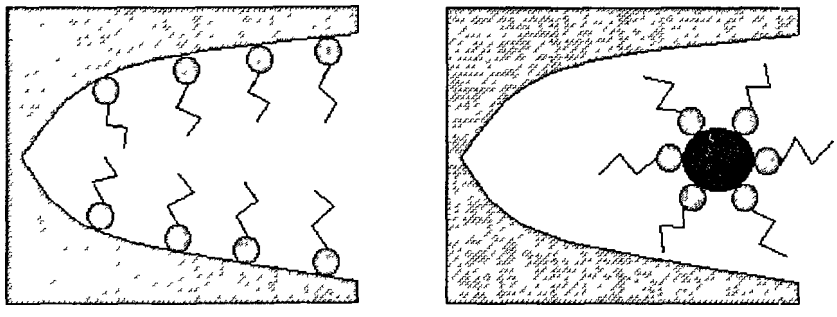

a b

Figure 2. Scheme of **SNF** and **OMP** action

High fluidity of the cement paste is related with an increase in the fine fraction content in cement and with the better conservation of **SNF** during grinding procedure.

Table 3 gives mechanical and structural characteristics of hardened cements. The measurements were carried out for the cement pastes of constant fluidity.

The best values of the compressive strength were obtained for the cements with **OMP** on the kaolin base. It should be noted that at the age of 1 and 3 days the compressive

strength of cements with **OMP** is less than the compressive strength of cement with 1 % **SNF**, but it is more than the one of the control cement.

Table 3. Compressive strength and porosity of cements

Cement	R_{28}, MPa	Total porosity, %	Open porosity, $cm^3 \cdot g^{-1}$
Control	46.8	18.0	0.057
+ 1 % SNF	54.2	15.1	0.039
+ 3 % OMP smectite 5:1	71.6	14.6	0.032
+ 3 % OMP kaolin 5:1	77.9	11.8	0.034

The cements with **OMP** have lower values of total and open porosity than the control cement and the cement with 1 % **SNF**, wich is related with a decrease in the w/c ratio and with a compaction of hydrated cement by fine clay particles.

There were no any changes in the phase composition of hydrated cements with **OMP** compared with the cement containing 1 % **SNF** observed.

CONCLUSION

The organo-mineral nanocomposites have a greater effect on grinding of cement, plasticity of a cement paste, mechanical and structural characteristics of a hardened cement than pure **SNF** superplasticizer. Besides clays other inorganic materials of an appropriate structure and slight hardness (amorphous silica, zeolites, $Ca(OH)_2$, etc.) show promise to be used for the syntesis of **OMP**.

REFERENCES

Babaev, S.T., Bashlykov, N.F. and Goldina, I.Y. "Raising the Strength of Cement Compositions", Cement, No 9, 1990, pp.13-15.

Batrakov, V.G., Babaev, S.T. and Bashlykov, N.F. "Concrete Based on Binders of Low Water Requirement", Concrete and Reinforcing Concrete, No 11, 1988, pp.4-6.

Durekovic, A. "Hydration in Very High Strength Cement Composites", Proceeding of 9-th International Congress on the Chemistry of Cement, New Delhy, India, 1992, Vol. IV, pp. 543-549.

Messersmith, P.B. and Giannelis, E.P. "Polymer-Layered Silicate Nanocomposites: *In-Situ* Intercalative Polymerisation of ε-Caprolactone in Layered Silicates", Chemistry of Materials, Vol.5, No 8, 1993, pp. 1064-1066.

Nanazashvili, V.I. and Babaev, S.T. "Decorative Binders of Low Water Requirement and Products Based on them", Cement, No 9, 1990, pp. 11-13.

Theng, B.K.G. " Clay-Polymer Interactions: Summary and Perspectives", Clays and Clay Minerals, No 1, 1982, pp.1-10.

Tunney, J.J. and Detellier, C. "Interlamellar Covalent Grafting of organic Units on Kaolinite", Chemistry of Materials, Vol.5, No 6, 1993, pp. 747-748.

Wang, M.S. and Pinnavaia, T.Y. "Clay-Polymer Nanocomposites Formed from Acidic Derivatives of Montmorillonite and Epoxy Resin", Chemistry of Materials, Vol.6, No 4, pp. 468-474.

Wu, J. and Lerner, M.M. "Structural, Thermal and Electrical Caracterisation of Layered Nanocomposites Derived from Na-Montmorillonite and Polyethers", Chemistry of Materials, Vol.5, No 6, pp. 835-838.

Kn o. 2 5. JAN. 2001 d o k 31784

2ii021
4 pp

THE THERMOKINETIC FACTOR IN CEMENT HARDENING

Alexander V. USHEROV-MARSHAK, Otar P. MCHEDLOV-PETROSSYAN, Anatoly G. SINYAKIN, State technical University of Building and Architecture, Kharkov, Ukraine

ABSTRACT The important role of the thermokinetic factor in the hardening of cement is established. The interrelation between parameters of time and temperature of hardening as a result of natural and artificial heat impact is marked. The necessity of quantitative evaluation and registration of thermokinetic characteristics of different cements within the range of informative (computer) technologies of concrete is shown.

KEY-WORDS: Calorimetry, Heat evolution, Hydration, Metod, Temperature

INTRODUCTION

In 1984 (Usherov-Marshak, 1984) a classification of hardening processes of binders by thermokinetic signs - velocity and fullness of heat evolution of hardening - into three types was suggested. Many of cement properties - setting velocity, hardening growth and others are determined by the type of thermokinetic regularities, presence and duration of the principal periods of the hardening (inductive, accelerated and decelerated) as well as the intensity of the hydration reactions. It is proved that for the regulation of the hardening process the parameters of heating impacts must be assigned with consideration for thermokinetic characteristics.

METHOD OF THERMOKINETIC ANALYSIS

In the chemistry of cement the calorimetry is widely used. The principal difference of our method which we call thermokinetic analysis is the possibility of computer registration and interpretation of dependences of $dQ/d\tau=f(\tau)$, $Q=f(t)$ and $dQ/d\tau=f(Q)$ kind with simultaneous interpretation of hydration periods and the prediction of heat evolution.

Earlier was given the description of calorimetric experiment methods with the interaction of disperse character and the original mathematic apparatus for building nonisothermal dependencies for different variants of heat impacts in the interval 20-180^0 C (Usherov-Marshak and Sinyakin, 1992). The development of the treatment brings about the formal and conceptual modelling of hydration reactions after the data of heat evolution. The obtained information is automatically directed in the computer banks of the thermokinetic knowledge.

WHAT IS THE THERMOKINETIC FACTOR ?

The thermokinetic factor of hardening (TKF) - is the reason which rules the process as result of interaction between two important and differing in their nature physical parameters - temperature and time. TKF is the result of manifistation of the mechanism and kinetics of elementary acts of hydration - adsorption, chemical reaction, dissolution, crystallization and others under the influence of temperature conditions.

The effect of TKF is obvious in the cases of hydration of highthermal monomineral binders - CaO and $3CaO \cdot Al_2O_3$. They belong to the first type of thermokinetic regularities. High indices of reaction velocity and heat evolution stipulate selfheating of hardening mixes. The discrepancy between the velocity and hydration degree destroys the structure of hydrates and does not allow the rise of strength at normal conditions (20^{0}C). In this case natural heat impact is manifested.

Lowering of hydration temperature to 0^0C and lower changes the degree of velocity and fullness of reactions and leads to the formation of stable new formations with enough strength.

Another example is the hydration of MgO. Low velocity of heat evolution at 20-50^0C changes into rough growth over 60-70^0C. The hydration becomes uncontrollable. The natural heat impact causes the change of the type of thermokinetic regularity and possible alteration in reactions mechanism.

The hydration of lowbasic binders of the third type regularities - slags, ashes, calciumoxide-silica-compositions is accompained by very low heat evolution. Activation of the hydratation by alkalies and sulfates insignificantly intensifies reactions. The contribution of endoeffects resulting from dissolving and break of the bonds of Ca-O, Al-O, Si-O type is high. Therefore TKF plays insignificant role in the evolution of hydration and formation of their nature. The natural heat impacts through hydration heat of cement raise the TKF meaning in massive concrete constructions. Therefore thereby we use low exotermal cement, introduce additives and cool the massives.

THERMOKINETIC FACTOR AND ARTIFICIAL HEAT IMPACTS

The coherence principle

Artificial heat impacts are stipulated through elevated (80-180^0C) or so called negative (0-20^0C) temperatures, chemical additives and others. They change the condition and character of hardening process, change the degree of use of the binders, the strength and durability. The character of the natural and artificial impacts is different but within any temperature interval is characterised by common time parameters, the moment, intensity and continuance of application. Earlier was shown (Mchedlov-Petrossyan, 1991) the necessity of the coordination of impact parameters with the hydration kinetics (the coherence principle).

To estimate the influence of time and temperature while assigning the regime of cements and concrete hardening different conditional indices, coefficients, "degree-hours" and others were offered. But they had no physico-chemical sense. The thermokinetics allows to overcome methodological complications. Principal physico-chemical indices of velocity and completeness of heat evolution are appraised. The apparatus of thermokinetic analysis allows to receive and interprete the results for any hardening regime.

The data of Fig1. are illustrating the truth of this conclusion by the example of the thermokinetic indices at the hardening of C_3S. The experimental data provide possibility according to calorimetric results to estimate the influence of alteration in the moment of heat impact within the interval of 2-6 hours, velocity - 10-30^0C/hour and duration of heating 0-8 hours. The heating temperature changes from 30^0C to 80^0C. As a matter of fact this is the search for the optimal regime for concrete hardening with consideration of TKF. With help of thermokinetic dependencies $dQ/d\tau=f(\tau)$ and $Q=f(\tau)$ the direct proportion between impact moment of heat treatment and maximum of the process velocity is marked. It is important that value of dQ/dt decreases with the rise of application time from 11 to 7 cal/g•h, the hydration completeness with the exception of short period (to 10 hours) is practically the same. The regulation of heating velocity from 10 to 30^0C/hour proportionally shifts the emergence time and data of maximum of heat evolution from 11 to 7.5 cal/g•h. This is quite explicable. But some slowering of the velocity of the initial reactions leads to the increase of $Q=f(\tau)$.

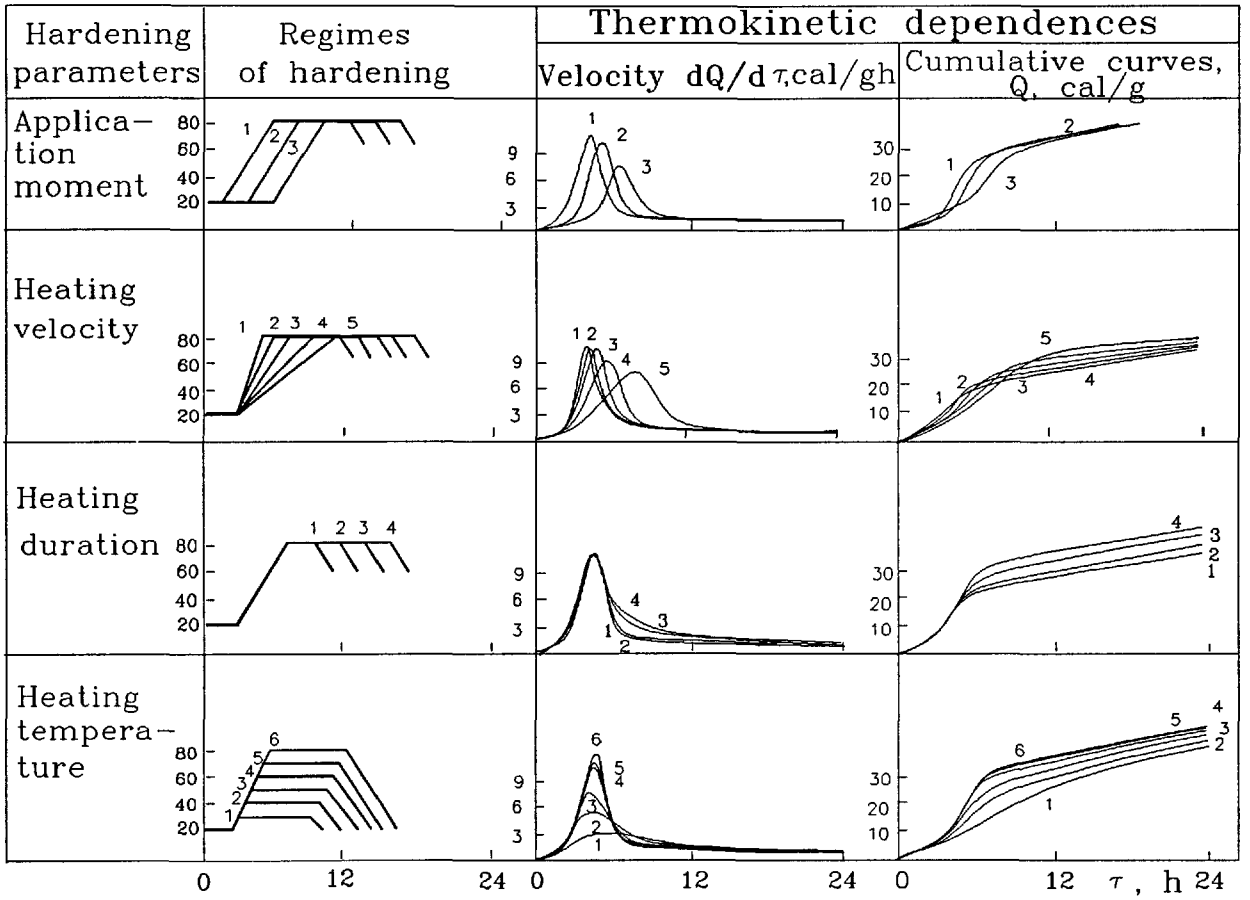

Figure 1 Non-isothermal heat evolution at the hardening of $3CaO \cdot SiO_2$

Earlier a discussion took place about the applicability of the Le-Chatelier principle for the substantiation of the parameters of the heat impacts. The jist of the discussion is that if before the end of heating of the hardening mix the process velocity does not reach the maximum the cooling must lower its completeness. If the principal exotherm appears before heating - the continuance of the isotherm does not essentially influence the growth of fullness of heat evolution. For the hardening C_3S the increase of duration of the heating in the studied interval contributes to the growth of the degree of the use of hardening properties.

Unlike this for cements the integral heat evolution depending on their activity, kinds of mineral or chemical additives can fall or rise. Especially evident is the rise of heat evolution by introducing surface active agents, hindering the initial hydration. In the nonisothermal thermokinetics most appreciable is the role of hardening temperature boundary (Fig 2). The absolute meaning of the maximum of exotherm rises proportional to the rising of these parameters. But the heat evolution falls. Principally important is that the information of TKF allows to formulate the bases of data and knowledge for expert systems and information technologies of cement and concrete (Frohnsdorff et al, 1988, Usherov-Marshak and Sinyakin, 1994).

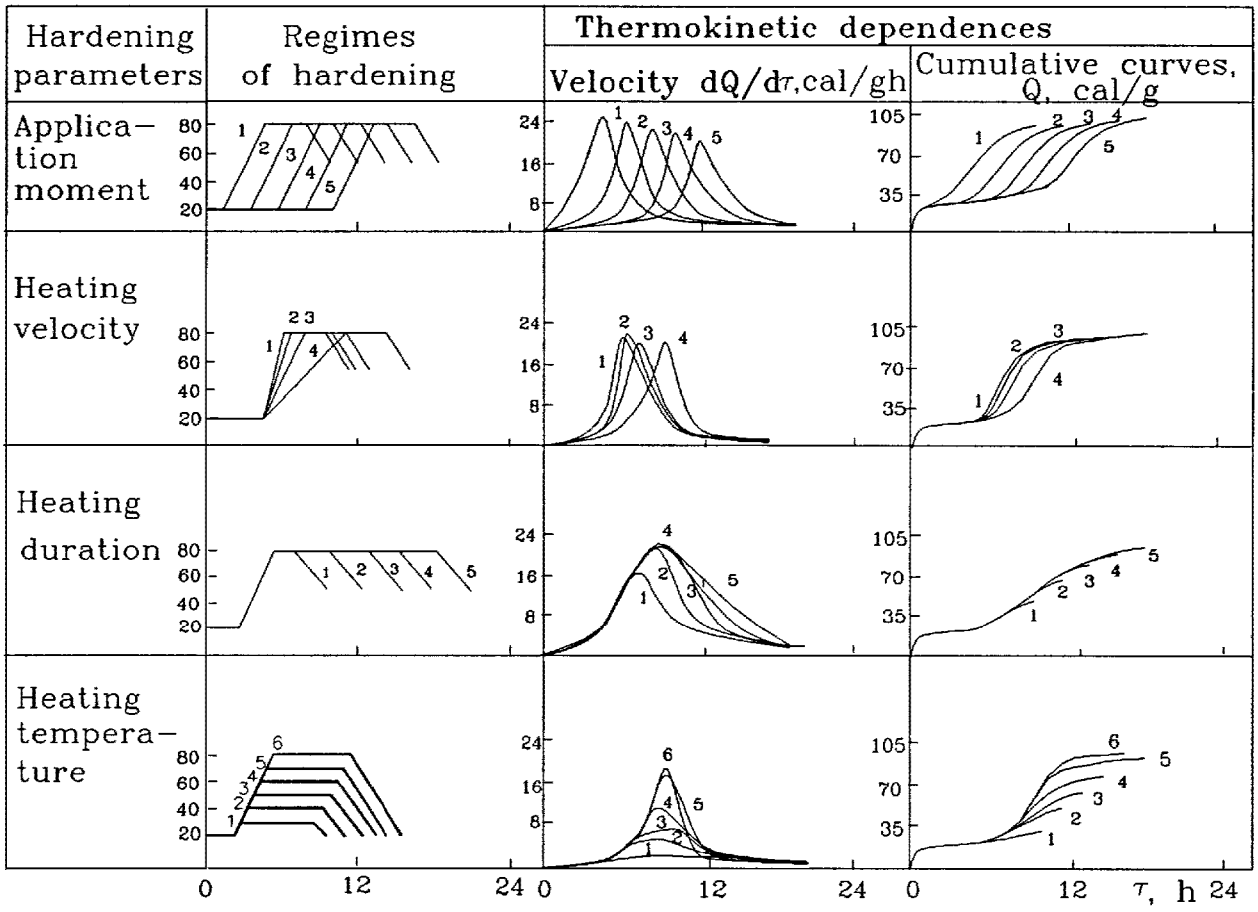

Figure 2 Non-isothermal heat evolution at the hardening of Portland cement

REFERENCES

Frohnsdorff, C.J. and Clifton, J.C., Pommersheim at st., "Implications of Computer - Based Simulation Models, Expert System, Data Bases and Networks for Advanced Cement Research",- Ceramic Bulletin, Vol. 67, N8 USA, 1988.

Mtschedlow-Petrossyan, O.P., "Das Entsprechungsprinzip in der Technologie der Silikate", Ibausil. Weimar, 1991, B.1.S 3-8.

Usherov-Marshak, A.V.,"Thermokinetics of hardening processes of cement", DAN USSR, 1984, N , pp. .

Usherov-Marshak, A.V. and Sinyakin, A.G., "Thermokinetics of cement hardening under non-isothermal conditions", 9th International Congress on the Chemistry of Cement, New Delhi, India, 1992, vol IV, pp. 175-180.

Usherov-Marshak, A.V. and Sinyakin, A.G., "Information technology of concrete", Moscow, "Concrete and reinforced concrete", 1994, N6, pp. 2-4.

Kno. 25. JAN. 2001 doki 31785

2ii022
8 pp

INFLUENCE OF $CaCO_3$ ON THE HYDRATION OF VARIOUS TYPES OF CALCIUM ALUMINATES WITH ANHYDRITE

Yoko OHBA*, Akinori NAKAMURA**, Jong Kyu LEE*,
Etsuo SAKAI*, and Masaki DAIMON*
* Dept. of Inorganic Materials, Tokyo Institute of Technology, Tokyo, Japan
** Cement & Building Materials Laboratory, Tokuyama Co., Ltd., Yamaguchi, Japan

ABSTRACT Limestone powders were investigated for the filler cement as ecological materials and as a functional cement for the flowing concrete. However, the reactions between limestone powders and calcium aluminates were not clear, quantitatively. In this study the reactions between the limestone powders and the calcium aluminates such as C_3A, $C_{11}A_7{\cdot}CaF_2$ and $C_{12}A_7$ glass, were examined and effects of anhydrite to above reactions were investigated, quantitatively.

Key-words: Calcium aluminates, Limestone powders, Hydration, Anhydrite.

INTRODUCTION

Various types of calcium aluminates were widely used for the main composition of super high early strength cements and rapid hardening cements, and additives. Recently, the amounts of the reinforcement of the bridge girder and so on, and the repairment increased, where calcium aluminates were used with $CaSO_4$. And $CaSO_4$ are used as additives for the high strength concrete. For such progressing technologies of construction, the fluidity must be required to the super high early strength cement. On the other hand, the limestone powders were used for the filler cement as ecological materials and for the flowing concrete as functional cement, and were investigated (Hosino et al, 1995). Therefore, the super high early strength and the high flow concrete used the super high early strength cement together with limestone powders will be important as advanced construction technology.

The reactions of the limestone powders ($CaCO_3$) during the hydration of cements were investigated for the filler cements (Sakai et al, 1993) and for portland cement (Asaga and Kuga, 1995, and Grandet and Olliver, 1980). It was cleared that C_3A was reacted with $CaCO_3$ and produced monocarbonate (Kuzel and Pollman, 1980, Manabe et al, 1961, and Hosokawa et al, 1995). However, the reactions of $CaCO_3$ between calcium aluminates $C_{11}A_7{\cdot}CaF_2$ and calcium aluminate glass of $C_{12}A_7$ composition ($C_{12}A_7$ glass) were not cleared quantitatively .

In this study, we investigated the reactions between $CaCO_3$ and calcium aluminates with and without $CaSO_4$, quantitatively.

EXPERIMENTAL

Materials

C_3A and $C_{11}A_7{\cdot}CaF_2$ were synthesized in a laboratory electric furnace at 1350 °C and 1300 °C, respectively, from chemical reagents ($CaCO_3$, Al_2O_3 and CaF_2). $C_{12}A_7$ glass was synthesized by quenching meltage at 1600 °C. Limestone powders ($CaCO_3$: calcite, Tsukumi Japan) and anhydrite ($CaSO_4$, Thailand) were granulated and their specific

surface areas were shown in Table 1.

Table 1 Specific surface areas of materials (Blaine's method)

Materials	C_3A	$C_{11}A_7 \cdot CaF_2$	$C_{12}A_7$glass	$CaCO_3$
Specific surface area (m^2/kg)	410	390	385	510

Sample preparation

Calcium aluminates and $CaCO_3$ were mixed, where the Al_2O_3 / $CaCO_3$=1 in molar ratio. $CaSO_4$ was added to the mixed powders, and the amount of $CaSO_4$ varied from 0 to ettringite composition. They were kneaded with distilled water at 20 °C, and the water / solid ratios in weight were 0.8 to form pastes. The pastes were poured into polystyrene bottles (5 ml), and sealed with polystyrene films. They were cured at 20 °C for 1 - 28 days. After the curing time, the samples were crushed in excess acetone, and were dried by an aspirator for 16 hours. The amount of the combined water was estimated by the ignition loss (at 1000 °C, for 30min.) and by the amounts of $CaCO_3$.

Measurement of reaction ratios and amounts of hydrated products by XRD

The phases in the hydrated samples were identified by XRD. The amounts of C_3A, $C_{11}A_7 \cdot CaF_2$, $CaCO_3$, C_3AH_6 and $C_3A \cdot CaCO_3 \cdot 11H_2O$ were decided by XRD (Isizaki et al., 1988). Pure C_3AH_6 and $C_3A \cdot CaCO_3 \cdot 11H_2O$ were synthesized by the hydration of pure C_3A. MgO as internal standard was added to the sample in 10 weight %, and the scanning speed was 0.02 deg. (2 θ) / 20sec..

RESULTS AND DISCUSSION

The reactions of between various type of calcium aluminates and $CaCO_3$

Table 2 shows the hydrated products and unhydrated materials at each reacting duration in C_3A, $C_{11}A_7 \cdot CaF_2$ or $C_{12}A_7$glass - $CaCO_3$ systems measured by XRD.

At 1 - 28 days, C_3AH_6 and monocarbonate were formed in the systems of C_3A - $CaCO_3$ and $C_{11}A_7 \cdot CaF_2$ - $CaCO_3$. In the system $C_{12}A_7$ glass - $CaCO_3$, C_2AH_8 and monocarbonate were formed at 1 -7 days, and at 28 day only monocarbonate existed as the hydrated product.

Table 2 Hydration products of various calcium aluminates with $CaCO_3$

	Hydration time (days)	1	3	7	28
C_3A $-CaCO_3$	Products	C_3AH_6 Mc	C_3AH_6 Mc	C_3AH_6 Mc	C_3AH_6 Mc
	Unhydrated materials	C_3A $CaCO_3$	C_3A $CaCO_3$	C_3A^* $CaCO_3$	$CaCO_3$
$C_{11}A_7 \cdot CaF_2$ $-CaCO_3$	Products	C_3AH_6 Mc	C_3AH_6 Mc	C_3AH_6 Mc	C_3AH_6 Mc
	Unhydrated materials	$C_{11}A_7 \cdot CaF_2$ $CaCO_3$	$C_{11}A_7 \cdot CaF_2$ $CaCO_3$	$C_{11}A_7 \cdot CaF_2^*$ $CaCO_3$	$CaCO_3$
$C_{12}A_7$glass $-CaCO_3$	Products	C_2AH_8 Mc	C_2AH_8 Mc	$C_2AH_8^*$ Mc	Mc
	Unhydrated materials	$CaCO_3$	$CaCO_3$	$CaCO_3$	$CaCO_3$

Mc : monocarbonate, * : small amount

Figure 1 shows relations between the reacting duration and the reaction ratios of C_3A and $C_{11}A_7{\cdot}CaF_2$ measured by XRD. The reaction ratios of both C_3A and $C_{11}A_7{\cdot}CaF_2$ increased till 1 day and increased to 28 day. At 28 day, both reaction ratios showed 100%.

Figure 2 shows the reaction ratios of $CaCO_3$ in each systems. In C_3A system, the reaction ratio of $CaCO_3$ was 53% at 1day, and 79% at 28day. In $C_{11}A_7{\cdot}CaF_2$ system, it was 25% at 1 day, and 30% at 28 day. In $C_{12}A_7$ glass system, 11% of $CaCO_3$ reacted 1 day and 47% at 28 day. The amount of the reacting $CaCO_3$ in $C_{12}A_7$ glass - $CaCO_3$ system was less than those of other calcium aluminates systems at 1day, and the results agreed with the earlier report about the hydration of $C_{12}A_7$ glass (Hosokawa et al., 1995).

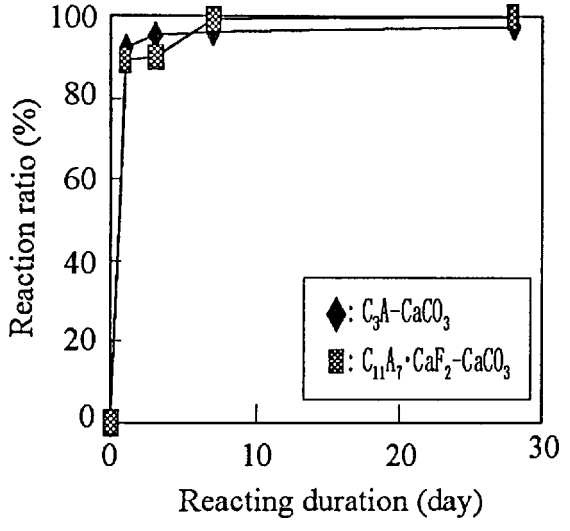

Figure 1 Reaction ratio of various calcium aluminates measured by XRD.

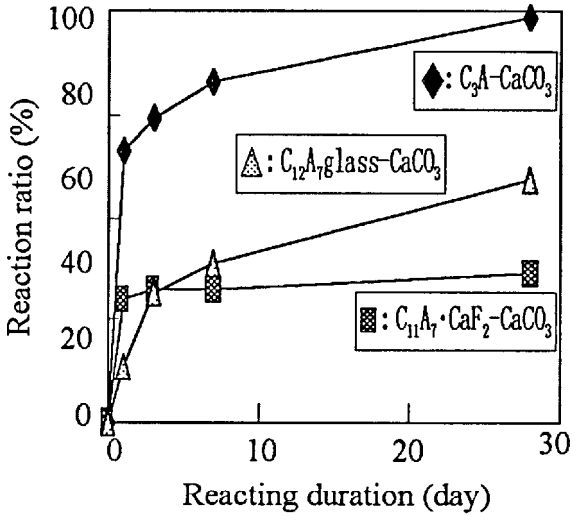

Figure 2 Reaction ratio of $CaCO_3$ measured by XRD.

Figure 3 shows the relations between the amount of reacted $CaCO_3$ (mol) and the amount of produced monocarbonate (mol). In C_3A - $CaCO_3$ system, the slope of the solid line is 1. The reaction formula for the formation of monocarbonate was written as Eq 1.

$$C_3A + CaCO_3 + 11H_2O \rightarrow C_3A{\cdot}CaCO_3{\cdot}11H_2O \quad [1]$$

In $C_{11}A_7{\cdot}CaF_2$ - $CaCO_3$ and $C_{12}A_7$glass - $CaCO_3$ systems, the slope of the dashed line is 0.53. The theoretical formula for the formation of monocarbonate in $C_{11}A_7{\cdot}CaF_2$ - $CaCO_3$ system was written as Eq 2.

$$C_{11}A_7{\cdot}CaF_2 + 4CaCO_3 + 52H_2O \rightarrow 4(C_3A{\cdot}CaCO_3{\cdot}11H_2O) + 2Al(OH)_2F + 2AH_3 \quad [2]$$

For the systems $C_{11}A_7{\cdot}CaF_2$ - $CaCO_3$ and $C_{12}A_7$glass - $CaCO_3$, the slope was 0.53 (dashed line), was not 1 (solid line). It was thought that the part of $CaCO_3$ existed as a gel. Then Eq 2 can be written as Eq 3.

$$C_{11}A_7{\cdot}CaF_2 + 4CaCO_3 + 52H_2O \rightarrow 2.12(C_3A{\cdot}CaCO_3{\cdot}11H_2O) + 1.88(C_3A_{2.1}{\cdot}CaCO_3{\cdot}11H_2O{\cdot}1.1Al(OH)_2F{\cdot}14.2H_2O)gel \quad [3]$$

The amounts of unhydrated $C_{12}A_7$ glass and produced C_2AH_8 were difficult to measure directly, so they were estimated as follows. The reaction formula for the formation of

monocarbonate in $C_{12}A_7$ glass - $CaCO_3$ system was written as Eq 4, theoretically.

$$C_{12}A_7 \text{ glass} + 4CaCO_3 + 53H_2O \rightarrow 4(C_3A \cdot CaCO_3 \cdot 11H_2O) + 3AH_3 \quad [4]$$

As $C_{11}A_7 \cdot CaF_2$ - $4CaCO_3$ system, the slope was 0.53 and the part of reacted $CaCO_3$ existed as a gel. Then Eq 4 can be written as Eq 5.

$$C_{12}A_7 \text{ glass} + 4CaCO_3 + mH_2O \rightarrow 2.12(C_3A \cdot CaCO_3 \cdot 11H_2O) + 1.88(C_3A_{2.6} \cdot CaCO_3 \cdot nH_2O)\text{gel} \quad [5]$$

In this system, unreacted $CaCO_3$ and the formed monocarbonate were observed, but C_3AH_6 or C_2AH_8 were not detected by XRD at 28 day. Supposing that the reactions except Eq 5 did not occur in the system, the combined water of the gel (n) was estimated. Then Eq5 was written as Eq 6. Therefore the amount of the reacted $C_{12}A_7$ glass was estimated from the amount of the reacted $CaCO_3$ given by Eq 6.

$$C_{12}A_7 \text{ glass} + 4CaCO_3 + 53.4H_2O \rightarrow 2.12(C_3A \cdot CaCO_3 \cdot 11H_2O) + 1.88(C_3A_{2.6} \cdot CaCO_3 \cdot 16H_2O)\text{gel} \quad [6]$$

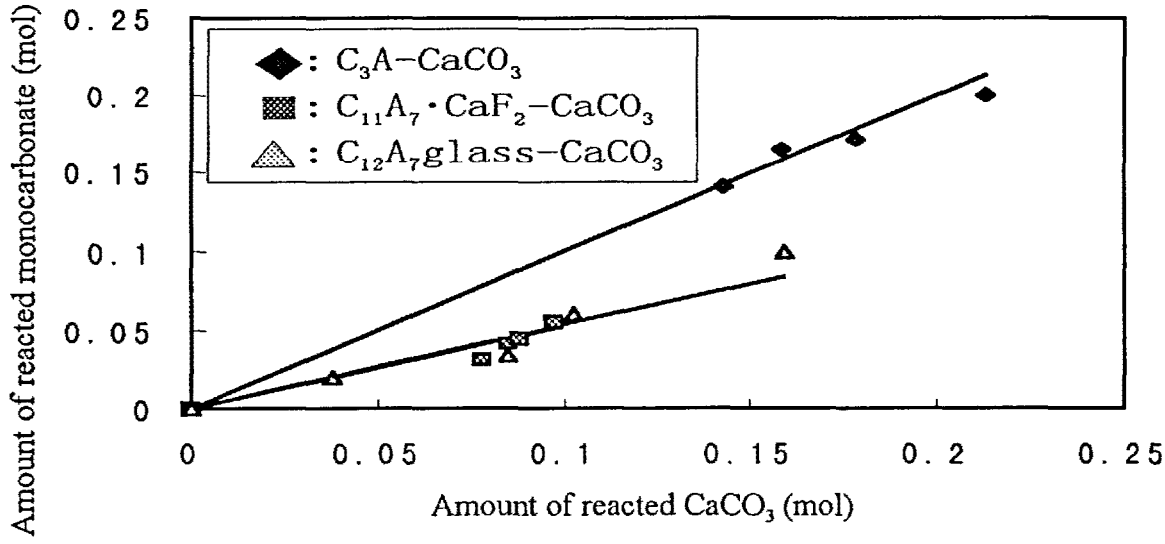

Figure 3 Relations between amount of produced monocarbonate and reacted $CaCO_3$.

In case of existing C_2AH_8 together, other reaction was also occurred. In this case, the amount of unreacted $C_{12}A_7$ glass was calculated from the amount of the combined water from Eqs 6 and 7.

$$C_{12}A_7 \text{ glass} + 51H_2O \rightarrow 6C_2AH_8 + 3AH_3 \quad [7]$$

Phase composition of hydrated various calcium aluminates - $CaCO_3$ systems

Changes in the phase compositions of the hydrated systems of C_3A, $C_{11}A_7 \cdot CaF_2$ and $C_{12}A_7$glass - $CaCO_3$ are shown in Figs 4, 5 and 6, respectively. The phase compositions are shown in weight percent of the unhydrated counts, (because the density of each compounds was unknown.)

In C_3A - $CaCO_3$ system, following reactions occurred;

$C_3A + 6H_2O \rightarrow C_3AH_6$ [8]
$C_3A + CaCO_3 + 11H_2O \rightarrow C_3A{\cdot}CaCO_3{\cdot}11H_2O$ [1]
$C_3AH_6 + CaCO_3 + 6H_2O \rightarrow C_3A{\cdot}CaCO_3{\cdot}11H_2O$ [9]

Till 1 day, the reactions of Eqs 8 and 1 proceeded simultaneously. Most of C_3A reacted for 1 day. After 1 day, while the reaction of Eq 9 proceeded until all C_3AH_6 or $CaCO_3$ was consumed, the amount of the produced monocarbonate kept on increasing.

In $C_{11}A_7{\cdot}CaF_2$ - $CaCO_3$ system, the following reactions were thought to proceed;

$C_{11}A_7{\cdot}CaF_2 + 31H_2O \rightarrow 4C_3AH_6 + 2Al(OH)_2F + 2AH_3$ [10]
$C_{11}A_7{\cdot}CaF_2 + 4CaCO_3 + 52H_2O \rightarrow 2.12(C_3A{\cdot}CaCO_3{\cdot}11H_2O)$
$+ 1.88(C_3A_{2.1}{\cdot}CaCO_3{\cdot}11H_2O{\cdot}1.1Al(OH)_2F{\cdot}14.2H_2O)$gel [3]

The same as the C_3A system, the reactions of Eqs 10 and 3 proceeded simultaneously till 1 day. Not so remarkable as the C_3A system, C_3AH_6 reacted with $CaCO_3$ to form monocarbonate. In this system, the reaction formula for the formation of monocarbonate was expressed as Eq 3.

In the $C_{12}A_7$ glass - $CaCO_3$ system, the following reactions were thought to occur;

$C_{12}A_7$ glass $+ 51H_2O \rightarrow 6C_2AH_8 + 3AH_3$ [7]
$C_{12}A_7$ glass $+ 4CaCO_3 + 53.4H_2O \rightarrow 2.12(C_3A{\cdot}CaCO_3{\cdot}11H_2O)$
$+ 1.88(C_3A_{2.6}{\cdot}CaCO_3{\cdot}16H_2O)$gel [6]

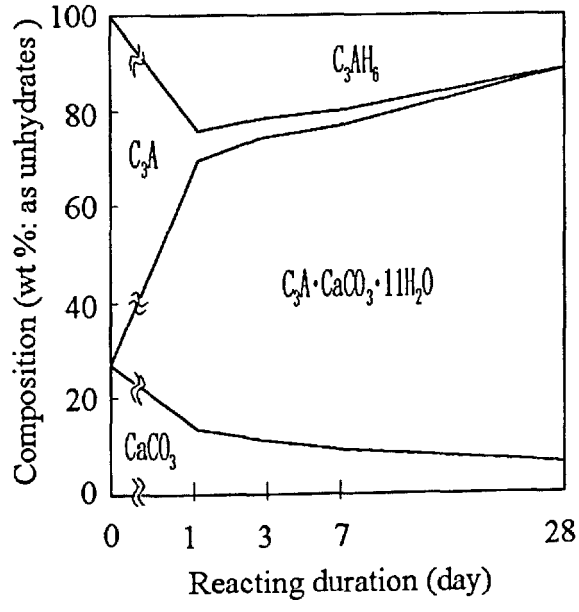

Figure 4 Composition change of hydrated C_3A-$CaCO_3$ system.

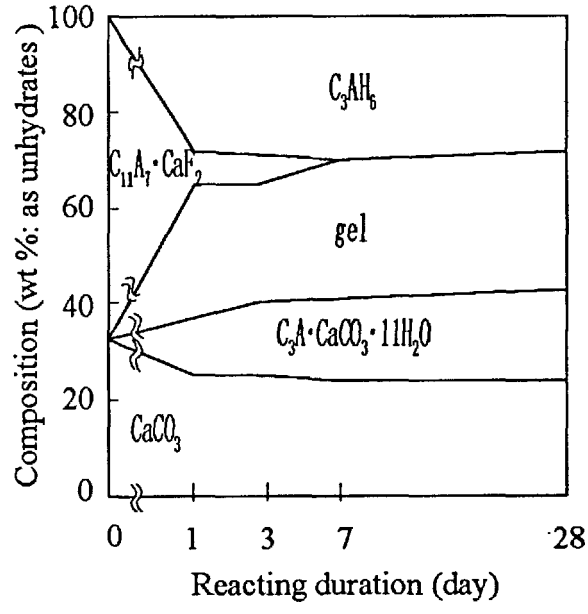

Figure 5 Composition change of hydrated $C_{11}A_7{\cdot}CaF_2$-$CaCO_3$ system.

In this system, at 1 day, most of C_2AH_8 produced and $CaCO_3$ hardly reacted. Therefore the reaction Eq 7 proceeded predominately. At 28 day, as mentioned above, the reaction in the $C_{12}A_7$glass - $CaCO_3$ system was written as Eq 6.

Calcium aluminate hydrates reacted with $CaCO_3$ and monocarbonate formed in the various calcium aluminates - $CaCO_3$ systems. In the hydrated systems of $C_{11}A_7 \cdot CaF_2$ - $CaCO_3$ and of $C_{12}A_7$glass - $CaCO_3$, $CaCO_3$ was suggested to be included in the gel. But the further experiment was necessary to discuss about it .

Reactivity of $CaCO_3$ in hydrated calcium aluminates - $CaSO_4$ - $CaCO_3$ systems

Figure 7 shows relations between the reaction ratio of $CaCO_3$ and the molar ratio of $CaSO_4$ / C_3A at 7 and 28 days in the C_3A - $CaSO_4$ - $CaCO_3$ system. Without $CaSO_4$, 79% of $CaCO_3$ reacted at 28 day sample. But with $CaSO_4$, the ratio of $CaCO_3$ decreased with the increasing of the ratio of $CaSO_4$ / C_3A. When the ratio of $CaSO_4$ / C_3A more than 2.5, $CaCO_3$ did not react until 28 day.

Figure 8 shows relations between the reaction ratio of $CaCO_3$ and the ratio of $CaSO_4$ / $C_{11}A_7 \cdot CaF_2$ at 7 and 28 days in the $C_{11}A_7 \cdot CaF_2$ - $CaSO_4$ - $CaCO_3$ system. Without $CaSO_4$, 30% of $CaCO_3$ reacted at 28 day sample. But with $CaSO_4$, the ratio of $CaCO_3$ decreased with the increasing of the ratio of $CaSO_4$ / $C_{11}A_7 \cdot CaF_2$. $CaCO_3$ did not react, where $CaSO_4$ / $C_{11}A_7 \cdot CaF_2 = 12$ of the ettringite composition, till 28 day.

Figure 9 shows relations between the reaction ratio of $CaCO_3$ and the ratio of $CaSO_4$ / $C_{12}A_7$ glass at 7 and 28 days in $C_{12}A_7$glass - $CaSO_4$ - $CaCO_3$ system. Similar to the other calcium aluminates systems, without $CaSO_4$, 47% of $CaCO_3$ reacted at 28 day sample. But with $CaSO_4$, the ratio of $CaCO_3$ decreased with the increasing of the ratio of $CaSO_4$ / $C_{12}A_7$glass. $CaCO_3$ did not

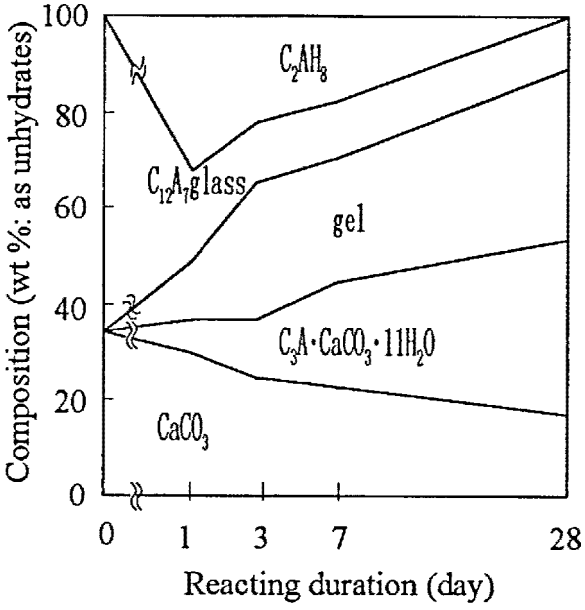

Figure 6 Composition change of hydrated $C_{12}A_7$ glass-$CaCO_3$ system.

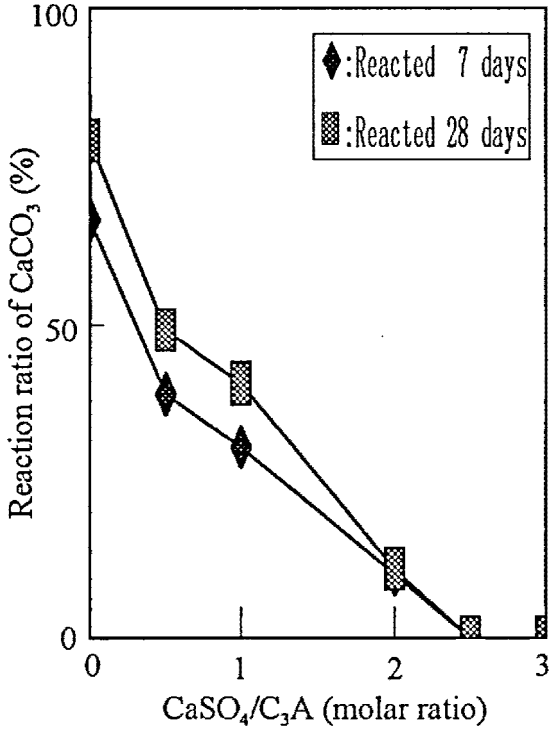

Figure 7 Relations between $CaSO_4/C_3A$ ratio and reaction ratio of $CaCO_3$.

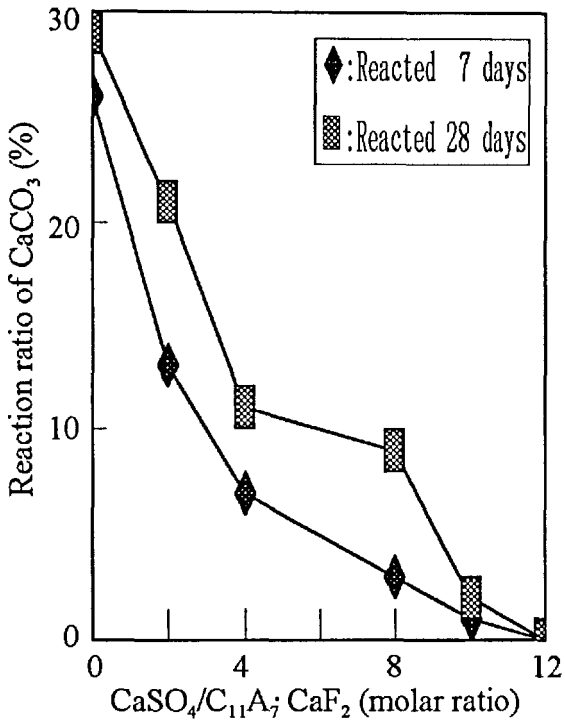

Figure 8 Relations between $CaSO_4/C_{11}A_7 \cdot CaF_2$ ratio and reaction ratio of $CaCO_3$.

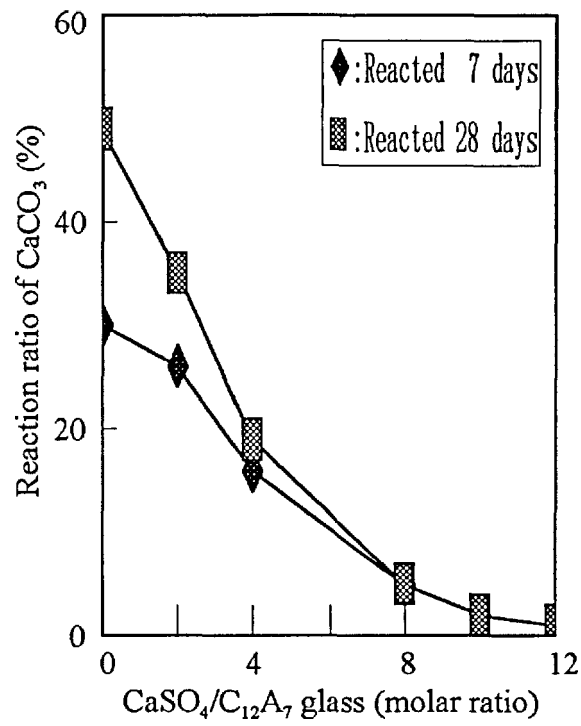

Figure 9 Relations between $CaSO_4/C_{12}A_7$ glass ratio and reaction ratio of $CaCO_3$.

react, where $CaSO_4$ / $C_{12}A_7$ glass = 12 of the ettringite composition, till 28 day.

In all the calcium aluminates - $CaSO_4$ - $CaCO_3$ systems, mentioned above, C_3A, $C_{11}A_7 \cdot CaF_2$ and $C_{12}A_7$ glass without $CaSO_4$, the reaction ratios of $CaCO_3$ showed the highest value.

The reaction ratios of $CaCO_3$ decreased with the increasing of the additional $CaSO_4$. $CaCO_3$ did not react when the amount of $CaSO_4$ closed to the composition of ettringite. But the ratio of $CaSO_4$ less than that of the composition of ettringite, $CaCO_3$ greatly influenced the hydration mechanisms of calcium aluminates - $CaSO_4$ systems.
As a results, in order to use the limestone powders as the inert filler, the required amount of $CaSO_4$ was near the composition of ettringite.

CONCLUSION

The hydration of the various types of calcium aluminates, C_3A, $C_{11}A_7 \cdot CaF_2$ and $C_{12}A_7$ glass, and the reactivity of $CaCO_3$ with or without $CaSO_4$ has been investigated. The following results were derived.

1) The reaction ratios of $CaCO_3$, in various types of calcium aluminates - $CaCO_3$ systems, C_3A, $C_{11}A_7 \cdot CaF_2$ and $C_{12}A_7$ glass, were 79%, 30% and 47%, respectively.
2) The molar ratio of produced monocarbonate / reacted $CaCO_3$ was 1 when C_3A-$CaCO_3$ system. But when the calcium aluminate was $C_{11}A_7 \cdot CaF_2$ or $C_{12}A_7$ glass, the ratio of produced monocarbonate / reacted $CaCO_3$ was 0.53. That might be caused by the gel including $CaCO_3$.
3) Various types of calcium aluminates reacted with $CaSO_4$ rather than $CaCO_3$ predominately, and the reaction of $CaCO_3$ was controlled by the amount of $CaSO_4$.

REFERENCES

Asaga, K. and Kuga, H., "Influence of $CaCO_3$ on the Rate of Hydration for Portland Cement", Proceedings of the 22nd JUCC Congress on Cement and Concrete, 1995, pp.79-84.

Grandet, J. and Olliver, J. P., "Etude de la Formation du Monocarboaluminate de Calcium Hydrate au Contact d'un Granulat Caraire dans une Pate de Ciment Portland", Cem. Concr. Res., Vol. 10. No. 6, 1980, pp.759-770.

Hosino, S. et al., "The Fluidity of Cement Paste with Various Classified Lime Stones and the Prepared Lime Stone", Extended Abstracts; The 49th Annual Meeting of JCA, 1995, pp.484-489.

Hosokawa, K., et al., "Hydration of C_3A, amor$C_{12}A_7$ or $C_{11}A_7{\cdot}CaF_2$ in the presence of Calcium carbonate", Annual Meeting of CSJ, 1995, p.488

Isizaki, T., "Measurement of Reaction Ratio for each Minerals no the Hydration of Portland Cement", CAJ Proceeding of Cement & Concrete, Vol.42, 1988, pp.40-43.

Kuzel, H.J. and Pollman, H., "Hydration of C_3A in the Presence of $Ca(OH)_2$, $CaSO_4{\cdot}2H_2O$ and $CaCO_3$", Cem. Concr. Res., Vol. 21. No. 5, 1991, pp.885-895.

Manabe, T. et al., "2 or 3 Experiment about Calcium Carbo Aluminate", CAJ Proceeding of Cement & Concrete, Vol.15, 1961, pp.54-60.

Sakai, E., et al., "Easily Cement Science" JCA, Tokyo, 1993, No.6:"Filler Cement", pp.54-61.

Kn o. 2 5. JAN. 2001 d o k 31786

2ii023
4 pp

SEQUENCE OF HYDRATION PROCESS DURING HARDENING OF HIGH ALUMINA CEMENT

Valeriy CHISTYAKOV, Kiev State Technical University of Construction and Architecture, Ukraine
Vladimir SERBIN, National Technical University of Ukraine, Kiev, Ukraine

ABSTRACT The results of experimental studies on hydration kinetics peculiarities of high-alumina cement minerals in the conditions of steam curing are summarized and discussed. The process of hardening of cement has been demonstrated to be characterized by a sequence under which the processes of hydration of minerals CA and CA_2 occur and different intensity of crystallization of C_3AH_6 and AH_3.

Key-words: High alumina cements, Hydration, Kinetics, Temperature

INTRODUCTION AND EXPERIMENTAL

With the use of a specially designed device "IG-IR" (Grankovskiy, 1984) allowing to determine the elastic characteristics of the system ($\omega_{res.}$) and change in degree of dispersion of the hardening system ($A_{res.}$) the processes of structure formation in the cement paste and stone have been studied at 70^0C (Fig 1). The increase in the resonance amplitude ($A_{res.}$) proves the prevalence of dispersing processes, while the decline of $A_{res.}$ is caused by the aggregation (condensation) processes (Chistyakov et al, 1986). In accordance with the structure formation curves $\omega_{res.}$ and $A_{res.}$ a selection of patterns of the hardening cements was made. Specially treated patterns were examined using X-ray diffraction (XRD), Differential Thermal analysis (DTA) and Infrared spectroscopy (IR). Points and figures on the structure formation curves (Fig 1) correspond to numbers of the patterns. The heating of the cell filled with cement paste was done in a steam-air medium with a velocity of 4^0C/ min. to simulate the heating regime of hot pressing technology of the compositions based on high alumina cement.

RESULTS AND DISCUSSIONS

An intensive increase of the interface surface (curve $A_{res.}$) caused by the dispersing of the primary particles of the cement and hydrolysis of clinker minerals CA and CA_2 are fixed immediately after cement is mixed with water.

The data of XRD prove that the primary weakly crystallized hydrates start to form from the moment when a cement is mixed with water and during mixing of the cement paste. In point 2 (Fig 1), when the temperature of the cement paste approaches 50^0C, the intensity of the line appropriate to AH_3 and C_3AH_6 increased to some extent. The interval 1-2, in accordance with character of the curves $\omega_{res.}$, $A_{res.}$ and Δm, corresponds to a first stage of structure formation of the cement paste, and the degree of hydration Δm increases insignificantly (from 2.28 for non-hydrated cement to 5.13%).

A sharp lowering of the values of $A_{res.}$ after point 2 proves the aggregation of disperse phase and intensive condensation processes. The inner stresses occurring in the structure being formed occur as a result of this process and a primary formed colloid network turned out to be disturbed as a result of their relaxation. This destructive process is fixed by a sharp loss of the elastic properties of the hardening cement paste (decline of values of $\omega_{res.}$ after point 2). The interval 2-3 with total duration 7 min. corresponds to the setting of the cement paste. A sharp increase of

rate of binding water (interval 2-3, curve Δm) is fixed at the moment of setting. The amount of water bound with new formations has increased twice: from 5.13% (pattern 2) to 11.5% (pattern 3). The elastic properties of the hardening system enhance greatly ($\omega_{res.}$= 550 Hz in point 2 and 900 Hz in point 3, Fig 1).

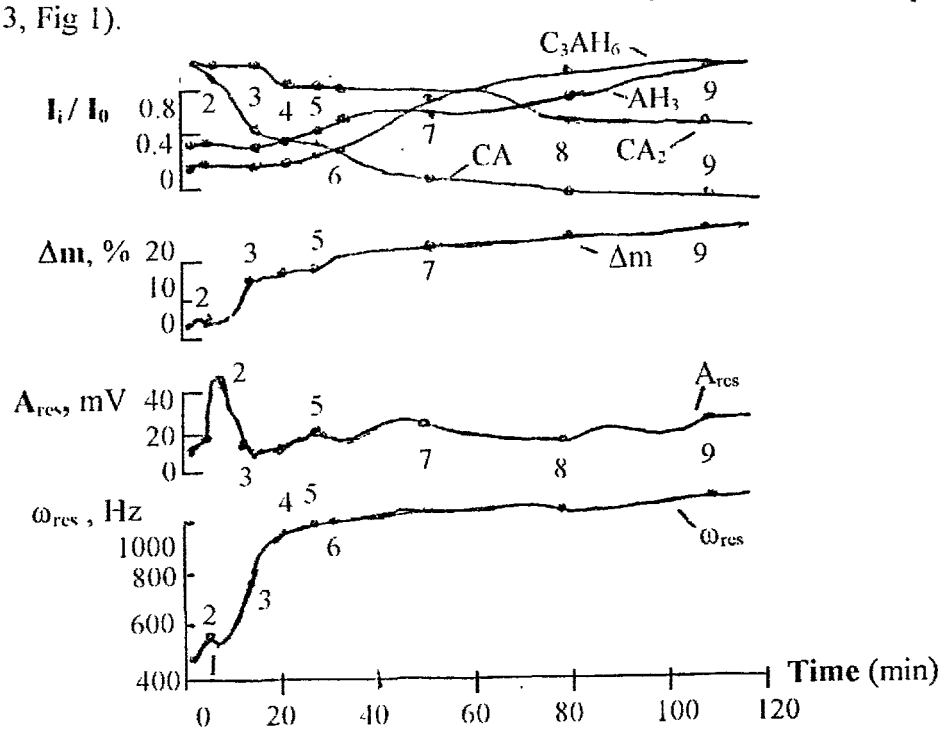

Figure 1 The kinetic curves of structure formation of the cement paste and stone at 70°C : $\omega_{res.}$- resonance frequency (Hz), $A_{res.}$- resonance amplitude (mV), Δm- degree of hydration (loss of mass by the pattern while heating up to 1000°C,%). Figures on the curves correspond to numbers and time of selection of XRD, DTA, and IR patterns.

I_i/I- the ratio of intensities of lines on X-ray diffractograms; I_i - the intensity of lines CA (d=0.295 nm), CA_2 (d=0260 nm), AH_3(d=0.482 nm), C_3AH_6 (d=0.55 nm) of a corresponding pattern; I- the intensity of a line characteristic of: CA-d=0.295 nm (non-hydrated cement); CA_2-d=0.260 nm (non-hydrated cement); AH_3-d=0.482 nm (pattern 9), C_3AH_6-d=0.515 nm (pattern 9).

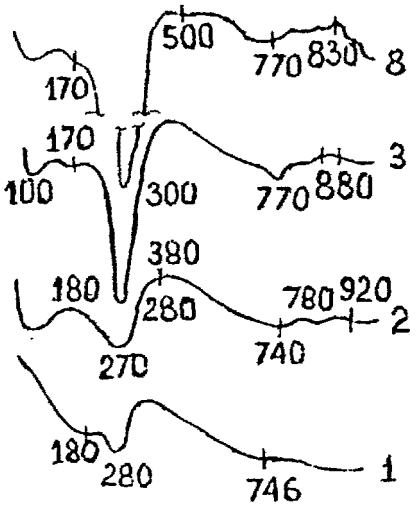

Figure 2 The DTA curves of the patterns selected according to structure formation development (designations as in Fig 1).

The hydration of clinker minerals and crystallization of hydrates was evaluated by variations in intensities of characteristic lines appropriate to above compounds on the X-ray diffractograms. The lines to be examined were selected for they would be characteristic only for one compound and to escape superposing of distances between the planes of other compounds. The line with d=0.295 nm was selected for CA, and 0.260 nm, 0.515 nm and 0.482 nm - for CA_2, C_3AH_6 and AH_3, respectively. The data produced testify to a more intensive hydration of CA as compared with CA_2. Was found that 50% of CA and 14% of CA_2 have reacted in point 3. After the setting is over (interval 3-4) the formation of hydrates slows considerably as compared with the previous period. After point 4 the CA_2 does not hydrate in practice and the hydrates are formed predominantly as a result of CA hydration The interval 4-6 is characteristic of the greatest intensity of AH_3 and C_3AH_6. The data of XRD demonstrate that gibbsite crystallizes with a greater velocity.

The interval 6-7 corresponds to the induction period for both CA and CA_2 (Fig 1). Meanwhile, the formation of hydrates is not over. C_3AH_6 is formed more intensively and is accompanied by retardation of crystallization of AH_3. A retardation of the processes of binding water is fixed within the interval 7-8 (Fig 1, curve Δm), and the hardening system is characterized by maximum values of ω_{res} reflecting elastic properties of the cement paste.

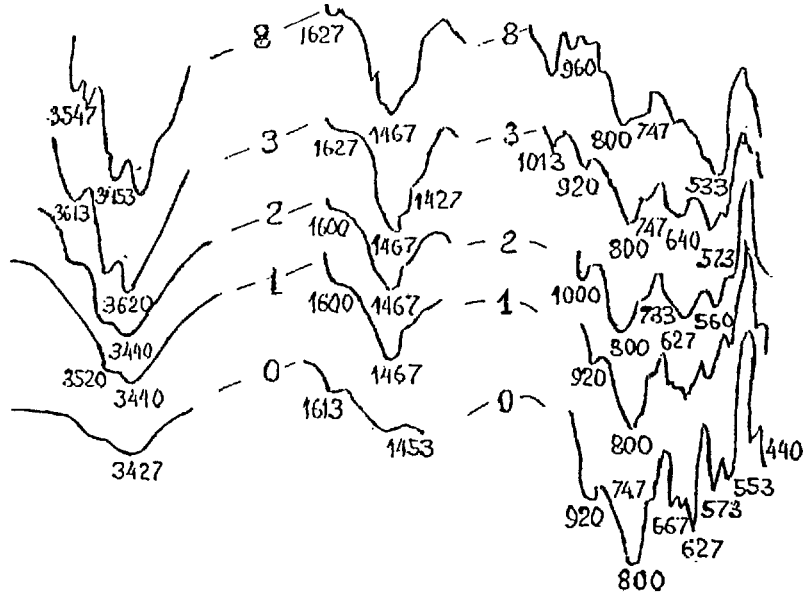

Figure 3 The IR- spectrums of the patterns selected according to structure formation development (designation as in Fig 1, the curve 0- infrared spectrum of non-hydrated cement).

The endotherm at 90°C appears on the DTA curve of the pattern 8 again, the intensity of endotherm at 170°C becomes weaker (Fig 2). Additional endotherm appears at 240°C, and testifies to the formation of carboaluminate of calcium $3CaOAl_2O_3$ $CaCO_3$ $12H_2O$. This conclusion correlates well with the data obtained using XRD.The endotherm within a field of 300°C on the DTA curve of the pattern 8 splits into 300 and 320°C. This effect is caused by the increase of the content of AH_3 and C_3AH_6 in the hardening system. The effect that appeared at 500°C may be referred to both AH_3 and C_3AH_6. Resulting from further heat treatment of the hardening system phase transformations of the hydrates take place what finds its reflection on the DTA curves and disappearance of some replicas on the X-ray diffractograms. Simultaneously, the intensive crystallization of AH_3 is observed.

The fragments of IR spectrums of the patterns of hardening cements selected according to a structure formation development (Fig 1) are given in Fig 3. Change in intensity of the bands 440cm^{-1} (bonds CaO-O in calcium-oxygen octahedrons) are fixed. The presence in the cement minerals of calcium- and alumino-oxygen polyhedrons initiates the superimposing of the Al-O- and Ca-O-bonds within an interval 400-600 cm^{-1} as well as the occurrence of "mixed" Al-O-Ca vibrations. A variation in intensities of the absorption bands 530 cm^{-1} which reflects the Al-O-Ca-bonds in the structure [(OH)O_4Al-O-CaO_4OH)] or [(OH)$_2O_3$Al-O-CaO_3(OH)$_2$] is fixed. This effect may be attributed to change in the degree of polymerization of the octahedrons and the degree of their hydroxylation. At the moment of setting, some growth of intensity of the bands of AH_3 (3660, 3625, 3540, and 1020 cm^{-1}) and C_3AH_6 (3628, 522 cm^{-1}) is fixed (Kuznetsova, Talaber, 1988).

During the hydration and increase of the interface surface, the adsorption of carbonic acid from the air to produce carbonate complexes (bands 1370-1480 cm^{-1}) takes place. At different stages of hardening the intensity of this process varies resulting from prevalence of the hydrates that are present. A maximum carbonization of aluminate complexes is reached after the setting of the cement (pattern 4). A cyclic change of degree of dispersing of the hardening system resulting from rearrangement of metastable forms of hydrates is observed at this period. The greatest changes in the IR-spectrums are fixed within a field 3000-4000cm^{-1} characteristic of stretching vibrations of hydroxyl-ions. According to structure formation development (Fig. 1), a positive effect of heat treatment on the hardening system is over near point 8. The prevalence of the condensation processes observed near point 7 (curve $A_{res.}$) and stabilization of the elastic properties (curve $\omega_{res.}$ before point 8) are changed by the strengthening of dispersing and destructive processes.

CONCLUSIONS

The process of hardening of high-alumina cement at 70^{0}C is characterized by a consequence of hydration of minerals CA and CA_2. At the moment of setting (interval 2-3) a sharp growth of the rate with which water is bound is fixed. This period is characteristic of the formation of calcium hydroaluminates detected by XRD in an amorphous state. An intensive joint crystallization of AH_3 and C_3AH_6 is observed after the setting. A heat treatment of the hardening high-alumina cement allows to minimize the formation of metastable hydroaluminates of calcium CAH_{10} and C_2AH_8 to produce at 70^{0}C a cement stone composed of stable hydrate phases AH_3 and C_3AH_6.

After 1.5 hrs of hydrothermal treatment, the processes initiating the strengthening of a cement stone become considerably slower (after point 8). Further heat treatment results in the intensification of phase transformations of hydrates, rearrangement of the cement stone structure formed and the development of destructive processes.

REFERENCES

Grankovskiy, I.G., Structure Formation in Mineral Cementitious Systems, Naukova Dumka Publish., Kiev, 1984, 300 pp.

Chistyakov, V.V., Grankovskiy, I.G., Gots, V.V, "The Formation of Structure of a Slag Alkaline Cement", Prikladnaya Himia Journal, 1986, Vol.59, No 3, pp. 590-595.

Kuznetsova, T.V., Talaber J., High Alumina Cement, Moscow, , Stroiizdat Publishers, 1988, 268 pp.

Kn o. 25. JAN. 2001 d o k 31787

2ii024
8 pp

CALCULATION OF THE MAXIMUM SUPERSATURATION CURVE OF C_2AH_8 IN THE $CaO-Al_2O_3-H_2O$ SYSTEM AT 20°C

Denis DAMIDOT, LAFARGE Laboratoire Central de Recherche, St-Quentin Fallavier, France
Pierre BARRET, Laboratoire de Recherches sur la Réactivité des Solides, Dijon, France

ABSTRACT The knowledge of the maximum supersaturation curves of the hydrates is of great importance in order to understand the hydration process. In the $CaO-Al_2O_3-H_2O$ system, only parts of the maximum supersaturation curve of C_2AH_8 have been determined experimentally. As it is very difficult to advance theories in order to calculate the maximum supersaturation values, we have developed a calculation method which is based on experimental data and thermodynamic calculations. This method which has been applied to the maximum supersaturation curve of C_2AH_8, can also be used for other systems.

Key-words: Calcium aluminate cement, Hydration, Thermodynamics, Phase diagram

INTRODUCTION

Hydraulic binders react through a dissolution precipitation mechanism whose driving force is based on a higher solubility of the solids that is dissolved relatively to the hydrate that precipitates. Thus during the dissolution process, the composition of the aqueous phase reaches supersaturated region with respect to the hydrate which precipitates after an induction period. The duration of the induction period mainly depends on the supersaturation value which is reached: higher supersaturation values decrease the duration of the induction period. As a consequence, if the induction period is less than 1 second, the precipitation seems to be immediate for human eyes. An hydraulic binder will have a setting time which is very closely related to the amount of hydrate formed and thus to the duration of the induction period before the start of the period of growth of the hydrates. Thus the setting time is linked with the ability of the solid which dissolves, to reach the highest supersaturation as possible in order to have the shortest induction period. This aptitude will mainly depends on the position of the equilibrium curve of the solid that dissolves relative to the region of supersaturation that induces a quasi-immediate precipitation of the hydrate (practically no induction period). This last region is delimited by a maximum supersaturation curve with respect to the hydrate that precipitates. It can exist two main cases that are represented on Fig 1:

- in case A, the equilibrium curve of the solid that dissolves is on the left of the maximum supersaturation curve. As a consequence, it is possible to reach the equilibrium curve of the dissolving solid during the hydration process. The aqueous phase is supersaturated with respect to the hydrate, but it exist an induction time before the start of the hydrate precipitation as the supersaturation value is not high enough to induce an immediate precipitation. This case represents hydraulic binders that do not induce a rapid setting such as CA.
- in case B, the maximum supersaturation curve with respect to the hydrate is reached first. This induces a rapid hydrate precipitation which prevents the aqueous phase to reach the equilibrium curve with respect to the solid that dissolves. This case corresponds to hydraulic binder that sets rapidly such as C_3A.

Most of the experimental and theoretical work on the hydration is generally based on the knowledge of the equilibrium curves of the hydrates and sometimes on the solids that dissolves, and also on the kinetic paths. However the determination of the maximum supersaturation curves did not find the same enthusiasm even if these are as important in order to understand the mechanism of the early hydration which is linked with the workability of hydraulic binders. This

may be due to the experimental difficulties in order to determine these curves but also to the impossibility to calculate them theoretically without any experimental data.

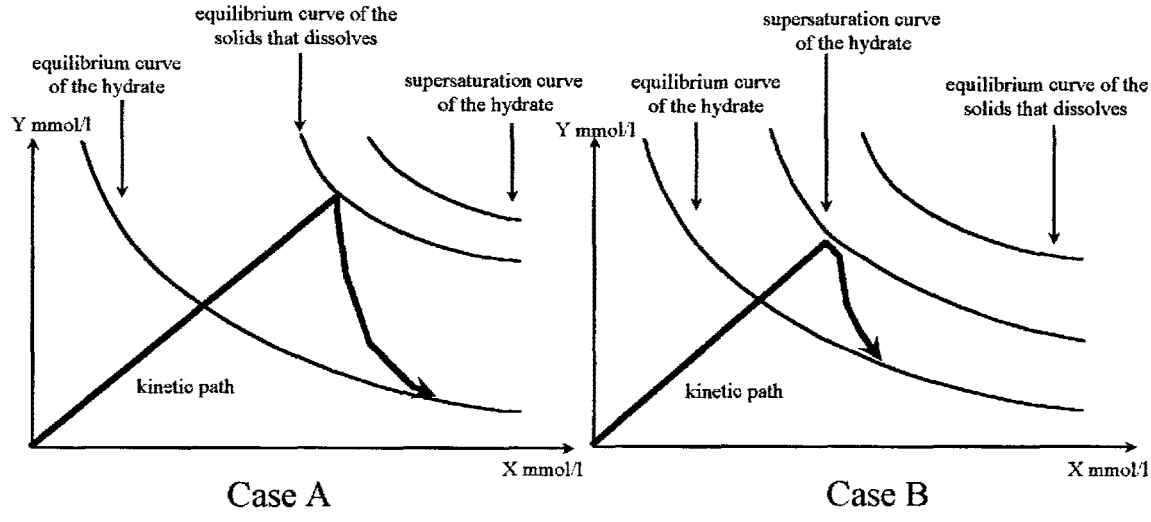

Fig 1. Schematic representation of the two major cases that can occur during the early hydration of hydraulic binders.

From our knowledge, some points of the maximum supersaturation curves have been defined experimentally for C-S-H (Barret, 1986) and for C_2AH_8 (Bertrandie, 1977, Barret, 1980). The maximum supersaturation curve of C_2AH_8 (named curve I) is very important in order to understand the hydration process in the $CaO-Al_2O_3-H_2O$ system. However curve I is not very well defined from the experiments (Fig 2).

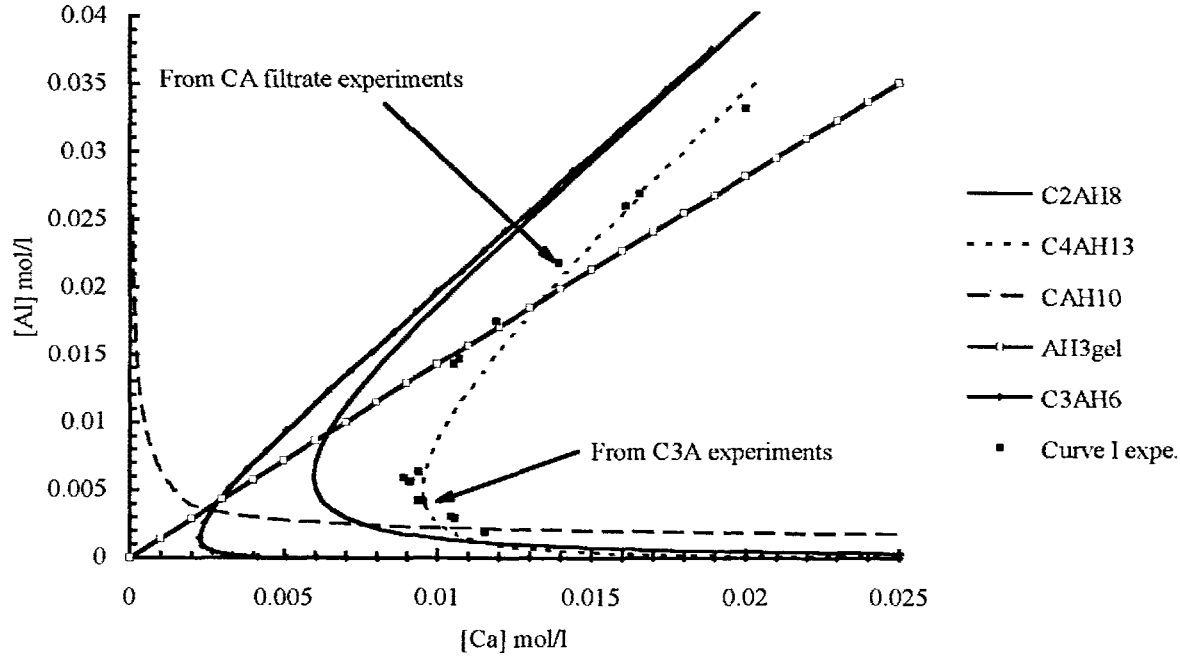

Fig 2. Experimentally determined points of the maximum supersaturation curve with respect to C_2AH_8 (curve I) added to the $CaO-Al_2O_3-H_2O$ phase diagram calculated at 20°C

It exists an unknown part between the two groups of points which correspond to two different types of experiments. The first group has been obtained by the modification of the composition of supersaturated solutions recovered during CA hydration (Bertrandie, 1977). The second group was defined during C_3A hydration in various lime solutions (Barret, 1980). It should be possible to reach experimentally the unknown part of curve I using $C_{12}A_7$ hydrated in various solutions. But we wanted to find a general method that enables us to calculate a maximum supersaturation curve by combining the data of some experimentally determined points of this curve and thermodynamic calculations.

EXPERIMENTAL: METHOD OF CALCULATION

In a first approach, Barret (Barret, 1994) dried to calculate the curve I from curve m (curve of iso-supersaturation with respect to C_2AH_8 and AH_3): curve I was similar to curve m but with a supersaturation value (βm) of 12. This method was accurate enough in the upper part of curve I (high aluminate concentrations) but could not describe the bottom part of curve I: curve I was crossing the equilibrium curve of C_2AH_8 and thus describing some aqueous compositions undersaturated with respect to C_2AH_8. This problem was the consequence of curve m equation which is similar to C_4AH_{13} but with a value of the solubility product divided by 2: C_2AH_8 and C_4AH_{13} equilibrium curves always cross whatever the value of the solubility product.

In the present approach, we started to calculate the supersaturation value of C_2AH_8 (β2) at the experimental points that define curve I using a speciation program derived from PHREEQE (Parkhurst, 1980). The following dissolution equation for C_2AH_8 was considered:

$$2CaO.Al_2O_3.8H_2O \Rightarrow 2\,Ca^{2+} + 2Al^{3+} - 10H^+ + 13H_2O$$

The use of Al^{3+} and H^+ as ionic species instead of $Al(OH)_4^-$ and OH^- respectively is due to the thermodynamic database which is associated to PHREEQE. As a consequence, the value of the solubility product of C_2AH_8 at 20°C differs from the usual value which is calculated with $Al(OH)_4^-$ and OH^- (Barret, 1994):

$$K_{C2AH8} = (Ca^{2+})^2(Al^{3+})^2(H^+)^{-10}(H_2O)^{13} \text{ with Log } K_{C2AH8} = 60.79 \text{ at } 20°C \qquad [1]$$

There is no obvious relation between the calcium concentration and β2 (Table 1). On the contrary, the value of β2 appears to increase monotonously with the aluminate concentration in the aqueous phase (Fig 2). This behaviour can be accurately fitted with an exponential growth function (Fig 2 and Table 1):

$$\beta 2 = 2.934156.10^{0.05235.[Al]} \quad \text{with [Al] in mmol/kg and T=20°C} \qquad [2]$$

For a given aluminate concentration it is possible to estimate the value of β2 using Eq. 2. Thus we can calculate the iso-supersaturation curve with respect to C_2AH_8 for the corresponding β2 value: Log $K_{\beta 2}$ has to be considered in Eq. 1 instead of Log K_{C2AH8}:

$$\text{Log } K_{\beta 2} = \text{Log } K_{C2AH8} + \text{Log } \beta 2 \qquad [3]$$

Two of these iso-supersaturation curves are represented on Fig 3 for β2 equal to 6.05 and 40.52 which correspond to [Al] equal to 6 and 21.78mmol/kg respectively. From these curves, it is possible to determine the calcium concentration which corresponds to the starting aluminate concentration:

- [Ca]=9.02mmol/kg for [Al]=6mmol/kg and β2=6.05

- [Ca]=13.95mmol/kg for [Al]=21.78mmol/kg and β2=40.52

Each pair of points, ([Ca],[Al]), represents one point of curve I. Thus if the same method is used for all [Al] concentrations ranging from 0.1 to 40mmol/l, it is possible to determine accurately curve I.

Table 1. Aqueous phase composition for experimentally determined points of curve I (Bertrandie, 1977, Barret, 1980) and value of the supersaturation with respect to C_2AH_8 (β2) obtained with the experimental points and from Eq. 2

[Ca] mmol/kg	[Al] mmol/kg	β2 experimental	β2 calculated with Eq 2
20.00	33.20	169.93	160.51
16.50	26.96	75.63	75.66
16.10	26.00	71.93	67.39
13.95	21.78	41.55	40.52
11.90	17.90	21.56	25.38
10.71	15.20	15.12	18.33
10.54	14.94	13.96	17.77
9.40	6.34	8.44	6.30
8.92	5.94	6.35	6.00
9.09	5.66	6.50	5.80
9.15	5.60	6.59	5.76
9.38	4.22	4.98	4.88
9.55	4.18	5.24	4.86
10.44	3.04	4.32	4.23
10.56	2.92	4.20	4.17
11.54	1.92	2.67	3.70

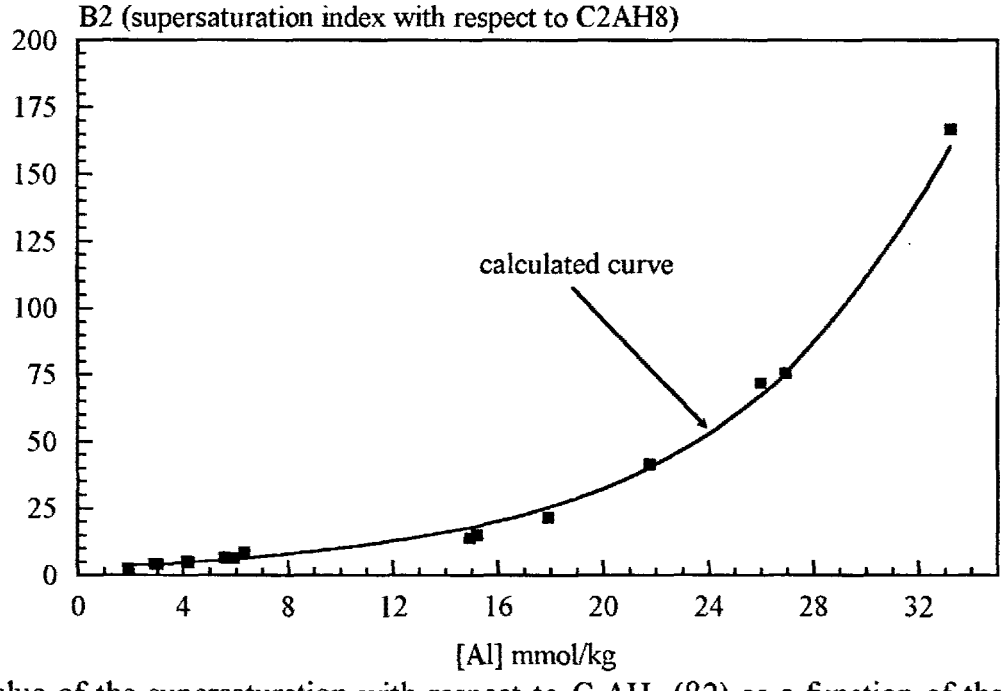

Fig. 3. Value of the supersaturation with respect to C_2AH_8 (β2) as a function of the aluminate concentration: experimental points and fitted curve using Eq. 2.

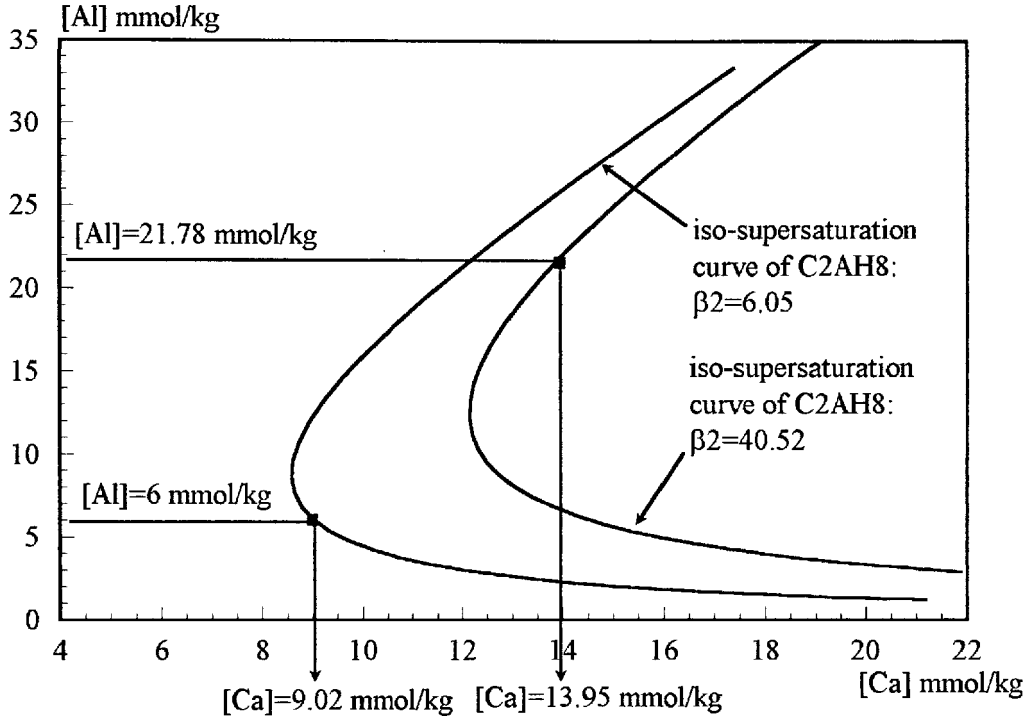

Fig. 4. Calculated iso-supersaturation curves with respect to C_2AH_8 and corresponding pairs of ([Ca],[Al]) concentrations which belong to curve I.

RESULTS & DISCUSSION

The results of the calculation of curve I at 20°C are given in Table 2. The calculated curve I was added to the $CaO-Al_2O_3-H_2O$ phase diagram (Fig 5): this curve is in good agreement with the experimental data. As expected, curve I remains in the supersaturated region with respect to C_2AH_8 and never crosses the equilibrium curve of C_4AH_{13}.

Table 2. Calculated pairs of ([Ca],[Al]) concentrations that define curve I at 20°C

[Ca] mmol/kg	[Al] mmol/kg	[Ca] mmol/kg	[Al] mmol/kg
22.75	0.75	11.6	16
18.87	1	12.06	17
12.78	2	12.47	18
10.69	3	12.94	19
9.68	4	13.39	20
9.22	5	13.88	21
9.02	6	14.39	22
8.97	7	14.87	23
9.08	8	15.39	24
9.22	9	16.42	26
9.47	10	17.52	28
9.76	11	18.6	30
10.03	12	19.71	32
10.41	13	20.85	34
10.9	14	22.07	36
11.17	15		

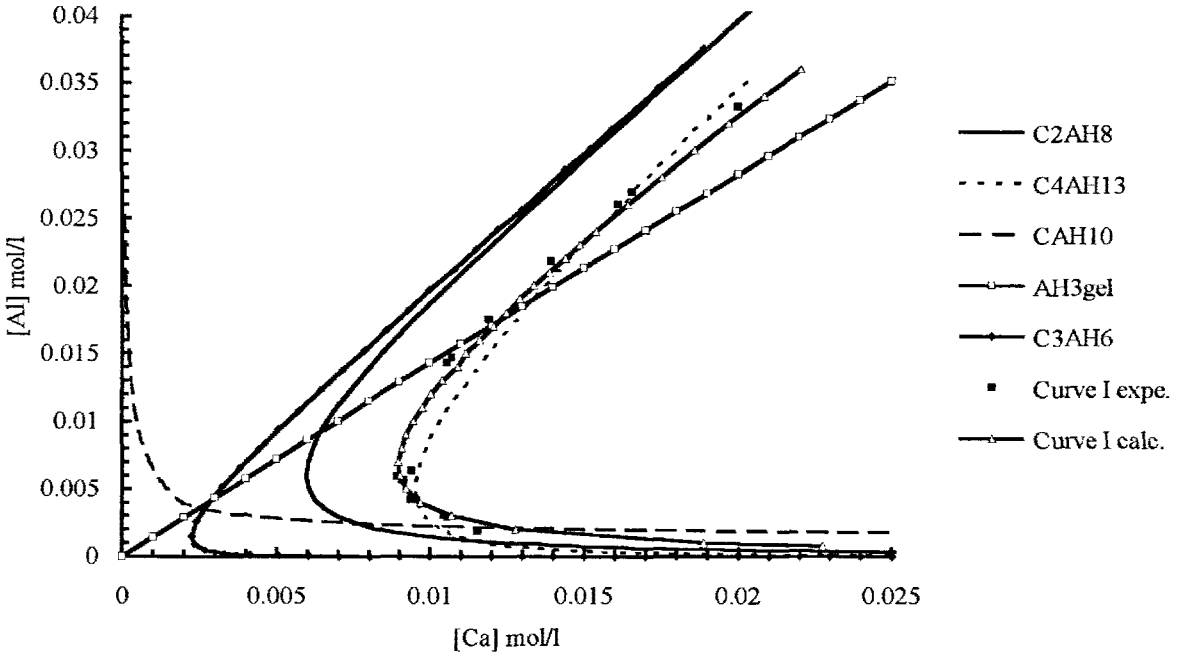

Fig. 5. Calculated curve I added to the phase diagram of the $CaO-Al_2O_3-H_2O$ system at 20°C

It is noticeable that the supersaturation values that have to be reached to induce an immediate precipitation of C_2AH_8 decrease markedly with a decrease of the aluminate concentration. This behaviour is expected to be linked to the increase of pH that occurs concomitantly. The position of curve I enables us to determine the systems that can lead to a rapid precipitation of C_2AH_8. We have to consider the calcium to aluminate molar ratio, $(C/A)_{dissol}$, of the ions accumulated in the solution by the dissolution of the anhydrous solid at the hydration beginning (this molar ratio can be different of the C/A ratio of the solid):

- If $(C/A)_{dissol}$ is lower than 1.25, curve I is never reached during the dissolution process and thus C_2AH_8 is never precipitated rapidly: an induction period is observed. In this last case, the aqueous phase can also be supersaturated with respect to other hydrates that can precipitate before or along with C_2AH_8 depending on their respective induction period. These systems are generally slow: case of CA hydration for example.
- If $(C/A)_{dissol}$ is higher than 1.25, curve I is reached and C_2AH_8 is precipitated rapidly. Once C_2AH_8 has been precipitated, the composition of the aqueous phase reaches some regions on the left part of curve I and other solids may precipitate if the aqueous phase is supersaturated with respect to them. In this case, an induction period with respect to these hydrates may be observed. However the initial precipitation of C_2AH_8 is often sufficient enough to induce a rapid setting of the system. These systems are representative of $C_{12}A_7$ and C_3A hydration.

Thus curve I is very important as it governs most of the early hydration in the $CaO-Al_2O_3-H_2O$ system. Moreover it can unable other maximum supersaturation curve of hydrates to be reached due to C_2AH_8 precipitation. As a consequence, these curves are never obtained experimentally. C_4AH_{13} seems to be an exception as it precipitates concomitantly with C_2AH_8 without any noticeable induction period during C_3A hydration.

Several factors can modify the nucleation and thus change the maximum supersaturation values that induce the immediate precipitation; temperature, presence of solids that provide nucleating sites, presence of foreign ions in the aqueous phase... The specific weight of these parameter is difficult to assess. However the influence of ions that only modify the ionic strength of the

solution without enabling some new solids to precipitate, can be estimated by thermodynamic calculations. For example, the influence of NaOH addition at different concentrations has been investigated. The main influence of NaOH is to shift the upper branch of the equilibrium curve of C_2AH_8, toward higher aluminate concentrations (Fig 6). If we consider a filtrate obtained during the induction period of CA hydration, the composition is close to [Ca]=20mmol/kg and [Al]=36mmol/kg. The filtrate lies in the supersaturated domain with respect to C_2AH_8 (Fig 6) and presents an induction of about 10 hours. Bertrandie (Bertrandie, 1977) reduced and even suppressed this induction period by adding a saturated lime solution ([Ca]=22mmol/l): the filtrate composition was shifted almost vertically to lower aluminate concentrations and as a consequence the supersaturation value was increased and curve I was reached. If a NaOH solution is added to the filtrate, the calcium and aluminate concentrations are not changed, but due to the shift of the equilibrium curve of C_2AH_8, the supersaturation value with respect to C_2AH_8 is increased. Thus if the increase of the supersaturation value is high enough, C_2AH_8 could precipitate immediately without any induction period (Fig 6).

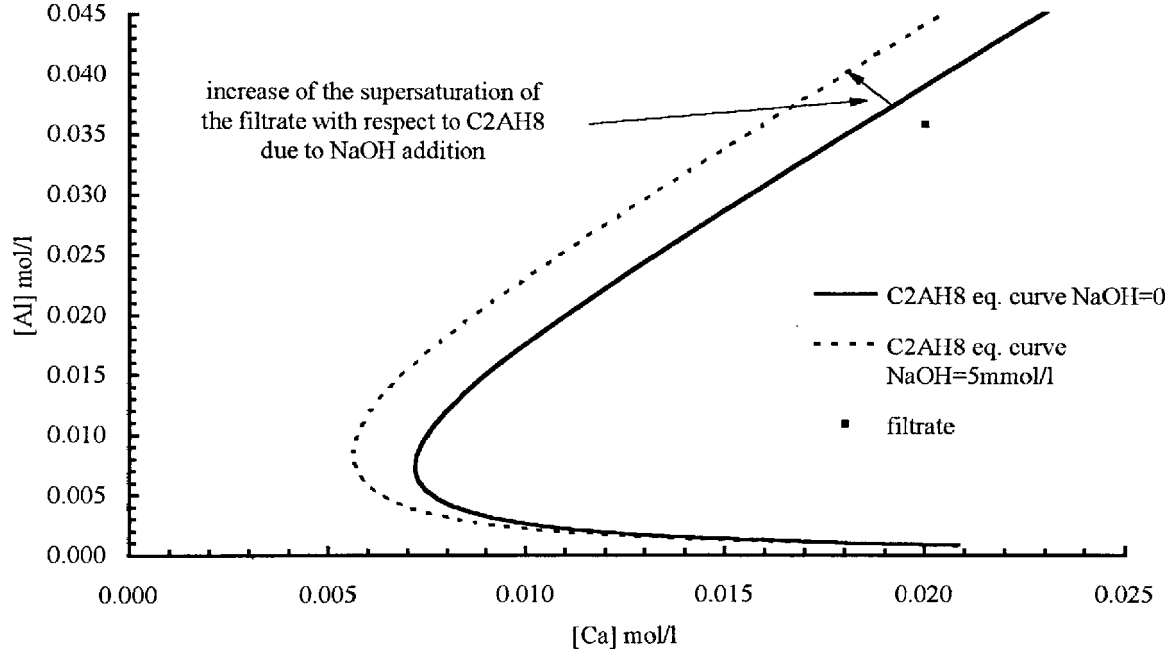

Fig 6. Influence of NaOH on the position of C_2AH_8 equilibrium curve.

We tested this hypothesis by following the electrical conductivity of stirred filtrate. The procedure was the following: 2ml of a given NaOH solution was added to 80 ml of filtrate. We used 41, 82 and 205mmol/l NaOH solutions in order to add 1, 2 and 5mmol/l NaOH to the filtrate. The induction period was reduced with 1mmol/l and suppressed with 2 and 5mmol/l (Fig 7) in a similar manner as observed with Bertrandie by just adding lime solutions to the filtrate (Bertrandie, 1977). The values of β2 were calculated for the different cases (Table 3).

Table 3. Calculated values of β2 for different compositions of the filtrate

[Ca] mmol/kg	[Al] mmol/kg	[Na] mmol/kg	β2	induction period
20	36	0	67	yes
20	36	1	104	yes
20	36	2	159	no
20	36	5	307	no
20	33	0	170	no

It is noticeable that the minimum β2 value which induces the immediate precipitation of C_2AH_8 in pure water (β2=170) is similar to the value of β2 found with 2mmol/l NaOH which is the first NaOH concentration that removes the induction period (β2=159). This point is very important as it enables us to calculate the curve I in the presence of sodium ions which are often brought by admixtures. In the presence of NaOH, the curve I calculated previously will be just shifted in a manner similar to the equilibrium curve of the hydrates as β2 values determined by Eq. 2 remain valid.

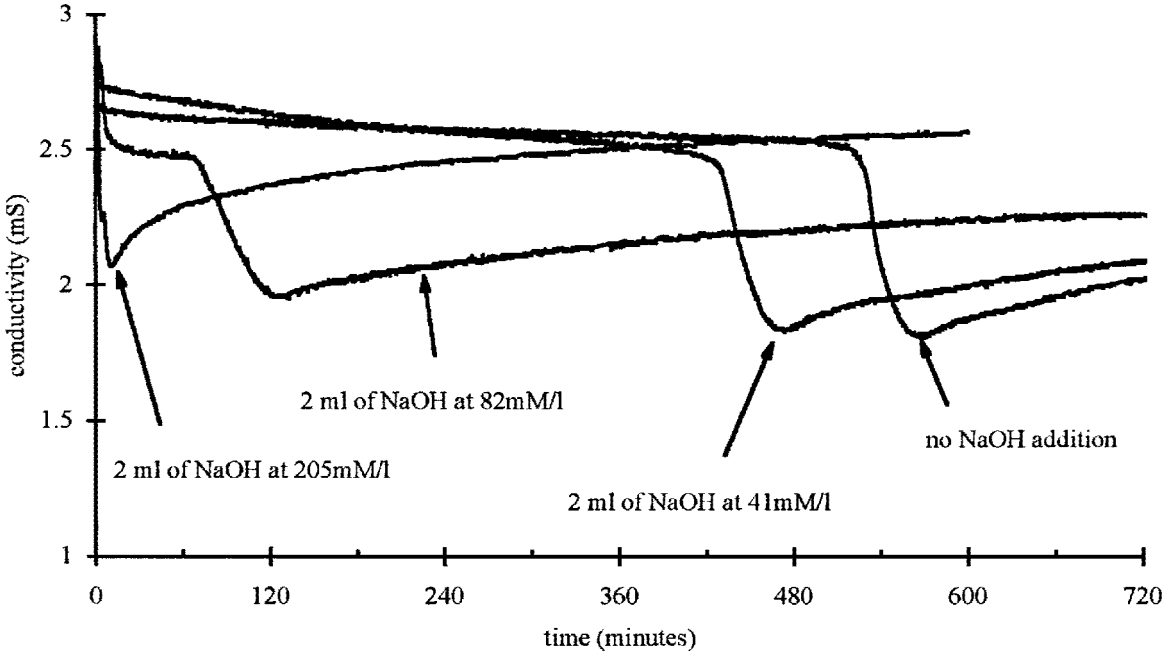

Fig 7. Conductivity of supersaturated filtrate in the presence of added NaOH solution.

CONCLUSION

A method to calculate the maximum supersaturation curve with respect to C_2AH_8 (curve I) at 20°C has been developed. This method is general and can be used for other systems. It also appears that the supersaturation value with respect to C_2AH_8 along curve I, is not markedly modified in the presence of NaOH. As a consequence, the method is still applicable in this case. However these kinds of calculation cannot take directly into account the influence of temperature or other parameters such as nucleating sites on solids added to the system: further experiments are crucially needed to bring new data on this important aspect of the hydration of cements.

REFERENCES

Barret, P. and Bertrandie, D., "Hydratation de C_3A en présence d'eau de chaux" 7th ICCC, Paris, Vol. 4, 1980, pp. 443.

Barret, P. and Bertrandie, D., "Fundamental hydration kinetic features of the major cement constituants: Ca_3SiO_5 and Ca_2SiO_4" Jour. Chimie Physique, 1986, pp. 765-775.

Barret P. and D. Bertrandie "Hydration of aluminate cements" Advances in cement and concrete, Proc of Engineering Foundation Conference, Durham, Grutzeck and Sarkar Ed.,1994, pp. 132.

Bertrandie D. "Contribution à l'étude cinétique de la formation des hydrates dans les solutions aqueuses obtenues à partir du ciment alumineux" Thesis, University of Burgundy, 1977.

Parkhurst, D.L., Thorstenson, D.C. and Plummer, L.N. "PHREEQE - A computer program for geochemical calculations" U.S. Geological Survey, USGS-WRI-80-96, 1980.

Kn o. 25. JAN. 2001 d o k 31788 2ii025 8 pp

MODIFICATION OF THE HYDRATION PROCESS FROM $C_{12}A_7$ TO C_3A AT 20°C

Denis DAMIDOT and François SORRENTINO, LAFARGE Laboratoire Central de Recherche, St-Quentin Fallavier, France

ABSTRACT

Mixtures ranging from $C_{12}A_7$ to C_3A have been obtained by a sintering process. The hydration of these mixtures has been studied in paste form by microcalorimetry and in diluted suspension by conductivity measurements. The hydration process of the mixtures can be classified in two groups depending on the C/A ratio of the mixtures. For mixtures having a C/A ratio lower than 2.3, the hydration advances through two steps which are separated by a short induction period. On the other hand, the hydration of mixtures having a C/A ratio higher than 2.3, proceeds through an unique step and therefore is very rapid. The differences in hydration behaviour have been explained in taking into account the precipitation of C_2AH_8.

Key-words: Hydration, Mechanism, Calcium aluminate, calorimetry.

INTRODUCTION

The hydration of both $C_{12}A_7$ and C_3A leads to short setting times at room temperature. This is a consequence of the rapid kinetic of hydration of both $C_{12}A_7$ and C_3A. However the hydration mechanisms at 20°C of $C_{12}A_7$ and C_3A are not similar. First the different stoechiometries of these two calcium aluminate induce different compositions for the aqueous phase and the precipitation of different hydrates at the hydration beginning (De Jong, 1968, Capmas, 1990): C_2AH_8 is observed with both $C_{12}A_7$ and C_3A whereas C_4AH_{13} is only obtained with C_3A. Moreover calorimetric experiments indicate that C_3A hydration proceeds through an unique step (only one exothermic peak) (De Jong, 1968), while $C_{12}A_7$ hydration displays two steps (two exothermic peaks) (Edmonds, 1988). These differences can be used to explain that the setting time of C_3A is shorter than the setting time of $C_{12}A_7$. This behaviour remains in mixtures of $C_{12}A_7$ and C_3A (Ménétrier-Sorrentino, 1986); the setting time of a mixture of 63% $C_{12}A_7$ - 28% C_3A (% by weight) is 1 minute whereas it is 45 minutes for a mixture of 85% $C_{12}A_7$ and 6% C_3A. In this previous example, the first mixture behaves more like C_3A and the second one is closer to $C_{12}A_7$. The aim of this study was to determine the composition in the $C_{12}A_7$-C_3A that delimits mixtures having a behaviour similar to $C_{12}A_7$ from mixtures behaving like C_3A. Thus the hydration of several mixtures of the system $C_{12}A_7$-C_3A was investigated in paste or in diluted suspension in order to determine their hydration mechanism relatively to $C_{12}A_7$ and C_3A.

EXPERIMENTAL

The sample were prepared by mixing the desired contents of pure ANALAR $CaCO_3$ and alumina in order to obtain the compositions given in Table 1. Then the mixtures were sintered at 1450°C in platinum crucibles and air atmosphere. The sintering process is followed by a slow cooling period. The samples were ground in order to have the same fineness of about 300m^2/kg SSA. Then the samples were checked by XRD and SEM using EDX analysis. Hydration was followed by isothermal calorimetry on paste having a W/C ratio of 1 but also on stirred suspension (W/C=10) with a specially designed calorimeter (D. Damidot, 1990). Conductimetry experiments were also performed on stirred suspensions (W/C=10). During these experiments, it was possible to recover 15 ml of the suspension in order to analyse the aqueous phase composition by ICP and the solids by XRD and SEM. The hydration was stopped by washing the solids by acetone and ether.

Table 1. Chemical compositions of the mixtures studied in the $C_{12}A_7$-C_3A system

Sample name	weight % CaO	weight % Al_2O_3	molar % $C_{12}A_7$	molar % C_3A	C/A molar
C48A52 ($C_{12}A_7$)	48	52	100	0	1.72
C50A50	50	50	88.4	11.6	1.86
C53A47	53	47	67	33	2.14
C56A44	56	44	45	55	2.42
C59A41	59	41	23.2	76.8	2.70
C62A38 (C_3A)	62	38	0	100	3.00

RESULTS

The calorimetry results are given in Figures 1 and 2 which correspond to two different cases. Calorimetry curves that present two exothermic peaks like $C_{12}A_7$ (Fig 1) and those that only contain one initial exothermic peak as C_3A (Fig 2). The scale of the two figures is similar in order to facilitate a comparison. However the intensity of the first exothermic peak varies significantly between the samples (Table 1).

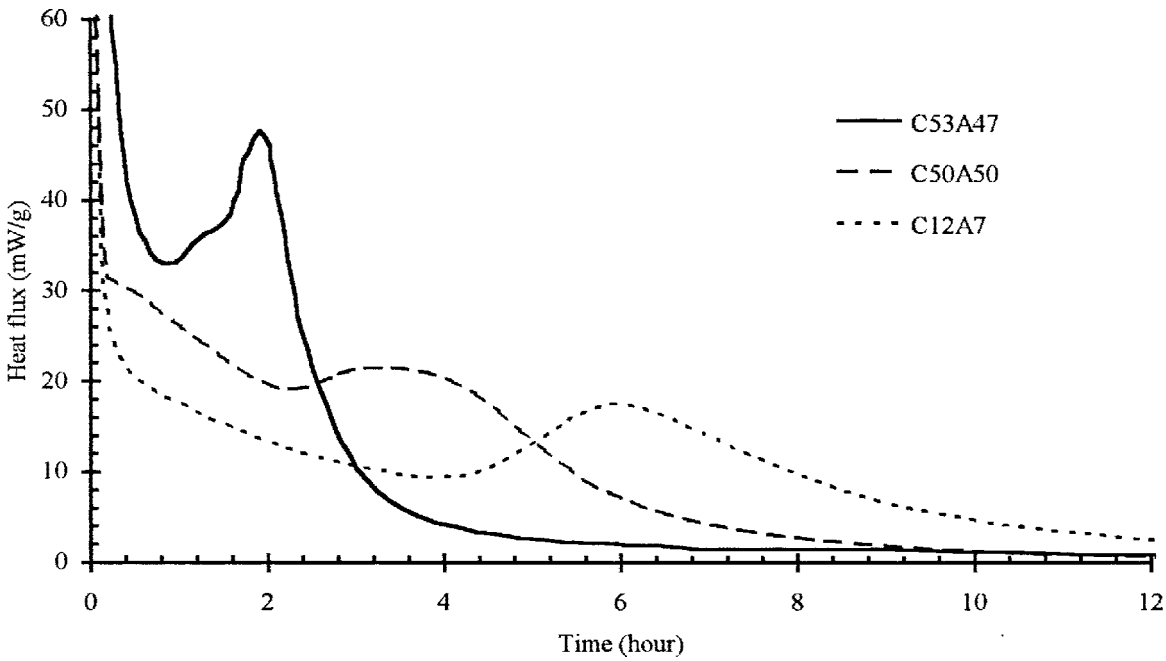

Fig 1. Calorimetry curves obtained with $C_{12}A_7$, C50A50 and C53A47 at 20°C and W/C=1

Table 2. Intensity and time at the maximum of the observed exothermic peaks

Sample name	first peak		second peak	
	heat flux (mW/g)	time	heat flux (mW/g)	time
C48A52	112.90	2 mn 20	17.60	5 h 55
C50A50	101.32	1 mn 45	22.99	3 h 25
C53A47	414.60	3 mn	44.97	2 h 07
C56A44	527.71	3 mn		
C59A41	439.83	2 mn 45		
C62A38	228.19	4 mn 40		

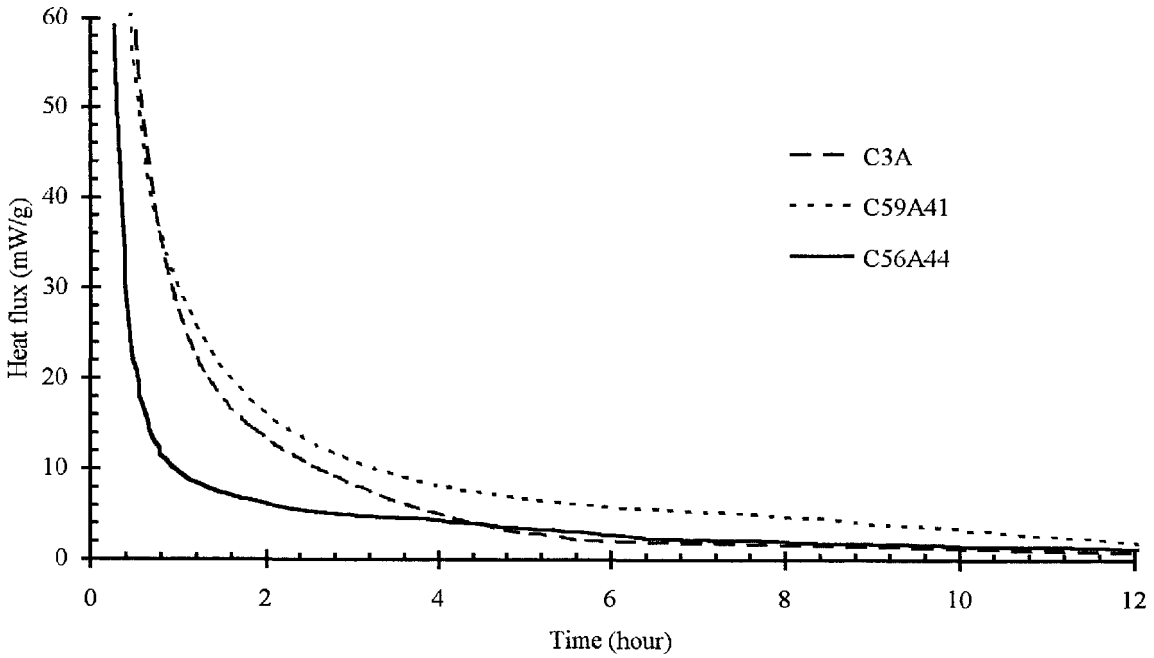

Fig 2. Calorimetry curves obtained with C_3A, C56A44 and C59A41 at 20°C and W/C=1

It is important to follow the changes in the aqueous phase in order to understand the mechanism of the hydration. However it is difficult to study the aqueous phase in paste and stirred suspensions are often used instead. As it is not obvious that pastes and suspensions behave in the same manner, calorimetry experiments were performed on suspensions for C50A50 and C56A44 (Figs 3 and 4).

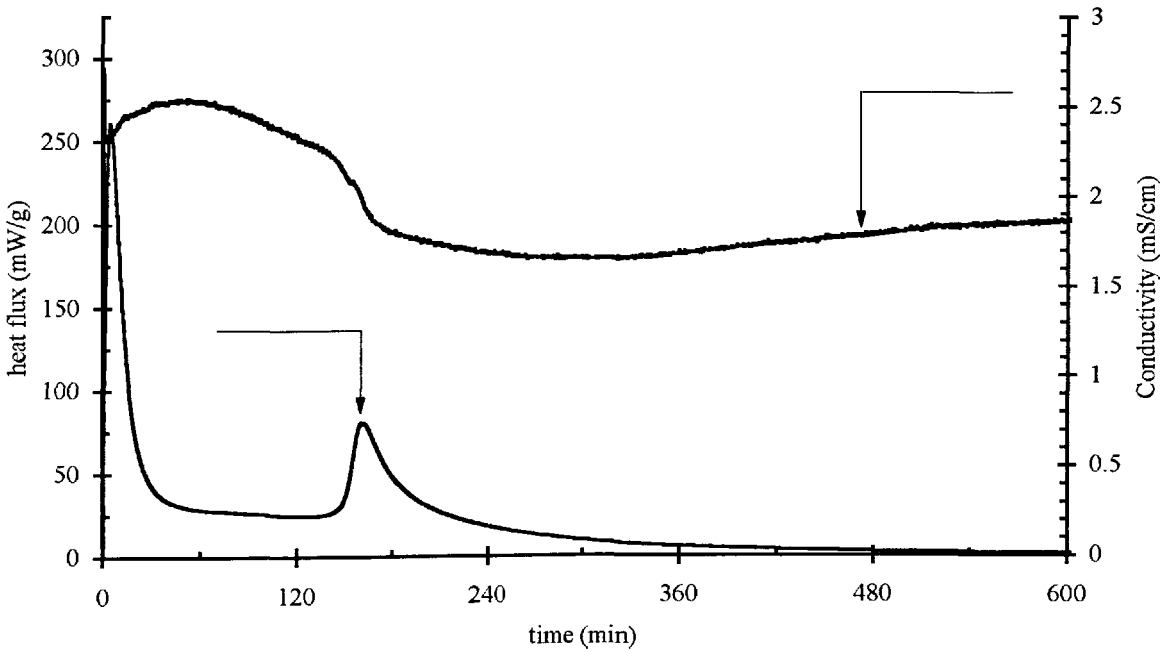

Fig 3. Conductimetry and calorimetry curves obtained simultaneously with C50A50 at 20°C in stirred suspension (W/C=10)

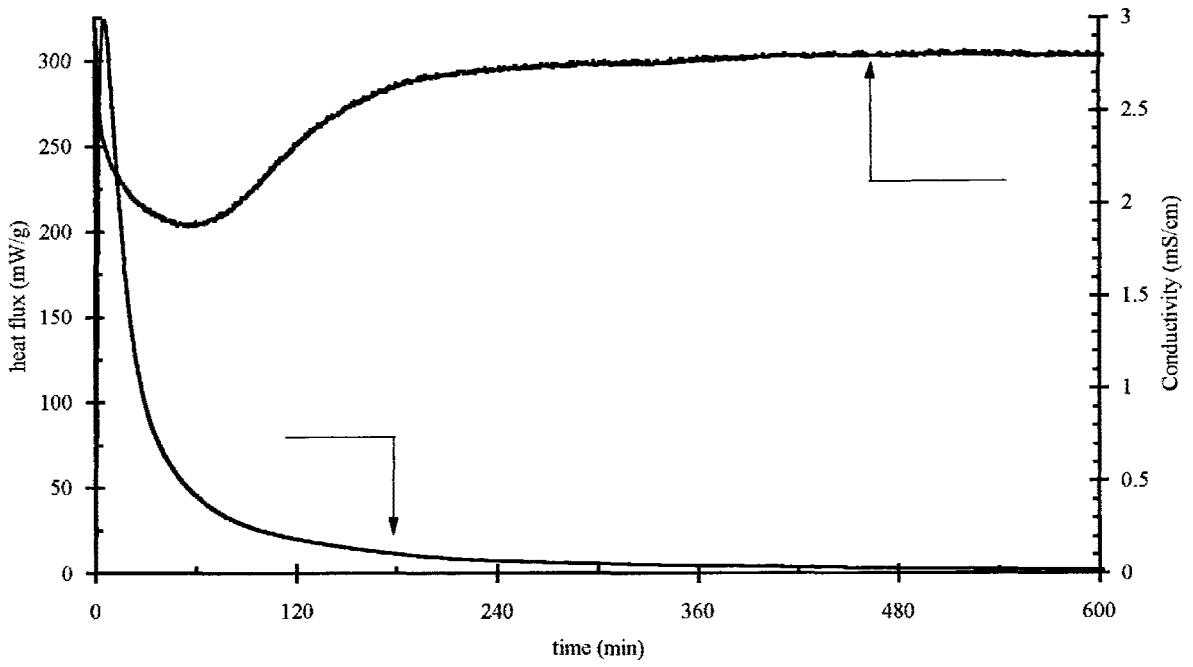

Fig 4. Conductimetric and calorimetric curves obtained simultaneously with C56A44 at 20°C in stirred suspension (W/C=10)

It appears that the calorimetric curves obtained in stirred suspensions maintain similar features than those recorded on pastes: presence of two exothermic peak for C50A50 and only one for C56A44. Thus the hydration mechanism in suspension is expected to be similar to the paste one. The evolution of the electrical conductivity of the aqueous phase, also enables us to differentiate the samples. The aspect of the conductivity curve of C50A50 is close to that of $C_{12}A_7$ (Capmas, 1990, Ménétrier-Sorrentino,1989) (Fig 3): a very rapid increase during the first minute, then a slight decrease during 5 minutes which is followed by an increase during 1 hour. This period corresponds to the first exothermic peak. Then the conductivity decreases slightly during a period of moderate heat flow and decreases more rapidly in the region where the second exothermic peak is observed. Finally a plateau of conductivity is observed when the liberated heat flow is very weak. The conductivity curve of C56A44 is simpler (Fig 4): a rapid increase of the conductivity during the first minute which is followed by a long decrease during the following first hour which corresponds to the main part of the exothermic peak. Then the conductivity increases again during two hours that coincides to the ending part of the exothermic peak. Finally the heat flow is very weak and a slightly descending conductivity plateau is observed.

The aqueous phase has been analyzed at different periods in order to understand further the evolution of the electrical conductivity. The samples C53A47 and C56A44 have been chosen as they delimit the two behaviours previously evidenced (Tables 3 and 4).

Table 3. Composition of the aqueous phase during C53A47 hydration at 20°C and W/C=10

Time (minute)	[Ca] (mmol/l)	[Al] (mmol/l)	pH	C/A
2	10.53	12	11.85	1.66
27	8.78	12.66	12.12	1.39
292	7.10	9.76	12.13	1.45
1440	5.16	6.62	12.20	1.56

Table 4. Composition of the aqueous phase during C56A44 hydration at 20°C and W/C=10

Time (minute)	[Ca] (mmol/l)	[Al] (mmol/l)	pH	C/A
2	9.30	9.12	11.60	2.04
58	9.85	3.40	11.76	5.77
180	8.03	2.70	12.08	5.93
1430	8.87	1.96	12.27	9.05

After 2 minutes of hydration, the composition is close between the two samples. However the C/A molar ratio of the aqueous phase is less than the C/A molar ratio of the solids. This may be due to a more rapid dissolution rate of $C_{12}A_7$ relative to C_3A. The precipitation of an hydrate can also be an explanation as the conductivity decreases between 1 and 2 minutes of hydration. The analysis of the solids confirms that C_2AH_8 is already formed in a detectable quantity by XRD after 2 minutes hydration (Tables 5 and 6). For hydration times longer than 2 minutes, C53A47 and C56A44 evolve differently; C/A ratio of the aqueous phase remains almost constant for C53A47 whereas it increases for C56A44. The precipitated solids also differ: C_2AH_8 is the main hydrate for both C53A47 and C56A44 but C_4AH_{13} and its carbonated forms, calcium hemicarboaluminate hydrate and calcium monocarboaluminate hydrate, are observed. After one day hydration, C_3AH_6 is also found for C56A44. Once more, these differences reflect perfectly the two behaviours derived from $C_{12}A_7$ and C_3A. For both samples, the hydration is fast; $C_{12}A_7$ and C_3A are almost completely consumed after 3 hours hydration. However the hydration seems to be faster for C56A44 compared to C53A47.

Table 5: Amount of solids relative to the intensity of the main peak of diffraction during C53A47 hydration at 20°C and W/C=10

Time (minute)	$C_{12}A_7$ d=4.9 Å	C_3A d=1.9 Å	C_2AH_8 d=10.45 Å	hemiC d=8.2 Å	monoC d=7.6 Å	C_4AH_{13} d=7.8 Å	C_3AH_6 d=2.04 Å
2	strong	medium	weak	---	---	---	---
27	medium	medium	medium	---	---	---	---
292	trace	weak	strong	---	---	---	---
1440	---	---	strong	---	---	---	---

Table 6: Amount of solids relative to the intensity of the main peak of diffraction during C56A44 hydration at 20°C and W/C=10

Time (minute)	$C_{12}A_7$ d=4.9 Å	C_3A d=1.9 Å	C_2AH_8 d=10.45 Å	hemiC d=8.2 Å	monoC d=7.6 Å	C_4AH_{13} d=7.8 Å	C_3AH_6 d=2.04 Å
2	strong	strong	weak	---	---	---	---
58	weak	medium	medium	trace	trace	weak	---
180	weak	weak	strong	weak	weak	medium	---
1430	---	---	strong	weak	weak	weak	medium

DISCUSSION

The mechanism of the hydration of $C_{12}A_7$ and C_3A has to be described in order to differentiate the samples of the $C_{12}A_7$-C_3A system. We have to consider first, the phase diagram of the system CaO-Al_2O_3-H_2O at 20°C (Fig. 5). This diagram contains the calculated equilibrium curves of C_2AH_8, C_4AH_{13} and C_3AH_6. The equilibrium curves of CAH_{10}, AH_3 and CH have been omitted to have a more readable diagram. The maximum supersaturation curve with respect to C_2AH_8 (curve I) has also been added. Curve I which has been determined experimentally by Barret et al. (Barret,1980a and 1980b), delimits the aqueous phase compositions which precipitate C_2AH_8

immediately without any induction period (on the right of curve I) from the compositions that produce an induction period before precipitating C_2AH_8 (part between the right of C_2AH_8 equilibrium curve and the left of curve I). The composition of the aqueous phase at various hydration time (kinetic path) hydration has been plotted on the $CaO-Al_2O_3-H_2O$ phase diagram for $C_{12}A_7$ (Fig 5). During the hydration of $C_{12}A_7$, the composition of the aqueous phase reaches the supersaturated domain with respect to C_2AH_8 and finally curve I. The C/A molar ratio of $C_{12}A_7$ which dissolves is 1.72 and the C/A ratio of C_2AH_8 which precipitates is 2. As a consequence, the aqueous phase is enriched in aluminate and the C/A ratio decreases as explained by Barret (Barret, 1994). The kinetic path follows approximately the curve I, until it intersects the equilibrium curve of $C_{12}A_7$ superficially hydroxylated (sh): [Ca]≈24mmol/l and [Al] ≈45mmol/l. During this process which takes about 10 minutes in our experimental conditions (20°C and W/C=10) and which corresponds to the first exothermic peak, an important quantity of C_2AH_8 is formed. Then the reaction rate is reduced due to an induction period originated by the nucleation of AH_3; the concentrations generally pass from 24 to 21mmol/l for calcium ions and from 45 to 42mmol/l for aluminate ions. This process corresponds to the period between the two exothermic peaks. As soon as the nucleation rate of AH_3 is high enough, the global reaction rate increases again and the second exothermic peak is observed. Finally $C_{12}A_7$ is exhausted and the aqueous phase evolves slowly toward the equilibrium state. It is important to notice that AH_3 is not detected by XRD as it firstly precipitates as a gel.

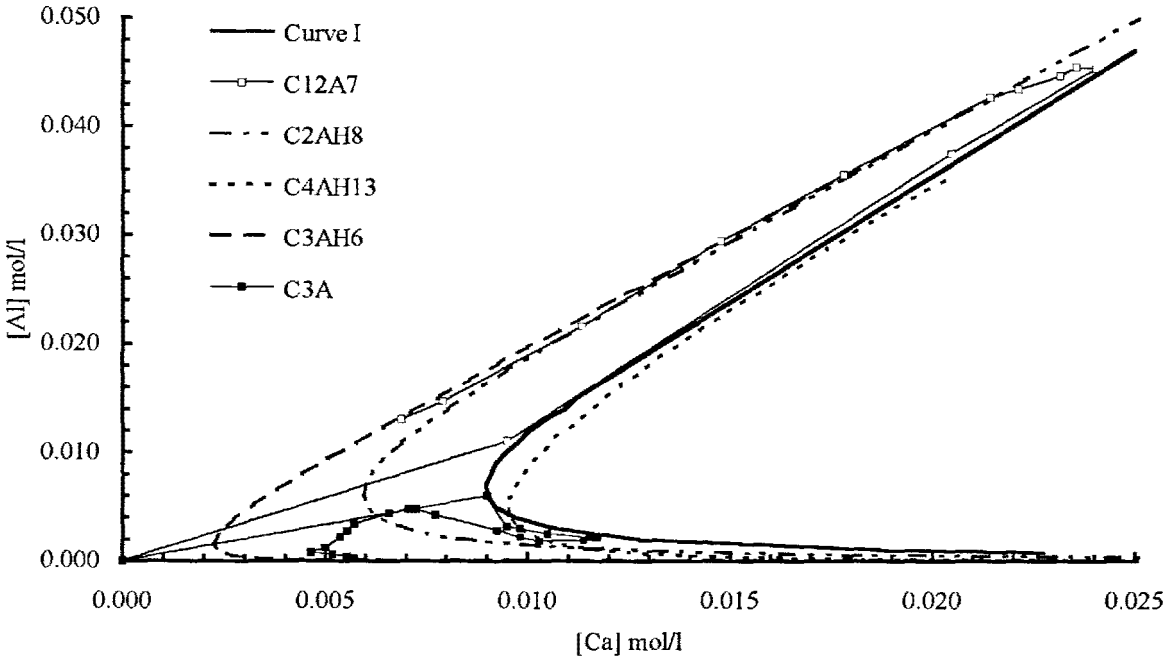

Fig 5. Kinetic path for the hydration of $C_{12}A_7$ and C_3A at 20°C

The kinetic path of C_3A hydration has also been drawn (Fig 5). Similarly to $C_{12}A_7$, C_3A dissolves congruently until it reaches curve I as demonstrated by Barret (Barret, 1980a). At this point C_2AH_8 precipitates but in this case, the C/A molar ratio of the aqueous phase increases; the C/A ratio of C_3A which dissolves is greater than the C/A ratio of C_2AH_8 which precipitates. Thus the aqueous phase can enter the supersaturated region with respect to C_4AH_{13} which precipitates as soon as a sufficient supersaturation is reached. This corresponds to the important exothermic peak observed at the hydration beginning. Once C_3A is almost completely consumed, the continuation of hydrate precipitation, reduces the concentrations in solution and leads the aqueous phase in the undersaturated domain with respect to C_4AH_{13}. From this point, C_4AH_{13}

can be transformed into C_2AH_8 but also into C_3AH_6 and the aqueous phase evolves slowly toward equilibrium. Calcium monocarboaluminate hydrate is often formed due to carbonation.

The previous discussion demonstrates that the different mechanism of hydration for $C_{12}A_7$ and for C_3A are linked to the precipitation of C_2AH_8 which depends on the position of curve I on the $CaO-Al_2O_3-H_2O$ phase diagram. This demonstration is also applicable to the $C_{12}A_7-C_3A$ system. The aqueous phase composition of samples having a C/A molar ratio lower than 2 is expected to move toward the upper part of the $CaO-Al_2O_3-H_2O$ phase diagram and thus behaves like $C_{12}A_7$: rapid precipitation of C_2AH_8, followed by a short induction period due to AH_3. On the contrary, for samples having a C/A ratio higher than 2, the precipitation of C_2AH_8 increases the calcium concentration and drives the aqueous phase composition toward the bottom part of the $CaO-Al_2O_3-H_2O$ phase diagram. This induces a rapid precipitation of C_4AH_{13} along with C_2AH_8 in one kinetic step. The kinetic paths for C53A47 and C56A44 are reported on Figure 6. The kinetic path of C56A44 evolves as suspected even if there is a restricted number of points that describe it: once curve I is reached, the C/A molar ratio of the solution increases (Table 4). The evolution of the kinetic path of C53A47 is less obvious with the 4 points that define it: the curve I is reached but the kinetic path does not really follows curve I toward higher calcium and aluminate concentrations. On the other hand, C50A50, displays the expected behaviour: the maximum concentrations are [Ca]=22mmol/l and [Al]=41mmol/l.

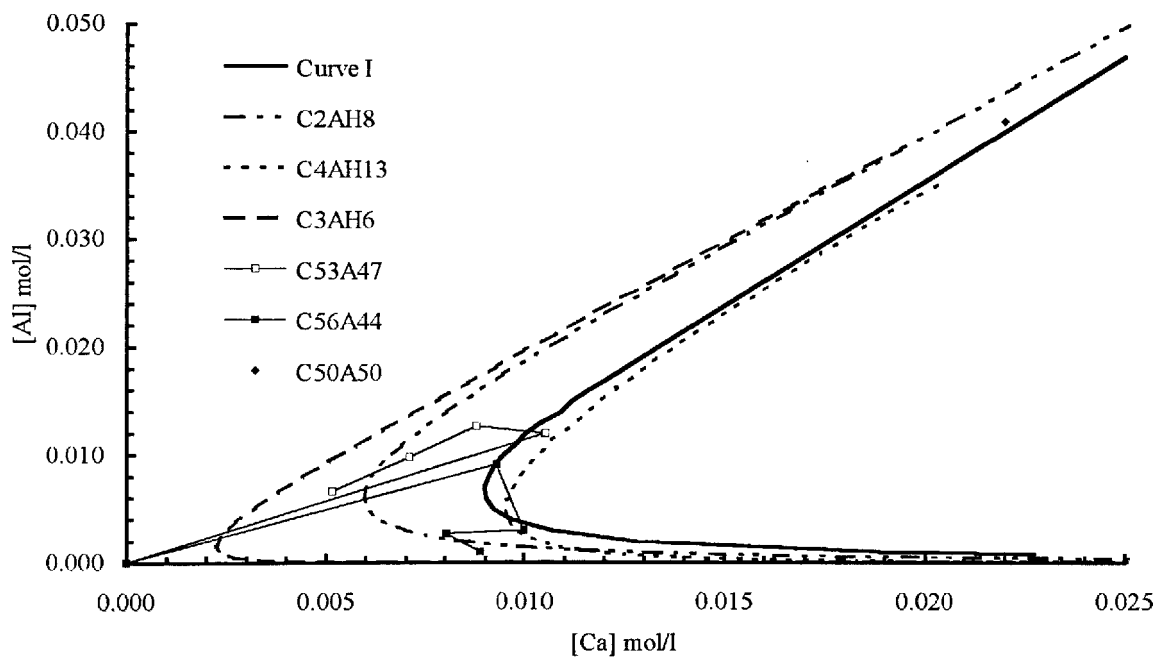

Fig 6. Kinetic path for the hydration of C53A47 and C56A44 at 20°C and maximum concentrations reached with C50A50.

From our previous hypothesis, C53A47, C56A44 and C59A41 which have a C/A molar ratio higher than 2, should behave as C_3A. This is correct except for C53A47 which behaves closer to $C_{12}A_7$ than to C_3A. In fact, this is not the C/A molar ratio of the solid which is important but the C/A molar ratio of the dissolution process. These two C/A molar ratios can be different even if the dissolutions of $C_{12}A_7$ and C_3A are congruent, if we consider different rates of dissolution between $C_{12}A_7$ and C_3A. For C53A47, the solid C/A molar ratio is 2.14 whereas the C/A molar ratio of the solution after 2 minutes of hydration is only 1.66. Similarly we are obtaining a C/A value of 2.42 for C56A44 and a value of 2.04 in solution after 2 minutes of hydration. This

suggests that the dissolution rate of $C_{12}A_7$ is faster than the one of C_3A. Moreover these differences of dissolution rate, induce a variable C/A ratio of the dissolution process during the hydration: C/A of the dissolving solids should be lower at the hydration beginning and then higher compared to the solid C/A molar ratio. This process may complicate the hydration mechanisms especially for samples which have a C/A molar ratio close to 2.

CONCLUSION

The hydration mechanisms of samples ranging from $C_{12}A_7$ to C_3A can be classified into two categories depending on the C/A molar ratio of the samples:

- if the C/A ratio is lower than 2.3, the hydration proceeds through two main steps in a similar way as $C_{12}A_7$,
- if the C/A ratio is equal or higher than 2.3, only one step exists at the beginning of the hydration as observed during C_3A hydration.

These differences can be explained by the precipitation of C_2AH_8 which occurs in all cases after less than 2 minutes of hydration:

- If the solid which dissolves induces a C/A molar ratio of the aqueous phase which is lower than 2, the precipitation of C_2AH_8 decreases the global C/A ratio of the aqueous phase. As a consequence, the kinetic path is expected to reach higher calcium and aluminate concentrations.
- On the contrary, if the C/A ratio of the dissolution is higher than 2, the precipitation of C_2AH_8 increases the C/A ratio of the aqueous phase. The kinetic path is expected to reach high calcium concentrations and low aluminate ones.

The fact that the limiting C/A molar ratio of the samples is 2.3 instead of 2, indicates that $C_{12}A_7$ dissolves more quickly than C_3A at the initial hydration.

REFERENCES

Barret, P. and Bertrandie, D., "Hydratation de C_3A en présence d'eau de chaux", 7th ICCC, Paris, vol IV, 1980, pp 443.

Barret, P. and Bertrandie, D. "Minimum instability curve in a metastable solution of CA" 7th ICCC, Paris, Vol. 3, 1980, pp 134.

Barret, P. and Bertrandie, D., "Hydration of aluminate cements", Advances in cement and concrete, Proc of Engineering Foundation Conference, Durham, Grutzeck and Sarkar editors, 1994, pp. 132-174.

Bessières, A., "Influence des ensemencements sur la vitesse de précipitation des aluminates de calcium hydratés" Thesis, University of Burgundy, 1972

Capmas, A., Ménétrier-Sorrentino, D. and Damidot, D. "Effect of temperature on setting time of calcium aluminate cements", Calcium Aluminate Cements, Ed. by R.J. Mangabhai, 1990, pp 65-80.

Damidot, D., Nonat, A. and Barret, P. "Kinetics of tricalcium silicate hydration in diluted suspensions by microcalorimetric measurements", Jour. Amer. Ceram. Soc., Vol. 73, No. 11, 1990, pp 3319-22.

De Jong, J. G. M., Stein, H. N. and Stevels, J. M. "Mutual interaction of C_3A and C_3S during hydration" 5th ICCC, Tokyo, Vol. 2, 1968, pp 311.

Edmonds, R. N. and Majumdar, A. J. "Hydration Of $12CaO.7Al_2O_3$ at different temperatures.", Cement and Concrete Research Vol. 18, No. 3, 1988, pp 473-478.

Ménétrier-Sorrentino, D., George, C.M., and Sorrentino, F. "The setting and hardening characteristics of calcium aluminate cements: studies of the systems $C_{12}A_7$-C_3A and $C_{12}A_7$-CA", 8th ICCC, Rio de Janeiro, Vol. 4, 1986, pp. 334.

Ménétrier-Sorrentino, D., Capmas, A., and Sorrentino, F. "Hydration of amorphous and crystallised compounds based on monocalcium aluminate" Unitech Congres, 1989, pp 189-192.

Kn o. 2 5. JAN. 2001 d o k 31789

2ii026
8 pp

STUDY OF THE HYDRATION OF MIXTURES OF CA AND α-Al_2O_3 AT DIFFERENT TEMPERATURES

Angelika RETTEL, Denis DAMIDOT and Karen SCRIVENER, LAFARGE Laboratoire Central de Recherche, St-Quentin Fallavier, France

ABSTRACT

Alumina which is added to calcium aluminate cements is not an inert material with respect to the hydration: the specific surface area and the soluble Na_2O content of alumina are the main parameters which influence CA hydration. Adding alumina most often increases the reaction rate. When mixtures of CA and alumina are hydrated at different temperatures, this accelerating effect is added to the effect of the hydration temperature. The anomalous increase of setting time for CA paste between 20 and 35°C is known, but can thus be reduced or even suppressed by adding alumina. This behaviour has been attributed to the increase of the nucleation rate of AH_3 in the presence of alumina.

Key-words: Calcium aluminate cement, Alumina, Hydration, Temperature, Mechanism.

INTRODUCTION

Alumina is often added to calcium aluminate cement in some refractory applications: for example mixtures containing 55% (by weight) of CA and 45% of α-Al_2O_3 have a total Al_2O_3 content of 80%. It has been previously demonstrated that the specific surface and the soluble Na_2O content of alumina are the main parameters which influence CA hydration at 20°C (Damidot, 1995). The effect of these two parameters is not similar on the dissolution and induction periods that precede the massive precipitation of the hydrates which leads to setting in the paste. The dissolution period is longer for the mixtures of CA and α-Al_2O_3, regardless of the alumina content in comparison to pure CA. This can be explained by the dilution of CA by Al_2O_3. The influence of CA dilution is reduced by high soluble Na_2O contents. Alumina accelerates the induction period: the higher the specific surface area, the greater the acceleration. This is due to the seeding effect of AH_3 contained on the alumina surface which increases the rate of AH_3 nucleation. On the other hand, sodium ions coming from soluble Na_2O, have a discontinuous effect on the duration of the induction period: it is longer at low Na^+ concentrations and shorter otherwise. The addition of the effects of soluble Na_2O and of the specific surface of Al_2O_3 on the dissolution and induction periods, generally results in a reduction of the setting time at 20°C for mixtures containing 45% α-Al_2O_3. The hydration of CA at different hydration temperatures is also complex and has been widely studied (Bushnell-Watson, 1986, Capmas, 1990, Edmonds, 1988, Murat, 1980, Rettel, 1985). Most of the explanations of this phenomenon rely on nucleation difficulties of the hydrates. We have recently proposed a new hypothesis based on changes in the nucleation rate: the CAH_{10} nucleation rate decreases with the temperature whereas the AH_3 nucleation rate would increase (Damidot, 1997). Thus the CAH_{10} nucleation rate would control the induction period for temperatures lower than about 27°C for pure CA, whereas the AH_3 nucleation rate does this for higher temperatures. The presence of alumina which modifies the nucleation rate of AH_3, is thus expected to modify the anomalous setting behaviour.

The aim of this work is to understand better the addition of the effects of soluble Na_2O and of the specific surface area of α-Al_2O_3 for different hydration temperatures. Previous results seem to indicate that a global accelerating effect remains (Rettel, 1993) and is able to suppress the anomalous increase of the setting time observed for CA pastes for hydration temperatures between 20 and 30°C. The hydration of CA and α-Al_2O_3 mixtures have been investigated on pastes (W/C=0.5) by calorimetry and also on diluted suspensions (W/C=10). The study of

suspensions instead of pastes gives us the possibility to study more accurately the dissolution and induction periods that occur before the massive precipitation of hydrates which induces the setting in paste.

EXPERIMENTAL

Pure CA was synthesised by heating a mixture of α-Al_2O_3 and $CaCO_3$ at 1500°C. The major phase was CA along with a trace of CA_2: no $C_{12}A_7$ was detected by XRD or by SEM on polished sections. The properties of the alumina used in this study are summarised in Table 1. The presence of Na_2O in the alumina comes from the Bayer process which involves sodium aluminate. Total Na_2O content of the alumina was determined by X Ray fluorescence spectroscopy but more important, the soluble Na_2O content was measured: alumina suspensions (alumina/water = 10) were stirred for 24 hours and then Na^+ concentration was determined. In order to avoid as far as possible, the influence of soluble Na_2O, washed alumina were also used.

Table 1. Characteristics of the alumina used in the mixtures

alumina name	specific surface area (m^2/g)	α-Al_2O_3 content (%)	total Na_2O content (%)	soluble Na_2O (mM/l)
A1	0.6	> 95	0.3	0.5
A2	9.2	> 70	0.2	2.11

Mixtures of CA and 30, 45 or 60% alumina were investigated. The hydration of these mixtures was followed by differential isothermal calorimetry at 15, 20, 25 and 30°C in paste W/C=0.5. The time at the maximum of the second exothermic peak was associated to the setting time. The hydration was also investigated on suspensions (W/C=10) by recording the electrical conductivity at 15, 20, 23, 27 and 35°C. The presence of alumina does not change the shape of the conductimetric curve for CA: Figure 1 gives as an example, the conductimetric curve obtained for CA hydrated at 20°C.

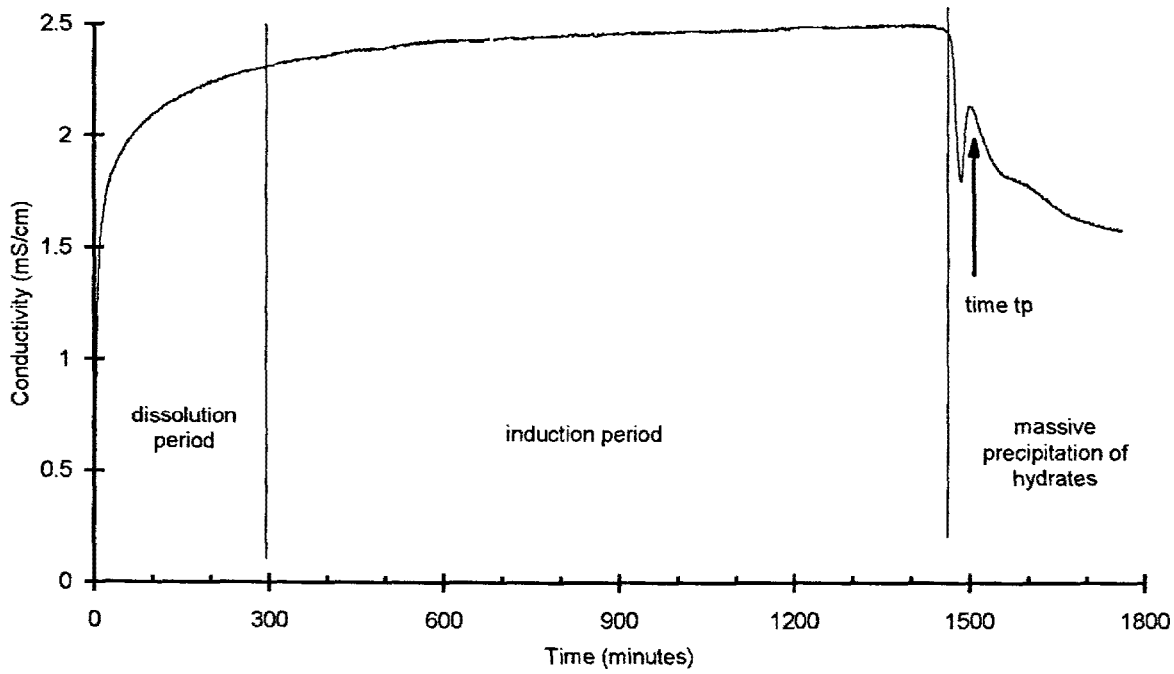

Fig. 1. Conductimetric curve obtained during the hydration of CA at 23°C in water at W/C=10.

The conductimetric curve of Figure 1 can be divided into three periods:

- dissolution period: this corresponds to the accumulation of ions in solution by the dissolution of CA: the conductivity increases rapidly at the beginning and then more slowly. This period ends when the composition of the solution comes into equilibrium with superficially hydroxylated CA (CA_{sh}) (Barret, 1994).
- induction period: the beginning of this period corresponds to a slightly increasing conductivity plateau during which the composition of the aqueous phase stays almost constant. During the induction period, the kinetics is governed by the rate of nucleation of the hydrates and not by the dissolution rate of the cement. The rate of nucleation increases slowly before reaching a critical number of nuclei that allows the growth.
- growth period: when growth starts, concentrations in solution such as the conductivity decrease markedly and the aqueous phase becomes more and more undersaturated with respect to CA_{sh}. In order to overcome this phenomena, the dissolution rate of CA increases and as a consequence a small increase of the conductivity is observed. However the growth rate of the hydrates becomes rapidly faster than the dissolution rate of CA and the conductivity decreases again. During this period, a massive precipitation of the hydrates occurs and this leads to setting in the paste. It is this period that corresponds to the second exothermic peak observed by calorimetry on paste. Thus in order to compare calorimetric and conductimetric results, the time at the maximum of the dissolution rate of CA during this period, tp on Figure 1, will be considered: it is the time at which the massive precipitation of hydrates occurs.

RESULTS

Calorimetry on paste (W/C=0.5)

Mixtures of 55% CA and 45% α-Al_2O_3 were used for paste experiments. Compared to pure CA, the hydration is quicker in the presence of alumina at all tested temperatures (Fig. 2).

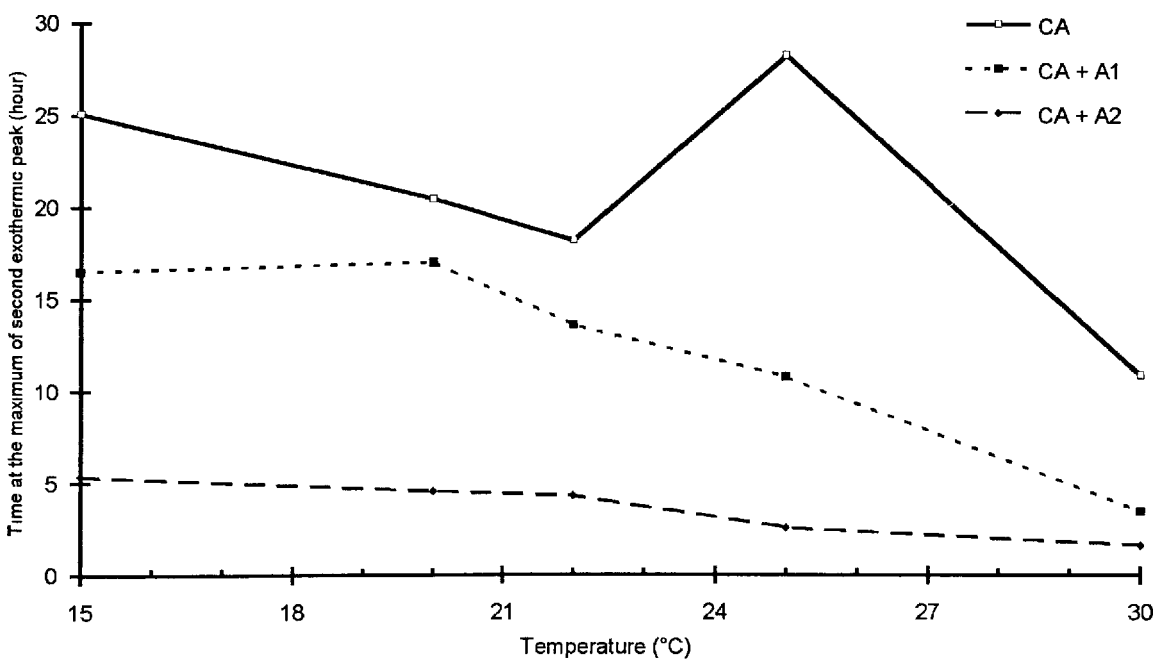

Fig. 2. Time at the maximum of the second exothermic peak recorded during calorimetric experiments on pure CA or mixtures of 55% CA and 45% alumina at different hydration temperatures

Furthermore, alumina A2, which has a higher specific surface area than A1, induces a greater acceleration of the hydration as we already demonstrated at 20°C (Damidot, 1995). The hydration rate is markedly modified for the mixture that contains A1: the setting occurs about 10 hours earlier at 30°C compared to 15°C, but we can still observe a maximum delay at 20°C. Compared to pure CA, this delay occurs at a lower temperature i.e. 20 instead of 25°C and the retardation is of lower intensity. On the contrary, a retardation of the setting temperature with an increase of the hydration temperature is no longer observed with alumina A2: the setting time decreases continuously with the temperature. It also appears that temperature has less effect on the setting time compared to alumina A1. As a consequence, an increase in the temperature reduces the difference of the hydration rate between the two mixtures.

Conductivity on suspensions (W/C=10)

The same mixtures as in paste experiments were also studied by conductimetry in order to verify that the behaviour was identical in paste or in suspensions. The massive precipitation of the hydrates observed during CA hydration still passes through a maximum delay for temperatures ranging between 20 and 35°C (Fig. 3) as already reported (Capmas, 1990). Mixtures of 55% CA and 45% A1 or A2 display a quicker hydration rate than pure CA and, similar to the paste experiments, A2 induces a greater acceleration. Thus, paste and suspension experiments are in perfect accordance despite the fact that the time, tp, of the massive precipitation of the hydrates defined by conductimetry does not correspond exactly to the time at the maximum of the second exothermic peak determined by calorimetry. For temperatures ranging from 20 to 35°C, the two mixtures increase their respective hydration rates continuously when the temperature is increased as was observed with the pastes. Unfortunately, we did not make some experiments at 15°C; this would have enabled us to confirm that a retardation could be observed with alumina A1 at 20°C.

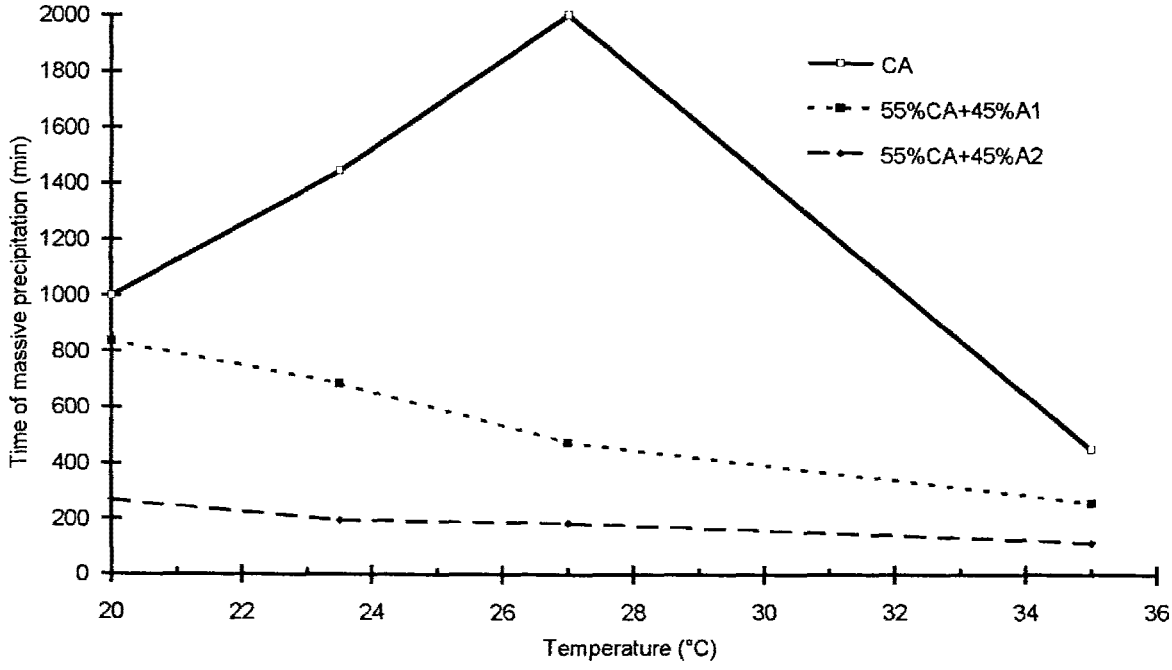

Fig. 3. Time of the massive precipitation for CA and mixtures of 55% CA and 45% of alumina (W/C=10) at different temperatures.

Some specific experiments were devoted to differentiate the effects of soluble Na_2O and of the specific surface area of alumina. First, CA was hydrated in a 10 mmol/l NaOH solution; this NaOH concentration is known to induce a marked acceleration of the hydration rate of CA or

mixtures of CA and alumina at 20°C (Damidot, 1995). The hydration rate remains accelerated for temperatures higher than 20°C relative to CA hydrated in water, but the time of the massive precipitation of the hydrate passes a maximum at 23°C (Fig. 4). As a consequence, the presence of NaOH due to the soluble Na_2O, does not seem to suppress the anomalous setting behaviour.

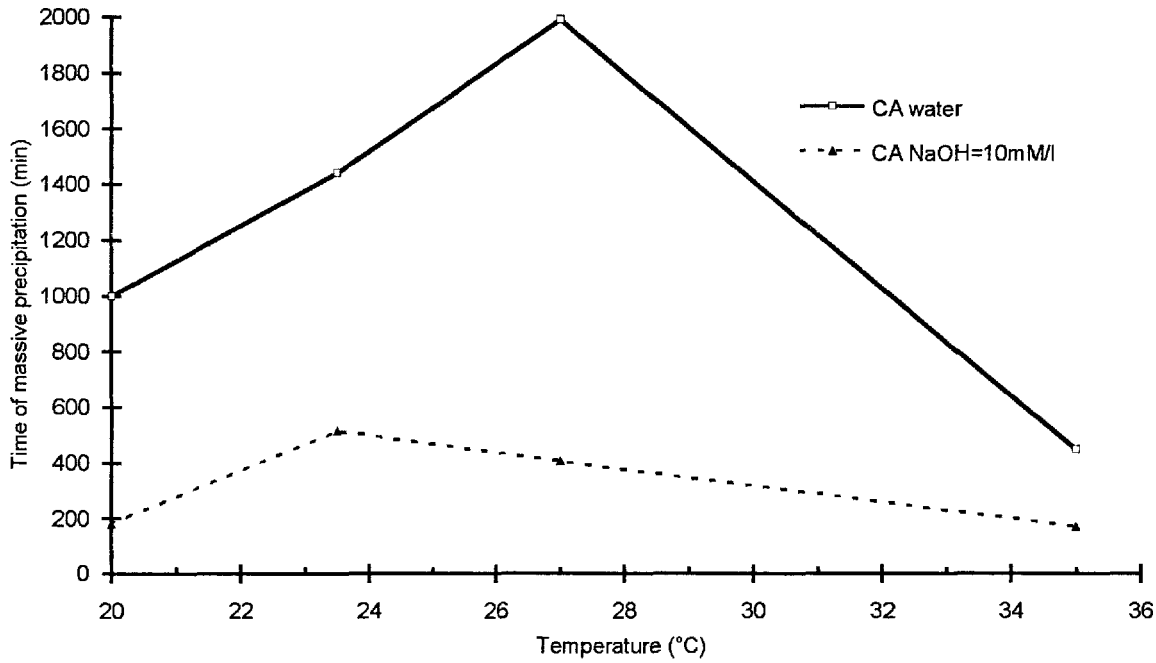

Fig. 4. Time of the massive precipitation for CA hydrated in 10 mmol/l NaOH (W/C=10).

Secondly, mixtures containing different amounts of washed alumina A2 were hydrated at different temperatures (Fig. 5).

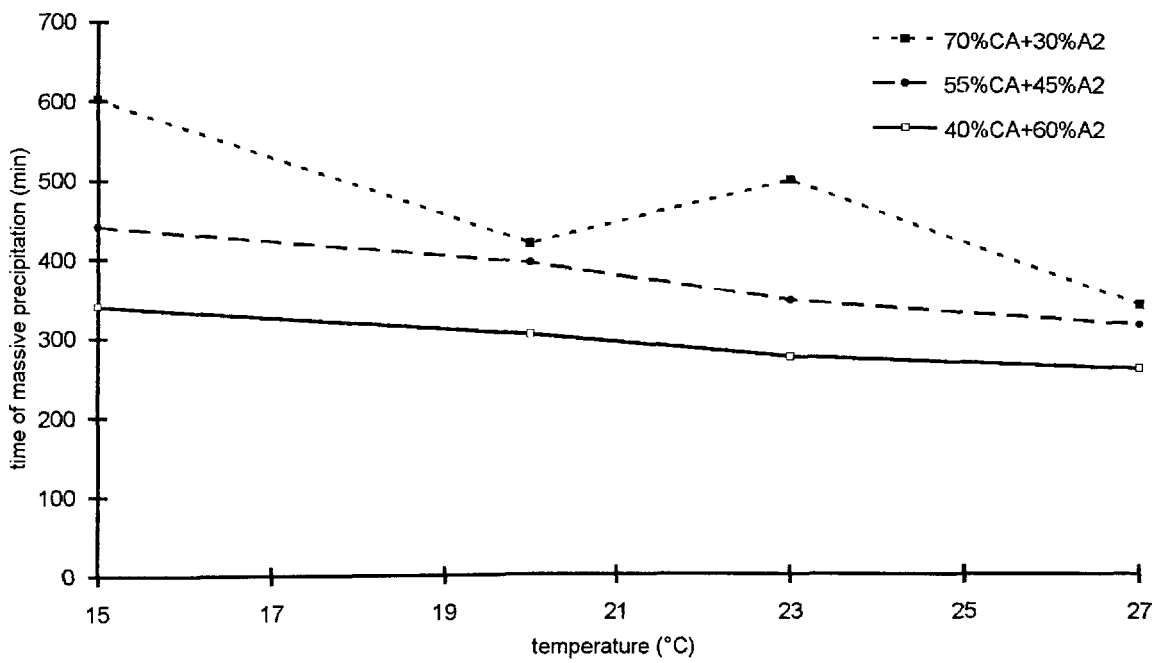

Fig. 5. Time of the massive precipitation for mixtures of CA and <u>washed</u> alumina A2 hydrated in water (W/C=10) at different temperatures.

The hydration is accelerated even more as the amount of alumina is high for all of the studied temperatures. It is also noticeable that with the lowest alumina content, 30%, a maximum delay is observed at 23°C whereas the time of massive precipitation decreases continuously for the other two mixtures (45 and 60%). Thus, the higher the alumina surface area is, the quicker the reaction rate is. This confirms what was observed with alumina A1 compared to alumina A2 in mixtures containing 45% alumina (Fig. 2). Temperature does not modify the difference of rate between mixtures containing 45 and 60% of alumina. The effect of the specific surface area is able to remove the anomalous setting behaviour observed with pure CA.

DISCUSSION

The anomalous setting behaviour observed for CA for temperatures between 20 and 30°C can be suppressed in the presence of alumina due to the effect of the specific surface area of the alumina. The Na_2O released by alumina into the solution as Na^+ and OH^- does not seem to remove the anomalous setting behaviour. This has been demonstrated previously (Damidot, 1995) and in this work, the alumina accelerates the induction period: the higher the specific surface, the greater the acceleration. These results are consistent with the effect of lithium salts on the hydration of calcium aluminate cement at different temperatures: lithium ions are able to suppress the anomalous setting behaviour depending on the concentration of lithium ions (Damidot, 1997). This behaviour is due to a strong increase of AH_3 nucleation rate by incorporating lithium ions in the structure of AH_3 (Damidot, 1996). Thus, the effect of lithium ions and alumina are similar, an increase of AH_3 nucleation rate, but their relative intensity are not equivalent due to two different mechanisms. Alumina acts on AH_3 nucleation rate due to a seeding effect: it exists some AH_3 on the surface of alumina that can be evidenced easily by diffuse reflectance Fourier transform infrared (DRIFT) (Fig. 6): The infrared bands at 3656, 3546-3550, 3465-3477 and 3427-3440 cm^{-1} are associated with the OH stretching modes of a bayerite-type species, while the bands at 3624, 3527, 3460 and 3380-3396 cm^{-1} are related with those of a gibbsite-type species (Lee, 1995). This seeding effect is expected to be all the more important with alumina having higher specific surface areas. This effect is not as effective compared to the incorporation of lithium ions in AH_3 and also may differ depending on the relative amount of bayerite versus gibbsite.

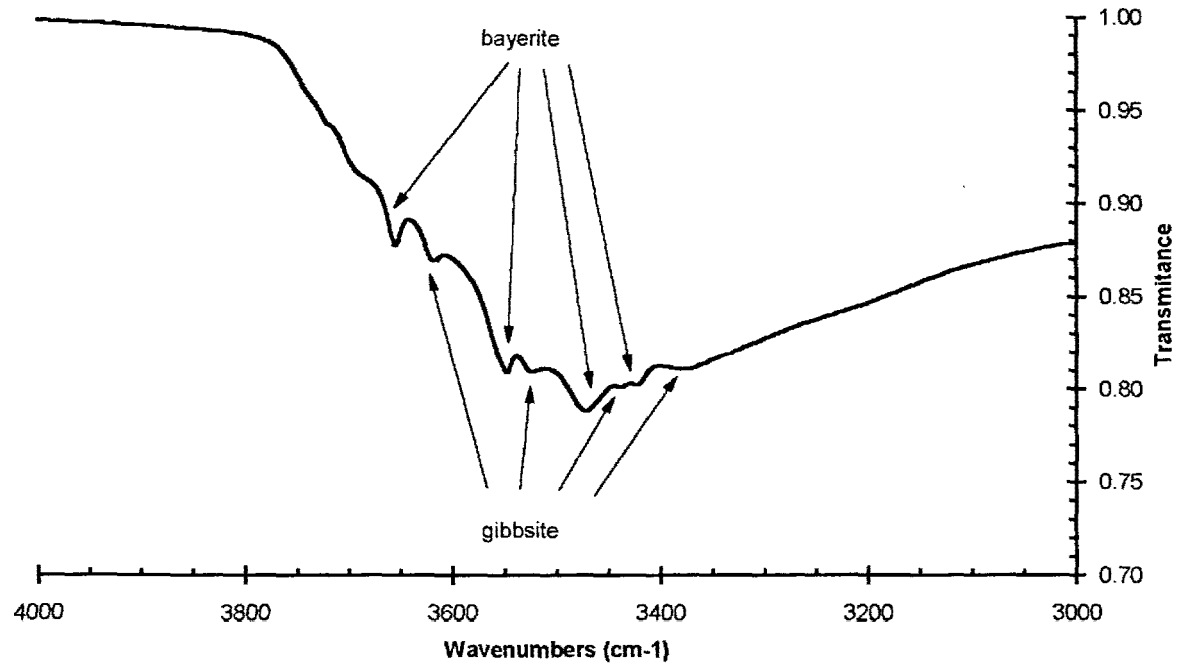

Fig 6. DRIFT spectrum obtained on washed alumina A2

The reduction of the intensity of the anomalous setting behaviour or its suppression by alumina can be explained in taking into account the hypothesis that we made to explain the action of lithium salts (Damidot, 1997): as it can seem on Figure 7, the nucleation rate of CAH_{10} decreases slowly with temperature up to 15°C and then decreases more rapidly. This would be a consequence of the decrease of CAH_{10} stability with an increasing temperature. On the other hand, the nucleation rate of AH_3 increases with temperature with a stronger increase from 22°C. Thus the controlling mechanism of the induction period passes from CAH_{10} to AH_3 at the maximum of the duration of the induction period (lowest nucleation rate) which corresponds to 27°C on Figure 7.

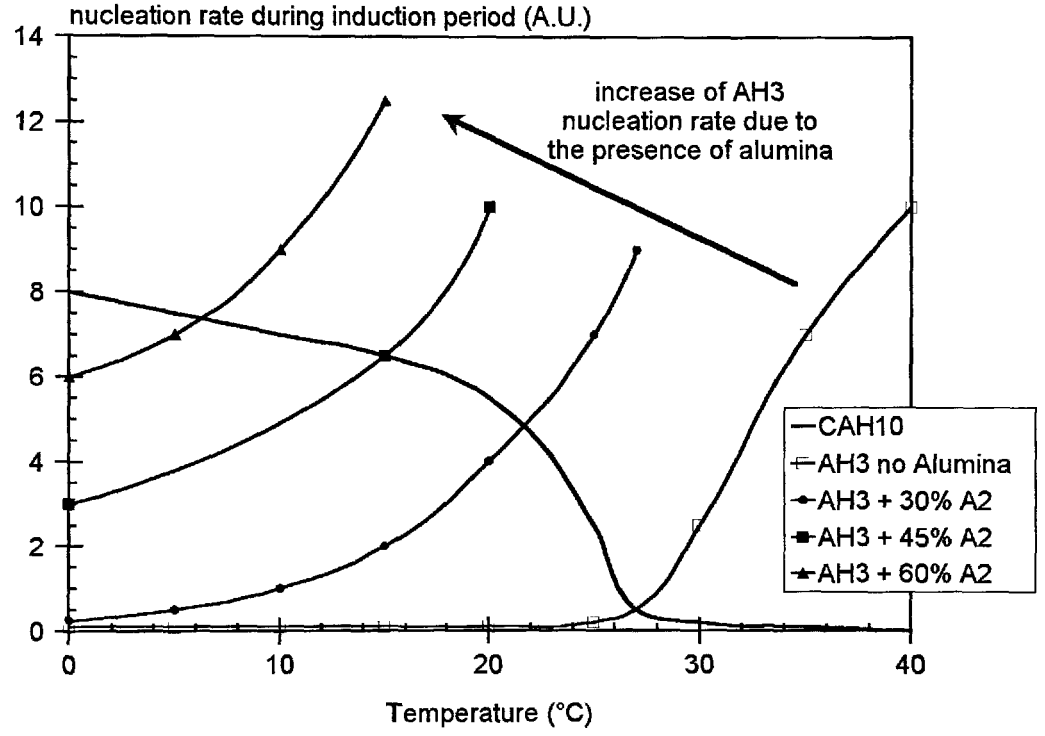

Fig 7. Relative nucleation rate for CAH_{10} and AH_3 as a function of the temperature and effect of alumina on AH_3 nucleation rate.

The change in the controlling hydrate, also induce a different chemical reaction for CA hydration. If CAH_{10} controls the induction period, CAH_{10} is the main hydrate and the chemical reaction of CA hydration can be simplified as: CA + 10H => CAH_{10}. On the contrary if AH_3 governs the induction period, AH_3 and C_2AH_8 are the main hydrates: 2 CA + 11H => AH_3 + C_2AH_8. C_2AH_8 is a consequence and not the cause of the suppression of the anomalous setting behaviour for CA hydration. On the other hand, the precipitation of C_2AH_8 before the induction which occurs in mixtures of CA + $C_{12}A_7$, induces the formation of some AH_3 which act as seed during the induction period and thus may accelerate this period depending on the amount of seeds: case of Fondu cement which also displays an anomalous setting time behaviour but of lower intensity compared to CA. This last example is very close to the effect of adding alumina if we except the diluting effect of alumina (less CA in a mixture compared to pure CA). If we consider the experiments with different quantities of washed alumina A2 (Fig. 5), AH_3 nucleation rate is expected to increase as a function of the alumina content of the mixture: this has been arbitrary represented on Figure 7. As a consequence of the increase of the nucleation rate of AH_3, the temperature which induces the change in the control of the induction period by either CAH_{10} or AH_3, is shifted to the left, i.e., to lower temperatures. Furthermore, the intensity of the decrease

of the nucleation rate during this period, is more and more reduced and globally the retardation is not observed as the dissolution period is continuously decreases with an increase of the temperature (Fig. 7).

CONCLUSION

The effect of alumina on CA hydration can be understood by taking into account two main parameters: the specific surface area and the release of Na^+ and OH^- ions due to soluble Na_2O contained in alumina. In order to understand the changes in the anomalous setting time behaviour of CA in the presence of alumina, these effects have to be added to the effect of the temperature. This corresponds in a first approach, to the evolution of the nucleation rate of CAH_{10} and AH_3 with temperature relatively to the same evolution in the presence of alumina. Compared to pure CA, the presence of alumina increases AH_3 nucleation rate and as a consequence the temperature shifts that induces a maximum retardation to lower temperature and also reduces the intensity of the retardation. As a consequence a marked anomalous setting time of CA behaviour between 20 and 30°C can be suppressed in the presence of alumina even if this behaviour can remain at temperatures lower than 20°C but with a very low intensity. The presence of admixtures can also induce variations of the nucleation rate of CAH_{10} and AH_3 and as a consequence can modify the behaviour of CA + alumina mixtures. But the additivity concept of the different effects remains and can be used to explain the complex behaviour of these systems.

REFERENCES

Barret, P. and Bertrandie, D. "Hydration of aluminate cements" Advances in cement and concrete, Proc of Engineering Foundation Conference, Durham, Grutzeck and Sarkar Ed., 1994, pp 132.

Bushnell-Watson, S.M. and Sharp, J.H. "The effect of temperature upon the setting behavior of refractory calcium aluminate cements" Cem. and Concr. Res., Vol 16, 1986, pp. 875.

Capmas, A., Ménétrier-Sorrentino, D. and Damidot, D. "Effect of temperature on setting time of calcium aluminate cements", in Calcium Aluminate Cements, Ed. R.J. Mangabhai, 1990, pp 65.

Damidot, D., Rettel, A. and Capmas, A. "Action of admixtures on Fondu cement. I. Lithium and sodium salts compared" Advances in Cement Research, Vol 8(31), 1996, pp 111.

Damidot, D., Rettel, A. and Sorrentino, F. "Action of alumina on calcium aluminate hydration. I: influence of specific surface area and soluble Na_2O content of alumina" World Cement, December Issue, 1995, pp 79.

Damidot, D., Rettel, A., Sorrentino, D. and Capmas, A. "Action of admixtures on Fondu cement. II. Addition of the effects of admixtures used to cancel the anomalous setting time observed with temperature" in press Advances in Cement Research (to be published in 1997).

Edmonds, R. N. and Majumdar, A. J. "The hydration of monocalcium aluminate at different temperatures" Cem. and Concr. Res., Vol. 18, 1988, pp 311.

Lee, D.H., Condrate Sr., R.A. "An FTIR spectral investigation of the structural species found on alumina surfaces" Materials Letters, Vol. 23, 1995, pp. 241.

Murat, M., Galtier, P., Guilhot, B. and Negro, A. "Etude, par calorimétrie isotherme, de l'influence de la température sur la réaction d'hydratation de l'aluminate monocalcique" (in fr.) C. R. Acad. SC. Paris, Vol 291 serie C, 1980, pp 113.

Rettel, A., Gessner, W., Müller, D., Scheler, G. "On the Hydration of $CaAl_2O_4$ at various temperatures" Br. Ceram. Trans. J., Vol 84, 1985, pp 25.

Rettel, A., Seydel, R., Gessner, W., Bayoux, J.P. and Capmas, "Investigations on the Influence of Alumina on the Hydration of Monocalcium Aluminate at Different Temperatures" Cem. Concr. Res., Vol 23, 1993, pp 1056.

2ii027
Kno. 25. JAN. 2001 dok 31790 3 pp

INFLUENCE SOLID SOLUTION OF CALCIUM ALUMINATE ON ALUMINA CEMENT PROPERTIES

Tamara V. KOUZNETSOVA, RCTU, Moscow, Russia
Adel A. ABDEL KADER, TIMS, Cairo, Egypt.

ABSTRACT: Solid solution of calcium aluminate with addition of CaF_2, MgO and ZrO_2 was investigated in order to correlate solid solution composition to hydration characteristics. Based on these results, sintering parameters for various high alumina cements have been recommended.

Key-words: **A**=Alumina **C**=Calcium aluminate cement **R**=Refractory

INTRODUCTION

In the last decade, the issue of increasing the efficiency of refractories use in metallurgical for their use in metallurigical, chemical, petrochemical industries and in the producing of building materials, has experienced a substantial advancement. Efficiency works and duration exploitation of refractory aggregates depend on refractory mixture (materials) which can be used as custom articles refractory lining and refractory concrete. Using refractory materials as a refractory concrete led to the speed-up of the rate of building refractory aggregates by 3-4 times, and the decrease in capital outlays by 2-3 times, in comparison with traditional refractory bricks. However, using concrete as a refractory material (Kouznetsova and Talaber, 1988) have some shortcomings. For example, as the decrease in its strength at high temperatures. High refractoriness properties of concrete manufactured from high alumina cement are of great interest and are always used in different industries.

EXPERIMENTAL

The main phases of alumina cement were synthesized such as 12 $CaO.7Al_2O_3(C_{12}A_7)$, $CaO,Al_2O_3(CA)$ and $CaO.2Al_2O_3(CA_2)$(Kouznetsova, 1986). Also these minerals have been prepared with the addition l and 5% CaF_2, 3 and 10% MgO and 2 and 10% ZrO_2.

Raw mixtures stoichiometrically prepared for $C_{12}A_7$, CA and CA_2 minerals production in pure state, as well as with above calculated additives. In these investigations we used the following materials, $CaCO_3$, Al_2O_3, CaF_2, MgO and ZrO_2 marke (h.d.a). Phase were synthesized by grinding stoichiometric proportions of given materials in fused alumina ball mill. Batch of each phases were moulded and pressed using a thrust of 30 MPa. The specimens were demoulded, dried and heated at 1200-1400°C for 60-120 minutes depending on the phase character. For preliminary check of complete sintering reactions, the fired mineral powders were tested for free lime and unreacted alumina.

RESULTS

The results indicate that, the synthesis of minerals depend upon the firing temperatures and on the soaking time at these temperatures. Complete dissociation of $CaCO_3$ happned at 850°C (Serry et al, 1987) then the heated minerals at this temperature contain CaO and Al_2O_3. XRD Patterns for sintered mixtures at 900°C confirm presence of CA (d = 0.297, 0.252, 0.241 and 0.190 nm) and its amount increases with increasing firing temperature up to 1150°C.

Addition of calcium fluoride in raw mixture causes besides the CA formation, $C_3A_3CaF_2$ was formed (d = 0.308, 0.288, 0.267 and 0.197mm). Also, the CA_2 synthesis is the presence of CaF_2 the CA_2 and C_3A_3. CaF_2 were formed. Activation energy of the aluminate phases synthesis with additives is 78 kj/mol, while is 110 kj/mol for calcium aluminates without additives (Saha and Paddar, 1984).

Analogous experiments were carried and using ZrO_2 as additives. Chemical analysis together with XRD showed that the sintered samples consisted of $C_{12}A_7$,CA, CA_2 and $C_7A_3ZrO_2$ at 1000°C. As the temperature increases from 1100 to 1400°C , the change ratio of the above mentioned phases are shown in Table 1.

Table 1 : phase composition of sintered samples containing ZrO_2

Firing	Diffraction maximum of minerals (nm)					
Temperature °C	$CaCO_3$	Al_2O_3	$C_{12}A_7$	CA	CA_2	$C_7A_3ZrO_2$
600	0.303	0.3860	-	-	-	-
700	0.303	0.3870	0.493	-	-	-
800	0.303	0.3870	0.493	0.298	-	-
900	0.303	0.3860	0.494	0.298	-	-
1000	0.303	0.3860	0.496	0.299	0.446	0.284
1100	-	0.3860	0.497	0.299	0.448	0.284
1200	-	0.3860	0.497	0.299	0.449	0.284
1300	-	0.3860	0.497	0.299	0.449	0.284
1400	-	0.3860	-	0.299	0.449	0.284

The compound $7CaO.3Al_2O_3.ZrO_2$, was determined using XRD and its X-ray power patterns:d = 0.284, 0.224,0.196 nm.

Results of investigations in all cases showed that, the addition of MgO in raw mixture, for $C_{12}A_7$, CA and CA_2 production, caused magnesium spinel and preclase to be formed. thus, the diffraction pattern of the basic minerals is different as a result of the formation of solid solution, as shown in Table 2.

Table 2: Phase composition of the sintered sample containing MgO

Temperature	Diffraction maximum of minerals (nm)			
°C	$C_{12}A_7$	CA	CA_2	MgO%
600	0.490	0.296	-	-
800	0.487	0.294	-	10
900	0.491	0.296	-	-
900	0.485	0.293	-	10
1000	-.490	0.297	0.446	-
1000	0.484	0.290	0.444	10
1100	0.490	0.297	0.446	-
1100	0.483	0.290	0.443	10
1200	0.490	0.297	0.447	-
1200	0.483	0.290	0.450	10
1300	0.490	0.297	0.446	-
1300	0.483	0.290	0.440	10

These showed the correlation between the phase composition of contents and their properties. For example, the compressive strength of cement paste reduces as a result of the presence of MgO. Al_2O_3. On other hand, the presence of these compounds caused an increase in the refractoriness of the cementstone.

The presence of $C_{11}A_7.CaF_2$ and $C_3A_3.CaF_2$ caused a reduction in the strength in early stages of hydration, but it rises constantly during the long time hardening.

Zirconium oxide contained cement have higher strengths both at early stages as well as at long time hardening. Also, the addition of ZrO_2 improves high alumina cement quality by increasing its strength and refractoriness of cementstone.

CONCLUSIONS

Aluminate Phases (CA, CA_2) form solid solution with MgO,ZrO_2, CaF_2, etc. Solid solution of CA and CA_2 hydrate faster and have better refractory properties.

REFERENCES

Kouznetsova, T.V. And Talaber, E., "Alumina Cement" -M.: GOSSTROIIZDAT 1988 pp. 58.

Kouznetsova, T.V., "Alumina and Sulphoalumina Cements" - M.: STROIIZADAT, 1985-205 pp.

Saha, S.K. and Poddar P.K., "Effect of Titania on Hydrolysis and Related Properties of High-Alumina Cement". Indian Jorn. technol. Vol. 22. No. 10, 1984, pp. 385-390.

Serry, M.A., El-Didomony, H. and Abdel-Kader, A.A., "Influence of calcination conditions on the Hydration of Metakaolin-lime". Silicates Industrials.-Tome LII-No. 5-6, 1987, pp. 83-87.

2ii028
8 pp

Кп о. 25. JAN. 2001 d o k 31791

ON THE POSSIBILITIES OF *IN SITU* STUDIES OF THE HYDRATION OF ALUMINATE CEMENTS USING ^{27}AL NMR AND PROTON RELAXATION RATE MEASUREMENTS.

Andrew. B. KUDRYAVTSEV. NMR Laboratory, D. Mendeleev University of Chemical Technology of Russia , Moscow, Russia
Tamara. V. KOUZNETSOVA. Cement Technology Dept., D. Mendeleev University of Chemical Technology of Russia , Moscow, Russia

ABSTRACT. Wideline ^{27}Al nmr spectroscopy and the measurements of means and variances of proton relaxation rate have been applied to the investigation of hydration of CA, CA_2 and C_3A. A selective fast hydration of one of the six non–equivalent AlO_4 tetrahedra in the crystal lattice of CA has been found from the deconvolution of nmr spectra. Difference nmr spectra were used to investigate the hydration of CA_2 and C_3A. The contents of free water were derived from the data on means and variances of proton relaxation rates. A significant release of water from the adsorption layer occurs at about 400 - 500 min. of hydration of CA.

Key-words: Calcium aluminate cement, Hydration, Kinetics, Nuclear Magnetic Resonance

INTRODUCTION.

Nuclear magnetic resonance has been successfully used in many studies of hydration of various cements and their components. Application of advanced solid state nmr methods (MAS, PE-MAS, *etc.*(see in J. Skibsted et al., 1993) is possible in the cases of comparatively stable samples, i.e. those hydrated for at least one or several days, or of artificially stabilized specimens of minerals hydrated for shorter times. In the latter cases the problem is that the liquid phase still present at earlier stages of hydration is destroyed and dissolved products are forced to crystallize under conditions far from normal. The *in situ* studies of cement hydration provide more reliable information on the state of cement pastes during the induction period and the initial crystallization of products. In many cases these stages are of short duration and the measurements must be fast. Proton magnetic relaxation measurements as well as ^{27}Al nmr spectroscopy comply with these requirements. These methods have been applied to the study of hydration of modified calcium sulphoaluminates (A.B. Kudryavtsev and T.V. Kouznetsova, to be published). A significant increase in the proton relaxation rate was observed during induction period which could not be unambiguously assigned due to the absence of the data on the dissolution of original grain. Such data can be obtained from the analysis of wideline ^{27}Al nmr spectra.

The lineshape of a ^{27}Al nmr spectrum of a powdered mineral is a convolution of a gaussian lineshape (caused by relaxation) and of a complicated lineshape arising from the averaging of quadrupolar shifted resonances over all orientations. In many instances such parameters as quadrupolar coupling constant, chemical shifts, electric field asymmetry factors can be estimated. In some cases, on the other hand, the lines are so broadened that they can be considered a collection of gaussian lineshapes.

Proton relaxation time measurements when used to study the hydration of cements are far from being a trivial experiment. These systems are heterogeneous from several points of view: water is distributed between bulk liquid and adsorption layer. The adsorption layer is inhomogeneous in

itself and contains centers with different relaxation efficiency. Powdered materials (when not specially fractionated) are polydisperse and multicomponent. The properties of corresponding pastes are dependent on the distribution of particles over the grain's size and composition. The exchange of water molecules between different states in such systems is usually slow which is reflected by a non–exponential relaxation of water protons. By analyzing non–exponential re–equilibration of longitudinal and transverse nuclear magnetization it is possible to identify several products in hydrated cement pastes. This method, known as *spin–grouping* (H. Peemoeller and M. Pintar, 1980), requires, however, prolonged measurements and could not be used in kinetic studies of hydration of fast setting cements. Recently a new method of nuclear magnetic relaxation studies (A.B. Kudryavtsev et al., 1994) has been suggested for the measurements of the means and variances of relaxation rates in heterogeneous systems. This method only requires the initial part of re–equilibration curve to be analyzed and is sufficiently fast to be used in kinetic studies. In the presented paper the possibilities of the wideline ^{27}Al nmr and the measurements of means and variances of relaxation rates have been explored using the samples of specially synthesized and fractionated (grain size 28 - 40 μm) CA, C_2A and C_3A. Water-to-cement ratio was 0.4.

^{27}Al MNR DATA.

Hydration of CA.

^{27}Al nmr spectra of CA obtained at various stages of hydration are shown in Fig. 1A. According to J. Skibsted et al. (1993) the line observed in the spectrum of anhydrous CA is a superposition of the lines from 6 non–equivalent AlO_4 tetrahedra in the crystal structure of CA. After the addition of water a new narrow line appears at 80 ppm which is connected (A.B. Kudryavtsev et al., 1990) with tetracoordinated Al species in liquid phase. The intensity of this line remains approximately constant during about 100 min of hydration and then starts to decrease. After 100 min of hydration another line (with a maximum around zero ppm) appears in these spectra (Fig. 1, curve t=102min) which reflects the well known formation of octahedrally coordinated hydrated aluminate species (D. Mueller et al., 1984). At approximately the same time the low–frequency part of the line of original solid begins to disappear (Fig. 1A). This means that the dissolution of original solid is selective concerning the nonequivalent species present in the crystal structure. At long hydration times this part of the original line seems to disappear completely. In order to follow quantitatively the growth of new solid and the disappearance of the initial grain the spectrum of *anhydrous* CA was approximated by a sum of 6 gaussians of *equal* integral intensities and their parameters were determined by non–linear regression. Spectra of hydrated CA were approximated by a larger number of gaussians. Positions of maxima, widths and normalizing factor were adjusted to achieve an adequate description of the experimental lineshape in the spectrum of anhydrous CA: The parameters of the spectra of hydrated samples were estimated adjusting the individual integral intensities of all the lines keeping fixed the positions and widths of the lines of original solid. Because of the overlapping of the lines of initial solid the estimates of their intensities were strongly correlated which was a source of several observed artifacts (e.g., the component #3 is 'vanish' immediately upon the addition of water, Fig. 1 B). The real changes in original solid may be represented by a set of lines the total intensity of which does not increase and/or smoothly runs downwards. For example, the total sum of the intensities of *all* original lines after being constant for 100 minutes of hydration decreases smoothly during the remaining period of observation (Fig. 2). The widest lines of the original solid are the inner lines and their behavior is the most correlated. However the sum of their integrals is approximately constant during hydration (Fig. 2).

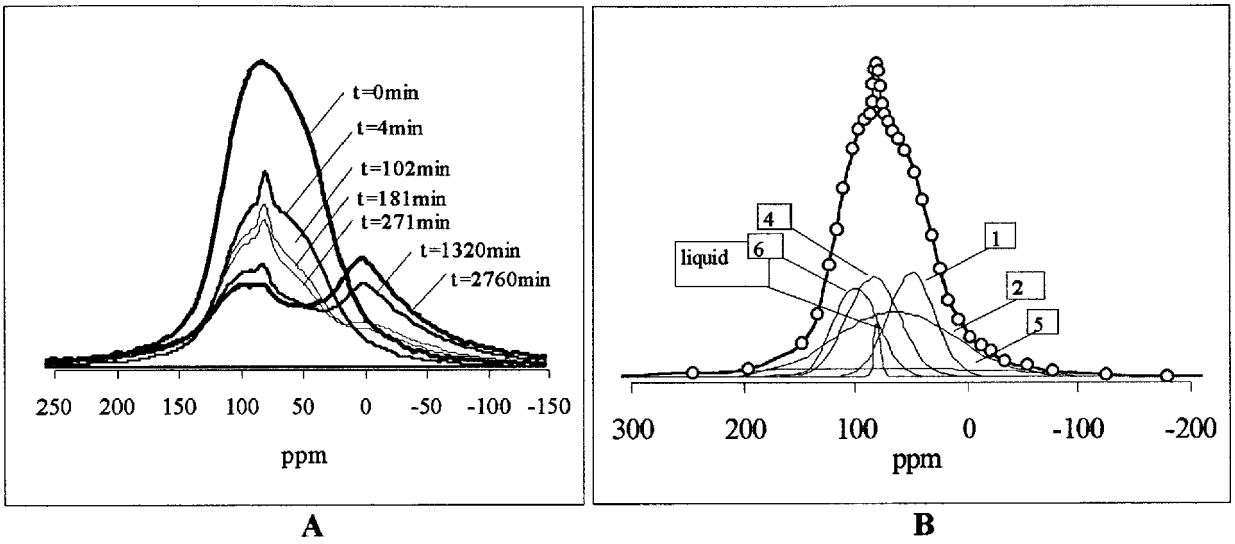

Figure 1. ^{27}Al nmr spectra (78 MHz) of hydrated CA(A) and deconvolution of the curve corresponding to 4 min of hydration (B).

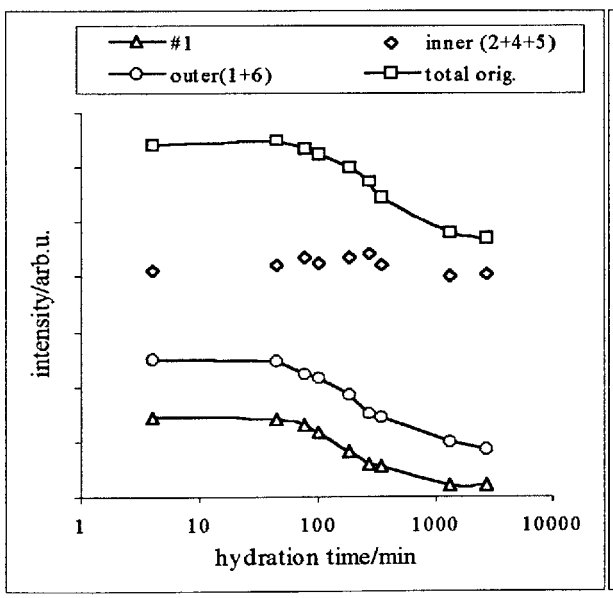

Figure 2. Development of the intensities of different sets of lines of original solid during the hydration of CA.

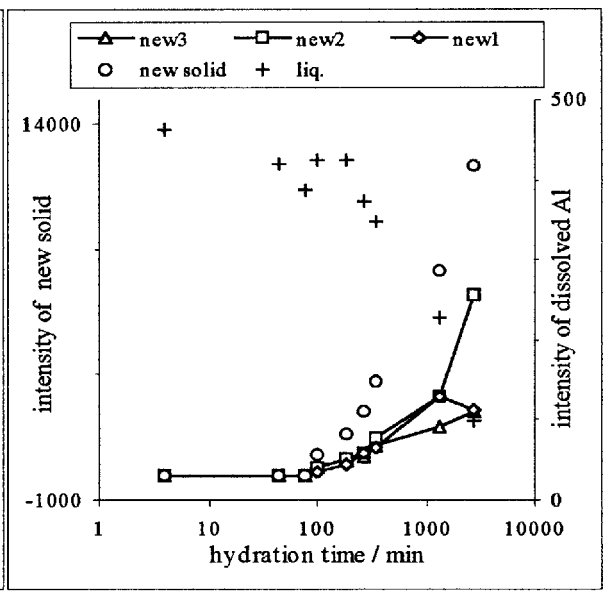

Figure 3. Development of the intensities of the lines of the products of hydration of CA.

The outer lines are comparatively narrow and one of them (having the lowest resonance frequency) shows an approximately exponential decay down to practically zero intensity at 2 days of hydration. Fortunately, the lines of *hydrated products* are significantly shifted from the lines of original solid and their intensities are not so strongly correlated. The line of aluminate in liquid phase is distinguished by its small width. From one to three lines of solid hydrated products were necessary for an adequate description of the experimental lineshapes at different stages of hydration. They overlap strongly, therefore it was impossible correlate these processes with the transformation of the primary product CAH_{10} (after approximately 10 hours of hydration) into C_2AH_8 (T. Kosmach et al., 1993). The total amount of new solid increases smoothly and is always much higher than the amount of aluminum in the liquid phase (mark the different scales

for these intensities in Fig. 8). The growth of a new hydrated phase is accelerated while the concentration of aluminum in the liquid phase is decreased. These facts indicate that the liquid phase should be considered not as a mother liquor but as an intermediate layer between the original solid and hydrated products. The amount of the *dissolved* aluminate ions is stationary during induction period. The total amount of *aluminum* in the original solid is also stable. What processes actually occur during this time is not clear from ^{27}Al nmr spectra.

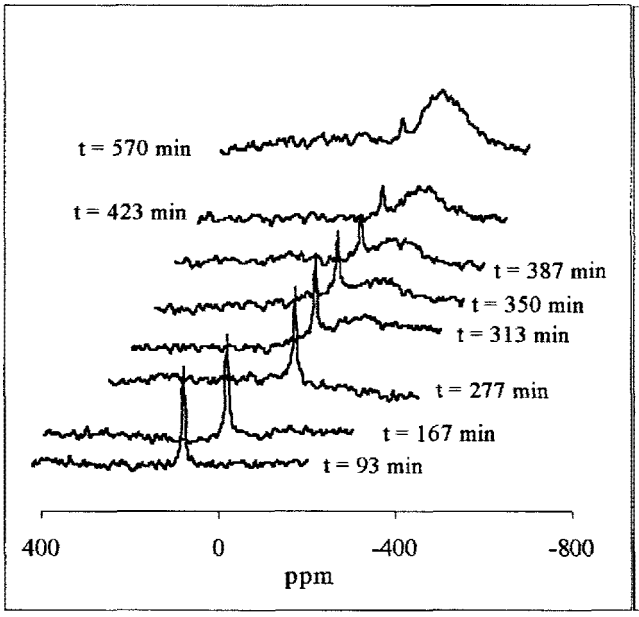

Figure 4. Difference spectra of hydrated and anhydrous CA_2.

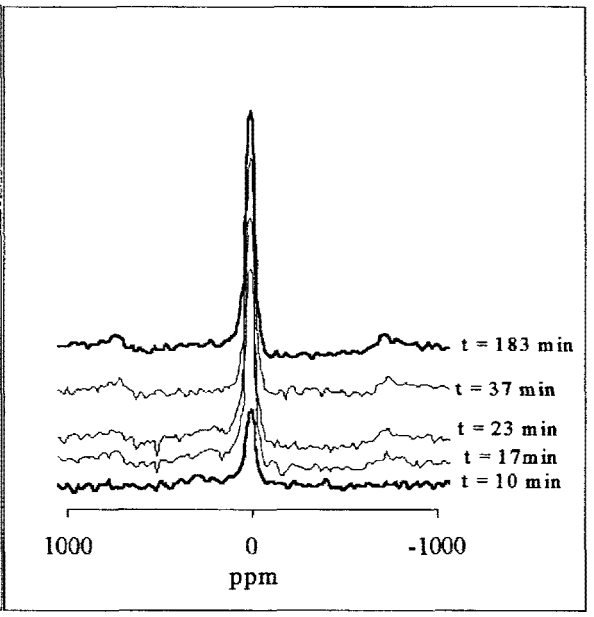

Figure 5. Difference spectra of hydrated and anhydrous C_3A.

Hydration of CA_2.

CA_2 is hydrated much slower than CA. At 10 hours of hydration the peak of hydrated products is barely visible as a shoulder to the central line in ^{27}Al nmr spectrum. However, the difference spectra, Fig. 4, of a hydrated sample and the original solid show a gradual decrease of the narrow signal at 80 ppm and a growth of the line at ca. 0 ppm (hydrated solid products). The moment of the first appearance of new solid can easily be determined from these spectra (between 277 and 313 min). The absolute amounts of the dissolved aluminum (as $[Al(OH)_4]^-$ ions) and of crystallized products of hydration are much smaller than in the case of hydrated CA.

Hydration of C_3A .

An intense line of new solid is visible in the spectra of hydrated C_3A at the shortest possible hydration times which can be investigated by ^{27}Al nmr. Difference spectra thus obtained (Fig. 5) contain one comparatively narrow central line of hydrated products, accompanied by broad satellites. Only three experimental points can be obtained before the intensity of the line of hydration product reaches a stationary level.

PROTON RELAXATION RATE MEASUREMENTS

Theoretical background.

In the presence of differently relaxing species nuclear magnetic relaxation is *multi-exponential irrespective* the rate of exchange between these species. However, at the rates of exchange higher than the difference of relaxation rates, the fraction of the fast relaxing component

decreases with increasing exchange rate and approaches zero. *Multi-exponentiality* of relaxation, i.e. a non–zero *variance of relaxation rate* indicates the presence of differently relaxing species the higher the precision of measurements the higher is the limiting exchange rate at which the multi-exponentiality may be observed. Small variance could therefore be a result of either a small content of one of the phases in slow exchange or a fast exchange between the phases present in comparable quantities. The parameters (relaxation rates and populations) of the experimentally determined (as in spin-grouping method) in such systems re-equilibration curves contain both the relaxation and exchange terms. For example in the case of slow exchange the experimental relaxation rates R_B and corresponding population, x_B, of one of the phases in a two-site system are (e.g. in: A.B. Kudryavtsev and W. Linert, 1996),:

$$R_B \approx R^0_B + p_A k - k^2/4\Delta R \qquad x_B \approx p_B + 2p_A p_B/\Delta R \qquad [1]$$

However it can be shown, that *means* and *variances* of relaxation rate are independent of the exchange rate and always are:

$$\langle R_1 \rangle = R_A x_A + R_B x_B = R^0_A p_A + R^0_B p_B \qquad [2]$$

and

$$V(R) = \langle R_1^2 \rangle - (\langle R_1 \rangle)^2 \qquad [3]$$

The parameters of a heterogeneous system derived from $\langle R_1 \rangle$ and V(R) do not contain therefore the contributions from exchange processes. The populations and and relaxation rates in the phases can be determined from $\langle R_1 \rangle$ and V(R) using certain models. If the distribution of water molecules over relaxation rates in adsorbed state is sufficiently narrow to be characterized by a single relaxation rate R_A then the average relaxation rate is:

$$\langle R_1 \rangle = xR_B + (1-x)R_A = R_A - x(R_A - R_B) = R_B + (1-x)(R_A - R_B) \qquad [4]$$

where x is the fraction of water molecules in bulk liquid ($x = p_B$), R_B is the relaxation rate of water protons in bulk liquid (for pure water R^0_B is about 0.3 sec^{-1} at 25°C). The variance of relaxation rates under the same conditions is:

$$V(R) = \langle R_1^2 \rangle - \langle R_1 \rangle^2 = x(1-x)(R_A - R_B)^2 \qquad [5]$$

The ratio, α, of the variance, Eq. 5, to $(\langle R_1 \rangle - R_B)^2$ is:

$$\alpha = V(R)/(\langle R_1 \rangle - R_B) = x/(1-x) \qquad [6]$$

and

$$x = \alpha/(1 + \alpha) \qquad [7]$$

The relaxation rate in adsorbed state can be calculated by substituting the fraction *x* in Eq. 4 by its value from Eq. 7:

$$R_A = R_B + (\langle R_1 \rangle - R_B)(\alpha + 1) \qquad [8]$$

The experimental values of means and variances of relaxation rates were obtained (according to A.B. Kudryavtsev et al., 1994) by fitting the re–equilibration curves of longitudinal magnetization to Eq. 9:

$$A = A_0(1 - \exp(-a\tau + b\tau^2)) \qquad [9]$$

where A is the amplitude of an nmr signal in a saturation-recovery sequence, $a = \langle R_1 \rangle$, and $b = 0.5$ V(R). The kinetics of hydration reflected by the changes in $\langle R_1 \rangle$ and V(R) in hydrated CA are shown in Figs. 6 and 7. The estimates of $\langle R_1 \rangle$ and V(R) depend on the region in which the curve was analyzed, i.e. on the number of points of experimental data used in regression, Figs. 6, 7. The shifting of the truncation point of experimental curve (imposed to obtain adequate descriptions at different stages of hydration) produces steps or breaks in the kinetic curves. A correct quantitative analysis can only be performed within the regions explored under identical experimental settings. Qualitatively such curves can be analyzed by 'pasting' these parts together.

Hydration of CA.

At the initial stage (0 -200 min. of hydration) both the means and variances of relaxation rate are not high. A sharp rise of $\langle R_1 \rangle$ and V(R) at t_{hydr} = 250 - 350 min. indicates the beginning of crystallization of hydrated phases. The mean relaxation rate passes through a maximum at about 350 min, whilst the variance proceeds to increase, although at a slower rate. This maximum was observed by T. Kosmach et al. (1993) and was attributed to the transformation of CAH_{10}, into CAH_8 and AH_3. Small initial variances if relaxation rates mean that either the amount adsorbed water is low or the exchange rate between bulk liquid and adsorbed state is high. Observed increase in V(R) may be connected with the increasing viscosity of liquid phase (slower exchange) and/or penetration of water molecules into micropores (higher fraction of adsorbed molecules).

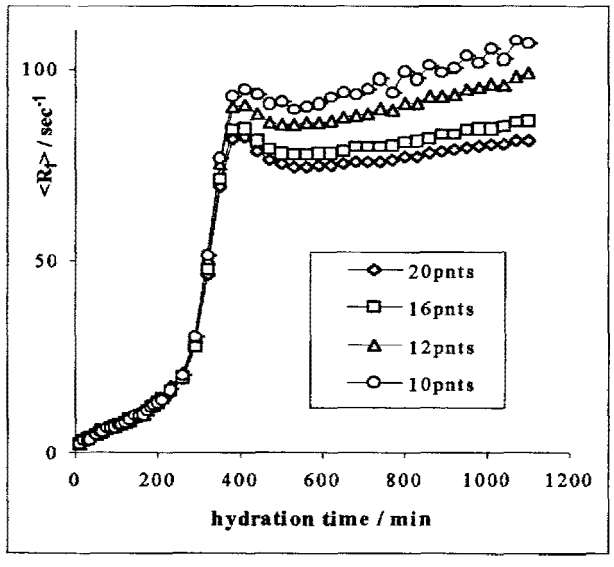

Figure 6. Development of $\langle R_1 \rangle$ during the hydration of CA.

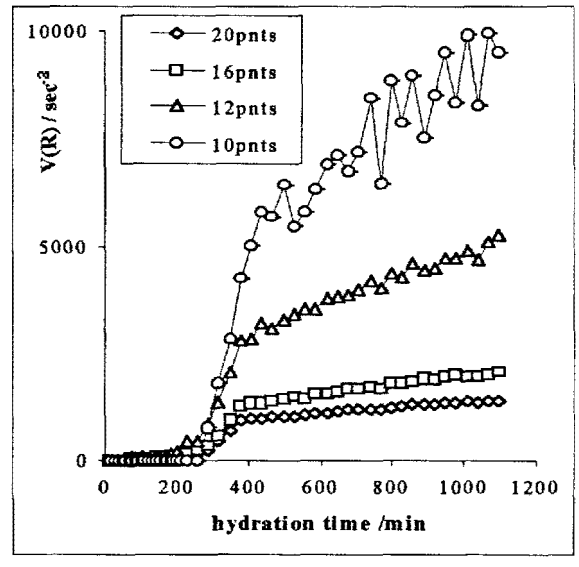

Figure 7. Development of V(R) during the hydration of CA.

Supposing that low initial variances were caused by a weak adsorption of water we assume implicitly that bulk water and adsorbed water exist in slow exchange. The relaxation rate R_B can then be identified with the relaxation rate in a solution separated from a suspension (0.366 sec^{-1} in the solution centrifuged from a freshly prepared paste of CA). The results of the calculations of α and x using this value of R_b are shown in Fig. 8A. Because $\langle R_1 \rangle$ and V(R) were measured using three different sets of re–equilibration delays three regions of the curve 'X' are observed in Fig. 8A). By shifting upwards the parts of this curve a continuous dependence of the fraction of 'free

water' can be obtained (curve 'Xcorr' in Fig. 8). Supposing that low initial variances were caused by a fast exchange the ratio α should be calculated using $R_B \approx \langle R_1 \rangle (t_{hydr} \dashrightarrow 0) = 2.0\ sec^{-1}$. In this case we implicitly assume that a polymolecular layer with fast exchange was initially formed with $R_B \approx 2.0\ sec^{-1}$. This layer yields upon hydration a kinetically distinct layer ('adsorbed state'). characterized by the relaxation rate R_A. Such calculations lead to α and x decreasing with hydration x, Fig. 8B, which reflects the diminishing amount of the initial polymolecular adsorption layer at the initial stage of hydration.

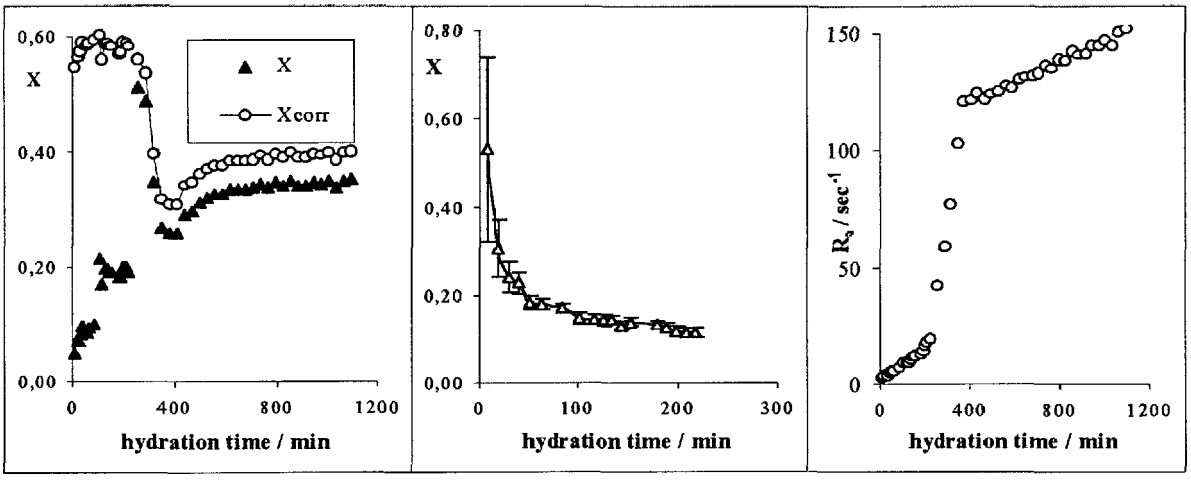

A ($R_b = 0.36\ sec^{-1}$) **B** ($R_b = 2.0\ sec^{-1}$) **C**

Figure 8. Kinetics of the conversion of free water molecules (A,B) and of the development of relaxation rate in adsorbed state (C).

The relaxation rates in adsorbed state, R_A, (calculated according to Eq. 8, Fig. 8C) are small comparing to the relaxation rates in a monomolecular layer on similar solid surfaces (about 100 sec^{-1}). This means that the phase 'A' is also a polymolecular adsorption layer. The observed increase in R_A shows that molecular mobility is decreased by a certain processes, which must be connected with nucleation because the other alternative: the increasing concentration of dissolved products, does not correspond with approximately constant intensity of the signal of dissolved products in ^{27}Al nmr spectra at this period (see above).

After the beginning of crystallization new solid phase attracts water from both the bulk liquid and polymolecular adsorption layer. The phase 'A' in this case is the adsorption layer of this newly formed crystals possessing of a high adsorption capacity. The water being more thinly distributed over the solid surface the calculated R_A approaches the values characteristic for a monomolecular adsorption. It is remarkable that the dependence of R_A on hydration time consists of three straight lines and does not contain either maxima or breaks of continuity (Fig. 8C). This shows that the influence of surface in the adsorption layer kinetically separated from 'bulk water' is continuously increasing.

Hydration of C_3A

The curves in Fig. 9A show that both the means and variances of relaxation rate are increasing steadily starting from comparatively high values. They pass through a flat maximum at about 500 min. of hydration. The fraction of free water, x, and the relaxation rate, R_A, reflect a release of adsorbed water and an increasing mobility of water in the 'adsorption layer' after 500 min. of

hydration (Fig. 9B). The release of water might be connected with the growing size of crystals and lesser specific surface. On the other hand the water within the phase 'A' can be transformed from adsorbed state into the water of crystallization. Such transformation can be accompanied with an increase of molecular mobility due to a free rotation along some axis in a crystal lattice.

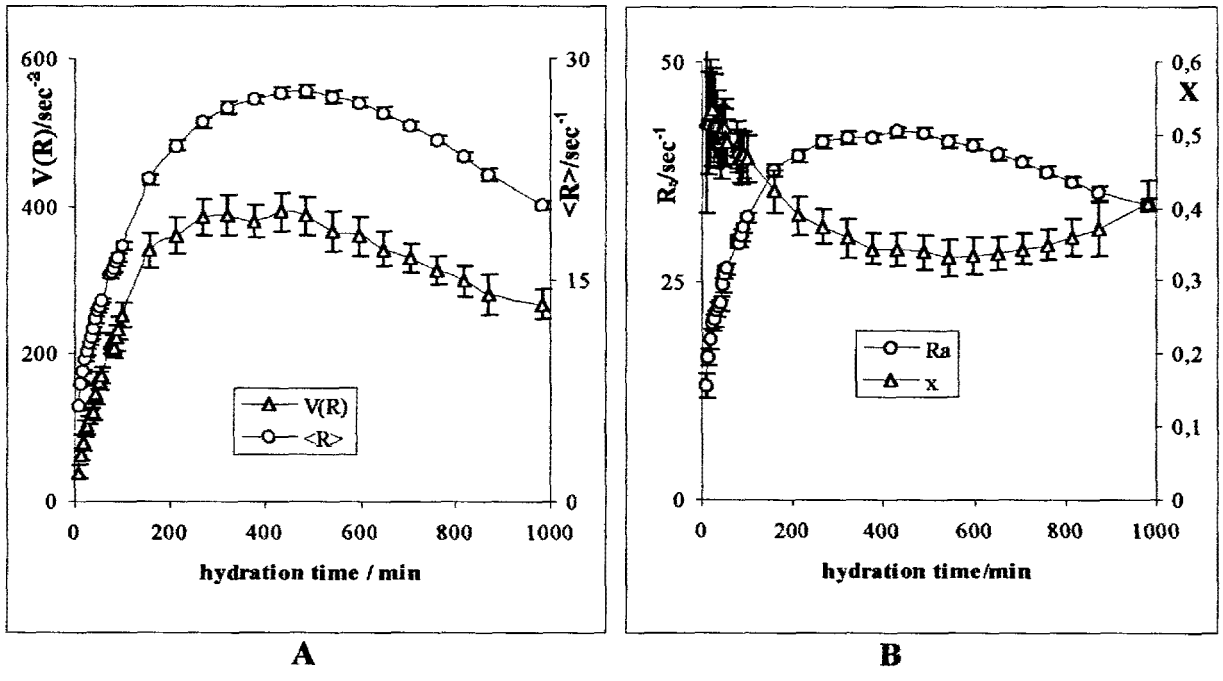

Figure 9. The development of the means and variances of relaxation rate (A) and of the free water content and relaxation rate in adsorbed state during the hydration of C_3A (B).

REFERENCES.

Kosmach, T, Lahajnar, G., Sepe, A., "Proton NMR relaxation study of calcium aluminate hydration reaction", *Cem. Concr. Res.*, Vol. 23, No 1, 1993, p. 1

Kudryavtsev, A.B., Kouznetsova, T.V., Pyatkova, A.V., "Proton relaxation and High Resolution Solid State Aluminium - 27 NMR study of hydration of calcium oxide sulphoaluminate", *Cem. Concr. Res.*, Vol. 20, 1990, p. 407

Kudryavtsev, A.B., Linert, W. and Pyatkova, A.V. "Determination of mean nuclear magnetic relaxation rates in multiphase systems in slow exchange", *Chem. Phys.*, Vol. 186, 1994, p. 53

Kudryavtsev, A.B., Kouznestova, T.V., "Hydration Kinetics of Modified Calcium Sulphoaluminate Oxides Studied by Aluminum-27 NMR Spectroscopy and Proton Magnetic Relaxation" *Cem. Concr. Res.* to be published.

Kudryavtsev, A.B., Linert, W., *"Physico-Chemical applications of NMR"*, World Scientific Publishers, Singapore, 1996, page 308.

Mueller, D., A. Rettel, A., Gessner, W. and Scheller, G., "An application of Solid State Magic Angle Spinning 27Al NMR to the Study of Cement Hydration", *J. Magn. Reson.* Vol. 57, 1984, p. 152.

Peemoeller, H., and Pintar, M.M., "Two-dimensional time-evolution approach for resolving a composite free-induction decay", *J. Magn. Reson*, Vol. 41, 1980, p. 358

Skibsted, J, Henderson, E., and Jakobsen, H., "Characterization of Calcium Aluminate Phases by 27Al MAS NMR Spectroscopy", *Inorg. Chem.* Vol. 32, No. 6, 1993, p. 1013

2ii029
8 pp
Kn o. 2 5. JAN. 2001 d o k 31792

EFFECT OF COMPOSITION ON THE HYDRATION PROPERTIES OF RAPID-HARDENING SULFOALUMINATE CEMENTS

Julius BERETKA and Natalie SHERMAN, Commonwealth Scientific and Industrial Research Organization D.B.C.E., P.O. Box 56, Highett, Victoria 3190, Australia
Milena MARROCCOLI, Antonella POMPO and Gian Lorenzo VALENTI, Dipartimento di Ingegneria e Fisica dell'Ambiente, Università degli Studi della Basilicata, Via della Tecnica 3, 85100 Potenza, Italy

ABSTRACT The influence of $C_4A_3\overline{S}$ and C_4AF on the properties of sulfoaluminate cements has been studied. Cements containing about 30-40% $C_4A_3\overline{S}$ hydrated with w/s ratios ranging from 0.35 to 0.50 showed the best behaviour. The resistance of sulfoaluminate cements to CO_2 attack was improved by the incorporation of C_4AF.

Key-words: Sulfoaluminate, Brownmillerite, Anhydrite, Hydration, Ettringite.

INTRODUCTION

The properties of calcium sulfoaluminate cements are influenced mainly by $C_4A_3\overline{S}$ which forms ettringite according to the following reactions:

$$C_4A_3\overline{S} + 8\,C\overline{S} + 6\,C + 96\,H \rightarrow 3\,(C_6A\overline{S}_3H_{32}) \quad [1]$$

$$C_4A_3\overline{S} + 2\,C\overline{S} + 38\,H \rightarrow C_6A\overline{S}_3H_{32} + 2\,AH_3 \quad [2]$$

The microstructure of ettringite is strongly dependent on the presence of lime (Metha, 1973). Ettringite produced by the reaction in Eq 1 is expansive and this property is exploited in special applications such as shrinkage-resistant and self-stressing cements (Kurdowski et al, 1986).

Ettringite formed in the absence of lime by the reaction in Eq 2 is non-expansive and generates high early strength in cementitious systems. Rapid hardening sulfoaluminate-based cements have higher mechanical strength and require lower synthesis temperature than ordinary portland cements (OPC) (Muzhen et al, 1992). It also allows the use of considerable amounts of industrial wastes and by-products as raw materials (Beretka et al, 1993).

According to the stoichiometry of the reaction (Eq 2) a $C\overline{S}/C_4A_3\overline{S}$ weight ratio of 0.45 and a relatively high water/solid ratio of 0.78 by weight are required for the full formation of ettringite. Hence the $C_4A_3\overline{S}$ concentration in cement and the amount of water in the mixture must be adjusted so as to ensure optimum properties. Accordingly, if the $C_4A_3\overline{S}$ content is too high, strength reduction may occur due to excessive porosity of the hydrated systems; on the other hand, when the $C_4A_3\overline{S}$ content is too low, the ettringite concentration within the hydration products is no longer sufficient to give adequate mechanical strength.

Sulfoaluminate clinkers can be conveniently diluted with blending components in order to lower the $C_4A_3\overline{S}$ concentration. However, they usually contain considerable amounts of other phases like C_2S, $C_5S_2\overline{S}$, C_3A and C_4AF, depending on the synthesis temperature as well as the composition and proportioning of the raw materials used. The positive role played by calcium disilicate C_2S in $C_4A_3\overline{S}$-based cements is clearly defined as in OPC, since it contributes to the strength and durability of the hydrated systems (Ikeda, 1980; Sudoh et al, 1980). Calcium

sulfosilicate $C_5S_2\overline{S}$ hydrates very slowly and can only contribute to the ultimate strength of the system (Sherman et al, 1995). The hydration of C_3A is fast, it competes with that of $C_4A_3\overline{S}$, and is responsible for early setting (Beretka and Sherman, 1992). C_4AF, like C_3A, gives hydration products which react with ettringite, and generate monosulfate ($C_4A\overline{S}H_{12}$) that is a phase more resistant to carbonation than ettringite (Belz et al, 1995). Due to its moderate rate of hydration, C_4AF does not cause the usual problems associated with the presence of C_3A and can enhance the durability of calcium sulfoaluminate cements, particularly at later ages.

Therefore, regarding the role played by the individual components of these cements, the effects of $C_4A_3\overline{S}$ content and of the presence of C_4AF need to be examined and are here discussed.

EXPERIMENTAL

Raw materials

Natural materials (limestone, bauxite), industrial byproducts (phosphogypsum, fly ash) and pure analytical grade reagents were used for the raw mixes. The commercial materials were the same as used previously (Beretka et al, 1993; Sherman et al, 1995). The pure reagents grade materials used were not analyzed.

Synthesis and procedures

The various cementitious compositions were prepared by firing them in an electric oven. The cements were obtained in a single firing or prepared by blending individually synthesized components. Then they were ball-milled dry to pass a 53 μm sieve with a residue of 5%.

Hydration

Small (2 g) specimens were mixed with the selected amounts of water, then placed in a plastic envelope and cured for various time intervals at a constant temperature (23 or 55°C). At the end of the hydration period the reaction was stopped with acetone and the material dried with ether (Beretka et al, 1993).

Qualitative and quantitative analyses

XRD, SEM, DTA and TGA were employed for the qualitative analysis of the cured specimens. XRD was also used for the qualitative analysis of the anhydrous systems; and TGA was also employed for the measurement of ettringite concentration in the hydrated cements.

Mechanical testing and carbonation studies

The compressive strength was determined on paste cubed specimens, 25 mm in size, which were cast, then cured at 23 °C and 100% RH for various times. Some of the samples were submitted to accelerated carbonation that was carried out in a carbonation chamber (4% CO_2, 60% RH) for different times to up to 28 days, before testing.

RESULTS AND DISCUSSION

Effect of $C_4A_3\overline{S}$ content

Five calcium sulfoaluminate cements, obtained by heating mixtures of limestone, bauxite, phosphogypsum and fly ash for 4 hours at 1200 ° C, have been investigated.

The proportioning of the raw mixes has been formulated so as to obtain products containing the

three components, $C_4A_3\overline{S}$, $C_5S_2\overline{S}$, $C\overline{S}$. The minor phases which may have formed were ignored. In the five cements the $C_4A_3\overline{S}/C_5S_2\overline{S}$ weight ratio was varied between 1:5 and 2:1; the ratio between $C\overline{S}$ and $C_4A_3\overline{S}$ was kept constant and equal to 0.5, that is a slightly higher value in respect to the stoichiometric ratio (0.45) fixed by Eq 2. This reaction is the only one that has been considered during the hydration process, since the calcium sulfosilicate contribution has been neglected due to its poor hydraulic behaviour. Table 1 shows the compositions examined.

Table 1 Compositions (wt %) of sulfoaluminate cements.

System / Component	A	B	C	D	E
$C_4A_3\overline{S}$	15.4	22.2	28.6	40.0	50.0
$C_5S_2\overline{S}$	76.9	66.7	57.1	40.0	25.0
$C\overline{S}$	7.7	11.1	14.3	20.0	25.0

Hydration has been carried out in two different sets of experiments: (i) the first one on compositions from B to E using a constant water/total solids ($C_4A_3\overline{S} + C_5S_2\overline{S} + C\overline{S}$) ratio of 0.4; (ii) the second one (compositions A to E) using a constant water/reactant ($C_4A_3\overline{S} + C\overline{S}$) ratio of 0.86, that is ~10% higher than that required by stoichiometry of Eq 2 (0.78). For the second set of experiments, in spite of the excess water, the use of a superplasticizer was required for improving the workability of systems A and B, characterized by the lowest w/s ratios (Table 2).

Table 2 Water/solid ratios, w/s, for the second set of hydration experiments (constant water/reactant ratio, 0.86).

System	A	B	C	D	E
parts of $C_4A_3\overline{S} + C\overline{S}$	1.50	1.50	1.50	1.50	3.00
parts of water	1.29	1.29	1.29	1.29	2.58
total solids	6.50	4.50	3.50	2.50	4.00
w/s	0.20	0.29	0.37	0.52	0.65

Values of compressive strength and ettringite concentration are plotted in Figs 1 and 2, respectively, as a function of time for compositions cast at the w/s ratio of 0.4. It is possible to notice that as the $C_4A_3\overline{S}$ content increases, the mechanical strength rises for all the four systems examined to up to 28 days curing. For longer hydration times the strength of B and C cements is about constant, while the strength of cement D slowly decreases, and cement E shows a rapid

drop in strength, due to expansion and cracking.

The ettringite content for the above compositions (Fig 2) increases with the amount of $C_4A_3\overline{S}$ present, and in fact after 1 day curing it reaches a remarkably high value, then slowly increases to an almost constant value, except for system E. This particular system (E) after 28-56 days hydration shows a further growth in ettringite content.

Such behaviour has to be related to the water content of the paste. System E would require a much higher water content for complete hydration (Table 2) than the one used here. As a consequence, when the gauging water has been consumed, the further hydration of $C_4A_3\overline{S}$ is achieved by the absorption of water from the curing environment (100% RH). This delayed hydration is responsible for the expansive phenomena, due to ettringite formation on the surfaces of hardened samples. The fact that this phenomenon does not occur at 67% RH, strengthens this hypothesis.

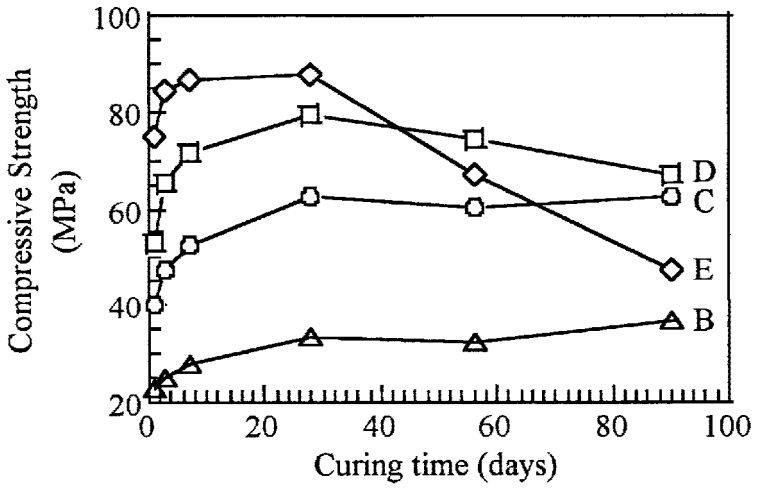

Figure 1 Compressive strength for compositions hydrated with w/s 0.4.

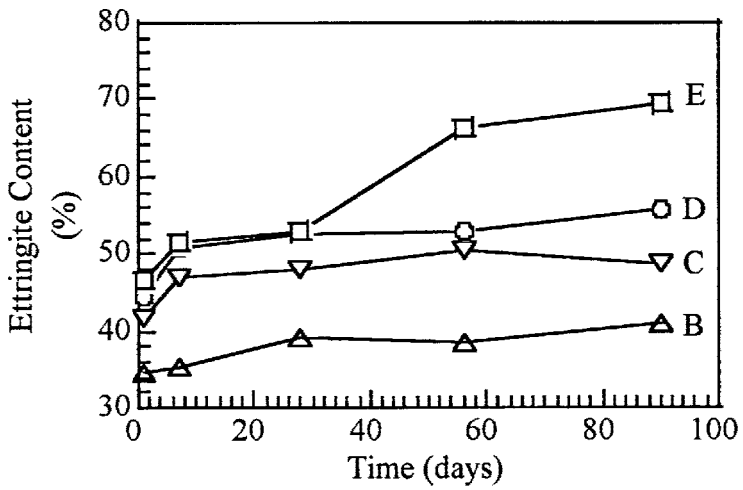

Figure 2 Ettringite content for compositions hydrated with w/s 0.4.

Table 3 confirms the critical role played by the water content (second set of experiments). The

compressive strength and ettringite content data are reported for different curing times for the five systems investigated. The highest mechanical strength is shown by cement B, followed by cements D, C, A and E respectively. Compositions A and E do not give a good compromise between the $C_4A_3\overline{S}$ content and the amount of water used. In fact, cement A has a low $C_4A_3\overline{S}$ (and ettringite) content while cement E has a high one. In spite of its high ettringite concentration, cement E gives lower strength due to the high porosity induced by the water content.

Table 3 Compressive strength, (MPa) (left upper corners) and ettringite content, wt (%) (right lower corners) for compositions hydrated with water/reactant ratio of 0.86.

Time(days) / System / w/s	1	3	7	28	56
A 0.20	35.7 22.7	42.3 24.2	45.0 25.5	57.9 27.6	61.5 29.7
B 0.29	55.4 35.2	72.3 38.5	81.0 40.3	79.4 40.9	90.0 37.0
C 0.37	36.3 39.7	48.7 43.6	59.4 46.4	61.8 49.1	66.8 48.5
D 0.52	35.8 48.8	49.5 53.0	59.7 56.7	70.7 60.3	70.5 60.3
E 0.65	27.8 53.6	41.0 58.2	46.2 62.4	54.6 65.2	57.3 66.7

Differently from the first set of tests, the systems hydrated with a water/reactant ratio of 0.86 were dimensionally stable, since the water content was sufficient to obtain complete hydration for all compositions.

Role of C_4AF

Samples of synthetic monosulfate ($C_4A\overline{S}H_{12}$) and samples of the systems F and G shown in Table 4 were also investigated. Monosulfate was obtained by hydrating a mixture of $C_4A_3\overline{S}$, C_3A and $C\overline{S}H_2$ (Beretka and Sherman, 1992). System G was prepared by blending a mixture of individually synthesized $C_4A_3\overline{S}$, $C\overline{S}$ and C_4AF in a stoichiometric ratio suitable for ettringite-monosulfate transformation (weight ratio 1:0.45:1.6).

Pure $CaCO_3$, Al_2O_3, $CaSO_4{\cdot}2H_2O$ and Fe_2O_3 were used as raw materials for each synthesis. $C_4A_3\overline{S}$ was obtained by heating at 1260 °C for 4 hours; $C\overline{S}$ at 850 °C for 1 hour and C_4AF at

1300 °C for 4 hours. Composition F was obtained in a similar way as the previous ones. Its composition is only slightly different from that of the system D reported previously in Table 1. The good resistance of monosulfate to CO_2 attack is demonstrated by Figs 3a and 3b, which show the XRD results of a sample before and after accelerated carbonation, respectively. The carbonation products present in minute quantities are attributed to traces of ettringite in the synthesized monosulfate samples.

Table 4 Compositions (wt %) of sulfoaluminate cements.

Component / System	$C_4A_3\overline{S}$	$C_5S_2\overline{S}$	$C\overline{S}$	C_4AF
F	42.9	40.0	17.1	—
G	32.8	—	14.7	52.5

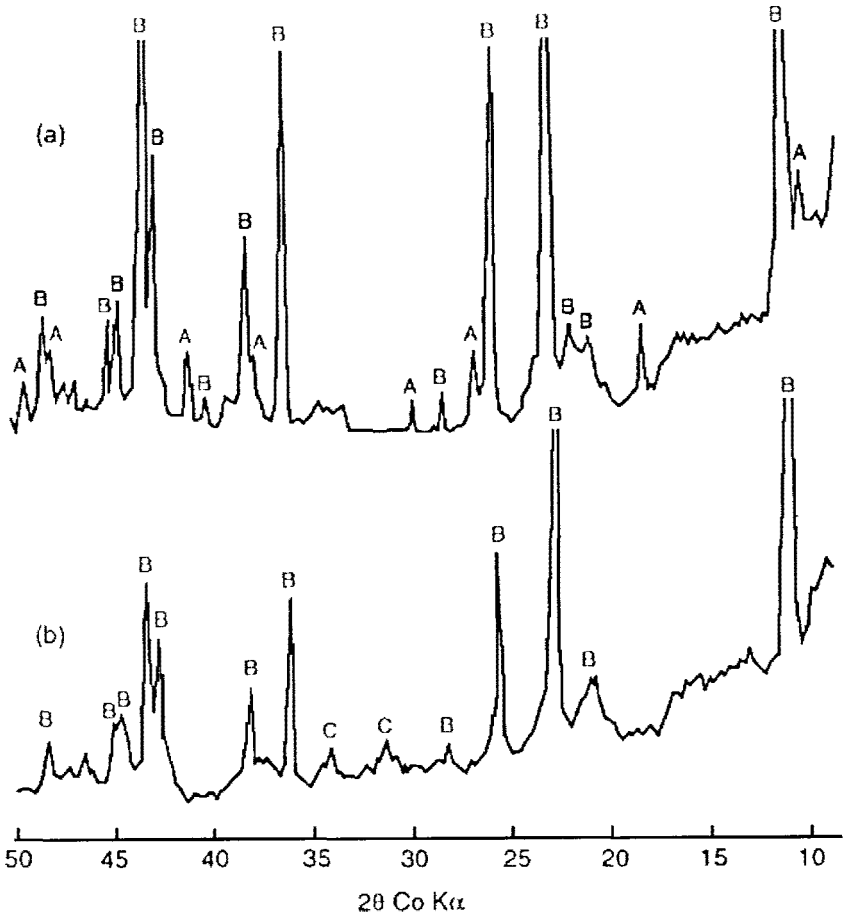

Figure 3 XRD diagrams for: (a) monosulfate before carbonation; and (b) monosulfate after 28 days exposure to CO_2 in a carbonation chamber (4% CO_2). A = $C_6A\overline{S}_3H_{32}$; B = $C_4A\overline{S}H_{12}$; C = calcium carbonates.

Fig 4 illustrates the ability of the C_4AF-containing system of generating monosulfate at the expense of ettringite.

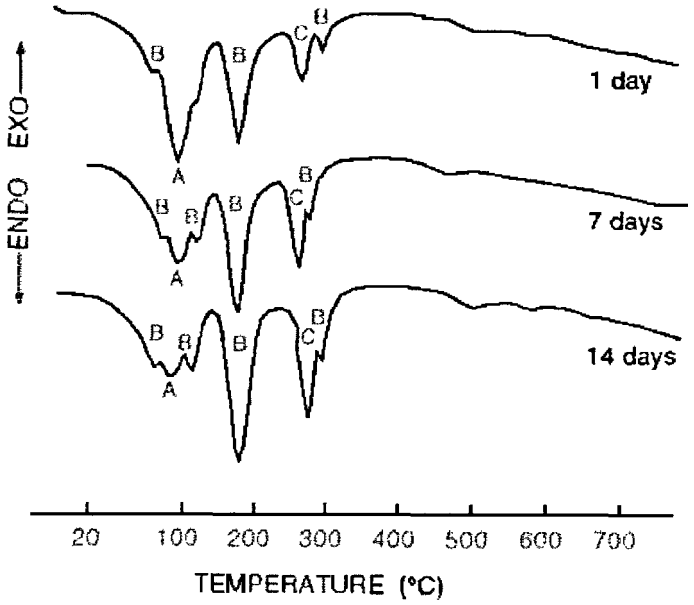

Figure 4 DTA traces for composition G hydrated at 55°C; w/s 0.5. A = $C_6A\overline{S}_3H_{32}$; B = $C_4A\overline{S}H_{12}$; C = alumina gel.

The positive effect of C_4AF in $C_4A\overline{S}$-containing systems can be demonstrated by the good compressive strength and resistance to carbonation of specimen G (Table 5).

Table 5 Retained compressive strength (%) for samples F and G after accelerated carbonation.

Days of carbonation / System	1	3	7	28
F	100.6	87.8	78.4	66.5
G	98.7	96.5	106.7	117.6

CONCLUSIONS

Non-expansive ettringite generated by the hydration of sulfoaluminate cements produces high mechanical strength. Since this hydration requires a relative high stoichiometric amount of water, it is necessary to optimize the $C_4A_3\overline{S}$ concentration and the water content of the mix. C_4AF incorporated in sulfoaluminate cements has a favourable influence on their resistance to carbonation.

REFERENCES

Belz G., Beretka J., Marroccoli M., Santoro L., Sherman N. and Valenti G.L., "Use of Fly Ash, Blast Furnace Slag and Chemical Gypsum for the Synthesis of Calcium Sulfoaluminate-Based

Cements", Proc. 5th CANMET/ACI Int. Conf.. Fly Ash, Silica Fume, Slag and Natural Pozzolans in Concrete, Milwaukee 1995, ACI, SP-153, Vol. 1, pp. 513-530.

Beretka J., de Vito B., Santoro L., Sherman N. and Valenti G.L., "Hydraulic Behaviour of Calcium Sulfoaluminate-Based Cements Derived from Industrial Process Wastes", Cem. Concr. Res., Vol. 23, 1993, pp. 1205-1214.

Beretka J., and Sherman N., Private Communication, 1992.

Kurdowski W., George C.M. and Sorrentino F.P., "Special Cements", Proc. 8th Int. Congr. Chem. Cem., Rio de Janeiro 1986, Vol. 1, pp. 292-318.

Ikeda K., "Cements Along the Join $C_4A_3\overline{S}$-C_2S", Proc. 7th Int. Congr. Chem. Cem., Paris 1980, Vol.2, Theme III, pp. 31-36.

Mehta P.K., "Mechanism of Expansion Associated with Ettringite Formation", Cem. Concr. Res., Vol. 3, 1973, pp. 1-6.

Muzhen S., Kurdowski W. and Sorrentino F.P., "Development in Non-Portland Cements", Proc. 9th Int. Congr. Chem. Cem., New Delhi 1992, Vol.1, pp. 317-354.

Sherman N., Beretka J., Santoro L. and Valenti G.L., "Long-Term Behaviour of Hydraulic Binders Based on Calcium Sulfoaluminate and Calcium Sulfosilicate", Cem. Concr. Res., Vol. 25, 1995, pp. 113-126.

Sudoh G., Otha Y., Harada H., Proc., "High Strength Cement in the CaO-Al_2O_3-SiO_2-SO_3 System and its Application", 7th Int. Congr. Chem. Cem., Paris 1980, Vol. 3, pp. 152-157.

2ii030
4 pp
Kno. 25. JAN. 2001 doc 31793

EFFECT OF CHLORIDE ON HYDRATION PROPERTIES OF ALINITE CEMENT

JI Lin, REN Xiantai and SU Muzhen, China Building Materals Academy, Beijing 10002, China

ABSTRACT Hydration of alinite cement is studied by calorimeter, TGA, XRD, and SEM/EDAX. Ion content in the hydration solution is determined by ICP and wet chemical analysis .The action of Cl^- in alinite cement hydration and its effect on the formation of hydration products are revealed. The hydration reactivity of alinite cement is quite high because of rather rapid hydration of minerals containing Cl^-.Forming $C_3A \cdot CaCl_2 \cdot 10H_2O$ will reduce soluble Cl^- and compose an intergrowth structure with CSH gel.So that strength of alinite cement is enhanced.

Key-Words : Alinite Chloride Hydration

INTRODUCTION

The main minerals containing Cl^- in alinite cement are alinite phase and $C_{11}A_7 \cdot CaCl_2$, which hydrate quickly due to Cl^- in the structure. $C_{11}A_7 \cdot CaCl_2$ phase in clinker must be limited in a content,e.g.10%,or quick setting may occur. When $C_{11}A_7 \cdot CaCl_2$ hydrates the product is the Friedel' s salt and no Cl^- is released, which prevents Cl^- being free.

Alinite has a higher reactivity with water and hydrates more fast than alite (Boikva,1986). It hydrates so fast that after 15 minutes of adding water large amount of Al^{3+},Ca^{2+},Cl^- solve into the liquid phase. Such a high reactivity of hydration is quite profitable to the early strength of cement.

Alinite cement is an energy-saving product and has a good strength characteristics. But its application is restricted because of soluble Cl^-.So it is necessary to investigate and recognize the regularity of Cl^- release

EXPERIMENTAL

Raw mixtures were made from limestone, Clay, flyash, as well as chemical agents, $CaCl_2$ and MgO. The burning temperature was 1250 ℃. Alinite cement was made by mining 95% clinker and 5% gypsum and its strength and the rate of hydration heat evolution were tested. Pure phases were made from chemical agents.

The hydration of alinite cement and the pure phases was studied with W/C=10 and by curing in sealed plastics bottles which was rotated for various ages. Samples were filtered ,of which the filtrate solution was determined by ICP and chemical analysis and the remaining was analysised by TGA, XRD, SEM/EDAX after drying in vacuum.

RESULTS AND DISCUSSION

Alinite content in the cement is about 50 ~ 60% and it plays an important role in cement properties Figure 1 gives the rate of heat evolution of alinite hydration, which reaches the first peak value, 0.0132J/s.g, in 15 minutes after adding water when a great number of Al^{3+},$Ca^{2+}$and Cl^- solve into the liquid phase (see Table 1). In 6 hours the second peak of heat evolution appears and the contents of ions in the solution come up to more than 70% of their final values. Figure 2 shows that the ions enter into the liquid fast during early ages, e.g, the contents of Al^{3+},Ca^{2+} and Cl^- are in the first day are 94%,82% and 76%, respectively, of their final values. Figure 3 reveals that the content

of Cl^- in the solution of hydrated alinite reaches the highest value after three days, It is much lower in that of hydrated alinite cement and its solving rate is slower and slowes with the period which is caused by the Friedel' s salt, $C_3A.CaCl_2.10H_2O$ that fixes Cl^-.

Table 1 Characteristics of alinite hydration in early ages (w/c=10)

	hydration heat reaction rate	Al_2O_3 * μg/ml	CaO * μg/ml	Cl^- * mg/ml	fixed wate %	Ca(OH) %	hydration rate %
15 min	0.0131 J/g.s	22.5	3.3	3.3	0.8	0	9.1
6 hour	0.0126 J/g.s	28.5	7.1	7.01	14.57	12.35	36.36
1 day		30	9.2	7.17	22.58	21.03	43.45

* ion contents in liquid phase determined by ICP

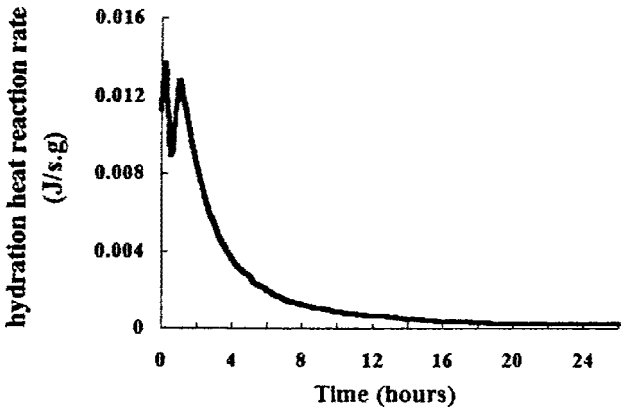

Fig 1 Heat evolution of alinite hydration

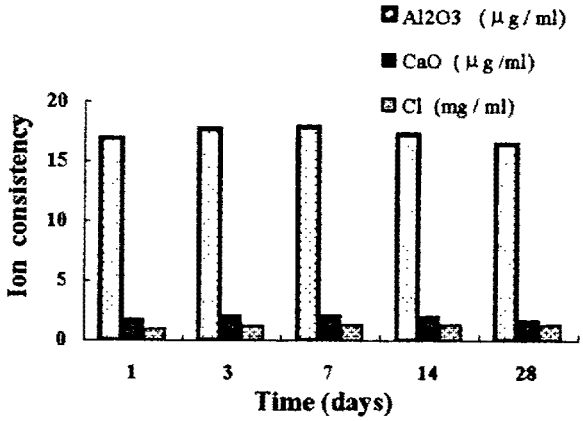

Fig 2 ion contents in the liquid phase of alinite cement hydration VS time

Table 2 lists the hydrated extent of cement and pure phases, from which no marked effect of W/C on the early hydration rate of alinite is observed. The hydration rate of alinite samples with different W/C are similar in the first three days and then slow down for lower W/C. It is the characteristics of alinite that its hydration may reach quite high extent even in rather low W/C, so the W/C needed by alinite cement is also quite low, which corresponds to the result by Ftikos(1991).

Table 2 Hydration extents of alinite cement and its pure phases (%)

	W/C	1 day	3 day	7 day	14 day	28 day
Alinite	10	43.45	51.19	78.57	>95	
	0.25		53.39	53.57		61.90
$C_{11}A_7 \cdot CaCl_2$	10	44.83	>90			
	0.25		34.47	47.73		54.55
$\beta-C_2S$	10	22.41	39.66	41.35	48.28	62.07
Alinite Cement	10	34.59	47.44	64.24		81.66

Figure 3 shows that the fixed water in hydrated alinite increases fast during the initial three days and then tends to increase slowly. while that of alinite cement increases smoothly. In TG curves (Fig 4) the fixed water of hydrated cement includes three parts: fixed water in CSH gel at below 250 ℃, combined water on hydrated aluminate phase at 250 ~ 450 ℃,and structural water of $Ca(OH)_2$ at about 450 ~ 550 ℃. XRD shows (Fig 5)that the main products of alinite cement hydration include $Ca(OH)_2$, AFT, CSH, $C_3A{\cdot}CaCl_2{\cdot}10H_2O$,ferrite phase as well as a little C_3AH_6 and CAH_{10}.

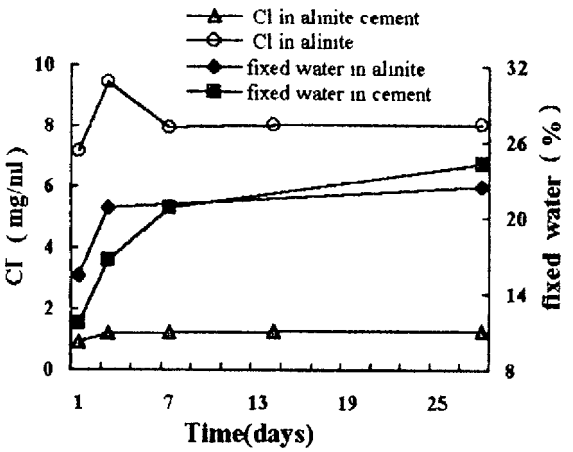

Fig 3 Fixed water and Cl^- solved in liquid of hydrated alinite cement VS ages

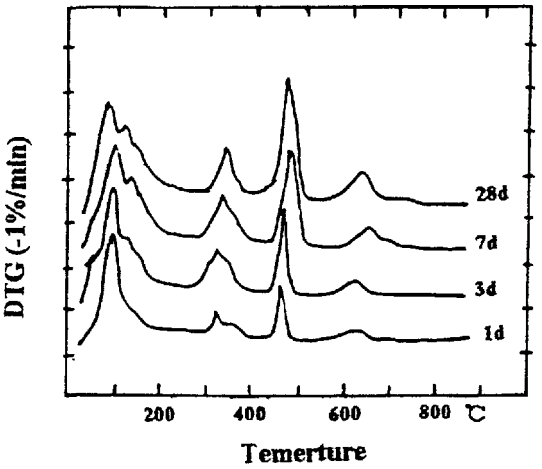

Fig 4 TGA curves of hydrated alinite cement

Addition of gypsum changes the hydration process of alinite cement: AFT is the prior product to $C_3A{\cdot}CaCl_2{\cdot}10H_2O$ because AFT is more stable in thermodynamics so delays $C_3A{\cdot}CaCl_2{\cdot}10H_2O$ formation (Richarty 1969). Rapid hydration of alinite increases Ca^{2+} in liquid phase, which retards the hydration of ferrite phase. In other hand, the raise of Cl^- concentration accelerates β-C_2S hydration producing additional $Ca(OH)_2$ (Ramachandran 1981). $C_{11}A_7{\cdot}CaCl_2$ hydrates to form $C_3A{\cdot}CaCl_2{\cdot}10H_2O$ which fixes some Cl^- coming from alinite hydration. Moreover, EDAX evidence shows that CSH gel may fix about 3.5% Cl^-.

By SEM analysis on cement pastes hydrated for 3 days, CSH gel is recognized around unhydrated minerals and on the hollow part of the crystal (Fig 6), Ettringite shaped as willow leaves is observed in the intervals of other crystals (Fig 7). CSH gel on alinite matrix and $C_3A{\cdot}CaCl_2{\cdot}10H_2O$ crisscross each other and become the inter growth (Fig 8). The reason to form such a structure is that Cl^- diffuse but of CSH gel and forms Friedel' s salt with aluminate on the surface of CSH gel. Such a crisscross and intergrowth structure can contribute an excellent strength to alinite cement, e.g. the compressive strength of alinite cement after 3 days is as high as 49.5 MPa (Table 3).

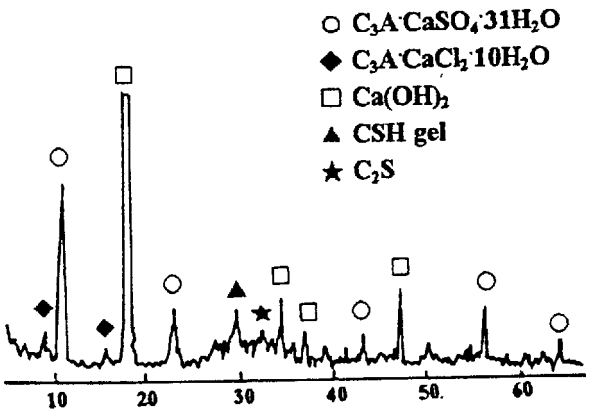

Fig 5 XRD spectrogram of alinite cement for 28 day

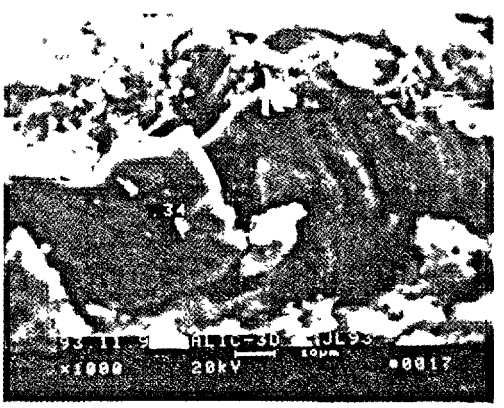

Fig 6 CSH, AFt as well as unhydrated crystals

Table 3 Compressive strength of alinite cement and the minerals containing Cl^- (MPa)

	W / C	3 day	7 day	28 day
Alinite Cement	0.25	49.5	57.1	69.3
Alinite	0.25	42.3	58.9	65.4
$C_{11}A_7.CaCl_2$	0.36	48.2	53.2	64 2

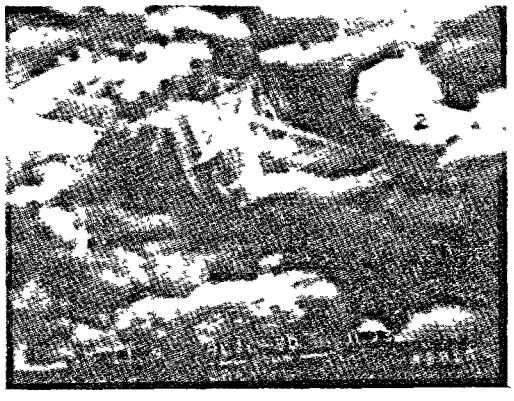

Fig 7 AFt crystals shaped as willow leaves



Fig 8 Intergrowth of CSH and $C_3A\,CaCl_2\,10H_2O$

CONCLUSION

During alinite cement hydration Cl^- combines with aluminate phase to form $C_3A\,CaCl_2\,10H_2O$ which brings out much lower level of free Cl^- in the hydrates of alinite cement than on alinite hydrates.

phases containing Cl^- may reach quite a high hydration extent in early ages and W/C does not markedly affect early hydration of alinite.

The main hydrates of alinite cement are $Ca(OH)_2$, $C_3A\,CaSO_4\,31H_2O$, $C_3A\,CaCl_2\,10H_2O$, CSH gel, ferrite phase as well as a little C_3AH_6 and CAH_{10}.

Cl^- releases out from CSH gel and combines with aluminate on the surface of CSH to form a crisscross and intergrowth constructure with Friedel' s salt, which leads to an excellent strength of hardened cement pastes.

REFERENCES

Boikva, A.I., Grish.L.V., Domansky.A.I., "Hydration Activity of Chlorine-containing Phases" 8th International Congress on the Chemistry of Cement, Theme.2, Vol. III, Paris, 1986, pp.271.

Ftikos, Ch., Georgiades.A., Philippou.Th., " Preparaton and Hydration Study of Alinite Cement " , Cement and Concrete Research, Vol. 21, No.6, 1991, pp.1129-1136 .

Ramachandran, V.S., Fedman, R.F., Beaudoin, J.J., "Concrete science", Chapter 4, Heyden & Son Ltd .,1981.

Richarty, Von.V., "The Combining of Chloride in the Hardening of Cement", Zement-Kalk-Gips,Vol. 22, No.10, 1969, pp.447-456 .

Kn a. 2 5. JAN. 2001 d o k 31799 2ii031 8 pp

RATE OF ETTRINGITE FORMATION FROM CALCIUM ALUMINOFERRITE HYDRATION

CHEN Yimin and SHI Liping, China Building Materials Academy, Beijing 100024, China

ABSTRACT Ettringite formation from hydration of the mixtures with mole ratio of $CaSO_4 2H_2O$ / C_4AF or C_6AF_2 from 1:3 to 4:1 is studied. Before exhaustion of gypsum the hydrates are AFt with Fe^{3+}, $Fe(OH)_3$ gel with Ca^{2+} and somewhat $Ca(OH)_2$. The first and main DTG peak of AFt dehydrates $26H_2O$ corresponding to its constitutional formula. The hydration equations are deduced and their rates are illustrated, which depends on Al / Fe and is not affected by the amount of gypsum but is retarded by lime.

Key–words: Ettrigite, Aluminoferrite, Hydration

INTRODUCTION

Calcium aluminoferrite is a solid solution series in which the ratio Al_2O_3 / Fe_2O_3 varies in a large range. A typical composition in cement clinker is C_4AF and in some cases it may be C_6AF_2 or C_6A_2F. It is well known (Taylor, 1990) that the first crystalline product of ferrite phase hydration in the presence of $CaSO_4$ is AFt containing Fe^{3+} and later is replaced by AFm. The rate of hydration reaction of the ferrite phaes decreases with the Fe / Al ratio in it and is retarded by CH. Metha (1973a,b) attributed the retardation to forming a fine AFt crystal covering on the unhydrated particles. Fukuhara et al (1981) concluded that the AFt phase formed from C_4AF in pastes at 20℃ had an Al / Fe ratio of about 3 and postulated that FH_3 was also formed. Brown (1987) indicated that the initial AFt phase made form C_4AF contains little or no Fe^{3+} and an iron oxide gel containing some Ca^{2+} is formed by C_4AF hydration in the presence of gypsum. The later products are similar to that introduced by Fukuhara et al(1981). Xi (1992) synthesised ettringite solid solutions with 0–100% substitution of Fe_2O_3 for Al_2O_3 in special conditions.

EXPERIMENTAL

C_4AF and C_6AF_2 were synthesized at 1380℃ and 1280℃, respectively, from chemical agents and ground into the size listed in Table 1. Their average diameters are 21.7μm and 21.4μm, respectively. These ferrite phases were mixed with $CaSO_4 2H_2O$ and CaO according to the ratio listed in Table 2 and then added with distilled water. Water / solid is 0.5 for most samples and water / $CaSO_4 2H_2O$ is 1.5～1.3 for the samples in which $CaSO_4 2H_2O$ / ferrite is 3 / 1 or 4 / 1 in order to meet the needs of forming AFt.

Table 1. Partical size distribution of C_4AF and C_6AF_2 (wt%)

Diameter(μm)	<1	<1.5	<2	<3	<4	<6	<8	<12	<16	<24	<32	<48
C_4AF	3.8	6.3	8.1	8.1	8.1	8.1	13.5	19.9	29.1	58.2	69.3	100
C_6AF_2	3.1	5.4	8.8	8.8	8.8	8.8	8.9	10.8	24.6	62.5	80.9	100

Table 2. Mole ratio in samples

No.	C4-1	C4-2	C4-3	C4-4	C4-5	C4-6	C4-9	C4-12	C4-30	C4-60	C4-90	C4-120
C_4AF	3	3	3	3	3	3	3	3	1	1	1	1
$CaSO_4 \cdot 2H_2O$	1	2	3	4	5	6	9	12	1	2	3	4
CaO	–	–	–	–	–	–	–	–	0.5	0.5	0.5	0.5
No.	C6-1	C6-2	C6-3	C6-6	C6-9	C6-12	C6-30	C6-60	C6-90	C6-120		
C_6AF_2	3	3	3	3	3	3	1	1	1	1		
$CaSO_4 \cdot 2H_2O$	1	2	3	6	9	12	1	2	3	4		
CaO	–	–	–	–	–	–	0.5	0.5	0.5	0.5		

Samples were cured at 25℃ for various periods and then ground in large amount of ethanol and dryed in vacuum. Determination is made by DUPONT 1090 Thermal Analyser for TG and DTG, Regago D_{max}-ⅢA X-ray Diffractor for XRD. A part of samples were obeserved by SEM and EDAX to analyse the composition of AFt.

RESULTS AND DISCUSSION

AFt formation from C_4AF hydration

Hydration products

Fig.1 and Fig.2 give DTG curves and XRD spectrograms, respectively, of some hydrated samples. On DTG curves, the temperature of main peaks of AFt, $CaSO_4 2H_2O$, AFm, $Fe(OH)_3$ gel is 100–140℃ , 150–160℃ , 180–200℃ , and 280–300℃ , respectively, in which the range of peak temperature is due to various contents of phases. In fact the main peak of AFt usually starts below 100℃ and ends at higher than 200℃ and its minor peaks locate at much higher temperature. So the main peaks of gypsum and $Fe(OH)_3$ gel always contain some water of AFt.

It is obvious that the products of C_4AF hydration in the presence of gypsum are AFt, which transforms to AFm after exhaustion of gypsum in the samples with raw $CaSO_4 2H_2O / C_4AF \leqslant 3$, and a $Fe(OH)_3$ gel phase. In the sample C4-12, AFt does not increase any longer after 21 days but $CaSO_4 2H_2O$ always exists and no any AFm appears, which means that C_4AF has been used up and the amount of $CaSO_4 2H_2O$ in the raw mixture is somewhat higher than that needed by AFt formation. It can also be believed that less than 25% Al_2O_3 in AFt is replaced by Fe_2O_3 and the raw mole ratio of $CaSO_4 2H_2O$ to C_4AF should be near 4 if both of C_4AF and $CaSO_4 2H_2O$ totally hydrates to form AFt.

Fixed water in AFt

Table 3 lists the DTG data at the time when $CaSO_4 2H_2O$ disappears and the main peak of AFt reaches the largest value. The number of fixed water included in the first and main DTG peak of AFt is calculated by:

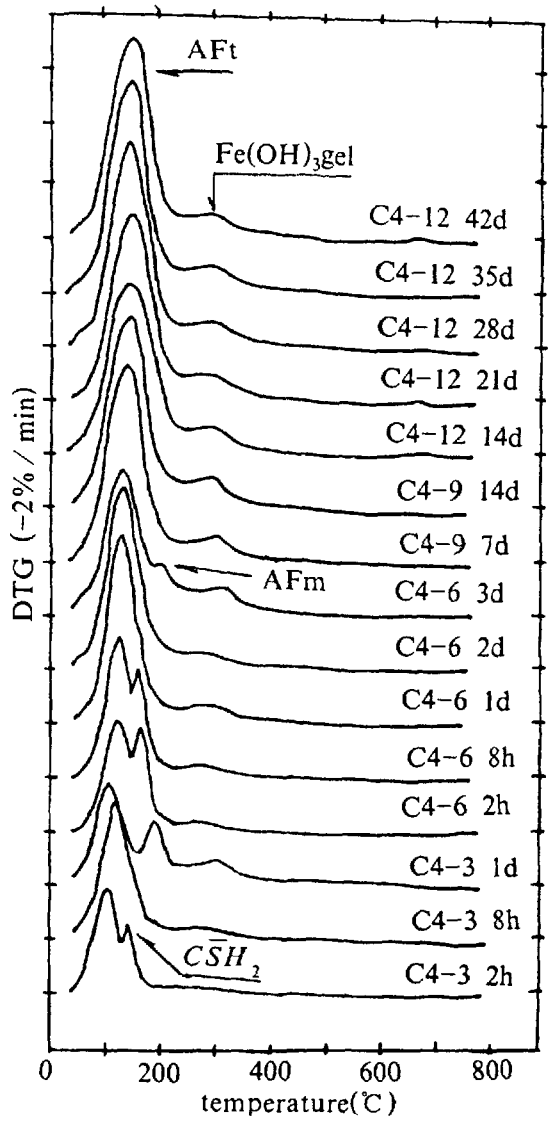

Figure 1 DTG curves of hydration products of C_4AF in the presence of gypsum (20℃ / min)

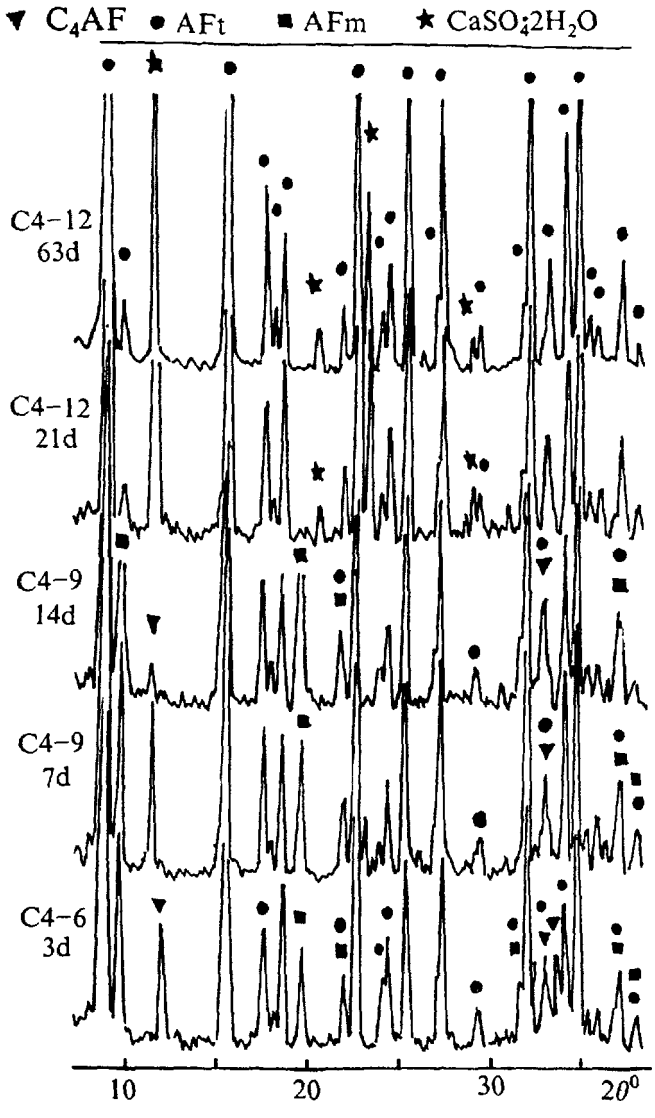

Figure 2 XRD spectrogram of hydration products of C_4AF in the presence of gypsum

$$n = (3 \times M_{CaSO_4} \times W_{H_2O}) / (M_{H_2O} \times W_{CaSO_4}) \quad [1]$$

where M_{CaSO_4} and M_{H_2O} are molecular weight of $CaSO_4$ and H_2O, respectively, and W_{H_2O} is the losing weight of AFt in its first peak and W_{CaSO_4} is the weight of $CaSO_4$ in the sample which can be calculated from both of the raw ratio of $CaSO_4$ to C_4AF and the residue weight of the sample after heating. The average value of n from the results in Table 3 is 25.9. Due to the sampling is not exactly at the time when all AFt forms, so it is reasonable to believe that n = 26 which is identical with the constitu-

tional formula, $[Ca_3(Al,Fe)\cdot(OH)_6\cdot 12H_2O]_2\cdot(SO_4)_3\cdot 2H_2O$ (Taylor, 1990), in which $26H_2O$ are weakly combined in the structure and easily released during heating.

Table 3 Calculation of dehydrated water in the first peak of AFt by DTG

No.	C4-1	C4-2	C4-3	C4-4	C4-4	C4-5	C4-6	C4-9	C4-9
time	1h	3h	8h	12h	1d*	1d	2d	7d	14d*
dehydration of AFt main peak(%)	8.80	14.82	19.41	22.18	19.37	24.87	26.73	31.48	31.72
residue(%)	89.29	80.15	76.34	73.02	72.69	70.46	66.37	60.65	59.67
$CaSO_4$(%)	7.62	12.61	16.69	19.84	19.75	22.41	23.82	27.70	27.23
n	26.2	26.6	26.4	25.3	26.0	25.2	25.4	25.8	26.4

* a little of AFm exists

Rate of AFt formation in samples with different ratio of $CaSO_4 2H_2O$ to C_4AF

The time all gypsum combining into AFt can be deduced from the main dehydration peak of AFt. In Figure 3 solid line is the result of six samples with the ratio of $CaSO_4 2H_2O$ to C_4AF from 1:3 to 2:1 and the points is the result of C4-6 in various periods. They are quite identical with each other, which reveals that there is a definite rate of AFt formation from C_4AF hydration in presence of gypsum which is independent of the ratio of $CaSO_4 2H_2O$ to C_4AF.

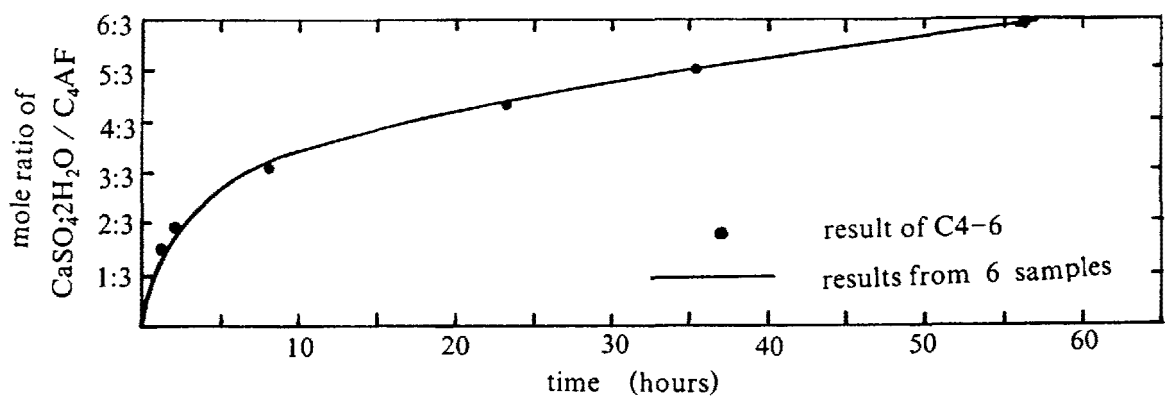

Figure 3 AFt formation rate vs $CaSO_4 2H_2O$ exhaustion time

Substitutional amount of Fe_2O_3 for Al_2O_3 in AFt

Both main dehydration peak of AFt and $CaSO_4 2H_2O$ end at about 210~220℃, in which 1 mol AFt contains 3mol $CaSO_4$ and 26 mol H_2O while 1 mol $CaSO_4 2H_2O$ contains 1mol $CaSO_4$ and 2 mol H_2O. It is not difficult to deduce the following formula:

$$G = \frac{CaSO_4(inAF_t)}{CaSO_4(total)} = \frac{3}{20}\left(\frac{W_{H_2O} \times M_{CaSO_4}}{W_{CaSO_4} \times M_{H_2O}} - 2\right) \qquad [2]$$

where W_{H_2O} is the weight of total water contained in the main peaks of AFt and $CaSO_4 2H_2O$ and W_{CaSO_4} is the weight of total $CaSO_4$ in the sample. G is the percentage of $CaSO_4$ entering AFt of total $CaSO_4$ in the sample.

If there is no Fe_2O_3 in AFt it needs 3 mol $CaSO_4 2H_2O$ for each mole C_4AF to hydrate and form AFt. On the other hand, if Fe_2O_3 is substituted for 25% Al_2O_3 in AFt the G of the sample will be 100% in the end. In fact, after 21 days, 28 days, 35 days and 63 days of hydration the G of C4–12 is always about 93% and less than 94%, which means that about 3.75 mol gypsum is needed for 1mol C_4AF to hydrate and form 1 mol AFt and that about 20 mol% Al_2O_3 in AFt is replaced by Fe_2O_3.

EDAX determination on a lot of points shows that the amount of Al_2O_3 substituted by Fe_2O_3 in AFt is about 18～30mol% and in most of detected points it locates in 20～25 mol% which supports above calculation result. In addition, EDAX shows that in hydration products there is a gel phase made mainly of Fe and small amount of Ca, i.e. $Fe(OH)_3$ gel containing $Ca(OH)_2$.

Chemical equation and reaction rate of C_4AF hydration to form AFt

Based on above experiment result, analysis and calculation, the chemical reaction equation representing C_4AF hydration in the presence of gypsum to form AFt can be put forward as following:

$$4C_4AF+15CaSO_4 2H_2O+140H_2O \rightarrow 5\,[C_3(Al_{0.8}Fe_{0.2})_3CaSO_4 32H_2O] +6Fe(OH)_3gel+Ca(OH)_2gel \quad [3]$$

where $Ca(OH)_2$ gel exists inside $Fe(OH)_3$ gel. The reaction rate determined from all samples is given in Figure 4.

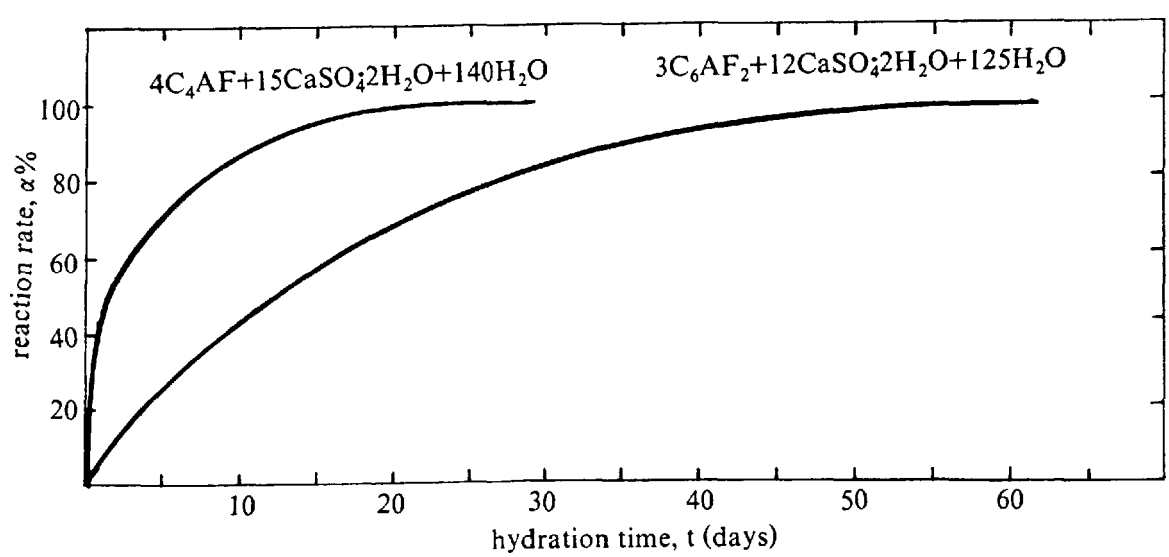

Figure.4 Reaction extent, α, of calcium aluminoferrite hydration to form AFt vs time,t

AFt formation from C_6AF_2 hydration

Figure 5 and Figure 6 present DTG curves and XRD spectrograms of C_6AF_2 hydration products in presence of gypsum, respectively. The process of

C_6AF_2 hydration is similar to that of C_4AF: The products includes AFt containing Fe^{3+} and $Fe(OH)_3$ gel containing Ca^{2+} before gypsum is exhausted and then AFt transforms to AFm. But some differences are recognized by DTG evidence: the gel phase is more in C_6AF_2 hydration products and there is an individual $Ca(OH)_2$ phase which has transformed to $CaCO_3$ during drying treatment. It is obvious that the rate of AFt formation from C_6AF_2 hydration is slower than that from C_4AF.

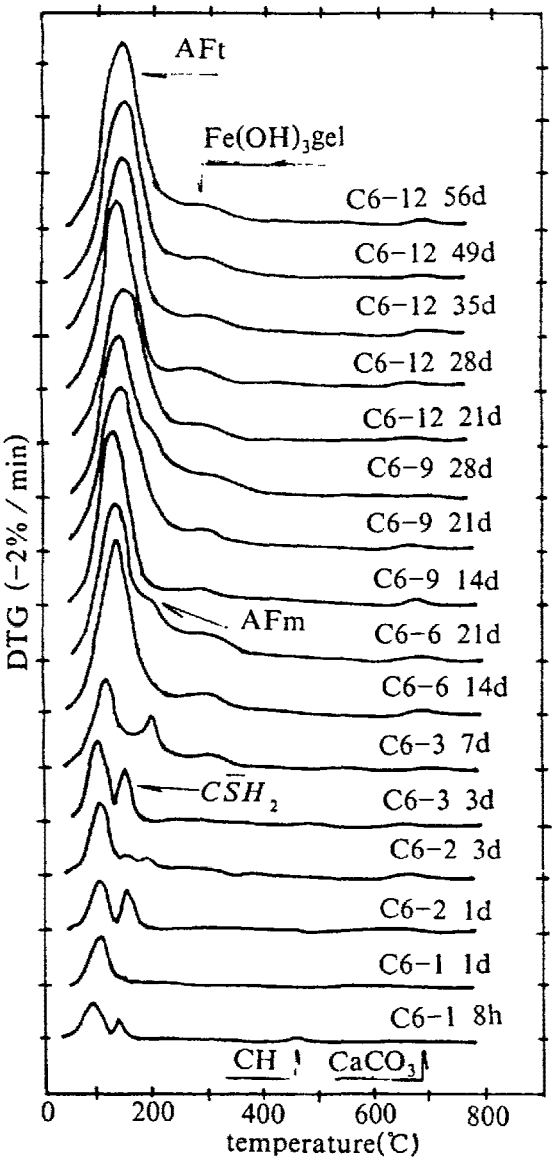

Figure 5 DTG curves of C_6AF_2 hydration products in the presence of gypsum (20℃ / min)

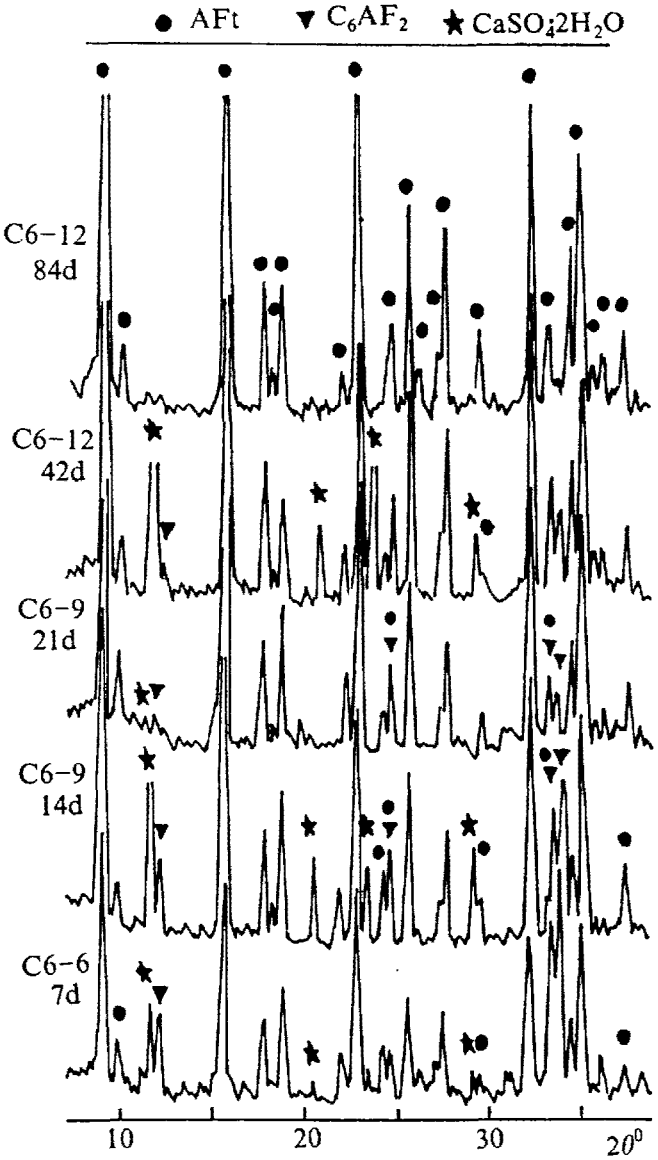

Figure 6 XRD spectrograms of C_6AF_2 hydration products in the presence of gypsum

In sample C6-9 AFm phase appears after 28days. In sample C6-12, after 56 days gypsum disappears, AFt will not increase any more and AFm will not apppear at even

longer time. The value of G calculate from Eq.2 reaches 100%. So the largest mole ratio of $CaSO_4 2H_2O$ to C_6AF_2 for all of them to hydrate and enter into AFt is 4, which means the substitution of Fe_2O_3 for Al_2O_3 in AFt is about 25mol% and is higher than that of $CaSO_4 2H_2O$ to C_4AF. Therefore the reaction equation may be expressed as:

$$3C_6AF_2+12CaSO_4 2H_2O+125H_2O \rightarrow 4[C_3(A_{0.75}F_{0.25})3CaSO_4 32H_2O]+10Fe(OH)_3gel+6Ca(OH)_2gel \quad [4]$$

where both $Fe(OH)_3$ gel and $Ca(OH)_2$ are more than that in Eq.3, which is one of reasons to delay ferrite hydration and AFt formation. The rate of this reaction, determined from all samples, is given in Figure 4.

Effect of CH on AFt formation from ferrite hydration

Figure 7 and Figure 8 give DTG curves of some hydrated samples of C_4AF and C_6AF_2, respectively, in the presence of both gypsum and lime. Comparing these with Figure 2 and Figure 5 introduces that $Ca(OH)_2$ retard AFt formation from ferrite hydration though does not change the products, which may also explain the slower rate of C_6AF_2 hydration than that of C_4AF to some extent.

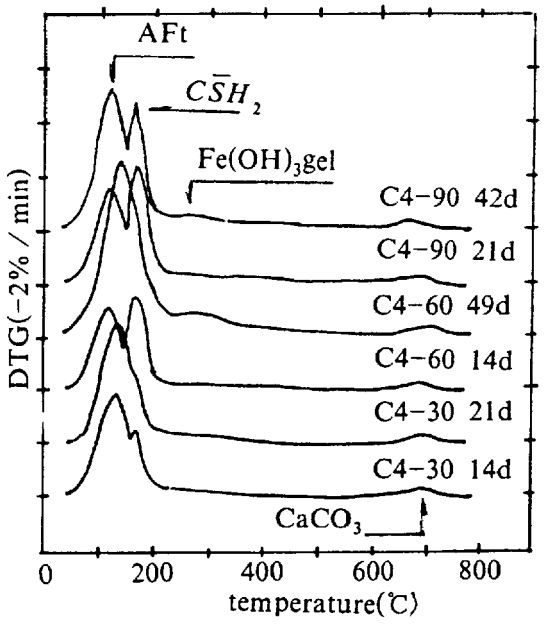

Figure 7. DTG curves of hydration products of C_4AF in presence of gypsum and lime

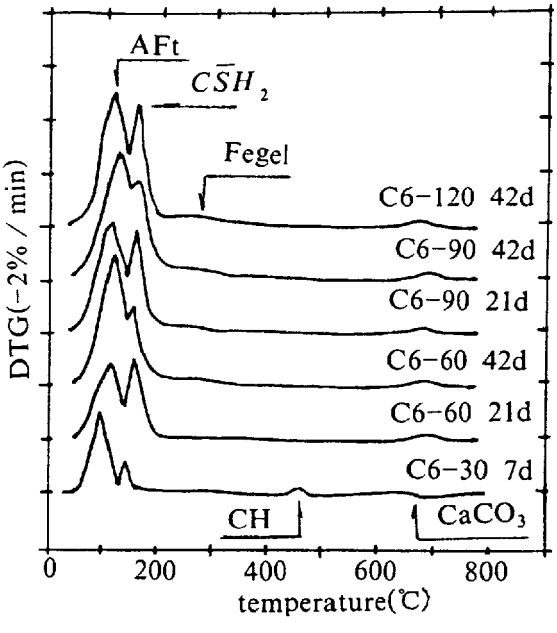

Figure 8. DTG curves of hydration products of C_6AF_2 in presence of gypsum and lime.

CONCLUSION

Products of calcium aluminoferrit hydration in the presence of gypsum include AFt containing Fe^{3+} and $Fe(OH)_3$ gel containing Ca^{2+} and, in the case of C_6AF_2, some $Ca(OH)_2$. After gypsum is used up, AFt will be gradully replaced by AFm.

In DTG curves the main peak of AFt dehydrates 26 H_2O, which corresponds to its constitutional formula, $[Ca_3(Al, Fe)(OH)_6 \cdot 12H_2O]_2(SO_4)_3 \cdot 2H_2O$ in which 26 H_2O are

conbined weakly. Other 5~6 H_2O will be released at higher temperature.

The reaction of ettringite formation from calcium aluminoferrite hydration can be represented by following chemical equations:

$4C_4AF+15CaSO_4{\cdot}2H_2O+140H_2O \rightarrow 5[C_3(A_{0.8}F_{0.2})3CaSO_4{\cdot}32H_2O]+6Fe(OH)_3gel+Ca(OH)_2gel$

$3C_6AF_2+12CaSO_4{\cdot}2H_2O+125H_2O \rightarrow 4[C_3(A_{0.75}F_{0.25})3CaSO_4{\cdot}32H_2O]+10Fe(OH)_3gel+6Ca(OH)_2gel$

As illustrated in Figure 4, the speed of AFt formation from C_4AF hydration is faster than from C_6AF_2, which is caused by the contents of $Fe(OH)_3$ gel and $Ca(OH)_2$ in the products. Under the present conditions in less than 1 month all C_4AF has hydrated and formed AFt but it need about 2 months for C_6AF_2 to totally hydrate. $Ca(OH)_2$ addition will markedly retard the hydration of both C_4AF and C_6AF_2 to form AFt.

REFERENCES

Brown,P.W., "Early hydration of Tetracalcium aluminoferrite in gypsum and lime-gypsum solutions", J.Am. Ceram. Soc., Vol.70, 1987, PP.493-496.

Fukuhara,M.,Goto, S., Asaga. K.,Daimon, M., and Kondo, R., "Mechanisms and Kinetics of C_4AF hydration with gypsum", Cem. Concr. Res., Vol.11, 1981, PP.407-414.

Mehta, P.K., "Effect of Lime on Hydration of Pastes Containing Gypsum and Calcium Aluminate or Sulfoaluminates", J.Am. Ceram. Soc., Vol. 56, 1973, p.315.

Mehta, P.K., "Mechanism of Expansion Associated With Ettrigite Formation', Cem. Concr. Res., Vol.3, 1973, p.1

Taylor, H.F.W., "Cement Chemistry", Academic Press Limited, London, 1990, PP.177-181, PP.196-197.

Xi, Yaozhong, "Fe_2O_3 Solid Solution of Ettrnigite", Proc. 9th Inter. Congr. on Cem. Chem., Vol.Ⅳ, 1992, PP.377-383.

Kn o. 2 5. JAN. 2001 d o k 31795

4 pp

SYNTHESIS AND CHARACTERIZATION OF CO_3 - CONTAINING Ca - Al - Fe - HYDRATES

M. ECKER* and H. PÖLLMANN**
* Bilfinger + Berger Umweltverfahrenstechnik GmbH
Theodor-Heuß-Anlage 12 68165 Mannheim, Germany
** Department of Mineralogy and Geochemistry
University of Halle, Germany

ABSTRACT
The hydration characteristics and properties of new hydrates containing iron and of solid solutions containing iron and aluminum are described. Especially the influence of CO_3^{2-} on formation conditions is investigated. The phase relations, the formation conditions from anhydrous compounds and the properties of the hydrates are given .

Key-Words: AFm phase, Brownmillerite, Carbon dioxide

INTRODUCTION
Calcium aluminate hydrates and calcium aluminoferrate hydrates have a great significance on the formation and the stability of concrete and on the immobilisation of pollutants. The hydration of aluminate phases under the influence of various anions has already been widely investigated and different hydrates are well known. Iron containing phases with varying anions, however, are only little known yet. For a better understanding of the meaning of AFm phases in cement chemistry and environmental chemistry, iron containig AFm phases vere investigated. Due to the importance of carbonate to all technical processes, the investigations applied especially to CO_3^{2-} containing phases.

EXPERIMENTAL
The synthesis were made by mixing the hydroxides of aluminum and iron with calcium oxide and sodium carbonate in excess water (saturated portlandite solution). The hydroxides were always freshly precipitated from solutions of aluminum chloride or iron chloride with an ammonia solution and afterwards carefully washed with hot water. For synthesizing calcium aluminoferrate hydrates, aluminum and iron hydroxide were always precipitated together. Additional synthesis were made by mixing calcium aluminoferrates of the Brownmillerite type with calcium oxide and sodium carbonate in excess water. The reactions were carried out in 50 ml high density polyethylene bottles. The reaction times lasted from 6 weeks to 6 month. The progress of the reaction of all samples could be observed at all samples by turning the colour from red to colourless. All synthesis were carried out at room temperature.

The originated phases were investigated by x-ray powder diffraction, scanning electron microscopy, thermal analysis and infrared spectroscopy. X-ray patterns of dry samples were recorded with a Siemens diffractometer D 5000 and patterns of wet samples with a Phillips diffractometer and a special climate camera. Some samples were additionally investigated by high temperature x-ray diffraction. The wet samples were dried at 35 % rel. humidity over a saturated solution of calcium chloride. All samples were carefully treated, wet samples were only handled in a glove box with CO_2-free atmosphere.

RESULTS AND DISCUSSION

Pure phases

For this investigation it was necessary, that the following pure phases had been characterized:
Monohydroxide $3CaO{\cdot}Al_2O_3{\cdot}Ca(OH)_2{\cdot}nH_2O$
Monocarbonate $3CaO{\cdot}Al_2O_3{\cdot}CaCO_3{\cdot}11H_2O$
Iron monohydroxide $`3CaO{\cdot}Fe_2O_3{\cdot}Ca(OH)_2{\cdot}nH_2O´$
Iron monocarbonate $3CaO{\cdot}Fe_2O_3{\cdot}CaCO_3{\cdot}12H_2O$
Monohydroxide and monocarbonate were already investigated by Fischer & Kuzel (1982) and Pöllmann (1984) and are well known. Iron monohydroxide is described by Negro & Stafferi (1979) and Rogers & Aldridge (1977). Own investigations show, that a phase with the composition $3CaO{\cdot}Fe_2O_3{\cdot}Ca(OH)_2{\cdot}nH_2O$ is not stable at room temperature. Iron monocarbonate was synthesized and investigated.

Iron monocarbonate

The reaction time for iron monocarbonate took 6 month. After that time in the scanning electron microscope hexagonal platy crystals with about 1 to 5 µm in diameter could be observed. The chemical analysis of the dried sample is in accordance with the formula $3CaO{\cdot}Fe_2O_3{\cdot}CaCO_3{\cdot}12H_2O$. The wet and the dried sample show the same lattice parameters: a_o = 591,7 pm; c_o = 4767,9 pm; SG: $R\bar{3}\,c$

Thermal analysis and high temperature x-ray diffraction show, that at temperatures higher then 135°C the main layer starts dehydrating and the structure gets destroyed. More particular data will be given in an extra paper.

Pseudobinary systems

The system $3CaO{\cdot}Al_2O_3{\cdot}Ca(OH)_2{\cdot}nH_2O$ - $`3CaO{\cdot}Fe_2O_3{\cdot}Ca(OH)_2{\cdot}nH_2O´$,
Synthesis with the following compositions were made:
$4CaO + (2x)Al(OH)_3 + (2\text{-}2x)Fe(OH)_3;\ 0 \le x \le 1$
No other AFm phase then $3CaO{\cdot}Al_2O_3{\cdot}Ca(OH)_2{\cdot}nH_2O$ was formed. In iron containing samples portlandite and iron hydroxide were always present.

The system $`3CaO{\cdot}Fe_2O_3{\cdot}Ca(OH)_2{\cdot}nH_2O´$ - $3CaO{\cdot}Fe_2O_3{\cdot}CaCO_3{\cdot}12H_2O$
The following synthesis were made:
$4CaO + 2Fe(OH)_3 + (x)Na_2CO_3;\ 0 \le x \le 1$
The only stable AFm phase at room temperature is $3CaO{\cdot}Fe_2O_3{\cdot}CaCO_3{\cdot}12H_2O$. In samples with a molar ratio Fe_2O_3 / CO_2 < 1 iron hydroxide and portlandite could always be found.

The system $3CaO{\cdot}Al_2O_3{\cdot}CaCO_3{\cdot}11H_2O$ - $3CaO{\cdot}Fe_2O_3{\cdot}CaCO_3{\cdot}12H_2O$,
For the investigation synthesis with the following compositions were made:
$4CaO + (2x)Al(OH)_3 + (2\text{-}2x)Fe(OH)_3 + Na_2CO_3;\ 0 \le x \le 1$
Samples containing both aluminum and iron are belonging to the solid solution series
$3CaO{\cdot}(x)Al_2O_3{\cdot}(1\text{-}x)Fe_2O_3{\cdot}CaCO_3{\cdot}nH_2O;\ 0 < x < 1$
In contrast to the pure phases monocarbonate and iron monocarbonate, the solid solutions are forming two different hydrates at room temperature:

A rhombohedral phase containig 12 H_2O per formula is stable at 100 % rel. humidity. A triclinic phase containing 11 H_2O is formed by drying at 35 % rel. humidity. The phase transformation is irreversible. Figs 1 and 2 show the lattice parameters of the rhombohedral phase and the d (0 0 1)-spacings of the triclinic phase.

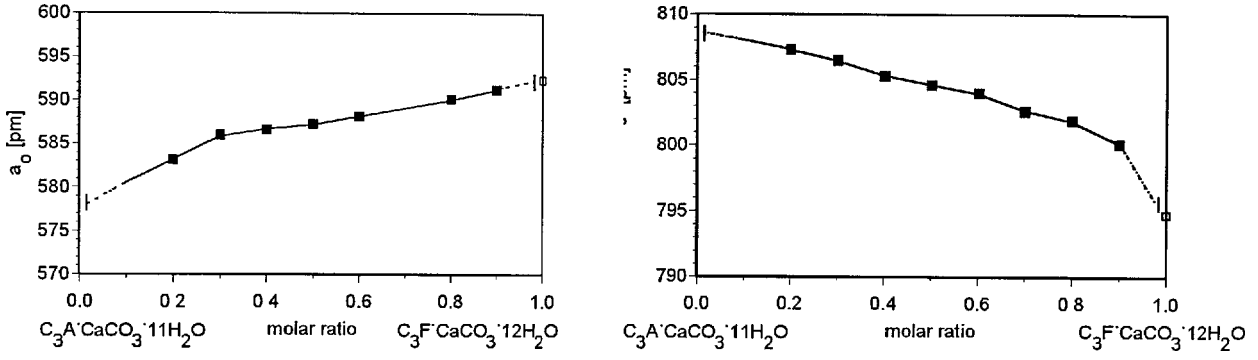

Figure 1: Lattice parameters of the rhombohedral phase in the system

$3CaO{\cdot}Al_2O_3{\cdot}CaCO_3{\cdot}11H_2O$ - $3CaO{\cdot}Fe_2O_3{\cdot}CaCO_3{\cdot}12H_2O$

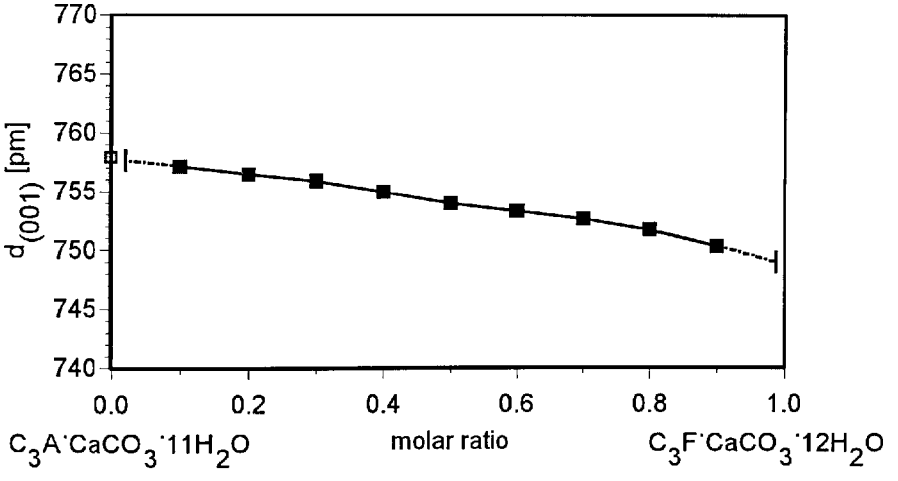

Figure 2: d (0 0 1)-spacing of the triclinic phase in the system

$3CaO{\cdot}Al_2O_3{\cdot}CaCO_3{\cdot}11H_2O$ - $3CaO{\cdot}Fe_2O_3{\cdot}CaCO_3{\cdot}12H_2O$

Pseudoternary system

For investigations in the pseudoternary system $3CaO{\cdot}Al_2O_3{\cdot}Ca(OH)_2{\cdot}nH_2O$ - `$3CaO{\cdot}Fe_2O_3{\cdot}Ca(OH)_2{\cdot}nH_2O$´ - $CaO{\cdot}Al_2O_3{\cdot}CaCO_3{\cdot}11H_2O$ - $3CaO{\cdot}Fe_2O_3{\cdot}CaCO_3{\cdot}12H_2O$ the following synthesis were made:

$4CaO + (2x)Al(OH)_3 + (2-2x)Fe(OH)_3 + (y)Na_2CO_3$; $0 \leq x \leq 1$; $0 \leq y \leq 1$

Additionally to the upon described AFm phases, in the pseudoternary system one additional solid solution series appeared:

$3CaO{\cdot}(x)Al_2O_3{\cdot}(1-x)Fe_2O_3{\cdot}0.5CaCO_3{\cdot}0.5Ca(OH)_2{\cdot}11.5H_2O$, $0 < x \leq 1$

Besides these phases no further AFm phases are stable in the pseudoternary system at room temperature. Fig 3 shows the d-spacings of the investigated AFm phases.

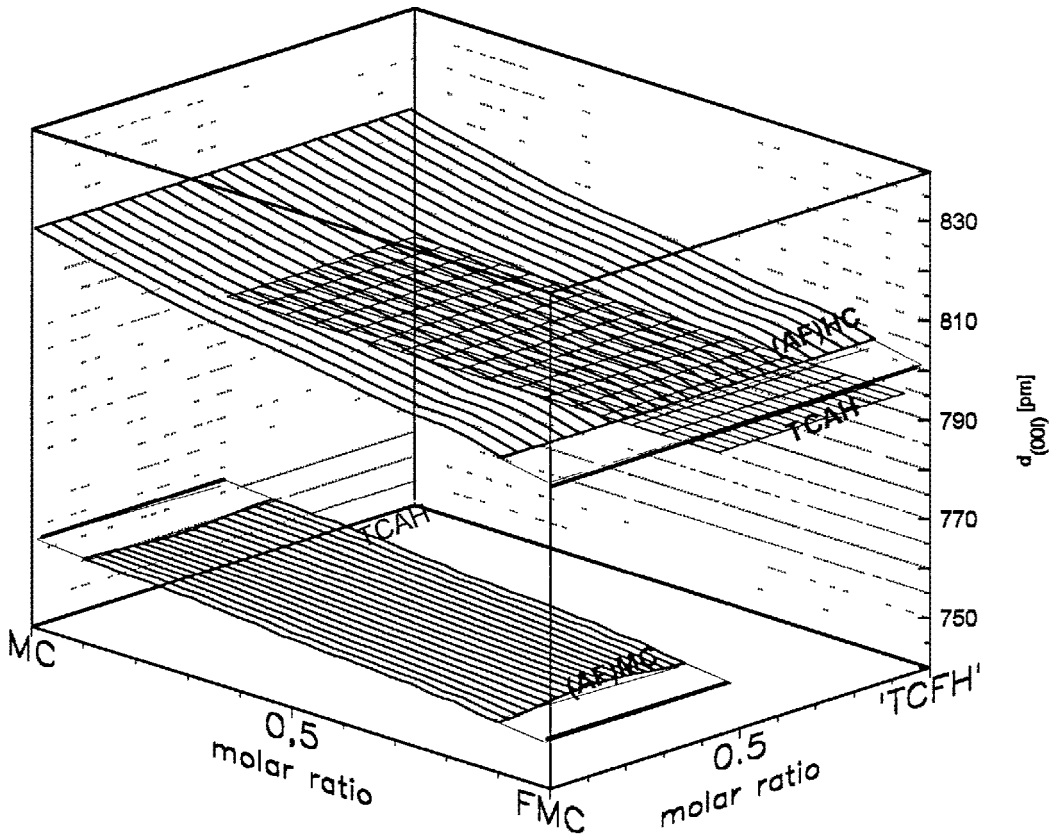

Figure 3: d-spacings of AFm phases in the system $3CaO\ Al_2O_3 \cdot Ca(OH)_2\ nH_2O$ - $`3CaO \cdot Fe_2O_3 \cdot Ca(OH)_2 \cdot nH_2O´$ - $CaO \cdot Al_2O_3\ CaCO_3\ 11H_2O$ - $3CaO \cdot Fe_2O_3 \cdot CaCO_3\ 12H_2O$ at room temperature and 35 % rel. humidity

MC:	$3CaO\ Al_2O_3\ CaCO_3 \cdot 11H_2O$
FMC:	$3CaO \cdot Fe_2O_3 \cdot CaCO_3 \cdot 12H_2O$
TCAH:	$3CaO \cdot Al_2O_3\ Ca(OH)_2\ 12H_2O$
`TCFH´:	$`3CaO\ Fe_2O_3\ Ca(OH)_2 \cdot nH_2O´$
(AF)MC:	solid solutions $3CaO\ (Al,Fe)_2O_3\ CaCO_3\ 11H_2O$
(AF)HC:	solid solutions $3CaO \cdot (Al,Fe)_2O_3 \cdot 0{,}5Ca(OH)_2\ 0{,}5CaCO_3 \cdot 11{,}5H_2O$

REFERENCES

Fischer, R. & Kuzel, H -J : Reinvestigation of the system $C_4A\ nH_2O$-$C_4A\ CO_2\ nH_2O$. - Cem Concr. Res. 12, 1982, pp. 517-526.

Negro, A. & Stafferi, L.: Über die Hydratation der Calciumferrite und Calciumaluminatferrite. - ZKG 2, 1979, p. 83.

Pöllmann, H.. Die Kristallchemie der Neubildungen bei Einwirkung von Schadstoffen auf hydraulische Bindemittel. - Dissertation, Erlangen 1984

Rogers, D.E. & Aldridge, L.P.: Hydrates of Calciumferrites and Calciumaluminoferrites. - Cem. Concr. Res. 7, 1977, pp. 399-410.

Kn o. 25. JAN. 2001 d o k 31796

2ii033
4 pp

ALKALINE ALUMINATE BINDERS

Pavel V KRIVENKO
Ekaterina K PUSHKARYEVA
Sergey V SHAPET'KO
Scientific Research Institute on Binders and Materials, Kiev, Ukraine

ABSTRACT Physico-chemical regularities of manufacturing alkaline aluminate binding systems with the use of aluminate raw materials like wastes and by-products, spinel-containing additives and sodium soluble glass with silicate modulus 1-2.8 have been revealed. Principles of synthesis of a paste made with the above binders featuring stable thermo-mechanical characteristics within a wide temperature range have been demonstrated and discussed.

Key-words: high alumina cement, soluble glass, srtrength development, hydration

INTRODUCTION

Strength of a paste and concrete composed of high alumina cements is known to be a function of temperature (Kravchenko, 1960) and sharply declines while transformation of hydroaluminates from hexagonal into cubic syngonia. Is found to be possible to regulate the ratio between hydroaluminates in the hardening product by changing pH of the mixture (Talaber J, 1976). According to known works (Zaldat et al, 1991), while adding to calcium aluminates the solutions with increased pH, the hydration processes accelerate and the processes of transformation of hexagonal hydroaluminates of calcium into cubic ones (C_3AH_6) intensify resulting in losses of strength. The possibility of manufacturing concrete having stable thermo-mechanical characteristics from aluminates of calcium and sodium metasilicate has been proved by Krivenko et al (1984). Other researchers (Berger et al; 1973) demonstrate that increasing pH of the solution suppresses hydrolysis and inhibits velocity with which a mineral CA hydrates, as well as results in dissolution of C_3AH_6 with the formation of hexagonal hydroaluminates of calcium. Thus, a question of how the alkaline solutions affect the intensity and directions of flow of hydration processes, synthesis of strength of a cement paste made with calcium aluminates remained open and initiated this study. Analyzing physico-chemical regularities of manufacture of concrete with stable thermo-mechanical characteristics from calcium aluminates revealed by Krivenko et al (1984), as well as the works in the field of regulation of structure and properties of a fire-resistant stone based on alkaline binding systems (Pushkaryeva, 1995), allowed to assume the possibility of producing alkaline aluminate binders (AAB) featuring enhanced thermo-mechanical characteristics within a wide temperature range by lowering intensity of the formation of calcium hydroaluminates while hardening in the presence of alkali metal compounds. This lead to synthesis of thermostable compounds to provide such structure of a material that changes its porosity insignificantly under action of thermal loads.

MATERIALS AND TESTING TECHNIQUE

Minerals $CaO{\cdot}Al_2O_3$ (CA), $CaO{\cdot}2Al_2O_3$ (CA_2) and $MgO{\cdot}Cr_2O_3$ (MCr) have been synthesized from chemically pure substances such as $CaCO_3$, Al_2O_3, MgO, and Cr_2O_3 that were taken in stoichiometric ratios. Used in the experiments were: a top quality (extra pure) high alumina cement with 72 % Al_2O_3 (HAC), standard high alumina cement with 39 % Al_2O_3 (AC) as an aluminate constituent of AAB, waste from production of chromo-magnesium refractories as a

fine additive, and sodium soluble glass with silicate modulus M_s=1.0-2.8 and density ρ=1100-1300 kg/m^3 as an alkaline component. Physico-chemical processes of hydration and dehydration were investigated with the use of a set of methods such as XRD, DTA, IR spectroscopy.

DISCUSSION OF RESULTS

A model system CA-CA_2-MCr-Na_2O·nSiO_2 synthesized from chemically pure compounds was studied to reveal a principal possibility of producing the AAB.

To determine the influence of such factors as silicate modulus and density of soluble glass, mineralogical composition of cement, curing conditions on strength characteristics the investigated field was restricted by vertexes of a triangle with the following content of minerals: V_1=7%CA + 43%CA_2 + 50% MCr; V_2=10%CA + 90%CA_2; V_3=45%CA + 45% CA_2 + 10% MCr. The investigations were directed by a specially synthesized MTQ-plan (in cooperation with Professor V. Voznesenskiy, Odessa, Ukraine), in which a mix triangle was shifted along a square indicating variations in modulus of soluble glass M_s =1-2 and density ρ of the solution from 1200 to 1300 kg/m^3 (Figure 1).

It was established that the increase in density of water glass solution always results in strength gain. The paste characteristic of the highest strength is formed when the solutions of low-modulus soluble glass (M_s=1.0-1.5) are added to the alumina binders with the increased content of mineral CA_2. When the use is made of alumina binders composed predominantly of mineral CA, the highest strength cement stone is formed with sodium soluble glass having Ms=2.0-2.8. Increasing the silucate modulus of soluble glass results in strength decline. The introduction into a binder composition of chromo-magnesium spinel in a quantity of 25-45 % promotes the enhancement of residual strength of the cement stone after firing to reach a level exceeding 70% of its initial strength.

The influence of change in silicate modulus and density of soluble glass is found affect 1.5-2 times stronger the strength of AAB as compared with that of minaral composition and curing conditions (normal hardening or steam curing).

The AAB made with AC (composed mainly of CA) and HAC (composed mainly of CA_2) were found to have quick strength gain at first stages of hardening and considerable retardation of strength gain with time as compared with the cements in which water was used as an admixture (Table 1).

The study's results indicate that an increased quantity of a gel phase of gibbsite composition is formed during hydration products of the AAB and the formation of low basic hydroaluminates of calcium occurs with a slower rate. The strength gain observed while drying the specimens (up to 70-120 MPa) may be attributed to a densification of the structure and crystallization of gibbsite what is accompanied by decline of the intensity of destructive phenomena associated with transformation of the hexagonal hydroaluminates of calcium into cubic ones (C_3AH_6).

Indicated in the model system CA-CA_2-MCr-Na_2O nSiO_2 insignificant variations in strength of the AAB at varying their mineralogical composition allows to replace up to 50 % of AC or cements hydrated with water. By the data of XRD, the interaction of sodium silicates with calcium aluminates occurs at T= 800-1000^{0}C with the formation of gehlenite, and the reaction

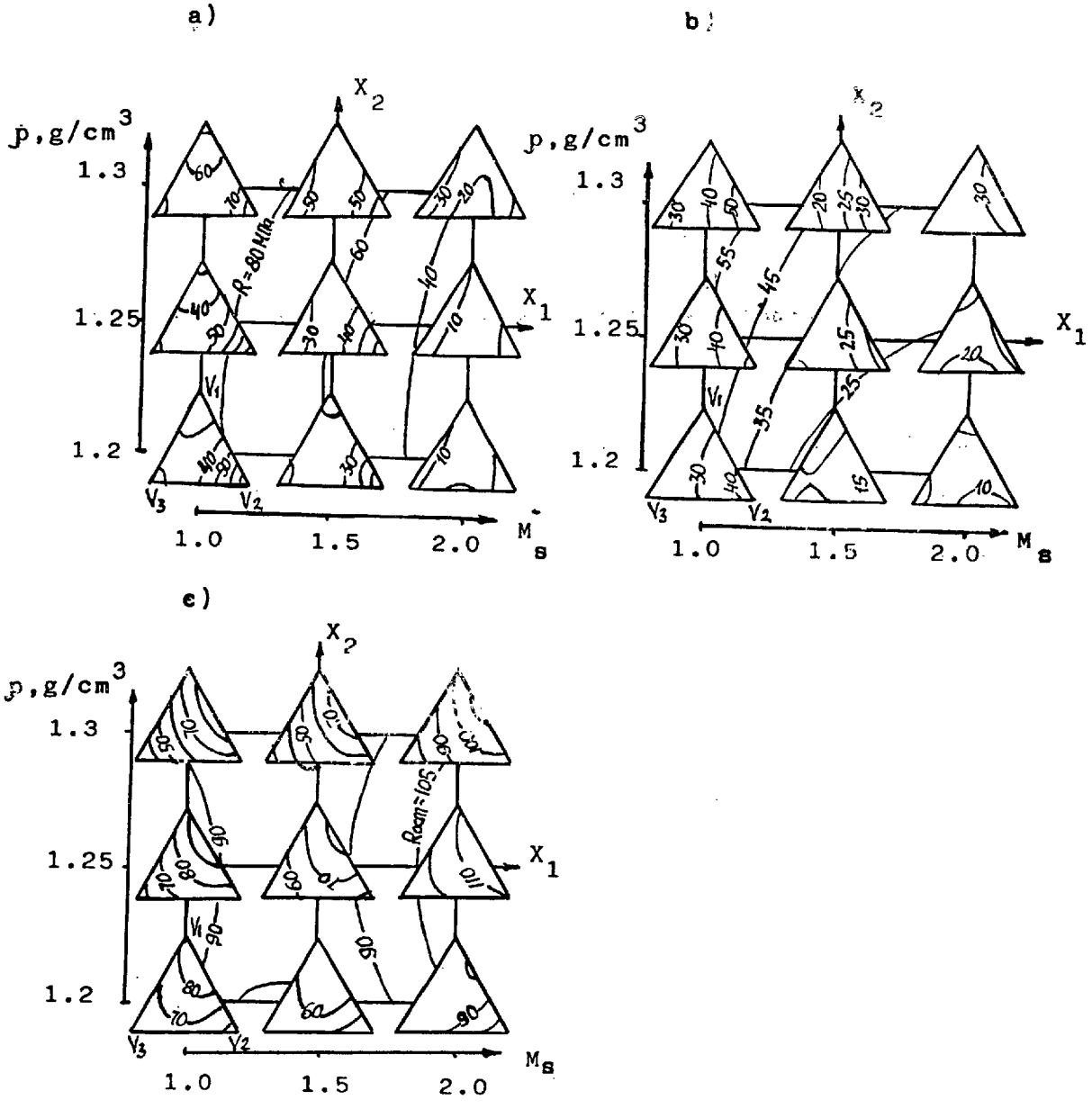

Figure 1. Isoparametric diagrams of variations in compressive strength (a, b) and residual strength after firing (c) for the binders of a system CA-CA_2-MCr-Na_2O nSiO_2 mH_2O after a) 7 days of curing; b) firing at T=800°C.

Table 1. Initial setting time and strength VS silicate modulus of water glass.

Type of cement	Silicate modulus	Initial setting	Compressive strength (MPa) after, days				
			1	3	7	14	28
High alumina cement	1.0	6 min	21.8	22.5	38.3	51.5	74.5
	1.5	9 min.	19.0	24.3	30.0	35.5	48.3
	2.0	3 hrs - 15 min	19.5	22.5	23.5	25.5	34.3
	2.8	more than 8 hrs	0.5	1.5	1.5	2.0	2.5
	water	3 hrs - 13 min.	24.5	54.5	62.8	66.5	96.3
Alumina cement	1.5*	momentary	-	-	-	-	-
	2.0*	15 min.	40.0	47.2	52.1	-	-
	2.8*	32 min.	38.9	47.0	53.4	-	-
	water	45 min.	22.7	43.2	58.1	-	-

NOTE: * 1.5 % Na_3PO_4 (by a cement mass) was introduced as a retarder.

HAC with a finely dispersed additive from used chromo-magnesium refractories. The developed binder compositions differ with a smooth flow of the processes of strength loss while firing, the residual strength enhances with increase of silicate modulus of soluble glass and reaches 60- 100 % of initial strength, exceeding considerably that of traditional aluminate cements hydrated with water. By the data of XRD, the interaction of sodium silicates with calcium aluminates occurs at T=800-1000°C with formation of gehlenite, and reaction between aluminate constituent of cement and chromo-magnesium additive resulted in formation of the alumo-magnesium spinel - $MgAl_2O_4$.These variations in mineralogical composition enhance stability of the AAB while heating.

Basing on the binders developed with a finely dispersed additive and chamotte aggregate the formulations of heat-resistant concretes have been developed. These concretes are characteristic of strength after drying 50-70 MPa, after firing 35-58 Mpa, thermo-resistance- 42 (on HAC) and 60 (on AC) water-heat cycles (12-15 cycles of conventional aluminate cement-based concretes).

CONCLUSIONS

1. The processes of formation of a heat-resistant paste based on AAB have been studied and the formulations to provide stable strength characteristics within a wide range of temperatures have been developed. The main factors determining strength of the paste have been revealed, namely: characteristics of soluble glass, curing conditions and basicity of calcium aluminates.
2. The hydration products of AAB are characteristic of the increased content of a gel phase of gibbsite composition and an insignificant content of hexagonal hydroaluminates of calcium thus providing lack of strength losses while drying and smooth course of dehydration processes while firing without deterioration of the cement structure.
3. A finely dispersed chromo-magnesium additive, not changing the composition of both hydration and dehydration products, while firing at a temperature exceeding 1000°C, interacts with an aluminate constituent of the cement to form an alumo-magnesium spinel $MgAl_2O_4$ providing stability of structure of the fired paste and concrete. By introdusing a spinel-containing additive in a quantity 10-50 % by cement mass the concretes featuring strength 56-81 MPa, residual strength after firing at T=800-1000°C- 60-80%, and thermo-resistance- 60 water-heat cycles may be produced.

REFERENCES

Bergen, A.S., Kotsupailo, N.P. and Pushnyakova, V.A, "About Metastable Solubility of Tricalcium Hydroaluminate in the Solutions of Alkali Metal Hydroxides, Izvestia, SO of Academy of Sciences of USSR, Chemical Sciences Series, 1973, No.9, Issue.4, pp.110-115.

Kravchenko, I.V., High Alumina Cement, Gosstroiizdat Publishers, Moscow, 1960, 175 pp.

Krivenko, P.V., Pushkaryeva, E.K. and Chirkova, V.V., "Studies of the Hydration Processes of Calcium Aluminates in the Presence of Alkali Metal Compounds", Izvestia VUZov, Chemistry and Chemical Technology Series, 1984, No.10, pp. 1204-1208.

Pushkaryeva, E.K., "Heat-resistant Materials Based on Alkaline Binding Systems", DrSc Thesis, Khar'kov, Ukraine, 1995, 32 pp.

Talaber, J., "High Alumina Cements", Proc. 6 Int. Congress on the Chemistry of Cement, Vol.3, 1976, pp.124-133.

Zaldat, I.G., Kukui, S.M. and Talisman, I.S., "The Hydration and Hardening of Aluminates of Calcium and High Alumina Cements in the Presence of Alkalies", Tsement Journal, Nos.3-4, 1991, pp.40-43.

2ii034
4 pp

Kn o. 25. JAN. 2001 d o k 31797

CEMENT FOR HPC CONCRETES

Stanisław PEUKERT, Institute of Mineral Building Materials (IMMB), Cracow, Poland

ABSTRACT In the paper the authors take up the subject of modification of cement properties for concretes of high strength and increased durability. They point up the possibility of obtaining HPC concretes from so called gypsum-free cements containing a complex additive stimulating rheological properties and hardening processes of concrete mixes. Possible application of silica fume additive and superplasticizers for said cements makes possible obtaining concretes with compressive strength higher than 100 MPa.

Key-words: composite cements, admixtures, hardening

INTRODUCTION

Technical, ecological and economic reasons have created an increased interest in the issue of making concrete objects of high strength and durability. In most cases the possibility of manufacturing high performance concrete HPC consist in admixtures of microsilica SF and superplasticizer SP added to concrete. Compacting of the concrete structure by the application of the mentioned above additives gives rise to an increase concrete strength and durability. The problems of design and practical implementation of low-porosity MDF and DSP concretes have been the subject of numerous publications. The principles presented in the major papers at the last Congress on the Chemistry of Cement (Roy, 1992, Collepardi and Ramachandran, 1992) continue to hold. Analysis of these data along with the recent experimental results (Gjørv, 1995) reveals that the question of the cement choice in design and practical application of MDF and DSP concretes is treated as a marginal issue. It is often assumed that these technologies yield HSC concrete in any conditions whatever on the application of OPC. However, many years of research by our Institute have shown the advantages of making the appropriate selection of special cements to make of HPC concretes according to the class of strength required and the specific areas of application (Peukert et al., 1996, Peukert, 1992). In the paper the phase composition of special cements and the additives required to modify their properties according to HPC technology requirements have been discussed.

PHASE COMPOSITION OF CEMENT

The results of research carried out by IMMB in the field of HSC concretes show that the best possibilities for design and making are obtained by the application of high-strength cement with a high calcium silicate content. This cement is produced from clinker with a high silicate module 3.0 or over (Peuketr, 1984). The silicate content in the clinker is over 80%. There is a corresponding limitation in the content of C_3A and C_4AF in the clinker. This type of phase composition of the clinker gives the best possibilities for the adaptation of the cement properties to modify parameters of HPC concretes. The enhanced silicate module in the clinker has an advantageous effect on the cement strength development, as shown in **Fig 1**.

The early and normative strength of the high silicate cement, and hence also of the cement matrix strength of HPC concrete, may be controlled very effectively by modification of cement lime saturation factor LSF and fineness of cement. Cement with a high silicate content also affords a good level of stimulation for the strength of HPC cement matrix through the addition of microsilica and a superplasticizer. A restricted C_3A content in the cement improves the fluidization effect of SP addition. On the other hand the composition of the cement ensures the

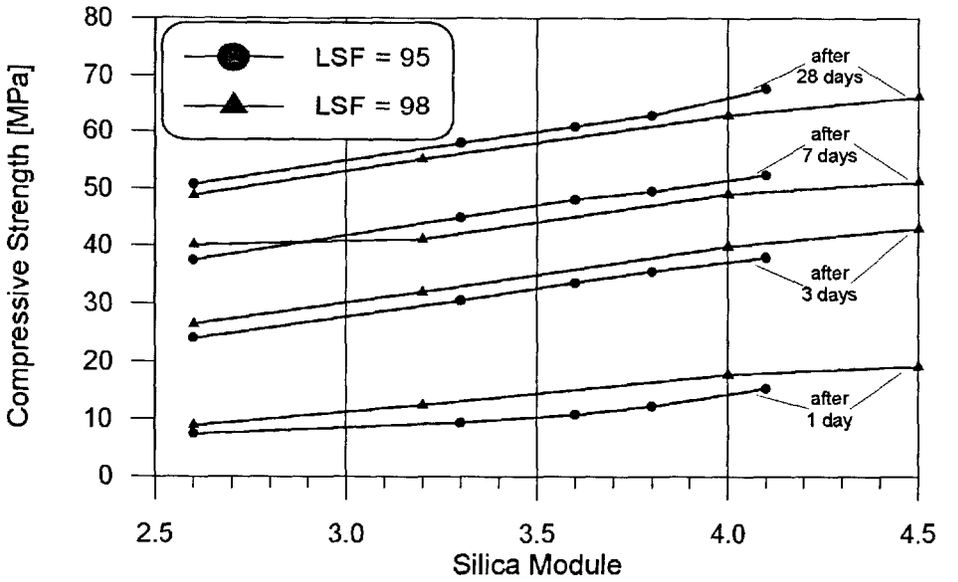

Figure 1 Influence of silica module on compressive strength of cement.

production of a greater amount of the CSH and CH phases during hydration process. The SF additive is thus particularly efficiently bonding in the pozzolana reaction with CH. The product of this reaction increasing amount of the CSH phase, which fills up the micropores of the hardening cement binder, enhances the compacting effect of the cement matrix. These phenomenons have been illustrated in **Figs 2 and 3**.

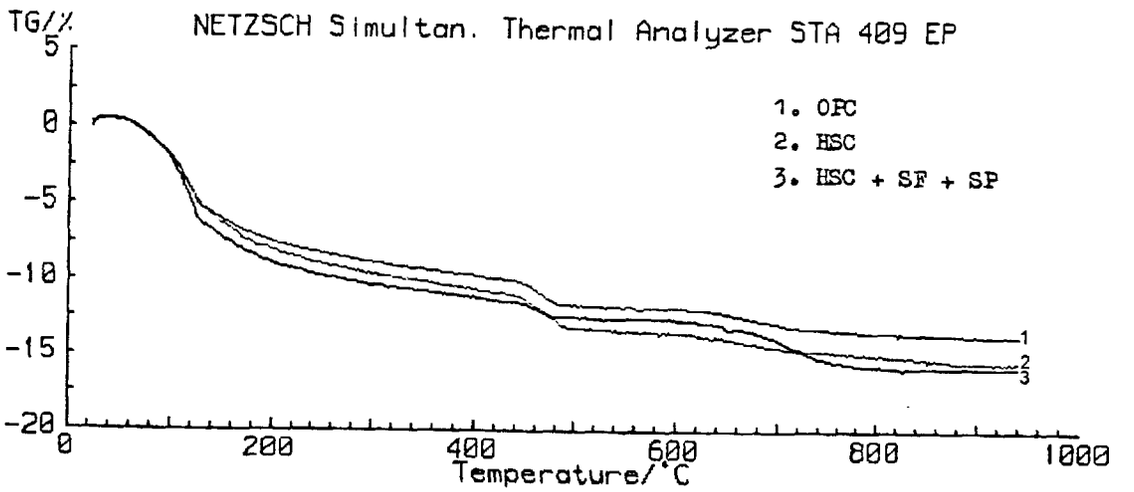

Figure 2 Thermogravimetric curves of cement pastes.

Thermogravimetric tests carried out on cement paste (Fig 2) confirm an increase of the C-S-H phase content in high-strength cement with SF additive (the first effect on TG curve). Already after 2 days of maturing the clear reduction of CH content which may be observed in cement with an SF additive confirms the great influence pozzolana reaction on hydration processes. This effect is least in cement with a microsilica additive due to the bonding of CH by SF (CH decomposition effect on TG curve at temperature of approx. 450°C). The great compacting effect of the paste structure from high-silicate cement with a microsilica additive is directly confirmed by measurements of porosity by means of mercury porosimeter (Fig 3). The reduced porosity of the matrix and the high density HPC concretes produced from cement with a high

silicate content gives a set of very good durability properties, such as frost resistance and resistance to sulphate and chloride corrosion (Peukert et al., 1996, Peukert, 1992).

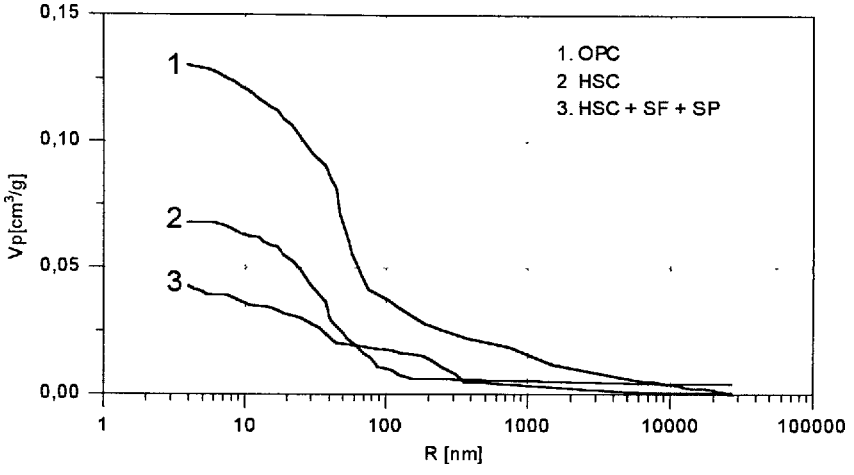

Figure 3 Porosity of cement pastes.

CEMENT SETTING REGULATOR AND HARDENING ADDITIVES

Alongside its mechanical properties, the high silicate cement is also recommended in HPC concrete technology for its increased potential to improve SP fluidization effect. In general, cements with a limited C_3A content are less water-requiring. On the other hand the use of anhydrite in these cements instead of the universally applied gypsum gives a particularly large lowering of the water demand of cement, **Table 1**. This fact has been applied in the technology for the production of the "gypsum-free" cements used for HPC concretes. The excellent workability of these cements creates the opportunity for the limitation of SP consumption in MDF and DSP concretes.

Table 1 Water demand of cements.

Type of cement	C_3A contents, [% by mass]	Control setting agent, [% by mass]	
		Gypsum, $CaSO_4 \cdot 2H_2O$	Anhydrite II $CaSO_4$
SRC, CEM I 42.5	2.5	25.0	22.0
OPC, CEM I 42.5	9	26.0	24.0
	11	26.5	25.0
	13	27.5	27.0

For the super-rapidly hardening HPC concretes it is essential to modify the kinetics of hardening in the cement through the addition of hardening activators. The effects of the alkaline activators, K_2CO_3 and Na_2CO_3, have been shown to be highly efficient in silicate cements. These additives give a very good early strength of the cement, with a simultaneous high normative strength.

The application of the mentioned above hardening activators reduces the setting time of cement then often needs to use the addition of setting retarders. Good retardation effects may be obtained by using SP of Ca-LS type with an extra additive, according to needs, of the hydroxycarboxilic acids. The potential for the modification of strength of the gypsum-free cements with described above complex additive of modifiers is shown in **Table 2**.

Table 2 Properties of cements modifying by complex additive.

Cement		Paste			Mortar					
Concentration of complex additive	Specific surface area	Water demand	Setting time		Consis-tency	c/w ratio	Compressive strength, after days, MPa			
			initial	final						
% by mass	m^2/g	wt. %	h^{min}		cm		1	3	7	28
5.5	0.45	23.5	1^{50}	2^{10}	18.0	2.86	20	45	52	61
7.5	0.45	22.5	1^{55}	2^{20}	18.2	3.03	22	47	54	63
5.5	0.55	21.5	1^{02}	1^{08}	18.3	3.03	37	58	71	81
7.5	0.55	20.5	1^{08}	1^{14}	18.2	3.03	43	61	72	83

The strength of concretes produced from describe above cements, granite aggregate and containing 10% additive of silica fume, is shown in **Table 3**.

Table 3 Mechanical properties of HPC concretes.

No of concrete sample	c/w ratio	Compressive strength, after days, MPa				
		0,25	1	3	7	28
1.	2.5	3.3	40.8	51.3	66.2	78.7
2.	3.5	7.7	58.5	68.5	81.4	94.2
3.	2.5	3.1	39.8	57.5	62.3	78.4
4.	3.5	6.3	49.5	61.2	78.4	97.8

CONCLUSIONS

Cements with a high silicate content appear to be particularly useful in design and production of HPC concretes. The cements applicated in the MDF and DSP technologies gives an extremely good means of controlling the rheological properties of concrete mixes and performance parameters of concrete.

Gypsum-free cements with a silicate content over 80% particularly favourable influence the fluidization effect of superplasticizers additive, also in the presence of the alkaline hardening activators, K_2CO_3 and Na_2CO_3.

REFERENCES

Collepardi, M., Ramachandram, V.S., "Effect of Admixtures", Proceedings of the 9-th Intarnational Conference on the Chemistry of Cement, 1992, Vol. 1, pp. 529-571.

Gjørv, O.E., et al., "Abrasion Resistance of Road Pavements", Proceedings of the International Seminar "Durable and Safe Road Pavements", May 12 1995, Kielce Poland, pp 105-112.

Peukert, S., Mierzwa, J., Mróz, H., "Cement and Special Composites for HPC Concrete and Structure Reconstruction", Proceedings of the International Congress "Concrete in the Service of Mankind", June 24-28 1996, Dundee Scotland, under Press.

Peukert, S., "Cements for High Performance Concretes", Przegląd Budowlany, No. 6-8 1992.

Peukert, J., Peukert, S., "Special Cements", Cement-Wapno-Gips, No. 11-12 1984.

Roy, D.M., "Advanced Cement Systems Including CBS, DSP and MDF", Proceedings of the 9-th Intarnational Conference on the Chemistry of Cement, 1992, Vol. 1, pp. 357-383.

2ii035
4 pp
Kno. 25. JAN. 2001 dok 31798

HYDRATION MECHANISM OF HIGH PERFORMANCE CONCRETE

Yeong N. SHEEN, National Taiwan Institute of Technology, Taipei, Taiwan.
Chao L. HWANG, National Taiwan Institute of Technology, Taipei, Taiwan.

ABSTRACT The hydration mechanism of HPC was studied in this paper. Setting behavior, ultrasonic pulse velocity, strength development and calorimetric curve were measured simultaneously. Among them a coincident trend was shown just as the result observed for blended cement paste. The heat evolution curve of HPC has delayed accordingly by the amount of cement and the transition zone appeared later than normal concrete.

Keywords: Hydration mechanism, High Performance concrete(HPC), Heat evolution.

RESEARCH SIGNIFICANCE

The hydration of high strength and high flowing HPC was studied. The HPC with fixed paste amount and three W/B compared with traditional high strength concrete (HSC). Heat evolution, penetrative resistance, pulse velocity, electrical resistivity and compressive strength were conducted to build up quality assurance and basic theory for the application of HPC.

TEST PLAN

The materials used in this study met the requirement of ACI 363. Based on the densified mixture proportion algorithm, HPC with different W/B was prepared to meet the requirement of f'c at 56 day > 56 MPa and slump > 230 mm. High strength concrete was designed by ACI 318. The material and mixture proportion are shown in Table 1.

Table 1. The Mixture of Concrete

Type	N	W/C	W/B	W/S (%)	Mixture Proportion (kg/m^3)							
					Fly Ash	Sand	Coarse aggregate	Cement	Slag	Water	SP	UW
HPC	1.3	0.43	0.28	7.2	177	929	738	376	20	126	35	2401
		0.50	0.32	7.8				342	18	158	14	2376
		0.67	0.40	8.9				285	15	183	8	2335
HSC	2.1	0.34	0.34	11.5	0	825	586	719	0	244	0	2374

After mixing with water, heat evolution, penetrative resistance and ultrasonic pulse velocity were measured during the first 100 hr. Also pulse velocity, electrical resistivity and compressive strength were measured at 28, 56, 120 and 180 days.

RESULT AND DISCUSSION

Cement content varies from 285 kg/m^3 of HPC to 719 kg/m^3 of HSC in this study. The main heat source of HPC is cement. Hence HSC has the highest heat with the rapidest hydration due to the largest amount of cement as shown in Fig. 1.

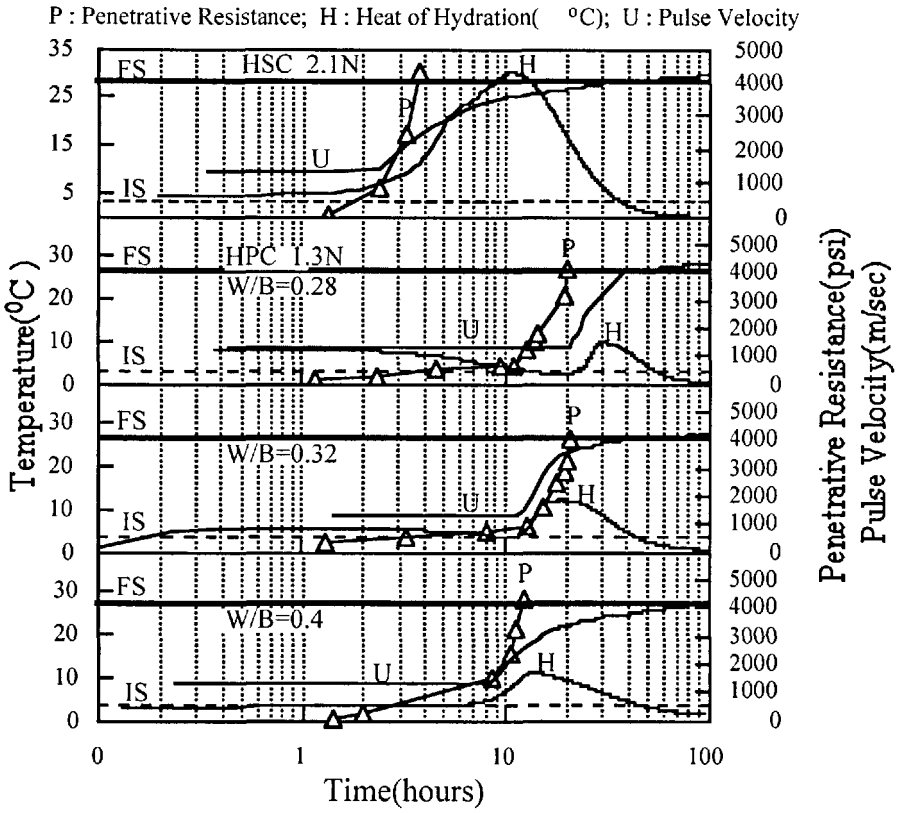

Figure 1 Hydration mechanism of HPC (1.3n) with various W/B

It is also shown that there is a close relationship among heat evolution, penetrative resistance and pulse velocity. Such behavior is quite similar to the observation of transition zone (TSZ) in the previous researches on paste. Large amount of calcium hydroxide (CH) grows during this period and ultrasonic velocity as well as penetrative resistance largely grows in TSZ. Heat peak also increases as the increment of cement. It may indicate there is same physiochemical variation in this zone. At same amount of paste, the smaller the W/B of HPC is, the higher the compressive strength will be. After 56 days the strength of HPC with W/B = 0.32 and 285 kg/ m^3 of cement exceeds that of HSC with W/C = 0.34 and 719 kg/m^3 of cement. Pulse velocity, compressive strength and electrical resistivity increase with time as shown in Fig. 2.

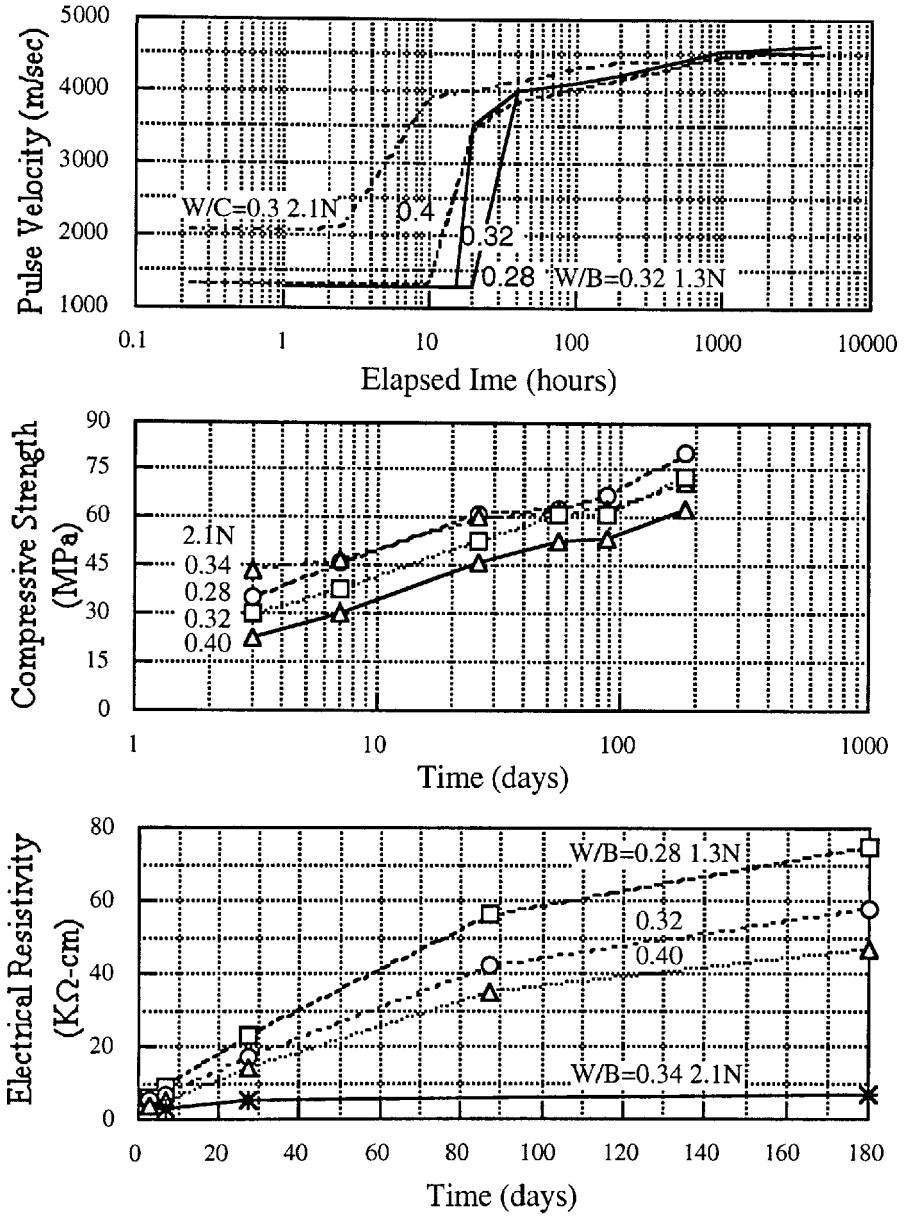

Figure 2 Development of pulse velocity, compressive strength and electrical resisitivity of HPC with various W/B

However, the ultrasonic pulse velocity and long-term strength of HSC with rich cement have shown degradation. Electrical resistivity at all ages is below 10 kW-cm mainly due to without pozzolanic material. The lower the W/B of HPC is, the higher the electrical resistivity will be. The electrical resistivity of HPC is ten times greater than that of HSC without pozzolan. And hence, it can be concluded that HPC with the addition of pozzolanic material would obtain better water penetrative resistance and durability.

CONCLUSION

Hydration behavior of HPC with different W/B is similar to that of cement paste with or without pozzolan. The peak of heat evolution curve increases as the increment of cement amount. The pulse velocity, penetrative resistance and heat evolution curves have transition zone in the same duration. The results have shown that the more cement there is, the worse the properties will be. Therefore, the addition of pozzolan is helpful to maintain long-term strength and durability of concrete for construction needs .

REFERENCES

ACI 363, State-of-the-Art Report on High Strength Concrete, American Concrete Institute, 1984.

Hwang, C. L., Liu, J. J., Lee, L. S., and Lin, F. Y., "Densified Mixture Design Algorithm of High Performance Concrete and Its Early Properties", Journal of the Chinese Institute of Civil and Hydraulic Engineering, Vol. 8, No. 1, Taiwan, 1996, pp. 207-219.

Hwang, C. L. and Shen, D. H., "The Effect of Blast-Furnace Slag and Fly Ash on the Hydration of Portland Cement", Cement Concrete Research, Vol. 21, 1991, pp. 410-425.

Mindess, S. and Young, J. F., Concrete, Prentice-Hall, Englewood Cliff, N. J., 1981.

2ii036
5 pp

Kno. 25. JAN. 2001 doc 31799

HIGH PERFORMANCE CONCRETE: STUDY OF MORTAR PORE SOLUTION

Jorge. D. SOTA, J., LEMIT - CIC. Techn. Univ. La Plata. Argentina.
Graciela M. GIACCIO, LEMIT - CIC. Nac.Univ. La Plata. Argentina.
Raúl L. ZERBINO, LEMIT - CONICET. Nac.Univ. La Plata. Argentina.

ABSTRACT Many studies have shown that the capilary porosity of concrete is strongly related with their physico mechanical properties specially its strength and durability. The knowledge of the characteristics of liquid phase, present in pores, enables to study the process of hydration of cementitious systems. In this case mortars corresponding to conventional and high performance concretes are compared. A pressure of 450 MPa was applied to express pore solution. Capilary porosity, testing ages and the presence of different mineral admixtures were included as variables.

Key-words: Admixtures, Hydration, Ions, Pore solution, Porosity.

INTRODUCTION

During the last 20 years several special concretes have been developed, most of them restricted to particular situations. However, the interest in High Performance Concrete (HPC) continuously increased as its use is extended to a wide range of field applications; HPC have been applied in the construction of many important structures and they were generally specified in order to assure long service life.

Concrete is a material where pores of different types and sizes are randomly distributed together with discontinuities in the microestructure such as interfaces. This porosity not only implies differences in mechanical properties but also affects the permeability, allowing the movement of fluids liable to produce material degradation.

HPC are characterized by its high strength and durability, obtained as consequence of their low water to cement ratio, high content of cement and the use of superplastizicers and many times mineral admixtures. Previous studies have shown that the matrices of high performance concrete have a higher amount of unhydrated cement than conventional concrete; at the same time some differences in the morphology of hydration products have been observed. These facts are strongly related with the significant reductions in the porosity of the cementitious system.

The knowledge of the characteristics of liquid phase present in pores results of interest to the study of the process of hydration of cementitious systems. In this case the characteristics of conventional and high performance concretes are compared. This paper shows some results from a research program on the microstructure of high performance concrete, particularly those related with the analysis of pore solutions. In this case the porosity of the system (conventional vs. high performance mortar) and the presence of mineral admixtures were included as variables.

EXPERIMENTAL PROGRAM

The pore solution of different mortars was analyzed (Na^+, K^+, Ca^{2+}, CO_3^{2-}, HO^-). The expression of pore solution from hardened mortars was realized applying a pressure of 450 MPa. The used methodology was refered in Longuet et al (1973), a general description of the apparatus (materials, operation, analytical procedures) can be found in Barneyback and Diamond (1981). In many papers this methodology was applied in order to discuss the development of alkali-silica

reaction in cementitious systems Struble and Diamond (1981), Diamond et al (1981), Diamond (1983), Sota et al (1995) or the chloride binding capacity of the hardened cement pastes Page (1983).

To compare the composition of pore solution of high performance and conventional concretes, mortars representative of their matrices were studied. Water to cement ratios (w/c) equal to 0.35 and 0.55 were selected. Different types of mixtures including several mineral admixtures (silica fume and natural pozzolans) were sudied. The physical and chemical characteristics of cement and pozzolan are given in Table 1.

Table 1. Fineness and chemical analysis of the natural pozzolan and the cement.

Test	Normal Portland Cement	Natural Pozzolan
Surface area, Blaine (m^2/kg)	350	700
Chemical analysis (%)		
Loss on ignition	3.50	6.40
Silicon dioxide (SiO_2)	20.90	68.50
Aluminum oxide (Al_2O_3)	3.10	14.20
Ferric oxide (Fe_2O_3)	4.30	2.40
Calcium oxide (CaO)	62.70	-----
Free lime	----	2.70
Magnesium oxide (MgO)	0.85	0.18
Sulphur trioxide (SO_3)	2.00	0.00
Sodium oxide (Na_2O)	0.11	2.40
Potasium oxide (K_2O)	0.79	3.12

Eight mortars were prepared using these materials and a siliceous natural river sand. No chemical admixtures were added. Two reference mortars, M-1 (w/c=0.35) and M-2 (w/c=0.55), with portland cement and without mineral admixtures were made. In mortars M-3 and M-4, 15 % by weight of cement was replaced by a natural pozzolan, while in mortars M-5 and M-6 the same percentage of pozzolan was added to cement content. In the same way, 15% (by weight of cement) of silica fume was added to cement content in mortars M-7 and M-8. Mix proportions are given in Table 2. Cylinders of 50 mm x 100 mm were cast; they were sealed and kept at 20 C until the age of testing (1, 3, 7, 28 and 90 days).

Table 2. Mortar mix proportions.

MIX	Proportions (gr.)						
	water	cement	natural sand	natural pozzolan	silica fume	w/c	w/(c+a)
M-1	157	450	700	-	-	0.35	0.35
M-2	165	300	805	-	-	0.55	0.55
M-3	157	382	700	67.5	-	0.41	0.35
M-4	165	255	805	45	-	0.65	0.55
M-5	157	450	626	67.5	-	0.35	0.30
M-6	165	300	756	45	-	0.55	0.48
M-7	157	450	612	-	67.5	0.35	0.30
M-8	165	300	746	-	45	0.55	0.48
w/c: water to cement ratio			w/(c+a): water to cement + mineral admixture ratio				

Test results

The results of the analysis of pore solution are given in Table 3. The variation with age of the concentration of calcium ion in pore solution of mortars with low and regular porosity is plotted in Fig 1. In a similar way, Figs 2 and 3 show the changes in sodium and potasium concentrations.

Table 3. Results of the analysis of pore solution. (expressed in meq/l)

	Age	Mortar							
	(days)	M-1	M-2	M-3	M-4	M-5	M-6	M-7	M-8
HO^-	1	496	394	404	261	608	350	462	310
	3	558	441	472	292	612	405	325	163
	7	509	429	525	326	632	442	310	145
	28	492	447	557	380	592	453	160	94
	90	405	261	500	309	570	447	106	72
CO_3^{2-}	1	45	29	34	23	22	13	15	10
	3	51	31	47	34	29	14	30	12
	7	58	51	61	35	19	12	22	7
	28	46	47	47	30	15	6	-	6
	90	34	21	54	35	12	8	14	6
K^+	1	554	432	420	258	621	332	448	301
	3	583	397	510	313	650	391	310	139
	7	525	486	582	346	709	437	207	141
	28	565	490	564	333	652	439	178	56
	90	420	258	546	328	640	431	118	42
Na^+	1	36	27	42	29	46	30	37	27
	3	36	33	52	38	49	34	54	19
	7	43	28	67	44	61	48	56	28
	28	41	35	46	42	72	57	82	63
	90	42	30	58	40	74	61	84	71
Ca^{2+}	1	11	10	7	4	8	10	11	9
	3	11	12	7	7	11	8	32	8
	7	15	11	7	6	21	9	48	15
	28	7	7	7	7	9	8	120	60
	90	8	12	7	9	26	9	116	58

DISCUSSION

Regarding the behaviour of reference mortars (M-1, M-2) in Fig 1 it can be seen that there are not significant differences of Ca^{2+} in pore solution when w/c varies from 0.35 to 0.55. Although there are important differences in cement content, calcium concentration is limited by the sparingly soluble calcium hydroxide. The higher porosity of 0.55 mixes makes easier the hydration of cement. For both w/c ratios Ca^{2+} ions concentration remains almost constant as age increases.

A different situation appears when silica fume was added, then Ca^{2+} ion content is notably higher in 0.35 than in 0.55, and it increases with time. This fact can be explained considering that silica fume enhances cement dispersion and then, hydration process. When cement is replaced by natural pozzolans (M-3 and M-4) no differences between w/(c+a)=0.35 and 0.55 mixes were detected, being calcium concentration almost constant along the time. When pozzolan is added to cement content, a similar behavior can be observed in M-6 but in M-5 (w/c=0.35) there is a tendency to increase calcium concentration with time.

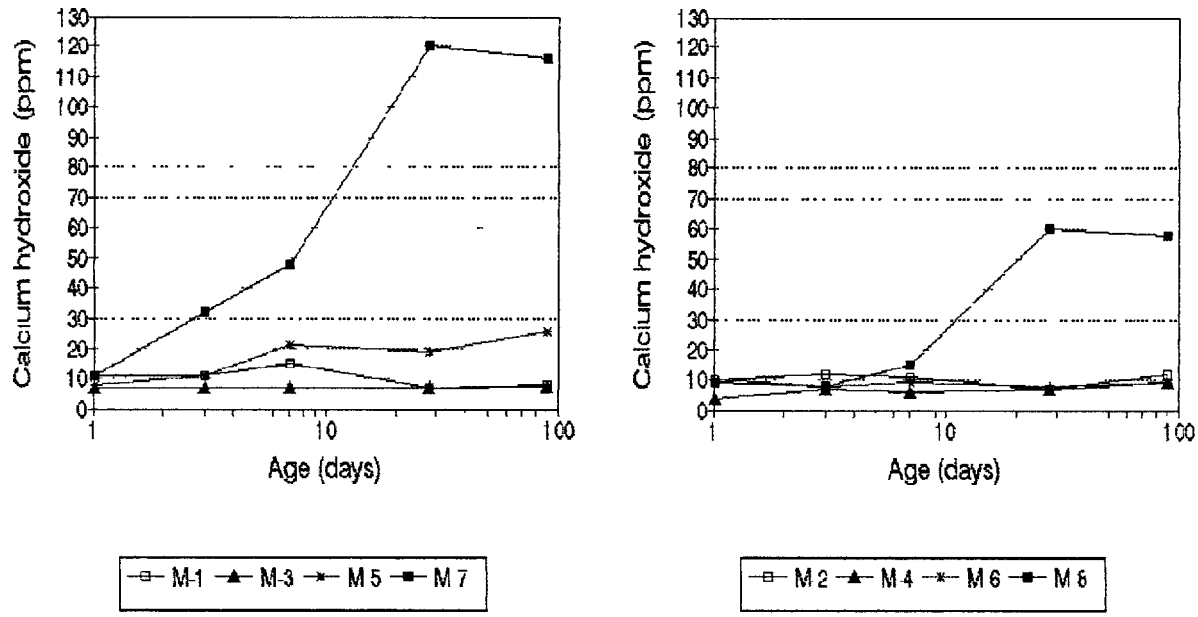

Figure 1 Variation with age of Ca^{2+} concentration of high performance and conventional mortars.

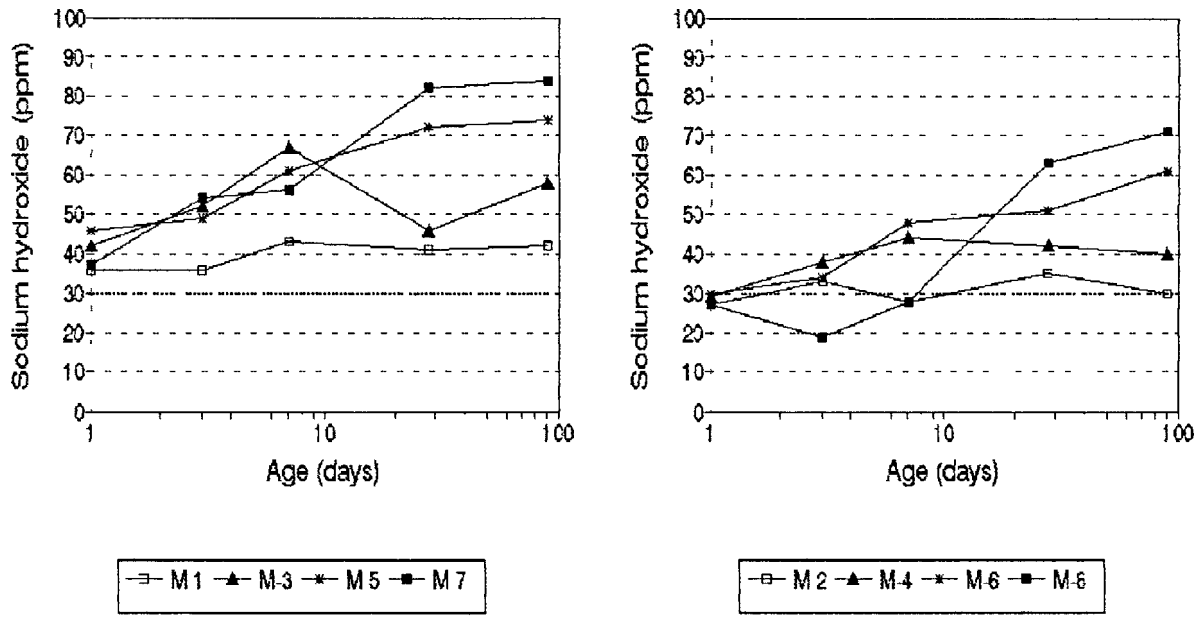

Figure 2 Variation with age of Na^{+} concentration of high performance and conventional mortars.

Fig 2 shows that Na^{+} contents are always higher in high performance (low w/c ratio) than in conventional mixes. This behaviour can be justified regarding the differences in cementitious material content of the mortars. In reference mortars Na^{+} sligtly increases with age. When mineral admixtures are used it tends to increase. The most significant increments with time take place when silica fume was added (M-7, M-8), followed by pozzolan addition (M-5, M-6) and finally pozzolan as partial cement replacement (M-3, M-4). In all cases Na^{+} is higher in mortars with silica fume or pozzolan than in plain mortars (no admixtures).This fact is attributed to the Na^{+} ions supplied by the mineral admixtures but also to the dispersion effect of the ultrafine particles which enhanced the solubility of the cations.

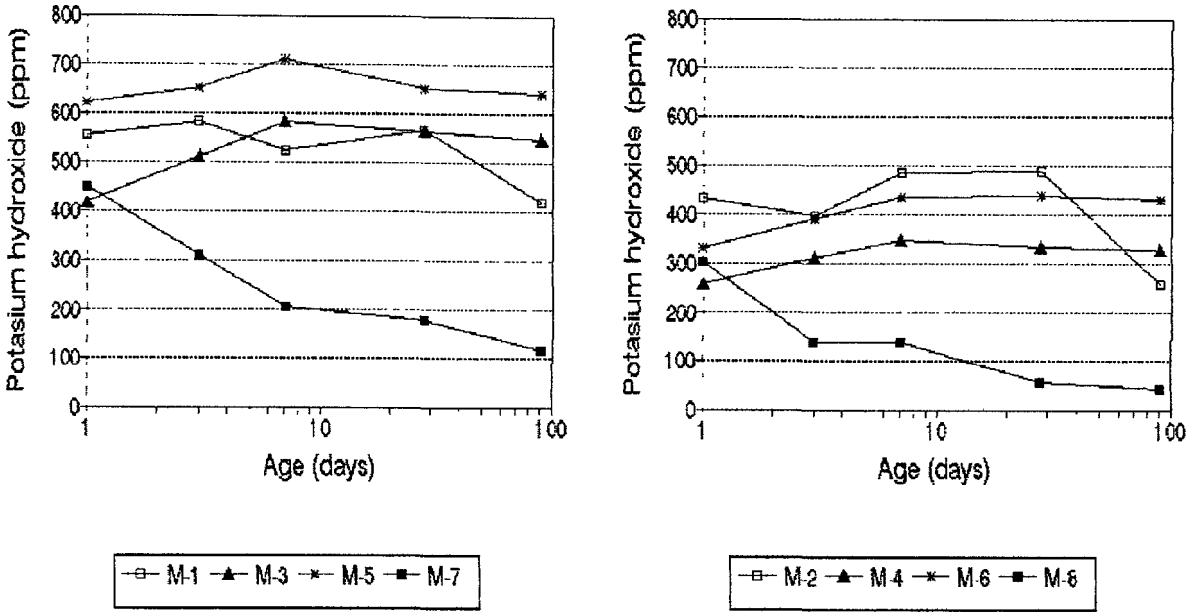

Figure 3 Variation with age of K^+ concentration of high performance and conventional mortars.

The variation of the concentration of K^+ with age of high performance and conventional mortars is represented in Fig 3. As in the case of sodium, K^+ contents are always higher in the mixes of lower porosity (w/c=0.35). In reference mortars K^+ remains relatively equal until the age of 28 days and then it starts to decrease. In pozzolan mortars it increases during the first days (probably due to the K^+ supplied by the admixture) and then they start to decrease slowly. On the contrary, when silica fume was added the content of K^+ is continously and strongly reduced since the begining. This reduction in K^+ can be justified considering that these ions are the first ones that are fixed by the silicates. This effect was more important in mortars of lower porosity.

Finally, regarding the variation of the different ion contents it can be thought that in M-7 and M-8 the rate of hydration of cement increases due to the dispersion effect of silica fume particles, then there is a higher capacity to fix K^+.

REFERENCES

Barneyback, R.S.(Jr) and Diamond, S. "Expression and analysis of pore fluids from hardened cement pastes and mortars". Cement and Concrete Research. Vol. 11, pp. 279-285, 1981.

Diamond, S., Barneyback R.S.(Jr) and Struble L.J., "On the physics and chemistry of alkali-silica reactions". Conf. on alkali-aggregate reaction in concrete. South Africa. March 30-April 3, 1981.

Diamond, S., "Álcali Reactions in Concrete-Pore Solution Effects" . Proc. 6th Int. Conf. Alkalis in concrete, Copenhagen, pp.155-165, 1983.

Longuet, P., Burglen, L. and Zelwer, A., La phase liquide du ciment hydrat. Revue des Matriaux de Construction et de Travaux Publics, 676, pp.35-41. 1973.

Page, C.L. and Vennesland, O, "Pore solution composition and chloride binding capacity of silica-fume cement pastes", Materials and Structures, RILEM, vol 16, n 91, 1983.

Sota, J.D., Iasi, R., Perez, R. and Batic, O.R., "Los iones presentes en el líquido de poros de los hormigones afectados por la reacción álcali-agregado". XXI Congreso Argentino de Química, B.Blanca Argentina, september 1996 (in spanish).

Struble, L. and Diamond S., "Unstable Swelling Behavior of Alkali Silica Gels". Cement and Concrete Research. Vol. 11, pp. 611-617, 1981.

2ii037
5 pp

Kn o. 2 5. JAN. 2001 d o k 31800

PROPERTIES AND MICROSTRUCTURE OF ULTRA HIGH STRENGTH CEMENT COMPOSITES

Hai Moon CHEONG, Jung Ryoul LIM and Dong Won CHO
Ssangyong Cement Industrial Co. Ltd., Taejon, KOREA

ABSTRACT The medium-sized and pozzolanic particles were favorable for DSP cement system, since they produced denser packing and their pozzolanic reaction reduced $Ca(OH)_2$ and formed C-S-H with lower C/S ratio. The suitable particles were slag. Curing temperature had great effect on the compressive strength development. High temperature curing promoted pozzolanic reaction as well as Portland cement hydration. Autoclave curing produced the best compressive strength.

Key-words : Microstructure, High strength, silica fume, Pore structure, Curing

INTRODUCTION

In recent years many studies for ultra high strength cement composites have been reported. Ultra high strength cement composites would be used extensively for the construction, chemical and mechanical materials(Wise, 1985 ; Yoshihiko, 1991 ; Young, 1991 ; Roy, 1992). DSP(Densified System containing homogeneously arranged ultra fine Particles) cements had the more densified system with ultra fine particles such as silica fume and superplasticizers. Since DSP cement was first described in H.H. Bache(1981), the studies of DSP cements have been widely applied in the area of high strength cement composites. DSP cement had good mechanical properties due to lower water-cement ratio(W/C) and denser, homogeneous microstructure(Lu, 1993).

For more compacted and homogeneous hydrated cement matrices, multi-components DSP cements with the medium size particles ranging from silica fume to cement would have been studied(Lu. 1993 ; Yokoyama, 1994). And silica fume was one of the pozzolanic materials, however its reaction was less active than Portland cement, and a large dosage of superplasticizers retarded the early cement hydration. To accelerate the early cement hydration the various curing conditions have been investigated. High-temperature and high-pressure curing were widely used to increasing the strength of DSP cements(Sun, 1993). Especially high-temperature curing at 200 ℃-400 ℃, in spite of some cracking and shrinkage, produced much higher strength. Until now many researches have been reported to optimize the curing conditions for the best properties.

In this study, using various medium size particles whose size distribution ranged from silica fume to Portland cement, the ultra high strength cement composites with more densely-compacted and homogeneous hydrated cement matrices were prepared, and the influence of curing conditions on the microstructure and physical properties was investigated.

EXPERIMENTAL PROCEDURE

Materials

Ordinary Portland cement(Ssangyong Cement Industrial Co., Korea) and Silica fume(Grade 940-U, Elkem Materials A/S, Norway) were used. As medium-sized particles, ggbf slag(granulated ground blast furnace slag with the blaine 8000cm^2/g, Pohang Steel Industrial Co., Korea), fly ash(classified fly ash, Boryoung Power plant, Korea), paper sludge ash(Ssangyong Paper Industrial Co., Korea) and calcined bauxite(ground red bauxite, China) were used. The chemical compositions are shown in Table 1.

Table 1. Chemical Compositions of Raw Materials.

Materials	SiO_2	Al_2O_3	Fe_2O_3	CaO	MgO	Na_2O	K_2O	SO_3	TiO_2	P_2O_5	f-CaO	LOI	Ave.Dia (um)
OPC	20.88	5.46	3.05	62.22	2.98	0.01	0.87	2.57	-	-	0.76	1.2	12.0
Silica fume	94.60	0.90	0.60	0.20	0.40	0.24	0.89	-	-	-	-	1.9	0.5
GGBF slag	31.40	14.20	0.50	44.20	5.60	0.20	0.54	2.20	-	-	-	1.2	4.8
Paper sludge ash	23.30	38.80	1.00	32.60	2.60	0.37	0.22	1.50	-	-	-	0.4	2.3
Fly ash	61.20	27.90	4.30	1.70	0.40	0.40	0.80	-	1.38	0.60	-	1.9	9.3
Calcined bauxite	10.11	84.00	0.70	0.10	0.40	0.10	0.10	-	4.22	0.11	-	0.2	4.1

The preparation and characterization of ultra high strength cement composites

The mix proportions(wt%) was cement/silica fume/medium size particle=7:1:2. The superplasticizers (Melment F10, melamine formaldehyde condensate) was added with 3wt% of this mixtures. The solid powders were mixed with water(water/solid=0.16 - 0.20) by the planetary mixer for 6 minutes. The specimens were cast in 50 x 50 x 50 mm mold and demolded after 1 day and cured in water at 20 ℃ for 28 days. For the characterization of the specimens, XRD, DT/TGA, SEM/EDS, mercury intrusion porosimetry and compressive strength test were employed.

To investigate the influence of curing conditions, the ultra high strength cement composites were prepared under various curing conditions as shown in Table 2 and their mechanical and hydration properties were analyzed.

Table 2. Curing Conditions

Notation	Curing condition	
W	. In water	. 20±5 ℃
AU	. Autoclave	. 180 ℃, 10atm., 24hrs.
DO	. Dry oven	. 200 ℃, 24hrs.
HT	. In water	. 80±5 ℃, 24hrs.
AU+DO	. Autoclave	. Autoclave(180 ℃, 24hrs.)→ 20 ℃ 24hrs. in air → Dry oven(200 ℃,24hrs.)
HT+DO	. Hydrothermal+dry oven	. Hydrothermal(80 ℃, 24hrs.)→ 20 ℃, 24hrs. in air → Dry oven(200 ℃,24hrs.)

RESULT AND DISCUSSION

Influence of medium size particles

Fig. 1 shows the compressive strength of the specimens cured in water for 28 days with various kinds of medium-sized particles such as ggbf slag, fly ash, paper sludge ash and calcined bauxite. Medium-sized particles made compressive strength increase. Especially the ggbf slag showed higher compressive strength than other particles. Water demand changed with the kind of medium-sized particles due to their particle size distribution and surface properties. Ggbf slag-containing composites could be mixed at a lower W/S ratio. It was considered that they had more densely packing than other composites. In general, it was well known that the compressive strength decreased with increasing W/S ratio. However there is no relationship between compressive strength and W/S ratio, because W/S ratio was lower compared with theoretical water demand (W/S=23.5%) and lower W/S(< 0.18) led to lower workability. The suitable W/S ratio was 0.18 - 0.20. Ggbf slag gave better compressive strength. It was assumed that they made more densely-packed structure in fresh state and better hydrated matrices by more active hydraulic reaction than other powders.

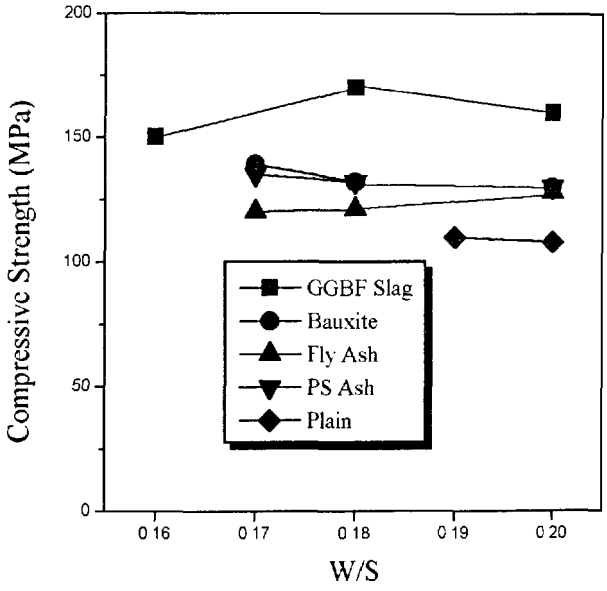

Fig. 1 Compressive strength of ultra high strength cement composites with various medium-sized particles. (Cured in water for 28 days)

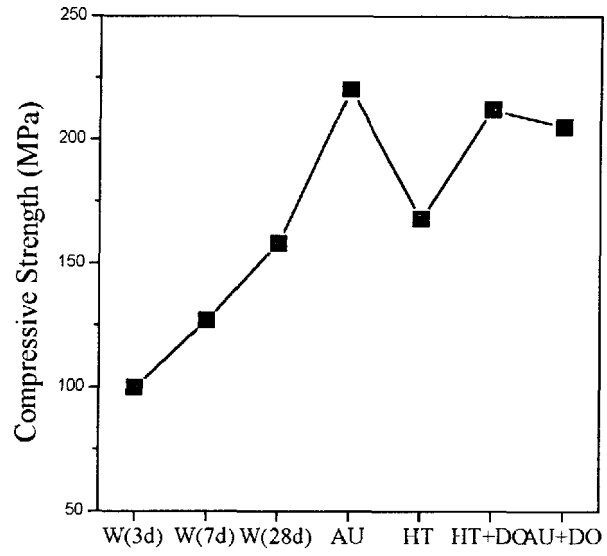

Fig. 2 Compressive strength of ultra high strength cement composites with various curing conditions.

The medium-sized and pozzolanic particles were favorable for DSP cements system, since they produced denser packing in fresh state and their pozzolanic reaction reduced $Ca(OH)_2$ and formed C-S-H with lower C/S ratio. The suitable particles were ggbf slag. The compressive strength seemed to be unaffected by the mechanical properties of medium-sized particles.

Influence of curing conditions

Fig. 2 shows the relationship between compressive strength and curing condition. As shown above, ggbf slag-containing composites showed better compressive strength, so they were chosen for investigation of curing condition. As the curing temperature was higher, the compressive strength increased. Curing temperature had great effect on the compressive strength. High temperature curing promoted pozzolanic reaction as well as Portland cement hydration. Autoclave curing produced the best compressive strength.

After hydrothermal+dry oven curing, the compressive strength increased remarkably. XRD data indicated that the autoclave curing showed higher degree of hydration. Under hydrothermal curing and water curing, only C-S-H was observed, and under autoclave and hydrothermal + dry oven curing, the tobermorite crystals as well as C-S-H were observed. Fig. 3 shows the pore size distribution of the specimens with various curing conditions. After autoclave and hydrothermal curing, the specimens contained lower total porosity. The specimens which showed higher compressive strength contained less macroporosity (over 15 μm). The small capillary pore (below 0.01 μm) did not greatly influence on the compressive strength. After dry oven curing, the medium capillary pore (below 0.05 μm) increased. Autoclave curing produced the best compressive strength because of the denser hydration products and tobermorite formation. Although hydrothermal + dry oven curing increases medium capillary porosity (below 0.05 μm) and total porosity slightly, the compressive strength increased. The reasons of this result were the tobermorite formation and reducing of macroporosity which influenced on the mechanical property.

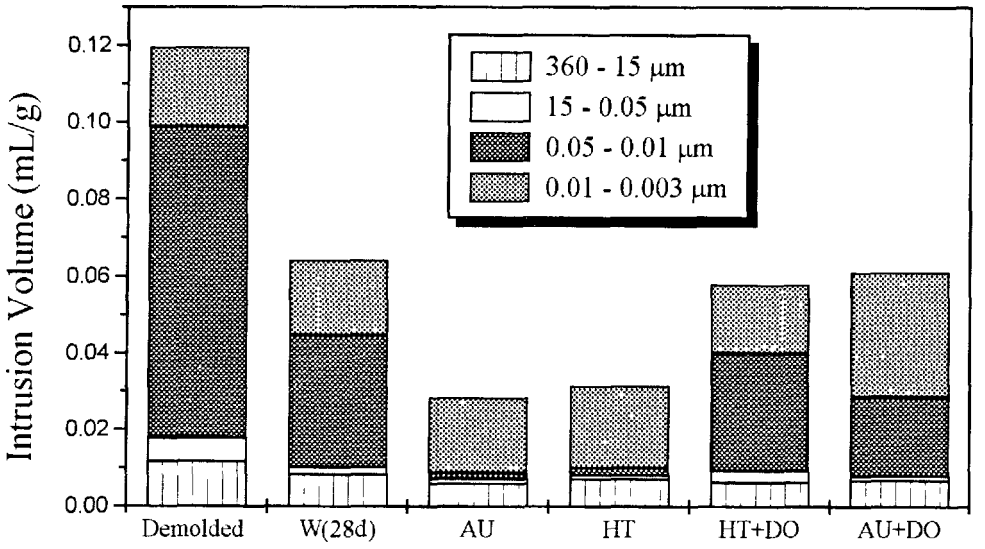

Fig. 3 Pore size distribution of the ultra high strength cement composites with various curing conditions.

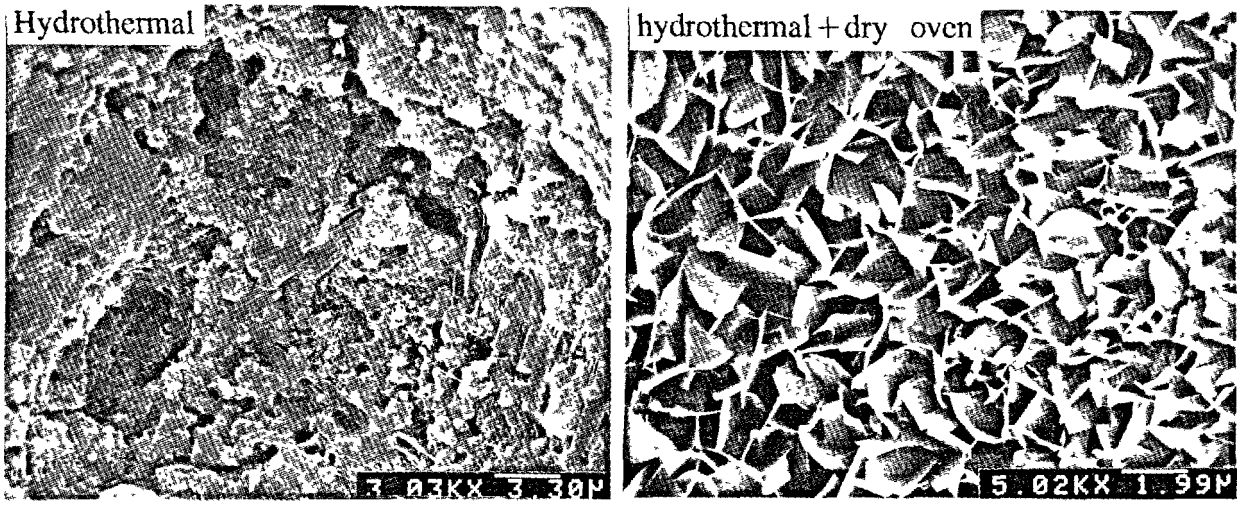

Fig. 4 SEM micrographs of macropores for the specimens with hydrothermal and dry oven curing.

Fig. 4 shows SEM micrographs of macropores for the specimens with hydrothermal and dry oven curing. After hydrothermal curing, the amorphous C-S-H was observed in the pores. After dry oven curing, tobermorite crystals were observed in the pores(this exhibited the same result as autoclave curing) Since denser microstructure by the hydrothermal curing had been heated at 200 ℃, the autoclave-like-reaction occured because dense matrix acted as the closed system(Wise 1985). In this case, tobermorite crystals were formed in the entrapped air and large capillary pores.

CONCLUSIONS

Using various medium-sized particles whose size distribution ranged from silica fume to Portland cement, the ultra high strength cement composites were prepared, and the influence of curing conditions on the microstructure and physical properties was investigated. The conclusions are as follows.

(1) The medium-sized and pozzolanic particles were favorable for DSP cements system, since they produced denser packing and their pozzolanic reaction reduced $Ca(OH)_2$ and formed C-S-H with lower C/S ratio. The suitable particles were ggbf slag.

(2) Curing temperature had great effect on the compressive strength. High temperature curing promoted pozzolanic reaction as well as Portland cement hydration. Autoclave curing produced the best compressive strength.

(3) After hydrothermal+dry oven curing, the compressive strength increased remarkably. It seemed that the microstructure became denser by the hydrothermal curing and tobermorite crystals were formed in macroporosity by the dry oven curing at 200 ℃.

REFERENCES

Bache, H. H., "Densified Cement / Ultra-fine Particle Based Materials", 2nd International Conference on Superplasticizer in Concrete, Ottawa, 1981.

Lu, P., Sun, G. K., and Young, J. F., "Phase composition of Hydrated DSP Cement Pastes", J. Am. Ceram. Soc., Vol. 76, No. 4, 1993, pp1003-1007.

Lu, P. and Young, J. F., "Slag-Portland Cement Based DSP Paste", J. Am. Ceram. Soc., Vol. 76, No. 5, 1993, pp1329-1334.

Roy, D. M., "Advance Cement System, including CBC, DSP, MDF", 9th ICCC, Vol 1, 1992, pp357-380.

Sun, G. K. and Young, J. F., "Hydration Reaction in autoclaved DSP Cements", Advances in Cement Research, Vol. 5, No. 20, 1993, pp163-169.

Wise, S., "The Development of a high strength Cementitious Tooling/ Molding Material", Mater. Res. Soc. Symp. Proc., No. 41, 1985, pp253-263.

Yokoyama, S., Fujimoto, I., Maruta, T. and Tanaki, E., "A consideration on Hydration Texture of Blended Cement Containing Silica fume and Super-pulverized Materials", JCA Proceedings of Cement and Concrete, No. 48, 1994, pp100-105.

Yoshihiko, O. et al, "Development of Super high strength mortars with compressive strength of $3000kg_f/cm^2$ or higher", Cement Concrete, No. 534, 1991, pp9-16.

Young, J. F. and Jennings, H. M., "Advanced Cement Based Materials" in "Cement and Concrete Science and Technology", edited by S. N. Ghosh ,1ST Ed. New Delhi. 1991.

2ii038
4 pp

Kn o. 2 5. JAN. 2001 d o k 31801

HIGH PERFORMANCE CEMENTOUS BINDER

Jun-Feng WANG, Schomburg & Co. KG, Detmold, Germany

ABSTRACT In comparison to a normal Portland cement (CEM I 52.5 R according to DIN 1164) shows the newly developed high performance cementous binder not only a good hydraulic property, but also a high strength development (ca. 45 N/mm² after 1 day and 105 N/mm² after 28 days according to DIN 1164 by a very low water cement ratio). The mortar and concrete which was improved with the high performance cementous binder show a very good chemical and mechanical resistance because of the very low porosity in hardened cement stone.

Key-words: High performance cementous binder (HPCB), Penetration, Low temperatur

INTRODUCTION

Portland cement, usually meaning Ordinary Portland Cement (OPC), are massive building material for normal constructional use. Specifications of Portland cement are based partly on chemical composition or physical properties such as setting time or compressive strength developed under standard conditions. In general, the setting time of a OPC is between 60 - 240 min. and its compressive strength between 32.5 - 52.5 N/mm² after 28d (determined in accordance with DIN 1164). In the following investigations on a newly developed high performance cementous binder - modified with chemical admixtures on the basis of Portland cement - is reported and its actions is discussed.

SAMPLE PREPARATION

For comparative purposes of comparison with the newly developed high performance cementous binder (HPCB) a commercially available Portland cement (CEM I 52.5 R) was also investigated. The corresponding properties of the fresh cement pasts, cement mortar and concrete of the HPCB and the Portland cement were tested in accordance with DIN 1164 and DIN 1048. Prisms (4x4x16 cm) were used in the tests of cement mortar and cubs (15x15x15 cm) were used for tests of concrete.

The mortar prisms and concrete cubes were removed from molds after 1d and then cured partly under water (20°C), in a climate room 20°C/65% RH. Partly prisms of cement mortar were cured in a deep freezer (ca. -20°C), in a fridge (ca. 5°C) and in a drying cabinet (ca. 50°C) until the testing term.

The resistance against chemical attack on the cement mortars were determined with diesel, 20% NaCl solution and 5% lactic acid.

RESULTS AND DISCUSSION

Properties of fresh cement pasts

The dates of fresh cement pasts which were determined according to DIN 1164 are presented in Table 1.

Table 1 : Properties of fresh cement pasts

samples	CEM I 52.5 R	HPCB
w/c ratio (standard stiffness)	0.285	0.200
initial setting min.	130	280
final setting min.	180	360

Table 1 shows that the w/c ratio of HPCB (0.200) by standard stiffness is lower than the w/c ratio of CEM I 52.5 R (0.285), the water demand can be reduced by about 42%. In comparison to the CEM I 52.5 R the setting time of HPCB is significantly retarded until to 280 min. (initial setting) and 360 min. (final setting).

Properties of cement mortars

The compositions of cement mortars and the resulting water cement ratio at approximately constant spread measure are given in Table 2.

Table 2 : Composition of cement mortars

Samples		A	B
CEM I 52.5 R	g	450	-
HPCB	g	-	450
Standard sand*	g	1350	1350
w/c ratio		0.500	0.300
Spread measure**	cm	16.0	16.0
Flexural strength after 16h	N/mm^2	2.11	5.70
Compressive strength after 16h	N/mm^2	8.15	28.8

* : According to DIN 1164 part 7
** : According to DIN 1060 part 3

The results in Table 2 show that the sample A with CEM I 52.5 R has a high w/c ratio of 0.500, at the similar water consistency the sample B with HPCB achieves a very low w/c ratio of 0.300. This means that in comparison to the reference mortar (sample A) a water reduction (sample B) of up to ca. 40% is achieved (Wang et al, 1995).

All test specimens after their demoulding were stored up to their testing in different curing conditions. The strength development of cement mortars determined according to DIN 1164 are presented in Fig 1.

The strength development of HPCB at early age is very positive, after 16h the compressive strength has achieved already 28.8 N/mm^2 (see Table 2) contrary to sample A only 8,15 N/mm^2. The results in Fig 1 show that the sample B achieves not only a high strength improvement during the initial phase of the hydration (45.5 N/mm^2 after 1d, curing in water), but also in the course of later strength development (105 N/mm^2 after 28d, curing in water).

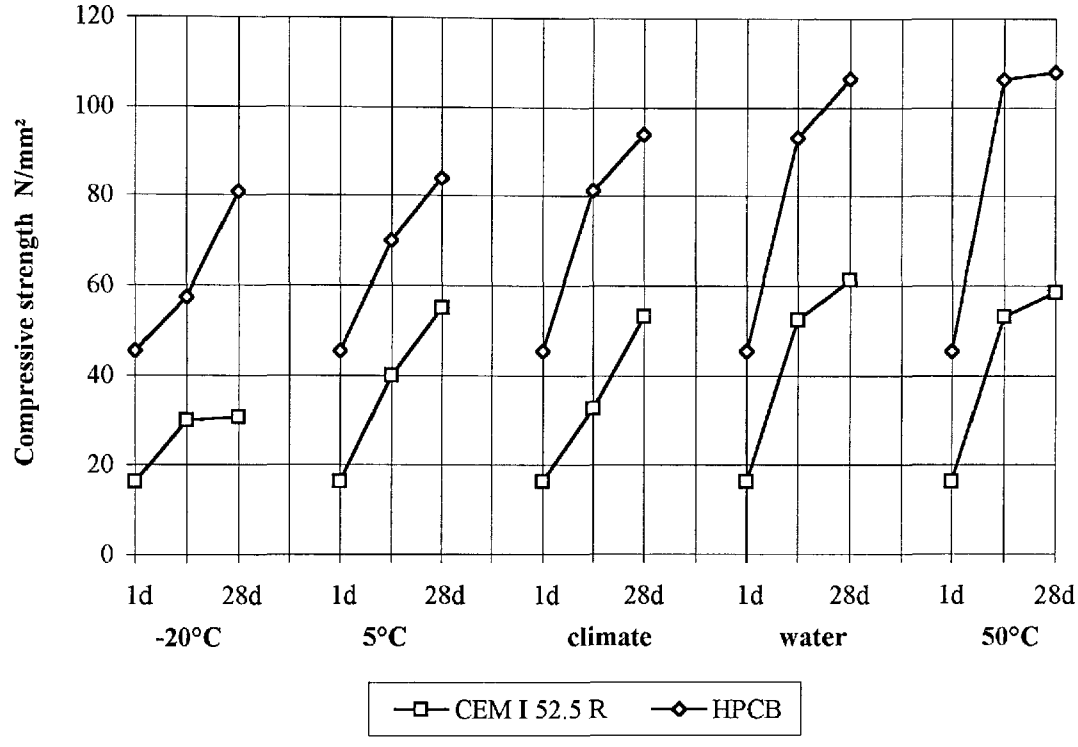

Figure 1 : Development of compressive strength of cement mortars in different curing conditions

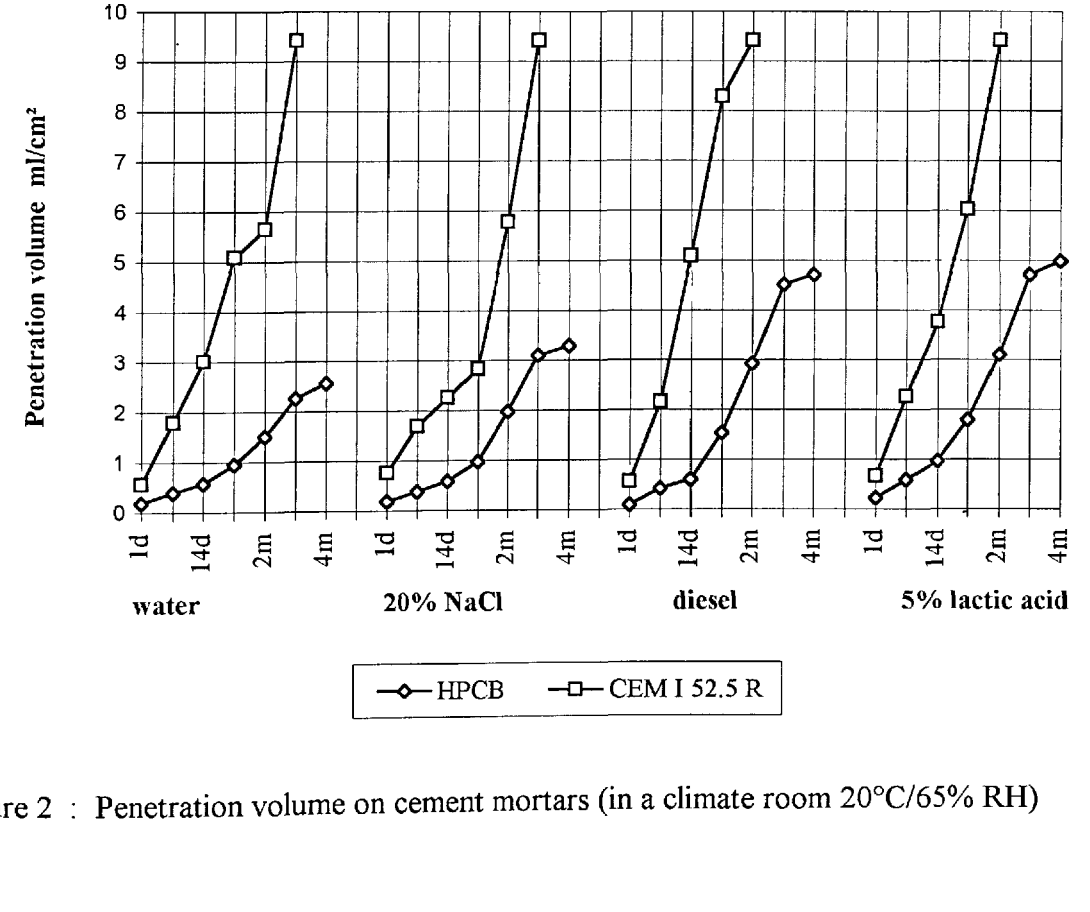

Figure 2 : Penetration volume on cement mortars (in a climate room 20°C/65% RH)

The strength development of cement mortars is appreciably influenced by the curing conditions (Fig 1), especially by the low temperature (-20°C) and high temperature (50°C). It is to see that the strength of HPCB increases further by -20°C from 57.4 N/mm² after 7d until 80.8 N/mm² after 28d, but the strength development of sample A, Portland cement is total stopped because of the low temperature from 30.0 N/mm² after 7d until 30.6 N/mm² after 28d. This means that the HPCB in comparison to Portland cement has a good hydration behavior by low temperature because of the lower water cement ratio and the dense microstructure (Wang et al, 1996) in hardened cement stone.

The compositions of cement mortar which were used for penetration tests are presented Table 3 Specimens of cement mortars were stored after demoulding until 7d in a moisture cabinet (20°C/95% RH) and then 1d in a climate room 20°C/65% RH for trying, the glass cylinder for penetration test were pasted over cement mortar with epoxy resin. The penetration volume on cement mortar were tested with different solutions (water, diesel, 20% NaCl solution and 5% lactic acid).

Table 3 : Compositions of mortars for penetration tests

Samples		A	B
CEM I 52 5 R	g	630	-
HPCB	g	-	630
Quartz sand 0-2 mm	g	1170	1170
w/c ratio		0.390	0.260
Spread measure*	cm	16.0	22.5

* : According to DIN 1060 part 3

The results of penetration tests are shown in Fig 2. It can be seen that the penetration volume on HPCB mortar are much lower than the Portland cement CEM I 52.5 R and the penetration rate of different solutions on HPCB mortar after 3 months tends to slow down.

CONCLUSIONS

The newly developed HPCB - a modification of Ordinary Portland Cement - has not only a very high early strength, but also a good strength development in course of the later hydration because of the very low water demand of the high performance cementous binder. In comparison to Portland cement the HPCB shows a very good strength development by the low temperature too The mortar and concrete which are improved with the high performance cementous binder have a very good resistance against the chemical and the mechanical attack because of the very dense microstructure of the hardened cement stone.

REFERENCES

Wang, J.-F., Adler, J., "Investigation on a new superplasticizer", Concrete Precasting Plant, (Betonwerk + Fertigteil-Technik), 11/1995, pp. 98-104

Wang, J.-F., Adler, J., "Microstructure and resistance against chemical attack of high performance concrete", 18th Inter. Con. on Cement Microscopy, April 1996, Houston/USA, pp. 205-214

2ii039
8 pp

Kno. 25. JAN. 2001 dok J/802

BLENDS OF BASIC CEMENTS OF DIFFERENT PHASE COMPOSITIONS HYDRAULIC BEHAVIOUR STUDIES

A.S. HEBLE, K. VISHWANATHAN, A.K. CHATTERJEE
Research & Consultancy Directorate
The Associated Cement Cos. Ltd.
Thane 400 604, India

ABSTRACT Generically different basic cements - Ordinary Portland Cement, Calcium Aluminate Cement, Calcium Sulpho Aluminate Cement and Calcium Fluoro Aluminate Cement are in production in company facilities. These cements have been studied in isolation or in combination to understand their complex hydraulic behavior. The setting and hardening,Volume change,Strength progression and Retrogression,Formation of hydrated phases etc. are features studied and reported in this paper.

KEY-WORDS Setting ,Hardening,Volume change,Hydration

INTRODUCTION

In India, under the auspices of the Associated Cement Cos. Ltd. a variety of special cements are in regular commercial production. In addition, a host of modified or composite cementitous formulations based on these cements are made and used in industrial applications like heavy machinery foundation, bolting of mineroofs, concrete structure repairs, etc. Depending on their end use, they differ in properties like setting and hardening, strength development, expansive properties, etc. A need was therefore, felt to undertake a study to understand the complexities of hydraulic behaviour of such formulations on account of the phases appearing in the basic cements and their influences in hydraulic reactions. The paper enumerates some of these aspects of study on setting and hardening, expansion, strength progression or retrogression, formations of hydrated phases, etc. In some formulation the effect of cold temperature on the strength development is also dealt with.

MATERIALS USED

The basic materials in the studies are from commercial production facilities. These are Ordinary Portland Cement (OPC), High Alumina Cement (HAC), High Purity Calcium Aluminate Cement (CAC), Calcium Sulpho Aluminate - Belite cement (CSA-B) as well as Calcium Sulphoaluminate Clinker (CSA-C), and Calcium Fluoro Aluminate Clinker (CFA).The chemical and phase compositions are given in Table 1. The present paper deals with the early age hydration studies of the following types of blend prepared from the above base materials

(a) : OPC blended with 10% & 50% of HAC, CAC, CSA-B and CSA-C separately ; OPC blends with 10% special cements have also been studied with additional gypsum mixing
(b) : HAC, CAC, CSA-B and CSA-C blended with 10% OPC
(c) : Two different low-temperature hydration blends
(d) : HAC blended with 10% & 50% CSA-B and CSA-C seperately,HAC with 10% special cements have also been studied with additional gypsum mixing.

Table - 1 : Chemico-mineralogical characteristics of basic ingredients of blends

	OPC (%)	HAC (%)	CAC (%)	CSA-B (%)	CSA*-C (%)	CFA* (%)
SiO_2	22.0	1.6	0.6	12.0	3.4	1.8
Al_2O_3	5.0	50.4	72.6	17.7	13.8	53.9
CaO	62.7	33.7	23.8	45.2	59.7	40.3
SO_3	2.3	-	-	9.3	17.2	<0.1
LOI	1.5	0.6	0.6	3.4	1.6	1.4
F^-	-	-	-	-	-	0.9
PHASES PRESENT						
	C_3S +++	CA ++++	CA +++	C_4A_3S ++++	C_4A_3S ++	$C_{12}A_7$ ++++
	C_2S +++	CA_2 ++	CA_2 +++	C_2S +++	$CaSO_4$ +++	$C_{11}A_7CaF_2$ +++
	C_3A +	$C_{12}A_7$ ++	$C_{12}A_7$ Traces	Gypsum ++	Free lime ++	
	C_4AF +					
	Gypsum +					

*** Indicating Clinker Samples**

METHODOLOGY

All the above formulations were subjected to different tests for evaluation which are indicated below :

a) Neat cement pastes (W/C 0.4) were cast and the hardened cement pastes were demoulded at designated period such as 1 day, 3 days and the samples were washed in alcohol and vacuum dried to prevent any continuance of hydration. These samples were subjected to X-Ray diffraction analysis with scanning speed of 0.2° two theta per minute using a Siemens D-500 X-Ray Diffractometer. Selected samples were also observed under Jeol JSM 5400 Scanning Electron Microscope to observe the presence/development of hydrated phases and their morphology.

b) Setting Time was determined with the help of a Vicat Apparatus.

c) Compressive Strength was determined on samples prepared with A/C 3.0 & W/C 0.4. As some amount of expansive property was expected in these mortars, prism of 40X40X160 mm were restrained from all sides till the age of the test.

d) Expansion Test was carried out with the same mortar that was used for strength test.

e) Low temperature effect was studied on the calcium sulpho aluminate and calcium fluoro aluminate cement formulations for the strength development at temperatures down to -5°C.

RESULTS

Ordinary Portland Cement Blends

The trends of variation of compressive strengths of OPC blends at early ages are depicted in Fig. 1(a) & (b). Considering the strengths of reference OPC as 100% at 1,3 & 7 day the relative quantitative variations of strengths of 10% and 50% blends are shown in Table 2. From this table it is evident that when 10% or 50% of HAC or CAC is blended with OPC, the fall in strength is seen right at 3 days hydration but the fall maintains thereafter at the same sort of level in both the situations. Increase in the percentage of the aluminate cements does not reflect in any detectable difference, although the purity of the aluminate cements does affect the magnitude of the strength deterioration.

Table 2 OPC System : OPC + Basic Cement :
Relative quantitative variation of strengths (% of OPC Strength)

OPC + Basic + Gypsum	50 : 50 : 00 Blend			90 : 10 : 00 Blend			86 : 9.5 : 4.5 Blend			10 : 90 : 00 Blend		
	1D	3D	7D	1D	3D	7D	1D	3D	7D	1D	3D	7D
OPC + HAC	108	74	71	108	101	72	65	116	87	29	56	50
OPC + CAC	91	85	85	91	100	73	96	120	96	64	70	70
OPC + CSA -B	129	44	30	129	108	91	94	126	98	200	135	117
OPC + CSA -C	129	109	100	129	152	104	84	144	139	139	128	122
OPC + CFA	168	117	97	168	133	107	100	139	144			

On the other hand the blending of 10% and 50% CSA-B and CSA-C indicates more erratic trend in strength characteristics.Fig.1(c) & (d).While immediately after 24 hours of hydration there is generally an increase but later there is progressive deterioration; the strength reduction in the case of 50% blends of CSA-B is quite precipitous.

The hydration related information of the above blend systems is summarised in Table 3 &4. The substantial reduction in setting time in all blends and progressively increasing expansions both in free and restrained state in blend with 50% CSA-B, 10% CSA-C & 50% CSA-C are worth noting. These properties need to be seen in the context of formation of hydrated phases in these blends.

Among the hydrated products the C-S-H gel phases, although seen with the help of SEM, could not be detected by XRD owing to their amorphous poorly crystalline nature. Only crystalline hydration products were identified by XRD. As can be seen from the Table 4, 50% & 10% CSA-C blends show major Ettringite phase both at 1 & 3 days. Whereas in the case of 50% CSA-B Ettringiee formed on 1 day gets partly converted to monosulphate on third day,further part of C_4A_3S phase still remains as unhydrated phase.

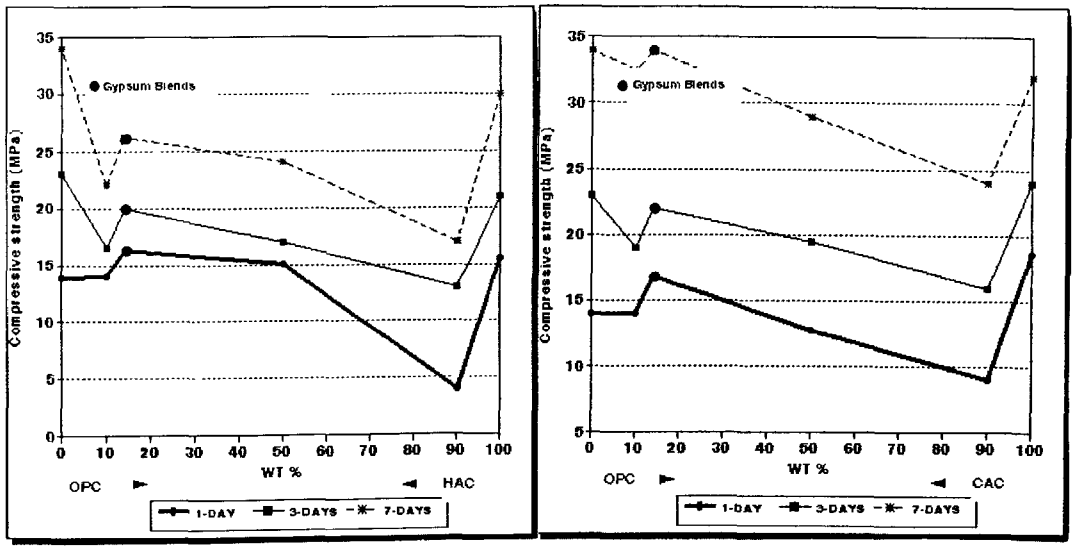

(a) (b)

Fig 1 : Variation of compressive strength of OPC blends (a). OPC & HAC, (b). OPC &CAC

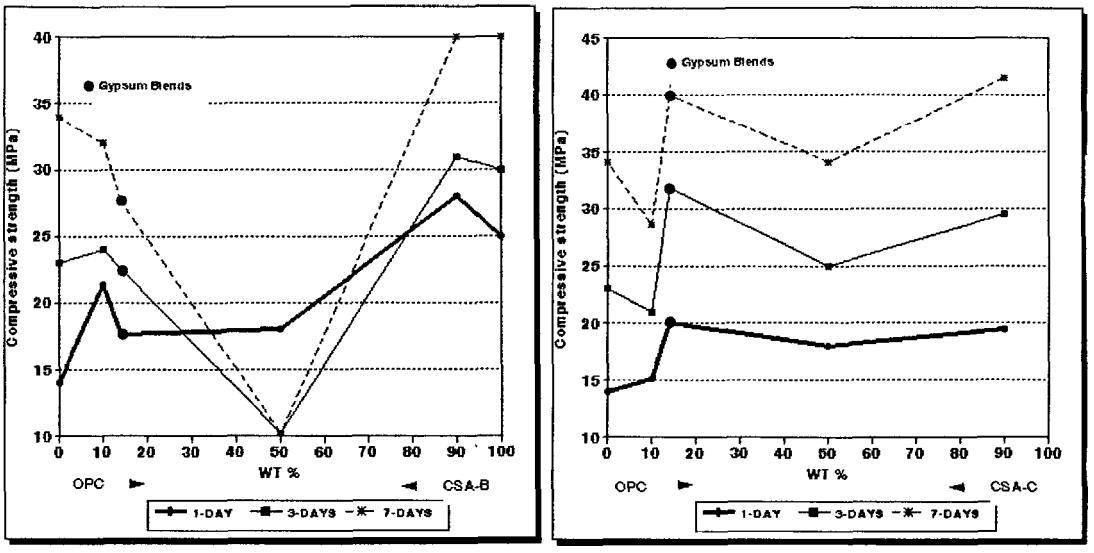

(c) (d)

Fig 1 Variation of compressive strength of OPC blends
(c) OPC & CSA-B blends (d) OPC & CSA-C blends

Table 3 Variation in setting time , & Expansion vis-a-vis Relative abundance of hydrated & unhydrated phases in OPC Systems.

	OPC + HAC + Gypsum								OPC + CAC + Gypsum							
	10:90:00		50:50:00		90:10:00		86:9.5:4.5		10:90:00		50:50:00		90:10:00		86:9.5:4.5	
	1D	3D	1D	3D	1D	3D	1D	3D	1D	3D	1D	3D	1D	3D	1D	3D
ST% (I)	91	-	94	-	94	-	94	-	18	-	82	-	79	-	79	-
reduction (F)	78	-	88	-	92	-	94	-	Nil	-	73	-	71	-	63	-
Expansion % Free	Nil	-	Nil	-	0.02	-	0.01	-	Nil	-	Nil	-	Nil	-	0.01	-
Restrained	Nil	-	Nil	-	0.01	-	0.01	-	Nil	-	Nil	-	Nil	-	0.01	-
a) Hydrated Phases																
P	L	L	L	M	L	H	H	H	M	L	M	M	H	H	H	H
E	M	-	-	L	L	L	L	M	-	-	-	-	-	-	H	M
MS	-	-	-	-	-	-	-	-	-	L	-	L	-	M	-	L
S	-	-	L	L	-	-	-	-	L	L	M	H	-	-	L	L
CAH_{10}	-	-	L	-	-	-	-	-	L	-	L	-	L	-	-	-
C_2AH_8	-	-	-	-	-	-	-	-	L	M	-	M	-	L	-	-
C_3AH_6	-	L	-	L	-	-	-	-	-	L	-	-	-	-	-	-
b) Unhydrated Phases																
C3S	M	M	L	L	H	M	H	M	M	L	M	M	L	L	M	M
C2S	H	H	H	H	H	H	H	H	H	M	H	H	H	H	H	H
C3A	-	-	-	-	-	-	-	-	-	-	-	-	-	-	-	-
C_4AF	-	-	L	L	L	L	L	L	-	-	L	L	L	L	L	L
C_4A_3S	-	-	-	-	-	-	-	-	-	-	-	-	-	-	-	-
CA	M	L	M	L	M	L	L	L	M	-	H	M	H	M	L	-
CA_2	H	M	L	-	-	-	-	-	M	M	H	L	H	-	L	-
$C_{12}A_7$	-	-	-	-	-	-	-	-	-	-	-	-	-	-	-	-
C_2AS	H	H	H	H	L	L	M	M	-	-	-	-	-	-	-	-

ST=Setting Time, (I) = Initial, (F) = Final ,H=High, M= Medium , L= Low, P=Portlandite, E= Ettringite, S= Stratlingite, MS=Mono Sulphate,

Table 4 Variation in setting time , & Expansion vis-a-vis Relative abundance of hydrated & unhydrated phases in OPC Systems.

	OPC + CSA-B Blends								OPC + CSA-C Gypsum							
	10:90:00		50:50:00		90:10:00		86:9.5:4.5		10:90:00		50:50:00		90:10:00		86:9.5: 4.5	
	1D	3D	1D	3D	1D	3D	1D	3D	1D	3D	1D	3D	1D	3D	1D	3D
ST % (I)	97	-	94	-	79	-	79	-	85	-	91	-	106	-	76	-
reduction(F)	96	-	94	-	76	-	51	-	82	-	90	-	92	-	57	-
Expansion % Free	0.06	-	0.03	-	0.01	-	0.01	-	4.0	-	0.8	-	0.4	-	0.2	-
Restrained	0.04	-	0.03	-	0.01	-	0.04	-	2.0	-	0.4	-	0.2	-	0.1	-
a) Hydrated Phases																
P	L	M	L	L	H	H	H	H	H	H	M	H	M	H	H	H
E	M	M	M	M	M	M	L	M	M	M	H	H	H	H	H	H
MS	-	L	-	L	-	L	-	-	-	-	-	-	-	-	-	-
S	-	L	-	-	-	-	-	-	-	-	-	-	-	-	-	-
CAH_{10}																
C_2H_8																
C_2AH_6																
b) Unhydrated Phases																
C_3S	M	L	M	-	M	M	M	M	-	-	M	M	H	M	H	M
C_2S	H	M	M	M	H	H	M	M	H	M	M	M	H	H	M	M
C_2A	-	-	-	-	-	-	-	-	-	-	-	-	-	-	-	-
C_4AF	L	L	L	L	L	L	L	L	L	L	L	L	L	L	L	L
C_4A_3S	L	L	L	L	-	-	-	-	-	-	-	-	-	-	-	-
CA	-	-	-	-	-	-	-	-	-	-	-	-	-	-	-	-
CA_2	-	-	-	-	-	-	-	-	-	-	-	-	-	-	-	-
$C_{12}A_7$	-	-	-	-	-	-	-	-	-	-	-	-	-	-	-	-
C_2AS	-	-	-	-	-	-	-	-	-	-	-	-	-	-	-	-

On addition of 1% Superplasticiser to OPC + CSA-C blend with 4.5% gypsum, complete rheology of the mix changed from a plastic to flowable, and gave a working time of 30 minutes and compressive strength rise of 20 - 25% at 1 & 3 days compared to blend without superplasticiser. A SEM photograph showing formation of Ettringite phase in the cement paste is shown in Fig 3.(a).The OPC blends with CSA-B & CFA set and gain strength even at low temperature although the rise is slow. This property is not observed in OPC as can be seen in Table 5.

Table 5: Effect of Low temperature on OPC & CSA-B and OPC & CFA mixes

Temperature degree C		Compressive strength (MPa)								
Mixing	Curing	OPC 100%			OPC+CSA-B 10% + 90%			OPC+CFA+GYP 50% + 35% + 15%		
		1D	3D	7D	1D	3D	7D	1D	3D	7D
27	27	25	35	60	41	45	48	42.5	46	47.5
15	-5	NO STRENGTH			5	6	16	6	10	21
10	-5	NO STRENGTH			3	6	16.5	8	12.5	21.5

High Alumina Cement Blends

The trends of variation of compressive strengths of HAC blends at early ages are indicated in Fig.2. Considering the strength of reference HAC as 100% at 1,3 & 7 day, the relative quantitative variations of strength of various blends with CSA-B & CSA-C are shown in Table 6. From Table 6 it is evident that all the HAC & CSA-B blends are more or less steady and higher strength potential right from 1 day to 3 days, hydration but in the case of HAC+ CSA-C blends fall in strength is seen right from 1st day in the case of 50% blend and the blend with gypsum.

Table 6 - HAC System with CSA-B & CSA-C. Relative variation in strength shown as % of HAC strength

HAC + Basic+ Gypsum	10 : 90 : 00			50 : 50 : 00			90 : 10 : 00			86 : 9.5 : 4.5		
	1D	3D	7D	1D	3D	7D	1D	3D	7D	1D	3D	7D
HAC + CSA-B	174	166	140	86	118	105	110	110	98	116	126	127
HAC + CSA-C	90	109	107	29	21	9	39	43	40	86	73	73

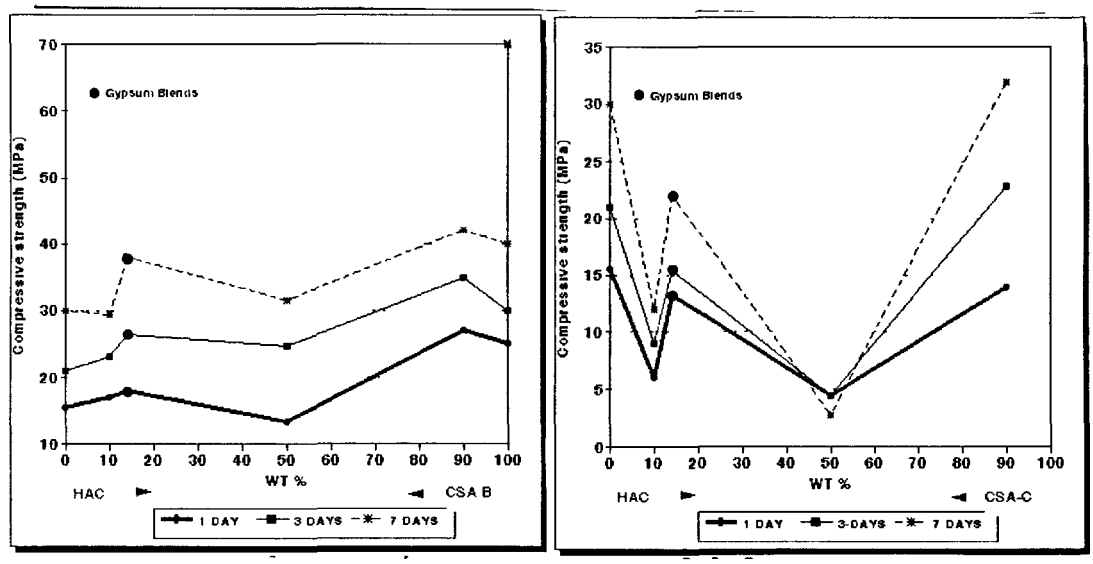

(a) **(b)**

Fig 2 Variation of compressive strength of HAC blends
(a) HAC & CSA-B blends (b) HAC & CSA-C blends

The hydration related information of the blend system is summarised in Table 7. In the case of 50% CSA-B Ettringite appears as a steady phase both at 1D & 3D hydration along with appearance of Monosulphate at 1 day, the latter slightly increases but the strength fall is not seen This may be due to substantial formation of Stratlingite right from one day which remain unchanged even after 3 days hydration (Fig. 3b) which may be responsible for slight gain in strength from 1 to 3 days, however, no evidence of conversion of aluminate phases was noticed. But in 50% blend with CSA-C no Ettringite is seen and Monosulphate appears right at 1st day and is responsible for the erratic trend in strength.

In these systems there appears substantial reduction in setting times in all the blends and progressive increase in the expansion values as the percent CSA-B or CSA-C increases in HAC and part conversion of Ettringite to Monosulphate is seen at 3day hydration in almost all the cases.

Table 7 Variation in setting time & Expansion vis-a-vis Relative abundance of hydrated & unhydrated phases in HAC Systems.

	HAC + CSA-B Blends								HAC + CSA-C Blends							
HAC + Basic + Gyp.	10:90:00		50:50:00		90:10:00		86:9.5:4.5		10:90:00		50:50:00		90:10:00		86:9.5: 4.5	
	1D	3D	1D	3D	1D	3D	1D	3D	1D	3D	1D	3D	1D	3D	1D	3D
ST (I)	77	-	77	-	69	-	62	-	92	-	92	-	92	-	85	-
reduction (F)	89	-	89	-	87	-	82	-	97	-	96	-	97	-	92	-
Expansion % Free	0.08	-	0.08	-	0.02	-	Nil	-	4.0	-	0.8	-	0.1	-	0.2	-
Restrained	0.04	-	0.06	-	0.02	-	Nil	-	1.8	-	0.4	-	0.2	-	0.1	-
a) Hydrated Phases																
P	M	M	M	L	L	-	L	-	M	H	H	M	M	M	M	-
E	H	H	M	M	-	-	-	-	H	M	-	-	L	L	M	L
MS	-	L	-	L	-	L	-	-	-	L	M	M	-	L	-	L
CAH_{10}	-	-	-	-	M	-	M	M	-	-	-	-	-	-	-	-
C_2AH_8	-	-	-	-	M	M	L	M	-	-	-	-	-	-	-	-
S	-	L	M	M	-	L	-	L	-	-	-	-	-	-	L	-
C_3AH_6	-	-	-	-	-	-	-	-	-	-	-	-	-	-	-	-
AH_3	-	-	-	-	-	-	-	-	-	-	-	-	-	-	L	L
b) Unhydrated Phases																
CA	-	-	-	-	-	-	M	M	M	M	-	-	M	L	M	M
CA_2	M	-	L	-	M	M	M	M	-	-	-	-	-	-	-	-
$C_{12}A_7$	-	-	-	-	-	-	-	-	-	-	-	-	-	-	-	-
C_2AS	-	-	H	H	H	H	H	H	M	M	H	H	H	H	H	H
C_2S	M	M	M	M	-	-	-	-	-	-	-	-	-	-	-	-
C_4A_3S	L	-	M	L	L	-	-	-	-	-	-	-	-	-	-	-
Gypsum	-	-	-	-	-	-	-	-	-	-	-	-	-	-	-	-

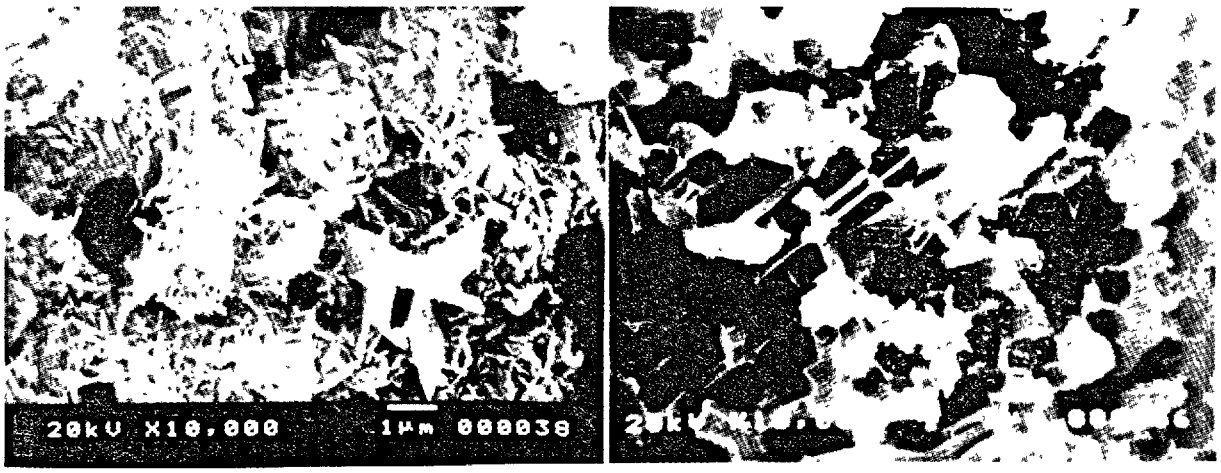

(a) (b)

Fig.3 SEM Photomicrograph showing (a) needles of Ettringite crystals in OPC+CSA-C+ Gypsum blend (b) stratlingite & $Ca(OH)_2$ in 50:50 blend of HAC+CSA-B both at 3 days hydration

CONCLUSIONS

- In the specially tailored blends of OPC with other binders like Calcium Aluminate or Calcium Sulphoaluminate based cements, the original phase assemblage of the latter assumes critical significance. The presence of aluminates other than CA in the aluminate cements or presence / absence of belite along with Calcium Sulphoaluminate requires a careful consideration in achieving the desired setting, hardening and expansion characteristics.
- The supplementary influence of gypsum separately incorporated in certain blends or the use of superplasticisers in some often significantly alter the strength properties and workability respectively.
- For low temperature applications appropriate blends can better be based on either sulphoaluminate or fluoroaluminate cements.
- In all OPC based blends there was virtual absence of crystalline CSH phase and in all HAC blends studied the nonappearance of C_3AH_6 is also worthy to note.
- The optmisation of setting characteristics, strength properties and expansion behaviour appears easier if the trend of appearance of hydrated phases are considered.

ACKNOWLEDGEMENT

The authors gratefully acknowledge the help rendered by Dr.J.Chitale & Dr.S.K.Jatty in experimental work and preparation of this paper.

REFERENCES :

Bayoux J.P., Bonin A., Marcdargent,Mathieu A & Verschaeve M "Study of the hydration propertiesof aluminous cement & calcium sulphate mixes". Proceedings of the Int. Sym. on Calcium Aluminate Cement, London, 9-11 July, 1990, Edt by R.J. Mangabhai, pp - 320 - 324.

Brooks S.A. & Sharp J.H., "Ettringite based cements" - Pro. of the Int. Sym. on Calcium Aluminate Cement, London, 9-11 July, 1990, Edt by R.J. Mangabhai, pp - 335 -350.

Mudbhatkal G. A., Parmeswaran P.S., Heble A.S., Pai B.V.B,Chatterjee A.K.,"Non-alitic cement from calcium sulphoaluminate clinker optimisation for high strength and low temperature application", 8th ICCC, Brazil, 1986,Theme 3 Vol IV PP 364-370

Fukuda Nobue "Fundamental studies on the expansive cement" - 1, Suppl. paper IV, 69, 5th Int, Symp. on the Chemistry of the Cement, Tokyo, 1968, pp 342 - 418.

2ii040
4 pp

Kno. 25. JAN. 2001 doc 31803

EFFECT OF GYPSUM ON THE HYDRATION OF ALITE AND BELITE

Hirotaka USHIYAMA Yoshiyuki SHIGETOMI and Yasushi INOUE, Cement/Concrete & Building Materials Research Laboratory, Tokuyama Corp., Tokuyama, Yamaguchi, Japan

ABSTRACT The effect of gypsum on the hydration of alite and belite was investigated. Mixtures of alite or belite with gypsum were mixed with water at 0.5 w/c. The experiment was carried out by means of XRD, DTA, EPMA and chemical analysis, and also the compressive strength developement of the paste was measured

INTRODUCTION

Gypsum in portland cement plays an important role for the hydration of C_3A, so there are many papers related to the hydration of C_3A clinker-gypsum system. And there are not so many papers related to the hydration of calcium silicate clinker-gypsum system(Yamaguchi et al, 1959, Benture, 1976), however it is also important to investigate the hydration of this system in order to make more clear the role of gypsum on the hydration of portland cement. In this paper the effect of gypsum on the hydration of calcium silicate clinker is investigated, comparing the effect on the hydration of alite and that of belite.

EXPERIMENT

Synthesis of alite and belite

Based on the paper by Yamaguchi(1968), the raw mixtures for synthesizing alite and belite were prepared respectively from chemical grade reagents and heated in electric furnace. Alite:Raw mixture for Alite was heated three times at 1500℃ for two hours with intermediate grinding and finally groud to 3000cm²/g of Blaine value. Belite:Raw mixture for belite was heated at 1500℃ for two hours, cooled and heated at 1000℃ for one hour. This product(Belite-1 or B-1) was found to be β-C_2S and not to contain interstitial phase like as C_3A by XRD. However, by EPMA analysis B-1 was found to contain a very small amount of interstitial phase. This phase was eliminated by KOSH solution (Gutterridge, 1978), and the product was heated at 900 ℃ for 1 hour , then Belite-2(or B-2) which did not contain interstitial phase was obtained. B-1 and B-2 were ground to 3000cm²/g of Blaine value respectively and B-2 was also found to be β-C_2S XRD. The chemical compositions of alite, belite-1 and belite-2 are shown in Table 1.

Experimental method

Chemical grade gypsum was added to alite and belite so as to get SO_3 content(=SO_3/alite or belite weight ratio)being 0, 1, 2, 3, 5 or 7%. Hydration temperature was 20℃, and water to solid ratio was 0.5 in all experiment. The hydration degree was determined by XRD internal standard method with Al_2O_3.

Table-1 Chemical Ccmposition (wt%)

	SiO_2	Al_2O_3	Fe_2O_3	CaO	MgO	Na_2O	K_2O
Alite	26.1	1.2	-	71.6	1.0	-	-
Belite-1	32.5	2.8	1.2	62.7	0.5	0.2	0.1
Belite-2	33.8	1.3	0.7	63.5	0.5	0.1	0.1

RESULTS AND DISCUSSION

Hydration of alite

As is shown in Fig 1 the hydration of alite was accelerated by addition of a small amount of gypsum, and was most accelerated in case of SO_3 content of 1～2%. The degree of hydration, however, shows an increase below 10%. In SO_3 content of more than 2% the hydration degree becomes smaller with increase of SO_3 content. This tendency was also seen

in the amount of $Ca(OH)_2$ produced as shown in Fig 2. But, as to combined water this tedency was not clearly seen as shown in Fig 3.

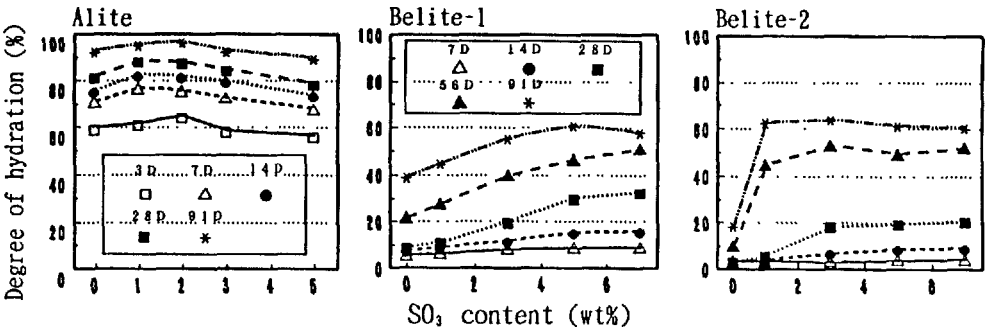

Fig. 1 Effect of gypsum content on the degree of hydration

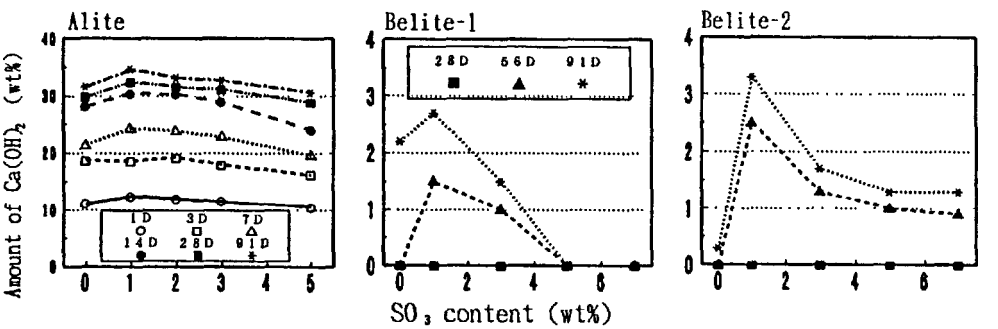

Fig. 2 Effect of gypsum content on the amount of $Ca(OH)_2$ produced

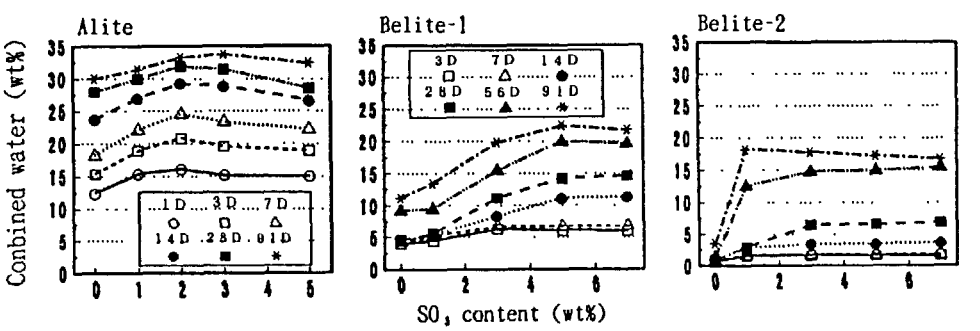

Fig. 3 Effect of gypsum content on combined water

Hydration of belite

As is shown in Fig 1 , even though the SO_3 content is increased to 7% the hydration of B-1 and B-2 in 7 days is not almost accelerated. In 28 to 91 days, however, the hydration is largely accelerated by addition of gypsum. This tendency is seen in combined water as shown in Fig 3. However, this tendency is not seen in $Ca(OH)_2$ produced, that is, in SO_3 content of more than 1% the amount of the produced $Ca(OH)_2$ is decreased with increase of SO_3 content as shown in Fig 2. This is considered to be due to formation of ettringite. By comparison of the hydration of B-1 and B-2 within small SO_3 content, B-2 is influenced more largely than B-1. That is, in SO_3 content of 1% the hydration of B-2 is largely accelerated in 56 to 91 days and even though SO_3 content is increase to more than 1% the hydration degree does not become larger than that in SO_3 content of 1%.

On the other hand the hydration degree of B-1 in 56 to 91 days was affected by SO_3 content, that is , the more the SO_3 content the larger the hydration degree. This means that gypsum added to B-1 was consumed for formation of ettringite and little amount of gypsum remains for accelerating the hydration of belite. It is considered that a small amount of gypsum is sufficient for accelerating the hydration of belite without interstitial phase.

Compressive strength of paste

The highest strength of alite paste is shown in SO_3 conten of 1 to 2 %, and in more than 3 % the strength lowers with the insrease in SO_3 content. The paste strength of belite becomes higher with the increase in SO_3 content as shown in Fig 4.

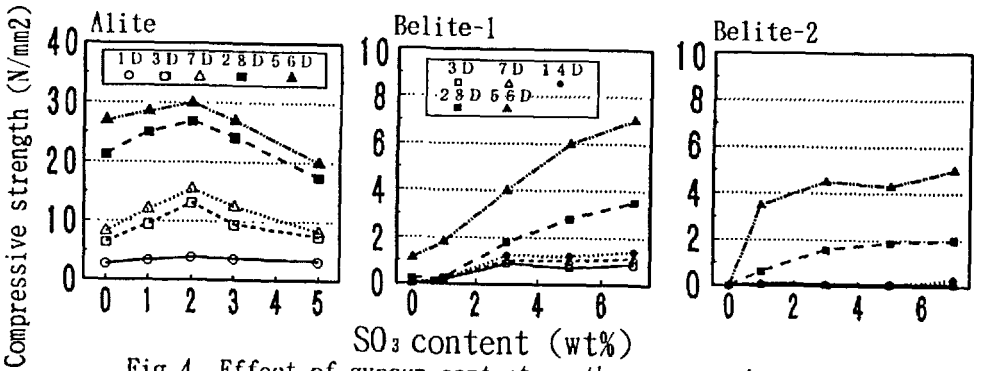

Fig. 4 Effect of gypsum content on the compressive strength

Results of EPMA analysis

Photo 1 shows the back scattered electron images and the EPMA images of S element distribution of the alite- and belite-paste (SO_3 content=5%) before and after hydration. For the alite, gypsum almost disappears already in 7 days and S disperses uniformly in the whole area. On the other, for the belite-2, gypsum remains in initial grain size even in 28 days. These results coincides with those of XRD analyses in Table 2.

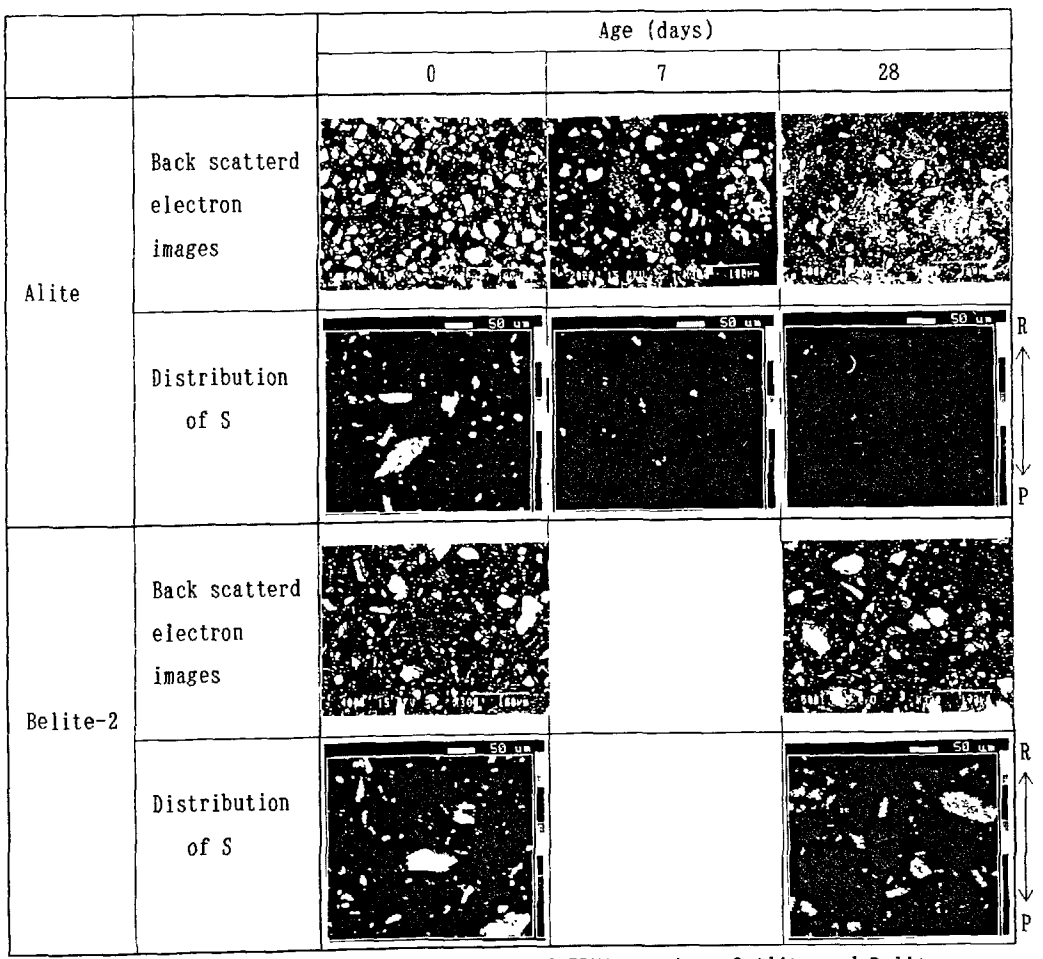

Photo. 1 Back scatterd electron images and EPMA mapping of Alite and Belite

(R:Rich P:Poor)

Discussion on the action of gypsum on alite and belite hydration

Odler(1980) investigated the interaction between gypsum and the CSH-phase formed in C_3S hydration and stated that SO_4^{2-} ions from gypsum are physically adsorbed to the surface of the CSH-phase and an equilibrium exists between the amount of SO_4^{2-} ions adsorbed and the calcium sulphate concentration in the liquid phase. It is also considered that in the hydration of alite-gypsum system amorphous gypsum is produced by combination of Ca^{2+} ion from the hydration of alite and SO_4^{2-} ion from gypsum added initially. In any case it is considered that SO_4^{2-} ion concentration in the liquid phase is rather high , even though not so high as that in the saturated gypsum solution. Consequently it is considered that relatively many SO_4^{2-} ions are liable to move in the liquid phase especially because of mutual diffusion of SO_4^{2-} and OH^-. It is also considered that through the gel pore a part of SO_4^{2-} ions are able to move to the surface of alite grain which have not yet hydrated, affects the surface and accelerates the hydration (Kondo, 1975).

Table2 XRD analyses of the hydration products

	SO3content	Age(days)							
	(%)	1	3	7	14	21	28	56	91
Alite	0	-	-	-	-		-	-	-
	1	-	-	-	-		-	-	-
	2	-	-	-	-		-	-	-
	3	-	-	-	-		-	-	-
	5	G	G	G	E, M		E, M	-	-
Belite-1	0		-	-	-	-	-	-	-
	1		-	-	-	-	E, M	E	M
	3		E	E	E	E	E	E	E
	5		G, E	G, E	G, E	E	E	E	E
	7		G, E	G, E	G, E	G, E	G, E	G, E	E
Belite-2	0		-	-	-	-	-	-	-
	1		G	G	-	-	-	-	E
	3		G	G	G	G	G, E, M	E	E
	5		G	G	G	G	G, E, M	G, E	G, E
	7		G	G	G	G	G, E, M	G, E	G, E

G:Gypsum E:Ettringite M:Monosulphate -:no detect

In case of much addition of gypsum:The hydration type of alite after accelerating period is rather diffusion-controlling (Fujii, 1978). If gypsum is added too much, the gel pore would be blocked with sulphate hydrate, therefore water would not be able to diffuse easily to the unhydrated surface and the hydration would be delayed. On the other hand the hydration type of belite after accelerating period is rather reaction-controlling. Thererfore even though gypsum is added too much the hydration acceleration would not be prevented.

CONCLUSION

Effect of gypsum on the hydration of alite and belite was studied. The results obtained are as follows.

(1) The hydration of alite is accelerated by addition of a small amount of gypsum. The hydration is most accelerated in SO_3 content of 1 to 2%, and in SO_3 content of more than 2 % the degree of hydration lowers with increase of SO_3 content.

(2)The hydration of belite is not almost accelerated in 7 days even though SO_3 content is increased to 7%. In 28 to 91 days the hydration was largely accelerated by adition of gypsum. SO_3 content of 1% is sufficient for accelerating the hydration of belite-2 which does not contain interstitial phase. SO_3 content of more than 1% does not prevent the hydration to be accelerated.

(3)The paste compressive strength of belite becomes higher with increase in SO_3 content.

REFFERENCES

Yamaguchi, G. et al., Semento gijutu nenpo vol. 13, 1959, pp. 62-75(in Japanese)

Bentur, A., Journal of The American Ceramic Society, Vol. 59, NO. 5-6, May-June, 1976, pp. 210-213

Yamaguchi, g. et al., Proc. of The 5th Intern. Symp. on the Chem. of Cement, Vol. I, 1968, pp. 210

Gutteridge, W. A., Cement and Concrete Research, Vol. 9, 1978, pp. 319-324

Ushiyama, H. et al, Semento Gjutu Nenpo, Vol. 30, 1976, pp. 77-81

Kondo, R. et al, Semento Gijutu Nenpo, Vol. 29, 1975, pp. 17-22(in Japanese)

Odler, I., 7th Intrnl. Cong. Chem. Cem., Paris, Vol. IV, 1980, PP. 493-495

Fujii, K., Semento Gijutu Nenpo, Vol. 32, 1978, pp. 22-28(in Japanese)

2ii041
4 pp

Kn o. 2 5. JAN. 2001 d o k 31804

THE EFFECT OF C_3S ON THE HYDRATION OF C_3A

E. EL AOUNI, CPR SOUISSI BP 6210 Rabat-Instituts 10101, Rabat, MOROCCO
M. BENKADDOUR, Département de Physique, Faculté des Sciences, Oujda, MOROCCO

ABSTRACT The cubic phase coming from the hydration of C_3A appears since the first minutes with the hexagonal phases. After 24 h, it is probable that some water is not only adsorbed, but strongly bound as in a hydrate. In the presence of C_3S, two new phases are observed by DTG. The calcium hydroxide coming from the hydration of C_3S is probably less crystalline, and less stable towards thermal decomposition, than that coming from hydration of free CaO.

Key-words: C_3A+C_3S, Hydration, DTG, X-ray Diffraction Analysis, Calorimetry

INTRODUCTION

It is usually admitted that the first products of C_3A hydration are the hexagonal hydrates C_2AH_8 and C_4AH_{13} which are metastable. They transform later into the cubic hydrate C_3AH_6 which is more stable. A disagreement exists between different researchers about the time of this conversion (Breval, 1976; Collepradi et al, 1978; Tashiro and Oba, 1980; Ramachandran and Mei, 1987). Ramachandran and Mei (1987) found a DTG and DSC peak at about 100°C which the attributed to the adsorbed water. However, we found only few investigations concerning hydration of C_3A+C_3S (Corstange et al, 1973; Ghorab et al, 1988). The aim of the present paper is a contribution to the C_3A hydration alone and in the presence of C_3S in comparison with the literature.

EXPERIMENTAL PROCEDURE

Materials

C_3A and C_3S are synthesized from reagent grade $CaCO_3$, Al_2O_3 and SiO_2, by heating the mixtures in appropriate molar ratios. Sometimes we have noted that C_3S was slightly green. Probably the platinum of the crucible (or its oxide) diffuses into C_3S causing this colour (Amossé and Allibert, 1991). Experiments are carried out to establish this hypothesis. C_3A+C_3S was prepared by grinding the sample in a laboratory mill to a Blaine specific surface of about 300 m^2/kg.

Methods

TG and DTG curves of pastes with w/s = 0.5 were obtained by a thermoanalysator G70 SETARAM. The heat development was measured by a Biocalorimeter BCP ARION for pastes with w/s = 1. XRD patterns of the samples were obtained by a Rigaku diffractometer completely automated.

RESULTS AND DISCUSIONS

Fig 1 shows TG and DTG curves of C_3A hydrated for 15 min. The peak at 100°C is attributed to the desorption of water. This result is not in agreement with the view of researchers who suggest that this peak is present only in the presence of admixtures (Milestone, 1977; Sersale et al, 1980). It is also in disagreement with the result of a work in which this peak is particularly evident in the presence of hexagonal hydrates (Monosi et al, 1983). This peak increases up to 16h, after which it decreases. Probably, water is strongly bound. But it is important to note that the cubic hydrate C_3AH_6 appears simultaneously with the hexagonal phases (peaks at 320 and 500°C). This result is not in agreement with a lot of workers (Breval, 1976; Collepardi et al,

1978; Tashiro and Oba, 1980). The formation of C_3AH_6 soon after is probably due to the important heat rate of hydration. Fig 1 depicts also the peak attributed to the hexagonal phases (180°C). XRD confirm the result of DTG (Fig 2).

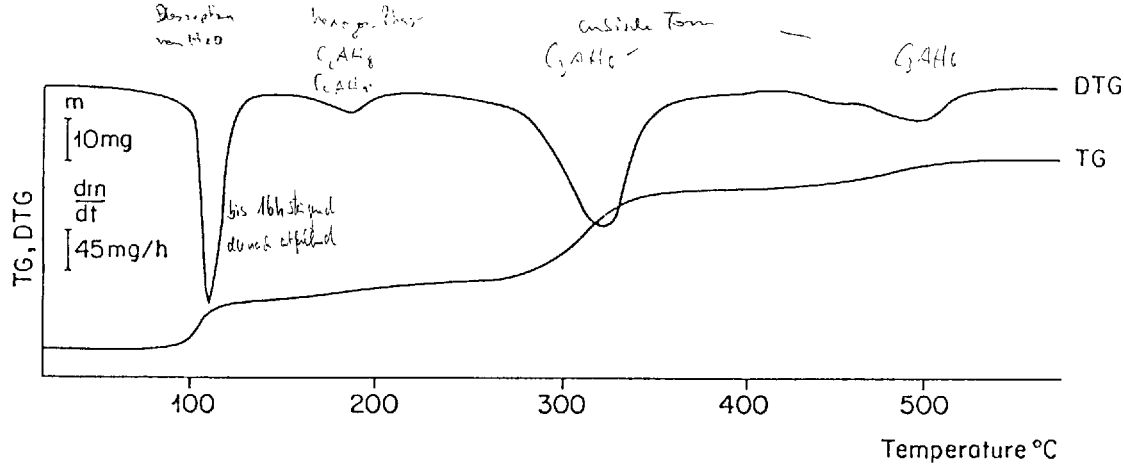

Figure 1 TG and DTG curves of C_3A hydrated for 15 min.

The rate of heat evolution as a function of time shows a large peak during the first 30 min (Fig 3). In the presence of C_3S this peak decreases when the amount of C_3S increases. When the time of hydration increases, two new phases are observed by DTG. The first one can be detected as a peak at 170°C. This peak present in the beginning, seems to disappear at 24h. The second one is observed by the splitting of the peak at 320°C (Fig 4). Water is not adsorbed. The dissolution of Ca^{2+} must be very important. The appearance of these two phases can be related to the work of other researchers (Regourd et al, 1976).

For certain mixtures two peaks were observed around 500°C corresponding to CH. We concluded that CH coming from C_3S hydration probably is poorly crystallized and less stable (Fig 5). Investigations on C_3A+C_3S synthesized simultaneously are carried out.

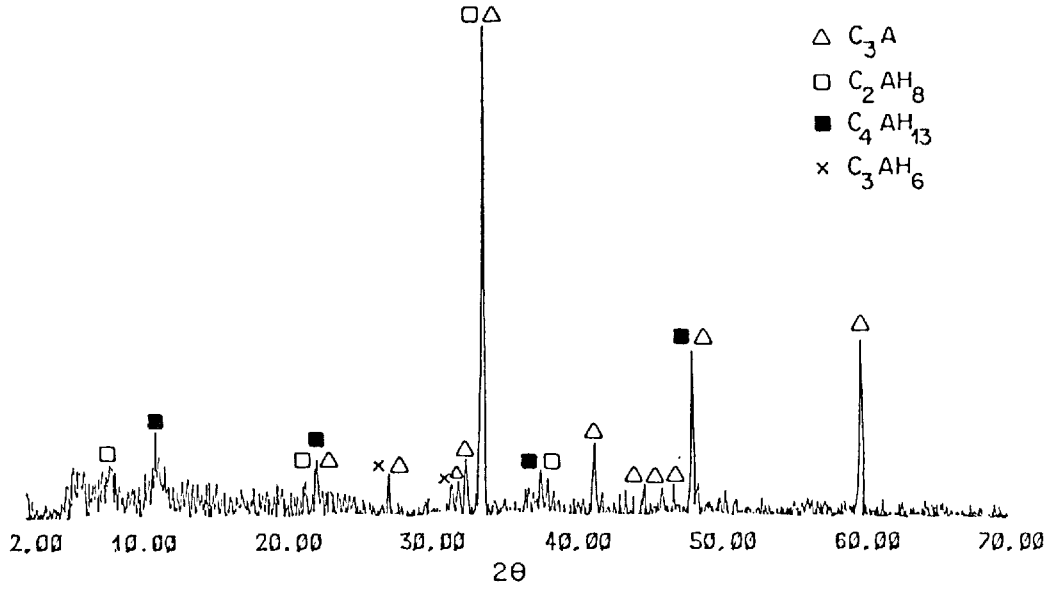

Figure 2 XRD pattern of C_3A hydrated for 15 min.

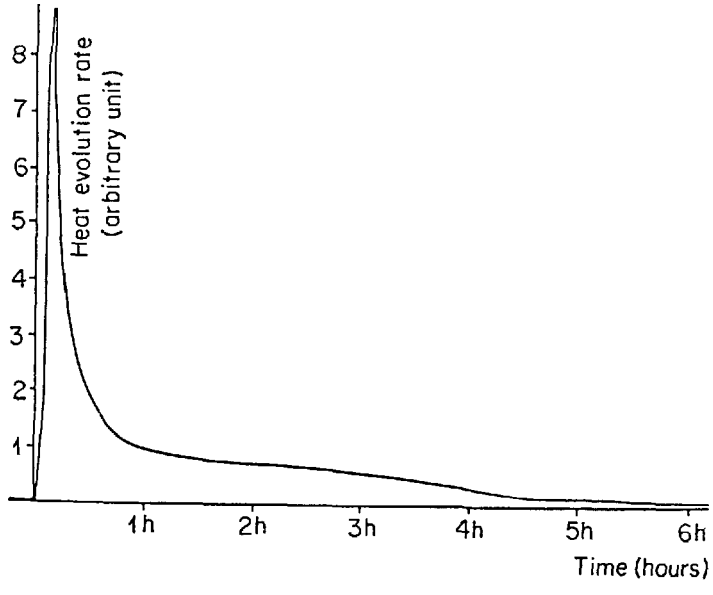

Figure 3 Rate of heat evolution for C_3A

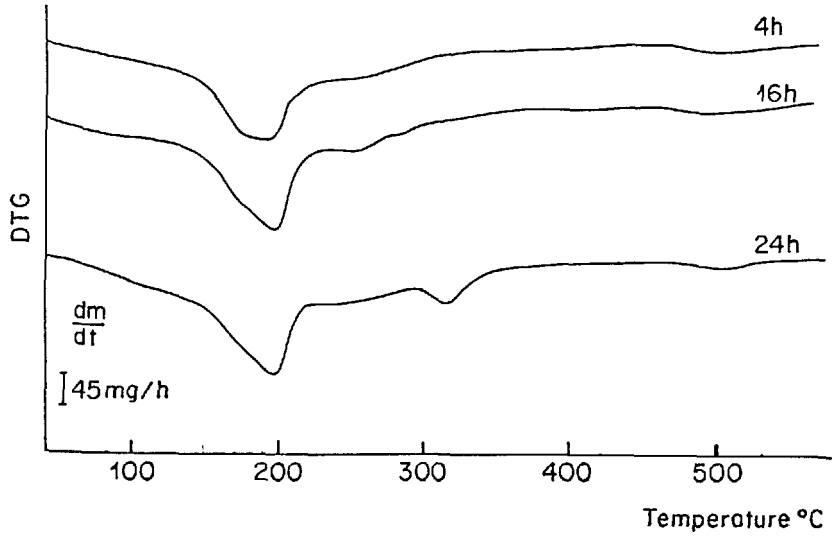

Figure 4a DTG curves of C_3A+50%C_3S hydrated for different times

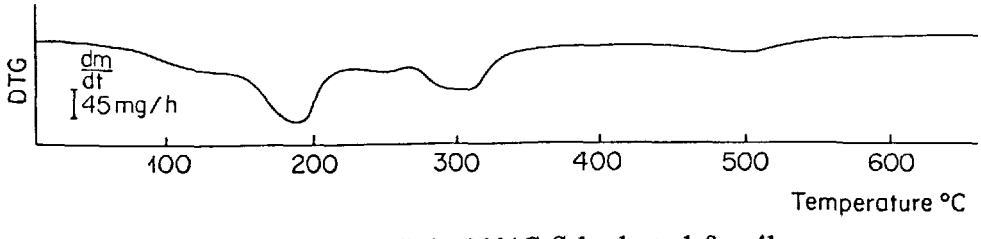

Figure4b DTG curve of C_3A+20%C_3S hydrated for 4h

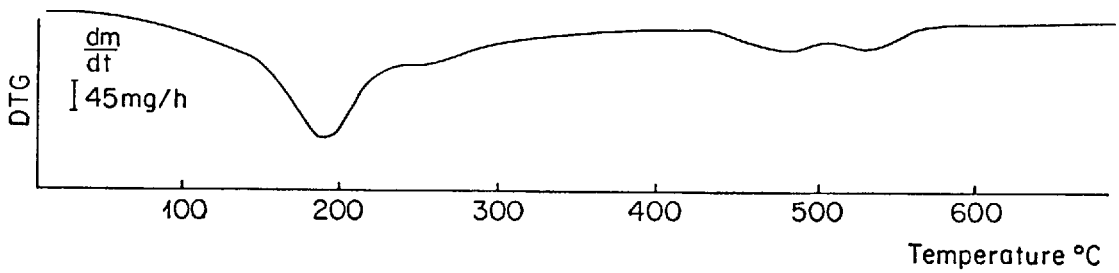

Figure 5 DTG curve of C_3A+100%C_3S hydrated for 8h.

REFERENCES

Amossé and Allibert: "Experimental Study on the Solubility of Pt and Ir in Basic Silicate Melt. Implication for the Differenciation of Platinum Group Elements During Magmatic Process", Chem. Geol. Vol. 81, 1991, pp. 45-53.

Breval, E.: "C_3A Hydration", Cem. Concr. Res., Vol. 6, 1976, pp. 129-138

Collepardi, M., Baldini, G. and Pauri, M.: "Tricalcium Aluminate Hydration in the Presence of Lime, Gypsum and Sodium Sulphate", Cem. Concr. Res., Vol. 8, 1978, pp. 571-580

Corstange, W.A., Stein, H.N. and Stevel, J.M.: "Hydration Reactions in Pastes C_3S+C_3A+$CaSO_4$·2aq+H_2O at 25°C", Cem. Concr. Res., Vol. 3, 1973, pp.791-806

Ghorab, H.Y., Abou El Fettouh, S.H. and Ahmed, H.M.: "New Aspects for the Hydration Reaction of Tricalcium Aluminate in the Presence of Alite", Zement-Kalk-Gips, No. 2, 1988, pp. 624-627

Milestone, N.B., Cem. Concr. Res., Vol. 7, 1977, pp. 45-52

Monosi, S., Moriconi, G., Pauri, M. and Collepardi, M.: "Influence of Lignosulphonate, Glucose and Gluconate on the C_3A Hydration", Cem. Concr. Res. , Vol. 13, 1983, pp. 568-574

Ramachandran, V.S. and Zhang Chun Mei: "Hydration Kinetics and Microstructural Development in the $3CaO·Al_2O_3·CaSO_4·2H_2O$-$CaCO_3$-$H_2O$ System", Matériaux et Constructions, Vol. 19, No. 114, 1987, pp. 437-444

Regourd, M. Hornain, H. and Mortureux, B.: "Evidence of Silicoaluminates in the Hydrated Mixtures of Tricalcium Silicate and Tricalcium Aluminate", Cem. Concr. Res., Vol. 6, 1976, pp. 733-740

Sersale, R., Sabatelli, V. and Valenti, G.L., Proc. VII Int. Congr. Chem. Cem., Vol. IV, 1980, pp. 546-551

Tashiro, C. and Oba, J., Proc. VII Int. Congr. Chem. Cem., Vol. II, 1980, pp. 58-63

ACKNOWLEDGEMENTS

The authors acknowledge with thanks the collaboration of Mrs. Kabbaj, Messrs Satour and Zakaria from the Spectroscopy Laboratory in the "Ministry of Energy and Mines".

2ii042
8 pp

Kno. 25. JAN. 2001 doc 31805

A STUDY ON THE HYDRATION ACTIVITY OF ALITE CONTAINING $\overline{F}$ AND $\overline{S}$

YE Qing,
Department of Civil Engineering, Zhejiang University of Technology, Hangzhou 310014, P.R.China

ABTRACT The hydration activity of Alite containing $\overline{F}$ and $\overline{S}$ in a series of Alite-CaF_2, Alite-$CaSO_4$ and Alite-CaF_2-$CaSO_4$ systems was studied by XRD, SEM/EXAD, QXDA, DTA, conductive calorimeter and chemical analysis. Results indicated that hydration activities of Alite ($\overline{F}$), Alite ($\overline{S}$) and Alite ($\overline{F}$, $\overline{S}$) were obviously influenced by the solid solubility of $\overline{F}$ and $\overline{S}$. The early hydration activity of Alite ($\overline{F}$) was very poor and could be improved by the substitution of $\overline{S}$ in Alite ($\overline{F}$). Furthermore the particularly combined substitution of $\overline{F}$ and Fe_2O_3 in C_3S was the source of reducing the early hydration activity of Alite ($\overline{F}$). The results suggest that as compound mineralizer both gypsum and fluorite may be used in manufacture of cement by low temperature burning technology.

Key-words: Alite, Calcium fluoride, Hydration

INTRODUCTION

Al_2O_3 and Fe_2O_3 act as fluxing agents in the CaO-SiO_2 system, thus reducing the appearance point of liquid phase to 1338 ℃ and quickening the reaction of C_3S synthesis. However, the introduction of fluxing agents cannot change the basic law of thermodynamics so that in this system C_3S can only be synthesized at a temperature higher than 1250 ℃. The introduction of mineralizer CaF_2 causes the formation of C_3S containing $\overline{F}$ and the appearance of liquid phase at 1185 ℃ (Tanaka, 1968). Hence, the presence of $\overline{F}$ leads to a variation of liquid phase characteristics in this system, and the solid solution of $\overline{F}$ causes the change of the thermodynamic performance of the C_3S crystal. Meanwhile, it will be definitely accompanied by a change of C_3S crystal texture and hydration activity (Gutt,1968 and YE, 1992). CaF_2 and $CaSO_4$ act not only as effective mineralizers, but also act as fluxing agents in the production of cement. It is possible to sinter portland cement clinker at a low temperature, in this way. The purpose of this study was to research the hydration activity of Alite containing $\overline{F}$ and $\overline{S}$, namely Alite ($\overline{F}$), Alite ($\overline{S}$) and Alite ($\overline{F}$, $\overline{S}$). This study was identified as being useful to the production of cement at a low temperature.

PREPARATION OF SPECIMENS AND TESTING METHODS

Preparation of specimens

Pure C_3S was synthesized at 1650 ℃ and its crystal type was T_1. Alite was synthesized from the above C_3S by addition of 1%Al_2O_3 ,1%Fe_2O_3 and 1%MgO at 1350 ℃ and its crystal type was M_2. Specimens of Alite or C_3S containing $\overline{F}$ and $\overline{S}$ [Alite ($\overline{F}$), Alite ($\overline{S}$) and Alite ($\overline{F}$, $\overline{S}$)] were synthesized from the above Alite or C_3S by addition of CaF_2 or $CaSO_4$ at 1350 ℃. The compounds used were all of analytical by pure grade.

Experimental methods

Microstructure analysis

The specimens were subjected to XRD, QXDA and chemical analysis. Parts were also analysed by XPS, SEM/EDAX and high temperature microscope in order to determine the crystal type, solubility and purity of these specimens.

Testing hydration activity during early hedration

Rates of heat evolution during the early hydration (36 hours) were determined by conduction calorimetry under the testing condition of specific surface area of samples 300-350m^2/Kg (Blain), water-cement ratio 0.80, and curing temperature 20±2 ℃.

Testing the degree of hydration

Hydration degrees of Alite containing $\overline{F}$ and $\overline{S}$ were tested by determing $Ca(OH)_2$ quantitatively by QXDA under the testing condition of the specific surface area 300-350 m^2/Kg,water-cement ratio 0.30, curing temperature 20±2 ℃ and relative humidity > 90%.

Testing strength development

The strength development was determined by testing compressive strength on cubic specimens with 20mm length under the testing condition of the specfic surface area 300-350 m^2/Kg, water-cement ratio 0.30 cruing temperature 20±3 ℃ and relative humidity > 90%.

Equipment and testing conditions

1. X-ray diffraction analyser: D/Max-A type, (Cu target used) tube electric current 100mA, tube voltage 40 KV.
2. X-ray photoelectron spectroscopy analyzer: KA-ES-300 type.
3. Scanning electron microscope: ASM-SX type, its energy spectrum is EDAX-9100.
4. Conduction calorimeter: made by Building Materials Academy of China.

Code names of samples

Code names AFi, ASj and iAj represent samples of Alite ($\overline{F}$) (Alite containing or added with i% CaF_2), Alite ($\overline{S}$) (Alite containing or added with j% $CaSO_4$) and Alite ($\overline{F}$, $\overline{S}$) (Alite containing or_added with i% CaF_2 and j% $CaSO_4$), respectively. Alite represent C_3S solid solution containing 1%Al_2O_3, 1%Fe_2O_3 and 1%MgO. $\overline{F}$ and $\overline{S}$ represents $F^-$and SO_3 respectively.

RESULTS AND DISCUSSION

Analysis of crystal structure

The crystal types of Alite ($\overline{F}$), Alite ($\overline{S}$) and Alite ($\overline{F}$, $\overline{S}$) are illustrated in Fig.1. The crystal type and coloring phenomenon of Alite ($\overline{F}$) show: M_2, greenish-grey (pure Alite) → M_3, deep iron red (Alite containing 1% CaF_2) → R, dark red (containing > 2%CaF_2). Therefore $\overline{F}$ was a stabilizer for high temperature crystal type of Alite. The solid solution of $\overline{F}$ made Alite ($\overline{F}$) colored and its color was changed from greenish-grey into dark red with the solubility of $\overline{F}$ increased. The limit solubility of $\overline{F}$ in Alite was 1.5% (namely 3.4% CaF_2). The crystal type and color of Alite ($\overline{S}$) show: M_2, greenish-grey (pure Alite) → M_2, greenish-grey (Alite

containing 1% $CaSO_4$) → M_1, greenish-grey (containing > 2% $CaSO_4$). The crystal type of Alite ($\overline{S}$) was decreased and the colors of all Alite ($\overline{S}$) samples were greenish-grey with the solubility of S increased. The limit solubility of $\overline{S}$ in Alite was 2.2% (namely 4.0% $CaSO_4$). The variable law of crystal type and coloring phenomenon of Alite ($\overline{F}$, $\overline{S}$) was determined mainly by $\overline{F}$ solubility, for instance, M_2, greenish grey [Alite ($\overline{F}$, $\overline{S}$) containing 0% CaF_2 and 1% $CaSO_4$] → M_3, pink (containing 1% CaF_2 and 1% $CaSO_4$) → R, iron red (containing 2% CaF_2 and 1% $CaSO_4$). The curve of limit solubilities of $\overline{F}$ and $\overline{S}$ in Alite was obtained (the imaginary line in Fig.1). The color of Alite ($\overline{F}$, $\overline{S}$) became lighter with the solubility of $\overline{S}$ increased.

Hydration activity of Alite ($\overline{F}$)

Rate of heat evolution during early hydration

Fig.2 and Tab.1 show the heat evolution curve for control sample Alite and Alite ($\overline{F}$) determined by conduction calorimetry. The final time of induction period of Alite was 3.0h and the final time (the main heat evolution peak) of acceleratory period 15.0h. The rate of main heat evolution peak $(dQ/dt)_m$ was 6.39 W/Kg and the heat evolved during early 36 hours Q_{36} was 3.80×10^5 J/Kg. But all samples of Alite ($\overline{F}$) (AF0.5, AF1, AF2 and AF3.5) did not reach the final time of induction period during early 36 hours. It indicates that the early hydration activity of Alite containing $\overline{F}$ was very poor.

Degree of hydration

Fig.3a shows degrees of hydration obtained by QXDA for Alite and Alite ($\overline{F}$). At the ages of 1, 3 and 7 days hydration degrees of Alite ($\overline{F}$) samples AF0.5, AF1, AF2 and AF3.5 were much lower than one of control sample Alite. At 1-day age hydration degrees of all Alite ($\overline{F}$) samples were 6%, much lower than one of Alite 30%. At 3-day age degrees of AF0.5, AF1, AF2 and AF3.5 were respectively 30%, 30%, 14% and 12%, lower than one of Alite 49%. At 7-day age, the distinction of hydration rate between low and high solubility of $\overline{F}$ was obviously shown, and the degrees of hydration for AF0.5, AF1 and AF3.5 were respectively 71%, 64% and 20%. At 28-day age the degrees of all Alite ($\overline{F}$) samples were almost equal to one of Alite. It is clear that the incorporation of $\overline{F}$ into Alite affected the early period of hydration and did not affect the later period.

Compressive strength

The hydration process of Alite ($\overline{F}$) sample AF3.5 was much unusual. At 3-day age AF3.5 had not completed its induction period. Its 7-day compressive strength was 17.6 MPa, much lower than the one of Alite 41.2 MPa. But its 28-day compressive strength was 66.7 MPa, higher than one of Alite 61.7 MPa (shown in Tab.2).

Hydration activity of Alite ($\overline{S}$)

Rate of heat evolution during early hydration

The final time of induction period of Alite ($\overline{S}$) sample AS4 was 5.5h, more than one of Alite 3.0h (shown in Fig.2) and its final time of acceleratory period 18.0h, more than one of Alite 15.0h. $(dQ/dt)_m$ of AS4 was 6.89W/Kg, more than one of Alite 6.39W/Kg. Because of its high heat evolution rate in deceleratory period, Q_{36} of AS4 was 4.51×10^5 J/Kg, much more than one of Alite 3.80×10^5 J/Kg. It is clear that the incorporation of $\overline{S}$ into Alite delayed the

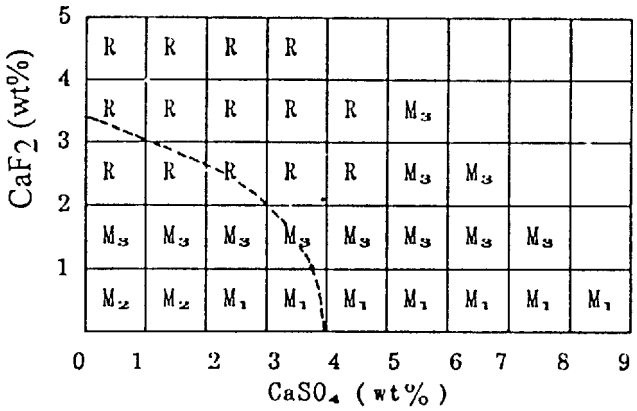

Fig.1 Variation of crystal types and limits of solubility of $\overline{F}$ and $\overline{S}$ in Alite with the amounts of $\overline{F}$ and $\overline{S}$ additives

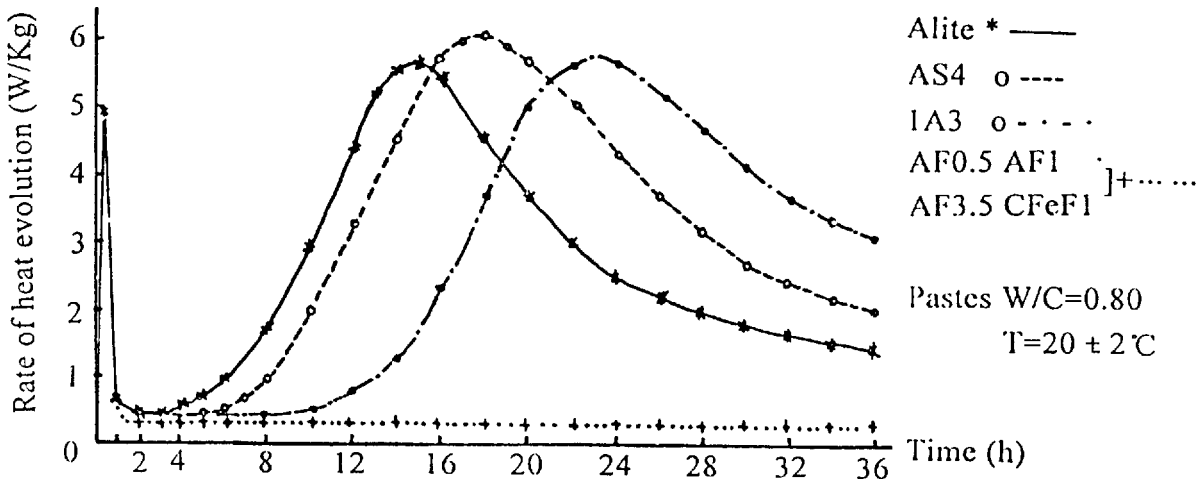

Fig.2 Heat evolution curves for Alite containing $\overline{F}$ and $\overline{S}$ determined by conduction calorimetry.

Tab.1 Rates of heat evolution of Alite containing $\overline{F}$ and $\overline{S}$ during early hydration

Code name of sample	Additive amount in Alite or C_3S (%)		Crystal type	The final time of (h)		(dQ/dt)m (W/Kg)	Q_{3d} ($\times 10^3$ J/Kg)
	CaF_2	$CaSO_4$		induction period	acceleratory period		
Alite	/	/	M_2	3.0	15.0	6.39	38.0
AF0.5	0.5	/	M_3	> 36	/	/	42.9
AF1	1.0	/	M_3	> 36	/	/	42.9
AF3.5	3.5	/	R	> 36	/	/	42.9
AS4	/	4.0	M_1	5.5	18.0	6.89	450.7
1A3	1.0	3.0	M_3	10.2	23.0	6.46	409.0
CFeF1	1.0	1% Fe_2O_3	R	> 36	/	/	42.3

acceleratory period 2 hours.

Degree of hydration

At 1-day and 3-day ages the hydration degrees of Alite ($\overline{S}$) sample AS1, AS3 and AS4 were almost equal to one of Alite. But at 7-day and 28-day ages their hydration degrees were a little lower than one of Alite (Fig.3b).

Compressive strength

The 3-day, 7-day and 28-day compressive strengths of Alite ($\overline{S}$) sample AS4 were respectively 28.3, 38.2 and 58.5 MPa, and were almost equal to one of Alite (Tab.2).

Hydration activity of Alite ($\overline{F}$, $\overline{S}$)

Rate of heat evolution during early hydration

The hydration reaction of Alite ($\overline{F}$, $\overline{S}$) sample 1A3 was delayed in comparison with Alite and Alite ($\overline{S}$) sample (shown in Fig.2). Its final time of induction period was 10.2h and its final time of acceleratory period 23.0h, and its $(dQ/dt)_m$ was 6.46W/Kg. Becaus of its high rate of heat evolution in deceleratory period, its Q_{36} was 4.09×10^5 J/Kg, more than one of Alite. In comparison with AS4, the heat evolution curve of 1A3 after induction period broadly resembled the curve of AS4 and was delayed for 5.0h. $(dQ/dt)_m$ 6.46W/Kg of 1A3 was almost equal to $(dQ/dt)_m$ 6.89W/Kg of AS4 and the time 12.5h of 1A3 undergoing acceleratory period was almost equal to the time 12.8h of AS4. The sample Alite ($\overline{F}$, $\overline{S}$) 1A3 had both hydration property of Alite ($\overline{F}$) and the one of Alite ($\overline{S}$). The induction period of Alite ($\overline{F}$, $\overline{S}$) was long due to the very poor hydration activity of Alite ($\overline{F}$) in early hydration. Q_{36} of 1A3 overtook the one of Alite due to $\overline{S}$ solution improving hydration activity of Alite ($\overline{F}$).

Degree of hydration

At 1-day age, the hydration degree of 1A3 (shown in Fig.3c) was 21%, lower than one of Alite 30%, and the degrees of 1A1, 1A2, 2A1 and 2A2 all were under 10%. At 3-day age the degrees of all samples Alite ($\overline{F}$, $\overline{S}$) were lower than one of Alite, but the gap of the degrees between Alite and Alite ($\overline{F}$, $\overline{S}$) was reduced. At 7-day and 28-day ages the degrees of all Alite ($\overline{F}$, $\overline{S}$) were almost equal to Alite.

Compressive strength

The 3-day, 7-day and 28-day compressive strengths of Alite ($\overline{F}$, $\overline{S}$) sample 1A3 were respectively 26.7, 39.2 and 65.3MPa and were almost equal to one of Alite (Tab.2).

Hydration activity of C_3S ($\overline{F}$,F)

Rate of heat evolution during early hydration

Sample $C_3S(\overline{F},F)$ (CFeF1, namely C_3S containing 1%Fe_2O_3 and 1%CaF_2) did not reach the final time of induction period during early 36 hours like Alite ($\overline{F}$) sample AF1 (Fig.2).

Degree of hydration

At 1-day, 3-day and 7-day ages the hydration degree of CFeF1 was respectively 6.7, 18.6 and 8.1%, much lower than one of Alite. And in comparison with AF1, the degree of CFeF1 was

Tab.2 Compressive strengths of Alite containing $\overline{F}$ and $\overline{S}$

Code name of sample	Additive amount in Alite (%)		Crystal type	Compressive strength (MPa)		
	CaF_2	$CaSO_4$		3d	7d	28d
Alite	/	/	M_2	27.6	41.2	61.7
AF3.5	3.5	/	R	0	17.6	66.7
AS4	/	4.0	M_1	28.3	38.2	58.8
1A3	1.0	3.0	M_3	26.7	39.2	65.3

Tab.3 Decolorizing phenomena of Alite ($\overline{F}$) in hydration period

Code name of sample	Additive amount in C_3S (%)				Crystal type	Color of sample	Degree of hydration (%) Color of hydration products			
	CaF_2	Al_2O_3	Fe_2O_3	MgO			1d	3d	7d	28d
CFeF1	1.0	-	1.0	-	R	DIR	6.7 IR	18.6 IR	28.1 LIR	65.5 GG
AF1	1.0	1.0	1.0	1.0	M_3	DIR	6.3 IR	29.9 IR	64.3 LIR	76.1 GG
Alite	-	1.0	1.0	1.0	M_2	GG	29.8 GG	49.1 GG	70.6 GG	76.5 GG

Note: DIR means Deep Iron Red, IR means Iron Red, LIR means Light Iron Red, GG means Greenish Grey.

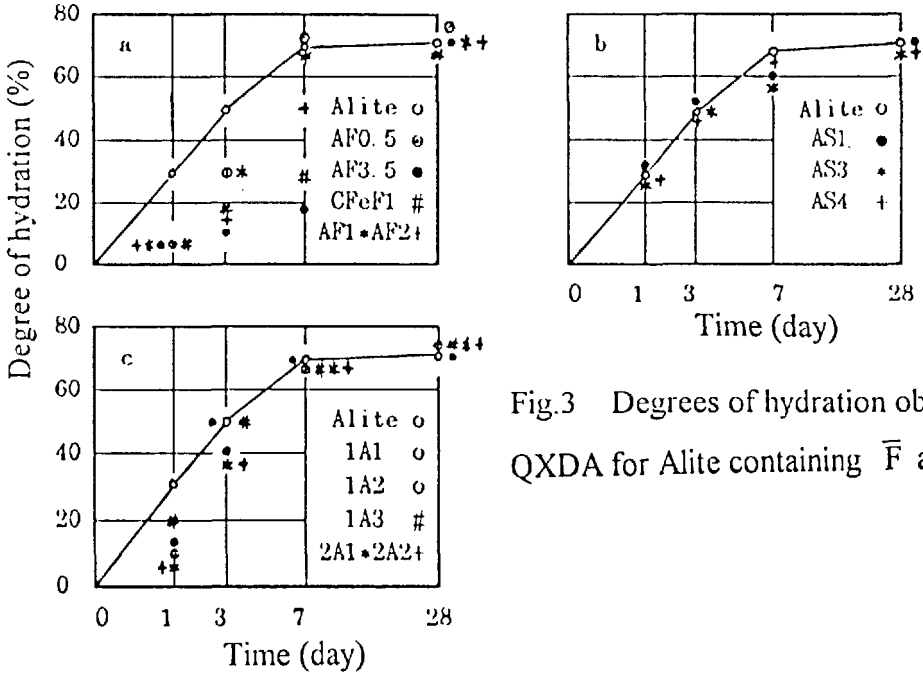

Fig.3 Degrees of hydration obtained by QXDA for Alite containing $\overline{F}$ and $\overline{S}$

almost equal to one of AF1 at 1-day age, and was much lower than one of AF1 at 3-day and 7-day ages. Till 28-day age the degree was almost equal to one of AF1 and Alite (shown in Fig.3a).

Decolorizing phenomenon of Alite ($\overline{F}$) in hydration period

With hydration degree increased, the color of sample Alite ($\overline{F}$) became lighter, from deep iron red into greenish-gey. For instance, the color of AF1 hydrate was iron red at 1-day and 3-day ages, and became light iron red at 7-day age and greenish-grey at 28-day age (show in Tab.3)

The soure of decreasing the hydration activity of Alite ($\overline{F}$) in early period

It is known that the early hydration activity of $C_3S(\overline{F})$, C_3S ($\overline{F}$,A) and C_3S ($\overline{F}$,M) was not obviously decreased (Aldous, 1983 and Nurse). In this study it was obtained that the early hydration activity of C_3S ($\overline{F}$,F) was very poor. Now it is clear that the source of very poor hydration activity of Alite ($\overline{F}$) in early period should be attributed to the particularly combined solution of $\overline{F}$ and Fe_2O_3 in C_3S. It is known in this paper that the solution of $\overline{F}$ and Fe_2O_3 in C_3S had a mutual effect, the incorporation of $\overline{F}$ into C_3S restrained the solution of Fe_2O_3 in C_3S , and the particularly combined solution of $\overline{F}$ and Fe_2O_3 made C_3S or Alite colouring. The colors of both Alite ($\overline{F}$) and C_3S ($\overline{F}$,F) were iron red whose early hydration activities were very poor and the color of their hydration samples had become lighter from iron red into greenish grey almost till 7-day or 28-day age when their hydration degrees were equal to one of Alite.

The solution of $\overline{F}$ and $\overline{S}$ in C_3S or Alite had a mutual effect and restraint. The incorporation of $\overline{S}$ into C_3S or Alite made Alite ($\overline{F}$) decoloring from iron red into pink. And according to the hydration activities of Alite ($\overline{F}$), Alite ($\overline{S}$) and Alite ($\overline{F}$, $\overline{S}$), the incorporation of $\overline{S}$ could reduce the particularly combined solution of $\overline{F}$ and Fe_2O_3, and could improve the hydration activity of Alite ($\overline{F}$).

CONCLUSION

1. The early hydration activity of Alite ($\overline{F}$) (Alite containing $\overline{F}$) was very poor and could be improved by the substitution of $\overline{S}$ (in Alite containing $\overline{F}$). The particularly combined substitution of $\overline{F}$ and Fe_2O_3 in C_3S or Alite was the source of reducing the early hydration activity of Alite containing $\overline{F}$.

2. The hydration activity of Alite ($\overline{S}$) was almost equal to one of Alite.

3. The early hydration activity of Alite ($\overline{F}$, $\overline{S}$) was poorer and its induction period was longer than one of Alite. With $\overline{F}/\overline{S}$ ratio reduced, its early hydration activity was improved.

REFERENCES

Aldous R.T.H., Cem. Concr. Res. Vol.13, PP.89-96, 1983.

Gutt W., Proc. of the Fifth Intern, Symp. on the Chem. of Cement, 1968, Vol.I (1968) 101.

Nurse R.W. et al, Symposium on structure of portland cement paste and concrete, Highway Research Board, Special Report 90, PP258-62, Washington.

Tanaka M. and Sodoh G., Proc. of the Fifth Intern. Symp. on the Chem. of Cement, Tokyo, 1968,Vol.I (1968)122
YE Qing, et al., Proc. of the Ninth Intern. Symp. on the Chem. of Cement, New Delhi, 1992, Vol,II (1992) 342.

2ii043
8 pp

Kno. 25. JAN. 2001 dok 31806

HYDRATION CHARACTERISTICS OF $11CaO \cdot 7Al_2O_3 \cdot CaF_2$

Qijun YU and Xiuji FENG, Institute of Materials, Wuhan University of Technology, China
Shuichi SUGITA, Dept. of Civil Engineering, Hachinohe Institute of Technology, Japan

ABSTRACT The effect of temperature, fineness and water solid ratio (w/s) on the hydration properties and hydrates of $11CaO \cdot 7Al_2O_3 \cdot CaF_2$ ($C_{11}A_7 \cdot CaF_2$) were studied. With the increase of hydration temperature and specific surface its early hydration is improved and setting time shortened. At different temperatures the hydration processes of $C_{11}A_7 \cdot CaF_2$ are all in accordance with the equation of $[1-(1-\alpha)^{1/3}]^N=Kt$ even though its hydrates are varied with temperature. As w/s is increased its hydration rate is enhanced but hydrates remains unchanged.

Key-words: Fineness, Fluoride phases, Hydration, Kinetics and Temperature

INTRODUCTION

$C_{11}A_7 \cdot CaF_2$ is an important constituent of fluorine-contained cement and has a great influence on cement properties, especially the setting and early strength of cement, to which much attention was paid and many studies on its formation in cement clinkering and its effect on cement properties have been done (Wang et al., 1985, Wang et al., 1988 and Klemm et al.), but the hydration and setting characteristics of itself under different conditions have not been profoundly investigated yet. As all the calcium aluminates, such as C_3A, CA, CA_2 and $C_{12}A_7$, are different from each other in hydration and setting properties, so a thorough investigation is necessary to fully understand the hydration characteristics of $C_{11}A_7 \cdot CaF_2$.

EXPERIMENTAL AND RESULTS

Preparation of $C_{11}A_7 \cdot CaF_2$ and its hydration samples

Analytical agents of $CaCO_3$, Al_2O_3 and CaF_2 were dried at 105°C for 2hr and then ground to wholly passing a 0.06mm seive. A homogeneous mix with a mole ratio of $CaCO_3$: Al_2O_3 : CaF_2=11.00 : 7.00 : 1.08, considering a loss of 8.01% CaF_2 during the formation of $C_{11}A_7 \cdot CaF_2$ at high temperatures (Yu, 1992), was burnt at 1250°C for 2hr, then quenched to room temperature in the air of R.H. <5%, and finally ground to 202 m^2/kg, 342 m^2/kg and 453 m^2/kg of Blaine specific surface after it was identified as $C_{11}A_7 \cdot CaF_2$ by the methods of XRD and chemical analysis. Samples of hydrated $C_{11}A_7 \cdot CaF_2$ for XRD, SEM and DTA tests were made by mixing the ground $C_{11}A_7 \cdot CaF_2$ of 342 m^2/kg with distilled and CO_2 free water at a w/s of 1.0. The samples were sealed and cured at 15°C, 25°C, 30°C, 40°C and 60°C respectively to definite ages (Table 1), then they were dried at 20°C in a vacuum drier after finely ground in the presence of ethylalcohol.

Analysis of hydrated $C_{11}A_7 \cdot CaF_2$ by XRD, SEM and DTA

Hydrates exsiting in the hydrated $C_{11}A_7 \cdot CaF_2$, detected by XRD, are shown in Table 1 and no other kinds of crystalline hydrate were observed. Figs 1 and 2 are the SEM photos and DTA curves of the hydrates. Within present observations it can be concluded that the hydrates of $C_{11}A_7 \cdot CaF_2$ at different temperatures are mainly as follows:

(1) Hydrates at 15°C: The initial hydrate is CAH_{10}, which is as same as that of CA (Edmonds and Majumdar, 1988a) but different from that of $C_{12}A_7$ (Edmonds and Majumdar, 1988b). After hydrated for 2hr C_2AH_8 and C_3AH_6 are formed in sequence, and after 3d unhydrated $C_{11}A_7 \cdot CaF_2$ can not been observed by XRD. In addition, Fig 1-a and Fig 2 (H_5 and H_8) show there is also alumina gel AH_x in the hydrates. The peaks nearby 90°C and 300°C in the DTA curves are respectively attributed to the loss of adsorbed and/or enveloped water in AH_x and the decompo-

Table 1 Phase exsiting in hydrated $C_{11}A_7 \cdot CaF_2$ samples as a function of hydration time and temperatures (w/s=1.0)

No.	Hydration		Phases present			
	Temp.(℃)	Time(hr)	$C_{11}A_7 \cdot CaF_2$(%)	CAH_{10}	C_2AH_8	C_3AH_6(%)
H_1	15	0.5	65	○*	—**	—
H_2	15	2	46	○	○	11
H_3	15	6	19	○	○	26
H_4	15	12	15	○	○	29
H_5	15	24	7	○	○	43
H_6	15	2×24	<5	○	○	45
H_7	15	3×24	—	○	○	49
H_8	15	7×24	—	○	○	52
H_9	25	0.5	53	—	○	4
H_{10}	25	2	27	—	○	19
H_{11}	25	6	15	—	○	33
H_{12}	25	12	8	—	○	48
H_{13}	25	24	<5	—	○	63
H_{14}	25	2×24	<5	—	○	68
H_{15}	25	3×24	—	—	○	71
H_{16}	25	7×24	—	—	—	82
H_{17}	30	0.5	16	—	—	74
H_{18}	30	2	14	—	—	77
H_{19}	30	6	13	—	—	79
H_{20}	30	12	11	—	—	80
H_{21}	30	24	10	—	—	83
H_{22}	30	2×24	9	—	—	85
H_{23}	30	3×24	7	—	—	86
H_{24}	30	7×24	6	—	—	88
H_{25}	40	0.5	17	—	—	66
H_{26}	40	2	15	—	—	68
H_{27}	40	6	14	—	—	71
H_{28}	40	12	12	—	—	72
H_{29}	40	24	11	—	—	74
H_{30}	40	2×24	10	—	—	77
H_{31}	40	3×24	9	—	—	79
H_{32}	40	7×24	8	—	—	80
H_{33}	60	0.5	20	—	—	67
H_{34}	60	2	19	—	—	68
H_{35}	60	6	17	—	—	69
H_{36}	60	12	16	—	—	71
H_{37}	60	24	14	—	—	72
H_{38}	60	2×24	13	—	—	76
H_{39}	60	3×24	13	—	—	77
H_{40}	60	7×24	12	—	—	78

* ○ --Present but less than 5% in amount, ** — --Nil.

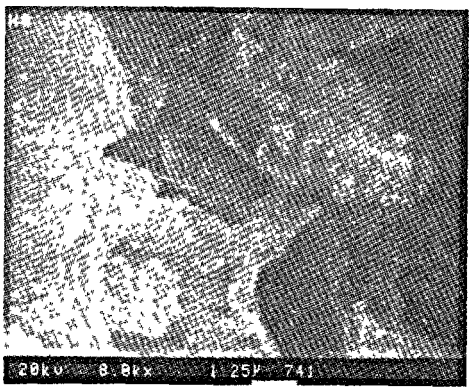

(a)



(b)

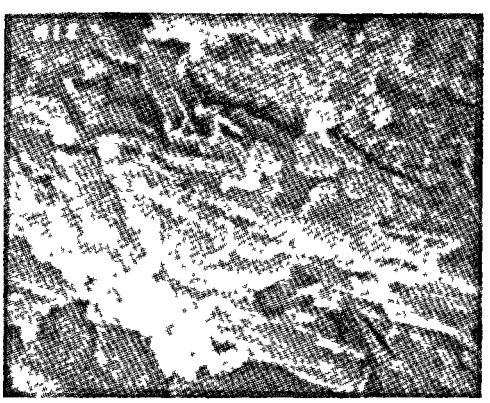

(c)

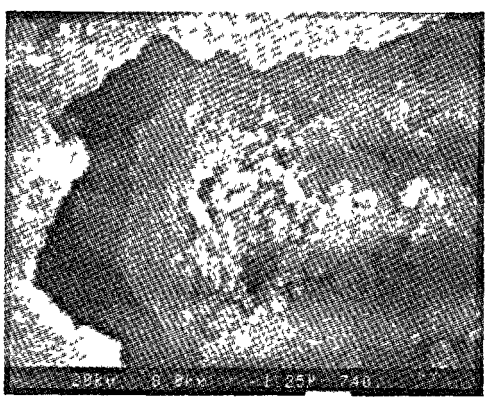

(d)

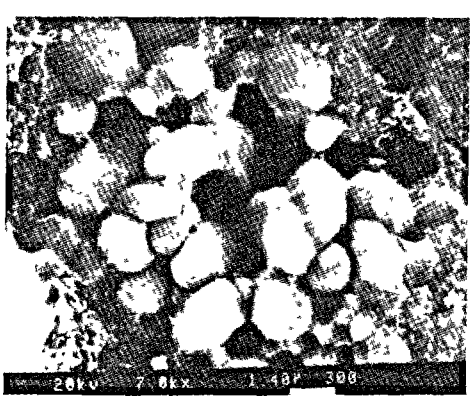

(e)

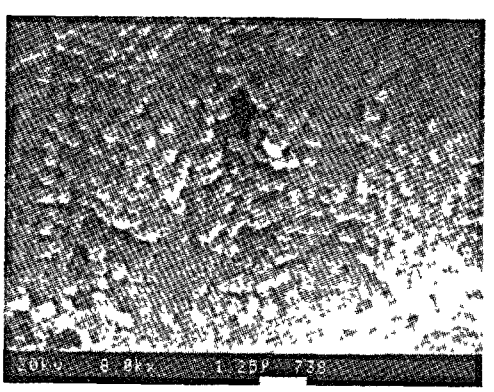

(f)

Figure 1 SEM photographs of hydrated $C_{11}A_7 \cdot CaF_2$ samples (w/s=1.0).
a --Alumina gel and irregular flakes (H_8);
b --Hexagonal flakes and cubes (H_8);
c --Irregular flakes (H_{12});
d --Alumina gel and C_3AH_6 grains (H_{16});
e --C_3AH_6 mostly as aggregates, its schematic outer shape is shown in the right (H_{16});
f --Compact structure formed by stacked cubes of C_3AH_6 (H_{25})

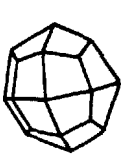

sition of C_3AH_6 in the form of: $7C_3AH_6 \rightarrow C_{12}A_7H + 9CH + 32H$. As hydration temperature rises this peak is drifted towards high temperature side. The peak ranged from 260°C to 270°C is due

to the conversion of AH_3 (gibssite) to AH. The transformation of C_2AH_8 to C_3AH_6 and AH_3 is characterized by the small band near 250°C.

(2) Hydrates at 25°C: The hydrates are C_2AH_8, C_3AH_6 and alumina gel (Table 1 and Fig 1-d). With the development of hydration the amount of C_2AH_8 is reduced and after 7d it disappears. Fig 1-e shows the well grown C_3AH_6 crystals of icositetrahedron.

(3) Hydrates at 30°C, 40°C and 60°C: The hydrates at these temperatures, whether the initial or final, are only C_3AH_6 and alumina gel, therefore larger peaks attributed to C_3AH_6 (300°C) can been observed in Fig 2 ($H_{25}-H_{36}$). Because of C_3AH_6 having a larger C/A ratio than that of CAH_{10} and C_2AH_8 more alumina gel will be formed at these temperatures, which is corresponded to the enlargement of the peak nearby 260°C in the DTA curve.

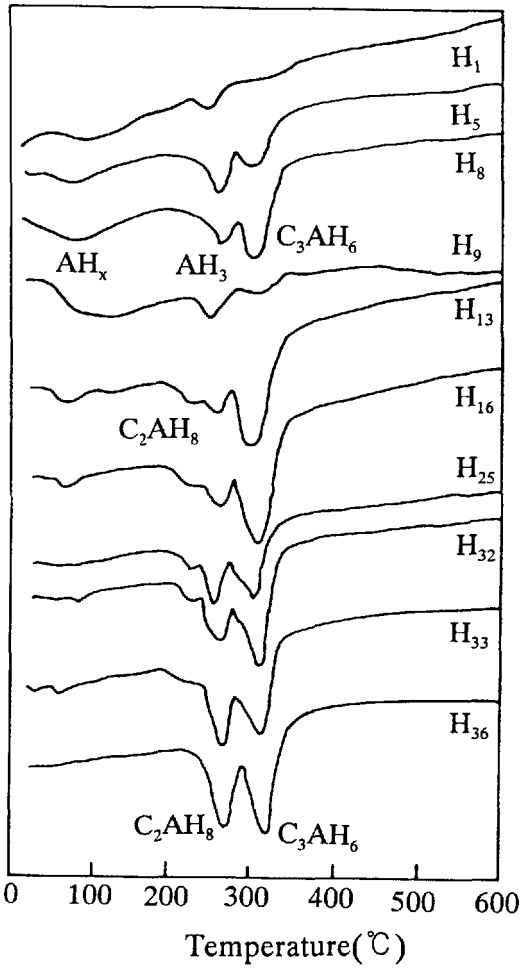

Figure 2 DTA curves of hydrated $C_{11}A_7 \cdot CaF_2$.

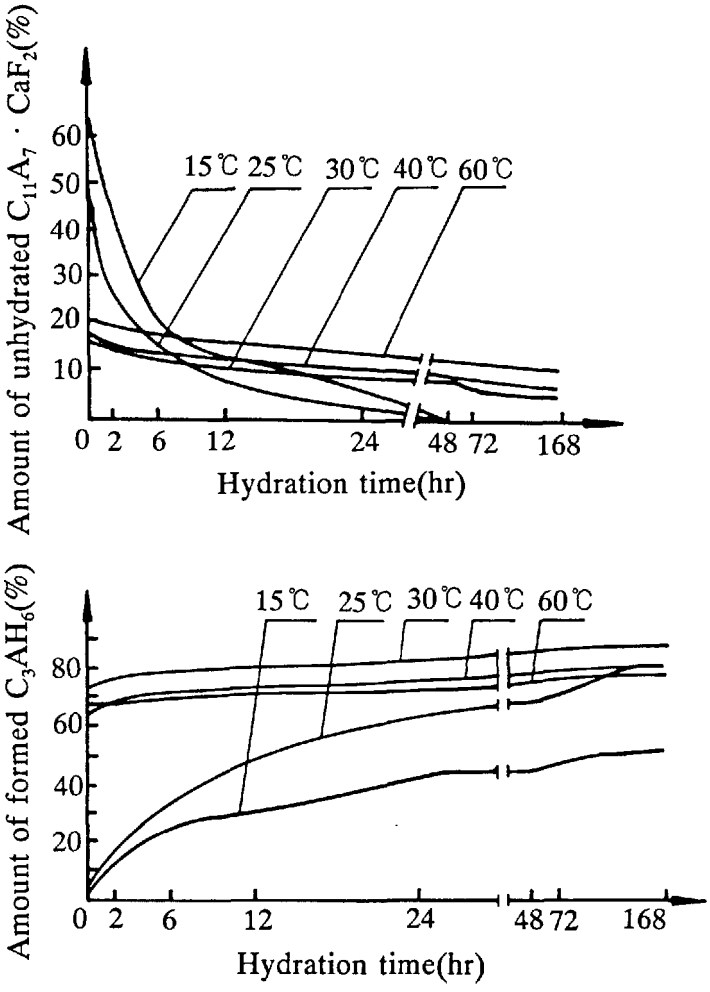

Figure 3 Amount of unhydrated $C_{11}A_7 \cdot CaF_2$ and formed C_3AH_6 vs hydration time at different temperatures.

Table 2 Dynamic parameters of the hydration of $C_{11}A_7 \cdot CaF_2$ at different temp.(w/s=1.0)

Temperature (°C)	15	25	30	40	60
N	2.6	3.8	19.7	23.0	34.5
K	10.6×10^{-3}	8.0×10^{-3}	2.1×10^{-7}	1.3×10^{-9}	1.3×10^{-13}

Kinetics of the hydration of $C_{11}A_7 \cdot CaF_2$

For the quantitative analysis of hydrated $C_{11}A_7 \cdot CaF_2$ the internal standard method in QXRD was adopted by using α-Al_2O_3 as reference and pure $C_{11}A_7 \cdot CaF_2$, C_3AH_6 and C_2AH_8 as standard samples. The results are also shown in Table 1, but in which the amount of C_2AH_8 is not listed because it falls short of 5% in all the samples. Fig 3 shows the variation of the amount of C_3AH_6 and unhydrated $C_{11}A_7 \cdot CaF_2$ with hydration time.

By defining the percentage of hydrated $C_{11}A_7 \cdot CaF_2$ as hydration degree α it was found that α satisfactorily fit to the following equation suggested by R. Kondo et al. (1968):

$$[1-(1-\alpha)^{1/3}]^N = Kt \qquad [1]$$

where α is the hydration degree of $C_{11}A_7 \cdot CaF_2$ at time t, K is the reaction rate constant and N is the constant related to reaction mechanism. Frequently, N<1 suggests that the reaction is controlled by automatically catalytic reaction, while $N \fallingdotseq 1$ is by boundary reaction and $N \geqq 2$ is by diffusion process. Fig 4 shows ln $[1-(1-\alpha)^{1/3}]$ is linear with ln t, and from which the N and K at different temperatures can be obtained (Table 2). From Table 2 it can be seen that the hydration of $C_{11}A_7 \cdot CaF_2$ between 15°C and 60°C is dominated by diffusion process for N>2 in all the cases.

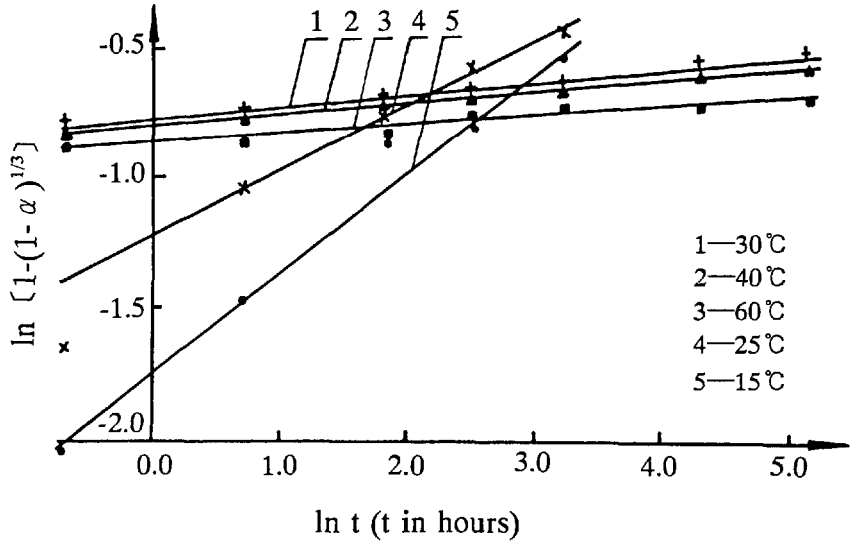

Figure 4 ln $[1-(1-\alpha)^{1/3}]$ vs ln t for hydrated $C_{11}A_7 \cdot CaF_2$ at different temperatures.

Effect of w/s and fineness on the set and hydration of $C_{11}A_7 \cdot CaF_2$

At 25°C the products of hydrated $C_{11}A_7 \cdot CaF_2$ with a w/s of 10.0 are C_3AH_6, C_2AH_8 and alumina gel. The relations between hydration time and the amount of formed C_3AH_6 and residual $C_{11}A_7 \cdot CaF_2$ are shown in Fig 5.

Table 3 Effect of fineness on the setting time (min) of $C_{11}A_7 \cdot CaF_2$ paste (w/s=0.6)

No.	Specific gravity	Blaine surface area (m^2/kg)	Initial set	Final set
S_9	2.69	202	13	23
S_{10}	2.69	342	0	10
S_{11}	2.69	453	0	5

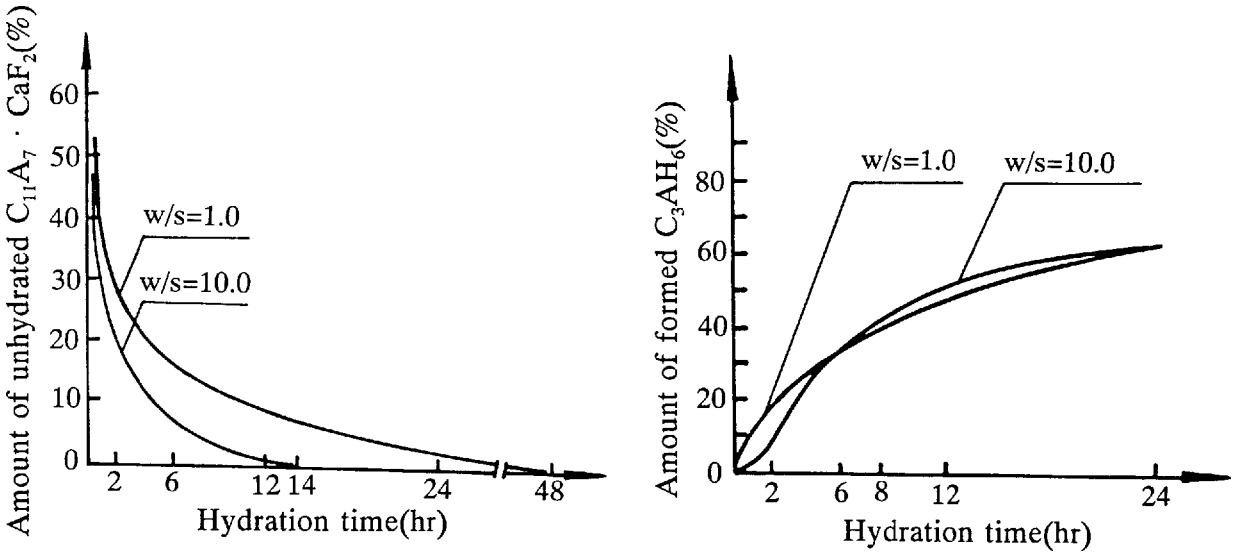

Figure 5 Amount of $C_{11}A_7 \cdot CaF_2$ and C_3AH_6 in hydrated $C_{11}A_7 \cdot CaF_2$ vs time at a w/s of 1.0 and 10.0.

The heat evolution profiles of hydrating $C_{11}A_7 \cdot CaF_2$ with different fineness are shown in Fig 6. The tests of setting time were conducted on the pastes with a w/s of 0.6 at 20°C by the Vicat apparatus. When initial set occurs within 3min after $C_{11}A_7 \cdot CaF_2$ is immersed to water the initial setting time was defined as 0min here (Table 3).

DISCUSSIONS

Effect of hydration temperature on the hydration of $C_{11}A_7 \cdot CaF_2$

Below 30°C the hydration degree of $C_{11}A_7 \cdot CaF_2$ is increased with temperature, while above 30°C it is decreased with the rise of temperature and after 5-20 hours it becomes less than those

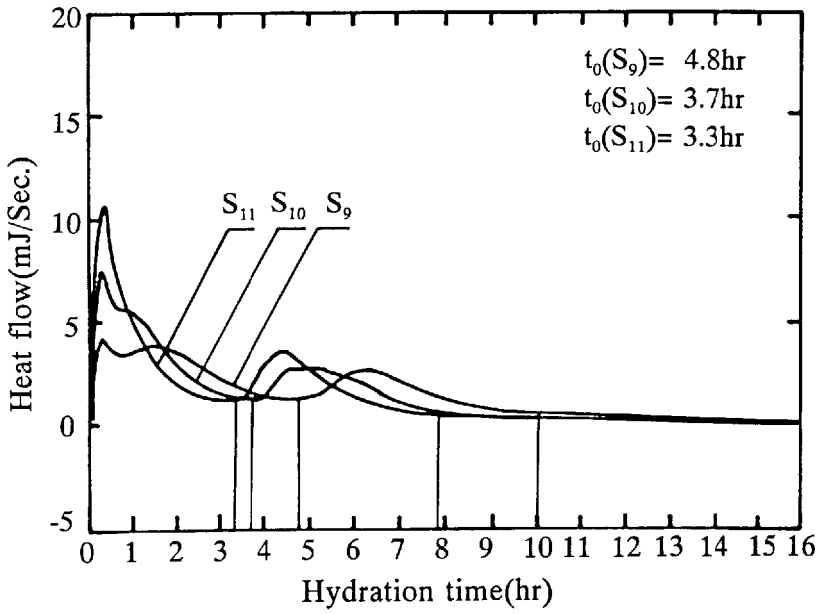

Figure 6 Effect of fineness of $C_{11}A_7 \cdot CaF_2$ on its heat evolution rate in hydration (30℃, w/s=10.0)

at 15℃ and 25℃ (Fig 3). For example, in the samples hydrated for 3d at 15℃ and 25℃ unhydrated $C_{11}A_7 \cdot CaF_2$ could not be found by XRD but in those hydrated at above 30℃ for 7d there yet exsited 6-12% of $C_{11}A_7 \cdot CaF_2$ even though at this time about 80% of $C_{11}A_7 \cdot CaF_2$ was hydrated only for 30min (Table 1). This phenomenon is similar to the variation of hydration rate of $C_{12}A_7$ with temperature observed by Edmonds and Majumdar (1988b). Why is the hydration of $C_{11}A_7 \cdot CaF_2$ retarded in adverse with temperature rise above 30℃? In our opinions this is because: (1) as hydration temperature rises its initial hydration is accelerated in a large scale and in a short time a lot of hydrates are produced, which constitute barriers on the surface of $C_{11}A_7 \cdot CaF_2$ grains and prevent the contact of them with water, (2) the increase of N in Eq 1 with temperature (Table 1). In Wu's (1988) opinion the N is dependent on reaction resistance, the larger the resistance, the bigger the N. Here the reaction resistance is primarily comprised of diffusion resistance for N>2. Thus the increase of N, i.e. the enhancement of diffusion resistance, necessarily results in the delay of hydration. The formation of compact hydrates shown in Fig 1-f gives direct evidence for the increase of diffusion resistance with temperature, (3) reaction rate constant K is decreased with the rise of hydration temperature, and (4) much water is consumed due to the formation of more amorphous alumina gel (AH_x), leading to the decrease of available water for further hydration.

On the contrary the amount of hydrated $C_{11}A_7 \cdot CaF_2$ and formed C_3AH_6 are increasing quickly with hydration time at 15℃ and 25℃, and $C_{11}A_7 \cdot CaF_2$ can hydrate completely after 3d. The reasons for this are: (1) at these temperatures no thick barriers envelope unhydrated $C_{11}A_7 \cdot CaF_2$ grains as the hydration rate is comparatively low, (2) the hydration products are large in size and with a porous structure, as shown in Fig 1-a—Fig 1-e, through which water can easily penetrate to the surface of $C_{11}A_7 \cdot CaF_2$ grains, and (3) large rate constant K is held at these temperatures.

Effect of water solid ratio(w/s) and fineness on the hydration of $C_{11}A_7 \cdot CaF_2$

From Fig 5 it can be found that the hydration of $C_{11}A_7 \cdot CaF_2$ is accelerated greatly when w/s is increased from 1.0 to 10.0. At a w/s of 10.0 $C_{11}A_7 \cdot CaF_2$ was completely hydrated only in 14 hours while there was about 8% residual $C_{11}A_7 \cdot CaF_2$ in the sample with a w/s of 1.0. The influence of w/s on the early hydration of $C_{11}A_7 \cdot CaF_2$ and portland cement was compared by Yu (1992), and greater accelerating effect of w/s on the hydration of $C_{11}A_7 \cdot CaF_2$ was observed. In the hydrating $C_{11}A_7 \cdot CaF_2$ with a w/s of 0.6-1.0 initial and final set occurred only in several minutes, coherently much water was rapidly consumed in the formation of hydrates. Furthermore, the hydrates adjacent to $C_{11}A_7 \cdot CaF_2$ grains hindered the further hydration. These phenomena have not been observed in the contorl samples of hydrated portland cement, but by rising w/s they can be greatly changed.

At 25℃ whether at a w/s of 1.0 or 10.0 the kinds of hydration products of $C_{11}A_7 \cdot CaF_2$ were the same and after hydrated for 24hr no difference in their amount of C_3AH_6 was found.

When the Blaine specific surface of $C_{11}A_7 \cdot CaF_2$ is increased from 202 m^2/kg to 342 m^2/kg its initial and final setting time are decreased from 13min to 0min and from 23min to 10min respectively (Table 3), and the first heat evolution peak, completed in 8-12 min, is enlarged evidently (Fig 6), which indicate that not only $C_{11}A_7 \cdot CaF_2$ can set very quickly but also its fineness does have a great effect on its hydration rate and setting time. The onset of the second peak in Fig 6, which corresponds to the end of induction period of the hydration, is possibly associated with the beginning of the accelerated hydration of $C_{11}A_7 \cdot CaF_2$ due to the fail of the barriers of hydrates on the surface of hydrating $C_{11}A_7 \cdot CaF_2$ grains. The relation between the heat evolution and hydration time of above samples are respectively in agreement with following equations:

S_9 : $1/P=1.54\times10^{-3} + 1.05\times10^{-2}(1/t-t_0)$, $t_0=4.8$, $\tau=6.83$, $P_\infty=705.4$, $r=0.98$ [2]

S_{10} : $1/P=1.98\times10^{-3} + 4.38\times10^{-2}(\ 1/t-t_0\ ),\quad t_0=3.7,\quad r=0.97$ [3]

S_{11} : $1/P=1.38\times10^{-3} + 6.02\times10^{-2}(\ 1/t-t_0\ ),\quad t_0=3.3,\quad \tau=4.36,\quad P_\infty=723.8,\quad r=0.98$ [4]

where P is the heat evolution (kJ/kg) at time t (hr), t_0 is the time in hours at which induction period of hydration ends, τ is the half life period (hr) of the hydration, P_∞ is the total heat output of hydrated $C_{11}A_7 \cdot CaF_2$ (kJ/kg) and r is the linear correlation factor, from which it can be known that the half life period (τ) and induction period of the hydration of $C_{11}A_7 \cdot CaF_2$ are gradually shortened with the increase of its fineness.

Hydration products of hydrating $C_{11}A_7 \cdot CaF_2$ at the time of initial and final set

At 25°C the products exsiting in the hydrated $C_{11}A_7 \cdot CaF_2$ with a w/s of 0.6 at the time when initial and final set occurred were determined by XRD and TG-DTA. Except for a large amount of unhydrated $C_{11}A_7 \cdot CaF_2$ there were only a small amount of C_2AH_8, C_3AH_6, $C_3AH_{8\text{-}12}$ and alumina gel in the both hydrates. It is just because of the rapid formation of these products that makes the paste set quickly.

CONCLUSIONS

1. At 15°C and at a w/s of 1.0 $C_{11}A_7 \cdot CaF_2$ can be nearly hydrated completely after 3d and the hydration products are mainly C_3AH_6, alumina gel and a small amount of CAH_{10}, C_2AH_8.
2. At 25°C the initial hydration products of $C_{11}A_7 \cdot CaF_2$ are C_3AH_6, C_2AH_8 and alumina gel. The C_2AH_8 will be gradually changed to C_3AH_6 with hydration time and disappear in the paste after 7d. Simultaneously amorphous alumina gel AH_x will crystallize to gibssite (AH_3).
3. At and above 30°C the hydrates of $C_{11}A_7 \cdot CaF_2$ are only C_3AH_6 and alumina gel, and its hydration degree is reduced with the rise of temperature.
4. Between 15°C and 60°C the hydration degree (α) of $C_{11}A_7 \cdot CaF_2$ is varied with hydration time (t) in the form of: $[1-(1-\alpha)^{1/3}]^N=Kt$, and after hydrated for half an hour its hydration enters the process controlled by diffusion.
5. The hydration degree of $C_{11}A_7 \cdot CaF_2$ is enhanced with water solid ratio but the kinds of hydrates are kept unchanged. As the fineness of $C_{11}A_7 \cdot CaF_2$ increases, its heat evolution rate in early hours is raised evidently, induction period is shortened gradually and initial, final set are further accelerated.

REFERENCES

Edmonds, R.N. and Majumdar A.J., Cem. Concr. Res., Vol. 18, No. 2, 1988, pp. 311-312.

Edmonds, R.N. and Majumdar A.J., Cem. Concr. Res., Vol. 18, No. 3, 1988, pp. 473-478.

Klemen, W.A. and Jawed I., 7th Intern. Cong. Chem. of Cem., 1980, Paris, Vol.II, p. I -150.

Kondo, R. and Ueda S., 5th Intern. Cong. on the Chem. of Cem., 1968, Tokyo, Vol.II, p. 224.

Wang, S.B. and Ding W.C., J. of Chinese Ceramics Society, Vol. 16, No. 4, 1988, p. 305.

Wang, T.D. and Chen W.Q., Proc. of 1985 Beijing Intern. Symp. on Cem. and Concr., Vol. I , 1985, p. 24.

Wu, X.Q., J. of Chinese Ceramics Society, Vol. 16, No.5, 1988, pp. 423-429.

Yu, Q.J., "On the Crystal Structure and Characteristics of $C_{11}A_7 \cdot CaF_2$", Ph.D.Thesis, Wuhan University of Technology, 1992, pp. 17-19, 82-87.

2ii044
8 pp

Kno. 25. JAN. 2001 doc 31807

INTERACTION BETWEEN GYPSUM AND C-S-H PHASE IN C_3S HYDRATION USING ESCA

Nam-Ho KIM, Young-Jin LEE Construction Materials Laboratory, Tong Yang Central Laboratories, 38-1 Jung-Ri, Kusung-Myun, Yongin Kyungki-Do 449-910, Korea
Woo-Sik UM, Hee-Soo LEE, In-Shik LEE, Material Testing Team, Korea Testing Laboratory for Industrial Technology, KAITECH, 222-13, Kuro 3-Dong, Kuro-Gu, Seoul 152-053, Korea

ABSTRACT We studied the hydrated reaction of C_3S and gypsum mixture using ESCA (electron spectroscopy for chemical analysis). The chemical shifts of Ca, Si, O and S binding energies were measured in the systems of gypsum, gypsum-free C_3S and C_3S-gypsum mixture after hydration. We find out from the observed chemical shift that SO_4^{2-} tetrahedron is bound by the C-S-H phase which is a main product of the hydrated C_3S in the presence of calcium sulfate from chemical shift. X-ray diffraction pattern, wavelength dispersive x-ray spectroscopy and differential scanning calorimetry analysis were also used to study the hydration reaction between C_3S and gypsum.

Key-words: CSH, ESCA, Gypsum, Hydration, Tricalcium silicate

INTRODUCTION

One of the most important technological parameters in the manufacture of portland cement is the addition of the optimum amount of gypsum to clinkers. Gypsum is added mainly to prevent flash set caused by the rapid hydration of C_3A phase, but the amount of gypsum added also affects the physical properties of mature cement paste. When portland cement clinker is blended with the optimum amount of gypsum, the paste has maximum compressive strength and minimum drying shrinkage (Lerch, 1946). It is generally believed that the optimum effect of gypsum is associated with its intensive reaction with the C_3A phase. However, there are many indications (Copeland et al., 1967, Copeland et al., 1969 and Kalousek, 1965) that gypsum may react with the silicate phase in portland cement, and alter the chemical constitution and microstructure of the C-S-H gel formed.

It has been reported that the increase in the amount of gypsum accelerates the hydration of the silicate phases but lowers the mechanical quality of the C-S-H gel (Ish-Shalom et al., 1972 and Bentur, 1976). Some papers have reported that it is caused by the replacement of the sulfate ion in the amorphous structure of C-S-H phase (Odler, 1979 and Ménétrier, 1980). Therefore, our study reports further attempts about the incorporation of sulfur ion in the C-S-H structure using the ESCA and other analytical tools.

EXPERIMENTAL PROCEDURE

The C_3S used for the hydration was made by mixing and calcining $CaCO_3$ and SiO_2. The gypsum ($CaSO_4 \cdot 2H_2O$) of 3.1 wt% was intermixed with the C_3S and

it was hydrated at room temperature for the selected periods of time in distilled water (50 wt% for the gypsum and C_3S mixture). The hydration was interrupted by washing the paste in acetone and drying in a desiccator. The hydration sample of C_3S without gypsum also was prepared. X-ray diffraction (XRD), differential scanning calorimetry (DSC), scanning electron microscopy (SEM) and wavelength dispersive x-ray spectroscopy (WDX) were used to study the phase transition during the hydration. The electron spectroscopy for chemical analysis (ESCA) was carried out at room temperature under the ultra high vacuum condition (-1×10^{-8} Pa) using a two-chamber spectrometer with the monochromatized x-ray source of Al-Kα ($h\nu = 1486.6$ eV).

RESULTS AND DISCUSSION

Fig. 1 represents the XRD patterns of the hydrated C_3S and gypsum mixture. The pattern at 15 minutes shows the peaks of $CaSO_4 \cdot 2H_2O$ and C_3S. By 6 hours, the peaks for the $CaSO_4 \cdot 2H_2O$ and the C_3S are reduced and $Ca(OH)_2$ starts to grow. The gypsum has completely reacted and the peaks for $Ca(OH)_2$ becomes much stronger in the hydrated samples after 19 hours. The C-S-H phase which may be formed could not be identified from XRD patterns because of its poor crystallinity. As the peak for $Ca(OH)_2$ in the hydrated C_3S without gypsum was detectable after 19 hours, the acceleration of C_3S hydration reaction by gypsum could be confirmed.

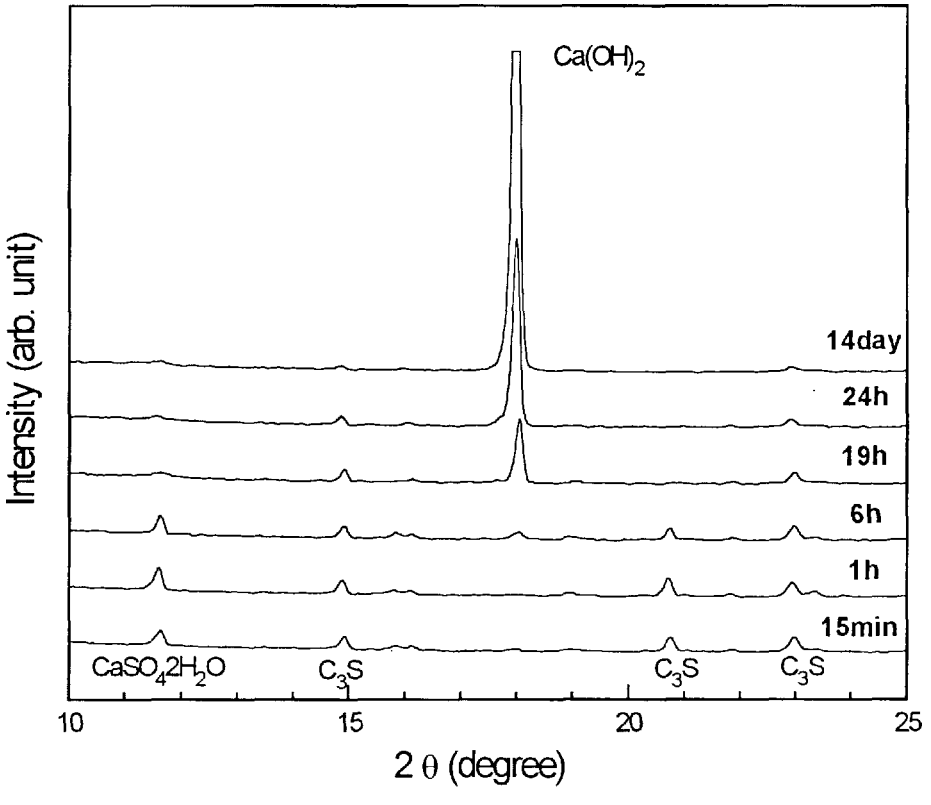

Fig. 1 XRD patterns of the C_3S and gypsum mixture with changing the hydration time.

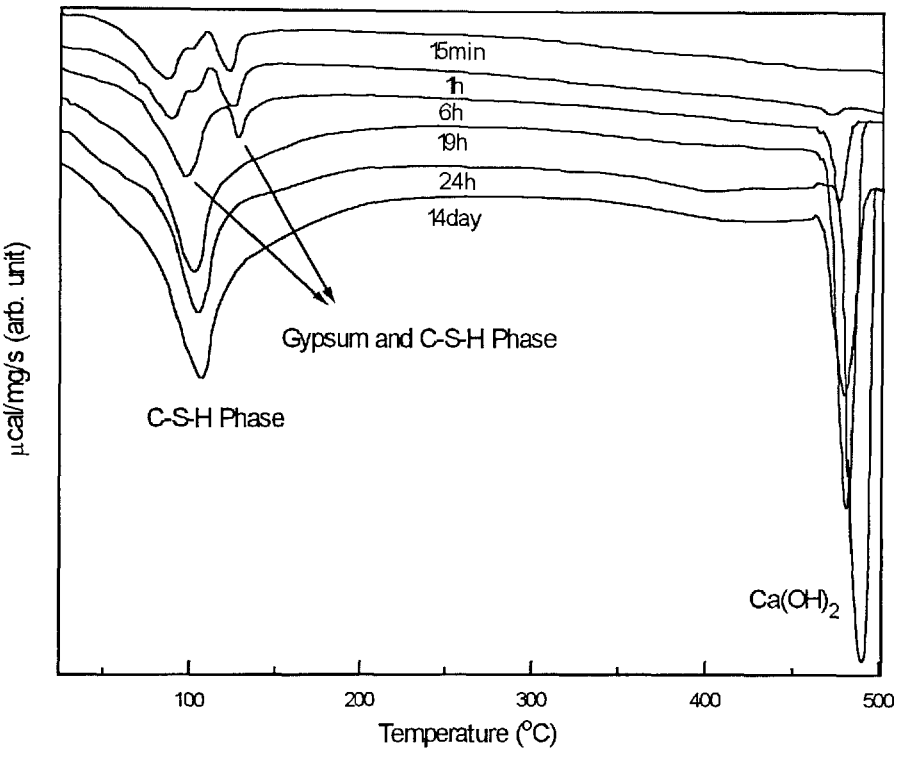

Fig. 2 DSC curves of the C_3S and gypsum mixture with changing the hydration time.

The phase transformation of C_3S during hydration reaction was also studied using DSC as shown in Fig. 2. As the hydration progresses, the gypsum content detectable by DSC decreases until no gypsum endotherm could be observed for the sample hydrated at 19 hours. The C-S-H and the $Ca(OH)_2$ phases were already detectable after 15 minutes and 1 hour hydration. The $Ca(OH)_2$ phase formed in the first one hour, not detectable by XRD, is believed to be amorphous or microcrystalline phase (endotherm at about 460-490°C), whereas the one formed after 1 hour is crystalline (Ménétrier et al., 1980). As hydration time advances, the endotherm for C-S-H phase shifts to higher temperatures (from 85 to 105°C) and broadens. XRD and DSC analysis results show indirectly that sulfate ion may replace the silicate ions in the amorphous structure of C-S-H. There is no possibility for sulfur ions to participate in $Ca(OH)_2$ phase and only small amount of Si are located in that phase (Ménétrier et al., 1980).

The incorporation of sulfate ion into C-S-H phase was also studied by observing the microstructure using SEM and WDX as shown in Fig. 3 and 4. Fig. 3 (a) shows the well-developed needle-like shape of C-S-H phase and the quantity of sulfur ions which may be incorporated in the C-S-H of the hydrate C_3S and gypsum mixture. Sulfur ions were detected in the several part of the microstructure and its quantity changed as shown in Fig. 3 (b). The quantity of sulfur ion increases and the ratio of Ca/Si decreases with moving WDX analysis

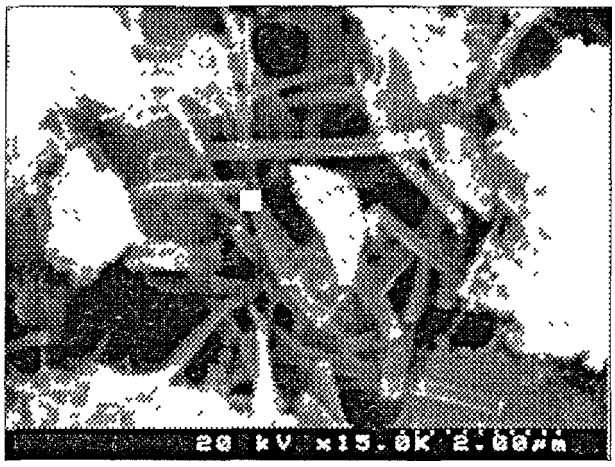

	■ area
Ca	71 2470 %
Si	25 9378 %
S	2 8152 %

(a)



	■ area	● area	◆ area
Ca	71 3795 %	74 6110 %	76 7643 %
Si	25 8280 %	23 4277 %	21 9670 %
S	2 7925 %	1 9613 %	1 2688 %

(b)

Fig. 3 SEM and WDX analysis in C-S-H phase (atomic percent) for the different parts of 14 days hydrated C_3S and gypsum mixture.

point toward the well-developed needle-like C-S-H phase, which originates from the C-S-H phase variation from the gel-like phase formed on the surface of unreacted C_3S grain to needle-like phase during the hydration (Melzer et al., 1989). The trend of Ca/Si ratio decrease agrees with the reported relationship between Ca/Si ratio and degree of hydration (Bentur, 1976). Therefore, this result indicates that the incorporated amount of sulfur ion grows with the phase transformation of C-S-H phase during hydration advancement. The microstructure of hydrated C_3S phase without gypsum shows fibrous bundles of C-S-H phase and Ca/Si ratio is higher than that of the sample in Fig. 3, meaning the lower degree of hydration.

	● area
Ca	79 1644 %
Si	21 8217 %
S	0 0139 %

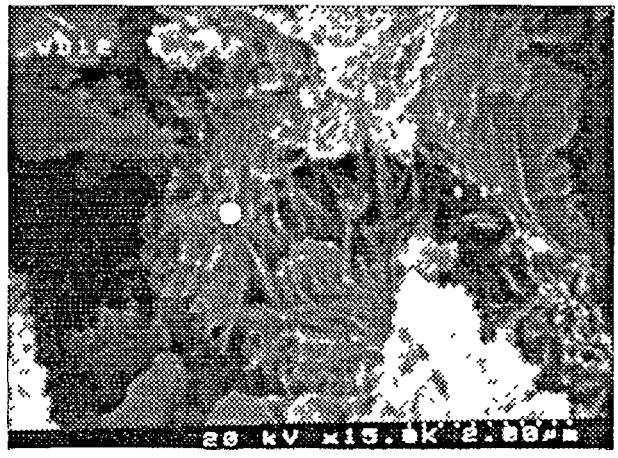

Fig. 4 SEM and WDX analysis in C-S-H phase (atomic percent) for 14 days hydrated C_3S.

In order to observe the sulfur ion behavior and the changes of the chemical environments of each ion in C-S-H phase, specimens of gypsum, 14 days hydrated C_3S and C_3S-gypsum mixture were studied using ESCA. The variation of atomic chemical environment can be identified by virtue of the chemical shift, resulting from variance of electrostatic screening experienced by core electrons as valence electrons are drawn towards or away from the atom of interest.

The wide scan spectra of ESCA for $CaSO_4 \cdot 2H_2O$ and hydrated C_3S and C_3S-$CaSO_4 \cdot 2H_2O$ is shown in Fig. 5. Narrow scan peaks for Ca 2p3, O 1s, S 2p and Si 2p in Fig. 6 were obtained from the wide scan spectra. After the deconvolution of each emission, binding energies were corrected by C 1s peak and summarized in Table 1. All the binding energies of Ca 2p3, O 1s, S 2p and Si 2p emissions for $CaSO_4 \cdot 2H_2O$, hydrated C_3S and C_3S-$CaSO_4 \cdot 2H_2O$ are nearly constant. This result means that chemical environment of each element does not change very much.

Ca in $CaSO_4 \cdot 2H_2O$ structure is surrounded by O and H_2O, and S by four O's resulting in the structure of tetrahedron (Evans, 1966). In imperfect tobermorite-like and jennite structures of C-S-H phase, Ca is known to be also bonded by O, OH and H_2O, and Si is located in the center of oxygen tetrahedron

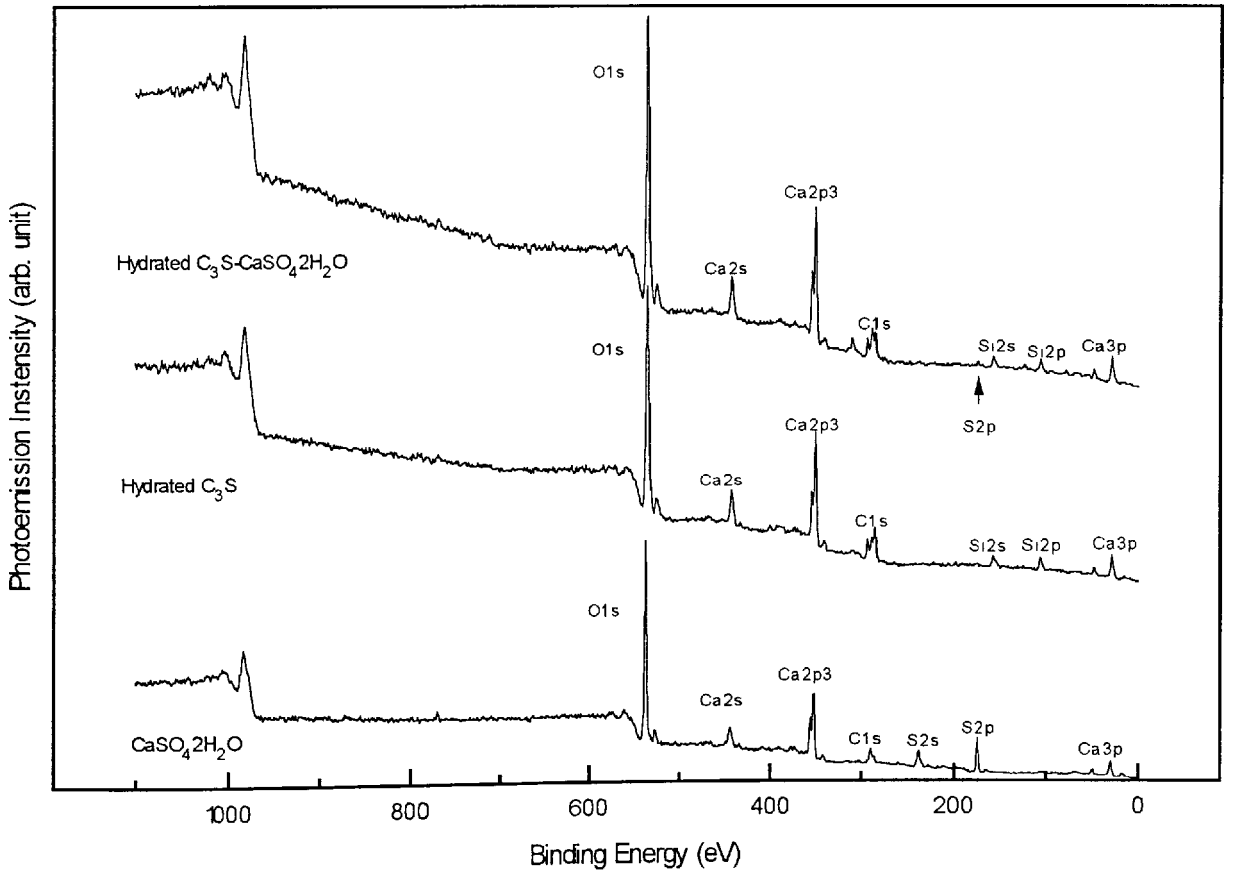

Fig. 5 ESCA wide scan spectra for $CaSO_4 \cdot 2H_2O$ and 14 days hydrated C_3S and C_3S-$CaSO_4 \cdot 2H_2O$

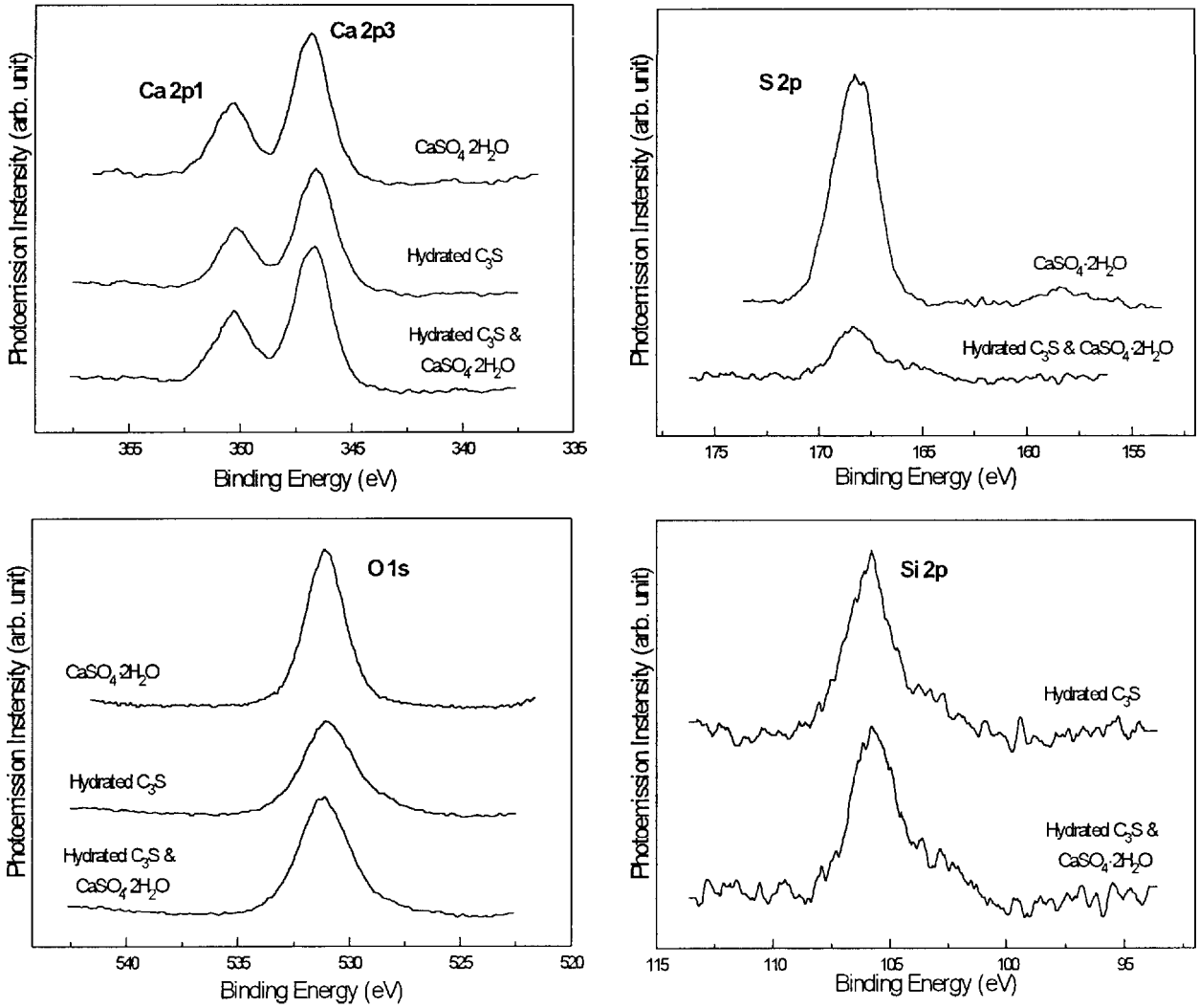

Fig. 6 ESCA narrow scan peaks of $CaSO_4 \cdot 2H_2O$, and 14 days hydrated C_3S and C_3S-$CaSO_4 \cdot 2H_2O$

Table 2-1-1 Binding energies of each element

Element \ Sample	$CaSO_4 \cdot 2H_2O$	Hydrated C_3S	Hydrated C_3S + $CaSO_4 \cdot 2H_2O$ (3.07wt%)
Ca 2p3	346.80	346.55	346.70
O 1s	531.15	531.05	531.15
S 2p	168.30	-	168.65
Si 2p	-	101.50	101.44

which consists of the finite chains (Taylor et al., 1980). Therefore, from no difference between Ca 2p3 and S 2p binding energies for $CaSO_4 \cdot 2H_2O$ and hydrated C_3S-$CaSO_4 \cdot 2H_2O$, it is assumed that Ca of $CaSO_4 \cdot 2H_2O$ is incorporated in C-S-H and $Ca(OH)_2$ phases, and that S does in the form of oxygen tetrahedron like SiO_4^{4-} tetrahedron because of the absence of $CaSO_4 \cdot 2H_2O$ in 14 day hydrated C_3S-$CaSO_4 \cdot 2H_2O$ mixture shown by XRD and DSC analyses (Fig. 1 and 2). It is also believed from constant binding energies of Ca 2p3, O 1s, S 2p and Si 2p emissions for hydrated C_3S and C_3S-$CaSO_4 \cdot 2H_2O$ that the addition of gypsum to C_3S does not affect the bonding of each ion consisting C-S-H phase.

CONCLUSIONS

It is observed that C_3S and gypsum react completely during the hydration, using XRD and DSC. WDX results show that the sulfur ion of the reacted $CaSO_4 \cdot 2H_2O$ is incorporated in C-S-H phase, and the participated amount of sulfur ion increases with the higher degree of C-S-H hydration which was verified by Ca/Si ratio variation. It is conceived from the same ESCA binding energy of sulfur ion in SO_4^{2-} tetrahedron of $CaSO_4 \cdot 2H_2O$ as that of sulfur ion incorporated in C-S-H phase that the sulfur ion in C-S-H phase is in the form of SO_4^{2-} tetrahedron similar to SiO_4^{4-} tetrahedron C-S-H phase

REFERENCES

Bentur, A., "Effect of Gypsum on the Hydration and Strength of C_3S Pastes", J. Am. Ceram. Soc. Vol. 59, No. 5-6, 1976, pp. 210-213.

Copeland, L. E., Bodor, E., Chang, T. N. and Weise, H. H., "Reactions of Tobermorite Gel with Aluminates, Ferrites and Sulfates", J. PCA Res. Devl.Lub., Vol. 9, No. 1, 1967, pp. 61-74.

Copeland, L. E. and Kantro, D. L., "Hydration of Portland Cement", pp. 387-420 in Proceeding of the 5th International Symposium on the Chemistry of Cement, 1968, Vol. II. The Organizing Committee, The Cement Association of Japan Tokyo, 1969.

Evans, R. C., edited 'An Introduction to Crystal Chemistry', 2nd Edition, Cambridge University Press, 1964, pp. 192-193.

Ish-Shalom, M and Bentur, A., "Effects of Aluminate and Sulfate Contents on the Hydration and Strenght of Portland Cement Pastes and Mortars", Cem. Concr. Res., Vol. 2, No. 6, 1972, pp. 653-662.

Kalousek, G. L., "Analyzing SO_3-Bearing Phases in Hydrating Cements", Mater, Res. Stand., Vol. 5, No. 6, 1965, pp. 292-304.

Lerch, W., "Influence of Gypsum on the Hydration and Properties of Portiand Cement Pastes", Proc. Am. Soc. Test, Mater., Vol. 46, 1946, pp. 1252-1292.

Melzer, R., and Eberhard, E., "Phase Idendification during the Early and Middle Hydration of Tricalciumsilicate (Ca_3SiO_5)", Cem. Concr. Res., Vol. 19, 1989, pp. 411-422.

Ménétrier, D., Jawed, I. and Skalny, J., "Effect of Gypsum on C_3S Hydration", Cem. Concr. Res., Vol. 10, 1980, pp. 697-701.
Older, I., "Interaction between Gypsum and the C-S-H Phase Formed in C_3S Hydration", Proc. 7th Int. Cong. on the Chem. Cem., Vol. 4, 1981, pp. 493-495.
Taylor, H. F. W. "Proposed Structure for Calcium Silicate Hydrate Gel", J. Am. Ceram. Soc. Vol. 69, 1980, pp. 464-467.

2ii045
4 pp

Kn o. 25. JAN. 2001 d o k 31808

HYDRAULIC ACTIVITY OF LOW TEMPERATURE DICALCIUM ORTHOSILICATE MODIFIED BY BaO ADDITION

Krystyna RAJCZYK, Institute of Mineral Building Materials, Opole, Poland

ABSTRACT The studies on the BaO influence on the structure and properties of dicalcium orthosilicate produced at 1300°C were carried out.The β polymorph was stabilized by excess BaO. The effect of $BaSO_4$ and $BaCO_3$ on the hydraulic activity and hydration products was investigated. The results give the possibility of the Ba containing by-products utilisation in the low energy cement technology.

Keywords: belite, activation, low energy, stabilization, additives

INTRODUCTION

Dicalcium orthosilicate is an important constituent of the low energy belite clinker, produced at lowered temperature. Despite of numerous research works, the problem of the belite hydraulic activity improvement is still unresolved. The studies on the active belite low temperature synthesis on the industrial scale are therefore of particular importance.

The technology of the low energy belite cementitious material has been worked up in the Institute of Mineral Building Materials, as a research project [Rajczyk, Nocuń 1992; Rajczyk, Kurdowski, Weryński 1992]. The belite phase was activated with barium addition, introduced to the raw mixture. The industrial by-product from barite plant was the source of Ba. It has been found that barium was incorporated to the dicalcium silicate structure thus modifying the hydraulic properties of this phase.

The role of BaO in clinker, particularly the question of the α' - dicalcium orthosilicate stabilisation was the subjest of many reports [Revergat, Choisnet 1981]. In the presented work the results of the studies on the BaO influence upon the dicalcium silicate structure and properties are shown.

EXPERIMENTAL

The silicate phase was synthesized from the chemically pure raw materials: calcium carbonate and siliceous acid at 1300°C. $BaSO_4$ or $BaCO_3$ were added as Ba-bearing components, at assumed BaO content corresponding to 3,0 % BaO in final product. The effect of BaO on the hydraulic properties of belite thus produced was investigated.

RESULTS AND DISCUSSION

The synthesized samples revealed some differences in phase composition as it has been found by XRD. Only in the barium sulphate doped sample some amount of admixture was detected. In all samples the β dicalcium silicate polymorph occurred as a main componenet. In the sample without admixture the γ polymorph was found. The XRD patterns of synthesized, unhydrous samples are presented in Fig.1. The peak d=0.282 nm at the plots for BaO doped samples is attributed to the α' polymorph. A substantial amount of free CaO was found both by XRD and chemical analysis.

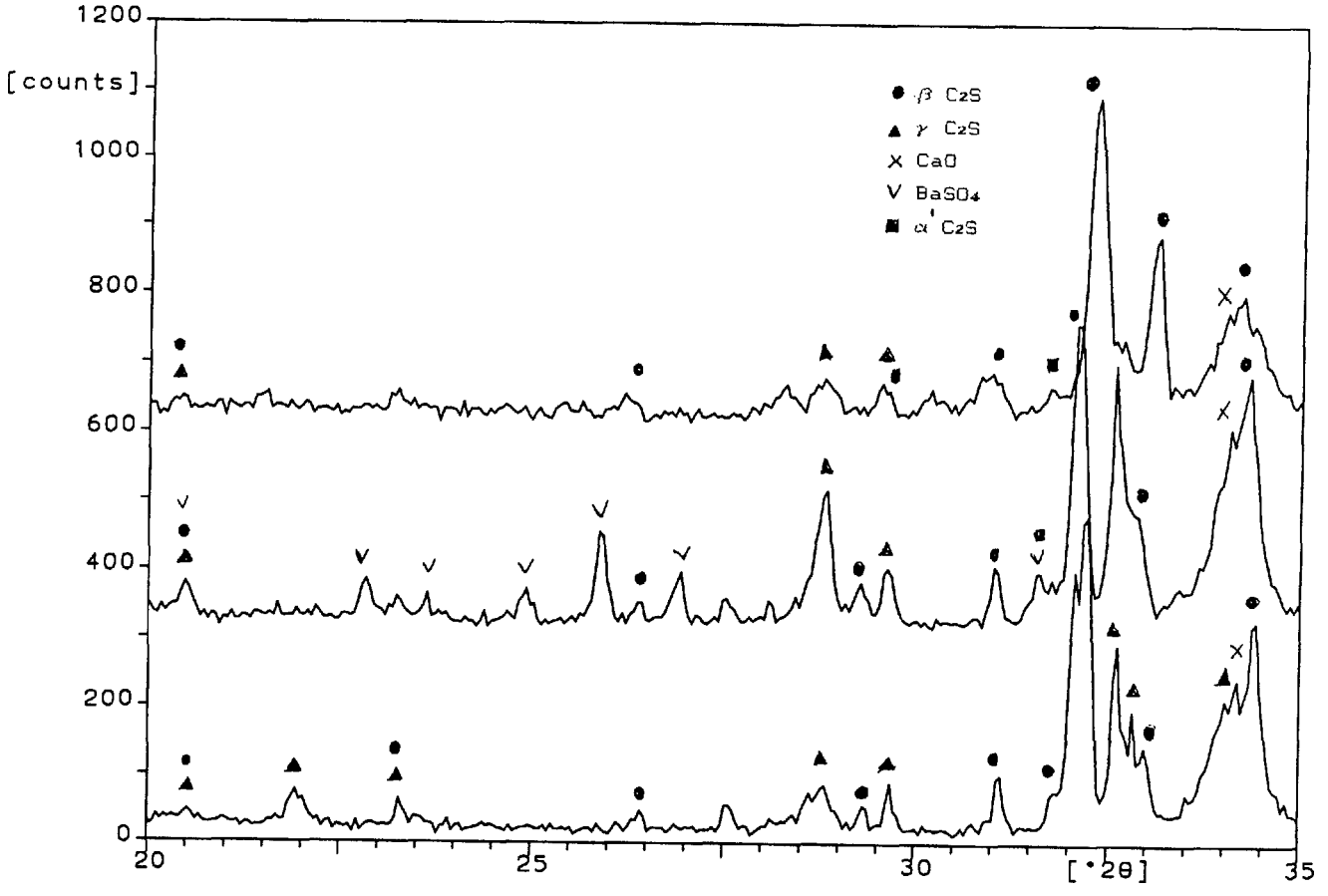

Figure 1 XRD patterns of dicalcium silicate samples.
a) - without admixture, b) - with $BaSO_4$, c) - with $BaCO_3$.

SEM observation revealed the effect of $BaSO_4$ and $BaCO_3$ on the microstructure of dicalcium silicate crystals. One should notice the presence of coarse belite grains with the free CaO inclusions. In the Ba doped samples the lamellar structure with the numerous fissures is evident. In the reference sample without admixture a significant amount of the γ - polymorph is observed (Fig.2). In Fig.2 the microstructure of samples after 90 days hydration is also presented. The progress of hydration is visible particularly in the case of the sample doped with $BaCO_3$. The belite grains are covered with the C-S-H of honeycomb structure. In the sample without additive the needle-like C-S-H is shown. The $BaSO_4$ long needles are detected on the grains on silicate grains doped with this compound.

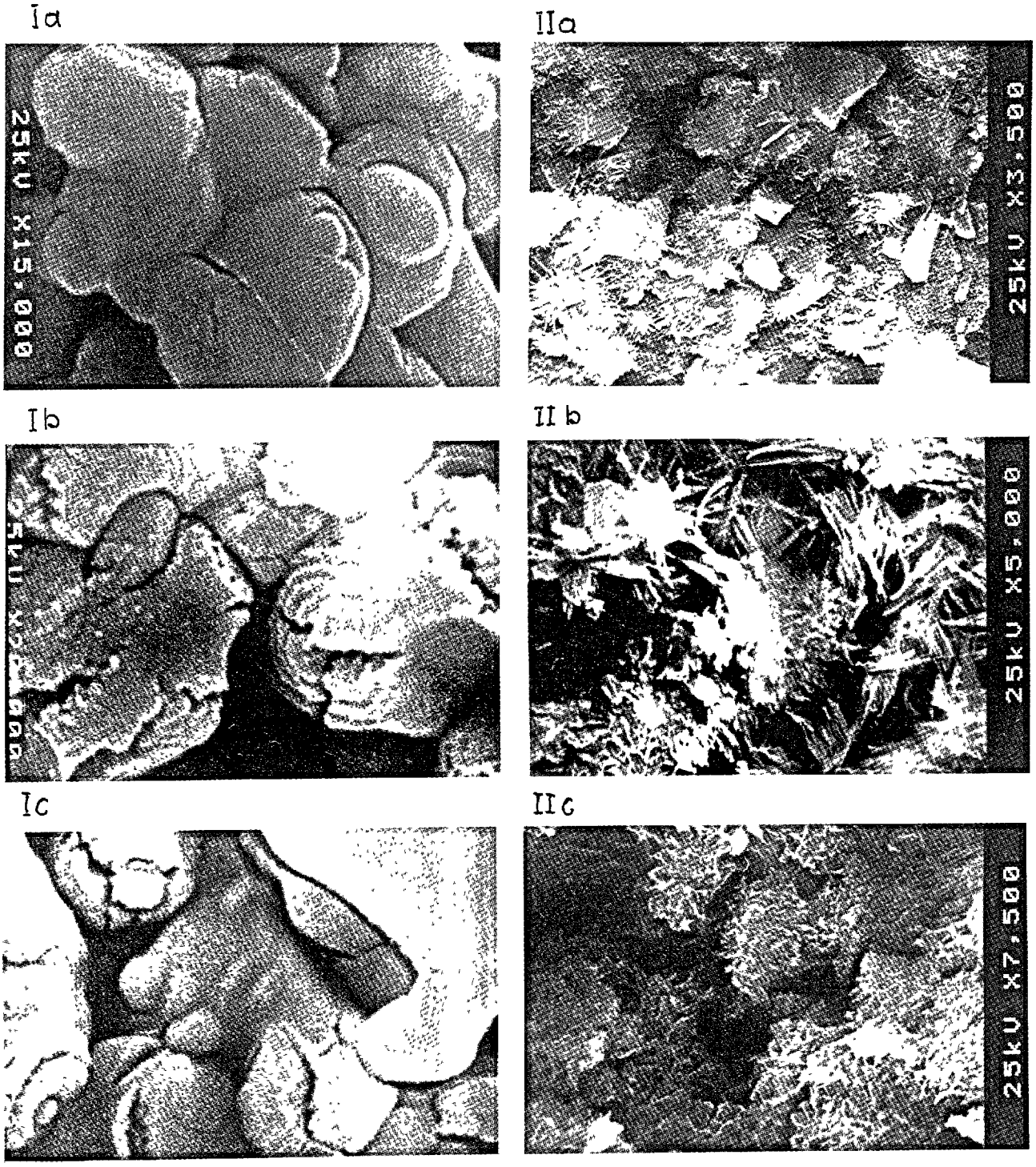

Figure 2 Microstructure of anhydrous belite sample [I]and hydrates after 90 days [II]. a) - without admixture, b) - with $BaSO_4$, c) - with $BaCO_3$.

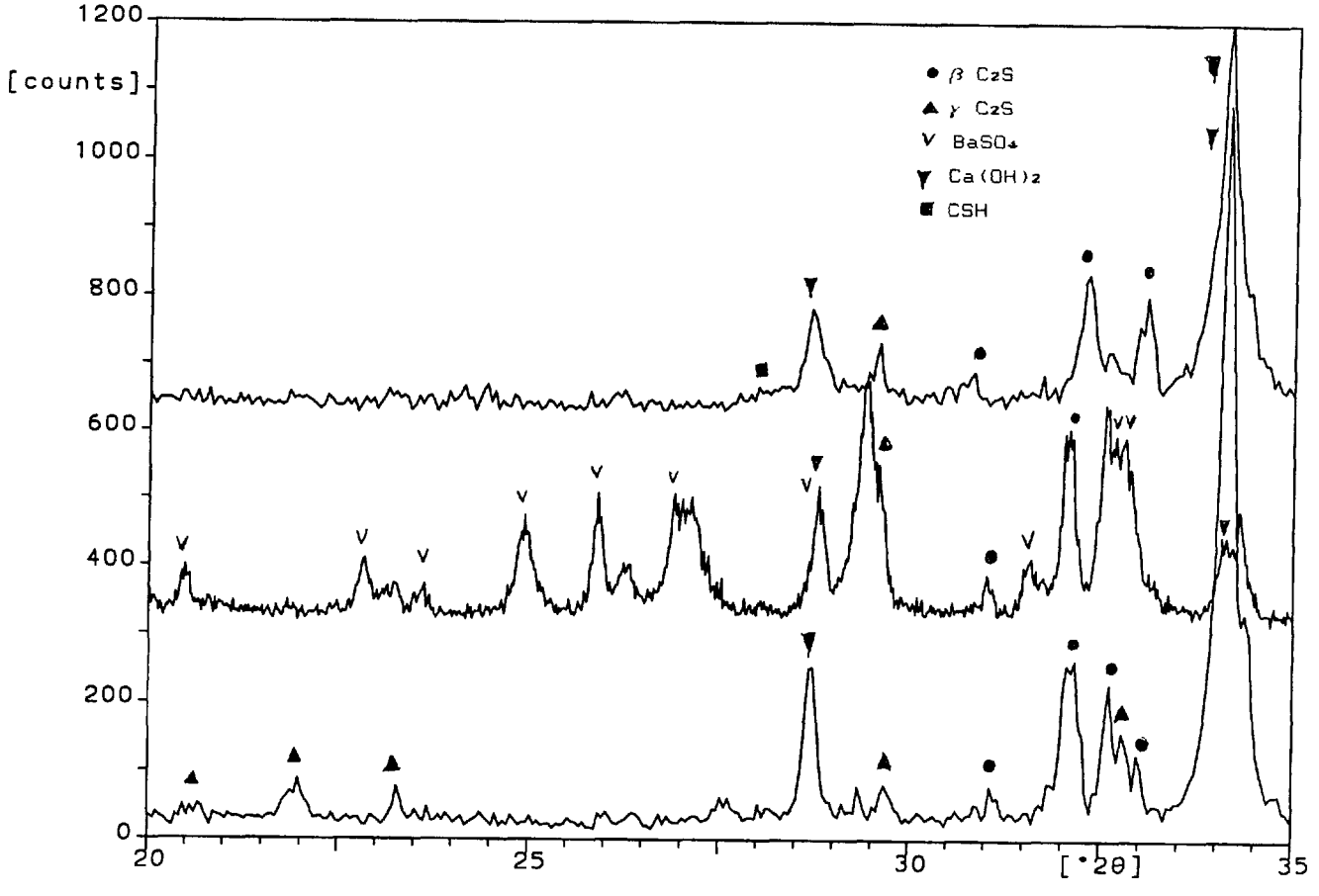

Figure 3 XRD patterns of hydrated dicalcium orthosilicate:
a) - without admixture, b) - with $BaSO_4$, c) - with $BaCO_3$.

SUMMARY

As it results from the data presented above, the structure of dicalcium orthosilicate can be modified by barium addition to the raw mixture, giving the material of better hydraulic properties. The effect is more pronounced when Ba occurs in form of $BaCO_3$.

REFERENCES

Rajczyk, K., Nocuń-Wczelik, W., "Studies of Belite Cements from Ba Containing Wastes", Proc. 9th International Congress on the Chemistry of Cements", Vol.II, 1992, New Delhi, India.

Rajczyk, K., Kurdowski, W., Weryński, B., "Belite Cement with BaO", Cement-Wapno-Gips, No1, 1992. (in Polish)

Revertegat, E., Choisnet, J., "Influence de l'oxyde de baryum sur les proprietes cristallographiques et technologiques du clinker de ciment portland", Ann.Chim.Fr., 6, 1981.

2ii046
4 pp

Kn o. 25. JAN. 2001 d o k 31809

THERMODYNAMICAL AND CRYSTAL-CHEMICAL ASPECTS OF INORGANIC BINDERS HYDRATION

Sh.M. RAKHIMBAEV, D.Sc., Professor.
Belgorod Technological Academy of Building Materials, Belgorod, Russia.

ABSTRACT The equation of the kinetics of heterogenous reactions with due account of kinetic and diffusion control has been proposed. The dependence of a hydration activity upon a salt basicity, the energy of atomization, ionization and hydration of a metal (cation), the affinity for an anion proton, has been established by the methods of chemical thermodynamics. The alkali activation of slags and ashes is connected with the dissociation constant of acids, the salts of which they are.

KEY-WORDS Hydration, Energy, Diffusion, Ions

INTRODUCTION

The best substantiated method to assess hydration activity of binders is by calculation of the difference of free energies of hydration products and initial nonhydrated compounds (Babushkin et al., 1962). However, this method is of no practical value because, to determine the thermodynamic properties of hydrated phases it is necessary to synthesize them in quite a pure state: this is difficult. It should be pointed out that the use of thermodynamic methods to characterise hydration processes meets with difficulties; most experts admit that reactions of clinker formation and binder hydration are mainly under diffusion control. But the use of thermodynamic methods of the calculation is based upon the assumption that the process is controlled in a kinetic field. It is necessary to confine the fields of thermodynamic application.

Kinetics of Hydration

The author suggested that kinetics of heterogeneous processes should be described by the equations (Rakhimbaev, 1990) :

$$(t/m) = (t/m)_o + k_1 m \quad [1]$$

$$(t/m) = (t/m)_o + k_2 t \quad [2]$$

where (t/m) is a value inverse to a current rate of a heterogeneous process; $(t/m)_o$ is an inverse initial rate; k_1 and k_2 are retardation coefficients.

The author's conception lies in the fact that a heterogeneous process starts at a maximum rate (m/t) under the given conditions. It is determined by kinetic factors, i.e. by binder reactivity with respect to water. When a binder particle is covered with a film of hydration product, diffusion resistance of which becomes quite high, the process passes into the area of internal diffusion control. The coefficients k_1 and k_2 in Eqs [1] and [2] characterize the intensity of the diffusion resistance of the film of reaction products which cover binder particles.

Eq [1] describes the kinetics of processes with extensive retardation when specific diffusion resistance of the reaction product film is constant throughout the whole process. A retardation coefficient has a measuring unit $[k_1] = sec/m^2$. It is inverse to a diffusion coefficient $[D] = m^2/sec$, i.e. Eq [1] is similar to the well-known equation of kinetics of processes with internal diffusion control and a constant diffusion coefficient in terms of time (Budnikov et al., 1965).

Eq [2] describes the processes in which specific diffusion resistance of the reaction product film increases with time. This process is characterized by a diffusion coefficient which apparently decreases with time.

The analysis of the experimental data on kinetics of hydration and the hardening of portland cement and other inorganic binders shows that at the initial stage hydration rates increase with time, as during this period its rate is determined by the processes of dissolution and hydrolysis, by the formation and the growth of hydrated phase nuclei and by heterogeneous crystallization under high supersaturation conditions, i.e. it is under kinetic control. Then the process passes into the area of internal diffusion control. The last stage is described well by Eq [2]. It follows from the above that thermodynamic methods can be used for the calculation of hydration processes of inorganic binders. They allow assessment of the maximum possible hydration activity of binders at the initial stage of their interaction with water when the diffusion resistance of hydration products may be neglected. It follows from Eqs [1] and [2] that if the initial rate $(m/t)_o$ is equal to 0, i.e. the process has a kinetic limitation, its current rate (m/t) is equal to 0 at any moment of time irrespective of diffusion characteristics.

Thermodynamics of the Initial Hydration Stage

In view of the above, the author used a chemical thermodynamic method for the calculation and prediction of hydration activity of inorganic salts of weak acids and strong bases, among these are portland cement, alumina cement, various slags, etc. (Karpov et al., 1968).

For this let us consider an elementary and easily-calculated equation of a hydration reaction of a salt having a composition of M_aRO_n (particular cases – Ca_2SiO_4, $Ca_3Al_2O_6$, etc.). At the first stage of the interaction with water these salts are dissolved and hydrolyzed, shown by the equation:

$$M_aRO_{n(sol)} + a\,H_2O_{(l)} = a\,M^{x+}_{(s)} + a\,OH^{-}_{(s)} + H_aRO^{ax-}_{n(s)} \qquad [3]$$

where (a) is a stoichiometric coefficient; (sol), (l), (s) are an aggregative state of compounds and ions; solid, liquid and solution states respectively in this case.

The free energy, ΔG, of dissolution and hydrolysis as per the equation is equal to:

$$\Delta G = a\Delta G_{M^{x+}_{(s)}} + a\Delta G_{OH^{-}_{(s)}} + \Delta G_{HaRO^{ax-}_{n(s)}} - \Delta G_{MaRO_{n(sol)}} - a\Delta G_{H_2O(l)} \qquad [4]$$

It follows from this equation that hydration activity of salts increases with increase of their basicity (a), free energies of the formation of a cation $\Delta G_{M^{x+}_{(s)}}$, an anion $\Delta G_{HaRO^{ax-}_{n(s)}}$ and with decrease of the free energy of the formation of an initial solid-state salt.

The free energy of salt formation characterizing its stability decreases from calcium silicate to calcium aluminate (when their basicities are the same), which is the main reason for the increase in the hydration activity in the same series. The free energy of the formation of various dicalcium silicate modifications drops from a gamma to alpha prime, which is the reason for the increase in their hydration activity in the same series, $\alpha' > \gamma$.

The reason for a higher hydration activity of glassy compounds as compared with crystals of the same composition is a lower free energy of the formation of the former ones. The measure characterizing the difference of the hydration activity of glass and crystals of the same composition is the free energy of crystallization.

The Effect of Cation and Anion Composition upon Hydration Activity

The author calculated free energies of dissolution and hydrolysis of the series of silicates, aluminates, ferrites, germanates, titanates of some univalent and bivalent metals. It was established that the activity of orthosilicates and metasilicates decreased in the series of Cs, Rb, K, Na, Ba, Li, Ca, Mg, Mn, Co, Fe, Pb, Be, Zn, Cu salts. The activity of calcium salts drops in the series:

$In_2O_6^{6-}, Ga_2O_6^{6-}, Al_2O_6^{6-}, PbO_4^{4-}, GeO_4^{4-}, Fe_2O_5^{4-}, SiO_4^{4-}, TiO_3^{2-}, SiO_3^{2-}$.

Based upon thermodynamics, calculations using Born-Haber cycles were formulated (Rakhimbaev, 1968, 1978) using the following equation for cation formation energy $\Delta G_{M_{(s)}^{x+}}$:

$$\Delta G_{M_{(s)}^{x+}} = \Delta G_{\text{hydration}M_{(g)}^{x+}} - \Delta G_{M_{(g)}} - \Delta G_{\text{ion}M_{(g)}} \qquad [5]$$

where $\Delta G_{\text{hydration}M_{(g)}^{x+}}$ – free energy of gaseous ion $M_{(g)}^{x+}$ hydration; $\Delta G_{M_{(g)}^{x+}}$ free energy of metal formation in a gaseous state – metal atomization; $\Delta G_{\text{ion}(g)}$ – metal ionization energy in a gaseous state.

It is seen from the last equation that the free energy of the cation formation in solution, which exerts a considerable effect upon the hydration activity of weak acid salts, grows with increase in the cation hydration energy but decreases as the atomization energy of the corresponding metal increases; also as its ionization potential increases.

The initial data and calculation results of free energies of dissolution and hydrolysis of some orthosilicates are given below:

	$-\Delta G_{M_aRO_{n(sol)}}$ (kJ/mole)	$-\Delta G_{H_aRO_{n(s)}^{ax-}}$ (kJ/mole)	$-a\Delta G_{M_{(s)}^{x+}}$ (kJ/mole)	ΔG (kJ/mole)
Ba_2SiO_4	2157.85	1039.12	1097.78	15.503
$Ca_2SiO_4(\beta)$	2199.75	1039.12	1110.35	56.565
$Ca_2SiO_4(\gamma)$	2203.94	1039.12	1110.35	60.755
Mg_2SiO_4	2057.29	1039.12	905.04	134.080
Pb_2SiO_4	1248.62	1039.12	-48.604	361.597
Zn_2SiO_4	1525.16	1039.12	278.216	251.819
Fe_2SiO_4	1386.89	1039.12	186.874	217.042

In going from alkali salts to alkaline-earth salts and then to univalent and bivalent metals of transition groups, a sharp drop in the hydration activity of silicates, aluminates, ferrites, germanates is explained by a considerable increase in the atomization energy and the ionization potential in the same series. At the same time the first Eq [5] component (i.e. the free energy of

the cation hydration $\Delta G_{hydration M^{x+}_{(g)}}$) of the elements of the main and secondary subgroups differs little and depends mainly upon a valency and a radius of ions. The free hydration energy of univalent ions of sodium, potassium and lithium is considerably less than the same of bivalent atoms of the second group including transition elements (zinc, manganese, copper, cobalt, iron). A higher hydration activity of barium and calcium silicates and aluminates, as compared with compounds of secondary subgroup elements (Zn, Mn, Pb), is explained by a higher free energy of the hydration of the former ones, which depends upon their little energy of the atomization and ionization potentials.

The calculations showed that in an alkaline medium the free energy of the hydrolysis of low-basicity silicates (components of slags and ashes) was higher than it was in water. At the same time the alkaline activation of slag may be considered as anion depolymerization with hydroxyl addition. The higher dissociation constant of a polyacid is, i. e. the stronger it is as an acid, the more readily it is depolymerized. Hence it follows that a tendency to alkaline activation grows in the series: aluminates, titanates, silicates, phosphates. This series agrees with the experimental data on alkaline activation of slags and ashes.

Thus, the experimentally determined regularities of the influence of a cation composition and an anion one and that of a compound phase state upon the hydration activity of inorganic salts find a theoretical explanation.

Let us consider the factors determining a high tendency to the hydrolysis of anions of silicates, aluminates and other salts of weak acids as compared with sulphates, phosphates and other salts of strong acids.

Effective Charges of Ions and Hydration

The author showed (Rakhimbaev, 1968, 1978) that the effective charge of an ion in anions RO_4^{a-} increased in the series of nitrates – sulphates – silicates – germanates – aluminates – gallates – indates. The higher the effective charge of an oxygen ion in an anion is, the higher its affinity for a proton is, the less a dissociation constant of the corresponding acid is, the weaker it is as an acid.

REFERENCES

Babushkin V.I., Matveyev G.M., Mchedlov-Petrosyan O.P., "Thermodynamics of Silicates", Moscow, Stroiizdat Publishers, 1962, p.266.

Rakhimbaev Sh.M., "Calculations of Rate Constants of Some Processes of Artificial Building Conglomerate Technology", "Materials Technology Problems and Improvement in the Building Material Production Tachnology", Belgorod, BTISM-MISI Publishers, 1990, p.184.

Budnikov P.P., Ginstling A.M., "Reactions in Mixtures of Solids", Moscow, Stroiizdat Publishers, 1965, p.474.

Rakhimbaev Sh.M., "Calculation of Effective Ion Charges in Some Oxyacid Salts Based upon Thermochemical Data", Journal of Physical Chemistry, 1968, vol.40, ¹ 12, pp. 3089-3091.

Rakhimbaev Sh.M., "Regulation of Technical Properties of Grouting Mortars", Tashkent, Fan Publishers, 1978, p.178.

Karpov I.K., Kashik S.A., Pampura V.D. "The Constants of Materials for Thermodynamic Calculations in Geochemistry and Petrology", Moscow, Nauka Publishers, 1968, p.142.

2ii047
4 pp

Kn o. 2 5. JAN. 2001 d o k 3186

HYDRATION AND STRUCTURE FORMATION OF INORGANIC BINDERS

Magdelinka RADENKOVA-YANEVA, University for Architecture, Civil Engineering and Geodesy, Sofia, Bulgaria

ABSTRACT Special features of structure formation during hydration of inorganic binders with salts and complex admixtures are considered. The processes of formation of a coagulation structure and its transition into a structure of condensation-coagulation type are discussed. The results received are explained on the basis on the above mentioned succession of the structure formation processes. A structure model of hydrated cement pastes in the early stages of hydration is proposed. The practical use of theoretical consideration is shown.

Key-words: Admixtures, binder, CSH, hardening, hydration.

INTRODUCTION

Hydration of inorganic binders in their practical use takes place in highly concentrated suspensions - cement pastes, mortars and concretes. This is a spontaneous process, which is subordinate to the regularities of the heterogeneous chemical reactions. The dissolution of the solid metastable phase (clinker minerals) is an obligatory stage and calcium hydrosilicates, hydroaluminates and hydroferrites are precipitated from the supersaturated solution.

The interaction between cement and water takes place on the surface of the cement particle and is controlled by diffusion. In the products of the reaction an inner and an outer part (Kondo, 1968) or even an intermediate layer are formed (Pommersheim, 1980). Hydration products have an irregular structure and inconstant composition. In the early stages of water - cement interaction calcium hydrosilicates have a colloid character. Gel from C-S-H phase is generated and the primary structure of the cement stone is formed - the system is setting and hardening. These processes are due to the coagulation of the cement particles and the hardening of the coagulated structure (Segalova and Rebinder, 1954; Rebinder, 1956; Shchukin et al, 1979, 1980; Jiang et al, 1995, 1996).

The present investigation aims to establish the influence of salts and complex admixtures on the hydration processes and on the structure formation of inorganic binders in the early stages of their interaction with water, and to formulate some additional considerations concerning the origin of coagulation - thixotropic and condensation - crystallization structures.

EXPERIMENTAL

Materials

The investigation is performed with pastes on the base of ordinary cements and binders containing no cement clinker. The mineral composition of the clinkers used (calculated according Bogue) is shown in Table 1. Binder without cement clinker is received from belite middling slime, which is a byproduct obtained in the production of aluminum oxide from nonbauxite materials and contains as a main component approximately 80 % β-$2CaO.SiO_2$. Its composition and properties are very close to those of dicalcium silicate in portland cement clinker (Bojenov et al, 1966). As the belite middling slime has a bad activity (low rate of interaction with water) it is activated with hydraulic lime.

Table 1 Mineral composition of the clinkers

Mineral composition, %	Clinker No 1	Clinker No 2
C_3S	35.45	40.08
C_2S	40.12	34.13
C_3A	6.50	11.26
C_4AF	1.15	0.46

In the investigated cement systems salts and complex admixtures are added, designated as **A**, **B**, **C**, **D** and **E**. Admixture **A** is a mixture from Na_2SO_4 and $NaNO_3$; admixture **B** contains $CaCl_2$, $NaNO_3$ and $NaNO_2$; admixture **C** consists of $CaCl_2$ and water-soluble methylolmelamine polycondensate; admixture **D** contains admixture **B** and water-soluble epoxy resin; admixture **E** is a mixture of water-soluble epoxy resin and water-soluble methylolmelamine polycondensate.

Experimental methods

Cement pastes are prepared by mixing with water according to EN 196-1. The setting time (initial and final) is determined by Vicat tests (EN 196-1). The shear strength (cohesion forces) is determined by using MGU device (Rebinder, 1949). From the curves shear strength versus time of hydration, the time for structure formation (t_{sf}) is determined.

RESULTS AND DISCUSSIONS

The results received are shown in table 2 and table 3 and characterize the structure formation processes in the early stages of hydration (up to 8 - 10 hours). They show that salts admixtures accelerate the beginning and the end of setting and decrease the time for structure formation. The complex admixtures have a lower influence on the mentioned properties.

Table 2 Setting time of the pastes with admixtures

Admixture	Type of binder					
	Binder without cement clinker		Cement No 1		Cement No 2	
	initial	final	initial	final	initial	final
	hour - min.		hour - min.		hour - min.	
Without admixture	2 - 55	6 - 30	2 - 00	4 - 25	1 - 15	3 - 10
2 % admixture A	2 - 20	5 - 50	1 - 30	3 - 55	1 - 00	2 - 30
3 % admixture A	2 - 15	5 - 05	1 - 15	3 - 25	0 - 45	2 - 15
Admixture B	0 - 50	2 - 05	1 - 10	2 - 15	1 - 05	2 - 40
Admixture C	2 - 40	6 - 05	1 - 45	3 - 55	1 - 25	3 - 05
Admixture D	1 - 25	2 - 45	1 - 50	4 - 20	1 - 10	4 - 55
Admixture E	1 - 15	3 - 30	1 - 25	3 - 15	1 - 20	5 - 10

The data obtained can be discussed in view of the specific character of the admixtures and their influence on the coagulation of the investigated systems.

The systems we have studied belong to the joined - dispersive microheterogeneous systems. They consist of water, fine binder particles and finedisperse hydrate products.

Table 3 Time for structure formation (t_{sf}) of pastes with chemical admixtures

Admixture	Type of binder		
	Binder without cement clinker	Cement No 1	Cement No 2
	hour - min.	hour - min.	hour - min.
Without admixture	7 - 20	7 - 30	8 - 40
2 % admixture A	5 - 20	6 - 45	7 - 10
3 % admixture A	4 - 45	6 - 05	6 - 45
Admixture B	5 - 35	5 - 30	6 - 40
Admixture C	5 - 10	5 - 20	6 - 05
Admixture D	4 - 50	6 - 10	6 - 10
Admixture E	5 - 45	5 - 15	7 - 05

The latter are received during clinker minerals dissolution with simultaneous passing of calcium (Ca^{2+}), silicate, aluminate and alumoferrite ions in the solution. The latter form the negatively charged nuclei of the colloid particles. Positively charged ions (H^+, Ca^{2+}, Na^{2+}, etc) are adsorbed on their surface and an electric double layer is generated. The kind and quantity of the ions in the adsorption layer determines the value of the electrokinetic potential (zeta potential) of the system, and consequently the interparticle interaction. The coagulation in such kinds of systems is provoked by adding of electrolytes. In this process the diffusion layer is diminishing proportionally to the concentration and the valency of the ions with a charge opposite to the ions determining the ζ - potential; the latter decreases gradually and the system comes near to its isoelectric condition. In the borderline case the ζ - potential is equal to 0 and as a result of the loss of the aggregative stability a coagulation occurs - coagulation contacts are generated. This is possible in case that the particles come close to a definite distance - h_{min}. In such a case we think that a short distance coagulation occurs and the structure formed has a coagulation-thixotropic character. For such a structure Van der Waals forces of interparticle interactions are typical.

In the evolution of the hydration processes due to the additional precipitation of the hydration products near the coagulation contacts and to the continuous changes in the solid and liquid phase of the system, a condensation - crystallization structure is formed. This structure is irreversible because of the valent bonds formed between the particles. The considerations pointed out, concerning the mechanism of structure formation, show that the coagulation in a short distance is an obligatory condition for the following crystallization contacts occurring and for the cement systems.

In accordance with the above exposed, the influence of the electrolytes added in the hardening cement pastes is connected with the diminishing of the size of the double electric layer of the colloid particles, with the decreasing of the value of the ζ - potential and with the creation of conditions for short distance coagulation. As a result the time for structure formation is shortened (see Tables 2 and 3).

At the same time the liquid phase (pore solution) becomes supersaturated regarding to Ca^{2+} and SO_4^{2-} and gypsum crystals are precipitated. Calcium ions are brought out of the adsorption layer

of the colloid particles. After a fast coagulation, crystallization contacts are formed and a condensation - crystallization skeleton is developed.

Complex admixtures, containing an organic component, have a weaker influence on the processes of structure formation. They decrease in a lower degree the time for structure formation and in some cases (cement No 2) they even increase the end of setting in comparison to the samples without admixtures (see Table 2). This can be explained with the mineral composition of the clinker, respectively the content of $3CaO.Al_2O_3$ and the behavior of the organic component of the admixture. The organic admixtures used make adsorption layers mainly on the aluminate component of the system. In this way the processes of short distance coagulation are retarded which results in decreasing of the time for structure formation.

The data obtained in our investigations, considered according to our theoretical concepts and the proposed model for structure formation, are different from some other authors' considerations (Jiang, 1995,1996) and explain more clearly the formation of a structure with coagulation - thixotropic character.

CONCLUSION

The processes of structure formation of the inorganic binders are discussed using the DLVO theory. It is pointed out that as a first stage of the hydration a coagulation structure with thixotropic character is formed, and this structure later on is transformed in a skeleton of condensation - crystallization type. The processes of coagulation are dealt with in detail and the problem of short distance coagulation and the factors, influencing it, is discussed.

The investigations conducted and the results obtained show that the used admixtures influence the cement systems structure formation according to their character and the type of the binder. They promote decreasing or even reduce to zero the coagulation process energy barrier, which is due to the double electric or adsorption layer. The experimental results conform well to the adopted model for short distance coagulation contacts formation during the structure formation in cement systems.

The practical value of the investigations performed is connected with the technology parameters of concrete manufacture. The time for setting and hardening determines the conditions for concrete mixtures processing, placing and compacting during building concrete structures.

REFERENCES

Bojenov, P. I., V. I. Kavalerova, Nefelin Slime, Publishers of Literature about Civil Engineering, Moscow, 1966.

Jiang, S. P., J. C. Mutin, A. Nonat, Cem. and Concr. Res., vol. 25, No 4, pp. 779 - 789, 1995.

Jiang, S. P., J. C. Mutin, A. Nonat, Cem. and Concr. Res., vol. 26, No 3, pp. 491 - 500, 1996.

Kondo, R., S. Ueda, Proc. 5th Int. Congr. Chem. Cem., Tokyo, II, Sess. II-4, p. 203, 1968.

Pommersheim, J. M., Proc. 7th Int. Congr. Chem. Cem., Paris, Theme IV, p. 195, 1980.

Rebinder, P. A., Proc. 3rd Int. Congr. Chem. Cem., Stroiisdat Publisher, Moscow, p. 125, 1956.

Rebinder, P. A., N. A. Semenko, Dokl. Acad. Nauk SSSR, 64, No 6, pp. 835 - 838, 1949.

Segalova, E. E., P. A. Rebinder and O. I. Lukyanova, Vestnik Moscow Univ., 9, Serie Phys., Math. and Nat. Sci., 1.17.1954.

Shukshin, E. D., E. A. Amelina, Adv. in Colloid and Interface Sci., 11, p. 235, 1979.

Shukshin, E. D., Microscopic Aspects of Adhesion and Lubrification, Tribology, Series 7, Elsevier, 1982.

2ii048
4 pp

Kn o. 2 5. JAN. 2001 d o k 31811

THE STRENGTH OF THE HYDRATED PHASES IN THE PORTLAND CEMENT PASTES

Vadim BABKOV and Ildar KARIMOV, Ufa State Petroleum Technological University, Russia

ABSTRACT A theoretical model for the strength of the hydrated phases in the Portland Cement pastes is proposed assuming that Portland Cement paste consist of separate crystals with contacts. The strength of model determined the main features, such us crystals size distribution, area of contact-section of crystal relationship, space direction of crystals. In this model, failure take place gradually breaking weak elements before strong elements. Two kind of failure through crystals, along contacts. The model is bases on theory of fracture mechanics and theory of probability.

Key-words: crystal structure, modelling, capillary porosity

INTRODUCTION

The main feature of the hardened of Portland Cement pastes is the structure-mechanical non-homogeneity which is characterized by different strengths of separate structural crystals and stress distribution to the crystals while loading. The different strengths of separate crystals is very dependent on the size distribution of crystals. The typical size of separate crystals of the hardened Portland cement paste (diameter of needle-shaped form crystals, thickness of lamellar form crystals) is in the range of 5-20 nm to 1 μm. A.F.Ioffe (1974) and G.V.Bereshkova (1969) have shown that the tensile strength R_k of separate crystals of rock-salt and quartz change in 100 time when the diameter of needle-shaped form crystals is in the range of 0.1-20 μm.

MODEL

To describe the function $R_k = f(a)$ proposed (Babkov and Polak, 1977):

$$R_k = R_m (a_* / a)^n, \qquad [1]$$

where R_m - theoretical strength of crystalline phase; a - typical size of separate crystals; a_* - non-defects crystal size; n - coefficient intensity lowering strength when increasing a.

The different strengths of separate crystals depend on area of contact - section of crystals relationship, different strengths contact and crystal as well. The stress distribution to the crystals while loading is linked with space direction of crystals and others. We considered a model for the crystalline phase of Portland Cement paste which consist of separate crystals united by contacts. The crystals are of difference size. All crystals have a space direction along three axies in the same probability. We considered two kind of failure: through crystals, along contacts.

If crystals have strong contacts then failure occur through crystals. In this case loading fracture weak crystals and redistributes on the strong crystals. If stress is lesser or of equal strength of weakest crystal, then the structure is stabile. For intermediate condition specific load is expressed by

$$R = \frac{1}{3} V_m R_m (a_* / a)^n \int_{a_0}^{a} \varphi(a) da, \qquad [2]$$

where $\varphi(a)$ - function size distribution of crystals; a - size the greatest remaining crystals $(a_0 \le a \le a_m)$; a_0, a_m - accordingly lesser and greatest characteristic size of crystals; V_m - relative volume of crystalline phase.

When loading is increased to break all crystals, this load corresponds to the strength crystalline phase R_{kc} which equal extremum to Eq 2 for a. For even distribution function $\varphi(a) = \frac{1}{a_m - a_0}$ when $a_0 \ge a_*$ it will be

$$R = \frac{1}{3} V_m R_m (a_* / a)^n \frac{a - a_0}{a_m - a_0}; \qquad [3]$$

$$\frac{dR}{da} = \frac{1}{3} V_m R_m \frac{a^n}{a_m - a_0}(a - na + na_0) = 0; \quad a_{cr} = \frac{na_0}{n-1};$$

$$R_{kc} = \frac{1}{3} V_m R_m (a_* / a_0)^n \frac{a_0}{a_m - a_0} \cdot \frac{(n-1)^{n-1}}{n^n}. \qquad [4]$$

Eq 4 take place by $a_* \le \frac{n+1}{n-1} a_0$, $n > 1$. For non-fulfilment of this conditions the strength is expressed by

$$R_{kc} = \frac{1}{3} V_m R_m (a_* / a_m)^n \qquad [5]$$

For even distribution and $a_0 \le a_*$, $a_* \le a_{cr} \le a_m$ the strength correspond to Eq 4. For non-fulfilment of this conditions the strength is expressed by

$$R_{kc} = \frac{1}{3} V_m R_m \int_{a_0}^{a_*} \frac{1}{a_m - a_0} da = \frac{1}{3} V_m R_m \frac{a_* - a_0}{a_m - a_0}. \qquad [6]$$

This calculations were carried out for other function distribution including the normal law distribution. The calculation strength through crystals for crystalline phase of Portland Cement pastes (at $V_m \approx 0.72$; $R_m \approx 4 \cdot 10^3$ MPa; $a_* \approx 50$-100 nm; a_0-a_m=5-1000 nm; $n \approx 1.2$-1.6) to carry out for several function distribution is given by tensile strength in the range 80-200 MPa. The analysis of Eqs 4-6 show that in order to increase the strength of crystals with strong contact, it is necessary to decrease large crystals size.

If crystals have weak contact then failure occurs along contacts. In this case the mechanism of failure and strength structure determine overload contacts with reference to stress of area section of crystals and heterogeneous tensity in contacts. Out of equilibrium case the stress in contact equal the stress in crystal divided by specific area contact η which equal area contact - section of crystal relationship. For intermediate condition specific load is expressed by

$$R = \frac{1}{3} V_m R_m \eta \int_{\eta}^{\eta_m} \varphi(\eta) d\eta, \qquad [7]$$

where R_m - the strength of contact; $\varphi(\eta)$ - function distribution of specific area contact η.

For even distribution function $\varphi(\eta) = \frac{1}{\eta_m - \eta_0}$ the strength of crystalline phase along contacts it will be

$$\text{- at } \eta_0 \le \eta_m / 2: \quad R_{kc} = V_m R_m \frac{\eta_m^2}{12(\eta_m - \eta_0)}, \qquad [8]$$

$$\text{- at } \eta_0 \ge \eta_m / 2,\ 0.5 \le \eta_m \le 1: \quad R_{kc} = \frac{1}{3} R_m V_m \eta_0. \qquad [9]$$

The calculations of strength along contacts for crystalline phase of Portland Cement pastes ($0.2 \le \eta_m \le 1$; $0.1 \le \eta_0 / \eta_m \le 0.5$) carried out for several function distribution gives tensile strength in the range 25-150 MPa.

The analysis of Eqs 7-9 show that in order to increase the strength of crystals with weak contact it is necessary to decrease number of contacts, to develop area of contacts, to increase the strength of contacts, levelling specific area contacts. In the latter case stress in contacts become homogeneous.

The second main factor of influence on the strength of the hardened Portland Cement pastes is capillary porosity which occupy of 10-40% total volume. The strength of Portland Cement stone R_c one can connect with concentration hydrated phase so-called "gel:space" F. If structure consist of separate structural elements with the same local densities then all elements will fail at the same time. In this case the strength of structure it will be

$$R_c = R_{kc} F^2. \qquad [10]$$

The real structure is inhomogeneous when the separate structural elements have a different local densities. The mechanism of failure of this structure is "stepped" when breaking overloaded structural elements (Babkov and Polak, 1980). For intermediate condition specific load is expressed by

$$R = R_{kc} v^2 \int_{0}^{v_m} \varphi(v) dv, \qquad [11]$$

where $\varphi(v)$ - function distribution of local density v; v_0, v_m - accordingly lesser and greatest value of v.

For even distribution function of local density $\varphi(v) = \frac{1}{v_m - v_0}$ (for the present instance

$F = \frac{v_m + v_0}{2}$) the strength of porous material, for example Portland Cement stone it will be

$$R_c = R_{kc} \frac{4v_m^3}{27(v_m - v_0)}. \qquad [12]$$

Eq 12 take place by $v_0 \le 2/3v_m$. For non-fulfilment of this condition the strength is expressed by $R_c = R_{kc} v_0^2$. The calculations by Eq 12 and other function distributions, including the normal law distribution (Babkov and Karimov, 1996), it is shown that Eq 12 correspond to expression proposed by Powers and Brownyard (1948)

$$R_c = R_{kc} F^s, \qquad [13]$$

where s=2.5-3.5 depending on $\varphi(v)$. This value s correspond with value s=2.6-3.0 received by Powers and Brownyard (1948) for Portland Cement stone.

CONCLUSION

The calculated strength of the hardened Portland Cement pastes shown that the structure-mechanical inhomogeneity decrease the theoretical strength by 50-100 times, while the capillary porosity decrease the strength by 3-10 times.

REFERENCES

Бабков В.В., Мохов В.Н., Полак А.Ф. Механика разрушения и прочность кристаллизационного сростка. - В кн.: Гидратация и структурообразование неорганических вяжущих. -М., 1977, -С.39-50.

Бабков В.В., Мохов В.Н., Ананенко А.А., Полак А.Ф. Структурная неоднородность и прочность пористых материалов //Изв.ВУЗов. Сер.Строительство и архитектура, 1980. -№12. -С.64-70.

Бабков В.В., Каримов И.Ш. Неоднородность пористости и ее связь с прочностью материалов типа цементного камня //Современные проблемы строительного материаловедения. Мат. междун. науч.-техн. конференции, часть 1. -Казань, 1996, -С.18-21.

Иоффе А.Ф. О прочности на разрыв тонких стеклянных нитей и слюдяных пластинах //А.Ф.Иоффе, Избранные труды. -Л.: Наука, 1974. -С.280-283.

Бережкова Г.В. Нитевидные кристаллы. -М.: Наука, 1969. -155 с.

Powers T.C. and Brownyard T.L. Studies of the Physical Properties of Hardened Portland Cement Paste. Portland Cement Association Bulletin 22, 1948, 101-992.

2ii049
6 pp

Kn o. 25. JAN. 2001 d o k 31812

AN INVESTIGATION INTO THE CHEMICAL NATURE OF THE REACTIVITY OF LIME

C. A. STRYDOM, Department of Chemistry, University of Pretoria, Pretoria 0002, South Africa
J. H. POTGIETER, PPC Technical Services, P O Box 40073, Cleveland 2022, South Africa

ABSTRACT
The hygroscopic nature of lime causes it to react with water vapour in the atmosphere to form $Ca(OH)_2$. In the presence of CO_2, any slaked lime immediately reacts with the CO_2 at temperatures above 300 °C to give $CaCO_3$. Loss in the reactivity of lime can both be attributed to rehydration and recarbonation. The mass loss curves of lime samples clearly show the percentage rehydration and recarbonation and it serves as an indication of the reactivity of the lime samples.

Keywords : Lime, reactivity, free lime, calcium hydroxide, thermogravimetry

INTRODUCTION
The thermal decomposition of limestone (mainly $CaCO_3$) has been the focus of many researchers, particularly those dealing with cement technology, as it is the most energy demanding reaction taking place during the clinkering process (Kasselouri, Dimopoulus and Parissakis, 1995). Masonry cements are also produced by intergrinding cement clinker, gypsum and limestone, which can be partially or totally replaced with hydrated lime. The limestone and lime improve the workability of the mix and also act as water retention agents to prevent too rapid drying when the cement is used for plastering purposes.

The percentage calcium content of lime containing samples is determined in the cement industry by the XRF method, and it is then directly expressed as the %CaO, which of cause, is not always correct, since $Ca(OH)_2$, $CaCO_3$ and other compounds could have formed also. The percentage free lime (CaO) is of particular importance for hydration and neutralization reactions. This percentage is determined using a method measuring the amount of CaO and $Ca(OH)_2$ simultaneously, and denoting it the "available free lime". The reactivity of the lime is tested using the DIN slaking test. Water is added to a lime containing sample in an adiabatic container, it is stirred and the time (in seconds) taken for the reaction mixture to reach a temperature of 60 °C is used to get the reactivity index:

$$R_{DIN} = {}^{2400}/_{t}$$

The reactivity index is thus an indication of the amount of CaO, available for hydration and/or neutralization, in the lime sample.

In industry it is sometimes found that lime samples with a high percentage "available free lime", give low reactivity values, or that the reactivity decreases dramatically with time (days) although the availability value remains constant. The hygroscopic nature of lime causes it to react with water vapour to form $Ca(OH)_2$, while any CO_2 in the atmosphere could react with lime to form $CaCO_3$. It was

found that the rate of uptake of CO_2 for this equilibrium reaction, is comparable to that of the decomposition reaction even at relatively small sample masses and high flow rates of an inert gas (Sinev, 1988).

It is the purpose of this study to determine whether there is any relationship between the reactivity of lime and the percentage $Ca(OH)_2$ and $CaCO_3$ in a sample. The rehydration and recarbonation of lime samples in the precence of water vapour and carbon dioxide were also investigated.

EXPERIMENTAL

Sample preparation

Pure $CaCO_3$ and $Ca(OH)_2$ were obtained from Merck to compare the thermogravimetric decomposition curves of the pure samples to that of the lime samples. The unslaked lime, received from Lime Acres, where it was burnt from limestone at 1200 °C, were crushed and screened into a -4.75 mm + 1.0 mm fraction. This fraction was divided into 5 equal parts of 200 g each. The first portion's reactivity was immediately measured on a LRT 60 reactivity meter according to the standard procedure. The remaining 4 samples were exposed outside the building to relatively dry atmospheric conditions and their reactivities were similarly measured on 1 day intervals (Table I). Immediately after measuring a sample's reactivity, XRF analysis was performed on the sample on a Siemens MRS 400 XRF spectrometer (Table II). The hydrated lime sample was obtained from Lime Acres, where the unslaked lime was passed through a commercial type hydrator.

Table 1 : Reactivity values (R_{DIN}) after exposure to atmosphere

Day number	Time (s)	Reactivity (R_{DIN})
0	80	30
1	1209	1.98
2	1413	1.70
3	∞	Never reached 60 °C
4	No analysis attempted	

Thermogravimetry

A Netzsch STA 409 simultaneous TG/DSC instrument was used to collect thermogravimetric data. Nitrogen was employed as a dynamic atmosphere, except in the case where the samples were subjected to a 50% CO_2 : 50% air mixture and an atmosphere where this mixture was purged through water at 20 °C. The flow rate in all cases was 20 $cm^3.min^{-1}$. Temperature calibration was achieved using the ICTAC recommended DTA standards. Sample masses varied between 20 and 50 mg. To relate all results a heating rate of 5 °C.min^{-1} was used throughout.

Table 2 : XRF Analysis of samples (H.Lime = Hydrated Lime; Av.Lime = Available Lime)

	Day 0	Day 1	Day 2	Day 3	Day 4	H.Lime
SiO_2	1.0	1.0	0.9	1.0	0.9	2.0
Al_2O_3	0.4	0.5	0.4	0.4	0.5	0.6
Fe_2O_3	0.4	0.4	0.4	0.3	0.3	0.5
Mn_2O_3	1.1	1.1	1.1	1.1	1.1	0.9
TiO_2	<0.1	<0.1	<0.1	<0.1	<0.1	<0.1
CaO	93.7	92.9	92.7	92.2	91.5	70.7
MgO	1.4	1.4	1.3	1.3	1.4	1.5
P_2O_5	0.0	0.0	0.0	0.0	0.0	0.0
SO_3	0.1	<0.1	0.1	0.1	<0.1	0.2
Cl	0.0	0.0	0.0	0.0	0.0	0.0
K_2O	<0.1	<0.1	<0.1	<0.1	<0.1	<0.1
Na_2O	0.1	0.1	0.1	0.1	0.1	0.1
LOI	1.7	2.7	3.0	3.6	4.1	24.3
TOTAL	99.9	100.1	100.0	100.1	99.9	100.7
Av.Lime	87.9	85.6	87.8	86.8	84.8	66.1

RESULTS AND DISCUSSION

Fig. 1 contains the thermogravimetric decomposition curves for pure $Ca(OH)_2$, pure $CaCO_3$ and the limestone samples. The mass loss of 22.5% between 350 and 460 °C, observed for $Ca(OH)_2$ indicates the persence of a small amount of impurities in the pure sample, as the theoretical value is 24.3%. The mass losses between 600 and 840 °C, of respectively 43.5 and 43.4 % observed for the $CaCO_3$ sample and limestone sample indicate that both mainly consist of calcium carbonate (the theoretical value being 43.97%). The hydrated lime sample shows a mass loss of 20.9% between 340 and 460 °C, indicating a 86% rehydration of the lime sample prepared as described under sample preparation and also a 1.8% mass loss between 560 and 800 °C, indicating a 4% recarbonation of the sample.

To determine the uptake and influence of CO_2 on the limestone and hydrated lime samples, both were heated in an atmosphere containing 50% CO_2 and 50% air, they were cooled down in this atmosphere for 90 minutes, the atmosphere was then switched to nitrogen and the mass loss curves measured to determine the amount of recarbonation of the samples. This was repeated with the addition of purging the gas mixture of CO_2 through water at 20 °C, to determine whether the presence of water vapour enhanced the uptake of CO_2 and/or H_2O.

In the presence of the 50% CO_2 - 50% air atmosphere, the decomposition of the carbonate occurs only between 850 and 950 °C, in comparison to the values of 600 and 840 °C for the sample in an inert atmosphere (Fig. 2). This clearly indicates the strong influence of any partial pressure of CO_2 on the decomposition

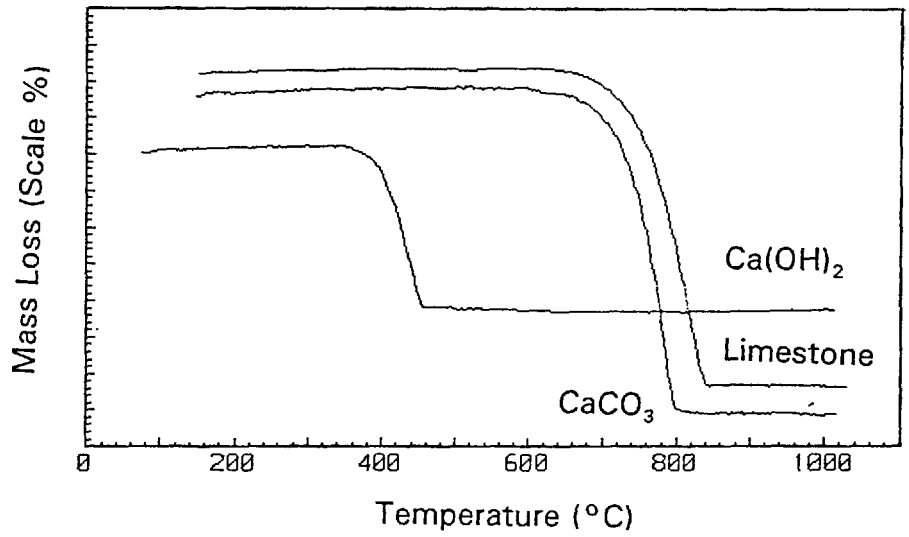

Fig 1 : Thermogravimetric decomposition curves for pure $Ca(OH)_2$, pure $CaCO_3$ and the limestone sample (heating rate 5 °C.min^{-1}).

of $CaCO_3$. On cooling down from 1000 °C to 25 °C in 90 minutes in the CO_2 gas mixture, in the presence and without the presence of water vapour, only recarbonation of the lime seems to occur, as no $Ca(OH)_2$ decomposition curves are observed on reheating the samples in nitrogen. The only difference between the presence and absence of water vapour being that an average recarbonation of 56% occurrs without water vapour and an average of 64% in the presence of water vapour. The presence of water vapour thus clearly enhances the uptake of CO_2.

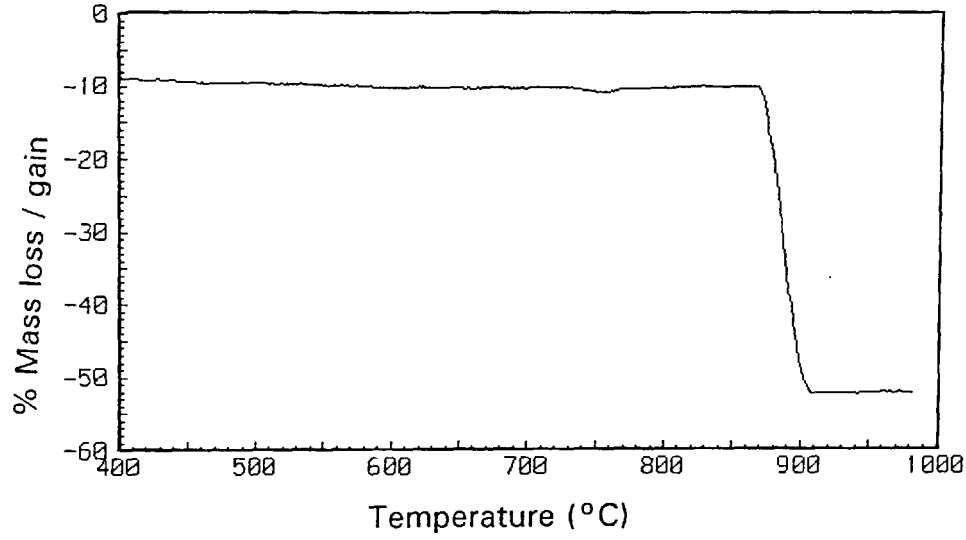

Fig. 2 : Thermogravimetric decomposition curve of $CaCO_3$ in a 50% CO_2 - 50% air atmosphere, using a heating rate of 5 °C.min^{-1}.

As was seen in Fig. 1, the hydrated lime sample starts to decompose to CaO at 340 °C under the conditions used. Heating the hydrated lime sample in the mixture of CO_2 and air, results in an increase in the mass from 300 °C to 520 °C. This can only be attributed to the immediate uptake of CO_2 as soon as CaO is formed from

the decomposition of $Ca(OH)_2$. The mass loss observed between 850 and 920 °C, indicates an immediate recarbonation of 93% at the temperatures between 300 and 520 °C. The same tendency was observed when heating the hydrated lime sample in the CO_2 mixture in the presence of water vapour (Fig. 3). In this case the immediate recarbonation was 94%.

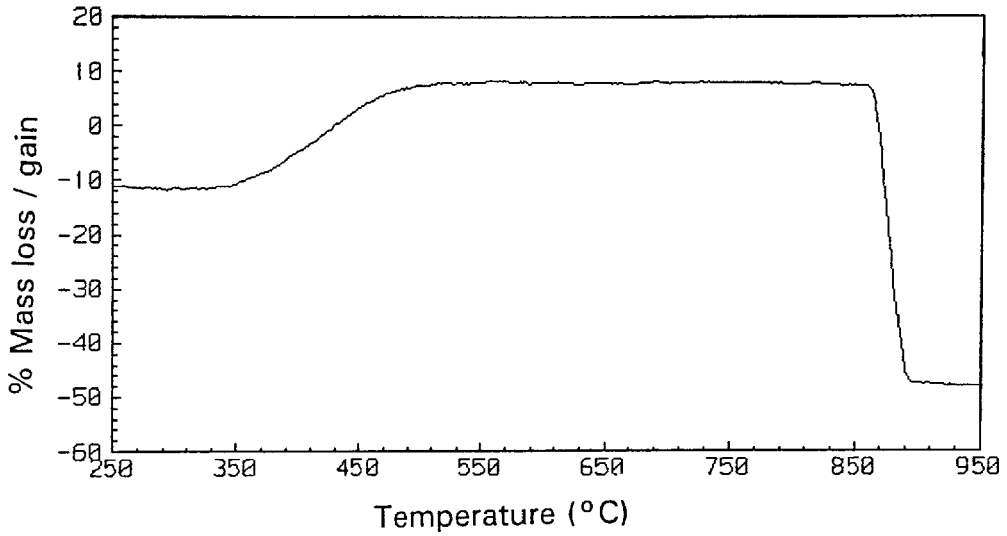

Fig 3 : Thermogravimetric curve of hydrated lime in a 50% CO_2 - 50% air atmosphere (heating rate 5 °C.min^{-1}).

Cooling down the samples in the various atmospheres, changing the atmospheres to nitrogen and obtaining the decomposition curves, gives approximately the same results as for limestone, i.e. a 57% recarbonation having taken place in the absence of water vapour and a 65% recarbonation in the presence of water vapour. Some of the decomposition curves of the lime samples with different reactivities are given in Fig. 4. It is clear that rehydration and recarbonation occurred. The samples being in the presence of a very low partial pressure of CO_2, only recarbonated to a maximum of 1.4% at the experimental conditions.

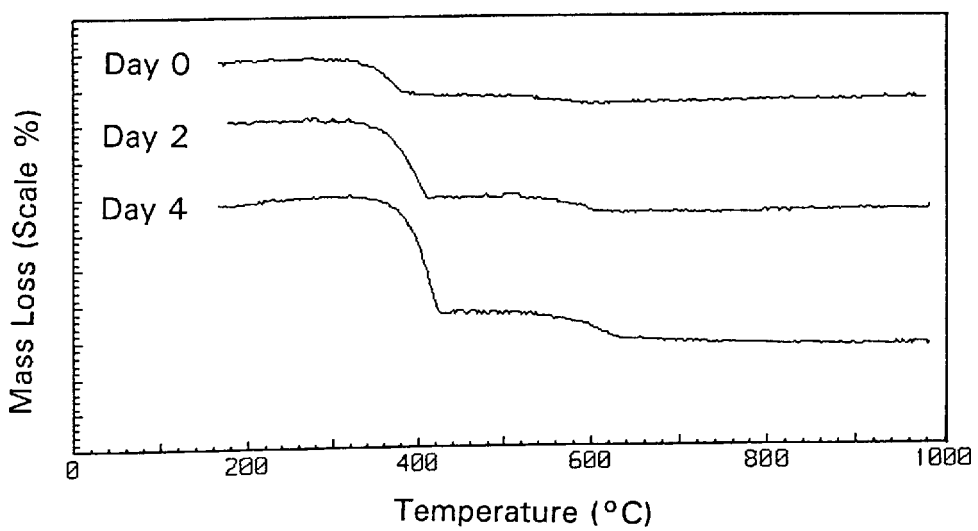

Fig 4 : Thermogravimetric curves of lime samples exposed to the atmosphere for days as indicated (heating rate 5 °C.min^{-1}).

Rehydration increased with time, starting at 4.1% for the sample with reactivity of 30, to 13.1% for the sample exposed to the atmosphere for 4 days (reactivity unmeasurably low). Fig. 5 gives an indication of the relation between reactivity and % rehydration and total % rehydration and recarbonation.

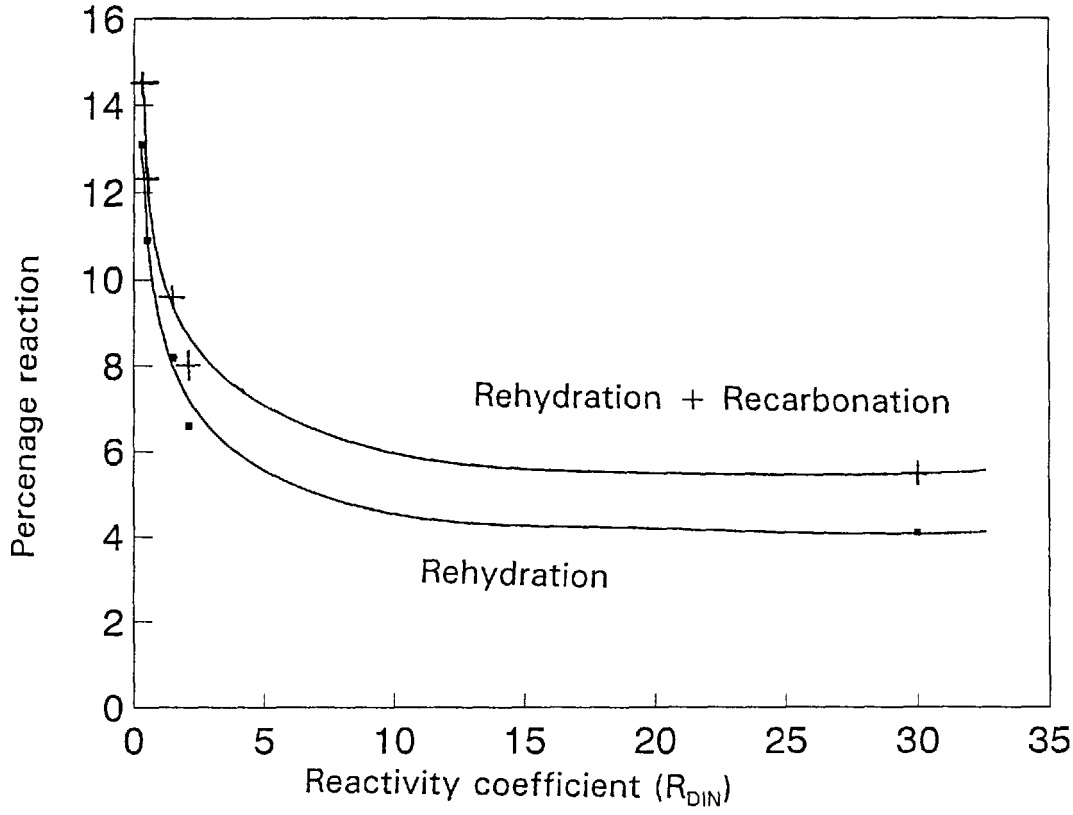

Fig. 5 : Plot of reactivity coefficient value versus the percentage rehydration and the total of the percentage rehydration and recarbonation.

CONCLUSIONS

The loss in reactivity of lime can be attributed to both the rehydration (formation of $Ca(OH)_2$) and the recarbonation (formation of $CaCO_3$) of lime. The extend to which these two occur, depends highly on the partial pressure of both water vapour and CO_2. The recarbonation reaction taking place at an increasing rate, to such an extend that as soon as CaO is formed from the dehydration of $Ca(OH)_2$, it immediately reacts with CO_2 at temperatures above 300 °C to form $CaCO_3$. In industry great care has to be taken to store reactive lime away from any moisture and carbon dioxide gas. The percentage rehydration and the total percentage rehydration and recarbonation, as determined by thermogravimetry give a good indication of the reactivity coefficient value. The reactivity coefficient R_{DIN} decreases sharply with increasing rehydration and recarbonation.

REFERENCES

Kasselouri, V., Dimopoulos, G. and Parissakis, G., "A Study on energy reduction during the thermal decomposition of limestone", World Cement Research and Development, Nov. 1995, pp. 72 - 74.

Sinev, M.Yu., "Methodological aspects of studying the kinetics of reverible reactions in solid-gas systems", J. Therm. Anal., Vol. 34, 1988, pp. 221 - 230.

2ii050
8 pp

Kn o. 2 5. JAN. 2001 d o k 31813

REACTIVITY AND MECHANISM OF HYDRATION OF CEMENT PHASES

Reinhard TRETTIN, Institute for Geosciences, University of Mainz, Mainz, Germany

ABSTRACT The main factors for the kinetics of the hydration of phases are primarily the potential reactivity, which depends on the crystal structure, and secondarily the qualities of a reaction layer forming on the surface of the anhydrous compounds at the beginning of the hydration (observable with the AFM). The potential reactivity of the structure increases with the basicity of oxygen induced by an increase of the number of calcium atoms in the coordination sphere of the oxygen.

Key-words: Reactivity, hydration, mechanism, calcium silicate, calcium aluminate

INTRODUCTION

The macroscopic kinetics of cement hydration is the result from very complex reactions. The degree of hydration with respect to time depends on the interaction of a number of various factors. The different clinker minerals have a very variable reaction behaviour with respect to water and are influenced themselves in their reaction with the ion concentrations in the common solution phase. In addition, the reaction is not predominantly continuous but is characterised by periods of various hydration rates.

Several reviews of models to the explanation the reactivity and the mechanism of hydration have been published in the literature (Taylor, 1990a, Massazza and Daimon, 1992). Until now the mechanisms of the hydration of the single clinker phases is not understood completely. This applies to the more complicated polyphase system of the cements to an even greater extent. Further research is therefore necessary for a better understanding of the causes of the various reactivity and the mechanisms of hydration of clinker phases.

REACTIVITY AND CRYSTAL STRUCTURE

The anhydrous calcium silicates and calcium aluminates show very different reactivities towards water. There are some theories to explain the different reactivities based on of the differences in the crystal structure, but most of them are not correct regarding modern structural data. This was demonstrated by Jost and Ziemer (1984) for the theories of openness of structure, distortion of polyhedra, and relations to the coordination number of calcium. Moreover, the theories do not explain the differences in reactivities of β- and γ-Ca_2SiO_4. Jost and Ziemer (1984) proposed a hypothesis, in which they suggest that the major factor for reactivity is building units of Ca-O polyhedra linked through face-sharing. The reactive calcium silicates contain such face sharing Ca-O polyhedra. However, the face sharing-polyhedra cannot be the main factor for the reactivity. In the reactive phase $CaAl_2O_4$ and in CaO no building units of face-sharing Ca-O polyhedra exist.

In order to understand the structural causes of the differences in the reactivity towards water it is necessariy to look at the mechanism of the initial reaction with water. In agreement with Barret et al. (1983) it is suggested that the first step in the reaction with water is a transfer of protons from water to the oxygen atoms in the solid phase. This means it is more probable that the oxygen basicity is the major factor for reactivity.

A differentiation of the reactivity of the clinker phases and other calcium silicates and calcium aluminates is possible in simplified form with the degree of hydration determined experimentally to same time of hydration:

$$C_3S > C_2S > C_3S_2 > CS$$
$$C_3A > C_{12}A_7 > CA > CA_2 > CA_6.$$

The hydraulic reactivity generally also increases with the CaO content per unit formula. This differential series does not make any distinction of reactivity differences possible between the reactive β-C_2S and the inactive γ-C_2S. Therefore it is better for a more realistic analysis of the reativity of the substances with water to examine the content of the calcium in relation to the volume. The density of the Ca atoms per unit volume of the substances should then be a measure for the oxygen basicity.

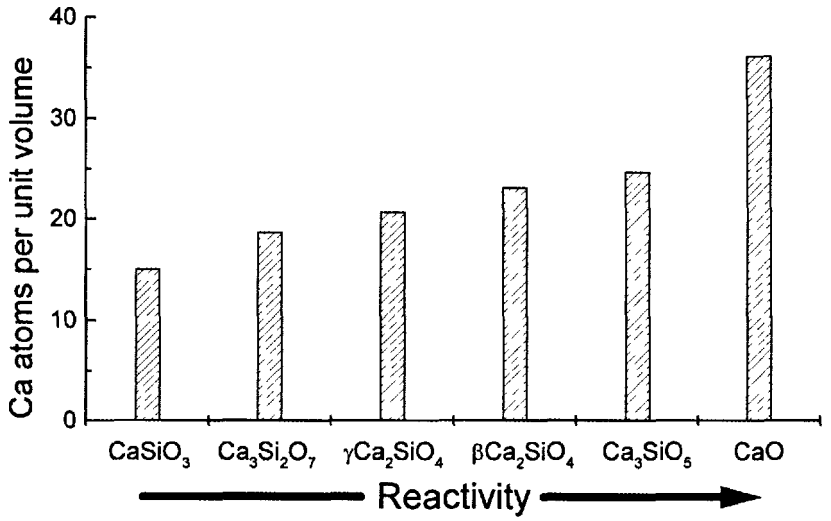

Figure 1 The density of the Ca atoms per unit volume of calcium silicates

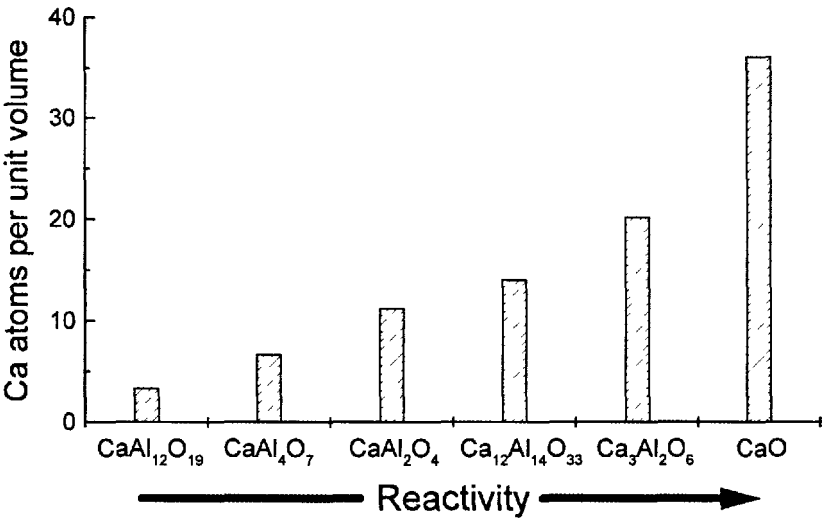

Figure 2 The density of the Ca atoms per unit volume of calcium aluminates

Indeed, it was found that with increasing number of Ca atoms per unit volume the reactivity of the calcium silicates and calcium aluminates increases; the results are shown in Figs 1 and 2. Also the differences in reactivities of β- and γ-Ca_2SiO_4 are pointed out and the results are in good agreement with the reactivity series of calcium aluminates.

On analysis of the nearest neighbours of the oxygen in the different compounds, it is seen that very different neighbour atoms are available here. The chemical composition of the clinker phases is in an area between SiO_2 and Al_2O_3 with very low reactivity with waters on one side and the highly reactive CaO on the other side. The environment of the oxygen also changes with respect to the chemical composition and crystal structure of the compounds. Oxygen atoms are linked only to calcium (Ca-O-Ca) in the highly reactive calcium hydroxide while oxygen atoms are linked predominantly to silicon or to aluminium and calcium (Ca-O-Si , Ca-O-Al) in the calcium silicates and calcium aluminates. In contrast, oxygen atoms are linked only to silicon or to aluminium in the unreactive SiO_2 and Al_2O_3.

The mean relationship of the different atoms also should show a connection with the basicity in the neighbourhood of the oxygen next to the integral density of the Ca atoms per unit volume. On the basis of the structural data (ICSD, 1996), the environment around the oxygen has been studied for the calcium silicates and calcium aluminates. It is shown in Figs. 3 and 4 that, with increasing reactivity, the ratios of Ca/Si and Ca/Al of the nearest neighbours of oxygen increase which induces an increase in the oxygen basicity. The grading of reactivity of calcium silicates and calcium aluminates are also in good agreement with the differences in experimentally estimated reactivities. Furthermore they show the differences in the reactivity of β- and γ-Ca_2SiO_4.

These results, with the correlation between reactivity and the ratios of Ca/Si and Ca/Al of the nearest neighbours of oxygen, support the hypothesis that the oxygen basicity is important for the transfer of protons from water to the oxygen atoms. This concept of the reasons for the reactivity is in a generalised form also applicable to other compounds.

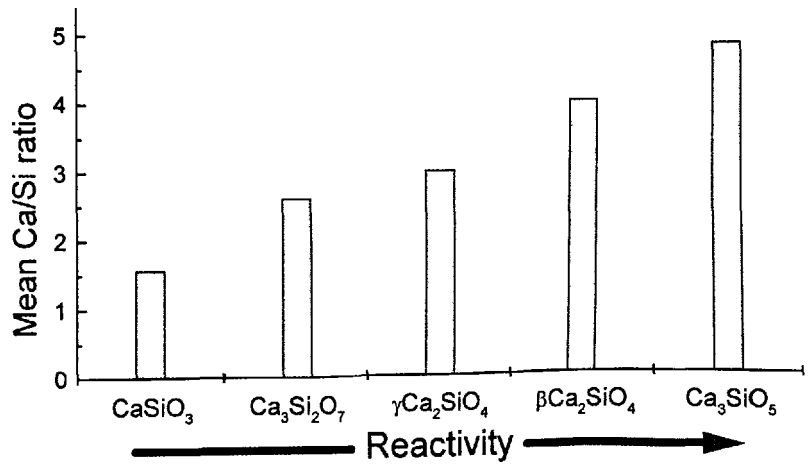

Figure 3 The ratios of Ca/Si of the nearest neighbours of oxygen in calcium silicates

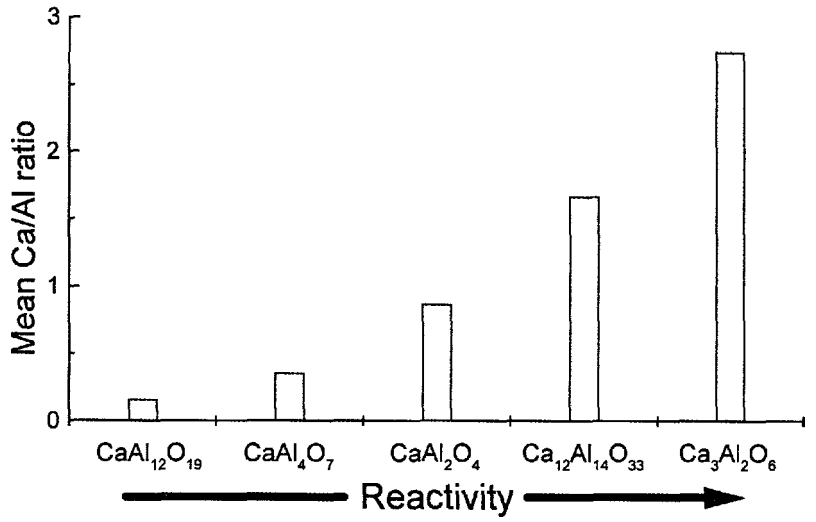

Figure 4 The ratios of Ca/Al of the nearest neighbours of oxygen in calcium aluminates

The calcium aluminates have a higher reactivity then the calcium silicates at the same density of calcium atoms per unit volume. This is caused by the smaller electronegativity of the Al with respect to Si, influences the oxygen basicity.

The distances between different ions and the polyhedra structures have also been investigated and a statistical analysis was applied but no additional generalisations for both calcium silicates and calcium aluminates were found.

The previous discussions to the structural causes of the reactivity only pertained to the ideal structure of the compounds. It has however to be taken into account that defects and foreign ions have an additional influence on the reactivity.

HYDRATION MECHANISM

In the first section, only the reactivity of the calcium silicates and calcium aluminates towards water on the basis of the crystal structure was discussed. The hydration of the single compounds however is not continuous. The reaction passes through different periods of various rates of hydration at which maximums and minimums partially appear. This means that the course of the reaction is still determined by other factors. In the literature there are numerous models to explain the kinetics the hydration, this have been summarising reviewed in Taylor (1990) or Massazza and Daimon (1992). But up until now the mechanism of the hydration is not sufficiently clear.

To obtain a better understanding of the causes of the kinetics of hydration, several early studies were carried out. Different methods were used such as isothermal heat-flow calorimetry, gas adsorption measurements, ESCA and analysis of the liquid phase. From the results it may be deducted based on the theory of Stein et al (1967, 1977) that the primary hydration products cover the surface of the anhydrous compounds and determine the continuation of the hydration by their permeability Trettin at al (1986, 1991). The permeability of the reaction layer depends on the chemical composition, the porosity and the kinetics of its formation. Generally reaction layers rich in calcium have little permeability in the hydration of calcium silicates. On the other

hand, if the formation of a reaction layer with low Ca/Si ratio is favoured then a more permeable reaction layer is formed and the hydration is accelerated.

The origin of the induction period in the hydration of C_3S is attributed to the formation of a reaction layer rich in lime, which exhibits a lower permeability. Former results of investigations indicate that a reaction layer already is formed immediately after contact with water at the beginning of the hydration. In order to get more information about the formation of the reaction layer on the surface the atomic force microscope (AFM) was used (Topometrix TMX 2000). Initially, examination of single crystals of the C_3S was performed. The single crystals of C_3S (triclinic) were grown using the method of Nurse (1949). The AFM images of the surface of C_3S after a time of hydration of 15 seconds is shown in Figure 5. It can be seen that an initially smooth surface already is covered by a reaction layer. The thickness of the reaction layer increases with time of hydration, these new reaction products become more increase and show a stronger height profile. Figure 6 shows the reaction product layer after a time of hydration of 15 minutes in the induction period. The observations made with AFM appear to support the protective layer hypothesis.

A specific influence of the hydration kinetics of a single clinker phase is possible through a corresponding change in the qualities of the reaction layer, which can be achieved by change of the chemical composition of the solution phase. The hydration of C_3S and C_2S is accelerated by reduction of the calcium ion concentration in the solution phase which produced a more permeable layer poor in calcium. Examples for a such acceleration mechanisms are additions which reduce the calcium ion concentration such as SiO_2 or an increase of the water/solid ratio which has a corresponding effect.

The hydration would be retarded by a high level of calcium ion concentration in the solution phase if the formation of a layer rich in calcium with low permeability is favoured. This is achieved for example by hydration in a previously saturated calcium hydroxide solution.

On examination of the influence of the grinding time on the hydration of C_3S, an agreement with Kondo et al (1968) was found in that after longer milling the hydration is retarded. The Induction period is longer and the second maximum is shifted to longer time (from 310 to 560 minutes).These results are surprising because acceleration of hydration by activation is more probable. By the investigation of the solution phase in the very early stage of hydration, it was found that the calcium ion concentration increased with time of milling. Therefore in agreement with the hypothesis of mechanism of hydration the retardation of the hydration is caused by a more impermeable reaction layer rich in calcium.

Similarly to the hydration of the calcium silicates, it was found that the hydration of calcium aluminates is also determined by formation of a primary reaction layer on the surface. It was shown for the hydration of CA (Trettin et al 1987), $C_{12}A_7$, CA_2, CA_6 (Trettin 1989) and C_3A (Trettin et al 1992). Fore instance, the origin of the induction period in the hydration of CA is also contributed to the formation of a reaction layer, which exhibits a lower permeability. From studies on the mechanism of C_3A hydration in the presence of gypsum it may be deducted that in agreement with the literature (Taylor 1990b) the retardation of hydration is caused by a reaction layer.

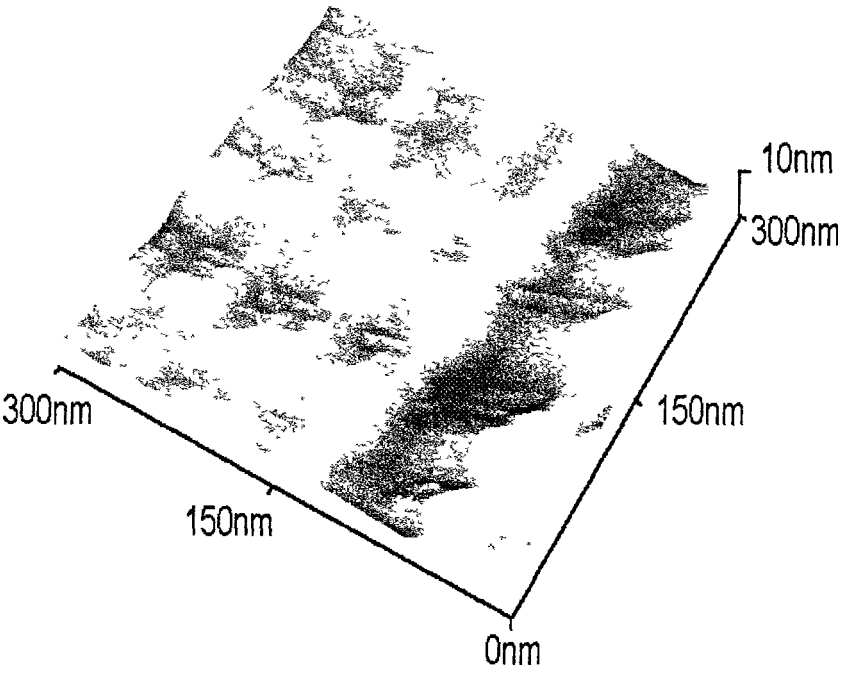

Figure 5 AFM images of the surface of a C_3S single crystal after 15 seconds of hydration

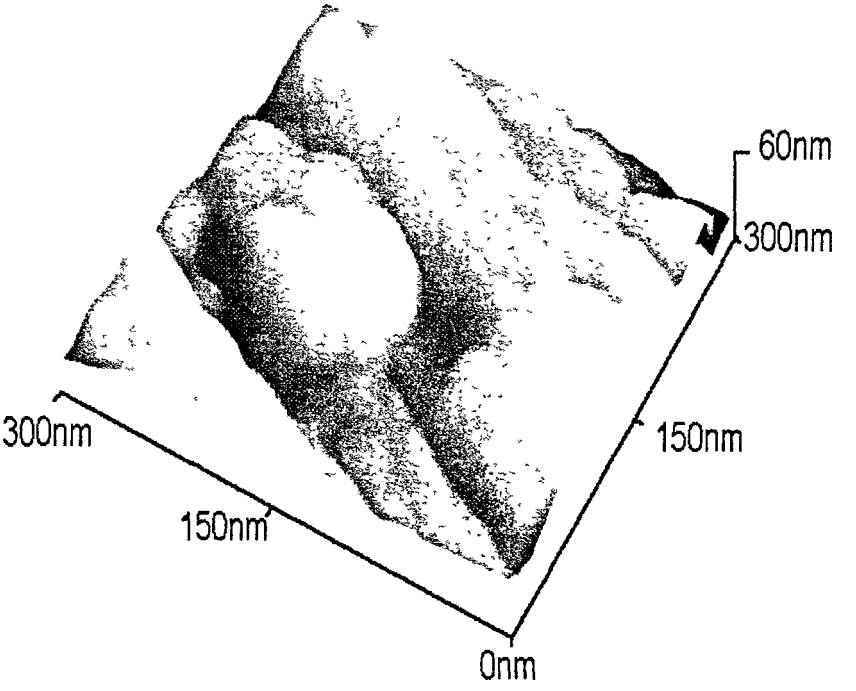

Figure 6 AFM images of the surface of a C_3S single crystal after 15 minutes of hydration

REACTION MODEL

The macroscopic kinetics of the hydration of cement clinker phases depends on several factors. The reactions are very complex and involve several processes. The most essential potential factor for the reaction with water is the crystal structure of the anhydrous compounds. This

means, a sufficient reactivity of the crystal structure is absolute necessary for the reaction. The potential reactivity is determined by the oxygen basicity. The reactivity of the crystal structure is the most essential factor for hydration which however is reduced by the formation of the reaction layer. This layer forms a physical diffusion barrier around the grains. Therefore the permeability becomes a further essential factor for the kinetic of the hydration. The permeability of the reaction layers depends on different factors such as chemical composition of solution, structure, kinetics of formation and transformation, solubility and stability.

It is possible that the different clinker phases can be summarised with respect to their structural potential reactivity, the kinetics of hydration and influence of the reaction layer into groups, see Tab. 1.

Table 1 Overview for relations between the kinetics of hydration, the potential structural reactivity and the influence of the reaction layer for different calcium silicates and calcium aluminates

	Degree of reaction (α)	Rate of heat liberation (dQ/dt)	Reactivity caused by structure	Influence of reaction layer	Compounds
1	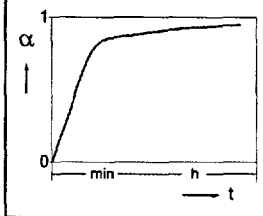	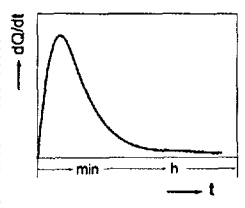	very high	initial low; increasing after longer times of hydration till diffusion determines the rate of hydration	C_3A $C_{12}A_7$ — C
2	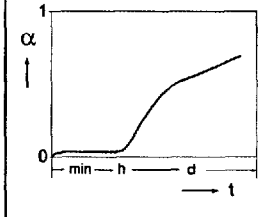	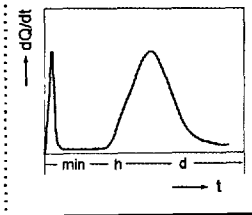	medium to high	primarily caused the induction period; increasing after the acceleration period till diffusion determines the rate of reaction	C_3S C_2S CA CA_2
3	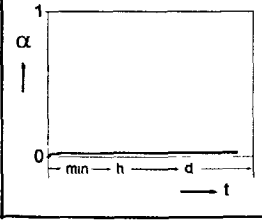	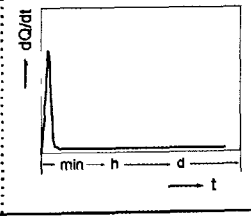	very small	not determinable	C_3S_2 CS CA_6

CONCLUSIONS

The various reactivity of the calcium silicates and calcium aluminates depends mainly on the crystal structure. It is suggested (in agreement with Barret et al., 1983) that the first step in the reaction with water is a transfer of protons from water to the oxygen atoms in the solid phase. Therefore the oxygen basicity must be the most essential factor for reactivity. The oxygen basicity depend on the environment around the oxygen atoms. Increasing electronegativity of the nearest neighbour atoms correspond with increasing of the reactivity. This means, that with increasing reactivity the ratios of Ca/Si and Ca/Al of the nearest neighbours of oxygen increase.

The structural reactivity do not, in general, determine the kinetics of the hydration. The course of hydration is influenced by the formation of the reaction layer. This layer forms a physical diffusion barrier. The origin of the induction period or retardation in the hydration of reactive calcium silicates and calcium aluminates is contributed to the lower permeability of the reaction layer.

A specific influence of the hydration kinetics of a single clinker phase is possible through a corresponding change in the qualities of the reaction layer, which can be achieved by change of the chemical composition of the solution phase.

ACKNOWLEDGEMENTS

The author is very grateful to Mrs. W. Rosenbusch for the sample preparation and Prof. H. Niehus, E. zur Mühlen and Mrs. K. Braune for their help in AFM measurements.

REFERENCES

Taylor, H.F.W., "Cement Chemistry", Academic Press, London, 1990a, pp. 123-242.

Massazza, F. and Daimon, M., "Chemistry of Hydration of Cements and Cementitious Systems", 9th Intern. Congr. On the Chemistry of Cement, Vol. II , 1992, pp. 383-446.

Jost, K.H. and Ziemer, B. "Relations Between the Crystal Structures of Calcium Silicates and Their Reactivity Against Water", Cem. Concr. Res., Vol. 14, 1984, pp. 177-184.

Barret, P., Ménétrier, D. and Bertrandie D. "Mechanism of C3S Dissolution and Problem of the Congruency in the Very Initial Period and Later On", Cem. Concr. Res. Vol. 13, 1983, pp.728-738.

ICSD - Inorganic Crystal Structure Database, FIZ Karlsruhe and Gmelin-Institut 1996/1.

Stein, H. N., Stevels, J. M., "Influence of Silica on the Hydration of $3CaO{\cdot}SiO_2$"J. Appl. Chem. (London), Vol. 14, 1964, pp. 338-346.

Stein, H. N., "The Initial Stages of the Hydration of C_3S", Il Cemento, Vol. 74, 1977, pp. 3-13.

Trettin, R., Wieker, W., "Zur Hydratation von Tricalciumsilicat I. Ursachen der Induktionsperiode", Silikattechnik, Vol. 37, 1986, pp. 75-78.

Trettin, R., Oliew, G., Stadelmann, C., Wieker, W., "Very Early Hydration of Dicalcium Silicate-polymorphs", Cem. Concr. Res., Vol. 21, 1991, pp. 757-764.

Nurse, R.W., "Summarised Proceedings of Conference on X-ray Analysis, London, April 1948", J. Sci. Instr., Vol. 26, 1949, pp. 102.

Ueda, S., Hashimoto, M., Kondo, R., "Study on the Hydration of Cement by Electron Diffraction", Semento Gijutzu Nenpo, Vol. 22, 1968, pp. 67-72.

Trettin, R., Rettel, A., Geßner, W., "Zum Verlauf der Hydratation von $CaO{\cdot}Al_2O_3$ in den Primärstadien", Z. anorg. allg. Chem., Vol. 547, 1987, pp. 133-141.

Trettin, R., "Zum Hydratationsverlauf von Calciumsilicaten und Calciumaluminaten", Habilitation, Berlin 1989.

Trettin, R., Wieker, W., "Zum Verlauf der Hydratation von $3CaO{\cdot}Al_2O_3$ in den Primärstadien" Z. anorg. allg. Chem., Vol. 613, 1992, pp 113-118.

Taylor , H.F.W., "Cement Chemistry", Academic Press, London, 1990b, pp. 194-196.

2ii051
8 pp

Kn o. 2 5. JAN. 2001 d o k 31814

DEVELOPMENT OF A KINETIC MODEL FOR HYDRATION OF CEMENT

Fuminori TOMOSAWA, The University of Tokyo, Tokyo, Japan

ABSTRACT A hydration model of cement is proposed to describe not only a microstructure formation of cement paste but also the time-dependent characteristics such as development of strength and rigidity, heat liberation, temperature rise, thermal stress, early age creep, setting phenomenon, etc. The model is expressed as a single equation composed of four rate determining coefficients which determine the rate of formation and destruction of initial impermeable layer, the activated chemical reaction process and the following relent diffusion controlled process.

Key-words: Unreacted core model, Degree of hydration, Heat evolution, Strength development

INTRODUCTION

The setting and hardening process of concrete where the concrete changes from fresh state to hardened concrete is an essential problem to be clarified for many features of concrete engineering, such as predicting strength development, temperature rise by heat of hydration, early age shrinkage and creep. However, researches on this process have been conducted so far rather on the basis of empirical methods than theoretical analysis, and in many cases only series of sets of experimental data could have expressed the time dependent behavior of the concrete in this process. Naturally, the process is dependant on the hydration process of cement, thus the hydration model is indispensable to deal with this problem theoretically.

A lot of hydration model has been proposed so far. Most of them were, in the beginning, simple applications of experimental data under constant curing conditions to empirical equations or applications of a first~order reaction equation which could not describe the actual change of rate of hydration in the whole stage. These empirical models could hardly describe the whole stage of the hydration or the changing rate of hydration, for example, under varying temperature curing conditions. The first order reaction model was too simple to describe the complicated phenomena like hydration of cement. Some of them described the reaction well, such as models developed by late Prof. R. Kondo (1968), but from the view point of practical application to concrete engineering, they had some difficulties to be effectively used.

As the hydration of portland cement is an extremely intricate and compound process, it might be impossible to make a perfect model which describes the whole reaction process accurately from the view point of chemistry of cement. However, to develop a model which can be applied to the problems of concrete engineering might be possible and that development of the model can contribute to better understanding of the hydration process from the engineering point of view. An engineering model does not mean a simple model, but it needs to simulate the hydration process as correctly as possible and can describe the effects of all the factors which come into the process.

A kinetic model of hydration of cement which has been developed from this standpoint (Tomosawa, 1974) is presented in this paper.

DESCRIPTIVE MODEL OF HYDRATION

Basic concept

To describe the process of hydration is in effect to express the changes in the degree and rate of reaction over time. In regard to the practical aspects of hydration as well, such as strength development and heat generation, the main concern is how they increase and change with time. However, this does not mean that the rate of hydration is directly determined as a function of time. The rate of hydration at a point in time is determined by the amount of cement that has gone through a hydration process by that time, amount of water available for hydration at that time, as well as temperature and pressure (this paper does not take pressure into account). Conventional

hydration models have tended to try to express the degree and rate of hydration directly as functions of time. However, such an approach cannot describe the phenomenon correctly. The hydration rate after 5 hours from the time of cement-water contact, for instance, widely varies depending on the curing temperature. Accordingly, the author proposes here a model that expresses the hydration rate using the degree of hydration.

Descriptive model

The hydration process of a cement particle that is assumed to be spherical is modeled as follows:

(i) The cement particle initiates hydration the moment it is brought into contact with water.
(ii) The hydrate formed by the reaction adheres to the cement particle, gradually covering it up. The cement particle remains spherical as a whole.
(iii) The hydrate has a volume twice the original cement volume.
(iv) The liquid phase, which is assumed to be water, diffuses through the hydrate layer and reaches the surface of the cement particle (reacting surface) and chemically reacts with cement there. This continues the reaction.
(v) Part of the hydrate produced at the reacting surface moves out through the formed layer of hydrate. Accordingly, nearly equimolar counter diffusion of water and hydrate (presumably ions) is assumed to be taking place in the hydrate layer.
(vi) It is assumed that, in the so-called dormant period in the initial stage, there is a process in which the reaction resistance increases in inverse proportion to the reaction degree (film formation) followed by a period in which the reaction resistance decreases in proportion to the square of the reaction degree (film breakage).
(vii) The rate of reaction decreases more rapidly than assumed in a normal diffusion-determined process. Several explanations are conceivable to account for this phenomenon. It is assumed here that the radial effective diffusion coefficient in the hydrate layer is reduced by the deposition of part of subsequently produced hydrate on the inner surfaces of pores in the hydrate layer. Another convincing explanation is the reduction in the amount of water which is present outside of the hydrate layer and is available for the reaction. Though this parameter is included in the model, it is tentatively assumed to be constant.

MATHEMATICAL MODEL OF HYDRATION

The outline of the mechanism of cement hydration is as stated above. In short, the hydrate as such inhibits subsequent reaction. The so-called unreacted core model (Yagi and Kunii, 1953) is often applied to the case where the reaction product deposits or remains between the reactants, inhibiting the reaction.

Basic equation

At time t, a cement particle covered by cement gel is represented by **Fig 1**. The origin of time is when the particle is brought into contact with water. Then the following equation holds:

$$4\pi r_t^2[N_w]_{r=rt}=4\pi r^2 N_w \qquad [1]$$

where r_t = radius of unhydrated cement particle
r = an arbitrary radius between r_t and R_t
R_t = total radius including the gel layer
N_w = flux of water at r towards the reaction surface

The following equation is obtained from the basic equation(s) of diffusion:

$$N_w=D_e(dC_w/dr) \qquad [2]$$

where D_e = effective diffusion coefficient of water in the cement gel
C_w = abundance concentration of water at r

Eq1 and **Eq2** lead to:

$$r_t^2[N_w]_{r=rt}=r^2 D_e(dC_w/dr)$$

This is integrated under the following boundary conditions:

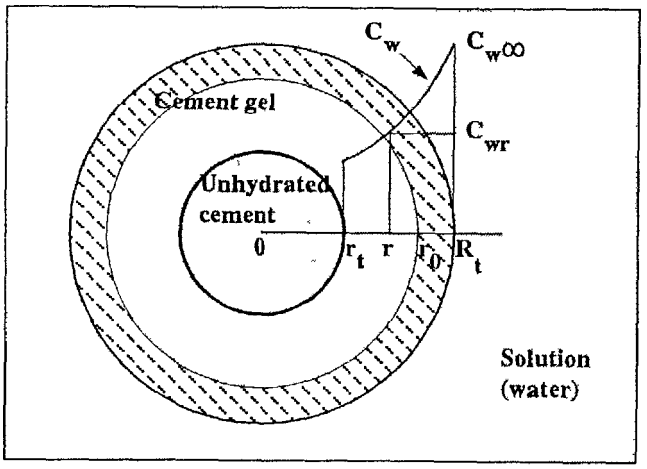

Fig.1 Unreacted core model for a particle of cement

When $r = r_t$, $C_w = C_{wr}$
When $r = R_t$, $C_w = C_{w\infty}$

Then the following equation is obtained:

$$r_t^2[N_w]_{r=rt}(1/r_t-1/R_t)=D_e(C_{w\infty}- C_{wr}) \quad [3]$$

As the overall reaction rate, R, equals the diffusion rate at the total area of the reaction surface,

$$R=4\pi r_t^2[N_w]_{r=rt} \quad [4]$$

Eq3 and **Eq4** lead to:

$$R = 4\pi D_e \frac{C_{w\infty} - C_{wr}}{\frac{1}{r_t} - \frac{1}{R_t}} \quad [5]$$

The overall reaction rate, R, also equals the chemical reaction rate of water and cement at the reaction surface. If the chemical reaction rate is assumed to be linear in regard to the abundance concentration of water, the following equation holds:

$$R=4\pi r_t^2 k_r C_{wr} \quad [6]$$

where k_r = coefficient of reaction rate per unit area of reaction surface

From **Eq5** and **Eq6**, C_{wr} is eliminated as follows:

$$R = \frac{4\pi C_{w\infty}}{\frac{1}{D_e}\left(\frac{1}{r_t} - \frac{1}{R_t}\right) + \frac{1}{k_r r_t^2}} \quad [7]$$

If it is assumed that the reaction surface shifts from rt to r_t-dr_t while t becomes t+dt, then the following equation holds in regard to unit area of the reaction surface:

$$dt[N_c]_{r=rt}=-dr_t \rho_c$$
$$\therefore dr_t/dt=-1/\rho_c[N_c]_{r=rt} \quad [8]$$

where $[N_c]_{r=rt}$ = flux of unhydrated cement into the reaction surface
ρ_c = density of unhydrated cement

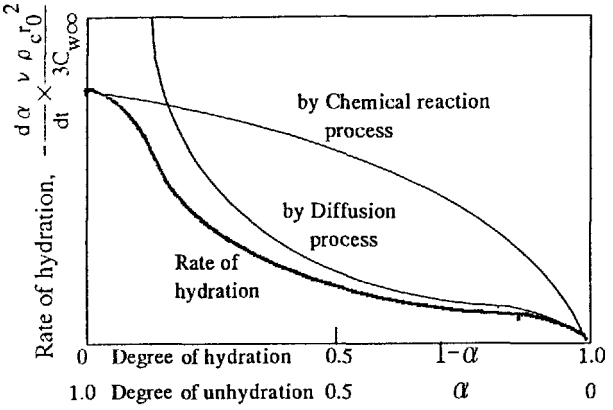

Fig.2 Rate of hydration determined by two different process

If the stoichiometric ratio by mass of water to cement is assumed to be ν, then:

$$[N_w]_{r=rt} = \nu\,[N_c]_{r=rt} \qquad [9]$$

From **Eq4**, **Eq8**, and **Eq9**:

$$R = -4\pi r_t^2 \nu\, \rho_c \cdot dr_t/dt \qquad [10]$$

Substituting this into **Eq7** and rearranging the equation lead to:

$$-\frac{dr_t}{dt} = \frac{C_{w\infty}}{\nu\rho_c r_t^2}\,\frac{1}{\frac{1}{D_e}\left(\frac{1}{r_t}-\frac{1}{R_t}\right)+\frac{1}{k_r r_t^2}} \qquad [11]$$

If it is assumed that $r_t=r_0$ when t=0 and that the ratio of the volume of unhydrated cement at t=t to that of t=0 is the degree of unhydration, α, then:

$$\alpha = \left(\frac{4}{3}\pi r_t^3\right)\Big/\left(\frac{4}{3}\pi r_0^3\right) = \left(\frac{r_t}{r_0}\right)^3 \qquad [12]$$

Also, if the hydrate has a volume twice as large as that of unhydrated cement, then:

$$\left(\frac{4}{3}\pi R_t^3\right)\Big/\left(\frac{4}{3}\pi r_0^3\right) = \alpha + 2(1-\alpha) = 2-\alpha$$

$$\therefore (R_t/r_0)^3 = 2-\alpha \qquad [13]$$

Eq12 is differentiated as follows:

$$\frac{dr_t}{dt} = \frac{r_0^3}{3r_t^2}\frac{d\alpha}{dt}$$

Consequently, **Eq11** is rearranged with respect to the degree of unhydration, α, as follows:

$$-\frac{d\alpha}{dt} = \frac{3C_{w\infty}}{\nu\rho_c r_0^2}\,\frac{1}{\frac{1}{D_e}\left\{\alpha^{-\frac{1}{3}}-(2-\alpha)^{-\frac{1}{3}}\right\}+\frac{1}{k_r r_0}\alpha^{-\frac{2}{3}}} \qquad [14]$$

This equation suggests that when α is near 1, or in an early stage of reaction, the reaction rate is determined by the chemical reaction (the k_r term governs), whereas when α is near 0, or in the final stage of the reaction, the reaction rate is determined by diffusion (the D_e term governs). In an intermediate stage, the reaction rate is determined by both (see **Fig 2**).

Introduction of dormant period model

Equation 14 does not express the dormant period in the beginning of hydration. The low reaction rate during the dormant period is not negligible, as reaction proceeds significantly in a few hours where high temperature curing is done, for instance. The characteristics of this early reaction can be considered as being caused by a certain substance whose mass transfer resistance suddenly increases from the state of zero and then suddenly decreases. It can be assumed that a layer having such a pattern of mass transfer resistance exists between the unhydrated cement particle and the external gel layer. If the abundance concentration of water at the outer and inner interfaces of the layer are assumed to be C_{wII} and C_{wIII}, respectively (see **Fig 3**), the overall reaction rate, R, can be considered similarly as follows:
R equals the rate of passing through the initial film. Therefore,

$$R=4\pi r_t^2 k_d(C_{wII}-C_{wIII}) \qquad [15]$$

where k_d = mass transfer coefficient

R also equals the diffusion rate within the gel layer and reaction rate at the reaction surface:

$$R = 4\pi D_e \frac{C_{w\infty} - C_{wII}}{\frac{1}{r_t} - \frac{1}{R_t}} \qquad [16]$$

$$R=4\pi r_t^2 k_r C_{wIII} \qquad [17]$$

Consequently,

$$R = \frac{4\pi C_{w\infty}}{\frac{1}{k_d r_t^2} + \frac{1/r_t - 1/R_t}{D_e} + \frac{1}{k_r r_t^2}} \qquad [18]$$

This is rewritten using the unhydrated degree, α:

$$-\frac{d\alpha}{dt} = \frac{3C_{w\infty}}{\nu\rho_c r_0^2}\left(\frac{1}{\frac{1}{k_d r_0 \alpha^{2/3}} + \frac{\alpha^{-1/3} - (2-\alpha)^{-1/3}}{D_e} + \frac{1}{k_r r_0 \alpha^{2/3}}}\right) \qquad [19]$$

The first term of the denominator in the brackets on the right side of the equation relates to the initial reaction, indicating its reaction resistance. This affects only a very early stage when $\alpha \fallingdotseq 1$, and therefore $\alpha^{2/3}$ is assumed to be 1. In this case, the reaction rate is determined by k_d. Here kd is assumed to be expressed as the sum of the term in inverse proportion to the reaction degree, $(1-\alpha)$, and the term in proportion to the square of $(1-\alpha)$:

$$k_d=B_d/(1-\alpha)+C_d(1-\alpha)^2 \qquad [20]$$

The first term indicates that the reaction resistance increases as the reaction proceeds (formation of impermeable film), and the second term indicates the reaction resistance suddenly decreases after hitting the peak (breaking of the film). Other forms of kd may be conceivable. It is necessary that the model agrees well with the measurements of the initial reaction including the dormant period.

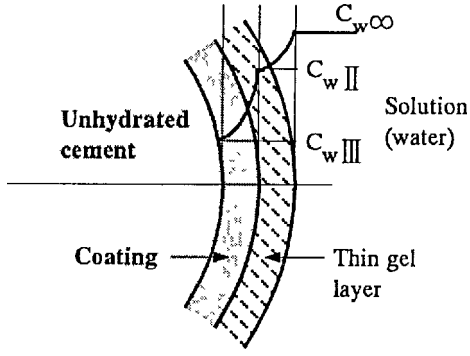

Fig.3 Schematic model of a cement particle in the dormant period

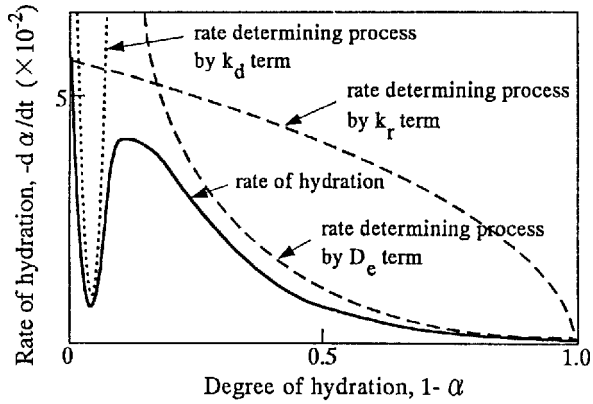

Fig.4 Rate of hydration expressed by the model and 3 types of rate determining processes

Changes in effective diffusion coefficient

The model up to the previous section does not agree well with the measurements. Higher reaction rates are calculated by this model in later stages of reaction. From among several options for correcting this, here the method mentioned in (vii) under "Descriptive model" above is adopted. As a result, the changes in the effective diffusion coefficient are expressed as follows:

$$D_e = D_E\left(\ln\frac{1}{1-\alpha}\right)^2 \qquad [21]$$

Whole process hydration model

Consequently, a mathematical model of hydration is obtained as follows:

$$-\frac{d\alpha}{dt} = \frac{3C_{w\infty}}{\nu\rho_c r_0^2}\left(\frac{1}{\frac{1}{k_d r_0} + \frac{\alpha^{-1/3}-(2-\alpha)^{-1/3}}{D_e} + \frac{1}{k_r r_0 \alpha^{2/3}}}\right) \qquad [22]$$

where k_d and D_e is defined by **Eq20** and **Eq21**, respectively.
By adequately selecting the coefficients, **Eq22** is plotted as the solid lines shown in **Fig 4**. The broken lines represent the rate-determining processes, indicating that the reaction rate is determined by them.

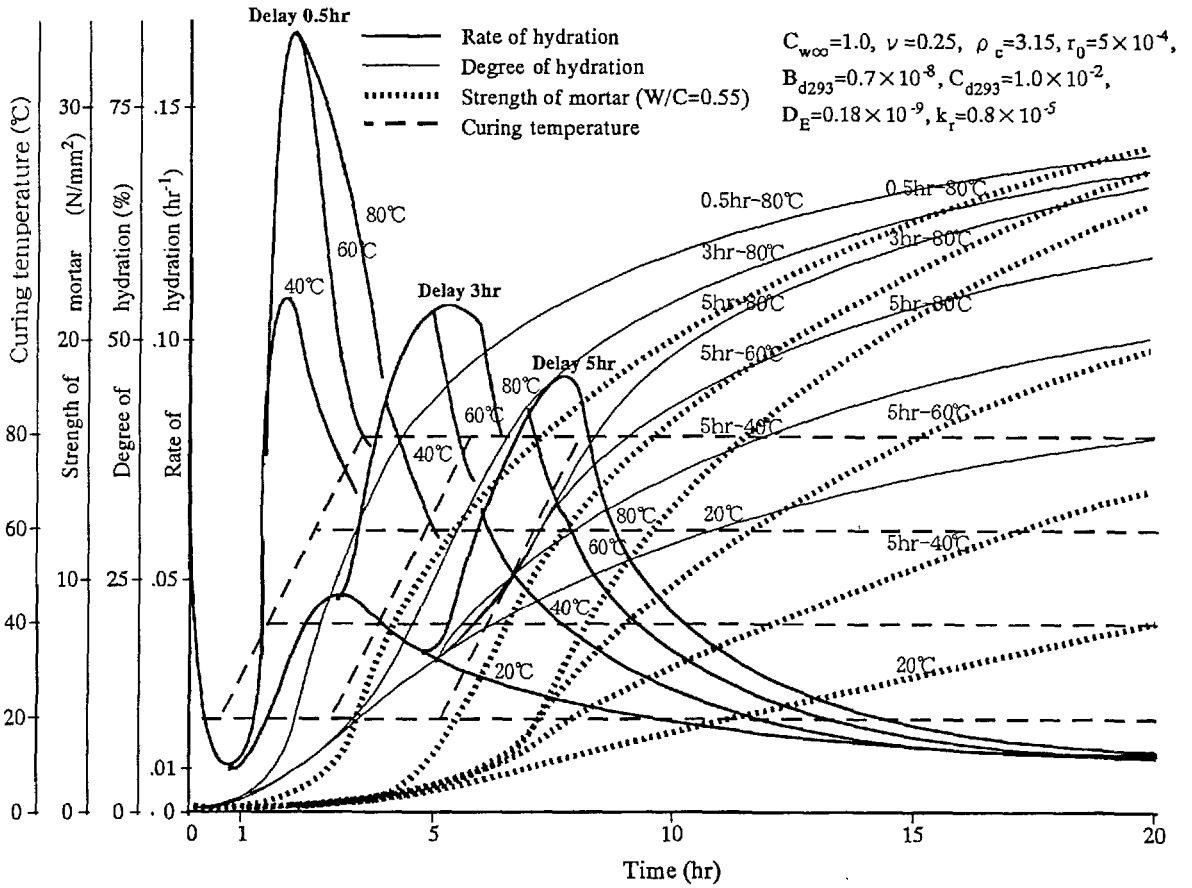

Fig.5 Simulation of hydration of cement under various curig conditions

Values of mass transfer coefficients

Coefficients k_r and D_E among the four mass transfer ratios contained in the model were determined so as to agree with the overall cement hydration degree obtained from the reaction degrees of minerals composing cement at 20℃ proposed by the PCA Group (Copeland et al., 1960). Coefficients B_d and C_d were determined so as to express the general characteristics of initial reaction. Also, the constants were selected as follows:

$C_{w\infty} = 1.0$, $\nu = 0.25$, $\rho_c = 3.15$, $r_0 = 5\times10^{-4}$ cm
$B_d = 0.7\times10^{-8}$ cm·hr^{-1}
$C_d = 1.0\times10^{-2}$ cm·hr^{-1}
$k_r = 0.8\times10^{-5}$ cm·hr^{-1}
$D_E = 0.18\times10^{-9}$ cm·hr^{-1}

Values of temperature coefficients

The effect of temperature on hydration is introduced to each mass transfer coefficient. Accurate relationships are considered to be obtainable by experimentally determining the changes in the reaction rate. Here it is assumed that B_d is in proportion to the square of absolute temperature, and that C_d, D_E, and kr follow Arrhenius' law. The values for the coefficients given in the previous section are those for 20℃. Therefore the coefficients at θ K are expressed as follows:

$$B_{d\theta} = B_d\sqrt{\theta/293}$$
$$C_{d\theta} = C_d\exp\{-\beta_1(1/\theta - 1/293)\} \quad [24]$$
$$k_{r\theta} = k_r\exp\{-\beta_2(1/\theta - 1/293)\}$$
$$D_{E\theta} = D_E\exp\{-\beta_3(1/\theta - 1/293)\}$$

The following values of β_1, β_2, and β_3 are considered appropriate from the strength development data of mortar during high temperature curing (Kishitani and Tomosawa, 1968), etc.

$\beta_1 = 0.3 \times 10^4$
$\beta_2 = 0.42 \times 10^4$
$\beta_3 = 0.40 \times 10^4$

SIMULATION OF HYDRATION AND STRENGTH DEVELOPMENT

Thus the mathematical model has been obtained with typical values of the constants. This makes possible the simulation of hydration under any changing temperature. An example of the calculation result is illustrated in **Fig 5**. This shows the rates and degrees of hydration with a fixed temperature of 20℃, as well as those with a precuring period of 0.5, 3.0, and 5.0 hr, maximum temperature of 40, 60, and 80℃, and curing at a temperature rise gradient of 20℃/hr. It represents well the increase in the reaction rate associated with the temperature rise, as well as the changes in the reaction rate when the temperature stops rising. The figure also contains a compressive strength development curves of mortar as an application example. These were calculated by assuming that the strength is proportional to the cube of the gel-space ratio (Powers, 1964) at a point of time, which is determined from the degree of hydration at that time.

Similarly, if the generation of hydration heat is assumed to be proportional to the degree of hydration, exotherm curves can be obtained as well. The model can also simulate the situation in which the heat generation in turn accelerates the reaction.

CONCLUSION

The author devised a simulation model that expresses the entire process of hydration of portland cement with a single kinetic equation. This model is characterized by the independence of rate-determining processes. This enables researchers to attempt other equations based on different assumptions for each rate-determining process, modify the values of mass transfer coefficients or temperature dependency, and conduct model experiments to assess their validity. The humidity dependency of the reaction rate may be introduced by modifying $C_{w\infty}$ in **Eq22**.

REFERENCES

Kondo, R., "Kinetics and mechanisms of the hydration of cements", Proc. of the 5th International Symposium on the Chemistry of Cement, V-ISCC, Tokyo, 1968
Tomosawa, F., "A Hydration model of cement", Proc. of Annual Meeting on Cement Technology, Cement Association of Japan, Vol.28, 1974, pp.53-57
Yagi, S. and **Kunii**, D., Magazine of Industrial Chemistry, No.56, pp131-134, 1953
Copeland, L.E., **Kantro**, D.L. and **Verbeck**, G., Proc.of the 4th International Symposium on the Chemistry of Cement, Washington, 1960, p.429; The Chemistry of Cements, Edt., H.F.W.Taylor, Vol.1, p.350, Fig.10
Kishitani, K. and **Tomosawa**, F., "Kinetics of strength development of concrete", Report of Annual Meeting of Architectural Institute of Japan, 1968, pp.105-106
Powers, T.C., Chapter 10, The Chemistry of Cement, Edt., H.F.W. Taylor, 1964

2ii052
7 pp

Kn o. 2 5. JAN. 2001 d o k31815

SIMULATION OF CEMENT-HARDENING IN THE PRESENCE OF CARBON USING HYDRA2D

R.J. van EIJK and H.J.H. BROUWERS University of Twente, Department of Civil Engineering and Management, P.O. Box 217, 7500 AE Enschede, The Netherlands

ABSTRACT In the present study the cement hydration simulation program Hydra2d is adjusted in order to simulate the influence of reaction-rate limiting contaminants such as carbon. The water absorbing effect of activated carbon is simulated and resulted, among other things, in high porosity microstructures and lower hydration degrees.

Key-words: modelling, hardening, hydration, immobilization, waste material utilization.

INTRODUCTION

The solidification of waste materials in a cement matrix has several advantages. A waste problem can be solved, the use of primary materials is decreased and in general recycling of materials will take place. Waste materials, however, can influence the hydration reaction by interacting with all components in the matrix that are involved in the cement reactions. One example of such an interaction is presented here, namely a water absorbing species such as active carbon. Active carbon can be added to the cement matrix in order to bind organic contaminants (Conner, 1990). However its presence during hydration causes extra porosity in the cement as it removes the water needed for the cement reactions. The carbon is able to bind water several times its weight (Capelle and de Vooys, 1983). In this paper the effect of carbon on hydration is demonstrated by numerical simulation of the hydration process.

HYDRA2D

Modelling of cement hydration can be done in many ways (Jennings et al., 1996). A digital-image-based cement paste microstructure model has been developed at the NIST (Bentz and Garboczi, 1990). The computer program in which this model is implemented has been used for simulation studies on the electrical conductivity of cement (Christensen et al., 1991) and the percolation of phases (Bentz and Garboczi, 1990). It can be used to study the development of the fine porosity and gel structure during hydration and to investigate the influence of the hydration conditions on the final microstructure.

In this study the two dimension version of this program, called Hydra2d, was used in which the cement mixture is presented as a 2 dimensional matrix of 200 x 200 pixels. Cement particles are presented as discrete spheres and filler particles can be added as 1 pixel elements. An aggregate can be placed in the middle and extends in one dimension. Every pixel in the system is assigned a phase including C_3S, CSH, CH, Inert and Porosity.

When all pixels are placed the hydration starts following the principle of dissolution-diffusion-precipitation (Bentz and Garboczi, 1992). A hydration cycle starts by the determination of all cement (C_3S) pixels that are in contact with porosity. These pixels perform a random move and when this move is into porosity the particle is dissolved. All dissolved pixels diffuse randomly until a reaction or precipitation takes place. The cement reaction in this model has the following volume stoichiometry (C =CaO, H=H_2O, S=SiO_2) (Young and Hansen, 1987):

$$C_3S + H => 1.7\ C_{1.7}SH_4 + 0.61\ CH \quad [1]$$

This means that 1 volume unit of cement reacts with water to produce 2.31 volume units of solid product. This volume expansion results in the moulding of a rigid microstructure. The present model does not take chemical shrinkage into account.
After the dissolution step all dissolved pixels perform random moves. Diffusing CSH precipitates into solid CSH upon contacting a solid C_3S or CSH surface. Diffusing CH has a chance, depending on its concentration, to nucleate spontaneously and precipitate into solid CH upon contacting a solid CH surface. When no more diffusing pixels are present a new hydration cycle is started. When hydration is completed after a given degree of hydration or number of cycles phase compositions can be determined by pixel counts on the final structure. Also the composition as a function of the distance to the aggregate can be determined in order to obtain information about the Interfacial Zone near the aggregate (Garboczi and Bentz, 1991).

ADJUSTMENTS

General adjustments in the program were made in order to be able to measure results during hydration without loosing the microstructure developed so far. An extra option was added for the addition of Portland C cement in one step. The amount of particles is adjusted automatically in the presence of aggregate or carbon particles in order to maintain a constant w/c ratio.

Next, the Hydra2d program was adjusted to simulate the influences of activated carbon. The presence of a water absorbing species is added to the program by introducing a new phase called Carbon. This phase can be introduced into the system as particles as well as aggregate or filler. This phase also will be detected for dissolution and when a random move into porosity takes place, the Carbon is converted into a phase called Carbon Water and stays in place. In this way the conversion is executed in the same way as the conversion of C_3S into diffusing CSH. Extra pixels of the Carbon Water phase are placed randomly in the simulation field replacing porosity and simulating overall water binding. Contrary to dissolved cement particles the Carbon Water particles do not diffuse but stay in place. Carbon Water pixels are counted separately, but will be regarded as extra porosity because they represent weak spots in the cement matrix.

SIMULATION RUNS

Simulations were executed using different compositions of the starting structures. In all structures an approximation of the particle size distribution of Portland C cement was used (Souwerbren, 1995). In all structures a w/c ratio of 0.45 was employed and the same initial cement particle distribution. In Table 1 the used particle size distribution is summarised.

Table 1. Particle size distribution of used cement.

d-size (μm)	particles (n)
5	318
10	53
15	16
25	4

In the center of the 200 x 200 matrix an aggregate of size 10 x 200 pixels was placed. Carbon particles were introduced as 10 μm spheres, representing the mean size of Powdered Activated Carbon particles (Capelle, 1983). All carbon was assigned a reactivity factor of 5, implying that every Carbon Water pixel generates 5 extra Carbon Water pixels. In order to keep a constant starting w/c ratio some of the 10 μm C_3S particles were replaced by the 10 μm carbon particles. Four simulations were executed in the presence of an inert aggregate and 0, 1, 3 and 7 % (v/v) 10 μm carbon particles. The 7 % Carbon simulation can be considered as an extreme case. Two simulations were executed in the presence of a Carbon aggregate with and without an extra 3 % (v/v) carbon particles to simulate the effect of a large Carbon particle in the cement. In Table 2 all these initial conditions are tabulated.

Table 2. Phase compositions of starting microstructures (%(v/v)).

Structure	a	b	c	d	e	f
Porosity	55	55	53	50	55	53
C_3S	40	39	38	37	39	38
Carbon	0	1	3	7	5*	8*
Aggregate	5	5	5	5	5	5

* Includes 5 % Aggregate.

All simulations were executed during 15 cycles. Compositions were measured after 0, 5, 10 and 15 cycles. At the same time w/c ratios and degrees of hydration were determined.

RESULTS

The final microstructures are presented in Fig. 1 (see end of volume). Carbon Water, implying weak spots, appear all over the microstructure as expected. Most Carbon Water is found around the carbon particles itself or near the carbon aggregate.

Table 3 presents the phase compositions in the simulated microstructures after 15 cycles

Table 3. Compositions after 15 cycles.

Structure	a	b	c	d	e	f
Porosity	18	14	9	3	10	4
C_3S	11	12	14	17	14	17
CSH	47	44	41	34	42	36
CH	17	16	14	12	15	12
Carbon	0	0	1	3	2*	4*
Carbon Water	0	6	14	24	14	25
Total porosity	18	20	23	28	24	29

* Includes remaining of aggregate.

Fig 1 is found in the colour photo section.

From Table 3 it can be seen that a small addition of water absorbing material has a relatively large effect on the final composition of the cement. For example, an addition of 1 % carbon causes a decrease of 3 % in the amount of CSH and 3 % extra porosity. So, though the initial amount of porosity was 1 % less (see Table 2), the final amount is 2 % higher. The hydration degree is decreased by 5 % after 15 cycles. Table 3 also learns that, comparing (d) with (f), that the final composition is nearly the same when the carbon is placed as particles (7% in structure (d)) or as aggregate and particles (5 + 3 = 8% in structure (f)).

Fig. 2 show the porosity fractions as function of the distance from the aggregate at the end of all simulations. The interfacial zones are relatively small (5 μm) compared to experimental results (Scrivener, 1989). When a carbon aggregate is present an extreme high porosity fraction is present near the aggregate, due to the Carbon Water that stayed in place after diffusion from the aggregate surface into the solution. It should be realised that for structures (e) and (f), the aggregate thickness is reduced by its dissolution (see Fig. 1). However, in Fig. 2 the distance is taken from the original aggregate boundary. In fact, the aggregate shrinked almost 1 pixel on both sides. The region immediately adjacent to this shifted reactive surface would correspond to an aggregate distance of -1 in Fig. 2 and here the porosity tends to unity. On the other hand, the thickness of the interfacial zone is hardly affected by the Carbon. This results from the fact that the presence of Carbon does not influence the particle packing near the aggregate.

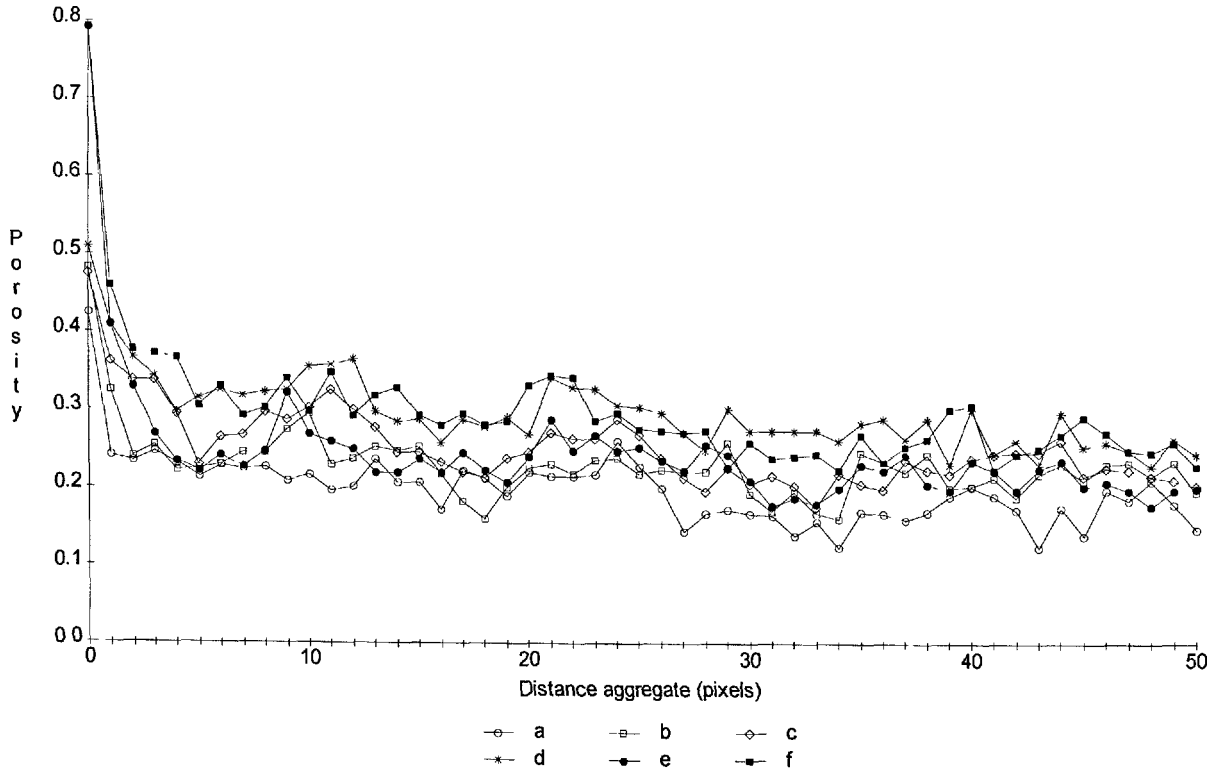

Figure 2 Porosity fractions as function of the distance from the aggregate (1 pixel is approximately 1 μm).

The overall porosity, determined by adding all porosity and Carbon Water in the total microstructure, increases strongly when Carbon was present in the initial structure. Fig. 3 shows the development of this total porosity during all simulations.

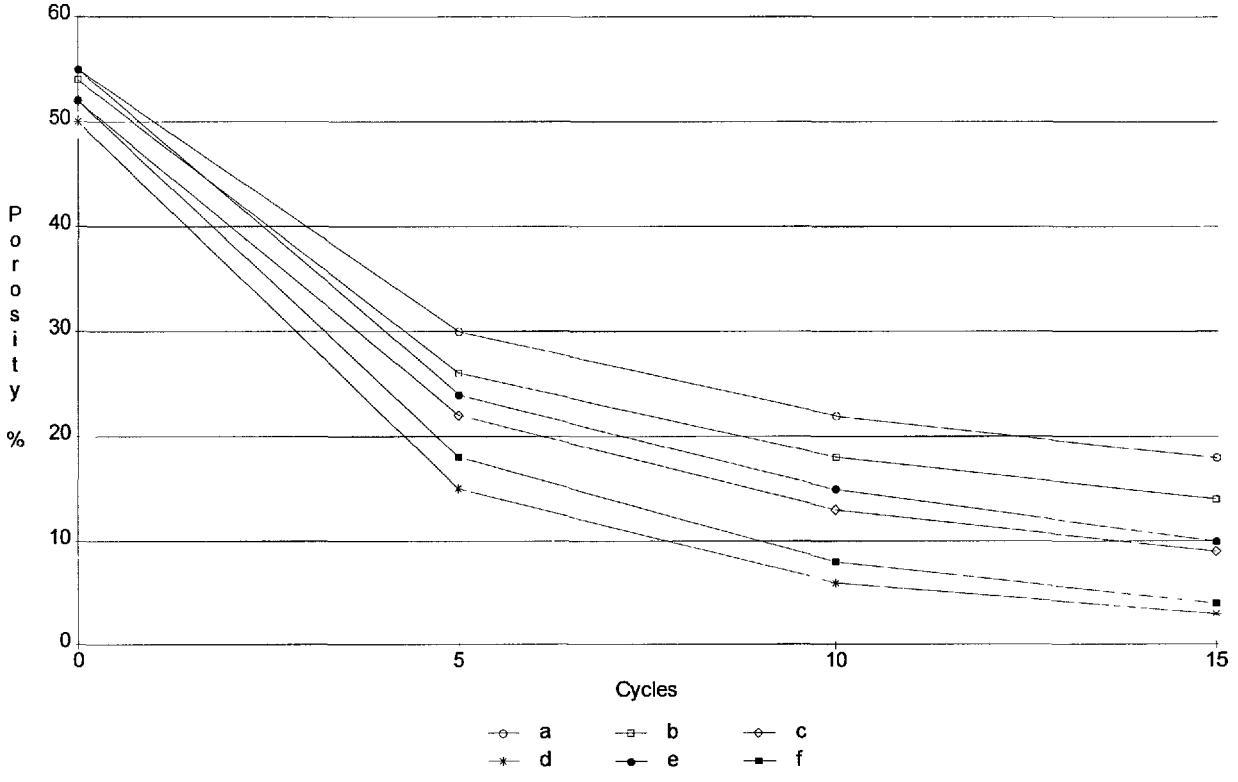

Figure 3 Total amount of porosity (%) during simulation.

Fig. 4 shows the hydration degrees during 15 cycles for all simulations. It is obvious that the hydration degree decreases strongly in the presence of carbon, which might be expected. Figs. 3 and 4 again illustrate that the d) and f) structures, which contain the same total amount of Carbon, closely correspond to each other. Though for the latter most Carbon is added as aggregate, the final result corresponds to the d) structure, in which the Carbon is placed as spheres.

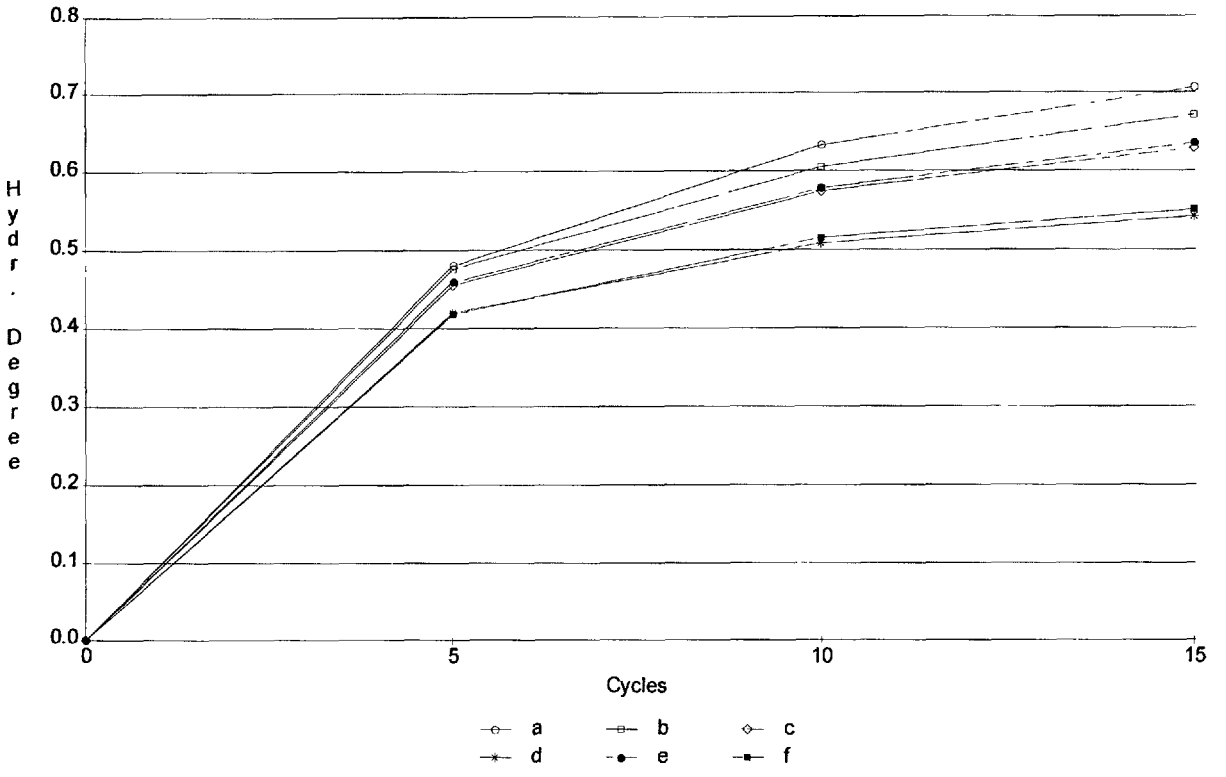

Figure 4 Hydration degrees during simulations.

CONCLUSIONS

The Hydra2d program appeared to be very suitable to simulate the hydration of cement in the presence of water absorbing species. A few adjustments in the program code were adequate in order to accomplish this. The microstructures formed in the presence of carbon as water absorbent showed high porosity. This follows directly from the introduction of extra porosity each time when Carbon is converted into Carbon Water. The hydration degrees decreased strongly in the presence of relatively small amounts of active carbon. This effect is caused by the increase of the replacement of porosity by Carbon Water resulting in a lower growing space for CSH. Also it is caused by the Carbon Water pixels that replace the porosity surrounding the cement particles, thereby decreasing the amount of possible moves into porosity and lowering the dissolution possibility for cement pixels.

The carbon pixels were assumed as static in the presented model. The effect of diffusion is considered minor because carbon pixels are already placed randomly into the system. The probability of a carbon pixel moving into the solution should be adjusted using experimental results. It is yet unknown whether this probability is the same as the probability of a cement particle going into solution.

Ongoing research comprises the modelling of cement hydration in the presence of contaminants or immobilisates. This can only be done when the most abundant influences of the contaminants on the hydration process are known and quantified. When this is done the corresponding necessary adjustments can be made. A new version of the model that takes into account more aspects of the hydration process will be used for this purpose because it offers more possibilities for adjustment.

ACKNOWLEDGEMENTS
The programming assistance by Messr. J.H. Alferink and G.H. Snellink is greatly acknowledged.

REFERENCES
Bentz, D.P. and **Garboczi,** E.J., A digitized simulation model for microstructural development, Cer. Trans., 16, 1990, pp 211-226.
Bentz, D.P. and **Garboczi,** E.J., percolation of phases in a three-dimensional cement paste microstructural model, Cement and Concrete research, Vol 21, 1990, pp 325-344.
Bentz, D.P. and **Garboczi,** E.J., Guide to using Hydra3d, NISTIR 4746, U.S. Department of Commerce, 1992, pp 3-5.
Capelle, A. **and de Vooys,** F., Activated carbon... a fascinating material, Norit, Amersfoort, 1983.
Christensen, B., **Mason,** T.O., **Jennings,** H.M. **Bentz,** D.P. and **Garboczi,** E.J., experimental and computer simulation results for the electrical conductivity of portland cement paste, MRS proc. 1991.
Conner, J.R., Chemical fixation and solidification of hazardous wastes, Van Nostrand Reinhold, New York, 1990, pp 41-43.
Garboczi, E.J. **and Bentz,** D.P., Digital simulation of the aggregate-cement paste interfacial zone in concrete, J. Mater. Res., Vol. 6(1), 1991, pp 196-201.
Jennings, H., **Kropp,** J. and **Scrivener,** K., The modelling of microstructure and its potential for studying transport properties and durability, Kluwer Acadamic publishers, Dordrecht, 1996.
Scrivener, K.L., Materials Science of Concrete (American Ceramic Society, Westerville, 1989), J. Skalny Ed. Vol. 1 pp 127-161.
Souwerbren, C., Betontechnologie, St. Betonprisma, Den Bosch, 1995, pp 126.
Taylor, H.F.W., Cement Chemistry, Acadamic Press, London, 1990, pp 345-349.
Young, J.F. and **Hansen,** W.,Volume relationships for CSH formation based on hydration stoichometries, Materials Research Society Symposium Proceedings, Vol. 85, Pittsburgh 1987, pp 313-322.

2ii053
8 pp

Rec'd 25 JAN. 2001 doc 31816

PHYSICO-CHEMICAL PARAMETERS DETERMINING HYDRATION AND PARTICLE INTERACTIONS DURING SETTING OF SILICATE CEMENTS.

André NONAT, Jean-Claude MUTIN and Shi Ping JIANG, Laboratoire de Recherches sur la Réactivité des Solides, CNRS-Université de Bourgogne, Dijon, France.

ABSTRACT Setting of tricalcium silicate results from interactions between anhydrous or very partially hydrated particles. Two fundamental steps have been identified : the coagulation of cement grains during the first minutes following the mixing, and the rigidification of the coagulated structure which arises simultaneously with the acceleration of the calcium silicate hydrates (C-S-H) formation. There exists a critical range of lime concentration required to coagulate cement particles and to enable C-S-H to stiffen the coagulated structure depends on their solubility.

Key-words : Setting, Strength development, Degree of hydration, CSH, Particle size distribution

INTRODUCTION

Hydration, setting and hardening are all related to the main properties of hydraulic binders, that is to say, the ability to get a hard material by mixing cement powders with water (eventually aggregates) but they involve different processes with different mechanisms. Hydration is a chemical process which, from the anhydrous cement powder and water, through several chemical reactions leads to the formation of hydrates. This complex process has thermodynamic, kinetic and structural features which depend on both chemical and physical parameters. Setting is a definite time event which corresponds to the transition from a soft state of the paste to an hardened state.

Hardening is certainly the less ambiguous term, it involves increase in the strength of the material. It depends on a lot of physicochemical parameters such as degree of hydration, water to cement ratio (W/C), curing conditions, etc.... There are reasons to believe the elementary processes during hardening and setting as being the same.

The purpose of this paper is to examine the interactions that may exist between these simultaneous processes, which all together contribute to build up the complex materials that are cement paste and concrete. The experimental investigation of the elementary processes involved in the chemical and physical evolutions of a system of hydrating particles has given answers to the following questions:

- What are the features of hydration, i.e., the chemical reactions, the nature of the products and the parameters determining thermodynamics, kinetics, and their structural and microstructural properties?
- What are the processes involved in setting and the determining parameters?
- What are the interactions between hydration and setting?

Taking into account that real Portland cement is a complex mixture of different phases, we focused our attention on Ca_3SiO_5, the main component of this cement, as a reasonable easier model system.

Considering the fact that both chemical and mechanical properties change the most during the earlier part of the temporal evolution of the solid-liquid system, we focused our attention on the period following the mixing to the setting of the paste, i.e., the first 24 hours of the evolution.

CHEMICAL AND MECHANICAL EVOLUTIONS OF A NORMAL TRICALCIUM SILICATE PASTE

Hydration of tricalcium silicate proceeds through three successive reactions becoming successively simultaneous (Barret et al, 1986) :
- the dissolution of Ca_3SiO_5 ,providing calcium, silicate and hydroxide ions in solution;
- the precipitation of calcium silicate hydrate (C-S-H).The stoichiometry of C-S-H given by the calcium to silicon ratio (Ca/Si, or C/S) depends on the lime concentration in solution;
- the precipitation portlandite ($Ca(OH)_2$).

Fig 1 shows the evolution versus time of the chemical compositions of the solid and liquid phases and the mechanical evolution of the system.

Based on this figure, two important remarks can be made:
- 1/ Setting, which corresponds to the time at which the Vicat needle does no more penetrate the paste, occurs when only less than 5% of tricalcium silicate has hydrated. This means that the set paste is a continuously connected network of very partially hydrated Ca_3SiO_5 particles.
- 2/ The most important changes of the lime concentration in the pore solution occurs between mixing and setting. Thus, the lime concentration may be an important parameter controlling both hydration and setting processes.

In order to investigate hydration and setting phenomena, we have developed experimental procedures allowing control of the ionic concentrations in a better way than in paste. They are based on conductimetric, calorimetric and granulometric measurements on more or less diluted suspensions of particles (0.5<W/C<300) (Damidot et al ,1990, Damidot and Nonat, 1992, Nonat and Mutin, 1992, Jiang et al,1995,1996).

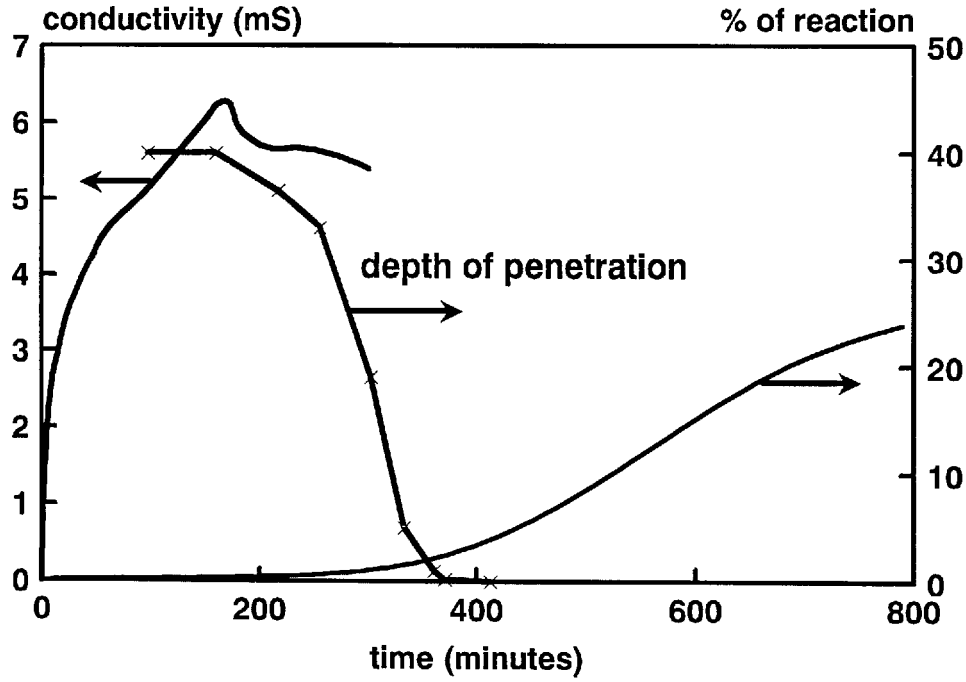

Fig 1. Chemical and mechanical evolutions versus time of a Ca_3SiO_5 paste (W/C=0.5, T=25°C) represented respectively by the electrical conductivity of the pore solution, the advancement of the hydration and the depth of penetration of the Vicat needle.

PARAMETERS CONTROLLING THE HYDRATION OF TRICALCIUM SILICATE

Kinetics of Ca_3SiO_5 hydration

The way how lime concentration controls the kinetics of hydration of Ca_3SiO_5 is described in detail in another report of these proceedings (Nonat et al, 1997). It is however useful to remind here that the kinetics of the reaction does not depend very much on the water to tricalcium silicate ratio. This result is illustrated in Fig 2 showing the advancement of hydration versus time for different liquid to tricalcium silicate ratios. In these cases Ca_3SiO_5 was mixed with a saturated lime solution. It is then possible to simulate the chemical conditions of hydration in paste in diluted suspensions.

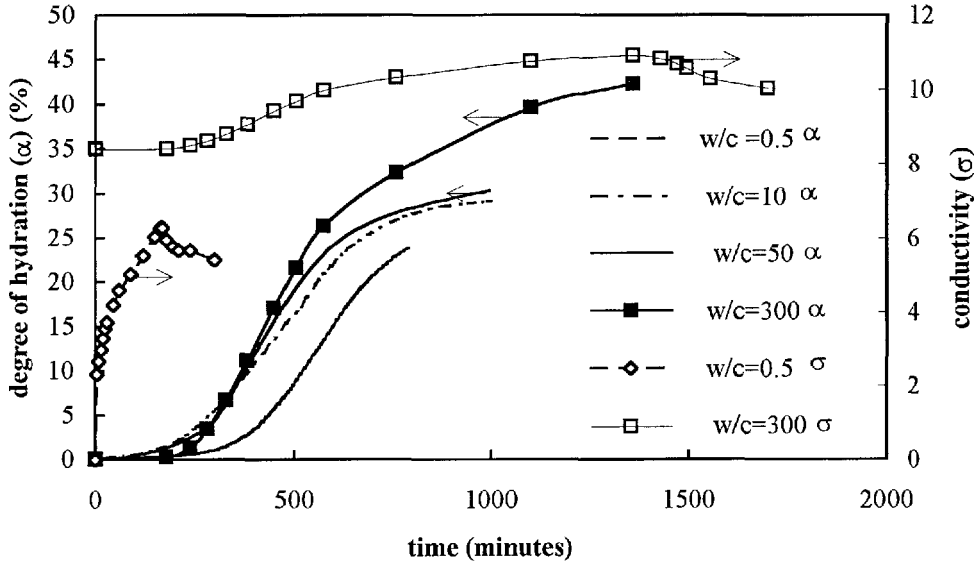

Fig 2. Comparison of the advancement of hydration of Ca_3SiO_5 in saturated lime concentration for suspensions with different water to tricalcium silicate (W/C) ratios.

The length of the period of low chemical activity (so-called dormant period) is fixed by the number of C-S-H nuclei which depends on the lime concentration and the W/C ratio. The percentage of reaction when the hydration rate decreases depends on the growing mode of C-S-H also fixed by the lime concentration.

PROCESSES AND PARAMETERS CONTROLLING THE SETTING OF TRICALCIUM SILICATE PASTE

Setting results from the transformation of a dense suspension of more or less dispersed particles in a mechanically irreversible network of connected particles. An understanding of setting depends on knowledge of the processes involved in that transformation and of the parameters that determine the mechanism. Using the ability to control hydration in dilute suspensions, we used a granulometric method to study the evolution of the particle suspensions dispersed or not by ultrasonic (US) waves (Nonat and Mutin, 1992, Jiang et al, 1995, 1996).

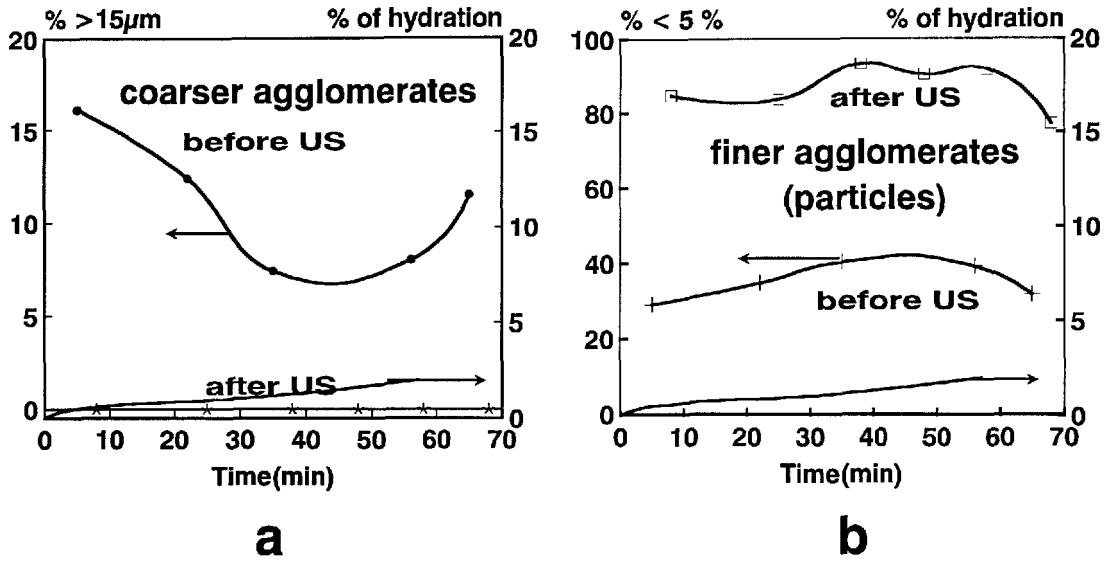

Fig 3. Evolution versus time of the percentage of coarser (a) and finer (b) granulometric classes of Ca_3SiO_5 suspension mixed in initially saturated lime solution (W/C=300). The corresponding advancement of the hydration is indicated. Granulometric measurements are performed with a photosedimentometer CAPA 500 (or 700) HORIBA. During the experiment the suspension was subjected continuously to a gentle stirring and periodically to a ultrasonic treatment (during 30s, power 300 W). The coagulation is indicated by the variation of the granulometric curves before and after ultrasonic (US) treatment.

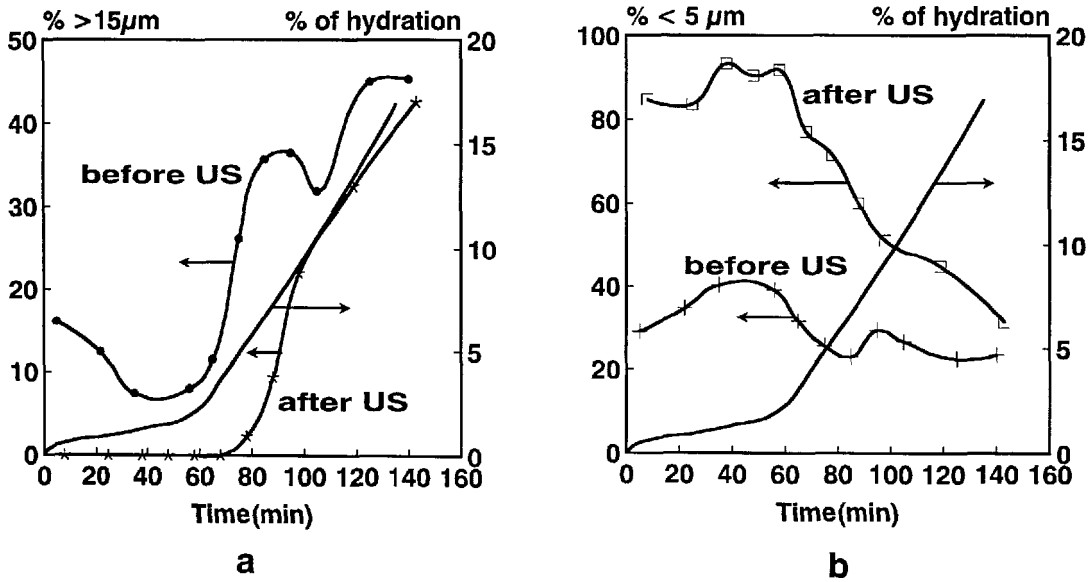

Fig 4. The evolution of the coarser (a) and finer (b) granulometric classes of the same suspension as Fig 6 are represented during the accelerated period of hydration (the percentage of hydration increase distinctly after 60 min.). The same ultrasonic (US) treatment becomes less and less dispersive: the coarser population increases as the finer one decreases, showing the irreversibility of contact interaction between particles due to the hydrates bridging effect.

The coagulation and rigidification processes

Fig 3 shows the case of a suspension of Ca_3SiO_5 in a lime saturated solution ([CaO]=22 mmol/l, W/C=300); it represents the evolution versus time, on one hand, of the percentage of the coarser (Fig 3a, D>15μm) and finer agglomerates (Fig 3b, D<5μm) in suspension and on the other hand, the percentage of hydration The time during which there is practically no hydrate formation (the nucleation period) is about 60 minutes. During this time, before initial dispersion by ultrasonic waves, Ca_3SiO_5 particles are aggregated, and distributed as 16% coarser agglomerates and 30% finer. Ultrasonic treatment disperses the agglomerates since the populations become 90% finer and 0% coarser agglomerates. About 10 minutes after ultrasonic treatment, the population becomes virtually as before, showing the mechanical reversibility of the interparticular bonds. Further sonication again destroys the aggregates and the particles again agglomerate when ultrasonic treatment is stopped . this is the **coagulation** phenomenon in terms of colloid science

Fig 4 shows that, after the nucleation period, as soon as C-S-H formation accelerates, the US treatment destroys less and less agglomerates. **C-S-H formed at the particle contacts rigidify them.** Only a significant increase of US power allows to break the rigidified aggregates. So, setting proceeds through, at least, two fundamental steps:

- the coagulation at the origin of the essential contacts between particles,
- the rigidification by hydrates at the contact points between anhydrous particles

Parameters determining the coagulation process.

Coagulation is due to attractive forces between particles. These forces may result from interactions from various origins, van der Walls forces, chemical interactions, electrostatic forces or solvation forces (Delville, 1992) in which the ionic constitution of the solution surrounding each particle plays an important role. In the present case, the respective concentrations of calcium, silicate and hydroxide ions are not independent, they are fixed by the solubility equilibrium of C-S-H.

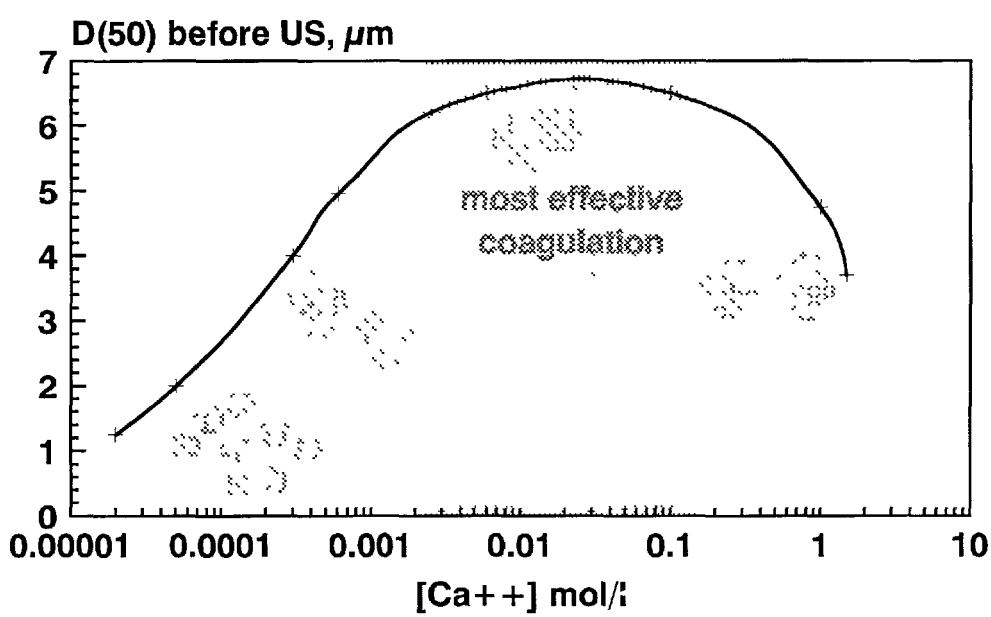

Fig 5 Value of the median diameter (D_{50}) of the agglomerates measured before ultrasonic treatment during the coagulation period versus the calcium concentration in solution.

By controlling these concentrations in solution, we have determined the evolution of the coagulation process. Fig 5 shows the variation versus calcium concentration, of the median diameter, D_{50}, of the agglomerates before ultrasonic treatment which corresponds to 50% of the cumulative granulometric distribution. This curve indicates that coagulation is most effective in the range 1-100 mmol/l. On an other hand, we have proved, by electrophoresis measurements, that the zeta potential of the Ca_3SiO_5 and C-S-H particles is the same and increases from -20 mV to + 20 mV in the same range of lime concentration than granulometric measurements. It equals zero when the lime concentration is about 3 mmol/l (Nachbaur et al, 1997). The coagulation of C_3S particles may then be explained by the evolution of surface charges of unhydrated compounds and hydration products. The high content of Ca^{++} near the surface of particles in suspension promote the coagulation either by adsorption on the surface from solution or by screening the electric double layers around the particles and bridging mechanisms. It must be noticed that during Ca_3SiO_5 hydration under normal conditions, calcium concentration is such as coagulation always occurs.

Parameters determining the rigidification process

Rigidification occurs as soon as hydrates rigidify the contacts between particles. It is revealed in diluted suspensions by the time at which the characteristic dimension of aggregates, after sonication, increases. A systematic study of rigidification in suspensions, having initial calcium and silicate concentrations in the ranges 0-22 mmol/l and 20-0 mmol/l, respectively, shows that rigidification occurs as soon as calcium concentration reaches about 10 mmol/l, whatever the percentage of precipitated hydrates. This is illustrated in Fig 6 where the evolution of the average

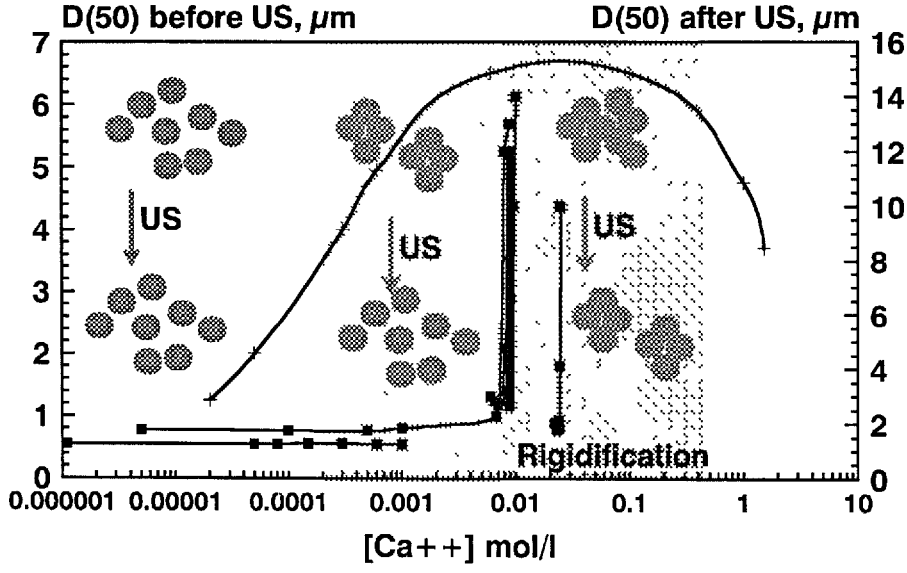

Fig 6 Evolution versus the calcium concentration in solution, of the median diameter of agglomerates measured after sonication.

diameter of the coagulates is plotted against the lime concentration in solution. Below 0.1 mmol/l, rigidification cannot occur, because the particles are always dispersed Between 0 1 and 100 mmol/l, particles coagulate but the coagulates are rigidified only when the lime concentration in solution is higher than 10 mmol/l. In fact, this threshold value corresponds to the concentration at which the solubility of C-S-H in solution becomes very low (Fig 7) Only in such conditions, does C-S-H precipitate on the surface of anhydrous grains, where it is able to bridge particles. In

the case where the calcium concentration cannot reach this threshold value at complete hydration of Ca_3SiO_5, rigidification never occurs. This clearly shows that hydration is not sufficient for setting.

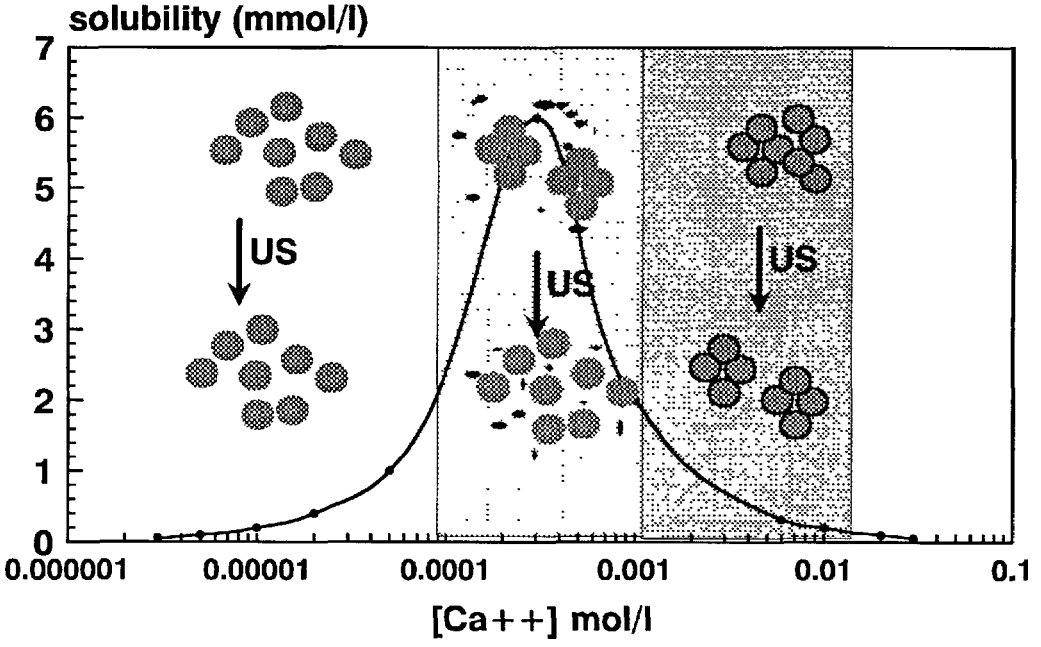

Fig 7. The evolution of the solubility of C-S-H with the calcium concentration in solution is compared with the calcium concentration in solution domains in which the coagulation and rigidification processes are most effective. Above the threshold concentration of 10 mmol/l, the solubility of C-S-H is very low, the coagulation is most effective, consequently does C-S-H precipitate on the surface of the coagulated particles and does rigidify the agglomerates.

CONCLUSION

A systematic study of the effects of lime concentration on the behaviour of suspensions of Ca_3SiO_5 during their hydration leads us to conclude that lime concentration in solution determines the particle interactions and the solubility of hydrates which control the coagulation and rigidification processes at the origin of setting. Coagulation which provides the contacts between particles results from particles interaction in accordance with DLVO theory. Rigidification is due to the strengthening of the contacts by hydrates. The nature of forces between C-S-H particles are not yet clearly identified but they may be the same as during coagulation.

Coagulation and rigidification must occur for setting of cement paste, but these conditions are not sufficient. The coagulated structure must lead to a continuously connected network of particles. This last condition depends on the solid volume fraction and the dimension of cement grains.

ACKNOWLEDGEMENTS

The authors thank the « Conseil Regional de Bourgogne » and the « Association Technique des Industries des Liants Hydrauliques » for their financial support.

REFERENCES

Barret P., Bertrandie D., J. Chim. Phys, (1986), pp. 765.

Damidot D., Nonat A. and Barret P., J. Am. Ceram. Soc., 73(11), (1990), pp.3319.

Damidot D., Nonat A., Proc of 9th Int. Congress on the Chemistry of Cement, New Delhy , III , (1992), pp. 227.

Damidot D., Nonat A., in Hydration and Setting of Cements, A. Nonat, J.C. Mutin Edrs, E&F Spon, London, (1992), pp. 23.

Damidot D., Nonat A., Advances in Cement Research, , 6(21), (1994) pp. 27.

Damidot D., Nonat A., Advances in Cement Research, (1994), 6(22), pp. 83.

Delville A., in Hydration and Setting of Cements, , A. Nonat, J.C. Mutin Edrs, E&F Spon, London, (1992), pp. 253.

Jiang S. P., Mutin J.C., Nonat A., Cement and Concrete Research, 25(4), (1995), pp. 779.

Jiang S. P., Mutin J.C., Nonat A., Cement and Concrete Research, 26(3), (1996), pp. 491.

Lecoq X., Thesis, Université de Bourgogne, Dijon, (1993).

Nachbaur L., P. C. Nkinamubanzi, A. Nonat, J. C. Mutin, J. Coll. Interface Sc., submitted for publication.

Nonat A., Mutin J.C., in Hydration and Setting of Cements, , A. Nonat, J.C. Mutin Edrs, E&F Spon, London, (1992), pp. 171.

Nonat A., Lecoq X., Gauffinet S., these Proceedings

Nonat A., Lecoq X., Proceedings of 2nd International Conference on NMR Spectroscopy of Cement Based Materials, Springer Verlag, In Press.

Taylor H.F.W., J. Am. Ceram.Soc., 69(6), (1986), pp. 464.

2ii054
4 pp

Kn o. 25. JAN. 2001 d o k 31817

THE COLLOID-CHEMICAL PRINCIPLES OF THE STRENGTH THEORY OF CONTACT HARDENING CEMENTS

Raisa F. RUNOVA, Kiev State Technical University of Construction and Architecture, Ukraine
Arkady N. PLUGIN, Kharkov State Academy of Railway Transport, Ukraine

ABSTRACT The contact hardening cements form strong waterresistant stone during heating-free pressing. To ensure development of such property the substance structure must be in disordered (amorphous) state. A model of strength of such systems is presented. The electrosurface properties and interactions in dispersed systems compose the basis of the model.

Key-words: binder, hardening, structure, strength development, crystallography.

INTRODUCTION

V.D.Glukhovsky and R.F.Runova (1976) have published some experimental results discovering the phenomenon of contact hardening of mineral disperse systems including the hydration products of cement. The products of pre-hydration of cement have the same properties (Glukhovsky et al, 1980). In the opinion of these authors, the amorphous state of a substance structure plays the principal role in the process of contact hardening. The hydrated industrial waste products may be used as cements of contact hardening as well (Glukhovsky et al,1986). It was shown by Glukhovsky et al (1991) that the silicate powders are compatible with the metal and polymeric ones. The heat emission under load was registered in the results of physico-chemical research on analysis of energy characteristics of the process of contact hardening (Runova,1992). The results included thermo-baro-graphical data. In this work, the next step of this complex research is presented. The authors offer experimental data analysis with the twofold goal: to extend knowledge of strength forming mechanism and to develop an analytical model of strength in binders of contact hardening.

The most important resulting conclusion was that the hydration and condensation processes in contact hardening cements can be separated in time. It means that the artificial stone formation procedure (structure formation) is a result of the physical and chemical processes in the contacts between the particles of high-dispersed system during their attraction under compression without a change in chemical composition. It allows to use physico-chemical theory of dispersed systems strength by Rehbinder-Schukin (1964) extended by A.N.Plugin (1988, 1989, 1995) in application to binding materials with regard to electrosurface properties and interactions for this purpose.

OBJECTS AND METHODS

The artificial monomineral substances of amorphous submicro-crystalline structure of calcium silicates and hydrosilicates, sodium and potassium hydroaluminumsilicates and their anhydrous compounds as well as metakaolinite were used as the binders of contact hardening. The hydrothermal synthesis and dehydration of hydrates technologies were used to obtain the substances. The X-ray analysis was applied to identify their structure. The dispersity of the specimens determined after D-drying was within the limits of 8-10,000m^2/kg. The cylindric samples for compression strength testings were 20 mm in diameter and height. They were made with the use of dry pressing techique at pressures 50-500 MPa . The testings for strength were carried out right after the pressing R_1 , and after 28 days of water storage R_2. The Rehbinder method was applied to evaluate the strength of bonding in the elementary contacts r_1 between the compressed particles.

The development of the analytical model of strength was based on the fact that structure and strength

of binders are the result of the rise of either electroheterogeneous contacts (EHC) between the oppositely charged surfaces of the structure forming particles (Plugin,1989) or concentration electro-homogeneous contacts (below concentration contacts CC) between the same charged surfaces. The latter contacts rise at high electrolyte concentration or when the surfaces are mechanically pressed together (Plugin and Plugin,1995). The bonds in such contacts are due to attraction between the oppositely charged potential determining ions in the active centers of the structure forming elements (SE) in the EHC and attraction between a potential determining ions of the SE and an anti-ions of a melt or solution in the CC. The distances between the elementary contacts depend on the surface concentration of the active centers of the SE $a=(1/n)^{1/2}$.

In view of it, the modified equation of tensile strength of dispersed systems by Rebinder-Schukin was used as an assumption to obtain the analytical model of strength $R_t = n \cdot P$, where n - the number of the elementary contacts (on the active centers) in a unit of stretched area, $1/m^2$; P - the strength of bond in the contact, N (Rehbinder et al.,1964; Plugin et al.,1995). Substituting the known expressions for ion-ion and ion-dipole interaction and for density of surface charge in double electric layer (DEL), the following formula of tensile strength of hardened cement paste was derived:

$$R_t = \left(\frac{z_2 e \psi_1}{32\pi^2 d_1 h^2} + \frac{z_2 \mu \psi_1}{8\pi^2 z_1 d_1 h_\mu^3}\right)\gamma = \left(\frac{508 z_2 \psi_1}{d_1 h^2} + \frac{773 z_2 \mu \psi_1}{z_1 d_1 h_\mu^3}\right)\gamma,$$

where ψ_1 -the electrosurface potential of the SE, V; e - the charge of electron, Kl; μ -the dipole moment of a molecule of water, Kl·m; z_1 , z_2 , h - the valences of the ions and the distance (m) between them in an elementary contact; h_μ -the distance between the ion and water molecule in an elementary contact, m; d -the distance between the ions which form dense DEL, m; γ - the share of the contacts of EHC or CC type in the total number of the contacts (for the systems considered $\gamma=1$). The method by A.N.Plugin (1988,1989) was used to evaluate the electrosurface potentials of the SE with account for their chemical compositions. The values of z_1 , z_2 , d_1 , h and h_μ were found with the help of the given schemes by the known crystalline structures of the considered or similar compositions.

EXPERIMENTAL AND CALCULATED RESULTS OF THE STRENGTH

The datas on strength of contact hardening cement paste are shown in the Tables 1 and 2.

Table1 The compression strength - to - chemical composition relationship (P_{pres}=200 MPa).

Sample No	Chemical composition	Compression strength, MPa, after:		$K_w = R_2/R_1$	r_1, N	R_t^{calc}, MPa
		pressing, R_1	28 days in water, R_2			
1	$CaO \cdot SiO_2 \cdot 2H_2O$	48.0	49.0	1.0	10^{-8}	49.0
2	$2CaO \cdot SiO_2 \cdot 1.5H_2O$	45.0	46.0	1.0	10^{-9}	46.0
3	$CaO \cdot SiO_2$	25.0	44.0	1.7	-	24.1
4	$Na_2O \cdot Al_2O_3 \cdot 2SiO_2 \cdot 2H_2O$	11.5	10.0	0.9	10^{-10}	11.5
5	$Na_2O \cdot Al_2O_3 \cdot 2SiO_2$	8.0	7.6	0.9	10^{-10}	7.5
6	$K_2O \cdot Al_2O_3 \cdot 2SiO_2 \cdot nH_2O$	7.6	7.5	1.0	-	10.0
7	$K_2O \cdot Al_2O_3 \cdot 2SiO_2$	6.0	5.5	0.9	-	6.4
8	$Na_2O \cdot Al_2O_3 \cdot 4SiO_2 \cdot 2H_2O$	11.4	10.5	0.9	10^{-9}	10.3
9	$Na_2O \cdot Al_2O_3 \cdot 4SiO_2$	7.0	6.0	0.8	10^{-10}	6.8
10	$Al_2O_3 \cdot 2SiO_2$	5.5	4.0	0.9	10^{-11}	5.9

Table 2 The strength - to - compression pressure relationship.

Chemical composition	R_c, MPa, after pressing under load P_{pr}						R_c^{calc}, MPa
	50	100	200	300	400	500	
$CaO{\cdot}SiO_2{\cdot}2H_2O$	22.0	30.5	68.0	143.0	192.5	275.6	507
$Na_2O{\cdot}Al_2O_3{\cdot}2SiO_2{\cdot}2H_2O$	9.4	22.2	50.0	52.5	58.8	68.0	82

In Table 1 strength of the pressed samples depends on the chemical compositions of substances. Particularly, it depends on the presence of alkali and, especially, alkali-earth (Ca) oxides (calcium containing hydrosilicates have maximum but metakaolinite $Al_2O_3{\cdot}2SiO_2$ - minimum strength) and water molecules in composition (hydrogel shows two times better results for calcium hydrosilicates than the anhydrous product). All the contact hardening binders are highly waterresistante.

The fact that the calculated and experimental results on strength are very close is evidence of the correctness of both the assumed theoretical prerequisites and the analytical model of strength. Based on such model, one can analyse how strength of the contact hardening binders depends on the structural and electrosurface characteristics. Besides, it allows to extend knowledge of strength forming mechanism. The data for analysis are given in the Table 3.The structural and electrosurface characteristics are assumed on the basis of the crystalline structures. The blocks (walls) of portlandite are the main SE in the structure of the calcium hydrosilicates (HSC) with potential determining ions (PDI) Ca^{2+} and the hydrosilicate gel with PDI $[Si_2O_7H_4]^{2-}$ and $[SiO_4H_2]^{2-}$. The bicalcium silicate strips of Ca-polyhedrons with PDI Ca^{2+} are the SP and the bivalence silica-oxygen tetrahedra are the anti-ions (AI) in dehydrated calcium silicates by Ilukhin. The particles with frame structure formed by aluminum silicate tetrahedral rings with complex anions $[Al_2Si_2O_8]^{2-}$, $[Al_2Si_4O_{12}]^{2-}$ or Na^+ as an active centers (AC) are the SE in alkali aluminumsilicates. At last, the silica-oxygen nets with AC formed by $O[SiO_3]^{2-}$ and dehydrated layers of alumo-oxygen tetrahedrons with AC formed by tetrahedral cations of $O_5[Al_2O_2]^{2+}$ are the SE in metakaolinite. The distances a between the AC vary within 14.3-32.1 nm.These data are coordinated with known experimental data about active centers.

Table 3 The calculated characteristics and strength of samples.

Sample No	SFE	PDI-PDI(AI)	h, nm	h_μ, A°	R_c, MPa	R_μ, MPa	ψ, v	a, nm	Con-tact
1	CH_2S	Ca^{2+}-H_2O-$[Si_2O_7H_4]^{2-}$	0.6	0.362	31.0	18.0	+0.53	20.3	EHC
2	$CH_2CSH_{0.5}$	Ca^{2+}-H_2O-$[SiO_4H_2]^{2-}$	0.6	0.385	29.0	17.0	+0.53	20.3	EHC
3	C_2S	Ca^{2+}-O-$O[SiO_3]^{2-}$	0.6	-	24.0	-	+0.55	18.2	CC
4	AS_2O	$[Al_2Si_2O_8H]^-$-H_2O-Na^+	0.86	0.62	7.7	3.8	-0.97	14.3	CC
5	AS_2O	Na^+-O-$[AlSiO_4]^-$	0.56	-	7.5	-	+0.26	22.2	CC
6	AS_2O	$[Al_2Si_2O_8H]^-$-H_2O-K^+	0.89	0.65	7.0	3.0	-0.97	14.3	CC
7	AS_2O	K^+-O-$[AlSiO_4]^-$	0.59	-	6.4	-	+0.26	22.7	CC
8	AS_4O	$[Al_2Si_4O_{12}H]^-$-H_2O-Na^+	0.885	0.65	7.1	3.2	-1.07	13.8	CC
9	AS_4O	Na^+-O-$[Al_2Si_4O_{12}H]^-$	0.58	-	6.8	-	+0.26	22.5	CC
10	S,A	$O[SiO_3]^{2-}$-O-$[Al_2O_2]O_5^{2+}$	0.92	-	5.9	-	+0.33	32.1	EHC

where: C - CaO , S - SiO_2, A - Al_2O_3, H - H_2O, O - oxygen atom.

Calcium silicates have higher strength, which is caused by the higher valency of cation as well as by smaller sizes of anion in the contacts. Furthermore, the ion-dipole interaction in hydrate compounds additionally contributes in strength. As the compression pressure Rpr increases beyond 50 MPa the water molecules are gradually displaced from the elementary contacts. In this case the chemical ion bonding h=2.4A° in length is established in the contacts. Correspondingly, strength increases. Its limit calculated values are equal to 507 and 82 MPa for the samples No2 and 4 correspondingly (the experimental values are 275,6 and 68 MPa). The behavior of R_1-R_{pr} relationship (Table 2) demonstrates that the limits of strength capabilities of contact hardening binders are far from being reached. The preliminary grinding of the source binders bares the active centers and the subsequent pressing restores the destructed contacts thanks to the long-range action of electrical field of the potential determining ions in the active centers. The binders with submicrocrystalline and amorphous structures and, therefore, with maximum specific surface of the SE have the maximum number of the bared active centers (and maximum of surface energy). It predetermines the necessity to provide the above-mentioned state of structure to the binders considered.

CONCLUSION

Disordering of substance structure which stipulates the presence of surplus surface energy can be considered as thermodynamic basis of contact hardening cements. This energy is realised during mutual approach of the particles with extremely developed surface. As a result, the condensation of a dispersed system with the artificial stone forming takes place. From the point of view of the physical-chemical theory of strength of dispersed systems with allowance for electrosurface interactions, strength of contact hardening binders is caused by the presence of the electroheterogeneous (EHC) or concentration (CC) contacts. The long-range action of bonds in the contacts ensures reducting of the destructed by grinding ones during pressing. The analytical model of strength of binding substances is presented. It can be effectively used in further research works and in the contact hardening binders manufacturing.

REFERENCES

Glukhovsky, V.D. and Runova, R.F., "Properties of Dispersed Products of Cement Hydration", Proc. of the VI ICCC, Vol. I, 1976, Moskow, pp. 90-93.

Glukhovsky, V.D., Krivenko, P.V. and Runova, R.F., "Condensation Properties of Dispersed Products of Portland Cement Hydration and Rehydration", Proc. of the VII ICCC, Vol. II, 1980, Paris, pp. 419-422. "Particularites de Structure le Ciment durci Contenant des alsalis", Proc. of the VIII ICCC, Vol. VI, 1986, Rio de Janeiro, pp. 614-616.

Glukhovsky, V.D., Runova, R.F. and Maksunov, S.E., "Binders and Composite Materials of Contact Hardening", 1991, Kiev, Vishya Shkola, 232 pp., (in Russian).

Rehbinder, P.A. et al., "About Mechanical Strength of Dispersed Bodies", RAS (Reports of Academy of Sciences) USSR, 1964, Vol. 154, No. 3, pp. 696-698, (in Russian).

Runova, R.F., "Contact-Condensation Binders Based on Calcium Hydrosilicates", Procceedings of the IX ICCC, Vol. III, 1992, New-Delhi, pp. 367-372.

Plugin, A.N., Vdovenko,N.V., Birukov,A.I. and Ovcharenko, F.D.,"About origination electrosurface potential of different substances in water solutions", RAS (Reports of Academy of Sciences) USSR, 1988, Vol. 298, No. 3, pp. 656-661, (in Russian).

Plugin, A.N., "Electroheterogeneous Interactions at the Process of Cement Binders Hardening", The DSc(Chem) degree thesis, 1989, Kiev, ICCCW, 282 pp., (in Russian).

Plugin, A.N. and Plugin, A.A. "Colloid-Chemical Aspects of Strength and Waterproofness of Various Binders and Composite Materials", Proc. of 4th Intern. Conf. "Modern Building Materials, Structures and Techniques", Vol. 1, 1995, Vilnius, Technika, pp. 206-211.

2ii055
8 pp

Kn o. 2 5. JAN. 2001 d o k 31818

CALCIUM HYDROXIDE CONCENTRATION IN SOLUTION : PARAMETER DETERMINING THE KINETICS OF THE EARLY HYDRATION OF TRICALCIUM SILICATE AND THE CHARACTERISTICS OF THE PRODUCTS.

Andre NONAT, Xavier LECOQ , Sandrine GAUFFINET, Laboratoire de Recherche sur la Réactivité des Solides, CNRS-Université de Bourgogne, Dijon, France.

ABSRACT The lime concentration in the solution is found to be the parameter controlling the kinetics of the hydration of tricalcium silicate. The lower the lime concentration, the shorter the duration of the induction period and the weaker the percentage of reaction corresponding to the limitation of the reaction rate by the diffusion of water and ions through the layer of C-S-H. The experimentally observed variations tend to prove that the axial growing rate of C-S-H increases with the lime concentration. The evolution of the growth mode is described from numerical simulations.

Key-words : Hydration, Kinetics, Calcium Silicate, CSH , Induction period

INTRODUCTION

In normal conditions, when cement powder is mixed with water, kinetics of reaction follows a sigmoïd law (**Fig 1**) with an induction period, an accelerated period and finally a period during which the reaction is drastically slowed down by the diffusion of water and ions through the layer of hydration products. Considering the large number of published papers, conflicting results appear with respect to both hydration products and hydration mechanisms (Taylor et al, 1984). In this paper we try to establish the processes limiting kinetics. The results on which the discussion is based are obtained by studying paste and more or less stirred diluted suspensions in water or lime solutions.

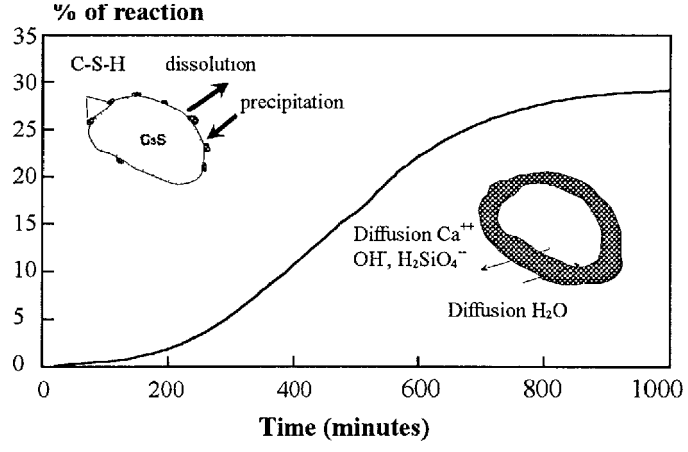

Figure 1 Typical evolution versus time of the percentage of hydration of tricalcium silicate in paste (water/C_3S =0.5) and schematic evolution of the grain covered by the product.

CHEMICAL REACTIONS

In normal conditions (w/c=0.5) hydration of tricalcium silicate proceeds through three reactions which become successively simultaneous :

- the dissolution of tricalcium silicate, C_3S
- the precipitation of calcium silicate hydrate, C-S-H,
- the precipitation of calcium hydroxide, CH.

C_3S dissolution

The first chemical interaction between C_3S and water occurs as soon as tricalcium silicate contacts water. It leads to the protonation of SiO_4^{4-} ions on the C_3S surface (Barret et al,1980, Damidot et al,1994). After this first interaction, protonated species can then pass into solution and C_3S dissolves congruently :

$$Ca_3SiO_5\ _{superf\ hydrox} + 3\ H_2O = 3\ Ca^{2+} + 4\ OH^- + H_2SiO_4^{2-} \qquad [1]$$

If the W/C ratio is greater than 3000, all C_3S dissolves in water. Conversely, when the W/C ratio is lower than 3000, [CaO] and [SiO_2] reach respectively a plateau and a maximum, lower values than the solubility of C_3S. The silica concentration decrease is due to the precipitation of C-S-H which limits the pure dissolution of C_3S. The critical concentrations of 5.5 and 1.7 mmol/l of CaO and SiO_2 respectively are the values at which C-S-H precipitates spontaneously corresponding to the maximum supersaturation with respect to this phase.

Precipitation of C-S-H

As mentioned above, when the supersaturation maximum with respect to C-S-H is reached, its precipitation starts.

$$x\ Ca^{2+} + H2SiO_4^{2-} + 2(x-1)\ OH^- + y\ H_2O = (CaO)_x\ SiO_2\ (H_2O)_{y+x-1} \qquad [2]$$

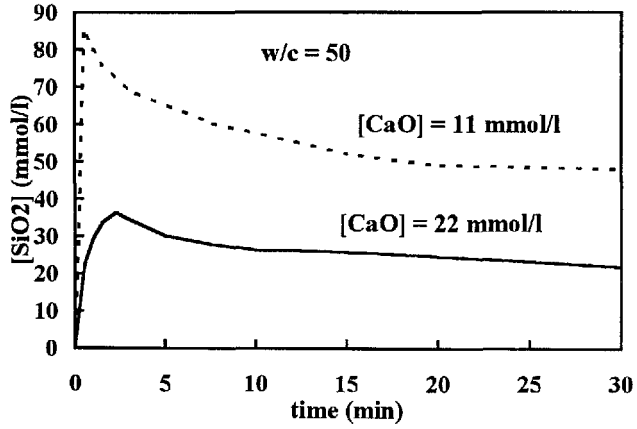

Figure 2 Variation of silicate concentration versus time during the earlier part of hydration in different lime solutions. The maximum value corresponds to the critical supersaturation with respect to C-S-H.

Table 1 : Variation of the quantity of nucleating C-S-H during the first 30 minutes with initial lime concentration of the solution in which C_3S is hydrated (W/C=50).

[$Ca(OH)_2$] mmol/l	quantity of nucleating C-S-H (µmol)
11	65
19.5	45
22	35
33	10

The stoichiometry of precipitating C-S-H, expressed by the calcium to silicon ratio (C/S) and the water to silicon ratio (H/S), depends on the lime concentration in solution. C/S varies between 1 and 2 when [CaO] varies between 1 and 30 mmol/l (Nonat, 1994). During this initial

precipitation, lime concentration remains constant while silica concentration decreases from its maximum value to a quasi steady state. The quantity of C-S-H nucleating after reaching the critical supersaturation depends on the lime concentration in solution (**Fig 2**), the higher the initial lime concentration, the lower the quantity of nucleating C-S-H (**Table 1**). It depends also on the W/C ratio since for a given concentration, higher the volume of solution, greater the number of mole of silica precipitating from the solution.

After this stage, silica concentration does not vary much whereas the lime concentration increases. The quasi-steady state with respect to the silica concentration is due to the fact that the rate of consumption of silicate ions by the precipitation of C-S-H is equal to the silicate release by the C_3S dissolution (Barret and Bertrandie, 1986). So, according to Eqs 1 and 2 and considering the dependence of the Ca/Si ratio in C-S-H with respect to the lime concentration in solution, the rate of accumulation of Ca^{2+} and OH^- in solution depends

i - on the lime concentration due to :

- the Ca/Si ratio dependence

$$Ca_3SiO_5(sh) + z\,H_2O = (CaO)_{C/S}\,SiO_2\,(H_2O)_{H/S} + (3\text{-}C/S)\,Ca^{2+} + 2(3\text{-}C/S)\,OH^- \quad [3]$$

- and probably to the evolution of the Ca/Si ratio of the already precipitated hydrates that Ca/Si ratio corresponds to a lower lime concentration :

$$(CaO)_{xi}\,SiO_2\,(H2O)_{yi} + (xf\text{-}xi)\,Ca^{2+} + 2(yf\text{-}yi)\,OH^- = (CaO)_{xf}\,SiO_2\,(H2O)_{yf} \quad [4]$$

ii - on the W/C , it is more rapid as the suspension is more concentrated i.e. small W/C ratio (**Fig.3**).

Precipitation of calcium hydroxide, portlandite

The increase of the lime concentration ends with the start of precipitation of portlandite $Ca(OH)_2$ revealed by the drop in the electrical conductivity of the solution when the maximum of supersaturation with respect to this phase is reached (about 36 mmol/l at 25°C- **Fig 3**).

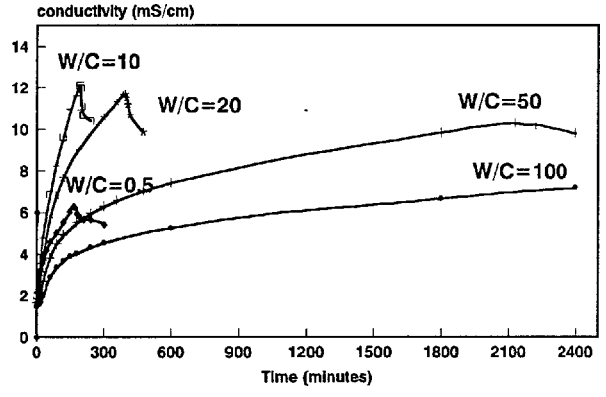

Figure 3 Evolution versus time of the electrical conductivity of the solution which is proportional to the lime concentration during C_3S hydration in water with different Water/C_3S ratios.

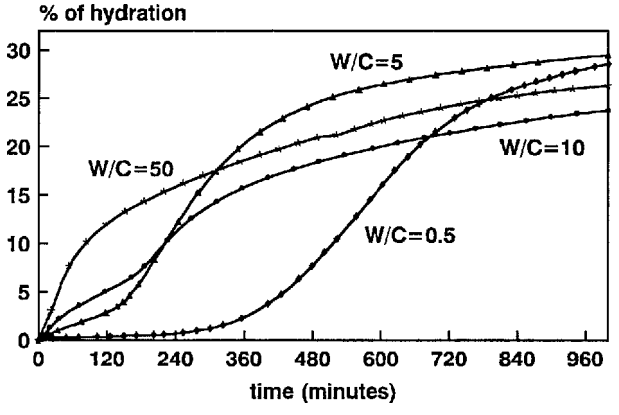

Figure 4 Evolution versus time of the percentage of reaction during C_3S hydration in water with different Water/C_3S ratios.

KINETICS OF REACTIONS

influence of W/C ratio

It was show in the previous part that the chemical reactions involved in the hydration process do not depend very much upon the experimental conditions (i.e. especially the W/C ratio). On the contrary, the kinetics of these reactions are influenced by W/C ratio when reaction begins in pure water. **Fig 4** shows the percentage of hydrated C_3S versus the time of hydration in pure water for W/C ratios ranging from 0.5 to 50. They were calculated from both calorimetric and conductimetric data (Damidot and Nonat, 1994) During the major time of hydration, the rate of C-S-H precipitation is equal to the rate of C_3S dissolution, these also are the evolution curves of the formed C-S-H quantity. Kinetic regime changes from a parabolic law for the highest W/C ratios to a sigmoïdal law for the lowest ones with the succession of two steps for the intermediate values. In the case of high W/C ratios, the reaction is the fastest at the beginning and it continuously decreases following a law characteristic of a limitating diffusion process. In the case of low W/C ratio (paste), the reaction rate is initially very weak, accelerated and finally decelerated in the same way as for high W/C ratios, but the limit is greater.

It has been shown in Fig 3, that depending on the W/C value, the lime concentration increases more or less rapidly from 6 mmol/l, corresponding to the critical supersaturation with respect to C-S-H, to 36 mmol/l, the critical supersaturation with respect to CH. Comparing the evolution of percentage of reaction and the lime concentration versus time lead to associate a rapid initial evolution with a low lime concentration and the high final percentage of reaction with a high lime concentration. Experiments where hydration begins in concentrated lime solutions confirm this view (**Fig 5**): kinetics do not depend very much on W/C ratio and the evolution of percentage of reaction is close to the one observed in water at low W/C ratio. These observations lead to conclude that it is not the W/C ratio, but the lime concentration which is the important parameter.

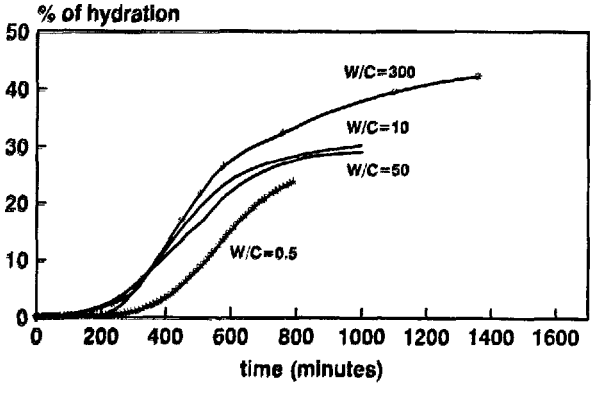

Figure 5 Evolution versus time of the percentage of reaction during C_3S hydration in saturated lime solutions with different Solution/C_3S ratios.

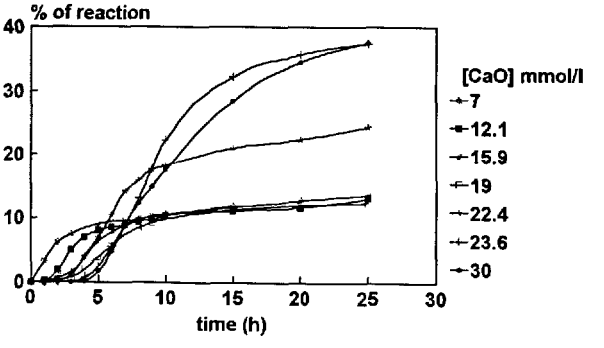

Figure 6 : Evolution versus time of the percentage of reaction during C_3S hydration in different lime solutions. The lime concentration is kept constant during all the process (W/C=57).

Influence of lime concentration

Hydrations of C_3S by keeping constant lime concentration in solution have been undertaken for different value of [CaO] ranging between 6.5 and 30 mmol/l. To maintain constant lime concentration in solution during the hydration process, the 3-C/S moles of $Ca(OH)_2$ not

consumed by the C-S-H precipitation (Eq.3 must be taken out); this is obtained by replacing a volume $V=(3-C/S)/C_0$, C_0 being the initial lime concentration to be keeped constant, by the same volume of pure water. The lime concentration is monitored by continuously measuring the electrical conductivity of the solution which is proportional to the lime concentration in the conditions of the experiments. **Fig 6** shows the evolution of the percentage of reaction corresponding to the hydration of C_3S keeping constant the lime concentration in solution at different values in the range 10 - 30 mmol/l. All these kinetic curves have a sigmoid shape. At high lime concentration, the kinetic curves look like a typical hydration of a C_3S paste. The main changes concern the duration of the induction period and the percentage of reaction at the end of the decelerated period, when hydrates completely cover the surface of anhydrous grains:
- the initial period of slow rate including the induction period is very short (few minutes) at low lime concentration and becomes longer and longer when the lime concentration increases,
- the percentage of the reaction at the end of the decelerated period increases with a drastic dicontinuity around 20 mmol of lime per liter of solution.

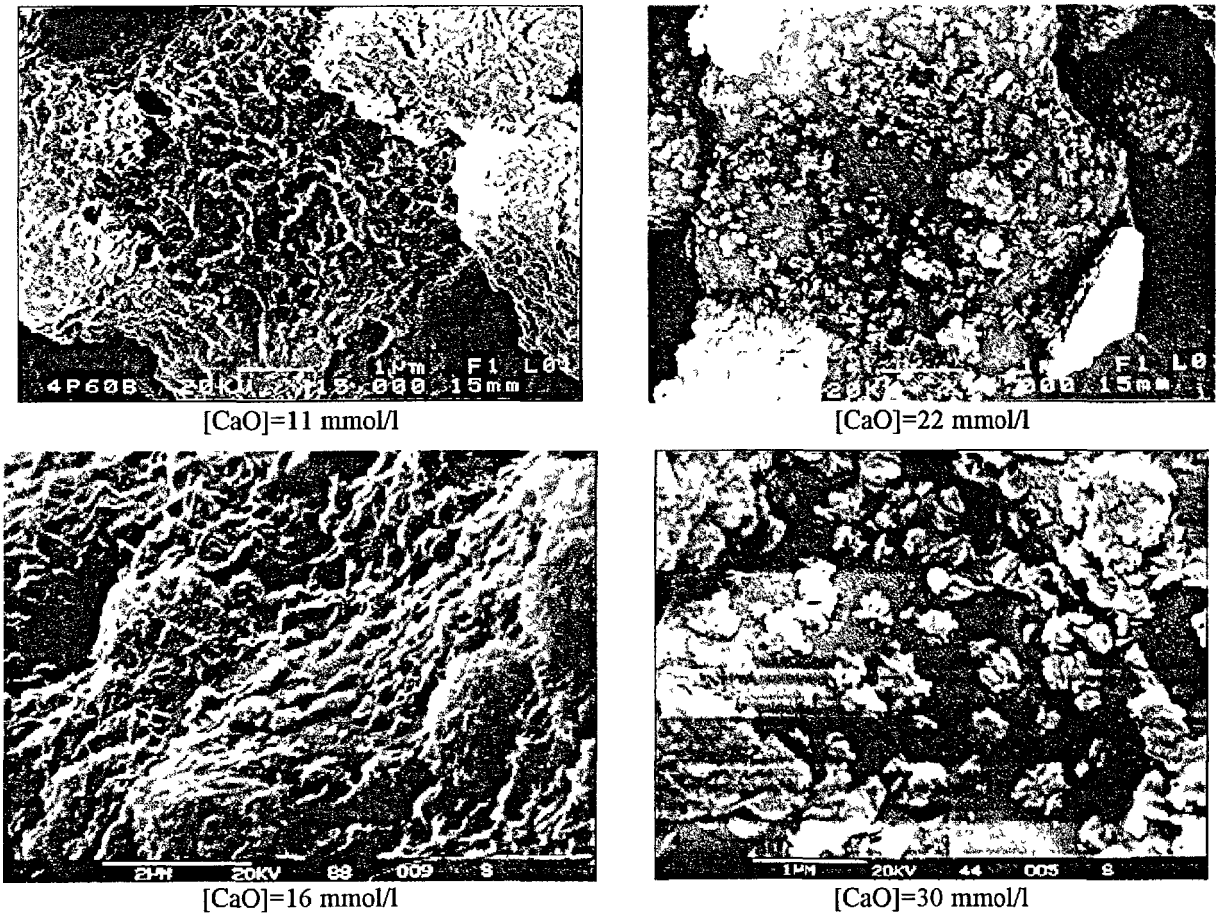

Figure 7 Morphology of C-S-H covering the surface of C_3S when it is hydrated increasing lime concentration solutions.

This behaviour may be associated to the fact that at low lime concentration, there are more nuclei than at high lime concentration (see Table 1). But the change of lime concentration is also associated with a change of morphology of C-S-H which precipitates as it appears on **Fig 7**; at low lime concentrations ($\leq$ 20 mmol/l) C-S-H has a typical honeycomb structure while at high lime concentration ($\geq$ 20 mmol/l), it precipitates with a denser structure as far as it may be

deduced from classical SEM. So the evolution of kinetics with lime concentration may be also due to the modification of growth mode of C-S-H with lime concentration. In order to make allowances for nuclei number and growth mode effects, two type of experiments have been made:

- in the first one (**Fig 8**) , different C_3S samples were prehydrated during 30 minutes in different lime solutions to get different number of nuclei, and then, prehydrated samples were hydrated in the same lime solution to fix the growth mode of C-S-H.
- in the second one (**Fig 9**), samples were prehydrated in same conditions i.e. have the same number of C-S-H nuclei on the surface of C_3S grains, and then hydrated in different lime solutions to vary the growth mode of C-S-H.

Whatever the growth mode, the effect of the number of nuclei essentially controls the acceleration of reaction while the growth mode controls the percentage of reaction for which the surface is completely covered by C-S-H.

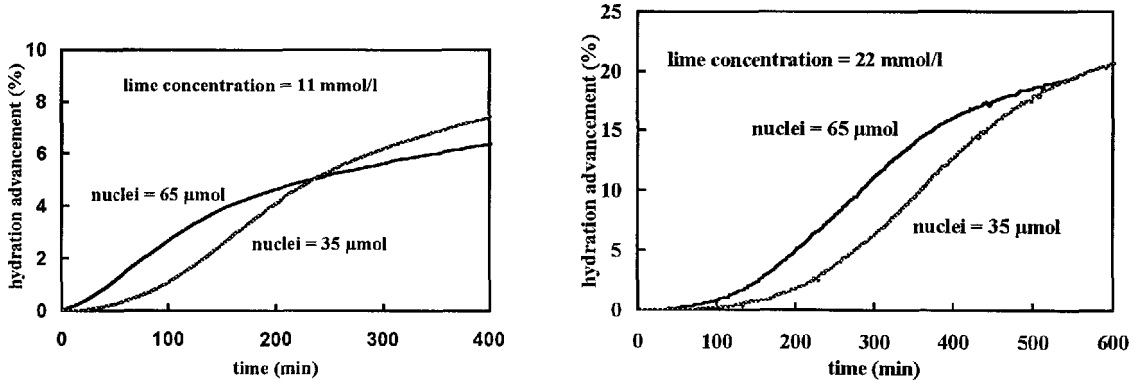

Figure 8 Evolution versus time of the percentage of reaction during hydration of seeded C_3S with different quantities of C-S-H. (a) at low lime concentration (b) at high lime concentration (W/C=57).

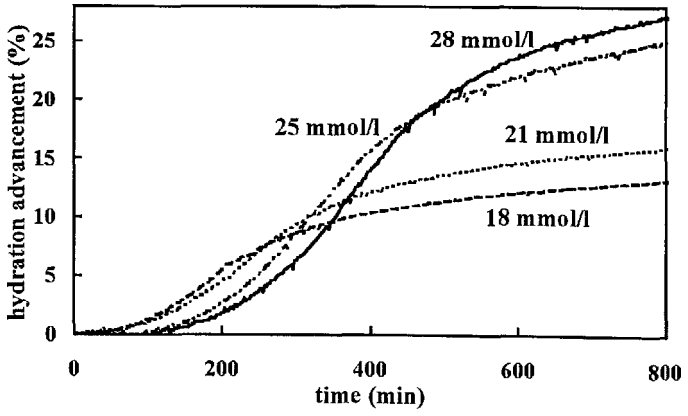

Figure 9 Evolution versus time of the percentage of reaction during hydration of a same seeded sample of C_3S in different lime solutions. The lime concentration is kept constant during all the process (W/C=57).

Morphology and growth mode of C-S-H

At low lime concentration, C-S-H have a morphology much more smoothed on the surface than at high lime concentration suggesting that C-S-H laterally grows faster than at high lime

concentration (**Fig 7**). This would be the reason why, in these conditions, the surface becomes completely covered by a lower quantity of hydrate than at high lime concentration. The quantification of « axial growth rate » and « lateral growth rate » of C-S-H has been attempted with numerical simulations. Nucleation of C-S-H on C_3S surface has been simulated by a randomly generated matrix in which each « 1 » represents a C-S-H nucleus and each « 0 » an element of free C_3S. The dimension of matrixes is 500 x 500 . The percentage of « 1 » with respect to « 0 » is proportional to the experimental number of nuclei per surface unit. The lateral growth is simulated by the convolution product of the « surface matrix » by a « growth matrix ». The dimension of the growth matrix is equal to the number of generated elements of C-S-H per element at each iteration. The axial growth is obtained by superposing, at each iteration, k layers identical to that got by lateral growth with the hypothesis of the growth is identical in each point of the surface. It is so a linear function of the number of iteration. This simulation of C-S-H growth is only valid while the diffusion through the layer of product does not limit the reaction. In this case, the model account well for the variation of the number of initial nuclei (**Fig 10**). It is then possible to find the dimensions of the growth matrix characteristic of the « lateral growth » and the values of k, characteristic of the « axial growth » to fit the experimental kinetics for the different values of the lime concentration (**Fig 11**). The variations of the lateral and axial growth rates versus the lime concentration are plotted on **Fig 12**. They are in accordance with the hypothesis of the variation of the growth mode with the lime concentration. The lateral growth is very fast at low lime concentration and its rate decreases rapidly when the lime concentration increases. Conversely, axial rate does not vary much with lime concentration, but its value shows a clear discontinuity at about 22 mmol/l, the second is about 1.5 times the first. The variation versus lime concentration of many properties of C-S-H shows such a discontinuity, for exemple Ca/Si ratio and structural properties. This is corresponding to two different C-S-H phases, β-C-S-H and γ-C-S-H, for which structural modifications are proposed (Nonat and Lecoq, 1997).

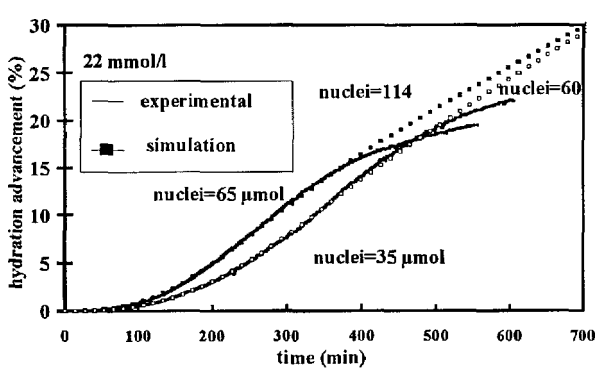

Figure 10 Evolution of the experimental and simulated percentages of reaction during hydration of seeded C_3S with different quantities of nuclei with a growth mode corresponding to a high lime concentration.

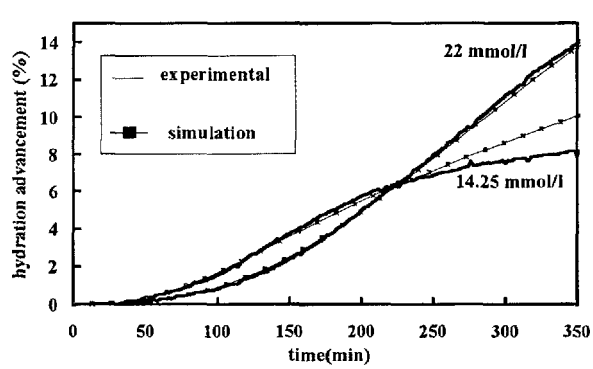

Figure 11 Evolution of the experimental and simulated percentages of reaction during hydration of seeded C_3S with growth modes corresponding to low and high lime concentrations in solution.

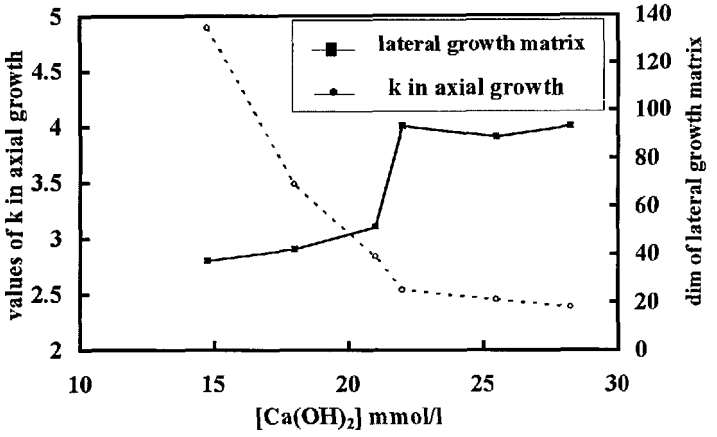

Figure 12 Variation versus lime concentration of the characteristics of the lateral and axial growth rates of C-S-H on the surface of C_3S.

CONCLUSION

Hydration of tricalcium silicate is a complex solid-liquid reaction during which the value of the main parameter controlling kinetics and the properties of the product varies. It has been identified by artificially maintaining constant its value and then its effects have been quantified. On the other hand, simple numerical simulations of the growth kinetics appear to be helpful to characterise the growth mode of a nano-crystalline product, C-S-H. It would be possible to also get data on the properties of the two different C-S-H phases with respect to diffusion by extending the numerical model to period limited by diffusion trough the C-S-H protective layer.

REFERENCES

Taylor et al, Rilem Committee 68 ."The hydration of tricalcium silicate". Mater. Struct., 102(17), (1984). pp. 457-468.

Barret P. "Mécanismes d'hydratation des silicates de calcium (C_3S,C_2S) constituants des ciments vus à travers les concepts de la réactivité des solides", in proceedings of 7th symp. chemistry of cement, Paris, I, (1980) pp. 86-92

Barret P., Bertrandie D. "Fundamental hydration kinetic features of the major cement constituants: Ca_3SiO_5 and Ca_2SiO_4". J. Chim. Phys., (1986) pp. 765-775.

Damidot D., Nonat A.. "C_3S Hydration in diluted and stirred suspension : II Properties of the two C-S-H precipitation steps". Advances in Cement Research, 1994, 6, 22 , pp. 83-91.

Damidot D., Rassem R., Zanni H., Barret P., Bertrandie D. and Nonat A.. "C_3S Hydration in diluted and stirred suspension : III 29Si NMR study of the two C-S-H precipitation steps". Advances in Cement Research, 1994, 6, 24 , pp. 27-35.

Nonat A.. "Interactions between chemical evolution (hydration) and physical evolution (setting) in the case of tricalcium silicate". Materials and Structure, 1994, 27, pp. 187-195.

Nonat A., Lecoq X., "Structure of C-S-H from fully hydration of C_3S in controlled lime concentrations". Proceedings of 2nd International Conference on NMR Spectroscopy of Cement Based Materials, Springer Verlag, In Press.

211056
8 pp

Kn o. 2 5. JAN. 2001 d o k 31819

HYDRATION KINETICS FOR THE ALITE, BELITE, AND CALCIUM ALUMINATE PHASE IN PORTLAND CEMENTS FROM ^{27}Al AND ^{29}Si MAS NMR SPECTROSCOPY

Jørgen SKIBSTED†, Ole Mejlhede JENSEN‡, and Hans J. JAKOBSEN†
† *Department of Chemistry, University of Aarhus, DK-8000 Aarhus C, Denmark.*
‡ *Department of Structural Engineering and Materials, The Technical University of Denmark, DK-2800 Lyngby, Denmark.*

ABSTRACT ^{29}Si magic-angle spinning (MAS) NMR spectroscopy is shown to be a valuable tool for obtaining the quantities of alite and belite in hydrated Portland cements. The hydration (1 - 180 days) of a white Portland cement with 10 wt.% silica fume added is investigated and the degrees of hydration for alite, belite, and silica fume are determined. It is demonstrated that ^{27}Al MAS NMR spectra of hydrated Portland cements can give quantitative information about the formation of ettringite and the conversion of this phase to monosulphate during hydration.

Key-words: Nuclear Magnetic Resonance, Alite, Belite, Ettringite, Monosulphate.

INTRODUCTION

Solid-state MAS NMR spectroscopy has become an important tool for studying the chemistry of cements and for obtaining new structural information about the crystalline and amorphous phases in cement-based materials. The majority of MAS NMR investigations of cementitious systems have employed the ^{29}Si nuclear spin as a probe to follow the formation of the C-S-H gel and to obtain its average chain length of SiO_4 tetrahedra in hydrated samples of C_3S (Lippmaa *et al.*, 1982), β-C_2S (Barnes *et al.*, 1985), and Portland cements (Barnes *et al.*, 1985 and Hjorth *et al.*, 1988). These studies utilized the fact that the ^{29}Si isotropic chemical shift reflects the degree of condensation of SiO_4 tetrahedra (Q^n, n = 0, 1, 2, 3, 4), a relationship which has also been used in ^{29}Si MAS NMR investigations on the structure of C-S-H gels (Brough *et al.*, 1994 and Cong and Kirkpatrick, 1996). Recently, Skibsted *et al.* (1995) showed that the content of alite and belite in anhydrous Portland cements can be determined from computer deconvolutions of the ^{29}Si MAS NMR spectra combined with elemental analysis of the bulk SiO_2 content. In the present work this method has been extended to include the ^{29}Si resonances from the Q^1 and Q^2 units in the C-S-H gel, thereby allowing the quantities of alite and belite in hydrated cements to be obtained. Combining these quantities with those from a similar analysis of the anhydrous Portland cement gives the degrees of hydration for alite and belite, which are of utmost importance to the cement chemist.

In a preliminary ^{27}Al MAS NMR investigation of a white Portland cement, before and after 40 days of hydration, Hjorth *et al.* (1988) showed the potential of this spin nucleus in following the hydration reactions for the small quantities of calcium aluminate (C_3A) in Portland cements. This employs the difference in ^{27}Al isotropic chemical shift of ca. 60 ppm for Al in tetrahedral (Al[4]) and octahedral (Al[6]) coordination. More recently, synthetic samples of the calcium aluminates present in Portland and high alumina cements have been accurately characterized by ^{27}Al MAS NMR (Skibsted *et al.*, 1993). In that study it was shown that first of all the variation in ^{27}Al quadrupole coupling parameters for these samples provides the tool (using MAS NMR) for identification of different phases containing Al in the same coordination state. Furthermore, it has been demonstrated that ^{27}Al MAS NMR represents a unique method for studying the nature of the incorporation of Al guest-ions in the alite and belite phases of Portland cements (Skibsted *et al.*, 1994). In the present work we investigate the hydration kinetics for the formation of ettringite during the early hydration stages of Portland cement and show that the subsequent conversion of this phase to monosulphate can be followed by ^{27}Al MAS NMR.

Table 1 Estimated phase compositions from Bogue calculations for the studied white (wPc) and ordinary (oPc) Portland cements.

	C_3S	C_2S	C_3A	C_4AF	$CaSO_4$	free CaO	Na_2O eq.
wPc	63.9	22.6	4.3	1.0	3.6	2.4	0.16
oPc	56.2	18.5	7.8	8.0	4.7	1.3	0.27

EXPERIMENTAL

Hydrated samples of a rapid-hardening white Portland cement (wPc) and an ordinary Portland cement (oPc), both obtained from Aalborg Portland A/S, Denmark, were studied by ^{29}Si and ^{27}Al MAS NMR, respectively. The blaine fineness of the cements were 426 m^2/kg (wPc) and 317 m^2/kg (oPc) and their estimated phase compositions from a standard Bogue calculation are given in Table 1. 10 wt.% of silica fume (specific surface of 23 m^2/g) and 3.5 wt.% of a melamin-based superplasticizer (Sikament FF) were added to the wPc. The hydration of the wPc mixture employed a water/cement ratio of 0.25. The water was added in two steps during the mechanical mixing in order to ensure dispergation of the silica fume. During hydration the cement paste was kept in sealed glas ampoules at 30° C. At appropriate time intervals the samples were crunched and the hydration process was stopped with ethanol followed by drying at 105° C. The hydration of the oPc was performed in a similar manner, however, employing a water/cement ratio of 0.5, no superplasticizer, and a hydration temperature of 20° C. After one day of hydration the hardened samples were transferred into a new set of sealed containers with high humidities. The hydration was stopped by grinding with acetone and the samples were dried in a desiccator filled with dry N_2.

^{27}Al and ^{29}Si MAS NMR spectra were obtained on a Varian XL-300 (7.1 T) spectrometer, equipped with a home-built CP/MAS probe for 7 mm o.d. zirconia rotors (Jakobsen *et al.*, 1988), employing spinning speeds of ca. 7.0 kHz. The ^{27}Al MAS NMR spectra were recorded using high-power ^1H decoupling, a 15° flip angle, a 2 s relaxation delay, and 2,000 - 16,000 scans, while the ^{29}Si MAS NMR experiments employed a 45° flip angle, a 30 s relaxation delay, and 2,000 - 10,000 scans. ^{27}Al and ^{29}Si chemical shifts are given in ppm relative to external samples of 1.0 M aqueous $AlCl_3$ and neat tetramethylsilane, respectively.

RESULTS AND DISCUSSION

Degrees of hydration for alite and belite from ^{29}Si MAS NMR.

^{29}Si MAS NMR spectra following the hydration over a time scale of three months for the white Portland cement (wPc), with 10 wt.% silica fume added, are shown in Fig. 1. In accordance with previous studies (Barnes *et al.*, 1985 and Hjorth *et al.*, 1988) these spectra display ^{29}Si resonances from the isolated SiO_4 tetrahedra in alite and belite (Q^0: -68 to -76 ppm), the end groups and middle chain SiO_4 units in the amorphous C-S-H gel (Q^1: -76 to -81 ppm, Q^2: -81 to -90 ppm), and from the fully condensed SiO_4 tetrahedra in the silica fume (Q^4: -95 to -129 ppm). The Q^0 region of the ^{29}Si MAS spectra shows a narrow resonance at -71.3 ppm from the unique SiO_4 tetrahedra in β-C_2S, which is superimposed on a broader peak originating from overlapping resonances from the 18 structurally different Si sites in the monoclinic M_{III} form of alite. A visual examination of the spectra in Fig. 1 indicates that the C-S-H gel is formed mainly at the expense of alite and silica fume, while the intensity of the resonance from β-C_2S decreases only slightly with increasing hydration time.

Improved information about the consumption and formation of the individual ^{29}Si species is obtained from numerical simulations of the individual ^{29}Si MAS spectra (cf. Fig. 2). The method for deconvolving the ^{29}Si MAS NMR spectra employs the approach recently used in similar analyses of anhydrous cements (Skibsted *et al.*, 1995), however, with the extension of including a

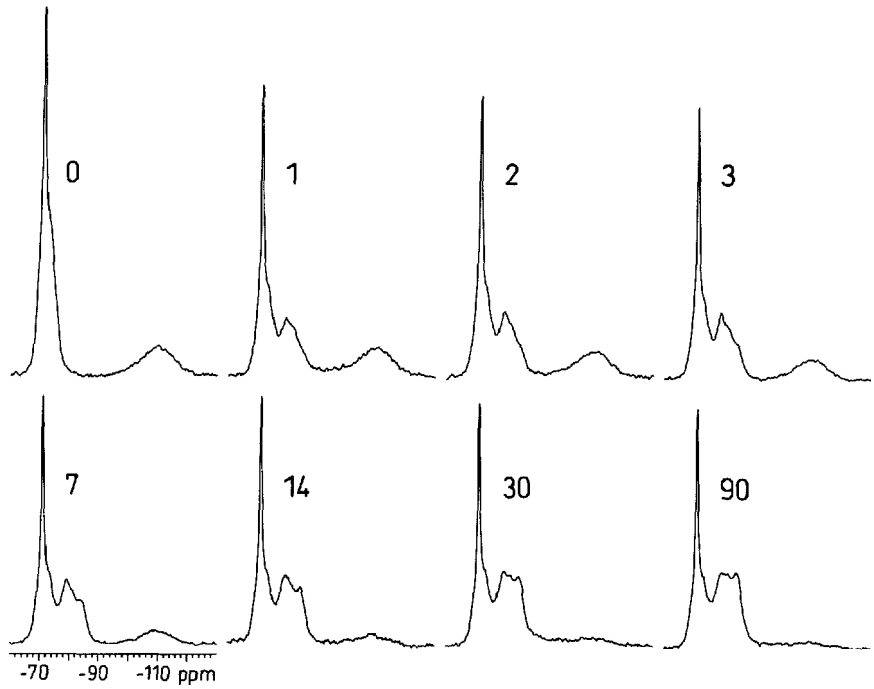

Figure 1 ^{29}Si MAS NMR spectra following the hydration of the wPc with 10 wt.% silica fume added. The time of hydration is indicated in days for the individual spectra.

simulated subspectrum of the ^{29}Si resonances for the Q^{1+2} units of the C-S-H gel. The subspectra of alite and belite are obtained from deconvolutions of ^{29}Si MAS spectra of synthetic samples of β-C_2S and the monoclinic M_{III} form of alite, while five resonances with Gaussian and/or Lorentzian line shapes are used for the Q^{1+2} units. The relative intensities for the individual components are obtained from least-squares optimization of the alite/belite subspectra and the five resonances for the Q^{1+2} units to the experimental spectrum. In addition to the intensities, the optimization allows the linewidths of the individual subspectra to be varied in order to account for variations in line broadening of the individual ^{29}Si MAS spectra. The optimization gives the relative molar intensities for Si in alite, belite, and the C-S-H gel. Combining these intensities with the bulk SiO_2 content of the anhydrous wPc (from an elemental analysis) and the relative intensity for silica fume allows calculation of the quantities of alite and belite in the hydrated sample and thereby a determination of the degrees of hydration for these phases. The relative intensity for silica fume is obtained by integration of the experimental spectra, since the broad resonance from this phase does not overlap with the peaks from the other components.

Optimization of the alite and belite subspectra to the ^{29}Si MAS NMR spectrum of the anhydrous wPc gives the molar intensity ratio $C_2S/C_3S = 0.334 \pm 0.021$. Assuming stoichiometric phase compositions for the calcium silicates this ratio corresponds to 17.5 ± 1.2 wt.% C_2S and 69.6 ± 1.6 wt.% C_3S, when combined with the bulk SiO_2 content (24.44 wt.%). The C_3S/C_2S quantities from ^{29}Si MAS NMR are somewhat lower/higher than those estimated from the Bogue calculation (Table 1). This observation is in general agreement with the earlier reflected light microscopy study by Kristmann (1977) and the recent ^{29}Si MAS NMR investigation (Skibsted *et al.*, 1995) of a series of Portland cements. Both studies find that the C_3S and C_2S values from Bogue calculations on average are ca. 8 wt.% lower and ca. 6 wt.% higher, respectively, than those determined experimentally. An improved estimate of the alite and belite contents in Portland cements may be obtained using the non-stoichiometric compositions for these phases proposed by Taylor (1990). Employing these compositions, along with the molar C_3S/C_2S ratio from ^{29}Si MAS NMR, give the quantities of 19.4 ± 1.6 wt.% belite and 72.7 ± 1.3 wt.% alite for the wPc.

The results of the deconvolution of the ^{29}Si MAS NMR spectra in Fig. 1 and a similar spectrum for the wPc after six month of hydration are illustrated in Fig. 3 by plots of the degrees of hydration for alite, belite, and silica fume as function of the hydration time. The graph for alite shows that ca. 40 % of this phase has been consumed after one day, indicating that the hydration stage, where the rate of hydration increases and the C-S-H and the remaining cement solidifies, is terminated. Thus, the studied time evolutions for the alite and belite hydration characterize the subsequent period, where the hydration rate decreases because the C-S-H gel covers the alite and belite grains. This leads finally to a stage of slow hydration, which is limited by the rate of diffusion of species through the dense C-S-H pore network around the alite and belite grains (Billingham and Coveney, 1993). Fig. 3 shows that the degrees of hydration for alite and belite display almost linear relationships with the logaritm of the hydration time for the final stage of hydration. Similar correlations have been observed by ^{29}Si MAS NMR for the hydration of synthetic samples of β-C_2S and C_3S employing a water/powder ratio of 0.5 (Barnes *et al.*, 1985). However, in that work higher degrees of hydration were reported for the synthetic phases relative to those observed here for alite and belite in the wPc. This difference is ascribed to the lower water/cement ratio used for the wPc and to the significant decrease in relative humidity (RH) in the pores of the cement paste, which has been measured for the studied samples of hydrated wPc (Jensen and Hansen, 1995). A lower RH in the pores reduces the chemical motive power of the hydration and reduces the size of the water-filled spaces. This hampers the diffusion of reacting species and nucleation and growth of the hydration products. The results from ^{29}Si MAS NMR (Fig. 3) indicate that the C_2S hydration is more hampered by the low RH than the C_3S hydration. This is in agreement with earlier reported RH measurements on Portland cement pastes (Patel *et al.*, 1988), which showed that the hydration rate for C_2S is very sensitive to variations in RH. The degrees of hydration for the silica fume (Fig. 3) appear to be less affected by the decrease in RH compared to the hydration of alite and belite. This is in accord with the ^{29}Si MAS NMR observations by Justnes *et al.* (1992) and may reflect the fact that the pozzolane reaction of silica fume in cement pastes only requires a small amount of H_2O to be present as an independent component (Sellevold *et al.*, 1982).

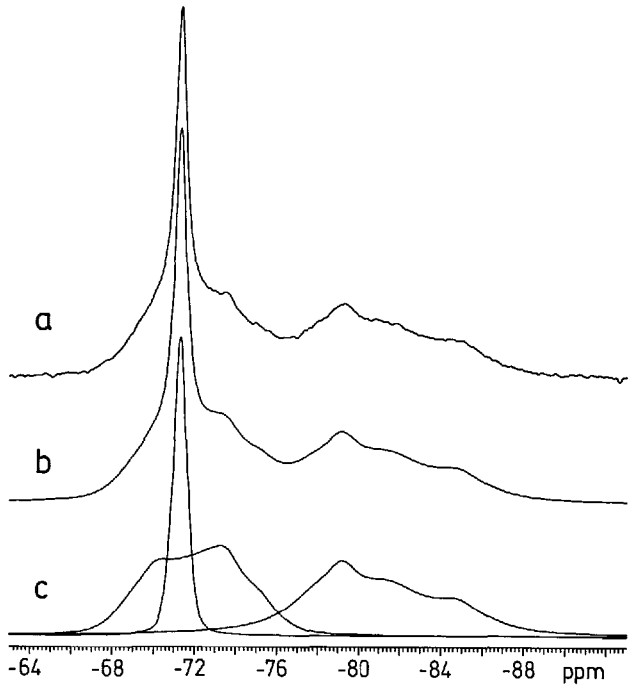

Figure 2 (a) ^{29}Si MAS NMR spectrum of the wPc after 3 days of hydration illustrating the spectral regions for the Q^{0-2} units only. (b) Deconvolution of the spectrum in (a) employing the optimized subspectra for alite, belite, and the Q^{1+2} units in the C-S-H gel shown in (c).

Portland cement hydration followed by ^{27}Al MAS NMR.

The bulk Al_2O_3 content in Portland cements is normally in the range 3 - 7 wt.%, where the major part is present in the so-called interstitial material, which contains the calcium aluminate (C_3A) and ferrite ($C_4A_xF_{2-x}$; $0 < x \lesssim 1.4$) phases. The calcium aluminate phase is the fastest hydrating component in Portland cements and the idealized hydration reaction for this phase in the presence of calcium sulphate can be described as

$$C_3A \xrightarrow[\text{fast}]{C\bar{S}+H} C_6A\bar{S}_3H_{32} \xrightarrow[\text{slow}]{C_3A+H} C_4A\bar{S}H_{12}. \qquad [1]$$

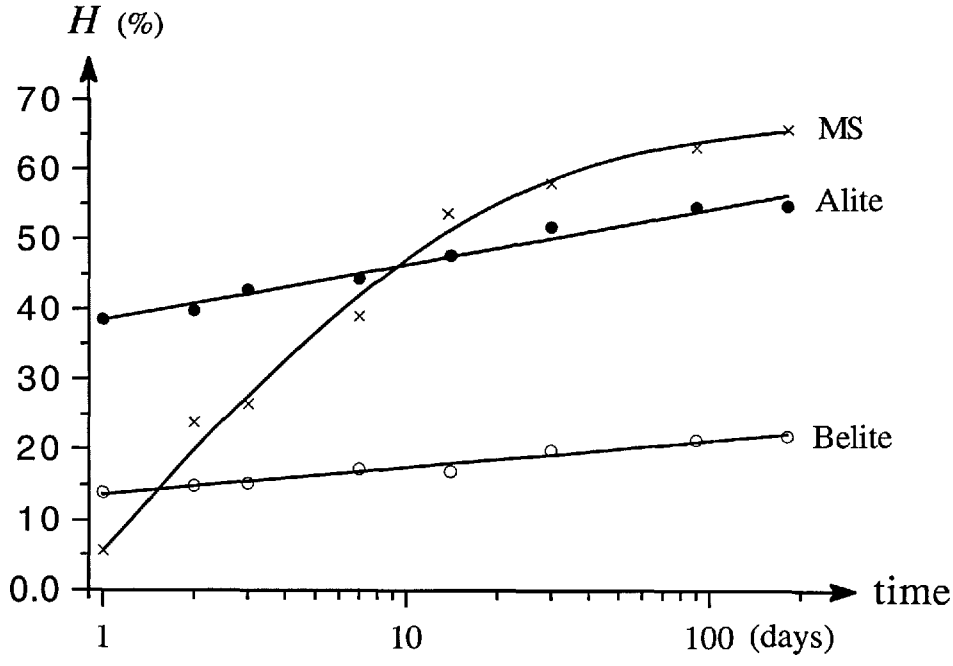

Figure 3 Degrees of hydration (*H*) for alite, belite, and silica fume (MS) for the wPc with 10 wt.% silica fume added as function of the hydration time.

The ferrite phase reacts more slowly with water and forms hydration products similar to those produced by C_3A. Although the basic reactions for these phases are well-known (Taylor, 1990), reliable quantitative studies of these hydration processes are still lacking. The principal aim of this work is to quantitatively characterize the hydration kinetics for the formation of ettringite ($C_6A\bar{S}_3H_{32}$) and its conversion into monosulphate ($C_4A\bar{S}H_{12}$) rather than directly investigating the consumption of the calcium aluminate phase. Thus, the ^{27}Al MAS experiments have been performed using a spinning speed of $\nu_r = 7.0$ kHz at a magnetic field of 7.1 T, which facilitate the observation and distinction of ettringite and monosulphate, because these phases have small (but different) quadrupole couplings (Skibsted *et al.*, 1993). On the contrary, the observation of C_3A by ^{27}Al MAS NMR requires considerably higher spinning speeds ($\nu_r \approx 20$ kHz at 7.1 T) in order to obtain undistorted central transitions because of the strong ^{27}Al quadrupole couplings for this phase (Skibsted *et al.*, 1991).

^{27}Al MAS NMR spectra following the hydration of the oPc from 10 min. to 28 days, and illustrating the spectral regions for the ^{27}Al central transitions, are shown in Fig. 4. The ^{27}Al MAS spectrum before hydration (Fig. 4) displays an asymmetric Al[4] centerband with the highest peak intensity at 79 ppm and a minor peak at ca. 10 ppm from Al[6]. The Al[4] resonance originates from the ^{27}Al guest-ions in the calcium silicate phases (Skibsted *et al.*, 1994), while the Al[6] centerband is ascribed to a minor quantity of a hydrated phase. The calcium aluminate phase is not observed due to its strong quadrupole couplings, which cause a large linebroadening of the central transition. The ferrite phase is neither observed because of the strong dipolar couplings between the ^{27}Al nuclear spins and the spins of the unpaired electrons of the Fe^{3+} ions, resulting in a severe linebroadening of the resonances from this phase. The ^{27}Al MAS spectra of the hydrated oPc demonstrate, even within 10 minutes of hydration, the observation of a narrow Al[6] resonance with the center of gravity at 12.9 ppm. This resonance is easily assigned to ettringite using the earlier reported ^{27}Al quadrupole coupling and isotropic chemical shift data for synthetic calcium aluminate hydrates (Skibsted *et al.*, 1993). The intensity of the central transition for ettringite increases during the induction period (0 - 12 hours) and the following period (12 hours - 2 days), where the major part of the C-S-H is formed and the cement paste solidifies. After one day of hydration a minor shoulder is observed at the low-

frequency side of the centerband from ettringite. During the following hydration the intensity of this peak increases significantly and at the expense of the ettringite resonance. The low-frequency resonance (center of gravity at 9.0 ppm) is easily assigned to Al in monosulphate (Skibsted *et al.*, 1993), and thereby the ^{27}Al MAS spectra in Fig. 4 illustrate the conversion of ettringite into monosulphate during the later stages of hydration. The formation of monosulphate is generally difficult to observed by techniques such as X-ray diffraction and thermal analysis. This is due to the fact that monosulphate is probably interstitified within or near the amorphous C-S-H gel (Taylor, 1990), resulting in a lack of long-range order, which may prevent a reliable observation by X-ray diffraction and lead to a somewhat different thermal behaviour compared to synthetic monosulphate.

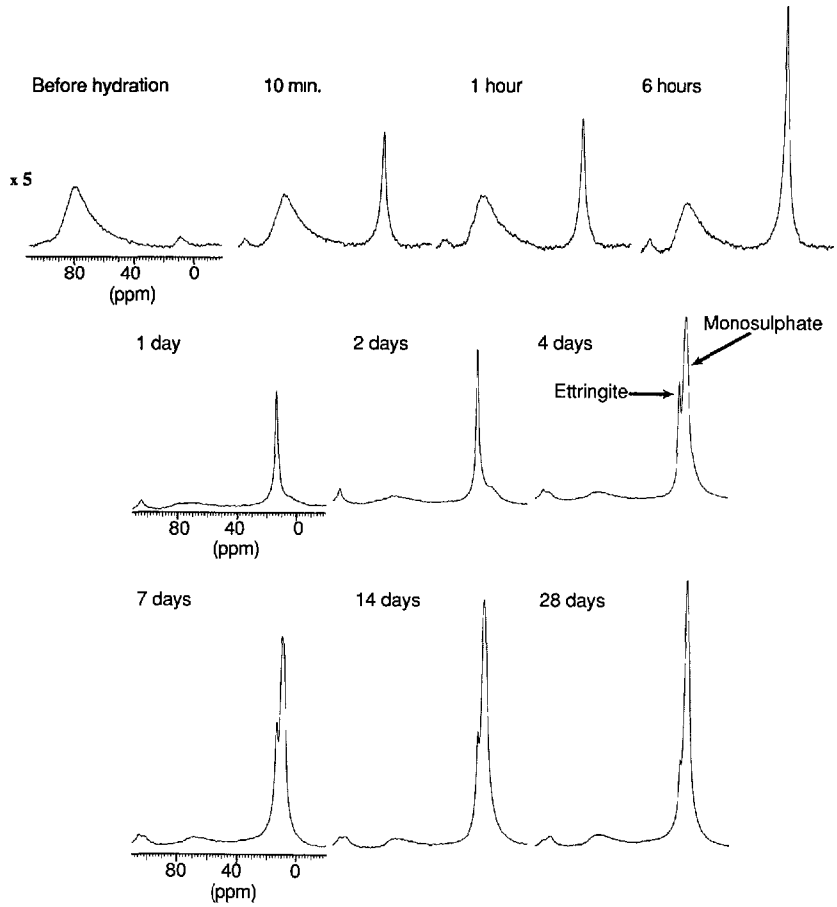

Figure 4 ^{27}Al MAS NMR spectra following the hydration of the oPc. The intensities for the upper row spectra are expanded by a factor of five relative to the other spectra.

The quantities of ettringite and monosulphate in the hydrated oPc samples can be determined from the ^{27}Al MAS spectra (Fig. 4), employing numerical simulations, spectral integrations, and the intensity observed for an external reference sample. The time evolution for the formation of ettringite (Fig. 5) shows a maximum following hydration for ca. two days. At this time the monosulphate formation initiates and the quantity of this phase increases considerably during the following hydration. After eight days of hydration the quantity of monosulphate exceeds the maximum amount of ettringite observed after ca. two days. The results summarized in Fig. 5 thereby indicate that the hydration of the calcium aluminate phase closely follows the mechanistic scheme given in Eq. [1]. This result is in good agreement with an earlier XRD study of the hydration of synthetic C_3A in the presence of gypsum and an excess of calcium hydroxide (Kuzel and Pöllmann, 1991), where the quantity of ettringite was observed to increase gradually until the SO_4^{2-} anions were consumed after hydration for ca. 65 hours. Following this period the remaining C_3A reacted rapidly with ettringite to produce monosulphate.

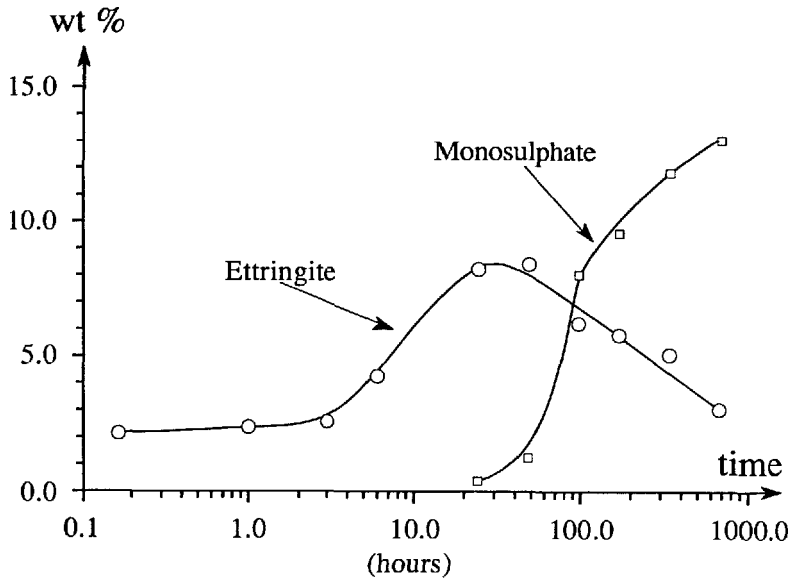

Figure 5 Quantities of ettringite and monosulphate in the hydrated oPc from ^{27}Al MAS NMR as function of the hydration time.

The quantitative analysis of the ^{27}Al MAS NMR spectra in Fig. 4 also allows a determination of the quantities of Al[4] guest-ions in the calcium silicate phases. Before hydration this concentration corresponds to a quantity of 1.0 ± 0.2 wt.% Al_2O_3 in alite and belite, in good agreement with earlier reported Al[4] impurity-ion concentrations in Portland cements (Skibsted *et al.*, 1994). During hydration the Al[4] resonance in the Fig. 4 spectra shifts ca. 10 ppm towards lower frequency. The resonance at lower frequency is assigned to Al^{3+} impurity ions in the C-S-H gel based on the result from an ^{27}Al MAS study of a semi-crystalline C-S-H gel, where an ^{27}Al resonance with a similar line shape and chemical shift was observed (Richardson *et al.*, 1993). A rough estimation of the Al guest-ions in alite/belite and in the C-S-H gel may be obtained from the ^{27}Al MAS spectra in Fig. 4. For example, for the oPc sample hydrated for 28 days we estimate an Al^{3+} impurity concentration corresponding to 0.2 wt.% Al_2O_3 in alite/belite and 0.9 wt.% Al_2O_3 in the C-S-H gel.

CONCLUSIONS

High-resolution ^{27}Al and ^{29}Si MAS NMR are valuable quantitative tools for characterization of the hydration kinetics for alite, belite, and the calcium aluminate phase in Portland cements. The quantities of alite and belite and the degrees of hydration for these phases in hydrated Portland cements can be obtained from ^{29}Si MAS NMR, employing spectral deconvolutions and the bulk SiO_2 content from an elemental analysis. For a white Portland cement with 10 wt.% silica fume added ^{29}Si MAS NMR reveals degrees of hydration for alite and belite, which display almost linear relationships with the logaritm of the hydration time. The measured decrease in relative humidity in the pores of the cement paste decreases the hydration rate for belite considerably, but only affects the reaction of silica fume slightly. ^{27}Al MAS NMR spectra following the hydration of an ordinary Portland cement show the formation of ettringite even within 10 minutes of hydration. The maximum quantity of ettringite is observed after ca. 2 days. After this period ettringite converts rapidly into the thermodynamically stable phase monosulphate.

ACKNOWLEDGEMENT

The authors wish to thank the Cement and Concrete Laboratory, Aalborg Portland A/S, Denmark for providing the white anhydrous Portland cement and the hydrated samples of the ordinary Portland cement. The use of the facilitites at the University of Aarhus NMR Laboratory, sponsored by Teknologistyrelsen, the Danish Research Councils (SNF and STVF), Carlsberg-fondet, and Direktør Ib Hensriksens Fond, is acknowledged.

REFERENCES

Barnes, J. R., Clague, A. D. H., Clayden, N. J., Dobson, C. M., Hayes, C. J., Groves, G. W., Rodger, S. A., "Hydration of Portland Cements followed by ^{29}Si MAS NMR Spectroscopy", *J. Mater. Sci. Lett.*, Vol. 4, 1985, pp. 1293-1295.

Billingham J., Coveney, P. V., "Simple Chemical Clock Reactions: Application to Cement Chemistry", *J. Chem. Soc. Faraday Trans.*, Vol. 89, 1993, pp. 3021-3028.

Brough, A. R., Dobson, C. M., Richardson, I. G., Growes, G. W., "Application of Selective ^{29}Si Isotopic Enrichment to Studies of the Structure of Calcium Silicate Hydrate (C-S-H) Gels", *J. Am. Ceram. Soc.*, Vol. 77, 1994, pp. 593-596.

Cong, X., Kirkpatrick, R. J., "^{29}Si MAS NMR Study of the Structure of Calcium Silicate Hydrate", *Adv. Cem. Based Mater.*, Vol. 3, 1996, pp. 144-156.

Hjorth, J., Skibsted, J., Jakobsen, H. J., "^{29}Si MAS NMR Studies of Portland Cement Components and Effects of Microsilica on the Hydration Reaction", *Cem. Concr. Res.*, Vol. 18, 1988, pp. 789-798.

Jakobsen, H. J., Daugaard, P., Langer, V., "CP/MAS NMR at High Speeds and High Fields", *J. Magn. Reson.*, Vol. 76, 1988, pp. 162-168.

Jensen, O. M., Hansen, P. F., "Autogenous Relative Humidity Change in Silica Fume-modified Cement Paste." *Adv. Cem. Res.*, Vol. 7, 1995, pp. 33-38.

Justnes, H., Sellevold, E. J., Lundevall, G., "High Strength Concrete Binders Part A: Reactivity and Composition of Cement Pastes with and without Condensed Silica Fume", ACI, CANMET, 4th International Conference on Fly ASH, Silica Fume, Slag and Natural Pozzolans in Concrete, Istanbul, May 1992, pp. 873-889.

Kristmann, M., "Portland Cement Clinker: Mineralogical and Chemical Investigations, Part 1: Microscopy, X-ray Flourescence and X-ray Diffraction", *Cem. Concr. Res.*, Vol. 7, 1977, pp. 649-658.

Kuzel, H.-J., Pöllmann, H., "Hydration of C_3A in the presence of $Ca(OH)_2$, $CaSO_4{\cdot}2H_2O$, and $CaCO_3$", *Cem. Concr. Res.*, Vol. 21, 1991, pp. 885-895.

Lippmaa, E., Mägi, M., Engelhardt, G., Grimmer, A.-R.,"A High Resolution ^{29}Si MAS NMR Study of the Hydration of Tricalcium Silicate", *Cem. Concr. Res.*, Vol. 12, 1984, pp. 597- 602.

Patel, R. G., Killoh, D. C., Parrot, L. J., Gutteridge, W. A., "Influence of Curing and Different Relative Humidities upon Compound Reactions and Porosity in Portland Cement Paste", *Mater. and Struct.*, Vol. 21, 1988, pp. 192-197.

Richardson, I. G., Brough, A. R., Brydson, R., Groves, G. W., Dobson, C. M., "Location of Aluminum in Substituted Calcium Silicate Hydrate (C-S-H) Gels as Determined by ^{29}Si and ^{27}Al NMR and EELS", *J. Am. Ceram. Soc.*, Vol. 76, 1993, pp. 2285-2288.

Sellevold, E. J., Bager, D. H., Jensen, E. K., Knudsen, T., "Silica Fume - Cement Pastes: Hydration and Pore Structure", Norwegian Institute of Technology, Trondheim, Report BML 82.610, 1982, pp. 19-50.

Skibsted, J., Bildsøe, H., Jakobsen, H. J., "High-Speed Spinning versus High Magnetic Field in MAS NMR of Quadrupolar Nuclei. ^{27}Al MAS NMR of $3CaO{\cdot}Al_2O_3$", *J. Magn. Reson.*, Vol. 92, 1991, pp. 669-676.

Skibsted, J., Henderson, E., Jakobsen, H. J., "Characterization of Calcium Aluminate Phases in Cements by ^{27}Al MAS NMR Spectroscopy", *Inorg. Chem.*, Vol. 32, 1993, pp. 1013-1027.

Skibsted, J., Jakobsen, H. J., Hall, C., "Direct Observation of Aluminum Guest-ions in the Silicate Phases of Cement Minerals by ^{27}Al MAS NMR Spectroscopy", *J. Chem. Soc. Faraday Trans.*, Vol. 90, 1994, pp. 2095-2098.

Skibsted, J., Jakobsen, H. J., Hall, C., "Quantitation of Calcium Silicate Phases in Portland Cements by ^{29}Si MAS NMR Spectroscopy", *J. Chem. Soc. Faraday Trans.*, Vol. 91, 1995, pp. 4423-4430.

Taylor, H. F. W., "Cement Chemistry", Academic Press, London, 1990.

2ii057
9 pp

Kno. 25. JAN. 2001 doc31820

PHASE DIAGRAMS RELEVANT TO HYDRATION OF C_3S. PART 1: A CASE FOR METASTABLE EQUILIBRIUM

Hamlin M. JENNINGS, Depts. of Materials Science and Civil Engineering, Northwestern Univ., Evanston, IL, US
Christopher M. NEUBAUER, Dept. of Materials Science, Northwestern Univ., Evanston, IL, US
Kathryn D. BRENEMAN, Dept. of Materials Science, Northwestern Univ., Evanston, IL, US
Bruce J. CHRISTENSEN, E. Khashoggi Industries, Inc., Santa Barbara, CA, US

ABSTRACT The possibility of interpreting the chemistry of the aqueous phase of C_3S pastes in terms of phase diagrams has been tested with experiments that first perturb the system and then follow its return to an equilibrium state. Other experiments using an environmental scanning electron microscope show the existence of a protective layer around C_3S during the induction period. Evidence suggests that at about the time of set, this layer undergoes a phase transformation with morphological and physical changes that could be associated with the end of the induction period.

Key-Words: Phase Diagram; Hydration; Thermodynamics; Equilibria; Mechanism

INTRODUCTION

The mechanism that controls the rate of hydration during the early stages of reaction between cement and water has been debated for more than a hundred years. Much attention has also been focused on pure tricalcium silicate (C_3S), the main component of portland cement, which follows rate laws similar to portland cement, and is generally less complex. The most difficult period to understand is the induction period, several hours when chemical activity is slow, followed by more rapid reaction. The length of the induction period can be shortened or lengthened by many hours with the addition of relatively small amounts of chemical admixtures. Two main schools of thought have focused on 1) the role of a protective layer and 2) delayed nucleation of product. Both of these possibilities could explain a slow reaction followed by a period of acceleration.

Interest in understanding the mechanism extends past academic curiosity. For example, developing new admixtures that control the rate of reaction is of both engineering and economic importance. Furthermore, the distribution of products throughout the microstructure as well as attempts to control the microstructure through chemistry are dependent on understanding and controlling the mechanism of reaction.

A question that has emerged in the last few years is whether or not the portland cement system, or even the pure C_3S system, can be analyzed with a phase diagram. As with other systems, such as metals and ceramics, once an equilibrium phase diagram is established, nonequilibrium conditions can be investigated For example, rates of phase change and associated grain size can be related to rates of transition across phase boundaries. The problem with cement-based materials is that they are always changing, especially during the early stages of reaction, and instantaneous measurements are difficult to make. Thus, the question becomes one of whether or not an equilibrium condition, that in principle must exist, can be achieved, or nearly achieved, in the reacting system. This is a question frequently considered by chemical engineers. This paper summarizes some recent results that may

help refine our understanding of the chemistry of the early reaction between tricalcium silicate (C_3S) and water.

EQUILIBRIUM

Because equilibrium has several different meanings, and criteria for evaluating whether or not a system is near equilibrium have evolved over the years, a few important points will be discussed here. First, equilibrium is seldom achieved. Rather, metastable equilibrium or equilibrium with a metastable phase that persists for a long time is common. Throughout this paper the word equilibrium will include the almost indistinguishable state of metastable equilibrium. Transformation to a more stable equilibrium with the passage of time is always a possiblility.

At time zero, as the C_3S starts to dissolve, the aqueous phase is undersaturated with respect to all the relevant phases discussed here. With dissolution, the concentration of the components increases and within minutes fall on a curve in the SiO_2-CaO-H_2O phase diagram, now referred to as C-S-H (M). The location of the curve is generally agreed upon, but the interpretation of the curve is a subject of debate, and thus is the subject discussed here.

A few important concepts are typically invoked when considering whether or not an equilibrium model is appropriate. These concepts are as follows (Smith and Missen, 1982):

1) Equilibrium can be interpreted in terms of forward and reverse reactions that proceed at the same rate. Therefore, the total amount of the reactants and products will not change with time. In the case of a dissolved solid, the amount of dissolved material can be represented by concentration, or more accurately the chemical potential.
2) The system should not change with time. If there is a disturbance which results in a shift out of equilibrium, the system will proceed in a direction which reverses the imposed changes, thereby moving back into equilibrium. This is known as Le Chatelier's principle.
3) Equilibrium occurs independently of the previous history of the system. In other words, equilibrium is a state function. This means that the conditions that define equilibrium do not depend on the path, or the direction, from which equilibrium is approached. In the case of solubility, equilibrium concentrations should not depend on whether or not the initial conditions were supersaturated or undersaturated.
4) Equilibrium can be considered in terms of global versus local conditions. Global equilibrium occurs when the entire system is in the same equilibrium state. During steady-state equilibrium, however, the system is subject to a potential gradient resulting in a flux of mass. In this case, part of the system will be close to equilibrium while another part will be either at a different equilibrium or out of equilibrium. Specifically, we consider that C_3S is never even close to equilibrium with the aqueous phase - equilibrium is between the aqueous phase and a surface layer. Thus, only local equilibrium can be considered here.

Equilibrium between a solid and an aqueous phase occurs between the solid and its dissolved components. When studying the hydration of C_3S, the aqueous phase is most easily analyzed. One of the fundamental issues in cement-based systems is whether the concentration of components in the aqueous phase can be interpreted in terms of equilibrium with a solid and, if so, what can be inferred about the solid. If the reaction simply involves solid C_3S and water going to other solid products,

then the concentrations of components in the aqueous phases would simply be the result of a competition between dissolution and precipitation and equilibrium is not relevant. This possibility has been considered (Barret and Bertrandie, 1988).

Because C_3S and water constitute a reacting system, and because C_3S is unstable when exposed to water, it is not obvious that equilibrium has much relevance. In other words, the system is always far from equilibrium and therefore in an unstable state. The reaction between C_3S and water is extremely slow during the induction period. If this is a result of waiting for product nuclei to form than the aqueous phase should approach a state of equilibrium with C_3S, but this is almost certainly not the case (Jennings, 1986, Jennings, 1988, Stein, 1972). It is difficult to believe that the rate of dissolution is intrinsically slow because dissolution occurs rapidly at the start of the reaction. If a protective layer causes such a slow reaction, it allows a local equilibrium between the aqueous phase and the layer to be established. This paper develops an argument in support of a protective layer.

As discussed below, there is considerable evidence for a layer of product forming around the unreacted solid which might serve to slow the dissolution of C_3S. The question now is whether the concentrations of components in the aqueous phase are the result of a competition between slowly dissolving C_3S and slowly forming product, or by a rapid adjustment to equilibrium with the layer?

If the system is approaching equilibrium with the layer and the layer has a solubility distinctly different from C_3S, then the layer must be considered a phase in itself. The main issue is whether or not the aqueous phase is moving towards any type of equilibrium, stable or metastable, with this layer. Thus, we are not considering global equilibrium but rather a local equilibrium with the aqueous phase. In a sense, equilibrium is being considered to describe the aqueous phase at a local level, while steady state describes the system on a global level.

THE INDUCTION PERIOD

Evidence for a local equilibrium comes from the aqueous phase when concentrations of components from a large number of experiments at different times and reaction conditions (including different mixing conditions) are plotted on a ternary SiO_2-CaO-H_2O diagram. These points typically form a smooth curve. At this point during the reaction, the system is undersaturated with respect to calcium hydroxide (CH). If we accept that the data falls on C-S-H(M), a curve with one degree of freedom, then invoking Gibb's phase rule with three components (at constant temperature and pressure) forces the conclusion that two phases are present, one is the aqueous phase. Since C_3S cannot be the other phase (much too soluble), then the surface of C_3S must be surrounded by another phase which is some form of C-S-H. Therefore, this system is being governed by equilibrium. In other words, any change brought about by slow dissolution of C_3S is adjusted for by precipitation of product. The system approaches equilibrium rapidly compared to these changes, and the equilibrium is between a product layer and the aqueous phase.

It is possible that extraordinary coincidence could explain the one degree of freedom with concentrations given the wide range of reacting and mixing conditions from which the data was taken (Jennings, 1986). Thus, the issue of kinetic competition is still not absolutely settled in that we could have a slowly dissolving reactant, whose rate is controlled by the layer, and a slowly forming product. Since there is scatter in the data, the idea of drawing a curve and calling it one degree of

freedom might be an oversimplification. The scatter could be the result of changing conditions in the kinetic competition, the system's inability to exactly achieve equilibrium, or experimental error, or a combination of two or more of these mechanisms. One test would be to disturb this balance and follow whether or not the aqueous phase remains in a new state or returns to the equilibrium state.

One type of experiment has been performed repeatedly to explore the system's ability to maintain equilibrium even if the system is altered. The object is to perturb the system and track the concentration of components in the aqueous phase to see if it stays perturbed or returns to the C-S-H (M). The addition of water or lime to the paste at various times throughout the induction period, imposes huge perturbations and then concentrations in the aqueous phase are followed. The brief experimental sequence and a typical result are described in Fig 1 and Fig 2 and, as can be seen, the system returns to the equilibrium concentrations very rapidly.

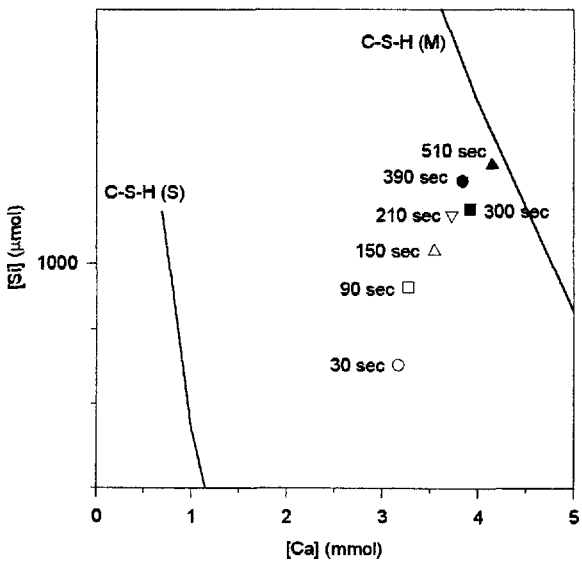

Figure 1: Typical results from dilution experiment. C_3S and de-ionized water were mixed at a water/cement (w/c) ratio of 0.5 by hand for 5 minutes. The sample was allowed to sit for 10 minutes and was then slowly poured into a de-ionized water batch which diluted the sample to a w/c=20. Following dilution, the aqueous phase was extracted at various times (indicated on the graph) using a pipet and filter paper (particle retention=5-10 µm). Ion concentrations in the extracted aqueous phase were analyzed using inductively coupled spectroscopy (ICP) analysis.

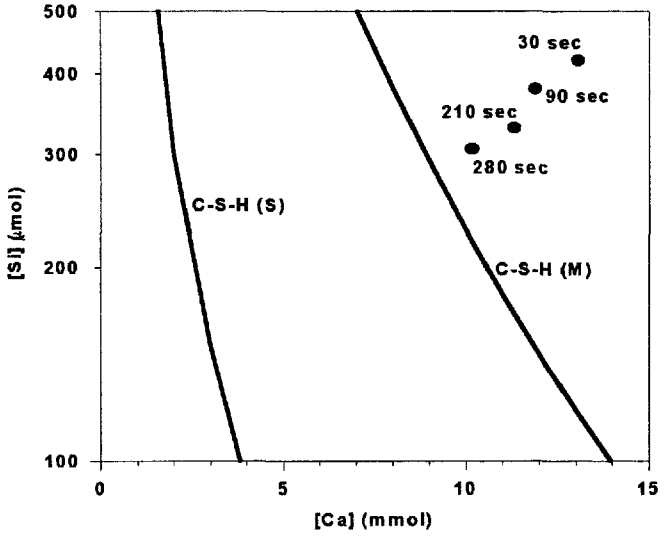

Figure 2: Typical results from CaO addition experiment. C_3S and de-ionized water were mixed at a water/cement (w/c) ratio of 0.5 by hand for 5 minutes. The sample was allowed to sit for 10 minutes and CaO was then added. Following CaO addition, the aqueous phase was extracted at various times (indicated on the graph) using a pipet and filter paper (particle retention=5-10 µm). Ion concentrations in the extracted aqueous phase were analyzed using inductively coupled spectroscopy (ICP) analysis.

There is also physical evidence for a metastable layer. An early surface layer has been observed on C_3S particles at high w/c ratios (Groves, 1983, Double and Hellawell, 1976, Ings et al, 1983). Additionally, Bergstrom and Jennings (1992) and, more recently, Meredith et al (1995) have used an environmental scanning electron microscope to note that the surface of C_3S particles in normal w/c pastes is covered with a gelatinous material very early in the hydration process. X-ray photoelectron spectroscopy studies also support the early formation of a layer on the C_3S surface. Regourd et al (1980) noted a sharp decrease in the C/S ratio of the C_3S surface, followed by an increase, and another decrease to a final value of 1.5-2. This seems to suggest two different types of early hydrate; the latter, with the C/S ratio ~ 1.5-2, is believed to be a metastable phase which controls the early hydration and gives rise to the induction period. In addition, Jennings (1986, 1988) suggests there are two phases, one stable with respect to the other.

Thus, both physical and chemical evidence suggests that both a layer forms and that it is in equilibrium with the aqueous phase. The question now is why does the induction period come to an end, or perhaps, why does the layer become ineffective.

A CASE FOR A LAYER--METASTABLE C-S-H

As discussed above, there are two types of C-S-H, one metastable with respect to the other. These have been designated C-S-H (M) and C-S-H (S). It is tempting to speculate that a conversion from one to the other is the basic mechanism that triggers the end of the induction period. Extensive investigation, however, found little or no change, either physical or chemical, at the end of the induction period as measured by calorimetry.

Environmental scanning electron microscope (ESEM) micrographs (Sujata and Jennings, 1992) have suggested that the texture of the surface layer begins to change only around the time of set. Typical results are shown in Fig 3. These are consistent with the surface area measurements.

Finally, the aqueous phase chemistry has been studied extensively and it is typically found that a transition occurs from the upper curve to the lower curve about the time of set. Data from this study can be seen in Fig 4. Again, this data is consistent with a phase change occurring at the time of set.

SUMMARY

All indications are that the C_3S-water system behaves as if it is nearly at equilibrium. It obeys Gibbs' phase rule and it responds to perturbations in a manner consistent with equilibrium. This equilibrium is with a C-S-H layer that is a distinct phase. Furthermore, at about 4-6 hours there appears to be a phase change associated with the nucleation of a more stable form of C-S-H. However, this phase change occurs at a time significantly later than the end of the induction period as defined by calorimetry.

ACKNOWLEDGMENTS

The authors wish to thank both the Department of Energy (award # DE-FG02-91ER45460/A01) and the National Science Foundation Center for Advanced Cement-based Materials. CMN wishes to thank the Department of Defense for financial support through a National Defense Science and Engineering Graduate Fellowship.



(a)

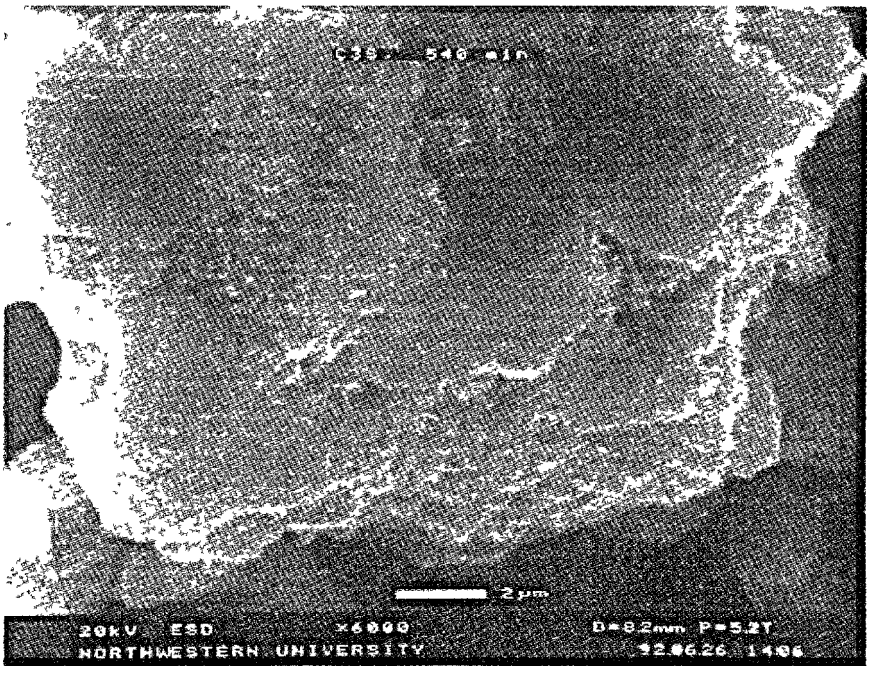

(b)

Figure 3: ESEM micrographs of C_3S paste taken at 60% relative humidity after (a) 7 and (b) 9 hours of hydration.

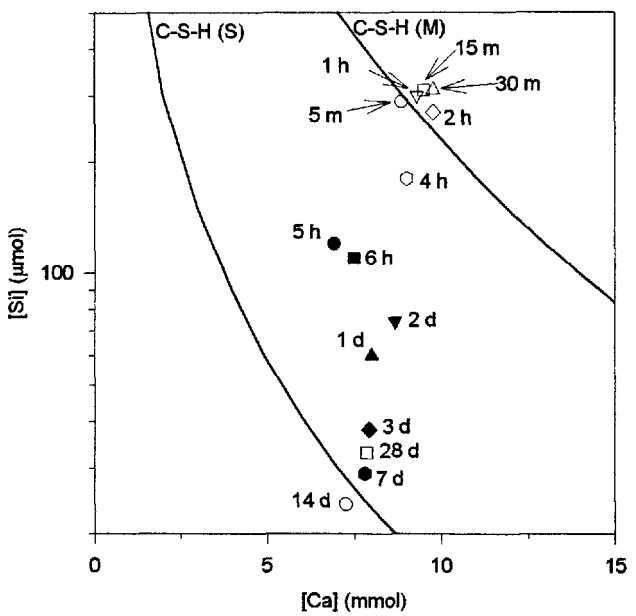

Figure 4: Trace of Ca and Si concentrations in extracted aqueous phase. C_3S and DI H_2O were mixed by hand for 5 minutes at a w/c=20. The aqueous phase was immediately filtered (filter paper with particle retention=5-10 µm) from the solid phases and stored in polystyrene bottles under nitrogen. At the selected times shown on the graph, the aqueous phase was analyzed using ICP analysis. In some later age samples, very small precipitates were visible.

REFERENCES

Allen, A.J., Oberthur, R.C., Pearson, D., Schofield, P., Wildings, C.R., "Development of the Fine Porosity and Gel Structure of Hydrating Cement Systems", Phil. Mag. B, Vol. 56, No. 3, 1987, pp.263 - 288.

Barret, P. and Bertrandie, D., "Comment on "Aqueous Solubility Relationships for Two Types of Calcium Silicate Hydrate", Comm. Am. Ceram. Soc., February 1988, pp. C-113 - C-115.

Bergstrom, T.B., and Jennings, H.M., "On the Formation of Bonds in Tricalcium Silicate Pastes as Observed by Scanning Electron Microscopy", J. Mat. Sci. Let., Vol. 11, 1992, pp. 1620-1622.

Double, D.D., and Hellawell, A., "The Hydration of Portland Cement", Nature, Vol. 261, 1976, pp. 486-488.

Groves, G.W., "TEM Studies of Cement Clinker Compounds: Their Hydration and Strong Cement Pastes", Phil. Trans. Roy. Soc. London A, Vol. 310, 1983, pp. 79-83.

Ings, J.B., Brown, P.W., and Frohnsdorff, G., "Early Hydration of Large Single Crystals of Tricalcium Silicate", Cem. Concr. Res., Vol. 13, No. 6, 1983, pp. 843-848.

Jennings, H.M., "Aqueous Solubility Relationships for Two Types of Calcium Silicate Hydrate", J. Am. Ceram. Soc., Vol. 69, No. 8, 1986, pp. 614-618.

Jennings, H.M., "Reply on "Aqueous Solubility Relationships for Two Types of Calcium Silicate Hydrate", J. Am. Ceram. Soc., Vol. 71, No. 2, 1988, pp. C-115 - C-116.

Jennings, H.M., at the Gordon Conference on the Chemistry and Physics of Cement-based Materials, Plymouth State College, Plymouth, NH, 1996.

Meredith, P., Donald, A.M., and Luke, K., "Pre-induction and Induction Hydration of Tricalcium Silicate: An Environmental Scanning Electron Microscopy Study," J. Mat. Sci., Vol. 30, 1995, pp. 1921-1930.

Regourd, M., Thomassin, J.H., Baillif, P., and Touray, J.C., "Study of the Early Hydration of Ca_3SiO_5 by X-ray Photoelectron Spectroscopy", Cem. Concr. Res., Vol. 10, No. 2, 1980, pp. 223-230.

Smith, W.R., and Missen, R.W., "Chemical Reaction Equilibrium Analysis; Theory and Algorithms", John Wiley and Sons, Inc., New York, 1982.

Stein, N.H., "Thermodynamic Considerations on the Hydration Mechanisms of Ca_3SiO_5 and $Ca_3Al_2O_6$", Cem. Concr. Res., Vol. 2, 1972, pp. 167-177.

Sujata, K., and Jennings, H.M., "Formation of a Protective Layer During the Hydration of Cement", J. Am. Ceram. Soc., Vol. 75, No. 6, 1992, pp. 1669-1673.

2ii058
15 pp

Kn o. 25. JAN. 2001 d o k 31822

PHASE DIAGRAMS RELEVANT TO THE HYDRATION OF C_3S. PART II: A PHASE DIAGRAM FOR THE CaO-SiO_2-H_2O SYSTEM

Christopher M. NEUBAUER, Dept. of Materials Science, Northwestern Univ., Evanston, IL, US
Jeffrey J. THOMAS, Dept. of Civil Engineering, Northwestern Univ., Evanston, IL, US
Maria C. GARCI, Dept. of Materials Science, Northwestern Univ., Evanston, IL, US
Kathryn D. BRENEMAN, Dept. of Materials Science, Northwestern Univ., Evanston, IL, US
Gregory B. OLSON, Dept. of Materials Science, Northwestern Univ., Evanston, IL, US
Hamlin M. JENNINGS, Depts. of Materials Science and Civil Engineering, Northwestern Univ., Evanston, IL, US

ABSTRACT A new phase diagram, based on a wide range of data, is presented for the CaO (C)-SiO_2 (S)-H_2O (H) system. This phase diagram provides important new insight into understanding the hydration of cementitious systems and supports the idea of a metastable C-S-H layer as the cause of the induction period. A mechanism for the end of the induction period is considered: a eutectic solidification reaction. First, a layer forms, and during the induction period a metastable equilibrium triangle is established between C_3S, the metastable C-S-H layer, and solution. When a sufficient level of calcium supersaturation is reached, CH and C-S-H begin to form cooperatively starting at the metastable layer, and two separate local equilibria are established at the product/solution interface and at the product/C_3S interface. Interpretation of this diagram in the β-C_2S system has also been made. Differences between C_3S hydration and C_2S hydration are accounted for by the proposed phase diagram.

Key-Words: Phase Diagram; Hydration; Thermodynamics; Equilibria; Mechanism

INTRODUCTION

The development of a phase diagram for the CaO (C) - SiO_2 (S) - H_2O (H) system has long been an elusive goal in cement and concrete research. A relevant phase diagram for cementitious systems must contain C_3S and C_2S, the major components of portland cement; water; and the products of the hydration reaction. Phase diagrams are a powerful tool and are frequently used to understand and design the microstructure of materials.

As noted by Brown (1989), it is difficult to describe the CaO - SiO_2 - H_2O system in terms of a phase diagram since traditional phase diagrams assume equilibrium. In the cement system the concept of absolute equilibrium has proven inadequate; one must instead consider constrained or metastable equilibria which control phase development and stability.

At the present time, only rough sketches of this phase diagram have been published. For example, Williamson (1968) has presented a ternary diagram showing where the C-S-H phase field must exist, and Taylor et al (1984) have presented a more extensive map of the major phase fields. While these are helpful in describing the process of hydration, they are not very useful for predicting or controlling reactions. Brown (1989) has presented a more detailed diagram accompanied by a series of proposed mechanisms for the hydration of C_3S. However, there is a

definite need for a more exact phase diagram consistent with the experimental data that has been accumulated to date.

One of the desirable characteristics of any phase diagram of this system is a logical explanation for the end of the induction period. Taylor et al (1984) have reviewed the four existing main hypotheses. Two of these hypotheses involve a protective surface layer on the C_3S surface which is either destroyed by osmotic bursting or rendered more permeable by aging or by a phase transformation The other two hypotheses cite nucleation of either the CH or C-S-H phase as the trigger which ends the induction period. In this case, growth of product relieves supersaturation and allows dissolution of unreacted cement. Much of the experimental evidence gathered to date seems to support the nucleation of C-S-H as the governing factor in the end of the induction period. However, there is also some evidence for the surface layer hypothesis (Taylor, 1990). Taylor (1990) notes that, in the most likely scenario, two or more of these mechanisms work in conjunction to ultimately end of the induction period.

As discussed in Part I, phase diagrams are very important tools for studying the hydration of cement-based materials. This paper presents a proposed phase diagram for the CaO - SiO_2 - H_2O system which appears to be consistent with most of the experimental evidence collected to date. It also can be used to help support a mechanism for the end of the induction period involving a eutectic solidification reaction. The hydration of C_3S is discussed throughout, and extensions to the hydration of β- C_2S are also made.

MAPPING THE PHASE DIAGRAM FOR THE C/S/H SYSTEM

The goal of our research was to create a ternary phase diagram consistent with all of the data observed to date. The major phases in portland cement, C_3S and C_2S, along with one of the major products, CH, can easily be placed on the phase diagram in their respective locations. Each was assumed to be a line compound[1] for the purposes of the discussion which follows. Mapping the phase field of the C-S-H phase was far more challenging. It was assumed that there are two separate types of C-S-H which form (see Part I): a metastable phase which controls the early hydration and causes the induction period, and a more stable phase which develops later and causes the material to set. Although this theory is not universally accepted, both phases are introduced here in order that they be included in discussion.

Metastable C-S-H Phase

There is evidence (see Part I) to state that the onset of the induction period is caused by a form of C-S-H which slows ion dissolution from hydrating C_3S and C_2S. Brown et al (1984) determined that this layer probably forms within 30 seconds of wetting the solid surface, moving the system toward a metastable equilibrium between C_3S, solution, and the slow growing C-S-H surface layer. Jennings (1986) referred to this phase as C-S-H (B) [subsequently C-S-H (M)] and showed that the solubility of this phase is significantly greater than that of the stable C-S-H phase, C-S-H (A) [subsequently C-S-H (S)].

---

[1] The concept of a line compound refers to the representation of its free energy vs. composition function as a vertical line located at the stoichiometric composition.

The metastable phase, C-S-H (M), has been placed on the phase diagram using an assumed composition of $C_{1.85}SH_{2.65}$. These values fall well within the range determined by the X-ray photoelectron spectroscopy studies (Regourd et al, 1980) and also support the idea of a supersaturated phase relative to the stable C-S-H phase boundary described in the next section. It is interesting to note that these values are very close to that determined for jennite ($C_9S_6H_{11}$), a mineral which can be synthesized from CH and hydrous silica in aqueous suspensions (Taylor, 1990). Whether any relations exist between jennite and this metastable C-S-H phase is a topic for future investigations.

Stable C-S-H Phase Boundary

The placement of the C-S-H phase boundary in Fig 1 (bounding its two-phase field with CH) is governed by the following assumption: the CH formed during this reaction is separate from the C-S-H phase. Other authors, notably Taylor (1990), have argued that the CH forming within the C-S-H layers is an integral part of that phase and they should be considered together. However, for the remainder of this paper, we will assume that the two phases are separate, though they may be intimately mixed.

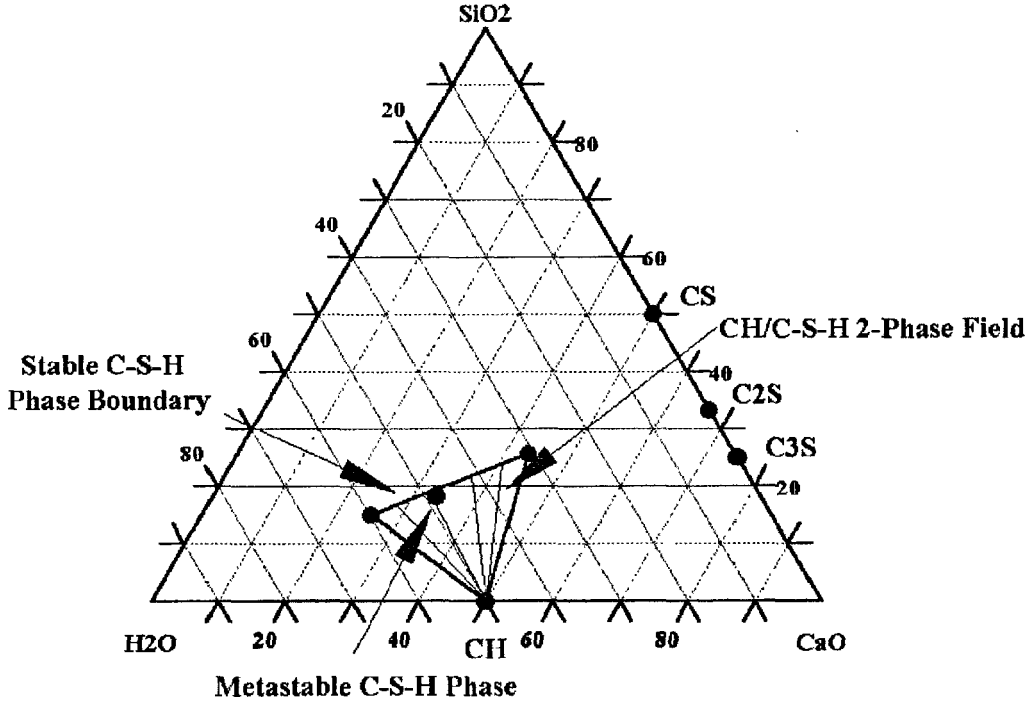

Figure 1: Ternary diagram for the $CaO-SiO_2-H_2O$ system showing the placement of the line compounds CS, C_2S, C_3S, and CH; the metastable C-S-H phase; and the stable C-S-H boundary limiting the C-S-H and CH two-phase field.

The first, easiest, and most obvious way to distinguish between these phases is via the stoichiometric reaction equations. Young and Hansen (1987) studied saturated C_3S pastes to arrive at a C-S-H composition of $C_{1.7}SH_4$. This result was compared with a composition of $C_{1.7}SH_{3.35}$ derived from the work of Locher (1966) and Brunauer and Kantro (1964). An additional comparison was made with the work of Jons and Osbaeck (1982), but there was doubt as to whether all of the capillary water had been excluded and this value will not be used in this paper.

Direct experimental data on the composition of C-S-H is more difficult to obtain when the C-S-H and CH are considered separately due to the difficulty in discretizing between the two mixed phases. Three main experimental techniques are used to separate the two phases: quantitative x-ray analysis (QXDA), thermal methods such as thermal gravimetric analysis (TGA), and extraction methods using aqueous media or free lime. In general, extraction methods detect more CH than either thermal methods or QXDA (Taylor, 1990). The lower values of thermal methods and QXDA are generally attributed to adsorbed, amorphous, or interlayer CH (Taylor, 1990), which is the exact value we are trying to quantify. Hence, we concentrated on values gathered from extraction methods. Only the work of Odler and Dorr (1979a) used an extraction method following D-drying, resulting in a composition of $C_{1.6}SH_{1.32}$. Their work cited many authors who found typical compositions of $C_{1.7}SH_{1.3\text{-}1.5}$ using D-drying techniques. It is important to note that not all of the cited results differentiated between C-S-H and CH in the hydration product; these results were included in our analysis because of their consistency with the results of Odler and Dorr (1979a). We take a final composition value of $C_{1.7}SH_{2.1}$ for C_3S equilibrated at 11% relative humidity from the work of Young and Hansen (1987).

Examining all of the data, a general consensus for a C/S ratio of about 1.7 was found, with differing H/S ranging from H/S=4 for saturated pastes to H/S=1.3-1.5 for D-dried pastes. The C-S-H phase boundary limiting the C-S-H and CH two-phase field was then mapped as a straight line of C/S=1.7 between the two H/S limiting values mentioned above. This is obviously an approximation and far more work into the position of this boundary is needed.

Gathering all of the data described above gives a good approximation of a phase diagram for the C-S-H system. Fig 1 shows this ternary diagram with the stable C-S-H and CH field represented by the tie lines, and the metastable C-S-H phase placed as described above. The implications of this phase diagram will be discussed in this next section.

IMPLICATIONS OF THE PROPOSED PHASE DIAGRAM

Early Hydration and Onset of the Induction Period

The early hydration period is marked by a rapid period of ion dissolution and an exothermic reaction (Gartner and Gaidis, 1989). The dissolution and reaction rates suddenly and rapidly decrease followed by a period of very slow reaction, the induction period. Approximately 1-2% of the C_3S is consumed during this time.

As noted above, there is sufficient evidence to state that the slowing of the ion dissolution is due to a surface layer of C-S-H which forms rapidly during this period. This surface layer is almost certainly a metastable phase. Calcium dissolution is subsequently controlled by this surface layer resulting in a nearly constant concentration of calcium during the induction period, as shown by experimental data (Taylor, 1990).

Insight into the physical properties of this layer is vital to understanding the early hydration process. It is probably a very thin layer which is non-uniform in thickness, being thicker around active dissolution sites on the C_3S surface (Fierens and Verhaegen, 1976a). Since its C/S ratio is less than 3, as more C_3S reacts, free calcium ions are generated. These ions then diffuse through the layer and dissolve into solution, accounting for the rise in calcium concentration with time (e.g. Brown et al, 1984). The layer correspondingly thickens as the reaction proceeds toward a metastable three-phase equilibrium state. This is consistent with several studies by X-ray photoelectron spectroscopy (Regourd et al, 1980, Jawed et al, 1980, Jawed and Skalny, 1982) and electron microscopy (Ings et al, 1983), as noted by Gartner and Gaidis (1989).

The phase diagram representing the metastable state, which we believe to be approached during the early hydration and induction periods, is shown in Fig 2. It shows the metastable three-phase triangle between C_3S, aqueous solution, and the metastable C-S-H phase which has a C/S ratio between 1.8 and 2. We believe that this phase diagram is consistent with all of the experimental evidence discussed above.

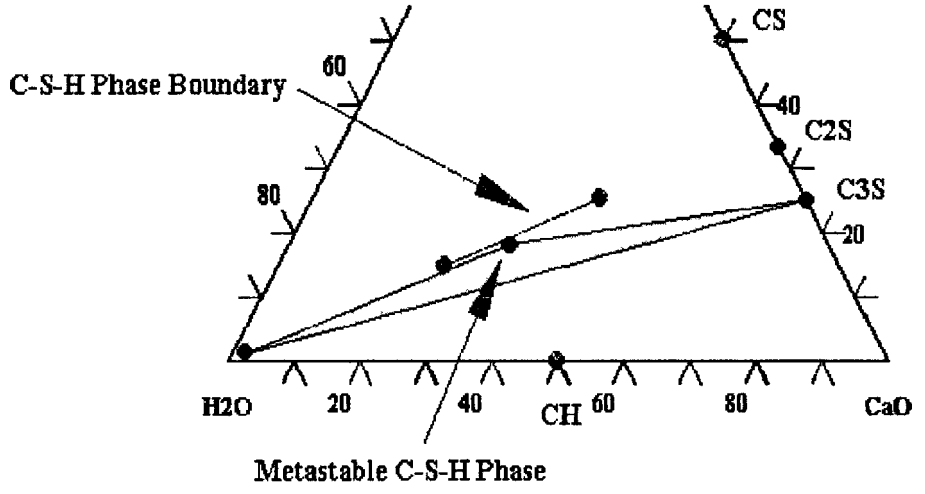

Figure 2: Metastable equilibrium phase diagram for the $CaO\text{-}SiO_2\text{-}H_2O$ system. The triangle indicates the metastable equilibrium between C_3S, solution, and metastable C-S-H.

Induction Period

During the induction period C_3S reacts at a very slow rate. As it reacts, the C-S-H surface layer thickens and the aqueous solution continues to become more calcium rich, eventually becoming

supersaturated with respect to CH (Taylor, 1990). The resulting supersaturation level is still too low, however, for homogeneous CH nucleation.

CH may precipitate at areas of local supersaturation in the solution (Odler and Dorr, 1979a, Odler and Dorr, 1979b, Fierens and Verhaegen, 1976b, Young et al, 1977). The presence of these crystals may not affect the local metastable equilibrium present at the surface of the C_3S, and thus would not affect the overall hydration process. Similarly, seeding the paste with CH crystals, as attempted by Uchikawa (1984), does not appear to influence the local equilibria present at the C_3S/solution interface. Thus, seeding does not accelerate the end of the induction period. Rather, the presence of these CH crystals may have a slight retarding effect, as noted by Uchikawa (1984), as they provide a surface upon which calcium ions in solution may precipitate. In this case, the calcium concentration in the solution drops, requiring more time to reach the supersaturated state necessary to induce the eutectic solidification reaction described below.

End of the Induction Period

As discussed in Section 1 and in Part I, there is still a great deal of debate about the end of the induction period. Each of the four main theories still offers an incomplete explanation for this phenomenon. Since this paper argues that a protective metastable layer is the cause of the induction period, the destruction or disruption of this layer must be explained. Additionally, as discussed in Section 1, the nucleation of both CH and C-S-H have been mentioned as possible triggers for the end of the induction period. We shall now set forth a mechanism which combines these hypotheses and is consistent with the phase diagram presented in Section 2: a eutectic solidification reaction.

Eutectic Solidification Reaction

A eutectic solidification reaction involves the nucleation of two solid phases cooperatively from the liquid according to the following equation:

$$L \rightarrow \alpha + \beta \qquad [1].$$

This phenomenon occurs in many metal systems such as Al-Cu and Al-Fe. Many different morphologies result, which are usually classified into either *normal* or *anomalous* reactions. In this paper we are discussing a normal eutectic solidification reaction; the resulting morphology from this reaction consists of lamellae of alternating phases, as shown in Fig 3a (Porter and Easterling, 1981).

Rapid cooperative growth in these systems is controlled by short range diffusion between neighboring lamellar tips as shown in Fig 3b. Material rejected from the α phase is incorporated into the β phase, and vice versa. The overall growth rate is controlled by the rate at which this diffusion can occur and is thus controlled by the spacing between lamellae, λ (shown in Fig 3b) (Porter and Easterling, 1981). For a spherical colony, λ will be very small initially and will tend to increase as the lamellae grow further away from the particle. Because λ is determined by supersaturation and remains constant, the lamellae often branch to shorten the inter-lamellar spacing.

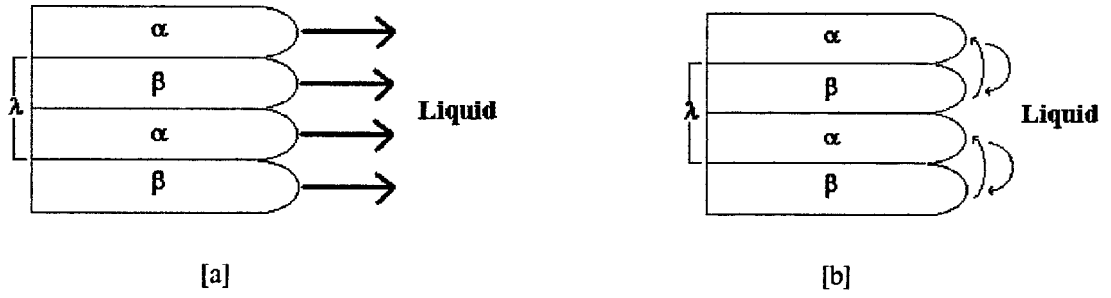

Figure 3: Morphology and mechanism of eutectic solidification reaction. [a] Alternating lamellae of α and β phases. Arrows indicate growth direction into liquid. [b] Diffusion controlled growth between adjacent lamellae. Arrows indicate diffusion of atoms in liquid to form α and β (after Porter and Easterling, 1981).

Extending this reaction to the C/S/H system gives the resulting nucleation equation:

Aqueous Solution → C-S-H + CH [2].

The C-S-H lamellae will contain interspersed micro-crystals of CH. As calcium is rejected from the C-S-H, it will be incorporated into the CH; similarly, as silicon is rejected from the CH, it will be incorporated into the C-S-H. Later, the CH may coarsen into larger particles elsewhere in the microstructure.

This reaction follows naturally from the phase diagram presented in Section 2. Fig 4 depicts the situation which we believe to be present at the end of the induction period. The left hand triangle (1) shows the equilibrium between solution, $C_{1.7}SH_4$, and CH. It represents the local equilibrium governing behavior at the product/solution interface. This triangle describes the ternary eutectic solidification reaction where solution decomposes into $C_{1.7}SH_4$ and CH. The right hand equilibrium triangle (2) between C_3S, $C_{1.7}SH_{1.3}$, and CH describes the slow reaction behavior at the C_3S/product interface.

It is important to note that the original C-S-H layer does not just disappear; rather it is converted from a metastable form of C-S-H with approximate composition $C_{1.85}SH_{2.65}$ to a stable form of the phase with a C/S ratio of approximately 1.7 and water content ranging from H=1.3-4.0. Fig 5 illustrates this change from a step function to a phase with a gradient of water contents. Additionally, the liquid phase moves from a point on the solubility curve for metastable C-S-H (M) (Jennings, 1986) (corresponding to point L on Brown's diagram (Brown, 1989)) to a point on the solubility curve for stable C-S-H (S) (Jennings, 1986) (corresponding to point I on Brown's diagram (Brown, 1989)). The relative positions of the metastable equilibrium triangle and the two stable equilibrium triangles are shown in Fig 6.

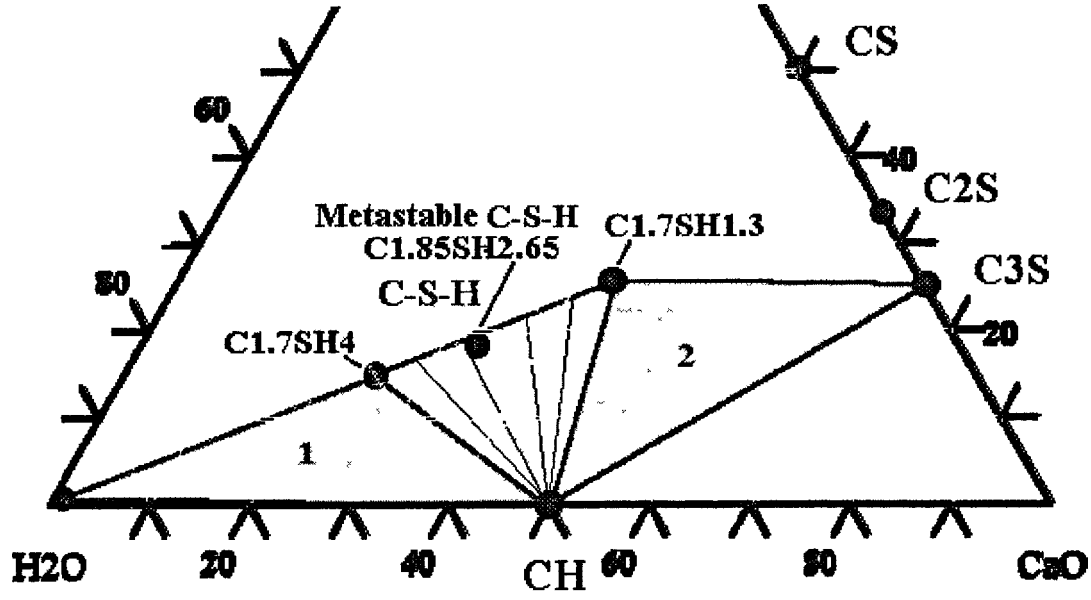

Figure 4: "Equilibrium" phase diagram for the $CaO-SiO_2-H_2O$ system. Equilibrium triangle number 1 is the equilibrium between solution, C-S-H, and CH. Equilibrium triangle number 2 is the equilibrium between C_3S, CH, and C-S-H.

The idea of an alternating layered structure consistent with that produced by the eutectic solidification reaction has been proposed by Williamson (1968). 'From both the morphology and the chemistry it is apparent that the calcium silicate hydrate can be thought of as a form of two phase material similar to a eutectic or eutectoid.' He proposed a *constitutional supersaturation* process to account for the resulting layer morphology in which the heat of hydration depresses the equilibrium concentration of calcium at the growth interface. A supersaturated state occurs at that point, which then leads to the growth of protuberances he called "sheafs of wheat". This idea, although different from what is proposed, supports the importance of supersaturated states in the hydration of C_3S.

Kantro et al (1962) have also proposed an alternating layer structure as the final result of the hydration process. However, they considered the CH to be a part of the C-S-H and not a separate phase.

Experimental Evidence

There is considerable experimental evidence to support the idea of a eutectic solidification reaction. First and foremost is the presence of microcrystalline CH in C-S-H pastes as noted by Groves. He found such crystalsin pastes of very low water/cement (w/c) ratio (Groves, 1981) and, more recently, pozzolonic cement pastes (Groves and Richardson, 1994) using transmission electron microscopy (TEM). The typical morphology of these crystals is a cluster of lamellae approximately 10 nm thick. The crystals also appear to align themselves locally, though the degree of alignment varies widely. Both studies imply the intimate mixing of CH and C-S-H on the nanometer level; this mixing would be the logical result of a eutectic solidification reaction.

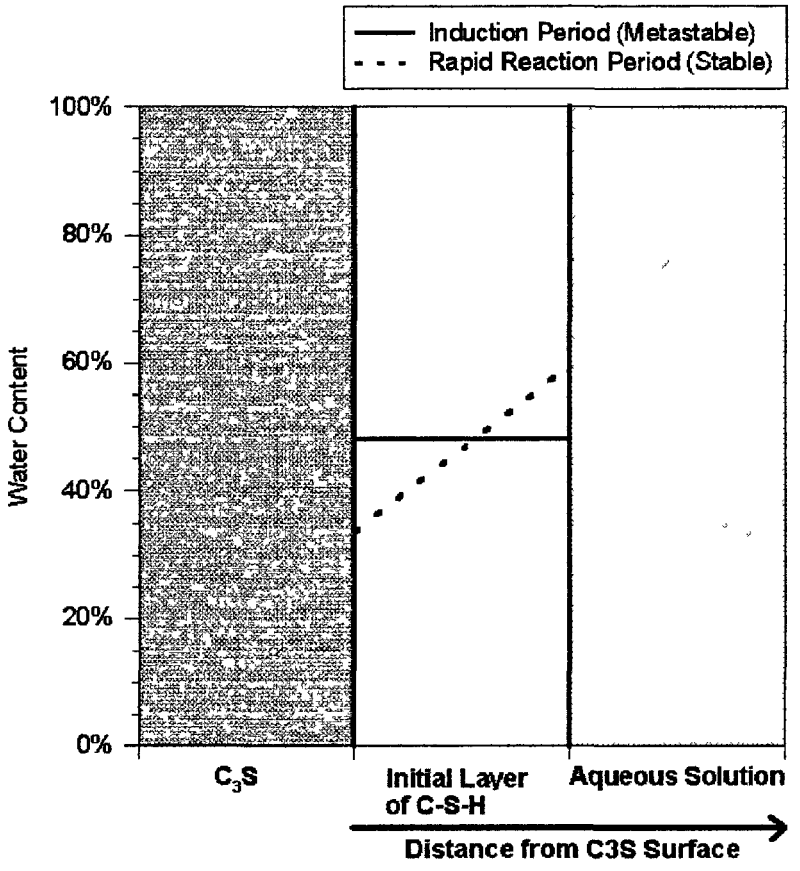

Figure 5: Transition from metastable C-S-H phase of constant water content to stable C-S-H with a gradient of water contents. The solid line represents the water content of the initial metastable C-S-H phase ($C_{1.85}SH_{2.65}$) The dotted line represents the gradient of water contents present in the C-S-H produced by the two equilibrium reactions $C_{1.7}SH_{1.3}$ at the C_3S/C-S-H interface, and $C_{1.7}SH_4$ at the C-S-H/aqueous solution interface.

However, no microcrystalline CH has been found in pastes of normal w/c ratios. This absence of CH may be the result of a leaching process from the inner to the outer C-S-H hydration product. No CH was observed under TEM examination in the inner product in a 26 year old C_3S paste of w/c=.45 (Groves, 1987). The outer product, on the other hand, has a very wide range of morphologies with substantial water-filled empty space. Outer C-S-H is probably the result of the left hand equilibrium triangle in Fig 4 along with CH crystals, and could explain the lack of microcrystalline CH in normal w/c ratio pastes As large crystals form, a coarsening process may occur, with smaller CH crystals dissolving and growing upon the larger CH crystals. Since the smallest CH crystals will be those which form in the dense inner product, these should be the first to be consumed by this coarsening process.

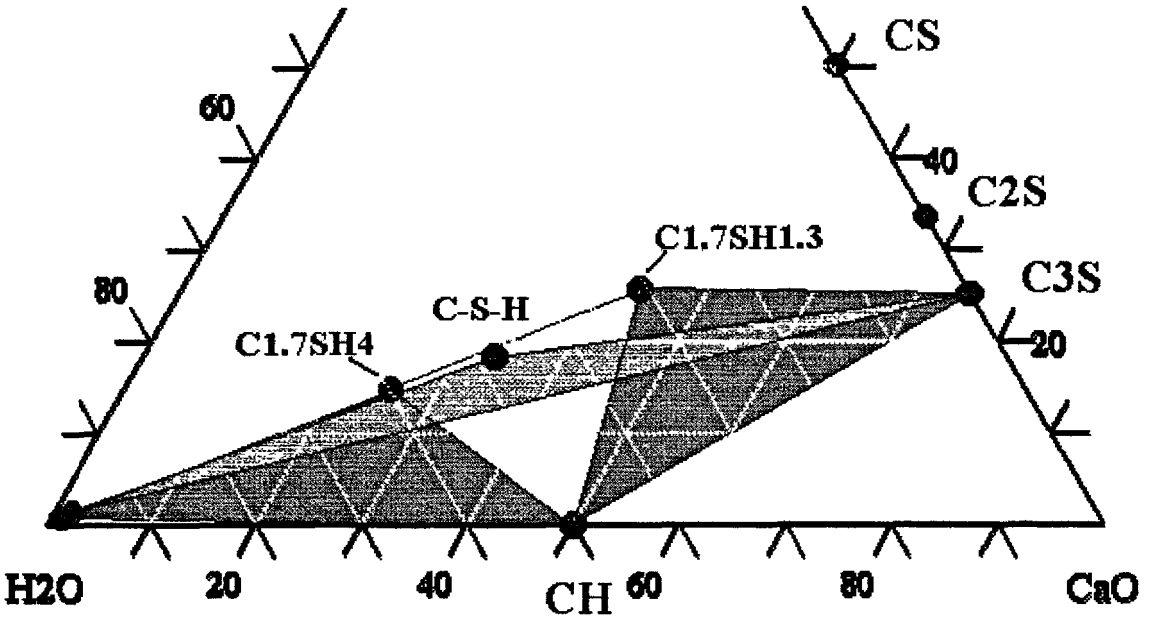

Figure 6: Phase diagram for the $CaO-SiO_2-H_2O$ system. Both stable and metastable equilibrium triangles are shown.

Groves (1987) has noted in the 26 year old C_3S paste mentioned above that there are large CH crystals which possess protuberances growing into the open space of the outer product C-S-H. These protuberances could easily be the result of a coarsening process. The crystals also appear to be very well bonded to the outer product C-S-H. Additionally, Groves notes the presence of plate-like CH crystal of only a few tens of nm in thickness. These smaller crystals suggest that very small CH specimens may have been present at some time in the past.

The C/S ratios for the inner and outer product of the 26 year old paste and a 2 year old C_3S paste support this hypothesis. The C/S values for the outer gel ranged from 1.25-2.07, with a mean of 1.72; the inner gel ranged from C/S=1.27 to C/S=1.78, with a mean of 1.66. Since these values do not discriminate between C-S-H and CH in the paste, it is likely that this higher C/S ratio can be attributed in part to the leaching effect described above. This mechanism would be independent of other proposed mechanisms for C/S ratio discrepancies, such as different silicate polymerization states (Taylor, 1990).

This leaching process is also consistent with the results of Stade and Wieker (1980) who found that CH could be leached from C-S-H with C/S ratios > 1.25. However, below this limit little or no CH could be extracted. Additionally, all of the leached pastes had a C/S ratio of 1.25 following the extraction process; this value may represent the lower extension of the C-S-H phase

boundary. However, since the C-S-H caused by the hydration of C_3S typically has a C/S ratio of approximately 1.7, it would be expected that CH could be extracted from this phase.

It is possible that this coarsening effect was also occurring in the very low w/c ratio pastes mentioned above in which microcrystalline CH was present. However, the very low amount of aqueous phase may have inhibited the diffusion of the smaller CH crystals to the large CH crystals.

This leaching effect could also partially explain why the inner product never fully densifies. As stated by Powers (1961) and noted by Groves (1987), there is no obvious explanation for silicon diffusing to the outer product area before reacting; rather, it should react in the inner product area to form a fully dense phase. Powers hypothesized that the pore spaces left in the inner product eventually become too small for further nucleation of hydrate and remain unfilled. A second mechanism could be the leaching effect described above, which would leave nanometer scale pores as the microcrystalline CH plates dissolve.

A final compelling piece of evidence is the proximity on the phase diagram of the metastable phase and phase boundary to phases which are believed to exist in cement-based systems. Using compositions from Taylor (1990), tobermorite and jennite were plotted on the phase diagram in several different forms: equilibrium composition (jennite and 1.4 nm tobermorite), de-hydrated composition (metajennite and 1.1 nm tobermorite), and an early form in which only dimeric polymerization of the silicon ions has occurred. Fig 7 shows the locations of these phases. Note that jennite with dimeric polymerization falls extremely close to the proposed metastable phase, while the other phases fall above the C-S-H phase boundary. This suggests that our proposed metastable phase may be a form of unpolymerized jennite. As the reaction proceeds, polymerization occurs and provides the driving force necessary to drive the system towards the stable C-S-H phase boundary. When this boundary is crossed, precipitation of C-S-H and CH occurs through the two stable equilibrium triangles indicated by the phase diagram.

Deceleratory Period and Final Slow Reaction

As the main reaction proceeds, it eventually reaches a point where the reaction rate is very slow. This is known as the deceleratory period, and it is not very well understood, as noted by Gartner and Gaidis (1989). They describe three main hypotheses for the slowed reaction rate: (1) the dissolution of C_3S becomes rate limiting; (2) the diffusion of reactants through the hydration products becomes rate limiting; or (3) the deposition of hydrates is prevented by a lack of free space. Gartner and Gaidis (1989) state that the most probable limiting step is the diffusion of the silicate ion through the reaction product layer. The conclusion of Gartner and Gaidis (1989) is also consistent with a eutectic solidification reaction.

EXTENSIONS TO β-C_2S

The hydration of β-C_2S is very similar to the hydration of C_3S in terms of its products and mechanisms except that it reacts much slower and there is much less CH (Taylor, 1990). A possible phase diagram for this system is shown in Fig 8. This phase diagram is consistent with both a slower reaction rate and less CH production. Again, CH seeding cannot be used to

supplement dissolution because only the chemistry present within the metastable C-S-H layer is important.

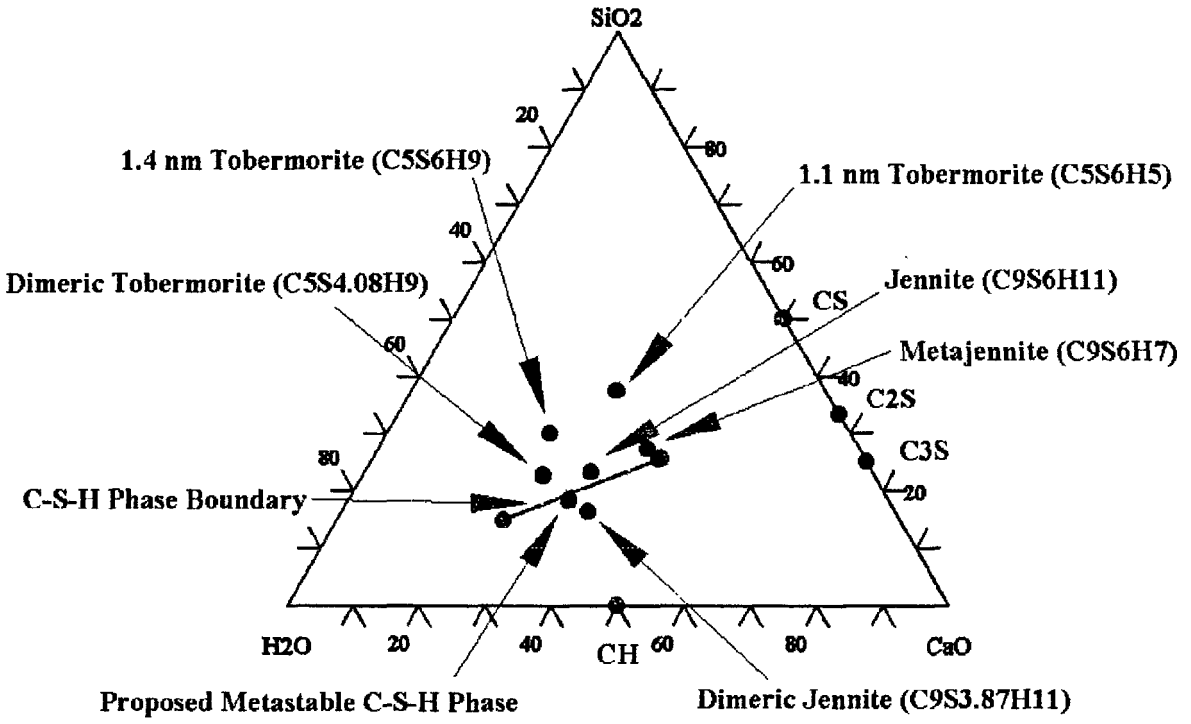

Figure 7: Proximity of various phases of jennite and tobermorite to proposed metastable C-S-H phase and C-S-H phase boundary.

The slower reaction rate could be the result of less calcium going into solution. Since the C/S ratio of C_2S is much closer to that of the proposed metastable C-S-H phase than is C_3S, there should be considerably less calcium going into solution because most of it is consumed in thickening the metastable layer. This thickening has been observed indirectly by electron spectroscopy for chemical analysis (ESCA) (M`en`etrier et al, 1980). As less calcium goes into solution, more time is required to reach the calcium supersaturation level necessary for the eutectic solidification reaction to begin.

A lower amount of CH produced is also predicted by the phase diagram. The lever rule for ternary alloys predicts that approximately twice as much CH should be produced in the hydration of C_3S than in C_2S. This is consistent with the accepted stoichiometric equations which predict three times as much CH production in the hydration of C_3S than in C_2S (Mindess and Young, 1981). The differences are probably due to the crudeness of the proposed phase diagram and the assumptions made in developing the stoichiometric equations.

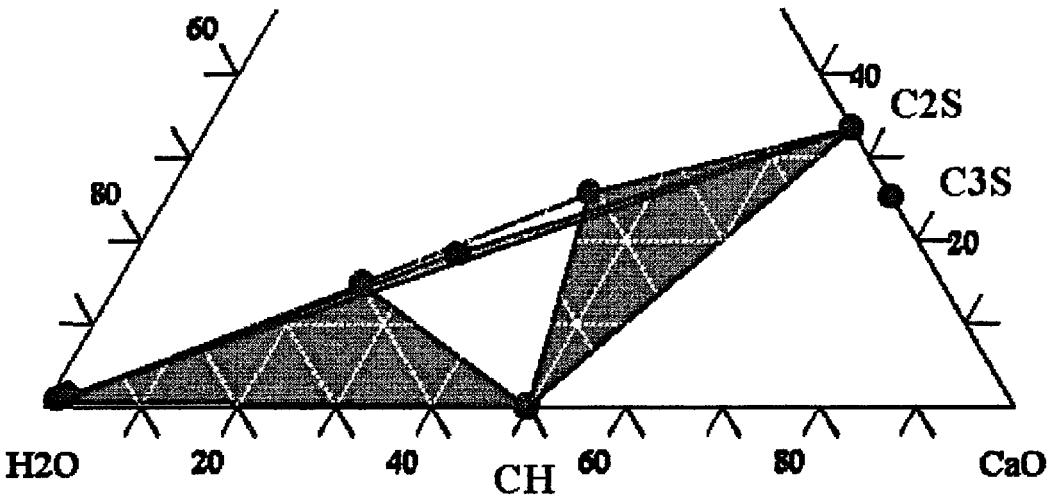

Figure 8: Phase diagram for the $CaO-SiO_2-H_2O$ system. The large left-hand triangle indicates the stable equilibrium between C-S-H, CH, and aqueous solution. The large right-hand triangle indicates the stable equilibrium between C_2S, CH, and C-S-H. The long skinny triangle indicates the metastable equilibrium between solution, C_2S, and metastable C-S-H.

Note that the phase diagram gives no insight as to why certain C_2S phases hydrate while others are inactive in water. This does not invalidate the proposed phase diagram since they may be the result of mechanisms which cannot be represented on a phase diagram. However, further study into the reasons why these phases do not hydrate is needed.

SUMMARY

A new phase diagram for the CaO (C)-SiO_2 (S)-H_2O (H) system is presented and discussed in terms of a very early reaction and later reaction. This phase diagram provides new insight into understanding the hydration of cementitious systems. The phase diagram is consistent with a rapid forming, semi-permeable C-S-H layer as the cause of the induction period. This phase has a C/S ratio of 1.8-2.0 and is almost certainly metastable.

A mechanism for the end of the induction period is proposed: a eutectic solidification reaction. This reaction occurs most commonly in metals and results in two lamellar phases growing cooperatively. It is proposed that the hydration of cement occurs via this reaction when the concentration of calcium achieves a sufficient level of local supersaturation to induce CH and C-S-H nucleation. As these phases are dependent upon the thermodynamic equilibria near the interface of C_3S and water, this reaction would explain the early presence of CH crystals in the bulk solution and why CH seeding does not accelerate hydration. This reaction results in an

equilibrium between $C_{1.7}SH_{4.0}$, CH, and solution at the product/solution interface and an equilibrium between $C_{1.7}SH_{1.3}$, CH, and C_3S at the product/C_3S interface.

ACKNOWLEDGMENTS

The authors wish to thank both the Department of Energy (award # DE-FG02-91ER45460/A01) and the National Science Foundation Center for Advanced Cement-Based Materials. CMN wishes to thank the Department of Defense for financial support through a National Defense Science and Engineering Graduate Fellowship. MCG wishes to thank the National Science Foundation for financial support through a graduate fellowship.

REFERENCES

Brown, P.W., Franz, E., Frohnsdorff, G., and Taylor, H.F.W., "Analyses of the Aqueous Phase During Early C_3S Hydration", Cem. Conc. Res., Vol. 14, No. 1, 1984, pp. 257-262.

Brown, P.W. (Skalny, J.P. (Ed)), "Phase Equilibria and Cement Hydration" , Materials Science of Concrete, American Ceramic Society, Westerville, OH, 1989, pp. 73-93.

Brunauer, S., and Kantro, D.L. (Taylor, H.F.W. (Ed)), The Chemistry of Cements, Academic Press, London, 1964, pp. 287-309.

Fierens, P. and Verhaegen, J.P., "Induction Period of Hydration of Tricalcium Silicate" Cem. Conc. Res., Vol. 6, No. 2, 1976a, pp. 287-292.

Fierens, P., and Verhaegen, J.P., "Hydration of Tricalcium Silicate in Paste: Kinetics of Calcium Ion Dissolution in the Aqueous Phase", Cem. Concr. Res., Vol. 6, No. 3, 1976b, pp. 337-342.

Gartner, E.M., and Gaidis, J.M. (Skalny, J.P. (Ed)), "Hydration Mechanisms I", Materials Science of Concrete, American Ceramic Society, Westerville, OH, 1989, pp. 95-125.

Groves, G.W., "Microcrystalline Calcium Hydroxide in Portland Cement Pastes of Low Water/Cement Ratio", Cem. Conc. Res., Vol. 11, 1981, pp. 713-718.

Groves, G.W., "TEM Studies of Cement Hydration", MRS Symp. Proc., Vol. 85, 1987, pp. 3-12.

Groves, G.W., and Richardson, I.G., "Microcrystalline Calcium Hydroxide in Pozzolanic Cement Pastes", Cem. Conc. Res., Vol. 24, No. 6, 1994, pp. 1191-1196.

Ings, J.B., Brown, P.W., and Frohnsdorff, G., "Early Hydration of Large Single Crystals of Tricalcium Silicate", Cem. Conc. Res., Vol. 13, No. 6, 1983, 843-848.

Jawed, I., M'en'etrier, D., and Skalny, J., "Early Hydration of Calcium Silicates: Surface Phenomenon", Proc. of 7th Intl. Cong. on the Chem. Cem., Vol. 2, Paris, 1980, pp. II/182-II/187.

Jawed, I., and Skalny, J., "Surface Phenomena During Tricalcium Silicate Hydration", J. Colloid Interface Sci., Vol. 85, No. 1, 1982, pp. 235-243.

Jennings, H.M., "Aqueous Solubility Relationships for Two Types of Calcium Silicate Hydrate", J. Amer. Cer. Soc., Vol. 69, No. 8, 1986, pp. 614-618.

Jons, E.S., and Osbaeck, B., "The Effect of Cement Composition on Strength Described by a Strength-Porosity Model", Cem. Conc. Res., Vol. 12, No. 2, 1982, pp. 167-178.

Kantro, D.L., Brunauer, S., and Weise, C.H., "Development of Surface in the Hydration of Calcium Silicates. II. Extension of Investigations to Earlier and Later Stages of Hydration", J. Phys. Chem., Vol. 66, 1962, pp. 1804-1809.

Locher, F.W., "Stoichiometry of Tricalcium Silicate Hydration", Symp. on Struct. of Portland Cement Paste and Concrete, Special Report 90, Highway Research Board, Washington, D.C., 1966, pp. 309-327.

M`en`etrier, D., Jawed, I., Sun, T.S., and Skalny, J., "Surface Studies of Hydrated β-C_2S", Cem. Conc. Res., Vol. 10, No. 3, 1980, pp. 425.
Mindess, S., and Young, J.F., Cement Chemistry, Prentice-Hall, Englewood Cliffs, NJ, 1981, pg. 77.
Odler, I., and Dorr, H., "Early Hydration of Tricalcium Silicate. I. Kinetics of the Hydration Process and the Stoichiometry of the Hydration Products", Cem. Conc. Res., Vol. 9, No. 2, 1979a, pp. 239-248.
Odler, I., and Dorr, H., "Early Hydration of Tricalcium Silicate. II. The Induction Period", Cem. Conc. Res., Vol. 9, No. 3, 1979b, pp. 277-284.
Porter, D.A., and Easterling, K.E., Phase Transformations in Metals and Alloys, Chapman and Hall, London, 1981, pg. 222.
Powers, T.C., J. PCA Res. Dev. Lab., Vol. 3, 47 (1961).
Regourd, M., Thomassin, J. H., Baillif, P., and Touray, J.C., "Study of the Early Hydration of Ca_3SiO_5 by X-ray Photoelectron Spectroscopy", Cem. Conc. Res., Vol. 10, No. 2, 1980, pp. 223-230.
Stade, H., and Wieker, W., "On the Structure of Ill-crystallized Calcium Hydrogen Silicates. I. Formation and Properties of an Ill-crystallized Calcium Hydrogen Disilicate Phase", Z. Anorg. Allg. Chem., Vol. 466, 1980, pp. 55-70.
Taylor, H.F.W., Barret, P., Brown, P.W., Double, D.D., Frohnsdorff, G., Johansen, V., M`en`etrier-Sorrentino, D., Odler, I., Parrott, L.J., Pommersheim, J.M., Regourd, M., and Young, J.F., "The Hydration of Tricalcium Silicate", Mater. Struct., Vol. 17, 1984, pp. 457-468.
Taylor, H.F.W., Cement Chemistry, Academic Press, London, 1990.
Uchikawa, H., "The Role of Free Lime in Early Hydration of Alite-Retarder or Accelerator", Am. Ceram. Soc. Bull., Vol. 63, No. 9, 1984, pp. 1143-1146.
Williamson, R.B., "Constitutional Supersaturation in Portland Cement Solidified by Hydration", J. Crystal Growth, Vol. 3, No. 4, 1968, pp. 787-794.
Young, J.F.,Tong, H.S., and Berger, R.L., "Compositions of Solutions in Contact with Hydrating Tricalcium Silicate Pastes", J. Am. Cer. Soc., Vol. 60, No. 5-6, 1977, pp. 193-198.
Young, J.F., and Hansen, W., "Volume Relationships for C-S-H Formation Based on Hydration Stoichiometries", MRS Symp. Proc., Vol. 85, 1987, pp. 313-322.

2ii059
8 pp

Kn o. 25. JAN. 2001 d o k 31823

THERMODYNAMIC AQUEOUS SOLUBILITY DIAGRAM FOR THE BINARY SOLID-SOLUTION SYSTEM C-S-H - H_2O

Michael KERSTEN, IOW Geology Section, Seestr. 15, D-18119 Rostock, Germany
(e-mail: kersten@io-warnemuende.de)

ABSTRACT A thermodynamic solid solution - aqueous solution model for a binary non-ideal mixing of the end-members portlandite and Ca-silicate, with known pK's and a miscibility gap at C/S > 3, predicts a maximum in Gibbs free-energy of mixing (ΔG^M) of -3.2 kJ/mol to occur at a C/S ratio of 1.6. Predicted Ca and Si solubilities and pH values agree with experimental data reported from the literature. It is also possible to predict the solubility of trace metals bound into the C-S-H host phase which will be exemplified for the case of Zn.

Key-words: CSH, Calcium hydroxide, Solid solution, Thermodynamics

INTRODUCTION

C-S-H gel dissolves incongruently in pure water, with aqueous Ca concentrations being much higher than those of Si. The extent of the incongruent dissolution behaviour is gradually increasing with the C/S ratio of the solid phase. In spite of this complex dissolution behavior, a close inspection of the data published over a period of 50 years revealed that the concentration of Ca and Si in the aqueous phase must be guided by a yet not well understood thermodynamic equilibrium (Jennings, 1986). A common approach to fit the relationship between the Ca vs. Si solubility curve and the C/S ratio of the C-S-H solids is based on the assumption of variable solubility products of the main components portlandite and calcium silicate as a function of the particular C/S ratio. This empirical approach enables to describe experimental data on equilibria in the C-S-H - H_2O system and speciation modeling involving ion association (using MINEQL: Berner, 1988, and Bennet et al., 1992) or ion interaction models (using Pitzer equations: Reardon, 1990). However, this approach has three major drawbacks: (i) it is not justified by thermodynamic principles, (ii) it does not incorporate any structural information such as the non-ideal mixing behavior due to mixing gaps known for the C-S-H solid solution system, and (iii) it is not possible to extend this approach to multi-component systems in a predictive sense, if the composite solubility product vs. composition relationships have previously not been measured for that systems. I will therefore introduce a new approach ("inverse modeling") based on both thermodynamic principles and structural information for the C-S-H gel, to derive a thermodynamic equilibrium relationship between the composition of the solid solution and the respective aqueous phase composition.

THE NEW THERMODYNAMIC MODEL

The C-S-H phase is essentially a solid solution of portlandite in an imaginary low-C/S-ratio calcium silicate component (Richardson and Groves, 1993). This widely accepted compositional model is based on a highly disordered layer structure comprising finite dreierketten silicate chains of length *3n-1* in solid-solution with a variable amount of $Ca(OH)_2$, where for individual structural units n = 1, 2, 3, etc. The simplest possible silicate endmember composition with integer stoichiometry (C/S = 1) can be formulated as $Ca_2H_2Si_2O_7 \cdot 3H_2O$. This endmember (abbreviated as CS) is assumed to be congruently soluble with a unique solubility product

given by Berner (1988) or Bennet et al. (1992). For the formulation of a solid-solution aqueous-solution (SSAS) equilibrium model, first the solubility products of the end-members assumed to compose the solid solution have to be determined by the mass action laws:

$$Ca_2H_2Si_2O_7 \cdot 3H_2O = \{H_3SiO_4^-\}^2\{CaOH^+\}^2 = K_{CS}^2 \quad [1]$$

$$Ca(OH)_2 = \{CaOH^+\}\{OH^-\} = K_{CH} \quad [2]$$

The solubility products have been recalculated with activities of the monovalent Ca-species $CaOH^+$ as a common cation to give values of $pK_{CH} = 4.0$ and $pK_{CS} = 7.8$, using the thermodynamic database listed in Table 1.

Table 1 The thermodynamic database: Formation constants of the aqueous species

aqueous species	formation reaction	logK
OH^-	$H_2O - H^+$	- 14.00
$H_3SiO_4^-$	$H_4SiO_4 - H^+$	- 9.86
$H_2SiO_4^{2-}$	$H_4SiO_4 - 2H^+$	- 22.91
$CaOH^+$	$Ca^{2+} + H_2O - H^+$	- 12.78

The thermodynamic equilibrium in this binary system is described by the equivalence of the chemical potentials of the solid and aqueous phase components:

$$\{H_3SiO_4^-\}\{CaOH^+\} = K_{CS}(1-X_{CH})\lambda_{CS} \quad [3]$$

and

$$\{CaOH^+\}\{OH^-\} = K_{CH}X_{CH}\lambda_{CH} \quad [4]$$

The solid phase activities are given as the product of their respective mole fraction, X, and solid activity coefficient, λ (not to mix up with the aqueous activity coefficient γ). Dividing Eq 3 by Eq 4 and removing the common cation yields the well-known Berthelot-Nernst distribution law:

$$X_{CH}/1\text{-}X_{CH} = D\{OH^-\}/\{H_3SiO_4^-\} \quad [5]$$

where D, the distribution coefficient, is given by:

$$D = K_{CS}\lambda_{CS}/K_{CH}\lambda_{CH} \quad [6]$$

Eq 5 is the classical expression of a SSAS system at thermodynamic equilibrium. Another expression for the SSAS equilibrium is obtained by simply adding Eqs 3 and 4 to give:

$$\Sigma\Pi_{eq} = (\{H_3SiO_4^-\}+\{OH^-\})\{CaOH^+\} = (a_{CH}K_{CH}) + (a_{CS}K_{CS}) \quad [7]$$

where the left term is the "total solubility product" variable $\Sigma\Pi$, which is fixed by the right term to the total solubility product constant $\Sigma\Pi_{eq}$ at thermodynamic equilibrium (Lippmann, 1980; Glynn and Reardon, 1990). The latter is dependent on the composition of the solid solution, while the variable $\Sigma\Pi$ does not depend on the solid phase composition. The $\Sigma\Pi_{eq}$ constant can be calculated (using Eq 7), if the individual activities of the components in the solid

phase (a_{CH} and a_{CS}) are known at thermodynamic equilibrium. Alternatively, $\Sigma\Pi_{eq}$ can be calculated if the activity fractions of the substituting ions in the aqueous phase are known. The activity fractions are defined as:

$$\chi_{OH^-} = \{OH^-\}/(\{H_3SiO_4^-\}+\{OH^-\}) \quad [8]$$

$$\chi_{H_3SiO_4^-} = \{H_3SiO_4^-\}/(\{H_3SiO_4^-\}+\{OH^-\}) \quad [9]$$

Substituting these two relations into Eq 7 and rearranging by expressing the activities of the solid phase components in terms of their activity coefficients and mole fractions yields:

$$\Sigma\Pi_{eq} = \frac{1}{\frac{\chi_{OH^-}}{K_{CH}\lambda_{CH}} + \frac{\chi_{H_3SiO_4^-}}{K_{CS}\lambda_{CS}}} \quad [10]$$

$\Sigma\Pi$ - X - χ phase diagrams can now be constructed from total solubility product expressions (Eqs 7 and 10) together with the appropriate mole and activity fractions as co-ordinates (Lippmann, 1980; Glynn and Reardon, 1990). Analogous to phase diagrams for binary solid - melt systems, a SSAS phase diagram is a plot of a "solidus curve" (the total solubility product defined by Eq 7) and a "solutus curve" (Eq 10), with the $\Sigma\Pi$ variable as the ordinate. Both the solidus and solutus curves form a characteristic loop common in phase diagrams involving (complete) solubility of two phases. The loop becomes wider when the difference in the solubility products of the end members increases. Horizontal tie-lines ("conodes") can be drawn between the solutus and solidus curves, thereby giving the solid-phase and aqueous-phase compositions for the series of possible thermodynamic equilibrium states.

The SSAS diagram differ from traditional phase diagram representations in that it uses aqueous activity products and activity fractions rather than elemental concentrations and mole fractions to define the composition of all phases in the system. For the present case, two different scales are used for the abscissa: an activity-fraction scale χ_{OH^-} relating to the aqueous-phase composition, and a mole-fraction scale X_{CH} defining the solid-phase composition. The benefit of the activity-fraction scale is that there is no necessity to consider the extent of ion pairing and/or complexation with other ions in the aqueous solution. The speciation effect is important in the alkaline solutions of cementitious systems, where ion pairs that form complete or nearly-complete solid-solution series may not have similar complexing affinities. As a consequence, a speciation model of ion complexation in the aqueous solution will be required for the construction of the diagrams from experimental total Si and Ca concentration data.

The solidus and solutus curves can be plotted and used to predict the solubility of any ideal solid-solution at thermodynamic equilibrium (i.e., at $a_i = X_i$). The description of the thermodynamic properties of a non-ideal solid-solution, and consequently of the solid-phase activity coefficients vs. solid composition relations, requires knowledge of the excess-free-energy of mixing of the solid solution, that is of the deviation of its free-energy of mixing from that of an ideal solid solution:

$$\Delta G^E = \Delta G^M + \Delta G^{M,id} \quad [11]$$

The Gibbs free-energy of mixing ΔG^M of a solid-solution can be considered to be the difference between the actual free-energy of the solid-solution and that of a compositionally-equivalent mechanical mixture of the endmember components. For an ideal binary solid-solution, the free-energy of mixing for endmember components *i* and *j* will be:

$$\Delta G^{M,id} = RT\ (X_i \ln X_i + X_j \ln X_j) \qquad [12]$$

No experimental data exist, however, on ΔG^M functions of the C-S-H composition, and therefore on solid-phase activity coefficients for that system. Empirical relationships for the compositional dependence of the solid-phase activity coefficients obtained from a Gibbs-Duhem integration, using the Guggenheim subregular model for the excess-free-energy of mixing of a binary solid solution, has been successfully used to fit laboratory solubility data for a variety of SSAS systems (Glynn, 1991):

$$\Delta G^E = RT\ (X_i \ln\lambda_i + X_j \ln\lambda_j) = X_i X_j RT\ [\alpha_0 + \alpha_1(X_i - X_j)] \qquad [13]$$

with the dimensionless empirical parameters α_0 and α_1, from which the following expressions for the solid activity coefficients in the C-S-H system can be derived:

$$\ln\lambda_{CS} = X_{CH}^2\ [\alpha_0 - \alpha_1(3X_{CS} - X_{CH})] = X_{CH}^2\ [\alpha_0 - \alpha_1(3 - 4X_{CH})] \qquad [14]$$

and

$$\ln\lambda_{CH} = X_{CS}^2\ [\alpha_0 + \alpha_1(3X_{CH} - X_{CS})] = X_{CS}^2\ [\alpha_0 + \alpha_1(4X_{CH} - 1)] \qquad [15]$$

Structural information of the C-S-H solid-solution behavior can be used to estimate the α_0 and α_1 parameters which is a better approximation than the commonly used assumption of an ideal solid solution (i.e., $\Delta G^M = 0$). Complete solid-solution series in the C-S-H system are not known; i.e., this system deviates from ideality, because the solubility of the two end-members is limited in the lime-rich part and the partial solid-solution series is not isomorphous. Although initial dissolution of C_3S may be congruent, the hydrated solid has always a C/S ratio less than 3, and no C-S-H can be synthesized beyond a C/S > 3 (i.e., $X_{CH} > 0.67$). This miscibility gap information can be exploited to calculate the Guggenheim α_0 and α_1 parameters using the MBSSAS computer program (Glynn, 1991). However, no information on the solubility of the silicate endmember in $Ca(OH)_2$ is available. It may be assumed to be negligible as a first approximation, because the portlandite lattice has no structural units where the silicate chains could fit in. The upper boundary was arbitrarily set to $X_{CH} = 0.95$, because the MBSSAS program becomes unstable at higher values. With this miscibility gap information for the C-S-H solid-solution system, a value of -2.3 for the α_0 and 3.4 for the α_1 coefficient at 25 °C can be obtained. Fig 1 shows the resulting SSAS equilibrium phase diagram.

DISCUSSION

Verification of the model can be done using experimental data published in the literature upon the necessary recalculations. As mentioned above, an aqueous speciation and activity coefficient model is required in order to determine aqueous phase compositions from the ion activity scale of the solutus (Eq 8) at a given solid composition (and, *vice versa*, solid-solution composition at a given aqueous phase composition for verification with experimental data). Experimental data published by Fujii and Kondo (1981) and Greenberg and Chang (1965) were

selected, because the authors used C-S-H precipitates for their solubility evaluations, obtained by stirring hydrated silica and calcium hydroxide in a suspended state for several weeks. The final aqueous equilibrium at 25-30 °C was determined under absence of any unreacted calcium silicates such as C_3S. The published total concentrations of the components were transferred to the respective species activities with the thermodynamic database listed in Table 1, and the reported pH and ionic strength data. Ion activity coefficients were calculated using the Davies equation by help of the speciation program MICROQL provided by Westall (1986).

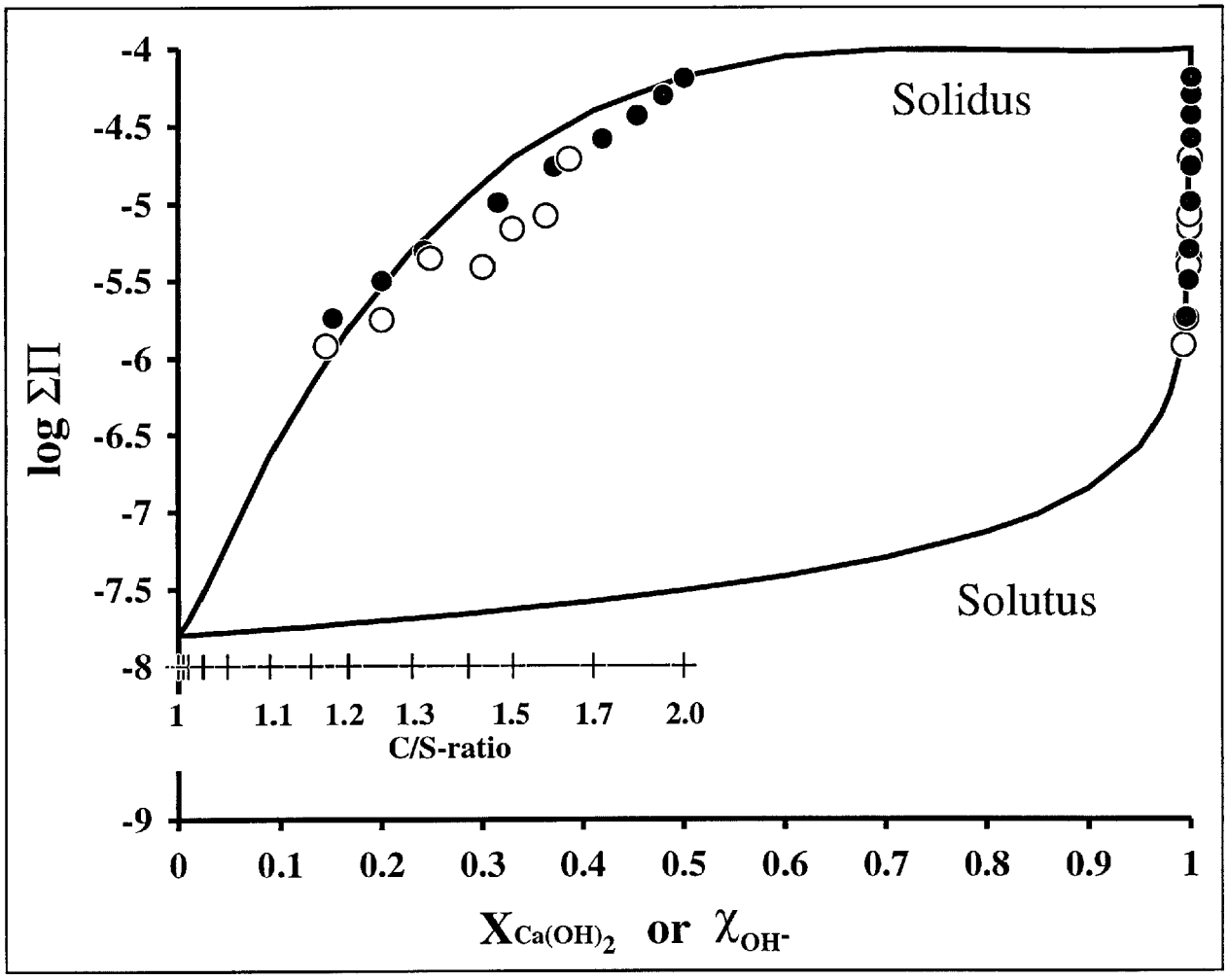

Figure 1. SSAS diagram for the pseudo-binary C-S-H - H_2O system. $\Sigma\Pi$ values for the solid and the aqueous phase are plotted on the ordinate against two superimposed scales on the abscissa: $X_{Ca(OH)_2}$ refers to the concentration of Ca in the solid (upper "solidus" curve calculated from Eq 7), and χ_{OH^-} refers to the activity of hydroxyl-ions in the aqueous solution (lower "solutus" curve calculated from Eq 10). The asymmetric, non-ideal mixing behavior is represented by a mixing gap at C/S > 3 ($X_{Ca(OH)_2} > 0.67$). The dots represent experimental data on aqueous suspensions of C-S-H components with varying C/S ratios for verification of this model (filled dots from Fujii and Kondo, 1981; open dots from Greenberg and Chang, 1965).

Both the solidus and solutus curves in the SSAS diagram constructed by the inverse modeling exercise are perfectly matched by the experimental data. Data pairs on solid and solution composition lie on the solidus and solutus curves, respectively, and can in fact be bound with a horizontal tie-line (not indicated in Fig 1). This verifies also the basic assumption of thermodynamic equilibrium for the selected experimental data. The C-S-H gel is a solid-solution system, capable of adjusting its composition in response to the aqueous solution composition within relatively short time. This is not surprising given the high reactivity of this amorphous solid with a very high specific surface (values of >100 m^2/g are common). Kinetic conditions that cause solid-solutions to react as metastable one-component solids of fixed composition as used in the stoichiometric or primary saturation concepts seem not to play a significant role.

The SSAS model is useful to explain some unique features of the C-S-H - H_2O system which have not yet been understood. In cement pastes, except in the very early stages of reaction, the average C/S ratio of the gel is constant at 1.5 - 1.7 (Taylor, 1992). The model predicts a minimum in the Gibbs free-energy of mixing (ΔG^M) of -3.2 kJ/mol to occur at a C/S ratio of 1.5 (Kersten, 1996). The gain in ΔG for solid solutions below or above that value must therefore decrease when approaching that mol ratio leading to a cease in further reactivity of the C-S-H gel formed. It is in fact difficult to prepare C-S-H gels with a C/S ratio of above 1.5 by reaction of, e.g., calcium hydroxide with silica gel or calcium nitrate and tetraethylorthosilicate.

The SSAS equilibrium approach enables also to predict the dependence of the incongruent solubility of C-S-H on the C/S ratio. The extremely low solubility of the Ca-silicate endmember compared to portlandite implies a strong preferential partitioning of Si in the solid phase. As a consequence, the solutus curve in the SSAS diagram shows a strong asymptotic behaviour due to the dominance of the hydroxyl ions in the activity fraction χ_{OH^-} (Eq 8). The total Si concentration in solution can be predicted given the C/S ratio of the solid (conode from the solutus) and the pH of the solution. In the same manner, total Ca concentrations can be calculated given the C/S ratio, the pH of the solution, and the total solubility product $\Sigma\Pi$ (Eq 7).

Only a narrow range of aqueous-phase compositions can coexist in equilibrium with solid mole fractions in the C/S range 1 - 2. The range of pH values, e.g., have been reported to lie in between 12.0 ± 0.3 (Berner, 1988). Within this range, small changes in the aqueous composition imply drastic changes in the solid equilibrium composition. This behaviour might explain the appearance of compositional variations on a micrometre scale recognized by SEM studies of C-S-H phases (Taylor, 1992). The much greater solubility of portlandite leads to the result that even from a Ca-rich solution (saturated with respect to portlandite), the equilibrium precipitate is low in C/S ratio. Only when the Si concentration in the aqueous solution becomes by more than three orders of magnitude lower than the corresponding Ca concentration, which occurs in later stages of C_3S reaction due a hindrance of Si diffusion into solution through the reactant rim, will a more Ca-rich C-S-H phase ($C/S \geq 1.5$) precipitate.

It should be stressed, that the total solubility product $\Sigma\Pi$ (Eq 7) gives the activities of the ions $CaOH^-$ and $H_3SiO_4^-$ from which the total Ca and Si concentrations have to be recalculated. Fig 2 shows a diagram of total dissolved Si concentrations (in µM on a logarithmic scale) vs. total dissolved Ca concentrations (in mM) in suspensions of C-S-H gels with solid compositions in the range $1.1 < C/S < 1.5$ at pH values of 11.7 and 12.3. The pH is a sensitive parameter which

has not been previously accounted for. The experimental data from various sources plot in between both curves. These data were chosen only from suspension experiments which yield tobermorite-like C-S-H as represented, e.g., by the lower solubility curve A published by Jennings (1986). However, both solubility curves A and B given by Jennings (1986) never cross and as a consequence, jennite-like C-S-H having the upper solubility curve B is always metastable with respect to tobermorite-like C-S-H having the lower solubility curve A. Both the pH-curves also bracket the model curve calculated by Gartner and Jennings (1987).

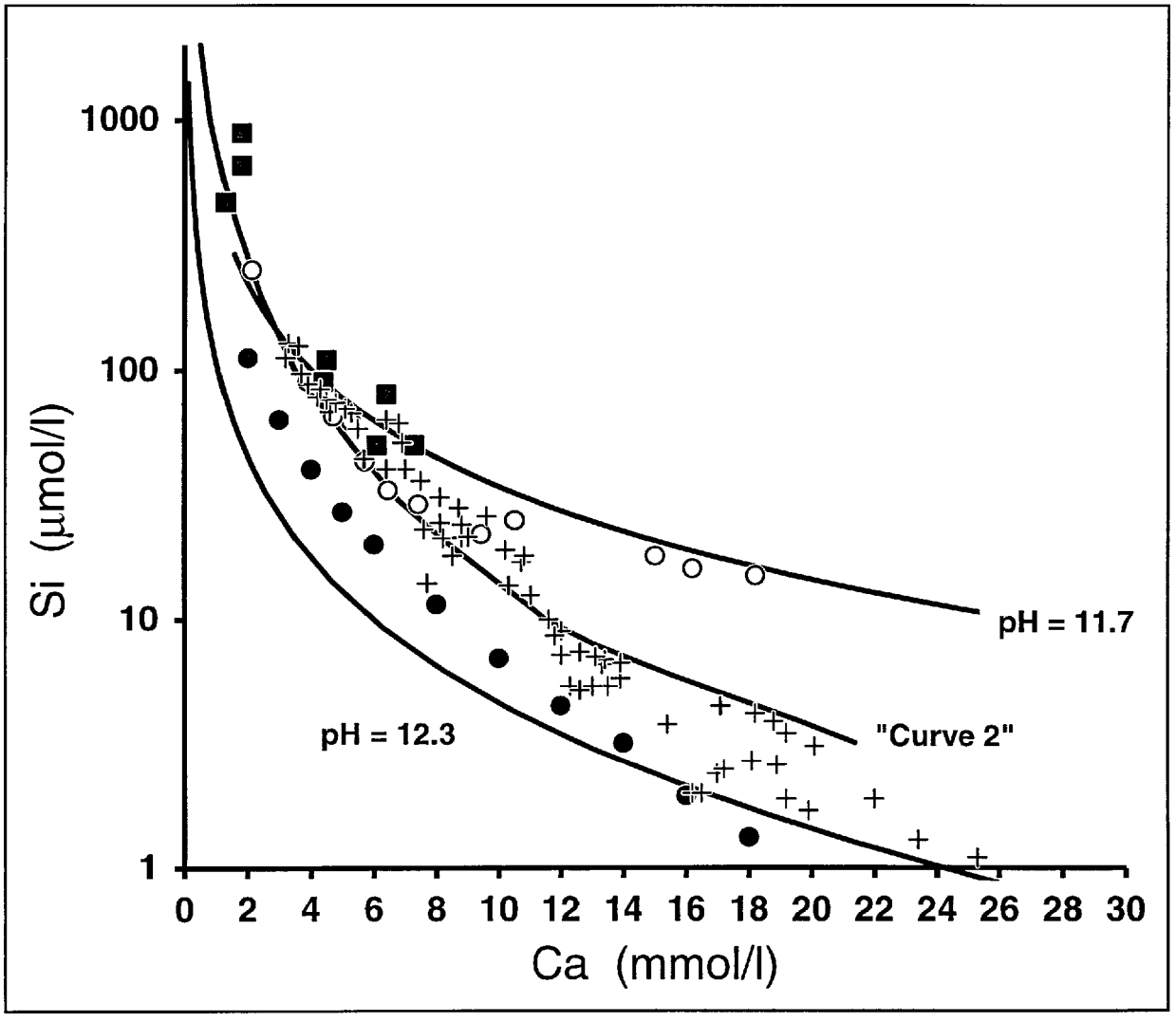

Figure 2. Plot of predicted total Si and Ca concentrations in an aqueous phase in equilibrium with C-S-H gel, calculated for two different pH values and a C/S range of 1.1 - 1.5. A speciation programme (MICROQL) has been used to calculate the aqueous activities by the Davies equation for an ionic strength of I = 0.04. The model curve for tobermorite-like C-S-H of Gartner and Jennings (1987, curve 2) plots in between both curves, as well as the many experimental data points taken from the literature (+ Brown et al., 1984, ● Fujii and Kondo, 1981, o Greenberg and Chang, 1965, and ■ Suzuki and Nishikawa, 1985).

There are two main applications for SSAS theory: (i) prediction of solid-solution solubilities as shown above, and (ii) prediction of the distribution of trace components between solid and aqueous phases for chemical modeling of cementitious solidification/stabilization (S/S) processes. The latter is the most promising application, because it is possible to extend this model to multi-component systems in a predictive sense, e.g. by calculation of ternary SSAS phase diagrams in the case of solid solution of a trace toxic element (heavy metal or radionuclide) into the C-S-H gel. In the brucite-type crystal structure of portlandite, the Ca^{2+} cation can be replaced isomorphously by, e.g., Zn^{2+} or Cd^{2+} ions without significant deformation of the lattice (Shpynova and Melnik, 1985). It would therefore be not surprising if these cations substitute at a crystal-chemical level in the octahedrally coordinated $Ca(OH)_2$-layers of C-S-H phases in later stages of the stabilization process after decomposition of the metastable Ca-metallate phases (i.e., within a few days: Lieber and Gebauer, 1969). The aqueous solubility of such trace metal "impurities" in the C-S-H host phase can therefore be represented by a SSAS diagram of the ternary metal hydroxide - Ca-hydroxide - Ca-silicate system which will be detailed in another paper (Kersten et al., in prep.). This finding is also important for the assessment of the long-term fate of cementitious S/S systems, because the carbonation effect may then be represented as a change from the ternary hydroxide to a binary carbonate SSAS system for a variety of bi-valent metals. Some minor but important hydrate phases like ettringite, monosulphate, hydrogarnet and hydrotalcite also form extended multi-component solid-solution series with trace metals. SSAS diagrams of these ternary or even quaternary systems may also be calculated, because most of the endmember components are congruently soluble and the mixing gaps are relatively well known.

REFERENCES

Bennet D.G., Read D., Atkins M. and Glasser F.P., J. Nucl. Mat., Vol. 190, 1992, 315-325.

Berner U.R., Radiochim. Acta, Vol. 44/45, 1988, 387-393.

Brown P.W., Franz E., Frohnsdorff G. and Taylor H.F.W., Cem. Concr. Res., Vol. 14, 1984, 257-262.

Fujii K. and Kondo W., J. Chem. Soc. Dalton Trans. Vol. 2, 1981, 645-651.

Gartner E.M. and Jennings H.M., J. Am. Ceram. Soc. Vol. 70, 1987, 743-749.

Glynn P.D., Comput. Geosci., Vol. 17, 1991, 907-966.

Glynn P.D. and Reardon E.J., Am. J. Sci., Vol. 290, 1990, 164-201.

Greenberg S.A. and Chang T.N., J. Phys. Chem., Vol. 69, 1965, 182-188.

Jennings H.M., J. Am. Ceram. Soc., Vol. 69, 1986, 614-618.

Kersten M., Environ. Sci. Technol., Vol. 30, 1996, 2286-2293.

Lieber W. and Gebauer J., ZKG No. 4/1969, 161-164.

Lippmann F. N., Jb. Min. Abh., Vol. 139, 1980, 1-25.

Reardon E.J., Cement Concr. Res., Vol. 20, 1990, 175-192.

Richardson I.G. and Groves G.W., Cem. Concr. Res., Vol. 23, 1993, 131-138.

Shpynova L.G. and Melnik S.K., Izv. Vyssh. Uchebn. Zaved. Khim. Khim. Tekhnol., Vol. 28, 1985, 83-85 (Abstract translated in CA 102:20837d).

Suzuki K. and Nishikawa T., Cem. Comcr. Res., Vol. 15, 1985, 213-224.

Taylor H.F.W., Z. Krist., Vol. 202, 1992, 41-50.

Westall J., Report No. 86-02, Dept. of Chemistry, Oregon State University, Corvallis, 1986.

211060
8 pp

RECD 25 JAN 2001 dok 31824

FACTORS AFFECTING CEMENT STRENGTH STUDIED BY MODEL CEMENTS MADE OF CLINKER MINERALS

György BALÁZS*, Margit BOROS*
Ferenc TAMÁS**

*Technical University, Dept. of Building Materials, Budapest, Hungary
**University of Veszprém, Dept. of Silicate- and Materials Engineering, Veszprém, Hungary

ABSTRACT Clinker minerals (of known chemical and phase composition) were produced and 57 different "Synthetic Cements" made of them by varying composition (primarily the C_3A, C_4AF and gypsum ratio) and grinding fineness. Compressive strength can be increased by increasing grinding fineness; splitting-tensile strength reaches highest value at 350 m^2/kg Blaine and decreases with increasing fineness. The C_3S/gypsum reaction precedes the C_4AF/gypsum reaction, irrespectively of the C_3A/C_4AF/gypsum ratio.

Key-words: Strength development Fineness Gypsum Aluminate phase Silicate

INTRODUCTION

The modeling of cement properties by using synthetic mixtures of clinker minerals is a common practice, although the validity of data for hardening mechanism and kinetics are often questioned. This paper deals with the the hardening of 57 sorts of such "Synthetic Cements"; mineralogical composition, grinding fineness and gypsum content were the variables. Investigated parameters included strength of pastes (at 20°C, ages ranging from 6 hours to 90 days), and their non-evaporable water (NEW) content (by TGA). Results are compared with those obtained by the linear combination of similar results obtained with the pure clinker minerals.

EXPERIMENTAL

Clinker minerals C_3S, β-C_2S, C_3A and C_4AF were produced at the University of Veszprém. Their purity was controlled by X-ray diffraction. The gypsum was pure $CaSO_4.2H_2O$, of theoretical composition.

Composition of paste samples was adjusted in a way that C_3S contents (with the exception of 2 series) was always 50%; C_3A, C_4AF and gypsum contents were changed systematically, finally the mixture was extended by β-C_2S to make 100%. In most experiments the synthetic raw materials (of 300 m^2/kg Blaine surface are) were weighed and subsequently homogenized in a ball mill for 40 mins. The surface area of the mixtures became 360 ± 5 m^2/kg by this treatment. In some cases, cements of different fineness (low ≅ 200, high ≅ 500 m^2/kg) have been used.

Pastes were made with 30% water (based on solid weight). 12 cubes (edge length = 20 mm) and 6 prisms (10×10×50 mm) were made of each set, stored (with the exception of the 6 hr. test) in the mould, and subsequently in 100% r.h. room temperature atmosphere. Tests were made at ages of 6, 24 and 48 hr., 7, 28 and 90 d. Compressive strength was measured on the cube specimens. To reduce deviation, a special spherical joint was made, where the geometric centre of the cube and the sphere were coincident. Splitting-tensile strength was measured on the prisms.

Thermal (TGA, DTA, DTG) tests were made immediately after strength testing, from the fragments, by a Derivatograph (type Paulik-Paulik-Erdey, manufactured by MOM, Budapest). Heating rate was 10°C/min, top temperature 1000°C, sample mass approx. 1000 mg. A Pt crucible was used, reference DTA material was Al_2O_3. Weight loss data refer to the anhydrous material (heated to 1000°C). Thermal weight losses up to approx. 170°C were considered as adsorptive and layer water; over that as NEW (exact temperature determined by the DTG curve). The CO_2, coming from the decomposition of $CaCO_3$ was calculated to the water content of $Ca(OH)_2$, and considered as portlandite.

Degree of hydration was calculated by the NEW content, but similar other indexes were calculated too (e.g. by water content of portlandite or of the ferrite phase). The following equation was used for C_3S hydration:

$$6\ C_3S + 18\ H \rightarrow C_5S_6H.H_4 + 13\ CH$$

The above formula corresponds to Taylor's "tobermorite" (Taylor, 1964); it has been adopted by testing the validity of five other formulae used for the evaluation of pure C_3S samples of different parameters, as grinding fineness, w/c ratio, age, etc. This formula proved to be most satisfactory.

The 1 mole of structural water of Taylor's tobermorite is lost between 560 and 800°C, i.e. after the dehydration of portlandite, but before the decomposition of $CaCO_3$.

The formula used for C_2S hydration is:

$$7\ \beta\text{-}C_2S + 14\ H \rightarrow C_5S_6H.H_4 + C_2S.H_2 + 7\ CH$$

adopted from Kurczyk and Schwiete (1963), who found a tobermorite-like phase as hydration products of both calcium silicates; hydrated β-C_2S however yields microcrystalline, nearly amorphous product, as proved by electron microscopy. This means the presence of uncertain peaks (rather bands) on both XRD and thermal patterns, even after more than 1 year of curing. In case of β-C_2S therefore total NEW was calculated, without making a distinction between the various hydrated phases.

Formulae for aluminate and ferrite hydration are the following (Š = SO_3):

$$3\ C_3A + 4\ CŠ + 50\ H \rightarrow C_3A.3CŠ.32H + C_3A.CŠ.12H + C_3AH_6$$

and

$$3\ C_4AF + 4CŠ + 53\ H \rightarrow C_3AF.3CŠ.32H + C_3AF.CŠ.12H + C_3AFH_6 + 3CH$$

Approx. dissociation temperatures (exact values by the DTG peaks): CH ≅ 460-560°C, $C_5S_6H.H_4$ ≅ 560-700 °C, $C_3A.3CŠ.32H$ ≅ 130-150 °C, $C_3A.CŠ.12H$ ≅ 150-250 °C, C_3AH_6 ≅ 280-430 °C, $C_3AF.3CŠ.32H$ ≅ 160-180 °C, $C_3AF.CŠ.12H$ ≅ 180-260 °C

RESULTS AND DISCUSSION

Results are not shown as tables, only as figures, constructed from the numerical data.

The effect of fineness

Formerly it has been determined (**Figs. 1. and 2.**) that by increasing the grinding fineness of C_3S, compressive strength and splitting-tensile strength increased and decreased, resp., while in case of β-C_2S, a strength optimum exists in case of medium fineness. More recent tests (**Fig. 3**) gave similar results: the splitting-tensile test, although it increases over a medium fineness (350

m^2/kg Blaine), but only insignificantly, while cube strength increase by increasing fineness varies, depending on the composition.

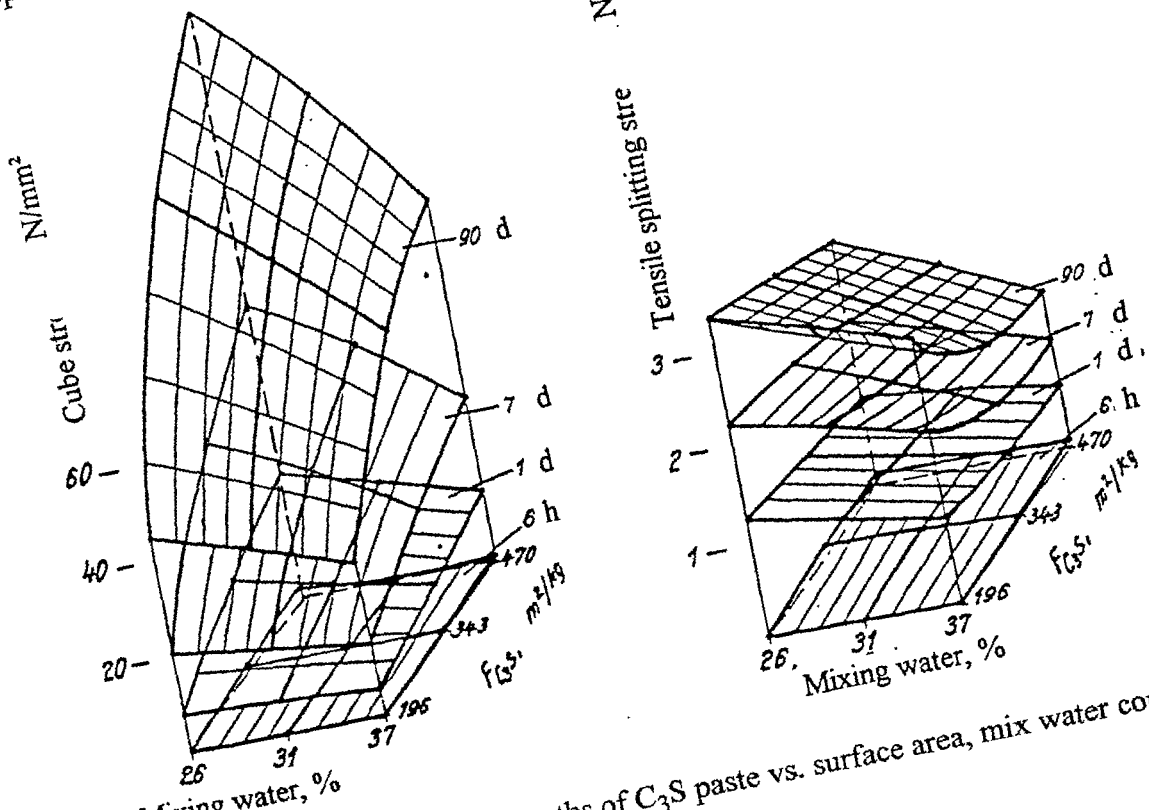

Fig. 1. Cube and splitting-tensile strengths of C_3S paste vs. surface area, mix water content and age of the paste

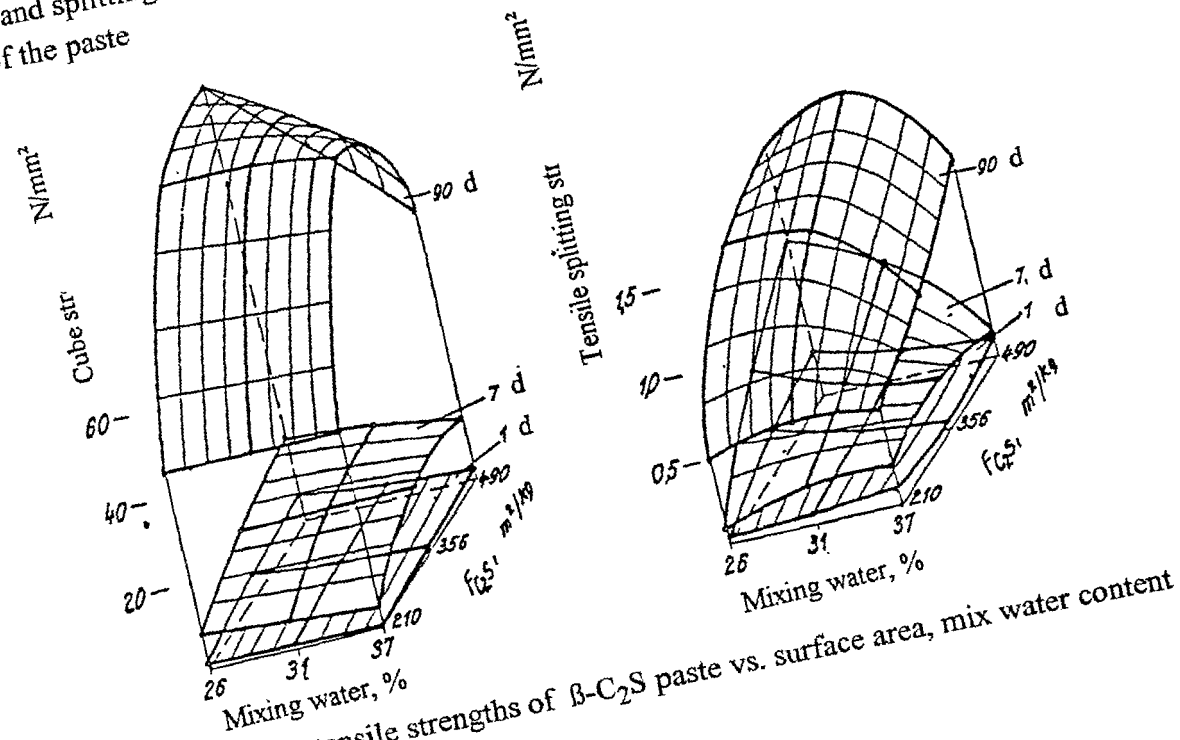

Fig. 2. Cube and splitting-tensile strengths of ß-C_2S paste vs. surface area, mix water content and age of the paste

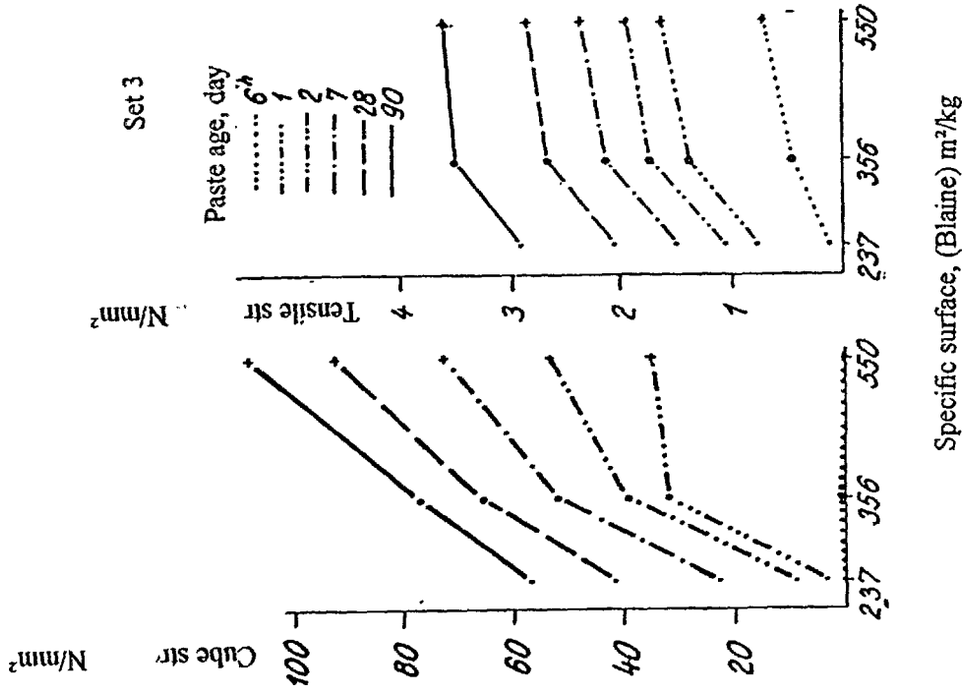

Fig. 3. Strengths of samples in Set 3. vs. age and surface area

The effect of mineralogical composition

Comparing actual strengths with those calculated by the proportional combination of clinker mineral strengths, it is obvious that actual strength is always higher than the calculated one. This can be explained by the fact that cement paste is a heterogeneous system, i.e. microstructure is formed in a different way than in the more or less homogeneous system of clinker minerals; in other words, cement hydration is more complicated than clinker mineral hydration, and alite is much more reactive than is pure tricalcium silicate. This might lead to a conclusion that experiments made with pure clinker minerals are superfluous. If, on the other hand, not absolute values, but trends are considered in case of "synthetic" cements (i.e. those artificially made of pure clinker minerals), such experiments are still of value as they doubtlessly help the interpretation of complicated processes taking place during cement hydration.

Differences between C_3S and β-C_2S hydration

Kinetic differences are the most important. This is due to the fact, that the structure of C_3S is less dense, thus hydration processes have a higher rate than in the case of densely packed β-C_2S. In case of mechanisms, both similarities and differences exist, as proved by NEW contents and hydration degrees. A topochemical mechanism exists in both cases; still quality, quantity and morphology of reaction products - as shown by the thermal tests - may differ considerably.

One of the hydration products of both C_3S and β-C_2S is $Ca(OH)_2$, portlandite; its crystallinity, however is very different: $Ca(OH)_2$, coming from C_3S is well crystallized, gives a distinct XRD pattern and is dehydrated at $\cong$ 500°C; C_2S-born $Ca(OH)_2$, on the other hand, is much less in quantity and is nearly amorphous, gives almost no XRD or DTA/DTG peaks. Well-crystallized portlandite, having crystallized in large hexagonal plates, reduces compressive strength. A common experience that the ratio of NEW contents of the two silicate minerals is higher than

the ratio of cube strengths (identical ages obviously presupposed). This means that by the quantity of strength-carrying phases (as established by the NEW contents) a higher cube strength could be expected in case of C_3S. This decrease can be attributed to the presence of the large portlandite crystals. However this strength reduction is not observed in case of high-fineness pastes; cube strength of β-C_2S does not increase proportionally with NEW, the majority of which is bound to gel hydrates. A similar comparison between splitting-tensile strength and NEW content shows a much better correlation, showing that a close connection exists between this sort of strength and the water contant bound in the gel.

The ferrite + gypsum reaction

Comparison of DTG curves definitely shows that no topochemical reaction takes place between C_4AF and gypsum (**Figs. 4.** and **5.**). It is clear by this comparison, that at the age of 6 hr. curves are similar, i..e. the C_4AF + gypsum reaction did not start yet at this age. Crystallization of iron-containing hydrates starts only after 7 days, and this goes continually on. This means that the reaction between C_3A and gypsum always precedes the reaction of C_4AF and gypsum, irrespectively of the C_3A/C_4AF/gypsum ratio of the system. The quantity of C_4AF has a much lesser effect on hydration than C_3A and gypsum.

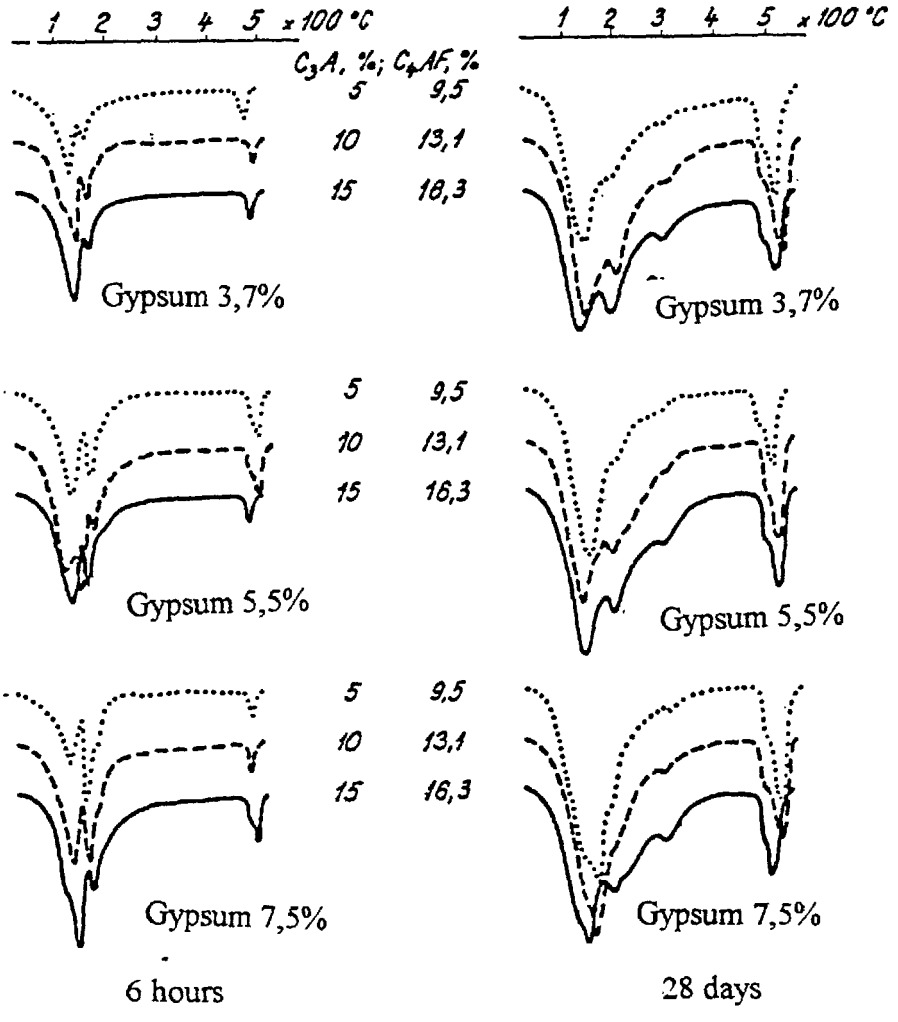

Fig. 4. DTG curves of samples with simultaneously increased C_3A and C_4AF contents at ages of 6 hr. and 28d.

These results corroborate the opinion expressed by Jawed at al. (1980) that a competition exists in hydration cement between C_3A and C_4AF for gypsum, and this is won by the more reactive C_3A.

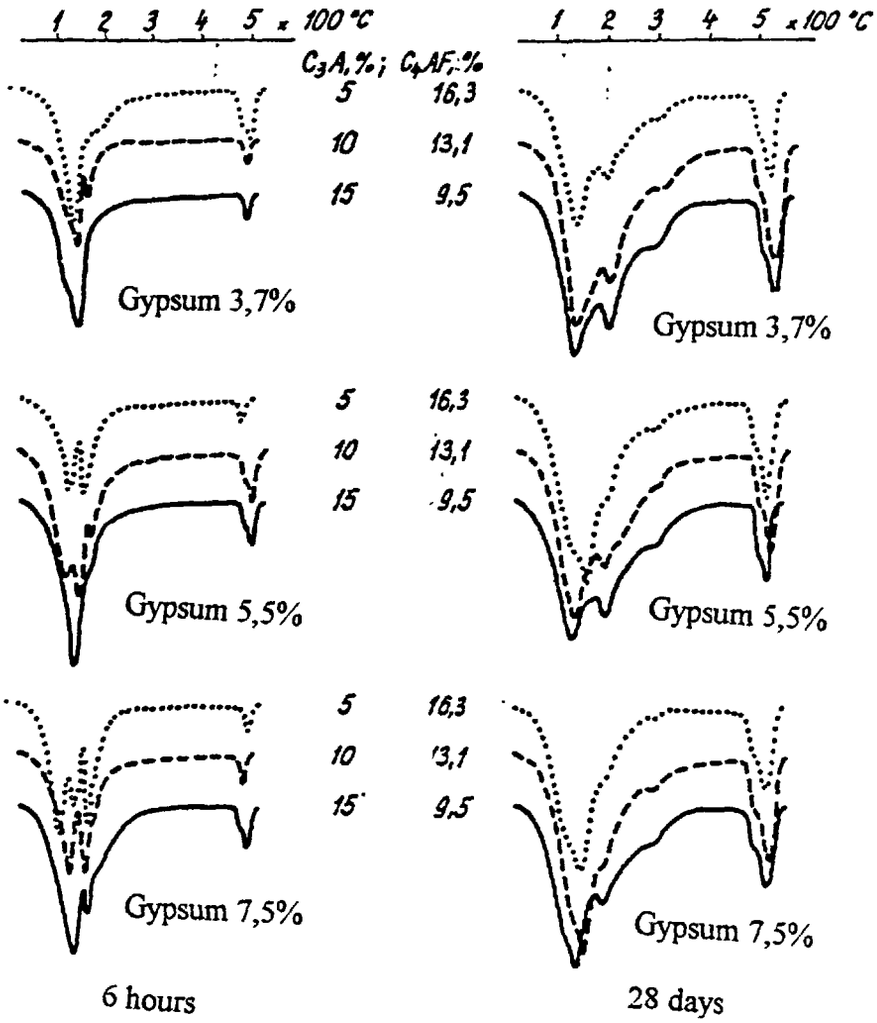

Fig. 5. DTG curves of samples with increasing C_3A and decreasing C_4AF contents at ages of 6 hr. and 28d.

When investigating the effect of Al-containing phases, the quantity of C_3S was kept constant (50 %), but the quantities of C_3A, C_4AF and gypsum had been changed. This necessarily involved the change of the quantity of β-C_2S too (10 to 30 %). The C_3A/C_4AF/gypsum ratio, has a considerable effect on strength, but this effect is quite different in case of compressive and tensile strengths, as indicated above. **Figs 6. - 8.** show a different approach: here the quantity of C_4AF was kept constant, while the quantities of C_3A and gypsum were changed. Cube strength was the highest at medium gypsum content (5.5 %), and the more, the higher the C_4AF content of the paste and the higher its age. In case of splitting-tensile strength, however, highest values were shown by pastes containing medium C_4AF and low C_3A.

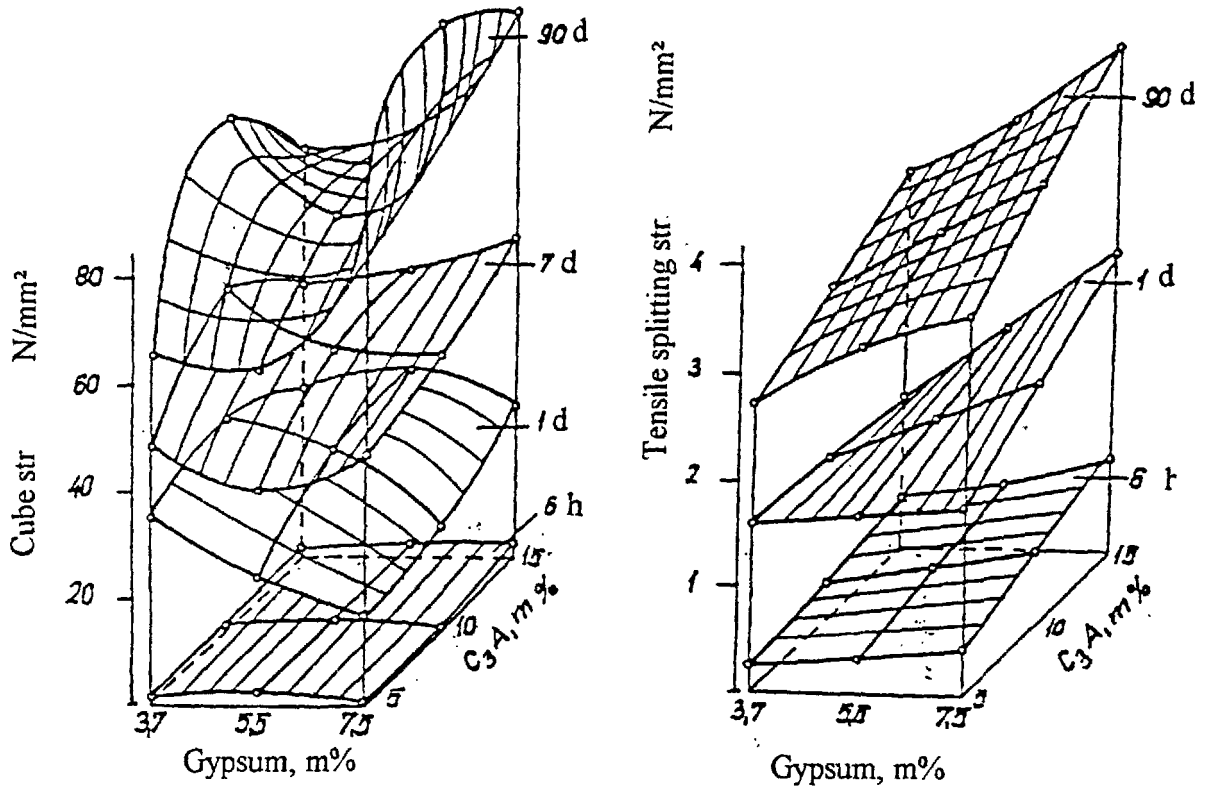

Fig. 6. Cube and splitting-tensile strengths of sets containing 9.5% of C_4AF vs. increasing gypsum and C_3A contents

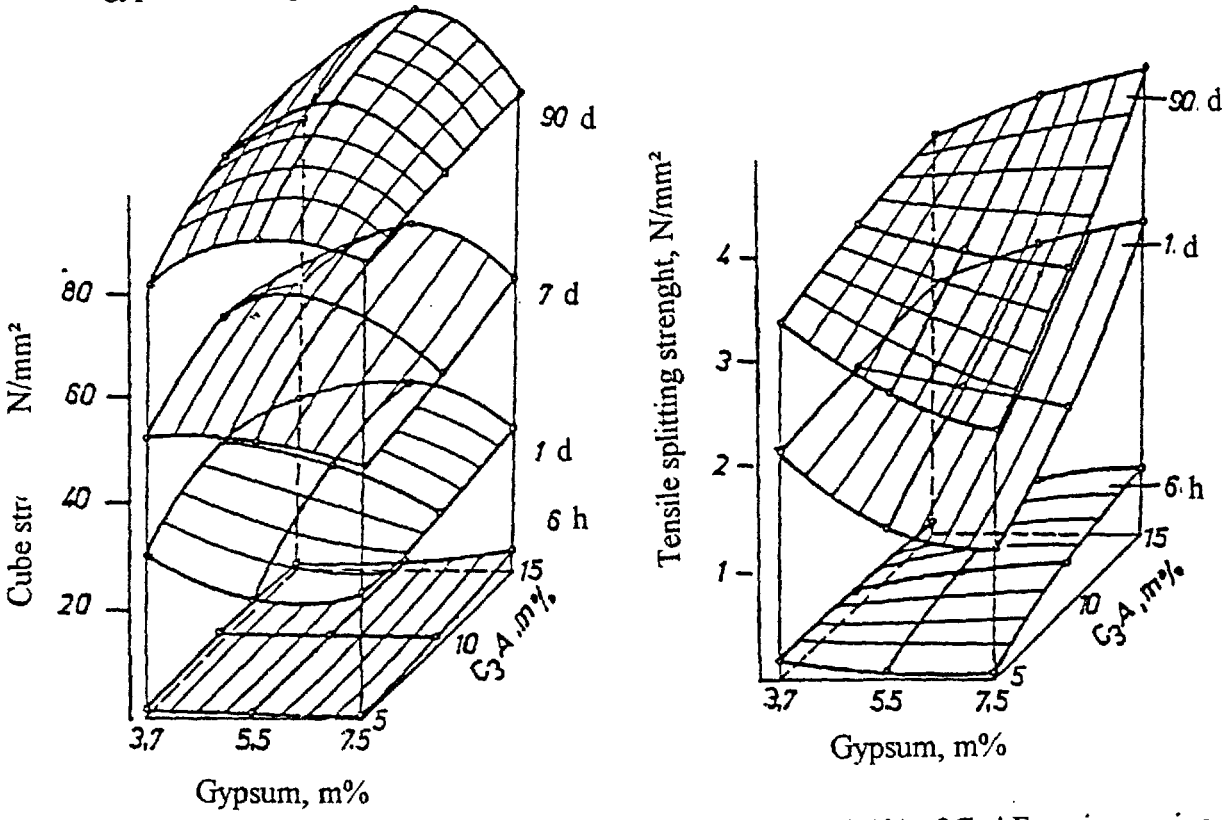

Fig. 7. Cube and splitting-tensile strengths of sets containing 13.1% of C_4AF vs. increasing gypsum and C_3A contents

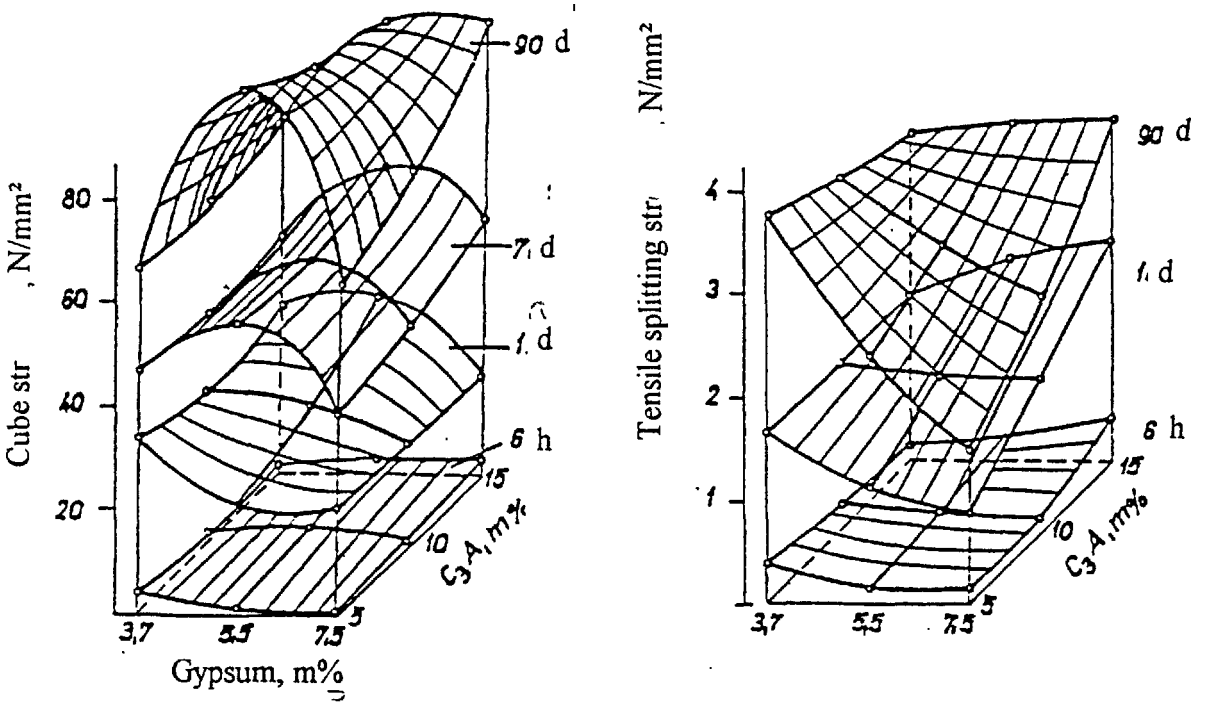

Fig. 8. Cube and splitting-tensile strengths of sets containing 16.3% of C_4AF vs. increasing gypsum and C_3A contents

CONCLUSION

Several formulae exist in the literature to calculate "optimum" or "minimum" gypsum content for cements to attain a high strength. These contain usually two variables only: C_3A-content and fineness. It is concluded that these two factors are inadequate to predict optimum gypsum content and the incorporation of C_4AF-content is necessary; and different formulae ought to be derived for compressive and tensile strengths.

ACKNOWLEDGEMENT

This research was supported by the Hungarian Academy of Sciences.

REFERENCES

Hobbs, D.W. (1977): "The influence of SO3 content on the behaviour of Portland cement mortars" World Cement Tech. **8** [5-6] 75-85

Jawed, I., Menetrier, D. and Skalny, J. (198): "Early hydration of calcium silicates: surface phenomena. 7. International Congress on the Chemistry of Cement, Paris, 1980. Vol. II, 187-87

Kurczyk, H.G. and Schwiete, H.E. (1963): ., "The calcium silicate hydrates". In: "The chemistry of Portland cement" pp.168-232 (1964)

Ost, B.W. (1974): "Optimum sulphate content of portland cements. Amer. Ceram. Soc. Bull. **53** [8] 579-84

Taylor, H.F.W. (1964), "The calcium silicate hydrates". In: "The chemistry of Portland cement" pp.168-232

2ii061
11 pp

Kn o. 2 5. JAN. 2001 d o k 31825

THE CEMENT HYDRATION EQUATION AND ITS APPLICATION TO SEVERAL HYDRATION CRITERIA ACCORDING TO THE LITERATURE

Konstantin SIDERIS. Building Materials, Democritus University of Thrace, Xanthi, Greece
Kosmas K. SIDERIS. Reinforced Concrete, Democritus University of Thrace, Xanthi, Greece

ABSTRACT The cement hydration equation $K = K_\infty \pm b*t^{-p}$ introduced by Sideris (1993) is represented. This equation is applied to 25 cements and clinker phases hydration criteria according to the literature (heat of hydration, non evaporable water, $Ca(OH)_2$ elimination, density, total porosity, porosity with pore diameter D> 75 Å, gas permeability, specific surface, vapor and water sorption, compressive strength of cement paste, mortar and concrete, flexural strength of mortar, pulse velocity, rebound hammer units). The same equation is also applied to the clinker phase's hydration criteria of C_3S, C_2S, C_3A, and C_4AF pastes' compressive strength and non evaporable water and to the $Ca(OH)_2$ elimination of C_3S pastes.

Key-words: Cement hydration equation, hydration.

INTRODUCTION

In order to determine the time dependence of cement hydration the exponential function $K = K_\infty \pm b*t^{-p}$ was introduced by Sideris (1993), where K is the value of the examined hydration criterion, t the age of hydration and p the hydration number.Although cement hydration equation is a usefull scientific tool for the understanding of the course of several hydration criteria, it is known mainly from its application to the criterion of pastes', mortars', and concretes' compressive strength.

Table 1 Hydration criteria.

Cement hydration criteria	**Equations**
1. Heat of hydration (cal/g)	Q: $Q=Q_\infty-bt^{-p}$
2. Non evaporable water (%)	W_n: $W_n=W_{n\infty} - t^{-p}$
3. $Ca(OH)_2$ elimination (%)	CaO: $CaO=CaO_\infty-bt^{-p}$
4. Density (g/cm^2)	d: $d=d_\infty+bt^{-p}$
5. Total porosity (%) 6. Porosity when D> 75 Å (cm^3/g)	P: $P=P_\infty+bt^{-p}$
7. Gas permeability	G_p $G_p=G_{p\infty}+bt^{-p}$
8. Specific surface (m^2/g)	O_s: $O_s=O_{s\infty}-bt^{-p}$
9. Vapor sorption (%) $V_s=V_{s\infty}-bt^{-p}$ 10. Water sorption (%)	W_s: $W_s=W_{s\infty}+bt^{-p}$
11. Compressive strength of cement paste (MPa)	β_D: $\beta_D=\beta_{D\infty}-bt^{-p}$
12. Compressive strength of mortar (MPa)	β_D: $\beta_D=\beta_{D\infty}-bt^{-p}$
13. Compressive strength of concrete (MPa)	f_c: $f_c=f_{c\infty}-bt^{-p}$
14. Flexural strength of mortar (MPa)	β_B: $\beta_B=\beta_{B\infty}-bt^{-p}$
15. Pulse velocity (km/sec)	V_t: $V_t=V_\infty-bt^{-p}$
16. Rebound hammer units	R_t: $R_t=R_\infty-bt^{-p}$
Clinker phases' hydration criteria	
Compressive strength of Clinker Phases (MPa): 17) C_3S, 18) C_2S, 19) C_3A, 20) C_4AF	β_D: $\beta_D=\beta_{D\infty}-bt^{-p}$
21. $Ca(OH)_2$ elimination of C_3S paste (%)	CaO: $CaO=CaO_\infty-bt^{-p}$
22-25. Non evapor. water of C_3S, C_2S, C_3A and C_4AF paste (%)	W_n: $W_n=W_{n\infty} - t^{-p}$

In this work the cement hydration equation is represented and applied to the hydration criteria indicated in Table 1. In each case the measured values were taken from the literature.

CEMENT HYDRATION EQUATION

The first and second phases of the hydration, characterized by a hydration criterion K in the co-ordinate system with K on the ordinate and $(1/t)^p$ on the abcissa, follow a straight line path (Fig 1, where K=Q). The quantitative relationship is given by the following equation (Sideris, 1993):

$$\mathbf{K = K_\infty \pm b*t^{-p}} \qquad [1]$$

in which: K: is the hydration criterion examined (Table 1).

K_∞: is a constant, which represents the intersection of the straight line of Eq. 1 with the ordinate

b: is the slope of the straight line of Eq. 1.

t: is the hydration time expressed in days (t>>0).

p: is the hydration number, depending only on the chemical composition of the cement type used.

Equation $K = K_\infty \pm b\, t^{-p}$ applies to the hydration criteria shown in Table 1. It is important to notice that the value of the hydration number p remains the same as long as the chemical composition of the cement type used also remains the same (Sideris, 1993).

The value of the hydration number p does not depend on:

1. the hydration criterion used
2. the curing temperature [5-60°]
3. the fineness of the cement
4. the ratio w/c
5. the aggregates' grading curve and the aggregates' quality when the hydration criterion of the compressive strength of mortar or concrete is examined.

The linear propotionality between two hydration criteria

The combination of the value pairs of any two hydration criteria for the same cement, show that there is a linear relationship between these hydration criteria (Fig 2, Sideris, 1993). This indicates that each linear correlation between two hydration criteria for a given cement or a clinker phase, specifies a functional relationship which is characterised by the same hydration number.

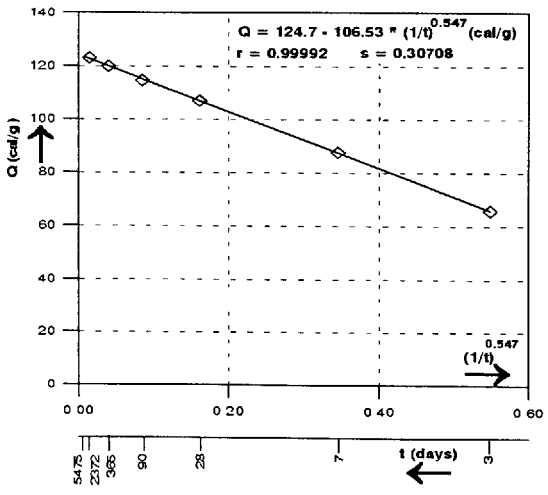

Figure 1 Heat of hydration as a function of hydration time [measured values taken from Verbeck et al (1964)]

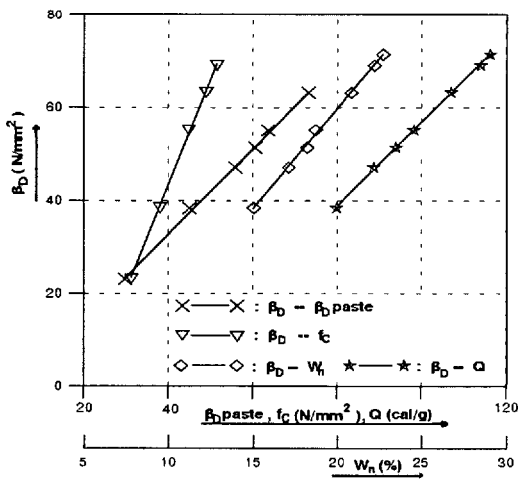

Figure 2: Correlation between the mortar compressive strength (β_D) and other hydration criteria (Sideris, 1993).

Final hydration time

Experimental determination of the final hydration using long-term trials is very difficult because of the very slow decay of the reaction and the inaccuracy of the methods of measurement, and has no practical significance as the results would only be available after several years. It is therefore proposed (Sideris, 1993) to take a period of 15 years as the end of hydration at storage temperatures between 5 and 60° C corresponding to the measured results of the long-term trials by Verbeck et al (1964) and Verbeck et al (1950). This final time was substituted in the hydration equation for all the application examples described in the present work.

Degree of hydration

To determine the true degree of hydration which gives the actual reaction conversion at any given hydration age, it is necessary to use a hydration criterion which is scientifically exact. The most suitable for this purpose is the heat of hydration determined with the heat-of-solution calorimeter. Table 2 contains an example of the calculation to determine the degree of hydration. The hydration equation was used to give the final heat of hydration approximately after 5475 days (15 years). The value of p=0.547 used here is determined by Sideris (1993).

Table 2 Determination of the hydration equation for the heat of hydration and of degree of hydration [measured values taken from Verbeck et al (1950)].

Hydraton age (days)	3	7	28	90	365	2372	5475
Q_{meas} (cal/g)	**65.8**	**87.7**	**107.1**	**114.7**	**120.0**	**123.1**	-
Linear regression	65.8	87.7	107.1	114.7	120.0	123 1	-
for the pairs	0.5483	0.3449	0.1616	0.0853	0.0397	0.0142	-
Q_{meas} - $(1/t)^{0.547}$	correlation coefficient **r = 0.99992** standard deviation s = 0.30708 (cal/g) hydration equation: **$Q = 124.27 - 106.53*(1/t)^{0.547}$ (cal/g), $t \geq 3$**						
Q_{calc} (cal/g)	65.86	87.52	107.05	115.18	120.04	122.75	123 31
Degree of hydration Q_{calc}/Q_{5475}	**0.534**	**0.710**	**0.868**	**0.934**	**0.973**	**0.995**	**1.000**

Evaluation of the hydration number p.

The value of the hydration number p can be estimated with the use of any hydration criterion shown in Table 1, as below. The accuracy of the determination of the value of p depends on the accuracy of the measured values of the hydration criterion used.

For the evaluation of the hydration number p of a particular cement with known chemical composition (or a clinker phase), two different methods may be used.

Method 1

The evaluation of the hydration number p may be obtained using the formula (Sideris, 1993):

$$\frac{(1/t_1)^p - (1/t_2)^p}{(1/t_1)^p - (1/t_3)^p} = \frac{K_2 - K_1}{K_3 - K_1} \qquad [2]$$

In this case three measured values (K1, K2, K3) of the hydration criterion used are needed. These values must be determined with high accuracy in order to obtain a reliable value of the hydration number p. Even a small deviation of one or more of the measured values leads to unreliable values of p. Such accuracy of the measured values K1, K2 and K3 may be obtained only using the hydration criterion of the heat of hydration. The use of the formula shown above is not recommended when the hydration criterion of the compressive strength of cement paste, mortar or concrete is used. In this case the second method mentioned below is suggested.

Method 2

This method can be used with any of the hydration criteria shown in Table 1. It is specially recommended though for the evaluation of the compressive strength, since the measured values in this case are not of high accuracy. In this case the use of 6-8 measured values is recommended. The value of p is estimated with higher accuracy if the criterion of the compressive strength of mortar is used, according to DIN 1164 or ASTM/C- 349.

Use of different values of p

Initially, the point of intersection of the hydration lines for the two phases is determined approximately by graphical means (Fig. 7). This is accomplished by substituting different p values, until the measured values lie on two straight lines. The best value of p is determined based on the measured values of the criterion examined (Table 3). The compensating computation (linear regression) of the Q_{meas} values versus the corresponding ages, expressed by the formula t^{-p}, leads to different values of the correlation coefficient (r) and the standard deviation (s). The best value of the hydration number, in the examined case, was estimated to be p=0.4166 (the same p value is also obtained by use of the formula 2) as shown in Figure 3 It is also noted that the best value of p corresponds to the maximum value of the correlation coefficient (r) and the minimum value of the standard deviation (s).

Table 3 Evaluation of hydration number p.[measured values taken from Verbeck et al, (1964)].

Hydration number p	correlation coefficient	standard deviation	Heat of hydration at the age of (days)							
p	r	s	days	7	28	90	365	2372	4745	5475
-	-	-	Q_{meas}	**60.9**	**79.6**	**88.1**	**95.4**	**98.4**	**100.7**	-
0.3166	0.995940	1.5099		62.27	78.18	87.10	94.24	99.96	101.36	101.61
0.3666	0.996983	0.9212		61.56	78.76	87.80	94.59	99.62	100.77	100.97
0.3766	0.998790	0.8233		61.44	78.88	87.93	94.66	99.55	100.65	100.84
0.3866	0.999030	0.7385		61.31	79.01	88.07	94.71	99.47	100.53	100.71
0.3966	0.999207	0.6680		61.19	79.13	88.20	94.77	99.40	100.42	100.59
0.4066	0.999305	0.6253		61.07	79.25	88.33	94.82	99.33	100.30	100.46
0.4166	**0.999365**	**0.60189**	Q_{calc}	**60.96**	**79.39**	**88.47**	**94.87**	**99.24**	**100.18**	**100.34**
0.4266	0.999339	0.60965		60.85	79.52	88.58	94.91	99.17	100.06	100.22
0.4366	0.999266	0.6424		60.74	79.64	88.72	94.96	99.09	99.95	100.10
0.4466	0.999136	0.6970		60.64	79.77	88.84	95.00	99.01	99.83	99.97
0.4566	0.998952	0.7675		60.54	79.90	88.97	95.04	98.93	99.72	99.86
0.4666	0.998720	0.8480		60.45	80.04	89.08	95.08	98.86	99.60	99.74
0.5166	0.996830	1.3337		60.03	80.70	89.65	95.20	98.46	99.06	99.16

Table 3 and figure 3 contain the values determined for r and s using the measured values for the heat of hydration taken from Verbeck et al, (1964) (cement type II, No 5, W/C = 0.4, hydration time from 7 days to 13 years). The values of Q calculated with the hydration equations for the corresponding p values show, that the error that arrises from the best value by ±0.05 is less than

1%. It is therefore not necessary to calculate the hydration number very accurately for the hydration equation or, in particular, for the strength equation.

Use of special PC program

The best value of the hydration number p is automatically estimated by the use of a special PC program. Table 4 contains an example of the estimation of the hydration number when 10 measured values of the mortar's compressive strength are used (Sideris K.K. et al, 1996). Linear regression is performed for the measured values β_D versus the corresponding hydration age (t), initially for the 6 last pairs up to the 10 pairs. The p value is estimated to be p=0.159≈0.16. The pairs β_{Dmeas} - t_{2-28} and β_{Dmeas} - t_{1-28} lead to unsuitable p values (p=0.001) since the measured values of days 1 and 2 belong to the first phase of the hydration.

Table 4 Use of special P/C programm.

Age (days)	**1**	**2**	**3**	**5**	**7**	**10**	**14**	**18**	**22**	**28**
β_{Dmeas} (N/mm²)	**26.1**	**28.0**	**29.1**	**33.2**	**35.7**	**38.3**	**40.6**	**42.2**	**43.3**	**44.9**
Linear regression	-	-	-	-	7	10	14	18	22	28
for the value pairs	-	-	-	-	35.7	38.3	40.6	42.2	43.3	44.9
β_{Dmeas} - t^{-p}	p=0.183, r=0.999838, s=0.062434									
Linear regression	-	-	-	5	7	10	14	18	22	28
for the value pairs	-	-	-	33.2	35.7	38.3	40.6	42.2	43.3	44.9
β_{Dmeas} - t^{-p}	p=0.167, r=0.9999099, s=0.062434									
Linear regression	-	-	3	5	7	10	14	18	22	28
for the value pairs	-	-	29.1	33.2	35.7	38.3	40.6	42.2	43.3	44.9
β_{Dmeas} - t^{-p}	**best value of p=0.159, r=0.999951, s=0.057869**									
Linear regression	-	2	3	5	7	10	14	18	22	28
for the value pairs	-	28.0	29.1	33.2	35.7	38.3	40.6	42.2	43.3	44.9
β_{Dmeas} - t^{-p}	p=0.001, r=0.997450, s=0.469371									
Linear regression	1	2	3	5	7	10	14	18	22	28
for the value pairs	26.1	28.0	29.1	33.2	35.7	38.3	40.6	42.2	43.3	44.9
β_{Dmeas} - t^{-p}	p=0.001, r=0.989928, s=1.019341									

The following example (Table 5) is intended to explain how the hydration equation is drawn up when the criterion of concrete's compressive strength is examined (K=f_c). In this case the p value is estimated from the measured values of concrete's compressive strength, taken from Hansen, (1990). The same values are used for the determination of the equation of concrete's compressive strength. The hydration equations plotted in Figures 4-25 were determined with the same procedure. The p value was estimated in each case as above.

Table 5 Determination of equation of compressive strength of concrete.

Hydration age (days)	14	28	112	1267	2534	5475
f_{cmeas} (N/mm²)	**8.80**	**13.40**	**25.20**	**39.80**	**42.20**	-
Linear regression	fc_∞ = 77.1401, b=97.8566, **r=0.999078**, s=0.746725 (MPa)					
for the pairs fc_{meas} - $(1/t)^{0.133}$	Compressive strength equation: **$fc = 77.1401 - 97.8566*(1/t)^{0.133}$** (N/mm²), t≥14					
$fc_{calculated}$	*8.2502*	*14.3171*	*24.8951*	*39.3027*	*42.6349*	*45.9953*

Figures 4-25 contain application exambles for 25 cement and clinker hydration criteria according to the literature.

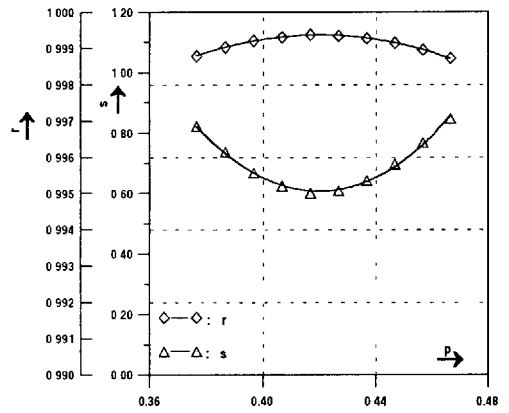

Figure 3: Correlation coefficient (r) and standard deviation (s) as a function of hydration number p.

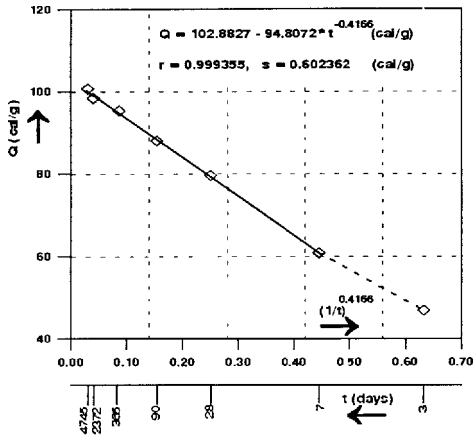

Figure 4: Q of cement paste [measured values taken from Verbeck et al, as table 3].

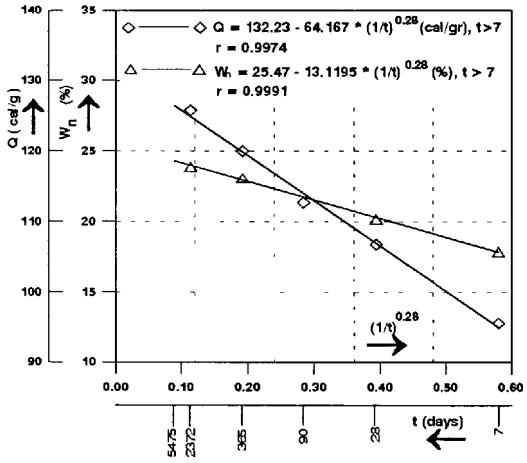

Figure 5: Q and W_n of cement paste [measured values taken from Verbeck et al, 1964].

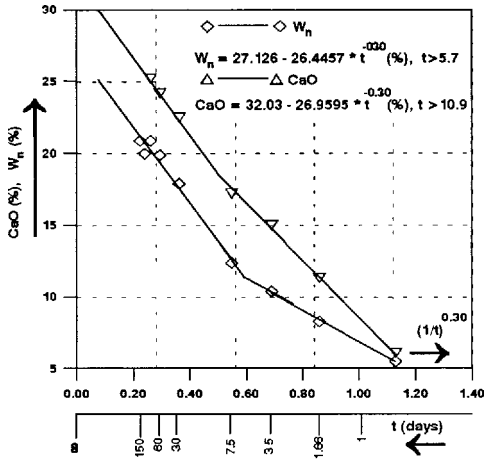

Figure 6: W_n and CaO elimination of C_3S paste [measured values taken from Schwiete et al, 1959].

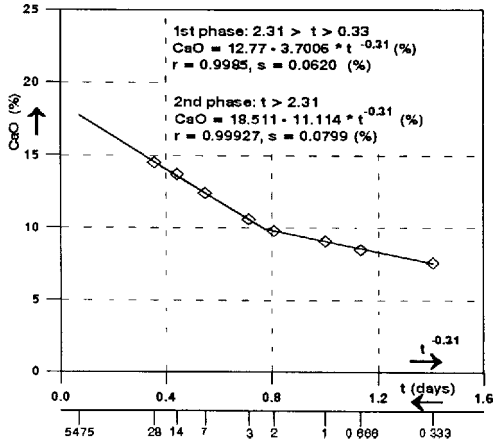

Figure 7: CaO elimination of cement paste [measured values taken from Schwiete et al, 1969].

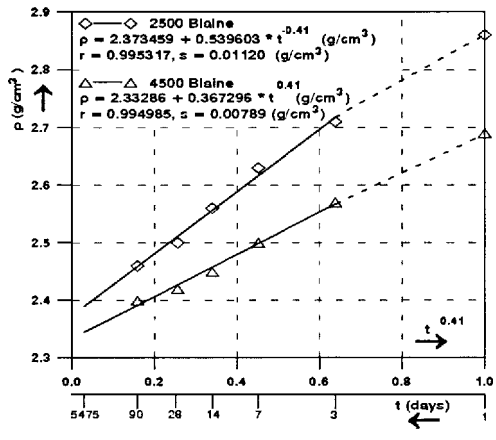

Figure 8: Density of hydrated cement [measured values taken from Krogbeumker, 1971].

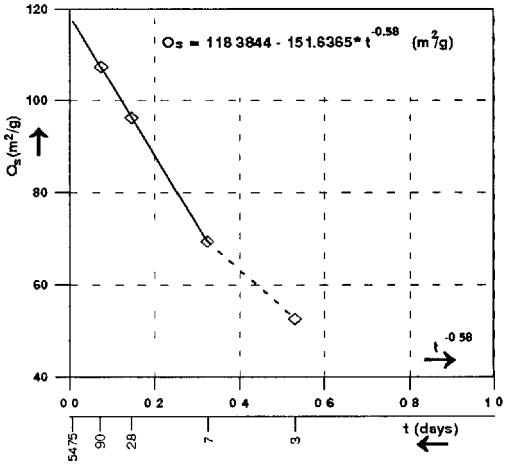

Figure 9: Specific surface of cement paste [measured values taken from Lehmann et al, 1965].

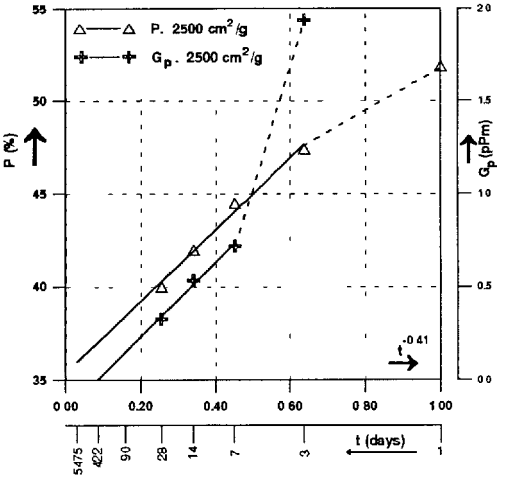

Figure 10: Total porosity (P) and gas permeability (G_p) of cement paste [measured values taken from Krogbeumker, 1971].

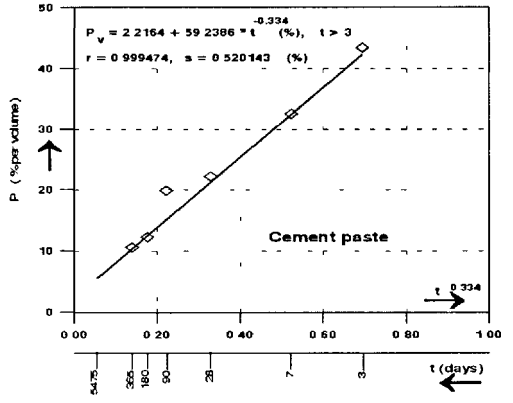

Figure 11: Porosity for pores with diameter D > 75 Å [measured values taken from Sideris et al, 1993].

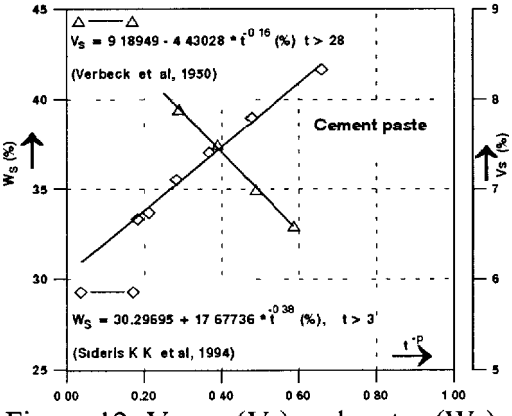

Figure 12: Vapor (V_S) and water (W_S) sorption [measured values taken from Verbeck et al, 1950 and Sideris K.K. et al, 1994].

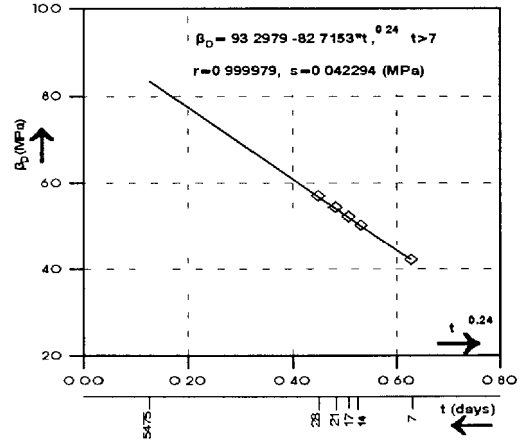

Figure 13. Cement paste compressive strength [measured values taken from Sideris K.K. et al, 1995].

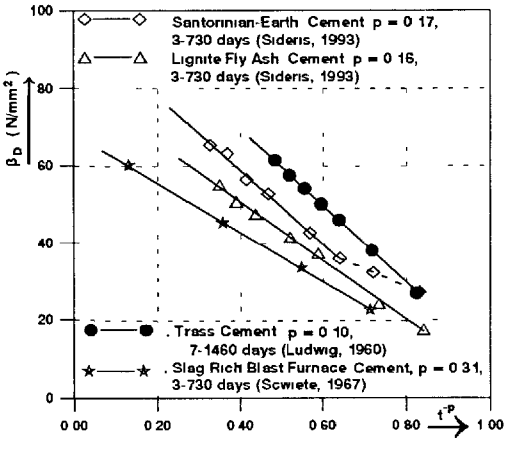

Figure 14: Mortar compressive strength [measured values taken from the literature]

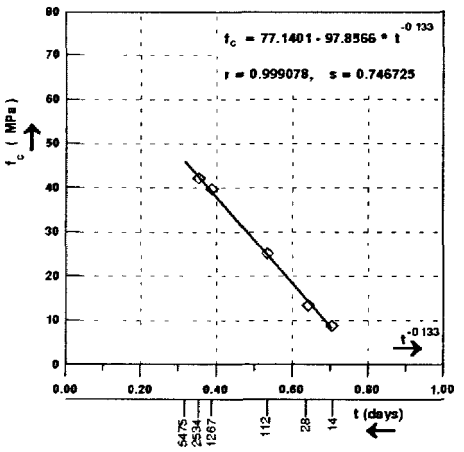

Figure 15a: Concrete compressive strength [measured values taken from Hansen, 1990].

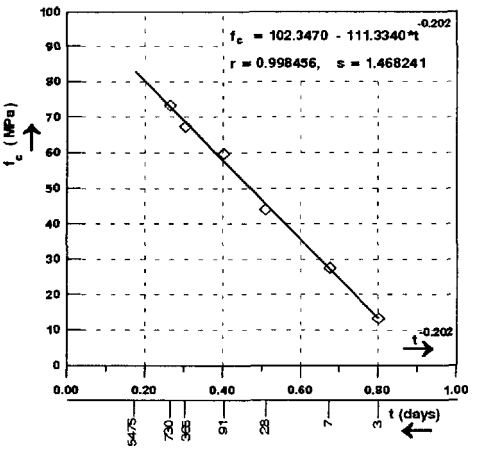

Figure 15b: Concrete Compressive strength [measured values taken from Sivasundaram et al, 1990].

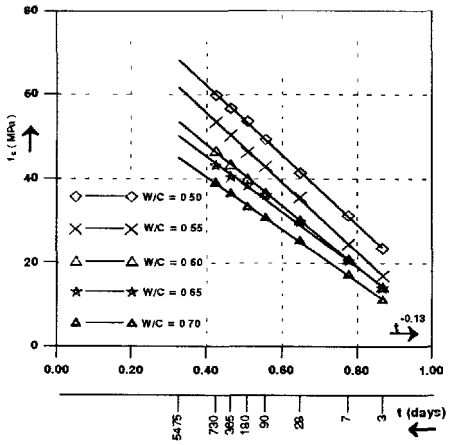

Figure 15c: Concrete compressive strength [measured values taken from Sideris K.K. et al, 1996].

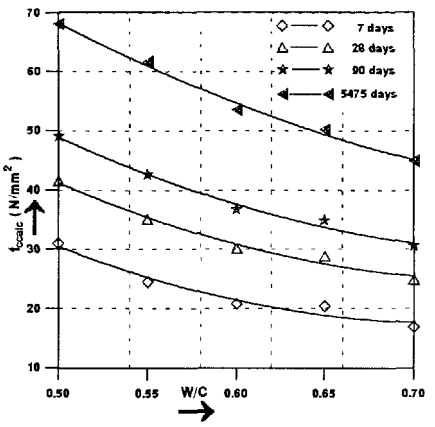

Figure 15d: Influence of the W/C ratio on the compressive strength of concrete [calculated values according to equations of fig. 15c].

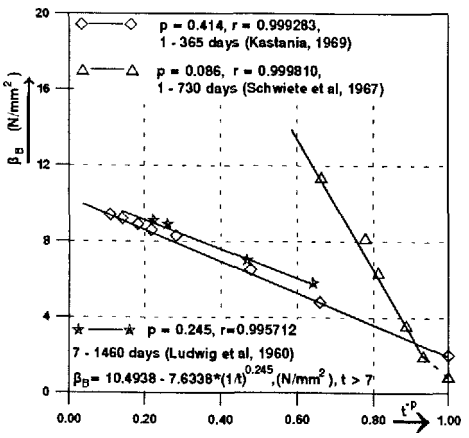

Figure 16: Mortar's flexural strength [measured values taken from the literature].

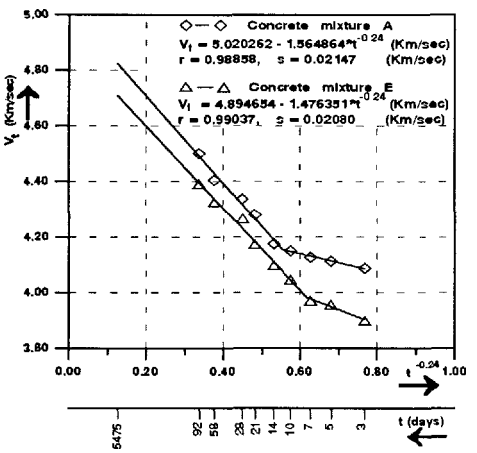

Figure 17: Concrete pulse velocity [measured values taken from Sideris K.K. et al, 1995].

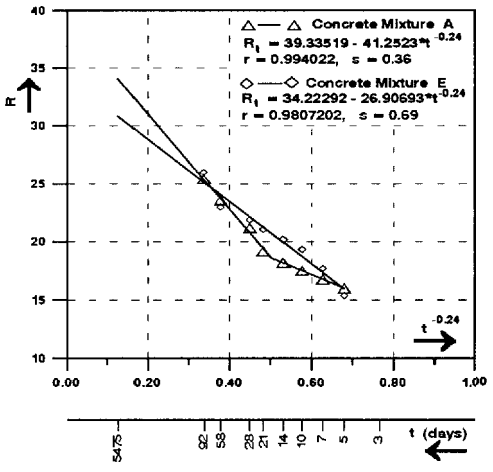

Figure 18: Rebound hammer units [measured values taken from Sideris K.K. et al, 1996].

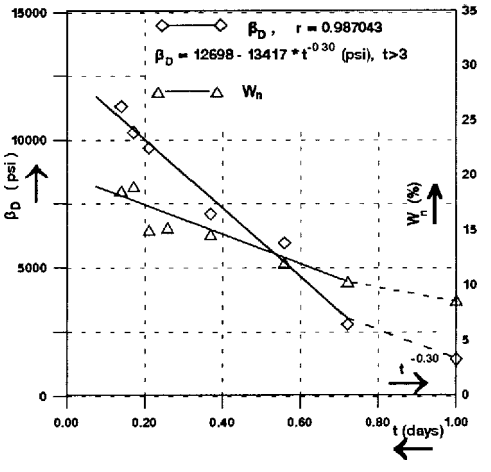

Figure 19: W_n and compressive strength of C_3S paste [measured values taken from Bogue et al, 1934].

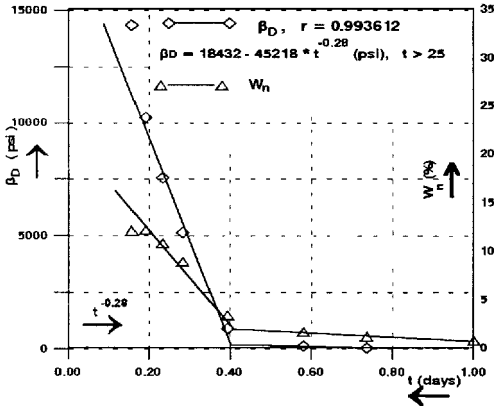

Figure 20: W_n and compressive strength of C_2S paste [measured values taken from Bogue et al, 1934].

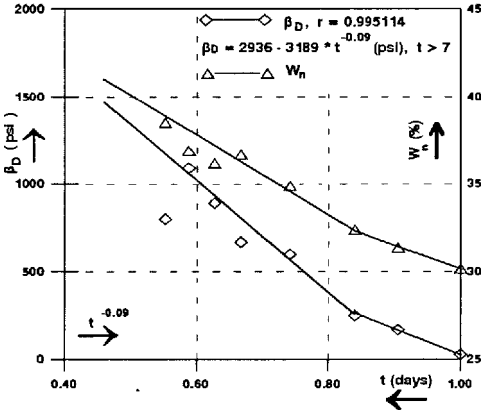

Figure 21:W_n and compressive strength of C_3A paste [measured values taken from Bogue et al, 1934].

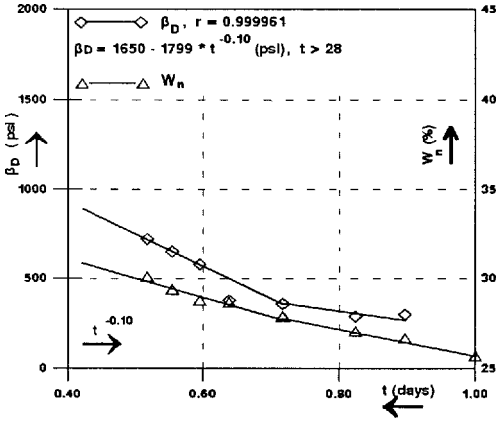

Figure 22: W_n and compressive strength of C_4AF paste [measured values taken from Bogue et al, 1934].

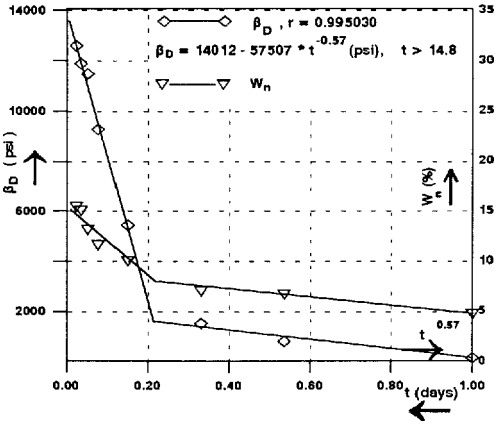

Figure 23: W_n and compressive strength of 50% C_3S and 50% C_2S mixture paste [measured values taken from Bogue et al, 1934].

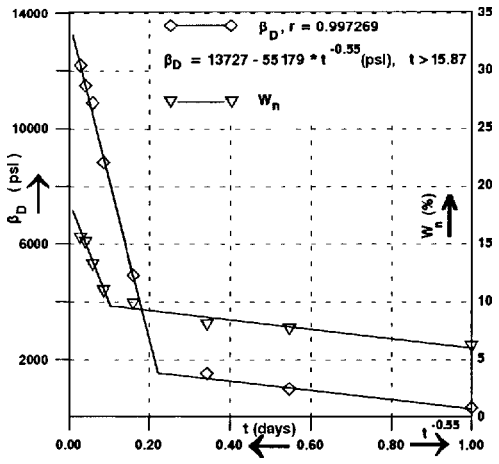

Figure 24: W_n and compressive strength of mixture paste (50% C_3S+50%C_2S+ 5% gypsum) [measured values taken from Bogue et al, 1934].

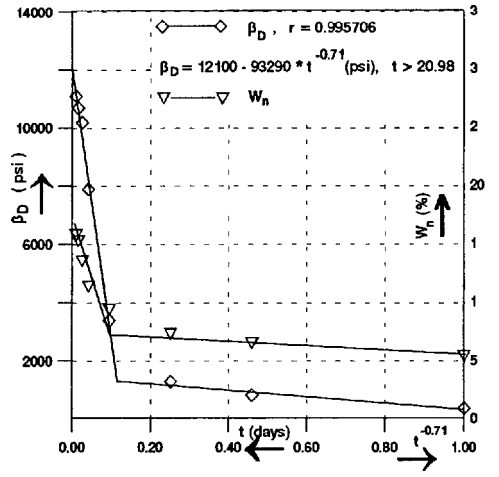

Figure 25: W_n and compressive strength of mixture paste (42.5% C_3S+42.5%C_2S+15% C_4AF+5% gypsum) [measured values taken from Bogue et al, 1934].

CONCLUSIONS

The application of the hydration equation to 25 cement and clinker phases hydration criteria indicates, that the equation with the general form $K = K_\infty \pm b*t^{-p}$ is applicable to all the established hydration criteria of cement and clinker phases.

The compensating computation (linear regression) of the Q values, measured for a hydration period of 6.5 and 13 years, over the corresponding hydration times, expressed by t^{-p}, gives rise to a correlation coefficient of 0.9999-0.9994. This correlation shows a very strong linear relationship between Q and t^{-p}, which signifies that the exponential hydration equation is linear with the heat of hydration criterion in the t^{-p} scale.

The equation $Q = Q_\infty - b*t^{-p}$ constitutes the exact equation which gives quantitavely the course of the chemical reaction of the cement hydration. This is because the heat of hydration is the singular scientifically exact criterion of the hydration of cement.

From the examples given for the pozzolanic and slag cements it can be seen that these cements have a similar hydration behavior to Portland cements. The hydration equation can therefore also be applied to these cements.

The applications of the hydration equation to compressive strength of cement paste, mortar and concrete for long hydration periods (from 28 days to 7 years) show that the correlation coefficient reach a value of 0.99 - 0.999. These results indicate that the hydration equation is generally applicable to the hydration criteria of the cement and concrete compressive strength. The hydration equation is also applicable in the cases of non-destructive tests.

REFERENCES

Bogue, R.H., Lerch, W.: "Hydration of Portland Cement Compounds", Ind. Emgmg. Chem. 26, Nr. 8, 1934, pp. 837-847.

Hansen, T.C.: "Long-Term Strength of High Fly Ash Concretes", Cement and Concrete Research, vol. 20, 1990, pp. 193-196.

Kastania, P.A.: "Das mörteltechnische und chemische Verhalten von Schmelzgranulaten", Dissertation Aachen, 1969.

Krogbeumker, G.: Beitrag zur Beirtlung des Zementsteingefüges", Dissertation Aachen 1971.

Lea, F.M.: *The Chemistry of Cement and Concrete,* Third Edition, Arnold, London (1970) Table 59, pp 392.

Lehmann, H., Roesky, W.: "Festigkeitsentwicklung und Hydratation von Portlant und HÜttenzementen dei 20, 5 und 1° C", Tonind - Ztg. 89, Nr. 15-16, 1965, pp. 337-350.

Ludwig, U., Schwiete, H.-E.: "Das Mörteltechnische, chemische und mineralogische Verhalten von Trasszement und Trasskalkgemischen", Veroffentlichung des Inst. f. Gesteinschuttenkunde der R.W.T.H. Aachen, Bd. 3, 1960.

Schwiete, H-E., Ludwig, U., Otto, P.: "Untersuchungen an hüttensand-reichen Hochofenzementen", Institut fÜr GesteinshÜttenkunde, TH Aachen, Tabelle 22, pp. 173, 1967.

Schwiete, H-E, Knoblauch H., Ziegler G.: "Die hydratation der Verbindungen $3CaO.SiO_2$ und â-$CaO.SiO_2$" Forschungsbericht des Landes Nordhein - Westfalen, Nr. 748, Westdeucher Verlag (1959), pp. 27-32.

Sideris, K.: "The cement hydration equation", Zement-Kalk-Gips, 12 (1993), Edition B, pp.E337-E344.

Sideris, K., Savva, A.E.: "Concrete Porosity", Bulletin of Association of Civil Engineers of Greece, 211, Jan-Feb 1993, pp.39-48 (in Greek).

Sideris, K.K., Baltzopoulou, K.D., Savva, A.E, Ekonomou, C.M., Sideris, K.: "A proposal for the evaluation of concrete strength using rebound hammer", Proceedings of 12th Greek Concrete Conference, Limasol, Cyprus, October 1996, Volume I, pp 310-319 (in Greek).

Sideris, K.K., Baltzopoulou, K.D., Karayannis, C.G.: "A proposal for the evaluation of concrete strength using ultrasonics", Proceedings of the First Joint Belgian - Hellenic Conference on Non Destructive Testing, Patras, Greece, May 22-23, 1995, pp. 259-265.

Sideris, K.K., Konsta, M.S.: "A new proposion for the estimation of the permeable porosity of cement paste and concrete", Proceedings of 11th Greek Concrete Conference, Corfu, Greece, May 1994, Volume I, pp 272-282 (in Greek).

Sideris, K.K., Konsta, M.S.: "Influence of the water to cement ratio on the compressive strength of concrete - An application of the cement hydration equation to concrete", Proceedings of the 4th Greek National Congress on Mechanics, Xanthi, Greece, June 26-29, 1995, Volume I, pp. 167-174, and Applied Composite Materials, vol. 3, No 5 (1996), pp. 335-343.

Sivasundaram ,V., Carette, G.G., Malhotra, V.M.: "Mechanical Properties, Creep and Resistance to Diffusion of Cloride of Concretes Incorporating High Volumes of ASTM Class F Fly Ashes from Seven Different Sources", ACI Materials Journal, vol. 88, pp. 407-416, July-August 1991.

Verbeck, G.J., Foster C. W.: "Long-Time Studies of Cement Performance in Concrete; Chapter 6: The heats of Hydration of Cements", Proceedings of ASTM, 50, 1950, pp. 1235-1257.

Verbeck, G.J., Hass, W.E.:Portl. Cem. Ass. Staff. Rep. (1951); Zitat in H.F.W. Taylor; The Chemistry of cements, vol. I, Academic Press, London and New York (1964), pp.356.

2ii062
6 pp

Kn o. 25. JAN. 2001 d o k 31826

ENERGY AND ELECTRONIC TRANSFORMATIONS IN THE PROCESS OF BINDERS SOLIDIFICATION.

Larisa B. SVATOVSKAYA, Saint-Petersburg University of Transportation, Russia

ABSTRACT Correlations between the energy of chemical reactions in the process of solidificating and strength of paste are evaluated, introducing the notions of thermodynamic reserve (TR) and coefficient of thermodynamic strengthening (CTS). Physicochemical categorization of binders and fillers is proposed, wich take in to account mechanisms of material and energy transformations on the electronic level. Donor-acceptor and energetical interactions are assumed as a basis of chemical design of physico-mechanical features of paste on the base of binders.

Activation, calcium silicate, characterization, degree of hydration, thermodenamics.

ENERGY TRANSFORMATIONS IN THE PROCESS OF BINDERS SOLIDIFICATION

Proposed energy aspect of toughness is based on following propositions by Svatovskaya (1996):

1. Correlation between energies of chemical reactions and mechanical properties of the system, reflected by toughness of stone. It can be a reaction, for instance,of hydration. Toughness of stone in such a case, depends on values of reaction energy changes in standard conditions. This value ΔH^0_{298} depends on nature of interacting materials and products of reaction. Considering the first law of thermodynamics, it is possible to claim that full energy, which is required for destroying of a material, received by the spontaneous chemical reactions, passed wholly, can not rise above the value of energy, liberated in these reactions ΔH^0_{298}. It is possible also to claim that value of energy, reflected in toughness, $\sigma^0 < \Delta H^0_{298}$ of reaction, and that the more negative ΔH^0_{298} of reaction, the more can be toughness of material σ^0, on one hand, and the more it stability in enviroment, on the other. Since the smaller is the value of ΔH^0_{298} of hydrates, the greater is the value of ΔH^0_{298} of the reaction, so the material toughness σ^0 is the function of products-hydrates enthropy changes.

2. In the binders, in which source phases are present in the majority by phases, having high share of a covalent bond (more than 50 %) and so, in the difference for instance from gypsum, not change completely in final products sufficiently long, energy of not yet passed reactions at a moment of the time τ_i is the reserve of toughness of the material. In such a cases, difference of enthalpy changes is a thermodynamic reserve TR_{II}:

$$TR_{II} = \Delta H^0_{298} - \Delta H^0_{298i}\,, \qquad [1]$$

where ΔH^0_{298}-is a full energy of reaction, liberated with the assumption that conversion of source products into final ones has occurred completly; ΔH^0_{298i} - an energy of already realized reaction at given time τ_i .The value of TR_n is the difference in enthalpy values, and is the base of increasing of material toughness, or otherwise thermodynamic reserve (TR) of toughness. If at a moment of the time τ_i, for instance 28 days, ΔH^0_{298i} provide energy of failure σ_i, but total energy content can provide the energy of failure σ_0, then

$$\Delta\sigma=\sigma_0-\sigma_i, \qquad [2]$$

provides by thermodynamic reserve (TR), i.e. energy of nonreacted substances, which are the system reserv at a given time τ_i.

Increasing in time the toughtness of cement systems on the base of materials by mainly covalent nature is connected with consumption of the energy reserves of these materials in reactions, for instance, of hydration. Thereby, thermodynamic reserve possess binders on the base of phases with high share of covalent bond, which are "alive" in the sense of going in them thermodynamic process justified by spontaneouse reactions ($\Delta G<0$), wich replenish the system by the energy. In ceramic or metallic materials there are no such a reserve of toughness .

3.Energy reserve of spontaneous strengthening at the cost of replenishing of the system by the energy of chemical reactions at different points can be described not only in terms of the energy content of the systems (enthalpy-parameters), but as well in terms of the free energy or the Gibbs free enrgy of the reaction ΔG^0_{298}:

$$TR_G=\Delta G^0_{298}-\Delta G^0_{298i} \qquad [3]$$

In such a case, while value $\Delta G_{298i}<0$, alongside with spontaneous chemical reaction, take place spontaneous strengthening of the systems in certain conditions and on certain mechanisms. The larger the amount of nonreacted substance, the larger is TR at a given moment of the time τ_i.

4. At a moment of the time, when thermodynamic reserve of toughness is exhausted, toughness takes a maximum value, which can increase or decrease at the cost of the contribution of other reactions or processes, for instance reactions of polycondensations.

5. Thermodynamic description of toughness of material, received by the realization of the spontaneous chemical reaction, allows to forecast strengthening of the materials on the base of binders, using not only parameter TR, as well as other parameter - coefficient of thermodynamic strengthening (CTS) in relative units or in percent. CTS represents a ratio between the TR and ΔH^0_{298}, whos energy can be evaluated in terms of enthalpy or free Gibbs energy (Eqs 4 and 5).

$$CTS_H = \frac{TRH}{\Delta H^0_{298}} \quad [4]$$

$$CTS_G = \frac{TRG}{\Delta H^0_{298}} \quad [5]$$

For systems on the base of phases with mainly ion bonds TR at an age of already one day is a zero and CTS material is a zero also, as far as share of conversions of substances is close to 100 %. For substances with mainly covalent nature of bond, CTS in same temporary intervals is more than zero and the larger is the covalent component, the larger is the value of CTS of the systems and the larger is strengthehing of the system in time. The value of CTS, evaluated in percent, gives information on that, what part of energy of chemical reaction is in the reserve and, accordingly, what energy reserve CTS and TR are to be found by the calculation of the reaction with provision for degree of reaction, definied for instance, on degree of hydration. Correction for spontaneous strengthening of "alive" systems in time allows to forecast the exploitation behaviour of materials in the environment in conditions of different sort of aggression. Calculations of TR and CTS are founded on experimental data of degrees of hydration of materials. Thermodynamic aspect of toughness allows to control energy content and toughness of the system at least one of following ways.

a). To orientate the process of hydration on forming the products with the smallest enthalpy of formation; in this case in accordance with the proposition 1 toughness of system will the largest. In the University of Transportation was designed new additives, which orientate hydration process to form the hydrates with the smallest enthalpy and thereby allowed to get a concrete, having under natural solidification toughness two times higher, than reference sample at an early age of 2-3 days.

b). The use of the reduction of temperature as a way of ordering of the system, accompany liberation of energy. As shown by Svatovskaya, Sychov, Smirnova (1989) at the temperature of 269 K the degree of hydration is increases, possible at the cost of of increase protons mobility at rapid mechanism of protron transfer and, besides, the amount of $CaCO_3$ increases under these conditions at the cost of the $Ca(OH)_2$ by carbonation. The degree of ordering of the system, growth of the hydration degree and forming of a carbonate has its energy share in total energy content of the system reduction, and accordingly, growing of toughness.

c). Injection in solidificating system fillers, including hydration-active, which reduce energy content of the system at the cost of the own chemical reactions or at the cost of catalysis of the main materials hydration.

The development of the thermodynamic aspect of toughness, considering energy nature and system toughness reserves, in which hard phases have mainly covalent

nature of bond, stipulates consideration of mechanisms of chemical reactions, which are to occur in the binder in the system of solids or quasisolids.

ELECTRONIC TRANSFORMATION LEVELS IN THE PROCESS OF BINDERS SOLIDIFICATION.

Electronic phenomenas in the process of binders solidification is a collection of phenomena with the transmission of electrons and electronic couples, exist in spontaneously solidificate systems and influence on processes of hydration, accordingly, solidification and on system toughness, on some mechanical characteristics also, such as flow and fragility. Electronic phenomenas of binders touch a construction of materials: on the level of realization of chemical bond, on the level of donor-acceptor bond, on the level of reduction-oxidation reactions and on the level of the reduction-oxidation and acid-base catalysis. The first level of electronic phenomenas accounting allows to get cements with flow characteristics (Svatovskaya, 1986), the second, the third and the fourth levels allow to control reactions in binder systems, using chemical categorization of binders and fillers (Svatovskaya, 1985).

Table 1 Categorization of binders according to the electronic family of Mendeleev table.

Binders	Examples	Acceptor of Electronic Couple	Electronic Level	Orbital Electronegativity, eV
s-cements	$2CaO*SiO_2*nH_2O$	Ca^{2+}	4s	2.33
p-cements	$Al_2O_3*nP_2O_5*mH_2O$	Al^{3+}	3p	6.01
d-cements	$ZnO*nP_2O_5*mH_2O$	Zn^{2+}	3d	-1.02

In Tables 1 and 2 are presented categorizations, which allow to consider cements, fillers, contact areas and interactions between them coming from the unified basis. Categorization in connection with the position in the Mendeleev table on the sign of belonging to the electronic family allows to forecast first; manifestation of binder characteristics as characteristics of electronic analogues s -, p - and d - elements; and secondly - toughness of chemical bond in hydrates.

The third particularity of binders categorizations consists of that, that it will allow to foresee a glue system ability, or otherwise, adhesive characteristics, for instance, p- and d- cements possess higher glue ability (adhesion) than s- cements, since energy of p-and d- orbital is higher than energy of s-orbitals, other things being equal.

Table 2 Categorization of fillers on the base of chemical nature.

Fillers	Place in Mendeleev Table		Electronic Construction		Nature of Chemical Bond	
	quantum numbers	type of filler	ΔE, eV	electrical propeties	Pirsons parameter, $r_k/r_a*\Delta x$	type
$CaCO_3$ $MgCO_3$	$4s^0$ 3sp	s-acceptor	>3.5	dielectric	0.6-1.5	ionic
$Al_2O_3*2SiO_2*H_2O$	$3sp^2$	p-acceptor	>3.5	dielectric	0.06-0.14	ionic-covalent
Fe_2O_3	$4s^03d^5$	d-acceptor	2.2	semiconductor	0.14-0.6	ionic-covalent
SiO_2	$3sp^3$	donor	>3.5	dielectric	0.06-0.14	covalent
Cu	$4s^23d^{10}$	donor	0	conductor	0	metallic
Fe	$4s^23d^6$	acceptor	0	conductor	0	metallic

The fourth particularity of this categorizations: it allows to forecast mechanical characteristics of artificial stones: more flexible, dumbbell-like directivity in the space, characteristic of p-cements, and fillers will promote more "flexible" structure of material , i.e. higher bending strength. In materials, the origin of toughness which lie in chemical reactions, forming new phase is capable to interact hereinafter with the surface of other solid (adhesion) by opening, donor-acceptor bond systems for instance. By classifying filler in the chemical system by its beloging to the electronic family, so depending on cation, it is possible to select s- , p- , d- fillers. Herewith, belonging of cation to the family, gives with provision for values of main quantum number information about energy and configuration of electronic orbital of cation. The use of such sort of notions, series of clay-materials are obtained, in which is used structure motive of silicates aluminum as well as are received composits, containing d-fillers, i.e. materials, having surface for instance, 3d-ferric (III) cations, distinguished by high energy of electronic configurations. As 3d-filler, slag can be used. However, structured - sp^2-motive can be present and in the source material - a reagent, not only filler; in this case it also dictates flat direct motive to the structure a material, brought about reduction of its fragility.

Categorization of fillers by particularities of solid electronic construction and nature of bond reflected by parameters of ΔE or $r_k/r_a*\Delta x$ allows to foresee influences of surface within the framework of notions reduction-oxidation and

acid-base catalysis. On this notions, materials which are mainly ion by nature, dielectrics are to shift balances of proton reactions on the principle of hard acids and bases; for metals (conductors) and semiconductors is also important ability to have a vacant electronic orbital.

REFERENCES

Svatovskaya L.B., "Cements with flowage characteristics", Cement, No.6, 1986, p.11.

Svatovskaya L.B., Smirnova T.V., Sychov M.M., "Activated solidification of nephelin slime", Cement, No.7, 1989, pp.9-10.

Svatovskaya L.B. "Thermodynamic aspect of toughness", Cement, No.1, 1996, pp.8-10.

Svatovskaya L.B. "Engineering chemistry", vol.1 Saint-Petersburg University of Transportation, 1995, pp.31-45.

2ii063
8 pp

Kn o. 2 5. JAN. 2001 d o k 31827

INVESTIGATIONS ON CALCIUM PHOSPHATE CEMENTS

Peter VANIS and Ivan ODLER, Technical University Clausthal, Clausthal-Zellerfeld, Germany

ABSTRACT: The setting and strength development of pastes made from blends of dicalcium and tetracalcium phosphate may be accelerated by using a Na- K- or NH_4- phosphate solution, rather than pure water, as mixing liquid. Similarly, the strength development of compacts made from these starting materials becomes accelerated by placing them into these solutions, or into a solution whose ionic composition corresponds to that of the human body fluid. This effect is due to an accelerated conversion of the starting Ca-phosphates to hydroxyapatite, the phase responsible for the cohesion of the material.

INTRODUCTION

Calcium phosphate cements have been widely studied in recent years [e.g. Brown 1986, 1991, 1992, Chow 1991, Monma 1984, 1988, Williams 1992, Xie 1991]. In all of them hydroxyapatite [$Ca_5(PO_4)_3OH$; abbr. HAp], the phase thermodynamically most stabile in the ternary system CaO-P_2O_5-H_2O at pH > 4,8, is fomed as the final reaction product of the cementing process. The great interest in calcium phosphate cements is mainly due to their excellent biocompatibility, based on the fact that hydroxyapatite, in a solid solution with fluorapatite, is the mineral component of human bones and teeth.

The starting compounds in most, though not all, calcium phosphate cementitious systems are dicalcium phosphate [$CaHPO_4$; abbr. DCP] or dicalcium phosphate dihydrate [$CaHPO_4.2H_2O$; abbr. DCPD] in combination with tetracalcium phosphate [$Ca_4(PO_4)_2O$; abbr. TeCP]. If suspended in water, both substances are dissolved in the liquid phase and hydroxyapatite, which is less soluble, precipitates.

$$CaHPO_4 + Ca_4(PO_4)_2O = Ca_5(PO_4)_3OH \qquad [1]$$

This dissolution/reprecipitation reaction forms the basis of the setting and hardening of calcium phosphate cements. In addition to hydroxyapatite, also β-tricalcium phosphate [$Ca_3(PO_4)_2$; abbr. β-TCP] and octacalcium phosphate [$Ca_8H_2(PO_4)_6.5H_2O$; abbr. OCP] may precipitate as intermediate reaction products, however, both of them eventually convert also to the more stabile hydroxyapatite.

Even though the conversion of DCP (or DCPH) and TeCP to HAp may take place in pure water, diluted phosphoric acid is being most widely used as the mixing liqud, to accelerate the rate of reaction. Also employed were some other mixing liquids, such as solutions of soluble fluorides, calcium hydroxide or sodium silicate. Other factors that may affect the rate of setting and the attained strength include the particle size of the starting materials and the addition of HAp-seeds to the mix.

As in the reaction between DCP (or DCPH) and TeCP neither an acid nor a base are liberated, the pH of the liqud phase is supposed to stay close to the singular point for DCP (or DCPH) and TeCP, i.e. at around pH=7.4. However, in performed experiments a time dependent variation of the pH value was observed, apparently due to differences in the dissolution rate of both starting substances.

In our previous work on cementing reactions in the system CaO-SiO_2-P_2O_5-(H_2O) we observed that the rate of setting depended greatly on the pH of the liquid phase and that the hardening

process could be accelerated by the presence of soluble phosphates [Vanis 1996]. Inspired by these observations, in the present work we studied whether and to what an extent the setting/hardening process of DCP+TeCP based Ca-phosphate cement may be controlled in a similar way. The experiments were performed both on pastes made from a DCP+TeCP blend as well as on compacts produced by isostatic compaction, that were kept in various phosphate solutions.

EXPERIMENTAL

Preparation of the starting DCP+TeCP powder

The employed DCP was a commercial product with at purity of >99.5%

To produce TeCP in the laboratory, stoichiometric amounts of pulverized $CaCO_3$ were introduced into a concentrated $(NH_4)_2HPO_4$ solution under stirring, at 70-80°C. The suspension was stirred still for additional 7 hours and then dried at 110°C. The obtained residue was burnt in an electric furnace for 3 hours at 1350°C, to obtain pure TeCP, with a residual free lime content of < 0.1%.

$$4\,CaCO_3 + 2\,(NH_4)_2HPO_4 = Ca_4(PO_4)_2O + 4\,NH_3 + 3\,H_2O + 4\,CO_2 \qquad [2]$$

Equimolar amounts of DCP and TeCP were comminuted and blended by grinding the material in a laboratory ball mill for three days. The characteristics of the produced DCP+TeCP powder were as follows:

Particle size distribution (laser granulometry):

$D_5 = 0.5\ \mu m$
$D_{50} = 7.0\ \mu m$
$D_{95} = 76.1\ \mu m$

Specific surface area (BET_{N2}) = 4.6 m^2/g

Performed studies

For studying the setting characteristics, Na-, K- ad NH_4- phosphate solutions with different pH values were prepared by dissolving pertinent amounts of XH_2PO_4 and X_2HPO_4, where X = Na, K or NH_4, in water. Such solution were mixed with the DCP+TeCP powder in a ratio: 0.5 ml of solution per 1 g of powder. Similar mixes were prepared also with pure water. The progress of setting of the obtained pastes was studied by the Vicat needle penetration method. The results were expressed as curves in which the needle penetration depth was plotted as function of time.

The strength properties of the produced Ca-phosphate cement were studied both on pastes and on compacts. In the preparation of the pastes pure water or saturated solutions of Na_2HPO_4, K_2HPO_4 and $(NH_4)_2HPO_4$ were employed as mixing liquids. In all instances the liquid was mixes with the DCP+TeCP powder in a ratio: 0.5 ml of liquid per 1 g of powder. Test specimens 10x10x60 mm^3 prepared from the paste were cured in humid air at 20°C and tested for flexural and compressive strengths after different times of curing.

The compacts to be tested were produced by isostatic compaction in which the DCP+TeCP powder was exposed to a maximum pressure of 200 MPa. This way the porosity was brought down from an initial value of about 0.38 ml/ml (in samples exposed to a pressure of 0.1 MPa) to about 0.12 ml/ml in the produced compacts. This compaction procedure was selected to obtain low porosity, a uniform degree of conpaction and a homogenious texture within the whole sample. From the produced compacts (cylinders about 17 mm in diameter) test specimens 10x10x60 mm^3 were produced by cutting with a diamond saw and subsequent polishing. The produced specimens were then stored in the folowing liquids until testing: 1-2: pure water at 20°C and 80°C ; 3-5: saturated solutions of Na_2HPO_4, K_2HPO_4 and $(NH_4)_2HPO_4$ at 20°C and 6: a liqud whose ionic composition corresponded to that of the human body liquid [biosolution: Na^+ = 142 mMol; K^+ = 5 mMol; Mg^{+2} = 1.5 mMol; Ca^{+2} = 2.5 mMol; Cl^- = 147.8 mMol; HCO_3^- = 4.2 mMol; HPO_4^{-2} = 1 mMol; SO_4^{-2} =

0.5 mMol]. The flexural and compressive strength, modulus of elasticity and fracture energy values shown in Figure 2 and inTable 1 were determined on five parallel specimens.

X-ray diffraction and thermoanalytical studies were performed on samples in which the hardening reaction was stopped and the free water removed by the d-drying procedure.

RESULTS

Setting

Pastes prepared with pure water did not exhibit setting for at least 10 hours neither at 20°C nor at 80°C. The setting characteristics at 20°C of pastes in which phosphate solutions were employed as mixing liquids are shown in Figure 1. It appears that the rate of setting depended greatly on the pH value of the liquid phase. Up to about pH=7-8 mixes produced with any of the phosphate solutions set almost instanteniously, whereas at higher pH the setting process became well controllable and slowed down as the pH value increased.

Compressive strength development of pastes

Pastes produced from the DCP+TeCP powder by mixing it with water did not exhibit measurable strength even after 28 days of curing, whereas those in which saturated phosphate solutions were used as mixing liquids attained distinct strengths within a few days.The results found in these pastes are shown in Figure 2. It appears that the obtained strength values depended greatly on the phosphate solution employed and increased in the order Na-phosphate < NH_4-phosphate < K-phosphate.

Compressive strength development of compacts

Figure 2 shows also the compressive strength development of DCP+TeCP compacts after storing them in different solutions for different periods of time and at different temperatures. It appears that the strength of the material depended greatly on the liquid in which it was stored. Remarkably, test specimens stored in the K-phoshate solution exhibited significantly higher strengths than those stored in solutions of Na- or NH_4-phosphate. Samples stored in pure water at 20°C exhibited also measurable strengths, however, the strength value found at any curing time were lower than those of samples stored in phosphate solutions. Expectedly, an increase of the water temperature from 20°C to 80°C resulted in a distinct increase of the strength values. Test specimens stored in the "bio-solution" developed their strength at the beginning rather slowly, however, they exhibited high strength value after 7 and 28 days.

Physico-mechanical properties of compact.

Table 1. shows the 28-day compressive and flexural strength, modulus of elasticity and work of fracture values of the compacted material. All these parameters varied in a wide range, depending on the liquid in which the test specimens were stored and on the employed temperature. They were highest in samples stored in the K-phosphate solution and lowest in those kept in plain water at 20°C.

Reaction products

The phase composition of the DCP+TeCP compacts stored in different solutions was studied by X-ray diffraction. After 28 days, in samples stored in the K-phosphate solution, just as in those stored in the "bio-solution" neither non-reacted dicalcium nor tetracalcium phosphate could be identified, indicating a complete consumption of these original calcium phosphates in the hardening reaction. Hydroxyapatite was found as the sole crystalline phase present. Contrary to that, distinct amounts of dicalcium phosphate and tetracalcium phosphate, besides of hydroxyapatite, were still found in all remaining samples. The amount of these phases was distinctly lower in the materal cured in water at 80°C than in that stored at 20°C.

Table 1. Physico-mechanical properties of DCP+TeCP compacts after curing 28 days in different solutions

	Compr. str. (MPa)	Flex. str. (MPa)	E-modulus (GPa)	Fract. energy (Nm/m^2)
H_2O - 20°C	29.4	5.8	22.3	37.9
H_2O - 80°C	50.3	14.6	29.9	146.2
Na_2HPO_4 - 20°C	36.4	14.5	31.3	129.5
K_2HPO_4 - 20°C	125.3	28.6	43.7	471.2
$(NH_4)_2HPO_4$ - 20°C	31.2	14.6	30.6	133.5
Bio-solution - 37°C	91.1	15.2	34.6	148.9

In thermogravimetry studies the hardened d-dried samples exhibited a thermal decomposition associated with an almost contineous weight loss at temperatures above about 50°C (Figure 3). The samples did not exhibit a noticeable shrinkage, as measured by thermodilatometry, up to about 1000°C, however, they shrank distinctly between about 1000°C and 1450°C.

DISCUSSION AND CONCLUSIONS

The obtained results revealed a significant accelerating effect of alkali and ammonium phosphates on the rate of the reaction between dicalcium and tetracalcium phosphate, yielding hydroxyapatite. It is remarkably, however, that the rate of the reaction depended not only on the presence of orthophosphate anions in the liquid phase, but also on the quality of the pertinent cation. Not unexpectedly, the rate of reaction was accelerated also by increasing the curing temperature.

Another factor that was found to exhibit an effect on the rate of setting and probably also on the overall rate of reaction was the pH of the liquid used in the preparation of the calcium phosphate cement pastes. Thus, the setting time of such pastes may be conveniently controlled just by altering the pH of the employed alkali or ammonium phosphate solution.

Expectedly, hydroxyapatite was identified as the sole crystalline reaction product by XRD. However, the way how the hardened material thermally decomposed suggests that, in addition to a well crystallized form that decomposes at temperatures of around 1300°C, some of it may have been formed in a highly dispersed form decomposing at distinctly lower temperatures. There exists also the possibility that some additional non-crystalline C-P-H products were formed in the hardening process.

The existing strength differences found after 28 days of curing appear to be mainly due to differences in the degree of DCP+TeCP conversion to HAp. The differences between strength values found in pastes and compacts are obviously mainly due to different degrees of porosity existing in both types of samples.

In the performed experiments we were also able to demonstrate a conversion of the prepared

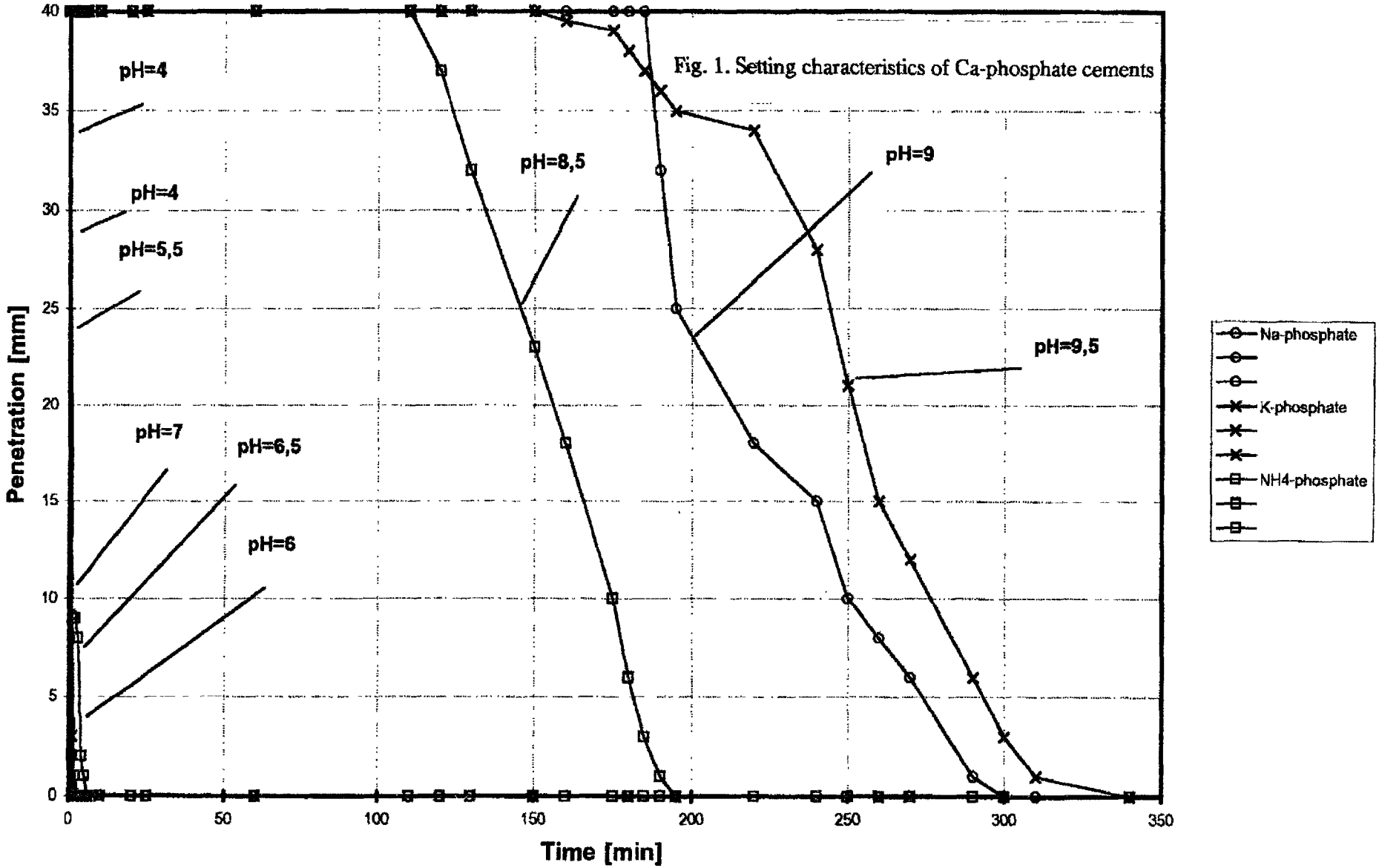

Fig. 1. Setting characteristics of Ca-phosphate cements

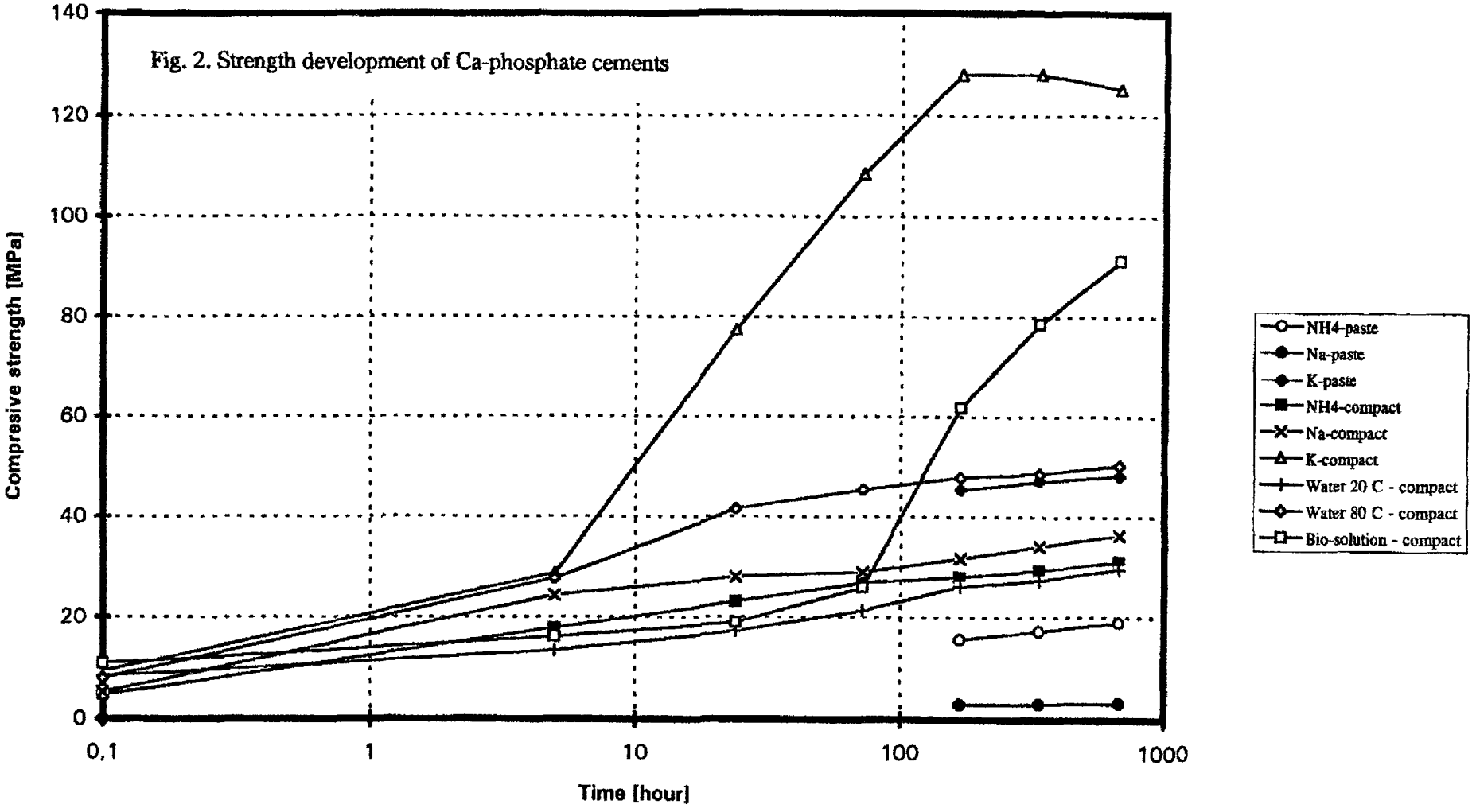
Fig. 2. Strength development of Ca-phosphate cements
Compresive strength [MPa]
140
120
100
80
60
40
20
0
0,1
1
10
100
1000
Time [hour]
NH4-paste
Na-paste
K-paste
NH4-compact
Na-compact
K-compact
Water 20 C - compact
Water 80 C - compact
Bio-solution - compact

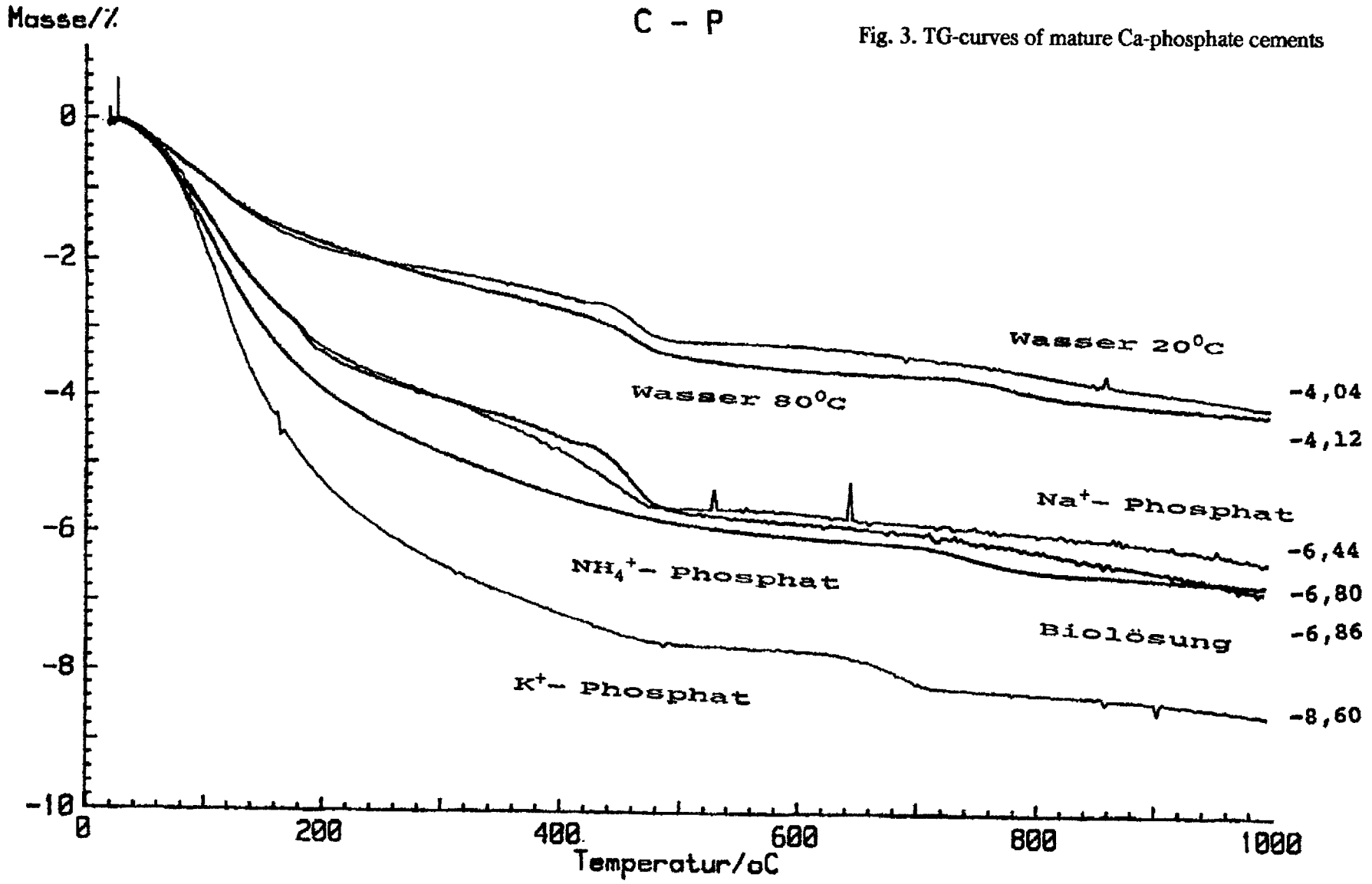

Fig. 3. TG-curves of mature Ca-phosphate cements

DCP+TeCP compacts to a high strength, hydroxyapatite based material in a solution whose ionic composition corresponded to that of the human body fluid. Such results suggest the possibility of using DCP+TeCP compacts in such surgical applications, where the in vivo conversion of the material to hydroxypatite, rather than a direct implantation of hydroxyapatite based implants, may be beneficial.

REFERENCES

Brown, P. W. and Chow, L.C., "A New Calcium Phosphate, Water-Setting Cement" , in.: P.W.Brown (ed.): Cement Research Progress, American Ceramic Society Westerville OH 1986, pp.353-379.

Brown, P.W., Sample, D. and Hocker, N., "The Low Temperature Formatiom of Synthetic Bone", Mat. Res. Soc. Symp. Proc., Vol. 179, 1991, pp. 41-49.

Brown, P.W., "Phase Relationship in the Ternary System CaO-P_2O_5-H_2O at 25°C", J. Am. Ceram. Soc., Vol. 75, 1992, pp. 17-22.

Chow, L.C., Takagi, S., Constantino, P.D. and Frieman, C.D., "Self Setting Calcium Phosphate Cements", Mat. Res. Soc. Symp. Proc., Vol. 179, 1991, pp. 3-24.

Monma, H., Goto, M. and Kohomura, T., "Effect of Hydration and Hardening of Tricalcium Phosphate", Gypsum and Lime, Nr. 188., 1984, pp. 11-16.

Monma, H.; "On Hydraulic Calcium Phosphates", in: Proc. Mat. Res. Soc. Internat. Meeting. on Advanced Materials, Vol. 13, Tokyo 1988, pp.15-19.

Vanis, P. and Odler, I.. "Hydration Reactions in the System CaO-P_2O_5-SiO_2-(H_2O)" J. Am. Ceram. Soc., Vol. 79., 1996, pp. 1124-1126.

Wiliams, D.F.(ed.), "Medical and Dental Materials", Material Science and Technology Vol. 14, VCH Weinheim 1992

Xie, l. and Monroe, A.A., "Calcium Phosphate Dental Cements", Mat. Res. Soc. Symp. Proc., Vol. 179, 1991, pp. 25-39.

Topic II.C

Structural models for hydrated cementitious pastes

2ii064
7 pp

Kn o. 2 5. JAN. 2001 d o k 31828

THE ROLE OF MgO IN THE SYNTHESIS OF C-S-H AND TOBERMORITE

Zdzisław PYTEL, Jan MAŁOLEPSZY, University of Mining and Metallurgy, Department of Material Science and Ceramics, Cracow, Poland

ABSTRACT The effect of Mg^{2+} on the reaction in the CaO, SiO_2 and MgO containing mixtures in hydrothermal conditions was investigated. It has been found that the magnesium ions are incorporated to the calcium silicate hydrate structures in a limited amount. The excess Mg admixture can produce the magnesium silicate hydrate phase. Additionally, the influence of Mg^{2+} ions on the morphology of tobermorite crystals was observed.

Key-words: CSH, tobermorite, magnesium oxides, synthesis, microstructure

INTRODUCTION

The calcium silicate hydrates are produced usually during the autoclaving of lime-sand or lime-silica mixtures. At temperatures not exceeding 180°C, C-S-H or tobermorite are formed as main hydration products, depending on the duration of thermal treatment (Taylor, 1964). These phases affect significantly the practical properties of autoclaved building materials.

Tobermorite was found by Heddley, as a naturally occurring mineral in Tobermory, Scotland, in 1880. In some other places (Ireland, California, Japan), tobermorite occurs as a component of the so-called contact zones. However, it is known mainly as a synthetic mineral produced from different lime- and silica-bearing components under the saturated steam pressure, at 110° to 180°C. The first synthesis of 1.13 nm tobermorite was carried out by Flint, McMurdi and Wells, in 1938 (Flint et al, 1938). It was subsequently synthesized and examined by Heller and Taylor (Heller, 1951) as well as by Kalousek (Kalousek, 1955a). The tobermorite phase was produced from lime or cement mixtures with quartz or amorphous silica.

The synthesis of tobermorite is carried out in heterogeneous lime-silica suspensions. The reactions proceeds through several intermediate stages in which the poorly crystalline materials are formed, with varying C/S molar ratio (Rademaker and Reiman, 1994). At temperatures close to 180°C calcium silicate hydrate transforms to crystalline 1.13 nm tobermorite, with definite chemical composition, given by the formula $C_5S_6O_{18}H_2{\cdot}4H_2O$. However, the tobermorite material is not stable, and undergoes further transition to xonotlite or gyrolite as the temperature or duration of hydrothermal treatment increases.

The foreign ions in the structure of tobermorite have been the subject of special interest. The substitution of Ca^{2+} by several cations, e.g. Co^{2+}, Pb^{2+}, Cd^{2+} and Ni^{2+} but not Cr^{6+} were reported (Komarneni et al, 1986). The possibility of Ca^{2+} replacement by Mg^{2+} was also reported (Shrivastava et al, 1991). However, it should be underlined that these substitutions were carried out by ionic exchange between the crystalline tobermorite and solution of concentration in the range 100 to 1000 ppm. On the other hand there are not many reports of substitution during the synthesis of tobermorite; this means the process in which tobermorite is produced from the mixture containing the substituting components.

There are different opinions dealing with the position of Mg^{2+} in the structure of 1.13 nm tobermorite. According to data reported by Petrovič (Pertovič, 1973a, 1974b) and Mitsuda (Mitsuda, 1973a), the isomorphous substitution of Ca^{2+} by Mg^{2+} does not occur. Only the paragenesis of calcium and magnesium silicate hydrates is possible on autoclaving. Another point of view was presented by Diamond (Diamond et al, 1966). This author confirmed the occurrence of isomorphous substitutions in tobermorite and determined their limits; a 7.5% limit of Mg^{2+} substitution was thus found.

EXPERIMENTAL

Sample preparation

The tobermorite was produced from silica and lime admixtured with periclase. The two siliceous components were used: colloidal SiO_2 and quartz. The CaO was produced by thermal dissociation of analytically pure $CaCO_3$ at 1150°C for 4 hours. The MgO-periclase was produced by $Mg(OH)_2$ dehydration at 1300°C for 1 hour. The materials were preliminary ground to pass a 63 μm sieve.

Two variant procedures of tobermorite preparation were applied. In the first, the initial mixture with constant C/S molar ratio equal 5:6=0.83 (denoted as M), i.e. corresponding to „theoretical" tobermorite was doped with variable amount of periclase. In this way samples containing 0, 5, 10, 15, 20 and 40% MgO added in relation to the CaO constant content in the basic batch were prepared. Thus a series of constant C/S and (C+M)/S varying in the range 0.83 to 1.27 was produced. In the second series, samples were prepared at constant (C+M)/S=0.83 molar ratio with variable C/S molar ratio respectively (denoted as KGM0). The C/S molar ratio decreased because of gradually lowered CaO content. Every 0.2 mole CaO was replaced by an equivalent MgO portion.

The particular components were carefully weighted, homogenized as dry materials and subsequently mixed with distilled water free of CO_2 to produce pastes. These pastes were placed in "Teflon" containers and autoclaved in laboratory autoclaves at constant temperature 180°C, for 2, 4, 8, 12, 48 and 72 hours respectively. The samples were subsequently treated with acetone, to stop the hydration process, and dried at 50°C. The materials thus obtained were subjected to the phase composition and microstructure determination. For this purpose the following techniques were applied: DTA, TG, XRD, FTIR, SEM and EDS.

Results and discussion

In the mixtures composed of CaO, MgO and SiO_2 at constant C/S=0.83 and variable (C+M)/S molar ratio, calcium silicate hydrate is produced as a basic material in hydrothermal conditions at 180°C. The transition of structure from nearly amorphous C-S-H to the crystalline tobermorite is a function of time. In short reaction times (2, 4 and 8 hours) amorphous C-S-H is a dominating product. A considerable amount of tobermorite is produced at longer autoclaving times. C-S-H is identified on XRD pattern from the strongest, broadened peak corresponding to d=0.307 nm. On the DTA curve, in turn, it is identified from the endothermic peak in the range 80° to 190°C, attributed to C-S-H dewatering (Fig. 1).The H_2O in the C-S-H structure is also seen on the IR curves, as 1640 and 3440 cm^{-1} bands (Fig. 2). The sharp exothermic peak on the DTA curve at 795°C, attributed to formation of wollastonite, proves additionally the formes presence of calcium silicate hydrate. In Fig. 3 the microstructure of gel-like C-S-H is shown. The C/S on the fractured surface was estimated to be 1.5; this implies that this product is C-S-H(I). For longer autoclaving times the tobermorite phase was produced, with characteristic, skeletal octahedral, plate-like crystals (Fig. 4). The C/S molar ratio for this phase was determined to be 0.8, it close to the theoretical value. The presence of tobermorite was also confirmed in the IR spectrum.

In the presence of MgO amorphous and crystalline hydration products are formed, depending on the time of thermal treatment. At 180°C for 8 hours synthesis time the C-S-H content increase is observed to the maximum value in M15 and subsequently, a reduction of C-S-H takes place with increase of tobermorite content. It means that magnesium ions lower the limit of stable tobermorite formation and thus accelerates the tobermorite crystallisation. A similar trend is observed in the products of 72 hour synthesis, in which the tobermorite phase dominates. In the presence of MgO, the morphology of tobermorite is strongly affected. The elongation of plate-

like crystals gives way to lath-like or needle-like forms; xonotlite fibrous crystals are also observed. These crystals are localized in the pores, as can be seen in Fig. 5.

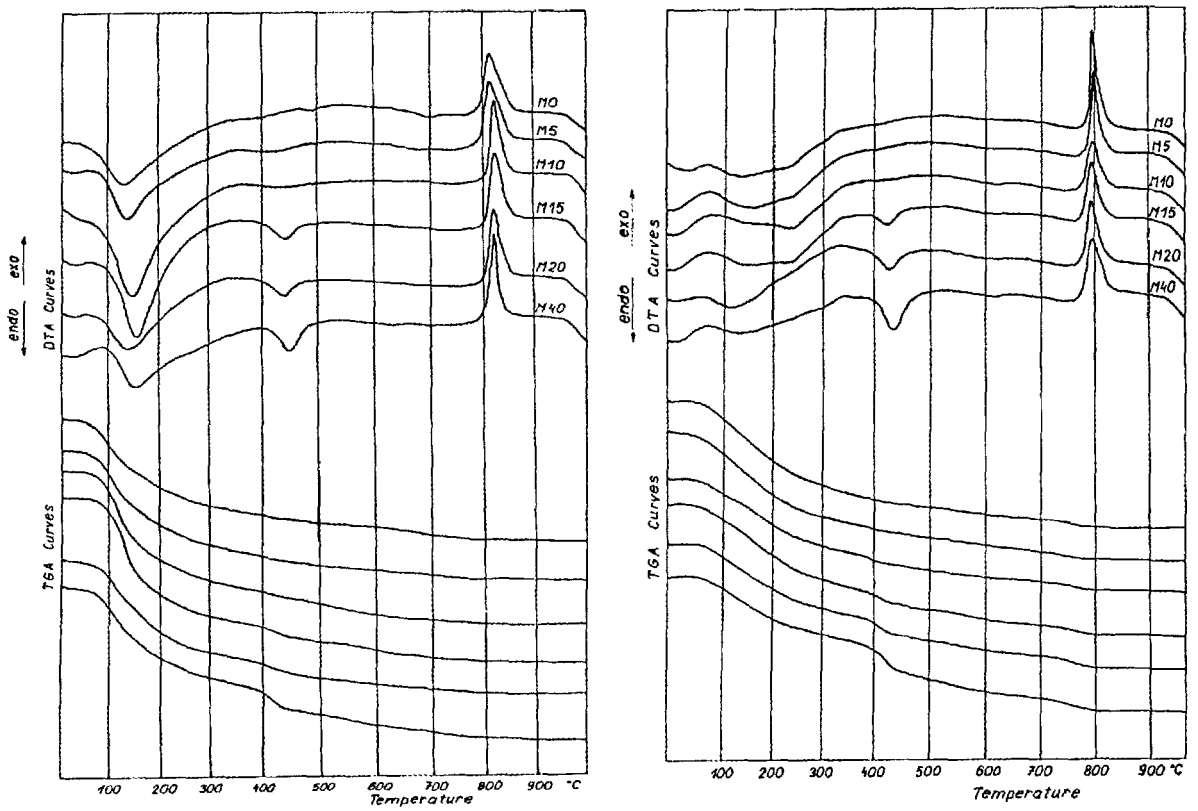

Figure 1. Thermal date of autoclaved samples with constant C/S and variable (C+M)/S ratio: after 8 hours hydrothermal treatment (left), after 72 hours hydrothermal treatment (right)

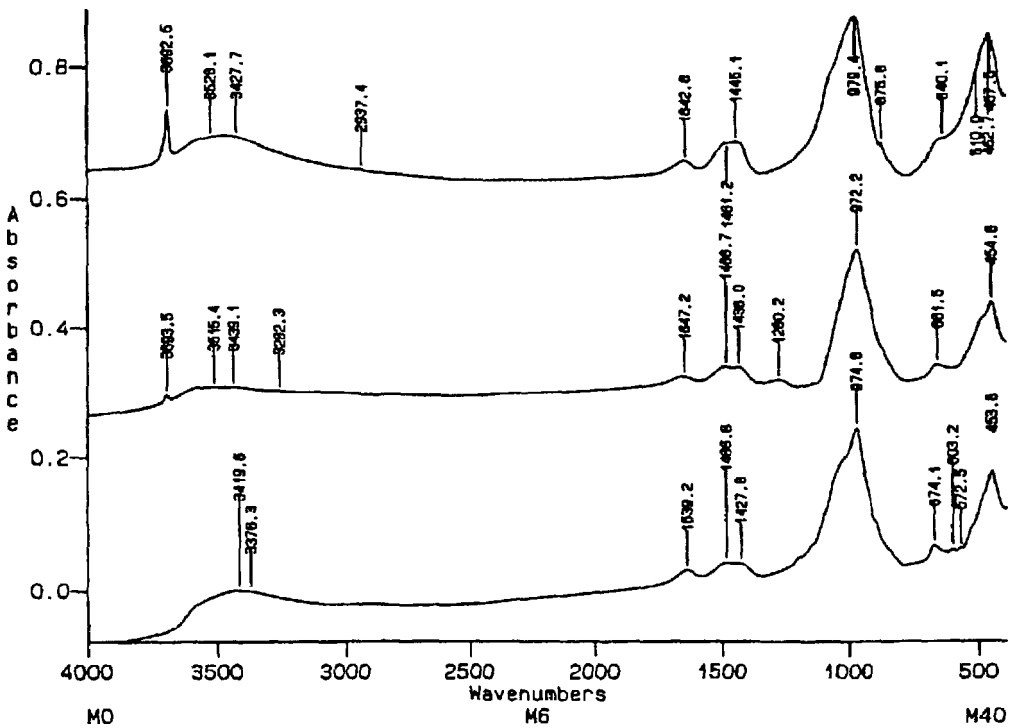

Figure 2. Infrared spectra of autoclaved samples with constants C/S and variable (C+M)/S ratio

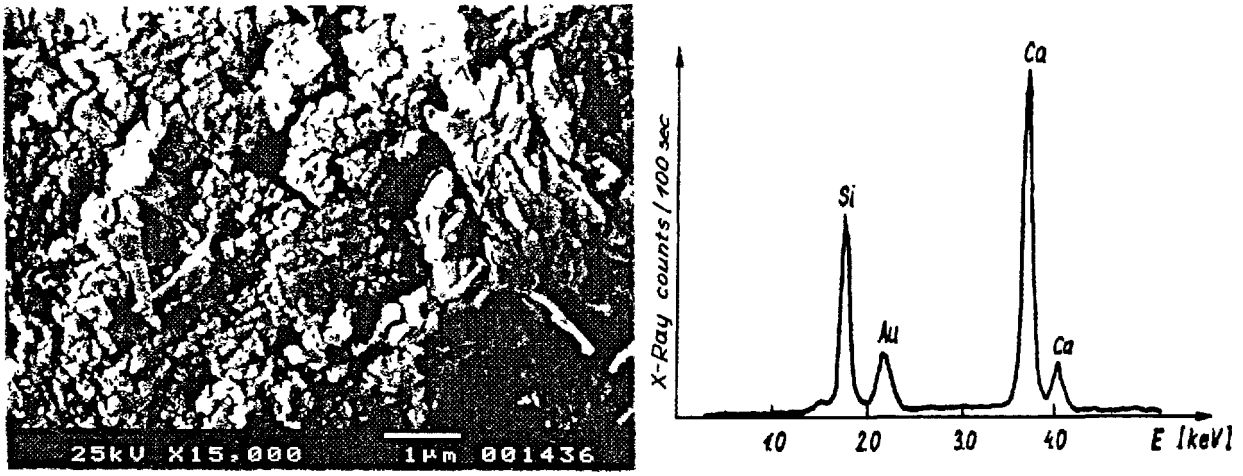

Figure 3. Scanning electron micrograph of C-S-H phase with EDS analyse

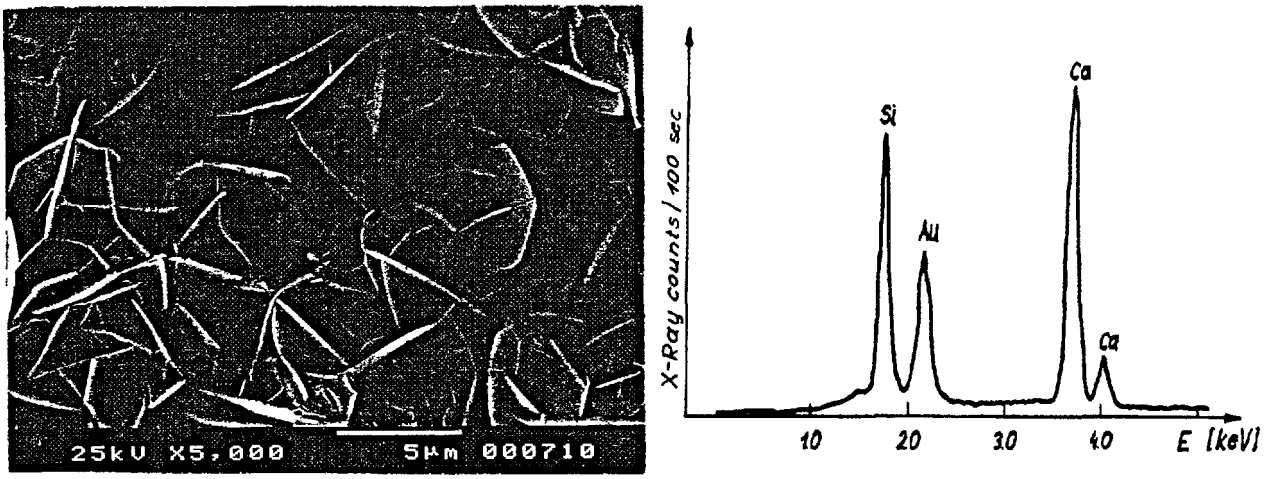

Figure 4. Scanning electron micrograph of tobermorite with EDS analysis

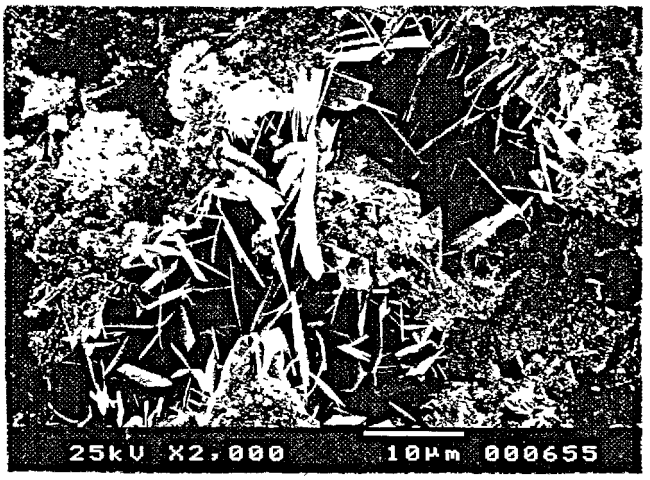

Figure 5. Scanning electron micrograph of tobermorite and xonotlite

In the mixtures prepared at constant (C+M)/S and variable C/S molar ratios similar results to those described above have been obtained only for the samples with higher CaO and low MgO contents. There are the samples of the following composition. $C_{0.8}/S_{1.0}$ (KGM0), $(C_{0.6}+M_{0.2})/S_{1.0}$

(KGM02) and $(C_{0.4}+M_{0.4})/S_{1.0}$ (KGM04). The DTA curves of these samples are plotted in Fig. 6. One can notice that the tobermorite is a main product in the Mg doped samples, irrespectively from the time of autoclaving.

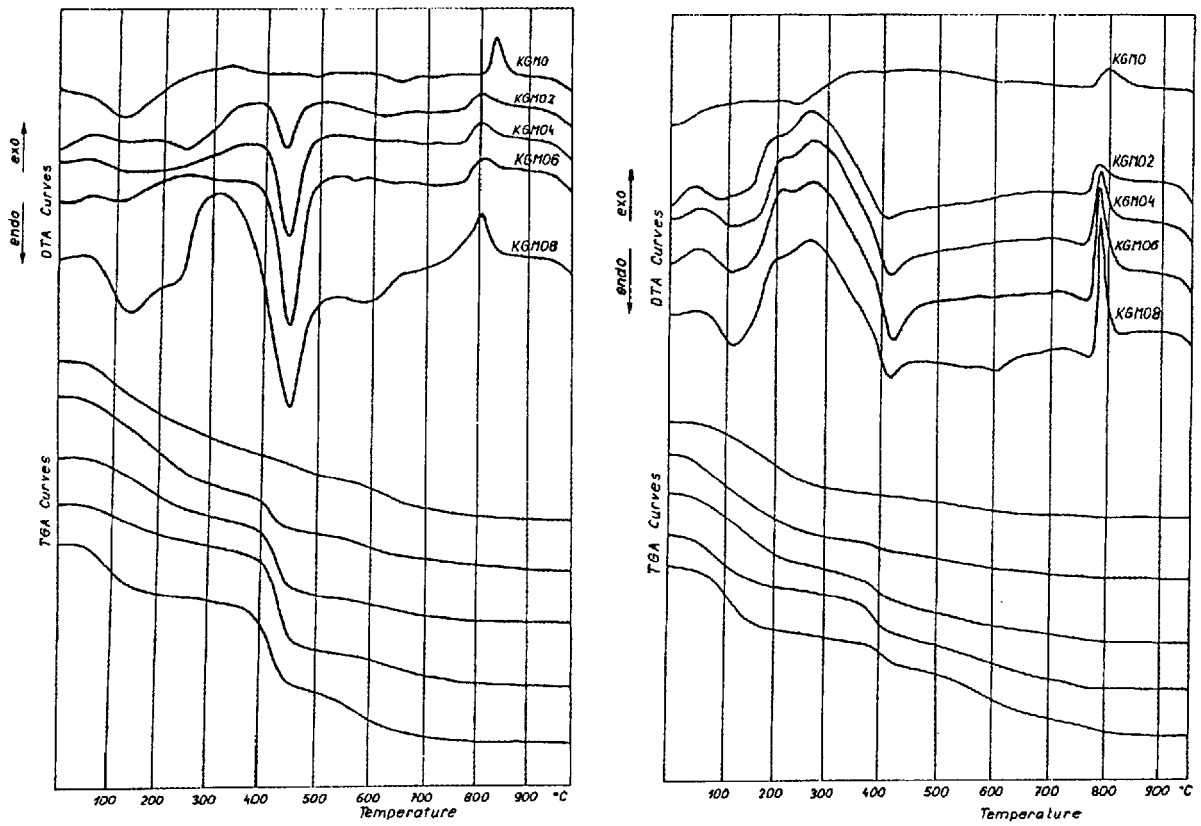

Figure 6. Thermal data of autoclaved samples with constant (C+M)/S and variable C/S ratio: after 8 hours hydrothermal treatment (left), after 72 hours hydrothermal treatment (right)

Unreacted $Ca(OH)_2$ was detected only in the KGM08 hours autoclaved sample, without MgO, in which the C-S-H of C/S=1.5 was produced. In turn, in the 72 hours autoclaved sample of the same composition the tobermorite was present exclusively. Therefore one can conclude that the Mg ions accelerate the transformation C-S-H → tobermorite in such a way that the Mg ions are incorporated to the structure of tobermorite and a solid solution is thus produced. The upper limit of tobermorite stability is also reduced by the presence of Mg. The tobermorite phase transforms more easily to xonotlite, as observed under SEM.

Quite different results were obtained for the samples with MgO content higher than CaO, i.e. in $(C_{0.2}+M_{0.6})/S_{1.0}$ (KGM06) and $M_{0.8}/S_{1.0}$ (KGM08). The rate of hydration in these mixtures is low - after 8 hours treatment an unreacted residue of quartz, brucite and portlandite is observed. The hydration products are composed of C-S-H and M-S-H in mixture without CaO, a product of amorphous character. The latter phase is evidenced by d=0.67 and d=0.304 nm XRD peaks. Obviously, the progress of reaction in the mixtures subjected to 72 hours autoclaving is clearly seen - the portlandite peaks on the XRD pattern disappear while those for brucite become significantly weaker. The magnesium silicate hydrate occurring as the main hydration product, identified from the set of XRD data, viz. d=1.022 to 1.134, 0.456 and 0.248 to 0.256 nm. These results correspond well with those reported by Kalousek (Kalousek, 1954b) and Mitsuda (Mitsuda, 1977b). The M-S-H gel is the first product between the magnesium hydroxide and silica, with M/S molar ratio 1.5. The cryptocrystalline magnesium silicate is formed as an

intermediate product in the synthesis of talc or chrysotile. In the presented study the M/S molar ratio was estimated for 0.7; the microstructure of M-S-H gel is shown in Fig. 7.

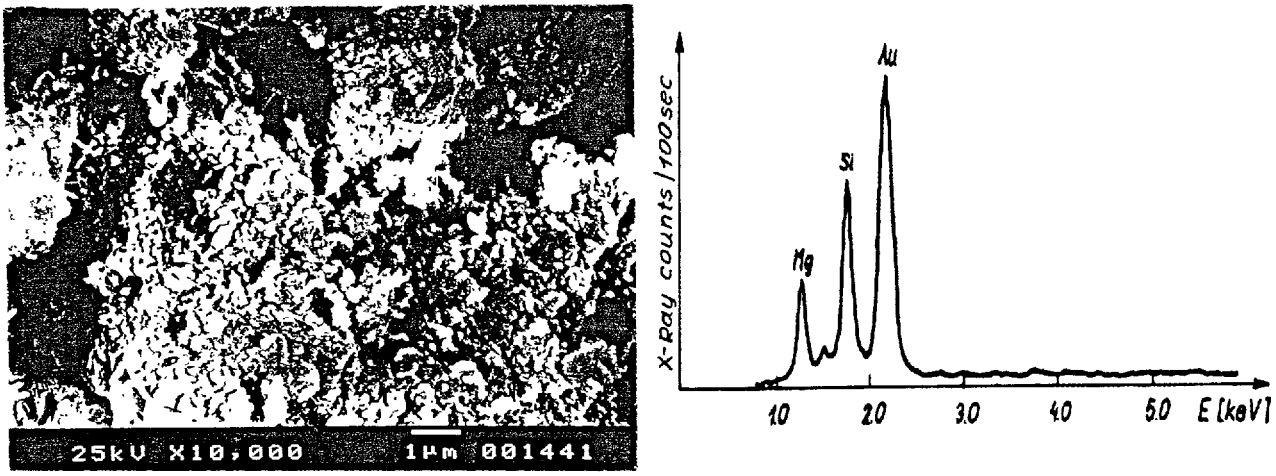

Figure 7. Scanning electron micrograph of M-S-H gel with EDS analyse

Irrespectively of time of thermal treatment, the brucite appears at MgO content not lower than 6% (sample M15). The free brucite content increases with MgO in the samples M20 and M40. At lower MgO content, i.e. in M5 and M10, brucite is not observed. This means that the Mg^{2+} from $Mg(OH)_2$ dissociation forms isomorphic substitutions in the structures of C-S-H and tobermorite, up to a certain limit; the excess occurs as brucite. The decreasing $Mg(OH)_2$ in samples M20 and M40 prove that Mg^{2+} reacts with the silicate component to produce a magnesium silicate phase. This is observed as a crystalline product only after at longer time of thermal treatment.

Summary

At 180°C, the crystallinity of final products depends on the duration of thermal treatment. At shorter times (2, 4, 8 hours respectively); nearly amorphous hydration products are observed, mainly so-called C-S-H. Crystalline tobermorite appears with time. The amount and structure of hydration products is influenced by Mg^{2+} ions. C-S-H synthesis is accelerated at MgO additions up to 6.03%, upon 8 hour autoclaving. Subsequently, an acceleration of tobermorite crystallisation occurs. The Mg^{2+} ions are incorporated to the structure of products. The limiting value for MgO diluted in the structure approximately 6.0%. Any excess MgO is hydrated to form brucite or, at longer times, react with the siliceous component producing a magnesium silicate hydrate of poorly developed structure. The morphology of tobermorite crystals is strongly affected by the presence of Mg^{2+} ions. The elongation of skeletal octahedral tobermorite plates disappears with increased MgO contents and needles or fibres appear.

REFERENCES

Diamond, S., White, J.L., and Dolch, W.L.,"Effects of Isomorphous Substitution in Hydrothermally-Synthesized Tobermorite", American Mineralogist, Vol. 51, 1966, pp. 388-401.

Flint, E.P., McMurdi, H.F., Wells, L.S., J. Res. Nat. Bur. Stand., Vol. 21, 1938, p. 617.

Heller, L., Taylor, H.F.W., J. Chem. Soc., 1951, p. 2397.

Kalousek, G.L.,"Tobermorite and Related Phases in the System $CaO-SiO_2-H_2O$", Journal of the American Concrete Institute, Vol. 26, No 10, June 1955, p. 989-1011.

Kalousek, G.L. and Mui, D.,"Studies on Formation and Recrystalization of Intermediate Reaction Products in the System Magnesia-Silica-Water", Journal of the American Ceramic Society, Vol. 37, No 2, 1954, pp. 38-42.

Komarneni, S., Roy, R., Roy, D.M.,"Pseudomorphism in Xonotlite and Tobermorite with Co^{2+} and Ni^{2+} Exchange for Ca^{2+} at 25°C", Cement and Concrete Research, Vol. 16, 1986, pp. 47-58.
Mitsuda, T., "Paragenesis of 1.1 nm tobermorite and poorly crystalline hydrated magnesium silicate", Cement and Concrete Research, Vol. 3, 1973, pp. 71-80.
Mitsuda, T., Taguchi, H.," Formation of magnesium silicate hydrate and its crystalization to talc", Cement and Concrete Research, Vol. 7, 1977, pp. 223-230.
Pertovič, J.,"The system $CaO-MgO-SiO_2-H_2O$ underhydrothermal conditions"-part I, Silicaty, Vol. 17, No. 4, 1973, pp. 311-317.
Petrovič, J.,"The system $CaO-MgO-SiO_2-H_2O$ at 150°C - 350°C under hydrothermal conditions" -part II, Silicaty, Vol. 18, No. 1, 1974, pp. 61-67.
Rademaker, P.D., Reiman, V.,"Autoclaving calcium silicate bricks", Zement-Kalk-Gips, Vol. 47, No. 11, 1994, pp. 636-642.
Shrivastava, O.P., Komarneni, S., Breval, E.,"Mg^{2+} uptake by synthetic tobermorite and xonotlite", Cement and Concrete Research, Vol. 21, 1991, pp. 83-90.
Taylor, H.F.W.,"The Chemistry of Cements", Academic Press, London and New York, Vol. I, 1964, Chapter 5: "The Calcium Silicate Hydrates", pp. 167-232.

2ii065
5 pp

Kn o. 2 5. JAN. 2001 d o k 31829

THERMAL BEHAVIOUR OF TOBERMORITE INTERCALATED WITH ALKALI IONS

Naomichi HARA, Norihiro INOUE and Hiroaki NOMA
Kyushu National Industrial Research Institute, Tosu, Japan

ABSTRACT Normal type 1.1 nm tobermorite could be transformed into anomalous or mixed type by immersing in aqueous alkali solutions such as NaOH, KOH, NaCl and KCl solutions. When the resulting anomalous or mixed type was rinsed in water, normality was recovered. These results suggest that alkali ions are reversibly intercalated between the layers of tobermorite to increase anomaly, where alkali ions function as hydrated ions binding water molecules in their immediate vicinity.

Key-words: Tobermorite, Alkali, Ions, Mobility, X-ray Powder Diffraction

INTRODUCTION

Tobermorite (1.1 nm) is classified into three types according to its thermal behaviour, viz. 1) normal type (Taylor, 1964), which is converted to 0.9 nm tobermorite by dehydration in heating in the air at about 300°C, 2) anomalous type (Gard and Taylor, 1957), which keeps the basal spacing at about 1.1 nm even after dehydration, and 3) mixed type (Chatterji, 1973), which shows an intermediate behaviour between normal and anomalous types. However, all the types are converted to β-wollastonite in further heating in the air at about 800°C.

Hara and Inoue (1980) investigated relationships among thermal behaviour, synthetic conditions and lattice parameters of hydrothermally synthesized 1.1 nm tobermorite and have clarified that factors which decrease the lattice parameter c_o, viz. decrease of Ca/Si and H_2O/Si mole ratios, increase of crystallinity and the presence or addition of alkalis accelerate the formation of anomalous type, but the presence or addition of aluminium ions, which increases the lattice parameter c_o, accelerates the formation of normal type. Normal type is transformed into anomalous type via mixed type in prolonging the reaction time, which results in the increase of crystallinity of tobermorite.

In an extension of these studies, the present authors found out that normal type tobermorite was easily transformed into anomalous or mixed type only in immersing in aqueous alkali solutions. This and some other findings are reported in this paper.

METHODS AND RESULTS

Preparation of normal type tobermorite

In hydrothermal preparation of 1.1 nm tobermorite, starting Ca/Si mole ratio and reaction time affect thermal behaviour of the resulting tobermorite as shown in Table 1 (Hara and Inoue, 1980).

Table 1 Basal spacing (nm) of tobermorite after heated at 400°C for 20 hours.

Reaction time hours	Starting Ca/Si mole ratio			
	0.6	0.7	0.8	0.9
6	1.09–0.98 m	0.99–0.96 m	1.13 a	–
12	1.13 a	1.03 m	0.97 n	0.96 n
24	1.13 a	1.13 a	1.13 a	1.10–0.97 m

n : normal type; a : anomalous type; m : mixed type.

Namely, low Ca/Si mole ratio is favourable for the formation of anomalous type but high Ca/Si mole ratio for normal type. Increase of reaction time increases the anomaly of tobermorite. Based on these results, the starting Ca/Si mole ratio and reaction time for the preparation of normal type 1.1 nm tobermorite to be used for the following experiments were set at 0.8 and 12 hours, respectively.

A slurry with Ca/Si mole ratio 0.8 and water/solid weight ratio 3 was prepared from quartz (Ig loss 0.38, SiO_2 98.13, Al_2O_3 1.16, Fe_2O_3 0.04, Na_2O 0.10, K_2O 0.14 %; Blaine specific surface area 319 m^2/kg), CaO obtained by calcining precipitated $CaCO_3$ at 1,100°C and water, and reacted in an autoclave at 180°C for 12 hours. The resulting slurry was dried and ground in an agate pot mill. The reaction product was 1.1 nm tobermorite. In heating in the air at 400°C for 20 hours, it was converted to 0.9 nm tobermorite with the basal spacing 0.96 nm, which was a typical normal type tobermorite.

A batch of thus prepared normal type tobermorite was divided into small portions and each portion was given for immersion-treatment under various conditions as follows:

Effect of immersing temperature and time

Firstly, normal type tobermorite was immersed in 50 times (by weight) 0.5 % NaOH and KOH aqueous solutions at temperatures ranging from 20° to 80°C for 24 hours. As a control, a portion of the same tobermorite was immersed in deionized water under the same conditions. After immersion-treatment, excess water was removed by decantation and each residue was freeze-dried. The resulting sample was heated in an oven at 400°C for 20 hours and then given for x-ray diffractometry. Thermal behaviour of tobermorite was discussed due to the change of basal spacing of heated tobermorite thus determined by x-ray diffractometry.

The relationship between immersing temperature and basal spacing of heated tobermorite is summarized in Fig 1. Tobermorite immersed in deioinized water showed a slightly larger basal spacing after heated compared with the untreated one (original) but still within the range

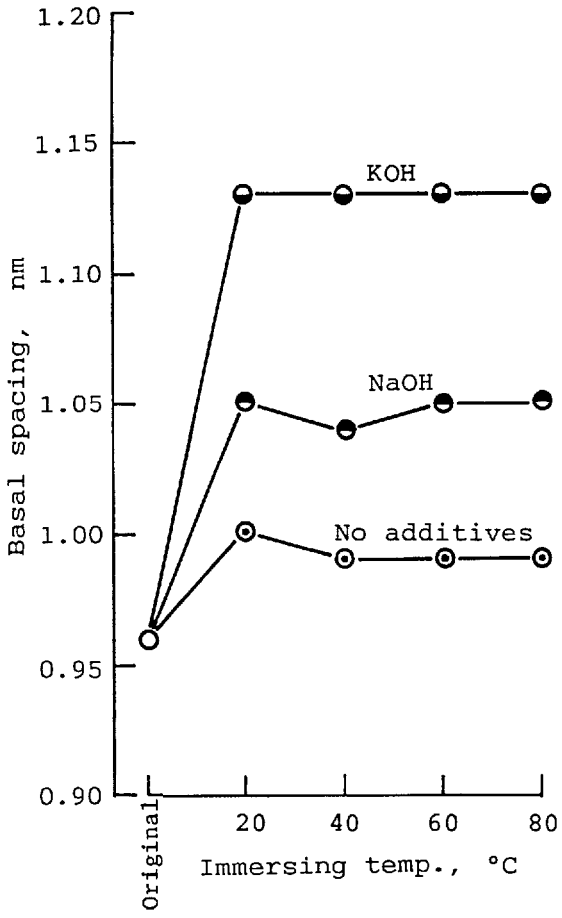

Figure 1 Immersing temperature vs basal spacing of tobermorite after heated at 400°C for 20 hours.

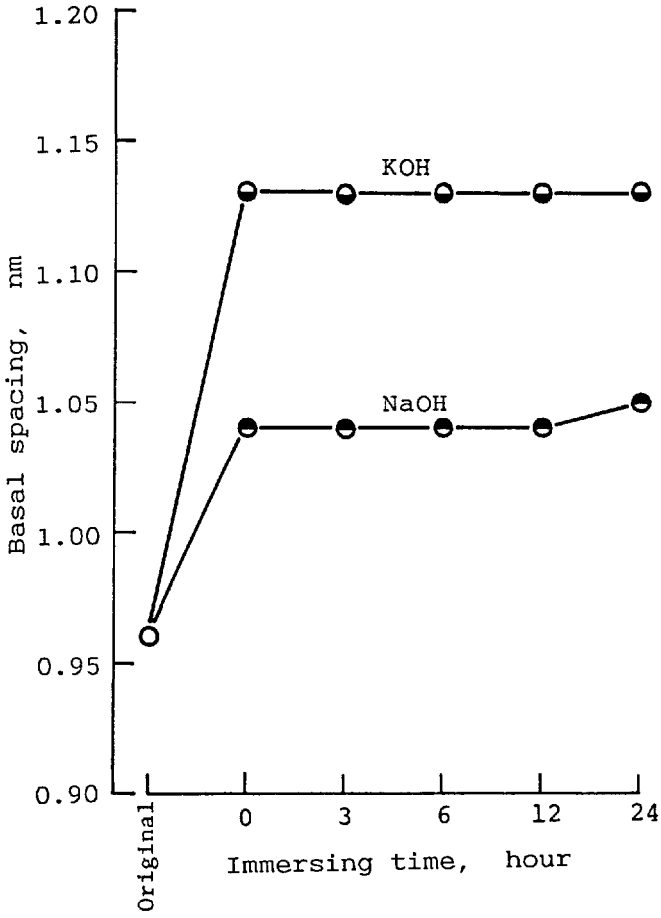

Figure 2 Immersing time vs basal spacing of tobermorite after heated at 400°C for 20 hours.

classified as normal type. Immersion in NaOH solution gave mixed type having the basal spacing after heated 1.05 nm and in KOH solution anomalous type having the basal spacing after heated 1.13 nm. Namely, the presence of alkali ions increased anomaly even at room temperature, and K^+ ions were remarkable in its effect.

Secondly, effect of immersing time was investigated in the range from 0 to 24 hours at temperature fixed at 20°C. The sample taken out from alkali solutions as soon as immersed was designated as "0 hour". The relationship between immersing time and basal spacing of heated tobermorite is summarized in Fig 2. In spite of the length of immersing time, short or long, normal type tobermorite was transformed into anomalous type in KOH solution and into mixed type in NaOH solution. In NaOH solution, anomaly of tobermorite was increased a little by prolonging the immersing time from 12 to 24 hours as shown in Fig 2 as increase of the basal spacing.

Effect of alkali concentration

In the above experiments, normal type tobermorite was immersed in 50 times (by weight) alkali solution, and then about 80 % alkali solution was removed by decantation before freeze-drying. As the result, about 5 % (by weight) alkali still remained in freeze-dried tobermorite. In order to clarify the effect of alkali concentration, immersion-treatment was carried out by using alkali solutions with various concentrations. NaOH and KOH aqueous solutions with various concentrations were prepared to have solid alkali/tobermorite weight ratio after freeze-drying ranging from 0.1 to 5 %. Immersing temperature was set at 20°C. Normal type tobermorite was immersed in 50 times (by weight) solution and taken out instantly. This procedure corresponds to "immersing time 0 hour" in the above experiment shown in Fig 2. The following procedures were the same as the abovementioned experiments. The relationship between alkali concentration and basal spacing of heated tobermorite is summarized in Fig 3. Vertical lines extending from circular dots in Fig 3 correspond to the broadening of x-ray diffraction line width of respective basal spacings, which was caused by low crystallinity of corresponding tobermorite. In both NaOH and KOH solutions, anomaly was increased according to increase of alkali concentration, where 2 % KOH was enough to give anomalous type and 1 % NaOH mixed type.

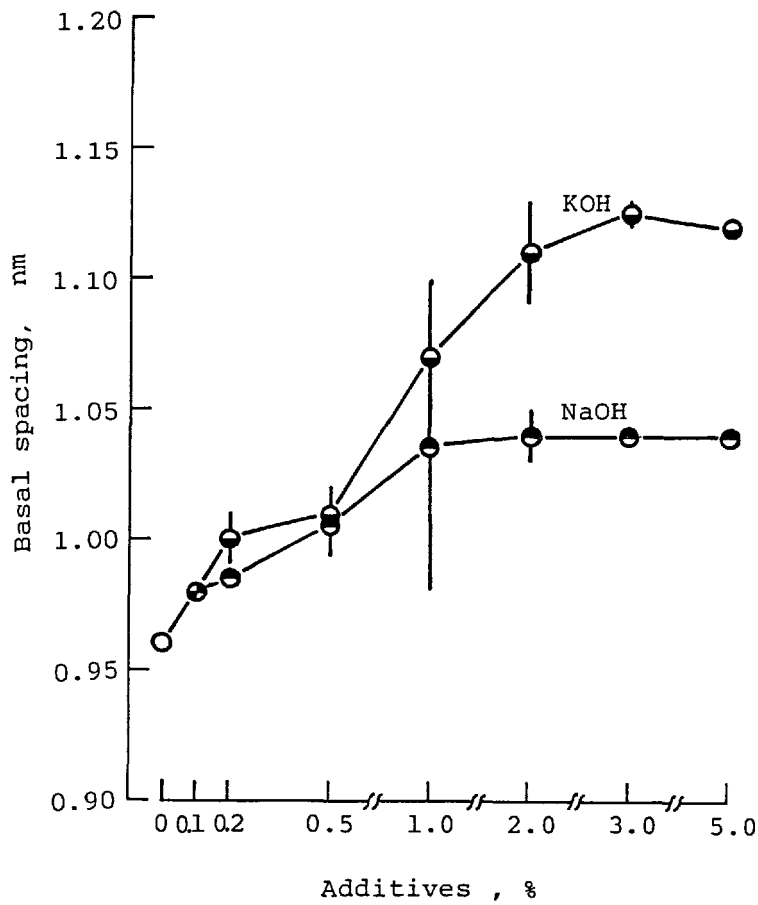

Figure 3 Concentration of alakli solution vs basal spacing of tobermorite after heated at 400°C fo 20 hours.

Removability of alkalis from tobermorite

If results obtained from the above experiments suggest that alkalis are intercalated between the layers of tobermorite, it may be possible to remove thus intercalated alkalis by rinsing in water. In order to confirm this possibility, immersion-treated tobermorite was rinsed in water under

various conditions. Results are summarized in Table 2.

Table 2 Removability of alkalis from tobermorite.
(Basal spacing after heated at 400°C for 20 hours, nm)

Processing conditions	1	2	3	4	5
a) 20°C, 0 hour					
NaOH 0.5 %	1.04 m	1.04 m	0.98 n	–	–
KOH 0.5 %	1.13 a	1.10 a	0.98 n	–	–
b) 20°C, 24 hours					
NaOH 0.5 %	1.05 m	1.05–1.03 m	0.97 n	1.03>0.99 m	1.03, 0.98 m,n
KOH 0.5 %	1.13 a	1.13–1.10 a	1.00–0.98 n	1.10 a	1.13 a
c) 20°C, 24 hours					
NaCl 0.5 %	1.03–1.01 m	–	–	–	0.98 n
KCl 0.5 %	1.13–1.10 a	–	–	–	1.00–0.96 n
d) 20°C, 24 hours					
NaCl 1.0 %	1.05–1.03 m	–	–	–	1.00–0.98 n
KCl 1.0 %	1.13–1.10 a	–	–	–	0.98 n

– : These processing conditions were omitted.
Processing conditions of samples after immersed in alkali solutions :
1. Freeze–drying. 2. Filtration. 3. Filtration and rinsing in water.
4. Freeze–drying and then rinsing in water.
5. Freeze–drying and then ultrasonic rinsing in water.

When normal type tobermorite was immersed in 0.5 % alkali solution at 20°C for 0 hour and freeze–dried, NaOH solution gave mixed type and KOH solution anomalous type with the basal spacing after heated 1.13 nm. However, when freeze–drying was replaced by filtration for tobermorite immersed in KOH solution, anomaly was slightly decreased to give the basal spacing after heated 1.10 nm as shown in Table 2, 2–a.

When 0.5 g tobermorite, which was immersion–treated for 0 hour and filtered, was rinsed in 50 ml deionized water three times, both mixed type obtained in NaOH solution and anomalous type in KOH solution were transformed to normal type having the basal spacing after heated 0.98 nm (Table 2, 3–a). Even for tobermorite immersion–treated for 24 hours and filtered, similar results were observed but recovered normality was inferior to that of tobermorite immersion–treated for 0 hour.

For freeze–dried samples, rinsing and ultrasonic rinsing in water were given, but only a slight recovery of normality was observed for tobermorite immersion–treated in NaOH solution (Table 2, 4–b, 5–b).

Similar experiments were tried by using NaCl and KCl aqueous solutions as shown in Table 2. Immersion at 20°C for 24 hours and freeze–drying gave mixed type in NaCl solution and anomalous type in KCl solution. These samples were freeze–dried ones, but normality was easily recovered by ultrasonic rinsing. These results suggest that alkalis from alkali chlorides are more easily removed by rinsing in water than those from alkali hydroxides.

CONCLUSIONS

Normal type tobermorite was easily transformed into mixed type or anomalous type when immersed in alkali solutions such as NaOH and KOH aqueous solution. KOH solution was higher in its effect to increase anomaly than NaOH solution. Thus obtained anomaly was recovered to a certain extent by rinsing in water. Similar phenomena were observed when immersed in alkali chloride solutions such as NaCl and KCl aqueous solution. However, alkali chlorides were inferior to alkali hydroxides in the effect to increase anomaly. These results suggest that alkali ions are reversibly intercalated between the layers of tobermorite.

When it comes to ionic radii of alkalies, K^+ is larger than Na^+. But when ionic radii are compared as hydrated ions which bind a certain number of water molecules in the immediate vicinity of alkali ions, hydrated K^+ is smaller than hydrated Na^+ (Ushio, 1976).

In addition, hydrated K^+, which is of "negative hydration", is more mobile than hydrated Na^+ in aqueous solutions (Samoilov, 1957). These seem to be the reasons why K^+ ions were more effective than Na^+ ions not only to increase anomaly by immersing in alkali solutions but also to recover normality by rinsing in water.

As for the reason why the presence of alkali is favourable for the formation of anomalous type, McConnell (1954) has suggested that alkali ions present between the layers of tobermorite may stabilize its basal spacing to increase anomaly, noticing similarity of tobermorite to vermiculite where the basal spacing of Na–vermiculite is more stable than that of Ca–vermiculite. Alkali ions intercalated by immersion–treatment seem to contribute similarly to enhance the stability of the basal spacing of tobermotire, which results in the increase of anomaly.

REFERENCES

Chatterji, S, "Hydration State of Tobermorite in Hydrothermal Lime–Silica Products", Cem. Concr. Res., Vol. 3, 1973, pp. 215–217.
Gard, J.A. and Taylor, H.F.W., "A further Investigation of Tobermorite from Loch Eynort, Scotland", Mineralog. Mag., Vol. 31, 1957, pp. 361–370.
Hara, N. and Inoue, N., "Thermal Behaviour of 11 Å Tobermorite and its Lattice Parameters", Cem. Concr. Res., Vol. 10, 1980, pp. 53–60.
McConnell, J.D.C., "The Hydrated Calcium Silicates Riversideite, Tobermorite, and Plombierite", Mineralog. Mag., Vol. 30, 1954, pp. 293–305.
Samoilov, O.Ya., "A New Approach to the Study of Hydration of Ions in Aqueous Solutions", Discussion of the Faraday Society, No.24, 1957, pp. 141–146.
Taylor, H.F.W., "The Chemistry of Cements, I", Academic Press, London and New York, Chapter 5: "The Calcium Silicate Hydrates", pp. 181–191.
Ushio, M., "Effect of Mineralizers on Growth of Foshagite Fiber", *Nippon Kagaku Kaishi*, No.1, 1976, pp. 83–87 (in Japanese).

2ii066
4 pp

Kn o. 2 5. JAN. 2001 d o k 31830

THE REGULARITIES OF FORMING AND MODELLING THE MICROSTRUCTURE AT THE EARLY STAGES OF CEMENT STONE HARDENING

Alexander V. USHEROV-MARSHAK, Victor P. SOPOV, State technical University of Building and Architecture, Kharkov, Ukraine, Valery I. KONDRASCHENKO, State Academy of railway transport, Kharkov, Ukraine

ABSTRACT The structure of cement stone has been classified in consideration of physical-chemical interaction of solid, liquid and gaseous phases. There has been done analysis by the method of thermoporometry, and regularities of microstructure development under the hardening of cement and its minerals were found. The model of the formation of cement stone structure has been computerised along with the graphical, stage-by-stage representation of the results of modelling.

KEY-WORDS: Calorimetry, Pore structure, Porosity, Structure, Temperature, Thermodynamics.

INTRODUCTION

Formation of the structure of a typical capillary-porous material (that of cement stone) takes place in the process of the complex interaction of hydration of solid, liquid and gaseous phases. It is, therefore, difficult to estimate the microstructure quantitatively. The availability of the very quantitative characteristics is principal for analysis of the properties of materials based on cement.

STRUCTURE OF CEMENT STONE.

The complication of the process of binding materials hydration, instability of a hardening system and continuous changing of phase constitution present difficulties in the studying of the structure and those of the process of its formation. The formation of the structure under the hardening of the cement paste is the process of development of polydispersed and polymineral systems. The true concept of it is based on the geometrical structure evolution and conversion of phases in hardening cement. Classification of the cement stone structure presumes the presence of several levels of the latter. This is conditioned by shapes and sizes of particles, their state of aggregation as well as by their location. Solid and liquid phases and porosity can be considered as the basic elements of the structure. As a result of analysis of the data given by literature, the classification of the structure of cement stone has been proposed (Fig 1). It emphasizes two structural levels: microstructure - the one of colloidal size (less than 10^{-7} m), and macrostructure (greater than 10^{-7} m). The increase of the number of molecules on the interphase surface and, consequently, the excess of free energy are characteristic for the first level. This influences significantly the changes in the properties of the cement stone. The size of cement hydrates belongs to this level. The structure of the products of hydration has not been well-explained. The reason for that is morphological variety of hydratied species and the many factors which influence formation of the structure. Development of the notion of the cement stone structure is due to the modelling (Garboczi and Bentz, 1991, van Breugel, 1992), when liquid phase and porosity have been considered as primary factors.

Methodologies including different impacts upon experimental material (pressure, dehydration-saturation, etc) are used for research of porosity of cement stone within a wide range of pores sizes. The method of thermoporometry (Brun et al., 1973, Usherov-Marshak and Sopov, 1994) is based upon the thermodynamical estimation of phase transitions of porous water under process of freezing

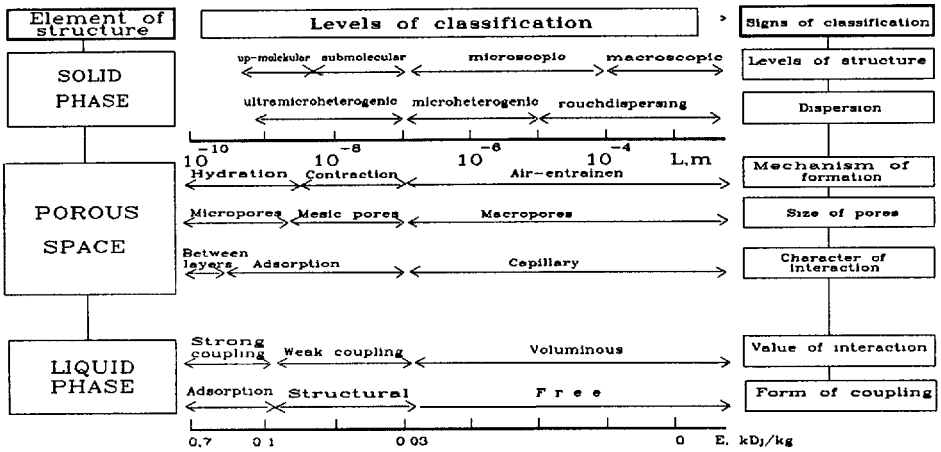

Figure 1 Classification of the cement stone structure.

of cement stone and, therefore, exludes coercive errors. The thermodynamically allowable transition from overcooled liquid to a crystal becomes possible only when a nucleus of the size greater then r_{cr} has been formed. The nucleus in porous materials can not reach its critical size under $t_0=0^0C$. It is originated in pores of the size corresponding to that of the critical nucleus under temperature t less than t_0. The temperature of crystallization and radius of pore are related by the equation:

$$\frac{1}{r} = \frac{1}{2\gamma}\int_{T_0}^{T}\frac{\Delta S}{V_l}dT, \qquad [1]$$

where: γ- free surface energy at the boundary between solid and liquid phases; V_1- molar volume of porous water; ΔS- changes of the entropy of crystallization; T- temperature of crystallization. Temperature of crystallization has been taken by the method of Differential Scanning Calorimetry. The cement stone samples of 10-50 mg of mass have been placed in alluminium air-tight capsules. The process of their cooling took place with the rate of 0.5 ^{0}C/min within the temperature range of +20...-60 ^{0}C. Liquid nitrogen was used as the cooling agent. A typical DSC plot is shown in Fig.2.

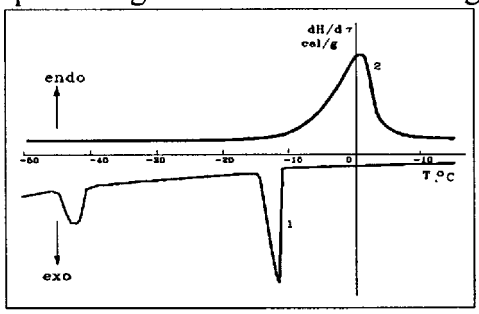

Figure 2 Typical DSC-curve of freezing 1 and thawing 2 for cement stone

TRICALCIUM SILICATE

Formation of the porous structure during the process of hardening of tricalcium silicate is conditioned by the originating and growth of amorphous calcium hydrosilicates of CSH- type. At the early stages, the number of hydrated phases is not substential. Calcium hydrosilicates grow among the particles of C_3S in the form of long fibres, together with thin plates of calcium hydroxide.The fibres of the hydrosilicates create space links. At this stage, an area of distribution of micropores by size from 7 to 12 nm is observed. New hydrates are continuously formed in micropores filled with water, so that the volume and size of pores decrease. The presence of two areas is noted on the second day: distribution of micropores by size is ranged from 2 to 2,5 nm in the first one, that in the

other is from 5,2 to 7,5 nm (Fig 3). Changes of micropores cause the decrease of size of hydrated phases located within. According to Locher and Richartz (1976) fibres of calcium hydrosilicates are on the first day 5-10 nm long with diametre of 0,1 - 0,2 nm. The size of the inner pores of fibrous hydrosilicates is approximately 2-2,5 nm. Primary calcium hydrosilicates are encrusted with the new ones and calcium hydroxides. Integrated microporosity of the hardening tricalcium silicate decreases from 0,21cm^3/g (Fig 3) - on the first day, to 0,043cm^3/g - on the 48th day. The most intensive changes of microporosity are observed during the first seven days. The volume of micropores decreases twice if compared to the specimen which was hardening in one day. During later terms - up to 48 days - changes in the micropores volume are insignificant.

ALUMINATE PHASE

Formation of microporosity of hydroaluminate and hydrosulphoaluminate phases differs substantially in character from that of calcium hydrosilicates. Their structure is conditioned cheifly by mutual location and size of the crystalls of the stable C_3AH_6. Microporosity of the hardening C_3A is characterised by the presence of an area of micropores ranged from 4 to 17 nm. Location and boundaries of microporosity are changing in the process of hydration. The total volume of micropores is decreasing from 0,56 cm^3/g (Fig 3) to 0,06 cm^3/g within 7 days. The main change is taking place during the first day. The following changes of the volume are caused by transformation of hexangonal hydroaluminates of C_4AH_{13} - type to cubical C_4AH_6. The change of the total volume of micropores C_4AF from 0,61 cm^3/g to 0,1 cm^3/g is obvious. Two areas of micropores in the interval of 9,5-17 nm are formed at the early stages. Later on they come closer and the interval of distribution of micropores narrows to 8 - 12 nm (Fig 3).

CEMENT STONE

Formation of the structure of cement stone is obviously more complicated because of development and interaction of hydroaluminate and hydrosilicate phases. Microporosity of cement stone was studied for three kinds of cement of different compositions. The results of the studying are presented by Fig.3.

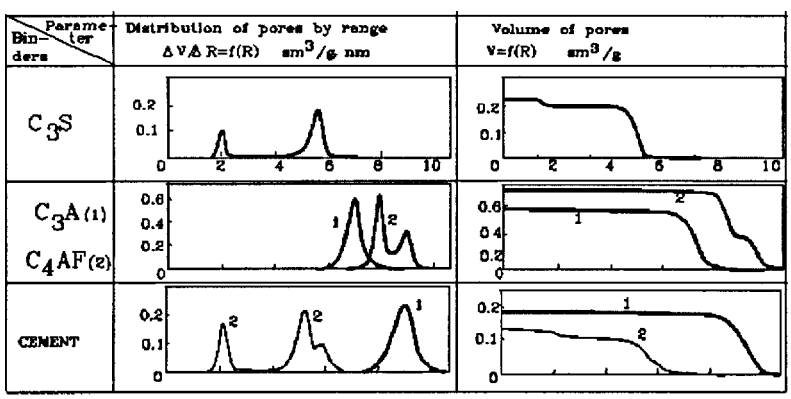

Figure 3 Microporosity of cement stone

Variations in the character of microporosity have been found (Fig.3). An area of distribution of range from 7 to 13,7 nm is observed when the presence of aluminate phase increases. Its width and location change as the process of hydration goes on. At the beginning, it is located in the range from 10-13,7 nm. By the end of the first day, its shifting to the area of range from 7,3 to 9,3 nm is observed. The total volume of micropores decreases three times. Two areas of distribution of micropores by size ranged between 2-10 nm are observed when the presence of aluminates decreases

and that of silicates increases. Cement stone of the increased content of β-C_2S (up to 30%) has an area of distribution of micropores ranged between 12-14,5 nm. Changes in the size of micropores during hydration are caused by the changes of morphology of new products. At the early stages - up to the end of the first day, the area of distribution of micropores is conditioned by aluminated phases. Development of microporosity is probably connected to destruction of the primary hydrosulphoaluminated carcass, to the process of origin and growth of smaller hydrosilicate phases which, in their turn form pores of smaller size (Usherov-Marshak and Sopov, 1995). The total volume of the micropores increases almost two times under the nonsignificant growth of aluminates content: of C_3A - up to 2,5% and of C_4AF - up to 2%. The decrease of pores size is conditioned by the acceleration of the processes of hydration of cement under the growth of content of aluminates. The structure of cement stone (Fig 3) represents hydrosilicate gel (pores size - 2- 4 nm) and phases of hydroaluminates, hydrosulfoaluminates, calcium hydroxides (pores size - 6-8 nm).

MODELLING OF STRUCTURE

The primary structure is represented by particles of irregular shape which are located randomly on a plate of unit thickness. Formation of the structure is conditioned by the changes of the size of each particle. The rate of changes in the particles size is computed by data of thermokinetic analysis. The basic elements of the structure are particles of cement which have not reacted, CSH-, AFm- and CH-phases and porous space of two types of pores. Interparticle porosity is estimated by the model. Porosity of CSH is determined by thermoporometry. Formal equations of particles size changings are set by structure-imitating analysis. The quantitative characteristics (size, volume, shape of pores, number of contacts, etc.) of the cement stone structure have been determined. The modelling data correlate with that done by Jennings and Tennis (1994). Modelling of the process of hardening of cement stone verified the validity of kinetic schemes of changings of crystalline and amorphous structures of hydrates.

REFERENCES

van Breugel, K.: "Numerical Simulation of Hydration and Structural Development of Cement-Based aterials". Proc. of the 9th Int. Congress of the Chemistry of Cement. New Delhi, India, 1992.

Brun M., Lallemand A., Quinson J.F., Eyrand C.J.: "New method of determination size and distribution pores: thermoporometry" , Thermochimica acta, Vol.21, No. 1, 1977, pp.37-45.

Frohnsdorf, G.I. et al.: "Implications of Computer -Based Simulation Models, Expert Systems, Data Bases, and Networks for Advancing Cement Research". Ceramics Bulletin, 1988, 67(8), pp.1368-1371.

Garboczi, E.J. and Bentz, D.P.: "Fundamental Computer-Based Models of Cement-Based Materials". Materials Science of Concrete II, Westerville, American Ceramic Society, 1991.

Jennings, H.M. and Tennis, P.D.: "Model for the Developing Microstructure in Portland Cement Paste", J. Am. Ceram. Soc., 77, [12], 1994, pp. 3161-3172.

Locher F.M., Richartz W., Sprung S. "Erstarren von Zement", Teil 1: Reaction und Gefäge, Zement-Kalk-Gips, 29, 10, 1976, pp.435-442.

Usherov-Marshak, A.V., Sopov, V.P.: "Calorimetric Analysis of interaction in dispersion systems by the sample of binding materials", Inorganic Materials, Vol.32, No.2, 1996, pp. 249-253.

Usherov-Marshak, A.V., Sopov, V.P.: "Termoporometry of Cement Stone", Colloid Journal, Vol.56, No 4, 1994, pp. 527-530.

2ii067
10 pp

Kn o. 2 5. JAN. 2001 d o k 31831

CHARACTERISTICS OF C-S-H GELS

Michael GRUTZECK, Judith LaROSA-THOMPSON and Stephen KWAN, Materials Research Laboratory, The Pennsylvania State University, University Park, PA 16802 U.S.A.

ABSTRACT Data are presented which reinforce a two phase model for the structure of calcium silicate hydrate (C-S-H). Recent ^{29}Si MAS NMR data on the nature and number of silicon's nearest neighbors in a variety of C-S-Hs suggests that 1.4nm tobermorite is a suitable model phase for C-S-H having C/S ratios ranging from 0.6 to 1.0, but not for the C-S-H normally associated with hydrated cement and concrete (C/S≥1.1). These C-S-Hs are better described as Ca-deficient derivatives of a sorosilicate-like phase having the general formula $Ca_4Si_2O_7.(OH)_2 \cdot xH_2O$.

Key-Words: CSH, C-S-H, Hydration, Structure, Nuclear Magnetic Resonance

INTRODUCTION

Calcium silicate hydrate (C-S-H) is an ill defined, cryptocrystalline material which, for want of a better descriptor, is often described as having gel-like characteristics. C-S-H develops as a function of time as anhydrous clinker phases found in portland cement react with water to form a characteristic network of interlocking plates and foils. Because of its gel-like character, the crystal chemical structure of C-S-H is not yet fully understood. Nevertheless, as a binder and matrix phase present in cementitious materials such as grouts, mortars and concrete, C-S-H has literally become the foundation of modern civilization. Portland cement is a readily available, rather inexpensive building material, which is adaptable for use under a wide variety of weather conditions and is relatively free of problems once placed in service. When the anhydrous clinker phases are mixed with water, the resulting slurry transforms into a solid. Although the physical and mechanical properties of cementitious materials are well documented, questions concerning the chemistry and potential chemical interactions of C-S-H with its environment (durability) still remain to be answered. If the structural model for C-S-H and its chemical performance were better understood, there is a strong possibility that long term performance could be increased and that the practice of over designing concrete structures for safety purposes might be better quantified.

The literature speaks of C-S-H as a single phase akin to a solid solution having a structure similar to tobermorite in which a fully occupied layer of CaO molecules are sandwiched between layers of silicate dreirketten. As the C/S ratio of the C-S-H increases from 0.6 to 1.7, it has been suggested that additional Ca ions are accommodated in the interlayers between small bits of randomly oriented layers of tobermorite-like material. An HOH molecule is replaced by CaO along an edge of a bridging tetrahedron for every incremental increase in C/S ratio. When fully loaded with Ca in interlayer positions (C/S≈1), it is then suggested that individual bridging tetrahedra are removed from the dreirketten, which has the effect of increasing the C/S ratio. The two most widely accepted models for single phase C-S-H have been promoted by Taylor (1990) and more recently Richardson and Groves (1992). In terms of substitution theory the models are related, but Taylor goes a bit further and also suggests that the single phase C-S-Hs seen in cementitious materials may actually be comprised of a mixture of nanosized bits of two different structures, structures possibly related to tobermorite and jennite. Unfortunately, at least in terms of recent ^{29}Si MAS NMR data for these mineral analogues, neither structure contains dimer. Both are made up of layers of dreirketten, and thus they can not be used to account for the extensive amount of dimer present in most C-S-Hs. Because of these inconsistencies, it is proposed that C-S-H is actually better described by a two phase model which embraces the idea of two atomic level structures rather than one.

Studies by Stein (1972), Stade and Wieker (1980), Stade (1980), Ramachandran and Grutzeck (1993), Grutzeck et al. (1989), Kwan et al. (1996) and others have suggested that two C-S-H phases rather than one might actually exist. Recent fixed pH studies in the system $CaO\text{-}SiO_2\text{-}H_2O$ and more recently $CaO\text{-}Al_2O_3\text{-}SiO_2\text{-}H_2O$ (Kwan and Grutzeck, 1994) coupled with morphologic investigations show that there is a distinct and sharp boundary occurring at a

CaO/SiO_2 ratio of ~1.0. If one goes through the exercise of recalculating Flint and Wells' (1934) and Roller and Ervin's (1940) data as a function of pH, these too suggest a discontinuous change at about C/S = 1. The observed discontinuities indicate that two distinct phases are present (invariant situation) and as one moves through the composition range represented by the discontinuity one C-S-H phase is replaced by another, the latter having a lower free energy of formation. Fig 1a represents a schematic representation of the phase relations in the system CaO-Al_2O_3-SiO_2-H_2O containing a single C-S-H. In constructing this figure, the compositions of the hydrated phases have been projected onto the anhydrous base of the system. Fig 1b represents the same system but it contains two C-S-Hs instead of one. Note that the figures are not that different in appearance because, the only significant change was to increase the number of C-S-H phases to two and add an invariant triangle between them.

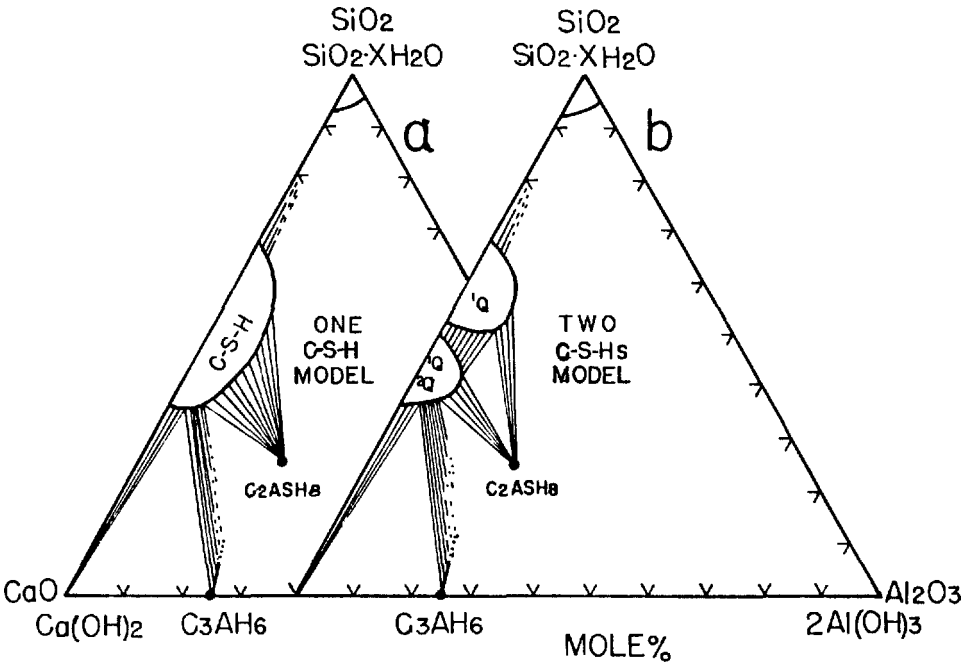

Figure 1 Schematic phase diagrams for the system CaO-Al_2O_3-SiO_2-H_2O showing the extent of a single C-S-H phase field (view a) and two C-S-H phase fields (view b).

The two C-S-H concept which is the topic of the current paper was an outgrowth of recent ^{29}Si MAS NMR data for C-S-H precipitated from lime silica slurries. The spectra given in Fig 2 are typical of the C-S-Hs studied. They represent data for 3 samples taken from either side of the proposed invariancy. Some data have been reported previously (Kwan et al., 1994) and four are taken from Kwan's Ph.D. thesis (1995). The spectra are for C-S-H samples containing 10 wt.% Al_2O_3 and reported upon later in the text. The spectra from either side of the discontinuity suggest that something out of the ordinary happens as one moves across the C/S 1.0 to 1.1 ratio of compositions. There is a noticeable jump in the Q^1/Q^2 ratio as one moves from the silica-rich group of three identified as 23-57.5, -52.5, and -50, to the calcium-rich group of three identified as 23-40,-35,-30.[1] A similar discontinuity is also reflected in the data of Cong and Kirkpatrick (1996). For discussion purposes, these data have been plotted as a compendium of ^{29}Si MAS NMR spectral data for C-S-H as a function of their Q^1/Q^2 ratios in Fig 3. Data points falling in the C/S range of 1.0 to 1.1 (stippled area) have been plotted, but not included in calculations of the best fitting straight lines representing the points. These points have been omitted because they fall within the invariancy and are thus a combination of both C-S-H phases. In toto, the data suggest the presence of a discontinuity occurring over the C/S ratio of 1.0 to 1.1.

[1]Throughout the paper a series of mind experiments are carried out in which Ca is gradually added to or subtracted from the structure. The experiments are akin to visualizing the structural consequences of a small change in composition, a change that in the thermodynamic sense does not change the state of equilibrium.

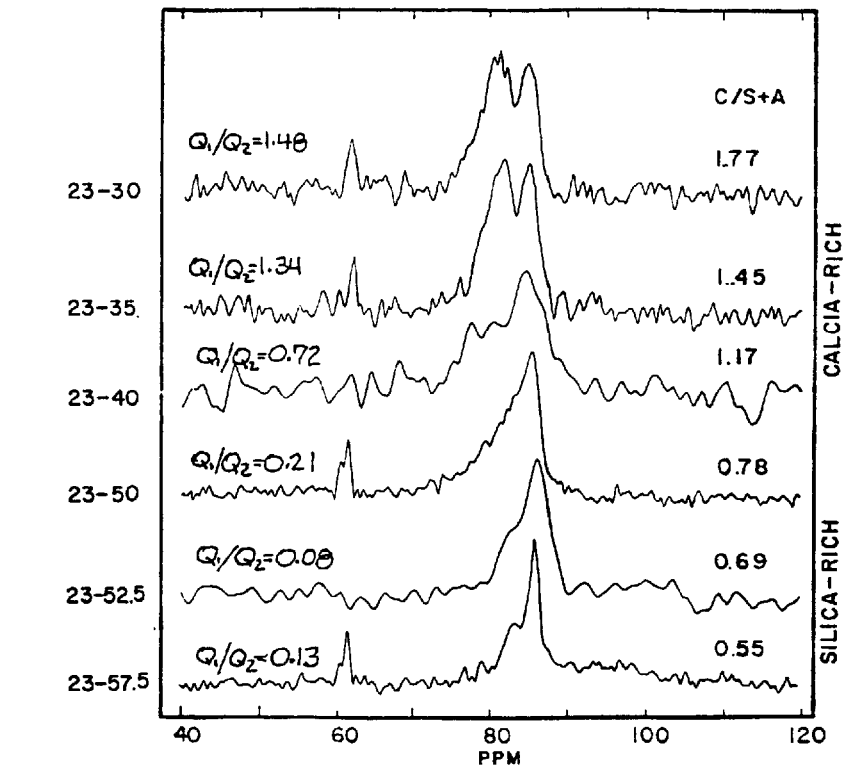

Figure 2 MAS NMR data for 6 mixtures highlighted in Fig. 3. Q^1/Q^2 ratios for each spectrum were calculated and are plotted beside their respective spectra.

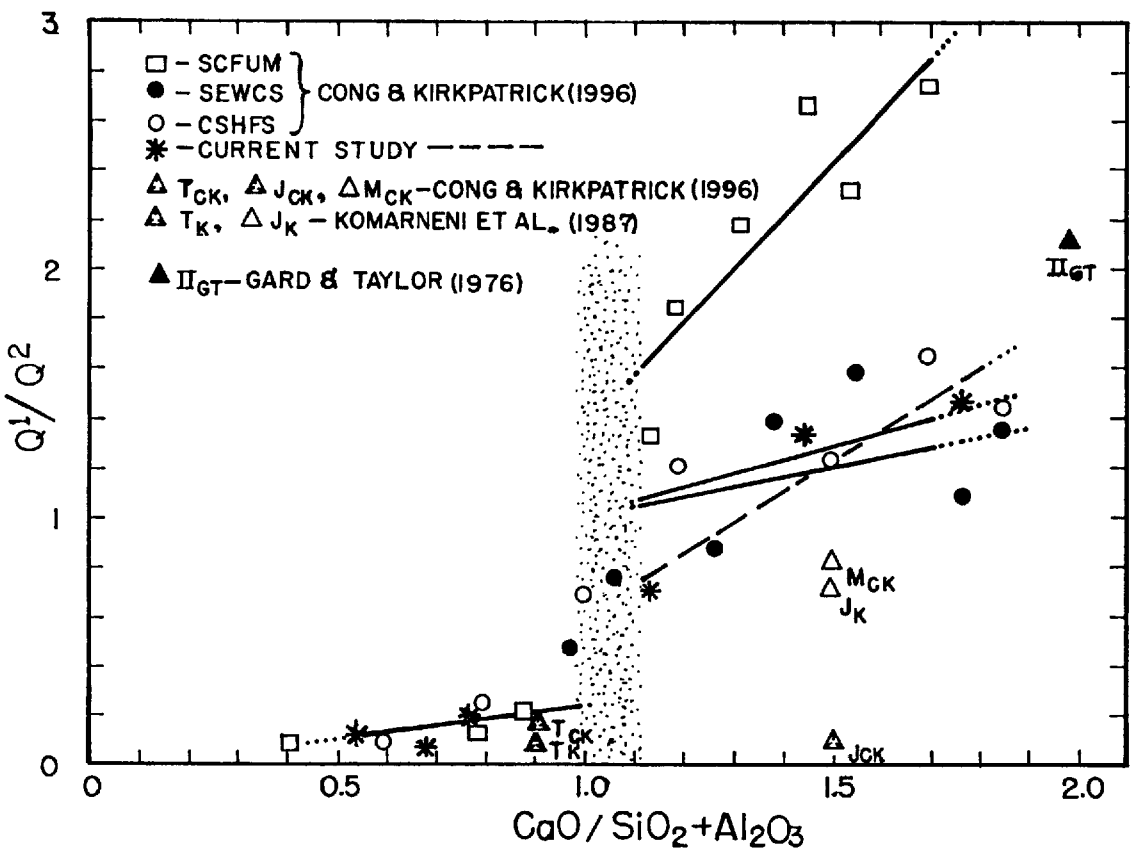

Figure 3 Plot of Q^1/Q^2 ratios for various C-S-H and related samples. Compared to Cong and Kirkpatrick's short term lime-silica data (SCFUM), the plot for our Ca-rich samples is offset to lower Q^1/Q^2 values. Our data are more in keeping with their dicalcium silicate data. Apparently lime-silica samples take longer to equilibrate than dicalcium silicate containing samples.

EXPERIMENTAL METHOD

The purpose of the current paper was to provide confirmatory data for the two phase model, to show that a discontinuity does in fact exist in the systems under study and thus strengthen the two C-S-H theory. It was hypothesized that if two C-S-Hs do exist, they should have distinctly different properties and that the properties should fit the proposed model. Ramachandran and Grutzeck (1993) demonstrated that C-S-H had different dissolution behavior and different morphologies depending on which side of the observed invariancy in the lime-silica systems they took their samples. MAS NMR data also reflect the presence of a discontinuity (Grutzeck et al., 1989). Results for X-ray, TGA, BET surface area, and SEM measurements for the same C-S-H samples used to gather the original ^{29}Si MAS NMR C-S-H data plotted in Fig 2 are reported upon in this paper. The samples were prepared from suspensions of lime, colloidal silica and highly reactive alumina. After mixing with freshly boiled deionized water the samples were sealed in HDPE bottles, placed on a shaking table where they have received continuous room temperature agitation (60cpm) for 8 years. The samples span the C/(S+A) molar range 0.6 to 1.8. Samples were separated from solution via centrifuging followed by freeze drying prior to examination.

RESULTS

X-ray

X-ray data are given in Fig 4. Two aluminate phases were found in two mixtures (23-35 and 23-30). See Figure 4a. One is of the AFm type, most likely containing carbonate, the other is hydrogarnet. The C-S-H which is present in both groups is poorly crystalline as reflected by the presence of 4-5 peaks. In addition, all samples have a characteristic peak(s) in the 1.4nm region. See Fig 4b. These spectra are partial scans of the low angle peaks (3-10°2θ) of the C-S-Hs taken at 1/2 degree 2θ/minute. The 23-40, -35 and -30 samples have a hint of a bimodal distribution which changes with composition as Ca is added to C-S-H.

Table 1. Values of bimodal peaks present in lime-rich C-S-H X-ray patterns.

Mixtures	C/S	d-spacing (nm)
23-40	1.17	1.66, 1.32
23-35	1.45	1.49, 1.26
23-30	1.77	1.40, 1.26

On the other hand, the silica rich C-S-Hs have a single broad peak centered about 6.3°2θ which is equivalent to 1.4nm. The broad peak gradually decreases in height as more silica is added to the C-S-H. The 23-57.5 pattern has just a trace of the 1.4nm peak, suggesting that we are approaching its limit of stability. Overall, the consistency of all of the patterns (Figs 4a &b) indicates that the long range order of all the C-S-Hs is similar, which in turn suggests that the presence of dreirketten must somehow be preserved even in the very lime rich material. The single 1.4nm peak in the silica-rich samples reinforces the tobermorite-derivative model for these phases, but the bimodal distribution of the more lime rich material suggests that a different structure exists, a structure containing dimeric silicate intermixed with dreirketten which has a spacing close to that of tobermorite.

TGA

TGA data for the same samples are given in Fig 5. View 5a represents the original data collected in flowing air with a 10°C/min heating rate. Our interpretation of the behavior of samples 23-35 and 23-30 is that they contained some type of AFm phase and thus lost some water in the 200-400°C range. Of the 2, the 23-30 sample lost more water, which is consistent with the larger amount of AFM seen in the X-ray diffraction pattern. The presence of AFM was unexpected. However, by taking the remaining four curves as a model (each is rather smooth with a major weight loss up to 200°C followed by a less intense loss that gradually lessens up to 1000°C) one can then assume that the 200-400°C loss observed in 23-35 and -30 is due to AFM and thus it should be possible to sketch AFM-free equivalents of 23-35 and -30. In effect we have connected the initial and final parts of these 2 curves to produce the curves given in Fig 5b. The latter were used to calculate total weight loss at 1000°C for each C-S-H phase (see Table 2).

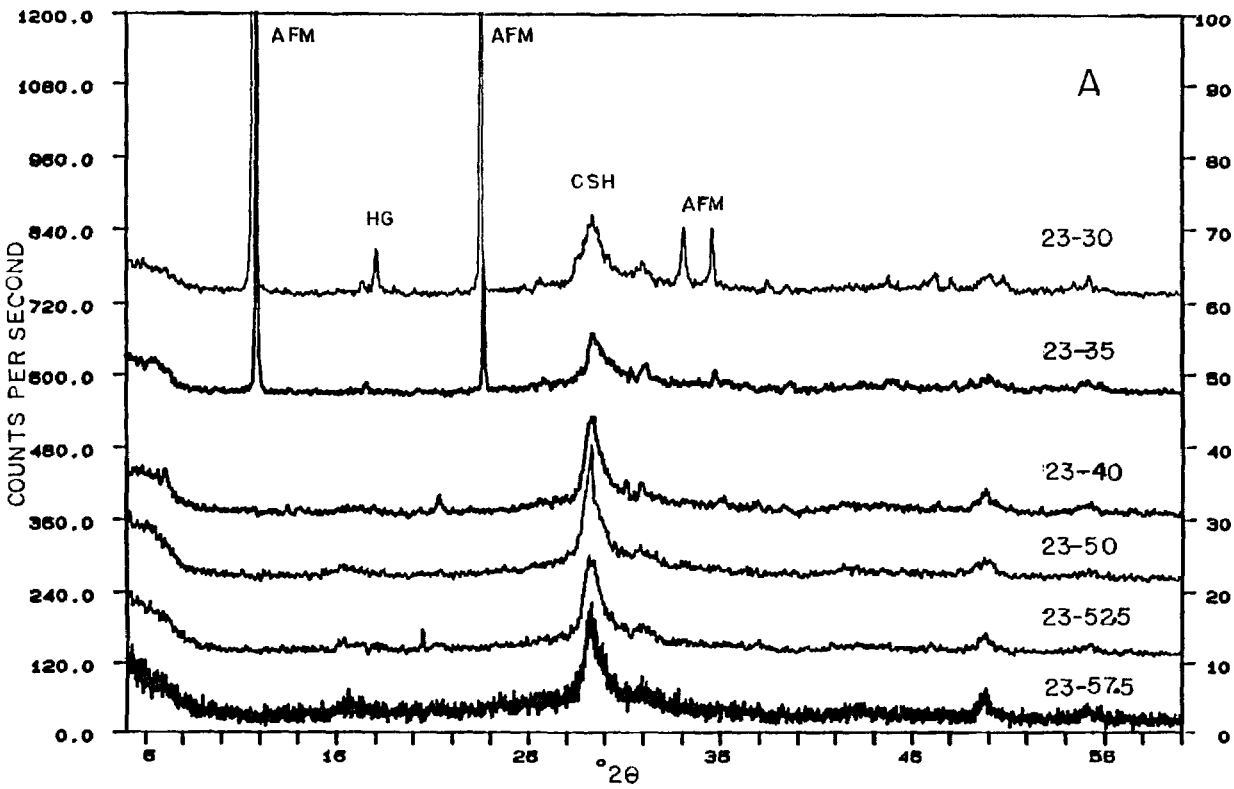

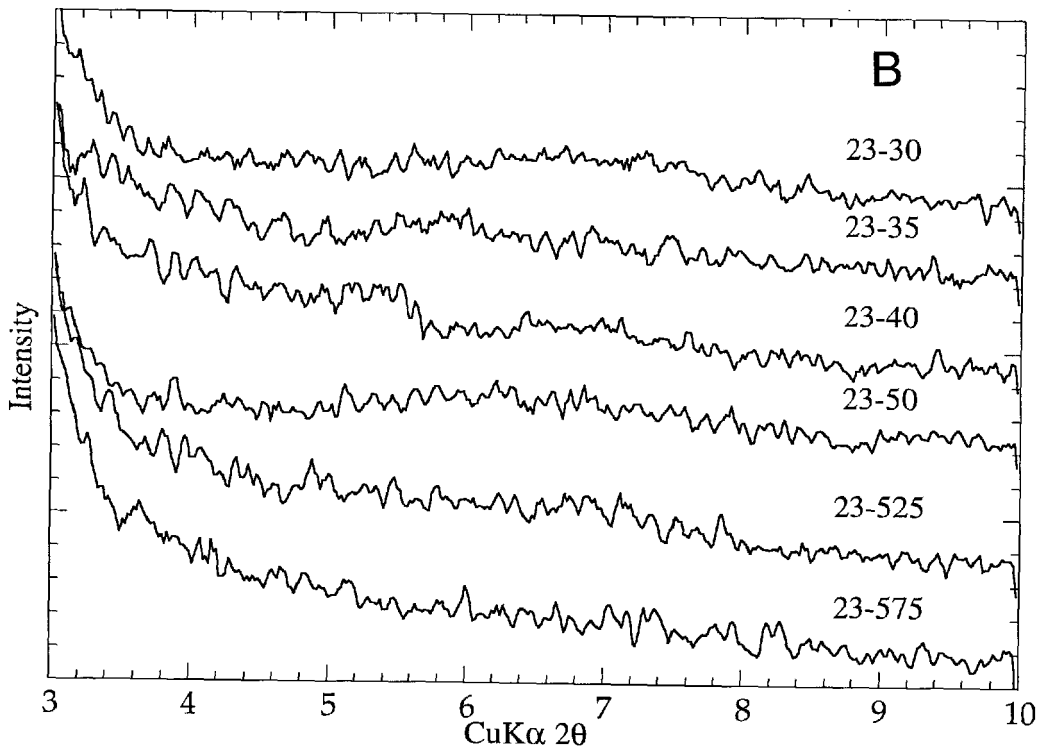

Figure 4 X-ray diffraction patterns of the 6 mixtures studied. View (a) = full pattern. View (b) = 3-10° 2θ.

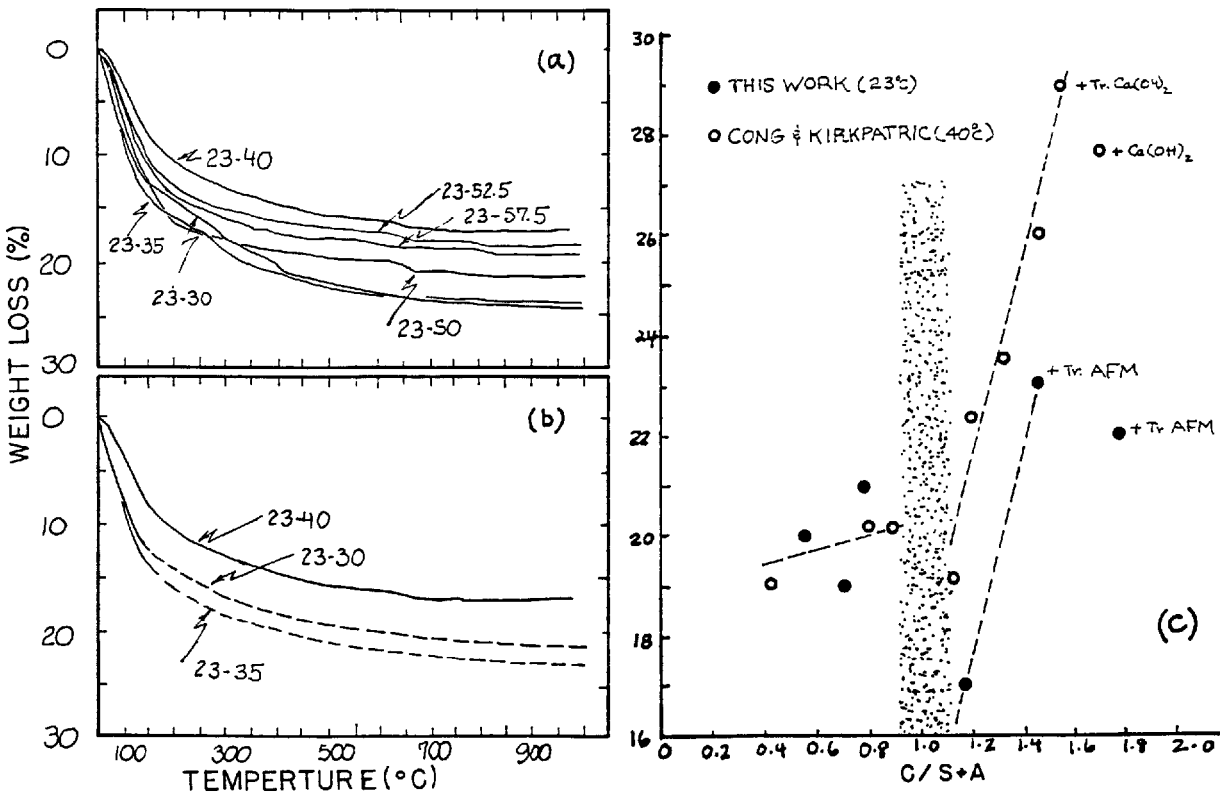

Figure 5 TGA data for the 6 mixtures studied. View (a) = raw data. View (b) = treated data. View (c) = plot of 1000°C weight loss versus C/(S+A).

Table 2. TGA weight loss of freeze dried samples at 1000°C

GROUP ONE (Si-rich)				GROUP TWO (Ca-rich)		
Mixture	C/(S+A)	wt.%		Mixture	C/(S+A)	wt.%
23-57.5	0.55	20		23-40	1.17	17
23-52.5	0.69	19		23-35	1.45	23
23-50	0.78	21		23-30	1.77	22

Plotting these data as well as those of Cong and Kirkpatrick (1996) as a function of C/S+A ratio (Fig 5c) one gets the impression that water content varies differently in the two groups. In the silica-rich C-S-Hs the water loss remains reasonably constant at 20wt.%±1. This would imply that the level of combined water in the C-S-H as C/S+A ratio varies from 0.6 to 1.0 is reasonably constant. As CaO enters interlayer sites, it is does so by displacing the equivalent one molecule of water. On the other hand, in the lime-rich C-S-Hs the water content seems to rise with increasing Ca content. This is reasonable behavior for the proposed Ca-deficient sorosilicate structure. As more Ca returns to the structure the dreirketten layers which had formed revert back to dimers and in doing so incorporate three additional water molecules for each Ca ion. Because dimer formation is linked to Ca^{2+} uptake as C/S increases from 1.1 to 1.7, the positive slope of the curve is justifiable. Note that Cong and Kirkpatrick's data mirror the same behavior as our data. In any case, the lime rich C-S-H contains more water than its silica rich counterpart. This has been observed in slurry systems produced with identical w/s ratios where samples of C-S-H >1.1 have formed "dry" powders whereas C-S-Hs having C/S ratios <1.0 have remained slurries.

BET Surface area

BET surface area data were collected on the identical freeze dried samples. The values for the six samples are listed in Table 3. Units are in square meters/gram.

Table 3. Surface area of freeze dried C-S-H samples.

GROUP ONE				GROUP TWO		
Mixture	C/(S+A)	m^2/g		Mixture	C/(S+A)	m^2/g
23-57.5	0.55	270		23-40	1.17	97
23-52.5	0.69	190		23-35	1.45	40
23-50	0.78	134		23-30	1.77	62

A plot of the data is given in Fig 6. Here more than anywhere else is the structural division between the two C-S-H phases most easily seen. The two straight lines intercept at C/S ~0.9, which is in keeping with the suggested location of the invariancy between the two C-S-H structures. There is however more scatter in the calcia-rich samples. Repeat measurements show that the value of 23-35 is always much lower than its neighbors. The cause of the low reading is not understood, but it may be more than coincidental that its C/S+A ratio is close to 1.5.

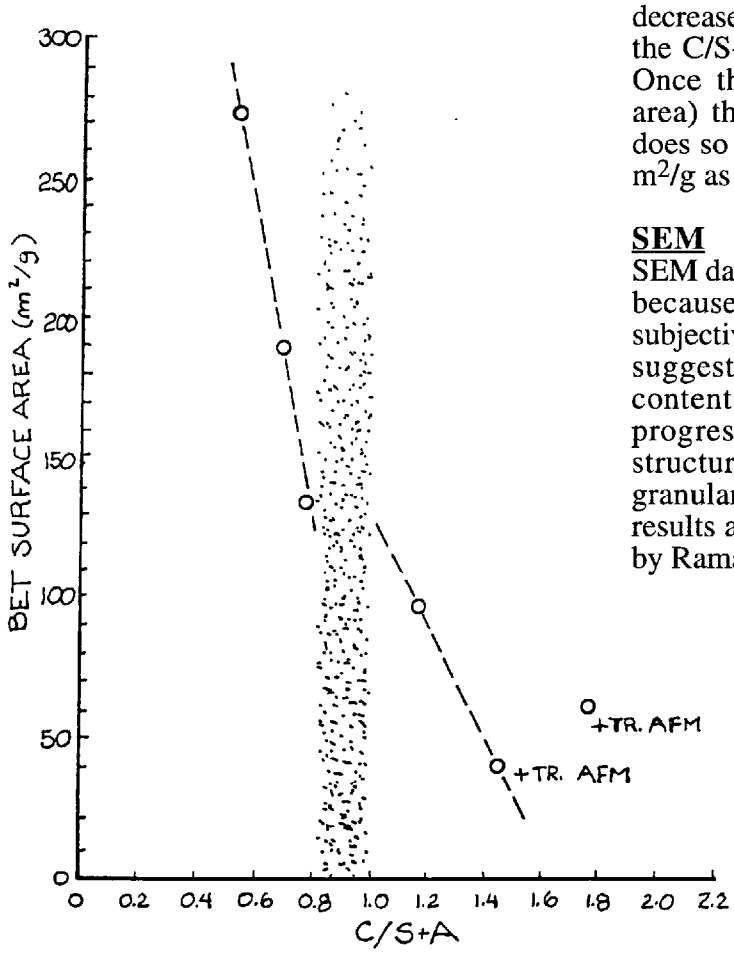

Figure 6. BET surface area of 6 C-S-H samples studied.

The surface area of the silica-rich C-S-Hs decreases almost 2 fold (270 to 130 m^2/g) as the C/S+A ratio increases from 0.6 to 2.0. Once the invariancy is crossed (stippled area) the surface area still decreases, but does so at a much lower rate, e.g. 100 to 50 m^2/g as C/(S+A) varies from 1.3 to 2.0.

SEM

SEM data are not as conclusive as other data because their interpretation can be quite subjective. Yet there seems to be a trend that suggests that, with increasing calcium content, the morphology of the C-S-H progresses from a very open foil-like structure to one which is denser, more granular, and more clustered looking. The results are similar to those noted previously by Ramachandran and Grutzeck (1987).

DISCUSSION

Apparently there are two C-S-Hs in the systems studied. This fact was suggested by an abrupt change in atomic level structure and chemistry of the coexisting solution phase. It was theorized that this discontinuity would also be reflected in other measured properties. Fortunately it has, but the picture is not yet entirely clear. Nevertheless, on the whole the experiment was a success. A discontinuous change first detected in ^{29}Si MAS NMR data was observed to occur in other properties as well. Using these findings, it is now possible to propose models for the two C-S-Hs described in this paper.

Silica-rich C-S-H

The high silica C-S-Hs reported in Fig 3 had C/S ratios ranging from 0.6 to 1.0. It is generally agreed that these C-S-Hs are tobermorite-derivatives probably consisting of layers of dreirketten with Ca^{2+} ions occupying more and more of the interlayer positions as C/S ratio increases from 0.6 to 1.0. This model is consistent with the current data and is essentially the same as other models in the literature. The Q^1/Q^2 ratios of the C-S-Hs are nearly constant (0.15 ± 0.05) as is the combined water content over this range of composition. The surface areas are extremely high and because there is no Q^3 present that can be attributed to C-S-H, these values suggest a lack of cross bonding between the interlayer silicate ions.

Calcia-rich C-S-H

At C/S $\geq$ 1.1 the C-S-H structure that forms has a Q^1/Q^2 ratio in the vicinity of 1 to 1.5 depending upon whether or not the system contained calcium silicate or lime, respectively (see Fig 3). This implies that the structure is radically different--now containing approximately 50% dimer and 50% dreirketten. Because jennite as well as tobermorite are composed of dreirketten chains (see plotted points from Komarneni et al., 1987, Cong and Kirkpatrick, 1996), where are the dimers coming from? One can shorten the chains only so much, but even a chain of 5 would have a Q^1/Q^2 ratio of 0.67. It is hard to fathom a complete disintegration of the tobermorite chain into one consisting mainly of dimers ($Q^1/Q^2 = \infty$), especially in light of TMS data which suggests the average chain length is around 8 (Taylor, 1990). The sorosilicate-derivative model we are proposing better accommodates ^{29}Si MAS NMR data as well as the data presented above. It is conceivable that amorphous gel-like precursors having sorosilicate structures similar to cuspidine [$Ca_4Si_2O_7(OH,F)_2 \cdot H_2O$] and lawsonite [$CaAl_2Si_2O_7(OH)_2 \cdot H_2O$] could form in cements. For example, if one replaces the fluoride ions in cuspidine with hydroxyl groups (which have identical sizes) one gets [$Ca_4Si_2O_7(OH)_2 \cdot H_2O$]. If one starts with lawsonite and replaces all of the aluminum ions in the octahedrally coordinated (AlOOH) layers with calcium, one also gets [$Ca_4Si_2O_7(OH)_2 \cdot H_2O$].

Sorosilicates normally contain dimers that are arranged in columns that radiate outward from a central octahedrally coordinated AlOOH/CaO layer with additional molecules of calcium hydroxide and H_2O occupying holes in the diametric portion of the structure (Liebau, 1985). In the calcium sorosilicate analogue we are proposing, we believe the dimers have three different orientations: parallel to, and at 30° and 120° angles to the central CaO layer forming a highly distorted diametric layer containing additional calcium ions. See Fig 7a for a schematic representation of the C/S=1.17 C-S-H end-member. Note that there are "holes" in the structure which can accommodate additional water and/or $Ca(OH)_2$ molecules. This arrangement is not inconsistent with Viehland et al., (1996) TEM data. The "secondary ring" (in their Figure 2a) is discontinuous, has a hexagonal/trigonal symmetry and a periodicity of ~0.18nm, which could be the repeat distance and spatial orientation of the $[Si_2O_7]^{-6}$ groups in the proposed sorosilicate structure.

By removing the molecular $Ca(OH)_2$ from the sorosilicate structure and replacing it with HOH, a predominantly Q^2 C-S-H with a C/S=1.5 can be obtained. Beyond that point continued removal of calcium down to C/S=1.1 causes the structure to become highly calcium deficient and as a result some of the dimeric layers between adjacent CaO layers are prone to collapse and convert to dreirketten; the sorosilicate has essentially "unzipped" to alleviate some of the instability and formed a tobermorite-like interlayer as depicted in Fig 7b.

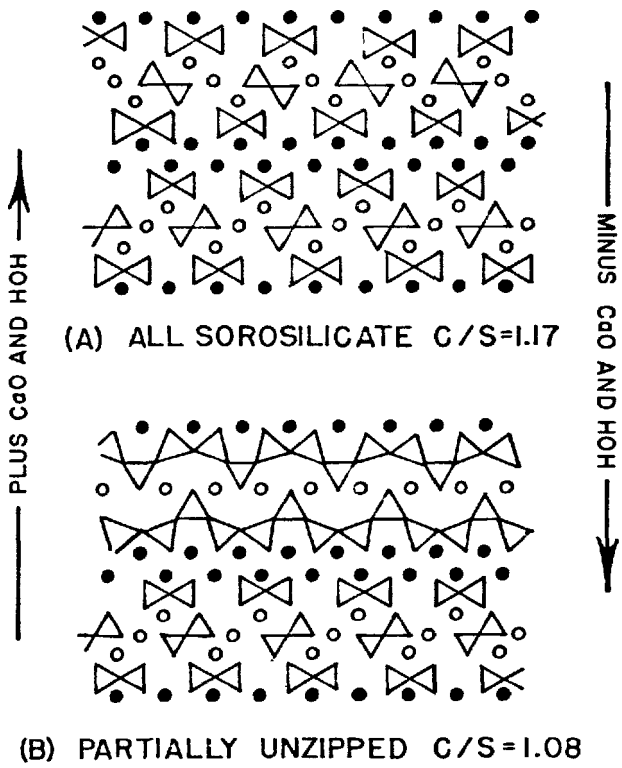

Figure 7. C-S-H structures. View (a) = sorosilicate C/S = 1.17. View (b) = partially converted sorosilicate C/S = 1.08.

The proposed sorosilicate structure would be extremely unstable under ambient conditions and thus constantly "teetering" on the verge of collapse. This would explain its extreme sensitivity to temperature and starting material composition. This sensitivity is clearly documented by Stade and Weiker's (1980) and Stade's (1980) work in which they demonstrate the existence of a completely dimeric C-S-H at 0°C. This preparation could be dried at -10°C, but it tended to "unzip" more and more as it was held at room temperature. They also found that the Q^1/Q^2 ratio of their calcia-rich C/S (1.1-1.7) C-S-H decreased with increasing temperature. Once again, the compositional variation exhibited by their di,poly C-S-H could be better explained in terms of a sorosilicate model rather than a tobermorite model.

In addition, a sorosilicate-derivative structure for C/S≥1.1 to 1.7 C-S-H seems to resemble Gard and Taylor's (1976) C-S-H (II) structure more so than a tobermorite in as much as it contained 68% dimer and 32% chains. See Fig 3. A sorosilicate-derived C-S-H also resembles Carpenter et al.'s first anionic structure for jennite (1966). Although they first suggested that jennite could contain $3[SiO_3]_n$ and Si_2O_7 units, in a subsequent paper (1977) Gard and Taylor suggest that jennite contains only dreirketten. If one plots Cong and Kirkpatrick's jennite on Fig 3 it would look very much like it falls on an metastable extension of the tobermorite-like C-S-H curve on the left side of the figure. What is even more interesting, however, are the locations of the points representing the stated Q^1/Q^2 ratios for Komarneni et al.'s jennite spectrum and Cong and Kirkpatrick's metastable intermediate phases. If one plots these, they are clearly more sorosilicate-like than tobermorite-like.

CONCLUSIONS

It is concluded that the observed discontinuous offset in the measured physical properties of C-S-H reflects a phase change in which C-S-H changes from a tobermorite-like structure to a sorosilicate-like structure. The latter structure is highly unstable (favoring low temperatures and high C/S ratios) and thus very sensitive to changes in composition and curing conditions. As both thermal and compositional instability increase, the dimers in the sorosilicate-like C-S-H will occasionally convert to "islands" of dreirketten similar to those shown by Viehland et al. (1996). Because C-S-H is normally heterogeneous, the phase change may often occur in what one may think is a random fashion. But there is a delicate balance between the two structures and either one can convert to the other based upon localized conditions. Given the instability of the sorosilicate structure, it now becomes rather easy to model the behavior of C/S≥1.1 C-S-H without invoking a tobermorite-derived structure (i.e. jennite).

ACKNOWLEDGMENTS

The support of the Department of Energy/Office of Basic Energy Science under Grant # DE-FG02-91ER45456 is gratefully acknowledged.

REFERENCES

Carpenter, A.B., Chalmers, R.A., Gard, J.A., Speakman, K. and Taylor, H.F.W. "Jennite, a New Mineral", Amer. Mineral, Vol. 51, 1966, pp. 56-74.

Cong, X. and Kirkpatrick, J., "^{29}Si MAS NMR Study of the Structure of Calcium Silicate Hydrate", Advn. Cem. Bas. Mat., Vol. 3, 1996, pp. 144-156.

Flint, E.P. and Wells, L.S., "Study of the System CaO-SiO_2-H_2O at 30°C and the Reaction of Water on the Anhydrous Calcium Silicates", J. Res. Natl. Bur. Standards, Vol. 12, 1934, pp. 751.

Gard, J.A., Taylor, H.F.W., "Calcium Silicate Hydrate (II) ('C-S-H(II)")," Cem. Concrete Res., Vol. 6, 1976, pp. 667-78.

Gard, J.A., Taylor, H.F.W., "A Reexamination of Jennite", Amer. Mineral., Vol. 62, 1977, pp. 365-368.

Grutzeck, M.W., Benesi, A, and Fanning, B., "Silicon-29 Magic Angle Spinning Nuclear Magnetic Resonance Study of Calcium Silicate Hydrates," J. Amer. Ceram. Soc., Vol. 72, 1989, pp. 665-68.

Komarneni, S., Roy, D.M., Fyfe, C.A., Kennedy, G.J., "Naturally Occurring 1.4nm Tobermorite and Synthetic Jennite: Characterization by ^{27}Al and ^{29}Si MASNMR Spectroscopy and Cation Exchange Properties," Cem. Concrete Res., Vol. 17, 1987, pp. 891-95.

Kwan, S., Structure and Phase Relations of Calcium Silicate Hydrate and Related Phases in the System Calcium Oxide-Aluminum Oxide-Silicon Oxide-Water, PhD Thesis in Materials, Penn State University, 1995, 185 pp.

Kwan, S., Grutzeck, M., "Hydration of Alite at Different pHs", in PAC RIM Conference Proceedings, Cement Technology, Ed. E. Gartner, Amer. Ceram. Soc., Westervill, OH., 1994, pp. 99-108.

Kwan, S.,LaRosa-Thompson, J.L. , Grutzeck, M.W., "Structures and Phase Relations of Aluminum Substituted Calcium Silicate Hydrate", J. Am. Ceram. Soc. Vol. 79, 1996, pp. 967-71.

Liebau, F., Structural Chemistry of Silicates, Springer-Verlag, N.Y., 1985, 347 pp.

Ramachandran, A.R. and M.W. Grutzeck, "Microstructural Development During Suspension Hydration of Tricalcium Silicate Under 'Floating' and Fixed pH Conditions," in Microstructural Development During the Hydration of Cement. Eds. C. Struble, P. Brown. Symp. Proc. Vol. 85, Materials Research Society, Pittsburgh, PA, 1987, pp. 33-38.

Ramachandran, A.R. and Grutzeck, M.W., "Effect of pH on the Hydration of Tricalcium Silicate," J. Amer. Ceram. Soc., Vol. 76, 1993, pp. 72-80.

Richardson, I.G. and Groves, G.W., "Models for the Composition and Structure of Calcium Silicate Hydrate (C-S-H) Gel in Hardened Tricalcium Silicate Pastes", Cem. Concr. Res., Vol. 22, 1992, pp. 1001-1010.

Roller, P.S. and Ervin, G., "The System Calcium Oxide-Silica-Water at 30°C. The Association of Silicate Ion in Dilute Alkaline Solution", J. Amer. Ceram. Soc., Vol. 62, 1940, pp. 461.

Stade, Von H., Wieker, W., "On the Structure of Ill-Crystallized Calcium Silicate Hydrates. I. Formation and Properties of an Ill-Crystallized Calcium Silicate Hydrate Phase" (in German), Z. Anorg. Allg. Chem., Vol. 466, 1980, pp. 55-70.

Stade, Von H., "On the Structure of Ill-Crystallized Calcium Silicate Hydrates. II. A Phase Consisting of Poly- and Disilicate Phase" (in German), Z. Anorg. Allg. Chem. Vol. 470, 1980, pp. 69-83.

Stein, H.N., "Thermodynamic Considerations on the Hydration Mechanisms of Ca_3SiO_5 and $Ca_3Al_2O_6$", Cem. Concr. Res., Vol. 2, 1972, pp. 167.

Taylor, H.F.W., Cement Chemistry, Academic Press, London, 1990, 475 pp.

Viehland, D., Li, J.-F., Yuan, L.-J., and Xu, Z., "Mesostructure of Calcium Silicate Hydrate (C-S-H) Gel in Portland Cement Paste: Short Range Ordering, Nanocrystallinity, and Local Compositional Order," J. Amer. Ceram. Soc., Vol. 79, 1996, pp. 1731-44.

2ii068
8 pp

Kn o. 2 5. JAN. 2001 d o k 31832

THE STRUCTURE OF C-S-H IN HARDENED SLAG CEMENT PASTES

Ian G. RICHARDSON
CEMU, Department of Civil Engineering, University of Leeds, Leeds LS2 9JT, U.K.

ABSTRACT The C-S-H gels present in hardened pastes of alkali-activated blast-furnace slags of varying composition and of both water- and alkali-activated white Portland cement / slag blends have been characterised by solid-state ^{29}Si NMR spectroscopy and analytical TEM. All of the C-S-H gels, whatever their chemical composition or degree of structural order, have aluminium substituting for silicon only in the central tetrahedron of pentameric silicate chains. The results strengthen confidence in dreierkette-based models for the structure of C-S-H.

Key-words: C-S-H; Structure; NMR; TEM, Blastfurnace slag

INTRODUCTION

The Al/Ca ratio of the calcium silicate hydrate (C-S-H) gels in ordinary Portland cement (OPC)/blast-furnace slag blends increases linearly with increasing Si/Ca ratio (Richardson and Groves, 1992a, 1993a). This has been interpreted in terms of a model for the C-S-H gel structure in which the mean silicate chain length increases as the Si/Ca ratio increases, with Al substituting for Si at bridging sites of a 'dreierkette' chain structure (Richardson and Groves, 1992b, 1993b). The model may be represented as formula 1,

$$\left\{Ca_{2n}H_w\left(Si_{1-a}R_a^{[4]}\right)_{(3n-1)}O_{(9n-2)}\right\}\cdot I^{c+}_{\frac{a}{c}(3n-1)}\cdot(OH)_{w+n(y-2)}\cdot Ca_{\frac{n.y}{2}}\cdot mH_2O \qquad [1]$$

where if $0\leq y\leq 2$ then $n(2\text{-}y)\leq w\leq 2n$, if $2\leq y\leq 4$ then $0\leq w\leq 2n$, and if $4\leq y\leq 6$ then $0\leq w\leq n(6\text{-}y)$. The model is based on a tobermorite-like core (that part of formula 1 contained within the braces) and consists of a highly disordered layer structure comprising finite silicate chains of average length $3n$-1. In immature cement pastes dimer is the most abundant silicate species (n=1). These are linked during polymerization by bridging tetrahedra to form pentamer (n=2) and higher polymers. $R^{[4]}$ is a trivalent cation, mainly Al^{3+}, in tetrahedral co-ordination and I^{c+} is an interlayer ion, either a monovalent alkali cation or Ca^{2+}, charge-balancing the R^{3+} substitution for Si^{4+}. Aluminium is assumed to only substitute for Si in the bridging tetrahedra of the dreierkette structure; since there are n-1 bridging sites,

$$0\leq a\leq\frac{n-1}{3n-1}$$

The model can be interpreted in terms of either of the two most common approaches to the structure of C-S-H, namely as a mixture of structural units based on the minerals jennite and 1.4nm-tobermorite (Taylor, 1986) or as tobermorite-based units in 'solid-solution' with $Ca(OH)_2$ (Greenberg et al. (1960,1965), Fujii and Kondo (1983), Kantro et al. (1962), Birchall and Thomas (1984)). This is most simply demonstrated for dimeric C-S-H: if we consider the model as a mixture of structural units based on jennite and tobermorite, then with w=n and y=1 we get,

$$\left[Ca_2HSi_2O_7\right]\cdot\tfrac{1}{2}Ca\cdot mH_2O$$ i.e. Taylor's tobermorite-based dimer, Ca/Si = 1.25,

or with w=n and y=5 we get,

$\left[Ca_4HSi_2O_7(OH)_4\right]\cdot\frac{1}{2}Ca\cdot mH_2O$ i.e. Taylor's jennite-based dimer, Ca/Si = 2.25.

From the tobermorite/$Ca(OH)_2$ viewpoint it is better to represent the model by formula 2,

$$Ca_XH_{(6n-2X)}\left(Si_{1-a}R_a^{[4]}\right)_{(3n-1)}O_{(9n-2)}\cdot I^{c+}_{\frac{a}{c}(3n-1)}\cdot zCa(OH)_2\cdot mH_2O \qquad [2]$$

where, $X=\frac{1}{2}(6n-w)$; $z=\frac{1}{2}\left(w+n\left(y-2\right)\right)$. When n=1 (i.e. dimer), formula 2 reduces to that used by Glasser et al. (1986) to describe the C-S-H predominant in young OPC pastes:

$$Ca_XH_{(6-2X)}Si_2O_7\cdot zCa(OH)_2\cdot mH_2O$$

The model successfully links the chemical composition and silicate anion structure of low Ca/Si ratio C-S-H phases (Richardson and Groves, 1992b) and is supported by Richardson et al.'s determination of the location of Al in semi-crystalline substituted C-S-H gels (Brydson et al., 1993, Richardson et al., 1993, 1994). These were formed by the reaction of a slag (SC in Table 1) and a synthetic slag-glass (AG) with 5*M* KOH solution. The single-pulse ^{29}Si and ^{1}H-^{29}Si cross-polarization (CP) magic-angle spinning (MAS) NMR spectra for these gels gave conclusive evidence that Al only substitutes for Si in the central tetrahedron of pentameric linear chains. Since there were no $Q_1(1Al)$* units on the ^{29}Si CP MAS NMR spectra Al could - assuming no chain terminating Al - only be substituted for Si in bridging tetrahedra. There were no chain terminating Al as this would have produced higher Al/Si ratios derived from NMR than from analytical transmission electron microscopy (TEM) which gives unambiguous compositions. This paper presents new data for slags of varying chemical composition and data for both water- and alkali-activated Portland cement / slag blends (Richardson and Groves, 1997).

EXPERIMENTAL

Results are reported for six commercial blast-furnace slags (supplied by Frodingham Cement Company and the AEA Technology Harwell Laboratory) with different chemical and mineralogical compositions and for one synthetic slag glass (AG). Powder X-ray diffraction showed that slags SC, HG and VL were >95% glassy whilst slags SM, PT and CP had varying amounts of merwinite and/or melilite. Chemical data for the glassy phase present in the slags and fineness data are given in Table 1. These data are given in greater detail elsewhere (Richardson et al., 1997). The cement used in the blends was a white Portland cement (WPC) from the Aalborg company (Bogue composition: 65% C_3S, 22% C_2S, 4% C_3A, 1% C_4AF). A white Portland cement was used because of its low Fe content; the presence of paramagnetic ions causes peak broadening in NMR. The commercial slags were activated with KOH solution (S/S=0.4) and blends of 1/9 and 1/1 WPC / VL slag with water (W/S=0.4) or 5*M* KOH solution (S/S=0.5). Freshly ground samples were used for X-ray diffraction and NMR.

---

* ^{29}Si MAS NMR can provide quantitative information on the fractions of silicon present in different tetrahedral environments, Q_n ($0 \le n \le 4$), where Q is a silicate tetrahedron and n is the number of oxygens which bridge to adjacent tetrahedra. Increased polymerization of the Q_n building units causes characteristic up-field chemical shifts. In aluminosilicates the shifts are further influenced by the replacement of Si by Al. There are 15 possible $Q_n(mAl)$ structural units where Q is a silicate tetrahedron connected via oxygen bridges to m Al and n-m other Si atoms, with n=0 to 4 and m=0 to n.

Table 1. Glass composition (determined by wavelength dispersive X-ray analysis) and fineness data. n and x_0 represent the particle size distribution (Rosin-Rammler constants): n is a measure of breadth of distribution (higher n → narrower); x_0 is a measure of average size (36.8% of particles are > x_0 μm).

	SC	SC1	SC2	HG	VL	SM	PT	CP	AG
Ca/Si	1.10	1.10	1.07	1.21	1.21	1.35	1.17	1.28	1.09
Al/Si	0.36	0.36	0.36	0.62	0.40	0.45	0.43	0.36	0.33
Mg/Si	0.32	0.32	0.32	0.53	0.44	0.44	0.33	0.05	0.30
n	0.99	1.10	-	0.99	0.89	0.97	0.97	0.94	1.01
x_0 μm	22.9	15.0	-	17.1	17.5	19.9	27.0	21.6	36.7
Median	16.9	12.2	89.3	11.7	9.7	14.0	20.6	13.8	27.1

Details of TEM sample preparation and analysis are given elsewhere (Groves et al. (1986), Richardson and Groves (1992a)). Specimens for NMR spectroscopy were ground to a powder and packed into zirconia rotors. The single-pulse ^{29}Si spectra for slags HG, SM, PT and CP were acquired using a Bruker MSL-400 spectrometer (magnetic field 9.4 T; operating frequency of 79.49 MHz for ^{29}Si). All other single-pulse ^{29}Si and ^{1}H-^{29}Si cross polarization (CP) spectra were acquired using a Bruker MSL-200 spectrometer (magnetic field 4.7 T; operating frequencies of 200.13 MHz for ^{1}H and 39.76 MHz for ^{29}Si). The single pulse spectra were acquired over 4000→42000 scans using flip angles (30→45°) and pulse recycle delays (2→20s) sufficient to minimize saturation effects. For CP, the Hartmann-Hahn condition was set using kaolinite (Rocha and Klinowski, 1990). ^{29}Si chemical shifts are given relative to tetramethylsilane (TMS) at 0 ppm, with kaolinite used as an external standard at -91.2 ppm. All spectra were apodized with 10 Hz of exponential line broadening and zero filled to 8192 points prior to Fourier transformation. The spectra were iteratively fitted to voigt line shapes using the software Igor (WaveMetrics, 1992&1996) with additional macros written by Brough (1993). The full procedure is outlined in Richardson and Groves (1997).

RESULTS AND DISCUSSION

Hydration products and microstructure

The microstructural features and hydration products present in all of the systems studied can be classified as either 'outer', forming within the boundaries of the original anhydrous grains - whether cement or slag - or 'inner', forming in the originally water- or solution-filled spaces. The microstructures of the water-activated WPC / VL slag blends are similar to those of the OPC / SC slag pastes described previously by Richardson and Groves (1992a,1993a). The main 'outer' hydration products are C-S-H and AFm with $Ca(OH)_2$ present in the blends. The $Ca(OH)_2$ in the water-activated blends generally occurs as large plates but in the KOH-activated pastes it is largely microcrystalline, being intimately mixed on a nanometer scale with layers of C-S-H; this is illustrated in Richardson and Groves (1997). The C-S-H is generally nearly amorphous but it is semi-crystalline in some of the KOH-activated systems giving electron diffraction patterns similar to the example for the SC slag / KOH paste in Richardson et al. (1994). Whatever its degree of structural order, C-S-H is present in all of the systems as two morphologically distinct forms: inner product (Ip) and outer product (Op). This is illustrated in Fig 1. Ip can be considered to be an intimate mixture of C-S-H and a Mg,Al hydroxide type phase.

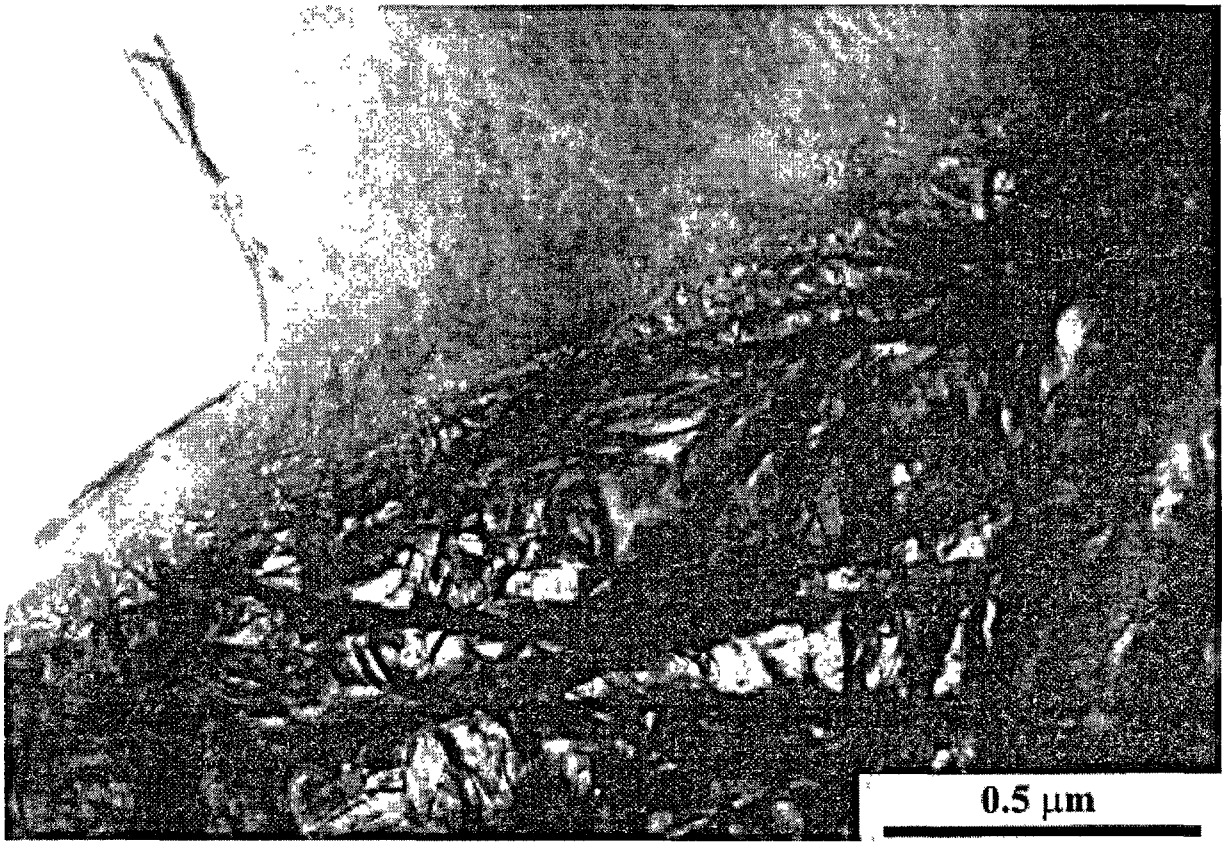

Figure 1. Transmission electron micrograph showing examples of fine-textured Ip (top) and foil-like Op C-S-H.

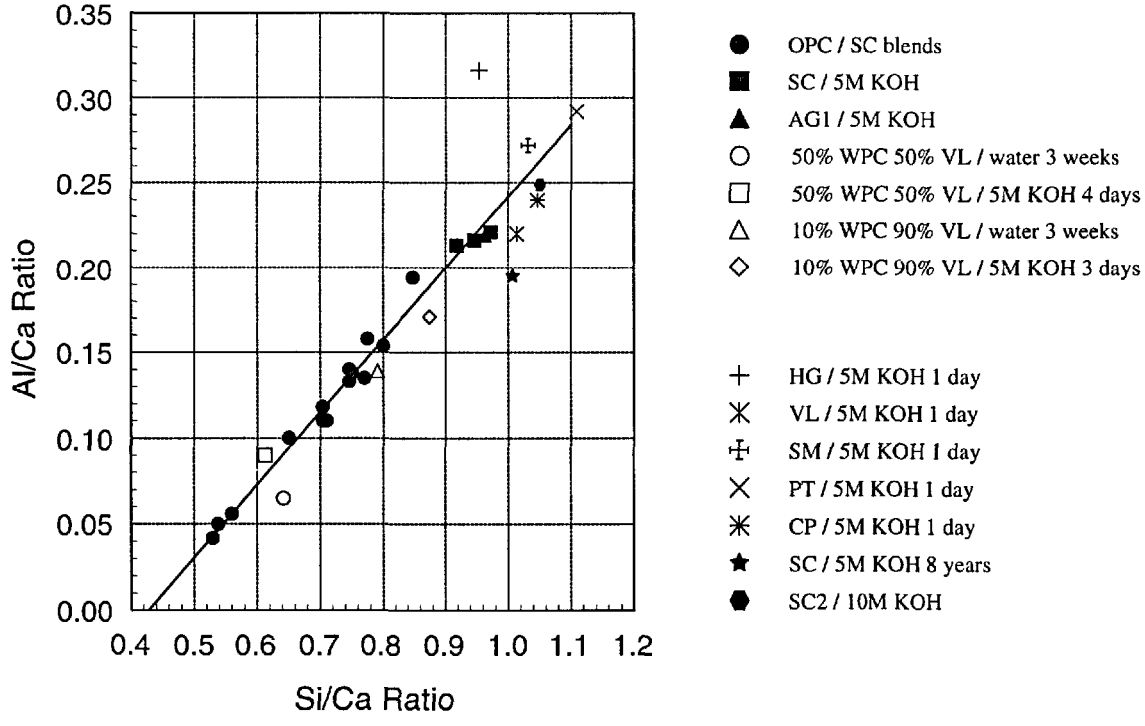

Figure 2. Al/Ca v Si/Ca for Op C-S-H gels in a range of slag-containing hardened cement pastes. Each point corresponds to a mean value of 20→50 analyses which are unambiguously of Op C-S-H.

Chemical composition of the C-S-H gels

Fig 2 is a plot of Al/Ca ratio against Si/Ca ratio for Op C-S-H gels present in a range of slag-containing hardened cement pastes: the Al/Ca ratio increases linearly with increasing Si/Ca ratio. The figure incorporates some earlier data of Richardson and Groves' (1992a,1993a,1994) for a range of OPC / slag blends (SC slag; hydrated at 20°C for 14 months (W/C=0.4) (●)), some slag / KOH pastes made with the same slag (■), and a synthetic slag / KOH paste (▲). The compositional trend line is derived from these data. The compositions of the Op C-S-H gels present in the WPC / VL slag blends (open symbols) are similar to those in the OPC / SC slag blends despite having different Portland cements and different blast-furnace slags. The C-S-H gels in all but one of the other KOH-activated slags fall on the same compositional trend line, suggesting an almost universal compositional relationship for the C-S-H phases present in slag-containing hardened cement systems. The HG slag has a very high aluminium content (Table 1) and this is reflected in the composition of the C-S-H present in the HG slag-KOH paste. Although its composition is off the trend line, the compositional and structural data are still consistent with formula 1.

Aluminosilicate anion structure

Fig 3 (top) shows the single-pulse ^{29}Si NMR spectrum for the PT slag-KOH paste which has particularly well-resolved peaks: the broad Q_0 peak at -73.0 ppm corresponds to unreacted slag and the three sharp hydrate peaks at -78.9, -82.0, and -85.2 to Q_1, $Q_2(1Al)$, and Q_2 respectively. Deconvolution of the spectrum (bottom) allows calculation of the mean Al/Si ratio of the C-S-H in the paste - i.e. in both the Op and Ip - and of the mean aluminosilicate chain length (MCL); the results are reported in Table 2. Fig 4 shows the single-pulse ^{29}Si NMR spectra for the water- (top) and KOH-activated 1/1 WPC / VL slag blend. The Q_0 peaks correspond to both unreacted slag and belite (the sharp component); it is assumed that all of the alite has reacted. Although the water-activated spectrum appears to have three hydrate peaks, Q_1, $Q_2(1Al)$, and Q_2, they are not well-resolved and so the results from deconvoluting the KOH-spectrum, where the hydrate peaks are very clearly defined, were used to aid in its deconvolution. This process, which was also done for the 9/1 blends, is discussed in greater detail in Richardson and Groves (1997). The compositional results are summarised in Table 2 and on Fig 5. The MCL of the C-S-H present in these systems increases with age but the chemical composition does not change very much; this is illustrated in Fig 6 for the VL slag / KOH system. It can be seen from Fig 5 that the compositions derived from the deconvolution of the NMR spectra are in excellent agreement with those from TEM. The assumptions that there are no chain-terminating Al, and that Al only substitutes for Si at tetrahedral bridging sites, would seem therefore to be well-founded. Al substitution in non-bridging sites would require the presence of $Q_1(1Al)$ units. The ^{29}Si chemical shift expected for $Q_1(1Al)$ units is ≈-75ppm; such peaks are not present on the ^{1}H-^{29}Si CP spectra - an example is given in Fig 7 - so it can be concluded that Al replaces Si only in the bridging sites of a dreierkette structure. The absence of $Q_1(1Al)$ units also supports the view that the higher polymers are formed by the linking of dimeric silicate units by silicate or aluminate monomers; there can be no aluminate-containing dimers. The number of occupied bridging sites that are occupied by Al and not Si is high in all cases of KOH-activation: 81, 86, 91, 72, and 83% for the C-S-H gels in Figs 3, 8, 9, and in the WPC / VL slag 1/1 and 1/9 blends respectively. Water-activation of the blends produces only ¾ as much Al substitution as does KOH.

Table 2. Composition of C-S-H in the pastes as determined by TEM and NMR. WPC / VL slag 1/1 and 1/9 blends activated with water (1W and 9W) or 5*M* KOH solution (1K and 9K); temperature (°C) of hydration and age as indicated. HT= hydrotalcite-type phase; N/Q = not quantitative; % hyd = % slag hydrated; MCL = mean linear aluminosilicate chain length.

		SC	SC2	HG	VL	SM	PT	CP	AG	1K	1W	9K	9W
	°C	20	20	25	25	25	25	25	60	25	25	25	25
Age	TEM	8y	8m	1d	1d	1d	1d	1d	1w	4d	3w	3d	3w
	NMR	8y	8m	3m	5m	3m	6m	5m	1w	4d	3w	3d	3w
Op	Ca/Si	0.99	0.95	1.05	0.99	0.97	0.90	0.96	1.04	1.63	1.56	1.14	1.26
	Al/Si	0.19	0.24	0.33	0.22	0.26	0.26	0.23	0.23	0.14	0.10	0.19	0.19
Ip	Ca/Si	1.18	1.22	1.14	1.11	1.10	1.05	0.94	1.17	1.47	1.56	1.16	1.27
	Al/Si	0.18	N/D	0.33	0.21	0.21	0.21	0.21	0.18	0.12	0.11	0.16	0.13
HT	Mg/Al	2.46	N/D	2.38	2.67	2.29	2.23	-	2.54	2.67	N/D	2.60	2.34
NMR	Al/Si	0.19	0.23	0.33	0.22		0.26		0.22	0.12	0.10	0.17	0.17
	MCL	7.1	7.4	11.5	6.1	N/Q	8.0	N/Q	4.8	3.6	4.1	4.2	6.5
	% hyd	78	13	48	60		70		33	-	-	-	-

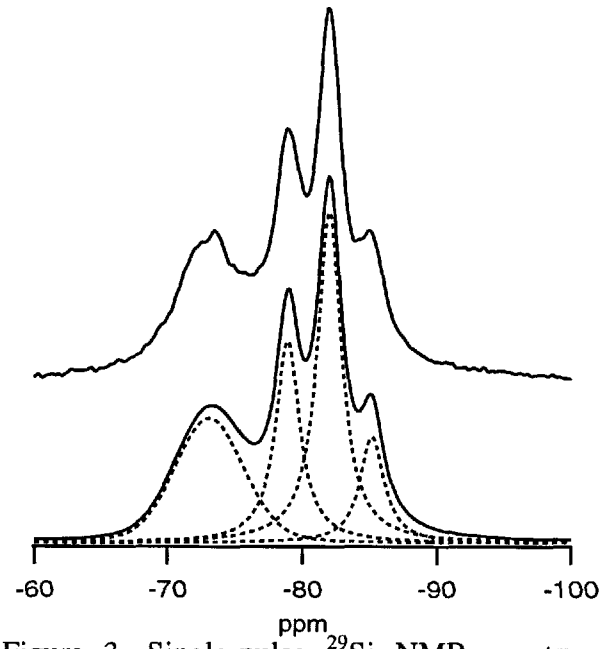

Figure 3. Single-pulse ^{29}Si NMR spectrum (top) for the PT slag-KOH paste and results of the deconvolution.

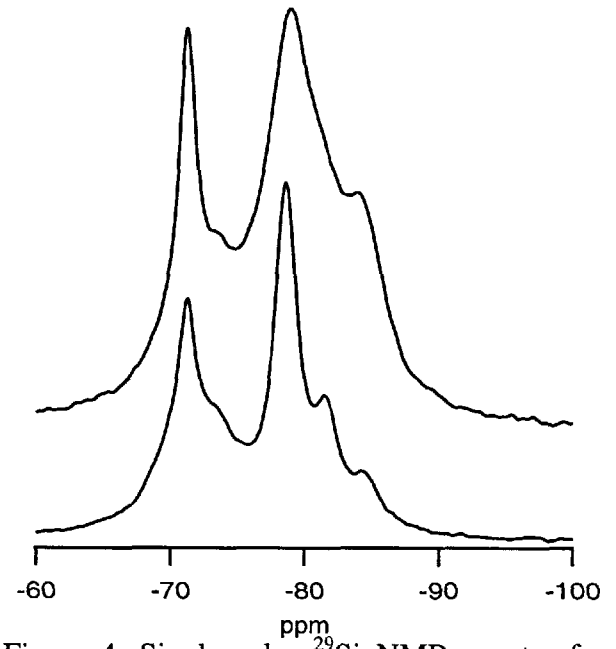

Figure 4. Single-pulse ^{29}Si NMR spectra for the water- (top) and KOH-activated 1/1 WPC / VL slag blend.

CONCLUSIONS

The C-S-H gels present in hardened pastes of alkali-activated blast-furnace slags of varying composition and of both water- and alkali-activated white Portland cement / slag blends - whatever their chemical composition or degree of structural order - all have aluminium substituting for silicon only in the central tetrahedron of pentameric silicate chains. The results give considerable confidence in models for the structure of C-S-H based on broken dreierkette chains with Al substituting for Si at 'bridging' sites only.

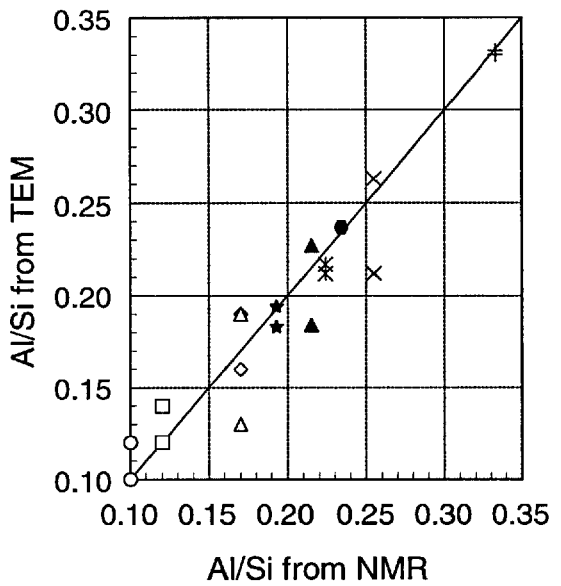

Figure 5. Al/Si ratio measured directly in the TEM (for both Ip and Op C-S-H) vs. the Al/Si ratio calculated from the NMR data.

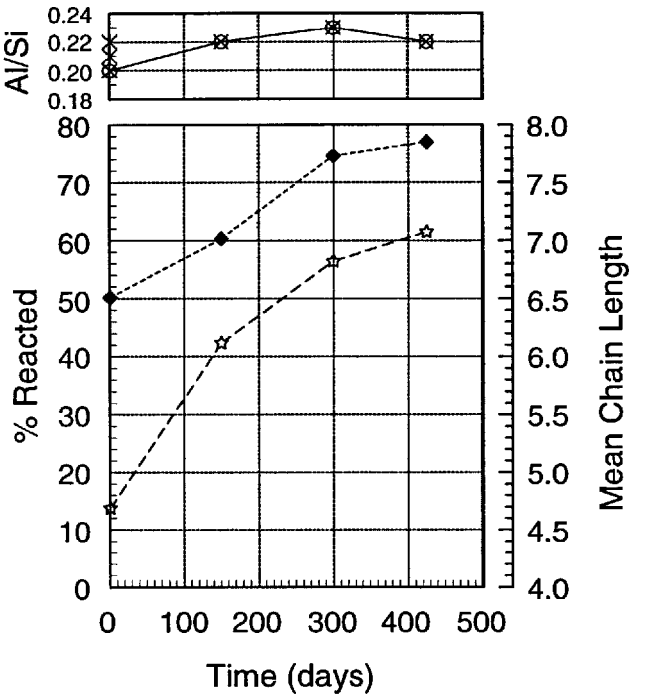

Figure 6. Variation in degree of slag reaction (◆), MCL, and Al/Si with age (from 1 day) for the VL slag / KOH system.

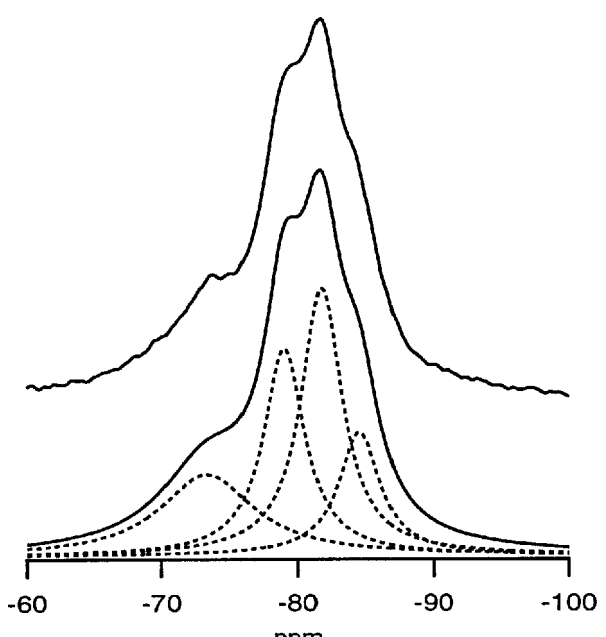

Figure 7A. Single-pulse ^{29}Si NMR spectrum (top) for the VL slag-KOH paste (hydrated for 14 months) and results of the deconvolution.

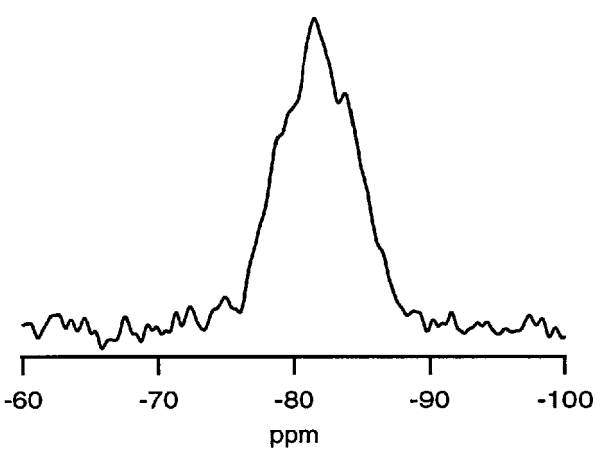

Figure 7B. ^{1}H-^{29}Si CP spectrum for the VL slag-KOH paste (hydrated for 14 months). Note the absence of a peak at ≈-75ppm.

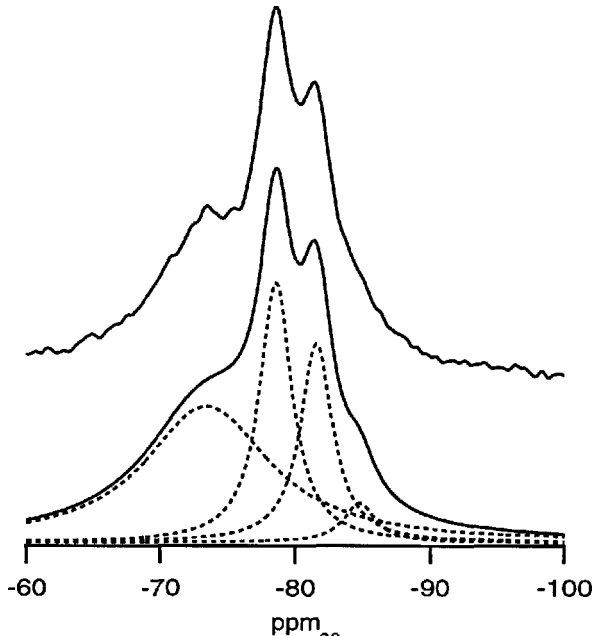

Figure 8. Single-pulse ^{29}Si NMR spectrum (top) for the VL slag-KOH paste (hydrated for 1 day) and results of the deconvolution.

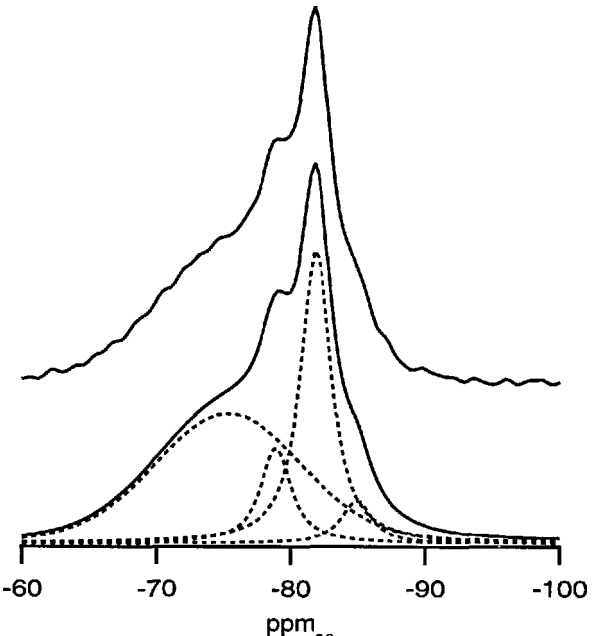

Figure 9. Single-pulse ^{29}Si NMR spectrum (top) for the HG slag-KOH paste (hydrated for 3 months) and results of the deconvolution.

REFERENCES

Birchall, J.D., and Thomas, N.L., Proc. Brit. Ceram. Soc., Vol. 35 (1984) 305.

Brough, A.R., D.Phil. Thesis, University of Oxford, (1993).

Brydson, R., Richardson, I.G., McComb, D.W. and Groves, G.W., Solid State Communications, Vol. 88 (1993) 183.

Fujii, K., and Kondo, W., J. Amer. Ceram. Soc., Vol. 66 (1983) C-220.

Greenberg, S.A., Chang, T.N., and Anderson, E., J. Phys. Chem., Vol. 64 (1960) 1151.

Greenberg, S.A. and Chang, T.N., J. Phys. Chem., Vol. 69 (1965) 182.

Groves, G.W., LeSueur, P.J., and Sinclair, W., J. Amer. Ceram. Soc., Vol. 69 (1986) 353.

Kantro, D.L., Brunauer, S., and Weise, C.H., J. Phys. Chem., Vol. 66 (1962) 1804.

Richardson, I.G. and Groves, G.W., J. Mater. Sci., Vol. 27 (1992a) 6204.

Richardson, I.G. and Groves, G.W., Cem. Concr. Res., Vol. 22 (1992b) 1001.

Richardson, I.G. and Groves, G.W., J. Mater. Sci., Vol. 28 (1993a) 265.

Richardson, I.G. and Groves, G.W., Cem. Concr. Res., Vol. 23 (1993b) 131.

Richardson, I.G. and Groves, G.W., J. Mater. Sci., (1997) in the press.

Richardson, I.G., Brough, A.R., Brydson, R., Groves, G.W. and Dobson, C.M., J. Amer. Ceram. Soc., Vol. 76 (1993) 2285.

Richardson, I.G., Brough, A.R., Groves, G.W. and Dobson, C.M., Cem. Concr. Res., Vol. 24 (1994) 813.

Richardson, Ou, D.L., and Cabrera, J.G., (1997) in preparation.

Rocha, J. and Klinowski, J., J. Magn. Reson., Vol. 90 (1990) 567.

Taylor, H.F.W., J. Amer. Ceram. Soc., Vol. 69 (1986) 464.

WaveMetrics, Inc., Igor (1992) and Igor Pro (1996), Lake Oswego, Oregon, 97035, USA.

Topic II.D

Chemical and physical shrinkage

2ii069
8 pp

Kn o. 2 5. JAN. 2001 d o k 31833

INFLUENCE OF MEASURING METHOD ON BLEEDING AND CHEMICAL SHRINKAGE VALUES OF CEMENT PASTES

Harald JUSTNES, SINTEF Civil and Environmental Engineering,
Cement and Concrete, Trondheim, Norway
Arne VAN GEMERT, K.U.Leuven, Belgium
Frank VERBOVEN, K.U.Leuven, Belgium
Erik SELLEVOLD, NTNU Trondheim, Norway
Dionys VAN GEMERT, K.U.Leuven, Belgium

ABSTRACT Hydration of cement paste causes a certain amount of chemical shrinkage. A distinction is made between chemical shrinkage and external or autogenous shrinkage. This paper discusses different measuring methods for the chemical and external shrinkage, their negative effects on the measured results and how the rotation method and the handling procedures of the samples were developed to overcome these problems.

Key-words: chemical shrinkage, autogenous shrinkage, hydration, structure.

INTRODUCTION

Shrinkage of a cement paste can be defined as a decrease in volume caused by a certain loss of water volume. This loss of water volume can be caused by physical or/and by chemical reasons. The physical processes which have an effect on the shrinkage can be easily recognized. Sedimentation of the solid particles and absorption by porous substances are two of them. Plastic shrinkage can occur when the water evaporates at the surface or is sucked up by dry cement paste below. Drying shrinkage occurs through evaporation when the hardened cement paste is stored in unsaturated air. A part of this shrinkage is irreversible and should be distinguished from the reversible part. If sufficient attention is given during the hardening period, most part of the shrinkage caused by physical reasons can be avoided.

However, even when there is no moisture movement possible to or from the cement paste autogenous shrinkage occurs. This external volume change is also called external chemical shrinkage. It is part a consequence of the chemical shrinkage. The chemical shrinkage during the hydration is caused by the smaller volume of reaction products compared to reactants. It may be calculated by assigning the total volume reduction to the water taking part in the hydration, with the value of 25.4 % reduction per cm^3 chemically bound water. The result is the rule of thumb, that chemical shrinkage at 100% hydration is about 6.00 ml/100g cement (Powers T.C. and Brownyard T.L.,1948, in Lea F.M.,1970). Autogenous shrinkage, a small volume change by itself, can cause cracks or may act as an initiator of processes. As a consequence, chemical shrinkage of the cement paste may influence the durability of concrete, particularly for low w/c-ratio concrete. It is therfore of importance to have reliable methods to measure the amount of autogenous shrinkage of cement pastes as a function of their composition, fineness, w/c etc., from as early as possible. It will be shown that the amount of autogenous shrinkage of a cement paste is very dependent on the adopted measuring procedure. A discussion of the effects of measuring procedures on the results is made, and a rotation method is presented to overcome most of the unwanted effects. The amount of autogenous and chemical shrinkage of cement pastes was measured for pastes in the w/c range 0.30 to 0.50 over a period of 48 hours. This paper only deals with the measuring methods. The shrinkage values as a function of w/c are discussed earlier (Justnes et al, 1996).

MATERIALS

All tests were performed with two commercially available Norwegian portland cements: Cement 1 with a setting time of 142-204 minutes, and Cement 2 with a setting time of 87-134 minutes. The cement characteristics were for Cement 1; 20.92% SiO_2, 4.60% Al_2O_3, 3.54% Fe_2O_3, 63.44% CaO, 3.06% SO_3, 1.80% MgO, 0.88% K_2O, 0.36% Na_2O, 0.94% Alkalis and fineness (Blaine) 358 m^2/kg, and for Cement 2; 20.84% SiO_2, 5.04% Al_2O_3, 3.30% Fe_2O_3, 63.61% CaO, 2.70% SO_3, 1.06% Alkalis and fineness (Blaine) 361 m^2/kg. Potential minerals according to Bogue calculations were for Cement 1; 19% C_2S, 55% C_3S, 6.2% C_3A and 10.8% C_4AF, and for Cement 2; 24.4% C_2S, 46.9% C_3S, 7.80% C_3A and 10.0% C_4AF. Distilled water was used in the experiments.

EXPERIMENTAL METHODS FOR CHEMICAL SHRINKAGE MEASUREMENTS

Chemical shrinkage

The addition of water to a cement results in hydration reactions. The hydration products will gradually fill the originally water filled spaces between the cement particles, resulting in reduced porosity. There are three main measuring techniques: 1) **Dilatometry.** The cement slurry is water saturated in a receptacle. A pipette reaches into the water in the receptacle and the total chemical shrinkage is measured by the change in water level in the pipette. 2) **Gravimetry.** This method is based on the principle of Archimedes. The cement paste is put in a container with flexible membrane together with an excess of water. The change in buoyance force of the sealed sample gives the total chemical shrinkage in time. 3) **Pycnometry.** The hydrating cement paste undergoes a volume decrease. The water level is kept constant by the addition of water. The change of weight measures the total chemical shrinkage.

In our experiments the total chemical shrinkage is determined by the dilatometry method. The cement paste was put into three 50ml Erlenmeyer flasks, forming a ± 10 mm thick layer. After weighting the samples, the Erlenmeyers were filled with distilled water. A rubber stopper closed the Erlenmeyer. A pipette was put through the stopper into the Erlenmeyer. This pipette was filled with water. On top of the water level an few drops of paraffin oil prevented evaporation which would disturbe the measurements. The Erlenmeyers were kept in a water filled bath at 20°C ± 1°C, Fig 1.

Autogenous (external) shrinkage

When water is added to the cement, hydration of the cement starts. The reaction products grow into the pores and build a structure between the cement particles. Initially, the chemical shrinkage is identical to the external shrinkage since the paste is fluid, but when a skeleton structure is formed the chemical shrinkage results in empty pores, and the external shrinkage becomes much smaller than the chemical shrinkage. The measurements of the external shrinkage of sealed specimens can be done using an unidimensional dilatometer method or using a volumetric dilatometer method.

1. Unidimensional dilatometer

By using a unidimensional dilatometer the distance variation between two studs which are fixed to a testbar, is followed (Fulton, 1963, and Baron, 1968, in Buil M. and Baron J., 1980). However, in the period that the cement paste has not yet set, it behaves liquidlike, and the deformation will mainly take place vertically. Hence, linear measurements are not reliable before setting.

2. Volumetric dilatometers

Measurements by volumetric dilatometry can be executed in various ways.

- The paste is put in a rubber balloon. This balloon acts as a barrier between the cement paste and a mercury column. The external shrinkage is given by the movement of the mercury which follows

the external shrinkage of the sample (Edmeades et al., 1966, in Setter N. and Roy D.M., 1978).

- Also common is to put the sealed sample in a water filled vessel which is connected to a beaker. Due to contraction of the cement paste, water migrates from the beaker to the vessel. By measuring the weight change of the beaker, the external shrinkage can be determined.
- Another method to determine the external chemical shrinkage is based on Archimedes' principle: external shrinkage of the sealed specimen leads to a decrease of the buoyance force and consequently an increase in weight is measured.

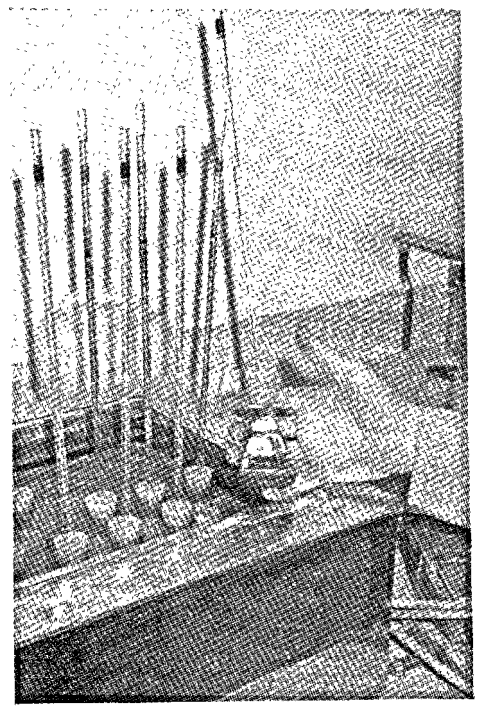

Figure 1 Equipment to determine total chemical shrinkage

In our experiments the Archimedes principle was used. Three parallel elastic rubber bags (condoms) were filled with cement paste. The rubber bags were closed by twisting the end and tying it with a thin copper wire. To be sure that the sample was sealed from the environment silicon glue was applied into the open end. The samples were kept in a water filled bath at a constant temperature of 20°C ± 1°C. One hour after water-cement contact, the weight measurements started.

BLEEDING EFFECT

The settlement of solids in a fresh, plastic paste is followed by the formation of a water layer at the paste surface known as "bleeding". Fig 2 shows that bleeding has an enormous effect on the measurements of autogenous shrinkage. The total chemical shrinkage vs time curve of Cement 2 paste with w/c = 0.50 is compared with the external chemical shrinkage curve of the same paste without and with rotation prior to setting. The external chemical shrinkage curve follows more or less the total chemical shrinkage curve within the observation time of 48 h, while the external chemical shrinkage curve for the rotated specimens flattens out at about 7 h as expected (i.e. a strong enough hydration network has been formed that can resist the contracting forces). The behavior of the static samples is caused by the "bleeding" water (can be seen through the transparent condom) formed by the segregation of the paste: After the skeleton of interconnecting hydration products is strong enough to resist the contracting forces created by the chemical shrinkage, the under pressure set up by the contraction pores will suck the bleeding water into the paste and the volume decrease (directly proportional to the volume of contraction pores) will erroneously be

interpreted as external chemical shrinkage. A secondary, false flattening out level will be registered when the imbibition of the bleeding water is complete.Therefore, in order to get correct results of the amount of external shrinkage, a new method had to be developed to avoid the bleeding effect.

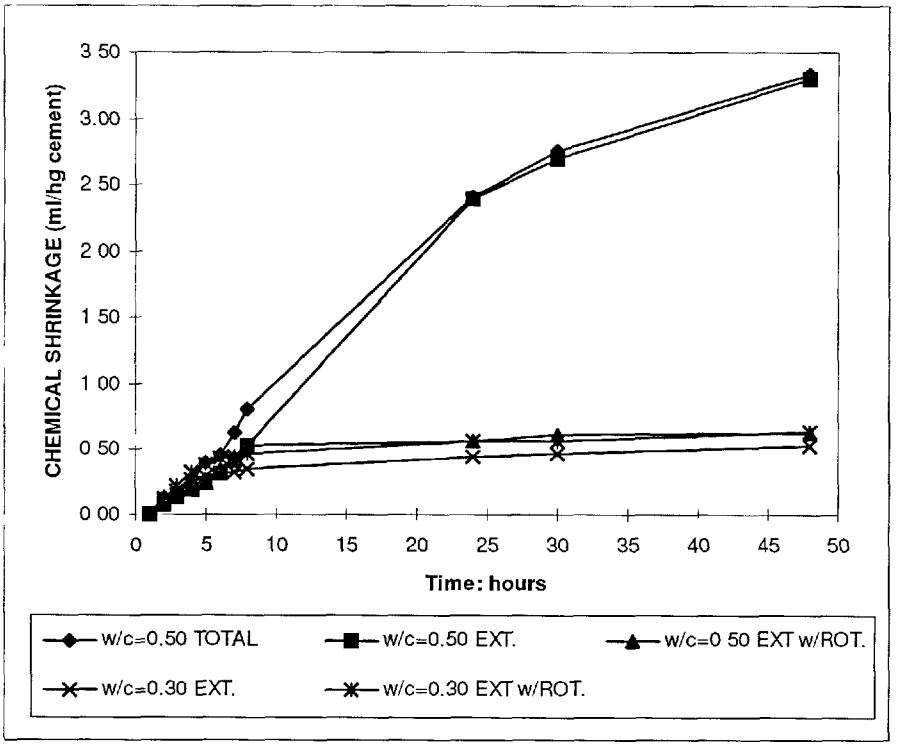

Figure 2 Comparison of total chemical shrinkage and external chemical shrinkage for static and rotated Cement 2 pastes.

In the beginning, the samples were turned around by hand every quarter of an hour. This experiment was done with 3 parallels of Cement 1 and a w/c ratio of 0.40. As can be seen in Fig 3 the shrinkage curves of the paste flattened out after about 10 hours if the samples were rotated by hand, but when the samples were not rotated (static test) there was still some bleeding water present after 48 hours, as demonstrated by the higher rate of shrinkage. Moreover the external shrinkage dropped with 60% (from 3.19 cm^3/ 100 g cement to 1.23 cm^3/ 100 g cement).

The first success at rotating the samples by hand had strenghened the idea to develop a system that would rotate the samples continuously. The rotating system consisted of an ordinary rotating table which was modified to function under water (Fig 4). This was done by a chain transfer between the motor and the rolling bars which were placed under water. A problem which occurred when using the rotating system was damage to the rubber bags when they were lying on the rolling bars. Because the form of the samples was not symmetric the samples moved to the outside of the rolling bars and were damaged by the gear or by the chain. A hole in the rubber would disturb the measurements because water from the bath would be sucked into the sample and the weight would increase. To avoid this problem the samples were put into a stiff plastic tube. This tube could withstand the friction and torsion forces which arise at rotation and which act on the sample. The extra advantage of using the tube is that the building up of the network of the cement paste will not be disturbed when the sample is manipulated for weighing.

But now another problem arised. The rubber bags were slided into the tubes in the air, above water. Once the tubes were filled, they had to be transported to the rotating system. A lot of air bubbles were hanging on the tube and some were located between the rubber bag and the tube. It was impossible to remove all the air bubbles without damaging the rubber bag. These air bubbles had a negative effect on the measurements, because the amount of air bubbles was not the same at the different measurements. To avoid this problem the samples were slipped into the tube just above the water surface, whilst the tube was always kept under the water surface. By filling the tubes in this way, the air bubbles were avoided. When the samples needed to be weighed they were transported from the rotating bath to the weighing bath in a big glass container to be sure that no air bubbles were trapped and could influence the measurements. The weighing had to be done in a separate water bath because the turbulence of the rotating system and of the stirrer, which assured an equal temperature in the water bath, disturbed the stability of the weight too much.

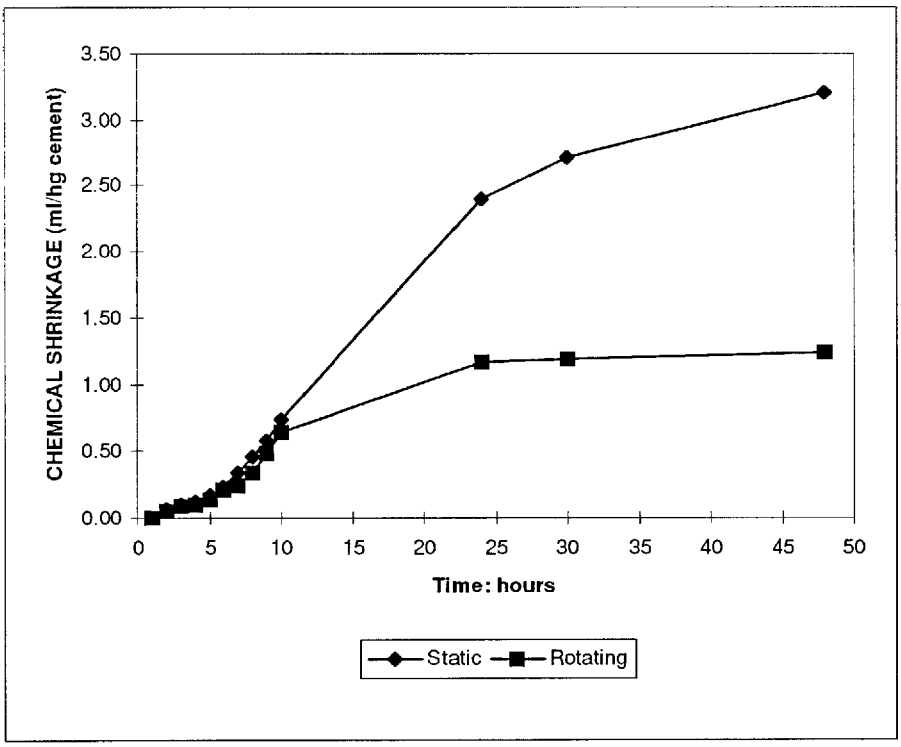

Figure 3 Average values of external chemical shrinkage of samples in static and hand rotated test. Cement 1, w/c = 0,40.

After the measurements the rubber bag was wiped dry and was stripped from the paste. The amount of cement paste had to be determined from the difference in weight of the paste + rubber bag + tube + silicone glue + copper wire and the weight of the tube + rubber bag + silicone glue + copper wire. The external shrinkage is calculated as the average value of three parallel samples and is given in ml/100 g cement.

RESULTS AND DISCUSSION

When the samples were rotated, bleeding water on top of the sample could be prevented even when the w/c ratio was 0.50. In Table 1 a comparison is made between the measured values of external chemical shrinkage of rotated and non-rotated samples.

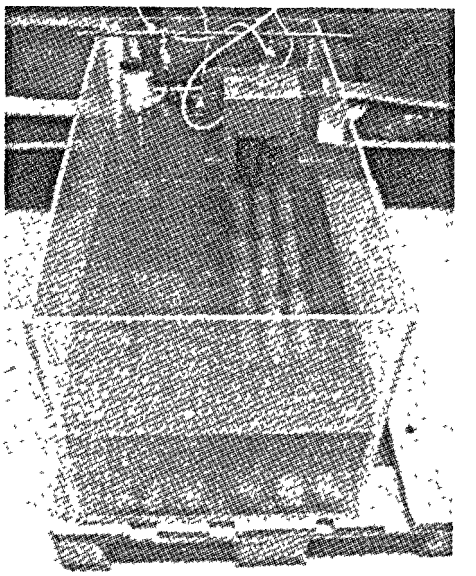

Figure 4 Water bath with automatic rotating system. 9 samples are being rotated.

Table 1 Results of the external chemical shrinkage after 48 hours of rotated and static samples (cm^3/ 100 g cement)

		w/c ratio				
Cement type	**procedure**	**0.30**	**0.35**	**0.40**	**0.45**	**0.50**
Cement 2	non-rotated	0.53	0.71	1.79	3.41	3.21
	rotated	0.50	0.68	0.61	0.64	0.63

The difference between the measured external chemical shrinkage of rotated and non-rotated samples becomes larger as w/c increases. This is evidently caused by the bleeding water that is present on top of the non-rotated samples. The greater the w/c ratio, the greater the amount of bleeding water. This could easily been observed through the transparant rubber bag. At a w/c ratio of 0.30 and 0.35 there is just a small difference of 0.03 cm^3/ 100 g cement between the rotated and non-rotated sample. This difference might be caused by manipulating the samples by hand for weighing when the paste had not yet set. This conclusion came after the observation of clear finger prints in the hardened samples. As mentioned earlier the handling of the rotated samples was easier because they were put in a hard plastic tube.

The shrinkage "flattening out" level for the rotated samples does not depend on the w/c-ratio (Fig. 3) in contrast to the static test (Fig. 2). This implies that the degree of hydration, which is proportional to the chemical shrinkage at the knee point, needed to produce a rigid skeleton allowing empty pores to form, is independent of the w/c-ratio. This is somewhat surprising, since the average distance to be 'bridged' by hydration products to produce a skeleton increases strongly with increasing w/c-ratio. Possibly the greater friction, and hence more energetic mixing, of low w/c-ratio pastes produces a less flocculated structure than for high w/c-ratio pastes. Thus, the skeleton of the two is formed at the same degree of hydration, but the bridging for low w/c-ratio is primarily particle-to-particle, while in high w/c-ratio the bridges are between flocs.

In order to get a better understanding of the different shrinkage behaviour of the rotated and non-rotated samples an electron microscope examination of a hardened sample of each type was done. Cement 2, w/c ratio 0.45, was used in the examination. Two small pieces were taken from each sample for the examination: one at the outside of the sample and one in the centre. The small pieces were dried and a graphite layer was deposited over the pieces on fracture surfaces.

The piece that was taken on the edge of the rotated sample which consisted of some layers that could be recognized bacause of their different colour. Alternatively bright and grey layers could be distinguished (Fig 5).

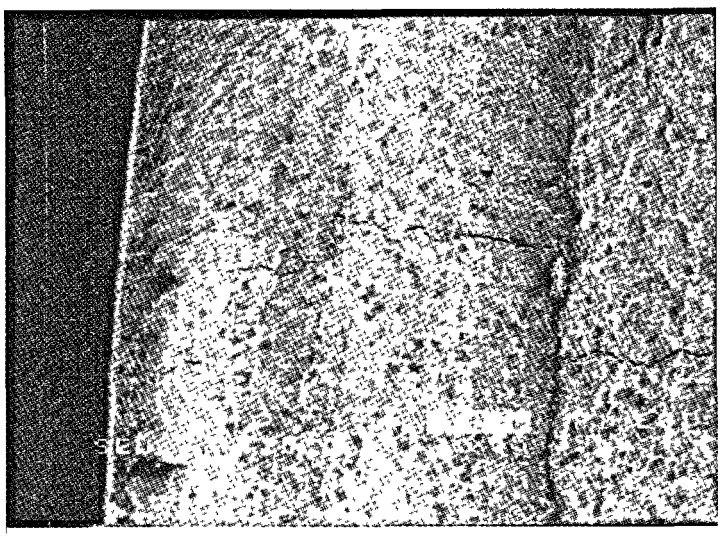

Figure 5 Cement 2, w/c = 0.45, layered structure at outside of rotated sample. Layer thickness about 0.3 mm.

The bright layer is probably rich in $Ca(OH)_2$ which is precipitated out of the water solution while the grey layers are mainly CSH-gel. This can indicate that at the edge of the samples ,when the paste is not set, some layers are rotating over each other divided by a small water layer. This layered structure was not found in the non-rotated sample.

The microstructure of the rotated sample seemed to have a less dense structure than the non-rotated sample. This confirms the observations that when bleeding water is present, the real w/c ratio is decreased and a denser structure will be formed. During the experiments a lot of bleeding water was present on top of the non-rotated sample. The microstructure of the rotated sample was a mix of plates, needles and pores, whereas the microstructure of the non-rotated sample contained more plates, less needles and less pores. Further research has to be carried out to determine the nature of the elements of the microstructure, as well as to check if the microstructure of the rotated cement paste still represents the structure of the corresponding cement paste in concrete or mortar.

A continuous external shrinkage measurement has been done to get an idea about the influence of the weighing manipulations during the normal procedure on the results. The measurement was done using a continuous registration of the buoyance force in a static balloon test. At a w/c ratio 0.40 the value of the external chemical shrinkage increased by more than 25 % due to the weighing manipulations, compared to the continuous measurement without manipulations. This observation again stresses the importance of the careful experimental handling procedure on the results of autogenous shrinkage measurements.

CONCLUSIONS

External chemical shrinkage values of hydrating cement pastes are highly dependent on the measuring procedure. This paper compares the usual balloon method under static and rotating conditions. The static method is unable to deal with the influence of bleeding at medium and high w/c ratios. The rotation method avoids bleeding of the cement pastes, and keeps the pastes at the desired w/c ratio. Thus, we believe that the rotating method is the best to obtain a "true" autogenous shrinkage curve, and in particular to establish the "knee" where the autogenous shrinkage curve "flattens out" and deviates from the chemical shrinkage curve, indicating that a skeleton is formed by the hydration allowing empty pores to form. We furthermore believe that this knee represents the transition from liquidlike to solidlike behavior in the paste, and that the crack sensitivity is very high during this transition when the skeleton has very low strength. It should be added that any physical manipulation during the experiment appears to influence the results, and of course the rotation itself represents a manipulation.

The present results illustrate quite clearly that the often used method to measure autogenous shrinkage linearly in a horizontal direction is a very questionable procedure.

ACKNOWLEDGEMENT

The study is partly a result of the collaboration between Katholieke Universiteit Leuven (Belgium) and Norwegian University of Science and Technology in Trondheim (Norway) within the framework of the european student exchange programme ERASMUS.

REFERENCES

Buil M., **Baron** J., Le Retrait Autogène de la Pâte de Ciment Durcissante, 7th Int. Conf. Chem. Cem., (1980), pp. VI-37-41.

Justnes H.,**Van Gemert** A., **Verboven** F., **Sellevold** E. J., Total and external shrinkage chemical shrinkage of low w/c ratio cement pastes, Advances in Cement Research, 1996, 8, No. 31, July, 121-126.

Lea F. M., The chemistry of Cement and Concrete, Third Edition, Edward Arnold Publishers Limited, London (1970), pp. 41-42, pp. 177-310.

Ramachandran V.S., Concrete Admixtures Handbook : Properties, Science and Technology, Noyes Publications, New Yersey (1984), pp. 116-201, pp. 211-268

Reyniers B., **Van Loo** D., Chemical Shrinkage of Cement, Thesis 1993, Erasmus Leuven-Trondheim

Setter N., **Roy** D.M., Mechanical Features of Chemical Shrinkage of Cement Paste, Cement and Concrete Research, vol. 8, pp. 623-634, (1978).

Soroka I., Portland Cement Paste and Concrete, The Macmillan Press Limited, 1979.

Van Gemert A., **Verboven** F., Chemical Shrinkage of Cement Pastes, Master's Thesis 1994, Erasmus Leuven -Trondheim

2ii070
8 pp

Kn a. 2 5. JAN. 2001 d o k: 31834

AUTOGENEOUS SHRINKAGE OF CEMENT PASTE DURING HYDRATION

Toshiyuki TAKAHASHI, Hideki NAKATA and Kozaburo YOSHIDA, R & D Department, Constructing Materials Division, Ube Industries, Ltd., Ube,Yamaguchi, Japan
Seishi GOTO, Department of Advanced Materials Science and Engineering, Yamaguchi University, Ube, Yamaguchi, Japan

ABSTRACT Autogeneous shrinkage of cement pastes with W/C=0.30 for low heat cements and ordinary portland cement has been measured. The development of shrinkage can be divided into 3 stages, that is (1) first shrinkage, (2) no shrinkage or expansion and (3) second shrinkage. The first shrinkage ended when the rigid structure was formed in each cement paste. The second shrinkage initiated when gypsum was consumed. It was suggested that second shrinkage initiated with reaction and/or recrystallization of ettringite.

Key-words : Autogeneous shrinkage, Chemical shrinkage, Hydration, Ettringite

INTRODUCTION

It is well known that the absolute volume of hydrates formed is less than the sum of the volumes of cement hydrated and water consumed. This phenomenon is called " Chemical shrinkage" or " Hardening shrinkage" (White, 1928). If the specimen is not in communication with an external water source, after the rigid structure has formed, chemical shrinkage causes the development of a gaseous volume, empty space, in the pore initially saturated with water. This phenomenon is called "Self desiccation" .

Autogeneous shrinkage is a macroscopic reduction in the volume of paste, which has kept in the condition of constant temperature, no moisture migration, no carbonation and so on (Davis, 1940). A recent study (Tazawa and Miyazawa et.al., 1991) has revealed that the amount of autogeneous shrinkage, in contrast to drying shrinkage, increases with a decrease in the water-cement ratio (w/c) and with densifying of the microstructure of cement. It becomes more significant when higher strength is required for concrete. There are many reports discussing the influence of the kind of cement and the mix proportion of concrete on autogeneous shrinkage(Tazawa and Miyazawa, 1994), but very few that have discussed the behavior of autogeneous shrinkage with the course of hydration of cement.

The purpose of this study is to understand the relationship between the behavior of autogeneous shrinkage and that of the hydration of cement. Autogeneous shrinkage of the cement pastes prepared with low heat cements and ordinary portland cement with w/c=0.30 was measured by a newly prepared apparatus which is able to measure the shrinkage from an early stage to a later stage of hydration.

EXPERIMENTAL PROCEDURE

In this experiment, an ordinary portland cement (OPC) and a low heat cements such as a moderate heat portland cement (MHC), a low heat portland cement (LHC) and a low heat portland cement based blastfurnace slag cement (LSC) were used. Synthesized alite was also used to investigate the effect of aluminate on the autogeneous shrinkage. Alite was prepared by Yamaguchi's method and 2% of gypsum was added to alite. Chemical composition and specific surface areas (Blaine) were shown in Table 1. Slag content in LSC was 60% in weight.

Cement pastes were prepared according to JIS R 5201. Water-cement ratio (w/c) was 0.30 for the measurement of autogeneous shrinkage and analysis of hydration process, and 0.40 for the measurement of chemical shrinkage. Setting time of cement was measured with w/c=0.30 according to JIS R 5201. The penetration time was also measured by using a needle loaded with 3000g.

Table 1 Fineness and chemical composition of cement, alite and slag used

Type	Braine (cm2/g)	Chemical composition (%)										Mineral composition(%)			
		ig loss	insol.	SiO_2	Al_2O_3	Fe_2O_3	CaO	MgO	SO_3	Na_2O	K_2O	C_3S	C_2S	C_3A	C_4AF
Ordinary poltland cement	3190	0.8	0.0	21.5	5.1	2.8	65.2	1.0	2.1	0.23	0.52	57	18	9	9
Moderate heat cement	3100	0.6	0.2	23.4	4.0	4.0	63.7	0.9	2.1	0.12	0.46	43	35	4	12
Low heat cement	3240	1.0	0.1	25.0	3.6	3.7	62.4	0.9	2.1	0.15	0.43	28	50	3	11
Alite	3200	0.1	—	24.4	1.1	0.1	70.2	0.9	1.9	0.02	—	—	—	—	—
Blastfurnace slag	4220	0.8	—	32.6	12.9	1.2	41.4	6.6	2.1	0.18	—	—	—	—	—

Measurement of autogeneous shrinkage

An apparatus for the measurement of autogeneous shrinkage strain of cement paste was made for this study. This apparatus can measure the change in length from an early stage of hydration(Takahashi et.al., 1996). The apparatus is shown in Fig. 1. We considered that vertical volume change by bleeding almost finished at initial setting time, and measured horizontal change in length, which is caused by the hydration of cement, after initial setting time. The change in length from initial setting time to 2 days was determined by measuring the displacement of gauge plugs attached to a specimen with non-contact type displacement sensors shown in Fig. 1 (a). A specimen was wrapped with a polyethylene film to reduce an adhesion force between specimen and mold, and to prevent water evaporation from the specimen. The hardened paste cured for 2 days was demolded from the apparatus shown in Fig. 1 (a), and wrapped with a polyethylene film and an aluminium film. Then the specimen was put on an apparatus shown in Fig. 1 (b) to measure the change in length after 2 days. These measurements were carried out at 20 ± 3℃. The strain of autogeneous shrinkage measured with this apparatus was a good reproducibility within ± 30 μ (3 σ) on repeated runs. The obtained value was not corrected by the thermal expansion coefficient because of little rise in temperature inside the specimens.

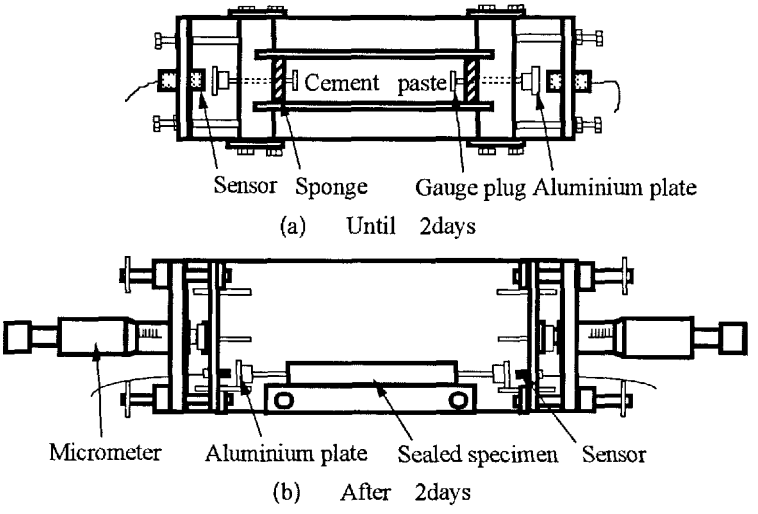

Figure 1 Apparatus for measurement of autogeneous shrinkage (Top view)

Measurement of chemical shrinkage

The chemical shrinkage was measured by Tazawa's method (Kasai and Tazawa, 1988) where a cement paste was placed in an Erlenmeyer flask with a depth of about 10mm and water was added on the top of the paste. The volume change of cement plus water was measured with a pipette mounted on the top of the water. The flask was immersed in a water bath controlled at 20 ± 3℃.

Analysis of hydration process

Cement paste for the analysis of hydration ratio was molded in a plastic container (ϕ 20mm × 40mm) and the sealed container was cured at 20 ± 3℃. The cured samples were crushed under 5mm and washed by acetone to stop the hydration.

For X-ray diffraction (XRD) analysis, the crushed samples were ground under 88 μ m. The ground samples were mixed with internal standard material (CaF_2) and dried at 11%RH under nitrogen atmosphere. A Rigaku X-ray diffractometer system (RU 200B, 50kV, 180mA) was used for XRD analysis. The XRD data was collected by step scanning (stepped width : 0.02deg, fixed time : 10sec).

The relative intensity of hydrates to that of internal standard material was determined where the ranges of scanning 2 θ (Cu K α ,deg) for gypsum, ettringite, monosulfate and CaF_2 were from 11.2 to 11.8 degree, from 8.7 to 9.4 degree, from 9.5 to 10.3 degree, and from 28.0 to 28.5 degree, respectively.

For transmission electron microscopy (TEM), the crushed samples were D-dried and then polished by dimpling and ion-thinning. A Nihondenshi TEM system (JEM-2010) was used for the observation of samples.

RESULTS AND DISCUSSIONS

Autogeneous shrinkage of cement pastes

The changes in length of pastes for OPC, MHC, LHC and LSC were shown in Fig. 2. For OPC, MHC and LHC pastes, two types of turning points appeared on the strain-time curve at the early stage of hydration. The initial shrinkage stopped at the first turning point (black arrow) and started again after the second turning point (white arrow). The times of these turning points for OPC were shorter than those of MHC and LHC. Cement pastes for MHC and LHC expanded during the first turning point and the second turning point. The

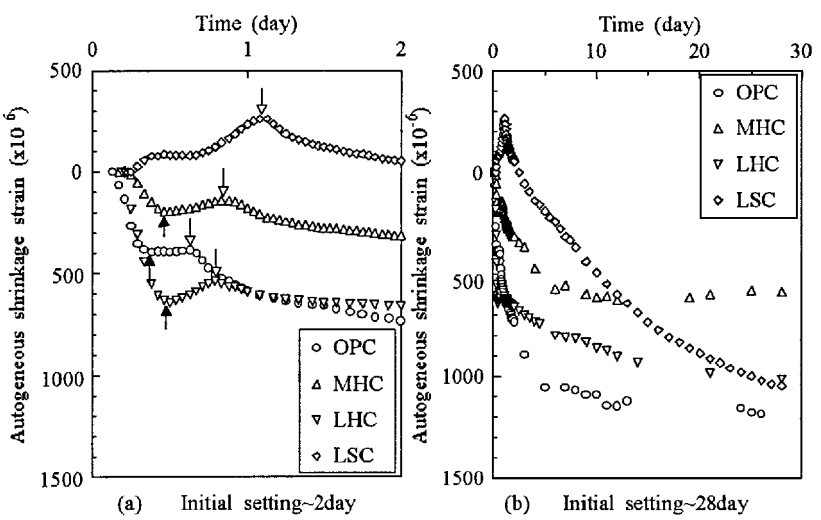

Figure 2 Autogeneous shrinkage of cement paste (W/C=0.30)

there were no autogeneous shrinkage during the first turning point and the second turning point. The slopes of curves for LSC and OPC paste after the second turning point were larger than that of MHC and LHC paste. These results suggested that the mechanism of autogeneous shrinkage could not be explained directly by chemical shrinkage.

The relationship between autogeneous shrinkage and the setting of cement

The development of autogeneous shrinkage could be divided into 3 stages, that is (1) the first stage with first shrinkage (before the first turning point) , (2) the 2nd stage with no shrinkage or expansion (between the first turning point and the second turning point) and (3) the 3rd stage with the second shrinkage (after the second turning point).

We investigated the reason why first shrinkage terminated in spite of progressive chemical shrinkage. Fig. 5 shows the relationship between the time of the first turning point (t_1) and the final setting time (t_s) of cement. Time (t_1) had a good correlation with the final setting time, but these times did not correspond to each other.

Fig. 6 shows the relationship between time (t_1) and the penetration time (t_p) of a 3000g loaded needle into paste. Time of t_1 and t_p for OPC, MHC and LHC pastes also had a good correlation of linearity, and corresponded to each other. These results show that first shrinkage ended when a rigid structures were formed in cement pastes. The shrinkage, is a result of the balance of contracting force and rigidity of paste. So, at the first turning point, the rigidity might overcome the force of contraction. The development of empty space in paste, that is self-desiccation, should start at the first turning point.

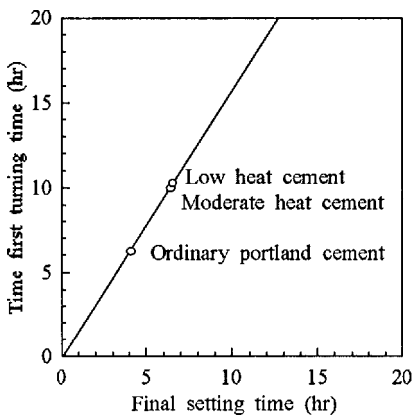

Figure 5 Relationship between setting time and time to first turning point

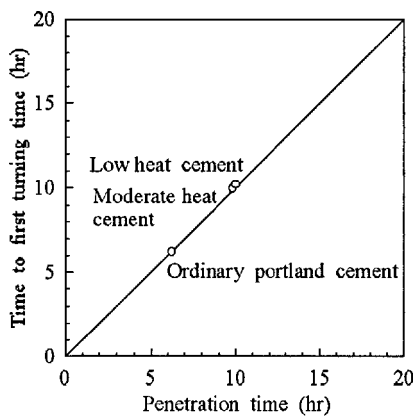

Figure 6 Relation between penetration time and time to first turning point

The influence of reaction of aluminate on autogeneous shrinkage

The influence of hydration of aluminate on autogeneous shrinkage was investigated to clarify the reason why the second stage (no shrinkage or expansion) terminated. Fig. 7 shows the result of XRD analysis for OPC, LHC and LSC paste. Gypsum was consumed at the second turning point in all cements paste. The amount of ettringite increased until the second turning point occurred and decreased after that, especially in LSC paste. There was little amount of monosulfate before the second turning point in all cement pastes. For LSC paste only, the amount of monosulfate increased with curing time after the second turning point .

TEM photographs of cement paste cured for the time of the second turning point (t_2) and for the time of t_2 plus 24 hrs are shown in Fig. 8. At the second turning point, prismatic crystals of ettringite elongated from the surface of cement particles. Some crystals made

magnitude of shrinkage strains at the first turning point were in the order of LHC, OPC and MHC, but the shrinkage strain after the second turning point for OPC paste was larger than that of LHC and MHC. The cement paste of LSC cement paste showed no shrinkage after the initial setting, but expanded greatly up to about 26 hrs. The shrinkage for LSC paste after the second turning point was largest of all.

The relationship between autogeneous shrinkage and chemical shrinkage of cement pastes

Fig. 3 shows the change in volume by chemical shrinkage. The turning points such as appeared in the curve of autogeneous shrinkage were not recognized in the chemical shrinkage curve. The changes in volume by chemical shrinkage were less in the order of OPC, MHC, LSC and LHC pastes.

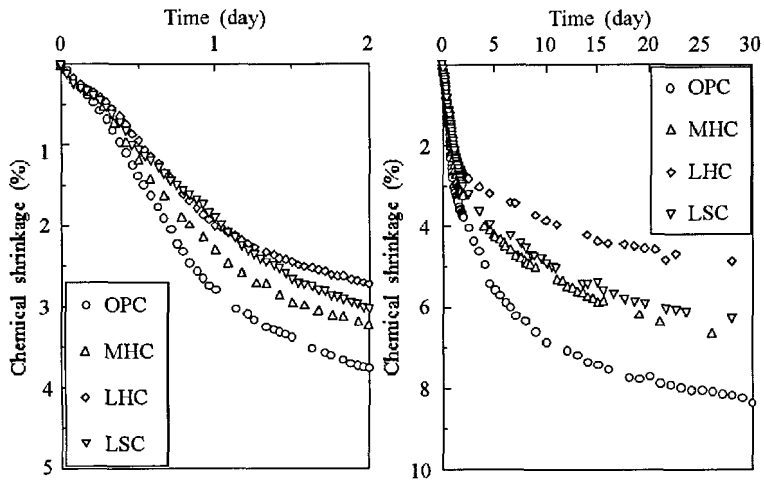

Figure 3 Chemical shrinkage of cement paste (W/C=0.40)

Fig. 4 shows the relationship between autogeneous shrinkage and chemical shrinkage. The turning points were recognized in these relationships. The time at which turning points appeared corresponds to that of the autogeneous shrinkage curve. The slope of curves differed with curing time and kinds of cement. In spite of progressive chemical shrinkage,

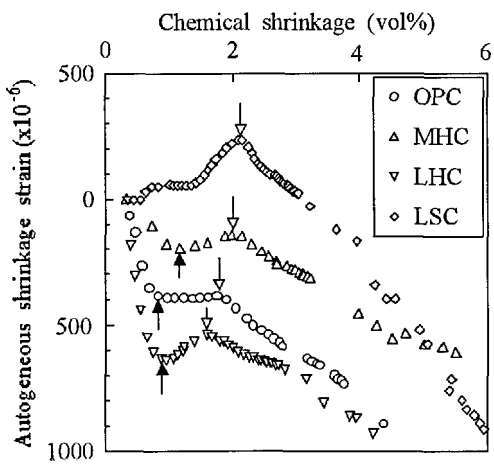

Figure 4 Relationship between chemical shrinkage and autogeneous shrinkage

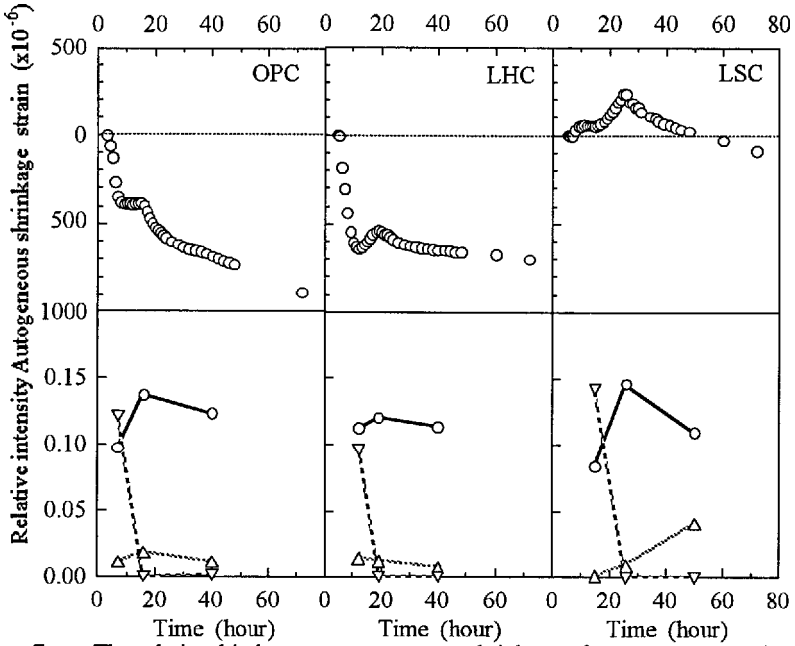

Figure 7 The relationship between autogeneous shrinkage of cement pastes and amount of calcium aluminate hydrate and gypsum
(○:Ettringite,△:Monosulfate,▽:Gypsum)

contact with other cement particles. The amount and crystal size of ettringite was larger for OPC and LSC paste. This is agreed with the result of XRD analysis. At t_2 plus 24 hrs, the number of ettringite crystals elongated from cement particles decreased and large crystals were observed between cement particles. These large crystals were identified as ettringite and monosulfate by element analysis. Plate crystals of monosulfate was rarely observed in the case of OPC and LHC, and more observed in the case of LSC.

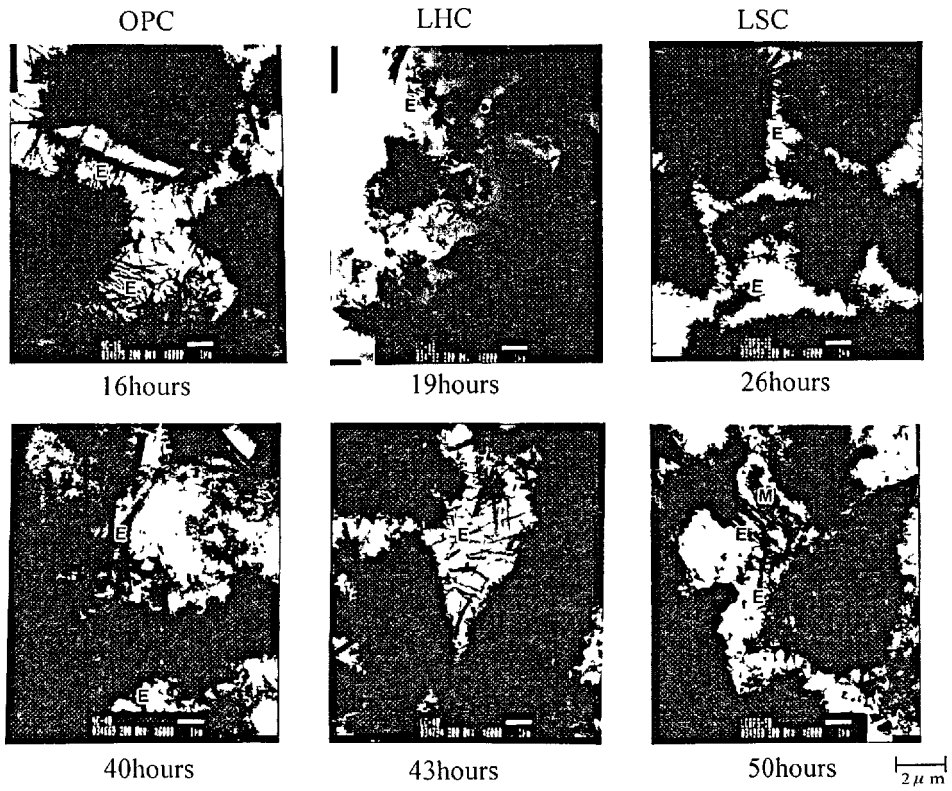

Figure 8 Transmission electron micrographs of cement pastes (W/C=0.30)
(E: Ettringite, M: Monosulfate)

Fig. 9 shows the change in length by autogeneous shrinkage of alite paste which contains no aluminate phase . Both the first and the second turning points were recognized in the curve , but the second turning point occurred at longer hydration times (about 2 days) than OPC, LHC and LSC.

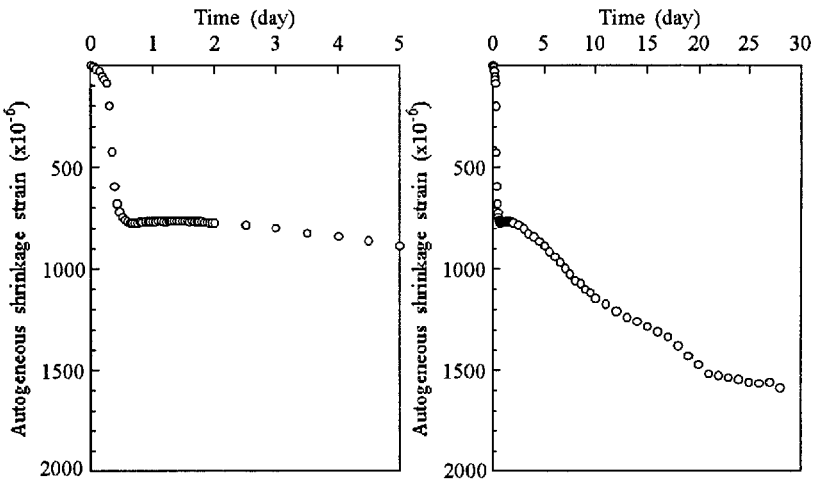

Figure 9 Autogeneous shrinkage of alite paste (W/C=0.30)

The following mechanism of autogeneous shrinkage at an early stage of hydration is suggested.

(1) first shrinkage ($\sim t_1$) in the 1st stage of autogeneous shrinkage

Autogeneous shrinkage is mainly caused by chemical shrinkage. The void produced by chemical shrinkage may be closed by vacuum pressure inside the void. The first shrinkage ends when a rigid structure is formed by progressive hydration.

(2) no shrinkage or expansion ($t_1 \sim t_2$) in the 2nd stage of autogeneous shrinkage

Ettringite is produced by the reaction between the aluminate phase and gypsum in cement. Prismatic crystals of ettringite elongate from the surface of cement particles. Some crystals make contact with other cement particles. Cement paste in which elastic modulus is low, expands by the formation of ettringite. The reason why no expansion occurs for OPC paste is probably attributed to the rigid structure made by large amounts of C-S-H produced by the reaction of alite.

(3) second turning point (t_2)

The consumption of gypsum results in the termination of ettringite formation. The time at which second turning point appears is often consistent with the time at which the third peak appeared in calorimetric curve of cement, e.g., 16 hrs for OPC and 26 hrs for LSC(Yoshida,1993).

(4) second shrinkage ($t_2 \sim$) in the 3rd stage of autogeneous shrinkage

Ettringite becomes unstable when the gypsum in cement paste has been consumed. XRD analysis and TEM observation shows that small crystals of ettringite elongated from cement particles are recrystallized to form large crystals in the space between cement particles at the 3rd stage of autogeneous shrinkage, and conversion from ettringite to monosulfate occurs, especially for LSC paste. Gartner and Gaidis(1991) assumed that solubility of ettringite crystal growing outside a C-S-H shell is sufficiently high to allow recrystallization of the previously existing small crystals into larger, more well-formed crystals. It is suggested that second shrinkage of cement, having an aluminate phase initiates with dissolution of ettringite crystals, which contributed to expansion, by recrystallization and conversion.

The recent study by Hirao and Uchikawa et. al.(1996) mentioned that self desiccation of ordinary portland cement and blastfurnace slag cement pastes prepared with W/C ratio of 0.25 occurs at about 2 days of hydration. It is therefore suggested that autogeneous shrinkage of ordinary portland cement and blastfurnace slag cement pastes after about 2 days of hydration is caused by capillary tension in meniscus which is formed by self desiccation.

The reason why second shrinkage initiated before 2 days during which capillary tension is small is attributed to rapid dissolution of ettringite crystals as described previously. The fact that second shrinkage for alite paste, which contains no ettringite, initiates after 2 days may support accelerated shrinkage by recrystallization and conversion of ettringite.

CONCLUSIONS

Autogeneous shrinkage of cement paste with W/C ratio of 0.30 has been measured. The cement paste was prepared with low heat cements and ordinary portland cement. An apparatus for measurement of autogeneous shrinkage strain of cement paste was made in this study. This apparatus can measure the change in length from early stage of hydration. The development of shrinkage can be divided into 3 stages, that is (1) the first stage with first shrinkage (before the first turning point) , (2) the 2nd stage with no shrinkage or expansion (between the first turning point and the second turning point) and (3) the 3rd stage with the second shrinkage (after the second turning point). These stages were not recognized in chemical shrinkage of cement pastes. The first stages of shrinkage ended when a rigid structure was formed in each cement paste. At the second stage, low heat cement pastes expanded, while ordinary portland cement paste did not expand. This expansion seemed to be attributed to the formation of ettringite. The 3rd stage of second shrinkage initiated when gypsum was consumed. It was suggested that second shrinkage initiated with reaction and/or recrystallization of ettringite.

REFERENCES

Davis, H.E. "Autogeneous Volume in Hydrated Portland Cement" , Proceeding of ASTM, 40, 1940, pp.1103-1110.

Gartner, E.M. and Gaidis, J. M. "Hydration Mechanisms 2" ,Materials Science of Concrete 1(edited by Skalny, J.P.) American Ceramic Society,1991,pp.9-39.

Hirao, H., Uchikawa, H. and Hanehara, S., "Influence of Humidity and Hardened Structure and Structure on the Autogeneous Shrinkage of Hardened Cement Paste" ,Proceedings of the Japan Concrete Institute, Vol.18,No.1,1996,pp.705-710.

Kasai, T. and Tazawa. E., " Degree of Hydration of Cement Estimated from Measurement of Shrinkage due to Chemical Reaction" , Bulletin of the Faculty of Engineering, Hiroshima University,Vol.37,No.1,1988,pp.23-29.

Takahashi, T., Nakata, H. and Goto, S., "An Apparatus for Measurement of Autogeneous Shrinkage of Cement Paste" , Proceedings of the Japan Concrete Institute, Vol.18,No.1,1996,pp.621-626.

Tazawa, E., Miyazawa, S., Shigekawa, K. and Miyake, H., "Macroscopic Shrinkage due to Chemical Reaction in Hardened Cement Paste" , CAJ Proceeding of Cement and Concrete,No.45,1991,pp.122-127.

Tazawa, E. and Miyazawa, S., "Influence of Binder and Mix Proportion on Autogeneous Shrinkage of Cementitious Materials" , Journal of Materials, Concrete Structure and Pavements,No.502/V-251994,pp.43-52.

Yoshida, K., "Structure Formation and Strength Development by Hydration of Low Heat Portland Cement" ,doctoral thesis(in Japanese),1993,pp.163-189.

White,A.H., "Volume Change in Hydrated Portland Cement" Concrete, Vol.33,No.2,1928,pp.41-45.

2ii071
8 pp

Kn o. 2 3. JAN. 2001 d o k 31835

INFLUENCE OF CEMENT COMPOSITION ON AUTOGENOUS SHRINKAGE OF CONCRETE

Ei-ichi TAZAWA, Department of Civil Engineering, Hiroshima University, Japan
Shingo MIYAZAWA, Department of Civil Eng., Ashikaga Institute of Technology, Japan

ABSTRACT Autogenous shrinkage was observed with cement paste and concrete with different types of cement, with different water to cement ratio and volume concentration of aggregate. It was proved that autogenous shrinkage was strongly dependent upon the content of C_3A and C_4AF, that the effect of volume concentration of aggregate could be estimated from an existing composite model. A practical equation for estimating autogenous shrinkage of concrete was proposed as the function of time elapsed, the type of cement and water to cement ratio.

Key-words: Autogenous shrinkage, volume change, composition, water-to-cement ratio

INTRODUCTION

Autogenous shrinkage of concrete, which was defined by Davis(1940) , is a macroscopic volume reduction caused by hydration of cement. It has recently been demonstrated that autogenous shrinkage is considerably large for high-strength concrete and it should be considered in the design of concrete structures, especially in the control of cracking(Paillere, 1989 and Tazawa, 1996). It was reported by Tazawa(1992) that autogenous shrinkage was considerably influenced by the type of cement, but the relationship between autogenous shrinkage and cement composition has not been quantitatively understood.

Studies on the prediction of autogenous shrinkage of concrete have recently been done by some researchers. A prediction model, which was a function of compressive strength of concrete was proposed by Roy(1996). However, a model which includes the effect of cement type has not been obtained yet.

EXPERIMENTAL PROCEDURES

For cement paste, two series of experiments were conducted; w/c=0.30 in series 1, w/c=0.23 and 0.40 in series 2. In order to study the effect of cement composition on autogenous shrinkage, number of cements with various composition were used. Physical properties and chemical composition of cements used in the experiments for cement paste are shown in Table 1. Mineral compositions of these cements calculated form Bogue's equations are shown in Table 2. Cement L1, L2, L4 and L5 are low heat cement with high C_2S content ranging from 56.3% to 74.1%. Cement N, M, H, S, W and O are commercial cements in Japan which contain some mineral powder up to 5% by weight. N0 is pure Portland cement. Cement N2, N3 and N4 have different fineness, which were prepared by milling cement N1.

For experiments for concrete, ordinary Portland cement, moderate heat cement and low heat cement with high C_2S content were used. Water to cement ratio was varied from 0.20 to 0.56. In some cases, volume concentration of aggregate was varied from 0 (cement paste) to 0.60.

Autogenous shrinkage was measured as horizontal length change of sealed cement paste and concrete beam specimens in a room at 20 ℃. For the first 24 hours after casting, measurement was done with mixtures in the mold by dial gauges(Fig 1). In order to eliminate the restraint by the mold, foamed styrol mold was used for cement paste, and Teflon plate 1 mm in thickness was

Table 1 Blaine Fineness and Chemical Composition of Cements

Series 1 (W/C=0.30)

Type	Blaine (cm^2/g)	Ig.Loss (%)	SiO_2 (%)	Al_2O_3 (%)	Fe_2O_3 (%)	CaO (%)	MgO (%)	SO_3 (%)	Na_2O (%)	K_2O (%)
N0	3270	0.6	21.3	5.3	2.6	64.4	2.2	1.9	0.28	0.60
N	3520	1.7	21.4	5.3	3.1	63.4	1.0	2.0	0.39	0.43
N1	3390									
N2	5570	1.7	21.4	5.3	3.1	63.4	1.0	2.0	0.39	0.43
N3	6230									
N4	7430									
M	2990	1.1	23.6	3.3	4.0	64.0	0.8	1.7	0.30	0.32
H	4250	1.0	20.4	5.1	2.8	65.4	0.9	2.9	0.33	0.40
S	3300	1.3	21.7	3.6	4.5	63.9	1.0	2.3	0.27	0.37
W	3700	2.9	21.6	4.5	0.2	66.1	0.6	2.5	0.07	0.48
O	3120	1.3	22.0	3.6	4.6	64.0	0.9	2.2	0.26	0.38
L1	3260	0.9	26.9	2.5	2.5	63.6	0.7	2.2	0.21	0.43
L4	3297	0.7	27.7	3.0	2.9	61.2	1.3	2.5	0.35	0.14
L5	3218	0.8	26.5	3.2	3.2	61.9	1.3	2.3	0.31	0.21

Series 2 (W/C=0.23, 0.40)

Type	Blaine (cm^2/g)	Ig.Loss (%)	SiO_2 (%)	Al_2O_3 (%)	Fe_2O_3 (%)	CaO (%)	MgO (%)	SO_3 (%)	Na_2O (%)	K_2O (%)
N	3390	1.1	21.5	5.2	2.9	63.8	1.6	2.0	0.30	0.48
M	3200	0.6	23.8	3.7	3.9	63.8	1.1	1.9	0.26	0.32
H	4590	1.1	20.6	4.8	2.8	64.9	1.4	3.0	0.24	0.43
S	3300	0.5	21.9	3.7	4.8	65.0	1.0	1.9	0.11	0.25
W	3890	2.5	21.8	4.7	0.2	65.3	0.6	2.5	0.31	0.45
O	3600	0.7	22.3	3.7	4.6	65.0	1.0	2.1	0.25	0.32
L2	3380	0.8	26.5	2.9	3.1	62.6	0.6	2.3	0.18	0.32

N0: Ordinary Portland cement without any mineral powder,
N, N1: Ordinary Portland cement, N2, N3, N4: Cement N1 milled. M: Moderate heat cement.
H: High-early strength cement, S: Sulfate resisting cement. O: Oil well cement,
W: White cement, L1, L2, L4, L5: Low heat cement

Table 2 Mineral Composition of Cements

Series 1 (W/C=0.30)

Type	C_3S (%)	C_2S (%)	C_3A (%)	C_4AF (%)
N0	55.5	19.3	9.7	7.9
N	49.7	23.9	8.8	9.4
M	48.4	31.2	2.0	12.2
H	64.6	9.7	8.8	8.5
S	58.0	18.5	1.9	13.7
W	67.2	11.2	11.6	0.6
O	56.2	20.7	1.8	14.0
L1	27.8	56.3	2.4	7.6
L4	7.1	74.1	3.1	8.8
L5	17.9	62.6	3.1	9.7

Series 2 (W/C=0.23, 0.40)

Type	C_3S (%)	C_2S (%)	C_3A (%)	C_4AF (%)
N0	55.5	19.3	9.7	7.9
N	51.5	22.9	8.9	8.8
M	42.9	35.9	3.2	11.9
H	62.8	11.8	8.0	8.5
S	61.0	16.9	1.7	14.6
W	61.1	16.5	12.1	0.6
O	57.6	20.5	2.2	13.7
L2	22.9	58.8	2.5	9.4
L4	7.1	74.1	3.1	8.8
L5	17.9	62.6	3.1	9.7

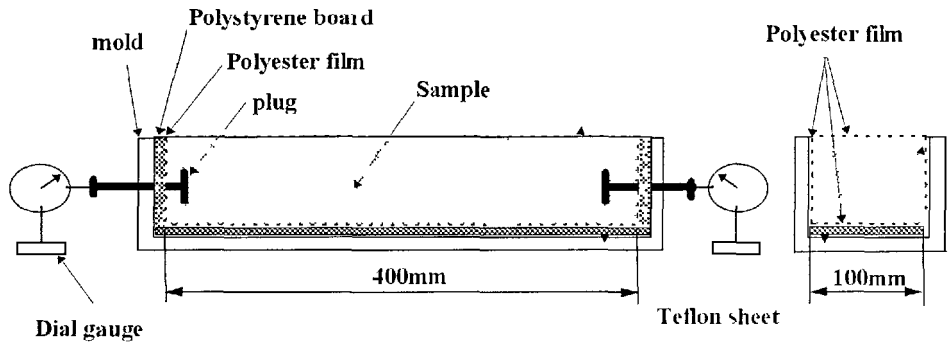

Figure 1 Measurement of autogenous shrinkage of concrete during first 24 hours

put on the bottom of steel mold for concrete In order to consider cracking, it is convenient to exclude volume change of fresh concrete, so the measurement was started at time of initial setting which was determined by Japanese Industrial Standard(JIS R 5201) for cement paste and JIS A 6204 for concrete During the first day, temperature of specimens rose due to hydration Therefore, thermal expansion was excluded from the measured strain on the assumption that thermal expansion coefficient of cement paste and concrete were $20\times10^{-6}/℃$ and $10\times10^{-6}/℃$ respectively.

After specimens were demolded at the age of 24 hours, the specimens were sealed with aluminum tape in order to prevent from evaporation, and length change was measured at specified ages The specimens were $40\times40\times160$mm beam for cement paste, and $100\times100\times400$mm for concrete.

RESULTS AND DISCUSSIONS

Autogenous Shrinkage of Cement Paste

Autogenous shrinkage of cement paste with various types of cement is shown in Fig 2. Autogenous shrinkage dose not reach the ultimate value even after two years from casting. Compared to normal Portland cement(N), autogenous shrinkage is larger for high-early strength cement(H) at early age, and it is lower for moderate heat cement(M). Autogenous shrinkage is very low for low heat cement with high C_2S content(L)

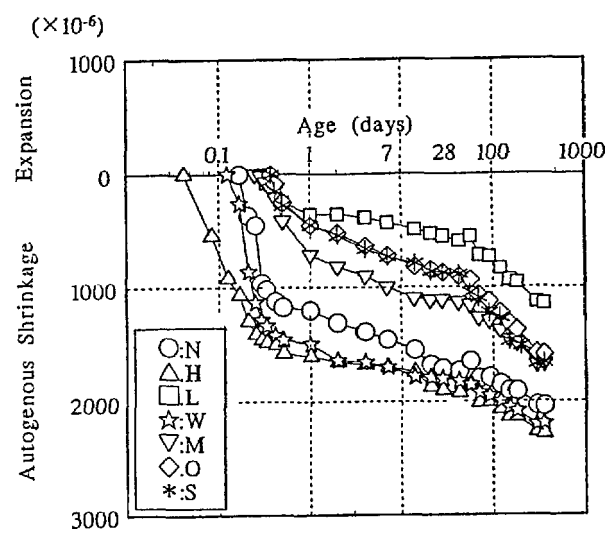

Figure 2 Autogenous shrinkage of cement paste (w/c=0 23)

Autogenous shrinkage is strongly dependent upon the type of cement. This may be due to the different composition of cement It is assumed that autogenous shrinkage strain of cement paste depends on the hydration of each mineral

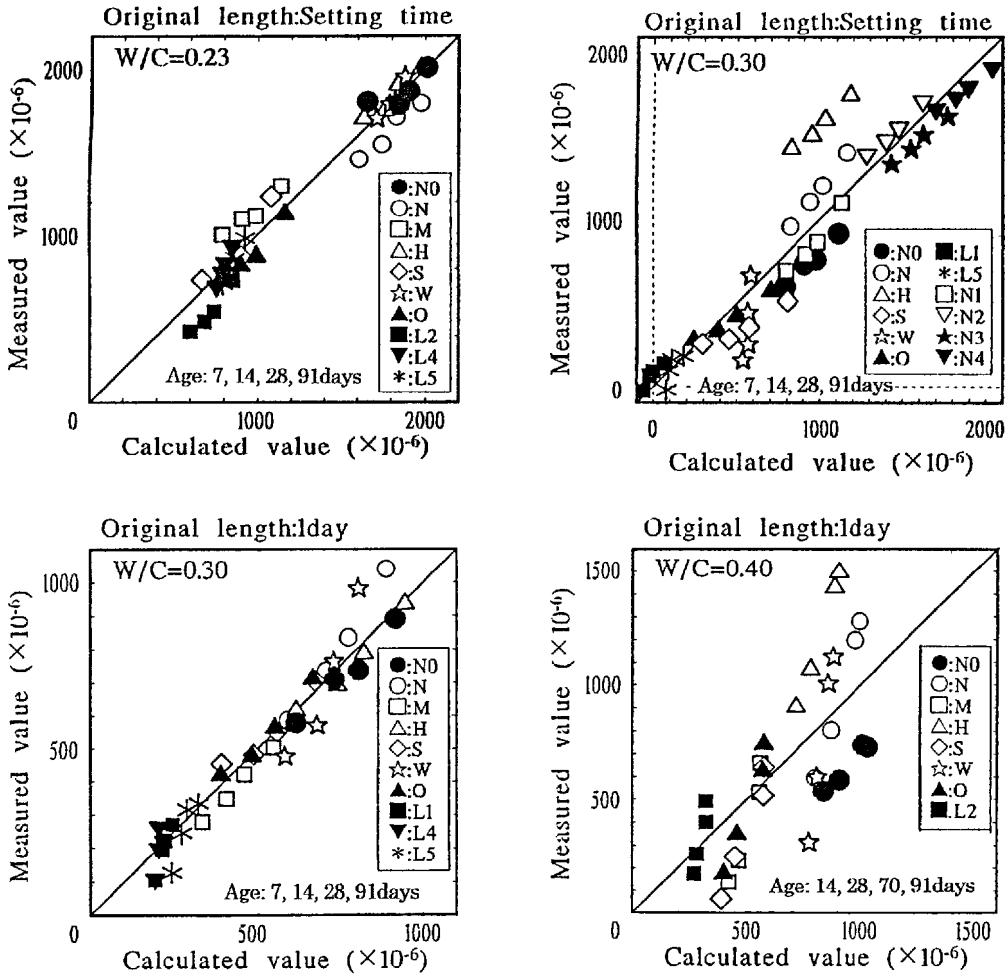

Figure 3 Relation between calculated and observed autogenous shrinkage of cement paste

compound and that it is equal to the sum of the strains due to these hydrations. Then, it is assumed that autogenous shrinkage of cement paste can be described by the next equation.

$$\varepsilon_p(t) = \mathbf{a}\cdot\alpha_{C3S}(t)\cdot(C_3S\%)+\mathbf{b}\cdot\alpha_{C2S}(t)\cdot(C_2S\%)+\mathbf{c}\cdot\alpha_{C3A}(t)\cdot(C_3A\%) +\mathbf{d}\cdot\alpha_{C4AF}(t)\cdot(C_4AF\%)+\mathbf{e}\cdot(\text{Blaine})+\mathbf{f} \quad [1]$$

where

$\varepsilon_p(t)$ is autogenous shrinkage of cement paste ($\times 10^{-6}$)
$\alpha_i(t)$ is hydration ratio of compound i (%)
t is age of concrete
(i %) is content of compound i (%)
i is mineral compound
(Blaine) is Blaine fineness of cement (cm^2/g)
a, **b**, **c**, **d**, **e** and **f** are constants

The constants **a**, **b**, **c**, **d**, **e** and **f**, which are dependent on water to cement ratio, are obtained by the least square analysis with observed autogenous shrinkage. In the calculation, mineral

composition shown in Table 2 and the hydration ratio shown in Table 3, which is obtained from data by Copeland(1960), are used. The values of α i(t) at the time of initial setting are assumed to be zero in the calculations.

The relations between observed values and the calculated ones from Eq 1, which are corresponding to ages of 7, 14, 28, 70 and 91 days, are shown in Fig 3. It can be seen that autogenous shrinkage of cement paste can be estimated by the proposed method. As shown in Fig 4, the absolute values of coefficients for C_3A and C_4AF are larger than those for C_2S and C_3S by one or two orders. This suggests that autogenous shrinkage depends on the hydrations of C_3A and C_4AF and it increases with increasing these compounds. When the original length is taken at initial setting time, **e**=0.195 and **f**=-960 for w/c=0.23, and **e**=0.224 and **f**=-1610 for w/c=0.30, which means autogenous shrinkage increases with fineness of cement. As the influence of fineness is not observed after 24 hours, **e** and **f** are taken to be zero when the original length is taken at 24 hours.

Table 3 Hydration ratio of cement compounds(%)

compound \ age(day)	0	1	7	14	28	91
C_3S	0	45	76	82	87	92
C_2S	0	10	38	53	65	82
C_3A	0	64	87	91	93	96
C_4AF	0	29	58	67	74	86

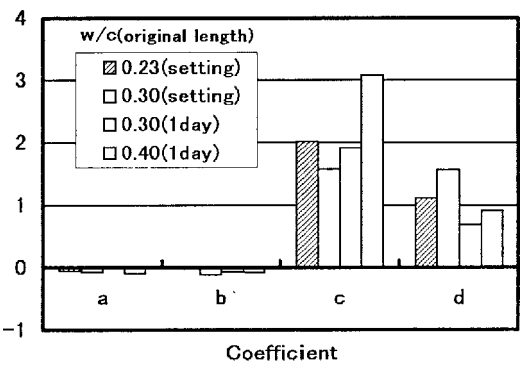

Figure 4 Coefficients in Eq 1

Influence of volume concentration of aggregate

Autogenous shrinkage of concrete occurs in cement paste phase. So autogenous shrinkage of concrete is less than that of cement paste itself because of the presence of aggregate particles. It is assumed that concrete can be expressed by a two-phase model, where aggregate particles are dispersing in cement paste matrix as inclusions. Hobbs' model(Hobbs, 1974), Eq 2, which was proposed for estimating drying shrinkage of concrete, is used to evaluate the effect of aggregate on autogenous shrinkage.

$$\varepsilon_c/\varepsilon_p = \frac{(1-V_a)(K_a/K_p+1)}{1+K_a/K_p+V_a(K_a/K_p-1)} \qquad [2]$$

where

ε_c is autogenous shrinkage of concrete

ε_p is autogenous shrinkage of cement paste

V_a is volume concentration of aggregate

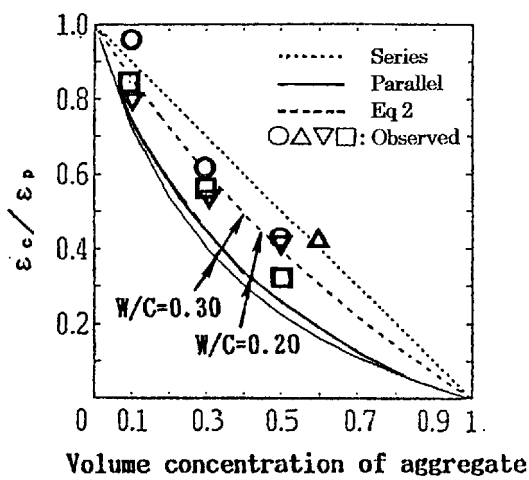

Figure 5 Effect of volume concentration of aggregate on autogenous shrinkage

K_p is bulk modulus of elasticity of cement paste

K_a is bulk modulus of elasticity of aggregate

$K = E / 3(1-2\upsilon)$, υ is Poisson's ratio, E is modulus of elasticity

Autogenous shrinkage observed for mortar and concrete after age of 24 hours is shown in Fig 5, with estimated curves given by Eq 2, parallel and series models. In the calculations, the values of K_a and K_p determined by experiments(Tazawa, 1992) are used. Estimation by Hobbs' model gives good agreement with the observed values. Therefore, the reason why autogenous shrinkage decreases with increasing aggregate volume concentration can be explained both by reduction in cement paste content and by the elastic deformation of aggregate particles.

Predicting model for autogenous shrinkage of concrete

Autogenous shrinkage increases with decreasing water to cement ratio, as shown in Fig 6. Therefore, water to cement ratio is taken as a main valuable in the predicting model of autogenous shrinkage. In order to take account the effect of cement type, a coefficient γ is introduced. Then the model for concrete with a normal volume concentration of aggregate is as follows.

$$\varepsilon_c(t) = \gamma \ \varepsilon_{c0} \ \beta(t) \qquad [3]$$

where

$\varepsilon_c(t)$ is autogenous shrinkage of concrete at age t

γ is a coefficient to describe the effect of cement type (γ =1.0 for ordinary Portland cement)

ε_{c0} is the ultimate autogenous shrinkage(Eqs 4 and 5)

$\beta(t)$ is a coefficient to describe the development of autogenous shrinkage with time(Eq 6)

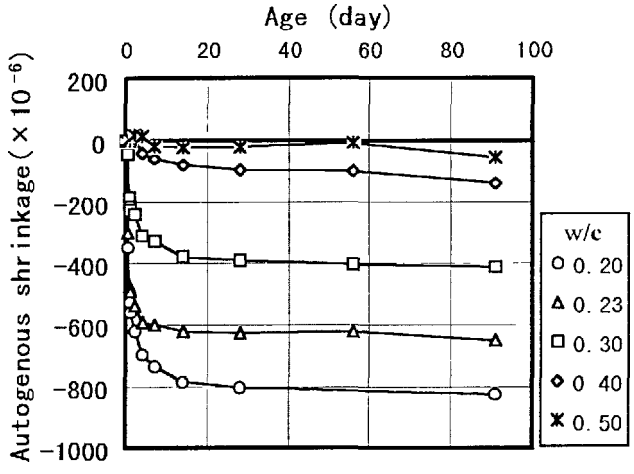

Figure 6 Influence of w/c on autogenous shrinkage (Ordinary Portland cement)

The ultimate autogenous shrinkage ε_{c0} and the development of autogenous shrinkage with time $\beta(t)$ are given by the next empirical equations Eqs 4, 5 and 6, which are obtained by the approximation of observed values.

0 2≦w/c<0.5:

$$\varepsilon_{c0} = 3070\exp\{-7.2(w/c)\} \times 10^{-6} \qquad [4]$$

0.5≦w/c:

$$\varepsilon_{c0} = 80 \times 10^{-6} \qquad [5]$$

Table 4 Coefficients a and b in Eq 6

w/c	a	b
0.20	1.2	0.4
0.23	1.5	0.4
0.30	0.6	0.5
0.40	0.1	0.7
more than 0.50	0 03	0.8

$$\beta(t)=[1-\exp\{-a(t-t_0)^b\}] \qquad [6]$$

where

w/c is water to cement ratio
a and **b** are constants
t is age in day
t_0 is initial setting time in day

Development of autogenous shrinkage with time, β (t), describes the shrinkage after initial setting time t_0. The rate of autogenous shrinkage at early ages increases with decreasing water to cement ratio. Autogenous shrinkage reaches the ultimate value at earlier ages, as water to cement ratio is lower. Therefore, the coefficients **a** and **b** in Eq 6 are strongly dependent upon water to cement ratio. Coefficients **a** and **b** obtained from observed values are shown in Table 4. Fig 7 shows the relationship between observed $\varepsilon_e(t)/\varepsilon_{e0}$ and calculated one from Eq 6. Relationship between observed and calculated autogenous shrinkage at 91 days is shown in Fig 8. The calculated values in these figures have a good agreement with the observed ones.

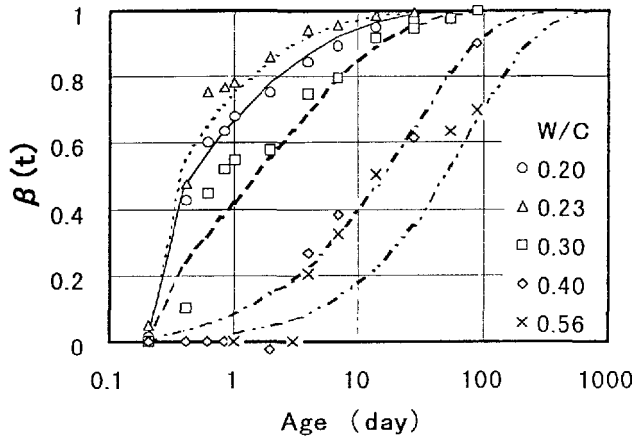

Figure 7 β (t) and observed value

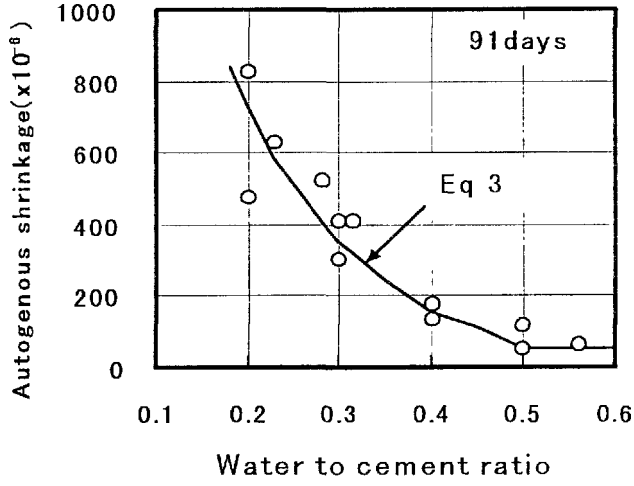

Figure 8 Autogenous shrinkage versus w/c

Table 5 Coeffidient γ in Eq 3

Water to cement ratio	Type of cement		
	N	M	L
0.23	1.0	0.84	0.61
0.30	1.0	0.37	0.30

The prediction model for autogenous shrinkage (Eq 3) is valid for concretes with water to cement ratio ranging from 0.2 to 0.56, and with volume concentration of aggregate ranging from 0.55 to 0.65, at an environmental temperature 20℃. It should be noted that autogenous shrinkage calculated from Eq 3 is the strain after time of initial setting t_0, and that the exact value of t_0 is necessary to make an accurate estimation for concrete with low water to cement ratio.

Autogenous shrinkage with different type of cement are shown in Fig 9. As is shown in the experiments for cement paste, concretes with moderate heat cement(M) and low heat cement(L) show lower autogenous shrinkage than concrete with ordinary Portland cement(N). By using γ in Table 5, autogenous shrinkage of concrete with different type of cement can be calculated from Eq 3.

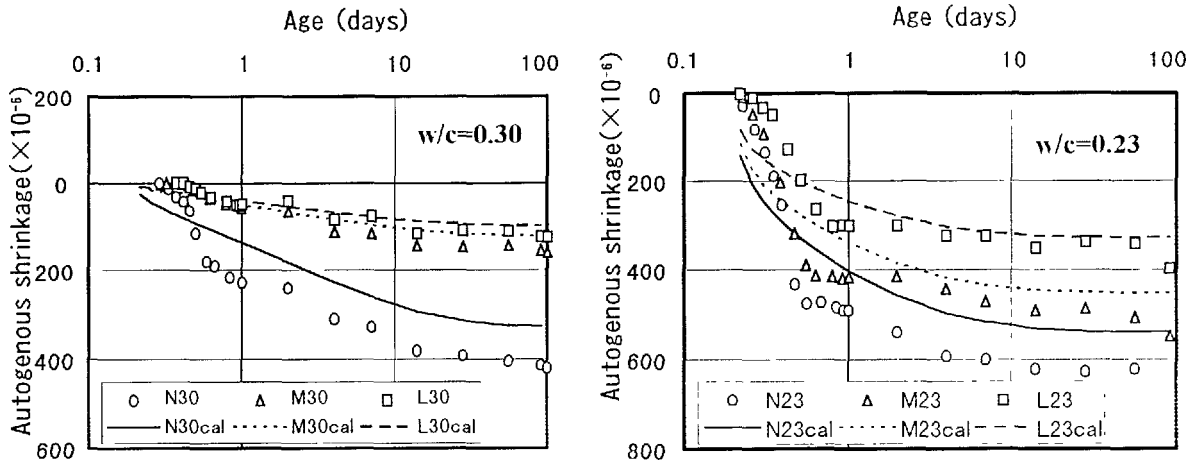

Figure 9 Autogenous shrinkage of concrete with different type of cement

CONCLUSIONS

In this study, influence of cement composition on autogenous shrinkage of concrete was investigated, and the following conclusions were obtained.

1. Autogenous shrinkage of cement paste at a certain age can be estimated by the mineral composition and the hydration ratio of each compound. Autogenous shrinkage increases with increasing C_3A and C_4AF content.
2. Influence of aggregate volume concentration on autogenous shrinkage can be estimated by an existing composite model.
3. Autogenous shrinkage of concrete with different type of cement and various water to cement ratio can be calculated from the proposed equation Eq 3.

REFERENCES

Copeland, L. E. and Kantro, D. L., "Kinetics of the Hydration of Portland Cement", Proceedings of the 4th International Symposium on the Chemistry of Cement, 1960, pp.443-453.

Davis, H.E., "Autogenous Volume Change of Concrete", Proc. ASTM 40, 1940, pp.1103-1110.

Hobbs, D.W., " Influence of Aggregate Restraint on the Shrinkage of Concrete", Journal of ACI, Vol.71,No.9, 1974, pp.445-450.

Paillere, A. M., Buil, M. and Serrano, J. J., " Effect of fiber Addition on the Autogenous Shrinkage of Silica Fume Concrete", ACI Material Journal, Vol.86, No.2, 1989, pp.139-144.

Roy, R. L, Larrard, F. D. and Pons, G., "The AFREM Code Type Model for Creep and Shrinkage of High-performance Concrete", Proceedings of the 4th International Symposium on Utilization of High-strength/High-performance Concrete, 1996, pp.387-396.

Tazawa, E. and Miyazawa, S., " Autogenous Shrinkage Caused by Self Desiccation in Cementitious Material", Proceedings of the 9th International Congress on the Chemistry of Cement, Volume IV, 1992, pp.712-718.

Tazawa, E. and Miyazawa, S., "Influence of Autogenous Shrinkage on Cracking in High-strength Concrete", Proceedings of the 4th International Symposium on Utilization of High-strength/High-performance Concrete, 1996, pp.321-330.

Tazawa, E., Miyazawa, S., Sato, T. and Konishi, K., "Autogenous Shrinkage of Concrete", Transactions of the Japan Concrete Institute, Vol.14, 1992, pp.139-146.

211072
8 pp

Kn a. 2 5. JAN. 2001 d o k 31836

CHEMICAL SHRINKAGE AS INDICATOR FOR HYDRAULIC BOND STRENGTH

Peter PAULINI, Institute for Building Materials and Material Testing, University of Innsbruck, Austria

ABSTRACT Hardening processes like cement hydration are exothermic and supply a bonding energy to the reacting system. Bonding forces cause a densification of the material which can be measured as chemical shrinkage. The strain work supplied to the material is described by using the bulk modulus and is applied to a strength model for hydraulic bond materials. Material tensile strength is defined with half of the strain work. The influence of porosity is considered by a linear strength reducing function.

Key-words: Chemical shrinkage, Volume change, Bound water, Porosity, Strength development

INTRODUCTION

Volume shrinkage is a natural phenomenon accompanying all hardening processes. It expresses the dominance of Coulomb attractive potentials over electrostatic repulsive potentials during the chemical reaction. The result of a hardening reaction is a material densification which can be measured as a volume loss. Therefore, volumetric measurements of cement hydration have been used for a long time together with calorimetric kinetic data to follow hydration developement.

Since the early measurements of Le Chatelier (1904) many other authors have used volumetric procedures to record the kinetics of cement hydration (Czernin (1956), de Haas et al (1975), Geiker and Knudsen (1982), Raffle (1984)). Compared with calorimetric methods, volumetric measures are possible over much longer periods. Accurate results can now be obtained with strain gauges and electronic scales applying dipping and weighing methods (Paulini, 1992a).

Chemical volume changes have direct physical significance for describing material strength. A volume strain work is supplied to the material during a hydraulic hardening reaction which must be overcome by a mechanical force. Attempts to define hydraulic bond energy by means of chemical shrinkage volume are described by Paulini (1992a,b).

CHEMICAL SHRINKAGE VOLUME AND KINETICS OF CEMENT REACTIONS

Chemical shrinkage volume of cement hydration is in a range of 55-69 cm^3/kg. It can be measured or can be calculated from stoichiometry of cement phase reactions. With mass fractions of cement phases the ultimate chemical shrinkage volume $V_{cs,u}$ becomes (Paulini, 1992a)

$$V_{cs,u} = -(53.2\cdot[C_3S] + 40.0\cdot[C_2S] + 178.5\cdot[C_3A] + 111.3\cdot[C_4AF]) \qquad [cm^3/\ kg\ Cement] \qquad [1]$$

In Table 1 some values are given for ASTM type cements which are reached after full hydration. They can be used to define the degree of hydration α according to Eq 2.

$$\alpha(t) = \frac{V_{cs}(t)}{V_{cs,u}} \qquad [2]$$

Fig.1 shows some kinetic plots of pure cement phases where chemical shrinkage has been measured by hydrostatic weighing. Reactions occurred isothermally at 20°C and with a water/solid ratio of 0.40 (Paulini, 1988). Negative volume changes are drawn with a positive sign in order to receive

conventional kinetic plots.

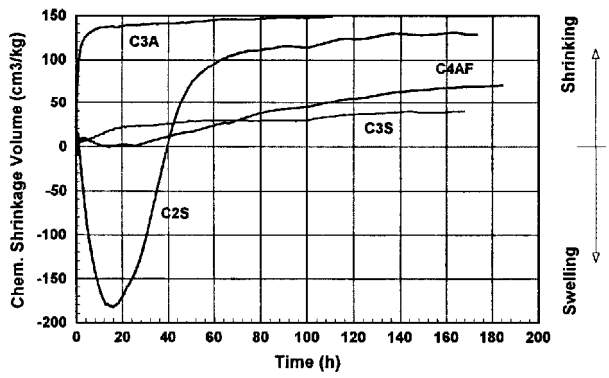

Fig. 1, Measured pure cement phase shrinkage volumes, T=20 °C, w/s=0,40

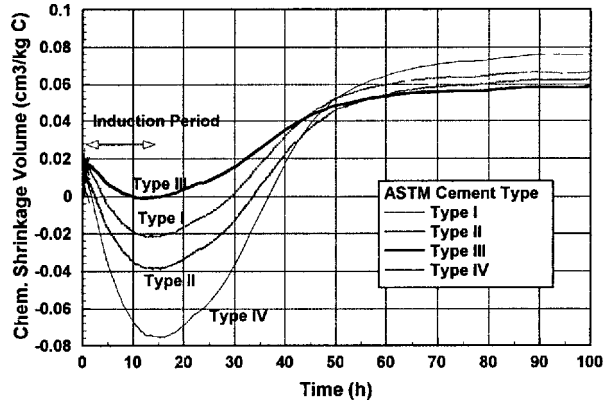

Fig. 2, Calculated shrinkage volumes for ASTM cement types

Table 1 Mean mass fractions of ASTM type cements and calculated chemical shrinkage volume and water demand factor

ASTM Cement	C_3S %-M	C_2S %-M	C_3A %-M	C_4AF %-M	Total %-M	$V_{cs,u}$ cm³/kg	$F_{wv,u}$ %-V
Type I	49	25	12	8	94	60.5	82.5
Type II	46	29	6	12	93	60.8	81.9
Type III	56	15	12	8	91	66.9	82.7
Type IV	30	46	5	13	94	57.7	81.2

Except for C_2S chemical shrinkage volumes of cement phases tend towards the ultimate values of Eq 1. In C_2S at the beginning a significant swelling occurs which changes after about 18 hours into a volume shrinkage. High Le Chatelier expansions are known for C_2S rich belite cements (Chatterjee, 1996). Fig.2 shows ASTM type cement reactions calculated as linear combinations from the kinetics of pure cement phases with the mass fractions in Table 1. Despite the fact that a linear combination of cement phase reactions may not be absolutely valid for a cement reaction and that variations of measured cement phase kinetics exist depending on burning conditions, the following conclusions can be drawn from Fig.2:

- the initial phase of cement hydration is characterised by the opposed reaction behaviour of C_3A and C_3S on the one side and C_2S on the other side
- growing fractions of C_2S lead to a dominance of early swelling in cement reaction
- the initial dormant period of setting is obviously defined by the swelling time of the cement reaction

An initial swelling behaviour has been found with blended cements (BFC, FAC), sulphate resistant cements (SRPC) and by addition of silica fumes. The use of concrete admixtures like retarders and plastizicers can also force an initial swelling (Paulini, 1990).

A stoichiometric calculation of ultimate shrinkage volume according to Eq 1 cannot be made for blended cements because the assumption of pure cement phase reactions does not hold. For such cements with an initial swelling period the ultimate chemical shrinkage $V_{cs,u}$ has to be extrapolated from long term measurements of shrinkage volume. A kinetic model based on chemical shrinkage volume has been presented by Paulini (1994).

The kinetic model assumes that volume changes occur basically during both the phase transitions of cement hydration. A first order serial reaction is taken to be

$$A \xrightarrow{k_x} X \xrightarrow{k_z} Z \qquad [3]$$

with constant reaction rates k_x and k_z. Reactant A is regarded as a solid mass of cement, the intermediate product X as solution product in pore water and the final product Z again as solid bound CSH-gel. The first phase transition solid-fluid $A \Longrightarrow X$ causes a volume gain while the crystallisation step fluid-solid $X \Longrightarrow Z$ leads to shrinkage. As a result of increased bond energies a shrinkage volume $V_{cs,u}$ remains in the final product Z (Eq 1). The solution of differential Eq 3 shows an interesting context for the total reaction rate (Eq 4)

$$\frac{dZ(t)}{dt} = k_z \cdot X(t) \qquad [4]$$

The solution product $X(t)$ becomes the dominant quantity for the total reaction rate. The function $Z(t)$ behaves steady convergent towards 1 and is defined as the degree of hydration α. Chemical shrinkage volume $V_{cs}(t)$ is expressed by the solutions $X(t)$ and $Z(t)$ of differential Eq 3

$$V_{cs}(t) = V_{cs,u} \cdot [Z(t) - X(t)] \qquad [5]$$

HYDRAULIC BOND ENERGIES AND STRAIN WORK

Chemical reaction energies set free in a system can be described with the internal energy U of the system

$$\Delta U = \Delta Q + \Delta W = \Delta(c \cdot T) + \Delta(p \cdot V) \qquad [6]$$

Under the pressure term p we understand for reactions in fluids and solids the internal bonding forces p_B between particles. These forces result from changes of energy potentials and lead to volume changes. The change of internal energy dU_R of a chemical reaction becomes

$$dU_R = dQ_R + dW_B \qquad [7]$$

Exothermic hardening of cement hydration supplies a positive heat of reaction dQ_R as well as a positive bonding energy dW_B to the system. According to the general understanding the total change of internal energy is positive ($dU_R > 0$).

In considering only the reacting system the exothermic heat of reaction dQ_R is regarded as an excess energy which is released from the system. This dissipative energy flux means an energy loss for the system. Instead, a positive bonding energy dW_B is supplied to the system. The first law of thermodynamics also holds true for the reacting system in the form $dU_R = 0$. Therefore, energy changes of chemical reactions are energies working in opposing directions according to Eq 8 (Paulini, 1988).

$$dW_B = -dQ_R \qquad (8)$$

This opposing behaviour of chemical reactions is known as the *Le Chatelier* principle. Dissolving reactions with negative bonding energies occur endothermically while exothermic reactions are hardening or densification processes. It is obvious from Eq 8 that volumetric as well as calorimetric reaction measurements will lead to the same kinetic rates. In Fig. 3 kinetic data of differential calorimetric (Wieker, 1995) and shrinkage volume measurements are shown for a cement reaction at 20 °C. Both methods result in very similar kinetic rates.

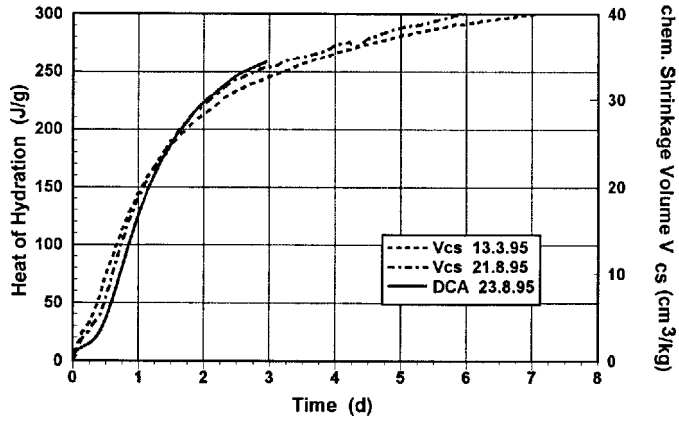

Fig.3, Cement reaction data, chemical shrinkage volume and heat of hydration, T=20 °C

Bonding forces p_B can be expressed by the bulk modulus K and relative volume changes e (Eq 9). The bonding energy W_B of the reacting material is obtained by Eq 10

$$p_B = -K \cdot \frac{\Delta V}{V} = -K \cdot e \qquad [9]$$

$$W_B = p_B \cdot V = -K \cdot \Delta V = -K \cdot e \cdot V \qquad [10]$$

Relative volume changes e can be calculated stoichiometrically for hydration of pure cement phases or can be measured (Paulini 1988, 1992a). It is more difficult to determine their bulk moduli K. Verbeck and Helmuth (1968) mention for cement values of K=54.5 GPa and E=74.5 GPa. Using these data, bulk moduli of CSH-gel were calculated with a composite model (Paulini and Gratl, 1995) applied to the water fraction of full hydration. Bulk moduli and bond energy of cement phases calculated with Eq 10 are shown in Table 2.

Table 2 Calculation of bond energy and strain work resulting from hydration of cement phases

Cement Phase	Heat of Hydration Q_R	rel.Volume Change e=Vs/Va	Density of CSH	Solid Mass Fraction	Water Content	calc.Bulk Modulus CSH-Gel	Hydration Strain Energy W_{IIT}	Hydration Bond Energy W_B	Ratio Q_R/W_B
	J/g	%-V	g/cm3	%-M	%-V	MPa	J/g	J/g	
C3S	490	-9.56%	2.457	80.86%	42.60%	23340	53.7	1123.3	0.44
C2S	222	-7.78%	2.549	82.70%	40.74%	24060	34.5	888.1	0.25
C3A	1373	-24.32%	2.520	71.43%	54.59%	19780	325.0	2672.6	0.51
C4AF	465	-17.78%	2.648	77.88%	48.86%	21620	165.7	1864.1	0.25

For all cement phases the ratio of heat of hydration to bond energy is smaller than 1 ($Q_R/W_B<1$). It is particularly low for slow reacting phases C_2S and C_4AF for which long term calorimetric measurements are inaccurate. More precise calculations of bond energies would have to be based on measured bulk moduli.

A positive bond energy W_B corresponds with a densification work, which results in a volume loss . According to a theory given by Paulini (1988,1992a,b), only the irreversible part of strain energy is responsible for material strengthening. The total work done during the irreversible chemical reaction from initial state 0 to final state 1 along the adiabate 0-2-1 (Fig. 4) is

$$\Delta W = (p_1 - p_0) \cdot (V_1 - V_0) = \Delta p_B \cdot \Delta V \qquad [11]$$

Assuming a possible reversible path between initial and final state, the irreversible strain work ΔW_{irr} remaining in the material becomes

$$\Delta W_{irr} = \Delta W - \Delta W_{rev} \qquad [12]$$

The reversible strain work ΔW_{rev} is obtained by integration over the volume changes V_s (chemical shrinkage volume)

$$\Delta W_{rev} = \int_0^{V_s} p_B \cdot dV = - V \cdot \int_0^{e} K \cdot e \; de = - \frac{K}{2} \cdot e^2 \cdot V \qquad [13]$$

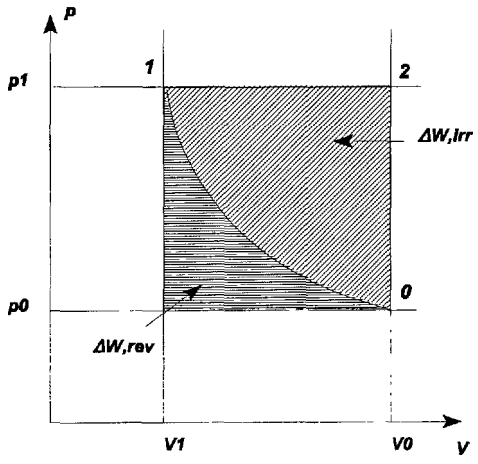

Fig.4, Strain work of an irreversible process from state 0 to 1

With Eqs 11, 9 and 13 the irreversible strain work ΔW_{irr} is obtained with the same expression as the reversible work

$$\Delta W_{irr} = - \frac{K \cdot e^2}{2} \cdot V \qquad [14]$$

Material tensile strength is considered as an all round stress, whose mechanical strain work is opposed directed to the irreversible strain work of the chemical reaction. The failure state is characterized by an equivalence of failure energy and resisting energy. Therefore, tensile strength f_t is defined by half of the supplied irreversible strain work (Eq 15).

$$f_t = - \frac{K \cdot e^2}{4} \qquad [15]$$

Integration of Eq 13 assumes a constant bulk modulus during the chemical reaction. Bulk moduli of concrete change from initially 3-6 GPa to finally over 20 GPa during cement hydration. Exact values depend to a large extent on the stiffness of aggregates. Nevertheless, Eq 15 remains valid if we consider the final values for K and e and if we count the reaction from an initial state without any bond pressure. To prove this, consider the total differential of bond pressure p_B (Eq 16)

$$dp_B = - (K \cdot de + e \cdot dK) \qquad [16]$$

An integration from initial state 0 to the state defined by the degree of hydration α leads to

$$p_B(\alpha) = - \int_0^{\alpha} \left(K \cdot \frac{de}{d\alpha} + e \cdot \frac{dK}{d\alpha}\right) d\alpha \qquad [17]$$

By partial integration of Eq 17 we obtain the bond pressure p_B

$$p_B(\alpha) = -[K(\alpha) \cdot e(\alpha)]_0^{\alpha} + p_{B0} = -K(\alpha) \cdot e(\alpha) + p_{B0} \qquad [18]$$

For engineering practice, the initial state 0 is considered to be the state when water is added to the mix, where an initial bond pressure p_{B0} can be neglected. Then, bond pressure $p_B(\alpha)$ is only dependent on bulk modulus $K(\alpha)$ and on the relative volume change $e(\alpha)$. The description of a hydration dependent tensile strength according to Eq 15 needs a formation function for the bulk modulus $K(\alpha)$. Such a stiffness model for concrete has been proposed by Paulini and Gratl (1995).

INFLUENCE OF CAPILLAR POROSITY

The dominant influence of porosity to strength properties is well known to concrete technologists through the wc-ratio. The same amount of cement C leads to the same shrinkage volume $Vs(\alpha)$

$$V_s(\alpha) = C \cdot V_{cs,u} \cdot \alpha \qquad [19]$$

but will result in different concrete strength depending on the wc-ratio. The most important factor is the strength development in cement paste. In this model a strength f_0 for cement paste with zero porosity is calculated and then reduced by a function considering the capillar porosity $P(\alpha,wc)$. In the literature different theories are known to reduce a strength depending on the porosity of a material. For cement pastes the linear model of Hasselmann has been found to hold true (Rößler and Odler, 1985). Accordingly, strength $f(P)$ is reduced by porosity P (Eq 20)

$$f(P) = f_0 \cdot \left(1 - \frac{P}{P_0}\right) \qquad [20]$$

Therein, P_0 is the maximum porosity where zero material strength occurs. Porosity of cement paste as a function of the degree of hydration and the wc-ratio is given in Eq 21

$$P(\alpha,wc) = \frac{v_{wc} - \alpha \cdot F_{wv}}{1 + v_{wc}} \qquad [21]$$

$$v_{wc}(wc) = \frac{V_w}{V_c} = wc \cdot \frac{\rho_c}{\rho_w} \qquad [22]$$

The constant v_{wc} represents the volume ratio of mix water to cement in the fresh mix (Eq 22). The volumetric water demand factor F_{wv} (Paulini, 1992a) is the ratio of chemical bond water V_{cw} to the binder solid volume V_s can also be calculated stoichiometrically (Eq 23) and is given for different cement types in Table 1.

$$F_{wv} = 0.7422 \cdot [C_3S] + 0.6874 \cdot [C_2S] + 1.2023 \cdot [C_3A] + 1.3754 \cdot [C_4AF] \qquad [23]$$

Fig. 5 shows porosities of cement paste over wc-ratio for limiting degrees of hydration α=0 and α=1. Zero strength porosity P_0 of Eq 20 is taken to be $P(0,wc)$ for α=0 according to Eq 21. The strength reducing function $(1-P/P_0)$ has a shape as shown for the degree of hydration α=1 in Fig.5.

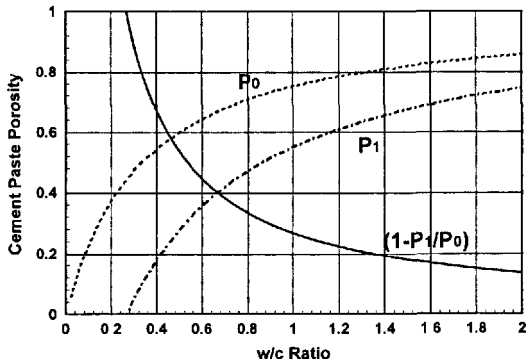

Fig.5, Limiting porosities in hydrated cement paste and strength reducing function

Hydrostatic tensile strength for zero porosity f_{t0} is calculated from Eq 15. With the cement content C_p of cement paste

$$C_p = \frac{\rho_c}{v_{wc}(wc) + 1} \qquad [24]$$

the relative volume change e in cement paste becomes Eq 25

$$e\ (\alpha,wc) = C_p \cdot V_{cs,u} \cdot \alpha \qquad [25]$$

Uniform tensile strength f_{ct} of a concrete mix with a cement content C_{con} is obtained with Eq 15 to

$$f_{ct}(\alpha,wc) = -\ e(\alpha,wc)^2 \cdot \frac{K(\alpha)}{4} \cdot \frac{C_{con}}{C_p} \cdot \left(1 - \frac{P(\alpha,wc)}{P(0,wc)}\right) \qquad [26]$$

Fig. 6 shows some model results of concrete tensile strength for different degrees of hydration calculated with Eq 26. A mix content of 300 kg/m^3 cement and an ultimate shrinkage volume of $V_{cs,u}$ = 60 cm^3/kg have been assumed. Bulk modulus has been calculated with Eq 27 and constants of K_0=5 GPa, B=3.5, C=0.4 and D=2 (Fig. 7)

$$K(\alpha) = K_0 \cdot (1 + B\cdot\alpha + D\cdot\alpha^C\cdot(1-\alpha)) \qquad [27]$$

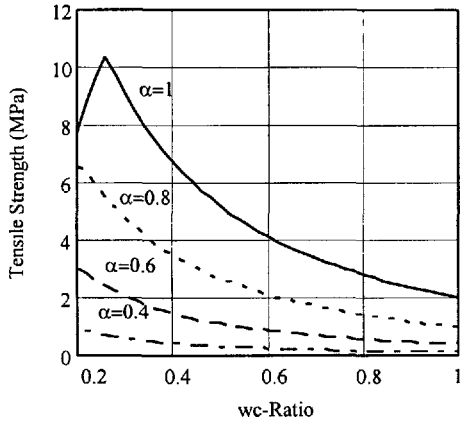

Fig. 6, Concrete tensile strength, model results, C_{con}=300 kg/m^3

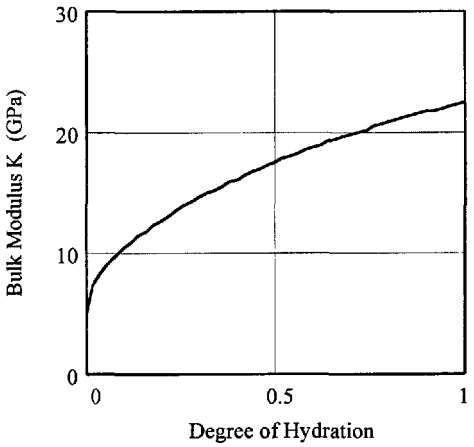

Fig. 7, Bulk modulus K(α)

Results obtained by Eq 26 are in normal strength ranges for concrete and exhibit the known dependence on the wc-ratio. Notice also the strength limiting behaviour for low wc-ratios and high degrees of hydration, resulting from incomplete hydration. Fig. 8 shows a similar calculation for different cement contents at a degree of hydration α=0.9 .

This strength model does not describe the relationship between tensile and compressive strength. Such a model must contain a description of internal material friction and is not yet finished.

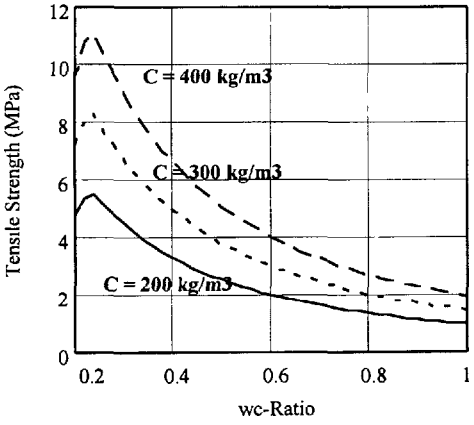

Fig. 8, Concrete tensile strength, model results, degree of hydration α=0.9

CONCLUSION

Exothermic hydration of cement is accompanied by a chemical shrinkage. Internal volume changes of cement hydration are very much dependent on the cement type especially during the initial reaction period. During early cement hydration a swelling behaviour can dominate over volume shrinkage. The swelling period is strongly influenced by the percentage of C_2S. The induction period of setting is defined by the swelling time.

Internal volume changes during a chemical reaction are generally not considered in physics. In this article an attempt is made to express bonding forces of a chemical reaction in terms of volume changes and bulk modulus. Heat of reaction and bond energy are considered as oppositely acting energies according to the principle of *Le Chatelier*. Bonding forces lead to a material densification and supply a strain work to the material. The uniform tensile strength resulting from chemical reaction is defined with half of the supplied strain work. A strength model based on chemical shrinkage volume is introduced for cement paste. The influence of porosity has been considered according to the linear Hasselmann theory. A few results prove the model to be applicable to the tensile strength of concrete.

REFERENCES

Le Chatelier, H., "Recherches experimentales sur la constitution des mortiers hydrauliques", Dunod, Pairs, 1904

Chatterjee A.K., "High belite cements - present status and future technological options: Part I", CCR, Vol.26, 1996, 1213-1225

Czernin, W., "Über die Schrumpfung des erhärteten Zements", Zement-Kalk-Gips, 9, 1956, 525-530

de Haas, G.D. et al, "The shrinkage of hardening cement paste and mortar", CCR, Vol.5, 1975, 295-320

Geiker, M., Knudsen, T., "Chemical shrinkage of Portland cement pastes", CCR, Vol.12, 1982, 603-610

Paulini, P., "Kinetik der Zementhydratation und ihr Einfluß auf die Festigkeit von Beton im jungen Alter", Dissertation, Universität Innsbruck, 1988

Paulini, P., "Reaction mechanisms of concrete admixtures", CCR, Vol.20, 1990, 910-918

Paulini, P., " A weighing method for cement hydration", 9th ICCC, New Delhi, 1992a, Vol.IV, 248-254

Paulini, P., "Thermodynamics of hydraulic hardening", RILEM Proc.16, in Hydration and setting of cements, E&FN Spon, London, 1992b, 323-330

Paulini, P., "A through solution model for volume changes of cement hydration", CCR, Vol.24, 1994, 448-496

Paulini, P., Gratl, N., "Stiffness formation of early age concrete", RILEM Proc.25, in Thermal cracking in concrete at early ages, E&FN Spon, London, 1995, 63-70

Raffle, J.F., "Volume changes during hydration of cement plasters", Proc.Brit.Ceramic Soc., 35, 1984, 295-303

Rößler, M., Odler, I., "Investigation on the relationship between porosity, structure and strength of hydrated portland cement pastes", CCR, Vol.15, 1985, 320-330

Verbeck, G.J., Helmuth, R.A., "Structures and physical properties of cement pastes", 5th ICCC, Tokyo, 1968, Vol.III, 1-32

Wieker, W., personal communication, 1995

2ii073
9 pp

Kn o. 2 5. JAN. 2001 d o k 31837

LONG-TERM SHRINKAGE OF HIGH-PERFORMANCE CONCRETE, HPC

Bertil PERSSON, Lund Institute of Technology, University of Lund, Division of Building Materials, Lund, Sweden

ABSTRACT In this article an extensive experimental and numerical study of shrinkage in HPC is outlined. For this purpose cylinders of eight qualities of concrete were studied. Parallel studies of autogenous, carbonation and drying shrinkage, hydration, internal relative humidity and strength were carried out. Previous research in the field is summed up. Finally the article presents the mechanisms of shrinkage in HPC by modelling correlations to the composition of the concrete and the physical properties. The project was carried out between the years 1992 and 1996.

Keywords: Autogenous shrinkage, Carbonation, Pozzolanic, Relative humidity, Self-desiccation.

GENERAL

Autogenous shrinkage caused by the self-desiccation in HPC with low water-cement ratio, w/c, has been pointed out by Persson (1997). Autogenous shrinkage as such is not a new phenomenon, but may be the driving force is self-desiccation. When the internal relative humidity decreases substantially the depression in the pore water also decreases, which causes compression in the aggregate and the cement paste (Persson, 1996) and self-stress in HPC.

PREVIOUS RESEARCH ON SHRINKAGE OF HPC

Roy and Larrard (1993) studied shrinkage of both HPC and normal concrete at different w/c, and also with different amounts of silica fume. They found that the autogenous shrinkage increased at lower w/c. At w/c $\approx$ 0.3 the autogenous shrinkage after 400 days was about 250 μm/m. However, they observed the total shrinkage (sorption shrinkage and autogenous shrinkage) to be larger at higher w/c; for example about 600 μm/m at w/c $\approx$ 0.6. Fig 1 shows the results of shrinkage versus w/c with different amounts of silica fume (Roy and Larrard, 1993). The specimens were 1 m long and 0.16 m in diameter. The following conclusions were drawn:

1) The autogenous shrinkage increased with decreasing w/c.
2) The autogenous shrinkage increased when the concrete contained silica fume.
3) The total shrinkage and the sorption shrinkage increased with increasing w/c.

Other French experiments were carried out on 0.12 m diameter cylinders with a length of 0.24 m (Sicard, 1993). In this case the water moisture losses were 1% by the weight of the concrete per year. The measurements of shrinkage started at an age of 1.2 days. In Fig 2 the result of the autogenous shrinkage is shown versus time. The following conclusions were drawn:

1) The autogenous shrinkage increased with decreasing w/c.
2) The autogenous shrinkage was larger with limestone aggregate than with sandstone.
3) The autogenous shrinkage was larger in a concrete with silica fume than without silica fume.

Tazawa and Miyazawa (1993) studied shrinkage at very early ages by cast-in strain gauges. The specimen was 0.1 x 0.1 x 1.2 m. The concrete was cast in vinyl polymer plastic moulds allowing for movements of the concrete at early ages. The measurements started at $\approx$ 0.2 days' age. Fig 3 shows the shrinkage versus time at different w/c. The shrinkage increased with lower w/c and higher content of silica. The difference between autogenous and drying shrinkage was small.

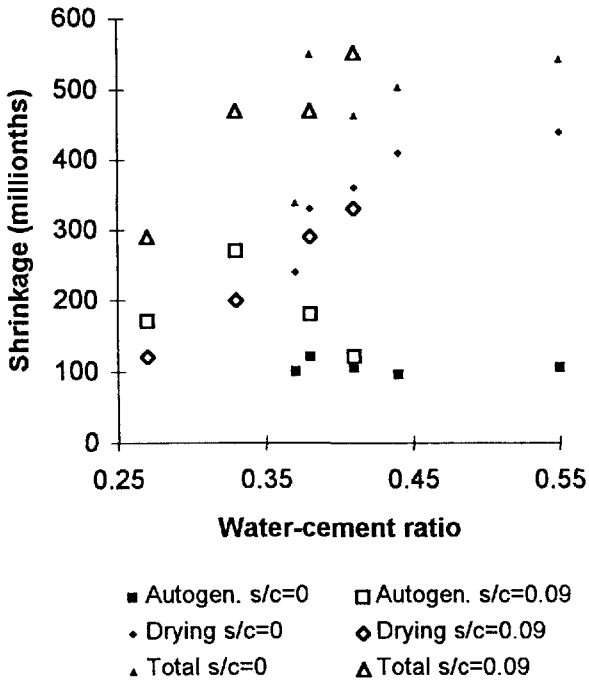

Figure 1 Shrinkage versus w/c with different amounts of silica fume (Roy and Larrard, 1993).

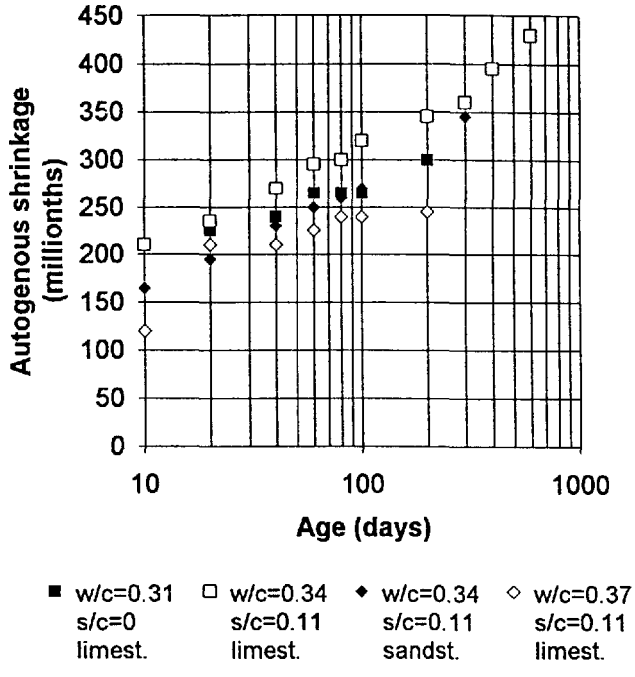

Figure 2 Autogenous shrinkage versus time, (Sicard, 1993). c = cement; s = silica fume.

EXPERIMENTAL METHOD

A total of 52 specimens for studies of autogenous shrinkage and 26 for studies of drying shrinkage were cast from 78 different concrete batches with compositions given in Table 1.

Table 1 Mix proportions and main properties of concretes (in kg/m^3 of dry material)

Material /Littera	1	1(3)	2	3	4	5	6	7	8
Quartzite sandstone, 11-16 mm	460	440	965	910		1010	985		1065
Quartzite sandstone, 8-11 mm	460	440							
Natural sand, Å 0-8 mm	800	780	820	790		750	755		690
Granite, N 11-16 mm								1030	
Pea gravel, T 8-16 mm					1095				
Natural sand, B 0-8 mm					780			780	
Cement, low-alkali (302 m^2/kg Blaine)	430	410	440	445	455	495	530	490	545
Granulated silica fume (≈ 17000 m^2/kg)	21	21	44	45		50	51		55
Silica fume slurry (≈ 22000 m^2/kg)					23			49	
Air-entraining agent (vinsole resin)	0.02	0.04		0.02					
Superplasticiser, (melamine formaldehyde)	2.6	2.8	4.5	3.8	5.1	4.6	7.6	8.6	10.8
Water-cement ratio	0.38	0.38	0.37	0.37	0.33	0.31	0.30	0.30	0.25
Air-content (% by total volume)	4.8	7.0	1.1	4.0	0.9	1.1	1.2	1.0	1.3
Density (kg/m^3)	2335	2245	2440	2360	2510	2465	2480	2500	2490
Slump (mm)	140	140	160	170	45	200	130	45	45
28-day strength, drying cube (MPa)	69	50	85	69	89	99	106	112	114
1-year strength, drying cube (MPa)	70	54	89	76	97	109	112	121	125
3-year strength, drying cube (MPa)	69		91		97		115	121	127
28-day strength, sealed cube (MPa)	89	62	105	95	101	121	126	122	129
1-year strength, sealed cube (MPa)	101	65	117	98	115	129	145	131	154
2-year strength, sealed cube (MPa)	112				115			131	
3-year strength, sealed cube (MPa)			123	102			141		145
4-year strength, sealed cube (MPa)	102				113			129	

After demoulding and insulation by 2 mm butyl rubber clothing (in case of studies of autogenous shrinkage), 6 stainless steel screws were fixed into cast-in items in the cylinder. Measurements were taken on three sides of the cylinder on a length of 250 mm within 1 h of demoulding (Bazant and Carol, 1993). After cooling the specimen was placed in a 20 °C climate chamber with a relative humidity, RH = 55%. The measuring was performed by mechanical devices.

SOURCES OF ERROR

In spite of all the careful precautions some faults existed causing unforeseen weight losses. The specimens were continuously weighed to detect this loss. Possible absorption of water in the butyl rubber insulation would affect the total weight of the specimen. Effects of hydration heat in particular were avoided by obtaining the first measurement at 20 °C. A thermocouple was cast in the specimen and the temperature was followed. The different materials of the mix design were carefully weighed to avoid variations. However, the moisture of the gravel (normally 4%) had to be calibrated after the batching as well, which may cause alteration in the mixed proportions.

RESULTS FROM PRESENT STUDY

In Fig 4 a summary of the shrinkage of concrete 6 is given versus age. Fig 5 shows the relative loss of weight (the ratio of weight loss, w_e, to the mixing water, w) versus time. Fig 6 shows the shrinkage versus the relative loss of weight. Symbols in use in Figs 4, 5 and 6:

6...	denotes the concrete type
....02	denotes a batch of the same type of concrete
c	denotes the content of cement (kg/m^3)
s	denotes the content of silica fume (kg/m^3)
w	denotes the mixing water of the concrete (kg/m^3)
w_e	denotes the evaporated water or the absorbed carbon dioxide (kg/m^3)
.B..	denotes autogenous shrinkage
.D..	denotes drying shrinkage (RH= 55%)

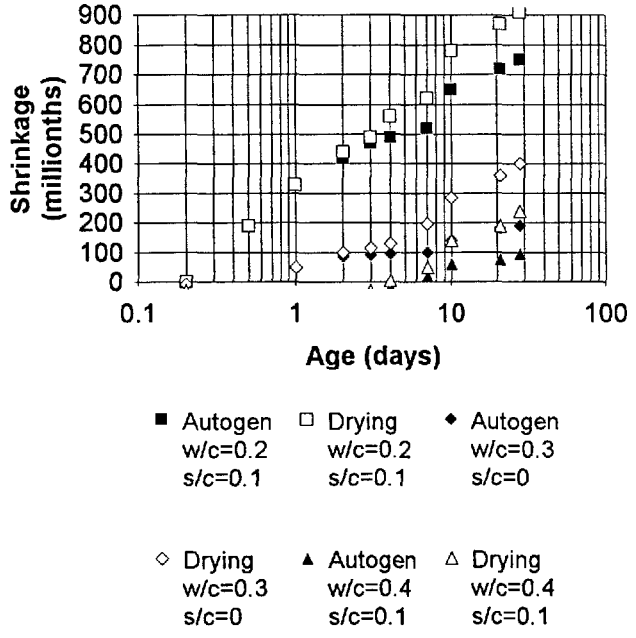

Figure 3 Shrinkage versus time at different w/c (Tazawa and Miyazawa, 1993)

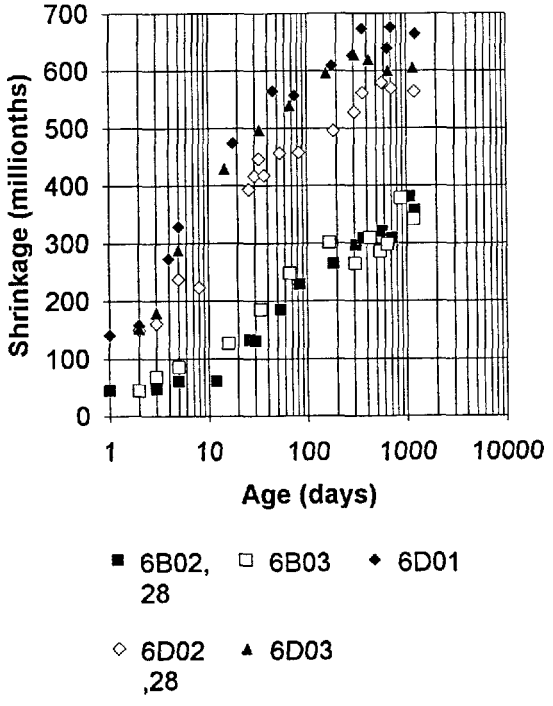

Figure 4 Measured shrinkage of concrete 6. 02 = concrete batch; B = autogenous; D = drying.

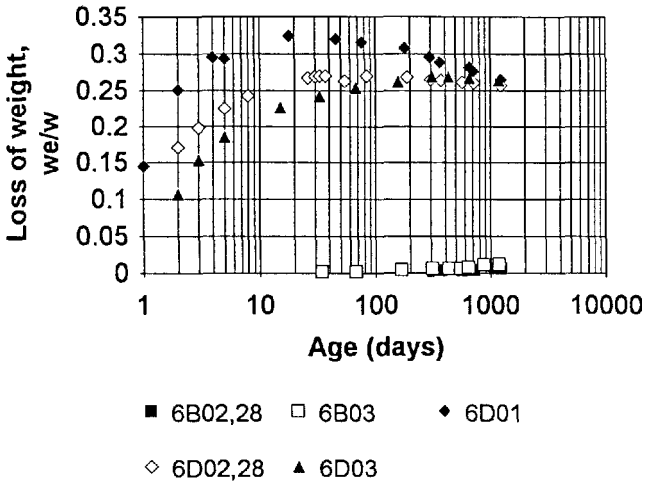

Figure 5 Loss of weight versus concrete age.

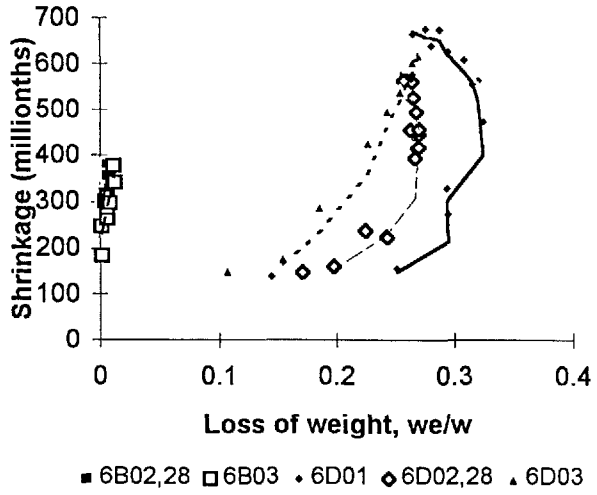

Figure 6 Shrinkage versus loss of weight.

ACCURACY

All results of shrinkage studies and weighing were presented in the same way as in Figs 4, 5 and 6. After about 1 months' age carbonation affected the weight of the drying specimens at w/c > 0.30, which caused a combination of drying and carbonation shrinkage. At low w/c = 0.25 no increase of the weight was observed within the period of measurement. Absorption of water in the butyl rubber insulation existed at a high relative humidity only. Three rubber insulation tubes were first placed in an ambient relative humidity, RH = 40%. After one week they were weighed and placed in RH = 55%. No change of weight was observed at RH = 55%. At RH = 95% the weight increased slightly but was hardly detectable, that is 0.1 g of increased weight. Since the specimen originally contained 120 g of mixing water the absorption was negligible.

A thermocouple was cast in the specimen and the temperature was followed as the first measurement was performed. The maximum faults would then have been $4 \cdot 8 \cdot 10^{-6} = 32$ μm/m, assuming the same effect of temperature on HPCs like on normal concrete. The temperature was followed as the first measurement was performed (± 1 °C of difference to 20 °C reducing the observed fault to ≈ 16 μm/m). The variations in the mixed design were normally very small, much less than stipulated w/c ± 0.01. Only for concrete 6 was a slightly larger difference observed; w/c≈ 0.285 instead of w/c = 0.30. Finally, the mechanical devices (Huggenberger and Proceq) were continuously calibrated with an INVAR rod and with a Mitutoyo micrometer. The reading of the device was within 0.005 mm, which was comparable to a maximum fault of 20 μm/m (the length of the device: 250 mm). The total fault of a temperature difference of ± 1°C and the fault of the mechanical device was fairly large i.e. ≈ 16 + 10 ≈ ± 25 μm/m.

ANALYSIS

Autogenous shrinkage

From a previous work on basic creep of HPC (Persson, 1995) it was observed that the loss of weight for 14 cylinders used in the long-term creep studied was less than 0.7 g per specimen over a period of at least 1 year. (A 0.7 g loss of weight equals to we/w= 0.006.) However, in the present study the joint between the side of the cylinder and the end rubber clothing did not perform perfectly, which may have increased the loss of moisture. Fig 6 show that very small loss of weight may affect the measured shrinkage. Linear regressions were performed to obtain the measured shrinkage at no loss of weight (autogenous shrinkage). In Fig 7 the autogenous shrinkage is given versus the w/c. The type and amount of silica fume affected the measured autogenous shrinkage, Fig 8, which has also been observed by others (Mejlhede Jensen, 1993).

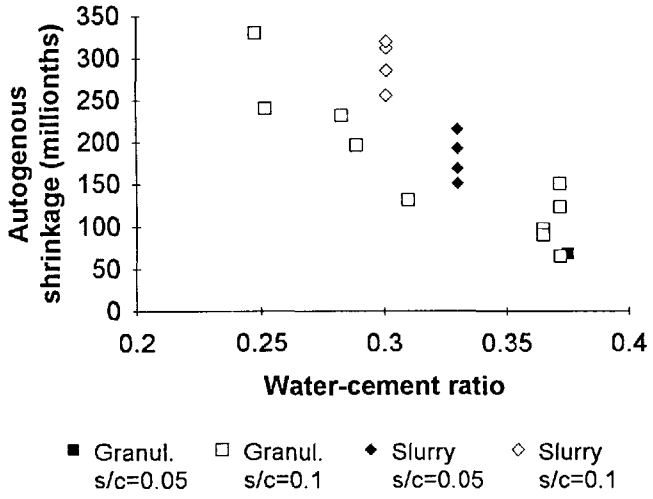

Figure 7 Autogenous shrinkage versus w/c. The concrete type is given.

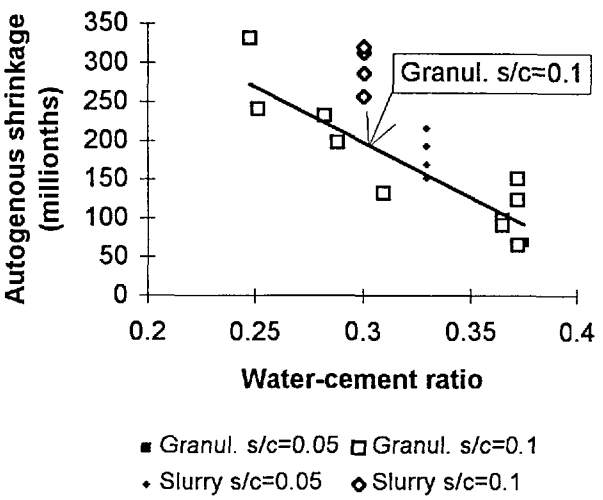

Figure 8 Autogenous shrinkage versus w/c. The type and amount of silica fume is indicated.

In Fig 9 the autogenous shrinkage is given versus the internal relative humidity. The autogenous shrinkage was affected by the type and amount of silica fume, Fig 10. (The internal relative humidity was obtained in the experiments). Silica fume slurry reacted more rapidly with the calcium hydroxide which caused a larger shrinkage. The following correlations were obtained to describe the autogenous shrinkage, ε_B (mm/m):

$$\varepsilon_B = k_s \cdot k_5 \cdot 0.624 \cdot [1 - 2.27 \cdot (w/c)] \quad [1]$$

$$\varepsilon_B = k_{s\varnothing} \cdot 1.75 \cdot (1 - 1.13 \cdot \varnothing) \quad [2]$$

k_s	= 1.5 for silica fume slurry; k_s = 1 for granulated silica fume
$k_{s\varnothing}$	= 1.3 for silica fume slurry; k_s = 1 for granulated silica fume
k_5	= 0.78 for 5% silica fume; k_5 = 1 for 1% silica fume
w/c	denotes the w/c $\{0.2 < w/c < 0.4\}$
$\varnothing$	denotes the internal relative humidity $\{0.7 < \varnothing < 0.9\}$

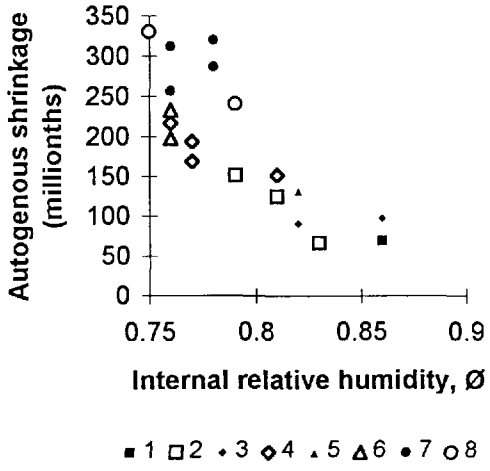

Figure 9 Autogenous shrinkage versus the internal relative humidity. Type of concrete.

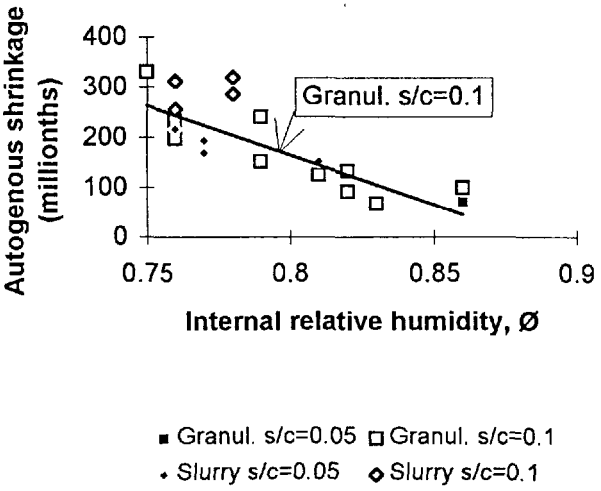

Figure 10 Autogenous shrinkage versus the internal relative humidity. Type of silica fume.

Drying shrinkage of mature concrete

Small loss of weight was observed of the sealed specimens of reasons mentioned above. Table 2 shows the loss of weight recorded during a period of at least 3 years from a 1.8 kg concrete specimen. Small loss of weight over a long period gave a good simulation of the shrinkage of a large specimen of mature concrete. The relationship between the relative loss of weight, i.e. the ratio of evaporated water to the mixing water made the study non-dimensional. Fig 11 shows the specific shrinkage versus the ratio of evaporated water to the mixing water, w_e/w:

$$\varepsilon_D = k_{sD} \cdot 20 \cdot [1.1 \cdot (w_e/w) - (w_e/c)] \qquad \{0 < w_e/w < 0.03\} \qquad [3]$$

c	denotes the cement content of the concrete (kg/m^3)
k_{sD}	= 0.4 for concrete with silica fume slurry; k_{sD} = 1 for granulated silica fume
w	denotes the mixing water of the concrete (kg/m^3)
w_e	denotes the evaporated water from the concrete (kg/m^3) $\{0 < w_e/w < 0.03\}$
ε_D	denotes the specific shrinkage related to the evaporated water (per mil)

Table 2 Loss of weight from 1.8 kg specimen (g).

Concrete	01	02	03	28
1	-	3.9	-	-
2	2.6	2.0	1.1	-
3	2.7	2.3	-	-
4[1)]	5.3	2.4	4.2	3.0
5	1.7	1.6	-	-
6	0.7	1.3		
7[1)]	3.9	2.5	2.9	5.2
8	0.9	1.0		

[1)] 4 years

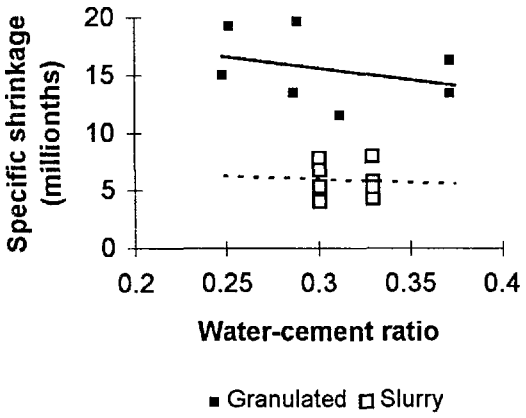

Figure 11 Specific shrinkage versus w/c.

Drying shrinkage of young concrete

The internal relative humidity, Ø, of the cylinder used for the measurements of shrinkage was obtained in the experiments. Between 5 and 28 days' age Ø became less than 0.70, which ceased the effect of hydration and thus the autogenous shrinkage in the specimens. However, at 28 days' age, Ø of the specimen was still about 5% larger than the ambient relative humidity. However, due to carbonation of the calcium hydroxide of the concrete, the loss of weight ceased at an age of the concrete that was dependent on w/c as shown in Fig 12. [The water in the calcium hydroxide (molecule weight 74) was replaced by the carbon dioxide (molecule weight 100)]. When sufficient silica fume was available in the concrete all the calcium hydroxide was consumed by the pozzolanic reaction according to Eq 4. In normal concrete about 16% silica fume is required to consume all the calcium hydroxide (Peterson, 1976):

$$3\ Ca(OH)_2 + 2\ SiO_2 = 3\ CaO.2\ SiO_2.3\ H_2O \qquad [4]$$

At lower w/c the required amount of silica fume, s_{rq}, to consume all the water in the calcium hydroxide became smaller (Powers & Brownyard, 1946-1948; Peterson, 1976):

$$s_{rq} \approx [(w/c)/0.39] \cdot 0.16 \approx 0.4 \cdot (w/c) \qquad [5]$$

According to Eq 5 carbonation does not occur at w/c = 0.25 and s/c = 0.10. This was confirmed by the experiments as shown in Fig 12. At w/c = 0.3 some of the concretes did not carbonate, which indicated the required amount of silica fume to be slightly lower than estimated in Eq 5. Eq 6 was evaluated for the age at carbonation of HPC with 10% silica fume, t_{ca} (days):

$$t_{ca} = 0.142 \cdot (w/c)^{-6.42} \qquad \{0.3 < w/c < 0.4\} \qquad [6]$$

For concretes with w/c < 0.3, when carbonation did not occur, the drying shrinkage, ε_{D1}, was correlated to the loss of weight by Eq 7 (μm/m):

$$\varepsilon_{D1} = 1600 \cdot [(w/c) - 0.22] \cdot e^{63 \cdot [0.42 \cdot (we/w) - (we/c)]} \qquad \{0 < w_e/w < 0.30\} \qquad [7]$$

c	denotes the cement content of the concrete (kg/m^3)
w	denotes the mixing water of the concrete (kg/m^3) {0.25< w/c<0.30}
w_e	denotes the evaporated water from the concrete (kg/m^3) {0< w_e/w<0.30}
ε_{D1}	denotes the specific shrinkage related to the evaporated water (μm/m)

However, for w/c > 0.3 the carbonation took place simultaneously with the drying of moisture In this case the shrinkage was correlated to time, which made Eq 8 dependent on the size of the specimen. (Eq 7 was non-dimensional.) The time of drying shrinkage was set according to Eq 6. Fig 13 shows the rate of shrinkage. The following equation was obtained [(mm/m)/day]:

$$\delta\varepsilon_{D2}/\delta t = k_s \cdot [5.65 \cdot (w/c)^2 - 3.28 \cdot (w/c) + 0.556]/t \qquad [8]$$

k_s	=0.85 for concretes with silica fume slurry; k_s= 1 otherwise
t	denotes the age (days)
$\delta\varepsilon_{D2}/\delta t$	denotes the rate of shrinkage [(mm/m) /day] (diameter: 55 mm; length: 300 mm)

Eq 8 indicates that the rate of drying was lower for concrete with silica fume slurry than for concrete with granulated silica fume, which seemed logical due to the autogenous shrinkage.

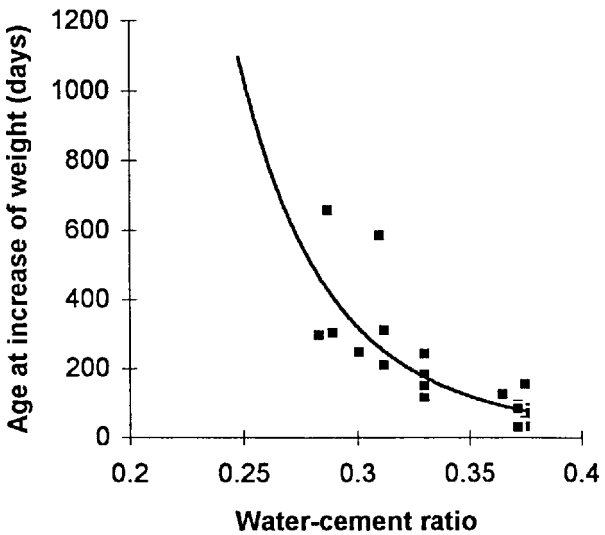

Figure 12 Age at increase of weight due to carbonation versus the w/c.

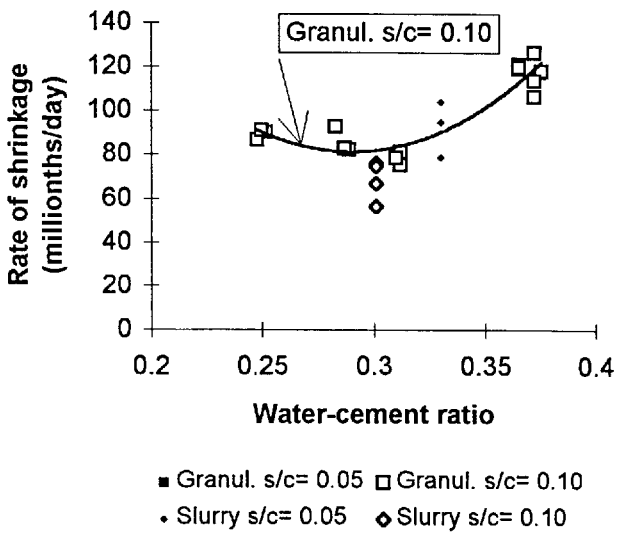

Figure 13 Rate of drying shrinkage versus the w/c. Type of silica fume is indicated.

Carbonation of mature concrete

At an age as described in Eq 6 the specimens began to carbonate, which was recorded by weighing. Once the carbonation started, no decline of the internal relative humidity occurred. Fig 6 shows the carbonation shrinkage versus the loss of weight. Fig 14 shows the carbonation rate versus w/c. The carbonation rate, $\delta(w_c/w)/\delta t$, was related to the mixing water, w [(kg/kg)/day]:

$$\delta(w_c/w)/\delta t = 0.25\ (w/c-0.25)/t \qquad \{0.25< w/c<0.40\} \qquad [9]$$

t denotes the age (days)
w_c denotes carbonated weight (kg/m^3) $\{0.2< w_c/w<0.35\}$

Eq 9 confirmed the previous results in Eqs 5 and 6 namely that no carbonation occurred in a concrete with 10% silica fume and a water-cement ratio less than 0.25.

Total shrinkage

From Fig 15 the shrinkage after at least 3 years (4 years for concretes 4 and 7) was correlated:

$$\varepsilon = k \cdot 34 \cdot [(w/c)^2 - 0.68 \cdot (w/c) + 0.13] \qquad [10]$$

$$\varepsilon_B = k_B \cdot 1.5 \cdot [0.43 - (w/c)] \qquad [11]$$

$$\varepsilon_C = 0.85 \cdot [(w/c) - 0.25] \qquad [12]$$

$$\varepsilon_D = 33 \cdot [(w/c)^2 - 0.65 \cdot (w/c) + 0.11] \qquad [13]$$

k =1.1 for 10% silica fume slurry; k=1 for 10 % granulated silica fume or 5% slurry
k_B =1.5 for 10% silica fume slurry; k_B=1 for 10 % granulated silica fume or 5% slurry
ε, ε_B, ε_C, ε_D denote total, basic (autogenous), carbonation, drying respectively (mm/m)

Comparison with other results

Table 2 shows a comparison with results according to other studies of the estimated shrinkage.

Table 2 A comparison of results of the estimated shrinkage (μm/m) for w/c= 0.3 and s/c= 0.1.

Study	le Roy and Larrard (1993)	Sicard (1993)	Tazawa and Miyazawa (1993)	Persson (1995A)	Persson (1995A)	Present study	Present study
Silica fume	Granulated	Granul.	Granulated	Granul.	Slurry	Granul.	Slurry
Age (days)	400	600	40	1000	1000	1200	1500
Autogenous	220	430	200	320	380	195	295
Drying	160	-	200	-	-	300	285
Carbonation	-	-	-	-	-	45	30
Total	380	-	400	-	-	540	610

CONCLUSIONS

The following conclusions were drawn from the experiments after studies for at least 3 years:

1) The autogenous shrinkage was dependent on the age, w/c and type and content of silica fume.
2) The autogenous shrinkage of HPC was related to the decline of internal relative humidity.
3) Estimations of drying shrinkage of mature HPC were made related to the evaporated water.
4) The conditions for carbonation of HPC were settled related to w/c and content of silica fume.
5) The age at start of the carbonation of HPC was related to w/c.

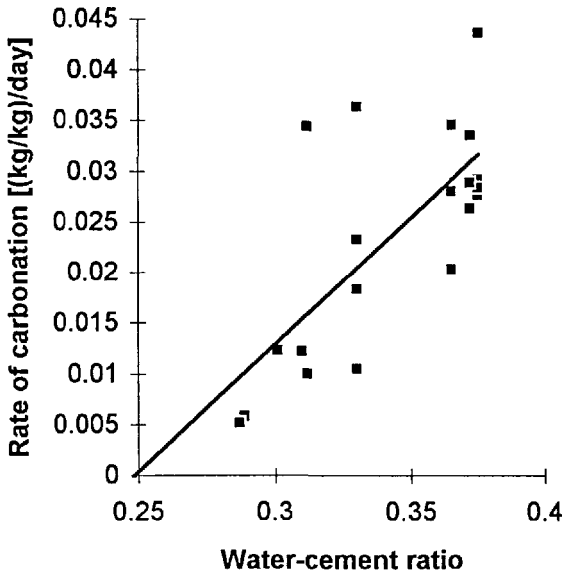

Figure 14 Rate of carbonation versus w/c.

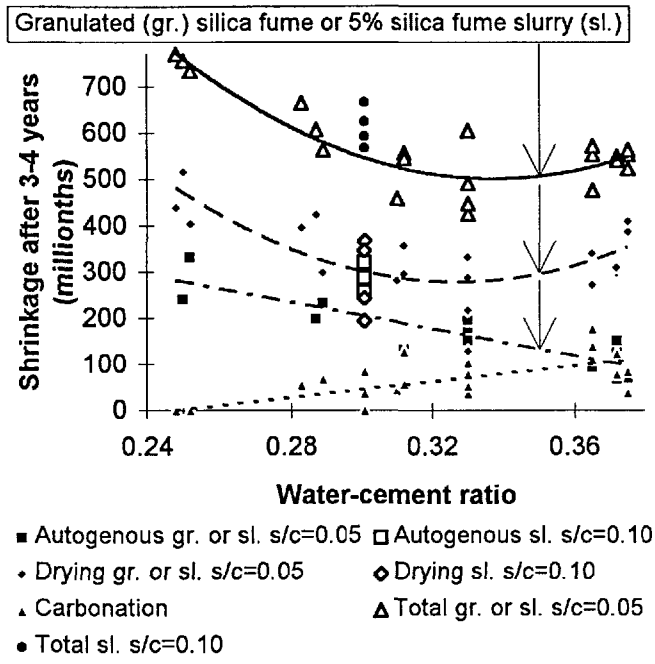

Figure 15 Type of shrinkage versus w/c.

6) The drying shrinkage of young HPC was related to the age and to the loss of weight.
7) The carbonation rate of HPC was related to age and w/c by a logarithmic relationship.
8) The total shrinkage after 3-4 years was related to age, w/c and type and content of silica fume.

ACKNOWLEDGEMENT

The study was financed by a Norwegian-Swedish consortium (Cementa, Elkem, Euroc Beton, NCC Bygg, SKANSKA, Strängbetong, BFR, NUTEK) which hereby is gratefully acknowledged.

REFERENCES

Bazant, Z.P., Carol, I., Guidelines and recommendations for characterising creep and shrinkage in structural design codes, Fifth International RILEM Symposium, E&FN Spon, pp. 805-829.

Mejlhede Jensen, O., Autogenous Deformation and Change of Relative Humidity - Self-desiccation and Autogenous Shrinkage, Report 284, Dep. of Building Materials, DTU, 1993.

Persson, B., Basic creep of High Performance Concrete, Report M6:14, Lund Institute of Technology, Division of Building Materials, 1995, pp. 1-292.

Persson, B., (Early) basic creep of High-Performance Concrete, 4th International Symposium on the Utilisation of High-Performance Concrete, Paris, 1996, pp. 405-414.

Persson, B., Self-desiccation and Its Importance in Concrete Technology, Materials and Structures, Vol. 30, RILEM, 1997.

Peterson, O., Interaction between Silica Fume and Standard Portland Cement in Mortar and Concrete, Cementa Ltd, Malmö, 1976, pp. 1-8.

Powers, T. C., **Brownyard**, T. L. (1946-1948). Studies of Physical Properties of Hardened Portland Cement Paste. Research Laboratories PCA, Bulletin 22. Pp 473-488, 845-864.

le **Roy**, R., de **Larrard**, F., Creep and shrinkage of High-Strength Concrete, Proceedings of the Fifth International RILEM Symposium in Barcelona, E&FN Spon, London, 1993, pp. 500-508.

Sicard, V., Origenes et proprites des deformations de retrait et de flauge de betons a Hautes Performances a partir de 28 heures de durcissement, Laboratorie Materiaux et Durabilite de Constructions, INSA-UPS no 201, Toulouse, 1993, pp. 55-81.

Tazawa, E., Miyazawa, S., Autogenous shrinkage of concrete and its importance on concrete technology, Fifth International RILEM Symposium, E&FN Spon, London, 1993, pp 159-168.

2ii074
8 pp

Kn o. 2 5. JAN. 2001 d o k 31838

INVESTIGATIONS ON SHRINKAGE COMPENSATED AND EXPANSIVE REPAIR MORTARS AND GENERAL BEHAVIOUR TO TYPICAL INFLUENCES

M. DEGENKOLB and D. KNÖFEL, Universität-GH Siegen, Labor für Bau- und Werkstoffchemie, Siegen, Germany

ABSTRACT Lime-based binders and mortars rich in blastfurnace slag were modified with expansion compounds on the basis of calcium aluminate, calcium aluminate sulphate and meta-kaolin in combination with gypsum. Compounds on the basis of CA and CAS show the quickest expansion. Meta-kaolin addition gives low swelling effects and causes a slower reaction. Generally, the course of expansion succumbs a strong interaction with chemical admixtures. The addition of slag improves the controllability of expansive systems, independently of the binder.

Key-words: Additives, Blastfurnace Slag, Ettringite, Expansion, Lime

INTRODUCTION

As repair mortars for masonry two basic binder systems have been developed: Lime-based mortars blended with blastfurnace slag and sulphate activated slag mortars (Trautmann, 1990). For the restoration of masonry, lime-based mortars offer a favourable distortability and water vapour permeability. The first problem encountered is the strong initial shrinkage of lime-based mortars. These negative volume changes affect for example the bonding properties of repair mortars. Expansive additives, well known from the expansive cement technology (Kurdowski, 1980), enables us to compensate this initial shrinkage and to produce low swelling mortars. Sulphate activated slag mortars own a high sulphate resistance and offer good conditions for expansion by controlled ettringite formation (Henkel, 1994). By use of expansive compounds affecting initial swelling phenomena, the bonding properties of joint mortars can be improved.

PROGRAM

The following binders were used:

- lime hydrate with low hydraulic contents
- lime hydrate with slag sand (75 % lime + 25 % slag sand by weight) and
- slag sand/gypsum/cement (85 % slag sand + 10 % gypsum + 5 % portland cement by weight).

As expansion compounds

- calcium aluminate cement/gypsum (CA-1/gypsum and CA-2/gypsun)
- meta-kaolin/gypsum (MK/gypsum)
- calcium aluminate sulphate/gypsum (CAS/gypsum)

were added to the various binders.

The analyses of the raw materials used are established in table 1; the composition of expansive compounds is shown in table 2. The binder/aggregate value is 1:4 in parts by weight for all mixtures. As test samples, mortars prisms 40 mm x 40 mm x 160 mm were produced, as well as small prisms made of binder paste with the dimensions 15 mm x 15 mm x 60 mm. The

consistency of the mortar mixtures was adjusted to a slump of 15 cm ± 0,5 cm, the binder pastes were produced with a water/binder ratio of 0,5.
The following investigations were carried out, according to Knöfel and Schubert, 1993:

- determination of length change on hardened test samples
- expansion immediately after production using a special measuring mould
- determination of setting time
- strength development and modulus of elasticity
- variation of storage conditions (conditions are mentioned in table 4)
- freeze/thaw-cycles
- liability to efflorescence
- x-ray diffraction
- scanning electron microscopy
- application of testing fields

Table 1 Chemical composition of materials used in weight-percentages
AC = Aluminous Cement

	Kaolin	Slag	Gypsum	Lime	AC-1	AC-2
CaO	0,1	41,1	35,9	86,4	38,0	27,1
MgO	0,2	7,6	1,1	0,8	1,2	0,2
SiO_2	47,8	35,6	-	8,9	5,0	0,7
Al_2O_3	36,3	11,2	-	2,7	39,0	70,1
Fe_2O_3	0,9	1,1	-	1,1	17	0,2
SO_3	-	3,5	47,8	0,4	0,2	0,2
CO_2	-	-	1,5	3,0	-	-
H_2O	-	-	13,5	-	-	-

Table 2 Composition of expansion compounds

Compound	Composition	Phases	Production	Specific Surface Area cm^2/g
Aluminous Cement-1/Gypsum (AC-1/G)	50:50 (weight-%)	**CA**, C_2A, $C_{12}A_7$, **$CaSO_4 \cdot 2\ H_2O$**	blending	4000
Aluminous Cement-2/Gypsum (AC-2/G)	30:70 (weight-%)	**CA**, C_2A, $C_{12}A_7$, **$CaSO_4 \cdot 2\ H_2O$**	blending	4700
Meta-Kaolin/Gypsum (MK/G)	70:30 (weight-%)	**$2\ SiO_2 \cdot Al_2O_3$,** **$CaSO_4 \cdot 2\ H_2O$**	burning (650 °C, 2 h)	11000
Calcium Aluminate Sulphate/Gypsum (CAS/G)	1:8 (molar ratio)	**$C_4A_3\bar{s}$,** **$CaSO_4 \cdot 2\ H_2O$**	burning (1300 °C, 2 h)	4000

RESULTS

Lime-Based Mortars

Lime-based mortars exhibit a strong initial shrinkage. The expansive potential of the expansive additives is consumed for the compensation of this early shrinkage. Figure 1 shows the compensation of the initial shrinkage by increasing addition of expansion compound. More than 20 % addition provides actual expansion. The figure clarifies the typical length change of lime based binders; the main part of the shrinkage process happens during the first days.
By comparison of the different expansion additives used - meta-kaolin, calcium-aluminate-sulphate and calcium aluminate cements in combination with gypsum - the following differences relating to their mode of working have been determined and the results are mentioned in table 3.
The addition of meta-kaolin provides low expansion and the reaction proceeds slowly. To accelerate the expansion process, microsilica and nanosilica were added. This results in higher expansion, so that it is possible to compensate the strong shrinkage and to produce low swelling mortars up to an expansion of 0,5 mm/m. The addition of pure calcium aluminate sulphate (CAS) affects strong expansion and it takes a rapid course. The setting and hardening of lime-based mortars were accelerated. By addition of aluminous cements a quick and strong expansion can be reached.

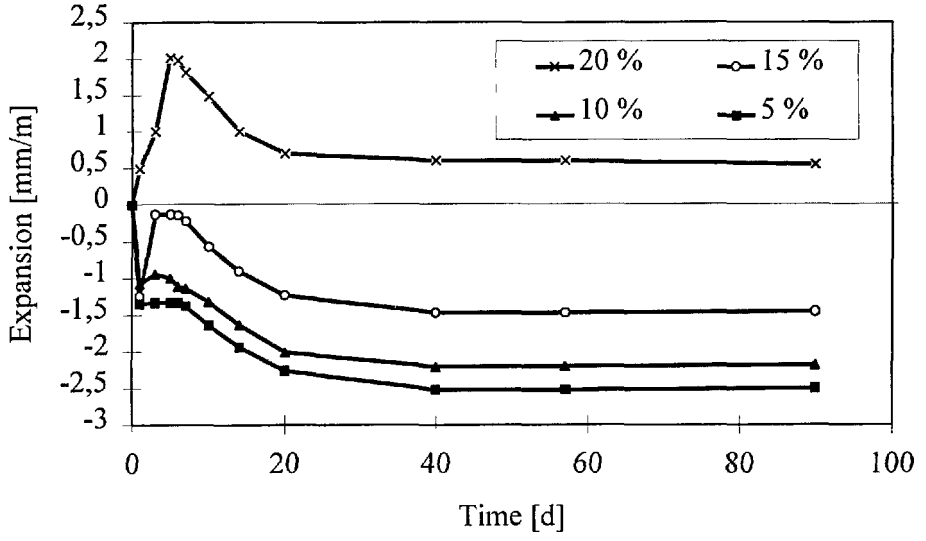

Figure 1 Length change of lime-based mortars, increasing addition (% by binder-weight) of expansive compound CA-1/Gypsum
Storage conditions 7 days 20/95 (20° C/95 % relative humidity), subsequently 23/50 (23° C/50 % r.h.)

After the end of the expansion period, lime-based mortars shrink to the same extent as unmodified binders. Normally, this is the usual behaviour of all expansion mortars, so that the term "shrinkage free" mortars is not correct strictly speaking.

Table 3 Comparison of different expansion compounds in different binder systems
MC = methyl cellulose

binder	expansive compound	additives	expansion	compressive strength 28 d
	25 % by weight		mm/m	N/mm^2
lime/slag	CA1/gypsum	-	2,5	18,8
lime/slag	CA2/gypsum	-	2,5	16,5
lime/slag	CAS/gypsum	-	4,5	15,8
lime/slag	MK/gypsum	-	0,5	14,1
		-		
slag/gypsum	CA-1/gypsum	-	0,3	8,3
slag/gypsum	CA-2/gypsum	-	0,7	5,5
slag/gypsum	CA-1/gypsum	polymer	0,7	4,5
slag/gypsum	CA-1/gypsum	polymer/MC	1,8	5,4
slag/gypsum	MK/gypsum	microsilica	0,3	15,3

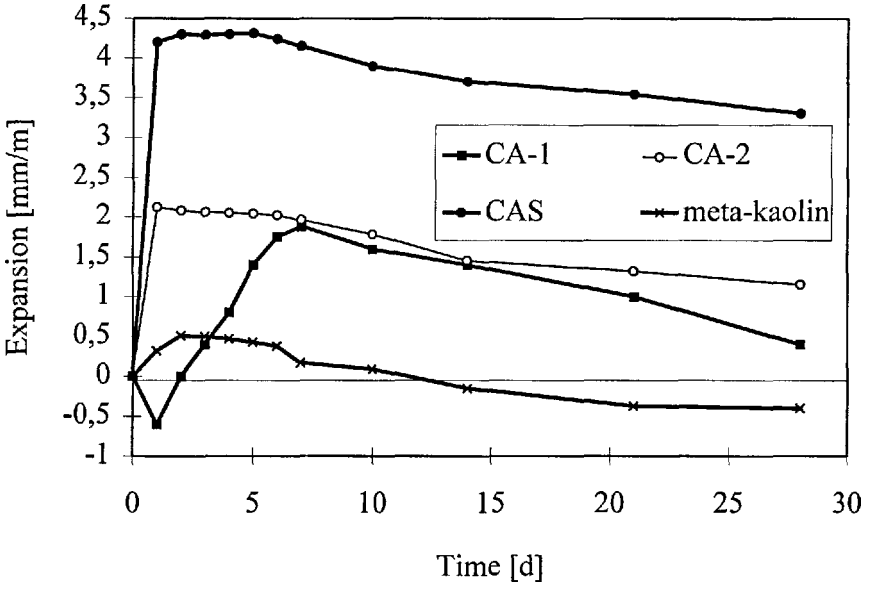

Figure 2 Lime/slag-mortars with different expansive compounds. Storage conditions 7 days 20/95, subsequently 23/50

Slag-Based Mortars

Unmodified mortars on the basis of sulphate activated blastfurnace slag don't succumb the initial shrinkage of lime mortars mentioned above. The hardening process is characterised by a low swelling period (0,2-0,3 mm/m) during the first days. The following shrinkage period takes a very slow course up to 90 days after production. Slag-based mortars offer excellent conditions for the modification with expansive additives, because the main hydration phases are AFt-phases like ettringite. By manipulation of quantity, speed or morphology of the ettringite formation a controlled expansion can be reached. Generally the addition of the expansive compounds affects

lower expansion values than in the lime-based mortars (see table 3). The reasons are the low $Ca(OH)_2$-content and accordingly lower pH-values.
A stronger expansion can be reached by adding $Ca(OH)_2$ to the slag-sulphate system. However, the excellent volume stability and the controllability of slag-mortars are impaired by adding $Ca(OH)_2$.
The addition of meta-kaolin affects low swelling phenomena. The further shrinkage doesn't differ from the normal shrinkage behaviour. Adding CAS/gypsum to slag-based mortars without an additional $Ca(OH)_2$-additive, low swelling effects are determined. By adding $Ca(OH)_2$ strong expansion is reached, but the controllability decreases.

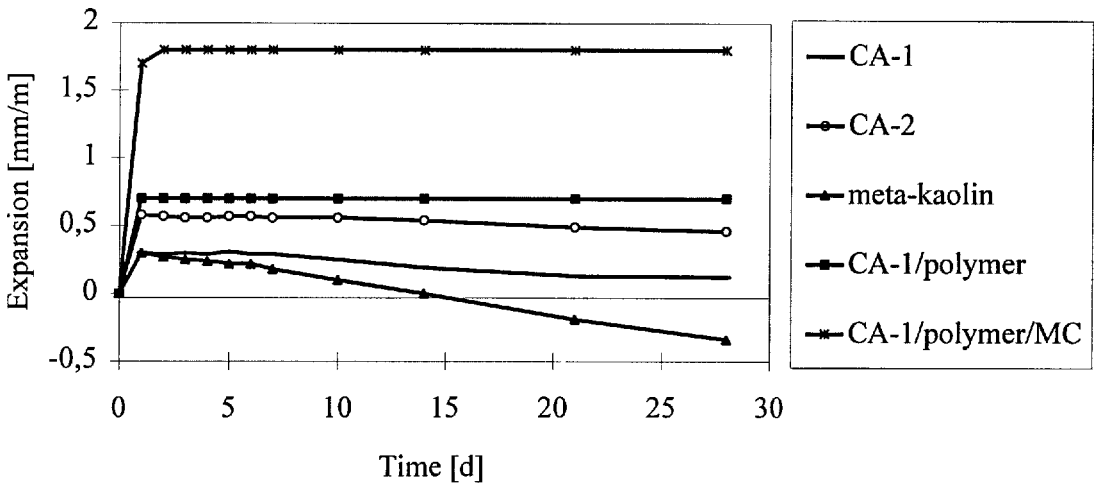

Figure 3 Sulphate activated slag mortars modified with various expansive compounds. Storage conditions 20/95, subsequently 23/50

The addition of CA-cements with varying Al_2O_3-contents in combination with gypsum enables the production of low and strong expansive mortars, which possess a long term shrinkage compensation due to a slow consumption of the sulphate compound (see figure 3).

Influence of storage conditions

The samples tested were stored until the 7th day after production in climate 20/95 (20 °C/95 % rel. air humidity). Thereafter, they were subjected to four different storage conditions until the testing date, temperature and air humidity being varied. Additionally one set of the samples was stored under water at 8° C immediately after production. The storage conditions are mentioned in table 4.

Table 4 Storage conditions

Storage	Temperature	Humidity	Weathering
	[° C]	[% relative humidity]	
wet (20/95)	20	95	-
dry (23/50)	23	50	-
CO_2	20	65-75	1 Vol.-% CO_2
under water	8	under water	-

The different storage conditions indicate the potential and the limits of practical applications of expansive mortars. The time progress and the ending of expansion is shown by a storage in wet climate with a humidity of 95 %; that means that for practical application the expansion of the mortars should be terminated during the first 7 days after production. The following change of storage to a temperature of 8° C under water shows remaining expansive compounds, that means, that undesired swelling phenomena after the 7th day of hydration can be detected. The "dry" storage in a climate of 23/50 shows the maximum of shrinkage. The weathering with 1 % carbon dioxide by volume indicates the resistance of the ettringite produced to carbonation. The additional storage in water at 8° C immediately after production determines the total potential of expansion at extreme conditions.

Generally the addition of blastfurnace slag has positive effects on the expansion behaviour of the mortars, which is expressed by quicker hardening, earlier expansion and easier controllability. Furthermore expansion is terminated after 7 days and during the following storage under water at a temperature of 8° C, no further expansion phenomena are observed - whereas, using pure lime mortars without slag addition, expansion may occur longer than 7 days. The slag can take over a regulating buffer function within the expansive system. The development of expansive mortars turned out to be complex using pure lime hydrate as binder.

By a storage in alternating wet/dry-cycles, liability of efflorescence and volume stability were detected. E.g., mortars containing expansion compounds with a CA-1/gypsum-ratio < 1 show damaging phenomena during the wet/dry-changing.

Further, the resistance to freeze/thaw-changing was tested. All samples remained without damaging after 45 cycles of freeze (-20° C, for 3 hours), thaw (+20° C for 3 hours) and respectively 1 hour of cooling and heating.

The behaviour of the mortars developed to natural weathering was tested by application on test fields as repair mortars on historic brickwork constructions in the north of Germany.

Main results of the storage variations:

- good controllability due to the presence of blastfurnace slag
- sulphate activated slag mortars are hardly influenced by changing of storage conditions
- critical sulphate contents are detected by wet/dry-cycles in climate 23/50
- during freeze/thaw-changing no damages were observed
- ettringite phase produced is being destroyed during CO_2-weathering, which has been determined by X-ray-diffraction

Influence of water/binder-ratio

With regard to practical application, the influence of mixing water on the course of expansion is an important parameter influencing length change. The following example shows this influence by use of a typical expansion mortar on the basis of a lime/slag-binder and addition of 25 % CA-2/gypsum by weight. The samples were stored in a climate of 20/95 and the water/binder-ratio was varied. The different ratios and mixing water contents are shown in figure 4. The increasing water content affects a linear decrease of expansion in the expansive mortar.

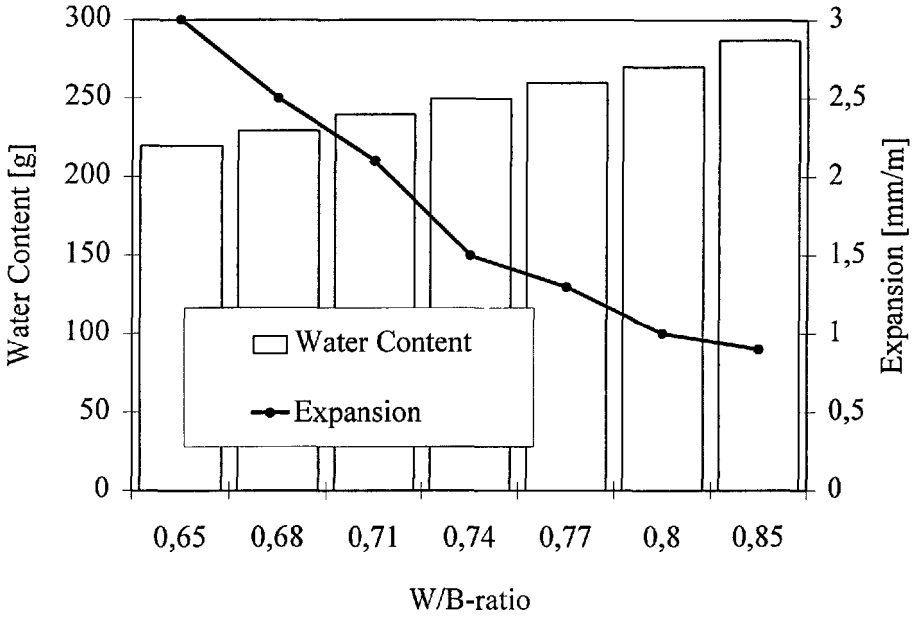

Figure 4 Influence of water content on expansion in lime/slag-mortars with 25 % expansive compound CA-2/gypsum

Influence of binder:aggregate-ratio

According to the variation of water/binder-ratio, the influence of the ratio of binder:aggregate (B/A-ratio) was investigated. By use of a standard expansive mortar (lime/slag-binder with 25 % CA-2/gypsum the binder:aggregate ratio was altered. Comparing the ratios 1:3, 1:4 and 1:5 the course of expansion differs decisively. The standard B/A-ratio 1:4 posses swelling effects of 2,5 mm/m. By increasing the ratio up to 1:5 the expansion is being reduced to 0,5 mm/m. On the other hand, using a B/A-ratio of 1:3 expansion remains on the same values of 2,5 mm/m.

Influence of fineness

The influence of fineness of expansive compounds was studied. The standard expansive compound CA-2/gypsum was added to ordinary portland cement by using a fineness of expansive compound of 4000 and 8000 cm^2/g (Blaine). The course of expansion was observed during a storage in 20/95 and at 8°C under water. Both storage conditions indicate no significant differences between the different grinding levels. Of course, technically used expansive cements basing on $C_4A_3\bar{s}$ show strong influences on fineness. However, the mortar compositions used in this investigation content amounts of expansive compound up to 25 % by weight related to binder. That means 5 % by weight related to the mortar, so that the influence of the specific surface of expansive additives on the course of expansion is quite low.

Influence of additives

Various chemical admixtures were added to the expansion systems, e.g. different types of polymers, air-entraining agents, accelerators or methyl-cellulose (see table 3). Polymers,

especially in the case of slag-based mortars, influence decisively the expansion. However, the effect of the polymer added depends on the type of polymer and on the binder used. Concerning the present treatise, the following effects of polymer addition occur:

- decreasing of expansion in lime-based mortars
- increasing and accelerating of expansion in slag-based mortars
- no influence on expansion by polymer addition in slag-based mortars

E.g., in the case of a slag based mortar with expansion compound CA-1/gypsum, the expansion increases by addition of 5 % polymer on the basis of vinyl acetate from 0,2 to 0,7 mm/m (see figure 3). An extra addition of MC, which is used to improve the water retentivity of slag-based mortars, accelerates and increases the expansion in this system to 1,8 mm/m.
By choosing the type of polymer, the course of expansion can be directed.
The mechanisms of the different admixtures influencing expansion are complex, consisting e.g. change of pH-value, change of setting and/or hardening during the first days after mortar production.

CONCLUSIONS

To reach a quick expansion process during the first 3 days after production, combined with a good controllability, availability and handling, calcium aluminate cements in combination with gypsum were preferred.
For the production of shrinkage compensated or low expansive mortars on the basis of lime, the blending with blastfurnace slag turned out to be a secure way to reach a good controllability of expansion.
Sulphate activated slag-mortars show a quick expansion during the first 3 days and subsequently a long lasting volume stability. Furthermore, the influence of different storage conditions, alteration of temperature and moisture on the course of expansion is quiet low.
Variation of storage conditions, especially the storage at low temperatures under wet conditions, indicates the mixing limits of expansive mortars.
The course of expansion is decisively influenced by technological and chemical parameters as e.g. water content, binder:aggregate ratio, setting time or additives. That means, that a reliable workmanship of expansive mortars must be guaranteed. Furthermore, it has to be kept in mind, that every change in mortar formula affects the expansion process.

REFERENCES

Henkel, S., Knöfel, D., "Zur Verträglichkeit von mineralischen Mörteln mit sulfatbelastetem Mauerwerk", 12. Internationale Baustofftagung Weimar, 2, 1994, pp. 58-66
Knöfel, D., Schubert, P., "Handbuch Mörtel und Steinergänzungsstoffe in der Denkmalpflege", Verlag Ernst und Sohn, Berlin, 1993
Kurdowski, W., "Ciments expansifs", 7e Congres International de la Chemie des Ciments, Vol. I, Paris, 1980
Trautmann, I., Knöfel, D., "Entwicklung eines Gipshüttensandzementmörtels", Fortschritte der Mineralogie, 68, p 264

Topic II.E

Influence of mixing techniques and curing conditions

2ii075
9 pp

Kno. 25. JAN. 2001 dok 31839

Mechanical Property/Microstructure Relationships in a Mortar Fabricated in a Microgravity Environment

Richard FIRST Master Builders, Inc., Cleveland, Ohio, USA
Andre' WALLISER Master Builders Technologies (Schweiz) AG Zurich, Switzerland

ABSTRACT The purpose of this study was to examine the effects of microgravity on the microstructure/property development of a portland cement mortar; in particular, compressive strength and wedge-splitting experiments were performed. The results indicated a 30% increase in compressive strength and better performance under tensile load for the microgravity mortar than for the control mortar. These mechanical property data are correlated with the micro-structural differences observed between the two mortar specimens.

Key-words: microgravity, strain softening, wedge splitting, fracture mechanics, microstructure

INTRODUCTION

It has been thoroughly documented in the literature and is well accepted that changing the microstructure of a material can lead to changes or differences in physical properties and/or materials performance (Melton, 1975; Park and Snyder, 1995) . Portland cement-based mortar and concrete are no exception. It is well known that pozzolanic mineral admixtures (i.e. pulverized fly ash, ground granulated blast-furnace slag and silica fume) lead to microstructural changes in the interfacial transition zone (ITZ) which correspondingly lead to enhanced physical properties of the composite material (Faran, 1956; Scrivener and Pratt, 1996; Mindess, 1988; Bentur and Odler, 1996). As such, it is plausible that other changes in the microstructure of these materials could also lead to enhanced properties and/or performance.

Master Builders, Inc. designed an experiment for flight in the NASA space shuttle program in order to study the effect of microgravity on a Portland cement mortar (First *et. al.*, 1995 and Miller, *et. al.*, 1995). A 50:50 (by weight) mixture of a type I (U.S.) Portland cement and ASTM C-109 silica sand were mixed at a water/cement ratio of 0.40; a water-reducing admixture was also used in the mix design. The mortar was mixed once the shuttle was in a microgravity environment. The mortar hardened within the mixing chamber and cured for 12 days under microgravity conditions. Upon return to earth, the hardened mortar was removed for analysis. A second mortar was mixed at the Master Builders Headquarters in Cleveland, Ohio, USA, under the same controlled conditions except, in this case, a normal 1-g gravity environment.

Among the analyses performed on these materials, optical and scanning electron microscopy (SEM) were used to examine the macro/microstructure of the samples. BET and mercury intrusion porosimetry (MIP) were also used to examine the pore size distribution in the samples. In addition, the compressive strength of several samples taken from each of the materials was measured. Wedge-splitting experiments were also performed to assess the fracture behavior of these samples, as well as obtain the fracture energy/toughness of the materials. From these data, it is also possible to extract tensile strength information. These results are the topic of this paper and will be correlated with microstructural features of the materials.

OVERVIEW OF MICROSTRUCTURAL OBSERVATIONS

Upon removal from the mixing canister, the shuttle sample was observed to exhibit color variations along its central axis. Upon further investigation, it was apparent that these variations

were brought about by a combination of the failed false bottom mechanism and the unaccounted for 3-g force the experiment sustained during the shuttle lift-off. The 3-g force led to a packing of the dry materials on one side of the canister during lift-off. Because the false bottom did not actuate during the mixing procedure, there was no driving force for the material in the bottom portion of the canister to be mixed. As such, the material hydrated, but did not become part of a homogeneous mixture with the mortar in the rest of the canister. This material exhibited a lower water/cement ratio than the mortar in the rest of the mixing canister. This difference in water/cement ratio accounted for the bulk color variation in the sample. Also, the void space appeared to be concentrated at the surface of the hardened mortar sample and was helically shaped.

Optical microscopy

For reflected light optical microscopy investigation, a polished cross-sectional surface from each sample was examined. Both of the samples appeared fairly homogeneous and well-mixed. Porosity was evident in the control sample, while none was found in the microgravity sample. The overall water/cement ratio appeared lower in the control sample than in the microgravity sample. Slight, local variations in the water/cement ratio were observed throughout the cross-sectional surfaces of both samples. Perhaps the most significant difference here between the two samples was the presence of what the authors term "mixing folds" in the microgravity sample (Figure 1). It is thought that, as the mortar gained consistency, the material was able to fold onto itself. In the absence of gravity, as no driving force for settling occurs, the material may harden in place, with these folds or seams left in-tact. An appropriate analogy to this would be the folding of pizza dough onto itself. As this occurs, a seam is created where the two halves meet.

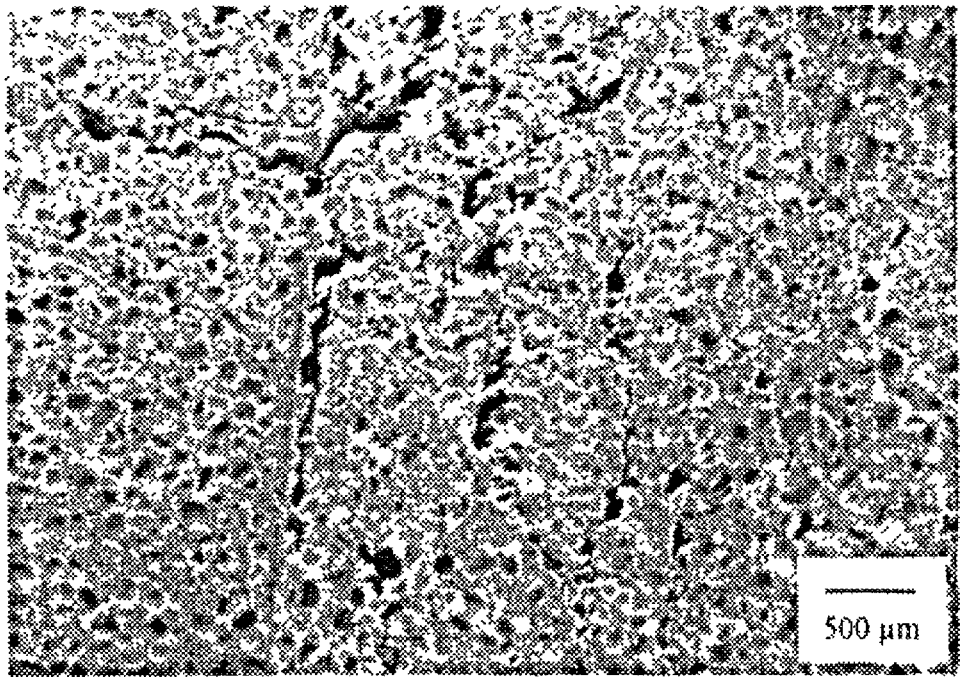

Figure 1 Normal-incidence, reflected light optical photomicrograph showing the "mixing folds" present in the microgravity sample microstructure.

The possibility that these features were merely cracks was discounted because of both the appearance of the features in cross section, as well as the fact the significant forces could not readily cause the features to propagate as crack would.

Thin-section and SEM analysis

The samples were also analyzed with transmitted light optical microscopy and SEM. The thin section optical microscopy work indicated the hydration (gel) products were more abundant in the microgravity mortar and that the $Ca(OH)_2$ crystals appears much larger (i.e. on the order of 2-3 times) in the control sample. SEM analysis on fresh fracture surfaces confirmed the above-mentioned observations. Furthermore, an abundance of ettringite crystals were observed in the microgravity mortar; whereas, no ettringite was observed in the control mortar. Also, there appeared to be no capillary pore space on any of the examined fracture surfaces from the control sample; whereas, the microgravity mortar contained many capillary pores, as evident by the plentiful amount of ettringite observed.

EXPERIMENTAL SYSTEM DESCRIPTION

Fracture tests carried out in an Environmental Scanning Electron Microscope allow us to observe the development of the fracture process zone and crack propagation under increasing load. The specimen chamber of the microscope is operated with a controlled environment (2-3 Torr, 25°C), while the optical column is kept under high vacuum.

Wedge splitting tests were conducted using a special in-situ testing machine developed at the Swiss Federal Institute of Technology, which was mounted on a coordinate table in order to control the position of observation. The test device consists of a stiff frame to support the specimen, as well as the loading wedge (wedge angle = 15°), a strain gauge and a load cell. The load was applied by means of this wedge, which allows fracture of the specimens under wedge displacement. Loading and unloading of the specimen was carried out by remote control. The position of the specimen is kept approximately constant via a contrarotating system. The splitting force and displacement were continuously recorded during testing.

The specimens were cut with a precision diamond saw from cores which were taken from the center of the space shuttle and control samples. Reference and space mortar specimens were further prepared by drilling holes for the load support and by cutting the notch with a diamond wire saw. As the drilling phase of the specimen preparation was too risky for the sample integrity, a piece of polymer concrete was glued on the top of the mortar (see Figure 2). Preliminary testing indicated that the polymer concrete pieces on the mortar specimens had no influence on their fracture behavior. A video recorder was also connected to the ESEM in order to follow, in full, the crack apparition and the crack opening pattern. For each specimen a scan over the surface was carried out in order to locate voids or macro defects before applying the load.

The fracture surfaces created during the wedge-splitting experiments were examined using SEM; the fracture surfaces were coated with gold to prevent charging.

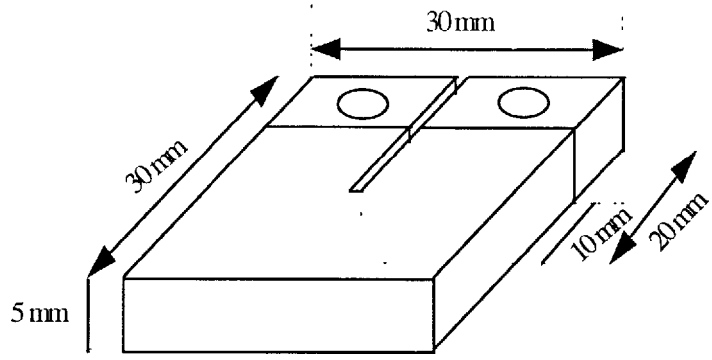

Figure 2 Schematic of wedge splitting sample tested *in-situ* using the environmental scanning electron microscope.

FRACTURE MECHANICS MODEL

Numerous fracture mechanics models have been presented for concrete (Elfgren, 1989). The two most prominent models are linear elastic fracture mechanics (LEFM) models and fracture energy models; only the fracture energy model will be discussed here. Fracture energy models are based on the concept that fracture energy is consumed for crack formation by the creation of two new surfaces. The material parameters for fracture energy models are: the specific fracture energy, G_f, the splitting force, F_{sp}, the crack mouth opening displacement, CMOD, and the softening diagram, which describes the relationship between the stress and the width of the fracture process zone by means of fitting graphical parameters from the fracture energy model with the experimental data.

The tensile softening diagram of concrete cannot be directly determined from fracture mechanics experiments other than uniaxial tensile tests. Roelfstra and Wittmann proposed a method (Roelfstra and Wittmann, 1985) to evaluate a bilinear softening diagram from the experimentally obtained force vs. displacement curve by means of a data fit. Their method is based on the Fictitious Crack Model (Hillerborg, Modeer and Peterson, 1976). In the above-mentioned method, the wedge splitting test is simulated by finite element analysis and the calculated force vs. deformation curve is compared to the experimental curve. The parameters of the input softening diagram are optimized until a good agreement between the calculated and experimental curves is obtained. The softening diagram leading to this result is considered to be the tensile softening diagram of the tested concrete/mortar.

A schematic representation of a tensile softening diagram is given in Figure 3. Here, the experimentally measured maximum splitting force is used to calculate the tensile force. The tensile strength of the material is calculated by the model. The other important parameters are denoted w_1 and w_2. w_1 denotes the softening point (displacement, CMOD) in the bilinear model and w_2 is the CMOD at the end of the wedge splitting test--that CMOD under a null load. These model parameters are adjusted to fit the experimental data and represent, in essence, a strain at a certain load.

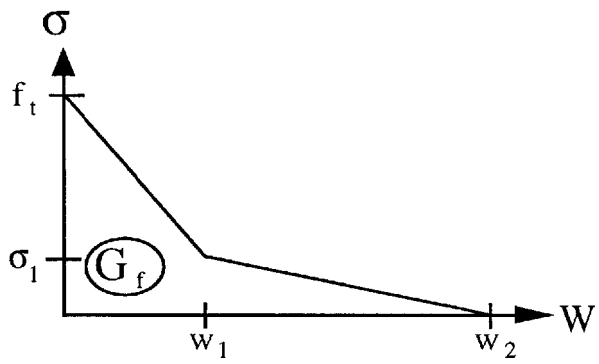

Figure 3 Schematic of the Bilinear Softening diagram used to calculate tensile parameters from the results of the wedge splitting experiments.

RESULTS

Porosity

The pore system was analyzed using Archimedes density (ASTM C-642), BET nitrogen absorption and mercury intrusion porosimetry (MIP). The ASTM C-642, BET nitrogen absorption and MIP data are summarized in Table 1 below:

Table 1 Summary of ASTM C-642 bulk specific gravity data

Technique	Property	Microgravity Mortar	Control Mortar
ASTM C-642	Bulk specific gravity	1.93	1.87
	Permeable voids (water)	24.5%	25.8%
BET nitrogen absorption	surface area	14 m^2/g	6 m^2/g
MIP	average porosity	18%	22%
	average pore diameter	0.020 μm	0.028 μm

Mechanical testing - compressive strength

The compressive strength measurement was performed on a single 25 x 25 x 25 mm cube taken from each sample at an age of 40 days. The compressive strength for the shuttle and control samples were 52 and 39 MPa, respectively. The compressive strengths were reevaluated at an age of 14 months by testing three (3) 10 x 10 x 10 mm cubes from each of the shuttle and control samples. The average compressive strengths for the shuttle and control samples at this age were 96.5 and 74.4 MPa, respectively.

Fracture mechanics - wedge splitting tests

Splitting force (F_{sp}), crack mouth opening displacement (CMOD) and elapsed time were simultaneously recorded. These data enable plots as shown in Figures 4,5. The F_{sp} vs. CMOD curve allows the calculation of the specific fracture energy, which is given by the area under curve. This specific fracture energy is then divided by the projected ligament area to obtain G_f.

The F_{sp} vs. time curve (Fig. 5) provides information regarding the stability of the performed test (i.e. if no sudden drop is observed on the recorded force, it can be said that cracking is occurring in a stable manner, Figure 4).

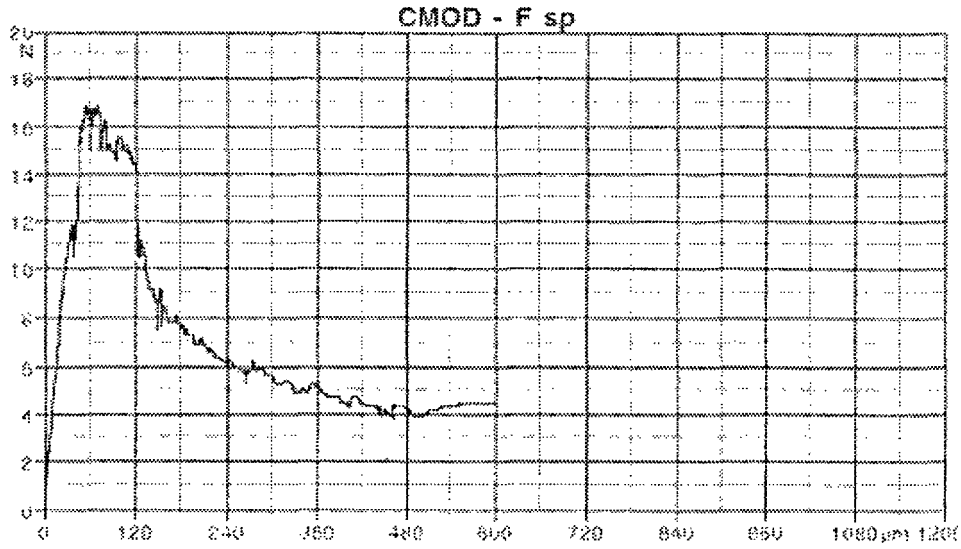

Figure 4 Experimental Splitting Force vs. CMOD Curve Obtained From the *In-Situ* Test.

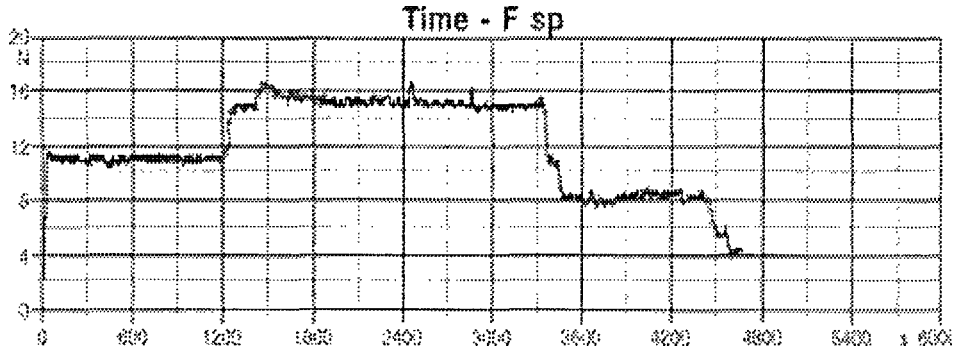

Figure 5 Experimental Splitting Force vs. Time Curve Obtained From the *In-Situ* Test.

Wedge splitting tests were conducted on four samples from each of the microgravity and control mortars. These data are summarized below in Table 2.

Table 2 Mean values based on four WST experiments

	Fspma (N)	G_f (N.m^{-1})	F_t (N.mm^2)	σ_1 (N.mm^2)	w_1 (mm)	w_2 (mm)
Microgravity mortar	15.6	79.5	2.86	0.33	0.029	0.272
Control mortar	15.7	77.3	2.52	0.31	0.047	0.356

DISCUSSION

In comparing the data produced in the present study, several significant differences in mechanical/physical properties are evident. Considering the pore size/distribution data, all of the results support the notion of the microgravity mortar sample exhibiting slightly less total porosity as well as a finer average pore diameter. The complete set of MIP data (not included here) also shows the pore size distribution for the microgravity mortar to be skewed toward the finer pore sizes (i.e. those pores in the 0.003-0.05 μm range. While there is much speculation regarding the accuracy with which these techniques define the actual pore size distribution, the data gathered in this investigation all support the implication that there exist a larger number of finer-sized pores

in the microgravity mortar than in the control mortar. The Archimedes data can be correlated with the original microscopical porosity determination, where it was found that the control mortar contained on the order of 5+% air voids; whereas, the microgravity mortar contained almost no optically observable pores. This could account for the 4% difference in average porosity as determined by ASTM C-642.

Considering both sets of compressive strength data, a 29.7% greater compressive strength average value was measured on microgravity mortar at an age of 14 months, which confirms the first compressive strength measurements of 52 MPa and 39 MPa (a difference of 33%) for the microgravity and control mortars, respectively, at an age of 82 days.

The experimentally obtained data from the in-situ wedge splitting tests were not markedly different for the two materials studied. Moreover, the in-situ observation of the propagating crack paths in all of the samples examined did not show a marked difference in the cracking behavior between the microgravity and control mortars. What is noteworthy are the data obtained from the strain softening diagram model. The computed tensile strength, f_t, was found to be ~13.5% higher for the microgravity mortar. Perhaps even more significant are the computed crack widths, w_1 and w_2, corresponding to σ_1 and a null stress at the end of the wedge splitting test. While the values of σ_1 are comparable for both sets of data, the computed crack widths are significantly different. The average crack width for the microgravity mortar at the same σ_1 is approximately 40% less than that computed for the control mortar. Moreover, at the end of the wedge splitting test, when there is a null load, the crack width in the microgravity mortar was ~24% less than that in the control sample. All of the above-mentioned modeled data from the strain softening diagram support the notion that the microgravity mortar exhibited better tensile properties than those of the control mortar. It should be noted again that this statement is inferred from the parameters of the fracture energy model/strain softening diagram and were not explicitly borne out in the experimentally obtained wedge splitting test data.

The microstructural features observed microscopically in previous investigations as well as those observed/measured in the present study support the mechanical property findings discussed above. The results of the compressive strength evaluation and the strain softening diagram obtained from the fracture mechanics experiments both indicate the microgravity mortar to have better overall mechanical properties that the control mortar. The porosity and pore size distributions of the two samples are somewhat different, as evidenced above by the BET, MIP, Archimedes density and SEM/image analysis results. All of the above-mentioned data indicate the microgravity mortar exhibited less total porosity and a finer average pore size. The MIP data specifically indicated the microgravity mortar contained more pores in the size range of 3-50 nm than did the control mortar. Furthermore, the microgravity mortar was found to contain almost no"macroscopic" porosity, as evidence by the optical microscopy analysis performed previously. The correlation between pore size distribution and compressive strength has been documented in the literature (Roelfstra and Wittman, 1985). It has been experimentally determined that a finer pore size distribution directly correlates with higher compressive strength--all other factors (including total porosity) being equal. Furthermore, a material having less total porosity may also have a lower compressive strength if it contains more larger-sized pores. Although the actual specific porosity size ranges which pertain to the above-mentioned relationships may be debatable, the general correlation likely exists within the present investigation. Moreover, the presence of a greater number of larger pores may serve to act as stress distributors during

fracture. The computed 13.5% greater tensile strength, f_t, for the microgravity mortar is evidence of this.

The previous SEM/thin-section optical microscopy analyses both concluded a significant difference in the $Ca(OH)_2$ crystals present in the two mortar samples; both studies documented a much larger average crystal size for $Ca(OH)_2$ present in the control mortar as well as more intergrowth of the crystals. As $Ca(OH)_2$ precipitates in pore space and at aggregate surfaces, its presence can typically be associated with areas or zones of weakness within the mortar. Furthermore, it is often the case in other materials systems that a finer grain size and/or a finer crystallite size also leads to an increase in physical properties. As such, it is plausible that these significant differences in $Ca(OH)_2$ crystal features may account, in part, for the lower compressive strength and modeled lesser tensile properties.

SUMMARY

Wedge splitting experiments were conducted on mortar mixed in a microgravity environment onboard a 1995 space shuttle mission using an in-situ device (in an ESEM) to facilitate observation of the crack propagation simultaneously with data gathering. The experimentally obtained fracture mechanics quantities and the observed crack behavior were not markedly different between the microgravity and control mortar samples; however, the modeled parameters obtained from the strain softening diagram indicate the microgravity mortar exhibits better tensile properties than that of the control sample. Indeed, the ~30% higher compressive strength for the microgravity mortar also indicates the microgravity mortar to exhibit better mechanical properties. Pore size distribution studies and microscopical analyses both provide useful information concerning the microstructure which appear to support the mechanical property findings.

Although not comprehensive, the intent of this article is to summarize the current status of the analyses performed on mortar samples mixed onboard the space shuttle in a microgravity environment. Although the results of the fracture mechanics model postulate better tensile behavior for the microgravity mortar, further investigation in this area as well as further SEM fractography of the wedge-split surfaces may help better define the actual role of microgravity in these experiments.

REFERENCES

Bentur, A. and Odler, I., RILEM Report 11, Ed. J.C.Maso, E&FN Spon, London, (1996), p.18.

Elfgren, L. (ed.), Fracture Mechanics of Concrete Structures- From theory to applications. State of the art report, RILEM TC 90-FMA, Chapmann & Hall, London (1989).

Farran, J., Thèse de Doctorat, Toulouse, in Revue des Matériaux de Construction, Paris, numbers 490, 491 and 492 (1956).

First, R. and Kovach, L., "Petrographic Analysis of a Concrete Mortar Mixed Onboard a Recent Space Shuttle Endeavour Mission", Proceedings of the 17th International Conference on Cement Microscopy, Calgary, Alberta, Canada (1995), pp. 311-329.

Hillerborg, A., Modeer, M. and Peterson, P., Cement and Concrete Research, **6**, (1976), pp. 773-792.

Melton, K., "The Structure and Properties of a Cold-Rolled and Annealed Al - 0.8wt% Zr Alloy", Journal of Materials Science, **10**, (1975), pp. 1651-1654.

Miller, P., Farrington, S. and Kovach, L., "Petrographic Thin-Section and Scanning Electron Microscope Analysis of a Mortar Mixed Fabricated in a Microgravity Environment:Preliminary

Studies", Proceedings of the 17th International Conference on Cement Microscopy, Calgary, Alberta, Canada (1995), pp. 330-343.
Mindess, S., Materials Research Society Symposium Proc. **114**, (1988), pp.3-10.
Park, C. and Snyder, R., "Structures of High-Temperature Cuprate Superconductors", Journal of the American Ceramic Society, **78** [12], (1995), pp. 3171-3194.
Roelfstra, P. and Wittmann, F., Fracture Toughness and Fracture Energy of Concrete, Elsevier, Amsterdam, (1985), pp. 163-176.
Scrivener, K and Pratt, P., RILEM Report 11, Ed. J.C.Maso, E&FN Spon, London, (1996), p.3.

ACKNOWLEDGMENTS
The authors acknowledge T. Steiger for useful discussions as well as for perfroming the ESEM in-situ experimental work at the Swiss Federal Institute of Technology, Institute for Buildings Materials, in Zurich headed by Prof. F.Wittmann. The optical microscopy thin-section analysis was performed by P. Miller and S. Farrington, Master Builders, Inc., Cleveland, Ohio, USA. The authors also wish to acknowledge Dr. H. Wang for his useful discussions.

2ii076
4 pp

RD 0. 2 3. JAN. 2001 d o k 31840

HARDENING OF CEMENTS, POLARIZED IN ELECTRIC FIELD

V.A. MATVIYENKO, N.M. ZAITCHENKO, Donbass State Academy of Civil Engineering and Architecture, Makeyevka, Ukraine

ABSTRACT The high-electric polarization of cement in the systems "solid-gas" and "solid-liquid" increases its hydrate activity as a result of surface and volume charging. Intensification of the condensed and crystallized stage of structure formation and increase of strength, modifying of microstructure of the hydration products, rebuilding of the cement paste's pore space are the peculiarities of the hardening processes of polarized cements.

Key-words: activation, hardening, heat evolution, strength development, structure

INTRODUCTION

Active centres in the cement structure play an important role in its hydration capacity. Electric polarization of cement in the system "solid - gas" is one of the ways of creating and exciting these active centres, which results in volume charging of dispersed particles. High electric polarization of cement pastes (systems "solid - liquid") thanks to low-voltage electric field doesn't cause volume charging in the conducting dispersed phase, but exciting of the surface of active centres according to electroadsorbtive mechanism and polarization of the double electric layer. Indicated phenomenons reduce the chemical bonds in cement, strengthen interphase and interparticle interactions during the hydration. Stimulation of hardening processes results in the creation of new non-equilibrium conditions in the system, which intencificate an increase of strength. So, electric polarization of cement systems allows to improve the physical-mechanical properties of the cement paste as a result of both increase of cement's degree of hydration (increase of concentration of active centres and speed of interphase diffusive processes), and modification of its structure (strengthening of interparticle interactions during the polarization of double electrical layer). Power consumptions for realization of polarization of cements are minimum, because density of electric current is limited for elimination of heat effects.

METHODS AND EQUIPMENT

Alumina, portland cements, cement pastes and concrete mixes have been examined by polarization. Electrodes from the constant current-source (5-25 kV) were placed in such a way that one of them had the contact with processing material, another (with opposite polarity) was isolated with high-resistance insulation for limiting of current density (less than 0.1 A/m^2). Duration of the exposition in electric field for the initial cements was 0.5-2 min and 2-30 min for the cement pastes. The hardening processes of cements were examined with the help of the methods heat of hydration, elastic properties of cement paste and plastometry. The hydration products were identificated by Infra Red Spectroscopy (IRS), DTA, X-ray examinations, electronic microscopy. Differential porosity of the cement stone was determined by a hydrodynamic method.

RESULTS AND DISCUSSION

It was established, that polarization of cements in the system "solid - gas" must be provided at intensity of electric field $(3\text{-}5)*10^5$ V/m during 2-3 min. Besides, portland cement must have contact with negative polarity electrode, but alumina cement with positive one. That is because of the different basicity of the minerals in the above-mentioned cements. As for the systems "solid - liquid" (e.g. cement pastes, building motars and concrete mixes) it is necessary to take into account the possibility of polarity change of the integrated charge of dispersed particles surface on the opposite one during hydration as a result of hydrate products

formation or adsorbtion of surface-active substances from dispersed environment also. Thus, while concrete mixes based on portland cement have an integrated negative charge prior to the setting at the given period of time this requires submission of the negative potential from an external source of high voltage on the contact electrode. When the setting has begun it is necessary to exchange the poles of electrodes in connection with the formation of highly dispersed hydrate of calcium oxide and calcium aluminate with the positive sign of the surface charge. Besides, concrete mixes on portland cement with additives of calcium or sodium nitrates, as well as containing lignosulphanates should be activated in the electric field of positive polarity. Cements preserve activated condition for a long-time period of curing after electroworking. It is described by the dependence of kinetics of heat evolution during hydration of polarized cement (Fig 1).

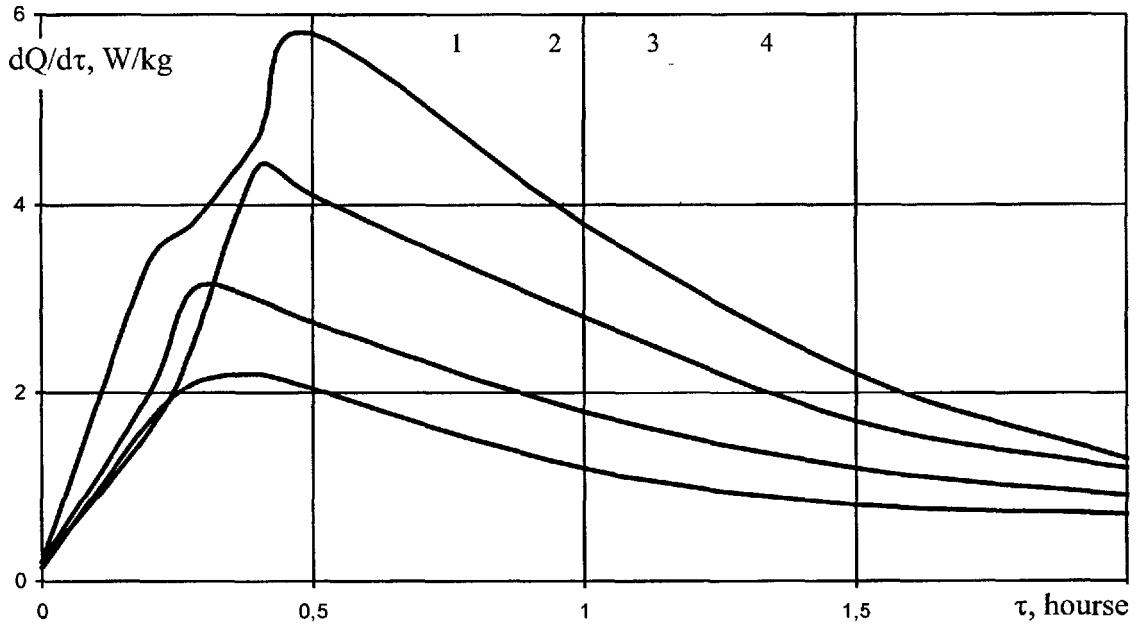

Figure 1 Kinetics of heat evolution during hydration of portland cement, activated in electric field of negative polarity.
1 - control cement; 2, 3, 4 - electric activation with voltage 3, 8 and 12 kV.

Intensive development of condensed and crystallized structure and growth of durability is explained by the acceleration of cement hydration on the early stages of hardening (Fig 2). By using a set of methods (X-ray diffraction analysis, IR spectroscopy and differential thermal analysis) to investigate the polarization-activated specimens, we determined high degrees of conversion of alite and polymerization of calcium silicate hydrates modified by sulfate ions and the content and stability of ettringite. We also noted an increase of the content of water belonging to hydrous aluminate components removable in the range 140-180 ^{0}C.

The polarization effectiveness is affected by electric-potential parameters and the structure of the electric double layer of the concentrated disperse system, which depends on many factors, namely the mineralogical and chemical composition of the binder, its particle-size distribution, the presence of additives, the solid-phase concentration, the temperature and hardening time of the system, etc. Electric voltage and current density are the main parameters of electroworking during the polarization of the cement-water systems (Fig 3).

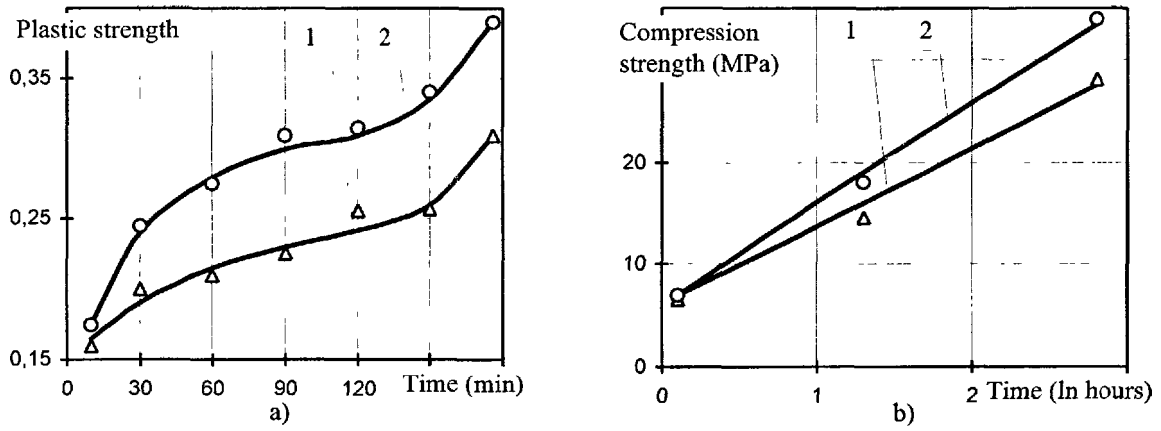

Figure 2 Increase of plastic strength t=20°C (a) and compression strength (b) during the hardening (t=85°C)of control (1) and polarized (2) cements.

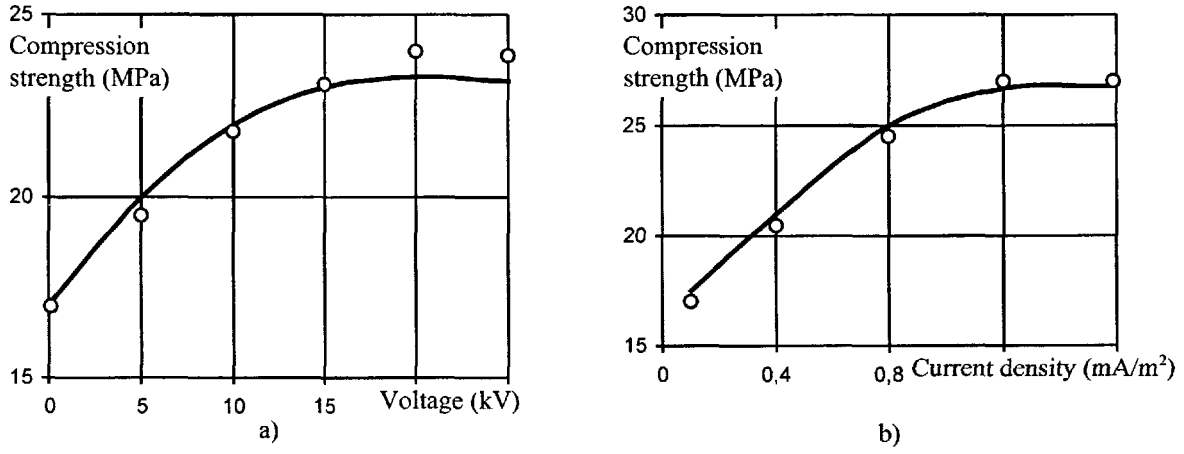

Figure 3 Dependence of concrete strength from the size of voltage (a) and current dencity (b)
during polarization of fine-grained concrete mix (at the age of 28).

An analysis of the relations σ=f(φpol) (a) and σ=f(Ipol/S) (b) shows that with increasing polarization potential and current dencity the strength of concrete increases. These relations are nonlinear, and in the high-potential range 20...25 kV (current density - 1.2...1.6 mA/m^2) they are flattening out. Investigations of structural characteristics of the cement paste and concretes on the base of polarized cements and cement-water systems indicate their common differences from control (non-activated) series. Their principal peculiarities are as follows:
- increase of the cement degree hydration by 15...30%;
- formation of small-crystalline structure of ettringite and portlandite;
- reduction of common porosity by 35...40% and redistribution of differential porosity: reduction of the quantity of pores with radius more than 10^3 nm and increase of the quantity of pores with radius less than 10^2 nm.

For the practical using of electric polarization different technological solutions have been developed. The developed ways of electrical processing of concrete mixes have comparable parameters of durability and energy costs (Table 1).

Table1 Technical characteristics of the activation posts of concrete mixes

Methods of electric activation	Technical characteristics of activation devices				
	electrical voltage, kV	duration of activation, min	specific energy costs, whr/m^3	relative increase of concrete strength,%	increase of strength on the unit of energy costs, %/whr
1.On the stage of concrete mix making	2.5...3	2...3	20...40	20...25	1...0.5
2.Before vibration seal of concrete mix in the curing bunker	15...20	2...3	50	20...50	0.4...1
3.Together with vibration seal	3...7	2...5	1.5...2	20...40	10...20
4.Curing products before heat treatment	15...20	15...120	150...200	15...25	0.1...0.2

CONCLUSION

As a result of modifying the cement paste microstructure by electrical polarization, mechanical (compression and tensile strength) and physical (frost resistance, deformations at drying shrinkage) properties improve. The specific power consumptions for the electroworking of cement or concrete mix do not exceed 50 whr/m^3 of concrete. Note that the polarity of external field must coinside with the sign of integral charge of solid phase surface and its voltage be within the limits of 15-20 kV and current density comes to 0.8-1.2 mA/m^2. The advantages of electric activation in concrete technology consist in hardening rate increase, strength increase, as well as in thermal treatment period reduction (1-5 hours) or cement saving (15-20%).

REFERENCES

Babushkin, V.I., Matviyenko, V.A. "Hydration of cement, activated by high-voltage current" [in Russion]. Izvestiya VYZov. Stroitelstvo, No.2, 1993, pp. 47-50.

Volkenshteyn, F.F. "Electronical processes on the surface of semiconductors by chemosorbtion" [in Russion], Moscow, Nauka, 1987, 431 pp.

Dukhin, S.S., Shilov, V.N. "Dielectric phenomena and double layer in dispersed systems and polyelectrolytes" [in Russion], Kiev, Naukova dumka, 1972, 206 pp.

Matviyenko, V.A., Veshnevskaya, V.G. "Electroimpulsive treatment of freshly-moulded units" [in Russion]/ Stroitelnie materialy i konstruktsii, No.3-4, 1992, pp.27-28.

Matviyenko, V.A., Gubar, V.N., Chereshnya, O.F., "Electric polarization in the technology of concrete [in Russion], New technological decisions for the building industry of Donbass, Kiev, 1989, pp.32-37.

Matviyenko, V.A., Sychev M.M. "Polarization activation of cement hardening", Journal of Applied Chemistry of the USSR, Vol.61, No 9, 1989, pp.1830-1835.

Sychev, M.M. "Nature of active centres and guiding of elementary acts of hydration [in Russion]/ Tsement, No 5, 6-10 (1990).

Timashev, V.V. Influence of physical structure of the cement stone on its durability[in Russion]/ Tsement, No.2, 6-8 (1978).

2ii077
8 pp
Kfn o. 2 5. JAN. 2001 d o k 31841

ADVANCED MODIFICATION TECHNOLOGIES OF THE PORTLAND CEMENT BASED BINDERS FOR DIFFERENT HIGH PERFORMANCE APPLICATIONS

Vladimir RONIN, Jan-Erik JONASSON and Hans HEDLUND, Luleå University of Technology, Sweden

ABSTRACT Portland cement-based binders with high performance properties regarding low clinker content, improved environmental parameters of production cycle, and higher durability can be produced with use of recently developed technology of Energetically Modification of Cement (EMC). Experimental results concerning EMC-cements containing up to 50% of quartz microfiller and application of the maturity concept for some EMC-concretes are presented.

KEY WORDS Degree of hydration, heat evolution, pozzolana, strength development

INTRODUCTION AND GENERAL ASPECTS

Solid-to-solid phase mechanical interactions of different levels of intensity in general terms gives significant influence on the interacted surfaces from the viewpoint of structural transformations and modification of surface properties known as mechano-chemical modification or activation, which plays an important role in a lot of technological processes. Milling equipments of different type should be considered as effective means for realisation of such processes, due to the wide range of mechanical force field parameters that could be created.

According to the latest experimental and theoretical data the mechanical (mechano-chemical) activation takes place when i) the particle size is lower than the size related to the though-brittle transition zone, and ii) the activated stress should exceed the yield stress of the powdery material, which depends on the dimension of the particle (Boldyrev et al, 1994 and Schönert, 1982 and 1990)The consequent significant increase in chemical reactivity (enthalpy gain) under mechanical action mainly associated with structural defects, irregularities and disturbances of the material, and with release of energy with following plastic alteration or degradation of the body. The main physical principals of the point stress generation, plastic deformation, temperature history in the areas of impact and friction of the solid phase, and movement of dislocations are discussed by Heinicke(1984)

Recently, it was discovered (Ronin et al, 1994 and 1995 and Jonasson et al, 1996) that considerable impact on the degree of activation of the Portland cement-type minerals can be achieved by a combined usage of cement grains and a superfine micro-filler, e.g. silica fume, in powdery form in a vibration mill with optimized mode of operation. Super high specific surface of this type of micro-filler (about 20 m^2/g, BET) and its much lower density in comparison with OPC provides a complete cover, in adsorbed form, of the surface of the commercially produced cements (specific surface about 1.8 m^2/g, BET), when introduced in the amount from 3 to 5% by weight of the cement. In this case the micro-filler starts to act as an additional component between the Portland cement particles and the grinding media of the mill, which transforms the flux of the kinetic energy of the vibrating grinding media preventing intensive grinding of the cement particles and creating surface zones with high concentration of micro-defects, see **Fig 1.**

An important feature of this stage of the process is a creation of the stress-strain conditions for partial disintegration of silica fume particles from agglomerated form with average size of 100 to 1000 nm to sub-micro level with size of 25 to 75 nm, which have been conformed by electron microscopy observations, see **Fig 2**, and corresponds to experimental results discussed by Lajnef

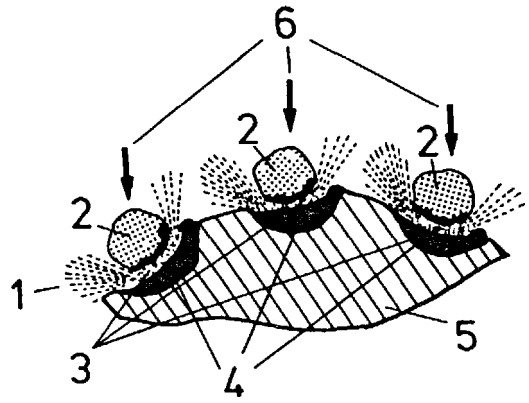

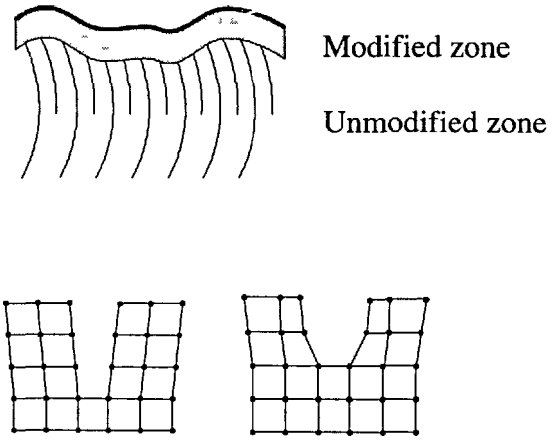

Figure 1 a) Hypothetical picture of the high intensive interaction of silica fume grains and Portland cement particles in the vibration mill. 1=exo-emission;2=initial silica fume grain; 3=newly developed sub-micro silica particles; 4=zones with distorted structure; 5=cement particles; 6=direction of impulses from the vibration grinding media.

b) Scheme of the surface of modified Portland cement particles deformation of mineral crystal lattice due to modification.

et al (1993). This means that the surface of cement particles, subjected to extremely intensive treatment (impact, shear, attrition) from vibrating media through sub-micro-metric silica particles, will also unclude some embedments of these particles in the surface layers of the Portland cement grains. As a result a significant increase of the surface energy of Portland cement minerals takes place, see **Fig 3**, and the obtained binder was called Energetically Modified Cement (EMC). The EMC-cements are characterised by increased rate of hardening, reduced porosity, increased rate of pozzolanic reaction and hydration of alite-component of cement, see **Figs 4, 5 and 6**, correspondingly.

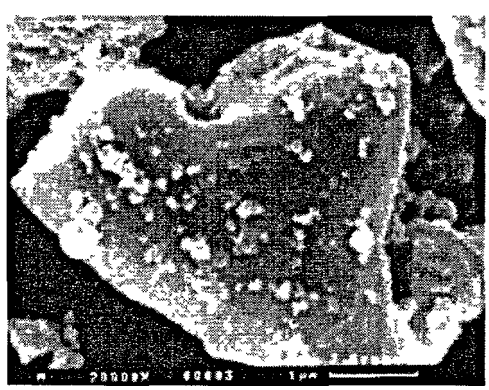

Figure 2 SEM micrograph of the surface of modified Portland cement particle with attached sub-micro silica grains.

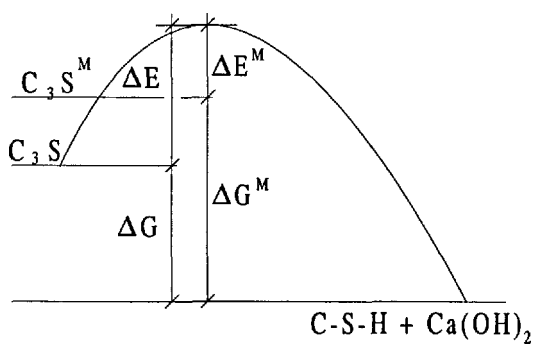

Figure 3 Surface energy (enthalphy) gain for the alite (C_3S) due to modification.

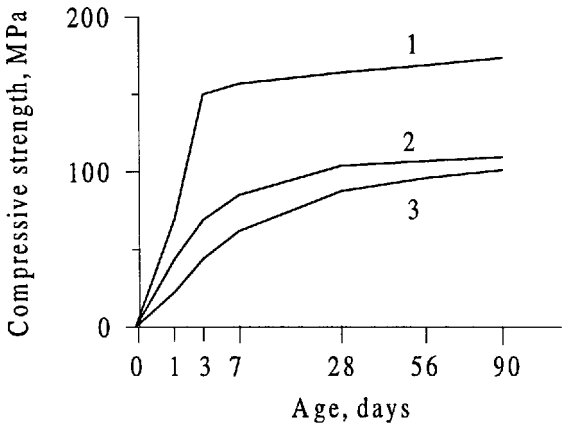

Figure 4

Strength development of cement paste with w/B = 0.20 containing 1% by weight of superplasticizer Mighty 100 and curing at 20 °C. 1 = EMC(Anl) incl. 5 % silica fume, 2 = Anl + 5 % silica fume, and 3 = Anl. "Anl" stands for a moderate heat liberating, sulphate resisting Portland cement.

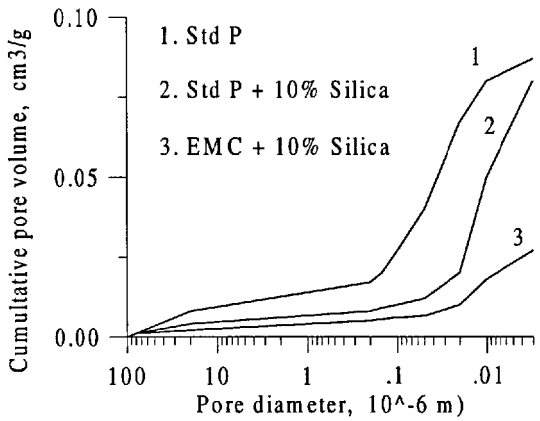

Figure 5

Pore size distribution measured by mercury intrusion in cement paste with w/B = 0.2 cured at room temperature in water for 28 days.

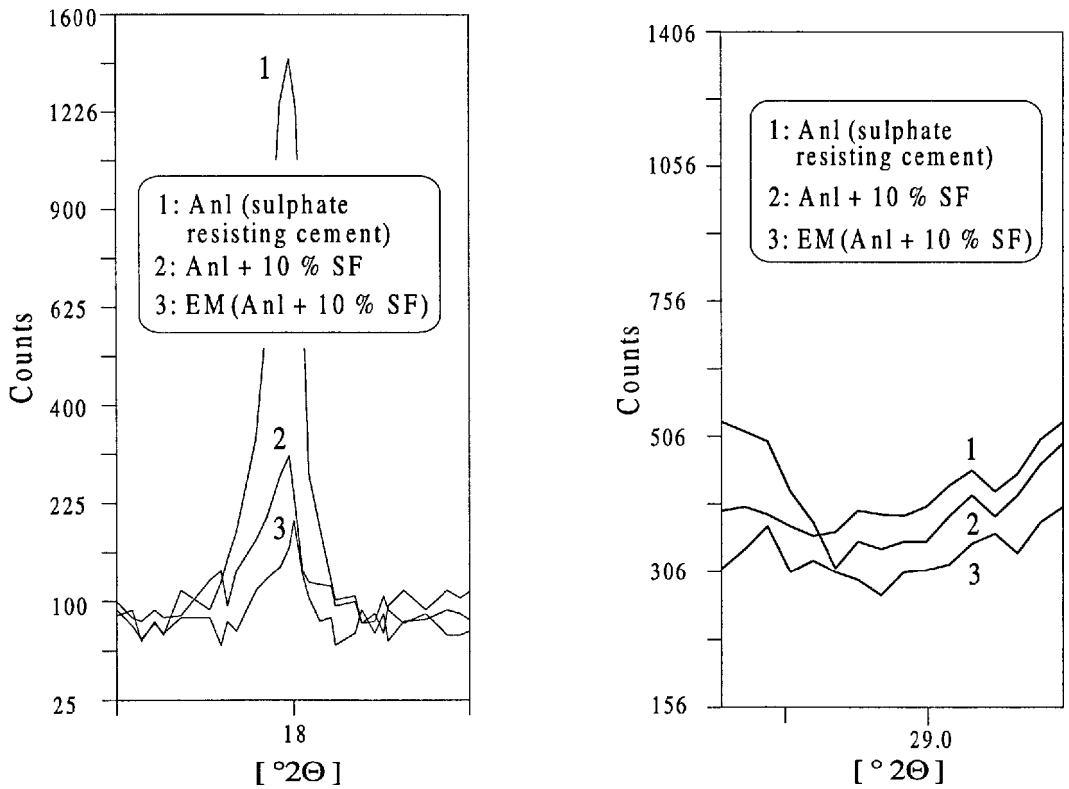

a) $Ca(OH)_2$ peaks b) C_3S peaks

Figure 6 X-ray diffractograms for cement paste with w/B=0.20 after 2 years of hardening at 20 °C.

EMC-BINDERS COMPRISING MICRO-FILLERS

Additional advantage of the EMC-cements is a significantly improved binding capacity (ability to produce a concretes of equal strength with reduced binder content) (Jonasson and Ronin, 1995a and 1995b). This gives a possibility to produce EMC-binders with low and super-low clinker content. The strength development has been measured for EN-mortars with standardized mixing proportions as well as for concretes produced with different amount of OPC and quartz microfiller. The microfiller had a SiO_2 content of 86%. The fraction before modification was 0 - 2 mm, and the fineness after modification was about 130 m^2/kg).

Tables 1, 2 and 3 represent clinker composition and strength development for the EN-mortar and concretes with binder (including modified microfiller) contents from 270 to 350 kg/m^3.

Table 1 Clinker composition of the binder types used.

Type of binder	Amount of microfiller, %	Clinker minerals, %			
		C_3S	C_2S	C_3A	C_4AF
OPC	0	59.0	13.0	8.0	7.0
EMC-20	20	47.2	10.4	6.4	5.6
EMC-30	30	41.3	9.1	5.6	4.9
ENC-50	50	29.5	6.5	4.0	3.5

Table 2 Compressive strength development of EN-mortars (max. aggregate size = 5 mm) with EMC-binders.

Type of binder composition	Compressive strength, MPa for the ages					Strength classification of the binder
	1 d	2 d	3 d	7 d	28 d	
OPC	16.5	21.6	36.1	43.1	54.2	CEM I 52.5
EMC-20	16.0	20.7	32.3	39.8	53.0	CEM 52.5
EMC-30	13.6	16.3	29.9	37.6	43.7	CEM 42.5
EMC-50	10.1	12.4	24.8	28.8	35.5	CEM 32.5R

Table 3 Compressive strength development of the concretes (max. aggregate size = 32 mm) with the binder EMC-50 cured at 20 °C. All mixtures had a slump of about 50 mm.

Concrete No.	Binder-to-Cement content ratio $(kg/m^3)/(kg/m^3)$	w_o/B	Compressive strength, MPa for the ages					Class of concrete
			1 d	2 d	3 d	7 d	28 d	
1	270/270 (ref. OPC)	0.58	9.9	14.8	15.8	21.1	28.6	K25
2	270/135	0.58	9.8	14.3	16.6	20.8	28.5	K25
3	300/150	0.56	10.4	14.9	17.6	22.4	33.2	K30
4	320/160	0.50	13.1	18.6	21.0	26.8	38.1	K35
5	350/175	0.47	13.9	19.4	22.3	30.1	42.8	K40

The gradual reduction of the clinker content and increase of the amount of microfiller (see **Table 1**) have very positive influence on i) sulphate resistance of the binder due to reduction of the C_3A content, ii) heat liberation and, most likely, the thermocrack generation mainly due to reduced amounts of C_3S and C_3A, iii) increased corrosion resistance of the reinforcement due to lower alkali content, and iv) environmental conditions of Portland cement production due to significant reduction of CO_2, SO_2 and NO_x emmisions.

Analysis of strength parameters of the EN-mortars containing different amounts of microfiller and the concretes with the binder EMC-50 (see **Tables 2 and 3**) clearly demonstrates the strong influence of the mechanochemical modification of blended binders on the strength development and ultimate 28-days strength. Especially, it is pronounced for the concretes (**Table 3**), where the substitution of half the clinker with microfiller has practically no significant influence on the strength gain for the whole range of studied cement contents. According to ENV-197 the EMC-binders containing microfiller are equivalent to the strength level from CEM 52.5 to CEM 32.5R depending on microfiller content (**Table 2**).

APPLICATION OF THE MATURITY CONCEPT FOR EMC-CONCRETES

Basic equations

The expending demands of the modern building practice require complex and flexible concrete technologies which can be adjusted and used for such purposes like assessing of stripping times and loading capacities at varying climate conditions and also comprehensive computer-based material simulations. The main purpose of the present investigation is to study whether the standard procedure to do calculations of temperature, maturity and strength development (Jonasson, 1994, Ekerfors, 1995 and Hedlund, 1996) can be applied to the EMC concretes. The concept used is based on an intrinsic parameter called equivalent time of hardening, t_{equ}, defined by

$$t_{equ} = \int \beta_T \, dt \qquad [1]$$

$$\text{with} \quad \beta_T = \begin{cases} \exp(\theta \cdot (1/293 - 1/(T+273)) & \text{when } T > -10\,^{\circ}\text{C} \\ 0 & \text{when } T \le -10\,^{\circ}\text{C} \end{cases} \qquad [2]$$

$$\text{and} \quad \theta = \theta_{ref} \cdot \left(\frac{30}{T+10}\right)^{\kappa_3} \quad [\text{K}] \qquad [3]$$

All notations and equation parameters in this chapter are in detail described and explained by Jonasson (1994), Ekerfors (1995) and Hedlund (1996). The compressive strength at a certain time is described by a fraction expressed in per mille of the 28 days strength by

$$f_{cc} = \frac{\eta}{1000} \cdot f_{28} \qquad \text{for } 4h \le t_{equ} \le 672h \qquad [4]$$

$$\text{and} \quad f_{cc} = 0 \text{ for } t_{equ} < 4h \qquad \text{and} \qquad f_{cc} = f_{28} \text{ for } t_{equ} > 672h = 28d\,. \qquad [5]$$

The strength development of **Eq 4** is given as a series of linear splines between a prechosen set of equivalent times of hardening according to

$$t_{equ} = [4h \quad 6h \quad 8h \quad 12h \quad 18h \quad 24h \quad 72h \quad 168h \quad 672h] \qquad [6]$$

$$\eta = [0 \quad \eta_2 \quad \eta_3 \quad \eta_4 \quad \eta_5 \quad \eta_6 \quad \eta_7 \quad \eta_8 \quad 1000] \qquad [7]$$

The use of **Eq 7** means that seven individual numbers per mixture, η_2 - η_8, are needed.

The heat of hydration is described in the following way

$$W = W_u \cdot \alpha^* \cdot B \qquad [J/m^3] \qquad [8]$$

$$\text{with} \quad \alpha^* = \exp\left(-\lambda_1 \cdot \left[\ln(1 + t_{equ} / t_1)\right]^{-\kappa_1}\right) \qquad [9]$$

The last parameter to be known for a specific mixture is the heat capacity per volume for the concrete mix, $\rho \cdot c$, which here is set to

$$\rho \cdot c = 2.35 \cdot 10^6 \quad [J/m^3] \qquad [10]$$

The use of exactly **Eqs 1 - 10** is necessary in calculations, as the applications must be done in the same way as the underlying evaluation.

Examined EMC concretes

Five recipes with EMC binders have been studied with respect to **Eqs 1 - 10**. The main mix parameters and the 28 days compressive strength are given in **Table 4**. The remaining parameters in accordance with **Eqs 3 - 9** are given in **Table 5.**

Table 4 Mix parameters and 28 days strength for studied EMC concretes. Maximum aggregate size is 16 mm.

Designation	Type of binder	w/B	B [kg/m^3]	f_{28} [MPa]
EMC21	EMC510*	0.21	528	166
EMC39	EMC510*	0.39	331	108
EMC58	EMC500**	0.58	303	55
EMC65	EMC500**	0.65	234	51
EMC73	EMC500**	0.73	180	42

Notes:
*) EMC510=94%OPC+ 5% SF+ 1% superpl.
**) EMC500=95%OPC+ 5% SF

Table 5 Parameters to the use of **Eqs 3-9** for the recipes presented in **Table 4**.

Denotation	**Eq 3**		**Eq 7**							**Eqs 8 and 9**			
	θ_{ref} [K]	κ_3	η_2	η_3	η_4	η_5	η_6	η_7	η_8	W_u [kJ/kg]	λ_1	t_1 [h]	κ_1
EMC21	5920	0.769	228	285	361	440	498	711	828	218	1.90	4.84	1.95
EMC39	3750	0.535	93	148	241	335	414	625	747	324	0.7	9.7	2.1
EMC58	4580	0.783	0	69	161	264	367	594	734	345	0.68	10.0	2.14
EMC65	4320	0.829	19	74	194	309	404	622	777	365	1.96	4.92	2.53
EMC73	4790	0.636	17	68	182	278	347	572	772	365	2.41	5.36	2.59

The description of the properties according to the parameters given here in comparison with the underlying test results are given in **Fig 7** for concrete mixes EMC21, EMC39 and EMC73, respectively. The scatter of test data and the agreement in accordance with the use of **Eqs 1 - 10** for EMC concretes are of the same nature as for the use of non-modified cement (Jonasson, 1994, Ekerfors, 1995 and Hedlund, 1996). One consequence is that calculation of the temperature field and assessments of strengths in hardening concrete for different applications can also for EMC concretes be made by the use of existing computer programs like for instance the Hett2DL program (Jonasson and Stelmarczyk, 1997).

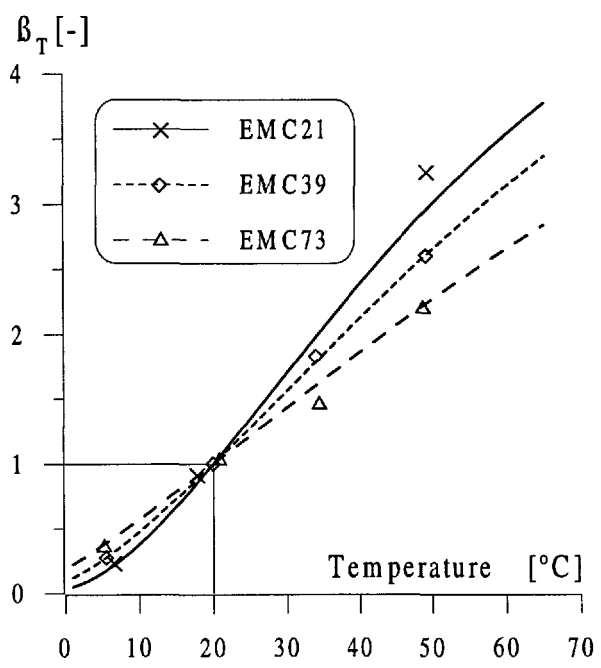

a) Temperature sensitivity (**Eq 2**)

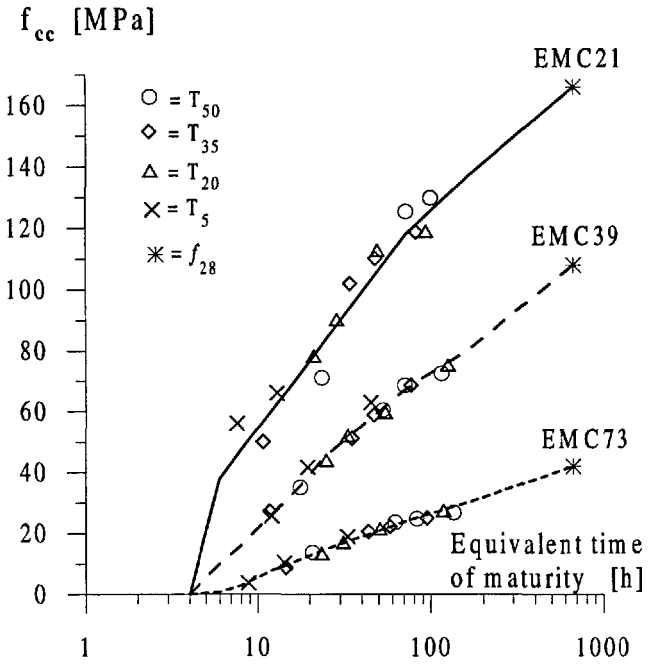

b) Strength development (**Eq 4**)

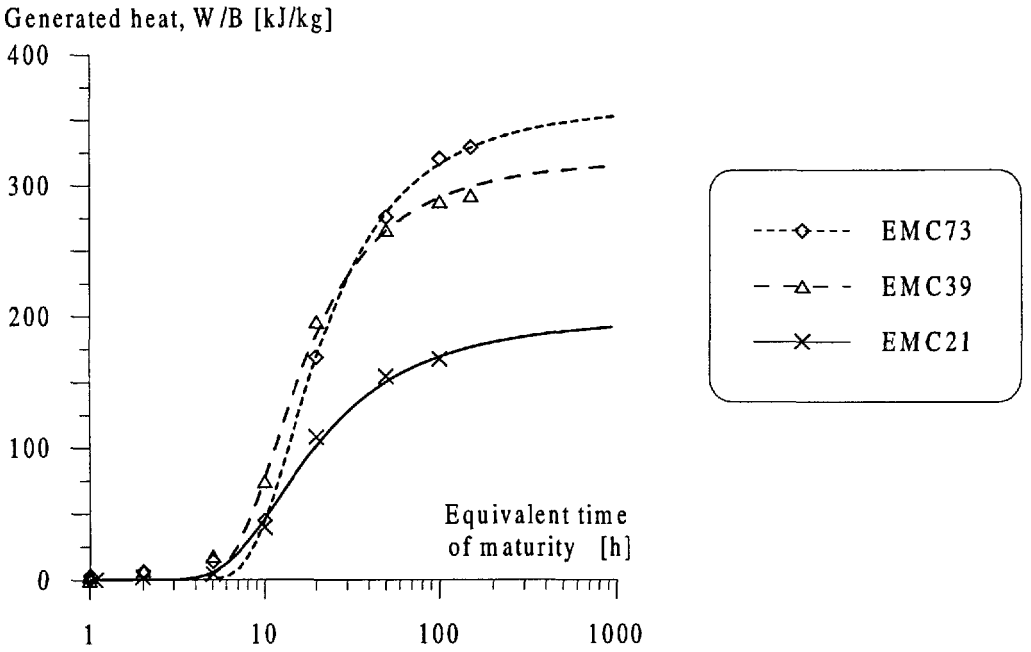

c) Liberated heat of hydration (**Eq 8**)

Figure 7 Comparison between evaluated properties (solid, long-dashed and short-dashed lines) and measured data (individual symbols) for three EMC concretes. Evaluated numbers are presented in **Tables 4 and 5**, and the basic relations are in accordance with **Eqs 1 - 10**. The indices (i for different T_i) in subfigure b) means curing temperature at level 5, 20, 35 and 50 °C, respectively.

CONCLUSIONS

- According to ENV-197 the EMC binders correspond to strength levels from CEM 52.5 to CEM 32.5 depending on the microfiller content. This shows that the use of a vibration mill as a EMC-processor is an effective way to produce EMC-cements containing quartz as a microfiller (SiO_2 content about 86%) with substitution ratio of the Portland clinker up to 50 %.
- The use of an ordinary maturity concept to describe the hardening process, the liberated hydration heat and the strength development has been shown to work equally well for EMC concretes as for the use of non-modified cements. This means that existing computer programs can be used in analysing early age behaviour even for EMC concretes.

REFERENCES

Boldyrev, V., Pavlov, S. and Goldberg, E., "Interrelation Between Fine Grinding and Mechanical Activation", Proceedings of the 8th European Symposium on Communition, May 17 - 19 1994, Stockholm, Vol. I, pp. 191-196.

Ekerfors, K., "Maturity Development in Young Concrete - Temperature Sensitivity, Strength and Heat Development", Luleå University of Technology, Division of Structural Engineering, Licentiate Thesis 1995:34L, (in Swedish).

Hedlund, H., "Stresses in High Performance Concrete due to Temperature and Moisture variations at Early Ages, Luleå University of Technology, Division of structural Engineering. Licentiate Thesis 1996:38L.

Heinicke, G., " Tribochemistry", Akademie Verlag, Berlin, 1984.

Jonasson, J-E., "Modelling of Temperature, Moisture and Stresses in Young Concrete, Luleå University of Technology, Division of Structural Engineering, Doctoral Thesis 1994:153D.

Jonasson, J-E. and Ronin, V., "Improved Concrete Properties with Energetically Modified Cement (EMC)", Journal "Betong", nr 2, pp. 8-10, May, 1995a, (in Swedish).

Jonasson, J-E. and Ronin, V., "Energetically Modified Cement (EMC) - a New Binder for thr Future", Journal "Bygga Framtid", 6:e upplagan, Väg - och Vatten, Luleå University of Technology, 1995b, Luleå, (in Swedish).

Jonasson, J-E., Ronin, V. and Hedlund, H., "High Strength Concretes with Energetically Modified Cement and Modelling of Shrinkage Caused by Self-Desiccation", Proceedings of the International Symposium on Utilisation of High-Strength/High-Performance Concrete, 29-31 May, 1996, Paris, France, pp.245-254.

Jonasson, J-E. and Stelmarczyk, M., Hett2DL and ConStre, JEJMS Concrete AB, Stockholm (Manual in progress 1997).

Lajnef, M.,Chaignon. J. et al., "Silica Fume Characterisation", Proceedings of the 3rd International Conference on High Strength Concrete, June, 1993, Norway, pp. 769-776.

Ronin, V. et al., "Method for Producing Cement", International Patent Application PCT/SE 94/00383, April 29, 1994.

Ronin, V. and Jonasson, J-E., "Energetically Modified Cement (EMC) for High Performance Concrete in Winter Concreting", Proceedings of the International Conference "Concrete Under Severe Conditions - Environment and Loading", CONSEC'95, August 1995, Sapporo, Japan.

Schönert, K., "About the Particle Breakage and the Possibilities and Limits for Improving Size-Reduction Processes", Proceedings of International Symposium on Powder Technology, Society of Powder Technology, 1982, Kyoto, Japan, pp. 331 - 345.

Schönert, K., "Physical and Technical Aspects of Very and Micro Fine Grinding", Proceedings of the Second World Congress Particle Technology, Society of Powder Technology, 1990, Kyoto, Japan, pp. 557 - 571.

2ii078
8 pp

Kn o. 2 ɔ. JAN. 2001 d o k 31842

HYDRATION OF PORTLAND CEMENT: THE EFFECTS OF CURING CONDITIONS

Dale P. BENTZ, Kenneth A. SNYDER and Paul E. STUTZMAN, National Institute of Standards and Technology, Gaithersburg, MD 20899-0001 USA

ABSTRACT In this paper, experimental and computer modelling studies of the effects of curing on hydration are presented. Degree of hydration has been quantified for saturated, sealed, and 90% relative humidity ambient environments, all at 25 °C. For both the saturated and the sealed curing conditions, experimental results for degree of hydration and scanning electron microscopy images are compared to those generated using the NIST cement paste microstructural model. Implications for the field curing of concrete are also addressed.

Key-words: Curing, Hydration, Modelling, Scanning Electron Microscopy, Simulation.

INTRODUCTION

Proper curing of concrete is paramount for obtaining optimum performance from a given set of mixture proportions. For high-performance concretes, curing becomes even more important, due to the typically lower water-to-cement (w/c) ratios and the increased propensity for early age cracking due to thermal and self-desiccation stresses (Henrichsen and Laugesen, 1995). Besides the water which is removed due to exposure to an ambient environment, additional empty capillary porosity is created within the cement paste component of the concrete due to the chemical shrinkage that accompanies the cement hydration reactions, quantified many years ago by Powers (Powers, 1935), but also the subject of much recent research (Geiker, 1983, Hua *et al.*, 1995, Tazawa *et al.*, 1995, and Justnes *et al.*, 1996).

The creation of empty capillary pore space has two major effects on the evolving cement paste system. First, the resultant capillary pressures induce shrinkage stresses within the cement paste microstructure, causing a measurable external physical shrinkage (Hua *et al.*, 1995 and Justnes *et al.*, 1996). The magnitude of these stresses (at relative humidities where some of the capillary pore space is still filled with water) will be influenced by the relative humidity (RH), in the following manner. The Kelvin-Laplace equation can be used to relate the relative humidity to the capillary condensation process:

$$\ln(\frac{\mathbf{RH}}{\mathbf{100}}) = -\frac{K\gamma V_m}{RT} \quad [1]$$

where γ is surface tension, V_m is the molar volume of water, R is the universal gas constant (8.314 J/(mol· K)), T is absolute temperature, and K is the average curvature of the surface of the condensed water (equivalent to $2/r$ for a spherical droplet where r is the radius of the droplet/pore). Thus, at a given RH, water will condense in all pores of curvature greater than or equal to K (pore radius less than or equal to r). The induced capillary pressure, $\sigma_{\text{capillary}}$, is then given:

$$\sigma_{\text{capillary}} = K\gamma = -\frac{\ln(\frac{\mathbf{RH}}{\mathbf{100}})RT}{V_m}. \quad [2]$$

According to Eq 2, the induced capillary pressure is directly proportional to ln(**RH**). The measured shrinkage should be a function of this capillary pressure and the moisture con-

tent (saturation) of the concrete (Mackenzie, 1950 and Bentz *et al.*, 1996). Indeed, field measurements have shown that both moisture content and measured concrete shrinkage are proportional to variations in ambient RH (Granger *et al.*, 1994). In the case of hydration under sealed conditions, the autogenous shrinkage stresses will be influenced by the internal RH reduction due to the chemical shrinkage. As first quantified in 1940 (Gause and Tucker, 1940), this RH reduction can be quite substantial, with RH values as low as 70% measured for low w/c (< 0.3) ratio cement paste and concrete systems (Mjornell, 1994 and Persson, 1996). According to Eq 2, the induced capillary pressures will be seven times greater in a system with an RH of 70% vs. one with an RH of 95%, which may be one reason why high-performance concretes are often more susceptible to early age cracking.

The second effect of the creation of empty capillary pores will be a change in the hydration kinetics for the cement paste (Powers, 1947 and Molina, 1992). Because cement hydration reactions generally proceed by a dissolution/precipitation mechanism, the empty pore space created due to drying or self-desiccation is no longer available to be filled with hydration products, so that the hydration will slow down and effectively terminate at a lower degree of hydration than that which could be achieved under saturated conditions. The remainder of this paper will focus on this latter effect, using a combination of experimental and computer modelling techniques to quantify the effects of curing conditions on the measured degree of hydration of a series of cement pastes.

EXPERIMENTAL PROCEDURES

Saturated and Sealed Specimens

Details for the two ASTM Type I portland cements used in this study, Cements 115 and 116 issued by the Cement and Concrete Reference Laboratory, can be found elsewhere (Bentz, 1997). In all cases, the cement and the necessary mixing water, w/c=0.3 or 0.4, were conditioned at 25 °C overnight and then mixed together by hand in a sealed plastic bag for two to three minutes. For hydration under saturated and sealed conditions, samples on the order of ten grams were stored in capped plastic vials at 25 °C until measuring the non-evaporable water content, typically after ages of 1, 3, 7, 14, 28, 56, and 90 days. For the saturated samples, approximately 1 mL of water was added on top of the cement paste to maintain saturation. Non-evaporable water was quantified as the weight loss between 105 °C and 950 °C, corrected for the loss on ignition for the dry cement powder. These values were converted to degrees of hydration based on measurements performed on fully hydrated specimens (w/c=3.0, continuously ground in a jar mill for 28 days), which yielded values of 0.226 and 0.235 g H_2O/g cement for Cements 115 and 116, respectively. For Cement 115, two samples, one saturated and one sealed hydration, were removed after 94 days curing and prepared for viewing in the scanning electron microscope (SEM).

Curing Under 90% RH

The companion controlled relative humidity experiments were performed using Cement 116. The paste samples were mixed in a sealed plastic bag for 5 minutes. The specimen holders consisted of two 1.6 mm-thick sheets of hydrophobic polytetrafluoroethylene (PTFE) cut to 127 mm $\times$152 mm. One of the sheets had been punched with twenty three 25 mm-diameter holes, and the two sheets were adhered together using a silicone sealant. The mixed cement paste was spread over the 25 mm holes, filling them to form discs of uniform thickness. The fresh specimens were then placed in a 25°C, 100% RH environment.

To assess the combined effects of RH and time on the hydration of cement paste, the specimens were stored at 100% RH for 6 and 12 hours, and 3 and 7 days before being placed into an environment of 25°C and 90% RH. Here, the specimens were maintained in an atmosphere free of CO_2, to avoid carbonation effects, achieved by using an overpressure of pure nitrogen. Prior to entering the 90% RH environment, the two sheets were pried apart, exposing both sides of the hardened specimens (the sheets for the 0.3 w/c pastes were pried apart after 24 hours, or sooner as required). Periodically, the degree of hydration was determined by measurement of the non-evaporable water content, as described above, from a sample consisting of two paste discs.

Computer Simulations

In addition to the experimental studies, computer simulations were performed using the NIST cement paste microstructural model (Bentz, 1997). For each of the two cements, initial 3-D cement particle images were created for w/c=0.3 and w/c=0.4, and then "computationally hydrated" under saturated and sealed conditions. In the case of sealed (self-desiccating) conditions, the computer model creates empty pore space as the hydration occurs to account directly for the chemical shrinkage. A previous calibration of model cycles to real time (Bentz, 1997) was then applied to create model degree of hydration vs. time curves to compare to the experimental counterparts. In addition, two-dimensional slices from the "fully hydrated" three-dimensional computer model microstructures were created to compare to the SEM images for the two curing conditions for Cement 115 with w/c=0.3.

RESULTS

Saturated and Sealed Specimens

Figure 1 shows a comparison of degree of hydration achieved under saturated and sealed conditions for the two cements studied, with w/c=0.3. In both cases, the sealed conditions are observed to reduce the achieved hydration, particularly at times exceeding 7 days (168 hours). At early times, the newly created empty porosity (from the chemical shrinkage) has only a minor effect on the hydration kinetics as a significant volume fraction of water-filled capillary pore space still exists. For a w/c=0.3 system, initially, about one half of the volume is filled with water. However, as more and more water is consumed by the hydration reactions, the fraction of empty pore space relative to that which is water-filled becomes significant, and a substantial reduction in the hydration rate is observed. The predicted results based on the NIST cement paste microstructural model are seen to closely follow the experimental values, particularly for Cement 115. Thus, it appears that the model is able to account successfully for the effects of self-dessication on hydration kinetics and may be useful as a predictive tool for anticipating the effects of different curing regimens on achievable hydration and physical properties, as the model has already been applied to predicting 7 and 28-day compressive strengths from 3-day values (Bentz, 1997).

It should also be noted that simulations performed for w/c=0.4 for the two cements have indicated much smaller differences in the hydration kinetics for saturated and sealed conditions. For Cement 115, the "final" achieved degrees of hydration after 5000 cycles of the hydration model were 0.88 and 0.83 for the saturated and sealed conditions, respectively. The corresponding values for Cement 116 were 0.90 and 0.85. In addition, the differences to be expected after 28 days of curing, for example, were less than for the w/c=0.3 systems (on the order of 0.01 for Cement 115 and 0.03 for Cement 116). Thus, the effects of sealed curing become more prominent at lower w/c (< 0.4) ratios.

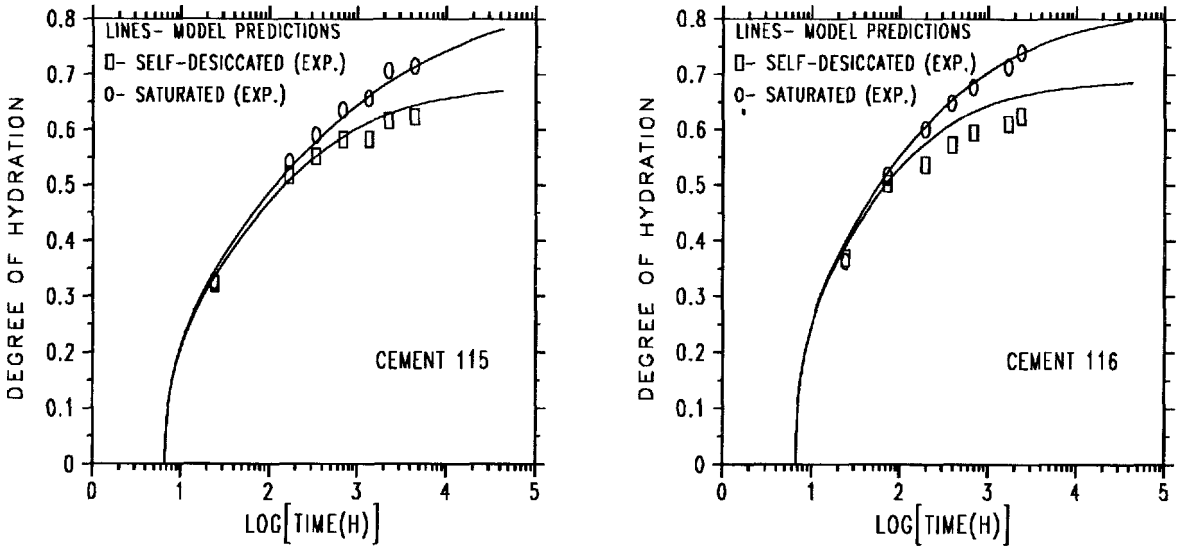

Figure 1: Comparison of saturated and sealed (self-dessicated) hydration for Cements 115 and 116 with w/c=0.3.

Microstructure

The model can be further validated against experiment by comparing SEM micrographs of real sample microstructures to two-dimensional images from the 3-D model. Figures 2 and 3 provide a comparison at similar scales for Cement 115. The two most distinguishing features between the sealed and saturated specimens are the amount and size of the unhydrated cement grains and the amount and size of the observable capillary pores. One can clearly observe that there are more and larger unhydrated cement grains in the sealed specimens (particularly in terms of the alite grains which are surrounded by a dense layer of calcium silcate hydrate gel), in agreement with their measured lower degrees of hydration. Based on quantitative SEM measurements of the unhydrated cement area fractions, after 94 days, the saturated sample has achieved a degree of hydration of 0.79 ± 0.03 while the sealed sample has only achieved a value of 0.66 ± 0.04, based on the averages from eleven fields of view (1024 pixels $\times$800 pixels, 0.25 μm/pixel) for each sample, and expressed with an uncertainty of one standard deviation. By constrast, the corresponding degrees of hydration for the two model systems shown are 0.80 and 0.69, respectively. In addition, due to the emptying of the capillary pores during chemical shrinkage, many relatively large pores remain in the sealed specimens. Once again, the effects observed in the real specimens are quite accurately duplicated by the model, as the real and model images exhibit many similar features.

Curing Under 90% RH

The results for the effect of the 90% RH environment on cement paste hydration are given in Fig 4. For the case of w/c=0.4, the 6 hour, 12 hour, and 3 day specimens show an effect due to hydration at 90% RH, while the 7 day specimen, over the first 28 days, does not appear to be affected by the change in environment. The data for the 0.3 w/c paste are similar, with the exception that the 3 day specimen also appears to be relatively unaffected by the change in environment.

These data, coupled with an understanding of the percolation of the capillary pore space, lead to a possible explanation for these effects. As the paste hydrates, the capillary porosity, and the characteristic capillary pore size, decrease. When the capillary porosity has been

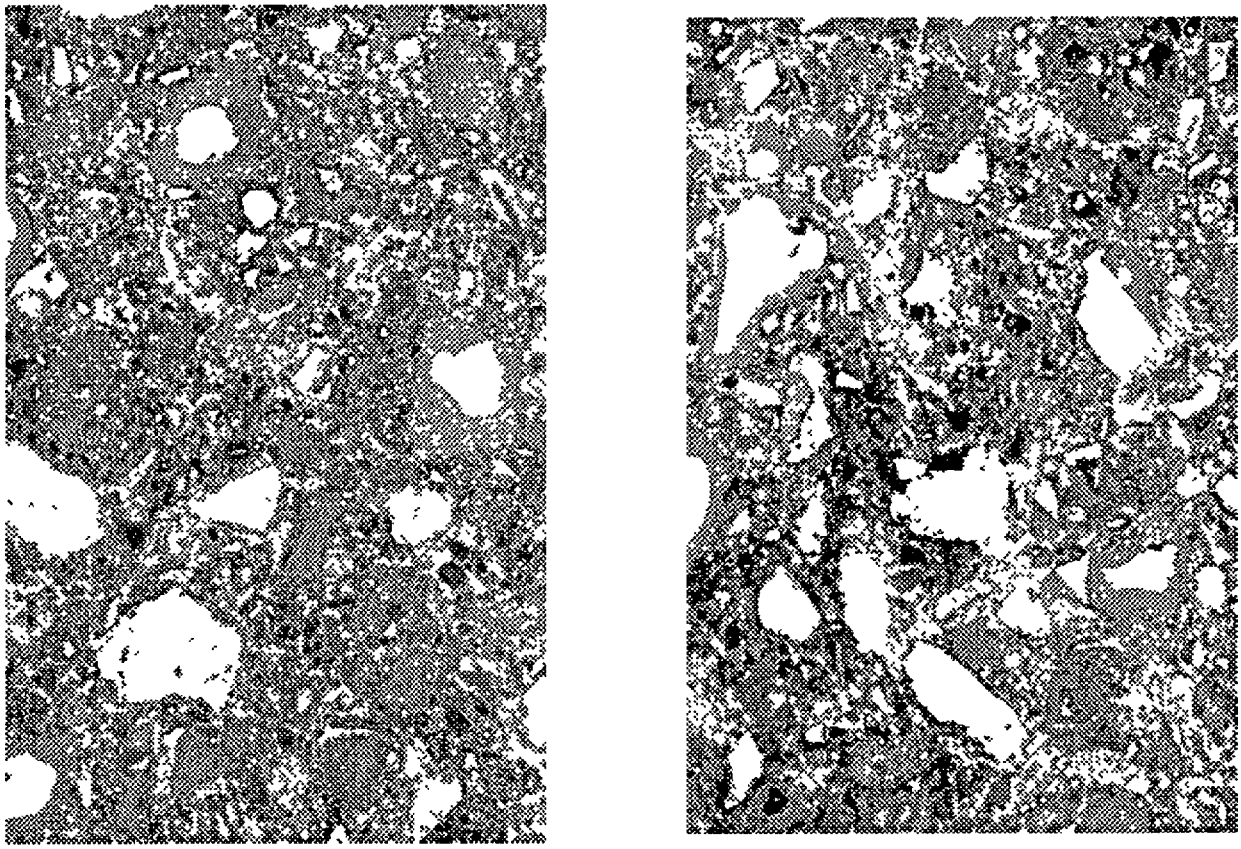

Figure 2: Comparison of real SEM images for saturated (left) and sealed (right) hydration for Cement 115 with w/c=0.3. Unhydrated cement is white, porosity is black, calcium hydroxide is light grey, and calcium silicate hydrate gel and other hydration products are dark grey. Areas imaged are approximately 128 μm $\times$190 μm.

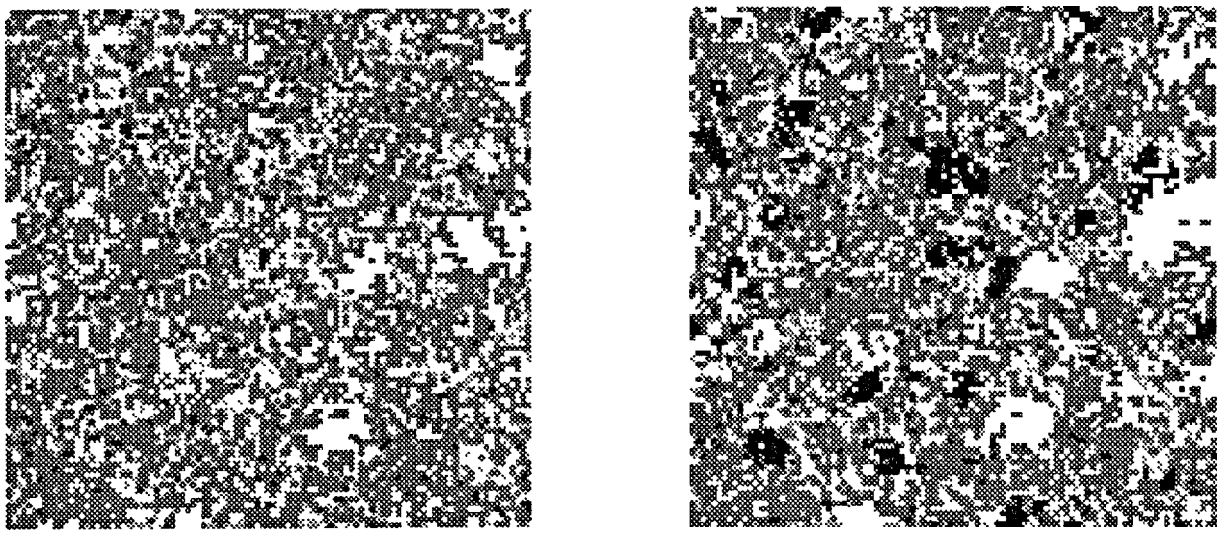

Figure 3: Comparison of model images for saturated (left) and sealed (right) hydration for Cement 115 with w/c=0.3. Greyscale assignments are the same as those given above for the real images. Areas represented by the images are 100 μm $\times$100 μm.

reduced to approximately 0.20, the capillary pore space is no longer interconnected throughout the paste (Powers *et al.*, 1959, and Bentz and Garboczi, 1991). When this occurs, vapor and moisture transport is restricted by the gel pore space, greatly reducing the transport coefficients. These gel pores, due to their small size (< 10 nm in diameter), will remain water-filled at RH values down to about 50% (Baroghel-Bouny, 1994). Any capillary pores connected to the exterior environment only via a path containing gel pores will also remain water-filled at RH > 50%. Thus, when the capillary pore space is no longer percolated, the moisture is, in effect, trapped inside the specimen, and if the specimen is placed in an environment at less than 100% RH, but greater than 50% RH, the specimen continues to hydrate. The estimated degrees of hydration needed to achieve a capillary porosity of 20% are 0.63 and 0.43 for the 0.4 and the 0.3 w/c pastes, respectively, as illustrated by the horizontal dotted lines in Fig 4.

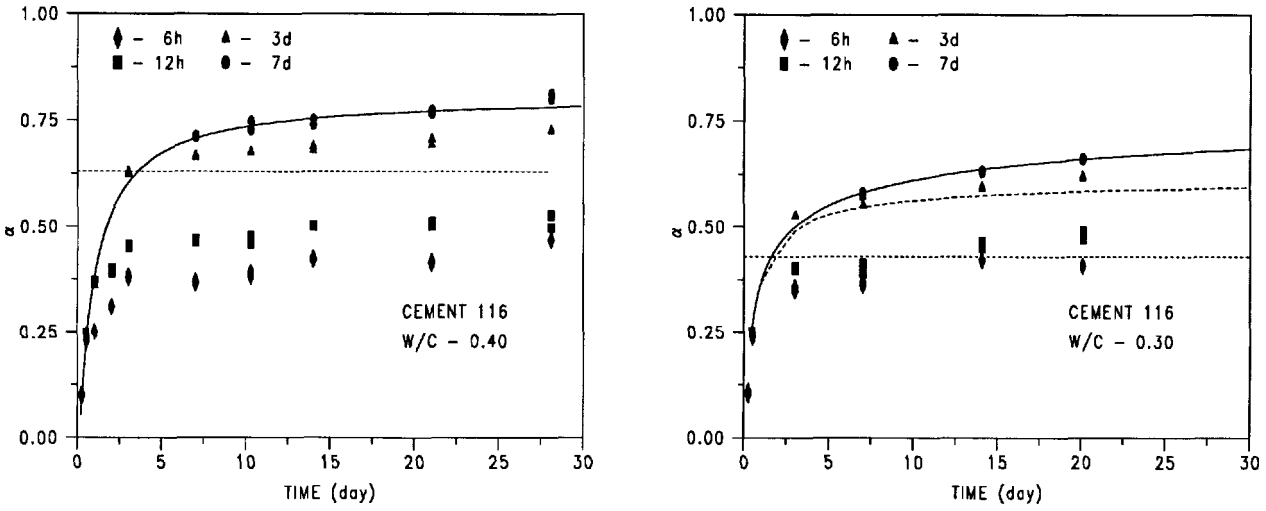

Figure 4: Effect of a 90% RH environment on the degree of hydration (α) for 0.4 and 0.3 w/c cement pastes after curing in 100% RH for 6 and 12 hours, and 3 and 7 days. The solid line indicates continuous hydration at 100% RH, the horizontal dotted line indicates the degree of hydration at which the paste achieves 20% capillary porosity, and the dashed line indicates hydration under sealed conditions for w/c=0.3.

For the w/c=0.3 data, while the 7-day data appear to directly track the saturated condition hydration data, the 3-day data fall slightly below this curve. This might be expected, since after 3 days exposure to 100% RH, the 3-day specimen is then exposed to 90% RH, where even if the capillary porosity has depercolated so that no water is removed, the hydration is continuing under sealed, as opposed to saturated, conditions. As hydration slowly continues beyond 3 days, this will lead to the creation of some empty capillary pores in the specimen due to the chemical shrinkage. Thus, the measured degrees of hydration are seen to fall between the curves for hydration under totally saturated and totally sealed conditions. Conversely, for w/c=0.4, where the saturated and sealed curves will nearly overlap (according to the computer model results discussed earlier), the 3-day system is not able to achieve the performance of a sealed environment. In this case, 7 days of curing are required to equal the performance of a sealed system.

In terms of practical implications, it may be important to realize that when the capillary

porosity depercolates, not only is it more difficult to remove water from the capillary pores in the specimen, but it is also more difficult to maintain saturation of the specimen via an external source of water. This effect has been observed during chemical shrinkage measurements on low w/c ratio cement pastes, where hydration as quantified by chemical shrinkage eventually falls below that measured by non-evaporable water content, as water can no longer be drawn into the specimen at a rate fast enough to maintain saturation (Powers, 1947, Geiker, 1983, and Bentz, 1997). This would imply that extended moist curing would be of limited benefit. However, moist curing during the first two to three days of hydration may be extremely important in maintaining internal saturated conditions to promote hydration, until depercolation of the capillary porosity is achieved. The situation will be even more complex in a concrete than in the cement paste specimens used in this study, due to the presence of the higher porosity interfacial transition zones surrounding each aggregate (Scrivener and Gartner, 1988). It is possible that when the capillary porosity depercolates in the "bulk" paste regions of the concrete, it may still remain interconnected in the interfacial zone paste regions (Winslow *et al.*, 1994 and Scrivener and Nemati, 1996). In this case, prolonged moist curing might be more valuable for a concrete than it would be for a cement paste specimen; more experimental measurements will be necessary to quantify the magnitude of this effect.

CONCLUSIONS

It has been shown that curing environments can have a significant effect on cement hydration kinetics. Even exposure to a 90% RH environment, after 6 or 12 hours of curing at 100% RH, can effectively terminate the hydration process as all remaining capillary water is removed from the specimen. While curing under sealed conditions may be adequate for systems with w/c ratios greater than 0.4, for lower w/c ratios, a significant reduction in the achieved degree of hydration has been observed. The best curing practice, similar to that originally suggested by Powers (Powers, 1947), may be to maintain surface saturated conditions until the capillary porosity depercolates, which will occur at different curing ages for different w/c ratios, and then seal the surface to prevent any moisture loss. The NIST cement paste hydration and microstructural model has provided valuable insights into the effects of sealed conditions and the resultant chemical shrinkage on hydration kinetics and microstructure.

REFERENCES

Baroghel-Bouny, V., "Microstructure and Moisture Characterization of Ordinary and Very High Performance Cement Pastes and Concretes (in French)," Ph. D. Thesis, Ecole Nationale des Ponts et Chaussees, Paris, 1994.

Bentz, D.P., and Garboczi, E.J., "Percolation of Phases in a Three-Dimensional Cement Paste Microstructural Model," Cement and Concrete Research, Vol. 21, 324-344, 1991.

Bentz, D.P., "Three-Dimensional Computer Simulation of Portland Cement Hydration and Microstructure Development," Journal of the American Ceramic Society, Vol. 80 No. 1, 3-21, 1997.

Bentz, D.P., Garboczi, E.J., and Quenard, D.A., "Modelling Drying Shrinkage in Porous Materials: Application to Porous Vycor Glass," to be submitted.

Gause, G.R., and Tucker Jr., J., "Method for Determining the Moisture Condition in Hardened Concrete," Journal of Research of the National Bureau of Standards, Vol. 25, 403-416, 1940.

Geiker, M., "Studies of Portland Cement Hydration: Measurements of Chemical Shrinkage and a Systematic Evaluation of Hydration Curves by Means of the Dispersion Model," Ph. D.

Thesis, Technical University of Denmark, 1983.
Granger, L., Torrenti, J.M., and Diruy, M., "Simulation Numerique du Retrait du Beton sous Hygrometrie Variable," Bulletin de Liaison des Laboratoires des Ponts et Chaussees, 1994.
Henrichsen, A., and Laugesen, P., "Monitoring of Concrete Quality in High Performance Civil Engineering Constructions," MRS Symposium Proceedings Vol. 370, 49-56, 1995.
Hua, C., Acker, P., and Erlacher, A., "Analyses and Models of the Autogenous Shrinkage of Hardening Cement Paste: I. Modelling at Macroscopic Scale," Cement and Concrete Research, Vol. 25 No. 7, 1457-1468, 1995.
Justnes, H., Van Gemert, A., Verboven, F., and Sellevold, E.J., "Total and External Chemical Shrinkage of Low w/c Ratio Cement Pastes," Advances in Cement Research, Vol. 8 No. 31, 121-126, 1996.
Mackenzie, J.K., "The Elastic Constants of a Solid Containing Spherical Holes," Proc. Phys. Soc., Vol. 683, 2-11, 1950.
Mjornell, K.N., "Self-Desiccation in Concrete," Publication P-94:2, Chalmers University of Technology, Goteburg, Sweden, 1994.
Molina, L., "On Predicting the Influence of Curing Conditions on the Degree of Hydration," CBI Report 5:92, Swedish Cement and Concrete Research Institute, Stockholm, Sweden, 1992.
Persson, B., "Hydration and Strength of High Performance Concrete," Advanced Cement-Based Materials, Vol. 3, 107-123, 1996.
Powers, T.C., "Absorption of Water by Portland Cement Paste During the Hardening Process," Industrial and Engineering Chemistry, Vol. 27, 790-794, 1935.
Powers, T.C., "A Discussion of Cement Hydration in Relation to the Curing of Concrete," Proc. of the Highway Research Board, Vol. 27, 1947.
Powers, T.C., "Capillary Continuity or Discontinuity in Cement Pastes," PCA Bulletin, No. 10, 2–12, 1959.
Scrivener, K.L., and Gartner, E.M., "Microstructural Gradients in Cement Paste Around Aggregate Particles," MRS Symposium Proceedings Vol. 114, 77-85, 1988.
Scrivener, K.L., and Nemati, K.M., "The Percolation of Pore Space in the Cement Paste/ Aggregate Interfacial Zone of Concrete," Cement and Concrete Research, Vol. 26 No. 1, 35-40, 1996.
Tazawa, E., Miyazawa, S., and Kasai, T., "Chemical Shrinkage and Autogenous Shrinkage of Hydrating Cement Paste," Cement and Concrete Research, Vol. 25 No. 2, 288-292, 1995.
Winslow, D.N., Cohen, M.D., Bentz, D.P., Snyder, K.A., and Garboczi, E.J., "Percolation and Pore Structure in Mortars and Concrete," Cement and Concrete Research, Vol. 24 No. 1, 25-37, 1994.

2ii079
4 pp

Kn o. 2 5. JAN. 2001 d o k 31843

IDENTIFICATION OF CAUSES OF LUMPS FORMATION IN INDUSTRIAL CEMENTS

Everaldo MARCIANO Jr., Sérgio Luiz CENTURIONE and Vagner MARINGOLO, Brazilian Association of Portland Cement, São Paulo - Brazil

ABSTRACT Portland cement is packed in papers bags prepared in such a way as to preserve the integrity of the hydraulic binder. Even by controlling the amount of alkali sulphates, monitoring grinding temperature and moisture, and storage in big silos, formation of lumps in cement bags or in bulk cement, whose causes are not directly related to pre-hydration of the cement, is likely to be observed. This phenomenon has been investigated on two cement samples of a Brazilian plant and compared with a non-problematic cement taken as reference.

Key-words: lumps, moisture, prehydration, packsetting

INTRODUCTION

The occurrence of alkali sulphates in portland clinker (Dreizler, 1986; Sprung, 1978; Kuhlmann et al, 1980), prehydration (due or not to gypsum dehydration) of cement inside the mill or silo (Hallick, 1980; Rott, 1987), fineness and electrostatic forces among particles after grinding (Thuler et al, 1988; Richartz, 1973), off-site vibrations, weight pressure on inadequately stored packs (ABCP, 1978) are some of numerous hypotheses that have been raised to explain the relatively common worldwide formation of lumps in packed and silo-stored cements.

In this work any causes, whether conventional or not, that might be acting on packsetting process occurring in cements produced by a Brazilian plant have been investigated.

METHODOLOGY

Samples

Three cement samples were chosen for experiment and analysis, two of them presenting lumps (A and B) and one pristine (R) which was taken as reference (Table 1).

Table 1 Characteristics of cement samples

Sample	Contents (%)			
	Clinker	Filler	Blast Furnace Slag	Gypsum [4]
A [1]	92	4	-	5
B [2]	86	10	-	3
R [3]	76	9	11	4

[1] High early strength cement, with little packsetting problems
[2] Cement with limestone filler with high incidence of lumps
[3] Reference cement, without occurrence lumps
[4] Calculated from chemical analysis

Experimental Work

All the three samples were packed in 7cm x 11cm x 2.8cm minibags (Kihara and Monteiro, 1993) in order to accelerate the cements hydration process. The minibags were further stored under laboratory conditions of temperature T = (23±1)°C and relative humidity = (68±1)%. After 7-, 14- and 21-day storage the samples were sieved (sieve #120) and thermodifferential-thermogravimetric and X-ray diffratometric analyses were carried out.

Sieving
Table 2 lists sieving residues of the three samples.

Table 2 Sieving residues

Sample	Residue >125μm		
	7 days	14 days	21 days
A	2.6	28.3	43.7
B	4.7	29.0	59.8
C	3.7	20.2	29.6

Results show that, under the same storing conditions, cements A and especially B tend to packset faster than R. This fact indicate that formation of lumps is not exclusively due to storage at the cement plant but also to some other distinct characteristic of the cement favoring the early packsetting.

Thermodifferential-Thermogravimetric (TD-TG) Analysis
The samples of the stored minibags and the here called *in-natura* samples, *i.e.* correspondent cements not exposed to laboratory storing conditions, were analysed for TD-TG. Figs 1 and 2 show the evolution of W_k (combined water) values (Theisen and Johansen, 1975) and calcite contents, respectively.

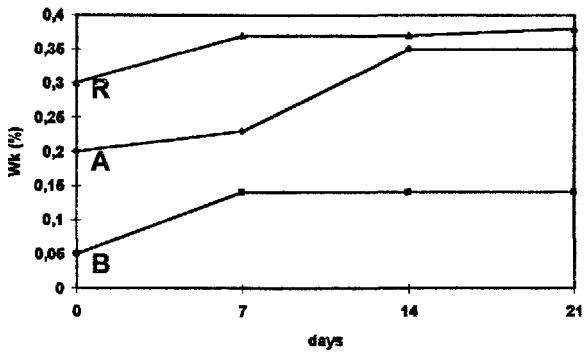

Figure 1 - Evolution of W_K values as function of storing time, under laboratory conditions

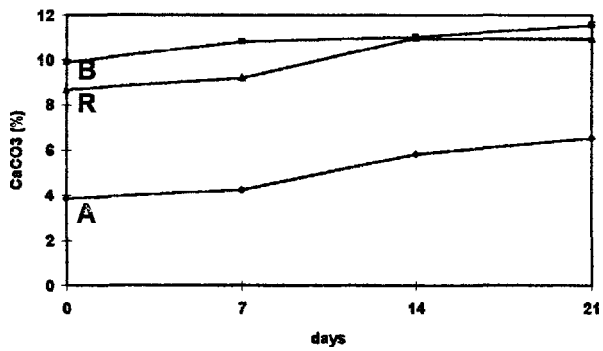

Figure 2 - Evolution of $CaCO_3$ contents as a function of storing time, under laboratory conditions

Smaller W_K values shown for samples A and B which have higher tendency to packset, as compared to sample R, allow us to affirm that lumps are being formed in those cements independently of significant prehydration of clinker components.

As for $CaCO_3$ contents, all the three samples went through a clear carbonation process.

X-Ray Diffratometry (XRD)
Residues from salicylic acid solution of laboratory-stored samples and the *in-natura* samples were also analysed for XRD. This analytical method was later on used to evaluate formation of hydration products and/or alkali sulphates in the samples. The minerals that make up the three samples are listed in Table 3.

Table 3 Samples mineral composition

Mineral component	Chemical composition	Sample		
		A	B	R
Alite+ Belite	$(Ca_3SiO_5) + (Ca_2SiO_4)$	*****	*****	*****
C_4AF	$Ca_4Al_2Fe_2O_{10}$	**	**	**
C_3A	$Ca_3Al_2O_6$	**	**	*
Calcite	$CaCO_3$	**	***	***
Gypsum	$CaSO_4.2H_2O$	8	*	*
Bassanite	$CaSO_4.½H_2O$	*	*	*
Quartz	SiO_2	tr	tr	tr
Syngenite	$K_2Ca(SO_4)_2.H_2O$	*	tr	*
Arcanite	K_2SO_4	tr	-	-
Ettingite	$Ca_6Al_2(OH)_{12}(SO_4)_3.26H_2O$	-	-	-

Note: * expresses comparatively a semiquantitative proportion of mineral phases according to diffraction peak intensity; tr = traces; - = not detected

The diffraction peaks comparatively shows that sample B has the lowest syngenite content in spite of its highest tendency to packsetting.

Along the laboratory storing process, no evidence of ettringite formation was found and incidence of syngenite was the same in the three samples.

CONCLUSION

The tendency to packsetting observed at the plant on samples A and especially B was evidenced in the laboratory tests through formation of lumps in minibags filled with these cements and stored for periods of 7, 14 and 21 days under laboratory conditions of temperature and relative humidity.

Cements A and B presented low prehydration, as compared to sample R, taken as reference for not showing packsetting problems. This evidence is indicative of lumps formation in those cements even at low W_K values what suggests that influence of prehydration was of little significance on this process.

A higher syngenite content was found in sample R followed by sample A and, in much smaller proportion, B. This curious fact indicates how little expressively alkali sulphates acted as packsetting agents on the cements analysed, especially sample B.

As to physical characteristics, very fine cement A (specific surface = $450 m^2.kg^{-1}$) presented less critical packsetting problems than coarser cement B (specific surface = $360 m^2.kg^{-1}$).

Based on data obtained, the evidences lead to the conclusion that formation of lumps in cement B and less intensively in cement A was actually due to their low W_K value, what for some physical-chemical reason makes the cement adsorb water. The reason for this adsorption must be related to grinding conditions, not only operational parameters but also the additive's nature and content.

From one point of view, W_K values higher than 0.35% in cements may affect negatively the mechanical strength performance of these cements (Theisen and Johansen, 1975), from another point, however, low values, normally lower than 0.10% may favour their susceptibility to

packsetting even under low humidity conditions. In case of high early-strength cements (sample A), W_K value was a little higher (0.20%), but its higher fineness must have contributed to its precocious lumps formation. In fact, the packsetting problems have been become more serious after water content in the mill was reduced.

REFERENCES

Associação Brasileira de Cimento Portland (ABCP). Armazenamento de cimento ensacado. 5 ed. São Paulo, 1978. (BT-67)

Dreizler, I. Formation of lumps and accretions in cement silos and measures to prevent and eliminate these phenomena. Cologne : KHD Humboldt Wedag, 1986. 32p.

Ghosh, S.N. Advances in cement technology. New York : Pergamon, 1994.

Hallick, K. Measurements of coating formation in cement silos. Zement-Kalk-Gips, v. 33, n. 9, p. 443-445, Sept. 1980. (Translation in English, v. 33, n. 11, p. 222-224, Nov. 1980)

Kihara, Y., Monteiro, J. B. Mecanismo de empelotamento em cimento portland ensacado. In: CONGRESSO BRASILEIRO DE CIMENTO PORTLAND, 3., São Paulo, 1993. Anais... São Paulo : ABCP, 1993. p. 519-537.

Kuhlmann, K., Ellerbrock, H.G. Changes in the flow behaviour of cement during storage. Zement-Kalk-Gips, v. 33, n. 9, p. 435-442, Sept. 1980. (Translation in English, v. 33, n. 11, p. 220-222, Nov. 1980)

Richartz, W. Effect of storage on the properties of cement. Zement-Kalk-Gips, v. 26, n. 2, p. 67-74, Feb. 1973.

Rott, C. Investigations for reducing incrustation build-up and improving the flowability of cement in silos. Zement-Kalk-Gips, v. 40, n. 4, p. 196-203, April 1987. (Translation in English, v. 40, n. 6, p. 146-149, June 1987)

Sprung, S. Effect of storage conditions on the properties of cement. Zement-Kalk-Gips, v. 31, n. 6, p. 305-309, June 1978. (Translation in English, v. 31, n. 8, p. 185-187, Aug. 1978)

Theisen, K., Johansen, V. Prehydration and strength development of portland cement. Ceramic Bulletin, v. 54, n. 9, p. 787-791, 1975.

Thuler, C.L., Melconian, R. Aglomeração (pack-set) do cimento, causas e meios de prevenção para obter eficiência na moagem e qualidade do produto. In: REUNIÃO DE TÉCNICOS DA INDÚSTRIA DE CIMENTO, 38., São Paulo, 1988. Anais... São Paulo : ABCP, 1988.

AUTHOR INDEX

A
M.S. Abdel-Aziz; 3v012
A.A. Abdel-Kader; 2ii027
A. H. Abedel-Reheem; 3ii124
A. Achmetov; 2ii013
F. Adenot; 3v003
A. D. Agnihotri; 1i003
S.C. Ahluwalia; 1i019, 1i031, 1i044, 1i045, 1i053, 2ii006, 3ii094, 4iv013, 4iv067
H. Ai; 3iii018
V.G. Akimov; 1i006
I. G. Al-Alm Rashed; 3ii124
B.S. Albats; 1i015, 1i007
A.H. Ali; 4iv014
M.M. Ali; 2ii006
M^{a}C. Alonso; 4iv004, 4iv082, 4iv083
V. Alunno Rossetti; 3v026
Ö. Andaç; 1i050
T. Ando; 2ii017
C. Andrade; 4iv004, 4iv082, 4iv083
M.V. Anufriev; 1i032
H. Anzai; 3v013
N. Arano; 4iv051
S. Argarwal; 4iv067
S.K. Argarwal; 4iv067
P. Arjunan; 3v020
V.K. Arora; 1i019
K. Asaga; 3ii107, 3iii022
E. Asakura; 2ii005
M.A. Aviles; 3v019

B
O. Baumanis; 3v025
Sh.T. Babaev; 3iii021
V. Babkov; 2ii048
V.I. Babushkin; 4iv039
P. Baccini; 4iv076
S. Bagosi; 4iv045
G. Balázs; 2ii060, 4iv002
K.D. Baltzopoulou; 4iv052
J.R. Baragaño; 3iii004
V.D. Barbanyagre; 1i011, 1i059
P. Barret; 2ii024
N.F. Bashlykov; 3iii021
A.F. Battagin; 3ii102, 3ii103
Y. Bazhenov; 4iv058
A. Beeldens; 4iv007
V. Belyaeva; 1i004
M. Benkaddour; 2ii041
J. Bensted; 3iii014
D.P. Bentz; 2ii078
J. Berekta; 2ii029
H. Bergqvist; 3ii106
A.F. Bernatsky; 4iv079
C. Bessada; 3v002
R. Bhargava; 1i031, 2ii006
K.N. Bhattacharjee; 3ii115
Y. Biryukovich; 4iv056
M^{a}T. Blanco-Varela; 1i034, 3ii096, 3ii113, 3iii004, 3iii015
A.I. Boikova; 1i057, 1i058
K. Bollmann; 4iv062
L. Bonafous; 3v002
D. Bonen; 4iv022
S. Bonnet; 4iv078
M. Boros; 2ii060
S. Bouraoui; 2ii012
P. Bowen; 3iii002
S. Boyko; 3v004, 3v022
M. Braiman; 3v022
K.D. Breneman; 2ii057, 2ii058
F. Brivot; 4iv074
A.R. Brough; 3v001
H.J.H. Brouwers; 2ii052
L. Brower; 3iii031
W. Brylicki; 3ii095
N. R. Buenfeld; 4iv070
T.A. Bürge; 3iii002

C
R. Cabrillac; 3v003
C. Caestecker; 4iv007
R. Caldwell; 4iv042
G. Camarini; 3ii102, 4iv063
L. Cassar; 1i027
P. Cassat; 3v014
M. Castellote; 4iv082
S.L. Centurione; 2ii079
W.-H. Chae; 1i036
J. Champa; 3iii027
S. Chanda; 3ii092
S. Chandra; 3ii106
P.K. Chang; 3v006
I. Chartschenko; 2ii010
A.K. Chatterjee; 1i008, 1i033, 2ii039

S. Chaturvedi; 4iv057
T. Chaussadent; 4iv074
M. Chen; 3iii016
Y. Chen; 1i010, 2ii031
H. M. Cheong; 1i049, 2ii037
V.L. Chernyavski; 4iv071
Y. Chi; 1i054, 1i055
V. Chistyakov; 2ii019, 2ii023
D.W. Cho; 2ii037
H. Choi; 3iii009
S.H. Choi; 1i036, 1i049, 4iv054
B.J. Christensen; 2ii057
M.A. Cincotto; 3ii102, 4iv063
R. Cioffi; 4iv017
P. Colombet; 3iii003, 3v002, 3v014
D. Constantiner; 3iii013
A.G. Constantinou; 4iv084
F. Corazza; 3iii003
U. Costa; 3iii003
J.-P. Coutures; 3v002, 3v005
T. Coverdale; 3iii027
N.J. Crammond; 4iv026
E. Csányi; 4iv002
L.J. Csetenyi; 4iv045
F. Curcio; 3v026, 4iv006
L. Cussino; 4iv006

D
M. Daimon; 2ii002, 2ii017, 2ii022, 3ii088, 3ii107, 3iii022
D. Damidot; 2ii024, 2ii025, 2ii026, 3iii007, 4iv066
T. Dashkova; 4iv056
B. De Blaere; 4iv007
B. De Vito; 4iv017
E. De Winne; 4iv007
M. Degenkolb; 2ii074
A.E. Degtyaryev; 2ii019
J. Deja; 4iv015
K. Demura; 3iii033
M. Deng; 4iv029
S.P. Dennington; 3iii008
R.K. Dhir; 4iv012
G. Diaz; 3v023
S. Dietz; 3ii087
J.M. Diez; 4iv040
S. Dimitrova; 3ii101
A.M. Dmitriev; 3iii021
C.M. Dobson; 3v001
A. Douy; 3v005
A. Dozono; 2ii001
M. Drabik; 3iii011
R. Dron; 4iv074
G.Ya. Drozd; 4iv039
V.Y. Dubnitsky; 4iv071
G. Dumitru; 3iii015
A.M. Dunster; 4iv026
S. Duszak; 4iv027

E
C.M. Economou; 4iv052
M. Ecker; 2ii032, 4iv044
L. Eckert; 3iii027
A.N. El-Afify; 3ii124
E.B. El Aouni; 2ii041
B.A. El-Sabbagh; 4iv014
H.A. El-Sayed; 4iv014
A. Emanuelson; 1i060
Z.B. Entine; 1i020, 1i046, 3v024
H. Ezirim; 3ii112

F
D. Fairhurst; 4iv008, 4iv009
V.R. Falikman; 3iii021
Y. Fang; 1i010
S.A. Farrington; 3iii013
P. Faucon; 3v003
X. Feng; 2ii043
A. Fernandez-Jimenez; 3ii098
V. Fernon; 3iii003
R. Ferrari; 4iv006
R.C. First; 2ii075
R. Flatt; 3iii002
O.I. Fomicheva; 1i057, 1i058
E. Forssberg; 3ii104
L.S. Fraiman; 3ii081
R. François; 4iv078
O. Francy; 4iv078
G. Frigione; 4iv017, 4iv050
X. Fu; 1i054, 1i055
H. Fujisawa; 2ii005
H. Fujiwara; 2ii001
K. Fukuda; 1i025, 1i052

G
L. Galikova; 3iii011
S.P. Gandhe; 1i033
A. Garbacik; 1i018

M.C. Garci; 2ii058
L. A. M. Garcia; 4iv037
S. Gauffinet; 2ii055
M. Gawlicki; 3ii089
Mª T. Gaztañaga; 4iv003
J. Geiseler; 4iv001
S. George; 1i003
W. Gessner; 3iii007, 3v018
D. Ghosh; 1i008, 1i033, 1i047
S.N. Ghosh; 3ii092
S.P. Ghosh; 1i030, 2ii018
G. M. Giaccio; 2ii036
Z. Giergiczny; 4iv019
C. Gilioli; 1i027
P. Gill; 3iii024
N. Giuliani; 1i051
G.K. Glass; 4iv070
F.P. Glasser; 1i050, 3ii091, 4iv066
V. Glukhovskiy; 4iv056
F. Goetz-Neunhoeffer; 1i056
L. Ya. Goldstein; 1i013
E. Gomez; 3v019
S. Goñi; 4iv003, 4iv004, 4iv024, 4iv040, 4iv083
J.W. Goodwin; 3iii008
V.K. Gore; 1i047
G. Goswami; 3v008
R.K. Goswami; 1i044, 1i045
S. Goto; 2ii070
A.M. Grabiec; 3iii019
M.L. Granizo; 3ii113
L.V. Grishchenko; 1i058
I. Grosvalds; 2ii009
G.W. Groves; 3v001
M. Grutzeck; 2ii067
G. Gu; 3iii016
A. Mª Guerrero; 4iv003, 4iv024
G.L. Guerrini; 1i027
R.S. Gupta; 1i053

H
H. Hagiwara; 3iii017
J. Han; 3ii122
K. S. Han; 1i049
M. Handa; 2ii017
S.K. Handoo; 3v019, 4iv013, 4iv067
S. Hanehara; 2ii014, 3iii001
F. Hanic; 3iii011
S. Hansen; 1i060
N. Hara; 2ii065
S. Harsh; 1i044, 1i045, 4iv013
M. Hasegawa; 3iii010
N.M. Hassanein; 4iv070
M. Hatano; 3iii009
A.S. Heble; 2ii039
H. Hedlund; 2ii077
D. Heidemann; Plen2
E. Henderson; 1i060
Mª S. Hernandez; 4iv003, 4iv024
A. Hidalgo; 4iv004, 4iv083
T. Higaki; 3iii022
M. Hilger; 1i009
H. Hirao; 2ii014
S. Hirose; 3iii022
F.J. Hofmann; 4iv038
H. Hofmann; 3iii002
S.-Y. Hong; 4iv068
K. Hormann; 4iv038
S. Hoshino; 2ii002
J. Houghton; 4iv025
Y.F. Houst; 3iii002
G. Hu; 1i023
S. Huang; 4iv032
Z. Huang; 4iv073
F.H. Hubbard; 4iv012
C.L. Hwang; 2ii035; 3ii108, 3v006, 3v021
C. Hübert; Plen2
C. Hyeon; 4iv072
R. Härdtl; 3ii082

I
M. Ichikawa; 3iii005
K.A. Idriss; 3v012
S.-i. Igarashi; 4iv051
T. Iisaka; 2ii003
T. Ikabata; 2ii007
K. Ikeda; 1i025
M.R. Ilić; 4iv023
N. Inoue; 2ii065
Y. Inoue, 2ii040
B.E. Ioudovitch; 1i020, 1i046, 3iii021, 4iv036
G. C. Isaia; 3ii110
A. Ishida; 3iii017
Y. Ishikawa; 2ii003
Y. Isojima; 3ii109, 3ii119
S. Ito; 1i052, 3ii121
J. Iwanciw; 1i022

H. Iwasaki; 3iii033

J
J.F. Jacquinot; 3v003
H.J. Jakobsen; 2ii056
S. Jalali; 3ii084
I. Y. Jann; 3v021
I. Jedda; 2ii020
H.M. Jennings; 2ii057, 2ii058
O.M. Jensen; 2ii056
M.-Y. Jeong; 4iv055
L. Ji; 2ii030
S.P. Jiang; 2ii053
W. Jiang; 3ii100, 3iii030
A.C. Johnson; 4iv076
J.-E. Jonasson; 2ii077
M. Jorda; 3v003
D.M. Joshi; 3ii092
H. Justnes; 1i038, 2ii069, 3iii012, 4iv064, 4iv081

K
K. V. Kalyani; 1i003
M. Kanaya; 3iii005
I. Karimov; 2ii048
A. Katz; 3ii083
S. Kawaguchi; 4iv051
M. Kawamura; 4iv051
T. Kawano; 3iii010
S. Kelham; 4iv060
M. Kersten; 2ii059
S.A. Khadilkar; 1i008, 1i047
Y. Kihara; 3ii085, 4iv048
H. Kikukawa; 2ii003
B.-K. Kim; 4iv068
N.-H. Kim; 2ii044
A. Kindness; 3ii091
P. Kittl; 3v023
V. Klassen; 1i004
J. Kļaviņš; 3v025
W.A. Klemm; 4iv041, 4iv059
A. Klusov; 2ii013
D. Knöfel; 2ii074
T. Kobayashi; 3iii010
M.M. Komljenović; 1i017
P.G. Komokhov; 2ii016
J. Komonen; 3iii029
N. Kondo; 2ii017
V.I. Kondrashchenko; 2ii066
Z. Konik; 1i022
G. Koprowski; 4iv018
H. R. Kota; 3ii104
M.V. Kougiya; 1i043, 3ii081
T.V. Kouznetsova; 1i001, 2ii027, 2ii028
J. Krištín; 3v009
É. Kristóf-Makó; 3v010
P.V. Krivenko; 2ii033, 4iv046
A.R. Krivoborodov; 4iv053
Y.R. Krivoborodov; 1i014, 1i040, 2ii013
D. Križan; 3ii085, 4iv020
R. Krzywobłocka-Laurów; 3iii019
A.B. Kudryavtsev; 2ii028
H. Kuga; 3ii107
W. Kurdowski; 4iv027
S. Kwan; 2ii067
L. J. Kyu; 2ii022
B. Ködderitzsch; 3v018
U. König; 1i039

L
E. E. Lachowski; 3ii091
A. Łagosz; 3ii089
S. Lagzdina; 1i035, 2ii009
A. Landa-Cánovas; 1i060
E. Lang; 4iv001
J. LaRosa-Thompson; 2ii067, 3iii024
C.K. Larsen; 4iv069
X. Lecoq; 2ii055
H.-S. Lee; 2ii044
I.S. Lee; 2ii044
S. H. Lee; 3ii088
Y.-J. Lee; 2ii044
P.G. Lele; 1i008, 1i047
M. Lewis; 4iv025, 4iv061
D. Li; 4iv029
P. Li; 1i028
R. Li; 4iv028
S. Li; 4iv030
V. Lilkov; 3ii116
J.R. Lim, 2ii037
L.K. Lin; 3ii108
J. Lindgård; 4iv064
C. Liu; 1i028
J.N. Liu; 3ii114
J.S. Lota; 3iii014, 4iv012
C. Lu; 1i012, 4iv028
H.M. Ludwig; 4iv034, 4iv035
I.G. Luginina; 1i029, 1i057

M. Lukach; 3v022
K. Luke; 3ii091
T. Lyashenko; 3v004

M
A. Macias; 4iv040
J. Madrid; 4iv040
N. Maeda; 3iii010
Y. Maejima; 2ii005
S. C. Maiti; 3iii020
J. Majling; 3v009
I. Maki; 1i052
R.I.A. Malek; 1i024
J. Małolepszy; 2ii064, 3ii089, 4iv043
S. Manjit; 3ii093
B. Marchese; 4iv050
E. Marciano Jr.; 2ii079, 3ii103
V. Maringolo; 2ii079
M. Marroccoli; 2ii029
V. Martinez; 3v023
D. Massiot; 3v002, 3v005
S. Matala; 3v017, 4iv005
V.K. Mathur; 1i053
V.A. Matviyenko; 2ii076
W.J. McCarter; 3ii112, 4iv011
O.P. Mchedlov-Petrossyan; 1i042, 2ii021
S.N. Mehrotra; 1i002
I. Meland; 4iv064
V.S. Melentyeva; 3ii117
E. Menendez; 4iv004
B. Meng; 3ii105
H.W. Meyer; 3v007
V. Michaud; 2ii011, 4iv049, 4iv065
A. Miezis; 3v025
T. Mihara; 3iii017
N. Mikhailishina; 4iv056
S.R. Miletić; 4iv023
F.M. Miller; 4iv041, 4iv059
K. Miskiewicz; 3ii087
S. Miyazawa; 2ii071
K. Mohan; 1i030, 2ii018
B.N. Mohapatra; 3v008
G.K. Moir; 1i041
G. Morales; 3ii123
M. Morioka; 3iii017
H. Motzet; 1i039
J.F. Muller; 3v014
A.K. Mullick; Plen1, 1i031, 3v019, 4iv047
D. V. Mundshtukov; 2ii020
J.C. Mutin; 2ii053
D. Müller; 3iii007
U. Mäder; 3iii002
S. Möhmel; 3v018

N
M. Nadu; 3v022
S. Nagataki; 2ii001
A. Nakamura; 2ii022
H. Nakata; 2ii070
S. Nakaya; 2ii017
D. Nazarsky; 4iv021
B. Nedumaran; 1i002
L.S. Nefyodova; 3v024
H. Nemoto; 3v013
C. M. Neubauer; 2ii057, 2ii058
J. Neubauer; 1i039, 1i056, 3v007
Y. Nikaido; 2ii017
T. Nishikawa; 3ii121
J. Nissenbaum; 3v022
W. Nocuń-Wczelik; 4iv043
T. Noguchi; 4iv072
H. Noma; 2ii065
A. Nonat; 2ii053, 2ii055, 4iv049, 4iv065
E.C. Nygaard; 3iii012

O
I. Odler; 1i026, 2ii063
H. Ogata; 2ii005
H.-K. Oh; 1i036, 4iv054, 4iv068
Y. Ohama; 3iii033
Y. Ohba; 2ii002, 2ii022
A. Ohno; 3v015
A. Olginsky; 2ii015
G.B. Olson; 2ii058
L. Opoczky; 1i009, 2ii004
A.P. Osokin; 1i005, 1i006, 1i014
Z. Owsiak; 4iv018

P
S. Pagliolico; 4iv006
A. Palomo; 1i034, 3ii096, 3ii113, 3iii004
J.G. Palomo; 1i034
M. T. Palou; 3v009
Y. Pan; 1i021, 1i054, 1i055
J.D. Panda; 3v008
P.K. Panigrahy; 3v008
I. Papayianni; 3ii086
A. Papo; 2ii004

C.-K. Park; 4iv068
P. Parmentier,; 3ii120
M. Pátkai-Horváth; 3v010
P. Paulini; 2ii072
S. Pavlenko; 3ii080, 4iv058
V. Penttala; 3iii029, 4iv033
J.L. Perez-Rodriguez; 3v019
B. Perrin; 4iv078
B. Persson; 2ii073
O.E. Petrov; 3ii116
S. Peukert; 2ii034, 3iii023
W.G. Piasta; 4iv018
A.K. Platten; 4iv008, 4iv009, 4iv073
A.A. Plugin; 4iv039, 4iv075
A.N. Plugin; 2ii054, 4iv075
A. Poltavtsev; 2ii019
A. Pompo; 2ii029
E.N. Potapova; 1i005, 1i006
J.H. Potgieter; 2ii049, 3v011
P.L. Pratt; 3iii014
I.G. Prokopova; 4iv075
J.R. Prusinski; 3ii090
F. Puertas; 1i034, 3ii096, 3ii098, 3ii113, 3iii004, 3iii015
E.K. Pushkaryeva; 2ii033
G.K.D. Pushpalal; 3iii010
R. Pyare; 1i016
Z. Pytel; 2ii064
H. Pöllmann; 1i039, 2ii032, 3iii032, 3v007, 4iv044

Q
V.A. Quarcioni; 3ii085

R
M. Radenkova-Yaneva; 2ii047, 3ii101
K. Raina; 1i002
K. Rajczyk; 2ii045
Sh. M. Rakhimbaev; 2ii046
X. Ren; 2ii030
A. Rettel; 2ii026, 3iii007
M. Ribas Silva; 4iv037
I.G. Richardson; 2ii068, 3v001
A. Risch; 4iv044
J. Roberts; 4iv073
E. Rodum; 4iv081
M^{a}.L. Romero; 3ii096
V. Ronin; 3ii104, 2ii077
G. Rosenthal; 3iii031
A. Rosić; 1i017
W. Roszczynialski; 3ii097
D.M. Roy; 1i010, 3ii100, 3ii114, 3iii030, 3v020
R. Roy; 1i010
R.F. Runova; 2ii054, 3ii117
O.V. Rybakova; 4iv053
P.F. Rymyantsev; 1i037

S
S. Sahu; 3v009
A. Saini; 1i051
E. Sakai; 2ii002, 2ii017, 2ii022, 3ii088, 3ii107
S.V. Samchenko; 1i014
G. Samuel, 4iv047
M.A. Sanitsky; 3iii025
R. Sanjaasuren; 1i037
S. Sano; 3iii005
S.L. Sarkar; 3ii090
L. Sas; 1i048
A.E. Savva; 4iv052
D. Sawaki; 3iii001
Z. Sawicz; 4iv018
B.E. Scheetz; 3ii111, 3iii024
M. Schieber; 3v022
P. Schiessl; 3ii105, 4iv016
M. Schmidt; 3ii087, 4iv038
C. R. Schweizer; 4iv076
K.L. Scrivener; 2ii026, 4iv025, 4iv061, 4iv084
H. Sedaira; 3v012
U. Sedmalis; 1i035, 2ii009
Y.P. Sehti; 1i019
K. Seki; 3iii009
Ž. Sekulić; 3iii028
M.M. Seleim; 3v012
E.J. Sellevold; 2ii069
V. Serbin; 2ii023
V.N. Serdyuk; 3iii021
R. Sersale; 4iv017
N.N. Shangina; 2ii016
S.V. Shapet'ko; 2ii033
K.M. Sharma; 1i053, 3ii094
P.S. Sharma; 3ii094
S.C. Sharma; 4iv057
M.A. Shater; 3ii124
Y.N. Sheen; 2ii035
A.L. Shein; 1i015

N. Sherman; 2ii029
V. Shevchenko; 2ii019
C. Shi; 3ii099, 4iv042
H. Shi; 1i012
L. Shi; 2ii031
Y. Shigetomi; 2ii040
H. Shima; 1i025
G.-Y. Shin; 4iv068
S.M. Shingote; 1i003
M. Shmelkov; 3ii080
M. Shoya; 3ii109, 3ii119
D. Shtakelberg; 3v004, 3v022
A.K. Shukla; 3ii115
K. Sideris; 2ii061, 4iv052
K.K. Sideris; 2ii061, 4iv052
M.R. Silsbee; 1i010, 3ii100, 3ii114, 3iii024, 3v020
N.B. Singh; 3ii115
Vinaya K. Singh; 1i016
Vipin K. Singh; 1i016
S.K. Sinha; 4iv047
A.G. Sinyakin; 2ii021
S.P. Sivkov; 2ii020
E. Sjöstedt; 1i060
J. Skibsted; 2ii056
R.C.T. Slade; 3iii011
S. Smeplass; 4iv064
K.A. Snyder; 2ii078
J.-T. Song; 4iv055
V.P. Sopov; 2ii066
D. Sorrentino; 4iv049, 4iv065
F. Sorrentino; 2ii025
J. D. Sota; 2ii036
J. Stark; 1i005, 2ii010, 4iv031, 4iv034, 4iv035, 4iv062
M. Stefanović; 3iii028
J. Stegemann; 4iv042
E.T. Stepkowska; 3v019
A. Stok; 1i022
J. Strigáč; 3v009
C.A. Strydom; 2ii049
P.E. Stutzman; 2ii078
S. Stürmer; 4iv031
St. Stöber; 3iii032
M. Su; 2ii030, 3iii026, 4iv029, 4iv030
L.G. Sudakas; 2ii008
R. Suderman; 2ii011
S. Sugita; 2ii043, 3ii109, 3ii119
L.M. Sulimenko; 1i007, 1i040
U. Sulser; 3iii002
T. Suzuki; 2ii005
L.B. Svatovskaya; 2ii062
K. Svinning; 1i038
R.N. Swamy; 4iv080
L.I. Sychova; 1i032
J. Szczerba; 3iii023

T
A. Tagnit-Hamou; 2ii012
S. Takahashi; 3ii107, 3v013
T. Takahashi; 2ii070
H. Takemura; 2ii007
Y. Takuma; 3ii118
F. Tamás; 2ii060, 3v010, 4iv002
C.E.S. Tango; 3ii085
E. Tazawa; 2ii071
J.J. Thomas; 2ii058
D.W. Thompson; 3iii008
F. Tomosawa; 2ii051, 4iv072
E.E. Toumbakari; 4iv010
B. Touzo; 3v005
R. Trettin; 2ii050
J. Tritthart; 3v010, 4iv069
D. Trumeau; 3v005
B. Trybalska; 4iv027
Y. Tsuchida; 3ii118
Y. Tsukinaga; 3ii109, 3ii119
N. Tsuyuki; 3iii009

U
S. Uchida; 3ii118
H. Uchikawa; 2ii014, 3iii001
T.S. Um; 4iv054
W.S. Um,; 2ii044
H.P. Unsworth; 4iv012
A. V. Usherov-Marshak; 2ii021, 2ii066, 3v016
H. Ushiyama; 2ii040
J.I. Ustimenko; 3ii117

V
H. Vaishnav; 3ii092
G.L. Valenti; 2ii029
K. Van Balen; 4iv010
C. Van Den Brande; 4iv010
R.J. van Eijk; 2ii052
A. Van Gemert; 2ii069
D. Van Gemert; 2ii069, 3ii120, 4iv007,

4iv010
M. Van Messem; 4iv007
F. Van Rickstal; 3ii120
K. Vanbelle; 3ii120
P. Vanis; 2ii063
L.B. Vasiliyeva; 2ii008
T. Vázquez; 1i034, 3ii096, 3iii004, 3iii015
F. Verboven; 2ii069
A. Vichet; 3iii003, 3v014
J. Virlet; 3v003
K. Viswanathan; 2ii039
V. Voznesensky; 3v004

W
A. Walliser; 2ii075
J.F. Wang; 2ii038
P. Wang; 3iii006, 3iii016
X. Wang: 3iii016
Y. Wang; 4iv029, 4iv030
R.C. Wason; 4iv047
D. Watson; 4iv011
J. Widmer; 3iii002
W. Wieker; Plen2
U. Wiens; 4iv016
S. Wild, 4iv075
J. Wu; 3iii006
K. Wu; 3ii122
X. Wu; 4iv032

X
Y. Xi; 3ii111
A. Xu; 4iv077
J. Xu; 4iv030

Y
D. Yadav; 3ii094
S. B. Yadav; 1i003
T. Yamamoto; 3v015
Q. Yang; 4iv032
Q. Ye; 2ii042
K. Yoshida; 2ii070
J.F. Young; 3iii018
Q. Yu; 2ii043, 3ii109, 3ii119
G.-C. Yum; 1i036

Z
N.M. Zaitchenko; 2ii076
M. Zdaniewicz; 3iii023
D.Yu. Zelensky; 4iv039
F. Zenone; 4iv017
R. L. Zerbino; 2ii036
F. Zhang; 4iv030
H. Zhang; 1i026
L. Zhang; 3iii026, 4iv029
X. Zhang; 3ii122
H. Zhuo; 1i028
B. Živanović; 3iii028, 4iv020
B.M. Živanović; 1i017
S.A. Zoubekhine; 3iii021, 4iv036

KEY-WORD INDEX

A
Accelerated test; 3iii033
Accelerators; 3ii103, 3iii005, 3iii012, 3iii014, 3iii022, 3iii027, 3iii032,
Acid attack; 3ii109, 4iv002, 4iv021, 4iv038, 4iv039, 4iv040
Activation; 1i006, 2ii016, 2ii045, 2ii062, 2ii076, 3ii083, 3ii092, 3ii094, 3ii098, 3ii099, 3ii100, 3ii103, 3ii104, 3ii113, 3ii114, 3iii028, 4iv047
Activation energy; 1i053
Activity coefficient; 4iv083
Additives; 1i009, 1i020, 1i035, 2ii003, 2ii009, 2ii045, 2ii074, 3ii116, 3iii017, 3iii032
Adiabatic temperature rise; 4iv072
Admixtures; 2ii012, 2ii034, 2ii036, 2ii047, 3ii087, 3ii095, 3ii097, 3iii001, 3iii002, 3iii004, 3iii009, 3iii018, 3iii019, 3iii023, 3iii024, 3iii025, 3iii026, 3iii029, 3iii030, 3iii031, 3v015, 4iv004
Adsorption; 2ii001, 3iii002, 4iv077
AFm phase; 2ii032, 3iii032, 3ii089, 4iv034, 4iv061
AFt phase; 1i060, 4iv034, 4iv041, 4iv059
Aggregate; 2ii015, 3v024, 4iv053, 4iv057
Air entraining; 4iv031, 4iv057
Air pollution; 4iv002
Alinite; 2ii030, 3ii118
Alite; 1i006, 1i015, 1i041, 1i050, 2ii040, 2ii042, 2ii056, 3ii107, 3ii117, 3iii005, 3iii031
Alkali; 1i002, 1i012, 1i028, 1i035, 1i049, 2ii012, 2ii065, 3ii083, 3ii098, 3ii100, 3ii103, 3ii113, 3ii114, 3ii117, 3iii025, 4iv003, 4iv028, 4iv055, 4iv066
Alkali aggregate reaction; 3iii033, 3v022, 4iv048
Alkali silica reaction; 4iv047, 4iv049, 4iv065, 4iv074
Alkali silicate solutions; 4iv049, 4iv065
Alkaline cement; 4iv046
Alumina; 2ii027, 2ii026, 3iii010
Aluminate phase; 1i001, 1i022, 1i051, 1i056, 2ii041, 2ii060, 3iii010, 3iii015, 4iv027, 4iv034, 4iv066
Aluminoferrite; 1i004, 1i005, 1i055, 2ii031
Aluminosilicate; 1i024, 4iv046
Anhydrite; 1i032, 2ii011, 2ii022, 2ii029, 3ii092, 4iv059
Aragonite; 1i042
Arc furnace dust; 4iv042
Asbestos; 1i027
Ash; 3ii080
Autoclavation; 3ii120, 4iv054
Autoclave soundness; 1i023
Autogeneous shrinkage; 2ii069, 2ii070, 2ii071, 2ii073

B
Backscattered electron image; 2ii014, 4iv061
Bacterial attack; 4iv038, 4iv039
Bamboo dust; 1i019

Barite; 1i036
Barium phases; 1i058
Belite; 1i006, 1i015, 1i018, 1i041, 1i052, 2ii007, 2ii040, 2ii045, 2ii056, 3v009
Belite cement; 1i036
Binder; 1i059, 2ii047, 2ii054, 3ii080, 3ii101, 3iii021, 4iv057
Blastfurnace slag; 2ii068, 2ii074, 3ii082, 3ii093, 3ii095, 3ii096, 3ii098, 3ii099, 3ii101, 3ii102, 3ii103, 3ii104, 3ii115, 3ii122, 3iii009, 3iii017, 4iv001, 4iv005, 4iv009, 4iv015, 4iv035, 4iv040, 4iv063
Blended cement; 1i020, 3ii089, 3ii091, 3ii111, 3ii114, 3ii115, 3ii121, 3v026, 4iv004, 4iv017, 4iv020, 4iv052,
Bogue calculation; 1i039, 3v007, 3v009
Borax; 1i036
Bottom ash; 3ii090
Bound water; 2ii072, 3iii019, 3v019
Brick; 3ii080
Brownmillerite; 1i022, 2ii029, 2ii032,
Burnability of raw mixes; 1i021, 1i030, 1i031, 1i034, 1i040, 1i041, 1i045, 1i048, 1i054
Burning conditions of clinker; 1i018, 1i023

C
Calcium carbonate; 1i042
Calcium aluminate; 2ii022, 2ii025, 2ii050, 3iii022, 3v005
Calcium aluminate cement; 2ii024, 2ii026, 2ii027, 2ii028, 3iii007, 3v018, 4iv003, 4iv025, 4iv026
Calcium aluminate sulphate; 2ii010, 4iv068
Calcium aluminozincates, 1i059
Calcium hydroxide; 2ii049, 2ii059, 3ii082, 3ii106, 3ii107, 3ii108, 3ii112, 3iii031, 3v019, 4iv067
Calcium fluoride; 1i032, 2ii042
Calcium langbeinite; 2ii011
Calcium nitrate; 3iii012
Calcium phosphate; 1i036
Calcium phosphate cement; 2ii063
Calcium silicate; 1i035, 1i055, 2ii055, 2ii050, 2ii062, 4iv054
Calcium sulphate; 1i012
Calorimetry; 2ii021, 2ii025, 2ii041, 2ii066, 3iii032, 3v016, 3v017, 4iv042
Capillary; 2ii048
Carbon dioxide; 1i024, 2ii032, 4iv010
Carbonation; 2ii073, 4iv003, 4iv004, 4iv005, 4iv006, 4iv010, 4iv017, 4iv026, 4iv035, 4iv048, 4iv070, 4iv084
Case studies; 4iv002
Cement; 3ii092
Cement hydration equation; 2ii061, 4iv052
Characterization; 1i008, 2ii062, 3ii088, 3v011, 3v020 3v023, 3v026, 4iv019
Chemical analyis; 3v012
Chemical attack; 4iv015, 4iv026, 4iv028, 4iv031
Chemical prestressing; 3iii016

Chemical shrinkage; 2ii069, 2ii070, 2ii072
Chloride; 1i002, 1i012, 2ii030, 3ii118, 4iv006, 4iv015, 4iv027, 4iv078, 4iv080, 4iv081, 4iv082, 4iv083
Chloride Binding; 4iv016, 4iv069, 4iv070, 4iv078
Classification; 4iv046
Clay; 2ii020
Clinker; 1i048, 1i058
Clinker composition; 1i028, 4iv036
Clinker formation; 1i004, 1i006, 1i008, 1i010, 1i011, 1i026, 1i031, 1i037, 1i043, 1i044, 1i046, 1i049, 1i054, 2ii006, 3ii118
Cluster; 1i003
Coal; 1i047, 3ii090
Composite cements; 1i009, 2ii016, 2ii034, 3ii122
Composition; 2ii007, 2ii071, 3v004, 3v011, 3v026, 4iv007, 4iv023, 4iv060
Concrete; 2ii035, 3ii108, 3iii024, 3iii029, 3v021, 3v022, 4iv025, 4iv035, 4iv073
Cooling of clinker; 3v005
Corrosion; 2ii006, 4iv014, 4iv020, 4iv023, 4iv027, 4iv028, 4iv030, 4iv038, 4iv039, 4iv071, 4iv082, 4iv084
Creep; 4iv018
Cross-linking; 3iii011
Crystal; 2ii015
Crystal size; 1i051, 3iii031
Crystal structure; 1i055, 2ii048
Crystallisation pressure; 4iv049
Crystallography; 2ii054
CSH; 2ii044, 2ii047, 2ii053, 2ii055, 2ii059, 2ii064, 2ii067, 2ii068, 3ii082, 3ii093, 3ii121, 3v001, 3v003, 4iv016, 4iv041, 4iv043, 4iv061, 4iv074, 4iv076
Curing; 2ii037, 2ii078, 3ii091, 4iv055, 4iv059, 4iv067

D

Deformation; 4iv021, 4iv058
Degree of hydration; 2ii051, 2ii053, 2ii062, 2ii077, 3v019, 4iv016
De-icing salts; 4iv006, 4iv035
Delayed ettringite formation; 4iv059, 4iv061, 4iv062, 4iv063, 4iv064
Delayed expansion; 3iii016
Design life; 4iv071
Dicalcium silicate; 1i017, 1i053
Differential thermal analysis; 2ii041, 4iv031
Diffusion; 2ii046, 3ii084, 3ii098, 4iv010, 4iv015, 4iv016, 4iv056, 4iv080, 4iv081
Diffusivity; 4iv008, 4iv009
Dilation; 4iv033
Dispersion; 2ii005
Disposal; 1i027
Dopant; 1i053
Drying; 3iii018, 3v018, 4iv011, 4iv077, 4iv079
Durability; 2ii011, 3ii095, 3iii024, 3v022, 4iv004, 4iv007, 4iv022, 4iv023, 4iv026, 4iv029, 4iv030, 4iv037, 4iv040, 4iv046, 4iv048, 4iv062, 4iv065, 4iv070, 4iv075, 4iv082

E
Economy; 1i036, 3ii114
Ecology; 1i043
Electron microscopy; 1i060
Electron spectroscopy for chemical analyses (ESCA); 2ii044
Electrical conductivity; 4iv011
Electrical impedance; 3ii112
Electrical properties; 4iv079
Electrical resistivity; 3v021
Energy; 2ii046
Environment; 1i003, 3ii093
Equilibria; 2ii057, 2ii058
Ettringite; 1i025, 2ii006, 2ii010, 2ii017, 2ii029, 2ii031 2ii056, 2ii070, 2ii074, 3iii022, 4iv012, 4iv018, 4iv031, 4iv060, 4iv062, 4iv065
Evaporable water; 3v019
Expansion; 2ii006, 2ii074, 3iii017, 3v022, 4iv057, 4iv060, 4iv062, 4iv064
Expansive cement; 1i001, 2ii010
Extraction methods; 3v020

F
False set; 3iii013
Ferrite phase; 1i008, 1i015, 1i060, 3iii005, 3v003
Ferroaluminate; 4iv029
Filler; 1i020, 2ii002, 2ii020, 3ii081, 4iv056
Fineness; 1i007, 2ii001, 2ii002, 2ii018, 2ii043, 2ii060, 3ii088, 3v008, 4iv060
Fingerprinting; 3v010, 3v011
Fire; 4iv073
Fire damage; 4iv067
Flow; 2ii017, 3v024
Flue gas desuphurisation product; 3ii090
Fluidity; 2ii001, 2ii002, 2ii012
Fluoride phases; 2ii043, 3v002
Fly ash; 3ii081, 3ii082, 3ii083, 3ii084, 3ii085, 3ii086, 3ii087, 3ii088, 3ii089, 3ii090, 3ii110, 3ii115, 3ii116, 3ii122, 3v006, 3v020, 3v021, 4iv004, 4iv009, 4iv012, 4iv019, 4iv020, 4iv023, 4iv058, 4iv077
Fracture mechanics; 2ii075
Free lime; 1i016, 1i045, 2ii049, 4iv036
Freeze-thaw damage; 2ii016, 3iii019, 4iv034, 4iv035
Freezing; 4iv033
Friedel's salt; 4iv027, 4iv080
Fuels for clinker making; 1i013, 1i019

G
Gel; 3ii105, 3iii007, 3iii022, 4iv074
Glass; 1i046, 1i051, 3ii088, 3ii119, 4iv030, 4iv055
Grinding aids; 2ii020, 3v014
Grinding technology; 1i009, 1i040

Ground silica; 3ii120
Grout; 2ii005
Gypsum; 2ii040, 2ii044, 2ii060, 3ii093, 3ii115, 3iii025, 3v008, 3v023, 4iv017

H
Hardening; 2ii008, 2ii034, 2ii039, 2ii047, 2ii052, 2ii054, 2ii076, 3ii112, 3v016, 4iv071
Heat capacity; 4iv033
Heat evolution; 2ii021, 2ii035, 2ii051, 2ii076, 2ii077, 3ii102, 3ii105, 3iii029, 3v016, 4iv042, 4iv072
Heavy metals; 1i043, 2ii014, 3v010, 3v013, 4iv041, 4iv043
High alumina cement; 2ii023, 2ii033, 3iii010, 3ii096, 4iv013, 4iv027, 4iv038
High performance; 2ii035, 2ii038, 3ii108, 3v006, 3v021
High strength; 2ii037, 3ii120
High sulphate clinker; 2ii011
High temperature; 3ii111, 3iii020, 4iv067
Humidity; 4iv011, 4iv079
Hydration; 1i022, 1i057, 1i059, 2ii004, 2ii006, 2ii008, 2ii007, 2ii012, 2ii013, 2ii015, 2ii019, 2ii021, 2ii022, 2ii023, 2ii024, 2ii025, 2ii026, 2ii028, 2ii029, 2ii030, 2ii031, 2ii033, 2ii035, 2ii036, 2ii039, 2ii040, 2ii041, 2ii042, 2ii043, 2ii044, 2ii046, 2ii047, 2ii050, 2ii052, 2ii055, 2ii057, 2ii058, 2ii061, 2ii067, 2ii069, 2ii070, 2ii078, 3ii089, 3ii094, 3ii097, 3ii099, 3ii100, 3ii101, 3ii102, 3ii107, 3ii116, 3ii118, 3ii119, 3iii008, 3iii014, 3iii015, 3iii019, 3iii025, 3v006, 3v016, 3v018, 4iv072, 4iv071
Hydrothermal synthesis; 1i017

I
Identification; 3v010
Image analysis; 4iv084
Immobilization; 2ii014, 2ii016, 2ii052, 4iv043, 4iv045
impact prediction; 1i003
Impact evaluation; 1i003
Induction period; 2ii019, 2ii055
Infra red absorption spectra; 3ii104
Inhibitor; 3iii033
Interfacial zone; 4iv050, 4iv051, 4iv053, 4iv056, 4iv084
Interground cements; 1i013, 3v026
Interstitials; 2ii007
Ion exchange resin; 4iv045
Ionic assocoiation, 4iv083
Ions; 2ii036, 2ii046, 2ii065, 3iii012, 3iii013, 4iv075, 4iv079
Iron mud; 1i021
Isomorphism; 1i059

K
Kinetics; 1i005, 1i035, 1i044, 1i052, 2ii019, 2ii023, 2ii028, 2ii043, 2ii055, 3ii098, 3iii008, 4iv076

L
Latex; 3iii008
Leaching; 2ii014, 4iv012, 4iv041, 4iv043, 4iv045
Light microscopy; 3iii031, 3v007
Lignosulphonates; 2ii004, 3iii013, 3iii021
Lime; 2ii049, 2ii074, 3ii084, 3iii005, 4iv010
Limestone; 1i047, 1i048, 2ii022, 4iv018
Long age; 2ii016, 4iv050
Low energy; 1i034, 2ii045
Low temperature; 1i018, 1i029, 1i037, 2ii009, 2ii013, 2ii038, 3iii014, 3v017
Lumos; 2ii079

M
Magnesium chloride; 4iv022
Magnesium sulphate; 4iv022
Magnesium oxide; 1i023, 2ii064, 3v012
Magnesium phases; 1i057
Mass spectroscopy; 3v014
Maturity; 3ii111
Macro Defect Free; 3iii010, 3iii011, 4iv013
Mechanical properties; 3v025
Mechanism; 1i046, 2ii025, 2ii026, 2ii035, 2ii050, 2ii057, 2ii058, 3ii100, 3iii003, 3iii006, 3iii012, 3iii025,, 3v014, 4iv074
Melt; 1i008, 1i011, 1i012, 1i014, 1i029, 1i046, 3v005
Mercury Intrusion Porosimetry; 3ii104
Metakaolin; 3ii113, 3ii114, 4iv011
Method; 2ii021, 3v011, 3v013, 3v016, 3v018, 3v022, 3v023, 4iv081
Microcrack; 4iv021
Microgravity; 2ii075
Microscopy; 1i029, 1i030, 1i039, 1i051, 1i052
Microstructure 1i038, 1i039, 1i047, 1i049, 1i052, 2ii008, 2ii014, 2ii018, 2ii037, 2ii064, 2ii075, 3ii091, 3ii095, 3ii096, 3ii099, 3iii014, 4iv005, 4iv015, 4iv025, 4iv037, 4iv047, 4iv050, 4iv051, 4iv053, 4iv055, 4iv068, 4iv084
Mineralisers in clinker making; 1i028, 1i030, 1i031, 1i033, 1i034, 1i037, 1i050, 3v002
Mineralogy; 1i046, 3ii087, 3ii105
Mineral phase; 1i015, 2ii009, 2ii015, 4iv028
Mixing procedure; 3ii120
Mobility; 2ii065, 4iv083
Modelling; 1i038, 1i044, 1i045, 2ii048, 2ii052, 2ii078, 3ii085, 3ii084, 3iii013, 3v004, 4iv005, 4iv070, 4iv071, 4iv073, 4iv078
Modified cement; 2ii004, 2ii020, 3ii085, 3ii097, 3ii104, 3iii021, 3iii023
Moisture; 2ii079, 3iii011,3v004, 4iv010, 4iv013, 4iv062
Molybdic compounds; 1i054, 1i055
Monosulphate; 2ii056
Mortar; 4iv033

N
Naphtalene Formaldehyde Sulphonate; 3iii003, 3iii009, 3iii030
Nitrate attack; 4iv002
Nodulization in clinker formation; 1i007
Non-equilibrium burning; 1i011
Nuclear Magnetic Resonance; 1i024, 2ii028, 2ii056, 2ii067, 2ii068, 3iii007, 3v001, 3v002, 3v003, 3v004, 3v005, 3v006

O
Oilwell cement; 2ii013, 3iii014
Organic; 3v015
Osmotic pressure; 4iv049

P
Packsetting; 2ii079
Particle size distribution; 1i009, 2ii018, 2ii053, 3ii110, 3v024
Pattern recognitin; 3v010
Penetration; 2ii005, 2ii038, 3ii109, 4iv080
Performance; 4iv073
Permeability; 4iv008, 4iv075
Petroleum coke; 3ii090
pH; 4iv065
Phase composition; 3ii091
Phase diagram; 1i050, 1i052, 2ii024, 2ii057, 2ii058, 4iv066, 4iv074,
Phase transition; 4iv033
Phase transformation; 4iv034
Phosphate; 4iv057
Physical properties; 3v025
Plasticizers; 2ii020
Polymer; 3iii008, 3iii009, 3iii010, 3iii027, 4iv013
Polymorphs; 1i053
Pore size distribution; 4iv077
Pore solution; 2ii036, 3iii003, 3iii013, 3iii022, 3ii091, 4iv040, 4iv069
Pore structure; 2ii037, 2ii066, 3ii111, 3iii009, 3iii018, 3v017, 4iv001, 4iv005, 4iv080
Porosity; 2ii036, 2ii048, 2ii066, 2ii072, 3ii085, 3ii119, 3iii023, 3v017, 4iv006, 4iv007, 4iv008, 4iv013, 4iv017, 4iv024, 4iv040, 4iv048, 4iv054, 4iv078
Portland cement; 3ii107, 3iii006, 3v025, 4iv012
Potentiometry; 4iv083
Powder; 2ii002
Pozzolana; 1i020, 2ii073, 2ii077, 3ii106, 3ii107, 3ii108, 3ii112, 3ii115, 3ii117, 3ii123, 3ii124, 3v001
Pozzolanic cement; 4iv036
Pozzolanic reaction; 3v006
Pozzolanic reactivity; 3ii088
Pre-calciners for clinker making; 1i028
Prehydration; 2ii079
Process parametres; 1i047

Q
Qualitative; 1i004, 3v010, 3v011, 3v015
Quantitative; 1i039, 1i056, 3v007, 3v012, 3v013, 3v015, 3v020
Quartz; 1i048

R
Rapid hardening cement; 2ii017
Rate equations; 1i044
Reaction products; 4iv049
Reactivity; 1i016, 1i018, 1i047, 1i060, 2ii049, 2ii050, 3ii082, 3ii109, 3ii110, 3v020, 4iv016, 4iv050
Refractory; 2ii027, 4iv053, 4iv057
Relative humidity; 2ii073
Residual silica; 4iv049
Retarders; 3iii007, 3iii020, 3iii032
Rheology; 2ii003, 2ii004, 2ii011, 3iii003, 3iii027
Rice husk; 1i019
Rice Husk Ash; 3ii108, 3ii109, 3ii110
Rietveld analysis; 1i039, 1i056, 3v007
Roller compaction; 3ii086
Rotary kiln; 1i007, 1i019

S
Salt scaling; 4iv001
Scanning Electron Microscopy; 1i002, 2ii078, 3ii083, 3ii120, 3iii008, 3v019, 4iv037, 4iv064
Sea water; 4iv025
Secondary ettringite formation; 4iv065
Self deccication; 2ii073
Setting; 1i038, 2ii019, 2ii039, 2ii053, 2ii063, 3ii101, 3ii112, 3iii006, 3iii012, 3iii023, 3iii026, 3v008
Sewage; 3ii123, 3ii124, 4iv038, 4iv039
Shotcreting; 3iii027
Shrinkage; 1i032, 3iii018, 4iv036, 4iv056
Silica; 3ii080
Silica colloid; 3ii106
Silica fume; 2ii037, 3ii105, 3ii106, 3ii110, 3ii116, 3ii120, 3v001, 4iv014, 4iv069
Silica modulus; 1i035
Silicate; 2ii060, 3iii027, 4iv065
Simulation; 2ii078, 3iii001
Sintering; 1i005, 1i007, 1i022, 1i032
Slag; 1i020, 3ii080, 3ii092, 3ii094, 3ii097, 3ii100, 4iv050, 4iv051, 4iv058
Slump loss; 3iii003, 3iii020
Sodium chloride; 4iv022
Solid solution; 1i014, 1i023, 1i057, 2ii059, 1i060, 3v009
Solid state reactions; 1i042
Solidification; 4iv042
soluble glass; 2ii033

Sorption isotherms; 4iv077
Specific surface; 3iii028
Spectrophotometry; 3v012
Stability; 4iv065
Stabilization; 1i016, 2ii045, 4iv041
Standards; 3v025
Steam curing; 3ii102, 4iv036, 4iv063
Steel; 4iv014, 4iv082
Steric repulsive force; 3iii001
Strain softening; 2ii075
Strength; 1i048, 1i058, 3ii109, 4iv057
Strength development; 1i029, 1i038, 1i041, 2ii007, 2ii017, 2ii018, 2ii033, 2ii051, 2ii053, 2ii054, 2ii060, 2ii063, 2ii072, 2ii076, 2ii077, 3ii085, 3ii089, 3ii097, 3ii111, 3ii117, 3ii119, 3ii121, 3iii004, 3iii026, 3iii028, 3iii029, 3v024, 4iv024, 4iv052, 4iv054, 4iv055, 4iv056, 4iv058, 4iv063
Strength retrogression; 4iv019
Stress; 4iv049
Structure; 1i005, 1i014, 1i056, 2ii054, 2ii066, 2ii067, 2ii068, 2ii069, 2ii076, 4iv007, 4iv025, 4iv042, 4iv043, 4iv075
Sucrose; 3iii006
Sulphate; 1i049, 2ii012
Sulphate attack; 4iv002, 4iv018, 4iv020, 4iv021, 4iv024, 4iv057, 4iv059
Sulphate resistance; 3iii004, 3iii015, 4iv017, 4iv019, 4iv023
Sulphoaluminate; 1i001, 1i025, 2ii029, 3iii026, 3v009, 4iv029, 4iv030, 4iv068
Sulphoaluminoferrite; 1i014
Superplasticizers; 2ii002, 2ii004, 3iii001, 3iii002, 3iii019, 3iii020, 3iii021, 3iii030, 4iv001
Support; 2ii015
Synthesis; 1i015, 1i024, 1i033, 2ii064, 3ii113

T

Temperature; 1i005, 1i007, 1i008, 1i012, 2ii021, 2ii023, 2ii026, 2ii043, 2ii066, 3iii002, 3iii029, 3v001, 4iv047, 4iv060, 4iv068, 4iv069
Terminology; 4iv046
Texture; 1i048
Thawing; 4iv033
Thermal stress; 4iv072
Thermal treatment; 1i027
Thermodynamics; 1i042, 2ii024, 2ii057, 2ii058, 2ii059, 2ii062, 2ii066, 4iv039, 4iv066
Thermogravimetry; 2ii049, 3ii105, 3iii011 4iv003, 4iv037
Thermoporosimetry; 3v017
Tobermorite; 2ii064, 2ii065, 3v003
Trace components; 1i021
Transmission Electron Microscopy; 2ii068
Tricalcium silicate; 1i049 2ii041, 2ii044

U

Unreacted core model; 2ii051

V
Vibration; 2ii017
Viscosity; 1i014, 1i032, 2ii001, 2ii003, 2ii005
Void spacing factor; 3v024
Volume change; 2ii009, 2ii039, 2ii071, 2ii072, 4iv031

W
Waste disposal; 4iv012
Waste material utilization; 1i010, 1i019, 1i022, 1i025, 1i026, 1i027, 1i033, 2ii052, 3ii081, 3ii093, 3ii101, 3ii116, 3ii118, 3ii119, 3ii121, 3ii123, 3ii124, 3v003, 3v013, 4iv014, 4iv024
Water; 4iv075
Water sorption; 4iv008
Water suction; 4iv008, 4iv011, 4iv078
Water-to-cement ratio; 2ii071
Waterglass; 3ii092
Wedge splitting; 2ii075
White Portland Cement; 3iii004
Workability; 2ii011, 3iii029

X
X-ray Diffraction Analysis; 1i051, 1i016, 2ii041, 3iii028, 3ii087, 3ii114, 3v008, 4iv003
X-ray Fluorescense Analysis; 3v011
X-ray Powder Diffraction; 1i002, 1i010, 1i056, 2ii065, 4iv018

Z
Zeolites; 1i020, 1i024, 4iv028, 4iv045, 4iv046
Zeta potential; 3iii001, 3iii002

S 424 -10.2-

Proceedings of the 10th International Congress on the Chemistry of Cement : Volume 2: Cement hydration
<Hrsg.>: Justnes, Harald
Göteborg (1997)

Inventarnr. 50205

Entleiher	Ausleihdatum
~~Dr. Wahlmann~~	~~05. SEP. 1997~~
~~Dr. Spanka~~	
~~Dr. Schneider~~	
~~Rickert~~	~~23.10.02~~
~~Rung~~	~~29.01.10~~

PROCEEDINGS OF THE 10TH INTERNATIONAL CONGRESS ON THE CHEMISTRY OF CEMENT
Gothenburg, Sweden, June 2-6, 1997

VOLUME 3

ADDITIVES
ADMIXTURES
CHARACTERISATION TECHNIQUES

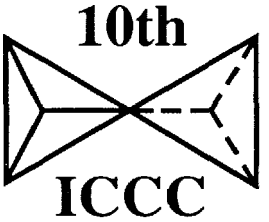

Göteborg 1997

Edited by

Dr. Harald Justnes
SINTEF Civil and Environmental Engineering, Cement and Concrete
Trondheim, Norway

Published by Amarkai AB and Congrex Göteborg AB in 1997

Copyright © Amarkai AB and Congrex Göteborg AB

All rights reserved. No part of this publication may be reproduced, stored in a retrieval system, or transmitted in any form or by any means, electronic, mechanical, photocopying, recording or otherwise without prior permission of the publishers.

Inform Trycket AB, Göteborg 1997
ISBN 91-630-5497-3

List of contents for Volume 3

II PORTLAND, BLENDED AND SPECIAL CEMENTS

II.F Effect of blends or additions of combustion ash, slag, silica fume or rice husk ash

S. Pavlenko, M. Shmelkov: "Cementless Binder and Silica Brick Based on it", 3ii080, 5 pp

M.V. Kougiya, L.S. Fraiman: "Hollow Microspheres of Ash and Binding, Compositions based on them", 3ii081, 4 pp

R. Härdtl: "The Pozzolanic Reaction of Fly Ash in Combination with Different Types of Cement", 3ii082, 8 pp

A. Katz: "Fly Ash Blended Cement Activated by a Strong Base", 3ii083, 4 pp

S. Jalali: "Modelling the Overall Rate of Reaction in Lime-Fly Ash Systems", 3ii084, 4 pp

D.M, Krizan, C.E.S. Tango, V.A. Quarcioni, Y. Kihara: "A Study on Time Behaviour of Fly-Ash Blended Cement Products", 3ii085, 8 pp

I. Papayianni: "Cooperation of Cement-Fly Ash System in High Paste Roller Compacted Concrete (RCC)", 3ii086, 4 pp

S. Dietz, K. Miskiewicz, M. Schmidt: "Properties of Cement Containing German Lignite Fly Ashes", 3ii087, 10 pp

S. H. Lee, E. Sakai, M. Daimon: "Characterization of Fly Ashes Directly Collected from Electrostatic Precipitator", 3ii088, 8 pp

M. Gawlicki, A. Łagosz, J. Małolepszy: "Utilization of Fly Ashes Containing Calcium Sulfite in Cement Production", 3ii089, 4 pp

S.L. Sarkar, J.R. Prusinski: "Microstructural Characterics of By-products of Petroleum Coke Blended Coal Combustion", 3ii090, 4 pp

E. E. Lachowski, F.P. Glasser, A. Kindness, K. Luke: "Compositional Development (Solid and Aqueous Phase) in Aged Slag and Fly Ash Blended Cement Pastes", 3ii091, 8 pp

S.N. Ghosh, D.M. Joshi, S. Chanda, H. Vaishnav: "Studies on Activation of Slag Cement", 3ii092, 4 pp

S. Manjit: "Effect of Blended Gypsum on the Properties of Portland Cement and Portland Slag Cement", 3ii093, 4 pp

K.M. Sharma, P.S. Sharma, D. Yadav, S.C. Ahluwalia: "Hydration Characteristics of Steel Slag in Ordinary Portland Cement Blends", 3ii094, 4 pp

W. Brylicki: "Modification of Alkali Activated Slag Pastes by Use of Mineral Admixtures", 3ii095, 4 pp

Mª.L. Romero, Mª.T. Blanco-Varela, A. Palomo, F. Puertas, T. Vasquez: "Activation of Blast Furnace Slag/High Alumina Cement Pastes: Mechanical and Microstructural Evolution", 3ii096, 8 pp

W. Roszczynialski: "Influence of Silico-Manganic Slag Additives on Cement Hydration and Properties",
3ii097, 4 pp

A. Fernandez-Jimenez, F. Puertas: "Kinetic Study of Alkali-Activated Blast Furnace Slag", 3ii098, 4 pp

C. Shi: "Early Hydration and Microstructure Development of Alkali-Activated Slag Cement Pastes", 3ii099, 8 pp

W. Jiang, M.R. Silsbee, D.M. Roy: "Alkali Activation Reaction Mechanism and its Influences on Microstructure of Slag Cement", 3ii100, 9 pp

M. Radenkova-Yaneva, S. Dimitrova: "Influence of Spent Blast Furnace Slag on the Properties of Cement Systems", 3ii101, 4 pp

A.F. Battagin, G. Camarini, M.A. Cincotto: "A Study of Early Hydration of Slag Cement Pastes Subjected to Thermal Curing", 3ii102, 4 pp

E. Marciano Jr., A.F. Battagin: "The Influence of Alkali Activator on the Early Hydration and Performance of Portland Blast Furnace Slag Cement", 3ii103, 4 pp

H. R. Kota, V. Ronin, E. Forssberg: "High Performance Energetically Modified Portland Blast-Furnace Slag Cements", 3ii104, 9 pp

B. Meng, P. Schiessl: "The Reaction of Silica Fume at Early Ages", 3ii105, 8 pp

S. Chandra, H. Bergqvist: "Interaction of Silica Colloid with Portland Cement", 3ii106, 6 pp

K. Asaga, H. Kuga, S. Takahashi, E. Sakai, M. Daimon: "Effect of Pozzolanic Additives in the Portland Cement on the Hydration Rate of Alite", 3ii107, 8 pp

L.K. Lin, C.L. Hwang: "The Characteristics and Hydration Mechanism of RHA Cement Paste", 3ii108, 4 pp

S. Sugita, Q.Yu, M. Shoya, Y. Tsukinaga, Y. Isojima: "On the Semi-Industrial Poduction of Highly Reactive Rice Husk Ash and Its Effect on Cement and Concrete Properties",
3ii109, 9 pp

G. C. Isaia: "Synergic Action of Fly Ash in Ternary Mixtures with Microsilica and Rice Husk Ash", 3ii110, 8 pp

Y. Xi, B.E. Scheetz: "Compressive Strength and Pore Structure of Slag-Silica Fume Cement Cured at 38-175°C", 3ii111, 4 pp

W.J. McCarter, H. Ezirim: "Characterising Reactivity of Alkali-Activated Pozzolans", 3ii112, 4 pp

M.L. Granizo, Mª.T. Blanco-Varela, F. Puertas, A. Palomo: "Alkaline Activation of Metakaolin: Influence of Synthesis Parametres", 3ii113, 8 pp

J.N. Liu, M.R. Silsbee, D.M. Roy: "Strength and Hydration of an Activated Alumino-Silicate Material", 3ii114, 6 pp

N.B. Singh, K.N. Bhattacharjee, A.K. Shukla: "Hydration of Portland Cement Blends in Presence of Bag House Dust from Calcium Carbide Furnace", 3ii115, 4 pp

V. Lilkov, O.E. Petrov: "Hydration of Cement Mixed with 'Pozzolit' Mineral Additive", 3ii116, 7 pp

R.F. Runova, V.S. Melentyeva, J.I. Ustimenko: "Peculiarities of Ukrainian Pozzolana Cements", 3ii117, 4 pp

Y. Takuma, Y. Tsuchida, S. Uchida: "Characteristics and Hydration of Cement Produced from Ash from Incinerated Urban Garbage", 3ii118, 8 pp

S. Sugita, Q.Yu, M. Shoya, Y. Tsukinaga, Y. Isojima: "The Effect of Waste Glass Powder on the Properties and Pore Structure of Normal Portland Cement Hydrates", 3ii119, 8 pp

F. Van Rickstal, D. Van Gemert, P. Parmentier, K. Vanbelle: "Addition of Ultra Fine Ground Sand for the Production of High Strength Autoclaved Mortars", 3ii120, 8 pp

T. Nishikawa, S. Ito: "Fracture Mechanics and Microstructure of Blended Cement Paste", 3ii121, 7 pp

X. Zhang, K. Wu, J. Han: "Research on a New Type of Composite Cement", 3ii122, 4 pp

G. Morales: "Utilization of Sewage Sludge as a Raw Material for Production of Pozzolanic Material", 3ii123, 5 pp

A. H. Abedel-Reheem, M.A. Shater, I. G. Al-Alm Rashed, A.N. El-Afify: "Utilization of Stored Cement. Part II: The Blending of Stored Cement by Fresh Cement", 3ii124, 4 pp

III UTILISATION OF ADMIXTURES; WATER REDUCERS, AIR ENTRAINERS, ACCELERATORS, RETARDERS AND POLYMERS

III.A Mechanisms; admixture chemical ↔ cement interaction

H. Uchikawa, S. Hanehara, D. Sawaki: "Effect of Electrostatic and Steric Repulsive Force of Organic Admixture on the Dispersion of Cement Particles in Fresh Cement Paste", 3iii001, 8 pp

R. Flatt, Y.F. Houst, P. Bowen, H. Hofmann, J. Widmer, U. Sulser, U. Mäder, T.A. Bürge: "Adsorption of Superplasticizers on Model Powders: Temperature Dependence, Effect of Zeta-potential and Role of Chemical Structure", 3iii002, 8 pp

U. Costa, F. Corazza, P. Colombet, V. Fernon, A. Vichet: "Mechanisms of Cement - Admixture Interaction", 3iii003, 12 pp

Mª.T. Blanco-Varela, A. Palomo, F. Puertas, T. Vazquez, J.R. Baragaño: "Effect of Superplasticizers on the Hydration of a Mineralized White Cement", 3iii004, 6 pp

M. Ichikawa, M. Kanaya, S. Sano: "Effect of Triisopropanolamine on Hydration and Strength Development of Cements with Different Character", 3iii005, 8 pp

P. Wang, J. Wu: "Influence of Sucrose on the Setting of Portland Cement", 3iii006, 4 pp

A. Rettel, D. Damidot, D. Müller, W. Gessner: "A NMR Study of Gels Formed during the Hydration of Calcium Aluminate Cements in the Presence of Citrate or Gluconate", 3iii007, 8 pp

S.P. Dennington, J.W. Goodwin, D.W. Thompson: "The Effect of Acrylic Polymer Latex Additions on the Hydration Kinetics of OPC and C_3S", 3iii008, 8 pp

N. Tsuyuki, H. Choi, K. Seki, M. Hatano: "The Hydration Behaviour of Converter Slag Admixed with Polymer Cement", 3iii009, 4 pp

G.K.D. Pushpalal, N. Maeda, T. Kawano, T. Kobayashi, M. Hasegawa: "The Efficacy of Calcium Aluminates in Producing High Flexural Strength Polymer Composite", 3iii010, 8 pp

M. Drabik, L. Galikova, F. Hanic, R.C.T. Slade: "MDF-related Systems based on Sulfobelitic Clinker / Hydroxypropylmethyl Cellulose / Polyphosphate Glass Compositions", 3iii011, 8 pp

H. Justnes, E.C. Nygaard: "The Mechanism of Calcium Nitrate as Set Accelerator for Cement", 3iii012, 8 pp

S.A. Farrington, D. Constantiner: "Effects of Cement/Admixture Interactions on the Early Stiffening Tendencies of Portland Cement Paste", 3iii013, 8 pp

J.S. Lota, P.L. Pratt, J. Bensted: "Effect of Sodium Aluminate on Class G Oil Well Cement Hydration at Low and Ambient Temperatures", 3iii014, 8 pp

G. Dumitru, T. Vázquez, F. Puertas, M^{a}T. Blanco-Varela: "Influence of $BaCO_3$ on the Hydration of C_3A", 3iii015, 5 pp

G. Gu, X. Wang, P. Wang, M. Chen: "Mechanism of Delayed Expansion and New Type Chemically Prestressed Concrete Filled Steel Tube", 3iii016, 8 pp

A. Ishida, M. Morioka, T. Mihara, H. Hagiwara: "Expansion of Slag Cement with Expansive Additives", 3iii017, 8 pp

H. Ai, J.F. Young: "Mechanism of Shrinkage Reduction Using a Chemical Admixture", 3iii018, 8 pp

III.B Influence of admixtures on microstructure development

A.M. Grabiec, R. Krzywobłocka-Laurów: "Influence of Melamine Superplasticizer on some Characteristics of Concrete", 3iii019, 6 pp

S.C. Maiti: "Performance of High-Range Water Reducers in Cement Concrete Mixes in Hot Weather Conditions", 3iii020, 4 pp

B.E. Ioudovitch, A.M. Dmitriev, S.A. Zoubekhine, N.F. Bashlykov, V.R. Falikman, V.N. Serdyuk, Sh.T. Babaev: "Low-water Requirement Binders as New-generation Cements", 3iii021, 4 pp

S. Hirose, T. Higaki, K. Asaga, M. Daimon: "Study on Hydration and the Properties of Hardening Accelerators Based on Calcium-Aluminate Glass", 3iii022, 8 pp

J. Szczerba, S. Peukert, M. Zdaniewicz: "Organosilicone Compound Effect on the Cement Matrix", 3iii023, 8 pp

J. LaRosa-Thompson, P. Gill, B.E. Scheetz, M.R. Silsbee: "Sodium Silicate Applications for Cement and Concrete", 3iii024, 8 pp

III.C Combined admixtures and their mixing techniques

M.A. Sanitsky: "Mechanism of Alkali-containing Complex Chemical Admixtures and Portland Cements Interaction", 3iii025, 8 pp

L. Zhang, M. Su: "Control Properties of Sulpho- and Ferro-aluminate Cement Concrete with Special Admixtures", 3iii026, 7 pp

T. Coverdale, J. Champa, L. Eckert: "Total Consistency Control for Wet Shotcrete - A Slump Killing System for Improved Performance", 3iii027, 7pp

Ž. Sekulić, M. Stefanović, B. Živanović: "Mechanical Activation of Ordinary Portland Cement and Cement with Additives", 3iii028, 5 pp

III.D Influence of type, dose, addition time and mixing time

J. Komonen, V. Penttala: "Influence of Admixture Type and Concrete Temperature on Strength and Heat of Hydration of Concrete", 3iii029, 8 pp

W. Jiang, D.M. Roy: "Interaction Mechanism of Chemical Admixtures and their Influences on Microstructure", 3iii030, 8 pp

G. Rosenthal, L. Brower: "Effect of Chemical Admixtures on CH Crystal Growth", 3iii031, 5 pp

H. Pöllmann, St. Stöber: "Hydration Characteristics and New Hydrates using Organic Additives (Carboxylates & Sulfonates)", 3iii032, 8 pp

Y. Ohama, K. Demura, H. Iwasaki: "Evaluation of Chemical Inhibitors for Alkali-Aggregate Reaction by Accelerated Tests", 3iii033, 8 pp

V DEVELOPMENTS IN CHARACTERISATION TECHNIQUES

V.A Nuclear Magnetic Resonance (NMR)

A.R. Brough, C.M. Dobson, I.G. Richardson, G.W. Groves: "^{29}Si Enrichment and Selectiv Enrichment for Study of the Hydration of Model Cements and Blended Cements", 3v001, 6 pp

L. Bonafous, P. Colombet, C. Bessada, D. Massiot, J.-P. Coutures: "High-Temperature ^{19}F NMR Observation of Fluorine Activity in Clinker Processing", 3v002, 6 pp

P. Faucon, F. Adenot, J.F. Jacquinot, J. Virlet, R. Cabrillac, M. Jorda: "Contribution of Nuclear Magnetic Resonance Techniques to the Study of Cement Paste Water Degradation", 3v003, 8 pp

T. Lyashenko, V. Voznesensky, S. Boyko, D. Shtakelberg: "Experimental-Statistical Modeling and Analysis of the Chain "Composition-NMR signal-Properties" of Cement Composite", 3v004, 8 pp

B. Touzo, D. Massiot, D. Trumeau, A. Douy, J.P. Coutures: "Cooling of Liquid Calcium Aluminates Monitored by ^{27}Al NMR Time Resolved Experiment", 3v005, 4 pp

C.-L. Hwang, P.K. Chang: "The Study of the Properties of High Performance Concrete Paste by Using NMR", 3v006, 7 pp

V.B X-ray diffraction (XRD)

J. Neubauer, H. Pöllmann, H.W. Meyer: "Quantitative X-ray Analysis of Clinker and OPC by Rietveld Refinement", 3v007, 12 pp

G. Goswami, B.N. Mohapatra, P.K. Panigrahy, J.D. Panda: "Application of X-ray Diffractometry in Communition of Gypsum", 3v008, 4 pp

V.C Other techniques

J. Strigáč, J. Krištín, S. Sahu, M. T. Palou, J. Majling: "An Approach to Refine the Bogue's Phase Composition of Sulfoaluminate Belite Cement", 3v009, 7 pp

F. Tamás, M. Pátkai-Horváth, É. Kristóf-Makó, J. Tritthart: "Qualitative Identification of Clinkers and Cements - Some Results and Possibilities", 3v010, 7 pp

J.H. Potgieter: "Fingerprinting S.A. Cements by Chemical Analysis", 3v011, 6 pp

H. Sedaira, K.A. Idriss, M.M. Seleim. M.S. Abdel-Aziz: "Use of Quinizarin as a Spectrophotometric Reagant for MgO Content Analysis of Portland Cement and Cement Clinker", 3v012, 9 pp

S. Takahashi, H. Anzai, H. Nemoto: "Analysis of the Trace Elements in Raw Materials and Cement by means of ICP-AES", 3v013, 4 pp

P. Cassat, J.F. Muller, A. Vichot, P. Colombet: "Direct Detection of Grinding Aids in a Cement Matrix", 3v014, 4 pp

A. Ohno, T. Yamamoto: "Qualitative and Qantitative Analysis of Organic Compounds in Cement and Hardened Cement", 3v015, 4 pp

A. V. Usherov-Marshak: "Calorimetric Analysis in Chemistry of Cement", 3v016, 8 pp

S. Matala: "Thermoporosimetry in the Pore Analysis of Concrete", 3v017, 9 pp

S. Möhmel, W. Gessner, B. Ködderitzsch: "A Comparison of Two Different Methods for Stopping the Hydration of Mono Calcium Aluminate at 20°C", 3v018, 7 pp

E.T. Stepkowska, A.K. Mullick, S.K. Handoo, J.L. Perez-Rodriguez, M.A. Aviles, E. Gomez: "Studies on Cement Hydration by Water Sorption and Static Heating", 3v019, 4 pp

P. Arjunan, M.R. Silsbee, D.M. Roy: "Quantitative Determination of the Crystalline and Amorphous Phases in Low Calcium Fly Ashes", 3v020, 4 pp

C. L. Hwang, I. Y. Jann: "Non-destructive Evaluation of Rich Fly Ash HPC", 3v021, 4 pp

M. Nadu, M. Schieber, J. Nissenbaum, M. Braiman, M. Lukach, S. Boyko, D. Shtakelberg: "Limitations of Standard Test Methods to Predict Delayed Damaging Alkali-Agregate Reaction (AAR) in Concrete", 3v022, 8 pp

G. Diaz, P. Kittl, V. Martinez: "On the Mechanical Properties of Compacted Neat Cement Paste, Cement Mortar and Gypsum Paste", 3v023, 8 pp

Z.B. Entin, L.S. Nefyodova: "Parameters Relevant for Standardization of Sand and Mortar", 3v024, 4 pp

O. Baumanis, J. Kļaviņš, A. Miezis: "Comparison of Physical and Mechanical Properties of Portland Cement according to LVS EN 197-1 and ГОСТ 10178-85", 3v025, 4 pp

V. Alunno Rossetti, F. Curcio: "A Contribution to the Knowledge of the Properties of Portland-Limestone Cement Concretes, with respect to the Requirements of European and Italian Design Code", 3v026, 6 pp

THEME II

PORTLAND, BLENDED AND SPECIAL CEMENTS

TOPIC II.F

Effect of blends or additions of combustion ash, slag, silica fume or rice husk ash

CEMENTLESS BINDER AND SILICA BRICK BASED ON IT

Stanislav PAVLENKO, SSAMM, Novokuznetsk, Russia
Michail SHMELKOV, SSAMM, Novokuznetsk, Russia

ABSTRACT A cementless binder based on high-calcium ash from brown coals of the Irsha-Borodinsky deposit has been developed by the SSAMM. High-calcium ash was previously ground to the fineness of 4500 to 4800 cm^2/g, and 10 to 15 percent silica fume was introduced into it. Hot water (60 to 80 degrees) was used for mixing. As a result, the binder obtained had a compressive strength of 20 to 35 MPa. Cohesion of the binder was improved by binding free lime (8 to 15%) with microsilica and by more complete hydration of the blended cement binder achieved through grinding and hot water treatment.

KEYWORDS: High-Calcium Ash, Cementless Binder, Ash-Slag-Silica Brick.

INTRODUCTION

The objective of this work was to develop a cementless binder based on high-calcium fly ash from the Abakanskaya thermal power plant and the technology of the production of a silica brick on the basis of this binder using slag sand from the same thermal power plant as an aggregate and silica fume as an admixture. Expensive materials such as lime, sand and cement were not required. Besides, the production of this brick would contribute to the solution of the environmental problem and satisfy the great need of the thermal power plant in concrete and brick. Technology of the production of non-autoclave ash-slag-silica brick, which uses an ash-slag blend as a binder and does not contain any lime or sand, has been developed.
The difficulty is that, so far, state standards for use of high-calcium ashes derived from brown coals of the Kansko-Achinsky deposit in various types of concretes and structural materials have not been developed. There are only specifications 34-70.10898-88 (1988) developed by several institutes.

MATERIALS

Fly ash

The ash from the Abakanskaya thermal power plant is produced by burning powdered brown coals of the Irsha-Borodinsky deposit. It is collected by electric filters and then delivered to landfills by water, binding properties of ash being-lost. Average grading fractions of the ash from all electric filters were taken for the investigation.
Physical properties of ashes from the Kansko-Achinsky deposit are standardised by two indices (1988), i.e., specific surface and residue on sieve No 008. They were determined in accordance with the State Standard 310.02-76 (1976 a) and 310.3-76 (1976 b). The data are given in Table 1.

Table 1 Physical Properties of Fly Ash

Indices	Standards		Data from Investigation
	First Grade	Second Grade	
Specific Surface, no less cm^2/g	2800	2000	2358
Residue on Sieve No 008, no more, %	12	15	7.5

As can be seen from Table 1, the ash is of the second grade due to its specific surface. To improve the ash grade, its physical properties, chemical activity and, consequently, to eliminate

spreading of concrete, the ash should be ground. Chemical analysis of the ash was made in accordance with the state Standard 5382-91 (1991). The data of the analysis are given in Table 2.

Table 2 Chemical Analysis of Ash

Oxides	Contents,%
Silicon dioxide (SiO_2) total	39.45
including SiO_2 free	24.2
Calcium oxide (CaO) total	31.20
including CaO free	8.96
Magnesium oxide (MgO)	6.31
Aluminium oxide (Al_2O_3)	7.11
Ferrous oxide (FeO)	0.87
Ferric oxide (Fe_2O_3)	9.92
Manganese oxide (MnO)	0.18
Sulphur trioxide (SO_3)	0.86
Titanium oxide (TiO_2)	0.9
Sodium oxide (Na_2O)	0.4
Potassium oxide (K_2O)	0.7
Loss on Ignition	1.85

Table 3 gives specifications for high-calcium ashes.

Table 3 Specifications For Ashes

Indices	Standards	
	First Grade	Second Grade
1. Coefficient of Quality (Q) $Q=(CaO+Al_2O_3+MgO)/SiO_2$	1.2	1.0
2. Contents, %		
2.1 Free Calcium oxide, CaO no more	6.0	9.0
2.2 Magnesium oxide, no more	3.0	7.0
2.3 Sulphur trioxide, no more	5.0	5.0
2.4 Loss of Ignition	3.0	5.0

Due to its coefficient of quality (Ignatova, 1990), the ash investigated is of the second grade (1.13) but it has good binding properties (Q>1). The high contents of free silica, free calcium oxide (8.96%) and magnesium (6.31%) increase the binding properties of the ash after its grinding and heat treatment. The ash investigated has a very low sulphur trioxide content (0.85%), and a loss on ignition is negligible (1.85%).

Slag sand

Slag from the Abakanskaya thermal power plant was ground to a sand with a particle size of 0 to 5 mm. Chemical analysis of the slag sand was performed in accordance with the State Standard 26644-85 (1985). The data on chemical analysis are given in Table 4.

The losses of the slag mass on determining the silicate and ferriferous decompositions were 6.38 to 6.7% and 4.46 to 4.6%, respectively. These meet the State Standard, requirements (no more than 8 and 5%) for use in concretes and brick.

Table 4 Chemical Analysis of Slag Sand

Oxides	Quantities,%	
	Standard	In Fact
Silicon dioxide (SiO_2) total	Non-standardised	56.47
including free SiO_2	Non-standardised	15.57
Calcium oxide (CaO) total	Non-standardised	29.92
including free CaO	no more than 1%	-
Magnesium oxide (MgO)	Non-standardised	3.50
Aluminium oxide (Al_2O_3)	Non-standardised	8.16
Ferrous oxide ($FeO+Fe_2O_3$)	Non-standardised	9.63
Manganese oxide (MnO)	Non-standardised	0.17
Phosphorus oxide (P_2O_5)	Non-standardised	0.05
Sulphur trioxide (SO_3)	no more than 3%	0.011
Loss on Ignition	no more than 3%	-

TECHNOLOGY OF THE PRODUCTION OF NON-AUTOCLAVE ASH-SLAG-SILICA BRICK

Mixture Proportions

To determine the optimum mixture proportions for the ash-slag-silica mixture, the following series of tests were carried out:

1. The influence of an ash-to-slag ratio on the strength of the ash concrete was determined (Fig.1). The mixing water had a room temperature (+18 °C). As can be seen from Fig. 1, the a/w = 4:1 gave the best results.

2. The effect of the temperature of mixing water on the strength of the ash concrete was determined (Fig. 2). The best results were obtained with the temperature of mixing water of 60 to 80 °C.

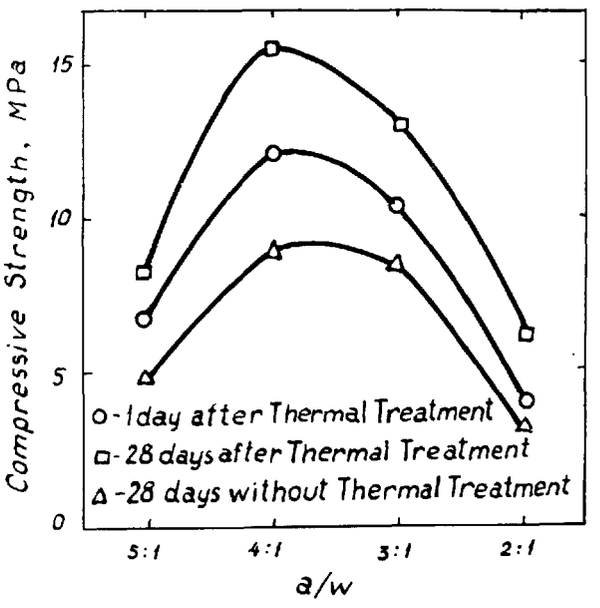

Figure 1 Strength of Ash Concrete Versus Ash-to-Water Ratio

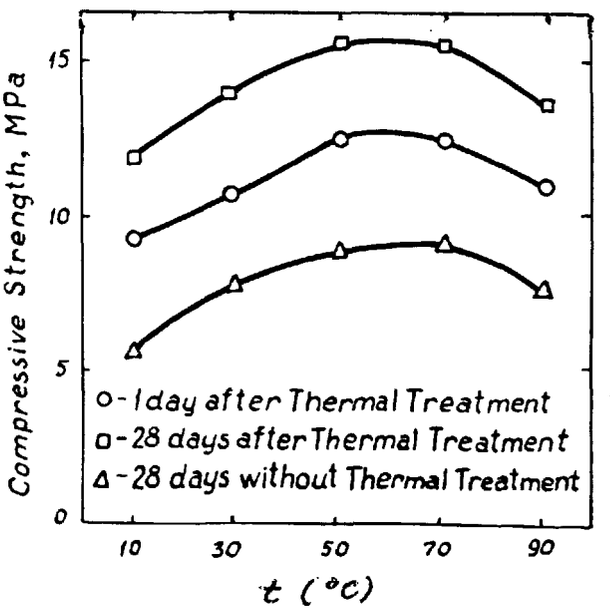

Figure 2 Strength of Ash Concrete Versus Water Temperature

3. The optimum amount of silica fume was determined. Table 5 shows the proportioning of the cementless concrete mixtures.

Table 5 Mixture Proportions and Properties of Fresh Concrete

Ingredients, kg/m^3			Slump, cm	Average Density kg/m^3	Compressive Strength, MPa
Fly Ash	Silica Fume	Water			
1540	- (0%)	420	4.6	1860	12.5
1460	73 (5%)	440	5.0	1885	13.8
1390	139 (10%)	400	4.0	1835	15.6
1237	186 (15%)	390	4.5	1750	15.2
1138	228 (20%)	380	4.8	1670	12.1

As can be seen from Table 5, the best results were obtained with 10 to 15% silica fume. The optimization of mixture proportions and technological parameters such as schedule of curing, temperature of mixing water etc, were performed using the mathematical method of the experimental planning (Voznesensky, 1972). The optimum mixture proportions of the ash-slag-silica mixture for the production of bricks were as follows:
High-Calcium Ash - 650-750 kg
Silica Fume - 70-80 kg
Slag Sand - 1000-1100 kg
Water - 180-210 kg
Superplasticizer - 0.7-2 kg (0.1-0.3% by weight of a binder)

Technology

The high-calcium ash collected by electric filters was ground in ball-tube mills to 4000 cm^2/g fineness which destroyed the glossy cover of the ash and sharply increased the degree of its hydration as well as accelerated the interaction of free calcium oxide and amorphous microsilica. This process was studied previously (Pavlenko, 1994).
The molten slag produced by the thermal power plant was granulated by water and ground to a particle size of 0 to 5 mm in roller crushers. The ash-slag-silica blend was mixed in a fixed-drum concrete mixer using hot water and at 12% humidity of the mixture. Brick was produced by the method of dri-pressing (P=20-25 MPa) and then cured in steam-curing chambers at 95 to 100 °C using a 3+10+3h cycle. The introduction of a high-molecular S-3 superplasticizer into the mixture (0.1 to 0.3% by weight of the ash) significantly improved its workability and increased the strength and durability of the brick. The variation of the free CaO content from 5 to 15% did not significantly affect the strength of the non-autoclave ash - slag- silica brick.

CONCLUSIONS

1. Non-autoclave slag-ash-silica brick having the compressive strength of 12.5 to 15 MPa, the average density of 1900 - 1950 kg/m^3 and frost resistance of 50 to 75 cycle has been produced. The brick meets the requirements of the State Standard 379-79 "Silica brick. Specifications".
2. The production cost of this brick is 35 to 40% lower than that of an ordinary autoclave silica brick.
3. The production of the ash-slag-silica brick directly at the Abakanskaya thermal power plant permitted to solve the problem of utilisation of by-products, to use steam and electrical energy of the plant.

REFERENCES

Ignatova, O.A., "Study of the Uniformity of High-Calcium Ash Derived from Kansko-Achinsky Coals and the Development of the Standard Requirements for Use in Concretes", Concretes Containing Ash and Slag from TPP and their Use in Construction, Conference Proceeding Edited by S.I. Pavlenko, V.1, Novokuznetsk, 1990, pp 145..150.

Pavlenko, S.I., "Structure Formation of Slag Ash Concrete on the Basis of High-Calcium Fly Ash and Silica Fume", Materials and Structures Journal, 1994, 27, pp.401-407.

Specifications 37-70-10898-88. "High-Calcium Ash Derived from Kansko-Achinsky Brown Coals Used as an Admixture for Concrete a Structural Materials", August 17, 1988, 43 pages.

State Standard 310.2-76* "Cements, Methods for Determining Fineness of Grinding", Gosstroy USSR, Puplishing Hause of Standards, Moscow, 1976.

State Standard 310.3-76* "Cements, Methods for Determining Normal Density, Setting Time and Uniformity of Volume Change", Gosstroy USSR, Publishing House of Standards, Moscow, 1976.

State Standard 5382-91 Gosstroy USSR, Publishing House of Standards, Moscow, 1991.

State Standard 26644-85, "Crushed Stone and Sand from Slag of Thermal Power Plants for Use in Concrete", Gosstroy USSR, Moscow, Publishing House of Standards, 1986.

Voznesenky, V.A., "Statistical Methods of the Experimental Planning in Technicoeconomical Investigations", Moscow, Izdatelstvo Statistiki, 1972, p192.

HOLLOW MICROSPHERES OF ASH AND BINDING COMPOSITIONS BASED ON THEM

Marina V. KOUGIYA, Giprocement, Phys.-Chem. Studies Lab., St. Petersburg, Russia
Lev S. FRAIMAN, Giprocement, Process Engineering Lab., St. Petersburg, Russia

ABSTRACT The properties of and possibilities for utilizing hollow microspheres, one of ash dump species formed when burning coals and oil shales, are described.

KEY-WORDS: Waste material utilization, Filler, Fly ash.

INTRODUCTION

Aluminosilicate hollow microspheres of coal ash have been studied by Raask (1968) and Redlov (1974). Kizilstein et al (1987) have investigated ash microspheres from burning coals of Russia. The hollow inorganic microspheres are an ideal filler and are used in many industry branches (Aslanova, 1981; Manual, 1981). Goberis et al (1990) have developed a heat-resistant concrete on a basis of hollow microspheres. Lalov et al (1990) have presented data of obtaining and utilizing hollow microspheres.

EXPERIMENTAL

For studies use was made of specimens of ash products obtained at the heat-and-power station of the town of Angarsk (the Irkutsk region) where the mix of coals of coalfields of the East Siberia was burnt. Ash products generated at the heat-and-power station of the town of Narva when burning oil shales in boiler furnaces have been also studied. Averaged samples of ash products and the most light weight fraction representing a foam material floating at the surface of the ash pond were taken. The chemical composition of samples is given in Table 1, their physical characteristics are listed in Table 2. Microscopic and X-ray phase analyses of all four samples have been performed. The X-ray phase analyses were done with the help of ДРОН-3 device. The grain size distribution of the samples was determined using the Analyzette-22 Sedimentograph of FritschGmbH.

Table 1 Chemical composition of hollow microspheres fractions and averaged samples of coal and oil shale ashes.

№	Specimen	Oxide content, %							
		LOI	SiO_2	Al_2O_3	Fe_2O_3	CaO	MgO	SO_3	K_2O
1	Averaged coal ash sample	3.61	52.92	23.82	6.66	8.92	2.19	3.19	1.77
2	Fraction of hollow microspheres of coal ash	0.95	58.50	30.93	3.65	3.15	2.03	-	1.80
3	Averaged oil shale ash sample	-	28.06	7.64	5.00	48.85	3.74	3.74	2.61
4	Fraction of hollow microspheres of oil shale ash	42.26	2.08	0.75	0.23	52.54	0.19	1.18	0.37

Table 2 Physical characteristics of hollow microspheres and averaged samples of coal and oil shale ashes.

№	Specimen	Apparent density, kg/cu.m	Bulk density, kg/cu.m	Glass density, kg/cu.m	Microsphere wall thickness μm	Melting temperature	
						t_B, °C	t_C, °C
1	Averaged coal ash sample	2600	960	2500	-	1320	1400
2	Fraction of hollow microspheres of coal ash	540	290	2500	5 - 10	1400	1480
3	Averaged oil shale ash sample	2450	800	2650	-	1330	1360
4	Fraction of hollow microspheres of oil shale ash	485	232	-	0 - 5	-	-

Besides, binding compositions with the use of fractions of hollow microspheres of coal ashes were prepared. For test specimen preparation the components were ground up to the proper size, but for fraction of hollow microspheres, weighed out in necessary ratios and mixed. On addition of the required water amount and mixing the paste prepared was placed into the forms and compacted. After one-day storing under moist conditions the paste was unmolded, and the further specimen hardening ran under several conditions simulating the actual conditions of lining works, wherever possible. Table 3 gives the results for specimens which were hardened under the following conditions: 7 days of air-moist storing and 3 days at temperature of 110°C. The microspheres ratio was 10%. The specimens were prepared with the use of alumina and portland cement. Crashed chamotte brick in fraction of 3-7 mm and 1-3 mm served as a coarse aggregate.

Table 3 Strength and thermal characteristics of binding compositions.

Specimen No	Specimen Name	Compressive strength, MPa			Shrinkage after heating at 1200°C	Refractoriness, °C
		upon 7 days of air-moist storing + 3 days at 110°C	on heating at			
			800°C	1200°C		
1	Fraction of hollow microspheres: alumina cement=0.32	39.6	35.4	50.3	1.2	above 1500
2	Fraction of hollow microspheres: portland cement=0.24	22.6	15.0	30.7	1.2	above 1300

DISCUSSION OF RESULTS

Peculiarity of the chemical composition and properties of hollow microspheres was noted. For specimens of coal ash this was in the higher SiO_2 and Al_2O_3 content and in the lower Fe_2O_3 and CaO content for hollow microspheres fractions as compared with the averaged sample which was an indication of the aluminosilicate composition of material. The same was observed by Raask (1968), Redlov (1974) and Kizilstein et al (1987). The microscope study showed that rounded particles were made up of glass the refraction index of which is characteristics of glasses of mullite composition, a fine-grained crystallization of mullite was found at the surface. The rounded particles floated up in immersion oils which pointed to the low density and was supported by experiments (Table 2). The main element of the diffraction pattern for the specimen of hollow microspheres of coal ashes was a wide diffuse maximum over an interval of angles $2\Theta = 8 - 20^0$ characteristic of highly disordered and glassy phases. The diffraction peaks of mullite and quartz were noted at its descending branch. The main size of globules for the hollow microsphere fraction was 80-120 μm. The enrichment of samples with a fraction of hollow microspheres improved their refractoriness.

For the specimens of the oil shale ash the CaO and LOI content of the hollow microspheres fractions increased, and the SiO_2, Al_2O_3 and Fe_2O_3 contents decreased. The composition of this fraction is closely approximating the calcium carbonate composition. This was confirmed by the X-ray analysis. At the X-ray diffraction photograph there were seen reflexes of calcite. The specimen heating up to 950^0C provided support to the fact that the bulk of it was made up of calcite since at the X-ray diffraction photograph of the product after the thermal treatment there detected only CaO reflections and SiO_2 relics. The main size of globules was 150-250 μm. In this case the suggestion has been made that in consequence of the high CaO content of gas because of its high concentration in the initial fuel (the Baltic oil shales) the secondary calcium carbonate was deposited in large quantities on the thin aluminosilicate walls of the microspheres. The carbonate composition of the hollow oil shale ash microspheres was observed by Goberis (1990). This kind of material was characterized by the least density. The strength of the specimens was moderate.

From the data of Table 3 it may be concluded that binding compositions with microspheres on alumina and portland cement met the requirements of the Russian standards for heat-resistant concretes both in regard to the initial strength and upon heating at 800^0C, in respect of shrinkage at 1200^0C and refractoriness.

CONCLUSIONS

The studies conducted showed the peculiarity of hollow microspheres fractions in comparison with averaged samples of ash products as to chemical and mineral compositions, density characteristics and thermal properties. Ligtweight heat-resistant concretes for lining works can be prepared with the use of hollow microspheres. The hollow microspheres of the oil shale ash are promising as adsorbents or as filling material forming the heat-insulating layer and so on.

REFERENCES

Aslanova, M.S. Stetsenko, V.L. and Shustrov, A.F., "Hollow Inorganic Microspheres", Ser.Khimicheskaya Promyshlennost za Rubezhom, Obzornaya Informatsiya, Trudy NIITEKhim, Moscow, 9, 1981, pp. 33-51.

"Fillers for Polymeric Composite Materials", (Manual), Khimiya, Moscow, 1981, 736 pp.

Goberis, S.Yu., Kizilstein, L.Ya., Pundene, I.I. and Spitzglus, A.L., "Heat-Insulating Refractory Concrete on a Basis of Aluminosilicate Hollow Microspheres of Ash of Coal-Fired Heat-and-Power Stations", Energeticheskoye Stroitelstvo, 5, 1990, pp. 36-38.

Kizilstein, L.Ya., Spitzglus, A.L. and Rylov, V.G., "Aluminosilicate Microspheres of Powdered Coal Combustion Ash", Khimiya Tvyordogo Topliva, 6, 1987, pp.122-126.

Lalov, D., Petsovska, A. and Stoyev, S., "Obtaining and Use of Microspheres - a Lightweight Fraction of Heat-and-Power Station Ash", Energeticheskoye Stroitelstvo, 3, 1990, p. 61.

Raask, E., "Cenospheres in Pulverized-Fuel Ash", Journal of the Institute of Fuel, 41, 332, 1968, pp.339-344.

Redlov, J., "Cenospheres", Bureau of Mines, 8640, 1974, pp.33-43.

3ii082
8 pp

THE POZZOLANIC REACTION OF FLY ASH IN CONNECTION WITH DIFFERENT TYPES OF CEMENT

Reiner HÄRDTL, Heidelberger Zement AG, Department for Research, Development and Consulting in Leimen, Germany

ABSTRACT Investigations into the chemico-mineral structure of hardened cement paste in mortars were conducted to examine the pozzolanic reaction of fly ash. Especially in this context, the interaction between fly ash and different types of cement (portland-slag cement, blast-furnace slag cement, portland-limestone cement) was investigated. The beginning and development of the fly ash reaction depend, to an extreme extent, on the content of clinker and slag in the cement. The higher the portion of slag in the cement, the slower the fly ash reaction. The main reason is the lower $Ca(OH)_2$ content available. In the initial phase of the pozzolanic reaction the strength contribution of the fly ash is higher than later on, resulting from the bond of the fly ash particles into the matrix of the hardened cement paste.

Key-words: Fly ash, Reactivity, Blastfurnace slag, Calcium hydroxide, CSH

INTRODUCTION

Concrete is not any longer only a simple three-component-system consisting of cement, water and aggregates. The choice of different cement types and various additives makes concrete a complex multi-component-system. From a technological and economic point of view, the selective use of mineral additives (e.g. slag, fly ash, limestone filler) during the production of cement and concrete allows a very flexible control of concrete properties depending on the specific application.

The trend in the past few years has been to combine the application of these materials. However, it is necessary to gather as much information as possible about the reaction mechanisms of the individual components in order to take optimum advantage of the effects of such combinations. Here, the interaction between the components is of special interest. For basic technological research, it is of minor importance whether the substances are applied as additives blended to cement or as additions to the concrete. This report takes a closer look at the development of the pozzolanic reaction of fly ash in connection with different types of cement (portland-slag cement, blast-furnace slag cement, portland-limestone cement).

EXAMINATIONS

Table 1 gives a general survey of the cements examined. For comparison, portland cements were also included in the investigations. All cements meet the requirements of ENV 197-1. A low-calcium fly ash conforming to EN 450 "Fly ash for concrete" and produced in a dry-bottom furnace was used (its properties are equivalent to ASTM Class F fly ash).This type of fly ash has a specific surface of 379 m^2/kg retaining 16.5 wt.% residue after passing a 40-µm-sieve. The amount of glass is approximately 80 wt.% and the loss of ignition is 1.7 wt.%.

First, standard mortars according to EN 196-1:1994 were produced. 20 wt.% of the cement was replaced by the same weight of fly ash (f/c=0.25). The ratio w/(c+f) = 0.60 was held constant for all mixes.

The mortars were demoulded after 24 hours and the samples were stored in water (20°C) until testing. For more detailed information on the composition of the substances used and the conduction of tests are documented in preceding publications (Härdtl, 1992 and Härdtl,1995).

Table 1 List of cements

Cement	Type of cement	Designation	slag content wt. %	specific surface m^2/kg
C1	CEM I 32,5 R	Portland cement	-	269
C2	CEM I 32,5 R	"	-	338
C3	CEM I 42,5 R	"	-	387
C4	CEM II/A-L 32,5 R	Portland-limestone cement	18[1)]	465
C5	CEM II/B-S 32,5 R	Portland-slag cement	26	349
C6	CEM III/A 32,5	Blastfurnace cement	50	370
C7	CEM III/A 32,5	"	49	353
C8	CEM III/B 32,5	"	74	390

[1)] limestone filler

$Ca(OH)_2$ CONSUMPTION DURING POZZOLANIC REACTION

Apart from its physical and rheological effect, fly ash is mainly applied in concrete for its pozzolanic reaction. The main feature of the pozzolanic reaction of fly ash is the consumption of $Ca(OH)_2$. $Ca(OH)_2$ is formed during the hydration of the portland cement clinker. In the course of the pozzolanic reaction, the glassy siliceous parts of the fly ash react with the free $Ca(OH)_2$ in the hardened cement paste, in the course of which new CSH phases are formed. The amount of $Ca(OH)_2$ in the hardened cement paste is reduced by this reaction. The amount of $Ca(OH)_2$ thus consumed is a significant parameter for describing the development of pozzolanic fly ash reaction.

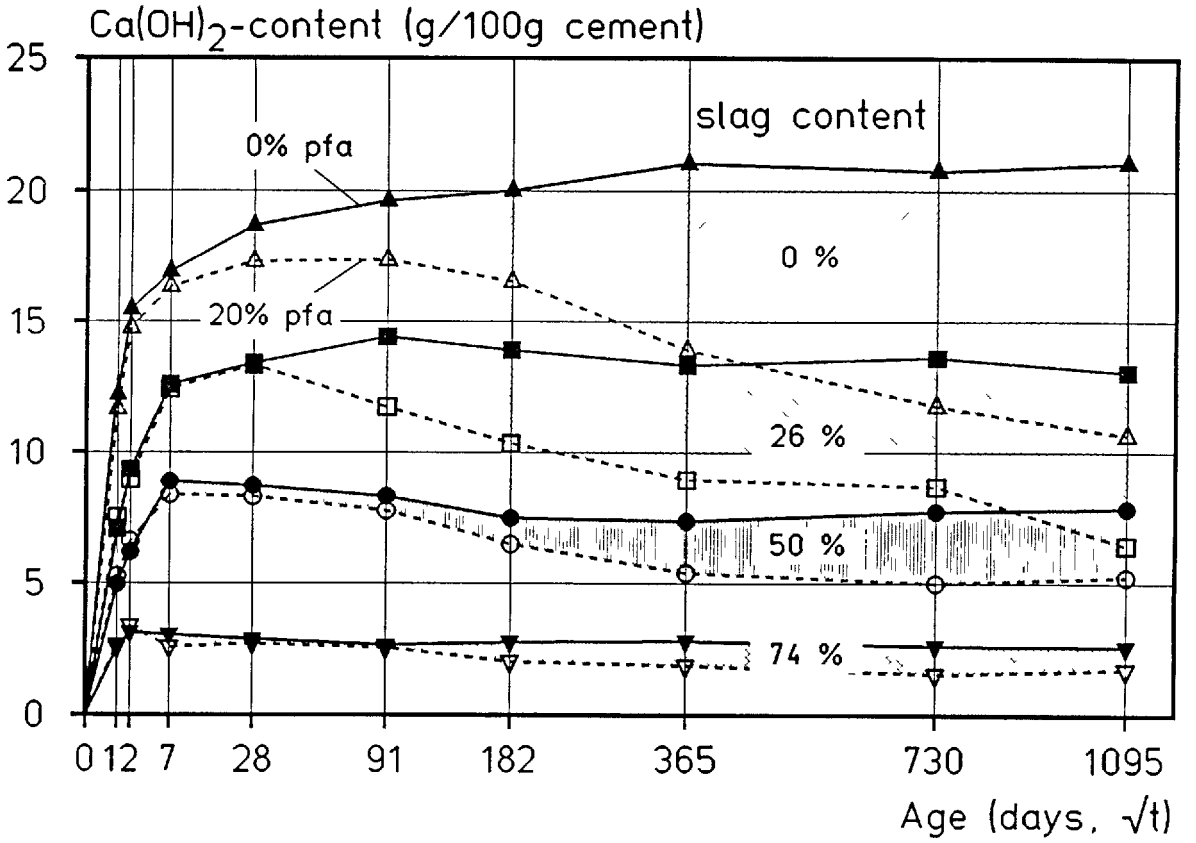

Figure 1 Development of $Ca(OH)_2$ content in mixes with different types of cement (mortar, w/(c+f) = 0.60; water curing)

In Figure 1 the development of the $Ca(OH)_2$ content for mixtures with 20 wt.% fly ash is contrasted to the corresponding reference mixes without fly ash. The amount of free $Ca(OH)_2$ in hardened cement paste was analysed by means of the Franke extraction method. This procedure not only determines CaO in free $Ca(OH)_2$, but also CaO components of other hydration products are extracted (Ramachandran, 1979; Shebl et al.,1983). By correcting the measured values by a factor of 0.85, these results correlated well to those obtained by thermogavimetrical analysis for all mixes.

The hatched areas show the reduction in $Ca(OH)_2$ by means of the fly ash reaction. Portland cement (C2) shows a slight consumption of $Ca(OH)_2$ at the early age of 7 days, indicating the start of the pozzolanic reaction. Increasing the amount of slag in cements causes the initial consumption of $Ca(OH)_2$ and thus the start of the fly ash reaction to occur at a later stage. Portland-slag cement (C5) containing 25 wt.% slag shows this reaction after 7 to 28 days, blast-furnace slag cement containing 50 wt.% slag (C6) after 28 to 91 days. After this period the $Ca(OH)_2$ consumption increases together with the reaction time, but it is still lower than the consumption occurring in portland cement. Given an extremely large amount of slag (C8), the cement generally reveals only a minor pozzolanic reaction of the fly ash.

The reduced pozzolanic reaction in connection with blast-furnace slag cements is caused by several factors. On the one hand, the alkalinity of the pore solution is slightly lower so that the glassy parts of the fly ash react at a lower rate. Furthermore, there is much less $Ca(OH)_2$ available as a reaction partner, which seems to be the main factor. Finally, the diffusion-related processes required for the pozzolanic reaction are hindered by the pore structure which becomes even denser as the amount of slag is increased.

This also explains why a pozzolanic fly ash reaction takes place at a slightly higher rate when the water-cement ratio is higher than when it is lower.

DEGREE OF FLY ASH REACTION

The determination of the cement hydration degree is relatively easy, e.g. by means of the amount of chemically bound water or by means of other parameters. With regard to fly ashes it is not possible to draw direct conclusions from the amount of $Ca(OH)_2$ consumed by pozzolanic reaction in proportion to the amount of reacted fly ash. Here, the amount of $Ca(OH)_2$ usually transformed during the development of the complete fly ash reaction must be known. Theoretical considerations based on simplified conditions for the chemico-mineral composition of the fly ash and the stoichiometry of the reaction products lead to the assumption that 1.0 g of completely reacted fly ash binds about 0.83 $Ca(OH)_2$ (Helmuth, 1987). Selected tests carried out so far show results of between 0.5 and 0.7 $Ca(OH)_2$ per 1 g reacted fly ash (Dalziel and Gutteridge 1986, Mohan and Taylor 1981, Taylor et al. 1985).

These investigations revealed a tendency of fly ash to bind a slightly decreasing amount of lime as the reaction time proceeded. There have also been, however, observations to the opposite effect (Dalziel and Gutteridge 1986). For the purpose of simplification, a constant lime consumption of 0.65 g $Ca(OH)_2$ per 1 g reacted fly ash is assumed independent of the reaction time, a ratio established during a number of experiments by the author. Yet these tests have only been carried out on the basis of portland cements so far.

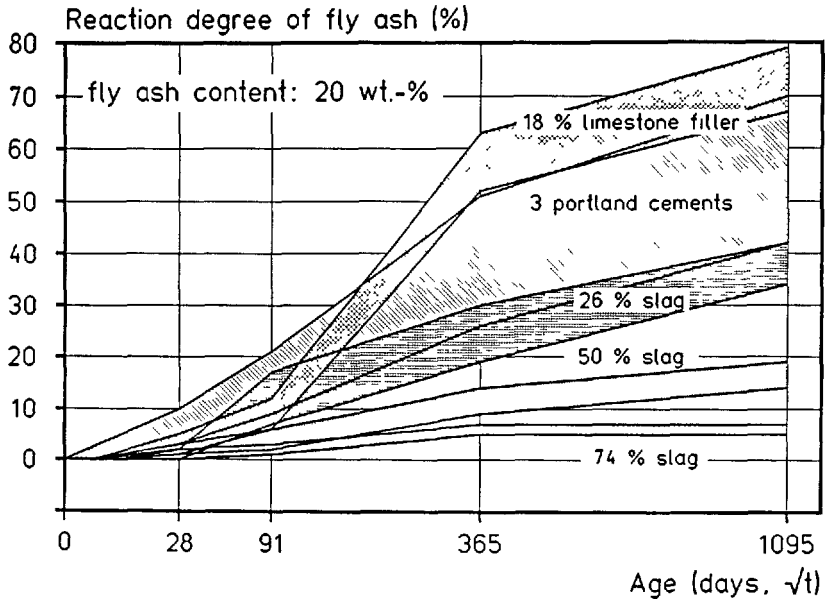

Figure 2 Degree of fly ash reaction dependent on the type of cement

Figure 2 shows the development of the degrees of fly ash reaction thus determined. With portland cements the degree of fly ash reaction at the age of 28 days is hardly more than 10 %, after 91 days slightly over 20%. Given sufficient moisture, the fly ash continues to react as the age of the cements increases. Consequently, the percentage of reacted fly ash after three years is between 40 and 70 %.

The increase in the amount of slag leads to a related decrease in values. Even after an extremely long reaction time, the degree of reaction is lower here. The degree of fly ash reaction with the extremely high slag portion of 74 wt.% is below 10%. In this context, it has to be verified if the assumed lime consumption of 0.65 $Ca(OH)_2$ per 1.0 g reacted fly ash can also be transferred to cements containing slag. Tests for orientation purposes indicate that the lime consumption of the fly ash is lower in these cements, leading to an effectively higher degree of fly ash reaction, as shown here. Further research is necessary to clarify the behaviour in slag cements.

The highest degree of reaction was observed for portland-limestone cement, where a degree of nearly 80% was reached after three years. In order to be able to generalise this result, further examinations have to be carried out. This can be an indication, however, that despite the reduced amount of clinker in the cement, enough $Ca(OH)_2$ is available for a complete pozzolanic fly ash reaction to take place.

CSH PHASES PRODUCED BY POZZOLANIC REACTION

As in the case of cement hydration, the pozzolanic reaction generates gel-like calcium silicate hydrate phases, abbreviated as 'CSH phases'. They are the main mineral phases in the hardened cement paste which determine the application properties of a concrete.

The absolute quantity of CSH phases, their stoichiometry and morphology influence, to a large extent, the pore system and the bond between the separate phases. In this publication, all hydrate phases that are not found in the hardened cement paste in form of unhydrated cement, unreacted fly ash, or $Ca(OH)_2$ are designated as CSH phases.

The investigations below were conducted to find out to what extent the pozzolanic degree of fly ash reaction has influence on the formation of CSH phases. For this purpose, the amount of CSH phases formed during the pozzolanic reaction was examined in relation to the specific amount of reacted fly ash (Fig. 3).

The amount of CSH phases formed during the pozzolanic fly ash reaction increases as the amount of reacted fly ash increases. This can be especially well observed in portland cements and portland-limestone cement. Considering the range of results there is an approximately linear relation between these two variables independent of the amount of fly ash. This can also be observed in blast-furnace slag cements, yet due to the reduced degrees of the fly ash reaction only in the lower region.

Proceeding from the above mentioned assumptions, about 1.5 g (± 0.5 g) CSH phases are formed per 1.0 g of reacted fly ash on average. On the basis of the same calculation methods, the hydration of portland cement leads to the formation of about 1.0 g CSH phases per gram hydrated cement. This deviation can be accounted to the fact that during hydration the lime and silicate portions are contained in the clinker, and only water needs to be integrated, forming not only CSH phases, but also $Ca(OH)_2$. During the pozzolanic reaction only the silicate portion is derived from the reacting substance (from the fly ash). The lime and water portion both come from $Ca(OH)_2$. This is why, relating to the amount of reacting fly ash, more CSH phases are formed here than during the cement hydration. This is also one reason why blast-furnace slag cements have a higher amount of CSH than portland cements, given the same hydration degree or age.

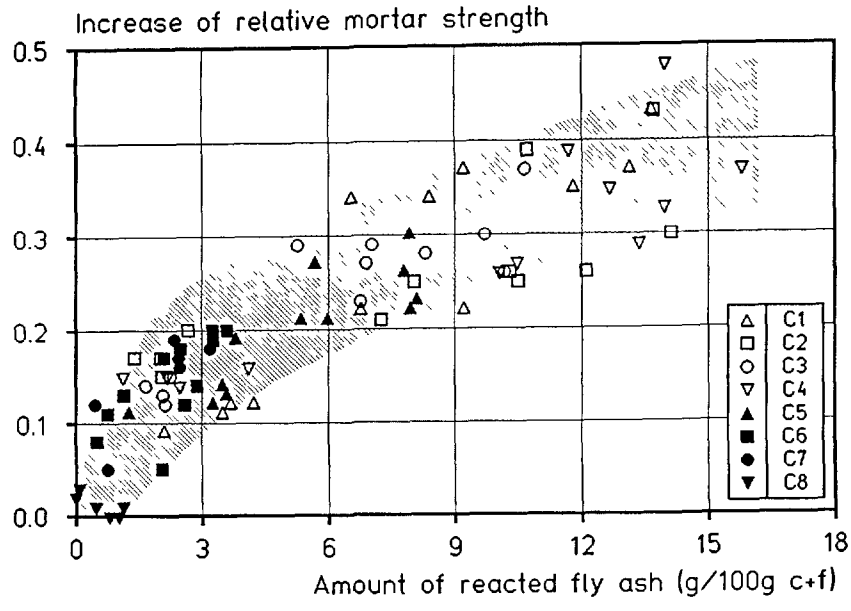

Figure 3 CSH phases formed during pozzolanic reaction dependent on the amount of reacted fly ash (mortar, w/(c+f) = 0.60, f/c = 0.25 and 0.50)

RELATIONSHIP BETWEEN DEGREE OF FLY ASH REACTION AND STRENGTH

The method of determining the course of fly ash reaction described in this report demands much work and effort. Thus, this procedure is not suitable as a standard test method for ordinary laboratories. The procedure usually used is the testing of the compressive strength. As to the cement hydration, a direct linear relationship between hydration degree and compressive strength is generally recognised and accepted. In order to determine fly ash efficiency, an activity index (relative strength) is usually established as a quotient of a mortar or concrete containing fly ash and a corresponding reference mixture without fly ash. Based on the well-known interaction in cements, it is assumed that the development of the fly ash reaction is reflected proportionally in strength development. It has not been verified so far, however, if this relation can be transferred to fly ashes as well.

The relationship between pozzolanic reaction and improvement in strength is shown in Figure 4. Here, the strength contribution of the fly ash is characterised by the increase of relative compressive strength. This contribution is derived from the difference to the relative compressive strength at the age of 28 days. At this stage, relative strength is not significantly influenced by the cement hydration any longer.

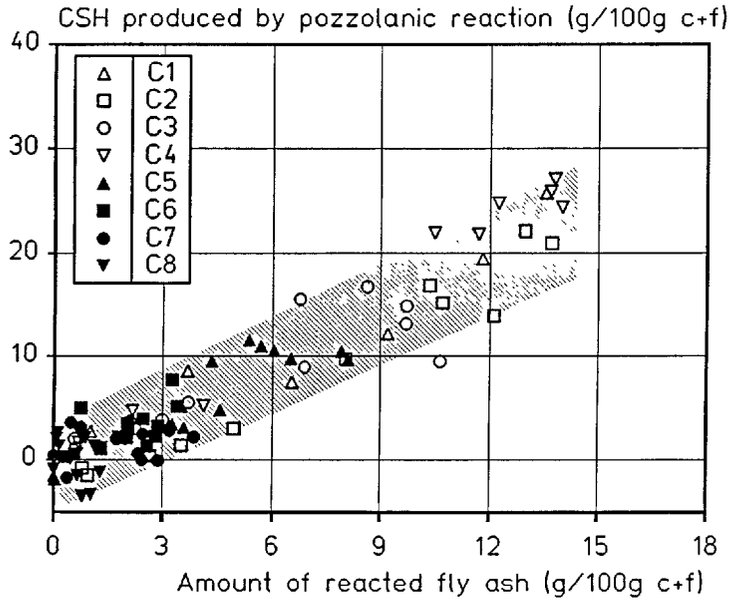

Figure 4 Increase of relative compressive strength dependent on the amount of reacted fly ash

The increase of relative compressive strength of mortar grows as the amount of reacted fly ash increases. This growth is somewhat more striking with lesser degrees of fly ash reaction than with higher amounts of reacted fly ash. This means, however, that the initial chemical reaction of the fly ash contributes more to the strength than the pozzolanic reaction at a higher age.

The fact that a higher strength contribution can be observed despite the smaller amounts of reacted fly ash can probably be accounted to the formation of a shell of CSH phases on the surface of the fly ash particles quite soon after the pozzolanic reaction has started (Pietersen 1993, Rodger and Groves 1988). This reaction shell generates a bond between fly ash particles and surrounding hardened cement paste. This integration of the fly ash into the matrix at this early stage causes a somewhat higher strength increase than the formation of additional CSH phases in the hardened cement paste itself.

CONCLUSIONS

Information gained about the variations of the chemico-mineral structure of hardened cement paste contained in cement mortars made it possible to observe the development of the pozzolanic reaction of fly ash in combination with different types of cement. Here, especially cements containing different amounts of slag were taken into consideration.

In the first 28 days the degree of the fly ash reaction is very low, that is below 10 %. The main pozzolanic reaction of the fly ash occurs only in an advanced age of the cement. A further progression can be expected far beyond the time period examined (3 years). As the amount of slag grows, the course of the fly ash reaction decreases. This can mainly be accounted to the fact that less $Ca(OH)_2$, the reaction partner for the fly ash, is available. Deviations in the alkalinity of the pore solution are of minor importance.

The investigations carried out did not produce any evidence on whether the hydration of slag is influenced by the application of fly ash or not.

The amount of CSH phases, most important in terms of strength and pore structure, increases proportionally to the degree of pozzolanic reaction. On the other hand, a non-linear relationship between improvement of strength and pozzolanic reaction was observed. In the first stage of the pozzolanic reaction, the fly ash particles are integrated into the hardened cement paste by reaction products on their surface. As a result, strength is improved to a larger extent at early ages than later on, when pozzolanic reaction only leads, so to speak, to 'pore filling' with a lesser gain in strength.

REFERENCES

Dalziel, J.A and Gutteridge, W.A., „The Influence of Pulverized Fuel Ash upon the Hydration Characteristics and certain Physical Properties of a Portland Cement Paste", Cement and Concrete Association - C&CA Technical Report Nr.560,1986

Rodger, S.A. and Groves, G.W., „Electron Microscopical Studies of Tricalcium Silicate-Fly Ash Blended Pastes", Mat. Res. Soc. Symp. Proc. „Fly Ash and Coal Conversion By-Products: Characterization,Utilization and Disposal IV", Vol.113, pp.117-118

Härdtl, R., „Chemical Binding of Water during the Hydration of Portland Cements and Blast-furnace Cements blended with Fly Ash, Delhi, 1992

Härdtl, R., „The Change of Concrete Structure by the Efficiency of Fly Ash and its Influence on Concrete Properties", Publication of Deutscher Ausschuß für Stahlbeton, No.448, Beuth, Berlin, 1995 (in German)

Helmuth, R.,"Fly Ash in Cement and Concrete", Skokie, Illinois, Portland Cement Association, 1987

Mohan, K. and Taylor, F.W., „Pastes of Tricalcium Silicate with Fly Ash - Anallytical Electron Microscopy, Triamthyl Silication and other Studies", Mat. Res. Soc. Proc., Symposium N: Effects of Flyash Incorporation in Cement and Concrete (Diamond, S. Ed.)), Boston, 1981

Pietersen, H.S., „Reactivity of Fly Ash and Slag in Cement", PhD-Thesis Technical University Delft/Netherlands, 1993

Ramachandran, V.S., „Differential thermal method of estimating calcium hydroxide in calcium silicate and cement paste. Cem. Concr. Res., Vol.9, No.6, 1979, pp.677-684.

Shebl, F.A. et al., „Investigations relating to the determination of calcium hydroxide by the Franke method. TIZ-International, Vol.107, No.7, 1983, pp.476-479, No.9, pp.646-648.

Taylor, H.F.W., et al., „Analytical Study of Pure and Extended Portland Cement Pastes, Part I: Pure Portland Cement Pastes; Part II: Fly Ash and Slad Cement Pastes", Jour.Am.Ceram.Soc. 68, No.12, 1985, pp. 680-690.

FLY-ASH BLENDED CEMENT ACTIVATED BY A STRONG BASE

Amnon KATZ, National Building Research Institute, Department of Civil Engineering, Technion, Haifa 32000, Israel

ABSTRACT The activation mechanism of fly ash in a basic environment was studied as a means to improve the reactivity of fly ash in blended cements. Experimental program included activation of fly ash by a strong base (NaOH) at different concentrations and water to fly ash ratio. Testing program included compressive tests, Scanning Electron Microscopy (SEM) and Mercury Intrusion Porosimetry (MIP).

Key-words: Fly ash, Alkali, Activation, Scanning Electron Microscopy

INTRODUCTION

Coal fly-ash from power plant is widely used as an additive or as partial replacement of cement (Helmuth, 1987) and its pozzolanic properties are known since Roman time. An increased interest in the activation of fly-ash came up lately (Roy and Silsbee, 1992, Larosa et al., 1992a,b and Brough et al., 1995). The motivation to these works came mainly from disposal of nuclear waste which is frequently of high alkalinity. Solidification of this waste in a cementitious material is one of the proposed methods for disposal of this material.

Studies done lately on the solidification of Low Level Waste (LLW) showed a high degree of reactivity of the fly-ash particles induced by the high alkalinity of the waste solution (Katz et al., 1995, 1996), when the process was performed at a relatively high water to binder (cementitious materials) ratio of 1.0 and at a curing temperature of approximately 90°C. Such temperature may develop adiabatically when solidifying wastes in large volumes (Lokken, 1991) though higher temperatures were used by others (Jiang et al., 1993) for better activation of fly-ash in the process.

In the studies by Larosa et al. (1992a,b) and Katz et al. (1995) a development of various types of zeolites and a relatively high compressive strength was reported when cement blended with flay ash had activated by a strong base at relatively low temperature (up to 90°C). The activating solution was a pure NaOH solution or a high alkalinity LLW solution. water glass ($Na_2O{\cdot}SiO_2$) is also common in works dealing with activation of blast furnace slag (Wang and Scrivener, 1995).

In this study the activation mechanism of fly-ash by highly alkaline solution was investigated, mainly the development of mechanical properties under different conditions and the microstructure of these systems.

EXPERIMENTAL

Fly-ash from local power plant was tested. The mineral composition of the fly-ash is presented in Table 1. All batches were of 250 gr. of d.i. water. The amount of NaOH and fly-ash was determined according to the experimental program shown in Table 2. Mixing was performed using a small Hobart mixer at a low speed. The mix was cast into a 25x25x25mm mold, sealed and stored in an oven in 90°C. After the mix had hardened sufficiently (usually one day) it was demolded and stored back in the oven in a sealed container, where a high humidity was maintained constantly.

Table 1: Mineral composition of the fly-ash (% by weight)

SiO_2	Al_2O_3	Fe_2O_3	CaO	TiO_2	K_2O	P_2O_5
55.1	26.1	9.3	3.1	1.3	1.9	0.4

The testing program was divided into two parts: *i.* studying the effect of NaOH concentration, *ii.* studying the effect of water/fly-ash (w/FA) ratio.

Four Sodium hydroxide concentrations were tested in the first part of the experimental program: 1M, 2M, 3M and 4M. Water to fly-ash ratio was 0.8 for all the mixes. Compressive strength was tested at the age of 7 days after curing at 90°C. According to the results it was decided to test the effect of water/fly-ash ratio on the 4M solution only. Three water/fly-ash ratios were tested: 0.4, 0.8 and 10. Due to technical difficulties the latter was tested in 80°C only. Summary of the testing program can be found in Table 2.

The fractured surface of all the specimens was observed by a Scanning Electron Microscope (SEM). Pore size distribution and compressive strength was tested for the low water/fly-ash mixes (0.4 and 0.8).

Table 2: Summary of the testing program.

water/FA ratio	NaOH concentration	Water (gr.)	NaOH (gr.)	Fly-ash (gr.)	Curing temperature (°C)
10.0	4M	10	4	1	80
0.8	4M	250	40	312	90
	3M	250	30	312	90
	2M	250	20	312	90
	1M	250	10	312	90
0.4	4M	250	40	325	90

RESULTS AND DISCUSSION

Effect of solution concentration

The effect of solution concentration on the compressive strength at the age of 7 days can be seen in Fig. 1. It can be seen that for the same water to fly-ash ratio and curing temperature the compressive strength increases as the concentration of the solution increases. The mixes of 4M exhibited good mechanical properties and a compressive strength of 6.1 MPa was obtained after 7 days, close to the compressive strength of a cement paste at the same age and water/ cement ratio. For the low concentration of 1M the specimens could hardly be demolded after 4 days of curing at 90°C and the compressive strength after 7 days was very low (0.2 MPa).

Other solution concentrations of 2M and 3M exhibited compressive strength values in between the 1M and 4M mixes (see Fig. 1) which indicates that the degree of reactivity increases as the NaOH concentration increases. Interesting to note that lowering the water/fly-ash ratio did not revealed a higher compressive strength as expected, but a lower compressive strength has observed as shown in Fig. 1 (6.1 and 4.9 MPa for the high and low w/FA ratios, respectively). A different microstructure was also seen by the SEM as will be discussed in the following.

Various modes of activation of the fly-ash were seen under the microscope. Fly-ash particles, as received from the power plant, seem round and smooth or appear as a cluster of particles. Fly-ash particles reacted by 1M solution of NaOH look similar to the unreacted fly-ash and only slight etching could be seen on the surface of the fly-ash reacted with 2M solution. An extensive etching was seen on the surface of the fly-ash reacted by 3M solution (see Fig. 2) and

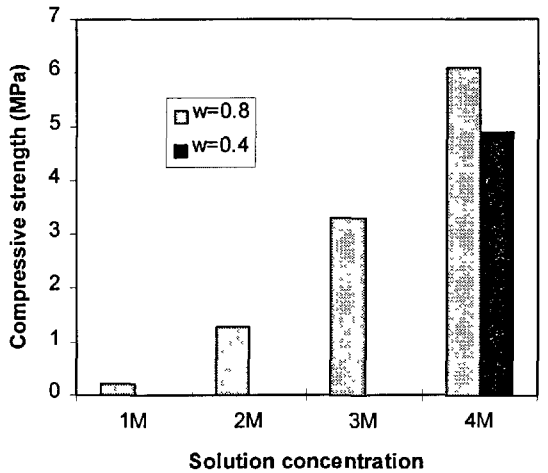

Figure 3: Effect of solution concentration on the compressive strength at the age of 7 days.

it seems as if most of the glassy phase was dissolved from the fly-ash, exposing the skeleton of the mullite crystals.

The fly-ash reacted by the 4M solution exhibited a different microstructure as seen in Fig. 3. A continuous matrix is seen between the particles and the material seems to be less porous. Higher magnifications showed needle like crystals between the fly-ash particles in the 3M system while cubic like crystals were seen on the surface of the particles of the 4M solution and non of needle like crystals were seen. Similar phenomenon of changes in the hydration products as the concentration of the activating solution increases was seen in the work of Katz et al. (1995) where Na-P1 (gismondine) was favored at one concentration and sodalite was favored at higher concentrations.

Effect of water/FA ratio

In addition to the change in the compressive strength discussed earlier, the microstructure as observed under the SEM was different when the water/fly-ash was lowered from 0.8 to 0.4 or increased to 10 as can be seen in Figs. 4 and 5, respectively. When lowering the water/fly-ash ratio the fly-ash particles seems to be separated form each other and no continuous matrix could be seen. The material over the particles of the w/FA of 0.8 seems more cubic while that of the 0.4 seems more plate like.

At the high w/FA ratio a different microstructure was formed as can be seen in Fig. 5. It seems as if an extensive etching took place, removing part of the glassy phase form the surface, while at the same time, sedimentation of another phase on the surface took place.

MIP tests on the samples showed that a threshold exist at a relatively large pore size in the range of 1-10μm. Changes in the solution concentration or w/FA ratio took place in this range accompanied by a reduction in the total porosity when lowering the w/FA ratio.

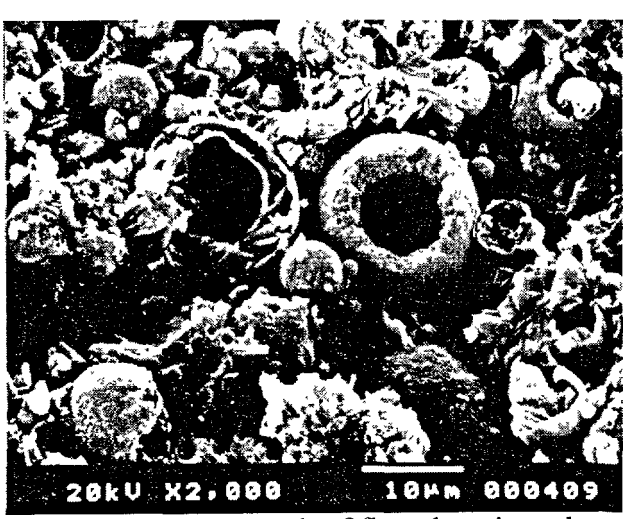

Figure 2: Micrograph of fly-ash activated by 3M of NaOH, water/fly-ash=0.8.

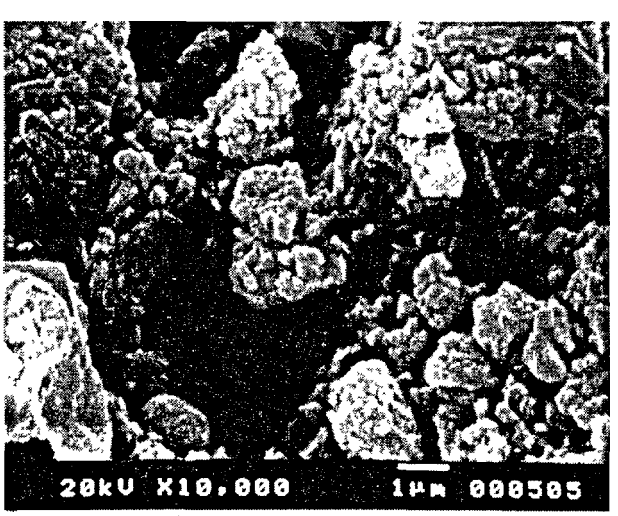

Figure 3: Micrograph of fly-ash activated by 4M of NaOH, water/fly-ash=0.8.

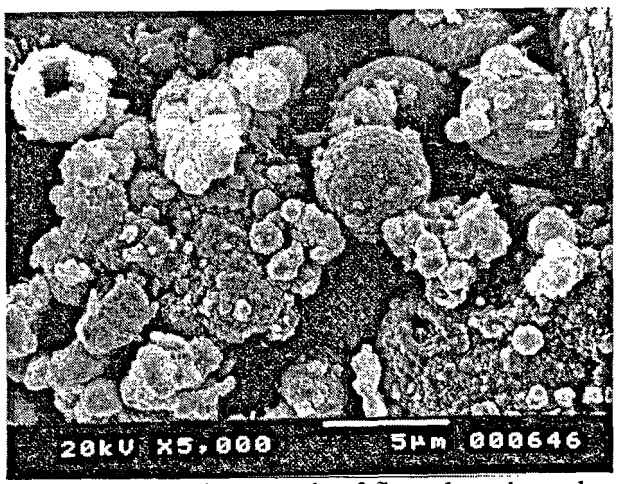

Figure 4: Micrograph of fly-ash activated by 4M of NaOH, water/fly-ash=0.4.

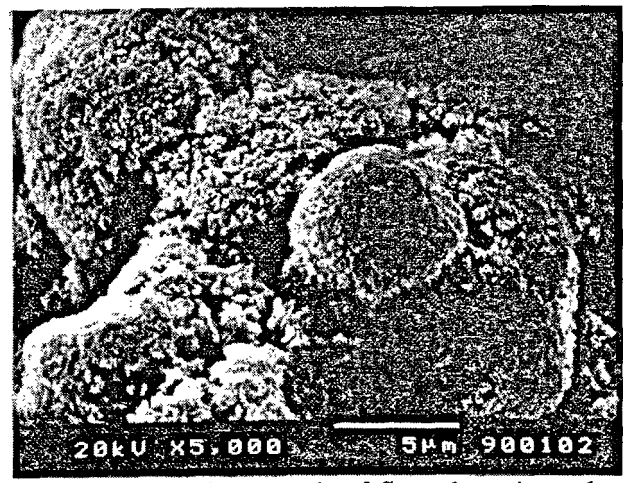

Figure 5: Micrograph of fly-ash activated by 4M of NaOH, water/fly-ash=10.

CONCLUSION

1. Increasing the concentration of the activating solution (NaOH) increased the compressive strength developed in a solution-fly ash system, indicating a higher reactivity. However, lowering the water/fly-ash ratio from 0.8 to 0.4 lowered the compressive strength.
2. SEM observations showed different microstructure of the systems affected by solution concentration and w/FA ratio. The differences were mainly in the etching manner and the type of crystals formed.
3. MIP showed that the changes in the pore size was mainly in the range of 1-10µm for the various systems.

REFERENCES

Brough, A., Katz, A., Bekharev, T., Sun, G.K., Kirkpatrick, R.J., Struble, L.J. and Young, J.F., "Microstructural Aspects of Zeolite Formation in Alkali Activated Cements Containing High Levels of Fly-Ash", Materials Research Society (MRS) Proc. Vol. 370, 1995, pp. 199-208.

Helmuth, R., "Fly-Ash in Cement and Concrete", Portland Cement Assoc, Illinois USA, 1987.

Jiang, W., Wu, X. and Roy, D.M., "Alkali Activated Fly-Ash Slag Cement based Nuclear Waste Forms", Materials Research Society (MRS) Proceedings Vol. 294, 1993, pp. 561-671.

Katz, A., Brough, A.R., Kirkpatrick, R.J., Struble L.J. and Young, J.F., "Cement Solidification of Solution from Off-Gasses of Vitrification of LLW", 1996, In preparation.

Katz, A., Brough, A.R., Bekharev, T., Kirkpatrick, R.J., Struble L.J. and Young, J.F., "LLW Solidification in Cement- Effect of Dilution", Materials Research Society (MRS) Proceedings Vol. 370, 1995, pp. 209-216.

Larosa, J.L., Kwan, S and Grutzech, M.W., "Self Generating Zeolite Cement Composites", Materials Research Society (MRS) Proceedings Vol. 245, 1992a, pp. 211-216.

Larosa, J.L., Kwan, S and Grutzech, M.W., "Zeolite Formation in Class F Fly Ash Blended Cement Pastes", J. American Ceramic Society, Vol. 75, No. 6, 1992b, pp. 1574-1580.

Lokken, R.O. and Martin, P.F.C., Report HGTP-91-0303-01, Pacific Northwest Laboratory, Richland, WA, 1991.

Roy, D.M. and Silsbee, M.R., "Alkali Activated Cementitious Materials: an Overview", Materials Research Society (MRS) Proceedings Vol. 245, 1992, pp. 153-164.

Wang, S.D. and Scrivener, K., "Hydration products of Alkali Activated Slag Cement", Cement and Concrete Research, Vol. 25, No. 3, 1995, pp. 561-571.

MODELLING THE OVERALL RATE OF REACTION IN LIME-FLY ASH SYSTEMS

Said JALALI, Universidade do Minho, Civil Engineering Department, Guimarães, Portugal

ABSTRACT Fly ash is the most widely used artificial pozzolan in concrete. It reacts with calcium hydroxide forming cementitious materials which enhance the strength and durability of concrete. A theoretical model for predicting the overall rate of reaction in lime-fly ash systems, based on nucleation, diffusional growth and the overlap of the growth centres is presented. Results from Differential Scanning Calorimetry (DSC) tests are used to evaluate the validity of the model.

Key-words: Modelling, Fly Ash, Lime, Diffusion

INTRODUCTION

Fly ash reacts with lime at ordinary temperatures in the presence of water, and cementitious materials are produced that are similar to the hydration products of ordinary Portland cement. Reactions which take place on the surface of fly ash are complex because of the complex chemical composition of fly ash particles. Furthermore, one reaction product may well influence the formation of others. Taking the individual reactions into account would make a model complex and thus impractical to use. Therefore, the cementitious materials are regarded as a single product and the aim is to estimate the overall rate of its formation.

Based on principles of nucleation and growth the mechanism of formation of cementitious material can be described in terms of the formation of small stable regions of product, i.e. nuclei. The growth of one centre, considered here to be diffusion controlled, will continue until it is limited by running into a nearby growing centre, i.e. impingement occurs. This type of impingement will physically inhibit the growth of the new phase in one direction (Christian, 1975). The process will continue until all directions of growth are blocked to all centres. A 'soft' type of impingement can also be visualised when gradual exhaustion of available reactants or when gradual 'soft' impingement of interweaving fibrils occur (Double, 1978). Hence, the proposed model considers nucleation and growth of the centres and their subsequent impingement on each other.

It can be seen that the morphology of the new phase plays an important role in the overall rate of the formation of cementitious materials. Scanning and transmission electron microscope provide direct means for observation of the morphology of the new phases. It is noticed (Jalali, 1991) that the new phase covers first the surface of the fly ash particles, which can be approximated to a two dimensional nucleation and growth. The second stage, which occurs apparently after the surface of fly ash particles are covered with the new phase, is the formation and growth of needle-like fibrous material. This can be assumed to be either one dimensional growth, if the radius of the needle is considered constant, or three dimensional if the radius of the fibres is also increased with time.

A conceptual model based on progressive nucleation is suggested and the equations governing the one, two and three dimensional diffusional growth of nuclei and their impingement are derived in the next section. A general form of these equations is suggested to predict the overall rate of reaction in lime-fly ash systems.

DERIVATION OF EQUATIONS FOR OVERALL RATE OF REACTION

The conceptual model, that will be published elsewhere, is based on the analysis of images obtained by SEM and TEM (Jalali, 1991). It is suggested that the cementitious material is formed by progressive nucleation, similar to what happens with the formation and growth of the new branches and twigs of trees. In such cases nuclei are formed gradually and growth occurs continuously.

Assuming a diffusional controlled growth process, the size of a transformed region in any direction is proportional to square root of time. Considering an isotropic growth rate constant k the area covered will have a circular shape with a radius proportional to $k(t)^{1/2}$. If a centre is formed at time u ($0<u<t$), at time t it will have an age equal to (t-u) and the radius will be given by $k(t-u)^{1/2}$. The contribution of one such centre to the total area will be $\pi r^2 = \pi k^2(t-u)$.

According to the general nucleation equation (Abyaneh, 1981 and Bewick, 1962), for progressive nucleation at preferred sites, when the product of A't remains small during the process, the number of nuclei (N) at a time t is given by

$$N = N_o A' t \qquad [1]$$

where N_o is the total sites available per unit area and A' is the rate of conversion of one site into a nucleus. In time δu the number of nuclei formed are $\delta N = N_o A' \delta u$. Thus the growth area in the absence of impingement, i.e. extended area (S_{ext}), of new material formed in the time interval between 0 and t will be

$$S_{ext} = \int \pi k^2 (t-u) A' N_o \delta u \qquad [2]$$

Considering that N_o, A' and k are constants, the integration yields

$$S_{ext} = (\tfrac{1}{2}) \pi k^2 N_o t^2 \qquad [3]$$

The actual area of growing centres (S) using Avrami's postulate (Avrami, 1939, 1940 and 1941) for overlap will be

$$S = S_{max} [1 - \exp[- (\tfrac{1}{2}) \pi k^2 N_o t^2] \qquad [4]$$

where S_{max} is the total area the new material can cover. For one dimensional growth, when A' is small, it can be shown that the volume of the new phase will be

$$V = V_{max} \{ 1 - \exp [- (\tfrac{2}{3}) \pi r^2 k' N' t^{3/2}] \} \qquad [5]$$

where N' is the number of sites available, r is the radius of the needle like material and k' is the growth constant for one dimensional growth. Likewise for three dimensional growth Eq 5 will become

$$V = V_{max} \{ 1 - \exp [- (\tfrac{2}{5}) \pi k"^3 N" t^{5/2}] \} \qquad [6]$$

It is suggested that Eqs 4-6 be represented in the following general form

$$V = V_{max} \{ 1 - \exp [- K t^n] \} \quad [7]$$

Eq 7 is suggested for prediction of the overall rate of reaction in lime-fly ash systems. Parameter K is the rate constant for growth and its temperature dependence can be shown by an Arrhenius equation. Parameter n, on the other hand, indicates the dominant morphology of the products. A value of 3/2 indicates a one dimensional growth while a value of 2 indicates a two dimensional growth and 5/2 indicates a three dimensional growth.

EVALUATION OF THE MODEL PROPOSED

In order to evaluate the validity of the proposed model Differential Scanning Calorimetry (DSC) tests were performed on lime fly ash mixtures at constant temperatures of 65, 75, 85 and 95 °C. In this mode, DSC tests provide the rate of heat flow while the reaction takes place, the integration of which indicates the degree of reaction at any given time.

The integral of the rate of heat flows obtained from DSC tests were used for evaluating the validity of Eq 7. A non-linear regression analysis was used to estimate the values of parameters K and n. Table 1 shows the values for these parameters as well as the sum of squared errors (SSE) estimated. Figs 1-4 show the DSC test results and the predicted values using Eq 7. It can be seen that the proposed model explains well the data.

Table 1. Parameters obtained using Eq 9 and DSC test results

Temperature (°C)	V_{max}	K	n	SSE
65	17.11	2.325E-6	2.328	0.35
75	18.73	4.348E-7	2.588	0.28
85	35.63	1.862E-6	2.548	3.65
95	33.96	8.228E-6	2.466	22.9

CONCLUSIONS

It can concluded that the proposed model explains the data from the DSC tests well and hence is able to predict the amount of reaction products at any given time. It can also be seen that the values of n are close to 2.5, which indicates that the nucleation and growth in the present case are predominantly three dimensional. Furthermore, it is seen that, except for the 65 °C, parameter K increases with temperature, which confirms the assumption of the diffusional growth of the reaction products.

REFERENCES

Avrami M., Journal of Chem. Phys., 7 (1939) 1103; 8 (1940) 212; 9 (1941) 177.

Abyaneh M.Y and Fleischmann M., J. Electroanal. Chem., 119 (1981) 187.

Bewick A. and Fleischmann M., Thirsk H.R., Trans. Faraday Sox. 58, 2200 (1962)

Christian J.W.; "The Theory of Transformation in Metals and Alloys", second edition, Perbamon Press, 1975.

Double D.D., Hellawell A., and Perry S.J.; "The Hydration of Portland Cement", Proc. R. Soc. London A.359, pp 435-451; 1978.

Jalali S., "A Study of Factors Affecting the Mechanical Behaviour of Lime-Fly Ash Mixtures", PhD thesis, Coventry University, 1991.

DSC Test Results and Prediction for 65 oC Curing Temperature

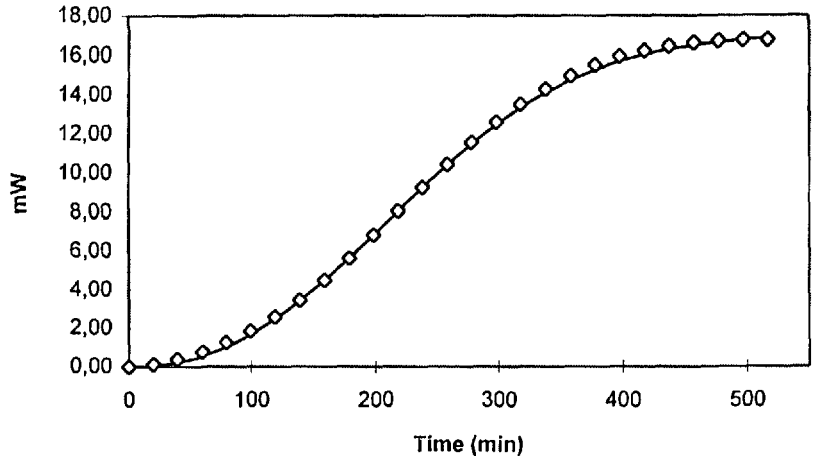

DSC Test Results and Prediction for 75 oC Curing Temperature

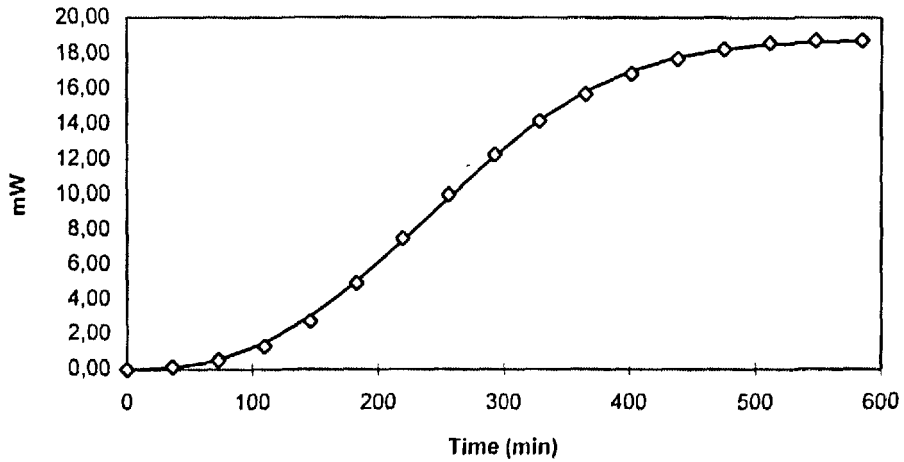

DSC Test Results and Prediction for 85 oC Curing Temperature

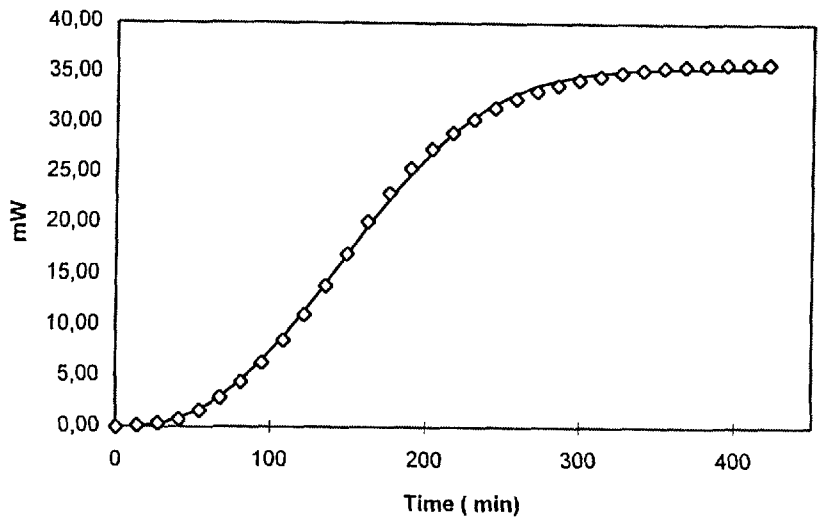

DSC Test Results and Prediction for 95 oC Curing Temperature

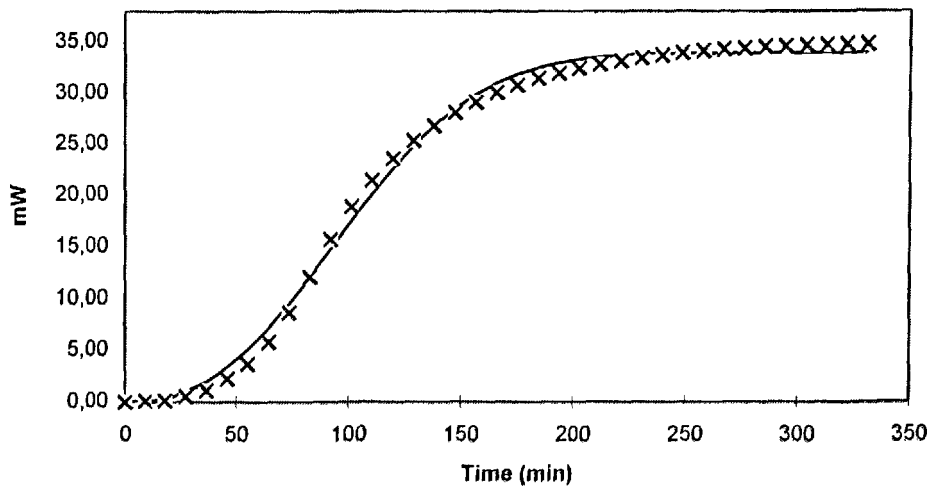

A STUDY ON TIME BEHAVIOUR OF FLY-ASH BLENDED CEMENT PRODUCTS

Darko M. KRIZAN, IMS Research Institute, Belgrade, Yugoslavia
Carlos E. S. TANGO, IPT Research Institute, São Paulo, Brazil
Valdecir A. QUARCIONI, IPT Research Institute, São Paulo, Brazil
Yushiro KIHARA, ABCP Cement Association, São Paulo, Brazil

ABSTRACT
Aiming to verify fly-ash addition influence on Portland cement paste, mortar and concrete, tests for compressive and tensile strength, porosity, chemical analysis of paste pore extracted solution, DTA and TGA were conducted at ages 7, 28, 63, 91 or 182 days. Proposed methods for accessing porosity by squeezing specimens at high compressive stress level and by acetone impregnation were compared with ASTM and Hg porosity with promising results. Good porosity/strength correlations were found, and a previous strength/time mathematical model always verified for cement without fly-ash was adjusted with success, in order to establish limit strengths or strength reserves for infinite ages, related with potential compaction and durability.

Key-words: Fly ash, modified cement, porosity, strength development, modelling

INTRODUCTION
This paper is a product of a co-operation program between IPT - Technological Research Institute (Brazil) and IMS Institute for Materials of Serbia (Yugoslavia) concerning laboratorial works developed in São Paulo, Brazil. The study was done with collaboration of Portland Cement Brazilian Association (ABCP) and participation of São Paulo University Polytechnic School (EPUSP).

The objective was to study Portland cement with fly ash addition. This subject is important for both countries since fly ash addition is an available and interesting common way to save energy in the manufacturing of cement for construction. Time evolution of paste, mortar and concrete properties was considered an adequate first approach of this subject, and Brazilian materials which characteristics are supposed acceptable for representing typical world-wide materials were used. The study is divided in characterisation of employed materials, study on paste, mortar and concrete, and conclusions.

CHARACTERISATION OF EMPLOYED MATERIALS
Brazilian Portland Cement CP V - ARI type (High Early Strength), with Standard strength 50.7 MPa at 28 days and Blaine Fineness 495 m^2/kg, was used. Pozzolan was a ground fly ash from Tubarão Coal Power Station, Santa Catarina State, Brazil, with Blaine Fineness 445 m^2/kg and Pozzolanicity Index with Lime 7.0 MPa. River sand with maximum grain size 2.4 mm was used as fine aggregate and crushed granite 9.5 mm maximum grain size as coarse. Potable water of São Paulo supply was used.

STUDY ON PASTE, MORTAR AND CONCRETE
Paste Study
Pastes with 0.6 water/binder weight proportion, pozzolan/binder amounts 0%, 35% and 55% were cured in moist conditions and standard ordinary temperature. Study was performed at 7, 28, 63, 91 and 182 days ages on cylinders 20 mm diameter x 40 mm height (compressive strength, acetone impregnation, modified ASTM voids by boiling water method, DTA, TGA) or 40 mm

diameter 80 mm height (squeezing for accessing porosity and pore solution extraction), or on prisms 40 x 40 x 160 mm^3 (ISO flexural tensile strength). Paste cylinders were cut with the shape of 4 or 5 coins (height 5 mm) for acetone impregnation.

Squeezing of specimens was performed with a special device in which specimen is highly confined, keeping a constant diameter, to compressive stress level 477 MPa, sufficient to destroy paste structure, deform specimen proportionally to voids volume, and expel pore water, collected for chemical analysis (OH^- by titration and Na^+, Ca^{2+} and K^+ by atomic absorption). Figs 1 to 5 present relations between paste's properties.

Acetone impregnation was made for interrupting hydration and obtaining a voids index by the following procedure: 1) Transversal diamond cutting obtaining at least 4 coins, 2) obtaining the Natural Weight of the coins, 3) vacuum (640+5 mmHg) of 1 hour for drying partially the water, 4) first immersion of the coins in acetone inside a closed glass, making vacuum during 10 min, 5) with the coins inside acetone, left liquid in atmospheric pressure 20 min (first impregnation), 6) submission of the coins to 2 hours of vacuum for drying the acetone and water, 7) obtaining "Weight after first Immersion and Vacuum", 8) second immersion of coins in acetone inside a closed glass, vacuum during 10 min, 9) with the coins inside acetone, left liquid in atmospheric pressure 20 min (2nd. impregnation), 10) obtaining "Weight after second Immersion" (W_s), 11) submission of the coins to 30 min of vacuum for drying the acetone, 12) obtaining "weight of the dry sample" (W_d), 13) immersion of coins in acetone for storage with interrupted hydration.

Calculations were made following the formula:

$$V_i = (100(W_s - W_d)/D_a)/(W_d/D_d) \quad [1]$$

where: V_i = Voids Index by acetone impregnation (%); D_a = Density of acetone (g/cm^3); D_d = ASTM bulk specific gravity of corresponding dry specimen (g/cm^3).

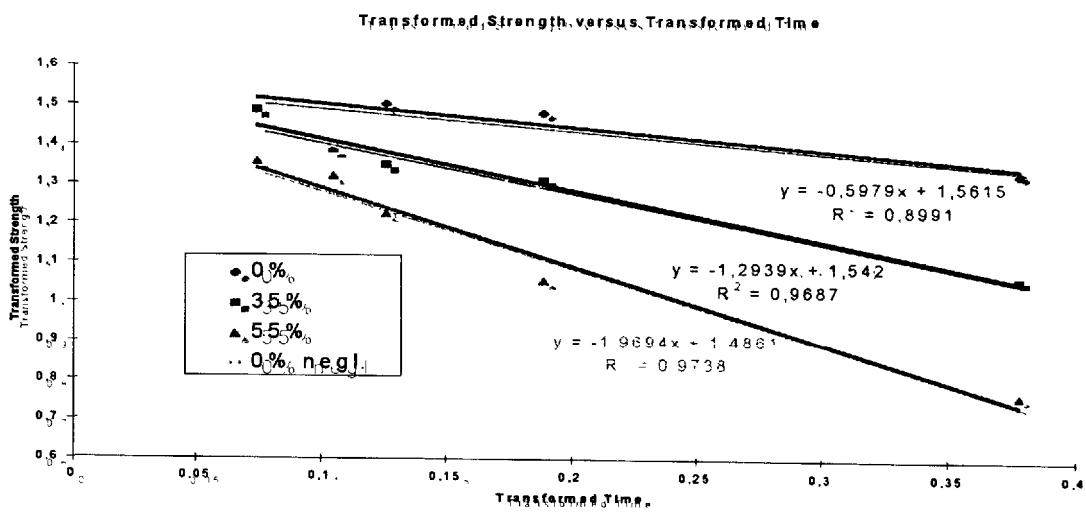

Figure 1: Transformed Strength versus Transformed Time for pastes. Acceptable linearisations, as proposed in a previous work (Tango, 1992) was obtained using $\log f_t$ instead of f_t (compressive strength in MPa) and $t^{-0,5}$ instead of t (time in days).

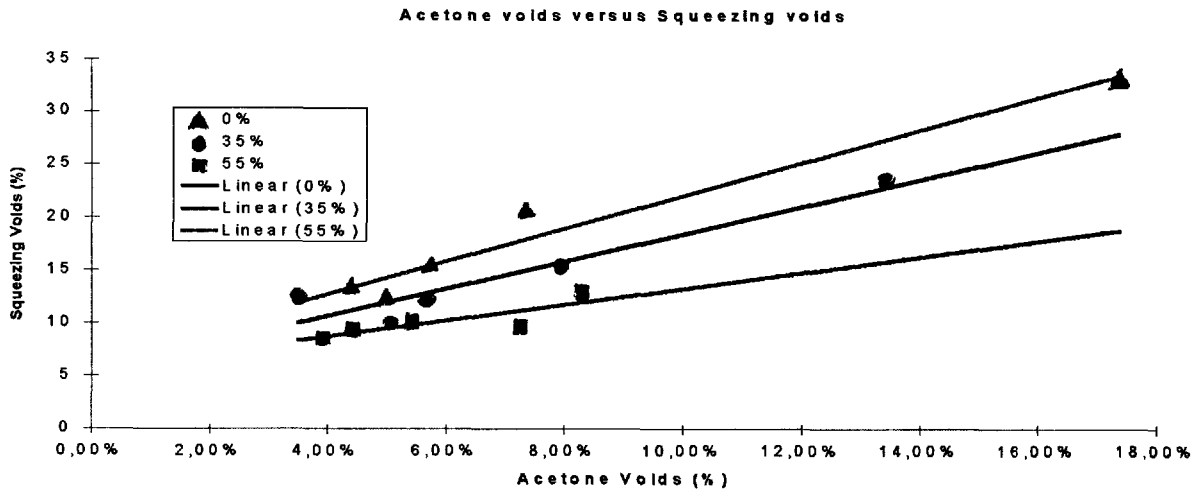

Figure 2. Acetone Voids versus Squeezing Voids for Pastes. There is influence of pozzolan amount in the correlation between these properties. Probably the method for acetone voids would be improved varying the time of acetone impregnation to obtain, for instance, constant weight and not using constant time.

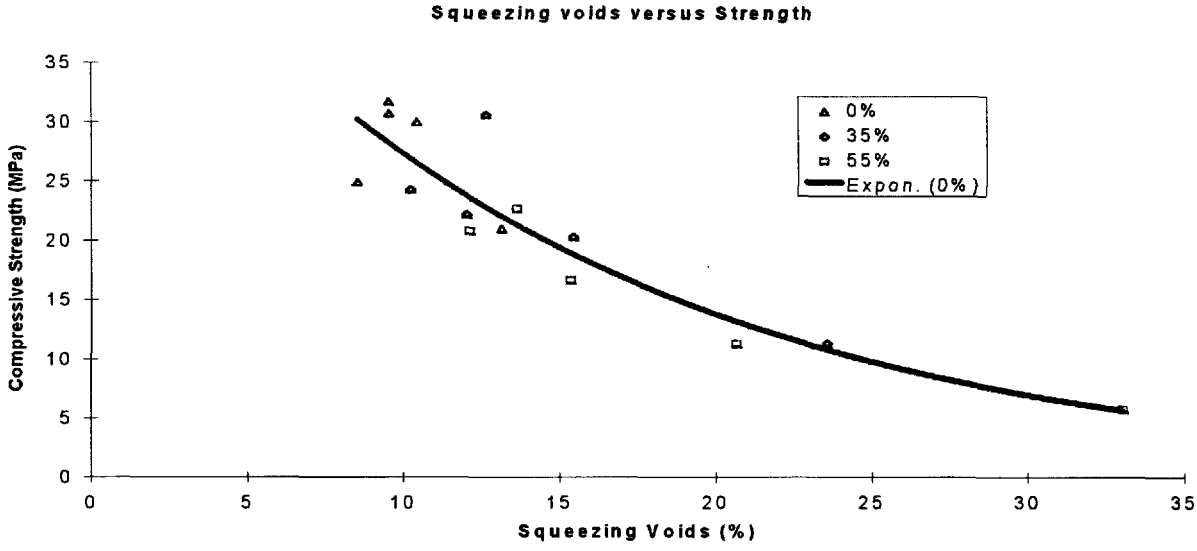

Figure 3. Squeezing Voids versus Strength for Pastes. A good correlation indicates Squeezing Voids as a good index for Compressive Strength, practically without influence of different pozzolan amounts.

Study on Mortar

Pozzolan amounts 0 %, 35 %, 55 % and fine aggregate/binder 1,00:2,00; 1,00:3,00; 1,00:4,00 were used. Ages were 7, 28, 63 (except for flexural strength test), 91 and 182 (except for flexural strength test) days. Thus, the number of different conditions for the mortar study was 45, except for flexural tests, which were 27. The amount or water of each mix proportion of mortar was determined by tentative, aiming a Brazilian flow table consistency ABNT MB-1 index of 210+10mm. Prismatic 40mm x 40mm x 160mm specimens were poured following ISO EN 196/1 for flexural strength and cylindrical specimens 50 mm (diameter) x 100 mm (height) were poured following Brazilian Standard ABNT MB-1 (modified from standard sand fixed aggregate

test to variable fine aggregate) for the rest of the tests. All specimens were cured following ABNT MB-1 procedure (submerged specimens in water with controlled pH and temperature).

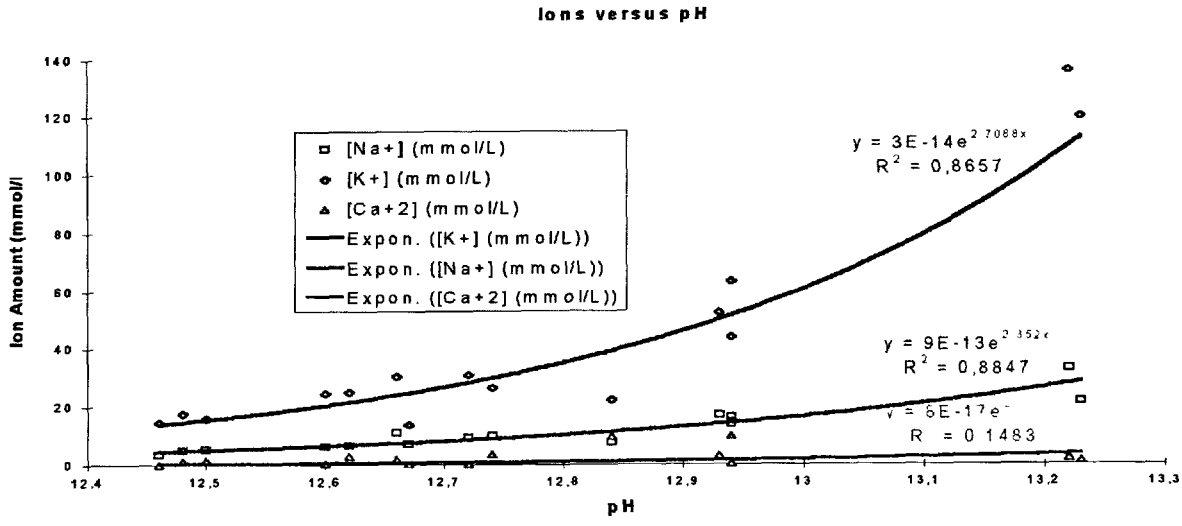

Figure 4. Ion molar concentrations versus pH_i for Pastes. Good correlation's between ions amounts (except Ca) and pH. The main influence on pH is not Calcium, but Potassium and Sodium ions.

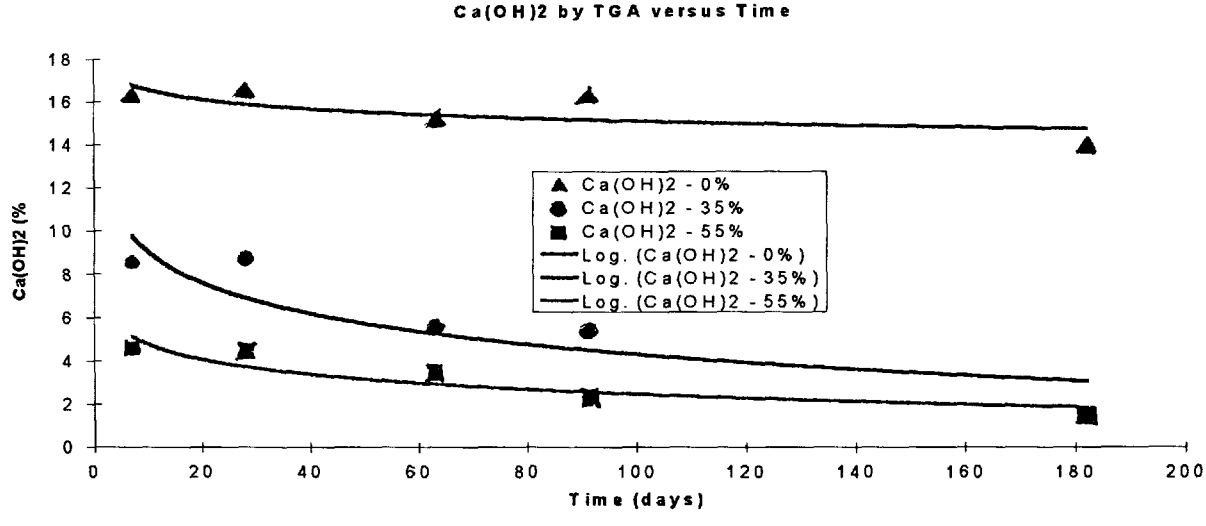

Figure 5. $Ca(0H)_2$ versus Time for Pastes. Expected behavior. Decreasing for cements with pozzolan and very slowly decreasing or practically constant for cements without it. According qualitatively to determinations of Ca Ion in pore solution extract.

Compressive strength tests were conducted following ABNT MB-1 procedure. The cylinders for hydration interruption and porosity by acetone impregnation were submitted to the same procedures and calculations for mortar disks as done for paste coins. The ASTM water boiling method C 642 originally used for concrete was adapted for mortars by the use of a balance with sufficient precision (0,5g division) for weighing parts of cylindrical 5-cm diameter x 10-cm height specimens. Only one specimen for each condition was tested.

A previous mathematical model (Tango, 1992) was aimed to adjust between the *dependent* variable *compressive strength* and *independent* variables *water/binder ratio* and *time*. The proposed model was:

$$f_c = A / (B^x \cdot D^{x/\sqrt{j}} \cdot E^{1/\sqrt{j}}) \quad [2]$$

where; f_c = compressive strength, x = water/binder ratio by weight, j = age of curing and A, B, D and E are constants. Eq 2 can be transformed to the linear form:

$$\text{Log } f_c = \log A - x \cdot \text{Log } B - (x/\sqrt{j}) \cdot \text{Log } D - (1/\sqrt{j}) \cdot \text{Log } E \quad [3]$$

which can be adjusted by linear correlation's algorithm available in microcomputer program Excel for Windows 95, using, as dependent variable, log f_c, and as independent variables, x, $x/\sqrt{j}$ and $1/\sqrt{j}$. Table 1 shows the values for the obtained constants and determination coefficients for each condition of this study on mortars.

Table 1. Compressive Strength Mathematical Model Constants for Mortars*

Pozzolan amount (%)	Log A	Log B	Log D	Log E	R^2**
0	2.3567	0.3222	0.5339	1.2309	0.9926
35	2.2734	1.0089	0.7661	0.5851	0.9961
55	2.2743	1.1093	1.0784	0.8582	0.9862

*Strength in MPa, Water/Binder Ratio adimensional (weight/weight), Age in days in Eqs 2 or 3.
**R^2 = determination coefficient.

Figs 6 to 8 show relations between mortar properties with comments.

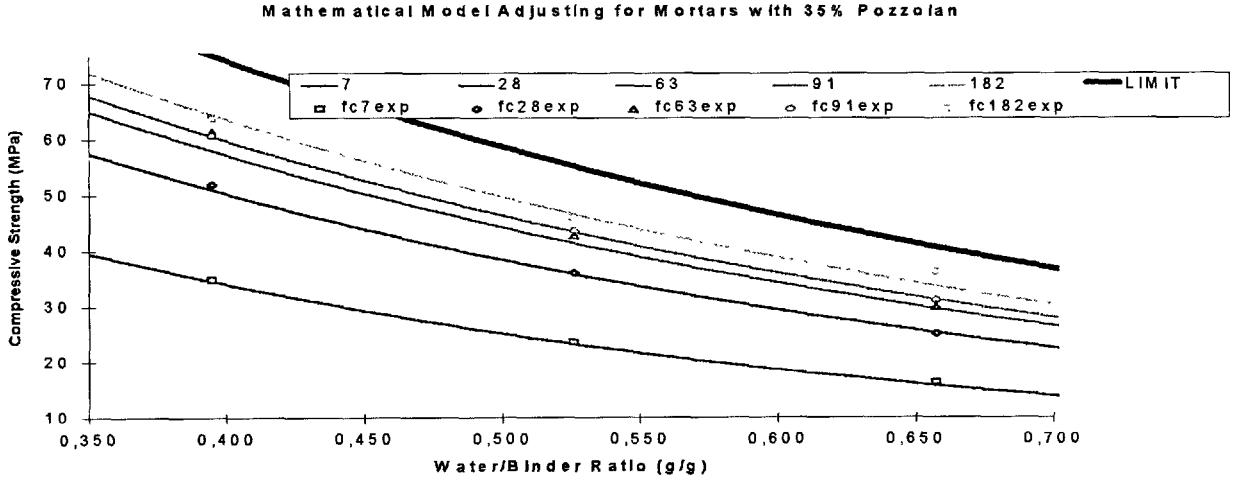

Figure 6. Generalization of Abrams' Law in the Time .for Mortars with 35% pozzolan binder. LIMIT means the theoretical curve inferred for infinite age. The mathematical model and its inferred constants are shown in Table 1 and Eq 3.

Study on Concrete

Concrete was made with a low maximum size coarse aggregate and can be classified as a plastic (not fluid) grout with Abrams' Slump Cone Consistency Index between (100±20) mm. Cement/Binder weight proportions 1/3.5; 1/5.0 and 1/6.5 were used. Dry mortar/Dry Concrete weight proportions were optimized for each pozzolan proportion by tentative method and maintained constant for the three Cement/Binder proportions. One-way cylindrical molds using PVC commercial tubes with polyethylene sheets fixed to the bottoms with a strong adhesive tape with 75 mm in nominal diameter and approximately 150 mm in height were used for the main part of the specimens. Exclusively for age 91 days, pozzolan proportion 0% (all aggregate proportions), and pozzolan proportion 35% (only 1/3.5 binder/aggregate proportion), eight

available metallic molds of the same nominal dimensions were used. Two specimens by condition of test were poured, remained 24 h in laboratory conditions covered by polyethylene sheets before demolding, and were cured in moist chamber (relative humidity over 95% and temperature between 24 $\pm$ 2 ^{0}C), following Brazilian ABNT method MB-2. Compressive tests were made following Brazilian ABNT method MB-3. Cylinders for hydration interruption and acetone voids index were submitted to the same procedures and calculations for paste, except for using slices of 10 mm instead of 5 mm. There was a procedure modification for 91 ages: the specimens were submerged into acetone at date of test for interrupting hydration, and after a few days as laboratory's schedule permitted, the test was normally carried. ASTM water boiling method C 642 was used in the remaining parts of specimens cut for acetone impregnation. As it was done for mortars, constants for eqs. 2 and 3 were inferred. See Table 2 and Figs. 9 and 10 with main results.

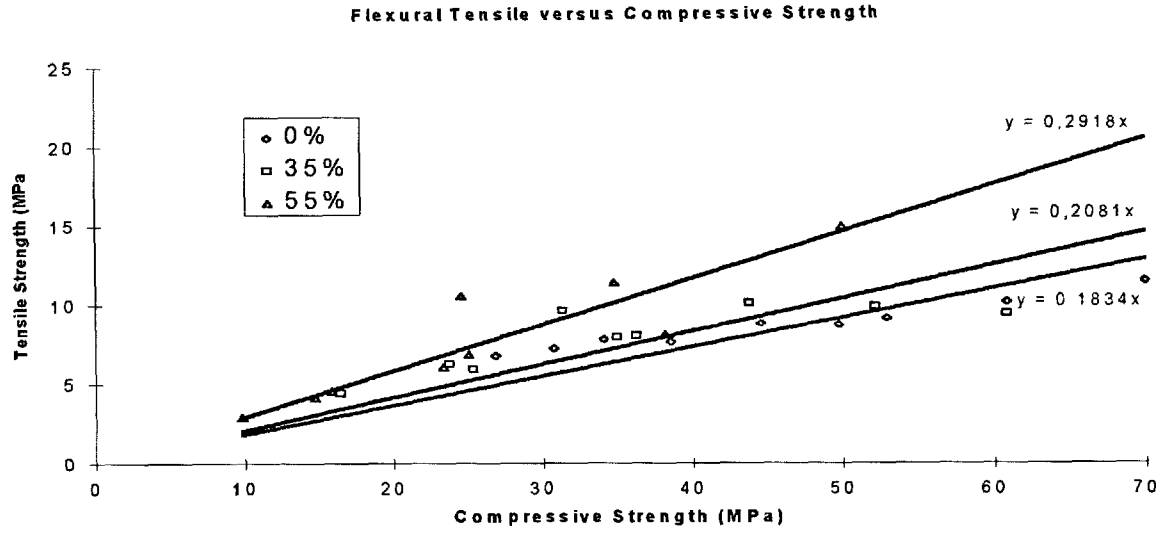

Figure 7. Tensile Strength versus Compressive Strength for Mortars. There is influence of pozzolan amount in the ratio between tensile and compressive strength. Binders with higher amounts of pozzolan reach higher ratios.

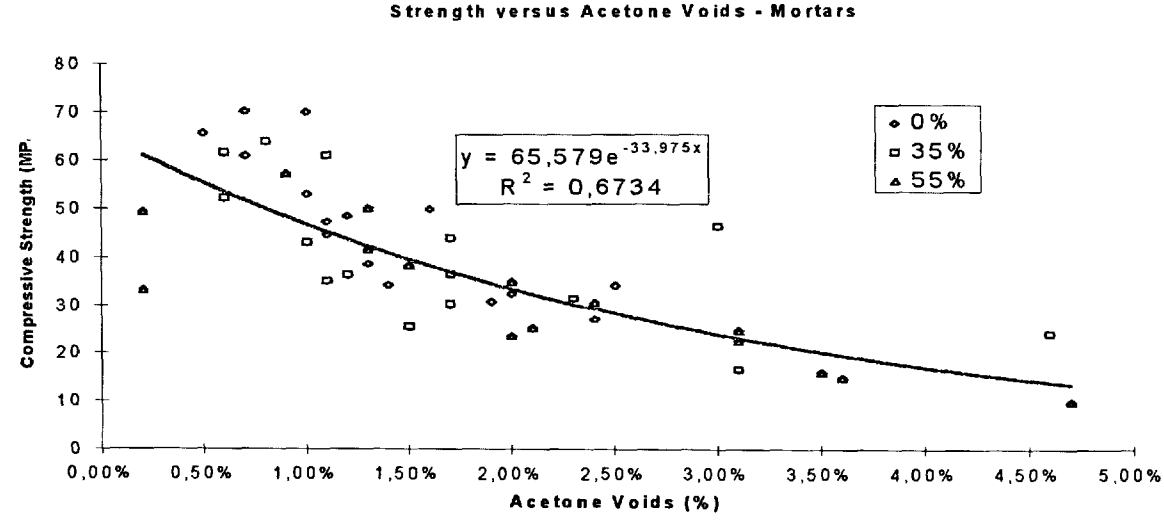

Figure 8. Compressive Strength versus Acetone Voids for Mortars. A not so good but the best correlation coefficient between strength and a voids index for mortars in this experience is shown in this figure, confirming paste's results. There is a very little influence of pozzolan amount but it appears negligible compared to the dispersion.

Table 2. Compressive Strength Mathematical Model Constants for Concretes*

Pozzolan amount (%)	Log A	Log B	Log D	Log E	R^2**
0	2.372	0.0915	1.1997	0.3484	0.9842
35	1.9947	0.6014	0.5752	0.5004	0.8814
55	2.0583	0.4646	0.7088	1.0136	0.9669

*Strength in MPa, Water/Binder Ratio adimensional (weight/weight), Age in days in Eqs 2 or 3.
**R^2 = determination coefficient.

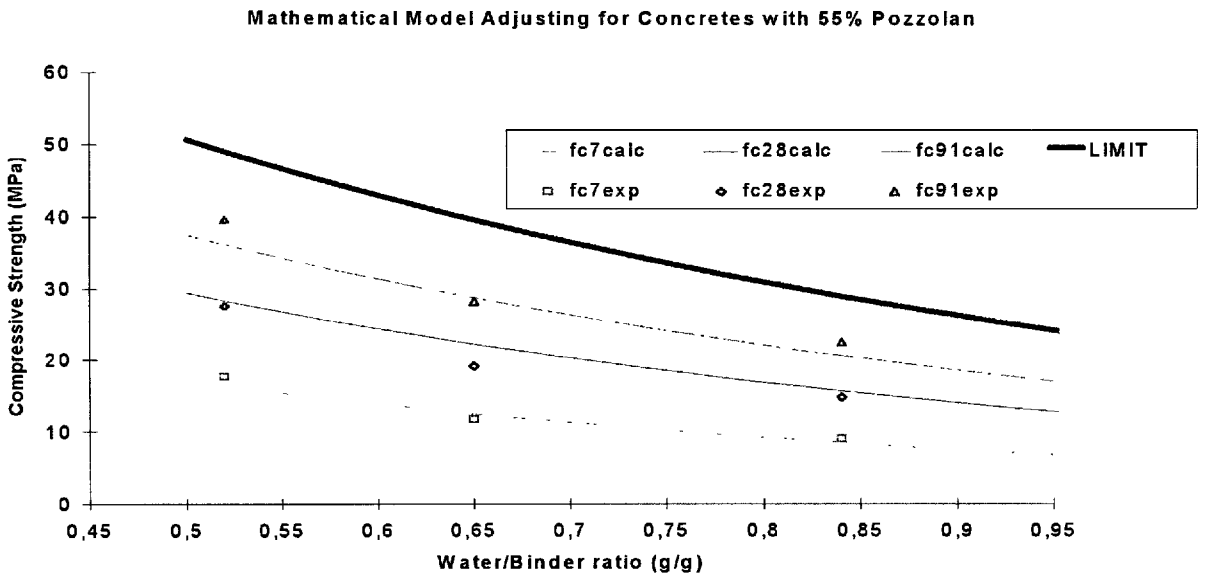

Figure 9. Generalization of Abrams' Law in the Time for Concretes with 55% pozzolan binder. LIMIT means the theoretical curve inferred for infinite age. Constants for the model are found in Table 2.

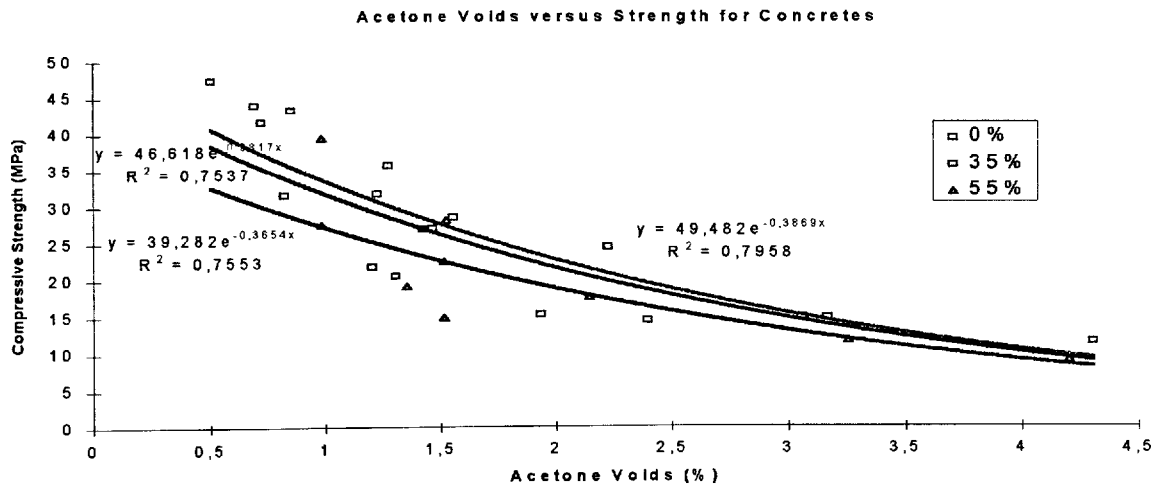

Figure 10. Compressive Strength versus Acetone Voids for Concretes. Relatively good determination coefficients and small influence of pozzolan amount on the curves' position.

CONCLUSIONS

In general, paste, mortar and concrete results agree qualitatively concerning compressive strength and porosity: binders without pozzolan reached higher strengths and higher speeds of developing strengths, with the inverted effect concerning decreasing of total pore volume.

Mathematical models for compressive strength as a function of water/binder ratio and age, proposed by equations 2 and 3, seems to be adequate for concrete or mortar both without or with pozzolan. These model permits to predict, for 35% and 55% pozzolan amounts in the binder, a theoretical limit strength, related to potential durability, which is lower than the corresponding for 0% pozzolan binder, for low water/binder ratios, and higher than the same, for high water/binder ratios. Keeping constant water/binder ratios, it is reasonably possible to linearize the curve strength versus time transforming the coordinates strength as logarithm of strength and age as inverse of age square root. This was confirmed for pastes, mortars and concretes with or without pozzolan.

For concretes, mortars and pastes it was found that acetone voids index is a good indicator of strength and probably of aggressive agents' accessibility. For pastes, the best index for compressive strength was squeezing voids, followed by acetone voids, modified ASTM boiling method voids and Hg intrusion voids. The ASTM method for voids index and its adaptations for mortars and pastes seem not to be adequate for low curing ages, probably because of leaching effect on soluble hydration products. Hg intrusion voids did not present good correlation with pastes' strength. Maybe paste structure destruction would have happened. It is recommended to research correlations between strength and various diameters cumulative pore volume amounts. It seems that acetone method gives better porosity indexes than ASTM and Hg intrusion total porosity, in spite of non realistic voids estimated percentages. The method for acetone impregnation must be improved reviewing the impregnation times in order to assure more complete pores' impregnation by acetone, giving more realistic estimated voids percentages. The method for squeezing voids in pastes must be improved by reviewing the maximum load in order to assure a more complete destruction of different binders' paste structures. Probably a not constant but a variable final load, in which it is noted a negligible displacement between compression machine plates, would assure the maximum paste structure destruction, giving more representative voids indexes as a consequence.

For the different pozzolan amounts in the binder, the relative tensile strength's development along time was different than the compressive strengths in mortars. Mortars with 55% of pozzolan exhibited a marked trend for higher tensile strengths at higher ages. Also in mortars, the ratio between tensile and compressive strength tended to be higher when the pozzolan amount increased.

Chemical analysis of paste extracted pore solution indicated that pH is very much more influenced by sodium and potassium ions than by calcium ions at the researched ages. As expected, decreasing of Ca ion with time was very marked in pastes with pozzolan, while not in pastes without pozzolan, and this was confirmed by $Ca(OH)_2$ amount obtained by TGA analysis. It is expected to continue this study not only by determinations on stopped hydration mortars and concretes stored in IPT Materials Chemistry Laboratory, but also by more discussions of results presented in this report, because of a presumable high number of non explored possibilities.

REFERENCE

Tango, C.E.S. "Modelling and Verifying Portland Cement Concrete Strength-Time Relationship up to 50 years ages. 9Th. International Congress on the Chemistry of Cements, New Delhi - India, November 1992.

ACKNOWLEDGEMENTS

To Dr., M.Sc., Chem. Maria A. CINCOTTO (São Paulo University Polytechnic School) for participation in the planning of study, Geol. Arnaldo BATTAGIN (Brazilian Portland Cement Association) for equipment, help and experience in the squeezing paste procedure, and Eng. Trainee Márcia C. TAKAHASHI, Chem. Trainee Marco A. MATAVELLI, Tech. Pedro C. BILESKY, Tech. Djalma NASCIMENTO and Tech. Sebastião R. de LIMA (Technological Research Institute IPT) for collaboration in performing the tests.

COOPERATION OF CEMENT-FLY ASH SYSTEM IN HIGH PASTE ROLLED COMPACTED CONCRETE (RCC)

Ioanna PAPAYIANNI, Aristotle University of Thessaloniki, Greece

ABSTRACT The use of cement - fly ash system (C/F) in RCC has started almost at the same time with the development of RCC. The effectiveness of it depends mainly on the type of fly ash. Low heat generation, slow strength development, low modulus of elasticity are the main advantages of C/F in mass concrete. The performance of C/F system with a high calcium fly ash was systematically studied during the construction of Platanovryssi RCC dam in Greece. Some of the results are presented here.

Key words: **Cement, high-calcium fly ash, cooperation, roller compacted concrete**

INTRODUCTION Mass concrete construction proved an unsuccessful field of application for the cement, a high energy enclosing material. Since the early 1970s (Dustan 1981) different types of mass concrete have been tried in gravity dams such as the rollcrete (cement content 110-200 Kg/m^3), the econocrete (cement content 120 Kg/m^3) and the high paste roller compacted concrete (RCC) in which large amounts of fly ashes contribute to cementitious phase. The proportioning of cement-fly ash system (C/F) depends basically on the tensile strength requirements of the RCC. The impact of fly ash inclusion on the properties of mortars and concretes (Malhotra and Mehta 1996) is closely related to its composition and origin (Low calcium fly ash from bituminous coal and high calcium from lignite coals). The combination of cement and fly ash, a high and a low potential material, constitutes a very clever system in which the by-product, fly ash, is upgraded. The fact, that 94 RCC dams (Dunstan 1994) all over the world have been constructed incorporating high content fly ash cementitious phase indicates that C/F system works quite satisfactory irrespective of variations in fly ash composition. This does not mean that fly ashes may exceed their own capacity for hardening. They need like provitamins activators and suitable climate to compensate for cement.

THE BEHAVIOR OF C/F IN HIGH PASTE RCC

One of the most characteristic cases of C/F system performance is the Platanovryssi RCC dam in Greece, the highest in Europe. It is being constructed with a paste consisting of 82% high lime fly ash and 18% portland cement I 42.5. The calcareous fly ash has been treated in a milling plant in order the free lime (CaOf) be reduced below 3% (Table 1).

Table 1. Chemical composition of cement, fly ash and cement/fly ash (C/F) system

Oxides	Cement I 42.5 (%)	Fly ash in oxides	C/F = 50/225 C+F = 275 kgr
SiO_2	19.80	33 - 88	32.65
Al_2O_3	4.65	16 - 18.5	14.91
Fe_2O_3	1.60	6 - 7.5	6.01
CaO	66.0	24.5 - 26.5	32
CaO_{Free}	-	1.96 - 2.17	1.60 - 1.77
MgO	2.62	2.05 - 3.5	2.15 - 3.33
SO_3	2.80	4.5 - 6.0	4.19 - 5.41
Insoluble residue	0.40	12.5 - 25.2	10.29 - 20.68
Loss of ignition	2.60	3.5 - 4.5	3.3 - 4.15

In the cementitious system there is an excess in $Ca(OH)_2$ and sulfates (SO_3), (Table 1), that implies unsuitability. However the main requirements of RCC for high VeBe density, low heat generation, slow strength development and as possible high deformability are fulfilled. Although for the low calcium C/F system the water demand in fresh RCC decreases up to 25% for the high calcium fly ashes, in RCC mixtures of the same VeBe time, the W/C+F increases with the content of fly ash (Papayianni 1992). This is also obvious in water demand of normal consistency pastes (Table 2). The retarding effect of the system on the setting and the low heat of hydration (Table 3) are very advantageous for RCC. It is worth mentioning that the heat of hydration of this fly ash should always be determined and varies with its reactivity. The slow rate of strength development (compressive and flexural) and the relatively low values of static modulus of elasticity are shown in Table 4 for mortars and in Table 5 for RCC.

Table 2. Setting times of C/F pastes (Vicat method)

C/F percentage	Initial h min	Water for normal consistency (g)
100/0	1 85	135
18/82	4 09	200
0/100	4 43	214

Table 3. Heat of hydration of D/F (ASTM C 186-82)

Binder	H_1 cal/gr	H_2 cal/gr	H cal/gr 7 days
cement I 42.5	589.1630	494.7858 507.2023	94.533 82.004
Fly ash 1) Liptol 2) UNIT II	402.9815 413.3010	383.1171 362.3868	20.0143 51.5474
C/F (1) 50/50 C/F (2) 21/79	417.2171 436.02	414.4095 404.0171	56.8076 32.0029

Table 4. Strength development of C/F mortars ASTM C 348-80, C 349-82

Binder	at 3-d compressive	Mpa flexure	at 7-d compressive	Mpa flexure	at 28-d compressive	Mpa flexure
cement I 42.5	28.5	3.65	34	7.8	42.25	8.1
Fly ash	8.5	0.38	10.5	2.01	18.2	4.2
C/F percentage 18/82	13	0.57	23.5	2.71	32.5	5.2

Table 5. Strength and elasticity development of concretes with C/F system

C/F percentage	VeBe density	at 7-d comp. MPa	flex. MPa	at 28-d comp. MPa	flex. MPa	Static modulus E GPa	at 91-d comp. MPa	flex. MPa	Static modulus E GPa	at 180-d compres. MPa
15/85	0.98	16.2	0.58	27.5	4.8	20.45	35.1	6	21	37.2
20/80	0.975	17.17	0.61	29.5	5.2	20.6	30.8	5.9	21.2	35.3
40/60	0.98	27	5.2	38.2	7.3	20.4	43.2	7.5	22.8	48.9

DURABILITY ASPECTS

Durability of RCC structures is governed by permeability which is affected by the achieved compactability (VeBe density), the bonding between successive layers and time dependent deformations due to drying shrinkage or thermal movement. A number of reports (Dunstan 1994) have shown that in high fly ash RCC higher than theoretical densities and very good bonding have been succeeded in the field. Very good volume stability of Platanovryssi RCC, was found after monitoring it for over a year (Papayianni 1992). The delayed ettringite formation due to the high sulfate content of C/F system is a question of great

concern. It was estimated that for 6% SO_3 in fly ash an amount up to 15% of ettringite could be formed. Ettringite is easily detected in X-ray diagrams of hardened RCC (Fig. 1). It seems that its gradual formation is unevitable. Needle crystals of ettringite are observed microscopically in the pores of RCC (Fig. 2). However the Dugan test applied in a number of cores taken from RCC did not show significant dilation. That leads to the thought that stresses developed are successfully balanced by existing restrainment in RCC mass. The crystal form of ettringite, in which less water is absorbed and less swelling is created is in favor of that stress balance (Mehta, 1973).

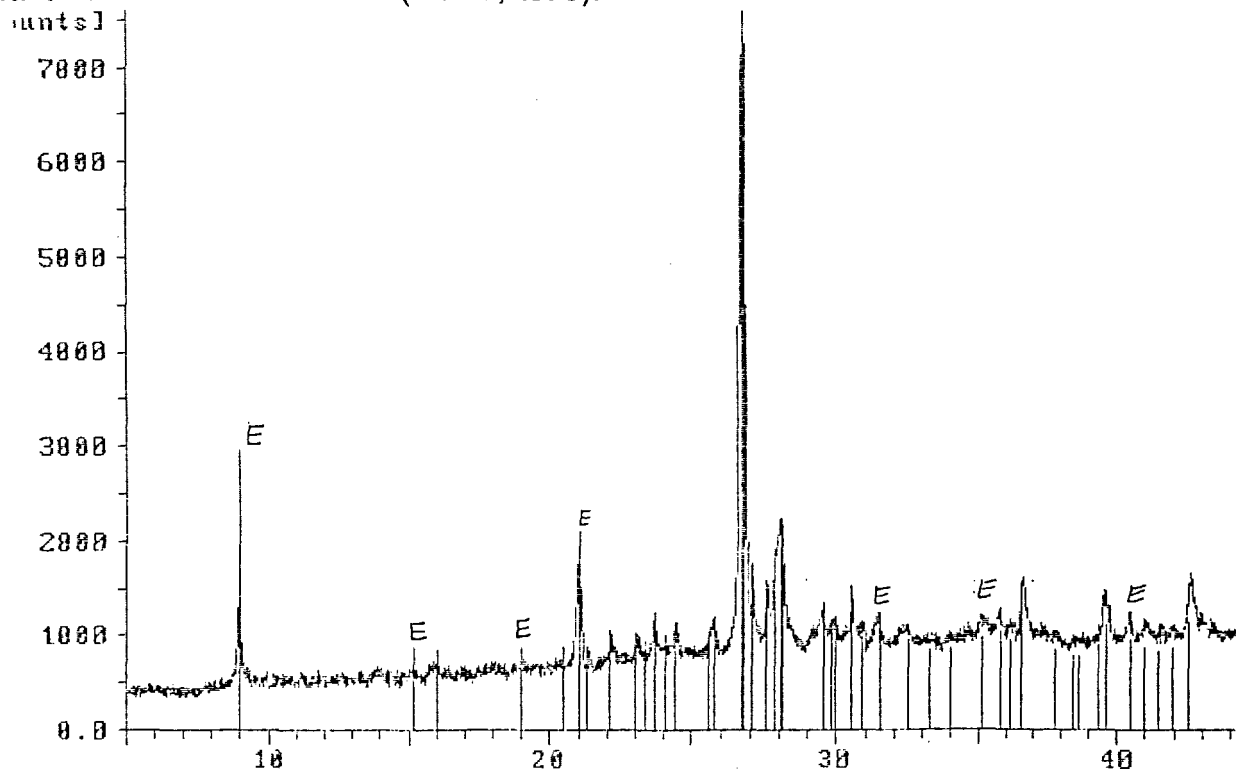

Figure 1. X-ray diagram of paste taken from RCC Sulfate content 13,5% E= Ettringite

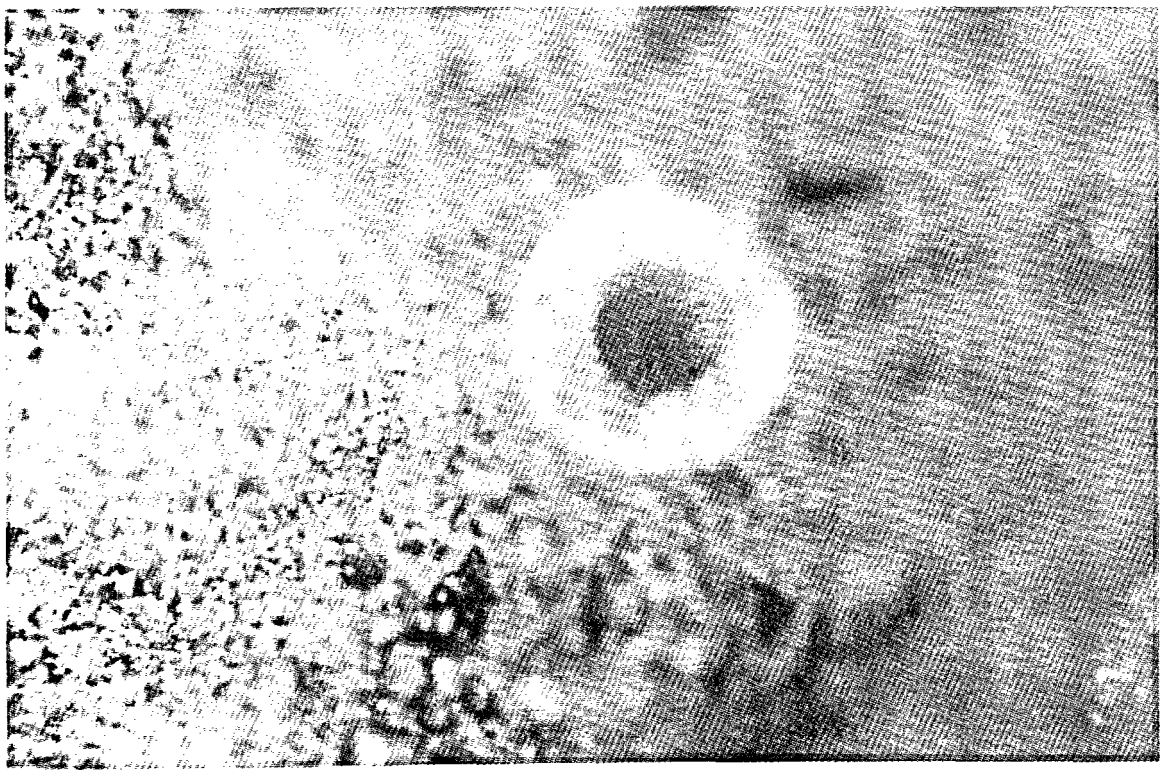

Figure 2. Ettringite crystals in pores of RCC

CONCLUSIONS

In C/F cementitious systems, the fly ash changes into an added value material by which the economy and the ecological profile of large projects are significantly improved. The proportion of fly ash in C/F system should be determined after trial mixes, taking into account the strength and elasticity requirements of the structure. The successful application of C/F high paste RCC in road construction could open new field in cement market in many countries. The good cooperation of cement fly ash system is a challenge for developing new blended type cement suitable for low strength concrete products.

REFERENCES

Dunstan M. R. H. "Roller Concrete for Dams. A Laboratory Study of the properties of high fly ash concrete" - Technical Note 105 - CIRIA May 1981

Dunstan M. R. H. "Future Trends in Roller Compacted concrete Dam Construction" - ACI SP 144-16 edited by P.K. Mehta - Detroit 1994 - pp. 307-325

Malhotra V. M. and **Mehta** P. K. "Pozzolanic and cementitious materials" - Gordon and Breach Publishers 1996 - pp. 45-103

Papayianni I. "Performance of a high Calcium Fly Ash in RCC" - ACI SP 132 Editor V. M. Malhotra - Detroit 1993 - pp. 367-387

Mehta P. K. "Mechanism of Expansion Associated with Ettringite Formation" - Cem. Concr. Res. 3 - 1973 - pp. 1-6

PROPERTIES OF CEMENT CONTAINING GERMAN LIGNITE FLY ASHES

Stefan DIETZ, University of Heidelberg, Germany
Krzysztof MISKIEWICZ, RWE-Gesellschaft für F und E mbH, Wesseling, Germany
Michael SCHMIDT, Heidelberger Zement AG, Leimen, Germany

ABSTRACT Lignite fly ash was tested as partial cement replacement on its properties and suitability. Lignite fly ashes represent a mixture of different binding type particles, whereas each fly ash possesses a specific reactivity. The fly ash-cement mixes showed strength contributions connected to the hydraulic activity of the fly ash. The fly ash-cement mixes had a good stability of volume and low expansion rates. Negative effects on the fly ash-cement-properties due to fly ash addition couldn't be observed with up to 10-15 % by mass fly ash content in most of the mixes.

Key-words: Fly ash, Admixture, Mineralogy, X-ray Diffraction Analysis

INTRODUCTION

In Germany about 180 million tonnes per year of lignite are fired for electricity supply. During the firing process about 10.9 million tonnes of fly ash are produced, of which 0.8-1.4 million tonnes are free for utilization.Today in Germany fly ashes from lignite fired power plants are mostly used to refill open pits in a mixture with FGD-process water.

In the last few years many projects were run by energy suppliers and building material producers about the properties, qualification and utilization options of lignite fly ashes. One of these projects was the „Utilization of Filter Ash from Coal Power Plants in the Federal Republic of Germany" cooperative research project („Ash Recovery", duration 1991-1995, over 30 different single projects) which was coordinated and financed with different shares by RWE AG, RWE Energie AG, VEAG, Rheinbraun AG, LAUBAG, NUKEM GmbH and RWE Entsorgungs AG. The investigation of fly ashes as a cement additive in blended cements was one of these projects carried out by the RWE-Gesellschaft für Forschung und Entwicklung mbH in cooperation with the Heidelberger Zement AG.

Several tests according to DIN-EN or other well-known testing methods for durability, carbonation, sulphate- or freeze-thaw-resistance were carried out, besides several mineralogical investigations.

PROPERTIES OF FLY ASH AND CEMENT

Chemical composition and physical properties

For the test programme fly ashes from two power plants in the main lignite mining regions in Germany, the Rhine region and the Lusatian region, were choosen. To ensure a representative composition of the fly ash 238 samples were taken from each power plant. The composition of the investigated fly ashes is close to the mean value of the fly ash samples tested. Table 1 shows the chemical composition and physical properties of the used fly ashes. BFA R represents a calcareous fly ash deriving from firing of lignite of the Rhine lignite mining region, BFA L a silica-rich fly ash from the Lusatian lignite mining region. BFA R is finer grained and has a higher specific surface (Blaine) than BFA L. BFA R can be described as a reactive latent-hydraulic fly ash, BFA L as a pozzolanic fly ash. As reference and mixing cement 2 Portland cements of a different strength class, PZ 45 F (CEM I 42,5 R) and PZ 35 F (CEM I 32,5 R) from the Heidelberger Zement AG were selected (Table 2).

Table 1 Chemical composition and physical properties of fly ashes

BFA	L	R
Chemical composition in % by mass [1]		
LOI at 850 °C	0,65	3,44
C	0,8	3,1
SiO_2	57,0	44,7
Al_2O_3	11,4	4,5
Fe_2O_3	8,5	8,7
CaO	15,7	27,4
free lime	1,0	6,5
MgO	3,1	7,0
S_{total}	1,4	3,2
K_2O	1,2	0,5
Na_2O	0,3	0,6
TiO_2	0,9	0,4
Cristalline phases in % by mass 2		
Quartz	41	42
Anhydrite	5	7
Hematite	5	7
Magnetite	n.n	1
Lime	1	7
Carbon	1	3
Cristalline share	53	67
Amorphous share	47	33
Physical properties		
Raw density [g/cm³]	2,7	2,9
Bulk density [kg/dm³]	1,1	1,3
Specific surface (BET) [m²/g]	2,7	19,7
Specific surface (Blaine) [cm²/g]	1900	3200

1 - according to DIN 51729 part 1-9
2 - detected by XRD

Table 2 Chemical composition and physical properties of Portland cements

Cement	CEM I 42,5 R (PZ 45 F)	CEM I 32,5 R (PZ 35 F)
Chemical composition in % by mass		
SiO_2	20,1	19,9
Al_2O_3	5,0	5,5
Fe_2O_3	3,1	2,1
CaO	65,3	61,9
free lime	1,0	0,6
MgO	1,0	3,0
K_2O	0,7	1,1
SO_3	2,7	3,1
LOI	1,0	1,0
Clinker phases calculated (BOGUE) in % by mass [1]		
C_3S	70,8	58,7
C_2S	4,3	12,8
C_3A	8,0	10,9
C_4AF	9,5	6,4
Physical properties		
Specific surface		
Blaine [cm²/g]	3260	2720
BET [m²/g]	1,1	1,0

1) C - CaO S - SiO_2
A - Al_2O_3 F - Fe_2O_3

PROPERTIES OF FRESH FLY ASH-CEMENT-MIXES

The following presentation of results is concentrated on mixtures with PZ 45 F. The same investigations were undertaken with PZ 35 F as well. The results are summerized in Table 3.

The indication of the raw material and fly ash-cement mixtures is as follows:

BFA L: Lignite fly ash from the **L**usatian lignite mining region
BFA R: Lignite fly ash from the **R**henish lignite mining region
PZ 45 F: Portland cement, strength class 45 N/mm² according to DIN 1164 (CEM I 42,5 R according to ENV 197)

Fly ash-cement-mixes (examples):

R 30-45 30 %(m/m) BFA R; 70 %(m/m) PZ 45 F

Water requirement

The water requirement, tested according EN 196 part 3, decreased cement was substituted by BFA L and increased with BFA R. Many parameters of BFA R like the higher surface area, the higher fineness, lower bulk density and the higher CaO-content compared to BFA L result in the different behaviour of the fly ash-cement-mixes. The water requirement of BFA R and of the fly ash-cement-mixes correlate with the calculated value (linear relation between water requirement

of OPC (27.6%) and water requirement of fly ashes (BFA R: 32.6%; BFA L: 25.6%)). BFA L-cement mixes show a minimum water requirement with 10 % by mass fly ash content but the same tendency as the calculated values (Fig 1).

Figure 1 Comparison of measured and calculated water requirement of BFA-PZ 45 F-pastes

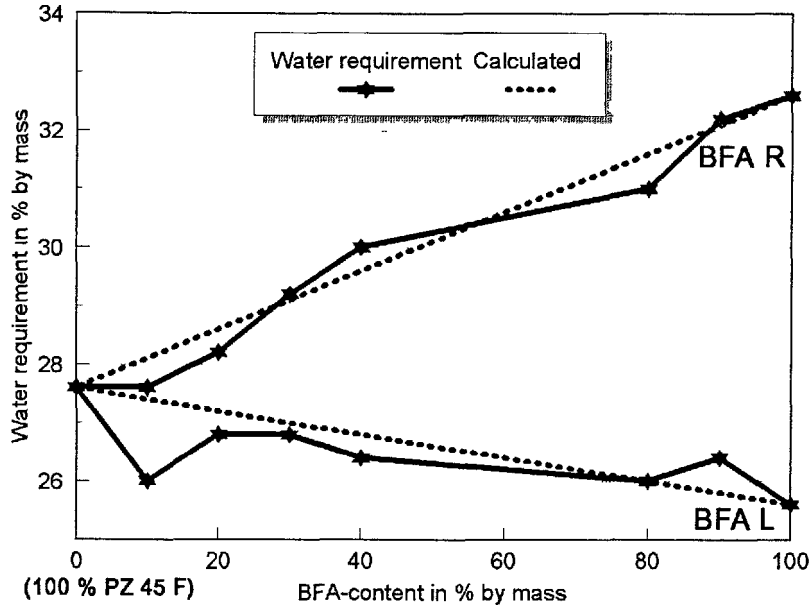

Setting time

The setting, determined according to EN 196, part 3, was generally accelerated with increasing amounts of BFA R and retarded by fly ash BFA L. The setting periods of all fly ash-cement-mixes range in the time period required in EN 196 part 3, setting starts not earlier than 1 hour after water addition and ends not later than 12 hours.

Flow table test

The flow diameter, determined according to DIN 1060, was decreased with increasing amounts of fly ash. BFA R-cement mortars had a stiffer consistence than the mixes with the same content of BFA L.

PROPERTIES OF HARDENED FLY ASH-CEMENT-MIXES

The hardened fly ash-cement mixes were tested as mortar bars (4x4x16 cm) manufactured according to EN 196 part 1. The Freeze-Thaw-resistance was tested on 10 cm concrete cubes.

Expansion

The mortar bars were stored according to DIN 52450 under water at 20°C. The expansion rates of the fly ash-cement mortar bars are mostly below 1 mm/m after 700 days. Only with a BFA R content of 90 % by mass the rates summed up to 3 mm/m (Fig 2). After 90 days of hardening the expansion rates remain constant, that means no delayed expansion reaction occurs due to fly ash-reactions. The expansion rates of BFA L-cement-mixes didn't exceed 1 mm/m with up to 90 % by mass fly ash content after 700 days.

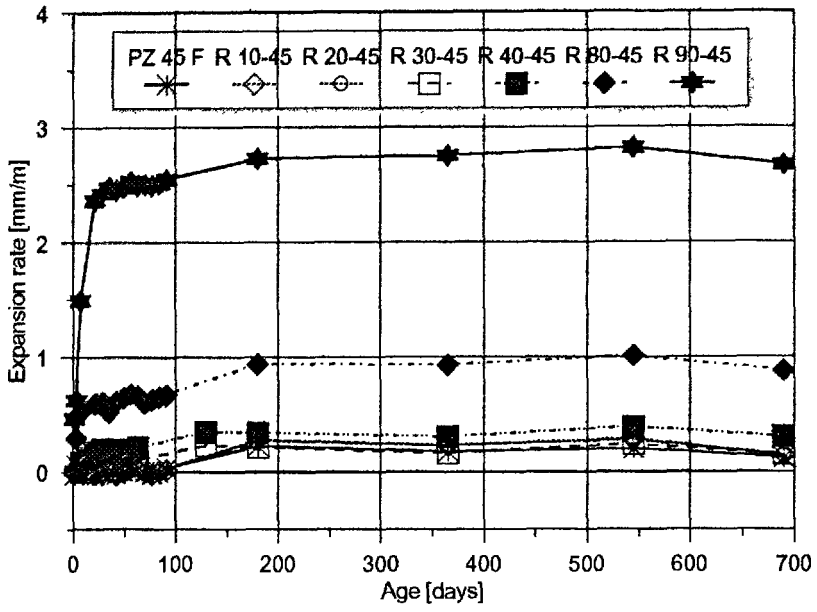

Figure 2 Expansion rates of BFA R-PZ 45 F-mixes depending on curing time (under water, 20°C)

Compressive strength

The compressive strength was determined according to DIN EN 196 part 1. Fly ash cement mixes with 10 % by mass fly ash content reached more than 90 % of the compressive strength of the reference cement mix at all ages. A strength contribution of the fly ash could be observed even for higher fly ash additions in most of the fly ash-cement mixes. The calcareous fly ash shows early strength contributions at 2 days because of their latent-hydraulic character, the silica-rich fly ash has a pozzolanic character, with increasing strength at higher ages (Fig 3).

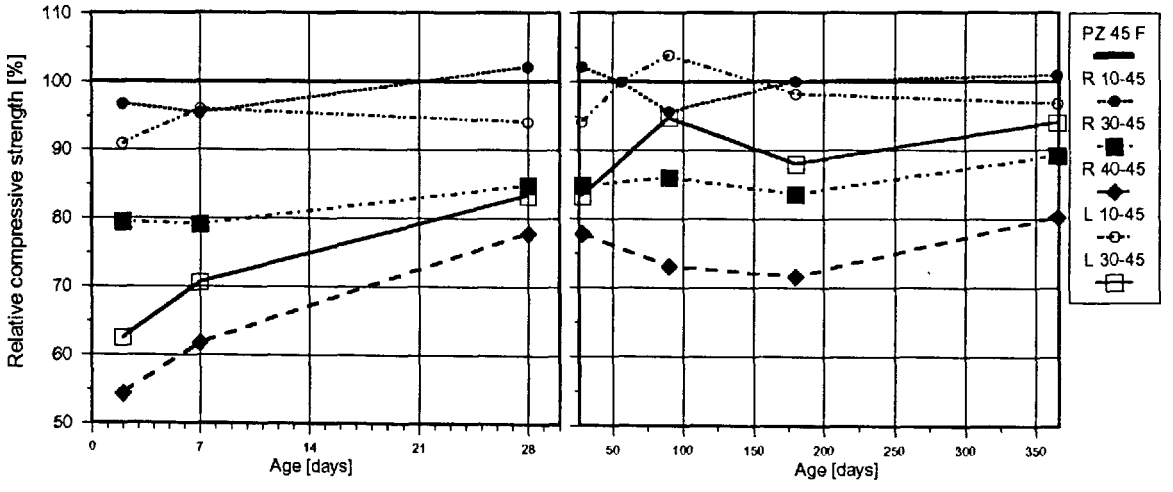

Figure 3 Compressive strength development of fly ash-cement-mortar bars related to reference mortar

Carbonation

After 2 days curing in 90 % rel. humidity, the mortar bars were stored in 20°C and 65 % rel. humidity. The short humid precuring represents very severe conditions.

Increasing carbonation depths could be observed with increasing fly ash contents (Fig 4). The carbonation depths of fly-ash-cement mortar bars with 10 % by mass fly ash content are in the range of the reference cement.

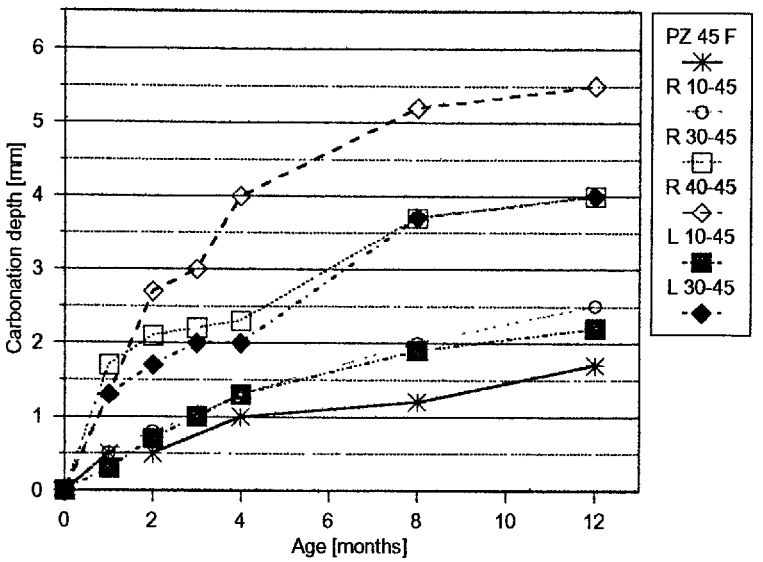

Figure 4 · Carbonation depth of BFA-PZ 45 F-mortar bars as a function of age

There was no difference between the two fly ashes concerning carbonation depth. Other test series with a longer wet curing of the mortar bars of 7 and 28 days under water before measurements started resulted in reduced carbonation depth.

The carbonation depth correlates with the compressive strength. The carbonation depth increases with decreasing compressive strength, that means the main influence factor on the carbonation is the compressive strength. Secondary the $Ca(OH)_2$-binding of latent-hydraulic and pozzolanic components e.g. Ca-Al-glass phases could reduce the alkaline potential in the fly ash cement mixes and lead to higher carbonation depths.

Freeze-Thaw-resistance of concrete

After defined Freeze-Thaw-cycles the concrete cubes were weighed according to the cube-method[1]. The decrease in weight is caused by scaling due to frost attack.

The Freeze-Thaw-resistance test showed an increasing scaling with increasing fly ash content (Fig 5). Concretes with BFA L-cement mixtures had a high freeze-thaw resistance up to 30 % fly ash content by mass and concretes with BFA R-cement-mixtures up to 10 % fly ash content (scaling of up to 5 % by mass is considered for good freeze-thaw-resistance).

Concretes with BFA R-cement-mixes showed significantly higher scaling than those with BFA L. As the concrete cubes were produced with a constant water content, the fresh concretes with BFA R had a stiffer consistency. Nevertheless the concretes containing fly ash had a higher raw density compared to the PZ 45 F concretes. Further investigation didn't show any relation between fly ash particles e.g. porous carbon particles and the decrease in Freeze-Thaw-resistance of fly ash containing concretes. From other investigation it was concluded that a reduction of compaction pores due to fly ash addition could lead to a higher scaling. Until there are no further

[1] Bunke N.: Prüfung von Beton, Empfehlungen und Hinweise als Ergänzung zu DIN 1048 - Heft 422, Beuth-Verlag,, p. 30-31 (1990)

information on the pore structure and distribution in cement paste future investigations are necessary.

More tests should be made with concretes of comparable workability and compressive strength to determine the influence of fly ash on the Freeze-Thaw-resistance. Air entraining agents can improve the Freeze-Thaw-resistance of concretes with higher fly ash contents.

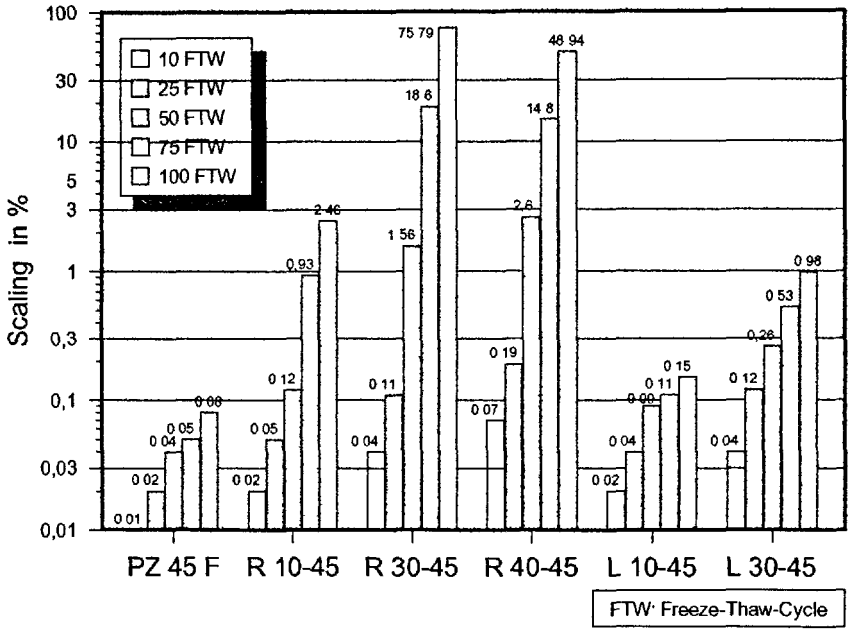

Figure 5 Scaling of BFA R-PZ 45 F containing concrete cubes due to frost-attack depending on the number of Freeze-Thaw-cycles

MINERALOGICAL INVESTIGATIONS

In addition to the mortar and concrete tests to determine macroscopic effects of fly ashes on cement properties, the mineralogical tests should show the effects on the microstructure as well as differences in the hydration reaction due to fly ash addition.

X-ray diffraction (XRD)

An important question for the durability of fly ash-cement mixes is the reactivity of free lime. In-situ XRD which allows the continous measurement of pastes during the early hydration (measurement starts 2 minutes after water addition) showed the nearly complete reaction of CaO forming $Ca(OH)_2$ within the first two hours of hydration. It can be concluded that there will be no expansion due to CaO-hydration in corresponding fly ash-cement mixes (Fig 6).

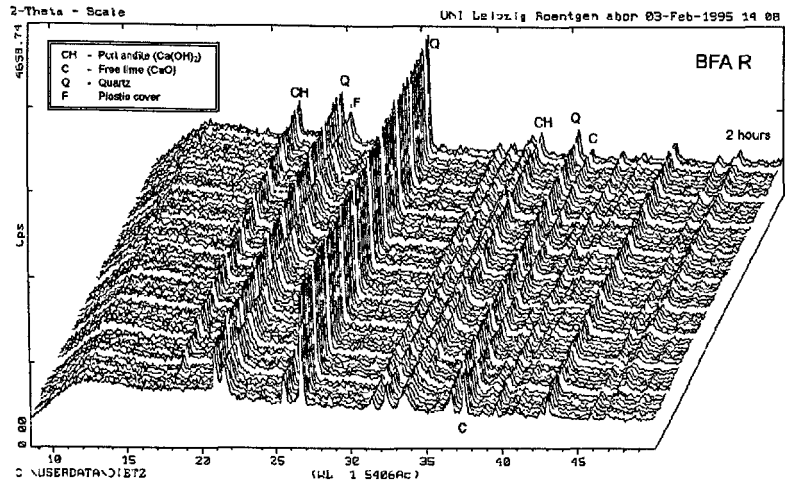

Figure 6 In-situ X-ray diffractogram of an BFA R-paste during the first 2 hours of hydration

Normal X-ray diffraction on fly ash-cement mix samples, hydration stopped with isopropanol and dried in a vacuum-dryer after certain hydration times showed a slightly higher Ettringite-concentration until 28 days of hydration in BFA R-cement mixes than in the cement-mixes.

Dynamic Scanning Calorimetrie (DSC)

The DSC showed the high reactivity of the fly ashes (Fig 7).

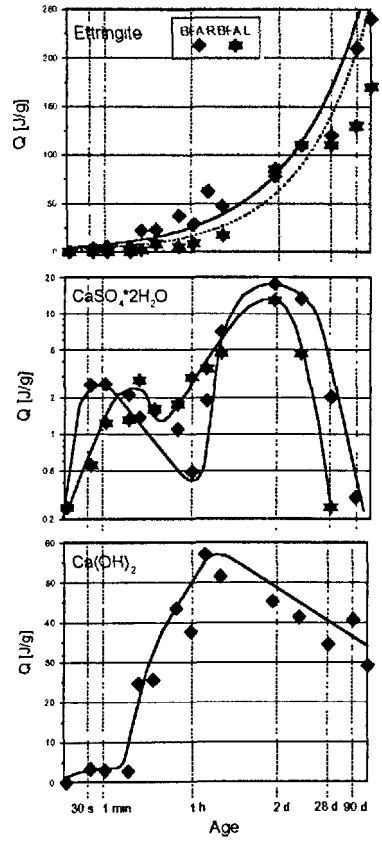

Figure 7 Quantitative DSC-determination of Ettringite, gypsum and portlandite during hydration

Ettringite was formed after the first minutes with increasing amounts during hydration. Anhydrite is highly soluble. Gypsum was formed in cycles depending on the saturation of the pore solution. Free CaO was hydrated very quickly so that $Ca(OH)_2$ could be formed in BFA R, with decreasing amounts due to the formation of Ettringite and other CSH-phases.

Scanning electron microscope (SEM)

For the SEM-investigations the samples, stopped with Isopropanol and dried, were coated with platinum. No major differences in the microstructure between the reference cement samples and the fly ash-cement-mixes could be observed. Fig 8 shows a reacting glass sphere (B) coated by a reaction cover (A). Fig 9 shows a pore filled with Ettringite and hexagonal Portlandite ($Ca(OH)_2$)crystals.

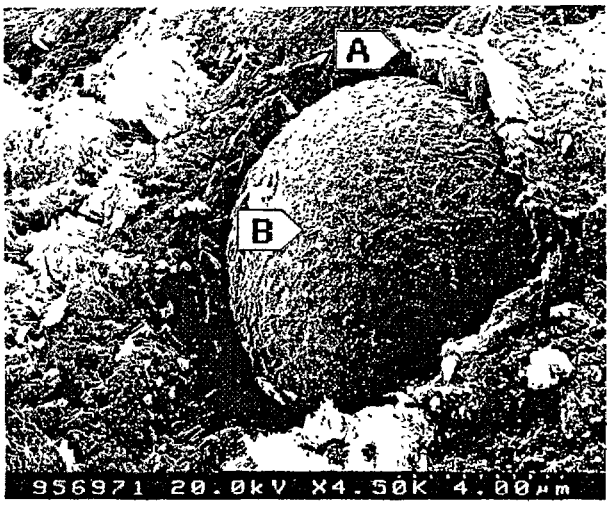

Fig 8 Reacting glass sphere of BFA R in a R 30-45-paste after 180 days of hydration

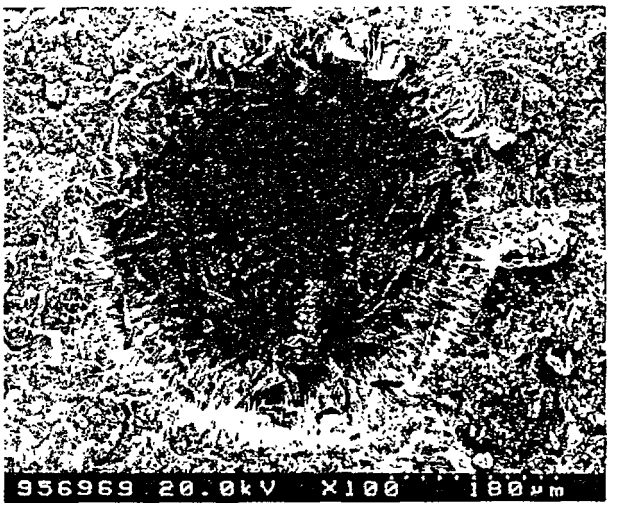

Fig 9 Ettringite and Portlandite in a pore of a R 30-45-paste after 180 days

DISCUSSION AND CONCLUSIONS

The investigation showed, that fly ashes are a reactive component in the fly ash-cement system. Early strength contributions even at early ages of hydration showed the high reactivity of the calcareous BFA R. The silica-rich BFA L reacts like a pozzolan with a „delution effect" due to low reactivity at the beginning of the hydration and a continous strength contribution with increasing hydration time.

The strength contribution of the fly ash in cement mixes could be observed for most of the mixes up to 40% by mass fly ash content.

Volume stability due to expansion-reactions is ensured with both fly ash types up to at least 40 % by mass fly ash content. Unsoundness couldn't be observed. The free lime in the calcareous fly ash BFA R is highly reactive and hydrates nearly completely after 2 hours of hydration.

The carbonation is increased with increasing fly ash content, no matter which type of fly ash is used. Reasons could be differences in pore structure and distribution and pozzolanic reactions of fly ash particles that lead to a decrease in the $Ca(OH)_2$-concentration. An extended curing time of the samples can decrease the carbonation depth of fly ash-cement-mixes. However extended wet curing is hard to realize in civil engineering.

Table 3 Maximum fly ash content in fly ash-cement mixes with no negative influence on the investigated properties

Properties of fly ash cement mixes	Maximum BFA content in fly ash-cement-mixes without obvious negative effects on cement and concrete properties *(BFA-content in % by mass)*			
	CEM I 42,5 R		CEM I 32,5 R	
	BFA R	BFA L	BFA R	BFA L
Pastes				
Water requirement				
higher than OPC	90	-	10	-
lower than OPC	-	90	20-30	30
Setting time compared to OPC				
retarded set	40	90	30	-
accelerated set	80-90	-	10	-
according to EN 196 part 3	90	90	30*	30*
Volume stability				
Le Chatelier (< 3 mm) accord. to EN 196 part 3	40	90	30*	30*
according to DIN 1164 part 6	40	90	30*	30*
modified DIN 1060	80	90	n.d.	n.d.
Fresh mortars				
Slump				
higher than OPC	-	10	-	-
> 140 mm	30	30	20	20
Bearing resistance				
higher than OPC	40*	-	30*	-
< / = OPC	-	10	-	30*
Hardened mortars				
Compressive strength (180d)				
cured under water at 5°C				
equal to OPC	-	-	10*	10*
> 80% of the OPC	20*	20*	-	-
Compressive strength (365d)				
cured under water at 20°C				
> 90% of the OPC	10	10	10	10
E-module (365d)				
higher than OPC	30	10	10	-
Expansion, mortar bars cured in				
water 5°C (180d) < / = OPC	20*	20*	10*	10*
water 20°C (690d) < / = OPC	40	40	n.d	n.d
20°C/ 65% r.H. (365d) </= OPC	40*	30*	-	-
Impermeability (k_r-value) < OPC	30*	30*	n.d.	n.d.
Sulfate resistance				
slightly weaker than OPC	n.d.	n.d.	10*	10*
Carbonation (365d)				
equal to OPC	10	10	-	-
> 3 mm	30	30	10	10
Concrete				
Freeze-Thaw-resistance (100 cycles)				
weight loss < 5 %(m/m)	10	30*	-	10

OPC: Ordinary Portland cement

* higher fly ash amounts were not tested

n.d. : not detected

- : the given value was not reached resp. fly ash contents < 10 % by mass were not tested

Freeze-thaw-resistance of fly ash containing concrete cubes decreases with increasing fly ash content. The reason for that phenomena could be an increasing capillary porosity and a reduction of air pores.

Table 3 shows the maximum contents of fly ash in fly-ash-cement-mixes which didn't show any negative effect on the cement and concrete properties.

The mineralogical investigations showed that lignite fly ashes represent a system of puzzolanic (Si-rich glassphases), latent hydraulic constituents (Al-Ca-rich glassphases) and CaO- and SO_3-suppliers. The reactivity of the fly ash and their influence on binding systems depends on the quantity of each category in the fly ash (Fig 10).

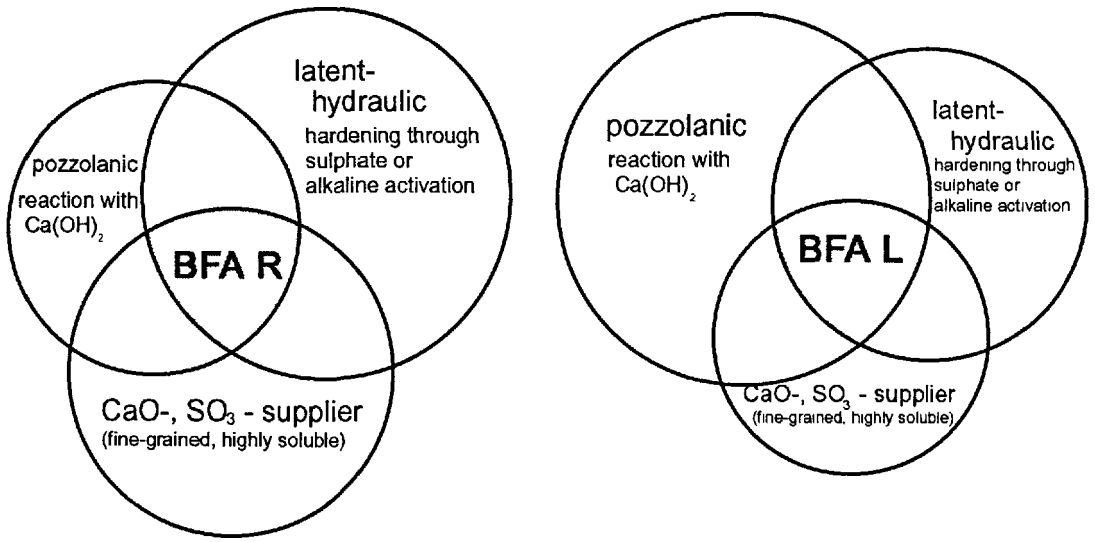

Figure 10 The binding character of the fly ashes as a combination of the three principle binding types

The differences in hydration of Portland cement compared to fly ash containing cement were very little. A slightly higher Ettringite concentration in BFA R-cement mixes could be observed without having any effect on the volume stability.

Finally it has to be pointed out that a fly ash content of at least 10-15 % by mass showed no negative effect on the properties of most of the fly ash-cement-mixes. Further investigation should be made on the effects of fly ash on the carbonation and the Freeze-Thaw-resistance of concrete.

CHARACTERIZATION OF FLY ASHES DIRECTLY COLLECTED FROM ELECTROSRATIC PRECIPITATOR

Seung Heun LEE, Kunsan Nat l. Univ., Kunsan, Korea
Etuo SAKAI, Masaki DAIMON, Tokyo Institute of Technology, Tokyo, Japan

ABSTRACT The test results show that fly ashes obtained from the hopper at the furthest point from the combustion boiler tend to have a finer particle size, larger density, lower carbon content and higher glass content. When the boiler is operated in full load running(600MW) in comparison with half load running (300MW) the glass content increases but the Blain specific surface area and carbon content decreases. And the fly ashes show that pozzolanic reactivity at 40℃ is related to the fineness. But the glass content has no significant influence on reactivity. there is a negative correlation between the apparent viscosity of cement paste with fly ashes and carbon content at addition of 1.6% superplasticizer.

Key-words: Characterization, Fly ash, Fineness, Pozzolanic reactivity, Glass content

INTRODUCTION

In coal-fired power plant, coal ashes passing through boiler are negatively charged by corona discharge in electostatic precipiator(ESP) system and attach to collection electrode and fall into hopper by rappers. ESP system has many collected fields in the direction of flue gases and hopper is installed in each collected field. In most coal-fired power plants, fly ashes collected from each hopper in ESP are transported to one line and stored in silo and the necessary amount is supplied to classifier. The supplied fly ashes are divided into coarse and fine particles by classifier to be stored in silo. However, since the properties of the fly ashes collected from each hopper in ESP system change as the farther the collected field gets from boiler the larger the Blaine specific surface area gets(Hemming and Berry, 1988), the hopper itself in ESP system is expected to have the effect of classifying fly ashes.

Based on the above background, this research investigated physical and chemical properties of fly ashes collected from hoppers in ESP system when boiler was operated either in full load running(600MW) and in half load running(300MW). Also the effect of the properties of such fly ashes on the apparent viscosity of paste following the reactivity with $Ca(OH)_2$ and the addition of superplasticizer has been examined.

EXPERIMENTAL METHODS

Materials

Fly ashes of six kinds collected per each load and hopper were used, when load of boiler in the capacity of 600MW in power plant was operated in 600MW and 300MW(at night), and when the locations of hoppers attached to ESP system were named 1st, 2nd and 3rd field in the moving direction of gases. $Ca(OH)_2$ of first grade reagent in evaluation of reactivity, and ordinary portland cement(Blaine specific surface area: 3560㎠/g, specific gravity: 3.15) and polycarboxylic acid superplasticizer in measurement of apparent viscosity were used.

Measurement of physical and chemical properties of fly ashes

Chemical properties of fly ashes, such as chemical composition, mineral composition, carbon content, loss on ignition and the adsorption amount of methylene blue(MB) were measured. And also physical properties, such as Blaine specific surface area, particle size distribution, residue on 45 μm sieve and specific gravity were measured. Mineralogical compositions of

fly ashes was obtained with powder X-ray diffraction analysis by the use of internal standard method.

Measurement of the amount of reacted $Ca(OH)_2$

After fly ashes and $Ca(OH)_2$ were mixed by the mole ratio of Ca/(Si+Al)=1 and water/powder was mixed with the mixture by weight fraction of 0.6, it was reacted in incubator of 40℃ for 3, 7, 28 and 56 days. The sample reacted for a certain period of time was deposited in acetone for 1 day and dried at 110℃ for 24 hours. The product was identified by powder X-ray diffraction analysis and the amount of unreacted $Ca(OH)_2$ was obtained from atmosphere of N_2 gas by TG-DTA. Reacted $Ca(OH)_2$ was obtained from the value and loss on ignition.

Measurement of apparent viscosity

Fly ashes were mixed by 20% of volume fraction in ordinary portland cement, and polycarboxylic acid plasticizer was added up to 2.0%. And then water/powder was mixed with the mixture by volume fraction of 0.6. This paste was made rise and fall between shear stress 0Pa and 200Pa at 20℃ by the use of viscometer, and the apparent viscosity at 200Pa was measured.

RESULTS AND DISCUSSION

Fineness of fly ashes

Table 1 shows the physical properties of fly ashes. It represents that as going from the 1st field to the 3rd one regardless of the load of boiler, the Blaine specific surface area of fly ashes increases and showes the value of 7,000cm^2/g or more in the 3rd field. The mean particle size of fly ashes was more than 30 μm in the 1st field but was 6.9 μm in the 3rd one. Most of fly ashes that obtained the 3rd field passed through 45 μm sieve. As the particle size distribution of fly ashes is shown in Fig 1, fly ashes going from the 1st field to the 3rd one, maximum particle size becomes smaller and the range of particle size distribution gets narrower and fly ashes in the 1st field represent multiple distribution with two maximum frequency diameters but, fly ashes in the 3rd one show normal distribution. In view of the differences in fineness by the load of boiler, the fineness was slightly better in half load running of 300MW than in full load running of 600MW. The presumed reason why it is so is because, in half load running of 300MW the amount of coal put into boiler has decreased to half in comparison with 600MW and thus cohesion by collision between pulverized coals at the time of combustion has decreased.

Table 1 Physical properties of fly ashes.

fly ash	load(MW)	collected position	specific gravity	Blaine specific surface area(cm^2/g)	residue on 45 μm sieve(%)	mean particle size(μm)
A-1	600	1st field	2.06	2760	22.8	34.6
A-2	600	2nd field	2.22	4180	3.8	18.6
A-3	600	3rd field	2.42	7360	1.7	6.9
A'-1	300	1st field	2.08	3580	16.6	30.4
A'-2	300	2nd field	2.23	4980	3.2	15.6
A'-3	300	3rd field	2.40	7920	0.2	6.9

Carbon content, loss on ignition and adsorption amount of methylene blue

carbon content, loss on ignition and adsorption amount of methylene blue are items used in evaluation of the amount of unburned carbon among fly ashes, as represented in table 2.

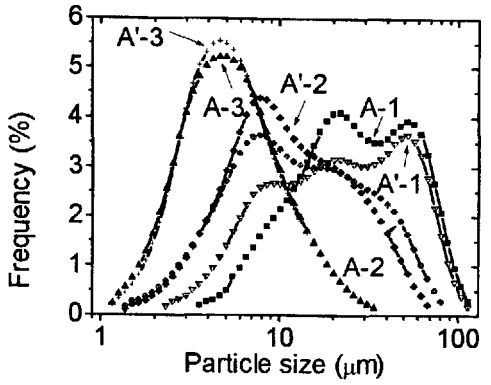

Fig. 1 Particle size distribution curves for fly ash

Carbon content and loss on ignition had overall low values in the range of 0.3-1.5% and 1.1-2.1%. carbon content was least in fly ashes of the 3rd field with least mean particle size but, loss on ignition did not show any such relation. Fly ashes collected from one and the same place had less total carbon and loss on ignition in full load running of 600MW than in half load running of 300MW. This may be because the combustion state is stable in full load running of 600MW appropriate to the capacity of boiler. As it was reported that adsorption amount of methylene blue, the blue coloring matter was linked to the adsorption amount of air-entraining agent on unburned carbon.(Tanosaki et al., 1995) However, in this experiment the correlation between the adsorption amount of methylene blue and carbon content, loss on ignition was not shown because the carbon content of fly ashes was small. But A'-1 and A'-2 with the most carbon content had more loss on ignition and adsorption amount of methyl blue.

Table 2 Ccarbon content and loss on ignition of fly ashes and adsorption amount of methylene blue(MB) on fly ashes.

fly ash	carbon content(%)	loss on ignition(%)	adsorption amount of MB(mg/g)
A-1	0.7	1.1	0.35
A-2	0.8	1.2	0.30
A-3	0.3	1.7	0.30
A'-1	1.5	2.1	0.50
A'-2	1.3	2.1	0.60
A'-3	0.4	1.8	0.30

Chemical and mineral characteristics of fly ashes

Table 3 represents the chemical compositions of fly ashes. It represents a typical composition of bituminous coal ashes as analytical SiO_2 and Al_2O_3 was more than 85% and analytical CaO had low value of 2.0-2.3%. In view of chemical composition of fly ashes depending on the place of collection, fly ashes going from the 1st field to the 3rd one, analytical SiO_2 decreased by 3.5% in full load running of 600MW and 2.5% in half load running of 300MW. But analytical Al_2O_3 increased to 1.6% and 1.5% in each running. The total amount of Fe_2O_3, alkali and alkali earth oxide which lower the melting temperature of coal ashes was about 10% and increased slightly as going from the 1st field to the 3rd one. There was little difference in chemical composition by load change of boiler. Fig 2 shows the results of X-ray diffraction of fly ashes. Major crystalline phase was mullite and α-quartz and minor crystalline phase was magnetite and hematite regardless of the place of collection and the load of boiler. Ca-containing phase could not be identified in X-ray diffraction analysis. As mentioned above, this may be because fly ashes used in this experiment had low value of 2.3% or less in the analytical CaO content and most acted as modifiers in glass formation.(McCrthy et al., 1988)

Table 3 Chemical analysis of fly ash(wt%).

fly ash	SiO_2	Al_2O_3	Fe_2O_3	CaO	MgO	SO_3	TiO_2	Na_2O	K_2O	C
A-1	63.8	24.8	4.6	2.3	0.9	0.3	1.0	1.2	0.7	0.7
A-2	62.0	25.5	4.3	2.2	1.2	0.4	1.1	1.3	0.8	0.8
A-3	59.5	26.4	4.8	2.3	1.2	1.0	1.1	1.3	0.8	0.3
A'-1	62.5	24.9	4.2	2.0	1.1	0.5	1.1	1.2	0.8	1.5
A'-2	60.9	25.4	4.2	2.3	0.9	0.6	1.1	1.2	0.8	1.3
A'-3	59.6	26.4	4.3	2.3	1.1	1.0	1.1	1.4	0.8	0.4

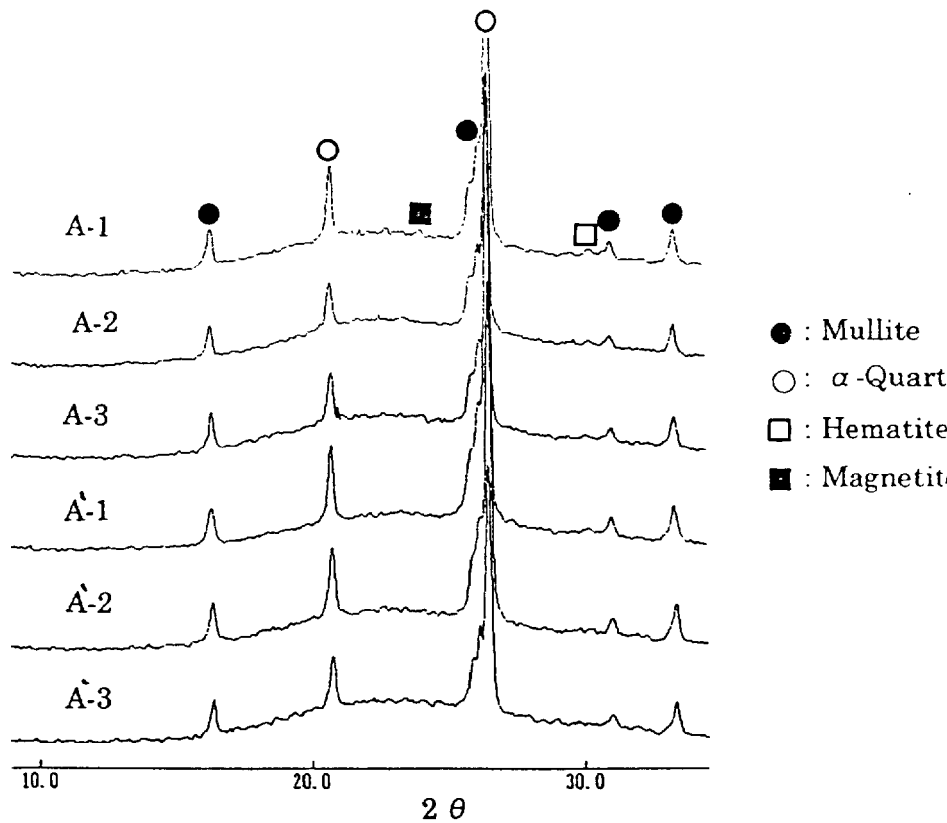

Figure 2 X-ray diffractograms of fractionated fly ashes.

As in Fig 2, fly ashes contain a considerable amount of glass phase as noncrystalline phase and thus a series of halo attributing to glass phase appears. This halo means long range order is lost. When the modifiers, alkali and alkali earth oxide enter random network structure, they break it and nonbridging oxygen is created, which in turn leads to discontinuous structure, and if the amount of modifiers increases, the structure becomes all the more discontinuous (Hemming and Berry, 1988,) and the maximum peak position of halo moves to high angle.(Diaond, et al., 1983) The maximum peak position of halo by X-ray diffraction represents the value approximate to 2θ =23.3 regardless of the kinds of fly ashes and may be considered to have a basically similar glass structure. Table 4 is mineral composition quantified by powder X-ray diffraction. Mullite, α -quartz, magnetite and hematite were obtained directly by internal standard method.(Alexander and Klug, 1948, Roode et al., 1987) SO_3 content was calculated on the assumption that they exist in the form of $CaSO_4$. The glass content deducted crystalline phase and loss on ignition from the total. The glass content had the value in the range of 65.9-76.8% and increased as going from the 1st field to the 3rd one. The amount of increase

was 6.2% in 600MW and 8.2% in 300MW. In other words, the finer the particles, the more the glass content has. The degree of glass content depends on the rate of quenching. If the rate of quenching is high, precipitation of crystalline phase is prohibited and the glass content is increase.(Freiman and Hench, 1969)

Table 4 Mineralogical compositions of fly ashes(wt%)

fly ash	α-quartz	mullite	hematite	magnetite	anhydrite	glass
A-2	8.7	12.4	-	0.4	0.7	76.6
A-3	7.2	12.6	-	-	1.7	76.8
A'-1	13.0	17.3	0.4	0.5	0.8	65.9
A'-2	11.3	16.5	-	0.4	1.0	68.7
A'-3	8.5	13.5	-	0.4	1.7	74.1

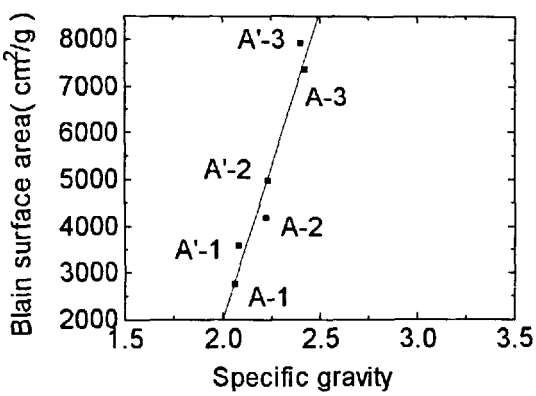

Figure 3 The relationship between Blaine specific surface area and specific gravity

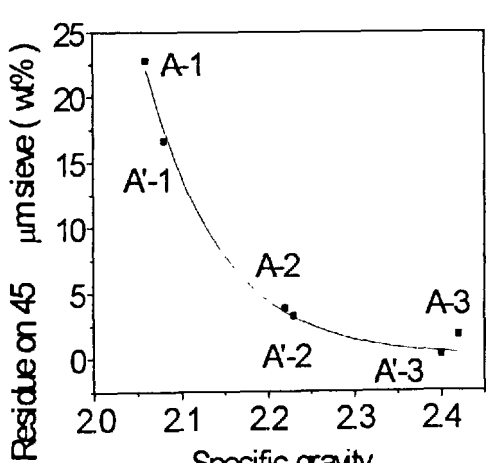

Figure 4 The relationship between specific gravity and residue on 45μm sieve

Ash particles are migrated by gases such as CO_2 , H_2 O generated in combustion and exit from the boiler. As the minimum fluidizing velocities of particles rely largely on particle diameter rather than density, small particles have high velocities of minimum fluidizing.(Kunii and Levenspiel, 1990) Accordingly fine particles have high rate of quenching. Fly ashes in the 3rd field composed of fine particles contain much glass content. The glass content in 600MW is larger than in 300MW. This may be attributed to the instability of combustion state following the load decrease of boiler. On the assumption that crystallines had stoichiometric composition, the chemical composition of fly ashes with deducted composition of crystallines was made the chemical composition of glass. The chemical compositions of glasses were mainly composed of SiO_2(63.3-67.6%) and Al_2O_3(18.9-22.6%) which can form a network structure and the modifier content was less than 10%. , the mole ratio of glass Al/(Si+Al) increases from 0.26 to 0.30 as going from the 1st field to the 3rd one, regardless of running conditions.

Specific gravity of fly ashes

As listed in Table 1, the specific gravity which is 2.06-2.42 takes the form of hollow spheres having a lower value than the theoretical value of mineral compositions. Fly ashes collected from one and the same location had similar values regardless of the load of boiler, and their increased as going from the 1st field to the 3rd one. The gravity of fly ashes is expected to decrease from the standpoint of the mass proportions of the mineral components because the finer the particles, the more likely the glass content of low gravity will increase. However, as this conflicts with the results of experiment, the mineralogical compositions may not greatly affect the specific gravity. In view of the relation between carbon content and specific gravity, carbon content are less than 1% and specific gravity and carbon content do not have any correlation, and thus gravity may not be affected by porous particles such as charcoal. Fine flyes ash may have thick shell wall because the finer the particles, the more the glass content has. However, in comparison, the fly ashes in the 3rd field of 300MW had 2.5% less glass content but bigger specific gravity than those in the 2nd of 600MW. Therefore, the shell wall thickness of fly ashes may not greatly affect the specific gravity. In hollow fly ashes, the finer the particles, the more likely the volume of closed pores will decrease. Fig 3 and Fig 4 show the relation between specific gravity and fineness. Specific gravity and Blaine specific surface area represent a good direct relation and an exponential correlation with residue on 45 μm sieve is shown. Therefore, the factors greatly affecting specific gravity may be the content of closed pores.

The tone of colors of fly ashes

The overall tones of fly ashes are bright gray. The brightness increases as going from the 1st field to the 3rd one. In other words, fly ashes collected from one and the same location represented the same tone of color regardless of the load of boiler. The color of fly ash is reported to depend on the amount of Fe_2O_3 (red) and unburned carbon(black).(Tanosaki et al. 1995) However, in this experiment such trend did not show. Moreover, Fe_2O_3 content had a similar value of 4.2-4.8% and carbon content had a low value of 0.3-1.5% A-1 and A'-1 with most differences in Fe_2O_3 and carbon content among all fly ashes represented the same tone of color. Presumably, in fly ashes produced from the same coal, the smaller the size of particles (glass content), the brighter they become.

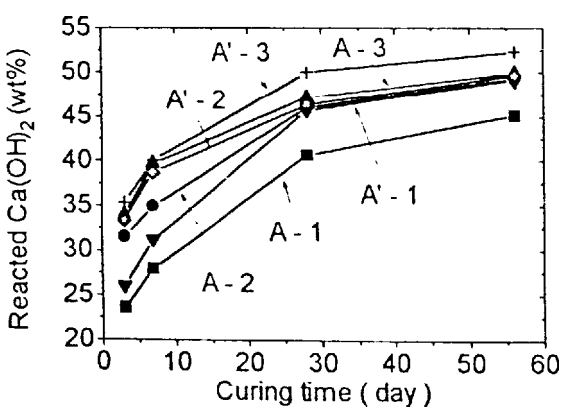

Figure 5 Amount of reacted $Ca(OH)_2$ with curing time at 40 C.

Reactivity with $Ca(OH)_2$

Fig 5 shows the relation between the aging time for fly ashes at 40℃ and the amount of reactivity with $Ca(OH)_2$. The longer the aging time, the more the amount of reactivity with $Ca(OH)_2$ increased and after 28 days there was virtually no change. The amount of reactivity of fly ashes with $Ca(OH)_2$ increased as going from the 1st field to the 3rd one, and fly ashes collected from one and the same location had slightly better reactivity with $Ca(OH)_2$ in load 300MW than

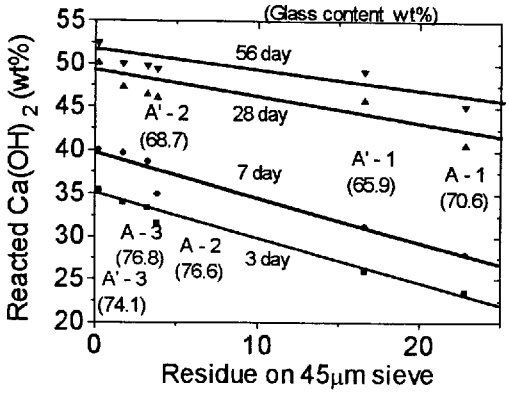

Figure 6 The relationship between reacted $Ca(OH)_2$ and residue on 45μm sieve

in 600MW. As a result of powder X-ray diffraction analysis, reacted products showed small amount of $CaSO_4 \cdot 2H_2O$ and C-S-H. Factors of fly ashes affecting the reactivity at 40℃ may include fineness and glass content. Fig 6 represents the relation between residue on 45 μm sieve and the amount of reacted $Ca(OH)_2$. A direct correlation between residue on 45 μm sieve of fly ashes and the amount of reacted $Ca(OH)_2$ was shown regardless of running conditions and the location of collection. In other words, as the residue on 45 μm sieve decreased, the amount of reacted $Ca(OH)_2$ increased and as aging time increased, the width of increase(tilt of direct line) decreased. Fig 6 did not show the correlation between glass content and the amount of reacted $Ca(OH)_2$. In conventional report(Sakurai et al., 1964), the more the glass content, the better the pozzolanic reactivity is in fly ashes where glass and crystallines are mixed. However, as the fly ashes used in this experiment had large difference in fineness, it might have been hard to show any effect of glass content.

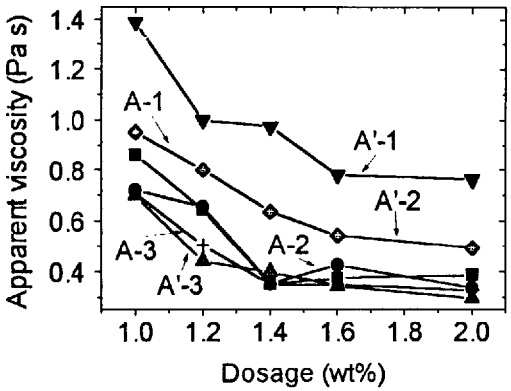

Figure 7 The influence of dosage of superplasticizer on the apparent viscosity of paste with fly ash.

Evaluation of apparent viscosity

Fig 7 shows the relation between the apparent viscosity of cement paste with 20vol% of fly ashes and the addition of superplasticizer. Up to 1.6% of superplasticizer, the apparent viscosity of paste decreased regardless of the kinds of fly ashes and in more admixture there was no change. This may be because the amount of admixture adsorbed on particles reached saturation around 1.6wt% of superplasticizer. The apparent viscosity is represented as $\eta = \tau / \gamma$ (τ : shear stress, γ : shear velocity) and counteracts to the reverse value of shear velocity generated under certain shear stress. From the standpoint of fluidity, the evaluation by $1/\eta$, the shear velocity itself is important rather than η counteracting to the reverse value of shear velocity. Fig 8 represents the relation between carbon content and the reverse value of apparent viscosity in 1.6% where the addition of admixture is saturated. The value $1/\eta$ linearly decreases as the carbon content increases.

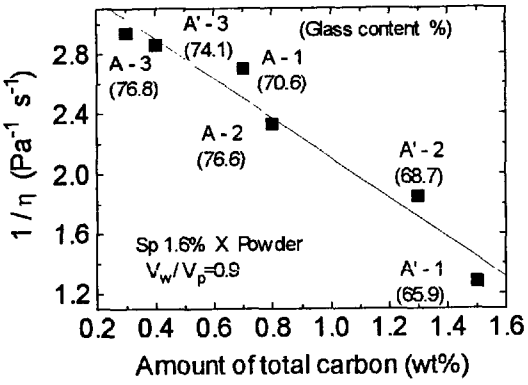

Figure 8 The relationship between amount of total carbon and 1 / η of pastes (η: Apparent viscosity)

CONCLUSION

The results obtained in this experiment can be arranged as follows.

1) Regardless of running conditions, the collected fly ashes increased in fineness, specific gravity and glass content as going from the 1st field to the 3rd one, but SiO_2 was decreased.

2) When the boiler is operated in full load running(600MW) in comparison with half load running(300MW) the glass content was increased, but the Blaine specific surface area and carbon content were decreased.

3) The reactivity of fly ashes at 40℃ with $Ca(OH)_2$ was more affected by fineness than by glass content.

4) In cement paste of 20vol% of fly ashes, the apparent viscosity represented constant value in 1.6% of superplasticizer, and at this time there was a linear correlation between carbon content and fluidity.

REFERENCES

Alexanders, L. and Klug, H.P., "Basic Aspects of X-ray Absorption", Anal. Chem., Vol. 20, No. 10, October 1948, pp. 886-889.

Diamond, S., "On the Glass Present in Low-Calcium and in High-Calcium Fly Ashes", Cem. Concr. Res., Vol. 13, 1983, pp. 459-464.

Frieman, S.W. and Hench L.L., "Further Analysis of Glass Crystallization Kinetics", J. Amer. Ceram. Soc., Vol. 52, 1969, pp. 111-112.

Hemming, R.T. and Berry, E.E., "On the Glass in Coal Fly Ashes: Recent Advances", Mat. Res. Soc. Symp. Proc., Vol. 113, 1988, pp. 3-36.

Kunii, D. and Levenspiel, O., "Fludization Engineering", Butterworth-Heineman Series in Chemical Engineering, 1944, pp. 68-71

MacCarthy, G.J., Johansen, D.M., Thedchanamoorthy, S.T., Steinwand, S.J., and Swansong, K.D., "Characterization of North American Lignite Fly Ashes-XRD Mineralogy", Mat. Res. Soc. Symp., Vol. 113, 1988, pp. 99-105.

Roode, M., Douglas, E. and Hemmings, R.T., "X-ray Diffraction Measurment of Glass Content in Fly Ashes and Slags", Cem. Concr. Res., Vol. 17, 1987, pp. 183-197.

Sakurai, M., Sato, K., Hasimoto, K. and Hukunaga, M., "Pozzolanic Reaction of Fly Ashes", CAJ Review of the 21th General Meeting, 1967, pp. 101-105.

Tanosaki, T., Nozaki, K., Tanigawa, K., Ashiyahara, S. and Manabe, K., "Characterization of Japanese Coal Ash in Recent Years", J. Res. of Chichibu Onoda Cem. Co., Vol. 46, No. 129, 1995, pp. 104-125.

UTILIZATION OF FLY ASHES CONTAINING CALCIUM SULPHITE IN CEMENT PRODUCTION

Marek GAWLICKI, Artur ŁAGOSZ and Jan MAŁOLEPSZY, University of Mining and Metallurgy, Cracow, Poland

ABSTRACT The research has been carried out on blended Portland cements containing fly ash and mixed gypsum and $CaSO_3 \cdot 0.5H_2O$ with different $CaSO_4/CaSO_3$ molar ratios. It was found that the fly ash cements containing calcium sulphite together with gypsum (molar ratio of $CaSO_4/CaSO_3 > 1$) gave a slightly slower setting. The increase of the amount of $CaSO_3 \cdot 0.5H_2O$ (molar ratio of $CaSO_4/CaSO_3 < 1$) results in a slow setting of cement mortars. It was also found that fly ash cements containing $CaSO_3 \cdot 0.5H_2O$ exhibit lower strengths.

Key-words: AFm phase, blended cement, fly ash, hydration, strength development.

INTRODUCTION

The desulphurization of non-dedusted flue gases in industrial fittings in which solid fuels are burned is carried out in a relatively low temperature. SO_2 sorbent and desulphurization produts do not react with the components of fly ash. The wastes acquired in the process are a mixture of fly ash, unreacted sorbent and calcium sulphates and $CaSO_3 \cdot 0.5H_2O$. The degree of hydration of calcium sulphates and the proportion of $CaSO_4/CaSO_3$ in the waste varies in quite a broad range and depends on the conditions in which desulphurization is conducted, as well as the conditions and time of waste storage. After some time both $CaSO_4$, $CaSO_4 \cdot 0.5H_2O$ and calcium sulphite change into gypsum (Grzeszczyk, 1995).

The present experiences in the utilization of ash sulphate/sulphite in building material industry are scarce. In Poland there has been an attempt in the production of pulverized fuel ash cellular concrete (Małolepszy et al., 1991). The majority of chemical components present in ash sulphate/sulphite wastes is active in a cement - water system and can influence the properties of hardening of cement pastes. It seems that a remarkable portion of these wastes can be utilized in the production of blended cements in which the wastes would play a double role: of a pozzolanic agent and of a regulator of setting time for cement. Such utilization is conditioned by the ability to perceive the role of particular waste components in the process of paste setting and the increase of strength in cement mortars. The functioning of those waste components seems to have synergic effects. Although the influence of calcium sulphate and calcium carbonate on cement hydration is widely known, the role of calcium sulphite in this process has been a subject of few publications. Their authors agree that $CaSO_3 \cdot 0.5H_2O$ in cement - water system gives AF_m phase but the authors describe them by means of different formulas: $3CaO \cdot Al_2O_3 \cdot CaSO_3 \cdot 8H_2O$ (Bloss and Odler, 1982) or $3CaO \cdot Al_2O_3 \cdot CaSO_3 \cdot 12H_2O$ (Yasue et al., 1981).

EXPERIMENTAL

The research has covered the determination of principal properties of blended cements containing fly ash with different amounts of $CaSO_4 \cdot 2H_2O$ and $CaSO_3 \cdot 0.5H_2O$. Those cements have been treated as model systems which allowed to determine the influence of calcium sulphite on the hydration of blended cements. Also, a series of analyses of reaction products in $3CaO \cdot Al_2O_3 - CaSO_3 - H_2O$ system have been carried out. Ordinary Portland clinkier (OPC) and fly ash (FA) acquired in a bituminous coal-fired power plant have been used in the preparation of blended cement samples. Chemical components of OPC and FA are presented in Table 1. Phase components of OPC were the following: C_3S - 58%, C_2S -18%, C_3A - 12 %, $C_2(A,F)$ -

- 8% and free CaO - 0.7%. The basic mineral components of fly ash were: quartz, glassy phase and mullite. Fly ash has also contained a limited amount of non-burned coal, hematite, magnetite, calcium sulphate and free CaO.

Table 1 Chemical composition of starting materials.

Compound	Composition [wt. %]	
	OPC	FA
LOI	0.15	2.21
CaO	66.06	4.86
SiO_2	21.48	51.43
Al_2O_3	6.12	25.21
Fe_2O_3	2.63	8.35
SO_3	0.19	0.52
MgO	1,46	3.06
K_2O	1.05	2.84
Na_2O	0.16	1.01

Portland clinker (85%) and fly ash (15%) were initially pulverized in a laboratory ball mill. Then gypsum or $CaSO_3 \cdot 0.5H_2O$ or the combination of these phases was added in the proportions presented in Table 2 in such amount that the total content of $CaSO_4/CaSO_3$ calculated as SO_3 amounted to 3% of total weight of every cement. The material was pulverized again until the acquisition of the cement with the specific surface equaling 320 ± 5 m^2/kg as measured by Blaine method. Calcium sulphate was added into cements as gypsum in its natural form ($CaSO_4 \cdot 2H_2O$ > 98%) and calcium sulphite - in the form of synthetic $CaSO_3 \cdot 0.5H_2O$.

Table 2 Molar ratio of SO_4^{2-}/SO_3^{2-} in blended cements.

Symbol of cement	Molar ratio of SO_4^{2-}/SO_3^{2-}	Symbol of cement	Molar ratio of SO_4^{2-}/SO_3^{2-}
BC-0	only SO_4^{2-}	BC-3	1:1
BC-1	4:1	BC-4	1:2
BC-2	2:1	BC-5	only SO_3^{2-}

Initial and final setting times (Vicat method) were determined in the pastes prepared from the above described cements. The analysis of compressive and flexural strength of mortars at w/c ratio = 0.5 was carried out on 4 x 4 x 16 cm samples kept in the water which temperature was 18 ± 2° C. The strengths of those mortars were determined after one day and after 3, 7, 28 i 90 days.

In order to explain what products are created in the reactions in $3CaO \cdot Al_2O_3 - CaSO_3 - H_2O$ system, two mixtures at molar ratios $3CaO \cdot Al_2O_3/CaSO_3$ equalling respectively 1:3 and 1:1 have been prepared. Tricalcium aluminate and $CaSO_3 \cdot 0.5H_2O$ were pulverized until the size of grains was smaller than 20 μm. The hydration of those mixtures was carried out in a normal temperature at a liquid to solid ratio equalling 1.0. Phase components of the samples were determined by an X-ray method in the range of the angles 5 - 40° $2\Theta CuK_\alpha$. DTA/TG and SEM/EDS studies were also performed.

RESULTS AND DISCUSSION

The resuts of the determination of BC paste setting time is shown is Table 3, and the determination of compressive and flexural strengths of mortars in Tables 4 and 5. The figures in parentheses include relative strengths (percentage of BC-0 cement strength).

Table 3 Setting time of BC pastes.

Symbol of cement	Normal consistency of pastes [w/c]	Setting time of cement pastes	
		Initial setting [h-min.]	Final setting [h-min.]
BC-0	0.28	2-05	3-10
BC-1	0.28	2-15	3-55
BC-2	0.27	2-35	3-55
BC-3	0.27	2-40	4-05
BC-4	0.26	2-00	3-00
BC-5	0.26	1-20	2-45

Table 4 Compressive strength of BC mortars.

Symbol of cement	Compressive strength of cement mortars [MPa]				
	1 day	3 days	7 days	28 days	90 days
BC-0	16.4 (100)	26.2 (100)	32.2 (100)	45.6 (100)	51.0 (100)
BC-1	12.6 (77)	25.1 (96)	31.7 (97)	44.8 (98)	50.8 (100)
BC-2	11.2 (68)	24.6 (93)	31.9 (97)	44.6 (98)	49.5 (96)
BC-3	9.0 (55)	21.7 (83)	27.3 (83)	42.3 (93)	50.8 (100)
BC-4	8.2 (50)	19.3 (74)	26.7 (82)	41.5 (91)	48.5 (95)
BC-5	7.7 (47)	17.0 (65)	26.3 (80)	39.6 (87)	47.9 (94)

Table 5 Flexural strength of BC mortars.

Symbol of cement	Flexural strength of cement mortars [MPa]				
	1 day	3 days	7 days	28 days	90 days
BC-0	4.3 (100)	5.9 (100)	7.2 (100)	8.4 (100)	9.2 (100)
BC-1	3.7 (86)	5.7 (97)	7.3 (101)	8.0 (95)	9.2 (100)
BC-2	3.2 (74)	5.2 (88)	6.4 (89)	8.7 (103)	9.4 (102)
BC-3	2.9 (67)	5.0 (85)	6.1 (89)	8.7 (103)	9.4 (102)
BC-4	2.6 (60)	4.6 (78)	6.0 (83)	8.1 (96)	8.9 (97)
BC-5	2.2 (51)	4.2 (71)	5.9 (82)	7.9 (94)	9.0 (98)

The XRD studies proved that in the process of chemical reactions between $3CaO \cdot Al_2O_3$ and calcium sulphite in the water environment, irrespective of the molar ratios of substrata, $3CaO \cdot Al_2O_3 \cdot CaSO_3 \cdot xH_2O$ phase is created. The attempt to determine an exact amount of water by means of DTA/TG turned out to be imprecise. The SEM/EDS studies showed that

$3CaO \cdot Al_2O_3 \cdot CaSO_3 \cdot xH_2O$ crystals created in a normal temperature are small and even after 28 days do not exceed 3 μm.

It seems that the differences in the setting time of BC pastes (Table 3) and the rate of increase in compressive and flexural strengths in cement mortars with different molar $CaSO_4/CaSO_3$ ratios (Tables 4 and 5) are probably the result of the fact that the $CaSO_3 \cdot 0.5H_2O$ dissolution is over 50 times smaller in comparison with $CaSO_4 \cdot 2H_2O$ dissolution and the fact that the gypsum in the cement - water system creates initially ettringite which quickly turns into monosulphate, and calcium sulphite creates only one phase - $3CaO \cdot Al_2O_3 \cdot CaSO_3 \cdot xH_2O$ (Bloss and Odler, 1982). In the cements containing enough $CaSO_4 \cdot 2H_2O$ (molar ratio of $CaSO_4/CaSO_3 > 1$), the setting of BC pastes is carried out in a typical way, but the layer of ettringite created on the grains of tricalcium aluminate is "insulated" by the tiny $3CaO \cdot Al_2O_3 \cdot CaSO_3 \cdot xH_2O$ crystals. Such layer prevents the hydration of $3CaO \cdot Al_2O_3$ for a period of time longer than the layer of "pure" ettringite. This causes that BC mortars containing gypsum together with calcium sulphite set slower than BC mortars containing only gypsum. The higher the amount of $CaSO_3 \cdot 0.5H_2O$ in relation to gypsum (BC-1, BC-2 and BC-3), the longer the setting time for BC mortars. The addition of too big an amount of $CaSO_3 \cdot 0.5H_2O$ in relation to gypsum causes the opposite process - the setting time for BC mortars is shorter. The reason for quick setting of BC mortars containing relatively small amounts of gypsum or containing no gypsum but only $CaSO_3 \cdot 0.5H_2O$ lies in the slow process of dissolution of $CaSO_3 \cdot 0.5H_2O$. It causes the creation of $3CaO \cdot Al_2O_3 \cdot CaSO_3 \cdot xH_2O$ in the amount not sufficient to delay the hydration of $3CaO \cdot Al_2O_3$ for a required period of time. The increase of the setting time for BC mortars influences mechanic properties of cement mortars. It causes the decrease of compressive and flexural strengths in the first day of hardening. The lower $CaSO_4/CaSO_3$ molar ratio in blended cement is, the higher a relative decrease of strengths of all BC mortars is. Within 3 - 7 days cement mortars, in which molar ratio of $CaSO_4/CaSO_3 > 1$, reach the strengths which are similar to the strengths of BC-0 cement mortars. In BC-4 and BC-5 ($CaSO_4/CaSO_3 < 1$) cement mortrars the decrease of strengths was greater. Those mortars had the strength similar to BC-0 mortars after 90 days.

CONCLUSIONS

Calcium sulphite is chemically active in the cement - water system and in the mixture with gypsum (molar ratio of $CaSO_4/CaSO_3 > 1$) can be used as a setting time regulator for blended cements containing fly ash.

The presence of $CaSO_3 \cdot 0.5H_2O$ in blended cements (molar ratio of $CaSO_4/CaSO_3 > 1$) prolongs the setting time of BC pastes and decreases compressive and flexural strengths of BC mortars in an initial period of their hardening.

Blended cements which contain a lot more calcium sulphite than gypsum set faster than cements containing only $CaSO_4 \cdot 2H_2O$. However, those cements have lower compressive and flexural strengths..

REFERENCES

Bloss, W. and Odler, I. "On the Possibilities of Utilization of Calcium Sulphite in Portland Cement Setting", Tonindustrie Zeitung, Vol. 106, No. 9. Sept. 1982, pp. 644-647 (in German).

Grzeszczyk, S. "The Binders Produced from Fly Ash and FGD Products from the Semi-dry Instalation", Cement Wapno Gips, Vol. 62, No. 1. January, 1995, pp. 8-12, (in Polish).

Małolepszy, J. et al.,."Cementitious Materials in the Production of Cellular Concrete", Polish patent No. 289854, April 10, 1991.

Yasue, T., Mihara, M. and Arai, Y. "Synthesis and Characteristics of New Compound in the System $CaO-Al_2O_3-CaSO_3 \cdot nH_2O$", Gypsum & Lime, No. 173, 1981, pp. 5-15 (in Japan).

MICROSTRUCTURAL CHARACTERISTICS OF BY-PRODUCTS OF PETROLEUM COKE BLENDED COAL COMBUSTION

Shondeep L. SARKAR, Sarkar & Associates, Inc., Houston, Texas, USA
Jan Richard PRUSINSKI, Portland Cement Association, Sugar Land, Texas, USA

ABSTRACT: Three by-products, namely fly ash (FA), bottom ash (BA) and flue gas desulfurization product (FGDP) from an experimental burn using a fuel mixture of 90% coal + 10% petroleum coke (PC) at a power plant in Texas, USA, were characterized microstructurally. The results demonstrate differences in particle size, sulfate and unburnt fuel contents. No significant difference in glass content was noted. The minerals produced were nearly the same, but their proportions varied. The coal + PC fuel blend imposed restrictions by way of sulfate content and unburnt fuel particles in the FA.

Key-words: Fly ash, bottom ash, flue gas desulfurization product, coal, petroleum coke

INTRODUCTION

An experiment to burn petroleum coke (PC) as a partial replacement for subbituminous Wyoming coal was initiated at a Texas power plant generating 2400 MW of electricity from four coal-fired units.

Higher calorific value of PC reduces energy cost. Additionally, its higher burning efficiency produces lesser amount of ash. Nonetheless, the higher sulfur content of PC is a major constraint for burning it without proper gas entrapment facilities. To meet the U.S. Environmental Protection Agency's regulation concerning maximum SO_2 emission, 10% PC by weight of total fuel was calculated as the permissible replacement value.

After a trial combustion using this fuel mixture, the three by-products, namely FA, BA, and FGDP that were collected for laboratory analyses, were compared with the three corresponding by-products of conventional coal combustion from the same power plant. The identifiable mineralogical, chemical, and microstructural differences that arise from this change in fuel are reported.

The chemical analysis results show that Class C FA with CaO >20% is produced. A conspicuous increase in its SO_3 level occurs with coal + PC combustion, but not in the corresponding BA. The LOI also increases noticeably in the FA and BA, indicating the presence of more unburnt fuel. The Al_2O_3 and SiO_2 contents do not change as a result of blended fuel. A decrease of nearly 1% Fe_2O_3 in both FA and BA when coal + PC is used is noteworthy. Higher LOI of the BAs suggests a concentration of unburnt carbon in this by-product, whereas it represents carbonate and loss of SO_2 in the FGDP when ignited. As expected, the FGDPs are mainly constituted of Ca and SO_3 (with minor variations) and very small amounts (<1.0%) of other oxides.

Bulk chemical analyses (Table 1) also supports this trend. Despite a lower amount of total SO_3 in FGDP of coal + PC combustion, its soluble form of SO_3 is higher, suggesting the possible presence

of more bassanite ($CaSO_4 \cdot 1/2H_2O$). Soluble Na is mostly concentrated in the FA. Though the total Na_2O in FGDPs is low, it is mostly in the soluble form. The mineralogical compositions of these by-products determined from XRDA are summarized in Table 3.

RESULTS

Table 1: Chemical analysis of coal and coal + petroleum coke combustion by-products (weight percent)

BP*	Fuel Type	SiO_2	Al_2O_3	CaO	K_2O	Na_2O	SO_3	Fe_2O_3	TiO_2	LOI
FA	Coal (C)	31.0	19.3	27.5	0.3	2.1	1.8	7.3	1.7	0.2
	C + PC	31.3	18.8	24.4	0.4	1.8	3.0	6.6	1.5	3.9
BA	Coal (C)	36.2	16.9	20.9	0.3	1.4	1.0	8.5	1.3	7.7
	C + PC	37.0	16.8	19.6	0.3	1.2	1.1	7.0	1.3	10.0
FGDP	Coal (C)	0.4	0.1	41.2	0.02	0.01	52.6	0.3	.01	8.9
	C + PC	0.8	0.4	42.8	0.05	0.02	45.4	0.3	.02	8.5

* BP - By-product

Table 2: Chemical analysis of soluble analytes (mg/L)

BP	Fuel	Ca	K	Na	SO_4
FA	Coal (C)	60.0	9.3	97.0	36.0
	C + PC	240.0	8.4	86.0	660
BA	Coal (C)	280.0	0.7	13.0	480.0
	C + PC	120.0	1.3	8.0	250.0
FGDP	Coal (C)	700.0	2.6	33.0	1480.0
	C + PC	810.0	1.6	36.0	1710.0

Soluble Ca and SO_3 ions in the three by-products of coal combustion follow the order:
FGDP >> BA >> FA (Table 2)

This trend, however, changes slightly in the case of coal + PC combustion to:
FGDP >>> FA > BA

Table 3: Mineralogical composition of by-products

Fuel	FA	BA	FGDP
Coal (C)	Quartz, anhydrite, merwinite, periclase, free lime	Quartz, graphite, calcite, anorthite, gehlenite	Hannebachite, bassanite, calcite
C + PC	Quartz, anhydrite, merwinite, periclase, free lime, magnetite	Quartz, graphite, calcite, anorthite, gehlenite	Hannebachite, bassanite, calcite

Though the glass content of the FAs did not appear to change with change in fuel type, the characteristic hump in the XRD pattern of BA for coal + PC combustion was higher. The mineral types did not change except for possible magnetite formation in the coal + PC fired FA. The contents, however, vary due to the change in fuel (Table 3).

Table 4: Thermal analysis of FGD products

Fuel	Peak 1		Peak 2		Peak 3	
	Temp.	Wt. Loss	Temp.	Wt. Loss	Temp.	Wt. Loss
	°C	%	°C	%	°C	%
Coal	140	3.82	390	1.93	740	1.54
Coal + PC	100	0.70	385	4.40	750	5.72

From thermal analyses (Table 4) it is postulated that slightly different forms of $CaSO_4$ hydrate are formed, represented by a difference in the first endotherm positions (100°-140°C). Hannebachite ($CaSO_3 \cdot 1/2\ H_2O$) and $CaCO_3$ exhibit greater weight loss at 385°C and 750°C respectively for coal + PC combustion. In the chemical analysis, however, there is negligible difference in ignition loss. From scanning electron microscopy, the FA particles of coal + PC combustion were observed to be more textured. Fused glass particles and unburnt fuel were clearly identified in the corresponding BA. The FGDPs were composed of two types of mineral, one which is highly geometric (prismatic, euhedral, thin platy), and the other occurs as lumps. No difference in their compositions could be established from microprobe analysis. The strong preferred orientation of bassanite suggests that the platy crystals are basanite, whereas the lumps represent hannebachite.

The particles in the coal + PC-fired FA are finer; in the corresponding BA only 30% particles are

finer than 10 μm versus 61% in the coal-fired one. The general particle size distribution pattern can be represented as: BA >> FA > FGDP

DISCUSSION

The FA produced from coal + PC combustion apparently is formed either under a hotter burning zone or under a cleaner and sharper flame resulting in smaller size of particles (Sarkar and Bonen, 1993). The larger hump in the XRD pattern of its BA can be attributed to higher amorphous phase; presence of unburnt coal, however, cannot be ruled out in view of its notably higher LOI. The higher calorific value of PC sets up a new crystallization regime. Not only does this affect the particle size, but also the amount of glass phase formation. Coal + PC combustion produces distinctly higher amount of sulfate due to less efficient heat transfer. Mullite was conspicuously absent in these ashes. According to McCarthy et al. (1988), low Al_2O_3 (10-15%) leads to the formation of other minerals. In the BAs investigated, gehlenite and anorthite were identified although, the Al_2O_3 content was slightly higher (16.8%). Gehlenite was also reported by Diamond, (1981).

Expansion and fracturing of $CaCO_3$ occurs in the scrubber during FGD sulfatization. Hannebachite is the first mineral to crystallize. Partial oxidation of this sulfite mineral converts it to the bassanite form of sulfate as observed in these FGDPs, whereas gypsum is formed from more complete oxidation. No gypsum was identified in either of the FGDPs.

The unburnt fuel particles in FA and BA from coal + PC combustion may be due to more rapid temperature rise of the higher calorific value PC, suggesting an incompatibility of conjunctive burning of these fuels; it is important to stabilize the calorific value when using fuels with varying heat generating capacity, and it is also necessary to control the balance of fuel streams.

From this study it appears that FA produced from this blend of coal + PC combustion will impose serious restrictions on its use in concrete because of its higher sulfate content and unburnt fuel particles; the latter is expected to increase the demand for air entraining agent when incorporated in concrete mixture.

CONCLUSIONS

The three by-products of coal + petroleum coke combustion, namely FA, BA and FGDP show differences in terms of particle size and unburnt fuel particles from those of conventional coal firing. Distinctly higher amounts of total and soluble sulfate in FA from this blended fuel combustion can impose restrictions concerning its use in concrete. The presence of unburnt fuel can be related to incompatibility in the blend, whose calorific value needs to be stabilized, in addition to controlling the balance of fuel streams.

REFERENCES

Diamond, S., "The Characterization of Fly Ashes", Materials Research Society Symposium N, 1981, pp. 12-23.

McCarthy, G.J., Johansen, D.M., Thedchanamoorthy, A., Steinward, S.J. and Swanson, K.D., "Characterization of North American Fly Ashes, II, XRD Mineralogy", Materials Research Society Symposium Proceedings, Vol. 113, 1988, pp. 99-105.

Sarkar, S.L. and Bonen, D., "The Effect of Burning Waste Fuel on Clinker Microstructure and Properties of Cement", PCA Symposium "Cement and Concrete in the Global Environment", Chicago, March 1993, 11 pp.

COMPOSITIONAL DEVELOPMENT (SOLID AND AQUEOUS PHASE) IN AGED SLAG AND FLY ASH BLENDED CEMENT PASTES.

E.E. LACHOWSKI, F.P. GLASSER, Department of Chemistry, University of Aberdeen, Old Aberdeen, Scotland, AB9 2UE
A. KINDNESS, Applied Chemistry Department, University of Natal, Durban, Dalbridge 4014, South Africa
K. LUKE, Canadian Fracmaster Ltd., Calgary, AB T2A 7H8, Canada

ABSTRACT A comprehensive compositional and microstructural examination has been made of cements, blended with fly ash (class 'F') and blast furnace slag, cured for 6 years. The evolution of the phase assemblage is continuing; some unreacted slag and fly ash remain. The reactivity of fly ash particles is particularly variable, ranging from completely unreacted to almost totally consumed. Pore fluid compositions were determined on solutions following extraction under high pressure.

Key-words: Blended cement, curing, microstructure, phase composition, pore solution

INTRODUCTION

Pozzolanic materials such as blast furnace slag and fly ash have been used as cement admixtures for many years. The composite matrix is dynamic in that there is continual change in the mineralogy, microstructure and aqueous phase chemistry with time. It is assumed that eventually the cement matrix will approach a steady-state in terms of the solid and aqueous chemistry. Studies to date have normally been carried out on laboratory samples aged up to 2 years (Taylor, 1990) or on aged specimens with undefined history (Thomas et al., 1992). Uncertainty exists concerning the impact of complete or nearly complete reaction on internal properties. Accelerated curing at temperatures in the range of 40-60°C have also been considered (Luke & Glasser, 1988) to accelerate reaction, though there has been question as to the relevance of elevated temperature cure to the steady-state attained at ambient temperature.

The present study reports the solid and aqueous chemistry of OPC and OPC blended pastes cured under controlled conditions for 6 years, at ~25°C, by which age it was assumed that most of the pozzolanic reaction would have taken place. Results have previously been reported for the same blends cured up to 2 years (Luke & Glasser, 1988, 1988a). The data generated can also be used to verify and develop models and to obtain a base-line from which the effect of environmental exchanges can be addressed.

EXPERIMENTAL

The ordinary portland cement (OPC) used in all preparations conformed to BS 12 specification and is comparable to that of an ASTM Type 1. Blending agents consisted of two commercially available class F fly ashes (FA) and one slag (BFS). The FA's were obtained from the British base-load power stations, Eggborough and Longannet. Their crystalline mineral content, as determined by X-ray diffraction and optical microscopy, included quartz, mullite, spinel close to magnetite and unburnt carbon. The BFS was supplied by Clyde Cement Ltd., and had a glass content of ~ 97% as shown by petrographic examination. Chemical and physical data for the raw materials have previously been reported (Luke & Glasser, 1988).

Cylinders of OPC and OPC blends, in the proportion of 30% admixture / 70% OPC (wt), were prepared as described previously (Luke & Glasser, 1988a) and stored at ~25°C and 100% RH. A 2g section from each cylinder was taken prior to pore fluid extraction, quenched in acetone to stop hydration, and oven-dried at 60°C. These sections were then subjected to solid phase analyses. Analytical electron microscopy (AEM) was carried out on argon-beam thinned sections using a JEOL 2000X EX Temscan electron microscope with LINK AN 1085/S analytical system. X-ray data were obtained using a Rigaku DMAXB diffractometer with $CuK\alpha$ radiation and Ni-filter. A sample of each section, not quenched in acetone, was analysed for $Ca(OH)_2$ content by thermogravimetry using a Seiko 320 SSC 5200 DTA-TGA thermoanalyser.

Pore fluid, ~5 ml, was extracted from the cylinders by a technique modified from that developed by Longuet et al. (1973). Mg and Ca contents were determined by atomic absorption spectroscopy while Na and K were determined by atomic emission spectroscopy using a Pye Unicam SP9 spectrophotometer. SO_4^{2-} content was obtained using a Dionex 2010i anion chromatograph. Spectrophotometric methods, using catechol violet (Dougan & Wilson, 1974) and molybdenum blue (Ramachandran & Gupta, 1985) reagents, were used to determine the Al and Si contents respectively. Total OH^- content was measured by titration with dilute HCl.

RESULTS

Solid Phase

SEM micrographs typical of the 6yr hydrated cement are shown in Fig 1 while those of the blended systems are shown in Figs. 2-4. Morphologies of the hydrated products in the neat cement paste are characteristic of those reported at earlier ages (Luke & Glasser, 1987). Fig 1a shows a somewhat open structure as expected for a W/S of 0.6, with CH platelets of variable dimensions well distributed throughout the specimen,. The C-S-H appears to be present principally in fibrous form, Fig 1b. In the case of the FA blended pastes the overall morphology is somewhat different. Less CH is present and the C-S-H is less well defined. Fig 2a shows the relict of an Eggborough FA particle; the outer section was determined to be of a mullite composition while the inner section was composed of a mixture of C-S-H, CH and fine needles of ettringite. A high percentage of almost totally unreacted particles were also observed of which Fig 2b is typical. The Longannet FA tended to have somewhat different morphological characteristics in comparison with the Eggborough FA, as seen in Fig 3a. The large micropores of the FA tend to become more evident on hydration and were a common feature in the Longannet FA blend. The structure remaining between the pores appeared to be composed of mullite crystals. In this case more of the FA particles seemed to have reacted although in many cases not completely, Fig 3b. The central particle in Fig 3b shows a reaction rim surrounding a central core; however the space between the rim and the core was atypical. The morphology of the slag blend, Fig 4, also differed considerably from that of the neat cement. Fig 4a shows formation of a more dense microstructure in which CH crystals are less well defined and unreacted slag grains persist as illustrated in Fig 4b.

Figs 5-7 are of argon-milled specimens of the pastes; numbers indicate areas selected for individual spot analysis. Characteristically, OPC cement pastes have C/S ratios in the range of 1.7-2.0 whereas in the present study ratios of up to 5 were observed This suggests that the some of the C-S-H analysed in Figs 5a and b (neat OPC) had embedded CH. Fig 8 shows a plot of Al/Ca ratio against Si/Ca. Ca-rich phases, Si/Ca~0.01, due undoubtedly to CH or calcite were also observed but were omitted from Fig 8 due to scaling factors. The fibrous phases in Fig 5a

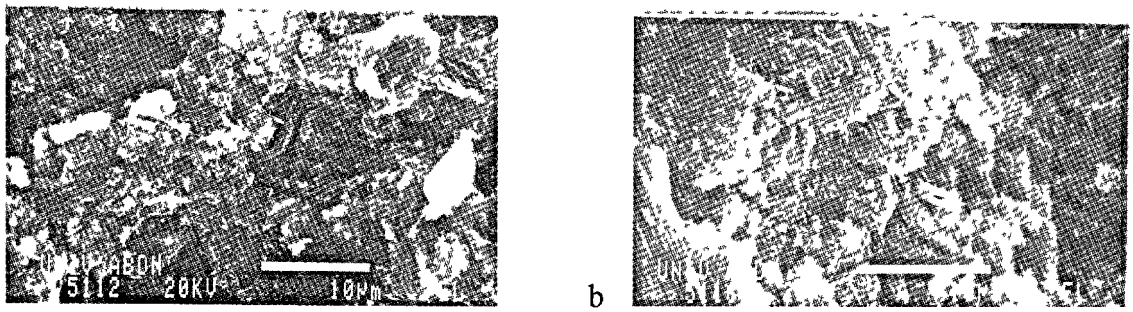

Figure 1 SEM micrographs of neat OPC paste cured for 6 years

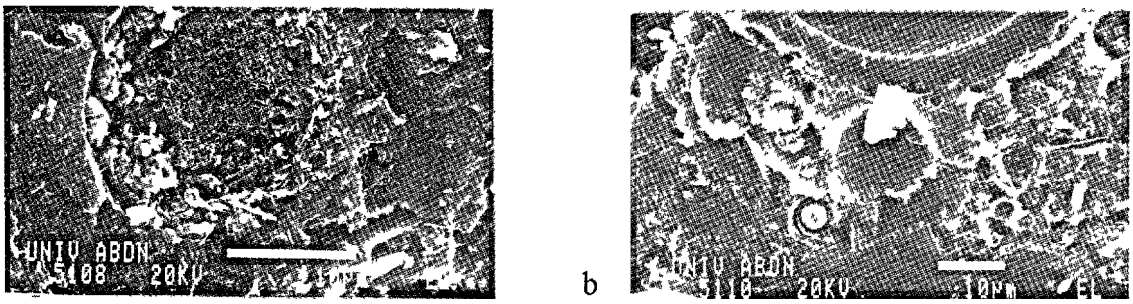

Figure 2 SEM micrographs of Eggborough FA/OPC blended paste cured for 6 years

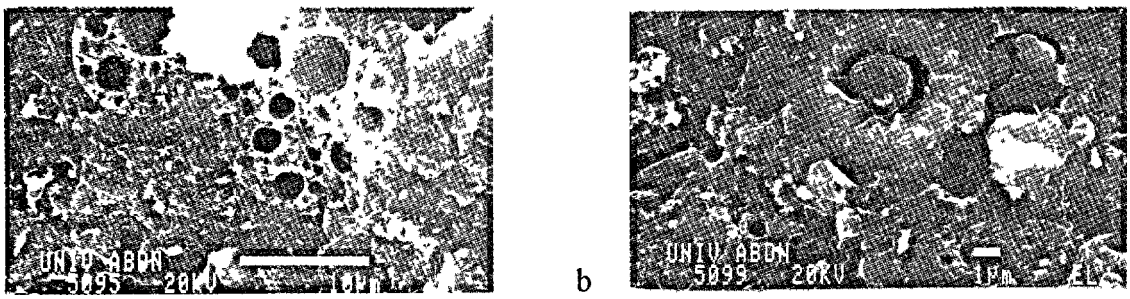

Figure 3 SEM micrographs of Longannet FA/OPC blended paste cured for 6 years

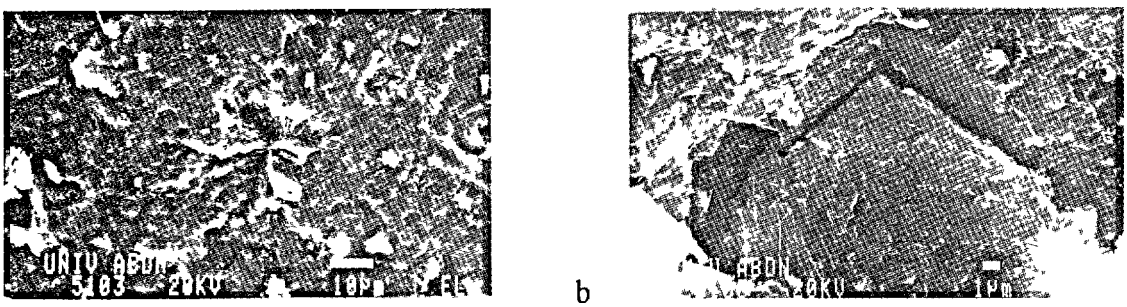

Figure 4 SEM micrographs of BFS/OPC blended paste cured for 6 years

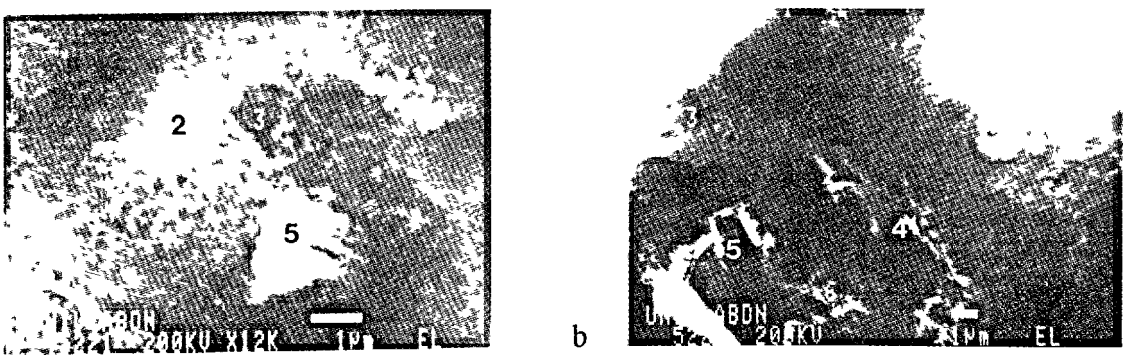

Figure 5 STEM micrographs of argon-milled neat OPC paste cured for 6 years

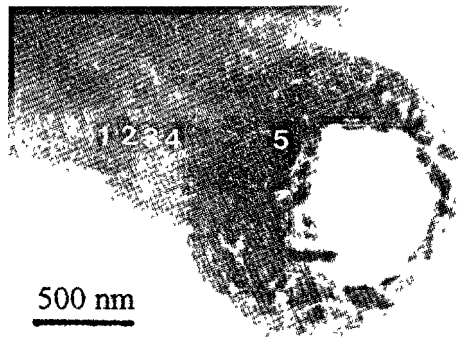

a

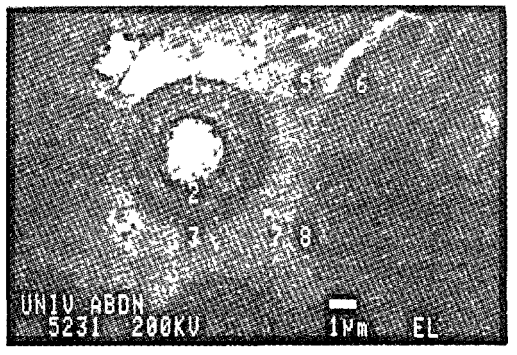

b



c

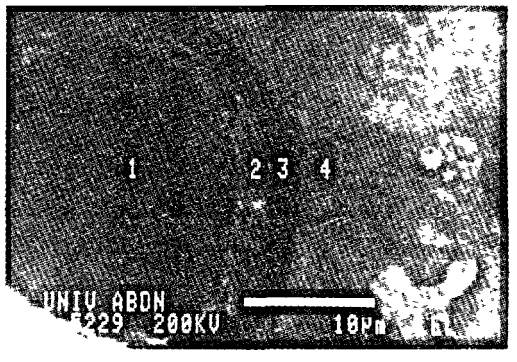

d

Figure 6 STEM Micrographs of Longannet (a,b) and Eggborough (c,d) FA/OPC blended pastes

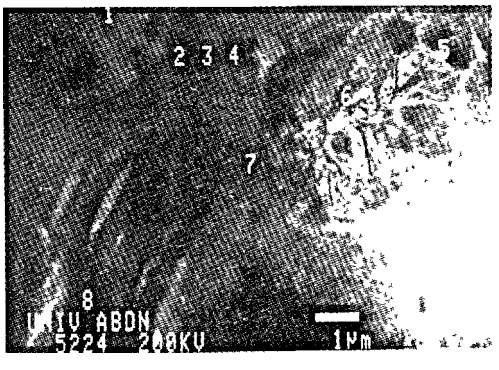

Figure 7 STEM Micrograph of BFS/OPC blended paste cured for 6 years

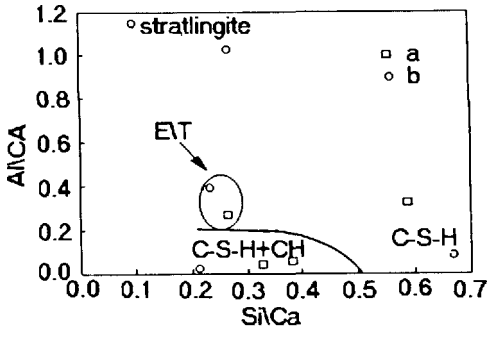

Figure 8 Al/CA vs Si/Ca ratios in OPC

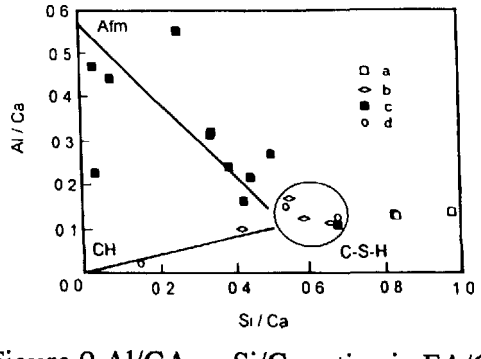

Figure 9 Al/CA vs Si/Ca ratios in FA/OPC blends

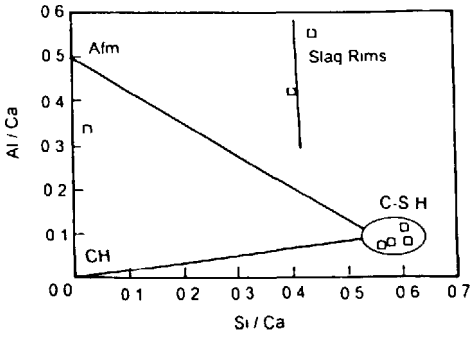

Figure 10 Al/CA vs Si/Ca ratios in BFS/OPC blend

and b at points 5 and 4 respectively, are of similar composition. Point 5 has a composition (based on hypothetical oxides and ignoring the presence of water or hydroxyl) of $Ca_{6.00}Si_{1.60}Al_{1.58}S_{1.59}Mg_{0.01}Fe_{0.01}O_{17}$ and is somewhat richer in Si and S and lower in Al compared

to point 4 which has a composition of $Ca_{6.00}Si_{1.41}Al_{2.35}S_{0.77}Mg_{0.01}Fe_{0.05}K_{0.03}Ti_{0.01}O_{15}$. It is believed that this fibrous phase, indicated in Fig 8 by the region E/T, is an ettringite/thaumasite solid solution. The phase rich in both Al and Ca as evidenced from Fig 8 and which corresponds to the lath-like crystals, 5, Fig 5b, has an atomic ratio Ca:Al:Si of 2:2:1, i.e. it is probably C_2ASH_8. Small fibrous particles, 6, situated adjacent to these lath-like crystals, had a similar composition though their Si content was much higher and are believed to be a mixture of C_2ASH_8 and C-S-H. Unreacted ferrite was also observed in the paste.

Figs 6a-d are representative of the FA blend. Analysis of the unreacted particles of Longannet FA, Fig 6a, b, shows it to be a mullite FA, whereas the Eggborough FA, Fig 6c, d, is primarily calcium-aluminium silicate having mean Si/Ca=0.34 and Al/Si=0.85. The C-S-H observed in the proximity of the Longannet FA, Fig 6a, has Si/Ca ratios of 0.83 -1.0 and is similar to that previously reported for C-S-H close to FA in a 10 year old mortar (Sato & Furuhashi, 1982). This is illustrated in Fig 9 where elemental ratios, Al/Ca versus Si/Ca are plotted. In general, Si/Ca ratios of the C-S-H from the hydrated cement lie between 0.56 to 0.67 while the Al/Ca is approximately 0.13 which is consistent with the results of Harrisson et al. (1986) for a 91 day old cement paste, with 28% FA and w/s=0.5. Interestingly in Fig 6b there appears to be no FA reaction product between the FA mullite crystals and the C-S-H. Fig 6c clearly shows reaction rims of FA hydration product, points 2, 3, 4 and 10. Elemental analysis gives a mean Si/Ca ratio of 0.34 and Al/Ca of around 0.30. The Si/Ca is lower than reported in the literature and could be due to inclusion of CH. Points 4 and 5, Fig 6a and points 1,2 and 6 Fig 6b have Al/Ca > 5.0 and are omitted from Fig 9 due to scaling factors. The elemental analyses of these points are consistent with mullite. Points 1, 2 and 3 in Fig 6d are Fe-rich: point 4 is a mixture of CH and C-S-H.

Fig 7 is a typical section of hydrated slag cement. Points 1 and 6 are representative of the internal composition of what appears to be completely hydrated slag grains. Oxide ratios (normalised to 10 oxygens for convenience) are $Ca_{2.61}Si_{1.16}Al_{1.44}Mg_{2.59}S_{0.05}K_{0.03}Ti_{0.04}Fe_{0.05}O_{10}$ and $Ca_{0.73}Si_{0.56}Al_{2.60}Mg_{3.98}S_{0.03}K_{0.12}Ti_{0.01}Fe_{0.03}O_{10}$, respectively, which are consistent with mixtures of C-S-H and hydrotalcite (Luke & Glasser, 1987a). The relict remaining in the hydrated slag particle, defined by point 5, is rich in both Ti and Fe and has the composition $Ca_{3.24}Si_{1.32}Al_{1.35}Mg_{0.54}S_{0.07}K_{0.01}Ti_{0.57}Fe_{0.14}O_{10}$. The large lath-like crystals at point 7 are ettringite, low in Si, unlike the high-Si thaumasite-like phase found in the neat OPC paste. Points 2, 3, 4 and 8 are indicative of C-S-H from cement paste between slag particles and have C/S of 1.82, 1.77, 1.68 and 1.66, respectively. Points 1-8 are illustrated in Fig 10 in terms of the Al/Ca ratio versus Si/Ca ratio. Si/Ca ratios of the slag relicts are considerably lower than the 0.62 value given by Harrisson et al. (1986) for blended pastes hydrated at 6 and 14 months.

XRD data for more crystalline components of the OPC and blended cement pastes are given in Table 1. Ettringite and AFm were observed in substantial amounts in both OPC and FA. XRD of the slag cement indicated only AFm while AEM also suggests the presence of trace amounts of ettringite. Hydrotalcite was clearly evident in the slag paste and was also observed but to a lesser extent in the FA blends. Mullite and quartz associated with FA particles were also detected. $Ca(OH)_2$ was observed in all pastes but was most prevalent in the neat OPC paste. This is further confirmed by the thermogravimetric analysis, Table 2, which shows the OPC to contain 32 wt% $Ca(OH)_2$ in comparison to ~11wt% in the FA blends and 19 wt% in the slag blend with $Ca(OH)_2$ content corrected for calcium present as $CaCO_3$.

Table 1 Phases observed by XRD in OPC and OPC-blended cements

Paste	C-S-H	AFt	AFm	Hydr	$Ca(OH)_2$	Calc	Vat	Mul	Qtz
OPC	+	++	++		+++	+			
OPC/Eggb	+	+	+	+	+	++		+	+
OPC/Long	+	++	+	+	+	++	++	++	+
OPC/Slag	++		++	++	++	+			

Calc=calcite, Vat=vaterite, Mul=mullite, Qtz=quartz + trace ++ minor +++ major

All samples showed some degree of carbonation, primarily as calcite, though the OPC Longannet blend also contained some vaterite. Unidentified peaks of weak intensity with d-spacings at 4.40, 2.27, 1.67 and 1.63 (Å) were observed in XRD of both OPC and OPC blended pastes and were most prevalent in the OPC paste.

Table 2. wt% $Ca(OH)_2$ in OPC and OPC blended cement pastes.

Paste	6 years	2 years $^{\phi}$
OPC	32.1	34.3
	*22.5**	*24.0*
OPC/Eggborough	11.3	15.3
OPC/Longannet	11.7	10.2
OPC/Slag	18.9	17.8

$^{\phi}$ Luke and Glasser (1988a)

* Values in italics relate to the dilution expected if 30% inert material were present. All values are corrected for Ca present as $CaCO_3$.

Aqueous Phase

Aqueous phase data for the OPC paste and OPC blended pastes are given in Table 3. Data given in italics represent values for the same pastes determined after 2 years under the same conditions of cure (Luke & Glasser, 1988). Na^+ and K^+ concentrations show a marked increase over the

Table 3. Pore fluid data for blended cements aged 6 years at 25°C and 98% relative humidity: equivalent 2 year data are given in italics.

System	Ion Concentration (mM)							
	Na^+	K^+	Ca^{2+}	$SO4^{2-}$	Al^{3+}	Si^{4+}	Mg^{2+}	pH
OPC	87.0	512	0.84	1.98	<0.3	-	<0.02	13.6
	47.0	*175*	*1.60*	*1.74*	*<0.3*			*13.2*
OPC/	45.7	120	1.41	4.47	0.71	4.1	0.068	13.1
Longannet	*31.0*	*106*	*0.38*	*1.83*	*<0.3*			*13.1*
OPC/	120	233	1.23	6.15	2.33	4.6	0.037	13.4
Eggborough	*77*	*175*	*0.47*	*2.11*	*1.1*			*13.3*
OPC/Slag	106	181	0.77	2.83	0.92	0.59	<0.02	13.3
	69	*125*	*0.99*	*0.67*	*<0.3*			*13.2*

intervening four year period, most noticeably in the neat OPC paste where there is a 85% increase in Na^+ and 193% increase in K^+. The OPC blends show a significantly lower increase, averaging 52% in Na^+ and ranging from 13 - 45 % in K^+. $SO4^{2-}$ concentrations are also notably higher in the 6 year old pastes with an increase of approximately 13% in the OPC paste and around 144-320% in the OPC blends. Aluminium concentrations also significantly increased though absolute concentrations remained low. Ca^{2+} concentrations increased in the OPC and OPC slag blends but decreased in the OPC FA blends which undoubtedly relates to the availability of $Ca(OH)_2$. pH in all cases was relatively constant between 2 and 6 years.

Pore fluid data for the 6 year old paste were run through the program MINEQL to give an indication on which solid phases are solubility-limiting for the components of the aqueous phases. Data are presented in Table 4 where a log saturation index (I) close to zero indicates close to saturation, <0 undersaturation and >0 oversaturation. Ca^{2+} solubility, as expected, is 'controlled' primarily by $Ca(OH)_2$ as it is the most soluble calcium-containing phase in all pastes. Sulphate solubility is not apparently limited by either gypsum, since the I values are all significantly negative, or AFt, where the high positive values indicate considerable supersaturation, in which case, AFt should precipitate spontaneously. This suggests some other phase(s) may be responsible for the observed sulphate solubility. The I values for C_3AH_6 indicate this could be the solubility "controlling" phase for aluminium but the notable absence of C_3AH_6 in both the XRD and SEM studies suggest this is questionable: clearly it is not $Al(OH)_3$. High positive I

Table 4. Log saturation indices (I) for pore fluids in Table 3, calculated by MINEQL with upgraded NEA/EIR database.

Cement	CH	AH_3	MH	CS	Si gel	C_3AH_6	AFt
OPC	+0.15	-	+3.0	-3.1	-	-	-
OPC/Longannet	-0.33	-1.8	+3.3	-1.6	-2.1	-0.32	+4.7
OPC/Eggborough	+0.01	-1.6	+3.4	-2.1	-2.8	+1.1	+4.9
OPC/Slag	-0.28	-1.9	+3.0	-2.5	-3.5	-0.43	+1.9

values for $Mg(OH)_2$ indicate that the pore fluids are supersaturated with respect to this phase: Mg contents should be < 0.001mM, the solubility product of $Mg(OH)_2$. Hydrotalcite which is known to exist in OPC pastes (Luke & Glasser, 1987a, Roger & Groves, 1989) is most likely the solubility "contolling" phase for Mg: solubilities for hydrotalcite were, however, not determined. Aqueous Si solubility would appear not to be determined by C-S-H gel, according to the high negative I values obtained. There are, however, substantial differences in the solubilities of pure C-S-H systems compared to 'real' pore solutions (Atkins et al. 1993).

DISCUSSION

Hydration of OPC and OPC blends is an evolving process controlled by both aqueous and solid phase chemistry. Processes such as a decrease in pore solution volume as hydration proceeds and liberation of alkalis from anhydrous cement grains, FA and slag, for which there is no distinct solubility limit are continuous. Other ionic species ultimately approach a 'steady state' equilibrium dependent on the rate of dissolution and precipitation of phases. Since the rate of dissolution of OPC and blending materials differs markedly, so does the time scale to approach the 'steady state' equilibrium. The present data suggest that for both OPC and OPC-FA blends the time to steady state exceeds 6 years. The microstructures of the pastes at 6 years still show the influence of the original fly ash microstructures.

It has been well established that the use of FA and slag can significantly reduce or eliminate the expansion due to alkali-aggregate reaction. However the evidence regarding the efficiency of the FA or slag in suppressing alkali-aggregate reaction is conflicting and it has proved difficult to produce a consensus on guidelines for their use. Inasmuch as the blending materials used in this study were typical, it is not difficult to understand this conflict. It is well known that slag hydration differs from that of FA (Luke & Glasser, 1987a) but the FA's themselves show considerable variation. SEM indicates a higher degree of reaction in the Longannet FA compared to Eggborough FA though $Ca(OH)_2$ contents are equivalent. The $Ca(OH)_2$ content of the Longannet FA at 6 years is similar to that for 2 years. This suggests that the pozzolanic reaction had ceased at around 2 years. Eggborough FA on the other hand shows a 35% decrease in $Ca(OH)_2$ between 2 to 6 years representing a considerable degree of ongoing reaction.

At 6 years, the aqueous alkali concentrations of the pozzolan blends was much reduced compared to the neat cement, even though aqueous alkali concentration had been increasing from 2 years. Although total alkali was lower, it should be noted that the Na^+ concentration was higher than in the neat cement for both the Eggborough and slag blends. The pH of the solution remains relatively constant and it may be assumed that the partitioning of the alkalis, their release characteristics from the solid phase and the alkali pore solution composition are the more important parameters in the beneficial though often unpredictable properties of blended cements. The concentration of alkalis in the OPC paste shows a substantial increase from 2 to 6 years and suggests continued hydration with release of alkalis from the remaining cement grains and associated decrease in the volume of pore solution upon the formation of hydration products: this differs, however, with data reported by Atkins et al. (1993), where no substantial difference was observed in the aqueous phase of OPC pastes hydrated from 90 days to 10 years.

REFERENCES:

Atkins M., Lachowski E.E. and Glasser F.P., Adv. Cem. Res., 5, 19, 97-102, 1993.

Dougan W.K. and Wilson A.L., Analyst, 99, 414-430, 1974.

Harrisson A.M., Winter N.B. and Taylor H.F.W., 8th International Congress on Chemistry of Cement, Vol 4., 170, Paris 1986.

Longuet P., Burglen L. and Zelwer A., Revue des Materiaux et Construction, 676, 35-41, 1973.

Luke K., and Glasser F.P., 4th International Conference on Durability of Materials and Components, Singapore, 1, 188-195, 1987.

Luke K. and Glasser F.P., Cem. Concr. Res., 17, 273-282, 1987a.

Luke K. and Glasser F.P., Cem. Concr. Res., 18, 495-502, 1988.

Luke K. and Glasser F.P., Il Cemento, 3, 179-192, 1988a.

Ramachandran R. and Gupta P.K., Anal. Chim. Acta., 172, 307-311, 1985.

Roger S.A. and Groves G.W., J. Am. Ceram. Soc., 72, 1073, 1989.

Sato T. and Furuhashi I., Review of the 35th General Meeting, Cement Association of Japan, 42, 1982.

Taylor H.F.W, Cement Chemistry, 290 -299, 1990.

Thomas M.D.A. et al., Proceedings of the Ninth International Conference on Alkali-Aggregate Reaction in Concrete, Concrete Society, Wexham Springs, U.K.1059-1066, 1992.

STUDIES ON ACTIVATION OF SLAG CEMENT

S. N. GHOSH, D. M. JOSHI, S. CHANDA and H. VAISHNAV
Gujarat Ambuja Cements Ltd., Ambujanagar
362715 Kodinar, Gujarat, India.

ABSTRACT An investigation on the feasibility of activating normal slag cement blend with alkali in the form of sodium silicate (waterglass) has been reported. In this multiple activators system, reasonable degree of improvement in early compressive strength development and reduction in setting time have been observed.

Key-words: Activation, Slag, Waterglass, Anhydrite, Cement.

INTRODUCTION

The production of slag cement in India is increasing but the use is limited to areas in the Eastern region of the country. The difficulty in acceptability of slag cement is mainly due to slow setting and lower early strength development compared to Ordinary Portland Cement (OPC). A market survey of slag cement showed the average compressive strenths are 11.86 (1d), 25.20 (3d) 37.94 (7d) and 53.04 MPa (28d) and average initial and final setting times are 165 min. (initial) to 220 min. (final). We conducted a detailed laboratory study on a steel plant slag and found that with the addition of alkali activator, improvement in properties can be achieved. For general acceptability all experiments were carried out on slag cement of conventional composition range and the present report is made out of these experiments.

EXPERIMENT

Materials

Granulated blast furnace slag (GBFS) was obtained from a steel plant in India. The chemical analysis is given in Table 1. The glass content of the slag is 96% as determined by optical microscopy. The basicity of the slag is 1.03 using (CaO + MgO + 1/3 Al2O3) / (SiO2 + 2/3 Al2O3). Cement clinker was obtained from our plant. The chemical composition is given in Table 1. Mineral gypsum or marine gypsum (Gyp) (after washing) was used along with anhydrite (gypsum heated to 150 deg.C for 3 hrs. in oven) in certain cases and marked as AG in the graph. Waterglass (WG) in solution of silicate modulus 3 was used. The chemical composition of the waterglass is SiO2 = 21.61%, Na2O = 7.20%, and its pH = 11.7.

Preparation and Testing

Compositions similar to normal slag cement i.e. slag, clinker & gypsum were used as base materials for making different batches. The percentage of slag was kept at 55, 65, 75 & 85. The water glass added in solution during grinding in a ball mill. (Gypsum and anhydrite were used at constant percentage). Preparation of batches (co-grinding) each about 6 kg. was made and the fineness (Blaine) was maintained around 400 m2/kg.

Normal consistency, setting time and mortar cubes (7.06 cm) were obtained as per IS-455 -1976. Autoclave Le-Chatelier tests were performed as per the above standard. The mortar cubes were cured in 100% RH at 27 +/- 1 deg. C for 24 hrs. and subsequently cured in water at the same temperature. Microscopic examinations (model Optiphot, Nikon) of hydrated slag cement samples (in powder mount, immersed in a liquid of suitable RI) were carried out after arresting hydration of the material. Particle size analysis of samples was done using Malvern Laser Beam

apparatus (Mastersizer-X model). X-ray diffraction (Rigaku D-Max 2000) and DTA (Rigaku Themoflex) studies of hydrated samples were undertaken.

Table 1 Chemical analysis of components.

OXIDE	CLINKER	SLAG	GYPSUM	OXIDE	CLINKER	SLAG	GYPSUM
SiO2	21.30	33.37	7.62	SO3	0.36	Tr.	40.71
Al2O3	5.64	19.62	0.68	Cl	0.003	-	0.57
Fe2O3	4.22	2.16		P2O5	0.14	-	-
CaO	65.30	33.64	28.90	MnO	-	0.76	-
MgO	1.62	9.60	Tr.	TiO2	0.50	-	-
K2O	0.42	1.00	0.22	IR	-	0.33	7.80
Na2O	0.21	0.20	0.36	LOI	-	-	21.88

RESULTS AND DISCUSSION

The addition of waterglass could lead to substantial gain in 1d and 3d compressive strength besides reduction in setting time. The increase was 91 to 42% (1d), 23 to 16% (3d) and marginally higher at 7d and 28d for 55 to 85% slag content. Fig 1 represents the increase of compressive strength of a 55% slag cement with different activators. The reduction in setting time (initial & final) was around 60 minutes.

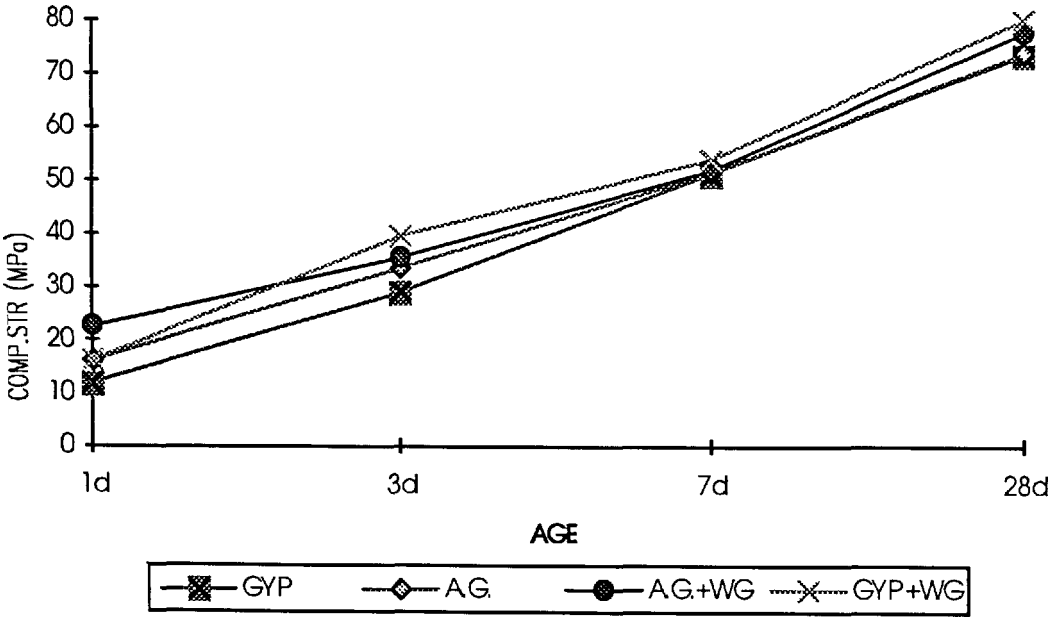

Figure 1 Effect of different activators on compressive strength.

In spite of the added alkali for activation of slag, compressive strength development above 65% slag containing batch, especially after 7d of hydration slowed down (Fig 2). This follows the pattern of normal slag cement hydration. Optical microscopy observation (X 400) of hydrated slag cement shows reacted slag pieces along the 'rims' in the initial stage of hydration i.e. even at 1d and later the surfaces of slag pieces were covered with this material (Fig 3). Similar observations of reacted rim of slag pieces had been reported earlier by Wilding and Mc Hugh (1986) and Richardson et al (1994). Formation of hydrotalcite type phase was indicated.

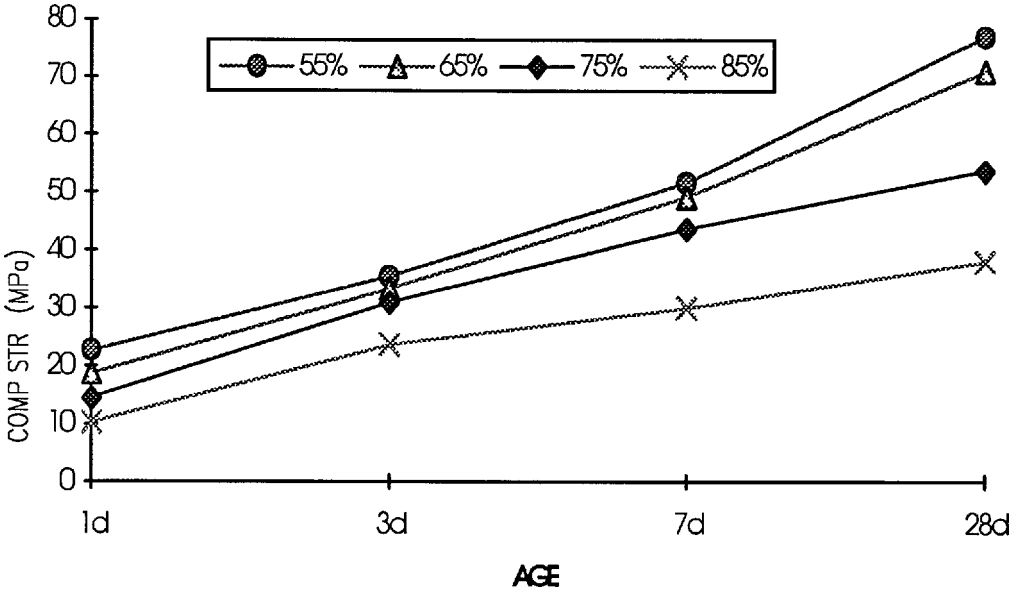

Figure 2 Compressive strength development with different percentage of slag addition.

There has been lot of research activity in the area of alkali activated slag in the Far East and in Europe. Wang et al (1994) reported the factors affecting the strength of alkali activated slag and recently Wang and Scrivener (1995) indicated presence of C-S-H(1), hydrotalcite and AFm type phases in NaOH/waterglass activated slag. The presence of C-S-H (82 deg.C, 112 deg.C), AFm type phase (150-200 deg.C), hydrotalcite type phase (384 deg.C), Ca(OH)2 (472 deg.C) can be identified by the DTA (Fig. 4) on the basis of hydrated OPC and alkali activated slag (Wang & Scrivener, 1995).

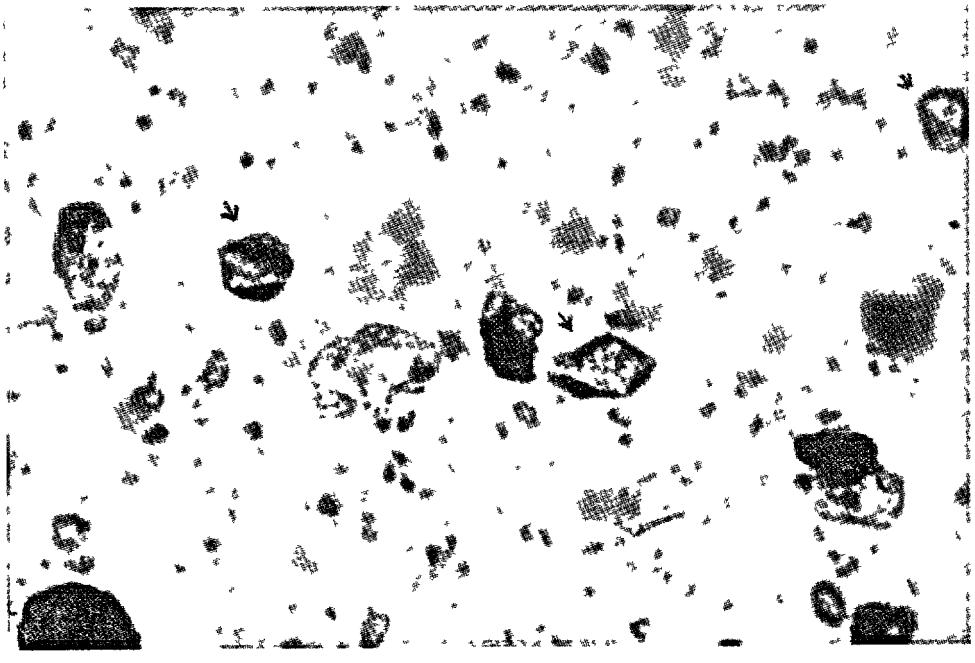

Figure 3 1d hydrated slag cement sample (x 400) - reacted slag (↑)

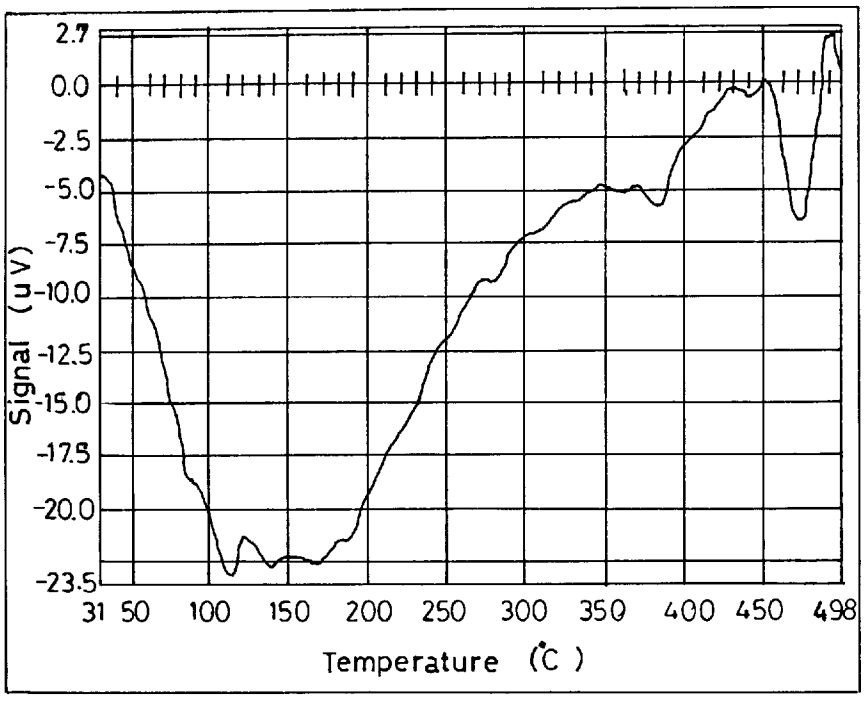

Figure 4 DTA patterns of activated slag cement (1d hydrated).

We carried out the detailed testing of one batch of our cement through our Concrete testing laboratory. Initial results appear satisfactory with respect to strength gain, workability, etc. In our system the content of alkali has been kept around 0.9 Na equ. Gifford and Gillott (1996) observed that increased alkali content for the activated BF slag cement concrete leads to a higher rate of consumption of reactive silica in the aggregates during the early stages of hydration. Hakkinen (1993) observed that with the increase of OPC content the number of micro cracks decreased in this type of cement.

REFRENCES

Gifford, P.M. and Gillott, J.E., "Alkali-Silica reaction and alkali-carbonate reaction in activated blast furnace slag cement and concrete", Cement and Concrete Research, Vol. 26, No. 1, pp 21-26 (1996).

Hakkinen Tarja, "The influence of slag control on the microstructure, permeability and mechanical properties of concrete". Cement and Concrete Research, Vol. 23, No. 2, 407-421 (1993).

Richardson, I.G., Brough, A.R., Groves G.W. and Dobson, C.M., "The characterization of hardened alkali-activated blast furnace slag pastes and the nature of the calcium silicate hydrate (C-S-H) phase", Cement and Concrete Research, Vol. 24 No. 5, 813-829 (1994).

Wang, S.D., Scrivener, K.L. and Pratt, P.L., "Factors affecting the strength of alkali activated slag", Cement and Concrete Research vol. 24, No. 6, 1033-1043 (1994).

Wang, S.D. and Scrivener, K.L., "Hydration products of alkali activated slag cement", Cement and Concrete Research, Vol. 25, No. 3, 561-571 (1995).

Wilding, C.R. and Mc Hugh, G., "Harwell Laboratory Report AERER-12297", (1986).

3ii093
4 pp

EFFECT OF BLENDED GYPSUM ON THE PROPERTIES OF PORTLAND CEMENT AND PORTLAND SLAG CEMENT

Singh MANJIT, Central Building Research Institute
Roorkee - 247 667 (India)

ABSTRACT The effect of unprocessed phospho and fluorogypsum both independently and in combination with natural gypsum on various properties of portland and portland slag cement was studied. The adverse effect of P_2O_5 and F impurities in phosphogypsum and those of fluorogypsum was offset by blending the natural gypsum with the by-product gypsum. The properties of cements conformed to the requirements of cement produced with natural gypsum. As compared to phospho and fluorogypsum the power consumption for grinding cement was reduced on using the blended gypsum.

KEY-WORDS : Blast furnace slag; CSH; gypsum; environment; waste.

INTRODUCTION

Large quantities of by-product gypsum are produced by the chemical industry which are currently disposed off by dumping into rivers, pond or onto waste land. Due to increasing concern about environmental pollution, it is essential to utilize these wastes as building material. Attempts have been made by Olmez and Erden (1989), Tabikh and Miller (1971) and Singh (1988) to use phospho and fluorogypsum (by-products of phosphoric acid and hydrofluoric acid industries) in the manufacture of cement. The impurities of P_2O_5, F, organic matter, alkalies present in the gypsum adversely affect the setting and hardening of cement (Singh, 1987). The effect of unprocessed phospho- and fluorogypsum was studied on the properties of portland cement and portland slag cement with and without natural gypsum. The natural gypsum was blended with the by-product gypsum to reduce the bad effect of obnoxious impurities of P_2O_5 & F present in the waste material. The role of blended gypsum vis-a-vis by-product gypsum on the grindability properties of cements was examined. The results of these findings are discussed in the paper.

RAW MATERIALS

The phosphogypsum (P_2O_5 0.42%, F 1.12%, $CaSO_4.2H_2O$ 96.75%, fluorogypsum (CaF_2 1.5%, $CaSO_4$. 93.5%, pH 5.0), cement clinker (SiO_2 24.19%, Al_2O_3 + Fe_2O_3 7.9%, CaO 64.04%, MgO 3.34%, SO_3 0.31% and loss on ignition 0.70%), granulated blast furnace slag (SiO_2 35.85%, Al_2O_3 + $Fe_2O_3$19.12%, MnO 0.63%, CaO 39.62%, MgO 4.09%, SO_3 0.13% and Sulphur 0.54%, glass 98.0%) and natural gypsum (SiO_2 8.80% Al_2O_3+ Fe_2O_3 0.66%, CaO 30.25%, MgO 0.10%, SO_3 39.60%, $CaSO_4.2H_2O$ 85.14%) were used to prepare the ordinary portland cement (OPC) and portland slag cement (PSC) respectively.

EXPERIMENTAL

Preparation and Testing of Cement

The ordinary Portland Cement (OPC) was produced by intergrinding cement clinker with unprocessed phosphogypsum (UPPG) and fluorogypsum (F.G.) with and without natural gypsum (N.G.) at 2.0% SO_3 content. The cement mixes were ground to a fineness between 317 and 421 m^2/kg (Blaine). The cements produced were tested for consistency, setting time and compressve strength as per relevant Indian Standards. The grindability of the cement samples was studied as per Bond's grindability test (Kannewurf, 1957).

RESULTS AND DISCUSSION

The physical properties of OPC and PSC reported in Table 1 show that setting time prolonged while the compressive strength reduced (Figures 1 and 2). However, on addition of blended gypsum

Table 1 Physical Properties of OPC and PSC in presence of Blended Gypsum

Sl. No.	Type of Gypsum	Fineness (m^2/kg) (Blaine)	Consistency (%)	Setting time (minutes)	
				Initial	Final
	OPC				
1.	Natural Gypsum (N.G.)	317	26.1	186	262
2a.	Unprocessed phosphogypsum (UPPG)	320	26.0	325	409
b.	UPPG + N.G.				
	40 60	323	26.3	188	270
	50 50	320	26.1	190	280
	60 40	330	26.4	191	286
3a.	Fluorogypsum (F.G.)	320	24.5	155	226
b.	F.G. + N.G.				
	40 60	320	26.9	132	198
	50 50	318	27.2	140	202
	60 40	326	26.8	150	220
	PSC				
4.	Natural Gypsum (N.G.)	416	22.8	238	305
5a.	Unprocessed phosphogypsum (UPPG)	421	23.7	270	380
b.	UPPG + N.G.				
	40 60	400	23.0	201	275
	50 50	418	22.8	208	290
	60 40	418	23.0	222	299
6a.	Fluorogypsum (F.G.)	417	22.2	190	226
b.	F.G. + N.G.				
	40 60	421	22.6	188	230
	50 50	420	23.0	200	240
	60 40	416	23.0	202	250

N.G. : Natural gypsum, UPPG : Unprocessed phosphogypsum,
F.G. : Fluorogypsum

Table 2 Grindability of OPC and PSC in presence of Blended Gypsum

Sl. No.	Type of Gypsum	Grindability (g/r)	Work Index (kwh/t)	Fineness (m^2/kg) (Blaine)	Power (kwh)
	OPC				
1.	Natural Gypsum	0.86	20.50	320	30.1
2a.	Fluorogypsum	0.90	21.50	320	32.6
b.	F.G. + N.G.				
	40 60	0.86	20.66	320	30.2
	50 50	0.84	20.40	320	30.2
	60 40	0.83	20.42	320	30.1
	PSC				
1.	N.G.	0.80	23.80	400	58.0
2a.	UPPG	0.88	24.90	400	59.1
b.	UPPG + N.G.				
	40 60	0.82	23.70	400	58.04
	50 50	0.84	24.20	400	58.10
	60 40	0.82	23.90	400	58.22

(UPPG/FG + natural gypsum), the setting time accelerated and the strength improved considerably (Figures 1 and 2). This may be ascribed to the dilution of impurities with the addition of natural gypsum. It is interesting to note that strength development of cement mortars were not affected by the impurities of fluoride of fluorogypsum, because most of the water soluble fluoride originate from fluoric acid, hence fluorogypsum does not so markedly retard the hydration of cement as the water soluble fluoride of phosphogypsum. The retardation is due to formation of silica gel or CSH (Na_2SiF_6 + $Ca(OH)_2 \longrightarrow CaF_2$ + C-S-H + NaOH) on the surface of cement grains. The power consumption for grinding cements (OPC & PSC) (Table 2) with fluorogypsum was mitigated on blending it with natural gypsum and found comparable to the values attained with natural gypsum.The presence of clay matter in natural gypsum apparently reduce the time of grinding thus, effecting power consumption.

REFERENCES

Kanneurf, A.S., Rock Products, Vol. 65, No. 5, 1957, p.86

Olmez, H and Erden, E, "The Effect of Phosphogypsum on the Setting and Mechanical Properties of Portland Cement and Trass Cement", Vol. 19, 1989, pp. 377-384.

Singh, Manjit, "Utilization of By-product Phosphogypsum for Building Materials", Building Research Note No. 9, CBRI Publication, Roorkee (India), March 1988.

Tabikh, A. and Miller, F.M., Cement and Concrete Research, Vol. 1, 1971, pp 663-678.

Singh, Manjit, "Influence of Phosphogypsum Impurities on Two Properties of Portland Cement", Indian Concrete Journal, Vol. 61, 1987, pp. 186-190.

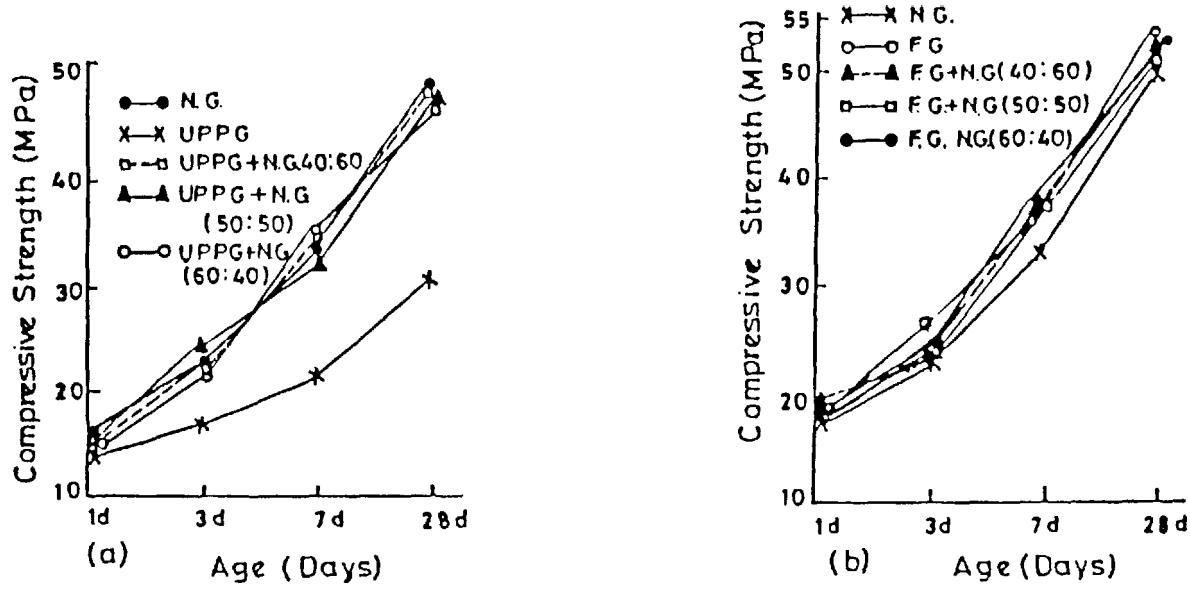

Figure 1 : Effect of blended gypsum (a) natural + phosphogypsum and (b) natural + fluorogypsum on the compressive strength of Portland Cement.

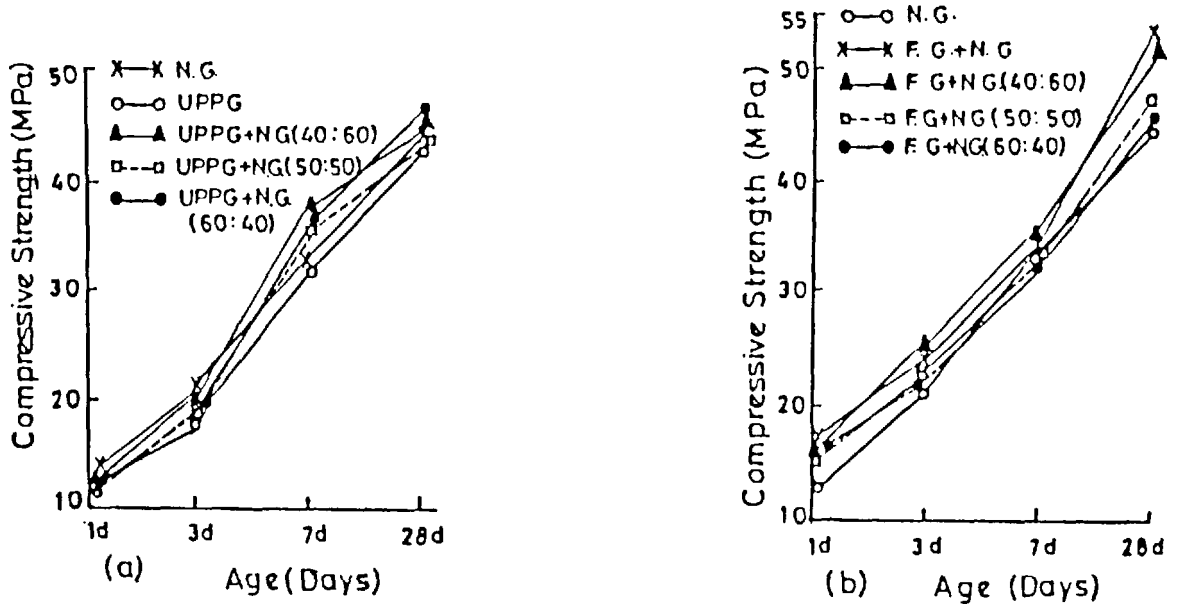

Figure 2 : Effect of blended gypsum (a) natural + phosphogypsum and (b) natural + fluorogypsum on the compressive strength of Portland Slag Cement.

HYDRATION CHARACTERISTICS OF STEEL SLAG IN ORDINARY PORTLAND CEMENT BLENDS

K. M. SHARMA, P. S. SHARMA and D. YADAV
National Council for Cement and Building Materials, New Delhi.
S. C. AHLUWALIA, OCL (India) Ltd., New Delhi, INDIA

ABSTRACT In view of the interest in the use of steel slag as a blending material for the manufacture of portland slag cement (PSC), investigations were carried out to explore the potentials of its use a reactive component by thermally activating it. Hydration of blends of air cooled steel slag and laboratory granulated steel slag with OPC over a period of six months under ambient and hydrothermal conditions have been studied and results reported.

Key-words : Activation, Hydration, Steel slag.

INTRODUCTION

Integrated steel plants produce two major slag wastes; blast furnace slag and steel making slag, more commonly known as steel slag. In India, presently about 1.8 million tonnes of steel slag is generated per year and an estimated 12 million tonnes of steel slag is accumulated. With the expansion of steel industry the volume of steel slag is likely to increase many times over creating a potential for a serious environmental problem and the requirement for a disposal site. The properties and use of blast furnace slag for making blended cements are widely known. A comparative evaluation with blast furnace slag indicates vital differences in terms of chemical, mineralogical and physical characteristics of the two slags. In view of the interest in the use of steel slag as a blending material for the manufacture of portland slag cement, investigations were carried out to explore the potential of its use as a reactive component by thermally activating it. Hydration characteristics of air cooled steel slag and the laboratory granulated steel slag have been studied and the results are presented in this paper.

EXPERIMENTAL

Steel slag, granulated blast furnace slag (GBF Slag), portland cement clinker and gypsum samples were obtained from the major steel and cement plants respectively and used for the preparation of cement blends. The elemental analysis of the raw materials are given in Table 1. Mineralogical characteristics of the raw materials were determined by X-ray diffraction and optical microscopic techniques.

TABLE 1 : Elemental Analysis of Raw Materials

S. No.	Sample Details	LOI/GOI*	Constituent (Percent) SiO_2	Fe_2O_3	Al_2O_3	CaO	MgO	Na_2O	K_2O
1.	Clinker	1.68	21.65	4.00	5.55	63.46	2.08	0.73	0.86
2.	Steel Slag	2.32	14.21	24.40	4.17	44.32	10.32	0.08	0.07
3.	GBF Slag	0.65	33.41	0.89	20.05	34.24	8.86	0.16	0.82
4.	Gypsum	14.22	18.55	0.83	1.40	23.83	0.97	-	-

Gypsum sample contains 34.95 % SO_3; purity works out to 75%
Clinker contains 0.27% CaO_f, Steel Slag contains 1.00 % TiO_2

*GOI = Gain on ignition

Activation of Steel Slag

Steel slag sample was melted in laboratory furnace at 1400°C and the molten slag was poured in water to granulate it (Sharma et al., 1992). The granulated slag so obtained was dried and ground to fineness of 400 m^2/kg and used for making blends with OPC.

Hydration Studies

The blends prepared air cooled with steel slag, granulated steel slag and granulated blast furnace slag were hydrated upto 180 days. The hydration was arrested by treating the hydrated samples with acetone and drying under vacuum. XRD and SEM techniques were employed for characterising hydration products.

Performance Studies

Blends of OPC-Steel slag, OPC- laboratory granulated steel slag and OPC-granulated blast furnace slag were prepared along with a control OPC sample maintaining the fineness level of all the samples at 350 m^2/kg Blaine. The performance characteristics of all the samples were determined as per the relevant Indian Standard and the data is presented in Table 2.

Table 2 : Performance cement blends prepared from air cooled and laboratory granulated steel slag and blast furnace slag (Fineness 350 m^2/kg Blain)

Sample No.	Composition %			w/c	Setting Time (min)		Compressive Strength (N/mm^2)		
	OPC	S.Slag	BFSlag		IST	FST	3d	7d	28d
Control OPC	100	Nil	Nil	0.37	34	65	23.7	40.2	53.2
PSC-1	75	25*	Nil	0.37	81	167	16.2	28.0	39.0
PSC-2	75	25*	Nil	0.36	75	151	18.2	32.5	46.3
PSC-3	75	Nil	25	0.36	72	149	20.0	34.2	50.5

* Laboratory granulated steel slag

RESULTS AND DISCUSSIONS

Evaluation of Raw Materials

The OPC clinker used in the present investigation contained 49.65 % C_3S, 24.61 % C_2S and had only 0.27 percent free lime.

The elemental analysis of granulated blast furnace slag indicates the presence of 34.24 and 33.41 percent of CaO and SiO_2 respectively. The sample also has 20.05 % Al_2O_3 and 8.86 % MgO. The optical microscopic analysis has indicated 92 % glass content in the sample. The elemental analysis of steel slag indicates the presence of 44.32 and 24.40 percent CaO and Fe_2O_3 respectively. Apart from CaO and Fe_2O_3 the sample also contains 14.21, 10.23 percent SiO_2 and MgO respectively. Optical microscopy has indicated the presence of only 34 % glass content in the air cooled steel slag.

Evaluation of elemental analysis data presented in Table 1 indicates that both the slags fulfill the chemical requirements laid down in Indian Standard Specification IS:12089-1987 for the slag to be used for the manufacture of portland slag cement.

However, steel slag does not fulfill the requirement of the glass content laid down in Indian Standard Specification. An attempt was therefore made to granulate steel slag in the laboratory by heating it to 1400°C and quenching in water. The results indicate an increase in glass content from 34 to 60 percent. These results are confirmed by X-ray diffraction analysis which shows higher amorphous material in laboratory granulated steel slag. The diffractograms are presented in Fig. 1.

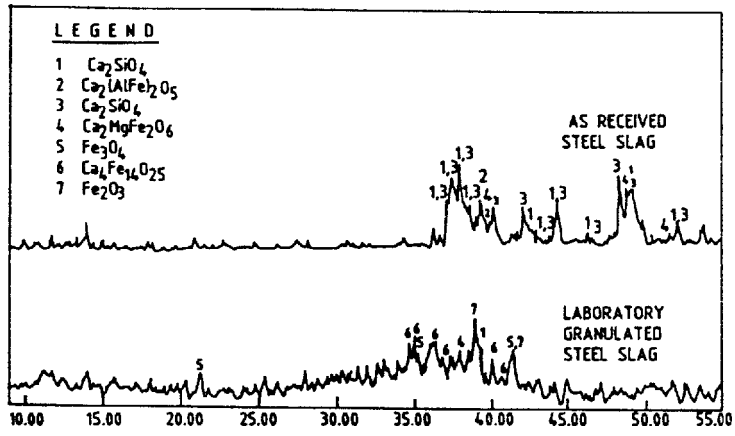

FIG. 1 : XRD OF AIR COOLED AND GRANULATED STEEL SLAG

Hydration Characteristics

The results of hydration studies indicate that the hydration of OPC starts immediately both in PSC-1 and PSC-2 prepared from air-cooled steel slag and laboratory granulated steel slag respectively. Presence of low quantities of $Ca(OH)_2$ and unhydrated ß-C_2S in blend prepared with laboratory granulated steel slag indicate faster hydration in it compared to the blend prepared with air cooled steel slag (Sharma et al., 1995). The diffractograms are presented in Fig.2.Scanning electron micrographs of hydrated samples of PSC-1 and PSC-2 under ambient conditions at 90 and 180 days have been presented in Plates 1 and 2. The results have shown the presence of unhydrated ß-C_2S upto 90 days and $Ca(OH)_2$ even upto 180 days alongwith C-S-H and other hydration products in PSC-1 where as in blend prepared with laboratory granulated steel slag (PSC-2) presence of cloud of C-S-H was noticed along with other hydration products as such as calcium aluminate hydrate etc. At 180 days hydration no $Ca(OH)_2$ was observed. Results indicate a higher degree of hydration for blend prepared with laboratory granulated steel slag. Performance studies of the blends (Table 2) confirm these findings. Autoclaved products however, were same: tobermorite, portlandite and α-quartz in both the cases. ß-C_2S was also fully hydrated under autoclaving condition.

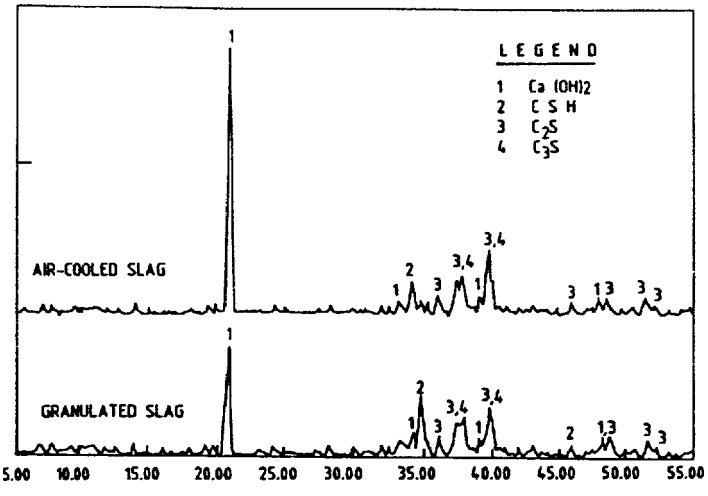

FIG 2 : XRD OF HYDRATED AIR COOLED & GRANULATED STEEL SLAG CEMENT BLEND

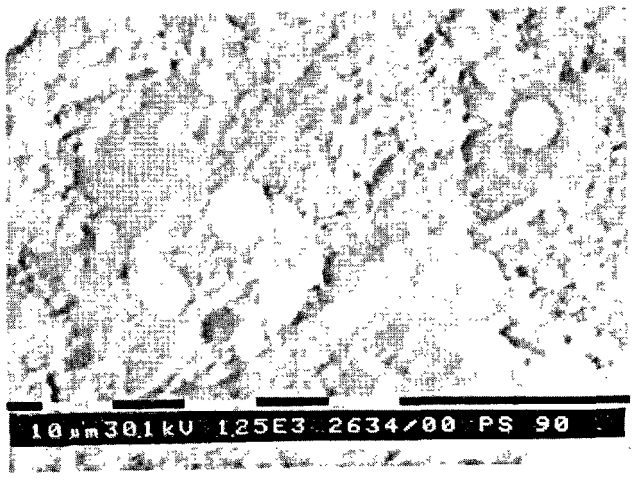

90 days

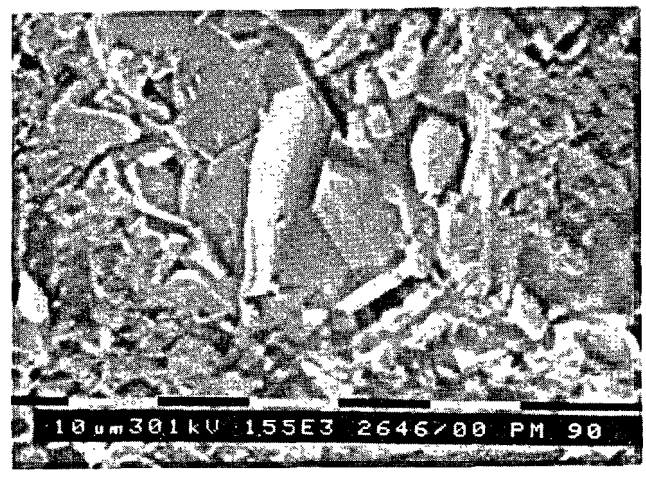

90 days



180 days

PLATE 1 : Hydrated PSC-1

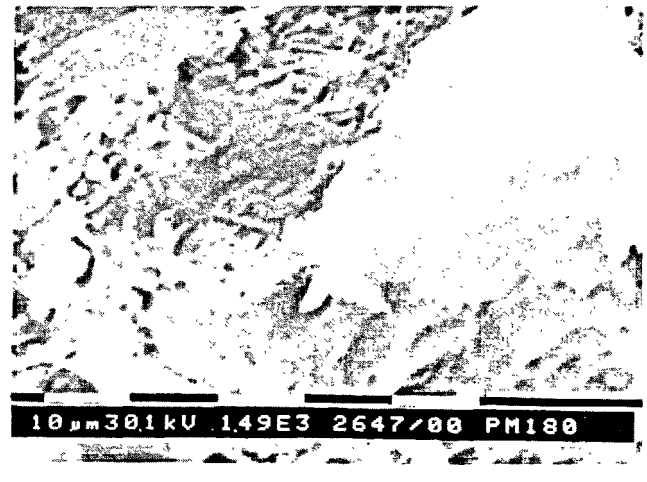

180 days

PLATE 2 : Hydrated PSC-2

CONCLUSION

1. Air cooled steel slag contains only 34 % glass content and shows poor hydraulicity. Steel slag granulated in the laboratory showed considerable improvement in glass content and the hydraulicity.
2. Results of hydration studies conducted at ambient temperature upto 180 days indicated much better and faster hydration for blend prepared from laboratory granulated steel slag. The findings have been confirmed by the performance data.

ACKNOWLEDGEMENT

The authors have freely drawn upon completed R & D work/status reports of NCB. The paper is being published with the permission of Director General, NCB, New Delhi, India.

REFERENCES

Sharma, K.M., Bhargava, R., Yadav, D. and Ahluwalia, S.C., "Metallurgical Slags as Blending Materials for Cement Manufacture", 9th Int. Cong. Chem. Cem, Vol. 3, 1992, pp. 121-127.

Sharma, K.M., and Ahluwalia, S.C., "Cement Blending Using Steel Slag", World Cement, Dec., 1995, pp. 74-77.

MODIFICATION OF ALKALI ACTIVATED SLAG PASTES BY USE OF MINERAL ADMIXTURES

Witold BRYLICKI, University of Mining and Metallurgy, Kraków, Poland

ABSTRACT The pastes produced from the ground, granulated blast furnace slag, activated with 5 % Na_2CO_3 additive and containing different mineral admixtures, such as ground portland cement clinker, portland cement, converter slag, bentonite clay and natural zeolite were studied at varying w/c ratio and curing conditions. The physical and mechanical properties of pastes were investigated as well as their phase composition, microstructure and porosity.

Key - words : admixtures, blastfurnace slag, durability, microstructure.

INTRODUCTION

The alkali activated slag binders show several good practical properties; particularly high corrosion resistance should be underlined. As a result of long term studies, these materials have been applied for many purposes; among them the injection - sealing works are particularly interesting (Brylicki, Malolepszy, Stryczek 1992, 1993, 1994). Mineral admixtures can succesfully improve the parameters of alkali activated slag paste - the results of investigations are the subject of presented work.

EXPERIMENTAL

Materials

The alkali activated slag binders were produced from the ground granulated blast furnace slag and 5 % Na_2CO_3 activator, 5 - 10 wt. % of the following admixtures were also used : ground portland cement clinker, portland cement class 45, ground converter slag, bentonite clay and natural zeolite. The pastes were cured in the following three ways : stored in standard conditions, at temperature 18 ± 2° C, RH > 90 %; heated at ambient pressure within 2 - 6 - 2 h cycle (max. 80° C); autoclaved at 180° C within 1 - 4 - 1 h cycle.

Methods

The following properties of slag - alkaline binders were studied : water demand, setting time, rheology, flexural and compressing strength, linear dimension changes using standarized procedures. The phase composition and microstructure were characterized by XRD, SEM and EDS as well as by porosimetry.

Results

The composition of pastes with admixtures are given in Table 1 together with the water demand (as w/c at standard consistency) and setting data. The fluidity, rheology and strength was measured on pastes of consistency used in sealing - injection works. The fluidity was evaluated by conus test, the relative viscosity was measured by Ford cup No 4 and rheology - by rotating viscosimeter Fann V - G 355. The results are shown in Table 2 and 3. The sample numbers correspond to the compositions given in Table 1. The linear dimension changes of 40x40x160 mm bars were measured in the Graf - Kaufman apparatus. The bars were produced from pastes of standard consistency. The results are presented in Table 4.

Table 1. Water demand and setting characteristics of slag - alkaline pastes with admixtures

Sample No	Compositttion of paste (in wt. %)	w/c at standard consistency	Initial setting [min.]	Final setting [min.]
1	95% bfs + 5% Na_2CO_3	0.29	155	320
2	85% bfs + 5% Na_2CO_3 + 10% PC cl	0.28	20	58
3	85% bfs + 5% Na_2CO_3 + 10% PC45	0.30	25	70
4	90% bfs + 5% Na_2CO_3 + 5% conv	0.26	65	169
5	85% bfs + 5% Na_2CO_3 + 10% bent	0.33	54	232
6	85% bfs + 5% Na_2CO_3 + 10% zeol	0.30	47	140

* following abbreviations are used : bfs - blast furnace slag; PC cl - portland cement clinker; PC 45 - portland cement class 45; conv - converter slag; bent - bentonite clay; zeol - natural zeolite.

Table 2. Fluidity and rheological properties of pastes

Sample No	w/c	Fluidity [mm]	Relative viscosity [s]	Plastic viscosity [m Pas]
1	0.45	160	65	237.45
	0.50	180	55	117.70
2	0.45	140	-	217.40
	0.50	210	50	112.96
3	0.45	150	-	236.64
	0.50	180	55	98.84
4	0.45	160	-	221.44
	0.50	200	65	90.26
5	0.45	130	-	237.64
	0.50	190	45	137.20

Table 3. Results of compressive and flexural strength test

Sample No	w/c	Flexural strength after 180 days [MPa]	Compress. strength after 180 days [MPa]	Sample No	w/c	Flexural strength after 180 days [MPa]	Compress. strength after 180 days [MPa]
1	0.45	11.5	23.7	4	0.45	8.2	31.0
	0.50	7.1	20.8		0.50	7.4	28.1
2	0.45	8.7	19.1	5	0.45	6.9	30.6
	0.50	8.0	17.7		0.50	6.5	30.0
3	0.45	7.2	21.3	6	0.45	10.9	32.4
	0.50	6.9	16.8		0.50	8.4	30.1

Table 4. Linear dimension changes of pastes

Sample No	Change of linear dimension in mm/m at age			
	3 days	7 days	28 days	90 days
1	- 0.19	- 0.52	- 0.53	- 0.53
2	- 0.18	- 0.41	- 0.42	- 0.52
3	- 0.01	- 0.12	- 0.30	- 0.35
4	- 0.13	- 0.14	- 0.24	- 0.24
5	+ 0.22	+ 0.24	+ 0.65	+ 0.78

The phase composition studies by XRD method on standard, 28 days cured samples revealed the presence of near amorphous C - S - H, calcite and calcium carboaluminate $C_3A\ CaCO_3\ 12H_2O$. In the 6 months stored samples the hydrogarnets were detected with varying Si/Al ratio as well as zeolites, such as thomsonite $CaNa_2\ [Al_5\ Si_5\ O_{20}]\ 12H_2O$ and natrolite $Na_2Al_2Si_3O_{10}\ 2H_2O$. The low pressure steam curing did not change the phase composition. In the autoclaved samples the better crystalized calcium silicate hydrates appeared (1.13 nm tobermorite). In Figure 1,2 the SEM micrographs and EDS plots of hydrogarnets and sodium - calcium zeolites are shown. These zeolites are modified by the presence of Mg^{2+} and K^+ ions being the components of pastes.

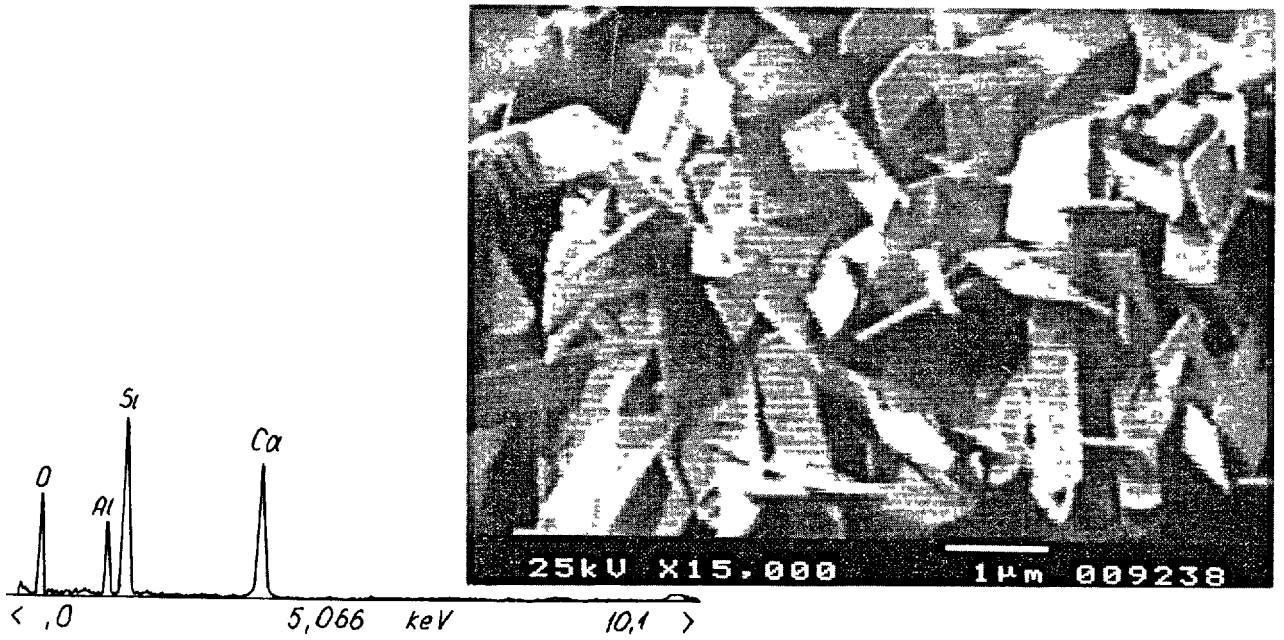

Fig.1. SEM : slag - alkaline paste with zeolite after autoclaving, the hydrogarnets crystals rich in Al are visible; EDS of hydrogarnets.

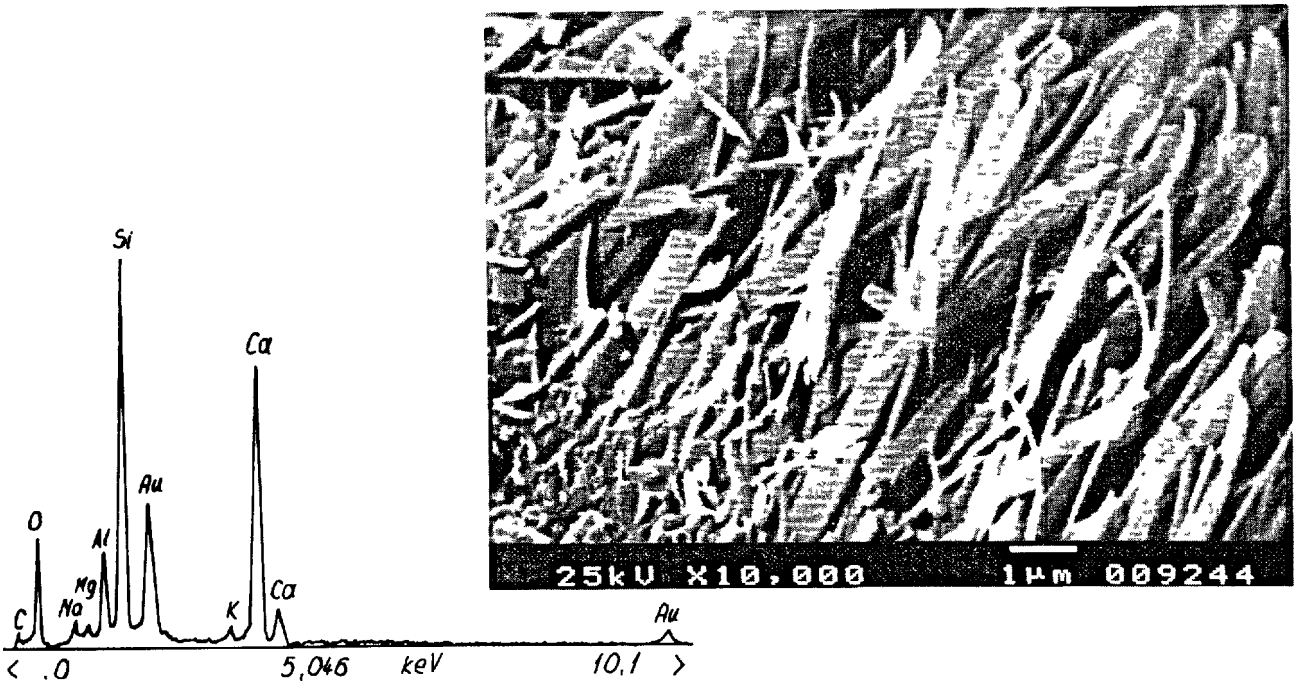

Fig.2. SEM : slag - alkaline paste with zeolite after autoclaving, the alongated zeolite crystals are visible; EDS of zeolite.

The results of porosity measurements are presented in Figures 3 and 4.

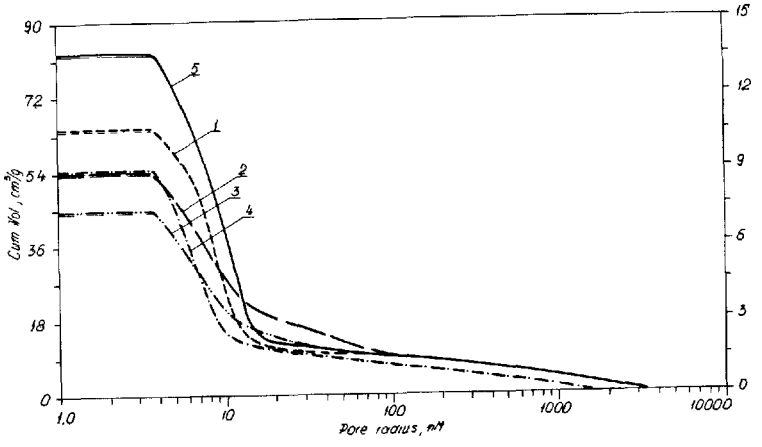

Fig.3. Porosity of hardened slag alkaline pastes 1 - 5 cured 6 months at standard conditions

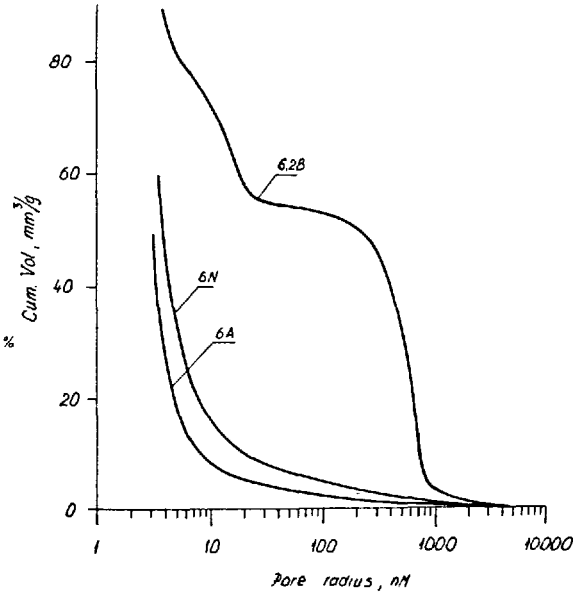

Fig.4. Porosity of hardened slag alkaline pastes admixtures with zeolite cured at standard conditions (sample 6,28) heated (6N) and autoclaved (6A).

CONCLUSIONS

1. Mineral admixtures improve substantially the properties of fresh and hardened slag - alkaline paste. This fact is of special, practical importance.

2. In the presence of mineral admixtures the water demand of slag - alkaline pastes does not change generally, setting time is significantly reduced, as well as shrinkage. In the presence of bentonite clay the expansion occurs.

3. Slag - alkaline pastes with mineral admixtures show very good flowability and rheology at w/c >0,45; simultaneously fairly good strength is maintained. From rheological point of view they correspond to the Casson's liquids.

4. Mineral admixtures do not alter significantly the phase composition but strongly affect the microstructure of hydrogarnets and zeolites.

5. Portland cement, clinker, converter slag bring about the reduction of total porosity and sealing of slag - alkaline pastes. Bentonite clay causes the porosity increase due to expansion.

Thermal treatment of pastes results in total porosity decrease with a significant change of pore structure.

REFERENCES

Brylicki W., Malolepszy J., Stryczek S., „Alkali Activated Slag Cementitions Material For Drilling Operation", Proc. 9 th Int. Congr. on the Chemistry of Cements, Vol. III, New Delhi, 1992, pp. 312 - 318.

Brylicki W., Malolepszy J., Stryczek S., „Properties and Use of Alkali Activated Slag Paste", Proc. 4 th International Symposium on the Reclamation, Treatment and Utilization of Coal Mining Wastes, Kraków, 1993, Vol. II, pp. 925 - 932.

Brylicki W., Malolepszy J., Stryczek S., „Industrial Scale Application of the Alkali Activated Slag Cementitions Materials in the Sealing Works", ed. J.J.J.M. Goumans, H.A. van der Sloat and Th.G.Aalbers, Elsevier Science Publishers, Amsterdam, 1994, pp. 841 - 849.

ACTIVATION OF BLAST FURNACE SLAG/HIGH ALUMINA CEMENT PASTES: MECHANICAL AND MICROSTRUCTURAL EVOLUTION

Mª Luisa ROMERO, Mª Teresa BLANCO-VARELA, Angel PALOMO, Francisca PUERTAS and Tomás VÁZQUEZ, Instituto Eduardo Torroja (CSIC), Spain.

ABSTRACT This study focuses the evolution of phases and the mechanical-resistant behaviour of high alumina cement (H.A.C.) mixed with granulated blast furnace slags (GBFS) and Na_2CO_3 2N as activator at 5 and 40ºC. Among other effects, the activator inhibits formation of C_2ASH_8 (at low temperature), induces carboaluminates formation and favours strengths.

Key-words: High alumina cements, Blastfurnace slag, microstructure.

INTRODUCTION

The hydration of high alumina cement (H.A.C.) mixed with slags produces different phases from those obtained by separate. The formation of hydrated gehlenite (C_2ASH_8) is of great interest, since it can result in a major phase (Fentiman et al., 1990)

The purpose of this work is to study the development of strengths, at different ages, in samples of high alumina cement with addition of slags in different proportions, and activator solution (dissolution of Na_2CO_3, 2N), and how the temperature affects their composition.

EXPERIMENTAL

Two types of hydration samples were prepared:
- High alumina cement + slags + standard solution (H_2O)
- High alumina cement + slags + activation solution (Na_2CO_3, 2N)

with three different mixtures:

A= 80% of high alumina cement + 20% of slags
B= 50% " " + 50% "
C= 20% " " + 80% "

The specific surface of the high alumina cement was 3.021 cm^2/gr, and that of the slag was 4.337 cm^2/gr. In Table 1 the chemical analysis of both samples is shown.

Table 1 Chemical Composition of High alumina cement and Slag

	SiO_2	Al_2O_3	Fe_2O_3	CaO	MgO	SO_3	H_2O comb.	S^{2-}
H.A.C	2.85	42.47	15.31	40.49	-	-	-	-
Slag	36.88	11.70	0.49	41.87	8.71	-	0.31	0.94

After drying at 100º C and homogenizing the mixtures, they were hydrated with distilled and deionized water and with a solution of Na_2CO_3 2N. Solution/powder ratio was 0.4.

All hydrated samples were stored in saturation chambers (100% RH) and kept at two different temperatures : 5ºC and 40ºC.

Samples were removed after 3, 7, 28 and 90 days. The process of hydration was interrupted in each case by "freezing" the sample with acetone and ethanol, and they were vacuum filtered. The pastes obtained were analyzed through XRD and FTIR.

Flexural strengths were determined at 28 and 90 days in two series of 1x1x6 cm prisms, one mixed with water, others with the alkaline solution. Samples were kept at 5ºC and 40ºC at 100% RH chambers. Samples were stripped off moulds 24 hours later and put again into their corresponding humidifying chambers, at the two chosen temperatures. Moreover, microstructural studies by SEM and EDAX were carried out on samples.

RESULTS AND DISCUSSION

Hydrated samples without activator, cured at 5ºC

In Table 2, results obtained by XRD are shown. At 3 and 7 days the major phase was CAH_{10}. In A samples (20% of slag) the most part of the anhydrous phases did not react during this period.

Table 2 XRD results of samples without activator (5°C).

AGE (DAYS)	CA			CAH_{10}			C_2ASH_8			C_4AcH_{11}			F F		
	A	B	C	A	B	C	A	B	C	A	B	C	A	B	C
3	-	-	-	-	+	o	-	-	-	-	-	o	-	+	-
7	*	-	-	*	+	*	-	o	+	-	-	o	+	+	o
28	+	-	-	*	*	o	-	o	+	-	-	*	+	+	*
90	+	-	-	+	o	-	-	+	+	-	-	o	+	+	-

+ : Abundant. o : Little, trace.
* : Moderate. - : None.

B Samples (with 50% slag) also showed hydrated gehlenite that became the major hydrated phase after 28 days, which agrees with Fentiman et al.(1990) and with Richardson et al. (1990). In the C samples (with 80% of slag), this was already a major phase at 7 days of hydration.The amount CAH_{10} in all samples decreased as slag amount was higher in the sample; that is, it showed a reciprocal evolution to this of the hydrated gehlenite. Thus, with 80% of slag, after 28 days hydration, samples were free of CAH_{10}.

IR absorption bands, typical of C_2ASH_8, used to be partly overlapped by those of aluminates and by those of the slag; however, in the IR spectra of the samples (Fig. 1) their presence could be clearly observed at 1130cm^{-1}. In samples with 80% of slag and 90 days of hydration, they gave broad, blurry bands in the region of OH stretching (3200-3600cm^{-1}) supposedly caused by the presence of amorphous (gel type) or poorly crystallized hydrates. A study by means of SEM and EDAX was carried out in samples with 80% of slag, at 28 and 90 days, in order to identify the hydrated gehlenite and the amorphous phase already detected through IR. Grains of slag are surrounded by plate-like hydration products growing perpendicular to their surface (Fig. 2). This product is hydrated gehlenite, as it was observed by EDAX analysis. Moreover, the presence of an amorphous phase surrounding the slag could be observed (Fig. 3), whose analysis through EDAX indicated that its composition did not correspond to any known hydrate and it also extended beyond from C-S-H gel phases or alumina gel. This amorphous phase detected through IR and observed through SEM, could

probably be a mixtureof C-S-H gel and other aluminum-rich gels, and even hydrated phase gels that did not have crystallized yet.

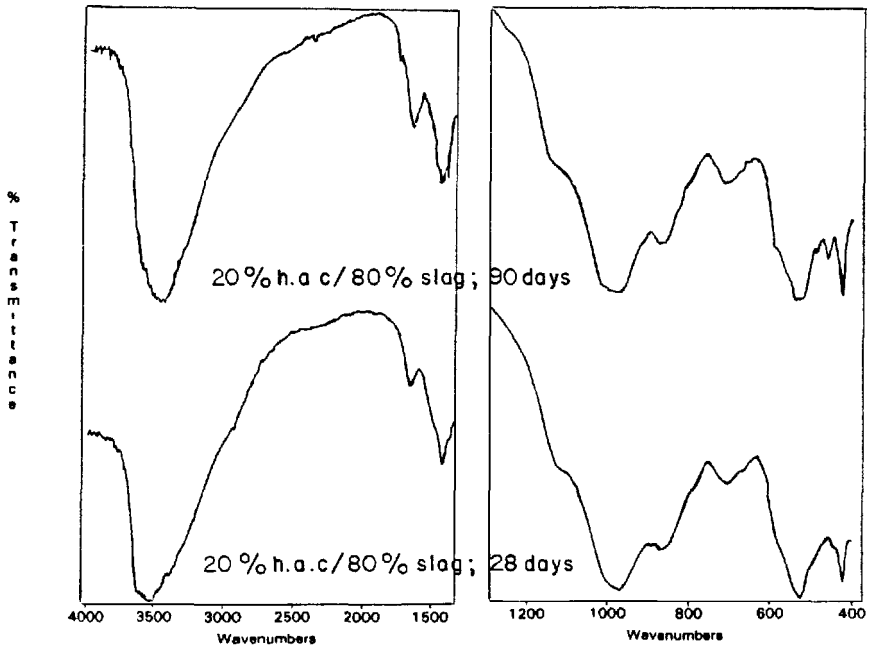

Fig.1. IR spectra of samples with 20% H.A.C. and 80% of slag

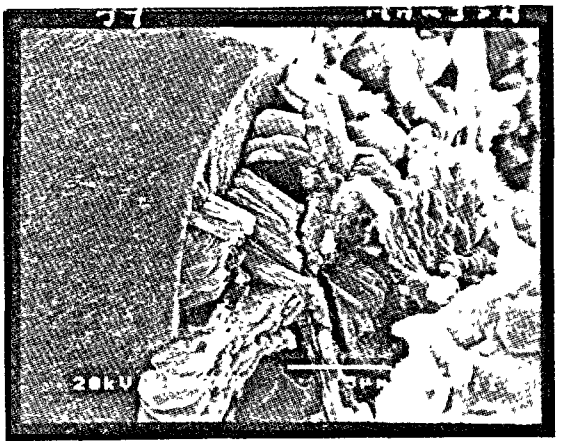

Fig. 2. Hydration products growing suround to slag grains.

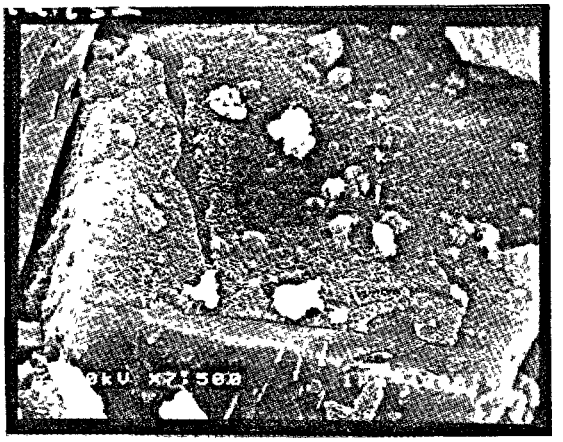

Fig. 3. Amorphous phase unknown

The formation of these gel type phases in reaction products of aluminous/slags mixtures has been proved by several researchers (Edmonds et al., 1989; Majumdar et al., 1989).
Flexural strength tests (Fig. 4) showed that at 28 days hydration, the paste with the highest strength (without act., at 5°C) was the one with 50% of slag. With 20% and 80% of slag, strengths at 28 days were lower but they increased with time. No doubt that initial low strengths in samples with higher content of slag were due to the low hydration rate of slags.
These results indicate that at low temperatures, and at 90 days, the reaction of the CAH_{10} with the slag silicates results in a diminish of strengths.

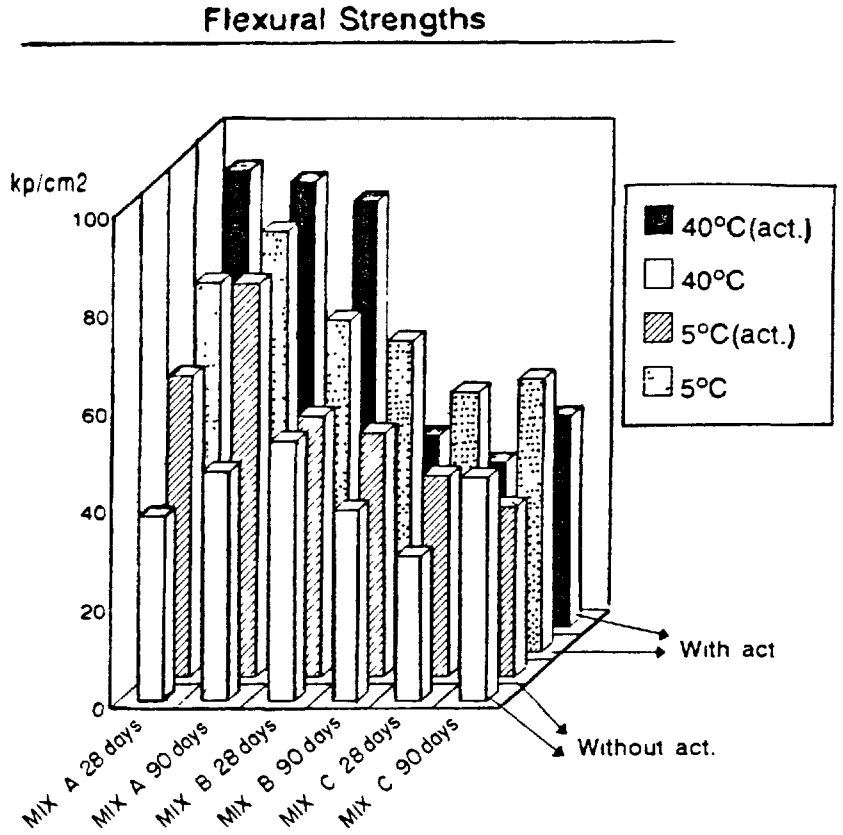

Fig. 4. Flexural strengths of specimens at 5 and 40°C with and without activator.

Hydrated samples with activator, cured at 5°C

Cement pastes hydrated with activator solution and kept at 5°C gave diffractograms which indicated, in all cases, the presence of CAH_{10} which decreased when the slag increased (Table 3). This hexagonal hydrate remains practically constant with time when the amount of slag was 20% and contained a small amount of monocarboaluminates (C_4AcH_{11}). When the amount of slag increased in the mixture, the CAH_{10} decreased with time, in the same proportion as C_4AcH_{11}. In the case of samples with 80% of slag, the amount of C_4AcH_{11} was negligible, but the increase of calcite was considerable.

Table 3 XRD results of samples with activator (5°C).

AGE (DAYS)	CA			CAH_{10}			C_4AcH_{11}			$CaCO_3$			F F		
	A	B	C	A	B	C	A	B	C	A	B	C	A	B	C
3	+	+	-	+	+	*	-	-	-	-	-	+	+	-	-
7	+	+	-	+	o	*	o	o	-	-	-	+	+	-	-
28	+	+	-	+	+	o	o	o	-	-	-	+	*	-	-
90	+	+	-	+	*	o	o	o	-	-	-	+	*	-	-

+ : Abundant. o : Little, trace.
* : Moderate. - : None.

Such results indicate that the activator induces carboaluminates formation, and prevents the C_2ASH_8 formation when there is a moderate amount of slag. When the amount of slag is high, $CaCO_3$ develops because the reaction of Na_2CO_3 from the activator with the Ca^{2+} of the slag released into solution.

Even though the presence of aluminum hydroxides was not detected through XRD, in the IR spectra corresponding to the samples with 20% and 50% of slag (Fig. 5), absorption bands at 3620-3525-3394-3376, 1024 and 970 cm^{-1}, which are characteristic of AH_3 (gibbsite), were clearly visible. The intensity of these bands in spectra is lower in older samples.

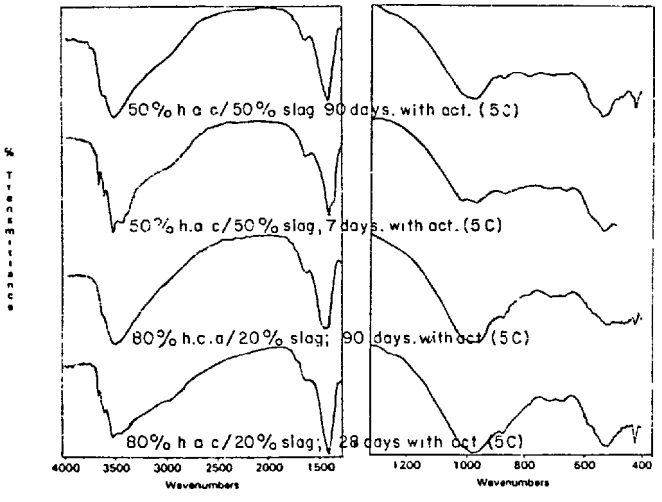

Fig.5 IR spectra of samples with act. (5°C)

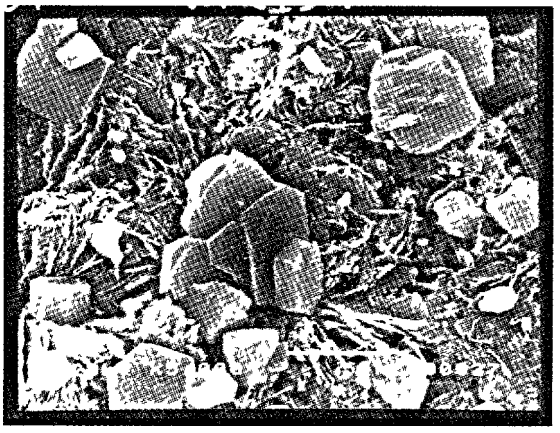

Fig.6 Crystal of CAH_{10}

This interpretation is verified by SEM studies carried out on these samples, where crystals of about 2 - 5 microns could be seen, and whose analysis by EDAX indicated that those were crystals containing almost exclusively aluminum (Fig. 6). Also, hexagonal crystals corresponding to CAH_{10} were seen.

The strenght of these samples made with addition of activating solution, were highly superior to those mixed only with water, which lead us think that the formation of carboaluminates confers these high, probably non-permanent, strenghts. The only exception is the 90 days hydration sample with the higher proportion of slag; this was precisely the case where no carboaluminates were detected, only calcite and the hexagonal hydrate.

The highest strengths were obtained when the proportion of slag was 20%.

Hydrated samples without activator, cured at 40%

XRD data (Table 4) indicates a logical absence of hexagonal hydrates. Diffraction lines, characteristic of cubic hydrate (C_3AH_6) and of hydrated gehlenite (C_2ASH_8) appeared instead.

Table 4 XRD results of samples without activator (40°C).

AGE (DAYS)	C_3AH_6			C_2ASH_8			$Al(OH)_3$			C_4AcH_{11}			F F		
	A	B	C	A	B	C	A	B	C	A	B	C	A	B	C
3	+	+	-	o	+	+	o	-	-	-	-	o	-	*	*
7	+	+	-	o	+	+	o	-	-	-	-	o	-	*	*
28	+	+	-	o	+	+	o	-	-	-	-	o	-	o	*
90	+	+	-	o	+	+	o	-	-	-	-	o	-	o	*

+ : Abundant. o : Little, trace.
* : Moderate. - : None.

The cubic hydrate was most abundant at early ages when the slag proportion was 20%; but it diminished when the proportion of slag increased, and was absent when slag amount reached 80%. Instead, C_2ASH_8 started to be noticeable in growing amounts.
These data indicated that slags, depending on their proportion in the mixture, prevent the formation of cubic hydrate, total or partially, because of the formation of hydrated gehlenite. The characteristic lines of AH_3 were only present in samples with 20% slag. Through IR (Fig. 7), spectra of samples with 50% and 80% slag, the broadening of absorption bands could be noticed, particularly in 3400-3600 cm^{-1}, presumably caused by hydrated amorphous compounds.

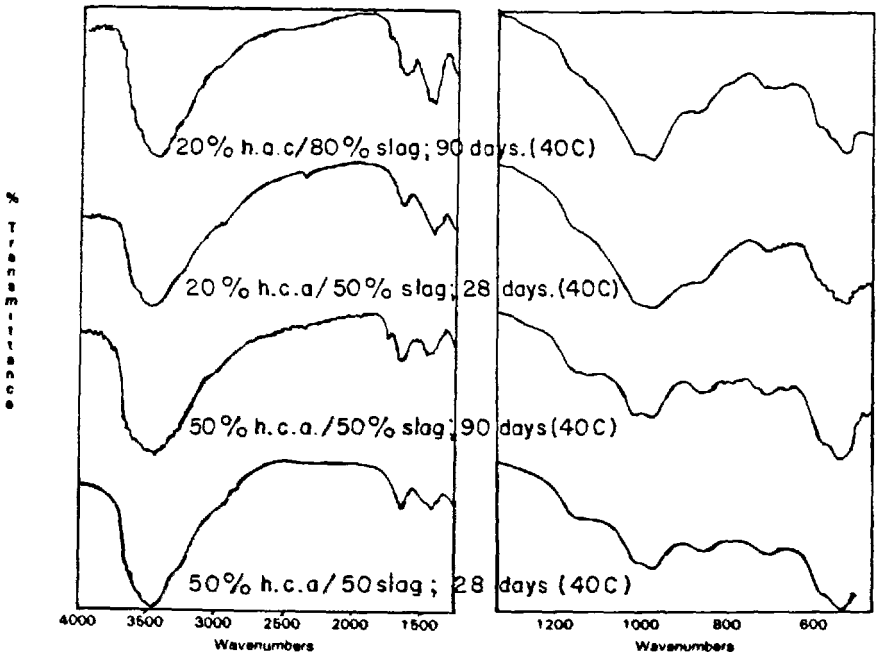

Fig.7. IR spectra of samples at 40°C

Therefore it is asssumed that absence of AH_3 bands is due to the fact that hydrated gehlenite does not only form from the reaction of hexagonal hydrates with the silica of the slag, but also

from aluminum hydroxide. Fetiman et al, (1990) support this hypothesis.
The evolution of the strength of these samples (Fig.4) indicates that a higher temperature favours a fast acquisition of mechanic strengths, at least along the ages studied in this work.

Hydrated samples with activator, cured at 40° C

Phases with silica incorporated in their structures were abundant in these samples as a consequence of a reaction of the cubic hydrates of the H.C.A. with the solubilized silica of the slag, which was favoured by rising temperatures.
The XRD of samples with 20% slag (Table 5) showed the simultaneous presence of C_3AH_6, katoite (hydrogarnet which formula is close to C_3ASH_4), and AH_3. This proportion (especially in the case of the katoite) increased with time. A small amount of hydrated gehlenite, was also observed. The katoite could be detected through IR because of the characteristic bands of the C_3AH_6; particularly, the intense sharp band of free OH, in 3663 cm^{-1}, diminished considerably and it is shifted to 3645 cm^{-1} (Fig. 8).

Table 5 XRD results of samples with activator (40°C).

AGE (DAYS)	C_3AH_6			C_2ASH_8			$Al(OH)_3$			C_4AcH_{11}			C_3ASH_4			$CaCO_3$			F F		
	A	B	C	A	B	C	A	B	C	A	B	C	A	B	C	A	B	C	A	B	C
3	*	-	-	o	o	-	o	-	-	o	o	-	*	-	-	-	-	+	*	*	-
7	*	-	-	o	o	-	o	-	-	*	o	-	+	-	-	-	-	+	*	*	-
28	+	-	-	o	o	-	*	-	-	o	o	-	+	-	-	-	-	+	*	*	-
90	+	-	-	o	o	-	+	-	-	o	o	-	+	-	-	-	-	+	*	o	-

\+ : Abundant. o : Little, trace.
* : Moderate. - : None

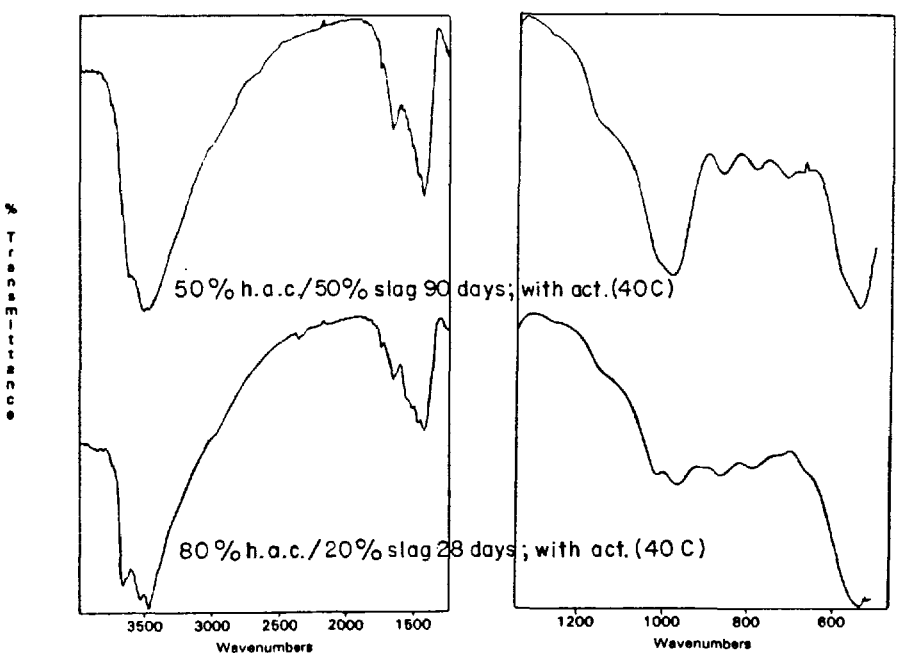

Fig. 8. IR spectra of samples with act. (40°C)

Samples with 50% slag had hydrated gehlenite as the only crystalline hydrate. The only crystalline compound in samples with 80% slag was calcite.

Bands with low definition, associated with gel type phases could be seen through IR (Fig. 8).
The presence of activator in samples cured at 40ºC favours the development of mechanical strengths (with 20% and 50% of slag) (see Fig. 4), while when 80% is added, the strength is decreased due to the scarcely reactive to the ages studied.

CONCLUSIONS

On samples cured at 5ºC

- Hydrated gehlenite (C_2ASH_8) is the major stable crystalline product which develops at low temperature in H.C.A. mixtures with a high proportion of slag, and hydrated with water. Its formation is mostly triggered by the reaction of the CAH_{10} and the dissolved silica from the slag. Amorphous phases, probably mixtures of C-S-H gel and other gels rich in aluminum, also appear.
- The activator prevents C_2ASH_8 formation. It also induces carboaluminates formation when amounts of slag are moderate. When the content of slag is very high, $CaCO_3$ appears due to the reaction of the activator with the Ca^{2+} of the slag, that is found in the solution.
- In samples manufactured with activator solution the resistances are higher than in samples mixed only with water. This indicates that formation of carboaluminates confers higher resistances which, in another hand, might not be permanent.

On samples cured at 40ºC

- The rise of temperature favours a fast strength increase.
- The slags, depending on their proportion in the mix, prevent total or partially the formation of cubic hydrates because of the formation of hydrated gehlenite, that, in another hand, is not only formed from the reaction of the hexagonal hydrates with the silica of the slag, but the aluminum hydroxide also influences its formation.
- The presence of activator in samples cured at 40ºC favours the obtention of mechanic resistances (with 20 and 50% of slag) while its effect is negative on those with 80%, due to their limited reactive character at the ages studied.

ACKNOWLEDGMENTS

The authors of the present work wish to thank to Subdirección General de la Promoción de la Investigación for funding this research through Programa Sectorial de promoción General del Conocimiento (PB94-0048) which was necessary to the realization of the present study.

REFERENCES

Edmonds, R.N. and Majumdar, A.J. "The hydration of mixtures of monocalcium aluminate and blast-furnace slag". Cem. Concr. Res. Vol 19, 1989, p. 779.

Fentiman,C.H., Rashid,S.,Bayoux,J.P.,Bonin,A. and Testud,M. "The effect of curing conditions on the hydration and strength development in Fondu:slag" Proc. of the Int. Symp. on Calcium Aluminate Cements. London, 9-11 July 1990, p. 272, Publ. E & FN Spon ISBN 0419 15200 8.

Majumdar,A.J.,Sing,B. and Edmonds,R.N. "Hydration of mixures of $C_{12}A_7$ and granulated blast-furnace slag". Cem. Concr. Res. Vol 19, 1989, p. 848.

Richardson, I.G. and Groves, G.W. "The microstructure of blast furnace slag/high alumina cement pastes". Proc. of the Int. Symp. on Calcium Aluminate Cements. London, 9-11 July 1990, pp 282-290, Publ. E & FN Spon ISBN 0419 15200 8 (HB).

INFLUENCE OF SILICO-MANGANIC SLAG ADDITIVES ON CEMENT HYDRATION AND PROPERTIES

Wojciech Roszczynialski, University of Mining and Metallurgy, Kraków, Poland

ABSTRACT Si-Mn slag is the mixture of different minerals with the akermanite as a predominant phase. In the granulation process almost all the Si-Mn slag transforms into the glassy substance. The investigation of the Si-Mn slag additives, from 1.5 to 15 %, on the standard properties of cement have been carried out. The effect of 15 % Si-Mn slag admixture on cement hydration was additionally studied by XRD and DTA methods. The results thus obtained prove the possibility of Si-Mn slag utilisation as cement admixture.

Key-words: admixtures, slag, modified cement, hydration, strength development.

INTRODUCTION

The silico-manganic slag (Si-Mn slag) is delivered as a by-product in the ferro-silico-manganese metallurgy. This slag has been used as cement admixture for a long time (Znaczko - Jaworski 1951), because of the similarity of chemical and phase composition to that for the blast furnace slag. However, the opinions about this material, as a component of cements, are not equivocal. The Si-Mn slags show much higher MnO content than the blast furnace ones. The effect of this component on the activity of slag and cement properties has not been understood until now. Generally, MnO is treated as an activity reducing agent (Smolczyk 1980). Among the numerous formulas, giving the factors of slag quality characterisation, the three following ones include the MnO component:

$$F_1 = \frac{CaO + 0.5MgO + Al_2O_3 + CaS}{SiO_2 + MnO}$$

$$F_2 = \frac{CaO + 0.5MgO + Al_2O_3}{SiO_2 + FeO + (MnO)^2}$$

$$F_3 = \frac{CaO + MgO + Al_2O_3 + BaO}{SiO_2 + MnO}$$

In all these indexes, MnO occurs in denominator; it means that MnO acts as an activity reducing component. On the other side, the applicability of slags as cement admixtures is determined not only on the basis of modulus, calculated from chemical composition but also by the structural disorder (Satarin 1974). MnO can favourize the formation of microheterogenity in the slag structure, as it would result from many experiments, in which the full applicability of slags with higher MnO content (5-20 %) was found (Datta and Lahiri 1972; Vylkova and Dagandzhieva 1974; Taneja et al. 1980; Roszczynialski et al. 1995).

EXPERIMENTAL

Materials

The crude Si-Mn slag from metallurgical plant was used in the studies. This slag was also granulated in laboratory. The granulated blast furnace slag was taken as reference. The chemical composition of slags is given in Table 1. In Figure 1 the XRD patterns of crude and granulated Si-Mn slags are plotted.

Table 1 Chemical composition of slags.

Component	Percentage (in weight %) in		
	crude Si-Mn slag	granulated Si-Mn slag	granulated blast furnace slag
SiO_2	42,5	42,4	39,2
Al_2O_3	7,0	7,0	8,3
Fe_2O_3	0,5	0,4	0,6
CaO	22,8	23,8	42,5
MgO	6,8	6,5	7,7
SO_3	0,1	0,1	1,1
MnO	8,5	8,9	0,2

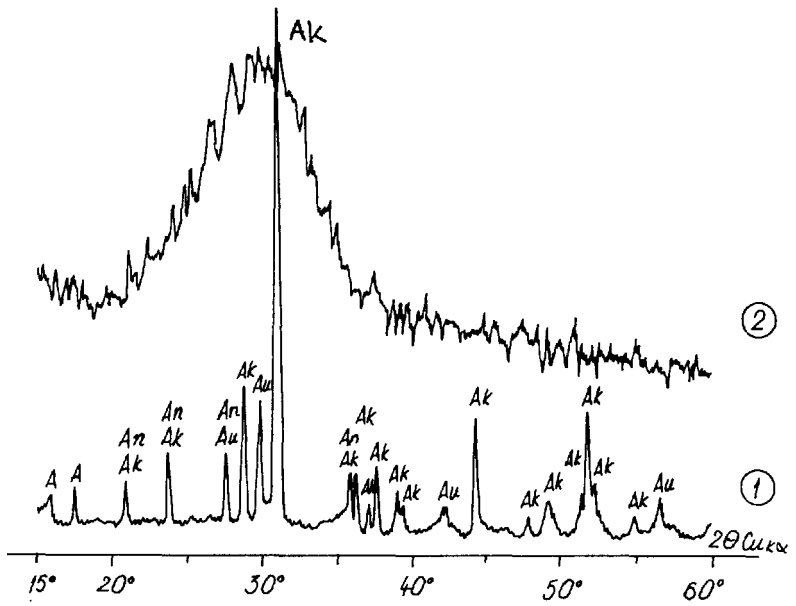

Figure 1 XRD pattern of crude and granulated Si-Mn slag (① crude Si-Mn slag, ② granulated Si-Mn slag, Ak - akermanite, Au - augite, An - anorthoclase).

Taking into account only the chemical compositions of slags and resulting values of modulus, one could presume much lower activity of Si-Mn slag as compared to the blast furnace slag (lower CaO and higher MnO content in Si-Mn slag). However, the XRD revealed the predominant occurrence of akermanite in crystalline Si-Mn material. This phase is of particular meaning as an active component of slags. Due the granulation process, practically all the crystalline phases transform into the microcrystalline or vitreous ones.

Cements with Si-Mn slag admixture

These cements were produced by grinding of portland cement clinker with Si-Mn slag in crude form or laboratory granulated and gypsum. The Si-Mn slag content was in the range of 1.5 to 15 % by weight of cement. The cement were ground to the Blaine specific surface about 300 m^2/kg. The two reference cements: portland cement without admixture and cement with 15 % blast furnace slag were prepared as references.

The cements thus produced were subjected to the standard tests in order to determine water demand, setting time, volume changes and strength. The reduction of water to attain the standard consistency was found for the Si-Mn slag containing cements. This reduction was in the range 1 - 12 %, depending on the slag content. Time of setting and volume changes were generally not affected by the presence of admixture. The results of compressive strength tests after 1, 3, 7 and 28 days curing are given in Table 2.

Table 2 Compressive strength of cements.

Admixture to cement	Compressive strength in MPa at age			
	1 day	3 days	7 days	28 days
-	8,6	20,0	29,3	41,1
1.5 % crude Si-Mn slag	8,1	19,1	28,9	39,9
1.5 % granulated Si-Mn slag	8,1	19,4	29,1	40,8
3 % crude Si-Mn slag	7,9	19,6	30,5	40,7
3 % granulated Si-Mn slag	8,2	19,8	30,4	41,8
5 % crude Si-Mn slag	7,7	19,2	29,6	38,1
5 % granulated Si-Mn slag	8,0	18,8	29,9	42,5
15 % crude Si-Mn slag	6,0	16,1	24,7	37,6
15 % granulated Si-Mn slag	6,8	17,2	26,8	39,2
15 % granulated blast furnace slag	6,0	16,4	25,6	36,8

Hydrated cements with 15 % granulated Si-Mn slag admixture and reference sample without admixture were subjected to the XRD and DTA measurements. The pastes were cured for 5, 10, 24, 72 hours and 28 days respectively. The acceleration of cement clinker minerals hydration in the presence of Si-Mn slag was observed after 10 hours from the beginning. The admixture plays a role of nucleating agent, thus facilitating the alite decomposition and calcium hydroxide crystallisation as one can notice from DTA results (see Figure 2). The admixture itself takes a part in the hydration products formation. Despite of 15 % clinker minerals content lowering the $Ca(OH_2)$ content between 10 and 72 hours is almost the same as for paste without admixture. After 28 days (see Figure 2) the $Ca(OH_2)$ content in the 15 % Si-Mn slag containing sample is about 10 % lower than in the reference one. It would result from the calcium ions consumption by active slag components. The accelerating effect of Si-Mn slag on cement hydration is additionally illustrated by XRD patterns of 28 days hydrated samples. In Figure 3, it is clearly seen, that the alite peak intensities are reduced more than it would result from only the "dilution" of cement with 15 % slag.

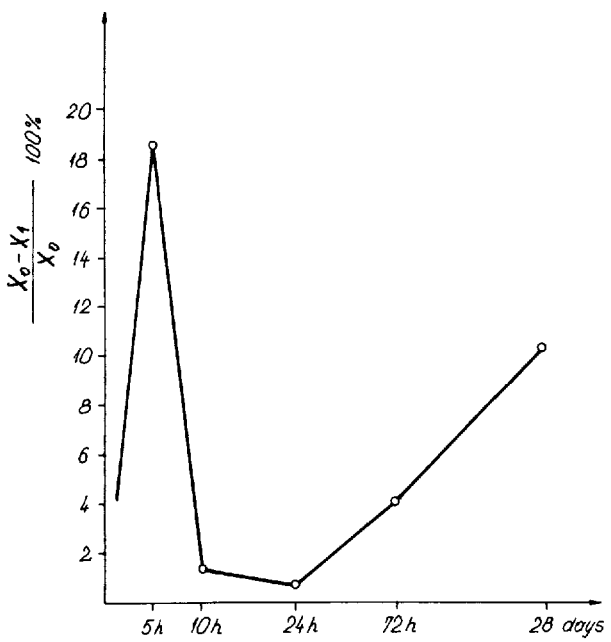

Figure 2 $Ca(OH_2)$ content evaluation in 28 days hydrating cement pastes calculated from TG measurements (X_0 - $Ca(OH_2)$ in paste without admixture; X_1 - $CA(OH_2)$ in paste with Si-Mn slag).

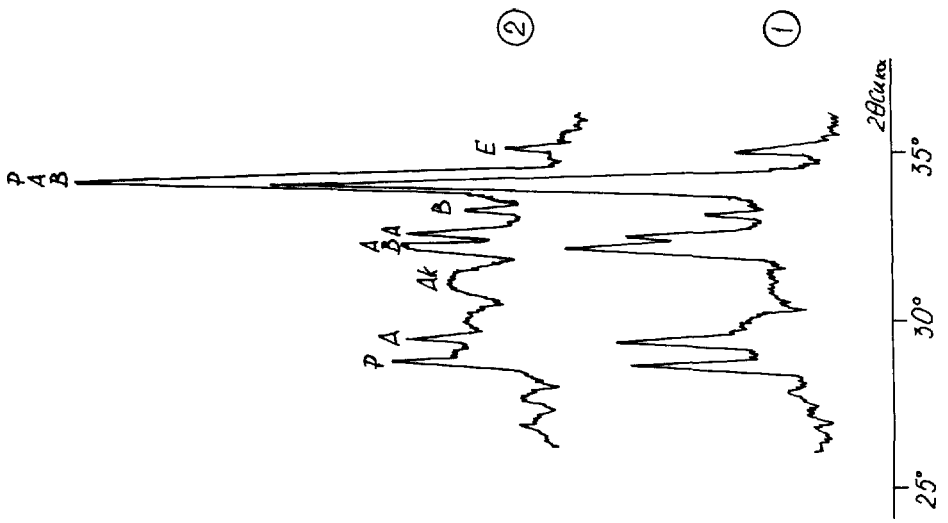

Figure 3 XRD patterns of pastes after 28 days hydration (① cement without admixture ② cement with 15 % granulated Si-Mn slag, A-alite, B-belite, P-portlandite, Ak-akermanite, E-ettringite).

CONCLUSIONS (SUMMARY)

From the data thus presented it results that the Si-Mn slag, added as 8-10 % of cement, is an active admixture. 1.5 - 15 % slag content can, of course, reduce the early strength (1-3 days), but at 28 days the strength values are similar to those for reference cements. The best results have been achieved at 5 % slag admixture. The granulated Si-Mn slag gives better parameters of cement, but the differences, as compared to the crude slag, are not significant. The results for Si-Mn slag are good as compared to those for the granulated blast furnace slag.

The good results achieved at Si-Mn slag admixtures can be explained as follows:

- Si-Mn slags reveal high content of active component, such as akermanite or akermanite glassy phase;
- Si-Mn slag acts as a modifying agent in clinker minerals (particularly alite) hydration.

REFERENCES

Datta R.K. and Lahiri D. „Einfluß kleiner Beimengungen auf die hydraulischen Eigenschaften von Hochofenschlacke. Teil 1. Einfluß von MnO", Zement Kalk Gips Nr 7, 1972, pp 344-346.

Roszczynialski W., Gładysz J. and Iwanciw J. „Badania nad wykorzystaniem żużli i pyłów krzemomanganowych jako dodatków do cementu", Cement Wapno Gips Nr 6, 1995, pp. 198-203

Satarin V. I. „Slag Portland Cement", The 6-th Int. Congr. on the Chem. of Cement , Moscow 1974, Vol III, pp. 45-56, Moscow-Stroyizdat 1976.

Smolczyk H. G. „Structure et caracterization des laitiers", 7-e Congres International de la Chimie des Ciments, Paris 1980, Vol I, pp. III 1/3 - IV 1/16.

Taneja C. A., Tehri S. P. and Singh M. „High Manganese High Alumina Slag for Cement Manufacture", 7-e Congres International de la Chimie des Ciments, Paris 1980, Vol II, pp III 48 - III 51.

Vylkova I.S. and Dagandzhieva R. G. „On Binding Properties of Blast Furnace Granulated Slag with High Content of Barium and Manganese", the 6-th Int. Congr. on the Chem. of Cement, Moscow 1974, Vol III, pp. 69-72, Moscow-Stroyizdat 1976.

Znaczko-Jaworski J. Ł. „Ob ispolzowanii w cemientnoj promyszlennosti mangancowistych szłakow", Cemient, Nr 3, 1951, pp. 9-12.

KINETIC STUDY OF ALKALI-ACTIVATED BLAST FURNACE SLAG

Ana FERNANDEZ-JIMENEZ. Instituto Eduardo Torroja (CSIC), Spain.
Francisca PUERTAS. Instituto Eduardo Torroja (CSIC), Spain.

ABSTRACT The alkaline activation process of granulated blast furnace slag (GBFS) has been studied. Activation degree (α) was determined from the data obtained by isothermal conduction calorimetry. The variables considered on the test were: temperature (25-60°C) and concentration of alkaline activator (Na_2O, 3-5% wt). For values of $\alpha \geq 0.5$ the process is controlled by diffusion. The equations that explain these kinetics are those of Jander (D_3, diffusion in sphere) and Ginstling-Brounshtein (D_4, surface diffusion).

Key-words: Alkali, Activation, Blastfurnace slag, Kinetic, Diffusion.

INTRODUCTION

The alkaline activation of granulated blast furnace slag (GBFS) leads to a cement material with low energy cost, high strength and good durability compared to portland cements (Glukhosky, 1980; Krivenko, 1992; Kutti, 1992; Wang, 1995). Nevertheless, the kinetic of the reactions has been little studied (Zhou, 1993). The objective of this work has been the determination of kinetic equations that explain the reaction processes of the slag with an alkaline activator. The activator solution was a mixture of water-glass and NaOH. The variables of the process were temperature (25, 35, 45, 60°C) of reaction and the concentration of Na_2O in activator solution (3, 4, 5% in weight).

EXPERIMENTAL

In Table 1 the chemical analysis of the GBFS from Avilés (Asturias, SPAIN) is shown.

Table 1 Chemical composition (% wt.) of the granulated blast furnace slag.

H_2O Comb	CO_2	*IR	SiO_2	Al_2O_3	Fe_2O_3	CaO	MgO	SO_3	**F	Blaine
0.10	1.23	0.14	36.10	11.22	0.49	42.80	8.40	0.0	1.72	440 m^2/kg

* IR= Insolubility Residue
**F= Hydraulic Index ($F=(CaO+MgO+Al_2O_3)/SiO_2$)

The activator solution was prepared with a mixture of commercial "water-glass" (SiO_2 =18.01%; Na_2O=8.53%) and NaOH. SiO_2/Na_2O ratio was maintained constant and equal to 1.5. The concentration of Na_2O was varied: 3, 4 and 5% wt respect to the weight of slag.

The degree of reaction (α), was determined according to the methodology of Stutter (1995), where $\alpha=Q(t)/Qmax$, (Q(t)= heat as a function of time; Qmax= total heat in kJ/kg). The mixtures were prepared to a constant ratio alkaline activator solution/slag = 0.4. The reaction temperatures were varied from 25 to 60°C and the time of reaction was constant and fixed at 45 hours.

RESULTS AND DISCUSSION

Figs. 1, 2 and 3 show heat evolution curves (kJ/kg) versus reaction time, for the different concentrations of activator solution and test temperatures. Figs. 4, 5 and 6 show the degree of reaction (α) versus time.

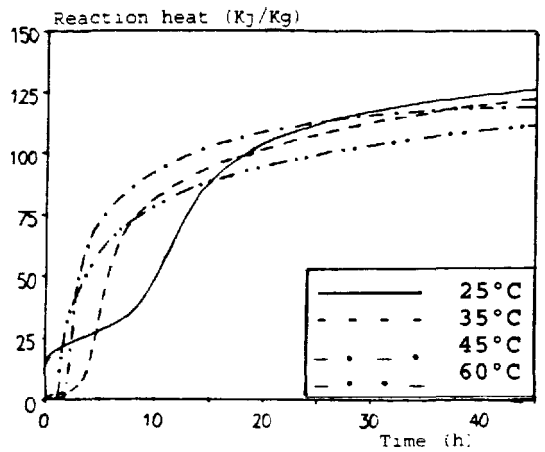

Fig 1 Reaction heat, 3% of Na_2O

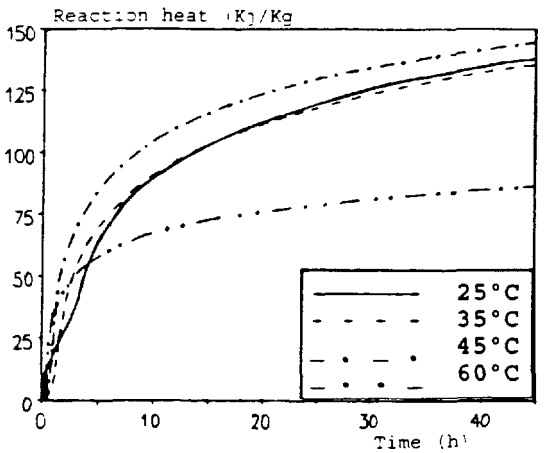

Fig 2 Reaction heat, 4% of Na_2O

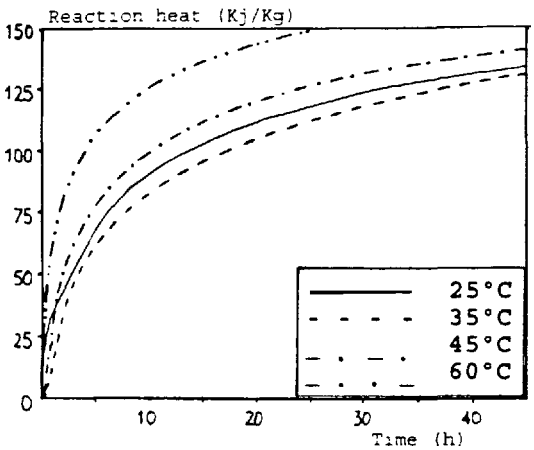

Fig 3 Reaction Heat, 5% of Na_2O

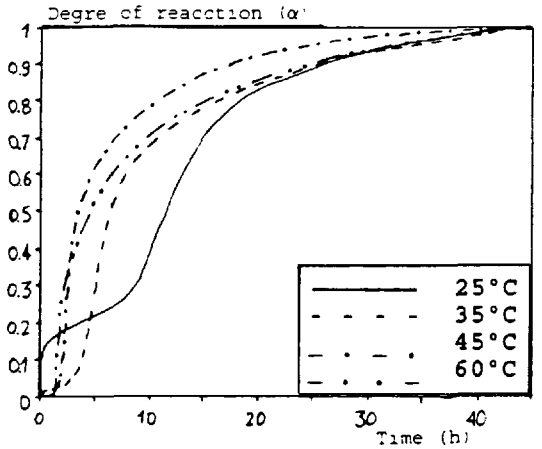

Fig 4 Degree of reaction, 3% of Na_2O

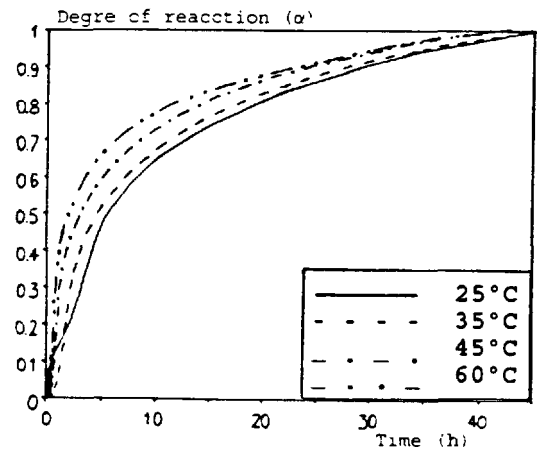

Fig 5 Degree of reaction, 4% of Na_2O

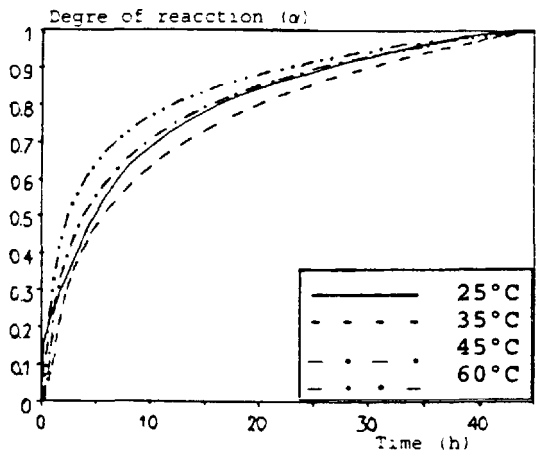

Fig 6 Degree of reaction, 5% of Na_2O

The kinetic of the process was studied through two complementary methods:

a) Mori and Minegishi method (1968). This method is based on determining the value of N on the Eq.1:

$$(1-(1-\alpha)^{1/3})^N = Kt \qquad [1]$$

Where α= degree of reaction; K = rate constant; t = reaction time; N is the value which is variable according to the reaction type. In the present case representing the $\log(1-(1-\alpha)^{1/3})$ versus the log(t), only two straight lines were obtained. These lines correspond to the periods of acceleration-deceleration and decay (dissolution and induction stages are so rapid that it is difficult to distinguish them).

The first straight line shows values of N less than 1 indicating that the reaction is autocatalytic, and the products that are being formed coat the slag grains without affecting the process of reaction. In Table 2 the values of N for the period of decay (second straight line) are shown, theses values are obtained for values of $\alpha \geq 0.5$.

Table 2 Values of N for Eq 1 (for $\alpha \geq 0.5$).

Na_2O (% weight)	Temperature (°C)			
	25	35	45	60
3	1.40	1.82	1.80	1.90
4	1.80	1.96	2.10	2.70
5	1.90	1.69	1.95	2.40

This process is phase boundary controlled when N=1. For N=2 it is controlled by pure diffusion, but for N>2 it is controlled by diffusion but the products formed around the slag grains are more dense and the diffusion rate decrease.

From the results of Table 2 it can be deduced that when the temperature of reaction increases the values of N increases too. Except for the samples with 3% Na_2O at 25°C at the time of test, N values are close to 2. It means that the process is controlled by diffusion.

b) Sharp method (1966). In this method the equations are expressed in the form $F(\alpha) = A(t/t_{0.5})$, where $t_{0.5}$ is the time for 50% reaction and A is a calculable constant depending on the form of F(x). With this methodology our values are fitted to the following equations:

The equation of Jander:

$$D_3 = (1-(1-\alpha)^{1/3})^2 = (k/r^2)t = 0.0426(t/t_{0.5}) \qquad [2]$$

This equation indicates that reaction is controlled by three-dimensional diffusion, in a sphere.

The equation of Ginstling-Brounshtein

$$D_4 = (1-2\alpha/3) - (1-\alpha)^{2/3} = (k/r^2)t = 0.0367(t/t_{0.5}) \qquad [3]$$

This equations indicates that reaction is controlled by diffusion starting on the exterior of a spherical particle of radius r, and the difference between the volume of the reaction product and that of the initial material is unity. Table 3 shows the equation followed in each activation process.

Table 3 Equations obtained according to Sharp method.

Na_2O (% in weight)	Temperature (°C)			
	25	35	45	60
3	--	D_4	D_3, D_4	D_3, D_4
4	D_4	D_3, D_4	D_3, D_4	D_3
5	D_4	D_4	D_3	D_3

These results confirm that for $\alpha \geq 0.5$ the alkaline activation of slags follows a diffusion kinetic (D_3 and D_4). But the kinetic equations vary depending on the temperature and the concentration of activator. The equation of Ginstling-Brounshtein (D_4) explain better the process at low temperature and concentration of activator. The equation of Jander (D_3) is more correct for high temperature and concentration of activator. In the same samples it was not possible to establish one of the equations.

The kinetic process depends mainly on the nature and the thickness of the hydration product around the slag grain. The temperature of reaction and activator concentration modify the nature and thickness of the diffusion barrier and this explain the change observed from D_4 to D_3.

CONCLUSION

The two methods applied are concordant. For values of $\alpha \geq 0.5$, kinetic equations controlling the alkaline activation slag are those of the diffusion (D_3 and D_4). When the temperature and concentration of activator increase the value of N increases too, and the kinetic equations change from D_4 to D_3.

ACKNOWLEDGMENTS

The authors of the present work wish to thank to DGICYT for funding this research through Program PB94-0048 which was necessary to the realization of the present study.

REFERENCES

Glukhovsky, V.D., Rostovskaja, G.S., Rumyna, G.V., "High Strength Slag-Alkaline cements", 7th. Intern. Congr. Chem. Cem. (Paris). Vol 3, 1980, pp. 164-168.

Krivenko, P.V., "Alkaline Cements", 9th. Intern. Congr. Chem. Cem. (New Delhi), Vol 4, 1992, pp. 482-488.

Kutti, T., "Hydration Products of Alkali Activated Slag", 9th. Intern. Congr. Chem. Cem. (New Delhi), Vol 4, 1992, pp. 468-474.

Mori, H., Minegishi, K., "Effect of the Temperature on the Early Hydration of the System $3CaO{\cdot}Al_2O_3$-$CaSO_4{\cdot}2H_2O$-$CA(OH)_2$-H_2O", 5th. Intern. Symp. Chem. Cem. (Tokyo). Vol II, 1968, pp. 349-361.

Sharp, J.H., Brindley, G.W., Narahari A.B.N., "Numerical Date for under me Commonly Used Solid State Reaction Equations", Journal of the American Ceramic Society. Vol 49, N° 7, 1966, pp. 379-382.

Shutter, G., Taerwe, L., "General Hydration Model for Portland Cement and Blast Furnace Slag Cement", Cem. Concr. Res. Vol 25, N° 3, 1995, pp. 593-604.

Wang, S.D., Scrivener, K.L., "Hydration products of Alkali Activated Slag Cement", Cem. Concr. Res. Vol 25, N° 3, 1995, pp. 561-571.

Zhou Huanhai, Xuequan, W., Zhongzi, X., Mingshu, T., "Kinetic Study on Hydration of Alkal-Activated Slag", Cem. Concr. Res. Vol 23, 1993, pp. 1253-1258.

3ii09
8 pp

EARLY HYDRATION AND MICROSTRUCTURE DEVELOPMENT OF ALKALI-ACTIVATED SLAG CEMENT PASTES

Caijun **SHI,** Water Technology International Corporation, Burlington, Ontario, Canada

ABSTRACT The early hydration and microstructure development of NaOH-, Na_2CO_3- and Na_2SiO_3-activated slag pastes were examined using calorimetry, scanning electron microscopy and X-ray diffractromery. The nature of activators played a crucial role during the hydration and microstructure development of alkali-activated slag pastes. C-S-H was the main hydration product regardless of activators, while minor phases varied with activators - C_4AH_{13} and C_2ASH_8 appeared in NaOH-, $C_3A.CaCO_3.12H_2O$ in Na_2CO_3- and C_4AH_{13} in Na_2SiO_3-activated slag pastes.

Key-words: Activation, Blastfurnace slag, Hydration, Microstructure

INTRODUCTION

Numerous studies have reported properties of alkali-activated slag cement and concrete [Gluhovsky, 1980; Shi et al 1992, Talling and Brandstetr, 1989]. Since the characteristics of slag vary from source to source, slags from different sources may be sensitive to different activators. Shi and Day [1996] have explained the selectivity of activators for the activation of slags from the aspect of hydration chemistry. However, very limited amount of work has been done on the hydration and microstructure development of alkali-activated slag pastes [Shi and Day, 1995, 1996; Wang and Scrivener, 1995]. An understanding of hydration characteristics and microstructure development will be beneficial to the explanation of the property development of hardened cement pastes and concrete, and to facilitate practical applications. The purpose of this work is to examine early hydration and microstructure development of NaOH-, Na_2CO_3- and Na_2SiO_3-activated slag.

EXPERIMENTATION

Raw Materials

A ground pelletized Canadian blast furnace slag was investigated. The characteristics of the slag have been reported previously [Shi & Day, 1995]. Chemical reagents NaOH, Na_2CO_3 and $Na_2SiO_3.9H_2O$ were used as alkaline activators. These activators were dissolved in mixing water first and then added at the dosage of 4% Na_2O by the mass of slag.

Measurement of Heat of Hydration

The heat of hydration of alkali-activated slag was measured at a constant temperature of 25±1°C using a Seebeck Isothermal Conduction Calorimeter. The sample container with 14 g of the slag sample and a syringe with the activator solution were heated to the testing temperature prior to mixing. A water-to-slag ratio of 0.45 was used. When thermal equilibrium was achieved, the slag and the activator solution were mixed by injecting the solution into the slag. The heat evolution was recorded by a computer as a voltage and then converted to kJ/kg.h through a calibration test. The calibration base line was established by recording the heat evolution of a mixture of water and ground quartz with the same water-to-solid ratio.

Scanning Electron Microscope (SEM) Observation

Pastes with the same mixing proportions as for calorimetry test were cast to SEM sample stubs directly and cured in a CO_2-free moisture desiccator. The samples were freeze-dried before SEM observations.

At testing ages, one sample from each batch was taken from the desiccator to cut the exposed surface, then, together with the sample stubs, placed in a bath of liquid nitrogen. After 3-5 minutes in the bath, these specimens were vacuumed for 24 hours to remove all free water. A Cambridge stereoscan 150 Scanning Electron Microscope was used to observe the morphology of raw materials and the microstructure of pastes.

X-Ray Diffraction (XRD) Analysis

For XRD examination, the pastes were cast into small plastic bottles and then cured in a CO_2-free moisture desiccator. At testing ages, one specimen from each batch was taken out from the desiccator and was ground in 2-propanol to arrest the further hydration. A Philips PW 1139 Diffractometer was used to perform the tests at a scanning rate of 2.10°/minute from 5 to 75° (2θ).

EXPERIMENTAL RESULTS

Heat of Hydration

It is well known that the hydration of portland cement can be classified into five periods based on the heat evolution curves: (I) initial (pre-induction) period; (II) induction period; (III) acceleration (post-induction) period; (IV) deceleration period; and (V) diffusion period. Heat evolution curves of alkali-activated slag in Fig.1 indicated that the classification was also suitable for the description of the hydration of alkali-activated slag.

Alkali-activated slag showed much lower initial heat evolution peaks than portland cement. The heat evolution features of alkali-activated slag varied with activators. NaOH-activated slag showed the lowest initial heat evolution peak, a negligible induction period and the highest accelerated hydration peak. Na_2CO_3-activated slag exhibited two obvious heat evolution peaks before the appearance of a induction period of 5 hours. Na_2SiO_3-activated slag also showed two heat evolution peaks before the very lengthy induction period, which lasted approximately 17 hours. However, the first peak was not so evident to be observed. Both Na_2CO_3- and Na_2SiO_3-activated slag pastes showed lower accelerated hydration peaks that the portland cement.

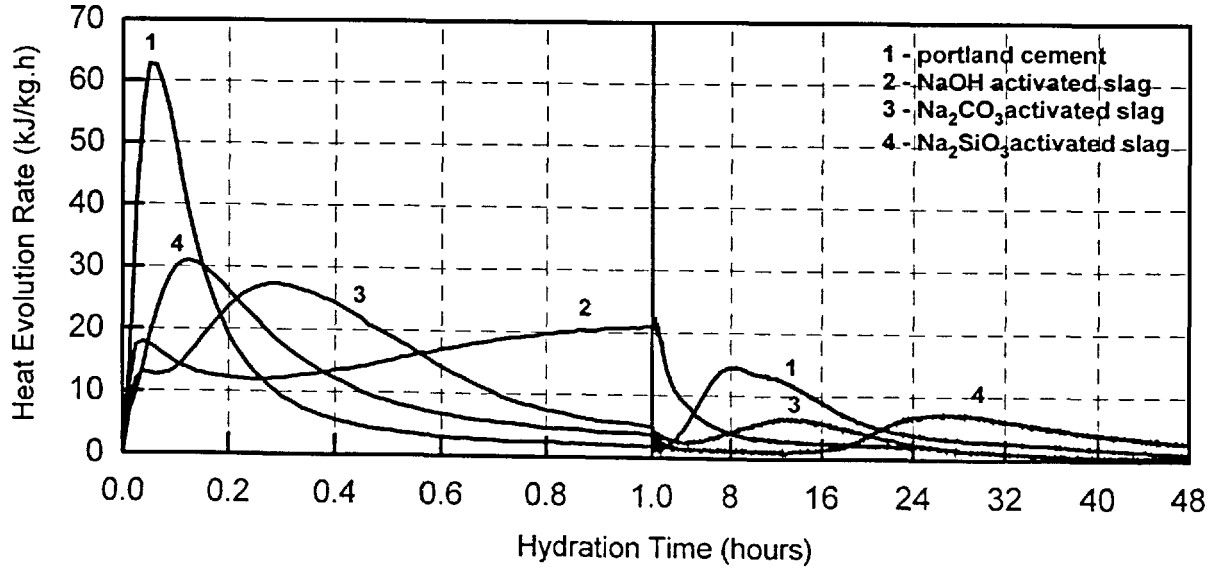

Figure 1 Heat Evolution Rates of Portland and Alkali-Activated Slag Cements

Microstructure Development

Fig.2 shows microstructure development of NaOH-activated slag pastes from 20 minutes to 3 days. At 20 minutes, it appeared that the surface of all slags particles were etched and coagulated products precipitated at some locations, as shown in Fig. 2-a. As time proceeded to 2 hours, most voids between slag particles were filled by coagulated products. Hexagonal plates, which were embedded in the coagulated products, appeared (Fig.2-b). However, the configuration of slag particles could still be identified. At 1 day, an uniform hardened structure was observed on fracture surface. At this time, although structure looked loose (Fig.2-c), it was impossible to identify the configuration of slag particles. Features of hydration products could only be notified in air voids. At 3 days, fracture surface of the activated slag paste appeared to be similar to but denser than that at 1 day. Features of hydration products in air voids are shown in Fig.2-d. In addition to coagulated particles, some hexagonal plates were also observed.

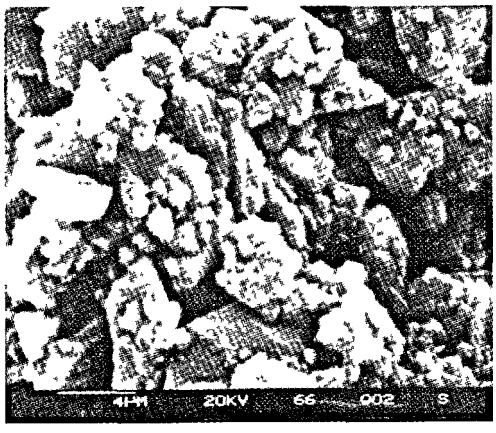

(a) at 20 minutes

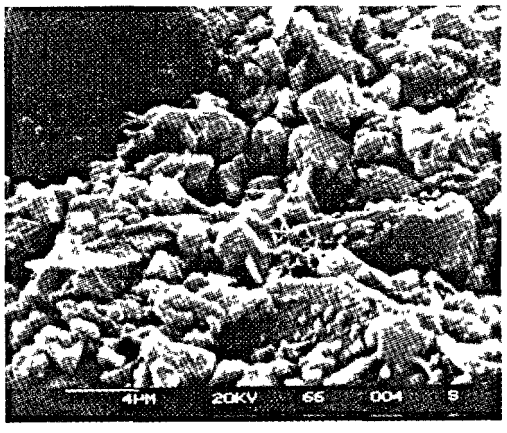

(b) at 2 hours

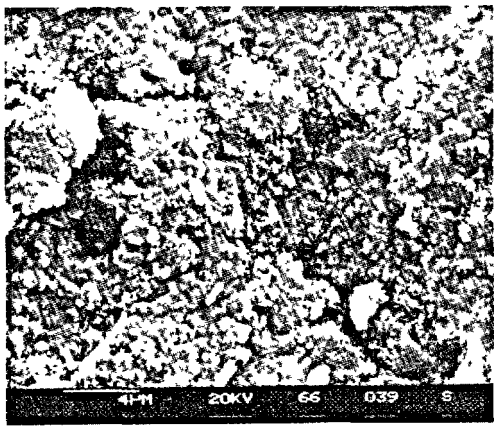

(c) at 1 day

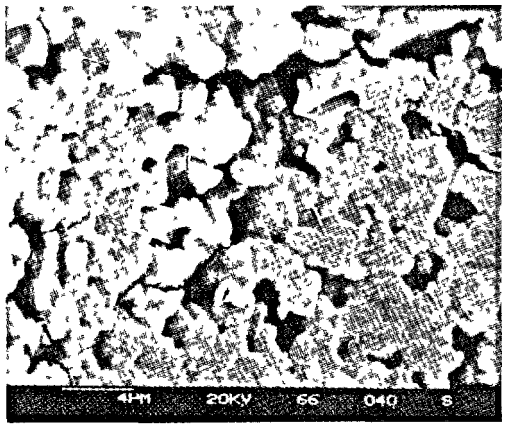

(d) at 3 days

Figure 2 Microstructure Development of NaOH-Activated Slag Pastes

Microstructure development of Na_2CO_3-activated slag pastes is shown in Fig.3. At 20 minutes, most slag particles were intact except for precipitated gel-like products on some slag particles (Fig.3-a). At 2 hours, all slag particles were etched and more gel-like products filled voids between slag particles (Fig.3-b). As time proceeded to 1 day, a foil-like product was observed, which had really different morphology from that either at early ages or in NaOH-activated slag. The foil-like product most spaces between slag particles (Fig.3-c). The configuration of slag particles was only identified at occasional locations. At 3 days, the fracture surface of hardened pastes showed a dense structure and the morphology of products could only be identified in voids (Fig.3-d). No well crystallized products were observed up to 3 days.

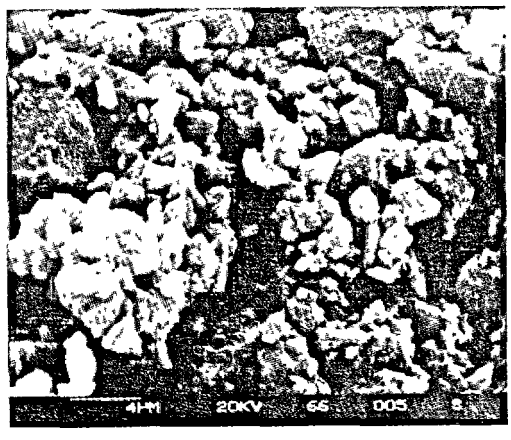

(a) at 20 minutes

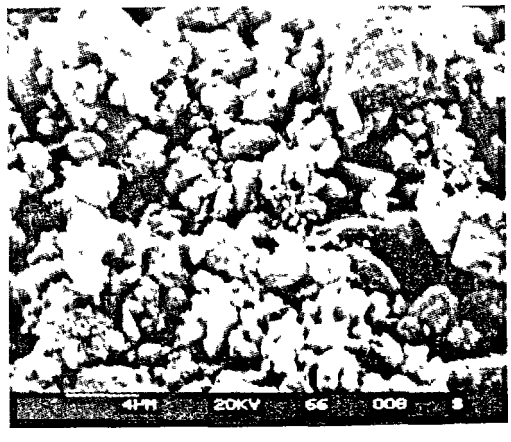

(b) at 2 hours



(c) at 1 day

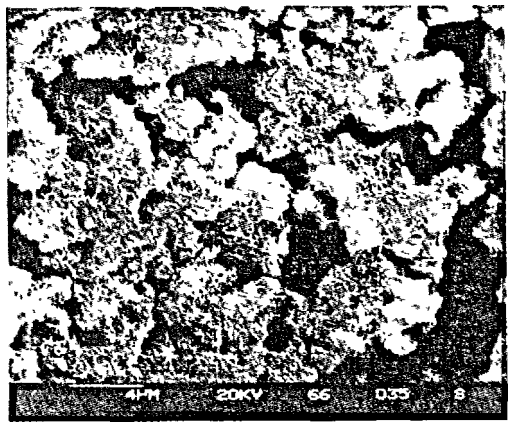

(d) at 3 days

Figure 3 Microstructure Development of Na_2CO_3-Activated Slag Pastes

Fig.4 shows the microstructure development of Na_2SiO_3-activated slag pastes. During the first two hours, the microstructure characteristics of Na_2SiO_3-activated slag pastes (Fig.4-a and 4-b) were very similar to those of Na_2CO_3-activated slag pastes. However, at 1 day, most slag particles were covered by a layer of coagulated products but still separated. The morphology of C-S-H was very similar to that observed at 2 hours. The SEM picture is not presented here due to the poor quality picture. At 3 days, the fracture surface appeared to be denser that that of Na_2CO_3-activated slag pastes.

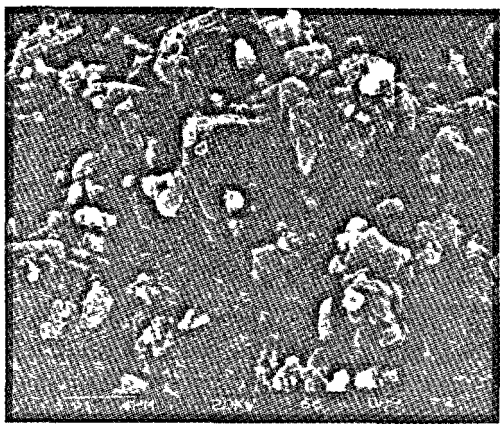

(a) at 20 minutes

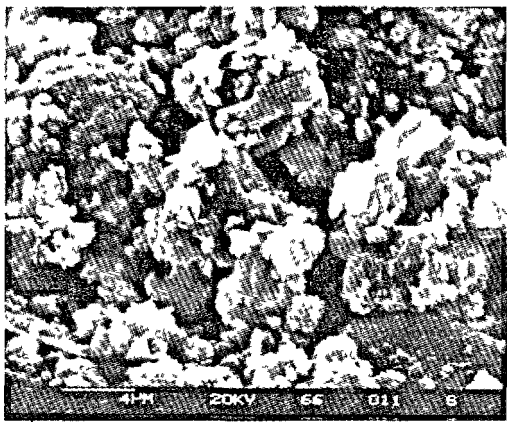

(b) at 2 hours

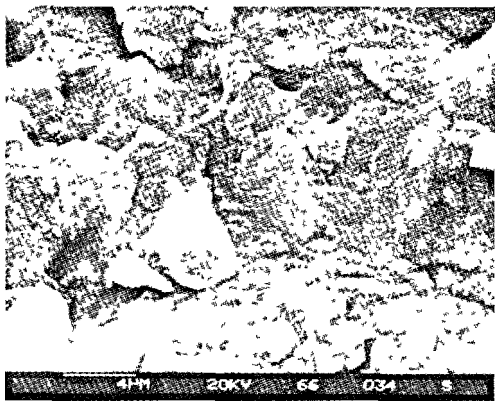

(c) at 3 days

Figure 4 Microstructure Development of Na_2SiO_3-Activated Slag Pastes

Hydration Products

Hydration products of alkali-activated slag pastes were analyzed by XRD since 20 minutes of hydration. The XRD patterns of alkali-activated slag pastes at 1 day are shown in Fig.5. Combining with the SEM observations, it could be concluded that the main hydration product of all three alkali-slag cement pastes was C-S-H gel, but minor products varied with type of activator: C_4AH_{13} and C_2ASH_8 in NaOH-activated, $C_3A.CaCO_3.12H_2O$ in Na_2CO_3-activated and C_4AH_{13} in Na_2SiO_3-activated slag pastes.

DISCUSSIONS

(a) in NaOH Solution

NaOH solution has a high concentration of OH^-, the Ca-O, Si-O and Al-O bonds on the surface of the glassy slag break under the polarization effect of OH^- [Teoreanu, 1991]. These dissolved species exist in water in the form of Ca^{2+}, $[H_2SiO_4]^{2-}$, $[H_3SiO_4]^-$ and $[H_4AlO_4]^-$. Since the Ca-O bond is much weaker than Si-O and Al-O bonds, the concentration of Ca^{2+} in the solution is much higher than $[H_2SiO_4]^{2-}$, $[H_3SiO_4]^-$ and $[H_4AlO_4]^-$, and a Si-Al-rich layer forms quickly on the

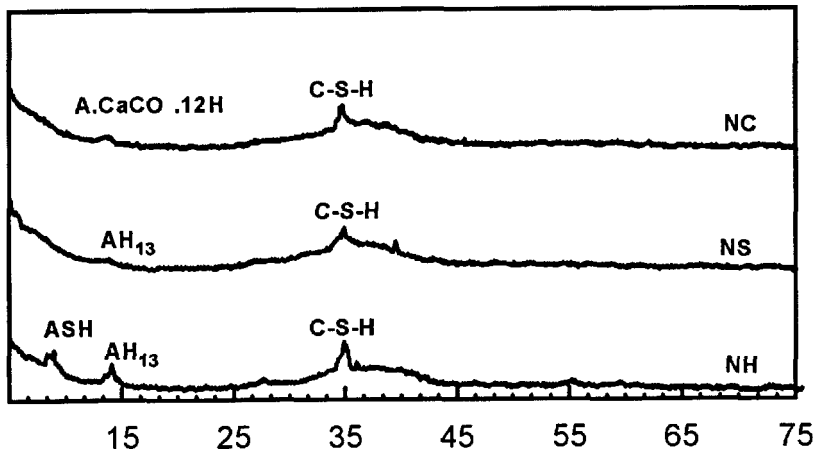

Figure 5 XRD Patterns of Alkali-slag Cement Pastes Hydrated For One Day at 23°C

Table 2 pH of Activator Solutions and Solubility Product of Relevant Ca-Compounds

Activator Solution	Measured pH	Ca-Compound	Solubility Product	Reference
NaOH	13.87	$Ca(OH)_2$	$5.5x10^{-6}$	[Yin, 1985]
Na_2CO_3	12.17	$CaCO_3$	$2.8x10^{-10}$	[Yin, 1985]
Na_3SiO_3	12.89	C-S-H*	$1.0x10^{-24\ to\ -14}$	[Glasser et al, 1987]

* the lower the C/S ratio of C-S-H, the higher the solubility product is.

surface of slag [Rajaokarivony-Andriambolona et al, 1990]. Table 2 lists these Ca-compounds associated with the anions or anion groups of alkaline activators investigated. Since $Ca(OH)_2$ has a much higher solubility than C-S-H, C-A-H and C-A-S-H, $Ca(OH)_2$ cannot precipitate from the solution. While C-S-H, C_4AH_{13} and C_2ASH_8 precipitates through the solution onto the surface of slag particles when concentration of Ca^{2+}, $[SiO_4]^{4-}$ and $[Al(OH)_4)]^-$ reach certain critical values. Thus, the initial peak was attributed to the wetting and dissolution of slag grains, adsorption of some ions onto the surface of slag grains and the formation of these products. 20 minutes of hydration correspond to the induction period on the heat evolution peak. At that time, all slag particles were etched, the gel-like product belong to C-S-H and some other products. Hexagonal hydration products can not be identified under SEM since they grow first as poorly crystallized compounds [Jawed et al, 1983].

The high concentration of OH^- enables OH^- to penetrate the precipitated layer of hydration products and to initiate the accelerated hydration of slag quickly. Thus, NaOH-activated slag does not show a noticeable induction period on the heat evolution curve. At time proceeds to 2 hours, it corresponds to the top of the accelerated hydration peak. Well crystallized hexagonal plates can be observed and C-S-H gel interlocks each other. Slag continues hydration and C-S-H fills most voids at 1 day.

(b) in Na_2CO_3 Solution

Two peaks are well identified during the initial hydration period on the heat evolution curve of Na_2CO_3-activated slag. Since the pH of Na_2CO_3 solution is significantly lower than that of NaOH solution (Table 2), the first peak corresponds to the wetting and dissolution of slag grains and adsorption of some ions onto the surface of slag grains, as stated above. Ca-O bonds at some active

centres on the surface of the glassy slag break first under the polarization effect of OH^-. The high concentration of $[CO_3]^{2-}$ in the solution results in the formation of poorly crystallized $CaCO_3$, which causes the second heat evolution (Fig.1). 20 minutes corresponds to the top of the second peak. the surface of most slag particles is intact at that time, and very limited amount of gel-like product, which is most likely $CaCO_3$, precipitates on the surface of slag particles (Fig.3-a).

The precipitation of $CaCO_3$ and low pH of the solution result in a lengthy induction period. After 2 hours of hydration, which corresponds to the middle of the induction period, the surface of most slag particles is etched and more gel-like product precipitates (3-b). Some gel-like product may belong to C-S-H in addition to $CaCO_3$ As OH^- continues attacking the surface of the slag particles, an accelerated hydration happen and more hydration products form. At one day, foil-like C-S-H fills most void space between slag particles and no other product can be observed (Fig.3-c). The difference in the morphology of C-S-H between NaOH- and Na_2CO_3-activated slag may be attributed to the difference in the pH of pore solution. While XRD analysis indicates the presence of $C_3A.CaCO_3.12H_2O$, instead of C_4AH_{13} and C_2ASH_8. $C_3A.CaCO_3.12H_2O$ can not be observed probably due to its limited amount.

(c) in Na_2SiO_3 Solution

Na_2SiO_3-activated slag exhibits two heat evolution peaks during the initial hydration period as Na_2CO_3-activated slag. However, the first peak of Na_2SiO_3-activated slag appears smaller and earlier than that of Na_2CO_3-activated slag. The first tiny peak corresponds to the wetting and dissolution of slag grains and adsorption of some ions onto the surface of slag grains, and the second peak to the formation of primary C-S-H [Shi and Li, 1989]. The difference in the heat evolution features between Na_2SiO_3-activated and Na_2CO_3-activated slag may be explained by the higher pH of Na_2SiO_3 solution than that of Na_2CO_3, and lower solubility of C-S-H than that of $CaCO_3$. By comparing the microstructure of between Na_2SiO_3-activated and Na_2CO_3-activated slag pastes at 20 minutes (Figs.3-a and 4-a)and 2 hours (Figs. 3-b and 4-b), they appear to be very similar but slight difference in the morphology of hydration product. While C-S-H and $CaCO_3$ exist in Na_2CO_3-activated slag and only C-S-H in Na_2SiO_3-activated slag pastes at these times.

The precipitation of the primary C-S-H results in a very long induction period. One day is almost on the top of the accelerated hydration peak of Na_2SiO_3-activated slag. Foil-like C-S-H fill most void spaces between slag particles at one day. C_4AH_{13} can be identified by XRD but not observed under SEM probably due to limited quantity. As time proceeds to 3 days, a very dense structure is observed.

CONCLUSIONS

1. In this study, it was found that the heat evolution peak of alkali-activated slag before the appearance of induction period was much smaller than that of portland cement. The heat evolution features of alkali-activated slag depended on the nature of activators. NaOH-activated alkali-slag cement showed the lowest initial heat evolution peak, but a negligible induction period and the highest accelerated hydration peak. Na_2CO_3-activated slag exhibited two obvious heat evolution peaks before the appearance of a induction period of 5 hours. Na_2SiO_3-activated slag also had two heat evolution peaks before the very lengthy induction period, which lasted 17 hours. However, the first peak was too small to be obviously observed.

2. The microstructure development of alkali-activated slag pastes was very consistent with the heat evolution characteristics. More hydration products were observed in NaOH-activated slag pastes and less in Na_2SiO_3-activated slag pastes. As time proceeded, more and more hydration products formed in Na_2SiO_3-activated slag pastes. Na_2SiO_3-activated slag pastes showed the densest structure at 3 days.

3. The main hydration product of the three alkali-activated slag pastes was C-S-H, but the minor products varied with activators: C_4AH_{13} and C_2ASH_8 in NaOH-activated, $C_3A.CaCO_3.12H_2O$ in Na_2CO_3-activated and C_4AH_{13} in Na_2SiO3-activated alkali-slag cements.

REFERENCES

Glasser, F. P., Lachowski, E. E. and Macphee, D. E., Compositional Model for Calcium Silicate Hydrate (C-S-H) Gels Their Solubilities, and Free Energies of Formation, Journal of American Ceramic Society, Vol.70, No.7, 1987, pp.481-485.

Gluhovsky, V. D., Rostovkaja, G. S., and Rumyna, G. V., High Strength Slag-Alkali Cement, Proceedings of 7th International Congress on the Chemistry of Cements, Vol.III, Paris, 1980, pp.V-164-168.

Rajaokarivony-Andriambololona, Z., Thomassin, J. H., Baillif, P. and Touray, J. C., Experimental Hydration of Two Synthetic Glassy Blast Furnace Slag in Water and Alkaline Solutions (NaOH and KOH 0.1 N) at 40°C: Structure, Composition and Origin of the Hydrated Layer, Journal of Materials Science, Vol.25, 1990, pp.2399-3410.

Shi, C. and Li, Y., Investigation on Some Factors Affecting the Characteristics of Alkali-Phosphorus Slag Cement, Cement and Concrete Research, Vol.19, No.4, 1989, pp.527-533.

Shi, C., Day, R. L., Wu, X. and Tang, M., Microstructure and Performances of Alkali-slag Cement Pastes, Proceedings of 9th International Congress on the Chemistry of Cements, Vol.3, New Delhi, India, November, 1992, pp.298-304.

Shi, C. and Day, R. L., Early Hydration Characteristics of Alkali-Slag Cements, Cement and Concrete Research, Vol.25, No.6, 1995, pp.1333-1346.

Shi, C. and Day, R. L., Some Factors Affecting Early Hydration of Alkali-Slag Cements, Cement and Concrete Research, Vol.26, No.3, 1996, pp.439-448.

Talling, B. and Brandstetr, J., Present and Future of Alkali-Activated Slag Concrete, Proceedings of Third International Conference on Fly Ash, Silica Fume, Slag, and Natural Pozzolans in Concrete, American Concrete Institute, 1989, pp.1519-1546.

Teoreanu, I., The Interaction Mechanism of Blast-Furnace Slags With Water: The Role of Activating Agents, IL Cemento, Vol.8, No.2, pp.91-97, 1991.

Wang, S.D. and Scrivener, K. L., Hydration Products of Alkali-Activated Slag Cement, Cement and Concrete Research, Vol.25, No.3, 1995, pp561-571.

Yin, Y., University Chemistry Handbook, Shandong Science and Technology Press, Shandong, 1985.

ALKALI ACTIVATION REACTION MECHANISM AND ITS INFLUENCES ON MICROSTRUCTURE OF SLAG CEMENT

Weimin JIANG, Michael R. SILSBEE and Della M. ROY, Materials Research Laboratory, The Pennsylvania State University, University Park, PA 16802, USA.

ABSTRACT This research constitutes a fundamental investigation of the reaction mechanisms in alkali activated granulated blast-furnace slag, and their influences on microstructure of slag cement. The microstructure of these materials was analyzed by SEM and ESEM. Also ^{29}Si MAS-NMR was performed to characterize the amorphous phase in these systems. A set of ordinary portland cement paste samples served as a control. Results of XRD, TGA, calorimeter, pore solution and Vicat penetration profiles were also reported.

Keywords: activation, alkali, hydration, mechanism, slag.

INTRODUCTION

This study is a part of research which deals with the microstructure and properties of alkali activated cementitious materials (AAC), the reaction mechanisms of which are still not properly understood, and remain one of the most difficult topics in the study of AAC. This is due to a number of theoretical and experimental problems encountered in the correct assessment of activation courses. Nevertheless it is understood that with the compositions studied the activation phenomenon is due to the attack of OH^- ions on the SiO_2 or Al_2O_3-SiO_2 bonds resulting in increased hydration rates. The primary focus of this study is on activation mechanisms, not only because knowledge of the mechanisms is essential to understanding activation processes but also because theories about activation mechanisms can explain diverse chemical phenomena in terms of a relatively small number of general principles.

This study also tried to emphasize the experimental evidence upon which mechanistic ideas are built and to point out areas of uncertainty and controversy where more work still needs to be done. The microstructural observations and properties test results presented in recent literature try to rationalize the factors which govern the course of alkali activation (Richardson *et al.*, 1993; Wang *et al.*, 1994; Wu *et al.*, 1990; Hong *et al.*, 1993; Shi and Day, 1995 and 1996; Roy and Silsbee, 1994, Krivenko, 1994; and Roy 1995). It is suggested by some researchers that R^+ (alkali) ions play a catalytic role in the early stages of hydration in a process involving interchange with Ca^{2+} cations, then in the later stage they are combined into the structure to form zeolite-like phases. Others believe that the alkaline cations may only have an effect of balancing and maintaining OH^- anions. Some controversy has been evoked over the identification of hydration products. Roy *et al.* (1992) reported their result, suggesting the reaction products were mainly varieties of C-S-H, $(C, M)_4AH_{13}$, and minor amounts of $Ca(OH)_2$ and C_2ASH_8 (strätlingite). Wang and Scrivener (1994) suggested that no zeolitic hydrates or other crystalline phase containing alkali cations or mica groups such as nepheline, natrolite, analcite, paragonite or gismondite could be identified in the pastes of slag activated with NaOH. Also there appears to be no convincing evidence for existence of a true solid solution $(M,C)_4AH_{14}$.

EXPERIMENTAL

The starting materials are granulated blast-furnace slag, and alkali activator expressed as R_2O. Some recent experiments reported were focused on pure slag activated with 4 or 5M NaOH (or KOH) at w/c = 0.4 (Richardson *et al.*, 1993; Wang *et al.*, 1994; and Wang and Scrivener, 1994). Ordinary Portland cement (OPC) was used as control. The chemical compositions of the OPC, and slag used in the current study have been reported in an earlier paper (Roy and Jiang, 1994). Formulations selected in this work are shown in Table 1. Two series (paste and mortar) were made. The specimens were cured under 98% relative humidity at 25°C. Hardened AAC paste hydration products from one hour to 16 months old were examined by means of x-ray diffraction (XRD). The morphologies of hydrates were observed by ESEM.

Table 1 Mixture proportions (by weight)

Paste	Mortar
Slag 100% + 5M NaOH or KOH solution at w/c= 0.4 casting in ø31.75 mm x 38.10 mm cylinders Control OPC (type I cement) + deionized water at w/c = 0.4	Slag:Sand (C 109 ASTM) : 1.0:2.25 (1) adding 5M NaOH or KOH solution w/c = 0.46 (2) adding sodium silicate solution (16.31 wt % SiO_2; 10.87 wt% Na_2O; 72.82% H_2O) at w/c = 0.46 casting 2 in. cubes or ASTM C490 prisms

Test Methods

NMR—^{29}Si NMR Spectra were recorded using a JEOL FX-90 instrument with a multinuclear probe covering the range 2.8-36.2 MHz.

DTA—Differential thermal analysis of materials was performed on a Perkin Elmer System 7/4 with a DTA 1700 unit. In all cases the heating rate was either 10 or 20°C/min and Pt/Pt 10 Rh thermocouples were used.

Isothermal conduction calorimeter—A thermostatically controlled Haake F3 water circulator with heating and cooling equipment was used in conjunction with a Thermonetics Corporation calorimeter. In each case 3 g of powder was placed in metal container, then 1.5 g of water was added. Setting time—was measure by Vicat needle (ASTM C191).

Pore solution—Samples of the aqueous phase in contact with alkali activated cement pastes were obtained by expression of the pore solution from hardened cement pastes under high pressures of 500 MPa at ages ranging from 15 minutes to 90 days.

Shrinkage—the length changes of the prisms were recorded as function of time. The preparation of mortar bar is in accordance with the requirements of ASTM C 490 (25/25/300mm). The stainless steel gage stud was used in each end. After mold has been filled, place the mold immediately in the moist cabinet. The specimens remain in the molds for 24 hours. Then the prisms are removed from the molds and measured for initial length. Following measurements are made at later ages as required, while specimens are stored in the air at temp. 30°C rh: 70%.

XRD—were performed on a Scintag Automated x-ray diffractometer (CuKα radiation, λ=1.540598Å) interfaced with a microVAX computer.

RESULT AND DISCUSSION

Hydration products

Fig. 1 is the XRD spectrum of a pure slag paste mixed with 5M NaOH after 2 days of curing. The main phases are C-S-H (JCPDS file No. 33-306), calcium carbonate (JCPDS file No. 5-586) and hydrotalcite. Although the intensity of those peaks increased with increasing cure time, the main peaks were formed after 2 days. These results suggest that the low-basic calcium silicate hydrate related to tobermorite is the major silicate hydration products of AAC. The hydrotalcite-type phase found is similar to formula $Mg_6Al_2CO_3(OH)_{16}{\cdot}4H_2O$ (JCPDS file No. 41-1428).

NMR—Schilling, *et al.* (1994) used the ^{29}Si NMR on NaOH-activated blast-furnace slag in order to better characterize the amorphous and poorly crystalline phases which occur in this system. The unreacted glass has a mainly dimeric silicate structure represented by a broad ^{29}Si

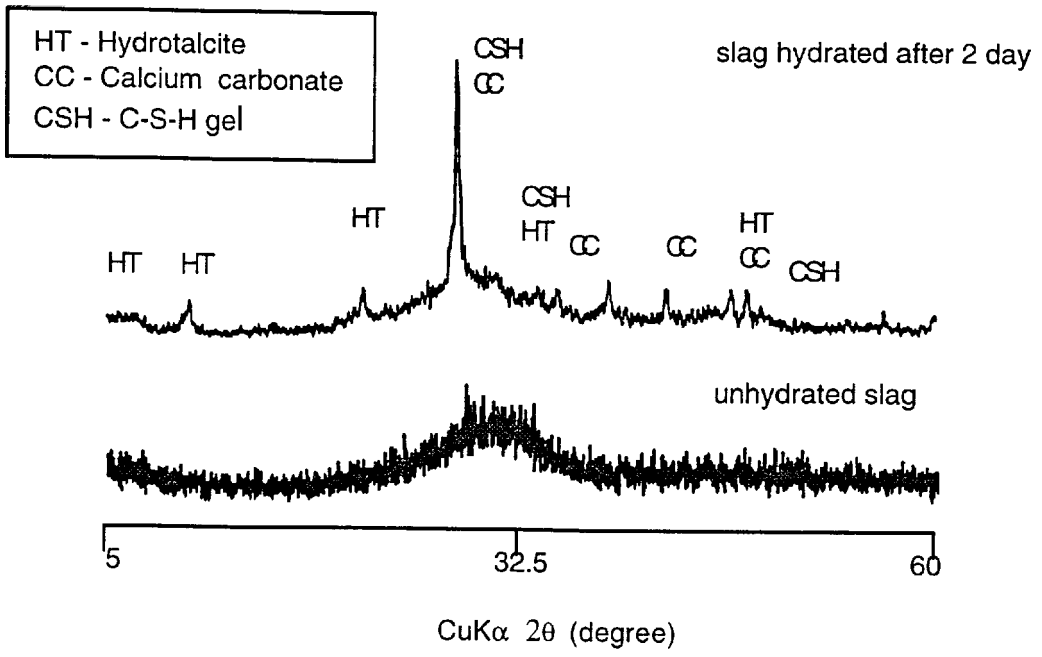

Figure 1 XRD patterns of slag pastes activated with 5M NaOH solution at w/c = 0.4 after 2 days hydration

peak centered at -74.5 ppm [Q^1], with aluminum present exclusively in tetrahedral coordination. ^{29}Si results indicate rapid initial consumption of glass, with roughly a third of the glass reacting within the first day and another third consumed over the following 27 days. Pietersen, *et al.* (1994) observed blended cement with 70% slag has a chemical shift to -73 ppm. Richardson *et al.* (1993) combined the solid-state ^{29}Si and ^{27}Al magic angle spinning NMR spectroscopy with electron energy loss spectroscopy (EELS) carried out in the transmission electron microscope to determine the location of Al substituting in a semicrystalline C-S-H gel present in a hydrated synthetic slag glass. Our ^{29}Si MAS NMR results (Fig. 2) show that unhydrated slag has peaks at -73.0 and -75.2 ppm. The hydrated KOH activated cement yields a peak near -78.3 ppm. After hydration, a shift is seen to a more shielded (more negative) position and the peak is much narrower, indicating a greater degree of short-range order. Two general observations can be immediately made from these ^{29}Si patterns. First, that the degree of structural modification around the Si nuclei during hydration is not great, as reflected by the minor shift in peak position. Second, extensive reaction is observed, with the broad glass peak greatly reduced in the pattern of the reacted materials. The result is similar to that reported by Schilling et al. (1994).

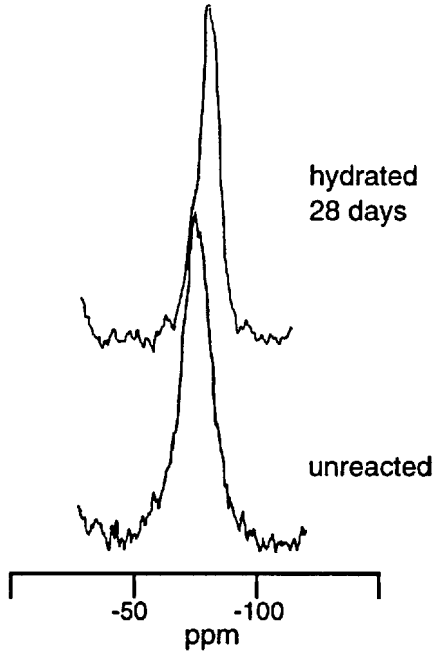

Figure 2 ^{29}Si MAS NMR spectra of slag with 5M KOH at w/c=0.4.

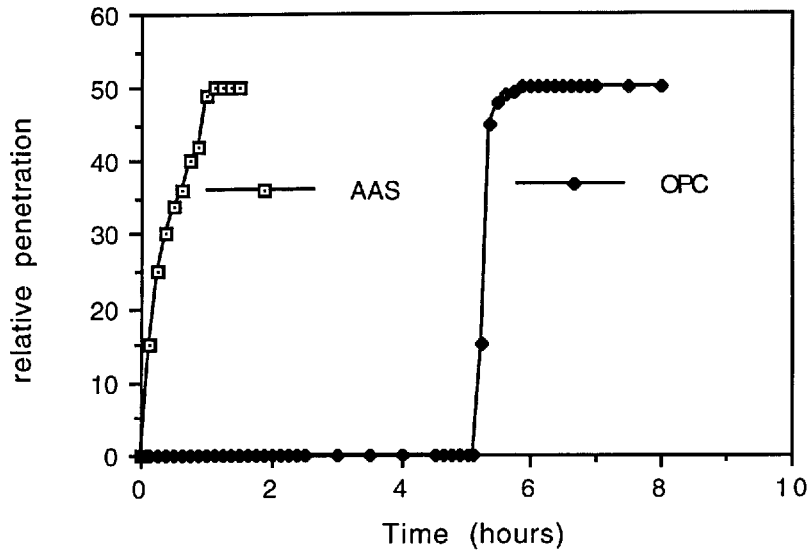

Figure 3 The Vicat penetration profiles for slag with 5M NaOH at w/c=0.4 compared with OPC at 25°C.

Setting time and DTA

The Vicat penetration profiles for AAC with different dosages of NaOH at 25°C shown in Fig. 3. The setting time for AAS is faster than OPC. Cheng and Sarkar (1994) also reported similar observations. The fast setting reaction may be described by dissolution and precipitation mechanisms during the early stages of reaction.

Fig. 4 shows a typical the DTA curve for slag paste activated with NaOH. In the pattern the endothermic peak at 130-150 °C is due to C-S-H(I), and the shoulder at 200-220 °C, superimposed on the right side of the main peak, indicates the presence of an AFm-type phase. The presence of the peak at 460-480 °C can be attributed to the hydrotalcite-type phase, corresponding to release structural water and CO_2.

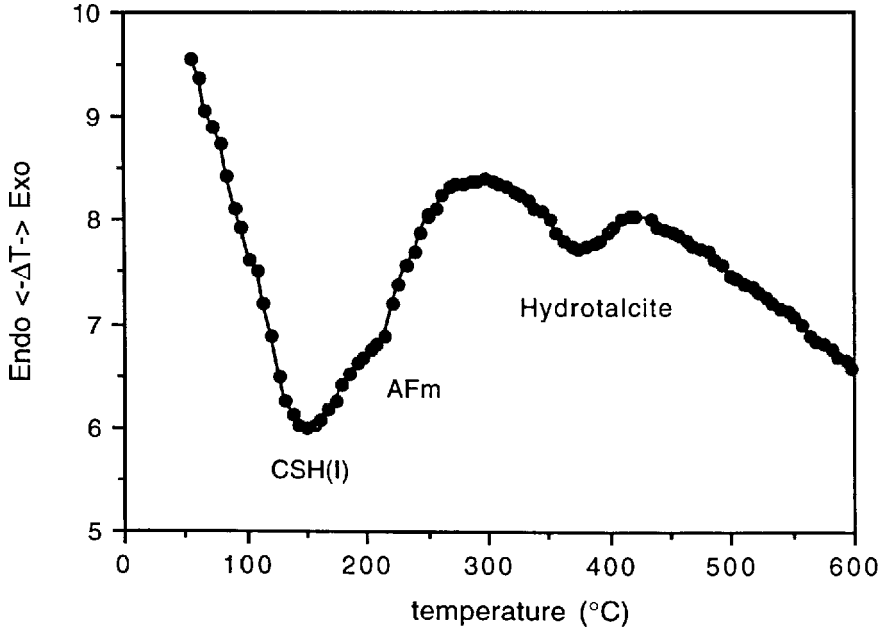

Figure 4 DTA pattern of slag activated 5M NaOH

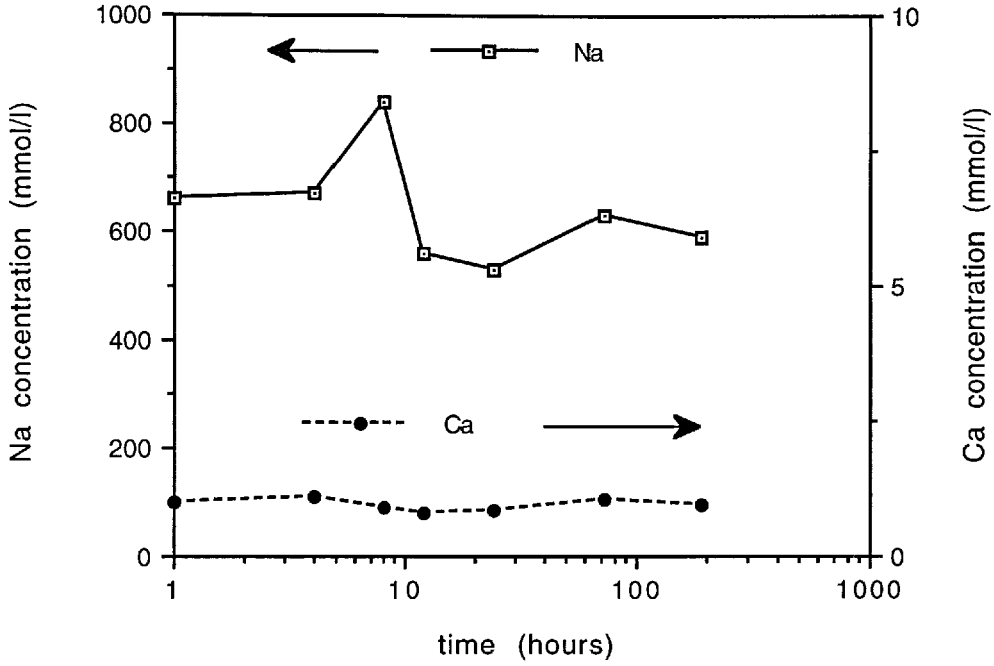

Figure 5 Pore solution composition of slag under activation by 2.5M NaOH at w/c = 0.4

Pore solution and hydration heat

Fig. 5 shows the pore solution compositionof slag under activation by 2.5M NaOH at w/c = 0.4. Condon (1992) showed that content of Na^+ in the pore solution of NaOH activated slag decreased by about 10% in 7 days. The content of Ca^{2+} was keeping unchange. Fig. 6 shows calorimetric curves of heat evolution as function of time for 5M KOH activated slag at w/c = 0.4 compared with OPC during first 24 hours of hydration. The increased reaction rates observed at early time is consistent with the increased rate of setting shown in Fig. 3.

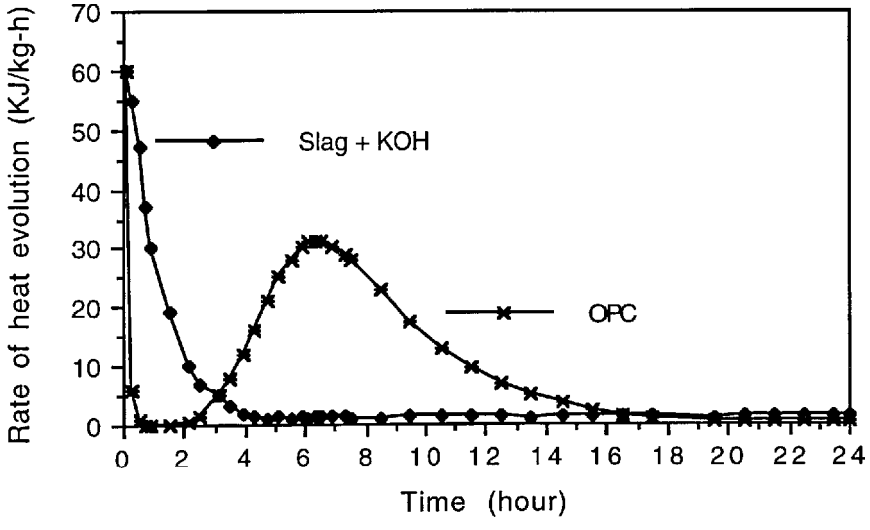

Figure 6 Calorimetric curves showing the heat evolution as function of time for 5M KOH activated slag at w/c = 0.4 compared with OPC during first 24 hours of hydration.

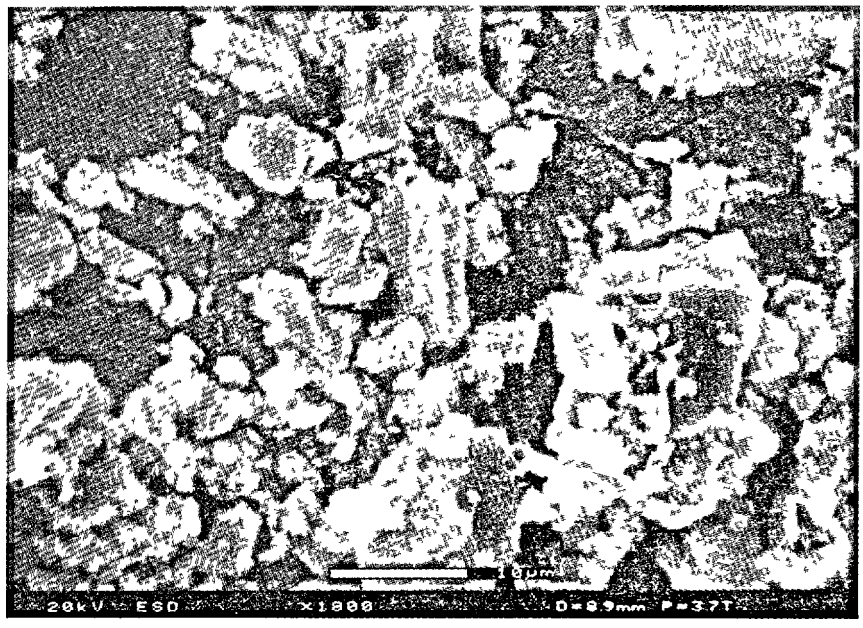

Figure 7 ESEM of 1g slag + 200 mL water after 24 hours.

ESEM

From direct observation of unconstrained samples under controlled humidity conditions, Fig. 7 shows that the slag particles remain relatively unhydrated 24 hour after adding deionized water. Fig. 8 in contrast shows that 1g slag added to 200 ml 5M NaOH solution after 24 hours, with gel-like reaction products.

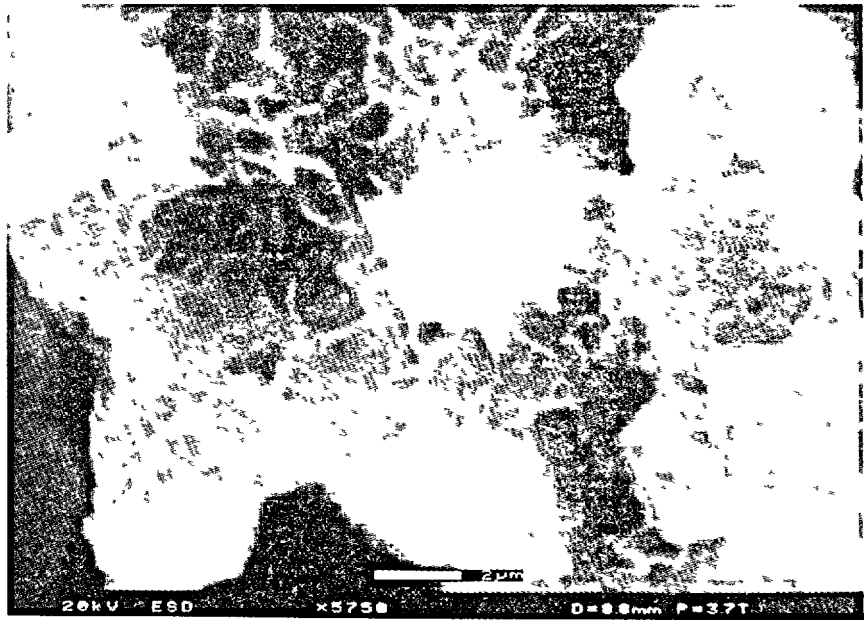

Figure 8 ESEM of 1g slag + 200 ml 5M NaOH solution after 24 hours.

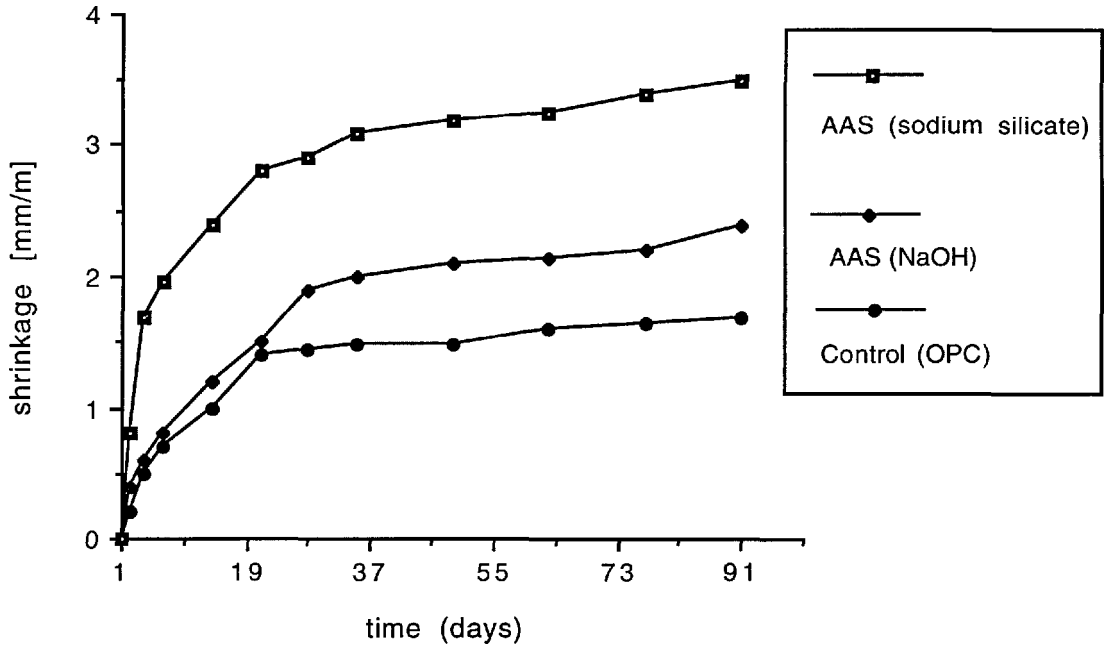

Figure 9 Shrinkage of slag mortar exposed in the air (rh: 70%, temp.: 30°C) at one day as reference state.

Shrinkage

Shrinkage is common measure of rate of a cementitious reaction. It also is used to investigate the stability of mature cement hydration products. The shrinkage of AAS mortars at rh 70% are shown in Fig. 9 in comparison with the control OPC. The shrinkage of slag paste and mortar involves different mechanisms, and is controlled by a number of factors that operate in various parts of the microstructure and at various length scales. The dimensional change due to drying is heterogeneous and each size range is controlled by its own mechanism. Some previous investigation reported that when waterglass was used, the strength is high (Wang et al. 1994), but those based on waterglass solution often undergo greater drying shrinkage due to the formation of silica or silica rich gel during hydration. Silica-rich gel has high water content and may dry with water loss. Drying shrinkage may result in microcracks.

Mechanisms

Activation mechanisms — The primary reaction is an attack on the SiO_2 or Al_2O_3-SiO_2 framework by OH^- ions. It may be postulated that the alkali activation effect could be described as a chemical acceleration of a more conventional pozzolanic reaction. In cementitious composites containing pozzolans the ratio [S+A]/C is high in comparison to conventional cements. Taylor (1990) stated that "the products formed in situ from the pozzolanic material are likely to reflect its composition and the situation in which SiO_2 and Al_2O_3 are readily available compared with CaO". Since slag differs sharply from portland cement in chemistry, it is not surprising that the properties of hardened pastes containing pure slag under alkali activation condition differs from those of cement. The effect of ordinary portland cement were excluded in this research. Perhaps the most common activator used for slag hydration is portland cement. The mechanism of anion removal ensures that even salts which have near-neutral aqueous solution often are able to activate slags.

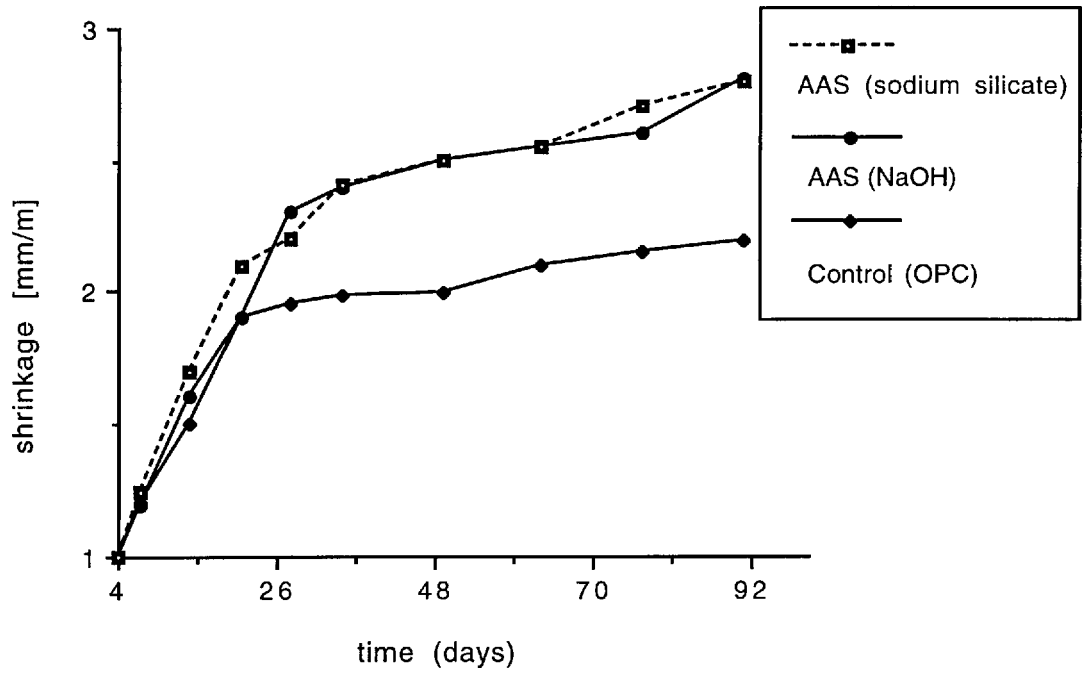

Figure 10 Shrinkage of slag mortar exposed in the air (rh: 70%, temp.: 30°C) at 4 days as reference state.

CONCLUSION

The results of this study show:

- From results of XRD and DTA, at room temperature the most possible hydrated products of alkali activated slag are CSH gel and a hydrotalcite-type phase.
- The results of NMR show that the degree of structural modification around the Si nuclei during hydration is not great, as reflected by the minor shift in peak position and also indicating a greater degree of short-range order.
- Calorimetric results show that a strong initial hydration peak appears. So it may that concluded the alkali (hydroxyl) acts strongly on slag at an early stage of hydration. The setting time is short. The fast setting reaction may be described by a dissolution and precipitation mechanisms during the early stages of reaction.
- ESEM revealed a gel-type reaction product observed after slag is reacted with NaOH for one day, showing the secondary fibrillar development of gel around the slag particles.
- Alkali activated pure slag showed larger shrinkage than those of OPC, when waterglass was used, the amount of shrinkage increased, showing increased reaction.
- The activation mechanisms proposed is that the primary reaction is an attack on the SiO_2 or Al_2O_3-SiO_2 framework by OH^- ions. However more direct experimental evidence still needs to be provided for understanding details.

Due to its rapid hardening and high ultimate strength, AAC have important applications; however, additional research is important to fully understand both "pure" and more complex alkali-activated cements

ACKNOWLEDGMENTS

This research was partly support by U.S. National Science Foundation.

REFERENCES

Brydson, R., Richardson, I.G., McComb, D.W. and Groves, G.W. (1993). "Parallel Electron Energy Loss Spectroscopy Study of Al-Substituted Calclium Silicate Hydrate (C-S-H) Phases Present in Hardened Cement Pastes". J. Solid State Commmunication, **88**, 183-187.

Cheng, Q.H. and Sarkar, S.L. (1994). "A Study of Rheological Properties of Mixed Alkali Activated Slag Pastes". Advn Cem. Bas. Mat. **1**, 178-184.

Condon, C. (1992). "Alkali Activated Cementitious Materials", Amercan Ceramic Annual meeting presentation, cement division, Cincinnati, OH., April, 1992.

Hong, S.Y., Kim, J.C., and Kim, J.K. (1993). "Studies on the Hydration of Alkali Activated Slag", in *Proceedings of 3rd Beijing International Symposium on Cement and Concrete.* (International Academic Publishers, Beijing), Vol. II, pp. 1059-1063.

Krivenko, P.V. (1994). "Alkaline Cements", in *Alkaline Cements and Concretes*, Proceedings of the First International Conference on alkaline cements and concretes. (Vipol Stock Company, Kiev, Ukraine), Vol. I, pp. 11-129.

Pietersen, H.S., Kentgens, A.P.M., Nachtegaal, G.H., Veeman, W.S. and Bijen, J.M. (1994). "The Reaction Mechanism of Blended Cements: A ^{29}Si NMR Study", in *Application of NMR Spectroscopy to Cement Science*, Ed. Colombet, P. and Grimmer, A. (Gordon and Breach Science Publishers, Amsterdam, Netherlands), pp. 229-238.

Richardson, I.G., Brough, A.R., Brydson, R., Groves, G.W. and Dobson, C.M. (1993). "Location of Aluminum in Sibstituted Calcium Silicate Hydrate (C-S-H) Gels as Determined by ^{29}Si and ^{27}Al NMR and EELS". J. Am. Ceram. Soc. **76**, 2285-88.

Richardson, I.G., Brough, A.R., Groves, G.W. and Dobson, C.M. (1994). "The Characterization of Hardened Alkali-Activated Blast-Furnace Slag Paste and the Nature of the Calcium Silicate Hydrate (C-S-H)". Cem. Concr. Res. **24**, 813-829.

Roy, A., Schilling, P.J., and Eaton, H.C., Malone, P.G., Brabston, W.N., and Wakeley, L.D. (1992). "Activation of Ground Blast-FurnaceSlag by Alkali-Metal and Alkaline-Earth Hydroxides". J. Am. Ceram. Soc. **75**, 3233-40.

Roy, D.M. and Jiang, W. (1994). "Microcharacteristics and properties of Hardened Alkali-Activated Cementitious materials", in *Cement Technology*, Ceramic Transactions, Vol. 40, Ed. Gartner, E.M. and Uchikawa, H. (Am. Ceram. Soc., Westerville, OH). pp. 257-264.

Roy, D.M. and Silsbee, M.R. (1994). "Novel Cements and Cement Products for Applications in the 21st century", in *Concrete Technology: Past, Present, and Future* — Proceeding of V. Mohan Malhotra Symposium, Ed. Mehta, P.K. (ACI, SP-144, Detroit, MI), pp. 349-382.

Roy, D.M. and Silsbee, M.R. (1995). "Overview of Slag Microstructure and Alkali-Activated Slag in Concrete", in *Supplementary Papers of Second CANMET/ACI Inttl. Symposium on Advances in Concrete Technology*, Las Vegas, Ed. Malhotra, V.M. pp. 699-716.

Schilling, P.J., Roy, A., and Eaton, H.C. (1994). *Reply to* "Comment on 'Activation of Ground Blast-Furnace Slag by Alkali-Metal and Alkaline-Earth Hydroxides.'" J. Am. Ceram. Soc. **77**, 1117-18.

Schilling, P.J., Butler, L.G., Roy, A., and Eaton, H.C. (1994). "^{29}Si and ^{27}Al MAS-NMR of NaOH-Activated Blast-Furnace Slag". J. Am. Ceram. Soc. **77**, 2363-68.

Shi, C. and Day, R.L. (1995). "A Calorimetric Study of Early Hydration of Alkali-Slag Cements". Cem. Concr. Res. **25**, 1320-1332.

Shi, C. and Day, R.L. (1996). "Some Factors Affecting Early Hydration of Alkali-Slag Cements". Cem. Concr. Res. **26**, 439-438.

Wang, S.D. and Scrivener, K.L. (1994). "Comment on 'Activation of Ground Blast-Furnace Slag by Alkali-Metal and Alkaline-Earth Hydroxides'". J. Am. Ceram. Soc. **77**, 1116.

Wang, S.D., Scrivener, K.L. and Pratt, P.L. (1994). "Factors Affecting the Strength of Alkali-Activated Slag". Cem. Concr. Res. **24**, 1033-1043.

Wang, S.D. and Scrivener, K.L. (1995). "Hydration Products of Alkali Activated Slag", Cement. Cem. Concr. Res. **25**, 561-571.

Wu, X., Jiang, W., and Roy, D.M. (1990). "Early Activation and Properties of Slag Cement" Cem. Concr. Res. **20**, 961-974.

INFLUENCE OF SPENT BLAST FURNACE SLAGS ON THE PROPERTIES OF CEMENT SYSTEMS

Magdelinka RADENKOVA-YANEVA, Sonya DIMITROVA, University for Architecture, Civil Engineering and Geodesy, Sofia, Bulgaria

ABSTRACT The paper presented deals with the application of spent blast furnace slag sorbents used for waste water cleaning from heavy metal ions. The influence of the type of the ions and the quantity of the spent sorbent on the properties of cement pastes are investigated. It is shown that the structure formation in cement systems and the strength properties of the cement stone are a result of the mutual action of the slag, which has lost its activity during the cleaning process, and ions Cr^{3+} and Zn^{2+}, incorporated in the slag. A possibility for application of useless spent blast furnace slag sorbents in the civil engineering practice is found out and materials saving and environment protection are achieved simultaneously.

Key words: binder, blast furnace slag, hydration, setting, waste material utilization.

INTRODUCTION

The sorption method is one of the most effective methods for drawing out heavy metal ions from waste waters, especially in the case of using cheap and accessible raw materials. In our previous investigations (Dimitrova, 1995; 1996) the sorption activity of blast furnace slag to the Cr^{3+}, Cu^{2+}, Ni^{2+}, Zn^{2+} - ions is established. Preliminarily conducted studies with the spent sorbent show that it is not an occasional case for environment pollution and can be disposed of or used additionally.

Recently a manner of inertization of wastes, containing heavy metals, is found (Malone, 1989; Conner, 1990; Rossetti et al, 1995). Different matrixes are used, including binders on the base of cement (Venkobachar et al, 1995). But more attention is paid there to the method for inertization of wastes while their influence on the hydration of binders is studied in a small scale.

It is known that the addition of inorganic salts in cement systems influences their hydration and properties (Ratinov, 1973; Babatschev, 1976). The possibility for application of blast furnace slag for production of slag cements and slag portland cements due to the hydraulic activity of the slag is ascertained (Ners, 1964). The possibility for additional use of slag applied for waste water cleaning and thus containing heavy metals ions is not still studied

The present study aims to establish the influence of the blast furnace slag sorbent on the physico-chemical and physico-mechanical properties of cement systems.

MATERIALS AND EXPERIMENTAL METHODS

The investigation is conducted using an ordinary portland cement type I (ENV 197-1). Blast furnace slag used as a sorbent has the following chemical composition (% by weight): SiO_2 - 36.0; CaO - 41.6; MgO - 2.7; MnO - 2.5; Al_2O_3 - 8.7; BaO - 3.0. The data from blast furnace slag studies (Dimitrova, 1995) show that it is a mixture of complex crystal calcium hydroaluminates, calcium silicates and oxides with sorption properties. The investigations are performed with ground blast furnace slag with a size of the grains below 0.25 mm ($d < 0{,}25$ mm) after its using as a sorbent for the cleaning of waste waters containing Cr^{3+}

and Zn^{2+} ions in dynamic condition. The spent sorbent contains approximately 1 % metal ions and is added in cement systems as a dry material.

From the cement and the spent sorbent, mixtures of binders are prepared. Their composition is shown in Table 1 and Table 2. The sorbent is added in quantities 5, 10, 15 and 20 % by the weight of the binder. From binders, pastes are prepared and using Vicat method (EN 196) the setting time is determined. The time for structure formation is reported from the curves of the shear strength change versus time of hydration.

Table 1 Setting time and time for structure formation for the pastes containing spent blast furnace slag sorbents

Binder			Setting time		Time for structure formation
Designation	Type	Spent slag, %	initial	final	
			hour - min.		hour - min.
A	Binders with pure slag - control	5	3 - 00	4 - 20	7 - 15
		10	3 - 05	4 - 25	8 - 40
		15	2 - 55	4 - 25	9 - 05
		20	2 - 55	4 - 45	9 - 20
B	Binders with spent sorbent, containing Zn^{2+} ions	5	2 - 55	5 - 00	8 - 05
		10	4 - 00	6 - 20	10 - 20
		15	9 - 45	14 - 50	18 - 40
		20	11 - 05	23 - 40	26 - 05
C	Binders with spent sorbent, containing Cr^{3+} ions	5	3 - 05	4 - 35	7 - 05
		10	3 - 15	4 - 55	8 - 20
		15	3 - 20	5 - 00	8 - 45
		20	4 - 25	5 - 30	9 - 05

Table 2 Strength properties of cement pastes containing spent blast furnace slag sorbents

Binder			Flexural strength, MPa, at the age, days			Compressive strength, MPa, at the age, days		
Designation	Type	Spent slag, %	7	28	90	7	28	90
A	Control	0	1.10	4.38	5.87	5.47	24.27	34.17
B	Binders with spent sorbent, containing Zn^{2+} ions	5	1.18	3.48	5.17	5.18	17.50	28.42
		10	1.10	3.67	4.39	5.17	22.17	23.52
		15	0.96	3.77	3.94	5.13	18.96	21.92
C	Binders with spent sorbent, containing Cr^{3+} ions	5	1.08	3.54	4.96	5.58	17.38	26.58
		10	1.04	3.58	4.71	6.39	19.46	26.88
		15	1.05	3.33	4.19	4.73	14.92	21.04
		20	0.93	2.68	4.06	4.75	11.83	18.75

The mechanical tests are performed using pastes with equal consistency. From the pastes samples prisms 2x2x8 cm are prepared. At a relevant age flexural and compressive strengths are determined.

RESULTS AND DISCUSSIONS

The data from the investigation performed are shown in Tables 1 and 2. The control in the mechanical testing is a pure portland cement without addition of slag (Table 2, composition A). For the other tests, characterizing setting and hardening, the control samples are of cement with a corresponding quantity of freshly ground slag (without heavy metal ions) (table 1, compositions A). The properties of the systems studied depend on the quantity of the spent blast furnace slag sorbent and the type of the contained in the slag metal ions. The spent sorbent, used in our investigations, has been in a prolonged contact with water during waste water cleaning. The appreciable finess of the material ($d < 0.25$ mm) and its peculiar composition determine some interaction with water (Dimitrova, 1995). That is why the spent blast furnace slag has a lower activity in comparison with the freshly ground slag. Metal ions, sorbed onto the surface of the slag grains, also influence the hydration process and on the properties of the hydrated systems.

The mixtures with addition of spent blast furnace slag have a retarded setting time and a prolonged time for structure formation (t_{sf}) (table 1, compositions B and C). This is explained with the kind of the ions sorbed on the surface of the slag grains and with the reduced quantity of the active component in the binders. The results received show, that the behavior of mixtures with two kinds of ions (Zn^{2+} and Cr^{3+}) is different. The retardation of structure formation (higher values for t_{sf}) is considerably higher for compositions containing Zn^{2+} ions (Table 1, samples B). In this case the retarding effect of heavy metal ions (Zn^{2+}) is summed with the generally lowered activity of the binders (the influences are unidirectional). For compositions containing Cr^{3+} (Table 1, samples C) the effect of the lower activity of the sorbent is summed with the accelerating action of the chromium ions, and the latter are predominant. The accelerating action of Cr^{3+} ions is sufficient to neutralize almost completely the effect of the lowered activity of the spent slag in the investigated compositions. The results received conform well to the literature data (Ratinov, 1973; Babatschev, 1976).

The flexural and compressive strengths of the mixtures studied are lower in comparison with those of the control (Table 2, sample A). These differences are greater in the later stage of investigation (29 and 90 days). The lowering of the strength properties is in accordance with the composition of the studied systems. The quantities of metal ions added to the binders with spent sorbents are not very high and their action is revealed in the early stages of hardening. The above mentioned can explain the almost equal flexural and compressive strengths at the age of 7 days for all the investigated compositions. The results obtained allow to propose the spent blast furnace slag for use as a component of cement systems where high strength properties are not required. The combination between retarded setting and enough strength could be suitable in special cases in civil engineering practice - the producing of "wash" concretes, decorative concrete products and others.

CONCLUSION

The investigations conducted and the results received show that the used spent blast furnace slag sorbent, containing metal ions (Zn^{2+} and Cr^{3+}), influences the hydration, the structure formation and the mechanical properties of the cement systems. The retarded time for setting and hardening and the sufficient strengths of the hardened cement systems enable us to recommend their use in specific cases in the civil engineering practice. The adding of spent blast furnace slag sorbent in cement systems results in the lowering of cement consumption and contributes to additional environment protection - the waste product from water cleaning is used and the area for its disposal is reduced.

REFERENCES

Babatschev, G., Chemistry in Civil Engineering, Technika Publishers, Sofia, 1976

Conner, J. R., Chemical Fixation and Solidification of Hazardous Wastes, Van Nostrand Reinhold, New York, 1990

Dimitrova, S., Metal Ions Removal from Water Solutions Using Blast Furnace Slag, Ph.D. Thesis, UASG, Sofia, 1995

Dimitrova, S., Metal Sorption on Blast Furnace Slag, Water Res., vol. 30, No 1, pp. 228 - 232, 1996

Ners, R. U., in The Chemistry of Cement, Edited by H. F. W. Taylor, Academic Press, London and New York, 1964

Malone, P. G., R. S. Jones, R. S. Larson, Guide to Disposal of Chemistry Stabilized and Solidified Wastes, SW - 872 US Environmental Protection Agency, New York, 1982

Ratinov, V. B., T. I. Rosenberg, Admixtures in Concrete, Stroiizdat Publishers, Moscow, 1973

Rossetti, V. A., F. Medici, Cem. and Concr. Res., vol. 25, No 6, pp. 1147 - 1152, 1995

Venkobachar, C., L. Iyengar, U. K. Mishra, M. S. Chauhan, Cem. and Concr. Res., vol. 25, No 6, pp. 1639 - 1646, 1995

A STUDY OF EARLY HYDRATION OF SLAG CEMENT PASTES SUBJECTED TO THERMAL CURING

Arnaldo Forti BATTAGIN, Brazilian Association of Portland Cement, São Paulo, Brazil
Gladis CAMARINI, State University of Campinas, Brazil
Maria Alba CINCOTTO, State University of São Paulo, Brazil

ABSTRACT A conduction calorimeter and DTA/TGA techniques were used to monitor hydration kinetics of mixtures of ordinary portland cement and granulated blast-furnace slag. It was found that at 23°C cement and slag have maximum hydration rates at different period. At 60°C only one peak occurs after a smaller period of hydration. Slag shows better behaviour under thermal curing than clinker and acceleration of slag hydration is confirmed by thermogravimetry and compressive strength results.

Key-words: blastfurnace-slag, heat evolution, hydration, steam curing

INTRODUCTION

Steam curing is a very useful technique employed in precast concrete with the aim of accelerating the concrete demolding. Cements at low hydration rate as the slag cements are known for a good behaviour under thermal curing.An attempt is made to explain the hydration characteristics of slag cements under thermal curing (60°C) in comparison to the same cements under normal curing (23°C).

EXPERIMENTAL PROCEDURE

The influence of curing temperature on hydration of slag cements were studied on mixtures of ordinary portland cement (OPC) and granulated blast-furnace slag (GBFS) representative of industrial production in Brazil. Proportions of OPC/GBFS were 100/0, 65/35, 50/50 and 30/70.

These mixtures were submitted to an isothermal conduction calorimeter (JAF model), w/c = 0.4, at both 23°C and 60°C and hydration products were analysed by DTA/TGA techniques. Mortar compressive strengths were determined according to the Brazilian method (NBR 7215) by using cylindrical test specimens Ø50 x 100mm height in proportion 1:3 (cement:sand), cured at 23°C, w/c = 0.48 and at 60°C according to a thermal cycle detailed in Camarini et al (1996).

Table 1 Characteristics of starting materials and mixtures

% mass	SiO_2	$A\ell_2O_3$	Fe_2O_3	CaO	MgO	SO_3	K_2O	Na_2O	LOI	IR
OPC	18.51	4.32	4.08	60.14	5.98	3.15	0.56	0.12	1.32	0.19
GBFS	33.25	11.29	0.53	44.93	6.28	1.60	0.36	0.19	-	-

	OPC	65/35 MIX	50/50 MIX	30/70 MIX	GBFS
Initial setting time (h:min) (Vicat test)	2:30	4:00	5:00	5:15	-
Specif surface area ($m^2.kg^{-1}$)	324	380	395	440	500

RESULTS AND CONCLUSIONS

Compressive Strength

Table 2 shows the mortar compressive strength results. RIC values were obtained just after an isothermal cycle of 9h at 60°C plus periods of both temperatures increasing and decreasing and setting time as schematized in Figure 1. RIC is abbreviation of "strength just after cycle", in portuguese.

Table 2 Mortar Compressive Strength (MPa) Camarini (1995)

Curing Temperature (°C)	Age (days)	OPC	65/35 Mix	50/50 Mix	30/70 Mix
60	RIC	21.2	22.3	22.9	22.2
23	2	21.9	14.1	11.3	9.0
	28	42.0	45.4	51.3	48.5
	90	44.4	49.0	62.9	50.0
60/23 (*)	2	30.0	28.4	26.8	26.4
	28	39.9	50.1	48.9	53.0

(*) thermal cycle at 60°C plus normal curing

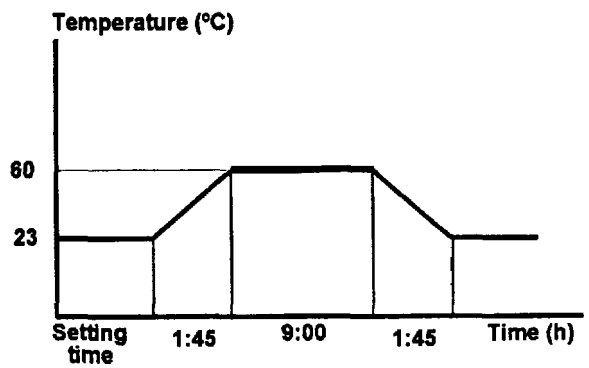

Figure 1 Thermal cycle characteristics

From Table 2 we can conclude that at early ages under normal curing, the higher the cement replacement by slag, the lower is the compressive strength. Slag hydration rate is lower than that of clinker and this fact can explain the strength reduction of mixtures when compared to the control. At 28 days and 90 days the highest values are found for 50% replacement. In this case, 50% seems to be the optimum content of slag and this proportion depends on the physical and chemical characteristics of both clinker and slag. Compressive strength values after initial 60°C cycle are almost the same for all mixtures moreover, these values are similar to the OPC specimens at 2 days under normal curing. The early strength gain of mixtures under thermal curing when compared to the same mixtures under normal curing is higher for higher the cement replacement by slag.

Heat of hydration

Figure 2 and Table 3 show the heat evolution rate. At 23°C, clinker and slag have maximum hydration rates at different time, represented by two peaks of heat evolution. One peak from 10:30h to 11:40h is due to clinker fraction and the other from 16:00 to 19:00h is due to slag hydration. At 60°C, only one peak occurs after a period between 3:25h and 4:30h, showing the acceleration of both clinker and slag hydration.

At 23°C, first peak of 50/50 and 65/35 mixtures is slightly retarded when it is compared to OPC but at 60°C it is slightly accelerated. However, kinetics of reaction of clinker and slag seems to be independent at 23°C as we can conclude from the experimental measures and calculated values presented in Table 4.

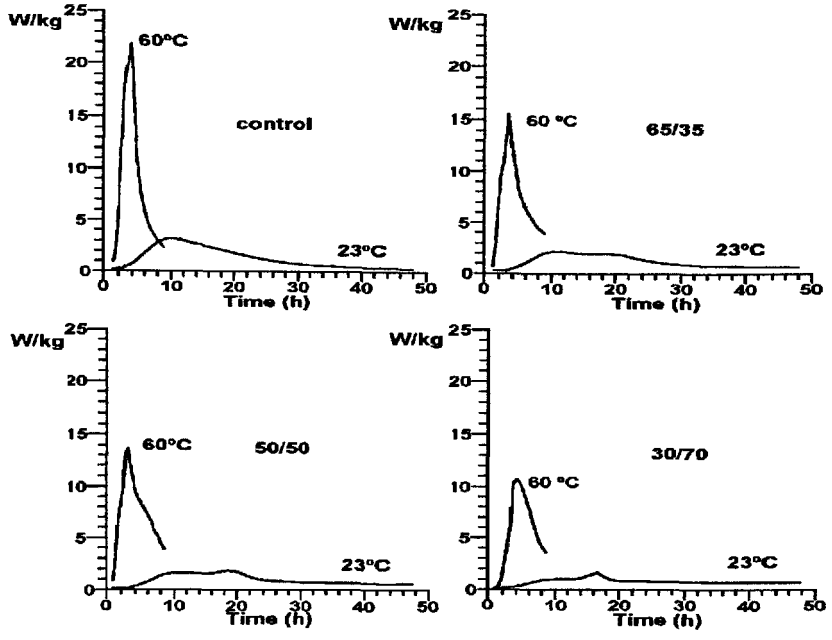

Figure 2 Calorimetric curves of OPC and slag cements at 23°C and 60°C

Table 3 Heat peak evolution of mixtures of OPC and GBFS at 23°C and 60°C

Mixtures	Heat peaks at 23°C				Heat peak at 60°C	
	W/kg		Time (h:min)		W/kg	time (h:min)
	First	Second	First	Second		
CONTROL	3.34	-	10:30	-	22.06	3:55
65/35	2.12	1.88	11:10	16:00	15.57	3:35
50/50	1.66	1.83	11:40	19:00	13.57	3:25
30/70	0.99	1.54	10:30	17:00	10.56	4:30

Table 4 Experimental and calculated values of heat liberation at 23°C

Mixtures	Peak of Heat (W/kg)		Total Heat Liberated After 48h		
			Experimental (J/g)	Contribution of Slag (Calculated)	
	Experimental	Calculated		J per gram of cement	J per gram of slag
OPC	3.34	3.34	239	-	-
65/35	2.12	2.17	180	25	70
50/50	1.66	1.67	152	32.5	65
30/70	0.99	1.00	114	42.3	60

DTA/TGA Results

In Figures 3 and 4 are presented thermograms of all mixtures cured at 23°C and 60°C, respectively. They exhibit an intense endothermic peak between 60°C and 100°C due to the loss of the free water. Another endothermic peak appears at 460°C and is due to $Ca(OH)_2$ decomposition. The lower the intensity of this peak, the higher is the contents of slag in the mix. In fact, increased amounts of $Ca(OH)_2$ are found at lower contents of slag, as we can conclude from the loss of mass values for the temperature interval of 440-500°C, shown in Table 5. These effects are indicative of the consumption of $Ca(OH)_2$ by the slag, mainly for the pastes cured at 60°C. Another endothermic peak of smaller magnitude also appears at 170°C in the pastes cured at 60°C and it is supposed to be due to hydrated aluminous phases. Sometimes an exothermal

peak is also found at 230°C probably due to the calorimeter oil contamination. From Table 5 we can also conclude that the contents of non evaporable water of mixtures cured at 60°C compared to those of the same mixtures cured at 23°C are higher, the higher the slag proportion.

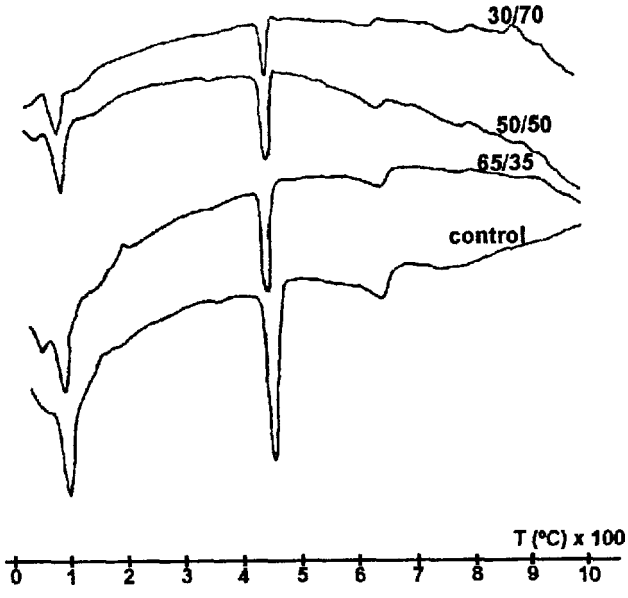

Figure 3 Thermograms of Mixes Cured at 23°C

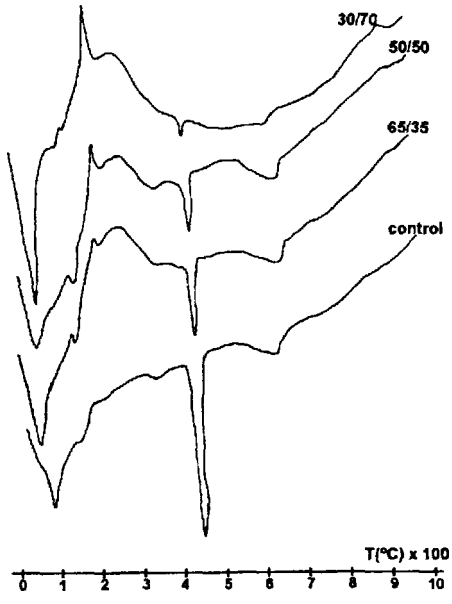

Figure 4 Thermograms of Mixes Cured at 60°C

Table 5 Loss of Mass (%) by Thermogravimetry

MIX	Curing Temperature	Curing Time (h:min)	Loss of Mass (%)		
			80-440 °C	440-500 °C	500-900 °C
CONTROL	23°C	9:00	7.95	2.03	2.97
65/35			6.55	1.32	2.24
50/50			5.51	1.01	1.56
30/70			4.81	0.68	1.54
CONTROL	23°C	48:00	10.45	3.18	2.87
65/35			8.85	1.72	1.78
50/50			7.89	1.18	1.77
30/70			7.55	0.68	1.86
CONTROL	60°C	9:00	9.40	3.16	3.05
65/35			11.90	1.16	3.17
50/50			11.75	0.65	2.62
30/70			9.72	0.51	2.29

REFERENCES

Camarini, G., "Performance of Mixtures of Ordinary Portland Cement and Granulated Blast Furnace Slag Subjected to Thermal Curing", PhD Thesis, University of São Paulo, 1995 (in portuguese).

Camarini, G., Cincotto, M.A., "Different Steam Curing Conditions Effects on Compressive Strength of Slag Cement". Proceedings of International Congress on High Strength Concrete and Performance and Quality of Concrete Structures, Florianópolis/SC Brazil, 1996 pp. 542-553.

3ii103
4 pp

Kn o. 26. JAN. 2001 d o k 31867

THE INFLUENCE OF ALKALI ACTIVATOR ON THE EARLY HYDRATION AND PERFORMANCE OF PORTLAND BLAST FURNACE SLAG CEMENT

Everaldo, MARCIANO JR.
Arnaldo Forti BATTAGIN, Brazilian Association of Portland Cement, São Paulo, Brazil

ABSTRACT This paper shows the best behaviour of Na_2SO_4 among other activators of portland blast furnace slag cement. Sodium silicate, extensively used in alkali activated slag, has a poorer performance than Na_2SO_4 in the presence of $Ca(OH)_2$. Depending on the characteristics of cement and activator, Na_2SO_4 can increase the early strength gain of blast furnace slag cements without significantly affecting long term compressive strength. A use of sodium sulfate - rich waste could be an environmental solution for waste disposal but further studies will be necessary.

Key-words: accelerators, activation, alkali, blastfurnace slag.

INTRODUCTION

Many publications have dealt with the role of chemical activators, mainly sodium silicates (water glass) on the slag hydration (Shao-Dong Wang et al, 1995). There is a general agreement about the good behaviour of these compounds as slag activators on so-called alkali-activated slag cements (AAS) but less work has been done about the study of alkaline activation of slag in portland cement.

In order to evaluate the most suitable slag activator we carried out preliminary tests based on compressive strength. Two blast furnace slag cement (BFSC) samples representative of industrial production in Brazil were chosen. Cements selected have different mechanical performance according to the Brazilian method by using 50 x 100mm cylindrical test specimens in proportion 1:3 (cement:sand), water cured at 23°C, w/c = 0.48. Both granulated blast furnace slag are basic, refractive index 1.65 and 95% vitrified. Mixes of 99% cement and 1% of six different chemical agents (Reagent Grade) were used with the aim of improving the early strength gain. Results are shown on Table 1.

Table 1 - Effects of different slag activators

Cement	Activator	Compressive Strength (MPa)			
		1 day	3 days	7 days	28 days
A	None	5.1	17.4	35.3	59.1
	K_2SO_4	8.1	21.2	35.2	49.8
	NaOH	7.2	15.7	23.0	33.8
	Na_2CO_3	6.9	17.3	26.7	37.4
	$A\ell_2(SO_4)_3$	5.5	18.3	32.3	52.1
	Na_2SO_4	8.6	21.0	32.7	47.1
	$NaSiO_3.nH_2O$	5.5	16.1	27.9	46.2
B	None	4.3	13.1	20.0	32.8
	K_2SO_4	7.2	15.7	22.4	34.7
	NaOH	6.5	14.1	19.1	29.5
	Na_2CO_3	5.6	14.1	18.7	30.6
	$A\ell_2(SO_4)_3$	4.0	13.0	21.3	36.0
	Na_2SO_4	7.6	16.1	22.5	33.8
	$NaSiO_3.nH_2O$	4.7	13.2	20.1	32.0

Based on the preliminary results it was decided to detail the investigation of the Na_2SO_4 activator, although Jawed and Skalny (1983) have shown it decrease the cement strength at long term age. Sodium silicate had a poorer and unexpected behaviour compared to those reported in literature for slag alone.

ACTIVATION WITH Na_2SO_4 (REAGENT GRADE)

Mixtures of BFSC and Na_2SO_4 at proportions in mass of BFSC/Na_2SO_4 of 100/0, 99.5/0.5, 99/1 and 98/2 were made. Compressive strengths were determined at 1, 3, 7, 28, 60 and 91 days and a conduction calorimeter was used to monitor hydration kinetics. Table 2 shows the results obtained as well as additional characteristics of materials.

Table 2 - Mechanical and Rheologycal Results

Cement	Na_2SO_4 (%)	Compressive Strength (MPa)						Setting Time (Vicat Test)		Soundness Le Chatelier
		1 day	3 days	7 days	28 days	60 days	91 days	Initial (h:min)	Final (h:min)	(mm)
A	0 (reference)	5.1	17.4	35.3	59.1	60.7	68.6	3:55	5:35	0
(58% slag , 5%	0.5	7.1	20.5	34.1	51.5	54.8	57.3	3:45	5:15	0.5
limestone and 419$m^2.kg^{-1}$	1.0	8.6	21.0	32.7	47.1	50.4	54.8	2:55	4:15	0
Blaine surface area)	2.0	10.7	21.9	29.5	39.9	44.3	46.5	2:35	4:15	0
B	0 (reference)	4.3	13.1	20.0	32.8	39.9	43.1	3:25	4:55	0
(44% slag, no	0.5	5.6	14.4	20.7	32.1	38.4	42.9	3:05	4:05	0
limestone and 342$m^2.kg^{-1}$	1.0	7.6	16.1	22.5	33.8	36.0	38.8	3:10	4:20	0
Blaine surface area)	2.0	8.5	17.0	22.0	33.1	37.1	39.5	2:40	4:00	0.5

From Table 2 we can conclude that at early ages (1 and 3 days) the higher the Na_2SO_4 content, the higher the compressive strength for both samples.For cement A, at 7 days and beyond, there is a remarkable decrease of strength with the increasing quantities of Na_2SO_4. It can be seen that strength values can reach only 68% of the reference at 91 days with 2% Na_2SO_4. However, a different behaviour was found for sample B showing smaller loss of strength. In fact, at 91 days a value of 90% of reference for 1% Na_2SO_4 was observed.

Tables 3 and 4 summarize the results of heat of hydration up to 72 hours, taking into account that the peak due to the first minutes of hydration was undetected due to operational conditions.

Table 3 - Heat Peak Evolution

Cement	Na_2SO_4 (%)	Heat peaks at 23°C (W/g)		Time (h:min)	
		First	Second	First	Second
A	0	2.32	-	12:25	-
	0.5	2.40	-	12:30	-
	1.0	2.42	-	12:15	-
	2.0	2.43	-	11:00	-
B	0	1.58	1.89	8:40	15:50
	0.5	1.69	1.78	8:30	17:00
	1.0	1.77	1.77	7:10	14:50
	2.0	1.73	1.74	8:20	15:20

Table 4 - Total heat liberation up to 72h

Sample	Na_2SO_4 (%)	Total heat liberated after (hour) (J/g)												
		2	4	6	8	12	16	20	24	30	40	50	60	72
A	0	1	4	12	22	50	76	91	103	118	139	156	169	182
	0.5	1	5	14	26	56	88	106	119	134	154	169	183	196
	1.0	1	5	13	26	57	90	111	125	140	159	173	184	193
	2.0	2	6	17	32	66	96	117	132	147	165	178	187	194
B	0	2	8	18	29	51	76	97	108	121	137	149	159	168
	0.5	2	9	19	31	55	80	104	120	135	152	164	174	184
	1.0	3	12	24	37	61	87	110	126	141	158	170	181	191
	2.0	2	9	20	32	56	81	105	123	139	156	169	180	190

From Table 3 we can conclude that first peak of 99/1 and 98/2 mixes is slightly accelerated compared to reference for both sample. The same phenomenon is found for the second peak of heat for sample B. First peak is supposed to be due to clinker fraction hydration and second peak is attributed to slag hydration. However, sample A exhibits only one peak. These atypical results indicate that, in this case, maximum hydration rate of both clinker and slag are simultaneous. Acceleration of both clinker and slag fraction by using Na_2SO_4 as activator is confirmed by results of total heat liberation listed on Table 4.

ACTIVATION WITH SODIUM SULFATE WASTE

The use of an activator is usually expensive and may impair its use in practice. Aiming the reduction of the costs and trying to find an environmental solution for waste disposal an attempt was made concerning the use of a waste as activator. So we replaced the Na_2SO_4 (Reagent Grade) by a glass - industry waste rich in this component (27.1% SO_3 and 47.5% Na_2O). Similar tests to those of compressive strength shown in Table 2 were carried out. Preliminary results are listed on Table 5.

Table 5 - Results of sodium sulfate waste as an activator

Cement	Waste Content (%)	Compressive Strength (MPa)			
		1 day	3 days	7 days	28 days
1	0	5.1	17.4	35.3	59.1
	0.5	3.0	16.0	30.9	55.5
	1.0	2.4	16.3	30.6	50.5
	2.0	1.1	16.7	28.5	43.8
2	0	4.3	13.1	20.0	32.8
	0.5	3.7	10.8	17.3	28.9
	1.0	5.1	13.2	18.6	29.5
	2.0	1.1	10.0	15.3	26.1

In spite of bad results for cement 1, the use of waste brought up some advantages to cement 2, mainly with 1% Na_2SO_4. This fact stimulates further studies to a better understanding of the behaviour of waste activated cement as a contribution for waste elimination.

DISCUSSION AND CONCLUSION

- Sodium silicate is the most used activator for alkali activated slag but its behaviour was not good in presence of $Ca(OH)_2$ liberated from clinker hydration.

- At 1% levels, Na_2SO_4 seems to be the most suitable activator among those used in this study.
- Unique heat peak found in cement 1 is probably not due to influence of activator because it also occurs in reference sample. In this case a higher specific surface area of slag and a poorer reactivity of clinker compared to sample 2 accelerated slag hydration and retarded clinker hydration.
- Compared to cement 1, cement 2 presented a higher heat liberation at first 12 hours probably due to its lower slag content in spite of being coarser than sample 1. At 24h and beyond (72 h) heat liberation was higher for sample 1. Results are in agreement with compressive strength results. Setting time is accelerated with the increase of Na_2SO_4 contents and unsoundness due to its use was not detected.
- At 1 and 3 days the behaviour of both samples activated with Na_2SO_4 was similar, with a strength gain of aproximately 100% and 25-30% respectively for 2% Na_2SO_4. However, a different behaviour was found after 7 days, with a harmful influence of Na_2SO_4 on the cement of better performance (sample 1). On the other hand, long term strength was little affected in cement of worse performance.
- Optimum contents of Na_2SO_4 depends on characteristics of both cement and activator and further studies will be necessary for supplementary consideration about the potential use of sodium sulfate-rich waste as activator.

REFERENCES

Jawed, I and Skalny, J. "The influence of alkali sulfates on the properties of cement and concrete." World Cement, 1983, Nov., p325.

Wang S.D. et alii, "Alkali-activated slag cement and concrete: a review of properties and problems." Advances in Cement Research, 1995, 7 nº 27, july, 93-102.

HIGH PERFORMANCE ENERGETICALLY MODIFIED PORTLAND BLAST-FURNACE CEMENTS

Hanumantha Rao KOTA[1], Vladimir RONIN[2] and Eric FORSSBERG[1]
[1]Division of Mineral Processing, [2]Division of Structural Engineering, Luleå University of Technology, S-971 87 Luleå, Sweden

ABSTRACT The mechano-chemical treatment in the milling equipment with vibrating grinding media of Portland cement-blast furnace slag blends has considerable impact on strength development, especially in the early-ages. The high shear/attrition treatment of solids increases the pozzolanic activity of microsilica by its disintegration and dispersion, increases the rate of hydration reactions due to the increase in surface free energy and increases the hydraulic activity of blast-furnace slag.

Key-words: Activation, Infrared absorption spectra, Mercury Intrusion Porosimetry, Modified cement.

INTRODUCTION

A new mechano-chemical activation method has been developed at Luleå University of Technology during the last years (Jonasson and Ronin, 1993; Ronin and Häggström, 1994), in which the ordinary Portland cement (OPC) in combination with silica fume is treated in a vibrating mill. The high shear/attrition environment is thought to have led an increased irregularities of the surface structure of the blends thereby increasing the surface electrostatic field and creating a new binder surface by coating silica fume on the cement particles. This newly obtained binder is called Energetically Modified Cement (EMC) and is found to have an extremely high chemical reactivity when compared to the reference blend of OPC and silica fume. The cement pastes and mortars obtained with the use of EMC show a pronounced increase of pozzolanic reaction rate with corresponding increase of C-S-H-gel amount and a significant decrease of the paste porosity, thereby the strength parameters at early ages and after prolonged curing times have greatly improved.

The EMC method is found to be effective for the development of high performance concretes with low-heat liberation. Compositions of the binders with various amounts of ordinary Portland cement, ground blast furnace slag and 5% of silica fume are investigated in order to understand the mechanisms underlying the improved properties of binding materials by the mechano-chemical activation method in a vibrating grinding mill. This paper describes the results of the efficiency of EMC method through particles characterisation, FT-IR studies, porosity of the pastes and strength development of the mortars at different stages of curing, while using the materials before and after the activation process.

EXPERIMENTAL

Materials

The ordinary Portland cement produced by Cementa AB, Sweden was used in this work. The condensed silica fume produced by Elkem A/S, Norway as a puzzolanic additive and the ground blast-furnace slag (MERIT 5000) manufactured by SSAB, Sweden as an admixture were used in the experiments. The chemical composition of the materials, according to the manufacturers, are given in Table 1.

Table 1. Chemical composition of the materials.

Oxide	OPC (wt%)	Silica fume (wt%)	Blast-furnace slag (wt%)
SiO_2	19.80	96.00	34.03
Al_2O_3	4.23	0.30	11.51
Fe_2O_3	2.21	0.20	0.42
CaO	63.00	0.95	35.46
MgO	3.43	0.30	13.54
SO_3	3.23	0.10	3.44
K_2O	1.28	0.30	0.56
Na_2O	0.27	0.20	0.54
MnO			0.44
TiO_2			1.90
Surface area, m^2g^{-1}	0.368 (Blaine) 1.830 (BET)	19.74 (BET)	1.21 (BET)

The following blends were investigated and referred in the text as 1 to 4:

1. 30% Ordinary Portland cement + 5% silica fume + 65% blast-furnace slag
2. 20% Ordinary Portland cement + 5% silica fume + 75% blast-furnace slag
3. 10% Ordinary Portland cement + 5% silica fume + 85% blast-furnace slag
4. 0% Ordinary Portland cement + 5% silica fume + 95% blast-furnace slag

Methods of investigation

The mechanical modification of the above mentioned blend mixtures was carried out in Humboldt Palla 20U vibrating mill. The blends of 2 kg material was subjected to milling ea time with porcelin cylindrical grinding media. Each blend was milled for three different perio (i.e., 5, 15 and 30 min) and the products before and after milling were used for the followi investigations:

Particles characterization

The particle size distribution was determined by Sedigraph (Micromeritics, model 5100) wh using Sedisperse A12 particle dispersion liquid. The particles in the suspension were dispers in a ultrasonic bath for about 30 seconds prior to the measurement. The specific surface areas the samples were determined by BET method (Micromeritics, flow sorb II 2300) using nitrog gas adsorbate.

FT-Infrared measurements

The spectra of the samples were recorded using a Perkin Elmer 1720X infrared Fouri transform spectrometer with diffuse reflectance attachment. The samples for diffuse reflectan were prepared by dispersing 25 mg of the sample in 200 mg of KBr. Typical measurement ti for recording the spectra was 2.4 min (32 scans) at a resolution of 4 cm^{-1}.

Porosity measurements

Porosity measurements were made by mercury porosimetry (Micromeritics, pore sizer 930 Cylindrical mortar specimens measuring 25 x 55 mm were produced with the water-binder ra of 0.25. For each blend, three specimens were prepared in a polyethylene container and th were heated at 105°C overnight after allowing a curing time of 7, 14 and 28 days respectively, order to stop the hydration process. Pore-size distributions were obtained at various times intruding mercury into the dried specimens at pressures up to 25 000 psi.

Mechanical strength properties

The mechanical strength tests, i.e., the compressive and bending strengths development, were performed on the mortar specimens containing 1 part by weight of binder of different composition and 3 parts by weight of EN standard sand. The water to binder ratio was maintained constant at 0.40. The mortars were mixed at room temperature of about 20°C in Horbart mixer for 3 min and cast in 40x40x160 mm steel moulds. After casting, the samples were compacted on the laboratory vibrating table for about 40 seconds. The density of the compacted mortars were 2250 to 2320 kg m^{-3}. The samples were sealed in plastic foil and put in curing chamber at 20°C for 24 hours. After one day curing, the samples were transfered to a thermostated water bath for the rest period of curing. The temperature was maintained constant at 20°C. Samples of each mortar were removed from moulds and tested for uniaxial compression and three-point bending for 1, 3, 7 and 28 days. Testing was done on the hydraulic press 506/200/10 DM1 (Germany). Loading speed rate was 2.4 kN/sec for compression and 0.5 kN/sec for bending. An average data of nine test results was presented.

RESULTS AND DISCUSSION

Particles characterization

Portland cement and slag materials consist rather broad size distributions extending from 2 to 40 μm size. The slag (d_{50} = 12.14 μm) is finer than Portland cement (d_{50} = 15.66 μm) but the BET surface area of the cement is found to be bigger (1.83 m^2g^{-1}) than slag (1.21 m^2g^{-1}). The results indicate the porous nature of cement grain when compared to the slag particle. The specific surface area of silica fume is determined to be 19.74 m^2g^{-1}.

The particle size distributions of the blends 1 to 4 after mechanical treatment at different time intervals have been summarized in Table 2. The vibration milling reduced the average particle size to 30-40% and increased the specific surface area to 10-20% at 30 min activation time. When the quantity of cement is proportionately decreased in the blends with an increase in the finer slag amount, the effect of treatment on decreasing the particle size is not that significant.

In vibration milling, the particles experience greater attrition/shear forces than impact forces, thereby the surfaces of the particles will become smoother leading to the shape of the particles close to sphere. The fluidity of the cement could be improved by bringing the shape of the particle close to sphere since the thickness of the free water film that exists between the particles increases with the increase of smoothness of surface (Uchikawa, 1994). High-strength concrete demands low water/cement ratio and at low water content, the particles will be closer in contact with each other and the viscosity is reduced. Thus, one of the beneficial effect of the present mechanical treatment is the improvement of the fluidity of cement paste at lower water contact by making the particles close to sphere.

The dosage of silica fume is an important parameter influencing the compressive strength of silica fume concrete. An optimum dosage is reported to vary in between 7 and 10 wt% of the total blend (Malhotra et al., 1992). Based on the specific surface area of cement and slag materials, the amount of 5 wt% silica fume used, is calculated to cover more than 86% fraction of the total surface area of matrix materials in any of the blends.

Table 2. Particle size and specific surface area of the blends before and after activation at different periods of time.

Admixture	0 min	5 min	15 min	30 min
1. Particle size, d_{80} (μm):	29.93	22.67	20.51	18.40
d_{50} (μm):	14.59	10.60	9.58	8.26
d_{20} (μm):	7.54	4.21	3.68	2.89
BET surface area, (m^2g^{-1}):	2.26	2.42	2.52	2.65
2. Particle size, d_{80} (μm):	25.60	23.38	19.69	18.61
d_{50} (μm):	12.06	10.57	8.98	7.64
d_{20} (μm):	4.99	3.98	3.27	2.41
BET surface area, (m^2g^{-1}):	2.17	2.35	2.46	2.60
3. Particle size, d_{80} (μm):	24.71	20.68	19.58	17.42
d_{50} (μm):	10.52	9.54	8.72	7.54
d_{20} (μm):	3.95	3.61	3.19	2.67
BET surface area, (m^2g^{-1}):	2.24	2.33	2.41	2.52
4. Particle size, d_{80} (μm):	23.96	22.88	18.42	16.90
d_{50} (μm):	11.12	10.24	8.20	7.59
d_{20} (μm):	4.77	4.55	3.00	2.90
BET surface area, (m^2g^{-1}):	2.14	2.21	2.30	2.41

FT-Infrared studies

The diffuse reflectance spectra of ordinary Portland cement (OPC), blast-furnace slag (BFS) and silica fume (SF) are presented in Fig 1. The spectrum of silica fume shows the strongest absorbance bands at 1122, 805 and 480 cm^{-1}, characteristic of silica gel where the four-coordinated silica absorbs at 1094, 800 and 470 cm^{-1} (Moenke, 1974). The silica gel nature can also be seen by the band at 3625 cm^{-1} due to OH stretching of SiOH, and the H-O-H bending vibration near 1630 cm^{-1}.

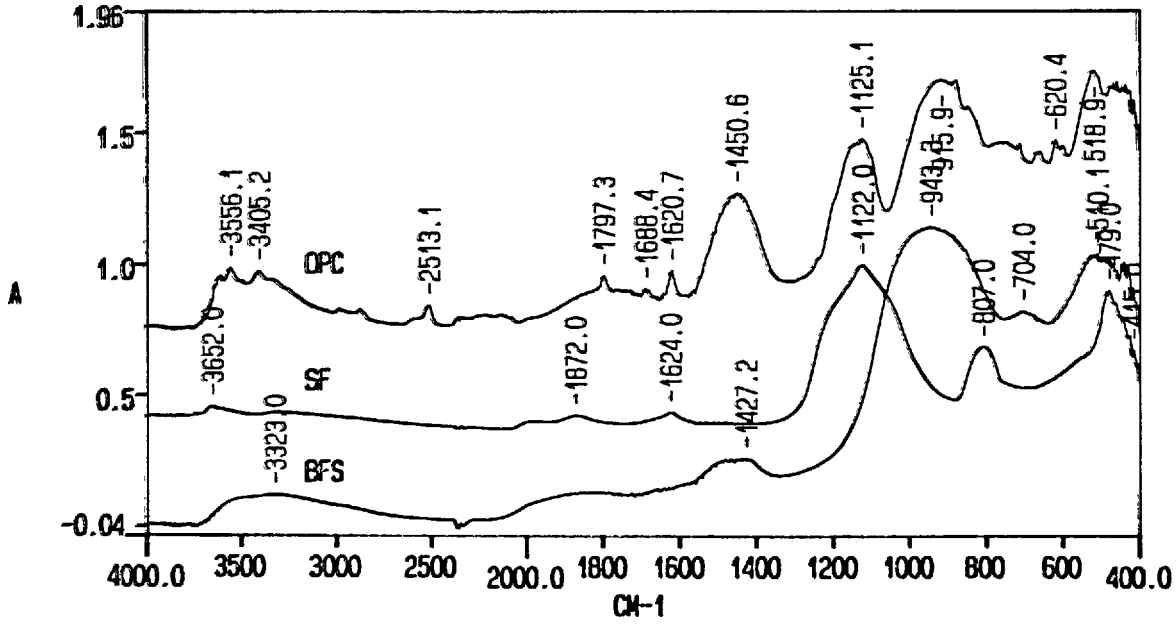

Figure 1 Diffuse reflectance spectra of ordinary Portland cement (OPC), silica fume (SF) and blast-furnace slag (BFS).

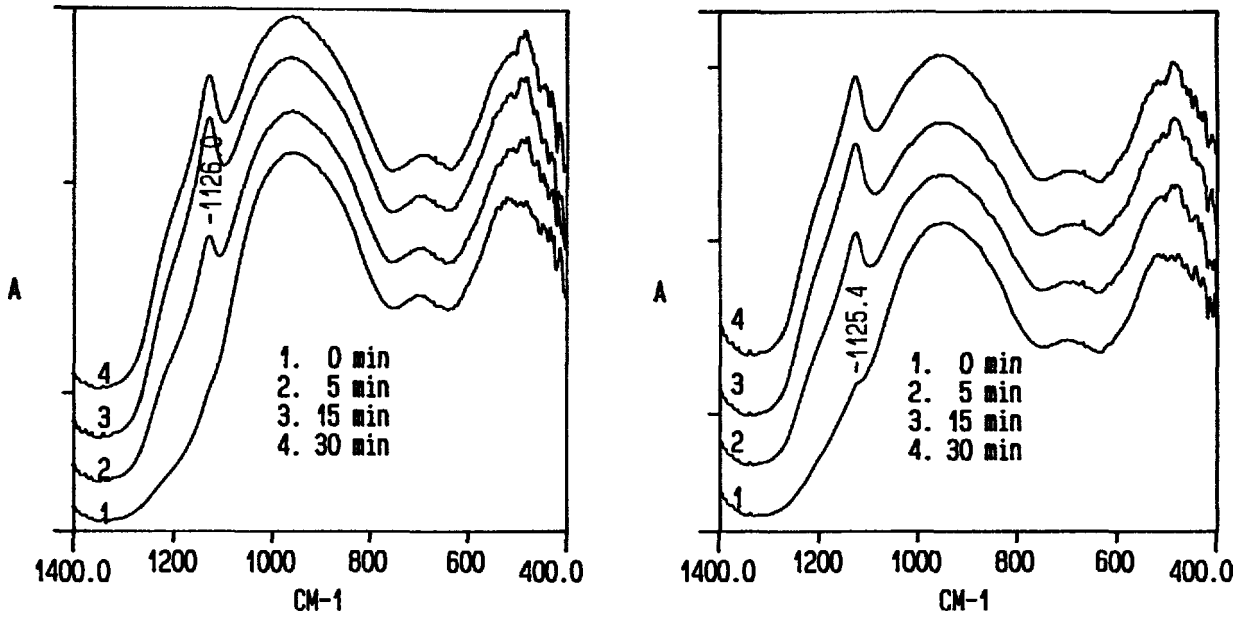

Figure 2 Diffuse reflectance spectra of the blends 2 (right) and 4 (left) before and after activation at different time intervals.

The spectrum of blast-furnace slag shows entirely different absorbance features than Portland cement, although the materials differ only in the ratio of chemical composition of the SiO_2, Al_2O_3, CaO and MgO. The main difference being that the CaO content is less in slag but with a proportionate increase in SiO_2, Al_2O_3 and MgO amounts. Since the materials consist of different mineralogical compositions, the different absorbance pattern is obviously expected. The antisymmetric Si-O-Si stretching band at 1125 cm^{-1} in the case of cement is shifted in slag with a broad high intensity band centering around 950 cm^{-1} due to its increased alumina content (Moenke, 1974). This low-frequency shift arises from the increasing contribution made by Si-O-Al linkages at the expense of Si-O-Si. The surface hydroxyl groups or the structural hydroxyl groups that present in gypsum component of cement can be seen from the OH stretch modes at 3610, 3556 and 3405 cm^{-1}, and from the H-O-H bending modes at 1687 and 1620 cm^{-1} in the spectrum of cement.

The spectral features of the blend containing only cement and silica fume are found to be exactly the same before and after vibration milling. However, the intensity of the band due to Si-O stretching vibration at 1127 cm^{-1} is seen to increase after the modification process. The beneficial effect of microsilica on the strength properties of concrete was reported by several authors, only when it is well dispersed in a concrete mixture. The efficient dispersion of microsilica can be noticed from the spectra of the blends in the presence (20 wt%) and absence of the cement component. These spectra before and after activation in vibration milling at different time intervals are presented in Fig 2. The spectrum of slag and silica fume mixture before activation show no absorbance bands characteristic of silica fume, but after the activation process, a sharp band characteristic of Si-O stretching vibration at 1127 cm^{-1} can be seen. It is worthwhile to point out here that the 0 min spectrum corresponds to the mixture before modification, but thoroughly homogenized in a rotating drum prior to recording the spectrum. With increasing time of activation process, the intensity of the band at 1127 cm^{-1} increases and also the silica fume characteristic band at 482 cm^{-1} became more predominant. The increase in the intensity of silica fume bands after vibration milling is obviously due to the increase in the

surface area of silica fume by deagglomeration and its dispersion. Thus, the intensity of the peak at 1127 cm^{-1} could be used as a measure of microsilica dispersion in the blend and the optimum time of activation process would equal to the intensity where it could no longer increase with increasing time of vibration milling.

Pore size distribution

The pore size distribution curves for the pastes made from the blends 2 and 4, before and after activation, are presented in Fig 3 for 7, 14 and 28 days curing age. In the case of cement-slag blend samples prepared from the blend 2, the unactivated samples have coarser pore sizes than activated samples at any of the curing age from 7 to 28 days. A discontinuity in the pore structure can be seen from the shape of the curves and with increasing curing age from 7 to 28 days, this disruption shifts to a lower pore size. The change in slope of these curves with age shows that large changes occur up to 28 days. These changes have been reported to take place with slag blends due to the silica fume reaction with $Ca(OH)_2$ (Cheng-yi and Feldman, 1985a).

A significant change in pore size distributions is observed with the pastes containing only slag and silica fume. The unactivated samples contain very large pores ranging from 0.37 to 10 μm and the distribution curves at 7 and 14 days are found to be the same. The activated samples after 7 days not only produced smaller pores but also fall within the narrow size range of 0.02 to 0.04 μm. This range is shifted to lower size end with increasing age and at 28 days, nearly 90% of the pores have sizes in between 0.01 and 0.02 μm. For the unactivated sample, there is a sudden change at 28 days and 70% of the pores are in between 0.02 and 0.03 μm size. The results show an increase in the hydraulic activity of slag pastes by the applied activation process.

The activation process in vibration milling has greater influence on the pore size distribution either for cement pastes or cement-slag blends or slag pastes. The pore sizes are always found to be more coarser for unactivated sample at any curing age in comparision to the activated sample. During the early stages of Portland cement hydration reactions, the C-S-H gel on the surface of cement particles and $Ca(OH)_2$ are formed (Cheng-yi and Feldman, 1985b). Silica fume is thought to accelarate hydration reactions by providing nucleation sites for $Ca(OH)_2$ within minutes after reaction commences, and also by reacting with the $Ca(OH)_2$ by pozzolanic reaction. The activation method allows the dispersion of microsilica around the cement grains and filling of the spaces between the cement grains to participate microsilica in pozzolanic reaction evenly in the entire matrix and thereby causing more refined capillary pore system. The development of smaller pores within 7 days shows that coagulation and bonding of C-S-H are considerably progressed in the case of activated samples.

Mechanical strength properties

The compressive and bending strengths of binders at various compositions of Portland cement, blast-furnace slag and silica fume (blends 1-4) for non-activated and activated samples as a function of curing age are presented in Fig 4. For the reference cement mortar not containing slag, the compressive strengths at 1, 3, 7 and 28 days are determined to be 24, 42.2, 49.5 and 62.6 MPa respectively. The strength is seen to decrease with decreasing cement composition during early days, but after 7 days, comparable strength has been developed with 30% cement component for the non-activated samples. After 28 days, the strength of the reference cement mortar is 62.6 MPa and the corresponding strengths for blends at 70 and 80% cement replacement are 57.23 and 51.71 MPa. For activated sample, a strength of 56.24 MPa has developed as early as 7 days for the 70% cement replacement sample and after 28 days, higher

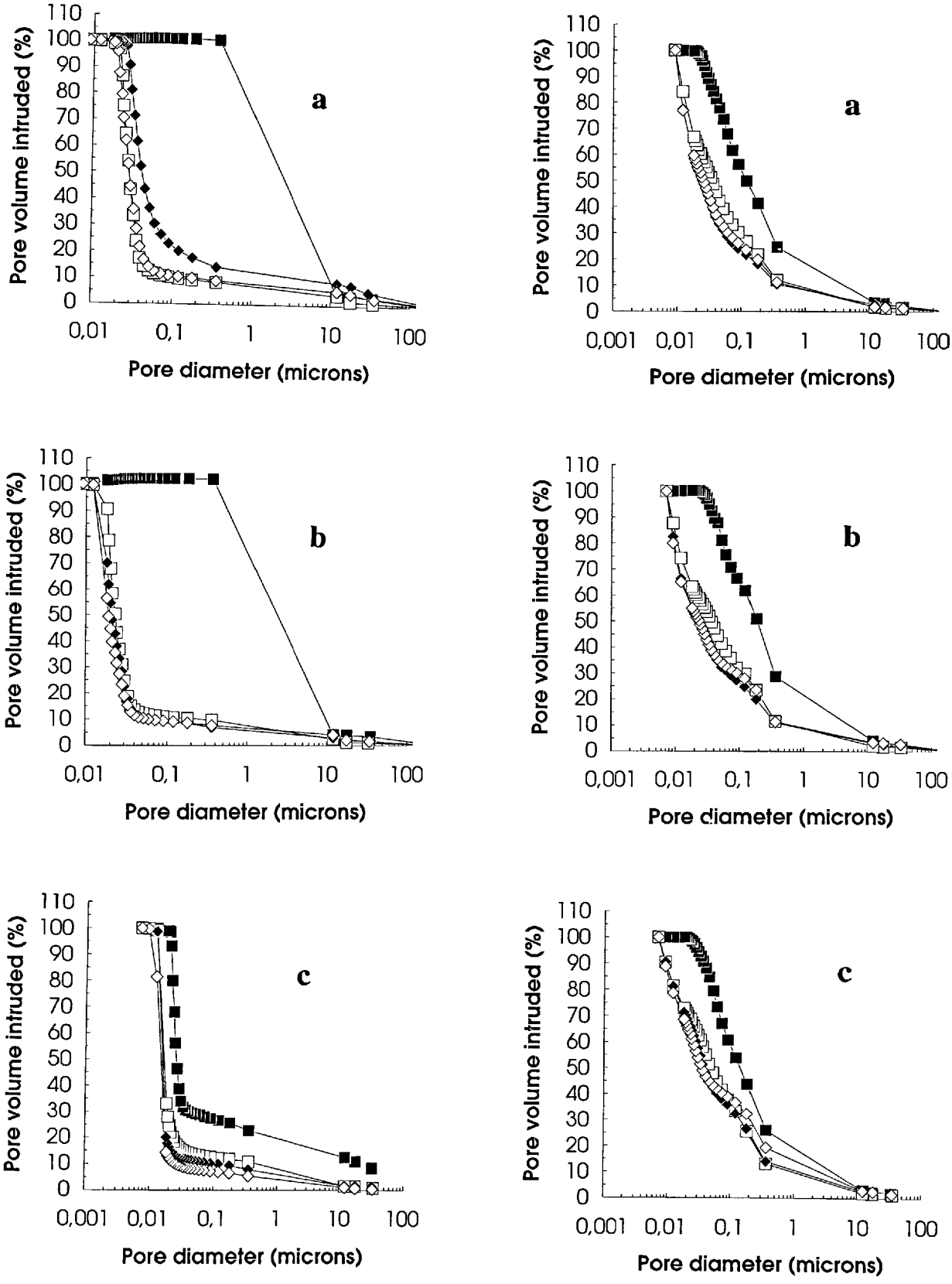

Figure 3 The pore size distribution of the pastes prepared from the blends 2 (right) and 4 (left) before and after modification at different time intervals and curing age. (a) 7 days (b) 14 days (c) 28 days; (■) 0 min (□) 5 min (♦) 15 min (◊) 30 min .

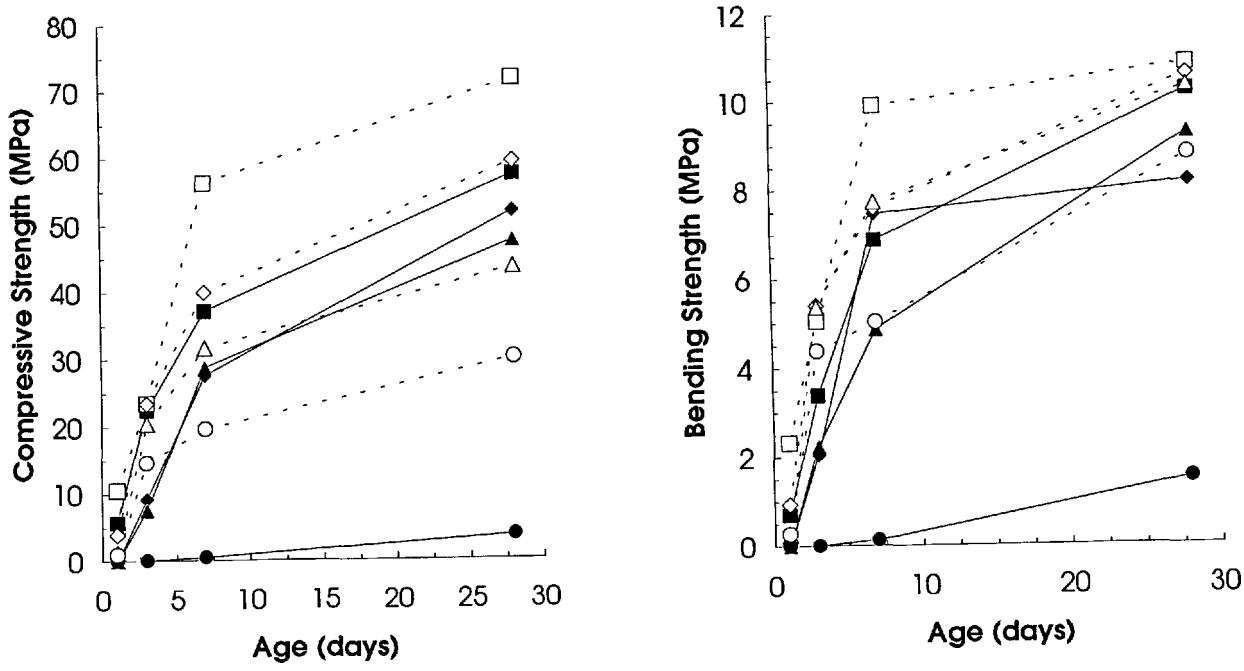

Figure 4 Compressive and bending strength results of the mortars prepared from the blends 1 (□), 2 (◊), 3 (Δ) and 4 (O) before and after modification. The dark symbols with lines represents the results before modification.

strength (71.62 MPa) than the reference cement mortar has been developed. It is especially important to note the strength development of blend 4, which do not contain OPC. The non-modified binder shows no strength up to 7 days of hardening and very low compressive strength of 3.6 MPa after 28 days. The corresponding compressive strengths for the modified binder are about 14 and 30 MPa after 3 and 28 days respectively, which directly reflects the increase of hydraulic activity of the slag. In the early age of hardening (1-3 days), the average strengths of the activated samples are three times higher in comparision to the non-activated samples. The increase in bending strengths for the activated samples are similar to that of the compressive strength results.

The strength increase of the hardened mortar leads to increased strength of the concrete. The strength of the mortar is closely related to the porosity and the first measure for increasing the strength is to reduce the porosity. The volume of gel pores in high- and ultra high-strength concretes is smaller than in ordinary concrete, though the combined water is higher. The mortars made from activated samples show smaller pores and hence the observed higher strength properties. The reduced amount, crystal size and crystallinity of $Ca(OH)_2$ could also increase the strength and the efficient dispersion of microsilica in matrix materials caused by the activation process would allow the pozzolanic reaction to take place at all calcium hydroxide crystal sites, thereby complete depletion of $Ca(OH)_2$ in the mortar may occur.

CONCLUSIONS

The activation of concrete blends in a vibration mill has the following beneficial effects:

(1) The hydraulic activity of blast furnace slag increases due to the increase in surface free energy and activity by the attrition and shear forces that experience in vibration milling.

(2) The rate of hydration reactions increases due to the increase in surface free energy of the particles. The increase in surface free energy allows faster dissolution of chemical species into

pore solution, which in turn, causes early $Ca(OH)_2$ and C-S-H formation, and thus an early strength development.
(3) The pozzolanic activity of silica fume increases due to its disintegration and thorough dispersion into the spaces between cement grains. The dispersion of microsilica allows the pozzolanic reaction to take place at all crystal nuclei sites of calcium hydroxide, leading to the depletion $Ca(OH)_2$ in the early curing ages and thus an early strength development.

ACKNOWLEDGEMENT
The financial support from the Norrbottens Forskningsrådet (NFR) is gratefully acknowledged.

REFERENCES
Cheng-yi, H. and Feldman, R.F., "The Influence of Silica Fume on the Microstructural Development in Cement Mortars", Cement and Concrete Research, Vol. 15, 1985a, pp. 285-294.
Cheng-yi, H. and Feldman, R.F., "Hydration Reactions in Portland Cement-Silica Fume Blends", Cement and Concrete Research, Vol. 15, 1985b, pp. 585-592.
Jonasson, J-E. and Ronin, V., "Energetically Modified Cement (EMC)", Proceedings of the Third International Conference on High-Strength Concrete, June 20-24, 1993, Lillehammer, Norway, Holand, I. and Sellevold, E. (Ed.), pp. 752-759.
Malhotra, V.M., Carette, G.G. and Sivasundaram, V., "Role of Silica Fume in Concrete: A Review", Advances in Concrete Technology, V.M. Malhotra (Ed.), CANMET, Canada, 1992, pp. 925-991.
Moenke, H.H.W., "Silica, the Three-Dimentional Silicates, Borosilicates and Beryllium Silicates", The Infrared Spectra of Minerals, Farmer, V.C. (Ed.), Mineralogical Society, Monograph 4, Adlard & Son Ltd., Bartholomew Press, Surrey, 1974, pp. 365-375.
Ronin, V. and Häggström, M., "Method for Producing Cement", International Patent Application, PCT/SE 94/00389, 1994.
Uchikawa, H., "Characterization and Material Design of High-Strength Concrete with Superior Workability", in "Cement Technology", Gartner, E.M and Uchikawa, H. (Eds.), Ceramic Transactions, 1994, Vol. 40, pp. 143-186.

THE REACTION OF SILICA FUME AT EARLY AGES

Birgit MENG, Peter SCHIESSL, Institute for Building Materials Research (ibac),
University of Technology, Aachen, Germany

ABSTRACT Investigations on the reaction mechanisms of silica fume in combination with cement were carried out. The results (rate of hydration heat, evolution of $Ca(OH)_2$ and bound water content) showed that the intense action of silica fume varies distinctly, depending on the type of cement. Principally, gel phases that are rich in water are formed at first and then later undergo phase transitions, expelling water.

Key-words: silica fume, mineralogy, heat evolution, thermogravimetry, gel

INTRODUCTION

The positive influence of pozzolanic additions on the properties of concrete is well known from research and practice. The long term effects have been studied extensively while only a few investigations on processes at early ages (the first 3 days) exist. The known increase in early strength shows that the silica fume reaction starts at very early ages. On the other hand, effects like an increased early shrinkage resulting in microcracking have been reported, when silica fume is added (Alfes, 1992, Al-Sugair, 1995, Cohen, 1990).

An addition of pozzolan affects the hydration mechanisms of the cement and possibly already leads to pozzolanic reactions at early ages. Some aspects of the reaction kinetics in combination with Portland cement (CEM I) are well understood by various investigations, but the more complicated mechanisms in combination with slag cement (CEM III/A) are widely unkown.

The investigations described in this paper were part of a research project dealing with the reaction mechanisms of fly ash and silica fume in cementitious materials (Schießl and Meng, 1996). Focusing on the reaction mechanisms affected by silica fume addition some results of practical interest, especially concerning the mineralogical phase evolution and the time-dependent progress of the reactions, will be discussed.

MATERIALS AND METHODS

The reaction behaviour of silica fume was investigated in combination with 2 different types of cement (CEM I 32,5 R and CEM III/A 32,5). All the tests were carried out on hardened cement paste specimens with a w/b value (b = total binder content = cement + silica fume = c + s) of 0.50. Silica fume was employed at an extremely high dosage in comparison with practical conditions (25 % by mass in relation to the total binder content), to enable clear identification of the influences on the reaction mechanisms in the hardened cement paste.

Measurement of hydration heat evolution

The tests were carried out according to the semi-adiabatic method (DIN prEN 196 - 9 : 1994). This method enables continuous tracing of the reaction processes which take place in the mortar or concrete at a young age (< 3 days). Evaluation of the results covered determination of the evolution of temperature and hydration heat as a function of time. To enable mathematical determination of the heat loss, cooling curves were measured on all specimens in an older state,

whereby the same test set-up was maintained throughout. With the aid of a maturity formula (Eq. 1), the time at which a certain heat of hydration was released was converted into the *reference time* at 20 °C. This is necessary because the course of hydration is accelerated by heat: at 35 °C, the reaction already takes place twice as quickly as at 20 °C. Consequently, quantitative comparison of the evolution of the heat of hydration of different specimens can only be achieved when the obtained results are converted back into constant temperature conditions (20 °C) by means of the reference time, (CEB, 1992).

$$\frac{v(T)}{v(20)} = \exp\left[\frac{E}{R}\left(\frac{1}{293} - \frac{1}{273+T}\right)\right] \qquad [1]$$

v = rate of reaction, T = temperature in °C,
E = activation energy (33500 J/mol) R = gas constant (8.314 J/mol).

For the purposes of assessment, the released heat of hydration was considered as a function of the reference time. These results show whether and in what manner changes result from replacing part of the cement with pozzolanas.

Measurement of $Ca(OH)_2$ and bound water content

At the time of testing, hydration of the cement was stopped by placing the cement in methanol. The specimen was subsequently dried at 105 °C and pulverised, prior to undergoing thermogravimetric (TG) examination. The analysis programme covered a temperature range from 30 to 894 °C. Fig. 1 shows the absolute weight losses (TG) and the appurtenant differential representation (DTG) over the entire temperature range, by reference to one representative cement paste specimen. The change in weight (TG) here represents a specific change in relation to the originally determined weight of the specimen concerned.

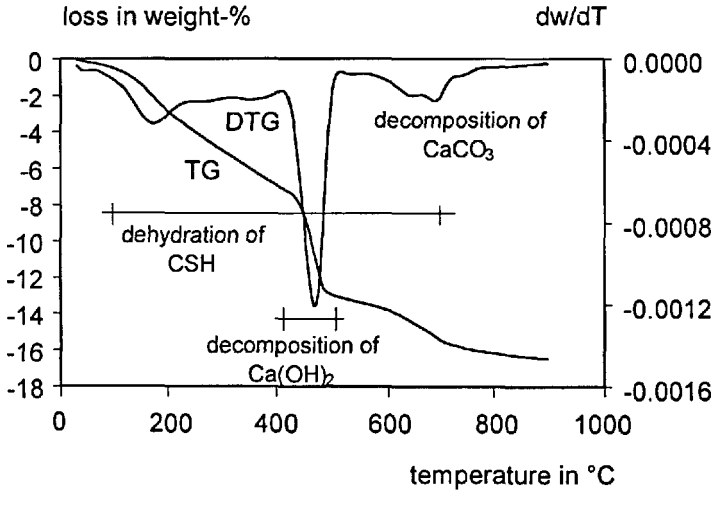

Figure 1:TG-Analysis of hardened cement paste (100 % CEM I 32,5 R, age: 28 days)

The hardened cement paste consists primarily of compounds containing hydration water, together with a small fraction of inorganic compounds containing carbonates. The most important compounds, the calcium silicate hydrates and calcium aluminate hydrates, occur in cement paste in a large number of composition variants, the decomposition reactions of which overlap. This makes quantitative evaluation more difficult, i.e. it is not possible to specify exact temperature ranges for the decomposition ranges.

The decomposition reactions can be explained by reference to Fig. 1. In the temperature range from around 100 to 750 °C, the CSH phases dehydrate relatively continuously. Between

approximately 400 and 500 °C, the water is removed from the $Ca(OH)_2$ in accordance with Eq. 2. $CaCO_3$ decomposes at a temperature of around 700 °C (separation of the CO_2).

$$Ca(OH)_2 \xrightarrow{\Delta T} CaO + H_2O \qquad [2]$$

The decomposition peak of the $Ca(OH)_2$ appears relatively sharp in comparison to the continuous decomposition of the CSH phases. According to Marsh (1984), during evaluation the $Ca(OH)_2$ content can be calculated from the TG curve by taking into account the CSH phases before and after the $Ca(OH)_2$ peak and, indirectly (via interpolation), during the $Ca(OH)_2$ peak. The $Ca(OH)_2$ content of the hardened cement paste specimen is obtained in accordance with Eq. 3.

$$Ca(OH)_2 = \frac{4.113 \cdot \Delta w}{w_{894\,°C}} \cdot 100 \quad \text{in weigth-\%} \qquad [3]$$

Δw = weight loss due to decomposition of $Ca(OH)_2$ in mg according to (Marsh, 1984); calculated from the TG curve (e. g. Fig. 1)

$w_{894\,°C}$ = weight of specimen at 894°C (final temperature of analysis) in mg.

As $Ca(OH)_2$ is consumed and CSH phases are formed in the course of the pozzolanic reaction, conclusions on the course of the pozzolanic reaction can be drawn from the results of the thermogravimetric investigation. The consumption of $Ca(OH)_2$ can be determined directly in comparison with a reference mixture. The formation of CSH phases can be determined only indirectly, via the bound water. By subtracting the water content of the $Ca(OH)_2$ from the directly measured total bound water (weight loss in the temperature range from 30 to 600 °C), the fraction of CSH phases can be deduced from the residual water, subject to several approximate assumptions. By way of approximation, the residual water is regarded as CSH water (i.e. water bound in the CSH phases), although it also contains the water bound in calcium aluminate hydrates and sulphate phases. The time-dependent development of the so-called CSH water fractions can only provide direct information on the development of the CSH phase fractions when the stoichiometry of the CSH phases remains constant.

RESULTS AND DISCUSSION

Heat of Hydration

The object of the investigations on the evolution of the heat of hydration was to establish at what point in time and to what extent silica fume influences the reactions in the cement paste. Differing, sometimes contradictory information, can be found in the relevant literature with regard to the extent and timing of silica fume's contribution to the evolution of hydration heat.

Contrary to the results specified in the relevant literature (Cheng-Yi, 1985, Meland, 1983), the test results presented in Figs. 2a and 2c demonstrate that the addition of silica fume does not inevitably reduce the specific release of heat in relation to the total binder mass (cement + silica fume). At a very young age (< 24 h) in particular, the heat evolution of the two types of cement is even markedly increased. In the medium term mixes of silica fume with CEM I release nearly the same quantity of heat as the pure cement. In the case of CEM III/A the hydration heat in the medium term is increasingly reduced by the addition of silica fume.

The specific heat evolution in relation to the cement mass is always greater when silica fume is added. Figs. 2a and 2c show that this applies not only in combination with CEM I, but also with CEM III/A. This contribution of the silica fume to the evolution of heat indicates that a pozzolanic reaction already occurs in the early phase. However, this effect cannot be separated beyond doubt from a possible promotion of cement hydration as a result of the addition of silica fume (higher level of hydration due to effect of nucleation substrate and inevitably higher w/c at constant w/b).

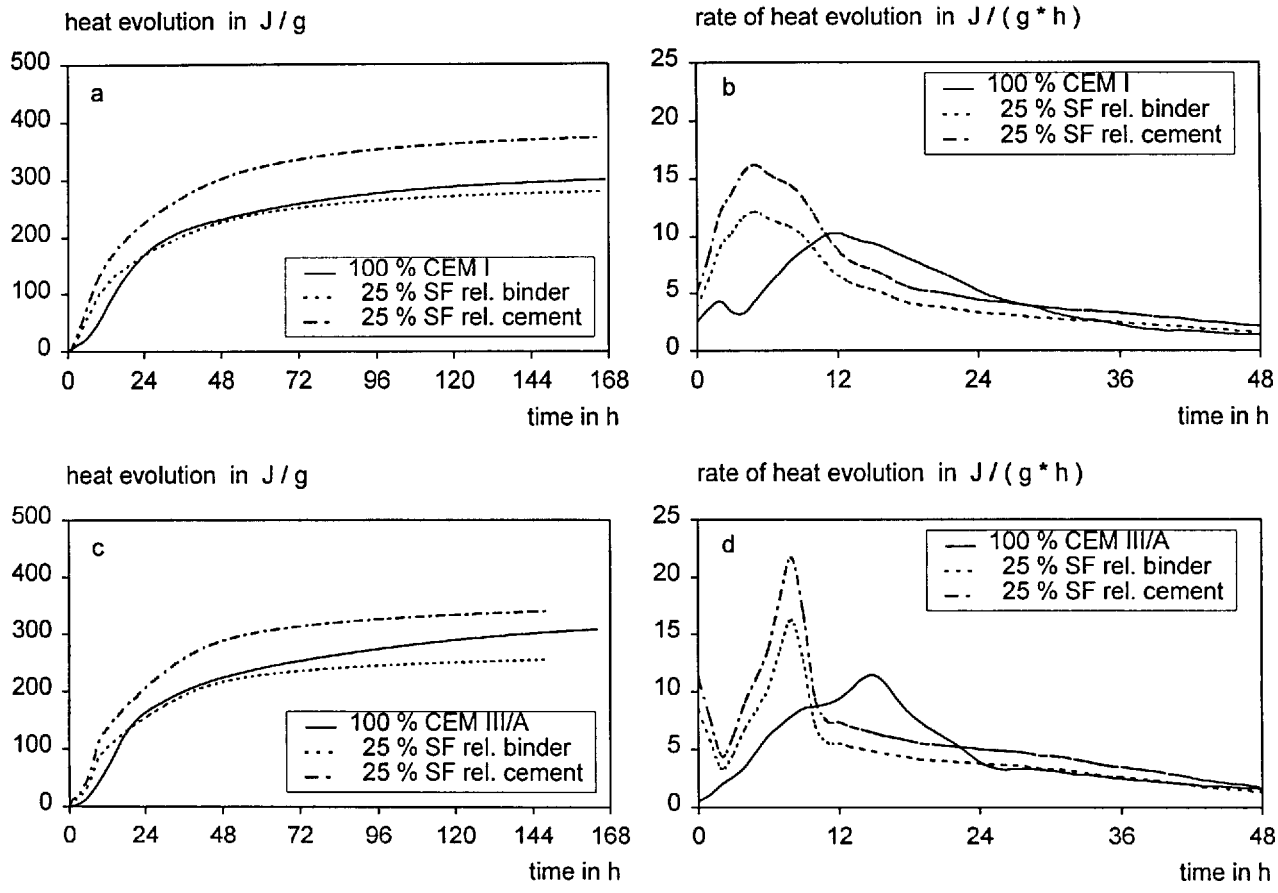

Figure 2: Heat evolution with and without silica fume

Different authors hold different views as to the influence of silica fume on the time at which the evolution of heat begins. It is generally assumed that the influence is only minor. There appears to be a general tendency for the onset of the evolution process to occur at an earlier point in time. The courses of evolution of hydration heat presented in Figs. 2a to 2d show that the evolution of heat commences substantially earlier when silica fume is added, in combination with both CEM I and CEM III/A. The maximum for the evolution of hydration heat also occurs markedly earlier. This is why the levels of hydration heat developed at an age of 12 hours are, in both cases, higher for the mixes containing silica fume than in the reference mixes without silica fume content. On the basis of these results alone, it is not possible to distinguish whether the strong evolution of heat is caused by the pozzolanic reaction, by other reactions of the silica fume (e.g. gel formation), by the promotion of cement hydration or by a combination of these three different processes.

The results do essentially show that the influence of the silica fume on the maximum rate of evolution of hydration heat is more pronounced with the employed CEM III/A than with the CEM I. The total quantity of heat released, on the other hand, is particularly high with CEM I: here, the reaction of the silica fume develops a quantity of heat which virtually corresponds tc the heat of hydration of the pure cement.

Reaction Products

Figs. 3 and 4 compare the $Ca(OH)_2$ and CSH water contents of mixes with and without silica fume at ages of 12, 24 and 48 hours. Both for the CEM I and CEM III/A mixes it can be seen that the $Ca(OH)_2$ contents of the specimens containing silica fume are significantly lower than those of the reference mixes without silica fume at all the investigated times. The reverse applies with regard to the so-called "CSH water" content. Conclusions regarding the pozzolanic reaction can be drawn from the consumption of $Ca(OH)_2$ and the bound CSH water.

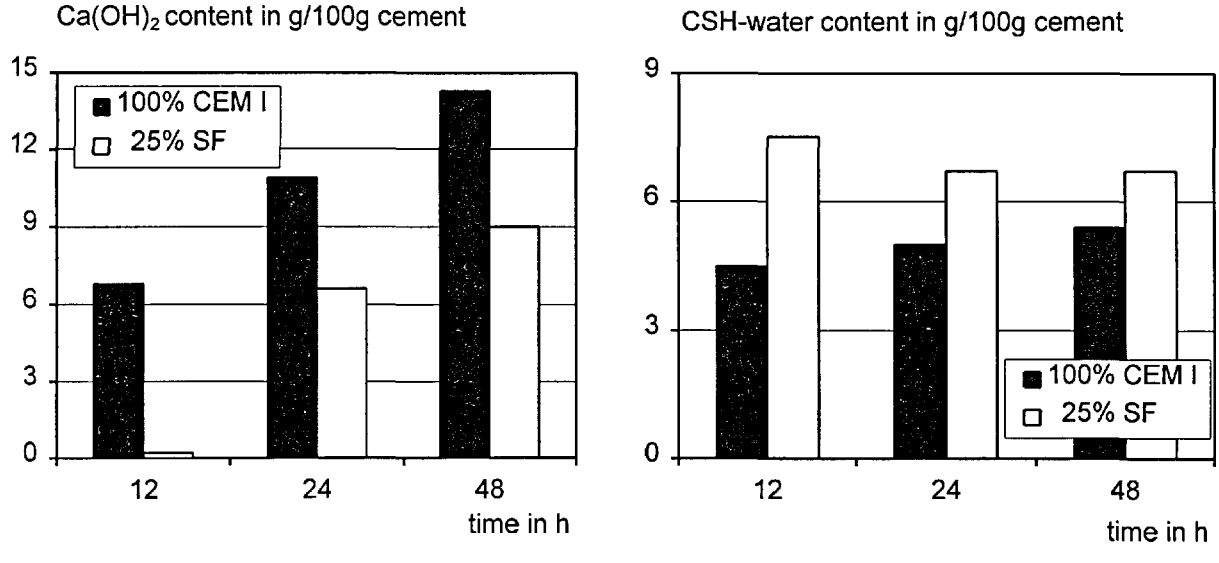

Figure 3: Influence of silica fume on $Ca(OH)_2$ and CSH-water contents for mixes with CEM I

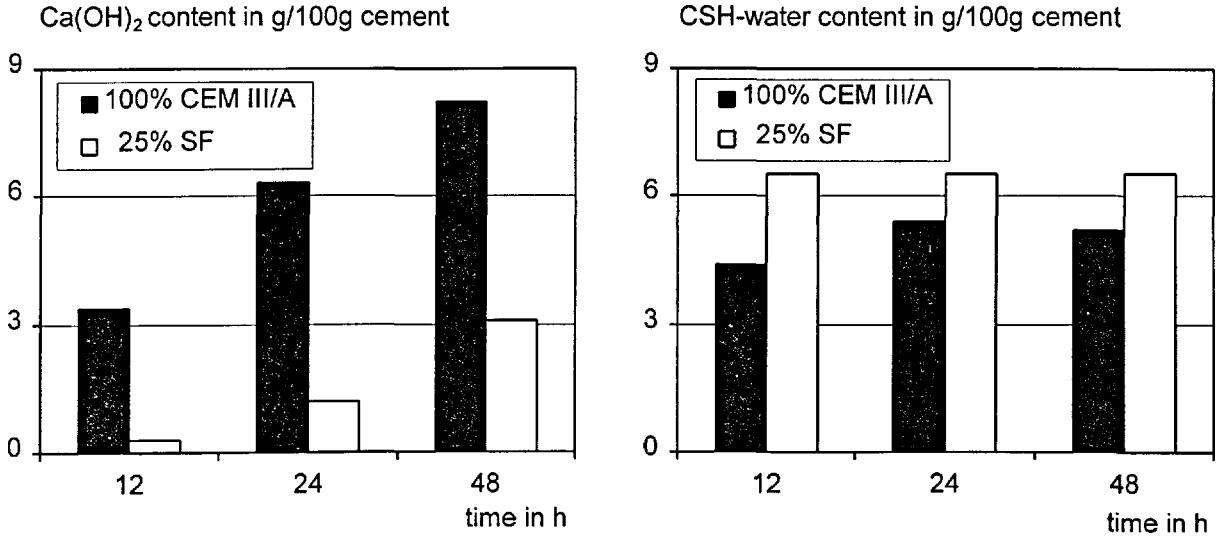

Figure 4:Influence of silica fume on $Ca(OH)_2$ and CSH-water contents for mixes with CEM III/A

It is notable that the mixes with silica fume contain only very minimal quantities of $Ca(OH)_2$ after 12 hours, while the reference mixes without silica fume already reveal a high level of $Ca(OH)_2$ content. The possibility of a delay in the cement hydration process can be excluded, as measurement of the heat of hydration rather revealed an accelerating effect (see Fig. 2). It would appear justified to assume that the quantity of $Ca(OH)_2$ corresponding to the difference involved here has already been consumed as a result of a very early reaction of the silica fume. Fig. 5 shows the differences in the $Ca(OH)_2$ content and in the CSH water content between the specimens with and without silica fume. If the difference between the $Ca(OH)_2$ content of the mixes containing silica fume and the mixes without silica fume is interpreted as the $Ca(OH)_2$ consumed by a pozzolanic reaction, in the case of the Portland cement this results in the paradox that the "$CaOH)_2$ consumption" is higher after 12 hours than after 24 hours. This can only be the case if the consumption of $Ca(OH)_2$ in the period between 12 and 24 hours is overcompensated by the new formation of $Ca(OH)_2$ (possibly accelerated cement hydration by the effect of silica fume as a nucleation substrate).

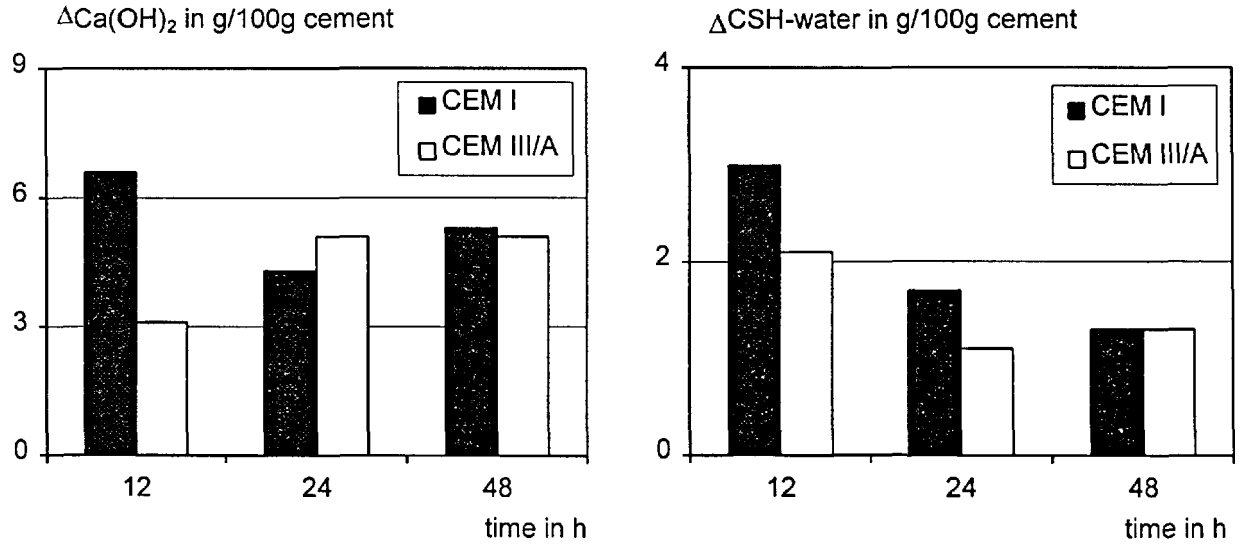

Figure 5: Influence of silica fume on $Ca(OH)_2$ and CSH-water contents (differences between the mixes with and without silica fume)

The course of development of the differences between the CSH contents of the mixes with and without silica fume, which is also presented in Fig. 5, supports the theory that a pozzolanic reaction already takes place at this stage. In all cases, the CSH water content of the mixes containing silica fume is greater than that of the mixes without silica fume. The blends containing silica fume reveal a higher surplus CSH water content after 12 hours than after 24 hours. This can only mean that primarily water-rich hydrate phases are formed, which release part of their water content again within several hours. Such dehydration is to be found with water-rich silica gels. It is possible that this dehydration may also take place with water-rich CSH gels.

This result is supported by different reports documented in literature. Specific examinations of the reaction products of silica fume in the early phase showed even when sufficient $Ca(OH)_2$ is available, CSH phases do not develop directly. Instead, a gel with high water content and low lime content is first of all formed (Grutzeck et al, 1983). This gel formation begins in the very first minutes after mixing. In turn, the gel then reacts to form CSH phases. This reaction takes

place predominantly with $Ca(OH)_2$, but it may also occur with CSH phases containing higher levels of lime from the cement hydration process (Wu and Young, 1984).

When silica fume binds large quantities of water in water-rich gel in the early phase, this water is interpreted (evaluating the TG curves) as a constituent of the so-called CSH water, with no possibility of differentiation. The dehydration characteristics of the thermogravimetry do not reveal any characteristic differences for the various investigated ages (12, 24, 48 hours). With this method, it is not possible to clarify whether a CSH gel or a silica gel (or both) forms.

At the age of 24 and 48 hours the results can be interpreted more clearly, after initially formed water-rich gel phases have released part of their water. A substantial quantity of $Ca(OH)_2$, of approximately the same magnitude in both cases, had already been consumed in both types of cement. This is accompanied by a higher CSH water content in the mixes containing silica fume, which supports the assumption that pozzolanic reactions are already taking place here.

SUMMARY

On the basis of the discussed results regarding the evolution of hydration heat and phase evolution, it was possible to determine the following influences of silica fume on the processes in the early phases of cement hardening:

- Replacing cement with silica fume does not inevitably lower the total quantity of hydration heat (in relation to the total binder mass) released in the early phase. An evident lowering is to be observed in combination with CEM III/A only, while in combination with CEM I nearly the same quantity of heat is produced as with the pure cement.
- When the quantity of heat developed in the early phase is considered in relation to the cement content, a substantial contribution of the silica fume to the evolution of hydration heat is to be observed with both types of cement. This is to be regarded as an indication that pozzolanic reactions already take place in the early phase of hydration. Without additional experiments, however, such effects cannot be clearly differentiated from a possible increase in the evolution of hydration heat as a result of an acceleration in clinker hydration (effect of nucleation substrate and higher w/c value).
- The course of phase evolution also indicates an early onset of the pozzolanic reaction. This is substantiated both by the consumption of $Ca(OH)_2$ and by the formation of additional CSH phases with regard to the reference mixes without pozzolanas. In the mixes containing silica fume, this formation process occurred very early, irrespective of the type of cement.
- The point in time at which the maximum level of hydration heat development occurs is brought forward by silica fume. The maximum is more pronounced than in the cement paste without silica fume. The latter effect is particularly pronounced in the employed CEM III/A.
- When silica fume is added, there are indications of other involved reactions, such as the primary formation of water-rich gels (CSH gel or silica gel). Thermogravimetry is unable to differentiate the bound water which results from these reactions and from the pozzolanic reactions, which consequently makes interpretation more difficult. This high level of water binding occurs primarily during the solidification phase of < 24 hours.

It can be deduced from these results that pozzolanic reactions occur with silica fume at an early age. Pozzolanic reactions are not the only reactions which take place, however: Water-rich gel phases develop very quickly within the first 12 hours, and these are accompanied by a high rate of evolution of hydration heat. These gel phases relatively quickly release a large proportion of

their water once again (stage between 12 and 24 hours). This phase transition could serve as a plausible explanation for the early shrinkage and the frequent ultrafine microcracking systems which are to be found in concretes containing a high level of silica fume.

REFERENCES

Alfes, Ch., „Modulus of Elasticity and Drying Shrinkage of High-Strength Concrete Containing Silica Fume", Detroit: American Concrete Institute, ACI SP-132, 1992.- In: „Fly Ash, Silica Fume, Slag, and Natural Pozzolans in Concrete", Proceedings 4th International Conference, Istanbul, May 1992 (Malhotra, V.m.(Ed.)), Vol. 2, 1651-1671

Al-Sugair, F.H., „Analysis of the Time-Dependent Volume Reduction of Concrete Containing Silica Fume", Magazine of Concrete Research 47 (1995), No. 170, 77-81

CEB; Comite Euro-International du Beton, „Durable Concrete Structures - Design Guide", Bulletin d'Information (1992), No. 183

Cheng-Yi, H., Feldman, R.F., „Hydration Reactions in Portland Cement-Silica Fume Blends", Cement and Concrete Research 15 (1985), No. 4, 585-592

Cohen, M.D., Olek, J., Dolch, W.L., „Mechanism of Plastic Shrinkage Cracking in Portland Cement and Portland Cement - Silica Fume Paste and Mortar", Cement and Concrete Research 20 (1990), No. 1, 103-119

Grutzeck, M.W., Atkinson, S., Roy, D.M., „Mechanism of Hydration of Condensed Silica Fume in Calcium Hydroxide Solutions", Detroit: American Concrete Institute, ACI SP-79, 1983. - In: Proceedings of the CANMET/ACI First International Conference on the „Use of Fly Ash, Silica Fume, Slag and Other Mineral By-Products in Concrete", Vol. 2 (1983), 643-664

Marsh, B.K., „Relationships Between Engineering Properties and Microstructural Characteristics of Hardened Cement Paste Containing Pulverized Fuel Ash as a Partial Cement Replacement", PHD Thesis, the Hatfield Polytechnic; Cement and Concrete Association, 1984

Meland, I., „Influence of Condensed Silica Fume and Fly Ash on the Heat Evolution in Cement Pastes", Detroit: American Concrete Institute, ACI SP-79, 1983. - In: Proceedings of the CANMET/ACI First International Conference on the „Use of Fly Ash, Silica Fume, Slag and other Mineral By-Products in Concrete", Vol. 2 (1983), 665-676

Schießl, P., Meng, B,. „Grenzen der Anwendbarkeit von Puzzolanen im Beton", Aachen: Institut für Bauforschung, (1994), Report No. F405

Wu, Z.-Q., Young, J.F., „The Hydration of Tricalcium Silicate in the Presence of Colloidal Silica", Journal of Materials Science 19 (1984), No. 11, 3477-3484

DIN prEN 196 - 9, „Methods of Testing Cements - Heat of Hydration - Semi-Adiabatic Method", 1994

INTERACTION OF SILICA COLLOID WITH PORTLAND CEMENT

CHANDRA,S*, BERGQVIST,H**
* Chalmers University of Technology, Götebrog, Sweden
** Eka Chemicals AB, Bohus, Sweden

ABSTRACT
Interaction of silica colloids with cement have been studied with the help of XRD and thermogravimetric analysis. It is shown that the reactivity of silica colloid with calcium hydroxide is much faster in comparison with the condensed silica fume. Small amount of colloidal silica is sufficient to produce the same pozzolanic effect as with the addition of higher doses of condensed silica fume at early ages.

Keywords: Calcium hydroxide, Silica fume, Interaction, Pozzolanic reaction, Silica Colloid.

INTRODUCTION
Silica fume is an industrial by product from ferro-silicium alloys producing units, and hence its availability is limited. Silica fume gives dark color to the concrete which is due to the unburnt coal contained in it, and is an aesthetical problem. However, specially treated silica fumes are available, but they are expensive. Besides this, being an industrial by-product homogeneity of the product can vary. This uncertainty in the quality can be overcome by using silica colloids which are man made in chemicals manufacturing companies. This makes its easy access worldwide. Special silica colloids have been developed by Eka Nobel AB, Sweden for use in cement mortars and concrete. These are tested in mortars and concretes at the Division of Concrete Structure, Chalmers University of Technology; Göteborg, Sweden. Interaction of condensed silica fume calcium hydroxide has been studied by many researchers (Buck et al, 1981, Costa and Massaza, 1983, Grutzeck et al, 1983). Interaction of silica colloid with portland cement during hydration is studied and comparison is made with condensed silica fume.

Silica Colloid
The silica colloids specially developed are stabilized for use in mortars and concrete. It is the aqueous silicic acid suspension which contains silicic acid particles expressed as silica, in an amount in the range from about 8% to 60% silica by weight of solution. The specific surface area of the particles is in the range of about 50 m^2/g to a 1000 m^2/g, but preferably in the range from about 50 m^2/g to about 200 m^2/g. Generally, the aqueous silicic suspension employed includes silicic acid particles which have a wide particle size distribution with particles ranging from 5 to 200 nanometers. Preliminary tests have been done with silica colloids having specific surface area ranging between 80 to 500 m^2/g. Some of the results are reported here. It was found that the silica colloid with specific surface area of 80 m^2/g behaved reasonably well. It was used therefore in further investigations.

MATERIALS AND METHODS
Standard Portland cement, supplied by Cementa AB, Slite.
Condensed silica fume (**SF**) was supplied by ELKEM, Norway. It has specific surface area of 20 m^2/g. It is in the dry powder form.

Colloidal silica (**KF**); was supplied by Eka Chemicals AB, Bohus, Sweden. It has specific surface area of 80 m^2/g.

Calcium silicates which are major constituents of Portland cement reacts with water and produce calcium hydroxide. Calcium hydroxide thus produced interacts with silica from condensed silica fume and silica colloid. This interaction is studied here. Portland cement, condensed silica fume/silica colloid and water have been mixed at the constant water to binder ratio. Total binder (portland cement + SF/KF) has also been kept constant. The mixes are shown in Table 1. The samples have been sealed in plastic beakers and were put with their lock on in water to avoid leakage to air and subsequent carbonation. These samples were used for XRD and thermogravimetric analysis.

X-ray Diffraction Analysis

The samples prepared have been analyzed after 1, 7, 28 and 48 days by X-ray diffractometry. The amount of calcium hydroxide detected at a particular time is calculated with respect to their intensities in cps (count per second). The results are summarized in Figure 1. Figure 2 shows the presence of calcium silicates at particular times. Calcium hydroxide (reflection at $2\theta = 18.10°$) decreases both with the addition of condensed silica fume as well as with silica colloid (Figure 1). The amount of calcium hydroxide is less in all the samples except with 4% SF, compared with the reference samples i.e without the addition of silica. This tendency is not very much pronounced with 4% SF even at the later stage. Whereas with the addition of 8 and 16% SF there is not much difference after one day but later on substantial decrease in the amount of calcium hydroxide is noted. In the case of silica colloid the amount of calcium hydroxide is significantly low compared to the other samples already after 1 day. 4% KF consumed 60% more calcium hydroxide after 7 days than 4% SF. It suggests that the silica colloid has reacted more and thus has consumed more calcium hydroxide. 8% and 16%
SF have shown more reaction than 4% KF assessed from the lower amount of calcium hydroxide presence, but have reacted less than 8% KF which has shown the lowest amount of calcium hydroxide at all ages. Consequently rate of reaction was highest for 8% KF.

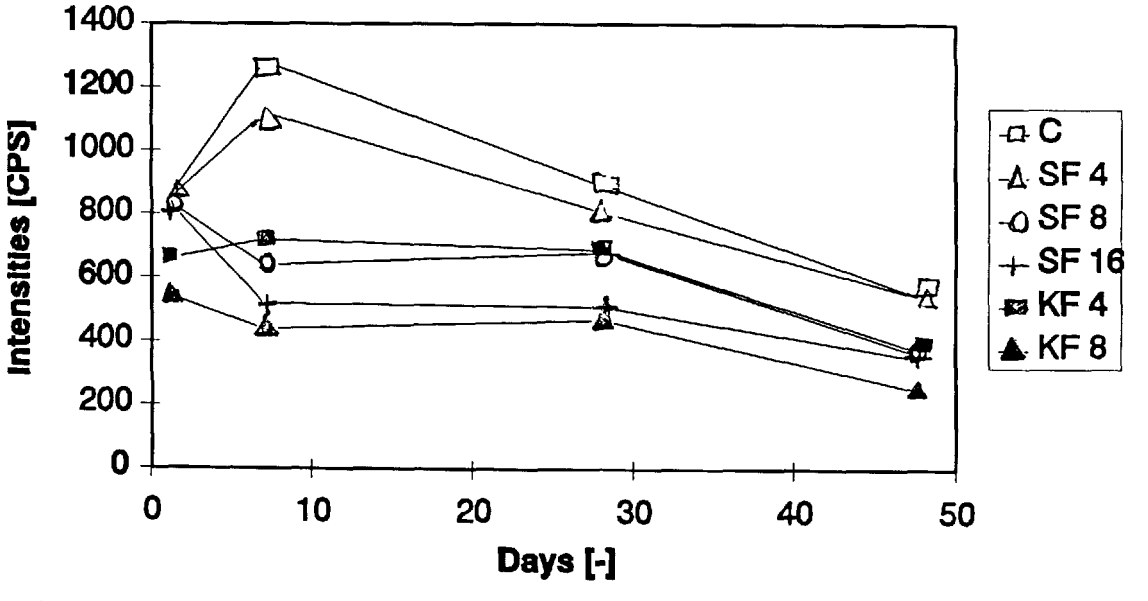

Figure.1, Quantity of calcium hydroxide calculated as counts per second (cps at $2\Theta = 18.10°$) at different curing times.

With increase in the reaction with calcium hydroxide and silica, more calcium silicate hydrate is produced in the early stage, which subsequently provides strength to the mortar. It may lead to higher early strength with the addition of silica colloid compared to the addition of condensed silica fume. On the other hand the content of di-calcium silicate (C_2S) and tri- calcium silicate

(C_3S) are a slightly higher in the case of 8% colloidal silica addition. It is speculated that the higher dose of silica colloid causes gelling, and some of the cement
particles become encapsulated and hydrate slower. It suggests that the higher dosages of silica colloid is difficult to mix. The limit seems to be 4-5% silica calculated on its solid weight in the dispersion to the weight of cement. Because of its high specific surface area very small amount of silica colloid is able to provide the same effect as with the addition of higher dosages of condensed silica fume at early ages.

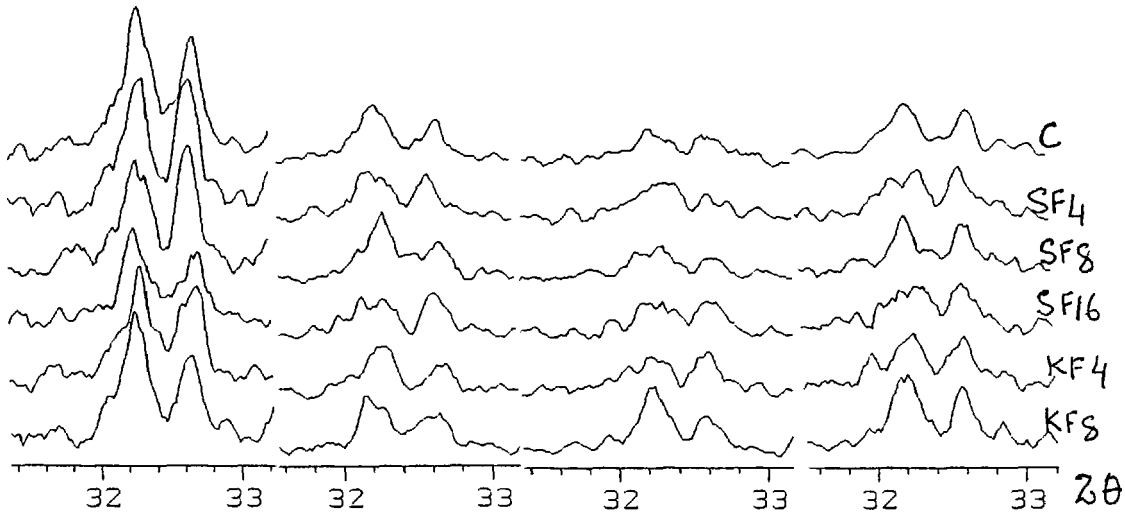

Figure 2, XRD of calcium silicate at different times a) 1 day, 148.92 cps, b) 7 days 280.98 cps, c) 28 days 280.98 cps, d) 48 days, 198.69 cps.

Thermogravimetric Analysis

The cement paste samples with the condensed silica fume and silica colloid addition (Table 1) have been analyzed by thermogravimetric method. The weight loss between 105-400°C have been calculated as non evoperable water to the weight of cement have been calculated. Weight loss between 400-500°C is on the otherhand considered mainly due to the loss of water from calcium hydroxide and is calculated as calcium hydroxide in percent to cement weight. Similar method have been used by Costa and Massaza (1983) for determining calcium hydroxide. The results are shown in the Figures 3 and 4 respectively.

Fig. 3 shows that the non evoperable water is higher in the case of 4 and 8% KF compare to the equal amounts of SF after one day. This tendency continues upto 7 days when its becomes on the same level. After 7 days the non evoperable water does not increase in the same proportion as in the case of SF and the reference sample. It means that there is less physically combined water and more chemically combined water, which suggests that the silica colloid has reacted more compare to the SF upto 7 days. After 7 days the reaction with SF becomes more progressive.

Water of calcium hydroxide is very low at 7 days with silica colloid addition (4% KF and 8% KF, Fig.4) compared to those made with silica fume addition. It shows that the reactivity of silica colloid to calcium hydroxide is much higher at early age compared with condensed silica fume. This confirms the measurements of the non evoperable water. Same tendency has been shown upto 28 days both with 4 as well as 8% addition. After which 8% addition continued to

show higher reactivity compared with 4% silica colloid addition upto 48 days.

Table 1., Mix proportions for X-ray diffraction and thermogravimetric analysis, number represents weight units.

No.	Description of Mix
1	Cement 100 + Water 35
2	Cement 96 + SF 4 + Water 35
3	Cement 92 + SF 8 + Water 35
4	Cement 84 + SF 16 + Water 35
5	Cement 96 + KF 4(Soln.8) + Water 31(4 water from KF solution).
6	Cement 92 + KF 8(Soln.16) + Water 27(8 water from KF solution).

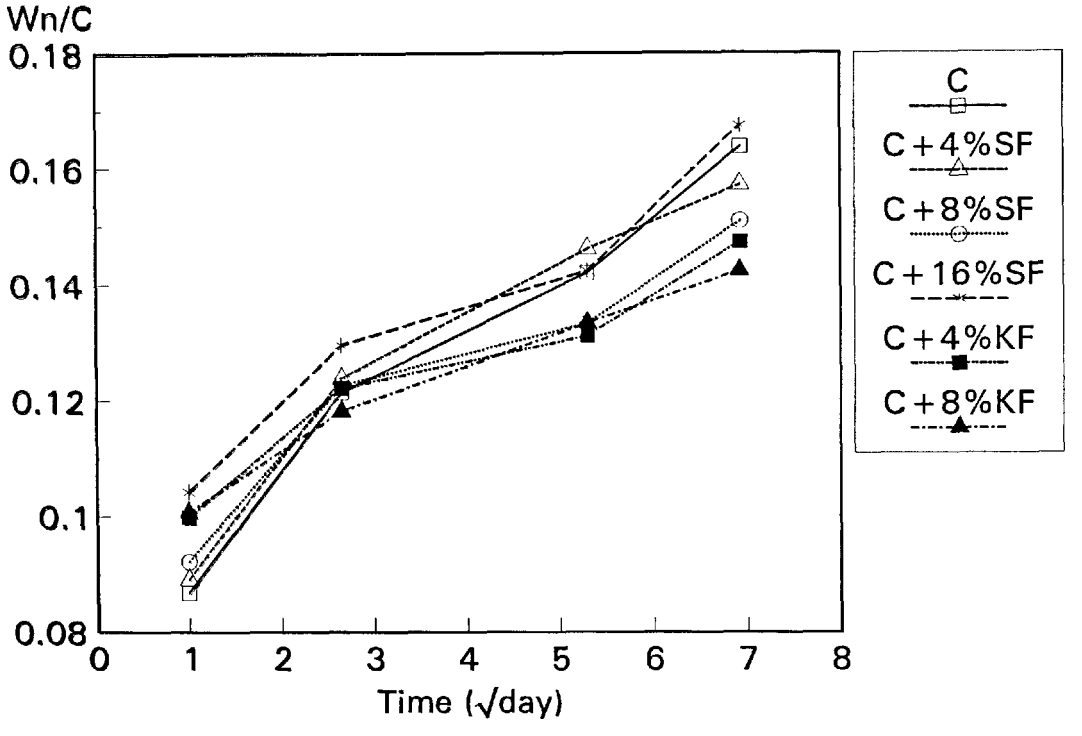

Figure 3, Weight loss between 105-400°C to the weight of cement with respect to curing time.

Thermogravimetric analysis results have shown low calcium hydroxide at 7 days both with the addition of 4 as well as 8% addition of silica colloid compare with the silica fume addition, suggesting more interaction with silica colloid than with condensed silica fume. Whereas XRD analysis has shown that the calcium hydroxide lies between 4% KF and 8% KF at 7 days. It shows that reaction with 8% SF and 16% SF at 7 days is more than 4% KF and less than 8% KF with calcium hydroxide, which is not in agreement with the thermogravimtric results. It may be due to the formation of silica rich layer around some of the cement particles with 8 and 16% condensed silica fume addition, causing hindrance in hydration, and thus resulting in less calcium hydroxide formation. This lower amount is subsequently interpreted

as due to the interaction with silica fume. Gel like layer formation is described by Grutzeck et al (1983).

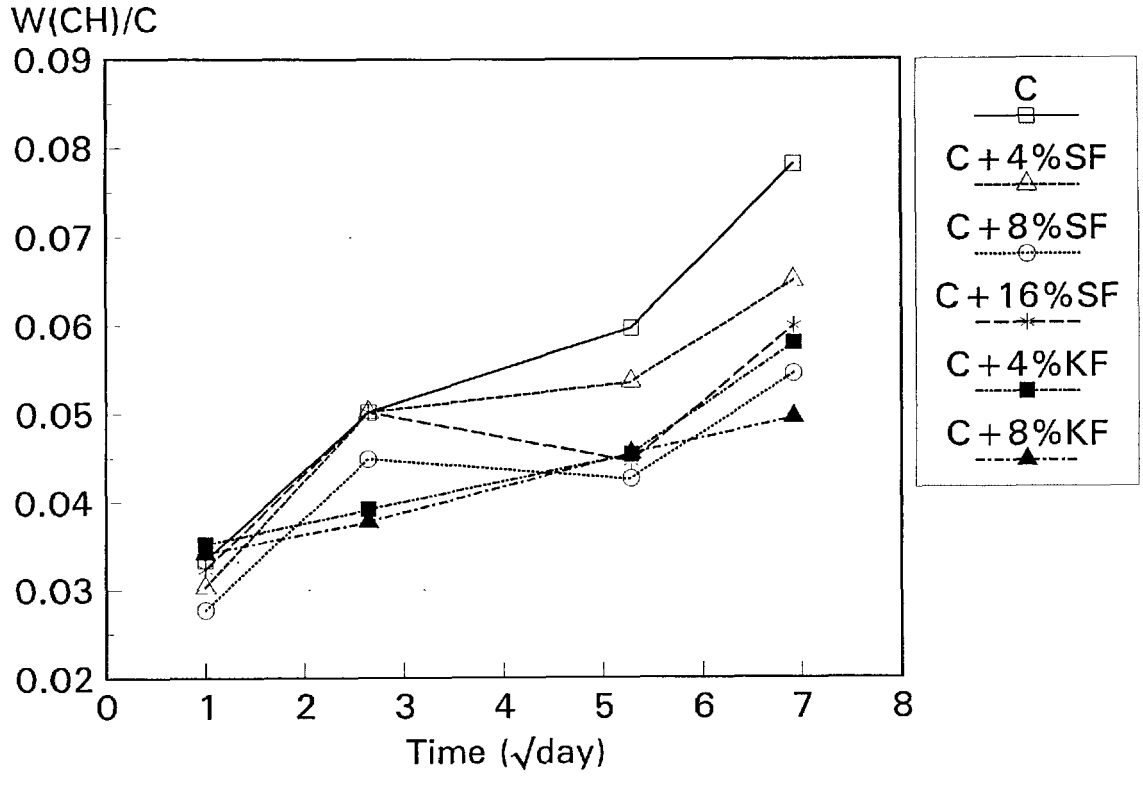

Figure 4, Weight loss between 400-500°C to the weight of cement with respect to curing time.

It clearly shows that there is more interaction of silica colloid with calcium hydroxide in comparison to condensed silica fume especially at early age. Similar observations have been made by Young et al (1984) during their study on the influence of colloidal silica on tri-calcium silicate hydration. One of the main reason of this is attributed to the fine particle size of silica colloid. Another factor involved may be that the silica colloid unlike condensed silica fume is in fine dispersion form which enables its quick access to the calcium hydroxide formed during portland cement hydration.

CONCLUSIONS

Tests performed reveal that the colloidal silica reacts with calcium hydroxide produced during the hydration of portland cement much faster than in the case of condensed silica fumes specially at early age. This may lead to the development of high early strength in mortar and concrete with its addition.

Small amount of silica colloid shows similar pozzolanic effect as with the higher doses of silica fume at early ages. This effect is attributed to the finer particle size of silica colloid.

REFERENCES

Buck A.D., and Burkes J.P., Characterization and reactivity of silica fume, Miscellaneous paper SL 81-13 US Army Engineer Waterways Experimental Station, Structural Laboratory, Vicksburg, USA 1981.

Costa U, and Massaza F., Some properties of pozzolanic cements containing fly ashes; In Proceedings First International Conference on The use of fly ash, silica fume, slag and other mineral admixtures in concrete, Montebello, 1983, ACI SP 79-11, pp 235-254.

Grutzeck M.W., Atkinson S., and Roy D.M., Mechanism of hydration of condensed silica fume in calcium hydroxide solution, in Proc. In Proceedings First International Conference; The use of fly ash, silica fume, slag and other mineral admixtures in concrete, Montebello, 1983, ACI SP 79-11, pp 643-664.

Kurbus B., Bakula F., and Gabrovsek R, Reactivity of silica fume from ferro-silicium production with calcium hydroxide under hydrothermal conditions, Cement and Concrete Research, vol. 15, 1985, 134-140.

Sanchez M.I de Rojas and M. Frias; The pozzolanic activity of different materials, its influence on the hydration heat on mortars, Cement and Concrete research., vol. 26, No.2, 1996, pp 203-213.

ZHAO-Q Wu and Young, J. F, The hydration of tri-calcium silicate in the presence of colloidal silica, J. Material Science 19, 1984, pp 3477-3486.

3ii107
8 pp

EFFECT OF POZZOLANIC ADDITIVES IN THE PORTLAND CEMENT ON THE HYDRATION RATE OF ALITE

Kiyoshi ASAGA, Teikyo University of Science and Technology
Hiroshi KUGA, Teikyo University of Science and Technology
Shigeru TAKAHASHI, Cement Association of Japan
Etsuo SAKAI, Tokyo Institute of technology
Masaki DAIMON, Tokyo Institute of technology

ABSTRACT Pastes of portland cement with pozzolanic additive in the water/solid ratio of 0.3–0.5 were hydrated at 20℃. The hydration percentage of alite was measured by means of quantitative X–ray analysis. It was observed that the standard deviation of reaction percentage of alite was about 1%. The hydration rate of alite in the portland cement is almost independent of water/solid ratio at initial stage, and reaction percentage in later stage is strongly affected by the water/solid ratio. Each pozzolan accelerates the hydration rate of alite.

Key–words Portland cement, Alite, Hydration, Pozzolana, Calcium hydroxide

INTRODUCTION

The hydration rate of portland cement is significantly affected by the water/cement ratio and pozzolanic additives. There are many studies on the effects of the water/cement ratio or pozzolanic additives on the hydration of portland cement (COPELAND,1968, UCHIKAWA,1986, TAYLOR,1990, MASSAZZA,1992). The hydration percentage of each compound is usually measured by means of quantitative analysis of XRD. But it is very difficult to get a sufficient accuracy. Then, there are little data of hydration percentage of cement compounds in the blended cement in spite of fundamental data of a mass concrete or high strength development concrete. To discuss the effect of pozzolanic additives on the hydration ratio of cement compounds, it is necessary to get a sufficient accuracy of XRD analysis. The authors discussed the method of measurement of hydration percentage of each compound by means of quantitative XRD analysis in their previous studies (ISHIZAKI,1988a, ASAGA,1992). The purpose of this study is to get more accuracy of measurement, and discuss the effect of water/solid ratio and pozzolanic additives on the hydration rate of cement compounds and hydration products by analyzing the precise hydration percentage of cement compounds.

The accuracy of the reaction rate of alite was improved, but was not improved for reaction ratio of belite and aluminate phase. The effect of water/solid ratio and pozzolanic additives on the hydration rate of alite in the blended cement are discussed in this studies.

EXPERIMENTAL PROCEDURES

SAMPLES

Ordinary portland cement used in the experiments was prepared by cement association of Japan, which did not include any pozzolan or filler particles. Chemical composition and physical test results of the ordinary portland cement are listed in Table 1. From the calculation of Bogue equation, there is 60% C_3S, 16% C_2S, 9% C_3A and 8% C_4AF in this portland cement. Specific gravity, Specific surface area and chemical compositions of used fly ash, blastfurnace slag and silica fume are listed in Table 2. Portland cement (PC) and the 3 types of blended cement were prepared by mixing the portland cement and pozzolan such as 80wt% of portland cement and 20wt% of fly ash (PF), 50wt% of portland cement and 50wt% of slag (PB) and 90wt% of portland cement and 10wt% of silica fume (PS).

Cement paste prepared with water to solid (W/S) ratio of 0.30, 0.40 and 0.50 was sealed in a test tube, and then cured in a incubator at 20℃ for 1, 3, 7 and 28 days, respectively. Hydration

was stopped by acetone and dried at 110℃ for 24 hours. In the case of preparation of paste with W/S=0.30, 0.6wt% of naphthalene–formaline condensates was added as the superplasticizer.

Table 1 Chemical composition and physical properties of the portland cement

Chemical compositions / wt%											
Ig.loss	Insol	SiO_2	Al_2O_3	Fe_2O_3	CaO	MgO	SO_3	Na_2O	K_2O	TiO_2	P_2O_5	MnO
0.4	0.1	21.3	5.0	2.6	65.0	2.0	1.9	0.21	0.67	0.34	0.14	0.11

specfic gravity	specific suface area (cm^2/g)	setting(h–m) inital	setting(h–m) final	flow	compresive strength 3d	7d	28d (M/Pa)	bending strength 3d	7d	28d (MPa)
3.17	3230	2–34	3–34	253	15	26	43	3.8	5.0	7.2

Table 2 Chemical composition and physical properties of the pozzolans

additive	specific gravity	specific surface area(cm^2/g)	Ig.loss	SiO_2	Al_2O_3	Fe_2O_3	CaO	MgO	SO_3	Na_2O	K_2O	TiO_2	P_2O_5	MnO
FA	2.49	2740	2.06	53.3	23.0	6.15	6.73	1.64	0.82	2.59	1.40	1.31	0.20	0.03
BFS	2.91	3910	0.10	32.4	13.6	0.20	42.8	6.60	2.00	0.19	0.28	0.60	0.02	0.34
SF	2.33	20.3*	4.57	8.87	0.90	1.45	0.30	1.22	0.42	0.49	1.58	0.01	0.08	0.05

*m^2/g, gas adsorption

MEASUREMENT AND ANALYSIS OF HYDRATION

Ignition loss of hydrated samples was measured by burning at 1000℃ for 1 hour. Amount of $Ca(OH)_2$ was measured by means of differential scanning calorimetry (DSC). Hydration ratio of each compound was measured using XRD. For XRD analysis, 10% of corundum was added as internal standard. Measurement was carried out after drying at 200℃ for 24 hours in order to dehydrate the AFm phase. This treatment was necessary to avoid to overlap between the peaks of AFt and belite. The condition of measurement was as follows. Target: Cu, 40kV, 150mA, 1 step: 0.02 deg./5 sec. More than eight measurements on each sample were carried out to avoid the statistical error and preferred orientation factor of minerals. Hydration ratio was calculated from the integrated intensity of selected peaks by means of pattern fitting calculation program using modified Lorentz function (ISHIZAKI, 1988b).

RESULTS AND DISCUSSION

Figure 1 shows the effect of water/solid ratio on the reaction ratio of alite in the samples of portland cement (PC). The standard deviation of reaction percentage of alite was about 1% in this study, which was smaller than that of previous study (ASAGA,1992). In the case of the samples with W/S=W/C=0.4 and 0.5, hydration of alite proceeded up to 28 days curing, but in the case of 0.3, it was very slow after 3 days curing. The reaction percentage of alite in the sample cured for 1 and 3 days was about 53% and 67% respectively, which was not affected by the water/solid ratio. But after 3 days curing, it was strongly affected by the water/solid ratio. The hydration rate of alite in the sample with W/S=0.3 decreased with curing time and then less than 75% of alite reacted at 28 day curing. On the other hand, it did not so decrease in the sample with W/S=0.4 and 0.5, the reaction percentage of alite at 28 days curing was about 90% and 92%, respectively. These results were in good agreement with the previous studies (ASAGA,1992).

From these results, it was considered that the amounts of water was sufficiently supplied to maintain the hydration of the cement until about 70% of alite reacted. In this range, hydration rate of alite in the cement did not depend on the amount of water/solid ratio. In the case of W/S=0.3, either supply of water or space for precipitation of hydrates was short to maintain the hydration, and then the ratio of hydration decreased remarkably after 70% of alite reacted.

Figure 2 shows the effect of water/solid ratio on the reaction ratio of alite in the samples with fly ash (PF). The reaction percentage of alite at 1 day curing was about 57%, which was almost same amount the samples with different water/solid ratio, and slightly greater than that of PC. It changed with water/solid ratio after 3 days curing. The hydration rate of alite in the

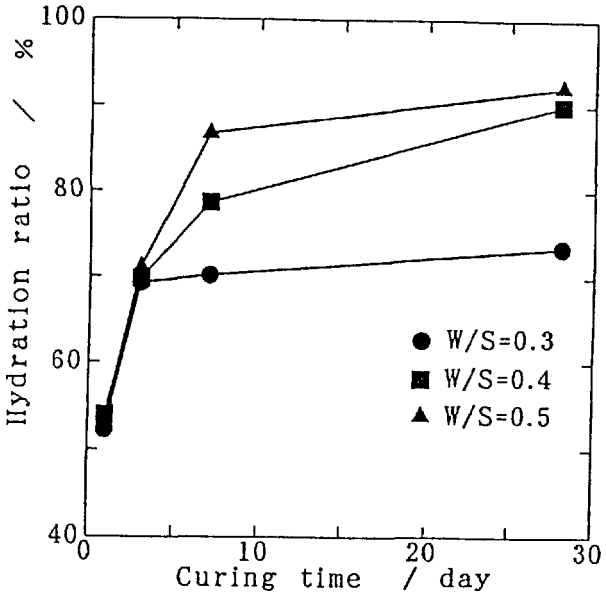

Fig.1 Effect of water/solid ratio on the reaction ratio of alite. sample: PC

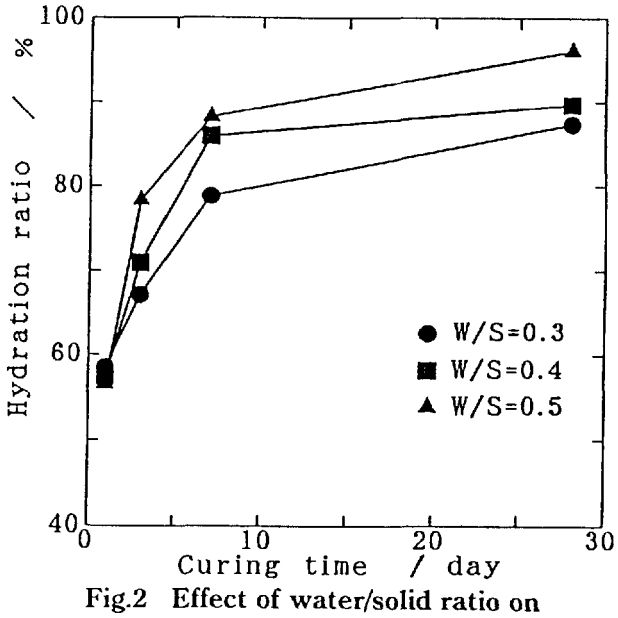

Fig.2 Effect of water/solid ratio on the reaction ratio of alite. sample: PF

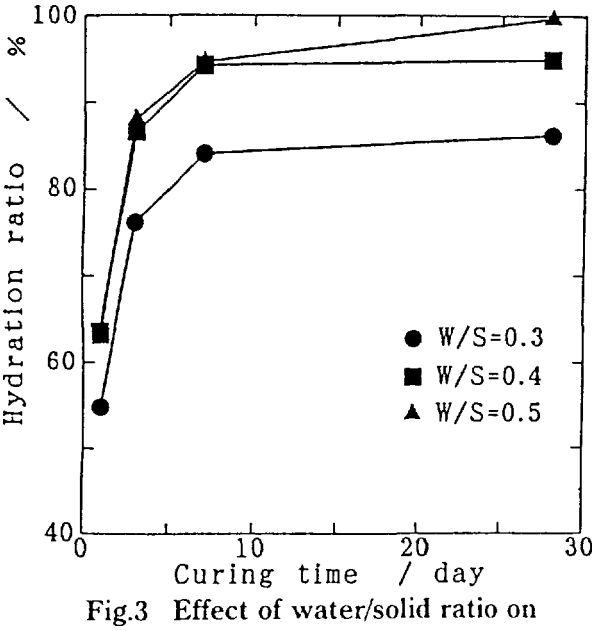

Fig.3 Effect of water/solid ratio on the reaction ratio of alite. sample: PB

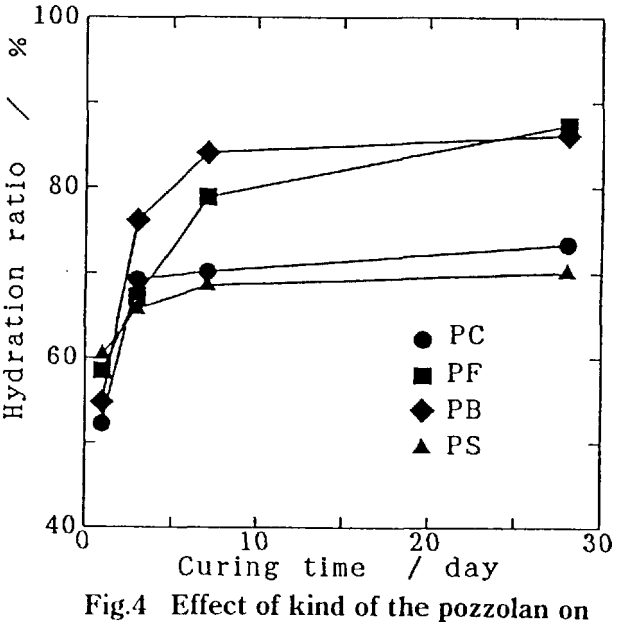

Fig.4 Effect of kind of the pozzolan on the reaction ratio of alite W/S=0.3.

sample with W/S=0.3 did not so much decreased with curing time compared to PC, and then about 87% of alite reacted at 28 day curing. In the case of W/S=0.4 and 0.5, the reaction percentage of alite at 28 days curing was about 90% and 96%, respectively.

Figure 3 shows the effect of water/solid ratio on the reaction ratio of alite in the samples with slag (PB). The hydration rate of alite in all of the samples was larger than that of PC. In the case of W/S=0.4 and 0.5, the reaction percentage of alite at 1 days curing was about 63% and 64%, respectively, which was about 10% larger than that of PC. But in the case with W/S=0.3, it was about 55%, which was slightly larger than that of PC. The hydration of alite continued with curing time, and then about 86% of alite was reacted at 28 day curing in the sample with W/S=0.3. In the case of W/S=0.4 and 0.5, almost of alite reacted, the reaction percentage of alite at 28 days curing was about 94% and about 99%, respectively.

Figure 4 shows the effect of kind of the pozzolan on the reaction ratio of alite in the samples

with W/S=0.3. At the 1 day curing, the reaction percentage of alite with pozzolan was larger than that of PC. In the case with silica fume, the reaction percentage of alite was largest at 1 day curing, but the hydration rate decreased with curing time and then less than 70% of alite reacted at 28 day curing, which was smaller than that of PC. On the other hand, it did not so much decrease in the sample with fly ash or slag, the reaction percentage of alite at 28 days was larger than that of PC.

The water/portland cement ratio (W/C) is different among the samples with the same water/solid ratio, because the amount of addition is different in the each pozzolanic materials. If the water/solid ratio (W/S)=0.3 is estimated in water/portland cement ratio (W/C), W/C is 0.375 in the case of PF, W/C is 0.6 in the case of PB, W/C is 0.33 in the case of PS. But the difference of the hydration percentage of alite among the samples within 3 days curing did not considered to the effect of water/solid ratio, because the reaction percentage of alite in the PC was not affected by the water/solid ratio within 3 days curing. The differences was considered to the effect of pozzolanic reaction.

The each pozzolan affected the reaction (UCHIKAWA,1986, MASSAZZA,1992). It is well known that silica fume accelerate the reaction of alite resulting the pozzolanic reaction (HUANG, 1985). In this study, it is clarified that the 10% of addition of silica fume accelerate the reaction of alite about 8% at 1 day curing. The microstructure changes by pozzolanic reaction resulted in the decrease of the reaction of alite at the later stage.

Figures 5 and 6 show the effect of kind of the pozzolan on the reaction ratio of alite in the samples with W/S=0.4 and 0.5, respectively. Within the 28 days curing, the reaction percentage of alite with pozzolan was larger than that of PC. Slag accelerated the alite reaction more than fly ash. In the both case of PF and PB, the hydration percentage did not change with W/S within the 7 days of curing. After 7 days curing, the reaction continued in the samples with 0.5, but slowed down in the samples with 0.4.

Water/portland cement ratio (W/C) is 0.5 (PF), 0.8 (PB) as W/S=0.4. and is 0.625 (PF), 1.0 (PB) as W/S=0.5, respectively. It is considered that the sufficient amount of water is existed in all the system. The acceleration of the hydration of alite did not result of the large water/solid

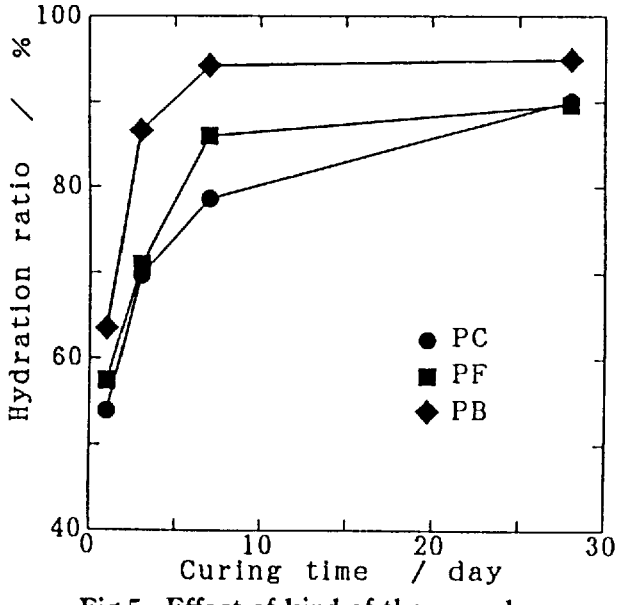

Fig.5 Effect of kind of the pozzolan on the reaction ratio of alite W/S=0.4.

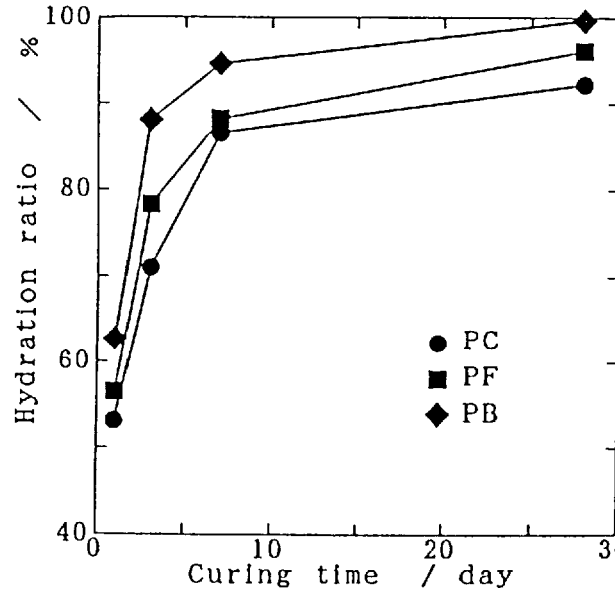

Fig.6 Effect of kind of the pozzolan on the reaction ratio of alite W/S=0.5.

ratio, because the reaction percentage of alite was the same value between W/S=0.4 and 0.5 within the 7 days curing. In the later stage, the retardation of the reaction in the case of W/S=0.4 was not due to the shortage of water but change of microstructure.

Figures 7–9 show the effect of water/solid ratio on the loss on ignition in the samples of PC, PF and PB, respectively. Figure 10 shows the effect of kind of the pozzolan on the loss on ignition in the samples with W/S=0.3. The each value was shown by the ignited base. In the case of PC , PF and PS, the loss on ignition increased with curing time almost the same manner of the hydration of alite. But in the case of PB, it increased much after 3 days curing compared to the reaction ratio of alite. It suggested the pozzolanic reaction of slag was much larger than that of fly ash.

In the case of W/S=0.5, the weight loss at 28 days curing of PC was about 25%, and the weight loss between 50℃ and 110℃ was about 13% of the initial solid, which was measured from sample weights dried at 50 ℃ for 24 hours and dried at 110 ℃ for 24 hours. About 12% of

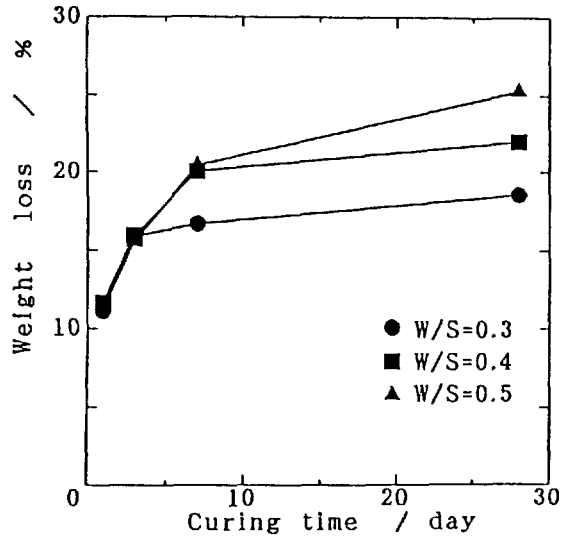

Fig.7 Effect of water/solid ratio on the loss on ignition samples: PC

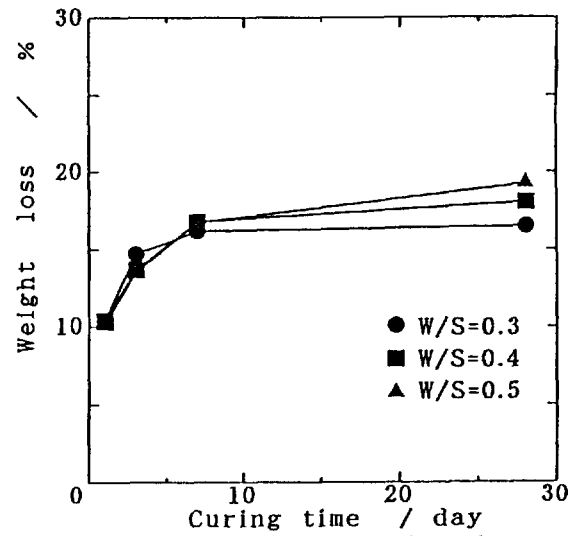

Fig.8 Effect of water/solid ratio on the loss on ignition samples: PF

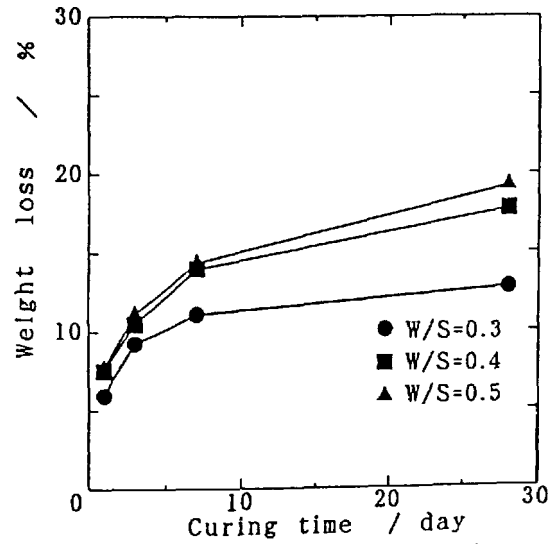

Fig.9 Effect of water/solid ratio on the loss on ignition samples: PB

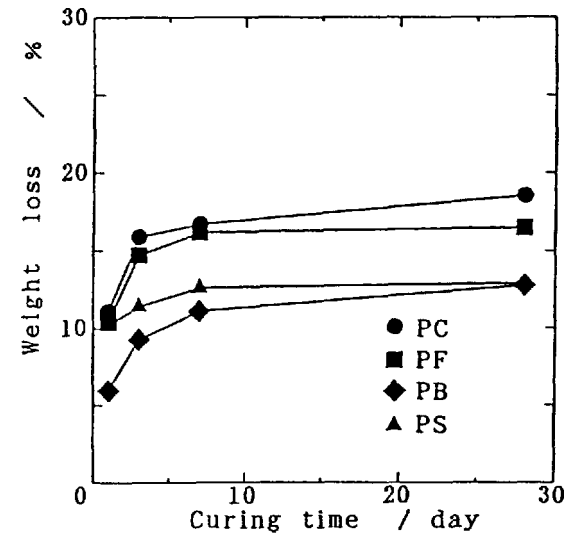

Fig.10 Effect of kind of the pozzolan on the loss on ignition W/S=0.3.

free water existed in the system at 28 days curing, In the case of W/S=0.3, the value of weight loss at 3 days curing of PC was about 16%, and the weight loss between 50℃−110℃ was about 7%. Less than 7% of free water existed in the system at 3 days curing, and same way, less than 3% of free water at 28 days curing. It is considered that the free water is too little to maintain the hydration in the sample of W/S=0.3 after 28 days curing.

Figures.11−13 show the effect of water/solid ratio on the amount of $Ca(OH)_2$ in the samples of PC, PF and PB respectively. Figure 14 shows the effect of kind of the pozzolan on the amount of $Ca(OH)_2$ in the samples with W/S=0.3. In the case of PC, the amount of $Ca(OH)_2$ increase with time as almost the same manner of the hydration of alite. But the values of W/S=0.3 were too small compared to the reaction ratio of alite. The shape of endothermic curve by decomposition of $Ca(OH)_2$ was observed slightly different from the sample with 0.4 or 0.5 in the measurement of DSC. The same phenomena were observed in the sample with pozzolan only at W/S=0.3. The superplasticizer might have affected the measurement, but, it was not clear that

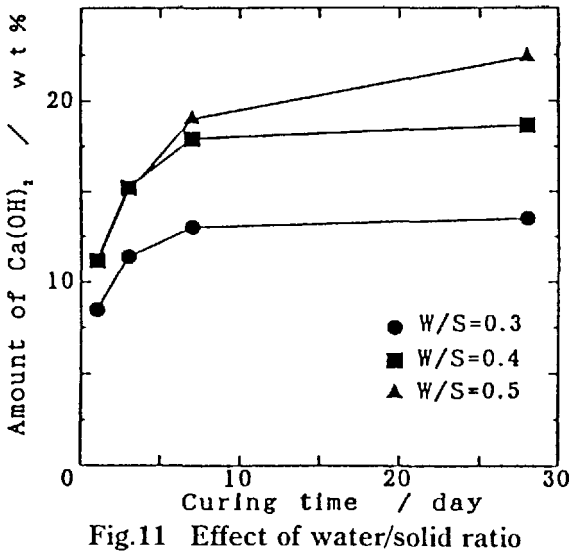

Fig.11 Effect of water/solid ratio on the amount of $Ca(OH)_2$ samples : PC

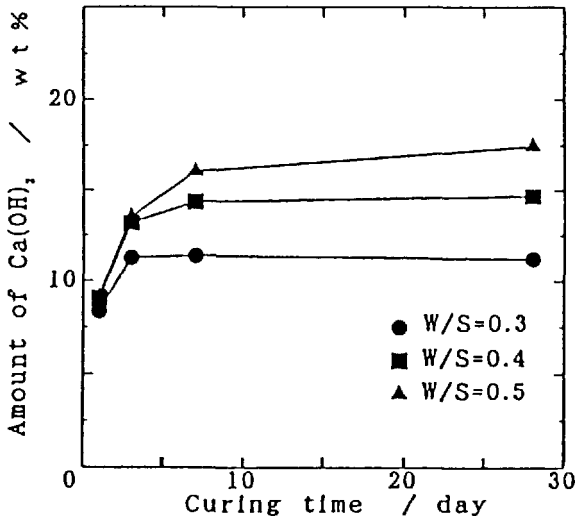

Fig.12 Effect of water/solid ratio on the amount of $Ca(OH)_2$ samples : PF

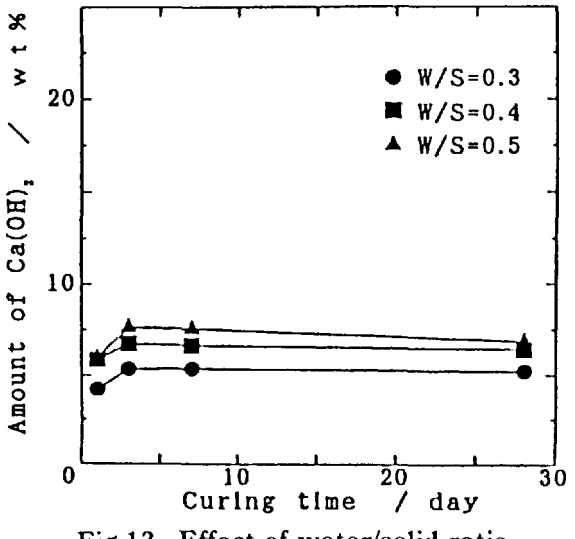

Fig.13 Effect of water/solid ratio on the amount of $Ca(OH)_2$ samples : PB

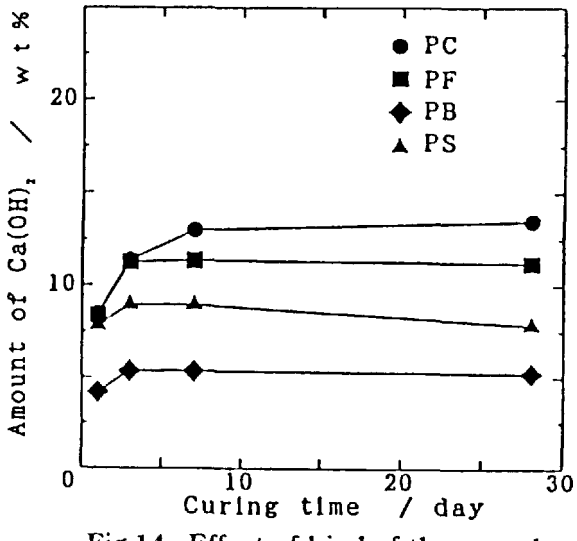

Fig.14 Effect of kind of the pozzolan on the amount of $Ca(OH)_2$ W/S=0.3.

the superplasticizer affected the formation of $Ca(OH)_2$ during the hydration or the only accuracy of the measurement.

In the case of PF, $Ca(OH)_2$ did not decreased within the 28 days curing, but $Ca(OH)_2$ decreased after 3 days curing in the samples of PB and PS.

The ignition loss and amount of $Ca(OH)_2$ of blended cement was smaller than that of PC within 28 days curing. Of course, these values depend on the content of portland cement, to compare the relation each others, the values need to change to per portland cement.

Figures 15 and 16 show the loss on ignition and amount of $Ca(OH)_2$ per portland cement respectively. In the case of W/S=0.4 and 0.5, loss on ignition of PB was remarkably larger than

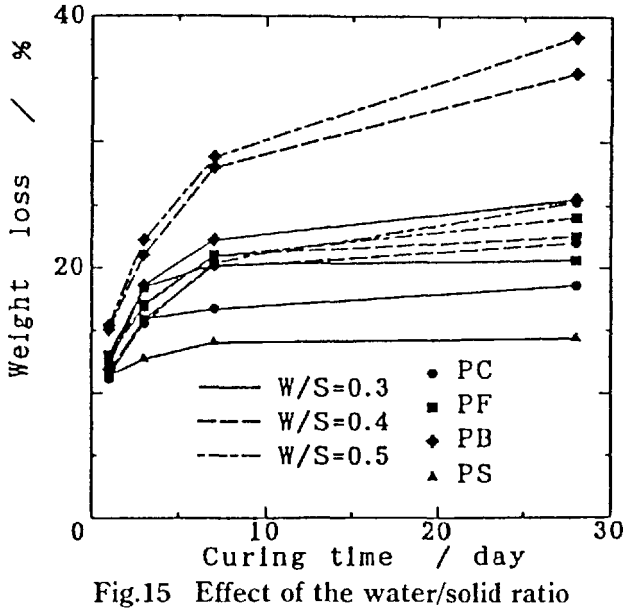

Fig.15 Effect of the water/solid ratio and kind of the pozzolan on the loss on ignition per cement

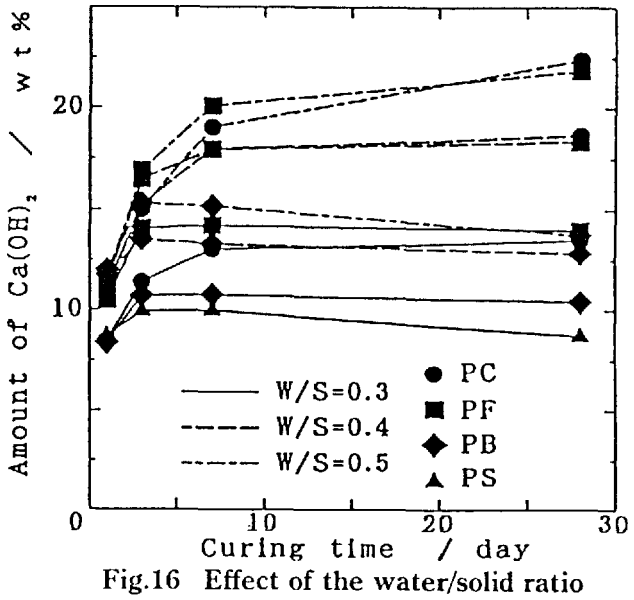

Fig.16 Effect of the water/solid ratio and kind of the pozzolan on the amounts of $Ca(OH)_2$ per cement

that of PC. On the other hand, it was not so much different between PB and PC. In the case of W/S=0.3, it was smaller in the sample of PS than that of the others.

The amount of $Ca(OH)_2$ in the PF samples was slightly large at early curing time, but at later stage it was not so much different from the sample of PC. It suggested that alite reacted more at early time, but fly ash reacted little within the 28 days curing. In the case of PB and PS,the amount of $Ca(OH)_2$ was remarkably less that of PC. Slag and silica fume considered to react from the early stage.

Figure 17 shows relation between the amount of $Ca(OH)_2$ and hydration ratio of alite in this experiments. In the case of W/S=0.3, the amount of $Ca(OH)_2$ is too small, it is discussed without the case of W/S=0.3. In the samples of PC and PS, the amount of $Ca(OH)_2$ increased almost proportionally

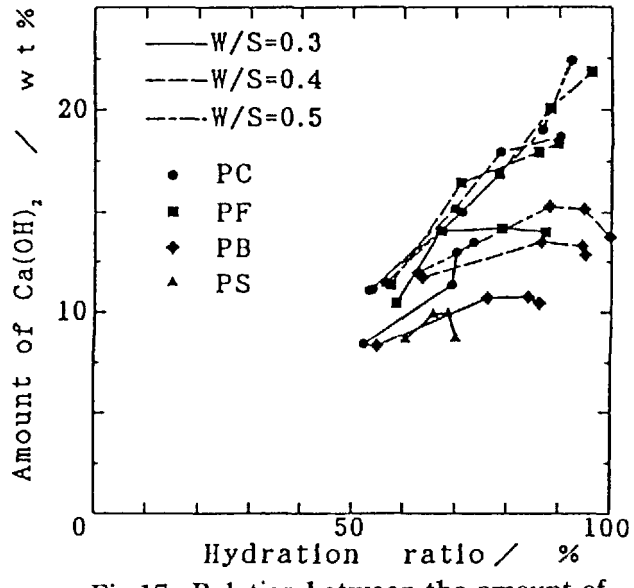

Fig.17 Relation between the amount of $Ca(OH)_2$ and hydration ratio of alite in the samples

with hydration ratio of alite, and it appears almost on the same line. In the samples of PB the amount of $Ca(OH)_2$ was remarkably below the line.

The mineral composition is assumed to the Bogue equation, the following experimental equation between the amount of $Ca(OH)_2$ and the amount of reacted alite was obtain from the sample PC and PB.

$$Y=1.15X$$

where, Y is the amount of $Ca(OH)_2$ shown as mole, X is the reacted alite shown as mole. The C/S ratio of C–S–H calculated was 1.85. It is the same result with the previous data (ASAGA,1992). In the case with fly ash, C/S ratio of C–S–H did not change remarkably within the 28 days curing.

It is pointed out that the mineral compositions are different from those obtained from Bogue equation and actual content of alite is larger than that from Bogue equation (YAMAGUCHI,1968, TAYLOR,1990). In the case, the C/S ratio of C–S–H might be larger than 1.85.

The value of C/S ratio of C–S–H produced from PB was not calculated because of the unknown of the hydration ratio of slag. The more studies will be needed to clarify the reaction of cement and pozzolanic additives, especially the improvement of the accuracy of analysis of the hydration rate of belite and aluminate.

CONCLUSIONS

(1) The hydration percentage of alite in the portland cement with the pozzolans was measured by XRD. It was observed that the standard deviation of reaction percentage of alite was about 1% .

(2) The hydration rate of alite in the portland cement is almost independent of the water/cement ratio at initial stage, and reaction percentage in later stage is strongly affected by the water/cement ratio.

(3) Fly ash accelerates the hydration rate of alite especially at initial stage, but fly ash reacts little at the initial stage.

(4) Slag accelerates remarkably the hydration rate of alite.

(5) Silica fume accelerates the hydration rate of alite especially at initial stage, but retards later.

REFERENCES

ASAGA, K.,ISHIZAKI, M., TAKAHASHI, S., KONISHI, K., TSURUMI, T. and DAIMON, M., "Effect of Curing Temperature on the Hydration of Portland Cement Compounds.", Proc. 9th Intl. Sym. Chem. Cement, New Delhi, 1992, Vol.4, pp. 181–187.

ISHIZAKI, M., ASAGA, K., DAIMON, M. and TAKAHASHI, S.,"Measurement of Reaction Ratio of Each Compound in the Hydration Process of Portland Cement", CAJ Rev., 1988, No.42, pp. 38–41.

ISHIZAKI, M. "Measurement of Reaction Patio of Each Compound in the Hydration Process of Portland Cement", Master of Theses, Tokyo Institute of Technology, 1988.

COPELAND, L.E. and KANTRO, D.L., "Hydration of Portland Cement", Proc. 5th Intl. Sym. Chem. Cement, Tokyo, 1968, Vol.2, pp. 387–421.

HUNG, C.Y and FELDMAN, R.F. "Hydration Reaction Cement–Silica Fume Blends", Cem. Conc. Res., 1985, Vol.15, pp. 585–592.

MASSAZZA, F. and DAIMON, M., "Chemistry of Hydration of Cements and Cementitious Systems", Proc. 9th Intl. Sym. Chem. Cement, New Delhi, 1992, Vol.1, pp. 383–446.

TAYLOR, H.F.W., "Hydration of Portland Cement", Cement Chemistry, Academic Press, London, 1990, pp. 199–241. UCHIKAWA, H., "Effect of Blending Components on hydration and Structure Formation" Proc. 8th Intl. Sym. Chem. Cement, Rio De Janeiro, 1986, Vol.1, pp. 249–280.

YAMAGUCHI, G and TAKAGI,S,, "The analysis of portland clinker", Proc. 5th Intl. Sym. Chem. Cement, Tokyo, 1968,
Vol.1, pp. 181–225.

3ii108
4 pp

CHARACTERISTICS AND HYDRATION MECHANISM OF RHA CEMENT PASTE

Lee K. LIN, National Taipei Institute of Technology, Taipei, Taiwan, ROC.
Chao L. HWANG, National Taiwan Institute of Technology, Taipei, Taiwan.

ABSTRACT Rice husk ash (RHA) produced by controlled incineration is a reactive pozzolan. Test results indicated active RHA are useful for making good concretes. Forming C-S-H gel by silicon ion from RHA with calcium hydroxide (CH) seemed to be one important hydration mechanism. Such hydration mechanism can be used for the R&D of high performance concrete (HPC) with solid waste.

Key words: Rice Husk Ash, Pozzolan, Calcium hydroxide, High performance concrete

INTRODUCTION

In each year, there are about 1.6 million tons of rice husk (RH) produced in the world (Lin, 1989). The treatment of RH has occurred as a severe waste problem due to such material is hard to disintegrate, so how to consume rice husk ash (RHA) effectively should be a significant study (Hwang, et al., 1990).

REVIEW ON R&D OF RHA

The beginning of burning RH into RHA and application as binding material was shown on the record of 1924 (Beagle, 1978). During 1950's RHA was only used in low-value applications (Mehta, 1986). Recent researches on the application of RHA as a supplementary cementing material in portland cement concrete have been made (Al-Khalf and Yousif, 1984, James and Subba, 1986, Boateng and Skeete, 1990, Hwang and Wu, 1989). However, the application is still limited.

RESEARCH PLAN

Acquired RH are treated by burning with Nabertherm furnace. The maximum heating temperature is about 1200°C. The process of heating in this research was maintained at heating rate of 5 °C/sec up to 700°C for 4 hours, and then naturally cooled down. The properties and characteristics of RHA and type I cement are shown in Table 1 (G represents "ground", UG represents "unground"). Cement paste and mortar specimens with W/B of 0.35, 0.47 and 0.59, and with 0, 10, 20 and 30 % RHA of cement, respectively, were studied.

Table 1. Properties of 700°C RHA and Cement

	Item		RHA	Cement
Chemical Ingredients	SiO_2		92.15	20.69
	Al_2O_3		-	6.04
	Fe_2O_3		-	3.29
	CaO		1.60	63.91
	MgO		0.51	2.04
	SO_3		0.79	1.81
	K_2O		3.94	-
	Na_2O		0.99	-
Physical Properties	Fineness (cm^2/g)		-	3200
	Specific gravity		2.22 (G), 2.04 (UG)	3.15
	Compressive strength(MPa)	3 days	-	17.6
		7 days	-	24.6
		28 days	-	36.4
	Setting time	initial	-	2 : 50
		final	-	5 : 30

RHA PROPERTIES AND HYDRATION BEHAVIOR

After burning up to 700°C, the properties of RHA are shown in Table 2.

Table 2. Basic properties of 700°C RHA

Item		Test result	Test method
Appearance color		light pink	visual observation
Weight loss ratio		86.0%(AD); 83.8%(OD)	average of 10 tests
Main ingredient		SiO_2	chemical analysis
Overall unit weight (kg/cm^3)	G	0.29(loose); 0.45(dense)	average of 6 test
	UG	0.14(loose); 0.20(dense)	
true specific gravity		2.22(G); 2.04(UG)	average of 2 tests
Microstructure		dense, straight crystal row	SEM
Pore structure		590 Å of average pore size	MIP

The appearance color of RHA is pink. Residual ash mainly contains SiO_2. Weight loss from combustion is over 80%. The overall unit weight of ground RHA is more than two times of unground RHA and with about 10% higher in density. Pore diameter lies within the range of 590 Å. Figure 1 illustrates the hydration behavior of cement paste with or without RHA. The first peak of heat evolution curve has dropped a lot as the addition of RHA to replace part of cement. This is caused by the large water absorption of RHA at an early stage, and then inadequate water contacts with the cement grain. The zeta-potential of RHA is -20~-30 mV, that is quite active to repeal water. As small amount of RHA may shorten setting time, however large amount may have worse effect on workability due to rough surface and light weight features. Proper use of RHA can obtain better properties, and is believed to help producing with high flowability HPC. On the 7th day, the C-S-H gel has partial growth only; and the

product on the RHA grain surface is not significant. On the 28th day, the C-S-H gel is observed with large formation which is connected with RHA grain as a continuous structure; pores are rapidly decreased; part of needle ettringite and calcium hydroxide (CH) laminar crystal are randomly heaped on the boundary, and therefore the strength is fully developed.

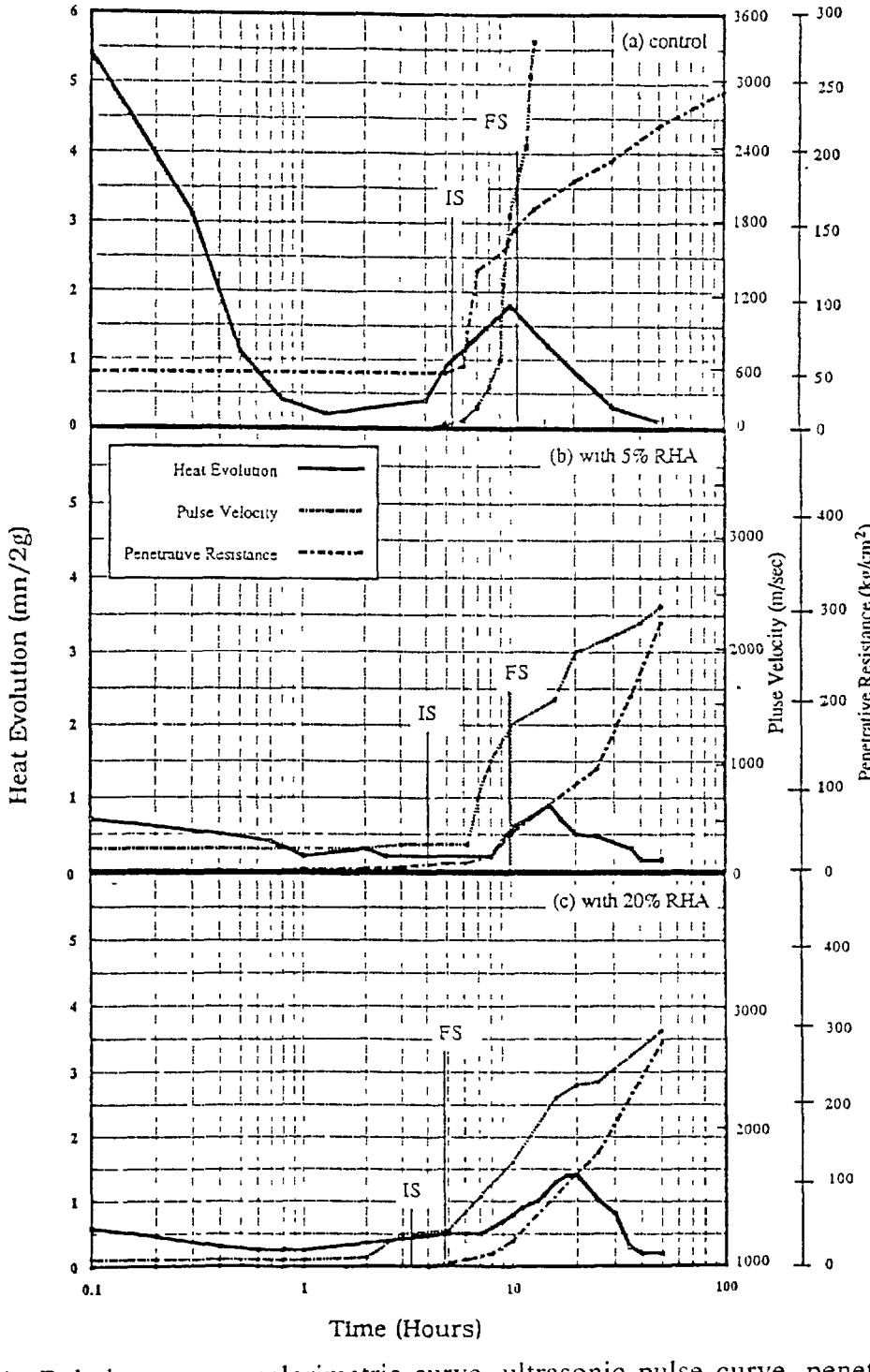

Figure 1 Relation among calorimetric curve, ultrasonic pulse curve, penetrative resistance curve and setting time (W/B=0.47). IS and FS are initial and final set, respectively.

HYDRATION MECHANISM MODEL OF RHA CEMENT

The addition of water with cement will react in the similar way with or without RHA. The water absorbed in the porous silica structure is released and aids the quick reaction of Ca^{++} with silica ion from RHA. Because the amount of hydrate in unit volume is increasing, the pore is decreased, so whole structure gets denser. Moisture is diffused for dissolving CH, therefore Ca^{++} has reacted with Si ion of RHA to form C-S-H gel. Such phenomenon is repeating over and over, so the strength is developed by the increasing age. The crystal is growing in accordance with the increasing of action energy and forms a continuous gel matrix finally.

CONCLUSION

Proper burning of RHA will have porous feature that will be highly active. The hydration mechanism of RHA paste is through silicon ion resolved and bound with CH to form loosen gel. In the future, large quantity of RHA in high quality can be produced in many rice-growing countries and could be effectively applied in HPC.

REFERENCES

Al-Khalaf, M. N. and Yousif, H. A., "Use of Rice Husk Ash in Concrete," J. Cement Composites, Vol. 6, 1984, pp. 241-248, 1984.

Beagle, E. C., "Rice-Husk Conversion to Energy," FAO Agricultural Services Bull 31, Food and Agricultural Organization of the United Nations, Rome, 1978.

Boateng, A. A. and Skeete, D. A., "Incineration of Rice Hull for Use as a Cementitious Material: The Guyana Experience," Cem. Concrete Research, Vol. 20, No. 5, 1990, pp.795-802

Hwang, C. L. and Wu, D. S., "Production of Cements Containing Rice Husk Ash," ACI SP-114 (Editor: V. M. Malhotra), 1989, pp.733-765.

Hwang, C. L., Peng, T. F. and Lin, L. K., "Effect of Burning Temperature on the Pozzolanic Reactivity of Rice Husk Ash", Journal of the Chinese Institute of Civil and Hydraulic Engineering, Vol. 2, No. 3, 1990, pp. 263-272.

James, J. and Subba Rao, M., "Characteristics of Silica in Rice Husk Ash," Amer. Ceram. Soc. Bulletin, Vol.65, No.8, 1986, pp.1177-1180.

Lin, L. K., The Application of Rice Husk Ash in Concrete, National Taiwan Institute of Technology, Taipei, Taiwan, 1989.

Meta, P. K., Concrete-Structure, Material and Properties, Prentice Hall, Englewood Cliffs, NM. J., 1986.

ON THE SEMI-INDUSTRIAL PRODUCTION OF HIGHLY REACTIVE RICE HUSK ASH AND ITS EFFECT ON CEMENT AND CONCRETE PROPERTIES

Shuichi SUGITA, Qijun YU*, Masami SHOYA, Yoichi TSUKINAGA and Yasuo ISOJIMA
Hachinohe Institute of Technology, 88-1, Myo, Hachinohe, 031, Japan
*Institute of Materials, Wuhan University of Technology, China

ABSTRACT Based on the further investigation on the relation between the pozzolanic activity of rice husk ash (RHA) and its burning, grinding processes, the authors proposed a method for the semi-industrial production of highly reactive RHA. It was found the burning and grinding conditions were the key to get active RHA. With the addition of the RHA obtained in the semi-industrial furnace to cement not only the strength of cement was increased but also the resistance of concrete to 2% HCl solution attack, Cl^- penetration and carbonation was improved greatly.

Key words: Acid attack, Penetration, Reactivity, Rice Husk Ash and Strength

INTRODUCTION

Just as the wide application of blast-furnace slag, fly ash and silica fume the possible utilization of rice husk ash (RHA) in concrete has received much attention since the end of 1970s and many positive results have been obtained (Mehta, 1977 and 1986, Karasudhi, 1979, Khan, 1985, Sugita, 1992 and 1996, Mazlum, 1992, and Inoue, 1996). RHA mainly contains 90-95% SiO_2 and 1−5% carbon residue, which is similar to silica fume in SiO_2 content but the SiO_2 in it can be in amorphous or crystalline form according to the manner in which it is burned. When over-burning occurs the amorphous SiO_2 will be changed to cristobalite, quartz and tridymite (Ibrabim and Helmy, 1981, James and Rao, 1986), and when it is burnt at low temperatures much carbon will exist in the product. In either case the pozzolanic activity of RHA will be decreased greatly. Although RHA of high quality has been obtained by many researchers in laboratories because the burning temperatures and cooling conditions can be well controlled at what as desired, yet it is difficult to get active and homogeneous RHA in an industrial scale. In an ordinary furnace for producing RHA in large quantities there always exists a heterogeneous temperature distribution due to the self-burning of rice husk and the heat loss from the surface of the burning rice husk, so the quality of RHA, sampled from the same furnace but at different parts or even at the same part but at different time, is often varied considerably. Now how to realize the production of active RHA with homogeneous quality in an industrial scale, in our opinion, becomes the key to the transformation of the study of RHA in laboratory to its industrial application, which is also the practical and final purpose of the research on RHA. As little detailed information on the above exists, the following work was therefore undertaken: 1) effect of burning temperature and grinding condition on the pozzolanic activity of RHA, 2) design of the furnace for producing RHA in large quantities and 3) the property of the RHA burnt in our semi-industrial furnace and its effect on the characteristics such as strength, resistance to acid attack, carbonation and penetration of portland cement mortar and concrete.

RAW MATERIALS

The used RHA was obtained by burning rice husk in an electric furnace or in the semi-industrial furnace designed by us. The cement and aggregates were: 1) Sumitomo ordinary portland cement, OPC for short, 2)Toyoura standard sand for preparing mortar specimens and 3) crushed stone with the nominal maximum size of 25 mm and river sand as the coarse and fine aggregate of concrete specimens (Table 1). In order to control the flow value of mortars with different RHA addition within 190−210 mm water reducer NL-1450 (highly polymarized aromatic sulphosalt) was adopted and for regulating the air volume and slump of various fresh concrete to about 5% and 12 cm both NL-1450 and air-entraining admixture (vinsol resin) were used.

Table 1 Properties of the aggregates used in this experiment

Sample	Specific gravity	F.M.*	Water absorption (%)	Solid volume (%)
Toyoura sand	2.65	0.96	0.78	57.0
River sand	2.66	2.46	1.26	66.2
Crushed stone	2.72	6.99	0.28	57.9

* F.M.--fineness modulus

EXPERIMENTAL AND RESULTS

Evaluation of the pozzolanicity of RHA

An exact evaluation of the pozzolanicity of any natural or artificial pozzolans should be based on the result of strength tests, but in which at least 28 days will be taken. We found the method for rapid evaluation of pozzolanic activity of natural products by conductivity measurement, proposed by Luxan et al. (1989), was also available to estimate the pozzolanic activity of RHA (Sugita, et al., 1992). The analysis procedures are mainly described as follows: 1) to measure the electrical conductivity of a saturated $Ca(OH)_2$ solution (E_0) of 40 ± 1°C, 2) to add 5.00g of the material to be tested to 200 ml of the $Ca(OH)_2$ solution and stir the solution continuously, 3) to read the electrical conductivity of the solution (E_1) after it is mixed with the material for 120 seconds, and 4) by subtracting E_1 from E_0 the change in conductivity of the solution is therefore obtained. The larger the change in electrical conductivity, the more active the tested material. In present work this method was also used.

Effect of burning temperature on the silica form in RHA and its activity

The effect of burning temperatures on the silica form in the RHA which was burnt in an electric furnace at 600°C, was investigated by high temperature XRD at a heating rate of 10°C / min (Fig 1). Fig 2 shows the change in conductivity of the $Ca(OH)_2$ solution after added with the RHA burned at different temperatures.

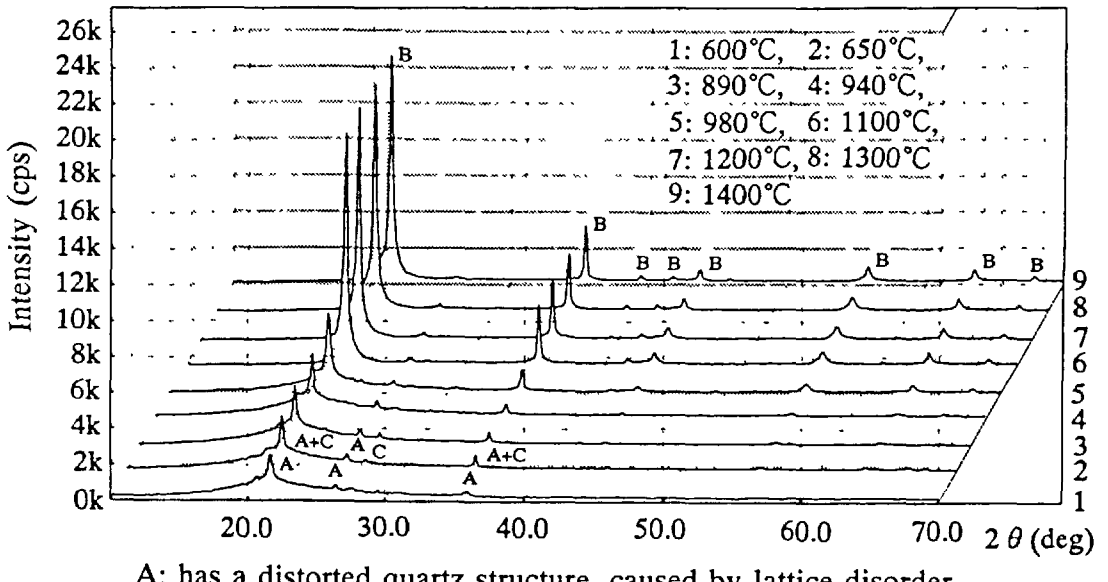

A: has a distorted quartz structure, caused by lattice disorder,
B: β - tridymite, C: β - quartz

Figure 1 XRD patterns of RHA at different temperatures

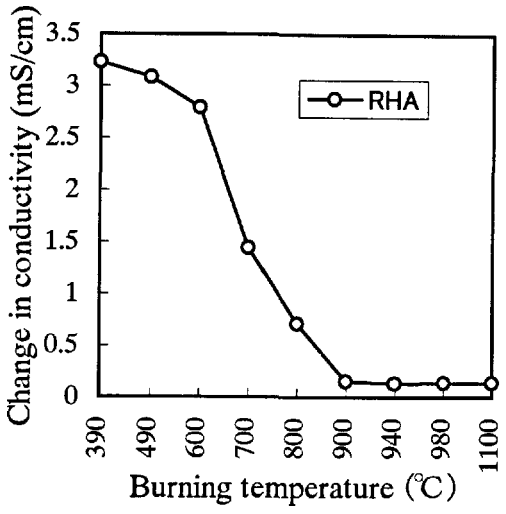

Figure 2 Relation between the change in conductivity and the heating temperature of RHA

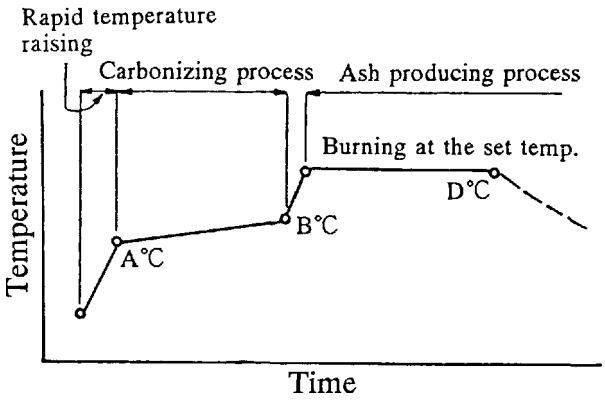

Figure 3 Schematic diagram of the "two step burning method"

Design of the furnace for producing highly active RHA

Based on the relation of the pozzolanicity of RHA with its burning processes and burning temperatures a new way to get highly active RHA, i.e. "two step burning method", has been proposed by the authors (Fig 3), the furnaces in respect to the method are shown in Figs 4 and 5 respectively. The "two step burning method" means that the whole process of burning RHA should be divided into two steps: one is to drive off the organic materials and water in the husk and carbonize the husk at a relatively low temperature under a reducing atmosphere, the other is to burn the carbonized husk to ashes at a proper temperature in a given time. Experiments showed the atmosphere and temperature at which the two processes occur and the time taken for each process were very important to the pozzolanicity of the final product (Sugita, 1996).

According to Luxan et al. (1989) the RHA produced by the furnace of either continuous system or batch system was very active: the change in conductivity of the saturated $Ca(OH)_2$ solution

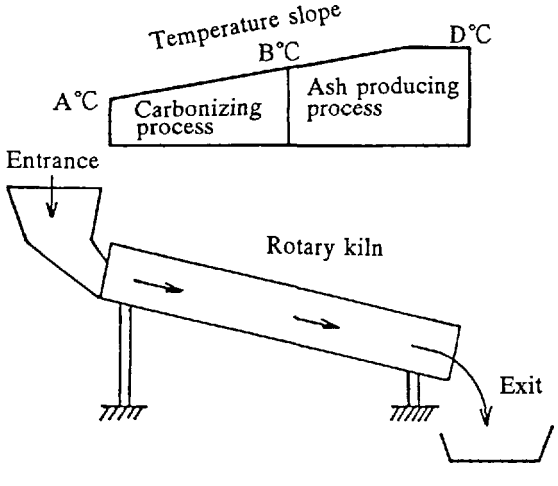

Figure 4 Continuous RHA production system with a rotary kiln

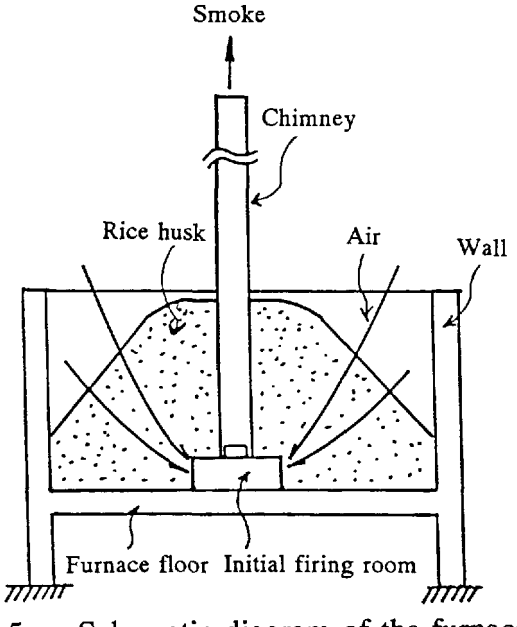

Figure 5 Schematic diagram of the furnace of batch production system

added with the RHA produced by the rotary kiln (Fig 4) and by the furnace as shown in Fig 5, called semi-industrial or batch furnace, was about 6.3 mS/cm and 2.4－3.0 mS/cm respectively. As small temperature difference yet exists in the batch furnace, now innovation upon it is being undertaken. With the addition of the RHA either from the kiln or from the furnace to cement the strength of concrete could be greatly enhanced (Sugita, 1996).

The effect of grinding on the pozzolanicity of RHA

Fig 6 are the SEM images of the corase and ground RHA burnt in the batch furnace. From Fig 6-b it can be found the corase RHA has a porous inner wall. In the presence of grinding agent (J=250) RHA can be finely ground to an average diameter of 15.4 μ m (Fig 6-c) with a high change in conductivity and a large N_2 specific surface (Fig 7), otherwise its specific surface and the change in conductivity are gradually decreased with grinding time, coherently large particles remain in the final product (Fig 6-d and Fig 7). Fig 8 shows the variation of the pore distribution of RHA with its grinding time.

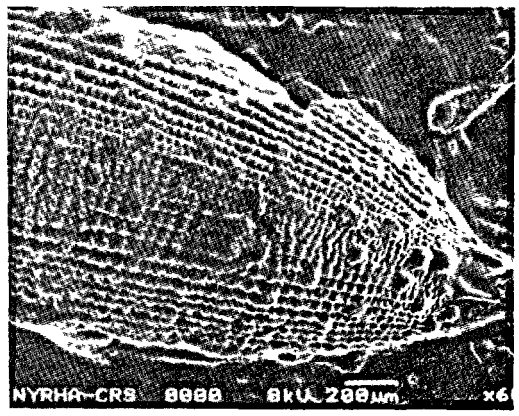

(a) coarse RHA, 60×

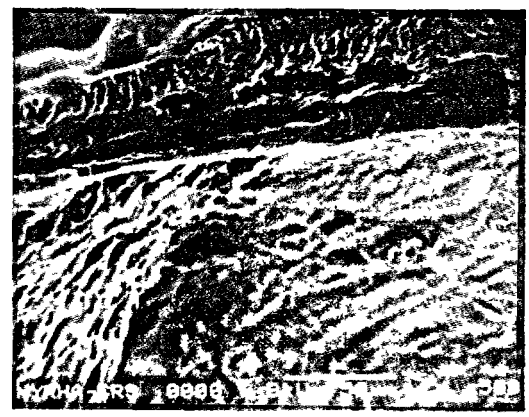

(b) the inner wall of the coarse RHA, 500×



(c) ground RHA with added grinding agent, 250×



(d) ground RHA without added grinding agent, 250×

Figure 6 SEM images of the coarse and ground RHA burnt in the batch furnace

Strength of RHA blended mortar and concrete

In the following experiments all the used RHA was from the batch furnace and ground in a ball mill for 60 min. with 0.025% grinding agent addition (J=250). It contains 91.2% SiO_2 and 1.48% residual C, with N_2 specific surface of 50 m^2/g, change in conductivity of 3.00 mS/cm and specific gravity of 2.17, and the silica in it is mainly in amorphous form.

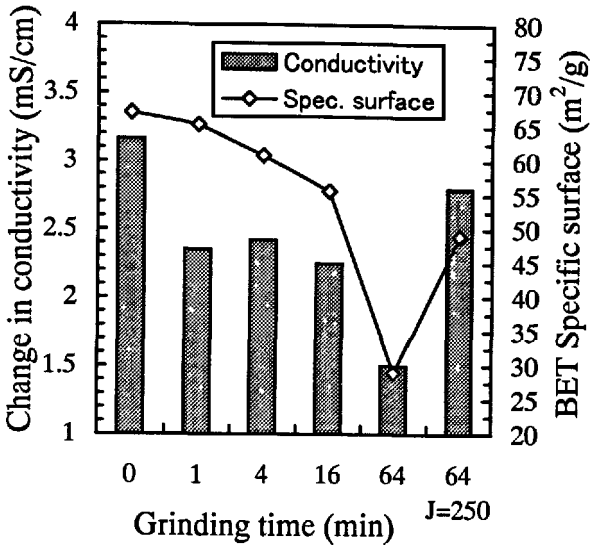

Figure 7 Variation in conductivity and specific surface of RHA vs grinding time

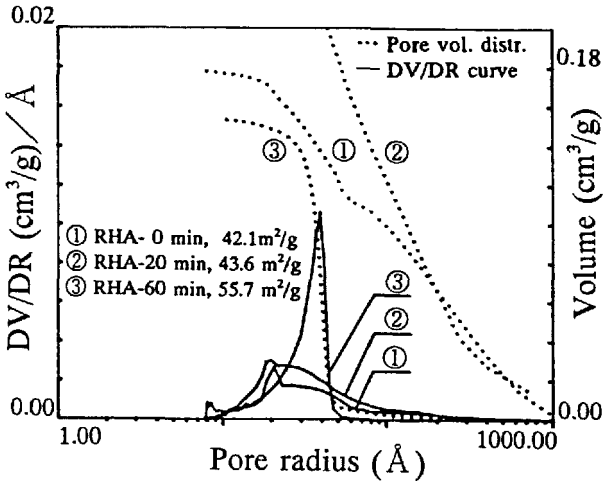

Figure 8 The effect of grinding on the pore distribution and cumulative pore volume of RHA

With adding 5%, 10%, and 15% of this RHA to OPC, mortar specimens of 40×40×160 mm were made at: 1) water cement ratios of 45%, 55%, and 65%, 2) sand cement ratio of 1.5 for the mortar at w/c = 45%, 1.8 for the mortar at w/c = 55%, and 2.0 for the mortar at w/c = 65%, and 3) flow values of 190−210 mm. Fig 9 shows their compressive strength variations relative to the control samples of OPC at 7d, 28d and 91d. According to JIS A 1132 concrete specimens of ϕ 100×200 mm were prepared at: 1) RHA blending ratios of 0%, 10%, 20%, 30%, and 50%,

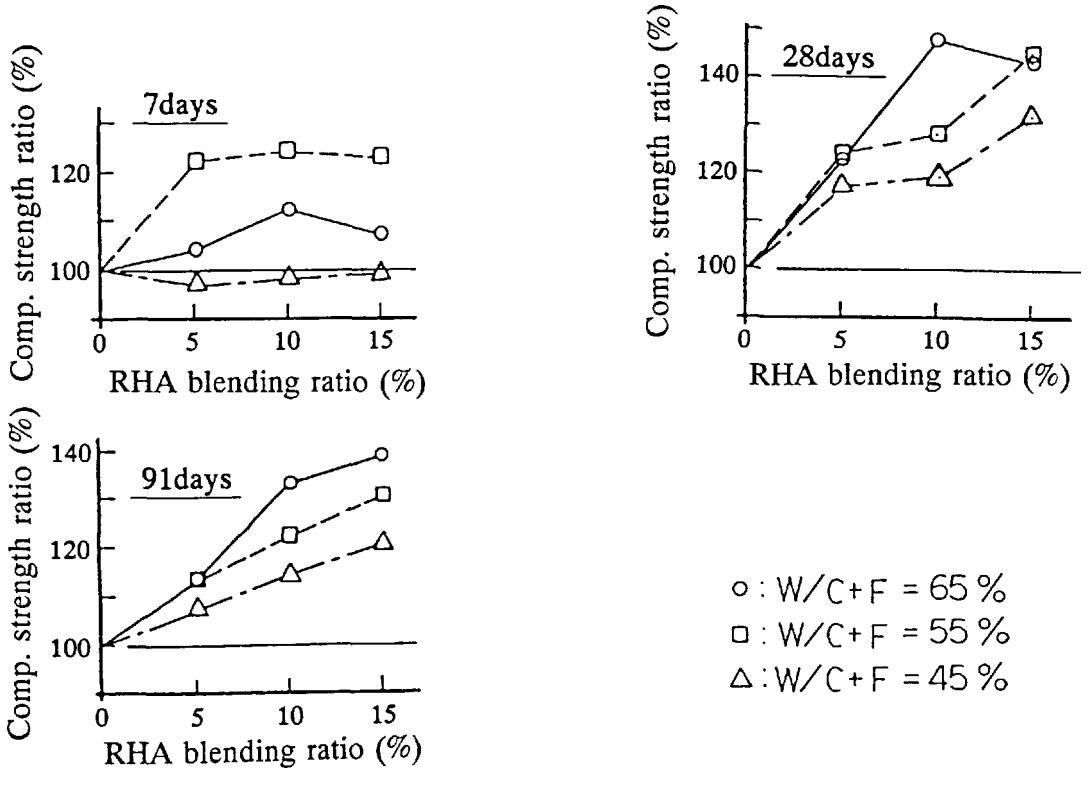

Figure 9 Relative compressive strength of RHA blended mortar vs RHA addition

2) water cement ratios of 70%, 75%, and 80%, and 3) slump of 12±1 cm and air volume of 5±1%. The relative compressive strength of the specimens is shown in Fig 10.

Resistance of RHA blended concrete to carbonation and to the attack by 2% HCl solution

As same as the above concrete cylinders of ϕ 100×200 mm were made at a water cement ratio of 75% and with 0%, 10%, and 30% RHA addition. After curing in water for 28 days the cylinders were dried at 60±2°C for 24 hrs, then dried at 20±2°C in the air of R.H.<40% for one week. Subsequently 3 slices of ϕ 100×50 mm were taken out from the middle portion of each of the cylinders. Finally the slices, with their top and bottom surfaces being tightly sealed with epoxy but with their outside surfaces being exposed, were cured in an accelerated carbonation chamber in which the conditions of 30°C, 60% R.H. and 5% CO_2 were set. Average carbonation depth was measured by a computer coordinating area-curvimeter at the ages of 2, 4 and 8 weeks using 1% phenolphthalein to distinguish carbonated portion from uncarbonated one. The result is as shown as Fig 11. In another aspect, some of the dried concrete cylinders were respectively immmersed to 2% HCl solution and water after their top and bottom surfaces were sealed with paraffin wax. Fig 12 and Fig 13 show their compressive strength and mass variations by percentage compared with the mass before cured in the HCl solution.

Resistance of RHA blended concrete to Cl^- penetration

The concrete cylinders of ϕ 100×200 mm with RHA blending ratios of 0%, 10%, and 30% were prepared at water cement ratios of 65% and 75%. After curing in water for 28 days they were cut to two parts of ϕ 100×100 mm and dried at 20±1°C in the air of 60% R.H. for one week. Afterwards they were immersed into 13% NaCl solution at 20°C for one week and then dried at the same condition for one week. After six immersion-drying recycles the average penetration depth of Cl^- was determined with the area-curvimeter by spraying 0.1% fluorescein sodium solution and 2% $AgNO_3$ solution on the freshly exposed surface, obtained by cutting the specimen along the direction of its diameter, to display the Cl^- penetrating region, the results are shown in Fig 14.

DISCUSSIONS

Fig 1 shows that with the increment of temperature the diffraction intensity of SiO_2 crystal is gradually increased. At 600°C the RHA is mainly consisted of amorphous SiO_2 (d = 4.04Å, JCPDS Card: 29-0085) and there is only a small amount of phase A in it. From 650°C β-quartz appears but disappears at 940°C. After 980°C the diffraction intensity of crystalline SiO_2 becomes

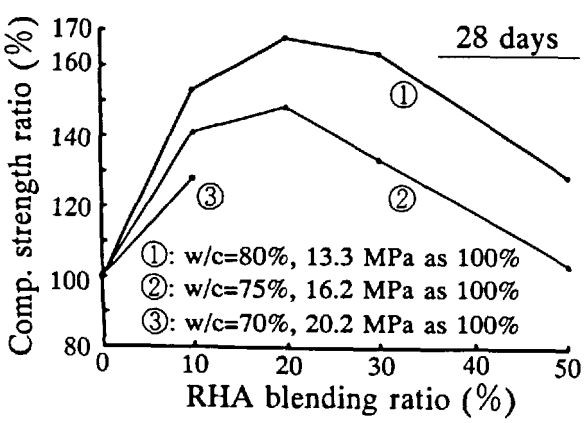

Figure 10 Relative comp. strength of RHA blended concrete vs RHA addition

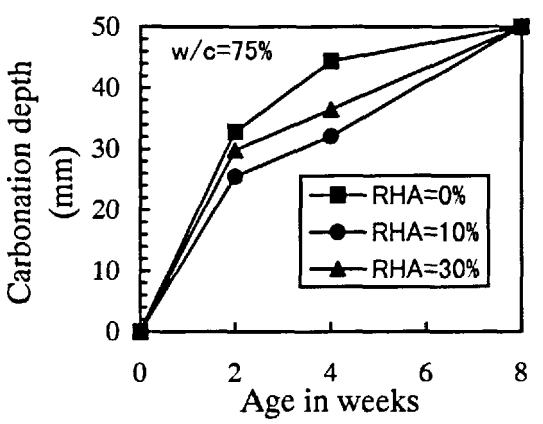

Figure 11 The effect of RHA addition on the carbonation of concrete

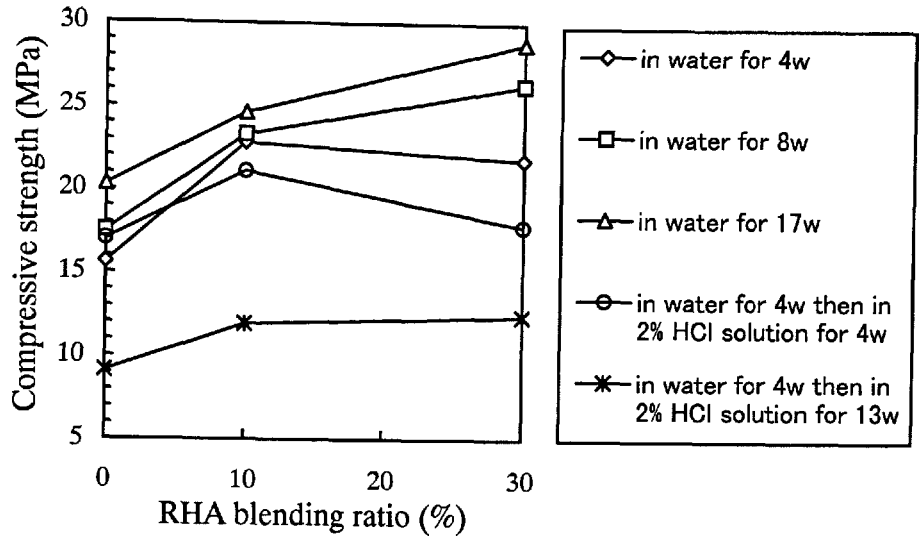

Figure 12 Compressive strength of RHA concrete cured in water and in 2% HCl solution

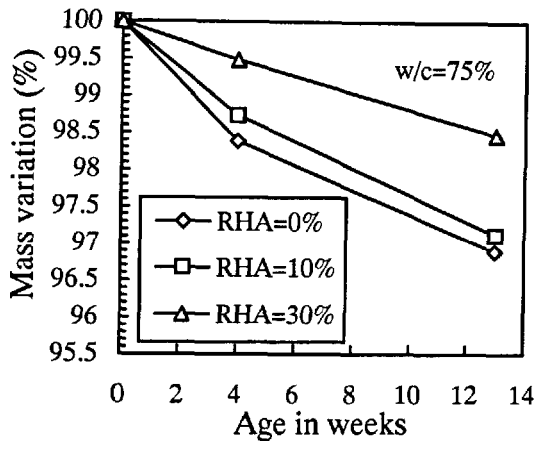

Figure 13 The variation of the mass of the RHA concrete specimens cured in 2% HCl solu. with curing time

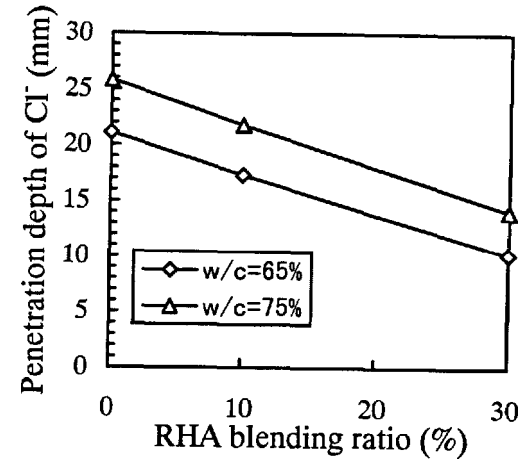

Figure 14 Penetration depth of Cl^- in concrete vs RHA blending ratios

much stronger than those of before and the peak of d = 4.04 Å disappears, which shows all the amorphous SiO_2 has been changed to crystalline SiO_2— a mixture of β-tridymite and phase A in which the former is the main constituent. As the result of the transformation of amorphous SiO_2 to crystalline SiO_2 the change in conductivity is decreased, especially there is an evident reduction of the change in conductivity between 600°C and 900°C (Fig 2). After 900°C the RHA will not behave any pozzolanic activity as the change in conductivity is less than 0.4 mS/cm (Luxan et al., 1989). On another hand if RHA is burnt at low temperatures, for instance below 500°C, much unburnt carbon will remain in it, which also leads it to have poor pozzolanic activity and have a negative influence on the long term properties of concrete. Hence after carbonizing process (Fig 3) it is suggested to controll the final burning temperature of RHA at about 600°C.

In the presence of much carbon in RHA, e.g. more than 4—5%, the change in conductivity of the saturated $Ca(OH)_2$ solution after adding the RHA to it can not give an exact evaluation of the pozzolanicity of the RHA as the carbon is active and can also cause a large change in

conductivity of the solution by physisorption and chemisorption.

It was observed even though RHA was appropriately burnt it was also inactive when it was inappropriately or over ground (Sugita, 1996). The reason for this is the secondary agglomeration occurred among the finely ground RHA particles caused by van der Waals attraction and the giant supersurface energy they have. The less the specific surface of the ground RHA, the poorer the pozzolanicity of it. In the presence of grinding agent (J=250) the specific surface of RHA is increased with grinding time (Fig 8). Therefore, in our opinion, in order to get active ground RHA grinding agent, for instance the by-product in the production of di-ethylene glycol, should be used in its grinding process.

From Fig 8 it can be also found the specific pore volume of coarse RHA is as much as 0.16 cm^3/g and the pores in it is mainly distributed in the region of 20 − 400 Å with an average radius of 123 Å. With a so large number of mesopores RHA has a characteristics of high water absorption (Inoue and Hara, 1996), which may directly worsen the workability of concrete. Before we tried to use unground RHA to cast concrete specimens but finally failed because the mix was too dry, but this phenomenon could be eliminated by grinding the RHA for a definite time in the presence of grinding agent (Sugita, 1996). Fig 8 shows the distribution of the pores in ground RHA is narrowed to the range of 20 − 50 Å with an average radius of 40 Å, at the same time its specific pore volume is decreased to 0.13 cm^3/g. As its pore volume and pore size are both decreased its ability of water absorption is certainly reduced as well. Therefore an appropriate grinding of RHA is not only advantageous to the enhancement of its pozzolanic activity but also to the improvement of the workability of RHA blended concrete.

With blending RHA with OPC at ratios of 5%, 10%, and 15%, the compressive strength of mortar at different ages are all increased. The more the added RHA the higher the strength of mortar, especially at 28d and 91d the RHA blended mortars show a higher strength increase than that of OPC mortars (Fig 9).

Fig 10 indicates that with an appropriate addition of RHA to OPC, for instance 20% by weight, the 28d compressive strength of concrete with different w/c is enhanced by more than 25%, in particular the strength of the concrete with a w/c of 80% is increased by as much as 65% compared with the control concrete.

From Fig 9 and Fig 10 it can be found that the higher the water cement ratio, the bigger the strength increase of either the mortar or concrete blended with RHA. This is possibly attributed to the reduction of effective water cement ratio in the mortar or concrete blended with RHA as free water has been absorbed by the added RHA and kept in its mesopores.

Regarding the strength increase mechanism of RHA blended concrete, the following results have been obtained: 1) at a definite age cement hydration degree is improved by the added RHA, 2) due to the reaction of the active SiO_2 in RHA with $Ca(OH)_2$ in the hydrates both the size and the amount of portlandite in RHA blended concrete is decreased, but the amount of C − S − H gel in it is increased and 3) with the addition of RHA the average pore size of concrete is reduced, especially the portion of pores greater than 200 Å in radius is evidently decreased instead of the increase of the amount of small pores.

With higher strength and smaller pores than reference concrete the resistance of RHA blended concrete to carbonation, to acid attack, and to Cl^- penetration is certainly improved (Figs 11, 12, 13 and 14).

Having the characteristics of continuous operation and a well controlled burning temperature the rotary kiln shown in Fig 4 can produce much more active RHA than the batch furnace (Fig 5) does. But the latter has the advantages of low investment and low production cost, and if it is operated in a proper manner active RHA can be obtained.

CONCLUSIONS

1. By using "two step burning method" proposed by the authors, RHA of high quality can be obtained with either the rotary kiln or the batch furnace when the burning conditions in them are well controlled.
2. The burning temperature of RHA has a great influence on the pozzolanicity of RHA. At the temperatures higher than 600°C the amorphous SiO_2 in RHA will be transformed to crystalline SiO_2, at the same time its activity is decreased greatly. At the temperatures below 500°C the quality of RHA is also poor due to the presence of much unburnt carbon in it.
3. RHA has a mesoporous structure with large N_2 specific surface. To prevent the secondary agglomeration among its finely ground particles, which will result in the decrease of its reactivity, grinding agent should be used in its grinding process.
4. With the addition of the ground RHA which was burnt in the batch furnace to ordinary portland cement not only the strength of cement was increased but also the resistance of concrete to the attack by 2% HCl solution, to carbonation and to Cl^- penetration was improved greatly. The higher the water cement ratio the bigger the strength increase of the RHA blended mortar and concrete respective to the control samples.

REFERENCES

Ibrahim, M. and Helmy, M., "Crystallization Growth of RHA Silica", Thermochimica Acta, 45, 1981, pp. 79-85.

Inoue, K. and Hara, N., "Thermal Treatment and Characteristics of Rice Husk Ash", Inorganic Materials, Vol. 3, July, 1996, pp. 312-318.

James, J. and Rao, S., "Silica from Rice Husk Through Thermal Decomposition", Thermochimica Acta, 97, 1986, pp. 329-336.

Karasudhi, P., Nimityongskul, P., "Use of Rice Husk Ash as Building Materials in Thailand", Div. of Structural Engineering and Construction, Asia Institute of Tech., Bangkok, Thailand, 1979, pp. 123-134.

Khan, M.H., Mohan, K., Taylor, H.F.W., "Pastes of Tricalcium Silicate with Rice Husk Ash", Cem. and Concr. Res., Vol. 15, No. 1, 1985, pp. 89-92.

Luxan, M.P., Madruga M. and Saavedra J., "Rapid Evaluation of Pozzolanic Activity of Natural Products by Conductivity Measurement", Cem. and Concr. Res., Vol. 19, No. 1, 1989, pp. 63-68.

Mazlum, F. and Uyan M., "Strength of Mortar Made with Cement Containing Rice Husk Ash and Cured in Sodium Sulphate Solution", Fly Ash, Silica Fume, Slag and Natural Pozzolans in Concrete, Proc. Fourth Int. Conf., Istanbul, Turkey, Vol. I, ACI SP 132-29, 1992, pp. 513-531. Editor: V. M. Malhotra.

Mehta, P.K., " Properties of Blended Cement Made from Rice Husk Ash", ACI Journal 74-9, 1977, pp. 440-442.

Mehta, P.K., "Concrete Structure, Properties and Materials", Prentice-Hall Inc., 1986.

Sugita, S., Shoya, M. and Tokuda, H., "Evaluation of Pozzolanic Activity of Rice Husk Ash", Fly Ash, Silica Fume, Slag and Natural Pozzolans in Concrete, Proc. Fourth Int. Conf., Istanbul, Turkey, Vol. I, ACI SP 132-28, 1992, pp. 495-512. Editor: V. M. Malhotra.

Sugita, "Fundamental Study on the Effective Utilization of Rice Husk Ash as Concrete Materials", Ph. D Thesis, Hokkaido University, 1996.

SYNERGIC ACTION OF FLY ASH IN TERNARY MIXTURES WITH SILICA FUME AND RICE HUSK ASH

Geraldo Cechella ISAIA, Federal University of Santa Maria, Santa Maria, RS, Brazil

ABSTRACT This paper presents the pozzolanic and physical effects of fly ash in addition with silica fume and rice husk ash, on substitution levels of cement ranging from 10 to 50%, by weight. The ternary mixtures with fly ashes showed synergic effects when the data was correlated with the remaining calcium hydroxide or unitary compression strength. It follows that when the fly ash was added to silica fume or rice husk ash, the performance of the reactivity depended on the amount of pozzolans in the mixture, besides the size of the grains less than 5 μm.

KEY-WORDS: fly ash, rice husk ash, silica fume, reactivity, particle size distribution

INTRODUCTION

The addition of pozzolans to Portland cement has the purpose to improve the concrete microstructure. According to Mehta and Aïtcin (1990), the small particles of pozzolans are less reactive than Portland cement and, when dispersed in the paste, they generate numberless nucleation sites for the precipitation of hydration products. Therefore, this turns the paste more homogeneous and dense in respect to fine pores distribution. In addition, through physical effect, the smallest grains bring on better packing with cement and decrease the wall effect at the transition zone. In consequence, there is reinforcement of this weaker zone due the higher adherence between paste and aggregate, increasing the concrete properties. Thus, the pozzolanic effect upon the cement paste performance depends on both the pozzolanic reactions as well as the filler effect of the small particles. Goldman and Bentur (1993) concluded that concrete strength increases when silica fume is added, due to the microfiller effect through the thickness of the transition zone, and this effect is even more relevant than the pozzolanic action.

The incorporation of fly ash or rice husk ash fine particles to the cement paste, even if not fully pozzolanic, as shown by Mehta (1987), causes the segmentation of large pores and increases the amount of the nucleation sites for the hydration products precipitation, accelerating the reactions and forming smaller calcium hydroxide crystals. The chemical action via pozzolanic reactions enhance the physical action, segmenting the pores in higher level and refining the CH grains, in extent the age increases. Research made by Berry et al. (1994) in CANMET, Canada, also followed that the particles of fly ash particles that are not completely hydrated are able to fill the voids, increase the denseness of the paste, and the result is more relevant if the amount of fly ash contained in the paste is higher.

Within this purpose, this paper investigates the fly ash action in ternary mixtures with silica fume or rice husk ash, through pozzolanic activity test, remaining CH, non-evaporable water and unitary axial compression strength. The results indicated that the fly ash presented synergic effect in the ternary mixtures, and this action was connected with the total pozzolans quantity of each mix, as well as the contents of the grains size smaller than 5 micrometers.

EXPERIMENTAL

A high early Portland cement (NBR 5733) was used and the fly ash came from Petrochemical Pole (Triunfo, RS) ground in laboratory for an hour and sieved in a #0.3 mm mesh sieve. A non-densificated silica fume was provided by a national supplier. The rice husk ash was constituted with 50%, by weight, burnt in a brick furnace factory, without temperature control, and

50% burnt in laboratory furnace at 650°C. The two parts were ground together for one hour and sieved in a #0,3 mm mesh sieve. Table 1 shows the physical and chemical characteristics of Portland cement and pozzolans. Figure 1 presents pozzolans XRD with quartz and mullite as crystalline phases in fly ash, and quartz and cristoballite in rice husk ash. Natural sand with FM = 2.83, Dmax = 4.8 mm, a basaltic coarse aggregate with FM = 6.97 and Dmax = 19 mm were used. The superplasticizer admixture was a ASTM C 494 Type F, with 1.18 kg/dm^3 density, 32.5% solid content and pH = 7.68.

Table 1 Physical and chemical characteristics of cement and pozzolans

	Cement	Fly ash	Silica Fume	Rice h. ash
Physical tests				
Specific mass kg/dm^3	3.08	2.33	2.17	2.11
Fineness Blaine m^2/kg	427	373	2576	1432
Fineness 45 μm residue %	0.3	2.3	0.7	0.9
Pozzolanicity with PC %	100	88	108	104
Grains Φ < 5 μm %	22	17	44	31
Chemical tests - %				
Ignition loss	3.60	0.70	1.70	11.80
SiO_2	18.20	61.40	91.40	78.60
Al_2O_3	5.80	27.70	1.80	2.30
FeO_3	2.80	6.10	n.a.	2.30
CaO	62.70	2.90	0.50	1.00
MgO	2.10	0.80	1.10	0.80
SO_3	3.30	0.30	0.40	0.04
Na_2O	0.08	0.02	0.25	0.01
K_2O	0.97	0.05	1.03	0.56
Equivalent Na_2O	0.72	0.05	0.93	0.38

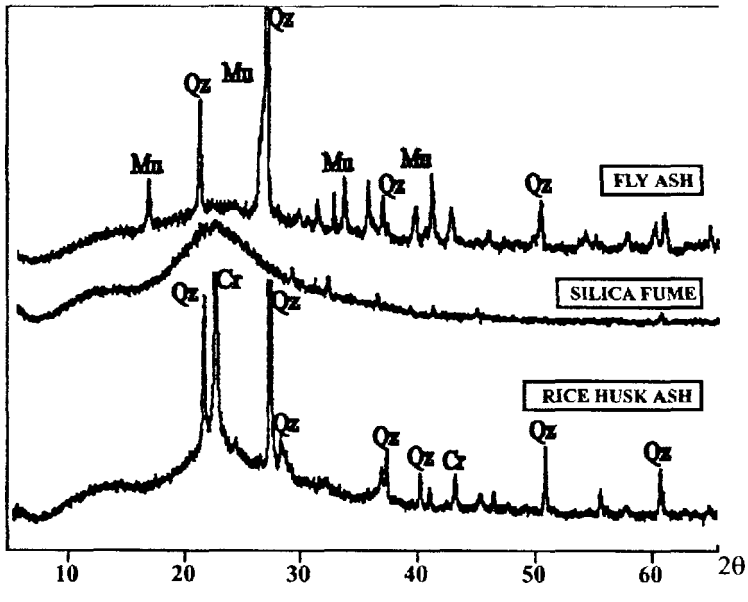

Figure 1 Pozzolans X-ray diffractogram

The concrete mixes were proportioned with 0.4 water-binder ratio, with the following amounts of pozzolans in the mixtures, by weight, with normal (N) and high (H) contents: i) ***binary mixtures***: fly ash (F) = 25 and 50%; silica fume (S) = 10 and 20%; rice husk ash (R) = 10, 20 and 30%; ii) ***ternary mixtures***: (F+S) = (15+10) and (30+20)%; (F+R) = (15+10), (30+20) and (20+30)%. A total of 13 binary and ternary mixtures were investigated. The following tests were

made: **a)** pozzolanic activity with pozzolanic PC, Fratini test (NBR 5753); **b)** non-evaporable water content, by mass difference between 105 and 550°C. In despite of this test not be a precise indicator, Sellevold and Justnes (1993) attest that this test provides adequate results to indicate the variations of the paste hydration degree; **c)** remaining CH (NBR 5748) and **d)** uniaxial compressive strength, NBR 5738, with 10x20 cm specimens.

TESTS RESULTS

Figure 2 and Table 2 show the results of the pozzolanic activity test (Fratini test). A Pozzolanic Activity Index (PAI) was calculated, representing the inverse of the distance (d), in cm, that separates each graphical point from the origin of the coordinates, multiplied by 100. Greater this index, higher was the pozzolanic activity, because the graphical points placed closer to origin means more consumption of CH and less total alkalinity. The PAI was higher to the fly ash ternary mixtures, with high total contents of pozzolans, followed by the mixtures with normal contents. It was established by this test that fly ash mixed with silica fume or rice husk ash increased the pozzolanic activity, in comparison with the binary mixtures, and it was more elevated as more elevated was the total amount of pozzolans in the mixture.

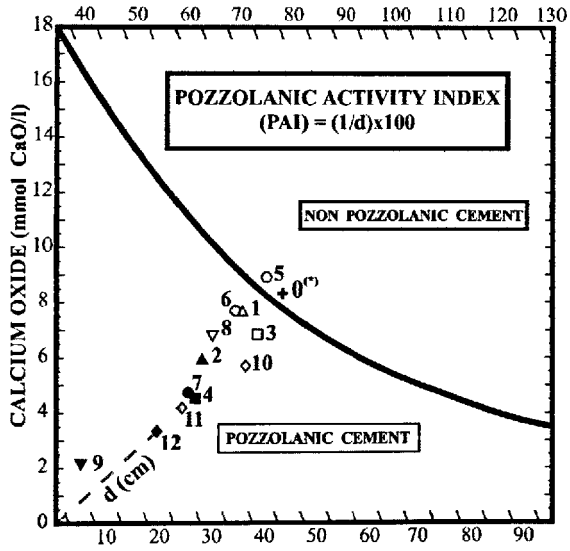

Table 2 Pozzolanic activity with cement

Nº	PC %	FA %	SF %	RHA %	PAI
0	100	-	-	-	**11.4**
1	75	25	-	-	**13.1**
2	50	50	-	-	**16.8**
3	90	-	10	-	**13.2**
4	80	-	20	-	**19.5**
5	90	-	-	10	**11.4**
6	80	-	-	20	**13.3**
7	70	-	-	30	**19.7**
8	75	15	10	-	**15.2**
9	50	30	20	-	**58.8**
10	75	15	-	10	**14.7**
11	50	30	-	20	**21.4**
12	50	20	-	30	**26.7**

Figure 2 Pozzolanic activity (Fratini test)

Figure 3 presents the results for the remaining CH, non-evaporable water and unitary axial compression strength located according to the decrescent sequence of the pozzolanic activity indexes. Segment a) shows the PAI, as well as the grains size contents smaller than 5 μm and the pozzolans quantity of each mixture, showing similar decreasing behavior with PAI, except for 25 and 50% fly ashes binary mixes. The segments b), c) and d) of Figure 3 show, respectively, the contents of the remaining CH, non-evaporable water and unitary axial compression strength. This figure shows that: **a)** the experimental mixtures arranged decreasingly related to pozzolanic activity, practically followed the same disposition of the pozzolans quantity, except for the fly ashes binary mixtures, likewise higher the pozzolans content was, more elevated was the PAI; **b)** the contents of pozzolans grains smaller than 5 μm strictly followed the same PAI sequence; **c)** to higher reactivities corresponded smaller remaining CH contents; **d)** the non-evaporable water and unitary compression strength decreased in the same sequence of PAI.

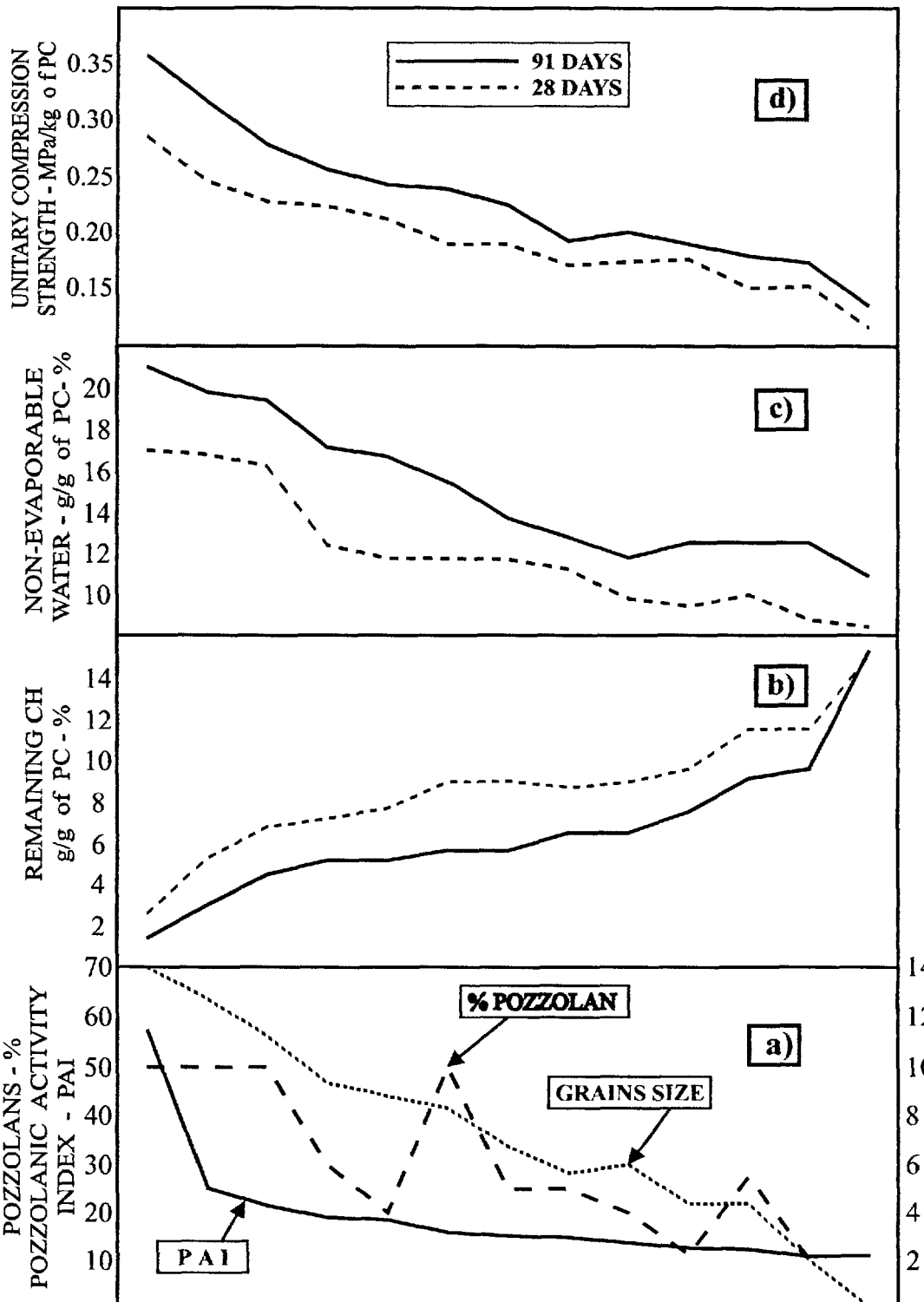

SERIES	FSH	FRRH	FRH	RRH	SH	FH	FSN	FRN	RH	SN	FN	RN	REF
FA %	30	20	30	-	-	50	15	15	0	10	25	-	-
SF %	20	-	-	-	20	-	10	-	20	-	-	-	-
RHA %	-	30	20	30	-	-	-	10	-	-	-	10	-
TOTAL	50	50	50	30	20	50	25	25	20	10	25	10	0
P A I	58.8	26.7	21.4	19.7	19.5	16.8	15.2	14.7	13.3	13.2	13.1	11.4	11.4
ORDER	1	2	3	4	5	6	7	8	9	10	11	12	13

Figure 3 Decreasing ordering, according to PAI, of the pozzolan contents, grains size < 5 μm, remaining CH, non-evaporable water and unitary axial compression strength (w/b = 0.4).

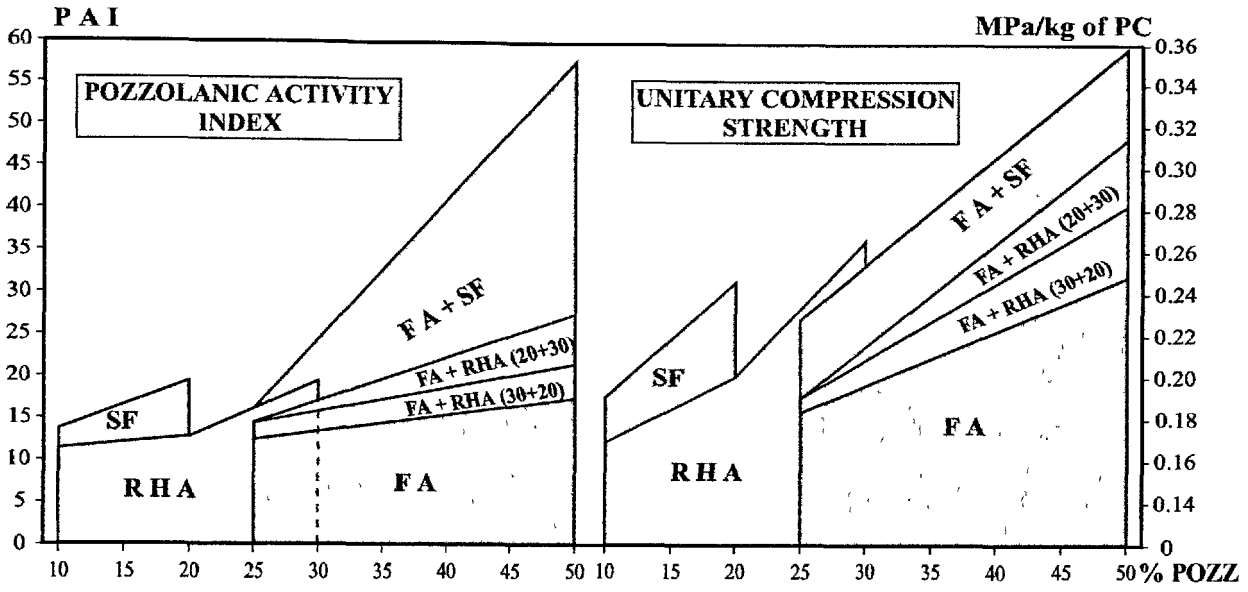

Figure 4 Variation of PAI and unitary strength with the content of pozzolans

DISCUSSION

The results show that concrete blended performances depended not only on the mineralogical composition or fineness, but also on the pozzolans quantity of each mixture, as well as the eventual aggregation with another pozzolan. Figure 4 shows that, as the content of the pozzolans increased in the mixture, the PAI and the unitary strength increased their performances too, that was higher to the ternary mixtures than to the binary ones.

The data make evident that, together the chemical activity, the physical parameters represented by the quantity of pozzolans and fine fraction of the grains also exercised influence upon the reactivity. Thus, it is possible to perceive the importance of small grains in this context, as shown by Scrivener (1989), when said that grains smaller than 5 μm react immediately while the bigger particles take more time to start the reaction. Besides the chemical action linked with the active grains size, the physical aspects concerned with the non-reactive grains are also important to the microstructure of the hydrated paste, with regard to packing, nucleation, microaggregate effects, etc. In a previous work Mehta (1985) pointed out that, besides the calcium content, the granulometric distribution of the pozzolans particles is an important parameter that governs the reactivity. In his experiment with fly ash, the reactivity was directly proportional to the particles contents smaller than 10 μm and inversely proportional to the particles amount bigger than 45 μm. The results of the present research is a claim fortified by the facts shown by the latter authors, as it is seen in Figure 5 where it is demonstrated the high statistical correlation obtained by regressions between the content of grains smaller than 5 μm and the contents of the remaining CH (r^2 = 94%) and the unitary axial compression strength (r^2 = 98%). The latter variable also had good correlation with the PAI as shown in Figure 6, based on complementary data of this research presented by Isaia (1995). The linear correlation is strong as from 28 days, when more than 72% of unitary strength variation is explained by the PAI. In earlier ages the coefficients r^2 are lower because, by that time, the pozzolanic reactions resulting from the CH consumption, only take place at older ages. It becomes evident, by the data submitted for consideration, that the reactivity matter it is not only linked with the crystalline or amorphous phases, as showed by XRD in Figure 1, but also to the quantity of pozzolans and the content of fine particles that may act synergicly, by physical effect, together with the pozzolanic reactions.

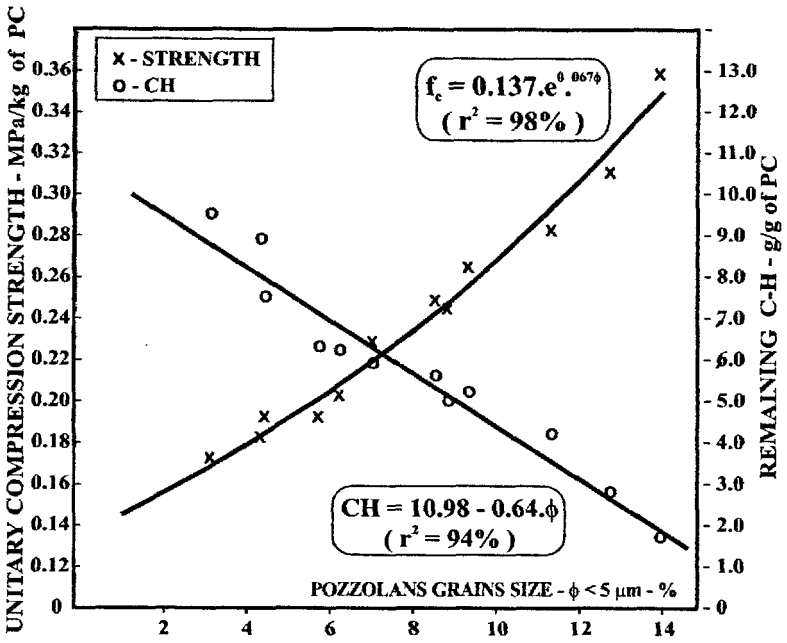

Figure 5 Correlation between $\phi < 5$ μm, unitary strength and remaining CH

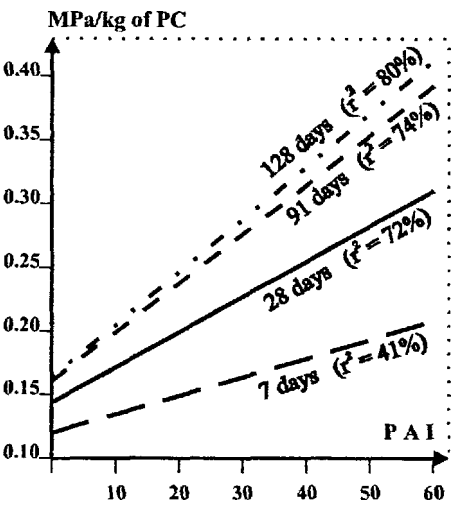

Figure 6 Correlation between PAI and MPa/kg

SYNERGIC EFFECT

It is possible to calculate the increment of the properties studied, like pozzolanic activity index and unitary strength, taking the Portland cement mix as reference. The increase of the pozzolanic activity due to the combined use of fly ash with silica fume or rice husk ash, is called **synergic effect** of the former pozzolan over the two latter ones, therefore, it can be shown by the formula: $P = (I_p/I_r).100$. P means the performance increment of a pozzolan with a given property, I_p and I_r show the increment of the considered property, respectively between the concrete with pozzolan and the reference mix. The synergic effect (SE) can be calculated by:

$$SE = P_{(FA + poz)} - (P_{FA} + P_{poz}) \qquad [1]$$

where $P_{(FA + poz)}$ represents the increment of the considered property of the fly ash ternary mixture with silica fume or rice husk ash; P_{FA} of the fly ash and P_{poz} of the silica fume or rice husk ash in binary mixtures. The influence of fly ash on the increment of the pozzolanic activity and unitary strength is shown in Table 3 and Figure 7. If had had only superposition of the effects when two pozzolans were mixed, the increase of the pozzolanic activity or unitary strength would be the arithmetic sum of the increments in the binary mixtures. In the case of PAI, the increase of the series SN and SH with 10 and 20% of silica fume was 15.8 and 71.1%, respectively. The increments for 15% (calculated by extrapolation) and 30% (calculated by interpolation) of fly ash series FN and FH were 8.9 and 21.4%, respectively, resulting in 24.7% to FSN (15+10 % of FA+SF) and 92.5% to FSH (30+20% of FA+SF) series. However, by the Fratini test, these two ternary series presented PAI increments of 33.3 and 415.8%, respectively, according to the sample of the Portland cement reference concrete. Therefore, there was an additional increase of 33.3 - 23.7 = 8.6% to the FSN and 415.8 - 92.5 = 323.3% to the FSH series, both called synergic effect of the fly ash on the two pozzolanic systems. The same calculations are valid to the increments of ternary mixtures of RHA in the FRN and FRH series, as well as to the unitary strength.

Table 3 Synergic effect of fly ash on PAI and unitary compression strength

Series	FA %	SF %	RHA %	Pozzolanic Activ. P %		f_{c91} - MPa/kg - P %	
				SF	RHA	SF	RHA
FN	15			- 8.9	-8.9	-21.2	-21.2
SN/RN		10	10	-15.8	-0.0	-42.5	-26.9
Sum				-24.7	-8.9	-63.7	-48.0
FSN/FRN	15	10	10	+33.3	+28.9	+68.7	+42.5
Difference				+8.6	+20.0	+5.0	-5.5
FH	30			-21.4	-21.4	-44.9	-44.9
SH/RH		20	20	-71.1	-16.7	-82.8	-52.0
Sum				-92.5	-38.1	-127.7	-94.9
FSH/FRH	30	20	20	+415.8	+87.7	+167.1	+110.4
Difference				+323.3	+49.6	+39.4	+15.5

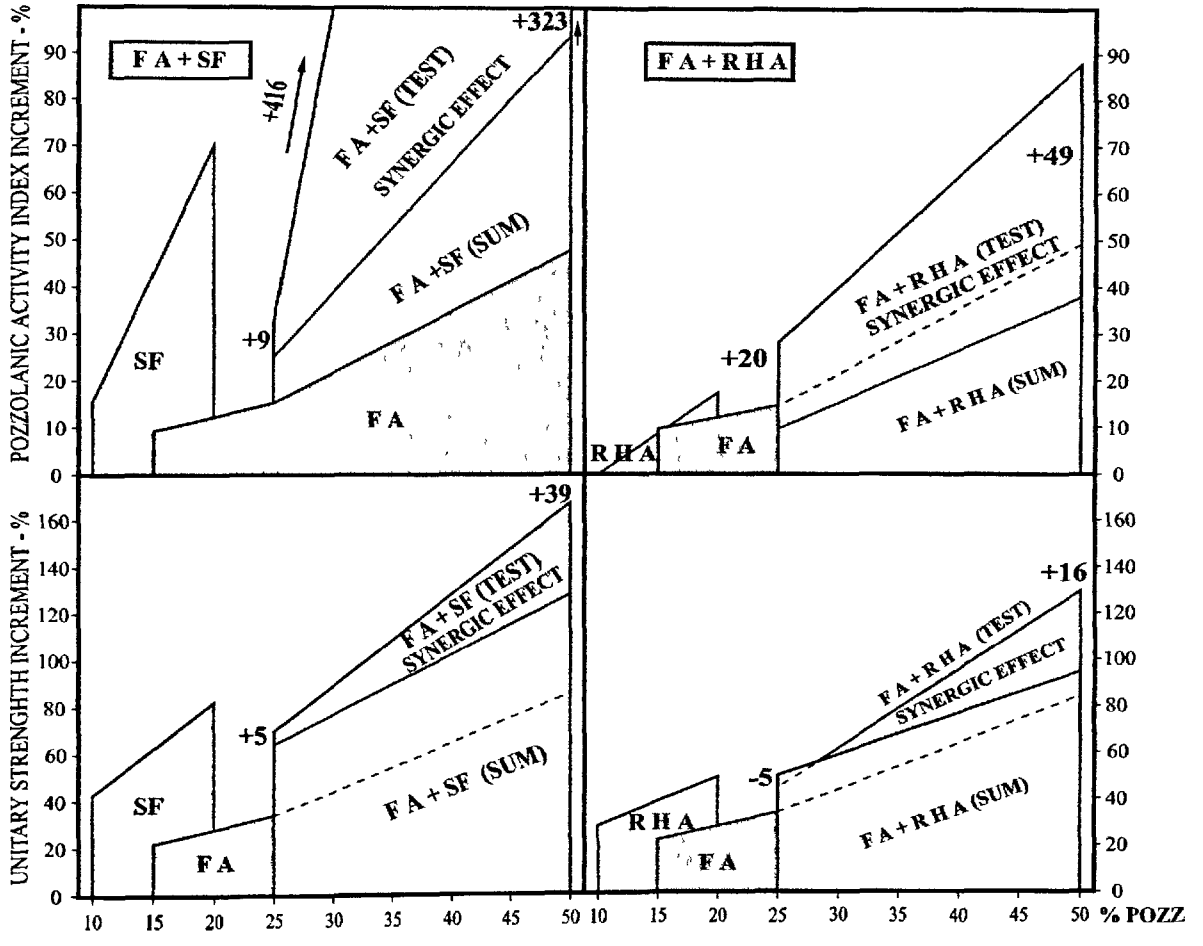

Figure 7 Synergic effect of fly ash on the silica fume and rice husk ash mixtures in the pozzolanic activity index and unitary axial compression strength at 91 days (w/b = 0.4).

The fly ash synergic effect could be explained by the higher physical action rather than the chemical one. Such behavior would be linked by the greater deflocculation of the cement grains provided by the fly ash, than to the silica fume or rice husk ash particles, increasing the surface of the cement grains in contact with free water, that would be more available by the

plasticizing effect of the fly ash, enhanced by its eletrocinetic potential (zeta potential). These mechanisms would propitiate more nucleation sites to start the reactions, and the final result would be an enlargement of the hydration reactions, consequently, higher CH consumption, pozzolanic activity and, finally, unitary compression strength gain. Similar performances were showed by Isaia (1996) to others properties related to concrete durability as chloride and water penetration, Cl^-/OH^- relationship and carbonation, with the same mixtures of this experiment.

CONCLUSIONS

It follows that the performance of pozzolans, in relation to chemical reactivity or mechanical strength, is not only a matter of crystalline or amorphous state but overall, the association with other pozzolans as the mixture of fly ash with silica fume or rice husk ash. The results presented in this research make evident that the fly ash added to the ternary mixtures presented a multiplier effect when associated to high total volumes of pozzolans, enhancing the idea that reactivity depends on the mineral addition quantity. The parameters tested as grains size content smaller than 5 μm, remaining CH, non-evaporable water and unitary axial compression strength reinforce the later conclusions. It was established that the synergic effect depended on physical action of the fly ash that, as well as the plasticizing admixtures, producing more deflocculation of the cement grains, and enabling higher quantity of sites to the hydration products nucleation. Thus, the resulting chemical effect was enhanced by physical action, and the general concrete performance was improved by means of grain and pore size refinement.

REFERENCES

Berry, E., E. et al. "Hydration in high-volume fly ash concrete binders". ACI Materials Journal, Detroit, v. 91, n. 4, p. 382-389, 1994.

Goldman, A, Bentur, A. "The influence of microfillers on enhancement of concrete strength". Cement and Concrete Research, v. 23, p. 962-972, 1993.

Isaia, G. C. "Effects of binary and ternary pozzolanics mixtures of high performance concrete: a durability study regarding rebars corrosion". São Paulo, 1995, 280p. PhD. Thesis. Escola Politécnica da Universidade de São Paulo (in portuguese).

Isaia, G. C. "Synergic effects of fly ash ternary mixtures with rice husk ash and silica fume on durability of high performance concrete". In: Prudencio, L. R., Helene, P., Dal Molin, D. (eds.). International Congress on HPC, and Performance and Quality of Concrete Structures, Florianopolis, Brasil, 1996. Proceedings. Florianopolis, Universidade Federal de Santa Catarina, 1996, p. 578-589 (in portuguese).

Mehta, P. K. "Studies on the mechanisms by which condensed silica fume improves the properties of concrete". In: International Workshop on Condensed Silica Fume in Concrete. Ottawa, 1987. Proceedings, 1987, p. 1-17.

Mehta, P. K., Aïtcin, P. C. "Microstructural basis of selection of materials and mix proportions for high strength concrete". In: Hester, W. (ed.) International Conference on Utilization of High Strength Concrete, 2nd, Berkeley. 1990. Proceedings. Detroit, American Concrete Institute, 1990, p. 265-287. (SP-121).

Scrivener, K. L. "The microstructure of concrete". In: Skalny, J. (ed.) Materials Science of Concrete I. Westerville: The American Ceramic Society, 1989, p. 127-162.

Sellevold, E. J., Justnes, H. "High strength concrete binders. Part B: non-evaporable water, self-desiccation and porosity of cement pastes with and without condensed silica fume". In: Malhotra, V. M. (ed.) International Conference on Fly Ash, Silica Fume, Slag, and Natural Pozzolans in Concrete, 4th, Istanbul, 1992. Proceedings. Detroit: American Concrete Institute, 1993, 2v., v.2, p. 891-902 (SP-132).

COMPRESSIVE STRENGTH DEVELOPMENT AND PORE STRUCTURE OF SLAG - SILICA FUME CEMENT CURED AT 38 -175 °C

Yaozhong XI, China Building Materials Academy, Beijing 100024, P. R. China
Barry E. SCHEETZ, Materials Research Laboratory, The Pennsylvania State University, PA, USA

ABSTRACT A PC-slag-silica fume cement paste was processed at 38 -175 °C for 1- 48 hours. The plots of f (compressive strength) - d (curing time) and f - t (curing temperature) translation are given. The cost effective d is 10 hours and the cost effective t is 90 °C. The regression analysis shows the logarithmic correlation of f - d at a certain t and of f - t at a certain d. The maturity equation is useful within certain ranges of t and d to predict an approximate strength. The strength-porosity data show the linear correlation of strength with porosity.

Key-words: blended cement; high temperature; maturity; pore structure; strength development

INTRODUCTION

Hooton (1980) reported the compressive strength of a pelletized slag cement and mortar with addition of 20-40% silica flour cured at 185°C for 4h, but recently the number of papers on the strength development and pore structure for a slag-silica fume cement (SS) at elevated temperatures and pressures is very limited. In engineering practice and production of prefabricated components it is very useful to be able to predict an approximate strength based on curing time and temperature, which are the two most important environmental factors determining strength gain. There have been simple and sophisticated ways to do this. In this paper the strength development and pore structures were tested for a slag-silica fume cement (weight percentage: PC 32.5%, slag 60.5%, SF 7%) cured at elevated temperatures. The strength data were processed using a computer software to establish strength expressions and correlation coefficients. The maturity (curing time × curing temperature) was calculated to determine whether the relationship of strength-logarithm of maturity is linear. In the last section critical pore radii and total porosities related to their compressive strengths are plotted and their correlation is discussed.

EXPERIMENTAL

ASTM Type-I portland cement of Ash Grove (PC), slag of Koch Minerals (ggbfs), silica fume of Elkem (SF) and superplasticizer Mighty-150 of Boremco Specialty Chemicals were used. The formulation of the neat paste: PC 100, ggbfs 186, SF 21.5, water 98.4, Might-150 4.7 (to control a flow of 110 ± 5). The superplasticizer was first mixed with water in the bowl of a paddle-mixer, then the raw materials were added and mixed for 1.5 min. The neat paste was placed in a 50× 50×50 mm mold and tamped with a 13×25×150 mm hard wood tamper. The molding plus precuring lasted nearly one hour. The molds with fresh paste were put into containers at 38, 60, 90, 125 and 175°C for 1, 10, 24 and 48 hours. The 38, 60 and 90°C containers accommodated saturated steam of atmospheric pressure. The 125 and 175°C curings were in a Chandler duplex curing chamber filled with water and kept at 1 ± 0.1 MPa (gauge pressure). The heating time was 1.5 h and the cooling was more than 1.5 h. The cooled cubes were tested for compressive strength. A Quantachrome scanning mercury porosimeter was used for pore data measuring. The samples with particle size < 6 mm were crushed from fragments of tested cubes and freeze-dried. The maximum intrusion pressure was 374 MPa, the canning rate 4, assuming a wetting angle of 140°.

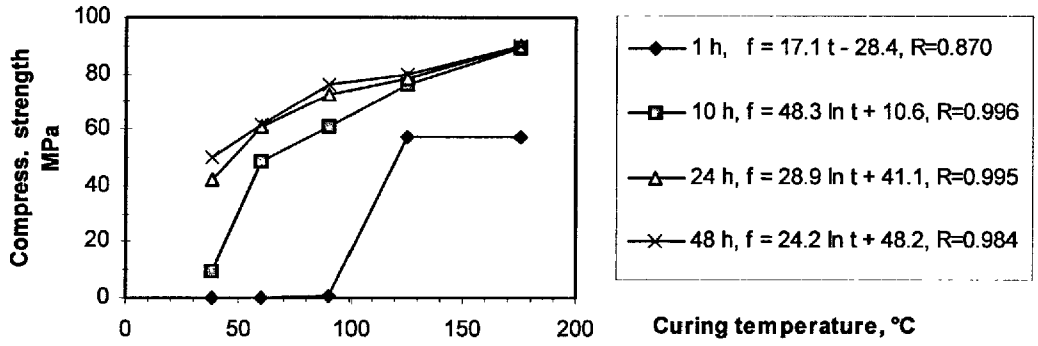

Fig.1A . Strength (f) ~ temperature (t)

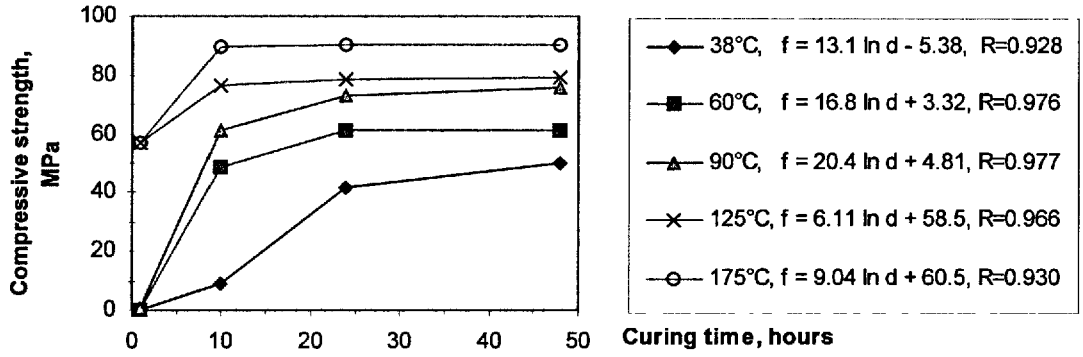

Fig.1B. Strength (f) ~ curing duraton (d)

LOGARITHMIC RELATIONSHIP OF f WITH t OR d

According to Fig. 1, for reaching a strength of 50 MPa, the following curing regimes can be chosen: 48 h at 38°C, 10 h at 60-90°C, and the quickest, one hour or less at or above 125°C. Fig.1A shows that the strength for 48 h curing is almost equal to that of 24h curing except at 38°C, i.e. a curing time longer than 24 h should not be selected. In Fig.1, regression equations and correlation coefficients are given to all the curves, indicating all curves are logarithmic except for 1 h curve since the paste had no strength after 1 h curing at 38°C and at 60°C. The 10 h curve in Fig.1A has the highest slope 48.3, suggesting the most effective curing time 10 h; the 90°C curve in Fig.1B has the highest slope 20.4, indicating the most effective curing temperature 90°C. The logarithmic relationship between strength - curing time and strength - curing temperature can be seen in other cement systems, e.g. in slurries of G class oil well cement plus silica flour and/or silica fume cured at 20°C 100% R. H. and 230°C 2.75 MPa (Grabowski et al, 1989a, 1989b), and in pastes of each of the four components for cement clinker (Bogue, 1934).

STRENGTH-MATURITY RELATIONSHIP

The early works by Nurse (1949, 1951) and Saul (1951) reported the maturity equation $M = \Sigma(T-T_0)\Delta t$, where T is the temperature of a concrete for the duration of Δt and T_0 is the datum temperature below which the concrete will not gain strength. T_0 has been defined by many researchers and ranges from 10 - 14°F for most concretes. Bergström (1953) accepted -10°C (14°F) as the datum temperature and gave the equation $M = \Sigma a_t (t + 10)$, where a_t is the duration at the temperature of t in degrees centigrade. Plowman (1956) found the relationship of strength with logarithm of maturity to be linear: $f = a \lg M + b$ ($\lg M$ is common logarithm). The maturity equation had been widely used, but later disagreements have been reported (Volz et al, 1981; Carino et al, 1983a and 1983b). Volz et al (1981) monitored the real temperature variation of a concrete cured at -1 , 21 and 43 °C by thermocouples to calculate maturity. They found that the

equation does not properly account for the effect of temperature occurring within about seven hours after placement on later strength. Kee (1971) suggested another strength-maturity relation—hyperbolic equation: S = M / (1/A + M/Su), where S = strength, M = maturity, Su = limiting strength as maturity tends to infinity and A = initial slope of the strength-maturity curve. Carino et al (1983a, 1983b) confirmed the equation is a good approximation for the actual strength - maturity relation.

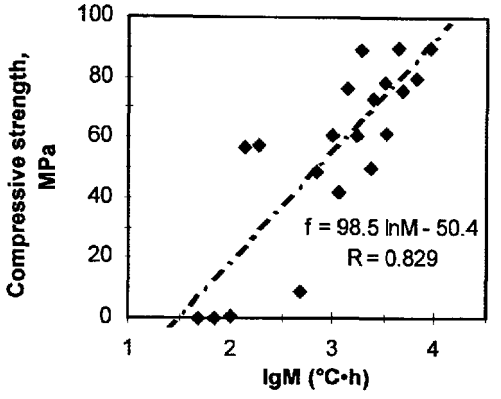

Fig. 2A. Strength (f) ~ all lg M(°C•h)

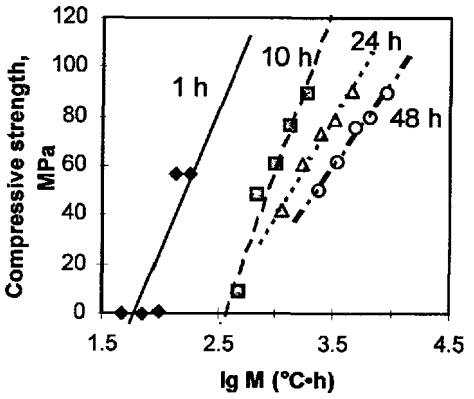

Fig. 2B.Strength(f)~grouped lgM(°C•h)

The maturities here are calculated for the SS paste (Table 1), neglecting molding and cooling periods from practical viewpoint of convenience. If all the strength - maturity data are plotted together, the linear relationship is not good (Fig.2A, R=0.829); if the data are group-plotted under 1, 10, 24 and 48 h, the linear correlation is satisfactory except for one hour " early" curing (Fig.2B). The correlation coefficients for lines of 10, 24 and 48 h are 0.975, 0.989 and 0.992 (Table 1), which is the situation similar to Fig.1A described in the previous section. Therefore the maturity equation is still a good approximate expression within certain range of time and temperature for a given concrete. However, the equation is inaccurate for a concrete with extensive or multiple curing history of time, temperature and pressure.

Table 1 Relationship of compressive strength (MPa in brackets) with lg M (°C • h)

	38°C	60°C	90°C	125°C	175°C	Regress. equatn	R
1 h	1.68 (0)	1.85 (0)	2.00 (0.7)	2.13(56.9)	2.27(57.1)	f = 115M - 205	0.851
10 h	2.68 (9.1)	2.85(48.5)	3.00(60.8)	3.13(76.1)	3.27(89.4)	f = 130M - 332	0.975
24 h	3.06(41.7)	3.23(60.8)	3.38(72.8)	3.51(78.6)	3.65(90.1)	f = 79.2M - 198	0.989
48 h	3.36(50.2)	3.53(61.4)	3.68(75.9)	3.81(79.4)	3.95(90.0)	f = 67.3M - 175	0.992

STRENGTH versus CRITICAL PORE RADIUS AND POROSITY

The mercury intrusion porosimetry provides a useful means for comparison of pore structures of hardened cement pastes (hcp), but it is not possible to obtain an actual pore size distribution of hcp because of its sensitivity to stresses introduced by sample pretreatment, resulting in pore coarsening (Moukwa et al 1988, Feldman et al 1991). The critical pore radii (r) and total porosities (p) of the hardened SS neat paste related to their compressive strengths are plotted in Fig.3. The paste has smaller critical pore radii down to 2 nm and lower porosities down to 14% than the hardened portland cement paste (typically, r~ 20 nm, p ~30% for 28 days curing at room temperature). Fig.3A shows an approximate linear relationship between f and p. This supports the finding by Watson (1981) that the compressive strengths of autoclaved aerated concretes with porosities 0.48-0.78 and portland cement pastes with porosities 0.26-0.45 is linearly related to the solid/pore volume ratio determined by helium pycnometry. Fig.3B shows

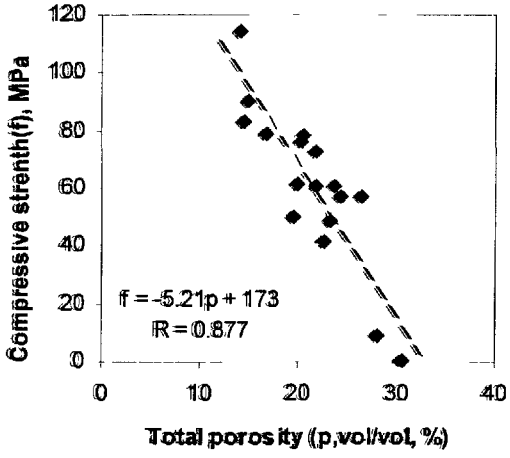

Fig.3A. Strength(f)~total porosity(p)

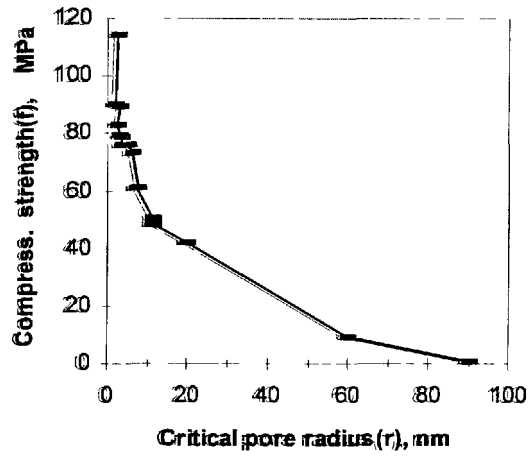

Fig.3B. Strength (f)~criti. pore radius(r)

that the critical pore radii of the SS paste having a strength greater than 79 MPa approach a constant value about 2.5 nm, possibly indicating that critical radii of dense pastes like SS pastes would not change much after reaching a certain small value. Jiang et al (1989) reported that the volume of small pores (radius 37-50 nm) for the 1:3 mortar of a slag cement composed of 20% clinker and 80% slag remains constant. Another explanation may be that the mercury intrusion method does not apply to a dense paste with critical pore radius $\leq$ 3 nm. Feldman (1987) indicated that cement pastes with SF contain discontinuous pores and mercury does not enter all the micropores.

REFERENCES

Bergström, S. G., Mag. Concr. Research, Vol. 4, No. 14, 1953, pp. 61-66.
Bogue, R. H. and Lerch, W., Industr. Engng Chem., Vol. 26, 1934, p. 837.
Carino, N. J., Lew, H. S. and Volz, C. K., J. A. C. I., March-April, 1983, pp. 93-101.
Carino, N. J. and Lew, H. S., J. A. C. I., May-June, 1983, pp.177-182.
Feldman, R. F., Proc. Int. Workshop on Condensed Silica Fume in Concr., CANMET, Montreal, May 1987, pp.1-9.
Feldman, R. F. and Beaudoin, J. J., Cem. Concr. Res., Vol. 21, 1991, pp. 297-308.
Grabowski, E. and Gillott, J. E., Cem. Concr. Res., Vol. 19, No. 3, 1989, pp. 333-344.
Grabowski, E. and Gillott, J. E., Cem. Concr. Res., Vol. 19, No. 5, 1989, pp. 703-714.
Hooton, R. D. and Emery, J. J., 7th International Congress on the Chemistry of Cement, Paris, 1980, Editions Septima, Vol. II, pp. III 43-47.
Jiang, Shi-ping and Grandet, J., Cem. Concr. Res., Vol. 19, No. 3, 1989, pp. 487-496.
Kee, Chin Fang, ACI Journal, Proceedings, Vol. 68, No. 3, Mar. 1971, pp. 196-203.
Moukwa, M. and Aïtcin, P. C., Cem. Concr. Res., Vol. 18, 1988, pp. 745-752.
Nurse, R. W., Mag. Concr. Research, Vol. 1, No. 2, 1949, pp. 79-88.
Nurse, R. W., Proc. Building Res. Cong., 1951, p.86.
Plowman, J. M., Mag. Concr. Research, Vol. 8, No. 22, 1956, p. 13-22.
Saul, A. G. A., Mag. Concr. Research, Vol. 2, No. 6, 1951, pp. 127-140.
Volz, C. K., Tucker, R. L., Burns, N. H. and Lew, H. S., Cem. Concr. Res., Vol. 11, No. 1, 1981, pp. 41-50.
Watson, K. L., Cem. Concr. Res., Vol. 11, No. 3, 1981, pp. 473-476.

CHARACTERISING REACTIVITY OF ALKALI-ACTIVATED POZZOLANS

W John McCARTER, Heriot-Watt University, Edinburgh, Scotland, UK.
Hubert EZIRIM, Heriot-Watt University, Edinburgh, Scotland, UK.

ABSTRACT The work detailed investigates the reactivity of replacement materials by direct activation with calcium hydroxide (CH) at ambient temperatures. Electrical impedance techniques are employed as a non-invasive method for investigating the pozzolanic reaction. Test results show that such a technique can be used to monitor the hydration process thereby following the stages of hydration and rate of chemical activity of replacement materials when blended with CH.
Key-words: Pozzolan; Calcium Hydroxide; Setting; Hardening; Electrical Impedance.

INTRODUCTION

Methods for quantifying pozzolanicity are varied including measurements on strength and lime consumption e.g. Chapelle test (Kostuch et al 1993). Regarding the latter, such a test gives no information on the rate of reaction at ambient temperatures. Electrical impedance methods have proved useful in monitoring and elucidating the early hydration characteristics of ordinary Portland cement (OPC) i.e. initial 24-hours (McCarter and Afshar, 1988; McCarter and Garvin 1989). It is over this period that the cement paste changes from a fluid to rigid state and results in significant changes in its electrical response. In a similar fashion, electrical resistance measurements have been made on pozzolans activated with solid CH and then subjected to elevated temperature (70°C) curing (Tashiro et al, 1994). In this instance, when used in conjunction with XRD studies, the electrical resistance of pozzolanic material measured at 72-hours was shown to correlate well with its CH consumption - a high resistance correlated with low CH consumption, whereas low resistance was indicative of high CH consumption.

A unified testing procedure is required for pozzolanic materials and electrical methods could offer a viable alternative for assessing setting and hardening; optimising CH content, or as a method for monitoring pozzolanic activity of natural materials (Luxan et al, 1989).

EXPERIMENTAL

Commercially available replacement materials were used in the current experimental programme and comprised pulverised fuel ash (PFA); ground granulated blast-furnace slag (GGBS) and metakaolin (MK). Materials were blended with reagent grade calcium hydroxide (CH) and mixed with sufficient water to obtain pastes of similar consistency. The mixes studied are summarised in Table 1; for comparative purposes, tests on plain OPC pastes were also undertaken.

Pastes were mixed in a planetary motion mixer and compacted into plexiglass *cube-type* cells with the contained sample being 50x50x45mm. Opposite walls of each cell had 50x50mm stainless-steel plate-electrodes. Four samples were tested for each of the mixes in Table 1. Leads from all four samples were connected to a multiplexing unit which, itself, was connected to an impedance analyser. A thermistor was embedded in one of the four replicate samples to monitor internal temperature changes. The complete monitoring system was controlled through a PC (486/66), with all tests carried out in a temperature controlled laboratory (22°C).

Table 1: Summary of materials and mix ratios.

Binder	Binder : CH ratio	ater : (Binder + CH) ratio
OPC	binder only	0.270:1
GGBS*	4:1	0.425:1
PFA	4:1	0.460:1
MK	4:1	1.000:1

* GGBS is more aptly termed a latent hydraulic binder

As the electrical response is frequency dependent (McCarter and Afshar, 1988), impedance measurements were recorded at up to 14 spot frequencies within the range 100Hz-100kHz. Both the in-phase (i.e. resistive) **and** quadrature (i.e. capacitive) components of the sample impedance were recorded at each spot frequency at 10 minute intervals over the test period, which extended over 55 hours in some instances.

RESULTS AND DISCUSSION

Since the geometry of the test cells (and hence samples) was fixed, the values of capacitance and conductance for the various binders can be compared and does not necessitate conversion of the results to conductivity and dielectric constant. In addition, results are presented in the form of *normalised* conductance and capacitance whereby the data recorded at time, t, after the start of the test (denoted G_t and C_t respectively) are divided by the respective conductance and capacitance value at time t = 0 (denoted G_o and C_o). The initial values of G_o and C_o and presented in Table 2.

Table 2: C_o and G_o values and frequency at which data are presented.

Binder	G_o $x10^{-3}$ (Siemens)	C_o $x10^{-9}$ (Farads)	Frequency (kHz)
OPC	72.7	1.55	30
GGBS	17.5	139	0.4
PFA	34.0	80.3	10
MK	21.0	59.5	1

The temporal change in normalised conductance and capacitance is displayed in Figures 1 and 2 respectively, for clarity only every 20th data marker is identified on these curves. Although data were recorded at a number of spot frequencies, for the current work, only those measurements at what is considered as the optimum response frequency are presented (this frequency is presented in Table 2). It should be emphasised that as far as absolute values are concerned, no direct comparison can be made between the various pastes as this parameter is frequency dependent (McCarter and Afshar, 1988) - as is conductance, although to a lesser extent.

General

The Portland cement response in Figures 1 and 2 is in agreement with published data (McCarter and Afshar, 1988; Christensen et al 1994). It is interesting to note that the overall trend in the electrical response of the alkali-activated pozzolanic materials is similar to the Portland cement paste, although the duration and prominence of specific features vary between the materials tested.

Figure 1: Normalised Conductance Response

As far as OPC is concerned, the conductance increases over the initial 30 minutes as the ionic concentration increases within the aqueous phase. For the GGBS, PFA and MK there is no discernible increase in conductivity over this time, indeed conductivity values reduce almost immediately after the start of the test.

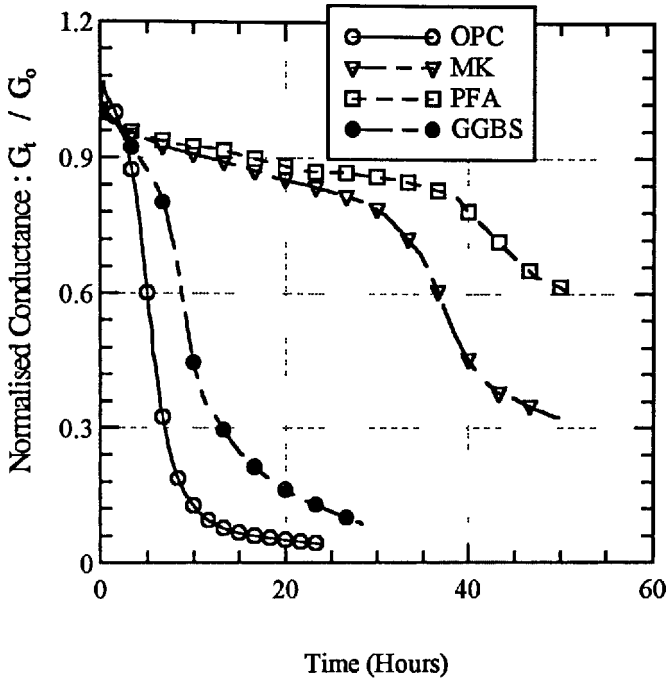

Figure 1: Change in normalised conductance over test period.

The conductivity for the pozzolanic materials decreases before undergoing a more rapid reduction, marking the end of the induction period. The more rapid decrease in conductance varies from approximately 8 hours for the GGBS; 32 hours for the MK to 38 hours for the PFA. This would signify an increase in rigidity, or setting, of the CH activated binder and the formation of an interconnected pore network. The rate of decrease over the setting period is in the order GGBS>MK>PFA. This result is not surprising as GGBS has a high lime content in its own right (≈ 41% for the material used).

After the setting period, the conductivity curves for GGBS and MK undergo a reduction in rate of change - at approximately 12 hours and 40 hours, respectively. This delineates the end of the acceleratory period and the beginning of the slower hardening process. This feature is not identified on the PFA curve as it lies outwith the 55 hour test period.

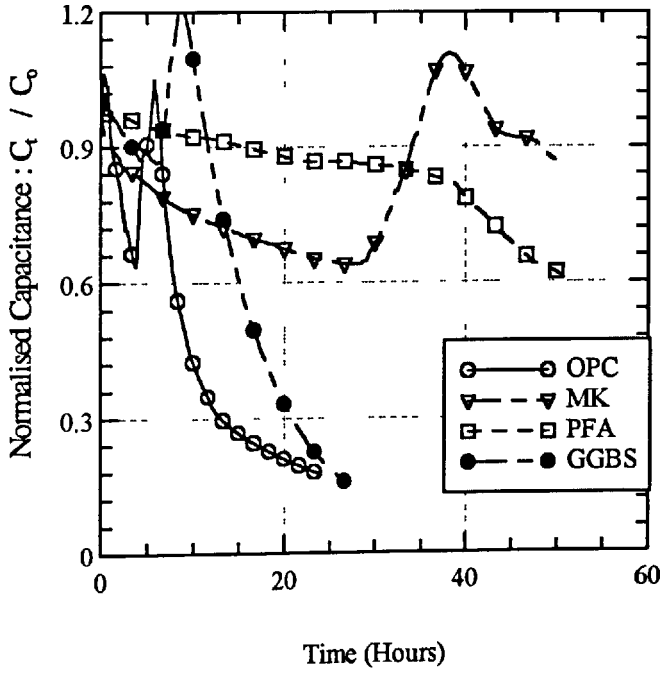

Figure 2: Change in normalised capacitance over test period.

Figure 2: Normalised Capacitance Response

For the most part the normalised capacitance almost mirrors conductance - an initial rapid decrease leading into a period of reduced chemical activity. The most interesting aspect of the capacitance response is just prior to the acceleratory period where a transient peak occurs.

Capacitance can be regarded as a movement or oscillation of charge in a applied electrical field. For example,

charges in the aqueous phase can move along the applied field and then get blocked at interfaces or boundaries within the system. Such charges take no part in the conduction process but manifests itself as a capacitive effect.

The increase in capacitance just prior to setting could be as a result of a phase change or transformation. The growth of fibrous gel layers from the grain surface could introduce thin blocking layers thereby enhancing capacitance in a transient way. The theory of *dielectric amplification* could be invoked to account for such behaviour (Christensen et al, 1994). After the peak in capacitance, solidification (thereby restricting charge movement) and irrotational binding of charges within the system results in the rapid reduction in capacitance values. The peak in capacitance is not observed in the PFA response and could be as a result of a lime deficient environment and hence much slower rate of gel formation.

Internal Temperature

Although not presented graphically, for OPC, setting is accompanied by liberation of heat with the internal temperature of the sample increasing to 30°C at approximately 10 hours. The internal temperature for all the pozzolanic materials fluctuated between 22±0.5°C in a gradual manner, representing no more than minor changes in laboratory temperature.

CONCLUDING COMMENT

Electrical impedance, when measured in terms of conductance and capacitance, has proved to be an effective testing technique for following the hydration of alkali-activated pozzolanic materials. The electrical response (the capacitance in particular) indicated a number of stages during early hydration and comparisons can be made with OPC in this respect.

ACKNOWLEDGEMENTS

The Authors acknowledge the financial support of the Engineering and Physical Science Research Council , UK (Grant GR/K65089).

REFERENCES

Christensen B J, Coverdale R T, Olson R A, Forde S J, Garboczi E J, Jennings H M, and Mason T O, 'Impedance spectroscopy of hydrating cement based systems: Measurement Interpretation and Application', J. Amer. Ceram. Soc., 77, 11, pp2789-2804, 1994.

Coverdale R T, Christensen B J, Mason T O, Jennings H M and Garboczi E J, 'Interpretation of the impedance spectroscopy of cement paste via computer modelling', J. Mater. Sci., 29, pp4984-4992, 1994.

Kostuch J A, Walters G V and Jones T R, 'High performance concretes incorporating metakaolin - a review', Proc. Concrete 2000 Conference, Dundee, 7-9 Sept., Vol. 2, pp1799-1811, 1993.

Luxan M P, Madruga F and Saavedra J, 'Rapid evaluation of pozzolanic activity of natural products by conductivity measurement', Cem. and Conc. Res., 19, 1, pp63-68, 1989.

McCarter W J and Afshar A, 'Monitoring the early hydration mechanisms of hydraulic cement' J. Mater. Sci., 23, pp488-496, 1988

McCarter W J and Garvin S, 'Admixtures in cement: a study of dosage rates on early hydration', Mater. and Struct.: Res. and Test., 22, pp112-120, 1989.

Tashiro C, Ikeda K and Inoue Y, 'Evaluation of pozzolanic activity by the electric resistance measurement method', Cem. and Conc. Res., 24, 6, pp1133-1139, 1994.

ALKALINE ACTIVATION OF METAKAOLIN: INFLUENCE OF SYNTHESIS PARAMETERS

M.L. GRANIZO, Instituto Eduardo Torroja (CSIC), Spain
M.T. BLANCO-VARELA, Instituto Eduardo Torroja (CSIC), Spain
F. PUERTAS, Instituto Eduardo Torroja (CSIC), Spain
A. PALOMO, Instituto Eduardo Torroja (CSIC), Spain

ABSTRACT Alkaline activation of metakaolin to produce inorganic polymers with high mechanical strengths has been studied. Two different metakaolins have been activated at 85°C during 2 hours. Four concentrations of NaOH solutions (5, 12, 15 and 18 M) were used as activator. Some metakaolin/liquid ratios were tested. A complete characterization of the products obtained was carried out. Flexural strengths were found to be between 2 and 16 MPa. Correlations among mechanical strength of specimens, activator concentration and metakaolin/liquid ratio have been found.

Key-words: Synthesis, Metakaolin, Alkali, Activation

INTRODUCTION

Metakaolin based cements result from an inorganic polycondensation reaction that occurs when metakaolin is activated by alkaline hydroxide solutions. These cements rapidly harden at temperatures below 100°C and provide high mechanical strengths. Both kaolin and metakaolin can be activated by alkaline hydroxides to give the inorganic polymer. The starting aluminosilicate and the different synthesis parameters directly influence the characteristics and properties of this polymer.

The synthesis of these binders can be compared to zeolite synthesis. The resulting binder network consists of SiO_4 and AlO_4 tetrahedra linked alternately by sharing all the oxygens where the alkaline cations from the activator solution are present in the structure balancing the negative charge of IV- coordinated Al. So, the structure of metakaolin cements can be also related to the structure of some zeolites. However, while in zeolite synthesis, to favour crystallization, an excess of liquid (activator dissolution) is used and the synthesised product can be separated through filtering, in metakaolin cements, a minimum of activator solution is desirable to obtain a paste with suitable workability. Thus, zeolites are very crystalline materials whereas metakaolin cements are almost amorphous. In the literature, there are some studies about alkaline activated metakaolin in which the influence of parameters such as temperature, curing time, reagents mix order, etc. have been studied (Palomo and Glasser, 1992, and Madani et al., 1990). Some composition limits to obtain optimum alkaline cements with high mechanical strength have been proposed, and the following ranges have been indicated: M_2O/SiO_2, 0.2 to 0.8; SiO_2/Al_2O_3, 3.3 to 4.5; H_2O/M_2O, 10 to 25; M_2O/Al_2O_3, 0.8 to 1.6 (Davidovits, 1985). Also, microstructural and mechanical characterisation studies of the obtained cements are found (Palomo et al., 1992). However, no references have been found about the influence of alkaline hydroxides solutions on final product properties. The influence of the starting kaolin characteristics on cement properties and its mechanical behaviour have not been studied.

The aim of this work is to study the influence of these parameters on the flexural strengths of metakaolin binders. For this purpose, two different metakaolins have been activated at 85°C during 2 hours. Four concentrations of NaOH solution (5, 12, 15 and 18 M) were used. Some metakaolin/liquid ratios were tested.

EXPERIMENTAL

Specimens of 1x1x6 cm were synthesised mixing MK1 and MK2 with 5M, 12M, 15M and 18M NaOH solutions and variable MK/liquid ratios. Specimens were cured during 2 hours at 85 ± 2°C. Then, the specimens were mechanically tested.

Rheological behaviour of MK1 and MK2 is very different (mainly due to their different fineness) so, MK1 specimens were mixed with 45-50 and 60 ml of solution by each 70 g of MK whereas those of MK2 were mixed with 20, 25, 30 and 35 ml of NaOH solution by each 70 g of MK. Specimens porosity was determined through mercury porosimetry.

The insoluble residue (I.R.) in acid of each paste was determined. The grounded sample is treated with cold diluted hydrochloric acid (1:10) and then with a 5% Na_2CO_3 solution. After this treatment the sample is calcined at 1000°C and the insoluble residue is calculated.

Soluble sodium was determined according to the following methodology: 3g of grounded sample dried in vacuum until constant weight are mixed with 200ml of deionized water, and stirred (magnetic agitation) during 3 hours. After this time, it is filtered and washed. The resultant liquid is taken to 500ml and Na^+ measured by ionic chromatography.

RESULTS

In a previous work (Granizo et al., 1996), a complete characterization of the two kaolins and their respective metakaolins was carried out (chemical and mineralogical composition, thermal behaviour, specific surface, particle size distribution, etc.).

Flexural strengths and insoluble residues of specimens elaborated with MK1 and MK2 mixed with different volumes of 5, 12, 15 and 18M NaOH are shown in Table I.

According to the results, 5M concentration is not enough to provoke reaction in the test duration. Specimens have no strength and this indicates that a higher solution concentration is required to provide reaction in the test time.

Regression analysis of flexural strength data of MK1 and MK2 is carried out in order to quantify the influence of the parameters (NaOH concentration and ml of dissolution in the mixes) on flexural strengths. Eqs 1 and 2 show the influence of NaOH solution concentration and the volume of NaOH solution on flexural strengths of the specimens with MK1 and MK2, respectively.

$$\text{F. Strength} = 124.73 - 1.5033\ \text{liquid (ml)} - 0.9575\ [\text{NaOH}] \quad (\text{R-SQ.} = 0.7560) \qquad [1]$$

$$\text{F. Strength} = 204.59 - 5.1317\ \text{liquid (ml)} + 1.9258\ [\text{NaOH}] \quad (\text{R-SQ.} = 0.8060) \qquad [2]$$

According to both equations, the sign of the coefficient affecting liquid amount (ml) is negative in both cases and as liquid amount increases, flexural strengths decrease. The sign of the coefficient affecting NaOH concentration is opposite in the two kaolins. Flexural strengths increase as NaOH concentration increases in MK2 while they decrease when NaOH concentration increases for MK1.

Table 1. Flexural strengths and insoluble residues of the compositions studied.

COMP.	METAKAOLIN (70g)	[NaOH] (M)	LIQ. (ml)	I. R. (%wt.)	Flex.Str. (MPa)
G2CB	MK1	5	50	60.56	------
G2CM			60	59.40	------
TCB	MK2		20	82.50	------
TCM			30	76.40	------
G2DBB	MK1	12	45	12.77	4.64
G2DB			50	9.10	3.69
G2DM			60	9.67	1.43
TDB	MK2		20	50.56	10.5
TDM			30	30.14	7.94
TDMM			35	24.95	5.92
GQBB	MK1	15	45	9.16	4.45
GQB			50	8.84	3.38
TQB	MK2		20	40.56	11.6
TQR			25	27.13	9.91
TQM			30	19.75	8.24
TQMM			35	20.77	5.12
G28BB	MK1	18	45	9.26	3.71
G28B			50	8.45	3.47
TD8BB	MK2		20	35.52	16.0
TD8B			252	32.69	11.2
TD8M			30	21.41	8.94
MK1				99.02	
MK2				98.50	

I.R. data can be taken as a measurement of reaction degree, because both metakaolins are very insoluble in acid medium while the polymers obtained are soluble in such medium. Thus, in the case of MK1, its reaction degree is already almost total for 12M concentration and the lowest liquid, varying little when these parameters increase. In the case of MK2, I.R. decreases, this means that reaction degree increases when the two parameters studied increase. Equation relating reaction degree of MK2, with NaOH concentration and liquid amount is the following:

I.R. = 90.3191 - 1.395 liquid ml - 1.4475 [NaOH] (R-SQ. = 0.8085) [3]

Soluble Na_2O content

Na_2O solubility tests were carried out through ionic chromatography in order to quantify the Na_2O percentage that remains in the product structure after water treatment. Results are shown in Table 2.

Table 2. Results of Na_2O solubility tests

COMPOSITION	SAMPLE INITIAL %Na_2O (%wt.)	FIXED %Na_2O (%wt.)	SOLUBLE %Na_2O (%wt.)	FIXED %Na_2O (%wt.(*)
G2DBB	12.90	10.86	2.04	84.19
G2DB	13.63	10.87	2.76	79.75
G2DM	14.88	11.07	3.81	74.40
TDB	7.71	6.56	1.15	85.09
TDR	9.01	7.93	1.08	88.02
TDM	10.15	9.03	1.12	88.97
TDMM	11.15	9.63	1.52	86.37
GQBB	15.69	11.34	4.35	72.28
GQB	16.55	11.51	5.14	68.95
TQB	9.48	8.35	1.13	88.08
TQR	11.05	9.93	1.12	89.87
TQM	12.41	10.91	1.74	85.98
TQMM	13.61	10.91	2.70	80.17
G28BB	18.40	10.83	7.57	58.86
G28B	19.38	9.46	9.92	48.82
TD8BB	11.22	10.11	1.11	90.11
TD8B	13.04	11.62	1.42	89.12
TD8M	14.62	12.62	2.00	86.33
TD8MM	16.10	10.78	5.32	66.96

* %Na_2O expressed with respect to the initial Na_2O.

These results indicate that soluble Na_2O increases as the Na_2O initial dosage increases. Hence, in MK1 compositions, where initial Na_2O amount is higher, there is a considerable increase in soluble Na_2O amount with respect to MK2 compositions. Thus, soluble Na_2O increases exponentially with the initial Na_2O amount dosage according to the following equation:

$$\text{Soluble \% } Na_2O = 0.097 \exp [(\text{\% initial } Na_2O)/4.1890] \qquad (\text{R-SQ.} = 0.9674) \qquad [4]$$

Hg porosimetry

Mercury porosimetry tests were carried out on dried specimens. Results are shown in Table 3. These results show that total porosity percentage is higher in samples obtained with MK1 than that of those made with MK2.

Table 3. Results of mercury porosimetry

	% TOTAL POROSITY (AREA)	% TOTAL POROSITY (VOLUME)	AVERAGE PORE DIAMETER (μm)
G2DBB	23.93	49.80	0.1331
G2DB	25.98	51.98	0.3061
G2DM	35.75	80.61	0.0857
TDB	15.31	35.48	0.0945
TDM	19.92	44.56	0.1262
TDMM	24.19	55.16	0.1201
GQBB	24.18	49.65	0.1458
GQB	23.00	57.59	0.2441
TQB	14.68	33.88	0.0814
TQR	17.45	39.52	0.1030
TQM	20.04	44.42	0.1709
TQMM	24.78	56.04	0.1087
G28BB	27.82	63.04	0.1060
G28B	27.98	64.18	0.0878
TD8BB	13.15	29.92	0.0796
TD8B	16.08	36.99	0.0899
TD8M	19.03	43.28	0.1302

The behaviour of both metakaolins is different, and a high relation between porosity of MK2 specimens with respect to NaOH concentration and amount of liquid is found. The equation governing this behaviour is the following:

$$\text{Porosity} = 7.6955 + 0.5622 \text{ liquid ml} - 0.3076 [\text{NaOH}] \qquad (\text{R-SQ.} = 0.9787) \qquad [5]$$

With respect to MK1 specimens, an increase in total porosity percentage is observed when liquid amount and NaOH concentration increase.

An exponential relationship between porosity and flexural strength of both MK specimens is found; strength increases as porosity decreases according to the following equation:

$$R = 565.25 \exp [(- \%\text{porosity})/9.8590] \qquad (\text{R-SQ.} = 0.9491) \qquad [6]$$

DISCUSSION

The starting kaolins present a similar chemical composition and they are mainly constituted by kaolinite with minor proportions of quartz (approximately 10%), also similar in both cases. K2 kaolin has also a minor proportion of anatase and pyrophyllite. The main difference between these kaolins is in their crystallinity index that is higher in the case of K1 and in their specific surface, also higher in K1.

Dehydroxilation of both kaolins by thermal treatment at 750°C during 24 hours leads to kaolinite structure destruction with metakaolin production. In this process, a decrease of specific surface is produced, being MK1 specific surface higher than MK2 one.

The behaviour of these metakaolins when they are alkaline activated is very different from the point of view of rheology, mechanical properties, etc.

Reaction degree reached by MK1 samples is practically constant and very high (of about 90%) in all the experiments, if the quartz proportion of the starting kaolin (close to 10%) is taken into account. Sodium fixing capacity in the final product is of about 11% with respect of the weight of such product and it remains almost constant in all the experiments.

On the other hand, specimens with MK1 have high porosity values. The porosity increases as activator solution concentration and volume increase.

Mechanical behaviour of specimens elaborated with MK1, described by Eq 1, can be justified if test conditions and measurements of porosity, fixed sodium and insoluble residue are taken into account.

Because of the high specific surface of MK1, the activator solution amount necessary to elaborate specimens is also high (45-60 ml /70g MK). This leads to a high Na_2O amount per gramme of MK in these samples and, thus, a practically complete reaction at the most soft test conditions is reached. When increasing the values of synthesis parameters ([NaOH], activator

liquid volume,) reaction degree and sodium fixing capacity (Na remains free in specimens) does not increase further, but, however, an increase in porosity is produced. As a consequence, specimens mechanical strengths decrease when solution volume and activator solution concentration are increased as it is described by Eq 1.

On the other hand, mechanical behaviour of specimens elaborated with MK2 and described by Eq [2] is also justified analyzing the results of insoluble residue determination, sodium fixed and specimens porosity as well as the conditions of the experiments.

So, the lower specific surface of MK2, permits the utilization of lower solution volumes (20-35 ml/70 g MK) in specimens mixing. This means that, in some of the experiments, sodium amount is not enough to provide a complete reaction degree and, thus, sodium fixed in the structure is not maximum. The sodium fixing capacity in MK2 specimens increases as initial $\%Na_2O$ increases and the maximum is of about 11-12% (expressed as Na_2O percentage).

The maximum reaction degree would be higher than 90% if minor compounds in the MK2 (quartz, anatase, pyrophillite) are taken into account.

However, an increase in reaction degree does not always involve higher mechanical strengths, but, as it is described by Eq 3, reaction degree increases as dosage of Na_2O increases , by mean of increasing NaOH concentration or by increasing activator solution volume. However, mechanical strengths (oppositely to porosity) increase as activator solution concentration increases, but they decrease when liquid/solid ratio increases.

Hence, higher strengths in specimens with MK2 will be obtained when porosity is lower, this is, when NaOH concentration is the highest and activator solution volume the lowest. In any case, mechanical strengths of specimens with MK1 are lower than those of MK2, but important values are reached if the high porosity of these samples is taken into account. Further investigations must be carried out in order to improve rheology and decrease liquid/solid ratio that will be translated in a porosity decrease and an improvement of mechanical strengths.

CONCLUSIONS

Metakaolin alkaline activation in hydrothermal conditions (85°C, 2h) leads to high strength cementitious materials. The synthesis parameters studied (activator solution concentration and the liquid amount of this activator) as well as the characteristics of the starting metakaolin have a decisive influence on the mechanical properties of the cements obtained.

Metakaolins specific surface condition their rheological behaviour and, subsequently, their mechanical strengths.

Metakaolins with a high specific surface need high liquid/solid ratios for their mixing. This leads to higher porosities and, thus, lower strengths of the specimens. Activator solution concentration necessary to obtain optimum strengths depends on metakaolin reactivity. So, in metakaolins with high specific surface (more reactive), more diluted solutions can be used in order to obtain reaction degrees similar to those obtained with metakaolins with lower specific

surface in the same hydrothermal conditions. To obtain the higher strengths the minimum activator solution amount providing reaction degrees higher than 90% must be used (in the curing conditions described above).

Later increases of activator solution concentration produce porosity increase and leave soluble alkaline hydroxides unreacted. All this leads to a strength decrease.

Materials obtained by metakaolin alkaline activation are extremely porous materials and their pore size is of about 0.1 μm.

An enhancement of pastes rheology would lead to higher mechanical strengths. Sodium fixing capacity in the polymer is of about 11% (expressed as Na_2O percentage).

ACKNOWLEDGEMENTS

The authors wish to thank to CICYT for funding this research through MAT93-0282 and MAT96-0598 programmes.

REFERENCES

J. Davidovits. "Early high strength mineral polymer" (1985). U.S. Patent 45009985.

M.L. Granizo, M.T. Blanco-Varela and A. Palomo. " Influence of the starting kaolin on alkali-activated materials based on metakaolin. Study of the reaction parameters by isothermal conduction calorimetry". J. Mat. Science (1996) (in press).

A. Madani, A. Aznar, J. Sanz and M. Serratosa. "^{29}Si and ^{27}Al NMR study of zeolite formation from alkali-leached kaolinites. Influence of thermal preactivation". Phys. Chem. Vol.94, 1990, pp. 760-5.

A. Palomo and F.P. Glasser. "Chemically-bonded cementitious materials based on metakaolin". Br. Ceram. Trans. J., Vol.91, 1992, pp. 107-112.

A. Palomo, A. Macías and E. Menéndez (1992). "Microstructure of geopolymers". Proceedings of the fourteenth Int. Conf. on cement microscopy. Costa Mesa, California.

STRENGTH AND HYDRATION OF AN ACTIVATED ALUMINO-SILICATE MATERIAL

J.N. LIU, M.R. SILSBEE and D.M. ROY, Materials Research Laboratory, Pennsylvania State University, University Park, PA 168021 USA

ABSTRACT This paper presents the results of a study of the behavior of an activated alumino-silicate material (metakaolin). The use of portland cement, $Ca(OH)_2$, gypsum and water soluble silicate ($Na_2O{\cdot}nSiO_2$) as activators of metakaolin were investigated. Compressive strength measurements along with X-ray diffraction studies were used to track hydration occurring in the system. The results of the study show that metakaolin has the potential to act as a supplementary cementitious material when the right combination of activators are employed to provide a suitable environment for hydration. In order to hydrate metakaolin, additional $Ca(OH)_2$ is required in order to form calcium silicate hydrate (CSH). Although, gypsum by itself cannot activate metakaolin, combinations of gypsum and $Ca(OH)_2$ or portland cement show promise as activators for metakaolin. Gypsum that consumes $Ca(OH)_2$ to form calcium aluminum sulfate hydroxide reduces $Ca(OH)_2$ significantly in the reaction product of a mixture of cement and metakaolin.

Keywords: activation, alkali, blended cement, economy, metakaolin, X-ray Diffraction Analysis

INTRODUCTION

It is well known that metakaolin has considerable potential for use as a cementitious material when mixed with calcium hydroxide. Metakaolin is kaolinite that has been calcined at a temperature in the range from 650-850°C (He et al., 1995; Murat and Comel, 1983). At this temperature range the interlayer water and hydroxyl in kaolinite is lost but the original network of a combination of SiO_4 tetrahedra and AlO_6 octrahedra or irregular polyhedra remain. During hydration the network first is attacked and bonds are broken by hydroxyl ions then new hydrates including CSH and other aluminate containing hydrates, such as C_2ASH_8, C_4AH_{13} and possibly zeolite precursors when alkalis are present are formed.

Calcium hydroxide is a very effective activator for metakaolin. For optimum strength development, 25% calcium hydroxide is needed (3). Metakaolin can be used to react with and eliminate calcium hydroxide in portland cement (4) in much the same manner as does silica fume. This is desirable since the excess calcium hydroxide forms as relatively soluble crystals that contribute much less to strength development and may cause durability problems (5). Using this approach some researchers have attempted to minimize calcium hydroxide formation in glass fiber reinforced cement composites by adding metakaolin to the composite (6).

The current study focuses on: 1) using combinations of calcium hydroxide and gypsum as activators; and 2) the characterizing the reduction of calcium hydroxide in cement matrixes with various metakaolin contents.

EXPERIMENTAL

Materials

Both Type III portland cement (PC) and metakaolin (MK) are commercial products and their chemical analysis are given in Table 1.

Table 1. Chemical Analysis of Type III Cement and Metakaolin

	SiO_2	Al_2O_3	TiO_2	Fe_2O_3	MgO	MnO	CaO	Na_2O	K_2O	P_2O_5	SO_3	L.O.I.
PC	20.2	2.32	0.11	4.47	3.54	0.05	63.9	0.12	0.49	0.21	3.0	0.85
MK	51.91	39.68	0.54	0.93	0.16		0.16	0.60	0.60			0.23

The $Ca(OH)_2$ and $Na_2O{\cdot}nSiO_2$ (Pine PQ Corporation) n=3.2] are chemical agents with 99.99% purity. Superplasticizer (Mighty 150, Boremco) is a dark brown solution containing 56% solid.

Mixture Proportions

Metakaolin (MK) was mixed with 0, 25, 50, and 65% Type III portland cement by weight respectively. Calcium hydroxide and gypsum dosages were 0, 5, and 10%. To maintain workability in the cementitious pastes, the water to solid ratios (W/S) and dosage of superplasticizer were adjusted from 0.45 to 0.65 and 1 to 3% respectively. The fluidity of the pastes was controlled within 150 - 175 mm flow by the use of a flow table. The mixture proportions are listed in Table 2.

Table 2. Mixture Proportions

No.	cement	MK	$Ca(OH)_2$	gypsum	SP	W/S	note
MK50-0	50%	50%			3%	0.45	
MK50-1	45%	45%	10%		3%	0.45	
MK50-2	45%	45%		10%	3%	0.45	
MK50-3	45%	45%	5%	5%	3%	0.45	
MK65-1	25%	65%	5%	5%	3%	0.60	
MK65-2	25%	65%	10%		3%	0.60	
MK65-3	25%	65%	5%			0.60	$Na_2O{\cdot}nSiO_2$ 5%
MK100-1		65%	35%		3%	0.65	
MK100-2		65%	25%	10%	3%	0.65	
MK20	75%	20%		5%	1%	0.45	
MK0	100					0.45	

Specimens and samples preparation

The solid materials were dry mixed in a paddle style mixer for 1 minute before the water was added; after the water was added, mixing continued for three minutes. The pastes were cast into 25 x 50 mm cylinder molds. After casting, all specimens were put into a curing chamber at 38 ± 2°C and 100% relative humidity for 24 hrs before being demolded for further curing.

On the test day the cylinders were cut into 25 x 25 mm specimens using a diamond saw and the bearing surfaces polished before the compressive strength tests were conducted. Samples of the broken specimens were ground to less than 100 μm and characterized by powder XRD using a Scintag diffractometer (Scintag, Sunny Vale, CA), with Cu Kα radiation.

RESULTS AND DISCUSSION

Compressive strength

The compressive strength development of hardened mixtures of cement and metakaolin is illustrated in Fig. 1.

In mixture MK50-0, the only activation is from the $Ca(OH)_2$ released from the cement during its hydration. A typical portland cement will produce about 20% $Ca(OH)_2$ or 10% in the mixture MK50-0. The 28 day strength of MK50-0 is 59.13 MPa. The strength of MK50-1 was higher than MK50-0 after 7 days curing since 10% $Ca(OH)_2$ was added. When the $Ca(OH)_2$ was replaced with 10% gypsum, (MK50-2) higher 7- and 14-day strengths than both MK50-0 and MK50-1, and equal 28-day strength as MK50-1, resulted. In mixture MK50-3, gypsum and $Ca(OH)_2$ (5% each) were added in combination. This combination of activators worked very well. The strength (78.38 MPa, 28 day) of MK50-3 is obviously higher than the others at both early and later age. When gypsum and $Ca(OH)_2$ were used the 28-day strengths of the mixture containing only 45% cement was nearly 85% of the pure cement paste.

Fig. 2 shows the effect of combined activators in mixtures with lower or zero cement contents. The strengths of MK65-1 and MK65-3 were improved compared with MK65-2. Soluble silicates ($Na_2O{\cdot}nSiO_2$) have been used to activate other pozzolanic materials, such as slag and fly-ash. It is very interesting that the combination of $Ca(OH)_2$ and soluble silicate resulted in MK65-3 having a lower early strength and significant strength increase at later ages.

In the mixtures which contained no cement, although the combined activators showed improved early strengths at 3, 7 and 14 days, the strengths decreased slightly after 14 days compared to the control.

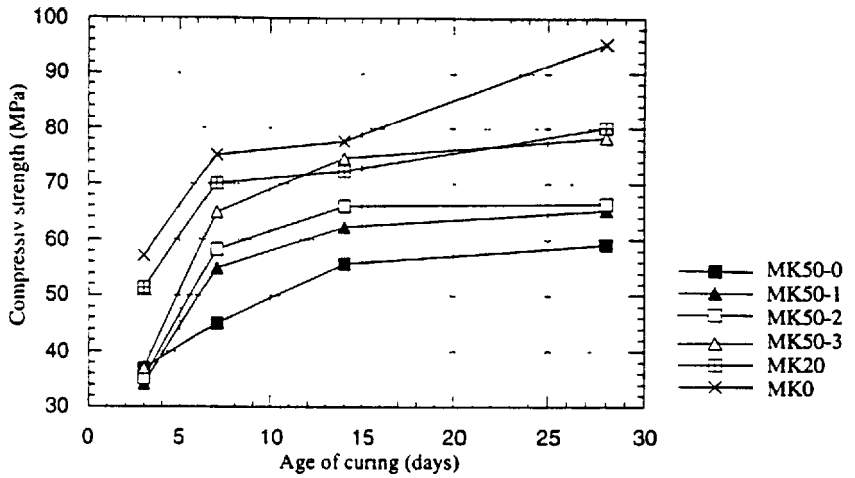

Fig. 1. Compressive strengths of metakaolin mixtures with high cement content

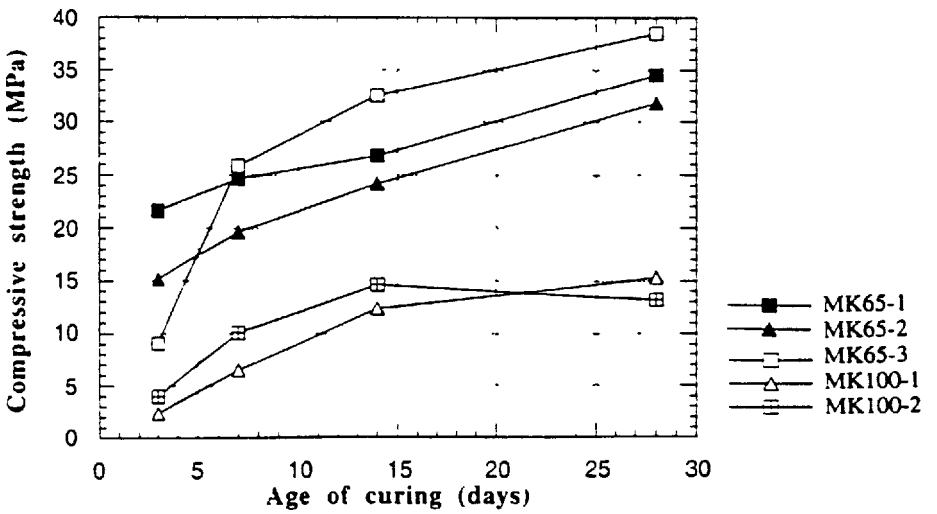

Fig. 2. Compressive strength of metakaolin mixtures with low cement content

Hydration of mixes

Fig. 3 shows the X-ray patterns gathered from samples of 50% metakaolin-50% portland cement paste (MK50-0) at various ages: The following observations can be made: 1) at all ages there was less $Ca(OH)_2$ than normally observed in portland cement pastes;

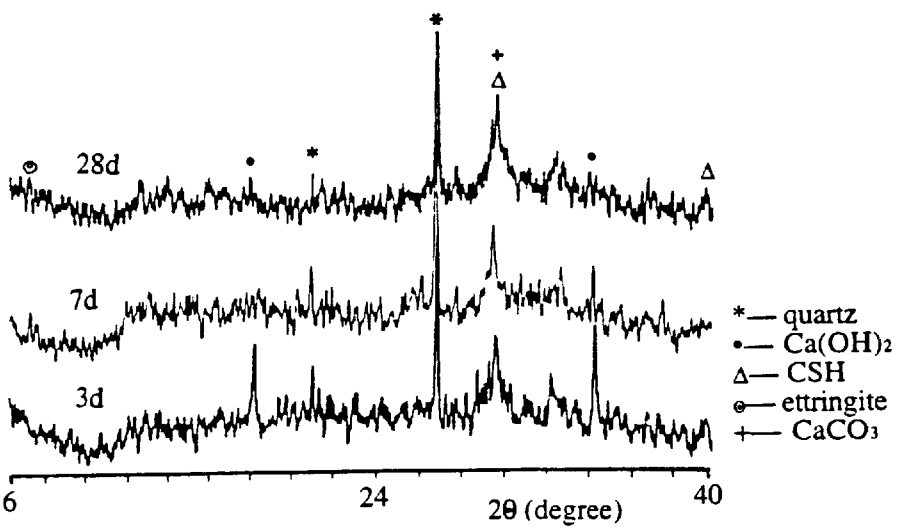

Fig. 3. The X-ray patterns of mixture MK50-0 (PC 50%, MK 50%)

2) there were several sharp peaks of quartz that was introduced as an impurity in the metakaolin and reacted very slowly; 3) $CaCO_3$ formed as the samples were exposed to the atmosphere.

Fig. 4 shows that metakaolin consumes $Ca(OH)_2$ during the hydration of MK50-1 (PC 45%, MK 45%, CH 10%). However, the metakaolin had not consumed all the $Ca(OH)_2$ at 28 days as evidenced by the peaks of $Ca(OH)_2$ that can be identified easily in the X-ray patterns of both MK50-0 and MK50-1.

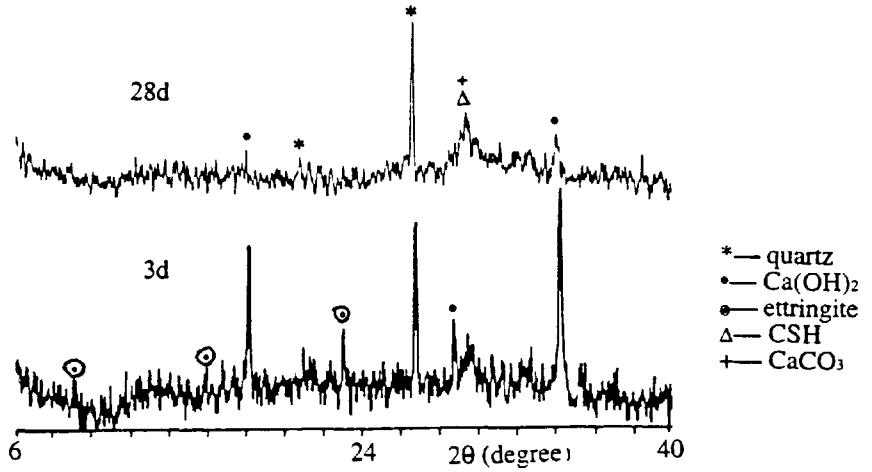

Fig. 4. The X-ray patterns of mixture MK50-1 (PC 45%, MK 45%, CH 10%)

When gypsum was added (MK50-3), very interesting results were obtained not only during strength development but also in the X-ray patterns (Fig. 5).

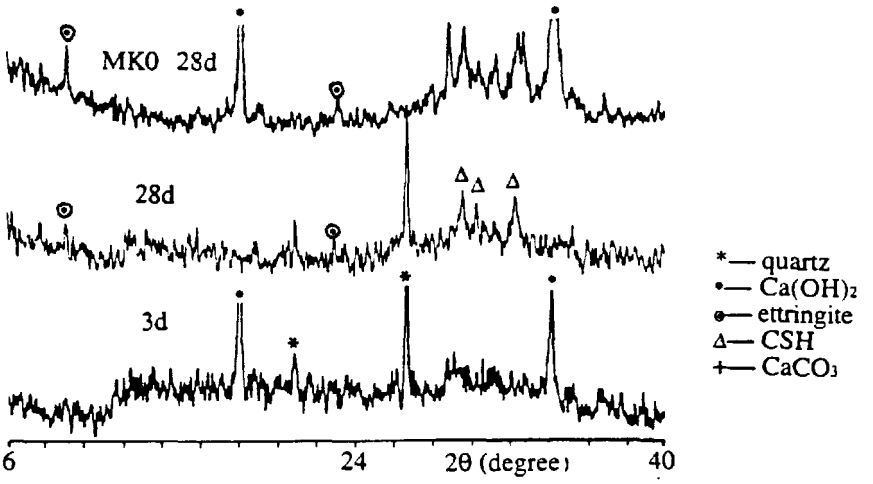

Fig. 5. The X-ray patterns of mixture MK50-3 (PC45%, MK45%, CH5%, gypsum 5%)

No $Ca(OH)_2$ peaks can be detected at age of 28 days. It indicated that $Ca(OH)_2$ was totally combined with gypsum and metakaolin to form calcium aluminum sulfate hydroxide hydrate (ettringite) and other hydrates. From Fig. 5 it also can be seen that the CSH peaks in MK50-3 were more like thatof pure cement paste than other mixtures and the quantity of ettringite was similar to that of cement paste at 28 days.

Fig. 6 shows X-ray patterns of mixtures MK65-1 and MK65-2 that are based on a 25% cement content. The peaks of ettringite were clearly found in both mixes, but more ettringite was in MK65-1 since 5% gypsum was added to the mixture. The peaks of $Ca(OH)_2$ did not appear in the mixture MK65-1 but can be observed in MK65-2 in which there was no gypsum added.

Mixtures MK100-1 and MK100-2 contained 35% $Ca(OH)_2$ or 25% $Ca(OH)_2$ and 10% gypsum respectively (no cement). At an early stage of hydration of MK100-2 (see Fig. 7), there were very sharp peaks of gypsum and $Ca(OH)_2$ present in the X-ray pattern. Ettringite

can not be identified from X-ray patterns at the age of 3 days. This means that the hydration processes occurring in this mixture was very slow. At the age of 14 days the peaks of ettringite were very clear and the peaks of gypsum were noticeably smaller than at 3 days. This phenomenon indicates that metakaolin, even when activated by $Ca(OH)_2$ and gypsum, has a very low hydration rate at early ages and then gradually accelerates. In contrast the X-ray pattern of MK100-1 at 28 days shows no peaks for ettringite or gypsum (as might be expected), the only evidence of hydration being a very broad peak indicative of CSH and the relatively low intensity observed for $Ca(OH)_2$.

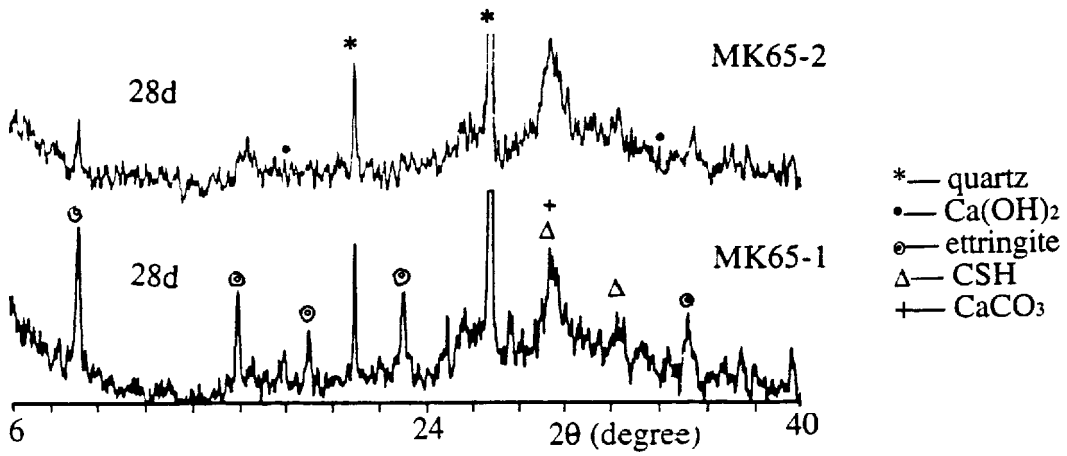

Fig. 6 The X-ray patterns of mixture MK65-1 and MK65-2

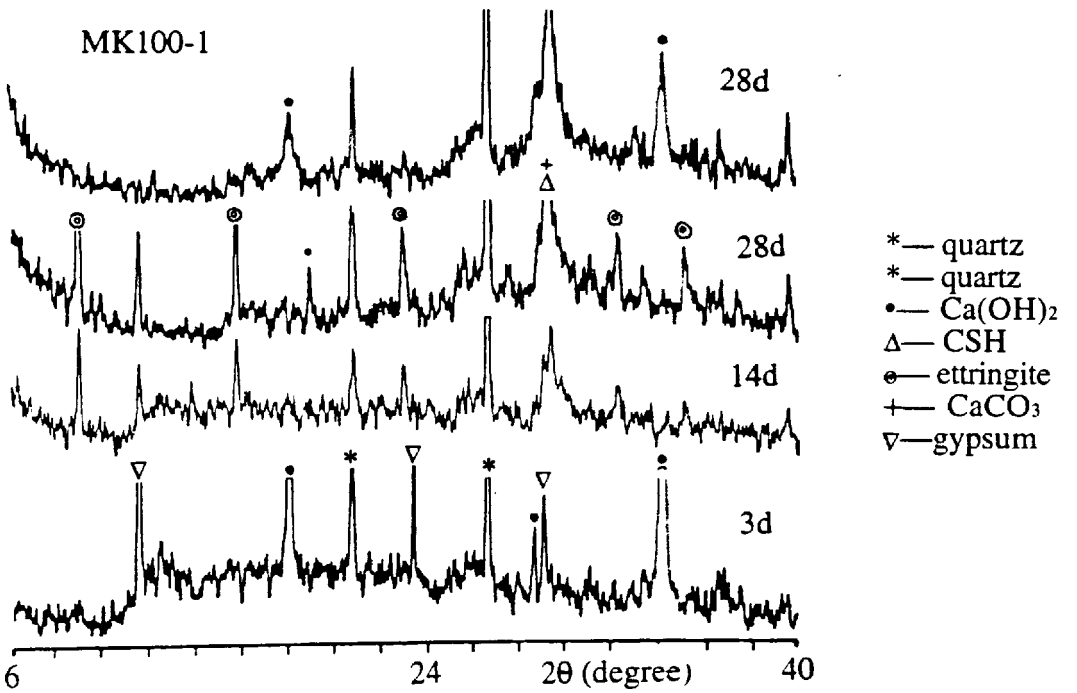

Fig. 7. The X-ray patterns of mixtures MK100-1 and MK100-2

DISCUSSION

The results above have shown that combinations of activators with metakaolin resulted in higher early and later strengths. The increase of early strength is mainly the result of the formation of ettringite. Ettringite is one of most easily formed crystalline phases found during cement hydration when Ca^{+2}, Al^{+3} and SO_4^{-2} are available at same time. It can be easily detected in a few hours, even in less than an hour, after cement is mixed with water. Ettringite that is formed quickly at early age of hydration builds up a skeleton in the fresh cementitious matrix and contributes to the early strength. The X-ray patterns indicated that Al^{+3} ions in the mixture at the beginning of hydration were from the C_3A in the cement not from the metakaolin. After three days, as the network was attacked by both hydroxyl and sulfate ions,

Al^{+3} ions dissolved gradually. The formation of ettringite consumed Al^{+3} ions from metakaolin and accelerated the dissolution reaction.

The average C/S ratio of CSH is about 1.5-1.7. If all the SiO_2 in the metakaolin was consumed by the formation of CSH (100% hydration), one mole of metakaolin would consume 3.0-3.4 moles of $Ca(OH)_2$. Based on silica alone metakaolin can theoretically consume an amount of $Ca(OH)_2$ equal to its weight. In fact calcium aluminum hydrates will also consume $Ca(OH)_2$ during their formation. In the short term metakaolin consumes less $Ca(OH)_2$ than the theoretical quantity since the hydration process is a slow one. The potential of using metakaolin to react with $Ca(OH)_2$ in blended cement pastes and form CSH has been demonstrated.. Gypsum when added to the mixture of cement and metakaolin resulted in higher composite strengths and also lower $Ca(OH)_2$ contents.

CONCLUSIONS

1) Although gypsum does not perform well as an activator by itself the combination of gypsum and portland cement or $Ca(OH)_2$ was effective in activating metakaolin.
2) Gypsum added to mixtures of cement and metakaolin results in not only an improvement in the strength of the mixtures but also lower $Ca(OH)_2$ contents.
3) Initially the rate of hydration of metakaolin is very slow, however, after 3 days the hydration begins to accelerate.

Acknowledgment
The authors would like to acknowledge their appreciation and the financial support from the National Science Foundation

REFERENCE

1. **He**, C., Osbæck B., and Makovicky E., Cem. Concr. Res. 25, 1691 (1995).
2. **Murat,** M. and Comel, C., Cem. Concre. Res. 13, 631 (1983).
3. **Ambroise** J., Murat M., and Pera, J., Cem. Concre. Res. 15, 83 (1985).
4. **Oriol**, M. and Pera, J., Cem. Concre. Res. 25, 265 (1995).
5. **Roy**, D.M. and Silsbee, M.R., Mat. Res. Soc. Symp. Proc. Vol. 245, 153 (1992).
6. **Murat**, M. and Al Cheikl, A., Cem. Concre. Res. 19, 16 (1989).

HYDRATION OF PORTLAND CEMENT BLENDS IN PRESENCE OF BAG HOUSE DUST FROM CALCIUM CARBIDE FURNACE

N.B. SINGH, K.N. BHATTACHARJEE and A.K. SHUKLA
Department of Chemistry, Gorakhpur University
Gorakhpur 273 009, India

ABSTRACT Hydrations of ternary and quarternary blends made from portland cement clinker, bag house dust, granulated blast furnace slag and gypsum were studied. It is found that in presence of an appropriate amount of bag house dust and gypsum, the deficiencies of slag cements can be removed and slags can be used in higher doses without diluting the quality.

Key-Words : Blast furnace Slag, Blended Cement, Fly Ash, Gypsum, Pozzolana

INTRODUCTION

In recent years considerable amount of work has been done on blended cements: Uchikawa (1986), Narang et al (1992), Chatterjee (1992), Singh et al (1995). Most of the blended cements presently commercialised are binary blends with either granulated blast furnace slag or pozzolans like fly ash, calcined clay or natural pozzolana. Multiblend systems with three or more components are gaining grounds in many countries. In this investigation the hydration characteristics of various ternary and quarternary cement systems have been studied in the presence of highly reactive calcareous particulate matter from the bag house of a calcium carbide furnace.

EXPERIMENTAL

Materials

Bag house dust (BHD) was procured from a specially designed calcium carbide furnace of M/S Bhutan Carbide and Chemicals Ltd. Pasakha, Bhutan. Portland cement clinker (PCC) was procured from a shaft kiln plant near Kanpur. Gypsum was procured from RSMDC Rajshthan. Granulated blast furnace slag was obtained from Indian Iron and Steel Co. Ltd. Burnpur. The chemical composition of the materials are given in Table 1.

Table1. Chemical composition of materials (Wt %)

Materilas	LOI	SiO_2	Al_2O_3	Fe_2O_3	CaO	MgO	Others
PCC	1.1	20.2	6.5	4.6	63.5	3.6	CaO=2.5
BHD	21.6	12.8	6.8	2.8	48.5	2.8	alk., sulphates-traces
GBFS	0.3	34.8	21.0	1.0	34.5	7.6	Sulphite = 0.5
Gypsum (Mineral)	13.6	10.3	5.6	1.1	28.8	1.2	SO_3 = 39.0

Methods

Blends of composition given in Table 2 were prepared in the laboratory.

Table 2. Composion of blends (wt%) with symbols

PCC	BHD	GBFS	Gypsum	Symbol
5	10	85		A
5	15	80		B
10	20	70		C
15	15	70		D
20	20	60		E
25	15	60		F
15	5	80		G
25	5	70		H
10	10	80		I
20	10	70		J
10	20	65	5	K
10	20	60	10	L

All physical testings were done in accordance with test methods prescribed in Indian Standard specifications IS 4031:1988 (Methods of physical tests for hydraulic cement) and chemical testing was done as per IS 4032:1985 (Methods of chemical analysis of hydraulic cement). Hydrations of cements (w/c=0.5) were allowed to continue for different intervals of time and were stopped with iso propyl alcohol and ether. Free lime and non-evaporable water contents were determined. Powder X-ray diffraction patterns of slected samples were recorded. M-15 concrete moulds were casted for few blended cements by taking one part cement, 2 parts sand and 4 parts aggregate. Compressive strengths were determined on a 150 x 150 x 150 mm^3 cube after 7 days. Some cement mortar cube samples were autoclaved after one day curing to assess the long term durability of the nonconventional blends.

RESULTS AND DISCUSSION

Results of physical testing and hydration studies are given in Tables 3 and 4. From Table 3 it is inferred that in absence of gypsum, with the increase of BHD, the setting time is shortened. This may be due to highly reactive calcium aluminate in BHD which tend to bring flash setting characteristics. Further the initial strengths are improved with BHD. This indicates that in addition to higher hydraulic activity of BHD, it might also act as a filler in the cement matrix due to high fineness. Addition of gypsum to the ternary blends reduces water demand and delays both initial and final setting characteristics. This might be due to the formation of ettringite which envelopes the grains of calcium aluminates initially and tends to reduce its flash setting characteristics. Blend L shows very high strength at 7 and 28 days indicating the formation of calcium sulphoaluminate hydrates. Such blends are expected to show high sulphate resistance.

From Table 4 it is seen that non evaporable water contents increase with hydration time but there is no correlation with the blends. The free lime values in all the blends increase upto 7 days and then there is a decrease at 28 days of hydration indicating pozzolanic activity of GBFS.

Table 3. Physical characteristics of ternary blends

Blends	w/c(%)	Setting time (min.)		Compressive strength (MPa)				7days CCS of M-15 Concr. (Mpa)
		IST	FST	1D	3D	7D	28D	
A	26.0	185	220	12.0	15.0	17.2	22.0	5.9
B	25.3	105	125	14.0	18.0	21.8	28.0	5.7
C	21.7	10	40	19.0	24.0	30.0	36.2	10.1
D	22.7	20	60	15.0	20.6	28.3	32.0	8.1
E	22.3	15	60	18.0	28.4	35.1	37.6	10.2
F	22.6	20	60	14.2	26.0	32.5	36.6	10.6
G	28.0	35	130	9.5	15.5	22.1	24.4	-
H	29.0	40	140	8.0	20.0	31.0	36.4	-
I	28.5	30	120	13.0	20.5	23.0	24.5	-
J	28.5	30	100	13.0	22.0	27.4	33.0	-
K	25.3	90	135	14.6	30.0	32.2	39.6	10.2
L	24.0	65	90	9.0	30.6	39.8	50.0	10.8

Table 4. Hydration studies of blends (w/c=0.5), Temp. 28°C

Blends	Free lime (%)				Wn (%)			
	1D	3D	7D	28D	1D	3D	7D	28D
G	4.2	7.0	7.8	4.1	6.5	11.8	14.9	15.9
H	3.8	5.2	5.8	3.1	10.3	13.3	16.6	19.8
I	4.5	6.5	7.5	4.3	7.8	9.5	14.8	16.2
J	4.0	5.8	6.2	3.5	9.7	12.7	15.2	17.5

Conclusion

Proper proportions of PCC, BHD, GBFS and Gypsum in the blended cement made it much better cement as compared to OPC and at the same time deficiencies of the slag cements are eliminated. In presence of suitable amounts of BHD and Gypsum, higher percentage of Indian GBFS (70%) can be used for making the slage cements without detoriating the quality of cement. BHD

activates GBFS and presence of gypsum form sulphoaluminate hydrates which makes significant contribution towards strength development.

REFERENCES

Chatterjee A.K. "Special and New Cements", Proc. 9th Int.Cong.Chem.Cem., New Delhi, I,1992.pp177-212.

Narang K.C., Sharma K.M., Sharma R.N. and Chopra S.K., "Technological Potentials of making unconventional blended cements using industrial wastes", National seminar on role of building materials industries in conversion of wastes to wealth, March 1985.

Singh N.B.,Bhattacharjee,K.N. and Shukla,A.K., Cem.Concr.Res.,25(5),1995,pp1023-1030

Uchikawa H,"Effect of blending components on hydration and structure formation"Proc.8th Int.Cong.Chem.Cem.,Rio,Brazil,1,1986,pp233-248.

HYDRATION OF CEMENT MIXED WITH "POZZOLIT" MINERAL ADDITIVE

Vili **LILKOV**, University of Mining and Geology, Sofia, Bulgaria
Ognyan E.**PETROV**, Centr. Lab. of Mineralogy and Crystallography, Sofia, Bulgaria

ABSTRACT Results from studies on the hydration process of cements mixed with fly ash, silica fume or a combination of both, called Pozzolit, are presented. The active role of the Pozzolit additive was revealed by DTA, XRD and IRS analyses. The effect of the additive is expressed in increased total amount of hydration products and decreased portlandite content.

Key-words: additives, fly ash, hydration, silica fume, waste material utilization

INTRODUCTION

The incorporation of silica fume-fly ash blend in the form of an additive in cement compositions results in decreased corrosion and permeability and increased strength of cement stone (Mehta and Gjørv., 1982; Matkovic et al., 1990; Stoichkov et al., 1994). The individual effect of fly ash and silica fume on cement hydration have been thoroughly studied (Ogawa et al., 1980; Marsh and Day, 1988; Fraay et al., 1989; Roy, 1989) and no substantial controversy regarding the mechanism of their action has been found. The hydration of cement in the presence of silica fume-fly ash blend has not been well described till now. The present work considers the results from studies on the hydration process of cement containing silica fume and low-calcium fly ash.

MATERIALS AND METHODS

Portland cement, PC 45, was tested. The silica fume (SF) is a by-product from the ferro-silicon steel production. The fly ash (FA) is a low-calcium one, class F. The blend of the two additives called Pozzolit (Pz) (Stoichkov et al., 1994) is prepared from equal quantities of fly ash and silica fume, and has a density of about 610 kg/m^3. The specific surface of SF, FA, and Pz determined by the BET-method is 19.2, 2.83, and 8.9 m^2/g, respectively. Four cements were studied - without additives (#1) and with addition of SF(#2), FA(#3), and Pz(#4) in amounts of 10% of the initial cement mass. The cement pastes (water/solid ratio of 0.33) were cured in plastic containers at a temperature of 20(±2)°C. The hydration was stopped at the respective time by consecutive soaking in acetone and ether and the samples were subsequently dried at 105°C for 3 hours in vacuum. The DTA studies were carried out on a MOM-3427 derivatograph (Hungary) at a heating rate of 10°C/min in the range 20 - 1000°C. The test samples were of equal mass of 200 mg each. The amount of non-evaporable water (the mass loss in the temperature interval 105 - 1000°C) was the estimate for the quantity of the hydration products in the cement pastes. The quantity of water released during portlandite dehydration, termed CH-water, was determined in the temperature range 460 - 520°C. The IR spectroscopic test was performed by IR spectrometer "Specord 75 IR" (Germany) in the frequency range 400 - 4000 cm^{-1}. The samples (1 mg mass and 0.5 mm thickness) were mixed with 300 mg KBr. The powder X-ray diffraction (XRD) phase analyses of the cement samples were performed on a DRON 3M diffractometer (Russia) with Ni-filtered Cu-α radiation. The patterns were recorded in the range 10-55° 2Θ. Before the XRD measurements the samples were dried, ground and pressed in standard sample holders.

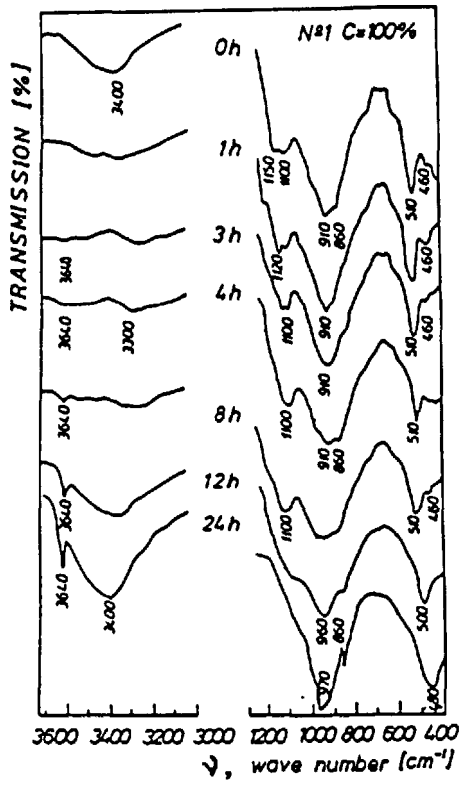

Fig.1 IR spectrum of plain cement paste

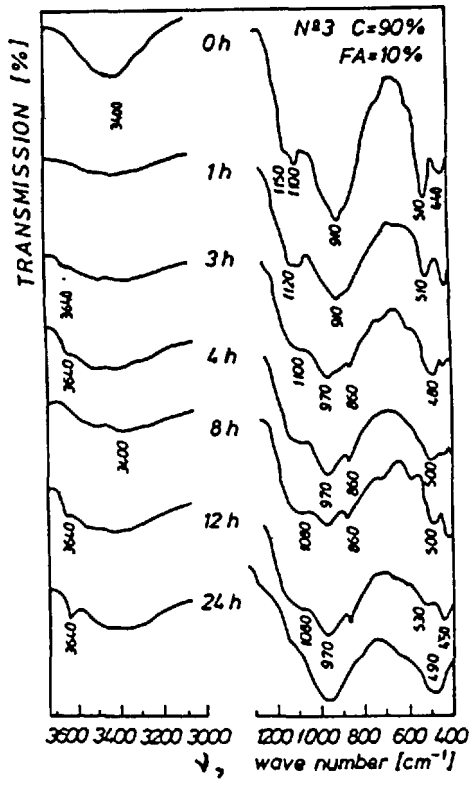

Fig.2 IR spectrum of FA-containing cement paste

RESULTS AND DISCUSSION

The IR spectra of all non-hydrated cements (0 h) (Figs. 1-4) contain the bands of the basic clinker minerals: alite - ν=460 and 910 cm^{-1}; belite - ν=510 and 860 cm^{-1} and gypsum-ν=465, 805, and 1100 cm^{-1}. The main changes in the plain cement spectrum in the first hours of hydration (Fig.1) are expressed in a decreased intensity of the gypsum and alite bands and emerging of the band characteristic for portlandite (ν=3640 cm^{-1}). The C-S-H band at ν=960-970 cm^{-1} gradually formed after the 4th hour. Parallelly, the intensity of the portlandite band increased and after the 8th hour the sulphoaluminate band with maximum at ν =3400 cm^{-1} was formed. The IR-spectra of FA-containing cement (Fig.2) repeat the above regularities for the plain paste, the only difference being that the band of C-S-H was formed earlier (between the 1st and 3rd hour of hydration)while the bands of portlandite and ettringite were not so clearly expressed. All the bands of the main hydration products (Fig.2) are broader than those in the plain cement which is, probably, due to the presence of distorted Si-tetrahedra in the fly ash portion causing variable frequency. The spectra in Figs.3 and 4 of SF- and Pz-containing cements show that SF participates actively in the hydration process from the first hour after the contact with water-the characteristic bands of amorphous silica at ν=1100 cm^{-1} fade with time, the spectral bands of C-S-H being formed at the same time (after 1 hour for Pz-containing paste and about the 4th hour for the SF-containing one). The SiO_2 band of cement #2 is preserved indicating that part of silica had not reacted and remained for further reaction in the later stages of hydration. The same band was not observed in paste #4 after the 8th hour, which was expected in respect to the lower SF quantity in it. The earlier formation of the C-S-H band in the spectrum of cement #4 is related to the easier C-S-H formation at lower SF-concentrations. The portlandite band is not displayed in the last two figures, probably, because of its small amount in both pastes and the screening effect of the ettringite band which is better shaped in the Pz-containing paste.

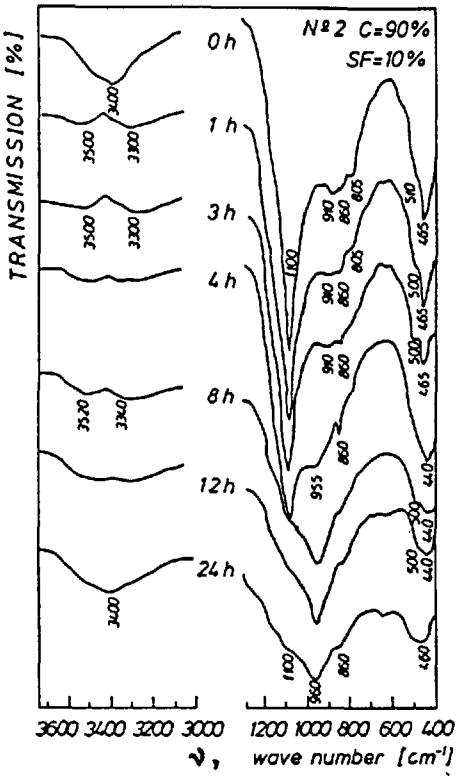

Fig.3 IR spectrum of SF-containing cement paste

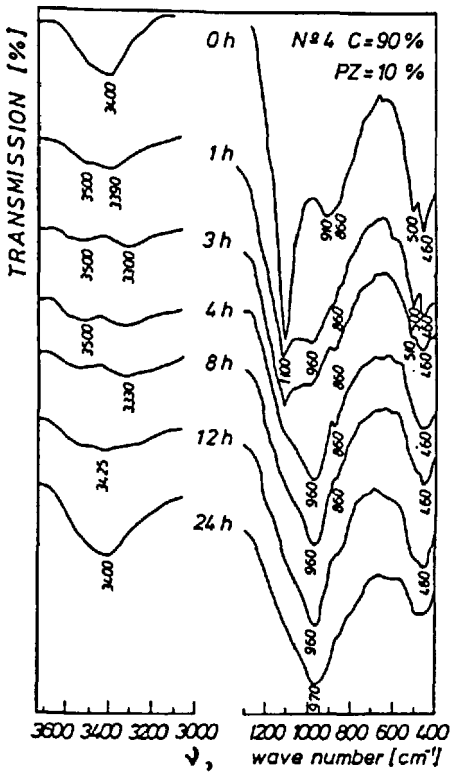

Fig.4 IR spectrum of Pz-containing cement paste

Summarized diffraction patterns of cement pastes (##1-4) showing the phase changes in the first 24 hours of hydration are given in Fig. 5. The lowest pattern in each case is of cement before hydration start. In the plain cement paste the portlandite (CH) formation is found to start around the 3-4th hour with gradual increasing crystallization followed up to the 24th hour. The most intense diffraction peak of CH (d=4.90 Å) in the pattern of FA-containing paste first was detected after the 6th hour then followed by a gradual intensity increase. For the case of SF-containing paste the formation of CH was obstructed up to the 12th hour (except a very small intensity trace at the 6th hour). Between the 12th and 24th hour the CH-content in this sample rapidly increased. For the cement paste with Pozzolit the crystallization of CH with time very much resembles that of cement #2 - up to the 12th hour of hydration no portlandite was detected.

DTA data showing the changes in the total amount of the newly formed hydrates in cement pastes during the first 24 hours of hydration are shown in Fig.6a. The amount of the hydration products for 1g cement in the pastes with SF and Pz is higher than the corresponding amount in the plain cement and FA-containing pastes. The CH-water content in the SF- and Pz-containing pastes till the 6th hour of hydration is in the range of the accuracy of the method - about 1.5 mg per gram cement, and it increases sharply after this age for both pastes (Fig.6b). After 1 hour of hydration the CH-quantity in the FA-containing pastes and in the plain cement paste is the same, rising more rapidly in consequence for the additive-free paste. The difference between the non evaporable water content and the CH-water, called H-water, is a measure for the hydrosilicate and hydroaluminate quantity in the cement pastes. Fig.7 shows the changes in the difference between the H- ($H-H_o$) and CH-water content ($CH-CH_o$) for the pastes with additives on one hand and for a plain paste on the other. The periods of accelerated hydration product formation and the period of relatively delayed hydration process in the additive containing pastes due to the specific effect of the additives are clearly observed from the curves.

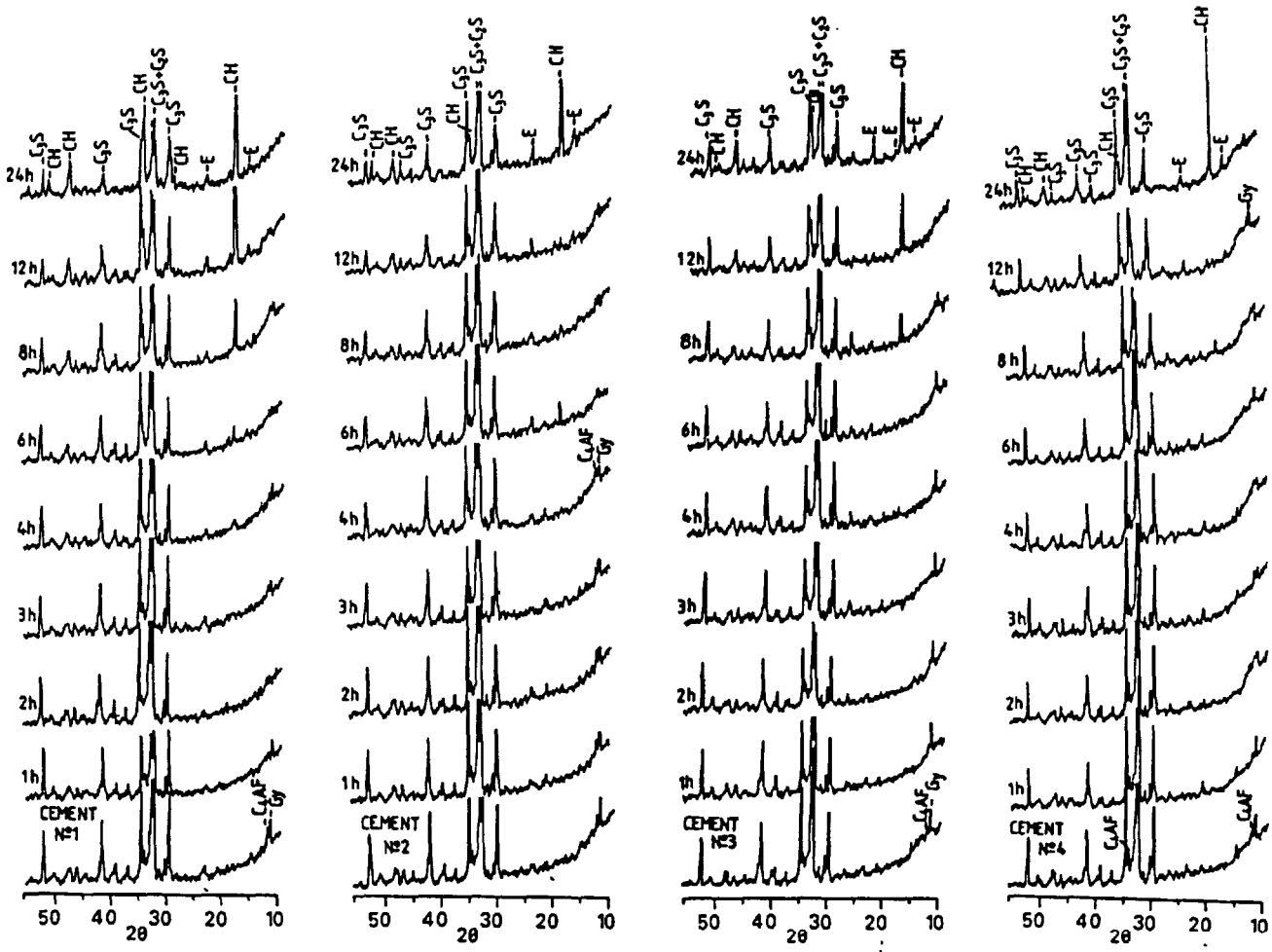

Fig.5 XRD patterns of plain cement paste (#1); with SF (#2), FA (#3) and Pz(#4)

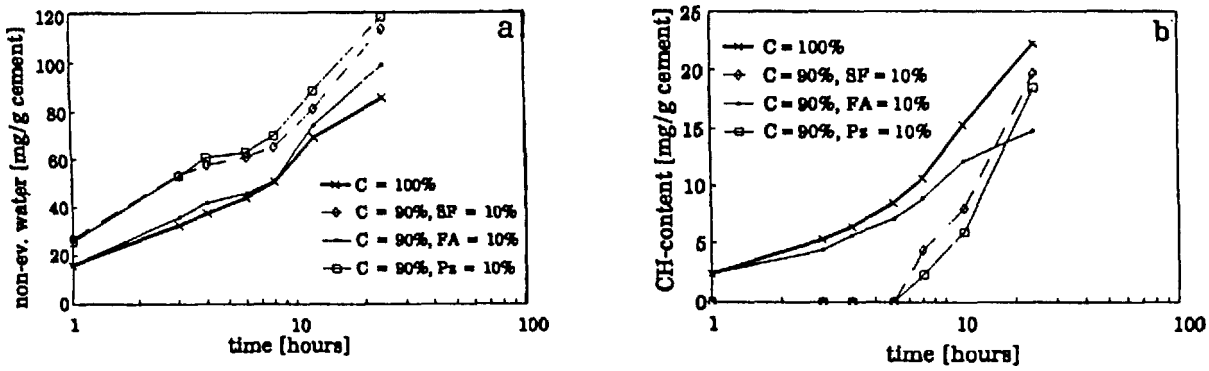

Fig.6 Changes in the amount of hydration products (a) and portlandite (b) in the cement pastes

The DTA, IRS, and XRD results prove that the manifestation of the chemical nature of the fly ash is negligible till the 24th hour of hydration and its effect can be considered rather as a physical one - the fly ash surface favours the nucleation mechanism of the hydration products. The SF particles participate actively in the hydration process of cement during the first 8 hours. They bind entirely the calcium ions in the solution and for this the amount of portlandite is very low. The absence of free calcium ions in the solution stimulates the dissolution of cement particles, the latter being gradually

covered by SF particles and hydrosilicate gel forming a diffuse layer which hampers their contact with water and slows down the dissolution rate. This period has a longer duration in the SF containing paste because of the high density of the SF particles around the cement grains. SF, FA particles, and complexes of FA-particles surrounded by SF ones exist separately in the Pz-containing paste. The lower SF-concentration and the last two types of aggregations make the diffusion layers around the cement grains in the Pz-containing paste more permeable for the water molecules. This is most probably the reason for the shorter period of retardation of the hydration rate in comparison with the SF-containing paste. Hydration is accelerated after the 8th hour due to breaking apart of the gel covers.

Table 1 presents results of determined CH-water contents from the 1st to 360th day of hydration. In cement pastes with mineral additives at all ages it is lower than in the plain paste. The CH-water content of SF- and Pz-containing cement pastes increases till the 28th and 90th day respectively, its decrease with time being clearly observed subsequently. The CH-content in FA-containing paste is low till the 28th day, then weakly increases and remains practically constant.

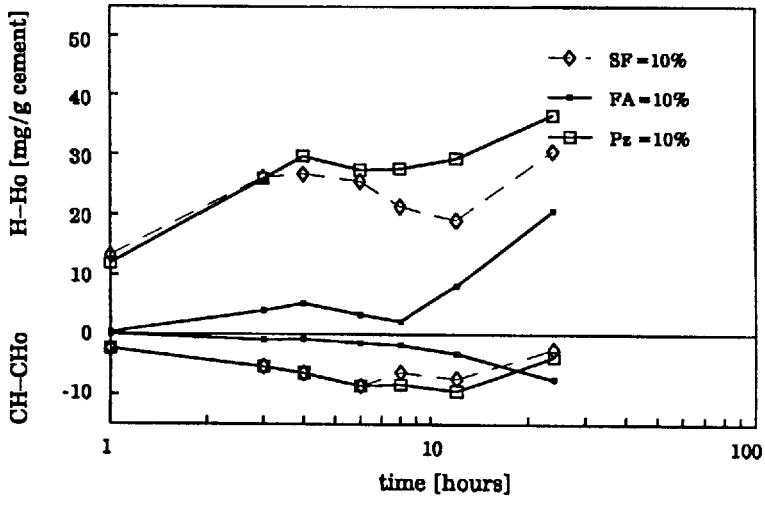

Fig.7 Differences between H- and CH- water contents in cement pastes with and without additives.

TABLE 1 CH-water content (mg/g cement) for age of hydration (days)

Cem. paste	Age	1	2	3	7	28	90	180	360
#1		22.2	28.7	31.0	36.6	39.9	43.2	41.9	42.6
#2		19.7	22.2	27.2	32.1	34.4	32.1	29.6	28.7
#3		14.8	19.7	22.2	25.9	30.7	33.7	34.4	35.0
#4		18.5	24.6	26.0	28.7	32.1	34.4	30.7	29.6

TABLE 2 H-water content (mg/g cement) for age of hydration (days)

Cem. paste	Age	1	2	3	7	28	90	180	360
#1		63.2	66.7	73.2	92.5	130.8	224.2	230.8	234.7
#2		93.7	119.4	121.8	152.7	177.3	273.8	278.3	280.0
#3		83.9	103.4	108.3	145.3	203.2	261.9	266.1	267.6
#4		99.7	118.2	121.8	164.0	195.8	263.6	270.4	273.4

The H-water content is growing with time for all tested specimens and at each age it is higher in the pastes with additives (Table 2). The hydrosilicate and hydroaluminate content in the Pz-containing cement paste is higher than in the SF-containing one till the 28th day of hydration, then this relation turning to be opposite till the 360th day. The paste with FA has the lowest H-water content among all additive containing pastes except for the age of 28 days.

The CH/H water content ratio was chosen as a criterion for the relation between the processes leading to portlandite formation on one hand and hydrosilicate and hydroaluminate formation on the other (Fig.8). The ratio of the plain cement paste is higher than the ratio in all other pastes at all investigated ages of hydration which is an evidence for the pozzolanic activity of the additives. A clearly expressed diminution of this parameter is observed between the 3rd and 90th day of hydration for all studied cements, the values being very slightly decreased till the 180th day reaching a constant value subsequently. The only exception is the FA-containing cement paste, where the equilibrium between CH- and H-water content is achieved as early as the 90th day of hydration. The maximum of this ratio is observed at the age of 3 days for cement with additive and at the age of 2 days for plain cement. The CH/H ratio for SF-containing paste is higher than the ratio of FA- and Pz-containing pastes (except for the 2nd day) till the 28th day and the relation turning to be opposite later on.

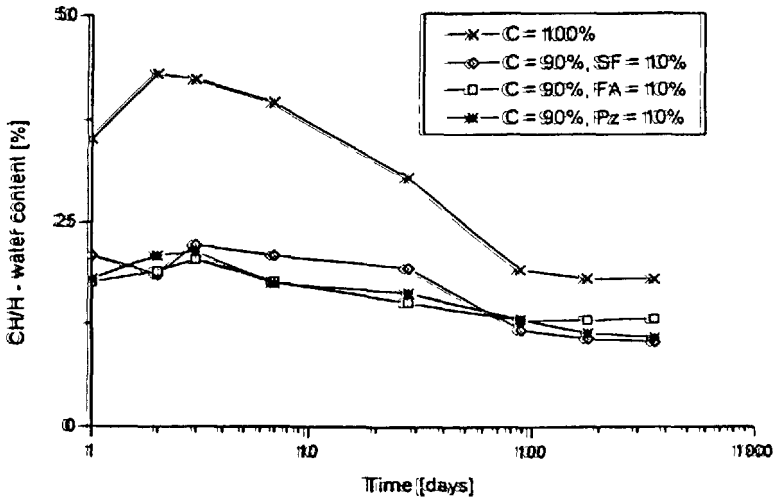

Fig.8 Changes of CH/H ratio

CONCLUSIONS

1. The effect of Pz mineral additive on the early hydration of cement is expressed in increased total amount of hydration products and in a decreased amount of calcium hydroxide.
2. The conditions of early hydration in the Pz-containing paste are more favourably in comparison with these of the SF-containing one where a part of the SF particles remains closed between the forming hydrates on the cement grain surface and do not actively participate in the cement hydration during the first 24 hours.
3. In the cement pastes with additive after the 3rd day the portlandite consumption prevails, although its total quantity continues to grow as a result of the proceeding hydration.
4. During the first days the effect of silica fume is in acceleration of the clinker minerals hydration and in consumption of portlandite in the cement paste. After the 28th day SF mainly bounds portlandite in insoluble hydrosilicates. Fly ash is not so active with respect to portlandite consumption till the 7th day of hydration but is

activated in the time between the 7th and the 90th day when the pozzolanic reactions of FA are dominant.

5. The effect of Pozzolit depends on the SF component during the first 7 days which is expressed in acceleration of cement hydration and binding of portlandite. The main processes in the Pz-containing paste later on depend in the FA-component.

ACKNOWLEDGEMENT

The authors thank Mr. M. Chr. Maleev for the help during the technical preparation of this manuscript.

REFERENCES:

Fraay, A.L.A., Bijen, J.M. and de Haan, Y.M., "The Reaction of Fly Ash in Concrete. A Critical Examination", Cem. Concr. Res., 19, 1989, pp.235-246.

Marsh, B.K.and Day, R.L., "Pozzolanic and Cementations Reactions of Fly Ash in Blended Cement Pastes", Cem.Concr.Res., 18, 1988, pp.301-310.

Matkovic, B., Grzeta, B. and Paljevic, M., "Hydrated Fly Ash with SiO_2 from and/or Portland Cement Addition. Reactions in Pastes and Strength Development in Mortars", Cem.Concr.Res., 20, 1990, pp. 475-485.

Mehta, P.K. and Gjorv, O.E., "Properties of Portland Cement Concrete Containing Fly Ash and Condensed Silica Fume", Cem.Concr.Res., 12, 1982, pp.587-595.

Ogawa, K., Uchikawa, H. and Takemoto, K., "The Mechanism of the Hydration in the System C_3S-Pozzolana", Cem.Concr.Res., 10, 1980, pp.683-696.

Roy, D.M., "Fly Ash and Silica Fume Chemistry and Hydration", Proc. of the Third Int. Conf. on Fly Ash and Silica Fume Chemistry and Natural Pozzolanas in Concrete. Trondheim, 1989, pp. 368-384.

Stoichkov, V., Abadjiev, P.A., Lilkov, V., Patsovska, A., "Physico-mechanical Properties of Blended Cements with Active Mineral Additives", Proc. of 7th Int. Conf on Mechanics and Technology of Comp. Materials, Sofia, Oct. 10-12, 1994, pp.468-473.

PECULIARITIES OF UKRAINIAN POZZOLANA CEMENTS

Raisa RUNOVA, Kiev State Technical University of Construction and Architecture, Kiev, Ukraine
Juriy USTIMENKO, "Horda Ltd.", Kiev, Ukraine
Victoria MELENTYEVA, Joint Stock Company "Podol'skiy tsement", Kamenets-Podolskiy, Ukraine

ABSTRACT Technical characteristics of cements made from clinkers produced by the plants situated in southern, central and western regions of Ukraine and natural pozzolana in a form of reactive silica (up to 55%), glassy rock (up to 70%) are given. The peculiarities of composition and structure of pozzolanas as well as their influence on properties of the cements are demonstrated. Technologies permitting to produce a concrete with a strength 1.5 times exceeding that of portland cement and frost resistance up to 900 cycles have been developed.

KEY-WORDS: alite, alkali, pozzolana, strength development.

INTRODUCTION

National standard of Ukraine and ENV-197-I prescribe the use of pozzolanic additives of different types and in different quantities in 4 from 5 types of cements. The advantages of Portland pozzolana cements is known to be caused by technical and economical reasons. In Ukraine with its well developed cement industry a problem of how to provide a competitiveness of cements on world and domestic markets may be solved successfully due to blended cements. As it follows from the reports (Narang, 1992; Sersale, 1992), the development of researches in the field of pozzolana cements is attributed, first of all, to possibility of utilisation of such industrial wastes as fly ashes and slags.This made attention to investigations of the compositions containing natural pozzolanas weaker. Undoubtedly, the use of natural pozzolanas is reasonable when properties of the obtained cements are equal to those of clinker cements or exceed them. The content of reactive silica may be considered as a determining requirement to quality of pozzolanas (even though this condition can not be easily provided)(Glasser et al, 1988). The modification of pozzolana cements properties is possible due to chemical additives in a form, first of all, of easily soluble salts (Tokemoto and Uchikawa, 1980). Simultaneously, other chemical and technological advantages can be achieved while using naturally occurring pozzolanas. This comes, first of all, from the researches on structure formation of alkaline cements which simulate the processes occurring in nature and new formations are represented by analogues to rock-forming minerals (Glukhovsky, 1957, 1971). The present study was dedicated at comparing the influence of natural pozzolanas on properties of the blended cements composed of clinkers manufactured by the main Ukrainian cements producers.

EXPERIMENTAL DETAILS

Used in the experiments were portland cement clinkers from 5 Ukrainian leading cement producers. Table 1 shows mineralogical composition of the clinkers.

Used as a pozzolanic additive was a reactive naturally occurring amorphous silica taken from deposits of western regions and perlite from the Carpethian Mountains (Table 2), a characteristic feature of natural silica composition was the presence, besides amorphous silica, of the increased content of quartz (up to 20%) as well as clay minerals and calcite. Perlite is itself a homogenous glassy mass consisting in chemical composition mainly of silica, alumina, and great quantities of alkalis.

Table 1 Mineralogical composition of the clinkers

Producer	Code	Content of minerals, %			
		C_3S	C_2S	C_3A	C_4AF
Open Joint Stock Company "Nikolaevtsement"	I	63.52	15.12	5.20	13.01
Open Joint Stock Company "Volyn' "	II	60.36	19.39	7.12	11.92
Joint Stock Company "Podol'skiy tsement"	III	55.82	17.13	9.38	13.44
Open Joint Stock Company"KTSGK",Krivoy Rog	IV	59.29	19.54	6.83	11.49
Open Joint Stock Company "Baltsement"	V	66.55	12.94	5.64	13.13

Table2 Chemical composition of pozzalanic constituent of the cements

Rock	Chemical composition, mass %					
	SiO_2	Al_2O_3	CaO	MgO	Fe_2O_3	R_2O
Natural silica	68.3	9.2	12.5	1.2	2.9	0.6
Perlite	73.0	16.4	2.5	0.9	1.9	6.6

The blended cements were made by grinding a clinker and pozzolana in certain ratios to produce a specific surface of 500-550m^2/kg was reached. The content of gypsum in all formulations was taken 5 %. When use was made of perlite a complex additive containing sodium sulfate in a quantity of 3 % by cement mass was introduced with a mixing water. The samples were prepared and tested under procedure specified in the USSR Standards 310.I-3-76 and 310.4-81. Strength development of the cement was observed while hardening in standard conditions and after steam curing (3+6+3 hrs, T=85^{0}C). Physico-chemical investigations were held with the use of XRD and DTA methods.

RESULTS AND DISCUSSION

High content of alite in clinkers of all the Ukrainian cement producers allowed to assume a possibility of introduction of pozzolana in rather great quantities. However, the results (Table 3) turned out to be unadequate, namely: the presence of 25% natural silica decreased the cement activity by 21-35 % .The cements with a higher content of alite ("Volyn", "Baltsement") demonstrated the higher strength both in 3 days and 28 days age. The cements from the Zdolbunov Plant demonstrated the strength of brand M400 if replacing 30 % clinker with natural silica. The cements with high content of alite demonstrated good results after steam curing. So, the cements from the Balakleya Plant, even with an additive of 55 % natural silica reached after steam curing 60 % of standard strength of additive-free cement.

The technological properties of the cement containing natural silica vary considerably. The initial and final setting times of all reference additive-free cements were found to be within 2hr.-40 min.-3 hr.-15 min. and 4hr.-00 min.- 4 hr.-30 min., respectively. The increase in pozzolana content in all commercially produced clinkers was accompanied by a shortening of the initial and final setting times to 1hr.-10 min.-1 hr.-30 min. and 4 hr.10 min.- 7hr.30 min., respectively, depending upon variations in mineralogy of clinkers. All the cements with a content of the natural silica within 30 % showed good results when tested for frost resistance (up to 50 cycles). Physico-chemical studies proved that in the cements containing the natural silica a free lime was absent, calcium hydrosilicates were found in a low-basicity form, and quartz present in the natural silica remained in an unbound state (Figure 1).

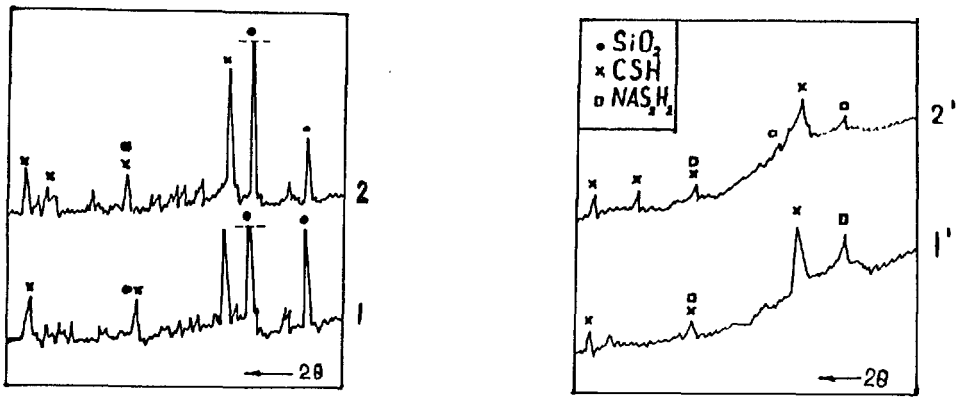

Figure 1 X-ray patterns of hydration products of the cements containing 25 % natural silica: (1) "Podol'skiy tsement"; (2)- "Nikolaevtsement" and 30 % perlite (1')- Podol'skiy tsement"; (2')- Nikolaevtsement".

Table 3 Strength characteristics of the cement stone containing natural pozzolana.

Content of pozzo-lana, %	Compressive/ flexural strength, MPa									
	Producer of clinker (codes from Table 1)									
	I		II		III		IV		V	
	R*	R**	R*	R**	R*	R**	R*	R**	R*	R**
0	55.9 7.3	39.3 4.9	56.5 6.8	37.0 4.8	51.5 6.7	29.9 4.5	52.5 6.6	37.0 4.7	63.4 6.8	30.5 4.8
with additive of natural silica										
10	52.3 6.9	31.1 4.5	55.1 6.8	32.0 4.8	47.1 6.4	25.4 3.9	49.8 6.0	32.3 4.4	52.4 6.2	24.4 4.1
15	42.4 6.2	23.5 4.3	52.9 6.7	27.8 4.8	43.4 6.2	23.4 3.6	42.1 6.1	28.7 5.0	49.4 6.5	23.2 4.1
20	40,8 5.7	23.7 3.9	49.2 6.7	26.8 4.5	39.7 5.3	23.3 4.0	40.8 4.9	28.5 4.5	48.4 6.0	21.8 3.4
25	36.5 5.5	20.3 4.0	44.1 6.5	26.0 4.1	36.8 5.9	22.1 3.9	36.3 4.8	24.2 4.0	46.2 6.2	23.1 4.1
30	32.1 4.8	16.7 3.2	39.1 6.1	24.0 4.3	34.7 5.9	20.6 3.8	33.8 5.0	23.0 3.0	32.1 5.5	19.0 3.2
35	23.8 4.3	14.4 3.1	35.5 6.0	22.0 3.4	32.7 5.7	20.5 3.7	29.0 4.9	23.6 4.1	35.5 5.5	18.5 3.1
45	22.5 4.8	11.5 2.7	27.9 5.5	22.9 4.6	25.5 4.8	20.4 4.0	23.5 4.4	22.3 3.8	29.3 5.2	18.8 3.9
55	-	-	24.1 5.1	22.1 4.3	19.5 4.3	20.1 3.6	17.7 4.0	22.5 3.8	24.4 4.8	22.0 4.1
with additive of perlite										
30	55.0 9.0	40.2 6.1	60.3 9.4	50.4 9.0	56.5 9.4	45.6 6.4	-	-	67.5 9.6	52.0 8.5
55	52.0 8.6	38.4 5.9	57.8 9.2	42.7 6.3	53.5 8.8	40.2 5.7	-	-	65.5 9.5	50.4 7.2
70	49.7 7.2	38.8 6.0	47.3 6.8	38.4 5.5	48.5 7.0	40.0 6.0	-	-	57.2 8.3	43.4 6.0

NOTE: R* -standard strength (in 28 days- age); R **- strength of steam cured cements.

The main reason of not satisfactory activity of the blended cements containing natural silica may be attributed to a presence of the quartz. The results differ greatly when use is made of a glassy aluminosilicate rock: a share of clinker may be decreased greatly (to 30 %) without decline of cement activity and by 1 year- age the cement strength reached 80 MPa. Of interest is the fact that even for these cements the best results were obtained with the clinker produced by the "Baltsement" Plant However, for all other Ukrainian clinkers, if using 50 % pozzolana, the activity corresponding to that of "pure" clinker cement may be provided. It is of importance because the plants in the western part of Ukraine are situated very close to sources of perlite.Worthy of particular mention is the fact that the use of a complex additive affects the initial and final setting times: 0 hr.-30 min.- 0 hr-.45 min. and 2 hr.-50 min.- 3 hr.-30 min., respectively.

The peculiarities of a perlite structure and large content of alkalis determined a different mechanism of strength development (Runova and Fundi, 1991). The alkaline hydroalumino-silicate of calcium analogous to natural hydronepheline were found to occur along with hydrosilicates of calcium. These alkaline hydroaluminosilicates create a main volume of new formations in a form of a gel phase. Nature of the gel, its increased density as well as capability to slow crystallization were found the main reason of good performance of the pozzolana cements.

CONCLUSIONS

The Ukrainian clinkers may be referred to a class of high alite cement and may be considered potential for manufacturing blended cements allowing to decrease a share of clinker to 30 % without corresponding decline of activity of the initial clinker cement. The peculiarities of composition and structure of natural reactive mineral additives determine a rather wide range of technical properties of the pozzolana cements such as activity in a 28 days-age varying from 40 to 70 MPa. The use of alkaline-alkali earth binder systems modified with glassy rocks and involvement of alkalis present in them in structure-forming processes may be considered as an advanced direction in manufacturing high performance pozzolana cements (high atmosphere-and frost resistance resulted in long-term durability).

REFERENCES

Glasser, F.P., Luke, K., Angus, M.J., "Modification of Cement Pore Fluid Compositions by Pozzolanic Additives", Cem.Concr.Res., No.18(2), 1988, pp.165-178.

Glukhovsky, V.D., "Soil Silicates," Gosstroiizdat Publish, Kiev, 1959, 196 pp.

Glukhovsky, V.D. and Runova, R.F., "Activity of Glass-like Alkaline Aluminosilicates," RAC USSR, Series B, No 5, 1971, pp.91-95.

Narang, K.C., "Portland and Blended Cement", Proceedings of the 9th International Congress on the Chemistry of Cement, New Delhi, Vol. I, 1992, pp.213-257.

Runova, R.F., Fundi, Y.A.S., "Activity and Properties of Alkaline Pozzolanic Cements", Fourth CANMET/ACI International Conference on Fly Ash, Istanbul, Part III,1992, pp.245-257.

Sersale, R., "Advances in Portland and Blended Cements," Proceedings of 9th Intern. Congr.. on the Chemistry of Cement, New Delhi, Vol.I, 1992, pp.261-302.

Tokemoto, K., Uchikawa, H., "Hydration of Pozzolanic Cement", Proceeding of the 7 th International Congress on the Chemistry of Cement, Paris, Vol.I, 1980, pp.210-229.

CHARACTERISTICS AND HYDRATION OF CEMENT PRODUCED FROM ASH FROM INCINERATED URBAN GARBAGE

Yasuhisa TAKUMA, Yoshiaki TSUCHIDA and Shun-ichiro UCHIDA, Chichibu Onoda Cement Corporation, Japan

ABSTRACT Three types of cement containing alinite or calcium chloroaluminate were produced from ash taken from incinerated urban garbage, and the characteristics of the clinkers and the hydration properties were investigated. Alinite turned to alite at about 1350℃, while calcium chloroaluminate remained stable at 900-1400℃. Each type of cement showed its own peculiar hydration characteristic and the microstructure of hardened body. Cement containing calcium chloroaluminate showed rapid setting and hardening property.

Key-words: Alinite, Chloride, Clinker formation, Hydration, Waste material utilization

INTRODUCTION

In Japan, urban refuse the main waste product of domestic life is rising owing to industrial development and the drift of population into cities. It is now becoming necessary to find practical applications that treat ash from incinerated urban garbage as a resource. Ash from incinerated urban garbage contains remarkable amounts of chlorine, primarily from plastics such as vinyl chloride and cooking salt, in addition to SiO_2, Al_2O_3, Fe_2O_3 and CaO, which are indispensable elements for producing Portland cement. Consequently, the ash cannot be used as a raw material for Portland cement as it is, although it can find practical application as a raw material for a special cement containing hydraulic materials such as alinite or calcium chloroaluminate ($C_{11}A_7 \cdot CaCl_2$). Cement containing alinite was examined as a potential energy-saving cement, since it could be burnt at lower temperatures, and was produced from steel refinery waste (Pradip et al, 1990). Several studies about the cement containing calcium chlorosilicate and calcium chloroaluminate were reported mainly from the environmental point of view, in Japan (Uchikawa; 1992, 1994a and 1994b, Uchikawa et al; 1995 and 1996).

In this study, three kinds of cement, each containing a quantity of alinite, $C_{11}A_7 \cdot CaCl_2$, belite (C_2S) and alite (C_3S), were produced from ash that was taken from incinerated urban garbage and other raw materials. The authors investigated the characteristics of the clinkers burnt under appropriate conditions, the hydration reactions and the physical properties of each cement produced.

EXPERIMENTAL

Raw material and cement preparation

Table 1 shows the target mineral composition of the clinkers, and the chemical composition of the raw meal of the three types of cement and the ash from incinerated urban garbage used as a raw material. The chemical compositions of ash from incinerators fluctuate with the season and the location where it was produced. Industrial grade $CaCO_3$, SiO_2, Al_2O_3, Fe_2O_3, $MgCO_3$ and $CaCl_2$ were used as raw materials for producing the cement clinkers, in addition to the incinerated ash. Since chlorine was vaporized in combination with alkali metals in the raw meal, the amount of chlorine, that was slightly more than the equivalent amount of alkali content, was added to the theoretical value.

Raw meal was burnt at between 900℃ and 1400℃ for 30 minutes in an electric furnace in order to determine the temperature range for the stable formation for each clinker mineral. Based on these results, clinkers were burnt at the most suitable temperature in a small rotary kiln which had a device to trap toxic gases such as hydrogen-chloride or dioxin. Three types of cement were manufactured from the clinkers : EC-1 clinker was ground with a 3% gypsum component as SO_3; EC-2 and EC-3 clinkers were ground alone, and mixed with anhydrite (II-$CaSO_4$) powder, the amount of which made the SO_3/Al_2O_3 molar ratio in the cement 1.0. Blaine's specific surface area of each ground powder was about 350m^2/kg.

Table 1. Mineralogical composition of clinkers, and chemical composition of raw meal and ash from urban garbage incineration.

	Mineralogical composition(%)					Chemical composition(%)*							
Sample	AL	C_3S	C_2S	C_{11}	C_4AF	SiO_2	Al_2O_3	Fe_2O_3	CaO	MgO	Na_2O	K_2O	Cl
EC-1	65	-	27	5	3	22.7	3.8	2.5	57.3	2.73	0.90	0.91	6.05
EC-2	58	-	20	20	2	19.5	14.4	1.4	55.5	2.90	0.74	0.43	6.17
EC-3	-	62	9	24	5	18.4	11.1	3.1	57.2	1.50	1.47	1.19	4.05
Ash						29.4	23.9	5.6	33.7	3.00	5.20	3.51	11.85

AL : Alinite, C_{11} : $C_{11}A \cdot CaCl_2$, * : LOI=0 base (LOI of Ash = 17.3%)

Investigation of clinker characteristics, hydration and physical properties

Quantitative analysis of trace elements of cement clinkers was performed using X-ray Fluorescence Spectrometry. The observation of back scattered electron image and analysis of composition for each clinker mineral were performed using Electron Probe Micro-Analyzer (EPMA), for the polished surface of each clinker.

The heat evolution in hydration of cement with a water-cement ratio (W/C) of 1.0 was measured using a conduction calorimeter. The pastes of these three types of cement were prepared with W/C=0.5 and were cured in water at 20 ℃. After the determined curing time, the pastes were cut to cubes of about 5 mm in size, washed several times with acetone and then dried under conditions of 11% relative humidity or D-dry. For these specimens, the measurement of combined water by ignition, and the identification and quantitative analysis of hydration products were performed by X-ray Diffraction (XRD) and Differential Scanning Calorimetry. For D-dried specimens, fracture surfaces and polished surfaces were observed using Field Emission Scanning Electron Microscope (FE-SEM) and EPMA, respectively. The setting time and compressive strength of each kind of cement were measured using a Japanese Industrial Standard (JIS) mortar, in which the W/C=0.65 and sand cement ratio (S/C) was 2.

RESULTS AND DISCUSSION

Clinker formation

Figure 1 shows the typical mineralogical phase-temperature relationships during the formation of the three types of cement clinkers, which were drawn up based on the results of XRD measurement of the clinkers burnt in an electric furnace. Alinite was not observed at 900℃, but was noted at 1000℃, despite the report by Agarwal et al (1986) that the formation of alinite became remarkable at about 900℃. As the temperature rose, the alinite increased, with a fall in C_2S and free lime, and began to change to C_3S, losing chlorine from about 1350℃ (EC-1 and EC-2) (Uchikawa, 1992 and Uchikawa et al, 1995). $C_{11}A_7 \cdot CaCl_2$ existed at a constant amount over a range of 900℃ to 1400℃, and the formation of tricalcium aluminate (C_3A)

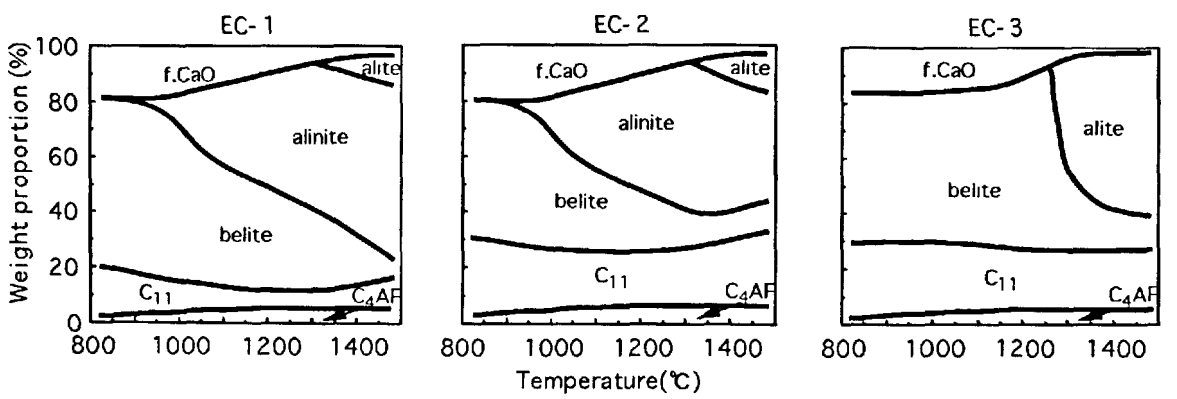

Figure 1. Schematic diagrams showing variations in typical contents of phases during the formation of prepared cement clinkers (C_{11}:$C_{11}A_7 \cdot CaCl_2$).

was not observed (EC-2 and EC-3). It is thought that at higher temperatures, $C_{11}A_7 \cdot CaCl_2$ is more stable (Sango et al, 1991) than $C_{11}A_7 \cdot CaF_2$ which declines rapidly and changes to C_3A from about 1380℃ (Uchikawa et al, 1983). In EC-3 clinkers, alinite did not appear prior to the formation of C_3S, it seems because $C_{11}A_7 \cdot CaCl_2$ was formed at still lower temperature range, consuming most of the chlorine and MgO, the contents of which in raw meal were small. On the basis of these results, EC-1, EC-2 and EC-3 clinkers were burnt in a rotary kiln at 1290℃, 1330℃ and 1360℃, respectively.

Clinker characteristics

Trace elements in clinkers

Table 2 shows the MgO, SO_3, Na_2O, K_2O and chlorine content in each clinker burnt in a rotary kiln. The amounts of alkalies and chlorine decreased remarkably, compared to those in raw meal (Table 1), because chlorine and alkalies combined and were vaporized. Measured chlorine content in EC-3 clinker was lower than the theoretical value, although the excess chlorine was added as a raw material.

Table 2. Result of chemical analysis of clinkers (trace elements).

Sample	Chemical composition(%) MgO	SO_3	Na_2O	K_2O	Cl	Cl*
EC-1	3.1	0.50	0.0	0.0	4.0	2.9
EC-2	1.9	0.28	0.0	0.0	4.2	3.4
EC-3	1.3	0.16	0.0	0.0	1.0	1.2

Cl : Calculated value from target mineral composition

Crystalline state of clinker minerals

Figure 2 shows the typical back-scattered electron images of polished surface of each clinker observed by EPMA. In the EC-1 clinker, alinite crystal is observed to be 15-40 μm in size, to be irregular shape and to include C_2S clusters. Alinite grains are supposed to have grown in contact with each other, because of the rapid burning reaction. C_2S grain is several μm in size, and has an elliptical cross section. Calcium alumino-ferrite phase (C_4AF) is needle-shaped and appears in minute quantities. In the EC-2 clinker, the C_2S grain is slightly larger than that in the EC-1 clinker, because the burning temperature was higher than that of the EC-1 clinker, and $C_{11}A_7 \cdot CaCl_2$ forms clusters which consist of small grains of 2-3 μm in size. In EC-3 clinker, C_3S grains grew to 10-20 μm in size, and to hexagonal plates in shape. C_2S and $C_{11}A_7 \cdot CaCl_2$ grains also grew larger. It is suggested that C_3S grains are large enough, considering the burning temperature of 1360℃, owing to the mineralizing effect of the chlorine.

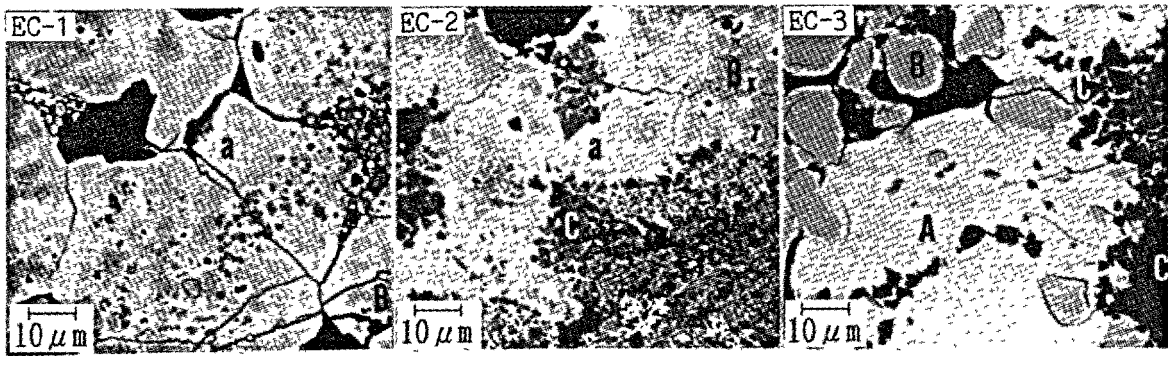

a:Alinite , C:$C_{11}A_7 \cdot CaCl_2$, A:C_3S , B:C_2S , F:C_4AF

Figure 2. Back-scattered electron images of burnt cement clinkers.

Chemical composition of clinker mineral

Table 3 shows the chemical composition of the principal minerals in each clinker, observed by EPMA. In alinite, the chlorine content was 4.2%, which conformed to the theoretical value (4.2%) calculated using the chemical formula. The amount of MgO was 3.2% (EC-1) and 3.5% (EC-2), which were closer to Lampe et al's (1986) theoretical value (3.7%) than to Bikbaou's (1986) value (2.3%).

In $C_{11}A_7 \cdot CaCl_2$, The chlorine content was 5.5% (EC-2) and 4.7% (EC-3), close to the theoretical value of 4.9%, and it is thought that the amount of chlorine fell as the burning temperature rose. Although it is generally reported that the $C_{11}A_7 \cdot CaX_2$ compound is apt to make solid solution with $C_{12}A_7$ or $C_{11}A_7 \cdot Ca(OH)_2$, and the X_2 content in $C_{11}A_7 \cdot CaX_2$ is smaller than the theoretical value, the results of this study suggest that $C_{11}A_7 \cdot CaCl_2$ in the EC-2 clinker has excess chlorine. This is because an excess amount of the chlorine was compounded to a raw meal, with the vaporization of the chlorine combining with alkalies taken into account.

C_2S has little chlorine and MgO. C_3S, the structure of which is similar to that of alinite, has little chlorine and has 1.2% composed of MgO, similar to the MgO component in C_3S in the OPC clinker. These results reconfirm that MgO as well as chlorine are, generally speaking, indispensable constituents in the formation of alinite.

Table 3. Chemical compositions of principal minerals in clinkers observed by EPMA.

Sample	Mineral	SiO_2	Al_2O_3	Fe_2O_3	CaO	MgO	SO_3	Na_2O	K_2O	Cl
EC-1	Alinite	22.7	2.7	2.4	64.9	3.2	0.03	0.02	0.00	4.1
	$C_{11}A_7 \cdot CaCl_2$	1.3	42.2	7.4	45.2	0.01	0.06	0.00	0.00	5.3
	C_2S	33.7	0.32	0.17	65.4	0.03	0.07	0.02	0.00	0.09
EC-2	Alinite	22.0	4.4	0.76	66.4	3.5	0.00	0.01	0.00	4.1
	$C_{11}A_7 \cdot CaCl_2$	1.0	47.1	2.7	46.6	0.02	0.06	0.00	0.00	5.5
	C_2S	33.5	0.52	0.15	66.0	0.05	0.04	0.00	0.00	0.07
EC-3	$C_{11}A_7 \cdot CaCl_2$	0.36	47.6	2.2	46.8	0.09	0.01	0.01	0.00	4.7
	C_3S	24.4	1.3	0.42	72.2	1.2	0.07	0.01	0.00	0.02
	C_2S	31.0	1.8	0.50	65.5	0.24	0.40	0.00	0.00	0.01

Hydration reaction

Heat evolution by hydration

Figure 3 shows the heat evolution rate curves and the cumulative heat evolution amount curves of three types of cement. In the case of EC-1, the initial heat evolution rate was lower than that in the other two, because the $C_{11}A_7 \cdot CaCl_2$ content in EC-1 was considerably small. In the case of EC-2, the initial heat evolution rate and the cumulative heat evolution amount up to one hour were larger than those observed in EC-3. In the case of EC-3, a small peak of heat evolution rate, owing to the formation of ettringite, appeared after the first peak. These results suggest a difference in hydraulic activity between $C_{11}A_7 \cdot CaCl_2$ in EC-2 and $C_{11}A_7 \cdot CaCl_2$ in EC-3.

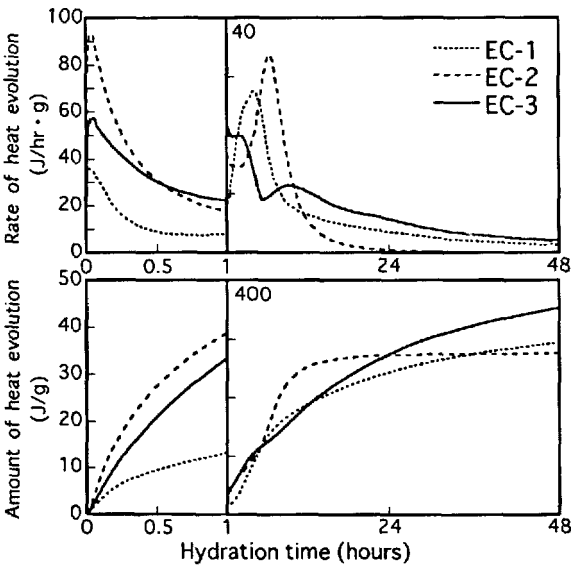

Figure 3. Heat evolution curves in hydration of cement pastes.

The second peaks of heat evolution rate of alinite in EC-1 and EC-2, and the third peak of C_3S in EC-3 appeared at 5-6 hrs, 7-8 hrs and 9-10 hrs, respectively. These results suggested that alinite was more active in hydration than C_3S. It is thought that the periods, in which alinite actively hydrates, differ depending on the concentration of Ca^{2+} in liquid phases (Uchikawa et al, 1985), between in EC-1 and in EC-2. The concentration of Ca^{2+} in liquid phase of EC-2 are

supposed to be considerably low, owing to the formation of ettringite or Friedel's salt caused by the active hydration of $C_{11}A_7 \cdot CaCl_2$. The cumulative heat evolution amount of EC-3 exceeded that of EC-2 after 24 hours, because of the hydration of C_3S, which was not abrupt but steady.

Amount of combined water and hydration products

Figure 4 shows the amounts of combined water and hydration products of each cement, depending on curing time. Three types of cement show distinct amounts of combined water and of hydration products. EC-1 formed $Ca(OH)_2$ and Friedel's salt, as well as the smallest amount of combined water and ettringite among the three types of cement. EC-2 formed a large amount of ettringite and Friedel's salt during the initial stage of hydration, but $Ca(OH)_2$ was not formed until seven days, since $Ca(OH)_2$ was consumed when ettringite and Friedel's salt were actively formed from alinite, $C_{11}A_7 \cdot CaCl_2$ and $CaSO_4$. EC-3 formed a medium amount of ettringite and $Ca(OH)_2$, and very small amount of Friedel's salt.

In case of the cement containing alinite (EC-1 and EC-2), the amount of combined water increased in proportion to the $C_{11}A_7 \cdot CaCl_2$ content, and $C_{11}A_7 \cdot CaCl_2$ formed Friedel's salt as well as ettringite (Uchikawa et al, 1995). In the case of the cement containing C_3S (EC-3), $C_{11}A_7 \cdot CaCl_2$ formed little Friedel's salt, and smaller amount of ettringite and combined water compared to the $C_{11}A_7 \cdot CaCl_2$ content. It is considered not only that the hydraulic activity of $C_{11}A_7 \cdot CaCl_2$ is depending on the crystal growth during the burning process, but also that the chloride ions, which remain excessively in the clinker and are released from alinite, promote the diffusion of water into $C_{11}A_7 \cdot CaCl_2$ (Kondo et al, 1977).

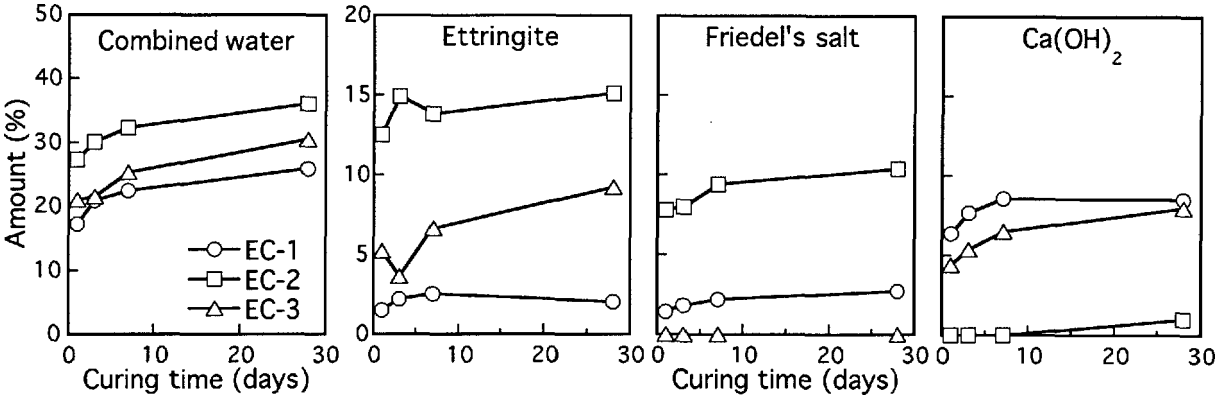

Figure 4. Change in the amounts of combined water and hydration products in cement pastes with curing time.

Microstructure of hardened cement pastes

Figure 5 shows the back-scattered electron images and the concentration mapping of each element of the polished surfaces of hardened cement pastes (seven days) observed by EPMA. In case of EC-1 and EC-2, the chlorine distributed to almost the entire hydrates. SiO_2 distributed to the hydrates more remarkably in the case of EC-1, while Al_2O_3 distributed to the hydrates more remarkably in the case of EC-2, than that in the case of the other, respectively. It is suggested that the chlorine exists not only in the Friedel's salt, but also in the ettringite and C-S-H. In the case of EC-3, the distribution of Al_2O_3 and chlorine are inferior to that in the case of EC-2, which supports the result that the degree of hydration of $C_{11}A_7 \cdot CaCl_2$ in EC-3 is considerably lower than that in EC-2. The amounts of the chloride ions, dissolved into the solution from the cement pastes hydrated in suspension, are 40%, 10% and 10% of the chlorine content in the cement of EC-1, EC-2 and EC-3, respectively. These results suggest that the chlorine is adsorbed to C-S-H, while the chlorine is chemically combined into ettringite and Friedel's salt.

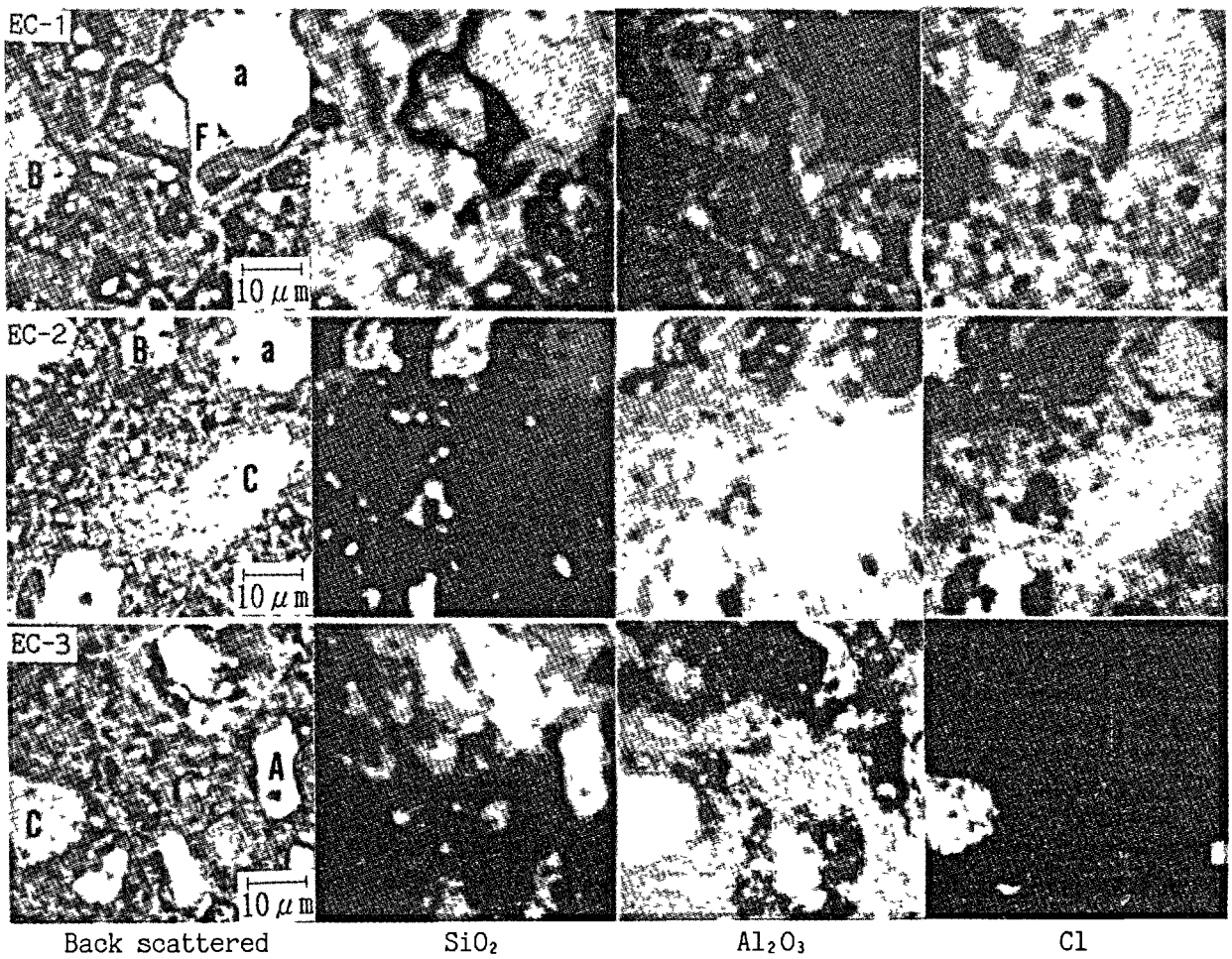

SiO_2	100.0	60.0	45.0	30.0	20.0	15.0	10.0	5.0	0.0
Al_2O_3	50.0	30.0	20.0	15.0	10.0	5.0	2.0	1.0	0.0
Cl	20.0	10.0	7.0	5.0	3.0	2.0	1.0	0.5	0.0

Figure 5. Back-scattered electron images and concentrations of three kind of elements on polished surfaces of hardened cement pastes.

Figure 6 shows the FE-SEM photographs of the fracture surface of each cement paste (seven days). In the case of EC-1, a needle-shaped ettringite, Friedel's salt in the shape of hexagonal plates and $Ca(OH)_2$ in the shape of layers are observed, in addition to large amount of calcium silicate hydrate gel (C-S-H). The C-S-H is more net-shaped (type II) than needle-shaped (type I). It is generally suggested that net-shaped C-S-H is formed when C_3S and C_2S are cured in heat (Diamond, 1976), and it is considered that alinite formed a net-shaped C-S-H, because alinite hydrated actively. On the other hand, EC-2 and EC-3 formed ettringite in the shapes of needles and pillars in large amounts. Friedel's salt in the shape of hexagonal plates was formed inside the ettringite in the case of EC-2, and C-S-H in the shape of small spheres (type III) filled the gaps in the both cases.

Physical properties

The setting time and compressive strength of the JIS mortar of each cement are shown in Table 4 and Figure 7, respectively. The setting property of EC-1 is earlier than that of Portland cement, owing to the hydration of alinite and $C_{11}A_7 \cdot CaCl_2$. The setting properties of EC-2 and EC-3 show rapid hardening because they contain more than 20% of $C_{11}A_7 \cdot CaCl_2$, which actively hydrates in the initial stage. It is necessary to add 0.5-1.0% retarder, such as citric acid, in order to use EC-2 and EC-3 practically (Uchikawa et al; 1995 and 1996).

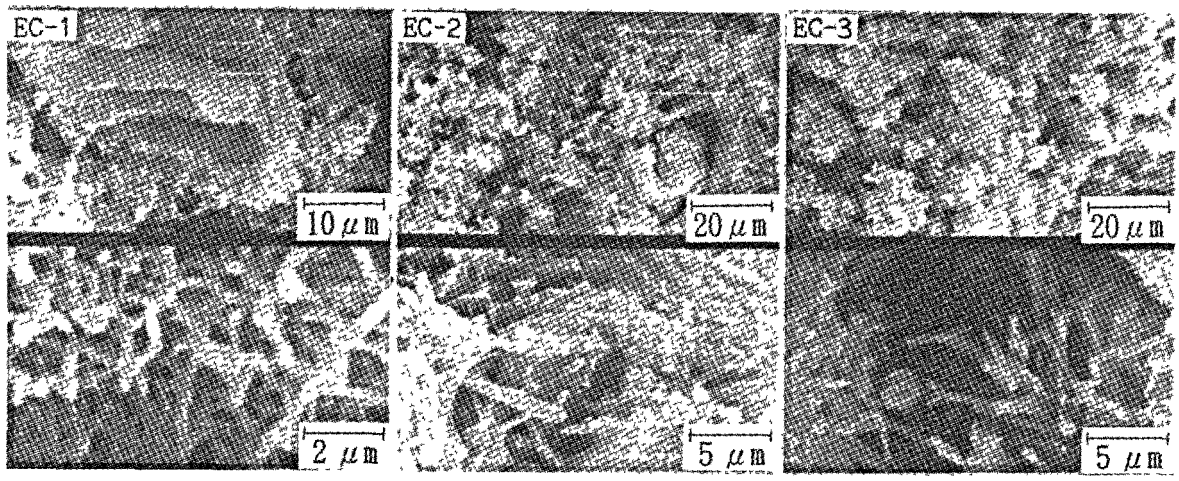

Figure 6. FE-SEM photographs of fracture surfaces of hardened cement pastes.

The strengths of EC-2 and EC-3 (three days and seven days) are significantly higher than those of EC-1, but are not as high as that of high early strength cement. The inferiority of the development of the strength of EC-1 is suggested to be owing to the lower degree of hydration and the greater amount of coarse pores. The strength of the three kinds of cement at 28 days were slightly lower than that of OPC. It is thought that the development of the strength of EC-2 containing alinite phase is smaller than that of EC-3 after seven days, as alinite encourage to form the Friedel's salts in the shape of hexagonal plates, which bring the coarse pores 0.2-1.0 μm in size. In the case of EC-3, these coarse pores remarkably decreased by 28 days.

Table 4. JIS mortar setting times.

Sample	Setting time (h:m) Initial	Final
EC-1	2:15	4:20
EC-2	0:37	1:04
EC-3	0:40	1:24

W/C=0.65, S/C=2

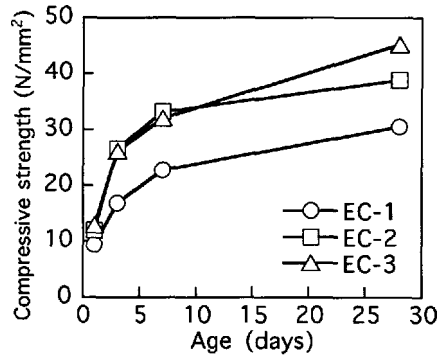

Figure 7. Development of compressive strength of each cement.

CONCLUSION

Three types of cement were produced from ash from incinerated urban garbage, and the characteristics of clinkers, hydration properties and the physical properties of each kind of cement were investigated. The following conclusions were obtained.

(1) Alinite was formed at about 1000℃ and began transforming to C_3S at about 1350℃ with the release of chlorine, although $C_{11}A_7 \cdot CaCl_2$ existed with stability at 900-1400℃. In the case of EC-3, alinite was not formed at lower temperature because chlorine in raw meal was largely consumed by the formation of $C_{11}A_7 \cdot CaCl_2$ at still lower temperatures.
(2) An almost stoichiometric chlorine component was included in alinite and $C_{11}A_7 \cdot CaCl_2$, but C_3S and C_2S had very little chlorine in any cement clinker.
(3) In the cement containing alinite, ettringite and Friedel's salt are formed with the hydration of $C_{11}A_7 \cdot CaCl_2$, and C-S-H and $Ca(OH)_2$ are formed with the hydration of alinite. The

amount of Friedel's salt increases and that of $Ca(OH)_2$ decreases in proportion to the $C_{11}A_7 \cdot CaCl_2$ content.
(4) The cement containing C_3S (EC-3) formed little Friedel's salt, and $C_{11}A_7 \cdot CaCl_2$ in that cement showed a lower hydraulic rate.
(5) The setting property of EC-1 is earlier than that of Portland cement, while those of EC-2 and EC-3 show rapid hardening because these cements contain more than 20% $C_{11}A_7 \cdot CaCl_2$. It is necessary to add 0.5-1.0% retarder, such as hydroxy-carboxylic acid, in order to use them.
(6) As a whole, the initial strengths of three kinds of cement are rapid hardening type, but the long term strengths of them are slightly lower than those of OPC. The developments of strengths are explained by hydraulic reactivity of the cement and the porous structure of hardened body.

ACKNOWLEDGMENTS
The authors are grateful to Mr. T. Nakano and Mr. T. Uwabo for DSC measurement and valuable discussions.

REFERENCES
Agarwal, R.K., Paralkar, S.V., and Chatterjee, A.K., "Chloride Salts as Reaction Medium for Low Temperature Clinkerisation - A Probe into Alinite Technology", 8th Int. Cong. Chem. Cem. (Rio de Janeiro), Vol.II, 1986, pp. 327-333.
Bikbaou, N., "Formation, Crystal Chemistry and Properties of Alinite and Jusmundite", 8th Int. Cong. Chem. Cem. (Rio de Janeiro), Vol.II, 1986, pp. 352-357.
Diamond, S., "Cement Paste Microstructure - An Overview at Several Levels", Proc. Conference on "Hydraulic Cement Paste and Their Structure and Properties", Held at Univ. Sheffield, 1976, pp. 2-30.
Kondo, R., Daimon, M., Sakai, E., and Ushiyama, H.,"Influence of Inorganic Salts on the Hydration of Tricalcium Silicate", J. Appl. Chem. Biotechnol., Vol.27, 1977, pp. 191-197.
Lampe, F.V., Hilmer, W. and Jost, K.H., "Synthesis, Structure and Thermal Decomposition of Alinite", Cem. Conc. Res., Vol.16, 1986, pp. 505-510.
Pradip, Vaidyanathan, D. and Kapur, P.C., "Production and Properties of Alinite Cements from Steel Plant Wastes", Cem. Conc. Res., Vol.20, 1990, pp. 15-24.
Sango, H., Miyakawa, T., Minamisawa, H., Machinaga, O. and Kasai, J., "Chemical Behavior of Chloride Ion on Formation and Hydration of $Ca_{12}Al_{14}O_{32}Cl_2$", Gypsum & Lime (in Japanese), No.233, 1991, pp. 13-19.
Uchikawa, H., "Present Problem in Cement Manufacturing", Invited special lecture of the 9th Int. Cong. Chem. Cem. (New Delhi), Vol.VII, 1992, pp. 23-57.
Uchikawa, H., "Management Strategy of Cement Industry in Technology Toward the Next Century", Proceedings of Engineering Foundation Conference (Durham), 1994a, pp. 524-561.
Uchikawa, H., "Cement Industry as Environmentally Compatible and Waste Recycling System" (invited), Proc. Int. Symp. Environmental Issues of Ceramics (Sapporo, Japan), The Ceramic Society of Japan, 1994b, pp. 12-37.
Uchikawa, H. and Kohno, K., "Ultra-rapid Hardening Cement (Jet Cement)", Concrete Technology and Design Vol.1, New Concrete Materials, Surrey Univ. Press, 1983, pp. 70-136.
Uchikawa, H. and Obana, H., "Ecocement - Frontier of Recycling of Urban Composite Wastes", World Cement, Vol.26, No.11, 1995, pp. 33-40.
Uchikawa, H. and Obana, H., "Ecocement - Environment Compatible Cement Manufactured from Urban Composite Wastes", Concrete Journal (in Japanese), Vol.34, No.4, 1996, pp. 57-63.
Uchikawa, H., Ogawa, K. and Uchida, S., "Influence of Character on the Early Hydration Process and Rheological Property of Cement Paste", Cem. Conc. Res., Vol.15, 1985, pp. 561-572.

THE EFFECT OF WASTE GLASS POWDER ON THE PROPERTIES AND PORE STRUCTURE OF ORDINARY PORTLAND CEMENT HYDRATES

Shuichi SUGITA, Qijun YU, Masami SHOYA, Yoichi TSUKINAGA and Yasuo ISOJIMA
Hachinohe Institute of Technology, 88-1, Myo, Hachinohe, 031, Japan

ABSTRACT Trials of using glass powder (GP) as admixture of cement under normal curing conditions have been made. With the addition of GP the strength of cement was decreased. After GP was ground for one more hour, nominated to NGP, it behaved differently on the properties of cement: 1) cement strength was increased, 2) porosity and average pore radius of mortars were reduced and 3) hydration degree of cement were enhanced. Moreover when 0.5% NaOH was introduced to NGP blended cements their strength and hydration were further developed.

Key-words: Glass, Hydration, Porosity, Strength development and Waste material utilization

INTRODUCTION

Now more and more waste such as blast-furnace slag, silica fume, fly ash and rice husk ash have been utilized as pozzolanic material in cement and concrete production (Mehta, 1983). With this not only the production cost is reduced but also the properties of concrete such as workability and strength can be changed so as to meet the various necessities of practical projects, and another benefit of this, possibly the most important one, is that the pollution by solid waste in now increasingly and seriously polluted world is decreased. Waste glass can be found everywhere, except the recycle of some glass bottles how to economically treat or reuse it is a practical problem ahead of us. The change in electrical conductivity of the saturated $Ca(OH)_2$ solution doped with the GP used in this experiment was determined to be -0.02 mS/cm but that added with one kind of silica fume (SF for short) was as high as 1.65 mS/cm. According to the evaluation standard for pozzolanic activity proposed by M.P. Luxan et al.(1989) GP did not exhibit any pozzolanic activity while the silica fume was very active. The difference of pozzolanic activity between GP and SF was also confirmed by mortar strength tests. With the increment of GP to ordinary portland cement (OPC) the final setting of cement was prolonged and cement strength was gradually decreased. Both GP and SF are amorphous and contain much silicon oxide (Fig 1 and Table 1) why they behave so much differently in pozzolanic activity? Can we utilize GP as an effective admixture of cement under normal curing conditions as we conducted on silica fume and rice husk ash (Sugita et al., 1992) and how can we improve the properties of GP blended cement? It is the focus of our attention. Fortunately it was found that with different fineness the glass powder did show different effects on the properties and pore structure of OPC hydrates. After GP was further ground for one hour in an effective ball mill, namely NGP, it was observed that the strength of NGP blended cement mortars was increased compared with that of GP blended cement. Moreover when 0.5% NaOH was introduced to NGP blended cement its hydration was accelerated and strength was further increased as well. This work is only a preliminary study on the utilization of waste glass but it does give us a hint, i.e. just as blast-furnace slag, fly ash and silica fume in the future waste glass can also be reused in the field of cement and concrete after more and further effort.

EXPERIMENTAL AND RESULTS

Raw material and mix proportions

Exhausted drink bottles were cleaned and dried, then ground in a vibration ball mill for one hour or two hours, the Blaine specific surface area and average particle size of the two products were respectively responding to 416 m^2/kg, 40 μ m (GP) and 656 m^2/kg, 8 μ m (NGP). Fig 2 are the SEM images of them. Sumitomo ordinary portland cement (OPC) was used as control sample

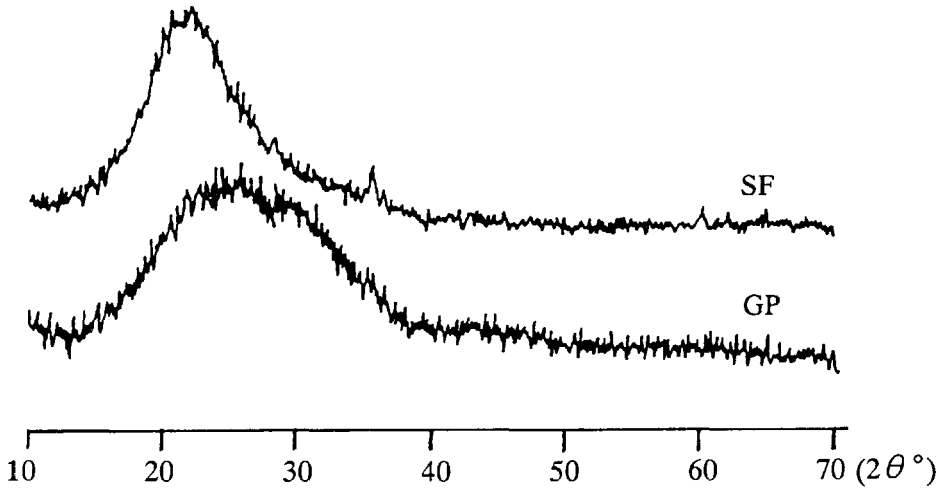

Figure 1 XRD diagrams of SF and GP

Table 1 Chemical compositions of glass powder and silica fume (%)

Sample	SiO_2	Al_2O_3	Fe_2O_3	CaO	MgO	K_2O	Na_2O	TiO_2	B_2O_3	I.L.
Glass	71.6	0.01	0.67	9.25	3.52	1.11	0.19	0.04	Tr.	0.00
SF	94.6	0.01	Tr.	Tr.	1.16	1.36	0.09	0.01	—	2.50

and Toyoura standard sand as fine aggregate in this experiment. The chemical composition of the glass and the mechanical properties of OPC are respectively shown in Table 1 and 2. GP and NGP blended cement were prepared by mixing x% GP or NGP with (100-x)% OPC by weight, where x=5, 10, 15 and 20 for GP blended cement (GP_1, GP_2, GP_3 and GP_4) and x=5, 10 for NGP blended cement (NGP_1 and NGP_2). In addition, 0.5% NaOH by weight was respectively incorporated into the cements added with 5% and 10% NGP, nominated to NGP_3 and NGP_4.

Electrical conductivity of GP, NGP and SF

A rapid evaluation of pozzolanic activity of natural products by electrical conductivity measurement was proposed by Luxan et al. (1989), which was proved to be also very effective and convenient in the evaluation of pozzolanic activity of rice husk ash and silica fume (Sugita et al., 1992, and Sugita et al., 1993). In this experiment two kinds of solution were adopted, one was saturated $Ca(OH)_2$ solution and the other was 0.5% NaOH solution. The analysis procedures of electrical conductivity are mainly described as follows: 1) the electrical conductivity of 200 ml of the $Ca(OH)_2$ solution or the NaOH solution at 40 ± 1°C (E_0) is measured at first, 2) 5.00g of the material to be tested is added to the solution and the solution is kept under constant stirring, 3) the electrical conductivity of the solution incorporated with the material (E_1) is taken over 120 seconds, and 4) by subtracting E_1 from E_0 the change in conductivity of the solution is therefore obtained. Table 3 shows the standard for the evaluation of pozzolancity by conductivity measurement (Luxan et al., 1989) and the electrical conductivity variation of the solution doped with GP or NGP or SF.

Normal consistency, setting time and strength of GP or NGP blended cement

Table 2 gives the effect of GP addition on the the normal consistency and setting time of cement. The $40\times40\times160$ mm strength specimens, which were made at a water binder ratio of 0.65 and sand binder ratio of 2.0, were cured at 20 ± 1°C in the air of R. H.>90% for one day after casting, then demoulded. Subsequently, the specimens were cured in water at 20 ± 1°C for 3d, 7d and 28d respectively. The strength of the tested mortars are shown in Table 2 and 4.



(a)-GP, 170×

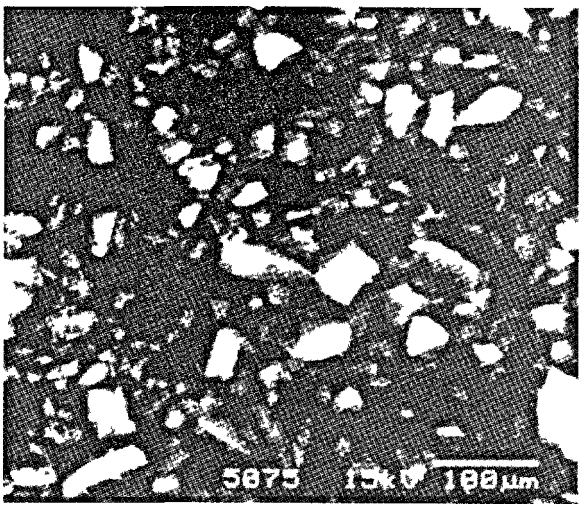

(b)-GP, 1000×

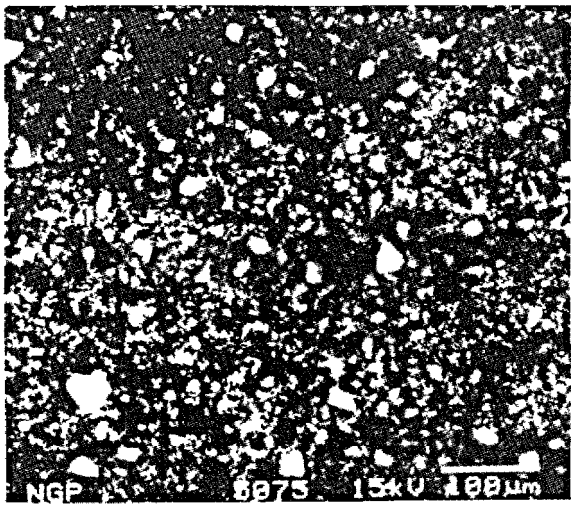

(c)-NGP, 170×

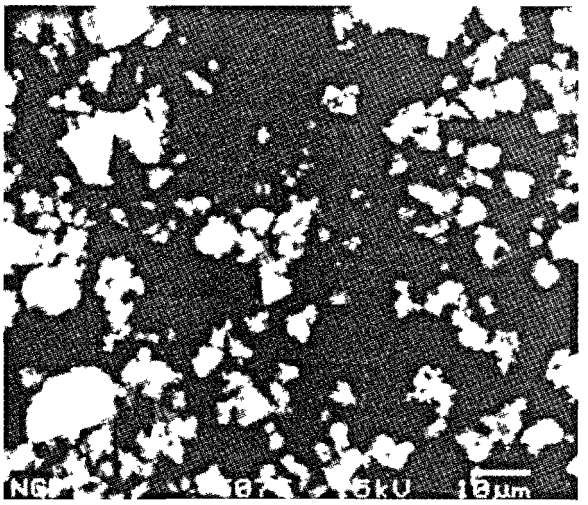

(d)-NGP, 1000×

Figure 2 SEM images of GP and NGP

Table 2 Influence of glass powder (GP) on the properties of normal portland cement (water/binder=0.65, sand/binder=2.0)

Sample	GP add. (%)	Nor. con. (%)	Setting time (h : m) Initial	Final	Flow value (mm)	Flexual strength (MPa) 3d	7d	28d	Comp. strength (MPa) 3d	7d	28d
OPC*	0	27.6	2 : 08	4 : 30	215	3.4	5.2	7.2	15.8	27.0	41.3
GP_1	5	28.4	2 : 03	4 : 46	217	3.0	4.3	6.5	12.5	21.8	35.8
GP_2	10	29.4	2 : 04	5 : 14	217	2.7	4.5	6.4	11.1	20.7	34.0
GP_3	15	28.4	2 : 06	5 : 04	224	3.1	4.9	5.8	12.9	23.1	38.2
GP_4	20	28.1	2 : 08	5 : 39	235	—	—	—	—	—	—

* The Blaine specific surface of NPC is 335 m^2/kg

Table 3 Evaluation of pozzolanic activity by electrical conductivity measurement and the conductivity of GP, NGP and silica fume

Pozzolancity	Change in conductivity (mS/cm)	Sample	Change in conductivity of sat. $Ca(OH)_2$ sol. (mS/cm)	Change in conductivity of 0.5% NaOH sol. (mS/cm)
Non pozzolanic	less than 0.4	GP	-0.02	0.35
Variable pozzolancity	between 0.4 and 1.2	SF	1.65	1.70
Good pozzolancity	larger than 1.2	NGP	-0.04	0.55

Non-evaporable water in the pastes

Pastes of OPC, GP and NGP blended cement were prepared at a water binder ratio of 0.65, then they were tightly sealed in glass bottle and cured in water at 20±1°C to 7d and 28d. The method for determining non-evaporable water in the pastes is shown in Eq 1 (Czernin, 1964) and the result is listed in Table 5.

$$W_c = \{(W_d - W_i)/W_d\} \times 100\% - W_o \quad [1]$$

where W_c is the amount of non-evaporable water of paste (%), W_d is the weight of the ground paste after dried at 105°C for one hour, W_i is the weight of the paste after calcined at 1000°C to constant weight and W_o is the ignition loss by weight percentage of the respective cement.

Pore size and pore volume distribution of cement mortars

After strength test the mortar specimens were carefully crushed and dried at 40°C in a vacuum drier for 48 hours, from which particles around 3×3×3 mm in size were selected for determining pore size and pore volume distribution with PASCAL 140 and 240 Porosimeter. The pressure of mercury intrusion was from 0.1 to 200 MPa and mercury penetration speed, in the both procedures of pressure increase and decrease, was all controlled at 4p. The results are respectively shown in Table 6 and Fig 3.

Table 4 Properties of the NGP blended cement mortars with or without NaOH addition

Sample	NGP (%)	NaOH (%)	Flow (mm)	Flexual strength (MPa)			Comp. strength (MPa)		
				3d	7d	28d	3d	7d	28d
NGP_1	5	0	265	3.4	4.6	6.7	14.4	24.6	39.9
NGP_2	10	0	274	3.4	5.0	6.9	14.1	25.2	40.6
NGP_3	5	0.5	243	3.9	5.3	6.8	19.0	28.6	42.6
NGP_4	10	0.5	256	3.6	5.2	6.8	16.2	27.1	38.4

DISCUSSIONS

Pozzolanicity of GP and NGP and the properties of GP and NGP blended cement

Table 5 Non-evaporable water in the pastes hydrated for 7d and 28d

Sample		OPC	GP_1	GP_2	NGP_1	NGP_2	NGP_3	NGP_4
Non-evapor.	7d	13.9	14.2	14.5	14.4	14.5	15.4	16.7
water (%)	28d	19.8	20.5	21.9	20.8	22.6	21.4	22.4

Table 6 Pore size distribution of the tested mortars cured for different ages

Sample	Relative volume (mm^3/g)					Pore radius av.(Å)	Total cumula. vol.(mm^3/g)
	<500 Å	500-10^3 Å	10^3-5×10^3 Å	5×10^3-10^4 Å	10^4-10^5 Å		
OPC	18.2	19.5	33.7	25.6	31.7	3709	128.9 (3d)
	59.5	20.3	28.0	10.4	8.9	566	127.1 (7d)
	82.2	9.6	2.6	0.7	1.0	284	96.0 (28d)
GP_1	63.1	34.9	6.3	1.0	1.6	387	107.0 (28d)
GP_2	61.0	28.8	12.2	2.5	3.8	421	108.0 (28d)
NGP_1	88.4	3.8	3.4	1.0	1.5	240	98.1 (28d)
NGP_2	89.3	4.5	5.1	1.2	1.2	241	101.2 (28d)
NGP_3	34.2	21.6	46.1	20.0	6.6	1300	128.4 (3d)
	75.7	8.9	8.0	2.0	3.3	251	97.9 (28d)
NGP_4	58.6	20.0	28.4	4.5	5.9	501	117.4 (7d)
	78.7	10.6	6.9	1.4	2.2	275	99.7 (28d)

The change in electrical conductivity of the saturated $Ca(OH)_2$ solution after adding GP or NGP to it was respectively equal to -0.02 mS/cm and -0.04 mS/cm, which showed that both of them would not have any pozzolanic activity according to Luxan, et al. (1989). But in our opinions the minus variation in electrical conductivity of the $Ca(OH)_2$ solution with GP or NGP may result in the rapid dissolution of partial CaO or other dissoluble oxides contained in them into the solution. The same phenomenon occurred for rich calcium fly-ash in the test conducted by us before. So only by this test it is yet difficult and not enough to give a precise estimation of the pozzolanicity of GP and NGP.

Table 2 indicates that with the addition of GP to NPC, from 5% to 20% by weight, the final setting of cement is prolonged, the flowability of mortar increased and the strength of cement decreased, only the initial setting of cement is kept unchanged. The more the added GP, the bigger the loss of the strength. In another hand SF, with a variation in electrical conductivity of 1.65 mS/cm, showed high pozzolanic activity and was proved able to greatly improve the strength of NPC (Sugita et al., 1992). Both GP and SF were rich in amorphous silicon oxide why GP exerted an adverse effect to SF on the properties of cement? It is known that silica fume is a by-product condensed in gas in the production of silicon or silicon alloys. The SF used here consisted mainly of spherical glass particles with an average diameter of 1500 Å and had

a N_2 specific surface area (BET method) of 24.06 m^2/g, while the N_2 specific surface area of GP which had an average particle size as high as 40 μ m was only 0.85 m^2/g. So in our opinions the main reason for the difference between the pozzolanic reactivity of GP and SF is that they have much different fineness and surperficial state, both of which are directly related to the reactivity of any material. So one possible way of improving the strength of GP blended cement is to increase the fineness of GP. This supposition has been proved true by experiments. NGP, which was obtained by grinding GP for one more hour, did show a higher conductivity variation in 0.5% NaOH solution than that of GP (Table 3), and Table 4 indicates with its addition both the compressive and flexural strength of cement mortars are increased compared with those of GP blended cement and at 28 days they come close to those of OPC. Even though at a same mix proportion the flow value of NGP blended cement mortar was higher than that of OPC and GP blended cement the phenomenon of bleeding has not been found.

Influence of NaOH addition on the strength of NGP blended cement

The stimulating effect of NaOH on the activity of slag and fly ash and other pozzolans as well has been observed by many other researchers. In this experiment the same phenomenon also occurred, that is after the addition of 0.5% NaOH to NGP blended cement its strength was improved and even became greater than that of NPC. Table 5, 6 and Fig 3 (b, c and d) give the direct reasons for the strength increment as follows: 1) non-evaporable water in the pastes of NGP_3 or NGP_4 at 7d and 28d are both enhanced compared with those in NPC pastes and 2) pore

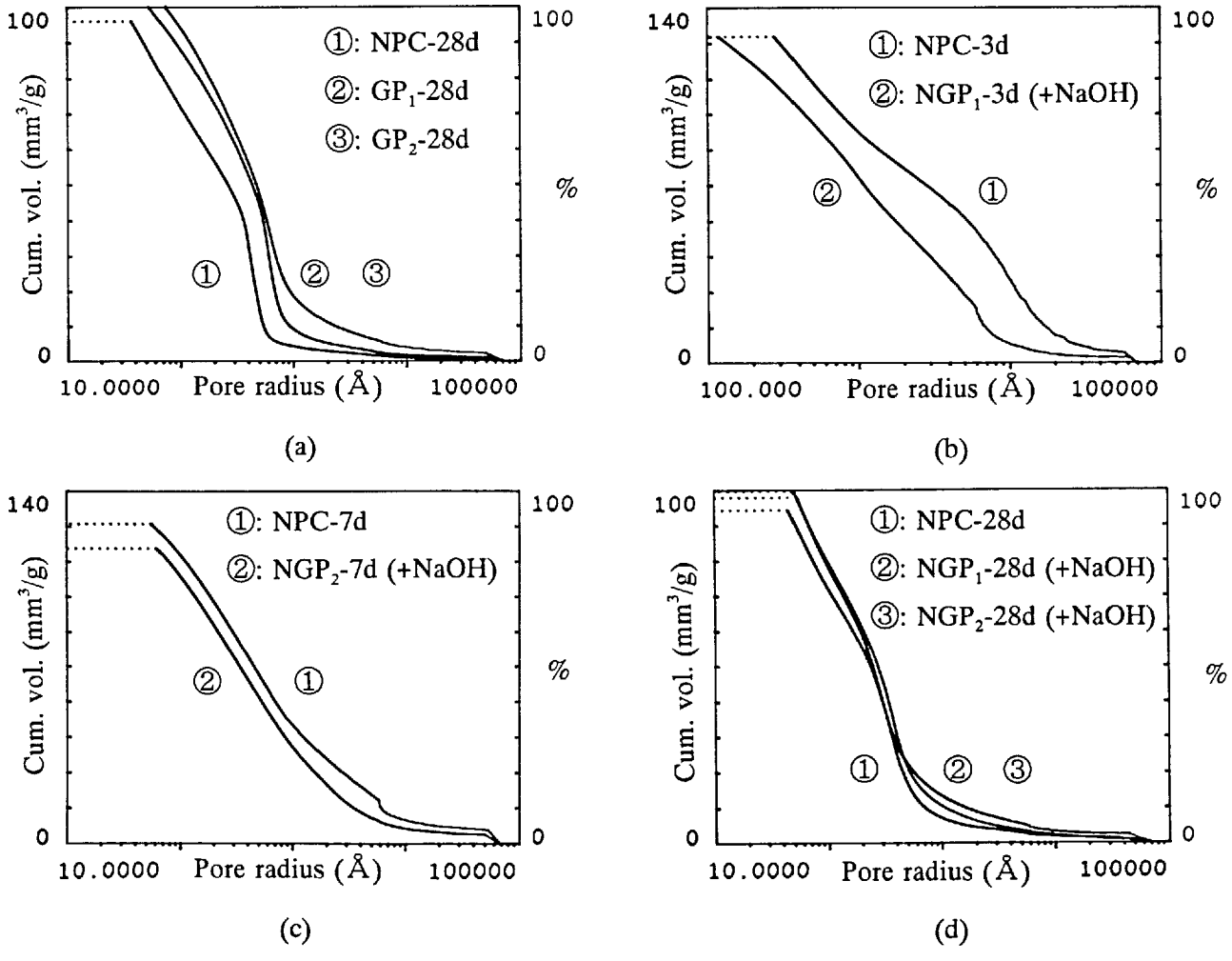

Figure 3 Pore size distribution of the tested mortars

size of their mortars at different ages are all reduced, in particular at 3d age the average pore radius of NGP_3 mortar shows a remarkable decrease in respect to that of NPC mortar.

Under the normal alkalinity produced by portland cement hydrates the potential activity possessed by glass powder could not be activated, therefore with the addition of either GP or NGP to OPC cement strength was gradually decreased. But in the presence of NaOH the dissolution of amorphous silica in the glass into the liquid phase of hydrating cement could be accelerated greatly, which possibly resulted from: 1) the activation of the surface of glass particles by the etching and damaging effect of alkali ions and 2) the early failure of Si-O network under the strong alkalinity circumstance produced by the added NaOH. As the result of this the silica in glass could react with $Ca(OH)_2$ in cement hydrates resulting in forming more C-S-H gel in the hydrates and accelerating the hydration of cement. So after adding NaOH to NGP blended cement the non-evaporable water in the hydrated pastes was enhanced and the pore structure of mortar was improved in favour of strength development, leading the strength of NGP blended cement to be increased finally.

In addition, Table 3 shows the change in electrical conductivity of the 0.5% NaOH solution added with glass powder was positive and increased with the fineness of glass powder, which also indicated that NaOH had a stimulating effect on the reactivity of glass powder.

Mechanism of the strength development of the cement blended with GP or NGP

Under a same hydration condition the strength of cement is closely related with the pore struture and hydration degree of its hydrate. Generally speaking the hydration degree of cement can be evaluated by the amount of non-evaporable water existing in its hydrate. Table 5 shows with the addition of GP to OPC the non-evaporable water in the paste, hydrated both for 7d and 28d, is increased. But from Table 6 and Fig 3-a it can be found the average pore radius and total cumulative pore volume of the mortars at 28d are adversely increased, especially the relative volume of mesopores (<500 Å in radius) is reduced by about 20% instead of the increment of the pores, ranged from 500 to 1000 Å in radius, by about 20%. Here the enlargement of pore size and total pore volume may plays the leading effect on the strength development, so cement strength is gradually decreased with the increased addition of GP.

NGP, with an average size of 8 μ m and a smooth surface, had a larger specific surface area than GP and NPC did. In both periods of specimen casting and cement hydration it probably played a dispersing role. With its addition to OPC instead of GP, at first compact specimens could be obtained by the increase of mortar flowability, in another aspect the hydration of cement was developed by improving the contact of cement particles with water. As the result of these the non-evaporable water in its paste was increased compared with that in GP cement paste, coherently the average pore radius and total pore volume of mortar were decreased, and particularly the volume proportion of the pores, greater than 500 Å in radius, was decreased evidently (Table 6), which certainly led the strength of NGP blended cement to be increased.

Now it is also difficult to say whether NGP has a high pozzolanicity or not as the strength of NGP blended cement is still inferior to that of OPC, there is also short of enough comparison data. But as far as the effect of NGP and GP on the properties of OPC it might be convinced that NGP is more active than GP. The influence of the fineness of glass powder on the hydration and strength properties of cement, and the effect of NaOH on the activity of glass powder should be investigated deeply in the future from the chemical or/and physical reaction of the finely ground glass with cement hydrates, and from the structure variation of both fresh and hardened cement paste and mortar after the addition of glass powder.

CONCLUSIONS

1. With the addition of glass powder to OPC the final setting of cement was prolonged and the strength was decreased.
2. The direct reason for the difference of pozzolanicity between silica fume and the glass powder used in this experiment was that they had much different specific surface areas. It was possible to improve the reactivity of glass powder by finely grinding it. The finer the glass powder, the higher the strength of glass powder blended cement. The increase of cement strength with the fineness of glass powder was mainly attributed to the improvement of cement hydration and the formation of compact structure of mortar.
3. After 0.5% NaOH was introduced to fine ground glass powder (NGP) blended cement its strength was further increased and became to greater than that of normal portland cement. The reason for this was the reactivity of NGP, which had a large specific surface area, was activated by the added NaOH and the pore size of mortar at different ages was decreased as well.

REFERENCES

Czernin, W., "Zementchemie fur Bauingenieure", Japanese version, Translated by Yoshio Tokune, Technology Information Press of Japan, 1969, p. 44.

Luxan, M.P., Madruga M. and Saavedra J., "Rapid Evaluation of Pozzolanic Activity of Natural Products by Conductivity Measurement", Cem. and Concr. Res., Vol. 19, No. 1, 1989, pp. 63-68.

Mehta, P.K., "Pozzolanic and Cementitious by-Products as Mineral Admixtures for Concrete", Fly Ash, Silica Fume, Slag and other Mineral by-Products in Concrete, Montebello, Vol. I, ACI SP 79, 1983, pp. 1-46. Editor: V. M. Malhotra.

Sugita, S., Shoya, M. and Tokuda, H., " Evaluation of Pozzolanic Activity of Rice Husk Ash", Fly Ash, Silica Fume, Slag and Natural Pozzolans in Concrete, Proceedings of the Fourth International Conference, Istanbul, Turkey, Vol. I, ACI SP 132-28, 1992, pp. 495-512. Editor: V. M. Malhotra.

Sugita, S., Shoya, M., Shi P., and Isojima Y., "Design of Furnace for Large Quantities of Highly Active Rice Husk Ash", Proceedings of the 3rd Beijing International. Symposium on Cement and Concrete, Vol. II, 1993, pp. 651-655.

ADDITION OF ULTRA FINE GROUND SAND FOR THE PRODUCTION OF HIGH STRENGTH AUTOCLAVED MORTARS.

Filip VAN RICKSTAL, K.U.Leuven, Belgium
Dionys VAN GEMERT, K.U.Leuven, Belgium
Petra PARMENTIER, K.U.Leuven, Belgium
Kris VANBELLE, K.U.Leuven, Belgium

ABSTRACT In concrete and in mortars, especially the weaker interfacial zones are determining the tensile and bending strength. To condense this interfacial zone, very fine ground sand, whose granularity is comparable to the one of cement, was added to the mix. By autoclaving the mortars, bending strength could be doubled from about 5 MPa to 10 MPa. The compositions were adjusted to a CaO/SiO_2 ratio of one, which is commonly known as the optimum, by adding silica fume. SEM- analysis showed that the interfacial zone of the autoclaved mortars became very dense and indicated reactivity of the ground sand.

KEYWORDS high strength mortars, silica fume, autoclaving, mixing procedure, SEM, ground silica

INTRODUCTION

For several years the Reyntjens Laboratory of the Civil Engineering Department of K.U.Leuven, has been involved in a research program about cement tiles. In this research program knowledge was built up about non standard curing cycles, i.e. autoclaving and steaming. Recently we focussed on the production of a mortar for the fabrication of small building components. The bending strength of these mortars should increase up to 15 to 20 MPa, to be competitive with ceramics.

Since in concrete and mortars the weaker interfacial zones are determining the strength, ultra fine ground silica sand, known as quartz flour, showing a granularity comparable to the one of cement (Fig 1), was added to the mix. Comparisons were made between the fine mixes and the coarser mixes regarding mechanical strength and shrinkage. For the mechanical testing of bending strength and compressive strength and also for the measurement of the shrinkage, standard mortar prisms (40 mm x 40 mm x 160 mm) are made, the strength is determined according to NBN B12-208. The E-dyn is calculated measuring the velocity of the sound through the samples according to NBN B15-229. The last part of this paper deals with the SEM analysis of the mortars, especially of the interfacial zone.

MATERIALS AND METHODS

Composition

Fig 1 shows the sieve curves of the M300, M2 and M32 sands, with the OP cement class 42.5 R. All three are nearly pure silica sands (> 99% SiO_2), which makes them very homogeneous, strong and hard. The shape of the M300 is very angular and irregular since it is ground quartz, providing good mechanical anchoring in the cement paste. Because of the very fine aggregates, a superplasticizer is absolutely necessary to obtain workability with an acceptable W/C ratio. Rheobuild 716 is used, a superplasticiser from the sulfonated naphthalene family. Without this superplasticizer, the W/C ratio would be too high to obtain a strong mortar. The silica fumes were added as a slurry.

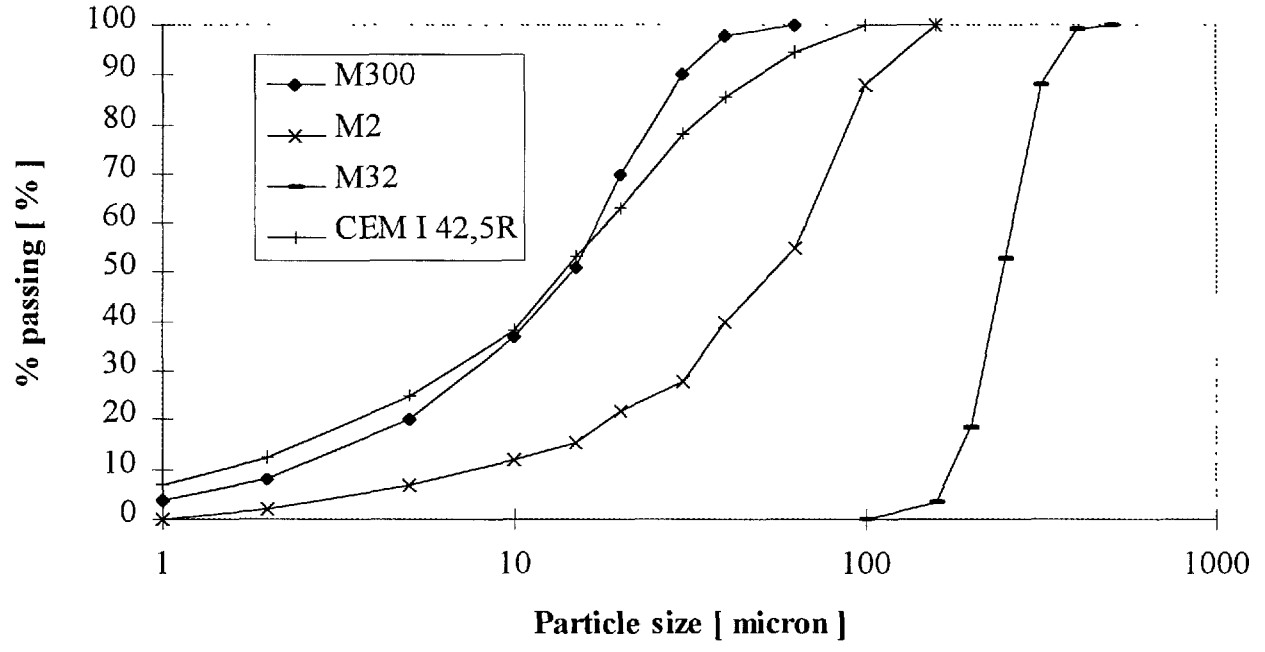

Figure 1 Sieve curves of the used sands and cement

The optimal mix was forced to meet the following requirements:
C/S ratio = 1, known as the optimum for steaming and autoclaving, taking into account the reactive silica and calcium in silica fume and cement
Cement/inert material = 1/3
Granularity of the mix fits close to the optimal granularity according to Bolomey's formula:
$y = A + (100 - A)\sqrt{d/D}$, where y = percentage passing, A = constant (= 10), d = sieve opening and D = max particle size.

The mix proportions for the above requirements are obtained with a least square solution for the granularity meeting the above boundary conditions:
M300 = 190 g, M2 = 1160 g, Silica Fume=142 g and CEM I 42.5 R = 308 g.

The initial W/C ratio for this mix to provide the necessary workability, equals 0.75. It will be explained further on how this W/C ratio was decreased by changing the mixing procedure without decreasing the workability. To be able to determine the influence of the amount of ultra fine ground sand, small variations in the content of M300 are used. In the same program several mixes containing the coarser M32 sand were tested, although these coarser mortar might not be suitable for certain building components.

Mixing procedure

In the first stage the mixing procedure of the Belgian code NBN B 12-108 was used. This means: mixing of silica fume slurry, water and superplasticiser for 5", adding the cement and mixing slowly for 30", adding the sand while slowly mixing in 30" and then switch to the high speed for another 30", stop mixing and scratch off the sides of the recipient, cover the recipient and wait for 1'30". Hereafter, mix for another 1' at high speed. The W/C ratio was adapted to 0.75 at which the flow of the mortar became 1.25.

Curing Cycles

In addition to the reference curing for 28 days at 60% R.H. and 20 °C, the mortars were steamed and autoclaved. Fig 2 shows both curing cycles. The temperature rising rate for the steaming is 18°C/hour, the isothermal period at 80°C lasts 20 hours. Thereafter the system is cooled by unforced heat exchange with the environment, since the autoclave, where the steaming and autoclaving are carried out, has no cooling abilities. From our experience, 180°C for the isothermal period is optimal for autoclaving. This isothermal period lasts only 5 hours, the rising rate to this temperature is 80°C/hour. The short isothermal period makes the curing cycle to obtain final strength very short, enabling a significantly shorter production period.

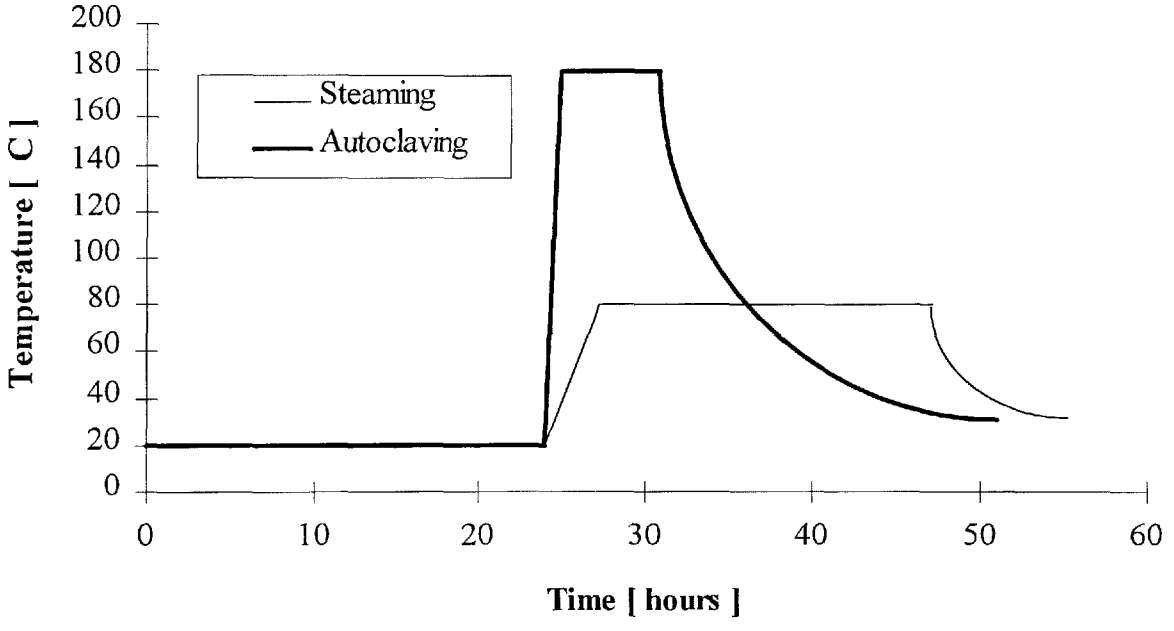

Figure 2 Temperature vs Time plot of autoclave and steam cycle

Initial Results

Although the W/C ratio was still too high, the results of the mechanical tests were promising, especially for the autoclaved samples. It appeared to be impossible to obtain the desired strength without autoclaving the mortars: steamed samples are significantly better than the reference cured ones concerning the shrinkage, but show no increased strength. The autoclaved samples perform very well for the mechanical strength and also for the final shrinkage. Table 1 lists the different mixes and their bending strength, compressive strength after 28 days and the E-dyn. The mortars are named after their composition: i.e. 36-64-00 means 36 % of the inert material = M300, 64 % = M2, 0 % = M32. As mentioned above, the W/C ratio of the mortars containing no M32 is 0.75, whereas the W/C for the mortars containing M32 is 0.65.

MODIFICATIONS AFTER FIRST RESULTS

Addition of SP in repeated doses decreases W/C ratio with 15 %.

The effect of the addition of ultra fine ground sand to increase the strength, is partly counteracted by the necessity to increase the W/C ratio up to 0.75. Adding more SP was no valid option, since the % of SP was already high (3.33 %). Addition in repeated doses of the same amount of SP could reduce the W/C ratio with 15 % down to 0.65 for the same workability. The mixing procedure to reduce the W/C ratio consists in the following steps: mixing the cement, the SF slurry and 3/4 of the water slowly for 1'; scratch off the recipient, mix for 1'30" at high speed; addition of half the

Table 1 Results of mechanical tests in MPa for three curing conditions

Mortar	Reference Curing			Autoclaving			Steaming		
	Bend.	Compr.	E-dyn.	Bend.	Compr.	E-dyn.	Bend.	Compr.	E-dyn.
36-64-00	5.6	39.0	20050	5.5	63.1	20879	9.4	68.1	24070
23-77-00	6.8	35.7	19803	-	-	-	-	-	-
18-82-00	4.9	38.8	19280	4.9	61.6	21279	10.7	67.0	23495
15-85-00	5.8	37.6	19194	-	-	-	-	-	-
13-87-00	5.4	36.6	19331	5.1	61.8	20198	11.2	68.8	24126
15-20-65	6.0	42.4	23396	4.5	67.1	22317	9.1	77.1	27619
15-10-75	5.7	37.9	22686	5.6	57.7	23219	8.8	80.7	28244
10-30-60	5.6	41.3	23784	5.1	66.7	22271	9.3	75.3	27852
10-20-70	5.3	38.1	21876	-	-	-	-	-	-
10-15-75	5.3	39.2	22646	6.3	54.2	23450	10.1	75.7	27511
10-10-80	5.7	37.5	21251	5.4	63.8	21169	8.3	74.5	26799

remaining water and half the SP, mixing for 3'; addition of the remaining water and SP and mixing for another 3'; add the sand in about 1'; after that, mix at high speed for 3' minutes. This mixing procedure takes about 15 minutes, but it seems to be the only way to reduce the W/C ratio with the materials and admixtures used.

The porosity after hardening will decrease because of the lower W/C ratio, the transition zone is still denser and so mechanical performance and drying shrinkage improves. **Table 2** lists the results of the mechanical tests for the mortars with the reduced W/C ratio.

Table 2 Results of the mechanical tests in MPa of the mortars with reduced W/C ratio

Mortar	Reference Curing			Autoclaving			Steaming		
	Bend.	Compr.	E-dyn.	Bend.	Compr.	E-dyn.	Bend.	Compr.	E-dyn.
23-77-00(0.7)	5.2	33.3	18097	4.4	62.3	26467	11.2	60.4	21964
13-87-00(0.65)	5.1	29.9	17548	4.9	69.6	27354	10.9	69.4	24480
15-20-65(0.6)	6.8	45.3	26323	6.9	79.9	33322	11.3	81.3	29660
15-10-75(0.6)	7.2	48.0	27061	6.6	79.9	32865	9.0	83.0	30806
10-10-80(0.6)	6.4	40.9	24630	6.3	72.5	31752	10.4	73.3	28641

Additional baking after autoclaving

Ohama (1991) indicated that additional baking immediately after autoclaving could increase the mechanical strength of the mortars. When the isothermal period of five hours is over, to pressure is released and the samples are put in a drying oven at 200°C and atmospheric pressure for 24 hours. Shrinkage was not checked and only one series of samples was produced this way. Since the average bending strength of these samples was up to 13.7 MPa and 14.7 MPa (Table 3), this curing procedure will be subject for investigation in a next program.

Table 3 Mechanical properties in MPa after additional baking.

Mortar			
	Bending	Compressive	E-dyn.
13-87-00 (0.65)	13.7	69.9	25923
12-20-65 (0.5)	14.7	86.5	28358

CORRELATION BETWEEN MECHANICAL STRENGTH AND E-dyn.

The research program provided a large amount of data from the different compositions and the different curing cycles. In this section, although somewhat separated from the rest of the paper, the correlation between the mechanical strength and the E-dyn is discussed. Fig 3 shows the correlation between the compressive strength and the E-dyn for each curing cycle. The correlation is good for the autoclaved samples, acceptable for the reference cured samples and poor for the steamed ones. The overall correlation of all samples, no matter what curing cycle, is 0.56. It is remarkable that the slopes of the steamed samples and the reference cured samples are nearly the same whereas the slope of the autoclaved sample is almost the double of that, probably caused by a different microstructure.

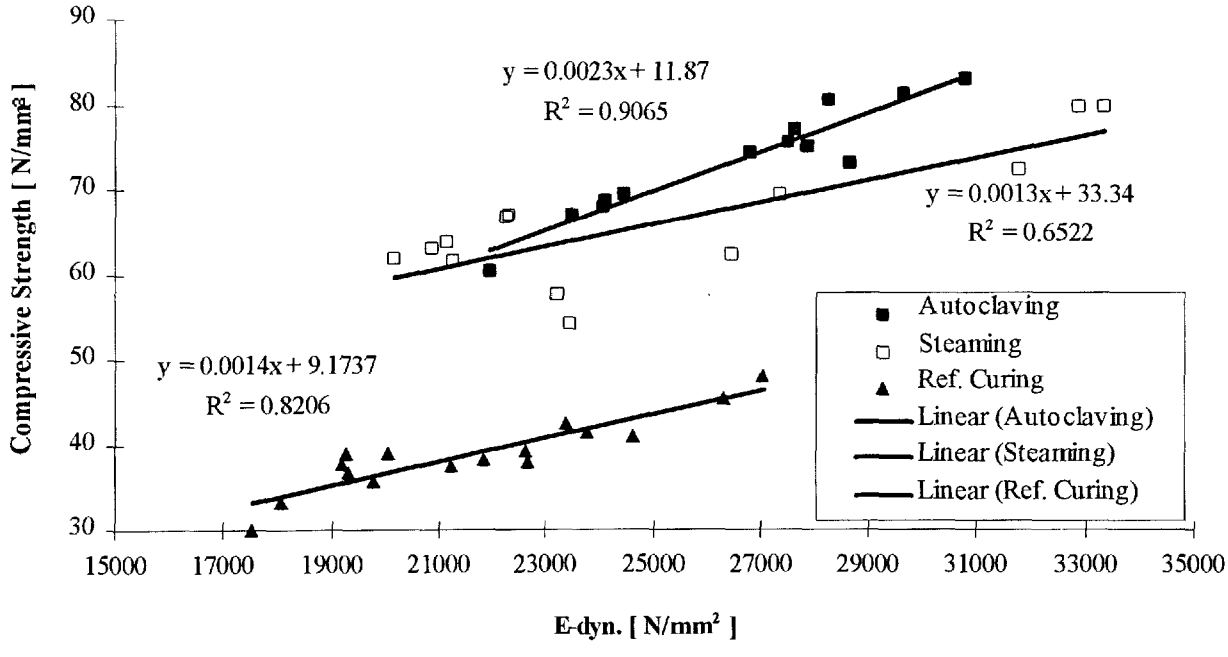

Figure 3 Correlation between compressive strength and E-dyn.

The correlation between the bending strength and the E-dyn. (Fig 4) is very poor. The overall correlation is only 0.19, meaning that there is no correlation at all. For the individual curing cycles, the correlation is a little better, but still very poor. It is worth investigating why the correlation forthe compressive strength is acceptable or even good and why this is not the case for the bending strength. Microcracking might be the reason for this fenomenon.

SCANNING ELECTRON MICROSCOPY FOR MICROSTRUCTURE ANALYSIS

General discussion of the SEM analysis

From the above results it is obvious that the production of high strength mortars without addition of polymers is impossible when reference or steam curing is applied. Only the autoclaved samples reach the desired strength and low shrinkage. SEM-analysis of the microstructure shows a big

difference in microstructure between reference cured and steamed samples on one hand and autoclaved samples on the other hand

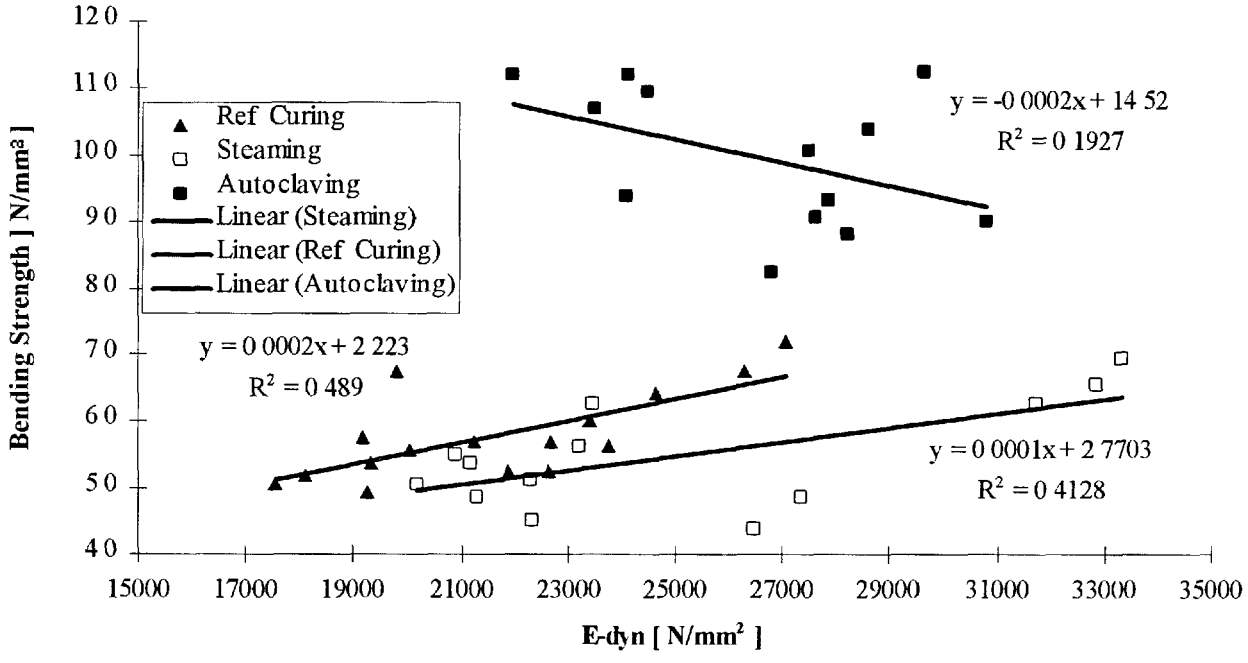

Figure 4 Correlation between bending strength and E-dyn

All reference samples show empty layers around sand grains (Fig 5) The big amount of water causes a thin water layer around every grain In case of a sand grain this water will not react and after evaporation an open layer between cement paste matrix and granulate is developed The same phenomenon can be seen in case of the reduced W/C ratio Although smaller there still exists an open space around each sand grain This interfacial zone will be the favorite place for cracks to develop due to shrinkage or mechanical load Cracks propagate around the sand grains via this interfacial zone (Fig 5) and do not pass through the grains

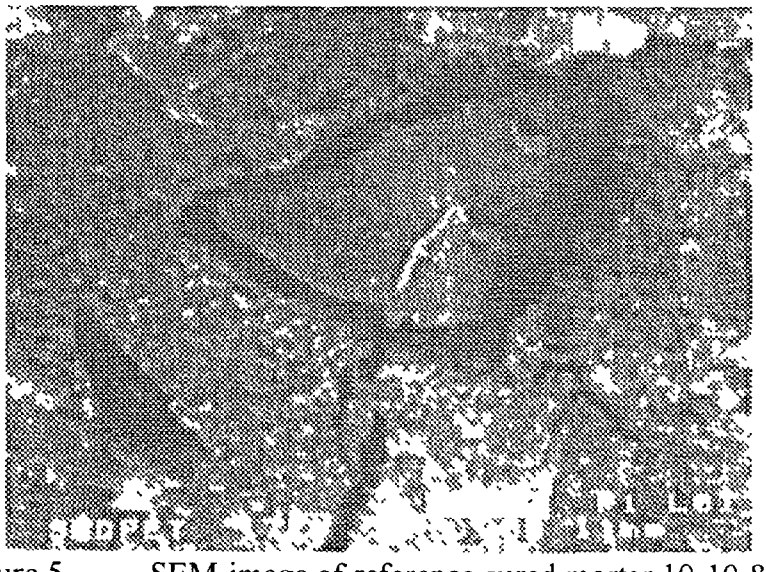

Figure 5 SEM-image of reference cured mortar 10-10-80

To analyze the hydration products, XRD-analysis is carried out, especially on the interfacial zone The reference cured samples have especially CH and $C_3S_2H_3$ crystals that have an open and amorphous structure With the addition of SF, the CH crystals are consumed by the reactive SiO_2 Autoclaved samples do not show any big CH-crystals that are well visible and detectable by XRD in case of the reference cured samples without silica fumes

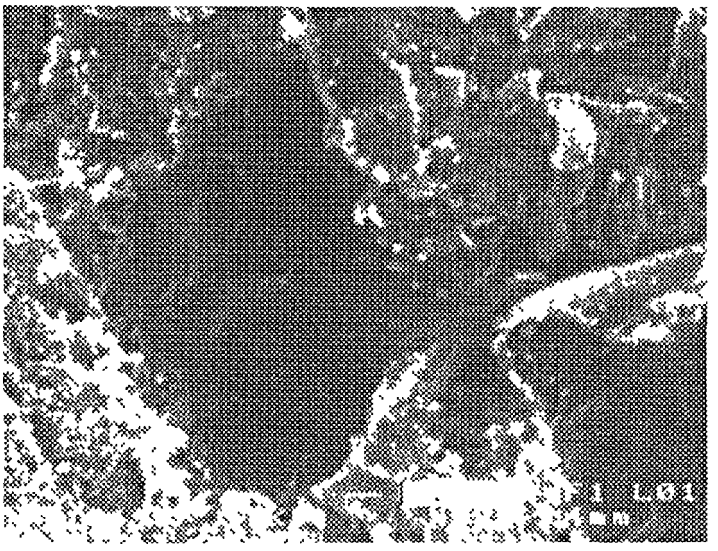

Figure 6 SEM-image of autoclaved mortar 10-30-60

Autoclaved samples (Fig 6) have a much denser structure The cement paste is much denser and the paste fits well to the sand grains. There is hardly any interfacial zone The open space between paste and grain has disappeared completely XRD-analysis indicates that the weak hydration products of the reference cured samples, CH and $C_3S_2H_3$, are less present and that the formation of tobermorite took place to form a dense and strong paste The hydration at higher temperature produces different hydration products and makes the interfacial zone more dense because of the high kinetic energy and hence the higher mobility of the hydration products Regularly cracks passing through the sand grains were found, whereas they passed through the transition zone in case of reference curing At last almost no cracks due to shrinkage occurred in the autoclaved samples, explaining the very low shrinkage values of the autoclaved samples

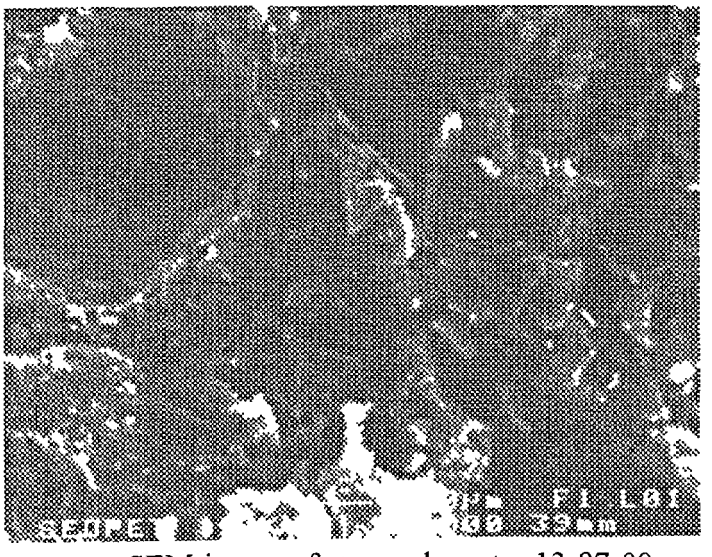

Figure 7 SEM-image of steamed mortar 13-87-00

The steamed samples (Fig. 7) are situated between the reference cured samples and the autoclaved samples. They show a finer microstructure, a denser transition zone than the reference cured samples, but do not perform as well as the autoclaved samples.

Was there any reaction between the ground quartz and the cement?

By analyzing the autoclaved samples with the fine ground quartz M300 a very good adhesion of the paste to the grains was detected. Cracks did not pass through the zone adjacent to the grain, but passed through the grain or passed by a little further away from the silica grains. We assume that the fine ground silica sand participates in the chemical reaction and is a little affected by the hydration forming an irregular surface where the hydration products are chemically and mechanically anchored at the grain. This makes the transition zone very strong and explains the good performance of this mortar. However, we were not able to find an increased amount of soluble SiO_2 in the mortar, to proove the assumption of reactive ground sand.

CONCLUSIONS

The aim of this research program was to check the possibilities of composing a high strength mortar for the production of prefabricated building components. When applying a cement mortar without polymer admixtures, autoclaving seems to be a necessity to obtain the desired 15 to 20 MPA bending strength. Actually, autoclaving doubles the mortars bending strength up to 11 MPa. Additional baking gives a bending strength up to 13.7 and 14.7 MPA.

The 28 days shrinkage values of the autoclaved mortars are very low with an average of 0.015 %. SEM-analysis provided the explanation for the good performances of the autoclaved mortars. A dense microstructure and different hydration products give a good adhesion between grains and paste. The low shrinkage and the absence of shrinkage cracks are confirmed by the SEM-analysis. XRD shows that the hydration products of the autoclaved samples are tobermorite. The amount of the weaker portlandite and $C_3S_2H_3$ have significantly decreased. Although it could not be confirmed by chemical analysis, there are some evidences that the very fine ground sand has taken part in the reaction. This can explain why the transition zone is strong enough to prevent cracks to pass through.

REFERENCES

Parmentier, P. and Vanbelle, K., Ontwikkeling van een performante mortel voor bouwcomponenten. Thesis at K.U.Leuven, 1996

Ohama, Y. and Demura, K., Development of superhigh strength portars using silica fume, 1991

Taylor,H.F.W., Cement Chemistry, Academic Press Limited, London 1990

Kolakowski, K. Et al., Low shrinkage based building components, International Journal of Cement and Concrete Research, Vol 24, No 4, pp 765-775, 1994

Menzel, C.A., Strength and volume change of steam-cured portland cement mortar and concrete, Proc. Am. Concr. Inst., Vol 31, No 2, pp 125-148, 1994

FRACTURE MECHANICS AND MICROSTRUCTURE OF BLENDED CEMENT PASTE

Tadahiro NISHIKAWA and Suketoshi ITO, Nagoya Institute of Technology, Nagoya, Japan

ABSTRACT Hardened cement pastes (HCP) were prepared with ordinary portland cement containing fine powder. Their fracture energy and strength were measured in relation to microstructure and hydrates formed. Effect of particle dispersion in cement matrix on the fracture mechanics was discussed with blended content, characteristics of powder, particle size or curing time. Bending strength for HCP was closely related to its fracture energy and critical crack length at fracture.

Key-words: Blended cement, CSH, Strength development, Waste material utilization

INTRODUCTION

Utilization of powder materials is necessary for enhancement of multiple functional properties for hardened cement paste(HCP). In particular, it is hoped to use waste materials or by-products in the development of chemical or mechanical properties. Blast furnace slag or silica fume is already used and results in lowering the heat evolution and developing the long-term strength. These inorganic materials are mainly prepared as a ground fine powder. Therefore, mechanical properties of blended HCP must be discussed in relation to the hydraulic properties and interaction of blended powder. Beaudoin et al (1985) already reviewed the factors influencing strength of porous cement systems, and took up the fracture energy together with the bending and compressive strength for mechanical properties. Fracture energy corresponds to the fracture toughness, which is an index of the resistance to crack propagation. Fracture energy is also important to evaluate the durability of HCP. However, it is difficult to measure the fracture energy for HCP or concrete, because of the preparation of large specimen having sharp and stable crack. Simultaneous development of bending strength and fracture toughness is required besides that of compressive strength. The HCP was prepared with ordinary portland cement containing fine non-reactive or reactive powder. The fracture mechanics and microstructure of blended HCP were investigated after curing at room temperature. The fracture energy of HCP was measured exactly by using compact tension specimen. Critical crack length, which controlled the strength and toughness for HCP, was estimated using Griffith (1920) equation. Optimum content or particle size of blended powder for durability and strength is also discussed.

METHODS AND MATERIALS

Mixing ratio and curing condition of HCP

The HCP was prepared with ordinary portland cement (Dai-ichi Cement Co.,Ltd.) and isotropic graphite (IG-11 Toyo Tanso Co.,Ltd.), good quality sand (Toyoura Standard Sand), glass waste or blast furnace slag (Dai-ich Cement Co.,Ltd.). Each additive powder, having Blaine of approx. 3000 ~ 4000 cm^2/g, average particle size of 20 μm, was replaced with cement up to 40 wt% (Nishikawa et al, 1995). For slag addition, gypsum of 5 wt% was added to promote hydration of slag. All components were added to distilled water containing a water reducer of 1 wt%, keeping a constant flow value in the water/solid ratio range of 0.28 to 0.32. The water/solid ratio increased with increase of additive powder content. Rectangular specimens 2x2x10 cm^3 were cast and cured in moist air above 1 month.

Hydrates and microstructure

Identification and quantitative analysis of hydrates were performed by XRD and DTA-TG analysis. The Ca/Si molar ratio of C-S-H was estimated by EDX after separation of hydrates with heavy liquid. The procedure for analysis (Nishikawa et al, 1994) is shown schematically in **Fig 1** . Microstructure of blended HCP was observed using SEM together with EDX near the propagated crack in HCP. The AFm and AFt phasaes were separated with ethylene glycol (Uchikawa et al, 1974).

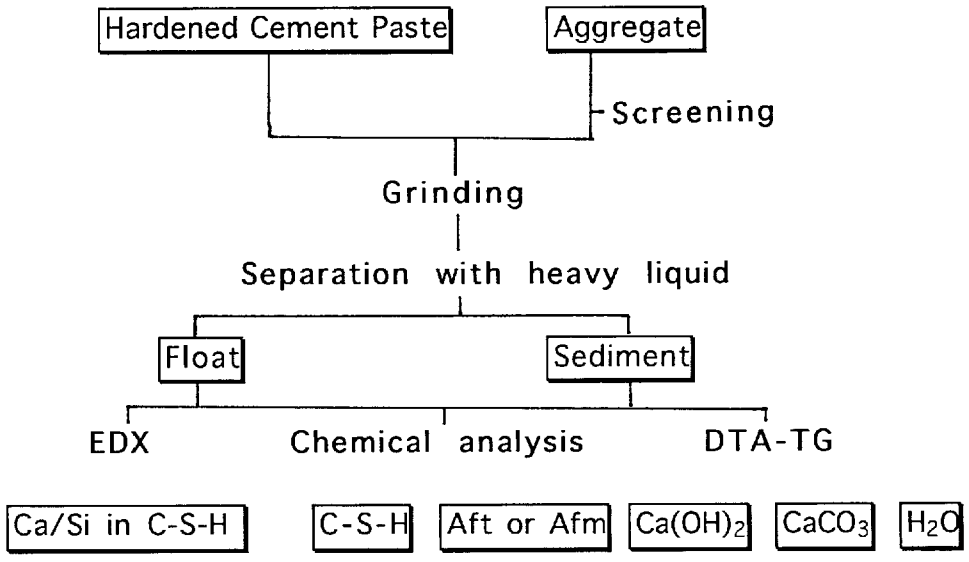

Figure 1 Procedure for analysis of C-S-H and other hydrates

Mechanical properties of HCP

Bending strength was estimated in the ten rectangular specimens by a three-point loading. The lower span width was 8 cm and cross head speed was 0.1 mm/min. Weibull's modulus of specimen for any mixed ratio was above 10, which showed a slight deviation in strength. The tensile strength of HCP was calculated from their bending strength and the Weibull's modulus (Davies, 1973). Compressive strength was measured at the contact area of 2x2 cm^2 after bending test. Ten specimens for each mixed ratio were used for the test. After the compressive test, cone-shaped scraps were observed at the upper and lower parts of specimens due to the fracture of only shear stress.

Fracture energy of HCP using compact tension specimen

A uniaxial tensile test was performed using compact tension specimen, which was cast according to ASTM E399/83, as shown in **Fig 2**. The crack mouth displacement (CMD) was measured by a strain gage on a bronze semicircular plate. The load-displacement (P-u) curve was measured by repetition of load and unload with a cross head speed 0.1 mm/min. The total fracture energy was calculated from the total area of P-u curve divided by double the

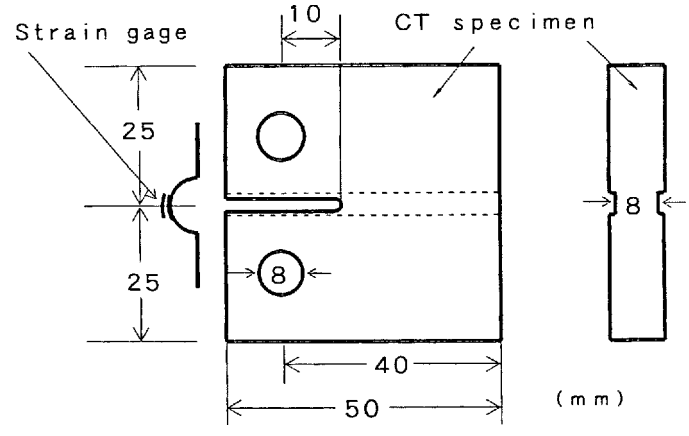

Figure 2 Compact tension specimen

fracture surface area. The obtained P-u curve showed the quasi-brittle fracture. Therefore, elastic fracture energy was obtained by shifting the irreversible residual displacement to the origin. The difference of above two kind of energy corresponds to the plastic energy dissipation (Sakai et al, 1986), which shows the plastic behavior of HCP.

RESULTS AND DISCUSSION

Formed hydrates and microstructure

In HCP subjected to load, the fracture origin and propagated cracks were observed mainly in the formed hydrates, calcium hydroxide and C-S-H. A few cracks propagated around unreacted mixed powder during early hydration. Therefore, fracture behavior mainly depended on the hydrates of HCP. The Ca/Si molar ratio of C-S-H in blended HCP, which was cured for 3 months, are shown in **Fig 3**. The C-S-H formed with unreacted graphite was approximately 2 to 3, which was normal ratio and similar to that in monolithic HCP. The amount of calcium hydroxide was in proportion to the initial amount of ordinary portland cement. Therefore, graphite powder did not participate in the hydration of cement or the formation of the hydrates. In the HCP with glass powder, the decrease in Ca/Si molar ratio was observed due to the sodium and soluble silicate ions dissolved from glass. A similar low-lime C-S-H was observed in HCP mixed with blast furnace slag or alkaline solution (Suzuki et al, 1986). The formation of calcium carbonate was also detected, which was explained by an increase in pH in the pore solution due to the alkaline ions dissolved. Glass or slag particles were not remarkably reduced in size even after 6 months, as shown in **Fig 4**.

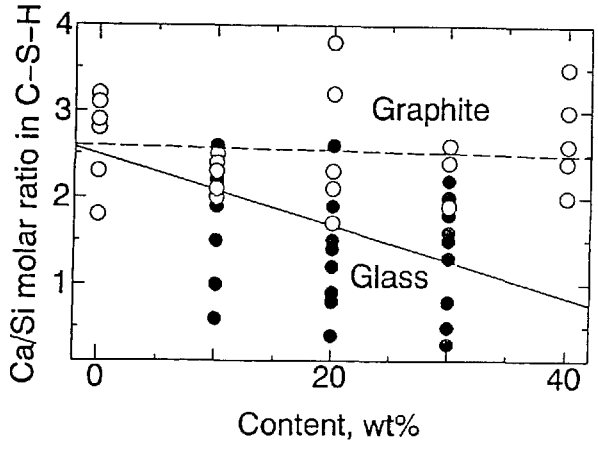

Figure 3 Ca/Si molar ratio of formed C-S-H

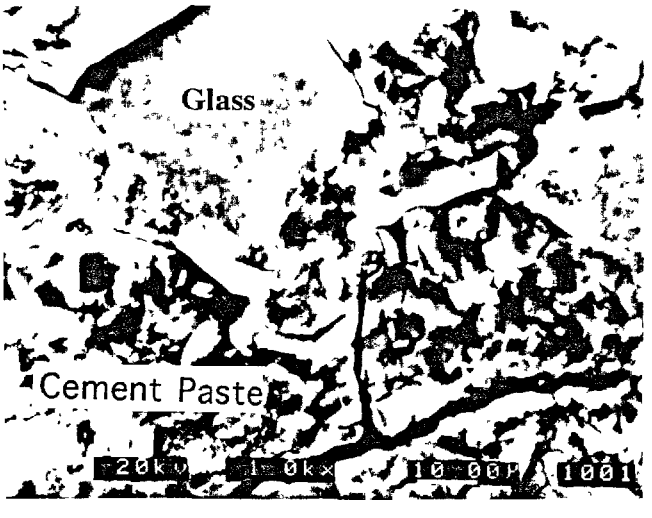

Figure 4 SEM photograph of HCP with glass cured for 6 months

Effect of mixed content on fracture behavior

Resistance to the propagation of a crack for cement based materials consists in a stress relaxation at the front of the crack and a crack shielding effect behind the crack tip, proposed by Cotterell et al (1987) and Jennings (1988). In this experiment, microcracks, which were mainly capillary pores in the cement paste, were observed in front of the propagated crack. The unhydrated cement and addition particles brought a refraction in the crack or grain bridging. This behavior was directly reflected in the fracture energy. Total fracture energy γ_{WOF}, elastic fracture energy γ_e and plastic energy dissipation γ_p were calculated from the P-u curves and shown schematically in **Fig 5** for blended content. Graphite does not react

with cement paste, only the dispersion effect of powder in cement paste can be discussed. In the HCP containing graphite, the hydration mechanism and Ca/Si molar ratio in C-S-H were similar to those for the monolithic HCP. The elastic fracture energy γ_e, according to the linear fracture mechanics, increased with blended content and depended solely on the crack refraction around the graphite particles (Hillemeier et al, 1977). However, bending and compressive strength were not developed by blending graphite. It was mainly due to the weak cementitious property between graphite particles and cement hydrates. The dispersion effect of the unreacted particles was not exhibited on the instantaneous fracture, that was bending or compressive strength. However, this effect increased slightly the fracture toughness, considering large total fracture energy.

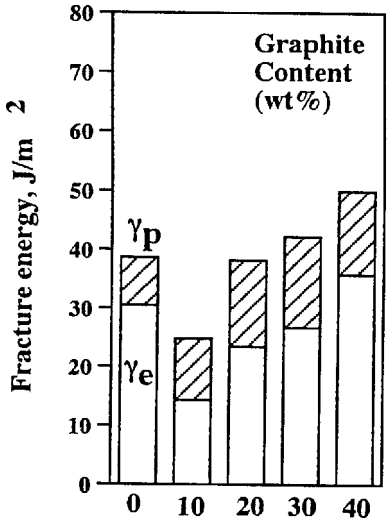

Figure 5 Fracture energy for HCP with graphite powder

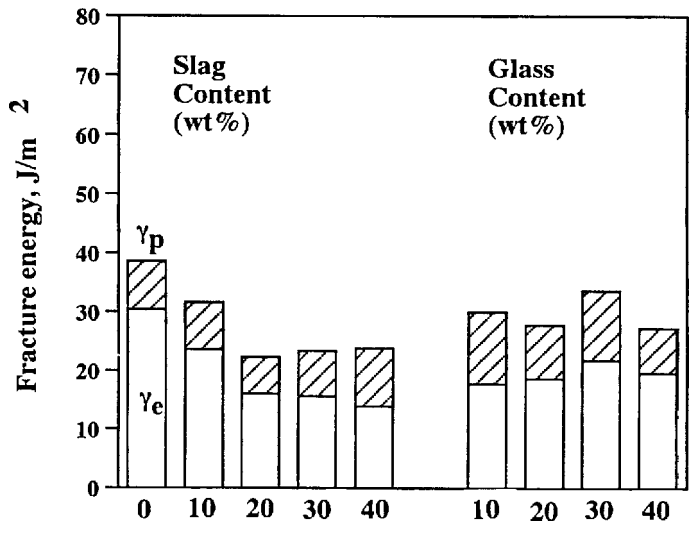

Figure 6 Fracture enegy for HCP with glass or slag powder

Effect of kind of powder on fracture behavior

Fracture energy of HCP containing reactive powder, glass powder or blast furnace slag, are shown in **Fig 6**. In the HCP containing glass powder, which reacted with cement in the same manner as blast furnace slag, a low γ_e was observed independent of mixed content. The lower Ca/Si molar ratio in C-S-H resulted in changes of the morphology and microstructure of C-S-H. Suzuki et al (1988) synthesized the various Ca/Si molar ratio of C-S-H by sol-gel method. The low-lime C-S-H had ill-crystalline phase and spherical shape, similar to silica gel. These chemical and crystalline change of C-S-H decreased the resistance to crack propagation. The friction among projected particles and grain bridging at the fracture surface are also important in discussing fracture behavior in HCP. High plastic energy dissipation γ_p was observed independent of kind of addition. Large unreacted particles remaining in HCP, independent of kind of powder, promote resistance to crack propagation to exhibit plastic behavior after the maximum load point in the P-u curve. Higher bending and compressive strength but lower fracture toughness were observed in HCP containing reactive powder due to the cementitious strength than those in HCP containing non-reactive powder. The formation of dense hydrates and a few large cracks at interface of powder can not disperse or consume the fracture energy of crack propagation at the crack tip.

Effect of curing time on fracture behavior

Fracture energy in HCP containing glass powder with curing time is shown in **Fig 7**. Elastic fracture energy γ_e in HCP containing glass powder showed double as much as that in monolithic HCP cured for1 month. The γ_e in HCP containing glass powder decreased with curing time, but that in monolithic HCP increased. The Ca/Si molar ratio in HCP did not change remarkably independent of curing time (Nishikawa et al, 1994). The formation of lower Ca/Si molar ratio C-S-H or calcium hydroxide with different morphology, and change of cement strength with time must be considered. However, total fracture energy did not decrease due to the increase of plastic energy dissipation. Therefore, fracture toughness did not drastically decrease with curing time, maintaining the high bending and compressive strength.

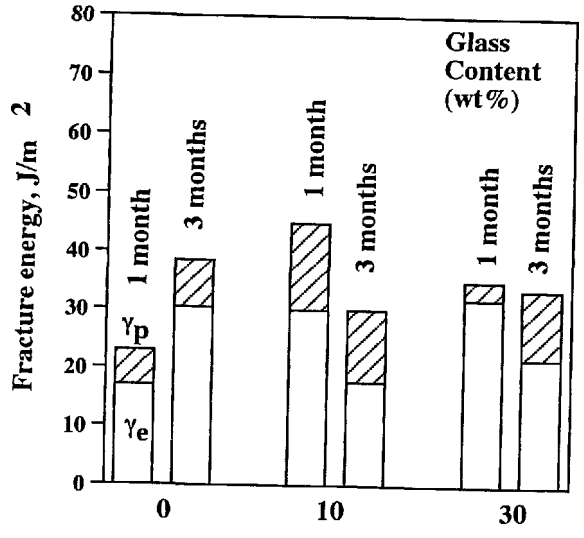

Figure 7 Fracture energy for blended HCP with curing time

Effect of particle size on fracture behavior

Fracture enegy in HCP containing large glass powder and sand (average particle size of 200 μm) after curing of 1 or 6 months were shown in **Fig 8**. Large particles in the cement matrix increased the fracture energy or fracture toughness at early hydration, but decreased the bending strength. In particular, thios increase of fracture energy was observed for HCP with

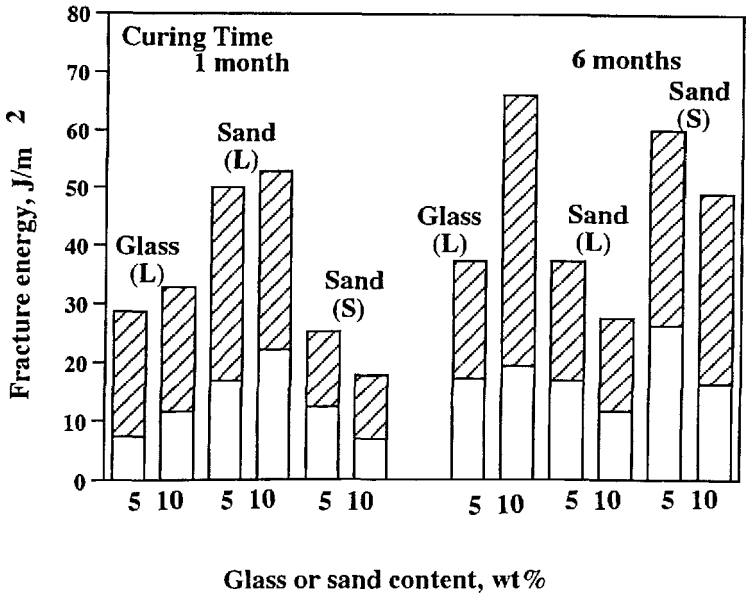

Figure 8 Fracture energy for blended HCP with particle size of powder

good quality sand. The large critical crack might grow along the interface between particle and cement paste. These cracks obstruct the propagation of main crack. After enough curing time, bending strength increased with slight decrease of fracture energy. While, for the HCP with reactive glass powder, this fracture behavior was not remarkable. Hydration of cement was promoted by the alkaline ions dissolved. The crack length grown along the interface might be small. These cracks do not become fracture origin.

Relationship between mechanical properties and fracture energy

For discussing the mechanical properties of HCP by fracture mechanics, tensile strength has been employed. Calculated tensile strength in HCP is shown in **Fig 9**, with their fracture energy. In Fig 9, the experimental data in HCP cured for 1 months are shown as square marks. Circle marks correspond to the HCP cured above 3 months. Closed and opened marks are the HCP with reactive powder and with non-reactive powder, respectively.

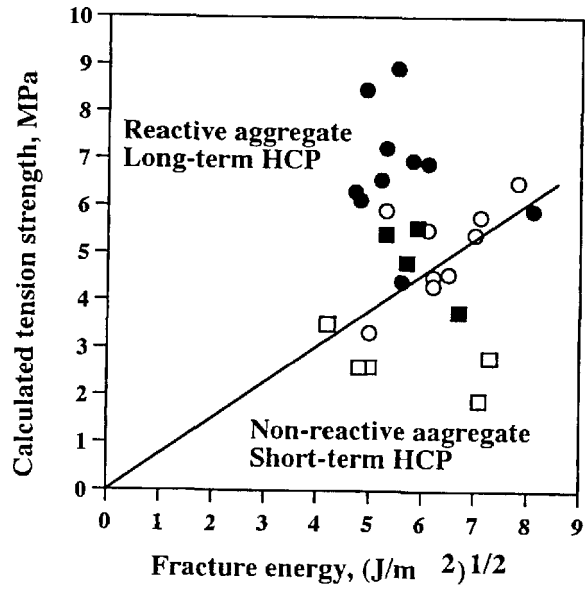

Figure 9 Calculated tensile strength for HCP with their fracture energy

Fracture in bending test is classified to mode I by fracture mechanics. Therefore, the tensile strength calculated from bending strength and fracture energy are formularized as Griffith equation, $\sigma_f=(\gamma_{WOF}E/\pi c)^{1/2}$. Here, σ_f is fracture strength, which corresponded to calculated tensile strength in this experiment. The E is Young's modulus and c is critical crack length at fracture. Fracturetoughness was in propotion to $(\gamma_{WOF})^{1/2}$. The linear relationship between σ_f and $(\gamma_{WOF})^{1/2}$ was observed in HCP containing graphite or in monolithic HCP. The similar relationship was also observed in HCP, which contained reactive powder cured for 1 month. If Young's modulus of HCP is constant independent of blended content and curing time (Glucklich et al., 1975), the slope in Fig 9 shows the critical crack length at fracture. The gentle slope corresponds to the large crack length. In particular, the existence of large crack was estimated for the HCP with large sand, curing for only 1 month. Large initial crack grew unstable along the interface between large sand particle and cement paste, which was proposed by Wittmann (1981). Adsorbed water on powder might also accelerate the peeling of hydrates. The critical crack length became small with curing time for HCP containing reactive powder. For HCP cured long time, the microcracks or capillary pore in C-S-H is considered to be fracture origin instead of interface of powder. Chemical and morphological difference of C-S-H formed in HCP has effect on the size of microcrack, which will become fracture origin. Compressive strength was important as structural materials. However, fracture in compressive test is classified to mode II (Davies,1987). Compressive strength could not be estimated from

the fracture energy, but a slight difference related to reactive and non-reactive powder was observed. For this fracture, frictional coefficient at fracture surface was considered besides the shear stress. The former may have relation to size and cementitious properties of powder.

CONCLUSIONS

Various powder materials have been blended up to 40 wt%, to improve its mechanical and chemical properties of hardened cement pastes (HCP). Fracture energy and bending strength of HCP were measured and discussed in relation to microstructure and hydrates formed. An improvement in fracture toughness and plastic fracture behavior were observed for HCP having non-reacted powder. Reactive powder, blastfurnace slag or glass waste, decreased the Ca/Si molar ratio of C-S-H to decrease fracture toughness. The critical crack length at fracture in HCP could be estimated from their bending strength and fracture energy.

REFERENCES

Beaudoin, J.J. And Feldman, R.F., "High-Strength Cement Pastes - A Critical Appraisal", Cement & Concrete Res., Vol.15, 1985, pp.105-116.

Cotterell, B. and Mai Y-W.,"Crack Growth Resistance Curve and Size Effect in the Fracture of Cement Paste", J. Mater. Sci., Vol.22, 1987, pp.2734-2738.

Davies, D.G.S., "The Statistical Approach to Engineering Design in Ceramics", Proc. Brit. Ceram. Soc., Vol22, 1973, pp.429-452.

Davies, J., "Fracture Behaviour of Mortar in Shear-Conpression Field", J. Mater. Sci., Vol.6, 1987,pp.879-881.

Glucklich, J. And Korin, U.,"Effect of Moisture Content on Strength and Strain Energy Release Rate of Cement Mortar", J. Am.Ceram.Soc., Vol.58, 1975, pp.517-521.

Griffith, A.A., "The Phenomena of Rapture and Flow in Solids", Vol.221A, 1920, pp.163-198.

Hillemeir, B. And Hilsdorf, H.K., "Fracture mechanics Studies on Concrete Compounds", Cement & Concrete Res., Vol.7, 1977, pp.523-536.

Jennings, H.M., "Design of High Strength Cement Based Materials:", Mater. Sci. & Tech., Vol.4, 1988, pp.277-300.

Nishikawa, T. And Suzuki, K., "Chemical conversion of C-S-H in Concrete", Cement & Concrete Res., Vol.24, 1994, pp.176-182.

Nishikawa, T., Takatsu, M. and Daimon, M., "Fracture Behavior of Hardened Cement paste Incorporating Mineral Additions", Cement & Concrete Res., Vol.25, 1995, pp.1218-1224.

Sakai, M., Goto, Y. and Inagaki, M., "Fracture Toughness of Graphite materials", Yogyo-Kyoukai-Shi, Vol.94, 1986, pp.153-158.

Suzuki, K., Nishikawa, T., Ikenaga, H. and Ito, S., "Effect of NaCl or NaOH on the Formation of C-S-H", Cement & Concrete Res., Vol.16, 1986, pp.333-340.

Suzuki, K., Nishikawa, T. and Ito, S., "Characterization of Low-Lime C-S-H", CAJ Proc. Of Cement Concrete, Vol.42, 1988, pp.36-39.

Uchikawa, H., Uchida S., "The Analysis of Ettringite in Hardened Cement Paste", Cement & Concrete Res., Vol.4, 1974, pp.821-834.

Wittmann, F.H., "Mechanisms and Mechanics of Fracture of Concrete", Adv. in Fracture Res., Vol.4, 1981, pp.1467-1487.

RESEARCH ON A NEW TYPE OF COMPOSITE CEMENT

ZHANG Xiong, WU Keru, HAN Jihong, State Key Laboratory of Concrete Materials Research, Tongji University, Shanghai, China

ABSTRACT The paper deals with the preparing technique of a new type of low energy -consumption composite cement by mixing fly ash and blastfurnance slag with composite activator and then grinding. The physical and mechanical properties of the composite cement meet the requirements of 525# quality grading (GB). Low hydration heat, micro -expansion and high long-term strength are its virtues . Concrete with high strength and excellent durability can be prepared by using it.

Key-words : Composite cement , Blast-furnace slag , Fly ash

INTRODUCTION

Fly ash and slag are different kinds of active blends with different hydration mechanism and rate. Compared with those prepared by single blend, the cementing materials prepared by mixing fly ash and slag with suitable activation exhibits "blends composite effect". Thus the composite cement with both fly ash and slag can be prepared.

EXPERIMENTS

The chemical composition of fly ash , slag and composite activator are listed in Table 1. The samples' fineness is controlled in the range of 360-380 m^2/kg and the proportion of samples Xn (n=0, 1, 2 . . 8) are shown in Table 2.

Table 1 Chemical Compositions of Raw Materials

Raw materials	Chemical composition (%)						
	Fe_2O_3	Al_2O_3	CaO	MgO	SiO_2	SO_3	Loss
Fly ash	6.24	30.36	3.25	0.16	47.07	—	8.65
Blastfunace slag	1.96	13.8	40.11	8.02	32.04	—	—
Composite activator	2.10	13.34	21.74	0.63	32.20	26.23	7.49

The physical and mechanical properties of the composite cement X4 such as compressive strength, setting time, soundness, fineness and expansion are tested. Strength, freeze resistance and carbonization of concrete prepared by using X4 are determined. Mix propotion of the concrete is as follows :

Cement (X4) :	Sand (Mx=2.8):	Gravel (5-25mm):	Water	Slump (cm)
1	1.46	2.97	0.48	13

Hydration heat evolution rate of X4 is measured by hydration heat of calorimeter. The hydration products and morphology are observed by SEM, XRD and DTA etc. The hydration degree of various ages is measured by water of combination test.

Table 2 Proportion and strength of samples

sample	Proportion (%)			Compresive strength (MPa)		
	Slag	Fly ash	Activator	3d	7d	28d
X0	75	0	25	22.6	33.3	56.8
X1	60	15	25	18.5	31.5	56.0
X3	45	30	25	18.1	31.1	66.0
X4	40	35	25	19.7	33.9	67.2
X5	30	45	25	17.0	24.0	60.7
X6	25	50	25	15.7	21.4	55.0
X7	15	60	25	16.0	22.4	56.o
X8	0	70	25	12.4	12.8	25.0

RESULTS AND DISCUSSIONS

The composite effect of fly ash and slag

The proportion between fly ash and slag is selected as main technical parameters of the composite cement. Table 2 shows the compressive strengthes of 3d, 7d and 28d of samples Xn (n=0, 1, 2. . 8) in different proportion of fly ash and slag. It indicates that the hydraulic activity of slag is higher than that of fly ash. Cement with single blend of fly ash has lower compressive strength at all ages. But with the increasing of slag content the strengthes of various ages are increased obviously. When the ratio between slag and fly ash (slag / fly ash) is in 1- 2. 5 the compressive strength of the composite cement reaches maximum . If the ratio exceeds 1% till only single slag the strengths of 3d and 7d changes a little but those of 28d drop markedly and generally 10 MPa lower than those in the optimum range. Thus the optimum proportion between fly ash and slag of composite cement is in the range of 1-2. 5. Within this range there exists a "blends composite effect".

Properties of the Cement and Concrete

The physical and mechanical properties of composite cement X4 are listed in Tables 3 and 4. Table 3 shows that composite cement possesses fine physical and mechanical properties . The strength develops slowly in early period but later increases rapidly and keeps on developing in long-term. Compared with 28d strength of 69.4 MPa , 3d, 7d and 14d separately reach to 13.4% 38.8% and 70.5% . Meanwhile flexural strength is also high with 9.9 MPa of 28d and expansive property is small and stable with expansion ratio of 28d nearly the same as that of 90d (Table 4). The physical and mechanical properties of concrete made from the composite cement are tested and showed in Tables 5 and 6.

Table 3 Physical and Mechanical Properties of the Composite Cement

Soundness Setting time (Ini. / Fin. Consistancy (%)	qualified 1: 31 / 3: 53 28.25					
Strength (MPa)	3d	7d	14d	21d	28d	180d
Flexural strength Compressive strength	1.6 9.3	4.7 26.9	6.9 48.9	8.4 57.0	9.9 69.4	10.4 74.5

Table 4 . Data of Expansion Ratio of Composite Cement

Sample	Expansion ratio (%)							Remark
X4	1d	2d	4d	7d	14d	28d	90d	specimen size 3x3x28 cm cement/sand=1/3
	0.014	0.039	0.046	0.042	0.046	0.046	0.045	

Table 5 Mechanical Properties of Concrete made from the Composite Cement

Compressive strength (MPa)	53.4
Tension splitting strength (MPa)	3.88
Flexural strength (MPa):	6.62

Table 6 Durability of the Concrete

Sample	Freezing resistance		Depth of carbonization (mm)				Impermeability
	loss of wt	Loss of Rc	3d	7d	14d	28d	(MPa)
X4	1.5 %	14.3 %	4.5	6.0	6.7	7.5	> 1.1

It can be seen that the composite cement can be used to prepare concrete with stength higher than 50 MPa and with all other mechnical properties nearly the same as the ordinary concrete of equivalent strength grading (Table 5). In the eye of durability (Table 5), the concrete with composite cement has satisfactory impermeability and freezing resistance but lower carbonization resistance, which can also meet the demands of construction engineering.

Hydration of Composite Cement

The curve of hydration heat evolution of the composite cement demonstrates that the

early hydration rate of composite cement is relatively low and the hydration heat at 1d is 144.6 J/g. The result of bond water (Table 7) shows that hydration degree of the cement of 3d is only 29.3% but that of 7d increases rapidly to 45.8% and that of 28d comes to 48.9% accounting for its strength development trend above-mentioned .

Table 7 Data of Bond Water and Hydration Degree

Sample	Bond water (%)					Hydration degree (%)			
	1d	3d	7d	28d	fully hydrated	1d	3d	7d	28d
X4	2.9	4.6	7.2	7.7	15.7	18.7	29.3	45.8	48.9

XRD diagrams of the composite cement at various ages indicate that hydration products in early period are AFt and $Al(OH)_3$. No characteristic peak of $Ca(OH)_2$ could be found in in XRD diagrams and DTA curve. The hydration process of the composite cement could be summarized as follows : shortly after composite cement mixed with water, Ca^{2+} dissolves quickly from the composite activator into water, forming the base liquid phase, and then dissolve SO_4^{2-}, Al^{3+} and Si^{4+} in proper order . When the concentrations of Si^{4+}, Al^{3+} and Ca^{2+} exceed the solubility of AFt, needle like AFt are deposited from the liquid phase. Then slag and fly ash commence hydrating in the base medium and sulphate, forming C-S-H gel and AFt. In the initial hydration process, the hydration activity of slag is much bigger than fly ash and the essential Ca^{2+} for forming AFT and C-S-H are offered mainly by slag but not by fly ash or activator, which contain fewer Ca^{2+}, so the early hydration products are mainly formed by slag while fly ash takes only micro-filler effect. Because of the lower hydration degree of slag , the amount of AFt and C-S-H are limited and the early strength is low. On the other hand, with more Al^{3+} and Si^{4-} dissolving from activitor into liquid phase , more $Al(OH)_3$ gel of high activity can be formed. Because of filling in the frame of cement paste, they can with the help of dissolving SO_4^{2-} stimulate the release of Ca^{2+} from slag, decrease the stability of slag glass network and improve the hydration degree of slag up to 45% at 7d. Moreover the hydration activity of fly ash is also increased, its hydration products intensify the density of the interface of fly ash and cement paste, leading to the densification of cement paste. So the later strength of composite cement is increased remarkablly.

CONCLUSIONS

1. The composite cements of GB525# grade could be prepared by mixing fly ash and slag with composite activator, which have fine physical and mechanical properties. The main technical parameter is slag/fly ash = 1 - 2.5 .

2. The composite cement has the properties of low hydration heat, micro- expansion and high later strength, Concrete with high strength and excellent durability is able to be prepared by using the composite cement. The results of microstructure experiments show that the main hydration products are AFt, hydrated calcium alminate, C- S- H and $Al(OH)_3$ gels.

3ii123
5 pp

UTILIZATION OF SEWAGE SLUDGE AS A RAW MATERIAL FOR PRODUCTION OF POZZOLANIC MATERIAL

Gilson Morales, PhD
Civil Engineer and Professor
STATE UNIVERSITY OF LONDRINA
University Campus - CTU - Department of Civil Construction
86051-990 LONDRINA / PARANÁ / BRAZIL

ABSTRACT

The sewage sludge is a residue deriving from the aerobic or anaerobic digestion in the purification plants. The utilization of this sewage sludge is restricted and, in many cities, it's simply cast on the solo as a sanitary embankment or as an organic fertilizer for agriculture. Meantime, these utilizations aren't very interesting for large cities because the large distances to the utilization place. In function of its chemical composition it's advisable to study the possibility of its utilization for production of pozzolanic material through the calcination process.

First of all, the sewage sludge needs to be dried, by centrifugation or other similar mechanism, then it's calcined under oxidant atmosphere about 750°C. After the calcination the ashes are grounded until the specific surface area about 800 m^2/kg. Their pozzolanic activity is determined by consumption of lime measured in milligrame for gramme of pozzolanic material.

It was verified that the sewage sludge presents pozzolanic activity when calcined above 500°C. The tests show that the ideal temperature for calcination is about 750°C and that garantees the adequate treatment of the present montmorillonite in this material, avoiding the possibility of expansion in the concrete. The sewage sludge presents pics of quartz and absence of diffuse band in the X-Ray Diagram, before and after the calcination. It shows the inexistence of the glass-phase or amorphous silica in this material. It shows that the pozzolanic activity is due of the montmorillonite presence. The ratios of ashes additionned in the concrete were: 15, 25 and 35% by weight of cement Portland and it was verified significant results on the compressive strenght and on the resistance of chlorides and sulphates attack. The fixation rate of lime by Modified Capelle Essay was about 600 mg/g of pozzolanic material showing an excellent performance of these ashes like pozzolana.

1. INTRODUCTION

The purification of the sewage sludge in the purification plants produces a lot of volum of solid residue which is simply cast on the peripheric cities places. This shows that it's urgent to meet a solution for this problem and we think that we have an excellent raw material for production of pozzolanic material in function of the chemical composition of the sewage sludge.

2. GENERAL CONSIDERATIONS

2.1. Calcination Process

The mineral clays need to be calcinated for to present satisfactories pozzolanic properties. However, the experience has showed that some calcinated clays present an excellent performance like pozzolanic materials.

2.2. Grinding Process

The specific surface area is very important for a good performance of the pozzolanic materials because they offer an appropriate place for the precipitation of the hydrated compounds of the paste of cement.

In first moment the specific surface area is fundamental to the pozzolanic activity and after others factors, like the presence of reactive silica and aluminium.

2.3. Pozzolanic Activity

With respect to the performance of the ashes like pozzolanic materials, the experience shows that its small particles present the maximization of the appropriate places for the precipitation of the hydrated compounds of the paste.
The development of the hydration of the cement results in the augmentation of the C - S - H and as a result of the presence of the pozzolanic materials, between others results, is the elevation of the mechanic resistance.

As more lime will be liberate for the paste, more C - S - H will be maden. Summarizing these comments, this consumption of lime by the pozzolanic materials characterize their pozzolanic activity.

2.4. The Sewage Sludge

The sewage sludge is a solid residue from the purification process of the sanitary sewer after the separation of the solid and liquid phases and still after the aerobic or anaerobic digestion of the solid fraction.

3. PRODUCTION METHODOLOGY

3.1. Drying Process

The usual drying process utilized in Brazil is the deposition of the sewage sludge in plane surfaces denominade "drying beds" whish have been an option that demand a minimum of investment costs. The "drying bed" is a very large basin with a small profoundity and having a permeable surface. The sewage sludge humidity is generally about 70 to 75%. It shows that is possible to calcine the sewage sludge immediately after its remotion of the "drying bed".

3.2 Thermic Activation

The sewage sludge is calcined under oxidant atmosphere and in temperature about 750°C because this temperature possibilitates the occurrence of the structural disorder in the crystalline structure of the material calcined. It was verified that the loss ignition is constant up to 600°C.
The samples were calcined staying in the furnace about three differents residence times. The effect of the residence time about the reduction of the original mass is showed in Table 1.

TEMPERATURE OF CALCINATION	MASS REDUCTION (%) RESIDENCE TIME (minutes)		
(°C)	30	60	90
600	17,62	20,31	20,55
650	19,18	21,39	23,56
680	17,79	21,60	22,43
730	18,48	19,18	18,95
790	20,09	21,61	21,68
980	23,21	22,34	22,01

TABLE 1 . Effect of the residence time in the reduction of the original mass of sewage sludge.

3.3. Mechanic Activation

The mechanic activation of the calcined sewage sludge by grinding promoves the mineralogical species separation and the elevation of the specific surface area about 800 m^2/kg.
The grinding systems more utilized were the ball mills and the disc mills.

4. SEWAGE SLUDGE ASHES

4.1. Physical and Chemical Analysis

The ashes presented specific mass by Blaine Test about 2,78 g/cm^3 and aparent mass about 0,75 g/cm^3. Table 2 shows the results of the chemical analysis of the ashes obtained from the calcination of the sewage sludge.

COMPOUNDS	PRESENCE IN %
SiO_2	41,20
Fe_2O_3	15,00
Al_2O_3	22,70
CaO	4,92
MgO	2,42
Na_2O	0,05
K_2O	0,28
SO_3	0,99
S^{2-}	0,35
Loss ignition	12,50
Equivalent alcaline (in Na_2O) (*)	0,23

(*) = % Na_2O + 0,658 (% K_2O)

TABLE 2. Chemical Analysis of the Ashes from Calcined Sewage Sludge

4.2. Diferential Thermic Analysis (DTA)

It was verified a very big endothermic peak at about 110°C possibily from the dehydration of the sodic montmorillonite. The DTA Diagram shows an endothermic peak at about 150°C from the dehydration. It was verified an exothermic peak at about 250 to 300°C possibily from the combustion of the organic material. It was verified an exothermic peak at about 300°C from the occurrence of organic material. At about 480°C it was verified an exothermic peak from the presence of sulfid or carbon. The occurrence of endothermic peaks at about 500 and 750°C amplify the possibility of the presence of montmorillonite. At about 550°C it was verified an endothermic peak from the loss of hydroxiles of the smectite. It was refused the possibilitiy of the occurrence of caulinite because in the Diagram of X-Ray Diffraction it was absent its maximum peak, (d=1,48). At about 750°C it was verified an exothermic peak from the graphite and at about 990°C it was verified an exothermic peak possibily from the recrystallization of the microscopical structure.

4.3. Thermogravimetry

The thermogravimetry analysis of the sewage sludge shows a very considerable loss of mass at about 270°C and a total loss of mass was verified at about 700°C.

4.4. Pozzolanic Activity Analysis

The minimum fixation rate of the lime by the pozzolanic material is 300 mg/g of pozzolanic material. For this analysis It was adopted the "Modified Chapelle Essay" which verified the consumption rate of lime by the pozzolanic material. Table 3 shows the results from these tests.

TEMPERATURE OF CALCINATION (°C)	CALCINATION TIME (horas)	SAMPLE	RESULTS MODIFIED CHAPELLE (mgCaO/g)
600	1:00	01	657,32
	2:00	02	685,32
700	1:00	03	732,92
	2:00	04	655,92
800	1:00	05	710,52
	2:00	06	685,32

TABLE 3. Results of Modified Chapelle Tests with Ashes from Calcined Sewage Sludge

4.5. X-Ray Diffraction

The results of the X-Ray Diffraction obtained with samples of ashes for about two years show a constancy in the diagrams which had the same pics. It shows a constant mineralogical composition and it was verified that the more evident pics present are from the quartz. The most important aspects verified in these tests were the absence of diffuse band on the X-Ray Diagram, before and after the calcination, showing that don't exist the glass-phase, or amorphous silica, in these ashes. The peaks at d=7, d=10 and d=12 Å are correspondent to clays and they disappear after the treatment for destruction of organic material and carbonate, probabily in function of the acid pH verified when is eliminated the carbonates. The disappearance of the clays peaks after the destruction of the organic material with H_2O_2 shows that is an organic mineral complex, probabily with the presence of montmorillonite. It justify the occurrence of pozzolanic activity althrough the absence of the amorphous silica.

4.6. Eletronic Microscopy

The sewage sludge calcined about 600°C during two hours shows, with amplifying of 3.000 times, two areas with different compositions: one presenting hexagonal plates with occurrence of calcium and potassium and other presenting spheric grains. With amplifying about 7.000 times it was verified very big hexagonal plates with occurrence of potassium from muscovite mica. It was still detected split plan that can be from the montmorillonite and a very porose structure.

5. CONCLUSIONS

The ash obtained presents a good performance like pozzolana and the results show that the process is technically viable. The cost of production equivale to the cost of the calcination of clays. The ratios of ashes additionned in the concrete were: 15, 25 and 35%about the cement weight and it was verified significant results in the compressive strenght and a good performance in presence of chlorides and sulphates attacks.
An important remark is the possibility to reduce the cost of production utilizing the own sewage sludge like a combustible because its high calorific power is about 3.000 kcal.
The next step will be a work to study the performance of ashes from calcined sewage sludge containning elevated levels of heavy metals.

6. BIBLIOGRAPHY

(01) KIHARA, Y. & SHUKUZAWA, J. K., "Contribuição ao Estudo de Pozolanas no Brasil", Publicação Técnica da ABCP-Associação Brasileira de Cimento Portland, São Paulo.

(02) LEA, F. M., "The Chemistry of pozzolans", Proceedings, Symposium on the Chemistry of Cement, Stockholm, 1938.

(03) MASSAZZA, F. "Chemistry of Pozzolanic Additions and Mixed Cements", International Congress on the Chemistry of Cement - 6th, Moscow, V.3, 1974.

(04) CARRASQUILLO, R. L. & TIKALSKI, P. J., "Fly Ash Evaluation and Selection for Use in Sulfate-Resistant Concrete", ACI Materials Journal, Nov.-Dec. 1993.

(05) MEHTA, P. K. & PIRTZ , D., "Use of Rice Hull Ash to Reduce Temperature in High-strength Mass Concrete", ACI Materials Journal, Feb. 1978.

(06) SANTOS, P. S., "Ciência e Tecnologia de Argilas", V.1, Edgard Blücher Ltda., São Paulo, 1989, 408p.

(07) THOMAS, M. D. A. & MATTHEWS, J. D., "Performance of Fly Ash Concrete in U. K. Structures", ACI Materials Journal, Nov.-Dec.1993, pp.586-593.

(08) XU, A. et alii, "Effect of Fly Ash on the Microstructure of Cement Mortar", Materials and Structures, V.26, No.161, 1993, pp.414-424.

(09) VON EUW, M., "Ciments contenant des Additions Minerales", International Congress on the Chemistry of Cement, 8th, V.4, Rio de Janeiro, 1986.

(10) MEHTA, P. K., "Concrete - Structure, Propierties and Materials", 1st.ed., Englewood liffis, Prentice - Hall Inc., 1986.

(11) BOMBLED, J. P., "Différents Moyens d'activation des matériaux potentiellement pouzzolaniques. Application aux Liants Chaux-Pouzzolane", International Congress on the Chemistry of Cement, 7th, V.4, Paris, 1980.

(12) LARGENT, R., "Estimation de l'Activité Pouzzolanique:Recherche d'un Essai", These de Doctorat, Université de Paris VI, Paris, 1975.

(13) MASSAZZA, F., "Structure of Pozzolan and Fly Ash and the Hydration of Pozzolanic and Fly Ash Cements", Int. Congress on the Chemistry of Cement, 7th, V.4, Paris, 1980.

(14) PERA, J. et alii, "Ciments à base de Latérites Thermiquement Activées. Rôle des Oxydes de Fer dansle Développement des Résistances Mécaniques", International Congress on the Chemistry of Cement, 8th, V.4, Rio de Janeiro, 1986.

(15) MORTUREUX, B. et alii, "Comparaison de la Réactivité de Différentes Pouzzolanes", International Congress on the Chemistry of Cement, 7th, V.3, Paris,1980.

(16) MALHOTRA, V. M., "Mechanical Properties of Concrete Incorporating High Volumes of Fly Ash from Sources in the U.S.", ACI Materials Journal, V.90, No.6, Nov.-Dec.1993.

(17) RAVERDY, M. et alii, "Appréciation de l'Activité Pouzzolanique des Constituants Secondaires", International Congress on the Chemistry of Cement, 7th, V.3, Paris, 1980.

(18) MORALES, G., "Caracterização do Agregado Leve Obtido a Partir do Lodo de Esgoto da Cidade de Londrina", Dissertação de Mestrado, EPUSP, São Paulo, 1989.

UTILIZATION OF STORED CEMENT, PART II: THE BLENDING OF STORED CEMENT BY FRESH CEMENT

ABEDEL-REHEEM. A . H , SHATER. M.A, AL-ALM RASHED.I.,GAR, EL-AFIFY.A.N

ABSTRACT: A suitable method, has been studed to improve the strength of stored cement, which may lose a percent of its strength during storage. This method includes the replacement of a part of stored cement by fresh cement. As the replacement ratio by fresh cement increases the strength of the stored cement is improved. The percent of improvement depends mainly on the storage conditions and on the age of storage.
Key words: Wast cement utilization,Strength fit, Reactivity,Long age of storage, Economy,

INRTODUCTION:

During the storage of cement, the storage conditions may cause the cement properties to deteriorate as the age of storage increses. The scope of this work is to find a suitable method to utilize stored cement. Prehydration may take place during cement storage. And as a result syngenite and ettrigite are formed, these products may cause false set and strength decline (El-Afify, 1994, Hunsen, 1954, and Hogan, 1981). So, it is required to reduce the effect of thses products on the strength development. The blending of cement with any material has a cementitious properties may reduce the effect of the prehydration products. ACI, (225R-91) reported that, the over all chemistry of blended cement is similar to that of portland cement. The blending ingredients contain the same major elements as portland cement, i,e. calium, granulated blast furnace slag, fly ashes and natural pozzolans. Many works have been carried out to use fly ash and slags as ingredient in blended cement for economy and to improve the strength of the concrete used for a certain application, such as the work of Hogan, and Meusel (1981). So, the method used in this work depends on the blending of stored cement by fresh cement to improve its strength (El-Afify 1994).

EXPERIMENTAL WORK

CASES OF STORAGE

a- Case I: The cement bags were stored inside the laboratory, they were placed over a woden base and covered with a tent cover. The average temperature inside the laboratory was 25°C. This case represents good storage conditions in the Egyptian sites.
b- Case II: The cement bags were placed in the open air over a wooden base without any cover. The cement bags were exposed directly to high humidity (rains and water vapour) and temperature.
The maximum temperature was about 40°C during summer. While the minimum was about 5°C in winter. This case represents bad storage conditions in the Egyptian sites.

STORES CEMENT SAMPLES

Storage compared in Table 1 includes the ages of storage that will be tested for both cases of with specification limit and the original values of the fresh cement. The method of maximum density of aggregate was used to design the proportions of concrete mix tested in this investigation. The mix proportions are (1:4.1:1.44) of cement: gravel: sand and w/c = 0.45

Table (1) The Compressive Strength of The Stored cement for (case I and II) At Differerent Ages For The Mortar And Concrete

compressive strength in kg/cm^2	compressive strength in kg/cm^2							
	case I			case II			limits	
	6	8	10	2	4	6	E.S.S. 373	fresh cement
1- mortar								
a- 3 days	195	164	160	177	137	110	180	250
b- 7 days	250	220	217	250	210	160	275	300
c- 28 days	312	275	260	300	275	260	---	395
2- concrete								
a- 7 days	245	203	195	230	185	174	---	280
b- 28 days	295	270	265	280	270	260	---	342

EXPERIMENTAL PROGRAM

The work is mainly designed to study the effect of blending the stored cement by fresh cement on the compressive strength. The study included samples from the two cases of storage (I,II). The program is mainly divided for two parts, the first part includes the tests of mortar specimens after 3,7 and 28 days. The second part includes the tests of concrete specimens after 7 and 28 days. The ratios of this work are chosen from 15% to 60% cover a wide range of study, and also to achieve the best utilization of stored cement.

RESULTS

THE COMPRESSIVE STRENGTH OF MORTAR

a-Case I

1- The results of 6 months stored cement indicate that the compressive strength after 3 and 7 days are nearly identical with that of fresh cement, about 98% from the original value, at a replacement ratio 60%. The results of the strength after 28 days show that, the percent of increase in the strength is less than that after 7 days. This result is acceptable, because the prehydration products may affect the strangth after 28 days more than that after 7 days.

2- The results of 8 and 10 months storage indicate that, the percent of increase in the strength after 7 days is more than that after 3 days. This result may be attributed to the effect of blending by fresh cement, which may increase the rate of hydration after 7 days more than that after 3 days. On the other hand, the percent of increase in the strength after 28 days is less than that at early after 28 days for 10 months is less than that of 6 months. So, it can be stated that, as the age of storage increases the formation of the prehydration products may reduct the effect of blending by fresh cement on the strength development after 28 days.

b- Case II

1- The results of 2 months storage, to some extent, give the same behavior of case I (6 months). But the effect of the prehydration products on the strength after 28 days is more than that on case I.

2- The results of 4 and 6 months storage indicate that the percent of increase in the strength after 28 days is considerably lower compared with that of case I (8 & 10 months). So, it can be seen that, for the cement which stored in bad storage conditions the formation of the prehydation products reduces the effect of blending by fresh cement after a short period of storage. Also, these result may give a restriction on the use of this method to utilize stored cement in bad storage conditions.

For all the tested samples, it can be seen that, the increase in the strength of mortar at 15 % replacement ranges between 5% -10%. While at 60% replacement, the increase in the strength ranges between 15% - 20%. Also, it can be seen that, a high percentage of increase in the strength is achieved at 15% replacement.

From the previous analysis of the results, it can be concluded that, if the cement does not loose a great percent of its properties during storage, a low replacement ratio (such as 15%) may be sufficient to gain most of its original strength. While cement which lost a great percent of its strength during storage, high ratios of replacements (such as 50%) may ensure that the blending with fresh cement will achieve safe and effective increase in the strength of stored cement.

THE COMPRESSIVE STRENGTH OF CONCRETE

The results of the tests show a significant increase in the strength as the replacement ratio by fresh cement increases. The results of both the two cases of storage can be indicated as following:

a- Case I

The resu;ts tend to have the same behavior of mortar after 7 days. In addition, an important note can be observed, the great value of the increase in the stength is achieved at 15% replacement, then a little change can be found between 15% and 60% replacement. This result may be attributed to the effect of the aggregate content on the concrete mix propertes (singh,1958). So, the aggregate content may reduce the effect of prehydration products on the strength of the concrete mix. And. the percent of increase in the strength after 28 days is more than or nearly equal to that after 7 days.

b- Case II

After 2 and 4 months of storage, most of the increase in the strength is attaind at 30% replacement. Then, a little change can be found between 30% and 60%. The percent of increase in the strength after 28 days is less than or nearly equal to that after 7 days.

For both the two cases (I,II), the percent of increase in the strength of concrete is greater than that of mortar after 28 days. This result may be attributed to, as discussed before, the effect of the aggregate content on the concrete mix properties.

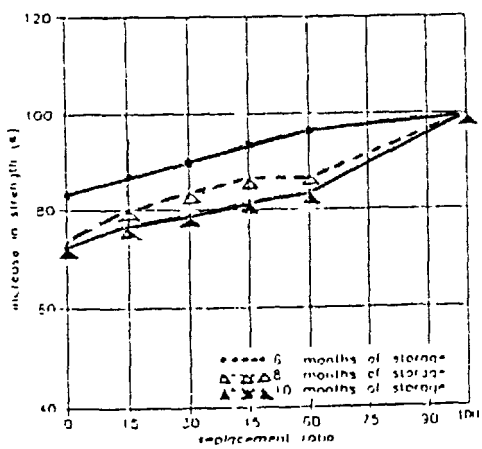

Fig (1) The percent of increase in the strength of 7 days due to blend- concrete (case I) after ing by fresh cement

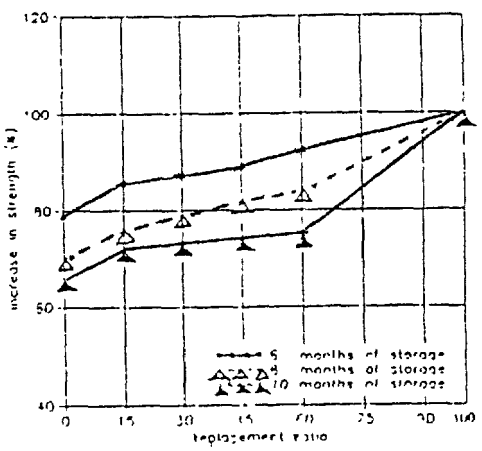

Fig (2) The percent of increase in the strength of concrete (case I) after 28 days due to blend- ing by fresh cement

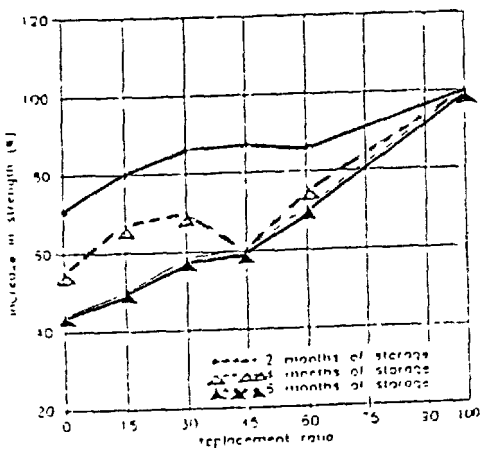

Fig (3) The percent of increase in the strength of mortar (case II) after 3 days due to blending by fresh cement

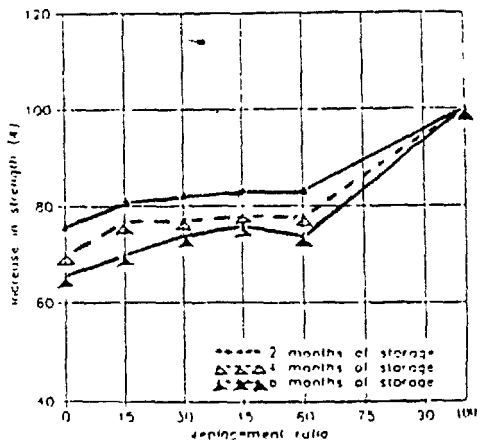

Fig (4) The percent of increase in the strength of concrete (case II) after 28 days due to blending by fresh cement

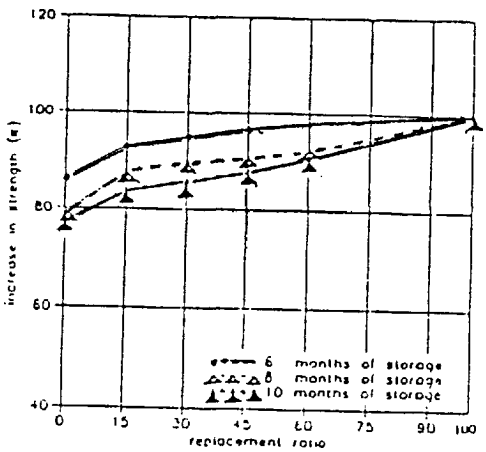

Fig (5) The percent of increase in the strength of concrete (case I) after 28 days due to blending by fresh cement

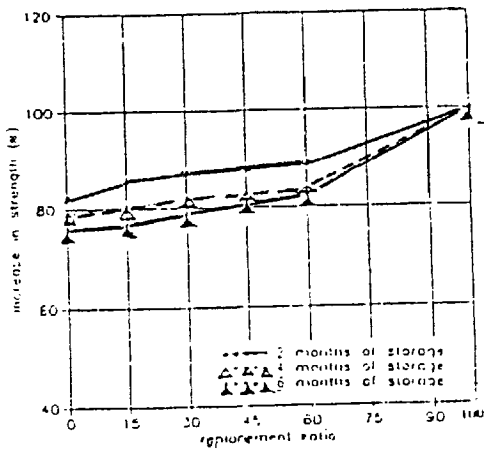

Fig (6) The percent of increase in the strength of concrete (case II) after 28 days due to blending by fresh cement

CONCLUSION

From the previous test results and discussions, the main conclusions can be summarizes as following:

1- The cement which is stored in good storage conditions and still within the specification limits, the blending by fresh cement may be sufficient to gain most of its original strength by blending with fresh cement.
2- The cement which is going to be out of specification and beyond, 50% replacement may ensure the effect of blending by fresh cement on the strength development. Also, the replacement retio by fresh cement must not be less than 30%.
3- In case of mortar, the results of blending stored cement by fresh cement showed that, the replacement ratio by 15% fresh cement may achieve an increase in the strength about (5-10%) of the original strength. while the replacement ratios between (45%-60%) an increase in the strength about (15%-20%) of that of the original strength.
4- In case of concrete, the results of blending by fresh cement showed that a great percent of the increase in the strength is achieved at 15% replacement. Then, a little change can be found between 15% and 60% replacements.

REFERENCES

ACI Committee 225R-91, "Guide to the Selection and Use of Hydraulic Cement".
Abdel-Reheem A.H. Shater. M.A, Gar Al-Alm Rashed, I. Elafify, A.N. "Effect of Storage Conditions on Cement and Concrete'Mix Properties", Military Technival College, Cairo, Second Conference on Civil Engineering. VI,P 54-63, 1994.
El-Afify, A.N. "Utilization of a Long Time Stored Cement in Concrete Mixes", Thesis Is Submitted to Mansoura Universuty, EGYPT, 1994.
Hansen, W.C., "Aeration Cause Flase Set in Protland Cement", ASTM. Proc., 58, (1958), 1044.
Hogan, F.J., and Meusel, J.W., 1981 "Evaluation of a Granulated Blast Furance Slag". Cement Concrete, and aggregates, V.3, No.1, Summer, pp40-52.
Singh. B.G., "Specific Surface of Aggregates Related to Compressive and Flexural Strength of Concrete" , Ptoc. Am. Concr. Jnst., 54, N o.10, 897-907, 1958.
Theisen, K., and Johansen, V., "Prehydration and Strength Development of Cement", Bulletin, American Ceramic Society, V.54, 1975, pp. 787-791.

THEME III

UTILISATION OF ADMIXTURES; WATER REDUCERS, AIR ENTRAINERS, ACCELERATORS, RETARDERS AND POLYMERS

TOPIC III.A

Mechanisms; admixture chemical ↔ cement interaction

EFFECT OF ELECTROSTATIC AND STERIC REPULSIVE FORCE OF ORGANIC ADMIXTURE ON THE DISPERSION OF CEMENT PARTICLES IN FRESH CEMENT PASTE

Hiroshi UCHIKAWA, Shunsuke HANEHARA and Daisuke SAWAKI, Chichibu Onoda Cement Corporation, Japan

ABSTRACT The authors proved for the first time that the existence of steric repulsive force acting on the surface of cement particles adsorbing the organic admixture by measuring the interactive force between surface of cement clinker adsorbing the admixture with an atomic force microscope and measuring the zeta potential of fresh cement paste under actual water to cement ratio by electrokinetic sonic amplitude method. It is also clarified that the rate of contribution of electrostatic and steric repulsive force to the dispersion of cement and hydrated cement particles differs by the kind of organic admixture.

Key-words: Admixture, Superplasticizer, Simulation, Zeta potential, Steric Repulsive Force

INTRODUCTION

The improved fluidity of concrete by adding the organic admixture is considered mainly caused by the dispersion of solid particles by the electrostatic repulsive force due to the increase of the surface potential caused by the admixture adsorbed to the surface of solid particles and by the steric repulsive force based on the interaction between the adsorption layers of admixture (Uchikawa, 1994). The electrostatic repulsive force has been proved by measuring the zeta potential of diluted suspension of cement, while the steric repulsive force is at present only estimated from the current knowledge of surface and organic chemistries and the existence of the steric repulsive force has never been evidenced by experimental determination.

This paper studies the relationship between the electrostatic and steric repulsive forces aiming at acquisition of the basic data for the material design and appropriate application of the organic admixture by proving the existence of the steric repulsive force in the dispersion of solid particles in concrete prepared by adding the organic admixture, and determining the contribution of it according to the types of admixture, and relationship of the contribution with the physical properties.

INTERACTIVE FORCE BETWEEN CEMENT PARTICLES COEXISTING WITH ORGANIC ADMIXTURE

The fluidity of concrete is strongly affected by that of cement paste, which correlates with the repulsive force between the cement particles. The force acting between the cement particles comprises van der Waals force (F_A) and the electrostatic repulsive force (F_{RE}) generated by the electric charge on the surface of particles. It is considered, however, that adding the organic admixture to the cement paste, in addition to those forces, the electrostatic repulsive force is increased by the organic admixture adsorbed to the surface of the cement particles and the steric repulsive force (F_{RS}) is generated from the osmotic pressure for relieving the local increase of density caused by overlapping of the adsorption layers of admixture. According to this idea, the force acting between the cement particles (F) in the coexistence of the organic admixture is represented as follows:

$$F = F_A + F_{RE} + F_{RS} \quad [1]$$

It is known that the force acting between the cement particles depends upon the distance between them, which is related to the interactive energy as illustrated in Fig 1 (Verwey et al., 1948).

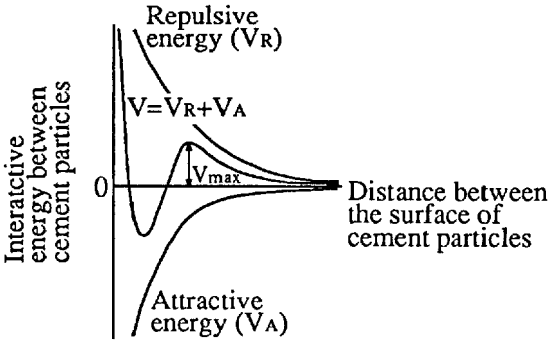

Figure 1 Relationship between distance and interactive energy of cement particles

Let the maximum repulsive energy on the potential

curve equal to Vmax, minimum Vmax required for keeping dispersion is considered to be 15kT (Verwey et al., 1948).

Since the working region of van der Waals force is within 1 nm from the surface of particles (Israelachvili, 1985) and the magnitude of it is approximately 0.5 nN (Israelachvili, 1985) assuming that the diameter of a cement particle is 2μm, it is negligible small compared with the force corresponding to Vmax and the compensated interactive force described later.

SELECTION OF MEASURING METHODS

Force acting between surfaces

Although Surface Force Apparatus (SFA) (Israelachvili et al., 1978) is applicable to measure the interactive force of solid sample, the sample must be transparent and the surfaces of them must be smooth at the molecular level. The sample applied to the method is, therefore, limited to a few kinds of solid.

The atomic force microscope (AFM) is used for measuring very little force acting between the sample and the probe brought close to it to approximately 1 nm (Uchikawa, 1992). The distance between the probe and the sample can be controlled at the accuracy of 0.05 nm with a piezo-electric element. The displacement of a cantilever caused by the force acting between the surfaces is determined at an accuracy of 0.1 nm at least by measuring the intensity of laser beams reflected from the back side of the lever with a position-sensitive photo-detector. The force acting between the surfaces is calculated by multiplying the displacement of cantilever by the spring constant of the lever and the lower limit of the measurement is 10^{-3} nN.

In this study, therefore, AFM was used for measuring the force acting between the solid surfaces since AFM is more easily operated than SFA and does not require so much smooth surface of the sample as that of SFA because the measuring region is as small as an order of μm^2 as well as can use an opaque sample though the measurements of the distance in the curve of the distance between the surfaces versus the force acting between the surfaces (F-D curve) with AFM are not so accurate as those with SFA.

Zeta potential

As mentioned before, one of the dispersion force of cement particles in fresh cement paste is the electrostatic repulsive force which is related to the surface potential of cement particle. Since the surface potential (ϕ_0) of bare particles and the Stern potential (ϕ_s) outside of the Stern layer cannot be measured, the potential on the slipping surface or zeta potential is substituted for the surface potential of the solid in solid-liquid suspension (Fig 2).

The electrophoretic method which has been used so far as a measuring method of zeta potential requires diluted concentration of particles in suspension because the migration speed of dispersed particles to which voltage is applied is directly observed. The streaming potential method is not only unsuitable for practical cement paste with a W/C of 0.5 or less because it requires the concentration of particles of 1vol% or less but also it has shortcomings including poor reproducibility and low accuracy. The zeta potential measured with conventional methods does not necessarily correspond to the fluidities of cement paste and concrete (Massazza et al., 1982).

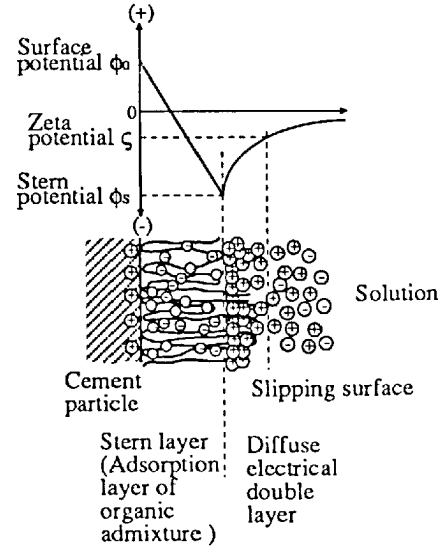

Figure 2 Schematic explanation of interfacial electrical double layer formed on the cement particle adsorbing organic admixture

In this study, therefore, the electrokinetic sonic amplitude method (Babchin et al., 1989) which has recently been developed for measuring zeta potential of cement paste with a practical W/C

as low as 0.3 is used. This method is applied to the measurement of zeta potential in such a way that the electrokinetic sonic amplitude (ESA) value caused by the particles moving between both electrodes by applying alternating voltage with higher frequency than 1 MHz to the charged particles is measured, and calculated according to the following formulas representing the relationship of ESA with dynamic mobility (μd) and zeta potential (ζ) of particle:

$$ESA = C \cdot V \cdot (\Delta \rho / \rho) \cdot \mu d \cdot (Zs / Zs + Zg) \quad [2] \qquad \mu d = \varepsilon \zeta G(\alpha) / \eta \quad [3]$$

where C = apparatus constant, V = volume fraction of particles, $\Delta \rho$ = difference of density between particle and disperse medium, ρ = density of disperse medium, Zs = acoustic impedance of solution, Zg = acoustic impedance of glass rod, ε = permitttivity of disperse medium, η = viscosity of disperse medium, and $G(\alpha)$ = correction term of inertia force.

SAMPLE AND EXPERIMENTAL METHOD

Cement and admixture

Normal portland cement shown in Table 1 was used. Polished surfaces of cement clinker produced at the time when the cement shown in Table 1 was manufactured were used for measuring the force acting between the surfaces of cement particles.

Three types of organic admixtures in total - a type of sulfonate based- and two types of polycarbonate based-admixtures - were used. Assuming that polycarbonate based-admixture, PC-A, has 40 branches of ethylene oxide in a molecule, it is inferred from the bond length of C-C and mean molecular weight that the lengths of the main chain and side chain will be approximately 30 and 20 nm, respectively. It is also inferred from the mean degree of condensation of 256 obtained from the mean molecular weight and the length of C-C bond of polycarbonate based-admixture, PC-B, that the molecular length of it will be approximately 154 nm. Ten percent (10%)-aqueous solutions of NS, PC-A and PC-B and 10^{-2} mol/l-aqueous solution of sodium sulfate similar to the concentration of ion in the liquid phase of cement paste were used as admixture or immersing solution.

Table 1 Character of normal portland cement

Chemical composition (%)								Free lime (%)	Blaine specific surface area (cm^2/g)
SiO_2	Al_2O_3	Fe_2O_3	CaO	MgO	SO_3	Na_2O	K_2O		
22.1	5.3	3.1	65.2	1.2	2.1	0.43	0.23	0.5	3,350

Table 2 Character of organic admixture

Kind	Main component	Structural formula of main component	Solid content (%)	Mean molecular weight	Sodium content (mol/l)
NS	Condensate of β-naphthalene sulfonate with formalin	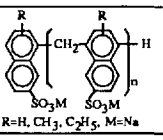 R=H, CH_3, C_2H_5, M=Na	41	1400	1.3
PC-A	Copolymer of acrylic acid with acrylic ester	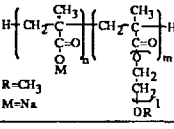 R=CH_3 M=Na	30	88000	0.8
PC-B	Copolymer of olefin with maleic acid	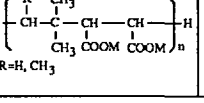 R=H, CH_3	34	59000	3.0

The characters of the organic admixtures used for the experiment are listed in Table 2.

Analysis of admixture

Solid content, mean molecular weight and sodium content were determined according to the procedures described in the previous paper (Uchikawa et al., 1996). The solid content was determined from the weight after drying the liquid admixture sample for an hour at 110°C. The mean molecular weight was determined by gel permeation chromatography. The sodium content was determined by high-frequency inductively coupled plasma emission spectrometry.

Measurement of force acting between surfaces of cement particles adsorbing admixture

Force acting between the surfaces of cement particles adsorbing the admixture was measured by immersing a polished surface of cement clinker sample or a silicon wafer in the admixture solution and determining the F-Dcurve of the adsorption surface of the admixture with the AFM.

Auto Probe CP manufactured by Nikon/Park Scientific Instruments Co. was used as the AFM which uses a quadrangular silicon nitride probe of approximately 100nm base length and a cantilever with the spring constant of 0.05 N/m. The dimensions of the polished sample of cement clinker are 5mm x 5 mm x 3 mm and the surface is finished with aluminum oxide of 0.05μm in diameter. The silicon wafer covered with silicon dioxide (SiO_2) supplied by Nikon was used. Prior to the measurement, the surface of the sample was washed by UV ozone cleaning to remove the contaminants including organic matter. The surface was carefully washed until it was evenly wetted by water. The working range and speed of the cantilever were zero to 750 nm and 1500 nm/sec, respectively.

Measurement of zeta potential of the surface of cement particle adsorbing admixture

Cement paste with the W/C of 0.3 was prepared by adding the admixture to it so as to make the weight ratio of the solid content of admixture to cement 0.6%. The zeta potential of the cement paste was determined with an electrokinetic sonic amplitude type zeta potential measuring apparatus (AcoustoSizer made by MATEC APPLIED SCIENCES Co.) five minutes after adding the mixing water.

Measurement of flow of cement paste

The value of flow of the same cement paste as used for measuring zeta potential was measured with the flow cone for mortar test specified by JIS R 5201 five minutes after the addition of water. The flow cone is 70mm in top diameter, 100 mm in bottom diameter and 60 mm high.

RESULTS AND DISCUSSION

Force acting between surfaces

A F-D curve of silicon wafer surface immersed in 10% aqueous solution of naphthalenesulfonate based-admixture (NS) is illustrated in Fig 3. The probe was brought close to the surface of sample at the speed of 1,500 nm/sec. The moving distance of the probe from the starting point and the interactive force calculated from the deflection of the cantilever are put on the X- and Y-axes, respectively. The point S at which the interactive force begins linearly increasing shows the point where the probe is brought into contact with the surface of sample. The force acting between the solid surfaces is determined as the difference of the interactive force between points S and P, and the range of the interactive force acting is determined from the moving time of probe. Fig 3 reveals that there is a difference between the F-D curve of the probe approaching the sample and that of the probe going away from it. In this study, however, the force acting between the surfaces was evaluated using the former force curve.

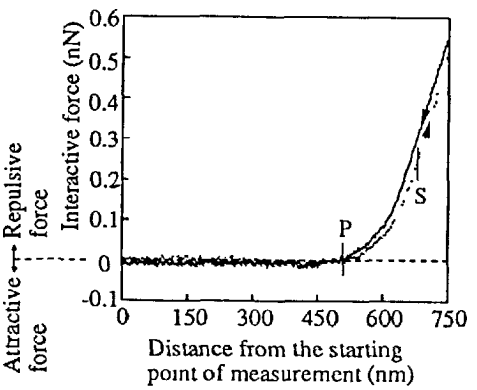

Figure 3 Interactive force-distance curve of silicon wafer surface immersed in the 10% solution of NS measured by AFM

The left side figure of Fig 4 is a figure drawn anew by transferring the point S in Fig 3 showing the actual measurements to the point of origin of distance. Since that figure is convenient for understanding the change of the interactive force perpendicular to the surface of cement particle, F-D curve will be illustrated such as this hereafter.

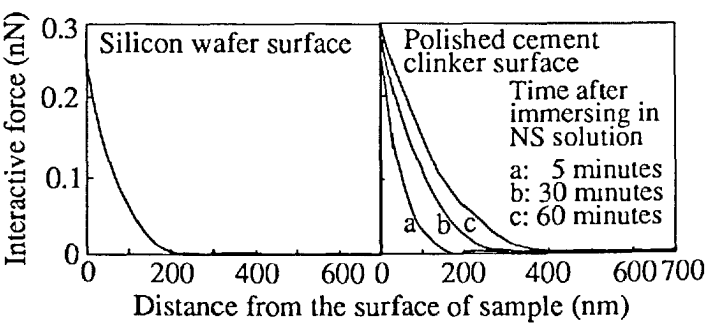

Figure 4 Influence of the time elapsed after immersing the cement clinker sample in organic admixture solution on the force-distance curve of it measured by AFM

The relationship between the distance of the probe from the surface of the

adsorption layer of admixture and the interactive force on the polished surface of cement clinker immersed in a 10%-NS aqueous solution is illustrated in the figure on the right side of Fig 4. The F-D curve varied according to the passage of time from the immersion in the aqueous solution of admixture. Maybe this is because the distance between the probe and the polished surface of clinker varied with time by the dissolution of component elements and the deposition of hydrates on the surface. It is, therefore, important to choose the measuring time in such a highly accurate study of a material progressing reaction during the measurement as this particular case. The F-D curve obtained in five minutes after the immersion was not so different from that of silicon wafer.

The relationships between the distances from the surfaces of the adsorption layer of admixtures determined from the F-D curves obtained in five minutes after immersing the polished surface of cement clinker in various organic admixtures and the interactive force are illustrated in Fig 5. The repulsive force on the polished surface of cement clinker immersed in pure water was 0.004 nN, while the maximum repulsive forces on the polished surface of cement clinker immersed in such aqueous solutions of admixtures as NS, PC-A and PC-B were 0.24, 0.60 and 0.19 nN, respectively. The distance beginning to work the repulsive force increased with increasing the repulsive force given from the admixture. It was approximately 10 nm for pure water, while approximately 160, 560 and 120 nm for the NS, PC-A and PC-B aqueous solutions, respectively. The interactive force logarithmically fell off in inverse proportion to the distance from the surface of the adsorption layer of admixture.

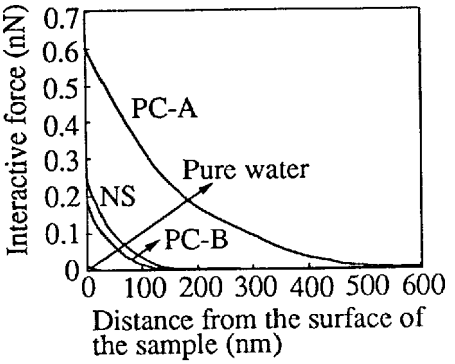

Figure 5 Relationship between interactive force and distance of polished cement clinker immersed in pure water and the 10% solutions of organic admixtures measured by AFM

Zeta potential of cement particle in fresh cement paste

The result of measurements of zeta potential of cement particle in fresh cement pastes with the W/C of 0.3 prepared by adding and without adding the organic admixture are listed in Table 3.

NS contains 64 mmol/l of SO_4^{2-} (Uchikawa et al., 1996) which is dissociated into anions. The zeta potential of cement particle in fresh cement paste prepared by adding NS was high. The PC-A contains as little as approximately 3% of carboxyl group and the hydrophobic group may enclose carboxyl group dissociated, so the zeta potential of cement particle in fresh cement paste prepared by adding PC-A was low. Meanwhile PC-B contains as high as approximately 60% of carboxyl group according to the calculation based on the molecular structure and maleic acid as a component is easily dissociated, therefore the zeta potential of cement particle in fresh cement paste prepared by adding PC-B was high.

In this experiment, even the zeta potential of well-dispersed cement particles in the fresh cement paste containing NS was -10mV. Maybe this is because the zeta potential is higher (lower in absolute value) than the surface potential.

Table 3 Zeta potential of cement particle in fresh cement paste prepared by adding organic admixtures measured by electrokinetic sonic amplitude method

Admixture	Zeta potential (mV)
NS	-11.0
PC-A	-1.5
PC-B	-9.1
No added	-1.8

Conversion of measured zeta potential to electrostatic repulsive force

It is necessary to convert electric potential to force for determining the electrostatic repulsive force from the measurements of zeta potential of cement particles in fresh cement paste. To the relationship in two spherical particles between the surface charge density (σ), Debye parameter (κ) and the electrostatic repulsive force (F), the following formula applies (Li et al., 1993):

$$F = [(2\pi\sigma^2 R)/(\varepsilon_r \varepsilon_0 \kappa)] \exp(-\kappa D) \quad [4]$$

where R = radius of spherical particle, ε_r = relative permittivity of water, ε_0 = vacuum permittivity, and D = distance between surfaces of particles.

The reciprocal number of Debye parameter (κ^{-1}) represents the thickness of an electric double layer. The following relationship exists between the concentration of electrolyte and κ^{-1}:

$$\kappa^{-1} = 0.304/C^{1/2} \quad [5]$$

where C= concentration of electrolyte. Since the concentration of electrolyte in the liquid phase of fresh cement paste is approximately 0.1mol/l, the thickness of diffuse electric double layer formed on the surface of cement particle adsorbing the admixture will be approximately 1 nm.

The surface charge density of the cement particle in cement paste can be calculated using the zeta potential instead of the surface potential from the following formula:

$$\sigma = (8n\,\varepsilon_r\,\varepsilon_0\,kT)^{1/2} \sinh (Ze\,\phi_0/2kT) \quad [6]$$

where n = concentration of electrolyte, k = Boltzmann constant, T = absolute temperature, Z = ionic charge number, e = elementary electric charge, and ϕ_0 = surface potential.

Values 1μm, 78.3 and 8.854 x 10^{-12} C^2/J m were used as the radius of cement particle, the relative permittivity of pure water and vacuum permittivity, respectively. Although the thickness of the adsorption layer of admixture corresponding to the Stern layer varies according to the types and concentrations of admixture (Uchikawa et al., 1992), 100 nm was used as the mean value of it in this study.

Taking the concentration of electrolyte as 0.1 mol/l, the temperature as 20°C, the ionic charge number as 1 and the elementary electric charge as 1.602 x 10^{-19}C, the electrostatic repulsive force of -15 mV equivalent to the minimum value of Vmax (=15kT) required for keeping the dispersion of cement particles 2μm in diameter in fresh cement paste is approximately 10 nN at the distance between the particles of 1 nm.

Factors affecting fluidity of fresh cement paste

The results of measurements of flow of cement paste with the W/C of 0.3 prepared with and without adding the organic admixture are illustrated in Table 4. The table reveals that the flow value is sharply increased by the addition of the admixture in such a manner that the fluidity is particularly much increased by adding PC-A, but the flow value is less increased by adding PC-B than by adding NS.

Table 4 Flow of fresh cement paste prepared by adding organic admixtures

Admixture	Flow (mm)
NS	248
PC-A	476
PC-B	182
No added	113

The relationship between the measured value of force acting between the polished surfaces of cement clinker immersed in an aqueous solution of organic admixture and the flow of fresh cement paste, and that between the zeta potential of the cement particle in cement paste containing the admixture and the flow of fresh cement paste are illustrated in Fig 6. The force acting between the surfaces are linearly related to the flow of fresh cement paste independently of what types of admixture is added and whether the admixture is added or not. The flow value increased with increasing the force acting between the surfaces. Meanwhile, the zeta potential is not necessarily linearly related to the fresh cement paste flow, especially the relation was remarkably separated from the linear relation by adding PC-A. This suggests that force other than the zeta

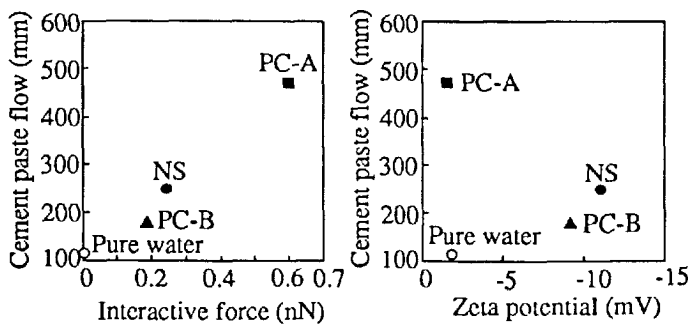

Figure 6 Relathionships between fresh cement paste flow and interactive force, and zeta potential

potential or electrostatic repulsive force contributes to the dispersion of cement particles, namely, the fluidity of fresh cement paste containing PC-A.

Effects of electrostatic and steric repulsive forces on fluidity

The steric repulsive force is considered to be one of the most important forces contributing to the fluidity of cement paste. The value of it can be calculated by subtracting the electrostatic repulsive force converted from the zeta potential measured according to the method described before from the force acting between the surfaces of cement particles in cement paste. Since no steric repulsive force acts in fresh cement paste without admixture, the electrostatic repulsive force converted from the zeta potential of it should be equal to the repulsive force measured with the AFM. The former value is, however, 1.5 nN, while the latter value is 0.004 nN. The former is, therefore, 375 times as much as the latter.

The repulsive force measured with the AFM is the force acting between the probe and the solid surface and the tip of probe is quadrangular with a side of 100 nm. Since the interactive force is proportional to the area, assuming that the tip of probe is a cement particle 2 μm in diameter, it will be 400 times [(2000 nm/100 nm)^2] as much as the force acting between the probe and the solid (cement clinker), which is nearly equal to the above-mentioned value of 375 times.

The relationship between the compensated interactive force of the surface of the adsorption layer of admixture on polished surface of cement clinker opposite to the cement particle 2 μm in diameter obtained by multiplying the value measured with the AFM by 400 and the distance is illustrated in **Fig 7**. A curve drawn by plotting the electrostatic repulsive force converted from the measured value of zeta potential versus the distance is illustrated together in the figure.

Fig 7 reveals that though the electrostatic repulsive force contributing to the dispersion of cement particles in fresh cement paste without admixture is extremely small and the working region is also narrow, the force acting on the surface of cement particle is increased by adding the admixture. The steric repulsive force predominates in the large repulsive force acting between the cement particles in fresh cement paste containing PC-A. Meanwhile, the steric repulsive force contributes only to the regions in the vicinity of cement particles in fresh cement paste containing PC-B and NS, but it disappears in the region exceeding 90 nm from cement particle and accordingly the mean contributions in the former and latter cases to total repulsive force are estimated to be 30 and 20%, respectively. Maybe this is because each molecule of PC-A with a long straight chain and side chains branched from it is adsorbed overlapping each other to the surface of cement particles and the adsorption layer containing many high-density regions are formed, thereby generating large steric repulsive force.

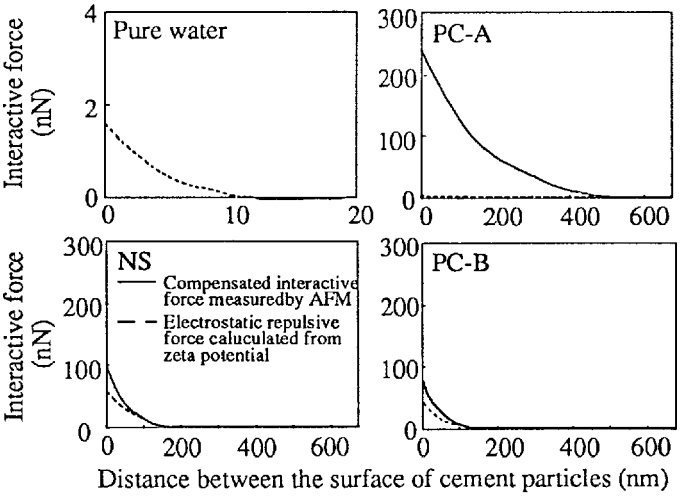

Figure 7 The rate of contribution of electrostatic repulsive force to total repulsive force

The results mentioned above prove for the first time that the steric repulsive force of the organic admixture, which has been a matter of speculation, acts on the dispersion of cement particles, and that the magnitude of the steric repulsive force is closely related to the molecular structure of the admixture. Most of the action dispersing the particles is attributed to the steric repulsive force in fresh cement paste containing a polycarbonate based-admixture mainly composed of acrylic acid-acrylic acid ester copolymer.

CONCLUSIONS

The conclusions obtained by investigating the function dispersing the particles of cement in concrete by the organic admixture are as follows:

(1) The force acting the polished surface of cement clinker adsorbing the admixture can be measured with good reproduciblity as a function of the distance from the adsorption surface of admixture with the atomic force microscope. The zeta potential of cement particles in fresh cement paste with low W/C can be reliably determined by measuring the magnitude of a pressure wave or an electrokinetic sonic amplitude value caused by the dynamic mobility of cement particles to which high-frequency alternating voltage is applied.

(2) Although the fluidity of fresh cement paste containing the organic admixture correlates with the repulsive force of cement particles, there is no constant relationship between the fluidity and the zeta potential. This suggests that force other than the electrostatic repulsive force acts on the dispersion of cement particles.

(3) Considering that van der Waals force is negligible small attractive force, it has been proved for the first time in this study that the cement particles adsorbing the organic admixture have the steric repulsive force besides electrostatic repulsive force by determining the difference between the compensated interactive force obtained from measured value of force acting between the surfaces and the force converted from the measured value of zeta potential.

(4) The repulsive force of the cement particles in fresh cement paste is increased by adding the organic admixture and the magnitude and working region of it depend upon the types of the admixture. The action dispersing the particles of a polycarbonate based-admixture mainly composed of an acrylic acid-acrylic acid ester copolymer is mainly attributed to the steric repulsive force, while that of naphthalene sulfonate based-admixture is attributed considerable part to the electrostatic repulsive force.

(5) The reason why steric repulsive force contributes predominantly to the dispersion of cement and cement hydrate particles in the addition of admixture composed of acrylic acid - acrylic acid ester is considered to be attributed to its molecular structure with a long straight chain of carbon atoms and the side chains branched from it. It forms an adsorption layer containing many high-density regions overlapping each other to the surface of cement particles. Less content of carboxyl group with electric charge ionized in water and the enclosure of carboxyl group with electric charge by hydrophobic groups may also be responsible to reduce the contribution of electrostatic repulsive force for the dispersion of particles.

REFERENCES

Babchin, A.J., Chow, R.S. and Sawatzky, R.P., "Electrokinetic Measurement by Electroacoustic Methods", Adv. Col. Int. Sci., Vol.30, 1989, pp.111-117

Israelachvili, J.N. and Adams, G.E., J. Chem. Soc., Faraday Trans.1, Vol.74, 1978, pp.975-1001.

Israelachvili, J.N., "Intermolecular and Surface Forces", Academic Press, London, 1985, pp.135-158.

Li, Y.Q., Tao, N.J., Pan, J., Garcia, A.A. and Lindsay, S.M., "Direct Measurement of Interaction Forces between Colloidal Particles Using the Scanning Force Microscope", Langmuir, Vol.9, No.3, 1993, pp.637-641.

Massazza, F, Costa U. and Barrila, A., "Interaction between Superplasticizers and Calcium Aluminate Hydrates", J.Am.Cer.Soc., Vol.65, No.4, 1982, pp.203-207.

Uchikawa, H., "Advances in Physico-chemical Characterization and Quality Control Techniques for Cement and Concrete", 9th Int. Cong. Chem. Cem. (New Delhi), Vol.I, 1992, pp.794-883.

Uchikawa, H., "Hydration of Cement and Structure Formation and Properties of Cement Paste in the Presence of Organic Admixture", Conference of Concrete Canada in Tribute to Micheline Moranville Regourd 'Importance of Recent Microstructural Developments in Cement and Concrete', Sherbrooke CANADA, 1994, pp.63-118.

Uchikawa, H., Hanehara, S., Shirasaka, T. and Sawaki, D., "Effect of Admixture on Hydration of Cement, Adsorptive Behavior of Admixture and Fluidity and Setting of Fresh Cement Paste", Cem. Concr. Res., Vol.22, 1992, pp.1115-1129.

Uchikawa, H, Sone, T and Sawaki, D., "Characters and Performances of Japanese and Canadian Organic Admixtures for Concrete", CEMENT & CONCRETE (in Japanese), No.589, Mar., 1996, pp.40-51.

Verwey, E.J. and Overbeek, J.TH.G., "Theory of the Stability of Lyophobic Colloids", Elsevier Publishing Company (Amsterdam), 1948, pp.135-199.

ADSORPTION OF SUPERPLASTICIZERS ON MODEL POWDERS: TEMPERATURE DEPENDENCE, EFFECT ON ZETA POTENTIAL AND ROLE OF CHEMICAL STRUCTURE.

Robert J. FLATT, Yves F. HOUST, Paul BOWEN, Heinrich HOFMANN, EPFL - Powder Technology Laboratory, Lausanne, Switzerland
Jürg WIDMER, Ueli SULSER, Urs MAEDER, Theodor A. BÜRGE, Sika A.G., Zürich, Switzerland

ABSTRACT It has been shown that the adsorption of superplasticizers on MgO and $Mg(OH)_2$, at pH 12.1 and 11.3 respectively, can strongly vary with temperature according to the chemical nature of the superplasticizer. MgO and $Mg(OH)_2$ were chosen as model powders because their surfaces and zeta potentials are similar to cement. The two polymers studied, of similar molar mass, contain the same ionic groups but have different charge spacing. The influence of this structural difference on adsorption and zeta potential was studied.

Key-words: Admixtures, Adsorption, Superplasticizers, Temperature, Zeta Potential.

INTRODUCTION

In the early 1960's, the first synthetic, high performance water reducing admixtures for concrete were developed. These admixtures were based on sulfonated naphthalene-formaldehyde, and, some years later, melamine formaldehyde polycondensates. In the eighties and nineties, new types of polymers, which form the chemical basis of a novel class of high range water reducers (HRWR), also called superplasticizers, were introduced. At present mainly three types of anionic polymers (anionic polyelectrolytes) are used in modern superplasticizers: Sulfonated Naphthalene-Formaldehyde-Polycondensates (SFNC), Polycarboxylic Acid Polymers (PCA) and Polycarboxylic Ester-polymers (PCE).
Such admixtures are today a valuable help in the production of high performance concrete exhibiting high flow and excellent workability which develope high density and durability on setting.
The effect that these polymers induce in cement suspensions, which permits high water reduction for the same workability, is linked to a change in interparticle forces [Horn (1990), Israelachvili (1992)]. However, the exact way in which these polymers modify interparticle forces in cement suspensions, whether it is by electrostatic, steric or entropic effects or a combination of these, is still a debated matter [Aïtcin et al (1994), Jolicoeur et al (1994)].
Our research aims to get new and additional information and knowledge about the mechanisms of the interaction of structurally different water-soluble polymers which are used or could be used as HRWRs. In this paper, we present results concerning the adsorption, at different temperatures, of a PCA and a PCE on model powders which bear many physical similarities to cement phases. We also look at the change in surface charge which these polymers induce on these model powders.

STRATEGY

When studying the effect of polymers on interparticle forces, it is important to know whether they adsorb on surfaces, and if so to what extent.
Because cement hydrates and its surface therefore changes with time, adsorption of HRWRs is commonly studied on inert model powders [Jolicoeur et al (1994), Nkinamubanzi (1994), Chapuis (1990), Pierre et al (1988), Girod et al (1988), Daimon and Roy (1978)]. This is believed to provide information on the initial steps of the interaction between HRWRs and cement. Such studies, carried out by Nkinamubanzi (1994) and Pierre et al (1988) have shown for instance that the adsorption of PNS on TiO_2 is strongly dependent on the pH of the suspension. At pH 3, where TiO_2 bears a strong positive surface charge, the adsorption is maximum, while it becomes non-existent in the alkaline region where the surface charge of TiO_2 is negative. From this example, we see that electrostatic interactions between a HRWR and a surface can be a determining factor for its adsorption.

The model powder must therefore have both a zeta potential and a pH similar to that of a cement suspension if we intend to relate adsorption on the model powder to that on Portland cement. Nägele (1985) found this potential to be positive by a couple mV. On the other hand, the behavior of a polymer in aqueous solution and its action at the interface of a solid is determined by specific structural characteristics of the solvated macromolecules. These characteristics, apart from depending on the polymer structure (electric charge, number, type, distribution and spacing of the functional side-groups), are strongly influenced by the solution pH.
This brings a second condition for adsorption experiments. It is to have a pH similar to that of cement (about 12.5). This can be quite a problematic condition, since at such a pH most powders have a negative surface charge. To the best of our knowledge, no adsorption experiments have so far been carried at pH 12 with model powders positively charged under those conditions.
In this study, the powders used are MgO dead burnt and $Mg(OH)_2$. Suspensions of MgO at pH 12 had positively charged surfaces since its Isoelectric Point (IEP) is at pH 12.4 [Parks (1964)]. $Mg(OH)_2$ is expected to have an IEP at pH 12 [Parks (1964)], therefore we used suspensions at pH 11.3 to obtain slightly positively charged surfaces. The small pH difference is not expected to alter results significantly. Another major interest for these powders is their chemical similarity to the major cement phases C_3S, C_2S and C_3A. The Mg-O bond is much stronger than the Ca-O bond because of the smaller size of Mg (it is above Ca in the periodic table). By dead burning, the reactivity of this powder is further decreased, making it almost insoluble.
The polymers used in this study (a PCA and a PCE) have the same ionic groups (carboxylate and sulfonate). However, the spacing of these groups is larger in the PCE, due to the inclusion of polyethylene glycol-ester (PEG-ester). This structural difference should allow us to get information concerning the importance of electrostatic interactions in the adsorption of such HRWRs.

EXPERIMENTAL

Powders

MgO dead burnt and $Mg(OH)_2$ from Martin Marietta Magnesia Specialties Inc. (type: P-98 and MH-10 respectively; Baltimore, USA) were carefully sampled. Half the MgO was sieved. The fraction below 50 µm, sampled with a spinning riffler, was used in our experiments.
The particle size was determined by laser diffraction (Malvern Mastersizer; Malvern, GB). The BET specific surface was determined by adsorption of N_2 (Micromeritics Gemini III 2375; Norcross, USA). XRD showed the $Mg(OH)_2$ contained a small amount of MgO, possibly formed at the surface by excess drying during the production. secondary phases were not observed in the MgO. Other powder characteristics are given in Table 1.

Table 1: Powder characteristics

	$Mg(OH)_2$	MgO
Specific Surface Area	11.8 ± 0.1 m^2 g^{-1}	0.77 ± 0.03 m^2 g^{-1}
Median Volume Diameter	10.5 ± 0.2 µm	15.0 ± 0.5 µm

Polymers

The polymers used for this study are laboratory test products produced by Sika A.G. (Zürich, Switzerland). Information as to their composition is given in Table 2.

Table 2: Characteristics of the polymers used.

	PCA	PCE
Chemical type	Na-polycarboxylate-polysulfonate	Na-polycarboxylate-polysulfonate, PEG-ester containing
Number Average Molar Mass	11'500 ± 2'000 g mol^{-1}	9'500 ± 1'500 g mol^{-1}

Adsorption

Adsorption measurements were performed on suspensions of 10 g of MgO or 5 g of $Mg(OH)_2$ in 20 ml NaOH 0.01M (pH 12 ± 0.1), previously thermostated in rotary bath at 200 rpm (different masses were taken to achieve similar volume fractions). The superplasticizers were added as concentrated aqueous solutions with a microdispenser. This makes dilution minimal and avoids possible hydrolysis due to a long exposure in an alkaline solution). After 30 min in the rotary bath, the suspensions were centrifuged for 5 min at 3'000 rpm. Five ml of the supernatant, buffered with 25 µl of CH_3COOH (30% V/V), were filtered at 0.45 µm through a filter mounted on a dispensable syringe. The first 2 ml were discarded and the rest was analyzed by reverse phase chromatography with an HPLC from Waters (mod. Alliance; Milford, U.S.A.) equipped with a diode array detector. The calibration standards, which apart from containing no powder and not being centrifuged, were submitted to the same treatment.

Zeta potential

Zeta potential was measured at 23-25° C by acoustophoresis (Penkem, system 7000; Bedford Hills, U.S.A.). Potentials were calculated from measured data using the method proposed by PenKem (Marlow et al 1988). The suspensions were prepared by dispersing 20 g of powder in 300 ml NaOH 0.01M under vigorous agitation and sonification for 15 min (150 W, 20 kHz). Prior to measuring, they were degassed for 5 min (≈20 torr). A slight vacuum was maintained in the measuring cell to avoid bubble formation which attenuates the signal. The superplasticizers were progressively added as concentrated aqueous solutions with a microdispenser.

RESULTS

Stability of powders

The pH of $Mg(OH)_2$ suspensions decreased from pH 12 to pH 11.3. This may be a result from the dissolution and/or precipitation of impurities not detected by XRD. Further pH decrease is hindered by the equilibrium:

$$MgOH^+ + OH^- \rightleftharpoons Mg(OH)_2$$

The suspensions containing dead burnt MgO however remained at pH 12, indicating this powder to be essentially non reactive.

Adsorption

The adsorption isotherms on MgO at 25, 32 and 40 °C for superplasticizers PCA and PCE are reported in Figs 1 and 2 respectively. These figures show that the adsorption of the PCE increases sharply with temperature, while adsorption of the PCA is uneffected by it. Figures 3 and 4 give the adsorption isotherms of the same polymers on $Mg(OH)_2$. In this case, neither polymer is effected by temperature.

The fact that on both powders adsorption of the PCA is not effected by temperature can be assumed to be due to a large adsorption enthalpy ΔH_{ads}. Indeed, over small temperature ranges, both enthalpy ΔH_{ads} and entropy ΔS_{ads} can be regarded as constant and the adsorption free energy ΔG_{ads} is therefore mainly effected by the $-T\Delta S_{ads}$ term, as $\Delta G_{ads} = \Delta H_{ads} - T\Delta S_{ads}$.

Understanding the behavior of the PCE is a more challenging task. However, we can gain some insight using similar considerations regarding its adsorption free energy. The PCE polymer is

similar to the PCA but has ionic groups which are further apart, due to the insertion in this polymer of PEG-ester segments which act as charge spacers. This anionic polymer will therefore have weaker electrostatic interactions with the positively charged surface and consequently a smaller heat of adsorption ΔH_{ads} than the PCA. Although this could explain a temperature dependent adsorption, it does not account for an increase as a function of temperature. Indeed, because of the decrease in configuration entropy linked with adsorption ΔS_{ads} is expected to be positive and adsorption to decrease with temperature. However, it could be that the PCE polymer would remain on the surface but be linked to it by less anchor points. This would then allow larger amounts of polymers to adsorb on the surface. Over a larger temperature range, these polymers would be expected to desorb. The reason why adsorption remains unchanged with temperature on the $Mg(OH)_2$ could be due to a larger ΔH_{ads} interaction with this powder.

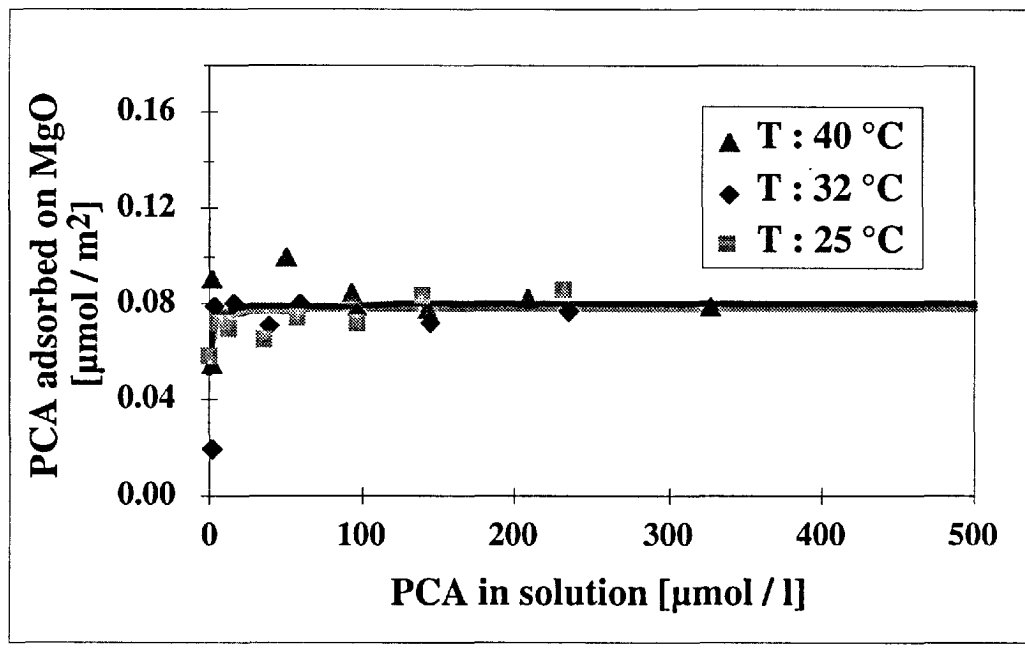

Figure 1 Adsorption isotherms of PCA on magnesium oxide at 25, 32 and 40°C.

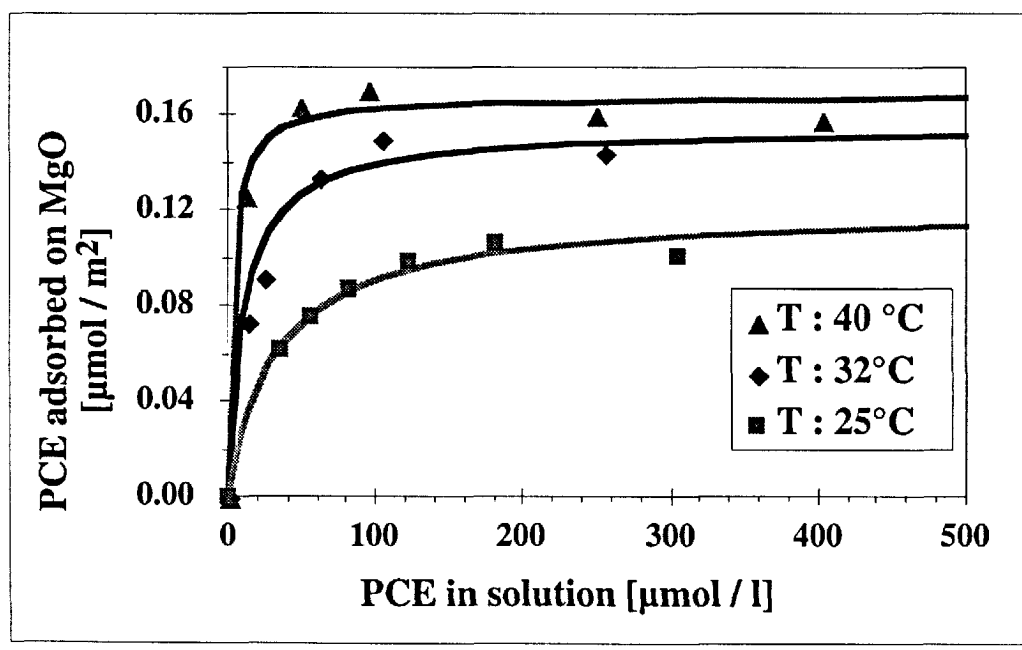

Figure 2 Adsorption isotherms of PCE on magnesium oxide at 25, 32 and 40°C.

Another possible consequence of the PCE having a smaller ΔG_{ads} than the PCA, would be to allow competitive adsorption of hydroxyl groups OH^-. These would be more easily desorbed by rises in temperature, allowing a higher surface coverage, especially on MgO. Adsorption on the $Mg(OH)_2$ might not be influenced by temperature because of the pH difference (12 and 11.3), which corresponds to a five fold concentration difference in OH^-.
On the other hand, it is known that PEO polymers, which are similar to our PCE, have increased polymer-polymer interactions with temperature rises over similar ranges (Claesson et al. 1986). This might lead to multiple layer adsorption (Klein 1997) on the MgO. This may not occur on the $Mg(OH)_2$ either because of different surface interactions, the pH difference or a larger porosity. We can point out that the interaction energy increase between PEO polymers is believed to be linked to the loss of a solvation layer (Israelachvili 1996). This in turn would lead to smaller surface occupation of the adsorbed polymers and would allow increased adsorption.

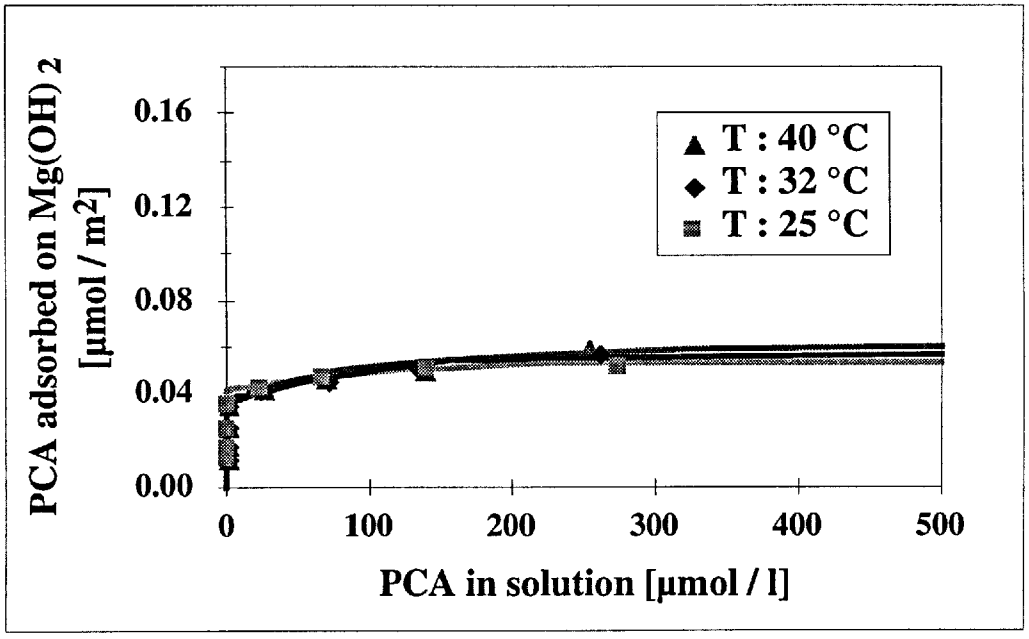

Figure 3 Adsorption isotherms of PCA on magnesium hydroxide at 25, 32 and 40°C.

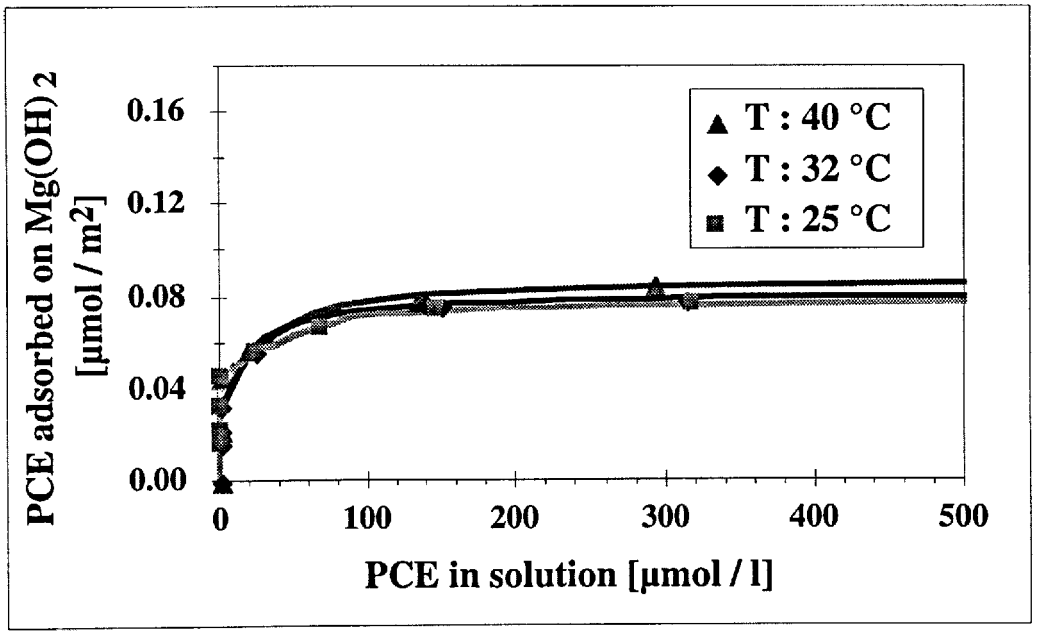

Figure 4 Adsorption isotherms of PCE on magnesium hydroxide at 25, 32 and 40°C.

Zeta potential

In Figs 5 and 6, we have reported the change in zeta potential (related to the surface charge) that the PCA and the PCE induce on MgO and $Mg(OH)_2$ respectively. In both cases, the PCA induces a larger negative zeta potential. This means that the larger adsorption of the PCE is not sufficient to overbalance the greater charge of the PCA. It is possible to compare absolute molar concentrations of these polymers because they have similar molar mass and similar mass distributions.

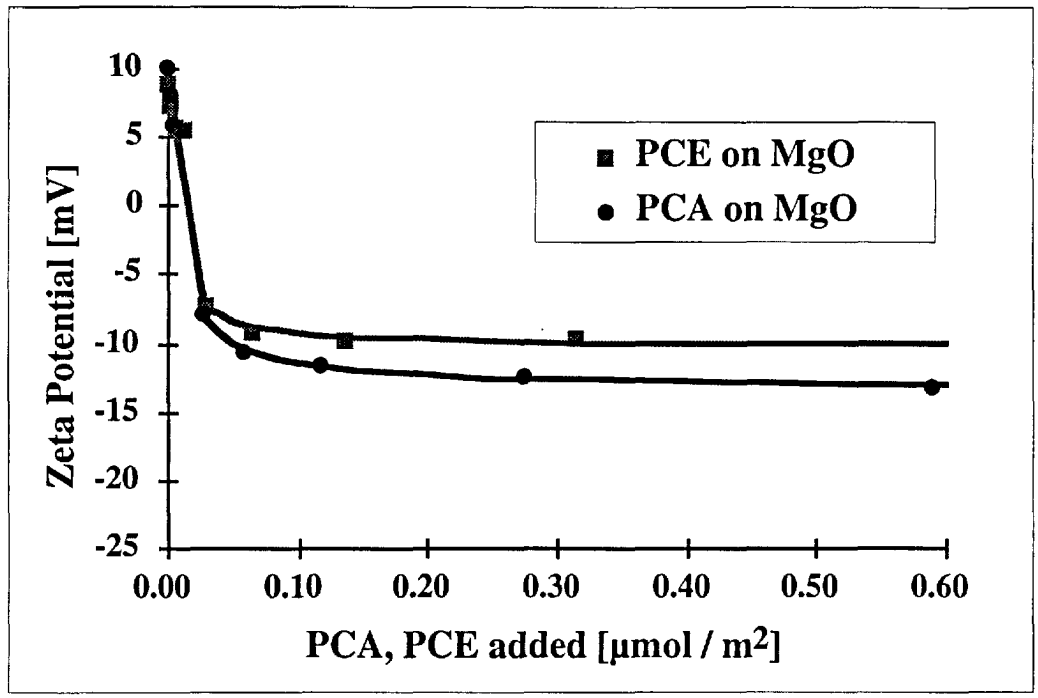

Figure 5 Zeta potential measured on magnesium oxide. The amount of superplasticizer added is given with respect to the surface of the powder in the suspension.

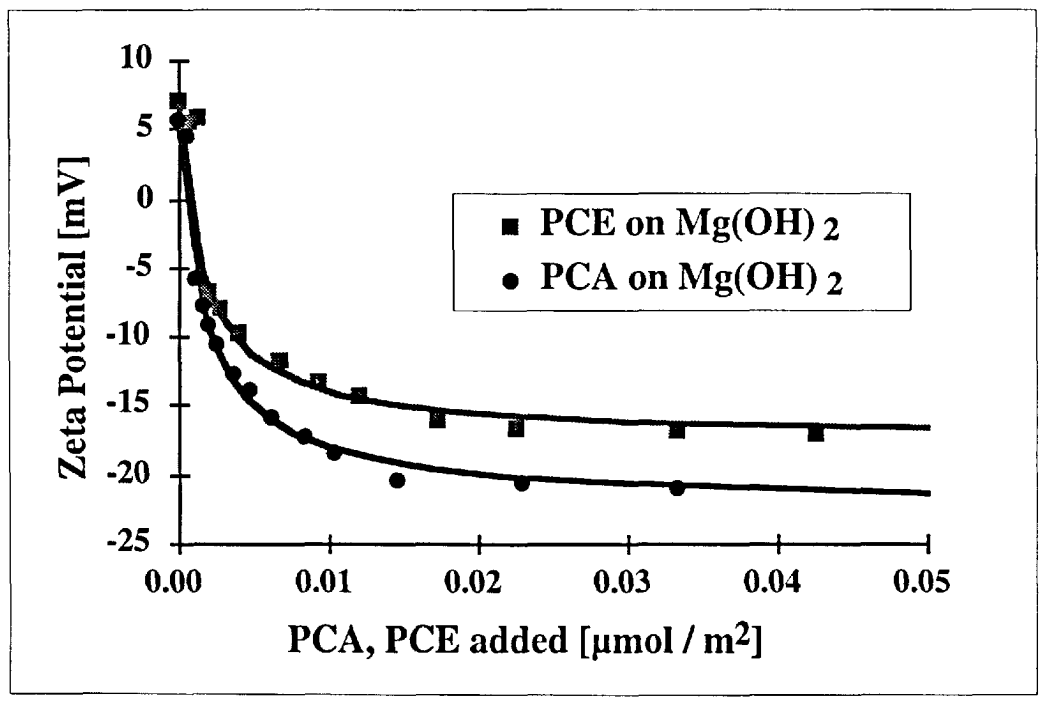

Figure 6 Zeta potential measured on magnesium hydroxide. The amount of superplasticizer added is given with respect to the surface of the powder in the suspension.

We also see especially in Fig 6, that the adsorption continues after the surface has acquired a negative charge. This might be due to either a non electrostatic interaction involved in the adsorption process, or to an inhomogeneity in the surface charge distribution. Hoogeveen et al (1996) in their study of the adsorption of cationic polyelectrolytes on oxides (TiO_2 and SiO_2) find the latter possibility the most likely in explaining a similar result with TiO_2.

CONCLUSIONS

The adsorption of the PCA polymer (a polycarboxylate, polysulfonate) on MgO does not depend on temperature, while it does for the PCE polymer (a polycarboxylate, polysulfonate, polyethylene glycol-ester containing). This may result from the PCA having a stronger interaction with the MgO surface, due to its larger number of ionic groups. On the $Mg(OH)_2$ no temperature dependence is observed. This can be due to the differences between the surfaces of both powders. More PCE than PCA can be adsorbed on either surface. However, the extra amount of adsorbed PCE is not sufficient to induce a larger negative zeta potential than the PCA.

When considering the dispersion effect of these polymers, we must therefore expect that the electrostatic effect of the PCA will be greater than for the PCE. However, due to its greater adsorption, the PCE will probably have a more important effect through steric repulsion or by entropic exclusion.

Rheological measurements must now be carried out to determine which of these polymers is the most efficient water reducer. From such measurements and with the above conclusions it may be possible to find out which effect is the most important. This knowledge will be an important help in the design and production of new even more efficient superplasticizers.

The strong temperature dependence for the adsorption of the PCE has shown that this factor could be a dominant issue concerning the use of some superplasticizers. Consequences on the rheology have still to be studied.

ACKNOWLEDGMENTS

This research was made in the frame of the EUREKA Project 1363 ICHRWR and received financial support from the Swiss Commission for Technology and Innovation (CTI) which is gratefully acknowledged. R. Oesch is thanked for having performed BET measurements of the specific surface of the powders used.

REFERENCES

Aïtcin, P.-C., Jolicoeur, C., MacGregor, J.G., "Superplasticizers: How they work and why they Occasionally don't", Concrete International, Vol. 16, No. 5, 1994, pp. 45-52.

Chapuis, J., "Physical Elementary Mechanisms of Fluidification by Superplasticizers or Water - Reducing Agents", Proc. 8th ICCC, Rio de Janeiro, Vol. 6, 1986, pp. 544-549.

Chapuis, J., "Rheological Measurements with Cement Paste in Viscosimeters: A Comprehensive Approach", Rheology of Fresh Cement and Concrete (P.F.G. Banfill, Ed.), E. & F.N. SPON, London, etc., 1990, pp. 3-12.

Claesson, P.M., Kjellander R., P. Stenius, H.K. Christenson, "Direct Measurement of Temperature-dependent Interactions between Non-ionic Surfactant Layers", *J. Chem. Soc., Faraday Trans. 1*, Vol. 82, 1986, pp. 2735-2746.

Daimon, M., Roy, D.M., "Rheological Properties of Cement Mixes: I. Methods, Preliminary Experiments and Adsorption Studies", Cem. Concr. Res., Vol. 8, 1978, pp. 753-764.

Girod, G., Lamarche, J.M., Foissy, A.,"Adsorption of Partially Hydrolyzed Polyacrylamide on Titanium Dioxide", J. Colloid Inter. Sci., Vol. 21, No 1, 1988, pp. 265-272.

Hoogeveen, N.G., Stuart, M.A.C., Fleer, G.J., "Polyelectrolyte Adsorption on Oxides. I. Kinetics and Adsorbed Amonts", J. Colloid Inter. Sci., Vol. 182, 1996, pp. 133-145 and "II. Reversibility and Exchange", ibid., pp. 146-157.

Horn, R.G., "Surface forces and their Action in Ceramic Materials", J. Am. Ceram. Soc., Vol. 73, No. 5, 1990, pp. 1117-1135.

Israelachvili, J., "Intermolecular & Surface Forces", Academic Press Ltd., Suffolk, 1990.

Israelachvili, J., Personal Communication, 1996.

Jolicoeur, C., Nkinamubanzi, P.C., Simard, M.A., Piotte, M.,"Progress in Understanding the Functional Properties of Superplasticizers in Fresh Concrete", Proc. of the 4th CANMET/ACI International Conference on Superplasticizers and Other Chemical Admixtures, Montreal, 1994, ACI SP 148, Detroit, 1994, pp. 63-87.
Klein, J., Personal Communication, 1997.
Marlow, B.J., Fairhurst, D., Pendse H.P., "Colloid Vibration Potential and the Electrokinetic Characterization of Concentrated Colloids", Langmuir, Vol. 4, 1988, pp. 611-626.
Nägele, E., "The Zeta-Potential of Cement", Cem. Concr. Res., Vol. 15, 1985, pp. 453-462.
Nkinamubanzi, P.-C., "Influence des dispersants polymériques (superplastifiants) sur les suspensions concentrées et les pâtes de ciment", Ph.D. thesis, Université de Sherbrooke, 1994.
Parks, G.A., "The Isoelectric Points of Solid Oxides, Solid Hydroxides and Aqueous Hydroxo Complex Systems", Chem. Rev., Vol. 67, 1965, pp. 177-198.
Pierre, A., Carquille, C., Lamarche, J.M., Foissy, A. and Mercier, R., "Adsorption d'un polycondensat d'acide naphtalène sulfonique (PNS) et de formaldéhyde sur le dioxyde de titane", Cem. Concr. Res., Vol. 18, No 1, 1988, pp. 18-28.

MECHANISMS OF CEMENT - ADMIXTURE INTERACTION

Umberto COSTA, Fabio CORAZZA, CTG Italcementi Group, Bergamo, Italy
Pierre COLOMBET, Valérie FERNON, Angélique VICHOT, CTG Italcementi Group, Guervillle, France

ABSTRACT Beside having physical effects which modify the bonds between the particles and therefore the rheology of cementitious mixes, some admixtures can act on the chemical processes of hydration and particularly on the nucleation and growth of crystals. When these interactions occur, final user describe the premature formation of chemical and physical bonds in the mixes as an inconvenience which is termed as "cement-admixture incompatibility" or "early thickening" of concrete. Such a too early loss of workability may have different origins. This paper is aimed at describing the basic mechanism of cement-admixtures interaction by considering the investigations of cases of practical interest.

KEY-WORDS: Mechanism, Naphthalene Formaldehyde Sulfonate, Pore solution, Rheology, Slump loss.

INTRODUCTION

The rheological behaviour of cementitious mixes depends on a number of chemical and physical factors, including the historic trend of the shear stresses occurring during preparation, haulage and casting operations (Bombled and Kalvenes, 1967; Locher et al., 1980; Massazza and Costa., 1982; Tattersall and Banfil, 1983; Costa and Massazza, 1986). Some admixtures have physical effects which modify the bonds between particles and can act on the chemical processes of hydration and particularly on the nucleation and growth of crystals. When these interactions occur, final user describe the premature formation of chemical bonds in the mixes as an inconvenience which is termed as "cement-admixture incompatibility" or "early thickening" of concrete. Such a too early loss of workability may have different origins that this paper is aimed at describing on the basis of studies carried out on some cases of practical interest.

RHEOLOGICAL BEHAVIOUR OF CONCRETE

Normal Workability Loss

The normal course of the chemical reactions occurring in the cement paste causes the progressive time-related increase in the yield value. Hydration has an evident effect in that it produces an increasing number of so-called "welding points" between the cement grains which constitute the very essence of setting and hardening. The chemical reactions occurring during the first phase of hydration (the dormant period) are the following:
- Formation of ettringite, whose nucleation starting from solution ions is the slow phase of the mechanism;
- C-S-H formation.

The natural loss of workability is therefore found in all cements, also when C_3A fails to be present, as is the case of pure C_3S, due to the formation of C-S-H bridges between the granules. This process is influenced by the mean distance between the particles which depends on the fineness and particle size distribution of the cement as well as on the water/cement ratio

(Blombed and Kalvenes, 1967). According to their different nature, admixtures can variously affect the natural loss of workability. Retarding agents, by slackening the chemical process, reduce the workability loss at a constant w/c ratio. Accelerating agents perform completely the opposite. Plasticizing and superplasticizing admixtures used as water reducing agents tend to accelerate the natural yield threshold increase as a consequence of a reduced w/c ratio.

The chemical processes related to the rheological behaviour have been investigated through isothermal calorimetry. The calorimetric curve of a portland cement, illustrated in Fig. 1, shows a first intense peak during the mixing period with ettringite being the prevailing product. The rate of reaction is subsequently slackened off (dormant period). After 2 hours, setting reactions make the rate increase again (second thermal peak). The speed is then reduced as soon as the hydrated layers surrounding the cement grains have become sufficiently thick (approximately 25 μm at 20°C) to slow down water and ion diffusion.

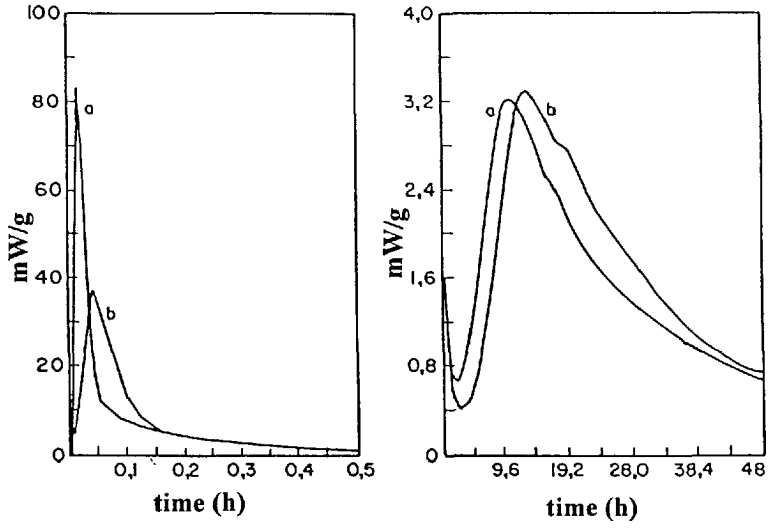

Figure 1 Calorimetric curves obtained on cement pastes: a) cement as received; b) cement with a 0,5% addition of Na-PNS

In the presence of superplasticizer the first thermal peak has lower intensity but the thermal flux is higher for a longer duration. In this case the admixture emphasises the retarding action of the calcium sulfate at the mixing period. The peak corresponding to the setting and hardening phases is not modified by the presence of the admixture. These results demonstrate that the intensification of workability loss caused by superplasticizer is principally linked to the reduction of the w/c ratio and not to particular interactions on hydration process.

Anomalous workability loss

In some cases concrete can show an anomalous trend of the rheology. The phenomena occurring in this case can be false or rapid setting.

False setting

False setting occurs when the rapid dissolution of hemihydrate produces a supersaturated solution from which gypsum crystals are formed, as in the case of the plaster of Paris. Bombled and Kalvenes (1967) determined the progress of the yield threshold in a paste affected by false setting and indicated also that the phenomenon is destined to disappear after remixing. False setting is not easily detectable in ready-mixed concrete on account of the large amount of energy

employed during mixing operations at the ready mix concrete plant. Admixtures containing strong electrolytes accelerate not only cement setting but also gypsum precipitation, which intensifies false setting. Weak electrolytes and most organic molecules with a retarding effect delay or inhibit the phenomenon inasmuch as they hinder nucleation of gypsum crystals and prevent these from precipitating.

Rapid setting

In less frequent cases of a too low gypsum content in cement, the retarding mechanism of C_3A by ettringite formation performs wrongly. Rapid setting is found to occur when the sulfate concentration gradient at the C_3A/solution interface is too small to inhibit the formation of hexagonal hydrates. The layer of aluminate hydrates covering the surfaces of C_3A contributes to stiffening the paste.

The size of hydrates thus formed, close to that of gels, is such that bonds cannot be broken by such typical mechanical actions as mixing or vibration. In the event that gypsum is not particularly underdosed, the situation is not so clear as that described above. In this case, however, a permanent increase in the yield value defined as "thickening" is found to occur.

The effects of the content and crystalline form of C_3A as well as the solubilisation rate of the mineralogical forms of gypsum have been covered exhaustively in literature (Locher et al., 1980). Fig. 2 shows the trend of the yield value of a cement paste as a function of the gypsum content and highlights the variable intensity of rapid setting.

Attenuated rapid setting (curve 5) manifests itself with a rapid increase in the yield value between 10 and 70 minutes.

Paradoxically, real set is delayed by the rapid one: in fact, the initial set is shifted from 100 to 500 minutes on account of the chemical effect of aluminate ions on the nucleation of portlandite. Also, the phenomenon of attenuated rapid setting is evidenced by conduction calorimetry (Fig. 3). An additional thermal peak, which is not observed in a normal cement, appears between 3 and 10 minutes due to the formation of aluminate hydrates.

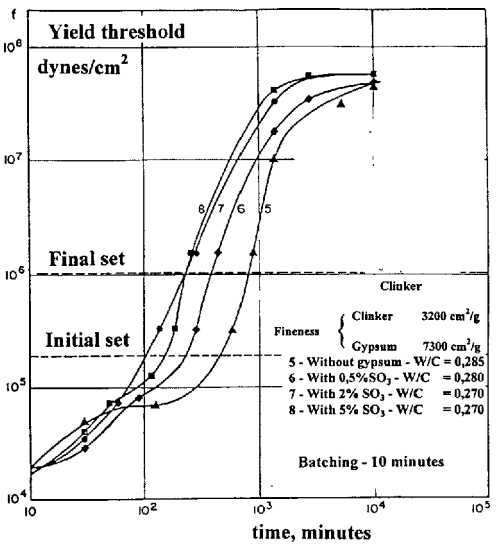

Figure 2 Attenuated rapid set: effect of gypsum addition (Bombled et al., 1967)

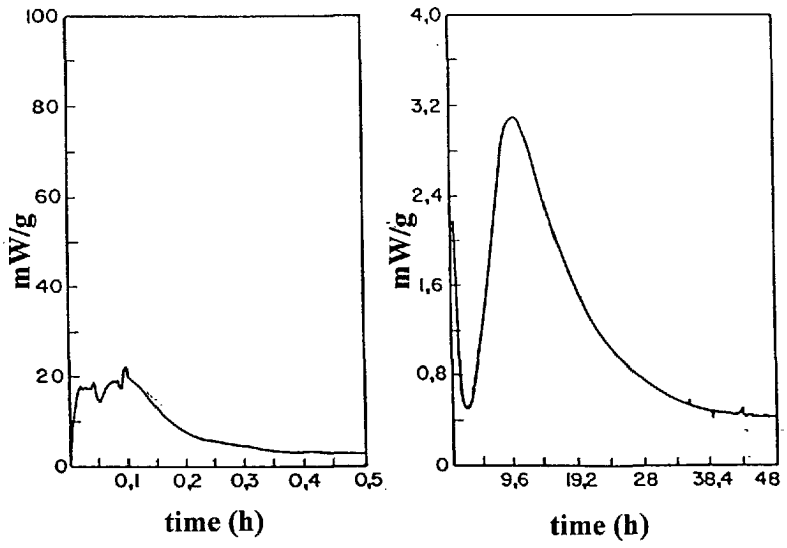

Figure 3 Calorimetric curve of a cement paste affected by an attenuated rapid set

As regards the influence of admixtures, a typical effect of attenuated rapid setting is sometimes found when using superplasticizers. Paste thickening becomes evident when the superplasticizers disturb the regulating mechanism of gypsum on C_3A hydration. With reference to set regulation mechanisms in the presence of superplasticizers, these items are considered in this study:

- The effect on the gypsum solubility
- The effect on ettringite nucleation
- The complex formation between superplasticizer and aluminate hydrates
- The modification of ionic equilibria of interstitial solutions.

POLYNAPHTHALENESULFONATE (PNS) - CEMENT INTERACTION

Materials

Cements - Five portland cements (A, B, C, D, E) were studied. Fineness, setting times, specific gravity and chemical analysis of those cements are given in Table 1.

Superplasticizers - The admixtures were sodium or calcium salts (Na-PNS, Ca-PNS) of a polydispersed naphthalene formaldehyde sulfonic acid. Two other sulfonates have also been tested, namely a sodium salt of β-naphthalene sulfonic acid (2NSA) and a disodium salt of 1,5-naphthalenedisulfonic acid (15NDS), both of which had been previously studied as far as the interaction with calcium aluminate hydrates is concerned (Fernon, 1994).

Calcium sulfates - The gypsum was an industrial set regulator (73% gypsum + 16% anhydrite + 11% impurities). Various other calcium sulfates containing various amounts of hemihydrate and anydrite (Table 2) were obtained from this set regulator via thermal treatments. Interaction between Ca sulfates and PNS was studied using a saturated lime solution to simulate the conditions of a cement paste. The water/solid ratio was 10, thus yielding a mixure with a consistency similar to that of a paste and the PNS concentration was 21.33 $g.l^{-1}$.

Table 1 Physical properties and chemical analysis of cements

	Cement A	Cement B	Cement C	Cement D	Cement E
SiO_2	21.21	21.26	20.99	20.57	21.45
$Al2O_3$	3.60	3.57	3.59	4.42	3.18
$Fe2O_3$	3.88	4.16	3.88	1.88	5.59
CaO	65.30	65.23	64.79	61.76	63.20
MgO	1.41	1.54	1.52	2.99	1.83
SO_3	1.90	2.07	1.89	2.59	2.41
Na_2O	0.09	0.11	0.11	0.33	0.21
K_2O	0.35	0.38	0.38	0.84	0.44
Loss on ignition	1.20	0.98	2.26	3.84	1.16
Fineness					
- oversize 40 µm, %	16	17	23	19	14
- Blaine, m^2/kg	372	377	387	416	352
Setting time					
- initial, min.	189	156	174	163	173
- final, min.	270	225	240	192	220
Specific gravity	3.14	3.18	3.14	3.10	3.20
Bogue composition %					
C_3S	69.42	68.07	69.11	55.26	57.97
C_2S	4.38	5.17	8.06	17.30	17.78
C_3A	2.98	2.43	2.96	8.54	0
C_4AF	11.80	12.65	11.80	5.72	17.00
Calcium sulfate composition %					
Gypsum	6	6	50	*	*
Hemihydrate	42	41	34	*	*
Natural anhydrite	49	46	12	*	*
Syngenite	3	7	4	*	*

* Not measured

Table 2 Thermogravimetric analysis of the calcium sulfate

	Sample 1 as received	Sample 2 after thermal treatment, 150°C, 24 hours	Sample 3 after thermal treatment, 800°C, 2 hours
% gypsum	73	0	0
% hemihydrate	0	61	0
% anhydrite	16	28	89
% impurities	11	not measured	not measured

Hydrates preparation - Pristine calcium aluminate hydrate (C_4AH_X) was prepared by reacting a small excess of a saturated $Ca(OH)_2$ solution ($[Ca^{2+}] = 21.45$ mM) with an aqueous solution of $NaAlO_2$ ($[AlO_2^{-1}] \approx 6.5$ mM). Coprecipitation products of calcium aluminate hydrate and PNS were obtained following the same procedure. PNS was first dissolved in the saturated $Ca(OH)_2$ solution together with various amounts of K_2SO_4. All the syntheses were perfomed using a continuous batch reactor with a sufficient residence time (an hour) to allow the equilibrium to be reached. After precipitation, the suspension was filtered. The solid phase was dried under vacuum at 80-100°C and stored in a CO_2 and H_2O- free atmosphere prior to characterization.

Methods

Solid products characterization - The structure of the precipitated solids was determined using X-ray diffraction, scanning electron microscopy and transmission electron microscopy.

Fluid pore analysis - PNS concentration was measured by UV spectrophotometry at the characteristic peak absorbance wavelength of 290 nm. Filtrate composition (SO_4^{2-}, Cl^-, Ca^{2+}, Na^+, K^+) was determined by capillary-ion analysis, ion chromatography and atomic absorption spectrophotometry along with its pH. The pore fluid was removed from fresh pastes by filtration and from mortars using a pressing-machine equipped with an adapted mold.

Mortar and pastes rheology - The flow behavior of mortars was studied using a flow table meeting ASTM specification C-230 (cement A, B and C), and a Fann rotation rheometer for pastes (cement D and E). The mortar flow was measured after 15 drops. All the tests were perfomed at 20°C and 75% RH. For pastes, yield value was estimated by measuring stress at various strain rates and extrapolating the stress at zero strain rate.

Results

Organomineral Compounds Formation

In the absence of sulfate anions

The elemental composition of the co-precipitated products is given in Table 3. They can all be considered as organomineral compounds, since they appear, at the scale of the SEM and TEM observations (Fig. 4), as homogeneously constituted of organic molecules or polymers intimately bound to a mineral skeleton made of calcium aluminate hydrate. In all cases, the Ca/Al molar ratio as measured using elemental analysis is not far from 2, suggesting the existence of $[Ca_2Al(OH)_6]^+$ units which are the principal layers from which C_4AH_X is built up (Hanic et al., 1989). From Table 3, it may be seen that the shorter the length of the polymer, the closer to 2 is the Ca/Al molar ratio which indicates a better ordered structural organization of the constitutive elements.

Table 3 Elemental composition of the organomineral compounds obtained by co-precipitation

Sulfonate precursor	Initial sulfonate concentrat. (gl^{-1})	Ca/S Initial molar ratio	% C	% S	% H	% Ca	% Al	Ca/Al molar ratio	Ca/SO_3 molar ratio	% organic part
none	-	-	3.8	-	3.1	9.9	24.7	1.7	-	
2NSA	2.5	2.00	25.6	6.6	3.9	16.4	5.7	1.9	2.0	42
15NDS	1.8	2.00	12.5	6.0	2.4	21.2	8.1	1.8	2.8	24
Na-PNS	2.0	2.60	31.1	6.5	4.1	13.6	3.9	2.4	1.7	57
Na-PNS	4.7	0.56	35.7	7.9	4 1	11.4	3.1	2.5	1.2	75
Na-PNS	10.0	0.26	35.0	7.8	4.1	11.1	3.2	2.3	1.1	75
Ca-PNS	2.7	1.95	28.9	7.0	3.7	14.2	4.3	2.2	1.6	80

This is confirmed by the XRD study which shows that the diffraction peaks become narrower. As the system becomes disordered both with increasing sulfonate molecular weight and initial concentration, the Ca/SO_3 molar ratio (SO_3 being the sulfonate group of the oligomers or polymers) decreases from ca. 2 to ca. 1. Simultaneously, the organic part amount increases from ca. 30% to ca. 75%. From these considerations, two formulae can be proposed. For the oligomers (2NSA and 15NDS), the organomineral compound can be described using the formula $< [Ca_4Al_2(OH)_{12}]^{2+}$, $2SO_3^-$, $nH_2O >$, whereas for the polydispersed high molecular

weight sulfonates it is described using $< [Ca_4Al_2(OH)_{12}]^{2+}$, $2SO_3^-$, x/2 Ca^{2+}, xSO_3^- $nH_2O >$. Also, the lamellar aspect of the organomineral compounds is confirmed by TEM showing well defined 002 lattice fringes (Fig. 4c).

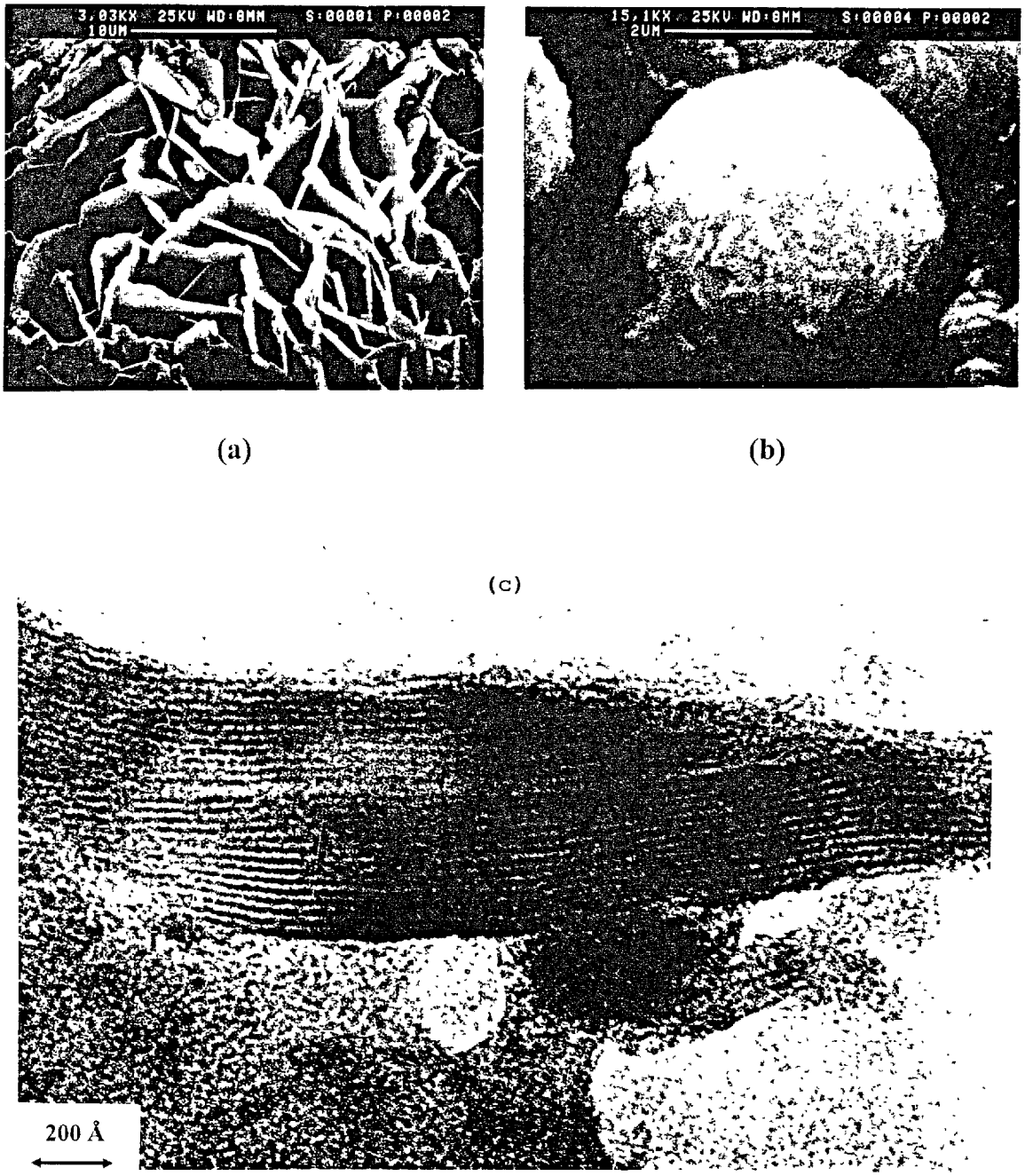

Figure 4 SEM Micrographs of the synthesized organomineral compounds obtained with 2NSA (a) and PNS (b); TEM micrograph of the 2NSA organomineral compound showing 002 lattice fringes (c)

In the presence of sulfate

When sulfate anions are present in the solution (this study is restricted to the case of Na-PNS), both ettringite and the organomineral compound are shown to be formed. Their proportions

depend on the initial SO_3^{-}/SO_4^{2-} molar ratio (Fig. 5). As this ratio decreases, the amount of ettringite increases. Interestingly, the morphology of ettringite in the presence of PNS is observed to be different from the one typically observed in cement pastes. Instead of long needles with an hexagonal section, small crystallites have grown. PNS may hence be suggested as acting as an inhibitor of crystal growth as previously stated by Luke and Aitcin, 1990.

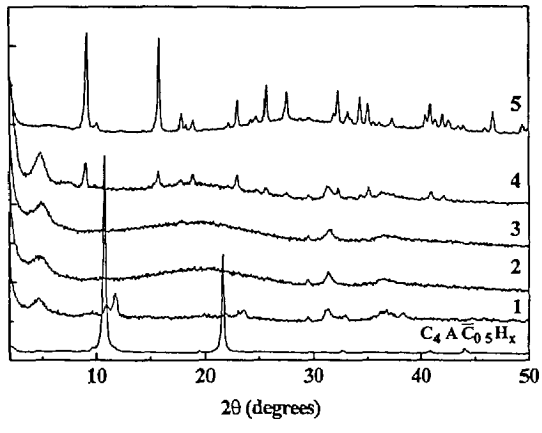

1 - $[SO_4^{2-}] = 0$ g l^{-1} and low initial $[SO_3^{-}]$ concentration
2 - $[SO_4^{2-}] = 0$ g l^{-1} and high initial $[SO_3^{-}]$ concentration
3 - 7.2 ≤ initial SO_3^{-} / SO_4^{2-} molar ratio
4 - 2.88 ≤ initial SO_3^{-} / SO_4^{2-} molar ratio ≤ 4.11
5 - 0 < initial SO_3^{-} / SO_4^{2-} molar ratio < 2.88

Figure 5 XRD patterns (λ_{Cu} = 1.54051 Å) of the organomineral compounds obtained from Na-PNS in the presence of K_2SO_4

PNS/sulfate interaction

The results of the analysis of the sulfates and PNS in the lime saturated solution as a function of time are shown in Fig. 6.

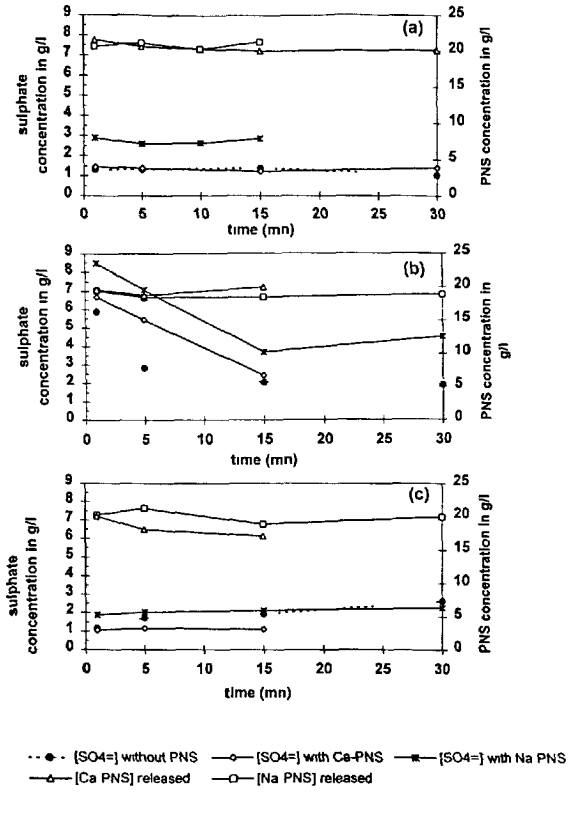

Figure 6 Effect of PNS-counter ions on the dissolution of set regulators of different nature: sample 1 (a), sample 2 (b) and sample 3 (c) (see Table 2)

It is clearly observed that Na-PNS greatly enhances the solubility of set regulators rich in gypsum or in hemihydrate, in agreement with the results obtained by Jolicoeur et al. (1994) for the same type of superplasticizer with Na as the counter ion, and only slightly that of anhydrite. To the contrary, Ca-PNS does not affect their solubilities except for anhydrite for which a decrease is evidenced. On the other hand, both Na- and Ca-PNS delay the gypsum precipitation subsequent to hemihydrate dissolution (15 minutes as compared to 5 minutes without superplasticizer). The important effect of Na-PNS on the gypsum and hemihydrate solubilities can be explained considering that ionized sulfonate groups in an alkaline medium are able to complex the free calcium ions present in the solution, increasing the dissolution of calcium sulfate due to an equilibrium shift.

The fact that the gypsum and hemihydrate solubilities in the presence of Ca-PNS are unchanged, as previously observed by Dodson and Hayden in the case of Ca-lignosulfonate (Dodson and Hayden, 1980), corroborates the hypothesis that calcium complexation by Na-PNS is actually at the origin of the solubility enhancement.

Pore fluid solution and rheology

As shown in Fig. 7 the plain pastes and mortars exhibit only a slight decrease of flow as a function of time (normal slump loss). This loss of fluidity is higher in the presence of the superplasticizer, except for cement E for which the yield value is practically zero. Cement A has a behavior markedly distinct from that of the other cements since the flow decrease from 5 to 15 minutes is much larger. As a matter of fact, cement A mortar is no longer workable after ca. 30 minutes, which leads us to consider that this cement exhibits early stiffening as it is superplasticized.

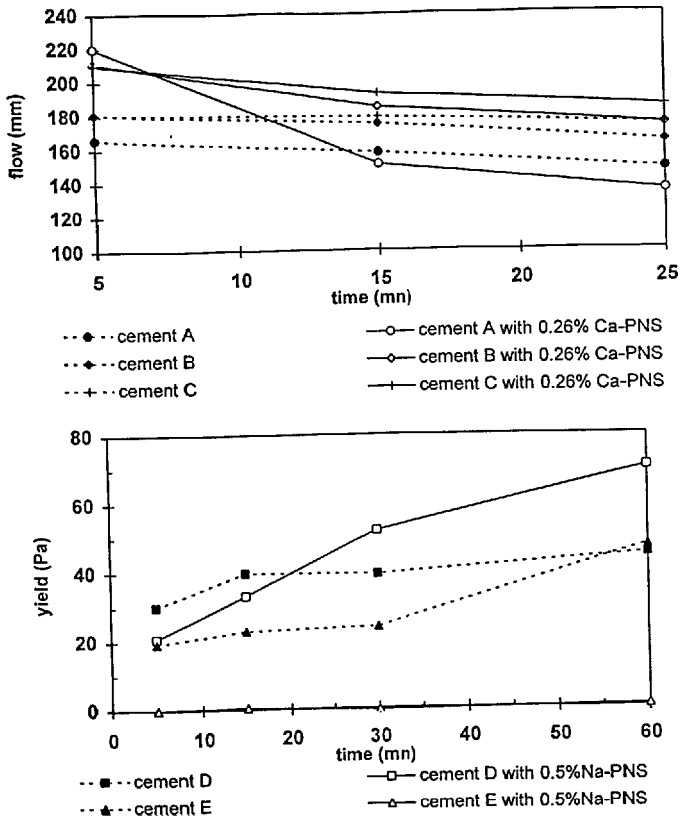

Figure 7 Rheological behaviour of the studied cements

As it can be seen from Tables 4 and 5, the peculiar behavior of cement A with respect to that of the others is also reflected in the chemistry of the pore fluid solution, as regards the sulfate concentration. That is to say, the above discussed stiffening for cement A is accompanied by an important increase in the sulfate concentration, which is not observed for cements B-E. For cement A specifically, the sulfate concentrations are 3.7, 5.9 and 7.0 $g.l^{-1}$ for initial PNS concentrations equal to 0, 5.4 and 14.8, respectively whereas they remain fairly constant and equal to 3.5 ± 0.5 (mortars, cements B and C) or 14 ± 1 (paste, cement D) or 6 ± 1 $g.l^{-1}$ (paste, cement E) i.e. dependent on the water/cement ratio (differing for mortars or pastes) and composition of the cement, but not on the absence or presence of superplasticizer. Note that for all the studied cements, including cement A, the concentrations of the other ions remain unchanged, within experimental accuracy, as the superplasticizer is added to the mixes, with reference to the concentrations measured in the absence of superplasticizer. On the other hand, whatever the flow behavior may be, about 80% of the PNS initial amount is observed to be consumed within 15 minutes.

Table 4 Ionic concentration ($g.l^{-1}$) evolution of the pore fluid solution of mortars during hydration

	time (mm)	[PNS]	$[SO_4^{2-}]$
A plain	12	-	3.7
	28	-	3.1
	58	-	2.9
A with [Ca-PNS] = 5.4 $g.l^{-1}$	12	0.6	5.9
	28	0.5	3.1
	58	0.5	2.9
A with [Ca-PNS] = 14.8 $g.l^{-1}$	12	1.9	7.0
	28	1.4	4.0
	58	1.3	3.5
B plain	12	-	4.3
	28	-	3.4
	58	-	3.2
B with [Ca-PNS] = 5.4 $g.l^{-1}$	12	0.6	4.6
	28	0.5	-
	58	0.5	3.3
B with [Ca-PNS] = 14.8 $g.l^{-1}$	12	2.9	5.3
	28	1.6	4.1
	58	1.5	3.7
C plain	12	-	3.7
	28	-	3.4
	58	-	3.2
C with [Ca-PNS] = 5.4 $g.l^{-1}$	12	0.6	3.7
	28	0.5	3.3
	58	0.5	3.1
C with [Ca-PNS] = 14.8 $g.l^{-1}$	12	1.6	4.0
	28	1.4	3.7
	58	1.4	3.2

DISCUSSION

The basic interactions of PNS with aluminate hydrates, calcium sulfate and pore solution can justify the different rheological behavior shown by the cements studied. It can be stated that the ability of C_3A hydration products to absorb PNS (yielding organomineral compounds of the type described earlier) prevents any positive effects of the admixture on the normal workability loss observed for cements B, C and D. The cement E has not an evident workability loss but

this cement is very easy to fluidify by PNS and that can be ascribed to peculiar minerological composition characterized by the absence of C_3A.

Table 5 Ionic concentration ($g.l^{-1}$) evolution of the pore fluid solution of pastes during hydration. The contribution from Na_2SO_4 present in PNS has been substracted.

	time (mm)	[PNS]	$[SO_4^{2-}]$	$[Ca^{2+}]$	$[Na^+]$	$[K^+]$
D plain	5	-	14.1	0.5	1.7	12.0
	30	-	13.1	0.6	1.8	12.7
	60	-	12.5	0.8	1.8	12.5
D with [Na-PNS] = 12.5 $g.l^{-1}$	5	1.6	15.3	1.0	2.7	11.5
	30	1.5	15.2	0.8	2.7	11.7
	60	1.5	14.2	0.9	3.0	11.4
E plain	5	-	5.9	1.0	0.9	4.3
	30	-	5.4	1.0	0.9	4.5
	60	-	4.7	1.1	1.0	4.4
E with [Na-PNS] = 12.5 $g.l^{-1}$	5	1.2	7.1	1.0	1.9	4.1
	30	0.8	5.8	0.9	2.2	3.5
	60	0.8	6.3	1.0	2.1	4.6

The cement A exhibits en abnormal early stiffening in spite of having chemical and minerological composition similar to that of cements B, C. It is important to note that the early stiffening of cement A can neither be related neither to false setting nor to attenuated rapid setting, otherwise the flow loss would have been observed in the absence of PNS.

The sulfate excess found in the pore solution of mortar of cement A in the presence of Ca-PNS cannot be attributed to an enhancement of the solubility of the set regulator (via e.g. calcium complexation), as it could have been inferred for Na-PNS taking into account the results presented in Fig. 6. Alternatively, it cannot be accounted for by assuming simply the formation of an organomineral compound, resulting from co-precipitation of PNS and C_4AH_X, because this cement has shown an absorption rate of PNS similar to that of the other cements. The only way to explain the observed phenomenon for cement A (early stiffening and excess of sulfates) hence turns out to invoke the insufficient supply of calcium and aluminate ions from aluminate phases ($C_3A + C_4AF$) to yield ettringite, due to a strong reduction of their reactivity to gypsum in the presence of PNS. The supply would however be sufficient in the absence of superplasticizer.

CONCLUSION

The previous studies dealing with early stiffening as a case of cement-admixture incompatibility evidence the fact that such a peculiar rheological behavior may be accounted for assuming that the presence of e.g. PNS leads to an insufficient supply of dissolved calcium sulfate to form ettringite (Jolicoeur et al., 1994; Dodson and Hayden, 1980; Tagnit-Hamou and Aitcin, 1993). This study does not confirm this hypothesis because the phenomenon appears to be related to an excess of dissolved calcium sulfate. Also in this case, the normal progress of hydration is not regular because no ettringite is formed. This statement corroborates the conclusion recently drawn by Bonen and Sarkar, 1995 stating that the higher the ionic strength (stemming from a higher ionic concentration), the faster the slump loss.

REFERENCES

Bombled, J.P. and Kalvenes O., "Comportement rhéologique des pâtes, mortiers et bétons: mesure, évolution, influence de certains paramètre", Revue des Matériaux de Construction 1967, (617), pp. 39-52

Locher, F.W., Richartz W., Sprung S., "Setting of Cement " Zement Kalk Gips 1980, 33, (6), 271-77

Massazza, F., Costa U., "Rheological problems related to the use of cement", Il Cemento 1982, (4), pp. 217-242

Tattersall, G.H. Banfil P.F.G., "The rheology of fresh concrete", Pitman Advanced Publishing Program, London, 1983

Costa, U., Massazza F., "Structure and properties of cement suspension", VIIIth ISCC, Rio de Janeiro 1986, Vol. VI, pp. 248-59

Wirquin, E., "Etude de l'évolution des résistances du béton très jeune en fonction de l'avancemeent de l'hydration - Role joué par la microstructure à l'état frais", Thèse, Université de Toulouse, 1993.

Fernon, V. "Etude de nouveaux solides lamellaires obtenus par coprécipitation d'hydrate aluminocalcique et de sulfonate aromatique"; Thesis, University of Orleans (France), 1994.

Hanic, F., Kapralik, I. and Drabik, M.. "Crystallochemistry and stability of monosulfoaluminate and aluminoferrite hydrates and their solid solutions"; Silikaty 1989, Vol. 33, pp. 203-214

Luke, K, and Aitcin P.C. "Effect of superplasticizer on TSA formation", Conf. on Advanced in Cementitious Materials, National Institute of Standards and Technology, Gaithersburg, 1990, Maryland, pp. 147-166

Jolicoeur, C., Simard, M.A., Aitcin, P.C. Baalbaki, M. "Cement-superplasticizer compatibility in high performance concretes: the role of sulfates"; Compilation of the most recent papers of University of Sherbrooke (Québec), Vol. II, 1994, pp. 103-128

Dodson, V.H. and Hayden, Th.D. "Another look at the Portland cement/chemical admixture incompatibility problem"; Cement, Concrete and Aggregates , CCAGDP, Vol. 11, n. 1, 1980, pp. 52-56

Tagnit-Hamou, A. and Aitcin, P.C. "Cement and superplasticizer compatibility"; World Cement 1993, pp. 38-42

Bonen, D., Sarkar, S.L. "The superplasticizer adsorption capacity of cement pastes, pore solution composition, and parameters affecting flow loss"; Cement and Concrete Research 1995, Vol. 25, (7), pp. 1423-34

3iii00
6 pp

EFFECT OF SUPERPLASTICISERS ON THE HYDRATION OF A MINERALIZED WHITE CEMENT

M.T. BLANCO-VARELA. Instituto de Ciencias de la Construcción Eduardo Torroja (CSIC)
A. PALOMO. Instituto de Ciencias de la Construcción Eduardo Torroja (CSIC)
F. PUERTAS. Instituto de Ciencias de la Construcción Eduardo Torroja (CSIC)
T. VAZQUEZ. Instituto de Ciencias de la Construcción Eduardo Torroja (CSIC)
J.R. BARAGAÑO. Consultant. Avda. Montecillo 7. Pozuelo, Madrid 28223 (SPAIN)

ABSTRACT The effect of two chemical admixtures (superplastizisers) on a normal white cement (16% C_3A) and on a mineralized cement (5% C_3A) has been studied. One of the admixtures is based on sulphonated naphthalene formaldehyde and the other on sulphonated melamine formaldehyde. Variations on setting times, on rheological properties as well as variations on mechanical strengths of mortars of both cements have been established.

Key words: Admixtures, White Portland Cement, Sulphate resistence, Strength development.

INTRODUCTION

Blanco-Varela et al (1981), Giménez et al (1991) described the procedure for obtaining new cements, using ordinary raw mixes partially substituted by fluorine and sulphates. One of the most interesting compositional characteristics of these cements are they contain a **new liquid phase** (Blanco-Varela et al., 1986) with low aluminate proportion.

The temperature of formation of the mentioned liquid phase is 1180°C and its approximated composition is :

CaO = 54%wt
Al_2O_3 = 4%wt
Fe_2O_3 = 3%wt
SiO_2 = 11%wt
CaF_2 = 4%wt
$CaSO_4$ = 24%wt

The validity of the mentioned melt for production of clinkers of low energy cost was verified in laboratory as well as in various Spanish cement factories.

The mineraliser pair F^- and SO_4^{2-} decreases alite stabilisation temperature, placing it at 1050°C.

As a function of the clinker desired (grey or white; or the same with little liquid phase that are more difficult to get), a suitable amount of mineralisers will be necessary.

As a consequence, this process provides clinkering with any type of raw mix and low energy cost, being its action more decisive in the so-called "very hard burning".

Most of the characteristics of the new raw mixes are similar to those of the traditional ones. So, the proportion of hydraulic calcium silicates (alite and belite) remains similar or even increased in the mineralised cement; however, mineralogical composition of the new cement is different

to that of the normal cement with respect to interstitial clinker phase, because aluminates and ferrites may be substituted, even totally by the phase called **fluorellesteadite** (Fell.) : $Ca_{10}(SiO_4)_3(SO_4)_3F_2$.

In these cases, because of the low aluminate content (as in the case of sea-water and sulphate resistant cements SR-MR of spanish standard UNE 80.305 and type V of ASTM), and with respect to normal white cements, they lead to longer setting times and lower mechanical strengths at early ages, although at longer times, the strengths are higher. There are little differences in microstructural developments in the pastes obtained from the two cements; with except of a considerably lower ettringite content in the case of the mineralised cement. Fluorellesteadite, an extremely stable phase, remains unaltered with cement hydration.

Other advantages of the new cements, with respect to that obtained according to the traditional process are:

- Decrease in environmental pollution caused by dust emission.
- Increase in specific clinker production
- Better performance in cement mills
- Low hydration heat
- Better strengths at long ages.

The effect of additions on mineralised cements have not been verified. The different nature of the liquid phase of said cements it is supposed to influence the effect of the chemicals when compared to the normal cement. At least, with respect to rheological characteristics, setting time and early age strengths.

The aim of the present work is to verify the effect of two commercial superplasticizers (hyperplasticising admixture) of general use, on a SR-MR white mineralised cement. One of the admixtures used is of sulphonated melamine formaldehyde type (S.M.F.) and the other is based on sulphonated naphthalene formaldehyde (S.N.F.).

EXPERIMENTAL

The normal clinker used in this work has been obtained in a spanish factory of white cement. The mineralised white clinker used has been obtained in the same factory, but modifying the raw mix with the mineraliser pair $CaF_2/CaSO_4$. The mineralised cement was obtained from this clinker, but after a period of time which generated on it to a partial meteorization.
The characteristics of the superplastizicers utilised are the following:

SNF: S.g. (specific gravity) = 1.21 g/cc
solid content = 40%
pH = 7.1± 0.5

SMF: S.g.= 1.24 g/cc
solid content = 40%
pH = 12 ±0.5.

The chemicals were used in proportion 1% in weight of the cement and they were added to mixing water. The settings has been carried out on pure paste by Vicat needle and workability

loss is measured with a mini-slump using mortars (1:3), and measuring the flow after 60 minutes rest.

To make the mechanical strength tests comparable in all cases, 1:3 mortars have been obtained at constat flow. This is, varying the european standard E.N. 197.1 that recommends that water remains constant (w/c = 0.5).
Compressive strengths have been tested at 1, 3, 7 and 28 days. Cements characteristics have been proved with and without the admixtures.

RESULTS AND DISCUSSION

The general characteristics of the clinkers which were the base for the cements studied are given in Tables 1 and 2, respectively.

Obviously, Bogue formulas and moduli cannot be applied to the case of mineralised clinker. For example, fluorellesteadite formation means to fixed certain proportions of Si and Ca that will not be integrated in phases hydraulically active. In this case modified Bogue formulas and LSF moduli are applied. Anyway, for their relative value, they are given in Table 2.

TABLE 1 CHEMICAL ANALYSIS OF THE INDUSTRIAL WHITE CLINKERS (% wt)

CLINKER	L O I	F LIME	SiO_2	Al_2O_3	Fe_2O_3	CaO	MgO	F^-	SO_3	K_2O	Na_2O	$(SO_3)s$ (*)	$(K_2O)s$	$(Na_2O)s$
NORMAL	0,50	0,63	23,1	6,2	0,28	67,8	0,83	0,24	0,89	0,14	0,05	0,31	0,02	0,01
MINERAL	0,90	0,84	23,8	2,3	0,27	68,0	0,48	0,85	3,5	0 12	0,04	0,65	0,01	0,01

(*) $(SO_3)s$-$(K_2O)s$-$(Na_2O)s$ - Water soluble

TABLE 2 RATIOS AND MAIN CLINKER PHASES

CLINKER	L S F	S/A+F	A/F	C_3S	C_2S	C_3A	C_4AF	FeII
NORMAL	92,4	3,6	22,1	55	25	16	0,85	--
MINERAL	93	9,3	8,5	66,7	10,5	5,6	0,85	14

The major difference between both clinkers is the moderate value of SO_3 (0.89%) and the high value of Al_2O_3 (6.2%) in the normal cement and the high SO_3 value (3.5%) and low Al_2O_3 value (2.3%) in the mineralised cement. C_3A content is of 16% in the first case and of about 5% in the second case. In spite of the different SO_3 proportion, water soluble sulphates are low in both cases. Likewise, both clinkers are "low -alkali". C_3S and C_2S sum is similar in both cases. Of course the mineralised clinnker contains the new phase Fluorellestadite.

After clinkers grinding in laboratory in the same conditions, normal clinker (with high C_3A content) gives higher initial strengths, having the mineralised clinker higher values at 7 days (Table 3).

TABLE 3 PHYSICAL CHARACTERISTICS OF THE INDUSTRIAL WHITE CLINKERS

CLINKER	WHITENESS	BLAINE	COMPRESSIVE STRENGTH (E N 1971)(N/mm²)			
			1 DAY	2 DAYS	7 DAYS	28 DAYS
NORMAL	83	3 900	18	33	57	67
MINERALIZED	83	3 900	12	27	58	75

The fineness and whiteness indexes are similar in both clinkers. The cements used in the present study were obtained from former clinkers, but, as it has been said, the mineralised cement was manufactured from a slightly meteorised clinker, which has negatively influenced strength development, mainly at early ages. This fact was thought would show better the admixture effect and by this reason, the use of this cement was considered suitable for this study. That effect shows why L.O.I. values (2,5%) and F. Lime values (1.0%) in the cement (Table 4), are higher than those of the clinker, showed in Table 1.

Optimum gypsum amount for normal cement is of 5% and it is of 2% in the mineralised cement.

TABLE 4 CHEMICAL ANALYSIS (%wt) OF HITE CEMENTS USED

CEMENT	L O I	F LIME	SiO_2	Al_2O_3	Fe_2O_3	CaO	MgO	F^-	SO_3	K_2O	Na_2O	$(SO_3)s$	K_2Os	Na_2Os
NORMAL	1,6	0,6	22,0	5,9	0,28	66,0	0,90	0,21	3,1	0,14	0,05	2,1	0,01	0,01
MINERAL	2,4	1,0	22,9	2,2	0,26	66,2	0,46	0,82	5,1	0 12	0,04	1,8	0,01	0,01

Setting times and rheological characteristics.

The effect of admixtures on setting time depends on cement type. The parameters with major influence are: fineness, alkalis, different sulphate forms and C_3A content.

In the cements here studied, fineness differences are inexistent; SO_3 soluble content is similar (approx. 2%) and alkaline sulphates are very low, hence, their influence on setting times is negligible. The most notable difference between both cements is the corresponding C_3A content.

Soluble SO_3 to C_3A ratio is 0.14 in the normal clinker an 0.36 in the mineralised clinker. So in the latter, C_3A hydration is blocked before - ettringite formation rate is higher- than in cement with higher C_3A content. This is, setting duration is longer than in normal cement.
The C_3A that has not reacted with sulphates, adsorb the admixtures acting these as regulators: as a consequence, setting duration is longer.

In the case of mineralised cement, admixtures shorten setting duration because they inhibit the sulphate reaction. Setting times of both cements after admixtures addition are similar and they correspond to normal values (Table 5).

TABLE 5 TIME OF SETTING (PASTE)

CEMENT	BLAINE	% ADM	I. SET	F. SET	% ADM	I. SET	F. SET	% ADM	I. SET	F. SET
NORMAL	3730	0	199'	159'	1% S.N.F.	174'	219'	1% S.N.F.	139'	179'
MINERAL	3690	0	169'	264'	1% S.M.F.	134'	234'	1% S.M.F.	139'	214'

Sometimes, admixtures fluidifying action is short and the time necessary for a determined work is not maintained. In Table 6, mini-slump loss is shown for both cements after 60 minutes rest.

TABLE 6 EFFECT OF TIME ON THE FLOW (MORTAR)

CEMENT	%ADMIXT.	w/c	FLOW 1'	FLOW 60'	%ADMIXT.	w/c	FLOW 1'	FLOW 60'	%ADMIXT.	w/c	FLOW 1'	FLOW 60'
NORMAL	0	0,578	110±5	32	1%S.N.F.	0,511	110±5	47	1%S.M.F.	0,518	110±5	36
MINERAL.	0	0,544	110±5	31	1%S.N.F.	0,453	110±5	15	1%S.M.F.	0,436	110±5	57

The same behaviour is observed in both cements when they have no admixture. Superplasticizing SNF addition enhances workability in normal cement, whereas SMF enhances that of the mineralised cement.

Mechanical strengths

In order to make comparable the tests, mortars were obtained at constant flow of 110±5, varying water proportion. Water content of specimens done with mineralised cement was always lower than in the case of mortars done with C_3A high content cement (Table 7). This also happens in mortars with admixture.

TABLE 7 COMPRESSIVE STRENGTH E.N. 1971 MODIFIED. - c/s = 1/3 W/C = VARIABLE; FLOW=k=110 ± 5

CEMENT	%ADMIXTURE	W/c	1 DAY %	3 DAYS %	7 DAYS %	28 DAYS %
NORMAL	0	0,578	100%	100%	100%	100%
MINERAL	0	0,544	69%	74%	76%	92%
NORMAL	1% S.N.F.	0,511	146%	126%	122%	117%
MINERAL	1% S.N.F.	0,453	114%	114%	113%	120%
NORMAL	1% S.M.F.	0,518	144%	120%	110%	98%
MINERAL	1% S.M.F.	0,436	132%	116%	116%	121%

In the same Table 7, values of compressive strength (in percentage) are shown, given at 100% value to results obtained with normal cement; it is observed that specimens elaborated with mineralised cement, with low C_3A content, present lower strengths at early ages than normal cement. Particularly, at 24 hours, they are 60% of those. Values are similar at longer ages.

In specimens elaborated with normal cement and SNF admixture, strengths are higher to those obtained with SMF, being generally more acute the strengths increase at early ages (146% with SNF at 24 h) than at long ages (98%, at 28 days with SMF).

Oppositely, with the mineralised cement, the highest strengths are reached with SMF admixture.

In general, the response of mineralised cement is very good with both admixtures, reaching percentage increases with respect to those of the cement without admixtures higher than those of the normal cement, specially at early ages, which was the weaker aspect of this cement (Table 8).

TABLE 8 EFFECT OF CHEMICAL ADMIXTURES ON COMPRESSIVE STRENGTH (CEMENT MINERALIZED)

% ADMIXTURE	w/c	1 DAY %	3 DAYS %	7 DAYS %	28 DAYS %
0	0,544	100	100	100	100%
1% SNF	0,453	165	154	150	131
1% SMF	0,436	192	158	153	132

SUMMARY AND CONCLUSIONS

The difficult burnability of the white clinker with low C_3A content is highly enhanced with the adequate dosage of the raw mix with the mineraliser pair gypsum-fluorite, saving more than 10% of the clinkering energy. Besides, a lower consumption in Kwh/T in the mills is reached because of an easier clinker grinding.

The cements elaborated with this clinker are resistant to aggressive agents (gypsum and sea water), although, as a consequence, setting time and strengths at early ages are somehow altered. They are lower than those corresponding to cements with high and moderate C_3A contents. The addition of superplastizicing admixtures based on SNF and SMF to the mineralised cement shortens setting time and considerable increases strengths, specially at early ages.

With SMF, flow is maintained for a longer time. Hence, with mineralised cement, concretes with equal or better rheological behaviours than those of white concrete of high resistance can be manufactured with the advantage that they will be resistant to aggressive agents (sulphates and sea water).

BIBLIOGRAPHY

Blanco-Varela, Mª T., Vázquez, T. "Ahorro de energía en la clinkerización empleando CaF_2 y $CaSO_4$ como mineralizadores. Estudio de la fluorellestadita· " Materiales de Construcción. nº181, 1981, pp55-64

Giménez, S., Blanco-Varela, Mª T., Palomo, A. and Puertas, F. "Production of cement requiring low energy expenditure - An industrial test". Zement-Kalk-Gips, nº1, vol.44, 1991, pp12-15

Blanco-Varela, Mª.T., Vázquez, T. and Palomo, A. "A studdy of a new liquid phase to obtain low-energy cements". Cement Concrete Research. Vol.16, 1986, pp97-104

EFFECT OF TRIISOPROPANOLAMINE ON HYDRATION AND STRENGTH DEVELOPMENT OF CEMENTS WITH DIFFERENT CHARACTER

Makihiko ICHIKAWA, Chicibu Onoda Cement Co., Ltd., Central Research Laboratory
Muneki KANAYA, Chicibu Onoda Cement Co., Ltd., Central Research Laboratory
Susumu SANO, Chicibu Onoda Cement Co., Ltd., Central Research Laboratory

ABSTRACT This study deals with the relation of cement characters to the effects of triisopropanolamine (TIPA) as an accelerator of hydration and strength development. TIPA enhanced the 28 day mortar strength development of the cement with ferrite phase. The content of alite and the fineness of cement were also concerned with the effects of TIPA; i.e., the increased degree of the strength development with TIPA became high with increasing the former and decreasing the latter. TIPA was further valuable for the cements containing high amounts of limestone and gypsum (SO_3) because of their reaction with ferrite phase during hydration.

Key-words: Accelerators, Alite, Ferrite phase, Lime, Gypsum

INTRODUCTION

Organic agents give a significant influence on the hydration of portland cement (Suzuki et al. 1959, Ramachandran 1976). E. Gartner et al. (1993a) have clarified that TIPA accelerates the hydration of ferrite phase as a result of increasing the solubility of ferric hydroxide which is produced by the hydration of ferrite phase and inhibits the subsequent hydration. Further, TIPA enhances the strength development of cement mortar because its effect on ferrite hydration leads to the promotion of the hydration of silicate phases which form a cement grain with ferrite phase.

The present study deals with the influence of cement characters such as mineral composition of the clinker used, fineness, amount of added limestone and SO_3 content on the strength enhancement of cement mortar with the addition of TIPA.

MATERIALS

Three types of cement clinkers N, L and W, of which mineral compositions are different as shown in Table 1, were ground with gypsum in a ball mill to a given blaine specific surface area. Limestone (Calcite) with the chemical composition shown in Table 2 was separately ground to blaine specific surface area of 392m²/kg. The characters of the prepared cements are listed in Table 3. TIPA used is a reagent with a purity of more than 95%.

Table 1 Mineral composition of clinker.

Clinker	Mineral composition (wt%)*			
	C_3S	C_2S	C_3A	C_4AF
N	58	20	11	9
L	30	57	3	8
W	60	26	12	1

* Calculated with Bogue equation

Table 2 Chemical composition of limestone.

Chemical composition (wt%)								
ig.loss	SiO_2	Al_2O_3	Fe_2O_3	CaO	MgO	SO_3	Na_2O	K_2O
43.2	0.8	0.4	0.2	54.6	0.6	0.0	0.1	0.1

Table 3 Characters of cements prepared.

Clinker	Blaine specific surface area (m^2/kg)	Limestone content (wt%)	SO_3 content (%)
N	260	0	2.0
	280	0	2.0
	325	0	2.0
		3	2.0
		5	1.0, 2.0, 3.0
		10	2.0
L	325	0	2.0
W	325	0	2.0

EXPERIMENTAL

Determination of compressive strength

The compressive strength of cement mortar after 3, 7 and 28 days was determined in accordance with JIS R 5201. Since TIPA is solid at room temperature, it was previously dissolved in the mixing water. The amount of TIPA added was 0.01wt% of the cement.

Observation of alite and belite crystals in cement

Microscopic observations have been made to examine the cement grains consisting of alite and belite crystals.

Identification of hydration products and determination of the hydration degrees of cement constituent minerals

The cements with blaine specific surface area of 325m^2/kg prepared from clinker N with and without limestone admixture were mixed with water at the W/C ratio of 0.4. The cement pastes were kept in small sealed glass jars at 20℃ for 3 and 28 days. TIPA was added in the same manner as in the compressive strength test. Hydration was stopped by grinding with acetone. It was then dried in a nitrogen atmosphere of 15% R.H. for 3 hours.

Using the prepared samples, the crystalline hydration products were identified with powder X-ray diffractometry. The X-ray diffractometer with CuKα radiation (40kV 150mA) was used at a scan rate of 5° 2θ/min. The DS, SS and RS are 1°, 1° and 0.15mm, respectively.

The degrees of hydration of alite, ferrite phase and limestone after 28 days were also determined. The measuring conditions of the X-ray diffractometer are the same as above except for carrying out the step scanning with each 2θ step 0.02° and fixed time 8 seconds. α-Al_2O_3 was used as the internal standard. According to Ishizaki et al. (1988) and Asaga (1995) the peaks used were 0 4 0,14 2 4 (d=1.76Å, 1.77Å) of alite, 0 2 0 (d=7.27Å) of ferrite phase, 1 0 4 (d=3.04Å) of limestone (Calcite) and 0 2 4 (d=1.74Å) of α-Al_2O_3.

RESULTS AND DISCUSSION

Fig. 1 shows the relation of the mineral composition and blaine specific surface area with the strength enhancement by TIPA. The compressive strength of mortar with the cement W*, which contains almost no ferrite phase, was not enhanced by TIPA. This indicates that the effect of TIPA as an accelerator of the ferrite phase hydration (Gartner and Myers1993a) is definitely concerned with the strength enhancement. However, a large difference in the above effect by TIPA was obtained even between the cements N and L in which the amount of ferrite phase was nearly equal; the ratio of the mortar strength with TIPA to that without it was obviously high in the cement N. The decrease in blaine specific surface area increased the difference. These are explained by taking into account the differences in the ratio of silicate phases (alite and belite) and in their grindability. Of four main minerals in clinker, belite shows the strongest resistance to fracture (Hornain and Regourd 1980), so that fractures are apt to occur along the crystal grain boundary of belite during clinker grinding (Maki et al. 1993b). In contrast, the high grindability of alite causes fractures to penetrate into the alite crystal, leading to the existence of alite as a

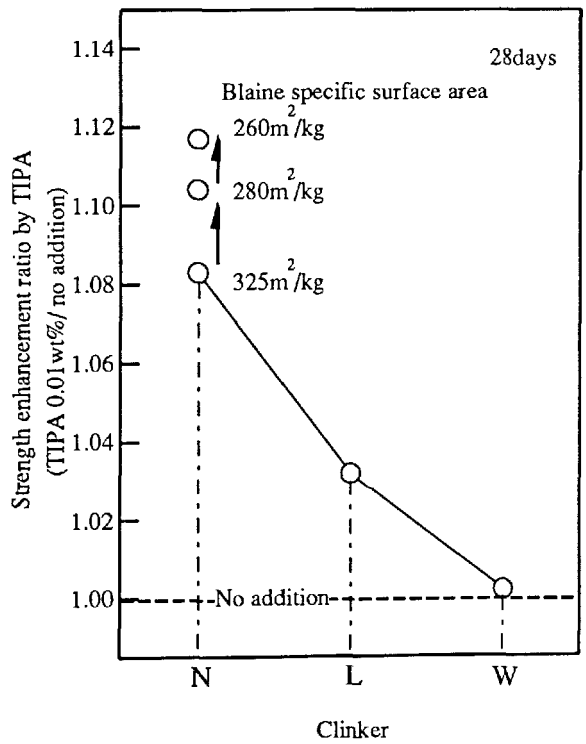

Fig. 1 Relation of the mineral composition and blaine specific surface area with the strength enhancement by TIPA. (SO_3: 2.0%)

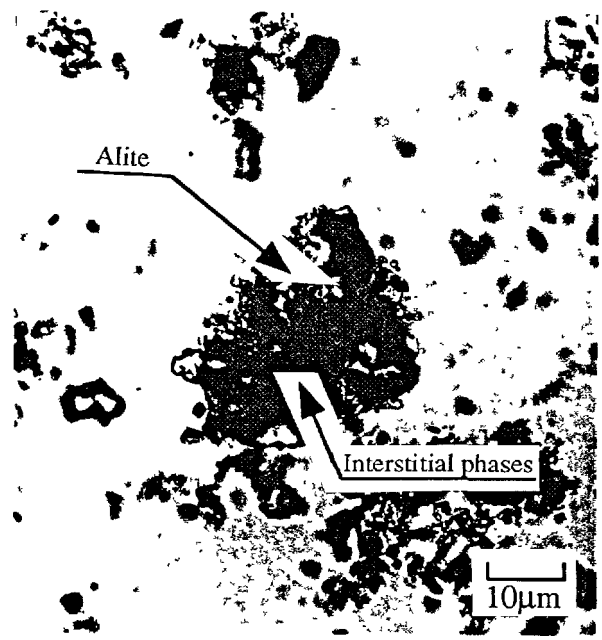

Fig. 2 Alite crystal coexisting with interstitial phases in a cement grain.

* Cement W (N and L) ; Cement prepared from clinker W (N and L)

polymineralic grain after grinding. According to our microscopic observations, belite in cement mostly existed as a single grain though some coarse clusters of belite in the fraction over 30μm in diameter were observed. Meanwhile, as shown in Fig. 2, alite frequently coexisted with interstitial phases including ferrite phase in a grain. Gartner et al. (1993a) suggested that in a polymineralic grain the accelerated hydration of ferrite phase by TIPA will expose surfaces of the adjacent silicate phases and consequently accelerate the hydration of them. The difference in strength enhancement of mortar by TIPA between the cements N and L is considered to be caused by the difference in the proportion of polymineralic grain; i.e., the cement N, which is abundant in alite, includes a high amount of polymineralic grains, resulting in a high strength enhancement by TIPA. It was easily understood that the decrease in blaine specific surface area increases the polymineralic grains and the strength enhancement by TIPA. In conjunction with belite content it took a longer time for grinding the clinker L to a given fineness compared to the other clinkers and thus fine single grains of alite were easily observed in the cement L. This is presumably one of the reasons why the strength enhancement by TIPA is limited in the cement L.

Fig. 3 shows the relationship between the limestone content in cement and the strength enhancement of mortar by TIPA. The strengths of mortar after 3 and 7 days were almost constant regardless of the limestone content and the addition of TIPA. On the other hand, the 28 day strength decreased to a considerable extent with the increase in the limestone content but the addition of TIPA depressed the decrease; i.e., the effect of TIPA was enlarged with the increase in limestone admixture.

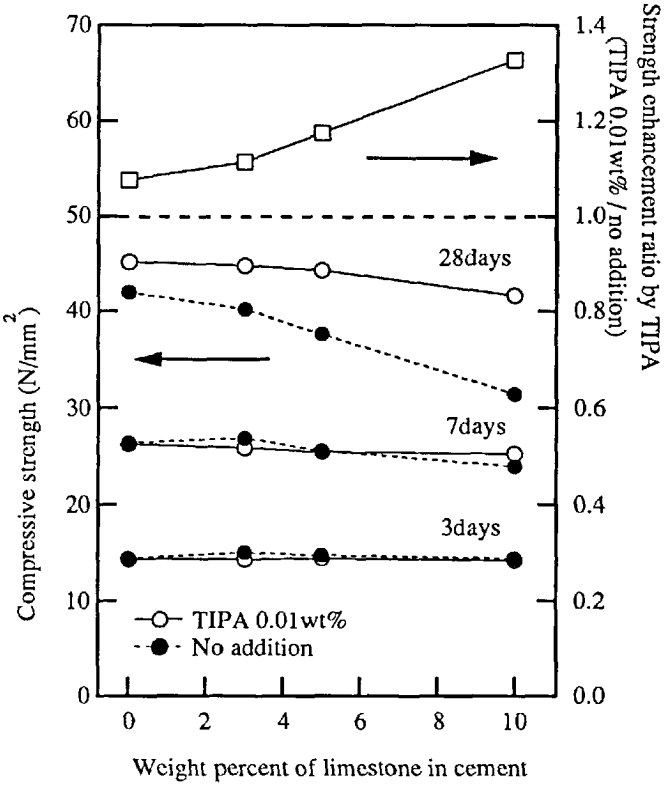

Fig. 3 Relationship between the limestone content in cement and the strength enhancement of mortar by TIPA. (Clinker: N, Blaine specific surface area: 325m^2/kg , SO_3: 2.0%)

Fig. 4 illustrates the X-ray diffraction patterns of cement hydrated for 3 and 28 days. The crystalline hydration product after 3 days was only ettringite, independent of the addition of TIPA and limestone and moreover, estimating from the peak height, no difference in quantity was confirmed. Gypsum in cement has already been consumed. These facts indicate that TIPA and limestone are not thoroughly concerned with the formation of such hydration products and the reaction in Eq. 1 preferentially proceeds. Because the solid solubility of Fe_2O_3 into hydrates is limited (Fukuhara et al. 1981) it is actually deposited as iron hydroxide in the same way as formulas in Eqs 2 and 3.

$$C_3A,\ C_4AF + 3CaSO_4 \cdot 2H_2O + 26H_2O \rightarrow C_3(A,\ F) \cdot 3CaSO_4 \cdot 32H_2O \quad [1]$$

This result is consistent with the experimental fact in Fig. 3 that the addition of TIPA, regardless of the limestone content, gives little effect on the initial strength of the mortar.

Meanwhile, the hydration products after 28 days remarkably varied in each cement. The ettringite changed to monosulfoaluminate hydrate in the cement without limestone and TIPA accelerated the change. No monosulfoaluminate hydrate was produced in the cement with limestone but calcium carboaluminate hydrates, which increase in amount with the addition of TIPA, were substitutionally produced. These indicate that TIPA and limestone definitely participate in the later stage of cement hydration and the acceleration of ferrite hydration with TIPA promotes the reactions in Eqs 2 and 3.

$$C_3(A,F) \cdot 3CaSO_4 \cdot 32H_2O + 2C_3A,\ C_4AF + 4H_2O \rightarrow 3C_3(A,\ F) \cdot CaSO_4 \cdot 12H_2O \quad [2]$$

$$C_3A,\ C_4AF + 3CaCO_3 + nH_2O \rightarrow C_{3.5}(A,\ F) \cdot 1/2CaCO_3 \cdot 12H_2O,\ C_3(A,\ F) \cdot CaCO_3 \cdot 11H_2O \quad [3]$$

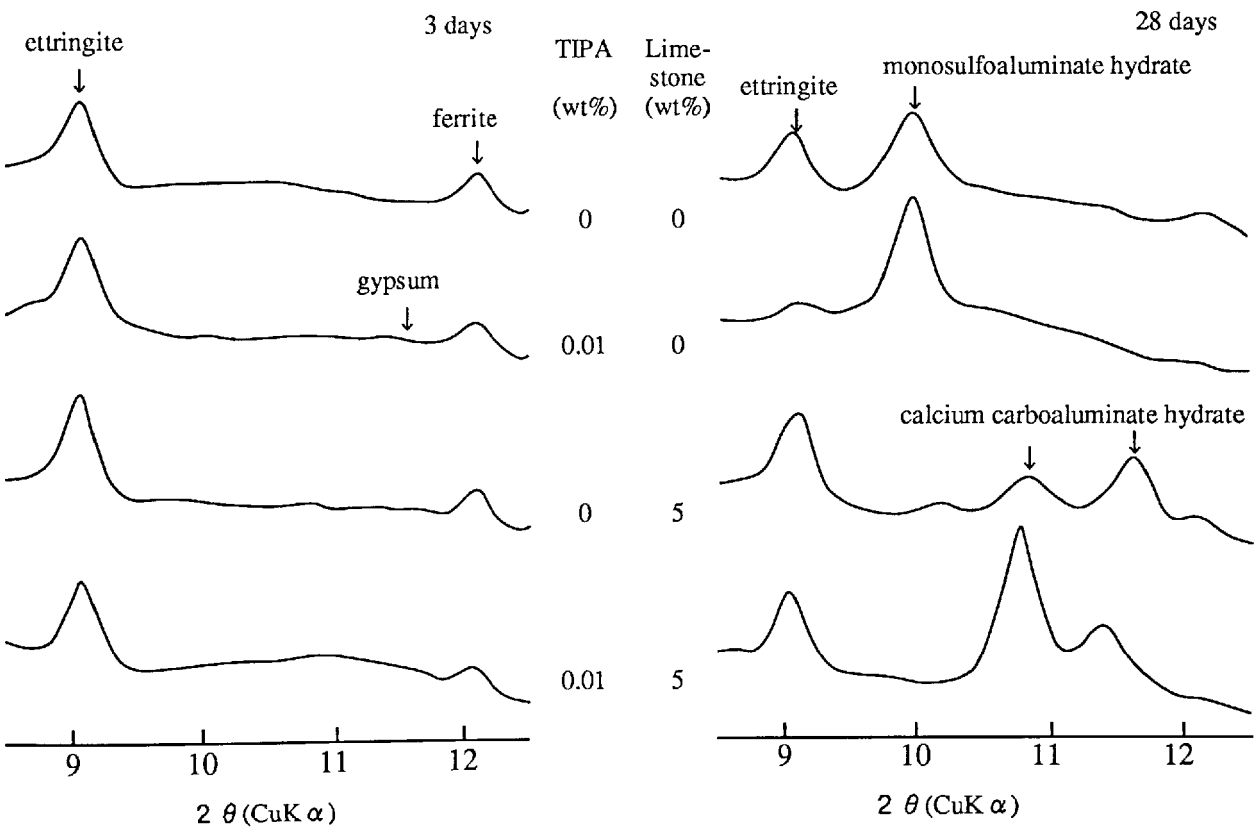

Fig. 4 X-ray diffraction patterns of cement hydrated for 3 and 28 days.
(Clinker: N, Blaine specific surface area: 325m^2/kg , SO_3: 2.0%)

Table 4 shows the hydration degree of cement constituent minerals after 28 days. As suggested from the variation in hydration products, the hydration degree of ferrite phase and limestone were evidently increased with the addition of TIPA. The hydration of alite was also promoted. The promotion of the hydration of limestone in addition to those of ferrite phase and alite is considered to be concerned with the experimental fact shown in Fig. 3 that the strength enhancement by TIPA increased with increasing limestone content in cement.

Table 4 Hydration degrees of cement constituent minerals after 28days.
(Clinker : N , Blaine specific surface area : 3250cm^2/g)

Limestone	TIPA	Hydration degrees (%)		
		C_3S	C_4AF	Limestone
—	—	79	40	—
	0.01wt%	86	73	—
5wt%		82	37	18
	0.01wt%	91	80	39

The strength enhancement by TIPA, as shown in Fig. 5(a), varied with SO_3 content in cement without limestone. The mortar strength after 28 days, when TIPA was not added, increased with decreasing SO_3 content in the range from 1.0% to 3.0%, while that was a maximum at the SO_3 content of 2.0% when TIPA was added. Accordingly, the strength enhancement ratio by adding TIPA was increased with SO_3 content. Khus (1959) confirmed that the optimum SO_3 content to obtain a maximum strength increases with increasing the amounts of interstitial phases such as the aluminate

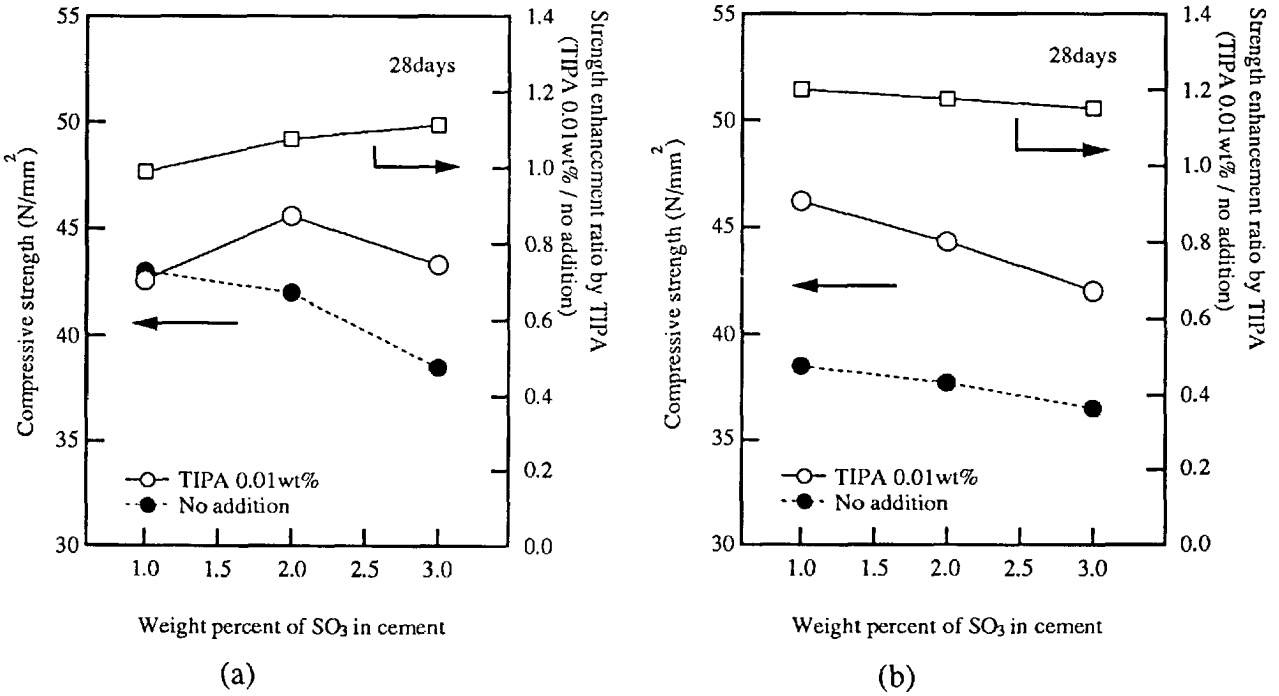

Fig. 5 Relationship between SO_3 content in cement and increase in the strength development with TIPA.
(a): Cement without limestone (b): Cement with 5wt% limestone (Clinker: N, Blaine specific surface area: 325m^2/kg)

and ferrite phase. Postulating that the acceleration of the ferrite hydration by TIPA is equivalent to the increase in the interstitial phases in cement, it can be explained that the optimum SO_3 content became high by adding TIPA. However, in case of the cement with limestone shown in Fig. 5(b), since limestone presumably compensates for the shortage of SO_3 (Bensted 1983), the 28 day strength monotonously decreased with SO_3 content even when TIPA was added, and so the difference in the strength enhancement ratio by TIPA with SO_3 content was not apparent. The increase in the hydration degree of limestone with decreasing SO_3 content, as shown in Fig. 6, supports this.

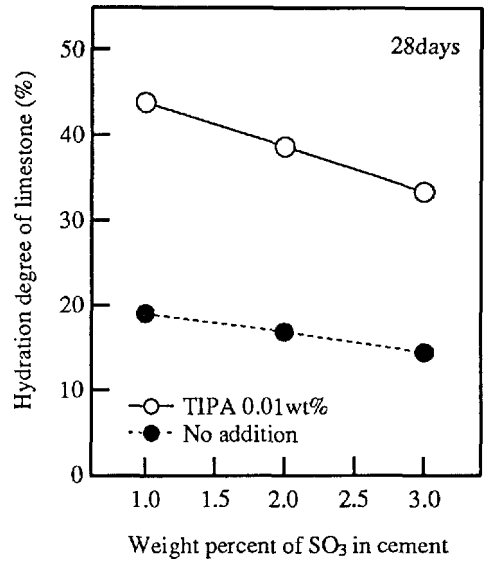

Fig. 6 Relationship between SO_3 content in cement and hydration degrees of limestone. (Clinker: N, Blaine specific surface area: 325m^2/kg, Limestone: 5wt%)

CONCLUSIONS

(1) The strength enhancement of cement mortar by TIPA depends on the quantity of ferrite phase. No effect was obtained on the cement prepared from the clinker without ferrite phase.
(2) Alite content and fineness of cement were also related to the above effect. An increase in the former and a decrease in the latter intensified it. These were understood by taking into account the grain properties of alite and belite in cement.
(3) When cement includes limestone admixture, the strength enhancement ratio with the addition of TIPA after 28 days became high because of the promotion of the limestone reaction in addition to that of ferrite and alite hydration.
(4) The promotion of ferrite hydration by adding TIPA increased the optimum SO_3 content in cement concerning the 28 day strength development. Limestone admixture depressed the increase.

REFERENCES

Suzuki, S. and Nishi, S., "Influence of saccharides and other organic additives on the hydration of portland cement", JAPAN CEMENT ENGINEERING ASSOCIATION Review of the 30th general meeting, May 1959, pp. 34.

Ramachandran, V.S., "Hydration of cement -- Role of triethanolamine", Cement and Concrete Resarch, Vol. 6, 1976, pp. 623-632.
Gartner, E. and Myers, D., "Influence of tertialy alkanolamines on portland cement hydration", Journal American Ceramic Society, 76[6], 1993, pp.1521-1530.
Ishizaki, M., Asaga, K., Daimon, M. and Takahashi, S., "Measurement of reaction ratio of each compound in hydration process of portland cement", JAPAN CEMENT ENGINEERING ASSOCIATION Revew of the 42nd general meeting, May 1988, pp. 38.
Asaga, K., Private communication.
Hornain, H. and Regourd, M., "Fissuration et broyabilite du clinker", 7th International Congress on the Chemistry of Cement, 1980, Vol. 1, pp. 276-281.
Maki, I., Ito, S., Tanioka, T., Ono, Y. and Fukuda, K., "Clinker grindability and textures of alite and belite", Cement and Concrete Resarch, Vol. 23, 1993, pp. 1078-1084.
Fukuhara, M., Goto, S., Asaga, K., Daimon, M. and Kondo, R., "Mechanisms and kinetics of C_4AF hydration with gypsum", Cement and Concrete Resarch, Vol. 11, 1981, pp. 407-414.
Kuhs, V. R., "Einflus des gipses auf klinker mit verschiedenem aluminatgehalt", TIZ-Zbl, Vol. 83, 1959, pp. 388-394.
Bensted, J., "Further hydration investigations involving portland cement and the sbstitution of limestone for gypsum", World Cement, December 1983, Vol.14, pp. 383-392.

INFLUENCE OF SUCROSE ON THE SETTING OF PORTLAND CEMENT

Peiming WANG, Jianguo WU, Tongji University, Shanghai, China

ABSTRACT The setting of portland cement in the presence of sucrose was studied.The amount of sucrose varied between 0.03% and 4.00% on the weight of cement.There exists a critical addition amount of sucrose to the maximal setting time.Sucrose as a retarder becomes a accelerator when its adding exceeds a given amount. The mechanism of regulation set of sucrose was discussed from the results of QXDA and SEM of hydrates and analysis of pore solution of cement paste. The influence of sucrose on setting is, most probably,dependent on the quantity of AFt crystals formed.

Key-words: cement; setting; sucrose; mechanism

INTRODUCTION

Sucrose is an effective set-retarding admixture for cement. Different addition methods, direct and delayed, result in different effect on set (Ludwig and Urrutia, 1989 ;Wang,1995). There have been theories of the set-retardation mechanism of sucrose. Those are adsorption of sucrose on the surfaces of hydrates(Thomas and Birchall 1983; Young, 1972)and inhibition of nucleation and growth of calcium hydroxide (Banfill and Saunders, 1986). However, these theories were deduced from results with a small dosage of sucrose, and through which, one can not explain the set-accelerating effect of surcrose. In this paper, we try to approach the set-regulation mechanism of sucrose on different exprimental data.

EXPERIMENTAL

525 II portland cement with 1.84% SO_3 was used to make cement pastes without and with sucrose of a w/c ratio varied with the standard consistancy,then they were cured under 20 °C. Setting times were measured using a Vicat needle.For determination of ion concentrations in pore solution of paste, the aqueous phase was extracted and analysed with a frame photometer for K^+ and Na^+ and with EDTA titration for $Ca^{2+}$and Al^{3+} after a given time. For SEM, after 40 d curing, the samples were immered in absolute alcohol for 24 h and dried under 40 °C for 48 h to stop their hydration. For the quantitative x-ray diffraction analysis, at the initial and final setting times, the samples immered with absolute alcohol were ground into fine powder and dried under 40 °C .

RESULTS AND DISCUSSION

Setting time

Fig 1 shows the setting times of the cement pastes with standard consistancy. We (Wang,1995) difined the addition amount at which the final setting time reaches maximal as the critical addition amount . In this experiment the critical addition amount lies in about 0.1%, the responding setting times are 7.4 h (initial) and 12 h (final), which agrees with our former results (Wang,1995) absolutely. When the content of sucrose is below the critical addition amount, the setting times increase with the adding; when the amount of sucrose exceeds the critical amount, setting times decrease with the adding, even become more shorter than that of the cement paste without sucrose, e.g. addition more than 0.4% makes the setting time less than 1 h. Sucrose can not only retard but also accelerate setting of portland cement, it deponds on the content of sucrose when the cement component is not considered.

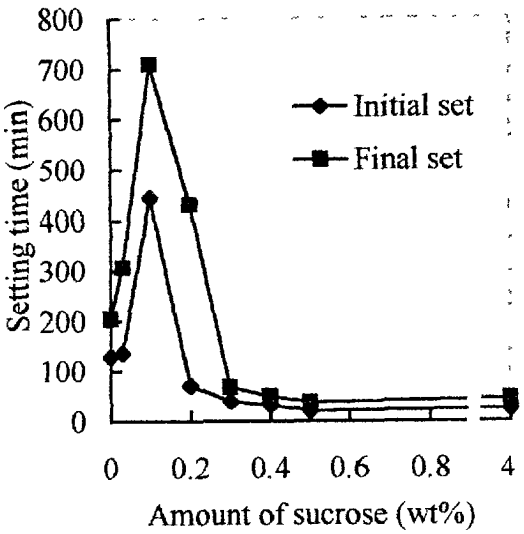

Fig 1 Change of setting times with amount of sucrose

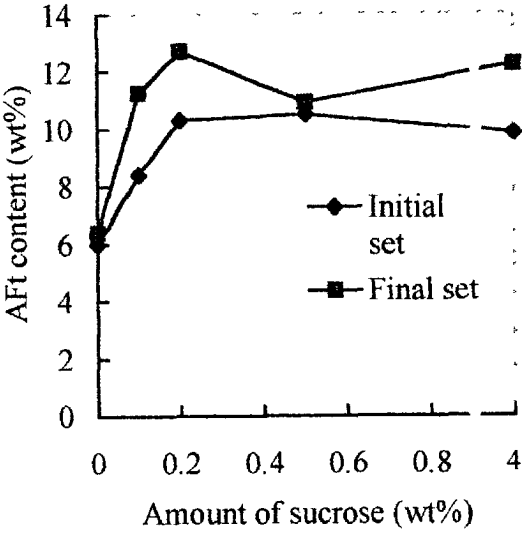

Fig 2 Change of AFt content with amount of sucrose

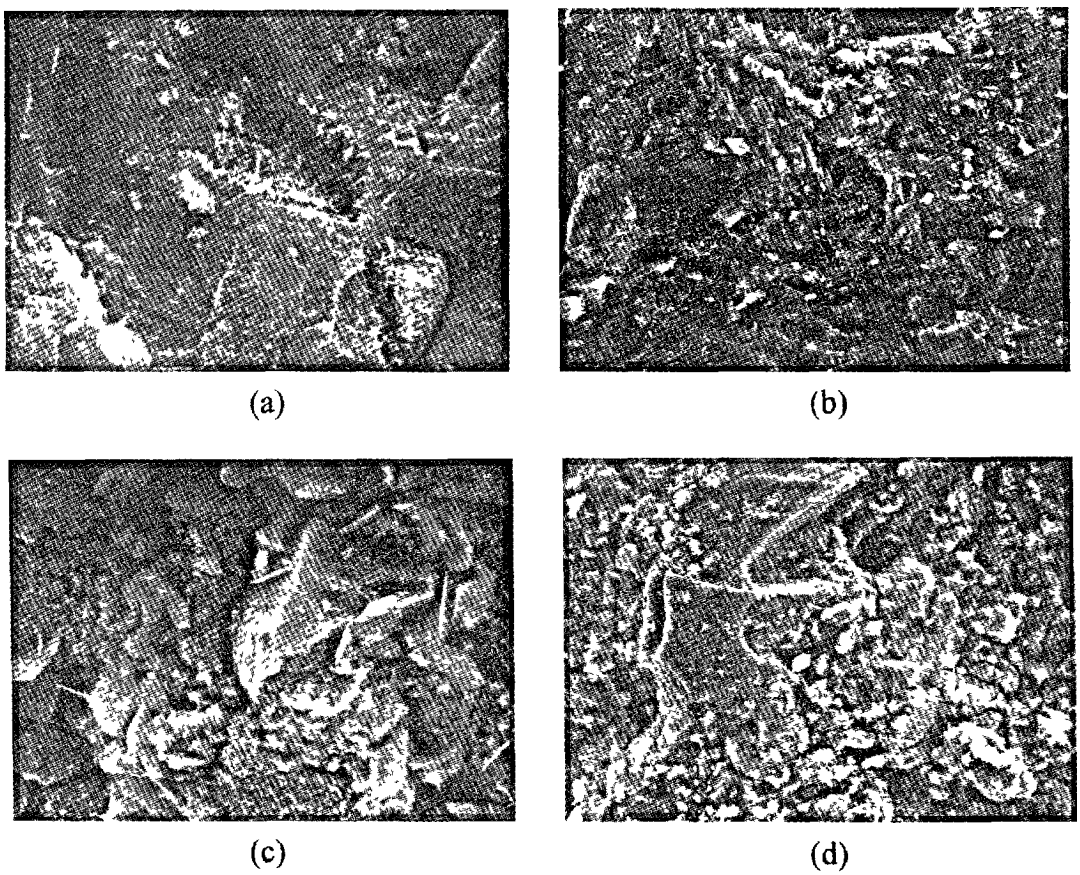

Fig 3 Morphologies of cement pastes with sucrose (a) 0%; (b) 0.2%; (c) 0.5%; (d) 4.0% 1000X

Hydrates

Fig 2 shows that the AFt contents obtained by QXDA,which increases with amount of sucrose at both initial and final setting times. This means that sucrose accelerates the formation of AFt crystals. Fig 3 gives morphologies of cement pastes by SEM. With pastes of more sucrose, the silicate phases yet maintain a distinct outline after 40 d (Fig 3(c) and (d)),the mittel phases have

hydrolysed and retain a cavity. This proves the inhibition action of sucrose on the hydration of silicate phases.

Ion concentrations

Fig 4 shows concentrations of K^+, Na^+, Ca^{2+} and Al^{3+} in pore solution of the cement pastes. It is evident that the concentrations of these ions vary with the amount of sucrose significantly. The K^+, Na^+ and Al^{3+} concertrations increase in line with the rise of sucrose almost at all curing times. The Ca^{2+} ions,however,decrease with the adding of sucrose, except at 0.2%, at early age. With the curing times the Ca^{2+} ions fall at almost all dosages, except 0.03%.The decrease of Ca^{2+} concertrations at early age is due to the inhibition of C_3S hydration, at late age to the complexing with sucrose. The increase of K^+, Na^+ and Al^{3+} proves a fact that the sucrose accelerates the hydrolyse of C_3A,because K_2O and Na_2O existed in C_3A phase of portland clinker,mainly.

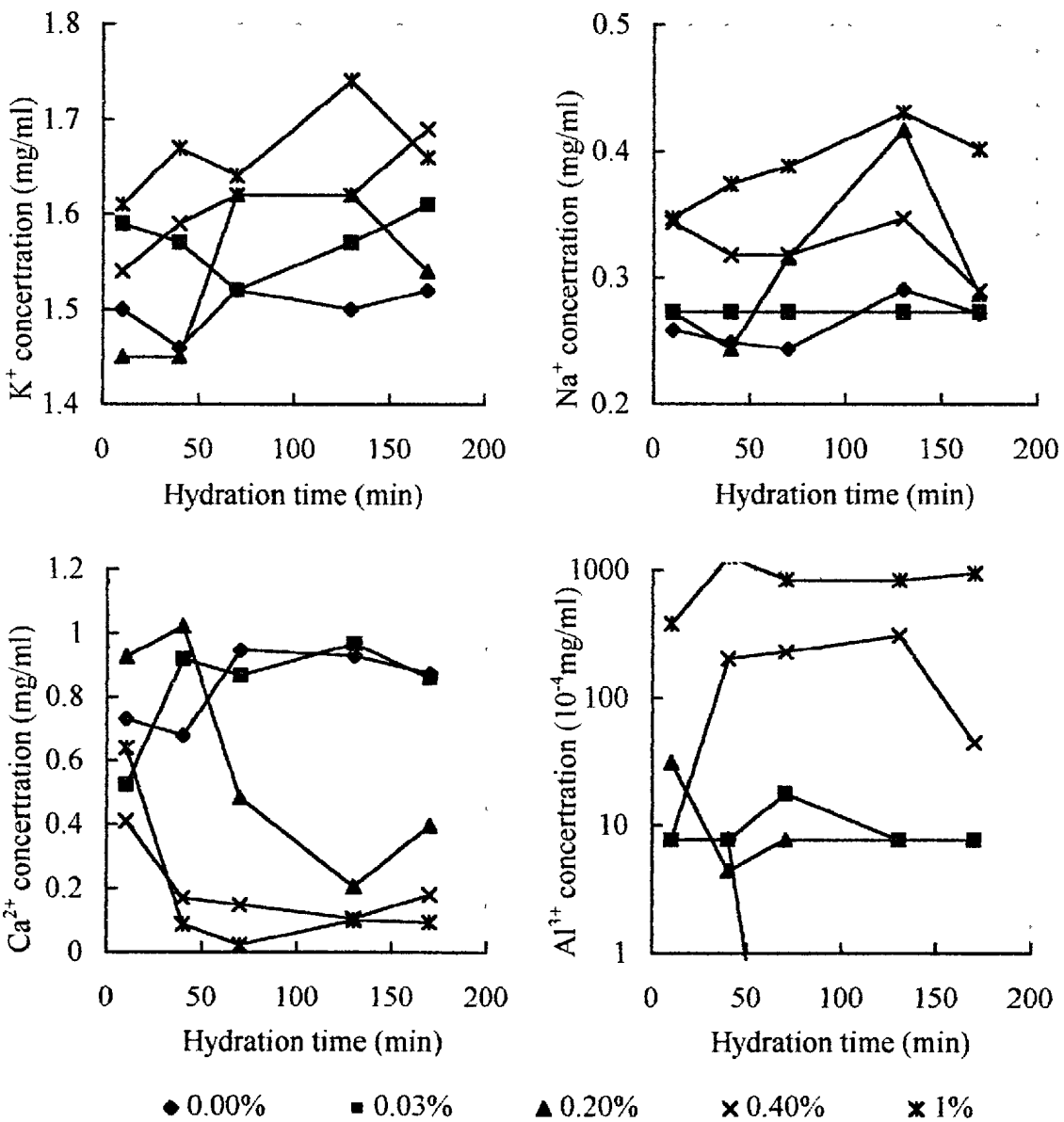

Fig.4 Change of ion concentrations in pore solution of the cement pastes with hydration time

Set-regulation mechanism

When sucrose comes to contact with Ca^{2+} ions, they react to form a spherical complex. The latter adsorbs the $Al(OH)_3$,forming $C_3A{\cdot}CH{\cdot}H_{31}$. This could be proved from our expremental results. The content of AFt determined by QXDA is more than that which form only from SO_3. The cement used here contains 1.84% SO_3 and the specimen with more than 0.2% sucrose for QXDA has 5% chemically bond water on average at final set according our determations. Corresponingly, those specimen possess 1.75% SO_3,which form at most 9.15% $C_3A{\cdot}3CS{\cdot}H_{32}$ on weight of specimen. The amount is far less than that of AFt determined by QXDA,12%, this means that there were other ions statt SO_3 to form AFt. These should be Ca^{2+} and OH^-, their content falls with the hydration time, rapidlier with more sucrose than without or with less sucrose. From this fact we can assume that large amount of AFt crystals, including $C_3A{\cdot}3CH{\cdot}H_{31}$ and $C_3A{\cdot}3CS{\cdot}H_{32}$, first form. So a large amount of water is consumed,the cement paste becomes thicker rapidly. In addition, AFt crystals having interlocking function make the setting time shortened. Therefore, in this case,AFt crystals play a crucial role in the setting of cement paste.

In the case of low dosage of sucrose, no complex forms. The $C_3A{\cdot}3CS{\cdot}H_{32}$ is formed rather than $C_3A{\cdot}3CH{\cdot}H_{31}$. The total AFt crystals are less in amount. Their interlocking is not enough to make the cement paste set, so that the setting time is prolonged. The paste does not set until more silicate hydrates form.

In addition, K^+ and Na^+ concentrations of the cement pastes with more sucrose are higher than those with less sucrose. These ions can precipitate syngenite $K_2Ca(SO_4)_2{\cdot}H_2O$ and arcanite K_2SO_4 which show platt-form or cylinder-form and may contribute to the setting.Besides,due to the removal of $CaSO_4$ from the system,AFm and AFm-CH solid solution are formed.This can cause rapid set.

It is seen that, in the presence of sucrose, abnormal setting occurs and is dominated by the quantity of AFt crystals formed. This supports Chen and Odler(1992) strongly, who reported that normal setting of portland cement appears to be controlled mainly by the amount of CSH, abnormal setting is associated with the formation of AFt and AFm.

REFERENCES

Banfill P.E.G., Saunders D.C., "The Relationship between the Sorption of Organic Compounds on Cement and the Retardation of Hydration", Cement Concrete Research, Vol.16, No.3, 1985, pp.399-410

Chen Y., Odler I. "On the Origin of Portland Cement Setting", Cement Concrete Research, Vol.22, No.6, 1992, pp.1130-1140

Ludwig U.,Urrutia C., "Zum Mechanismus der Wirkung von Saccharose auf das Erstarren und Erharten von Zementen", Zement-Kalk-Gips, Vol.42, No.8, 1989, pp.431-436

Thomas N.L.Birchall J.D., "The Retarding Action of Sugars on Cement Hydration", Cement Concrete Research, Vol.13, No.6, 1983, pp.830-842

Wang Peiming, "Effect of Sucrose on Setting of Portland Cement".Proceeding of the International Symposium on New Development in Concrete Science and Technology, Sep.1995, Nanjing, pp.263-269

Young J.F., "A Review of the Mechanism of Set-Redardation in Portland Cement Pastes Containing Organic Admixture", Cement Concrete Research, Vol.2, No.44, 1972, pp.415-433

A NMR STUDY OF GELS FORMED DURING THE HYDRATION OF CALCIUM ALUMINATE CEMENTS IN THE PRESENCE OF CITRATE OR GLUCONATE

Angelika RETTEL, Denis DAMIDOT, LAFARGE Laboratoire Central de Recherche, St-Quentin Fallavier, France
Dirk MÜLLER, Wolfgang GESSNER, Institut für Angewandte Chemie Berlin-Adlershof, Berlin, Germany

ABSTRACT At 20°C, high concentrations of trisodium citrate and sodium gluconate can induce a massive formation of gels that contain citrate or gluconate and calcium and aluminate. The formation of the gel can be simulated by adding sodium gluconate or sodium citrate solutions to a metastable solution obtained by the filtration of a Fondu cement suspension. The gels synthesised by this method, have been studied by ^{13}C and ^{27}Al NMR. These gels consist in finely combined mixtures of either calcium di-gluconate or tricalcium di-citrate, with CAH_{10} and may be with the corresponding AFm phase.

Key-words: Calcium aluminate cement, Retarders, Nuclear magnetic resonance, Gel.

INTRODUCTION

Sodium gluconate and trisodium citrate, are often used with calcium aluminate cements in order to improve the rheological properties of the paste at the beginning of hydration. These organic salts and their derivatives are known retarders of calcium aluminate cements (Tsuyuki, 1981, Rodger, 1984, Currell, 1987, Sharp, 1990, Damidot, 1996). Thus it appears to be surprising that high concentrations of these salts can induce a degradation of the rheological properties of Fondu cement pastes during the initial period of the hydration. The shear-stress measurements with a rotating coaxial cylinder on a paste after 18 minutes of hydration show a strong increase with the retarder content (Fig. 1)

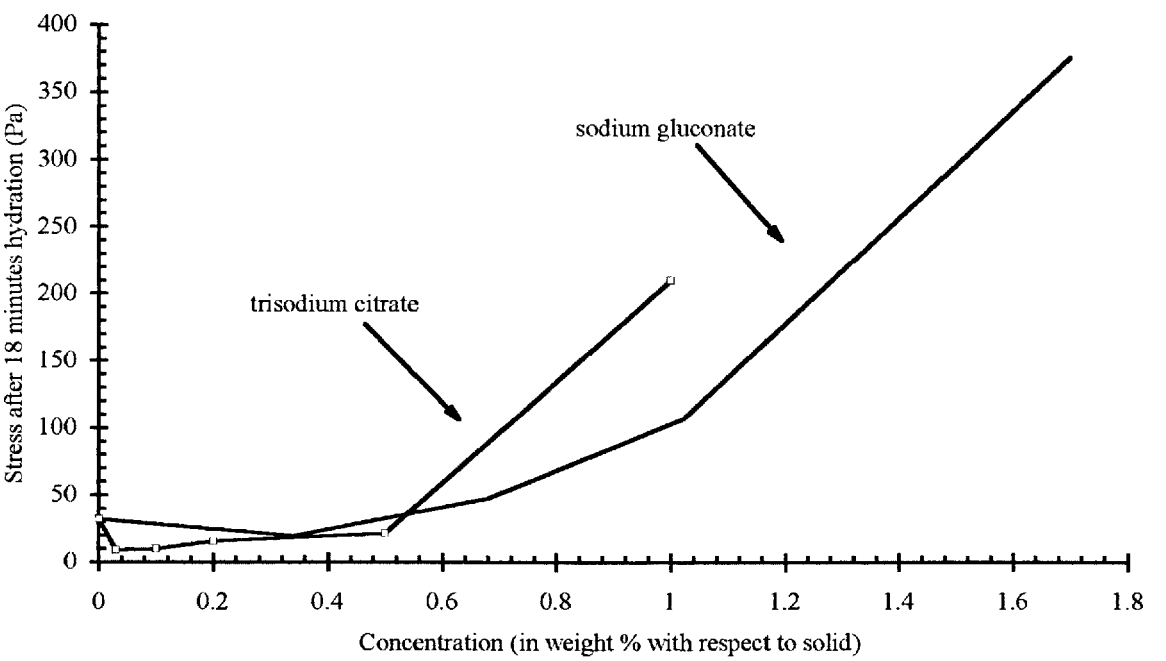

Fig 1. Shear-stress of Fondu cement paste (W/C=0.3) after 18 minutes hydration, in sodium gluconate and trisodium citrate solutions of increasing concentrations at 20°C

If the paste is mixed again after 30 minutes hydration, the structure of the paste is destroyed and the stress returns to the usually low value that characterises the beginning of hydration. Then the stress increases slowly as hydration proceeds. The aim of this study was to understand the mechanism of action of high concentrations of trisodium citrate or sodium gluconate on the hydration of the Fondu cement.

EXPERIMENTAL

The cement used in this study was a commercial Lafarge Ciment Fondu which contains mainly CA along with small quantities of $C_{12}A_7$, C_4AF and C_2S. Sodium gluconate and trisodium citrate were AnalaR grade reagents that were dissolved in distilled water prior to mixing with Fondu cement. The hydration was followed in stirred suspension in order to be able to study the aqueous phase more easily (W/C=10). Sodium, calcium and aluminium concentrations were determined by ICP. Citrate and gluconate were analysed by liquid chromatography. The NMR spectra were recorded on a Bruker solid-state NMR spectrometer running at 9.4 T. The corresponding resonance frequencies for ^{13}C were 100.6 MHz and for ^{27}Al 104.2 MHz, respectively. Additional ^{13}C MAS NMR spectra were recorded on a Varian Unity-plus 300 NMR spectrometer at 76 MHz. For line-narrowing magic-angle spinning (MAS) technique was applied using a double bearing 4 mm MAS probe. Spinning rates of 10 kHz were used. Up to 22000 scans with recycle delays of 6 s were accumulated in the case of the ^{13}C MAS NMR spectra of the treated cement gels. For the ^{27}Al MAS NMR spectra 100 scans with a recycle delay of 6 s were sufficient. Excitation pulses of 1 μs were applied. The chemical shifts refer to TMS and an aqueous solution of $AlCl_3$, respectively.

RESULTS

The aqueous phase composition was analysed during the hydration of Fondu in presence of 10mmol/l of sodium gluconate (Fig. 2). During the beginning of Fondu cement hydration, a decrease in gluconate ions and an increase in calcium and aluminate ions are observed.

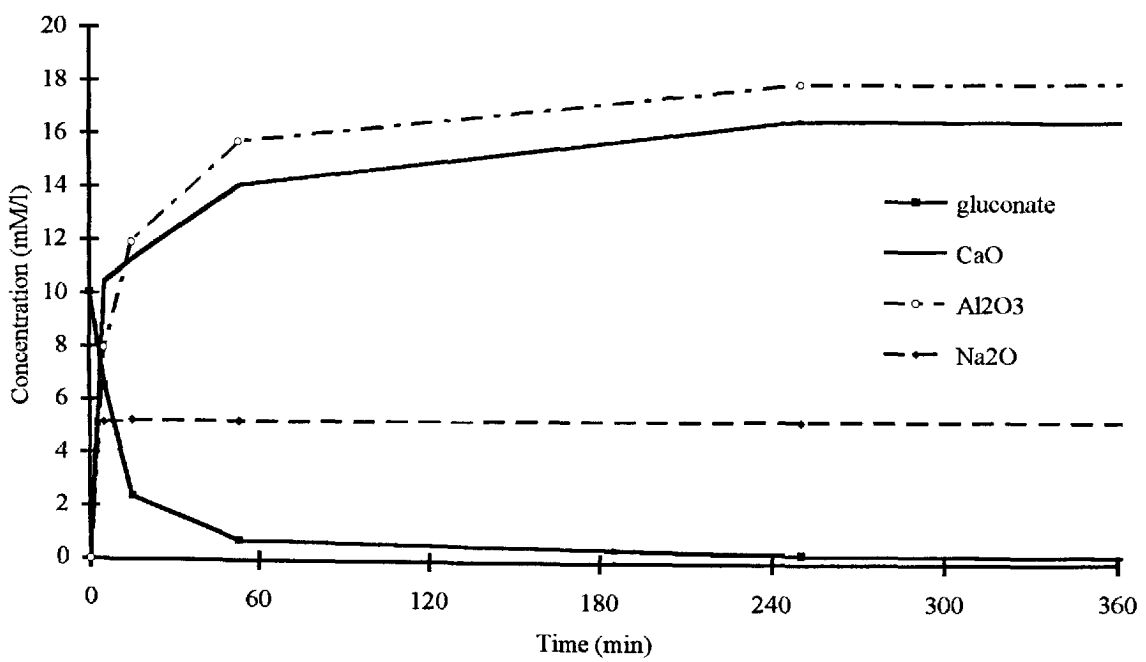

Fig. 2. Aqueous phase composition for Fondu cement hydrated in 10mmol/l sodium gluconate solution at 20°C and W/C=10

Experiments with C_3A, instead of Fondu cement, also indicated the gluconate ions are consumed (Casu, 1980). The sodium concentration remained constant at 10mmol/l. At first, there is a higher concentration of Ca^{2+} (expressed as CaO) than of $Al(OH)_4^-$ (expressed as Al_2O_3). After 15 minutes of hydration an inversion of these concentrations is also observed: the C/A ratio of the aqueous phase is higher than 1 during the first 15 minutes and then it stays close to 0.9. This effect is expected to be linked to the consumption of gluconate ions: as gluconate ions are consumed, they are replaced by OH^- ions in solution to keep the electrical balance of the aqueous phase. This mechanism could be explained by several chemical reactions; OH^- could come from the cement dissolution or the formation of AH_3 as described in the following chemical equation:

$Ca^{2+} + 2Al(OH)_4^- + 2[OH\text{-}CH_2[CH(OH)]_4COO.Na] \Rightarrow [OH\text{-}CH2[CH(OH)]_4COO]_2.Ca + Al(OH)_3 + 2Na^+ + 2OH^-$

Thus the calcium concentration is reduced by the common ion effect with sodium ions as it is observed when Fondu cement is hydrated in NaOH solution. The C/A molar ratio of the aqueous phase of Fondu cement hydrated in 10mmol/l NaOH is 0.86 at the beginning of the hydration.

If calcium and aluminate concentrations are compared between Fondu cement hydrated in water and in 10mmol/l sodium gluconate, it is obvious that the rate of increase of the concentration of these ions is less in the presence of gluconate ions (Fig. 3). Sodium ions did not reduce the rate of dissolution of Cement Fondu. Thus gluconate ions act on the surface of the dissolving solids either by an absorption process on cement Fondu and/or by the precipitation of solids that contain gluconate.

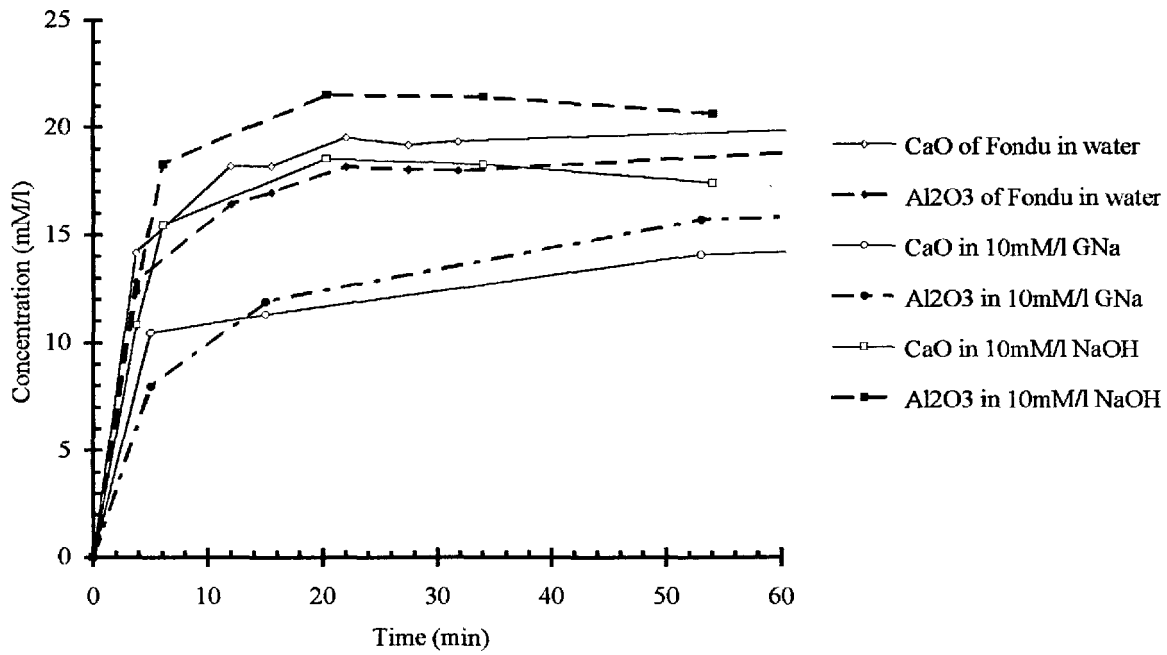

Fig. 3. CaO and Al_2O_3 concentrations in the aqueous phase during Fondu cement hydration in water, 10mmol/l sodium gluconate and 10mmol/l NaOH solution at 20°C and W/C=10

In order to investigate the possibility of the precipitation of solids, some specific experiments were carried out on a Fondu suspension filtered after 20 minutes hydration. 2ml of 41 or 205 or 410mmol/l sodium gluconate solutions were added to 80ml of clear filtrate in order to obtain 1, 5 or 10mmol/l sodium gluconate concentrations. A white precipitate appeared as soon as the sodium gluconate was added. The solid was recovered after one hour and dried with an acetone ether washing. The aqueous phase was also analysed (Table 1) and thus the global composition of the precipitated solid could be calculated: $C_{4.38}A_{3.91}Glu$ (1mmol/l), $C_{2.11}A_{1.45}Glu$ (5mmol/l) and

$C_{1.60}A_{1.03}Glu$ (10mmol/l). Higher gluconate concentrations lead to higher gluconate content in the solid compared to C and A. The solids appeared to be amorphous by XRD. NMR experiments were carried out on the solid precipitated in the presence of 10mmol/l sodium gluconate. ^{13}C MAS NMR showed some broad bands indicating a gel structure (Fig. 4). The three main bands can be assigned with the help of sodium gluconate and calcium di-gluconate NMR spectra (Figs. 5-6).

Table 1. Concentrations in the aqueous phase

	[Ca] mmol/l	[Al_2O_3] mmol/l	[Gluconate] mmol/l	[Na] mmol/l
initial filtrate	18.90	16.80	0.00	0.00
1mmol/l GNa added	16.84	14.96	0.53	1.00
5mmol/l GNa added	10.09	10.75	0.84	5.00
10mmol/l GNa added	5.63	8.28	1.72	10.00
	Δ[Ca]	Δ[Al_2O_3]	Δ[Gluconate]	Δ[Na]
1mmol/l GNa added	2.06	1.84	0.47	0.00
5mmol/l GNa added	8.81	6.05	4.16	0.00
10mmol/l GNa added	13.27	8.52	8.28	0.00

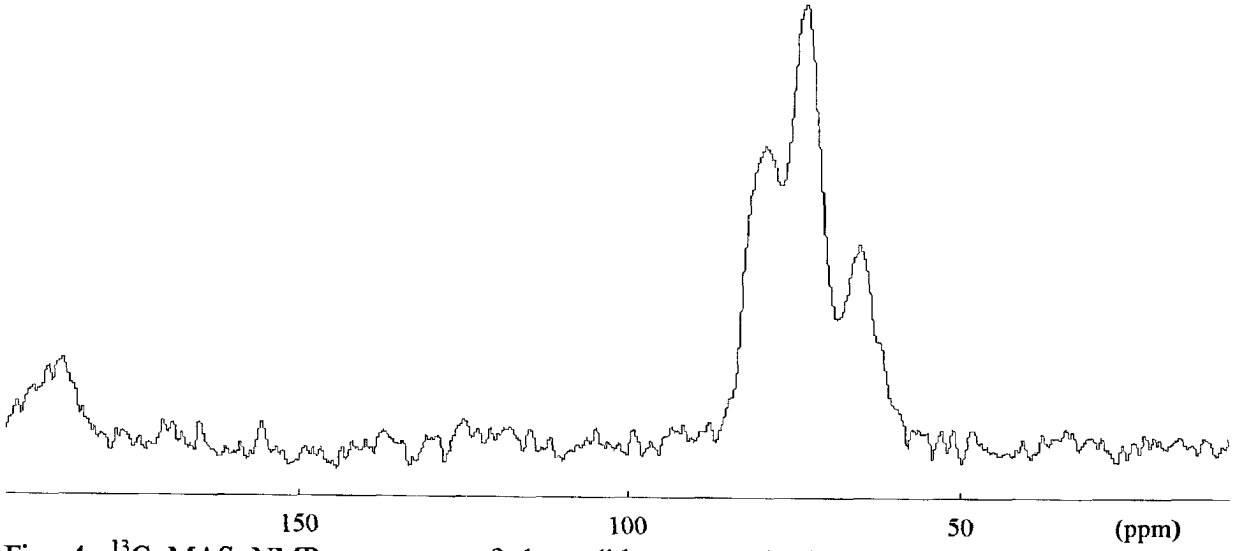

Fig. 4. ^{13}C MAS NMR spectrum of the solid recovered after adding 10mmol/l of sodium gluconate to a solution that contains 18.9 mmol/l CaO and 16.8mmol/l Al_2O_3.

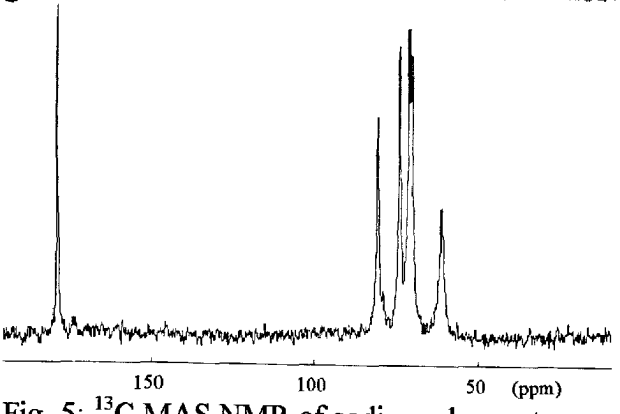

Fig. 5: ^{13}C MAS NMR of sodium gluconate

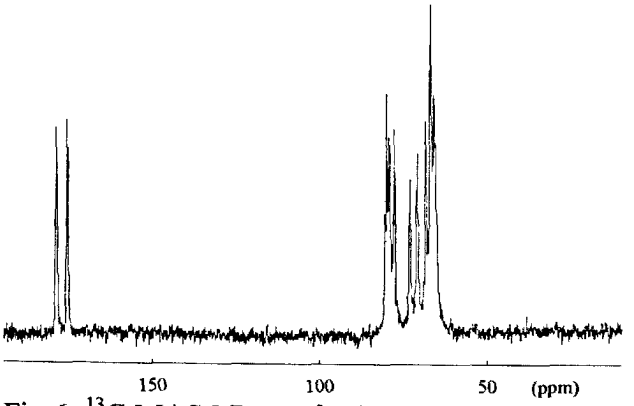

Fig 6. ^{13}C MAS NMR of calcium di-gluconate

The band at 185ppm corresponds to the signal of the carboxyl group. The signal at 65ppm is due to the other end group. The four carbon atoms of the middle chain give the bands in the region

between 70 and 80ppm. It can be noted that for calcium di-gluconate, the bands are more numerous than for sodium gluconate as the two gluconates do not occupy equivalent sites in the structure: two bands for the carboxyl groups exist. The ^{27}Al MAS NMR spectrum that is shown in Fig. 7, exhibits a strong signal representative of Al VI and a shoulder that may be induced by Al contained in a gel structure. Due to the width of the band, it is not possible to assign this peak to alumina gel, CAH_{10} or C_2AH_8 (Müller, 1992) or even an AFm phase.

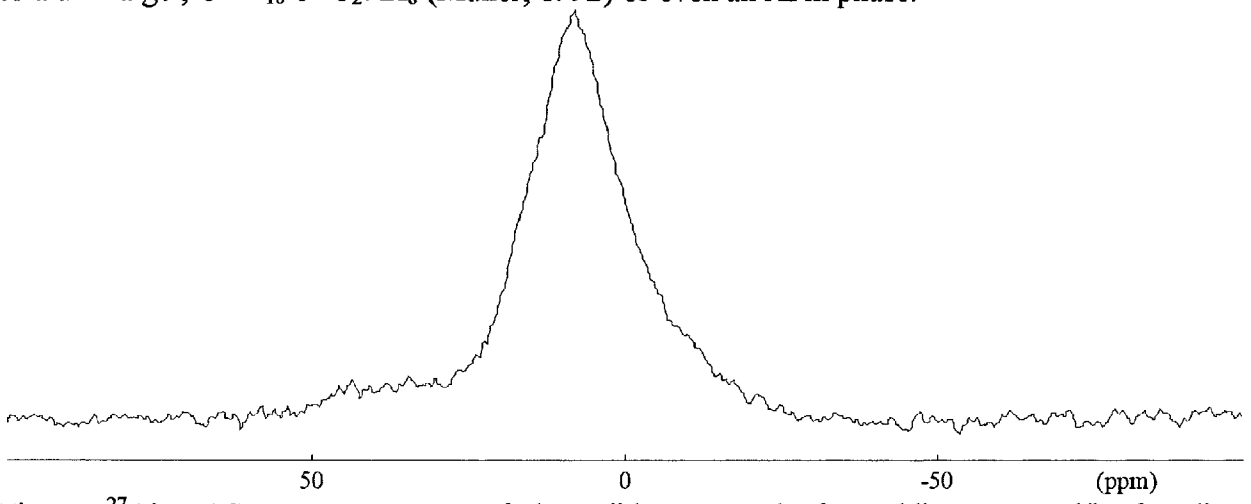

Fig. 7. ^{27}Al MAS NMR spectrum of the solid recovered after adding 10mmol/l of sodium gluconate to a solution that contains 18.9 mmol/l CaO and 16.8mmol/l Al_2O_3.

Similar experiments were carried out with trisodium citrate. First the composition of the aqueous phase was followed for Fondu cement hydrated in the presence of 1.7mmol/l trisodium citrate (Fig. 8). The citrate ions are consumed during the first 30 minutes which is a relatively long time compared to the initial citrate concentration. Rodger (Rodger, 1984) also reported that citrate ions were consumed in paste experiments.

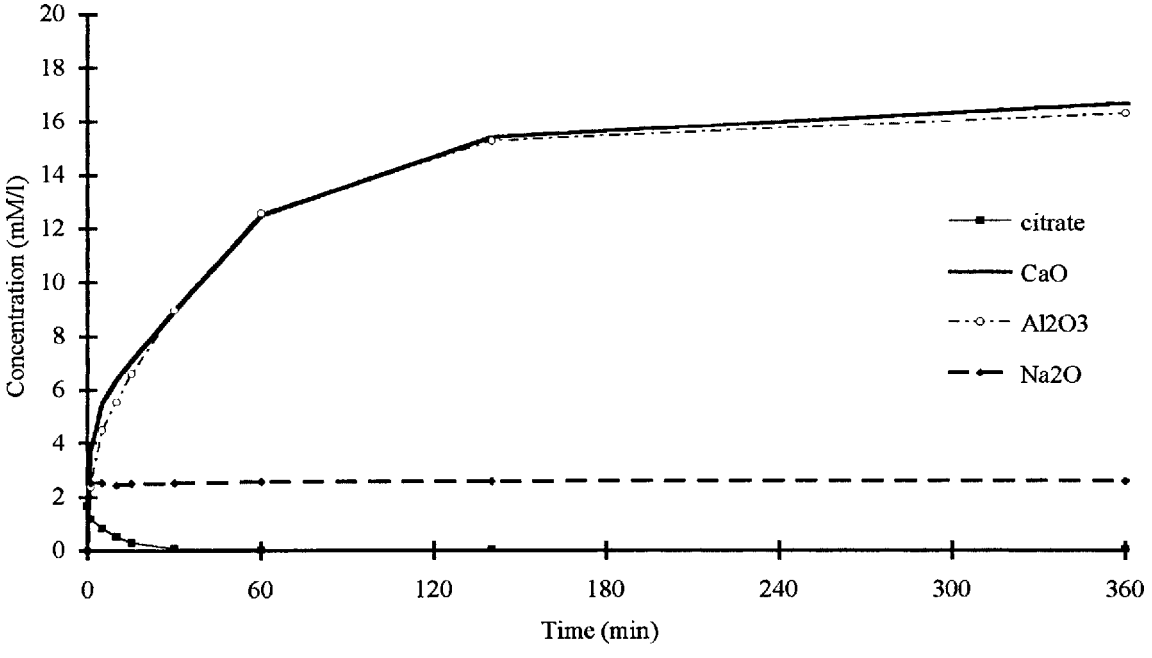

Fig. 8. Aqueous phase composition for Fondu cement hydrated in 1.7mmol/l trisodium citrate solution at 20°C and W/C=10

In order to study the possible precipitation of solids, 2ml of a 205mmol/l trisodium citrate solution were added to 80ml of filtrate containing 18.9 mmol/l CaO and 16.8mmol/l Al_2O_3. As with sodium gluconate, a white precipitate appeared as soon as the sodium citrate was added. The solid recovered after one hour was also amorphous by XRD. ^{13}C MAS NMR spectrum of the solid is presented on Fig 9. This spectrum contains three main broad bands that can be attributed by comparison with the chemical shifts of trisodium citrate and tricalcium di-citrate (Figs. 10-11). The carboxyl groups induce a band at 181ppm. The band at 47ppm corresponds to the two CH_2 groups and the signal at 76ppm is due to the carbon linked to OH. The ^{27}Al MAS NMR spectrum is very similar to the spectrum obtained with sodium gluconate (Fig. 12); an important broad band is observed in the Al VI region and also a small shoulder is found between 25 and 50ppm.

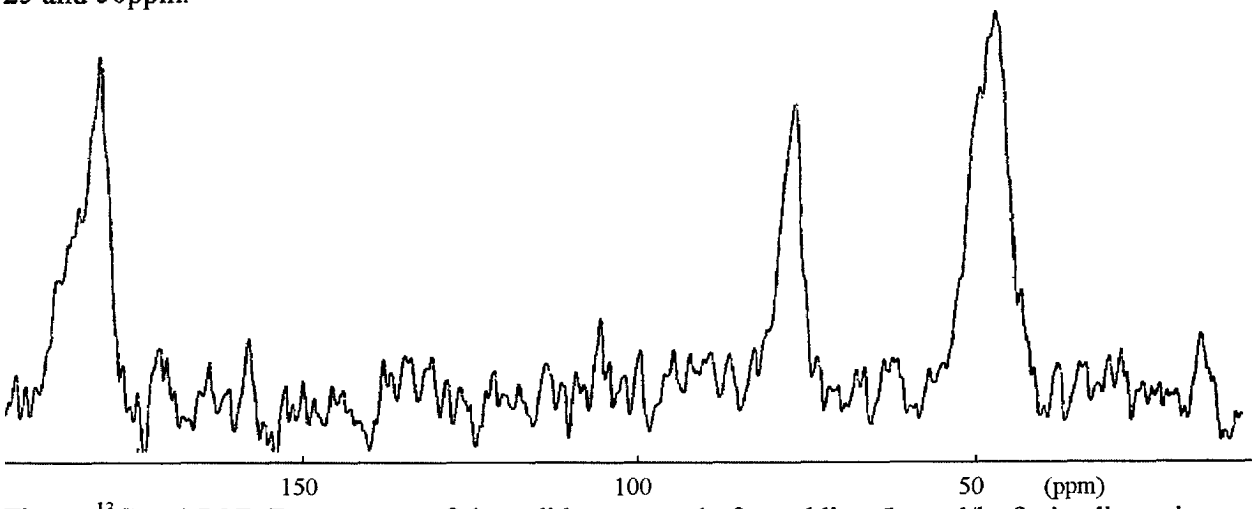

Fig. 9. ^{13}C MAS NMR spectrum of the solid recovered after adding 5mmol/l of trisodium citrate to a solution that contains 18.9 mmol/l CaO and 16.8mmol/l Al_2O_3.

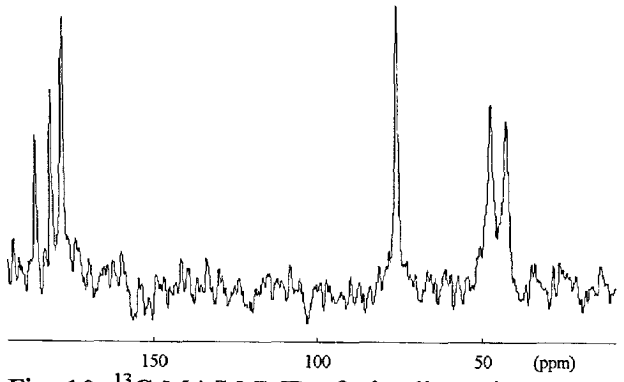

Fig. 10: ^{13}C MAS NMR of trisodium citrate

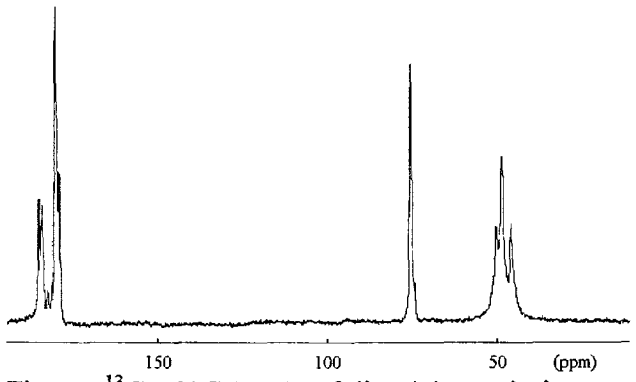

Fig 11. ^{13}C MAS NMR of di-calcium tri-citrate

DISCUSSION

In a sodium gluconate or a trisodium citrate solution, gluconate and citrate ions are completely dissociated: Cit^{3-} and Glu^{-}. As soon as cement hydrates, calcium, aluminate and OH- ions are introduced in the solution and can interact with citrate and gluconate ions. The pH is immediately higher than 11, and complexes with aluminium and citrate or gluconate ions do not exist (Motekaitis, 1984): $Al(OH)_4^-$ is the only aluminium containing species. On the contrary there can be aqueous complexes between calcium ions and gluconate or citrate ions (Amico, 1982). However the concentration of these complexes in solution is rapidly limited by the low solubility of $Ca_3(C_6H_5O_7)_2.4H_2O$ and of $Ca(C_6H_{11}O_7)_2$.

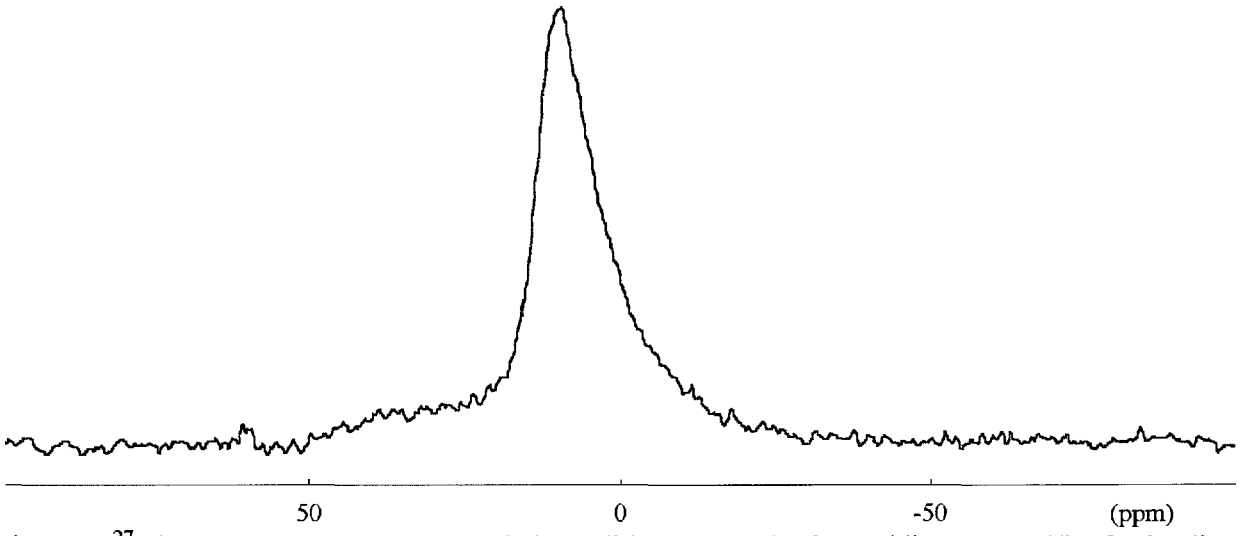

Fig. 12. ^{27}Al MAS NMR spectrum of the solid recovered after adding 5mmol/l of trisodium citrate to a solution that contains 18.9 mmol/l CaO and 16.8mmol/l Al_2O_3.

Experiments reported in the literature done with C_3A instead of Fondu cement, can give supplementary information. The hydration of C_3A in the presence of citric acid (Poellmann, 1990) indicates that a gel of citrate is formed at first. This gel that covers C_3A grains could be composed of $Ca_3(C_6H_5O_7)_2.4H_2O$ and AH_3. Then $Ca_3(C_6H_5O_7)_2.4H_2O$ would react further with C_3A in order to form an AFm phase having a composition close to $C_3A.0.33Ca_3(C_6H_5O_7)_2.nH_2O$ (AFm-Cit).

Casu et *al.* (Casu, 1980) indicate that aqueous complexes are formed during C_3A hydration in the presence of sodium gluconate. Then the complex precipitates on the surface of C_3A grains and should reduce the dissolution rate of C_3A. These authors suggested that aluminium is essential to rapidly form the complexes in which all hydroxyl groups of the gluconate are involved.

In our experiments (Table 1), aluminate ions are also consumed during the formation of the gel, thus the gel may be a coprecipitate of badly crystallised $Ca_3(C_6H_5O_7)_2.4H_2O$ or of $Ca(C_6H_{11}O_7)_2$ and an amorphous aluminium containing phase, which could be an alumina gel (AH_3), CAH_{10}, or an AFm phase; the AFm containing gluconate ions could be written as $C_3A.0.5[Ca(C_6H_{11}O_7)_2].0.5[Ca(OH)_2].xH_2O$ (AFm-Glu). The presence of citrate ions delay the nucleation and growth process of AH_3 (Van Straten, 1985) and a similar behaviour was found for gluconate ions (Rossiter, 1996). Thus it is not likely that the gel could contain AH_3. Moreover if AH_3 would be formed, the induction period should be accelerated (Damidot, 1996), instead of being retarded as found experimentally. AFm phases, AFm-Glu or AFm-Cit, which are generally well crystallised are not detected by XRD. On the other hand CAH_{10} is often badly crystallised and thus may not be observed by XRD.

Taking into account all the previous remarks, we can hypothesise that the solid formed could be a badly crystallised mixture of $Ca_3(C_6H_5O_7)_2.4H_2O$ or of $Ca(C_6H_{11}O_7)_2$ and of CAH_{10}. However, a gel-like structure containing randomly Ca, Al and gluconate could not be ruled out with our results: Sugama *et al.* (Sugama, 1989) indicate that electrostatic bonds formed by charge transfer from the Al as an electron donor to the electron accepting oxygen portion of COOH and C=O, exist, concomitantly with chemical bond between Ca and COOH.

CONCLUSION

Gluconate or citrate ions concentration decreases rapidly during the hydration of Fondu cement. This is a consequence of the precipitation of the aqueous gluconate or citrate complexes as soon as their concentrations reach a sufficient value. The precipitate covers the surface of the grains of Fondu cement and induces a decrease in the dissolution rate of the cement. If the concentration

of gluconate or citrate is high, the precipitate can create a thick gelatinous layer around the grains but also can form isolated gels. These gels are believed to be responsible for the bad rheological properties reported in Fig. 1 of the introduction. On the other hand, low concentrations of these organic salts, just form a thin layer around cement grains and give better rheological properties as the hydration rate is reduced.

It is not easy to determine the structure of the gels that are formed. It appears that the gluconate and citrate structures persist in the gels with some differences that are induced by different environments. Aluminium is octahedrally coordinated in the gel but the chemical shift does not allow us to determine accurately the solids that contain Al. Chemical analysis of the gel also indicates that calcium is present. It is believed that at 20°C, these gels are finely combined mixtures of either calcium di-gluconate or tricalcium di-citrate with CAH_{10} and may be with the corresponding AFm phase: $C_3A.0.5[Ca(C_6H_{11}O_7)_2].0.5[Ca(OH)_2].xH_2O$ and $C_3A.0.33$ $Ca_3(C_6H_5O_7)_2.nH_2O$ respectively. Note that CAH_{10} is not stable for temperatures higher than 30°C and that the aluminium containing phase could differ at these temperatures.

REFERENCES

Amico, P., Daniele, P.G., Rigano, C. and Sammartano S. "Stability of calcium and magnesium-citrate complexes in aqueous solution", Annali di Chimica , Vol. 72, 1982, pp 1-24.

Casu, B., Chiruzzi, M., Tegiacchi, F. and Zoppetti, G. "Interaction of aluminates with carbohydrates and aldonates", 7th ICCC, Paris, Vol. IV, 1980, pp 558-563.

Currell, B.R., Grzeskowiak; R., Midgley, H.G., and Parsonage, J.R. "Acceleration and retardation of set high alumina cement by additives" Cem. and Concr. Res., Vol. 17, 1987, pp 420-432.

Damidot, D, Rettel, A. and Capmas, A. "Action of admixtures on Fondu cement: Part 1. Lithium and sodium salts compared", Advances in Cement Research, Vol. 8, No. 31, 1996, 111-119.

Massiot, D, Thiele, H. and Germanus, A. , Bruker Report, Vol. 140, 1994, pp. 43-46.

Motekaitis, R.J. and Martell, R.J. "Complexes of aluminium (III) with hydroxy carboxylic acids" Inorg. Chem., Vol.23, 1984, pp. 18-23.

Müller, D., Rettel, A., Gessner, W, Bayoux, J.P. and Capmas, A. "Progress in the ^{27}AL MAS NMR Spectroscopy: Monitoring the Hydration of Calcium Aluminate Cements" 9th ICCC, New Delhi, Vol. 6, 1992, pp 148.

Poellmann, H. "Study of the influence of citric acid on the retardation and formation of new hydrates in cement" Proc. Conf. Cement Microscopy, Vancouver, 1990, pp 303-322.

Rodger, S.A. and Double, D.D. "The chemistry of hydration of high alumina cement in presence of accelerating and retarding admixtures" Cem. and Concr. Res., Vol 14, 1984, pp 73-82.

Rossiter, D.S., Ilievski D., Smith, O.G. and Parkinson, G.M. "The mechanism of sodium gluconate poisoning of gibbsite precipitation" Trans. IChemE, Vol 74, Part A, 1996, pp 828-34.

Sharp, J.H., Bushnell-Watson, S.M., Payne, S.M. and Ward, P.A. "The effect of admixtures on the hydration of refractory calcium aluminate cements" in Calcium Aluminate Cements, Ed by R.J. Mangabhai, 1990, pp. 127.

Sugama, T., Kukacka, L. E., Carciello, N. and Hocker, N. J., "Study of interactions at water-soluble polymer / $Ca(OH)_2$ or Gibbsite interfaces by XPS." Cem. and Concr. Res., Vol 19, 1989, pp. 857-867.

Tsuyuki, N., Hisashi, O., Miyakawa, T. and Kasai, T. "The Behaviors of Gluconic Acid Derivative in Hydration of $CaO.Al_2O_3$" Yogyo-Kyokai-Shi, Vol. 89, 1981, pp. 471-479.

Van Straten, H.A., Schoonen, M.A. and De Bruyn, P.L. "Precipitation from supersaturated aluminate solutions: IV influence of citrate ions" J. of Colloid and Interface Science, Voll 106, 1985, pp. 175-185.

THE INFLUENCE OF ACRYLIC POLYMER LATEX ADDITIONS ON THE HYDRATION KINETICS OF OPC AND C_3S

Simon P. DENNINGTON, Borvi AS, Sarpsborg, Norway
James W. GOODWIN, University of Bristol, Bristol, UK BS8 1TS
Dudley W. THOMPSON, University of Bristol, Bristol, UK BS8 1TS

ABSTRACT The effect of additions of acrylic polymer dispersions (latexes) on the hydration of OPC and synthetic C_3S has been studied by conduction calorimetry. Scanning electron microscopy showed that carboxylated polymer particles adsorb on OPC and C_3S, and to an even greater degree on C_3A. These latexes produced markedly different hydration exotherms compared to non-carboxylated particles, which do not adsorb. Two different mechanisms appear to be involved.

Key-words: Polymer, Latex, Hydration, Kinetics, SEM

INTRODUCTION

Ordinary Portland Cement (OPC) is a complex mixture of inorganic mineral phases which shows characteristic hydration kinetics (Double, 1983). The hydration exotherm can be divided into an immediate and vigorous evolution of heat followed by a prolonged and less intense main exotherm after an intervening quiescent period (the induction period). Tricalcium silicate (C_3S) is the major hydraulic component of OPC and its hydration exotherm shows the same essential features as that of OPC (Tadros, 1976). For this reason it is often taken as a model compound for hydration studies. Possible reasons for the induction period are the subject of much debate (Grutzek, 1987)(Fierens, 1976)(Odler, 1979). Many water-soluble additives modify the hydration kinetics of C_3S and OPC (Ramachandran, 1987). Dispersions of sub-micron sized polymer particles (or latexes) can also effect the course of hydration. Many studies have been reported on latex additives (Kuhlmann, 1990)(Ohama, 1987)(Lavelle, 1988) but the precise nature of the polymer and any incidental components of the latex (surfactants, salts) are seldom reported. Well-characterised acrylic latexes of varying compositions using the same stabilising system and having similar particle size distributions were synthesised for use in this study.

MATERIALS

Polymer latexes

The latexes were polymerised at a solid content of 50% using a standard pre-emulsion technique as described elsewhere (Justnes, 1988). The monomers used were methyl methacrylate (MMA), butyl acrylate (BA) and methacrylic acid (MAA). Polymer compositions and calculated glass transition temperatures (T_g) are given in table 1. The stabilising system consisted of 2 parts active material (by weight of monomer) of each of two surfactants, the sodium salt of nonyl phenol ether sulphate (9 moles ethylene oxide) and nonyl phenol ethoxylate (40 moles ethylene oxide).

Particle sizes were measured with a Leeds and Northrup Microtrac Ultrafine Particle Analyzer. Excluding two of the latexes, all the particle size distributions were highly monodisperse with the overall mean particle diameter 176 ± 3 nm. The exceptions were compositions a1 (100% BA, 223 nm) and c5 (80/0/20 MMA/BA/MAA, broad, polydisperse). The pH of the finished latexes was between 3.0 and 3.5. The latexes were used as prepared in some hydration experiments, while for others the polymerisation surfactants and ionic impurities were removed by extensive dialysis against distilled water.

Table 1 Polymer compositions. T_g calculated according to eq.1 in Anwari (1992)

	Composition	Calc. T_g		Composition	Calc. T_g
Ref:	MMA/BA	°C	Ref:	MMA/BA/MAA	°C
a1	0/100	-56	c1	0/80/20	-34
a2	20/80	-36	c2	20/60/20	-9
a3	40/60	-11	c3	40/40/20	21
a4	60/40	18	c4	60/20/20	60
a5	80/20	56	c5	80/0/20	110
a6	100/0	105	-	-	-

Ordinary Portland Cement

The OPC used was P-30, produced by Norcem, Norway, and had the following composition:

$C_3S = 54\%$ $C_2S = 17\%$ $C_3A = 7\%$ $C_4AF = 11\%$ Other = 11%

Tricalcium silicate

Synthetic C_3S was prepared by firing a stoichiometric mix of calcium hydroxide and silica at 1500°C followed by grinding and pelletizing before re-firing. The free lime, measured by the modified Franke method (Pressler, 1961), stabilised at 6% and was not reduced by re-firing.

Tricalcium aluminate

The sample of pure C_3A for microscopy was synthesised by Dr. G. Nickless (Univ. of Bristol).

CALORIMETRY

The conduction calorimeter used was based on a design by Dr. C. J. Wormald (Univ. of Bristol), shown diagramatically in Fig 2. Heat from the sample is conducted to the heat sink via a Peltier semi-conductor device, thus generating a voltage. The voltage output from the calorimeter was fed to an IBM PC fitted with a 20-bit analog to digital converter. The output from an identical blank calorimeter was simultaneously recorded and subtracted from the sample signal,providing a perfectly flat baseline. The data was stored on disc for subsequent calculation and analysis.

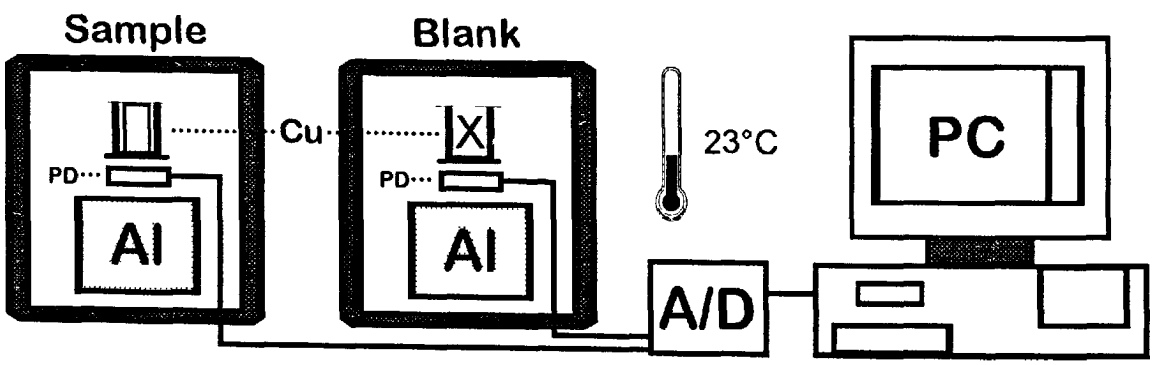

Figure 1 Diagram of conduction calorimeter.
PD = Peltier Device, Al = Aluminium heat-sink, Cu = Copper sample holder

Hydrations were carried out with the calorimeter placed in a temperature controlled room, at 23±1°C unless otherwise stated. The w/c ratio was 0.40 in all cases; polymer was taken in addition to the water and cement components and the amount is quoted as percent of cement weight (10g) or C_3S weight (5g) used. The calorimeter was calibrated electrothermally.

RESULTS

Scanning electron microscopy

Samples of cement minerals were affixed to grids and suspended upside down in dilute polymer latexes. Examination by SEM showed that not even the softest polymers formed films. The non-carboxylated polymer particles did not attach to OPC, C_3S, or C_3A. By contrast the 20%-MAA polymer particles did adsorb rapidly (in ≤1 minute). The coverage on OPC and C_3S was similar - a moderate, evenly spaced, covering of particles - while very much greater coverage was observed on C_3A, with the particles clustered in dense layers (see Fig 2):

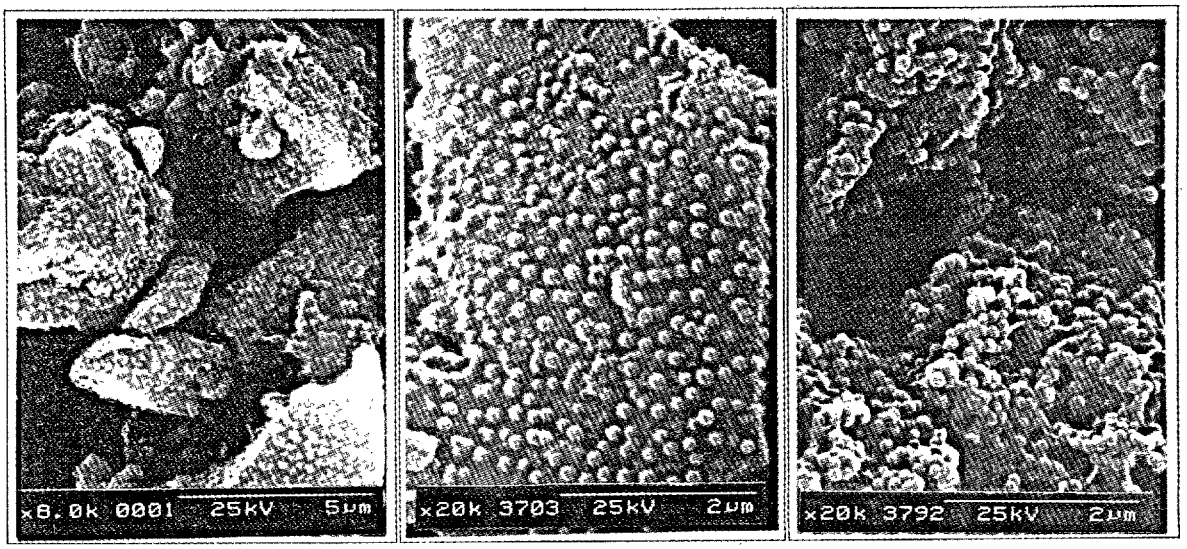

a) OPC b) C_3S c) C_3A

Figure 2 Adsorption of latex c4 particles on cement mineral phases by SEM

Calorimetry

The exotherm from hydrating OPC was extremely reproducible. Fig 3 shows traces from four runs superimposed, and they all coincide closely:

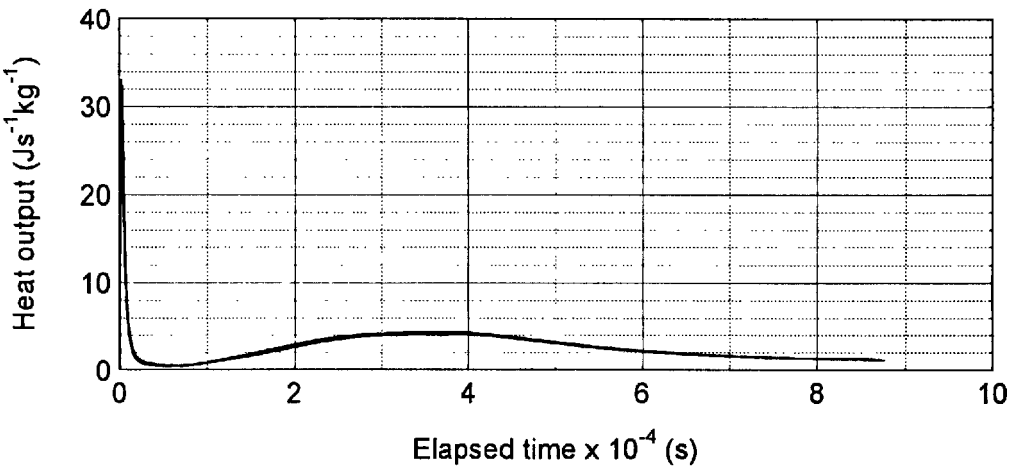

Figure 3 Linear plot of four superimposed standard OPC hydration exotherms

In Fig 4 the average of these four traces is shown plotted on log-log axes. This form of presentation allows comparison of hydrations lasting from a few minutes to several days, and is preferred in this work. Fig 5 shows the very slight retardation produced by the surfactants used.

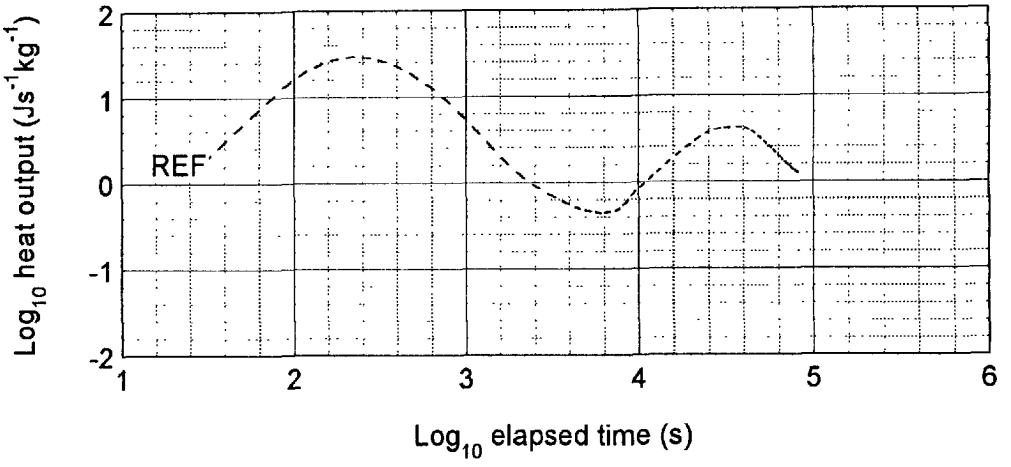

Figure 4 Log-log plot of standard OPC hydration exotherm (average of four traces)

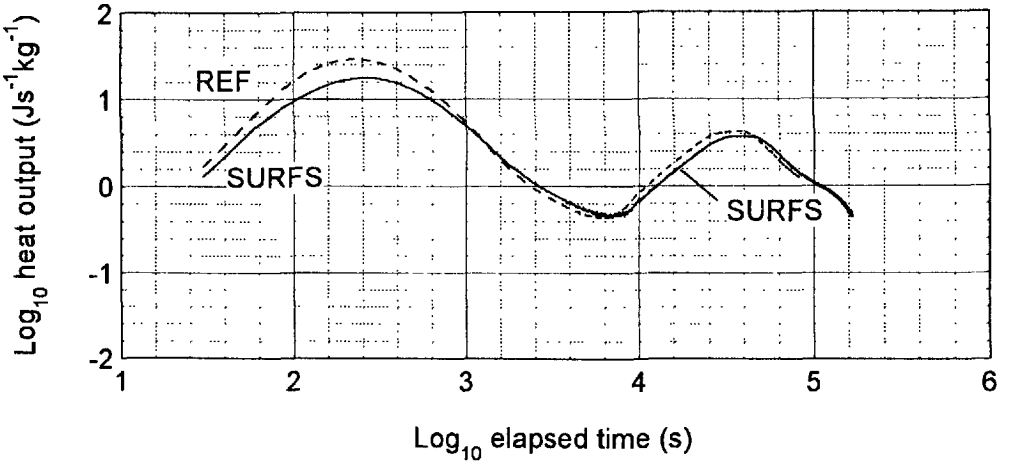

Figure 5 OPC hydration in a 2% solution with respect to each polymerisation surfactant

Hydration of OPC with the addition of the uncarboxylated latexes (a1-a6) as prepared (i.e. containing surfactants) showed a corresponding slight retardation combined with a progressive reduction in peak height of the main exotherm that depended on the composition of the polymer:

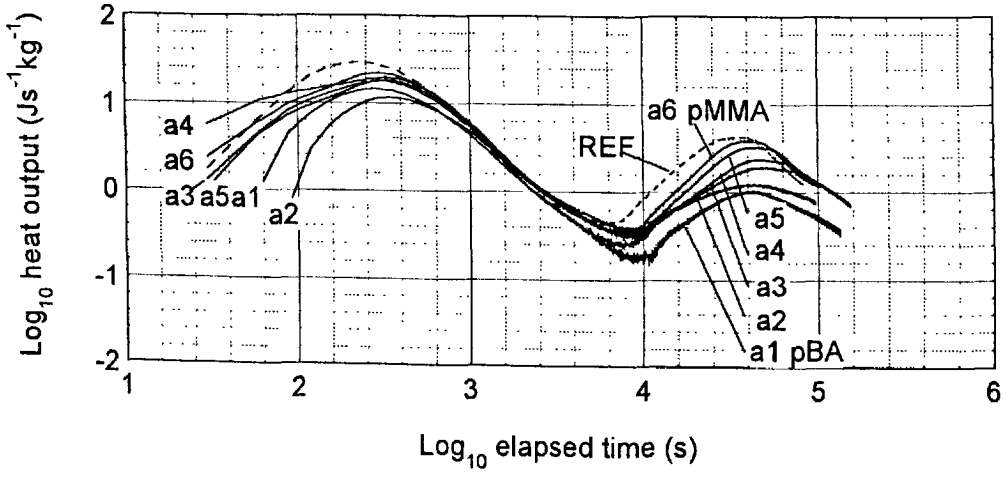

Figure 6 OPC hydration with BA/MMA copolymer latexes at P/C = 0.10

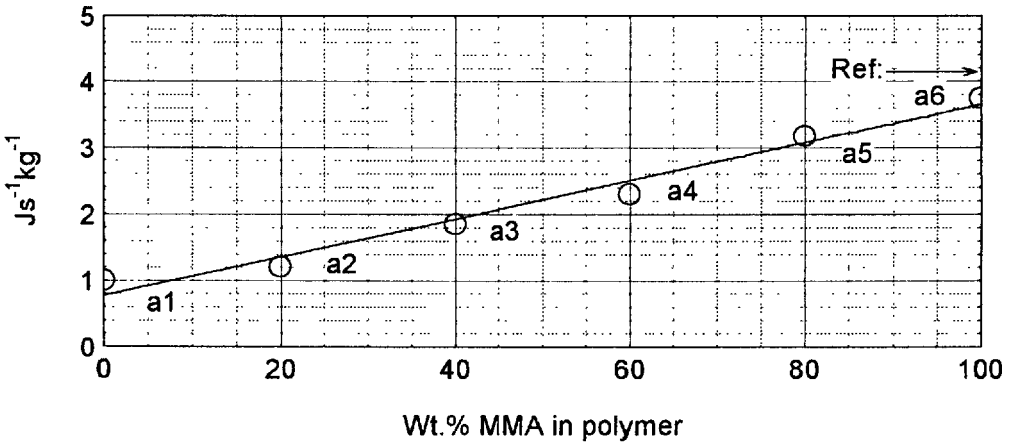

Figure 7 Peak height after 12 hours for OPC hydration with BA/MMA latexes

The slight reduction in peak height compared to the reference even with latex a6 (100% MMA) can be attributed to the presence of the surfactants. This was confirmed by hydrating OPC with the dialysed latex, when the trace coincided with the reference with no polymer. As these MMA homopolymer particles are hard (the glass transition temperature, T_g, of p-MMA is 105°C) and lacking chemical functionality, they may be considered simply as inert filler. Therefore they would not be expected to have a significant effect on the course of the hydration exotherm. However, softening the polymer particles by introducing the comonomer BA (T_g -56°C) did lead to a progressive reduction in the maximum vigour of the main exotherm, as shown by Fig 7. As BA is similarly without chemical functionality this effect can be attributed to the increasing softness of the polymer particles. In the high ionic strength aqueous environment produced during hydration of OPC the colloidal latex particles will become destabilised and tend to flocculate. The softer they are, the more strongly they will adhere to each other and form continuous networks of coagulum that restrict the diffusion of water-soluble species. This would account for the observed reduction in exotherm intensity without an accompanying delay in its occurrence.

The presence of carboxylated latexes in hydrating OPC systems resulted in a significant increase in the length of the induction period and also a marked reduction in the rate of heat evolution during the main hydration exotherm (Fig 8). These effects were found to increase with decreasing BA content of the polymer and also with increasing amount of polymer additive (Fig 9):

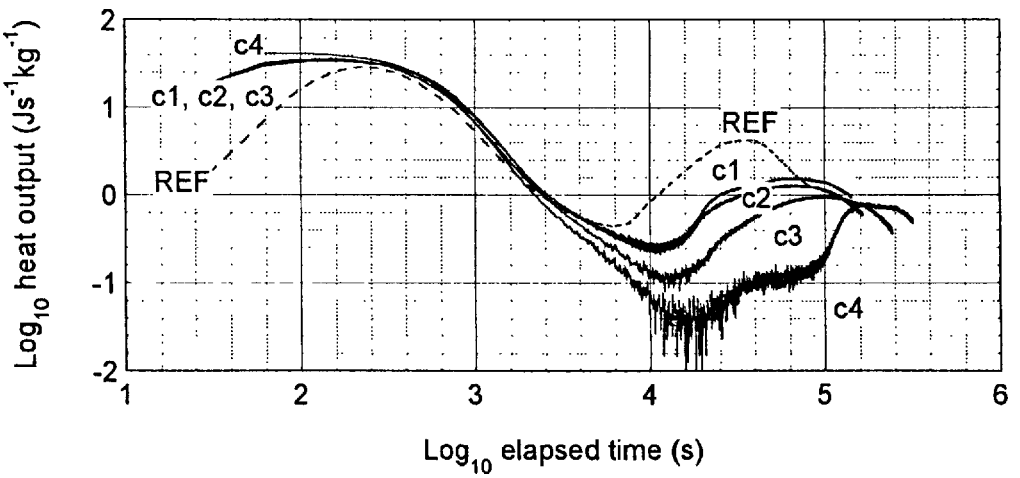

Figure 8 OPC hydration with undialysed 20%-MAA latexes at P/C = 0.10

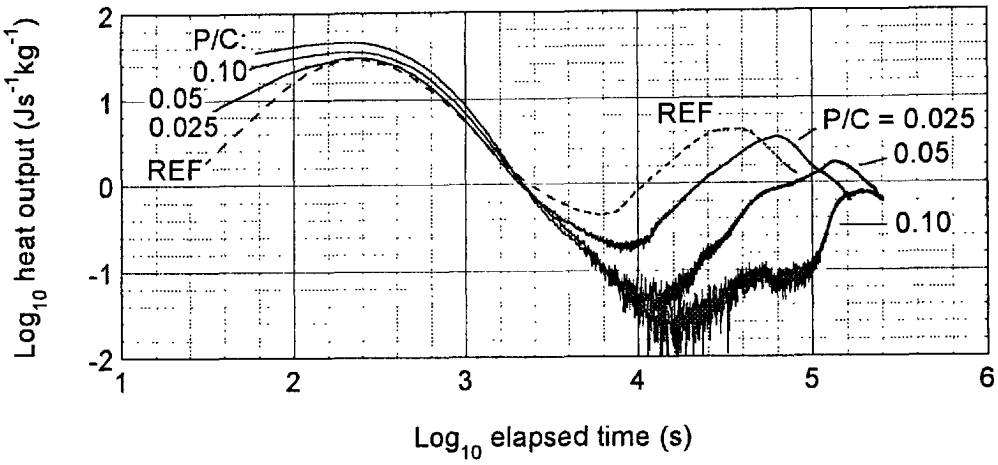

Figure 9 OPC hydration exotherm with varying amounts of dialysed latex c4

A dialysed sample of latex (c4) was centrifuged to remove the polymer particles and hydration carried out using the clear serum obtained. This had no retarding effect on the exotherm at all, so the inhibition produced by the carboxylated latexes must be due to the presence of the polymer particles themselves, rather than to any material remaining in the aqueous phase after dialysis.

Hydration of synthetic C_3S in the presence of the carboxylated latexes gave very similar results to those with OPC, indicating that this compound is a satisfactory model for investigating hydration:

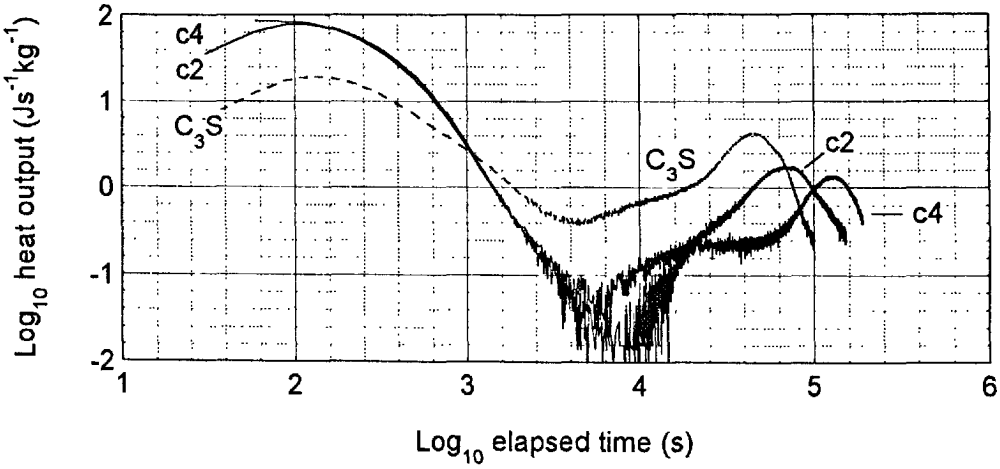

Figure 10 C_3S hydration with dialysed carboxylated latexes at P/C = 0.10

A sample of poly(methacrylic acid), p-MAA, of molecular weight ca. 80,000 was prepared. Hydration of OPC in a 0.1 M solution of this polyelectrolyte produced severe retardation of the main exotherm, even greater than that observed with polymer c4 (Fig 11). Monomeric methacrylic acid (MAA) produced only a slight reduction in the intensity of the main exotherm, with no significant retardation. The difference may be explained by the fact that calcium methacrylate is water-soluble, while the calcium salt of poly(methacrylic acid) is insoluble. Addition of p-MAA solution will therefore cause an insoluble precipitate of the polymeric calcium salt to form instantaneously around cement or C_3S grains, smothering their surfaces.

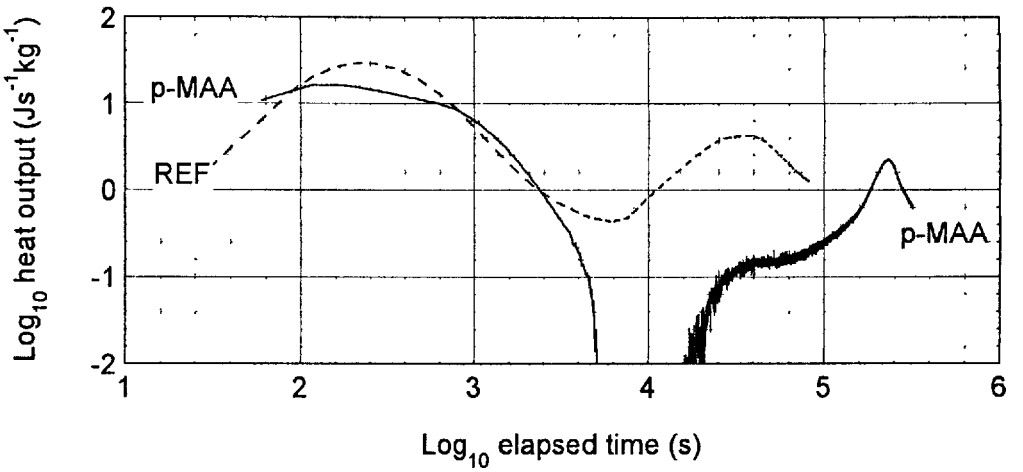

Figure 11 OPC hydration in 0.1 M poly(methacrylic acid) solution

The possibility that a methacrylic acid rich, water-soluble, polymer phase is present in the carboxylated latexes, and which could be responsible for their observed retardation, must therefore be considered. The extensive dialysis the latexes were subject to (at pH 3 as prepared) should have removed any free oligomers from the water phase; this was confirmed by the result of centrifuging the dialysed carboxylated latexes c2 and c4 and carrying out OPC hydration in the resulting clear supernatant fluids. No difference from the reference hydration in water was found, indicating a total absence of interfering oligomers.

One remaining possibility is that if any such carboxylated oligomers were present they would only be released at high pH, such as encountered in hydrating OPC. The carboxylated particles were found not to swell at all in saturated calcium hydroxide solution, although they do swell greatly when neutralised with sodium or ammonium hydroxide solutions (to three times their original diameter at pH 12). The lack of swelling with calcium hydroxide is undoubtedly due to ionic crosslinking of the polymer chains by divalent calcium ions which prevents their expansion (Han, 1991). This makes it unlikely that carboxylated oligomers would be able to escape from the particles in this case, even assuming they were not immediately precipitated by calcium ions. The interaction of calcium hydroxide and polymer latexes has been discussed by Chandra and Flodin (Chandra, 1989).

CONCLUSIONS

The addition of polymer latexes to hydrating OPC or C_3S affects the main hydration exotherm. Non-functionalised copolymer particles consisting only of methyl methacrylate and butyl acrylate were shown by SEM examination not to adsorb on OPC, C_3S, or C_3A. Nevertheless, these latexes reduced the intensity of the main exotherm but did not significantly delay its occurrence. The effect varied with T_g of the copolymer and is ascribed to the increasing tendency of the softer polymer particles to coagulate on flocculation, resulting in physically hindered diffusion of ionic species through the paste.

Polymer particles containing copolymerised methacrylic acid (at 20% by weight) showed much stronger effects and delayed the appearance of the main exotherm peak for many hours (or days). SEM observations showed that these carboxylated polymers adsorb rapidly onto OPC or C_3S grains, and to an even greater extent on to C_3A surfaces. However, as C_3S and OPC hydrations responded similarly to the presence of polymer, the retardation is unlikely to be associated with

the modification of the C_3A phase. The effect depended on the amount of polymer latex added, and was similar in form to that produced by hydrating in a solution of poly(methacrylic acid), which forms an insoluble precipitate on neutralising with calcium hydroxide, resulting in a strongly retarded exotherm. No water-soluble species were detected in the latexes dialysed as prepared, indicating that the retardation observed is due to the polymer particles themselves. Possible reasons for this are the subject of ongoing research.

REFERENCES

Anwari, F., et al, "Changes in hiding during latex film formation: Part III. Effect of coalescent level and latex properties", Journal of Coatings Technology, Vol. 64, No. 804, 1992, pp. 79-86.

Chandra, S., and Flodin, P., "Interaction of polymer with calcium hydroxide and tricalcium silicate", Proc. 3rd. Int. Conf. Superplasticizers and other Chemical Admixtures in Concrete, Ottawa, Canada, 1989, Ed. Malhotra, V. M., pp. 263-272, Publ. ACI, SP-119

Double, D.D., "New developments in understanding the chemistry of cement hydration", Philosophical Transactions of the Royal Society of London, Series A, No. 310, 1983, pp. 53-66.

Fierens, P. and Verhaegen, J.P., "Hydration of tricalcium silicate in paste - kinetics of calcium ions dissolution in the aqueous phase", Cement and Concrete Research, Vol. 6, 1976, pp. 337-342.

Grutzeck, M.W. and Ramachandran, A.R., "An integration of tricalcium silicate hydration models in light of recent data", Cement and Concrete Research, Vol. 17, 1987, pp. 164-170.

Han, K. and Williams, H.L., "Ionomers: Two formation mechanisms and models", Journal of Applied Polymer Science, Vol. 42, 1991, pp. 1845-1859.

Justnes, H., and Dennington, S.P., "Designing latex for cement and concrete", Nordic Concrete Research, Publ. No. 7, 1988, pp. 188-206.

Kuhlmann, L.A., "Styrene-butadiene latex-modified concrete: The ideal concrete repair material?", Concrete International, Vol. 12, No. 10, 1990, pp. 59-65.

Lavelle, J.A., "Acrylic latex-modified portland cement", ACI Materials Journal, Title no. 85-M6, January-February 1988, pp. 41-48.

Odler, I. and Dörr, H., "Early hydration of tricalcium silicate. I. Kinetics of the hydration process and the stoichiometry of the hydration products", Cement and Concrete Research, Vol. 9, 1979, pp. 239-248.

Ohama, Y., "Principle of latex modification and some typical properties of latex-modified mortars and concretes", ACI Materials Journal, November-December 1987, pp. 511-518.

Pressler, F.E., et al, "Determination of the free calcium hydroxide contents of hydrated Portland cements and calcium silicates", Analytical Chemistry, Vol. 33, No. 7, 1961, pp. 877-902.

Ramachandran, V.S., "Use of superplasticizers in concrete", Il Cemento, Vol. 84, No. 3, 1987, pp. 273-298.

Tadros, M.E., Skalny, J., and Kalyoncu, R.S., "Early hydration of tricalcium silicate", Journal of the American Ceramic Society, Vol. 59, Nos. 7-8, 1976, pp. 344-347.

HYDRATION BEHAVIOR OF CONVERTER SLAG ADMIXED WITH POLYMER CEMENT

Naomitsu TSUYUKI, Hyunkuk CHOI, Kazuhiro SEKI and Makoto HATANO
College of Science and Technology, Nihon University, Funabashi, Japan

ABSTRACT Hydration of portland cement - dephosphorized slag with reduced free lime - gypsum - SBR system is investigated. Hydration mechanism is studied with the help of XRD, SEM and calorimetry and the strength of hardened mortar is discussed in terms of pore structure. Effect of hydration mechanism on the strength development is discussed.

Key-words: Admixtures, Blastfurnace slag, Naphtalene Formaldehyde Sulphonate, Polymer, Pore Structure

INTRODUCTION

Method to utilize converter slag as a construction material has not been established so far. The authors proposed a method to utilize dephosphorized slag (Choi et al, 1993), the major components of which are di-calcium silicate (ß-C_2S) and fluoroapatite ($Ca_5F(PO_4)_3$), for construction materials by reducing free lime (CaO) present in it. It is well known that the component of human bone and tooth is hydroxyapatite ($Ca_5OH(PO_4)_3$) and what is included in the dephosphorized slag is a component in which OH of hydroxyapatite is substituted by F. This component can greatly contribute to bending strength of concrete as an admixture (Choi et al, 1995).

This paper will deal with a cement composite materials of high bending strength using dephosphorized slag with a high-range AE water-reducing agent and styrene-butadiene rubber (SBR) latex. The hydration mechanism is also discussed.

EXPERIMENTS

Materials used

The dephosphorized slag is a by-product of steel manufacture, whereby iron components were magnetically separated and crushed so as to pass through 75 µm sieve. The chemical components are shown in Table1. The dephosphorized slag was further burnt at 500 °C for 2 hours to reduce free lime less than 0.065% (Choi et al, 1993). The improved dephosphorized slag defined as to have free lime less than 1 %, hereinafter referred to as IDS, is used for the following experiments. The X-ray diffraction pattern of IDS is shown in Fig. 1, where the main minerals can be identified as ß-C_2S and $Ca_5F(PO_4)_3$. The total mineral components calculated from Table.1 is shown in Table. 2.

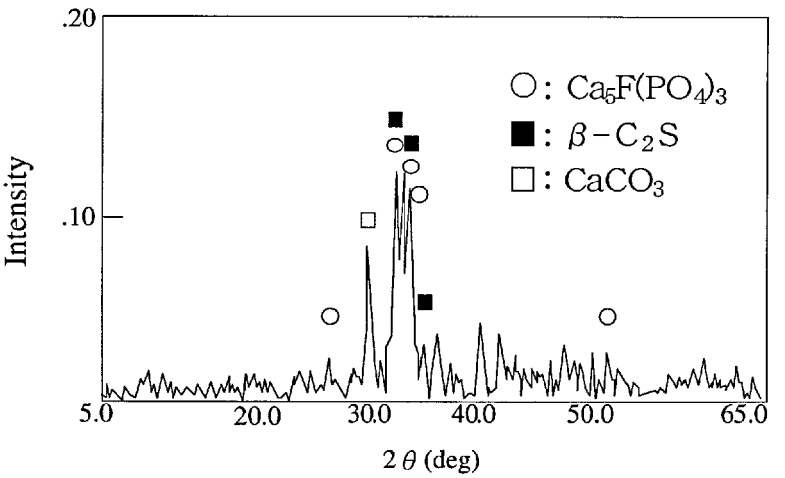

Fig.1 XRD of IDS (Improved dephosphorized slag)

Table 1 Chemical composition of IDS (wt%)

Ig.loss	SiO_2	Al_2O_3	FeO, Fe_2O_3	CaO	TiO_2	P	F
4.3	17.3	2.5	6.0>	50	1.8	1.4	1.5

Table 2
Mineral composition of IDS (wt%)

β-C_2S	$Ca_5F(PO_4)_3$	CaF_2
49.6	14.9	5.2

Table 3 XRD intensity of $Ca(OH)_2$ and $CaSO_4 \cdot 2H_2O$ in the presence of chamical admixture

Alkaline condition (d=2.46)		Neutral condition (d=4.29)	
Specimen (solid phase)	Relativ intensity	Specimen (solid phase)	Relativ intensity
$Ca(OH)_2$	100	CaSO4·2H2O	100
$Ca(OH)_2$ + NSN	23.10	CaSO4·2H2O + NSN	89.63
$Ca(OH)_2$ + PCN	35.15	CaSO4·2H2O + PCN	97.66
$Ca(OH)_2$ + SBR	74.85	CaSO4·2H2O + SBR	99.37

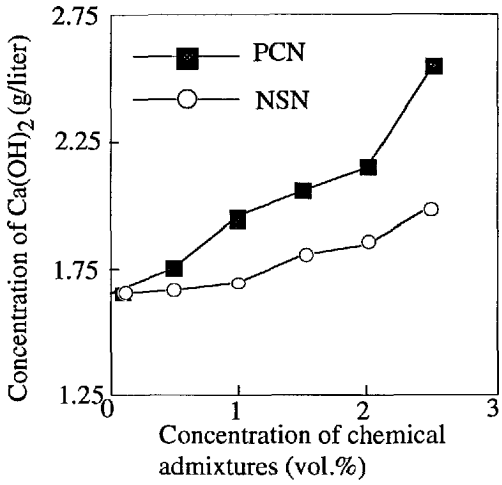

Fig.2 Solubility of $Ca(OH)_2$ vs. concentration of chemical admixtures

Testing methods

Since the SBR contains a high-range AE water-reducing agent which may affect the hydration of cement, reactivity with $Ca(OH)_2$ which may be released from portland cement and the IDS has been examined.

(1) Solubility of $Ca(OH)_2$ in chemical admixtures of naphthalene sulfonate (NSN) and polycarboxylate (PCN) was obtained by measuring the concentration of Ca^{2+} in the filtrate of well - stirred solution of over dispersed $Ca(OH)_2$ and 0 to 2.5 mass % of NSN and PCN. XRD of residue after chemisorption of NSN and PCN on $Ca(OH)_2$ was made and compared to that of gypsum ($CaSO_4 \cdot 2H_2O$).

(2) Hydration products of mixtures of portland cement, IDS and SBR (0 to 2.5 mass %) were identified by XRD and observed by scanning electron microscope (SEM). The same analysis was adopted when gypsum ($CaSO_4 \cdot 2H_2O$) is added.

(3) Total pore volume, specific surface area, mean pore diameter, total porosity, compressive strength and bending strength of the hardened material were measured.

RESULTS AND DISCUSSION

Solubility of calcium hydroxide in the high-range AE water-reducing agent solutions

Solubility of $Ca(OH)_2$ in the high-range AE water-reducing agent (NSN, PCN) solutions of 0 to 2.5 mass % was measured and expressed in terms of concentration of $Ca(OH)_2$ in Fig.2.
It is shown that the solubility of $Ca(OH)_2$ is higher in PCN solution than in NSN solution, and is always higher than 1.60 g/liter. This may be attributed to formation of a soluble complex at terminal groups and to chemisorption. XRD measurements of insoluble solid phase of $Ca(OH)_2$ and $CaSO_4 \cdot 2H_2O$ are given in Table. 3 where the diffraction intensity of $Ca(OH)_2$ at d=2.46 and $CaSO_4 \cdot 2H_2O$ at d=4.29 was normalized in 100. Table 3 shows that $Ca(OH)_2$ is likely to be a gel-like structure in the $Ca(OH)_2$ - NSN and $Ca(OH)_2$ - PCN system as seen in the depression of XRD intensity, while crystallinity is normal in the SBR system which contains no surfactant and in gypsum system. This characteristics may be dependent on the pH value of solutions.

Crystallinity of IDS

The crystallinity of IDS is substantially poor as shown in Fig.1 due to its glassy structure. The chemical composition implies the presence of a glass of the system of CaO - Al_2O_3 - CaF_2 or system of CaO - Al_2O_3 - SiO_2 (Tsuyuki et al, 1995), whereby the rapid formation of ettringite can be seen at hydration in the presence of gypsum. The exothermal rate of hydration of IDS in the presence of gypsum is shown in Fig.3. where the first exothermal peak reflecting the rapid formation of ettringite is recorded earlier than that without gypsum.

Hydration products in the hardened material

Hydration products of portland cement - IDS - gypsum - SBR system at the age of 28 days were identified by XRD. Since the crystallinity of IDS itself is poor and has much glass phase, the XRD shows low intensity when IDS is admixed. The major crystal components are ettringite and C-S-H group, and unreacted gypsum cannot be detected as it may react with CaO Al_2O_3 - CaF_2 glass phase to form ettringite. No substantial influence due to addition of SBR was detected.

Pore size distribution of the hydration products

Pore size distribution of the hardened mortar specimen at the age of 6 months measured by mercury porosimetry (Simazu Auto-pore 9220) is shown in Table. 4. Total pore volume and total porosity become smaller in the system OPC - IDS than in OPC, however in the presence of SBR, addition of 5 and 15 mass % of SBR resulted respectively larger and smaller pore volume than that of OPC. This may be attributed to the water reducing effect due to bleeding at mixing in the presence of larger

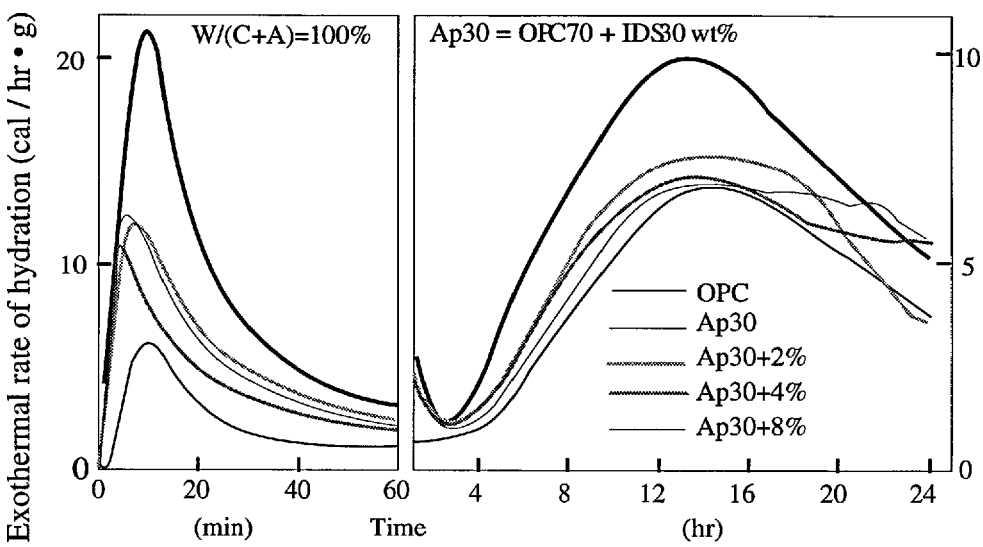

Fig.3 Exothermal rate of hydration of OPC-IDS-$CaSO_4$•$2H_2O$ system

Table 4 Pore structure (diameter below 30 μm)

Specimen	Total pore volume (cc / g)	Specific surface area (m^2 / g)	Mean pore diameter (μm)	Total porosity (%)
OPC	0.098	36.66	0.011	18.7
OPC+IDS	0.079	34.11	0.009	16.1
OPC+IDS+SBR5%	0.172	42.28	0.016	27.8
OPC+IDS+SBR15%	0.090	25.81	0.014	17.2
OPC+IDS+CaSO4·2H2O	0.088	32.62	0.011	17.3
OPC+IDS+CaSO4·2H2O+SBR5%	0.166	35.78	0.019	28.2
OPC+IDS+CaSO4·2H2O+SBR15%	0.101	30.77	0.013	18.8

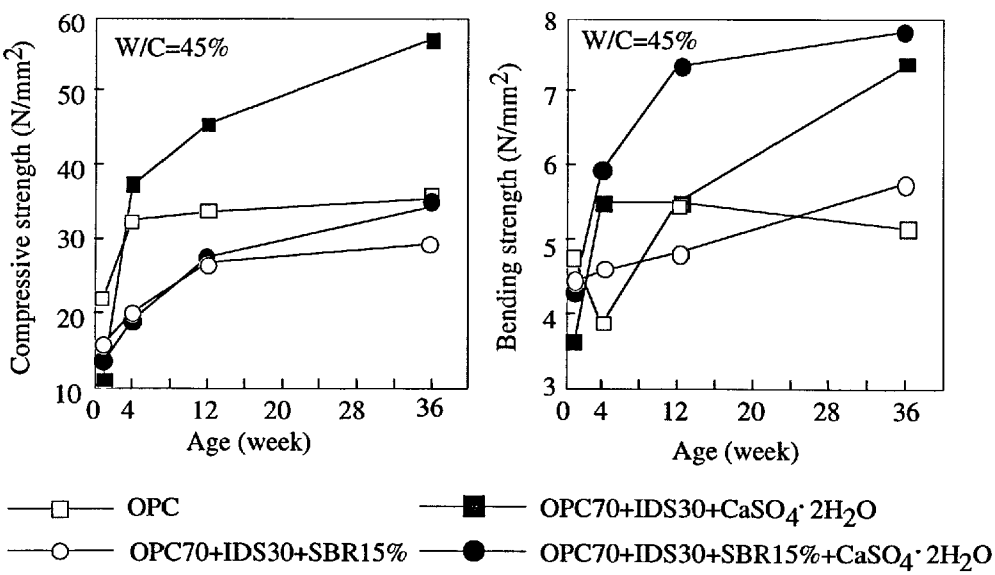

Fig. 4 Strength of hardened mortar

amount of SBR. Addition of gypsum also resulted in a dense structure with smaller pore volume thanks to the formation of ettringite.

Strength of the hydration products

Compressive strength and bending strength of mortar made of portland cement, IDS of 30 inner %, SBR, gypsum and standard fine aggregate are shown in Fig.4. Improvement of strength can be obtained by adding gypsum and SBR for 15 mass %.

Hydration mechanisms of IDS blended cement

IDS contains ß-C2S and $Ca_5F(PO_4)_3$. The former may contribute to the long term development of strength while the latter may play a role in fixing free lime in IDS as an apatite group, whereby major hydration products are C-S-H group and ettringite. With addition of SBR, the surfactant in the SBR forms a complex Ca^{2+} originated from the powder materials and the surface of the hydration products may be covered by the gel. In the presence of gypsum, pore volume may be reduced where interparticle pore space may be filled with SBR as schematically shown in Fig. 5.

CONCLUSIONS

A cement composite material with a high bending strength has been developed by blending the improved dephosphorized slag. The major findings are as follows.

(1) The surfactant in the SBR forms a complex in the $Ca(OH)_2$ - NSN and $Ca(OH)_2$ - PCN system and the surface of the hydration products may be covered by the gel.

(2) Development of strength of cement - IDS mortar with SBR and gypsum is greater than that without gypsum thanks to the formation of ettringite form the glass phase in IDS.

(3) Pore structure of a mortar admixed with SBR for 15 mass % shows more dense structure than that with 5 mass % due to the bleeding effect.

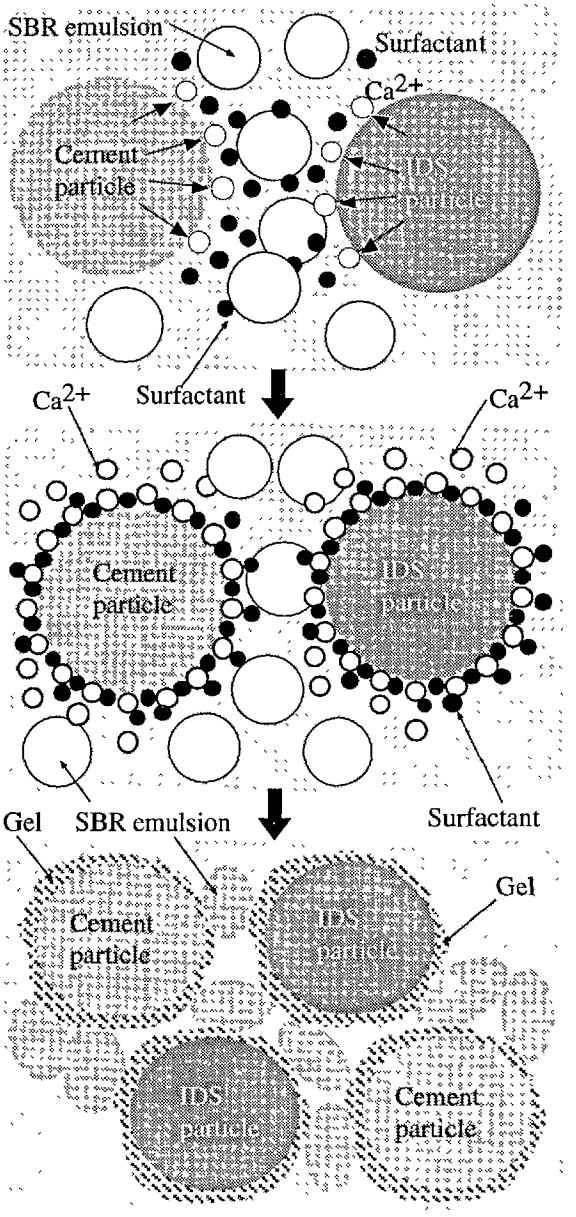

Fig.5 Hydration process of IDS in the presence of SBR

Acknowledgment

The authors would like to thank Foundation of the Environment Preservation Technology in the Steel Industry for the 1996 research grant (No. 17).

REFERENCES

Choi, H., Tsuyuki, N., Shimizu, G. and Sakuta, M, "Development of New Admixture Using Dephosphorized Slag and Its Properties", Annual Report of CAJ, 47, pp. 190-195, 1993

Choi, H., Tsuyuki, N., Shimizu, G. and Sakuta, M, "Study on Utilization of Dephosphorized Slag as Building Materials", 4th Japan International SAMPE symposium and Exhibition, vol. 2, pp. 1407-1412, 1995

Tsuyuki, N., Choi, H. and Sakuta, M., "Effect of Dephosphorized Slag on the Hydration of Portland Blast - Furnace Slag Cement", Annual Report of CAJ, 49, pp. 102-107, 1995

THE EFFICACY OF CALCIUM ALUMINATES IN PRODUCING HIGH FLEXURAL STRENGTH POLYMER COMPOSITE

G.K.D. PUSHPALAL, N. MAEDA, T. KAWANO, T. KOBAYASHI
Maeta Techno-Research, Inc., 6-7 Kamihoncho, Sakata, Yamagata, 998 Japan
M. HASEGAWA
Department of Materials Science and Technology,
Toin University of Yokohama, Yokohama, 225 Japan

ABSTRACT High alumina cement based high flexural strength polymer composite developed recently is investigated in this paper to understand interactions of polymer and cement. This innovation raised a concept that making a high strength cement paste including no water, but utilizing generated water by phenol resin precursor during heat curing to hydrate the surface of cement particles. The authors discuss the role of calcium aluminates to make a strong organic-inorganic three-dimensional network, which gives high flexural strength higher than 120 MPa.

Key-words: Alumina, Aluminate phase, High alumina cements, Macro Defect Free, Polymer

INTRODUCTION

High alumina cement (HAC) consists chiefly of calcium aluminates, though not tricalcium aluminate, but alumina compounds relatively poor in lime. Depending on the lime content of the raw mixture, high alumina cement consists mainly either of monocalcium aluminate ($CaO.Al_2O_3$), or of a compound poorer in lime, with the formula of $CaO.2Al_2O_3$ or of an aluminate richer in lime, $12CaO.7Al_2O_3$(Czernin, 1980). The strength losses due to "conversion" of hydration products to which high alumina cement concrete is subject have led to the use of this cement for load bearing structures being banned, in Japan and in some other countries. However, innovation of high flexural strength Macro Defect Free (MDF) cement have renewed the use of high alumina cement for high flexural strength polymer cement composites. Although many hydraulic cement/water soluble polymer combinations could be used to make MDF cement composites, high alumina cement /polyvinyl alcohol (PVA)/water system has attracted much attention because of superior mechanical properties (Birchall et. al.; 1983). Several authors studied the role of calcium aluminates in making strong HAC/PVA Macro Defect Free cement and proposed chemical interaction mechanisms between calcium aluminates and PVA; Rodger et. al.(1985), Edmonds and Majumdar (1989), Popoola et. al.(1991).

In contrast to high alumina cement /polyvinyl alcohol (PVA)/water system, we discuss recently developed high alumina cement/phenol resin/alcohol system in this paper. This new composite is made by combining high alumina cement, alcohol soluble phenol resin precursor, a little amount of N-methoxymethyl 6-nylon and glycerol under high shear mixing to produce viscoelastic cement paste through a twin roll mill (Kobayashi et.al.; 1992, 1993). This innovation raised a concept that making a high strength cement paste including no water, but utilizing generated water by phenol precursor during heat curing to hydrate the surface of cement particles. The highest mechanical and durability properties are only achieved by composite made with resole-type alcohol soluble phenol resin precursor and high alumina cement. The strength loss after immersion in water at 20°C and after outdoor exposure for one year is only 9% and 6%,

respectively, and the elastic modulus remains almost unchanged. Linear expansion and weight increase of high alumina cement - phenol resin composite are 0.12% and 0.82%, respectively, after immersion in water at 20°C (Pushpalal et. al., 1997a). Within several mineralogical components present in the high alumina cement, phases with higher Al^{3+} concentration and the higher hydraulic property were the best in performances. The evidence of possible calcium aluminate - resin interaction has been experimentally found in processing, during curing and in the final product. We discuss here the efficacy of calcium aluminate to interact with phenol resin, based on the observations in processing, experimental data of differential scanning calorimetry and electron probe microanalysis.

MATERIALS

Particulate Fillers

Two types of commercially available high alumina cements (Secar 71 and 51); ordinary Portland cement (OPC); synthesized $CaO.2Al_2O_3$ (CA_2), $12CaO.7Al_2O_3$ ($C_{12}A_7$) and $CaO.6Al_2O_3$ (CA_6); calcined alumina, $Al(OH)_3$, $Ga(OH)_3$, CaO, $Ca(OH)_2$ were used in this study as particulate fillers. The chemical compositions and physical properties of the cements are listed in Table 1.

Table 1. Chemical compositions and physical properties of the cements

Type of cement	Chemical composition (wt%)							Blaine's specific surface area (cm^2/g)
	Al_2O_3	CaO	SiO_2	TiO_2	Fe_2O_3	MgO	SO_3	
Secar 71	70.22	28.30	0.27	0.26	0.15	0.14	0.03	4010
Secar 51	53.75	36.52	4.22	2.52	0.74	0.39	0.01	4017
OPC	5.30	63.40	21.40	0.26	3.10	1.00	2.0	3260

Calcium aluminates (CA_2, $C_{12}A_7$,CA_6) were prepared in our laboratory by reacting appropriate molar amounts of $CaCO_3$ and Al_2O_3 powders. These materials were thoroughly mixed in a mechanical agate mortar, and fired for 5h at 1350°C-1500°C in a electric furnace in air. Pellets were refired for 5h at 1350°C-1500°C with intermediate crushing, until finally producing the intended calcium aluminate, with no other substances remaining.

Organic Components

Methanol soluble resole-type phenol resin precursors have been shown to have the best results among the several formaldehyde resins. The nature of the hydroxyl group in the phenol moiety seems to be the leading factor that controls the resultant strength. The resole type phenol resin precursor used in the present experiments has the following physical and chemical properties.

Viscosity (25°C)	340 cps
Specific gravity (25°C)	1.09
Nonvolatile matter (135°C)	61.3%
Gel time (150°C)	3.8 (min.)
M_w	6319

N-methoxymethyl 6-nylon was incorporated to modify the phenol resin and to develop the rubbery consistency of the paste. N-methoxymethyl 6-nylon remarkably improves viscoelastic properties of the cement paste and processing details have been given elsewhere (Pushpalal, 1997b). Glycerol was used as a plasticizer.

FORMULATION AND PROCESSING

Formulation

Mix proportions are categorized into two main groups as shown in Table 2.

Table 2. Mix proportions

Mix type	Resin+ Methanol+ modifier/ Solid (%)	Mix proportions (parts by weight)						
		Solid substances			Resin	Methanol	Modifier	Plasticizer
		HAC	Al_2O_3	$Al(OH)_3$				
Standard	23	100			13.06	8.24	1.70	2.30
Comparison	23		66	40	13.06	8.24	1.70	2.30

High alumina cements, OPC and calcium aluminates (CA_2,$C_{12}A_7$,CA_6) were proportioned according to "standard" mix proportion, disregard of slight differences of their specific gravities. The mix proportion called "comparison" is used in this study to compare the properties of cement-based composites with non cement-based composites. All non cement-based mixtures (calcined alumina, $Al(OH)_3$, $Ga(OH)_3$, CaO, $Ca(OH)_2$) were designed considering differences of specific gravities; i.e. total particulates in non cement-based mixtures is equal in volume to particulates in "standard" mix proportion.

Processing

The paste containing organic/inorganic compounds was prepared by mixing inorganic compounds, the modified methanol solution of phenol resin precursor and plasticizer in a kneader-style mixer. The general method of roll milling is nearly equal to the MDF technology, except in its attempt to cool the rolls to minimize rising temperature (Young, 1991). When the paste is mixed in the roll, temperature rises due to the work of the rollers and the viscosity of the paste also rises to become moderately hard. Then the paste is condensed into a thin layer and twined around the faster roller. This sheet is scraped away, folded and re-rolled several times until it becomes a homogeneous sheet. The resulting mass is allowed to cure at 200°C for 18 h. If the sheet is further densified by pressing (6 MPa at 80°C) after the calendering, considerable increment in final strength can be obtained. To ensure the highest strength, it is necessary to elevate the temperature slowly and keep it at 65°C or above for more than 30 minutes under pressure. The heat pressing step can be skipped if necessary, depending on property requirements.

RESULTS AND DISCUSSION

Interaction During Processing

The ability to make a sheet through a twin roll mill is highly dependent on the base powder used. All hydraulic cements perform considerably well in the roll milling process regardless of the main mineralogical component contained. Young and Berg (1992) concluded that a controlled cross-linking action is needed to develop the rubbery characteristics which are suitable for roll-milling;

we also observed the same tendency. Table 3 shows processing characteristics of cements, pure calcium aluminates, metal oxides and hydroxides with the addition of phenol resin precursor.

Table 3. Processing characteristics of several inorganic powders with the addition of phenol resin precursor

Type of powder		Forming ability
High alumina cements	Secar 71	Good
	Secar 51	Good
Ordinary Portland cement		Fair
Calcium aluminates	CA_2	Poor
	$C_{12}A_7$	Fair
	CA_6	Very poor
$Al(OH)_3$		Good
$Ga(OH)_3$		Good
$Ca(OH)_2$		Immediately hardened
Al_2O_3		Did not harden
CaO		Immediately hardened
$Al(OH)_3/Al_2O_3$ ("comparison")		Fair

High alumina cement showed good processing characteristics among all the powders tested. When OPC and $C_{12}A_7$ are used, roll milling is difficult because of rapid hardening during the milling. CA_2 and CA_6 were poor in combining during roll milling, hence stiffness of the sheet is low and difficult to handle. Our experiments showed that the cement can be replaced by inert fillers for up to 50% of the volume but higher than 50% influences negatively on processing; i.e. sheet-making is unsuccesful. However, complete replacement of the cement by Group III (Periodic Table) hydroxides provided good processing characteristics but was of lower strength. The paste consisting of calcined alumina and resin did not combine properly in roll milling, sheet making ability is poor, like with calcium hexaluminate.

The paste of calcium oxide and resin underwent a highly exothermic reaction shortly after mixing in the twin roll mill and hardened rapidly, thus sheet forming became impossible. Calcium hydroxide also showed the same features as calcium oxide. The different behavior of calcium and aluminum can be explained by their ionization potentials. Oxidation potentials of calcium and aluminum are +2.87 and +1.66 volts, respectively [Dean, 1979], thus calcium should have a higher oxidation tendency in the phenol resin system. Moreover, hardened calcium oxide or hydroxide dough can be softened by dipping it in acetic acid, thus occurrence of ionic-type interaction (rapid and reversible) is confirmed. It is reasonably expected that such an ionic reaction also occurs between phenol resin and cement phases in the cement to a certain extent; the ionic-type reaction corresponds to the development of a rubbery consistency which is essential for making a good sheet. This idea has been confirmed by the different processing characteristics showed by different calcium aluminates; i.e. highly reactive Ca ion rich phases ($C_{12}A_7$) hardened rapidly, while the low reactive (CA_6) phases combined poorly in roll milling.

Interaction During Heat Curing

Hardening of the phenol resin cement sheet occurs with a polycondensation reaction of phenol resin to form a three dimensional crosslinking structure between 130°C -170°C; in this temperature range water is released from the phenol resin. Fig. 1 shows the development of flexural strength of the composite during various stages of thermal curing. The flexural strength was measured on the specimens kept at each temperature level for 2 hours and with the temperature elevating rate at 20°C/hr. The strength of a standard specimen was compared with a non-cement based composite made according to mix proportion "comparison". The standard specimen showed a significant strength increment in between 140°C and 160°C.

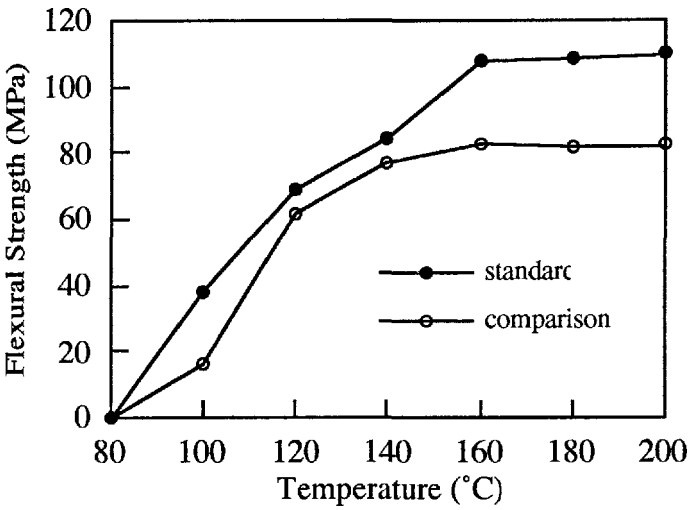

Fig. 1. Development of flexural strength of the composite during various stages of the thermal curing.

Hasegawa and coauthors (1995) have investigated the thermal behavior of phenol resin and several powder/phenol resin mixtures by Differential Scanning Calorimetry. The resole type phenol resin precursor shows sharp endothermic peak around 162°C, that certainly corresponds to the cross-linking formation accompanied with releasing the water molecules. The addition of HAC or CA to phenol resin precursor converts that endothermic peak to broad exothermic peak, while inert fillers (Al_2O_3 and SiO_2) do not show any response.

Strength Dependence on Base Powder

Table 4 shows flexural strengths and bending modulus results of specimens made with several inorganic powders. Mechanical properties are heavily dependent on the method of processing. Two processing routes were followed; one was calendering/heat curing (Route 1) and the other was calendering/heat press/heat curing (Route 2).

Secar 51 has recorded highest flexural strength among all the inorganic powders tested. With regard to the strength results of processing Route 1 of Table 4, Secar 71 gave slightly lower strength than Secar 51. To understand the reason of different behavior, mineralogy of both cements were analyzed by the X-ray diffractometer. Fig. 2 shows the X-ray profiles of Secar 51 and Secar 71 cements. Secar 71 contained more CA_2 than Secar 51. Moreover, pure CA_2 gave lower strength than Secar 51 cement, thus it is logical to conclude that slightly lower strength of Secar 71 is due to the lack of calcium monoaluminate. Neither phases like $C_{12}A_7$ which has higher hydraulic properties, nor CA_6 which is richer in Al^{3+} ions directly affects the strength

development. Moreover, the "comparison" formulation with non-cement powders shows moderate strength when processed by Route 1, however, further strength improvement by heat pressing was not possible. Pushpalal et. al. (1995) have shown that porosity and pore size of the specimens made by the same mix proportion was lower than that of the "standard," still, strength was lower than the "standard." Thus it can be inferred that both the hydraulic property, and a high concentration of aluminum ions in the base powder are essential for high strength and durability. In addition, OPC shows lowest strength in both processing routes regardless of its fair processability through the roll mill. Thus it can be inferred that aluminum ion plays a more essential role during heat curing than calcium ion, which enables it to produce a high strength and water resistant composite.

Table 4. Flexural strengths and bending modulus of specimens made with different inorganic powders.

Type of powder	Calendering/heat curing (Route 1)		Calendering/heat press/heat curing (Route 2)	
	Strength (MPa)	Modulus (GPa)	Strength (MPa)	Modulus (GPa)
Secar 51	134	29.57	198	39.08
Secar 71	123	30.34	167	34.85
OPC	74	25.10	86	27.19
CA_2	105	28.05	---	---
$C_{12}A_7$	81	31.48	---	---
CA_6	96	31.19	---	---
$Al(OH)_3$	76	18.36	97	25.43
$Ga(OH)_3$	73	18.05	---	---
$Al(OH)_3/Al_2O_3$ ("comparison")	88	28.10	heat press is ineffective	

--- data not obtained

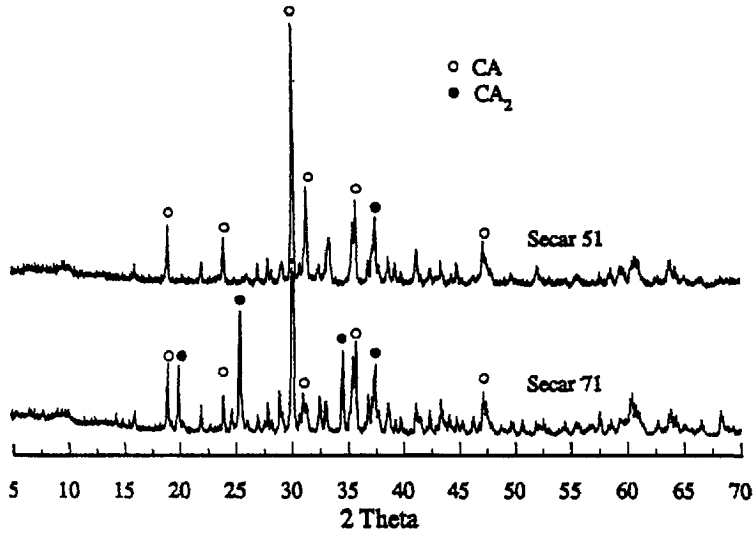

Fig. 2. The X-ray profiles of Secar 51 and Secar 71 cements.

Electron Probe Microanalysis

Samples of high alumina cement-phenol resin composite were investigated with an Electron Probe Microanalyzer. Wave Dispersive Spectrometer (WDS) in the electron microscope was used to quantify calcium and aluminum. Fig. 3 shows a back scattered electron image of a CA grain surrounded by the polymer matrix and an overlaid graph of the A/C ratio versus distance from the interface. A/C ratios were measured along the line of analysis at the distances indicated by bold circles. The A/C ratio of the center of the particle is 1.5 and decreases as it approaches the interface, where the ratio was found to be 1.36. In addition, certain amounts of calcium and aluminum were also traced in the polymer matrix.

Edmonds and Majumdar (1989) have suggested on the HAC/PVA system that the polymers (PVA) complex more readily with aluminum than with calcium ions to result in the removal of aluminum ions from the grain surfaces and the formation of a calcium-rich perimeter. Moreover, according to their suggestion, the calcium-rich hydration shells around CA and CA_2 grains suggest that the hydration involves first the removal of aluminum ions from the grain surfaces, followed later by the calcium ions. Thus we prefer to suggest that the aluminum-poor perimeter found by EPMA is due to the hydration which occurred by utilizing released water from the resin during the methylene bridge formation reaction. However, we have not detected any hydration products by Electron Probe Microanalysis.

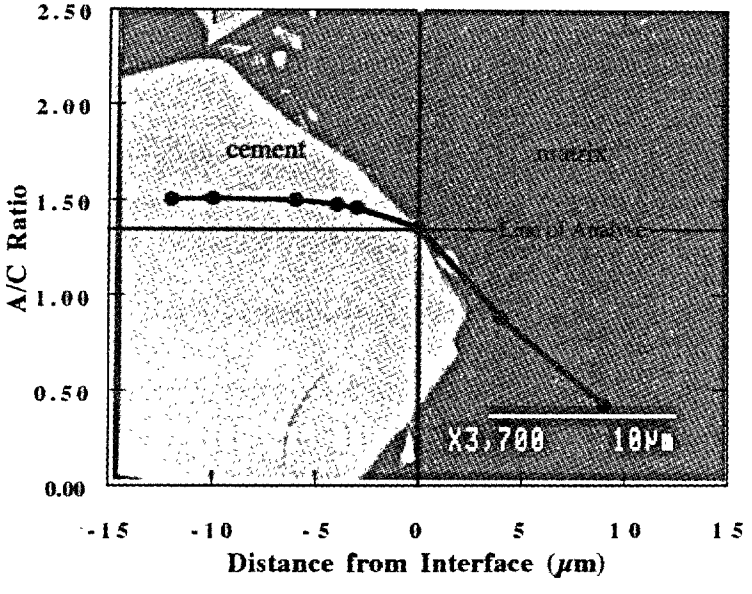

Fig. 3. Back scattered electron image of a CA grain surrounded by the polymer matrix and an overlaid graph of the A/C ratio versus the distance from the interface.

CONCLUSIONS

It is clear from the above results that calcium aluminates and resole type phenol resin precursor interact with each other through the whole process, beginning from the twin roll milling up to the final product to make it a stronger material. The authors prefer the mechanism in which the phenol resin complexes with Ca^{2+} ions through an ionic cross-linking reaction during the roll milling and

then with Al^{3+} ions through a chemical cross-linking reaction during heat curing. The schematic representation of crosslinking reaction is presented elsewhere (Pushpalal et. al., 1997c)

Acknowledgments

The authors wish to thank Mr. Tokuhiko Shirasaka and Mr. Takayoshi Okamura (Central Research Laboratory, Chichibu Onoda Cement Corporation) for their assistance on chemical analyses and useful discussions. The support of Dr. Bruno Espinosa, Mr. Vincent Mages and Mr. Arnaud Boussemart of Lafarge Aluminates, by providing samples and information to prepare this paper is appreciated.

REFERENCES

Birchall, J. D., Howard, A.J., Kendall, K., "Cement Composition and Product," U. S. Patent No. 4,410,366, (1983).

Czernin, W., "Cement Chemistry and Physics for Civil Engineers", Georg Godwin Limited, London, p. 161, (1980).

Dean, J. A., "Lange's Handbook of Chemistry", McGraw-Hill, Inc., USA, p. 6-5, (1979).

Edmonds R. N., Majumdar A. J., "The hydration of an aluminous cement with added polyvinyl alcohol-acetate", Journal of Material Science **24**, pp. 3813-3818, (1989).

Hasegawa, M., Pushpalal, G.K.D., Takata, T., Maeda, N., Kobayashi, T., Mat. Res. Soc. Symp. Proc., Vol. 385, Materials Research Society: Pittsburgh, pp. 167-172 (1995).

Kobayashi, T., Pushpalal, G.K.D., Hasegawa, M., Japanese Patent Application No. JP 301514 / 92 to Maeta Concrete Industry Ltd., Japan (1992).

Kobayashi, T., Pushpalal, G.K.D., Hasegawa, M., European Patent Application to Maeta Concrete Industry Ltd., Japan, Publication No. 0590948 A1 (1993).

Popoola, O. O., Kriven, W. M., Young, J. F., "Microstructural and microchemical Characterization of a Calcium Aluminate-Polymer Composite (MDF Cement)," J. Amer. Cer. Soc., 74(8), pp. 1928-1933, (1991).

Pushpalal, G. K. D., Maeda, N., Kawano, T., Kobayashi, T., Hasegawa, M., Takata, T., "Properties and flexural failure mechanism of a high strength phenol resin-cement composite," Proceedings of the VIIIth ICPIC Congress, Belgium, pp. 631-636, (1995).

Pushpalal, G. K. D., Kawano, T., Kobayashi, T., Miura, S., Maeda, N., Hasegawa, M., Takata, T., "Durability of high flexural strength alumina cement-phenol resin composite," In *Polymers in Concrete*, Edited by Ohama, Y., Kawakami, M., Fukuzawa K., Chapman & Hall: London, Proceedings of The Second East Asia Symposium on Polymers in Concrete, Koriyama, Japan, May 1997. (in press)

Pushpalal, G. K. D., Doctoral Thesis, Toin University of Yokohama, Japan, 1997.

Pushpalal, G. K. D., Kawano, T., Kobayashi, T., Hasegawa, M., "Chemical characterization of calcium aluminate-phenol resin composite," Journal of Advanced Cement Based Materials, Elsevier Science Inc., 1997. (in press)

Rodger, S. A., Brooks, S. A., Sinclair, W., Groves, G. W., Double, D. D., "High strength cement pastes, Part 2: Reactions during setting," Journal of Material Science **20**, pp. 2853-2860, (1985).

Young, J. F., "Macro Defect Free Cement: A Review," Specialty Cements with Advanced Properties, Ed. B. Scheetz, et al., Mat. Res. Soc. Symp. Proc., Vol. 179, pp. 101-121, (1991).

Young, J. F., Berg, M., "Macro-Defect-Free Cement: A novel organoceramic composite", Mat. Res. Soc. Symp. Proc., Vol. 271, pp. 609-619, (1992).

3111011
8 pp

MDF-RELATED SYSTEMS BASED ON SULFOBELITIC CLINKER / HYDROXYPROPYLMETHYL CELLULOSE / POLYPHOSPHATE GLASS COMPOSITIONS.

Milan DRABIK, Lubica GALIKOVA, Frantisek HANIC , Institute of Inorganic Chemistry, Slovak Academy of Sciences, 842 36 Bratislava, Slovak Republic
Robert C.T. SLADE , Department of Chemistry, University of Exeter, Exeter EX4 4QD, United Kingdom

ABSTRACT Model MDFs have been fabricated using (1) low-energy sulfobelitic clinkers (C_4AF and $C_4A_3\bar{S}$, with 25 % β–C_2S) or (2) sulfobelitic plant cement, with hpmc or polyphosphate glass as polymer component. Atomic level cross-links are demonstrated by nuclear (NMR and Mössbauer) spectroscopies and thermal analysis. The moisture resistance of these models is similar to that for PC-based MDFs. The use of polyphosphate glass enhances moisture resistance.

Key-words : Cross-linking , Macro Defect Free , Moisture , Thermogravimetry .

INTRODUCTION

A range of different clinker/polymer combinations have been said to have potential as regards formation of MDF materials. In an early patent in this field Birchall et al. (1988) outlined the use of aluminous, Portland (PC) and sulfate clinkers, and a wide range of water-soluble carbonaceous polymers. Studies comparing the properties of MDFs with hydraulic cements have attributed the improved mechanical characteristics to the partial filling of the pore structure by polymer gel and to the adhesive action of polymer, linking fibrils of hydrated cement. Several models involving atomic-level cross-linkages have been postulated (Rodger,1985; Edmonds,1989; Desai,1992) as explanations of the chemical origin of the exceptional properties of MDFs fabricated from aluminous cements and polyvinylalcohol-acetate (PVA/Ac). These models are complementary and evidently provide a realistic chemical view of the reactions occurring. Principles governing the chemistry and its transfer to bulk properties of PC-based MDFs have resulted from the studies of Roy's group, which performed MDF-related studies of Portland cement and polyacrylamide (Roy, 1992). More recently, Ma and Brown (1992, 1994) reported the use of polyphosphates (poly-P) in some model systems. We have reported MDF-processibility of particular components/phases arising in potential sulfobelitic clinkers in combination with hydroxypropylmethyl cellulose (hpmc) and polyphosphates (poly-P) (Drabik,1994a,b, 1995). The results have pointed to (i) the involvement of *Al, Fe, P* and *C* atoms in cross-links within amorphous AFm-like reaction products/intergranular gel, and (ii) the influence of that chemistry on porosity, a. c. electrical impedance and microstructure.

An exceptionally important task (for both scientists and technologists) is the control of moisture resistance of MDFs. The incompleteness of conversion of clinkers is obvious at the given w/s ratios, and this incompleteness exerts a negative effect - low (or undefined)

moisture resistance. Studies on the moisture resistance of MDFs are not uniform in their results. Igarashi (1992) differentiates effects of moisture below and above a relative humidity of 65%; the lower humidity environment does not deteriorate MDF material, whilst the upper does. That study was performed on PC-based MDFs. Results have also been presented for aluminous MDFs (Lewis,1994); moisture resistance was believed to be high. Percolative principles controlling the kinetics of degradation by moisture have been generally discussed by Chu and Robertson (1994), but the effects are not satisfactorily defined for MDFs. There are two contradictory tendencies evident in the results of these early studies: low percolation results in high moisture resistance (Lewis,1994; Chu,1994), but decomposition of PVA/Ac occurs in concretes and mortars (Zivica,1965) and especially in MDFs (Birchall,1988; Edmonds,1989; Rodger,1985).

The aim of present study was to investigate the MDF-related properties of model systems of the type sulfobelitic clinker / hydroxypropylmethyl cellulose (hpmc) / polyphosphate glass (poly-P). Particular interests are the processibility and cross-linking during MDF fabrication, and also the moisture resistance of the MDF models. Clinkers originating both from laboratory synthesis and from a cement plant have been investigated.

EXPERIMENTAL

Clinkers, cements and preparation of MDF probes

Laboratory clinker phases (C_4AF, $C_4A_3\bar{S}$) and physical mixtures of these (1:1, 1:2, 2:1) were prepared by reactions of chemical grade compounds at 1250 °C, as reported elsewhere (Drabik, 1994a). More complex sulfobelitic clinkers (in which the individual clinker phases were present along with C_2S, belite, 25 % by mass) were synthesized at 1250 °C (Drabik, 1994c). Low-energy sulfobelitic plant cements were produced at 1240 - 1270 °C in standard medium size rotary kilns (Cimus, Romania).

Processing to obtain model MDF materials was as follows : (i) Dry pre-mixing of clinker phases (or mixtures of clinker phases, or cement) with hpmc (5 % of total mass). (ii) Addition of water to give w/s = 0.2, or addition of an aqueous solution of sodium polyphosphate to incorporate 5 % (by mass) of poly-P and give w/s = 0.2 (s includes clinker and mass equivalent of the dissolved poly-P). (iii) Twin-rolling until the mixture reaches the consistency of dense dough (up to 5 min). (iv) Static 5 MPa pressure in a pellet die (diameter 10 mm) applied for intervals ranging from 30 minutes to 6 hours. (v) Chemical reactions kinetically frozen by air drying at 50 °C. Hydroxypropylmethyl cellulose (Aldrich) was p.a. purity, viscosity of 2 % aqueous solution 80 - 120 centiPoise. Sodium polyphosphate glass (Budit 9, approximate stoichiometry of a tetraphosphate) samples were supplied by Chemische Fabrik R.A. Oetker (Budenheim, Germany).

Methods of the treatment of MDF probes

For each model MDF composition 2 - 4 separate MDF disk samples were synthesized and investigated. In spectroscopic examination (multinuclear ^{27}Al, ^{13}C, ^{31}P high resolution MAS NMR, ^{57}Fe Mössbauer) and thermal analyses, ground samples were studied. ^{57}Fe Mössbauer spectra were recorded at -196 °C ($N_2(l)$) using a standard constant acceleration spectrometer and cryostat. Simultaneous TG and DTA were conducted on a T.A.I. sdt 2960 instrument (from ambient temperature to 1000 °C, 10-20 mg, 10 °C min^{-1}, in air).

MAS NMR spectra were recorded at ambient temperature using a Varian Unity 300 spectrometer. ^{27}Al (78.15 MHz) spectra were recorded with spin rates ~ 12 kHz. Short (1 μs) pulses were employed, a small background arising from the Doty probe was subtracted, and spectra were referenced to $Al(H_2O)_6^{3+}$ *(aq)*. ^{13}C (75.4 MHz) and ^{31}P (121.4 MHz) spectra were recorded with sample spinning rates 4.0 - 4.5 kHz, and were referenced to TMS (^{13}C) and concentrated (85%) H_3PO_4 (^{31}P). ^{13}C spectra were recorded with cross-polarization (^{1}H - ^{13}C), and ^{31}P spectra were recorded with gated decoupling.

In impedance studies the faces of an MDF disk were coated with conductive silver paint (Acheson Electrodag 915) and copper disks were then attached using the silver paint as adhesive. Pellets were equilibrated in a desiccator over saturated $NaHSO_4(aq)$ (relative humidity RH = 52 % at ambient temperature).

The moisture resistance of model MDFs was investigated at two different relative humidities (RH); mass increases of samples kept in the environments RH = 52% (above saturated $NaHSO_4(aq)$) and RH = 100% (above deionised water) were followed as a function of time. Sample changes after equilibration at those RHs were evaluated thermoanalytically.

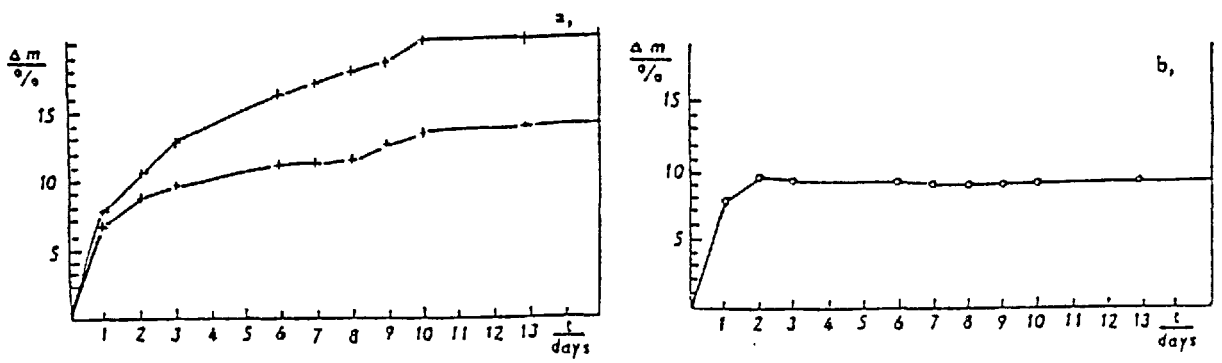

Figure 1 Δm = f (t), for MDFs formed from sulfobelitic clinker: (a) with hpmc and stored at RH = 100% (upper trace MDF pressing 1h, lower trace 6h), (b) with poly-P and stored at RH = 100% (independent of pressing time)

RESULTS AND DISCUSSION

Very good processibility is achieved across the whole composition range, with twin-rolling being an unavoidable step if proper dough consistency is to be achieved. Application of pressure for any interval between 30 min to 6 h results in well shaped test pieces, frequently with a semi-gloss surface. The test pieces do not all behave similarly under moisture-resistance testing (see later also). As regards the degree of atomic level cross-linking interactions and consequent moisture resistance, for MDFs made with hpmc as sole polymer a lengthy (5 - 6 h) pressing is preferable, whereas for systems with poly-P alone a shorter pressing (1 h) is sufficient.

Atomic level changes due to MDF fabrication procedures were monitored by nuclear (NMR and Mössbauer) spectroscopies and thermal analysis. Values of chemical (NMR) and isomer (Mössbauer) shifts of probe nuclei and assigned cross-linking interactions are summarized in Table 1. Indicative TG intervals and DTA events of MDF test pieces, both before and after moisture-resistance testing, are given in Table 2.

Table 1 Chemical shifts in MAS NMR (^{27}Al, ^{13}C, ^{31}P) and isomer shifts in Mössbauer (^{57}Fe) spectra, together with relevant local structures in (**a**) polymer-free systems, (**b**) MDF test pieces (cross-links in ***bold*** type) and (**c**) pure polymers.

	a	**b**	**c**
^{27}Al	δ = 13.4 *Al(6) - OH*	δ = 9.4 ***Al(6) - OX***	-
^{57}Fe	δ_{iso} = 0.50 mm s^{-1} *Fe(6) - OH*	δ_{iso} = 0.70 $\pm$ 0.05 mm s^{-1} ***Fe(6) - OX***	-
^{13}C	-	δ = 67 ***CH - O - Me***	δ = 66 *CH - O - R*
^{31}P	-	δ = - 5.1 ***P(4) - O - Me***	δ = 1.7, - 15.7 $P(4)_t$ - O $P(4)_b$ - O

Note : ^{29}Si m.a.s.-n.m.r. spectra revealed Q(0) of C_2S only, under all reaction conditions.

The resulting picture is fully in line with the accepted hydration kinetics of individual clinker phases ; $C_4A_3\bar{S}$ (containing *Al*) ~ C_4AF (containing *Al* and *Fe*) >> C_2S (containing *Si*). Cross-links are formed by *Al* and *Fe* originating in more reactive clinker phases. The results on *P* atom incorporation within the cross-links provide further evidence of the increasing value of the phosphate compounds in various branches of cementitious/ceramic materials, *cf.* Ma and Brown (1992, 1994), Connaway-Wagner (1991). ^{31}P MAS NMR spectra clearly show extensive chemical reaction and formation of *Al/Fe - O - P* cross-links during MDF procedures (Drabik,1995), and thus the attempt to use poly-P in this class of chemically bonded ceramics is very promising.

Thermal analysis of MDFs before and after moisture attack provides further useful information. Two (for models with hpmc alone) or three (for models with poly-P alone) steps of weight loss are seen in TG traces. When comparing these results with thermal events for polymer-free AFm hydrates (Nishikawa,1992) and for polymers alone, model MDFs have systematically higher decomposition temperatures, this being consequent on cross-links and clusters of those when polymers are incorporated. A significant exotherm at 300 °C in DTA traces of samples with hpmc indicates structural change of the carbonaceous network during the breakdown of cross-links containing *C* atoms. Mass loss between 500 - 700 °C in samples with poly-P alone is connected with chemical transformation of cross-links where the *P* atom is present. An additional mass loss and exotherm is seen for samples equilibrated at RH = 100 % (Fig. 2). These features coincide with literature reports for portlandite ($Ca(OH)_2$) dehydroxylation, and demonstrate the formation of secondary

portlandite at high relative humidities. Similar results were obtained for MDFs made with low-energy plant cement.

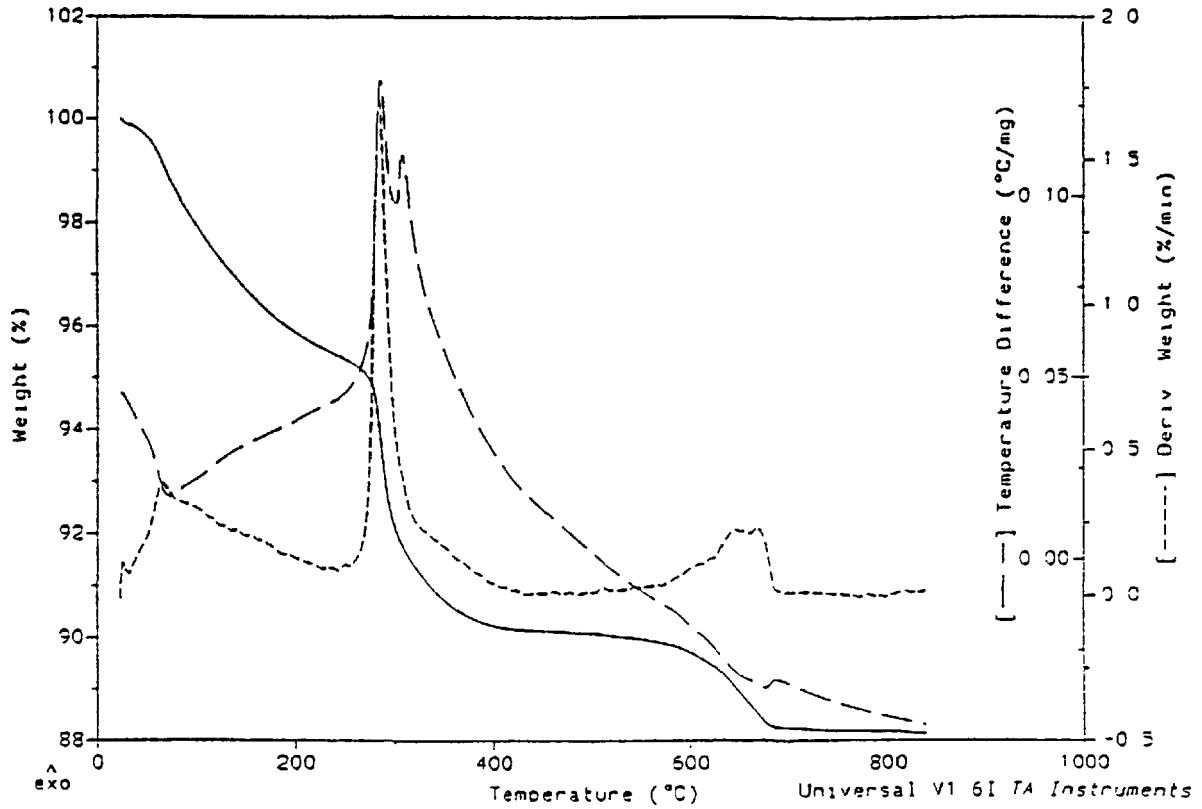

Figure 2 TG, DTG and DTA traces for the model MDF synthesized from sulfobelitic clinker + hpmc and after equilibration at RH = 100%.

Table 2 TG intervals (°C) and DTA events (°C) for model MDFs and those equilibrated at RH = 52 and 100 %.

polymer	RH = 52 %				RH = 100 %	
	TG	DTA	TG	DTA	TG	DTA
hpmc	100-200 250-400	100 300	100-200 250-400	320	100-250 250-350 500-700*	100 300 670*
poly-P	100-200 250-350 500-700	100	100-200 200-350 400-700	100 350	100-400 450-750	100 350 670*
hpmc + poly-P	100-200 200-400 500-700	100 300	100-200 250-400 500-700	100 300	100-250 250-400 400-700	100 300 670*

* feature due to portlandite

We have recently (Drabik, 1996a) given a diagrammatic representation of the formation of *Al/Fe - O - C/P* cross-links in this MDF system. The detailed atomic-level model accounts for next nearest neighbor interactions as detected by nuclear spectroscopies. Several features of that model are related to the principles governing the chemistry of aluminous MDFs (Rodger,1985; Edmonds,1989; Desai,1992). The schematic outline of clusters in the cross-linking section of the local structure of sulfobelitic MDFs has been very valuable in the consideration of moisture resistance and conductivities (Drabik, 1996b) in that system. Impedance spectra are typical of electronically-insulating materials functioning as solid electrolytes, with conductivity values depending on polymer component as well as the temperature of the measurement. Conductivity differences between the various model MDFs arise from the atomic level details of the pore-filling by AFm-like intergranular gel, different polymers giving chemically different gels. Conductivities vary only slightly with "MDF reaction time".

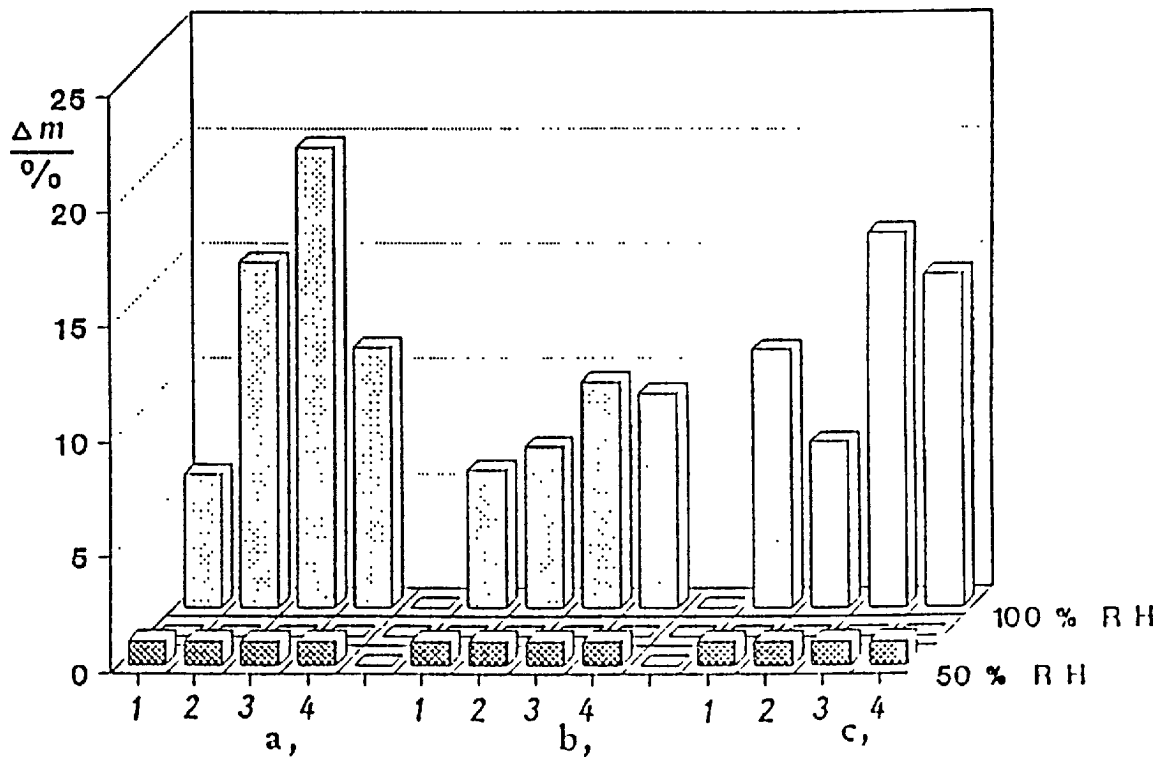

Figure 3 Mass increases of model MDFs after equilibration at RH = 52% and 100%. Polymer additions: (a) hpmc, (b) poly-P, (c) hpmc + poly-P. Clinker compositions: (1) $C_4A_3\bar{S}$ + C_4AF, (2)-(3) sulfobelitic laboratory clinkers, (4) Cimus sulfobelitic low-energy cement.

Mass increases of test pieces stored in moist atmospheres show that the behavior of MDFs within sulfobelitic clinker/hpmc/poly-P is similar to that of PC-based MDFs (Igarashi, 1992). In the current study, the moisture resistance is controlled by percolation through the AFm-like intergranular mass, in which clusters of cross-links hinder percolation for RH $\leq$ 52 %.

Those clusters are, however, attacked at higher relative humidity; an atmosphere with RH = 100 % exerts a fatal influence, degrading the surface of test pieces and leading to secondary portlandite (overall mass increase ~ 10 %, Figs. 1 and 3). Test pieces made with poly-P (Figs. 1b, 3b) appear more moisture resistant, with a lower mass increase and a mass plateau (equilibration) being achieved after 3 days (independent of MDF pressing time). For samples made with hpmc, the duration of pressing during fabrication is crucially important: the upper trace in Fig. 1a is for a sample fabricated with 1h pressing, the lower trace (with lower mass increase) is for 6h. Closely similar results were obtained for MDFs made with the low-energy plant cement (clinker No. 4 in Fig. 3). Percolation of MDFs by water and consequent surface corrosion by formation of $Ca(OH)_2$ (see above) clearly have technological consequences, and reinforce the need for very thorough improvement / impregnation of this type of material.

The results of this study demonstrate, as in simpler model systems related to sulfobelite-based MDFs (Drabik, 1994a,b, 1995), a link between the atomic level chemical interactions and bulk properties for a complex clinker mixture. We obtained similar results (in terms of moisture resistance and thermal events) with the low-energy plant cements. MDF processing leads to formation of *Al/Fe - O - C/P* cross-links; these represent the particular chemical bonds [generally postulated to be necessary in chemically bonded ceramics (Tan,1987)] and add the atomic scale viewpoint to the rheological knowledge of MDF materials. Cross-links are transferred into the bulk and affect the properties of the MDF test pieces. Control of the details of this synergism will improve the technologically important properties of such systems in the future. The system sulfobelite clinker / hydroxypropylmethyl cellulose / polyphosphate glass (especially compositions with polyphosphates incorporated) should be considered as an alternative to high alumina MDFs (Birchall,1988; Edmonds,1989; Rodger, 1985; Desai,1992; Young,1996) and PC-based MDFs (Igarashi,1992; Roy,1992; Ma,1992, 1994; Ohama,1996), when exploring the potential range of MDF materials.

CONCLUSIONS

1. The system studied exhibits a suitable processibility during MDF fabrication. Inorganic polymer (poly-P) reacts extensively to give cross-linking bonds to atoms originating in the clinker. Atomic level studies have demonstrated the AFm-like composition of hydrated intergranular mass.

2. Both nuclear spectroscopies and thermal analysis demonstrate the presence and rôle of *Al/Fe - O - C/P* cross-links. An increase of decomposition temperatures in MDFs is assigned to the existence of clusters of cross-links, which will be crucial in affecting thermal stability and bulk properties.

3. Moisture resistance is similar to that reported for PC-based MDFs, and is controlled by percolation of the AFm-like intergranular mass. The resistance is sufficient at RH $\leq$ 52%, but surface corrosion (portlandite formation) occurs at RH = 100%.

4. This study demonstrates the potential of low energy clinkers and cements for the MDF process. Further developments (*e.g.* use of the enhanced moisture resistance of systems containing poly-P, full evaluation of mechanical properties) are necessary if these compositions are to find technological application.

ACKNOWLEDGEMENTS

This research is funded by the Slovak Grant Agency for Science (VEGA 2070 project) and by the R&D Directorate of EC (as the part of Copernicus project ERB CIPA CT 94 0105). Low energy plant cements were produced by Cimus (Romania) within the Copernicus project. Part of the study was carried out under a collaborative agreement linking the University of Exeter and the Institute of Inorganic Chemistry (SASci, Bratislava). We thank the Royal Society and the British Council for the funds in support of that collaborative agreement. We thank the EPSRC National Solid State NMR service (Durham, UK) for recording MAS NMR spectra.

REFERENCES

Birchall J.D., Howard A.J., Kendal K. and Raistrick J.H, European Pat. Spec. No. 0055035, B1 (1988).

Chu T.J. and Robertson R.E., J. Mater. Sci. 29 2683 (1994).

Connaway-Wagner M.C., Klemperer W.G. and Young J.F., Chemistry of Materials 3 5 (1991).

Desai P.G., Young J.F. and Wool R.P., Proc. Mat. Res. Soc. Symp. 245 179 (1992).

Drabik M., Galikova L., Kubranova M. and Slade R.C.T., J. Mater. Chem. 4 265 (1994a).

Drabik M., Frtalova M., Galikova L. and Kristofik M., J. Mater. Chem. 4 271 (1994b).

Drabik M., Galikova L. and Odler I., Silikaty - Ceramics 38 127 (1994c).

Drabik M. and Slade R.C.T., Brit. Ceram. Trans. 94 242 (1995).

Drabik M., Galikova L., Slade R.C.T., Proc. of MAETA Workshop on High Flexural Polymer-Cement Composite (Sakata, Japan), 107 (October 1996a).

Drabik M.,. Galikova L., Hix G.B.,. Pearce A.G, Slade R.C.T. and Young K.E., Cement and Concrete Research, in press (1996b).

Edmonds R.N. and Majumdar A.J., J. Mater. Sci. 24 3813 (1989).

Igarashi H. and Takarashi T., Proc. Mat. Res. Soc. Symp. 245 173 (1992).

Lewis J.A., Boyer M. and Bentz D.P., J. Amer. Ceram. Soc. 77 711 (1994).

Ma W.P. and Brown P.W. , Proceedings of 9th International Congress on Cement Chemistry (New Delhi), 4 424 (1992).

Ma W.P. and Brown P.W., J. Mater. Res. 9 1291 (1994).

Nishikawa T., Sato K., Ito S. and Suzuki K., Proceedings of 9th International Congress on Cement Chemistry (New Delhi), 4 437 (1992).

Ohama Y., Demura K., Kobayashi T., Proc. of MAETA Workshop on High Flexural Polymer-Cement Composite (Sakata, Japan), 69 (October 1996).

Rodger S.A., Brooks S.A., Sinclair W., Groves G.W. and Double D.D , J. Mater. Sci. 20 2853 (1985).

Roy D.M., Silsbee M.R. and Wolfe D., Proc. Mat. Res. Soc. Symp. 245 309 (1992).

Tan S.R., Howard A.J. and Birchall J.D., Philos. Trans. Roy. Soc. (London) A322 479 (1987).

Zivica V., Bulletin RILEM 28 121 (1965).

Young J.F., Proc. of MAETA Workshop on High Flexural Polymer-Cement Composite (Sakata, Japan), 1 (October 1996).

THE MECHANISM OF CALCIUM NITRATE AS SET ACCELERATOR FOR CEMENT

Harald JUSTNES, SINTEF Civil and Environmental Engineering, Cement and Concrete, N-7034 Trondheim, Norway
Erik C. NYGAARD, Norsk Hydro A.S., R&D, N-3901 Porsgrunn, Norway

ABSTRACT Technical quality calcium nitrate (CN) is widely used as set accelerator for Portland cements and concrete. However, its efficiency may vary strongly with the cement type. In order to find the reason for this, a thorough analysis of the water in cement pastes from mixing to past setting was undertaken with respect to the ions; Ca^{2+}, SO_4^{2-}, OH^-, NO_3^-, NO_2^-, K^+ and Na^+, together with the elements Al, Si and Fe. Two extreme cases was investigated; one Portland cement with setting virtually unaffected by CN and another very much accelerated by CN. The difference was due to the high content of alkali sulphate of the former, precipitating active calcium as gypsum. A negative linear correlation between setting efficiency and increasing alkalies in the initial water phase of paste was found based on 9 different Portland cements.

Key-words: Accelerator, calcium nitrate, ions, mechanism, pore water, setting

INTRODUCTION

Technical calcium nitrate (CN) has been used for some time as set accelerator for Portland cements and concrete. However, in several studies (Justnes, 1993; Justnes and Nygaard, 1993, 1995, 1996a and 1996b) the efficiency of CN as set accelerator has been found to vary strongly with the cement type. In order to find the reason for this, and possibly the mechanism of CN as set accelerator for cement, a thorough analysis of the water in cement pastes from mixing to past setting was undertaken with respect to a number of ions.

The Vicat-needle setting profiles of the two extreme cases investigated; P30 cement virtually unaffected by CN and HS65 cement which is very much accelerated by CN, are previously published by Justnes and Nygaard (1995).

EXPERIMENTAL

Components

Technical quality calcium nitrate (CN) may in general be written as $xNH_4NO_3 \cdot yCa(NO_3)_2 \cdot zH_2O$. The CN used in the present work had x = 0.092, y = 0.500 and z = 0.826, or in other words 19.00 % Ca^{2+}, 1.57 % NH_4^+, 64.68 % NO_3^- and 14.10 % H_2O. The nitrite (NO_2^-) content was below the detection level (= 0) and the pH of a CN solution was ≈7. The technical quality CN was delivered by Norsk Hydro A/S, Porsgrunn, Norway.

The technical quality calcium nitrate (1.55 % CN by weight of cement) was added to cement pastes (distilled water-to-cement ratio 0.55) based on two different cements; ASTM type I (ordinary Portland cement = P30) and ASTM type II (moderate sulphate resistant = HS65). The contents (%) of CaO (C), SiO_2 (S), Fe_2O_3 (F), Al_2O_3 (A), SO_3 (S), MgO (M), Na_2O (N), K_2O (K) and free lime were 63.56&64.32, 20.31&22.13, 3.52&3.39, 5.02&4.05, 2.88&3.07, 2.34&1.03, 0.39&0.23, 1.18&0.42 and 1.87&?, while the specific surfaces (Blaine) were 290&418 m^2/kg for the P30&HS65 cements, respectively. The Bogue calculation based on the analyses resulted in a potential mineral content (%) of C_3S (alite), C_2S (belite), C_4AF (ferrite) and C_3A (aluminate) of 57&53, 15&24, 10.7&10.3 and 7.4&5.0 for P30&HS65, respectively. The cements and their analyses were all obtained from Norcem A/S, Brevik, Norway.

Methods

Water analyses

Each of the two cement pastes with w/c = 0.55 was made as one mix and distributed in plastic cups after two minutes manual mixing. At each of the termins 10, 30, 60, 120 and 480 minutes the "gelled" cement pastes was rapidly stirred and poured onto a black bond filter paper on a Büchner funnel attached to a "water pump" through a Erlenmeyer flask. The fluid filtrate was poured through a blue bond filter into small plastic bottles before they were sent for ion analyses performed by Norsk Hydro A/S, Porsgrunn, Norway.

The filtrates were diluted with doubly distilled and de-ionized water before they were analysed by ICP-AES (Atomic Emission Spectroscopy) with respect to the following elements; Ca, K, Na, Si, Al, Fe and S. The content of nitrate (NO_3^-) and nitrite (NO_2^-) ions were determined by DIONEX ion chromatography. The hydroxyl (OH^-) concentration was measured by a pH meter directly on the filtrate.

Cement interstitials

The cement silicates, C_3S and C_2S, of the cements were removed by the following extraction procedure: 1) 5 g pre-dried (300°C) cement was dispersed in 150 ml water-free methanol. 2) 15 g dry maleic acid was added, followed by stirring for 10 minutes. 3) The filtrate was washed with methanol and dried at 60°C. The filtrate then contain the clinker interstitials (C_4AF, C_3A and alkali sulphates) + added gypsum.

The X-ray diffractograms of the filtrates from the P30 and HS65 cements were recorded by a diffractometer after an internal reference consisting of 10 % anatas (TiO_2) was interground. Cu K_α-radiation with wavelength λ = 1.5418 Å and a Ni-filter were used.

RESULTS AND DISCUSSION

The ion concentrations (mM) for Ca^{2+}, SO_4^{2-}, OH^-, NO_3^-/NO_2^-, K^+ and Na^+, together with the elements Al and Si (potential complex ions), in the paste fluids are listed as a function of time in Tables 1, 2, 3, 4, 5, 6, 7 and 8, respectively, while the concentration vs time profiles for calcium and sulphate are plotted in Figs 1 and 2, respectively. The content of iron is negligible since it at all times was < 1 mg Fe/l. The uncertainty in the ion analyses is estimated to ±10%.

Table 1 The calcium concentration (mmol/l = mM) in the fluids of P30 and HS65 cement pastes with 0.00 and 1.55 % CN as a function of time (min) from mixing.

Time (min)	P30, 0.00 % CN	P30, 1.55 % CN	HS65, 0.00 % CN	HS65, 1.55 % CN
10	14.4 mM Ca^{2+}	23.0 mM Ca^{2+}	18.5 mM Ca^{2+}	90.1 mM Ca^{2+}
30	16.1 mM Ca^{2+}	23.5 mM Ca^{2+}	20.0 mM Ca^{2+}	86.8 mM Ca^{2+}
60	16.2 mM Ca^{2+}	23.2 mM Ca^{2+}	20.7 mM Ca^{2+}	80.8 mM Ca^{2+}
120	17.5 mM Ca^{2+}	23.7 mM Ca^{2+}	20.5 mM Ca^{2+}	73.4 mM Ca^{2+}
480	12.5 mM Ca^{2+}	17.7 mM Ca^{2+}	15.5 mM Ca^{2+}	51.7 mM Ca^{2+}

Table 2 The sulphate concentration (mmol/l = mM) in the fluids of P30 and HS65 cement pastes with 0.00 and 1.55 % CN as a function of time (min) from mixing.

Time (min)	P30, 0.00 % CN	P30, 1.55 % CN	HS65, 0.00 % CN	HS65, 1.55 % CN
10	178.3 mM SO_4^{2-}	78.9 mM SO_4^{2-}	50.8 mM SO_4^{2-}	13.4 mM SO_4^{2-}
30	180.8 mM SO_4^{2-}	72.3 mM SO_4^{2-}	45.2 mM SO_4^{2-}	13.1 mM SO_4^{2-}
60	176.4 mM SO_4^{2-}	70.1 mM SO_4^{2-}	39.3 mM SO_4^{2-}	13.1 mM SO_4^{2-}
120	171.5 mM SO_4^{2-}	83.2 mM SO_4^{2-}	43.6 mM SO_4^{2-}	13.4 mM SO_4^{2-}
480	153.4 mM SO_4^{2-}	76.1 mM SO_4^{2-}	40.5 mM SO_4^{2-}	13.7 mM SO_4^{2-}

Table 3 The hydroxyl concentration (mmol/l = mM) in the fluids of P30 and HS65 cement pastes with 0.00 and 1.55 % CN as a function of time (min) from mixing.

Time (min)	P30, 0.00 % CN	P30, 1.55 % CN	HS65, 0.00 % CN	HS65, 1.55 % CN
10	63.1 mM OH^-	50.1 mM OH^-	63.1 mM OH^-	25.1 mM OH^-
30	100.0 mM OH^-	63.1 mM OH^-	79.4 mM OH^-	31.6 mM OH^-
60	100.0 mM OH^-	63.1 mM OH^-	79.4 mM OH^-	31.6 mM OH^-
120	125.9 mM OH^-	79.4 mM OH^-	79.4 mM OH^-	31.6 mM OH^-
480	79.4 mM OH^-	39.8 mM OH^-	31.6 mM OH^-	31.6 mM OH^-

Table 4 The nitrate/nitrite (NO_3^-/NO_2^-) concentration (mmol/l = mM) in the fluids of P30 and HS65 cement pastes with 0.00 and 1.55 % CN as a function of time (min) from mixing.

Time (min)	P30, 0.00 % CN	P30, 1.55 % CN	HS65, 0.00 % CN	HS65, 1.55 % CN
10	0.18/<0.02 mM	290/0.46 mM	0.40/<0.02 mM	290/0.91 mM
30	0.16/<0.02 mM	274/0.39 mM	0.13/<0.02 mM	258/0.96 mM
60	0.13/<0.02 mM	258/0.57 mM	0.16/<0.02 mM	258/1.22 mM
120	0.27/<0.02 mM	274/0.63 mM	0.16/<0.02 mM	210/1.22 mM
480	0.10/<0.02 mM	210/0.67 mM	0.13/<0.02 mM	177/1.17 mM

Table 5 The potassium concentration (mmol/l = mM) in the fluids of P30 and HS65 cement pastes with 0.00 and 1.55 % CN as a function of time (min) from mixing.

Time (min)	P30, 0.00 % CN	P30, 1.55 % CN	HS65, 0.00 % CN	HS65, 1.55 % CN
10	309 mM K^+	340 mM K^+	118 mM K^+	118 mM K^+
30	340 mM K^+	350 mM K^+	118 mM K^+	115 mM K^+
60	350 mM K^+	330 mM K^+	113 mM K^+	115 mM K^+
120	353 mM K^+	366 mM K^+	115 mM K^+	120 mM K^+
480	304 mM K^+	307 mM K^+	105 mM K^+	118 mM K^+

Table 6 The sodium concentration (mmol/l = mM) in the fluids of P30 and HS65 cement pastes with 0.00 and 1.55 % CN as a function of time (min) from mixing.

Time (min)	P30, 0.00 % CN	P30, 1.55 % CN	HS65, 0.00 % CN	HS65, 1.55 % CN
10	89.6 mM Na^+	91.3 mM Na^+	27.4 mM Na^+	27.8 mM Na^+
30	95.3 mM Na^+	91.3 mM Na^+	27.4 mM Na^+	27.0 mM Na^+
60	96.6 mM Na^+	87.0 mM Na^+	26.1 mM Na^+	27.4 mM Na^+
120	95.7 mM Na^+	96.1 mM Na^+	27.4 mM Na^+	28.3 mM Na^+
480	81.8 mM Na^+	85.7 mM Na^+	25.2 mM Na^+	29.1 mM Na^+

Table 7 The aluminum concentration (mmol/l = mM) in the fluids of P30 and HS65 cement pastes with 0.00 and 1.55 % CN as a function of time (min) from mixing.

Time (min)	P30, 0.00 % CN	P30, 1.55 % CN	HS65, 0.00 % CN	HS65, 1.55 % CN
10	0.19 mM Al	0.25 mM Al	0.28 mM Al	0.13 mM Al
30	0.34 mM Al	0.29 mM Al	0.42 mM Al	0.26 mM Al
60	0.33 mM Al	0.29 mM Al	0.13 mM Al	0.00 mM Al
120	0.37 mM Al	0.43 mM Al	0.21 mM Al	0.00 mM Al
480	0.36 mM Al	0.26 mM Al	0.22 mM Al	0.00 mM Al

Table 8 The silicon concentration (mmol/l = mM) in the fluids of P30 and HS65 cement pastes with 0.00 and 1.55 % CN as a function of time (min) from mixing.

Time (min)	P30, 0.00 % CN	P30, 1.55 % CN	HS65, 0.00 % CN	HS65, 1.55 % CN
10	5.9 mM Si	3.9 mM Si	8.8 mM Si	6.4 mM Si
30	5.0 mM Si	12.1 mM Si	4.6 mM Si	8.8 mM Si
60	8.9 mM Si	8.2 mM Si	6.4 mM Si	0.0 mM Si
120	12.8 mM Si	8.9 mM Si	5.0 mM Si	0.0 mM Si
480	10.5 mM Si	10.2 mM Si	3.6 mM Si	0.0 mM Si

In order to control that all ions in the aqueous phase of the cement pastes in the present investigation are accounted for, the sum of positive and negative charges are listed in Table 9. Note that since OH^- is measured by pH-meter, the charge pr Al is -1 due to the complex $Al(OH)_4^-$, while the charge pr silicon is assumed to be -1. If the hydroxyl concentration was determined by titration, the Al and Si charge should be +3 and +4, respectively, due to the decomposition of the complex hydroxy ions. With the exception of one fluid (from HS65 without CN after 480 minutes), the difference between the sum of charges is within the accuracy of ion determination (±10%). The accuracy of the pH determination is assumed to be ±0.1 unit, which correspond to an accuracy in OH^- concentration of ±25%. The "error" in the one low sum of negative charge seems to be a too low hydroxyl concentration.

Table 9 The sum of positive (Σ_+) and negative (Σ_-) charges (Σ_+/Σ_-) for the ions (mM) in the fluids of P30 and HS65 cement pastes with 0.00 and 1.55 % CN as a function of time (min) from mixing.

Time (min)	P30, 0.00 % CN	P30, 1.55 % CN	HS65, 0.00 % CN	HS65, 1.55 % CN
10	427/426=1.002	477/503=0.948	182/174=1.046	326/349=0.934
30	468/467=1.002	488/494=0.988	185/175=1.057	316/326=0.969
60	479/462=1.037	463/470=0.985	181/165=1.097	304/317=0.959
120	484/482=1.004	510/528=0.966	183/172=1.064	295/270=1.093
480	411/397=1.035	428/413=1.036	161/117=1.376	251/237=1.059

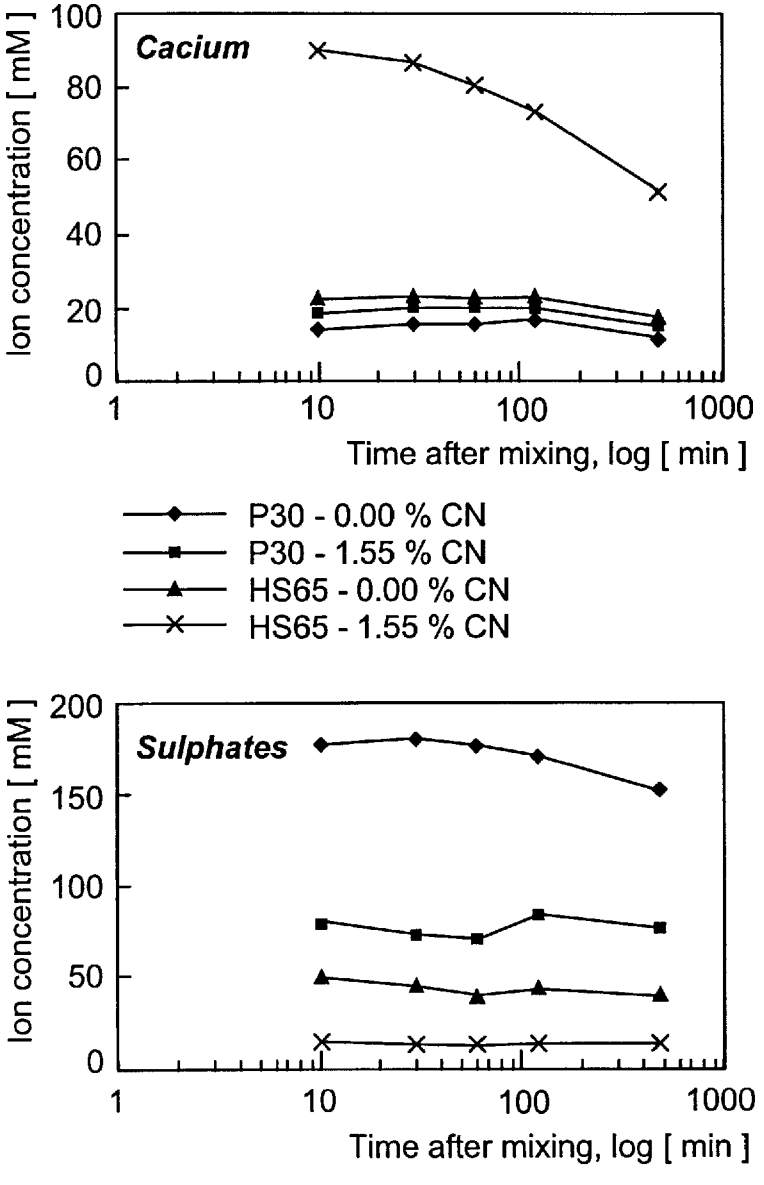

Fig. 1 The calcium (upper) and sulphate (lower) concentration as a function of time from mixing in the water of cement pastes.

For both cement pastes (w/c = 0.55), the most noticeable change when 1.55 % CN of the cement weight is added (except for the increase in nitrate concentration), is that the calcium concentration increases (see Table 1 and Fig 1) and the sulphate concentration decreases (see Table 2 and Fig 1). In addition, the hydroxyl concentration (see Table 3) is decreased in order to maintain the solubility product of calcium hydroxide.

The reason why the concentration of sulphates in the fluid of P30 is much higher than in HS65 paste, is the higher content of alkali sulphates (may also be seen from the potassium and sodium concentrations in Tables 5 and 6, respectively). Alkali sulphates may be detected by XRD of the residue after the extraction procedure enriching the interstitials if present. Alkali sulphates appear usually as the mineral Aphthitalite, $K_3Na(SO_4)_2$ (cement chemist's short hand notation; $K_3N\bar{S}_4$).

Aphthitalite is an excellent example of the solid solution phenomena, and the formula may be written $KK_{3-x}Na_x(SO_4)_2$, where x may vary from 1 to 3 without disturbing the crystal structure. The lattice distances for the two strongest reflections with hexagonal indices <110> & <102> will be 2.839 & 2.940, 2.804 & 2.889 and 2.778 & 2.841 Å for x = 1 (ASTM card 20-928), 2 (ASTM card 20-927) and 2.66 (ASTM card 20-926), respectively. The position of reflections (i.e. the unit cell axes) changes linearly with the composition according to Vegard's law of solid solution. For Aphthitalite, the linear correlation for the <110> reflection is $x = -27.319 \cdot d_{<110>} + 78.570$ and $x = -16.967 \cdot d_{<102>} + 50.921$ for the <102> reflection. The Portland cement P30 ("Standard" clinker) contain Aphthitalite with $d_{<110>}/d_{<102>} = 2.8355/2.9330$ Å, while the XRD of the interstitial residue from HS65 cement ("High strength" clinker) only shows weak indications of these reflections (see Fig 3 for reflections marked "A"). The observed lattice distances give x = 1.13±0.04 in the formula $KK_{3-x}Na_x(SO_4)_2$ for the P30 Portland cement.

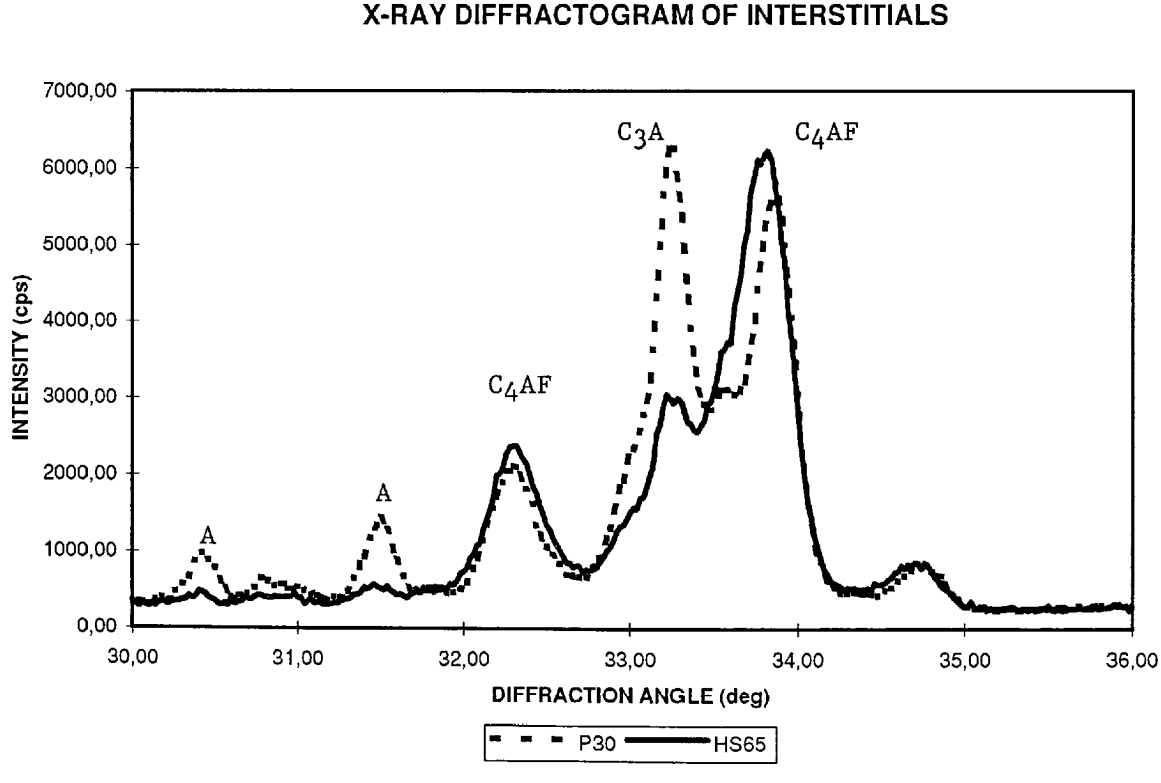

Figure 2 X-ray diffractogramme of the extracted interstitial phases from clinkers of P30 and HS65 Portland cements. The two reflections of the mineral Aphthitalite, $K_3Na(SO_4)_2$, are marked with an "A".

The alkali content of the cement paste fluids is not affected by CN additions (Tables 6 and 7). The K/Na ratio is about 3.5 for P30 and about 4 for HS65. In particular potassium may occur in other phases like syngenite and solid solution in belite (ß-C_2S). Assuming ideal composition of Aphthitalite (K/N=3), 100 mM Na^+ and w/c = 0.55 corresponds to 1.82 % $K_3N\bar{S}_4$ of the cement weight.

Justnes and Nygaard (1995, 1996a and 1996b) found a linear correlation between the belite content of different cements and the set accelerating efficiency of CN. Since belite is a slowly reacting mineral, it was concluded that this must be due to an indirect effect. This may now be understandable since belite can incorporate a portion of the total alkalies in its structure and consequently prevent them from taking part in the early fluid chemistry. Hence, for a series of cements with about equal total alkali content and increasing belite content, it is expected that the set accelerating efficiency of CN will increase. On the other hand, El Didamony et al (1996) investigated the influence of calcium acetate, chloride and nitrate on belite hydration. They found that after 1 day (first data point), the chemical bound water was increased 6 times when 2 % $Ca(NO_3)_2$ was mixed in the water, while 2 % $Ca(CH_3COO)_2$ and 2 % $CaCl_2$ only increased the 1 day chemical bound water by 30 % compared with the reference. Thus, a special influence of CN on β-C_2S can not be excluded.

When the alkali content (eqvivalent Na_2O) in the fluid of cement paste (w/c = 0.55) 20 minutes after mixing for 4 (of 5) Norwegian and 5 French portland cements investigated by Justnes and Nygaard (1995 and 1996a) is plotted against the reduction in setting time (i.e. measure of efficiency for set accelerator since the setting time without accelerator may vary widely for the cements) when 1.55 % CN is dissolved in the mixing water, a negative linear correlation with regression factor r^2 = 0.8196 is obtained as shown in Fig 3. This correlation supports the idea that the content of initially soluble alkalies (e.g. aphthitalite) is the most important characteristic of the cement influencing the efficiency of CN as set accelerator.

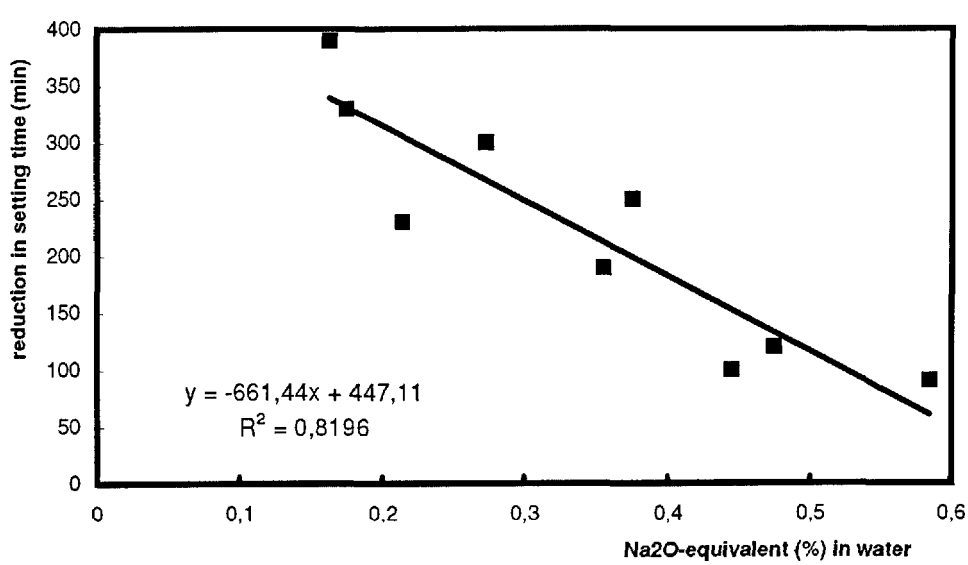

Figure 4 The reduction in setting time for portland cement pastes when 1.5 % calcium nitrate is added vs the alkali content of the liquid phase 20 minutes after mixing.

CONCLUSION

The mechanism for accelerated setting of cement by calcium nitrate (CN) is two-fold; 1) an increased calcium concentration lead to a faster super-saturation of the fluid with respect to calcium hydroxide, $Ca(OH)_2$, and thereby shorter time to initial crystallization and renewal of alite hydration, and 2) a lower sulphate concentration will lead to slower/less formation of ettringite which will shorten the onset of the aluminate, C_3A, hydration.

The reason why P30 is not accelerated by CN, is that P30 contain much more of the mineral Aphthitalite, $K_3Na(SO_4)_2$ from the clinker process, which will lead to a high sulphate concentration in the fluid. When CN is added, much of the calcium precipitates as sparingly soluble gypsum. Even when 1.55 % CN is added to the P30 paste, the sulphate concentration in the fluid is higher than in the water of HS65 paste without CN. The calcium concentration in the fluid of P30 with 1.55 % CN is only slightly higher than for HS65 without CN, while the Ca^{2+} concentration in the water of HS65 paste is increased with about 4 times when 1.55 % CN is added.

Generally speaking, the set accelerator calcium nitrate will be most effective for Portland cements high in belite and low in alkalies.

REFERENCES

El-Didamony, H., Sharara, A.M., Helmy, I.M. and Abd El-Aleem, S.: "Hydration Characteristics of β-C_2S in the Presence of Some Accelerators", Cement and Concrete Research, Vol. 26, No. 8, 1996, pp. 1179-1187.

Justnes, H.: "The Influence of Technical Calcium Nitrate (CN) on the Setting Time, Heat Evolution, Strength Development and Durability of Cement, Mortar and Concretes", SINTEF Report STF70 F93138, 1993-12-27, 40/4 pp.

Justnes, H. and Nygaard, E.C.: "Technical Nitrate as Set Accelerator for Cement", Nordic Concrete Research, Publication No. 13 (1993) pp 70-87.

Justnes, H. and Nygaard, E.C., "Technical Nitrate as Set Accelerator for Cement at Low Temperatures", Cement and Concrete Research, Vol. 25, No. 8, 1995, pp. 1766-1774.

Justnes, H. and Nygaard, E.C., "Technical Nitrate as Set Accelerator for Cement at Low Temperatures", Advances in Cement Research, Vol. 8, No. 30, Apr. 1996a, pp. 1-9 .

Justnes, H. and Nygaard, E.C.: "Calcium Nitrate - A Multifunctional Concrete Admixture", Proceedings of the International Conference on High-Performance Concrete, and Performance and Quality of Concrete Structures", June 05-07 1996b, Florianopolis, Brazil, pp. 514-525.

EFFECTS OF CEMENT/ADMIXTURE INTERACTIONS ON THE EARLY STIFFENING TENDENCIES OF PORTLAND CEMENT PASTE

S.A. FARRINGTON and D. CONSTANTINER, Master Builders, Inc., Cleveland, Ohio, USA

ABSTRACT The goal of this study was to correlate changes in pore solution composition with changes in workability of cement pastes. Two mechanisms of false set were investigated. Pore solution compositions were found to be significantly different for G-type and lignosulfonate-type false set. Experimental equilibrium constants and saturation indices were calculated with the Pitzer ion-interaction model. This approach indicates that G-type false set is related to gypsum precipitation, but does not indicate the mechanism of lignosulfonate-type false set.

Key-words: False set, Ions, Pore solution, Lignosulfonates, Modeling

INTRODUCTION

Early stiffening of Portland cement materials, known as false set, can occur under a variety of circumstances. The effect is traditionally attributed to the rehydration of calcium sulfate hemihydrate upon addition of mixing water to form The acicular gypsum crystals which interlock (Taylor, 1990). The presence of dehydrated sulfate phases other than gypsum in the cement powder is often due to improper final grinding or high temperature storage. This type of early workability loss has been referred to as G-type false set (Murakami, 1957).

In some cases, the addition of dispersing agents based on salts of lignosulfonic acid has been known to induce early workability loss in cement-based materials. This has been linked to the formation of increased levels of ettringite at early ages (Kalousek, 1974). Recent experience in our laboratory has shown that this effect does not occur with other dispersant chemistries (e.g. sulfonated naphthalenes) and therefore can not be attributed to a water reduction effect. This type of early workability loss will be referred to as lignosulfonate-type false set.

There exists very limited pore solution concentration data for false-setting cement systems (Kawada, 1966), and none was found for false-setting cement and lignosulfonate combinations. This study attempts to improve the understanding of false set mechanisms by examining the ionic concentrations in pore solutions of cement pastes at very early ages. In addition, it explores the possibility of explaining the mechanisms in cement paste through the chemistry of the pore solution. This has been carried out for cement paste with and without lignosulfonate.

EXPERIMENTAL

PORTLAND CEMENTS AND ADMIXTURES

The cement was a Type I Portland cement with the following oxide analysis: SiO_2=22.13%, Al_2O_3=4.50%, Fe_2O_3=2.99%, CaO=63.66%, MgO=2.12%, SO_3=2.68%, K_2O=0.80%, Na_2O=0.11%, Na_2O equiv.=0.64%, free CaO=0.50%, and LOI=1.16%. Blaine fineness was measured as 343 m^2/kg. Suggested Bogue potential phase composition: C_3S=48.8%, C_2S=26.6%, C_3A=6.9%, and C_4AF=9.1%. Suggested modified Bogue potential phase composition (Taylor, 1989): C_3S=62.8%, C_2S=17.8%, C_3A=4.0%, and C_4AF=10.2%.

X-ray powder diffraction analysis of this cement, following selective dissolution of the silicate phases by methanol/salicylic acid extraction, indicated that gypsum was the primary calcium

sulfate phase present in the normal cement. A portion of this cement was heat-treated for 16 hours at 160°C to induce G-type false setting behavior, and will be referred to as heated cement. X-ray powder diffraction analysis of the heated cement after methanol/salicylic acid extraction indicated that nearly all of the gypsum was dehydrated to calcium sulfate hemihydrate. Completely dehydrated calcium sulfate was not found.

Two commercially available lignosulfonate additives were used to induce lignosulfonate-type false set. These can be found in many water reducing admixtures for concrete. An analysis of these additives is displayed in Table 1.

Table 1 Chemical analysis of the lignosulfonate additives used in this study

	Calcium lignosulfonate	Sodium lignosulfonate
Reducing sugars	2.85%	4.21%
Sodium	0.96%	4.76%
Calcium	4.64%	1.92%

EXPERIMENTAL PROCEDURES AND RESULTS

The aim of this study was to correlate early age workability of cement paste with the chemistry of its pore solution. Six cement pastes mixes were prepared as shown in Table 2. For each of the mixes studied, workability was measured and pore solutions were collected over time. A detailed schematic of the experiment is shown in Fig 1. All experiments were carried out in the laboratory at approximately 20°C.

Table 2 Mix preparation data for the cement pastes

Cement	Mix	Additive (by weight of cement)	Paste w/c
	1	none	0.28
Normal	2	0.2% calcium lignosulfonate	0.26
	3	0.2% sodium lignosulfonate	0.27
	4	none	0.28
Heated	5	0.2% calcium lignosulfonate	0.26
	6	0.2% sodium lignosulfonate	0.26

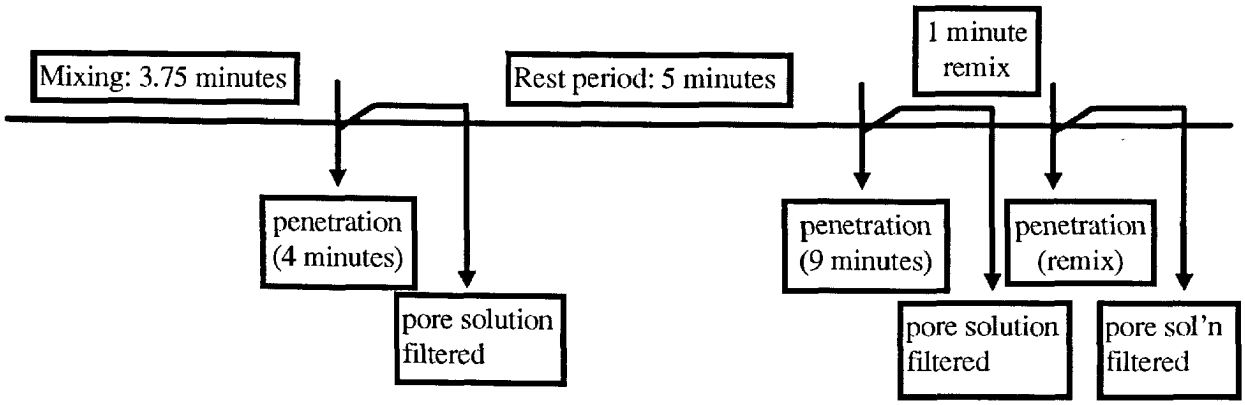

Figure 1 Experimental methodology

The mix procedure which evaluated the early stiffening of paste is outlined in Test Method C-451 (ASTM, 1991), in which workability is evaluated by penetration of a weighted plunger. The pore

solution was separated from the paste by pressure filtration through a polyethersulfone membrane with 0.8 μm opening. Details of the filtration apparatus are described elsewhere (Ong, 1993). The pressure-filtered pore solutions were analyzed for the following ions: OH^-, SO_4^{2-}, Na^+, K^+, Ca^{2+}, Al^{3+}, Mg^{2+}, Fe^{3+}, and SiO_4^{4-}. Hydroxide ion concentration was measured by titration with HCl and a methyl red indicator. Sulfate ion concentration was measured by ion chromatography. The remaining ionic concentrations were measured by inductively-coupled plasma (ICP) spectroscopy.

Early Stiffening Results

The results of the early stiffening measurements are shown in Figs 2 and 3. Fig 2 shows that the normal cement paste stiffened slightly after the rest period. Upon remixing, most of the workability was recovered. This pattern was present in all of the pastes studied, however, the degree of stiffening that occurred during the rest period and the subsequent increase in workability after remixing varied. False set is defined by significant stiffening during the rest period followed by workability increase after remixing. Based on this definition, the normal cement pastes experienced false setting only when lignosulfonates were added, i.e. lignosulfonate-type false set (Mixes 2 and 3). Although not reported here, studies on mortars (using the same cements and additives) followed similar stiffening trends.

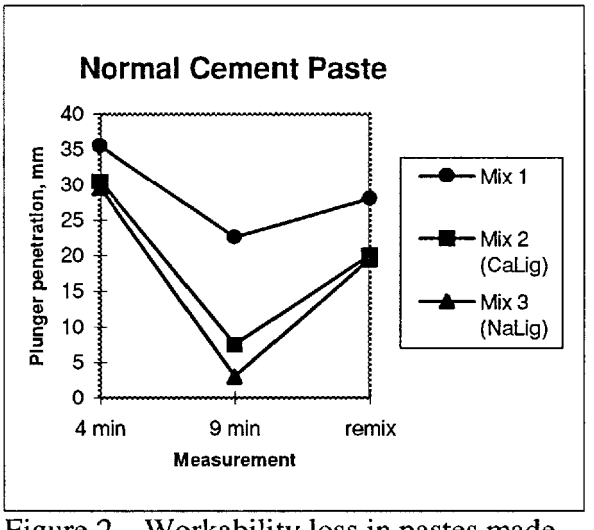

Figure 2 Workability loss in pastes made with normal cement

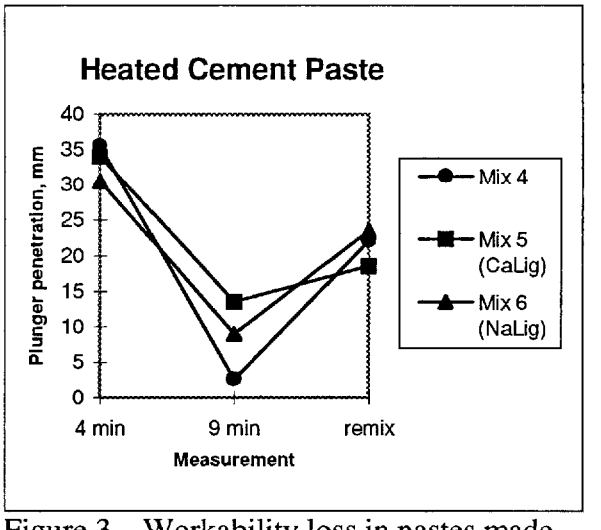

Figure 3 Workability loss in pastes made with heated cement

It can be seen from Mixes 1 and 4 that heating the cement produced a paste with definitive false setting tendencies. However, the addition of lignosulfonate to the pastes containing the heated cement resulted in a reduction of the early stiffening behavior relative to the paste without additive, although the pastes with lignosulfonate (Mixes 5 and 6) are also false-setting.

Pore Solution Results

The results of all pore solution analyses are included in Tables 3 for the highly concentrated ions and Table 4 for the ions of lower concentration. The net charge balance (summation of normality of all cations and anions) for all ions in each solution is also included in Table 4.

It can be seen that the pore solutions contain mainly Ca^{2+}, K^+, Na^+, OH^-, and SO_4^{2-}, with the concentrations of other ions being more than an order of magnitude lower. Early age concentrations reported elsewhere (Gartner, 1985) are in good agreement with these results. The

charge imbalances are significant in some cases and are attributed to experimental error. This paper addresses the highly concentrated ions in the pore solutions (Table 4), the other concentrations are included only for completeness.

Table 3 Highly concentrated ions in the pore solutions (in mmol/L)

	Ca^{2+}	K^{+}	Na^{+}	OH^{-}	SO_4^{2-}		Ca^{2+}	K^{+}	Na^{+}	OH^{-}	SO_4^{2-}
Mix 1						**Mix 4**					
@5 min.	19.3	466.8	91.3	150.0	280.8	@5 min.	52.4	326.1	81.6	82.8	241.8
@10 min.	21.2	466.8	92.4	161.7	273.0	@10 min.	47.4	326.1	85.9	95.4	241.8
post-remix	21.2	460.4	94.6	156.8	257.4	post-remix	29.9	390.0	91.3	109.1	234.0
Mix 2						**Mix 5**					
@5 min.	20.6	422.0	88.1	120.8	265.2	@5 min.	45.5	332.5	82.6	82.8	218.3
@10 min.	21.8	498.7	102.2	145.1	257.4	@10 min.	46.8	345.3	89.2	80.8	234.0
post-remix	18.7	454.0	96.8	134.4	265.2	post-remix	44.3	351.7	89.2	75.0	226.2
Mix 3						**Mix 6**					
@5 min.	20.6	447.6	108.7	135.4	273.0	@5 min.	48.0	351.7	104.4	84.7	226.2
@10 min.	18.7	473.2	119.6	134.4	273.0	@10 min.	45.5	351.7	107.7	78.9	218.3
post-remix	21.2	473.2	119.6	137.3	280.8	post-remix	48.7	370.9	119.6	81.8	218.3

Table 4 Trace ion concentrations in the pore solutions (in mmol/L), and net ionic charge balance in the solution (Σ+/-, in mN/L)

	Fe^{3+}	SiO_4^{4-}	Al^{3+}	Mg^{2+}	Σ+/-		Fe^{3+}	SiO_4^{4-}	Al^{3+}	Mg^{2+}	Σ+/-
Mix 1						**Mix 4**					
@5 min.	0.05	0.67	<0.05	<0.05	-0.117	@5 min.	0.11	0.54	<0.05	<0.05	-0.056
@10 min.	0.05	0.68	<0.05	<0.05	-0.109	@10 min.	0.09	0.67	<0.05	<0.05	-0.075
post-remix	0.08	0.82	<0.05	<0.05	-0.077	post-remix	0.07	1.1	<0.05	<0.05	-0.040
Mix 2						**Mix 5**					
@5 min.	0.08	0.61	<0.05	<0.05	-0.102	@5 min.	0.12	0.49	<0.05	<0.05	-0.015
@10 min.	0.07	0.79	<0.05	<0.05	-0.018	@10 min.	0.11	0.74	<0.05	<0.05	-0.023
post-remix	0.06	0.87	<0.05	<0.05	-0.080	post-remix	0.13	0.40	<0.05	<0.05	+0.001
Mix 3						**Mix 6**					
@5 min.	0.07	0.52	<0.05	<0.05	-0.086	@5 min.	0.24	0.4	<0.05	<0.05	+0.014
@10 min.	0.06	1.2	<0.05	<0.05	-0.055	@10 min.	0.17	0.4	<0.05	<0.05	+0.034
post-remix	0.10	0.52	<0.05	<0.05	-0.065	post-remix	0.17	0.3	<0.05	<0.05	+0.069

Comparing all pore solution ion concentrations, it can be seen that heating the cement resulted in a large increase in $[Ca^{2+}]$, a large decrease in $[K^{+}]$, a large decrease in $[OH^{-}]$, and a decrease in $[SO_4^{2-}]$. Of additional note is that the ratio of $[K^{+}]/[Na^{+}]$ from the cement analysis was on the order of 5:1. This ratio appears to hold in Mixes 1 and 2, and falls to 4:1 in Mix 3, likely due to additional Na^{+} from the lignosulfonate. In Mixes 4 and 5, the ratio is on the order of 4:1, which falls closer to 3:1 in Mix 6, likely a result of sodium lignosulfonate addition.

Solid-Phase Saturation Indices

In addition to simple comparisons of ionic concentrations in solution, the pore solution data was used to assess the state of the pore solution with respect to the solid phases present. This is accomplished by calculating saturation indices from ionic activities for expected solid phases. The Pitzer ion-interaction approach (Pitzer, 1991) for calculating activities of ions in solution has been successfully applied by geochemists to determine the solubility of minerals in solutions of very high ionic strength. This method has been applied to cement pore solutions for the same purpose (Reardon, 1990, Duchesne, 1995). In this study, the ionic concentration data from Table

3 was used to calculate activity coefficients based on the Pitzer model using the software package PHRQPITZ (Plummer, 1988), with one exception: the software requires pH values instead of [OH^-]. An iterative approach was followed to find the correct pH input value, to find a match between the measured and calculated [OH^-]. The software converted concentration to units of molality for calculation of activity coefficients. The calculated activity coefficients and water activity are presented in Table A1 in the appendix. The input temperature used for all calculations was 20°C.

The tabulated ionic activities were used to calculate experimental equilibrium constants, i.e. ion activity products (IAP_{20}), for the following solids: $Ca(OH)_2$, $CaSO_4$, $CaSO_4 \cdot 0.5H_2O$, $CaSO_4 \cdot 2H_2O$, $K_2Ca(SO_4)_2 \cdot H_2O$, K_2SO_4, and $Na_2SO_4 \cdot 10H_2O$. The saturation index of each solid (log $IAP_{20}/K_{sp,20}$) was determined using values of the solubility product constant ($K_{sp,20}$) included in the software which are internally consistent. Since the $K_{sp,20}$ for $CaSO_4 \cdot 0.5H_2O$ is not included in the software, and to further maintain internal consistency of the data, it was necessary to input published solubility data (Linke, 1965) into PHRQPITZ and use the calculated IAP_{20} as the $K_{sp,20}$. The saturation indices and reference $K_{sp,20}$ values appear in Table 5. With respect to each solid phase, positive saturation index values indicate that the solution is oversaturated, negative values indicate undersaturation, and values close to zero indicate equilibrium. K_2SO_4, and $Na_2SO_4 \cdot 10H_2O$ were significantly undersaturated and are not tabulated.

Table 5 Saturation index values of relevant solid phases (log $IAP_{20}/K_{sp,20}$)

		$Ca(OH)_2$	$CaSO_4$	$CaSO_4 \cdot 0.5H_2O$	$CaSO_4 \cdot 2H_2O$	$K_2Ca(SO_4)_2 \cdot H_2O$
	Mix 1 @ 5 min.	0.25	-0.13	-0.09	0.11	0.30
	@ 10 min.	0.37	-0.11	-0.07	0.13	0.32
	post-remix	0.36	-0.11	-0.07	0.13	0.29
Normal	**Mix 2** @ 5 min.	0.13	-0.08	-0.04	0.16	0.27
Cement	@ 10 min.	0.30	-0.11	-0.06	0.13	0.36
	post-remix	0.17	-0.14	-0.10	0.10	0.26
	Mix 3 @ 5 min.	0.21	-0.10	-0.06	0.14	0.29
	@ 10 min.	0.16	-0.15	-0.11	0.09	0.29
	post-remix	0.23	-0.09	-0.05	0.14	0.35
	Mix 4 @ 5 min.	0.22	0.37	0.41	0.61	0.48
	@ 10 min.	0.29	0.32	0.36	0.56	0.43
	post-remix	0.22	0.08	0.12	0.32	0.34
Heated	**Mix 5** @ 5 min.	0.18	0.29	0.33	0.53	0.41
Cement	@ 10 min.	0.16	0.31	0.35	0.55	0.46
	post-remix	0.08	0.28	0.32	0.52	0.45
	Mix 6 @ 5 min.	0.20	0.30	0.35	0.54	0.46
	@ 10 min.	0.14	0.28	0.32	0.52	0.43
	post-remix	0.18	0.29	0.33	0.53	0.48
Reference $K_{sp,20}$		6.46E-06	4.66E-05	4.20E-05	2.62E-05	3.56E-08

Another study (Gartner, 1985), not concerned with false set, which examined saturation indices for $Ca(OH)_2$, $CaSO_4 \cdot 2H_2O$, and $K_2Ca(SO_4)_2 \cdot H_2O$ in pore solutions at early ages showed relatively close agreement with saturation indices measured for $CaSO_4 \cdot 2H_2O$ in Mix 1 of this study. However, the saturation indices measured for $Ca(OH)_2$ and $K_2Ca(SO_4)_2 \cdot H_2O$ in Mix 1 of this study indicate significant oversaturation while those previously reported indicated undersaturation or slight oversaturation (saturation index ~ 0.1).

DISCUSSION

The saturation index calculations for the normal cement without admixtures (Mix 1) indicates two things: that the solutions were oversaturated with respect to $Ca(OH)_2$, $CaSO_4 \cdot 2H_2O$, and $K_2Ca(SO_4)_2 \cdot H_2O$, and undersaturated with respect to $CaSO_4$ and $CaSO_4 \cdot 0.5H_2O$. This is in agreement with the X-ray powder diffraction analysis for this cement which indicated the presence of gypsum and the absence of calcium sulfate hemihydrate and anhydrite. Similar saturation states are shown for all solid phases in the normal cement pastes containing lignosulfonates, regardless of their false-setting tendencies. This indicates that the explanation for lignosulfonate-type false set does not appear to be found in the saturation state of the solution.

Using pore solution experiments, a particular case of false-setting cements has been related to the solubility product of $Ca(OH)_2$ (Kawada, 1965 and 1966). The saturation indices for $Ca(OH)_2$ were reported to be on the order of 0.5-0.7 for the normal cement and 0.2-0.4 for the false-setting cement, concluding that false set occurred when the saturation index for $Ca(OH)_2$ was in the range of 0.3-0.37. It must be noted that solubility products were calculated using activity coefficients based on Debye-Hückel theory in a range of ionic strength (>0.1M) where such an approach is questionable. Such trends in the saturation index for $Ca(OH)_2$ were not seen in this study.

The saturation index calculations for the heated cement show significant differences. First, the solutions are oversaturated with respect to $Ca(OH)_2$ and all of the calcium sulfate phases. This is in partial agreement with the X-ray diffraction analysis which indicated the presence of gypsum and hemihydrate and the absence of $CaSO_4$. Although $CaSO_4$ was not detected, the saturation state suggests that it should be present. Second, the saturation index for gypsum is on the order of four times higher than in the normal cement case. Finally, the saturation index for syngenite is also higher than in the normal cement case. Based on this data, the early stiffening of the heated cement paste appears to be a result of the precipitation of sulfate phases, most likely gypsum. This is the expected definition of G-type false set.

Role of Ettringite in Early Stiffening

An attempt was made to determine the role of ettringite in the early stiffening primarily because previous work (Kalousek, 1974) suggested that ettringite precipitation is the cause of early stiffening in pastes containing lignosulfonates. In addition, the calculated saturation indices provide no clear explanation of lignosulfonate-type false set. It was not possible to directly determine saturation indices for ettringite because the aluminum concentrations in solution fell below the detection level of the ICP (after an initial dilution of the pore solution) and PHRQPITZ does not include parameters for interactions involving aluminum species. Therefore, the measured data was used to calculate the aluminum activity required for equilibrium with solid ettringite. This activity is calculated for the $Al(OH)_4^-$ species since most of the aluminum should be ionized to this state. This calculation used a $K_{sp,20}$ for ettringite which was determined using the Pitzer equations as 1.23E-45 (Warren, 1994). The results of the aluminum hydroxide activities calculations are listed in Table 6.

The values of these $Al(OH)_4^-$ activities are extremely low when compared to the concentrations of the trace ions measured, such as Fe^{3+}. Since the activity coefficients for $Al(OH)_4^-$ are likely to be in the neighborhood of those in Table A1, it is likely that all of the pore solutions are oversaturated with respect to solid ettringite. The difference (greater than an order of magnitude)

between the $Al(OH)_4^-$ activities in the normal and heated cement pore solutions are significant but are unlikely to have an effect on this saturation state.

Table 6 Aluminum hydroxide activities calculated for equilibrium with solid ettringite

	a: $Al(OH)_4^-$		a: $Al(OH)_4^-$
Mix 1		Mix 4	
@5 min.	3.23E-10	@5 min.	3.74E-11
@10 min.	2.18E-10	@10 min.	3.98E-11
post-remix	2.30E-10	post-remix	1.33E-11
Mix 2		Mix 5	
@5 min.	3.44E-10	@5 min.	5.72E-11
@10 min.	2.53E-10	@10 min.	5.54E-11
post-remix	4.11E-10	post-remix	7.55E-11
Mix 3		Mix 6	
@5 min.	3.09E-10	@5 min.	5.04E-11
@10 min.	4.37E-10	@10 min.	6.52E-11
post-remix	2.87E-10	post-remix	5.55E-11

There are some difficulties with the pore solution approach. First, during early hydration, a single pore solution provides only a snapshot of a dynamic process. Some solid phases are dissolving while others simultaneously precipitate. The kinetics of each process strongly influence the chemical composition of the pore solution, with the solution acting merely as a transfer medium in some cases. Therefore, observations based on ion concentrations may be difficult to interpret correctly. Second, there is uncertainty in the degree of oversaturation necessary for solids to precipitate, such that conclusions may not be drawn from saturation indices with certainty. Finally, if solids precipitate in a pore solution containing a water-reducing additive, the result may be an adsorption of the admixture and a corresponding drop in dispersing effectiveness, i.e. stiffening.

CONCLUSIONS

1. G-type false set, most likely caused by precipitation of gypsum, was confirmed by saturation states determined with an ion-interaction model.

2. Differences in saturation states observed with G-type false set and lignosulfonate-type false set cases indicate that the mechanisms are different.

3. The chemistry of the pore solution is significantly different when early stiffening of cement paste arises from lignosulfonate addition rather than the presence of dehydrated forms of gypsum in the cement.

4. Lignosulfonate additions can aggravate the early stiffening tendencies of cement.

5. Lignosulfonate-type false set can not be explained solely by examining the pore solution chemistry.

REFERENCES

ASTM, "C-451 Standard Test Method for Early Stiffening of Portland Cement (Paste Method)", in *1991 Annual Book of Standards*, Section 4.01, pp. 220-222, American Society for Testing and Materials, Philadelphia, 1991.

Duchesne, J. and Reardon, E.J., "Measurement and Prediction of Portlandite Solubility in Alkali Solutions", *Cem. Concr. Res.*, Vol. 25, No. 5, 1995, pp.1043-1053.

Gartner, E.M., Tang, F.J., and Weiss, S.J., "Saturation Factors for Calcium Hydroxide and Calcium Sulfates in Fresh Portland Cement Pastes", *J. Am. Ceram. Soc.* Vol. 68, No. 12, 1985, pp. 667-673.

Kalousek, G.L., "Hydration Processes at the Early Stages of Cement Hardening", The VI International Congress on the Chemistry of Cement, pp. 3-42, 1974.
Kawada, N., Nishiyama, M., and Nemoto, A., "Chemical Analysis of Liquid Phase in Hardened Portland Cement Paste", Semento Gijusto Nenpo XVIII Synopses, pp. 55-56, 1965.
Kawada, N. and Nemoto, A., "C-type False Set", Semento Gijusto Nenpo XIX Synopses, pp.115-117, 1966.
Linke, W.F., in *Solubilities of Inorganic and Metal Organic Compounds* 4th edition Vol. 1, p. 661, American Chemical Society, Washington, 1965.
Murakami, Y., "On the Consistency of Concrete Made from False Set (Type G) Cement", Semento Gijusto Nenpo XI Synopses, pp. 60-61, 1957.
Ong, S., "Studies on Effects of Steam Curing and Alkali Hydroxide Additions on Pore Solution Chemistry Microstructure, and Alkali Silica Reactions", p. 76-79, Ph.D. Thesis, Purdue University, 1993.
Pitzer, K.S., "Ion Interaction Approach: Theory and Data Correlation", in *Activity Coefficients in Electrolyte Solutions*, 2nd Edition, pp.75-153, CRC Press, Boca Raton, 1991.
Plummer, L.N., Parkhurst, D.L., Fleming, G.W., and Dunkle, S.A., "A Computer Program for Incorporating Pitzer's Equations for Calculation of Geochemical Reactions in Brines", U.S. Geological Survey Water-Resources Investigations Report 88-4153, Reston, 1988.
Reardon, E.J., "An Ion Interaction Model for the Determination of Chemical Equilibria in Cement/Water Systems", *Cem. Concr. Res.* Vol. 20, 1990, pp. 175-192.
Taylor, H.F.W., "Modification of the Bogue calculation", *Adv. Cem. Res.* Vol. 2, No. 6, 1989, pp. 73-77.
Taylor, H.F.W., in *Cement Chemistry*, p.233, Academic Press, San Diego, 1990.
Warren, C.J. and Reardon, E.J., "The Solubility of Ettringite at 25°C", *Cem. Concr. Res.* Vol. 24, No. 8, 1994, pp. 1515-1524.

APPENDIX

Table A1 Activity coefficients and water activity

	H^+	Ca^{2+}	Na^+	K^+	$SO4^{2-}$	OH^-	a:H_2O
Mix 1 @ 5 min.	0.174	0.073	0.619	0.612	0.079	0.568	0.986
@ 10 min.	0.178	0.072	0.620	0.614	0.080	0.571	0.986
post-remix	0.182	0.073	0.620	0.615	0.083	0.578	0.986
Mix 2 @ 5 min.	0.177	0.077	0.623	0.613	0.085	0.570	0.987
@ 10 min.	0.181	0.071	0.612	0.606	0.084	0.586	0.986
post-remix	0.178	0.074	0.619	0.611	0.083	0.576	0.987
Mix 3 @ 5 min.	0.176	0.074	0.618	0.609	0.082	0.571	0.986
@ 10 min.	0.176	0.072	0.613	0.605	0.082	0.577	0.986
post-remix	0.174	0.072	0.612	0.604	0.080	0.572	0.986
Mix 4 @ 5 min.	0.188	0.085	0.621	0.607	0.094	0.552	0.990
@ 10 min.	0.188	0.084	0.624	0.610	0.093	0.554	0.989
post-remix	0.188	0.080	0.623	0.613	0.093	0.577	0.988
Mix 5 @ 5 min.	0.195	0.085	0.624	0.611	0.099	0.569	0.990
@ 10 min.	0.189	0.084	0.620	0.606	0.095	0.563	0.989
post-remix	0.191	0.084	0.619	0.606	0.098	0.570	0.989
Mix 6 @ 5 min.	0.193	0.082	0.616	0.603	0.097	0.569	0.989
@ 10 min.	0.195	0.083	0.617	0.604	0.099	0.575	0.989
post-remix	0.196	0.080	0.611	0.599	0.099	0.578	0.988

EFFECT OF SODIUM ALUMINATE ON CLASS G OILWELL CEMENT HYDRATION AT LOW AND AMBIENT TEMPERATURES

Jasbir S. LOTA, Birchall Centre for Inorganic Chemistry and Materials Science, Department of Chemistry, Keele University, Keele, Staffordshire ST5 5BG, U.K.
John BENSTED, Birchall Centre for Inorganic Chemistry and Materials Science, Department of Chemistry, Keele University, Keele, Staffordshire ST5 5BG, U.K.
Peter L. PRATT (the late), Department of Materials, Imperial College of Science Technology and Medicine, Department of Materials, Prince Consort Road, London SW7 2BP, U.K.

ABSTRACT Sodium aluminate accelerates Class G oilwell cement hydration in a different way from other accelerating admixtures by not forming a hydration shell boundary around the cement grains. This causes the hydration to be rapid and more uncontrolled in comparison. More ettringite (AFt phase) is formed at 5°C than at 20°C, unlike for CSH. Significant morphological differences are found at these two temperatures.

Key-words oilwell cement, accelerators, hydration, microstructure, low temperature

INTRODUCTION

Oilwell cements are used in the oil industry both in exploration and in the production of oil and gas. Their primary use is to seal the annular space between the walls of a bore hole and the steel casing that lines the well (Bensted, 1987). Normally in oil- and gas-well cementing, the temperatures are mostly above ambient and pressures above atmospheric, often considerably so, which necessitates the use of retarders in the cement slurries to produce workable thickening or setting times. However, during the casing cementing of well sections at or near the surface under cold conditions, where the temperatures may be as low as around 0-5°C, typically in Arctic regions and in the Northern North Sea, the cement hydration reactions are slowed down and "accelerating" admixtures are used to promote hydration and give a successful cementing job. The work presented here was part of a research programme (Lota, 1994) in which other accelerating admixtures were used in addition to sodium aluminate ($NaAlO_2$). A greater understanding of the effect of low temperature and of accelerating admixtures upon the developing cement microstructure and properties should lead to improved and more efficient cementing of wells.

EXPERIMENTAL METHODS AND TECHNIQUES

The cement was supplied by Blue Circle Industries with a potential phase composition (Bogue %) of C_3S-56.6, C_2S-19.3, C_3A-1.5 and C_4AF-15.9. The $NaAlO_2$ was supplied by Fosroc Technology, U.K. Cement paste specimens were prepared using molar concentrations (0, 0.1, 0.3, 0.5 and 1.0M) of $NaAlO_2$ with distilled water and a water-to-cement ratio of 0.44 as recommended by the American Petroleum Institute (1995).

For examination by scanning electron microscopy (SEM), thermal analysis (differential thermal analysis (DTA) and thermogravimetry (TG)), infrared (IR) spectroscopy and x-ray powder diffractometry (XRD), cylindrical specimens, 11 mm diameter and 35 mm height, were cast after mixing in a Waring blender for three minutes and subsequently cured in water baths maintained at either 5°C and 20°C. Prior to casting at 5°C the cement and mix water were chilled at 8°C for 1 day.

At appropriate curing times the specimens were frozen in a slurry of solid carbon dioxide and ethanol mixture and then freeze-dried under vacuum. A JEOL-35CF scanning electron microscope was used to examine fracture surfaces. A solid state backscattered electron (BSE) detector linked to a Kontron SEM image processing system was used to obtain images from polished surfaces cut from the cement pastes after freeze drying.

The heat evolution from freshly prepared samples was measured using an isothermal conduction calorimeter supplied by Wexham Developments Limited (Forrester, 1970). Compressive strength measurements were obtained by crushing ten 12.7 mm side cubes, in an Instron testing machine, which had been cured at either 5°C or 20°C for a specified time.

RESULTS AND DISCUSSION

The heat evolution curves of the cement with additions of $NaAlO_2$ at 5°C or 20°C are shown in Figures 1 and 2 respectively. The concentration key in Figure 1 also applies to Figure 2.

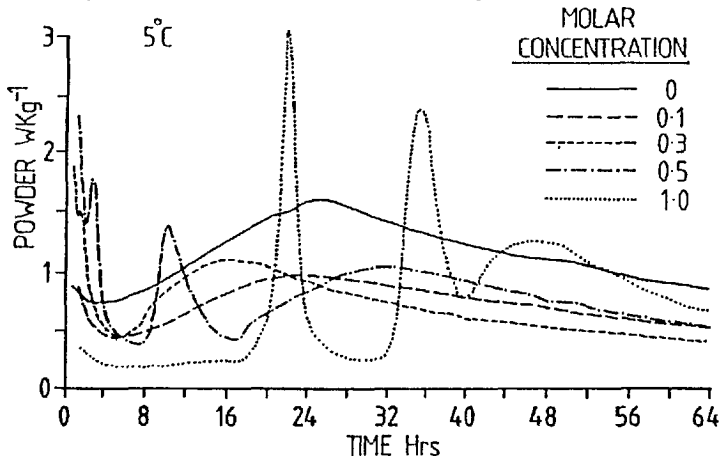

Figure 1. Heat evolution of cement paste hydrated with addition of $NaAlO_2$ at 5°C.

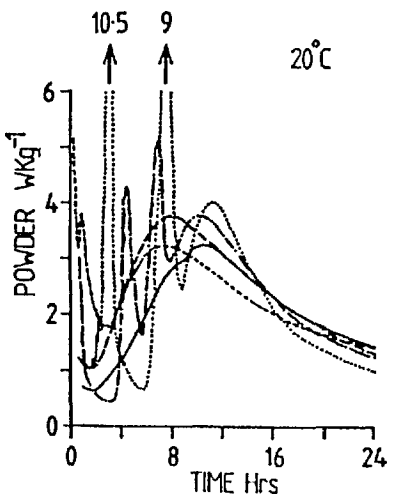

Figure 2. Heat evolution of cement paste hydrated with addition of $NaAlO_2$ at 20°C.

In addition to the peaks produced by the control paste, with increasing addition of $NaAlO_2$ two supplementary peaks appear at both temperatures during the "induction period". These supplementary peaks increase in intensity as the dosage is raised. At 5°C, 0.1M and 0.3M additions advance the main heat peak due to the alite phase hydration, whereas the 0.5M and 1.0M addition retard this peak significantly. At 20°C only the 1.0M addition retards the onset of the alite peak. Clearly, from these curves it can be deduced that the normal or "expected" cement hydration processes are not occurring with $NaAlO_2$ present.

Typical fracture surfaces and BSE images of the control paste and paste with 1.0M addition of $NaAlO_2$ that had been hydrated for 1 day at 20°C are shown in Figure 3. The fracture surfaces and BSE images of the control paste are typical of those hydrating Portland cement where CSH (calcium silicate hydrate) covers the cement grain surfaces and, amongst these, AFt phase

(ettringite) rods and calcium hydroxide (CH) are seen (Taylor, 1990). This is in contrast to the fracture surface of the paste containing $NaAlO_2$, which shows little evidence of CSH on the surfaces of the hydrating cement grains. Furthermore, there are thin and elongated rod-like crystals, probably AFt phase and an abundance of well defined hexagonal platelets of AFm/CAH (calcium aluminate hydrates) phases similar to those reported by Breval (1976). The surrounding CSH has an unrecognisable morphology, which appears to be ill-defined and not distributed throughout the paste thus creating large regions of porosity.

Control 1d 20°C, Fracture Surface

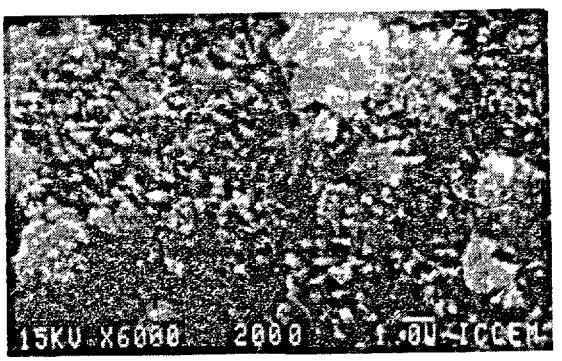

$NaAlO_2$ 1d 20°C, Fracture Surface

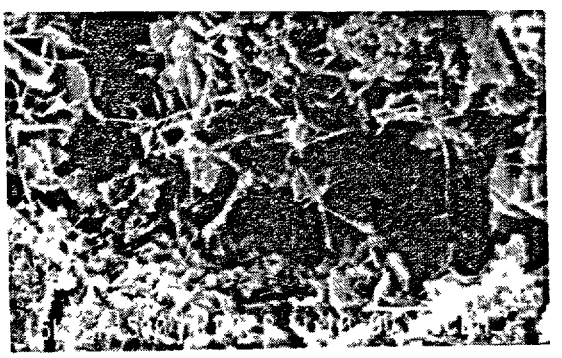

Control 1d 20°C, BSE image

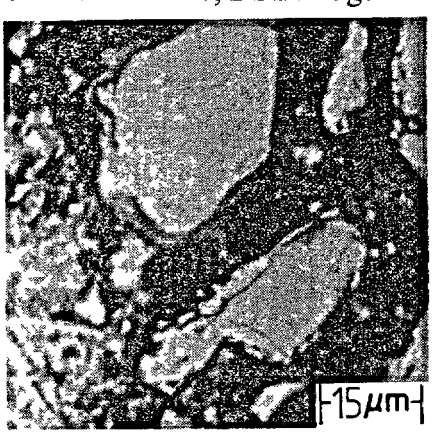

$NaAlO_2$ 1d 20°C, BSE image

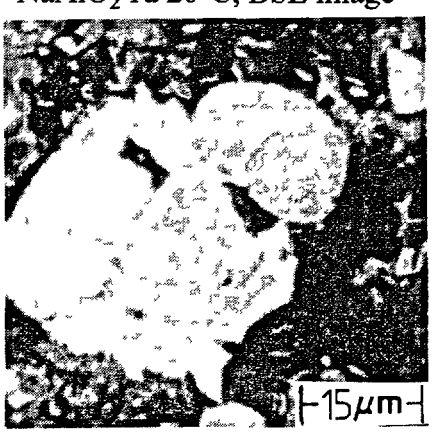

Figure 3. Fracture and BSE images of paste with/without 1.0M $NaAlO_2$ addition at 1d & 20°C.

The BSE images also show marked differences. In the control paste all the hydrating cement grains have hydration product shells, some forming hollow shells, and calcium hydroxide is clearly present. In comparison with the $NaAlO_2$-containing paste, there is no sign of a hydration product layer around any of the cement grains; clusters of CH are not clearly seen and the alite phase shows preferential signs of dissolution. It appears as if the presence of sodium and aluminate ions have interfered with the development of the CSH around the cement grains and consequently the mix water has had more opportunity to reach the anhydrous cement grains. As a result of this erratic process, there is much porosity within the paste.

The first supplementary peak in the heat evolution curves could be due to the formation of CAH in which the source of calcium ions come from the hydrating calcium silicate phases and the aluminate from the admixture. The removal of calcium ions from the developing hydration shell will prevent its forming similar to the manner in which EDTA (ethylenediaminetetraacetic acid) and sugars function (Thomas and Double, 1981 and Birchall and Thomas, 1984). Lack of

availability of calcium ions will have an influence on the Ca/Si ratio of the CSH and consequently upon the properties of the paste in its wet, set and hardened states.

With the absence of a hydration product shell enveloping the hydrating cement grain and easy access of the mix water to the anhydrous cement, there would be rapid dissolution of the aluminate phase. These aluminate ions from the dissolution of the aluminate and the ferrite phases will react further with calcium ions from the dissolution of the calcium silicate phases (especially alite) to form calcium aluminate hydrates. There are relatively smaller quantities of AFt phase in the $NaAlO_2$-containing paste probably because the high alkalinity of the mix water and the early surge of calcium ions in the aqueous phase would decrease the solubility of gypsum simply due to the common-ion-effect. It is probable (Iler, 1955) that when aluminium is co-ordinated with four oxygens in a silicate structure, an Al atom essentially replaces a Si atom giving a negative charge at the site on the aluminosiloxane structure, so that here:

$$3\,(\text{-O})_3\text{Si-OH} \;+\; \text{Al(OH)}_4^- \longrightarrow [(\text{-O})_3\text{Si-O}]_2\text{Al(OH)(O-Si-O-)}^- \;+\; 3\text{H}_2\text{O}$$

In this way, the structure of the CSH is disrupted and hence explains the absence of a hydration product layer completely covering the hydrating cement grain surface. This means that the mix water is not hindered in coming into contact with the anhydrous cement grain surface. Eventually, the remaining cement grains will begin to hydrate in the "normal" manner as the quantity of aluminate ions from the admixture diminish, provided that there is ample free water. This effect is seen by the emergence of the acceleratory peak due to the alite phase hydration. It appears that several processes are taking place simultaneously.

The CH of the paste measured by TG is shown in Table 1 and the measured non-evaporable water (loss-on-ignition, LOI) content of the paste is shown in Table 2.

Table 1. Volume % CH in the paste hydrated at 5°C and 20°C with and without $NaAlO_2$

	5°C			20°C		
	Molar Addition of $NaAlO_2$					
Hydration Time	**Control**	**0.3M**	**1.0M**	**Control**	**0.3M**	**1.0M**
3 Hours	1.13	0	0.61	0.70	3.26	3.69
6 Hours	1.19	0	1.47	1.18	1.10	0.62
12 Hours	2.42	1.67	0.74	3.93	4.02	3.20
1 Day	5.30	4.74	0.25	5.43	5.69	2.51
28 Days	9.01	12.28	8.34	10.99	10.21	4.24

Table 2. Non-evaporable water expressed as % weight loss referred to the ignited cement at 1000°C the paste hydrated at 5°C and 20°C with and without $NaAlO_2$

	5°C			20°C		
	Molar Addition of $NaAlO_2$					
Hydration Time	**Control**	**0.3M**	**1.0M**	**Control**	**0.3M**	**1.0M**
3 Hours	3.27	4.91	6.08	2.35	10.51	11.27
6 Hours	4.42	4.98	6.71	3.32	5.81	7.56
12 Hours	5.99	7.19	7.54	8.50	9.89	11.06
1 Day	7.47	12.58	6.91	8.99	12.17	10.78
28 Days	17.05	18.07	17.70	16.87	17.14	11.06

The LOI shows a pattern broadly similar to the CH content of the paste in Table 1. At 5°C, with 1.0M addition, the amount of CH that is formed up to 1 day is erratic. Beyond 1 day hydration the 0.3M addition produces the greatest amount of CH. At 20°C, with 0.3M and 1.0M addition there appears to be much more CH at 3 hours than in the control. The 1.0M addition does not significantly influence the formation of CH after 12 hours hydration and the quantity of CH remains low at least up to 28 days.

IR spectra of the control paste hydrated from 15 minutes to 1 year and the paste with 1.0M $NaAlO_2$ addition hydrated from 15 minutes to 28 days are shown in Figure 4.

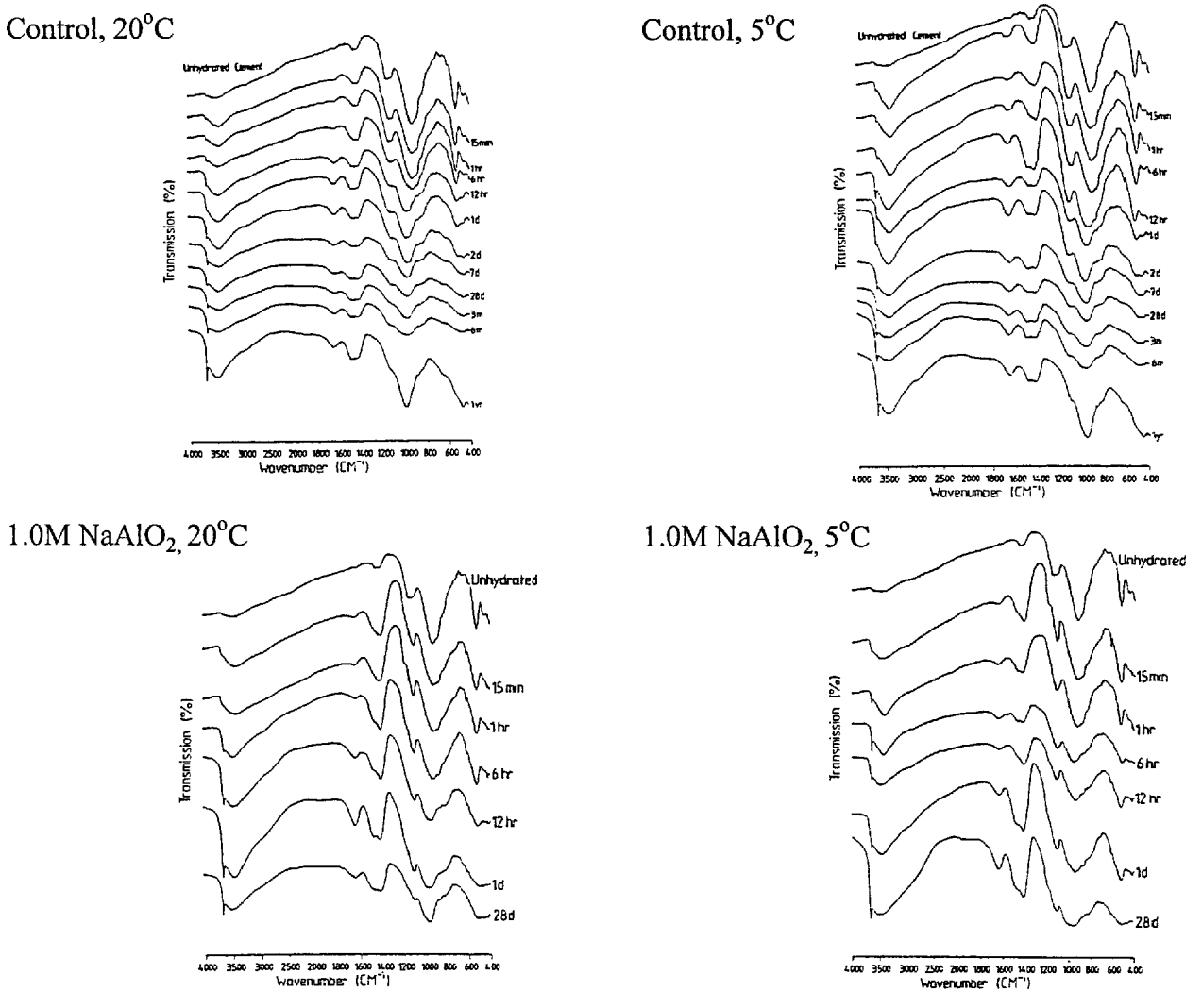

Figure 4. IR spectra of paste with/without 1.0M additions of $NaAlO_2$ hydrated at 5°C and 20°C.

The main differences in the paste hydrated at 5°C compared to that at 20°C are that greater quantities of AFt phase are formed up to 12 hours as indicated by the shape and sharpness of the water wavebands at 1600-1650 cm^{-1} and 3100-3500 cm^{-1}. The AFt phase is present from early ages (15 minutes) and persists up to 1 year. TG implies that greater amounts of water are retained within the paste when it is cured at 5°C than at 20°C. This may be due to the increased amount of AFt phase which incorporates a potential of 32 water molecules in its structure. At ages greater than 3 months AFm (monosulphate) phase is formed, as shown by the broadening of the water wavebands above 3000 cm^{-1}. The IR spectra of the paste hydrated with 1.0M

addition of $NaAlO_2$ at 20°C are similar to those of the control paste hydrated at 20°C and similar comments apply. The only exception is that the sulphate wavebands at 1000-1145 cm^{-1} remain much clearer up to 28 days. This may be as a consequence of the effect of the $NaAlO_2$ upon the hydration of the cement as discussed earlier.

The main difference between the XRD traces of the control paste hydrated at 20°C and at 5°C is that AFt phase at 20°C is detected from 28 days and at 1 year. In contrast, at 5°C AFt phase is present at all ages from 6 hours to 1 year hydration. The presence of AFt phase also is seen to persist in a sulphate resisting Portland cement (Gollop and Taylor, 1994) and may by due to the chemical composition of the ferrite phase being different from ordinary Portland cement (Lota et al, 1995) and hence more reactive. Furthermore, in the XRD traces there are small peaks or shoulders probably due to hydrogarnet phase. This phase is not normally observed in a Portland cement (Taylor, 1990). XRD traces of the paste with additions of $NaAlO_2$ at 5°C and 20°C are shown in Figure 5.

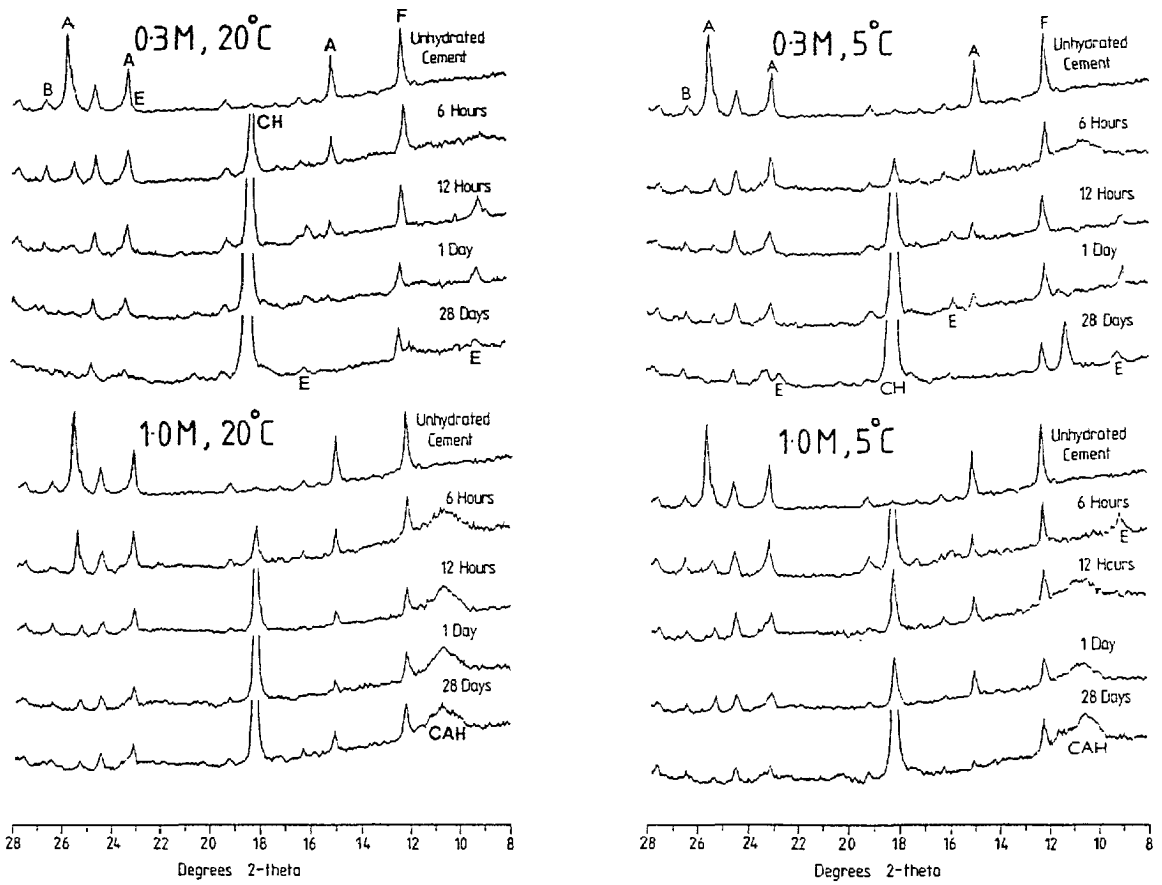

Figure 5. XRD traces of paste hydrated with additions of $NaAlO_2$ hydrated at 5°C and 20°C.

At 20°C, the 0.3M addition reveals AFt phase (9.28 and 15.95°2θ) at 12 hours; at 1 and 28 days its intensity decreases. The CH peak at 18.05°2θ becomes more intense as the paste ages. This indicates the continuing hydration of the calcium silicate phases. In contrast with the 1.0M addition, from 6 hours to 28 days hydration, a broad band is centred at 10.60°2θ suggesting the presence of AFm phase, $C_4(A,F)H_{13}$. The CH peak here is stunted at respective ages to that of the paste hydrated at 5°C and may be due to Ca^{2+} and OH^- ions being consumed to form CAH. At 5°C, with 0.3M addition a similar situation occurs to that at 20°C. However, at 6 hours CAH

is detected and there is the appearance of a sharp peak at 11.21°2θ possibly due to $C_4(A,F)H_{13}$ or other AFm phases. With 1.0M addition, AFt phase is detected at 6 hours and at later ages CAH is present. The intensity of the CH peak varies. This may be due to the consumption of Ca^{2+} and OH^- ions for the formation of CAH. These observations by XRD complement the SEM, TG and IR data. More AFt is formed at 5°C than at 20°C unlike for CSH, apparently because the slowness of CSH formation at 5°C means that there is much less competition for space, water and SO_4^{2-} ions here.

It is not known as to what the exact nature of the CSH in the paste with $NaAlO_2$ is and it may have Fe^{2+}, Al^{3+}, plus SO_4^{2-} from gypsum incorporated in its structure. The mode of action of $NaAlO_2$ in altering the paste hydration is depicted diagrammatically in Figure 6.

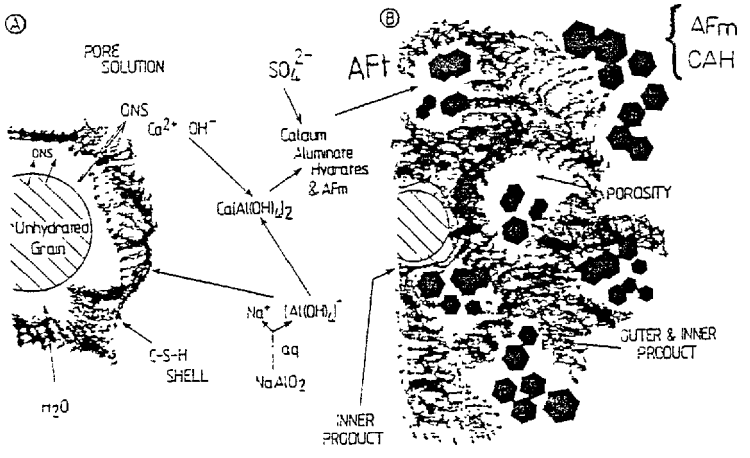

Figure 6. Development of cement microstructure of cement paste in the presence of $NaAlO_2$.

$NaAlO_2$ upon dissolution in water (initial pH 7.6) hydrolyses with release of OH^- ions to give higher pH values, viz. 11.0 for 0.1M and 12.7 for 1.0M solutions after 8 hours. Such release of OH^- ions and dissolution of aluminate in the aqueous phase would facilitate accelerated hydration of all the major cement phases, giving more CSH, CH (less crystalline) and aluminate hydrates including AFt at early ages. Due to rapid competition for space between the rapidly hydrating phases, overall hydration is not well controlled and "normal" hydrate formation suffers some disruption. This is typified by observations that a complete hydration product layer does not surround the hydrating cement grains and also that, since increased ferrite hydration will further raise silicate hydraulicity, the two characteristic supplementary conduction calorimetry peaks can be tentatively assigned as C_3A_{aq} from $NaAlO_2$ and C_3A_{aq} from ferrite phase.

Fracture surfaces and BSE images reveal that a distinct hydration product shell is not clearly discernible (see B in Figure 6). The consequence of this ill-developed shell boundary is that the AFm phase forms randomly and is not confined to the inner regions of the hydration shell. This is in complete contrast to the control paste where AFm phase only occurs within the intact hydration shell boundary and not in the aqueous/pore solution. The hydration shell appears to have become part of the surrounding CSH and no longer acts as a suitable barrier between the aqueous solution and the unhydrated cement core, thus exposing a greater surface area of unhydrated cement phases to the mix water. This results in an inhomogeneous hydration causing the paste to prematurely set by increasing the rate of hydration locally.

CONCLUSIONS

The hydration of the oilwell cement with additions of $NaAlO_2$ at 20°C and 5°C is different from that of the control paste. Rate of heat evolution curves show the emergence of supplementary peaks in addition to the typical peaks expected from the control paste with addition of $NaAlO_2$. This implies that different hydration processes are taking place in the paste with addition of $NaAlO_2$ as compared to the control paste. There is no well defined hydration product boundary around the hydrating cement grains and there are regions in the paste with preferential dissolution of the cement phases. $NaAlO_2$ appears to accelerate early hydration by not allowing formation of a hydration shell which completely surrounds the cement grain. Consequently, the lack of a hydration shell causes the hydration to be rapid and uncontrolled. It appears that $NaAlO_2$ accelerates the early hydration of the cement to such an extent that further hydration is stifled. AFt phase formation is erratic, but appear to be greater at 5°C than at 20°C, presumably because CSH formation is lower and there is thus less competition for space, water and sulphate ions, the majority of which end up in the CSH. Morphologies of the hydration products at 5°C and 20°C reveal significant differences. Such behaviour with $NaAlO_2$ is different for calcium chloride and calcium formate (Lota, 1994) and demonstrates that there is no universal mechanism for cement hydration.

ACKNOWLEDGEMENTS

The authors are grateful to the Science and Engineering Research Council and to the Sunbury Research Centre of British Petroleum plc for the support of Jasbir S. Lota who was then on a SERC/CASE studentship and to Dr Karen L. Scrivener for helpful assistance.

REFERENCES

American Petroleum Institute, "Specification for cements and materials for well cementing", API Specification 10A, 22nd Edition, American Petroleum Institute, Washington D.C., 1995.

Bensted, J., "Cements with specific applications-Oilwell cements", World Cement, Vol. 18, pp.72-78, 1987.

Birchall, J. D. and Thomas, N. L., "The mechanism of retardation of setting of OPC by sugars", British Ceramic Proceedings, No. 35, pp. 305-315, 1984.

Breval, E., "C_3S hydration", Cement and Concrete Research, Vol. 6, No. 1, pp. 129-138, 1976.

Forrester, J. A., "A conduction calorimeter for the study of cement hydration", Cement Technology, Vol. 1, pp. 95-99, 1970.

Gollop, R. S. and Taylor, H. F. W., "Microstructural and microanalytical studies of sulfate attack. II. Sulphate-resisting Portland cement: Ferrite composition and hydration chemistry", Cement and Concrete Research, Vol. 24, No. 7, pp. 1347-1358, 1994.

Iler, R. I., "The colloid chemistry of silica and silicates", Chapter VIII, Cornell University Press, Ithaca, New York, 1955.

Lota, J. S., "The hydration of Class G oilwell cement", Ph.D. Thesis, Imperial College of Science Technology and Medicine, University of London, 1994.

Lota, J. S., Pratt, P. L. and Bensted, J., A discussion of the paper "Microstructural and microanalytical studies of sulfate attack. II. Sulfate-resisting Portland cement: Ferrite composition and hydration chemistry", by Gollop, R. S. and Taylor, H. F. W., Cement and Concrete Research, Vol. 25, No. 8, pp. 1811-1813, 1995.

Taylor, H. F. W, "Cement chemistry", Academic Press, London, San Diego, 1990.

Thomas, N. L. and Double, D. D., "Calcium and silicon concentrations in solution during the early hydration of Portland cement and tricalcium silicate", Cement and Concrete Research, Vol. 11, No. 5/6, pp. 675-687, 1981.

INFLUENCE OF $BaCO_3$ ON THE HYDRATION OF C_3A

George DUMITRU, Universidad Craiova, Targu-Jiu, Romanie
Tomás VÁZQUEZ, Instituto Eduardo Torroja (CSIC), Spain
Francisca PUERTAS, Instituto Eduardo Torroja (CSIC), Spain
Mª Teresa BLANCO-VARELA, Instituto Eduardo Torroja (CSIC), Spain

ABSTRACT When gypsum is not present in the reaction, $BaCO_3$ retards the C_3A hydration. The mineral composition of the hydration products presents a specific peculiarity which is the formation of a hemicarboaluminate like $C_8A_2cH_{24}$[1] having 6 %wt of Ba in its composition. When gypsum is present $BaCO_3$ accelerates the hydration reaction of C_3A. Ettringite formation is inhibited.

Key-words: Aluminate phase, hydration, sulphate resistance.

INTRODUCTION

The utilisation of natural minerals as inexpensive substitution materials for cement manufacturing is a valid choice to get energy savings. Some authors have studied the influence of limestone, dolomite or magnesium carbonate additions on the behaviour and properties of cements, mortars and concretes (Ramachandran, 1986), (Negro et al, 1986), (Vernet, 1986), (Massazza et al, 1992). The role played by that limestone addition consists in a slight delay of hydration reactions of aluminate phases and the formation of carboaluminates of various nature. Limestone filler addition to cements is col ndards.
In some countr kia, Austria, England, Russia and those of other continents as Namibia, USA, Canada and China, have important witherite ($BaCO_3$) geological quarries. The aim of the present work is to know $BaCO_3$ influence on C_3A hydration process, in gypsum presence and absence.

EXPERIMENTAL

Tables 1 and 2 show the different mixes prepared, likewise water/solid ratios used for their preparation.

Table 1 Sample compositions.

SAMPLE	$C_3A/BaCO_3$ RATIO	WATER/SOLID RATIO	$Ca(OH)_2$(*)/SOLID RATIO
A	1/1	0.6	--
B	1/1	1	--
C	9/1	0.6	--
D	9/1	1	--
A_1	1/1	--	0.6
D_1	9/1	--	1

(*) $Ca(OH)_2$ saturated dissolution

[1] A= Al_2O_3, C= CaO, c= CO_2, H= H_2O

Table 2 Sample compositions.

SAMPLE	C_3A/GYPSUM/$BaCO_3$	WATER/SOLID RATIO	$Ca(OH)_2$(*)/SOLID RATIO
E	3/1/0	0.6	--
F	3/1/1	0.6	--
E_1	3/1/0	--	0.6
F_1	3/1/1	--	0.6

(*) $Ca(OH)_2$ saturated dissolution

The hydration of pastes obtained was stopped at different ages (1h, 3h, 24h, 3 days and 7 days) with acetone-ethanol. Resulting samples were analysed by XRD. On some pastes, SEM/EDX microstructural analyses were carried out.

RESULTS AND DISCUSSION

Reactions in gypsum absence

Table 3 shows the results obtained when analysing the pastes through XRD.

$BaCO_3$ delays C_3A hydration reaction as well as $CaCO_3$ does (Ramachandran, 1986). $BaCO_3$ delays C_3AH_6 formation, stabilising hexagonal hydrated calcium aluminates (C_2AH_8) and favouring the formation of C_4AcH_{11} and $C_8A_2cH_{24}$ type carboaluminates. $Ca(OH)_2$ presence in mix water inhibits C_3AH_6 formation until the ages studied.

C_2AH_8 is a metastable specie (Damidot and Glasser, 1994) in CaO-Al_2O_3-CO_3-H_2O system. The excess of $BaCO_3$, supposing that it acts similar to $CaCO_3$, would react with C_2AH_8 to form hydrated calcium-barium carboaluminates.

The hemicarboaluminate $C_8A_2cH_{24}$ is an stable specie until CO_2/Al_2O_3 ratios close to 0.8 (Fisher and Kuzel, 1982). In Fig.1, the microstructural aspect of this carboaluminate is shown. It presents a morphology of hexagonal plates. EDX analysis on these plates shows Ba presence (in proportion close to 6% wt.) in the hydrate composition.

Reactions in gypsum presence

In Table 4, results obtained analysing the pastes by XRD are shown. From these results, it is deduced that $BaCO_3$ presence accelerates C_3A hydration reaction.

In samples with $BaCO_3$ (F and F_1) ettringite formation is inhibited and high amounts of $BaSO_4$ are formed. In these samples, the presence of hydrated calcium carboaluminates is also detected.

Table 3 XRD Results.

SAMPLE	MINERALOGICAL COMPOSITION	1 HOUR	3 HOURS	1 DAY	3 DAYS	7DAYS
C_3A SYNT.	C_3A	+	O			
	$BaCO_3$	--	--			
	C_2AH_8	--	--			
	C_3AH_6	+++	++++			
	C_4AcH_{11}	--	--			
	$C_8A_2cH_{24}$	--	--			
A	C_3A	++	++	+	+	+
	$BaCO_3$	++++	++++	++++	++++	++++
	C_2AH_8	--	O	O	O	+
	C_3AH_6	++	--	--	O	+
	C_4AcH_{11}	O	O	--	--	--
	$C_8A_2cH_{24}$	--	--	O	+	+
B	C_3A	++	++	+		--
	$BaCO_3$	++++	+++	+++		+++
	C_2AH_8	--	--	++		++
	C_3AH_6	--	--	--		++
	C_4AcH_{11}	+	+	+		++
	$C_8A_2cH_{24}$	--	--	+		+++
C	C_3A	++	++	++	++	--
	$BaCO_3$	+++	++	++	++	++
	C_2AH_8	--	--	--	--	--
	C_3AH_6	++	+++	+++	+++	+++
	C_4AcH_{11}	--	O	O	O	+
	$C_8A_2cH_{24}$	--	--	--	--	--
D	C_3A	+++	+++	+		--
	$BaCO_3$	++	++	++		++
	C_2AH_8	O	+	++		O
	C_3AH_6	--	--	--		+++
	C_4AcH_{11}	+	+	+		O
	$C_8A_2cH_{24}$	O	+	+		+
A_1	C_3A		++	++	+	O
	$BaCO_3$		++++	++++	++++	++
	C_2AH_8		--	--	--	++
	C_3AH_6		--	--	--	--
	C_4AcH_{11}		+	+	+	++
	$C_8A_2cH_{24}$		--	--	--	--
D_1	C_3A		++	+	+	O
	$BaCO_3$		++	++	+	+
	C_2AH_8		O	+	++	++
	C_3AH_6		--	--	--	--
	C_4AcH_{11}		+	O	--	--
	$C_8A_2cH_{24}$		+	++	+++	++++

++++ abundant, +++ much, ++ moderate, + little, o traces, -- absent



Fig. 1 Calcium hemicarboaluminate containing Ba in its composition

Table 4 XRD Results.

SAMPLE	MINERALOGICAL COMPOSITION	7 DAYS OF HYDRATION
E	C_3A	+++
	ETTRINGITE	++
	$BaCO_3$	--
	$BaSO_4$	--
	C_4AcH_{11}	--
	$C_8A_2cH_{24}$	--
F	C_3A	+
	ETTRINGITE	--
	$BaCO_3$	--
	$BaSO_4$	+++
	C_4AcH_{11}	+++
	$C_8A_2cH_{24}$	--
E_1	C_3A	++
	ETTRINGITE	+++
	$BaCO_3$	--
	$BaSO_4$	--
	C_4AcH_{11}	--
	$C_8A_2cH_{24}$	--
F_1	C_3A	+
	ETTRINGITE	--
	$BaCO_3$	--
	$BaSO_4$	+++
	C_4AcH_{11}	+++
	$C_8A_2cH_{24}$	+

In $CaO-Al_2O_3-CaSO_4-CaCO_3-H_2O$ system, ettringite is the stable phase when $[SO_4]$ concentrations are between 1.52 x 10^{-2} mol/Kg and 7.60 x 10^{-1} and for carbonate concentrations inferior to 8.39 x 10^{-6} mol/kg (Damidot and Glasser, 1995). In this concentration range, ettringite becomes compatible with all phases present in the system. From data obtained in this work, $BaCO_3$ amount added is enough to react with all the gypsum and form $BaSO_4$, highly insoluble salt. This makes very low the SO_4^{2-} level in solution and ettringite cannot be formed.

$Ca(OH)_2$ presence in mix water accelerates ettringite formation rate (E and E_1 samples comparison). However, the presence of saturated solution of calcium hydroxide does not seem to induce alterations in mineralogical composition of pastes (from samples with $BaCO_3$).

CONCLUSIONS

1.- $BaCO_3$ delays C_3A hydration reaction, as well as $CaCO_3$ does.

2.- When C_3A hydration occurs in $BaCO_3$ presence, hydrated calcium carboaluminates are formed. Hemicarboaluminate $C_8A_2cH_{24}$ contains Ba in proportion close to 6 %wt.

3.- $BaCO_3$ accelerates C_3A hydration reaction in gypsum presence. Ettringite formation is inhibited and high amounts of $BaSO_4$ precipitates. The main hydration product of these pastes is a C_4AcH_{11} type carboaluminate.

4.- From results obtained, $BaCO_3$ addition is proposed to those cements and concretes exposed to sulphate attack. $BaCO_3$ would act as a reserve for the fixing of sulphates coming from the external medium.

ACKNOWLEDGEMENT

The authors wish to thank to the Spanish Education Ministry to the financial support given to Dr G. Dumitru for carried out this research.

REFERENCES

Damidot, D., Stronach, S., Kindness, A., Atkins, M., Glasser, F.P., "Thermodynamic investigations of the $CaO-Al_2O_3-CaCO_3-H_2O$ closed system at 25°C and the influence of Na_2O". Cem. Concr. Res., Vol 24, n° 3, 1994, pp. 563-572.

Damidot, D., Glasser, F.P., "Thermodynamic investigations of the $CaO-Al_2O_3-CaSO_4-CaCO_3-H_2O$ closed system at 25°C and the influence of Na_2O". Adv. Cem. Res., Vol 7, n° 27, 1995, pp. 129-134.

Fischer, R., Kuzel, H.J., "Reinvestigation of the system $C_4A.nH_2O-C_4A.CO_2.nH_2O$". Cem. Cocr. Res. Vol, 12, 1982, pp. 517-526.

Massazza, F., Daimon, M., "Chemistry of hydration of cements and cementitious systems". 9th Intern. Congr. Chem. Cem. Vol I, 1992, pp. 383-446.

Ramachandran, V.S., Zhang Chun-mei, "Cement with calcium carbonate additions". 8th Intern. Congr. Chem. Cem. Vol VI, 1986, pp. 178-182.

Vernet, C., "Sequence et cinetique des reactions d´hydratation de l´aluminate tricalcique en presence de gypse, de chaux et de fillers calcaires". 8th Intern. Congr. Chem. Cem. Vol III, 1986, pp. 70-74.

3iii016
8 pp

MECHANISM OF DELAYED EXPANSION AND NEW TYPE CHEMICALLY PRESTRESSED CONCRETE FILLED STEEL TUBE *

GU Ganshen[1],WANG Xinyou[2],WANG Peiming[2],CHEN Meizan[1]
1 Suzhou Concrete and Cement Products Research Institute,Suzhou 215004,China
2 Tongji University,Shanghai 200092,China

ABSTRACT The mechanism of delayed expansion for improving self—stressing level of the confined expansion concrete are studied, exemplifying the chemically prestressed concrete. The results show that the self—stressing level can be more than 21 MPa. The bearing capacity of chemically prestressed concrete filled steel tube is compared with that of ordinary concrete filled steel tube at different curing ages. Finally, QXDA, DSC and SEM data are presented to interpret the mechanism.

Key—words: delayed expansion; chemically prestressed concrete filled steel tube

INTRODUCTION

It is known that concrete has a very small elastic modulus, typical brittleness, low tensile strength. Researchers have tried to achieve the most favourable triaxial stress state by exerting confining binding factors on concrete in order to eliminate the inherent defects of concrete. The typical examples for application are the traditional concrete filled steel tube and high strength concrete filled steel tube.

Generally, the prestress can be exerted by mechanical and chemical methods. The former has good effects, but the process is too complicated and expensive. The latter is to make concrete obtain self—stress by adding expansive agent. According to former Soviet's method of stress correction, only when the self—stress reaches 20 MPa can it have the similar effect to mechanical prestress. Although the total expansive energy stored in expansion components is high and the process of self—stress is simpler than that of mechanical prestress, the self—stress is below 10 MPa for a long time, so the application of self—stressing concrete has been limited to low self—stressing members (Wu, 1990). The loss of lots of expansive energy is the essential cause to affect the improvement of self—stressing level in the traditional expansion mode. In view of this, a new mechanism of delayed expansion is proposed in this paper, exemplified by chemically prestressed concrete filled steel tube.

DELAYED EXPANSION MECHANISM AND TEST

Traditional expansion mechanism and mode

With the confined expansion concrete type ettringite, the major expansive source is ettringite phase (AFt) whose formation requires 45. 94% bound water. The mode of the traditional expansion is illustrated in Fig 1. It is obvious that a great amount of expansion occurs in the early stage and the confined expansion ratio reaches the maximum at 14 days, some at 7 days (Wu, 1990). When cured in air concrete will contract and become steady. When AFt phase grows, the strength structure of concrete undergoes a changing process of formation, plastic state, half—plastic state and elastic state. It is found that, under the curing condition of both enough water supply and moist air or water curing, a

* Project Supported by National Nature Science Foundation of China

large amount of AFt has formed when the strength structure is still in the plastic and half—plastic state,and expansion developes faster than strength. So along the expansion energy is absorbed by its working on the condensable strength structure,lots of expansion energy is consumed invalidly. In another aspect,the excessive water supply will increase the porosity of concrete and the size of pores,which influence the development of the elastic strength structure,lengthen the condensable process of the plastic and half—plastic stage,and increase the loss of expansion energy. In the past,the expansion mode above was widely used in the confined expansion concrete,where a large quantity of expansion produced before the formation of the elastic strength structure. Therefore,the self—stress did not exceed 10MPa on an average. This means that it is important to reform the traditional expansion mode for improving the self—stressing level.

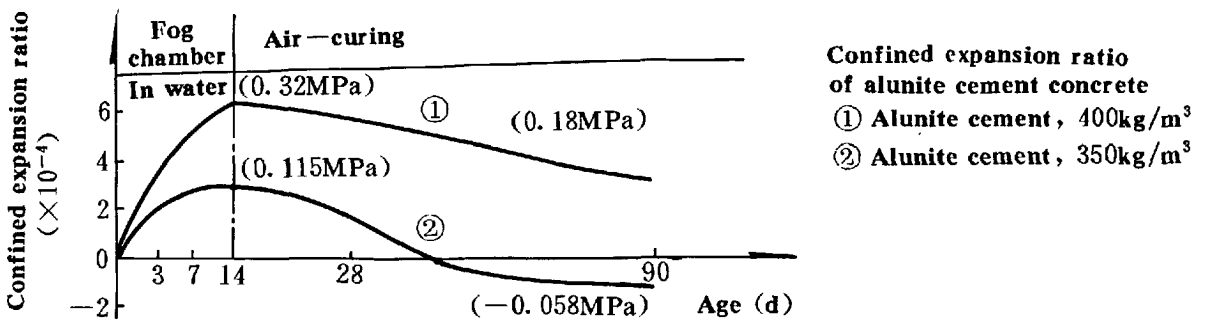

Fig 1 confined expansion ratio of alunite cement concrete

Delayed expansion mechanism and mode

The ettringite phase in the hardened cement paste will result in expansions which transform into self—stress,either because of the increase in volume of solid phase during the course of crystal growth,or because of the ion swelling by absorbing water only after the silicate phases have hydrated and the cement paste has a certain degree of strength. That is,the amount and rate of effective expansion depend on the amount and rate of the effective AFt formed after the formation of elastic strength structure. Therefore,the way to improve the self—stressing level of the confined expansion concrete is,in one hand,to improve its strength,especially the early strength,in the other hand,to restrict its expansive amount in the early age properly,so that the development of expansion and the improvement of strength as restricting factor can coordinate each other.

According to the analysis above,a new delayed expansion mechanism and mode are proposed in this paper. That is to allow maximal expansion of the confined expansion concrete to take place after the formation of the elastic strength structure. The quantity of AFt formation is restricted until the elastic strength structure of concrete founds,in order to reduce the invalid expansion energy as far as possible and to store the effective expansion energy as much as possible. The corresponding expansion mode is that the confined expansion ratio is restricted in the early age,rises up greatly in the middle age,and then goes down slightly and becomes steady in steps.

In order to reduce the expansion energy used for compacting concrete itself as far as possible,and to make more effective expansion energy form a strong active restricting force needed by high self—stress,the confined expansion concrete should possess the least porosity and the best strength in paste.

Physical and mechanical test of delayed expansion mechanism

The restricting condition of the specimen was offered by a steel tube of Φ88. 5mm×4mm ×164mm. The concrete core was mixed with 525 OPC, sand, gravel and water of 1 : 0. 46 : 1. 57 : 0. 4 proportion. Alunite expanding agent of low expansion and special water reducer were added. A combined temperature compensating strain gauge was embedded horizontally on the middle section of the concrete core, to test the variation of the confined expansion ratio of the concrete core in radial direction at different ages continually. The compressive strength of concrete at different ages was tested by six groups of 10mm ×10mm×10mm cubic specimen. The correspondent elastic modulus was obtained from the relation between the strength and the elastic modulus according to the concrete structure designing standard of China (GBJ10—89). The results are shown in Fig 2.

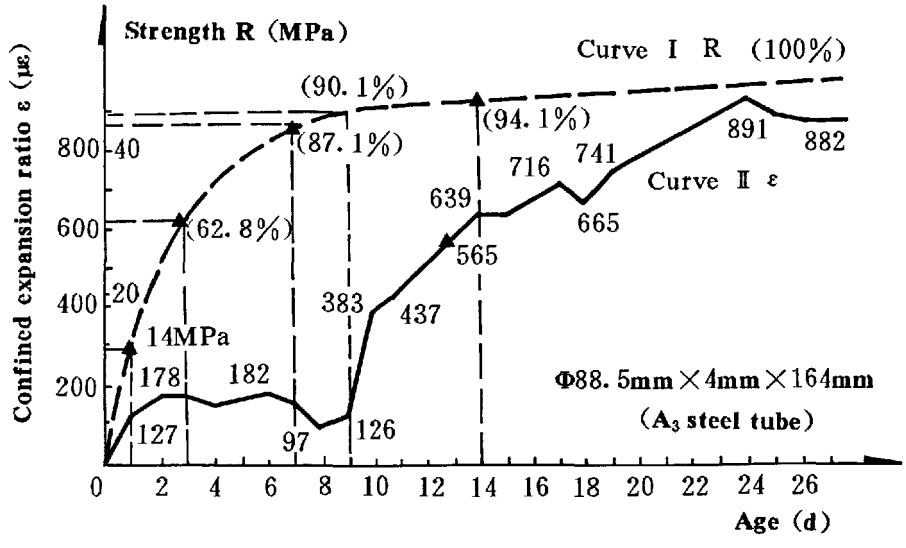

Fig 2 Mode of delayed expansion

It is shown that the strength of concrete reaches 14 MPa at age of 1 day when the self—stress has grown (curve I). In the early age (1～9 days) a low and flat area appears, which shows that the early expansion is restricted (curve Ⅱ). The strength of concrete at 9 days has increased quickly to 90. 1% of R28, and then the curve of the confined expansion ratio goes up rapidly, which shows that the confined expansive amount increases speedily and that there is a good coordination among the restricting factors, expansion and strength development. At age of 17 days, the confined expansion ratio is 716 με and the corresponding self—stressing level exceeds 21 MPa due to the delayed expansion (Gu, 1995).

Phase determination by QXDA, DSC and SEM

Two groups of cement pastes with same w/c ratio were made. For group A the condition of necessary mixing water was simulated, for group B the curing condition of keeping enough water supply. At the given ages, the content of AFt was determined by the quantitative X—ray diffraction analysis (QXDA). Whether the specimen contains the AFm was determined by the differential scanning calorimetry (DSC). The existing form of AFt and AFm on the pore wall of the sample section was observed by the scanning electron microscopy (SEM). The results are shown in Table 1 and Fig 3.

In the initial phase of hydration, the formation of AFt in group A is restricted, and then accelerated with the age. This is consistent with the development curve of concrete

strength with that of the confined expansion ratio. In addition, the formation of AFt is restricted before the formation of the elastic strength structure of concrete, while a certain amount of AFt crystals still grows after the foundation of the elastic strength structure, which indicates that the reduction of the invalid expansion energy in the early stage results in the later increase of the effective expansion energy stored in concrete, becoming the source of improving the self—stressing level.

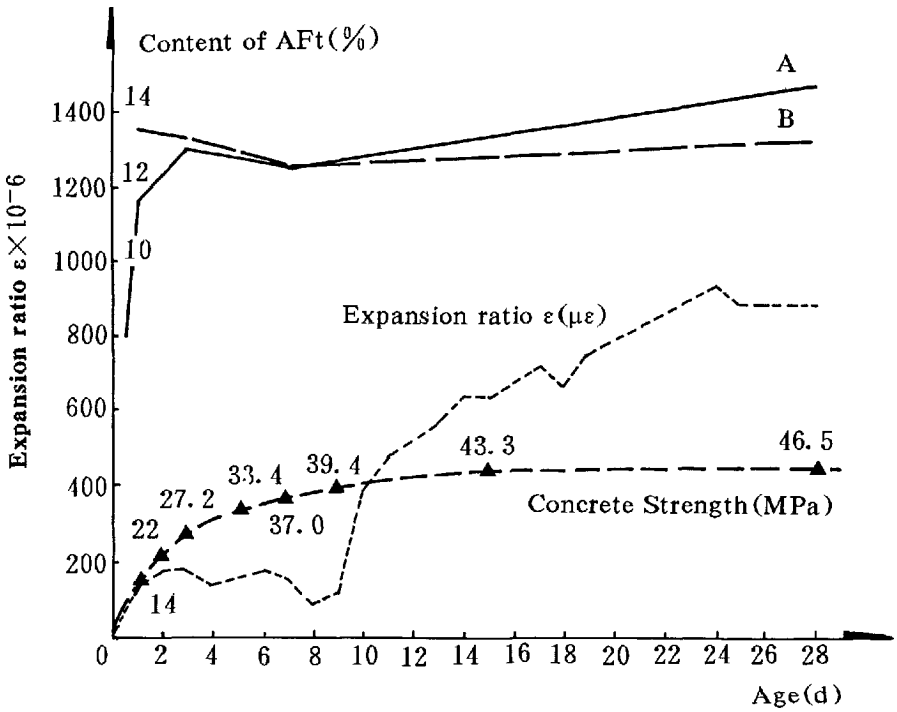

Fig 3 Curve of expansion, AFt formation and strength via ages

With group B, the amount of AFt reaches the maximum at 1 day, and then goes down slowly. It reflects that all AFt was formed during the stage when the strength structure is in the plastic and half—plastic state. Therefore, the invalid expansion energy at the early age is so big that the amount of the AFt can not increase after the elastic strength structure of concrete has formed. This essentially affects the magnitude of the later expansion energy and reduces the self—stressing level. If the amount of the mixing water is raised according to the traditional expansion mode, the formation of AFt will increase and the invalid expansion energy will increase in the early stage too, respondingly. Hence, it is difficult to improve the self—stressing level of the confined concrete made according to the traditional expansion mode.

It can be seen from the results of the SEM observation that only AFt crystals exist on the pore wall of the section of group A, while both AFt and AFm on that of group B.

The observation and analysis above prove that the mechanism of the delayed expansion is feasible, and that the corresponding mode is the only way to achieve the high self—stressing level of the confined expansion concrete.

Law of restricting concrete developing the high self—stress by delayed expansion

The self—stressing level of the confined expansion concrete is a measure of effective expansion energy stored in the expansion concrete under the confined conditions. Take the

example of the expansion concrete confined by steel tube into account. First, the expansion energy acts on the elastic strength structure of concrete, extruding the strength structure. The work can be transformed into the elastic recovering deformation energy of the elastic strength structure and be stored in concrete, when strength structure reaches a certain degree of strength (about 9.8 MPa), that is, when the structure changes from the plastic, half—plastic state to the elastic state. This will make concrete bear compression and become compact, compensating the microstructure defects of concrete itself. At the same time, the expansion energy acts on the steel tube and is transformed into its elastic recovering deformation energy, storing in the steel tube and acting on the concrete. Thus the concrete will be pressed further. Abiding by the delayed expansion mode, the expansion, the strength development of concrete and restricting factors can be coordinated, so that the process of storing energy above is accomplished effectively and the high self—stressing level is achieved.

The test proves that, when the inner expansive force acts on the steel tube, the stress relation on the inner and outer wall of the steel tube accords with the equation as follows:

Table 1 Phase determination by QXDA, DSC and SEM

Sample number		Content of AFt determined by QXDA, %	Existence of AFm tested by DSC	Existence of AFt and AFm observed by SEM *
Group A	C6h	8.1	none	AFt
	C1d	11.6	little	AFt
	C3d	13.0	little	AFt
	C7d	12.5	little	AFt
	C28d	14.6	little	AFt
Group B	W1d	13.5	none	AFt
	W3d	13.3	little	AFt+AFm
	W7d	12.6	little	AFt+AFm
	W28d	13.2	little	AFt+AFm

* Observed results on the pore wall of the sample section

$$P=\frac{2t\sigma_0}{D-t}=\frac{2TE\varepsilon_\theta}{D-t} \qquad [1]$$

Where P is radial expansive pressure (MPa); t is wall thickness of steel tube (mm); σ_0 is circular stress of steel tube (MPa); ε_θ is its circular strain; D is outside diametre of steel tube (mm); E is elastic modulus.

Therefore, given the circular strain of outer wall of steel tube measured by a resistance strain gauge, self—stress for extruding steel tube can be calculated from Eq[1]. In addition, using the embedded temperature compensating strain gauge, the confined expansion rate is measured directly continuously. Then total self—stress of concrete core is obtained by multiplying the measured strain and the elastic modulus according to its strength. The curve of confined expansion ratio via ages is shown in Fig 4. Considering the yielding of steel tube, we decrease the quantity of alunite expansive agent. Here we call the composite material as chemically prestressed concrete filled steel tube because its self—stressing level has the similar effect to mechanical prestress.

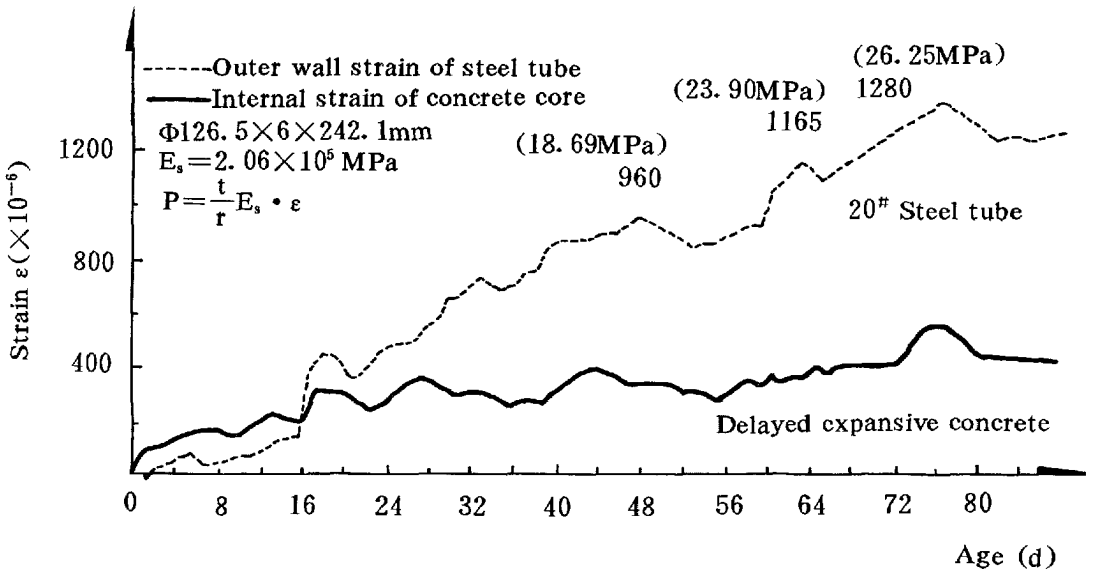

Fig 4 Curve of strain of chemically prestressed concrete filled steel tube via ages

Table 2 Self—stress value of concrete core at different ages

Classification	Age(d)			
	3	9	14	28
Internal strain of concrete ($x10^{-6}$)	97	136	190	344
Outer wall strain of steel tube ($x10^{-6}$)	26	66	133	582
Total self—stress of concrete core produced from effective expansion energy (MPa)	2.84	4.32	6.56	12.5
Self—stress for expanded steel tube (MPa) (fraction to total self—stress, %)	0.53 (18.7)	1.35 (31.2)	2.73 (41.6)	11.9 (95.2)
Self—stress for compacting concrete (MPa) (fraction to total self—stress, %)	2.31 (81.3)	2.97 (68.8)	3.83 (58.4)	0.6 (4.8)

It can be seen from Fig 4 that the curve of internal confined expansion ratio of concrete is above that of outer wall strain of steel tube before the two curves cross. It demonstrates that lower strength and elastic modulus make concrete core consolidate further. On the other side, the majority of expansion is restrained, the effective expansion energy produced is small and acts mainly on compacting concrete core itself. Furthermore, the elastic strength structure is developed gradually, and the expansion energy transmitted to steel tube is very small. As a result, it turns out that the internal strain of concrete is larger than outer wall strain of steel tube. After the two curves cross, a large amount of expansion occurs with the increasing of the consolidibility of concrete core and improving of the concrete strength structure. Therefore, more effective expansion energy is transformed into elastic deformation energy through the strength structure and then acts on steel tube while that used for self—compacting decreases. Meanwhile, the outer wall strain of steel tube increases rapidly. The increase of the internal strain of concrete is

slower than the outer wall strain of steel tube,but the self—stress of concrete grows still faster because its elastic modulus increases accordingly.

Table 2 shows the results calculated from the experimental data which fits the tendency of the strain curve,the total self—stress of concrete at 28 days is near the confining force of steel tube. In addition,the maximal self—stressing value more than 21 MPa occurs not at 28 days.

Table 3 Mechanical properties of chemically prestressed concrete filled steel tube

Specimen number	Ultimate elastic load (kN)	Ultimate yield load (kN)	Increase of ultimate elastic load (%)	Increase of ultimate elastic yield (%)
A_{21}	900	1100	73	29
A_{22}	900	1164	73	37
A_{23}	914	1200	76	41
A_{24}	890	1100	71	29
A_{25}	870	1010	67	19
A_{20}	520	850	0	0

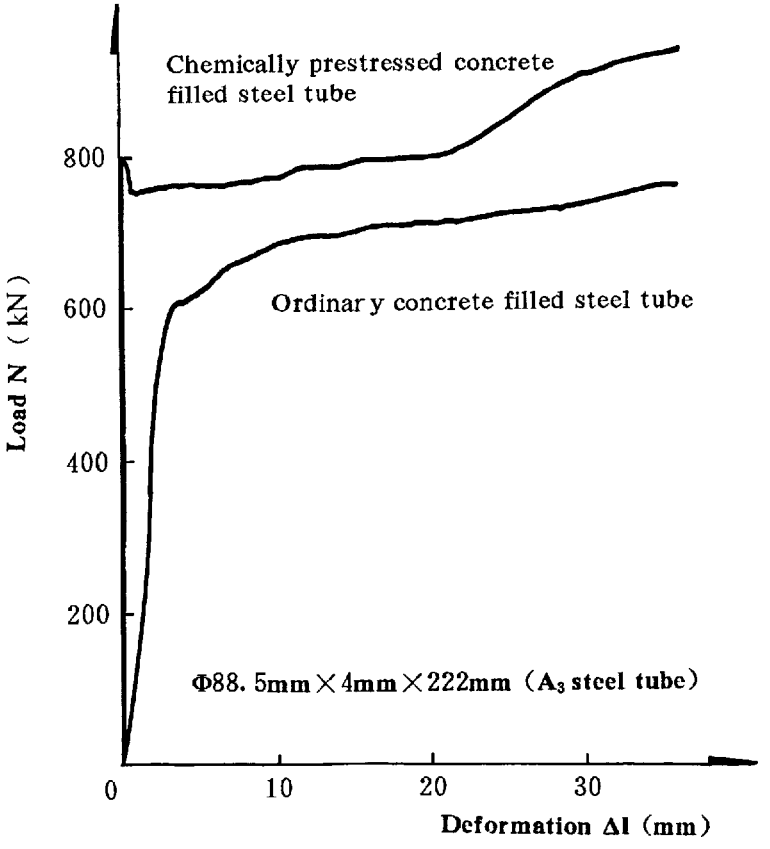

Fig 5 Curve of load—deformation of chemically prestressed concrete and ordinary concrete filled steel tube

Axial compressive test of chemically prestressed concrete filled steel tube

Table 3 gives the test results on the mechanical properties of delayed expansion on chemically prestressed concrete filled steel tube with 5 different dosages of expansive agent. Here a steel tube of Φ126. 5mm×6mm×241. 8mm (20#), was used as limiting condition. Of the specimen numbers, A_{20} is for the ordinary concrete filled steel tube. Compared to that, the property of chemically prestressed concrete filled steel tube at 28 days is a lot better.

Fig 5 shows the curve of load—deformation for chemically prestressed concrete filled steel tube and corresponding ordinary concrete filled steel tube at 60 days prepared by a same kind of cement. Strengthened under high self—stressing level, the chemically prestressed concrete filled steel tube has turned into strengthened elastic—plastic body with typical behavior of triaxial stress concrete of large bearing capacity and small deformation.

CONCLUSION

The mechanism of delayed expansion presented in this paper believes that the high self—stressing level can be obtained only when a large amount of expansion occurs after the establishment of elastic strength structure of concrete. It is proved that the mechanism can be not only put into practice, but also applied to all kinks of confined expansive concretes and make them as high self—stressing materials. Meanwhile, the matching between limiting conditions and maximal expansion should be taken into account in application.

The self—stress value of concrete core of chemically prestressed concrete filled steel tube, which is prepared by applying the mechanism of delayed expansion, is more than 21 MPa and its self—stressing level effects similarly as mechanical prestress. Compared to the corresponding ordinary concrete filled steel tube, the chemically prestressed concretes with 5 different dosages of the expansive agent used here at 28 days increase 72% of ultimate elastic load capacity and 31% of ultimate yield load capacity on an average.

The mode of delayed expansion can restrain the growth of AFt crystals before the establishment of elastic strength structure of concrete. According to this mode, the time and rate of AFt formation and the development of concrete strength can match each other, which allow to produce a large amount of effective expansion energy and then lead to high self—stressing level.

REFERENCES

Wu Zhongwei, "Expansive Concrete". China Railway Publishing House, Beijing, China, 1990, pp. 89—90, 164—165

Gu Ganshen, "Mechanism of Delayed Expansion for Confined Expansion Concrete and Its Practical Significance", Proceedings of the International Symposium, "New Development in Concrete Science and Technology". Nanjing, China, 1995, pp. 1017—1022

EXPANSIVE BEHAVIOR OF SLAG CEMENT WITH EXPANSIVE ADDITIVES

Atsumu ISHIDA, Minoru MORIOKA, Toshio MIHARA and Hirotoshi HAGIWARA
Cement & Special Cement Additive Laboratory, Denki Kagaku Kogyo Co., Ltd., Japan

ABSTRACT Expansive behavior of slag cement with expansive additives was investigated. Length change of slag cement with a new expansive additive was about three times larger than that with conventional type-K or type-O additive. Heat evolution curve of slag cement altered with the additives, which seemed to be reflecting the change of reaction behavior between slag and additives. Formation and morphology of calcium hydroxide and conversion rate of ettringite to monosulphate differed depending on the kinds of additives, suggesting that different expansive behavior took place.

Key-words: Additives, Expansion, Blastfurnace slag,

INTRODUCTION

Recently, the preservation of natural environment is strongly advocated, and is an important matter in the staple industries. In cement industry, a blended cement is one of the answer to the above statement. Blended cements are concerned with utilization of industrial wastes and reduction of CO_2 gas generated by the burning process of cement clinker, eventually decreasing overall energy consumption. Blastfurnace slag (BFS hereafter), pulverized fuel ash and microsilica, which are classified into pozzolanic materials, are well-known inorganic materials used in blended cements. In Japan, the amount of blended cements has increased up to 20% of total cement production in recent years.

With increasing use of blended cements, various additives, such as accelerators, water reducers and superplasticizers are applied to blended cements. An expansive additive is one of the widely known additive and is used to compensate a shrinkage of concrete or to produce self-stressing concrete. Two types of expansive additives are now placed on the market in Japan. One is type-K (ACI 223R-90, 1992) which contains hauyne as an essential ingredient, and the other is type-O (Neville, 1994) with free lime as an expansive ingredient. As ettringite and calcium hydroxide (CH hereafter) are considered to be the major expansive ingredients, their formation and morphology are important factors in producing expansion. At present, stress generated by the crystal growth or by swelling of colloidal form of the expansive ingredients are the most widely accepted mechanism for expansive behavior.

In applying expansive additives to blended cements, however, it has been pointed out that conventional expansive additives reduce their expansive activity when combined with blended cements (Tsuji et al, 1979, Mehta, 1995 and Min et al, 1995). Under such circumstances, present authors have developed a new expansive additive consisting of hauyne, anhydrite and high content of free lime, with improved expansive activity when applied to blended cements (Ishida et al, 1996).

In this paper, expansive properties of the new additive are reported compared with those of conventional type-K and type-O additives. As main expansive ingredients are CH and ettringite, studies of hydrates are focused on these two components.

EXPERIMENTAL

Materials

Commercially available BFS and ordinary Portland cement (OPC hereafter) were mixed by four

to six by weight to prepare slag cement (BFSC for blastfurnace slag cement, hereafter) used in the experiments. Three kinds of expansive additives, (A) new product, (B) type-K and (C) type-O were employed in the experiments. Their chemical composition and physical properties are shown in Table 1, along with OPC and BFS. In preparing mortar, ISO standard sand was used as an aggregate.

Table 1 Chemical composition and physical properties of expansive additives (A, B, C), ordinary Portland cement (OPC) and blastfurnace slag (BFS).

	ig-loss	SiO_2	Al_2O_3	CaO	SO_3	f-CaO	blaine (cm^2/g)	density (g/cm^3)
A	0.7	0.5	10.5	68.6	18.7	49.0	3200	3.03
B	1.8	1.5	14.5	51.7	28.3	19.8	3300	2.86
C	3.5	8.4	2.4	67.4	15.6	30.9	4100	2.99
OPC	1.9	20.8	4.7	64.7	2.0	-	3340	3.16
BFS	0	33.9	14.3	42.5	-	-	4070	2.91

A; new product, B; type-K, C; type-O

Preparation of specimens

Specimens were made of mortar and paste, with water/cement ratio of 50%, and as for mortar, cement/sand ratio was 1/2. BFSC or OPC was replaced by expansive additives. Replacement ratio was set to 8 or 10 wt% in mortar, and 10 wt% in paste. Specimens of mortar were cast in 4x4x16 cm and cured under condition of 20°C and 80% RH for the first 24 hours, and then in water of 20°C for the next six days, and finally at 20°C and 60% RH. Each set of mortar consisted of three specimens. Pastes were stored and cured in closed vessels at 20°C.

Evaluation

Compressive strength and expansive behavior of mortar were measured for different period of curing time from one day to 28 days, according to JIS R 5201 and JIS A6202, respectively.
The following procedure was employed to study paste specimens hydrated for different period of curing time. The paste specimens were crushed and lightly ground in a porcelain mortar with excess acetone in order to stop the process of hydration. The resulting suspensions were filtered and dried at 40°C for one day. In succession, X-ray diffraction (XRD) method and differential scanning calorimetry (DSC) were conducted to evaluate the hydrates, such as CH, ettringite and monosulphate. Microstructure of paste specimens was observed by scanning electron microscopy (SEM), and pore size distribution was measured by mercury intrusion porosimeter. Additionally, heat evolution curve of pastes was measured by conduction calorimeter.

RESULTS AND DISCUSSION

Expansive behavior

Figure 1 shows the length change of mortar with different expansive additives as a function of age. 10 wt% of BFSC or OPC was replaced by each expansive additives. As shown in the figure, length change of mortar with additive-A is about three times larger than that with additive-B or -C in both cements. Comparing the two cements, length change of mortar with BFSC is lower than that with OPC, except for mortar with additive-C which shows nearly the same length change for both cements. In mortar with additive-A, large difference of length change was observed from age of one day to two days in the two cements.

The reason for low expansive activity due to replacement of OPC by BFS may be considered as follows. As the major expansive ingredients are considered to be ettringite and CH, two reasons are considered. One is the acceleration of conversion of ettringite to monosulphate due to the existence of BFS. The other is the reduction of CH formation. Concerning CH formation, BFS will decrease the concentration of OH^- ions in the pore solutions, as is generally accepted, thus lowering the supersaturation of pore solution of cement paste with respect to CH and partly inhibiting in-situ formation of CH crystals (Min et al, 1995). The experimental results are shown and discussed later concerning the two expansive ingredients.

Some papers have discussed " autogenous shrinkage", that BFSC paste shows larger autogenous shrinkage than OPC paste (Tazawa and Miyazawa, 1992 and Tazawa, 1994). In this study, the influence of autogenous shrinkage on expansive behavior is not unambiguous, and further investigation should be undertaken to clarify the relationship between the mechanisms of autogenous shrinkage and expansive behavior.

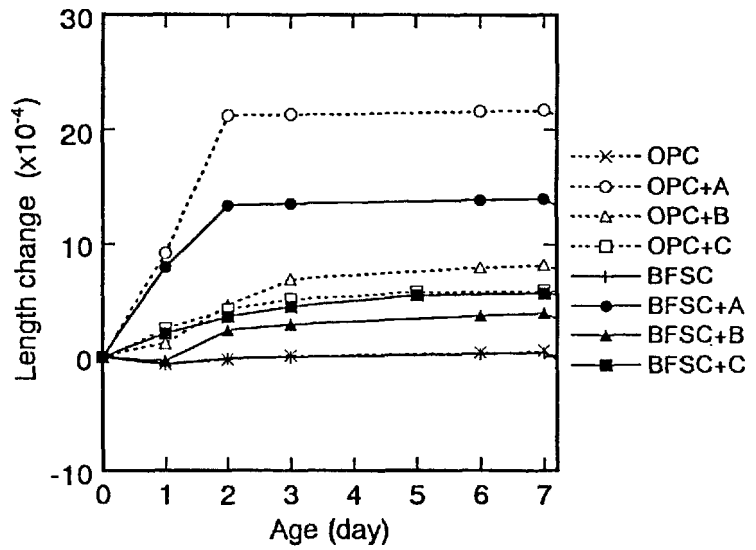

Figure 1 Length change of mortar as a function of age. additive replacement; 10wt%

Mechanical strength

Compressive strength of mortar as a function of age is shown in Fig 2. In both cements, significant loss of compressive strength was not observed by adding expansive additives with replacement ratio of 8 wt%. The exception is for mortar consisting of OPC and additive-A within age of 7 days. While mortars with BFSC resulted in lower compressive strength than that with OPC within age of 7 days, all mortars regardless of cement or additive, resulted in compressive strength of the same level after 28 days.

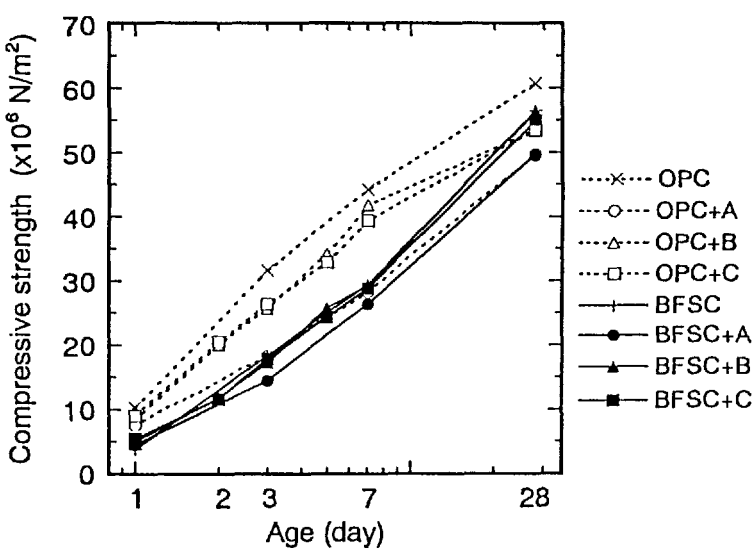

Figure 2 Compressive strength of mortar as a function of age. additive replacement; 8wt%

Heat evolution curve

Figures 3 and 4 show the heat evolution curve of pastes with OPC and BFSC containing 10 wt% of expansive additives. Comparing the exothermic peaks around 10 hours, the peaks of BFSC pastes were about 20% lower than that with OPC pastes.

While OPC pastes with and without expansive additives resulted in nearly the same heat evolution curves, additional exothermic peak was observed at around 30 hours in BFSC pastes with expansive additives. The additional exothermic peak was observed at around 25 hours in case of BFSC paste with additive-A. On the other hand, the additional exothermic peaks in BFSC pastes with additive-B and -C were observed at around 30 to 35 hours with lower heat evolution compared with that with additive-A. The additional exothermic peak suggests the reaction between the expansive additives and the BFS. The reaction between the expansive additives and BFS was confirmed by method using salicylic acid and acetone-methanol solution reported by Kondo et al (1969).

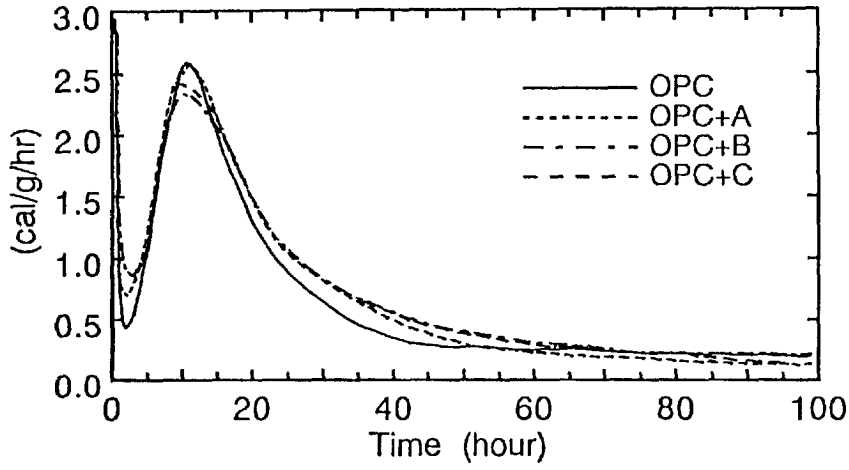

Figure 3 Heat evolution curve of pastes with OPC. additive replacement; 10wt%, W/C=60%, Temp.=20$_o$C

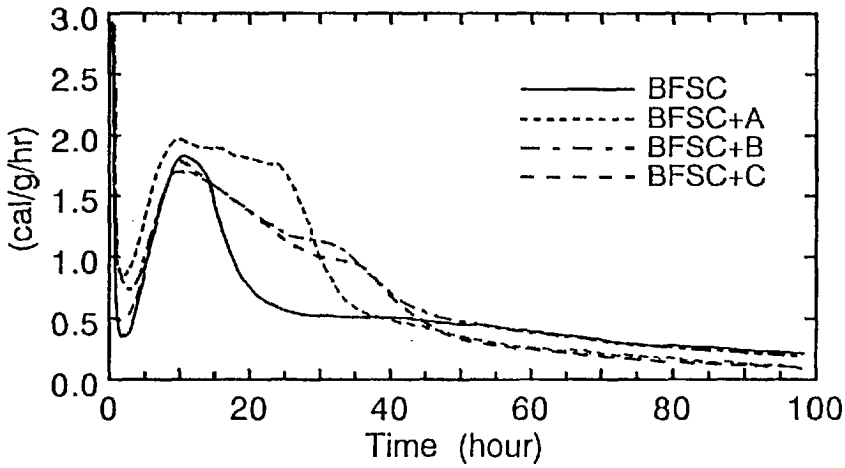

Figure 4 Heat evolution curve of pastes with BFSC. additive replacement; 10wt%, W/C=60, Temp.=20$_o$C

Composition and quantity of hydrates

Calcium hydroxide

Figure 5 shows the change of CH by DSC measurement as a function of age. DSC measurement has a feature of evaluating both crystalline and amorphous forms together, while XRD evaluate only the crystalline form. Comparing the cements, BFSC pastes have lower CH content than that of OPC pastes.

Comparing the expansive additives, pastes with additive of high free lime content (additive-A and -C) have higher CH content than that without additive, and pastes with additive of low free lime content (additive-B) have lower CH content. Although a total amount of CH during hydration from 1 day to 7 days is nearly the same between additive-A and -C, the expansive behavior is quite different as seen in Fig 1. As a conclusion, CH content by DSC measurement

does not show one-to-one correspondence with expansive behavior concerning expansive additives.

In XRD measurement, crystal morphology of crystalline CH was investigated. Figure 6 shows the change of (110)/(001) ratio of CH as a function of age. The ratio of paste with additive-A increases during the age from 1 day to 3 days. As the change of the ratio reflects the change of morphology in crystalline CH, large length change of mortar with additive-A may be related to the change of morphology of the hydrate.

Crystal shape of CH is reported to be influenced by co-existing additives, curing temperature and water/solid ratio (Berger and McGregor, 1973). In case when additive-A, containing 50% free lime, is employed in the system, relatively high degree of supersaturation is presumably maintained in pore solutions with respect to CH. Thus a width/thickness ratio of crystalline CH should be larger compared to the case when additive-B or -C is employed. It seems probable that the difference of crystal shape reflect the degree of supersaturation of pore solutions, and the development of expansive force is correlated to the degree of supersaturation of pore solutions.

At present, the mechanism most widely accepted for expansive behavior is based on the crystal growth pressure or swelling pressure of colloidal form of expansive ingredient (Min et al, 1995). Regarding additive-A or -C, it is conceivable that free lime first forms colloidal CH in supersaturated pore solutions of cement paste and subsequently these colloidal crystallites recrystallize or grow to macro-crystals. The size of very fine crystals of CH is reported as between 10 and 20 nm (Chatterji, 1995). Further study is needed to clarify the relation between the morphology of CH and the expansive behavior.

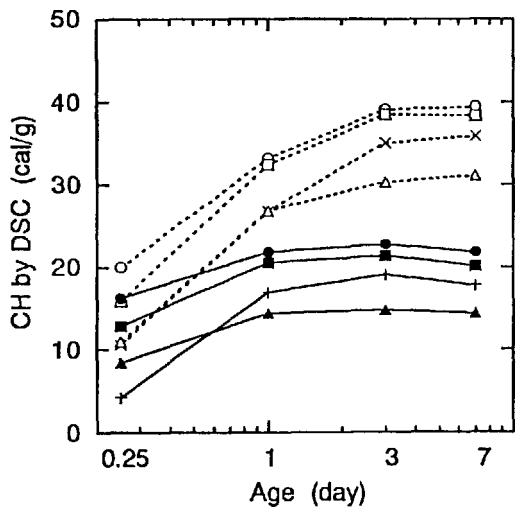

Figure 5 Change of CH in pastes by DSC measurement as a function of age. additive replacement; 10wt%

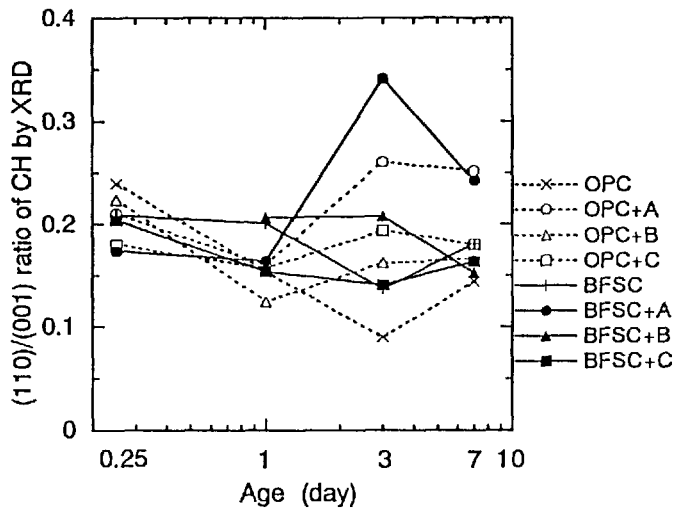

Figure 6 Change of (110)/(001) ratio of CH in pastes by XRD measurement as a function of age. additive replacement; 10wt%

Ettringite and monosulphate

Amount of ettringite and monosulphate measured by DSC as a function of age are shown in Figs 7, 8, 9 and 10, respectively. While BFSC pastes with expansive additives show decrease of ettringite and formation of monosulphate after age of one day, OPC pastes with expansive additives show gradual increase of ettringite with age and no monosulphate is observed within 3 days. Low expansive behavior of mortar with BFSC seems to be partly explained by conversion of ettringite to monosulphate. Furthermore, pastes with expansive additives resulted in higher content of ettringite than that without additive, and among these pastes, paste containing

additive-B which has high hauyne content showed higher ettringite content than other pastes. As seen in Fig 7, at age of 6 hours (0.25 day), higher content of ettringite is observed in paste with additives containing hauyne (additive-A and -B) compared with paste without additive or paste with additive-C.

Remaining peaks of additives were also evaluated in XRD measurements. While XRD peak of free lime was not observed within 6 hours in every paste, hauyne and anhydrite remained in pastes after 6 hours. In paste containing additive-B with high hauyne content, hauyne was observed within 1 day after the hydration started. The high content of ettringite at age of 1 day in paste with additive-B may be related with the remaining hauyne.

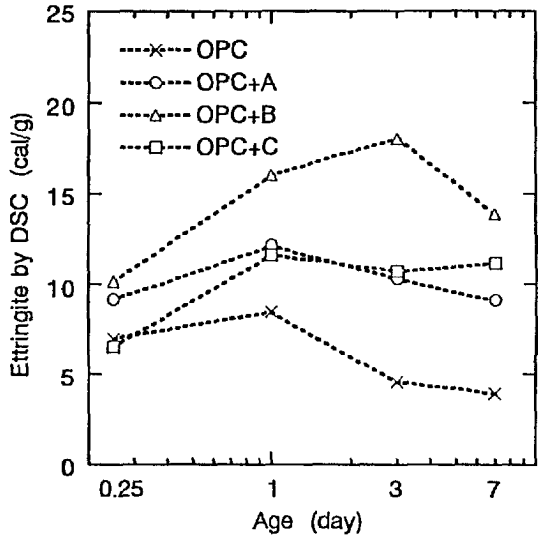

Figure 7 Change of ettringite in pastes by DSC measurement as a function of age. additive replacement; 10wt%

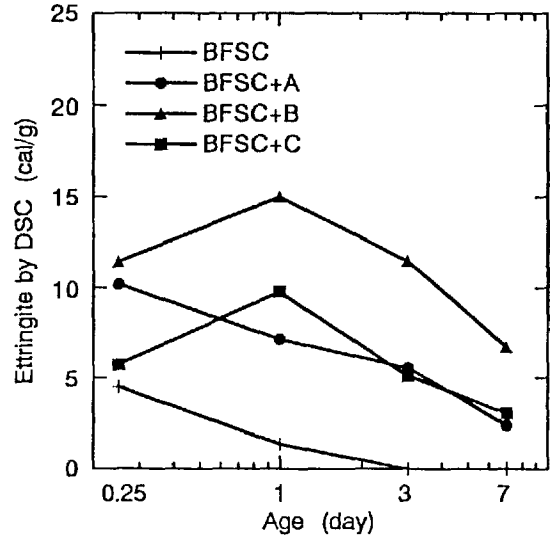

Figure 8 Change of ettringite in pastes by DSC measurement as a function of age. additive replacement; 10wt%

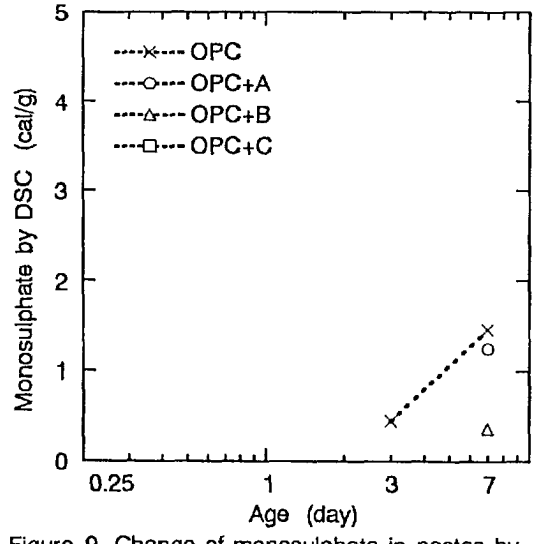

Figure 9 Change of monosulphate in pastes by DSC measurement as a function of age. additive replacement; 10wt%

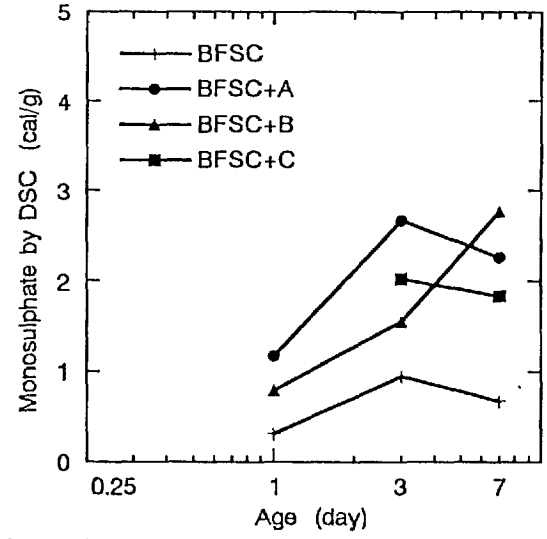

Figure 10 Change of monosulphate in pastes by DSC measurement as a function of age. additive replacement; 10wt%

Microstructure

Figure 11 shows SEM observations of the pastes at age of 3 days. While few needle-shaped hydrates were observed in BFSC pastes with additives, needle-shaped hydrates of several

micron in length, which seems to be ettringite, were clearly observed in OPC pastes with expansive additives. Sharp platelet hydrates of submicron size, which seems to be monosulphate, were observed in pastes with additive-B in BFSC. These observations are in good agreement with the evaluation of ettringite and monosulphate by XRD and DSC measurements.

Change of pore size distribution of hardened BFSC paste specimens with age are shown in Fig 12. The samples were prepared and cured under unrestrained condition. In paste with high length change, namely BFSC paste with 10 wt % of additive-A (BFSC+A), high portion of pores from 1000 to 20000 nm, and high total pore volume were still measured at age of 7 days. On the other hand, in pastes with low length change, namely BFSC paste with 10 wt% of additive-B and -C (BFSC+B and BFSC+C), decrease of total pore volume and pores over 100 nm, along with increase of pores under 100 nm were measured within 7 days. This phenomenon may be explained by the aggregates of colloidal CH in pore solution of (BFSC+ A).

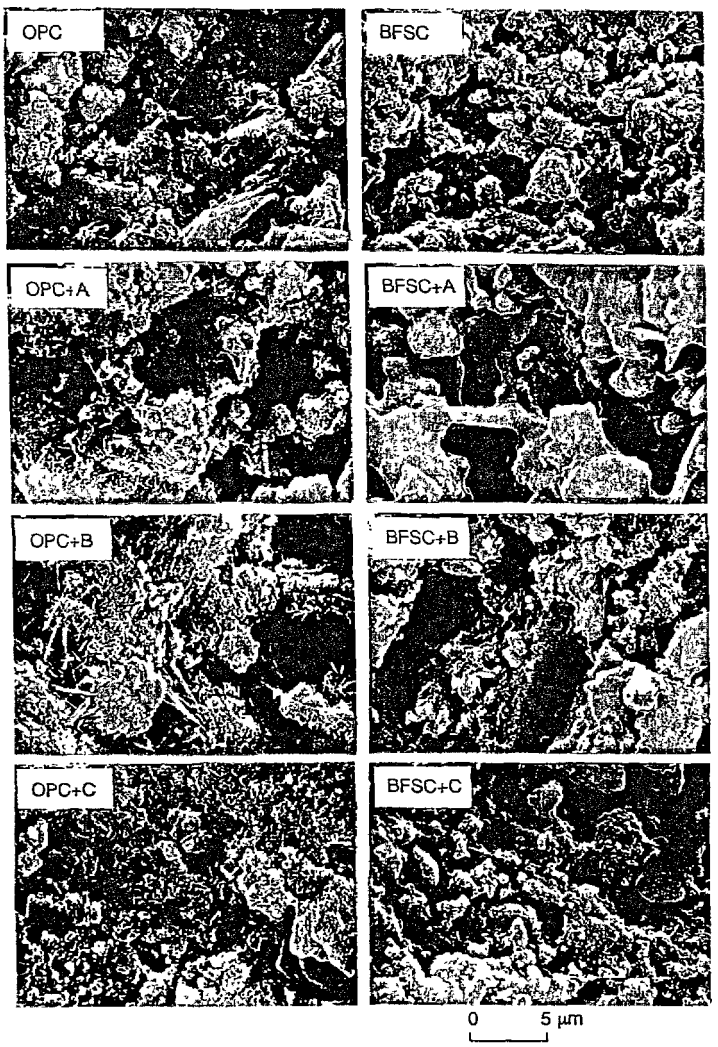

Figure 11 SEM observation of pastes at age of 3 days.

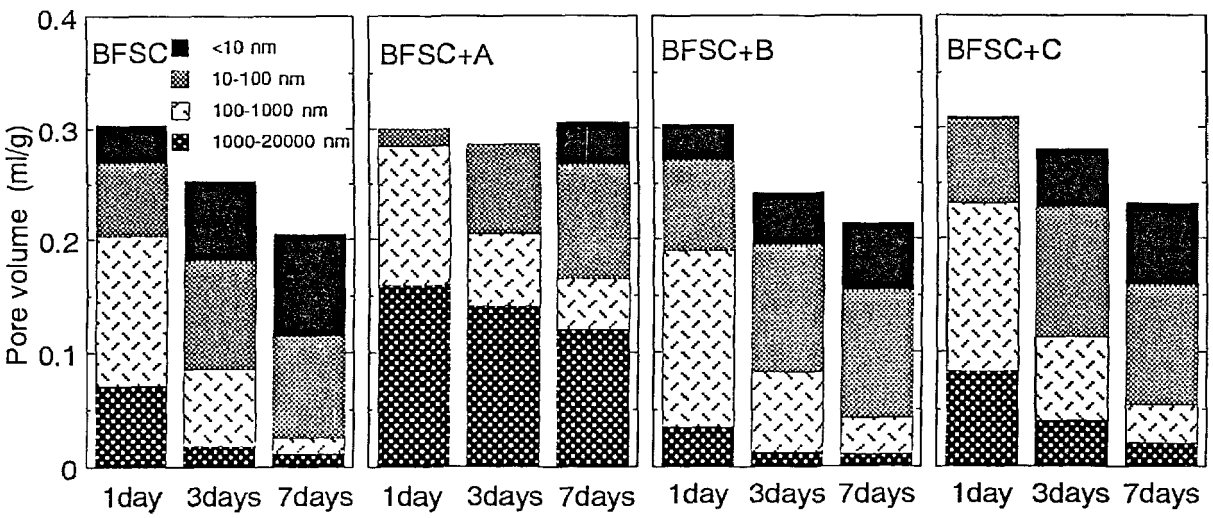

Figure 12 Change of pore volume in pastes as a function of age.

CONCLUSIONS

(1) Large expansion was achieved concerning the new expansive additive which consists of hauyne, anhydrite and free lime, when it was applied to OPC or to BFSC which contains 40 wt% of BFS.

(2) The new expansive additive manifests no harmful effect on strength development of cement matrix, which is similar to the conventional additives.

(3) Low expansion of BFSC paste with conventional type-K additive is considered as a result of high conversion rate of ettringite to monosulphate, and less amount of CH.

(4) The difference of expansive behavior between type-O and the new additive is suggested by the difference of crystal morphology of CH.

REFERENCES

ACI 223R-90, "Standard Practice for the Use of Shrinkage-Compensating Concrete," *ACI Manual of Concrete Practice*, Part 1, 26 (1992)

Berger, R. L. and McGregor, J. D., "Effect of Temperature and Water-Solid Ratio on Growth of Ca(OH)2 Crystals Formed During Hydration of Ca3SiO5," *J. Am. Ceram. Soc.*, **56** [2], 73-79 (1973)

Chatterji, S., "Mechanism of Expansion of Concrete Due to the Presence of Dead-Burnt CaO and MgO," *Cement and Concrete Research*, **25** [1], 51-56 (1995)

Ishida, A., Morioka, M., Mihara, T., and Yamada, H., "Expansion and Hydration Behavior of Slag Cement with Expansive Admixtures," *Proceedings of 50th Semento Gijyutsu Taikai (Japan)*, 56-57 (1996)

Kondo, R. and Ohsawa, S., "Studies on a Method to Determine the Amount of Granulated Blastfurnace Slag and the Rate of Hydration of Slag in Cement," *Yogyo-Kyoukai-Shi*, **77** [2], 39-46 (1969)

Mehta, P. K., "Mechanism of Expansion Associated with Ettringite Formation," *Cement and Concrete Research*, **3** [1], 1-6 (1973)

Min, D., Dongwen, H., Xianghui, L., and Mingshu, T., "Mechanism of Expansion in Hardened Cement Pastes with Hard-Burnt Free Lime," *Cement and Concrete Research*, **25** [2], 440-448 (1995)

Neville, A., "Whither Expansive Cement?," *Concrete International*, **16** [9] 34-35 (1994)

Tazawa, E., "Autogenous Shrinkage of Cement Paste Caused by Hydration," *Cement & Concrete*, **565**, 35-44 (1994)

Tazawa, E. and Miyazawa, S., "Autogenous Shrinkage Caused by Self Desiccation in Cementitious Material," *9th International Congress on the Chemistry of Cement (New Delhi)*, IV, 712 (1992)

Tsuji, Y. and Kawamura, I., "Expansion Characteristics of Expansive Concrete Using Pulverized Blast-Furnace Slag," *Semento Gijyutsu Nenpou*, **33**, 189 (1979)

MECHANISMS OF SHRINKAGE REDUCTION USING A CHEMICAL ADMIXTURE

Hua AI and J. Francis YOUNG Center for Cement Composite Materials, University of Illinois at Urbana-Champaign, Urbana, IL 61801

ABSTRACT Recently a chemical admixture was developed that reduces drying shrinkage of Portland cement paste by about 30%. The origins of this shrinkage reduction were investigated by studying changes associated with the admixture. Microstructure characterizations such as XRD, MIP, and N_2 adsorption were conducted and shrinkage-weight loss curves were also examined. It was concluded that a change in the surface tension of the pore liquid is the most likely cause of the shrinkage reduction.

Key-words: Admixtures, drying, pore structure, shrinkage

INTRODUCTION

The volume change of hardened Portland cement paste caused by moisture loss has significant effect on the service of concrete structures. Designs must allow for dimensional change caused by drying in order to minimize the stress generated by the external constrains. Shrinkage is a paste property, which is internally restrained by aggregate in concrete (Mindess and Young, 1981). The drying shrinkage behavior of hardened cement paste depends on parameters such as w/c ratio, the age of the paste, curing conditions, cement composition, the drying condition, and the addition of admixtures (Mindess and Young, 1981). These factors determine the microstructure of hardened cement paste and the state of moisture within the paste, which in turn determines the drying shrinkage characteristics of the paste [(Young et al., 1978; Bentur et al., 1980). The pore size distribution and C-S-H characteristics are the primary factors affecting drying shrinkage of pastes.

Many admixtures conventionally used in concrete have shown to have the effect of increasing the drying shrinkage through various mechanisms (Feldman and Swenson, 1975; Young et al., 1978; Bentur et al., 1980). However, a chemical admixture (Eclipse™) was recently developed that reduces drying shrinkage of concrete by about 30% on first drying. The purpose of this investigation is to study the effects of the chemical admixture on the microstructure of hydrated cement and the hydration chemistry, its effect on the shrinkage behavior of cement paste, and identify the origins of this shrinkage reduction.

EXPERIMENTAL PROCEDURES

Sample Preparation

Type I, white Portland cement from Lehigh Portland Cement Co. was used for all sample preparation throughout this investigation. The active ingredient of the shrinkage reducing admixture Eclipse™, designated DPTB, was obtained from ARCO Chemical Company. All samples were prepared at a water to cement ratio of 0.4. The admixture (2 wt% DPTB by the weight of cement) was dissolved in deionized water and mixed with cement powder in a Hobart mixer for 10 minutes. The slurry was then degassed by vibrating under vacuum for 1 min. to eliminate entrapped air bubbles, followed by casting.

Two types of specimens were cast for the purpose of different measurements. For drying shrinkage measurement, thin slabs of 2 mm x 20 mm x 100 mm in dimensions were used. Specimens were cast individually into Plexiglas molds, stored in 100% rh environment at room temperature, demolded after 24 hours and cured in saturated lime water for 1 or 10 days before the shrinkage measurements. Companion samples were also made for microstructure characterizations. They were cast as small cylinders in plastic vials (12.5 mm dia. x 50 mm ht.) and cured at 100% rh. The curing conditions were 1-day, 3-day, 7-day, and 28-day at room temperature.

Shrinkage and Weight Loss Measurements

The thin slabs specimens were used for drying shrinkage measurement and simultaneous weight change due to water loss. Previous experience and reports in literature have shown that

the choice of thin specimens is important in maintaining an equilibrium state of moisture content inside the specimens (Hansen, 1982; Hwang and Young, 1984). Specimens were dried in sealed desiccators maintained at 48% rh, over saturated KNO_2 solution. The length and weight of each specimen were monitored during the course of drying. Micrometer calipers with a resolution of 0.0025mm were used to measure the length of each sample, and an electronic analytical balance with a resolution of 0.0001g was used for weight measurements. Every data point is the average of three replicated measurements.

Qualitative X-ray Diffraction Measurements

At the end of curing period, part of a cylindrical specimen was crushed by hand into a fine powder passing #100 sieve, then immediately put in 105 °C oven to be dried for 48 hours. A Rigaku x-ray powder diffractometer (model D-max II) was used to perform qualitative powder XRD. The measurements used Cu (K_α) radiation, at a scanning speed of 1° 2θ/min., and scanning range from 5° to 65° of 2θ. Ten scans were collected and added together for each spectrum. Powder samples were packed from the back of sample holder to minimize preferred orientations of particles.

Microstructural Characterization

Small pieces (approximately 3-6 mm in dimensions) crushed from a cylindrical specimen were selected for the measurements. A solvent exchange procedure was used to replace pore water with methanol in order to minimize the stress on the solid network induced by drying procedure necessary for this technique. Samples were immersed in methanol for 14 days, with the solvent replaced every 1-3 day. Methanol-exchanged samples were dried at 105 °C in oven for 48 hours prior to testing.

Nitrogen adsorption measurements were carried out using an automated Micromeritics adsorption apparatus (model ASAP 2400). Data were taken on both the adsorption and desorption loop. Surface area was determined by BET analysis of adsorption data, and pore size distribution calculated using the BJH analysis based on Kelvin adsorption theory. The presence of micropores was assessed from v-t plots.

Mercury Intrusion Porosimetry (MIP) Measurements were conducted with the Micrometric Autopore II 9220 using 5cc penetrometers. The maximum intrusion pressure used in the experiment was 415 MPa.

Adsorption of Admixture By Cement

This experiment was designed to examine the possibility of DPTB adsorbing onto the solid surface of cementitious materials. Both unhydrated white cement and the powder made from materials hydrated for 28-day were mixed with DPTB water solution (~0.2 wt% in concentration) at a water to solid ratio of 10 (by weight). At this w/s ratio, the total DPTB available to solid is 2g of DPTB corresponding to 100g of cementitious materials, which is the admixture proportion in the paste.

For up to three days, portions of slurry were taken out of the mixture periodically and filtered to collect liquid for up to three days. The concentration of admixture DPTB in the liquid was analyzed by gas chromatography.

RESULTS

The Drying Shrinkage Characteristics

Figure 1 shows the weight change and drying shrinkage as functions of drying time for admixture added specimens and control. (Three replicates were run for each specimen). The specimens containing DPTB showed more weight change (and hence higher water loss) than control samples after drying for the same length of time. Rapid water loss occurs up to about 50 hours and then gradually slows, although considerable weight change was still observed after 300 hours. In the control samples, rate of the water loss slowed down considerably after the first 20 hours, and an nearly constant weight was reached at around 300 hours.

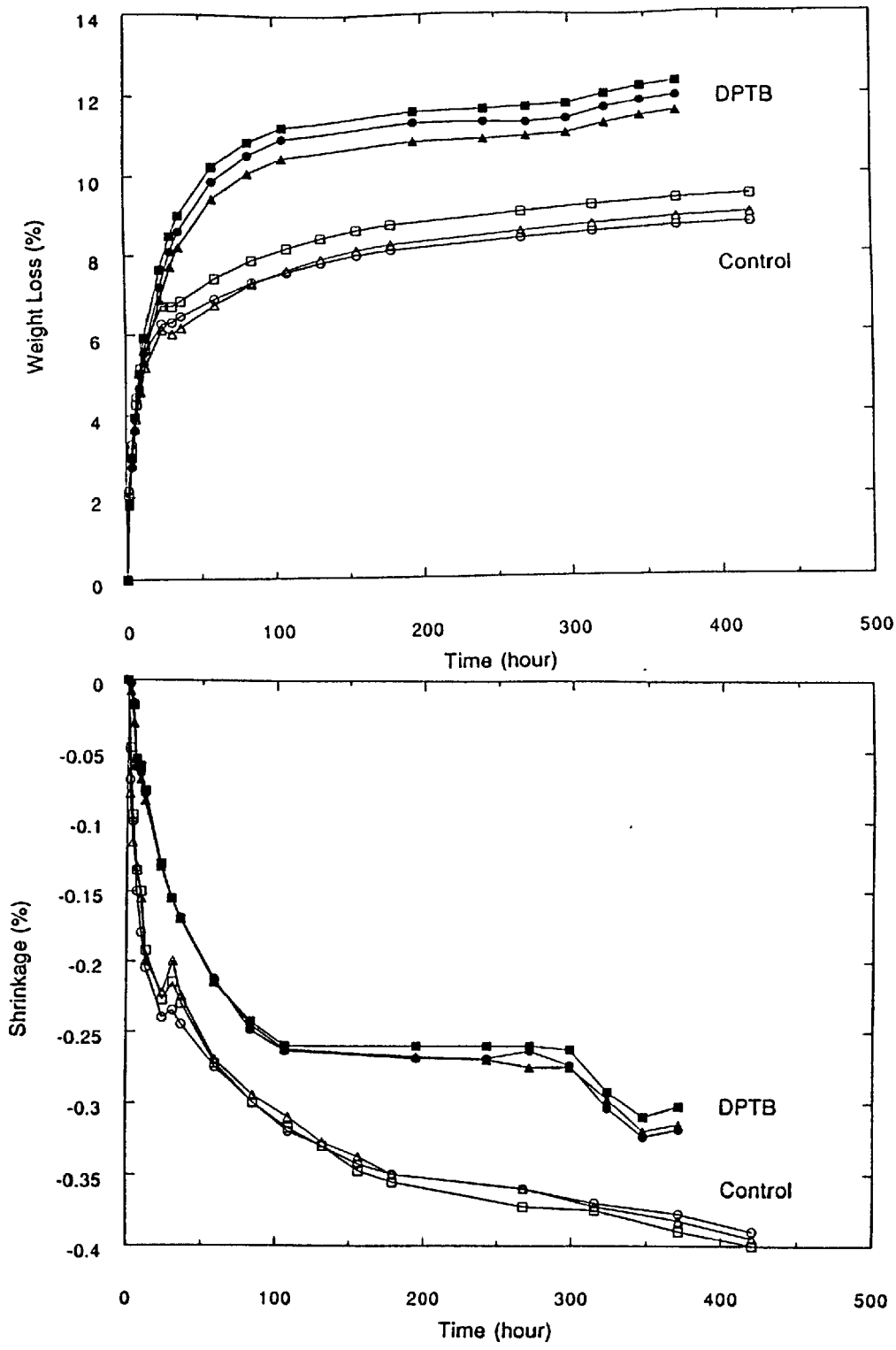

Figure 1. Effect of DPTB on drying of cement paste: a) drying shrinkage v. time; b) weight loss v. time. (10 day old sample).

However the higher water loss in the samples with admixture did not translate into greater drying shrinkage; on the contrary the magnitude of their drying shrinkage is smaller than that of control samples. The rate of length change for the control is greater at all ages. A plot of drying shrinkage versus weight loss is given in Figure 2 to compare directly the effect of water loss on the shrinkage behavior of different samples. For the same amount of moisture removed, paste containing DPTB produces less shrinkage than control sample. The amount of reduction increases as more water removed and is greater in more mature pastes.

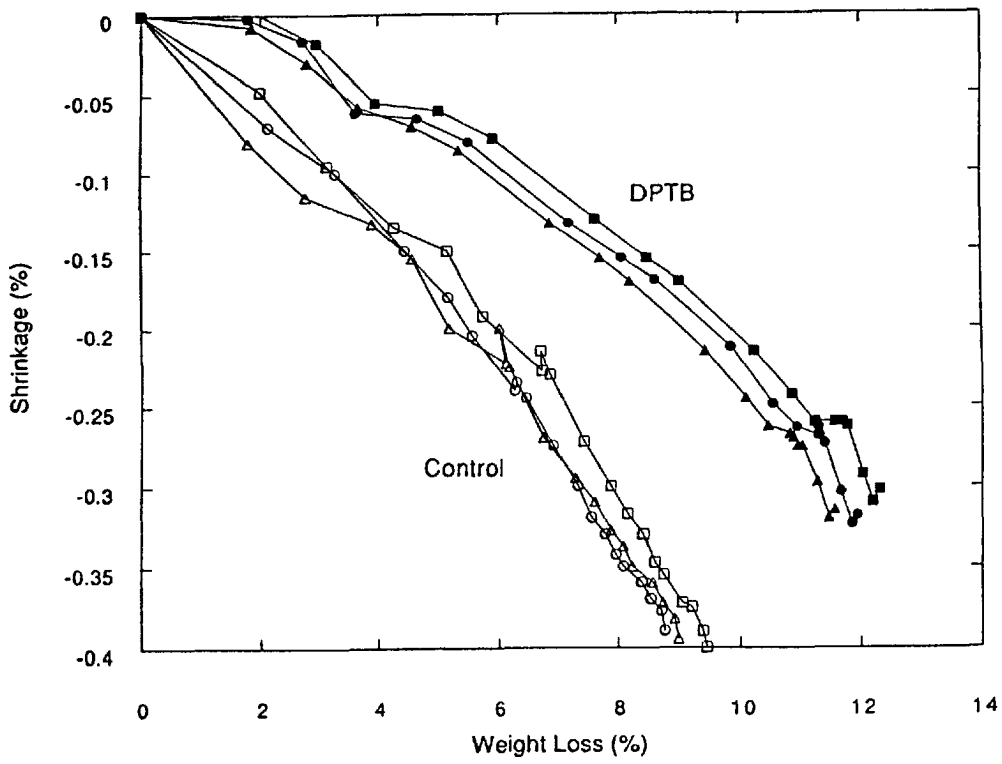

Figure 2. Shrinkage-weight loss curves for cement pastes with and without DPTB.

Phase Compositions

The XRD patterns are essentially identical at both 1 and 28 days indicating that the presence of admixture does not significantly alter the hydration chemistry. Calcium hydroxide (CH) and unhydrated cement are the only crystalline phases detectable in both materials. Similar results were found for more mature paste (28 days old). Qualitative estimations did not reveal any significant changes in the degree of hydration in the presence of DPTB. Thus the admixture does not influence the rate or nature of hydration.

Pore Structure

The Washburn equation was used to calculate the size of the pores from MIP data, using a value of 485.0 dyn/cm for the surface tension of mercury, and a contact angle of 130°. The maximum intrusion pressure used corresponds to a minimum pore size of about 30Å in diameter. Therefore, only those pores in the macropore and mesopore range are accessible by this technique. Figure 3a shows the effect of admixture on the pore size distributions of 1 day and 28 days old pastes obtained by MIP. The difference in the pore size distributions caused by the admixture in one day old cement pastes mainly lies in the macropore range (>500Å in diameter) which are not important for determining shrinkage characteristics (Bentur et al., 1979, 1980). The pore structure in the mesopore range is essentially the same, as suggested by that part of curves being parallel to each other (<500Å in diameter).

Representative mesopore size distributions obtained from nitrogen adsorption data are given in Figure 3b and some additional data reported in Table 1. The nitrogen adsorption measurements confirm the absence of changes on the pore structure in the mesopore range in the presence of admixtures Analysis of v-t curves did not reveal the presence of significant microporosity in any of the samples studied.

The Effect of Surface Adsorption of Admixture

The DPTB concentration remaining in the solution after in contact with cement was measured over time from 1 hr to 3 days. There was no evidence of adsorption of admixture by cement. The concentration of DPTB is constant under various experimental conditions, remaining at its original value.

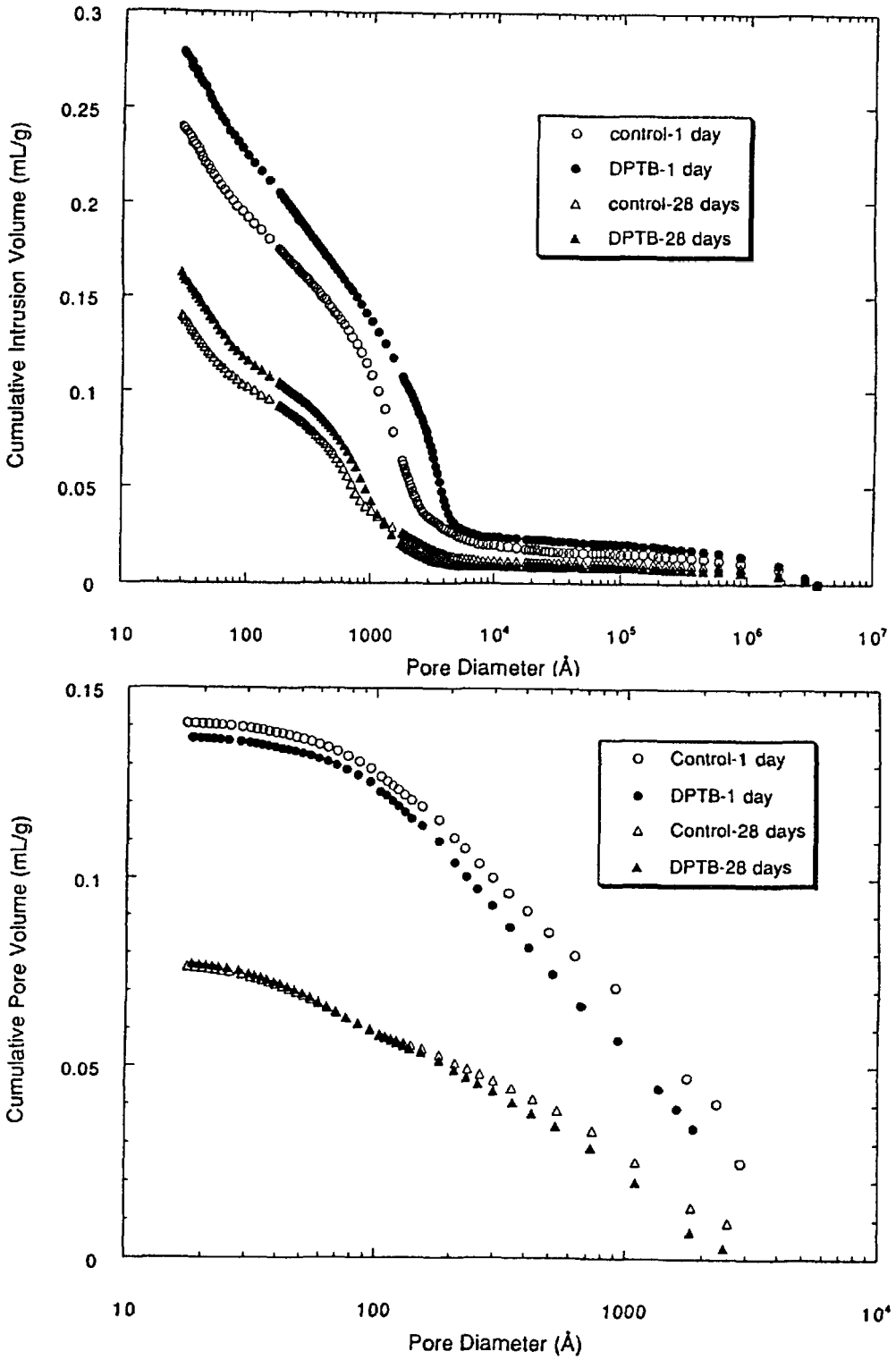

Figure 3. Capillary pore size distribution of cement pastes with and without DPTB. Calculated from (a) MIP data; (b) nitrogen adsorption data.

DISCUSSION

In the past, several microstructural parameters have been correlated with the dimensional change in hardened cement paste upon drying (Young et al., 1978, Bentur et al., 1980.) Shrinkage originates both from induced capillary stress and from changes in disjoining pressure within C-S-H gel. X-ray diffraction reveals no significant changes in either the rate or stoichiometry of hydration when DTPB is added. This, combined with similarities of the nitrogen adsorption measurements, suggests that no significant changes in C-S-H are occurring. Both MIP and

Table 1. Pore statistics of the specimens as measured by nitrogen absorption analysis

Curing Time	Measured parameter	Control	DPTB
1 day	BET surface area (m^2/g)	19.8	20.2
	Total pore volume (cm^3/g)	0.12	0.12
	Micropore volume (cm^3/g)	---	---
3 days	BET surface area (m^2/g)	19.0	18.0
	Total pore volume (cm^3/g)	0.09	0.10
	Micropore volume (cm3/g)	---	---
7 days	BET surface area (m^2/g)	21.0	20.1
	Total pore volume (cm^3/g)	0.09	0.10
	Micropore volume (cm^3/g)	---	---
28 days	BET surface area (m^2/g)	19.6	24.2
	Total pore volume (cm^3/g)	0.08	0.09
	Micropore volume (cm^3/g)	---	---

nitrogen adsorption show no significant change in capillary pore distribution in the mesopore range.

The shrinkage-weight loss curves show an high initial loss of water, that causes little shrinkage when DPTB is present. This agrees well with the higher macroporosity observed by MIP, particularly at early ages. Most of the shrinkage is associated with removal of water from the mesopore system, and in this case shrinkage is less in the presence of DPTB. Since shrinkage is related to the induced hydrostatic capillary stress, this implies that the induced stress is lower in the presence of DPTB. Given that the capillary stress (P_{cap}) is given by:

$$P_{cap} = 2\gamma/r \qquad [1]$$

the only way that the stress can be reduced for a given pore radius (r) is by a reduction in the surface tension of pore solution (γ).

The direct measurements for surface tension of DPTB solution were carried out by Wilhelm slide method (Adamson, 1982) in this study. Figure 4 shows the surface tension of solution as a function of DPTB concentration in water. Since DPTB has a much lower surface tension value, a monolayer of DPTB molecules is formed first on the surface of water when a small amount is added. This monolayer of DPTB will drastically reduce the surface tension of solution from that of pure water (72 Dynes/cm) as illustrated in Figure 4. With more DPTB addition, the surface tension continued to decrease but gradually approaches a constant value. In the real hydrated mix, as water participates in the hydration, the concentration of DPTB in the pore solution is likely to increase to a higher value than the initial concentration. Therefore, the reduction of surface tension provided by DPTB might exceed that expected from a 2% solution. We estimate that surface tension of the pore solutions will drop to about 50 dynes/cm, which is about a 30% reduction in γ and hence in P_{cap}.

The effectiveness of DPTB and related molecules in reducing shrinkage is thought to relate to their lack of adsorption by the hydrating cement. Other molecules that lower surface tension can be removed from solution by adsorption in the early hydration products C_3A and thus are no longer effective at the time water-loss begins. Adsorption of DPTB by hydrates of C_3A was not observed in this study. Therefore, the surface tension of the pore water will remain low during the time water is lost from the paste.

CONCLUSIONS

The effect of chemical admixture DPTB on hydrated cement paste was investigated through the characterization of microstructure and its interactions with the admixture. The results suggest that the presence of chemical admixture did not significantly change the hydration chemistry, the intrinsic structure of C-S-H, and the pore structure of the hydrated paste. The most likely cause for the shrinkage reduction is the reduction in the surface tension of pore solution, acting through the capillary effect, and this is supported by the evidence of direct surface tension measurements. DPTB is not adsorbed by the hydrating cement so that the surface tension will remain low during drying.

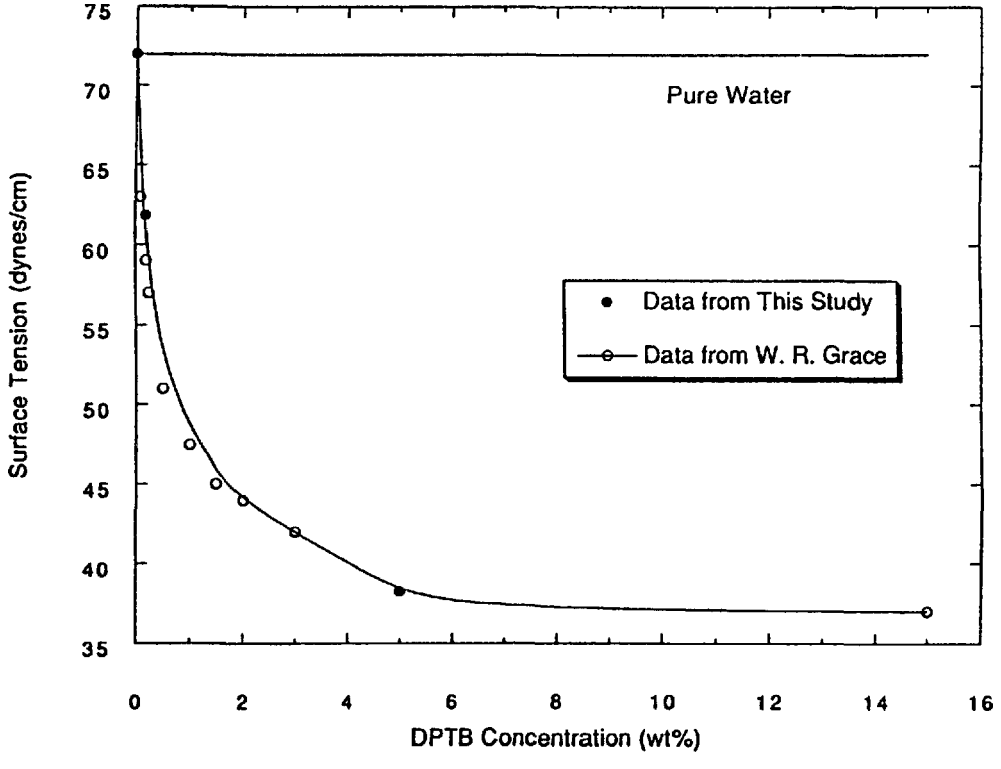

Figure 4. Effect of DPTB concentration on the surface tension of aqueous solutions.

ACKNOWLEDGMENTS

This work was supported by W. R. Grace & Co. We thank Dr. E. Shawl, ARCO Chemical Company for the chromatagraphic analyses of DPTB in solution. Surface tension measurements were carried out with the help of Ms. Lijun Coi, and we thank Prof. S. Granick for the use of the equipment. Additional surface tension data was kindly supplied by Dr. A. V. Kerkar, W. R. Grace & Co.

REFERENCES

Adamson, A. W., "Physical Chemistry of Surfaces"

Bentur, A., N. B. Milestone, J. F. Young, and S. Mindess, "Creep and Shrinkage of Calcium Silicate Pastes, IV. Effects of Accelerated Curing", Cement Concr. Res., Vol. 9, No. 2, pp. 161-170, 1979.

Bentur, A., J. H. Kung, R. L. Berger, J. F. Young, N. B. Milestone, S. Mindess and F. V. Lawrence, "Influence Of Microstructure On The Creep And Drying Shrinkage Of Calcium Silicate Pastes", Proc. 7th Int. Congr. Chem . Cement, Paris, 1980, Vol. III, Vl. 26-31.

Feldmen, R. F. and E. G. Swenson, "Volume Change On First Drying Of Hydrated Portland Cement With And Without Admixtures", Cement Concr. Res., Vol. 5, No. 1, pp. 25-35, 1975.

Hansen, W. "Investigation of Shrinkage Mechanisms in Hydrated and Carbonated Tricalcium Silicate Systems", Ph.D. Thesis, Univ. Illinois, 1983.
Hwang, C-L. and J. F. Young, "Drying Shrinkage Of Portland Cement Pastes, I. Microcracking During Drying", Cement Concr. Res., Vol. 14, No. 4, pp. 585-594, 1984.
Mindess, S. and F. Young, Concrete, (Prentice-Hall, 1981).
Young, J. F., R. L. Berger, and A. Bentur, "Shrinkage of Tricalcium Silicate Pastes: Superposition of Several Mechanisms", Il Cemento, 3/1978, pp. 391-398.

TOPIC III.B

Influence of admixtures on microstructure development

INFLUENCE OF MELAMINE SUPERPLASTICIZER ON SOME CHARACTERISTICS OF CONCRETE

Anna M. GRABIEC, Agricultural University, Poznań, Poland
Róża KRZYWOBŁOCKA-LAURÓW, Building Research Institute, Warszawa, Poland

ABSTRACT The influence of the superplasticizer on the some characteristics of concrete was determined. Compressive strength after 28 and 360 days, water absorbability and frost-resistance after 200 days of freezing and thawing were tested. The content of bound water in concrete was determined. It was found that there was a decrease in the strength of concrete with superplasticizer after longer periods in relation to the strength of this concrete after 28 days, after testing frost-resistance reaching 29%. This was accompanied by an increase in the bound water content.

Key-words: Admixtures, Bound water, Freeze-thaw damage, Hydration, Superplasticizers

INTRODUCTION

From the point of view of building material technology, both the influence of the superplasticizer on the properties of fresh concrete and the effect of admixture on hardened concrete characteristics changing with time, such as strength parameters as well as water absorbability and frost-resistance - being in a sense durability indicators, are important. In literature we find relatively few well-documented data on the changes of strength and structural characteristics of concrete with superplasticizers, maturing under different conditions of temperature and humidity for longer than 28 days. To evaluate the influence of superplasticizer on concrete it was suggested to use complex tests of physical-mechanical and structural characteristics of concrete. These include determining the compressive strength, water absorbability, frost-resistance, volume density of concrete, as well as determining the bound water content in hydration products and cement hydrolysis and the content of calcium hydroxide. The characteristics of concrete after 28 days are a reference point for comparing their changes after longer periods of concrete hardening.

MELAMINE SUPERPLASTICIZER

Introduction

Superplasticizers are widely used as effective admixtures improving the workability of the mix or reducing the water content in concrete, which should lead to higher compressive strengths and improved durability (Yilmaz and Glasser, 1989). SMF-type superplasticizers consist of salts of sulphonated melamine formaldehyde polymers, with quite large molecular weights, which are most effective with a molecular weight of about 30000. Next to salts of sulphonated naphthalene formaldehyde polymers (SNF) and preparations containing modified sulphonate they form the most numerous group (Masazza, 1983, Taylor, 1990).

Action mechanism

Literature points to three basic physical-chemical phenomena influencing the fluidifynig effect of superplasticizers. These are: dispersion, adsorption and intermolecular repulsion - potential zeta (Taylor, 1990, Collepardi and Ramachandran, 1992). It has not been conclusively determined whether superplasticizers are adsorbed on the surface of the cement grains or on the hydration products as well, particularly on the surface of the hydrated phase of aluminates and sulphates (Masazza, 1981). Not always a higher (in absolute values) zeta potential and what follows, a more effective dispersing action is tied to a greater adsorption of superplasticizers on the surface of cement grains. This results from

various forms of calcium sulphate in the cement - dihydrate, bassanite or anhydrite (Collepardi and Ramachandran, 1992).
There is little data from tests of the microstructure of cement composites with superplasticizers. From the available literature we see that the use of superplasticizers gives a denser structure of the cement paste (Ramachandran et al., 1984, Collepardi and Ramachandran, 1992, Ping Gu et al., 1994). According to Masazza (1983) changes in the morphology and size of cement hydration products affected by superplasticizers apply mainly to ettringite crystals. The admixture causes that in place of the thicker needle-like crystals, smaller and shorter ones are formed, measuring about 1/10 of those obtained in the absence of the superplasticizer and in smaller amounts. These observations are confirmed by Ping Gu et al., (1994), pointing to a cube-like shape of the ettringite crystals modified by superplasticizers. According to Yilmaz and Glasser (1989), ettringite crystals are more distinct and thicker in configurations with the superplasticizer. The size of portlandite crystals is decreased with the addition of the admixture, and their form changes from blocky to a thin, plate one.

RESEARCH

Materials, range and methods

Two series of concrete with natural aggregate were tested, with and without superplasticizer. The cement content in concrete was 350 kg/m^3. Cement with a 4% content of C_3A was used. The content of calcium sulphate calculated for SO_3 was 2.4%. An X-ray analysis showed in this cement the presence of a dihydrate calcium sulphate - gypsum, hemihydrate - bassanite and anhydrous - anhydrite. The content of alkalis in cement calculated for Na_2O was 0.5%, the specific surface of cement according to Blaine was 3003 cm^2/g. The melamine superplasticizer was added to the mix water in the amount of 2.2% with respect to cement mass. The value of the water-cement ratio was 0.43 in the concrete mix without and 0.35 in the mix with the superplasticizer. The consistency of concrete mixes was 7 s according to VeBe. The amount of mix water from the series with superplasticizer decreased by 18%. The tests were conducted on cubes a = 10 cm. The dates and hardening conditions of concrete were as follows: 28 days in standard conditions, 360 days in air-dry conditions, 360 days in water and after 200 cycles of freezing and thawing (freezing in air and thawing in water). The content of bound water in cement hydration products - silicates, aluminates and calcium aluminate-sulphates (HI) and cement hydrolysis - calcium hydroxide (HII) were determined in the concrete, using the thermal differential analysis method (DTG, DTA and TG). The microstructure of the concrete was examined in a scanning electron microscope. Specially prepared fresh fractures of concrete were subjected to observation. The range of magnification was from 20 to 10000x. The analyses had a qualitative character. Qualitative X-ray analysis was conducted on selected samples.

Results

The results of tests of physical-mechanical, and structural characteristics of concrete are given in table 1.Tests of microstructure on fresh fractures of 28-day concrete show a more compact structure in concrete with superplasticizer than in the concrete without the admixture. It should be stressed that in the concrete with superplasticizer there are numerous clusters of ettringite. After 360 days of maturing in air-dry conditions the concrete continues to show a more compact structure than the concrete without the admixture. The occurring hydrates silicates CSH-type have very indistinct, as if washed out contours. In the sample of concrete without superplasticizer CSH have as a rule the structure of crumpled foil, and only in some places they have a fibrous structure. In both types of concrete there are small ettringite crystals. In the sample of concrete with superplasticizer after 360 days in water there are signs of washing out of paste and small cracks. Numerous, unhydrated cement grains have surface etchings. CSH with indistinct contours, similar to those appearing after 360 days in air-dry conditions, are found.

Table 1. Physical-mechanical and structural characteristics of concrete with and without superplasticizer

Tested characteristic of concrete		Result of concrete test	
		without	with superplasticizer
Volume density after days (kg/m^3)			
28 - in standard conditions		2350	2380
360 - in air-dry conditions		2409	2385
360 - in water		2392	2403
200 freezing-thawing cycles		2381	2409
Compressive strength after days (MPa):			
28 - in standard conditions		34.9	34.9
360 - in air-dry conditions		35.5	35.5
360 - in water		38.5	38.5
200 freezing-thawing cycles		31.3	31.3
Water absorbability (%)		4.6	3.4
Frost-resistance - drop in compressive strength (%)		18.5	7.7
Bound water content in products of hydration (HI) and hydrolysis (HII), after days (kg/m^3):			
28 - in standard conditions	HI	49.4	45.2
	HII	9.4	7.1
360 - in air-dry conditions	HI	67.5	57.2
	HII	9.6	7.2
360 - in water	HI	69.4	50.5
	HII	12.0	7.2
200 freezing-thawing cycles	HI	64.3	55.4
	HII	9.5	7.2
Calcium hydroxide content after days (kg/m^3):			
28 - in standard conditions		37.6	28.6
360 - in air-dry conditions		38.5	28.6
360 - in water		50.2	28.8
200 freezing-thawing cycles		38.1	28.9

The occurring ettringite crystals are clearly shorter than those observed in concrete after 28 days. Worth noting is the very rich crystallization of ettringite, in single form and in clusters, apparent only in deep pores. After 200 cycles of freezing and thawing in the concrete with admixture we find micro-cracks passing not only through the pores, but also between them. In these micro-cracks we find ettringite crystals and large table-like crystals, most probably hydrated calcium aluminates. Ettringite crystals are also found in the entire cement paste. In the sample without superplasticizer the surface of the paste shows signs of carbonatization. The micro-cracks pass mainly through air pores. There are many ettringite crystals in them. But in the paste mass there is much fewer of them than in the concrete with admixture. The X-ray analysis of the paste separated from concrete with superplasticizer showed the presence of diagnostic three reflexes of ettringite in all the samples examined (d = 0.973, 0.561 and 0.388 nm). The most distinct is the d = 0.388 nm reflex. Its intensity is greatest in the concrete with superplasticizer, maturing in air-dry conditions, the smallest in concrete after 200 cycles of freezing and thawing. In the concrete without admixture there is only one diagnostic reflex for ettringite (d =

0.388 nm), whose intensity is also lowest in concrete after 200 cycles of freezing-thawing and slightly lower than in concrete with admixture.

DISCUSSION

In order to evaluate the influence of superplasticizer on the physical-mechanical and structural characteristics of concrete we examined the changes of values both in the concrete without, as well as with the superplasticizer. The volume density of concrete without the admixture is contained within 2350 to 2409 kg/m^3. The diversification of the volume density for the various samples of concrete from this series does not exceed 2.5%. In the case of concrete with superplasticizer the volume density is within the range from 2380 to 2409 kg/m^3. The diversification of density does not exceed 1.5%. The water absorbability of concrete with admixture is lower by 26% compared to concrete without the superplasticizer. Frost-resistance expressed in the drop of compressive strength of samples after 200 cycles with respect to strength of control samples - kept in water, is 18.5% for the series of concrete without admixture, and for concrete with superplasticizer it is much lower and stands at 7.7%. It must be noted that in these samples there were no macroscopic signs of damage or loss of mass. At the same time the bound water content (HI) in concrete samples without admixture clearly falls (by 7.3%) with its increased content (by 9.7%) in the samples with the superplasticizer. Other characteristics of the analyzed concretes change depending on the hardening conditions in a diversified way in both series. In concrete without the admixture the values of the tested strength and structural characteristics support the hitherto data. The greatest compressive strength, bound water content and calcium hydroxide is found in concrete maturing 360 days in water. Lesser values are found in concrete maturing in air-dry conditions for 360 days, and the smallest in concrete after 28 days. Freezing-thawing cycles lead to a drop of strength of 8.3% with respect to strength at 28 days and quite a significant increase in bound water content in hydration products (HI) and a slight increase in hydrolysis products (HII). Concrete with superplasticizer shows maximum compressive strength after 28 days of maturing in standard conditions with a minimal for this series bound water content in cement hydration products (HI). After 360 days of hardening in air-dry strength drops by 20%, which is accompanied by an increase in bound water in hydration products (HI) by 26.5% with an unchanged calcium hydroxide content. The same concrete after 360 days of maturing in water is characterized by an even greater drop of strength, at 25% and an increase in the bound water content (HI) by 12% with a constant calcium hydroxide content. The greatest drop in strength in this concrete of 29% was found after 200 cycles of freezing and thawing. At the same time there is an increase in the content of bound water (HI) by 23% with an unchanged amount of calcium hydroxide. In order to compare the degree of cement hydration in both concrete series we used the bound water content in hydration products - HI and hydrolysis products - HII (Fig. 1). According to Yilmaz and Glasser (1989) the $Ca(OH)_2$ content after longer periods of hardening is a reliable indicator of the degree of cement hydration. The ratio of the bound water content in hydration products - HI, i.e. in hydrated aluminate sulfates, aluminates and calcium silicates to the bound water content in hydrolysis products HII, that is in calcium hydroxide, may indirectly characterize the degree of reacting of the cement in concrete. This indicator was used to characterize the changes taking place in both series of concrete. In the concrete without admixture the value of the ratio of bound water in hydration products to water found in hydrolysis products is within 5.3 to 7. Maximum strength in this series of concrete is found in samples with the HI to HII ratio equal to 5.8. Samples with the least strength in this series have the HI/HII ration equal to 6.8. In concrete with superplasticizer the value of the HI/HII ratio is within 6.4 to 7.9. Maximum strength is found in samples with HI/HII equal to 6.4, minimal - 7.7. From the data presented above we see that in samples with the superplasticizer after longer periods of hardening changes take place in the bound water content in hydration products. HI with small hydration of the remnants of unhydrated cement.

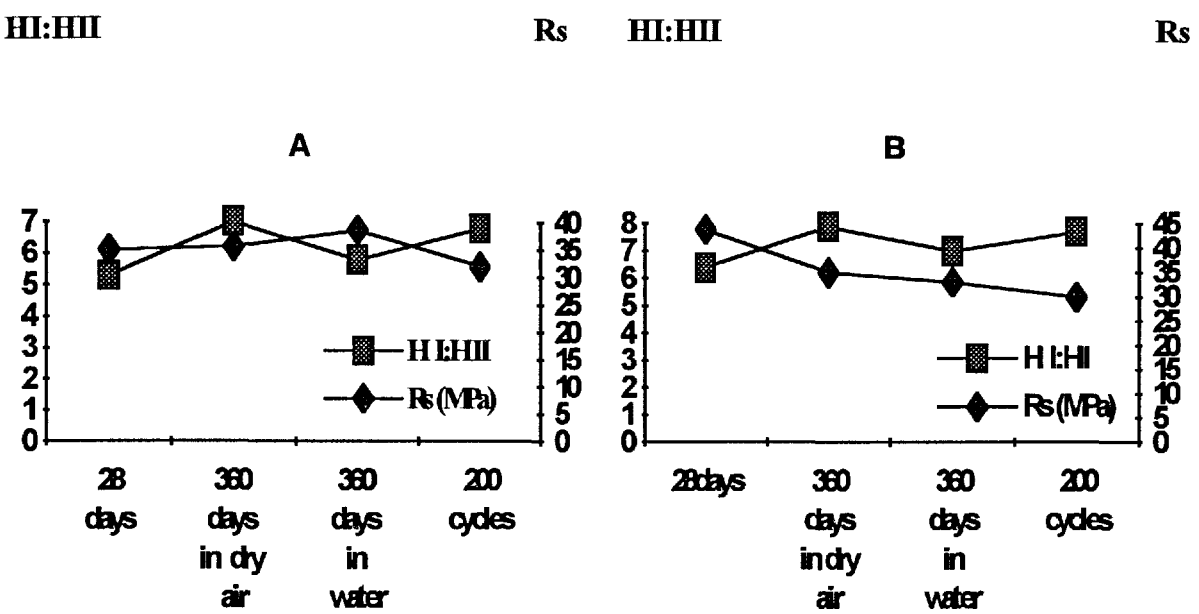

Figure 1 Value of the HI/HII ratio in concrete without (A) and with admixture (B) with respect to the compressive strength of concrete.

This is shown by both the growth of bound water content in hydration products HI, as well as the constant $Ca(OH)_2$ content. In the series without admixture, on the basis of calcium hydroxide content, the degree of hydration of cement is much greater. On the basis of observations in a scanning microscope we find that the microstructure of concrete with superplasticizer is more compact. On the basis of X-ray analysis it was found that the most ettringite is found in the sample of concrete with the superplasticizer after 360 days of hardening in air-dry conditions.

CONCLUSIONS

1. The influence of the superplasticizer is expressed by an increase in the compressive strength after 28 days, lowering of water absorbability and improved frost-resistance compared to concrete without the admixture.
2. The influence of the superplasticizer after 360 days of hardening in air-dry conditions and in water is expressed by a significant lowering of the compressive strength compared to the same concrete after 28 days.
3. The greatest drop in strength with respect to 28-day concrete with superplasticizer is found after 200 cycles of freezing and thawing.
4. The decreases of strength of concrete with superplasticizer are most probably tied to the changes taking place in cement hydration products. This is shown by the significant increase in the amount of bound water in these products in concrete after 360 days of hardening and after 200 cycles of freezing and thawing with an almost constant calcium hydroxide content.
5. In evaluating the effectiveness of the superplasticizer it is not enough to measure the strength after 28 days.
6. For the comparative evaluation of the course of hydration in cement without and with the superplasticizer it is recommended to determine the content of bound water in hydration and hydrolysis products and the calcium hydroxide content.

REFERENCES

Collepardi, M., Ramachandran, V.S., "Effect of Admixtures", Proceedings of the 9th International Congress on the Chemistry of Cement 1992, New Delhi, pp. 529-568.

Masazza, F., "Admixtures in Concrete. Advances in Cement Technology. Critical Reviews and Case Studies on Manufacturing. Optimization and Use", Cement and Research Institute, Pergamon Press, New Delhi, 1983.

Ping, Gu. et. al., "Investigation of the of the Retarding Effect of Superplasticizers on Cement Hydration by Impedance Spectroscopy and other Methods", Cement and Concrete Research, Vol. 24, No. 3, 1994, pp. 433-442.

Ramachandran, V. S. et. al., "Concrete Admixtures. Handbook", Division of Building Research National Research Council Canada, Ottava, Ontario, Canada, 1984.

Taylor, H.F.W., "Cement Chemistry", Academic Press, London, 1990.

Yilmaz, V.T., Glasser, F.P., "Influence of Sulphonated Melamine Formaldehyde Superplasticizer on Cement Hydration and Microstructure", Advances in Cement Research, No. 7, 1989, pp. 111-119.

PERFORMANCE OF HIGH-RANGE WATER REDUCERS IN CEMENT CONCRETE MIXES IN HOT WEATHER CONDITIONS

S C MAITI, National Council for Cement and Building Materials, New Delhi.

ABSTRACT The initial workability and slump-retention period for concretes with Indian superplasticizers are similar to those for concretes with superplasticizers from other countries. The type of cement did not make any difference. The rapid slump-loss of superplasticized concrete in hot weather condition could be checked using the retarder Sodium gluconate. For high-strength concrete mixes, the higher dosage of the superplasticizers enabled the workability to be retained for a comfortable period of time without any retarder.

KEY - WORDS : Superplasticizers, Slump loss, High temperature, Retarders

INTRODUCTION

Superplasticizers require to be evaluated before they are used in concrete construction, as they have to be compatible with the materials of construction, specially with the type of cement used. Addition of superplaticizer to concrete of medium workability renders the mix flowing, within minutes of addition. However, the extreme workability so obtained is transient and depends upon factors like the initial workability, type and dosage of the superplasticizers, atmospheric temperature, addition of retarders etc., apart from cement characteristics. At higher temperature, which is a general feature of many countries, the problem gets aggravated and the high workability of concrete is lost within a short period of time. This is a common feature of all kinds of superplasticizers. The rate of slump-loss gets accelerated when such concrete is subjected to prolonged mixing in ready mixed concrete plants (Ravina and Soroka, 1994). Others controlled the slump-loss by using a polymer (Ramachandran, Beaudoin and shihua, 1989).

SCOPE OF THE INVESTIGATION

The investigation aimed at evaluation of superplasticizers with different types of cement in hot weather condition. The experiments were conducted to evolve a method to check the slump-loss of superplacticized concrete. The mix design aspects of superplasticized flowing concrete were also looked into.

Materials

The performance of two Indian commercial naphthalene-based superplasticizers was compared with that of two imported superplasticizers (one melamine-based and the other naphthalene-based). The cements used are ordinary Portland cement (OPC) and three types of blended cements [two pozzolana-based: PPC-1 (flyash-based) and PPC-2 (burnt clay pozzolana-based) and one blast furnace slag-based: PSC]. The cements conformed to the relevant Indian Standard Specifications. The chemical constituents and the physical properties of the cements used are given in Tables 1and 2 respectively. The coarse aggregate (20mm maximum size crushed rock aggregate) and a natural fine aggregate were used. The retarders used are a commercial product, Sucrose, Citric acid and Sodium gluconate.

Table 1 Chemical Constituents (%) of cements used

Constituents	OPC	Blended cements		Slag cement
		PPC-1	PPC-2	PSC
SiO_2	25.94	28.74	26.76	25.63
CaO	59.86	51.60	50.80	53.47
Al_2O_3	5.21	6.88	9.18	9.43
Fe_2O_3	3.65	3.77	4.34	2.55
MgO	1.77	2.23	1.04	3.97
SO_3	1.50	2.49	-	1.49
Loss on ignition	1.69	2.10	2.52	2.43
Insoluble residue	3.97	16.63	16.31	2.60

Table 2 Physical properties of cements

Properties	OPC	PPC-1	PPC-2	PSC
Fineness, cm^2/gm	3137	4133	3235	3485
Specific gravity	3.15	3.02	3.00	2.87
Setting time (minutes):				
Initial	148	112	130	187
Final	275	207	235	316
Compressive strength: (N/sq mm)				
at 3 days	27.0	23.8	-	23.3
at 7 days	34.5	29.3	31.5	28.0
at 28 days	46.0	40.2	41.8	34.0

EXPERIMENTS CARRIED OUT

Experiments were conducted on high-workability superplasticized concrete mixes of M20 and M 40 grades. The control concrete mix had a medium workability of 25-50 mm slump. Concrete was mixed in a mechanical mixer. Superplasticizer was added to the mix with the last part of the mixing water. The retarder was added along with the cement with the first part of the mixing water.

TEST RESULTS AND DISCUSSIONS

About 0.75 % (by weight of cement) superplasticizer was required to convert 25mm slump concrete to flowing concrete of M20 grade. M 40 grade concrete required about double the dose for producing high-workability concrete mix. This was also observed by others (Rixom and

Mailvaganam, 1986). The dosage requirement in blended cement concrete was the same as in concrete with OPC. The M20 grade superplasticized flowing concrete in general required about 5% (%by weight of total aggregate) more fine aggregate in order to make the concrete mix cohesive. At normal temperature conditions (27°C, 65% RH), there was no rapid workability loss, and the control slump could be obtained even after 2.5 to 3 hours time. In hot weather conditions (40°C, 20% RH), the flowing characteristics of M 20 grade superplasticized concrete were retained only for about 30 minutes. The type of cement (OPC,PPC or PSC) did not make any difference. The initial workability and slump-retention period for concrete with Indian superplasticizers were similar to those for concrete with superplasticizers from other countries. There was no special trend observed for the type of superplasticizer or the type of cement used. The workability of superplasticised concrete could be maintained in hot weather conditions in case of M 20 grade concrete with the retarder Sodium gluconate (0.1% by weight of cement) for all types of concrete (Fig 1). Not all retarders were effective to control the slump-loss of superplasticized concrete mixes. A commercial set-retarder could not alleviate slump-loss. Sucrose although could alleviate the slump-loss at high dosage (0.5% by weight of cement), retarded the setting time of concrete considerably, and was not found useful. Citric acid did not perform well in the case of concrete with PPC.

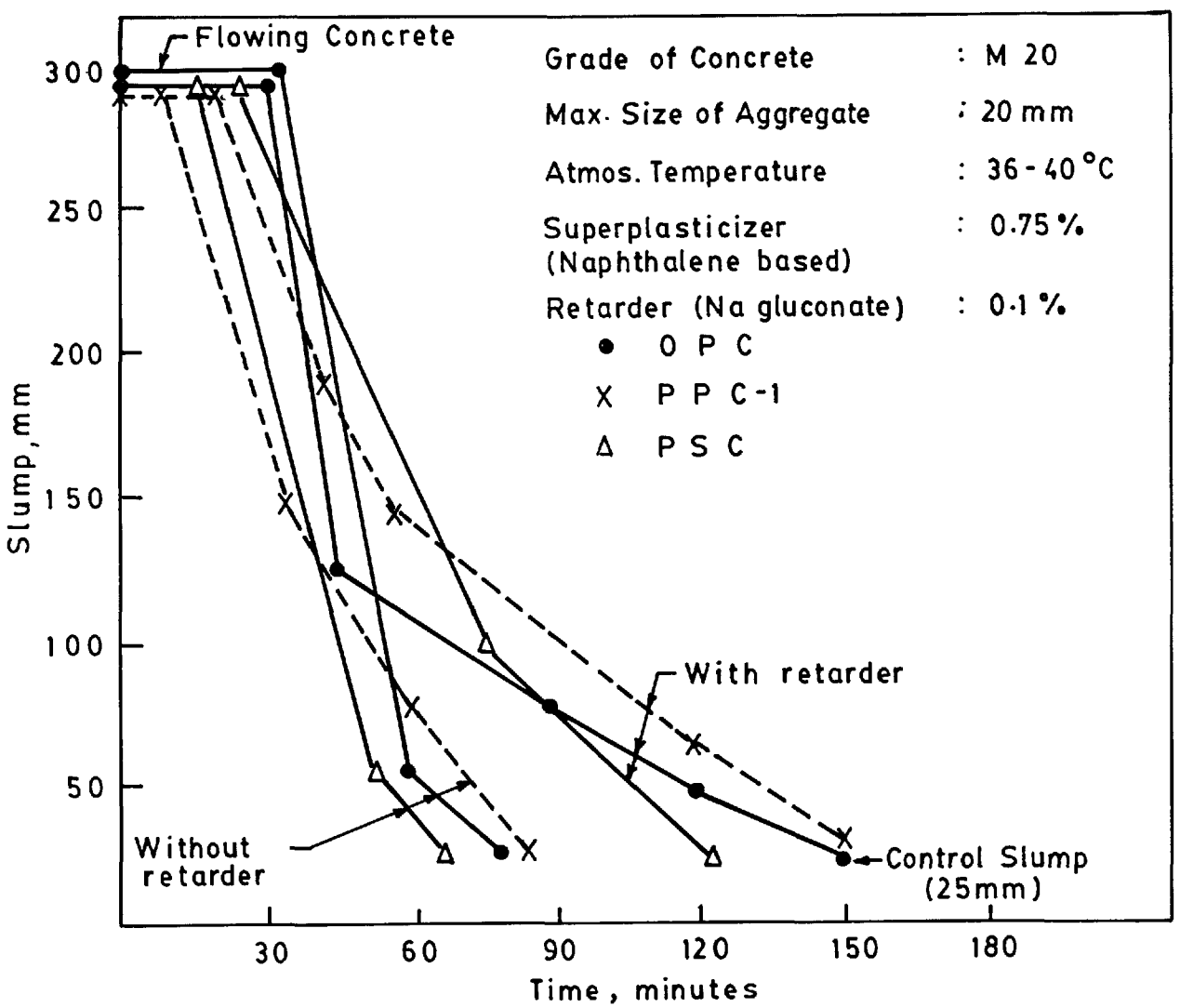

Figure 1 Slump retention of retarded superplasticized concrete in hot weather

For M 40 grade concrete, the comparatively higher dosage of the superplasticizer enabled the workability to be retained for the desired period of time, upto about 3 hours, without any retarder, even at 36-38°C temperature. The blended cement concrete did not make any difference. This is probably because of a cohesive concrete mix of high cement content holding a smaller quantity of mixing water efficiently, and not allowing it to expose to the surroundings causing evaporation. That the higher cement content in concrete reduces the rate of slump-loss, was also observed by others (Mailvaganam, 1979).

REFERENCES

ASTM C494-92 standard specification for Chemical Admixtures for concrete. 1995 Annual Book of ASTM Standards, American Society of Testing and Materials, Philadelphia.

Mailvaganam, N.P. "Factors Influencing Slump Loss in Concrete", American Concrete Institute SP-62,1979, pp. 389-403.

Ramachandran, V.S. et al., "Control of Slump Loss in Superplasticized Concrete", Materials and Structures, Research and Testing, Vol.22, No 128, March 1989, pp 107-111.

Ravina, D. and Soroka, I. "Slump Loss and Compressive Strength of Concrete Made With WRR and HRWR Admixtures and Subjected to Prolonged Mixing", Cement and Concrete Research, Vol.24, No.8, 1994, pp 1455-1462.

Rixom, M.R. and Mailvaganam, N.P. Chemical Admixtures for Concrete, E. & F.N. Spon, 1986, p.218.

ACKNOWLEDGEMENT

The paper is based on the R&D work carried out at the National Council for Cement and Building Materials, New Delhi. The paper is published with the permission of the Director General of the Council.

LOW-WATER REQUIREMENT BINDERS AS NEW-GENERATION CEMENTS

B. E. IOUDOVITCH, A. M. DMITRIEV, S. A. ZOUBEKHINE, NIICEMENT,
N.F.BASHLYKOV, V.R.FALIKMAN, V.N.SERDYUK, ``POLYMOD`` Association - NIIZhB,
Shahveran T. BABAEV, all from Moscow, Russia

ABSTRACT Low water requirement binders (LWBs) are modified cements Portland types consisted of interground Portland cement clinker (PCC), modifier (M), gypsum and active or inert mineral additions. Their history, chemistry, technology and properties are the objective of this report.

Key-words: Binder. Modified cement. Superplasticizers. Lignosulphonates.

INTRODUCTION AND HISTORY OF LWB

LWBs (Russian name - VNV) were invented in 1984 by Babaev and Bashlykov. They interground ordinary PC (OPC; variant: PCC) with dry M (included water lowering agent based on naphtalensulphonate, regulator of cement setting, intensifier of hardening etc.) and in concrete found the unprecedent water demand fall and strength growth - by minus 30-40% (here and below all % by weight) and by plus ≥3 classes of strength (≥30 MPa) accordingly in compare with high early strength PC (HPC) of 600 mark - the better by Russian standard (GOST 10178). LWB with slag or fly ash had also plus ≥ 2 classes of strength in compare with PCC based cement of such types. These results could not be obtained with M dissoluted in mixing water of mortar and concrete with decreasing of water demand by 18-25% and increasing of their strength under 2 classes. But sometimes mentioned positive effect of dry M-intergrinding (``intergrinding effect``, abbr. IE) is decreased to that of M, dissoluted in mixing water (``plasticizing effect``, abbr. PE). It delayed working out of binder and based products. In 1986 Tarnarutsky and Ioudovitch apart from previous authors made LWB by the same way with M based on lignosulphonates. They got reproducibility of data. After meeting in sci. conference (1987) mentioned authors had been decided to work jointly and in 1-2 years - together with other authors of this report and had established that the time of component intergrinding and high energy of mill charge/ground material impacts is essential for IE and is the *first condition* of IE>>PE. Review of patents had shown that m-lle Peiron (1982) had ground PCC + dry superplasticizer (S) + gypsum + retarder of cement setting and fixed cement disaggregation and PE. Collepardi (1987) introduced dry powdered S in OPC *after* grinding; the result was improving the PE reproducibility. Novelty of IE stipulated LWB research by three ways simultaneosly: 1) producing of LWB parties in pilot and plant mills; testing them in concrete and reinforced concrete with technological, mechanical, construction and environmental experiments and sanitary inspections of LWB producing and using; 2) studies of mechanochemical reactions of LWB formation during grinding in large mills; 3) analysis of hydration / hardening processes and strengthening different types of LWB-based concrete - from high strength to cellular. During 1988 - 1991 in these studies 24 leading research institutes on concrete and building took part with coordination from Ministry of Building (Gosstroy of USSR, namely B. N.Yeltzin, 1988-89, as official) and in 1989 - 1991 - 6 cement plants, some building industry plants and works of M production too. The purpose is to create new range of cement types based on LWB. Publications were not encouraged. In 1991 the prestandard for LWB (USSR Technical Conditions for VNV) and ``Technical Regulations for Concrete Producing and Using on VNV base`` were worked out (not published in the open editions). But after well known circumstances military consumers of super high strength cements (neat LWB) were disappeared and state granted studies were stopped. Further research had been conducted by 3 organizations named in title. This is the first open publication on LWB as a whole from authors of binder. The lack of place determines a conspectiveness of text.

ABOUT LWB FORMATION IN GRINDING PROCESS

It was demonstrated (1992) that the mechanochemical process of LWB formation in plant mill (2.9 x 8.6 m) is *endothermal* (versus *exothermal* for known surface-active matters acc. Rehbinder, 1931) by control of necessary present-position data with Link-system in grinding regimes without and with M. PCC from ring store had initial temperature 88°C, neat OPC had av. sp. surface 400 m^2/kg. The temperature of aspirated air at once after mill outlet after M introducing and regime stabilization had been lowered from 108 without to 104-105°C with M and cement (LWB) temperature - from 137 to 135°C when av. sp.surface raised to 450 m^2/kg. Sp. endotermal effect (EE) estimated was much over 100 J/mol of M. This is the first sign of chemical reaction (RA)``PCC+M``. Other components - gypsum and mineral additions - are passive because there is linear lowering EE during their content increasing. Water adding in the first mill chamber interrupts RA versus it introducing to the last chamber by F.L.Smidth pulverizing method which does not stop RA. It has been concluded that water in mill cannot solve product after high degree of RA. The quick method of RA degree estimation is obtaining the free M in ground material along mill. Ioudovitch and Srl'arenko had worked out optical micromethod of free M estimation in said material and in finish LWB. By this method it have been demonstrated that *IE is obtained only in absence of free M in LWB* (Ioudovitch,1989, unpublished report). This is the *second* technological *condition* of LWB production. Naturally, with increasing free M content in LWB said IE transformes to PE. Unreproducibility of IE, as it is obvious, are concerned to cases of RA interruption by some technological factors - from glassy clinker nodules and phases surfaces during kilns' dusting to over moist cement components etc. Practically by RA reason LWB producing is closely connected with all technological peculiarities of cement production process beginning from raw materials and PCC burning. The phenomenon of difference between PCC composition and properties in *surface* and in *volume* is especially important to LWB production.

Using range of physical and chemical methods among them Auger-spectrometry and gel-chromatography, as main interaction stages (st.) of RA were established: 1) molecular-dense aggregation; 2) chemisorption; 3) implosion (term by Wislozky, 1971, used in tribology) of organic matter of M into the PCC surface layers to the depth abt 1-2 μm during mutual contacting between comminuting PCC particles with M adsorbed on as a solid lubricant in friction pairs; 4) throttling (organic M constituents structure alteration in st.4 of process by chain length and molecular mass); 5) cladding of the active zones on PCC surfaces by M. Necessary precondition for st.1 is free valencies propagation on PCC particles' surfaces what is possible only after the beginning of dislocations motion on PCC surface during grinding. That is the reason of namely *mechanochemical* character of RA and impossibility of LWB obtaining by intimate component mixing. Analysis with help of microstamp contact mechanism of fine fraction formation during cement grinding (Ioudovitch et al., 1981) testifies that initial sp.surface level of dislocation motion and simultaneously minimal level for the RA beginning is 300-330 m^2/kg and real LWB cannot have sp.surface lower than 380-400 m^2/kg. But during the grinding to this min. sp.surface only small quantity of M can take part in RA. To prevent free M residue in LWB and IE $\Rightarrow$ PE the *conformity between M quantity in LWB* (with known M reactivity in relation to given PCC) *and sp. surface of LWB must be maintained.* That is the *third condition* of LWB production. Constancy of PCC and M quality and rational approach to mill charge and working regimen are necessary for obtaining LWB. If on the st.5 said conformity was achieved *LWB* obtained *can be keeping any time* in sacks or in silo *without losses of hydraulic activity* and for 6 months - without losses even early strength too independently of sp.surface values. This is *fourth* and the last *condition* of high quality LWB production. It is based on coordination compounds effect: hydrophobization of external active zones of LWB particles is the result of blockade of potential layers over their surfaces (from this layers water vapour molecules can be attracted to surface in Polanyi adsorbtion theory sense) by organic molecules whose passivity to water vapour in atmosphere explains by electron transition (as in coordination compounds) from external organic surface to

internal chemisorption contacts (RA zones) between M and PCC. Thus LWB hydrophobization is achieved without addition of hydrophobic matter proper that is very important for cement with such high fineness level as LWB.

M itself acc. st.5 can change under the influence of grinding attacks - depolymerize or polymerize if at the early stage of comminution it ``hide itself`` from grinding attacks into the inside of the clinker surface layer, or if it ``flew`` under the action of aspiration through the whole mill without alterations. The second variant is undesirable - this is one of the ways to leave the free M. In the rest cases modifier particles, while undergoing plastic deformations in the grinding process, predominantly shear deformations, apparently are also ``incrusted`` by calcium cations passing into the M from the calcium-enriched dislocation zones of the surface of clinker particles, in which calcium is known to be superstoichiometric (Tarnarutsky, 1977). This fact is diminish the strictness of demands to cation composition of water lowering organic constituent of M. In general, one would think all such conditions are too strict and LWB production is too much complicated process. Really it is not so - all these peculiarities demands knowledge of, careful preparation of all stages of cement technological process and then only habit of the personnel.

ABOUT THE IE FOR INDIVIDUAL MINERALS AND DIFFERENT CLINKERS

The participation of individual clinker minerals and different PCC in the interaction processes with the modifier and the peculiarities of the subsequent hydration and hardening are displayed in Table 1.

Table 1 Interaction of components and clinkers during intergrinding with M and hydration[1] (av. data)

Interaction of minerals and PCC + M	Minerals of PCC				PC clinkers			
	C_3S	βC_2S	C_3A	C_4AF	high-alite	belite	alite-aluminate	Ferrari-type
1. Solid-phase interactions during intergrinding								
Molecular-dense aggregation | Graf-	v.str	v.str	none	str.	v.str	wk	str.	v.str
Chemisorption | ting	str.	none	none	med	str	wk	med	wk
Implosion	+	-	-	+	+	v.wk	+	+
Throttling	+	-	-	-	+	-	+	v.wk
Cladding	+	-	-	+	+	-	+	+
2. Phenomena during hydration and hardening (as compared with unmodified cements or binders)[2]								
1-st exothermal effect of wetting[3]	sgl	sgl	sgl	dbl	dbl	sgl	dbl	dbl
Water requirement decrease[4], %	30	25	20	35	35-40	25-30	30-35	35-40
Strength increasing, after 3 days, MPa	20	15	30	25	30-35	20-25	25-30	35-40
Ditto, after 28 days, MPa	30	20	50	40	40-45	25-30	35-40	35-40

[1]Legend: (str) strong, (wk) weak, (med) medium, (v.) very, (+) present, (-) absent, (sgl) single, (dbl) double.
[2]Free M being absent. [3]With the mixing water. [4]At constant flowability.

ABOUT THE TECHNICAL PROPERTIES OF LWB

Water requirement of equally flowable fresh mortar and concrete (and, in general, of identical consistency, irrespective of the method of its measurement) reduced by 25 to 40%.
Water content of the major hydrated phases lowered in about the same degree, with the exception of portlandite whose amount in the hardened LWB paste is insignificant, but the amorphous $Ca(OH)_2$ content is fairly high, though lower than in the hardened HPC paste.
Strength of both neat (pure-clinker) LWB and LWB with mineral additions (Table 2) is higher, on the whole; this enabling the specific consumption of aggregates (SCA) by the binders (in the project of new Russian standard they have named ``cements of low water demand``) in concrete to be increased

in an unprecedent manner for an inorganic binder and, accordingly, the clinker consumption per 1 m^3 of concrete and per 1 MPa of strenght as well as specific energy inputs per 1 m^3 of concrete to be brought down to an extraordinary low level. Said Russian standard foresees variable W/C to LWB.

Table 2 Strength characteristic of LWB etc. in mortars (by new Russian std.) and in concretes

Cement type	Sp.surface, m^2/kg	Cement composition, wt.%			Modifier=Na-naphtalensul-	Mortar stren. on Russ. std.[2]			Concrete str (sl.3-4 cm)[4]		
		PCC	slag	sand[1]	phonate based	1d.	28d	St.c[3]	1d.	28d	St.c
HPC,mark 600(GOST 10178)	370	100	0	0	-	18	62	35	20	40	35
Composite cement(Eu.type V)	470	50	25	25	-	12	55	28	10	37	27
Ditto	470	50	25	25	in mixing wat.	20	65	37	20	40	36
LWB (comp.Eu.Type I)	470	100	0	0	within binder	52	93	68	45	88	64
LWB (comp.Eu.Type V/A)	470	50	25	25	ditto	23	77	59	30	76	51
LWB (comp.Eu.Type V/B)	550	30	35	35	ditto	17	67	48	22	44	36

[1])Quartz. [2])Sp.4x4x16 cm. [3])Std curing (h): 2+3+6(85°C)+3. [4])Cement consumption 375 kg/m^3, sp. 15^3 cm.

Modulus of elasticity lowered by 5-15% versus reference cement of the same mineralogical and material composition in concretes of identical composition.
Lowered exotermicity.
Frost resistance (expressed as the number of freezing/thawing cycles withstood by concrete without noticeable loss of strength) enhanced by a factor of 2 to 3.
High sulphate resistance, with which the corrosion stability of LWBs made of clinker with 9% C_3A is not inferior to the parameters of sulphate resisting PC (GOST 22266) holding no C_3A at all.

CONCLUSION

F. L.Wright maxim ``Each material speaks its own language with us`` is more than true for LWB. The LWB language is unusual for the time being. No wonder too: the SCA difference between OPC and LWB (max. 13 vs. max 27) is so great that it enables to regard LWBs as a new generation of binders. As almost all binders can be produced in the form of LWBs this is a new generation not only for PC, but also of lime, gypsum, slag cements and others. If the expensiveness of M will be lowered, in the XXI century many binders will prevail exactly in the form of LWB.

ACKNOWLEDGEMENTS

Authors are grateful to all former colleagues and among them especially to Ph.D. G.M.Tarnarutsky and Dr. Enrique F. Molina for their valuable contribution to this work.

REFERENCES

Collepardi, M. Private Communication: at Lection in Institute NIIZhB, Moscow, May, 1987.
Ioudovitch, B.E. et al. (the first family transcription was Yudovich). XII Conference of silicate industry and silicate science (Siliconf-XII). Ed. Akad. kiado, Budapest, 1981, sect.C-III, pp.11-15 (in English)
Peiron, J. European Patent No. 0081861, priority 1982 (Belgium), publ. June, 1983.
Rehbinder, P.A.Zeitschrift für Physik,1931, B.72, H.2, s.191. (Next refs. in Russian and Poland acc.)
Tarnarutsky, G.M., et al., Trudy (Proc. of) NIIcement, Moscow, 1977, No. 32, p. 134-146
Wyslocki, M. ``Systemy smarewnicze w przemysle ciezkim``, wid. Slask, Katowice, 1971, s. 174

STUDY ON HYDRATION AND THE PROPERTIES OF HARDENING ACCELERATORS BASED ON CALCIUM-ALUMINATE GLASS

Satoru HIROSE and Toru HIGAKI, Nihon Cement Co., Ltd., Tokyo, Japan
Kiyoshi ASAGA, Teikyo University of Science and Technology, Yamanashi, Japan
Masaki DAIMON, Tokyo Institute of Technology, Tokyo, Japan

ABSTRACT Hardening accelerators based on calcium-aluminate glass with different CaO-Al_2O_3 molar ratios were added to cement, and the behavior of setting and strength, amount of hydration product and ion concentration in the solution were measured. It is shown that a higher CaO-Al_2O_3 molar ratio of calcium-aluminate glass, the mortars came to final setting faster, but strength in the early stages was lower. These characteristics were significantly connected with the formation of ettringite and aluminum-rich gelatinous hydrated product.

Key -words: Accelerators, Calucium aluminate, Ettringite, Gel, Pore solution

INTRODUCTION

For the purpose of improving the efficiency of emergency repair work and shotcrete for tunnel excavation, the use of some kind of admixture to accelerate the hardening of cement is required. For this purpose, $12CaO{\cdot}7Al_2O_3$, $11CaO{\cdot}7Al_2O_3{\cdot}CaF_2$, $3CaO{\cdot}3Al_2O_3{\cdot}CaSO_4$ and some amorphous materials of similar chemical composition to those minerals are popular as quick-setting or rapid-hardening materials. In particular, calcium-aluminate glass (hereinafter referred to as C-A glass), with a CaO-Al_2O_3 molar ratio of approximately 12:7, hydrates more rapidly than the other materials mentioned above (Nakagawa et al, 1990) and is utilized as the main ingredient in quick-setting agents for shotcrete and hardening accelerators for concrete. Alkali carbonates are also effective in promoting the hydration of cement. A quick-setting agent for shotcrete made from C-A glass and sodium carbonate has been developed in Japan (Hirose & Yamazaki, 1993). But there are few papers concerning the relationship between hydration and the hardening properties of these accelerators.

Therefore, for this study, samples of C-A glass of different CaO-Al_2O_3 molar ratios were prepared. Hardening accelerators were made experimentally from these glasses, plus anhydrite and sodium carbonate. Setting, strength, amount of hydrate product and concentration of ions in the extracted solution were measured to investigate the influence of C-A glass on the properties of cement mixed with accelerator.

EXPERIMENTS

Materials

Calcium-aluminate glass: Three samples of C-A glass were prepared, that is, glass of intermediate composition between $CaO{\cdot}Al_2O_3$ and $12CaO{\cdot}7Al_2O_3$ (hereinafter referred to as C-A glass L), of equivalent composition to $12CaO{\cdot}7Al_2O_3$ (C-A glass M) and of intermediate composition between $12CaO{\cdot}7Al_2O_3$ and $3CaO{\cdot}Al_2O_3$ (C-A glass H).

Each mixture was melted in an electric furnace at about 1750℃. The molten material was quenched using a twin-roller quenching apparatus made of stainless steel.

Cement: Ordinary Portland cement was used. Table 1 shows the results of chemical analysis of the cement.

Table 1 Results of chemical analysis of the ordinary Portland cement(mass%).

ig.loss	insol.	SiO_2	Al_2O_3	Fe_2O_3	CaO	MgO	SO_3	Na_2O	K_2O	Total
1.2	0.2	21.1	4.5	2.7	64.3	1.6	2.4	0.38	0.46	98.8

Anhydrite: Commercially available anhydrite was used. Specific surface area measured by Blaine's method was 390 m^2/kg.

Sodium carbonate: Commercially available sodium carbonate was used.

Preparation of accelerator

C-A glass clinker was ground to 500±10 m^2/kg as Blaine's specific surface area. C-A glass, anhydrite and sodium carbonate were mixed in the proportion of 45:45:10 by mass to prepare the accelerators.

Mix design and preparation method of paste and mortar

The proportion of cement and accelerator was fixed at 90:10 by mass. The water-cement ratio for mortar and paste was 0.5:1, and the sand-cement ratio was 3:1. The sand used was prepared from three kinds of natural silica sand, with particle diameter of approximately 0.15-2.23 mm. Citric acid was added to maintain workability of the paste and mortar as a retarder at the rate of 0.25 mass% to the total amount of cement and accelerator.

Preparation of paste and mortar was carried out according to the flowchart shown in Fig.1. Preparation and curing of samples were done at 20℃.

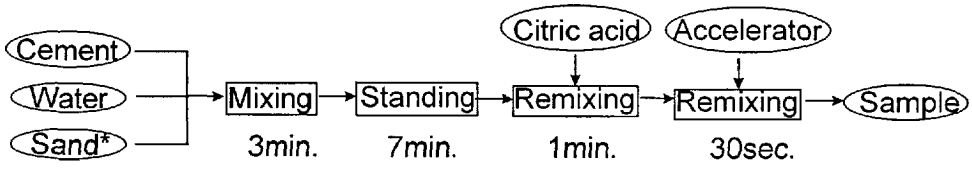

Fig.1 Flow-chart to prepare paste or mortar samples.
*:not mixed when preparing paste sample.

Method

Analysis of the C-A glass: The chemical composition of the C-A glass was measured by X-ray fluorescent analysis. The heat of crystallization of the C-A glass was measured by DSC.

Setting and strength: The hardening properties were measured from final setting time measured by Procter's penetration method. Development of compressive strength was measured using 4×4×16 cm mortar prisms.

Analysis of hydration products: DSC, quantitative X-ray analysis and loss on ignition were determined using paste samples. Hydration of the samples for test was stopped by soaking in acetone to remove excess water.

Pore size Distribution: Pore size distribution was measured by Mercury intrusion porosimetry, using the same sample as mentioned above.

Concentration of ions in the extracted solution: Suspension was extracted from paste sample at particular times by suction or pressing, and filtered with a 0.45 μm mesh to remove fine

particles. A small quantity of hydrochloric acid was added to the solution to adjust pH to about 4, and the concentration of ions was measured. Ca^{2+} and Al^{3+} were measured by ICP, Na^{+} and K^{+} by atomic absorption analysis, SO_4^{2-} by ion chromatography and OH^{-} by neutralization analysis.

RESULTS AND DISCUSSION

Characteristics of the C-A glass

Table 2 shows the results of chemical analysis and $CaO\text{-}Al_2O_3$ molar ratio calculated from the results. Figure 2 shows the relationship between $CaO\text{-}Al_2O_3$ molar ratio and heat of crystallization.

It is observed that the heat of crystallization was highest for C-A glass with a $CaO\text{-}Al_2O_3$ molar ratio of 1.70.

Table 2 Results of chemical analysis of the calcium-aluminate glass.

Sample	Chemical compositions(mass%)				CaO/Al_2O_3
	CaO	Al_2O_3	SiO_2	Total	(molar ratio)
C-A glass L	41.0	53.0	48	98.8	1.41
C-A glass M	45.5	48.7	48	99.0	1.70
C-A glass H	52.2	42.0	49	99.1	2.27

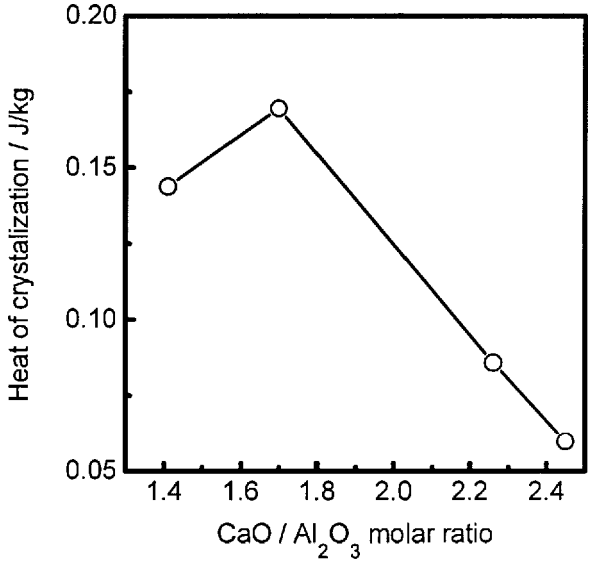

Fig.2 Relationship between heat of crystallization and CaO/Al_2O_3 molar ratio of C-A glass.

Hardening and development of strength

Figure 3 shows the relationship between time of final setting of mortar and $CaO\text{-}Al_2O_3$ molar ratio of the C-A glass.

The time of final setting was shorter with increased $CaO\text{-}Al_2O_3$ molar ratio. According to this result, it appears that the behavior of rapid hardening caused by accelerator consisting of C-A glass was mainly a function of the $CaO\text{-}Al_2O_3$ molar ratio, and is little affected by the heat of crystallization.

Figure 4 shows the compressive strength of the mortar.

At 3 hours and 6 hours, the strength when using C-A glass H, for which $CaO\text{-}Al_2O_3$ molar ratio

was highest, was lower than when using C-A glass L or M, for which $CaO\text{-}Al_2O_3$ molar ratio was lower. The strength at 24 hours when using C-A glass M, for which $CaO\text{-}Al_2O_3$ molar ratio was similar to $12CaO{\cdot}7Al_2O_3$, was a little higher than in the other cases. Later the influence of C-A glass on strength was negligible.

Nakagawa (1990) studied the strength development of cement mixed with C-A glass and anhydrite, and showed that the hydration of Alite in cement was retarded and that the strength in the early ages was suppressed when the $CaO\text{-}Al_2O_3$ molar ratio of the C-A glass was lower than 12:7. He suggested that alumina-gel or other kinds of aluminum-rich gelatinous hydrate product were formed on the surface of cement particles and suppressed their hydration. However, in our study using also sodium carbonate as a component of the accelerator, the results were different from those described in Nakagawa's paper, and strength increased as $CaO\text{-}Al_2O_3$ molar ratio decreased.

One reason for this difference was thought to be that the pH of the interstitial solution was raised by sodium carbonate and that the formation of gelatinous hydration product was suppressed, and the other presumed reason was that the suppression of hydration caused by gelatinous hydration product was diminished as sodium carbonate accelerated the hydration of cement. And from this study, it is suggested that gelatinous hydration product would contribute to the development of strength if formed.

On the other hand, as the hydration of cement progressed and the structure of cement hardened itself was formed after 24 hours, it is observed that the influence of the C-A glass on strength was small [Fig.4].

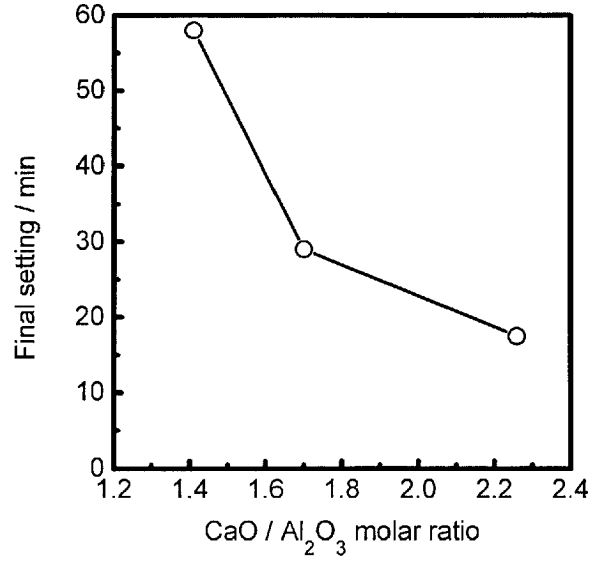

Fig.3 Relationship between time of final setting of mortar and CaO/Al_2O_3 molar ratio of C-A glass.

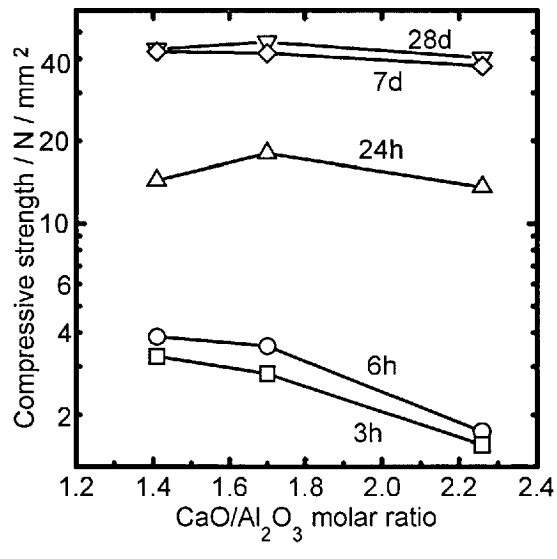

Fig.4 Relationship between compressive strength of mortar and CaO/Al_2O_3 molar ratio of C-A glass.

Change of hydratation products

Figures 5 and 6 show the change in the amount of ettringite and loss on ignition, respectively. Monosulfate and calcium hydroxide were detected after 6 hours by XRD, but quantitative analysis could not be carried out, as the quantities were too small. Further calcium carbonate could not be verified by XRD, because the main peak overlapped with Alite peak.

The hydration rate of cement was measured by quantitative XRD analysis, and it was concluded that the influence of variation of C-A glass on the hydration rate of cement was small, as there

was little diffrence in the decreasing tendency of Alite peak between samples within 6 hours. In the early stages, the amount of ettringite and loss on ignition increased faster when the CaO-Al_2O_3 molar ratio of C-A glass was higher. The increase in loss on ignition at an early stage was mainly attributed to the formation of ettringite. Subsequently, the amount of ettringite increased gradually after reaching about 10 % by mass, and the difference amongst the various C-A glasses became smaller at later stages. On the other hand, loss on ignition increased with time, while the rapid increase of amount of ettringite had stopped. The tendency towards an increase in loss on ignition was different with the C-A glasses tested; i.e., amount of Ettringite began to increase earlier when using C-A glass H than when using C-A glass L or M, but loss on ignition at 3 hours and 6 hours was less when using C-A glass H than when using C-A glass L or M. It is thought that there is excess of Al_2O_3 when ettringirte forms from C-A glass whose CaO-Al_2O_3 molar ratio is low. Material balance was calculated, assuming that same amount of ettringite formed from C-A glass L (CaO-Al_2O_3 molar ratio of 1.41) or C-A glass H (CaO-Al_2O_3 molar ratio of 2.26). For convenience sake, it was assumed that no Al_2O_3 remains when using C-A glass H.

C-A glass L: 1.00 g + CaO:0.28 g + $CaSO_4$:1.68 g → Ettringite: 5.16 g + Al_2O_3:0.11 g
C-A glass H: 1.00 g + CaO:0.17 g + $CaSO_4$:1.68 g → Ettringite: 5.16 g

As calculated above, 0.1 g of Al_2O_3 per 1 g of C-A glass is in excess when the CaO-Al_2O_3 molar ratio is 1.41, compared with when the CaO-Al_2O_3 molar ratio is 2.26. From these calculations, it is thought that the difference in loss on ignition at 3 hours or 6 hours referred to the fact that accelerator consisting of C-A glass L or M produced more aluminum-rich gelatinous hydration product than did C-A glass H, and that the gelatinous hydration product retained greater water content.

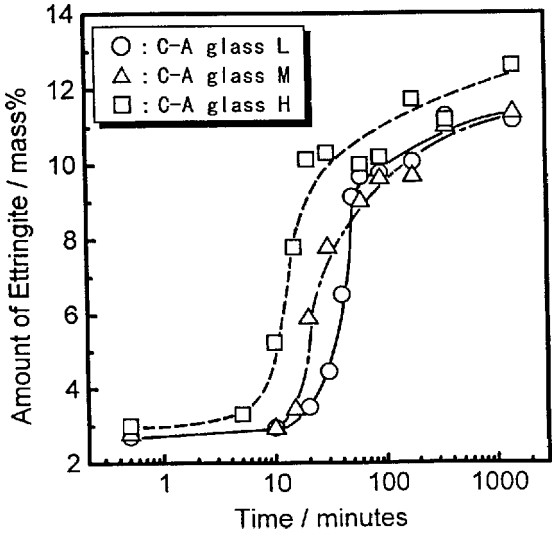

Fig.5 Changes in the amount of ettringite formed in the cement paste mixed with accelerator.

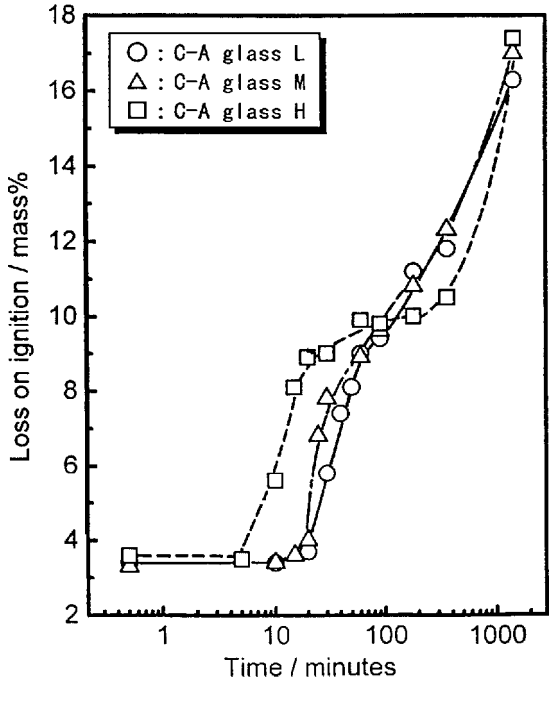

Fig.6 Changes in the loss on ignition of the cement paste mixed with accelerator.

According to the observations made, changes in hydration products relative to the properties of

mortar; the faster the increase in the amount of ettringite, the more rapidly mortar containing accelerator hardened. That is, the behavior of rapid hardening of mortar mixed with the accelerator is attributed to the formation of ettringite. On the other hand, the strength of such mortar at 3 hours or 6 hours was related to loss on ignition. It was mentioned before that for variation in $CaO-Al_2O_3$ molar ratio there was no obvious difference in the decrease in the unhydrated Alite peak by XRD at 3 hours or 6 hours, but there was obvious defference in loss on igniton. That is, a greater amount of some kind of aluminum-rich gelatinous hydration product formation, and this contributes to development of strength when using C-A glass with a lower $CaO-Al_2O_3$ molar ratio.

Change in the pore size distribution

Figure 7 shows the pore size distribution of hardened paste mixed with the accelerator.

There was little difference in total pore volume at each age, even if the $CaO-Al_2O_3$ molar ratio of the C-A glass varied. And the difference between pore volume at three hours and six hours was negligible amongst the various formulations of C-A glass.

Comparing pore size, there was a greater amount of large pores (1.0-10 μm) in the sample using C-A glass H. It is suggested that it was the reason that the strength of mortar using C-A glass H was lower than those using other C-A glasses at 3 hours and 6 hours. At 24 hours, the amount of the large pores decreased, and there was little difference in the amount of large pores amongst the hardened pastes using different formulations of C-A glass.

It is suggested that these results were obtained by the formation of aluminum-rich gelatinous hydration products; i.e., more gelatinous hydration product formed and filled in the pores of the hardened structure when the $CaO-Al_2O_3$ molar ratio was lower, but when the $CaO-Al_2O_3$ molar ration was higher, less gelatinous hydration products were formed, because there was less excess of Al_2O_3.

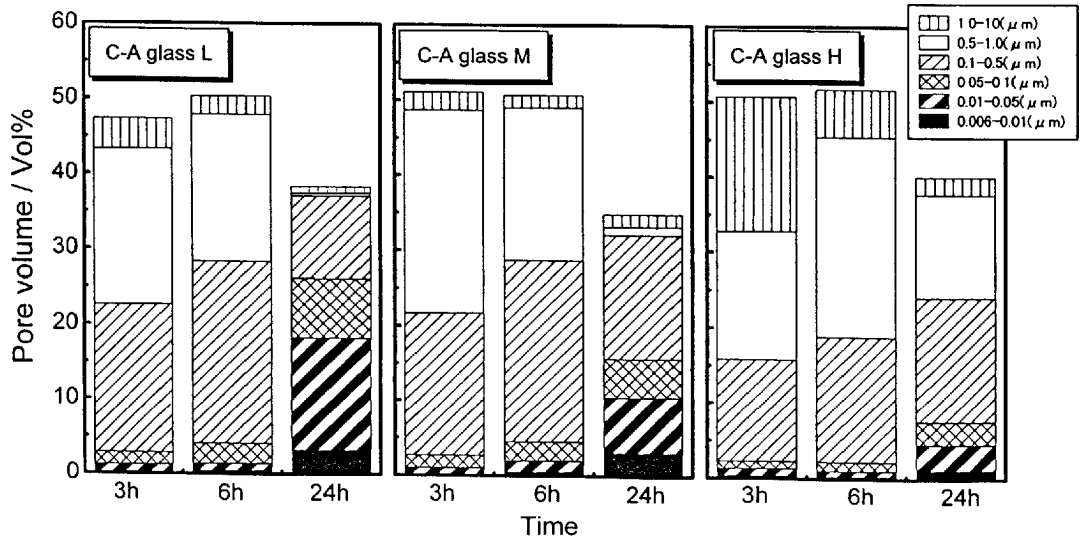

Fig.7 Pore size distributions of hardened cement mixed with accelerator.

Change in the concentration of ions in the solution

Figure 8 shows the changes in the concentration of ions in the solution extracted from paste samples.

While the change in the concentration of ions in plane cement paste was small, in the paste

mixed with accelerator, they varied significantly, regardless of the $CaO-Al_2O_3$ molar ratio of C-A glass.

Considering the relationship between the changes in concentration of ions and the properties of mortar, the time of final setting of mortar corresponded closely with the time when Al^{3+} increased temporarily and decreased subsequently, and Ca^{2+} and SO_4^{2-} decreased.

The concentration of each ion in the solution is an indication of balance between the amount dissolved from cement plus accelerator and the amount consumed to form hydration product. Therefore it is thought that Ca^{2+} and SO_4^{2-} were consumed and their concentration fell, while excess Al^{3+} remained in the solution, with respect to the dissolution of C-A glass and anhydrite and the formation of ettringite.

Noticing the accelerator, Al^{3+} increased to highest level and took the most time to fall when using C-A glass L for which the $CaO-Al_2O_3$ molar ratio was lowest. On the other hand, when using C-A glass M or H for which the $CaO-Al_2O_3$ molar ratio was higher, Al^{3+} changed at a lower level and was consumed rapidly. It is thought that, as the proportion of Al_2O_3 in C-A glass L was higher and the rate of formation of ettringite was lower than those in other formulations of C-A glass, as shown in Fig. 5, the concentration of Al^{3+} reached a high level temporarily. As the amount of ettringite and loss on ignition increased when the concentration of Al^{3+} changed significantly, as shown in Fig. 5 and 6, it is thought that Al^{3+} was consumed to form not only ettringite but also some kind of aluminum-rich gelatinous hydration product. As the $CaO-Al_2O_3$ molar ratio decreased, excess of Al^{3+} was dissolved and the amount of gelatinous hydration product increased.

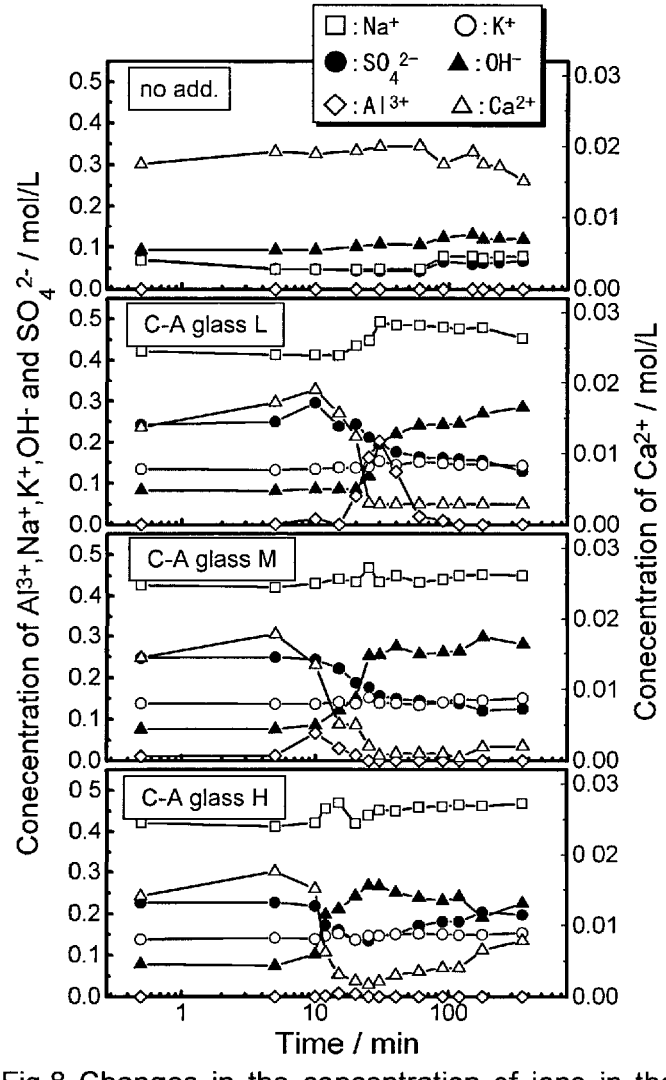

Fig.8 Changes in the concentration of ions in the solution extracted from the cement paste mixed with accelerator.

CONCLUSIONS

Rapid hardening of mortar mixed with accelerator based on calcium-aluminate glass is controlled by the $CaO-Al_2O_3$ molar ratio of calcium-aluminate glass, and the higher the ratio, the more rapidly the mortar hardens. This is caused by ettringite formed from the reaction of calcium-aluminate glass and anhydrite.

The concentration of ions in solution changes significantly when mortar mixed with accelerator hardens rapidly. Beginning with the rapid formation of ettringite, Ca^{2+} and SO_4^{2-} are consumed, and the concentration decreases, while excess Al^{3+} remains temporarily in the solution and is

consumed to form some kind of aluminum-rich gelatinous hydration product.

The compressive strength of mortar at 3 hours and 6 hours is higher when the CaO-Al_2O_3 molar ratio of C-A glass is lower than when the ratio is higher. On the basis of these results, it is suggested that gelatinous hydration products form from the excess of Al^{3+} and contribute to the development of strength when sodium carbonate is a component of accelerator based on calcium-aluminate glass.

ACKNOWLEDGEMENTS

The authors would like to thank Mr.S.Kikuchi, Ms.M.Takahashi, Mr.N.Ozawa and Ms.S.Tanaka of Nihon Cement Co., Ltd. for their assistance in this study.

REFERENCES

Hirose, S. and Yamazaki, Y., "Hydration Properties of Shotcrete with an Accelerator based on Calcium Aluminate", Proc. of the Engineering Foundation Conference "Shotcrete for Underground Support Ⅳ", May 2-6 1993, Niagara-on-the-Lake, American Society of Civil Engineers, pp. 25-32.

Nakagawa, K., Terashima, I., Asaga, K. and Daimon, M., "A Study on Hydration of Amorphous Calcium Aluminate by Selective Dissolution Analysis", Cem. Concr. Res., Vol. 20, No. 4, 1990, pp. 655-661.

Nakagawa, K., Thesis for a doctorate at the Tokyo Institute of Technology, 1990 (in Japanese).

ORGANOSILICONE COMPOUND EFFECT ON THE CEMENT MATRIX

Jacek SZCZERBA, Institute of Mineral Building Materials (IMMB), Cracow, Poland
Stanisław PEUKERT, Institute of Mineral Building Materials (IMMB), Cracow, Poland
Marzena ZDANIEWICZ, Institute of Mineral Building Materials (IMMB), Cracow, Poland

ABSTRACT The use of chemical admixtures reacting with cement matrix is considered to improve concrete durability. In the paper the effect of methylosilicone resin solution on cement pastes properties is presented. The rheology, setting time, heat of hydration and porosity of cement pastes made from different types of cement have been investigated. Depending on admixture content very differentiated influence on cement pastes was observed.

Key-words: modified cement, admixtures, setting, porosity

INTRODUCTION

The traditional cement mortars and concretes have properties limiting their application to special constructions, where enhanced durability is required. The main requirements on high performance concrete include mechanical strength, resistance to frost, abrasion properties and resistance to chemical aggression. Designs and construction methods of very durable buildings are realised by maximum densification of concrete structure. Compacting of the concrete structure can be obtained by using various additions. Generally silica fume with superplasticizers are applied. Other additives influencing on rheological properties of concrete mixture and performance properties of concrete are used. In the last decades very considerable progress is observed in research about admixtures and additives to concrete mixes like that; microaggregates, reducers, accelerators, plasticizers, superplasticizers, retarders, air entraining agents and polymer admixtures (Collepardi and Ramachandran, 1992, RILEM, 1995). The least attention has been devoted to the organo-silicone compounds. Effect of organo-silicone compounds in the hardening process of binding material has been the subject of publications in professional literature: Manżurnet et al (1963), Alentjev et al (1965), Artemenko (1989), Domin et al (1995). Nevertheless the problem has not yet been fully recognized. This article presents the effect of resin admixture on the properties of cement pastes. Additive of methylosilicone resin solution was used. The experimental research carried out has been concentrated particularly on the rheological properties.

EXPERIMENTS

The following three types of cement were used for the experiments: Portland cements CEM I 42.5 and CEM I 32.5, which have similar phase compositions but different specific surfaces. Blastfurnace slag cement CEM III/A 32.5 and pozzolanic cement CEM IV/A 32.5 were also investigated. The properties of the cements are represented in **Table 1**.

A 20% solution of methylosilicone resin in potash lye with density 1.27±0.02 g/cm^3 was used as the modifier. It was mixed with water and added into the pastes in appropriate quantities corresponding to the mass of the cement. The resin solution addition to cement paste was ranged from very low quantity of 0.05% up to very large concentration of 5% by mass.

The rheology of pastes, their setting times, kinetics of hydration, porosity of hardened pastes and water requirement of cements was investigated.

Table 1 Properties of cements

Composition	Type of cement			
	CEM I 42.5	CEM I 32.5	CEM III/A	CEM IV/A
	Composition content (% by mass)			
L.O.I.	0.63	1.03	1.10	2.90
SiO_2	21.68	21.02	30.62	32.41
Al_2O_3	4.15	4.51	6.41	13.85
Fe_2O_3	1.87	2.08	1.32	4.54
CaO	67.23	65.21	51.90	40.47
MgO	0.80	2.39	4.62	1.66
SO_3	2.88	2.33	1.96	1.92
Na_2O	0.25	0.11	0.32	0.30
K_2O	0.46	0.97	0.50	1.28
Na_2O_{eq}	0.55	0.75	0.65	1.14
Phase composition				
C_3S	70.0	65.5		
C_2S	9.3	10.9		
C_3A	7.8	8.4		
C_4AF	5.7	6.3		
Physical properties of cement				
Specific surface area (Blaine) (cm^2/g)	4500	3200	3200	3900

The relation between the apparent viscosity and organosilicone compound content in cement pastes was determined by means of a rotational viscometer. Apparent viscosity was estimated for cement pastes at a constant w/c ratio of 0.5 and 0.4 at a shear rate of $27s^{-1}$. Cement pastes for viscosity determination were mixed during 5 minutes.

Investigations of the physical properties of the cement pastes were conducted in accordance with the European Standard EN 196 series. The initial and final setting time was determined for cement pastes at normal consistency.

The heat of cement hydration was determined using semi-adiabatic calorimetry in compliance with pr. EN 196-8.

The porosity of the tested pastes was determined by the mercury porosimeter method, using a high-pressure measurement to estimate pores size in a diameter range from 3.7 to 6300 nm, and measurement at a low pressure for the 6300 - 53600 nm diameter range. Determination of the pores size distribution was carried out for paste samples with and without resin admixture at normal consistency. The porosity of the cement paste was determined for samples after 3, 7 and 28 days of curing at standard conditions.

RESULTS AND DISCUSSION OF EXPERIMENTS

Viscosity

The apparent viscosity of the cement pastes is presented in **Fig 1**. Investigations of the fresh pastes showed that methylosilicone resin solution influenced the rheology of the cement pastes depending on the type of cement, w/c ratio and resin additive concentration. Adding of resin up

to 0.1% did not change significantly the viscosity of pastes regardless of the cement types and w/c ratio. Further increase in the amount of resin added brought about a variety of effects on the paste rheology depending on the cement types. For resin concentration over 0.2% the apparent viscosity of the Portland cement CEM I 42.5 at w/c ratio 0.4 and 0.5 started to increase rapidly. The behaviour of Portland cement CEM I 32.5 was observed to be quite different. For w/c ratio of 0.5 and 0.4 increments of the resin concentration up to 2% caused a constant decreasing of cement paste viscosity (Fig 1).

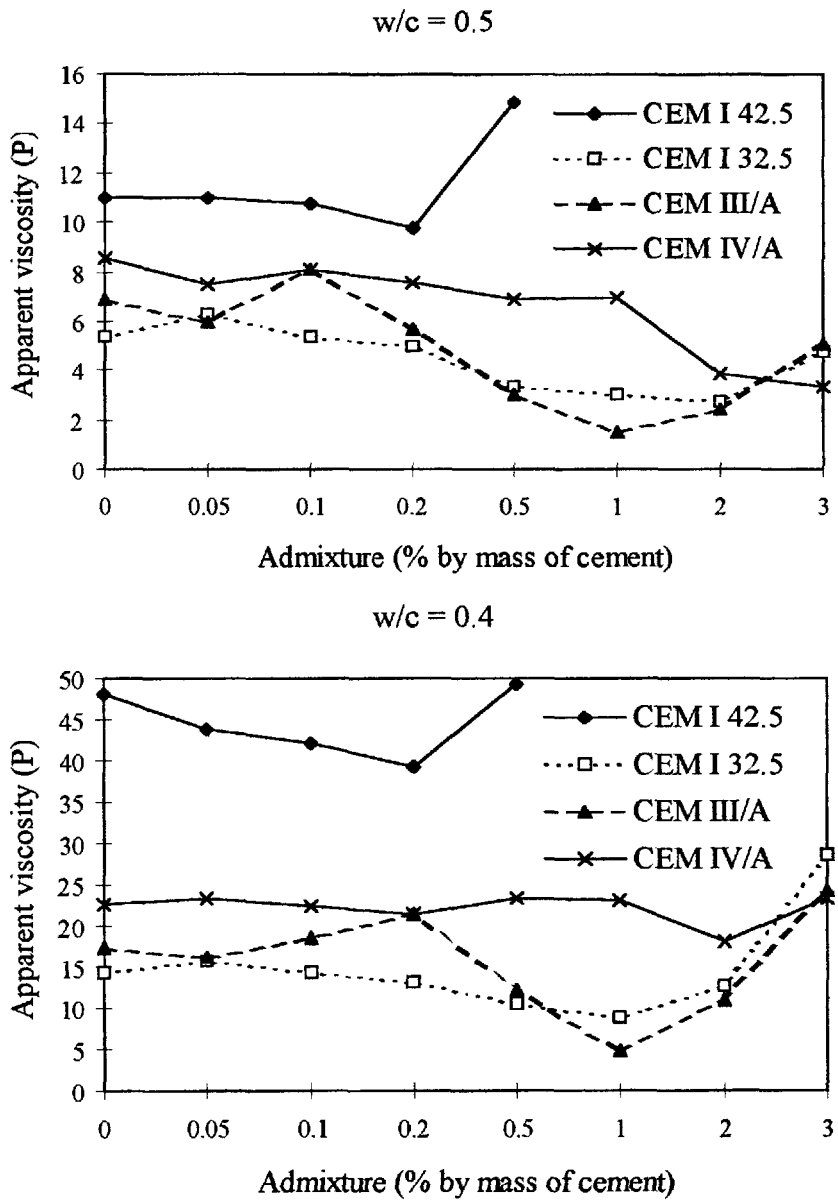

Figure 1 Effect of admixture on viscosity of the cement paste at shear rate 27 s^{-1}

Effect of methylosilicone resin solution on change of paste viscosity for blastfurnace slag cement CEM III/A is similar at both w/c ratio. In this case there was observed strong reducing of cement paste viscosity at 1% resin admixture. The least influence of admixture on paste viscosity was observed for the pozzolanic cement CEM IV/A irrespective of w/c ratio. For all range of the resin concentration the viscosity of pozzolanic cement appeared to be about the same value.

Water demand

The results of water demand tests are presented in **Table 2**. It can be seen that amounts of the methylosilicone resin solution of up to 0.5% in the cement lowered the water demand by approximately 5% for OPC CEM 32.5 and 2% for CEM I 42.5 and CEM III/A. For Portland and blastfurnace cements more than 0.5% admixture caused rapid increasing of cement water demand. It is interesting that no influence of admixture on water demand was observed for pozzolanic cement practically for total range of additive concentration in cement paste.

Table 2 Cement water demand

Quantity of admixture (% by mass of cement)	Water demand (% by mass)			
	CEM I 42.5	CEM I 32.5	CEM III/A	CEM IV/A
0	27.5	27.0	27.0	31.5
0.05	26.0	27.0	27.0	31.5
0.1	26.5	26.0	25.0	31.0
0.2	25.5	24.0	25.0	31.0
0.5	26.5	21.5	25.0	31.5
1	28.0	22.5	25.5	31.5
2	29.0	28.0	26.0	31.5
3	33.0	28.5	27,5	31.5
5	44.0	29.0	28.0	33.0

The test results of the cement water demand determination explain very well changes in the rheological properties of the pastes searched as the influence of the admixture on paste viscosity. As could be presumed the changes of the cement water demand caused by resin admixture influenced on the fluidity and therefore apparent viscosity of cement paste.

Setting time

Effect of the organo-silicone resin admixture on setting time of cement is shown in **Fig 2 and 2a**. The resin solution addition was found as a strong retarder of the initial and final setting time for OPC and blastfurnace slag cements. That retardation effect was accelerated when resin concentration was increased but only up to some limit. After this limit concentration accelerating effect of setting time was observed. That correlation was stated for all types of cements investigated. The highest changes of the setting time was stated for paste made from pozzolanic cement.

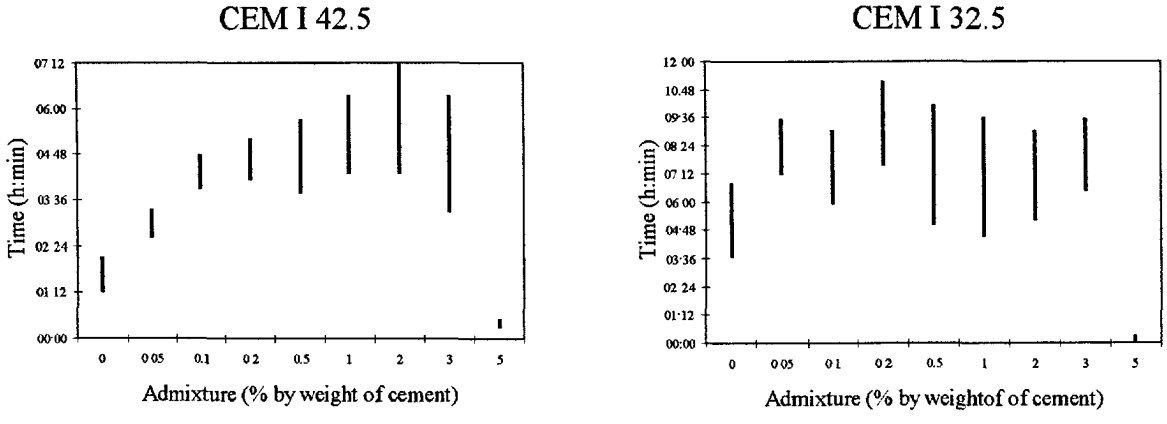

Figure 2 Effect of admixture on setting time of OPC cements

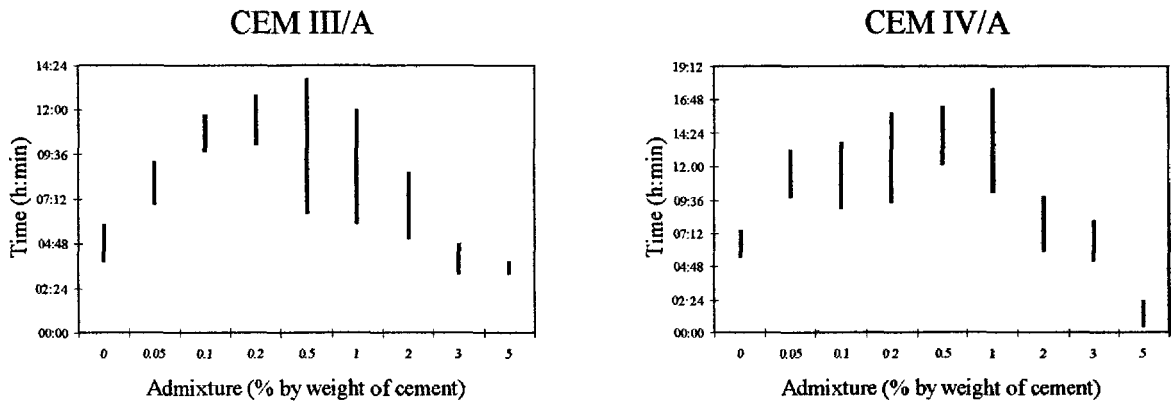

Figure 2a Effect of admixture on setting time of blastfurnace slag and pozzolanic cements

Heat of hydration

OPC, blastfurnace slag cement and pozzolanic cement containing different resin admixture amounts were subjected to tests. The results are shown in **Fig 3, 4 and 5**.

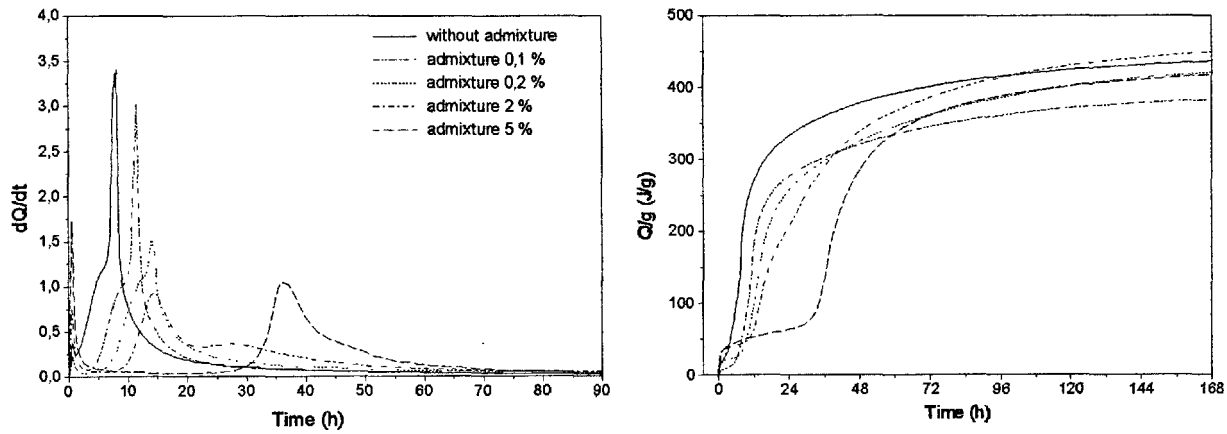

Figure 3 Heat of hydration of OPC CEM I 42.5

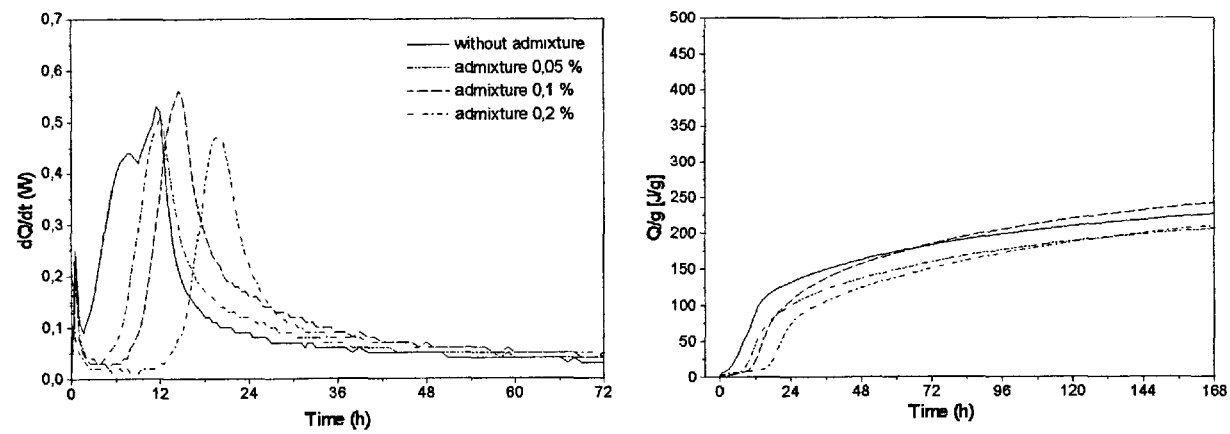

Figure 4 Heat of hydration of blastfurnace slag cement CEM III/A 32.5

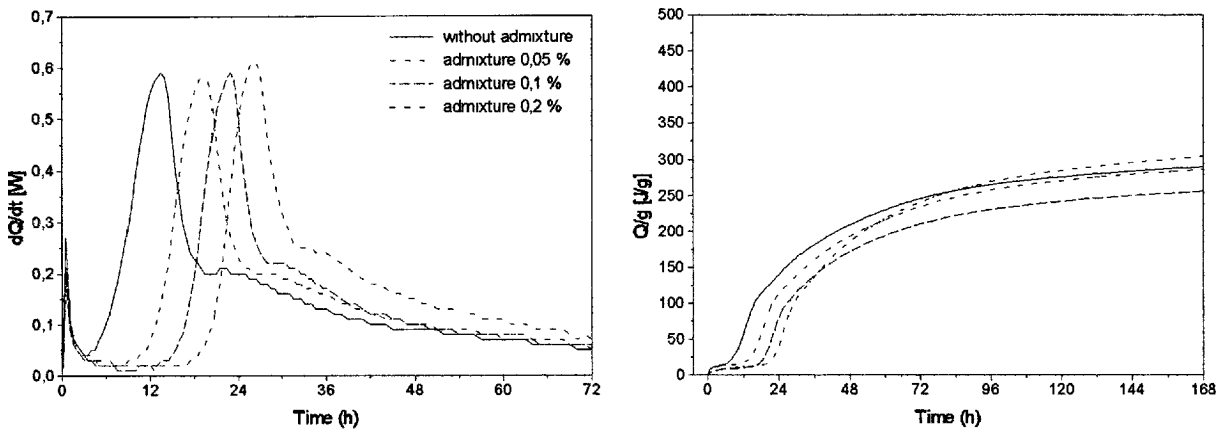

Figure 5 Heat of hydration of pozzolanic cement CEM IV/A 32.5

Analysis of heat of hydration investigations leads to conclusion that the kinetics of cement hydration was clearly influenced by the amount of methylosilicone resin addition. It appeared that heat of hydration value strongly depends on the amount of additive regardless of cement type tested. There was a clear delay effect of the maximum rate of heat emission at low resin addition. In this case a decrease of total heat of hydration value was also observed. Contrary, admixture over 1% was found to increase cement heat of hydration. For blastfurnace slag cement and pozzolanic cement that limit value of admixture addition was 0.1 and 0.2% respectively.

Porosity

The pores size distribution in hardened pastes are shown on **Figs 6, 7 and 8**. Pastes made at normal consistency from Portland cement CEM I 42.5, blastfurnace slag cement CEM III/A 32.5 and pozzolanic cement CEM VI/A 32.5 were investigated.

Analysis of pores size distribution in pastes made from OPC cement shows that the total porosity of the paste with and without admixture decreased with curing time (Figs 6 and 7). However, the pastes with the organo-silicone admixture showed that smaller size pores are predominant. The following conclusions may be drawn from the comparison of the pores size distribution in pastes of OPC cement with and without the methylosilicone resin:

- after 3 and 7 days of curing samples containing the polymer addition up to 0.1% and over 1% were found to increase total porosity. Addition of 0.2 to 1% of polymer was found to decrease the porosity.
- after 28 and 180 days of curing changes of porosity were quite different. In these cases the addition of the organo-silicone compound reduced total porosity in all addition concentrations range. There was a clear shift in the predominant pores size to the lower range of 3.7 - 100 nm. That pore size distribution is considered to guarantee higher tightness and density.

The quite different influence of admixture on pores size distribution in pastes was noticed for blastfurnace slag cement and pozzolanic cement. In comparison to the OPC, blastfurnace slag and pozzolanic cement pastes were found to be more porous (Fig 8). Higher total porosity for blastfurnace slag cement is connected with increasing the number of pores diameter over 100 nm but for pozzolanic cement with increasing porosity in all measuring range.

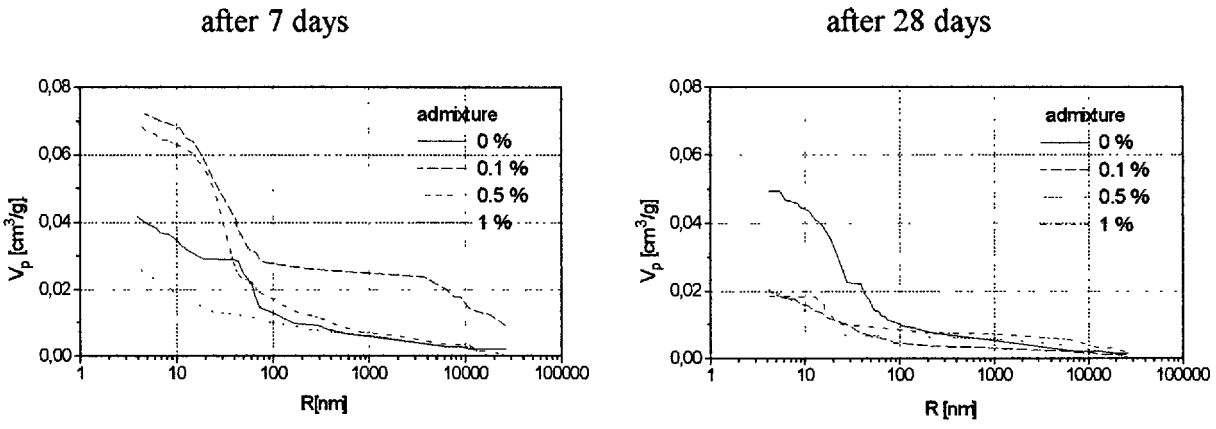

Figure 6 Porosity of cement paste for OPC

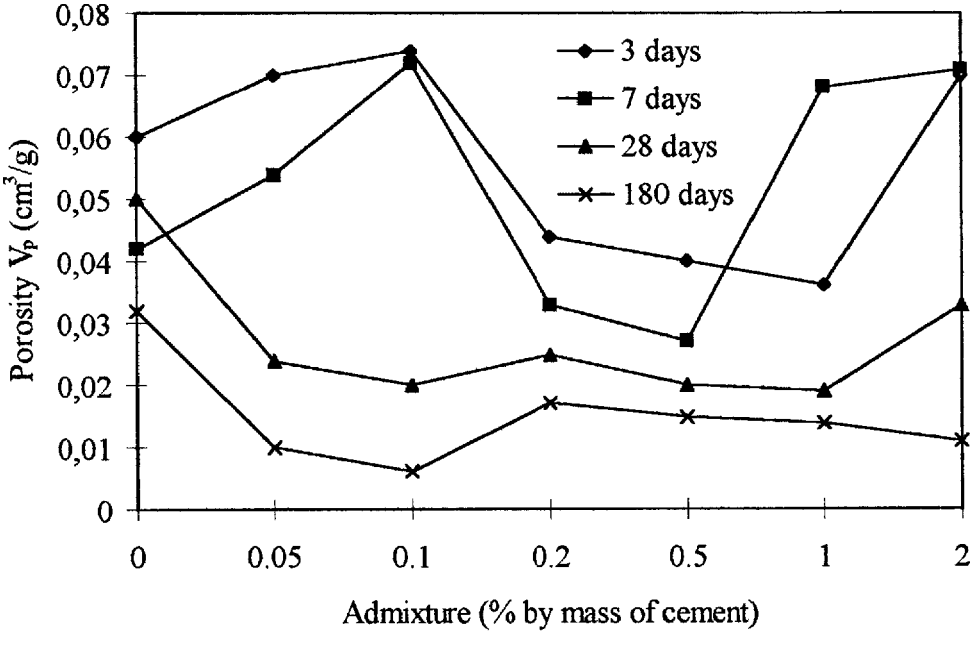

Figure 7 Effect of admixture on total porosity of the cement paste for OPC for different curing time

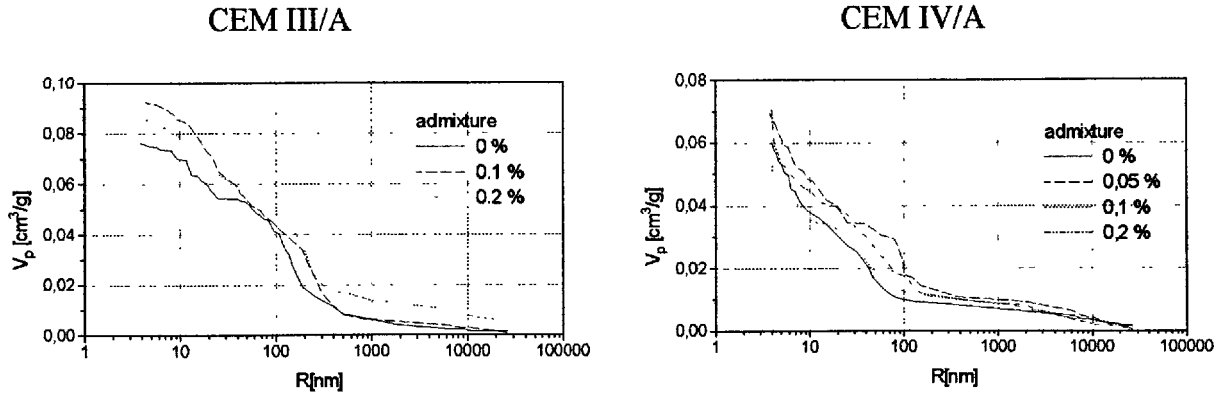

Figure 8 Porosity of cement paste for CEM III/A and CEM IV/A cements

CONCLUSION

The tests conducted to determine the effect of methylosilicone resin admixture on cement paste showed that:

- a silicone resin added to a cement binding material may act either as a plasticizer or as a retarder; the effect depends on the type of cement;
- the addition of up to 0.5% of the admixture contributes the best effect on rheological properties of fresh pastes and also on structure of hardened cement pastes;
- the favourable effect of methylosilicone resin on the porosity structure of cement pastes suggests that it may prove useful in the design and production of high performance concretes HPC.

REFERENCES

Alentjev, A.A., Paszczenko, A.A., Kalejnikova N.M., "Organosilicone solutions hydrofobic cement", Stavivo, No. 9, 1965, pp. 336-338.

Artemenko, A.I., "Application of polymers and organo-silicones in building", Scientific Bulletins of the High Engineering School in Opole, Opole 1989, Bul. 24.

Collepardi, M., and Ramachandran, V.S., "Effect of Admixtures", Proceedings of the 9-th International Conference on the Chemistry of Cement, 1992, Vol. 1, pp. 529-568.

Domin, T., Luchter, E., Maj, R., "Hydrofobic cement mortars", Cement-Wapno-Gips, No. 5, 1995, pp. 162-164.

Manżurnet, W.W., Paszczenko, A.A., Tereszczenko, N.P., "Investigation of properties of organosilicone solution hydrofobic cement", Cement, No. 4, 1963, pp. 13-14.

RILEM, "Application of admixtures in concrete", Edited by A.M. Paillere, RILEM Report 10, First edition 1995, Published by E & FN Spon, London SE1 8HN, UK.

SODIUM SILICATE APPLICATIONS FOR CEMENT AND CONCRETE

J. LAROSA-THOMPSON[1], P. GILL[1], B.E. SCHEETZ[2], and M.R. SILSBEE[2]
[1]The PQ Corporation, Valley Forge, PA 19482, [2]The Pennsylvania State University, University Park, PA 16802

ABSTRACT Soluble sodium silicates have been used in industry for a wide variety of applications. From detergents to adhesives, and deflocculant aids to corrosion inhibitor, these simply manufactured products have shown great versatility since their initial development in the early 19th century. This paper reviews the use of sodium silicates as cement sealer, integral admixtures for construction, and in specialty formulas for waste disposal.
KEYWORDS: admixtures, concrete, durability

INTRODUCTION

The raw materials for sodium silicate manufacture are soda ash and sand. Heated to 1100-1200°C, the materials fuse and a glass forms upon cooling. This glass is sometimes sold as anhydrous powder that can be dissolved later by the user, or the glass may be dissolved in water at the manufacturing plant. The resulting solution, also known as "water glass," may be sold as it is, or it may be causticized to form more alkaline solutions. Silicate solutions can also be dried to form hydrous powders, or they may be further processed to form hydrous and anhydrous metasilicates. The SiO_2/Na_2O weight ratio of the products typically falls in the range 1.0-5.0, and the liquids typically have an SiO_2 content of 24-36%. Soluble silicates are polymeric materials which are classified by the SiO_2:Na_2O ratio[7]. Diluted in water, the soluble silicates depolymerize to form negatively charged oxygen sites which react with positively charged metal ions in solution to form "metal silicates." These metal silicates are not soluble species but are combined polymeric species, the molecular weight of which varies depending upon pH and ionic strength. Table 1 contains descriptions of the sodium silicates used for this study.

Table 1 - Compositions of sodium silicates used in this study.

ID*	SiO_2/Na_2O wt. ratio	Wt. % water	Comments
N	3.22	62.4	aqueous liquid
D	2.00	55.9	aqueous liquid
OW	3.22	61.4	aqueous liquid with surfactant
SS-65	3.22	-.-	anhydrous powder
G	3.22	18.5	hydrous powder

Sealer

Within the cement and concrete industry, soluble silicates have varied uses. One of the foremost is as a sealant, providing chemical and physical durability to concrete surfaces such as bridges, walls, storage tanks, building blocks, warehouse floors, traffic barriers, slabs, and countertops. The porous nature of the cement matrix and of aggregate/cement interfaces cause such structures to be susceptible to chemical attack by acid or deicing salts and to freeze/thaw damage.

* Supplied by the PQ Corporation, Valley Forge, Pennsylvania USA

Therefore, an effective surface treatment must provide some means of inhibiting the transport of deleterious components.

Among the commercially available concrete sealers, three classes may be defined according to their means of protection. Some sealers are water repellents and include silanes, siloxanes, silicones, and stearates. Others, such as epoxies, polyesters, and vinyls, provide a barrier coating on top of the surface. Those in the third group, which includes aqueous sodium silicates, urethanes, linseed oil, and mineral gums, block pores near and at the surface but do not coat the top of the surface. Lea (1971) reports that sodium silicates have been found useful for protection against aqueous solutions and organic liquids.

The unique feature of the sodium silicate is that it chemically reacts with portlandite to form C-S-H[a] . The presence of CH is detrimental to both the cement's chemical and mechanical durability. CH is water soluble and susceptible to acid attack, and the interfaces around the CH are typically highly porous, thereby increasing permeability while decreasing strength. Penetrating the concrete surface with aqueous sodium silicate, provides the silicate needed to convert CH to C-S-H. As a result, the density and strength increases and the permeability decreases near the surface.

Controlling the penetration depth of the aqueous sodium silicate is critical to its performance as a sealant. On the one hand, the aqueous sodium silicate must penetrate about 3 to 6mm to affect a significant enough volume. However, if the penetration is very deep the aqueous sodium silicate may be too diffuse to be effective. The permeability and moisture content of the substrate are therefore extremely influential in the proper application of an aqueous sodium silicate sealer. Penetration depths may be greater with porous concrete, which would require multiple applications to prevent the aqueous sodium silicate from becoming too diffuse; while a 6mm depth may not be possible with a dense concrete.

Several factors control the penetration depth of aqueous sodium silicate. These include the following: 1) concentration of the aqueous sodium silicate; 2) the moisture content of the substrate; 3) condition of the substrate surface; 4) temperature; 5) mechanical force used during application of the aqueous sodium silicate (e.g., via a high pressure sprayer, brushing, etc.); and 6) presence or absence of wetting agents.

A typical liquid sodium silicate sold for this application would have a SiO_2/Na_2O ratio of ~3, ~30% SiO_2, a density of 1.4g/cc, pH ~11, and viscosity ~180cp. Before using the liquid sodium silicates are typically diluted by 3 parts (on a weight basis). Also, since the moisture content of the concrete is critical, it is best if the aqueous sodium silicate is applied at least four weeks after new concrete is placed. Preparing the surface to be coated is another important factor. For example, preparing a floor for coating includes sweeping, scrubbing with strong cleaning compounds using a scrubbing machine or wire brush to expose the true wearing surface, scrubbing again with soapy water, and then allowing the floor to dry for at least 24 hours depending on the humidity.

---

[a] Typical cement notation us used here, i.e. C=CaO, S=SiO_2, A=Al_2O_3, F=Fe_2O_3, etc.

Absorption is a measurement of a concrete's ability to contain liquid. Absorption is an important property to consider when evaluating the durability of hardened cements and concretes. For instance, Litvan (1992) reported a correlation between absorption and freeze thaw durability of coated concretes. To measure the effect of a surface coating of aqueous silicate, concrete blocks were coated with N and OW silicate in varying weight ratios and were allowed to dry for 24 hours before testing (The OW silicate contains surfactants to improve wetting.). ASTM Standard Method C642-90 was used to test the blocks for absorption.. Concrete specimens were immersed in water for a time not less that 48 hours and until they reached a constant weight. The blocks were then placed into boiling water for 5 hours and weighted again. The voids are calculated from these weights. As shown in Figure 1 the blocks coated with aqueous sodium silicate always absorbed less than the uncoated control. For instance the 3/1 N (silicate/water weight ratio) decreased the water absorption by 30% over the control sample. The 1/1 OW absorbed slightly less water than the 1/1 N suggesting that the surfactant is effecting the penetration of the aqueous sodium silicate into the concrete.

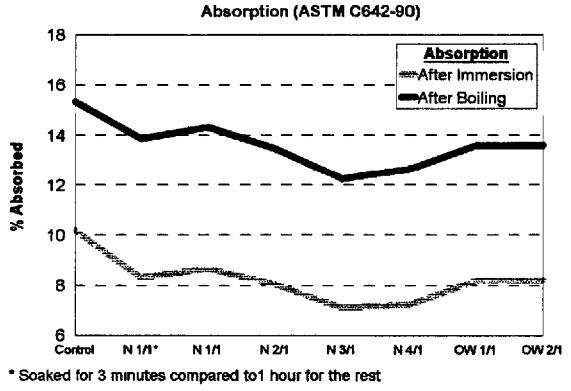

Figure 1 Water Absorption as a Function of Silicate/Water Ratio

Figure 2 shows the percentage voids or degree of porosity of the concrete samples after being coated with aqueous sodium silicate. Again, the 3/1 N sample outperformed the other samples, and showed a 5% decrease in percentage voids over the control. The decrease in percentage voids is directly related to a decrease in permeability and a decrease in the amount of water that can be absorbed. It should be noted that the trend of Figure 2 is the same as the trend in Figure 1. This data suggests that the strength and permeability of the samples will follow the same trend.

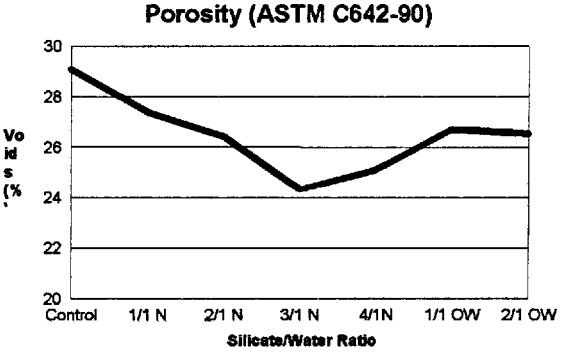

Figure 2 Apparent void space in coated concrete blocks.

The abrasion resistance of coated and uncoated concrete blocks was determined by ASTM Standard Test Method C418. The abrasion coefficient is determined by sand blasting the blocks for one minute and then measuring the volume of concrete removed from the block. A lower abrasion coefficient denotes a more abrasion resistance material. Figure 3 shows that as with the two previous measurements, the 3/1 N coating performed significantly better than the rest. The decrease in abrasion coefficient from the control to the 3/1 N coating is 67%. The other coatings follow the same trend that the percentage absorption and percentage voids data showed. The 1/1 OW has the same abrasion coefficient as the 3/1 N and may be due to the increased degree of penetration achieved with the surfactant in OW.

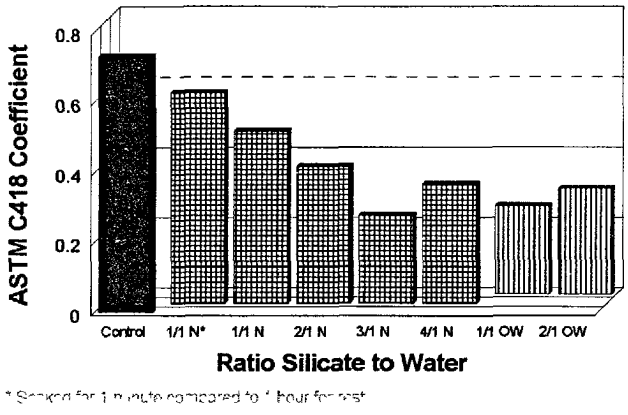

Figure 3 The effect of aqueous silicate coatings on the abrasion resistance of concrete blocks.

In the work of Litvan (1992), the freeze-thaw resistance of 8 types of mortar specimens treated with 57 concrete sealers was measured according to ASTM C666 procedure. Litvan's work is summarized in Figure 4. Litvan concluded that the ability of certain sealers to reduce expansion due to freeze-thaw cycling was directly related to the ability of a sealer to restrict movement of water through the surface region. The silicate based sealers exhibited the lowest degree of expansion in contrast to many sealers that caused greater expansion.

Integral Admixtures for Construction

Sodium silicates are also used as integral admixtures. An excellent example of this use is shotcreting in which liquid silicate is sprayed into a stream of concrete that is being "shot" at a wall or ceiling. The effect of the sodium silicate additions is two fold. The soluble SiO_2 is immediately available to react with the CH and form C-S-H as shown in Figure 5 where powder x-ray diffraction results illustrate the reduction in the CH content as liquid silicates are added to the portland cement paste. As the silica is consumed the alkalis associated with the soluble silicates raise the pH further accelerating hydration. Figure 6a shows the that set times(determined by ASTM C191) are decreased significantly when liquid silicates are used in portland cement pastes. Figure 6a shows that small dosages reduce the set times while higher

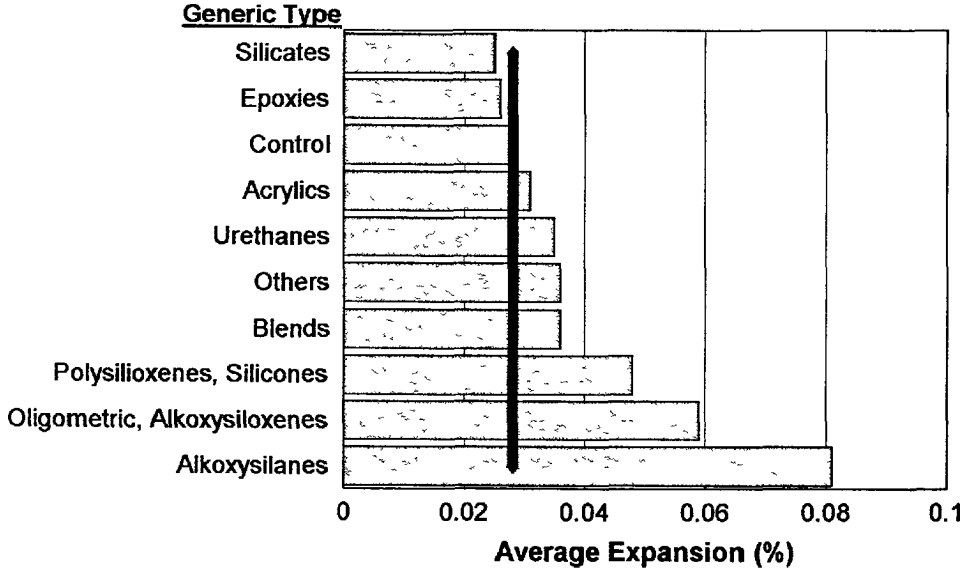

Figure 4 Ultimate average expansion of specimens treated with sealers of various generic types after 300 freeze-thaw cycles (after Litvan (1992)).

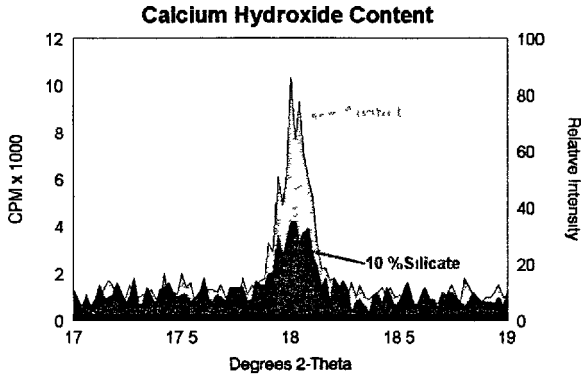

Figure 5 Effect of 10% N silicate addition on calcium hydroxide content in portland cement pastes. The pattern was taken from a 28 day old cement pastes with W/C = 0.4, cured at 25°C.

However, in spite of higher strengths at 1 day the anhydrous (SS-65) silicate containing pastes exhibited 28 day strengths similar to the control. In contrast to the hydrous (G) sodium silicates that result in higher 1, 7 and 28 day strengths compared to the control.

Waste Applications

Nine companies, world-wide, offer a chemical fixation system based on portland cement and soluble sodium silicate (Connor (1990)). These stabilization systems are used with a wide range of hazardous materials from heavy metals, organic to nuclear wastes. The objectives of these solidification and stabilizaton (S/S) systems is to eliminate all free liquids, improve handling and physical properties of the wastes, reduce mobility, toxicity and leachability of the hazardous components (PQ Corp. (No date)).

Soluble sodium silicate serves several functions in S/S systems. As shown in Figure 6 silicates can be used as an effective set regulator. The presence of soluble sodium silicate in freshly mixed portland cement has the effect of raising the pH of the pore fluids as well as maintaining a elevated level of dosages do not proportionately further reduce the set times. Figure 6b shows that modest dosages of soluble silicates increase the compressive strength of portland cement pastes. Apparently at higher dosages the rapid setting caused by the soluble silicates results in a more disorder structure and lower strengths.

Figure 7 examines the effect of additions of hydrous (G) and anhydrous sodium silicate (SS-65) powders on the strength developed in portland cement pastes. Regardless of the type of silicate used higher 1 day strengths, compared to the control, were observed. At the levels tested, the smallest additions resulted in the highest gain in 1 day strengths.

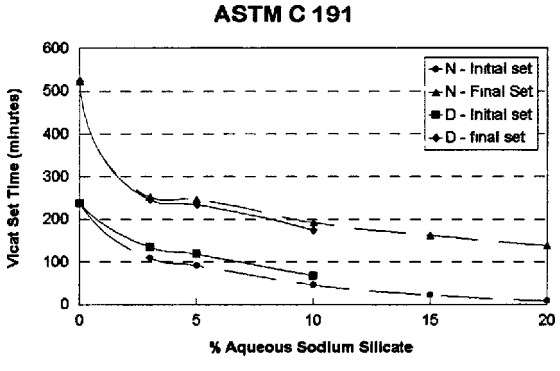

(a)

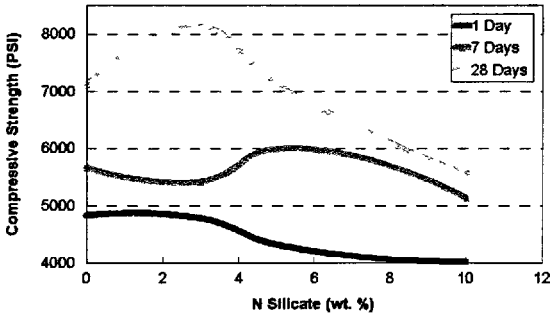

(b)

Figure 6 The effect of aqueous sodium silicate additions on (a) Vicat set times and (b) compressive strengths in portland cement pastes (w/c= 0.40).

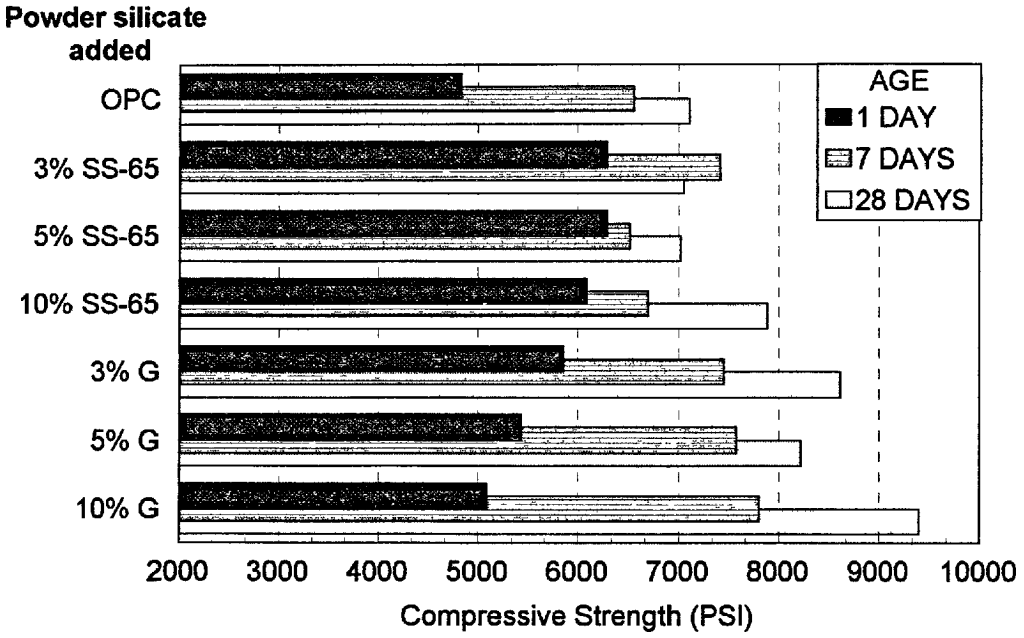

Figure 7 Effect of hydrous (G) and anhydrous (SS-65) sodium silicate powder on 28 day strengths in portland cement pastes.

labile silicon ions in these fluids (Hoffer 1990)). In, cement fly ash, lime and fly ash and kiln dust-based stabilization systems, the gelling time can be controlled from a half minutes to a half hour instead of 24 to 48 hours and still maintain pumpability (Scheetz and Hoffer (1996)).

Secondly, most heavy metals are least soluble at elevated pH ranges generally precipitating as metal hydroxides. In an extensive study, Silsbee and Scheetz (1993) have demonstrated lead extracted from the pore fluids of lead-bearing portland cement/soluble silicate waste forms was solubility limited in the form of lead hydroxide, figure 9.

Finally, as noted above, the reaction of soluble silicate with portlandite formed during the progressive hydration of both di- and tri-calcium silicate contributes to the enhanced formation of C-S-H in the waste form matrix. Effectively there is more "glue" per unit volume, therefore, physical properties of the composite are improved. C-S-H can act as an encapsulant for waste species, as a template for chemisorption of waste species or as a crystal chemical host . The most comprehensive model for C-S-H as a crystal chemical host was presented by Richardson and Groves (1993):

$$\mathbf{Ca_xH_{(6n-2x)}(Si_{1-a}R_a^{[IV]})_{(3n-1)}O_{(9n-2)} \cdot A^{c+}_{a(3n-1)/c} \cdot zCa(OH)_2 \cdot mH_2O}$$

where:

$x = 0.5(6n-w)$

$z = 0.5[w+n(y-2)]$

$for\ 0<y<4;\ n(2-y)<w,2n$

$2<y<4;\ 0<w<2n$

$4<y<6;\ 0<w,n(6-y)$

and $0<a<(n-1)/(3n-1)$

$R^{[IV]}$ = trivalent, tetrahedrally coordinated cation (usually Al or Fe)

A^{c+} = interlayer ion which charge balances the R^{3+} substitution for Si^{4+}.(M^{+})

Ni, Co (Atkins et al (1993)), U, I and Sn are reported to be substituted for Ca^{2+} on the surface of C-S-H. Cr^{3+} is reportedly exchanged for Al^{3+} in poorly crystalline C-S-H. Both Ni and Cd are reported to precipitate as $M(OH)_2$ species.

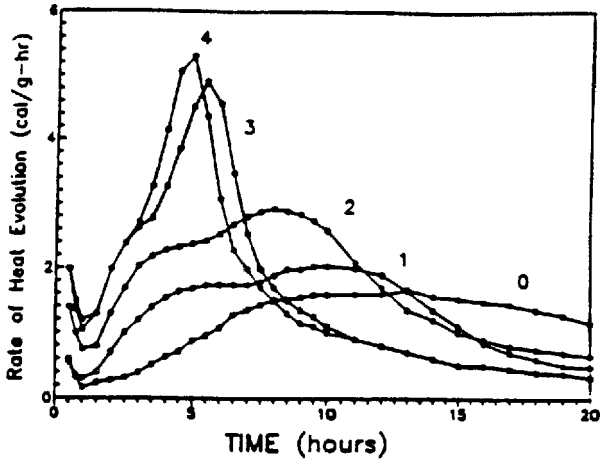

Figure 8. Heats of hydration of a portland cement paste (w/c = 0.5) with 0,1,2,3,4 g of soluble silicate added to 50 g of cement.

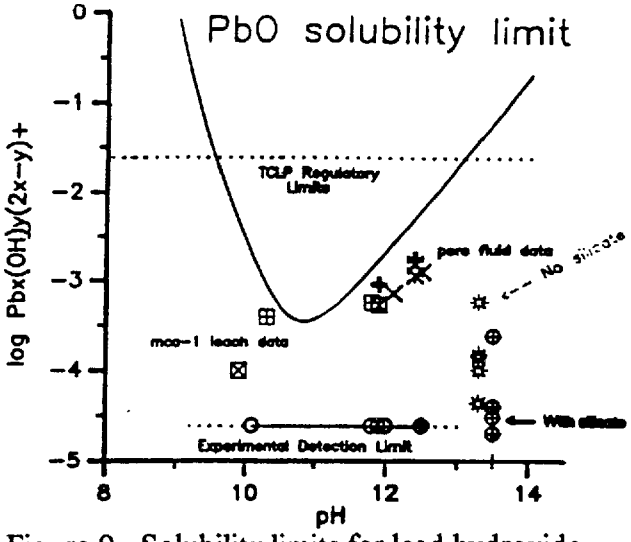

Figure 9. Solubility limits for lead hydroxide established by expressed pore fluids from lead-bearing portland cement waste forms.

SUMMARY

Soluble sodium silicate has a long history as an industrial chemical with a wide variety of used outside of cement and concrete application. This review has focused on its applications as an external sealant and as a reactive chemical admixture that controls has the ability to control both physical and chemical properties of hardened cementitious solids.

REFERENCES

Atkins, M., F.P. Glasser, L.P. Moroni and J.J. Jack, "Thermodynamic Modelling of Blended Cements at Elevated Temperature (50-90°C), DOE/HMIP/RR/94.011 (1993).

Conner, J.R., "Chemical Fixaton and Solidification of Hazardous Wastes," Von Nostrand Reinhold, NY, (1990).

Hoffer, Jefferson, M.S. Thesis, The Pennsylvania State University (1990).

Lea, F.M., The Chemistry of Cement and Concrete, Chemical Publishing Company, Inc., (1971).

Litvan, G.G, "The Effect of Sealers on the Freeze-Thaw Resistance of Mortar", Cement and Concrete Research, Vol 22, pp. 1141-1147, 1992.

PQ, Corp. "Treatability Study Manual for Solidifiaction and Stablizaton," Valley Forge, PA (no date).

Richardson, I.G. and G.W. Groves, "The Incorporation of Minor Trace Elements into Calcium Silicate Hydrate (C-S-H) Gel in Hardened Cement Pastes," Cem & Concr. Res, Vol 23, pp 131-139 (1993).

Scheetz, Barry E. And Jefferson Hoffer, "Characterization of Sodium Silicate Activated Portland Cement:1. Matrices for Low-Level Radioactive Waste Forms, Concrete and Grout in Nuclear and Hazardous waste Disposal," American Concrete Institute, ACI SP-159, pp 91-110 (1996).
Silsbee, M.R. and Scheetz, B.E., Annual Report to the PQ Corporation, (1993).

TOPIC III.C

Combined admixtures and their mixing techniques

MECHANISM OF ALKALI-CONTAINING COMPLEX CHEMICAL ADMIXTURES AND PORTLAND CEMENTS INTERACTION

Myroslav A.SANITSKY, State University "Lviv polytechnic", Ukraine

ABSTRACT Chemistry of hydration and hardening processes cement pastes with a multifunctional complex admixtures which include surface-active substances and alkali metals salts at ambient and negative temperatures is given. The destructive role of dihydrate gypsum in the portland cement pastes containing carbonates, silicates, sulphates sodium and potassium is established.

Keyword: hydration, mechanism, admixtures, alkali, gypsum.

INTRODUCTION

One of the ways of portland cement systems effectiveness increase is the activation by complex chemical admixtures of polyfunctional action containing surface-active substances and alkali metal salts. Alkali compounds are rather strong activation agents of cement systems hardening and widely used as antifreezing admixtures.So far, the results of alkaline admixtures on the setting characteristics of cement, on the effect of freezing of concrete and on the durability of reinforced concrete construction have been published as following reports: Collepardi and Ramachandran (1992), Krivenko (1992).However, some papers have been published as well: on the influence of alkali metals salts on the compressive strengh of slag-alkaline cements (Glukhovsky, 1989), a phase composition of the hardening products in a system Me_2O-MeO-Me_2O_3-SiO_2-H_2O (Krivenko, 1994) and the effect anti-freeze admixtures have on the setting characteristics of áoncrete at negative temperatures (Mironov and Lagojda, 1975).

SETTING

Introduction

In concrete practice a number of alkali admixtures (soda, potash) in amounts exceeding 1 mass.% lead to the sharp stiffening of concrete mixes. At the same time other salts (sodium nitrite and chloride) may be used in increased amounts (up to 10 mass.%) and they do not exert destructive effect on concrete mixes. That is why it is nessesary in frames of this work to investigate the reason of different effect nature alkali metals salts on portland cement structureforming processes and to classify the alkaline admixtures by mechanism of action on the time of setting of portland cements.

Results and Discussion

Due to the effect of alkali-bearing compounds on the time setting of ordinary portland cement (OPC) they can be divided into two groups.The first group consists of sodium salts such as chloride, nitrate, nitrite not affesting strongly on time of setting. The second group consists of sodium carbonate and silicate, and potassium salts. Even small dosage of these compounds results to the sharp acceleration of grout setting and the loss of the system plastic properties.

Due to the action mechanism the alkali metals salts are attributed to the admixtures undergoing exchange reaction with products of portland cement hydration. Therefore they are to react first of all with calcium hydroxide which is the product of alite phase hydrolysis of portland cement clinker. As a results anion part of admixtures in the process of hydration is bound aluminobearing phases and cations are retained in porous fluid. At the same time it is worthy to take into account the possibility of chemical interaction of alkali-bearing compounds with gypsum dihydrate.

In studying the alkali metals salts additives effect on properties of finely grounded gypsum dihydrate it was ascertained that additives of the second group greatly accelerate its settingtime. X-ray phase analysis data show that following types ofinteraction between gypsum and these additives take place: sodium carbonate and silicate undergo exchange reactions with gypsum forming calcium carbonate or hydrosilicate and mirabilite; potassium sulphate and gypsum form less soluble compound syngenite, which is complex double salt $K_2Ca(SO_4)\ H_2O$; other potassium salts also results to the formation of syngenite instead of low-soluble part of gypsum dihydrate. Syngenite is characterized by fine fibrous crystals and this leads to rapid grout setting. Admixtures of the first group - NaCl, $NaNO_2$, $NaNO_3$ do not interact with gypsum dihydrate and do not effect on paste setting time.

Therefore at large oversaturatios of cement paste liguid phase at the very initial hydration period due to tendency of coarse-grained potassium cation to complex formation with calcium on the one hand and alkali metals carbonates and silicates exchange reactions on the other hand gypsum is removed out of the process of early structure formation and doesn t serve its main function - to be inhibitor of threecalcium aluminate setting in portland cement. Fibrous syngenite crystals which are formed reduce the thixotropic properties of paste in great extern and it causes cement stone destruction, lack of concrete strength and its structure-technical properties. Given results affirm the expediency of alkali metals salts of the second grope usage as admixtures to portland cement without gypsum dihydrate.

As can be seen from Fig.1 the admixtures of the first group even in complex with enhanced content surface-active substances (lignosulphonate and so on) up to 1,0 mass.% do not delay gypsum-free portland cement (GFPC) setting and system stiffens rapidly. But admixtures of the second group together with surface-active substances permit to obtain GFPC with specified setting time. It is significant that potassium salts have more strong effect than sodium salts so cations together with anion part of alkaline metals salts admixtures effect essentially on early structure formation of fine grounded portland cement clinker.

As a result of synergism the alkaline admixtures significantly improve the plastisizing effect of the surface-active substances like LS etc. These complex chemical admixtures have a multifunctional effect and during application of GFPC they exibit the superplastisizer properties. In addition there is the possibility of introduction of alkali metals salts in increased ammounts which are the hardening accelerator and anti-freezing admixtures.

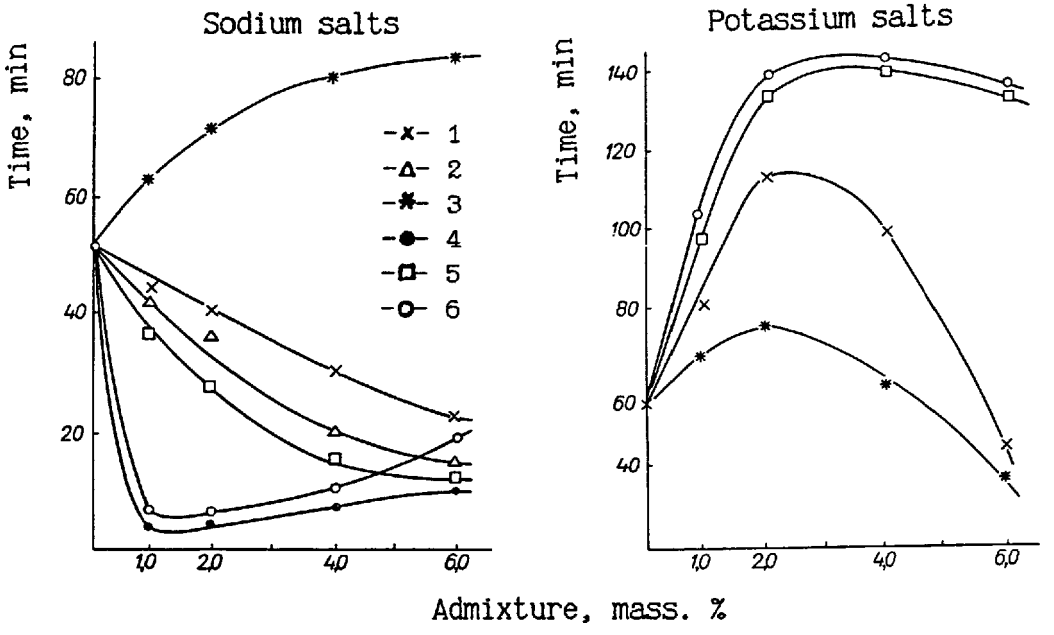

Figure 1 The start of setting GFPC (0.3 % LS) with sodium or potassium salts (carbonate, silicate, sulphate, nitrite, nitrate, chloride corresponding to curves 1-5 respectively)

HARDENING ACCELERATOR

Results and Discussion

The establishment of the causes of destruction phenomena, frequently appearing due to the alkaline admixture effect, allowed to form a group of special portland cements with regulated setting period and accelerated hardening at different temperatures.

The properties of the alkali metal carbonates and sulphates (with plasticizing/inhibiting admixtures) as high-effective hardening activators are fully discovered in GFPC in the process of its utilization. They are also serve as a setting times regulator for binding material which makes it possible to obtain rapid hardening portland cements (Skvara, 1984; Chistiakov and Myasnikova,1992). The properties of GFPC can be determined based on the type and the amount of plasticizing, inhibiting, alkali-bearing and mineral admixtures (Sanitsky and Sobol, 1992).

Among the second group alkali metal salts sodium sulphate became the most wide-spread as a hardening accelerator and potash - as an antifreeze. With the purpose of investigation of the potash and sodium sulphate on the portland cement hardening the admixtures influence on strength, phase composition and minerostructure of monomineral paste was studied.

The strength testing results showed (Fig 2) that 2-10 mass.% sodium sulphate admixture furthers to considerable intensification of the C_3S paste strength increase (in 2,8-4 times at 24 hours). The maximum strength is achieved with the Na_2SO_4 5 mass.% batehing (after 1

and 28 days according to 83% and 138% from the R_{28} C_3S paste strength without admixtures). The complex admixture 0,5 mass. % of LS and 5 mass.% of sodium sulphate or potash leads to the tricalcium silicate early strength reducing. The activation action effect of alkali compounds on -C_2S hardening is slower in a long-term age.

The investigation of the admixtures influence of the alkali metal salts on the aluminate and aluminoferrite phasis hydraulic activity change has been carried out on the C_3A and C_4AF minerals (Fig 2). When adding 5 mass.% Na_2SO_4 the considerable increase of C_3A stone strength is being observed: in early terms - 3 times as much, after 28 days - 4 times as much. 5 mass.% of potash admixture in pure condition increases the paste

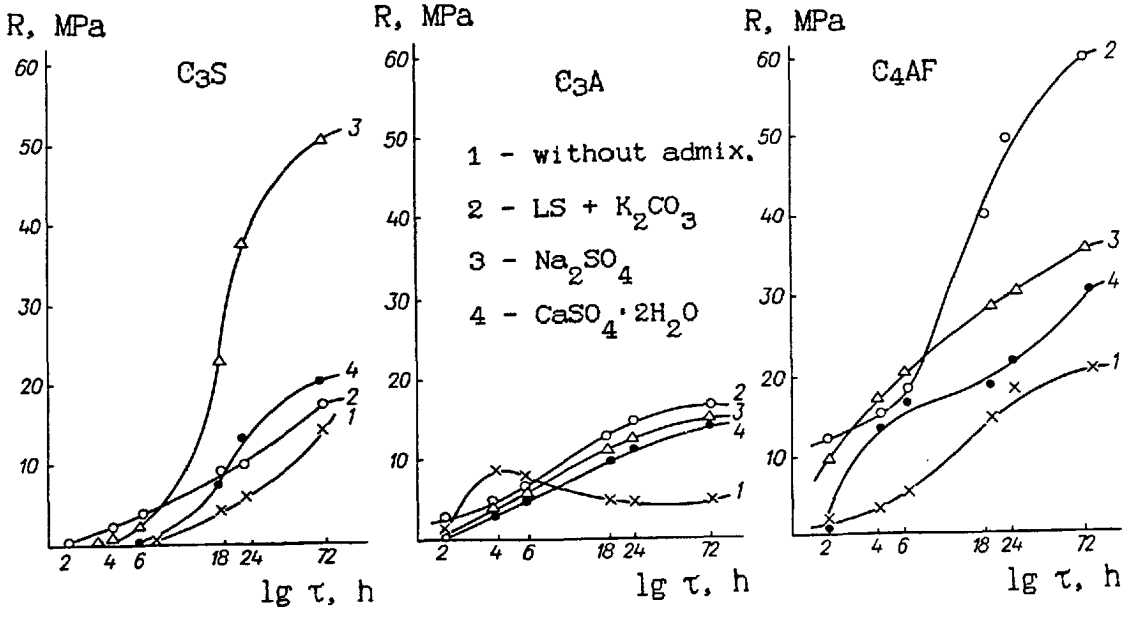

Figure 2 The early strength of monomineral stone with admixtures

strength C_3A only a little. But the complex admixture 0,5 mass.% LS and 5 mass.% potash allows to get the highest inerease of the paste strength in its early hardening period and maximum strength in the long-term age of hardening. Alkali-containing admixtures - sodium sulphate and potash - cause also the C_4AF monomineral paste strength increase. From the said data it follows that sodium sulphate activates the C_3S hardening stronger and potash activates aluminocontaining clinker phases. In this case after 1 day the C_3S hydratation stage increases in two times, C_3A and C_4AF, on the contrary, - reduces. In the case of aluminate phasis the reducing of hydration speed prevents the development of destructive phenomena during the forming of the early cement paste strength.

According to the data of the flame photometry in C_3S suspension just after the gating the alkali-containing admixtures reduce the calcium ions concentration in the liguid phase in 3-5 times, and with the passage of time - much more. With the adding of sodium sulphate in the C_3S suspension considerable calcium and sodium ions concentration reducing is firstly noted.That is connected with the forming of phase $4CaO\ 0{,}9Al_2O_3\ 1{,}1SO_3\ 0{,}5Na_2O\ 16H_2O$. Its building is like those of calcium monohydrosulfoaluminate.

In the processes of early structure-forming in portland cements incorporating alkali-bearing admixtures in amounts exceeding 2 mass.%, the liquid phase has a lower concentration of calcium ions as compared to ordinary portland cement. According to X-ray spectral microanalysis data, the alkali metals salts admixtures are mainly concentrated on the outer hydrates composition. Therefore, scanning electron microscopy shows formation of more fine crystalline microstructure of stone, whereas the trimethylsilylation method shows considerable increase in the polymerization rate of silicon-oxygen anions in hydrosilicates. In the process of C_3A hydration with the said admixtures, crystals of hexagonal AFm-phases are formed which can tightly fit in to each other. So, there is less of cement grains moving apart in the early period of hydration than in the period of ettringite acicular crystals formation. Besided, breakdown effects which occur during the transition of the high-sulphate form of calcium hydrosulphoaluminate into the low-sulphate one and which are accompanied by change in crystal habit and density,do not occur with the increase of hardening time. Together, the factors contribute to the forming of a dense, strong but least stressed structure of the cement paste.

For the model system (75 mass.% C_3S + 25 mass.% C_3A) it is showed that alkalicontaining admixtures considerably intensificate its hardening during the early period (after 1-3 days the strength is reached egually R_{28} of the stone with dyhidrate gypsum admixture). The slowing increase of model system strength with gypsum admixture in the period of 6-18 hours is stipulated by the general porosity increase by 20 %, according to the mercury poroumetry, as much as the result of overcrystalization of ettringite into calcium monohydrosulfoaluminate.

The mechanism of the setting and hardening processes proceeding in GFPC give really picture of alkali-containing chemical admixtures and clinker minerals interaction. The above mechanism is based on the leading part of a big calcium cation in making structures of new hydrate formations. The main processes of the early period in cement pastes are the primery formation of $[Ca_2Al(OH)_6]$ packs which predetermine AFm-phases formation due to the decrease of Ca ions concentration in the cement slurry liguid phase; making of protective shell out of AFm-phases on C_3A and aluminoferrites surface, their structure stabilization with $[CO_3]$, $[SO_4]$ bicharged anions. As a result of rejects polarization effects in the cement slurry owing to the difference in charge of the silicate and aluminum-bearing hydrating mineral surfaces cement particles do not aggregate into coarse clusters even if water requirements are reduced and cement slurry remains plastic.

The directed formation of the cement paste microstructure at early period of hydration including replacement of the acicular AFt-phases by hexagonal AFm-phases and subssequent stabilization of the structure makes for its compaction and prevents development of break-down effects in the hardened paste which accompany transition of ettringite to a low-sulphate form. As a result, the strength of the paste based on GFPC with surface-active substances and alkali metal salts carbonates or sulphates begin to increase considerably.

Technological methods of control over the portland cement systems properties presuppose a direct influence on the processes of their early structure formation and liquid phase

composition. They are determined by selection of mineralogical composition of the Portland cement clinker, type and member of retarders, plastisizers, alkaline metals salts and mineral additions as well as temperature.

The concrete prepared on the rapid-hardening cement systems bases possesses an intensive strength increase (70-80 % of the designed strength is reached in 24 hours at the ambient temperature).

ANTIFREEZING ADMIXTURES

Results

The introduction of gypsum dihydrate (5 mass.%) at frost results to the degradation of C_3S paste with LS and potash admixtures strength at the expense of reduction of its hydration at factor 1,5-2,0 and porosity structure formation caused by transition of potash admixture part (4 mass.% to arkanite not possesing the antifreezing effect.

Potash used as a highly effective hardening accelerator as well as an anti-frost admixture (eutectic temperature -36.5^0 C) for gypsum-free portland cement allows us to obtain binders with accelerated strength ,improved frost resistance and water-proofness as well as gain at negative temperatures. The expensive stress of these binders ability to hardening at negative temperatures (up to -35^0 C). is 5 to 10 times lower at early freezing as compared to OPC with NaCI, $NaNO_2$, K_2CO_3 admixtures.

GFPC with carbonate additives exhibit increased effectiveness when hardening at ambient, low and negative tenperatures. It is due to modifing effect of $CaCO_3$ on aluminobearing phases in the presence of gypsum is exhibited not fully. Two charge plane anions [CO_3] are set out parallel to the layers of [$Ca_2AI(OH)_6$] in the structure of AFm-phases, they compensate the charges of layers and stabilize these phases. Due to hexagonal packing of atoms in crystalline structure such AFm-phases grow together with calcite and other aggregates.

When hardening at lower positive temperatures and at frost up to -10^0 C the possibility of construction monolithic structures with terms of loading which are nearly to summer loading is created. At temperatures -15^0 C such concrete attains 80-100 % of branding strengh in 28 days and posses the capabi ity of hardening at frost -35^0 C. The compressive strength of concrete after 28 days at temperature -15^0 C and after 90 days at ambient temperature are listed in Table 1 for OPC and GFPC with LS and potash admixtures.

In case of using rapid-hardening blended cements prism strength, modulus of concrete elastisity and its adhesive strength with reinforcement is not less than similar indecies for ordinary concrete which harden under normal conditions even if it was affeced by negative temperatures. Besides concrete is characterized by high value of frost resistivity (F 300 and greater) and increased water-proofness.

Table 1. Compressive strength of concrete based on OPC and GFPC with LS and potash admixture at ambient and negative temperatures

CONCRETE based on	TEMPERATURE ^{0}C	COMPRESSIVE STRENGTH, N/mm^2 7 day 28 day 90*day
OPS	+20	20.4 22.5 22.8
	-15	12.9 17.5 21.0
GFPS	+20	25.7 30.0 31.2
	-15	18.4 29.6 32.0

* - 28 days at temperature -15^0 C, than 62 days at temperature +20^0 C

CONCLUSIONS

The establishment of the causes of destruction phenomena, frequantly appearing due to the alkaline admixtures effect, allowed to form a group of high early portland cement binders with regulated setting period and accelerated hardening at different temperatures. Technological methods of control over the binding systems properties presuppose a direct influence on the processes of their early structure formation and liquid phase composition.

It was also shown that rapid-hardening portland cement systems with multicomponent alkali-containing chemical admixtures are characterized by a reduced water consumption. The concrete prepared on their bases possesses an intensive strength increase, improved frost resistance and water-proofness as well as ability to hardening at negative temperatures (up to -35^0 C).

ACKNOWLEDGEMENTS

The author gratefully acknowledge Dr.-Ing. G.Shevchuk for her assistance in the experiments, and also Dr.-Ing. V.Melnyk for his improving the manuscript.

REFERENCES

Glukhovsky V.D.,"Durability of Concrete. Aspects of Admixtures and Industrial By-Products". Proceedings of the Internatoinal Seminar, Gotenborg, Sveden, 1989, pp. 53-62.

Chystyakov V.V. and Myasnikova, Ye.A.,"Gypsum-free high Early-strength Cement",Proceedings of the 9th Internarional Congress on the Chemistry of Cement,New Delhi, 23-28 November 1992.

Collepardi M. and Ramachandran V., "Effect of Admixtures", Proceedings of 9th Internarional Congress on the Chemistry of Cement, 23-28 November 1992,New Delhi, Vol. 1, pp. 529-567. Krivenko, P.V.: Special Slag-alkaline Cements. Kyiv, Budivelnyk, 1992, 192 p.

Krivenko P.V. "Alkaline Cements", Proceedings of the First International Conference on Alkaline Cements and Concretes, October 11-14 1994, Kyiv, Ukraine, pp. 11-129.

Mironov S.A. and Lagojda,A.V."Concretes hardening at frost", Moscow, Stroyizdat, 1975, 265 p.

Sanitsky M.A., Sobol,H.S.,"Gypsum-free Rapid Hardening and Mixed Portland Cements", Proceedings of the 9th Internarional Congress on the Chemistry of Cement, 23-28 November 1992, New Delhi, Vol.3, pp.438-443.
Skvara F.,"Nove typy bez adrovcovych portlandskych cementy", Stavivo, Vol.62, 1984, pp. 297-303.

CONTROL PROPERTIES OF SULPHO- AND FERRO-ALUMINATE CEMENT CONCRETE WITH SPECIAL ADMIXTURES

Liang ZHANG, Muzhen SU, China Building Materials Academy, Beijing 100024, P.R.China

ABSTRACT The setting time and the workable time of sulpho/ferro-aluminate cement concrete can be effectively controlled with special admixtures without reduction of its early mechanical properties. The setting and hardening regularity of the sulpho/ferro-aluminate cement with the special admixtures was studied at different temperature and the mechanical properties of the hardened concrete tested. In civil engineering practice, good results have been achieved by using these special admixtures.

Key-words: sulphoaluminate, admixtures, setting, strength development

INTRODUCTION

The sulpho-aluminate cement series(SAC) and the ferro-aluminate cement series(FAC), which were both developed by China Building Materials Academy(CBMA) and put into industrial production in 1970's and 1980's respectively, have been well received by civil engineers for the properties of rapid hardening, early-strength, good impermeability, rapid strength development at minus temperature and good corrosion resistance just after they came out in China. In the 3rd Beijing International Symposium on Cement and Concrete held in Oct., 1993, Professor WANG Yanmou, director of State Administration of Building Materials Industry and Professor SU Muzhen, vice-president of CBMA, named sulpho- and ferro-aluminate cement series as the third cement series to make the difference from the first cement series—Portland cement (its major mineral component is C_3S) and the second cement series cement—high-alumina cement (its major mineral is CA).

After 80's, the self-stressing cement in the third cement series was occupying the market step by step for producing self-stressed water pipe, but the application of rapid-hardening cement was still in its narrow applied fields such as repairing, anchoring, structural components joint construction in winter and some small size concrete products. Besides the problem of the production capacity, the most important reason was that the workability of concrete was not able to meet the requirement of construction in situ due to its rapid setting time. At that time, increasing W/C ratio was the only way to prolong the workable time of concrete that resulted in lowering compressive strength and poor durability although the strength of cement itself was higher according to the Standard. For this reason, the rapid hardening cement had not been used in civil engineering in a large scale. After 90's, with the development of the production technology and capacity of the third cement series, the task to develop its market and to enlarge its application fields becomes more and more important. Therefore, controlling the workability of its fresh concrete and the performances of its hardened concrete is the essential prerequisite for the cement to enter into large construction projects.

It is well-known that the successful applications of Portland cement series in civil engineering in recent decades are attributed to the admixtures, which have made concrete meet the requirements for its different performances. By using this experience as reference, we have realized that the third cement series also need to be modified with admixtures in order to bring its excellent performances into full play.

RESEARCH ON THE COMPOSITION OF SPECIAL ADMIXTURES

Designing idea

In order to solve the disadvantages of the third cement series and avoid to bring trouble to on-the-spot construction, the admixtures added should solve the following three problems in particular: the first one is to be able to control setting time and workable time of concrete; the second is to ensure consistency of concrete required for construction and the third is to improve strength and durability of concrete. It is obviously impossible to settle all the problems above mentioned with only one single admixture. Therefore, we selected some varieties of suitable retarder, superplasticizer and air-entrainer to make different compound admixtures with the comprehensive actions of retarding, water-reducing and air-entraining etc. The retarder is the key component in the admixtures.

The effects of many different retarders on setting time, rheological factors, flowability and strength of the pastes and mortars have been tested for picking up the best retarder finally. From our testing results we found the retarder selected has the following three actions for SAC/FAC:

- Retarding setting time effectively;
- Improving workability and prolonging workable time;
- Not affecting early strength and improving later strength at reasonable dosage.

Variety of special admixtures

China is a country with a vast territory and with complicated climate. According to the different aims and requirements, the special admixtures mainly include the following varieties:

①**High-range retarding water-reducer (special superplasticizer),** divided into two types:
Standard(S)—used for preparing high-strength concrete, suitable for the concrete construction at the temperature of 0～25℃ and at the positive and minus temperature in turn.

Retarding(R)—used for preparing high-strength concrete, suitable for the concrete construction at the temperature of above 25℃ in the hot summer.

Considering the difference of temperatures in different areas and in different seasons and the effect of different construction situations, S and R type superplasticizers can meet the different requirement of practical engineerings for setting time and workable time.

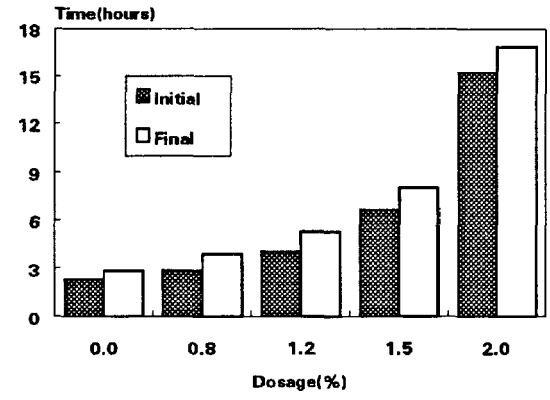

Fig.1 Setting time of the mortar with R type superplasticizer

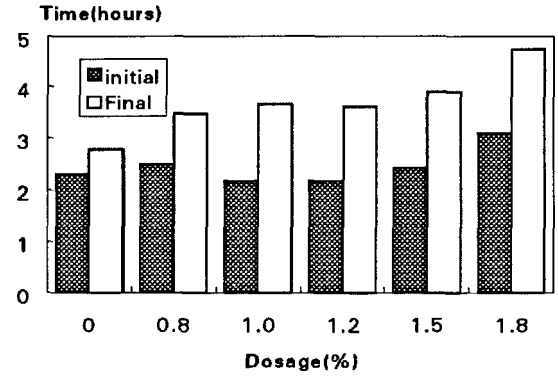

Fig.2 Setting time of the mortar with S type superplasticizer

②**ZB-2 anti-freezing admixture**—used for the winter construction at the temperature of -5 ℃～-30℃.

③**ZB-3 retarding water-reducer**—used for normal concrete to increase workable time, suitable for the construction at positive and minus temperature in turn.

④**ZB-4 pumping aid**—used for commercial concrete transported from ready-mixed concrete plant far away and pumping on-the-spot, capable to control the loss of slump in about 3 hours.

EFFECT OF SPECIAL ADMIXTURES ON PROPERTIES OF FRESH MORTAR AND CONCRETE

Effect of dosage on setting time

Fig.1 and Fig.2 show the effect of the dosage of R and S type of special superplasticizer on setting time of the cement at the temperature of 20℃. By using the special admixture, we can control the initial setting time within 2-15 hours to meet the normal requirement of concrete engineerings. It should be noted that all the setting times of mortar are tested under the same flowability.

The special admixtures are composed of two major compositions, i.e. water-reducing composition and retarding composition. The setting and hardening of SAC/FAC mortar and concrete are mainly controlled by the two factors of water-reducing and retarding which mean that retarder can prolong setting and water-reducer accelerate hardening. For the R type superplasticizer, prolonging setting time and workable time are its leading role because only under this prerequisite, we can get dense and good-qualified concrete thus bring water-reducing and strengthening into full play. For the S type superplasticizer, its purpose is to further develop the early-strength of SAC/FAC concrete which means water-reducing is its leading role at lower positive temperature and positive/minus temperature in turn because under these circumstances, the requirement for setting time is relaxed compared with higher positive temperature.

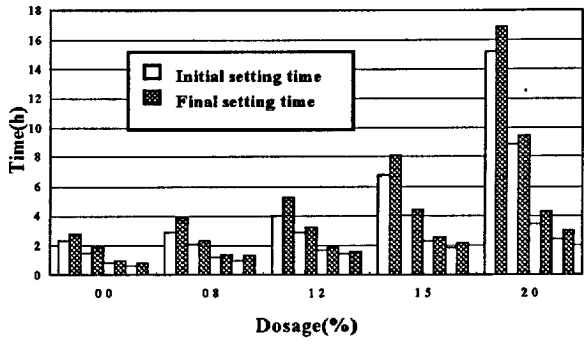

Fig.3 Setting time of concrete at 20, 30, 40 and 50 ℃ with R type superplasticizer.

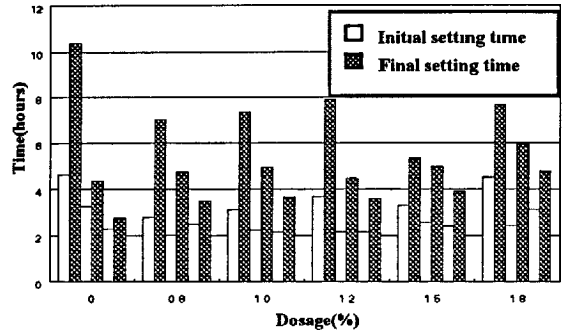

Fig.4 Setting time of concrete at -5, 12 and 20 ℃ with S type superplasticizer

Effect of Ttemperature on setting time

The effects of temperature on setting time of the mortar with R type are shown in Fig.3. Obviously, the setting and hardening of SAC/FAC are very sensitive to temperature. At room temperature, the R type superplasticizer can very effectively prolong the initial and final setting time of the cement but with the increase of temperature, its retarding action on setting time is reduced sharply and the difference between initial and final time is becoming smaller and smaller.

Therefore, it is effective for the retarder to control the setting before the hydration of the cement but once hydration heat is released, the temperature inside of concrete will significantly be increased to cause very quick development of strength

The effects of temperature on setting time of the mortar with S type are shown in Fig.4. Compared with the setting time of the control sample, little change of the ones takes place in the samples with S type superplasticizers though w/c ratios are reduced, that means that water-reducer is playing a main role. That is very advantages for the normal strength development of concrete at lower temperature.

Control slump loss

The curves in Fig.5 and Fig.6 show that the slump loss of SAC/FAC concrete can be effectively

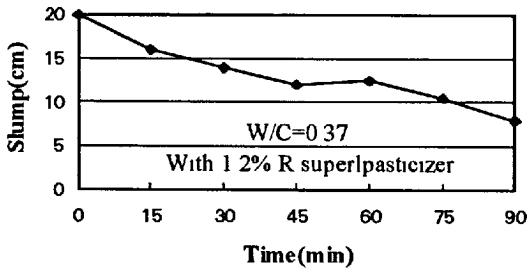

Fig.5 Slump loss of the concrete with the special R superplasticizer

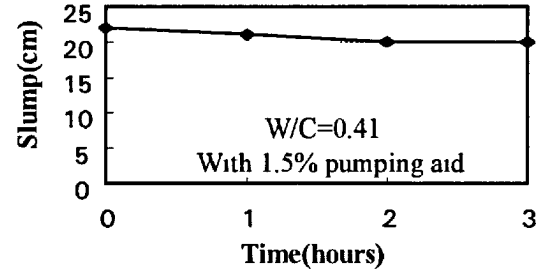

Fig 6 Slump loss of the concrete with the special pumping aid

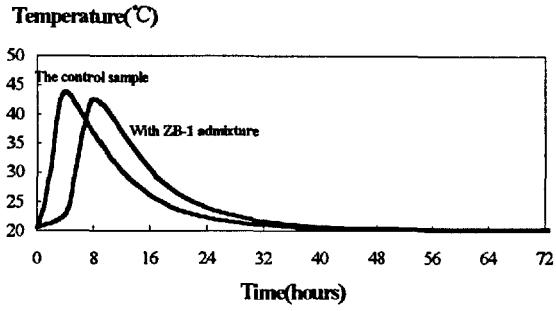

Fig.7 Hydration heat evolution curves

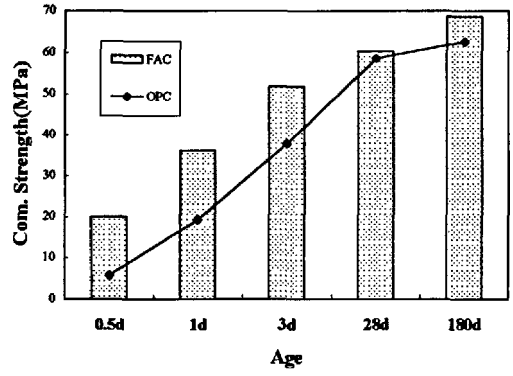

Fig.8 Development of compressive strength

ontrolled by the special admixtures, thus making the concrete meet the requirement of construction in situ and long-distance transportation. By using the special admixtures, we can get the SAC/FAC concrete whose setting time and workable time are able to be controlled.

Effect of special admixture on hydration heat

The hydration heat evolution curves as shown in Fig.7 show that only the time of appearance of the hydration heat peak is postponed but that the shape of the peak is not changed when the special admixture is added, thus retaining the properties of high early-strength and high-strength of SAC/FAC concrete.

PROPERTIES OF HARDENED CONCRETE WITH SPECIAL ADMIXTURES

Strength development at positive temperature

The contras test was made at 20℃ to investigate the strength development of FAC concrete and OPC concrete. FAC and OPC were adopted. The same concrete proportion was used in which the cement content is 450kg/m^3, the dosage of admixture is 1.2% R type special superplasticizer for FAC concrete and 1% sulfonated naptalene superplasticizer for OPC concrete. From the strength development with age(Fig.8), not only does the early-strength of FAC concrete develop much more quickly, but also its later strength goes up steadily.

Strength development at minus temperature

Compared with Portland cement concrete, one of the most excellent performances of the concrete with SAC/FAC is good anti-freezing ability at minus temperature especially at early age. The concrete constructed in winter with SAC/FAC can make use of the hydration heat released concentratedly by the cement itself to cure the concrete itself to gain its strength development, therefor, there is no restriction on the critical strength for this concrete at minus temperature. But the concrete prepared with SAC/FAC without other additives is still not be able to completely resist its freeze injury under fresh condition, so the aim of using special anti-freezing admixture is to keep the fresh concrete with good workability and from its freeze injury before its hardening so as to make the concrete with the admixture to be constructed with simple heat curing measures in winter and ensure the strengths and durability of hardened concrete. With the special

Table1 The strength development at minus temperature

Temperature (℃)	W/C	Slump (cm)	Admixture	Compressive strength (MPa)				
				-7d	-7+3d	-7+7d	-7+28d	-7+56d
-5℃	0.32	17.0	S type superplasticizer	6.7	55.7	61.5	67.2	79.1
-15℃	0.31	9.0	3% Anti-freezing admixture	3.6	43.7	54.2	58.5	70.4
-25℃	0.30	6.0	4% Anti-freezing admixture	56.5		65.8	69.7	70.0

Table 2 Strength development of the FAC concrete (MPa)

Age	1 day	3 days	28 days	6 months	1 year
Compressive strength	44.6	61.9	69.2	80.7	81.0
Splitting strength	2.85	4.24	5.38		5.74
Flexural strength		7.23	8.70		8.81
Elastic modulus($\times 10^4$)	34.2	35.6	37.8		

Note: Cement content=480kg/m^3, W/C=0.335, with R type superplasticizer.

anti-freezing admixture, we can prepare not only low and medium grade concrete, but also high-strength concrete. Part of the results are shown in Table 1. -7+3d means that the specimens are cured at given minus temperature for 7 days and then for 3 days under standard condition (20±3 ℃, RH>90%).

Effect On Other Mechanical Properties

Splitting strength, flexural strength, elastic modulus and creep of SAC/FAC concrete have the same development trend with its compressive strength when added the special admixtures as shown in Table 2. By using the admixtures, the high early-strength is not only kept, the other mechanical properties are also improved.

Freezing-Thaw Carbonation Resistance

The loss of the strength of concrete only with the special superplasticizer after 300 freezing-thaw cycles is only 1.62% and the carbonation depth also significantly reduced, as shown in Table 3 and Table 4.

APPLICATIONS IN PRACTICAL CIVIL ENGINEERINGS

At present, the special admixtures for SAC/FAC have been put into production and used in civil engineering. For example, in a cement products plant in Guangdong province, grade C80 centrifugal pretensioning prestressed high-strength concrete pile was pilot manufactured with the special superplasticizer. In the construction of the rebuilt projects of Eastern and Northwestern Third-ring-road, Jing-Shi Highway and Beijing New Railway Station, large span post-tensioned pre-stressed concrete beams with grade C50 ferro-aluminate cement high-strength concrete with the R and S types of special superplasticizer were used in about

Table 3 Freezing and thawing resistance

Admixture	W/C	Slump (cm)	Compressive strength after 300 cycles (MPa)	Control compressive strength (MPa)	Loss of strength (%)
S type	0.4	18	66.6	67.7	1.62

Table 4 Carbonation resistance

Cement	Admixture	W/C	Slump (cm)	Carbonated depth (mm)	Control strength (MPa)	Carbonated strength (MPa)	Coefficient of carbonation
FAC from Tangshan	\	0.52	7	1.29	51.4	49.3	0.96
FAC from Tangshan	R type	0.4	18	0.98	69.4	64.5	0.94
FAC from Lengshuitan	R type	0.3	5	0.26	73.6	71.8	0.976

Note: The results in the Table were obtained with the specimens carbonated 28 days under the standard condition.

20 overflys. Grade C60 concrete was successfully poured in Shenyang Long Distance Telecommunication Hub with R and S type superplasticizers in the summer and the autumn and with the special anti-freezing admixture in winter at the lowest temperature of -25°C. Grade C50 commercial concrete produced in Tianjin Hangbao Ready-mixed Concrete Plant was used in pumping construction with the special pumping aid. It is worthy to be noted that in the construction of Liaoning Products Building in 1994, grade C70 and C80 concrete with ferro- and sulpho-aluminate cement were applied for the first time in high-rise building in China. The special retarding water-reducer has been used in many concrete products plants for the production of varieties of concrete elements of C20～C40. The special admixtures have played an important role in the applications of SAC/FAC.

CONCLUSIONS

Setting time and workable time of SAC/FAC can be effectively controlled by the special admixture and simultaneously, the mechanical properties of SAC/FAC concrete at the early age are not affected and the durability also improved. The applications of the special admixtures in practical engineering have achieved good results.

REFERENCE

Liang ZHANG, et al., "Properties and application of high-strength concrete with ferro-aluminate cement", China Concrete and Cement Products (Chinese), pp.11-15, No.6, Dec. 1994.

3iii027
7 pp

RHEOLOGY CONTROL FOR WET SHOTCRETE - A SLUMP KILLING SYSTEM FOR IMPROVED PERFORMANCE

Tate COVERDALE, Jeff CHAMPA, and Larry ECKERT
Master Builders, Inc.
Cleveland, OH, 44122
USA

ABSTRACT
A chemical admixture system for changing the rheology of wet shotcrete as it is applied to vertical and overhead surfaces is described. The method is part of an overall approach to wet shotcreting called Total Consistency Control, and consists of an admixture system utilizing a high molecular weight polyethylene oxide, napthalene formaldehyde sulfonate condensate, and a modified sodium silicate. Using application thickness as a basis of equivalence, the new approach is compared to traditional wet shotcrete chemistries.

Key-words: accelerators, polymer, rheology, shotcreting, silicate

TRADITIONAL ACCELERATORS
Sprayed concrete uses different types of accelerators (Melbye, 1996). The most common types include sodium silicates and sodium or potassium aluminates. Silicates bind the water in the concrete and contribute little to the early hydration process. The water binding results in an immediate loss of slump providing a rapid initial "set" of the sprayed concrete (<10 seconds). Final sets are not typically rapid (>30 minutes depending upon temperature) when compared to aluminate based accelerators. The typical dosage of these accelerators is 3 to 6% of the binder weight as specified. In practice, however, the use of standard grade silicates typically results in dosages of 8% or higher to achieve necessary stiffening. Such an overdose can result in severly limited strength development and various other associated problems. Silicates typically work with all cement types, reduce ultimate strengths less than aluminate based accelerators and are less aggressive to the skin and eyes than the aluminates. Sodium silicates are sensitive to water/cement ratio and temperature. Increasing water/cement ratios and lower temperatures require higher dosages to achieve the same amount of stiffening. Temperature also affects the reactivity and viscosity of sodium silicate admixtures.

Aluminate based accelerators take part in the hydration process and contribute to early strength. They provide a sudden increase in the alkali available to the cement, promoting tricalcium aluminate hydration, and overwhelming the calcium sulfate that moderates the cement hydration. Rapid set and strength development occur. Final set of the sprayed concrete occurs within the first 9 minutes. After 20 to 30 minutes, the strength is usually high enough for the sprayed concrete layer to bear its own weight. The typical dosage of these accelerators is 4 to 8% of the binder weight. The set and strength gain properties enable an increase of layer thickness for the sprayed concrete and also make the aluminate based accelerators more effective in water problem areas. Aluminates can be sensitive to cement type and checking the reactivity of these accelerators with the cement before spraying is a necessity. Aluminate based accelerators reduce final strengths more than silicate based accelerators, and are very aggressive to the skin and eyes requiring greater precautions for safe handling. Potassium aluminate tends to be less sensitive to cement type and generally promotes faster setting and higher early strength when compared to sodium aluminate.

RHEOLOGY CONTROL SYSTEM

Master Builders Technologies (MBT) has developed a Total Consistency Control (TCC) system to control the rheology of shotcrete. This technology is a two component admixture system utilizing incompatible chemistries to produce an instant loss of slump, and, in combination with a modified sodium silicate, set acceleration. The MBT Underground Construction Division developed the system and introduced it throughout Europe in 1994. It has been used worldwide for projects in many countries including Sweden, Norway, Italy, U.K., Saudi Arabia, India, Malaysia, Hong Kong, Australia, Mexico, Venezuela, and, most recently, the United States.

Component A of the TCC system is a plasticizing admixture which contains a high molecular weight polyethylene oxide. This component, added to the concrete as it is batched, improves the workability and pumpability of the concrete. The increased workability of the concrete reduces the water content required for pumping, providing better concrete properties, improved layer thickness when spraying, and lower accelerator consumption. a high molecular weight polyethylene oxide also imparts improved pumping qualities to concrete with a low cement content, with aggregate gradations lacking fines, and with fiber reinforced concrete.

Component B of the TCC system, which is added at the shotcrete nozzle, is a modified sodium silicate and napthalene sulfonate blend that acts as a set accelerator and as the TCC activator. The modified sodium silicate is more effective than traditional silicates in that a lower amount is required to achieve the same performance. The TCC activator reacts with the a high molecular weight polyethylene oxide of Component A providing instant slump loss. The modified sodium silicate acts as a slump killer and a set accelerator.

The consistency control of this system enables the use of a lower accelerator dose to attain the same build thickness of sprayed concrete. The two polymer components of the TCC System react together to cause an instant loss of slump. In combination with the already lower water/cement ratio, the sharp slump loss allows a lower accelerator dose. This provides a thixotropic consistency to the sprayed concrete, leaving it more plastic as it hits the substrate yet able to build thickness. This thixotropic behavior provides better bonding properties, less rebound, and increased build thickness. The low accelerator dose keeps any decrease of the final strength due to the accelerator to a minimum, and provides a longer finishing window when shotcrete is to be used as a final lining or cover. The effects of this system also serve to reduce ultimate drying shrinkage. Through these methods the quality of the in place sprayed concrete is significantly improved.

IN HOUSE STUDY

A series of experiments was performed at an outdoor testing facility to demonstrate the performance of the TCC system for wet shotcrete. These experiments consisted of using a very high quality bagged concrete as the base material, and several different combinations of accelerators and a single water reducing/thixotropic admixture.

Basis for experiment

The underlying premise for these experiments was to compare different shotcrete systems on the basis of equivalent vertical build up thickness. In the experiments described here, three different accelerators were used: 1) modified sodium silicate (SA430), 2) modified sodium silicate containing a a high molecular weight polyethylene oxide (TCC 766), and 3) sodium aluminate (SA100). These accelerators were combined with a high quality concrete both with and without

the use of a thixotropic, water reducing admixture (Polyheed SG). Each system was calibrated to achieve the same vertical build up thickness, and then measurements of required accelerator, set time, and compressive strength were taken.

Experimental description

Materials and curing

The mix design for the concrete used in this evaluation is shown in Table 1. This material was manufactured in 25 kg bags to ensure accurate admixture dosing and operational convenience. Concrete was continuously produced in 8 - 10 bag batches in a stationary paddle mixer attached to a concrete pump. For both the plain concrete, and the concrete containing admixtures, the following parameters were measured on the first batch produced: slump, DIN flow, unit weight, and concrete weight per pumped stroke. Material from subsequent batches was assumed to have maintained the same plastic properties. Care was taken to ensure that shooting of test specimens utilized fresh material, as in some cases concrete had to sit in the lines for nozzle cleaning, etc.

Table 1 - Concrete Mix Design

	wt. %	kg/m^3
cement	22.3	455
silica fume	1.8	37
sand	52.2	1070
stone (10 mm)	23.7	490

Test specimens for set time and compressive strength were taken from 610x610x90 mm panels which were shot after measuring the build up thickness. These panels were cured under wet burlap and black plastic sheets for 24 hours, then cored for compressive strength samples.

Equipment

Concrete was mixed and pumped using a dual piston, swing tube pump (Powercreter 10) with an estimated output of 7.6 m^3 per hour, through 30.5 m of 38 mm diameter hose. The spray application utilized a typical air/admixture injection nozzle (WSN 100). Compressed air was supplied to the nozzle at a pressure of 6.8 ATM and volume of 5 m^3 per minute. Accelerating admixtures were delivered using an air diaphragm pump at a pressure of 6.8 ATM, and the volume was controlled using a manually adjusted needle valve near the nozzle.

Shotcreting conditions and accelerator measurement

As mentioned before build up thickness was used as the point of comparison in this study. In order to somewhat accurately measure build up thickness, a build up platform was utilized as a shooting substrate (Beaupre, 1994, pp 137). This platform, along with the general shooting setup is depicted in Figure 1. The platform was made of hardened concrete with dimensions of 305x305x25 mm, and was positioned approximately 100 mm from a supporting concrete wall. The shooting surface was treated to have exposed aggregate with a profile of approximately 6 mm. Build up thickness was measured by shooting continuously onto the platform with the same nozzle position until the concrete fell under its own weight. Since this measure was taken visually, it is considered to be accurate to only the nearest 10 mm. The nozzle was held

approximately 1.2 m from the platform. The purpose of this platform was to limit the variability of build up thickness due to the area of the base build up of concrete.

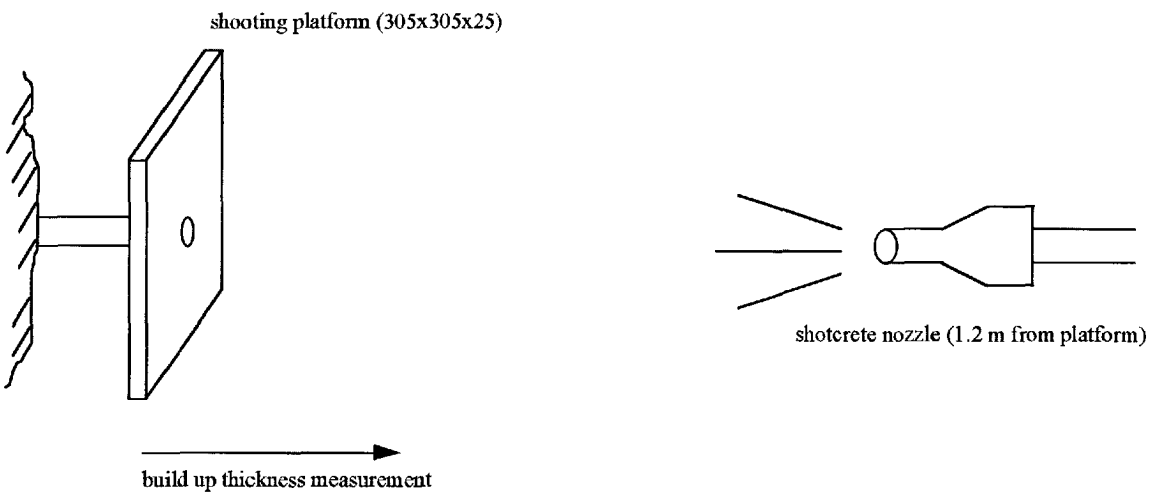

Figure 1 - Shooting setup for build up thickness measurement

Once the needle valve setting on the nozzle was determined, specimens were shot, allowing the determination of the accelerator dosage by measuring the amount of concrete sprayed, and the amount of accelerator used. The reported accelerator dosages are based on the total cementitious content of the concrete (cement and silica fume). With the equipment employed, calibrating to the desired build up thickness turned out to be a significant practical challenge, and in some cases, comparisons can be drawn only on equivalent accelerator doses.

Experimental results

The results from the seven test conditions are shown in Table 2. In these tests, initial set was determined using a penetration device, with 3.4 MPa as the criterion for initial set. All mixes were performed on the same day after two days of trial work. Mixes 1 and 2 were performed in the early morning, and the subsequent mixes were performed in the afternoon in a 3.5 hour time span.

Discussion of results

The results described in the table above will be discussed as two basic experiments: those without a nozzle added accelerator, and those with a nozzle added accelerator. Although all of the shooting was done on the same day, the conditions under which the first two mixes were made were quite different than the last five. Mixes 1 and 2 were made in the early morning as stated above. The bagged concrete had been stored under cover and was relatively cool, as was the ambient temperature (~ 18.3 C). The mixes used with accelerator were performed in the afternoon when the sun was out and the ambient temperature was about 29.4 C. This difference is evident in the water required to produce essentially the same slumps between the morning and afternoon mixes. Because of this difference, comparisons between mixes 1 and 2 and the mixes utilizing accelerator (3 - 7) should be made with caution.

Table 2 - Experimental Results

mix #	1	2	3	4	5	6	7
water reducer	none	SG	none	SG	none	SG	SG
accelerator	none	none	100	100	430	430	766
w/c	0.465	0.321	0.490	0.383	0.490	0.383	0.383
slump (mm)	170	160	190	180	190	180	180
DIN slump (mm)	85	50	95	85	95	85	85
DIN flow (mm)	450	445	480	470	480	470	470
unit weight (kg/m^3)	2270	2215	2285	2255	2285	2255	2255
gravimetric air	2.6%	8.7%	1.4%	5.3%	1.4%	5.3%	5.3%
thickness (mm)	180	330	405	480	330	405	380
accelerator. (%)	0.0%	0.0%	3.2%	2.3%	1.6%	2.1%	1.5%
initial set (min.)	120	210	2	3	90	90	80
Comp. Strength (MPa)							
1 day	33.7	44.6	17.3	24.4	20.6	32.8	36.8

Mix number one was a plain concrete that was pumped and sprayed without any water reducer or accelerator. The richness of the concrete is evident by the relatively low water to cement ratio needed to achieve the measured slump and flow. The unit weight and gravimetric air content are consistent with the mix design of this concrete. This mix was easily pumped and surprisingly built up to a thickness of 180 mm. The curing conditions favored a faster setting material, being in the sun and covered with black plastic sheeting. The quality of the concrete mix is again evident in the compressive strength achieved.

Mix two contained a lignosulfonate based water reducing and thixotropic admixture at a dosage rate of 980 ml per 100 kg of cement. With this dosage the water content was reduced by 31% from mix one while still achieving essentially the same slump and flow.The admixture also increased the air content which has been shown to have a slump killing effect (Beaupre, 1994, pp 146). Since most of the air entrained in the concrete is lost due to the turbulence and mixing action of the shotcrete nozzle, the concrete that passes through the nozzle loses slump that is caused by the entrained air. Perhaps of more importance, the concrete attains thixotropic characteristics due to the thickening chemistry in the admixture. This is evident by the fact that the vertical build up thickness was almost double that of the plain even though the slump and flow were the same. The lower water to cement ratio also resulted in excellent compressive strength.

The third mix was a plain concrete similar to mix 1, but a sodium aluminate accelerator was added at the nozzle. The required dosage to achieve 380 mm of build thickness was 3.2%, which is at the low end of what is probably used in the field (typical ranges of 4 - 8%). This material achieved initial set in 2 minutes, which is also long compared to what is typical for these accelerator chemistries (< 60 seconds). Even at this low dose, the strengths were drastically lower than mix 1, even considering the higher water to cement ratio.

Mix number 4 was a concrete containing water reducer, similar to mix 2, which used the sodium aluminate accelerator as did mix 3. At a lower dosage of accelerator the material had a

surprisingly high build up thickness of 480 mm. The combination of the lower accelerator dose, and the retarding effect of the lignin based water reducer extended the initial set to 3 minutes. The high build up thickness can be attributed to the thixotropic nature of the admixture, since more build was achieved with less accelerator than in mix 3, even though the slumps of the pumped concrete were about the same.

The fifth mix utilized the plain concrete and the modified sodium silicate accelerator at a dose of 1.6% by weight of cementitious material. At this dosage, the build up of 380 mm was not achievable, and the compressive strengths were somewhat lower than mix 1, but not as reduced as mix 3 which utilized the aluminate accelerator.

The sixth mix was made from a concrete containing water reducer and was accelerated using the modified sodium silicate. The required dose of accelerator to build up 380 mm (actually 400 mm) was 2.1%. The addition of the silicates at this dosage level does appear to lower the compressive strength of the concrete, but the strength levels are still very high in comparison to the aluminate accelerator and typical 24 hour design criteria. The longer setting times, also allow the concrete surface to be finished if this is desired.

The seventh and last mix described in this study utilized the complete TCC system; concrete containing water reducer and the modified sodium silicate containing the slump killing agent. With this system a very modest 1.5% accelerator was necessary to achieve a build up thickness of 380 mm. The lower amount of silicate required due to the slump killing agent resulted in a 12% increase in 1 day compressive strength over the straight silicate (mix 6).

The underlying trends from this study confirm much of what is already common knowledge in the shotcrete industry. The use of a water reducer provides significant improvement in compressive strength and to some extent the ability to hang thicker layers of shotcrete.The use of both silicate and aluminate accelerators results in decreases in compressive strength, and that trend is proportional to the accelerator dosage.

This study has also shown that for equivalent build up thickness, the modified sodium silicate appears to be as effective as sodium aluminate in terms of the dosage required (compare mixes 4 and 6). At equivalent doses, however, the aluminate accelerator gives a much greater loss in compressive strength than the modified sodium silicate. This study has also shown that by utilizing a slump killing system in addition to the modified sodium silicate accelerator, even less accelerator is required to achieve the same build up. This results in even less compressive strength reduction.

A significant advantage of the water reducing/thixotropic admixture that was not addressed in this study is the lubricating effect of the thixotrope. All concretes in this study were made with similar slumps to analyze the effect of the acceleration/slump killing systems. Since the thixotropic agent used with the water reducing chemistry provides excellent lubrication, significantly lower slumps may be pumped than what is usually observed with plain or otherwise plasticized concrete. The advantage of pumping concrete with lower slump is that higher build up thickness may be achieved. Thus, the ultimate advantage of the TCC system was not fully demonstrated in this study.

CONCLUSIONS

The TCC system represents the results of years of R&D and constitutes a new direction for shotcrete that provides improved performance without affecting or sacrificing the strength of the end product. In the past, increased early strengths meant increased dosages of accelerators and significant reduction in long term strength and quality. With this new technology increased performance can be achieved without increasing accelerator dosages.

ACKNOWLEDGMENTS

The authors would like to acknowledge Tom Bobrowski, Tim Gallagher, Frank Gay, Bill Hanley, Kevin Hutchings, and Mike O'Brien for help with the experimental process, and George Yoggy for reviewing and editing this document.

REFERENCES

Melbye, T.A.: "Sprayed Concrete for Rock Support". 4th ed. MBT International Underground Construction Group, 1996.

Meyco[R] **SA 430**, Master Builders, Inc. 23700 Chagrin Blvd., Cleveland, OH 44122.

Meyco[R] **TCC 766**, Master Builders, Inc. 23700 Chagrin Blvd., Cleveland, OH 44122.

Meyco[R] **SA 100**, Master Builders, Inc. 23700 Chagrin Blvd., Cleveland, OH 44122.

Polyheed SG, Master Builders, Inc. 23700 Chagrin Blvd., Cleveland, OH 44122.

Powercreter 10, Master Builders, Inc. 23700 Chagrin Blvd., Cleveland, OH 44122.

WSN 100, Whiteman Conspray 255 Woodford Ave., Elyria, OH 44035.

Beaupre, Denis. "Rheology of High Performance Shotcrete." Ph.D. thesis, University of British Columbia, 1994.

MECHANICAL ACTIVATION OF ORDINARY PORTLAND CEMENT AND CEMENT WITH ADDITIVES

Živko SEKULIĆ, Institute for Technology of Nuclear and Other Mineral Raw Materials, Belgrade, Yugoslavia
Miodrag STEFANOVIĆ, Cement Factory "Novi Popovac", Popovac, Yugoslavia
Branislav ŽIVANOVIĆ, Center for Multidisciplinary Studies, University of Belgrade, Belgrade, Yugoslavia

ABSTRACT
In this work, mechanical activation of ordinary portland cement (OPC) and cement with additives (PC 30d) in vibro mill was investigated. The analyses of cement specific surface area and X-ray diffractometry were performed. Besides, physico-mechanical properties of cements, before and after mechanical activation, were investigated. It was found out that mechanical activation results in increase of specific surface area, but also in change of mineralogical composition. The final consequence is increase of compression strength in activated cements. The compresion strength of OPC before activation (specific surface area 288 m^2/kg) was 43 MPa; after mechanical activation during 3 minutes (specific surface area 420 m^2/kg), it was 55.2 MPa. Compression strength of cement with additives, PC 30d (specific surface 380 m^2/kg) before the treatment was 43.1 MPa, while after mechanical activation, it was 51.1 MPa (specific surface 540 m^2/kg). Obtained results show that mechanical activation improves the mechanical properties of cements under investigation.

Keywords: Activation, specific surface, X-ray Diffraction Analysis, strength development.

INTRODUCTION
The investigation results in the area of mechanical activation of the silicate systems indicated that it could also be applied on standard portland cement (OPC) and cement with mineral additives (tuff and limestone). It was assumed that induced physical and structural changes in mechanically activated cements would cause certain energy changes in clinker minerals and mineral additives contained in cement which might improve mechanical characteristics of cements and their overall quality (1-4).

EXPERIMENTAL
The experiments of mechanical activation were performed in vibro mill with rings (Humboldt Wedag AG 954/3). The cement samples were obtained from the cement factory "Novi Popovac", Yugoslavia. In Table 1 the characteristics of used samples such as chemical composition, specific surface area (obtained by Blain method) and modules, are presented. Portland cement (OPC) contains 95 % of the portland cement clinker and 5 % of plaster. Cement with additives contains 75 % of the portland cement clinker, 5 % of plaster, 16 % of tuff and 4 % of limestone. The objective of our investigation was to obtain, by mechanical activation, specific surface area of 400 m^2/kg (for OPC) and 500 m^2/kg (for PC 30 d). In order to determine the time of mechanical activation necessary to reach reqired surface area, a great number of time dependent experimens was performed.

It was found out that optimal time of mechanical activation was 3 minutes for OPC and 4 minutes for PC 30 d.

Table 1 Characteristics of the starting cements

Characteristics	PC	PC 30d
SiO_2	19.59	16.11
Al_2O_3	5.22	4.71
Fe_2O_3	2.59	2.39
CaO	62.64	53.27
MgO	2.62	2.42
SO_3	2.49	2.41
Insoluble residue	0.46	12.38
loi	2.60	5.04
Free CaO	1.26	0.23
Humidity, at 105°C	0.80	1.30
Specific surface, (m^2/kg)	288	380
Saturation degree (SD)	94.97	97.39
Silicate modul (SM)	2.50	2.27
Aluminate modul (AM)	2.01	1.97
Hydraulic modul (HM)	2.28	2.29

RESULTS AND DISCUSSION

During the investigations, the analyses of specific surface area and X-ray analyses of investigated cements, prior and after mechanical activation, were performed. Physico-mechanical investigations of unactivated and activated cements were also carried out. The X-ray analyses of the starting and mechanically activated cements are presented in Fig.1. The maximal peak intensities are given in Tab.2. As can be seen from Fig.1 and Tab.2, maximal peak intensities characteristic for all investigated mineral decreased for both OPC and PC 30 d cements. This indicates that mechanical activation caused certain changes on the level of the mineral microsturucture.

In Tab.3, physico-mechanical characteristics of both starting and activated cements are presented. On the basis of these results, it can be seen that desired specific surface areas were produced, with cca 10 % discrepancies. Oversize per 1 cm^2 of 4900 mesh screen was lowered from 4.4 % to 0.6 % for OPC, from 4.0 % to 0.8 % for PC 30 d. After mechanical activation of investigated samples water, demand remained almost unchanged; the beginning of binding period was promoted in both cement types, while it's ending for

activated PC 30 d was slightly postponed (2h,40 min : 3 h). Bending strength and compression atrength of activated cements were improved after three days, remaining like that till the 28 th day of solidification (Tab.3).

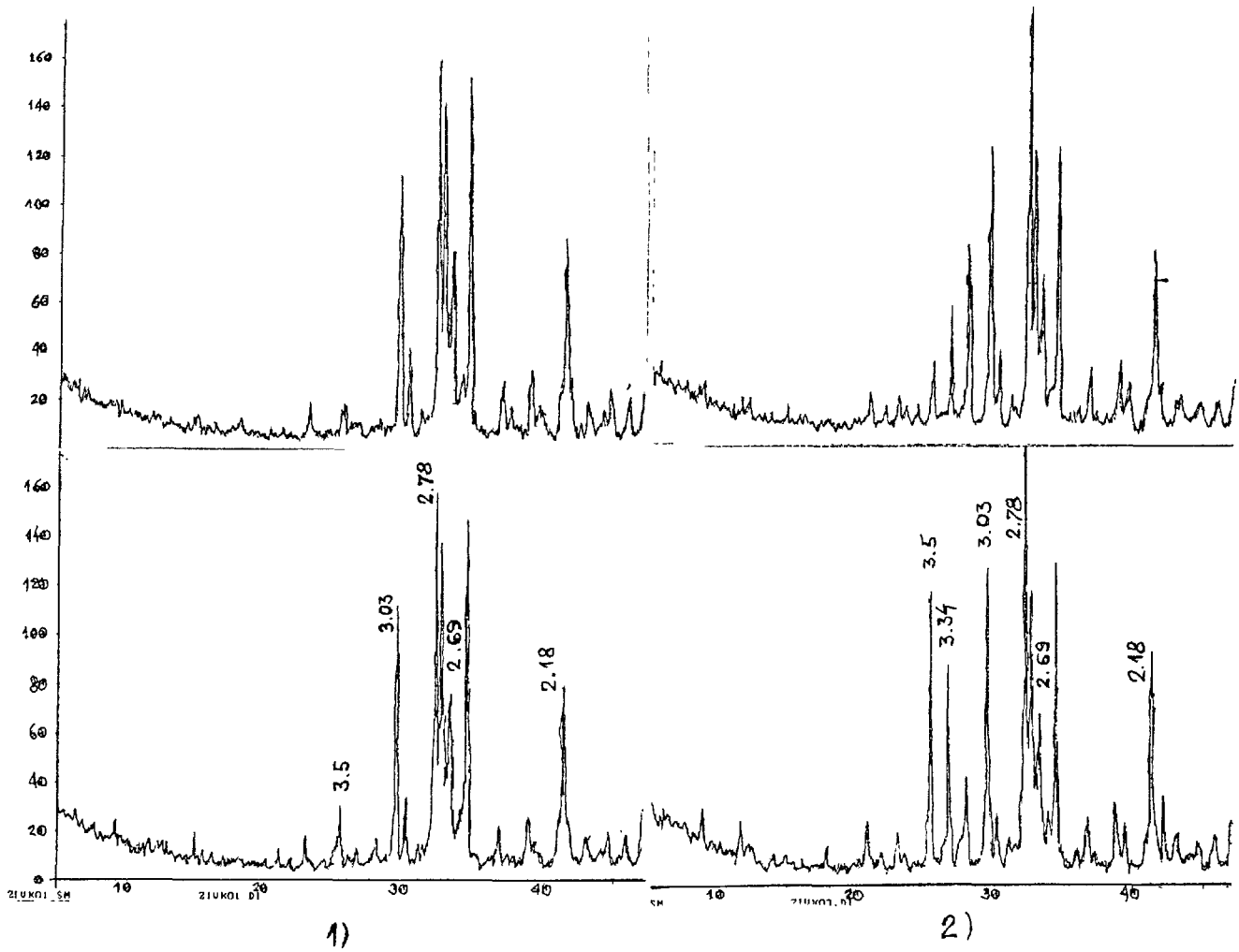

Figure 1 Diffractograms of starting and mechanically activated cements: 1- OPC; 2- PC30d

Table 2 Maximal peak intensities in x-ray diffractograms

Cement type		$C_3S + C_2S$ d = 2.78	C_3A d = 2.69	Anhydrite d = 3.5	Calcite d = 3.03	Quartz d = 3.34
PC	starting	177	83	32	125	
	activated	166	71	16	119	
	change,(%)	7	15	50	5	
PC 30d	starting	250	71	135	125	100
	activated	193	69	29	114	58
	change,(%)	23	3	79	7	

By comparing results of the x-ray analysis (Tab.2) and mechanical investigations (Tab.3), one can see that: a) mechanical activation od OPC caused increase of the specific surface area from 288 m^2/kg to 420 m^2/kg and increase of the compression strength in the 28 day solidification period of 28,4 % b) mechanical activation of PC 30 d caused increase of the specific surface area from 380 m^2/kg to 540 m^2/kg within 4 minutes, thus causing increase of the compression strength, in 28 days, of 18,6 %.

Table 3 Physico-mechanical properties of cement prior and after mechanical activation

Sample	4900 mesh screen oversize per 1 cm^2, (%)	Specific surface area, (m^2/kg)	Water demand, (%)	Binding time, (hours)	
				beginning	ending
starting OPC	4.4	288	27.00	2^{10}	3^{45}
activated OPC	0.6	420	24.70	1^{00}	2^{30}
starting PC 30d	4.0	380	28.00	1^{20}	2^{40}
activated PC 30d	0.8	540	27.80	1^{00}	3^{00}

	Bending strength after (MPa)			Compee-sion strength after (MPa)		
	3 days	7 days	28 days	3 days	7 days	28 days
starting OPC	5.7	6.9	7.5	25.6	31.2	43.0
activated OPC	6.2	8.0	9.0	33.0	40.8	55.2
increase, (%)	8.8	15.9	20	28.9	30.7	28.4
starting PC 30d	5.5	6.9	7.8	24.0	34.4	43.1
activated PC 30d	6.0	6.9	8.3	30.2	41.7	51.1
increase, (%)	9.1	0	6.4	25.8	21.2	18.6

CONCLUSION

Mechanical activation of portland cement and cement with additives caused increase of bending strength and compression strength after 28 day solidification. In other words, mechanical acitvation in vibro mill with rings of only 3 mins (for OPC) and 4 mins (for PC 30 d) significantly improved quality of investigated cements. This quality improvement is, in our opinion, the consequence of the microstructural changes in the minerals present in investigated cements, increased free energy and intensified hydration process.

REFERENCES

[1] G. Heinicke, Tribochemistry, Academie-Verlag, Berlin, 1987.

[2] L.Z.Jinyu, F.Yeming and Y.Jiazhi, The mechanical Activation of belite, Dept Inor. Mather., 9th Int. Cong. on the Chem. of Cement, New Delhi, India, 1992. Vol III

[3] Ž. SEKULIĆ, Investigation of mechanical activation influences on properties of portland cement clinker, M.Sc. thesis (in Serbian), Center for Multidisciplinary studies, University of Belgrade, 1995.

[4] K.Tkačova, Mechanical activation of minerals, Mining Institute of the Slovakia, Academy od Sciences, 1992, Košice, Slovakia.

TOPIC III.D

Influence of type, dose, addition time and mixing time

INFLUENCE OF ADMIXTURE TYPE AND CONCRETE TEMPERATURE ON STRENGTH AND HEAT OF HYDRATION OF CONCRETE

Juha KOMONEN and Vesa PENTTALA
Helsinki University of Technology, Concrete Technology, Espoo, Finland

ABSTRACT Twelve admixtures (plasticizers, non-chloride accelerators, retarders), four mixing temperatures, three cement contents, and three retarder dosage procedures influencing hydration heat of in-situ concretes were measured. Heat evolutions were compared by units kJ/kg-cement and MJ/m³-concrete. Mixing temperature was the most significant variable. Plasticizer based on modified polycondensate of cyanureamide and formaldehyde was more efficient than SMF and SNF based ones. Strength was measured by 150 mm cubes from the age of 14 hours onwards.

Key-words: concrete,admixtures,temperature,workability, heat evolution, strength development.

INTRODUCTION

This article deals with the methods by which early compressive strength of ready-mixed concrete can be reliably assured (Komonen and Penttala, 1997). There have been numerous studies on the subject and the basic factors which govern the early compressive capacity are known but when good workability of concrete is strived at the same time very few articles are found. At least in Finland, there is scarce information available on the properties of various ready-mixed concretes during the first 24 hours.

EARLY STRENGTH GAIN

The evolution of early strength of concrete can be affected in many ways but the most common methods are changing of the composition or temperature of concrete. Almost all concrete properties, including the strength, can be shown to be a function of water cement ratio. Lower water cement ratios give usually better properties in question. However, when extended workability is needed the decrease of w/c is restricted. Naturally, the rate of cement hydration accelerates as a function of temperature but if the rate is advanced too much, special measures have to be taken into consideration in order to achieve the desired workability.

Admixtures are mainly used to modify the properties of concrete and to make them more suitable for concreting works due to economical reasons or such other purposes as saving energy. In many instances an admixture might be the only feasible means of achieving the desired result. The dosage level of different plasticizers required to achieve certain workability varies from product to product. Also due to differences in chemical compositions the effects of superplasticizers on the hydration rate of cement differ significantly. It is very risky to model the effect for different types of products in general, and it is not unusual to find, that a particular superplasticizer works well in one concrete mixture but behaves rather strangely in another, Aïtcin et al. (1994).

SCOPE OF THE RESEARCH

The aim of the investigation was to compare various methods to accelerate strength development of concrete and to get information about its benefits and disadvantages. Additional aim is to give recommendations of different methods in enhancing the strength development at early age. The concretes investigated had a workability time so that they could be properly placed even after 120 minutes after mixing.

MATERIALS, METHODS, AND TESTS

The binder used in the tests was a rapid hardening cement CEM II A 42.5 R of local origin produced by Finnsementti Oy, **Table 1**. City tap water was used. The admixtures investigated are shown in **Table 2**. Aggregate was rounded granite with a particle density of 2670 kg/m³. The aggregate grading was combined from nine fractions (up to 32 mm) and had sieve passing values 3, 7, 12, 20, 28, 43, 56, 76, and 100 % with sieve sizes 0.125, 0.25, 0.5, 1, 2, 4, 8, and 32 mm, respectively.

Table 1 The binder properties.

Binder	CEM II A 42.5 R
Chemical analysis (%)	
SiO_2	18.7
Al_2O_3	5.2
Fe_2O_3	2.6
MgO	3.6
CaO	57.3
Na_2O	0.7
K_2O	0.9
Ignition loss	3.7
Insoluble SO_3	3.6
Free CaO	2.0
Additives in clinker production (%)	
Lime stone	7
GBFS	11
Clinker mineral Bogue analysis (%)	
C_3S	67
C_2S	9
C_3A	8
C_4AF	8
Specific surface area (m^2/kg)	
Blaine	465
Setting time (hours.minutes)	
Initial	3.35
Final	4.25
Compressive strength (MPa)	
1d	26
3d	39
7d	43
28d	54

Table 2 The admixture properties.

Report code	ADMIXTURE TYPE Active ingredient
P1	WATER-REDUCER modified lignosulfonate
P2	WATER-REDUCER lignosulfonate
P3	SUPERPLASTICIZER modified naphthalene-formaldehyde polycondensate
P4	SUPERPLASTICIZER modified polycondensate of cyanureamide and formaldehyde
P5	SUPERPLASTICIZER modified naphthalene-formaldehyde polycondensate
P6	SUPERPLASTICIZER sulphonated melamine-formaldehyde resin
P7	SUPERPLASTICIZER sulphonated melamine-formaldehyde resin
ACC1	NON-CHLORIDE ACCELERATOR organic sodium salts
ACC2	NON-CHLORIDE ACCELERATOR amines
R1	RETARDER alkali metallic salts of hydroxy acid
R2	RETARDER inorganic phosphates
R3	RETARDER watersoluble alkali salts of orthophosphoric acid and alkyl aryl sulphonates and saccharides

Proportioning and mix design

Workability was defined by Vebe test, which is a common test of consistency in Finland. The concretes were proportioned with respect to workability (Vebe time less than 5 seconds after 120 minutes from mixing). The cement amount was decreased when plasticizers were used. The dosage amount of an expensive non-chloride accelerator was determined by using the equal

relative cost with plasticizer. The concretes were proportioned using the basic volumetric equation of concrete. Mix design of the test concretes is given in **Table 3**.

Table 3. Mix design and some test results of the concretes.

Mix code = variable investigated	Mix design				Fresh concrete		Compressive strength			
	cem. (kg)	wat. (kg)	agg. (kg)	adm. (kg)	Air (%)	Vebe (s)	14 h (MPa)	24 h (MPa)	7 d (MPa)	28 d (MPa)
Mix temperature										
40°C	400	215	1698	-	1.1	5.0	15.1	21.1	31.2	38.7
30°C	400	200	1738	-	0.6	3.6	15.4	24.1	36.5	45.6
23°C	400	185	1778	-	1.3	3.0	16.3	28.2	44.4	52.7
18°C	400	200	1738	-	0.4	-	-	17.2	-	-
Cement content										
500kg	500	210	1653	-	0.8	2.6	22.0	33.4	45.3	54.8
400kg	400	185	1778	-	1.3	3.0	16.3	28.2	44.4	52.7
300kg	300	165	1917	-	1.2	4.2	9.1	20.5	35.9	43.7
Plasticizer type										
P1	375	165	1842	4.9	3.1	5.1	-	17.3	46.1	54.5
P2	375	165	1842	4.9	2.7	6.5	-	20.0	42.2	50.8
P3	375	165	1842	4.9	1.5	5.5	13.4	29.1	44.5	52.2
P4	375	165	1842	4.9	1.1	4.9	22.5	32.2	47.1	52.9
P5	375	165	1842	4.9	0.4	4.3	18.0	31.8	46.9	55.3
P6	375	165	1842	4.9	0.7	5.3	17.6	30.5	45.7	54.2
P7	375	165	1842	4.9	0.9	5.5	17.8	30.6	45.3	54.1

Mix code = variable investigated	Mix design			Total heat	Max rate of heat gain		Comp.
	cem./wat./agg. (kg)	P4 (kg)	adm. (kg)	evolution/24 h (kJ/kg-cem)	Rate/30 min (kJ/kg-cem)	Time (h)	24 h (MPa)
Accelerator type							
ACC1	375/180/1805	-	2.6	261	27	10.5	29.4
ACC2	375/180/1805	-	2.6	252	23	10.5	26.2
P4a	375/175/1813	4.9	-	254	26	10.5	27.9
Retarder type							
R1	375/165/1840	4.5	0.75	241	24	12.5	30.8
R2	375/165/1840	4.5	0.75	244	24	13	29.4
R3	375/165/1840	4.5	0.75	236	24	14	29.3
R3 amount							
0 %	375/165/1842	4.9	-	239	26	9	32.2
0.1 %	375/165/1840	4.5	0.38	242	26	11.5	30.0
0.2 %	375/165/1840	4.5	0.75	236	24	14	29.3
R3 dosaging							
Type A	375/165/1840	4.5	0.75	240	25	12.5	30.1
Type B	375/165/1840	4.5	0.75	233	23	13.5	30.7
Type C	375/165/1840	4.5	0.75	236	24	14	29.3

Abbreviations: cem.=cement/m³, wat.= water/m³, agg.=aggregate/m³, adm.=admixture/m³, Air=air content of concrete after mixing, Vebe=result of the Vebe test at 120 minutes after mixing, Time=the time of the maximum heat gain, Comp.=compressive strength.

Heat of hydration

The heat of hydration was calculated by means of temperature measurements in concrete in a semiadiabatic condition. A similar arrangement was utilized by Smeplass and Maage (1990). In every batch about 3.5 liters of fresh concrete was isolated from the surroundings by a disposable box of expanded polystyrene at the age of 15 minutes. The temperature of concrete was measured with a copper/constantan thermocouple (K-type) which was placed in the middle of the specimen. The temperature development of isolated concrete and ambient air were registered by a data logger at 15 minutes intervals for at least 24 hours. Due to the semiadiabatic nature of the apparatus, the heat flow through the polystyrene box had also to be taken into account in the calculations. This heat loss was evaluated by means of fully hydrated test specimens and is noticed as a heat liberation term in **Eq 1**. The rate of total heat energy generated in the hydration was determined from the temperature measurements by the following equation:

$$\frac{dQ}{dt} = \frac{dT_c}{dt} \cdot c_{fresh} \cdot m_c + \lambda_b \cdot (T_c - T_a) \qquad [1]$$

where Q is the total heat generated (J), t is the time (s), c_{fresh} is the specific heat of fresh concrete (1050 J/kg•K), m_c is the mass of concrete in the calorimeter (kg), λ_b is the thermal conductivity of container (0.30 J/s•K), T_c is the temperature of concrete (K), and T_a is the temperature of ambient air (K).

The rate of heat hydrated per kilogram binder is given by dividing **Eq 1** by the mass of binder (kg) in the calorimeter. This unit is a good indicator when the properties of cement are in question, but the definition like this does not indicate the real differences between mixes. More illustrative one is the hydration heat per cubic meter concrete, the definition of which the cement content in concrete is taken into account in the comparisons. The rate of heat hydrated per cubic meter concrete is obtained when **Eq 1** is divided by the mass of concrete (kg) in the calorimeter and multiplied by the density of fresh concrete in kg/m^3. This semiadiabatic method, by which the hydration heat was calculated by means of the heat loss through the container, was found efficient for comparative studies of in-situ concretes.

Concrete manufacturing, fresh and hardened concrete tests, curing

All the aggregate fractions were pre-heated (max 65° C) or cooled when the concretes were produced at various temperatures. The dry ingredients were mixed for 30 seconds before the water was added into the rotating mixer and thereafter mixing was continued for three minutes. When admixtures were used the addition procedure of water was changed. First ¾ of water was added into the rotating mixer and mixed for one minute. Then ¼ of water blended with the admixtures - plasticizer or non-chloride accelerator or retarder together with plasticizer - was added and mixing was continued for additional three minutes. This was dosaging type C. The properties of admixture R3 were also investigated by two other mixing procedures A and B. In type A the retarder was blended with ¾ of water. In type B the retarder blended with water was mixed at first with cement. Next the aggregates were added and mixing continued for one minute. Thereafter the plasticizer was added and the mixing was continued for three additional minutes.

The workability loss was measured by a Vebe consistometer test, a slump test, and a flow test. The air content and density were measured after mixing. Compressive strength was tested using three 150 mm cubes at the age of 14 hours and 1, 7, and 28 days. The specimens were cured at

20° C and 45% relative humidity after demoulding from the age of 24 hours onward if not tested before.

RESULTS

In **Table 3** the most important fresh and hardened concrete properties of the concretes are presented. The cumulative heat of hydration of the first 24 hours after mixing and the rate and time of maximum heat gain of some concretes are also shown. The cumulative heat gains are presented in megajoules per cubic meter concrete in **Fig 1**. The initial hydration heat peaks - the rapid first reactions of cement after contact with mixing water - were not registered by this measurement procedure because the reactions took already place in the mixer. The evolutions of heat of hydration of cement during 24 hours after mixing are presented in **Figs 2 and 3**.

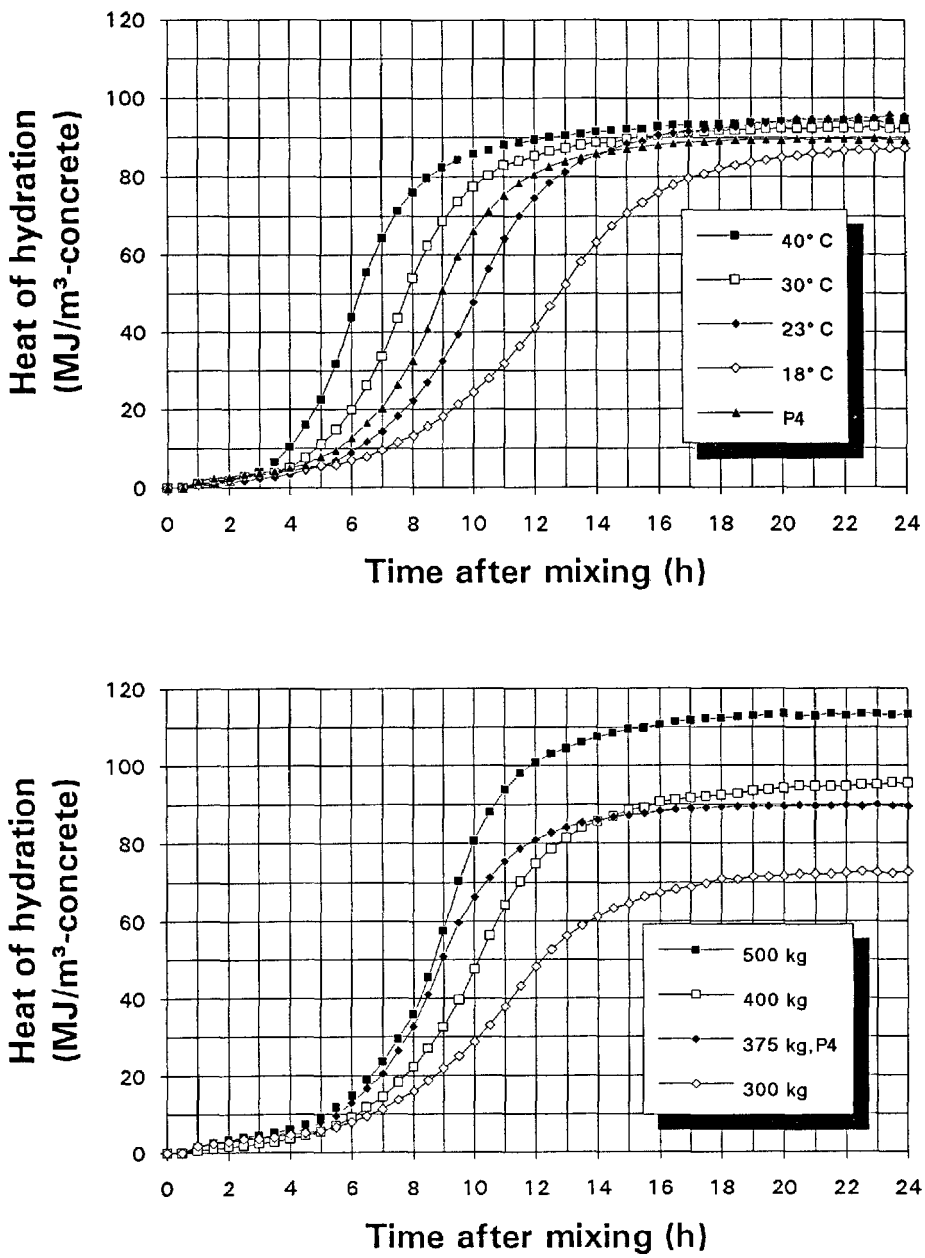

Figure 1. Effects of mixing temperature and binder amount on the heat of hydration of concrete. Hydration heat of concrete made with plasticizer P4 is also shown.

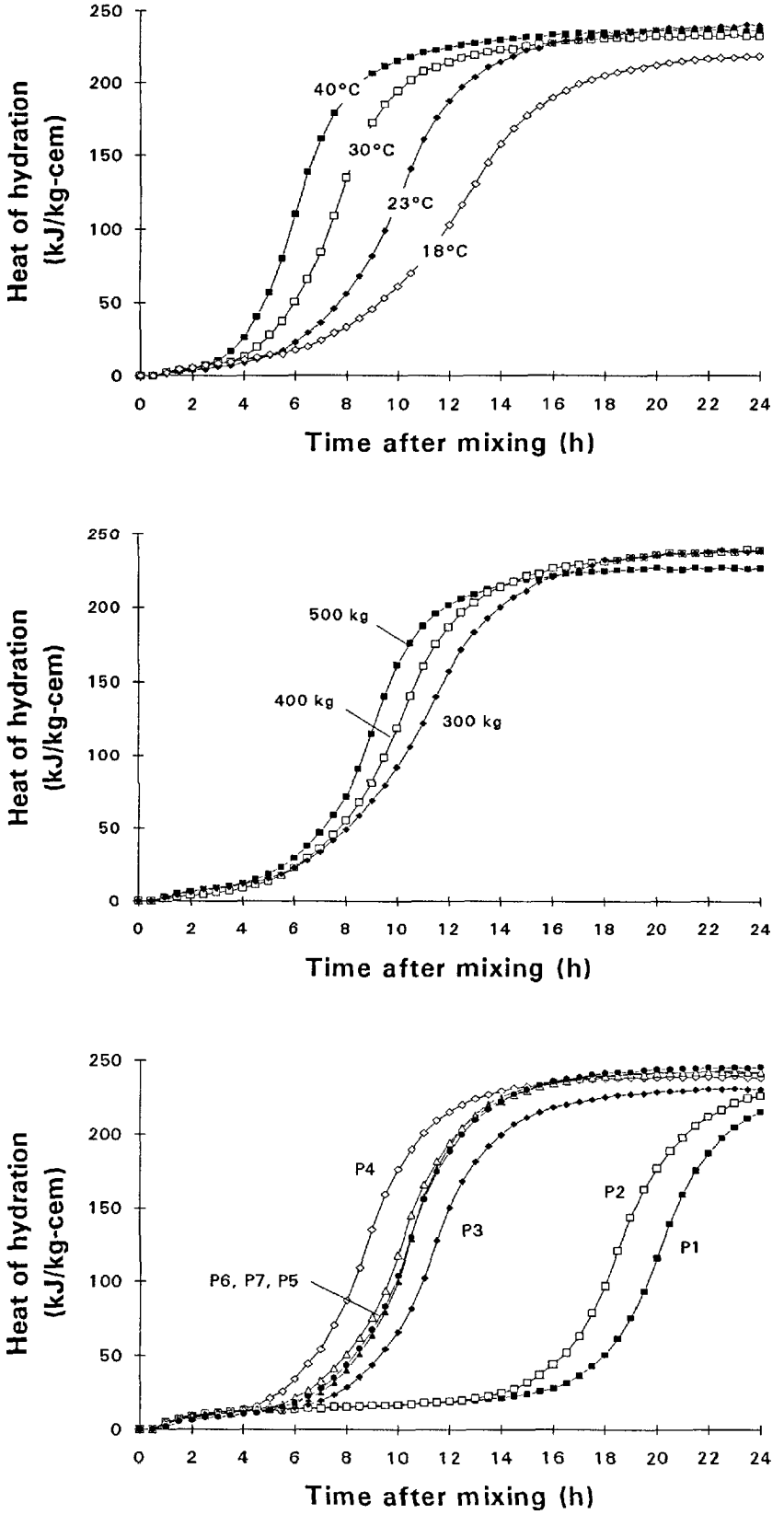

Figure 2. Effect of mixing temperature, binder amount, and plasticizer type on the heat of hydration of cement.

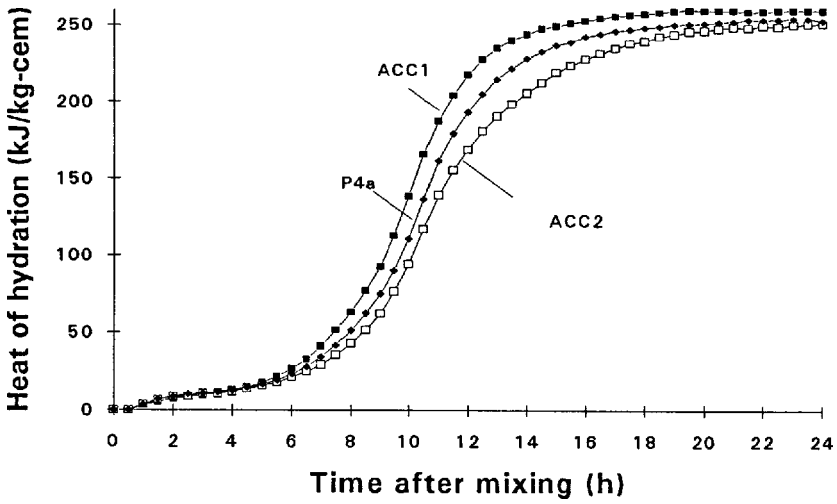

Figure 3. Effects of non-chloride accelerators and plasticizer on the heat of hydration of cement.

CONCLUSIONS

All the results and discussions are given in detail in Komonen and Penttala (1997). This presentation focuses only on the conclusions.

1. Mixing temperature was the most significant variable. The higher the mixing temperature was the earlier the heat gain took place. In spite of the higher water cement ratio the hydration reactions were advanced when the mixing temperature was increased.

2. High mixing temperature did not ensure early compressive strength. It did not accelerate the strength gain enough to compensate for the strength loss originating from water increase to ensure the workability desired. These effects cancelled each other at the age of 14 hours after mixing and the compressive strength of concretes mixed at 23, 30 and 40° C did not differ from each other at this age. At later ages the effect of water-cement law was dominant. The desired workability was obtained without retarders even at mixing temperature of 40° C.

3. The high cement content of the test concretes increased the rate of heat gain but had no effect on the induction period of cement. High cement content assured early strength gain. Compressive strength correlates with the cement content between the ages of 14 and 24 hours after mixing.

4. The efficiency of the different plasticizers varied considerably at early ages. The most efficient plasticizer was based on modified polycondensate of cyanureamide and formaldehyde. The second best plasticizers were based on sulphonated melamine-formaldehyde or modified naphthalene-formaldehyde polycondensate and the most inefficient plasticizer studied in this research project was lignosulfonate-based. Plasticizers based on lignosulfonates delayed the hydration reactions more than 9 ½ hours. The retarding and air-entraining effects of the admixtures based on lignosulfonate are in a good agreement with data generally accepted (e.g. Aïtcin et al. 1994 and Collepardi, 1984).

5. The chemical composition of plasticizer effected on the early strength gain but had very little effect on later strength. The plasticizers could be classified according to compressive strength after 14 and 24 hours from mixing.

6. The application of plasticizer together with a decrease of 25 kg in the cement content was equivalent to an addition of 100 kg cement content when an increase in the early strength gain of concrete was strived at.

7. The most effective non-chloride accelerator was based on organic sodium salts. This non-chloride accelerator and the reference plasticizer used gave quite equal evolutions of hydration heat and compressive strength. However, it has to be kept in mind that both concrete types were designed with respect to equal cost and equal workability, which governed the admixture dosage amounts.

8. The most efficient retarder was based on the water soluble alkali salts of orthophosphoric acid and alkyl aryl sulphonates and saccharides. This retarder delayed hydration reactions 2 ½ and 5 hours by dosages of 0.1 and 0.2 % of the weight of cement, respectively.

9. The efficiency of the retarders can be assured with the right mixing procedure. The best was the procedure in which cement, aggregates and three quarters of the total water amount were first mixed for one minute after which one-quarter of the total water amount including both plasticizer and retarder was added. It seems to be advantageous if the early reactions between cement and water take place before the retarder or other admixture is added.

10. All three retarders investigated gave equal compressive strengths after 24 hours from mixing. The method by which the retarder was added into the concrete had no effect on the compressive strength at the age of 24 hours after mixing. However, the effect of retarder amount (0, 0.1, and 0.2%) on the compressive strength was statistically significant at the age of 24 hours after mixing.

11. When hydration heat properties of various concretes are compared the definition megajoules per cubic meter concrete should be applied in the comparison. In this respect the accelerating effect of plasticizer P4 was found to be impressive. Concrete with cement content 375 kg and with plasticizer P4 (1.3%) gave much more earlier heat evolution than the concrete having a cement content of 400 kg and better early strength than the concrete having a cement content of 500 kg.. However, the total heat evolution at 24 hours after mixing correlated significantly with the cement content.

REFERENCES

Aïtcin, P.-C., Jolicoeur, C., MacGregor, J. G. 1994. Superplasticizers: How They Work and Why They Occasionally Don't. Concrete International. 16, 5, pp. 45-52.

Collepardi, M. 1984. Water Reducers/Retarders. In: Ramachandran, V.S., Concrete admixture handbook. United States of America, Noyes Publications. pp. 116-210.

Komonen, J., Penttala, V. 1997. Rapid hardening cast-in-place concretes. Helsinki University of Technology. Faculty of Civil and Environmental Engineering. Concrete Technology. Report 8. xxx p.

Smeplass, S., Maage, M. 1990. Heat of hydration of high-strength concretes. The second international symposium on utilization of high strength concrete, May 1990. Berkeley, California, U.S.A. Hester, W. T. pp 433-456.

3iii030
8 pp

INTERACTION MECHANISM OF CHEMICAL ADMIXTURES AND THEIR INFLUENCES ON MICROSTRUCTURE

Weimin JIANG and Della M. ROY, Materials Research Laboratory, The Pennsylvania State University, University Park, PA 16802, USA

ABSTRACT This study examines the interaction mechanisms between the chemical admixture and hydrating cement and influences of admixture on microstructure development. The mechanism of action of chemical admixture was explained by the interaction effects and the synergistic effects. The properties of cements and chemical admixture were studied using TGA, IR, zeta-potential, viscometry, chemical analysis and SEM-EDX. This study also attempts to discuss effects which contribute to hydration of the cement/admixture combination.

Keywords: admixtures, naphthalene formaldehyde sulphonate, superplasticizers.

INTRODUCTION

The emergence of chemical admixtures as a modern technique has resulted in advancements in concrete production, and for this reason a bright future is predicted for this technique in the 21st century. There is now general recognition that chemical admixtures provide a cost effective method of producing high-performance concrete which also has other merits of improving various properties of fresh concrete and markedly increasing the strength and durability of hardened concrete. Experts predicted that the most recent technological developments in concrete technology rely on enhanced admixture efficiency rather than on improvements in cement manufacturing (Nawy, 1996 and Aïtcin and Baalbaki, 1995). The progressive general contractor would be willing to pay the cost of admixtures, and derive great benefit from them, especially where innovative construction techniques are involved. McFarland et al. (1990) described that superplasticizers (also known as high range water reducers-[HRWR]) can be distinguished from water reducers by the effective deflocculation and the high dispersion of cement particles when used in the mix design. Collepardi (1994) stated that 1970's superplasticizers could join air entraining agents of the 1930's as two of the revolutionary developments in concrete technology in the century.

It is somewhat surprising that cement-admixture compatibility problems are becoming more and more frequent, especially in the field of superplasticizers (Aïtcin, 1994). From engineering practice, various cases have led to recognition of cement/admixture incompatibility, or "abnormal concrete performance in the presence of admixtures" (Helmuth et al., 1995). Different superplasticizers will behave quite differently with different cements, or when combined with a second admixture. The compatibility between cement and admixture could be identified as a result produced by interaction mechanisms (Hewlett and Young, 1987 and Ramachandran, 1995). In addition, the compatibility significance of this problem was recognized as a requirement which needs to be met with the development of new generation chemical admixtures. This also is due in part to the fact that the acceptance standards for superplasticizers themselves now are not very tightly written. Among the benefits to be derived from this research is a better understanding of the factors that modify concrete properties when adding an admixture deliberately to the concrete, and by controlling the chemistry and processing to produce the desired microstructures and properties. It should be noted that the superplasticizers exert their action by decreasing the surface tension of water and by equidirectional charging of cement particles (Nawy, 1996). However, the method of addition of superplasticizer can affect the increase in slump significantly. In the immediate mode, admixture is mixed with water; in the delayed mode either admixture was adding after 1 min of mixing or waiting for the last minute of mixing. Jawed et al. (1979) suggested that the combination of a lignosulfonate with either an alkali carbonate or bicarbonate in conjunction with cement and water gives rise to several unusual effects which appear to be the result of a synergistic interaction. One goal of this study is to attempt to discuss the similar synergistic effects which contribute negatively to cement/admixture incompatibility.

EXPERIMENTAL PROCEDURE

Materials and mixing

Ordinary portland cement (OPC) type I (The chemical composition in Table I), MRL code# I-35, was obtained from Keystone Cement Co. It has a density of 3.12 g/cm^3 and BET surface area of 0.88 m^2/g. The particle size distribution range determined by micromeritics sedigraph is 1.2 - 50 μm. The superplasticizing (SP) chemical admixture, Mighty-150 (sulfonated naphthalene formaldehyde condensate), specific gravity 1.213, solid content 42%. was used in some formulations (Table II). Pastes and mortars were first prepared by adding admixtures and water, resting for 3 min, again mixing for 2 min (2-3-2 mix sequence). In order to check slump loss, the superplasticizer was added during the last minute of mixing in several cases.

Table I The chemical composition of Type I OPC (wt. %)

Type I	Code#	SiO_2	Al_2O_3	CaO	Fe_2O_3	MgO	K_2O	Na_2O	SO_3	L.O.I
OPC	I-35	20.30	5.67	60.43	6.23	3.14	0.90	0.36	2.8	2.5
AC*	Z-61	3.28	39.63	37.36	12.79	0.79	—	—	1.54	2.0

*Ciment Fondu (Lafarge Aluminous Cement Co.) containing 1.95% TiO_2.

Table II Mixture proportions (by weight)

Paste	Mortar
OPC (type I cement) + deionized water at w/c = 0.22, 0.25, 0.3, 0.35, 0.4 adding Mighty 1%, 2%, 2.5% by cement wt% casting in ø1.25 in.x 1.5 cylinders	OPC:Sand (C 109 ASTM) ::1.0:2.25 at w/c = 0.3, 0.35, 0.44 adding Mighty 1%, 2%, 2.5% by cement casting 2 in. cubes

Experimental Methods

BET surface area—Nitrogen adsorption and desorption isotherms were measured using a Quantachrome Autosorb-1 Automatic Sorption Analyzer.

SEM-EDX—An International Scientific Instruments ISI-DS 130 dual stage Scanning Electron Microscope (SEM) with a Kevex Energy Dispersive X-ray analyzer (EDX).

ESEM—An ElectroScan ESEM with a cooling stage was used. The specimen was observed using a beam voltage of 20 keV, a beam current of 100 μA, at chamber pressure of 4 torr at temperature of 9°C, and a working distance of about 8 mm.

Zeta-potential of cement (in presence and absence of superplasticizer) was measured by the microelectrophoretic technique; more detail is given elsewhere (Malek and Roy, 1993).

IR—Infrared Spectrophotometer used was a Perkin-Elmer (model 283B). The sample preparation method followed the KBr disc method.

DTA-TGA—Differential thermal analysis of materials was performed on a Perkin Elmer System 7/4 with a DTA 1700 unit. In all cases the heating rate was either 10 or 20°C/min and Pt/Pt 10 Rh thermocouples were used. A Harrop Laboratories Thermogravimetric analyzer (TG 716) was used in this study with a Cahn balance.

Viscometer—A Haake Buchler coaxial cylinders rotational viscometer, Rotovisco™ RV 12 with the standard M 500 Measuring Drive, was selected.

Isothermal conduction calorimeter—A thermostatically controlled Haake F3 water circulator with heating and cooling equipment was used in conjunction with a Thermonetics Corporation calorimeter. In each case 3 g of powder was placed in metal container, then 1.5 g of water was added.

Pore solution—Samples of the aqueous phase in contact with alkali activated cement pastes were obtained by expression of the pore solution from hardened cement pastes under high pressures of 500 MPa at ages ranging from 15 minutes to 90 days.

RESULTS AND DISCUSSION

Effects of admixture adsorption on cement and rheological properties

BET data are given in Table III, and the setting time is in Table IV. There is little difference between results with or without Mighty-150 (SP), if w/c is unchanged. However, when reducing w/c to 0.22, BET surface is down to 1.96 m^2/g. The Ca^{2+} concentration in the cement-mighty-150 system is higher than in the control only. Fig 1 show the concentration of calcium ion and superplasticizer (SP) during hydration the first 24 hours in pore solution. The concentration of superplasticizer was determined by absorbance measurements (Jawed et al., 1979). When Mighty-150 was used, the rheological changes associated with setting time change of paste were determined to investigate the effects of admixture adsorption on cement and flow, yield value, plastic viscosity and zeta-potential. Setting is a poorly defined phenomenon (Struble and Lei, 1995). It is important to understand both the changes associated and physical (microstructural) changes associated with setting under superplasticizer's effect. Fig. 2 shows Haake flow curves of fresh paste of OPC (type I) with Mighty-150 1% (a/c wt%). The results indicated that although addition of superplasticizer decreases the yield stress and apparent viscosity in the early stage in the superplastizer-cements system, the magnitude of such decrease is qualitatively proportional to the amount of superplasticizer added and the water to cement ratio. However, with time elapsing the situation of "slump loss" may happened. After 30 min, the yield stress increased slightly is corresponding to a "slump loss". The negative zeta potential generated on the cement particles is illustrated in Fig. 3, which is consistent with those reported by Roy and Daimon (1980). The zeta potential of control (OPC only) is around +5 mV (Malek and Roy, 1993), which will shift to negative with a very small admixture addition, 0.1%, indicating that the dispersant was adsorbed on the particle surfaces. The increase in zeta-potential will cause cement particles to deflocculate (minimizing the yield stress) and setting the immobilized water free.

Table III BET specific surface area of OPC type I

unhydrated	hydrated (7 days) at w/c = 0.35	OPC + 1% Superpla. at w/c = 0.35	OPC + 1% Superpla. at w/c = 0.22
0.88 m^2/g	3.22 m^2/g	3.07 m^2/g	1.96 m^2/g

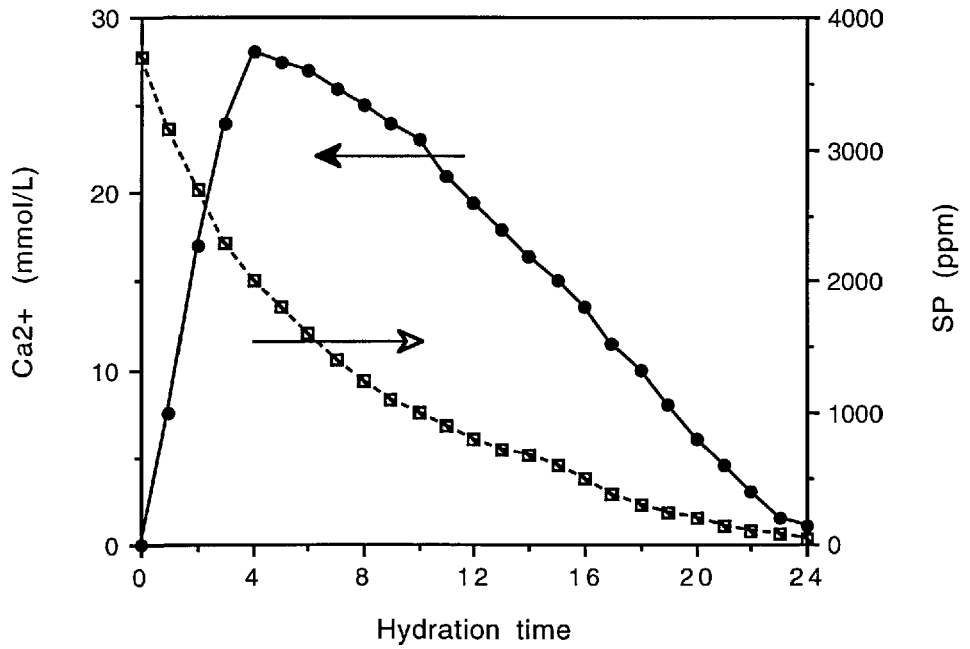

Figure 1 Concentration of calcium ion and superplasticizer(SP) in pore solution during hydration the first 24 hours.

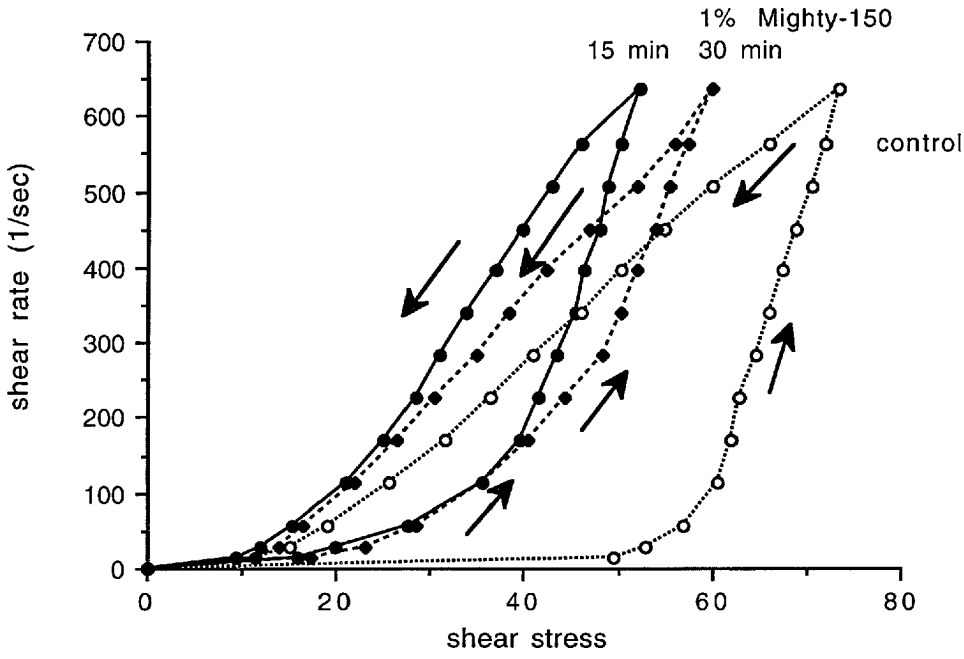

Figure 2 Haake flow curves of fresh paste of OPC (type I) with mighty-150 1% (a/c wt%)

Mode of interaction

The superplasticizers is a surfactant which acts by the way of adsorption predominantly at the solid-water interface (Hewlett and Young, 1987). Adsorption occurs via the polar backbone rather than the negatively charged end group causing the highly charged end to be thrust towards the solution. In this way, cement grains and small particles acquire an increased negative charge—any entrained air will also be negatively charged—and hence the mixture becomes mutually repulsive. Fig. 3 shows the tendency for zeta potential of OPC and Ciment Fondu to increase (negative magnitude) as a result of superplasticizer adsorption. Although, Ciment Fondu has a relatively larger negative zeta potential, the desired benefits of improved workability in the presence of Mighty-150 are not obtained to the expected degree, which will be reported elsewhere, and is consistent with data of Banfill and Gill (1993).

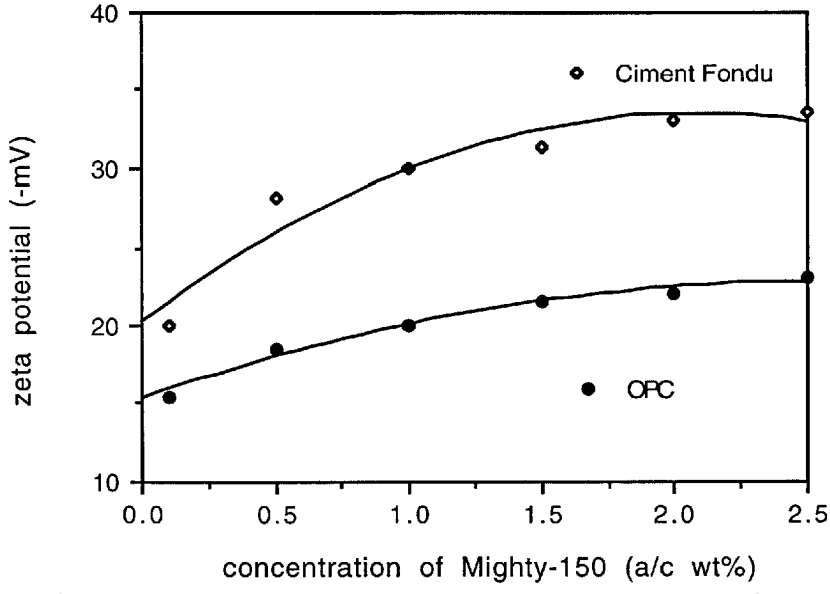

Figure 3 Zeta-potential of cement at different concentration of superplasticizer.

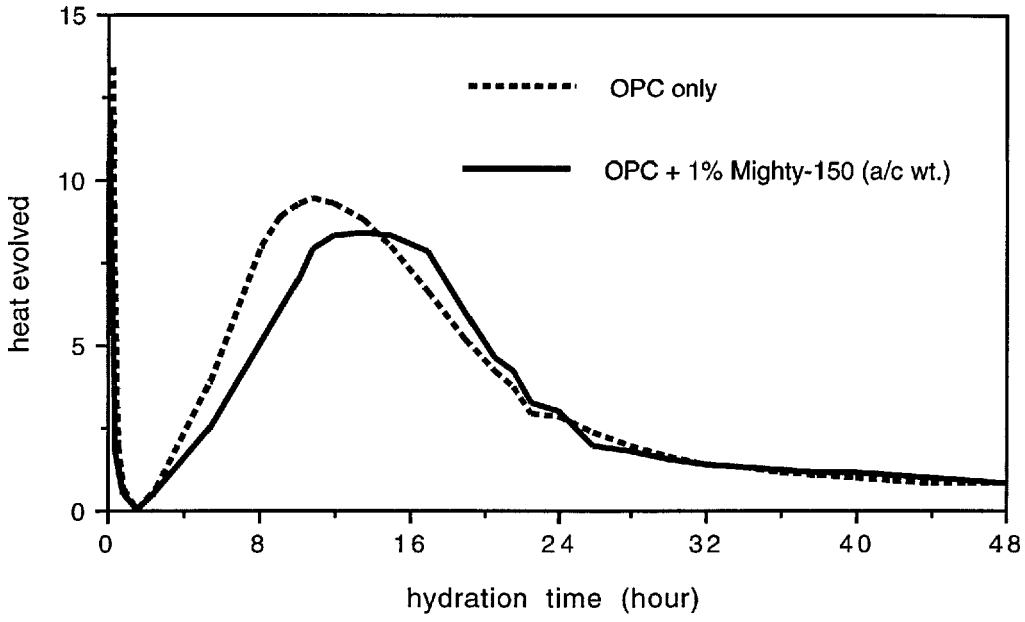

Figure 4 Calorimetric curves showing the rates of heat evolution as functions of time for portland cement + 1% SP at w/c = 0.5 during the first 24 hours of hydration.

Influences of admixture on hydration and microstructure development

Fig. 4 gives calorimetric curves showing the rates of heat evolution as functions of time for portland cement + 1% Mighty-150 at w/c = 0.5 during the first 24 hours of hydration. It seems that superplasticizers delay sightly OPC hydration, as in previous results (Dodson, 1990). Table IV of setting time also shows that when the w/c is unchanded, adding Mighty-150 delays setting slightly. However, when w/c ratio is decreased, setting time is reduced. The effect on microstructure of paste is based on the considerable ability to facilitate reducing the water content, with a consequent improvement in related characteristics of concrete (increased of compressive and flexural strength, decrease of permeability, creep, shrinkage).

Synergistic interaction

Fig. 5(A) is an SEM image of an OPC paste with 1% Mighty-150 after 18 hours hydration. It is shown that the better dispersion of cement particles in a superplasticized concrete produces a finer capillary structure. Fig. 5(B) x-ray sulphur map around the hydration products is shown. When compared with control (OPC only), extra sulphur is derived from Mighty-150. The sulphur-bearing products are also verified by EDX analysis, with results indicating that those kinds of product exist on the surface of cement particles. Fig. 6 illustrates the IR spectra in KBr disc.of Mighty-150. A series of spectrum of extracted Mighty-150 also made followed method described by Hime et al (1965). Those results will be reported elsewhere. It can be seen that both the composition of cement and the constitution of admixture must be known if the potential interactions are to be under stood (Hewlett and Young, 1987). The original compound from Mighty may converted into other substances by interaction with the cement components. The action of water reducers involves adsorption in the cement-superplasticizer system. In several cement/admixture incompatibility cases, successful analysis requires that results be related back to the original compound by "chemical intuition". The rate and amount of adsorption of superplasticizers on cement may identify the synergistic interaction of different factors. For instance, the solid-water interface (Stumm, 1992) may refer to the cement-superplasticizer, cement-set-accelerator (Justnes and Nygaard, 1995), or cement-corrosion-inhibitor (Nmai, 1995). According to this research, it seems that the adsorption reactions affect the surface charge of suspended cement particles and influence their aggregation and transport. However, more research is needed.

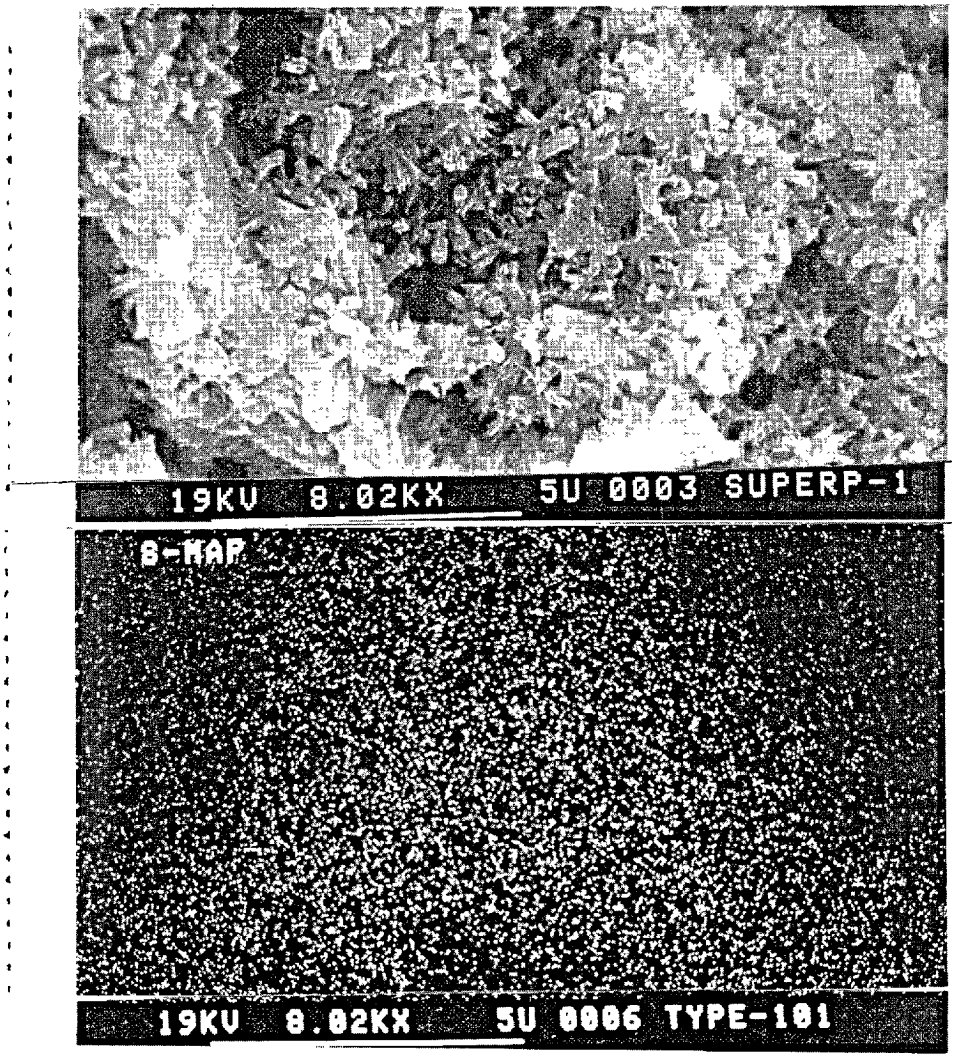

Figure 5 (A) SEM image of a OPC paste (w/c = 0.35) with 1% Mighty-150 after 18 hours hydration. (B) x-ray sulphur map around the hydration products.

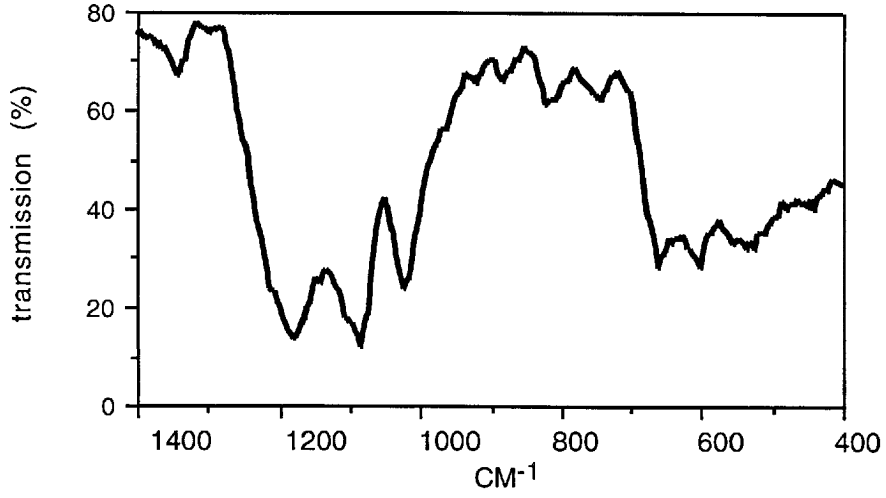

Figure 6 IR spectrum in KBr disc of Mighty-150.

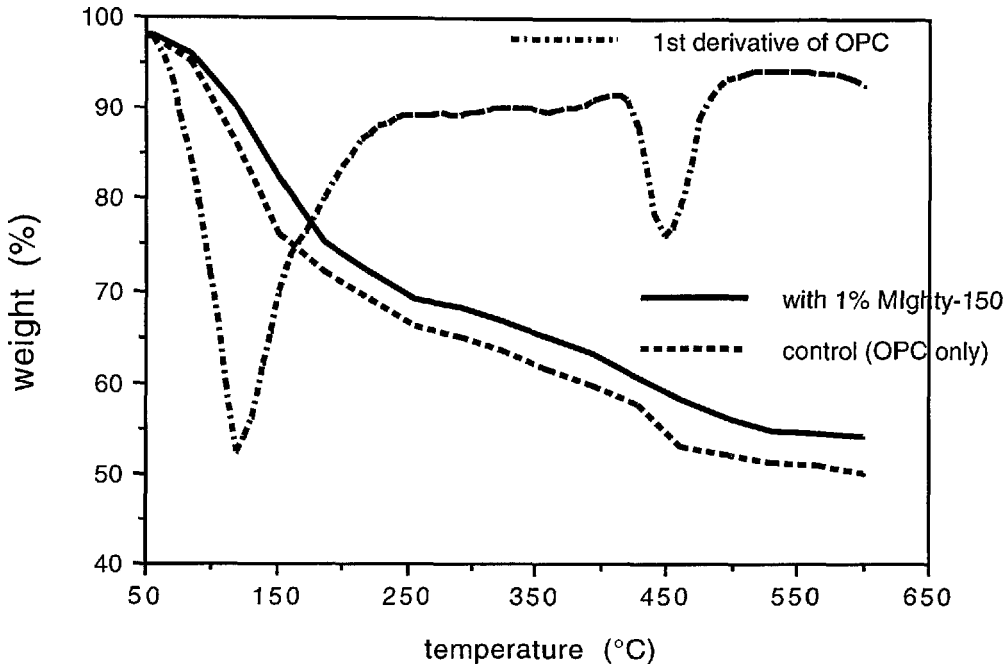

Figure 7 TGA data for OPC + 1% (a/c wt%) after hydration 7 days.

Table IV setting time

Setting time	OPC only at w/c = 0.35	OPC+1% SP at w/c = 0.35	OPC + 1% SP at w/c = 0.3	OPC + 1% SP at w/c = 0.22
Initial	4:17	4:30	3:53	2:56
Final	4:34	5:12	4:10	3:15

Combination of chemical admixture and mineral admixture

The influences of the actual combinations of chemical admixture and mineral admixture is a practical subject which attracts intensive attention. Uchikawa (1996) pointed out that increased chemical admixture is required with increasing fineness of mineral powder. Fly ash requires approximately 1.5 times as much chemical admixture as limestone powder. The more the adsorbed quantities of admixture, the larger of requirements are. Fig. 7 shows thermogravimetric (TGA) data for OPC + 1% (a/c wt%) and 5% silca fume after hydration 7 days. The content of combined water in paste with 1% Mighty-150 is lower than that of the control. TGA data shows two endothermic peaks, the first peak, 110°C, is due the capillary water, the second peak, 420-480°C, is due to portlandite. No major difference is suggested between the two TGA patterns. Increase of the strength of OPC with superplasticizer may be caused by densification of the structure under effect of admixture.

CONCLUSION

From this study the following conclusions may be drawn:

- Results shows the increased negative zeta potential of OPC and Ciment Fondu as a result of superplasticizer adsorption. Ciment Fondu has a relatively larger negative zeta potential. IR spectra in KBr disc.of Mighty-150 (reference) were illustrated.
- The present study shows that superplasticizers delay slightly OPC hydration, and setting time, when the w/c is unchanged.
- The adsorption reaction affects the surface charge of suspended cement particles, which influences their aggregation and transport.
- The content of combined water in paste with 1% Mighty-150 is lower than those of control. It is suggested that no major difference exists between both TGA patterns.

REFERENCES

Aïtcin, P.-C , Jolicoeur, C., and MacGregor, J.G. (1994). "Superplasticizers: How They Work and Why They Occasionally Don't". J. Concrete International, May, pp. 45-52.

Aïtcin, P.-C and Baalbaki, M. (1995). "Concrete Admixtures - Key Components of Modern Concrete", in *Concrete Technology New Trends, Industrial Applications*, Ed. Aguado,A., Gettu, R., and Shah, S.P. (E & FN Spon, London), pp. 33-47.

Banfill, P.F.G. and Gill, S.M. (1993). "Superplasticizer for Ciment Fondu, Part 1: Effects on Rheological Properties of Fresh Paste and Mortar". Advn in Cem. Res., **5**, 131-138.

Collepardi, M. (1994). "Superplasticizers and Air Entraining Agents: State of the Art and Future Needs", in *Concrete Technology Past, Present, and Future*, Ed. Malhotra, V.M., SP-144 (American Concrete Institute, Detroit, MI), pp. 543-564.

Dodson, V. (1990). *Concrete Admixture.* (Van Nostrand Reinhold, New York).

Helmuth, R., Hills, L.M., Whiting, D.A., and Bhattacharja, S. (1995). *Abnormal Concrete Performance in the Presence of Admixtures* (Portland Cement Association, Skokie, IL).

Hewlett, P.C. and Young, J.F. (1987). "Physico-Chemical Interactions between Chemical Admixtures and Portland Cement". J. Materials Education, **9**, 389-435.

Hime, W.G., Mivelaz, W.F., and Connolly, J.D. (1965). Use of Infrared Spectrophotometry for the Detection and Identification of Organic Additions in Cement and Admixtures in Hardened Concrete, in Analytical Techniques for Hydraulic Cements and Concrete, STP 395 (ASTM, Philedelphia), pp. 18-29.

Jawed, I., Klemm, W.A. and Skalny, J. (1979) "Hydration of Cement-Lignosulfonate-Alkali Carbonate System. J. Am, Ceram. Soc.**62**, 461-464.

Justnes, H. and Nygaard, E.C. (1995). "Technical Calcium Nitrate as Set Accelerator for Cement at Low Temperatures". Cem. Concr. Res. 25, 1766-1774.

Malek, R.I.A. and Roy, D.M. (1993). "Effect of Superplasticizers on the Workability of Concrete as Evident from Apparent Viscosity, Yield Stress and Zeta-Potential", in *Flow and Microstructure of Dense Suspensions*, Ed. Struble, L.J., Zukoski, C.F., Maitland, G.C. (Mat. Res. Soc. Symp. Proc. Vol. 289, Pittsburgh, PA), pp. 191-198.

Miller, K.T., Shi, W., Struble, L.J., and Zukoski, C.F. (1995). "Compressive Yield Stress of Cement Paste", in *Microstrcture of Cement-Based Systems/Bonding and Interfaces in Cementitious Materials*, Ed. Diamond, S., Mindess, S., Glasser, F.P., Roberts, L.W., Skalny, J.P., Wakeley, L.D. (Mat. Res. Soc. Proc. Vol. 370, Pittsburgh, PA), pp. 285-291.

McFarland, M.A., R.E. Carperter, S.A. Farrington, Motz, R.E., Volk, R.E., and Youn, D.J. (1990). "Admixtures" in Cements Research Progress, Ed. Brown, P.W. (American Ceramic Socity, Westerville, OH). pp. 131-164.

Nawy, E.D. (1996). *Fundamentals of High Strength High Performance Concrete.* (Longman Group Limited, Essex England), pp. 53-57.

Nmai, C.K. (1995) "Corrosion-Inhibiting Admixtures : Passive, Passiveactive versus Active Systems", in Advances in Concrete Technology, Ed. Malhotra, V.M., SP-154 (Amercian Concrete Institute, Detroit, MI), pp. 565-586.

Ramachandran, V.S. (1995). "Interaction of admixtures in the cement-water system", in *Application of Admixtures in Concrete*, Ed. Paillere, A.M. (E & FN Spon, London). pp. 1-15.

Ravina, D. and Soroka, V. (1994). "Slump Loss and Compressive Strength of Concrete Made with WRR and HRWR Admixtures and Subjected to Prolonged Mixing". Cem. Concr. Res. **25**, 1475-1484.

Roy, D.M. and Daimon, M. (1980). "Effect of Admixtures upon Electro-Kinetic Phenomena During Hydration of C_3S, C_3A and Cement". 7th ICCC. Paris, Vol. II, Theme II-242-246.

Schramm, G. (1994). *A Practical Approach to Rheology and Rheometry.* (Gebrueder HAAKE GmbH, Karlsruhe, Germany).

Struble, L.J. and W.G. Lei. (1995) "Rheological Changes Associated with Setting of Cement Paste". J. Advn. Cem. Bas. Mat. **2**, 224-230.

Stumm, W. (1992) *Chemistry of the Solid-Water Interface.* (J. Wiley & Sons, New York).

Uchikawa, H. Hanehara, S. and Hiro, H. (1996). "Influence of Microstructure on the Physical Properties of Concrete Prepared by Substituting Mineral Powder for Part of Fine Aggregate". Cem. Concr. Res. **26**, 101-111.

EFFECT OF CHEMICAL ADMIXTURES ON CH CRYSTAL GROWTH

Guy ROSENTHAL and Lynn BROWER, Master Builders Technologies, Cleveland, OH 44236 USA

ABSTRACT

A variety of small organic molecules have been examined in alite and OPC pastes for their effects on crystallization kinetics and crystal morphologies in the early stages of hydration. Admixtures were observed to remarkably affect $Ca(OH)_2$ (CH) size and morphology in alite paste, with aspect ratios (a/c) ranging from greater than 50 to less than 1. Differences were far less pronounced in cement paste. Computer modeling of interactions between organic molecules and CH surfaces showed a consistent preference for adsorption on the denser 001 surfaces over 100 surfaces.

Key-words: admixtures, alite, calcium hydroxide, crystal size, light microscopy

INTRODUCTION

The strength of a structural member is determined by the most efficient failure mode. For ordinary, moderate-strength concrete, crack propagation in compression or in tension occurs along the interface between paste and aggregate. The interfacial transition zone (ITZ) is thus considered to be the weakest aspect of concrete, and efforts to make significant gains in strength, as well as durability, have focused upon producing physical and chemical changes within the ITZ (Ahmed and Struble, 1995).

The disposition of $Ca(OH)_2$ (CH) crystals within the ITZ is a matter of some disagreement. CH crystals appear to precipitate preferentially within the ITZ (Patel, et.al., 1995) and, due to their plate-like habit, tend to self-orient with their ab crystallographic planes parallel, suggesting a mechanism for crack propagation and for fluid ingress between the oriented crystals. The lamellar nature of the individual crystals also provides a ready cleavage plane parallel to the ab plane.

Some disagreement persists, however, as to the orientation of the CH tablets relative to the aggregate surfaces. On the basis of microscopic observations, some investigators have concluded that the plates are oriented parallel to the aggregate surface (Maso, 1980), and some have concluded just the opposite (Afridi, et.al., 1990). Intuitively, one might conclude that a preferred orientation of plates perpendicular to the aggregate surface would result in a stronger ITZ (Groves, 1981, Barker, 1984), but in order for CH crystals in this orientation to effectively interfere with crack propagation, they would need to make contact, or even bond, with the aggregate surface. Irrespective of the orientation, however, it follows that removing the preferred orientation of the precipitating crystals, if not removing the CH entirely, from the ITZ can result in an increase in strength, and even a decrease in permeability, of a concrete or mortar sample.

Previous work by Berger and McGregor (1972) focussed upon the effect of inorganic admixtures on CH crystal morphology. Much is known about CH morphology in crystal grown from solution (Tadros, et.al., 1976, Barker, et.al., 1987) In this work, the crystal growth of CH from cementitious media is studied in the presence of a variety of organic modifiers which may have the effects of complexing calcium ions in solution and/or adsorbing preferentially upon specific crystal surfaces, thus influencing both the kinetics and morphology of CH growth. In concert

with the crystal growth experiments, a series of modeling studies were performed to investigate the possibility of preferential interaction of organic molecules with CH surfaces.

CRYSTAL GROWTH MODIFICATION

CH crystal growth was studied using the method of Berger and MacGregor, which involves spreading a thin layer of paste on a quartz microscope slide, beneath a cover slip, and placing the slide in 100% relative humidity for curing. Alite (C_3S) provides a paste which is more transparent than OPC, as well as a chemically simpler system.

Samples were prepared by combining alite or OPC (Type I) with water containing 0.5% by weight organic modifier, with a water/solids ratio of approximately 1.2. The thin paste was then spread on a microscope slide, covered, and cured at room temperature in a sealed Petri dish over water. The thickness of the samples averaged about 200 μm. Samples were examined under a polarizing microscope at 1, 4, 7 and 14 days.

After 24 hours, CH crystals were quite small, when observed, with largest dimensions usually less than 5 μm. 4-day observations yielded the best combination of optical transparency and contrasting results. By 7 days, most samples appeared quite opaque under the polarizer. The crystals were generally viewed down the crystallographic a axis, thus the basal (ac) plane is perpendicular to the slide. This was inferred from the pronounced striations observed in nearly all crystals, parallel to their longest observed dimensions. It was assumed that the crystals that were observed either spanned the thickness of the sample, from cover slip to slide, or occurred in microvoids, without significant amounts of amorphous paste above and below.

In alite, the reference CH crystals after 4 days of curing were relatively isotropic. Interestingly, while the aspect ratios (a/c) of measured crystals averaged around 2, no crystal was ever observed with an aspect ratio less than 1, i.e. the striations always appeared parallel to the longest observed dimension. Many organic modifiers had significant effects on CH growth habit (Table 1), and some resulted in extremely small crystals, rather than the normal case with several observed crystals of longest dimension greater than 50 μm.

In OPC, the results were more uniform. In almost every case, CH plates with aspect ratios greater than 5 resulted. Often the crystals were extensively twinned, resulting in star-like configurations in two dimensions. While this result is not surprising, it provides further evidence that C_3S has a pore solution chemistry which is not representative of Portland cement for the purposes of studying CH crystal growth. Only naphthalic acid, 2-carboxycinnamic acid and 2-ketoglutaric acid yielded relatively isotropic crystals.

MODELING OF MOLECULE-SURFACE INTERACTIONS

Modeling studies were conducted using the Cerius^2 program, minimizing interaction energy between a single molecule of organic modifier and a calcium-rich 001 (hexagonal) or 100 (rectangular) surface. Charges were assigned using semi-empirical and/or Qeq-based calculations. Molecules were given an initial impulse toward the surface and interaction energy was allowed to minimize over 5000 steps (5 ps) at 300 K.

Table 1. Alite CH growth habit results.

Isotropic (a/c < 3):
[reference]
iminodiacetic acid
2-carboxycinnamic acid
3,3' iminobis(N,N-dimethylpropylamine)
fumaric acid
succinic acid
oxalic acid
1,4 cyclohexanedicarboxylic acid
1,3,5 cyclohexanetricarboxylic acid
Anisotropic (3 < a/c < 10):
trans-glutaconic acid
glutamic acid
1,3-cyclohexanedicarboxylic acid
Highly anisotropic (a/c > 10):
2-aminoadipic acid
3-aminoadipic acid
benzenepropanoic acid
glutaric acid
malonic acid
1,2 diaminocyclohexane;
naphthalic acid
2-ketoglutaric acid

Note: Maleic acid, 2,2'-iminodibenzoic acid, 1,1-cyclopropanedicarboxylic acid and 1,2,3,4,5,6 cyclohexanehexacarboxylic acid all resulted in many very small crystals after 4 days.

Using all of the molecules in the optical microscopy study, interaction energies were calculated to be 50-75% lower (more negative) on the 001 surface than the 100, due to the higher positive charge density on that surface. The calculated interaction energies for energy-minimized configurations, corrected for base energies of the free organic molecules, are summarized in Table 2. All of the molecules studied oriented themselves with at least two close (<2.4 A) Ca-X (X = O,N) contacts per X atom. Thus, in the absence of covalent molecule-surface interactions or unsymmetrical charge distributions around basic atoms, all organic bases found a minimum energy configuration which simply maximized nearest-neighbor opposite charge interactions and minimized intramolecular repulsions. In molecules containing π bonds, the carbon backbone preferred to lie flat in order to maximize interaction of the positive surface charge with the π cloud.

Table 2. Interaction energies of molecules with $Ca(OH)_2$ surfaces.

Molecule	E(001)	E(100)	E(001)/E(100)
malonic acid	-456	-296	1.54
maleic acid	-439	-272	1.61
succinic acid	-466	-285	1.64
fumaric acid	-440	-274	1.61
aspartic acid	-483	-295	1.64
iminodiacetic acid	-482	-309	1.56
t-glutaconic acid	-461	-293	1.57
glutaric acid	-473	-285	1.66
glutamic acid	-478	-308	1.55
2-aminoadipic acid'	-473	-285	1.66
3-aminoadipic acid	-480	-310	1.55
2-aminobenzoic acid	-242	-144	1.68
3-aminobenzoic acid	-247	-135	1.83
4-aminobenzoic acid	-264	-146	1.81
2-carboxycinnamic acid	-441	-277	1.59
2-carboxybenzenepropanoic acid	-441	-279	1.58
2,2'-iminodibenzoic acid	-389	-247	1.57
naphthalic acid	-396	-252	1.57
cis-1,2 cyclohexanedicarboxylic acid	-456	-239	1.91
cis-1,3 cyclohexanedicarboxylic acid	-245	-150	1.63
cis-1,4 cyclohexanedicarboxylic acid	-182	-102	1.78
trans-1,2 cyclohexanedicarboxylic acid	-416	-260	1.60
trans-1,3 cyclohexanedicarboxylic acid	-300	-197	1.52
trans-1,4 cyclohexanedicarboxylic acid	-201	-114	1.76
cis-1,2 diaminocyclohexane	-63	-40	1.58
trans-1,2 diaminocyclohexane	-83	-55	1.51
cis-1,3,5 cyclohexanetricarboxylic acid	-561	-400	1.40

Clearly, the model also neglects the interactions of solvent molecules with crystal surfaces or with solvated basic molecules. While the model can examine negatively-charged or rough surfaces, it cannot account for competition at nucleation sites between precipitating ions and organic species in solution. Further work will involve development of the crystallization model.

CONCLUSIONS

The potential exists to substantially influence CH crystal growth from solution, using small organic molecules as modifiers. However, CH crystal growth in alite paste is markedly different from growth in OPC paste. Ions and/or nucleation surfaces present in the two environments act as morphology modifiers themselves.

Computer modeling indicates that organic bases will preferentially adhere to the close-packed 001 surfaces, due to coulombic factors. This interaction leads to growth perpendicular to the basal plane and plate-like crystals. Further development of the model is necessary to account for directional interactions, solvation and crystallization kinetics.

REFERENCES

Afridi, M.U.K., Ohama, Y., Iqbal, M.Z., Demura, K. "Morphology of $Ca(OH)_2$ in Polymer-Modified Mortars and Effect of Freezing and Thawing Action on its Stability," Cement and Concrete Composites, Vol. 12, 1990, pp.163-173.

Ahmed, A., Struble, L., "Effects of Microstructure on Fracture Behavior of Hardened Cement Paste", Proceedings of the Materials Research Society Symposia, Vol. 370, 1995, pp. 99-106.

Barker, A.P., "Structural and Mechanical Characterization of Calcium Hydroxide in Set Cement and the Influence of Various Additives", World Cement, January-February, 1984, pp. 25-31.

Barker, A.P., Brett, N.H., Sharp, J.H., "Influence of organic additives on the Morphology and X-ray Diffraction Line Progiles of Synthetic Calcium Hydroxide," Journal of Materials Science, Vol. 22, 1987, pp. 3253-3260.

Berger, R.L., McGregor, J.D., 'Influence of Admixtures on the Morphology of Calcium Hydroxide Formed During Tricalcium Silicate Hydration", Cement and Concrete Research, Vol. 2, No. 1, 1972, pp. 43-55.

Groves, G.W., "Microcrystalline Calcium Hydroxide in Portland Cement Pastes of Low Water/Cement Ratio," Cement and Concrete Research, Vol 11, No. 5, pp. 713-718.

Maso, J.C., "La Liason Entre les Granulats et la Pate de Ciment Hydrate," Proceedings of the Seventh International Congress on the Chemistry of Cement, 1980, Th. VII-1, pp. 1-14.

Patel, H.H., Bland, C.H., Poole, A.B., "The Microstructure of Concrete Cured at Elevated Temperatures," Cement and Concrete Research, Vol. 25, No. 3, pp. 485-490.

Pratt, P.L., Ghose, A., "Electron Microscope Studies of Portland Cement Microstructures During Setting and Hardening", Phil. Transactions of the Royal Society A, Vol. 310, 1983, pp.93-103

Tadros, M.E., Skalny, J., Kalyoncu, R.S., "Kinetics of Calcium Hydroxide Crystal Growth from Solution", Journal of Colloid and Interface Science", Vol. 55, No. 1, April 1976, pp. 20-24.

Hydration characteristics and new Hydrates using organic additives (carboxylates and sulfonates)

Pöllmann,H. & Stöber, St. Department of Mineralogy, University of Halle / Germany.

Abstract The use of organic additives is common in cement chemistry. In this study the use and the interaction of carboxylates and sulfonates were investigated. Different salts and compounds were used and the hydration mechanisms and formation of new hydrates due to the concentration were studied. A crystallochemical comparison due to properties of the organic compounds used as additives is given. Chain length, rings, substitution of carbon atoms and the change in hydration characteristics are described by heat flow calorimetry. New phases were synthesised purely for comparison purposes. Reaction mechanisms as a result of impurities of additives were included in the study. An improvement of additive usage and better understanding of reactions can be given. The fixation of organic ions in lamellar hydrates will be described.

Key-words: Accelerators, Additives, Afm phase, Calorimetry, Retarders

Introduction

The use of additives (Table 1) in cement industries plays an important role in manipulating a raw material in its physical and chemical abilities. To improve the knowledge of the basic mechanisms it is important to do fundamental scientific work on the main compounds of OPC, calcium aluminates C_3A, (C_4AF) and calcium silicates C_3S, C_2S. Mostly, only the resulting effect of additives is documented. Therefore the observation of the course of hydration by heat - flow calorimetry and combined XRD was done. On the other hand it is important to determinate the hydration products under equivalent conditions at special temporary hydration stages too. Pöllmann, Kuzel and Auer described new solid solutions and pure phases of calcium aluminate salts with different organic and inorganic ions.

Table 1 Organic acids used additives

Methane sulfonic acid	CH_3SO_3H
Ethane sulfonic acid	$C_2H_5SO_3H$
Propane sulfonic acid	$C_3H_7SO_3H$
Calciummethanesulfonate	$Ca(CH_3SO_3)_2$
Calciumethanesulfonate	$Ca(C_2H5SO_3)_2$
Benzene sulfonic acid	$C_6H_5SO_3H$
Toluene p-sulfonic acid	$C_7H_7SO_3H$
Xylol sulfonic acid	$C_8H_9SO_3H$
Formic acid	CH_2O_2
Acetic acid	$C_2H_4O_2$
Propionic acid	$C_3H_7O_2$

With the influence of additives retardation and acceleration occurs, depending on concentration, temperature and specific substances. Acids and salts give a retarding effect on the hydration of silicate phase forming a new hydration maxima. The heat evolution of the cement hydration changes as a function of additive concentration. Furthermore gel structures and chelates with different crystallinity were detected. At high additive concentrations precipitates of the organic compound were formed. The organic cations can enter the

interlayer of TCAH - like structures forming solid solution series (A) and pure phases (B) (Table2:)

Table 2: Table of new calcium aluminum hydrates with organic ions

A $[Ca_4Al_2(OH)_{12}]^{2+}$ $[(R)_2 \cdot nH_2O]^{2-}$	R = H-(CH_2)n-COO^- R = (C_6H_5)-(CH_2)n-COO^-
B $[Ca_4Al_2(OH)_{12}]^{2+}$ $[2x(OH)_2$ $(2-2x)(R)_2 \cdot nH_2O]^{2-}$ 0<x<1	R = CH_3-(CH_2)n-SO_3^- R = (C_6H_5)-(CH_2)n-SO_3^-

Experimental

1. The synthesis of lamellar salts had been done by preparing freshly synthesised educts $CaO \cdot Al_2O_3$ (CA), CaO and respective acids (Table 1) with CO_2 free H_2O W/F - Value = 10 in a glove box. In order to reach better homogeneity an get an higher reaction degree, the pastes were kept in a shaking tool.
Investigations had been done after 3 months of reaction time. Using a special sample holder for wet samples hydration stages at 100% r.F. and 35% r.F. could be exactly determinated.
The metric parameters of the new phases were refined by least squares method using cell parameter values of isotypical structures in combination with 2 Theta - values of the different XRD pattern. In addition the stability of the products will be tested concerning heat resistance and binding strength of organic ions and water molecules in the interlayer by using thermal methods. Optical methods, such as SEM and polarisation microscopy were used too.

2.The course of hydration of several pastes was investigated by using heat flow calorimetry in combination with XRD. As a commercial sample material OPC 42,5 R was used to demonstrate the influence of organic acids. 1g of cement was mixed with 1 ml water or an organic solution was added by injection method. The measured curves were used to determinate quantitative and qualitative effects of development and temporary changes of the hydration of OPC as a function of concentration, C - chainlength of acids, and arrangement of functional groups.

Crystallography

Mechanisms of hydration with respect to crystallography and chemical admixtures were determined. The Afm-Phases were synthesised using carboxylic or sulfonic acids or Ca- salts (Fig.1). Some reactions are described exemplary.

1. $CA + 2CaO + Ca(C_6H_5SO_3)_2 + nH_2O \longrightarrow C_3A \cdot Ca(CtH_5SO_3)_2 \cdot nH_2O$
2. $CA + 3CaO + CH_3SO_3H + nH_2O \longrightarrow C_3A \cdot Ca(CH_3SO_3)_2 \cdot nH_2O$
3. $C_3A + Ca(HCOOH)_2 + nH_2O \longrightarrow C_3A \cdot Ca(HCOOH)_2 \cdot nH_2O$

After 3 months the pastes were investigated by XRD with a special sample holder tool for humidity. The crystallinity was not equal in all samples. Beside well crystallised calcium aluminates containing acid ions with short C-chains (methane-, ethanesulfonates), precipitates with toluene p-sulfonic xylolsulfonic ions of minor crystallinity were developed. It was proofed that at 100% of relative humidity several hydration stages of calcium aluminate hydrates were stable.

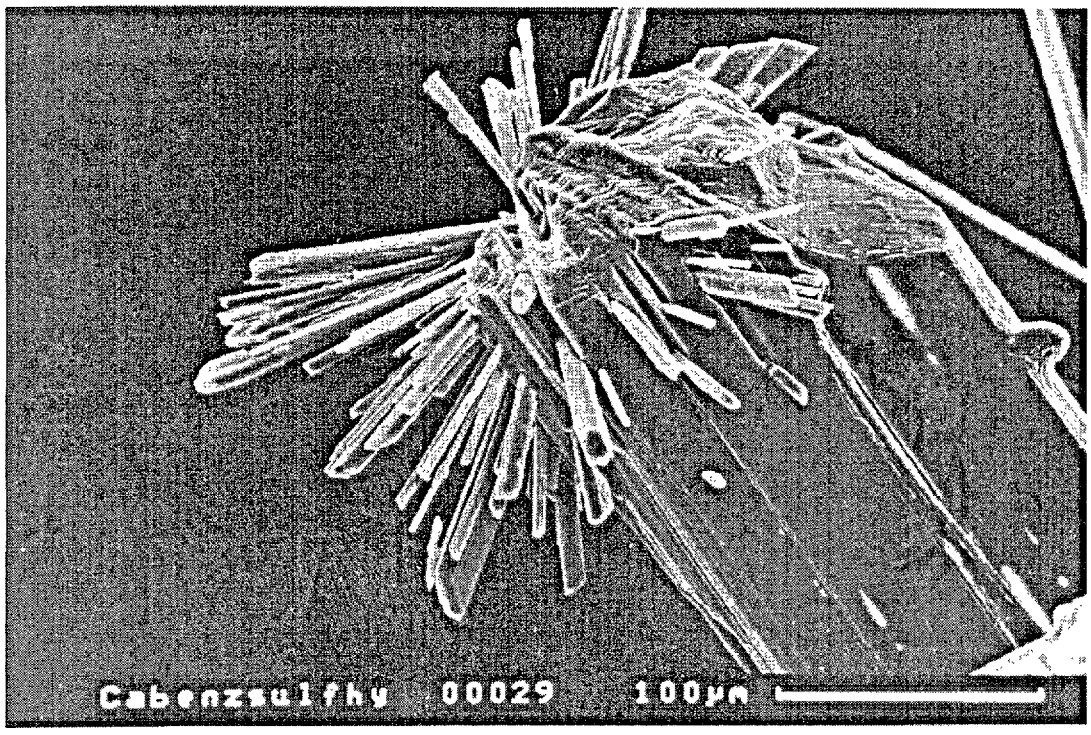

Fig.1 SEM Photography: Crystals of Calciumbenzenesulfonate Monohydrate

Drying until 35% r.F. water molecules were forced to leave the interlayer. The exchange of water between interlayer and surrounding is a reversible process. The formed crystal-structures are not isotypical with the TCAH structure at 100% and 35% r.F.. X-Ray investigations of calcium aluminate hydrates (Fig.2) with interlayered aliphatic - or aromatic sulfonate ions demonstrate, that the c_o-Dimension is equal to the layer thickness c'. Moreover structures with different triclinic or monoclinic crystal systems especially of calcium aluminate carboxylates were formed.

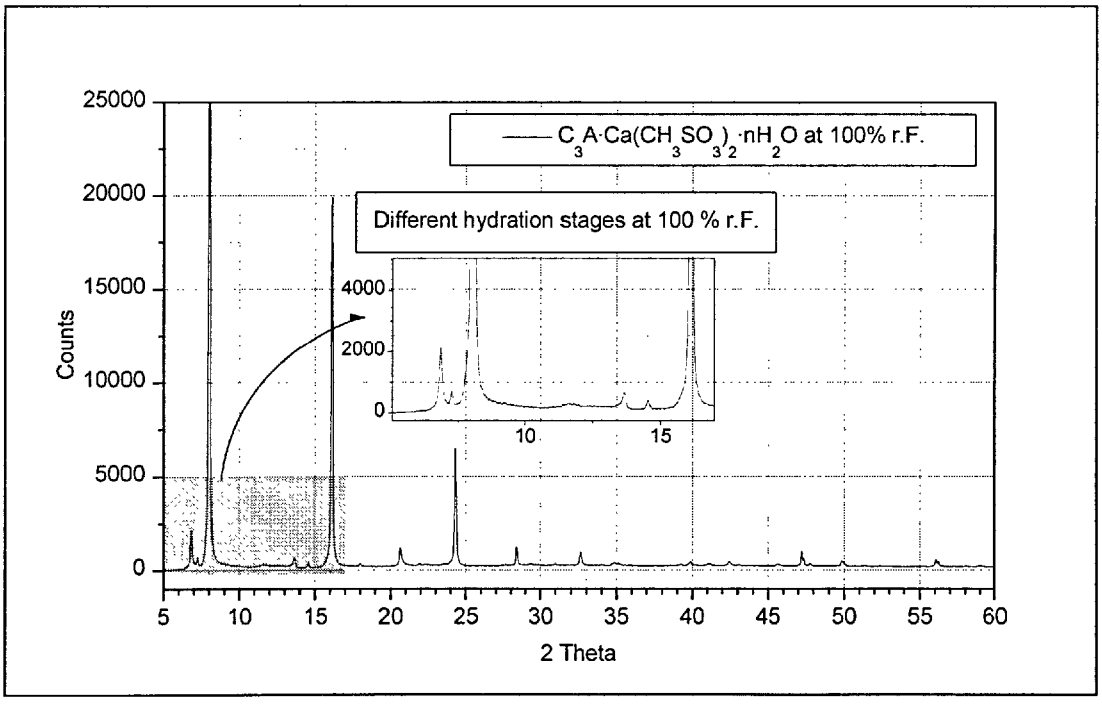

Fig.2 XRD - Pattern of $C_3A{\cdot}Ca(CH_3SO_3)_2{\cdot}nH_2O$

The system TCAH - Monobenzenesulfonatehydrate is illustrated in Figure 3. Neither at 100% r.F. nor at 35% r.F. solid solutions are stable in the range of 10 to 90% $Ca(C_6H_5SO_3)_2 \cdot nH_2O$. The quantity of the phases $C_3A \cdot Ca(CH_3SO_3)_2 \cdot nH_2O$ and $C_3A \cdot Ca(OH)_2 \cdot 18H_2O$ (TCAH) changes linear. Solid solutions were not formed in the system $C_3A \cdot Ca(CH_3SO_3)_2 \cdot nH_2O$ - $C_3A \cdot Ca(OH)_2 \cdot nH_2O$ at 35% and 100% r.F.. At 100% r.F. several coexisting hydration stages are stable too.

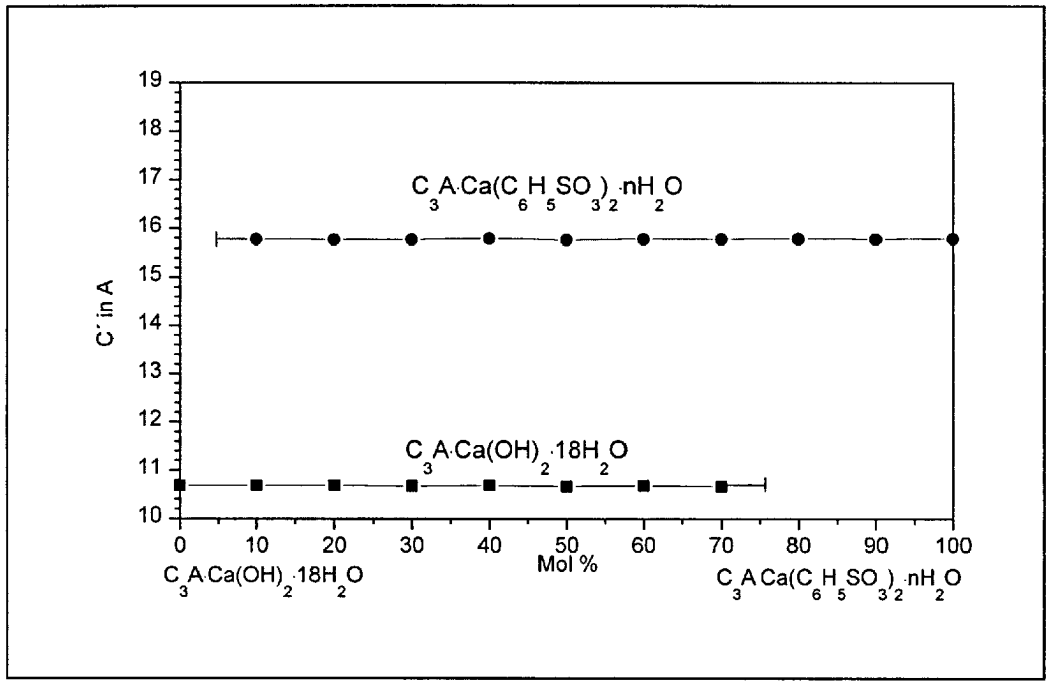

Fig.3 Solid solution system TCAH - $C_3A \cdot Ca(C_6H_5SO_3)_2 \cdot nH_2O$ 100% r.F.

The crystallographic data is given in Table 3. Furthermore gel structures of minor cristalinity are stable in the precipitates of the system TCAH - Monoetanesulfonatehydrate in the range of 20-70% $Ca(C_2H_5SO_3)_2$. Drying of these structures forces conversion to Portlandite, Hydrogrossular and organic calciumsalts.

Table 3: Crystallographic Data of Calcium Aluminium Sulfonate Hydrates and Carboxylates

Composition	Lattice parameters					
	a [Å]	b [Å]	c [Å]	α [°]	β [°]	γ [°]
$C_3A \cdot Ca(CH_3SO_3)_2 \cdot nH_2O$*	5.74	5.74	12.85	90	90	120
$C_3A \cdot Ca(C_2H_5SO_3)_2 \cdot nH_2O$*	5.73	5.73	13.65	90	90	120
$C_3A \cdot Ca(C_6H_5SO_3)_2 \cdot nH_2O$*	5.78	5.78	15,76	90	90	120
$C_3A \cdot Ca(C_6H_5SO_3)_2 \cdot 12H_2O$*	5.76	5.76	15,75	90	90	120
$C_3A \cdot Ca(C_7H_7SO_3)_2 \cdot nH_2O$*	5.72	5.72	17.15	90	90	120
$C_3A \cdot Ca(C_8H_9SO_3)_2 \cdot nH_2O$*	5.72	5.72	16.19	90	90	120
$C_3A \cdot Ca(HCOO)_2 \cdot 11H_2O$**	8.21	5.76	16.85	90	105.3	90
$C_3A \cdot Ca(CH_3COO)_2 \cdot nH_2O$*	5.77	5.77	65.60	90	90	120
$C_3A \cdot Ca(C_2H_5COO)_2 \cdot 11H_2O$*	5.76	5.76	13.77	90	90	120
$C_3A \cdot 3Ca(HCOO)_2 \cdot 32H_2O$	10.91	10.91	21.33	90	90	120

*100% r.F.

**35% r.F.

With longer chain length of the aliphatic carboxylic acids the distance c´ increased.
The fact is, that increasing c´ interlayer dimensions are not linear, because the organic ions are not fixed in the in c_o-direction.

Heat flow calorimetry
The hydration reaction of OPC was studied under the influence of several additives with special subject.

1. Sulfonic acids with increasing C_nH_{2n+1}-chain.
2. Influence of Calciummethane - and Calciumethanesulfonates.
3. Carboxylic acids with increasing amounts of C_nH_{2n+1}-chain.
4. Aromatic sulfonates with increasing amounts of C_nH_{2n+1}-groups.

The influence of aliphatic sulfonic acids show that retardation occurred with increasing chain-length (Fig.4). The Hydrationmaxima of methanesulfonic - and propanesulfonic acid roses up about 15 h. The integration of the heat of reaction over 72h indicated an exponential decrease o heat with increasing chain length. Carboxylic acids did not retard the cement reaction. With reference to the additive-free sample the hydration was accelerated up to 1h 20 min. Longer C_nH_{2n+1} chains caused retardation.

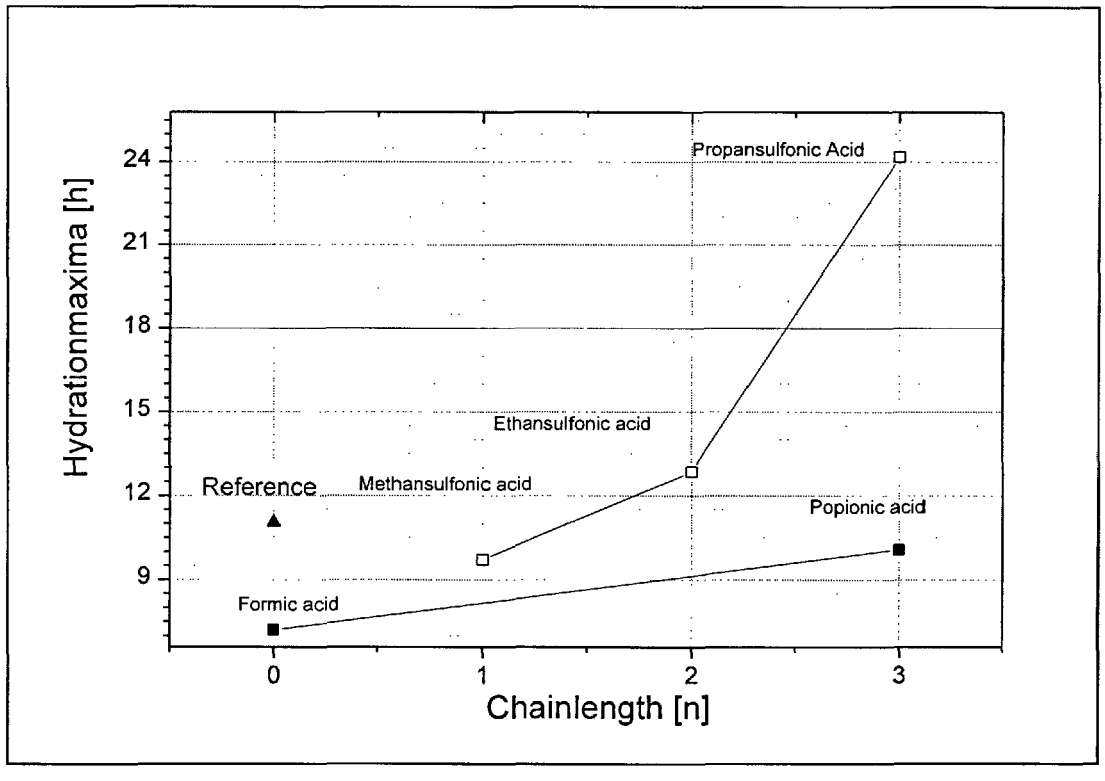

Fig.4 Hydration effects as a function of increasing chain length

The temporary influence of methanesulfonic and ethanesulonic acids (Fig.5) on the OPC hydration behaviour was quite similar. Increasing additive amounts caused retardation. The effect was much stronger using methanesulfonic acid. High concentrations of these acids caused different effects. The use of calcium salts for example calciummethanesulfonate and calciumetansulfonate (Fig.6) forced a secondary hydrationmaximum which is well developed with decreasing additive concentration.

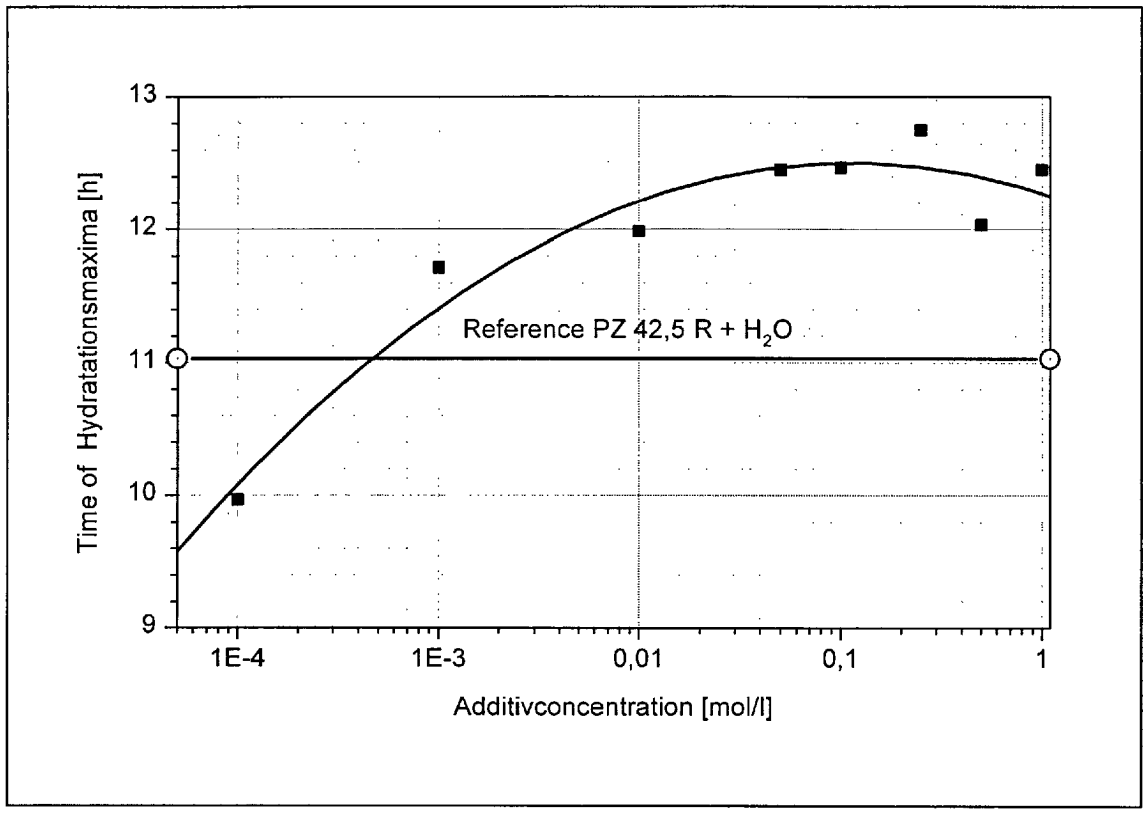

Fig.5 Influence of Ethanesulfonic acid on the hydration of OPC

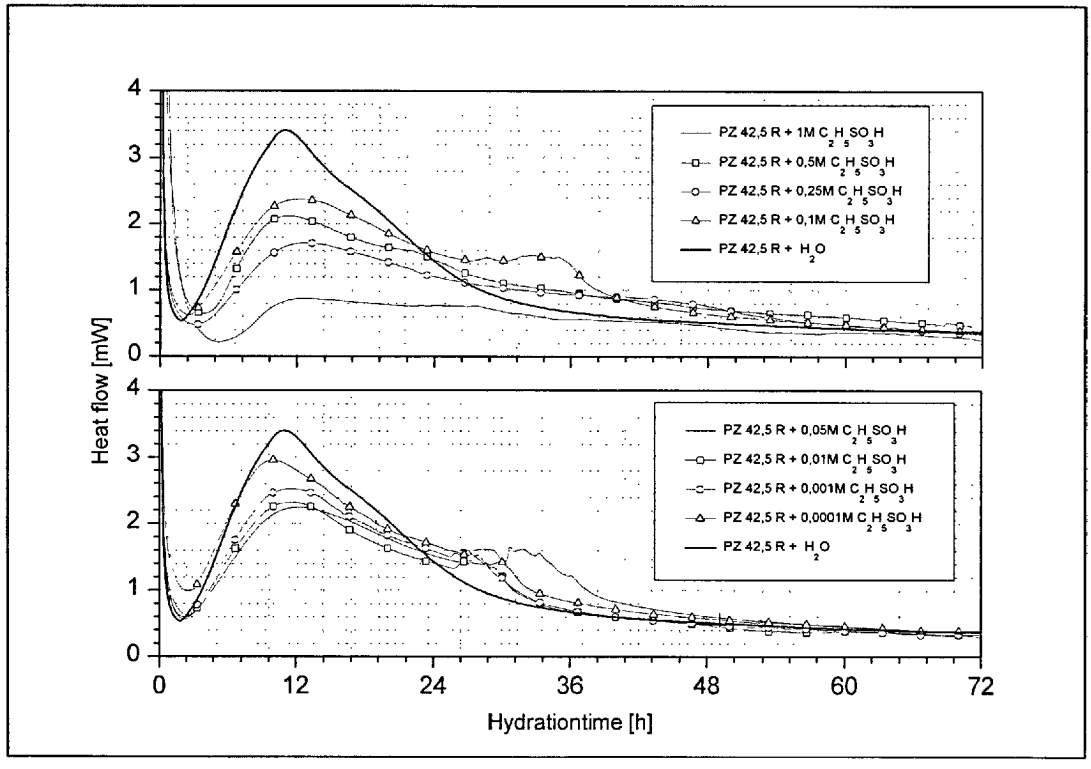

Fig.6 Heat flow calorimetry: Addition of Calciumethansulfonate to OPC

Calciumions in combination with acid ions using $Ca(C_2H_5SO_3)_2$ (Fig.7) retarded the hydration exponentially about 1 h relative to the additive free sample. Concentrations of Calciummethanesulfonate show acceleration and retardation which belongs to specific concentrations.

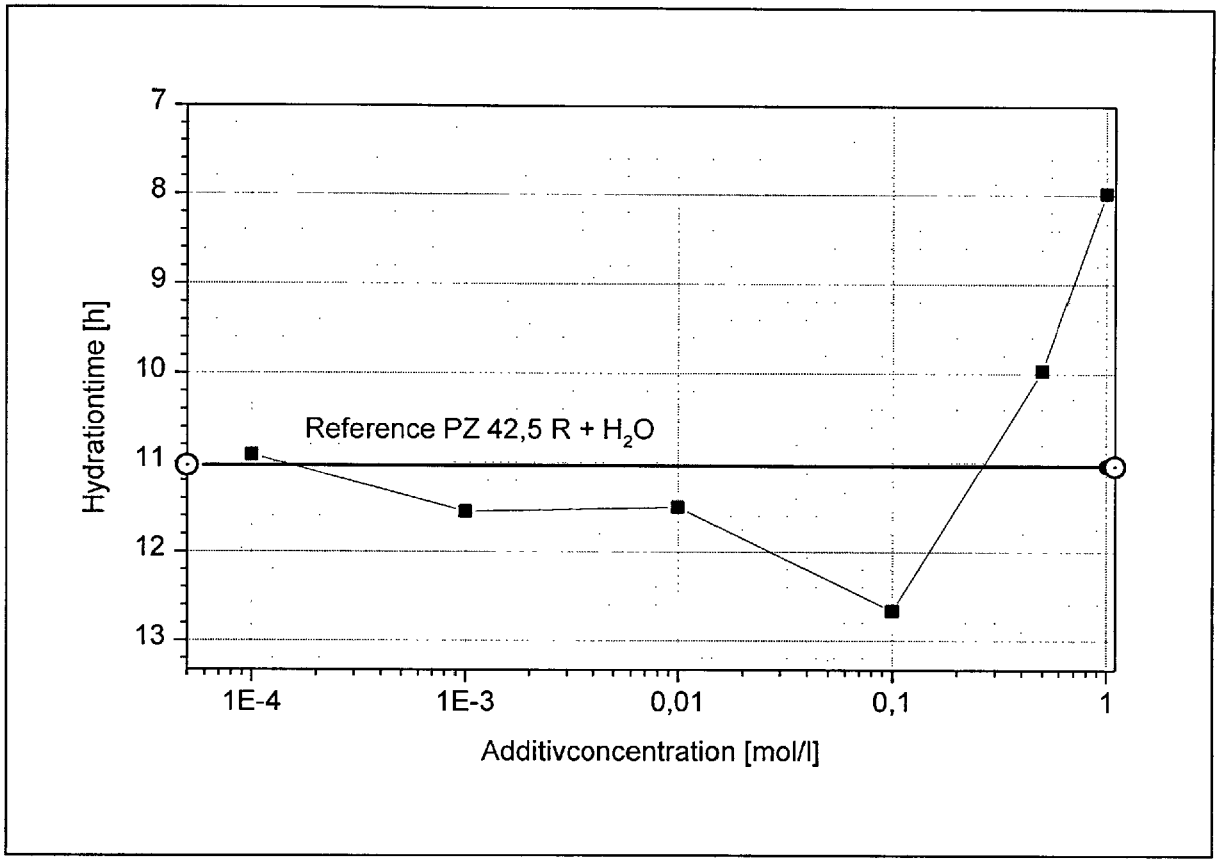

Fig.7 Hydrationmaxima as a function of the Calciumethansulfonate concentration

Aromatic sulfonic acids have a strong influence on the heat of hydration until 72 h. After a long induction period, especially of toluene p-sulfonic acid, the OPC hydration was slowed down.

Discussion and summary

The results of the addition of carboxylic and sulfonic acids and salts to OPC indicate that acceleration, retardation and heat suppression can occur as a function of concentration, chain length and functional groups ($-SO_3H$, -COOH, C_6H_5-). The different existing salts of various carboxylic acids and acids itself were used as additives. The crystallochemical change of bond mechanisms and delayed setting and hardening was tested using a model OPC. Using the size of organic molecules as well as functional groups and cations the influence on setting and hardening can be described. Besides well crystallised hydration products, chelates, gel-structures and semi crystalline phases occurs. The reactionproducts stand in relation with TCAH (tetracalcium aluminate hydrate), partly with different crystal system and structure. Because of fixation of organic ions in the interlayer the c_o- distance c´ will grow with increasing size of the molecules. A linear increase with different C-chainlength was not observed. Phases with ettringite structure containing organic ions were not observed. Only the small formate ion enters the structure of ettringite and forms formate-ettringite.

References

Ahmend, S.J.& Taylor,H.F.W. (1967):"Crystal Structures of the lamellar Calcium Aluminate Hydrates."Nature215,622-623

Allan,R.(1968):" Die Doppelschichtstruktur der plättchenförmigen Calcium-Aluminium-Hydroxisalze am Beispiel des $3CaO{\cdot}Al_2O_3{\cdot}CaSO_4{\cdot}12H_2O$" N.Jb.Min.Mh.,140-144

Auer,S. (1992):" Bindung umweltrelevanter Ionen in Ettringit und in Schichtstrukturen vom Typus TCAH" Dissertation- Mineralogisches Institut der Universität Erlangen-Nürnberg.

Meyer, H.W., Pöllmann, H. und Kuzel, H.-J. (1992): „Die Wirkung der Zitronensäure als Additiv hydraulischer Bindemittel" Europ.J.Min., Beihefte, 193."

Meyer, H.W. (1992):"Die Hydratation der Calciumaluminate im Portlandzement in Gegenwart von CO_3^{2-}"Dissertation-Mineralogisches Institut der Universität Erlangen-Nürnberg

Meyn, M., Beneke, K. & Lagaly,G. (1990):" Anion-Exchange Reactions of Layered Double Hydroxides." In.Chem.Vol.29 No.26 5201-5207

Monosi, S. Moriconi, G. & Collepardi, M. (1981):" Combined Effect of Lignosulfonate and Carbonate on Pure Portland Clinker Compounds Hydration. III: Hydration of Tricalcium Silicate alone and in Presence of Tricalcium Aluminate". Cem.ConcrRes. 12, 425-435

Pöllmann, H. (1989):" Mineralogisch-Kristallographische Untersuchungen an Hydratationsproduktn der Aluminatphase hydraulischer Bindemittel" Habilitationsschrift, Erlangen

Pöllmann, H. (1989):"Study of the hydration mechanisms and Formation of new Hydrates applying organic Additives to the Aluminate Phase of Cement" Proc.11th.Conf.on Cem.Micr., New Orleans, Louisiana, 324-343.

Pöllmann, H. (1988):"Calciumaluminathydroxisalze mit anorganischen und organischen Anionen - ein Vergleich" Z.Krist.182, 209-210.

Pöllmann, H., Michaux, M. und Nelson, E.B. (1990):"Study on the Influence of citric acid on the retardation and formation of new hydrates in cement" Proc.12th.Conf.on Cem.Micr.,Vancouver, 303-322.

Pöllmann, H. (1989):"Organische Derivate des TCAH mit Schichtstrukturen vom Typus $[Ca_2Al(OH)_6]^+[RCOO{\cdot}nH_2O]^-$"Z.Krist.186, 236-237

Satish,C. (1987):" Interaction of Polymers and Organic Admixtures on Portland Cement Hydration" Cem.Concr.Res. 17,875-890

Stöber, St., Wenda,R. & Pöllmann, H. (1995): Einfluß der Alkali- und Erdalkalibenzolsulphonatsalze auf das Hydratationsverhalten eines Portlandzementes PZ 45" Eur.J.Min.Bh., Vol.7, 240

Stöber, St. & Pöllmann, H. (1995): „Untersuchungen zur Kristallographie der Alkali- und Erdalkalibenzolsulphonate." Dt.Ges.Krist., 322

Taylor, H.F.W. (1973):" Crystal Structures of some double hydroxide minerals" Min.Mag. 304 39 378-389

EVALUATION OF CHEMICAL INHIBITORS FOR ALKALI-AGGREGATE REACTION BY ACCELERATED TESTS

Yoshihiko OHAMA, Katsunori DEMURA, Hiroyuki IWASAKI, Department of Architecture, College of Engineering, Nihon University, Koriyama, Fukushima-ken, 963 Japan

ABSTRACT The effectiveness of the addition of chemical inhibitors such as hexyl trimethoxy silane, lithium nitrite and hydrogen peroxide to mortars containing reactive andesite and opal for inhibiting alkali-aggregate reaction is tested by applying three accelerated tests in which mortar specimens are stored at 40°C and 100%RH, fully and partially immersed in a 2.5% NaCl solution for 189 days. It is concluded from the test results that the hydrogen peroxide and hexyl trimethoxy silane are considerably effective for inhibiting alkali-aggregate reaction, but the lithium nitrite is ineffective.

Key-words : Alkali-aggregate reaction, Inhibitor, Accelerated tests

INTRODUCTION

An alkali-aggregate reaction problem in reinforced concrete structures has drawn worldwide attention in the construction industry in recent years. However, effective measures for inhibiting the alkali-aggregate reaction have not been found till now, and it is most important in the current concrete technology to find out such measures for improving the durability of the concrete structures. It has been reported that alkyl alkoxy silane, lithium nitrite and hydrogen peroxide can be used as chemical admixtures to inhibit the alkali-aggregate reaction by the authors (Ohama, Demura & Kakegawa, 1989) and other researchers (Hibino, Tsuyuki & Ishida, 1994). However, the inhibition of the alkali-aggregate reaction by the addition of these admixtures has been evaluated under different test conditions. On the other hand, it was reported by some papers (e.g., Kawamura, Takeuchi & Sugiyama, 1994) that the alkali-aggregate reaction is promoted by alkalis from the outside of concrete. In the present study, the partial and full immersion tests of mortars in a chloride solution are discussed as the test methods to check up on this fact.

In the present paper, mortar specimens containing a reactive andesite or opal with chemical inhibitors such as hexyl trimethoxy silane, lithium nitrite and hydrogen peroxide are prepared, and evaluated for alkali-aggregate reaction by applying three accelerated tests due to storage at 40°C and 100%RH, full immersion and partial immersion in a 2.5% NaCl solution. The effects of the inhibitors on the expansion due to alkali-aggregate reaction are examined. Furthermore, the effectiveness of the partial and full immersion tests as rapid tests is also discussed.

MATERIALS

Cement

Ordinary portland cement as specified in JIS (Japanese Industrial Standard) R 5210 (Portland Cement) was used in all the mortar mixes. The properties of the cement are listed in Table 1.

Aggregates

Toyoura standard sand (size, 0.3mm or finer) as specified in JIS was used as a nonreactive aggregate for all the mortar mixes. Takayama crushed andesite (size, 5mm or finer) and Iou-island opal (size, 5mm or finer) were employed as reactive aggregates for the mortar mixes. The properties of the reactive aggregates, tested according to Appendix 7 [Method of

Table 1 Physical Properties and Chemical Compositions of Cement.

Specific Gravity	Blaine's Specific Surface (cm^2/g)	Setting Time (h-min)		Compressive Strength of Mortar (MPa)		
		Initial Set	Final Set	3d	7d	28d
3.16	3250	2-14	3-08	16.0	26.3	41.5

Chemical Compositions (%)			Total Alkali Content (%)
MgO	SO_3	ig.loss	
1.7	2.1	1.2	0.63

Testing Alkali-Silica Reactivity of Aggregate (Chemical Method)] of JIS A 5308 (Ready-Mixed Concrete) are listed in Table 2.

Table 2 Properties of Reactive Aggregates, Checked by Chemical Method.

Type of Reactive Aggregate	Dissolved Amount of Silica (Sc) (mmol / l)	Decrease in Alkali Concentration (Rc) (mmol / l)	Interpretation of Results
Andesite	461	121	Deleterious
Opal	1608	224	Deleterious

Chemical inhibitors

Hexyl trimethoxy silane [$C_6H_{13}Si(OCH_3)_3$: HTMS], lithium nitrite ($LiNO_2$) and hydrogen peroxide (H_2O_2) were used as inhibitors.

TESTING PROCEDURES

Preparation of specimens

In accordance with Appendix 8 [Method of Testing Alkali-Silica Reactivity of Aggregate (Mortar-Bar)] of JIS A 5308, mortars containing reactive aggregates were mixed with a cement-aggregate ratio of 1 : 2.25 (by mass) and inhibitor contents of 0, 0.5 and 1.0% of cement. The water-cement ratio of the mortars was adjusted to be a flow of 170±5, and the total alkali content of the mortars was adjusted to be 2.5% as Na_2O equivalent by using a 2N aqueous solution of the sodium hydroxide specified in JIS K 8576 (Sodium Hydroxide). A mixture of 20wt% nonreactive aggregate and 80wt% reactive andesite or a mixture of 90wt% nonreactive aggregate and 10wt% opal was used as an aggregate for the mortars. Gauge plugs for measuring the length change of the mortars were installed in molds. Mortar specimens 40×40×160mm were molded, and then subjected to a 1-day-20°C-80%RH-moist plus 1-day-20°Cwater cure.

Measurement of expansion

The measurement of the expansion of mortar specimens was conducted according to the dial gauge method specified in JIS A 1129 (Methods of Test for Length Change of Mortar and

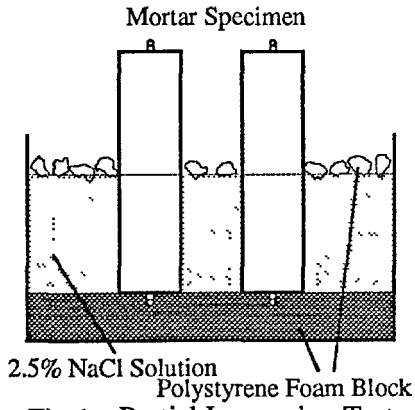

Fig.1 Partial Immersion Test of Mortar Specimens in 2.5% NaCl Solution.

Concrete). After water cure, the initial length of the mortar specimens was measured, and then the mortar specimens were stored at 40°C and 100%RH, or fully and partially immersed in a 2.5% NaCl solution as shown in Fig.1. Their expansion was measured at storage or immersion periods of 7, 14, 21, 28, 35, 42, 49, 56, 63, 70, 77, 84, 91, 105, 119, 133, 147, 161, 175 and 189 days.

TEST RESULTS AND DISCUSSION

Fig.2 shows the expansion of mortars containing reactive aggregates with inhibitors during storage at 40°C and 100%RH. The expansion of the mortar containing a reactive andesite without any inhibitor is increased with additional storage period, and becomes nearly constant at a storage period of 84 days. Its expansion at a storage period of 189 days is 0.36%. On the other hand, with additional storage period, the expansion of the mortar containing an opal without any inhibitor is increased, and attains 0.47% at a storage period of 189 days. The expansion of the mortars containing the reactive andesite with HTMS is slightly increased with additional storage period regardless of HTMS content, and becomes nearly constant at a storage period of 84 days. The expansion of the mortars containing the opal with HTMS is changed to a less extent up to a storage period of 49 days, and then is slightly increased. Such a

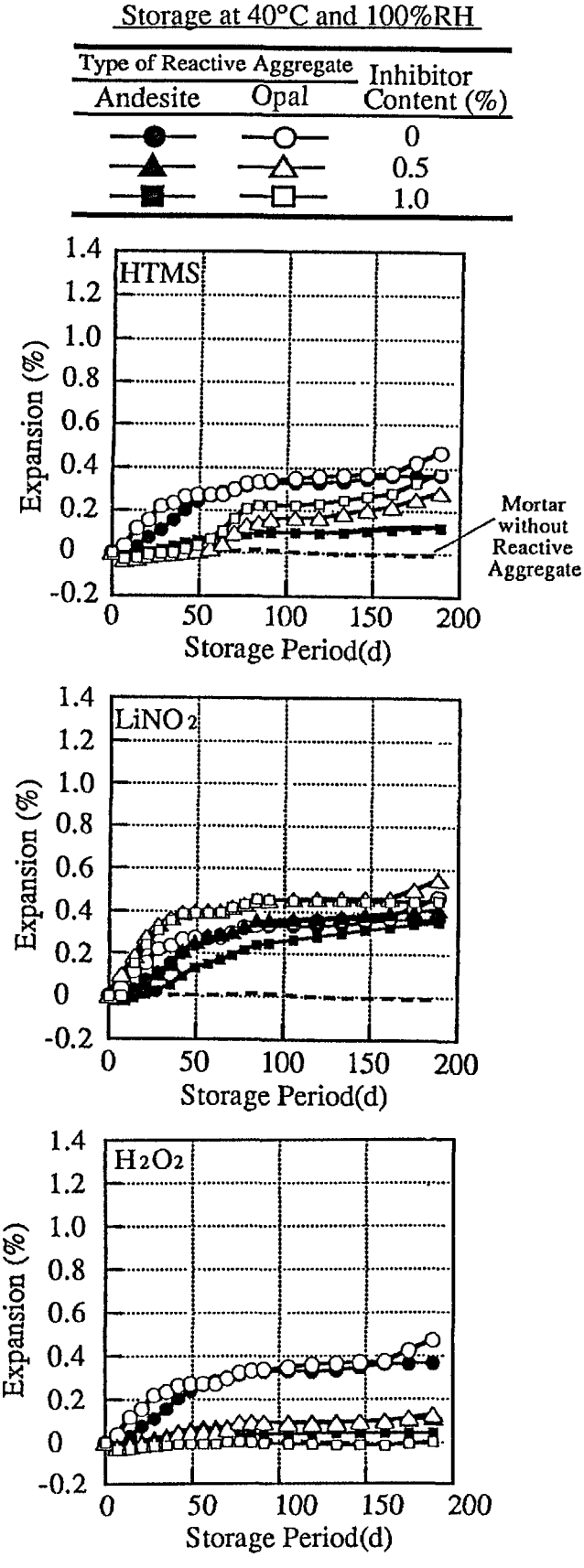

Fig.2 Expansion of mortars containing reactive aggregates with inhibitors during storage at 40°C and 100%RH.

marked reduction in the expansion by use of HTMS is ascribed to the water repellency which is given to the surface layers of the reactive aggregates, cement hydrates and alkali-silica gel in the mortars ; moreover, an increase in the entrained air content of the mortars due to the surface activity of HTMS contributes to a reduction in the expansion. With additional storage period, the expansion of the mortars containing the reactive aggregates with $LiNO_2$ is increased regardless of the type of aggregate and inhibitor content, and is nearly equal to that of the mortars containing reactive aggregates without any inhibitor. In a previous paper (Saito, Kitagawa & Hasaba, 1992), $LiNO_2$ in the mortar is found to form waterproof layers on the reactive aggregate surfaces, and inhibit a reaction between pore solution in the mortar and the reactive aggregates. However, no effectiveness of $LiNO_2$ against the expansion is recognized in this study because of its low content. The expansion of the mortars containing the reactive aggregates with H_2O_2 is changed to a less extent regardless of the type of aggregate and inhibitor content. It is reported that H_2O_2 attacks the reactive aggregate surfaces by strong oxidation action, and inhibits the alkali-aggregate reaction (Hibino, Tsuyuki & Ishida, 1994). The marked effectiveness of H_2O_2 against the expansion is also recognized in this study.

Fig.3 represents the expansion of mortars containing reactive aggregates with inhibitors during full immersion in a 2.5% NaCl solution. The expansion of the mortar containing a reactive andesite without any inhibitor is increased to some extent with additional immersion period, and becomes 0.18% at an immersion period of 189 days. With additional immersion period, the expansion of the mortars containing an opal without any inhibitor is markedly increased up to 0.68% at an immersion period of 189 days. The expansion of the mortars containing the reactive aggregates with the inhibitors is increased with additional immersion period. The expansion of the mortars containing the opal is much larger than that of the mortars containing the reactive andesite irrespective of the addition of the inhibitors. In the mortars containing the reactive aggregates, their expansion is reduced with increases in the contents of HTMS and H_2O_2 as inhibitors. However, the expansion of the mortars containing the opal tends to increase with an increase in $LiNO_2$ content. Such a tendency is not recognized in the mortars containing the reactive andesite with $LiNO_2$.

Fig.4 illustrates the expansion of mortars containing reactive aggregates with inhibitors during partial immersion in a 2.5% NaCl solution. The expansion of the mortars containing a reactive andesite without any inhibitor is increased to some extent with additional immersion period, and becomes 0.07% at an immersion period of 189 days. With additional immersion period, the expansion of the mortars containing an opal without any inhibitor is increased, and becomes nearly constant at an immersion period of 161 days. Its expansion at an immersion period of 189 days is 0.50%. Such an expansion of the mortars containing the reactive aggregates without any inhibitor is smaller than that of the same mortars fully immersed in the 2.5% NaCl solution. The effects of the inhibitors on the expansion behavior of the mortars containing the reactive aggregates in the partial immersion are similar to those in the full immersion. The expansion of the mortars containing the reactive aggregates is considerably decreased by the addition of HTMS and H_2O_2.

Figs.5 and 6 show the relation between inhibitor content and the expansion and reduction in expansion of mortars containing reactive aggregates after 189-day storage at 40°C and 100%RH, 189-day full immersion and 189-day partial immersion in a 2.5% NaCl solution. The relative reduction in expansion of the mortars is calculated as follows :

$$\text{Reduction in expansion (\%)} = [(Ero - Era) / (Ero - Eno)] \times 100 \quad [1]$$

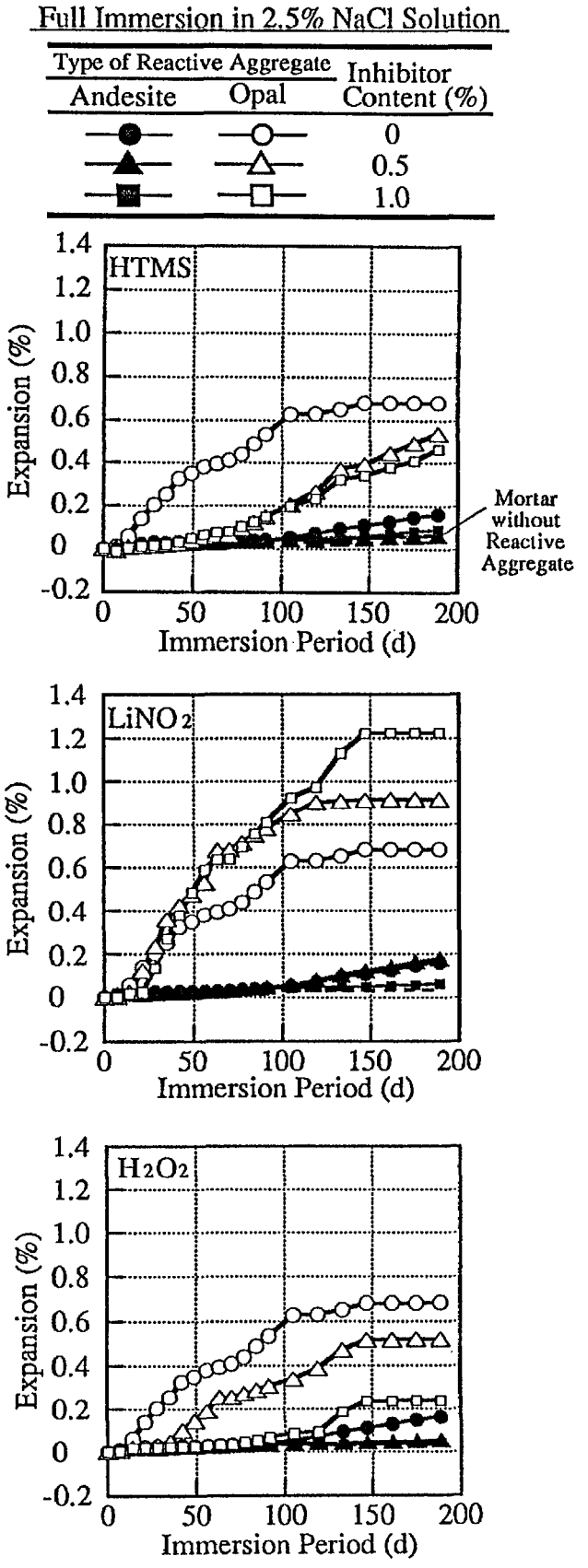

Fig. 3 Expansion of mortars containing reactive aggregates with inhibitors during full immersion in 2.5% NaCl solution.

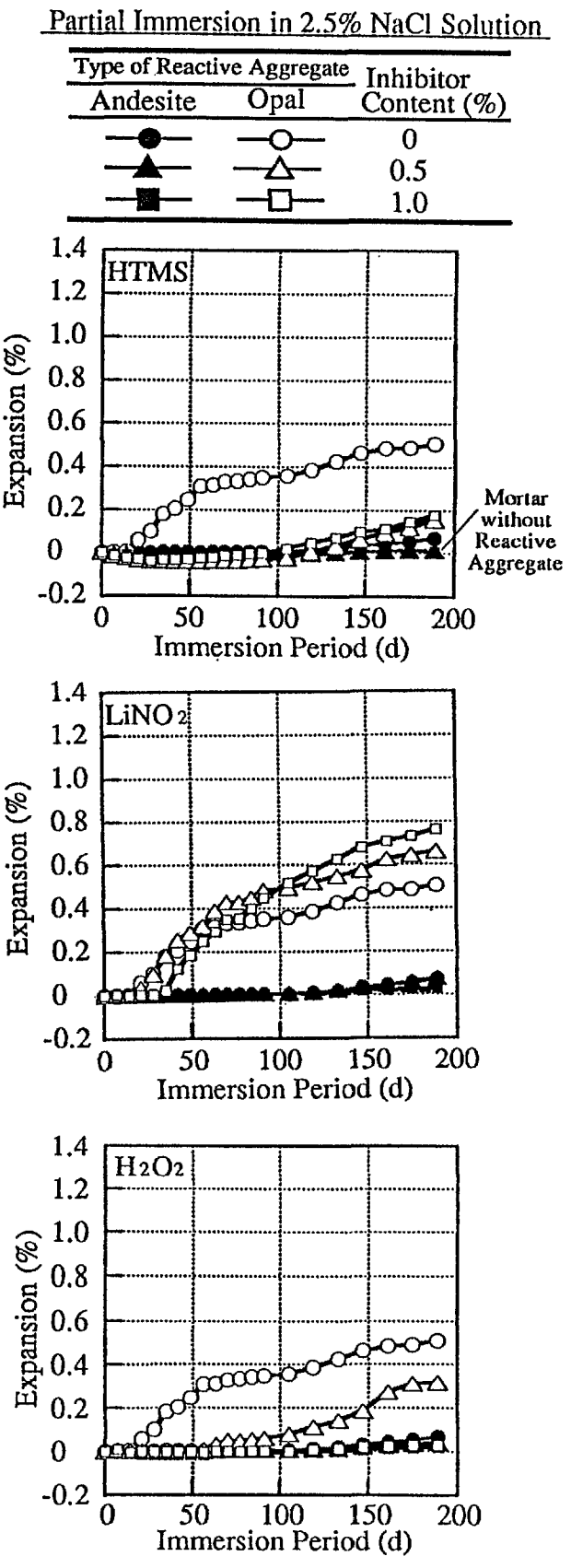

Fig. 4 Expansion of mortars containing reactive aggregates with inhibitors during partial immersion in 2.5% NaCl solution.

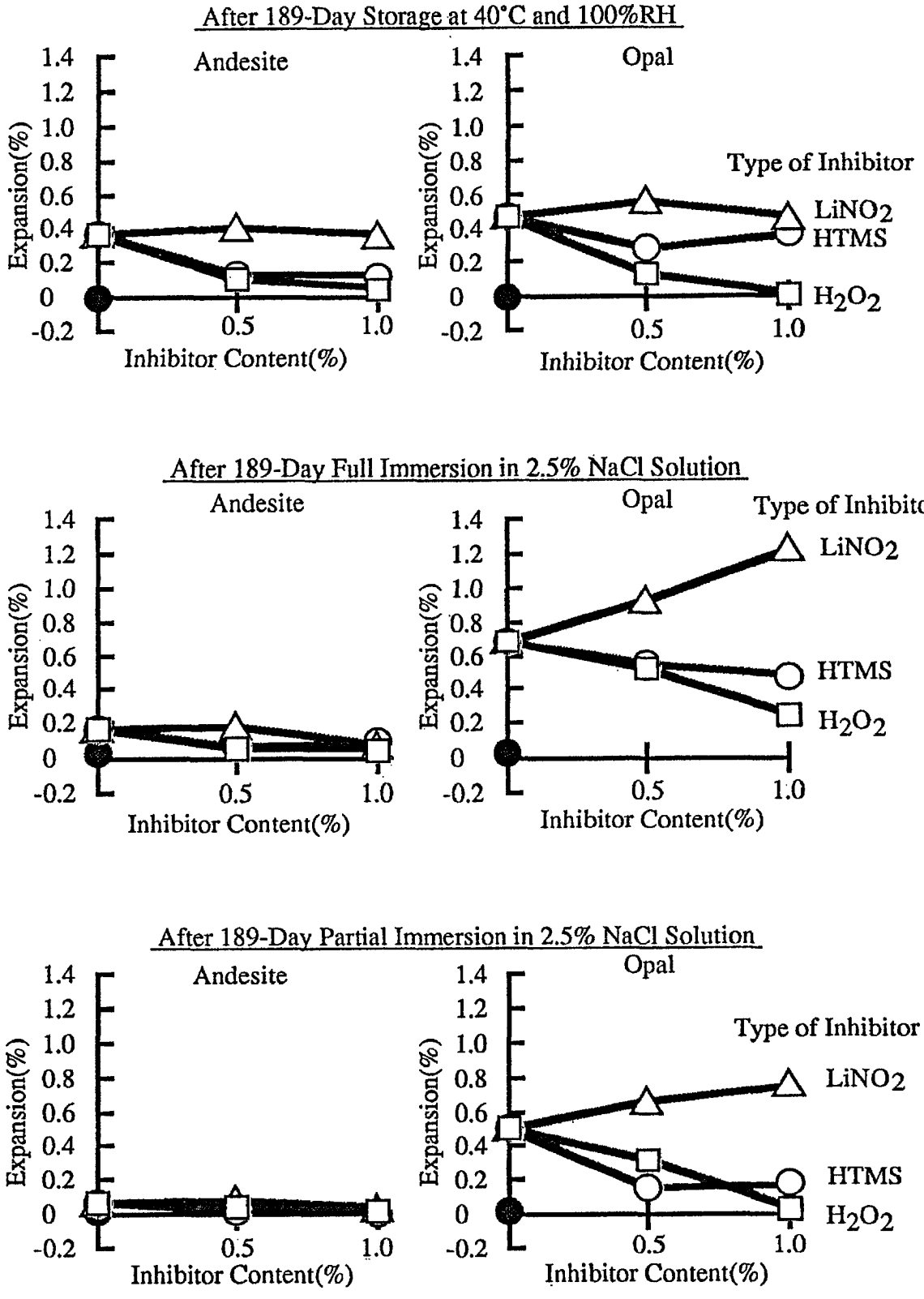

Fig.5 Inhibitor content vs. expansion of mortars containing reactive aggregates with inhibitors.

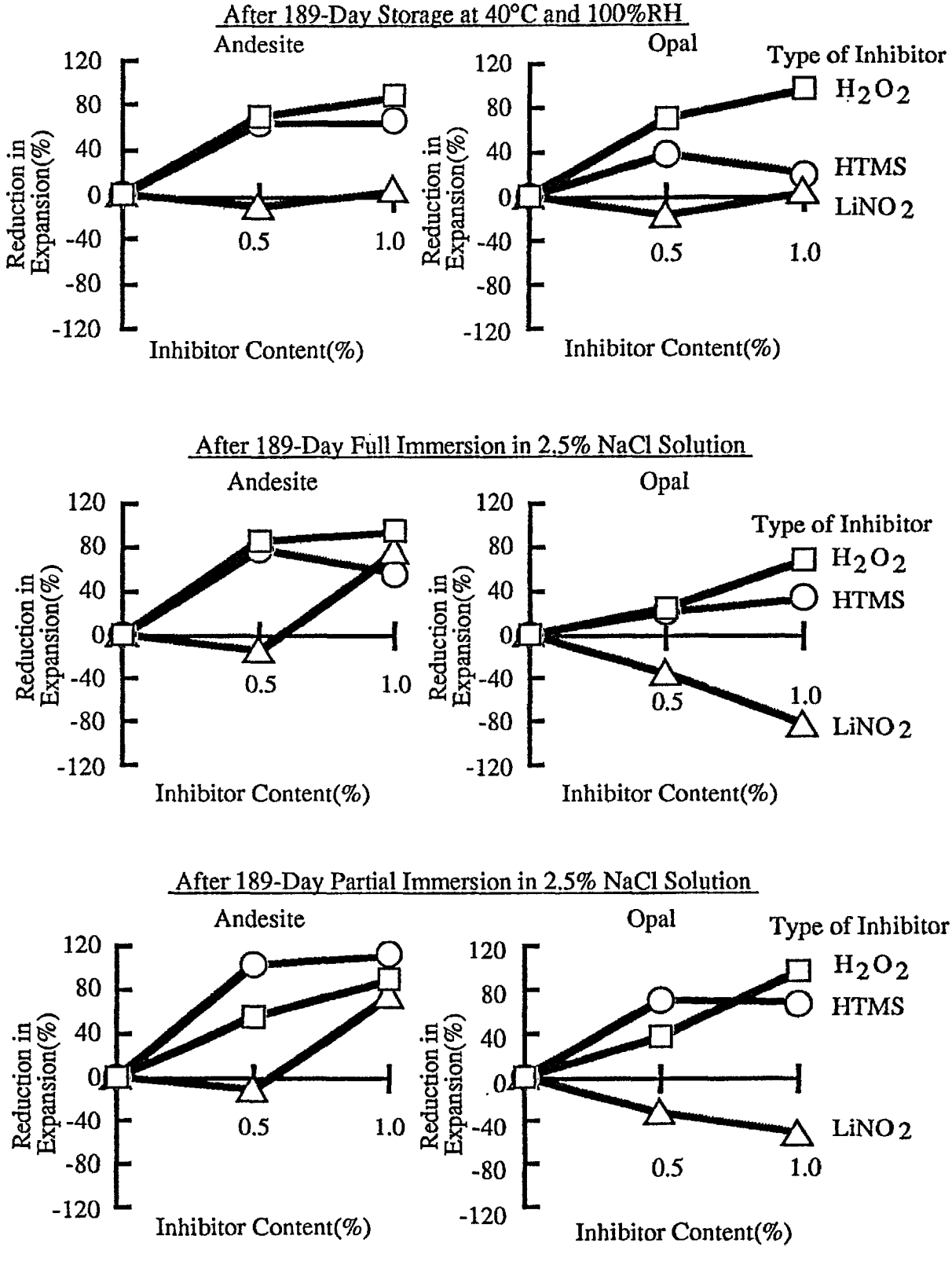

Fig.6 Inhibitor cotent vs. reduction in expansion of mortars containing reactive aggregates with inhibitors.

where Era is the expansion of the mortars containing the reactive aggregates with inhibitors at an immersion period of 189 days, Ero is the expansion of the mortars containing the reactive aggregates without any inhibitor at an immersion period of 189 days, and Eno is the expansion of the mortars without any reactive aggregate and inhibitor at an immersion period of 189 days. In the full and partial immersion tests, an increase in the expansion of the mortars containing an opal due to the addition of $LiNO_2$ is observed. Except for such a case, the expansion of the mortars containing the reactive aggregates is reduced with an increase in the inhibitor content. The addition of 1.0% of HTMS or H_2O_2 to the mortars containing the reactive aggregates provides a 60% or more reduction in the expansion regardless of the type of reactive aggregate and test conditions. From the above-mentioned test results, the effectiveness of the inhibitors to prevent alkali-aggregate reaction is influenced by the test conditions and the type of the reactive aggregate used to prepare mortar specimens. However, HTMS and H_2O_2 can be used as chemical inhibitors for inhibiting alkali-aggregate reaction.

CONCLUSIONS

The conclusions obtained from the above-mentioned test results are summarized as follows :
(1) In general, the expansion of mortars containing reactive aggregates with and without inhibitors is increased with additional storage period at 40°C and 100%RH, and full or partial immersion period in a 2.5% NaCl solution. However, the effectiveness of the inhibitors to prevent alkali-aggregate reaction is influenced by the test conditions and the type of the reactive aggregate used to prepare mortar specimens.
(2) Except for some cases, the expansion of mortars containing reactive aggregates is reduced with an increase in the inhibitor content. The addition of 1.0% of HTMS or H_2O_2 to the mortars containing the reactive aggregates gives a 60% or more reduction in the expansion regardless of the type of reactive aggregate and test conditions. HTMS and H_2O_2 can be used as chemical inhibitors for inhibiting alkali-aggregate reaction.

REFERENCES

Hibino, T., Tsuyuki, N. & Ishida, H., 1994, "Effect of Treatment of Reactive Aggregate by H_2O_2 on the Alkali-Silica Reaction", Journal of the American Ceramic Society, 77 (6), 1522-1524.

Kawamura, M., Takeuchi, K. & Sugiyama, A., 1994, "Mechanisms of the Influence of NaCl Externally Supplied on the Expansion of Mortars Due to the Alkali-Silica Reaction (in Japanese)", Journal of Materials, Concrete Structures and Pavements, Japan Society of Civil Engineers, V-25 (502), 93-102.

Ohama, Y., Demura, K. & Kakegawa, M., 1989, "Inhibiting Alkali-Aggregate Reaction with Chemical Admixtures", Proceedings of the 8th International Conference on Alkali-Aggregate Reaction, eds K.Okada, S.Nishibayashi & M.Kawamura, Kyoto, Japan, 17-20 July, Elsevier, London, 253-258.

Saito, M., Kitagawa, A. & Hasaba, S., 1992, "Effectiveness of Lithium Nitrite in Suppressing Alkali-Aggregate Expansion (in Japanese)", Journal of the Society of Materials Science, Japan, 41 (468), 1375-1381.

THEME V

DEVELOPMENTS IN CHARACTERISATION TECHNIQUES

TOPIC V.A

Nuclear Magnetic Resonance (NMR)

^{29}Si ENRICHMENT AND SELECTIVE ENRICHMENT FOR STUDY OF THE HYDRATION OF MODEL CEMENTS AND BLENDED CEMENTS.

Adrian R. BROUGH[1] and Christopher M. DOBSON, Inorganic Chemistry Laboratory, University of Oxford, S. Parks Rd., Oxford, OX1 3QR, UK
Ian G. RICHARDSON[2] and Geoffrey W. GROVES, Dept. of Materials Science, University of Oxford, Parks Rd., Oxford, OX1 3PH, UK
[1] Present Address, Dept. of Materials, Imperial College, London, SW7 2BP, UK
[2] Present Address, Dept. of Civil Engineering, University of Leeds, Leeds, LS2 9JT, UK

ABSTRACT ^{29}Si enrichment has been used to enable acquisition of multiple high quality ^{29}Si NMR spectra from samples of C_3S hydrating *in situ* in a MAS NMR probe. The growth of silicate chains in the hydrate was consistent with progressive linking together of dimeric hydrate with monomers. The pozzolanic reaction of C_3S with SiO_2 produced hydrate that was much more ordered and contained longer chains; selective ^{29}Si enrichment of the SiO_2 showed that hydrate formed from the SiO_2 was more ordered, and contained longer chains than the remainder of the hydrate.

Key-words: C-S-H, Nuclear Magnetic Resonance, Pozzolana, Silica fume, Temperature.

INTRODUCTION

This paper describes studies of the kinetics of calcium silicate hydration by ^{29}Si MAS NMR. It summarises results published elsewhere (Brough *et al.*, 1994a and 1995), and the reader is referred to the original papers for full experimental details, and more complete analysis of the data. The notations of cement chemistry and silicate NMR assignments are also detailed in Brough *et al.* (1994a). The aim of this paper is to demonstrate the power of ^{29}Si enrichment and selective enrichment for the study of the kinetics of cement hydration. Simple C_3S hydration and pozzolanic reaction with amorphous silica were chosen as model systems where the materials required are easily synthesised, but the techniques would be equally applicable to other systems.

RESULTS AND DISCUSSION

C_3S Hydration

For the hydration of C_3S, the relative rates of reaction were studied at a range of temperatures. The use of ^{29}Si enrichment and the aquisition of a series of spectra from a single sample gave rise to data of very high quality. The good signal to noise ratios enabled accurate quantification of the spectra. The lack of quenching avoided the possibility of the quenching procedure changing the nature of the sample. All the data were acquired from the same sample (not from separate portions taken from a larger sample). Thus uneven reaction of the sample will not introduce noise into the data.

In order to acquire results *in situ* it was necessary to acquire spectra quickly, since the polymerization of the system was changing rapidly with time, and NMR of conventional samples is relatively slow (perhaps 3-12 hours to obtain a typical spectrum.) Thus it was necessary to use ^{29}Si enriched material. 95%+ enrichment was chosen to obtain the best possible spectra as quickly as possible (line broadening due to dipolar interactions was minimal.) During in situ acquisition, the samples needed to be spun (to obtain MAS spectra).

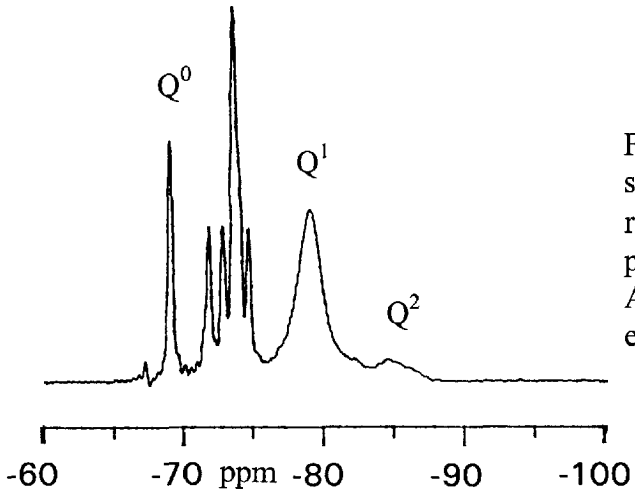

Figure 1 Representative ^{29}Si MAS NMR spectrum of C_3S hydrated at a water to solids ratio of 0.5 for 1 day at 20°C. The isotropic peaks are labelled with the peak assignments. A time series of spectra were acquired from each sample.

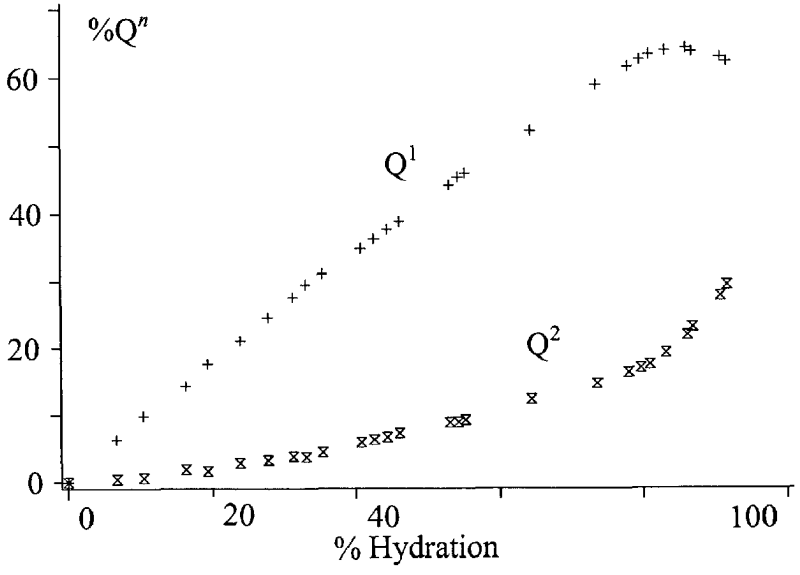

Figure 2 Q^n intensities for C_3S hydration plotted with respect to percentage of hydration (calculated from NMR as the percentage of silicate units no longer remaining as Q^0 species) at 20°C.

They were sealed in small plastic inserts in order to avoid loss of liquid. Control experiments were performed, and it was found that the MAS process had little effect upon the hydration kinetics, or the nature of the majority products.

It is possible to investigate the overall degree of reaction, but this is more readily studied by calorimetry. In this study we concentrate upon the evolution of product structure. C_3S was hydrated at temperatures from 20°C to 75°C and the polymerization of the products studied by ^{29}Si MAS NMR (Figure 1). The results are in agreement with previous studies (Lippmaa *et al.*, 1982, Clayden *et al.*, 1984). The product C-S-H contained only linear chains (Q^1 and Q^2 silicate species). In none of these systems were Q^3 or Q^4 species observed. The relative amounts of the Q^n species present were quantified, and the results for hydration at 20°C are shown in Figure 2. Note the low noise values in these two figures, due to the use of C_3S enriched in ^{29}Si.

The average chain lengths were calculated from the Q^1/Q^2 ratio, and are shown in Figure 3. At all three temperatures, the initial hydrate (by extrapolation to 0% hydration) is essentially dimeric. With hydration, the chain length increases. Various models for the growth of chain length can be proposed, but only some of them are consistent with the observed data.

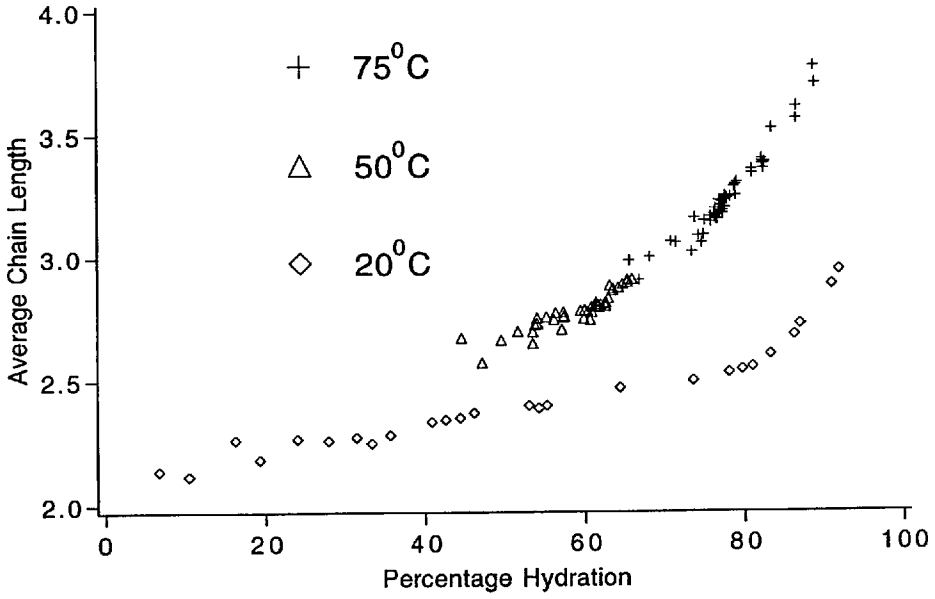

Figure 3: Average chain lengths (calculated as $2 + 2(Q^1/Q^2)$) plotted with respect to degree of hydration at temperatures of 20, 50 and 75°C. Data are only available at later stages of hydration for the hydration at higher temperatures due to the very rapid nature of the earlier hydration.

For hydration at 20°C the initial hydrate is dimeric, and contains Q^1 species, but at later stages of reaction, Q^1 species are consumed and additional Q^2 species are formed. It appears that the dimeric hydrate is being converted to polymeric hydrate. This rules out the possibility that monomers react to form Q^2 species directly at late ages; such a mechanism cannot account for the fall in Q^1 intensity. There must be additionally a conversion of dimeric hydrate to polymer, by joining of chains. A mechanism linking dimers with monomers is consistent with the drierketten structural units believed to be present in C-S-H (Richardson and Groves, 1992), and with previous TMS studies which found silicate anions as follows: dimer, pentamer, octamer, etc. (Hirljac *et al.*, 1983, Dunster *et al.*, 1989) On the basis of this model, the observed results can be extrapolated to complete hydration. A chain length of approximately 4 to 5 is expected, which is consistent with studies of very old samples of C-S-H. (Rodger *et al.*, 1987, Macphee *et al.*, 1988)

Arrhenius energies for the two stages of reaction were calculated assuming a two stage reaction. For the formation of Q^1 species, an energy of $35 kJmol^{-1}$ was found while for the formation of polymer, an energy of $100 kJmol^{-1}$ was determined (this includes the formation of dimer and subsequent polymerization.)

In addition to MAS NMR spectra, ^{29}Si CPMAS spectra were obtained. These enabled the observation of traces of hydrated monomeric species (obscured in the MAS spectra by the large peaks due to anhydrous monomeric species). CP spectra are not directly quantitative, but by comparison with the MAS spectra, and study of the CP dynamics, it was estimated that 2% of monomer was formed during the induction period at 20°C with a larger amount at 75°C. The hydrated monomeric species persisted through to late stages of hydration.

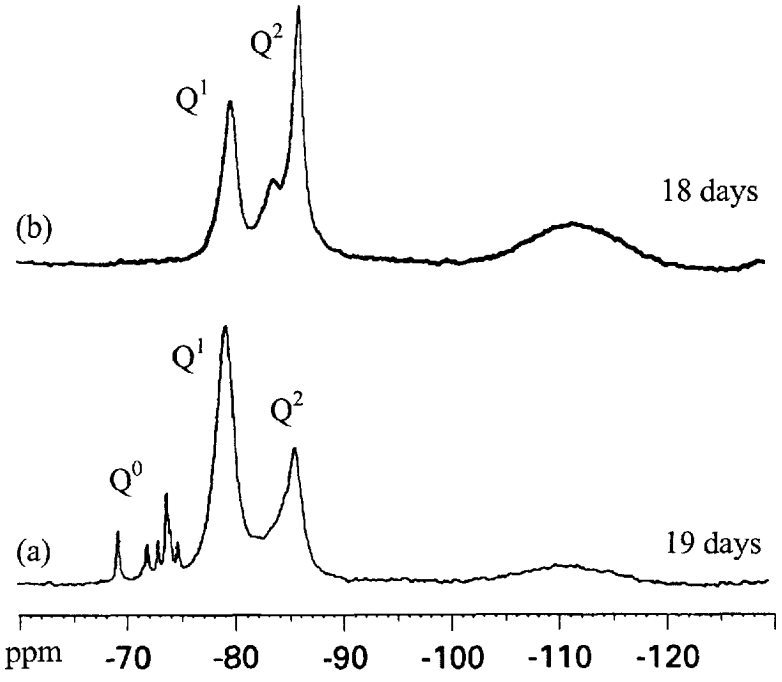

Figure 4: Selected ^{29}Si MAS NMR spectra showing the hydration of a mixture of SiO_2 and C_3S and having an overall Ca/Si atomic ratio of 1 with a water to solids ratio of 0.5. 5Hz exponential line broadening was applied to these spectra. (a) Both reagents enriched in ^{29}Si to 95%+, (b) Only the SiO_2 is enriched.

Pozzolanic Reaction

The pozzolanic reaction takes place in blended cements, where the lime liberated during the hydration of the calcium silicates reacts with a source of silica. The amount of free lime is reduced, leading to increased durability of the cements under some circumstances. In addition, the Ca/Si ratio of the hydrates may be reduced.

In this reaction, there are two reagents, the cement and the silica source, which release silicate groups into the system. In this study we used C_3S and silica. Enrichment of just one of these silicate sources makes it possible to observe selectively silicate groups that originated from that starting material. For useful comparisons to be possible, the ^{29}Si enriched and natural abundance reagents must be of the same reactivity. It was not possible to obtain silicas having the same reactivity, but ^{29}Si enriched and natural abundance samples of C_3S were prepared by the same route. Thus a pozzolanic paste in which both reagents were ^{29}Si enriched was compared with a paste in which only the silica was enriched.

The hydration of the doubly enriched system (Figure 4a) was found to be similar to that observed previously for pozzolanic pastes. The silica resonance could not be reliably quantified, due to an excessively long T_1. This made it impossible to determine the degree of reaction of either the silica or the C_3S. The chain length was significantly longer at all ages, and the hydration of the C_3S was somewhat accelerated. In addition, the peaks were sharper than those formed in the hydration of C_3S, indicating that there was a smaller range of silicate environments in the products. Either they were more crystalline, or more homogeneous.

Analysis of the spectra in which only the silica was enriched (Figure 4b) is more complex. It is no longer possible to assess an average chain length, because the degree of enrichment of

the Q^1 and Q^2 species is not known. The enriched portion of the hydrate contains many more Q^2 groups, and that contains even more well defined peaks than the doubly enriched system, indicating that the enriched ^{29}Si species end up in hydrate that is more crystalline or more homogeneous than the bulk hydrate in this system. Two possibilities arise for the greater prevalence of the ^{29}Si species in the Q^2 sites.

1) The ^{29}Si species from the silica might be preferentially distributed into the Q^2 sites within a homogeneous hydrate with a relatively short average chain length. This might arise if the hydrate formed initially from unenriched C_3S, with dimeric C-S-H, and then later polymerized by insertion of linking silicate bridges from enriched SiO_2. In this case these Q^2 sites would be preferentially observed. This can be discounted in this system, since the degree of preferential reaction required would be implausibly large.

2) Alternatively, the hydrate may be zoned, with the areas containing silicate species from the silica having a significantly longer chain length. Such regions would be rather more ordered, due to the very long chains, and might be expected to give rise to more sharply defined resonances as is indeed observed.

In the spectra of the pozzolanic materials, the Q^2 region contains not just one peak but two. The origin of the splitting is not clear, but it probably arises from different sites within the drierketten chains. The tentative assignment by Brough *et al.* (1994b) of the downfield peak to bridging or linking tetrahedra in the chains seems reasonable, and can explain the observed intensities. Cong and Kirkpatrick (1994) have noted that in the crystal structure of Hamid (1981), only one of the chains appears to have the distinct geometry required to produce this shift, giving a 1:5 ratio to the main Q^2 peak. More recent results by Klur *et al.* (1997) (for synthetic C-S-H's) support the assignment of the extra peak to bridging sites. It is unlikely that the two peaks result from hydroxylated and non-hydroxylated species, since they are excited to a similar extent in CP spectra. Q^3 species are also observed in the pozzolanic hydrate. The very large peak width of the Q^3 species suggests that they are associated with the silica resonance, perhaps with a Ca modified silica gel.

TEM studies could not be carried out on the very small samples used for this work, so that parallel compositional information is not available. Overall the Ca/Si atomic ratio is 1.0, but complete reaction did not occur within the timescale of the experiments, so that the Ca/Si ratio of the C-S-H cannot be calculated. The initial hydrate from both the silica and overall consists largely of dimer. On current models of C-S-H (Richardson and Groves, 1992) it is likely that this material has a Ca/Si ratio of at least 1.25, so that more polymerized hydrate which forms later might have a much lower Ca/Si ratio. However, significant amounts of silica may also remain unreacted. Also, the change of silicate polymerization in the C_3S system suggests that significant changes to the polymerization of the early hydrate may occur as hydration proceeds.

CONCLUSIONS

^{29}Si enrichment is an excellent tool for the study of hydration kinetics by ^{29}Si MAS NMR. For C_3S hydration, the kinetic data strongly support the drierketten model for C-S-H and also enable the calculation of Arrhenius energies. For the pozzolanic system, full quantification was not possible, since the silica was found to have a long T_1 as supplied. In future however, dissolution and reprecipitation in the presence of low levels of paramagnetic impurities could be used to synthesise a silica with a shorter T_1.

The use of selective enrichment proved to be very useful in studying the mechanism of the pozzolanic reaction of microsilica in the presence of C_3S. Silicate species from the silica formed a hydrate that had significantly longer chains than the bulk hydrate in the system, and that also contained a smaller range of silicate environments.

REFERENCES

Brough, A.R., Dobson, C.M., Richardson, I.G. and Groves, G.W., "*In Situ* Solid State NMR Studies of Ca_3SiO_5; Hydration at Room Temperature and at Elevated Temperatures using ^{29}Si Enrichment," J. Mat. Sci., Vol. 29, 1994a, p3926.

Brough, A.R., Dobson, C.M., Richardson, I.G. and Groves, G.W., "Application of selective ^{29}Si isotopic enrichment to studies of the structure of CSH gels", J. Am. Ceram. Soc., Vol. 77, 1994b, p593.

Brough, A.R., Richardson, I.G., Groves, G.W. and Dobson, C.M., "A study of the pozzolanic reaction by solid state ^{29}Si NMR using selective isotopic enrichment," J. Mat. Sci., Vol. 30, 1995, p1671.

Clayden, N.J., Dobson, C.M., Groves, G.W., Hayes, C.J. and Rodger, S.A., "Solid State NMR studies of cement hydration", Proc B. Ceram. Soc., Vol 35, 1984, p55.

Cong, X. and Kirkpatrick, .R.J., private communication, 1994.

Dunster, A.M., Parsonage, J.R., and Vidgeon, E.A., "Silicate anion analysis in Portland cement pastes", Mater. Sci. Tech., Vol. 5, 1989, p708.

Hamid, S.A., "The crystal structure of the 11A tobermorite $Ca_{2.25}Si_3O_{7.5}(OH)_{1.5}.H_2O$", Z. Krist, Vol. 154, 1981, p189.

Hirljac, J., Wu, Z.-Q., and Young, J.F., "Silicate polymerization during the hydration of alite", Cem. Concr. Res., Vol. 13, 1983, p877.

Klur, I., Pollet, B., Virlet, J., and Nonat, A., "C-S-H structure evolution with calcium content by multinuclear NMR. Use of ^{29}Si and ^{43}Ca enrichment and 2D correlation experiments" in "Nuclear Magnetic Resonance Spectroscopy of Cement Based Materials", ed. P. Colombet *et al.*, Springer Verlag in press (1997).

Lippmaa, E., Magi, M. and Tarmak, M., "A high resolution ^{29}Si NMR study of the hydration of tricalcium silicate", Cem. Concr. Res., Vol 12, 1982, p597.

Macphee, D.E., Lachowski, E.E., and Glasser, F.P., "Polymerization effects in CSH: implications for Portland cement hydration", Adv. Cem. Res., Vol. 1, 1988, p131.

Richardson, I.G. and Groves, G.W., "Models for the composition and structure of calcium silicate hydrate (C-S-H) gel in hardened C_3S pastes", Cem. Concr. Res., Vol. 22, 1992, p1001.

Rodger, S.A., Groves, G.W., Clayden, N.J., and Dobson, C.M., "A study of C_3S hydration from very early to very late ages", Mater. Res. Symp. Proc., Vol 85, 1987, p13.

HIGH-TEMPERATURE ^{19}F NMR OBSERVATION OF FLUORINE ACTIVITY IN CLINKER PROCESSING

Laurent BONAFOUS and Pierre COLOMBET, CTG Italcementi group, Guerville, France
Catherine BESSADA, Dominique MASSIOT and Jean-Pierre COUTURES, CRPHT, Orléans, France

ABSTRACT A sample of an industrial raw-mix containing 1% CaF_2 has been heated in a specially designed probehead of a NMR spectrometer, which allows signal recording as a function of sample temperature from room temperature to ca. 1500°C. ^{19}F NMR spectra analysis indicates that CaF_2 disappears at about 1000°C to form at least two other phases which grow simultaneously as the temperature increases above 1000°C. From the values of the isomer shifts, these two later phases are suggested to be $Ca_3(Si_{1-x}Al_x)O_{5-x}F_x$, with $x<0.10$, and $C_{11}A_7.CaF_2$, solid solutions, confirming the mineralizing effect of CaF_2 in clinker formation.

Key-words : Nuclear Magnetic Resonance, Mineralizers in clinker making, Fluoride phases.

INTRODUCTION

High-temperature multinuclear (^{29}Si, ^{27}Al, ^{19}F, ^{17}O) NMR study of the clinkering process has recently been carried out for the first time using a model raw-mix made of laboratory reagents, with weight composition: 64.3% CaO, 21.2% SiO_2, 5.0 % Al_2O_3, 2.0% Fe_2O_3, 5.0% $CaSO_4$, 1.5% K_2O, and 1.0% CaF_2 (Bonafous et al., 1997). Concerning fluorine, the thermal evolution of the NMR response was characterized by the appearance of a relatively narrow line from 1000°C, specifically in the vicinity of the temperature where C_3S was observed to start to be formed (ca. 1050°C). This line was suggested to be the signature of a phase involving « mobile » fluorine (not necessarily a liquid), in agreement with the absence of dipolar and chemical shift anisotropy broadenings which usually render unobservable ^{19}F (I=1/2) in solid state compounds. This line was observed to be present as the sample temperature was raised from 1000°C to 1450°C.

In order to contribute to illucidate further the role of fluorine as a mineralizer or/and flux for the formation of C_3S in the process of clinkerization, which is a question which has given rise to controversy (see for instance Shame and Glasser, 1987, and Taylor, 1990a), a different raw-mix with 1% CaF_2 addition has been studied using the same NMR apparatus. This second raw-mix was a sample of an industrial raw-mix taken at one of the french plants of Italcementi Group. Based on the comparison with the signals recorded for various fluorine containing silicates and aluminates, as explained below, it is confirmed that a significant amount of fluorine is involved in solid solutions from ca. 1000°C to the highest temperature that can be afforded using this set-up (ca. 1450°C).

EXPERIMENTAL

Materials

The studied industrial raw-mix was composed of a mixture of marly limestone and brown clay with addition of 1 wt.% CaF_2. As detemined using X-ray fluorescence analysis, the bulk composition of the as-obtained industrial clinker is 65.1% CaO, 19.9% SiO_2, 5.6% Al_2O_3, 2.8% Fe_2O_3, 2.4% MgO, 1.1%SO_3 (3.4% eq. $CaSO_4$) 1.0% K_2O, 1.0% CaF_2, 0.3% TiO_2 and minute amounts of various other oxides (total equal to 0.8%). To reproduce the presence of sulfates arising from the fuel, as evidenced from the above clinker bulk composition, an equivalent amount of calcium sulfate has been added to the raw meal.

Known reference fluorine containing phases (see Table 1) were synthetized from reagent grade CaF_2 and relevant oxides. The mixtures were ground in an agate ball-mill and moulded into tablets prior to allowing them to react at high temperature in a holed sealed platinum crucible. The reaction steps and final phases were controlled using powder X-ray diffraction at room temperature (Philips PW 1729 with Ni filtered CuKα radiation) and electron scanning microscopy (Cambridge Stereoscan 100). Spurrite $2C_2S.CaCO_3$ and potassium containing apatite-type phases such as $K_3Ca_2(SO_4)_3F$ (Triviño Vásquez, 1985) were not considered in this work, since they are usually evidenced as sedimentary coating of obstacles or cooler surfaces in preheater or kiln (via condensation of volatiles), which cannot occur in the present experiment.

NMR spectroscopy

The NMR experiments were performed using a Bruker MSL 300 spectrometer operating at 7.04 T. The ^{19}F spectra (I=1/2, 100% abundant), obtained at 282 Mhz with a single pulse excitation sequence, have been measured in static conditions for high temperature experiments and under Magic Angle Spinning (MAS) at room temperature for reference compounds. The reported chemical shifts are referenced to ^{19}F resonance in trichlorofluorocarbonate ($CFCl_3$).

High Temperature Experiments

The high-temperature device is an evolution of the previously described high temperature NMR setup (Taulelle et al., 1989, Coutures et al., 1994 and Bonafous et al., 1995). This setup is based on the heating of a MgO capped sample container, placed in the probehead and irradiated both from the top and the bottom by two CO_2 lasers (λ=10.6 μm). The container is thermally insulated from the axial Helmholtz coil (diameter 15 mm) tuned to the resonance frequency of fluorine, by a ceramic shield. The temperature gradient inside the container was measured to be less than 10 and 25°C at 1000 and 1500°C, respectively. As the use of a thermocouple is impossible during a NMR experiment, the temperature has been calibrated outside the magnet. The heating protocol was the following. A 5 minutes equilibration time was taken after each increase of the laser power. A typical 25 minutes duration was necessary to obtain a signal with satisfactory signal-to-noise ratio. With temperature increments of 50°C, the overall experiment from room temperature to 1450°C lasted about 10 hours.

It has to be noticed that there exists a strong ^{19}F probe signal arising from the probe radio frequency components themselves which clearly shows up at room temperature. This background signal has not been suppressed in the spectra presented in Fig 1. It even shows some evolution with increasing temperature.

Reference phases

In static conditions, which is the case for the experiment described above in which the heating device does not allow the spinning of the probehead, the room temperature solid phase ^{19}F signal is in general not visible, due to dipolar broadening and chemical shift anisotropy. This is the case for the studied materials. ^{19}F chemical shift data at room temperature were hence obtained for reference fluorine containing phases (see Table 1) using MAS (Magic Angle Spinning). Then, the dependence of the chemical shift upon temperature was investigated using the static high temperature NMR device described above.

RESULTS

Raw-mix

For the raw-mix the most illustrative spectra obtained as a function of temperature are shown in Fig 1. In the lower temperature domain, i.e. in the temperature range where the decompositions of limestone and clay occur to give then belite and aluminate from decomposition products, a sharp signal (located at -97 ppm) can be observed. It appears at ca. 300°C and remains observable at the same position up to about 900°C and slightly shifted to -105 ppm between ca. 950 and ca. 1050°C. In the higher temperature range (above 1050°C), this signal disappears for the benefit of two broader signals. These two signals are located at -82 (poorly defined) and -119 ppm, respectively, and their intensities increase simultaneously as the temperature increases.

Reference phases

The ^{19}F room temperature line chemical shift values for the most relevant fluoride compounds for this study are given in Table 1. Concerning CaF_2, both industrial and pure samples exhibit a line at -105 ppm. The other studied compounds are those that can be expected to be formed owing to the bulk composition of the mix, in particular the known C_3S stabilized solid solutions and fluor-ellestadite $3C_2S.3CaSO_4.CaF_2$ (Gilioli et al., 1979). $Ca_{6-x/2}Si_2\ O_{10-x}\ F_x$ is one of the possible explicite formulae of $3C_3S.CaF_2$ with a structure related to that of C_3S via partial substitution of F^- for O^{2-} and concomitant omission of half the same quantity of Ca^{2+} (Pérez-Méndez et al., 1985; Ye Qing et al., 1992). $Ca_3\ (Si_{0\,85}\ Al_{0.15}\ )\ (O_{4\,85}\ F_{0\,15})$ is the solid solution synthesized by Shame and Glasser (1986), where Al replaces Si in the structure of C_3S as F substitutes for O, to balance the electrical ionic charges. The former C_3S based solid solution shows two resonance lines of nearly equal intensity at -111 and -116 ppm, whereas the latter shows a single line at -120 ppm. All compounds exhibit broader lines in the high temperature spectrometer, visible only at temperatures higher than 500°C, as explained above, within their respective stability temperature range, the average tendency being a shift towards slightly less negative values for the chemical shift as the temperature increases (+2 ppm at 1000°C, with respect to room temperature) except fluor-ellestadite which was observed to show a single line from 700°C (-103 ppm) to 1200°C (-102 ppm) instead of two lines at room temperature (-87 and -100 ppm).

Table 1 ^{19}F room temperature MAS NMR chemical shift values (ppm vs. $CFCl_3$) for various fluorine containing phases prepared from reagent grade CaF_2 and oxides.

Composition	chemical shift
CaF_2	-105
$C_{11}A_7.CaF_2$	-82
$Ca_{6-x/2}Si_2\ O_{10-x}\ F_x$ with x=0.15	-111; -116
$Ca_3\ (Si_{0\,85}\ Al_{0\,15}\ )\ (O_{4\,85}\ F_{0\,15})$	-120
$3C_2S.3CaSO_4.CaF_2$ (fluor-ellestadite)	-87; -100

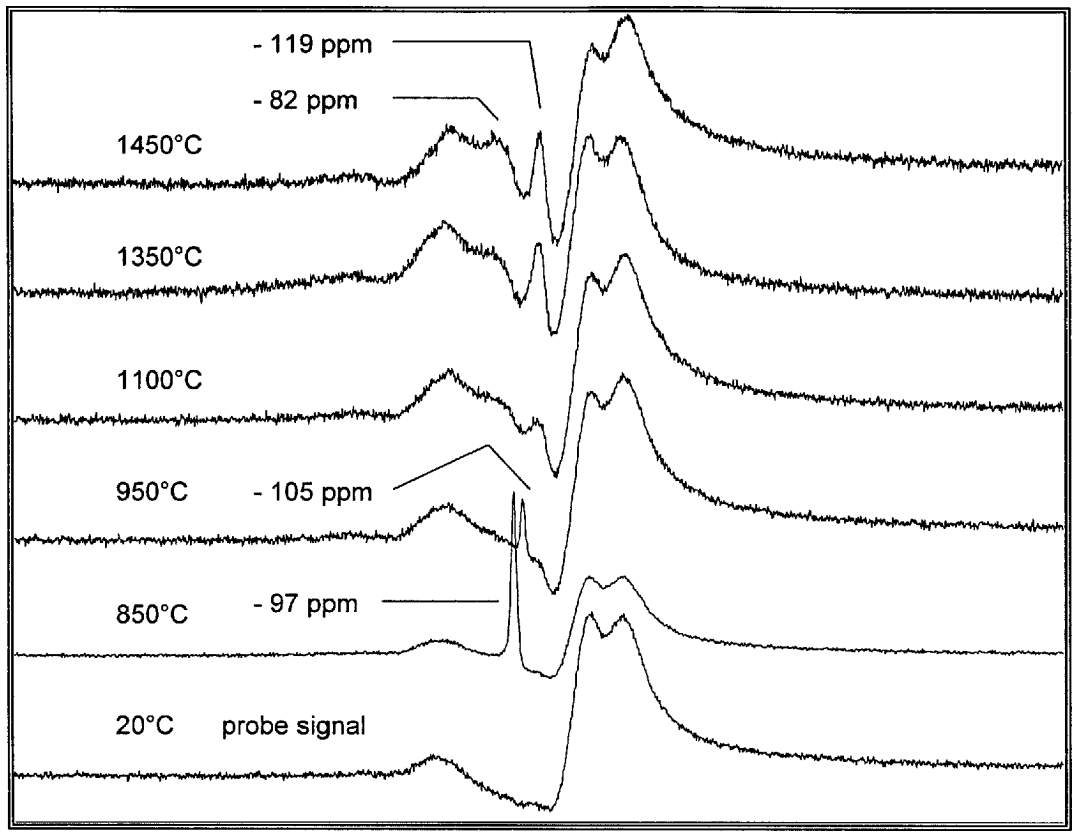

Figure 1 ^{19}F (static) NMR spectra for the studied raw-mix, as a function of temperature.

DISCUSSION

As far as the lower temperature range is concerned, where CaF_2 is known to favour limestone decomposition (Taylor, 1990b), the observed signal can be assigned only to CaF_2, since no other fluoride is expected to be formed in this range. The fact that the signal is visible from a much lower temperature (300°C) than that from which it was observed for the previously studied model raw-mix (Bonafous et al., 1997), which contained lime instead of limestone, may thus be considered as indicative of a reactivity-correlated mobility of fluorine (allowing line narrowing) in the process of limestone decomposition. It may be noted that another difference between the two mix is the presence of water traces in the presently studied industrial mix (including bound water in clay) whereas the previous one was totally dry. Specifically, it may be assumed that water plays a role to promote fluorine activity for limestone decomposition via intermediate formation of HF and subsequent reaction of HF with $CaCO_3$ to yield CaF_2, H_2O and CO_2. HF formation would then in turn favour F mobility in bulk CaF_2 due to vacancy production in the vicinity of its surface leading to F diffusion. This mobile fluorine would therefore give rise to the observed line at -97 ppm, i.e. slightly shifted from the position observed for CaF_2 taken alone (-105 ppm, see Table 1). Once the carbonate decomposition is completed at higher temperature, normal CaF_2 signal appears again at -105 ppm, in agreement with what is observed at ca. 950°C (Fig 1).

In the higher temperature range, the chemical shift values of the two observed signals (-82 and -119 ppm) are nearly identical, within experimental accuracy, to those observed at room temperature for $C_{11}A_7.CaF_2$ and Ca_3 $(Si_{0.85}$ $Al_{0.15})$ $(O_{4.85}$ $F_{0.15})$, i.e. -82 and -120 ppm, respectively

(Fig 1 and Table 1). Knowing that the ^{19}F chemical shift values are almost insensitive to temperature variations as discussed above (the variation is less than 2 ppm in the studied temperature range), it may thus be inferred that the above solid phases are simultaneously formed in the conditions of the present experiment, above ca. 1050°C. This interpretation is further supported by the observed larger width of these two lines, consistent with envolvement of fluorine in solid solutions. Note that the (Al,F) content in the studied synthetized C_3S solid solution has been choosen equal to the limit of (Si,O) substitution (0.15) determined by Shame and Glasser (1987). Obviously, the true content in the studied raw-mix is somewhat lower. Considering that all the fluorine is involved in this phase, x can be calculated equal to 0.10 from the mix composition. Since $C_{11}A_7.CaF_2$ is also assumed to be formed, then it may be deduced that $x<0.10$. Accordingly, we shall consider the general formula $Ca_3(Si_{1-x}Al_x)O_{5-x}F_x$ ($x<0.10$) as representative of the observed solid solution. The same kind of remark can be done as regards $C_{11}A_7.CaF_2$, which forms a continuous range of solid solutions with $C_{12}A_7$, that is to say, the present results do not allow its precise composition.

As a consequence, it may be stated that fluorine acts as a mineralizer in the present circumstances, i.e. using the studied mix composition and at the heating rate employed in this experiment, and avoiding condensation and reaction of volatiles. These findings are in fair agreement with the results obtained by Shame and Glasser (1987) who demonstrated that mixtures of $Ca_3(Si_{1-x}Al_x)O_{5-x}F_x$ solid solutions and $C_{11}A_7.CaF_2$ can be formed from ca. 1050°C, thus lowering the limit of C_3S thermodynamic stability.

No signals corresponding to fluor-ellestadite nor $Ca_{6-x/2}Si_2\ O_{10-x}\ F_x$ ($3C_3S$-CaF_2) are evidenced in this study, as opposed to the conclusions of Gilioli et al. (1979) who suggested that those phases might be of interest in the firing process of clinker. This discrepancy may be explained by considering that the mix they studied was free of Al_2O_3, which is not the case here.

CONCLUSION

This work supports the previous conclusions by Shame and Glasser (1987) concerning both the fluorine mineralizing action to promote C_3S formation and the predominant F/Al synergetical effect in the formation of solid solutions at high temperature. In addition, it gives evidence that such a mechanism does occur, not only in the simplified mix they use (CaO-SiO_2-Al_2O_3-CaF_2), but also in a real more complicated mix, as the one used in a kiln. We finally stress the fact that the present experiment does not reproduce exactly the conditions of a kiln as regards both heating rate and volatiles cycle. In particular, the heating rate used in the present in-situ NMR study, is much lower by at least 10 times, which implies conditions closer to reaction reversibility.

REFERENCES

Bonafous, L., Ollivier, B., Auger, Y., Chaudret, H., Bessada, C., Massiot, D., Farnan, I. and Coutures, J.P., "High Temperature Observation of Mobile Phases up to 1500°C ", J. Chim. Phys., Vol. 92, 1995, pp. 1867-1870.

Bonafous, L., Bessada C., Massiot D., Coutures, J.P., Le Rolland, B. and Colombet, P. (Colombet, P., Grimmer, A.-R., Zanni, H. and Sozzani, P. (Eds)): "In Situ High Temperature Multinuclear NMR Study of Clinker Formation", NMR Spectroscopy of Cement-Based Materials, Springer-Verlag, Heildelberg, 1997, in preparation.

Coutures, J.P., Massiot, D., Florian, P. and Coté, B. (P. Colombet and A.R. Grimmer (Eds)) : "High and Very High Temperature ^{17}O and ^{27}Al Nuclear Magnetic Resonance on Liquid Alumina

and Silica Bearing Oxides", : Application of NMR to Cement Science, Gordon and Breach Science Publishers, 1994, pp. 429-454.
Gilioli, C., Massazza, F. and Pezzuoli, M., "Studies on Clinker calcium silicates bearing CaF_2 and $CaSO_4$", Cem. Concr. Res., Vol. 9, 1979, pp. 295-302.
Pérez-Méndez, M., Fayos, J. Howie, R.A., Gard, J.A. and Glasser, F.P., "Calcium Fluorosilicates: the $Ca_{6-x/2}Si_2O_{10-x}F_x$ phase", Cem. Concr. Res., Vol. 15, 1985, pp. 600-604.
Shame, E.G. and Glasser, F.P., "Stable Ca_3SiO_5 Solid Solution containing Fluorine and Aluminium made between 1050°C and 1250°C", Ceram. Trans. J., Vol. 86, 1987, 13-17.
Taulelle, F., Coutures, J.P., Massiot, D ., Rifflet, J.C., "High and Very High Temperature NMR", Bull. Magn. Reson., Vol. 11, 1989, pp. 318-320.
Taylor, H.F.W., "Cement Chemistry", Academic Press, London, 1990a, Chapter 2: "High-temperature Chemistry", pp. 56-58.
Taylor, H.F.W., "Cement Chemistry", Academic Press, London, 1990b, Chapter 3: "The Chemistry of Portland Cement Manufacture", p. 94.
Triviño Vásquez, F., "A new compound: $K_3Ca_2(SO_4)_3F$, Identified in Coatings of Heat Recover Cyclones", Cem. Concr. Res., Vol. 15, 1985, pp. 581-584.
Ye Qing, Kong Jianmin and Liu Baoyuan, "Effect of Fluorite-Gypsum Composite Mineralizer on the Microstructure and Properties of Portland Cement Clinker Phase", Proceedings of the 9th ICCC, New Delhi, India, 1992, Vol. II, pp. 342-350.

CONTRIBUTION OF NUCLEAR MAGNETIC RESONANCE TECHNIQUES TO THE STUDY OF CEMENT PASTE WATER DEGRADATION

Pascal FAUCON, Service de Chimie Moléculaire, C.E.A. Saclay, 91191 Gif sur Yvette, France
Université Cergy-Pontoise, Laboratoire Matériaux et Sciences des Constructions, I.U.P. Génie Civil et Infrastructures, Rue d'Eragny, Neuville sur Oise, 95031 Cergy Pontoise Cedex, France
Frédéric ADENOT, Service d'Entreposage et de Stockage des Déchets, C.E.A. Saclay, 91191 Gif sur Yvette, France
Jacques F. JACQUINOT, Service de Physique de l'Etat Condensé, C.E.A. Saclay, 91191 Gif sur Yvette, France
Joseph VIRLET, Service de Chimie Moléculaire, C.E.A. Saclay, 91191 Gif sur Yvette, France
Richard CABRILLAC, Université Cergy-Pontoise, Laboratoire Matériaux et Sciences des Constructions, I.U.P. Génie Civil et Infrastructures, Rue d'Eragny, Neuville sur Oise, 95031 Cergy Pontoise Cedex, France
Michel JORDA, Agence Nationale pour la Gestion des Déchets Radioactifs, 92298 Châtenay-Malabry, France
Université Cergy-Pontoise, Laboratoire Matériaux et Sciences des Constructions, I.U.P. Génie Civil et Infrastructures, Rue d'Eragny, Neuville sur Oise, 95031 Cergy Pontoise Cedex, France

ABSTRACT Surface dissolution of the solid-aggressive solution interface has been demonstrated during leaching of cement pastes by water. The rate of degradation is initially governed by the laws of diffusion, and in the longer term by the surface dissolution. Nuclear magnetic resonance techniques (^{29}Si MAS-NMR and ^{57}Fe Mössbauer spectroscopy) show that substitution of iron for calcium in CSH greatly slows surface dissolution.

Key-Words: CSH, Ferrite phase, Nuclear Magnetic Resonance, Tobermorite, Waste material utilization

INTRODUCTION

Short-lived, and possibly long-lived, radioactive waste is stored in concrete containers (casks, disposal structures, etc.). It is therefore essential to predict the behaviour of these containers in aggressive medium. One of the worst-case scenarios is leaching of cement paste by flowing water of low ionic content.

In cement structures, hydrates are in equilibrium with an interstitial solution of approximate pH 13. Contact with a demineralized solution of pH=7 creates a degraded zone between the core and surface of the leached structure. The resulting decreasing concentration gradient of hydroxyls alters the chemical equilibria in the degraded zone, thereby inducing dissolution and precipitation of secondary phases: Faucon et al. (1997a). Adenot (1992) has shown that in the degraded zone dissolution-precipitation occurs much faster than diffusion. The surface of the cement cannot be at equilibrium since it is in contact with a demineralized solution. Its behaviour must therefore be hypothesized. If it is assumed that the cement surface does not dissolve, the rate of degradation is governed by the diffusion of ionic species in the degraded layer. The long-term behaviour of the cement can be modelled by solving Fick's equations for a semi-infinite medium, taking account of

the different solid-liquid equilibria: Adenot and Faucon (1997). This yields a $\sqrt{t}$ law predictive of degradation (where t is time).
However, the $\sqrt{t}$ diffusive regime is only valid if there is no surface dissolution. If the hydrate resulting from dissolution-precipitation in the surface layer is finally attacked by the aggressive solution, the solution of Fick's equations will yield erroneous results. We have studied the rate of surface dissolution in different cement pastes. Nuclear magnetic resonance techniques (^{29}Si MAS-NMR and ^{57}Fe Mössbauer spectroscopy) clarified the mechanisms underlying the slowing of surface dissolution.

EXPERIMENTAL CONDITIONS

Three cement pastes each containing the same C_3S, synthesized by Ciments Français, were studied (Table 1). Aluminium and iron were added in the form of C_3A and iron nitrate (FN), respectively, in order to study their influence on the rate of degradation. When introduced, FN was neutralized by addition of lime.

Table 1 Sample composition (% per unit mass)

Sample	% C_3S	% C_3A	% FN	% CaO
1	100.0	-	-	-
2	85.0	15.0	-	-
3	81.3	-	15.5	3.2

Samples (7 cm diameter, water/cement ratio 0.38) were kept for one month in a solution saturated in portlandite, and were then placed in a solution kept deionized at pH 7 by recirculation through a mixed bed of ion-exchange resins. Tests were performed under an inert atmosphere (N_2). After six months of leaching, the degraded layer (thickness 50 to 100 microns) was removed for study by NMR and Mössbauer spectroscopy. X-ray diffraction spectroscopy was first used to identify the crystallized phases of each degraded layer.

Table 2 X-ray diffraction of surface layer specimens

Sample	Sound zone	Surface layer
1	CH, CSH	CSH
2	CH, C_3AH_6, C_4AH_8	CSH, C_3AH_6, AH_3
3	CH,	CSH, C_3FSH_4

The Mössbauer study was performed using a ^{57}Co:Rh γ-ray source, the spectrometer comprising an electromagnetic vibrator with a triangular velocity signal. All spectra were recorded at ambient temperature. Each sample was exposed to the ^{57}Co source for about two days. The isomer shifts are given with reference to α-Fe. Each spectrum consisted of several doublets whose relative intensities, isomer shift, quadrupolar splitting and half-widths (HWHM) of lorentzian lines were determined using a least square fit procedure.
Solid-state NMR experiments were performed on a Bruker MSL 300 NMR spectrometer, in a 7.03 Tesla field, at a ^{29}Si frequency of 59.617 MHz. ^{29}Si MAS-NMR spectra were recorded with a spinning rate of approximately 4 kHz in double-bearing 7-mm ZrO_2 rotors. Spectra were accumulated using single-pulse excitation and high-power 1H decoupling with a 60-kHz rf field. A recycle time of 59 s was used. The number of scans varied from 800 to 2000 for the superficial layer. $[Si(CH_3)_3]_8Si_8O_{20}$ was used as a secondary standard, the major peak being at 11.6 ppm relative to tetramethylsilane (TMS, $Si(CH_3)_4$).

RESULTS

Rate of degradation

Figure 1 shows the dissolution of the solid-liquid interface as a function of time. Thinning of the surface layer occurred as a linear function of time, reflecting dissolution of the sample in contact with the aggressive solution. Degradation was accelerated by the presence of aluminium and slowed by iron.

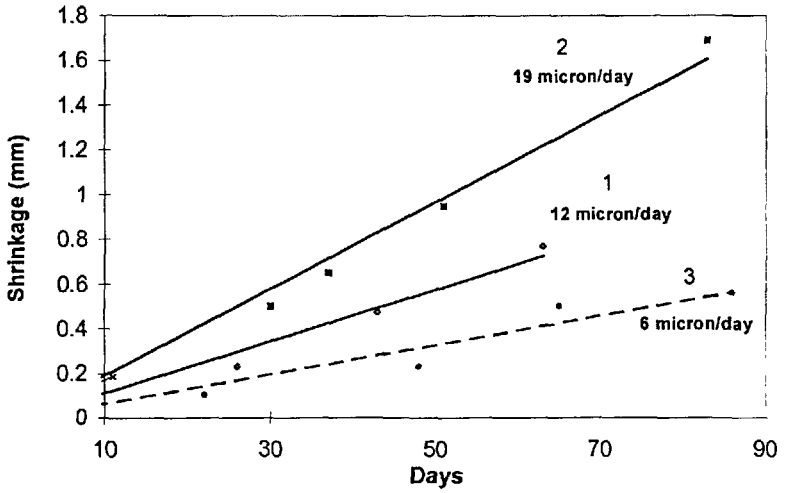

Figure 1 Surface dissolution of samples.

These data clearly show that surface dissolution may be considerable, and should be taken into account in predictions of behaviour of cement structures, independently of diffusion.

Silicon NMR (Samples 1& 2)

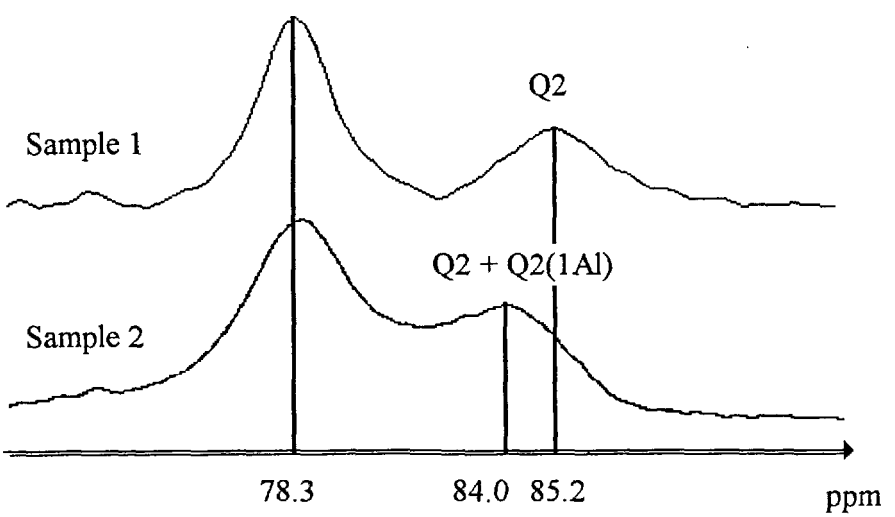

Figure 2 ^{29}Si MAS-NMR spectra of sound cement pastes.

Only samples 1 and 2 could be studied by NMR (Fig 2). The third contained iron, which is paramagnetic and partially destroyed the silicon signal.
In the sound paste of samples 1 and 2, the ^{29}Si MAS-NMR spectra were characteristic of that of

CSH of Ca/Si ratio 1.7 (Klur, 1996). The percentages of Q1 tetrahedra (linked to a single tetrahedron) and Q2 tetrahedra (linked to two other tetrahedra) indicates that the CSH of the sound paste comprise short chains of silicon tetrahedra (2 to 5 tetrahedra).
The chemical shift of the Q2 tetrahedra of sample 2 was smaller than that for pure C3S paste. Mägi et al (1984) have shown that the chemical shift of a Q2(1Al) tetrahedron for which one of the second neighbour silicons is substituted by an aluminium is 5 ppm less than that of a Q2 tetrahedron.

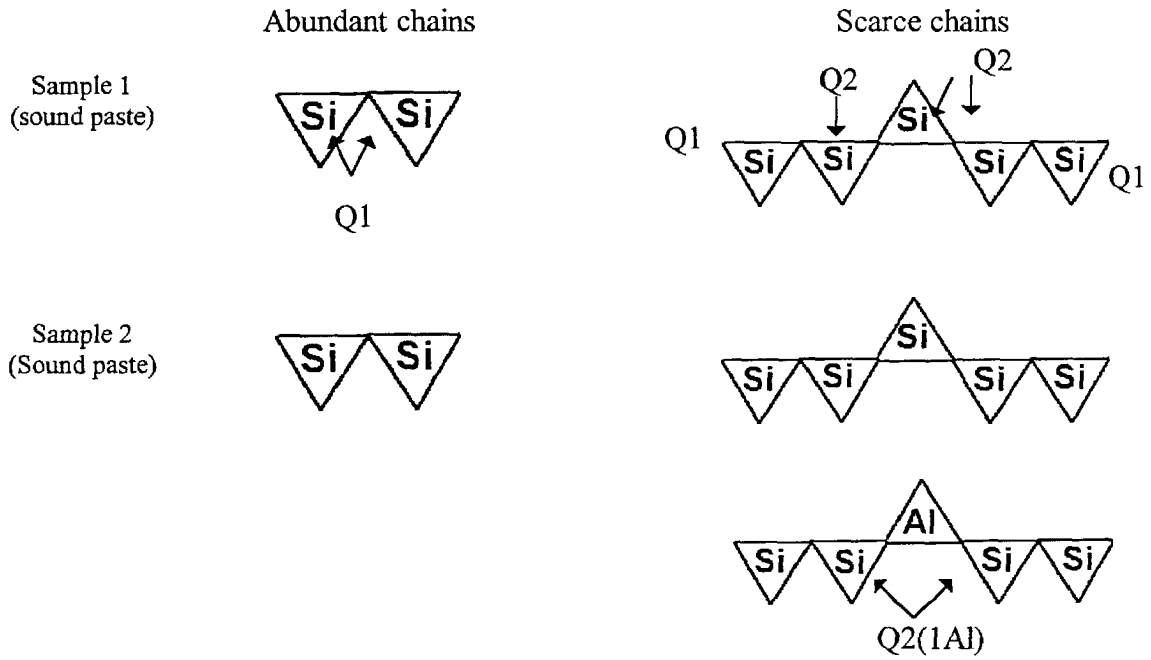

Figure 3 Types of chains of tetrahedra of the CSH in two sound cement pastes.

Aluminium introduced into sample 2 in the form of C_3A is therefore partially incorporated into the CSH. However, the percentage of silicon Q2 tetrahedra substituted by aluminium remains very low since the between-sample difference in chemical shift of the Q2 peak is small. Figure 3 shows the types of chains seen in the CSH of the two pastes.
The ^{29}Si MAS-NMR spectra of the degraded layers (Fig 4) are characteristic of those of CSH. The absence of Q0 silicon tetrahedra (no silicon as second neighbour) shows that no $4H^{+} \Leftrightarrow Si^{4+}$ substitution occurred in the C_3AH_6 structure in sample 2.
The percentage of Q1 has decreased in the two samples and that of Q2 has increased. The chains of tetrahedra of the CSH are therefore lengthened. The mean chain length increased from 2.5 in the sound zone of the two samples to 5 in the surface layers.
In sample 2, chain lengthening is accompanied by marked incorporation of aluminium in the CSH network since most of the Q2 silicons are, in fact, Q2(1Al) silicons. The latter have an aluminium as their second neighbour. This therefore yields the chains of tetrahedra of the "degraded" CSH shown in figure 4.
Leaching of cement pastes therefore results in "polymerization" of the CSH. In sample 2, the aluminium released by the dissolution of C_4AH_8 (Table 2) is in part incorporated into the CSH where it partially substitutes for silicon in the tetrahedral position.

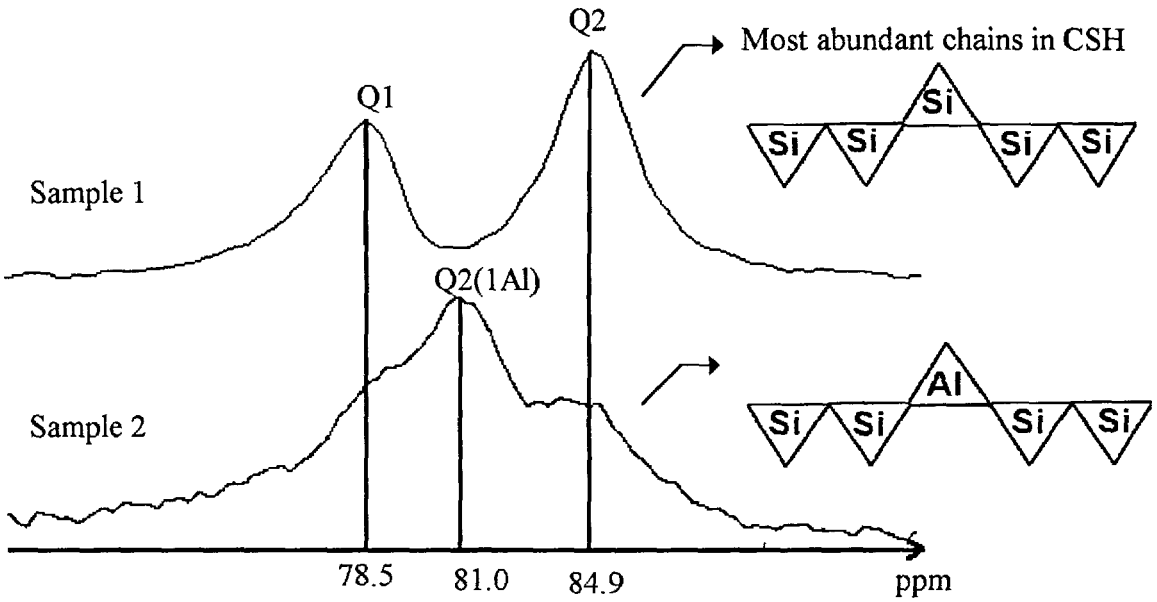

Figure 4 ^{29}Si MAS-NMR spectra of surface layers.

^{57}Fe Mössbauer spectroscopy (sample 3)

Sample 3 contained iron introduced in the form of iron nitrate, which dissolves on contact with water, thereby allowing incorporation of iron into hydrates. In sound paste (Figure 5), the isometric shifts, characteristic of the environment of iron, were all above 0.40 mm/s, i.e. characteristic of octahedrally coordinated Fe^{3+}. Iron is therefore not substituted for silicon. The quadrupolar coupling constants are characteristic of the symmetry of the incorporation sites and are close to the values determined by Labhasetwar et al (1991). for iron substituting for labile calcium (Δ_{labile} = 0.8 mm/s) and nonlabile calcium ($\Delta_{nonlabile}$ = 0.4 mm/s) in tobermorite, the structure of which is similar to that of CSH (Taylor, 1986). The band widths are characteristic of crystallized or nano-crystalline structures. It therefore appears that trivalent iron partially substitutes for the labile and nonlabile calciums of the CSH.

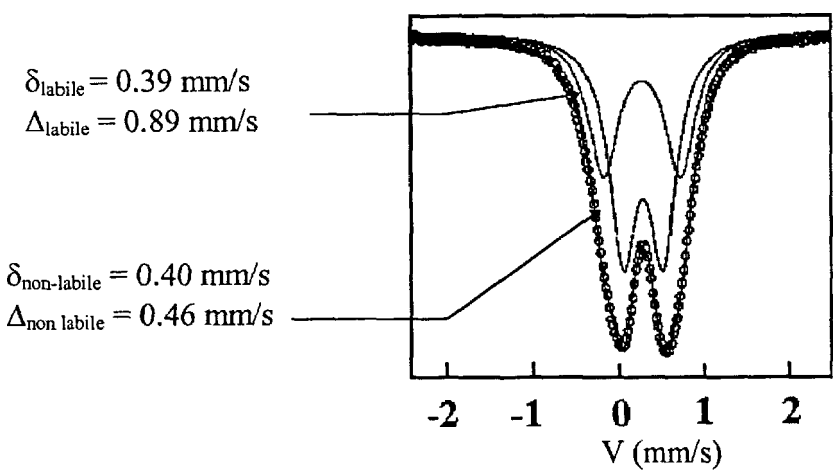

Figure 5 ^{57}Fe Mössbauer spectroscopy of sample 3 (surface layer).

DISCUSSION

Competition between diffusion and surface dissolution

Interface shrinkage occurred as a linear function of time (Fig 1). Two degradation mechanisms competed: degradation provoked by diffusion of the ionic species through the interstitial solution of the paste, and dissolution of the surface layer. It is vital for the prediction of long-term behaviour of cement structures to know which mechanism predominates over the stipulated storage period.
Rate of degradation in the diffusive regime
Assuming no shrinkage of the interface, solution of Fick's equations for a semi-infinite medium indicates that the thickness of the degraded layer, e, can be expressed in the following form:

$$e = \sqrt{D_{app} t}$$

where D_{app} is a constant with the same units as a coefficient of diffusion.
The following expression is then obtained for V_1, the rate of degradation in the diffusive regime:

$$V_1 = \frac{\sqrt{D_{app}}}{2\sqrt{t}}$$

V1 will therefore be large in the early stages of degradation, but small for longer times.
Limit time, t_0, of the validity of the diffusive regime
Figure 1 indicates that the interface shrinks at a constant rate V_2:

$$V_2 = K_2$$

where K_2 is a time-independent constant.

The limit time, t_0, of the validity of the diffusive regime will be reached when V_1 is equal to V_2, i.e.

$$t_o = \left(\frac{\sqrt{D_{app}}}{2K_2} \right)^2$$

D_{app} was approximately 15,000 µm2/day for each sample. The results given in figure 1 allow calculation of t0 for each sample.

Table 3 Time (t_0) after which the surface dissolution will govern degradation

Sample	1	2	3
V_2 (µm/day)	19	12	6
t_0 (days)	10	26	104

After t_0, surface dissolution will occur faster than diffusion-induced degradation. Dissolution of the surface in contact with the aggressive solution will determine the rate of degradation, and should therefore be minimized.

Effect of Al^{3+} and Fe^{3+} on the rate of degradation

Figure 1 (like table 3) shows that the surface layer of sample 1 dissolved quicker than that of sample 2. The ^{29}Si MAS-NMR results (Fig 2) and X-ray diffraction findings show that the CSH contain chains of five silicon tetrahedra on average. C_4AH_8 initially present in the surface layer of

sample 1 dissolved. The aluminium released precipitated in the form of AH_3 of low solubility at pH near neutrality (Damidot and Glasser, 1995) and was partially incorporated into the CSH, substituting for the Q2 silicons in the chains. This substitution creates a charge deficit compensated by the protonation of one of the oxygens of the tetrahedra (Fig 6). The resulting surface layer therefore dissolves much faster. The aluminium-substituted CSH therefore dissolve faster than nonsubstituted CSH. In contrast, partial replacement of divalent calcium by trivalent iron slowed the CSH dissolution (Figs 2 and 5). The excess charges introduced by the substitution are compensated this time by the loss of a proton (Labhasetwar et al., 1991, and Faucon et al., 1996, 1997b), yielding the structure shown in figure 6.

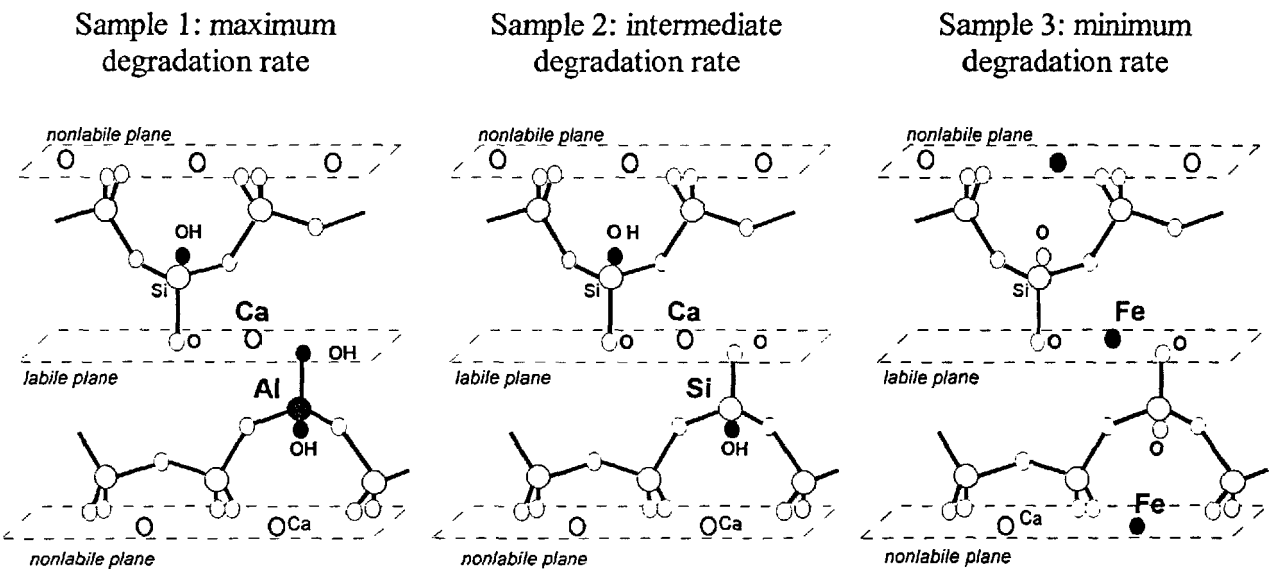

Figure 6 Structures of the different CSH of the degraded surface layers

The incorporation of iron reduced the solubility of CSH at pH near neutrality, whereas the presence of aluminium had the opposite effect. We are currently studying the solubility of the different CSH.

CONCLUSIONS

The degradation of cement by leaching with water results from the combined action of diffusion and dissolution of surface matter. In the short- and medium-term ($t < t_0$), degradation results from the diffusion of ionic species from the interstitial solution of the cement paste to the aggressive solution. The rate of degradation is governed by the rate of diffusion in the degraded layer. In the long-term ($t > t_0$), the rate of surface dissolution outstrips diffusion and therefore governs degradation.

These observations are fundamental for the prediction of the long-term behaviour of cement structures. The diffusive properties of the materials are important, but in the long term the rate of dissolution of the material at pH 7 is crucial.

NMR shows that that this dissolution is linked to that of the CSH, the main constituents of cement paste. Contact with a demineralized solution induces surface precipitation of short-chain CSH. Cationic substitutions in the CSH may increase or reduce their solubility and hence affect the rate of surface dissolution. Degradation is accelerated when aluminium substitutes for silicon in CSH and is slowed when iron replaces calcium.

ACKNOWLEDGMENTS

We would like to thank F. Pineau of ANDRA without whom this study would not have been possible.

REFERENCES

Faucon, P., Le Bescop, P., Adenot,F., Jacquinot, J.F., Pineau, F., and Felix, B., "Leaching of Cement: Study of the Surface Layer Cem. Concr. Res, 26 [11], 1996, pp. 1707.

Faucon, P., Adenot, F., and Cabrillac, R., "Behaviour of Crystallised Phases of Portland Cement upon Water Attack", Materials and Structures, 1997, in press.

Adenot, F., "Durabilité du béton : Caractérisation et Modélisation des processus physiques et chimiques de dégradation du ciment", Thèse, Université d'Orléans, 1992.

Adenot, F., and Faucon, P., "Modélisation du comportement à long terme des bétons utilisés dans le stockage des déchets radioactifs", Materials and Structure , 1997, in press.

Klur, Y., Thesis, Université de Paris VI, 1996.

Mägi, M., Lipmaa, E., Samoson, A., Engelhardt, G., and Grimmer, A.R., "Solid State High-Resolution ^{29}Si Chemical Shifts in Silicates", Journal of Physical Chemistry, 88, 1984, pp. 1518-1528.

Labhasetwar, N.K., Shriwastawa, O.P., and Medikov, Y.Y., "Mössbauer Study on Iron Exchanged Calcium Silicate Hydrate. $Ca_{5-x}Fe_xSi_6O_{18}H_2.nH_2O$." J. Sol. State. Chem., 93, 1991, pp. 82-87.

Taylor, H.F.W., J. Am. Ceram. Soc. 69 [6], 1986, pp. 464-467.

Damidot, D., and Glasser, F.P., "Investigation of the $CaO-Al_2O_3-SiO_2-H_2O$ system at 25°C by thermodynamic calculations", Cem. Conc. Res, 25, 1995, pp. 23-28.

Faucon, P., Bonville, P., Adenot, F., Genand-Riondet, N., Jacquinot, J.F., and Virlet, J., "^{57}Fe Mössbauer Study on Cement Water-Degradation", Advances in Cement Research, 1997, in press.

EXPERIMENTAL-STATISTICAL MODELING AND ANALYSIS OF THE CHAIN "COMPOSITION - NMR-SIGNAL - PROPERTIES" OF CEMENT COMPOSITE

Tatiana LYASHENKO and Vitaly VOZNESENSKY, Odessa State Building and Architecture Academy, Odessa, Ukraine
Shimon BOYKO and David SHTAKELBERG, Standard Institute of Israel, Jerusalem, Israel

ABSTRACT Nuclear Magnetic Resonance (NMR) has been used to determine moisture content of colloid and capillary-pore structure in hardening composites. Quantities of 4 composition ingredients have been varied according to optimal design of experiment, 18 composites being studied. Polynomial models "composition - strength", "composition - moisture content", and "moisture content - strength" have been built and used for analysis of structure formation and prediction of composite quality.

Key-words: Composition, Modeling, Moisture, Nuclear Magnetic Resonance.

INTRODUCTION

The progress of research physical methods makes it possible to include NMR-signals (S_{NMR}), as intervening informative element, into traditional chain "composition X - properties R" of composite. The analysis of "from X to S_{NMR}" links might serve adding to knowledge of structure formation mechanisms. Studying the links "from S_{NMR} to X" might help in developing the methods of compositions identification. Mathematical description of "S_{NMR} - R" relations would present the base for prediction and express-control of products quality.

The purpose of this work has been to analyze the influence of composition of cement composite hardening for τ days ($1 \le \tau \le 28$) on composite strength $R(\tau)$ and parameters $U(\tau)$ of moisture content determined with NMR-method.

Two basic engineering situations have been considered. The first is the case of "full" information on $R(\tau)$ and $U(\tau)$ being available, that would be useful primarily when studying structure formation process. In the second case available is only 1-3 days information about structure formation, on which strength R_{28} must be predicted and water dosage at concrete mixing plant be controlled.

METHODS OF STUDYING AND RESULTS OF MODELING THE STRENGTH OF CEMENT COMPOSITES (CONCRETES) AT AGE OF 28 DAYS

Design and methods of experiment

Eighteen cement composites (concretes) have been studied, their four components varied according to D-optimal experimental design (Voznesensky et al, 1989), allowing four-factor quadratic experimental-statistical models (ESM) to be built and analyzed. Concretes base composition and raw materials (save fine filler especially introduced into study) have corresponded to those used by one of leading Israel firm manufacturing concrete mixtures.

The levels of varying the composition factors (with water content in mixtures, W=200 dm^3/m^3, being constant) and their normalization rules are shown in Table 1. Non-linear transformation is used for factor x_4 varied non-proportionally. Quality indices - properties of technological mixture and hardened concrete (compression, tensile and bending strength, modulus of elasticity, shrinkage, and others) were determined to Israel and International standards.

Table 1 The levels of composition factors in the experiment.

	Level			
	lower	basic	upper	Normalization Rule
	x_i= -1	x_i=0	x_i= +1	-1 ≤ x_i ≤ +1
X_1= C = Cement (C_3S=62.0, C_3A=8.4%, Sp.s.=290 m^2/kg), kg/m^3	250	280	310	x_1 =(X_1-280)/30
X_2 = CA/S - crushed aggeregate (4.75-19 mm) and sand ratio	1.98	2.23	2.48	x_2 =(X_2-2.28)/0.25
X_3= A - Admixture (D-G type, synthetic polymer suspension), kg/m^3	0.42	0.56	0.7	x_3 =(X_3-0.56)/0.14
X_4 = F - Filler (dolomite, Sp.s=190 m^2/kg), kg/m^3	10	50	60	x_4 =[(X_4-10)/40]$^{3.11}$ -1

The method to estimate structure-formation parameters has been based on well known fact that changes in relaxation times of protons and amplitudes on NMR-spectrograms characterize the process of cement hydration. Cumulative curves obtained upon integrating the spectrograms give additional index, integrated NMR-signal, that has proved to be proportional to amount of free moisture in hardening system (correlation coefficient being 0.99).

The spectrograms for the fixed times of hardening (from 0 to 504 h) were taken with CORESPES spectrometer. Diameter of cuvette to be sealed and placed between electromagnets being restricted to 20 mm, so crushed aggregate was removed from technological mixture (x_2 not included into corresponding models). At the same hours the amounts of chemically bound water were also determined.

Models for concrete strength R_{28}

The analysis of composition influence on concrete mix and concrete quality indices after 28 days has been carried out on adequate models with significant estimates (at 10% risk) of their coefficients. Got for R_{28} has been model [1].

$$R_{28} = 24.7 + 4.3x_1 - 0.7x_2 + 1.9x_2^2 + 1.6x_1x_2 + 1.2x_2x_3 + 0.8x_2x_4 + 0.7x_3x_4 \quad [1]$$

This ESM describes, with error of 1.0 MPa, "composition - strength" field (Voznesensky and Lyashenko, 1989) that has following parameters: $R_{28.max}$ = 34.4 (at C/W=1.55, CA/S=2.48, A=0.7, F=60), $R_{28.min}$ = 18.1 (at C/W=1.25, CA/S=2.30, A=0.42, F=60), ΔR_{28}=16.3 MPa, K_R=($R_{max}/R_{min})_{28}$ = 190%. Three-factor ESM [2] describes the composition field of strength without considering x_2 (CA-S ratio).

$$R'_{28} = 25.2 + 4.3x_1 + 1.1x_4^2 + 1.4x_1x_4 + 0.8x_3x_4 \quad [2]$$

Its error of 1.45 MPa including disregarded influence of large-size aggregate is naturally greater than that of [1]; coordinates of extrema ($R'_{28.max}$ =32.8, $R'_{28.min}$=19.8) also shift. Such models, however, are necessary in simultaneous analysis with the models for structure formation parameters of cement composites, determined by NMR. Solved with ESM of type [1] for each property has been the complex of engineering problem (Voznesensky et al, 1989). Effect of each ingredient of composition on service and structural characteristics has been analyzed on one-factor curves passing through extremum points. Shown in Fig 1 are such functions of factor influence on R_{28} (fine lines) and R'_{28} (thick lines).

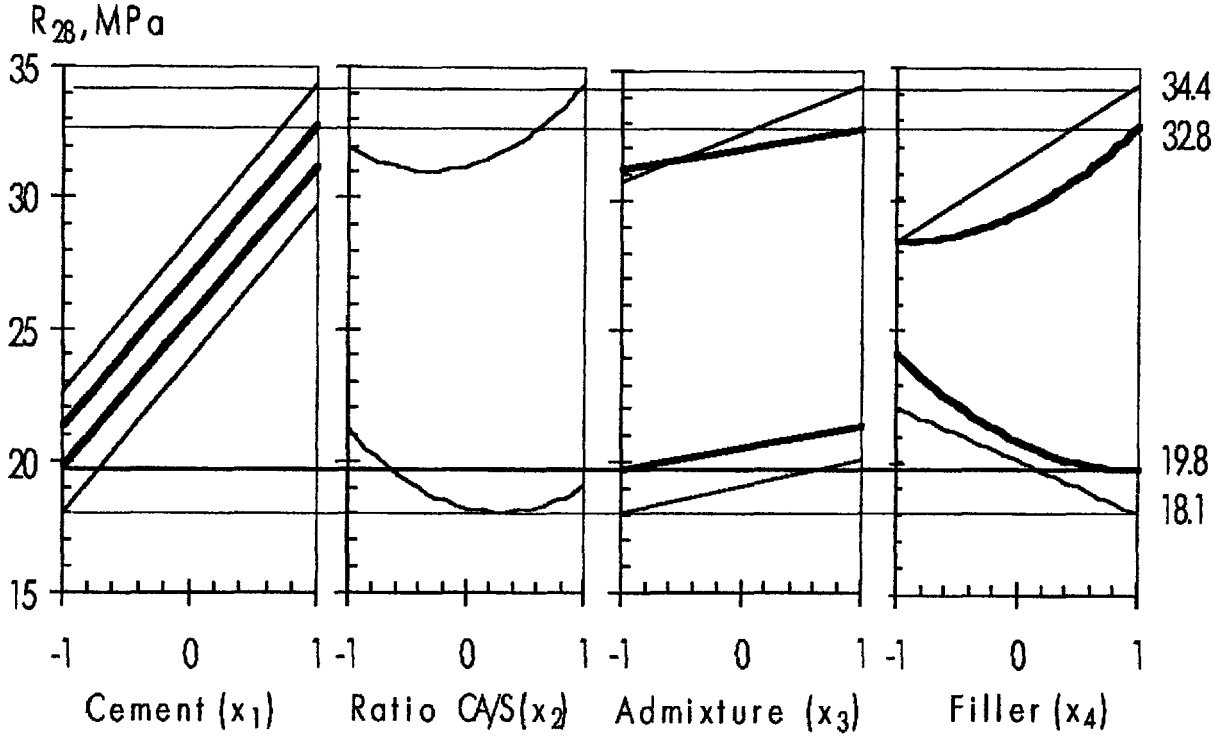

Figure 1 One-factor models of the influence of composition ingredients on concrete strength R_{28} at zones of its maximum and minimum.

There is no need to comment the effect of C (x_1), identical to that of C/W with W=const. The influence of polymer-containing additive is positive in extremum zones.

Non-trivial is the fact of ambiguous effect of filler. If the composite was prepared with increased dosages of cement and admixture (the region of $R_{28.max}$), then raising filler concentration from 3 to 20% would increase composite strength. But the same variation in composition would cause the strength to decrease, if composite contained little admixture and cement (i.e., at high W/C).

ANALYSIS AND USE OF NMR-RESULTS

Estimation of moisture state of cement composite over first month of hardening by parameters determined with NMR

Moisture content U has been estimated on the base of its linear relation with integrated NMR-signal (automatically got from cumulative curves after integrating NMR-spectrograms). Initial content of moisture U_0, i.e., free water amount (g/kg.dried) was determined in fresh mixture ($\tau = 0$ hardening days).

During hardening for $\tau > 0$ days the quantity of moisture goes down to U_τ (Fig 2, plots corresponding to averaged values for 18 compositions). The difference $\Delta U_\tau = U_0 - U_\tau$ characterizes the outflow of free moisture from "heavy" water films onto arising hard surfaces of gel and capillary components of developing structure of cement paste. Part of physically bound water switches to higher energy level of interaction with material. NMR-parameters reflect sufficiently well the variations of pore radii from 20 to 2000 A° as cement stone structure develops (Halperin et al, 1994).

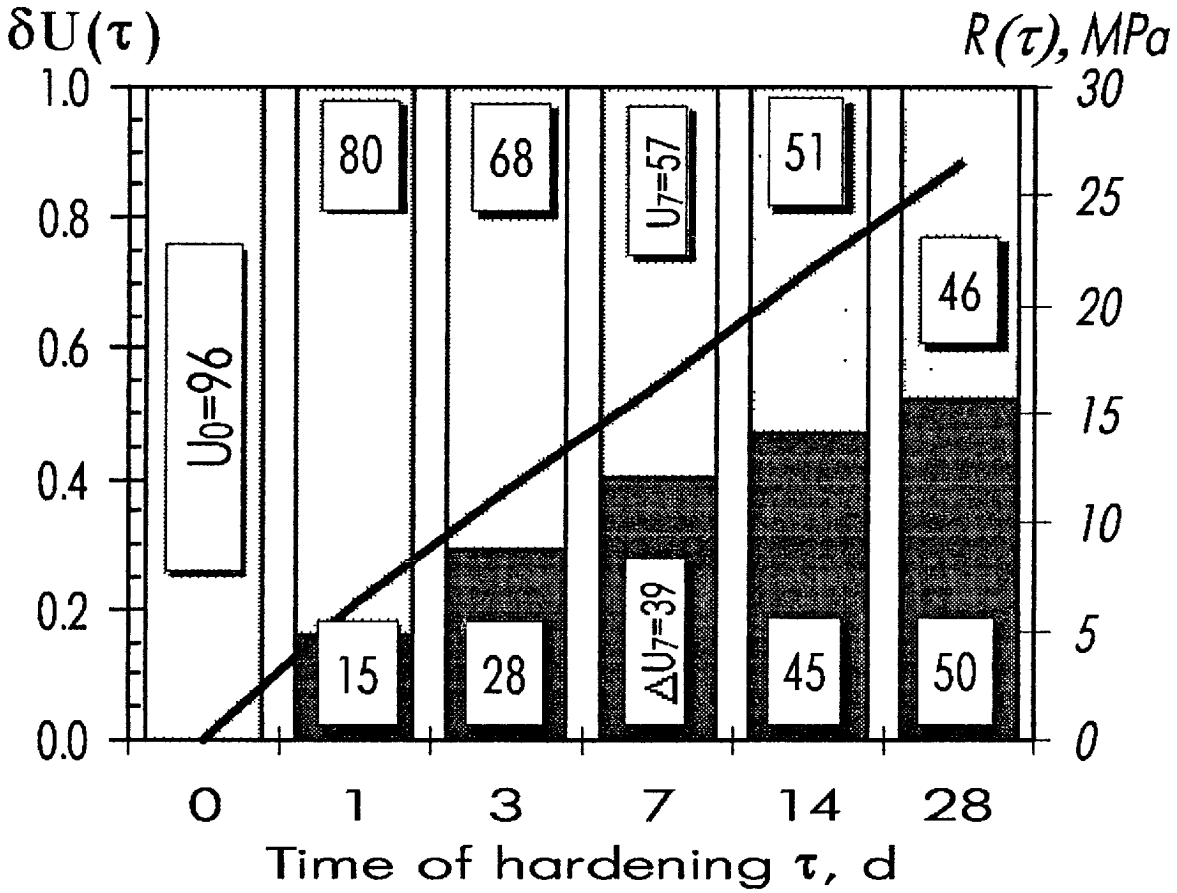

Figure 2 Variations of parameters determined by NMR and cement composite strength during 28 days of hardening.

For each of 18 concretes at age of τ = 1, 3, 7, 14, and 28 days compression strength R_τ was determined. For corresponding composites (with X_2=0) obtained from NMR-analysis was the information on time parameters U_τ characterizing moisture content:

- in colloidal structure, of low energy level of bond - $U_{1(3,7,14,28)}$,
- in capillary-pore structure, of high energy level of bond - $\Delta U_{1(3,7,14,28)}$.

The level and forms of moisture content define structure formation in hardening cement composite to a large degree (Shtakelberg and Sychev, 1990). Increasing of moisture content of capillary-pore structure in hardening cement composite, $\Delta U(\tau)$, proportional to decreasing of $U(\tau)$, proceeds similarly to a rise of strength, as can be seen in Fig 2.

Relation between varying content of moisture and growing strength of hardening composite

Similarity of $\Delta U(\tau)$ and $R(\tau)$ processes leads reasonably to linear relation between ΔU and R at any fixed time $1 \leq \tau \leq 28$. For all composites, irrelative to their compositions, model [3] has been calculated, that, with correlation coefficient 0.86 confirming linearity hypothesis at risk less then 0.1, has the error of 4.0 MPa. Linear relations of $\Delta U(\tau)$ and $R(\tau)$ for each of 18 composites studied are more deterministic (Fig 3), coefficients of correlation for the most part are over 0.98.

$$R(\tau) = k_0 + k_1 \Delta U(\tau) = -1.16 + 0.504\, \Delta U(\tau) \qquad [3]$$

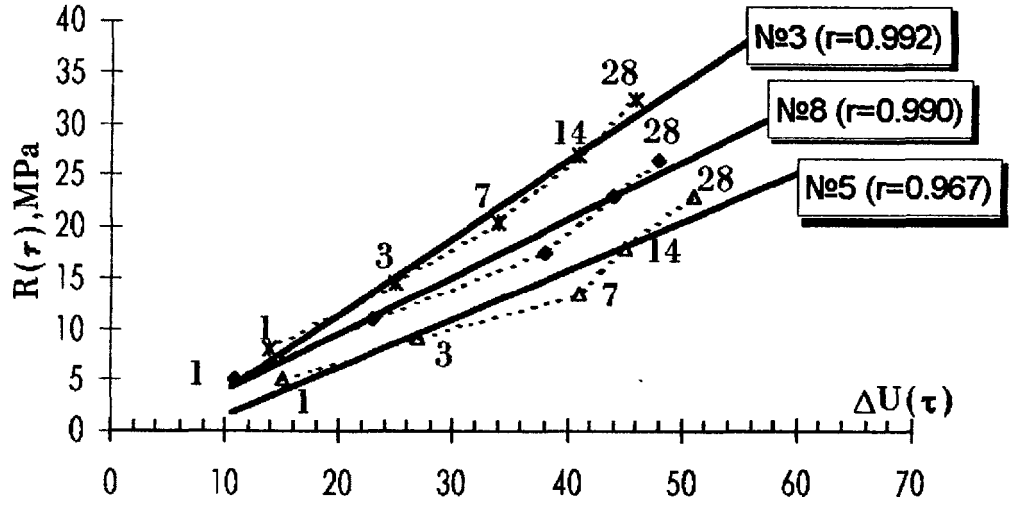

Figure 3 Linear relations of strength R(τ) and moisture content ΔU(τ) in hardening concretes (numbers of days indicated alongside labels).

Numeric estimates of coefficients in these models depend on concrete composition (as seen in Fig 3), that is, k_0 and k_1 are functions of factors C, A, F. The models $k_0(x_1, x_3, x_4)$ and $k_1(x_1, x_3, x_4)$ make it possible to analyze the influence of composition factors on parameters of structure formation process determined with NMR. Yet analysis has shown that ESM for other variables, following from [3], are more convenient for technological interpretation.

Effects of composition factors on structure formation parameters defined through NMR-analysis

The complex of ESM of type [3] describing relationship of R(τ) to ΔU(τ) for 18 composites (their compositions varied to optimal design) allows a number of non-trivial technological problems to be solved with the aid of computational experiments.

Problem 1 - about effects of amounts of cement, admixture, and filler on strength of hardening composites with equal content of moisture in capillary-pore structure.

It is too complicated to provide given level of moisture content at high energy level, determined with NMR, for each of 18 composites in real, physical experiment. It is rather simple (Voznesensky et al, 1989) to solve the problem through computational experiment with statistical models (with reasonable risk defined by non-adequacy errors of the models).

Fig 4 illustrates the way by which 18 "experimental" values of strength of capillary-pore structure, R{ΔU = 50} MPa, for 18 cement composites of equal structure-moisture level ΔU = 50 g/kg.dried (achieved clearly during different time of hardening - see Fig 3) has been determined.

On these results model [4] has been built describing the influence of composition factors on strength R{ΔU = 50}, for 18 cement composites of equal structure-moisture level ΔU = 50, with error of 2 MPa.

$$R\{\Delta U=50\} = 22.6 + 3.8x_1 - 1.2x_3 - 2.6x_3^2 + 5.7x_4^2 + 1.4x_1x_3 + 1.7x_1x_4 + 2.4x_3x_4 \qquad [4]$$

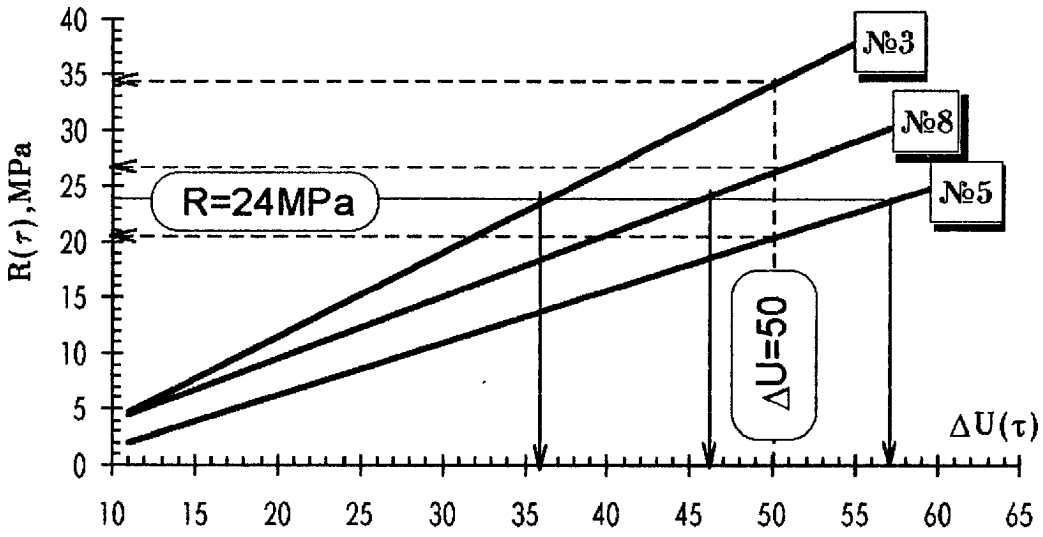

Figure 4 Determination of moisture content $\Delta U(\tau)$ in equally strong concretes (continuous lines) and strength $R(\tau)$ of concretes with equal content of moisture (dash lines).

One-factor models passing through extremal points of this ESM are shown in Fig 5. Upper curves relate to composite with high amounts of cement and filler and optimal concentration of admixture (A=0.56 kg/m^3), whereas lower curves correspond to composite of low content of cement and admixture with introducing great quantity of filler (about 18% of cement mass).

Variations in cement dosage for both composites have practically the same effect on $R\{\Delta U=50\}$; corresponding plots in Fig 1 demonstrate full analogy. Similarity is not observed, however, when comparing effects of filler on $R\{\Delta U=50\}$ and R_{28} at extremal points of Eq 4.

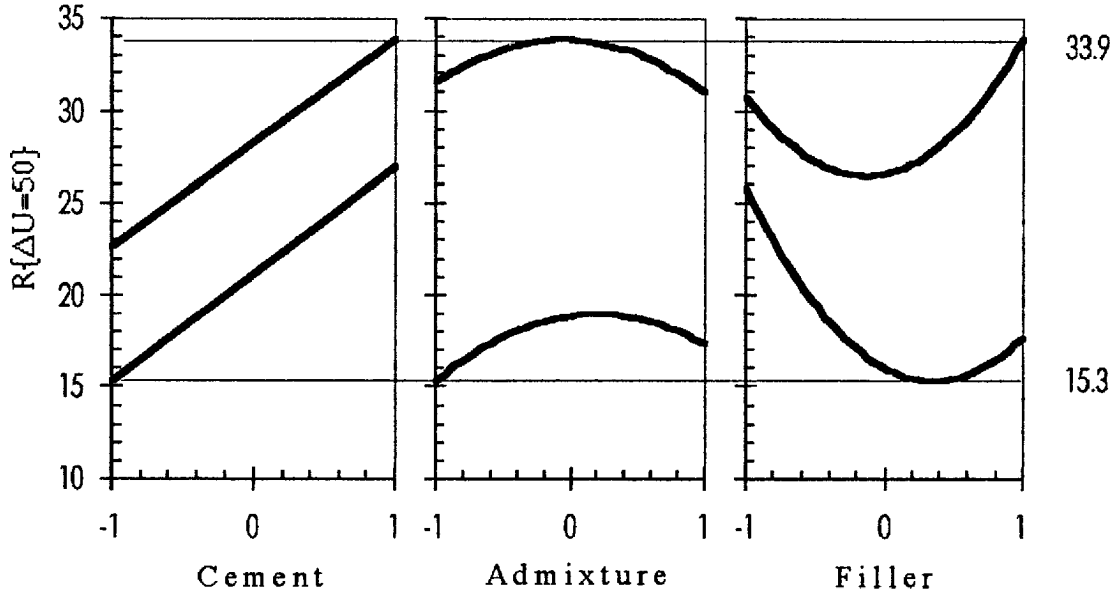

Figure 5 One-factor models of component effects on composite strength in maximum and minimum areas under condition of equal content of moisture.

In composites with increased cement content small concentrations of filler merely augment the quantity of non energy-saturated ("parasite") contacts of solid elements in hardening system, the strength of which falls. As concentration increases this negative effect might be overridden by growing "cramped conditions" (Sychev, 1974) of cement hydration, that would give rise to composite strength by 10% (when moving from -1 to +1). Negative effect of filler "parasite contacts" prevail in composites with low content of cement, for its volume concentration is almost 20% less than in the fist case. As a result the strength reduces by 33%.

Problem 2 is about composition factors influence on moisture content in capillary-pore structure, $\Delta U\{R = 24\}$, for composites of equal compression strength (24 MPa).

Initial information is got analogously to problem 1, as shown by continuous lines in Fig 4. It is logical to assume that variables $\Delta U\{R=const\}$ and $R\{\Delta U=const\}$ are inversely proportional. Three-factor ESM [5] describes (with 6% error) the influence of C, A, and F on this structure formation parameter.

$$\Delta U\{R=24\} = 51.7 - 6.4x_1 + 2.4x_3 + 2.8x_1^2 + 3.6x_3^2 - 9.4x_4^2 - 2.3x_1x_3 - 2.3x_1x_4 - 3.8x_3x_4 \qquad [5]$$

One-factor models passing through extremal points of Eq 5 are presented in Fig 6. In contrast to Fig 5 upper curves correspond to low-cement composites with increased content of filler. Lower row of curves characterizes compositions with large amount of cement , A and F at low levels.

For 5 curves the hypothesis of $\Delta U\{R=const\}$ and $R\{\Delta U=const\}$ being in inverse proportion may be accepted. Yet for composites with high level of C different phenomenon comes to light. With increasing concentrations of polymer-containing admixture far greater part of physically bound water must switch to upper energy level to provide equal strength of composites.

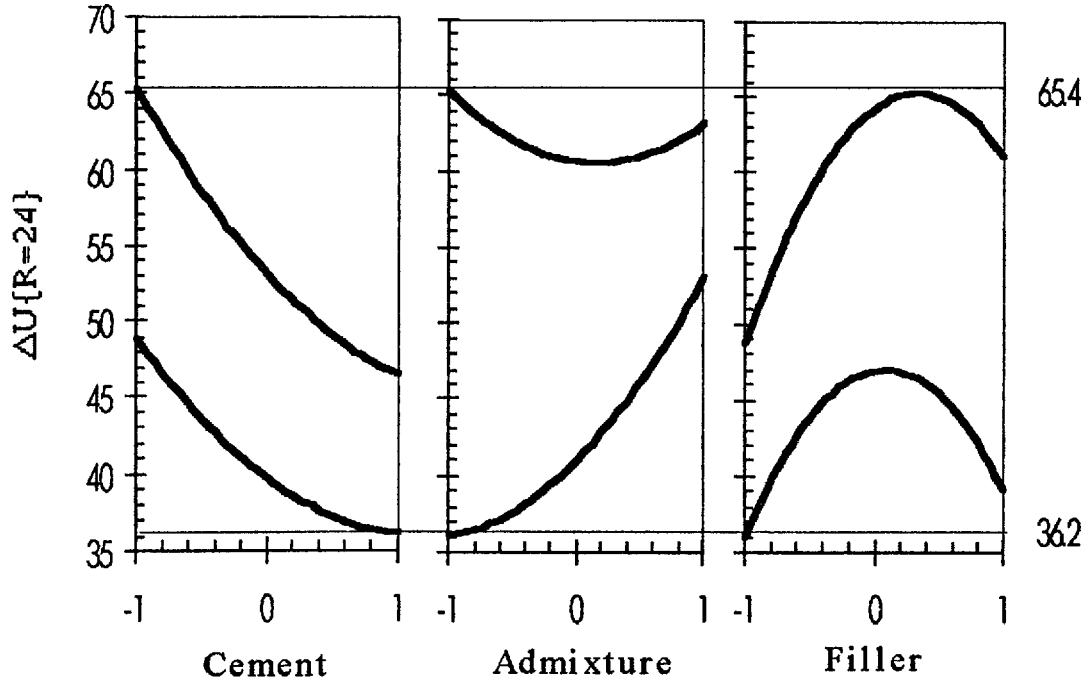

Figure 6 One-factor models of ingredient effects on moisture content ΔU of equally strong concretes (R=24 MPa) in maximum and minimum regions.

Using the results of NMR-analysis of young cement composites to predict concrete strength at age of 28 days

Comparison of various ways of building the models for predicting R_{28} has shown that it is reasonable to include into these models the normalized arguments, $-1 \leq w \leq 1$, comprising determined with NMR parameters of cement composites over 1-3 days of hardening. From the "fan" of models obtained ESM [6], in particular, might be considered sufficiently useful (prediction error about 18%).

$$R_{28}(w_1,w_3,w_{10}) = 26.0 + 11.9\, w_3 - 4.0\, w_{10} + 3.2\, w_1^2 + 3.4\, w_3^2 + 3.1\, w_1 w_{10} + 3.4\, w_3 w_{10} \qquad [6]$$

Eq 6 accounts for initial content of moisture, $w_1 = (U_0 - 112)/34$, moisture content of capillary-pore structure after 1-day hardening, $w_3 = (\Delta U_1 - 19)/9$, and moisture transformed to this high energy level between 1st and 3rd days, $w_{10} = [(\Delta U_3 - \Delta U_1) - 12]/4$.

If in addition to NMR results the information on chemically bound water could be incorporated in models of type [6], then prediction error for R_{28} would reduce approximately 20%. The error might be sharply decreased if technologist was assured of accurate dosage of all components (but water). In this case taking account of CA, S, D, and F amounts in conjunction with express physic-chemical data makes it possible to predict R_{28} with accuracy not worse than that on results of concrete compression tests, $R_1,\ldots, R_3$.

CONCLUSION

Optimal design of experiment offers substantial savings in resources when studying cement composites (especially with application of complex physic-chemical methods). Experimental-statistical models therewith allow most fully engineering information to be derived from experimental data.

It has been found on the base of ESM that polymer-containing admixture and the filler, modifying the character of structure formation (changing properties of thin film water, setting "cramped" conditions of hydration, increasing a number of parasite micro-contacts, etc.), affect ambiguously on composite quality indices.

Moisture content parameters of hardening concrete have been determined and the influence of composition factors on them estimated with the help of NMR. This has made possible to build multi-factor models for predicting 28 days concrete strength (with 15% error) on results of NMR-analysis of 1-3 days cement composites.

REFERENCES

Halperin, W.P., Jehna Jyh-Yuar and Song Yi-Qiao, "Application of Spin-Spin Relaxation to Measurement of Surface Area and Pore Size Distributions in a Hydrating Cement Paste", Magnetic Resonance Imaging, Vol. 12, No 2, 1994, pp. 169-173.

Shtakelberg, D.I. and Sychov M.M., Self-Organization in Dispersed Systems, (in Russian), Riga, Zinatne, 1990, 175 pp.

Sychov M.M., Hardening of Binder Systems, (in Russian), Moscow, Stroiizdat, 1974, 79 pp.

Voznesensky, V.A. and Lyashenko, T.V., "Modeling, analysis and optimization of brittle matrix composites properties fields", Brittle Matrix Composites 4 : Proc. IV Int. Symp. BMC 4, Eds. A.M. Brandt, V.C. Li and I.H. Marshall, Woodhead Publ. Ltd., 1994, pp. 255-263.

Voznesensky, V.A., Lyashenko, T.V., Ivanov Ya.P. and Nikolov I.I., Computers and Optimization of Composites Materials, (in Russian), Kiev, Budivelnick, 1989, 240 pp.

COOLING OF LIQUID CALCIUM ALUMINATES MONITORED BY ^{27}Al NMR TIME RESOLVED EXPERIMENT

B. TOUZO, D. MASSIOT, D. TRUMEAU, A. DOUY and J.P. COUTURES
CRPHT / CNRS, 1D, Av. de la Recherche Scientifique, 45071 ORLEANS CEDEX 2 FRANCE

ABSTRACT The free cooling of aerodynamically levitated liquid calcium aluminates droplets has been monitored by time-resolved ^{27}Al NMR. The results allow characterisation the structure and dynamics of these liquids from 2400K via the supercooled state, and to observe crystallisation. For liquid CA, the NMR relaxation time and the macroscopic shear viscosity appear to be related to the same microscopic fluctuations. Liquid CA_6 behaves as predicted by the phase diagram, and allows us to propose incongruent fusion for CA_2.

Key-words: Calcium aluminates, Nuclear magnetic resonance, cooling, melt

INTRODUCTION

Nuclear Magnetic Resonance of ^{27}Al is well known to provide characterisation of the local environment of aluminium in the solid state. As previously shown (Coutures, 1990, Massiot, 1995) it is still sensitive at very high temperature in the liquid phase. It is thus possible to characterise the average structure as well as the the dynamics of the liquids from chemical shift and relaxation time measurement. Furthermore, as ^{27}Al spectra can be obtained in one scan and as relaxation times are short, the evolution of the NMR parameters can be followed in real time even for fast dynamical process like quenching. In the experimental design used in this study an aerolevitated sample placed inside the NMR probe is heated by lasers (Massiot, 1995). When the laser heating is stopped, the sample cools freely, and NMR spectra can simultaneously be recorded. We report here some of the results obtained for the CaO-Al_2O_3 binary system.

EXPERIMENTAL

The experimental design for NMR measurements is described in **Fig 1**. A spherical sample (2 mm ∅) of calcium aluminate is placed in a convergent-divergent nozzle in which it levitates on an adjustable air jet. The whole is placed in the RF-coil of a vertical NMR probe. The sample is heated from the top and the bottom of the cryomagnet by two continuous wave CO_2 lasers. The levitation regime is checked by video and the infra red emission ($\lambda = 0.85$ µm) of the sample is monitored via an optical fiber and externally calibrated for temperature. With this setup temperatures above 2400 K can be reached . ^{27}Al NMR spectra of liquid calcium aluminates can be obtained in only one scan and show a single narrow line (80-100 Hz). As measured in previous works (Massiot, 1995, Touzo 1995), the spin system undergoes an extreme narrowing regime (high temperature), where $T_1 = T_2 \approx 4$ ms at 2400 K. These conditions make it possible to follow in real time, by ^{27}Al NMR, the cooling of the sample. When the lasers are shut down, the sample cools freely to room temperature. Simultaneously ^{27}Al NMR spectra and IR emission are recorded every 50 ms. Triggering of the recording is set one second before the interruption of the laser heating to check the high temperature steady state. In these experimental conditions, only the liquid part of the sample leads to a significant signal.

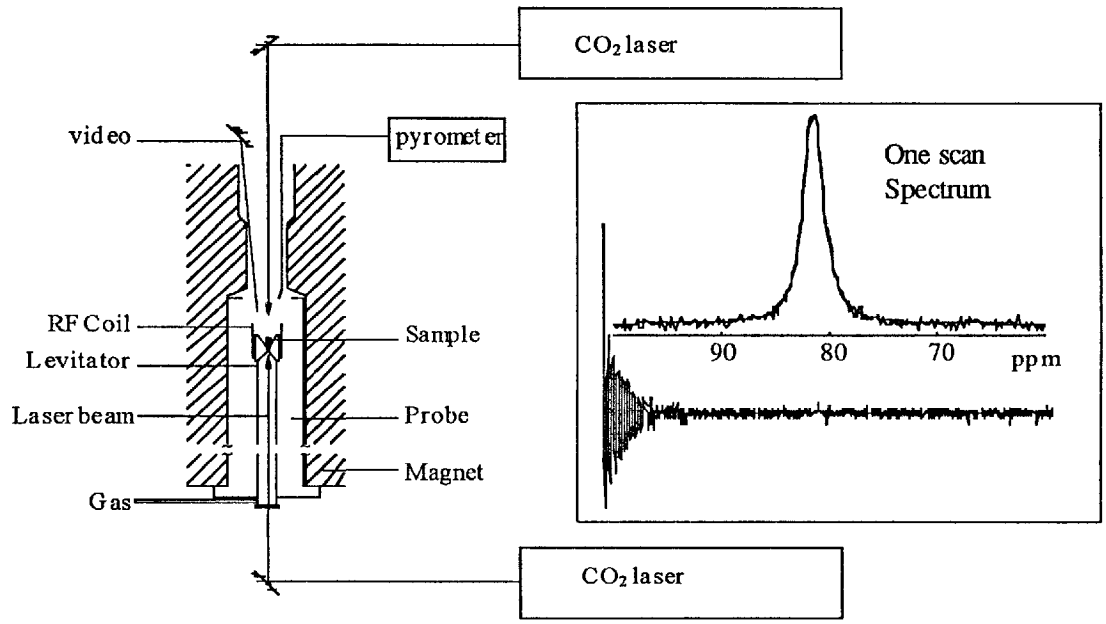

Figure 1: Schematic drawing of the high temperature experimental setting with double laser irradiation of an aerodynamic levitated sample. Inset : One scan ^{27}Al spectrum of liquid C_3A (adapted from Massiot, 1995)

RESULTS AND DISCUSSION

Liquid compositions ranging from 0 to 84 mol% CaO have been observed. there was no weight change of the sample during the experiments. Results obtained for the composition CA_6 are shown in **Fig 2** as an example. Before laser shut down, temperature, chemical shift (δ), full width at half maximum ($\nu_{1/2}$) as well as magnetisation (M) are constant, show the stability of the system. Then liquid behaviour is monitored over a range of ~700 K (2400-1700K) down to supercooled liquid. The magnetisation increases with decreasing temperature according to Curie's law, proving that we observe all the ^{27}Al spins of the sample. When the sample crystallises, the temperature increases sharply and the magnetisation drops. This recalescence (Coutures, 1994) can be observed by ^{27}Al NMR of the residual liquid in favourable cases. When the amount of liquid phase decreases, the signal-to-noise ratio decreases and the results obtained from fitting the spectra scatter. In these experimental conditions (absence of heterogenous nucleation, 200 $K.s^{-1}$ cooling rate), liquid calcium aluminates in the composition range 40-75 %mol CaO can vitrify. For those compositions, a smooth continuous evolution is observed for all the NMR parameters from liquid to the supercooled state.

Liquid calcium aluminates

At 2400 K, δ is a linear function of the composition and takes values from 58 ppm for Al_2O_3 to 85 ppm for the 84%mol CaO composition. This has been interpreted as an increase of the average Al coordination number with increasing Al_2O_3 content, in agreement with MD computations (Poe, 1994). Those liquids were proposed to consist of AlO_4, AlO_5 and AlO_6 polyhedra with rapid exchanges between different configurations. This has been partly confirmed from a glass of $C_{40}A_{60}$ composition in which ^{27}Al MQ-MAS spectrum clearly evidences the existence of AlO_4 and AlO_5 species (Massiot, 1996).

As δ and T are measured at the same instant, we can observe the thermal dependance of the chemical shift, δ, versus temperature. For all compositions of the $CaO-Al_2O_3$ binary system, we observe a linear correlation: dδ/dT depends on the liquid composition and has been related to structural evolution in the liquid. Al_2O_3 (dδ/dT = +2 ppm/1000K) is expected to undergo only small structual change with temperature (Florian, 1995), while CA (-4.6 ppm/1000K) shows the strongest evolution. The latter is estimated to be +0.2 increase in coordination number per 1000K (Massiot 1995). It is also worth noting that all liquids having a slope less than -2 ppm per 1000K vitrify ; chemically, this corresponds to compositions around CA (Touzo, 1995).

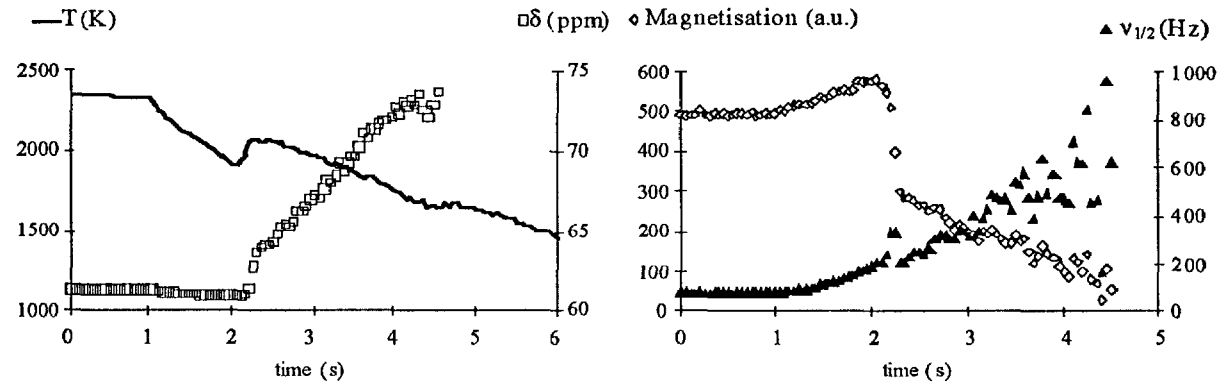

Figure 2 : Time resolved experiment for the CA_6 composition liquid

As these liquid are in extreme narrowing regime, the relaxation times T_1 and T_2 are equal and linked to the line width $\nu_{1/2}$ by the relation $T_1 = T_2 = 1/(\pi.\nu_{1/2})$. Linewidths then give access to the dynamics of these liquids during cooling. Quadrupolar interaction is the dominant interaction when observing ^{27}Al in solid state. A most sensible hypothesis is then that relaxation is induced by the fluctuations of this interaction and we can estimate a correlation time, τ_C, for atomic movements in the liquid, which are the origin of the NMR relaxation. In a similar way it is also possible to compute a correlation time τ_S for the shear viscosity from the Maxwell equation (Dingwell, 1990): τ_C and τ_S computed from the viscosity measurement made by Urbain (1983) are shown in **fig. 3**. The two sets of fully independent data are remarkably similar ; they both have the same magnitude and temperature dependance. Furthermore, the NMR data acquired in the supercooled liquid state follow the extrapolated curved proposed by Urbain. We thus consider that both ^{27}Al relaxation and viscous flow have the same microscopic origin, in the interconversion of AlO_4, AlO_5 and AlO_6 species (Massiot, 1995).

Crystallisation of CA_6

As mentioned above, crystallisation can be observed as long as liquid remains in the sample and its viscosity is not too high. This is the case for the CA_6 composition (**fig 2**). According to the phase diagram (Nurse, 1965), CA_6 presents a peritectic solidification. The evolution of the measured NMR data are very different from that observed for the congruent solidification of Al_2O_3 (Florian, 1995). In the case of CA_6, ^{27}Al NMR spectra shows an evolution in two steps : there is first a rapid change within 250 ms with a 48% magnetisation loss, i.e. 48% of the aluminium atoms go into the solid phase. By this time δ increases from 61 to 63.8 ppm and the

temperature goes up (recalescence). Then the temperature starts to decrease again, while M and δ shows continuous evolution until the signal disappears. The chemical shift evolution is large compared to that observed for liquids with temperature, and implies a chemical modification. Comparison of the δ value after the sharp increase to the values obtained for liquid calcium aluminate at constant temperature leads to the composition of $C_{24}A_{76}$ (Touzo, 1996). A similar composition can be computed by considering the magnetisation loss and assuming that

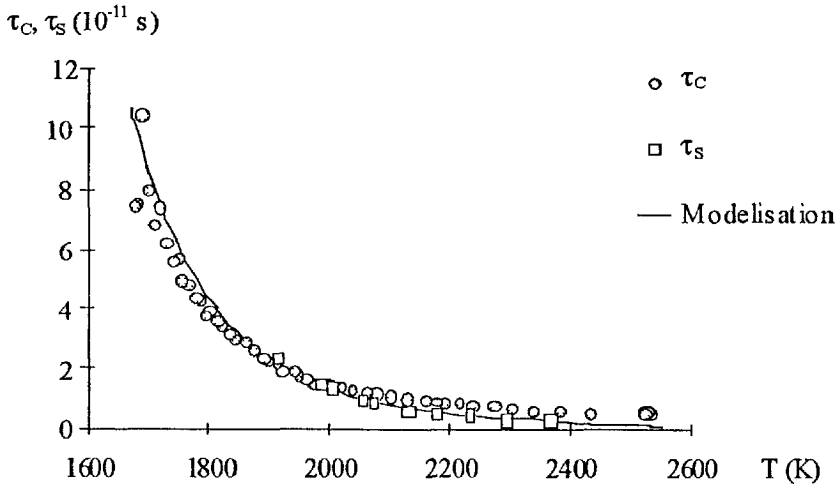

Figure 3 : Evolution of the correlation times τ_C (NMR) and τ_S (shear vicosity) and modelisation (Urbain, 1983) with temperature.

aluminium oxide first crystallises. This is in argreement with the peritectic solidification of CA_6 as described by the phase diagram of the $CaO-Al_2O_3$ binary system, where liquid CA_6 first transforms to solid Al_2O_3 + Liquid. After the rapid evolution step, the chemical shift increases rapidly and continuously, again evidencing a change of the chemical composition of the remaining liquid, while the magnetisation decreases. The chemical shift continues to increase far beyond the values for CA_2 (67.3 ppm). In these conditions, CA_2 appears to melt incongruently, in agreement with the experimental determination proposed by Nurse *et al.* (1965).

REFERENCES

Coutures, J.P., Massiot, D., Bessada, C., Echegut, P., Rifflet, J.C., Taulelle, F., C. R. Acad Sci., Vol. 310, 1990, pp. 1041-1045.

Coutures, J.P., Rifflet, J.C. Florian, P. Massiot, D., Rev. Int. Hautes Temp. Réfract., Fr., Vol. 29, 1994, pp. 123-142.

Dingwell, D.B., Webb, S.L., Eur. J. Mineral., Vol. 2, 1990, pp. 247

Florian, P., Massiot, D., Poe, B. T., Farnan, I., Coutures, J. P., Solid State NMR, Vol.5, 1995, pp. 233-288.

Massiot, D., Trumeau, D., Touzo, B., Farnan, I., Rifflet, J. C., Douy, A., Coutures, J. P., J. Phys. Chem. , Vol. 99, No 44, 1995, pp. 16455-16459.

Trumeau, D, Touzo B., Montouillout V., Farnan I. Coutures J.P. Massiot D., to be submitted to J. Phys. Chem.

Nurse, R.W., Welch, J.H., Majumdar, A.J., Trans. Br. Ceram. Soc., Vol. 64, 1965, pp. 409-418.

Poe, B.T., McMillan P.F., Coté, B., Massiot, D., Coutures, J.P., J. Am. Ceram. Soc., Vol. 77, No 7, 1994, pp 1832-1838.

Touzo, B., PhD Thesis, Orleans, France, December 20th 1995.

Touzo, B., Trumeau, D., Coutures, J.P., Massiot, D., 1996, to be submitted to J. Am. Chem. Soc.

Urbain, G, Rev. Int. Hautes Temp. Refract., Vol. 20, 1983, pp. 135-139.

3v006
7 pp

The Study on the Properties of High Performance Concrete Paste by Using NMR

Chao L. HWANG, National Taiwan Institute of Technology, Taipei, Taiwan, R.O.C..
Ping K. CHANG, Private Van Nung Institute of Technology, Jungli, Taiwan, R.O.C..

ABSTRACT In this study, solid ^{29}Si-NMR and compressive test were used to analyze macro and micro structure properties and hydration models of high performance concrete (HPC) paste. Test results showed that the replacement of fly ash for cement made the polysilicate forming reaction prominent. The decrement of cement affected the packing density and hence diminished the early strength. In addition, the contribution of fly ash to the ultimate strength of HPC is also acknowledged.
Key Words : NMR, Hydration Model, HPC, Pozzolanic Reaction, Fly Ash

PREFACE

The ingredient of High Performance Concrete (HPC) is same as the traditional concrete, but their design algorithms have some difference (Hwang, 1994). Hydration mechanism of traditional concrete has been explained through heat evolution, setting time, penetrative resistance, pulse velocity, compressive strength, X-ray defraction analysis and micrograph observation (Mindess, et al, 1981). NMR, an advanced method, will be helpful to understand the characteristics of HPC hydration behavior to discuss macroscopic correlation of paste hydration with help of the aforementioned traditional measuring techniques.

HYDRATION BEHAVIOR

In ^{29}Si-NMR (spectrogram), the chemical shifts of Trialcium silicate clinker and its hydrate C-S-H gel were Q^0 (-70 ppm), Q^1 (-80 ppm) and Q^2 (-87 ppm) (Lipma, et al., 1980). Due to the increment of signal (peak) intensity, the hydration mode of paste might be obtained. NMR has an advantage for the analysis of amorphous (noncrystal) components in the specimen, and this is good for C-S-H product analysis (Pietersen, et al., 1992).

TEST METHOD

Fly ash content and age were adopted as hydration parameter in this research. Test material such as local class F fly ash and type I OPC were used to make various paste specimens with W/B = 0.35. Upon completion of compressive test, the representative specimens were taken

for the performance of ^{29}Si-NMR NMR test (Bruker MSL 200 HMz). The condition, data and method of spectrogram test were shown in the literatures (Hwang, et al., 1994).

RATE OF HYDRATION

The hydration rate of paste has inverse proportion to the degree of hydration (doh). While the doh is lower, the hydration rate is quite fast. The initial hydrolysis has an extremely fast reaction. As the doh is more complete, the hydration rate nearly stops (Justnes, et al. 1990). The initial hydrolysis is a fast but unbalanced "chemical reaction", and later it is converted to "diffusive reaction" as hydration mechanism, so it is possible to apply "diffusion" formula for calculating the reaction rate of paste after the first day as follows:

$$\dot{\alpha} = d\,\alpha/dt = \alpha\, e^{-Q/RT} \quad \text{---------- [1]}$$

In this formula [1], Q is activation energy and is a constant for certain cement material. R is also a constant, and T is an absolute temperature. Therefore, $\alpha\, e^{-Q/RT}$ on the right side of formula [1] is a fixed value and has a right ratio to α^{-n}, i.e., formula [1] may be changed into formula [2], and k and n are coefficients.

$$\dot{\alpha} = d\,\alpha/dt = k\,\alpha^{-n} \quad \text{---------- [2]}$$

$$\text{i.e. } \alpha^{n} d\,\alpha = k dt \quad \text{----------[3]}$$

$$(\alpha_1^{n+1} - \alpha_0^{n+1}) / n+1 = k\,(t_1 - t_0) \text{ Integral may obtain} \quad \text{----------[4]}$$

The relationship for doh (α) and age (t) can be obtained from ^{29}Si-NMR information. The relationship between C-S-H reaction rate ($\dot{\alpha}$) and doh (α) in the paste can be obtained from regression as shown in formula [5]. The result may be explained when calcium silicate contacts moisture, the surface immediately produces extreme contact reaction. Clinker in the solution appears irregular hydrated rather than a hydrated crystal, and such reaction is violent surface reaction. Exothermal hydration also appears extremely fast discharge. When Ca^{+2} ion in the solution has reached the maximum concentration, i.e. chemical-controlled acceleration reaction (Justnes, et al., 1990), hydration acceleration is converted to "diffusive control" upon reaching the peak. Because ion movement in the solution is limited, cement grains not hydrated is engaged in hydration in a solid, and hence hydration velocity decreases sharply. At an later and stable stage diffusive hydration becomes much slower, so the curve is nearly horizontal and the doh will be nearly zero after 50% attained. The above formula is mainly influenced by cement fineness and C_3S and fly ash content.

$$\dot{\alpha} = d\,\alpha/dt = 44.69 * 10^{-4.54e^{-2\alpha}} \quad [5]$$

HYDRATION MODEL

The doh (α) of paste, degree of pozzolanic reaction (α_p), polysilicate length (Psi) and compressive strength (fs) all have a right proportion to the age.

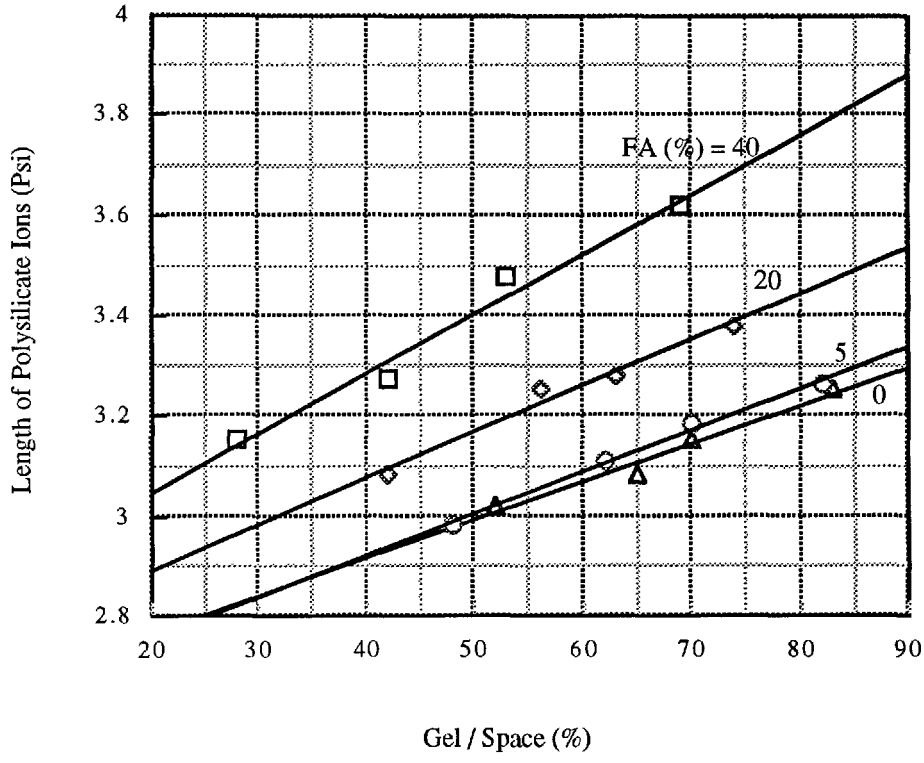

Figure 1 Relationship between the length of polysilicate ions and gel-space ratio of cement paste

Fig.1 shows there is a right proportion between polysilicate length (Psi) and gel-space ratio (G/S), i.e. in the paste the greater the silicon anion length is, the bigger the G/S will be; the higher the fly ash content is, the curve tends to move toward the left top. These explains that under same G/S, the more the fly ash content increases, the greater the polysilicate length will be. The fly ash is helpful to pozzolanic reaction , and while more fly ash is added, the reaction becomes more significant. It shows fly ash is good for long term strength and durability for HPC.

Under the same polysilicate legnth, G/S is reduced with the increase of fly ash content, i.e. under the same polysilicate length, the structure of pure paste is denser than the structue of paste added with fly ash. G/S means space gel packing density, and the higher the G/S

value is, the greater the polysilicate legnth will be. In other words, the addition of fly ash is helpful to have "pozzolanic reaction" which would br directly shown on silicon reaction.

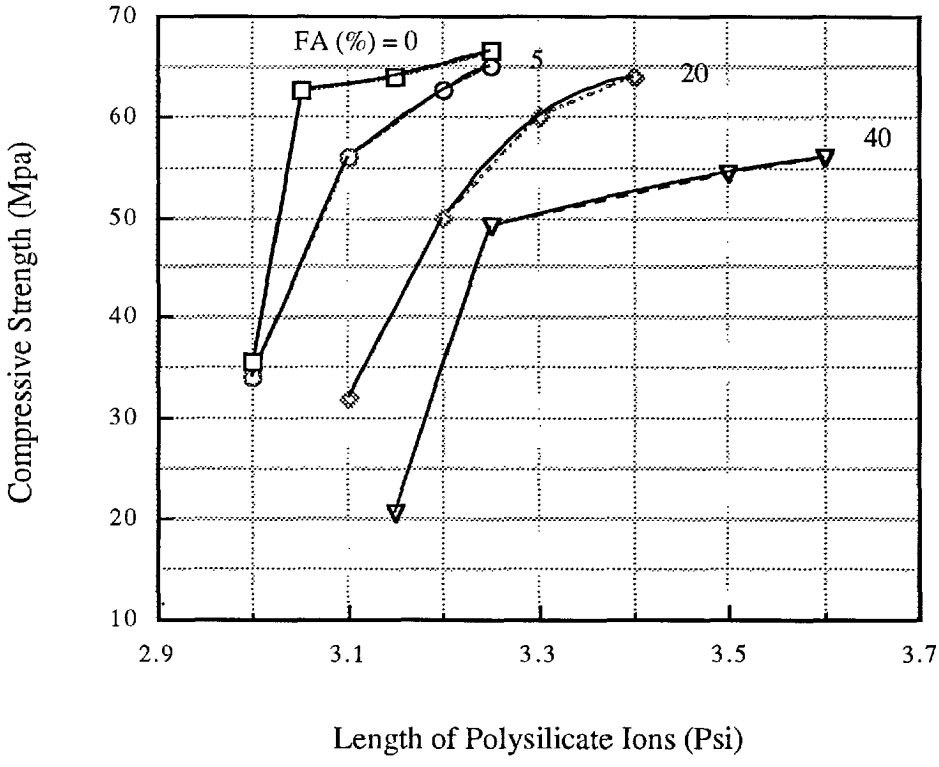

Figure 2 Relationship between the length of polysilicate anions and compressive strength of cement paste

When fly ash content is greater, the curve tends to move toward the right bottom. Silicate anion length of the paste with fly ash is greater than that of pure cement paste, because its stucture is looser, i.e. gel space is smaller as shown in Fig.1, and therefore the strength of paste with fly ash is less than that of pure cement paste. It is thus known the paste strength, except for polysilicate length, should depend on packing density of hydrant growth (i.e. G/S) and it may achieve better strength (γ^2>0.97). Fig. 2 shows the relationship between polysilicate length and strength. From the point of inflection, basically the higher the fly ash content is, the larger the strength in Fig.1 will be, and it is related to system C-S-H gel.

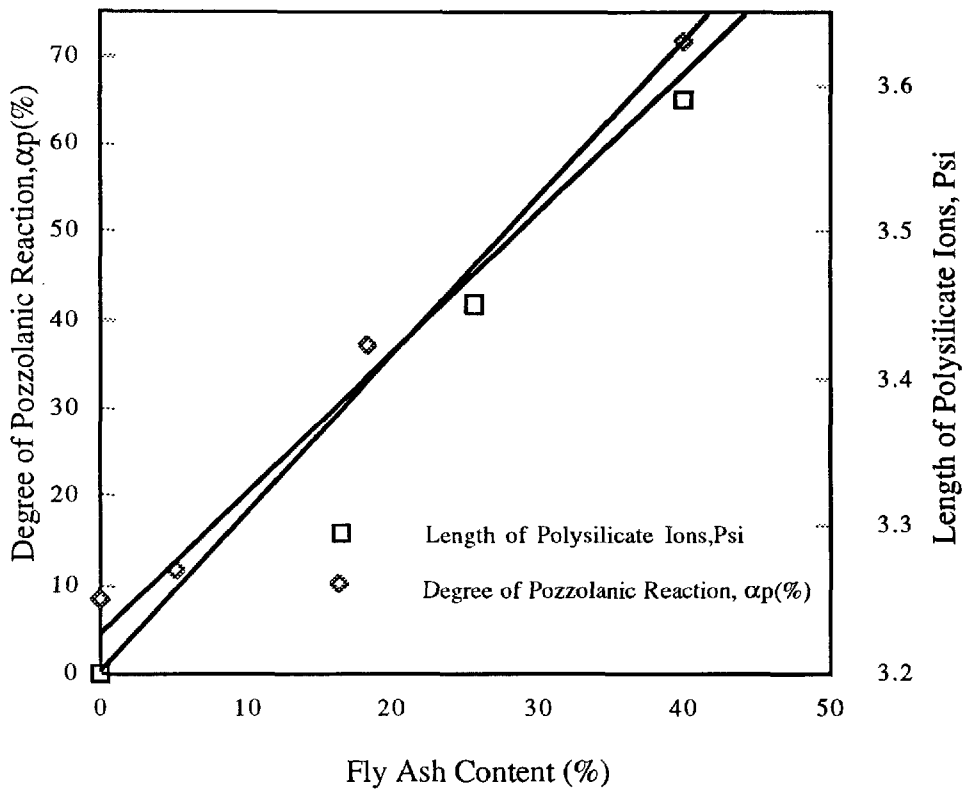

Figure 3 Relationship among the length of polysilicate anions, fly ash content and pozzolanic reaction of cement paste with age of 120 days.

Figure 3 shows the relationship among fly ash content, polyilicate length and pozzolanic reaction of the paste at the age of 120 days. It indicates while the fly ash content increases, the pozzolanic reaction (α_p) increases as well as the polyilicate length (Psi), i.e. pozzolanic reaction and polysilicate length have a right proportion to fly ash content. According to previous experiences, the excess of fly ash content is not good to hydration space density,. because the total volume of hydrated gel is reduced, so the strength will decrease accordingly. However, from physical and chemical viewpoint, proper fly ash content would promote cement strength efficiency to produce HPC (Malhotra, 1994). Figure 4 shows the relationship between pozzolanic reaction and doh of paste. According to ^{29}Si-NMR specter of pure cement paste and paste with 5% of fly ash, there is no fly ash peak, i.e. no pozzolanic reaction, so no corresponding curve appears, but only the relationship of paste with 20% and 40% of fly ash is shown. It also shows pozzolanic reaction has a right proportion to hydration because the hydration is necessary for cement to produce $Ca(OH_2)$ which enables fly ash to produce pozzolanic reaction. Therefore, the doh of paste is necessary for the degree of pozzolanic reaction. Accordig to the above result, it may indicate NMR is a good tool for the analysis of hydration reaction. Further, it implies in the HPC the paste has more

significant influence than the aggregate, but on the analysis it can not be ignored the reaction between the interface of paste and agregate is important for the long-term properties of HPC.

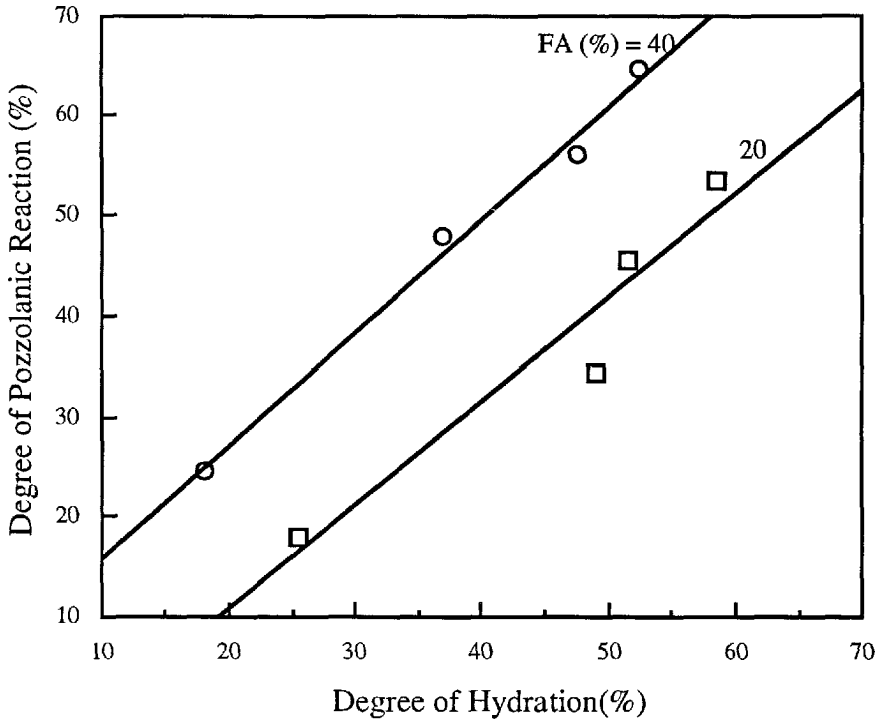

Figure 4 Relationship between the degree of pozzolanic reaction and hydration of cement paste

CONCLUSION

(1) NMR can give semi-quantative data to unhydrated cement content, C-S-H gel, doh polysilicate length and degree of pozzolanic reaction and to establish hydration model of paste in HPC through hydration rate analysis with various parameters.

(2) The doh for the paste is increasing in company with the increase of age and its polysilicate length has a right proportion to the age.

(3) At the same age, polysilicate length of fly ash paste is greater than that of pure cement paste, and pozzolanic reaction is larger, too. Polysilicate anion length has the right proportion to G/S. This gives positive effect to the boundary and may improve long-term strength of HPC with less paste.

ACKNOWLEDGMENT

We, all the authors give our deep thanks to Mr. Y. N. Sheen for assistance in data analysis.

REFERENCE

Hwang, C. L., "Material Selection and Properties of HPC-View from Kaoshiung 85-Story T&C Tower" Proceedings of Research, Development and Application of High Performance Concrete, Kaohsiung, 1994, pp. 83-124 .

Mindess, S. and Young, J. F., "Concrete" Prentice-Hall, Englewood Cliffs, N. J., 1981, pp.. 26-110.

Jackson, N., "Civil Engineering Materials," the MacMillan Press, London, 1985, pp.115-123.

Lipma, E., Magi, M., Samoson, A., Engelhardt, G. and Grimmer, A. R., "Structural Studies of Silicates by Solid-State High Resdution ^{29}Si Magic Angle Spinning NMR in Solid, " J. Amer. Chem. Soc., Vol. 120, 1980, pp. 2890-4893.

Pietersen, H. S., Kentgens,A. P. M., Nachetegaal, G. H., Veeman, W. S., Biuen, Nand J. M., "The Reaction Mechanism of Blended Cement: A ^{29}Si NMR Study," 1992 Istanbul Conference, ACI SP. 132-144, 1992, pp. 795-812.

Justnes, H., Meland, I., Bjorgum, J. O. and Krane, J., "A ^{29}Si NAS NMR Study of the Pozzolanic Acitivity of Condensed Silica Fume and the Hydration of Di-and Tricalcium Silicates," SINTEF FCB Report, Norway, 1990, pp.1-26.

Malhotra, V. M., "High-Performance Concrete Incorporating Large Volumes of ASTM Class F Fly Ash," Proceedings ACI International Conference, Singapore, 1994, pp. 177-193.

Hwang, C. L., Liu, J. J., Lee, L. S. and Lin, F. Y., "Densified Mixture Design algorithm of High Performance Concrete and its Early Properties," Journal of the Chinese Institute of Civil and Hydraulic Engineering, Vol. 8, No. 1, Taiwan, 1996, pp. 207-219.

Gartner, E. M., Gaidis, J. M. and Grace, W. R., "Hydration Mechanisms, I," Materials Science of Concrete I, the American Ceramic Societ, Inc., OH, 1989, pp. 95-126.

Hwang, C. L., Hsieh, H. C. and Chang, P. K., "The Measurement Technology of Cement Paste Micro Structure and Property," The 10th Technological and Vocational Education Conference of Republic of China, 1995, pp.71-80.

TOPIC V.B

X-ray diffraction (XRD)

QUANTITATIVE X-RAY ANALYSIS OF OPC CLINKER BY RIETVELD REFINEMENT

J. NEUBAUER, Mineralogical Institute, University Erlangen-Nürnberg (Germany)
H. PÖLLMANN, Department of Mineralogy and Geochemistry, University Halle, (Germany)
H.W. MEYER, KHD Humboldt Wedag AG, Cologne (Germany)

ABSTRACT

Samples of Portland cement clinker were taken at various operating conditions from two clinker production lines. Quantitative phase distribution was investigated by XRF (Bogue calculation), by microscopy (point counting) and by XRD (Rietveld analysis). Evaluation and comparison of the results, the Rietveld - and microscopic quantification yield a very high degree of accuracy. Therefore Rietveld calculation can be introduced as a high performance instrument in automatic quality control systems of the clinker- and cement production.

Key-words: Rietveld analysis, quantitative, Bogue calculation, light microscopy

INTRODUCTION

A main challenge in efficient and reliable quality control of Portland Cement production is the development of a practical and quick method to determinate the mineralogical composition of clinker and cement. Until nowadays the most frequently applied method to estimate the mineralogical composition is the procedure according to Bogue (1929). The disadvantage of this method is that the phase composition is calculated on basis of the chemical composition. Even if it is assumed that the chemical composition of the four main phases (alite, belite, tricalcium aluminate and ferrate) is well known, thermal equilibrium for a complete crystallization has to be realized. However in the technical process of cement clinker production thermal equilibrium is practically not existing. Therefore the results of the Bogue calculation do not exactly represent the real mineralogical composition of a clinker or cement.

Microscopical techniques of point or line counting are scientifically well recognized methods to determine alite and belite content. Furthermore information about the microstructure of the clinker can be obtained. Determination of the so called interstitial phases ferrate and tricalcium aluminate is problematic as the crystals of these phases are usually of submicroscopic size. Moreover this technique offers no reliable potential for automatization and is too time-consuming for practical applications in on-line quality control. The development of new computer aided image analysis do not meet the requirements and standards of technical usability yet.

During the last few years since digitalization of the Bragg-Brentano powder diffraction equipment efforts were made to determine phase composition by XRD methods. The most difficult problem for this method of quantification is the wide range of overlapping reflections of the main components, especially alite and belite and preferred orientation of some phases. Figure 1 presents the patterns of calculated mixtures (Rietveld method) with different ratios alite/belite.

For this reason standard XRD phase quantification by single peak measurement can not be applied successfully in the case of alite and belite because the only reflection of belite free from overlapping is of low intensity (31.1° 2θ Cu Kα).

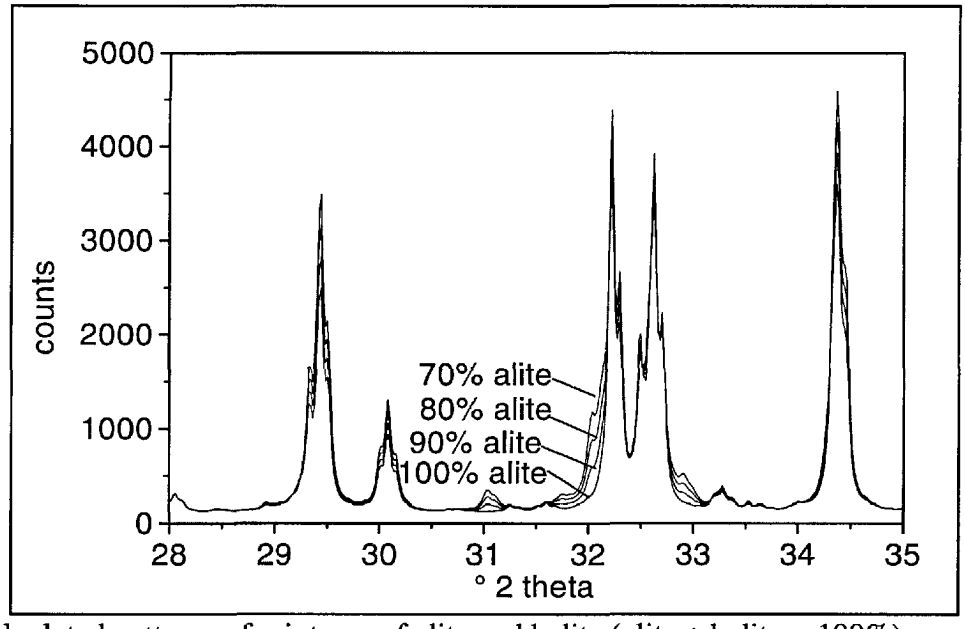

Fig. 1: Calculated patterns of mixtures of alite and belite (alite + belite = 100%)

Advances in electronic data processing enable the application of a method which calculates, compares and refines X-ray patterns from even very complex structure data. This method was initially by Rietveld (1969) for neutron diffraction and has been transcripted to X-ray diffraction a few years later. So-called full profile refinement is able to deal even with phasé mixtures up to 15 compounds. Increasing calculation performance of modern PC's allows quantification of a complex mixture within one minute. This method offers a large potential for automatization in quality control. Applications concerning OPC clinker quantifications are reported by Klaska (1996), Möller (1995), Mumme (1995), Neubauer et al. (1996) and Taylor & Aldridge (1993).
Described investigations in the following article were carried out to evaluate performance and accuracy of Rietveld quantification in comparison to Bogue and microscopic methods. Based on the results development and introduction of a practical application of the method is planned as an integrated part of the quality- and process control system of modern cement plants.

EXPERIMENTAL

Investigations were initiated and coordinated by KHD Humboldt Wedag AG. Three different quantification methods were applied at three independent laboratories to minimize subjective influences by the investigator. Sampling, primary preparation and chemical analysis were carried out by Humboldt Wedag AG in Cologne. Microscopic investigations were done at the Mineralogical Institute at the University Halle. XRD investigations including Rietveld quantifications were performed at the Mineralogical Institute, University of Erlangen-Nuernberg.

Sampling and preparation

Investigations of sample series A and B were carried out on seventeen representative clinker samples taken after the clinker cooler at different operating conditions during a period of one month. 1 kg of each clinker sample was crushed in a laboratory impact crusher to a fineness of < 4mm. The fraction ranging from 2 - 4 mm was received by hand screening of this material. This homogenized and divided material was used for all further analyses. Portions of this ma-

terial were finely ground to meet the requirements of XRF and XRD and wet chemical analysis.

Chemical analysis and Bogue calculation

XRF specimen discs were prepared in a flux by fusing a mixture of finely ground clinker and sodium-tetra-borate. For this reason the volatile compounds, such as chlorine, sulfate and alkalis had to be analyzed separately. Chlorine was directly quantified by coulometric titration. Sulfate was determined as total SO_2 with the aid of an IR-detector installed after an induction furnace. Alkalis (K_2O, Na_2O) were determined by flame photometrical analysis using reference solutions. Determination of free lime content of a clinker was carried out according to the method of Schläpfer & Bukowski (1933)

Based on the results of a chemical analysis the potential phase composition of the clinker was calculated according to the method of Bogue. The total CaO-content of clinker was reduced by the amount of free lime. As the degree of sulfatization of clinker is < 100, no further correction of total CaO was necessary. Following formulas are valid (clinker with an alumina ratio > 0.638):

$$c(C_3A) = 2.650*Al_2O_3 - 1.692*Fe_2O_3$$
$$c(C_4AF) = 3.043*Fe_2O_3$$
$$c(C_3S) = 4.071*CaO - 7.600*SiO_2 - 6.718*Al_2O_3 - 1.430*Fe_2O_3$$
$$c(C_2S) = 8.600*SiO_2 + 5.068*Al_2O_3 + 1{,}079*Fe_2O_3 - 3{,}071\ CaO$$

A standardization of the results of the Bogue calculation to a total of 100 % was carried out, to enable the comparison with Rietveld analysis and microscopical determination.

Microscopic Investigation

Crushed and screened clinker was homogenized. 6 to 8 grains of the particle size fraction 2 - 4 mm were embedded in epoxy resin and polished. The surface of this polished section specimen was treated for 30 seconds with a solution of 1 g salicylic acid in 125 ml destilled water and 125 ml ethyl alcohol.

Depending on etching time the clinker phases appear in different colors according to their different interaction with the acid solution. After 30 seconds alite is colored blue and belite is colored brown. The tricalcium aluminate and the ferrate-phase are not affected within this 30 s and appear colorless. By this etching technique an optical discrimination of alite, belite and the interstitial phase (tricalcium aluminate plus ferrate) is possible. Due to crystal size and the crystallinity a quantitative, microscopical differentiation of the interstitial phase into tricalcium aluminate and ferrate is not possible. Small amounts of periclase and free lime were recorded as subordinate compounds.

Quantitative analysis was performed by point counting with a 100x air lens and a step width of 0.4 * 0.05 mm. 10 000 points were counted of each section specimen. Mass contents of clinker phases were calculated from the resulting vol.% by the average specific weights (alite: 3.20 g/cm³, belite 3.28 g/cm³ interstitial phase 3.60 g/cm³). Subordinate compounds (approx. 1-2% by mass) were disregarded by calculation of alite, belite and interstitial phase. Finally a standardization of the results to a total of 100% was carried out.

Rietveld quantification

Rietveld refinement is based on comparison of an observed X-ray pattern and a pattern calculated from structure data of one or more phases. Calculation is finished successfully when the residual error is minimized by the refinement of global and structural parameters.

Prior to the investigation of clinker samples, the accuracy of the quantification by Rietveld refinement was verified on different synthetic clinker which were mixed from pure synthetic OPC phases. Chemical composition of clinker phases was chosen according to H.F.W. Taylor (1990) and modified to receive synthesis products free from additional phases. Rietveld refinement of synthesis proofed a purity larger than 99%. In table 1 the chemical composition of the main phases is summarized.

Table 1: Chemical composition of the synthetic clinker phases (in wt.%)

Phase	CaO	SiO_2	MgO	Fe_2O_3	Al_2O_3	Na_2O
Alite	72.6	25.6	1.1	0.7	-	-
Belite	64.0	34.2	0.5	0.9	-	0.4
C_3A	62.3	-	-	-	37.7	-
C_4AF	46.2	-	-	32.8	21.0	-

Pure alite, belite, tricalcium aluminate and brownmillerite were ground simultaneously at different ratios, examined by X-ray diffraction and quantified by the PC software of Wiles and Young (1981) modified by Howard. All mixtures were prepared and measured 5 times for calculating the standard deviation. In Table 2 the results are listed.

Table 2: Quantification of different synthetical mixtures with standard deviation.

Physical Mixture	**actual quantity**	**Alite** calculated	**Belite** calculated	**C_3A** calculated	**C_4AF** calculated	**standard deviation**
Alite	65	64.8				0.9
Belite	20		20.8			0.8
C_3A	10			9.6		0.6
C_4AF	5				4.8	0.6
Alite	55	55.3				1.1
Belite	25		25.4			1.2
C_3A	10			9.7		0.6
C_4AF	10				9.6	0.6
Alite	70	69.9				0.7
Belite	15		15.7			0.8
C_3A	5			5.0		0.6
C_4AF	10				9.4	0.9

values in wt.%

Average values of quantification indicate the excellent agreement with the real mineralogical phase composition. Deviations from the real composition is in any case below 1 wt.%. A maximum standard deviation of 1.2 % was found for 5 repeating experiments. Therefore a

single measurement of a technical clinker should deviate not more than 2 wt.% from the actual composition.
In figure 2 a powder diffraction pattern of a mixture of the four synthetic main components, a calculated pattern and an actual cement clinker pattern are plotted. A good agreement of the results was achieved.

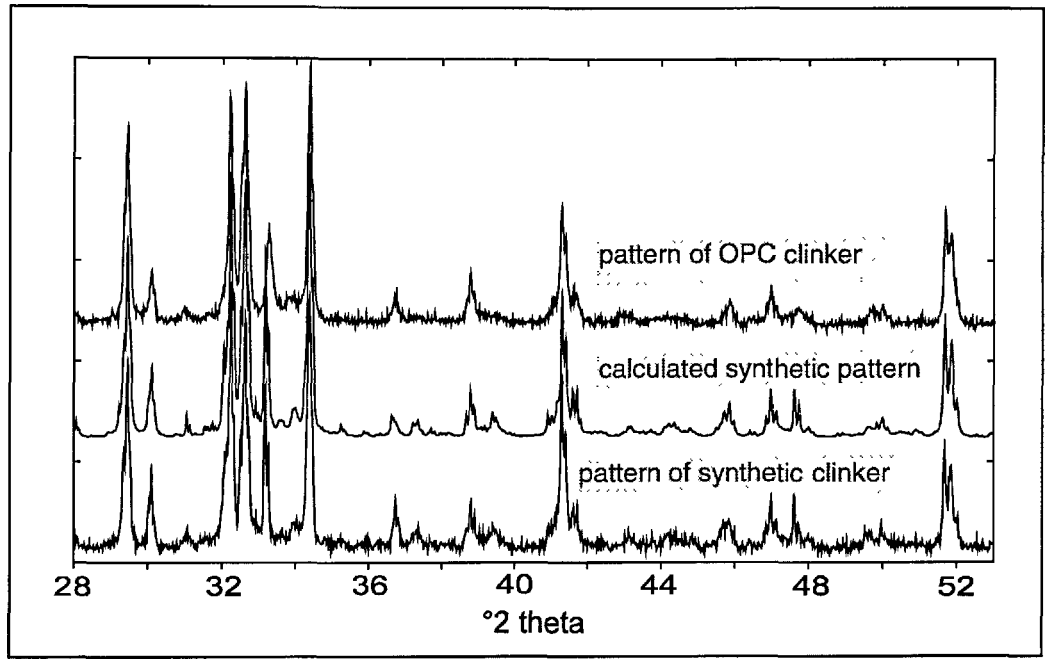

Fig. 2: Comparison of the X-ray pattern of a mixture of the four synthetic main components, the calculated pattern and an actual cement clinker pattern

Based on the above results a Rietveld control file had to be created and tested for its accuracy to quantify technical Portland cement clinker samples.
The crushed and screened Portland cement clinkers were ground for another 2 minutes in a disc mill. Samples were prepared in a front loading sample holder. All measurements were carried out with a Siemens D5000 X-ray diffractometer using Diffrac-AT software with the following adjustments:

Generator: 50 mA, 40 kV
Tube: fine focus
X ray: Cu Kα
Slits: fixed 0,5°, 0,5°
Detector slit: 0,1°
Detector: scintillation
Step/Time: 0.02° 2θ / 2s
Range: 10° - 55° 2θ

The following structure data were used after modification:

alite: Nishi & Takeuchi (1985)
belite: Jost et al. (1977)
C_3A: Mondal & Jeffrey (1975)
C_4AF: Colville & Geller (1971)

Rietveld refinement was carried out on a PC with a P200 processor using software of Wiles and Young (1981) modified by Howard. The control file for refinement was standardized and adapted for each clinker sample series - this allows refinement by a "press button" method. Calculation time for each quantification was approximately one minute. Besides the four main clinker phases periclase and free lime were evaluated. Again a standardization of the results to a total of 100% was calculated for comparison purposes.

RESULTS

A first series of 12 clinker samples (series A), taken under various operation conditions from a clinker production line was analyzed and evaluated to determine the accuracy and performance of Rietveld full pattern refinement. The variation of the phase composition of clinker samples, which is influenced by the operating conditions of the kiln line is evaluated and a comparison of the three described quantification methods is given. A second set of data from clinkers of another cement plant was sampled while firing different fuels and wastes (series B). No microscopical analysis could be carried out on sample series B.

1. Operating conditions

In table 3 general information on the quality of clinker samples and some essential operation parameters concerning the sampling periods are summarized.

Table 3: Required clinker quality and operation conditions of the kiln.

sample	clinker quality	typical operating conditions of the kiln
A1	Cem I class 52.5	normal operation, T (sintering zone) 1284°C
A2	Cem I class 32.5 and 42.5	Kiln starting period, T (sz) 1116°C
A3	Cem I class 32.5 and 42.5	4.5 h after operation start, T (sz) 1100°C
A4	Cem I class 32.5 and 42.5	normal operation, T (sz) 1299°C
A5	Cem I class 32.5 and 42.5	normal operation, T (sz) 1218°C
A6	Cem I class 32.5 and 42.5	conversion from HS to normal clinker T (sz) 1131°C
A7	Cem I class 32.5 and 42.5	start of kiln operation, T (sz) 1100°C
A8	Cem I class 32.5 and 42.5	normal operation T (sz) 1188°C
A9	Cem I class 32.5 and 42.5	normal operation T (sz) 1232°C
A10	Cem I class 32.5 and 42.5	operation not at optimum, T (sz) 1100°C
A11	Cem I class 32.5 and 42.5	normal operation T (sz) 1143°C
A12	Cem I class 32.5 and 42.5	normal operation T (sz) 1162°C

sample	typical operating conditions of the kiln
B1	1,9% O_2, 1400°C, fuels(in t/h): 2,6 waste oil, 5,7 coal, 0,5 photo sewage
B2	2,5% O_2, 1430°C, fuels(in t/h): 4,6 waste oil, 3,1 coal, 0,33 photo sewage
B3	3,8% O_2, 1400°C, fuels(in t/h): 2,7 waste oil, 5,8 coal, 0,5 photo sewage
B4	3,9% O_2, fuels(in t/h): 9,2 coal, 0,4 photo sewage
B5	2,6% O_2, 1300°C, fuels(in t/h): 6,4 waste oil, 0,5 photo sewage

O_2 partial pressure measured at kiln exit. Due to the measurement techniques the sintering zone temperature has to be considered as relative.

2. Comparison of quantification data

An overview and comparison of the results achieved by Bogue calculation, microscopical determination and Rietveld quantification is plotted in Figures 3-8.

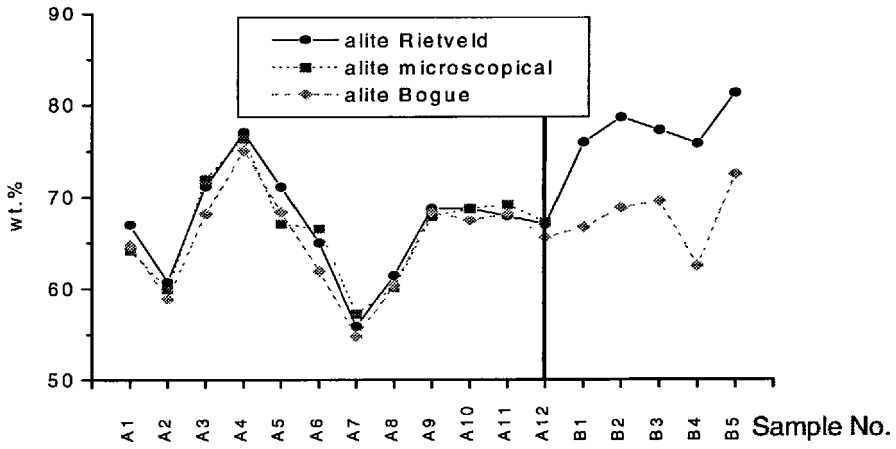

Figure 3: Alite content in samples

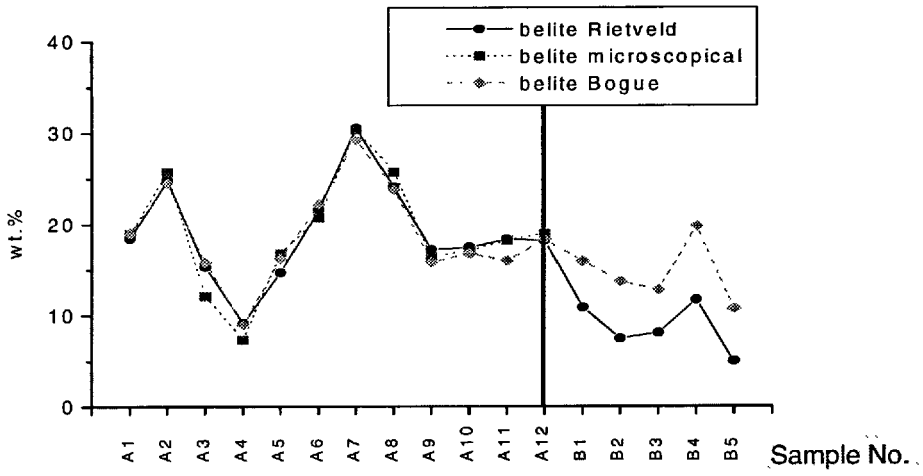

Figure 4: Belite content in samples

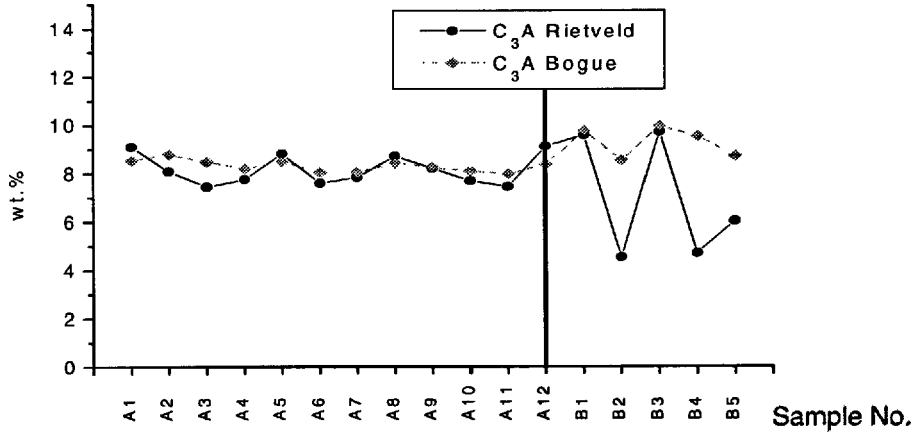

Figure 5: C_3A content in samples

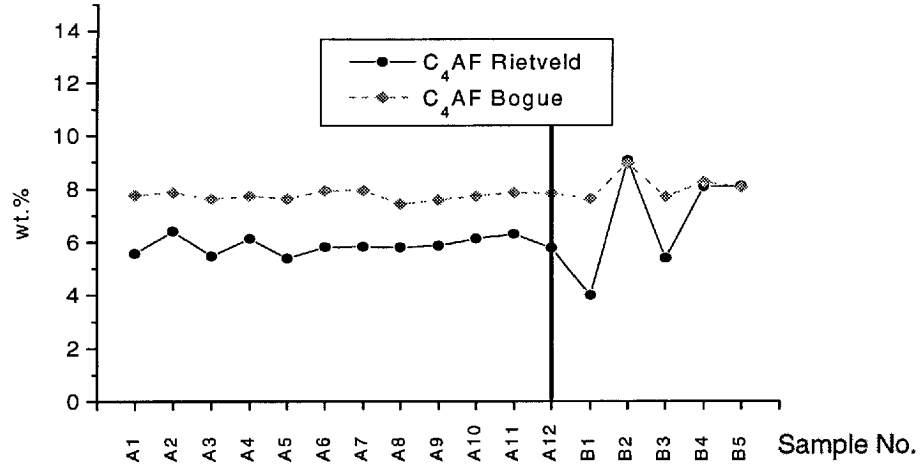

Figure 6: C_4AF content in samples

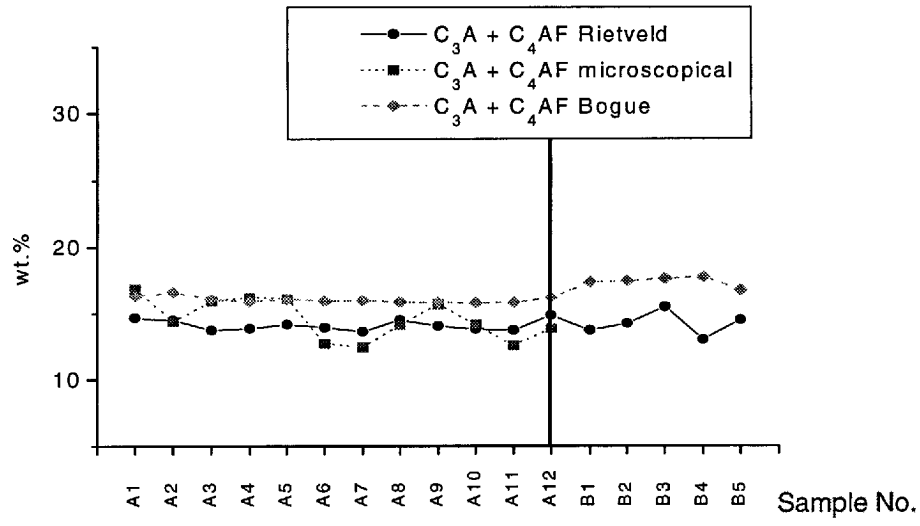

Figure 7: $C_3A + C_4AF$ content in samples

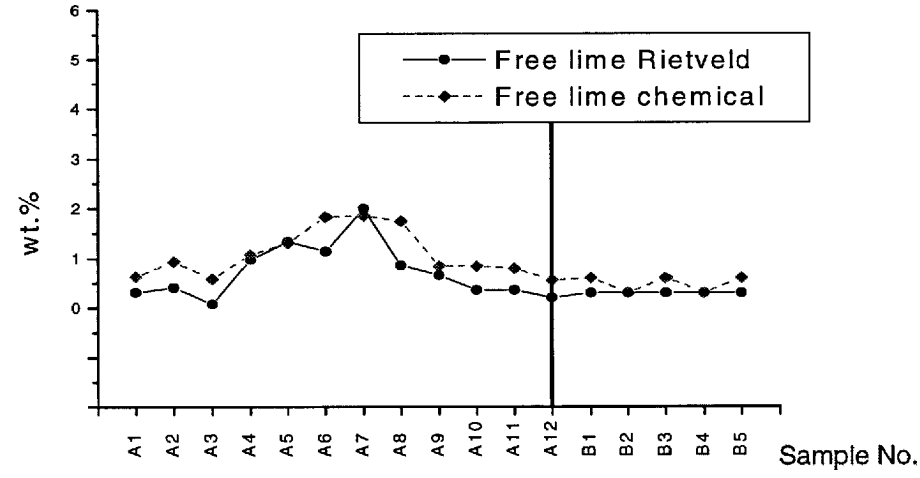

Figure 8: Free lime content in samples

Detailed results of the quantification are given in the appendix.

2.1 Sample series A

A comparison of sample series A indicate a good agreement of quantification results for alite and belite determined by Bogue calculation, microscopic examination and Rietveld analysis respectively (Figures 3 and 4). Concentration of C_3A are in well agreement comparing Bogue calculation and Rietveld analysis (Figure 5). In contrast, a significant difference in the quantity of brownmillerite determined by Bogue calculation and Rietveld analysis (Figure 6) was found. This difference is attributed to the incorrect assumption of the Bogue calculation the chemical composition of brownmillerite is C_4AF. As a consequence total iron content of clinker are calculated as brownmillerite of this composition. For this reason solid solution series of alite, belite and C_3A towards iron containing crystals are not taken into account by the Bogue calculation. According to detailed investigations by Rietveld refinement, the actual chemical composition of brownmillerite is $C_4(A,F,M,S,T)$. Furthermore, dependent on concentration and availability of iron, a variation in the chemistry and the amount of brownmillerite occur. Comparison of the quantification of the interstitial phase (C_3A + C_4AF) indicates a significant difference between the results of Bogue calculation and Rietveld analysis (Figure 7). This is again a consequence of the fixation of iron and aluminum in alite and belite structures. Therefore higher amounts of silicate phases were detected at the expense of interstitial phase by the Rietveld method. Due to the distribution of interstitial phase even in small pores, results obtained by microscopic examination of the quantity of interstitial phase have to be judged as intermediate in relation to Rietveld quantification and the Bogue calculation. In case of the interstitial phase the accuracy of a microscopic quantification is limited. Furthermore, the quantity of the additional clinker components, like free lime and periclase are simultaneously determined by the Rietveld method. In figure 8 the results of free lime concentration of clinker samples indicated by the Rietveld quantification and a wet chemical analysis are compared. A satisfying correlation of the results of both methods with regards to the low concentrations of free lime was achieved.

2.2. Data Set B

For sample series B only a comparison of the results obtained with Bogue calculation and Rietveld quantification was carried out. With respect to sample series A correspondence of both methods is poorer. Concerning alite and belite a similar trend as in sample of series A was found. In contrast absolute values differ up to 10 %. In case of C_3A and brownmillerite relative quantification differs up to 50 %. Therefore a selective solution of clinker material in K(OH) and salicylic acid followed by chemical analysis and Rietveld refinement of the residue was carried out. It was found out, that the results of the Rietveld quantification are accurate (Sieber, 1996 in print). Sintering of clinker under varying oxygen fugacities in the kiln atmosphere and variation of burning conditions caused by different fuels (waste oil, photo sewage, coal) result in differences in the chemical composition and crystallographical properties of clinker. In such cases Bogue calculation fails because of its inflexibility to adjust the variability of chemical compositions of clinker minerals.

DISCUSSION

As demonstrated by this investigation the Rietveld quantification method is an efficient tool in clinker - and cement characterization. Once a refinement strategy (the control file) is adjusted to a cement and/or clinker routine measurements are carried out by the „press button“ method.

During the adjustment work an accuracy test done by comparison of the clinker with the physically mixed synthetic clinker guarantees excellent quantification results.
In further study reduction of counting time by using a variable slit configuration for the X-ray equipment was reached. Detection of pattern and Rietveld calculation can be done within 15 minutes. Hence Rietveld quantification method could be introduced in on-line process control management.
An application of Rietveld quantification method to quality control of cements containing sulfates (gypsum, bassanite, anhydrite) and/or other additives (e.g. calcite, quartz etc.), as well as the process control of the cement mill is feasible. Generally the minimum concentration determinable is dependent on phase configuration. Usually the compounds can be detected down to a range of approximately 0,3 wt.% without any deterioration of the accuracy.
The Rietveld quantification method offers a plenty of advantages:

- very high potential for automatization
- fast method (analyzation and calculation within 6 minutes)
- determination of a huge number of phases in one step:

alite	anhydrite
belite	bassanite
aluminate	gypsum
brownmillerite	calcite
lime	quartz
periclase	

- high accuracy
- easy documentation
- simple handling
- low investment

ACKNOWLEDGMENTS
The authors wish to thank Walter Mayerhofer for carrying out the XRD investigations very accurately. Mr. Hubert Motzet was responsible for microscopic investigations. The very time consuming point counting was done by Uwe König.

REFERENCES
Bogue, R.H., Ind. Engnrg Chem (Anal.), 1, 192, (1929).
Colville, A.A. and Geller, S., „The Crystal Structure of Brownmillerite, Ca_2FeAlO_5", Acta Cryst. B27, 2311-2315 (1971).
Jost, K.H., Ziemer, B. and Seydel, R., „Redetermination of the Structure of ß-Dicalcium Silicate" Acta Cryst. B33, 1696-1700, (1977).
Klaska, R., „Rietveld-Analyse von Klinker-Mineralien. Problematik der Quantifizierung von Portlandzementphasen", 7. Philips-Symposium „Röntgenbeugung", Bernried Germany, (1996).
Möller, H., „Standardless Quantitative Phase Analysis of Portland Cement Clinkers", World Cement, 9, 75-84, (1995).
Mondal, J.W. and Jeffery, P., „The Crystal Structure of Tricalcium Silicate, $Ca_3Al_2O_6$" Acta Cryst. B31, 689-697, (1975).
Mumme, W.G., „Crystal Structure of Tricalcium Silicate from a Portland Cement Clinker and its Application to Quantitative XRD Analysis", N.Jb.Miner.Mh., 4, 145-160, (1995).

Neubauer, J., Kuzel, H.-J and Sieber, R., Rietveld Quantitative XRD Analysis of Portland Cement: II. Quantification of Synthetic and technical Portland Cement Clinkers", Proceedings of the Eighteenth International Conference on Cement Microscopy, Houston, Texas USA, (1996).

Nishi, F. and Takeuchi, Y., „Tricalcium Silicate $Ca_3O[SiO_4]$: The monoclinic superstructure", Z. Krist. 172, 297 - 314, (1985).

Rietveld, H.M., „A Profile Refinement Method for Nuclear and Magnetic Structures", J.Appl.Cryst.2, 65-71 (1969).

Schläpfer & Bukowsk, Ber. Eidgen. MPA. - Nr. 63, 1-39, Zürich, (1993).

Taylor, H.F.W., „Cement Chemistry", Academic Press pp. 475 (1990).

Taylor, J.C. and Aldridge, L.P., „Full-profile Rietveld quantitative XRD Analysis of Portland Cement: Standard XRD Profiles for the major Phase Tricalcium Silicate", Powder Diffraction, 3, 138-144, (1993).

Sieber, R., „Untersuchungen zur Konstitution eines Portlandzementklinkers bei unterschiedlichen Brennbedingungen." Thesis Erlangen in preparation.

Wiles, D.B. and Young, R.A., „A new Computer Program for Rietveld Analysis of X-ray powder diffraction patterns", J. Appl. Cryst. 14, 149-151, (1981).

APPENDIX

Table 4: Bogue calculation and free lime (chemical) (total of four main phases is 100%)

Sample	alite	belite	C_3A	C_4AF	CaO
A1	64.7	19.0	8.5	7.8	0.63
A2	58.8	24.5	8.8	7.9	0.93
A3	68.3	15.6	8.5	7.6	0.58
A4	75.1	9.0	8.2	7.7	1.07
A5	67.9	16.0	8.5	7.6	1.31
A6	61.9	22.2	8.0	7.9	1.83
A7	54.7	29.3	8.0	8.0	1.85
A8	60.3	23.8	8.4	7.5	1.74
A9	68.4	15.8	8.2	7.6	0.66
A10	67.5	16.7	8.1	7.7	1.19
A11	68.1	16.0	8.0	7.9	0.79
A12	65.5	18.3	8.4	7.8	0.56
B1	66.7	15.9	9.8	7.6	< 0.3
B2	68.8	13.7	8.5	9.0	< 0.3
B3	69.6	12.8	9.9	7.7	< 0.3
B4	62.4	19.8	9.5	8.3	< 0.3
B5	72.0	10.6	8.6	8.8	< 0.3

Table 5: Rietveld quantification for samples A and B (total of four main phases is 100%)

Sample	alite	belite	C_3A	C_4AF	MgO	CaO
A1	66.9	18.4	9.1	5.6	0.08	0.32
A2	60.7	24.8	8.1	6.4	0.22	0.39
A3	74.4	11.9	7.7	6.0	0.28	0.07
A4	77.1	9.1	7.7	6.1	0.09	0.98
A5	71.1	14.7	8.8	5.4	0.43	1.34
A6	65.0	21.6	7.6	5.8	0.08	1.14
A7	55.9	30.5	7.8	5.8	0.12	2.00
A8	61.4	24.1	8.7	5.8	0.23	0.86
A9	68.7	17.2	8.2	5.9	0.17	0.67
A10	68.8	17.4	7.7	6.1	0.46	0.36
A11	68.0	18.3	7.4	6.3	0.08	0.36
A12	67.0	18.1	9.1	5.8	0.30	0.20
B1	75.9	10.5	9.6	4.0	0.98	0.03
B2	78.7	7.7	4.5	9.1	0.48	0.03
B3	77.3	7.6	9.7	5.4	0.97	0.03
B4	75.8	11.4	4.7	8.1	0.73	0.03
B5	81.4	4.5	6.0	8.1	0.91	0.03

Table 6: Microscopic quantification (total of alite + belite + interstitial phase is 100%)

Sample	alite	belite	interstitial phase
A1	64.2	18.9	16.9
A2	59.9	25.7	14.4
A3	72.0	12.1	15.9
A4	76.4	7.4	16.2
A5	67.1	16.8	16.1
A6	66.5	20.8	12.7
A7	57.2	30.4	12.4
A8	60.1	25.7	14.2
A9	67.9	16.4	15.7
A10	68.7	17.1	14.2
A11	69.2	18.2	12.6
A12	67.2	18.9	13.9

3v008
4 pp

K n o. 0 5. APR. 2001 d o k 32823

APPLICATION OF X-RAY DIFFRACTOMETRY IN COMMINUTION OF GYPSUM

G.GOSWAMI, B.N.MOHAPATRA, P.K.PANIGRAHY AND J.D.PANDA
Dalmia Institute of Scientific and Industrial Research, Rajgangpur-770017, India.

ABSTRACT The paper demonstrates that during comminution of cement, the degree of crystallinity of gypsum as determined by X-ray diffraction (XRD) decreases with increase of grinding time and in the process increases the setting times of the cement. From a large number of experimental tests, it has been established that XRD can be applied to control gypsum grinding to achieve desirable setting times of cement.

Key - word : Gypsum, X-ray Diffraction Analysis, Setting, Fineness.

INTRODUCTION

Recent studies have shown that comminution of gypsum plays an important role in determining the cement properties, particularly setting times. Bensted (1982) and Goswami et.al (1990) studied the effect of comminution on early hydration of Portland cement. Soroka et.al (1986) determined the effect of gypsum contents and fineness on mechanical properties of cement. Theisen (1983) examined the relationship between gypsum hydration and strength development of cement. Although variations on the effects of gypsum comminution on cement properties are generally regarded to be due to the morphological changes in the calcium sulphate, Kanare et.al (1984) and Menetrier et.al (1980) failed to find discrete particles of any form of calcium sulphate in commercial cement and in an integrated mixture of gypsum and C3S respectively. This suggests the possibility of loss of crystallinity of calcium sulphate phase during comminution. Keeping this in view, the present study examines the loss of crystallinity of gypsum during comminution by X-ray diffractometry (XRD) and consequently the application of XRD in controlling the comminution process in order to achieve desirable setting times of cement.

MATERIALS EXAMINED AND EXPERIMENTAL PROCEDURES

An industrial Portland cement clinker containing - 64.2% CaO, 21.4% SiO2, 5.8% Al2O3, 3.5% Fe2O3, 3.8 % MgO, 0.92% K2O and 0.08% Na2O and a by-product gypsum with 39.5% SO3, 0.85% P2O5 and 0.25% F^- were taken for the study. For preparation of blended Portland slag cement (PSC) an Indian Blast Furnace Slag having 32.0% SiO2, 26.1% Al2O3, 0.5% Fe2O3, 30.0% CaO, 7.5% MgO, 1.1% TiO2, 0.61% Na2O and 0.46% K2O was used. For preparation of normal cement a mix containing 95% clinker and 5% gypsum was ground in a laboratory ball mill. Slag content in the examined PSC was kept at 30% level. For the controlled experimental cements, gypsum was ground for different times, either with the clinker or separately. In case of separate grinding, ground clinker and gypsum were later mixed in a ball mill.

Normal cement properties including setting times and compressive strength were determined according to the Indian Standard 4031 - 1988. X-ray Diffraction (XRD)

patterns of the samples were obtained using Ni-filtered Cu-Kα radiation at 40 kV, 20 mA. Crystallinity of gypsum was determined by recording XRD pulse counts for gypsum at 2θ 11.7 (dA$\circ$=7.56) after background correction.

RESULTS

Fig.1 shows the XRD peaks for gypsum in ordinary Portland cement ground for different times. Gypsum XRD pulse counts with the properties of the corresponding cement sample are recorded in Table-1. It is found that with increase of grinding time, XRD pulse counts decrease and along with that setting times increase. It is also found that with decrease of grinding time and hence increase of gypsum XRD intensity, cement sample shows in general,a marginal increasein strength. In a similar experiment with PSC, it was found that in almost identical fineness, while cement with gypsum XRD counts 300 recorded initial and final setting times 415 and 455 minutes respectively, that with XRD counts 1550 recorded initial and final setting times 145 and 240 minutes respectively, strengths remaining almost similar.

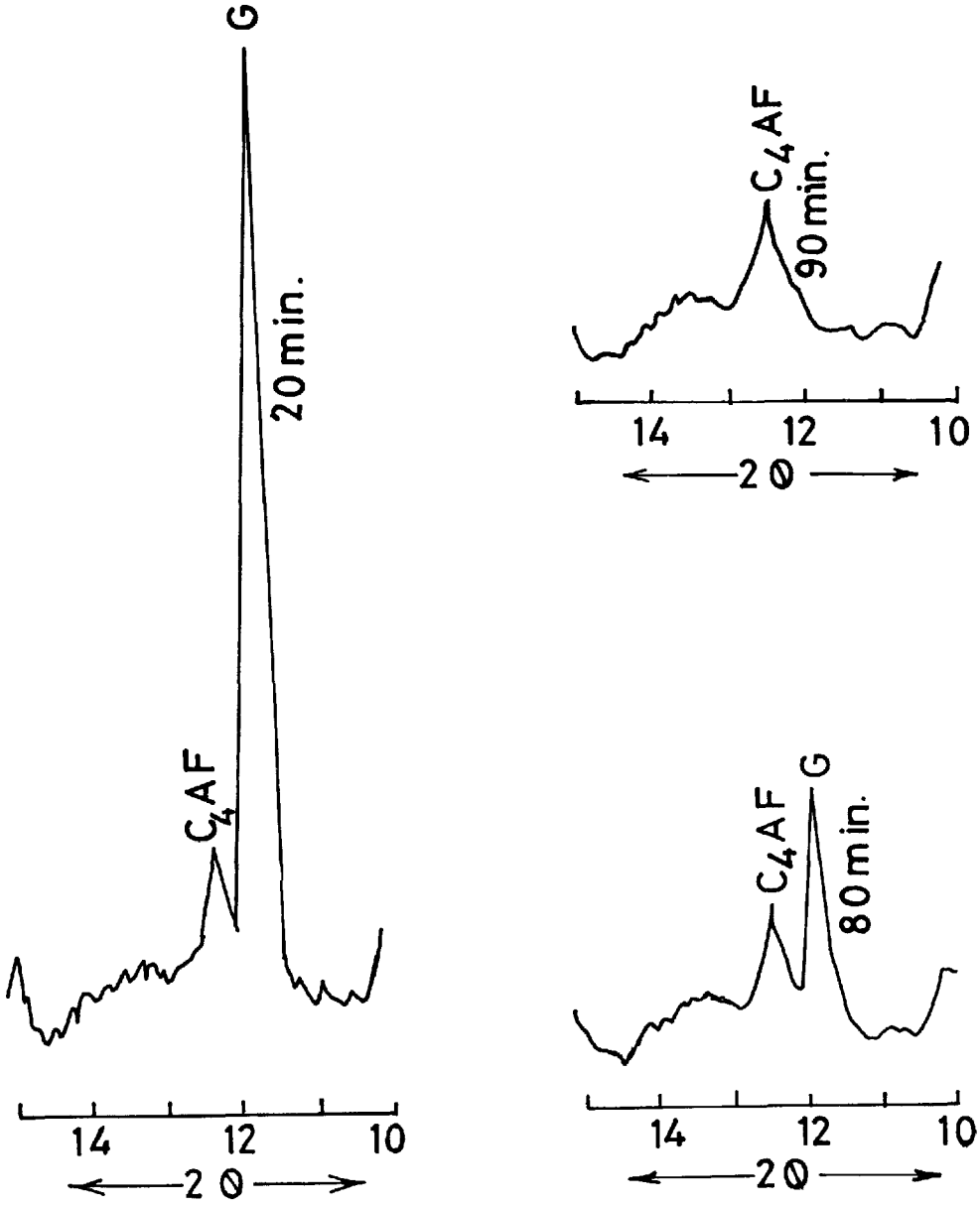

Figure 1 XRD peak intensities (Cu-Kα) of gypsum (G) ground for 20, 80 and 90 minutes in identical cement fineness

DISCUSSION

Table 1 shows that with increase of grinding time, XRD pulse counts or crystallinity of gypsum decreases. In a similar study on amorphism, Anderson (1975) has shown that on grinding silica material an amorphous layer forms around the original crystal. It is conceivable that with the increase of fineness relative volume of amorphous layer increases, although the thickness of the layer remains same. For example, Anderson (1975) calculated that with a constant 0.03 micron thickness of amorphous layer, volumes of amorphous material would be 1.8 and 93% of 10.0 and 0.1 micron spheres respectively. This explains the decrease of XRD pulse counts of gypsum with increase of cement grinding time.

Table 1 XRD pulse counts for Gypsum at $2\theta=11.7$ (Cu-Kα) and corresponding cement properties

GYPSUM				
Grinding time in minutes	20	30	40	90
XRD pulse counts	1060	880	620	NIL
CEMENT				
Sp.Su. Blaine (cm^2/g)	2932	2925	3000	2988
Setting times (minutes)				
Initial	175 (38)	270 (59)	325 (71)	456 (100)
Final	263 (51)	334 (65)	400 (78)	516 (100)
Compressive strength (kg/cm^2)				
3-Days	307 (113)	290 (107)	280 (103)	272 (100)
7-Days	350 (99)	325 (92)	347 (99)	352 (100)
28-Days	505 (116)	438 (100)	457 (104)	437 (100)

(Figures in parentheses, are in percentage of setting times and compressive strengths of cement with gypsum ground for 90 minutes).

In normal cement grinding, gypsum being much softer (Mohs Hardness - 2) than clinker gets ground to much finer state than the latter. That in identical grinding condition gypsum becomes finer and loses its crystallinity more rapidly than the clinker phases is evident from the fact that after grinding for 90 minutes of the cement samples examined, while crystallinity of gypsum got lost completely, producing no XRD pulse, the cement clinker phases including C4AF showed distinct XRD peaks (Fig.1). Effect of grinding on amorphisation of gypsum was also reported by Juhasz and Opoczky (1990). It might be that because of this fineness and amorphism, it is often difficult to find discrete particles of any form of calcium sulphate in commercial cement (Kanare et. al. 1984, and Menetrier et. al 1980). It is conceivable that with increase of and consequently formation of ettringite increases, leading to retardation of setting times. Accordingly amorphism, the reactivity of calcium sulphate with the cement phases gets intensified and consequently formation of ettringite increases, leading to retardation of setting times. Accordingly whenever it becomes necessary to reduce the setting times, as in the case of the use of by-product gypsum known to extend the setting times, it is desirable to retain some portion of the gypsum in crystalline state.

During the present study a large number of tests were conducted for different cement composition having identical fineness but made with gypsum ground to different fineness adopting both the process of intergrinding of clinker and gypsum and separate grinding followed by intermixing of the two components. In all cases it was found that setting times decreased with increase of XRD intensity of gypsum, without much change in other properties of cement. Thus it is found that XRD intensity of gypsum can be used successfully to control the comminution of gypsum in order to achieve desired setting times of the corresponding cement.

REFERENCES

Anderson P.L., Free silica analysis of environmental samples - a critical literature review, Am. Ind. Hyg. Assoc., J. Vol 36, 1975, pp.767.

Bensted, J., "Effects of the clinker gypsum grinding temperature upon early hydration of Portland Cement", Cem. Concr. Res. Vol.12, No.3, May, 1982, pp 341-348.

Goswami, G., Mohapatra, B. and Panda J.D., "Gypsum dehydration during omminution and its effect on cement properties", J. Am. Cerm. Soc., Vol. 73, No.3 , March 1990, pp.721-723.

Juhasz, Z.A. and Opoczky, L. "Mechanical activation of minerals by grinding, pulverizing and morphology of particles". Ellis Horwood Ltd., Chichester, England. 1990.

Kanare, M and Gartner, E.M., "Optimum sulphate in Portland cement", Cement Res. Pogress, Chapter 13, 1984, pp.213-251.

Menetrier, D., Jawed, I., and Skalny, J., "Effect of gypsum on C3S hydration, "Cement Cocr. Res. Vol.10, No.5, September, 1980, pp.697-702.

Soroka, I. and Abayneh, M., "Effect of gypsum on properties and internal structure of Portland cement paste", Cem. concr. Res. Vol.16, No.4, July, 1986, pp.495-504.

Theisen, K."Relationship between gypsum dehydration and strength development in Portland cement", Zem.-Kalk-Gips, Vol.36, No.10, October, 1983, pp.571-577

TOPIC V.C

Other techniques

AN APPROACH TO REFINE THE BOGUE'S PHASE COMPOSITION OF SULPHO-ALUMINATE BELITE CEMENT

Július STRIGÁČ*, Department of Ceramics, Glass and Cement, Faculty of Chemical Technology, Slovak Technical University, 812 37 Bratislava, Slovak Republic
Jozef KRIŠTÍN, Central Laboratory of Electron-Optical Methods, Faculty of Natural Sciences, Comenius University, 842 12 Bratislava, Slovak Republic
Sadananda SAHU, School of Civil Eng., Purdue University, West Lafayette IN 47906, USA
Martin T. PALOU*, Ján MAJLING*

ABSTRACT Pt-encapsulated sulphoaluminate-belite (SAB) cement samples were heated up to 1450°C, slowly cooled and partially equilibriated at 1200°C. Chemical composition of coexisting solid solutions was measured on polished sample surfaces by the electron probe microanalysis. Bogue phase composition of two test SAB cements prepared at usual conditions (1200°C, 1 hr) calculated for the nominal chemical composition of phases is in better agreement to their experimental phase composition than Bogue phase composition calculated for the chemical composition of phases determined in this work (taken as solid solutions). Non-equilibrium nature of the prepared SAB cements is a reason for this discrepancy.

Key-words: Sulphoaluminate, Belite, Solid solutions, Bogue calculation.

INTRODUCTION

The phase composition of ordinary portland clinkers is usually calculated according to Bogue's method, which is a flexible (Taylor, 1989) and a practical procedure satisfying the need for a simple and sufficiently reliable estimation of the clinker phase composition. In principle, such calculation can be extended to any mineralogical or ceramic system, if the identity of phases present in the system is known beforehand. In a more general sense it can also be applied in cases in which the relevant phase assemblages are established in the course of computation (Majling et al, 1989).

At usual conditions five crystalline phases would create a simple phase assemblage in a case of sulphoaluminate belite (SAB) cement belonging to the five component oxide system CaO-SiO_2-Al_2O_3-Fe_2O_3-SO_3. The most thoroughly studied SAB cements are those based on the mineral phase assemblage composed of C_2S, $C_4A_3\bar{S}$, C_4AF, $C\bar{S}$ and C. Recent computations of the phase composition of SAB cements are based on clinker phases taken as stoichiometric minerals (Metha, 1977 and Majling et al, 1993), because of the lack of underlying data. The results of Muzhen et al (1992) and Andac and Glasser (1995) are filling this gap partially. They refer however to complex solid solutions including K_2O, Na_2O, MgO, TiO_2 oxides and are applicable to clinkers prepared from the corresponding raw materials.

The aim of the present work is to establish the chemical composition of coexisting solid solutions inside the specified phase assemblage and to use it for the Bogue calculation of clinker phase composition of clinkers prepared inside the mentioned five component oxide system from pure chemicals.

EXPERIMENTAL

Initially two clinkers having the nominal phase composition: SAB 1; 20% C_2S, 20% $C_4A_3\bar{S}$, 40% C_4AF, 20% $C\bar{S}$, and SAB 2; 30% C_2S, 20% $C_4A_3\bar{S}$, 30% C_4AF, 20% $C\bar{S}$ were selected for experimentation. The phase composition was converted to the corresponding oxide contents. For the preparation of clinker samples analytical reagent grade $CaCO_3$, Al_2O_3, Fe_2O_3,

$CaSO_4.2H_2O$ and silica gel were used in the appropriate weight ratios. The mixtures were homogenised in an agate mortar and calcined in an electric furnace at 1000°C for 1 hr. The calcined products were again homogenised, pelleted into short cylinders and heated again to 1000°C for 0.5 hr. The obtained pellets were encapsulated into Pt-tubes (ϕ = 5.25 mm) by welding the ends of tubes.
The encapsulated samples were heated up to 1450°C and hold at this temperature for 15 minutes. They were then continuously cooled to 1200°C at a cooling rate of approx. 0.6°C/min (the sample SAB 2 with a soak at 1200°C for 4 hrs).
The phase composition of the products was examined by XRD by a Philips powder diffractometer using CuKα radiation. The chemical composition of solid solutions was determined by electron probe microanalysis (EPMA) JSM 840. For the EPMA study the samples were impregnated with epoxy resin, polished and coated with carbon. SEM imaging was carried out by backscattered electrons.

In the second part of the study two clinkers were prepared from chemicals by their heating at 1200°C in a bed of $C_4A_3\bar{S}$, for 1 and 3 hrs. Their mineralogical composition was checked by XRD.

RESULTS AND DISCUSSION

Establishment of the chemical composition of coexisting solid solutions

The objective of sealing the samples in platinum tubes was to prevent the loss of sulphates at high temperatures. Slow cooling of samples from 1450°C was applied to ensure the melt assisted growth of crystals which was expected to result in their increased size and the fairly developed morphology suitable for the EPMA.
XRD analysis of samples SAB 1 and SAB 2 showed the presence of small amount of free lime besides the expected phases β-C_2S, $C_4A_3\bar{S}$, C_4AF and $C\bar{S}$ respectively.
Microstructural examination of phase distribution of the clinker SAB 1 is shown in Figs 1 and 2 and of SAB 2 is shown in Fig 3.

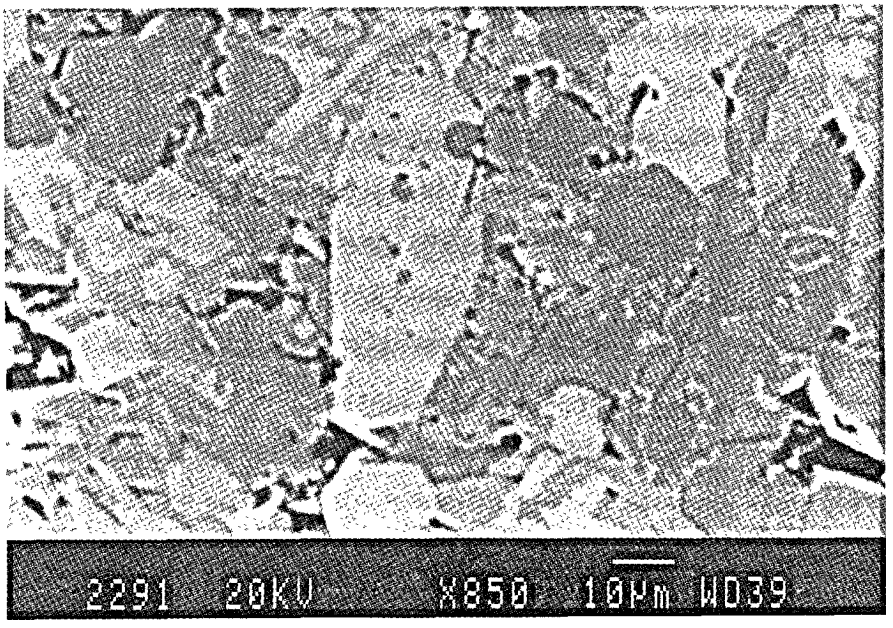

Figure 1 The backscattered SEM micrograph of clinker polished section of sample SAB 1.

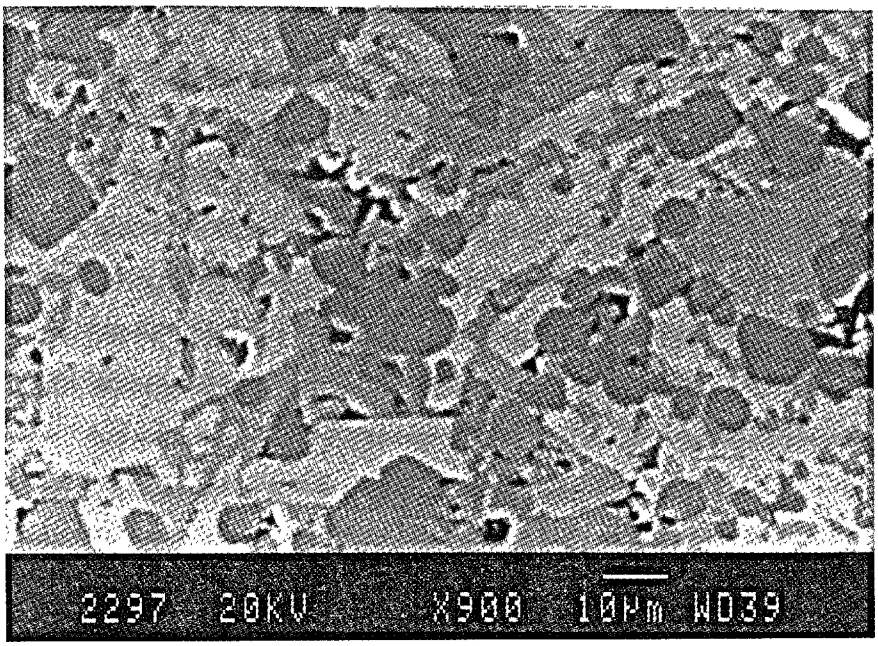

Figure 2 The backscattered SEM micrograph of clinker polished section of sample SAB 1.

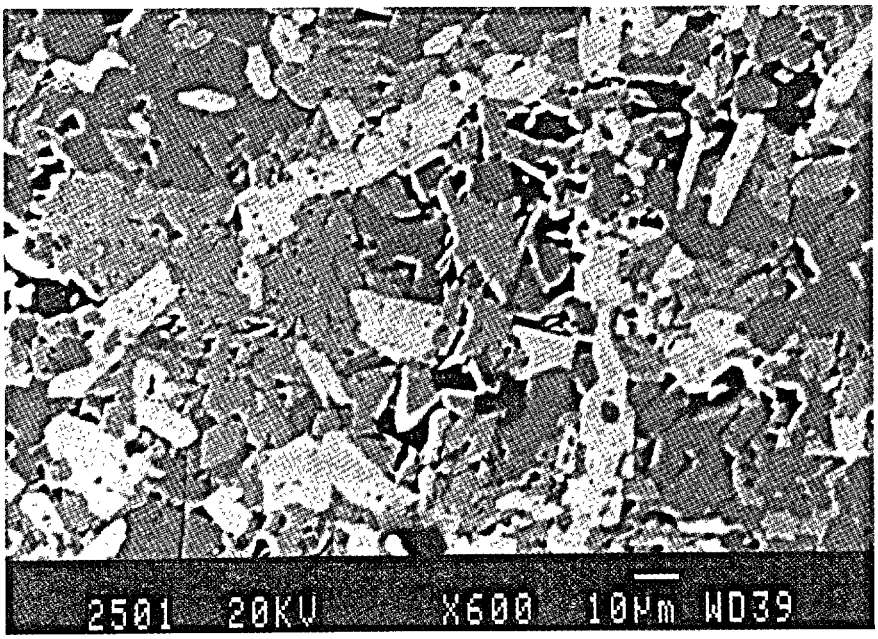

Figure 3 The backscattered SEM micrograph of clinker polished section of sample SAB 2.

The C_2S, $C_4A_3\bar{S}$, C_4AF and $C\bar{S}$ phases in SEM micrographs are well identified. The phase $C_4A_3\bar{S}$ is found in angular hexagonal dark grey crystals surrounded mainly by C_2S and C_4AF. The ferrite phase appears as large bright crystals with clean margins. The C_2S forms grey regions with a clear margins too. The $C\bar{S}$ appears as a dark grey regions with not quite well developed morphology, fuzzy margins and the crystals exhibit parallel cracks.

The chemical composition of clinker minerals from microprobe analysis is summarised in Table 1 and Table 2.

Table 1 Chemical composition of clinker minerals in sample SAB 1.

		CaO	SiO_2	Al_2O_3	Fe_2O_3	SO_3
C_2S	wt %	65.45 ± 0.03	29.34 ± 0.50	2.19 ± 0.04	1.07 ± 0.01	1.98 ± 0.43
	mol %	68.32 ± 0.11	28.59 ± 0.45	1.26 ± 0.03	0.40 ± 0.01	1.45 ± 0.32
$C_4A_3\bar{S}$	wt %	38.62 ± 1.83	0.11 ± 0.18	50.68 ± 1.32	2.20 ± 0.16	8.41 ± 2.88
	mol %	52.72 ± 2.28	0.14 ± 0.23	38.06 ± 1.11	1.05 ± 0.07	8.05 ± 2.80
$C\bar{S}$	wt %	48.05 ± 2.46	0.16 ± 0.03	0.14 ± 0.05	0.37 ± 0.10	51.28 ± 2.32
	mol %	56.97 ± 2.38	0.18 ± 0.03	0.10 ± 0.04	0.16 ± 0.05	42.60 ± 2.30
C_4AF	wt %	44.22 ± 4.82	1.12 ± 1.37	15.35 ± 1.34	38.71 ± 3.40	0.60 ± 1.03
	mol %	65.26 ± 4.51	1.53 ± 1.80	12.49 ± 1.32	20.11 ± 2.70	0.63 ± 1.13
C-S-$\bar{S}$	wt %	52.62	6.66	0.57	0.60	39.57
	mol %	60.43	7.14	0.36	0.24	31.83

Table 2 Chemical composition of clinker minerals in sample SAB 2.

		CaO	SiO_2	Al_2O_3	Fe_2O_3	SO_3
C_2S	wt %	65.69 ± 1.61	29.96 ± 0.56	1.41 ± 0.32	0.78 ± 0.07	2.15 ± 1.31
	mol %	68.28 ± 1.46	29.07 ± 0.64	0.81 ± 0.18	0.29 ± 0.03	1.57 ± 0.96
$C_4A_3\bar{S}$	wt %	38.04 ± 1.46	0.18 ± 0.18	48.64 ± 4.40	1.99 ± 0.76	11.14 ± 3.22
	mol %	51.80 ± 1.40	0.22 ± 0.22	36.42 ± 3.82	0.95 ± 0.36	10.61 ± 3.00
$C\bar{S}$	wt %	44.20 ± 1.86	0.04 ± 0.02	0.10 ± 0.03	0.26 ± 0.15	55.40 ± 1.67
	mol %	53.13 ± 1.70	0.05 ± 0.03	0.07 ± 0.02	0.11 ± 0.08	46.65 ± 1.81
C_4AF	wt %	45.19 ± 0.76	1.38 ± 1.30	13.75 ± 3.67	39.32 ± 2.38	0.37 ± 0.37
	mol %	66.36 ± 0.88	1.89 ± 1.80	11.11 ± 3.00	20.28 ± 1.32	0.38 ± 0.38
C-S-$\bar{S}$	wt %	59.45	24.35	4.61	6.59	5.02
	mol %	65.66	25.10	2.80	2.56	3.88

These tables contain arithmetic means of about fifteen analyses with the maximum deviations of measurement. Table 3 contains oxide percentage of stoichiometric clinker minerals for comparing it with analytical results.

Table 3 Chemical composition of stoichiometric clinker minerals.

		CaO	SiO_2	Al_2O_3	Fe_2O_3	SO_3
C_2S	wt %	65.12	34.88			
	mol %	66.67	33.33			
$C_4A_3\bar{S}$	wt %	36.76		50.12		13.12
	mol %	50.00		37.50		12.50
$C\bar{S}$	wt %	41.19				58.81
	mol %	50.00				50.00
C_4AF	wt %	46.16		20.98	32.86	
	mol %	66.67		16.67	16.67	

The ferrite phase C_4AF contains an increased amount of Fe_2O_3 which brings it essentially close to the C_6AF_2 stoichiometry. It also contains small quantity of SO_3 and SiO_2. The calcium sulphoaluminate phase $C_4A_3\bar{S}$ contains very small amount of SiO_2 and Fe_2O_3 substituting Al_2O_3 to about 2 wt % in both the cases. The dicalcium silicate, β-C_2S has a little increased ratio

of CaO/SiO_2 needed to compensate SO_3, Al_2O_3, and Fe_2O_3 admixtures. The anhydrite $C\bar{S}$ contains very small quantities of SiO_2, Al_2O_3 and Fe_2O_3. Comparison of the chemical composition of solid solutions determined with a data given for corresponding phases in literature will be published elsewhere (Strigáč et al, unpublished results).
Besides these main phases there were two another phases found in SAB 1 and SAB 2, containing simultaneously CaO, SiO_2 and SO_3 as major oxides. Moreover, an additional phase in SAB 2 was observed containing increased contents of Al_2O_3 and Fe_2O_3. The referred phase from SAB 1 has ratio CaO/SO_3 equal to 1.9. This ratio indicates $C\bar{S}$ phase and increased ratio is required to compensate for Al_2O_3, Fe_2O_3, SiO_2 admixtures. The phase from SAB 2 has CaO/SiO_2 ratio equal to 2.6. The ratio indicates C_2S phase modified with about 10 % admixtures Al_2O_3, Fe_2O_3 and SO_3. This phase is not considered to be related to $C_5S_2\bar{S}$ phase because of the too low content of SO_3. The chemical composition of these two phases needs to be confirmed in a next study. These results are therefore not taken into further account.

A comparison of the calculated and the experimental phase composition of model SAB clinkers

Two clinkers were prepared for the given purpose. Their chemical composition can be found in Table 4.

Table 4 Chemical composition of experimental clinkers prepared at 1200°C for 1 hr.

wt %	CaO	SiO_2	Al_2O_3	Fe_2O_3	SO_3
SC	60.32	23.63	10.74	2.28	3.03
SD	57.78	19.43	8.31	12.64	1.83

The XRD patterns of clinkers prepared at 1200°C, 1 hr, are given in Figs 4 and 5.

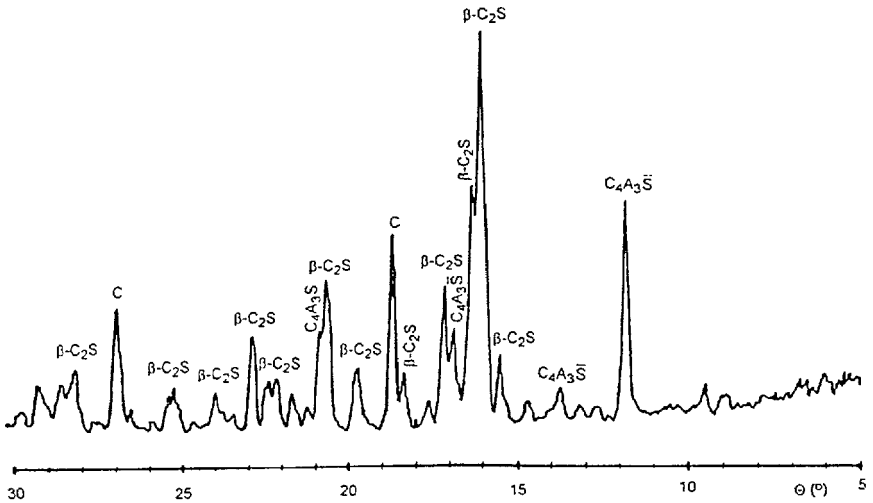

Figure 4 XRD pattern of the clinker SC prepared at 1200°C for 1 hr.

Bogue phase composition of these clinkers calculated for stoichiometric phases is given in Table 5 and the phase composition calculated for the phases taken as solid solution (referenced in Table 1) is given in Table 6. It is seen now that the chemical composition of clinkers (Table 4) was not taken arbitrarily but it was deduced from the presumed singular (three phases, C_2S, $C_4A_3\bar{S}$ and C_4AF) composition, at which the composition of phases was expected to comply the data given in Table 1.

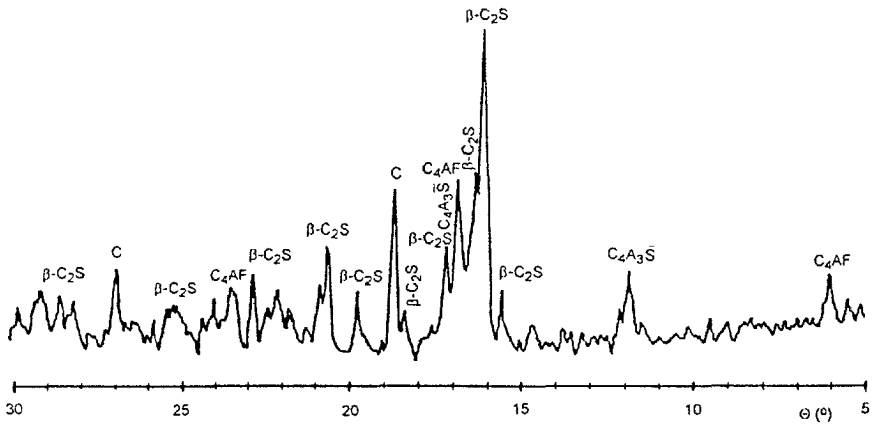

Figure 5 XRD pattern of the clinker SD prepared at 1200°C for 1 hr.

Table 5 The phase compositions of experimental clinker calculated for stoichiometric clinker phases.

wt %	C_2S	$C_4A_3\bar{S}$	C_4AF	$C\bar{S}$	C
SC	67.7	18.5	6.9	1.0	5.7
SD	55.7	0.4	38.4	3.0	2.3

Table 6 The phase composition of experimental clinker calculated for clinker phases taken as solid solutions.

wt %	C_2S_{ss}	$C_4A_3\bar{S}_{ss}$	C_4AF_{ss}	$C\bar{S}_{ss}$	C
SC	80.4	16.8	2.6	0.0	0.0
SD	65.0	4.2	30.5	0.0	0.0

The present comparison of results relies only on the visual inspection of powder patterns and comparison of their diffraction intensities and number of phases identified with the forecasted (calculated) phase quantities given in Tables 5 and 6. It is seen by this comparison that the powder patterns in Figs 4 and 5 show the presence of free calcia, a phase which should not be present, if solid solutions were formed in an extent corresponding to those present in the encapsulated sample slowly cooled from the high temperature. On a qualitative scale there is therefore a better agreement between the X-ray phase composition and calculated phase composition for stoichiometric clinker minerals than a phase composition calculated for solid solutions. By prolonged heating of cement samples the free calcia decreases. We may conclude therefore that the phase composition of solid state sintered cement samples (no mineralising effect of impurities or alkalis) is away from the equilibrium phase composition, after 1 and 3 hrs burning of the clinker at 1200°C and in this case the phase computation may be preferred which relies on the stoichiometric composition of phases.

The chemical composition of solid solutions determined in this work may be used to predict the phase composition of clinkers in order to get the idea about the limit the phase composition would approach at the not quite common burning conditions. On the other hand the stoichiometric composition of phases gives quite satisfactory estimation of phases present at usually burning regimes.

CONCLUSIONS

Chemical composition of coexisting solid solutions was determined inside the phase assemblage C_2S, $C_4A_3\bar{S}$, C_4AF, $C\bar{S}$ and C. The stoichiometry of ferrite phase established for slowly cooled samples from 1450°C strongly differs from its usually accepted stoichimetric composition (C_4AF). Its stoichiometry can be more adequately represented by the composition corresponding to C_6AF_2. In a course of equilibration of the clinker system the change in the Fe/Al ratio of the ferrite phase is the one of the dominant changes.

The model clinkers synthesised at usual burning conditions (1200°C, 1 and 3 hrs) are not equilibrium products and their phase composition is in better agreement to Bogue composition calculated for stoichiometric clinker phases than the phase composition calculated for phases taken as solid solutions.

ACKNOWLEDGMENT

This research was supported by COPERNICUS CIPA CT 94-0105.

REFERENCES

Andac, O. and Glasser, F. P., "Microstructure and Microchemistry of Calcium Sulfoaluminate Cement", Mat. Res. Soc. Symp. Proc., Vol. 370, 1995, Mat. Res. Soc., pp. 135-142.

Majling, J., Jesenák, V., Roy, D. M. and Roy, R., "Generalised Bogue Calculations for Determining Phase Compatibility/Equilibria, Assessing Potential Use of Inorganic Industrial By-Products", J. Mater. Res., Vol. 4, No. 2, Mar-Apr, 1989, pp. 447-451.

Majling, J., Sahu, S., Vlna, M. and Roy, D. M., "Relationship between Raw Mixture and Mineralogical Composition of Sulphoaluminate Belite Clinkers in the System CaO-SiO_2-Al_2O_3-Fe_2O_3-SO_3", Cement and Concr. Res., Vol. 23, 1993, pp. 1351-1356.

Mehta, P. K., US Patent 4036657, 1977.

Muzhen, S., Junan, D., Zongdao, W. and Xioxin, L., "Research on the Chemical Composition and Microstructures of Sulfoaluminate Cement Clinker", 9th Int. Congr. on the Chem. of Cem., New Delhi India, 1992, pp. 94-100.

Strigáč, J., Krištín, J., Palou M. T. and Majling, J., "Microstructure and Chemical Composition of Clinker Minerals inside the Phase Assemblage C_2S-$C_4A_3\bar{S}$-C_4AF-$C\bar{S}$ of Sulphoaluminate Belite Cements", Unpublished.

Taylor, H. F. W., "Modification of Bogue Calculation", Advan. in Cem. Research, Vol. 2, No. 6, 1989, pp. 73-77.

QUALITATIVE IDENTIFICATION OF CLINKERS AND CEMENTS — SOME RESULTS AND POSSIBILITIES

Ferenc TAMÁS*, Márta PÁTKAI-HORVÁTH*, Éva KRISTÓF-MAKÓ*
Josef TRITTHART**

* University of Veszprém, Veszprém, Hungary
** Technical University of Graz, Austria

ABSTRACT The qualitative identification of clinkers and cements is based on the fact that trace elements contained in them, and their proportion, retain the characteristic "chemical fingerprint" of the raw materials. The selection of trace elements requires care: best "fingerprint" elements are Mg, Mn, Sr, Ba, Ti and Zr. Clinkers and cements manufactured in Hungarian and Austrian cement factories had been analysed for the above elements (by ICP-ES). Results are interpreted statistically, by „pattern recognition" methods. Dendrograms constructed of analytical data show the possibilty of differentiation by unsupervised learning.

Key-words: qualitative, identification, fingerprinting, pattern recognition, heavy metals

INTRODUCTION

The problem: how to determine the *origin of cement* in concrete. This is a challenging problem, both scientifically and practically (even in case of criminal investigation).

The problem can be solved by the analytical determination of certain elements contained in cements, and the statistical processing ("Pattern Recognition") of analytical data. These elements act as „chemical fingerprints", by which the identification of the manufacturer can be done. As an extension, isotopic distributions can help too, but this is beyond the scope of this paper.

SELECTION OF "FINGERPRINT" ELEMENTS

Not all elements are good for identification. Several aspects should be taken into consideration, when selecting the „fingerprint" (dactylogrammatically relevant) elements. Some important aspects: dactylogrammatically relevant elements *A.* should not be main elements, as cements, manufactured all over the world contain same main elements, and even their ratio is very similar, depending only on cement type, and not cement origin; *B.* should come from the main raw materials (limestone, marl, clay, etc.) an not from the fuel, from refractories, from grinding media wear; *C.* should be thermally stable, as volatile ones evaporate at hot zones and condense at cooler places, thus their amount may vary by kiln conditions; *D.* should be present in measurable quantities; *E.* should not form soluble ions at pH > 10, as in the highly basic environment of concrete this ions can migrate.Above considerations exclude several elements. A list of elements which are definitely inadequate: *A.* Main elements (Ca, Si, Al, Fe, S, alkalies). *B.* Fuel may contain V (fuel oil), Zn, Pb (waste tyres), etc. Older kilns are frequently lined with magnesite-chrom refractories, thus excluding Cr. Grinding media contain steel alloy elements, excluding W, Mn and Cr. *C.* .Alkali-, Tl- , Sn-compounds (esp. chlorides) are easily volatilized. Point *D.* excludes rare earths, noble metals, etc., while point *E.* excludes Cr, Mn, U.

What remains after that? Sr, Ba, Mn, Mg, Ti, Zr, and possibly some others, not investigated yet. Sr and Ba are always present in limestones; their quantity and ratio is fairly constant,

depending on their geological origin, thus they are dactylogrammatically reliable. Mn, although mentioned above (points B and E), can still be used. To investigate the effect of grinding media wear, pure quartz has been ground in a ball mill with steel media for extended time (3 days), but its Mn content was less than 20 ppm; besides the presence of manganates or permanganates have never been reported.. The Mn content of cement is usually higher by 1 or 2 magnitudes. Goguel and StJohn (1993) have used the Ca-Sr-Mn plot for identification.

Our experience (Tamás, 1996; Tamás and Kristóf-Makó, 1996) has shown that the Sr-Ba-Mn 3-element approach (3EA) is not fully adequate, esp. in case of sulfate resistant clinkers, having a high iron content. For the time being, three more elements (Mg, Ti and Zr) are added. According to recent experiences, this 6-element approach (6EA) gives a possibility of a more satisfactory identification.

The knowledge of the concentration of the "fingerprint" elements can be used, in itself, for a rough estimation only. For a more satisfactory resolution, analytical data should be statistically processed, using "pattern recognition" methods. These are described in detail in our priveious publications (Tamás, 1996; Tamás and Kristóf-Makó, 1996)

EXPERIMENTAL

Materials

This paper gives results of clinkers and cements made in two Hungarian cement factories, as well as 27 cements made by various Austrian factories. In case of Hungarian materials, the origin and the type of the sample was known; Austrian factories gave sample numbers only, without describing details. (One of the samples, No. 16 has an extraordinary trace element composition, with all concentrations higher than in any other sample).

Sample preparation

Clinker samples were crushed to 2 mm, reduced to approx. 20 g and hand-ground in an agate mortar to pass sieve 0.045 mm. In case of cement samples there was no need of grinding. Small, but hopefully representative samples were used for further tests.

1 g, exactly weighed sample was dissolved in concentrated hydrochloric acid, SiO_2 removed by precipitation (evaporating in the presence of gelatin) and the precipitate washed out several times. The filtrate was analysed by ICP-ES (Inductively Coupled Plasma Emission Spectrography). This method is advantageous when absolute ppm values are needed, as standardization can be done by reagent grade chemicals of known concentration. The simpler, less time-consuming "slurry method", where the sample, of fineness < 50 μm is suspended in de-ionized water, nebulized in a spray chamber and introduced directly in the plasma unit proved to be insatisfactory. (A NIST standard cement sample was used for standardization, although, for our purposes, where only relative values are needed, unstandardized concentration data can be applied too).

Analytical method

An ARL/3410 type ICP spectrometer was used, with a mini-plasma torch, using a radiofrequency generator, 27.17 MHz of 650 W power. The spectrometer contains a Czerny-Turner vacuum monochromator. Spectral range 165-800 nm. Computation: EPIC (Evolutionary Program for Instrument Control) software, IBM PS/2 computer, with a PC DOS 3.0 system. The wavelengths used in this study (in nm): Mn = 257.610, Mg = 279.553, Sr = 407.771, Ba = 455.403, Ti = 336.121, Zr = 349.621.

Results

Analytical results are shown in **Table 1.** one of two parallels. If deviation between parallels was higher than 5%, a third, decisive analysis was made.

Table 1. Analytical data

Number	Symbol	Group	Mn	Mg	Sr	Ba	Ti	Zr
1 (33)	D/O	2	346	6020	134	214	1314	46
2 (35)	D/O	2	327	5236	130	154	1234	45
3 (37)	D/O	2	323	5677	128	163	1340	46
4 (39)	D/O	2	331	5845	126	243	1358	49
5 (41)	D/O	2	343	5853	128	213	1280	51
6 (43)	L/O	1	356	11775	211	127	1383	39
7 (45)	L/O	1	330	11742	186	121	1480	43
8 (47)	L/O	1	355	11631	201	119	1461	35
9 (49)	L/O	1	318	11876	200	124	1551	44
10 (51)	L/O	1	373	12516	221	124	1641	35
11 (53)	L/S	2	269	8270	165	108	1143	37
12 (55)	L/S	2	322	8591	181	118	1197	37
13 (25)	D/O	2	409	5989	127	193	1519	52
14 (27)	D/O	2	384	5220	131	224	1469	55
15 (29)	D/O	2	407	6834	139	181	1493	55
16 (31)	D/O	2	418	7091	143	181	1589	56
17 (33)	D/OPC	4	936	14771	289	292	1459	59
18 (35)	D/OPC	4	993	16684	325	331	1433	62
19 (37)	D/BFSC	2	417	6394	182	227	1564	54
20 (1)	11	2	631	6467	211	185	1563	59
21 (3)	12	1	1374	10312	288	320	2120	89
22 (5)	13	1	1657	11254	303	327	1894	88
23 (7)	14	1	512	10138	522	381	1773	55
24 (9)	15	3	3194	20079	512	482	2093	93
25 (13)	17	1	1227	10606	337	226	1609	62
26 (15)	18	2	336	6779	209	150	1560	50
27 (17)	19	4	812	17913	1252	219	1206	51
28 (19)	20	4	257	17631	1233	342	1142	49
29 (21)	21	3	3638	24019	1070	478	1391	87
30 (23)	22	4	543	18628	1306	207	1206	48
31 (25)	23	4	1034	16882	920	192	1142	42
32 (27)	24	1	1268	11343	287	230	1379	66
33 (29)	25	1	871	10034	1864	196	1302	50
34 (31)	26	2	1149	10468	1564	218	1256	50
35 (33)	27	2	537	6327	1727	103	1102	38
36 (35)	1	3	684	21888	453	306	1172	44
37 (37)	2	3	846	21646	529	388	1554	51
38 (39)	3	3	828	24519	458	338	1483	53
39 (41)	4	4	1715	15784	473	226	1218	53
40 (43)	5	3	1358	23614	616	215	1220	71
41 (45)	6	3	1296	21860	550	179	1241	64
42 (47)	7	3	551	19474	624	142	1041	44
43 (49)	8	3	1160	20512	512	178	1076	46
44 (51)	9	2	1859	7965	424	104	1021	35
45 (53)	10	4	1808	15632	443	255	1608	50

Explanations to Table 1.

- All analytical data are expressed in (μg/g) units.
- Two numbers are seen in Col. "Number". The first refers to actual sample No, as shown in the coming Figures; the second (in brackets) is an older number, for internal use only, and to facilitate finding of already published data
- Col. "Symbol" contains alphanumericals. Samples 1 - 19 come from 2 Hungarian factories, (D for Dunai Cement, L for Lábatlani Cement), and are clinker or cement samples. The symbol after the shilling stroke (/) gives type: O for ordinary portland cement clinker, S for sulfate resistant portland cement clinker, OPC for ordinary portland cement, BFSC for blastfurnace slag cement. Samples 20 - 45 come from Austrian factories, without giving any details. Here the sample No., as given by the factory is shown in this column. Austrian sample No. 16 was left out of this table. Its extraordinary composition (all 6 constituents higher than those of any other sample) suggests that it was neither clinker nor cement.
- Col. "Group" gives the grouping by statistical processing. The number can be 1, 2, 3 or 4 (see later, in figures, and under heading "Results and Discussion").

Discussion of results

Statistical data evaluation shows that all samples are similar over $S > 0.8$, as shown by the the dendrogram and by the Karhunen-Loeve transformation (from 6 to 2 dimensions). Detailed results are shown in **Figs. 1.**, **2.** and **3.**

Four groups can be seen in the dendrogram, constructed by "distances" in the six-dimensional space **(Fig. 1)**. (The grouping is indicated also in **Table 1**, Col. 3). S (similarity) values of the groups: $S_1 > 0.90$, $S_2 > 0.88$, $S_3 > 0.81$ (this is the lowest), $S_4 > 0.86$. A very distinct group (1a in Fig. 4) is formed by the Lábatlan ordinary clinkers, with $S > 0.95$. Some Austrian materials belong to this group too, but less significantly. In Group 2, the Dunai ordinary clinkers form a distinct group, with $S_3 > 0.96$. Here again an Austrian group is intermixed in a less significant way. The two L/S samples belong to this group too. Nothing is known of the origin of samples in Group 3 and 4. These are Austrian samples (although two Hungarian OPC's, No. 17 and 18) also belong to Group 4. The two extremes, No. 24 and 29, shown by the KL transformation (referred to above) are members of Group 3, but at rather low similarity levels ($S < 0.85$).

In **Fig. 2.** (KL transformation of results), the four cluster groups can be easily separated by a quasi-horizontal line (dotted). In **Fig. 3.** the Sample No. is shown. From this it is evident that the two samples, belonging to the extreme left part of the figures are due to samples 24 and 29. These are Austrian samples, where the exact origin is not known. But it is striking that these two samples are very high in Mn; this is why they are rather far for the other KL-transformed points belonging to Group 3.

Possibilities

The research described in this paper is necessarily only a beginning step, to be continued in three directions:

1. Analysis of already investigated and new samples for still more elements, which may be dactylogrammatically relevant.

2. Continuation of research to study cement identication and finally the same in case of concrete (here the separation of the effects of hydraulic additives and aggregates will cause serious problems).

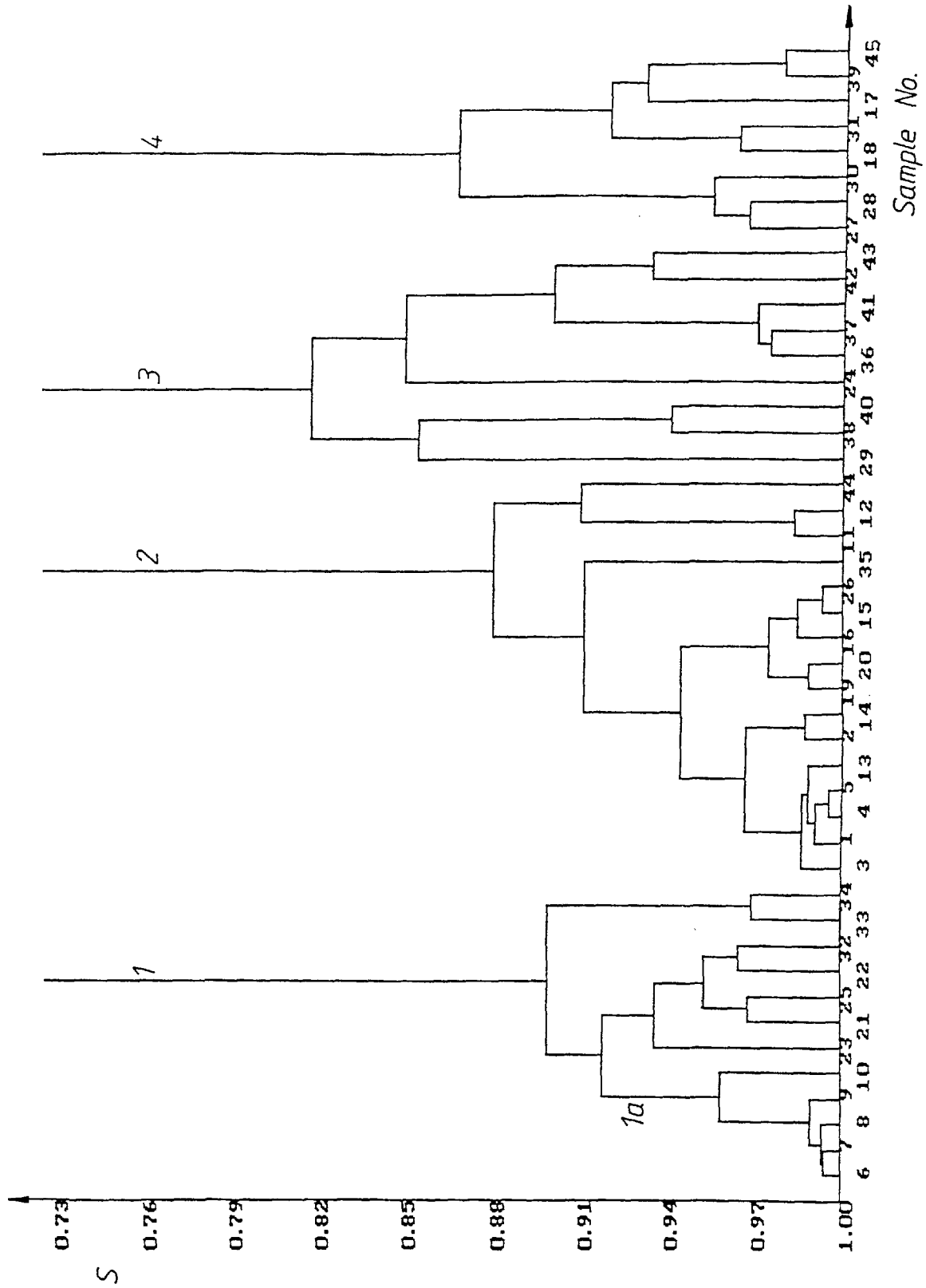

Figure 1. Dendrogram for the 45 investigated samples

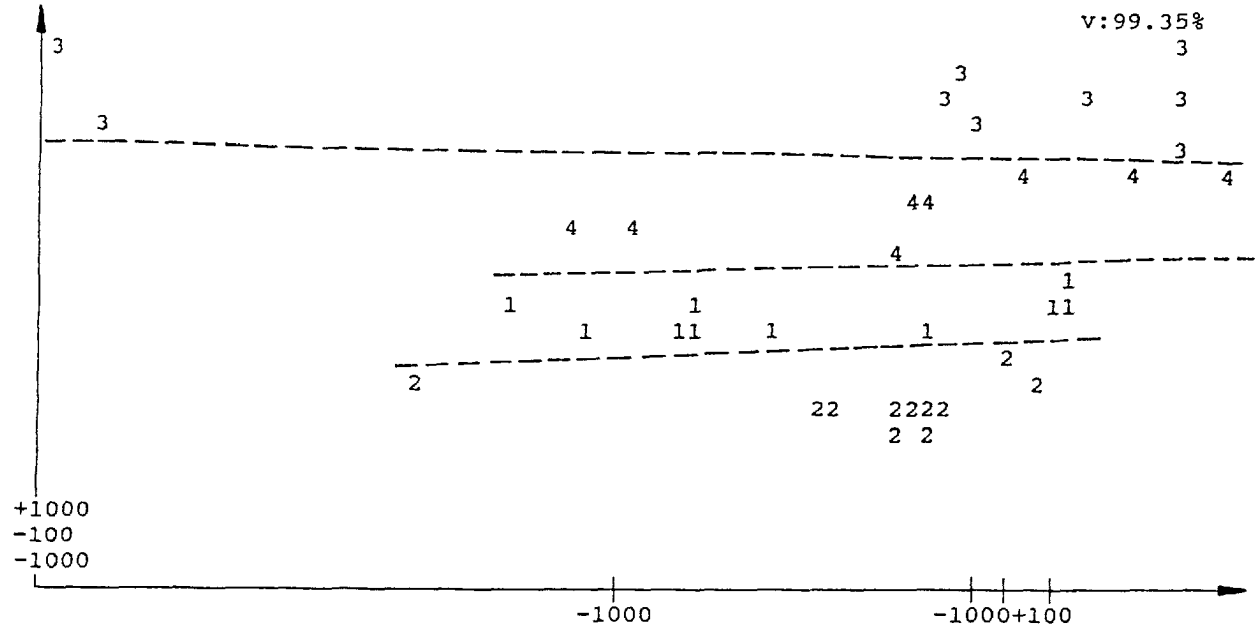

Figure 2. KL transformed data from 6 to 2 dimensions. Numbers refer to Group numbers

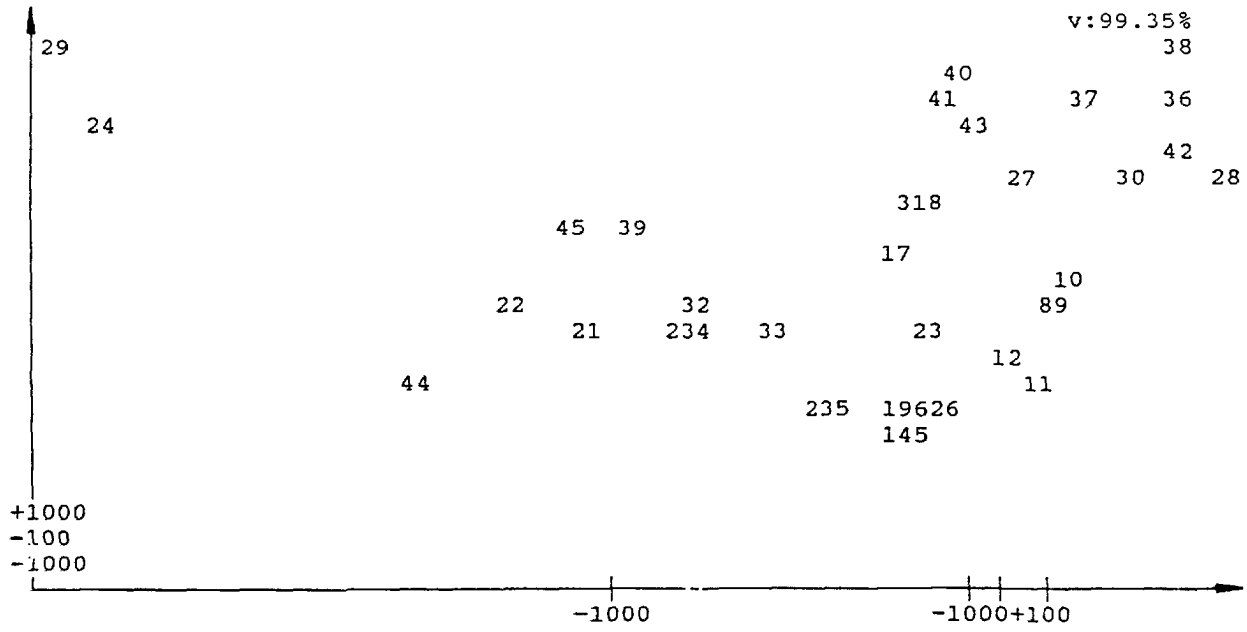

Figure 3. KL transformed data from 6 to 2 dimensions. Numbers refer to Sample numbers

3. The establishment of national, then regional and finally worldwide databases. This sort of research definitely needs international cooperation.

REFERENCES

Goodall, P., Foulkes, M.E. and Ebdon, L (1993): "Slurry nebulization inductively coupled plasma spectrometry - The fundamental parameters discussed". Spectrochimica Acta, Vol. 48B pp. 1563-77

Goguel, R.L. and StJohn, D.A. (1993): "Chemical identification of Portland cements in New Zealand concretes, Part I. Characteristic differences among New Zealand cements in minor and trace element chemistry". Cem. & Concr. Res., **Vol.** 23, pp. 59-68, "Part II. The Ca-Sr-Mn plot in cement identification and the effect of aggregates". Cem. & Concr. Res., Vol. 23, pp. 283-293

Tamás, F.D. (1996): "Pattern recognition methods for the qualitative identification of Hungarian clinkers". World Cement / Res. & Development Vol. 27, pp. 75-79

Tamás, F.D. and Kristóf-Makó, É. (1996) "Chemical fingerprints in Portland cement clinkers". Advances in Building Science — Wittmann Festschrift (Gerdes, A., Ed.) Aedificatio Publishers, Freiburg pp. 217-28

ACKNOWLEDGEMENTS

The financial support of OTKA (Hungarian National Scientific Research Fund), Project No. **T14257** is gratefully acknowledged. Exchange visits between the senior and Austrian author have been financed by the Hungarian-Austrian Intergovernmental S & T Cooperation Program, Project No. **47.**

FINGERPRINTING S.A. CEMENTS BY CHEMICAL ANALYSIS

J. Herman POTGIETER, Pretoria Portland Cement Technical Services, P.O. Box 40073, Cleveland, Johannesburg, South Africa

ABSTRACT There are three cement manufacturers in South Africa, having plants in various parts of the country. Due to geological differences in their raw materials, as well as different quality assurance systems and kiln configurations/operations, the various cements produced differ from one another. From a marketing point of view, as well as in the case of some customer queries, it is necessary and useful to be able to distinguish cements made by the various producers. This paper presents a graphical representation of the respective chemical analyses as well as some typical chemical parameters employed to accomplish these distinctions.
KEY-WORDS Composition, Characterization, Method, Qualitative, X-ray Fluorescence Analysis

INTRODUCTION

The South African cement industry owed its beginnings to the demand created by the discovery of gold in 1886 and the subsequent development of the mining industry. The industry today consists of three players: Pretoria Portland Cement Co. Ltd. (PPC), Blue Circle Ltd. (BC) and Alpha Ltd. (AC). The major deposits of limestone, which is the main raw material in the manufacture of cement, lie in the North West and Northern Cape Provinces, and vary in distance from about 250 to 500 km from Johannesburg, the centre of the industrial and economic area of the country, known as the Gauteng region. Cement compositions are governed by, amongst others, raw material constraints, kiln configurations and operating procedures and quality assurance systems. Therefore the chemical compositions of the cements produced by the different producers vary significantly.

In South Africa the chemical composition of cement must conform to the requirement of the South African Bureau of Standards (SABS) specification 471-1971. This specification only limits the MgO content to a maximum of 5%, the SO_3 content to a maximum of 3.5% for OPC and 3% for SRC and the loss on ignition (LOI) to a maximum of 4.5%. From a marketing perspective, as well as in the case of customer queries, it is often necessary and convenient to be able to distinguish between the cements from the various producers. This matter is becoming increasingly important world wide and only a limited amount of work has been done in this area(Goguel et al., 1993; Tamas et al., 1996).

EXPERIMENTAL

Samples of OPC from the various producers and also different geographical locations in South Africa were analysed on a Siemens MRS 400 X-Ray Fluorescence spectrometer after suitable preparation into pressed pellets and fused glass beads, using an appropriate calibration set up from standard reference materials. The elements which have been found to be most useful for characterisation purposes are Al, Fe, Mn, Ti, Mg, S, K, and Na. The two major elements Si and Ca are of little use. The results obtained are summarised in Table 1. The compositions of the various cements are ratioed against a set of reference values which lie midway between the average compositions of the various producers, as shown in Table 2.

RESULTS

A schematic representation of the ratio values of PPC cements from the Jupiter (Johannesburg) and Port Elizabeth plants on an ordinary x,y graph is given in Figure 1. However, the emerging shape has little impact in illustrating the significant difference between the two cements from a chemical

Table 1 XRF chemical analysis of various South African cements

Element	Reference values	PPC Hercules Plant	PPC Jupiter Plant	PPC Port Elizabeth	PPC Rie-Beeck Plant	PPC De Hoek Plant	PPC Slurry Plant	BC Lichtenburg Plant	Alpha Dudfield plant
SiO2	23.00	21.27	23.21	23.10	21.35	21.59	20.71	21.73	21.84
Al2O3	4.00	4.18	4.95	4.25	4.20	3.17	3.83	4.77	4.18
Fe2O3	3.00	1.71	2.60	4.38	3.44	4.03	3.31	2.85	2.59
Mn2O3	0.50	0.86	0.75	0.08	0.04	0.09	0.24	0.23	0.07
TiO2	0.40	0.23	0.40	0.20	0.21	0.18	0.41	0.40	0.35
CaO	64.00	62.63	60.11	61.87	65.80	63.02	63.16	61.69	62.61
MgO	3.00	4.08	3.72	0.62	0.91	1.06	2.52	2.77	2.02
P2O5	0.30	0.13	0.05	0.16	0.14	0.05	0.03	0.08	0.06
SO3	1.80	1.54	1.77	1.45	1.91	1.91	1.61	1.19	1.29
K2O	0.40	0.70	0.65	0.60	0.52	0.44	0.55	0.18	0.28
Na2O	0.20	0.10	0.13	0.19	0.19	0.29	0.10	0.13	0.10
SrO(ppm)	-	319	219	1224	2619	3328	177	166	192

Table 2 XRF chemical analysis of various South African cements ratioed against their refence composition values

Element	Reference Values	PPC Hercu-les Plant	PPC Jupiter Plant	PPC Port Elizabeth	PPC Rie-beeck Plant	PPC De Hoek Plant	PPC Slurry Plant	BC Lichten-burg Plant	AC Dud-field Plant
SiO2	1.00	0.92	1.01	1.00	0.93	0.94	0.90	0.94	0.95
Al2O3	1.00	1.05	1.24	1.06	1.05	0.79	0.96	1.19	1.05
Fe2O3	1.00	0.57	0.87	1.46	1.15	1.34	1.10	0.95	0.86
Mn2O3	1.00	1.72	1.50	0.16	0.08	0.18	0.48	0.46	0.14
TiO2	1.00	0.58	1.00	0.50	0.53	0.45	1.03	1.00	0.88
CaO	1.00	0.98	0.94	0.97	1.03	0.98	0.99	0.96	0.98
MgO	1.00	1.36	1.24	0.21	0.30	0.35	0.84	0.92	0.67
P2O5	1.00	0.43	0.17	0.53	0.47	0.17	0.10	0.27	0.20
SO3	1.00	0.86	0.98	0.81	1.06	1.06	0.89	0.66	0.72
K2O	1.00	1.75	1.63	1.50	1.30	1.10	1.38	0.45	0.70
Na2O	1.00	0.50	0.65	0.95	0.95	1.45	0.50	0.65	0.50

point of view.

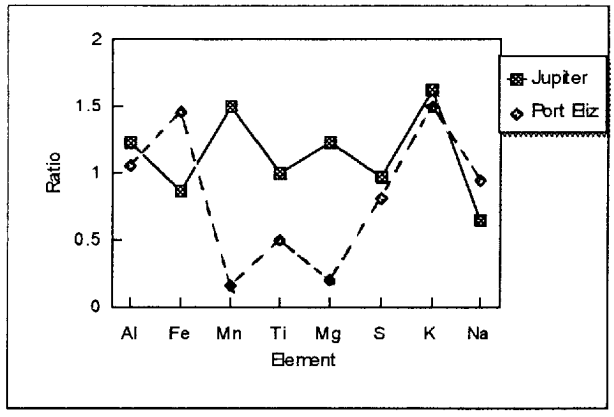

Figure 1 Representation of the ratio values of PPC cements from Jupiter and Port Elizabeth

When one represents the ratio values of the various cements, including these two, in radial fashion at 45^0 angle to one another as "star plots", the visual impact of their chemical differences are much more striking, as can be seen in Figure 2.. If the chemical analyses of the different cements are kept in a regularly updated data base, a library of cement "star plots" can be built up. This could enable one to speedily overlay a standard against an unknown, thus facilitating identification of the unknown cement. The big advantage of the "star plots" is that it utilise a whole suit of elements instead of just one or two to accomplish identification.

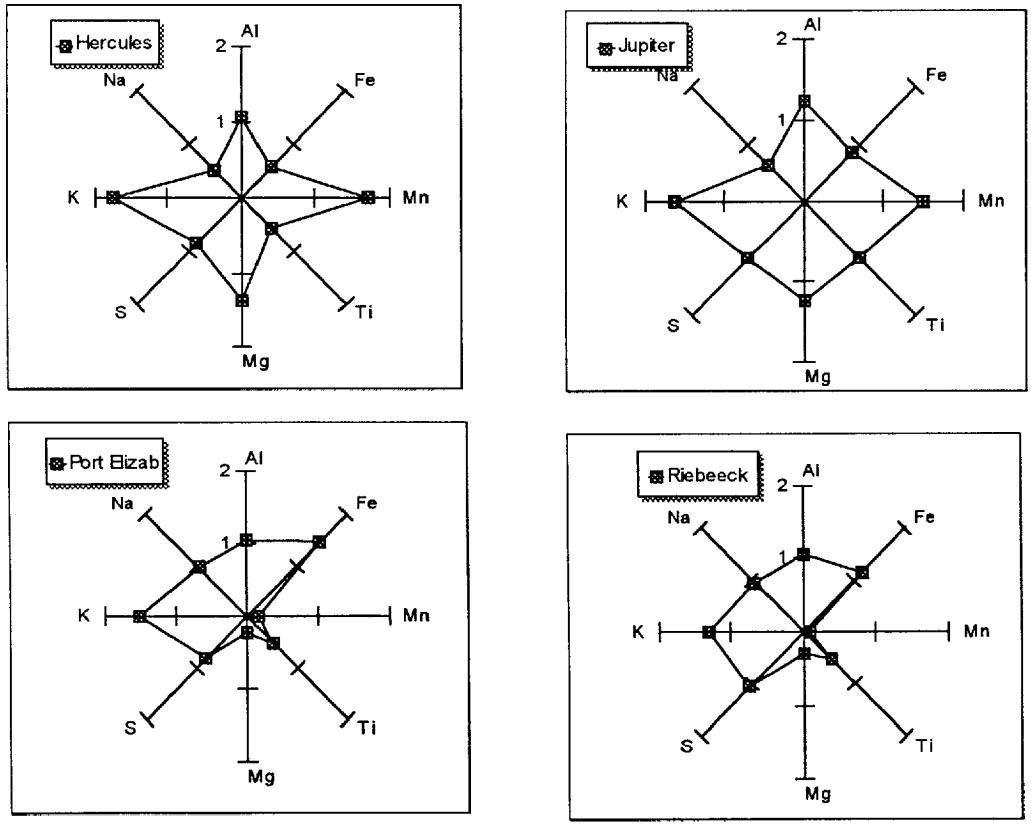

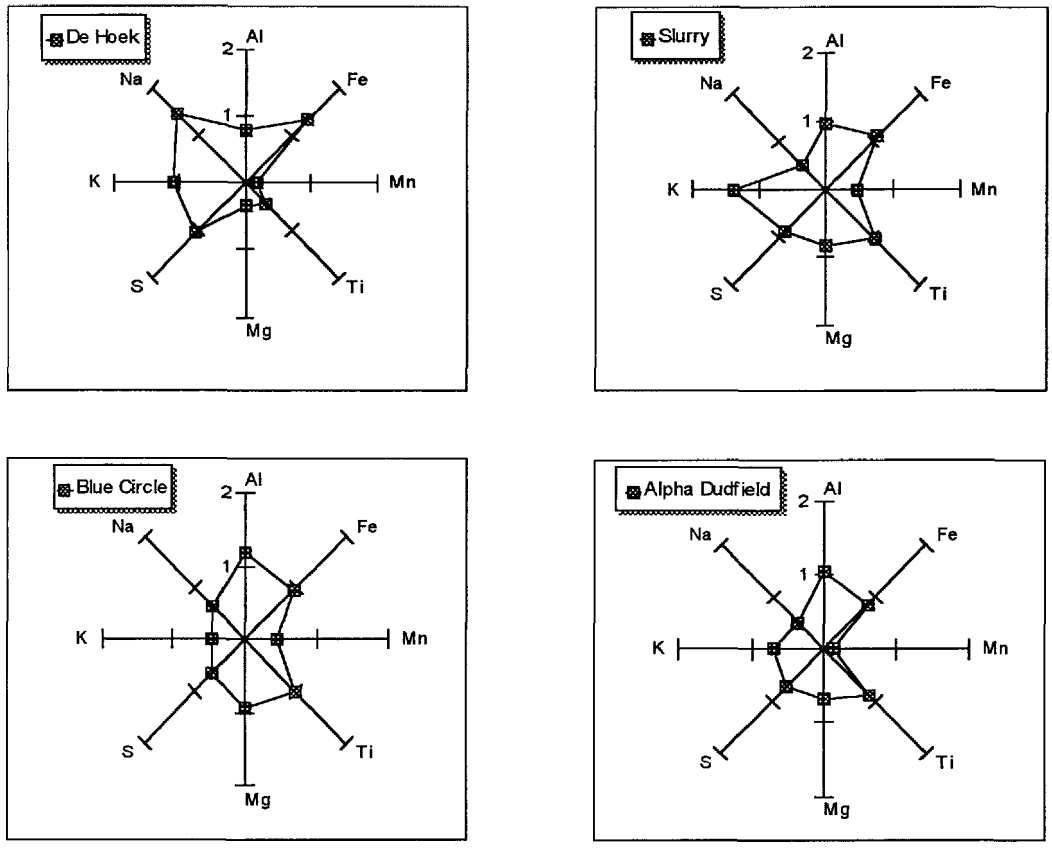

Figure 2 Star plots of the chemical composition of various South African cements

Alkalies are quite important constituents of cement, especially when strength development and possible alkali-silica reactions in concrete made of different cements are considered. The alkali contents, as well as the Sr content, of the various cements produced in South Africa varies significantly among the different producers and also among the different geographical areas in which the cement is produced. This feature can be used as an additional identification tool to determine from which area and producer a cement originate. The alkali equivalents together with typical Sr

Table 3. Alkali equivalents of various South African cements.

Producer	Geographical Area	SrO value (ppm)	Na_2O Equivalent Alkalies(%)	K_2O Equivalent Alkalies(%)
PPC Hercules	Gauteng	319	0.56	0.85
PPC Jupiter	Gauteng	219	0.56	0.85
PPC De Hoek	Western Cape	3328	0.58	0.88
PPC Riebeeck	Western Cape	2619	0.53	0.81
PPC P. Elizabeth	Eastern Cape	1224	0.59	0.89
PPC Slurry	North West Prov.	177	0.46	0.70
Alpha Dudfield	North West Prov.	192	0.28	0.43
BC Lichtenburg	North West Prov.	166	0.25	0.38

values of the various cements are indicated in Table 3 below.

It is clear that there are major differences between the various alkali equivalents and SrO values of the various geographical areas as well as between the different factories and also producers in one specific area. These parameters could therefore be utilise for discrimination and identification purposes.

CONCLUSIONS

A useful way of uniquely identifying cements from various geographical locations and made by different producers in South Africa have been presented. The main advantage of this method is that it utilises not just one or two chemical characteristics of a cement, but of whole suite of elements. The proposed method is furthermore visually striking and easy to use.

ACKNOWLEDGEMENTS

The author gratefully acknowledges Prof. James Willis of the Department of Geology, University of Cape Town who introduced the basic concept in South Africa, as well as the work done by his colleague Mr. Barrie Butcher in this regard. Mrs. Karen van der Merwe of the Council for Geosciences is aknowledged for analysis of SrO in the various samples used. This paper is published by permission of Pretoria Portland Cement Co. Ltd.

REFERENCES

Goguel, R.L. and StJohn, D.A., "Chemical identification of Portland Cements in New Zealand Concretes. I. Trace Element Chemistry", Cement & Concrete Research, Vol.23, 1993, pp. 59-68

Goguel, R.L. and StJohn, D.A., " Chemical identification of Portland Cements in New Zealand Concretes. II. The Ca-Sr-Mn Plot in cement identification and the effect of aggregates", Cement & Concrete Research, Vol. 23, 1993, pp. 283-293

Tamas, F.D., "Pattern recognition methods for the qualitative identification of Hungarian clinkers", World Cement, Vol. 27, 1996, pp. 75-79

Tamas, F.D. and Kristof-Mako, E., "Chemical fingerprints in Portland cement clinker", Wittmann Festschrift, 1996, pp. 217-228

Tamas, F.D. Patkai-Horvath, M., Tritthart, J. and Tagnit-Hamou, A., " Trace elements in clinker and cement for qualitative identification", Gordon Research Conference on Physics and Chemistry of Cement-based Materials, Plymouth, New Hampshire, U.S.A., 28 July-2 Aug. 1996, Poster No. 14

USE OF QUINIZARIN AS A SPECTROPHOTOMETRIC REAGENT FOR MgO CONTENT ANALYSIS OF PORTLAND CEMENT AND CEMENT CLINKER

H. SEDAIRA[a] , K.A. IDRISS[*a] , M.M. SELEIM[a], and M. Shafei ABDEL-AZIZ[b].
[a] Chemistry Department, Faculty of Science, Assiut University, Assiut, Egypt.
[b] Assiut Cement Company, Assiut, Egypt.

ABSTRACT A new direct spectrophotometric method for the determination of magnesium oxide in Portland cement and cement clinker is proposed. The method is based on the reaction of Mg with quinizarin(1,4-dihydroxyanthraquinone) in water-ethanol solution at pH 9.5-10.3. Fundamental study of the complexation reaction of magnesium(II) with this reagent is described. The mono-ligating complex formed under the optimum conditions, allows the determination of 0.5-3.9 $\mu g\ ml^{-1}$ of magnesium. The determination is not affected by any of the other constituents normally present in Portland cement materials .

Keywords : cement analysis, MgO determination, spectrophotometry .

INTRODUCTION

In a dry process cement plant the production of Portland and other types of cement can be divided into two segments, namely (a) processing of the raw materials to raw meal/kiln feed and (b) pyro-processing of the kiln feed to give cement clinker. The raw meal is pre-heated, pre-calcined and clinkerized by a combination of endothermic and exothermic reactions. Clinker is the basic component in the production of cement, which when combined with other elements, results in the formation of various cement types. Portland cement clinker consists substantially of four crystalline clinker 'phases' in close interpenetrating association. MgO and other foreign oxides are usually incorporated in clinker phases. MgO-rich clinker may also contain free magnesium oxide (periclase) which is undesirable because if it is present in substantial amounts, it may cause expansion of concrete, similar to that caused by lime, but more surreptitious. The damage it causes may remain undetectable for years. The magnesium expansion effects are commonly referred to as "unsoundness" of the cement. The high proportion of MgO favours the dissolution of "C_2S" and free lime at higher temperatures and lets "C_3S" form more quickly. It reduces viscosity and surface tension of the clinker melt and increases ionic mobility.

Inside the cement plant, on-line control of the composition of raw meal is needed to maintain the composition of cement to within strict requirements. In addition, the variability of the raw materials used is continuously and constantly traced. The development of new procedures for elemental analysis of cement constituents is desirable because the increasing demand for more analytical results requires faster, selective and precise methods which offer some measure of quality. There must be a method to determine the magnesium oxide content of cement materials. It is the main objective of this work to make use of visible spectrophotometry in the determination of magnesium. Selective determination of Mg^{2+} in presence of Ca^{2+} using common reagents is difficult to performe and several methods have the drawback of the interference from excessive amounts of Ca^{2+} (Sugawara et al, 1973 ; Jimenez et al, 1975 ; Banerjee et al, 1976 ; Sinha et al, 1978,1982 ; Ying-Quan et al, 1982 ; Robiseh et al, 1983 ; Lopez et al, 1986 ; Pal et al, 1992,1994). The standard methods (BS, 1985 ; ASTM - C 114, 1994) for magnesium-content analysis of Portland cement are complicated and require a long time to carry out the determination. It is aimed in the present study to develop a new spectrophotometric method for

the rapid analysis of MgO content of Portland cement and cement clinker, which is superior to other recommended methods in terms of selectivity and sensitivity. The instrument used is cheaper and the running cost lower than those for XRF, AAS or ICP-AES techniques.
In this paper fundemental study of the complexation reaction of magnesium(II) with quinizarin is described and a direct spectrophtometric method for the determination of MgO content of cement materials is presented. The validity of the method was thoroughly examined. MgO content analysis of SRM cement samples of the US NIST have been used to illustrate the results which can be achieved.

EXPERIMENTAL

Apparatus

A Perkin Elmer Lambda 12 spectrophotometer and Radiometer pH meter (M210) with a Radiometer combined glass electrode were used for measurement of absorbance and pH respectively. The pH meter was calibrated regularly befor use with standard buffer solutions. All the spectrophotometric and pH- metric measurements were performed in 50% (v/v) ethanol at 20°C. The pH values in water-ethanol medium were corrected as discribed elsewhere(Douheret, 1967).

Chemicals and Solutions

Standard Magnesium Solution : A stock solution (1 ml = 0.49 mg Mg) was prepared using high purity $MgCl_2$ in 0.05 M HCl and standardized against EDTA.
Quinizarin (QUIN) stock solution : 10^{-3}M in ethanol. Prepared directly using the purified reagent (E. Merck). Other reagents include sodium perchlorate, perchloric acid and sodium hydroxide standard solutions. Solutions of the foreign ions used for interference studies were prepared using the chloride, sulphate or nitrates of the metal cations and potassium or sodium salts of the anions to be tested. pH adjustment of solutions investigated was performed by the addition of either dilute perchloric acid or sodium hydroxide. The ionic strength was kept constant at I = 0.1 mol l^{-1} ($NaClO_4$).

Standard Procedures:

Procedure for Magnesium(II):

In a 25 ml calibrated flask, place a suitable volume of magnesium solution containing less than 80 µg of magnesium, 6 ml of 10^{-3} mol l^{-1} QUIN solution in ehtanol and 2.5 ml of 1 mol l^{-1} $NaClO_4$ solution. Adjust the pH to 10 and dilute to volume with doubly distilled water, keeping the ethanol content at 50% v/v. Mix the solution thoroughly and measure the absorbance at 630 nm against a reagent blank, similarly prepared but containing no magnesium.

Magnesium Oxide Content Analysis of Portland Cement, Clinker and Raw Meal

Step 1 : Dissolution of Sample. Weigh accurately 1.0 gm of the sample (dried at 110°C) into a beaker and dissolve it in the minimum volume of hydrochloric acid. Heat to dryness, add 25 ml of HCl (1+1) to the residue, digest and filter the insoluble residue into a 250 ml calibrated flask and then dilute to volume with bidistilled water.

Step 2 : Procedure for MgO determination in cement materials. Transfer a 2.5 ml aliquot of the sample solution into a 25 ml calibrated flask. Add 6.0 ml of 10^{-3} mol l^{-1} QUIN solution. After mixing with 6.5 ml of ethanol and 2.5 ml of $NaClO_4$, adjust the pH to 10 using NaOH solution added dropwise and mixing thoroughly after each addition. Dilute to volume and mix. Measure the absorbance of the solution at 630 nm against a reagent blank of the same pH as the reference.

RESULTS AND DISCUSSION

Acid-base properties of the reagent

The absorption spectra of QUIN solution in 50% (v/v) ethanol and at various concentrations of $HClO_4$ or NaOH were recorded as the dependence $A = f(\lambda)$ for various pH (see Fig. 1). The reagent yields three coloured acid-base forms in solutions of pH 1.5-11.2 : LH_2, LH^- and L^{2-}. There is a pronounced transformation from the yellow form (LH_2) to the orange red species (LH^-) at pH 8.2-9 . The red form is converted to violet (L^{2-}) at pH > 10.8 . The protonation scheme of the reagent indicate that gradual association of protons with the oxygen of the bis(hydroxyl) substituents is carried out at pH $\leq$ 10.8 and $\leq$ 8.2. It has been spectrophotometrically determined at the working pH region of solutions and 50% (v/v) ethanol that pK_{a1} (LH_2/LH^-) = 8.5 $\pm$0.03 and pK_{a2} (LH^-/L^{2-}) = 10.65$\pm$ 0.05 at I = 0.1.

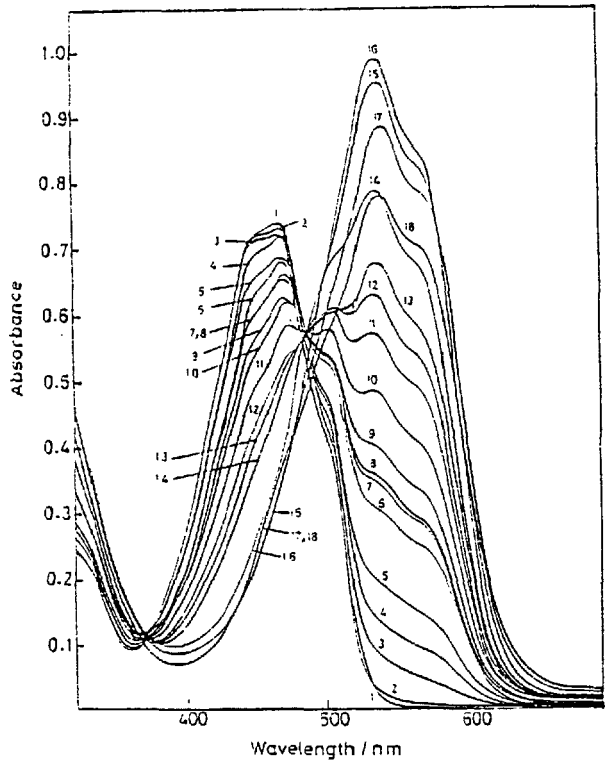

Figure 1. Absorption Spectra of $2x10^{-4}$ mol l^{-1} QUIN at different pH values, 50% (v/v) ethanol, pH : 1) 1.5; 2) 3.8; 3) 6.35; 4) 6.60; 5) 6.8; 6) 7.20; 7)7.3; 8) 7.4; 9) 7.6; 10) 7.9; 11)8.1; 12) 8.25; 13)8.45; 14) 8.7; 15)10.1; 16) 10.6; 17) 10.9; 18) 11.1

Complexation Equilibria of Mg^{2+} with QUIN

An aqueous Mg^{2+} solution reacts with ethanolic solution of QUIN in alkaline medium (optimum pH 9.5-10.3) to form a blue complex species . The absorption spectrum of the magnesium complex shows an absorbance maxima at 630 nm, where the reagent does not absorb. The magnesium complex is completely formed within 5 min of mixing of the reagents and remains stable for at least 4 hr .

The complexation reaction of Mg^{2+} with QUIN is investigated in 50% (v/v) ethanol over the pH range 8-10.8. The solution spectra are recorded in the presence of an excess of the metal ion, in equimolar solutions and in the presence of an excess of the reagent. For all solutions investigated, the absorption spectra are analogous and exhibit an abosprtion band at 630 nm irrespective of the component ratio (C_L/C_M) in solution. The absorption spectra of the Mg-QUIN system with reagent blank as reference are shown in Fig.2 .

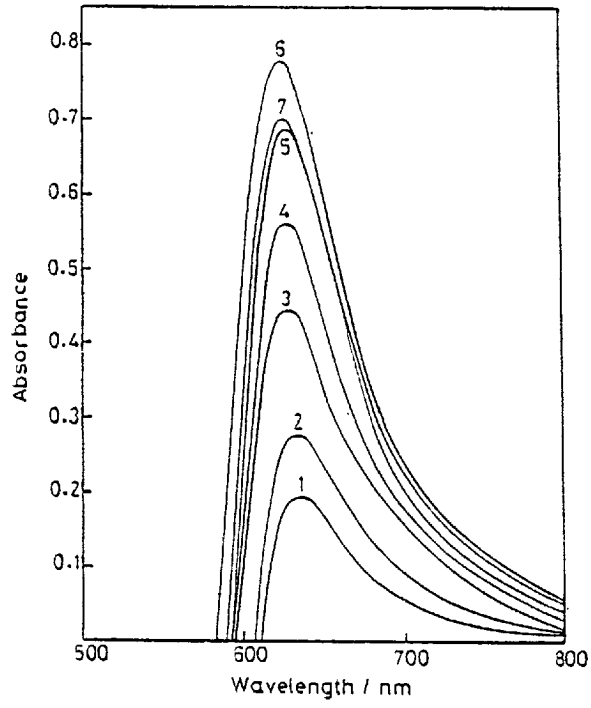

Figure 2. Absorption Spectra of Mg^{2+} - QUIN Complex . $C_L = 2.5x10^{-4}$ mol l^{-1}, $C_M = 1.5x10^{-4}$ mol l^{-1}. 50% (v/v) ethanol, pH : 1) 8.05; 2)8.2; 3) 8.45; 4) 8.7; 5) 9.2; 6) 10.15; 7)10.65 .

The absorbance *versus* pH graphs for solutions of different component ratio show the range of formation of Mg-QUIN complex species and indicate a single chelate equilibrium (c.f. Fig.3). The complexation reaction in the pH 8.2-10.3 is assumed to be carried out according to the general equilibrium

$$mMg^{2+} + nLH_x \rightleftharpoons Mg_m L_n H_b^{(2m-q)+} + qH^+$$

(where b = xn-q)

The absorbance versus pH graphs for the Mg-QUIN system were interpreted using the relations derived earlier (Sommer et al, 1976; Idriss et al. 1988) and the generalized approach described previously (Voznica et al, 1980) .

The following equilibria were assumed during the analysis of the absorbance versus pH graphs.

$$Mg^{2+} + LH^{-} \rightleftharpoons MgL + H^{+} \qquad [1]$$

$$Mg^{2+} + LH_2 \rightleftharpoons MgL + 2\,H^{+} \qquad [2]$$

By considering the acid-base equilibria of QUIN in 50% ethanol and the distribution ratio of the reagent species at different pH (c.f. Fig. 4.)one can assume that the monoionized form of this reagent (LH^{-}) is the prevalent ligand species in the pH range of complexation. The analysis of the ascending part of the absorbance - pH graphs gives the best fit for equilibrium in Eq. 1 and the formation of MgL complex species. The existence of this equilibrium was confirmed in solutions containing excess of one component and in equimolar solutions.
For equilibrium (1), in solutions containing excess of QUIN, it holds that:

$$\Delta A = \varepsilon_1 C_M - \Delta A\ [H]^q / {}^*K_{11} C_L^n \qquad [3]$$

$$\text{Log}\,[\,\Delta A / (\,\varepsilon\, C_M - \Delta A)\,] = q\,pH + \log {}^*K_{11} + n \log C_L \qquad [4]$$

The following equations are valid for equilibrium (1) in solutions with excess of metal ions:

$$\Delta A = \varepsilon_1 C_L - (\Delta A - \varepsilon\, C_L)\,[H]^q / {}^*K_{11} C_M \qquad [5]$$

$$\log\,[\,(\Delta A - \varepsilon\, C_L) / (\varepsilon_1 C_L - \Delta A) = q\,pH + \log {}^*K_{11} + \log C_M \qquad [6]$$

with the values n = q = 1

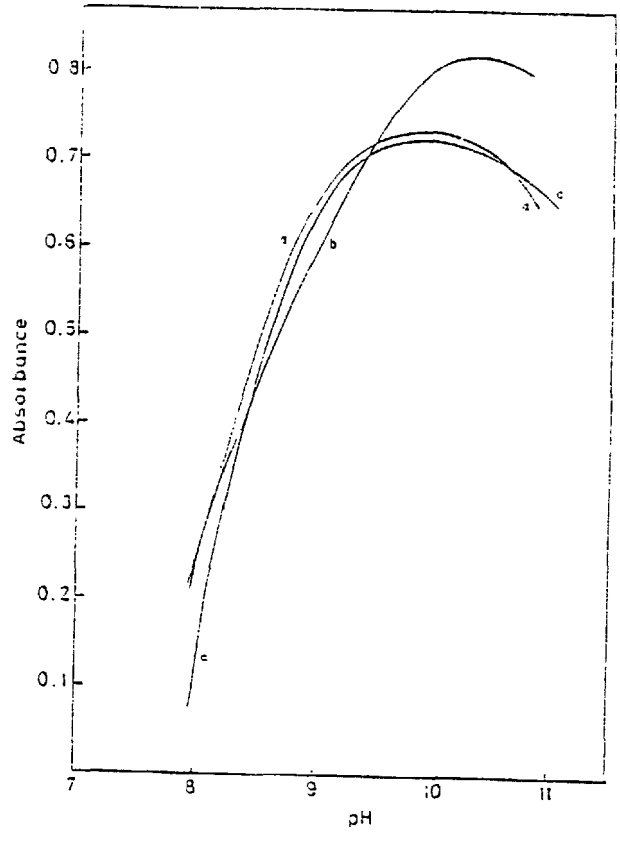

Figure 3 : Absorption versus pH graphs for Mg^{2+} - QUIN system of various concentrations of components, λ = 630 nm, I = 0.1 mol l^{-1} $NaClO_4$, 50% (v/v) ethanol. a) $C_M = 2\times10^{-3}$ mol l^{-1}, $C_L = 2.5\times10^{-4}$ mol^{-1}; b) $C_M = C_L = 2.5\times10^{-4}$ mol l^{-1}; c) $C_M = 1.5\times10^{-4}$ mol l^{-1}, $C_L = 2.5\times10^{-4}$ mol l^{-1} .

The metal : ligand ratio and the number of hydrogen ions liberated were further confirmed by the method of Betteridge and John (Betteridge et al, 1973).

The results obtained indicate that only one proton is liberated during the complex forming reaction and Eq. (1) is predominant. On the other hand, the coordination of a single Mg^{2+} with QUIN at pH 10.2 is confirmed independently by analysis of the $A = f(C_M)$ dependence at $\lambda = 630$ nm by using the relations given elsewhere (Idriss et al, 1993).

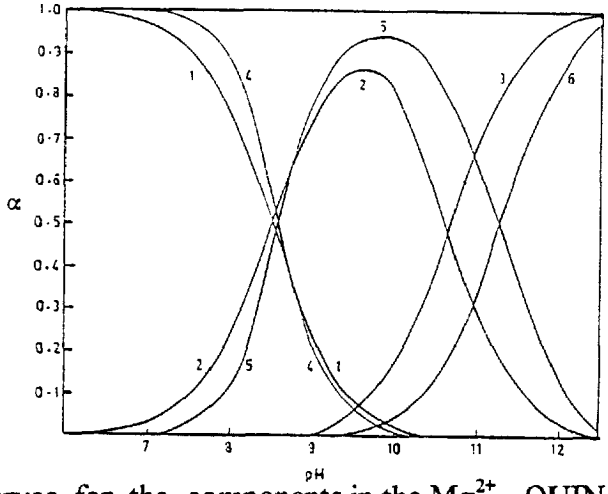

Fig 4. Distribution curves for the components in the Mg^{2+} - QUIN system, 50% (v/v) ethanol. I = 0.1 mol l^{-1} $NaClO_4$. Curves 1-3; $C_L = 2x10^{-4}$ mol l^{-1}, α = 1) $[LH_2]/C_L$; 2) $[LH]/C_L$; 3) $(L^-]/C_L$ Curves 4-6; $C_L = 2.5x10^{-4}$ mol l^{-1}, $C_M = 1.5x10^{-4}$ mol l^{-1}, α = 4) $[Mg]/C_M$; 5) $[MgL]/C_M$; 6) $[MgL(OH)_2]/C_M$

Side reactions involving the formation of hydroxo complexes prevent the appearence of definite plateaux on the absorbance versus pH graphs . The analysis of the descending branch of the graphs, above pH 10.6 for solutions of different component ratio confirms the existence of hydrolytic reaction of the MgL complex :

$$MgL + 2H_2O \rightleftharpoons MgL(OH)_2 + 2H^+ \qquad [7]$$

The stoichiometry of the Mg-QUIN complex was further verified by the method of continuous variations. In solutions having $C_o = C_M + C_L = 2.4 \times 10^{-4}$ mol l^{-1} at pH 10, a component ratio of 1:1 (metal to ligand) was obtained.

The calculated values of the equilibrium (log $^*K_{11}$) stability constant (log β_{11}) and molar absorptivity of the magnesium-QUIN complex are listed in Table 1.

Table 1. Mean value of equilibrium constant (log $^*K_{eq}$)[a], stability constant (log β)[b] and molar absorptivity of Mg-QUIN complex (50% v/v ethanol, I = 0.1 mol l^{-1} $NaClO_4$), 20°C .

Equilibrium[c]	Constant	Log constant	Molar absorptivity $l\ mol^{-1}\ cm^{-1}$
[MgL] [H]/[Mg][LH]	$^*K_{11}$	- 4.69	
[MgL]/[Mg][L]	$^*\beta_{11}$	5.95	4700 (λ = 630 nm)

a- From the absorbance versus pH graphs, b- $^*\beta_{11} = {}^*K_{11} / K_{a2}$, c- Charges are omitted .

Effect of foreign ions

The tolerance of the method to foreign ions was investigated with solutions containing 60 µg of Mg per 25 ml and various amounts of foreign ions. Magnesium was then determined as Mg

(QUIN) under the optimum conditions as described in the given procedure . The tolerance criterion for a given ion was taken to be the deviation of the absorbance values by more than ± 2% from the value expected for Mg alone . The determination of magnesium as the Mg(QUIN) complex was possible in the presence of Al^{3+}, V^{5+}, Mn^{2+}, Fe^{3+},Hg^{2+}, Mo^{6+}, Cu^{2+} (about 25 - fold excess). Also, Ni^{2+}, Cd^{2+}, Zn^{2+}, Pb^{2+}, Ba^{+2} , Sr^{2+} and Ca^{+2} are tolerated at about 40 fold excess. The presence of SO_4^{-2}, Cl^-, Br^-, NO_3^-, ClO_4^- , PO_4^{-3} up to about 100-fold excess caused no interference. The alkali metal ions have no interferring effect on the determination .

Calibration graph, detection limit and precision

Under the optimum conditions cited above, a linear calibration graph for the Mg-QUIN system was obtained up to a concentration of 3.9 μg ml^{-1} of Mg^{2+} with a molar absorptivity of $4.7x10^3$ l mol^{-1} cm^{-1} at 630 nm. A Ringbom plot showed that the optimum concentration range for the determination of magnesium was 0.85-3.2 μg ml^{-1}. The Sandell's sensitivity of the reaction was found to be $0.88x10^{-3}$ μg cm^{-2}. The reproducibility of the method was checked by analyzing a series of five solutions each having a Mg concentration of 2.4 μg ml^{-1}. The relative standard deviation was found to be 0.81% .

MgO content analysis of Portland cement

The potential of QUIN as a reagent for direct spectrophotometric determination of magnesium(II) prompted us to explore further the applicability of the method for the determination of MgO in Portland cement and cement clinker. The results of our study indicate that the determination of magnesium content of cement can be achieved precisely under the optimum conditions adopted (c.f. Fig. 5).

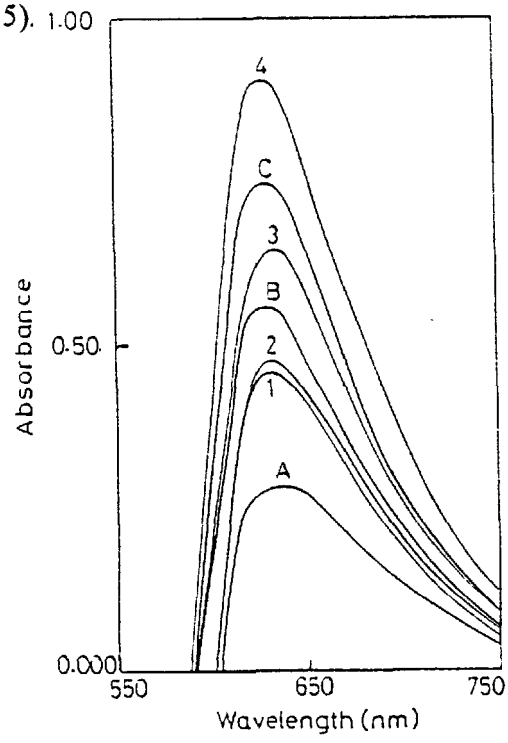

Fig 5. Spectrophotometric determination of magnesium with QUIN; $C_L = 2x10^{-4}$ mol l^{-1}, pH = 10, 50% (v/v) ethanol. Curves A,B and C ; Absorption spectra of Mg-QUIN complex; $C_{Mg} = 6x10^{-5}$ (A); $1.17x10^{-4}$ (B) and $1.55x10^{-4}$ mol l^{-1} (C) Curves 1-4 : Solution spectra of cement materials (1,2,3 = 10 mg sample; 4 = 7.5 mg sample); 1) clinker; 2) cement; 3) SRM (1889); 4) SRM (1880). MgO found (%) = 0.98 (1), 1.04 (2), 1.38 (3) and 2.59 (4)

Replicate MgO content analysis of SRMs of the US NIST : 1880, 1881, 1886, and 1889 were performed. In the precision study, five determinations were carried out for each sample, statistical evaluation of data indicated good precision of the proposed method which make it possible to apply it to the routine analysis of cement. Analysis of samples of cement materials containing various proportions of magnesium is feasible over the concentration range 0.85-3.2 $\mu g\ ml^{-1}$ of Mg^{2+}. The detection limit (at 95% confidence level) of the method for the mean of five analysis was calculated as 25.3 $ng\ ml^{-1}$ for Mg. Some results obtained for the analysis of cement standard reference materials are given in Table 2

Table 2 Application of the proposed method to the direct spectrophotometric determination of MgO in some Portland cement materials .

Sample*	Statistical term	Magnesium determination, % MgO
Cement	$\bar{x}$	1.03
	s	1.64×10^{-2}
	95% CL	$\bar{x} \pm 0.020$
Clinker	$\bar{x}$	0.99
	s	2.01×10^{-2}
	95% CL	$\bar{x} \pm 0.024$
Raw meal	$\bar{x}$	0.63
	s	1.80×10^{-2}
	95% CL	$\bar{x} \pm 0.022$
Clay	$\bar{x}$	2.65
	s	2.70×10^{-2}
	95%	$\bar{x} \pm 0.033$
	NIST SRMs Portland Cement^{++}	
SRM 1889	$\bar{x}$	1.37
	s	2.10×10^{-2}
	95%	$\bar{x} \pm 0.026$
SRM 1886	$\bar{x}$	1.61
	s	2.2×10^{-2}
	95% CL	$\bar{x} \pm 0.027$
SRM 1881	$\bar{x}$	2.62
	s	3.14×10^{-2}
	95% CL	$\bar{x} \pm 0.039$
SRM 1880	$\bar{x}$	2.63
	s	2.85×10^{-2}
	95% CL	$\bar{x} \pm 0.035$

* Number of determinations for each sample (n) = 5, $\bar{x}$ = mean recovery (%), s = standard deviation (%), CL = confidence limit (%), Test solution of the samples investigated contained 5-10 mg of cement material per 25 ml ($^{++}$) certified amounts : MgO = 1.38% (1889), 1.6% (1886), 2.63% (1881), 2.61% (1880) .

CONCLUSION

The proposed spectroscopic method utilizing quinizarin allows precise and accurate determination of MgO content of cement . The method has reasonable selectivity and is inexpensive . It save a lot of time in determining magnesium oxide in cement, clinker and raw meal samples and could replace the present test methods for cement analysis .

Acknowledgement : The authors acknowledge the financial support of Assiut Cement Company and the facilities provided which made it possible to undertake the work .

REFERENCES :

ASTM Annual Book of standards, American Society for Testing and Materials C-114, 1994 .
Banerjee, G., Kanji, S.K., and Mandal, S., Z. Anal Chem. 282, 1976, 47 .
Bello Lopez, M.A., Callejon Mochon, M., Gomez Ariza, J.L., and Guiraum Perez, A., Analyst 111, 1986, 429 .
Betteridge, D., and John, D., Analyst, 98, 1973, 390 .
British standard, British standard Institution, BS, 1985, 6588 .
Douheret, G., Bull. Soc. Chem Fr., 1967, 1412 .
Jimenez, M.D., Bustamante, J.A. and Marti, F.B., Anal Chem. 47, 1975, 521 .
Idriss, K.A., and Saleh, M.S., Analyst, 118, 1993, 723 .
Idriss, K.A., Seleim, M., Saleh, M., Abu-Bakr, M., and Sedaira, H., Analyst, 113, 1988, 1643 .
Pal, T., Jana, N.R. and Das, P.K. Analyst, 117, 1992, 791 .
Pal, T. and Jana, N.R., Talanta, 41 (8) 1994, 1291 .
Robiseh, G., and Rericha, A., Anal Chim. Acta, 153, 1983, 281 .
Sinha, B.C. and Dusgupta, S., Talanta 25, 1978, 693 .
Sinha, B.C. and Roy, S.K., Analyst, 105, 1980, 720; Analyst, 107, 1982, 965 .
Sugawara, M. and Kambara, T., Bull. Chem. Soc., Jpn, 46, 1973, 3789 .
Sommer, L., Langova M. and Kuban, V., Collec. Czech. Chem. Commun., 41, 1976, 1317 .
Voznica; P., Havel, J., and Sommer, L., Collec. Czech Chem. Commun.,, 45, 1980, 54.
Ying-Quan, Z. and Lijun-Yi, Analyst, 107, 1982, 957 .

ANALYSIS OF THE TRACE ELEMENTS IN RAW MATERIALS AND CEMENT BY MEANS OF ICP-AES

Shigeru TAKAHASHI, Hiroyuki ANZAI, Hiroyuki NEMOTO
Japan Cement Association, R&D Laboratory

ABSTRACT The trace elements in cement and raw materials were determined by means of ICP-AES. The elements analyzed are V, Cr, Ni, Cu, Zn, Sr, Cd and Pb.
The samples were decomposed by alkali fusion used lithium metaborate or hydrofluoric acid-hydrochloric acid-hydrogen peroxide. The concentrations in sample solution were determined by calibration curve method or addition method. The recoveries of each element in coal fly ash (the standard reference material of NIST, 1633b) were examined.

Key-words : Heavy metals, Method, Quantitative, Waste material utilization

INTRODUCTION

In the cement industry, various waste and sludge have been used for a part of raw materials of cement clinker recently. In this case, the trace elements in raw materials or cement should be analyzed quickly because it is necessary to judge whether the amount of trace elements in waste and sludge is suitable for raw materials of cement.
The multielement is analyzed high sensitively by means of ICP-AES. This analytical method is applied to soil and coal fly ash (Yamashige, 1984 and Haraguchi, 1984), etc.. But, ICP-AES analysis has been hardly applied to the trace elements of cements and raw materials.
This paper describes the rapid analytical method of the trace elements both on raw materials and cement by means of ICP-AES.

EXPERIMENTAL

Instrument

The instrumentation, operating parameters and analytical lines for the emission measurements are summarized in Table 1. The calibration curves were made by joining the points for the blank and standard with straight lines.

Chemicals and standard solutions

Lithium metaborate used was special grade reagent. Hydrofluoric acid and hydrogen peroxide used were spectrochemical grade reagent. Hydrochloric acid used was ultrapur for trace analysis. Standard solutions for calibration curves were prepared by adding diluted the commercially available standard solutions(1000mg/ml) for atomic absorption spectrometry to blank solution.

Table 1 Instrumentation, operating conditions and analytical lines

ICP spectrometer	Seiko Instruments Inc. SPS-1700	Element	Wavelength (nm)
Frequency	27.12MHz	V	292.402 II
Output power	1.3kW	Cr	267.716 II
Coolant gas	argon 16.0 l/min	Ni	231.604 II
Auxiliary gas	argon 0.5 l/min	Cu	327.396 I
Carrier gas	argon 0.45 l/min	Zn	213.856 I
Nebulizer	concentric type	Sr	346.446 II
Monochrometer	Czerny-Turner type (100cm focal length)	Cd	228.802 I
Grating	3600 grooves/mm	Pb	220.353 II
Entrance slit width	20μm		
Exit slit width	30μm		

Procedure

The procedures of alkali fusion decomposition(AFD) and hydrofluoric acid decomposition(HAD) are shown in Fig 1.

The concentrations of elements in final solutions were determined by caliblation curve method and addition method. The final solution (I) and (III) were prepared for caliblation curve method, and the final solution (II) and (IV) were prepared for addition method.

In addition method, the concentrations of elements in final solutions were calculated from **Eq 1.**

$$\text{Concentration} = I_c \times C_{ass} / (I_a - I_c) \quad [1]$$

where C_{ass} : Concentrations of added elements in final solution (II) or (IV)

I_c : Net intensity of final solution (I) or (III)

I_a : Net intensity of final solution (II) or (IV)

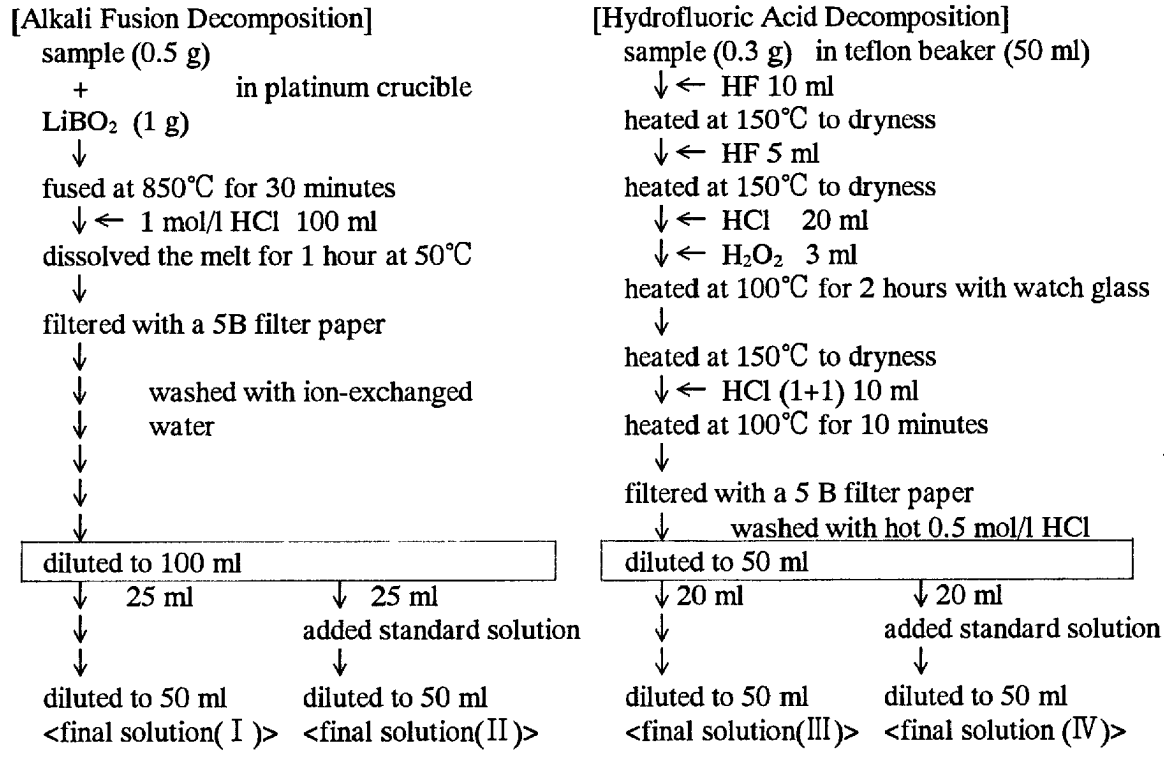

Figure 1 The procedures of alkali fusion decomposition and hydrofluoric acid decomposition

RESULTS AND DISCUSSION

Insoluble residue

Insoluble residues of samples are shown in Table 2. Insoluble residues were 0.05-0.62%. These insoluble residues were influential in determining track elements and all samples were able to be decomposed by both alkali fusion and hydrofluoric acid decompositions.

Table 2 Insoluble residues of samples (%)

Sample	Decomposition	
	Alkali fusion	Hydrofluoric acid
Coal fly ash(*)	0.20	0.20
Portland cement	0.62	0.35
Lime stone	0.19	0.19
Clay	0.17	0.22
Silicious rock	0.12	0.05

(*) Standard reference material of NIST,1633b

Lower limit of determination

The lower limits of determination of each element were calculated from **Eq 2**, and are shown in **Table 2.**

$$\text{Lower limit of determination} = C_s \times (10 \times S_b / I_s) \quad [2]$$

where C_s : Concentration of standard solution for calibration curve method

S_b : Standard deviation of the measured intensities of blank solution at analytical line

I_s : Net intensity of standard solution for calibration curve method

Table 2 The lower limits of determination of each element

Element	Final solution (ng/l)		Sample (mg/kg)	
	Alkali fusion	Hydrofluoric acid	Alkali fusion	Hydrofluoric acid
V	3.33	2.33	1.33	0.97
Cr	3.33	2.33	1.33	0.97
Ni	6.66	5.00	2.66	2.08
Cu	6.66	4.00	2.66	1.67
Zn	1.66	1.66	0.66	0.69
Sr	8.32	6.66	3.33	2.78
Cd	2.33	1.33	0.93	0.55
Pb	16.6	15.0	6.64	6.25

Recoveries of coal fly ash

The recoveries of each element were examined with coal fly ash (standard reference material of NIST, 1633b). The results are shown in **Table 3.** In AFD, the recoveries determined by calibration curve method were 92.2 - 105.2% and by addition method were 93.7 - 100.3% on V,Cr,Ni,Zn,Sr and Pb, and there was no difference between both methods. The recoveries of Cu were 66.1% and 71.6% respectively, and the evaporation of copper during fusing were found in AFD.

In HAD, the recoveries determined by addition method were 95.3 - 100.8% except Cd. But, the recoveries determined by calibration curve method were lower than addition method, and it is recognized that the determination by the calibration curve method is influenced by the physical interference in hydrofluoric acid decomposition(Hiraguchi, 1986).

The recovery of Cd were larger than 100% in all analytical conditions. It is neccessary to be concentrated by solvent extraction for determining the near content of lower limit of determination, because the intensity at the analytical line(228.802nm) of Cd is affected by spectral interference of major elements in sample.

Table 3 Determined values and recoveries of coal fly ash

Element	Certified value (mg/kg)	Alkali fusion decomposition		Hydrofluoric acid decomposition	
		Calibration curve	Addition	Calibration curve	Addition
V	295.7±3.6	284.6 (96.2%)	296.6 (100.3%)	278.2 (94.1%)	296.7 (100.3%)
Cr	198.2±4.7	198.6 (100.2%)	195.7 (98.7%)	173.7 (87.6%)	188.8 (95.3%)
Ni	120.6±1.8	121.6 (100.8%)	117.0 (97.0%)	106.6 (88.4%)	120.7 (100.1%)
Cu	112.8±2.6	74.6 (66.1%)	80.8 (71.6%)	109.7 (97.3%)	112.9 (100.1%)
Zn	(210)	209.4 (99.7%)	206.4 (98.3%)	187.6 (89.3%)	211.6 (100.8%)
Sr	1041 ±14	1095 (105.2%)	1028 (98.8%)	956 (91.8%)	1041 (100.0%)
Cd	0.784 ±0.006	1.33	1.67	1.2	1.6
Pb	68.2 ±1.1	62.9 (92.2%)	63.9 (93.7%)	58.1 (85.2%)	67.9 (99.6%)

The number of tests is 3 and the determinated values are average. Values in parentheses are the recoveries.

Analysis of cement and raw materials

The average contents and the standard deviation of reproducibility are shown in **Table 4**. The maximum of the standard deviation gave 1.60mg/kg on V,15.2mg/kg on Cr, 2.61mg/kg on Ni, 3.39mg/kg on Zn, 3.77mg/kg on Sr and 2.25mg/kg on Pb. From these results, the alkali fusion decomposition and the hydrofluoric acid decomposition are able to be applicable to the anlysis of these elements in addition method.

For the analysis of Cr in cement and raw materials, the averages of HAD were lower than AFD. But the analysis of coal fly ash did not show this tendency remakably (**Table 3**). Though it is known generally that Cr^{3+} products chromyl chloride in perchloric acid solution and chromyl chloride evaporates above 150℃, (Haraguchi, 1984 and Vandecasteele, 1993) it is a doubtful whether the chromyl chloride evaporates during hydrofluoric acid decomposition procedure, and so the HAD is not suitable for determining chromium.

For the analysis of Cu in cement and raw materials, the maximum of standard deviation of reproducibility gave 10.2mg/kg on AFD and 1.34mg/kg on HAD. The averages on AFD were larger than those on HAD, and these results were different with the result ot coal fly ash.

Table 4 The average contents in cement and raw materials and the standard deviation of reproducibility

(mg/kg)

Element	Alkali fusion decomposition				Hydrofluoric acid decomposition			
	Cement	Lime stone	Clay	Silicious rock	Cement	Lime stone	Clay	Silicious rock
V	107.7	5.2	96.2	10.3	105.9	5.1	94.4	9.3
	(1.60)	(0.17)	(1.05)	(0.06)	(0.72)	(0.00)	(0.52)	(0.29)
Cr	100.6	19.3	74.1	611.6	87.7	16.0	66.9	466.0
	(1.40)	(0.35)	(0.65)	(15.2)	(1.02)	(0.35)	(0.15)	(2.55)
Ni	33.4	5.2	20.6	21.4	31.2	3.2	16.9	20.6
	(2.26)	(2.61)	(1.85)	(0.25)	(1.35)	(0.25)	(1.97)	(0.49)
Cu	64.3	15.4	40.9	33.0	59.0	4.2	30.5	27.1
	(6.01)	(3.19)	(10.2)	(5.57)	(1.34)	(0.93)	(0.91)	(0.82)
Zn	230.0	20.2	83.5	24.1	216.6	15.8	80.1	21.2
	(3.39)	(6.23)	(2.24)	(1.11)	(2.20)	(3.37)	(1.67)	(1.55)
Sr	262.8	95.2	39.7	16.4	262.2	96.2	32.8	17.0
	(3.77)	(3.29)	(3.48)	(0.17)	(1.44)	(0.50)	(0.35)	(1.31)
Pb	13.5	<LLD	16.9	<LLD	17.2	<LLD	17.6	<LLD
	(0.14)	(−)	(2.25)	(−)	(1.01)	(−)	(1.51)	(−)

LLD is the lower limit of determination. Values in parentheses are the standard deviations of reproducibility (N=3)

REFERENCES

Haraguchi, H., "Basic and Application of ICP Spectrometry", Kodansya, Tokyo, 1986.

Haraguchi, H., **Kurosawa**, M. and **Iwata**, Y., "Bunseki Kagaku", Vol.34, 1984, pp.252-257

Vandecasteele, C. and **Block**, C.B., "Modern Methods for Trace Element Determination", John Wiley & Sons, Chichester, 1993

Yamashige, T., **Yamamoto**, M., **Shigetomi**, Y. and **Yamamoto**, Y., "Bunseki Kagaku", Vol. 33, 1984, pp.106-119

[This study has been conducted by the Committee on Cement Chemistry of Japan Cement Association. The members of committee are S.Hanehara, T.Takahashi, H.Morooka, T.Yamamoto, T.Iida, Y.Ochi, T.Hirose and S.Kuba.]

DIRECT DETECTION OF GRINDING AIDS IN A CEMENT MATRIX

Pierre CASSAT and Jean François MULLER.
Laboratoire de Spectrométrie de Masse et de Chimie Laser, University of Metz, France.
Angélique VICHOT and Pierre COLOMBET.
Centre technique Groupe Italcementi-Ciment français, 78931 Guerville Cedex, France.

ABSTRACT The present study is devoted to the enhanced detection of grinding aids into a cement matrix. The utilized method was the Laser Desorption Fourier Transform Mass Spectrometry without preconcentration step. It is shown that triethanolamine could be accurately detected at a dosage as low as 350 ppm. This molecule and triisopropanolamine were also detected on each of the pure mineral phases of clinker. The experiments suggest that both molecules exhibit different affinities for each of those phases.

KEY-WORDS : Grinding aids, Mechanism, Mass spectrometry

INTRODUCTION

In many cases, grinding aids are used in clinker grinding to decrease the energy consumption to obtain a given fineness or flow of cement. It is supposed that their positive effect stems from the fact that they interact with the surface of the anhydrous phase particles to form a film which prevents agglomeration. However direct evidence and analysis of such an interaction is not straightforward because only minute amounts of grinding aids are added to clinker (< 500 ppm). Hence, so far, precise investigation and deep knowledge of their mechanism of action, with the aim of improving clinker grinding, are rather limited. To achieve a direct route for such an analysis, the Laser Desorption Fourier Transform Mass Spectrometry (LD-FTMS) technique has been used.

EXPERIMENTAL

Chemical

Clinker pure phases (C3S, C2S, C3A and C4AF) were first prepared from laboratory grade calcium carbonate and the relevant oxides mixed in stoichiometric amounts and subsequently sintered at high temperatures. Then they were ground separately in a lab mill, in presence of triethanolamine (TEA) or triisopropanolamine (TIPA) both at the concentration of 500 ppm. The Blaine area values obtained for each sample are indicated in Table 1. The same grinding operations were carried out for an industrial clinker to which 5 weight percent of gypsum had been added. However, in this case, only the detection of TEA (at various concentrations : 350, 500, 1000 ppm) has been investigated.

	C_3S	C_2S	C_3A	C_4AF
TEA	2850	2758	1363	1204
TIPA	2900	2850	1263	1136

Table 1 :Blaine area values (cm^2/g) of the different mineral phases ground for 1 hour in presence of 500 ppm TEA or TIPA.

Fourier Transform Ion Cyclotron Resonance (FT-ICR) laser microprobe

The utilized laser microprobe set-up allows to analyse solid samples. Studied cement and clinker pure phases, which are finely divided powders, were pressed into pellets (5 tons during 20 minutes) for analysis. The obtained samples which were ca. 0.5 mm thickness and ca. 10 mm diameter were fixed on the holder. Analyses were performed on a laser microprobe Fourier Transform mass spectrometer (Muller et al., 1989 and Pelletier et al., 1988). This instrument is a modified, differentially pumped dual-cell Nicolet Instrument FTMS 2000 (nowadays Extrel FTMS millipore, Madison, WI, USA) operating at a 3 Tesla magnetic field strength and coupled with a reflexion laser interface and special sample manipulation hardware.The ionization step was performed using an excimer laser charged with ArF mixture (λ = 193 nm, pulse duration = 23 ns, output energy = 250 mJ) or KrF mixture (λ = 248 nm, pulse duration = 23 ns, output energy = 250 mJ). The laser beam was focused on the sample, which was placed inside the source cell, by means of several internal lenses and an external adjustable telescope. This configuration allows the adjustment of the laser beam diameter from 5µm to several hundreds of µm corresponding to a power density varying between 10^{10} and 10^5 W/cm^2 with an energy at the sample surface of approximatively 60 µJ per pulse. The viewing system, using an inverted Cassegrain optics design, allows sample visualization with X300 magnification (Muller et al., 1989 and Pelletier et al., 1988). A large sample surface can be swept and analysed (ca. 1 cm^2). Coarse and fine *x, y, z* manipulations of the sample stage can be achieved by micromanipulators with the spacial resolution attainable by micrometers.

The experiment sequence used for these analyses was as follows :

- At first, ions are formed by a laser induced ionization in the source cell (residual pressure : $5x10^{-8}$ Torr).
- During the ionization event, the conductance limit is kept as the trap potential (typically +1V) to confine ions to the source side. This conductance limit can eventually be grounded to transfer ions to the analyser side (residual pressure : 10^{-9} Torr) to achieve better resolution in heterodyne mode (Marshall, 1990).
- A variable delay period follows, during which ion/molecule reactions can occur.
- Ions are then excited by a frequency-excitation chirp and the ions image current is detected, amplified, digitized and Fourier transformed to produce a mass spectrum.

RESULTS AND DISCUSSION

At the laser wavelength of 193 nm, the grinding aids (TEA and TIPA) were detected in each of the four pure constitutive phases of clinker. Spectra (fig 1) show the unquestionable detection of TEA in C_2S via the presence of the peak at m/z=118 uma. Concerning TIPA, it could also be undoubtedly detected from the apparition of the peak at m/z=146 uma (fig 1). Indeed, at this wavelength value, the incident photon energy is 6.14 eV and the desorption process of organic molecules is known to be based essentially on a gazous photoionization step. Accordingly, both peaks correspond to the homolytic fragmentation of the alkanolamine βc-c bond as illustrated in figure 2.

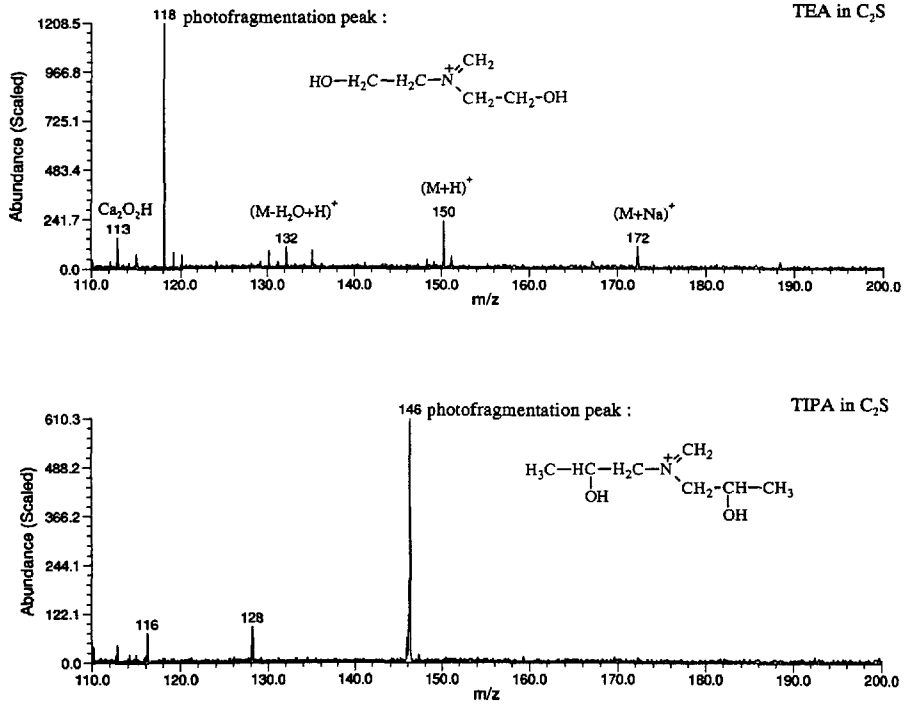

Figure 1 : Mass spectra of TEA and TIPA (500ppm) in C2S.

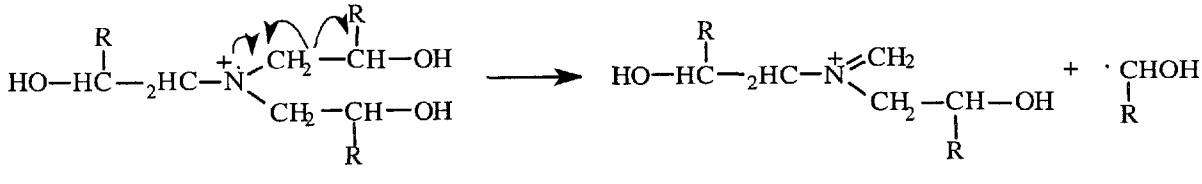

Figure 2: Proposed fragmentation scheme for the studied alkanolamines (For TEA R=H ; For TIPA R= CH_3)

Analysis of the other clinker different constitutives phases (C3S, C3A and C4AF) reveals similar spectral stamps. Observation of the peak intensities of TEA and TIPA (table 2) shows a major difference between C2S and C4AF from one hand, and C3S and C3A from the other hand. For the latter phases, the intensity is an order of magnitude larger than for the former phases, implying a smaller surface affinity for both TEA and TIPA.

	C2S	C3S	C3A	C4AF
TEA	1208	**4969**	**5220**	619
TIPA	610	**4204**	**5210**	661

Table 2 : Comparison of the grinding aid peak intensities in the four studied phases.

As for the industrial clinker, the ionization step has been done at λ = 248 nm (fig. 3). TEA was observed to be detectable at all studied concentrations. Its presence was evidenced by the apparition of a peak at m/z= 188 uma corresponding to the cationized $(TEA+K)^+$ peak, typical of a laser desorption process at this wavelength.

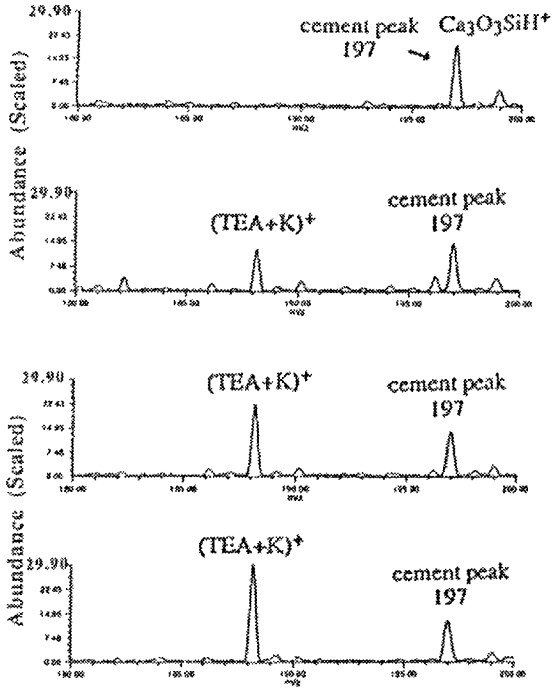

a) cement without grinding aids

b) cement with 350 ppm TEA

c) cement with 500 ppm TEA

d) cement with 1000 ppm TEA

Figure 3 : Mass spectra of TEA in a cement grounded in a lab mill.

It can be shown that the intensity ratio $(TEA+K)^+$ peak / cement peak ($Ca_3O_3SiH^+$, m/z=197) is a linear function of TEA concentration (y = 0.188+0.0024 x ; r=0.98) from which the detection threshold can be estimated at ca. 150 ppm.

REFERENCES

Marshall, A.G. and Verdun, F.R., "in Fourier Transforms in NMR, Optical and Mass Spectrometry. A User's handbook", 1990, Elsevier.

Muller, J.F., Pelletier, M., Krier, G., Weil, D. and Campana, J., Microbeam Analysis, 1989, p 311, Ed by P.E. Russel, San Francisco Press.

Pelletier, M., Krier, G., Muller, J.F., Weil, D. and Johnston, M., Rapid Commun. Mass Spectrom. , 1988, 2, p 146.

QUALITATIVE AND QUANTITATIVE ANALYSIS OF ORGANIC COMPOUNDS IN CEMENT AND HARDENED CEMENT

Akira OHNO and Takanori YAMAMOTO, Sumitomo Osaka Cement CO. LTD.,
Cement/Concrete Research Lab., Japan

ABSTRACT An analytical system using a pyrolysis - gas chromatography / mass spectrometer (pyro - GC / MS) was developed for qualitative and quantitative analysis of organic compounds in cement and concrete. Alkylation treatment was useful for detection of polar compounds which were difficult to analyze by GC. A cryogenic N_2 oven controller was used for analysis of the low molecular weight compounds.

Key-words: Admixtures,Organic,Qualitative,Quantitative

INTRODUCTION

There are many reports about quantitative analysis of organic compounds in hardened cement; Kroone(1971), Commolly(1980), Yilmaz(1989) etc. These methods show good sensitivity and good precision. But these methods usually need complex treatments to separate the organic compounds from the hardened cement. Moreover, these methods are valid only for specific components. We developed a new method using pyro - GC / MS; Ohno(1993). This method is applicable to a multicomponent system and also to qualitative analysis.

THEORY OF PYRO-GC/MS

Organic compounds in hardened cement are pyrolyzed in the Pyrolyzer and move from solid phase to vapor phase. The pyrolysis products in the vapor phase pass through a GC column at a different speed. Then at the detector, each product is detected at a different retention time. When MS is used as a detector, each product is ionized. The mass spectra of each peak is obtained by measurement of the mass of each ion. Each product shows a different mass spectra. Therefore, we can analyze a sample qualitatively from the mass spectrum and quantitatively from the peak area. However, the concentration of admixture in cement is usually very low, and can not be detected by the SCAN mode. In this case, the selected ion monitor(SIM) mode is used. Table 1 shows the analytical conditions of pyro - GC / MS.

Table1 Analytical Conditions

Pyrolyzer	JHP-3(Japan Analytical Industry)
Pyrolysis Temp.	764℃ 10seconds
Gas Chromatograph	HP5890A(Hewlett Packard)
Column	DB-1701(J&W) 30m×0.25mm i.d.
Column Temp.	50～300℃ 25℃／min.
Carrier Gas	He 1ml／min.
Mass Spectrometer	HP5970B(Hewlett Packard)

ANALYSIS OF ORGANIC COMPOUNDS IN CEMENT AND HARDENED CEMENT

Analysis of naphthalene sulfonate formaldehyde condensate(NSF) in hardened cement

Figure 1 shows the chromatogram of NSF solution(1.0wt%). A strong peak is observed at 5.7 min. Figure 2 shows the mass spectra of the peak. The ion with mass / charge = 128 shows the highest

intensity. This means that the mass / charge of the ion which is suitable for SIM of NSF is 128.

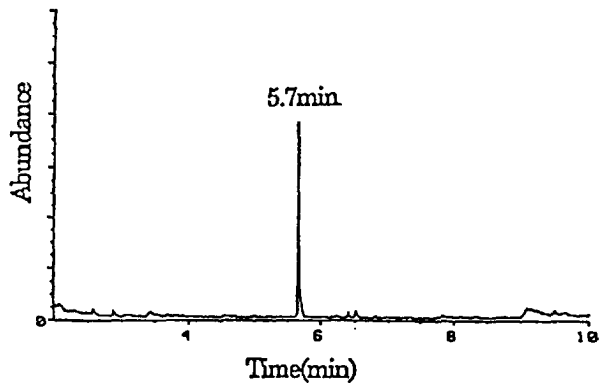

Figure 1 Chromatogram of NSF solution monitored by SCAN mode

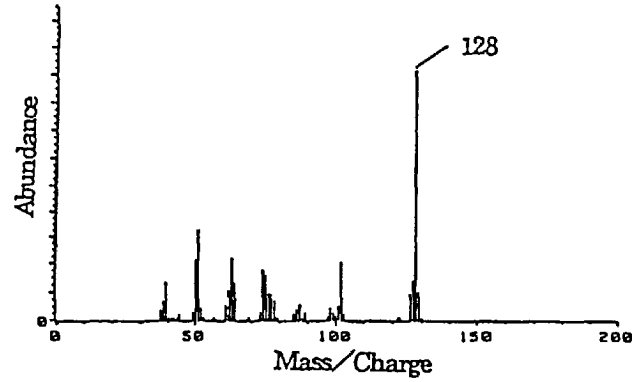

Figure 2 Mass Spectra of the peak at 5.7min

Figure 3 shows the calibration curve of NSF in cement paste monitored by SIM mode. It shows a good linearity. The amount of NSF in hardened cement can be analyzed by using this calibration curve. The kind of admixture also can be analyzed by using a data base of mass / charge for SIM and retention time of available admixtures.

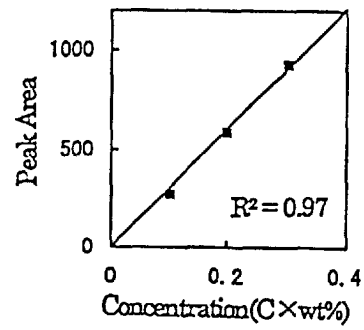

Figure 3 Calibration curve of NSF in cement paste monitored by SIM mode (Mass/Charge = 128)

Analysis of polar compounds

Methylation treatment of polar compounds

The compounds which have many hydroxyl or carboxyl groups, such as a sodium gluconate(SG) are usually difficult to analyze by GC due to their high polarity. Many organic admixtures contain such polar compounds. Alkylation of these polar compounds was effective treatment for analysis; Challinor(1989) etc. We used tetramethylammonium hydroxide(TMAH) as an alkylation aid. Eq 1 shows the methylation reaction of polar compounds by TMAH.

$$\text{R-OH} \xrightarrow[\text{heating}]{\text{TMAH}} \text{R-OCH3} \qquad [1]$$

$$\text{R-COOH} \xrightarrow[\text{heating}]{\text{TMAH}} \text{R-COOCH3} \qquad [2]$$

Analysis of SG in hardened cement

Figure 4 shows the chromatogram of the SG solution(1.0wt.%) and mass spectra of the main peak monitored by SCAN mode. No peak was observed without treatment. However, a large peak was obtained by methylation of SG. Figure 5 shows the calibration curve of methylated SG in cement paste monitored by SIM mode(mass / charge = 159). It shows a good linearity. These findings show that the methylation is effective treatment for analysis of polar compounds in hardened cement.

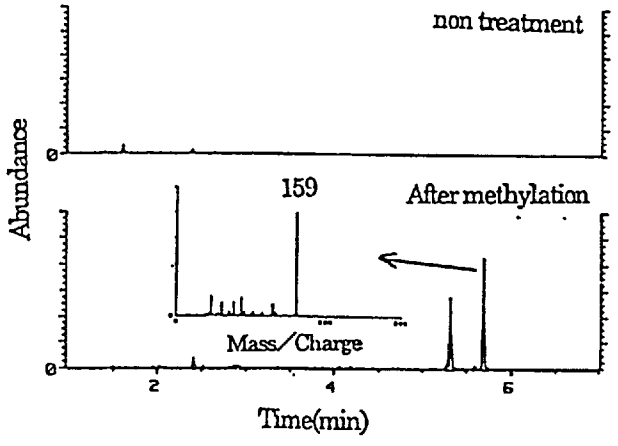

Figure 4 Chromatogram and Mass spectra of the main peak of SG solution monitored by SCAN mode

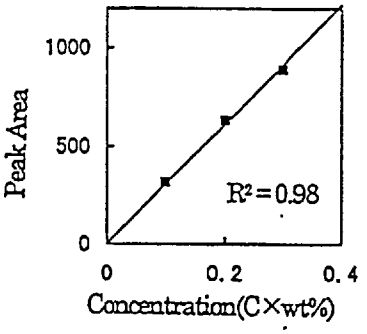

Figure 5 Calibration curve of SG in cement paste monitored by SIM mode (Mass/Charge = 159)

Analysis of low molecular weight compounds

Use of cryogenic N_2 oven controller

The boiling temperature of the pyrolysis products of the low molecular weight compound is very low. The retention time of these products is very short and peaks overlap with the. peak of CO_2 gas. Decrease of column temperature delays the retention time of product. However, usually analysis by GC is impossible under room temperature. We used cryogenic N_2 oven controller to separate the peak of products from that of CO_2. This apparatus can cool the column under 0 ℃.

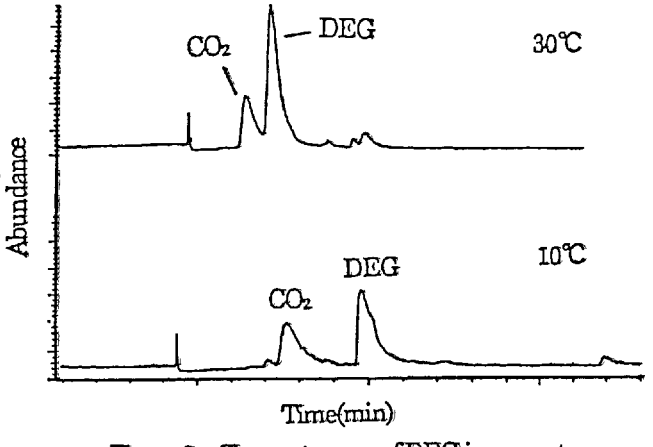

Figure 6 Chromatogram of DEG in cement monitored by SIM mode (Mass/Charge = 31)

Analysis of diethylen glycol(DEG) in cement

DEG is usually used as a grinding aid of

cement clinker. Figure 6 shows a chromatogram of DEG in cement(0.02wt%) measured at 30℃ and 10℃ using a cryogenic N_2 oven controller. Partially overlapped peaks of DEG and CO_2 were completely separated into each peak at a low temperature.

CONCLUSION

The pyro - GC / MS method is superior for qualitative and quantitative analysis of organic compounds in hardened cement. Polar compounds can be detected by methylation of samples. The cryogenic N_2 oven controller is useful for the analysis of low molecular weight compounds.

REFERENCES

Challinor, J. M., "A pyrolysis - derivatisation - gas chromatography technique for the structure elucidation of some synthetic polymers", Journal of Analytical and Applied Pyrolysis, Vol.16, No.4, 1989, pp. 323 - 333.

Connolly, J. D., Hime, W. G., Erlin,B., "Analysis for admixtures in hardened concrete", Proc. Int. Congr. on admixture construction press, London, 1980, pp. 114 - 129.

Kroone, B., "A method of detecting and determining lignin compounds in mortars and concretes", Magazine of Concrete Research, Vol. 23, No.75 -76, 1971, pp. 132 - 134.

Ohno, A., Tai, Y., Inokawa,H.,, "Qualitative and quantitative analysis of organic admixtures contained in concrete", Sement Konkurito Ronbunshu, Vol. 47, 1993, pp. 232 -237.

Yilmaz, V. T., Kindness, A., Glasser, F. P., "Quantitative analysis of sulfonated melamine formaldehyde superplasticizer in cement", Advances in Cement Research, Vol. 2, No. 7, 1989, pp. 107 - 110.

CALORIMETRIC ANALYSIS IN THE CHEMISTRY OF CEMENT

Alexander USHEROV-MARSHAK, State technical University of Building and Architecture, Kharkov, Ukraine

ABSTRACT There has been carried out the analysis of the possibilities of employing calorimetry in the cement chemistry and technology at the stages of its production and hardening. There are discussed some results of the thermokinetic and thermodynamic approaches to the studying of the early cement hydration stages and formation of cement stone microstructure. An accent is put on the necessity to solve some conceptual problems of cement chemistry within informative technologies and expert systems.

KEY-WORDS: Calorimetry, Heat evolution, Hardening, Method, Hydration

INTRODUCTION

Calorimetry is one of the most objective and informative methods of research in chemistry and technology of cement (Schwiete and Roth, 1973, Mchedlov-Petrossian et al, 1984). The cement binding properties are predetermined by thermodynamic instability and crystal-chemical nature of minerals. Hydration is a typical slow-going unbalanced process with exothermal nature of reactions. Heat evolution at phenomenological level depicts the effect of technological factors at the stages of manufacturing and hardening of cements.

In spite of essential importance and great volume of the stored calorimetric information the cement chemistry still remains incomplete. Estimation of the technological factors effect, approximation to the description of hydration mechanism and kinetics, creation of the computer data and knowledge bank on the hardening process and properties of cements - are just the main objects of calorimetry.

METHODS OF CALORIMETRIC ANALYSIS

To study hydration heat data, rate and completeness of heat evolution use is made of isothermal, adiabatic (thermos) and scanning calorimetric methods (Hemminger and Höhne, 1984). Chemical thermodynamic and heterogeneous kinetics, modelling and information science are also applied to interpret experimental data.

The most widely used method now is differential microcalorimetry, i.e. highly sensitive method of continuous measurement of minor quantities of hydration heat. The specifics of the dispersion interaction in "cement-water" system makes it necessary to consider thermodynamic instability of the reagents. Before the reaction they are isolated from one another. There should be provided equally accessible despersion phase and dispersion condition, total wetting of cement irrespective of W/C. To meet the requirements there were elaborated special loading devices to locate, isolate, bring into contact and mix reagents (Usherov-Marshak, 1984).

Fulfilment of the above conditions makes it possible to carry out correctly the thermokinetic analysis (TKA). In doing so (Fig 1) we can solve problems at 5 and even more levels (Usherov-Marshak and Sopov, 1995). The first one is to form the basic thermokinetic dependences - $dQ/d\tau=f(\tau)$ and $Q=f(\tau)$. The second level is the conceptual discrimination of induction, accelerated and retarded periods of reactions. This approach makes its possible to classify

the reactions as fast or slow-going on a non-formal basic. A long-term prediction of heat evolution depending on Q=f(τ) refers to the third level of TKA.

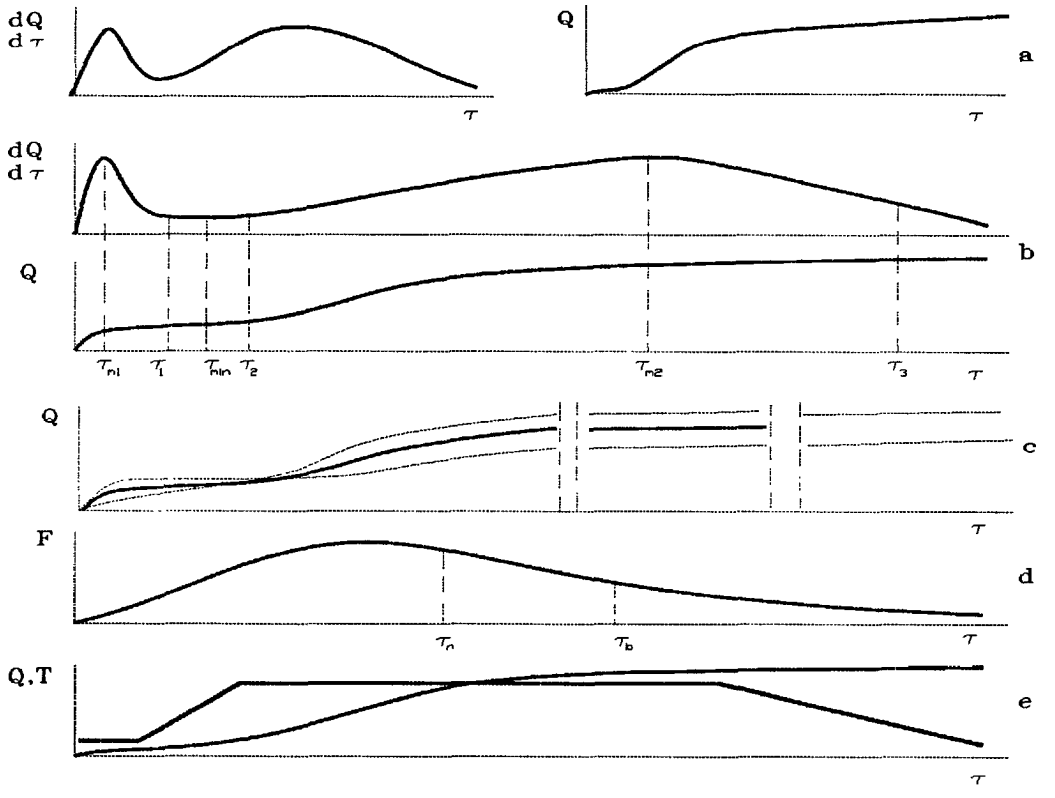

Figure 1 Levels of Thermokinetic analysis.
a - Treatment of the experimental results. Thermokinetic dependences.
b - Pick-out of the typical stages.
c - Prognosis of the heat evolution.
d - Building of the kinetic models.
e - Nonisothermal dependences.

The three level data are required to calculate the cement hydration (transformation) rate and degree in case of kinetic modelling and description of reactions at the 4th level. Its development provides for plotting of selfcoordinated models (Usherov-Marshak and Korobov, 1990) since it lacks a common mechanism monitoring the hydration at any stages of hardening. Here it is necessary to mention the incomplete and insufficient character of the works by Kondo and Ueda (1968), Pommersheim and Clifton (1979). Their approach to the problem is based on simplification, physical and mathematical description of a period selected formally by means of a single law, i.e. that of crystallization, diffusion, etc. The classical selection of the hydration stages according to Kondo (1968) is not universal.

The fifth level of research solves the problem of obtaining the thermokinetic dependences for nonstationary temperature conditions of any hardening mode (Usherov-Marshak and Sinyakin, 1992). At the successive levels of TKA it is expedient to find out quantitive interrelation of heat evolution readings with the structural strength and durability.

Attempts were made to use the differential scanning calorimetry (DSC) for estimation of the phase transformations, icebuilding, parameters of microstructure within the range of 2-10 nm. We have employed the lowtemperature poremetric method (Usherov-Marshak and Sopov, 1994) on the basis of concepts of the surface phenomena thermodynamics. The dependence of water crystallization, temperature (T) in pores and capillars of cement stone on their radius (Rn) is estimated accounting for the thermodynamic balance of water and ice. The experimental results help to determine the temperature of "water-ice" phase transitions, the apparent crystallization energy, the volume and distribution of micropores with respect to their dimensions and under certain assumptions the shape of pores (Fig 2).

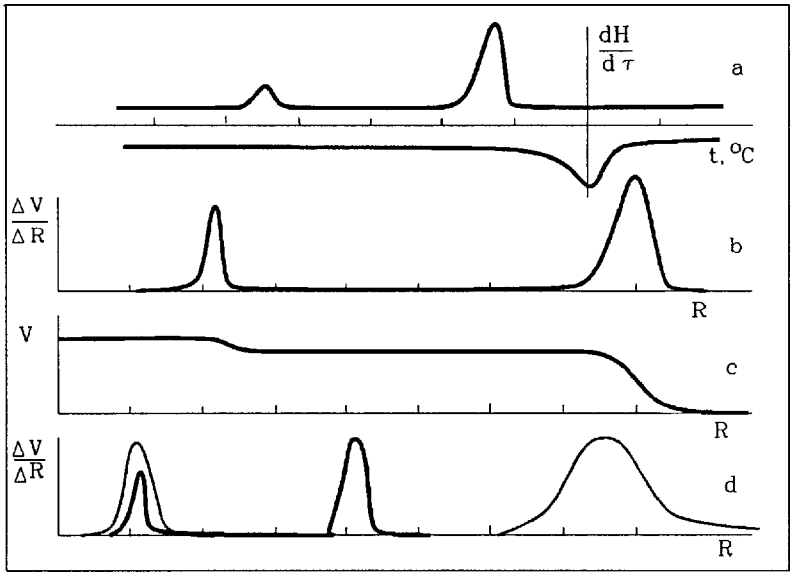

Figure 2 Levels of thermodynamic analysis.
a - Water crystallization (1), melting of the ice (2).
b - The pore-distribution by their dimensions.
c - Volume of the micropores.
d - The pore-distribution on their forms.

THERMOKINETICS OF THE HYDRATION EARLY STAGES

One of the advantages of the calorimetric research consists in obtaining reliable results without interfering with the processes of hardening, without stopping them, destroying the samples, etc. This is essentially important at the earliest stages when the hydratation degree is rather small and identification of the reaction products is difficult.

The hydration of minerals and polymineral cements is not equally studied. Comparative analysis of the results of thermokinetic experiments made by various authors is rather complicated due to non-identity of the studied samples. There are no standard samples in the cement chemistry. Therefore reproduction of results even for the "model" binding agent $CaSO_4 \cdot 0.5H_2O$ is rather low.

The physical and chemical peculiarities of the hydration of α and β modifications of semihydrate of calcium sulphate, the constancy of Q/α ratio during the whole process (1.5-3 hours) enable to use the conceptual modelling. The well-known models of Avraami-Yerofeev, Ridge and Schiller had been tested for fitness to experimental data. The position of Q_{max} (α_{max}) on the

dQ/dτ=f(Q) dependence proves the validity of the concept of the nucleus formation limiting stage. Its rate varies according to the exponential law with regard to "compressing" sphere model. Other models proved to be nonvalid.

Previously we have shown certain limitation in accepting Avraami-Yerofeev model to describe C_3S hydration within α=0.03-0.13 narrow interval. Calculation of the values of ΔG^+ apparent energy activation and ΔS^+ free entropy activation proved the nucleus formation limiting function. By its behaviour the C_3S solid solution hydration is analogous to estimated (test) dependences (Fig. 3). But the value of first exoeffect is lower which correlates with the replacing ion hydroxide solubility. It is quite probable that in the process of transition into a solution the modelling ions make up nucleus formation, i.e. the centers of $Ca(OH)_2$ early crystallization. Duration of induction period becomes shorter. The utmost hydration completeness is typical for C_3S solid with Ca^{2+} and Ba^{2+} ions. The data analysis using Avraami-Yerofeev model had proved heterovalency substitutions of Ca^{2+} ions with Fe^{3+}, Mn^{3+}, Al^{3+}, S^{6+} do not change the reaction rate constsant. In case of isovalency substitution with Cd^{2+}, Ba^{2+}, Ni^{2+}, Co^{2+} ions the reaction rate constant increases in proportion to the admixtured ion radius value. TKA makes it possible to quantitatively estimate the effect of the modifying oxides.

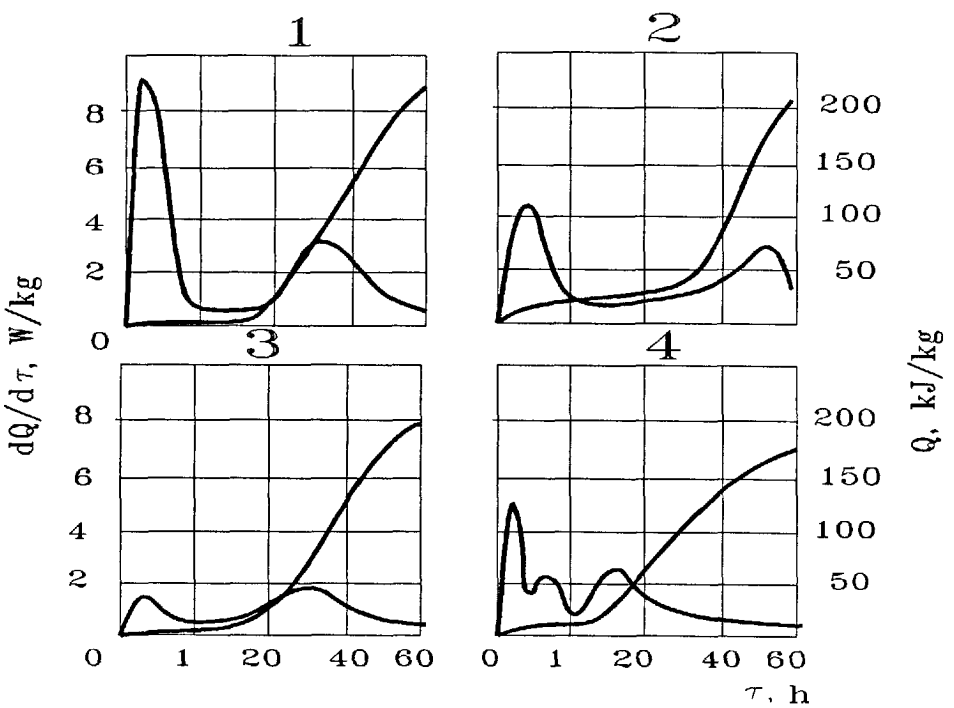

Figure 3 Thermokinetics of hydration of the solid solution.
1 - C_3S; 2 - C_3S + CaO; 3 - C_3S + Fe_2O_3; 4 - C_3S + Al_2O_3

Heat evolution of clinker aluminate phases is studied not so well. Reactivity of $CaO-Al_2O_3$ system minerals decreases in the $C_3A > C_2A_7 > CA > CA_6$ series. The $dQ/d\tau=f(\tau)$ dependence behaviour is complex and diverse (Fig. 4). This is linked with formation and recrystallization of the C_4AH_{13}, C_2AH_8 and C_3AH_6 type hydroaluminates, temporary existence of $Al(OH)_3$ as gibbsite and bemite. During C_3A hydration no induction period is fixed. The $C_{12}A_7$ hydration is determined by C_4AH_{13} recrystallization into C_3AH_6. Additional exoeffect is marked. The CA hardening thermokinetic curves are typical for the processes with clearly manifested induction period. This is explained by certain difficulties of hydroaluminate crystallization in $Al(OH)_3$ gel medium. The experiment had manifested differences in the kinetics of early hydration of the crystal and amorphous structure calcium aluminates obtained as a result of clinkering or melting. The reaction intensity of the minerals resulting from melting is somewhat lower.

The thermokinetics of hardening of certain minerals in which $CaSO_4 \cdot 2H_2O$ is present as well as of their mixtures is naturally more complicated. Yet their phase transitions are easily evident and identified. For instance, transformation of the calcium highsulphate hydrosulphate aluminate into monosulphate.

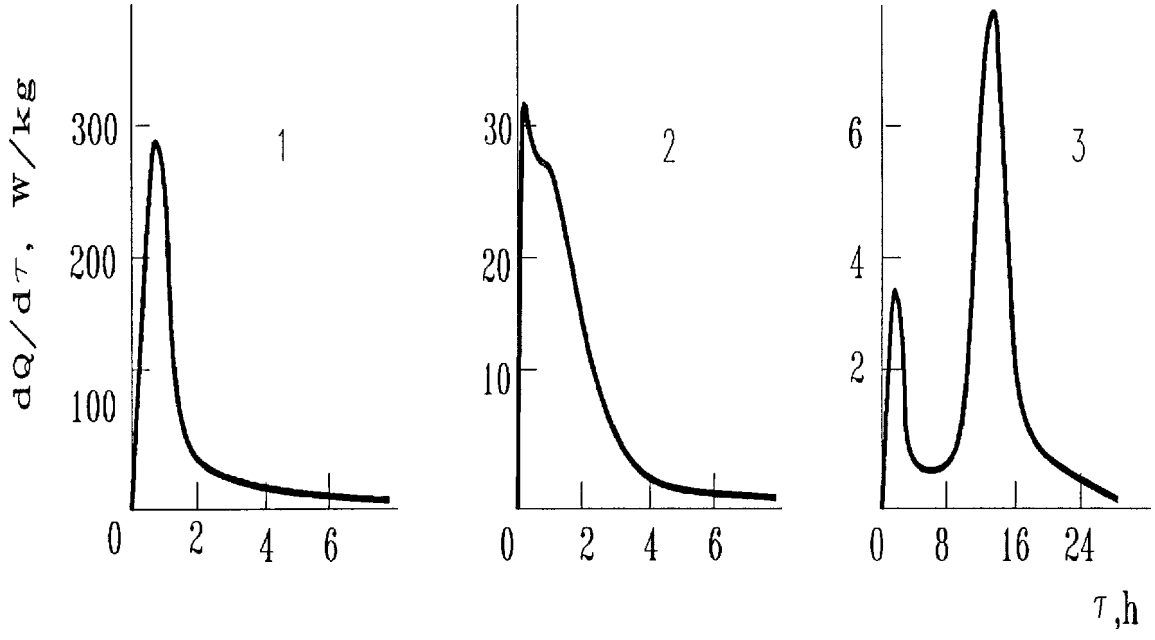

Figure 4 Thermokinetics of hydration of the calcium-aluminates.
1 - C_3A; 2 - $C_{12}A_7$; 3 - CA

Theoretically and practically the TKA of cement hydration with chemical admixtures like plasticizers, hardening promoters or inhibitor introduced at the stages of cement and concrete production is highly effective (Ramachandran, 1984, Wilding et al, 1984). Technological results of their effect are associated with manifistation of exoeffects as well as intensity and duration of early hydration major stages.

It is known that the surface-active substances, i.e. the base of plasticizers and superplasticizers, change to a great extent the process of the hydration elemental acts, namely, adsorption, nucleus formation, crystallization, etc. The plastification mechanism consists in surface-active substances adsorption by hydrates and its effect is determined through the molecular mass and the degree

of polycondensation of the oligomers of which the plasticizer is composed. An increase in polynaphthalenesulphonates molecular mass results in the proportional growth of the first exoeffect value at the expense of the dispersive action and better wetting conditions of C_3S. The time of the second exoeffect is displaced by a few to 350h. An increase in duration of the induction period from several up to 300 hours is quite natural. The intensity of reactions is reduced, the hydration is actually blocked, and, simultaneously the mixture water consumption falls down.

TKA provides for a better understanding of this mechanism and motivation of the new methods of obtaining highly effective binding substances by implementing surface-active agents when grinding cement. This results in mechanochemical activation of cement (Usherov-Marshak and Bondar, 1992) although the C_3S and C_3A initial hydration intensity and completeness are reduced (Fig.5). It is evident that some changes of the hardening elemental acts, shown by calorimetry, are the reason for increasing the binding properties efficiency. They are termed as low-water-requirement binder. In this case up to 70% of the clinkers can be replaced with the inert dispersive components.

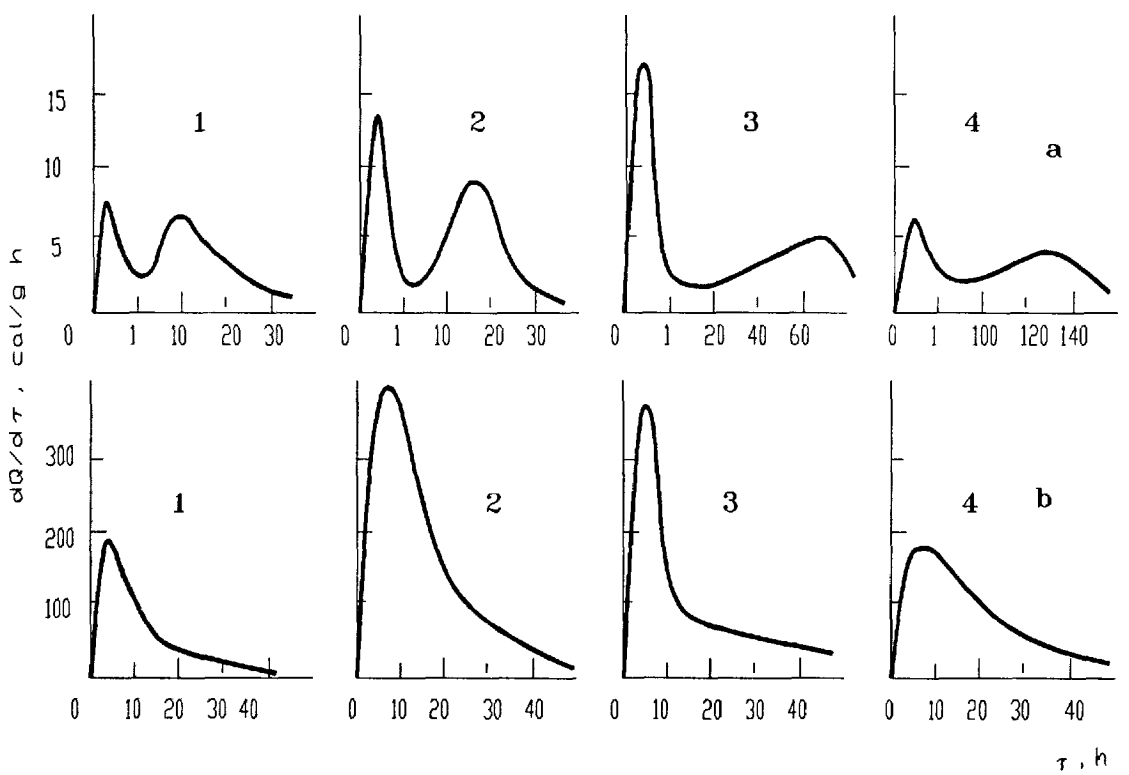

Figure 5 Thermokinetics of hydration.
a - tricalcium silicate; b - tricalcium aluminate
1 - initial mineral; 2 - post-grinding mineral;
3 - the same with surfactant, added with water of mixing;
4 - mechanoactivated binder.

The kind and concentration of the cement and concrete admixtures define the manifistation moment, intensity and duration of the heat effects. This phenomenon is termed by us as the "thermokinetic selectivity" of the admixtures effect and allows to classify the admixtures quantitatively.

The temperature factor is of special importance in hardening. Calorimetry provides for studying the early hydration within the interval of 5-180 ^{0}C. This is the hardening interval of the accelerated hardening cements under higher temperatures, in steam-and-pressure cured conditions, for grouting cement (Bensted and Ankett, 1990). At this the hydration scope decrease was recorded. For C_3S it equals 60-70 ^{0}C, for CA it is 40-50 ^{0}C. It was demonstrated that a somewhat retarded hydration of minerals and cements due to surface-active substances does not affect the binding properties at 80-90 ^{0}C. The effect estimation of the isothermic and nonstationary conditions of the cement hardening will be considered in a special report to be delivered at this Congress.

In recent years a new impulse has been given to the TKA hydration of the slagcontaining substances including slag-alkaline and binding ones (Usherov-Marshak et al, 1994, Shi and Day, 1995). The initial endoeffect - the result of the presence of the primary part of solution - fixed at the thermokinetic dependences. But this is a matter of special research. The experiment results interpretation is not always correct (Schutter and Taerwe, 1995). It is caused by the uncorrect interpretation of the 3 rd exo-effect on the dependence $dQ/d\tau = f(\tau)$.

THERMOCHEMICAL AND THERMODYNAMIC ANALYSIS

Thermochemical analysis of cements has not undergone any substantial changes as compared with the classical works by Eitel. Definition of the cement hydration heat with the help of the solution calorimetry methods, as was proved by CemBuro's research, does not exclude substantial errors in the results. This is caused by methods of the samples preparation, calibration of the calorimeters used, etc. Yet, the method is approved as the international one.

The potential of the above said thermodynamics of phase transitions and of scanning calorimetry is still poorly employed in the cement and concrete chemistry and technology. The method of differential scanning calorimetry is more often used instead of thermal analysis to identify icebuilding and the hydration degree. The differential scanning calorimetry as a method of thermoporometric research is more perspective in studying the cement stone structure. Microporosity and the laws of its formation also make a topic for a report at the Congress. Here we should mention high effectiveness of the microporosity calorimetric analysis from the viewpoint of the quantitive confirmation of correctness (validity) of the known kinetic diagrams of formation, interactions and changes in hydrosulphatealuminate, hydroaluminate and hydrosilicate structure types in the process of cement hardening. At some previous Congress the researchers dealt only with the morphology description and the material composition of new formations.

CONCLUSION

The further development of calorimetry is associated with the conceptual problems of cement and concrete chemistry. This includes standardization of samples, uniformity of the experimental conditions and interpretation.

From year to year the importance of calorimetric data to be stored in international computer data banks and informative storing systems will gain even greater value in data processing technologies and expert systems (Fronsdorff and Clifton, 1988, Usherov-Marshak and Sinyakin, 1994). The calorimetric centre of Kharkov Civil Engineering and Architecture University is willing and ready to cooperate.

REFERENCES

Bensted, J. and Ankett, P., "Applications of Higher Temperature conduction calorimetry to oilwell cementing ", World Cement, July, 1990, pp.308-320.

Fronsdorff, G. and Clifton, J., "Implications of Computer - Based Simulation Models, Expert Systems, Data Bases, and Networks for Advancing Cement Research" Ceramic Bul., Vol. 67, No 8., 1988, pp.1368-1371.

Hemminger, W. and Höhne, G., "Calorimetry. Fundamentals and Practice". Verlag chemie, 1984, p. 276.

Kondo, R. and Yeda, S., "Kinetics and mechanism of hydrations of cements", Proc. 5 Intern. Symp. Chem. Cem., Tokyo, 1968, Bd. II, pp.203-255.

Mchedlov-Petrossian, O., Usherov-Marshak, A., Urzenko, A., "Heat evolution during binders and concretes hardening", Moscov, Stroyizdat, 1984, p.224.

Pommersheim, J. and Clifton, J.R., "Mathematical models of cement hydration", Cements Research Progress, 1979, pp.281-307.

Ramachandran, V. "Concrete Admixture Handbook. Properties, Science and Technology". Noves Publications, Ney Jersey, 1984.

Schutter, G. and Taerwe, L., "General Hydration Model for Portland Cement and Blast Furnace Slag Cement", Cement and Concrete Research, vol. 25, N3, 1995, pp.593-603.

Schwiete, H. and Roth, W., "Beitrag Zur Hydratationswärme von Portlandzementen und deren Bestimmungsmethoden". Westdeutscher Verlag Opladen, 1973, p.100.

Shi, C. and Day, R., "A Calorimetric of early Hydration of Alkali-slag cements", Cement and Concrete Research, vol.25, N6, 1995, pp.1333-1346.

Usherov-Marshak, A., "Thermokinetics manufactur and hardening inorganic binders", Charkov, 1984, p.24.

Usherov-Marshak, A. and Bondar, E., "Calorimetric examination of Mechanochemical Activation of the Cement hardening processes". Proc. of the 1st Intern. Conf. on Mechanochemistry, Koshize, 1992, pp.172-175.

Usherov-Marshak, A. and Korobov, A., "Self-consisten model of kinetic heat evolution "Hydration of neorganic binders", norganic Materials, vol.26, N2, 1990, pp.423-425.

Usherov-Marshak, A., Krivenko, P., Domanskaya, N., "Early stages of Hydration of slag-alkaline binders", Inorganic Materials, vol.30, N10, 1994, pp.1341-1342.

Usherov-Marshak, A. and Sinyakin, A., "Information technology of concrete accelerate hardening", Concrete and Reinforced Concrete, N6, 1994, pp.2-4.

Usherov-Marshak, A. and Sinyakin, A., "Thermokinetics of cement hardening under nonisothermal conditions", 9th Intern. Congr. of the Chemistry of Cement, New Delhi, India, 1992, vol.IV, pp.175-180.

Usherov-Marshak, A. and Sopov, V., "Calorimetry in the science of Building Materials" Journal of Thermal Analysis, vol.43, 1995, pp.497-504.

Usherov-Marshak, A. and Sopov, V., "Thermoporometry of Cement Stone", Colloid Journal, vol.56, N4, 1994, pp.527-530.

Wilding, C., Walter, A., Double, D., "A classification of Inorganic and Organic Admixtures by Conduction Calorimetry", Cement and Concrete Research, vol.14, pp.185-194.

THERMOPOROSIMETRY IN THE PORE ANALYSIS OF CONCRETE

Seppo MATALA, Helsinki University of Technology, Concrete Laboratory, Finland

ABSTRACT A calculation method to analyze the pore volume and pore size distribution in concrete based on thermoporosimetry was developed. A hypothetical pore size distribution typical for concretes was used in the determination of the correction factor of the entropy changes due to the superficial phase transformations. The paper presents theoretical background of the method, and discusses on the validity of the method.

Key-words: Porosity, Pore structure, Thermoporosimetry, Low temperature, Calorimetry

INTRODUCTION

In studies of the pore structure, the selection of the testing procedure is of great importance. Each method has its own limitations. The conventional mercury intrusion method used mostly in the characterization of pore structures able to detect pore sizes over 2 to 4 nm in radius. This method, however, is quite sensitive to the preparation of samples, and the need to dry the sample beforehand obviously changes the pore structure of the finest pore range. During the last twenty years, thermoporosimetry has been used in the characterization of pore structure of cement based materials, e.g., by Fagerlund (1973), Sellevold (1980), Bager (1984), Beddoe and Setzer (1990) and Setzer (1990). These methods are based on the utilization of Kelvin's equation, and in the entropy of phase transformation, the effect of the superficial phase transformations on the entropy changes were neglected. Brun et al. (1977) included these factors in the method. On the basis of the aforementined research the calculation method was further developed. In this paper theoretical background of the method is presented and discussed. A full description of the method is presented in the reference Matala 1995.

THERMOPOROSIMETRY IN THE PORE ANALYSIS

Theoretical basis

Brun et al. (1977) have derived a differential equation for the triple point temperature dependent on the entropies and volumes of three phases (liquid, solid and gaseous) and on the free surface extension energies and curvatures of two interphases (solid-gas and solid-liquid) as follows:

$$\left(\frac{S_s - S_g}{V_s - V_g} - \frac{S_l - S_s}{V_l - V_s}\right) dT = \frac{V_g}{V_g - V_s}\, d\left(\gamma_{sg} \frac{dA_{sg}}{dV_g}\right) - \frac{V_l}{V_l - V_s}\, d\left(\gamma_{sl} \frac{dA_{sl}}{dV_l}\right) \qquad [1]$$

where S and V are the specific entropy and the volume of phases, subscripts l, s and g denote the phases liquid, solid and gas, γ is surface tension and dA/dV is the curvature of the interphase. Eq 1 shows that the curvatures of two of the three interphases should be known in order to calculate the triple point temperature in a general case. In the special case where the solid-gas interphase is plane and its curvature is zero, as in the case of full saturation, the Eq 1 can be presented in the form:

$$\Delta S_f\, dT + V_l\, d\left(\gamma_{sl} \frac{dA_{sl}}{dV_l}\right) = 0 \qquad [2]$$

where ΔS_f is the solidification entropy of the condensate. Assuming that solidification takes place by nucleation in a porous saturated material, the curvature of the nucleus equals that of the

pore radius subtracted by the thickness of the layer where phase transformation cannot take place. If the interphase has a spherical shape, the curvature dA_{sl}/dV_l equals $-2/R_n$, where R_n denotes the radius of the nucleus and Eq 2 can be expressed as:

$$R_n = 2 \cdot \gamma_{ls} \Big/ \int_{T_0}^{T} \frac{\Delta S_f}{V_l} dT \qquad [3]$$

Numeric formulation of the solidification energy

The measurable solidification energy of pore water can be evaluated theoretically if the change of entropy during phase transformation can be formulated. In a fully water saturated porous system the solid-gas interface is plane, and the change in entropy of the water-ice system of pores for temperature change $T_0 \rightarrow T$ and for the corresponding changes in pressure of liquid phase $P_0 \rightarrow P_l$ and solid phase $P_0 \rightarrow P_s$ can be expressed by the equation:

$$\Delta S_f = \Delta S_{f0} + \int_{P_l}^{P_0} \left(-\frac{\partial v_l}{\partial T} \right)_P dP + \int_{T}^{T_0} \left(\frac{c_l}{T} \right) dT + \int_{T_0}^{T} \left(\frac{c_s}{T} \right) dT + \int_{P_0}^{P_s} \left(-\frac{\partial v_s}{\partial T} \right)_P dP \qquad [4]$$

The first term in Eq 4 is the basic entropy and the second and the fifth term represent the effects of the compression heat of phases due to the change in pressure, assuming that the phases are incompressible. The third and the fourth term take into account the changes in the specific heat of the liquid and solid due to the depression of temperature. Eq 4 can be rearranged into the following form :

$$\Delta S_f = \Delta S_{f0} + \int_{T_0}^{T} \left(\frac{c_s - c_l}{T} \right) dT + \left[\left(\frac{\partial v_l}{\partial T} \right)_P - \left(\frac{\partial v_s}{\partial T} \right)_P \right]_T \cdot (P_s - P_0) + \left[\left(\frac{\partial v_l}{\partial T} \right)_P \right]_T \cdot (P_l - P_s) \qquad [5]$$

In Eq 5 P_s is the vapor pressure of ice at temperature T, and P_l-P_s can be expressed by Laplace's equation:

$$P_l - P_s = -\frac{\gamma_{ls}}{R_n} = -\int_{T_0}^{T} \left(\frac{\Delta S_f}{v_l} \right) dT \qquad [6]$$

Brun et al. (1977) noticed that Eq 5 is not fully accurate when the solidification of ice is considered. It does not take into account the effect of the entropy of superficial phases. During the solidification of ice there occur changes of interphase between the layers that do not freeze and the adjacent phase (water before solidification and ice afterwards). Brun (1977) derived the correction factor of entropy due to this additional entropy variation by considering the equality of chemical potentials and the equilibrium of three interphases at triple point. We derived a new relationship between the temperature depression and the enthalpy in the solidification of pore water. The comprehensive derivation of the solidification enthalpy is presented in the reference Matala (1995b). It is based on the numeric formulation of Eq 5, but the effect of superficial phase transformations on the total entropy has been considered in a way that is more convenient for the pore structure of concrete. Since this increase in entropy is a function of the pore geometry, the correction factor was derived in our study by utilizing a hypothetical pore size distribution corresponding to the finest capillary pore structure of cement pastes and mortars. In thermoporometric approaches of the first generation, the effect of the superficial phase transformations on the total entropy has been neglected although its influence may be within the

limits of 20% to 40% of the total entropy, depending on the pore structure (Matala 1995b). The finer the pore structure and the lower the temperature, the higher this effect is.

Using the linearized correcting factor due to the entropy changes of the superficial phase transformations and multiplying this by the equation derived by Brun, the numeric expression for the entropy at the nucleation point was developed into the following form:

$$\Delta S_{f\,np} = \frac{(1+0.004\cdot\theta)\cdot\left[-1.2227-4.889\cdot\ln\left(1+\frac{\theta}{T_0}\right)+10.124\cdot10^{-3}\cdot\theta+1.265\cdot10^{-5}\cdot\theta^2\right]}{1-4.556\cdot10^{-5}\cdot\left(\theta-0.227\cdot\theta^2\right)}, \qquad [7]$$

where θ is the freezing point temperature in °C. The enthalpy at nucleation point $W_a=(273.15+\theta)$ $\Delta S_{f,np}$ has been presented in Fig 1 together with the enthalpy values proposed by other investigators. Numerically, the solidification energy W_a based on Eq 7 can be expressed within the temperature range $0 > T > -60°$ C by a quadratic equation:

$$W_a = 334+4.83\cdot\theta+0.0125\cdot\theta^2\,, \qquad [8]$$

where W_a is expressed in J/g and θ in °C. The enthalpy proposed by Fagerlund in Fig 1 differs from the values given by Eq 8 and proposed by Brun since Fagerlund's expression neglects the effects of superficial phase transformations and compression heat of phases. The difference between Eq 8 and Brun's expression is due to different assumptions in the determination of the entropy of superficial phase transformations. Brun's correcting factor is a function of surface tension of liquid-solid interface and temperature depression. At a specified nucleation point, it corrects the entropy values of the superficial phases in previously frozen pores by an amount dependent on the surface tension of the nucleating pore. Obviously, this overestimates the effect of superficial phase transformations on the entropy values for the wide range pore structure normally observed in cement pastes, but Brun's equation gives correct values with the pore structure in the vicinity of the nucleation point. The hypothetical pore structures used in the testing of Brun's equation were very fine for ordinary cement pastes and mortars observed by different testing methods. A coarser pore size distribution resulted in an increase of 20% at -50° C for the entropy at the nucleation point, and the curve was approximately linear. Theoretically, the way by which the correction factor was determined is not absolutely correct since it is a function of pore size. However, this approximation must be used for the calculations. Otherwise, the calculations consist of a very complicated iterative process, where the correct pore size distribution must be derived step by step and the entropy of the previous pore system should be taken as a starting value for the next calculation step.

Pore size distribution in thermodynamic approach

The relation between an ice sphere R_n and freezing point temperature θ can be calculated using Laplace's equation [6], which gives the relationship between the difference in the vapor pressures of the liquid and solid and the surface tension of liquid-solid interface and its curvature. In the literature, there are many contradictory proposals for the values of surface tension between water and ice. Eq 9 is derived from experimental values presented in the literature at temperatures from 0 to -30° C. In that γ_{ls} is expressed in N/m and θ in °C. The relation between the ice sphere R_n and freezing point temperature θ can be calculated directly from Eq 3 by applying the

relationships derived before and inserting the equations of γ_{ls} (Eq 9), $\Delta S_{f,np}$ (Eq 7) and v_l (Eq 10) into Eq 3 and setting $T\text{-}T_0 = \theta$.

$$\gamma_{ls} = (36 + 0.25 \cdot \theta) \cdot 10^{-3} \qquad [9]$$

$$v_l = 1.000132 \cdot (1 - 9.1 \cdot 10^{-5} \cdot \theta + 1.035 \cdot 10^{-5} \cdot \theta^2) \qquad [10]$$

Since all the parameters in Eq 3 are expressed as a function of temperature, the numeric integration is possible. The relationship between ice sphere radius and temperature according to Eq 3 is presented in Fig 4, and it can be expressed by quadratic Eq 11 with good accuracy.

$$R_n = \frac{-2 \cdot (36 + 0.25 \cdot \theta)}{1.222 \cdot \theta + 0.0068 \cdot \theta^2 - 8.67 \cdot 10^{-7} \cdot \theta^3} \qquad [11]$$

The ice sphere radius as a function of nucleation temperature is strongly dependent on the assumptions taken in the evaluation of the surface tension of the water-ice interphase. It gives clearly smaller values for the ice sphere than the equations based on the surface tension of the liquid-vapor interphase, e.g., Fagerlund's expression (Fig 2).

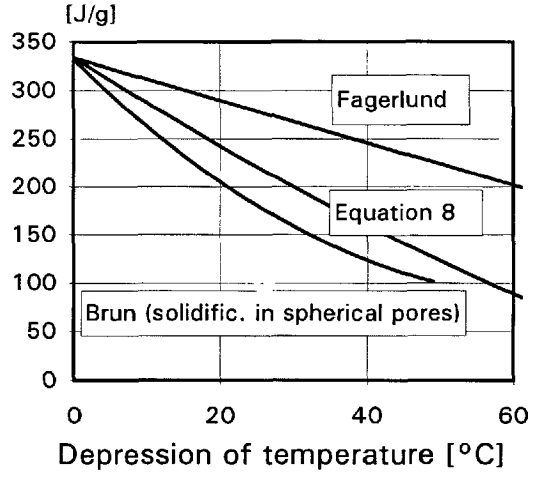

Figure 1. Enthalpy at nucleation point for spherical pore structure.

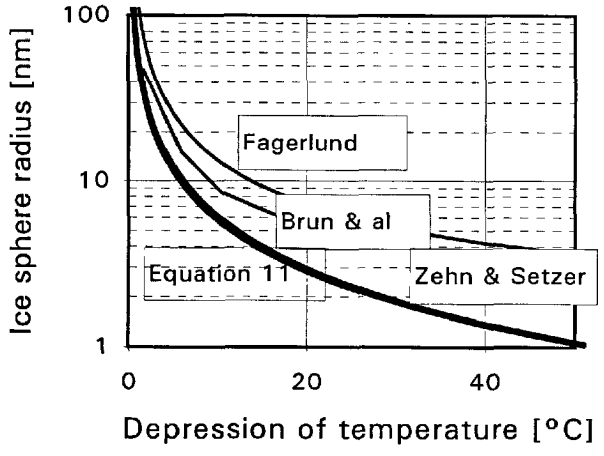

Figure 2. Different expressions for the size of ice sphere radius.

Fig 2 shows that the curves calculated by Eq 11 and by the method presented by Brun deviates only somewhat from each other. This is due to the fact that, although the entropy in Brun's equation differs markedly from the entropy value used in Eq 7, this effect is compensated by the higher value of surface tension .

When the ice sphere radius R_n has been formulated as a function of temperature depression, the pore size R_p can be calculated if the thicknesses of the adsorbed water layer and the liquid-like layer are known. Fagerlund (1973) has derived Eq 12 for the adsorbed water layer:

$$t_{ad} = 1.97 \cdot \sqrt[3]{1/(-\theta)} \ , \qquad [12]$$

where t_{ad} is expressed in nm and θ in °C. A new formula for the thickness of the liquid-like layer was derived starting from Takagi's quintic equation (Takagi 1990). A general

approximation for the thickness of the liquid-like layer δ [nm] as a function of the radius of ice sphere r_{ice} [nm] and temperature depression θ [°C] is as follows:

$$\delta = \frac{0.9 + 0.1 \cdot \log r_{ice}}{\frac{3}{(\log r_{ice})^{0.938}} + \theta \cdot \left(0.07 \cdot \log r_{ice} - 0.0365 + \ln \sqrt[3]{\frac{\log r_{ice} + 0.12}{\log r_{ice} - 0.12}} \right)} \quad [13]$$

The total thickness of the adsorbed water and the liquid-like layer of ice sphere can be calculated by summing Eqs 12 and 13. Fig 3 shows the magnitude of this layer as a function of temperature depression at the nucleation point.

Now, the pore size R_p can be calculated by adding the values of the adsorbed water layer and the thickness of the liquid-like layer to the value of ice sphere radius (Eq 11). For a spherical pore shape and always during nucleation, R_n is taken directly from Eq 11. In fusion, for a cylindrical pore, the multiplier 2 in the numerator of Eq 11 vanishes according to Laplace's equation. The curves for the spherical and cylindrical pore radii in nucleation and for the cylindrical pore radius in fusion are presented in Fig 4. The direct relationship between the temperature depression and pore radius in nucleation and in fusion is given by Eqs 14 and 15.

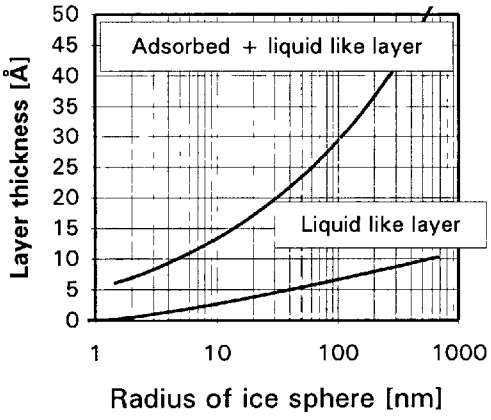

Figure 3. Thickness of the non frozen layers at nucleation point.

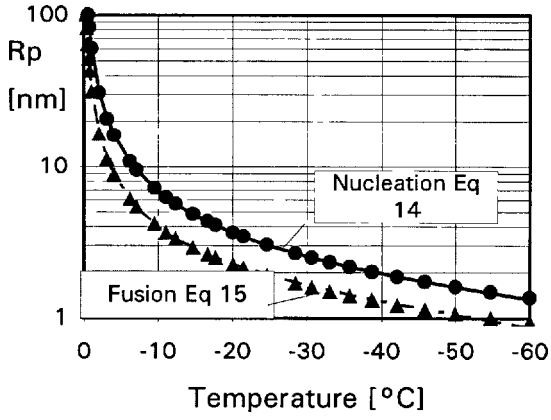

Figure 4. Pore radius R_p in nucleation and in fusion for a cylindrical pore.

$$R_{p_n} = 0.584 + 0.0052 \cdot \theta - \frac{63.46}{\theta} \quad [14]$$

$$R_{p_f} = 0.757 + 0.0074 \cdot \theta - \frac{33.45}{\theta} \quad [15]$$

In Eqs 14 and 15, $R_{p,n}$ and $R_{p,f}$ are the values of pore radius in nucleation and in fusion in nm and θ is temperature in °C.

Calculation method

Determination of the porosity and pore size distribution of saturated material using water as condensate by an iterative calculation method is presented e.g. in the references Matala 1995b.

DISCUSSION OF THE METHOD

Theoretical considerations

The principle behind thermoporosimetry is very simple: The phase transformation energy evolved during freezing or melting of the condensate in pores between the specified temperatures is measured calorimetrically, and corresponds to the pore volume in the pore ranges which relate to the solidification or fusion temperature of the condensate.

Although the principle is simple, there are many approximations in the theory on which the method is based. The energy evolved during phase transformation can be measured with high accuracy, but the correct evolution of entropy of the applied condensate before, during and after solidification and fusion is more difficult to calculate. Entropy changes in the adsorbed water layer, in the ice sphere, and in the interphases must be known. Supercooling of water lowers its freezing temperature and these thermodynamic properties are poorly understood.

The second difficulty lies in the phase state of the pore water. Pure pore water in cement paste is generally assumed in this context, but various impurities are known to exist. The effect of these substances on the entropy of water and ice, and on the entropy due to curvature of the water-ice interphase, are usually neglected. The values of surface tension for the solid-gas interphase, solid-liquid interphase and/or liquid-gas interphase must be known. One of these can be expressed as a function of the others, but in a case of incomplete saturation two of these must be formulated, and the surface tension of solid-liquid interface must be known in a state of full saturation. Unfortunately the reported values in the literature are mostly based on calculations using homogeneous nucleation theory or on the tests with samples having large pore diameters.

The third category of uncertainties lies in the freezing phenomenon in the porous system. The volume change during solidification affects the changes in the strain state of the matrix if the developed pressure cannot be released through the non-frozen pore space. If the matrix is unable to resist these strains it breaks down, and the calorimetric readings may include part of the fracture energy. How significant for analysis of the fusion thermogram are the changes in pore structure due to freezing pressure? Further, if the matrix is strong enough and transport through the pore space is prevented, what really occurs in the pores? Is solidification possible at all? These phenomena may play a certain role especially in the gel pore range.

Hysteresis between solidification and fusion thermograms

As a phenomenon, hysteresis is known to exhibit in the imperfectly elastic material systems, in which the reaction of the system to changes is dependent upon its past reactions to change. The phenomenon is clearly noticeable in the characterization of porous systems, especially, by the sorption and capillary methods; e.g. the adsorption-desorption and MIP tests. The facts causing hysteresis in porous cementitious materials are not comprehensively explained, but generally they are associated with the pore geometry and pore continuity. Obviously, the inelasticity and viscoelasticity of concrete have influence on this behavior.

According to Eqs 14 and 15 and Fig 4 the pore geometry explains some part of a strong hysteresis between the solidification and fusion thermograms seen in Fig 5. If the pore shape is strictly spherical the curvature of ice sphere remains the same when fusion takes place as it was when solidification took place, and the fusion and solidification temperatures are the same. On

the other hand, if the pore shape is cylindrical the curvature of ice-water interface becomes equal to the inverse of radius in fusion, but in solidification the spherical nucleus grows spontaneously through the cylindrical pore hence the curvature of ice-water interface is two times the inverse of radius. E.g. Eq 11 gives the radius of 1.37 nm for the nucleating ice at -40° C. In fusion, the same ice in cylindrical pore melts at -20.8° C. Obviously, the irregularity of pore system; likely layered than cylindrical shape, may give even higher hysteresis. Another feature in pore geometry which causes hysteresis can be derived from the differences in solidification and fusion energies. Solidification enthalpy (Eq 8) is dependent on the enthalpy caused by the entropy changes due to the superficial phase transformations. This, on the other hand, is strongly dependent on the pore geometry. If this effect is included in the consideration above, the ice formed in cylindrical pore at -40° C melts at -17° C.

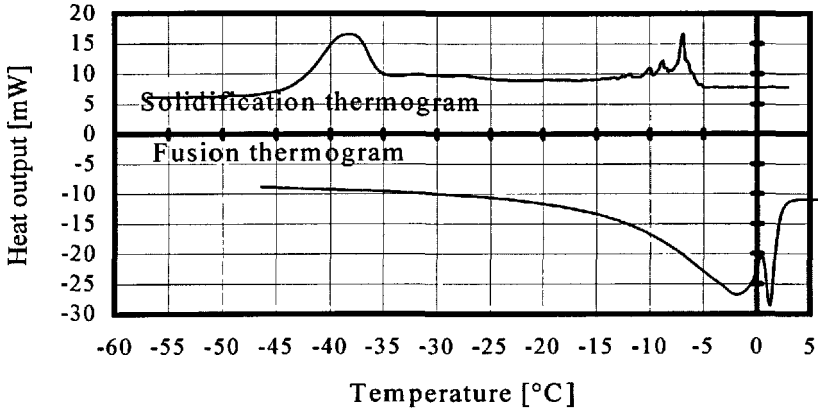

Figure 5. Solidification and fusion thermograms.

Although the pore shape explains a quite representative part of hysteresis there exist possibly also other facts. Enüstün et al. (1978) proposed that melting is controlled by the radii of cavities and the freezing by the radii of openings between the cavities. They state that since, by geometric necessity, the latter radii are on the whole smaller than the former, the model may form a basis for a theory to explain the observed freezing-melting hysteresis. In terms of this plastic ice theory, capillary freezing and melting take place by virtual movement of the ice-water interface along the capillary channels. The same type of hypothesis for the freezing-melting hysteresis is proposed by Sellevold and Bager (1980). They present that the spreading of the ice front through a pore system with variable cross sections would be controlled by the pore necks and the melting by the sizes of pores rather than of the necks, and hence, the hysteresis gives information about the continuity of the pore system.

Whatever the reasons for the hysteresis are; the pore shape, the pore continuity or some other reasons, the fact is that the direct calculation of pore size distribution from the fusion thermogram is unrealistic. This is shown by examples in the reference Matala (1995b). However, Setzer (1990) has presented a cyclic scanning method for DSC to analyze the fusion thermograms. Hence, the effect of supercooling of pore water being evident in solidification could be eliminated. Setzer found that ice, formed in freezing from -40° C to -55° C, melts in a very large temperature range giving a detected fusion heat at -35° C to -5° C in the DSC run. Further, the difference of the fusion thermograms with the reversal temperatures of -40° C and -38° C has a distribution between the temperatures from -25° C to -3° C and a peak at - 10° C. Setzer's results gives evidence of the effect of pore shape on hysteresis discussed above and supports the theory used in the evaluation of Eqs 14 and 15.

Validity of the Laplace's equation at small pore sizes

In the determination of the pore sizes according to Eq 14 it was assumed that the Laplace's equation is valid also at small pore sizes. The solidification thermograms in Fig 5 shows that the secondary peak exists at around -40° C. This peak denotes the pore radius of 2 nm and the radius of nucleating ice about 1.4 nm.

In the literature, e.g. Sellevold and Bager (1980) and Sidebottom and Litvan (1971, it is discussed that application of the capillary theory in small pore sizes may be questionable. These suspicions are based on the theories to explain the freezing phenomenon in porous saturated material. However, two strong evidences of the solidification by nucleation and of the relationship between the temperature depression and pore size can be found in the literature. First, it is widely accepted that all the gel water except for a couple molecular layers on internal solid surfaces is freezable in temperatures used in this study (Litvan 1972, Tada 1987, Zech and Setzer 1989 and Setzer 1990). Tada's finding that third to sixth layers are able to change their thermodynamic state already at around -40° C fits nicely on the estimated gel pore radius of 2 nm presented above. Further it is stated that an *in situ* freezing in gel pores is possible since there is an unfrozen adsorbed layer between the surface of the matrix and the pore ice which reduces the change in surface energy on freezing (Setzer 1990, p.417). Some evidence of the freezing of gel pore water can be found from the study where the gel pore volume of high strength pastes were determined by the LTC method and by the N_2-gas adsorption method. Both methods gave the same pore range for gel porosity (Matala 1995a).

Perhaps the strongest evidence of the applicability of the Laplace's equation also at gel pore range can be found from the investigation in which the solidification temperature of water was studied with materials of the known pore sizes; Vycor glass and five alumina porous plugs with the pore radii of 2.4 to 10.5 nm (Brun et al. 1977). The results are given in Fig 6 which shows that calculated pore radii by Eq 14 are extremely well in accordance with the experimental values.

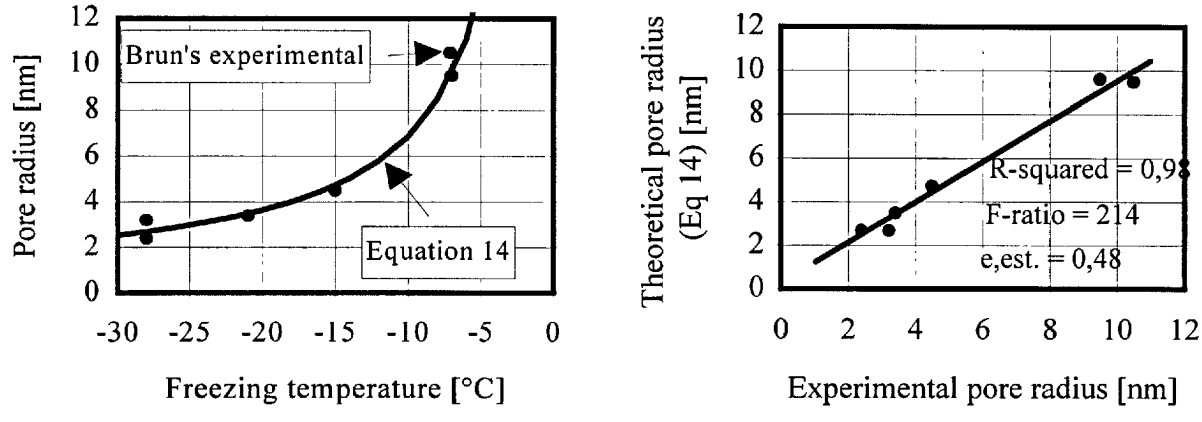

Figure 6. Comparison between experimental (Brun 1977) and theoretical (Eq 14) values of pore radii.

Consideration above shows the validity of Eq 14 in the calculations of pore size distribution by solidification thermograms and that the gel porosity is possible to estimate by the LTC method. However, it should be remembered that the whole solidification heat observed at -40° C does not consist of the heat caused by the nucleation of gel pore water. It comprises also the heat output of

the superficial phases; i.e., the adsorbed water layer of larger capillary pores, the thickness of which decreases in temperatures below the pore nucleation temperature.

Experimental uncertainties

Sample used for low temperature calorimetry are quite large. This, and although a temperature rate is slow, causes a lag in temperature over the sample. In addition, the pore space is measurable only within the limits of its saturation. If total porosity is of interest, there must be some certainty of water saturation in the sample. The aforementioned theoretical and experimental uncertainties should be taken into account as limiting factors when analyzing the results of thermoporometric measurements and when drawing conclusions about pore structure on the basis of any thermoporometric approach.

REFERENCES

Bager, D.H., "Ice formation in hardened cement paste", Technical University of Denmark. Ph.D. Thesis. Technical Report 141/84, 1984, 66 p.

Beddoe, R E., and Setzer, M.J., "Phase transformations of water in hardened cement paste, a low-temperature DSC investigation", Cement and Concrete Research, Vol 20, 1990, pp. 236-242.

Brun, M., Lallemand, A., Quinson. J-F. and Euraud. C., "A new method for the simultaneous determination of the size and the shape of pores: The thermoporometry", Thermochimica Acta, 21, 1977, pp. 59-88.

Enüstün, B.V., Sentürk, H.S. and Yurdakul, O., "Capillary Freezing and Melting", Journal of Colloid and Interface Science, Vol. 65, No. 3. 1978, pp. 509-516.

Fagerlund, G., "Determination of pore-size distribution from freezing-point depression", Matériaux et Constructions, Vol.6-No 33, 1973, pp. 215-225.

Litvan, G.G., "Phase Transitions of Adsorbates, III. Heat Effects and Dimensional Changes in Nonequilibrium Temperature Cycles", Journal of Colloid and Interface Science, Vol. 38, No. 1, 1972, pp. 75-83.

Matala, S., "Thermoporometric approach in the determination of pore structure in concrete", Proc. Int. Conf. on Concrete under Severe Conditions, Sapporo, Japan 2-4 August 1995, Ed. by K.Sakai, N. Banthia and O.E. Gjørv, Publ. E & FN Spon, Vol. 2., pp. 1087-1096.

Matala, S., "Effects of carbonation on the pore structure of granulated blast furnace slag concrete", Helsinki University of Technology. Concrete Technology. Report 6. Dissertation. 1995. 161 p. + app. 49 p.

Tada, S., "Pore structure and moisture characteristics", Proceedings of the First International RILEM Congress; Vol 1. Pore Structure and Material Properties. Versailles 1987. pp. 85-91.

Takagi, S., "Approximate Thermodynamics of the Liquid-like Layer on an Ice Sphere Based on an Interpretation of the Wetting Parameter", Journal of Colloid and Interface Science, Vol. 137, No. 2., 1990, pp. 446-455.

Sellevold, E.J., and Bager D.H., "Low temperature calorimetry as a pore structure probe", Proceedings of 7th Int. Cong. on the Chemistry of Cement. Vol.IV. Paris 1980. pp. 394-399.

Setzer, M.J., "Interaction of Water with Hardened Cement Paste" Ceramic Transactions, Advances in Cementitious Materials, Ed. S. Mindess. Vol. 16, Gaithsburg 1990, pp. 415-439.

Sidebottom, E.W. and Litvan G.G., "Phase Transitions of Adsorbates, Part 2. Vapor Pressure and Extension Isotherms of the Porous Glass+Water System Below 0° C", Transactions of the Farady Society. No. 585, Vol. 67, Part 9, 1971, pp. 2726-2736.

Zech, B. and Setzer, M.J., "The dynamic modulus of hardened cement paste. Part 2: Ice formation, drying and pore size distribution", Materials and Structures, 22., 1989, pp. 125-132.

A COMPARISON OF TWO DIFFERENT METHODS FOR STOPPING THE HYDRATION OF MONO CALCIUM ALUMINATE AT 20°C

Steffen MÖHMEL, Wolfgang GESSNER, Barbara KÖDDERITZSCH
Institut of Applied Chemistry Berlin-Adlershof e.V., Berlin, Germany

ABSTRACT
The influence of two different methods commonly used to stop the hydration of cements (freeze drying and washing with acetone and diethylether, respectively) on the reaction of mono calcium aluminate with water is compared. Investigations by XRD, N_2 adsorption (specific surface area), DTA-MS and ^{27}Al-NMR (degree of hydration) have shown that washing with the organic solvents effects both the surface of CA* grains and the hydration products formed. In view of this fact freeze drying would appear to be the preferred method for stopping the hydration of CA.

Key-words: Calcium aluminate cement, Hydration, Drying, Method

INTRODUCTION
For a better understanding of the hydration of a cement it is often desirable to stop or quench the reaction at a particular point during the hydration process to examine the extent of hydration and the nature of the hydrates formed at the samples obtained in this way.
Various methods may be used to eliminate uncombined water and to stop the hydration. But only little is published about the influences of these methods on the hydrated cement. Although it is known that several of the hydration products of calcium aluminates are able to incorporate organic compounds - for example C_4AH_{13} (Lavanant, F., 1965, Massazza, F. et al., 1982), C_2AH_8 (Young, J.F., 1971) and AH_3 (Kee Kwong, K.F.N. and Huang, P.M., 1978) - the most common and suitable method is grinding and washing the material with organic solvents (Bachiorrini and Guilhot, 1982). An other usual procedure to stop the hydration of cements is freeze drying. Chandra et al. (1980) noticed by SEM investigations that freeze drying is an effectiv and useful method to study cement hydration. However Vernet and Noworyta (1992) found that the dissolution rate of C_3S is influenced by both, washing with organic liquids and freeze drying as well. In addition the latter causes a cracking of the unhydrated C_3S grains.
Because of these different statements investigations were carried out to compare the influence of freeze drying and washing with acetone and diethylether, respectively, on the course of hydration of monocalcium aluminate after times between 8 hrs up to 28 days at 20°C.

EXPERIMENTAL
The CA used was free of $C_{12}A_7$ and shows a specific surface area of 0,80 m^2/g (BET).
The hydration experiments were carried out in an atmosphere free of CO_2 with a water/solid phase ratio of 0,5 at 20°C. For details of the experimental conditions see Geßner et al. (1993) and in literature quoted there.
To stop the hydration process after given (identical) times the samples were either ground in acetone, washed with acetone and ether and then dried in vacuum over silica gel or frozen in liquid N_2 and then dried in a freeze dryer (CHRIST ALPHA 2-4).
The hydrated and stopped samples were characterized by using the following methods:

- ^{27}Al NMR	:	hydration degree
- X-ray powder diffraction	:	semi - quantitative determination of the hydrate phases
- Adsorption of N_2	:	specific surface area
- DTA-MS	:	decomposition of the hydration products

* shorthand notation is used; C=CaO, A=Al_2O_3, H=H_2O

RESULTS AND DISCUSSION

The course of hydration of the CA in the range between 8 hrs and 28 days is illustrated in **Figs 1 - 3**, showing the development of the hydration products related to the degree of hydration **(Fig 1 and 2)** and that of their specific surface area **(Fig 3)** for the samples stopped with the different methods. A comparison of the samples stopped with acetone / ether on the one hand and with freeze drying on the other hand indicates several effects. Firstly there seems to be a higher degree of hydration in case of the material stopped with the organic solvents. Secondly the proportion of crystalline hydration products is higher in case of the freeze dried samples (especially the amount of CAH_{10} and C_2AH_8) - this may be in connection with the significant higher amount of amorphous products in the samples treated with acetone / ether (see **Fig 2**) - but the kind of the occuring hydration products is not influenced by the stopping procedure.

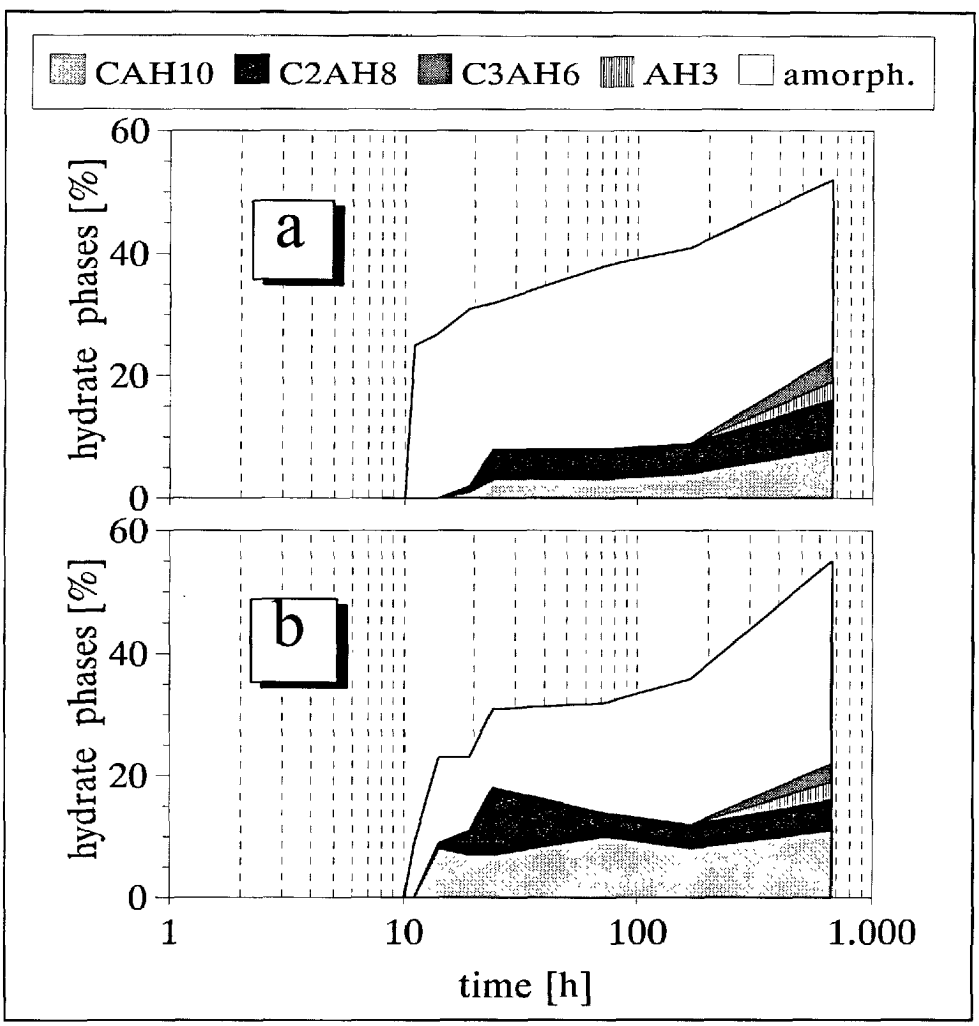

Figure 1 The development of the hydration products by stopping hydration with acetone / ether (a) and freeze drying (b), respectively

Thirdly, the specific surface area of the hydration products **(Fig 3)** also varies in dependence on the method for stopping the hydration. The freeze dried samples usually show a higher surface area during the investigated period than those stopped with acetone / ether. Nevertheless the course of the specific surface area seems to be the same for both series.

Thus it is evident that the method for stopping the reaction of CA with water influences the course of hydration. Compared with freeze drying stopping the hydration with acetone /ether leads to a higher degree of hydration, a higher amount of amorphous and a smaller part of crystalline products and finally to a lower specific surface area of the hydration products.

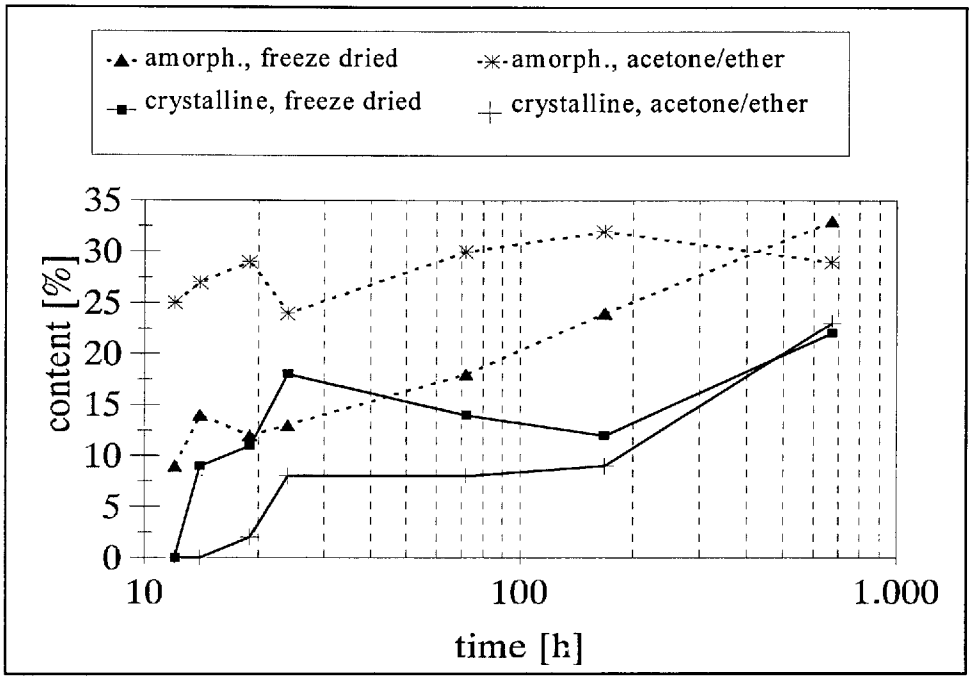

Figure 2 Comparison of the crystalline and amorphous parts of the hydration products in dependence on the method for stopping hydration

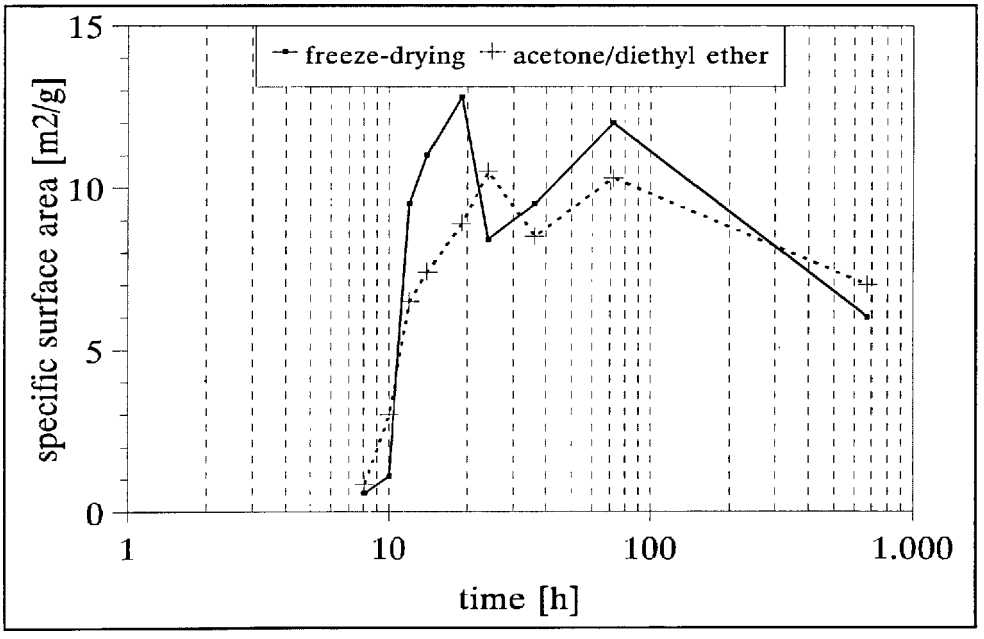

Figure 3 The course of the specific surface area of the hydration products in dependence on the method for stopping hydration

These differences are especially pronounced in the range between 10 hrs and 1 day. After longer times (7 - 28 days) the observed differences diminish and seem to disappear.
Supposing that especially the treatment with the organic solvents leads to changes in the characteristics of the hydration products investigations were carried out to study the influence of acetone and ether on mono calcium aluminate and calcium aluminate hydrates.
Therefore first of all DTA and DTA-MS investigations were made to find out whether there are organic compounds detectable in the hydrated specimens or not. **Fig 4** shows the DTA curves for the samples hydrated 14 hours and stopped with freeze drying and organic solvents,

respectively. The results largely agree with those of the XRD measurements. The CA sample stopped with freeze drying shows a large and broad endothermic peak in the range 120-160°C, indicating a relative high proportion of CAH_{10} and/or C_2AH_8. The smaller peak at about 280°C is attributable to the coinciding effects caused by the decomposition of AH_3 and C_3AH_6. Whereas the peak at the lower temperature is smaller in case of the sample stopped with acetone / ether that at 280°C is much higher. Considering the XRD results and because of the fact that C_3AH_6 is not known to occur in an amorphous state this second peak is likely related to AH_3 (possible with small amounts of C_3AH_6).

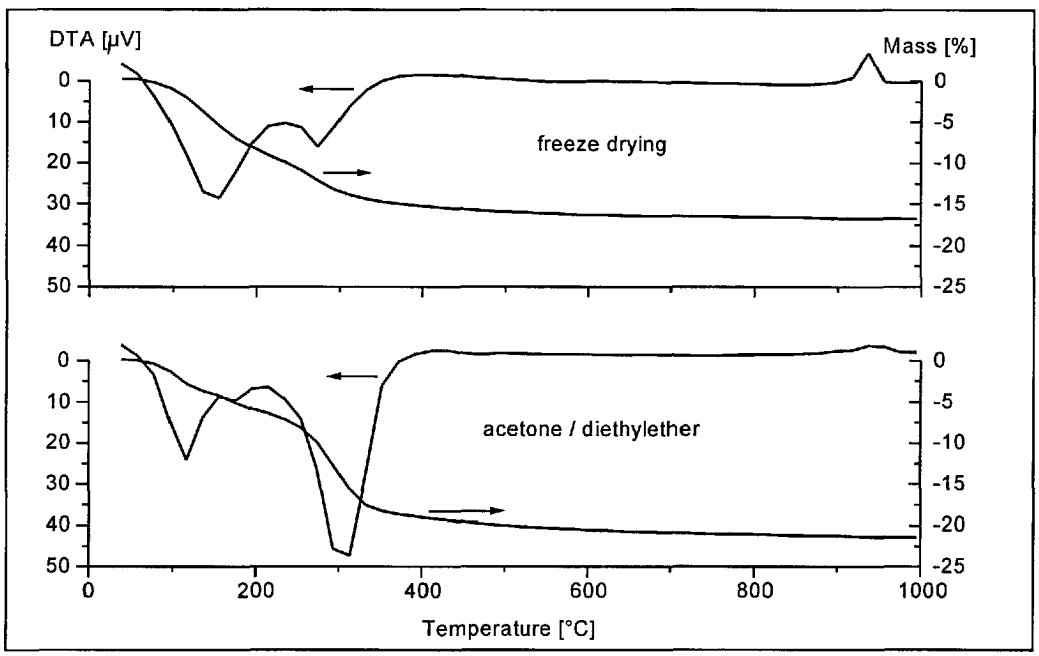

Figure 4 DTA/TG for the samples hydrated 14 hours at 20°C

The results of investigations with a combination of the DTA equipment with a mass spectometer show that traces of both acetone and ether are detectable in the samples stopped with the organic solvents (**Fig 5**).

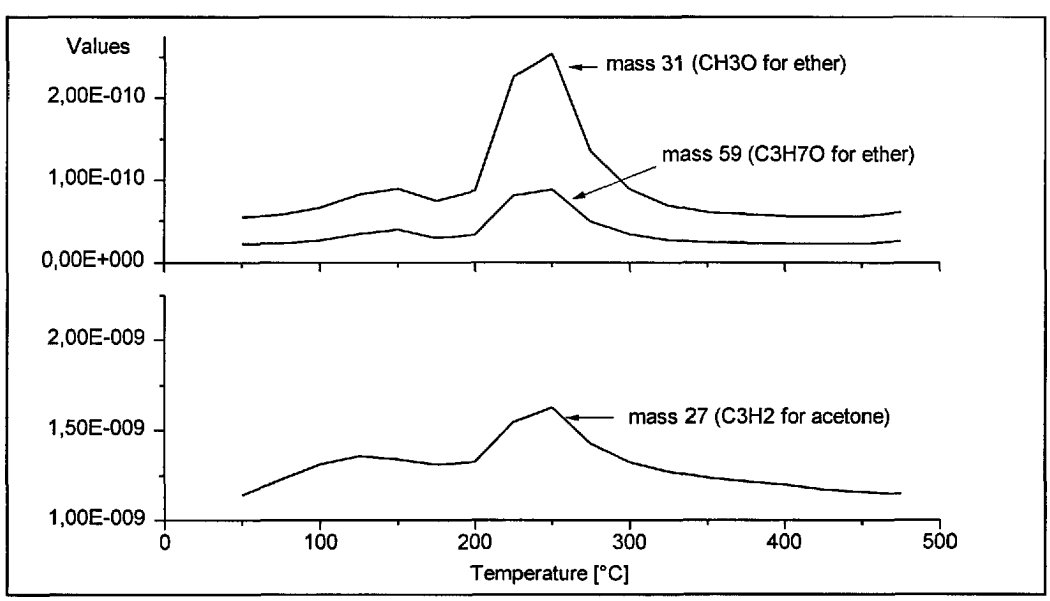

Figure 5 Mass-spectrometry for the sample hydrated 14 hours at 20°C and treated with acetone / diethylether

It is evident that a relative high amount of organic compounds is released in the range 200-300°C. In addition a small effect at about 120°C can be observed which is in good agreement with the endothermal decomposition of CAH_{10} and/or C_2AH_8 indicated in the DTA pattern. The more pronounced peak is in accordance with the beginning of the AH_3/C_3AH_6 peak. Therefore the organic compounds seem to be connected with the hydration products of the CA especially with the AH_3 but in an lower extend also with the CAH_{10} and C_2AH_8, respectively. Because of the drying procedure in vacuum over silica gel for at least 24 hours after grinding and washing with the organic solvents it could be concluded that these organic components are not only adsorbed but incorporated in the structure of these hydration products.
Further investigations were carried out with synthetic calcium aluminate hydrates to analyse the influences of a posttreatment on these phases. For that purpose pure samples of CAH_{10}, C_2AH_8, C_3AH_6 and AH_3 (gibbsite) were washed with acetone / ether and freeze dried, respectively, and then examined by XRD and N_2 adsorption. An inner standard was used for the XRD examination to compare the crystallinity (calculated from the area of the peak with the highest intensity in the XRD pattern) of the untreated phase (always 100%) with that of the stopped samples. The results of these investigations are summarized in **Table 1**.

Table 1 Comparison of the specific surface area (s.s.a.) and crystallinity of the hydration products untreated, treated with organic solvents and freeze dried

phase	untreated		treated with acetone / ether		freeze dried	
	s.s.a. [m^2/g]	crystallinity [%]	s.s.a. [m^2/g]	crystallinity [%]	s.s.a. [m2/g]	crystallinity [%]
CAH_{10}	33,3	100	31,3	86	39,9	76
C_2AH_8	8,9	100	9,0	88	8,5	92
C_3AH_6	4,9	100	244,5	181	2,9	96
AH_3	111,9	100	120,7	112	101,3	106

It can be seen from **Table 1** that the treatment with acetone / ether influences the crystallinity and specific surface area of the hydration products of CA. The crystallinity of CAH_{10} and C_2AH_8 appears to decrease whilst that of C_3AH_6 and AH_3 increases. The specific surface area shows an astonishing increase in case of the C_3AH_6 and a small one for AH_3. Especially the significant increase in the specific surface area and crystallinity of the C_3AH_6 is remakable and should be further investigated.
In contrast to the treatment with the organic solvents freeze drying appears to modify only CAH_{10} in a significant manner.
To examine a possible influence of the stopping procedure on the calcium aluminate itself a CA sample was treated for 1 hour in running water (to dissolve the CA surface but to prevent the precipitation of hydration products on the grains) and after that washed with the organic solvents and freeze dried, respectively. The results of the investigations of these materials are shown in **Table 2**.
It is evident from **Table 2** that also the unreacted CA is influenced by the method of stopping the hydration. Especially differences in the cristallinity of the treated samples are observed whereas their specific surface area is nearly the same. The crystallinity is lower in case of washing the samples with the organics than for those stopped with freeze drying. The apparent higher degree of hydration of the specimens treated with acetone / ether (see **Fig 1**) may be in connection with this stronger amorphisation of the unreacted CA.

Table 2 Comparison of the specific surface area and crystallinity of the washed CA in dependence on subsequent treatment

phase	subsequent treatment	sp. surface area [m^2/g]	crystallinity [%]
CA	/	0,8	100
CA	freeze drying	2,9	83*
CA	washing with acetone / ether	3,0	74*

* no hydration products were detectable

Taking all the results together it is evident that especially the treatment with the organic solvents leads to changes of the unreacted CA and the hydration products as well. Thus the observed smaller proportion of crystalline phases and the corresponding higher amount of amorphous products in the samples washed with the organics may be caused by a partial interaction of acetone and ether with the hydration products. This is deduced from the behaviour of the pure hydrates by contact with acetone and ether. Obviously an incorporation of these solvents take place leading to a partial amorphisation especially of CAH_{10} and C_2AH_8 and so to the observed smaller proportion of crystalline phases and higher amount of amorphous products. This assumption corresponds with the results of the DTA-MS investigations showing that organic compounds are released from the specimens in connection with the decomposition of the hydrates. However there is no evidence for a crystallisation of hydrates initiated by the treatment with aceton as mentioned by Murat (1988).
The higher degree of hydration of the samples stopped with acetone / ether could be attributed to changes of the unreacted CA as it is reflected by the results shown in **Table 2**. Only the lower specific surface area of the specimens of the series treated with acetone / ether can't be explained by changes caused by the organic solvents. Therefore the differences in the course of the specific surface area may be attributed to the freeze drying. Although there is no clear evidence for the occurance of microcracks caused by freezing - as described by Vernet and Noworyta (1992) - the higher specific surface area of the freeze dried specimen may be due to that.
The observed diminishing of the differences after longer times (28 days) may be attributed to contrary influences of the organic solvents on the different hydration products.

CONCLUSION

A comparison of two methods used to stop the hydration of mono calcium aluminate shows that at ages up to 7 days the quantity of crystalline hydrates, especially CAH_{10} and C_2AH_8, observed after freeze drying was larger and less amorphous products were found than in specimens washed with organics. Furthermore freeze dried samples also have a higher specific surface area and a lower degree of hydration. These different influences are obviously caused by an incorporation of the organics in the hydration products and by changes of the surface of the unhydrated CA grains.
At longer hydration times (28 days) the differences caused by the method used to stop the hydration seem to decrease.
Though also freeze drying seems to effect the hydration the described results show that this method appears to be more suitable for stopping the hydration of calcium aluminates than a treatment with organic solvents.

REFERENCES

Bachiorrini, A., Guilhot, B., „Premieres echeances de l'hydratation de láluminate monocalcique Influence du protocole de stoppage", Cem. Concr. Res., Vol. 12, 1982, pp. 559-567
Chandra, S., Hedberg, B. and Berntsson, L., „Freezing as a method of study the early cement paste hydration", Cem. Concr. Res., Vol 10, 1980, pp. 467-469
Geßner, W., Möhmel, S., Trettin, R., Oliew, G. and Müller, D., „On the influence of alumina on the hydration behaviour of mono calcium aluminate"Proc. 3rd UNITECR, Sao Paulo, Brazil, 1993, pp. 265-273
Kee Kwong, K.F.N. and Huang, P.M., „Nature of hydrolytic precipitation products of aluminum as influenced by low-molecular weight complexing organic acids", Proc. Int. Clay Conference, Oxford, 1978, pp. 527-536
Lavanant, F., „Contribution à l'étude de quelques aluminates de calcium hydratés", Rev. Mat. Constr., No. 595, 1965, pp. 193-207
Massazza, F., Costa, U. and Barrila, A., „Interaction Between Superplasticisers and Calcium Aluminate Hydrates", J. Am. Ceram. Soc., Vol. 65, 1982, pp. 203-207
Murat, M., „A Comment on the paper 'The Hydration of CA at different temperatures' by Edmonds and Majumdar", Cem. Concr. Res., Vol. 18, No. 5, 1988, pp. 830-834
Vernet, C. and Noworyta, G., „Comparison of two methods for stopping hydration: application to the study of the initial dissolution rate of C_3S", Proc. 9th Int. Congr. Chem. Cem., New Delhi Vol. IV, 1992, pp. 208-213
Young, J.F., „Effect of organic compounds on the interconversions of calcium aluminate hydrates. Hydration of monocalcium aluminate", Cem. Concr. Res., Vol. 1, 1971, pp. 113-122

STUDIES ON CEMENT HYDRATION BY WATER SORPTION AND STATIC HEATING

Ewa T.STĘPKOWSKA, Institute of Hydroengineering PAS, Gdańsk, Poland
Ajoy K. MULLICK, Surrinder K.HANDOO, National Council for Cement and Building Materials, New Delhi, India
Jose-Luiz PÉREZ-RODRIGUEZ, Miguel Angel AVILES and Eduardo GOMEZ
Instituto de Ciencia de Materiales de Sevilla, Spain.

ABSTRACT Quantitative study of hydration products of a cement powder and a cement paste by water sorption and weight loss on static heating is presented. Evaporable water was 2.5-3 times higher in paste, portlandite content was only by 1/3 higher and non-evaporable water content increased more than twice. XRD, SEM and DTA study of cement powder and paste is also reported.

Key-words: Bound water, Degree of hydration, Evaporable water, Scanning Electron Microscopy, Calcium hydroxide.

INTRODUCTION

The estimation of specific surface and hydration products in the cement powder was suggested by measurement of water sorption and weight loss on static heating (Stępkowska et al., 1996). Therefrom were estimated: the specific surface both in air dry state and in hydrated state, the content of evaporable water (at 110°C), of non-evaporable water (composed of zeolitic water and chemically bound water) and of portlandite. The influence of certain parameters on cement hydration products was evaluated, such as age of cement, sorption time (representing setting time), water availability (representing water/cement ratio), cement pretreatment and container material (representing the reinforcement).

Here the hydration of a Portland cement powder is presented and compared with the cement paste stored for two years.

MATERIALS

Ordinary Portland Cement (OPC) indicated the chemical composition (in form of oxides) as: SiO2 21.48%, Al2O3 4.50%, Fe2O3 3.40%, CaO 60.03%, MgO 6.08%, SO3 1.73%, free CaO 0.20%, LOI (1000°C) 1.56%. Cement paste prepared at w/c = 0.4 was stored for two years, ground to pass 100 mesh sieve and it was studied simultaneously with the cement powder.

METHODS AND RESULTS

Water sorption/retention test

5 g samples both of the cement powder and of the powdered paste either air dry (WS) or predried at 110°C (WSo) were placed in aluminium containers (3x2x1 cm), successively for two weeks at normal atmospheric pressure, at 30°C in desiccator over a suitable solution: in water sorption at R.H.= 50%, 95% and 100%, in water "retention" (WR) at R.H. = 100%, 95% and 50%. This was followed by heating successively (including untreated samples) at 110°C (1d), 220°C (8h), transferring to ceramic dishes, which resulted in contact with air, and heating farther at 400°C (4h) and 800°C (1h). Weight changes were measured and calculated in percent referring to the final weight at 800°C. Weight balance, DTA and XRD indicated decomposition of $CaCO_3$ at this temperature (Stępkowska et al., 1996). Results are presented in Fig. 1. The standard deviation was generally 0.1-0.4%. Exceptionally in three cases of high R.H. it was 0.8-1.0%.

SEM

JEOL JSM-5400 Scanning Electron Microscope was used, equipped with EDXR unit. Fig. 2 shows the similarity of microstructure after WR measurement and of the paste as known from the literature. The gel is exceptionally well hydrated; it contains calcium silicate aluminate, including some Fe and K. Irregular plates enclose pores of several micrometers size. After wetting-drying procedure many calcite crystallites on the sample surface were found.

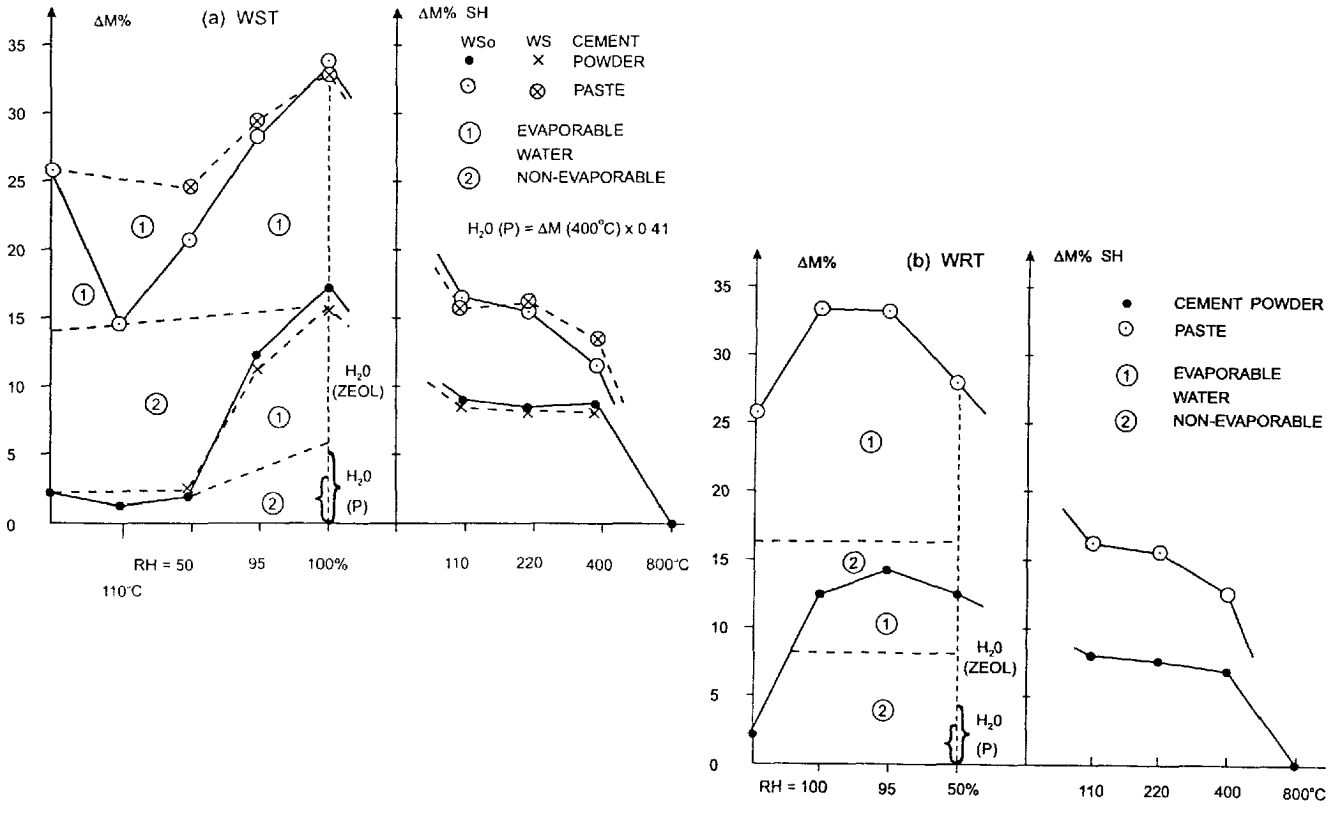

Figure 1. Change in sample weight (ΔM) during the WS test (a) and WR test (b) and static heating (SH).

XRD

Siemens Kristalloflex D 501, equipped with graphite monochromator CuKa and the computer SICOMP PC 16-20 was used. Important portlandite peaks were found in cement paste and no calcite was present. Similar was the XRD pattern of the WR sample with lower portlandite peaks. No calcite was found after heating at 800°C. Peaks were interpreted according to Taylor (1990), Fig. 3.

DTA

Thermal study was performed on Derivatograph MOM Budapest (mgr. Z. Sułek). The total weight loss in cement powder was 3.71 %, as compared to 2.5% measured in static heating (SH). In cement paste it was 28.82 % wherefrom 6.19 % escaped between 500 and 1000°C; in SH of cement paste it was 26.6% and 6.82%, respectively.

A pronounced dehydration endotherm was found in the paste at 120°C (with secondary minima about 70 and about 200°C), a smaller one was observed at 510°C corresponding to dehydration of portlandite and the smallest - at about 790°C, due to calcite decomposition, ending abruptly before 800°C.

DISCUSSION

Water sorption/retention is proportional to the specific surface. which was calculated in cement powder as 2.75 m^2/G (coefficient used was 585 m^2/G H_2O), whereas in hydrated state it was 44 m^2/G for cement powder and 96 m^2/G for cement paste (assuming six-molecular sorbed water layer and the coefficcient 556 m^2/G H_2O, Stępkowska et al., 1996). Cement powder after oven drying at 110°C (WSo) sorbed more water at R.H.= 95% and 100%, than the air dry one. This was observed also in some calcareous soils (unpublished data) and it was interpreted that oven drying disturbed some cementing bonds (there - carbonate cementation, here lime cementation) and thus the water sorption could proceed more freely.

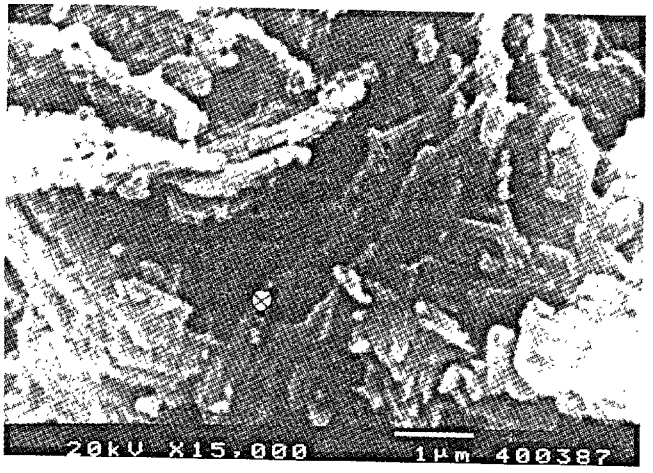

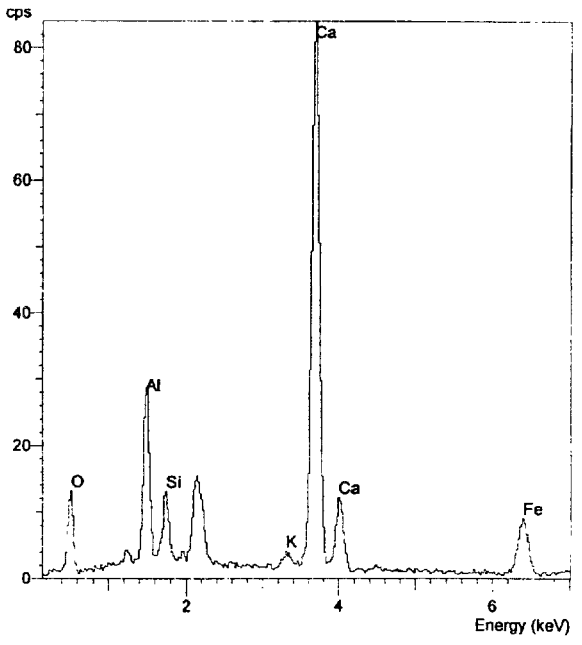

Fig. 2. Cement powder after WRT ; SEM 15,000x (387). Point EDXR indicates Ca:Al:Si = 5:2:1

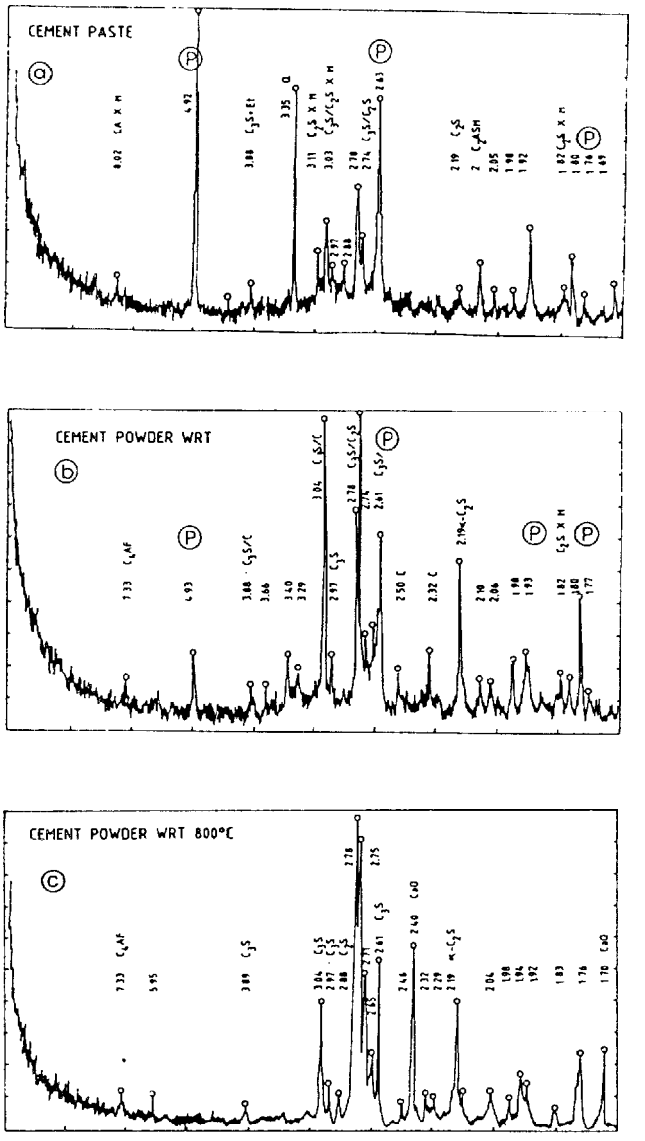

Fig. 3. XRD traces of cement paste (a) and cement powder after WR test (b) and after heating at 800°C

The total increase in weight was by more than one half lower after hydration in water vapour (WS/WR test) than after hydration in liquid water (paste), due to the difference in the hydration time: one month at R.H.= 95% to 100% as compared to two years in paste. In cement powder a full hydration was observed in selected places only as in Fig. 2. In Fig. 1a it is shown that the total increase in weight of cement powder reached about the value of non-evaporable water in cement paste.

Contributions of the evaporable water and non-evaporable water in the total weight increase were in the paste approximatelly equal: about 17% (evaporable) + 16% (non-evaporable) = 33%.

In WS test the contribution of the evaporable water was somewhat lower, but still both were almost equal. On the other hand in WR test the ratio of their contributions was exactly 1:2. The arrangement of grains was frequently more compact in WR test than in WS test, due to the surface tension of

water films at the saturated water vapour pressure (R.H.=100%). Thus spacial hindrances were preventing full hydration and the contribution of evaporable water content was lower.

A negligible change in weight was observed between 110 and 220°C (<1%). This represented the residual sorbed water in interlayer spaces and/or ettringite. Only in untreated cement paste (SH) this amounted to 2.8%.
Portlandite which developed on hydration during the WS/WR test, transformed up to 400°C into calcite, which decomposed at 800°C evolving CO_2 [Taylor, 1990, Ramachandran et al., 1964, Stępkowska et al., 1996].

Multiplying the weight loss beween 400 and 800°C [-ΔM(400- 800°C)] by the stoichiometric coefficient 0.41 = $M(H_2O)/M(CO_2)$ the amount of water chemically bound in portlandite is evaluated.This calculation is correct if the total portlandite transforms at 400°C into calcite and if no calcite is formed below 110°C. Both were proved by XRD in a previous paper (Stępkowska et al., 1996).
Subtraction of [H_2O (portlandite)] from the non-evaporable water content results in evaluation of the other part of stongly bound water, which could be described as "gel" water or "zeolitic" water according to the definitions used in soil science and in cement science (Powers and Brownyard, 1947, Bensted, 1983).

The amount of portlandite water measured in WS test was not much lower than in the paste rehydrated in water vapour (3.4-3.6% as compared to 4.8-5.4%, i.e. increase by about 1/3) in spite of the big difference in hydration time. Also some geometrical hindrances prevented the full formation of portlandite in WR test resulting in a lower value: for cement powder it was 2.9% and even in the paste it was somewhat lower, i.e. 4.6%.

Bigger differences were observed in formation of zeolitic water: it was more than twice as high in paste than in WS test. This means that the reactive centers to form portlandite are used quicker than the reactive centers to promote hydration.
The minor dependence of portlandite content on the hydration time (1-28 days) was observed by Handoo et al.(1996). Taylor (1990) indicates that 70% C3S transforms within 28 days into portlandite and within 1 year only 10% unreacted compound remains. Correspondingly a low C_3S peak was observed by XRD in the paste (Fig. 3).

CONCLUSIONS

Hydration of cement powder in water vapour proceeds in a similar way as in liquid water. Portlandite forms quickly and its content increases only marginally with time. Sorbed water content and zeolitic water content depend strongly on hydration time. Specific surface and contents of water in these states can be evaluated from water sorption and weight loss on static heating.

REFERENCES

Bensted, J., "Hydration of Portland Cement" in S.N.Gosh Ed. "Advances in Cement Technology", Pergamon Press, 1983, pp.307-347
Handoo, S.K., Shri Gopal and Gupta, R.S., "Investigation on the Hydration Characteristics of Multicomponent Cement Blends", Proc. 5th NCB Internat. Seminar, New Delhi Nov. 1966, V. 3, pp.XI-40-52
Powers, T.C. and Brownyard, T.L., "Studies of the Physical Properties of Hardened Portland Cement Paste", J. Amer. Concrete Inst., Proc. Vol. 43, 1947, pp. 971-992.
Ramachandran, V.S., Feldman, R.F. and Sereda, P.J.,"Application of Differential Thermal Analysis in Cement Research", Highway Res.Rec.No 62 (1964),Res.Pap.No 249, Div.Build.Res.,Ottawa, 1965.
Stępkowska, E.T., Pérez-Rodriguez, Justo, A. and Sánchez-Soto, P.J., "The Estimation of Cement Hydration Products by Water Sorption and Thermal Weight Change", Proc. 5th NCB Internat. Seminar, New Delhi Nov. 1996, V. 3, pp. XII-79 to XII-92.
Taylor, H.F.W., "Cement Chemistry", Academic Press, 1990.

QUANTITATIVE DETERMINATION OF THE CRYSTALLINE AND AMORPHOUS PHASES IN LOW CALCIUM FLY ASHES

P. ARJUNAN, M.R. SILSBEE and D.M. ROY, Materials Research Laboratory, The Pennsylvania State University, University Park, PA 16802.

ABSTRACT Glassy/amorphous phases and crystalline phases present in low calcium fly ashes were quantitatively extracted by hydrofluoric acid and phosphoric acid respectively using a new chemical phase analysis technique. The results of this chemical phase analysis technique are compared with 1) a conventional x-ray diffraction(XRD) method using an internal standard and 2) quantification using full spectra x-ray diffraction analysis technique. The result of the chemical phase analysis technique compare well with the results obtained using QXRD.

Key-words: Fly ash, Characterization, Extraction methods, Quantitative, Reactivity

INTRODUCTION

The reactivity of low calcium fly ash in concrete is determined to a large extent by amorphous phases. The crystalline phases are also known to be reactive though at a slower rate. It is very important to determine the quantity of crystalline and amorphous phases present in fly ash in order to evaluate their behavior in concrete. A number of studies have appeared concerning the evaluation of glassy content using various acid leaching techniques as following reports: Watt and Thorne (1966), Hulett et al. (1980), Hemmings and Berry (1988), Berry et al. (1987). However, a quantitative method for determining both crystalline and amorphous phases in fly ash never has been established. The purpose of the present study is to develop an accurate chemical procedure for measuring the various crystalline and glassy contents of the fly ash.

Basis of the method

Glass/amorphous phases were removed from the crystalline phases by etching with 1 % HF. In the case of the crystalline phases, orthophosphoric acid is used for selective removal of mullite and iron oxide phases from quartz. Mullite and iron oxide phases are calculated as difference from soluble silicates and quartz. Phosphoric acid forms water soluble complexes with both silicic acid and metallic oxides(Young (1974), Talvitie (1951)). Upon heating a silicate material with 85% phosphoric acid, vigorous boiling takes place accompanied by an increase in temperature. The boiling subsides as the acid approaches 100% concentration at about 220° C. With further heating between 230° C to 250° C the orthophosphoric acid, by loss of water, converts to pyrophosphoric acid as shown in Eq 1 and simultaneously dissolves the silicates.

$$\underset{\text{Orthophosphoric acid}}{H_3PO_4} \xrightarrow{>230^\circ C} \underset{\text{Pyrophosphoric acid}}{H_4P_2O_7} \xrightarrow{>315^\circ C} \underset{\text{Metaphosphoric acid}}{HPO_3} \qquad [1]$$

The clear, viscous solution obtained remains stable upon dilution with water, permitting a simple separation from quartz by filtration through paper.

EXPERIMENTAL PROCEDURE

Chemical phase analysis

Two types of low calcium fly ashes, American and Australian in origin were used for the study. A two step chemical phase separation is adopted. A number of probe experiments were conducted with different concentration of HF solution at different contact time for the removal of glassy phase. Similarly a number of preliminary experiments were conducted with ortho phosphoric acid for the separation of quartz and other crystalline phases.

Quantitative x -ray diffraction using single peak calibration.

In a sample containing glassy and crystalline phases, the mass fraction of each crystalline phase can be determined by measuring the integrated intensities of peaks at selected 2Θ values as ratios to the integrated intensity of an added internal standard(Popovic and Greta 1987). The samples were sieved to pass 325 mesh and paste mounts were prepared on a zero background quartz plate using ethanol. X-ray diffraction patterns were obtained for the original fly ash. The powder patterns were gathered over the range of 5° 2Θ to 60° 2Θ at the scanning rate of 2° 2Θ per minute. In the second instance, the fly ash samples were doped with known amounts of pure quartz and mullite in different weight fractions. The XRD powder patterns were gathered over the same range for the doped samples. In the third instance, the powder pattern for 100% quartz and mullite samples were obtained using the same measurement conditions. The weight fractions of the unknown samples were calculated from the calibration curve.

Quantitative x -ray diffraction using full spectra calibration.

A quantitative x-ray powder diffraction (GMQUANT) computer program developed by Smith et al.(1987) has been used in this study. The unique approach employed in this method is the utilization of the full diffraction pattern of a mixture and its reconstruction as a weighted sum of diffraction patterns of the component phases. The fly ash sample was mixed intimately with corundum in the ratio of 1:1 and sieved to pass through 325 mesh. The powder pattern was gathered over the range of 5° 2Θ to 75° 2Θ at a scanning rate of 2° 2Θ per minute. The intensities of the unknown pattern were fitted with the already available known working data base using the menu-driven interactive computer programs known as GMQUANT.

RESULTS AND DISCUSSION

Chemical phase analysis

A number of preliminary experiments were conducted to optimize the contact time and concentration of HF solution. The powder x-ray diffraction pattern for 1%HF treated ash clearly indicates(Fig 1b) the removal of all the glassy phase which was indicated by a broad hump in the original fly ash(Fig 1a). Similarly, the pattern for ortho-phosphoric acid treated ash(Fig 1c) confirms the removal of all the phases except quartz. The SEM micro structure for untreated fly ash (Fig.2a) shows the typical smooth faced round fly ash particle. The SEM for the ash after treatment with HF indicates(Fig.2b) the complete removal of glassy content and the presence of skeletons of quartz and mullite particles.

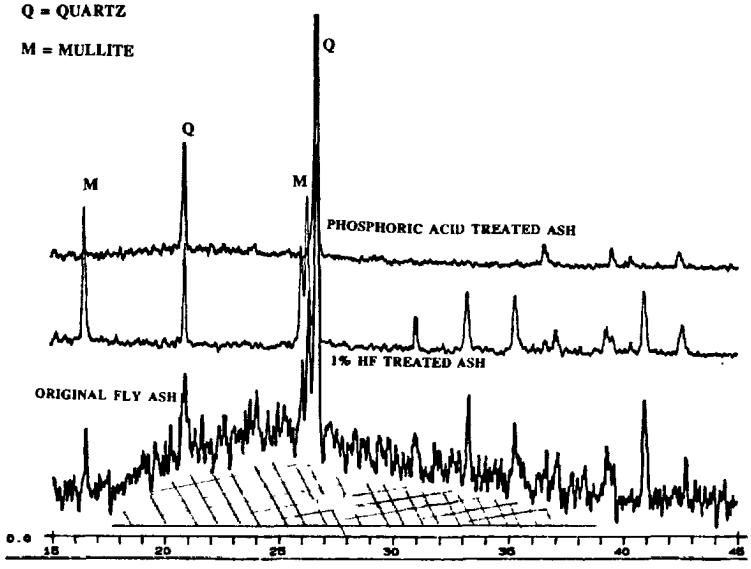

Figure 1. The X-ray diffraction pattern for a) the original fly ash, b) the fly ash treated with 1% HF and c) the fly ash treated with Orthophosphoric acid.

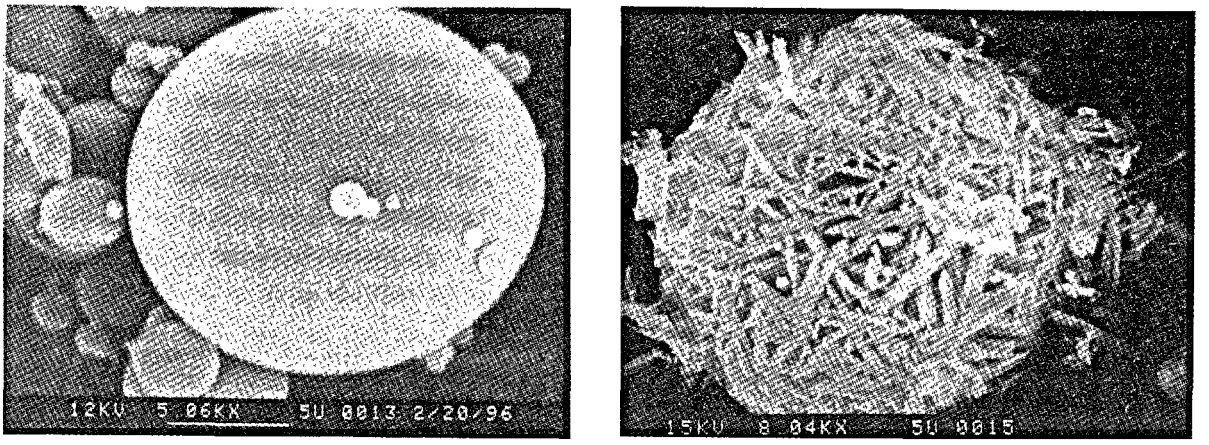

Figure 2. SEM picture showing the fly ash a) before and b) after HF treatment

Rate of dissolution of quartz and mullite in ortho phosphoric acid

In order to determine the rate of dissolution of mullite in pyrophosphoric acid and the extent of quartz dissolution during this period, known amounts of pure quartz and mullite were treated with orthophosphoric acid. The results indicate (Fig.3) that about 15 to 17 minutes of refluxing time is required for the complete removal of mullite. The results also indicate that about only 0.8 to 1.0% quartz is dissolved during this period.

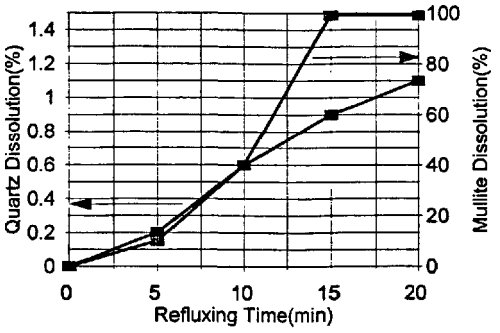

Figure 3. Rate of dissolution of quartz and mullite in pyrophosphoric acid.

Chemical phase analysis procedure

The procedure is as follows: To 1.0g of very fine(<325 mesh) fly ash sample 100 mL of 1% HF was added in an polythene container. The container was placed on an agitating table and agitated for 4 to 6 hours at room temperature. The contents were filtered using Whatman filter paper (pore size 5.4μm) and washed thoroughly with water. The residue was first dried at 100°C for 2 hours and ignited to incinerate the filter paper. The loss in weight was estimated as the soluble silicates. In the second step, 25mL of 85% orthophosphoric acid was added to the residue and the flask was placed directly on a preheated electric heater. When boiling subsides, the flask was swirled for 3 seconds at 1 minute intervals in order to minimize superheating and to keep the sample distributed throughout the acid. At the end of 15 minutes the flask was removed from the heater and placed on the cool surface. After cooling to room temperature, 125mL of hot(60 to 70°C) water was added to the flask and swirled vigorously until the syrupy phosphoric acid is completely dissolved. The contents were filtered using Whatman filter paper (pore size 5.4μm) and washed thoroughly first with cold water and 2 or 3 times with 1:9 HCl and followed by one or two washings with cold water. The filter paper with the residue was ignited in a tarred platinum crucible, first at low heat to char the paper, and finally at about 950° C. The crucible was cooled in a desiccator and weighed.

The residue was moistened with 1 : 1 sulfuric acid and hydrofluorized with 5 mL or more of 48% HF. The difference in weight after hydrofluorization was calculated as quartz.

Comparison of chemical phase analysis results with XRD methods

The quantitative amounts of amorphous and crystalline phases present in the fly ash estimated by the three methods are given in Table 1. In the chemical method, the amounts of quartz and soluble silicates were determined as mentioned earlier and the amounts of mullite and other crystalline phases were calculated as mass difference. In the case of QXRD by single peak calibration, quartz and mullite were calculated from the calibration curves and soluble silicates were obtained as mass difference, whereas in the case of GMQUANT, all the phases were calculated from the background corrected full diffraction pattern.

Table 1. Amount of crystalline and amorphous phases obtained using three methods.

PHASE	WEIGHT PERCENTAGE(%)		
	Chemical	Qxrd	GMQUANT
QUARTZ	17	12	18
MULLITE	11*	13	12
HEMATITE	NIL	NIL	NIL
SOLUBLE SILICATES	70	73*	69†

* By difference; †: Unaccounted phases;

The chemical phase analysis and GMQUANT technique show similar results. The degree of difference in results obtained for QXRD single peak calibration may be attributed to either preferred orientation of the crystals present in the fly ash or variation of crystallite perfection between the sample and standard.

CONCLUSION

A novel two step chemical phase analysis technique is proposed for the estimation of both amorphous and crystalline phases present in the low calcium fly ashes. The results of this technique compare well with the results obtained using full spectra quantitative X-ray diffraction. The chemical phase analysis technique is simple and can be performed with ordinary laboratory glassware. This technique can be used for the quick evaluation of potential pozzolanic reactivity of low calcium fly ashes.

ACKNOWLEDGMENT

The authors would like to thank USEPA for the financial support provided to carry out this work.

REFERENCES

Berry, E.E., Hemmings, R.T., and Golden, D.M., Materials Research Society Symposium, Proceedings, Vol-86, pp 365-380, 1987.
Hulett, L.D, Weinberger, A.J., Northcutt, K.J., and Marian Ferguson, Science, 210, pp 1356-13458, 1980.
Hemmings, R.T., and Berry, E.E., Materials Research Society Symposium, Proceedings, Vol-113,, pp 3-38, 1988.
Popovics, S., and Greta, B.,in "X-ray and neutron structure analysis in material science", Edited by J.Hasek, Plenum press, New York, pp.29-41, 1989.
Raask, E. and Bhaskar, M.C., Cement and Concrete Research, Vol-5, pp 363-376, 1975.
Smith, D.K., Gerald G.Johnson Jr, and Alexander Scheible, Powder Diffraction, Vol-2, No-2, pp.73-77, 1987.
Young, Roland.S. "Chemical Phase Analysis", p 94, 1974.
Talvitie, N.A., Analytical Chemistry, Vol-23, No.4, pp.623-626, 1951.
Watt, J.D. and Thorne, D.J., J. Appl. Chem., Vol-16, pp 33-39, 1966.

NON-DESTRUCTIVE EVALUATION OF RICH FLY ASH HPC

Chao L. HWANG, National Taiwan Institute of Technology, Taipei, Taiwan
Iuan Y. JANN, National Taiwan Institute of Technology, Taipei, Taiwan

ABSTRACT HPC with large amount of pozzolan has been successfully applied. Due to the densified mixture proportion algorithm (DMDA) and under the strict quality control the bleeding and segregation problems have disappeared. By NDT (V-meter) the strength at the designed age of 56 days could be predicted. Large variation of pulse velocity and electrical resistivity (another NDT) showed the deficiency in the conventional rich-mix concrete, and were harmful to long-term durability.

Key words: High performance concrete (HPC), Fly ash, Electrical resistivity.

INTRODUCTION

In Taiwan, the HPC with the designed strength of 56 Mpa at 56 days was successful used in the steel columns of Kaohsiung T&C Tower. Another, the basic limitation was imposed upon cement content less than 400 kg/m^3, water content less than 200 kg/m^3, with slump=230~270 mm, slump flow spread=500 mm and without bleeding and segregation occured(Chern, Hwang, and Tsai, 1996). The designer applied DMDA and introduced a large amount of pozzolans into HPC, of which fly ash and slag aimed to partially replace sand and cement, respectively. The typical mixture proportion is shown in Table 1. Upon completion of pouring HPC with V_p = 1.3n and W/B = 0.32, V-meter was used to evaluate the uniformity of concrete, and the strength was measured at the age of 56 days to build the relationship. The pulse velocity and electrical resistivity of HPC were compared with those of conventional concrete.

Table 1. Typical mixture proportion and fresh concrete property of HPC

V.P (n)	W/B	W/C	Binder (kg/m^3)			Aggregate (kg/m^3)		Mixing Water (kg/m^3)		Slump (cm)		Flow (cm)	
			Cement	Slag	Fly Ash	Coarse	Sand	Water	SP (%)	0 min	45 min	0 min	45 min
1.1	0.32	0.39	312	16	139	873	928	123	23.10	-	-	-	-
1.2	0.32	0.42	364	19	141	942	801	152	15.31 (4.2)	25	24	55	56
1.4	0.32	0.41	434	23	132	882	750	174	13.04 (3.00)	25	26	57	57
1.6	0.32	0.39	497	26	123	822	699	199	8.71 (1.75)	25	26	56	55
2.1 (ACI)	0..32	0.32	719	0	0	586	825	244	0	-	-	-	-

n : the least void

UNIFORMITY EVALUATION

Pulse velocity along pouring and perpendicular direction of the specimen is shown in Fig. 1. It shows no significant difference in any direction under different paste amount due to uniformly mixed HPC without segregation problem (Hwang, et al, 1996), fewer defects in transition zone of aggregate and paste, and pozzolanic reaction by fly ash with lower cement and water content.

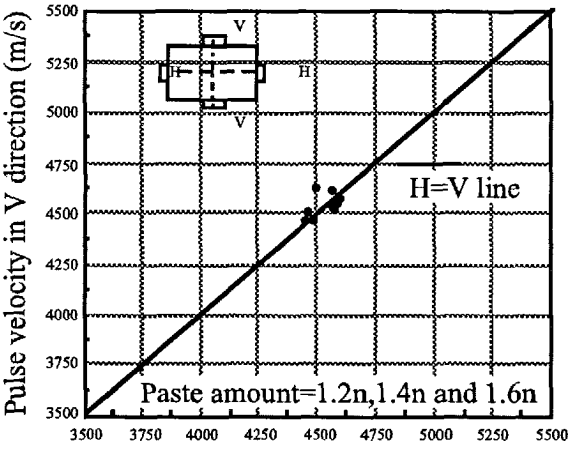

Figure 1 The relationship of pulse velocity in V and H direction of HPC

STRENGTH PREDICTION

Ultrasonic pulse velocity has been used for strength prediction and also is a feasible NDT method (Anderson Seals, 1981). The relationship between ultrasonic velocity and strength of NDT is as shown in Formula (1). The data prepared with various mixture proportions and cored specimens in the laboratory were collected to obtain the correlation constants a, b as shown in Formula (2). It successfully predicts the designed strength of HPC at 56 days as shown in Fig. 2.

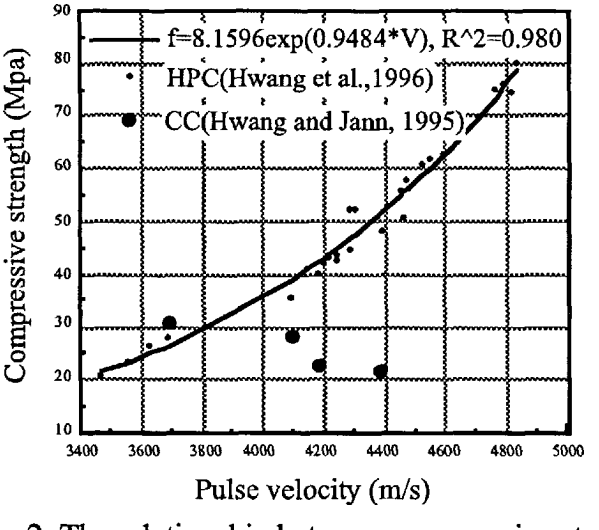

Figure 2 The relationship between compressive strength and pulse velocity of CC and HPC

$f = a\, e^{bv}$, where a, b are constants ---------- (1)

$f = 8.1596\, e^{0.9484v}$, $R^2 = 0.980$ ---------- (2)

Because of limited cement content in use, HPC is different with the conventional concrete. Under DMDA, cement paste is used only to fill the porosity among aggregates. High flowing HPC is achieved by the addition of pozzolan and chemical admixture to reduced water and cement amount. Referring to Fig. 3, the early strength of HPC was dominated by cement content. Concrete with lower cement content would obtain higher strength after 56 days, and hence it shows long-term strength was governed by W/B (water cementitious material ratio), but not W/C. The concept is accepted by ACI 318-95. Although conventional concrete without pozzolan could reach high strength, according to Fig. 2 it shows low pulse velocity occured by microstructure defects, which would cause durability problem (Hwang and Jann, 1996).

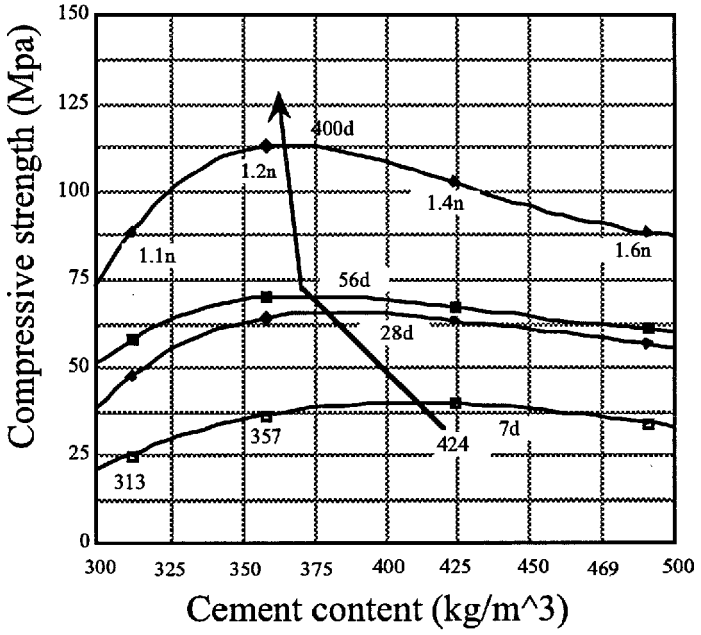

Fig 3. The effect of cement content on pulse velocity and compressive strength of HPC

DURABILITY EVALUATION

Resistivity can be used as an indication for durability of concrete. The electrical resistivity of HPC and conventional concrete at 56 days were measured as shown in Table 2. It shows high paste amount and high W/B may obtain lower resistivity because more capillary pores from pre-existing water in concrete can conduct ion migration, but harmful to long term durability. The addition of pozzolan can refine

the pore size and reduce pore volume, and the resistivity is about 6 times higher than that without any pozzolan.

Table 2. The comparison of electrical resistivity in HPC and CC

Type	n	W/B	Electrical Resistivity (kΩ-cm)			
			3d	28d	90d	180d
HPC	1.3	0.28	4	21	58	75
		0.32	4	16	42	58
		0.40	4	13	35	48
CC (ACI)	2.1	0.32	4	6	8	9

CONCLUSION

In this study the two NDT of ultrasonic pulse velocity and resistivity were conducted to evaluate the properties of concrete. It is found that by DMDA the quality of HPC can be evaluated accurately. The concrete with rich cement paste and without any pozzolan would has the strength as same as that of HPC, but has lower pulse velocity and resistivity. The NDT hence is a useful tool for measuring the soundness and durability of concrete. It also reveals that proper amount of fly ash in HPC under low cement content is helpful to its durability.

REFERENCES

Anderson, David A. and Seals, Roger K., "Pulse Velocity as a Predictor of 28 and 90 day strength," ACI Journal, March-April 1981, pp. 116~122.

Chern, J. C., Hwang, C. L. and Tsai, D. H., "Research and Development of High Performance Concrete in Taiwan", Concrete International, Vol. 17, No. 10, 1995, pp. 71~76.

Hwang, C. L., and Jann, I. Y., "Inspection and Research of Taitung Sanhsien Tai Sightseeing Bridge", Anti-Corrosion 001, R.O.C. Anti-Corrosion Engineering Society, Taiwan, 1995.

Hwang, C. L., Liu, J. J., Lee, L. S. and Lin, F. Y., "The Study on the Densified Mixture Design Algorithm of High Performance Concrete and its Early Properties", Journal of the Chinese Institute of Civil and Hydraulic Engineering, Vol. 8, No. 2, 1996, pp. 207~219.

3v022
8 pp

K n o. 0 6. APR. 2001 d o k 32870

LIMITATIONS OF STANDARD TEST METHODS TO PREDICT DELAYED DAMAGING ALKALI-AGGREGATE REACTION (AAR) IN CONCRETE

Mihai NADU, Michael SCHIEBER, Jacob NISSENBAUM ,Michael BRAIMAN and Michael LUKACH, School of Applied Science of the Hebrew University, Jerusalem 91904 Israel. Shimon BOYKO and David SHTAKELBERG, Standard Institution of Israel 7, Yad Harutzim St., P.O.B. 10258, Jerusalem , Israel.

ABSTRACT Length measurements on concrete prisms, stored in 100% humid air at 38°C, made with a limestone aggregate sample containing ~ 4% SiO_2 with 410 kg cement and 5 kg Na_2O equivalent per 1 m^3 of concrete, show the following expansions: insignificant prior to 5-6 month , 0.05% after 11 month, 0.14% after 12 month and 0.20% after 2 years. The expansion kinetics suggests a "late expanding alkali-silicate/silica reaction".The same aggregate did not show any reaction when tested according to the ASTM C227, C289 or C1260.
Key-words: Alkali-aggregate reaction, methods for AAR, expansion, durability of concrete

INTRODUCTION

An Alkali-Aggregate Reaction (AAR) research, taking into account the specific Israeli conditions, started for the first time in Israel some four years ago (Nadu et al,1996). The present paper deals with an aggregate sample that turned out to be particularly interesting for alkali reactivity research. This aggregate sample, supplied from a quarry situated in the north of Israel, was known as a "pure limestone" and was considered to be a comparative blank (non alkali - reactive) sample. Considerations based on the chemical analysis corroborates the assumption of non-reactivity. The different grain sizes of the aggregate were analyzed by the the Central Laboratory of Nesher Cement Ltd., by induction coupled plasma. (Table 1).

Table 1 Chemical parameters of the limestone aggregate sample, wt%

	Fine aggregate				Coarse aggregate
	0.3-0.6 mm	0.6-1.1.8 mm	1.18-2.36mm	2.36-4.75mm	4.75-19 mm
SiO_2	**4.00**	**3.90**	**4.20**	**4.40**	**3.60**
Al_2O_3	**0.14**	**0.15**	**0.16**	**0.19**	**0.19**
CaO	**53.00**	**53.00**	**52.80**	**53.10**	**51.00**
MgO	**0.26**	**0.28**	**0.28**	**0.28**	**2.12**
CaO:MgO ratio	**204**	**189**	**189**	**190**	**24**

The chemical analysis corroborates the assumption of non-reactivity: a) The sample is not suspected of alkali-silica reactivity (ASR) since it contains less than 5% SiO_2 insoluble residue in HCl (Fournier & Berube,1993); b) The sample is not susceptible to alkali-carbonate reactivity (ACR) according to a new CSA A23.2-26A-94 test, consisting of plotting on a graph, the CaO/MgO ratio as function of the Al_2O_3 content. For a CaO/MgO ratio $\geq$ 24 and for a content of $\leq$ 0.19% Al_2O_3 the sample is placed on the non ACR zone of the graph..

The limestone sample was studied by several AAR methods which led to inconclusive results but the non-reactivity assumption was finally refuted when our investigations comprised simultaneously: (1) high alkali containing concrete specimens, stored in warm and humid air; (2) late ages (11 month and more) measurements; (3) testing by the AS/SR version of the concrete prism expansion method (former 1990 Canadian CSA & 1990 French AFNOR-NF;

Hooton,1996). For the above conditions, concrete containing this aggregate, does show a strong late-expanding alcali-silicate/silica reaction (AS/SR).

Note: The former 1990 CSA Standards was replaced in June 1994 when our concrete specimens were 18 month old. The new 1994 CSA looks like the combined former CSA & French standards (410 kg cement /m3 of concrete) The AS/SR designation no longer exists.

EXPERIMENTAL PROCEDURE AND STANDARD REQUIREMENTS

Introduction

The samples have been tested for AAR using five known standard methods : **(I)** The 24 hour chemical method; **(II)** The two week "NBRI" mortar bar test; **(III)** The long term (2 years) mortar bar expansion method, at 38°C in 100% relative humidity; **(IV)** The same as in **"(III)"** but on concrete prisms; **(V)** The same as in **"(IV)"** but at 22°C. The test methods **I, II, III and V** gave inconclusive results or gave results that did not show alkali-reactivity for this investigated concrete aggregate sample. Only test method **IV** showed under certain conditions deleterious alkali- aggregate reactivity.

(I) The 24 hour ASTM C289,1994 chemical test with an altered graph (Fig.1)

The test consisting of the immersion of graded aggregate sample in 1N NaOH solution at 80°C for 24 hours, is followed by chemical analysis of the filtered solution for dissolved silica (Sc) and for reduction of alkalinity (Rc). The results are plotted on a graph showing four regions of

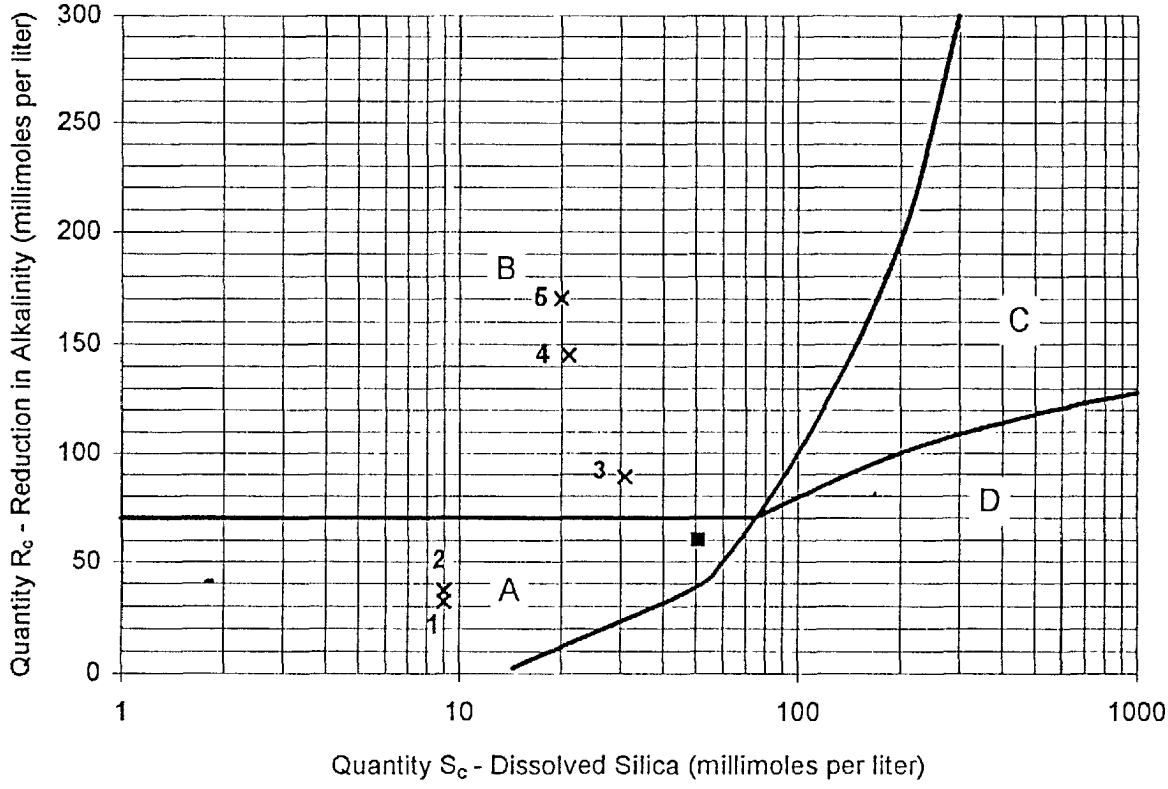

Figure 1 Evaluation of the AAR results by the 24 hour chemical method ASTM C289 with an altered graph. Sc is plotted on a logarithmic scale (Bredsdorf et al,1960; Romanian Standard STAS 5440,1970): **x1...x5** - Limestone aggregate samples, ■ - Sea sand sample from Ashdod

aggregates: (A) "innocuous"; (B)"generally non-reactive", but in this field the interference of carbonates in the reaction between SiO_2 and NaOH leads to inconclusive results requiring long term mortar bar or concrete prism expansion methods; (C) "highly reactive, potentially deleterious", but if the pessimus (worst) percentage of reactive silica is exceeded, the mortar bars might display non significant expansions; (D) "deleterious reactive". The original ASTM graph comprises three regions, the (A+B) region being considered innocuous. The chemical test was excluded from the last CAN/CSA. We think that it should be considered an alternative method for future AAR test of siliceous limestone. The alternative method consists of performing the ASTM procedure on the insoluble residue obtained by dissolution of the carbonates in hydrochloric acid (Dron,.1992; Berube & Fournier,1993; Barisone & Restivo,1996). In order to find the worst proportion of reactive particles the chemical method has been altered becoming a "kinetic" test (French NF-P18-589; Sorentino et al 1992). The kinetic test is criticized e.g., by Barisone & Restivo (1996) as nonreliable for the petrography of Italian aggregates

(II) The 2 week NBRI mortar bar test (ASTM C1260,1995, or CSA A23.2-25A,1994).
Mortar bars, 25 by 25 by 285-mm ASTM C227, are maintained at 80°C, one day in water up to the zero reading and afterward in 1N NaOH solution. Fournier&Berube (1993) and CAN/CSA A23.1-94.Appendix B suggested the following mortar bar expansion limits in 14 days: <0.10% for innocuous aggregates and ≥ 0.15% for deleterious aggregates. Shayan et al (1988) suggested that:(i) mortar bar expansion of 0.10% in 10 days and 0.10% in 22 days are to be taken as indicating reactive aggregate of short induction period and long induction period, respectively; (i,i) for some slowly reacting carbonate rocks a concrete prism test is more suitable than mortar bars for assessing the reactivity. Unfortunately, we performed measurements for only 2 weeks.

(III) The long term mortar bar test. (ASTM C227,1990 & CAN/CSA A23.1-90.Appendix B).
The reactivity limits are 0.05% at 3 months or 0.1% at 6 months or more, for mortar bars with high alkali content(1.25% Na_2O equivalent relative to the cement weight or 7.5 kg Na_2O equivalent per $1m^3$ of mortar) maintained at 38°C, in wet air . According to Hooton & Rogers (1989) the absorbent material used in the ASTM containers might cause diminished expansions due to the alkali-leaching of the mortar bars. The test is not included in the 1994 edition of CSA Standard.. For our future work we consider an alternative method which would replace the mortar bars 25 by 25 by 285 mm with mortar prisms 40 by 40 by 160 mm according e.g., to the European experience (Grattan-Bellew,1989) and to the Japanese standard JIS A 5308.

(IV,V) The long term concrete prisms expansion method

Generalities
Two versions (ACR and AS/SR) of the former CSA A23.2-14A,1990 and the French Standard NF P18-587,1990 were applied. Each former version of the CSA was intended to test concrete aggregate suspected to suffer from alkali carbonate reaction (ACR) or Alkali Silicate/Silica Reaction (AS/SR).The main difference between the two former versions is the storage temperature of the specimens in moist air, being 23°C for ACR and 38°C for AS/SR. The former CSA was replaced in June 1994 with the new CSA A23.2-14A-M94. The main modifications are: (i) the cement content increased from 310 to 420 kg/m^3 and an alkali content of 1.25 %Na_2O equivalent (eq.) by mass of cement, resulting in an increase of the alkali content in concrete from 3.90 to 5.25 kg. Na_2O eq./m^3 ; (i,i) a 38°C storage temperature in moist air is

required for all the specimens, independent of the AAR type. The French standard and the experimental variant M4/38 (Table 2) look like the new CSA (Portland Cement content in concrete of 410 kg/m^3, corresponding to 5.13 kg Na_2O eq/m^3).

Experimental conditions (CSA A.23.1 & A.23.2 & , A.23.2-14,1990 and Table 2)
Specimens: Three prisms of 75-mm by 75-mm by 285-mm, having a 250- mm- gauge length, with studs, were used for each experimental variant.

The aggregate contained 16% very fine, 24% fine and 60% coarse grains. The 0.15-0.60 mm aggregate was a quartz sand extracted from the Mediterranean seaside, frequently used in the manufacture of concrete. The sample of the sea quartz-sand are placed in region A "innocous aggregate" of the reactivity graph (Fig.1) It was graded together with the 0.60-4.75 mm limestone aggregate according to the grading requirements of ASTM C 227,1989. The coarse limestone aggregate was separated by 19, 14, 9.5 and 4.75 mm sieves and recombined taking equal portions by mass of the three sizes of the material.

The cement: A low alkali Portland cement, containing 0.47% alkalis.

Mixing water and slump: The amount of water (with optional addition of NaOH) should correspond to an 80 mm fresh concrete "slump" (CSA A.23.1 & A.23.2,1990) however the fresh concrete with 310 kg cement/m^3 (mixtures M1 and M2 in table 1) was "no slump" since a small increase of the water/cement ratio causes the fall of the concrete cone, immediately after the mold removal. For a cement content of 410 kg/m^3, (mixtures M3 and M4 in Table 1) the desired slump was easily obtained.

The compressive strength of the concrete was determined for each mixture on 100mm cubes. Comparing the mixtures M1 with M2 and M3 with M4, it appears obvious that NaOH addition in the mixing water acts as a strong retarder of the hardening especially for early ages (7 and 28 days). At 6 months, the retarder effect is diminished (Table 2)

Table 2 Concrete mixtures and experimental variants for AAR testing

Name of the concrete mixture	M1	M2	M3	M4
Water- cement ratio (w/c)	0.63	0.62	054	0.52
Portland Cement content in concrete (kg/m^3)	310	310	410	410
Additional alkalis through the mixing water	No	Yes	No	Yes
Alkali content (as Na_2O equivalent) provided from the cement and from the mixing water				
-Relative to the cement weight (%)	0.47	1.25	0.47	1.25
-Relative to the concrete (kg/m^3)	1.46	3.90	1.93	5.13
Slump of the fresh concrete (mm)	0	0	~80	~80
Density (kg/m^3)	2360	2350	2350	2370
Compressive strength (MPa): -7 days	31	21	38	23
-28 days	42	34	55	34
-180 days			66	59
Average expansion at 2 years (%):				
-Storage in 100% humid air at 22±2°C	-0.005	-	-0.008	0.002
-Storage in 100% humid air at 38°C	0.007	0.011	-	0.188
Negative (-)values represent shrinkage changes				

Standard requirements

CSA and ASTM requirements: **(a)** The former CSA considers that ACR expansions are deleterious, if the length change exceeds 0.010% after 3 months or 0.025-0.040% after 12 months (depending on the micro-climate to which the structure is to be exposed). **(b)** ASTM C1105,1989 considers deleterious ACR expansions of >0.015% after 3 months or 0.025% after 6 months or 0.030% after 12 months (independent of the micro-climate). **(c)** The former CSA considers that AS/SR expansions are deleterious, if the length change exceeds 0.040-0.075% after 12 months (depending on the micro-climate to which the structure is to be exposed). **(d)**The new Canadian Standard considers that expansions are deleterious, independent of the AAR type, if the length change exceeds 0.040% after 12 months , noting that "in critical structures such as those used for nuclear containment or large dams, a lower expansion limit may be required" (CAN/CSA A23.1-94. Appendix B).

French requirements. To the best of our knowledge there are no French standard limits for critical AAR expansions,of the concrete prisms NF-P18-587,1990. It seems to be accepted a 0.040% limit at 8 months, to indicate reactivity, but it is still being discussed (Corneille & Bollotte.1994). However it seems that the interpretation of the French test results is covered by the Canadian standard limits. In the future, significant AAR compositions for mortar bars and concrete prisms methods are to be prepared taking into account the experimentally found worst ("pessimum") content of the reactive particles (NF-P18-589,1992; Corneille & Bollotte, 1994).

EXPERIMENTAL RESULTS

(I) AAR studies by the 24 hours chemical test

On the graph (Fig.1) five tested samples are placed as follows: two samples in region **A**, three others on the doubtful region **B**, due probably to the presence of carbonates interfering with the reaction between NaOH and the dissolved silica. In order to clarify if the tested aggregate is reactive, long term tests are required by ASTM C33.

(II) AAR studies by the 2 week mortar bar test

After 14 days of storage at 80°C in 1N NaOH solution, an average expansion of 0.08% was recorded showing no alkali reactivity for the tested concrete aggregate.

(III) AAR studies by the long term mortar bar test

Even for mortars with high alkali content ,obtained by adding NaOH in the mixing water, the length changes were small (up to 0.013 % in 2 years), sensibly less than the reactivity limits

(IV) AAR studies by the long term concrete prism method

These studies comprise four concrete mixtures and six experimental variants (Table 2). Each experimental variant was labeled with the name of the concrete mixture (M1, M2, M3 or M4) and the temperature (in °C) of the wet air environment in which the specimens were stored. Storage. temperatures were 22°C or 38°C. According to the specifications of the ACR version of the former Canadian standard, the small length changes recorded for specimens M4/20, prove that the tested aggregate is not alkali carbonate reactive (CSA A 23.1.App. B & A 23.2-14, 1990). The same fact results logically from the chemical analysis according to the new CSA requirements(CSA A 23.2-26A, 1994). Fig. 2 shows the length changes vs. time up to 2 years for each specimen (#151, #152, #153) of the M4/38 experimental variant. The length changes (up to 2 years) for each specimen of the experimental variants M1/22, M1/38, M2/38, M3/22

and M4/22 are insignificant small, sometimes within the error of measurement, consequently the length changes are not placed on Fig.2. Trying to distinguish (at different ages), the non-reactive, the marginally or the very reactive aggregates, the expansion kinetics of each of the three specimens of the experimental variant M4/38 is compared with the Canadian typical AAR expansion curves comprised in the 1990 CSA A.23.1 App.B. For a better understanding, a comparison is made between the expansion kinetics of the M4/38 specimens and the values obtained by interpolation in the expansion curves comprised in the 1990 CSA A.23.1 App.B (Table 3). Figure 2 and table 3 show that the tested aggregate generates inside the concrete a very strong late-expanding alkali-silicate/silica reaction. It is also obvious that in comparison with the Canadian limits the beginning of the expansions appears much later and in a sudden manner at ~11 month, with subsequent expansions developing abruptly to high values.

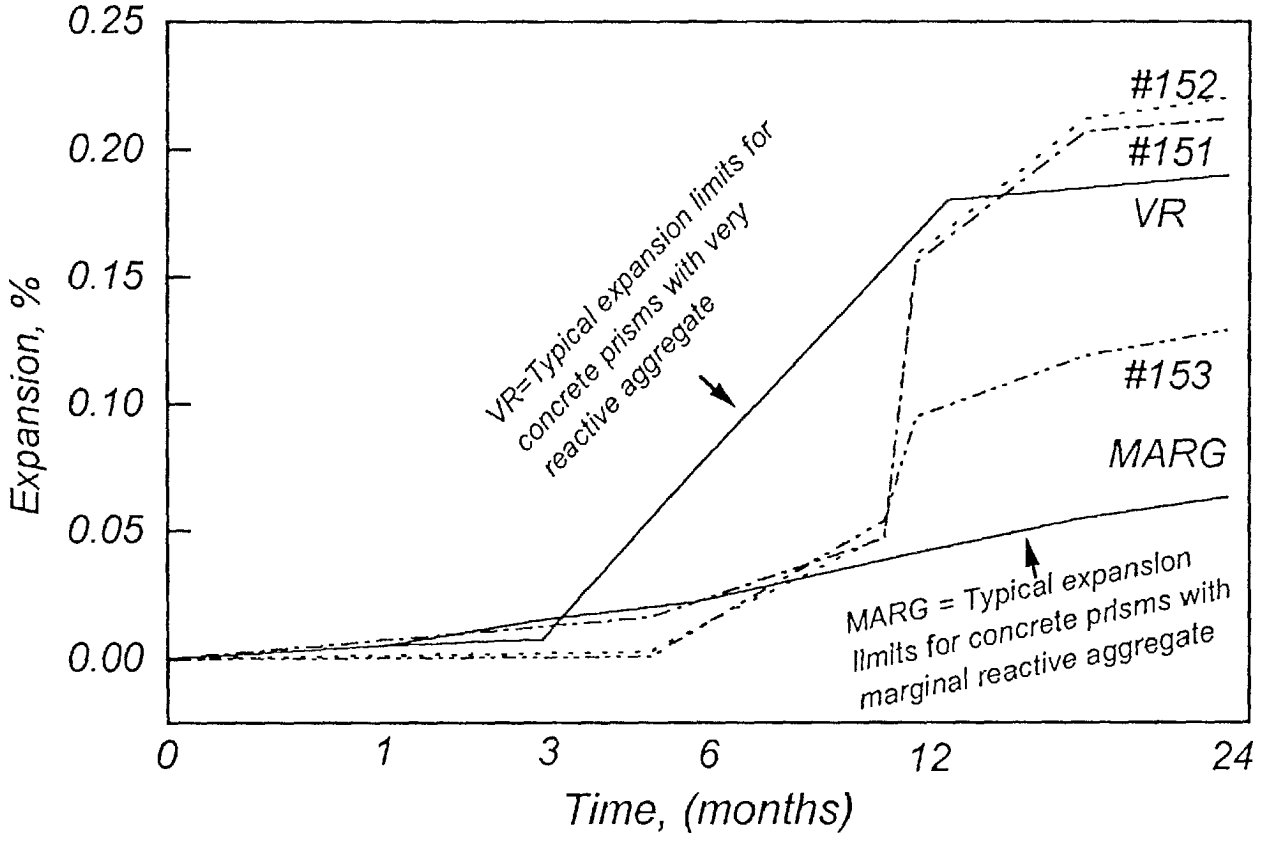

Fig 2 Expansion kinetics for each of the three M4/38 studied specimens (**#151,#152,#153**) are shown as dotted lines and are compared with solid lines **"VR"** and **"MARG"** representing the Canadian "characteristic expansion curves for concrete prisms made with the greywacke-slow/late-expanding alkali-silicate/silica reactive aggregates" adopted from page 100 of the former CSA A23.1. App B-90. The time is plotted on a square cubic root.

DISCUSSION

The long term expansion kinetics of concrete prisms with the limestone aggregate suggests a new case of " strong late expanding alkali-silicate/silica reaction". This behavior was not foreseeable by accelerated test methods and becomes obvious after some 11 months of measurements. Based on a detailed AAR study of Quebec rock-quarries, Fournier & Berube (1993) concluded that carbonate aggregates containing less than 5% insoluble residue or

involving expansions less than 0.1% after 14 days in the NBRI method are innocuous. However, our limestone concrete aggregate sample which passed both requirements is a deleterious aggregate. Unfortunately, the field of validity of each accelerated test method depends on the chemical, physical and geological peculiarities of the tested aggregate. International reputed AAR test methods, have sometimes limitations, e.g., turn out to be unable to predict delayed damaging reactions, as in the present paper described behavior of a certain Israeli limestone aggregate containing apparently insignificant quantities of residue insoluble in HCl, and tested according to the above mentioned non altered standard methods **(I, II, III, IV, V)**.

Table 3 Expansion kinetics of the M4/38 concrete specimens, compared to interpolated values from the expansion curves comprised in the 1990 CSA A.23.1 App B (%)

AGE (Month)	5	11	12	24
Expansion of the specimens of the experimental variant M4/38				
Concrete specimen #151	0.016	0.047	0.156	0.201
Concrete specimen #152	0.003	0.048	0.159	0.212
Concrete specimen #153	0.001	0.050	0.095	0.129
Average expansion	0.007	0.050	0.136	0.188
Reactivity limits by interpolation on the 1990 CSA curves				
Very reactive	>0.05	.>0.13	>.0.15	>0.18
Marginal reactive	0.03-0.05	0.035-.015	0.04-0.15	0.06-0.18
Non reactive	<0.03	<0.35	<0.40	<060

The Israeli cement users are generally unaware of AAR and its possible effects on the durability of the concrete structures. In the near future, our AAR research must drive to the appearance of AAR Israeli standards to avoid the repetition of structure failures similar to the ones which appeared 12 years ago in Belgium (Van Gemert.1989 and 1996), in the United Kingdom [Hoobs.1989 and 1996], in Japan (Okada.1989; Okada and al.1996) and in other countries where awareness on AAR arose. According to Oberholster (1996), "in most instances where ASR have been diagnosed in structures , the durability and serviceability have been greatly affected and the service life in many cases significantly reduced...owners of such structures are hard pressed for funds for the high costs of reparation and maintenance".

CONCLUSIONS

The present paper shows that concrete aggregates considered to be non reactive according to accepted testing procedures are in fact potentially deleterious for concrete structures due to their late AAR attack. Therefore it is very important to develop new methods of testing (or to improve the classical methods) which should identify such late AAR attacks. So for example it is possible to predict the AAR behavior of slowly reacting aggregates by an improved NBRI mortar bar expansion method according to Shayan et al.(1988) and by the use of autoclave methods (Fournier & Berube, 1993; the French standard NF P18-590-1993) which accelerate the AAR It is possible to test the reactivity of carbonate aggregates by use of alternative methods to the 24 hours chemical method ASTM C-289 (Dron,.1992; Berube & Fournier,1993; Barisone & Restivo,1996; French NF-P18-589; Sorentino et al 1992).

ACKNOWLEDGMENT

The AAR studies in the Hebrew University of Jerusalem were financially supported by the Israeli Cement Foundation and were performed in cooperation with the Jerusalem Branch of the

Israeli Standard Institution. Thanks are given also to the Nesher Cement Ltd., for their collaboration in some of the laboratory works.

REFERENCES

Barisone G. & Restivo G., 1996, "The ASTM C289 method and the kinetic test in the study of alkali-silica reactivity of Italian alluvial deposits" , Proc. 10th Int. Conf. on AAR, Melbourne, Edited by A. Shayan, p.288

Bredsdorff P.,. Idorn G. M, Kjaer A., Plum N. M. & Poulsen E. 1960, "Chemical reactions involving aggregate", Proc. 4th Int. Symp. Chem. of Cem.,Washington p.749.

Corneille A.and Bollotte.B.1994 ,"French recommendations for AAR concrete damage prevention", Proc. 3d Int. Conf. "Durability of Concrete", Nice, France, p. 725.

Dron R. 1992, Personnel communication, Central Laboratory for Highways and Bridges, Paris, France

Fournier B. and Berube M.A., 1993, "Canadian experience with alkali-aggregate testing", Cement & Concrete Composites, 15, 27.

Grattan-Bellew P. E. 1989, "Test methods and criteria for evaluation of potential reactivity of aggregates" Proc. 8th Int.Conf.on AAR ,Kyoto, eds K.Okada ,S.Nishibayashi & Kawamura, Elsevier, London , p.279; 1996, "A critical review of accelerated AAR tests", Proc. 10th Int. Conf. on AAR, Melbourne, Edited by A. Shayan, p. 27

Hobbs D.W.1989, "Cracking and Expansion Due to ASR in the United Kingdom" Proc.8th Int.Conf.onAAR,Kioto,Japan,edsK.Okada,S.Nishibayashi&M.Kawamura,,Elsevier,London, p.31; 1996, "Diagnosis of the cause of cracking in four structures in which ASR is occuring", Proc. 10th Int. Conf. on AAR, Melbourne, Edited by A. Shayan, p.209.

Hooton R.D.,1996, "Recent developments in testing for ASR in North America", Proc. 10th Int. Conf. on AAR, Melbourne, Edited by A. Shayan, p. 280.

Hooton R.D.and Rogers C.A.1989, "Leaching of alkalis in AAR testing", Proc.8th Int. Conf.on AAR" , Kyoto ,eds K.Okada, S. Nishibayashi & M.Kawamura, ,Elsevier,London p 327.

Nadu M., Schieber M. , Nissenbaum J., Braiman M., Lukach M., Boyko S., Shtackelberg D., 1996, "Alkali-Aggregate Reaction Experiments in Israel", Proc. 10th Int. Conf. on AAR, Melbourne, Edited by A. Shayan, p.271.

Oberholster R.E., "Case studies of the practical and economical impact of ASR in South Africa", Proc. 10th Int. Conf. on AAR, Melbourne, Edited by A. Shayan, p.123.

Okada K.1989, *Preface,* Proc. 8th Int. Conf. on AAR, eds K.Okada, S. Nishibayashi & M.Kawamura ,Kyoto, Japan, 17-20 July, Elsevier, London, p. 37.

Okada K., Sonoda K., Kojima T., Seki K., Murayama Y. ,1996, "Deterioration of reinforced concrete slabs with Alkali-Aggregate Reaction", Proc. 10th Int. Conf. on AAR, Melbourne, Edited by A. Shayan, p.1033.

Shayan A., Diggins R.G., Ivanusec I. and Westgate P.L.,1988, "Accelerated testings of some Australian and overseas aggregates for alkali-aggregate reactivity", Cement & Concrete Research, 18, p. 843-851.

Sorrentino D., Clement J.Y., Golberg J.M.,1992, "A new approach to characterize the chemical reactivity of aggregates",Proc. 9th Int Conf. on AAR, London

Van Gemert D., 1989, AAR in Belgium, Proc. 8th Int. Conf. on AAR, Kyoto, Japan, 17-20 July, eds K.Okada, S. Nishibayashi & M.Kawamura , , Elsevier, London, p. 43; 1996, Personnel communication (letter of 18/01/1996 to the Hebrew University of Jerusalem)

ON THE MECHANICAL PROPERTIES OF COMPACTED NEAT CEMENT PASTE, CEMENT MORTAR AND GYPSUM PASTE

Gerardo DIAZ, Departamento de Ingeniería de los Materiales, IDIEM, Facultad de Ciencias Físicas y Matemáticas, Universidad de Chile, Casilla 1420, Santiago, Chile.
Pablo KITTL and Víctor MARTINEZ, Departamento de Ingeniería Mecánica, Facultad de Ciencias Físicas y Matemáticas, Universidad de Chile, Casilla 2777, Santiago, Chile.

ABSTRACT The critical stress intensity factor, K_{IC}, was determined in cement paste and cement mortar. The correlation factor between K_{IC} and the fracture stresses in cement mortars under compression was 0.98. The splitting test was made in neat cement paste and neat gypsum paste. The results for K_{IC} and for splitting were analysed by Weibull's statistics determining then the corresponding parameters and mean values. For K_{IC} Weibullian two-parameter functions were obtained whereas for splitting Weibullian two- and three-parameter functions were obtained.

Key-words: Characterization, Gypsum, Method.

INTRODUCTION

The traditional method for obtaining the critical stress intensity factor in mode I of fracture, K_{IC}, requires the generation, by fatigue, of an initial crack. This procedure, owing to its laborious application, implies a limited number of samples for determining K_{IC}. When dealing with brittle materials the problem even becomes more complex. For these reasons, a simplified method to determine K_{IC} in brittle materials has been developed and successfully applied to glass, cement mortar and compacted neat cement paste, where some results have been obtained (Díaz et al, 1994a; Díaz et al, 1994b; Kittl et al, 1996). The said method consists in making a pseudocrack in samples of rectangular cross-sectional area which later are subjected to the three-point bending test. Then, the first scope of this work is the statistical analysis of K_{IC} in paste and mortar of cement, studying thereof the size effect and the correlation between K_{IC} and the compressive fracture stress, in the case of cement mortar.

In order to characterise brittle materials from the probabilistic standpoint, diverse method may be employed (Weibull, 1939; Kittl et al, 1988). In this work the splitting test is used to characterise cement paste and gypsum paste. Thus, the second scope of this work is to obtain the Weibull's parameters in neat cement paste and in neat gypsum paste under splitting.

EXPERIMENTAL PROCEDURE

In the manufacturing of the samples of compact cement paste used for obtaining K_{IC}, commercial portland cement devoid of additives was employed. The cement was mixed with a 4%, in weight, of water and was introduced in a steel rectangular mold with the dimensions 55x20 mm and then a compacting pressure of 35 MPa was applied to it in order to obtain samples of 4 mm high. The samples were stored in a moist room, with 99% of humidity and at 23° C, during 24 hours. After concluding the 24 hours, the samples were submerged in water until saturation in order to the process of hydration of the same ones could advance as rapid as possible. Afterwards, the samples were again introduced into the moist room until completing 7 days of hydration. The process of hydration was stopped by putting the samples into a furnace at 110° C during 24 hours, later they were stored into a desiccator until the moment of preparing them for testing. In this way, 50 samples were made. A half

of the samples were transversely cut at the middle of the length by using a diamond saw. One of the transversal edges of these little pieces were polished by using a mechanical polishing disk, edges that, later, were going to generate the profile of the crack induced. Then, two little pieces were sticked to a complete sample by using epoxy resin, as is shown in Fig. 1. Hence, the epoxy resin was left to polymerise during 24 hours at room temperature. Afterwards, the samples were subjected to the three-point bending test which allowed to obtain 25 samples with L=39 mm long, b=20 mm wide and W=10 mm high and a crack size a=5 mm. The precedent process for the generation of the crack is analogous to the one employed in the preparation of the glass samples (Kittl et al, 1996), except that in the samples of compact cement paste it was not necessary to make a transversal scratch because in the internal constitution of the cement there are a great number of cracks which are very easy to be observed by electron microscopy and that, for reasons of space, are not shown here.

In the case of portland cement mortar, 54 samples of 160 mm long, 40 mm wide and 40 mm high and 32 samples of 160 mm long, 40 mm wide and 25 mm high were prepared. A transversal crack was induced to every sample along all its width and in the middle of its length, with a size of 15 mm and 9.4 mm for the first and second set, respectively. The samples were fabricated according to the RILEM's procedure. Afterwards, the samples were stored into a moist room, with 99% of humidity, at temperature of 25° C, until to complete 7 days. The crack was generated by introducing a steel lamina into the samples, in the fresh state. The steel lamina was retirated after the first day of curing in a moist room. Two thicknesses of lamina were employed: 0.5 mm and 1.0 mm. From the group of 54 samples, a half was made with the lamina of 0.5 mm and the remaining one with lamina of 1.0 mm thick. From the group of 32 samples of 25 mm high, all of them were made with lamina of 0.5 mm thick. All samples were subjected to the three-point bending test, with a testing span of 100 mm, in moist state, immediately after completing the 7 days of curing.

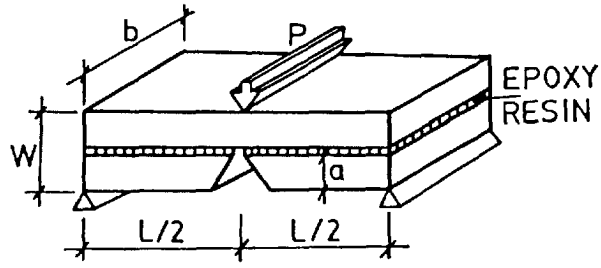

Figure 1 Form of addition with the epoxy resin used in the fabrication of the cement paste samples tested by the three-point bending test.

The critical stress intensity factor K_{IC} was determined by the expression:

$$K_{IC} = \sigma Y\sqrt{a} = \frac{3}{2}\frac{PL}{bW^2}Y\sqrt{a}; \quad Y = Y\left(\frac{L}{W}, \frac{a}{W}\right) \qquad [1]$$

where Y is a function depending on the geometry of the sample obtaining from tables (Chermant, 1975), a is the crack size and σ is the expression of the maximal stress of fracture for the case of the three-point bending test and P is the fracture load.

In order to perform the splitting test in neat cement paste and neat gypsum paste, the following methodology was adopted. Commercial cement and gypsum devoid of additives was employed. The cement was mixed in a steel cylindrical mold with 0.019 m length and 0.019 m diameter and then a compacting pressure of 25 MPa was applied. The process of hydration was similar as samples used in order to obtain K_{IC}, but the treatment into the moist room was until completing 14 day of hydration. In this way, 29 samples were made.

In the case of compact gypsum paste the gypsum was mixed with 20%, in weight, of water and was introduced in a steel cylindrical mold obtaining samples with 0.017 m length and 0.019 m diameter and then a compacting pressure of 12 MPa was applied. The samples were stored at room temperature during 24 hrs. After concluding the 24 hrs., the samples were stored for 24 hrs in a dessicator. The process of hydration was stopped by placing the samples into a furnace at 60^0 C during 2 hrs, later they were stored into a dessicator until the moment of testing. In this way, 39 samples were made.

In the splitting test the strength at fracture was determined using the following expression:

$$\tau = \frac{2P}{\pi L d} \qquad [2]$$

where P is the splitting load at fracture, L and d are the length and diameter of cylinder, respectively, and τ is the maximal splitting stress at fracture.

The probabilistic analysis of data obtained for K_{IC} and for fracture stress by splitting τ was made by using respective Weibull's diagrams.

THE PROBABILITY DISTRIBUTION FUNCTIONS

According to Probabilistic Strength of Materials (Weibull, 1939; Kittl et al, 1988), if the critical stress intensity factor K_{IC} follows a Weibull's distribution, this can be pointed out as follows:

$$F(K_{IC}) = 1 - \exp\left\{-\frac{B}{B_0}\phi(K_{IC})\right\} \qquad [3]$$

where F is the cumulative probability, ϕ is the Weibull's specific risk function, B_0 is the unit length and B is the crack width which, particularly in this work, is equal to beam width b, as can be seen in Figure 1. The Weibull's specific risk function, when assuming some analytical expression known a priori for it, can be expressed as follows:

$$\phi(K_{IC}) = \begin{cases} \left(\frac{K_{IC} - K_{ICL}}{K_{IC0}}\right)^m & K_{ICL} \le K_{IC} < \infty \\ 0 & 0 \le K_{IC} \le K_{ICL} \end{cases} \qquad [4]$$

where m and K_{IC0} are the Weibull's parameters depending on the process of generation of the crack and on the material manufacturing and K_{ICL} is the lower limit value for the critical stress intensity factor under which no crack propagation occurs. When $K_{ICL}=0$ the Weibull's specific risk function of two parameters is obtained, being them m and K_{IC0}.

According to Probabilistic Strength of Materials (Weibull, 1939; Kittl et al, 1988), the cumulative probability of fracture for splitting, when the function ϕ is of two parameters and of form similar to the one set forth in Eq 4, is given by:

$$F(\tau) = 1 - \exp\left\{ -\frac{Ld^2}{V_0}\left(\frac{\tau}{\tau_0}\right)^m \int_0^1 \int_0^{\sqrt{1-\eta^2}} \left[f(\xi,\eta)\right]^m d\xi d\eta \right\} \quad [5]$$

where V_0 is the unit volume, L is the cylinder length, d is its diameter and τ is the maximal stress of fracture. The function $f(\xi,\eta)$ is determined from Elasticity theory and it defines the stress field acting in the splitting test. As in the case of K_{IC}, m and τ_0 are the Weibull's parameters depending on manufacturing process of the material but now for splitting. When ϕ is a three-parameter function then one has:

$$F(\tau) = 1 - \exp\left\{ -\frac{Ld^2}{V_0}\left(\frac{\tau_L}{\tau_0}\right)^m \int_{V(\xi,\eta)} \left(\frac{\tau}{\tau_L} f(\xi,\eta) - 1\right)^m d\xi d\eta \right\} \quad [6]$$

where τ_L is the stress under which no splitting fracture of the material occurs and $V(\xi,\eta)$ is the volume given by $\tau f(\xi,\eta) \geq \tau_L$.

ANALYSIS OF RESULTS

Determination of K_{IC}

Figs. 2 and 3 show the respective diagrams for compact cement paste and cement mortar. Weibull's specific risk functions of two parameters, in a first approximation, were respectively obtained, given by the form of the curves shown in Figs. 2 and 3. In Fig. 3, Weibull's diagrams for the mortar cement samples identified by M1, M2 and M3 are shown. M1 is the curve corresponding to those 27 samples of 40 mm height whose crack was generated by a steel lamina of 1 mm thickness and M2 is the curve corresponding to those 27 samples of 40 mm height and whose crack was generated by a steel lamina of 0.5 mm thickness. In both curves the samples are of the same size. Likewise, M3 is the curve corresponding to the 32 samples of height 25 mm and for which the crack was generated with the lamina of 1.0 mm thickness. In these three curves, the size effect due to the thickness, or the crack width between M1 and M2 and, also, the same effect between M2 and M3 can be studied. When comparing the curves M1 and M2, in the Weibull's diagram, there is a shift to the left when the thickness of lamina generating the crack is increased, i.e., the cement mortar behaves as a Weibullian material when considering the critical stress intensity factor. However, if considering the height of the beam, an inverse Weibullian shift is observed because the curve moves to the right when the height of the beam is increased, as can be observed when comparing curves M1 and M3.

In Table 1, the respective parameters and the mean values of the critical stress intensity factor are shown. According to Table 1, the values found for the mean values of the critical stress intensity factor in the mode I are within the ranges of magnitude that appear in the literature when they are determined by the traditional method. Therefore, the procedure described herein and then put

into practice becomes efficient in the determination of the critical stress intensity factor in the mode I when applying in brittle materials, as was made here for portland cement paste and portland cement mortar.

From each one of the 32 samples of portland cement mortar, M3, two pieces, which were tested in compression, were obtained. The mean strength, σ_C, was determined for every sample and it was correlated with the respective value of K_{IC} associated. In Fig. 4 is shown the result of plotting the pairs (σ_C,K_{IC}) which allows to obtain a factor of correlation of 0.98. In accordance with the high value of this factor of correlation, the determination of the compressive mean strength in portland cement mortars is an excellent and indirect indicator in the determination of the critical stress intensity factor in the mode I.

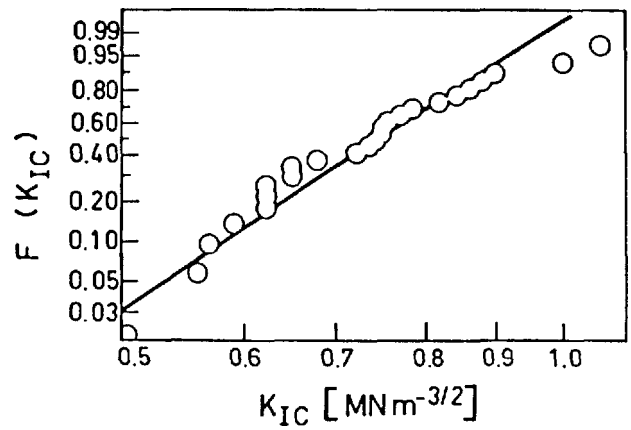

Figure 2 Weibull's diagram for the cumulative probability of K_{IC} for samples of portland neat cement paste.

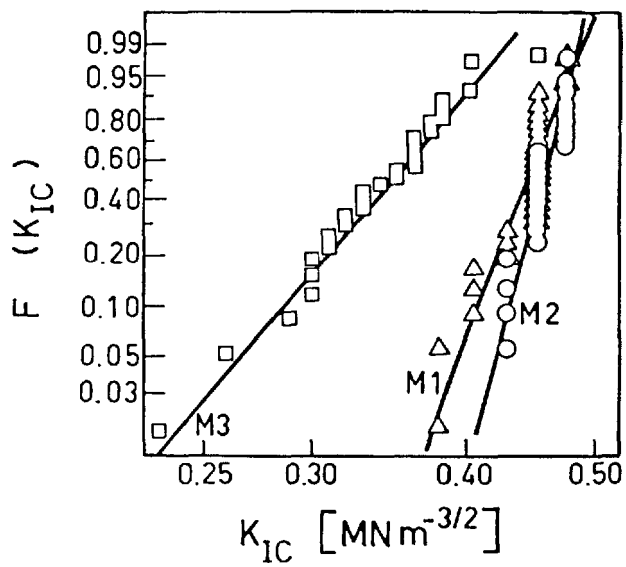

Figure 3 Weibull's diagram for the cumulative probability of K_{IC} for samples of portland cement mortar M1, M2 and M3.

Table 1 Parameters of the Weibull's functions and mean critical stress intensity factor in the mode I for the cement paste and cement mortar.

Material		m	K_{IC0}	$\overline{K_{IC}}$
			$MNm^{-3/2}$	$MNm^{-3/2}$
Cement Paste		6.60	0.79	0.74
Cement Mortar	M1	19.70	0.36	0.44
	M2	29.00	0.40	0.45
	M3	3.98	0.13	0.33

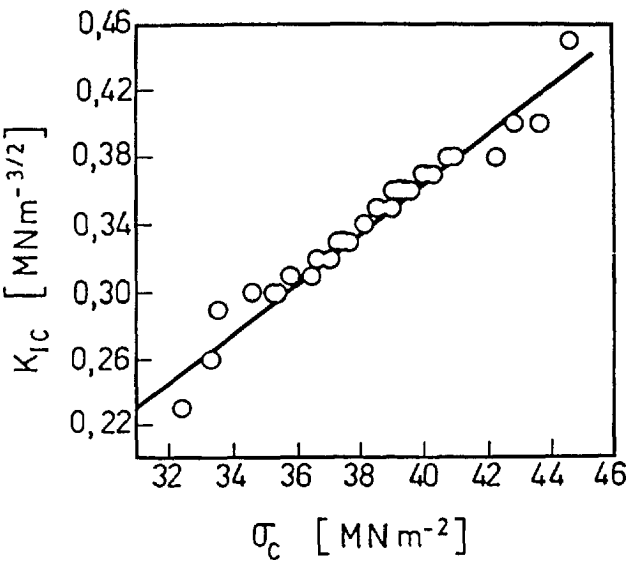

Figure 4 Correlation between the mean compressive strength, σ_C, and the critical stress intensity factor for the cement mortar (M3).

Determination of splitting fracture stress

In Figs. 5 and 6 are shown the Weibull's diagrams for the compacted pastes of cement and gypsum, respectively. Both diagrams were made with the experimental results of the splitting tests performed to both groups of samples. The mean strengths of fracture for the pastes of cement and gypsum were 14.5 MPa and 7.7 MPa, respectively. In view of the form adopted by the distribution of experimental data, as can be observed in Figs. 5 and 6, both materials present different Weibull's specific risk functions. The expression of this function is given by Eq 4 which for the case of our interest, splitting, the parameters are m, τ_0 and τ_L and the random variable is the fracture stress by splitting, τ. The parameters m and τ_0 are parameters depending on manufacturing process of the material and τ_L is the stress under which there is no fracture. When observing Fig. 5 is deduced that curve is adjusted with a Weibull's function of two parameters, i.e., $\tau_L=0$, whereas in Fig. 6 the corresponding curve follows one of the same type but of three parameters, i.e., $\tau_L\neq0$. Therefore, in the case of compacted paste of gypsum, the value of τ_L, obtained in a first approximation by a graphic interpolation, was 5.8 MPa. The

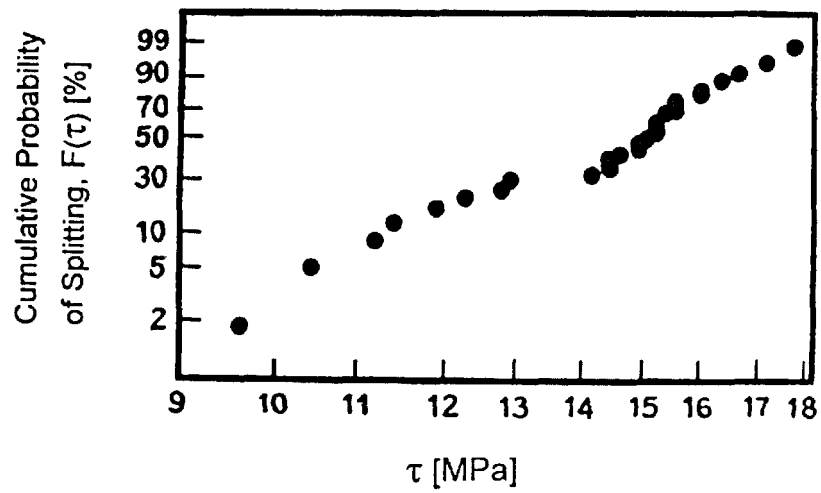

Figure 5 Weibull's diagram for the cumulative probability of splitting fracture stress for samples of neat cement paste.

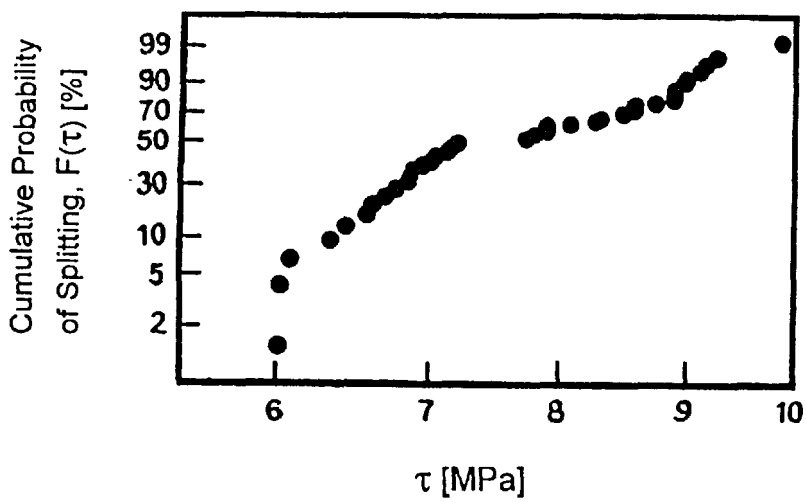

Figure 6 Weibull's diagram for the cumulative probability of splitting fracture stress for samples of neat gypsum paste.

parameter m, which is inversely related to dispersion, was 7.2 and 8.5 for cement paste and gypsum paste, respectively. Thus, the experimental data of the compacted cement paste exhibited a greater dispersion.

In preliminary results, which are not shown due to lack of space, the size effect has been studied in both pastes, determining thereof in the case of gypsum a shift to the left in the Weibull's diagram. This means the greater the size the lesser the splitting fracture stress, which fact is in accordance with Weibull's statistics theory. On the other hand, in the case of compacted cement

paste the size effect is not verified, as was already observed in samples tested under compression (Kittl et al, 1983).

CONCLUSIONS

A simplified method to determine K_{IC} in compacted neat cement paste and cement mortar was developed and proved by means of the generation of a pseudocrack. The values obtained thereof are in accordance to the ones obtained by the traditional methods. When the functions of probability distribution of K_{IC} were studied, Weibull's specific risk functions of two parameters were obtained in cement paste and cement mortar. A good correlation between the mean compressive strength and the critical stress intensity factor in mode I was established. The values are within the ranges of magnitude that traditional method produces. This reveals the efficiency of the method developed here and the possibility to apply it successfully to the determination of the critical stress intensity factor in mode I in other kinds of brittle materials. The method applied here is important because it allows to obtain a large number of samples in order to determine K_{IC} with a minimal cost, making thus sure a statistical analysis with a Weibull's diagram.

According to splitting tests performed in cement paste and gypsum paste Weibull's functions of two and three parameters, respectively, were obtained. In the case of gypsum paste is important to consider the existence of parameter τ_L=5.8 MPa, since it defines the stress limit under which no splitting fracture is produced. The size effect could be observed in gypsum samples whereas in cement samples the same was not observed.

ACKNOWLEDGEMENTS

The authors wish to thank the Fondo Nacional de Desarrollo Científico y Tecnológico, FONDECYT, for Grant N° 1961105.

REFERENCES

Chermant, J. L., "L'essai de K_{IC} Pour Les Matériaux Fragiles", Bull. Societé Française de Cerámique, Vol 108, 1975, pp. 39-52.

Díaz, G., Kittl, P. and Martínez, V., (a) "A Simplified Method to Determine K_{IC} in Brittle Materials", Proceedings of the 8th CIMTEC, World Ceramic Congress, Florence, Italy, 1994.

Díaz, G., Martínez, V. and Kittl, P., (b) "Determination of K_{IC} in Compacted Neat Cement Paste and Mortar of Cement", Proceedings of the 4th NCB International Seminar On Cement and Building Materials, New Delhi, India, 1994.

Kittl, P. and Aldunate, R., "Compression Fracture Statistics of Compacted Cement Cylinders", J. Mater. Sci., Vol 18, 1983, pp. 2947-2950.

Kittl, P. and Díaz, G., "Weibull's Fracture Statistics, or Probabilistic Strength of Materials: State of the Art", Res Mechanica, Vol 24, 1988, pp. 99-207.

Kittl, P., Díaz, G. and Martínez, V., "A Simplified Method for Determining K_{IC} in Glass with Liquid Solutions Impregnation", J. Mater. Sci., 1996, In press.

Weibull, W., "A Statistical Theory of the Strength of Materials", Ing. Vetenskaps Akad. Handl., Vol 151, 1939, pp. 1-45.

PARAMETERS RELEVANT FOR STANDARDIZATION OF SAND AND MORTAR STRENGTH

Z. B. Entin, L.S. Nefyodova, CEMISCON, Moscow, Russia

ABSTRACT. Properties of sands (void factor and specific surface values) which affect characteristics of a standard cement mortar like flowability, average mass of specimens after demolding and the corresponding strengths have been tested and analyzed using four standard polyfractional sands from Germany, Spain, England and Poland. It is shown that the effect of certain factors on the strength of mortars can be substantial enough even for the standardized methods. These are to be taken into consideration while standardizing the sand.

KEY-WORDS: aggregate, flow, particle size distribution, strength development, void spacing factor.

INTRODUCTION. The particle size distribution of a sand with established values is a necessary condition, but it is, by no means, the only one making the vulnerable for standard testing of cement mortars. The universally accepted criterion, in this instance will be, the comparison of 28 days strength values with the use of sand under test and the reference sand. The difference for 20 mixes using 3 cement types has not to exceed 5% for at least in 95% cases.

The void factor is not subject to normalization usually with regard to the standard sands used for cement testing, whereas with regard to building sand it is one of the quality criteria. It is common opinion that the quality of building sand with particle size distribution of 2.5 to 0.14 mm has void factor not less than 38% in loosely bulk state. An optimal combination of big, average and small grains which ensures the void factor of such polyfractional sand, it can be reduced to 30%. In this work typical properties of several polyfractional sands have been considered and the flowability of mortars, average mass after demolding of the specimens and strengths were measured.

EXPERIMENTAL. Several standard polyfractional sands which confirm EN-196-1 requirements for particle size distribution from Germany DIN EN 196-1, Spain UNE 80.101-88/CEN 196-1, England CEN 196 Part 1 and Poland PN-68/B-11000 have been used. The void factors of these standard sands in loosely packed state after compaction by shaking and after compaction by vibration have been determined. The results are shown in Table 1.

Table 1. Void factors of standard sands

Description	loosely packed	after compaction by shaking	after compaction by vibration
German	36	29	29
Spanish	40	35	34
English	39	30	28
Polish	37	32	31

Specific surface areas of monofractions of German, Spanish and Polish sands was determined by low temperature nitrogen adsorption. The results are shown in Table 2.

Table 2. Specific surface values of monofractions of standard sands , cm^2/g

Description	monofraction size, mm					for sand as a whole
	2.00 - 1.60	1.60 - 1.00	1.00 - 0.50	0.50 - 0.16	0.16 - 0.08	
German	2272	4352	1528	1331	1258	2305
Spanish	2109	1439	2091	3953	1973	2713
Polish	952	2879	832	1250	1489	1695

The variation in the specific surface values may affect the mechanical strengths of the mortars. In order to see this effect mortars specimens have been made with different types of cements. The properties of the cements used are shown in Table 3.

Table 3. Properties of cements used

Cement	Initial clinker, oxide content, %					Cement			
	SiO_2	Al_2O_3	Fe_2O_3	CaO	R_2O	SO_3, %	Additive, type-%	Grinding fineness	
								Residue on a 008 sieve	S_{sp} (Blaine)
SEM II/A-S 32.5 Belgorod	22.50	4.72	4.62	66.51	0.56	2.30	slag-19	3.4	2400
SEM I 42.5 Spasskcement	20.82	6.30	3.98	66.90	0.57	3.08	-	3.8	2890
SEM II/B-S 32.5 Krasnoyarsk	20.86	6.01	4.91	65.76	0.74	2.03	slag-22	9.4	2880
SEM II A/P 32.5 Maltsov	22.00	5.19	4.41	66.16	0.64	2.94	tripolite-7	11.2	3720
SEM II/A-S 42.5 Gornozavodsk-Cement	21.40	5.64	4.18	64.77	1.04	2.72	slag-8	3.4	3850

The flowability of the standard mortars made with different sands and cements have been determined by measuring the spread of a standard cone on shaking table according to Russian State Standard GOST 310.4-81. The water to cement ratio was kept constant at 0.50. The specimens were prepared and hardened in accordance with the EV 196-1 standard. Mass of the specimens was measured immediately after demolding. The results are shown in Table 4.

Table 4. Properties of mortars for various standard sand and cements according to EN 196-1.

Cement	Standard sand taken for comparison	Cone spread for w/c = 0.50, mm	Average specimen mass after demolding, g	Compressive strength after 28 days, N/mm^2
SEM II/A-S 32.5	German	209	589	42 5
Belgorod	Spanish	179	583	38.1
SEM I 42.5	German	213	600	60.1
Spasskcement	English	187	594	54.3
SEM II/V-S 32.5	German	153	605	41.1
Krasnoyarsk	Polish	222	585	34.8
SEM II/A-R 32.5	German	135	589	43.5
Maltsov	Polish	191	561	31.4
SEM II/A-S 42.5	Spanish	162	578	52.6
Gornozavodsk-Cement	Polish	240	567	41.4

While cleaning the natural sand various chemical reagents can be used. It is marked that these reagents affect the strengths of the mortars made with the sands thus obtained. English sand was treated with the water solution of $Al_2(SO_4)_3$, $CaCl_2$, and $FeCl_3$. After multiple washing followed by subsequent drying, these were used in comparative tests. The results are shown in Table 5.

Table 5. Effect of residual reagents used for precipitating slams on the properties of standard mortars.

Reagent dosage, g/l	Cone spread, mm	Average mass of specimens after demolding, g	Compression strength after 28 days N/mm^2
-	192	591	56.1
$0.25Al_2(SO_4)_3$	206	567	43.5
-	182	588	45.3
$20CaCl_2$	196	583	43.7
$20FeCl_3$	186	579	42.1

DISCUSSIONS OF RESULTS. Standard sands used from different countries have shown differences in the void factors which varies from 36% to 40% in loosely bulk state, from 29 to 35% after compaction by shaking and 28% to 34% after compaction by vibration. This observed difference in the void factor of standard sands being identical in the particle size distribution probably relates to the variation of grain form (shape) and predominance of rounded or angular form in monofraction (Table 1).

Substantial differences in the specific surface values in the same monofraction size have been noticed for the sands from different countries. (Table 2). The maximum total surface value calculated by specific surface of monofractions with regard to their mass % was observed for Spanish sand (2713 cm^2/g with monofractions varying from 1439 to 3953 cm^2/g) and the minimum one for the Polish sand (1695 cm^2/g with monofractions varying from 832 to 2879 cm^2/g).

It is seen from Table 2 and 4 that the difference in the void factors and specific surface values of sand caused differences in the characteristics of the standard mortars and their strength properties. This can be attributed to the difference in the shape of the particles, which subsequently affects the adhesion between the sand particle and the cement. Consequently it influences the strength. On the average for all the cements tested, the flowability of mortars under w/c 0.50 was 197 mm for German sand, 173 mm for Spanish and English sand and 229 mm for Polish sand.

Average mass of specimens after demolding was 594, 583, 585 and 570 g, correspondingly for German, Spanish, English and Polish sand. Difference in strength values for the mortars based upon Polish sand as compared with other sand under investigation reaches 10-12 N/mm^2 after 28 days.

According to the results of approximately 200 samples of mortar testing the average value of mass of specimens after demolding for German and English sands which have comparable mortar strengths is 587g and the probable lowest values about 575g with 90% probability. These factors can be considered as indirect characteristics while assessing the suitability of polyfractional sands for the use as standard ones according to EN 196-1.

It is also noted that besides the peculiarities of the sand grains shape the residual reagents used to accelerate precipitation of impurities (slams) when washing and beneficating natural sands during the production of standard polyfractional sands according to EN 196-1 significantly influence the strengths (Table 5). Out of the 3 reagents used as coagulants for the precipitation of slams , the most unfavourable results are obtained when using aluminium sulphate. In that case the reduction in strength reaches 12.6 N/mm^2.

CONCLUSIONS

On the basis of the tests done, the following conclusions are drawn:

Particle size distribution of sand can not be taken as reliable factor in assessing the suitability of standard sand.

For developing standard sands according to EN-196-1, it is reasonable to make a comparative tests measuring the flowability at w/c =0.50, average mass of the samples after demolding and strength.

The residual reagents used for precipitating slams have also detrimental effect on the strength of mortars made from the sands thus produced.

COMPARISON OF PHYSICAL AND MECHANICAL PROPERTIES OF PORTLAND CEMENT ACCORDING TO LVS EN 197-1 AND ГОСТ 10178-85

Ojārs BAUMANIS, Riga Technical University Institute of Silicate Materials, Rīga, Latvia
Jānis KĻAVIŅŠ, A/S (Joint-Stock Company) "Brocēni", Latvia
Aigars MIEZIS, A/S (Joint-Stock Company) "Brocēni", Latvia

ABSTRACT

As a result of research, a comparison of physical and mechanical properties of cement was made, according to two standards : Latvian standard LVS EN 197-1 which is identical with the European Standard and former USSR: ГОСТ 10178-85, which was in force in Latvia until the year 1995. The kinetics of hardening of the Portland cements CEM I 42,5 R and CEM I 32,5 R, by the methods defined in both of said standards, were investigated. The physical and mechanical properties of various samples of composite Portland cements, according to both standards, were determined.

Key-words: Portland cement, Mechanical properties, Physical properties, Standards

INTRODUCTION

Since 1995, the quality of Portland cement in Latvia is tested according to the standard EN 197-1 which fully meets the requirements of the European standard EN 197-1:1995. Because of this, the question becomes important what are the relations between the physical and mechanical properties of Portland cements prepared according to standards EN 197-1 and ГОСТ 10178-85.During the period from March 1994 through March 1996, A/S Brocēni carried out parallel tests of physical and mechanical properties of Portland cements CEM I 32,5 R and CEM I 42,5 R produced by the A/S Brocēni according to the standard EN 197-1 and standards of the former USSR: ГОСТ 10178-85. Altogether more than 70 parallel batches of samples of CEM I 32,5 R were produced and more than 30 parallel batches of samples of CEM I 42,5 R. The samples according to EN 197-1 were produced using the compression device : vibration table with the amplitude of 0.75 mm. To prepare the samples according to the standard ГОСТ 10178-85, a vibration table with the amplitude of 0.35 mm was used. The vibration frequency in both cases was the same: 3000 vibrations per minute.

As raw material for the production of the Portland cement, A/S Brocēni uses the Portland cement clinker of its own make, as well as gypsum from the deposite of Saurieši (Latvia). For the clinker produced by A/S Brocēni, it is typical to have medium high density coefficient according to Kühl - 97±2, contents of Al_2O_3: 4.8 - 5.5%, contents of C_3A: 6.0 - 7.5%, medium high contents of Na_2O eq (0.7 - 1.1). A/S Brocēni produces CEM I 32,5 R and CEM I 42,5 R from one and the same clinker. The difference is only in the fineness of grinding : for CEM I 32,5 R -- on average 320 - 350 m^2/kg after Blaine, but for CEM I 42,5 R -- 370 - 400 m^2/kg after Blaine.

EXPERIMENTAL PART

Introduction

The results of investigations of physical and mechanical properties of the Portland cements produced according to EN 197-1 and ГОСТ 10178-85 allow the conclusion that there is significant difference in methods of testing of both standards. As it is known, the hardness of cement is influenced by two factors: the fillers used in production and the ratio between water

and cement (w/c). To assess the hardness of cement, concrete prisms are made according to the methods of both standards, where the corresponding sand is used as the filling substance to make these prisms. The granulometric contents of this sand, as seen in Table 1, is very different. 10178-85 provides the use large-grain sand which meets the requirements of ГОСТ 6139-86. On the other hand, the EN 197-1 standard provides the use of multi-fraction sand.

Table 1. The requirements for sand used in cement testing

Requirements	ГОСТ 10178-85	EN 197-1
Content of SiO_2	>98.0	>98.0
Loss on ignition	<0.3	<0.5
Humidity	<0.2	<0.2
Admixtures	<1.0	-----
Cumulative sieve residue 2.0 mm	------	0
Cumulative sieve residue 1.6 mm		7 ± 5
Cumulative sieve residue 1.0 mm		33 ± 5
Cumulative sieve residue 0.9 mm	< 1.0	
Cumulative sieve residue 0.5 mm	> 92.0	67 ±5
Cumulative sieve residue 0.16 mm		87 ± 5
Cumulative sieve residue 0.08 mm		99±5

It must be noted that when using the sand which corresponds to the requirements of ГОСТ 10178-85, for preparation of concrete samples with w/c relation and compressing methods according to EN 197-1, the obtained results of compressive strength are significantly lower than when using the sand required by the standard EN. The results are given in Table 2.

Table 2. The influence of sand of different standards on compressive strength (N/mm^2)

	Compressive strength (N/mm^2)				
Sand used	1 day	2 days	3 days	7 days	28 days
ГОСТ 10178-85	2.6	5.9	9.3	14.3	24.0
EN 197-1	14.4	26.0	30.7	40.2	51.2

There are also differences in production of samples according to the water added. As it is known, the water quantity influences the compressive strength at the beginning of the process of hardening. Increasing the w/c ratio, the resistance against pressure at the beginning of the hardening process usually decreases. According to the EN 197-1 standard, the w/c ratio is constant : 0.5, while according to the ГОСТ 10178-85, this ratio is variable, depending on the normal consistency of cement and usually falls between 0.37 to 0.41. The results of comparative examinations made in the laboratories of A/S Brocēni show that there is still a correlation the between the results of tests according to both methods. The difference in compressive strength after 2 days of hardening is 5 - 6 N/mm^2 in favour for ГОСТ 10178-85. The correlation of compressive strength between samples prepared by both methods after 2 days of hardening is much better for cement CEM I 42,5 R (0.815) than for cement CEM I 32,5 R (0.565). The compressive strength after 7 days of hardening differes not so much, according to ГОСТ 10178-85 it is on average only by 2 - 3 N/mm^2 higher than the hardness of samples made according to the EN 197-1. Correlation between the two methods in this case is 0.755. The average after 28 days is by 0.5 - 2 N/mm^2 higher for EN 197-1 cement samples, as compared with samples made according to the ГОСТ 10178-85. The results of resistance against pressure for samples made by both technologies are given in Tables 3 and 4.

Table 3 The comparison between compressive strength of the Portland cement CEM I 32,5 R according to ГОСТ 10178-85 and EN 197-1

Time of hardening (days)	Average compressive strength according to EN 197-1 (N/mm^2)	Average compressive strength according to ГОСТ 10178-85 (N/mm^2)	Standard deviation (EN 197-1)	Standard deviation according to ГОСТ 10178-85	Correlation between resistance against pressure
2	21.9	27.5	1.06	1.97	0.565
28	46.9	45.9	2.14	2.54	0.477

Table 4 The comparison between compressive strength of the Portland cement CEM I 42,5 R according to EN 197-1 and ГОСТ 10178-85

Time of hardening (days)	Average compressive strength according to EN 197-1 (N/mm^2)	Average compressive strength according to ГОСТ 10178-85 (N/mm^2)	Standard deviation (EN 197-1)	Standard deviation according to ГОСТ 10178-85	Correlation between resistance against pressure
2	24.8	30.2	2.11	2.68	0.815
7	39.1	41.4	2.15	3.06	0.755
28	50.4	50.3	3.47	2.08	0.661

There is no certain correlation between both methods of standards as regards other physical and mechanical properties. Thus, for example, the correlation between the initial and final setting time according to both standards is 0.31-0.38. The initial setting time for the cement made according to the EN 197-1 is approximately 30 minutes delayed as compared with ĆĪŃŅ samples, while the end of setting does not actually differ. These differences can be explained in connection with the fact that according to the LVS EN 197-1 standard the samples, during the examination period, must be kept in moisture cabinet with relative humidity above 90%, while there is no such requirement according to the ГОСТ technology. The results of setting time tests are given in the Table 5.

Table 5 The comparison of initial and final setting time

Cement type	setting time	LVS EN 197-1	ГОСТ 10178-85	Coef. of correl.
CEM I 32,5 R	initial (min)	187.5	159.5	0.375
	final (min)	279.4	271.9	0.31
CEM I 42,5 R	initial (min)	191.5	157.7	0.22
	final (min)	283.9	271.5	0.14

The methods of determining the fineness of cement are incomparable. The specific surface of Portland cement in the case of the EN 196-6 standard and ГОСТ 10178-85 is different. The correlation coefficient between the two methods is < 0.7 which is an evidence that both methods are incompatible.

The physical and mechanical tests of properties of composite Portland cements

During the period from March 1994 through March 1996, in A/S Brocēni laboratory the samples of composite Portland cement were made, using fly ash of burnt shale from the Narva Power Plant (Estonia), Brocēni limestone and fly ash from the Riga Power Plant as an addition. By grinding these additives to the Portland cement clinker, in the amounts of 5, 15, 25 and 35%,

samples of the composite Portland cement were obtained which correspond to following types of EN 197-1 : CEM II/A-T; CEM II/B-T; CEM II/A-L; CEM II/B-L; CEM II/A-Q; CEM II/B-Q.

The results of investigation of the kinetics of hardening of the composite Portland cement show that when the share of additives in cement increases, the differences between the hardness (N/mm^2) of samples made according to technologies of EN 197-1 and ГОСТ 10178-85 decreases.

In samples, with the amount of additives of 5 and 15 %, the compressive strength after 2 days of hardening, is higher by 2 - 5 N/mm^2 as compared with cement without additives, when testing the hardening according to both standards. However, after 28 days of hardening, there is practically no difference, if testing is done according to ГОСТ 10178-85, but the compressive strength is much lower (by 4 - 12 N/mm^2) if tested according to EN 197-1. When the proportion of additives reaches 25% and more, the compressive strength in both cases is much lower when tested according to both standards. The results of tests are shown in Table 6.

Table 6 Comparison between various composite Portland cements

Type of s additives	Proportion of additives	Compressive strength (N/mm^2)					
		after 2 days		after 7 days		after 28 days	
		EN	ГОСТ	EN	ГОСТ	EN	ГОСТ
none	0	20.5	16.5	38.6	42.4	46.3	59.6
fly ash from the Riga Power Plant	5	22.1	15.4	38.6	38.4	46.7	54.2
	15	20.1	13.6	36.7	36.5	45.2	47.0
	25	18.7	13.4	33.9	31.3	40.9	45.8
	35	15.5	11.7	30.1	26.0	36.3	36.0
Brocēni limestone	5	21.5	18.2	46.1	44.0	47.0	58.2
	15	21.1	16.6	43.0	37.6	48.3	47.5
	25	18.8	14.2	32.5	30.5	39.5	38.6
	35	14.1	11.0	24.0	22.3	31.8	28.4
fly ash of burnt shale from the Narva Power Plant	5	22.1	21.7	39.5	42.1	45.8	53.0
	15	19.8	18.8	31.1	30.7	46.8	48.4
	25	17.2	14.2	27.7	29.4	40.6	42.3
	35	16.6	11.5	21.7	25.3	33.9	32.2

REFERENCES

ГОСТ 10178-85 : 1985 Cement - composition, specifications and comformity criteria.

LVS EN 197-1 : 1995 : Cement - composition, specifications and comformity criteria.

Kikas, V. and Piksarv, E. On hydratation of the finest fractions of fly ash of kukersit shale, Tallin Plytechnical Institute, Vol. A,1972, No. 272, pp. 49 - 67.

Richter, R., The methods of statistical analytics, University of Latvia, Rīga, 1995, pp. 1 - 28.

Schiller, B. and Ellerbrock H.G., "The grinding and properties of cements with several main constituents",Cement Lime Gypsum Journal, No.7, July,1992, pp.325-334.

Sprung, S. and Siebel E., "Assessment of the suitability of limestone for producing portland limestone cement (PKZ)", Cement Lime Gypsum Journal, No.1, Januar,1991, pp.1-11.

Timashev, V. V.and Kolbasov, V. M. "The properties of cements with carbonate additives" , Journal on Cement, Moscow, No. 10, 1981, pp. 10 - 12.

A CONTRIBUTION TO THE KNOWLEDGE OF THE PROPERTIES OF PORTLAND-LIMESTONE CEMENT CONCRETES, WITH RESPECT TO THE REQUIREMENTS OF EUROPEAN AND ITALIAN DESIGN CODE

Vito ALUNNO ROSSETTI, University "La Sapienza", Rome, Italy
Francesco CURCIO, Unicem Centro Ricerche, Guidonia, Italy

ABSTRACT The properties of Portland Limestone cements produced in two italian factories, conforming the new italian standard on cement UNI-ENV 197-1, have been tested, both on cement and on concrete, in comparison with Portland Cements. The aim of the test program was to verify the suitability of these new cements for structural concrete design, with reference to European and Italian Codes.

Key-words: blended cement, interground cement, composition, characterization

INTRODUCTION

The adoption of the European standard on cement ENV 197-1 in Italy as the new national standard UNI ENV 197-1, has introduced in this country the production and utilization of Portland Limestone cements, wich were not allowed by the previous regulations (and obviously not utilized and known).

Although such cements had already been used for the production of structural concrete in several countries abroad, and some literature was available, see for example Albeck and Sutej (1990) and Baron and Douvre (1987), the italian designers felt the need to verify the properties of structural concrete made with Portland Limestone cements of national production and the relationships of such properties whith those given by the design Codes.

To such purpose the authors have performed an intensive laboratory testing program with the aim to characterize the performances of Portland-Limestone cement concrete with respect to all physical and mechanical properties and their relationships contemplated by the national Code of Design and by European standard EN 1992. The results have been compared to reference concretes made with Portland Cement.

Tests have been done regarding compressive, flexural and tensile strengths, shrinkage elastic modulus, fracture energy, monotone and cyclic compression curves, creep. Some evaluation of the durability of the same concretes by means of water permeability, chloride and sulphate penetration, carbonation and sulphate attack have been performed. The experimental results confirm that concretes made with Portland Limestone cement behave consistently whith the recalled Codes of design.

MATERIALS

Cements

Industrial cements produced in two different plants (named B and G) have been utilized. For each plant, two samples have been collected: a Type I 42,5 R Portland cement (named respectively PB or PG, depending on the production plant) and a Type II/A-L 42,5 R Portland-limestone cement (named LB or LG), both produced with the same industrial clinker and gypsum; no other costituent has been utilized, apart from limestone in LB and LG. One commercial TEA-based grinding aid has been used in all cases.

In the aim to strenghten the influence on concrete properties given by the presence of limestone into Type II/A-L cements, the amount of limestone in the two samples has been increased up to the limit of 20 % by mass established by the standard for the composition of that type of cement. Actually, Type II/A-L 42,5 R Portland-limestone cements today available on the Italian market (B's and G's products included) are produced with a consistently reduced amount of limestone and differ much less than LB and LG from the corresponding Type I cements in terms of fineness, setting time and EN 196-1 mortar compressive strength. In the Authors' intention, if LB and LG perform satisfactorily, it is to be expected that any commercial Type II/A-L product will do the same: its behavior should in fact be somehow inbetween LB's (or LG's) and the corresponding PB's (or PG's) ones. Physical and mechanical properties of the four cements used in the present testing program are reported in Table 1.

Table 1 Physico-mechanical properties of the cements (according to test methods UNI EN 196)

	PCB	LCB	PCG	LCG
Retained at 0.063 mm sieve (%)	2.03	1.05	4.60	2.30
Retained at 0.090 mm sieve (%)	0.56	0.20	1.05	0.60
Blaine specific surface, m^2/kg	345.0	482.5	362.0	489.5
Water demand (%)	26.6	27.6	27.6	26.2
Initial setting time (minutes)	100	125	115	140
End of setting (minutes)	150	190	195	205
Compressive strength (MPa)				
1 d	16.8	15.2	14.1	16.0
2 d	25.1	24.3	25.9	24.9
3 d	30.5	29.2	30.2	29.3
7 d	38.5	38.1	37.2	35.9
28 d	49.4	46.5	48.6	45.9

In Table I are presented the properties of the cements. It can be observed that the limestone cement from factory B presents a slightly higher water demand with respect to its "parent" portland cement; the contrary holds for the G factory products; this can be explained with differences due to the hardness and grindability of clinkers and limestones (expecially Blaine surface, overall fineness and, even if not measured, a greater fineness of the clinker fraction). The mortar properties are practically the same up to 7 days; at later age the PC mortars show a compressive strength appreciably higher (about 10%), due to the dilution effect of the limestone.

Concretes

Concrete mixes, of the same consistence and with two cement dosages, such to obtain characteristic strengths Rck of about 25 and 30 MPa on cubes, were proportioned in the laboratory, using the standard siliceous laboratory aggregates, with a Bolomey grading. In Table 2 the compositions and characteristics of the fresh concretes are reported, and the 28 days compressive strength. The favourable effect of the limestone addition on the water demand of concrete can be appreciated, both at lower and at higher cement dosages, so that the difference in strength measured on mortars at 28 days is almost recovered in concrete at the same age. Also small differences in compaction index can be noticed, that seem to indicate a favourable influence on the response to vibration of limestone cement concrete.

Table 2 Composition and characteristics of concretes

CEMENT FACTORIES B, G	PCB	LCB	PCB	LCB	PCG	LCG	PCG	LCG
Cement dosage (kg/m3)	270	270	330	330	270	270	330	330
Water/cement ratio	0.65	0.64	0.55	0.53	0.63	0.62	0.54	0.53
Air (%)	2.0	2.0	1.7	1.8	2.0	1.8	2.0	1.8
Density (kg/m^3)	2399	2399	2409	2399	2399	2399	2409	2409
Slump(cm)	10	11	10	11	10	10	10	10
Compaction index	1.05	1.03	1.05	1.02	1.07	1.05	1.05	1.05
Compressive strength Rc, 28 d, MPa	30.7	30.0	39.7	38.0	31.6	29.1	37.5	36.5

TEST RESULTS

Mechanical properties taken into consideration in the design standards have been determined.

Compressive strength

Fig. 1 and 2 show the evolution of *compressive* strength measured on *150 mm cubes* up to 1 year. For the cements B the values at the first days show a substantial equivalence, whilst at later ages (from 180 days) the limestone cement strength results are about 30 % lower, due to the reduced presence of clinker; for the G cements the results are practically equivalent.

The compressive strength at 28 day has been also measured on 150x300 mm *cylinders (fc)*; the mean ratio Rc/fc is 1.40; this value, higher than the values normally found for portland cement concrete has to be verified.

Splitting tensile strength (fct,sp) has been measured on cylinders (150x300 mm), according to UNI 6135-72; three point Flexural strength (fct,fl) has been measured on concrete prisms (10x10x50 cm) according to UNI 6133-83 . Table 3 presents the results; the values obtained on limestone cement concrete are generally lower than on the corresponding portland cement concrete.

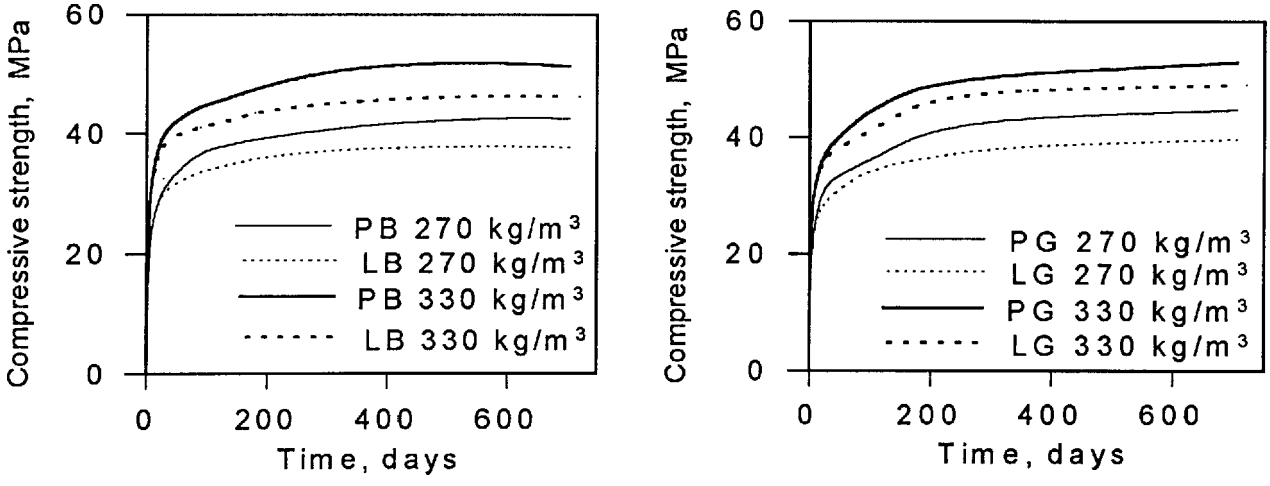

Figures 1 and 2. Compressive strength in time

The values of fct,sp and fct,fl have been compared with the corresponding values calculated from Rc, by means of the relationships given by the EC 2; the differences between experimental and calculated values are on average about ±15 % of the experimental value; the difference looks acceptable, taking into account the sensitivity of the method.

Table 3 Splitting and flexural strength, MPA

Cement and dosage kg/m^3	PCB 270	LCG 270	PCB 330	LCB 330	PCG 270	LCG 270	PCG 330	LCG 330
Splitting 28 days	2.3	2.7	2.9	2.7	3.2	2.1	4.1	2.6
Splitting 365 d	2.8	2.6	3.0	3.0	3.0	2.5	3.8	2.9
Flexural 28 days	5.0	4.8	6.4	5.3	3.6	4.7	4.7	4.7
Flexural 365 days	6.6	5.4	7.6	7.0	5.4	5.8	6.4	6.1

Elastic moduli of the concrete have been determined at 28, 60 and 90 days following UNI 6556; the results, shown in Table 4 indicate that no substantial differences exist between portland cement and limestone cement concretes.

Table 4 Elastic moduli, MPa .10^{-3}

Cement and dosage kg/m3	PCB 270	LCB 270	PCB 330	LCB 330	PCG 270	LCG 270	PCG 330	LCG 330
28 days:	26.0	24.5	28.0	27.5	25.1	25.4	27.2	27.1
60days	28.5	26.2	29.1	28.4	26.1	26.7	29.6	28.6
90 days	29.3	28.1	30.2	29.3	27.2	27.2	30.2	29.7

The experimental E moduli have been compared with those calculated by means of the expression $Ecm = 9.5(fck+8)^{1/3}$ given by EC 2; fck has been evaluated from the Rc values at 28 days, taking into account the coefficient fc/Rc=0.83 given by the code, and a k value of 6 MPa. The experimental values are always greater than those calculated, the average difference is about 10 %.

Fracture energy

The fracture energy has been determined following the draft recommendation 50 - FMC, by means of three-point bend tests on notched beams, 100x100x840 mm.

The results obtained (averages of two samples) are reported in Table 5; considering the sensitivity of the method the pairs of values for corresponding mixes of portland and limestone cement can be deemed to be alike, the only exception being the very low value of the sample LCB 270.

Table 5 Fracture energy

Cement and dosage kg/m3	PCB 270	LCB 270	PCB 330	LCB 330	PCG 270	LCG 270	PCG 330	LCG 330
Fracture Energy, N/m	176	123	216	197	145	162	201	207

Shrinkage

The shrinkage of the concretes has been measured following the standard UNI 6555 at a R.H. value of 50% ; the final results are reported in Table 6. Both shrinkage evolution and final values show no differences between the limestone cement and portland cement concretes. The

experimental values (between 0.54 and 0.67) are in satisfactory agreement with the indications of EC2 Code (0.6) and greater than the value given in the italian standard (0.3).

Table 6 Shrinkage at one year

Cement and dosage kg/m3	PCB 270	LCB 270	PCB 330	LCB 330	PCG 270	LCG 270	PCG 330	LCG 330
Shrinkage, μm/m	635	640	680	690	540	560	615	595

Creep

Creep tests have been performed by loading at 28 days the prismatic specimens (150x150x600 mm) at 1/3 of their compressive strength, at a R.H. of 50 ± 5%. In Table 7 are reported the observed values of creep (subtracting elastic deformation and shrinkage from the total deformation). The results give evidence to an appreciable difference in behavior of portland cement and limestone cement concretes, the first showing on average a creep about 17 % smaller than the latter; a possible cause could be that there is less cement gel on which the compressive stress develops its action.

Table 7 Creep results (m/m . 10^6)

Cement and dosage kg/m^3	PCB 270	LCB 270	PCB 330	LCB 330	PCG 270	LCG 270	PCG 330	LCG 330
Creep at 360 days	718	1102	778	914	824	972	756	869
Creep coefficient ($\varepsilon v / \varepsilon e28$)	1.43	2.10	1.24	2.56	2.02	2.19	1.48	1.66

The experimental creep coefficients have been calculated as the ratios between the observed creep values and the elastic deformation at 28 days; the values vary from 1.24 to 2.19 and result appreciably smaller than the corresponding values given by EC2 and the italian regulations .

Durability

To assess the behaviour of limestone cement concrete from the point of view of durability related properties, tests of water absorption at atmospheric pressure, according to UNI 7699, carbonation (UNI 9944), chloride (UNI 7928) and sulphate penetration (UNI 8019) have been performed.

Table 8 Durability related properties..

Cement and dosage	PCB 270	LCB 270	PCB 330	LCB 330	PCG 270	LCG 270	PCG 330	LCG 330
Water absorption % UNI 7699	4.8	4.8	4.2	4.5	5.5	5.5	5.3	5.1
Carbonation at 900 days, mm	20	10	18	13	19	21	15	16
Chloride penetration 28/60 days, mm	43/63	102/113	38/49	48/79	212/281	197/264	115/183	146/182
Sulphate penetration 28/60 days, mm	98/116	105/126	73/106	87/107	200/300	181/242	170/190	132/152

The data reported in Table 8 do not show great differences between the different types of cement; on the contrary the data could indicate some difference between cements from different factories. Water absorption, chloride and sulphate penetration are indeed greater, both for portland and limestone type, for the G factory cements.

One difference between cements that can be envoked to explain the different behaviour is to be find in the residue to the sieves; being the same the overall Blaine fineness, the greater fineness of the B factory cements (smaller residue) causes a lower permeability and a smaller water penetration. Another difference that can influence both chloride and sulphate penetration, is a slightly higher (about 2 %) content of C_3A in the B cement.

CONCLUSIONS

Taking into account what has been observed in the introduction about the peculiarity of the limestone cements used in the present tests, containing the maximum limestone dosage allowed by the cement standard, the results of the tests on the portland cements and limestone cements show that the difference in performances is very small and that the two types of cement are practically equivalent. In particular it can be observed that:

- the properties of fresh concrete confirm the favourable effect of limestone cement on the water demand in concrete; this is reflected also by the mechanical strength;
- the differences in mechanical strengths of concrete at 28 days, taking into account the differences in cement strengths, are very small; at longer ages the strength of limestone cement concretes are about 10 % lower than those of the corresponding portland cement concretes; the differences in elastic moduli are very small; the values evaluated from the EC2 expression are about 10 % lower than the experimental ones;
- the fracture energy does not appear to depend clearly on the type of cement: for the limestone cement produced at the B works Gf is greater than for the corresponding portland cement; the opposite holds for the G production;
- the shrinkage behaviour of the portland and limestone cement is the same;
- the creep results are the only case of apparent difference among the two cements oberved in this test program;
- chloride and sulphate penetration, water absorption, carbonation depth, chloride and sulphate penetration are not different for the two types of cement; differences noticed between the two factories are related to the different sieve residues and C_3A content.

REFERENCES

Albeck, J. and Sutej, B., "Neue Zemente - Eigenshaften von Betonen aus Portlandkalkstainzement". Vortragsreferat. Zement-Kalk-Gips 43 (1990) No. 4, pp. 216

Baron, J. and Douvre, C., "Technical and economical aspects of the use of limestone filler additions in cement", World Cement, April 1987, pp. 100-104

AUTHOR INDEX

A
M.S. Abdel-Aziz; 3v012
A.A. Abdel-Kader; 2ii027
A. H. Abedel-Reheem; 3ii124
A. Achmetov; 2ii013
F. Adenot; 3v003
A. D. Agnihotri; 1i003
S.C. Ahluwalia; 1i019, 1i031, 1i044, 1i045, 1i053, 2ii006, 3ii094, 4iv013, 4iv067
H. Ai; 3iii018
V.G. Akimov; 1i006
I. G. Al-Alm Rashed; 3ii124
B.S. Albats; 1i015, 1i007
A.H. Ali; 4iv014
M.M. Ali; 2ii006
Mª C. Alonso; 4iv004, 4iv082, 4iv083
V. Alunno Rossetti; 3v026
Ö. Andaç; 1i050
T. Ando; 2ii017
C. Andrade; 4iv004, 4iv082, 4iv083
M.V. Anufriev; 1i032
H. Anzai; 3v013
N. Arano; 4iv051
S. Argarwal; 4iv067
S.K. Argarwal; 4iv067
P. Arjunan; 3v020
V.K. Arora; 1i019
K. Asaga; 3ii107, 3iii022
E. Asakura; 2ii005
M.A. Aviles; 3v019

B
O. Baumanis; 3v025
Sh.T. Babaev; 3iii021
V. Babkov; 2ii048
V.I. Babushkin; 4iv039
P. Baccini; 4iv076
S. Bagosi; 4iv045
G. Balázs; 2ii060, 4iv002
K.D. Baltzopoulou; 4iv052
J.R. Baragaño; 3iii004
V.D. Barbanyagre; 1i011, 1i059
P. Barret; 2ii024
N.F. Bashlykov; 3iii021
A.F. Battagin; 3ii102, 3ii103
Y. Bazhenov; 4iv058
A. Beeldens; 4iv007
V. Belyaeva; 1i004
M. Benkaddour; 2ii041
J. Bensted; 3iii014
D.P. Bentz; 2ii078
J. Berekta; 2ii029
H. Bergqvist; 3ii106
A.F. Bernatsky; 4iv079
C. Bessada; 3v002
R. Bhargava; 1i031, 2ii006
K.N. Bhattacharjee; 3ii115
Y. Biryukovich; 4iv056
Mª T. Blanco-Varela; 1i034, 3ii096, 3ii113, 3iii004, 3iii015
A.I. Boikova; 1i057, 1i058
K. Bollmann; 4iv062
L. Bonafous; 3v002
D. Bonen; 4iv022
S. Bonnet; 4iv078
M. Boros; 2ii060
S. Bouraoui; 2ii012
P. Bowen; 3iii002
S. Boyko; 3v004, 3v022
M. Braiman; 3v022
K.D. Breneman; 2ii057, 2ii058
F. Brivot; 4iv074
A.R. Brough; 3v001
H.J.H. Brouwers; 2ii052
L. Brower; 3iii031
W. Brylicki; 3ii095
N. R. Buenfeld; 4iv070
T.A. Bürge; 3iii002

C
R. Cabrillac; 3v003
C. Caestecker; 4iv007
R. Caldwell; 4iv042
G. Camarini; 3ii102, 4iv063
L. Cassar; 1i027
P. Cassat; 3v014
M. Castellote; 4iv082
S.L. Centurione; 2ii079
W.-H. Chae; 1i036
J. Champa; 3iii027
S. Chanda; 3ii092
S. Chandra; 3ii106
P.K. Chang; 3v006
I. Chartschenko; 2ii010
A.K. Chatterjee; 1i008, 1i033, 2ii039

S. Chaturvedi; 4iv057
T. Chaussadent; 4iv074
M. Chen; 3iii016
Y. Chen; 1i010, 2ii031
H. M. Cheong; 1i049, 2ii037
V.L. Chernyavski; 4iv071
Y. Chi; 1i054, 1i055
V. Chistyakov; 2ii019, 2ii023
D.W. Cho; 2ii037
H. Choi; 3iii009
S.H. Choi; 1i036, 1i049, 4iv054
B.J. Christensen; 2ii057
M.A. Cincotto; 3ii102, 4iv063
R. Cioffi; 4iv017
P. Colombet; 3iii003, 3v002, 3v014
D. Constantiner; 3iii013
A.G. Constantinou; 4iv084
F. Corazza; 3iii003
U. Costa; 3iii003
J.-P. Coutures; 3v002, 3v005
T. Coverdale; 3iii027
N.J. Crammond; 4iv026
E. Csányi; 4iv002
L.J. Csetenyi; 4iv045
F. Curcio; 3v026, 4iv006
L. Cussino; 4iv006

D
M. Daimon; 2ii002, 2ii017, 2ii022, 3ii088, 3ii107, 3iii022
D. Damidot; 2ii024, 2ii025, 2ii026, 3iii007, 4iv066
T. Dashkova; 4iv056
B. De Blaere; 4iv007
B. De Vito; 4iv017
E. De Winne; 4iv007
M. Degenkolb; 2ii074
A.E. Degtyaryev; 2ii019
J. Deja; 4iv015
K. Demura; 3iii033
M. Deng; 4iv029
S.P. Dennington; 3iii008
R.K. Dhir; 4iv012
G. Diaz; 3v023
S. Dietz; 3ii087
J.M. Diez; 4iv040
S. Dimitrova; 3ii101
A.M. Dmitriev; 3iii021
C.M. Dobson; 3v001
A. Douy; 3v005
A. Dozono; 2ii001
M. Drabik; 3iii011
R. Dron; 4iv074
G.Ya. Drozd; 4iv039
V.Y. Dubnitsky; 4iv071
G. Dumitru; 3iii015
A.M. Dunster; 4iv026
S. Duszak; 4iv027

E
C.M. Economou; 4iv052
M. Ecker; 2ii032, 4iv044
L. Eckert; 3iii027
A.N. El-Afify; 3ii124
E.B. El Aouni; 2ii041
B.A. El-Sabbagh; 4iv014
H.A. El-Sayed; 4iv014
A. Emanuelson; 1i060
Z.B. Entine; 1i020, 1i046, 3v024
H. Ezirim; 3ii112

F
D. Fairhurst; 4iv008, 4iv009
V.R. Falikman; 3iii021
Y. Fang; 1i010
S.A. Farrington; 3iii013
P. Faucon; 3v003
X. Feng; 2ii043
A. Fernandez-Jimenez; 3ii098
V. Fernon; 3iii003
R. Ferrari; 4iv006
R.C. First; 2ii075
R. Flatt; 3iii002
O.I. Fomicheva; 1i057, 1i058
E. Forssberg; 3ii104
L.S. Fraiman; 3ii081
R. François; 4iv078
O. Francy; 4iv078
G. Frigione; 4iv017, 4iv050
X. Fu; 1i054, 1i055
H. Fujisawa; 2ii005
H. Fujiwara; 2ii001
K. Fukuda; 1i025, 1i052

G
L. Galikova; 3iii011
S.P. Gandhe; 1i033
A. Garbacik; 1i018

M.C. Garci; 2ii058
L. A. M. Garcia; 4iv037
S. Gauffinet; 2ii055
M. Gawlicki; 3ii089
Mª T. Gaztañaga; 4iv003
J. Geiseler; 4iv001
S. George; 1i003
W. Gessner; 3iii007, 3v018
D. Ghosh; 1i008, 1i033, 1i047
S.N. Ghosh; 3ii092
S.P. Ghosh; 1i030, 2ii018
G. M. Giaccio; 2ii036
Z. Giergiczny; 4iv019
C. Gilioli; 1i027
P. Gill; 3iii024
N. Giuliani; 1i051
G.K. Glass; 4iv070
F.P. Glasser; 1i050, 3ii091, 4iv066
V. Glukhovskiy; 4iv056
F. Goetz-Neunhoeffer; 1i056
L. Ya. Goldstein; 1i013
E. Gomez; 3v019
S. Goñi; 4iv003, 4iv004, 4iv024, 4iv040, 4iv083
J.W. Goodwin; 3iii008
V.K. Gore; 1i047
G. Goswami; 3v008
R.K. Goswami; 1i044, 1i045
S. Goto; 2ii070
A.M. Grabiec; 3iii019
M.L. Granizo; 3ii113
L.V. Grishchenko; 1i058
I. Grosvalds; 2ii009
G.W. Groves; 3v001
M. Grutzeck; 2ii067
G. Gu; 3iii016
A. Mª Guerrero; 4iv003, 4iv024
G.L. Guerrini; 1i027
R.S. Gupta; 1i053

H

H. Hagiwara; 3iii017
J. Han; 3ii122
K. S. Han; 1i049
M. Handa; 2ii017
S.K. Handoo; 3v019, 4iv013, 4iv067
S. Hanehara; 2ii014, 3iii001
F. Hanic; 3iii011
S. Hansen; 1i060
N. Hara; 2ii065
S. Harsh; 1i044, 1i045, 4iv013
M. Hasegawa; 3iii010
N.M. Hassanein; 4iv070
M. Hatano; 3iii009
A.S. Heble; 2ii039
H. Hedlund; 2ii077
D. Heidemann; Plen2
E. Henderson; 1i060
Mª S. Hernandez; 4iv003, 4iv024
A. Hidalgo; 4iv004, 4iv083
T. Higaki; 3iii022
M. Hilger; 1i009
H. Hirao; 2ii014
S. Hirose; 3iii022
F.J. Hofmann; 4iv038
H. Hofmann; 3iii002
S.-Y. Hong; 4iv068
K. Hormann; 4iv038
S. Hoshino; 2ii002
J. Houghton; 4iv025
Y.F. Houst; 3iii002
G. Hu; 1i023
S. Huang; 4iv032
Z. Huang; 4iv073
F.H. Hubbard; 4iv012
C.L. Hwang; 2ii035; 3ii108, 3v006, 3v021
C. Hübert; Plen2
C. Hyeon; 4iv072
R. Härdtl; 3ii082

I

M. Ichikawa; 3iii005
K.A. Idriss; 3v012
S.-i. Igarashi; 4iv051
T. Iisaka; 2ii003
T. Ikabata; 2ii007
K. Ikeda; 1i025
M.R. Ilić; 4iv023
N. Inoue; 2ii065
Y. Inoue, 2ii040
B.E. Ioudovitch; 1i020, 1i046, 3iii021, 4iv036
G. C. Isaia; 3ii110
A. Ishida; 3iii017
Y. Ishikawa; 2ii003
Y. Isojima; 3ii109, 3ii119
S. Ito; 1i052, 3ii121
J. Iwanciw; 1i022

H. Iwasaki; 3iii033

J
J.F. Jacquinot; 3v003
H.J. Jakobsen; 2ii056
S. Jalali; 3ii084
I. Y. Jann; 3v021
I. Jedda; 2ii020
H.M. Jennings; 2ii057, 2ii058
O.M. Jensen; 2ii056
M.-Y. Jeong; 4iv055
L. Ji; 2ii030
S.P. Jiang; 2ii053
W. Jiang; 3ii100, 3iii030
A.C. Johnson; 4iv076
J.-E. Jonasson; 2ii077
M. Jorda; 3v003
D.M. Joshi; 3ii092
H. Justnes; 1i038, 2ii069, 3iii012, 4iv064, 4iv081

K
K. V. Kalyani; 1i003
M. Kanaya; 3iii005
I. Karimov; 2ii048
A. Katz; 3ii083
S. Kawaguchi; 4iv051
M. Kawamura; 4iv051
T. Kawano; 3iii010
S. Kelham; 4iv060
M. Kersten; 2ii059
S.A. Khadilkar; 1i008, 1i047
Y. Kihara; 3ii085, 4iv048
H. Kikukawa; 2ii003
B.-K. Kim; 4iv068
N.-H. Kim; 2ii044
A. Kindness; 3ii091
P. Kittl; 3v023
V. Klassen; 1i004
J. Kļaviņš; 3v025
W.A. Klemm; 4iv041, 4iv059
A. Klusov; 2ii013
D. Knöfel; 2ii074
T. Kobayashi; 3iii010
M.M. Komljenović; 1i017
P.G. Komokhov; 2ii016
J. Komonen; 3iii029
N. Kondo; 2ii017
V.I. Kondrashchenko; 2ii066
Z. Konik; 1i022
G. Koprowski; 4iv018
H. R. Kota; 3ii104
M.V. Kougiya; 1i043, 3ii081
T.V. Kouznetsova; 1i001, 2ii027, 2ii028
J. Krištín; 3v009
É. Kristóf-Makó; 3v010
P.V. Krivenko; 2ii033, 4iv046
A.R. Krivoborodov; 4iv053
Y.R. Krivoborodov; 1i014, 1i040, 2ii013
D. Križan; 3ii085, 4iv020
R. Krzywobłocka-Laurów; 3iii019
A.B. Kudryavtsev; 2ii028
H. Kuga; 3ii107
W. Kurdowski; 4iv027
S. Kwan; 2ii067
L. J. Kyu; 2ii022
B. Ködderitzsch; 3v018
U. König; 1i039

L
E. E. Lachowski; 3ii091
A. Łagosz; 3ii089
S. Lagzdina; 1i035, 2ii009
A. Landa-Cánovas; 1i060
E. Lang; 4iv001
J. LaRosa-Thompson; 2ii067, 3iii024
C.K. Larsen; 4iv069
X. Lecoq; 2ii055
H.-S. Lee; 2ii044
I.S. Lee; 2ii044
S. H. Lee; 3ii088
Y.-J. Lee; 2ii044
P.G. Lele; 1i008, 1i047
M. Lewis; 4iv025, 4iv061
D. Li; 4iv029
P. Li; 1i028
R. Li; 4iv028
S. Li; 4iv030
V. Lilkov; 3ii116
J.R. Lim, 2ii037
L.K. Lin; 3ii108
J. Lindgård; 4iv064
C. Liu; 1i028
J.N. Liu; 3ii114
J.S. Lota; 3iii014, 4iv012
C. Lu; 1i012, 4iv028
H.M. Ludwig; 4iv034, 4iv035
I.G. Luginina; 1i029, 1i057

M. Lukach; 3v022
K. Luke; 3ii091
T. Lyashenko; 3v004

M
A. Macias; 4iv040
J. Madrid; 4iv040
N. Maeda; 3iii010
Y. Maejima; 2ii005
S. C. Maiti; 3iii020
J. Majling; 3v009
I. Maki; 1i052
R.I.A. Malek; 1i024
J. Małolepszy; 2ii064, 3ii089, 4iv043
S. Manjit; 3ii093
B. Marchese; 4iv050
E. Marciano Jr.; 2ii079, 3ii103
V. Maringolo; 2ii079
M. Marroccoli; 2ii029
V. Martinez; 3v023
D. Massiot; 3v002, 3v005
S. Matala; 3v017, 4iv005
V.K. Mathur; 1i053
V.A. Matviyenko; 2ii076
W.J. McCarter; 3ii112, 4iv011
O.P. Mchedlov-Petrossyan; 1i042, 2ii021
S.N. Mehrotra; 1i002
I. Meland; 4iv064
V.S. Melentyeva; 3ii117
E. Menendez; 4iv004
B. Meng; 3ii105
H.W. Meyer; 3v007
V. Michaud; 2ii011, 4iv049, 4iv065
A. Miezis; 3v025
T. Mihara; 3iii017
N. Mikhailishina; 4iv056
S.R. Miletić; 4iv023
F.M. Miller; 4iv041, 4iv059
K. Miskiewicz; 3ii087
S. Miyazawa; 2ii071
K. Mohan; 1i030, 2ii018
B.N. Mohapatra; 3v008
G.K. Moir; 1i041
G. Morales; 3ii123
M. Morioka; 3iii017
H. Motzet; 1i039
J.F. Muller; 3v014
A.K. Mullick; Plen1, 1i031, 3v019, 4iv047
D. V. Mundshtukov; 2ii020
J.C. Mutin; 2ii053
D. Müller; 3iii007
U. Mäder; 3iii002
S. Möhmel; 3v018

N
M. Nadu; 3v022
S. Nagataki; 2ii001
A. Nakamura; 2ii022
H. Nakata; 2ii070
S. Nakaya; 2ii017
D. Nazarsky; 4iv021
B. Nedumaran; 1i002
L.S. Nefyodova; 3v024
H. Nemoto; 3v013
C. M. Neubauer; 2ii057, 2ii058
J. Neubauer; 1i039, 1i056, 3v007
Y. Nikaido; 2ii017
T. Nishikawa; 3ii121
J. Nissenbaum; 3v022
W. Nocuń-Wczelik; 4iv043
T. Noguchi; 4iv072
H. Noma; 2ii065
A. Nonat; 2ii053, 2ii055, 4iv049, 4iv065
E.C. Nygaard; 3iii012

O
I. Odler; 1i026, 2ii063
H. Ogata; 2ii005
H.-K. Oh; 1i036, 4iv054, 4iv068
Y. Ohama; 3iii033
Y. Ohba; 2ii002, 2ii022
A. Ohno; 3v015
A. Olginsky; 2ii015
G.B. Olson; 2ii058
L. Opoczky; 1i009, 2ii004
A.P. Osokin; 1i005, 1i006, 1i014
Z. Owsiak; 4iv018

P
S. Pagliolico; 4iv006
A. Palomo; 1i034, 3ii096, 3ii113, 3iii004
J.G. Palomo; 1i034
M. T. Palou; 3v009
Y. Pan; 1i021, 1i054, 1i055
J.D. Panda; 3v008
P.K. Panigrahy; 3v008
I. Papayianni; 3ii086
A. Papo; 2ii004

C.-K. Park; 4iv068
P. Parmentier,; 3ii120
M. Pátkai-Horváth; 3v010
P. Paulini; 2ii072
S. Pavlenko; 3ii080, 4iv058
V. Penttala; 3iii029, 4iv033
J.L. Perez-Rodriguez; 3v019
B. Perrin; 4iv078
B. Persson; 2ii073
O.E. Petrov; 3ii116
S. Peukert; 2ii034, 3iii023
W.G. Piasta; 4iv018
A.K. Platten; 4iv008, 4iv009, 4iv073
A.A. Plugin; 4iv039, 4iv075
A.N. Plugin; 2ii054, 4iv075
A. Poltavtsev; 2ii019
A. Pompo; 2ii029
E.N. Potapova; 1i005, 1i006
J.H. Potgieter; 2ii049, 3v011
P.L. Pratt; 3iii014
I.G. Prokopova; 4iv075
J.R. Prusinski; 3ii090
F. Puertas; 1i034, 3ii096, 3ii098, 3ii113, 3iii004, 3iii015
E.K. Pushkaryeva; 2ii033
G.K.D. Pushpalal; 3iii010
R. Pyare; 1i016
Z. Pytel; 2ii064
H. Pöllmann; 1i039, 2ii032, 3iii032, 3v007, 4iv044

Q
V.A. Quarcioni; 3ii085

R
M. Radenkova-Yaneva; 2ii047, 3ii101
K. Raina; 1i002
K. Rajczyk; 2ii045
Sh. M. Rakhimbaev; 2ii046
X. Ren; 2ii030
A. Rettel; 2ii026, 3iii007
M. Ribas Silva; 4iv037
I.G. Richardson; 2ii068, 3v001
A. Risch; 4iv044
J. Roberts; 4iv073
E. Rodum; 4iv081
M^{a}.L. Romero; 3ii096
V. Ronin; 3ii104, 2ii077
G. Rosenthal; 3iii031
A. Rosić; 1i017
W. Roszczynialski; 3ii097
D.M. Roy; 1i010, 3ii100, 3ii114, 3iii030, 3v020
R. Roy; 1i010
R.F. Runova; 2ii054, 3ii117
O.V. Rybakova; 4iv053
P.F. Rymyantsev; 1i037

S
S. Sahu; 3v009
A. Saini; 1i051
E. Sakai; 2ii002, 2ii017, 2ii022, 3ii088, 3ii107
S.V. Samchenko; 1i014
G. Samuel, 4iv047
M.A. Sanitsky; 3iii025
R. Sanjaasuren; 1i037
S. Sano; 3iii005
S.L. Sarkar; 3ii090
L. Sas; 1i048
A.E. Savva; 4iv052
D. Sawaki; 3iii001
Z. Sawicz; 4iv018
B.E. Scheetz; 3ii111, 3iii024
M. Schieber; 3v022
P. Schiessl; 3ii105, 4iv016
M. Schmidt; 3ii087, 4iv038
C. R. Schweizer; 4iv076
K.L. Scrivener; 2ii026, 4iv025, 4iv061, 4iv084
H. Sedaira; 3v012
U. Sedmalis; 1i035, 2ii009
Y.P. Sehti; 1i019
K. Seki; 3iii009
Ž. Sekulić; 3iii028
M.M. Seleim; 3v012
E.J. Sellevold; 2ii069
V. Serbin; 2ii023
V.N. Serdyuk; 3iii021
R. Sersale; 4iv017
N.N. Shangina; 2ii016
S.V. Shapet'ko; 2ii033
K.M. Sharma; 1i053, 3ii094
P.S. Sharma; 3ii094
S.C. Sharma; 4iv057
M.A. Shater; 3ii124
Y.N. Sheen; 2ii035
A.L. Shein; 1i015

N. Sherman; 2ii029
V. Shevchenko; 2ii019
C. Shi; 3ii099, 4iv042
H. Shi; 1i012
L. Shi; 2ii031
Y. Shigetomi; 2ii040
H. Shima; 1i025
G.-Y. Shin; 4iv068
S.M. Shingote; 1i003
M. Shmelkov; 3ii080
M. Shoya; 3ii109, 3ii119
D. Shtakelberg; 3v004, 3v022
A.K. Shukla; 3ii115
K. Sideris; 2ii061, 4iv052
K.K. Sideris; 2ii061, 4iv052
M.R. Silsbee; 1i010, 3ii100, 3ii114, 3iii024, 3v020
N.B. Singh; 3ii115
Vinaya K. Singh; 1i016
Vipin K. Singh; 1i016
S.K. Sinha; 4iv047
A.G. Sinyakin; 2ii021
S.P. Sivkov; 2ii020
E. Sjöstedt; 1i060
J. Skibsted; 2ii056
R.C.T. Slade; 3iii011
S. Smeplass; 4iv064
K.A. Snyder; 2ii078
J.-T. Song; 4iv055
V.P. Sopov; 2ii066
D. Sorrentino; 4iv049, 4iv065
F. Sorrentino; 2ii025
J. D. Sota; 2ii036
J. Stark; 1i005, 2ii010, 4iv031, 4iv034, 4iv035, 4iv062
M. Stefanović; 3iii028
J. Stegemann; 4iv042
E.T. Stepkowska; 3v019
A. Stok; 1i022
J. Strigáč; 3v009
C.A. Strydom; 2ii049
P.E. Stutzman; 2ii078
S. Stürmer; 4iv031
St. Stöber; 3iii032
M. Su; 2ii030, 3iii026, 4iv029, 4iv030
L.G. Sudakas; 2ii008
R. Suderman; 2ii011
S. Sugita; 2ii043, 3ii109, 3ii119
L.M. Sulimenko; 1i007, 1i040
U. Sulser; 3iii002
T. Suzuki; 2ii005
L.B. Svatovskaya; 2ii062
K. Svinning; 1i038
R.N. Swamy; 4iv080
L.I. Sychova; 1i032
J. Szczerba; 3iii023

T
A. Tagnit-Hamou; 2ii012
S. Takahashi; 3ii107, 3v013
T. Takahashi; 2ii070
H. Takemura; 2ii007
Y. Takuma; 3ii118
F. Tamás; 2ii060, 3v010, 4iv002
C.E.S. Tango; 3ii085
E. Tazawa; 2ii071
J.J. Thomas; 2ii058
D.W. Thompson; 3iii008
F. Tomosawa; 2ii051, 4iv072
E.E. Toumbakari; 4iv010
B. Touzo; 3v005
R. Trettin; 2ii050
J. Tritthart; 3v010, 4iv069
D. Trumeau; 3v005
B. Trybalska; 4iv027
Y. Tsuchida; 3ii118
Y. Tsukinaga; 3ii109, 3ii119
N. Tsuyuki; 3iii009

U
S. Uchida; 3ii118
H. Uchikawa; 2ii014, 3iii001
T.S. Um; 4iv054
W.S. Um,; 2ii044
H.P. Unsworth; 4iv012
A. V. Usherov-Marshak; 2ii021, 2ii066, 3v016
H. Ushiyama; 2ii040
J.I. Ustimenko; 3ii117

V
H. Vaishnav; 3ii092
G.L. Valenti; 2ii029
K. Van Balen; 4iv010
C. Van Den Brande; 4iv010
R.J. van Eijk; 2ii052
A. Van Gemert; 2ii069
D. Van Gemert; 2ii069, 3ii120, 4iv007,

4iv010
M. Van Messem; 4iv007
F. Van Rickstal; 3ii120
K. Vanbelle; 3ii120
P. Vanis; 2ii063
L.B. Vasiliyeva; 2ii008
T. Vázquez; 1i034, 3ii096, 3iii004, 3iii015
F. Verboven; 2ii069
A. Vichet; 3iii003, 3v014
J. Virlet; 3v003
K. Viswanathan; 2ii039
V. Voznesensky; 3v004

W
A. Walliser; 2ii075
J.F. Wang; 2ii038
P. Wang; 3iii006, 3iii016
X. Wang: 3iii016
Y. Wang; 4iv029, 4iv030
R.C. Wason; 4iv047
D. Watson; 4iv011
J. Widmer; 3iii002
W. Wieker; Plen2
U. Wiens; 4iv016
S. Wild, 4iv075
J. Wu; 3iii006
K. Wu; 3ii122
X. Wu; 4iv032

X
Y. Xi; 3ii111
A. Xu; 4iv077
J. Xu; 4iv030

Y
D. Yadav; 3ii094
S. B. Yadav; 1i003
T. Yamamoto; 3v015
Q. Yang; 4iv032
Q. Ye; 2ii042
K. Yoshida; 2ii070
J.F. Young; 3iii018
Q. Yu; 2ii043, 3ii109, 3ii119
G.-C. Yum; 1i036

Z
N.M. Zaitchenko; 2ii076
M. Zdaniewicz; 3iii023
D.Yu. Zelensky; 4iv039
F. Zenone; 4iv017
R. L. Zerbino; 2ii036
F. Zhang; 4iv030
H. Zhang; 1i026
L. Zhang; 3iii026, 4iv029
X. Zhang; 3ii122
H. Zhuo; 1i028
B. Živanović; 3iii028, 4iv020
B.M. Živanović; 1i017
S.A. Zoubekhine; 3iii021, 4iv036

KEY-WORD INDEX

A

Accelerated test; 3iii033
Accelerators; 3ii103, 3iii005, 3iii012, 3iii014, 3iii022, 3iii027, 3iii032,
Acid attack; 3ii109, 4iv002, 4iv021, 4iv038, 4iv039, 4iv040
Activation; 1i006, 2ii016, 2ii045, 2ii062, 2ii076, 3ii083, 3ii092, 3ii094, 3ii098, 3ii099, 3ii100, 3ii103, 3ii104, 3ii113, 3ii114, 3iii028, 4iv047
Activation energy; 1i053
Activity coefficient; 4iv083
Additives; 1i009, 1i020, 1i035, 2ii003, 2ii009, 2ii045, 2ii074, 3ii116, 3iii017, 3iii032
Adiabatic temperature rise; 4iv072
Admixtures; 2ii012, 2ii034, 2ii036, 2ii047, 3ii087, 3ii095, 3ii097, 3iii001, 3iii002, 3iii004, 3iii009, 3iii018, 3iii019, 3iii023, 3iii024, 3iii025, 3iii026, 3iii029, 3iii030, 3iii031, 3v015, 4iv004
Adsorption; 2ii001, 3iii002, 4iv077
AFm phase; 2ii032, 3iii032, 3ii089, 4iv034, 4iv061
AFt phase; 1i060, 4iv034, 4iv041, 4iv059
Aggregate; 2ii015, 3v024, 4iv053, 4iv057
Air entraining; 4iv031, 4iv057
Air pollution; 4iv002
Alinite; 2ii030, 3ii118
Alite; 1i006, 1i015, 1i041, 1i050, 2ii040, 2ii042, 2ii056, 3ii107, 3ii117, 3iii005, 3iii031
Alkali; 1i002, 1i012, 1i028, 1i035, 1i049, 2ii012, 2ii065, 3ii083, 3ii098, 3ii100, 3ii103, 3ii113, 3ii114, 3ii117, 3iii025, 4iv003, 4iv028, 4iv055, 4iv066
Alkali aggregate reaction; 3iii033, 3v022, 4iv048
Alkali silica reaction; 4iv047, 4iv049, 4iv065, 4iv074
Alkali silicate solutions; 4iv049, 4iv065
Alkaline cement; 4iv046
Alumina; 2ii027, 2ii026, 3iii010
Aluminate phase; 1i001, 1i022, 1i051, 1i056, 2ii041, 2ii060, 3iii010, 3iii015, 4iv027, 4iv034, 4iv066
Aluminoferrite; 1i004, 1i005, 1i055, 2ii031
Aluminosilicate; 1i024, 4iv046
Anhydrite; 1i032, 2ii011, 2ii022, 2ii029, 3ii092, 4iv059
Aragonite; 1i042
Arc furnace dust; 4iv042
Asbestos; 1i027
Ash; 3ii080
Autoclavation; 3ii120, 4iv054
Autoclave soundness; 1i023
Autogeneous shrinkage; 2ii069, 2ii070, 2ii071, 2ii073

B

Backscattered electron image; 2ii014, 4iv061
Bacterial attack; 4iv038, 4iv039
Bamboo dust; 1i019

Barite; 1i036
Barium phases; 1i058
Belite; 1i006, 1i015, 1i018, 1i041, 1i052, 2ii007, 2ii040, 2ii045, 2ii056, 3v009
Belite cement; 1i036
Binder; 1i059, 2ii047, 2ii054, 3ii080, 3ii101, 3iii021, 4iv057
Blastfurnace slag; 2ii068, 2ii074, 3ii082, 3ii093, 3ii095, 3ii096, 3ii098, 3ii099, 3ii101, 3ii102, 3ii103, 3ii104, 3ii115, 3ii122, 3iii009, 3iii017, 4iv001, 4iv005, 4iv009, 4iv015, 4iv035, 4iv040, 4iv063
Blended cement; 1i020, 3ii089, 3ii091, 3ii111, 3ii114, 3ii115, 3ii121, 3v026, 4iv004, 4iv017, 4iv020, 4iv052,
Bogue calculation; 1i039, 3v007, 3v009
Borax; 1i036
Bottom ash; 3ii090
Bound water; 2ii072, 3iii019, 3v019
Brick; 3ii080
Brownmillerite; 1i022, 2ii029, 2ii032,
Burnability of raw mixes; 1i021, 1i030, 1i031, 1i034, 1i040, 1i041, 1i045, 1i048, 1i054
Burning conditions of clinker; 1i018, 1i023

C
Calcium carbonate; 1i042
Calcium aluminate; 2ii022, 2ii025, 2ii050, 3iii022, 3v005
Calcium aluminate cement; 2ii024, 2ii026, 2ii027, 2ii028, 3iii007, 3v018, 4iv003, 4iv025, 4iv026
Calcium aluminate sulphate; 2ii010, 4iv068
Calcium aluminozincates, 1i059
Calcium hydroxide; 2ii049, 2ii059, 3ii082, 3ii106, 3ii107, 3ii108, 3ii112, 3iii031, 3v019, 4iv067
Calcium fluoride; 1i032, 2ii042
Calcium langbeinite; 2ii011
Calcium nitrate; 3iii012
Calcium phosphate; 1i036
Calcium phosphate cement; 2ii063
Calcium silicate; 1i035, 1i055, 2ii055, 2ii050, 2ii062, 4iv054
Calcium sulphate; 1i012
Calorimetry; 2ii021, 2ii025, 2ii041, 2ii066, 3iii032, 3v016, 3v017, 4iv042
Capillary; 2ii048
Carbon dioxide; 1i024, 2ii032, 4iv010
Carbonation; 2ii073, 4iv003, 4iv004, 4iv005, 4iv006, 4iv010, 4iv017, 4iv026, 4iv035, 4iv048, 4iv070, 4iv084
Case studies; 4iv002
Cement; 3ii092
Cement hydration equation; 2ii061, 4iv052
Characterization; 1i008, 2ii062, 3ii088, 3v011, 3v020 3v023, 3v026, 4iv019
Chemical analyis; 3v012
Chemical attack; 4iv015, 4iv026, 4iv028, 4iv031
Chemical prestressing; 3iii016

Chemical shrinkage; 2ii069, 2ii070, 2ii072
Chloride; 1i002, 1i012, 2ii030, 3ii118, 4iv006, 4iv015, 4iv027, 4iv078, 4iv080, 4iv081, 4iv082, 4iv083
Chloride Binding; 4iv016, 4iv069, 4iv070, 4iv078
Classification; 4iv046
Clay; 2ii020
Clinker; 1i048, 1i058
Clinker composition; 1i028, 4iv036
Clinker formation; 1i004, 1i006, 1i008, 1i010, 1i011, 1i026, 1i031, 1i037, 1i043, 1i044, 1i046, 1i049, 1i054, 2ii006, 3ii118
Cluster; 1i003
Coal; 1i047, 3ii090
Composite cements; 1i009, 2ii016, 2ii034, 3ii122
Composition; 2ii007, 2ii071, 3v004, 3v011, 3v026, 4iv007, 4iv023, 4iv060
Concrete; 2ii035, 3ii108, 3iii024, 3iii029, 3v021, 3v022, 4iv025, 4iv035, 4iv073
Cooling of clinker; 3v005
Corrosion; 2ii006, 4iv014, 4iv020, 4iv023, 4iv027, 4iv028, 4iv030, 4iv038, 4iv039, 4iv071, 4iv082, 4iv084
Creep; 4iv018
Cross-linking; 3iii011
Crystal; 2ii015
Crystal size; 1i051, 3iii031
Crystal structure; 1i055, 2ii048
Crystallisation pressure; 4iv049
Crystallography; 2ii054
CSH; 2ii044, 2ii047, 2ii053, 2ii055, 2ii059, 2ii064, 2ii067, 2ii068, 3ii082, 3ii093, 3ii121, 3v001, 3v003, 4iv016, 4iv041, 4iv043, 4iv061, 4iv074, 4iv076
Curing; 2ii037, 2ii078, 3ii091, 4iv055, 4iv059, 4iv067

D

Deformation; 4iv021, 4iv058
Degree of hydration; 2ii051, 2ii053, 2ii062, 2ii077, 3v019, 4iv016
De-icing salts; 4iv006, 4iv035
Delayed ettringite formation; 4iv059, 4iv061, 4iv062, 4iv063, 4iv064
Delayed expansion; 3iii016
Design life; 4iv071
Dicalcium silicate; 1i017, 1i053
Differential thermal analysis; 2ii041, 4iv031
Diffusion; 2ii046, 3ii084, 3ii098, 4iv010, 4iv015, 4iv016, 4iv056, 4iv080, 4iv081
Diffusivity; 4iv008, 4iv009
Dilation; 4iv033
Dispersion; 2ii005
Disposal; 1i027
Dopant; 1i053
Drying; 3iii018, 3v018, 4iv011, 4iv077, 4iv079
Durability; 2ii011, 3ii095, 3iii024, 3v022, 4iv004, 4iv007, 4iv022, 4iv023, 4iv026, 4iv029, 4iv030, 4iv037, 4iv040, 4iv046, 4iv048, 4iv062, 4iv065, 4iv070, 4iv075, 4iv082

E
Economy; 1i036, 3ii114
Ecology; 1i043
Electron microscopy; 1i060
Electron spectroscopy for chemical analyses (ESCA); 2ii044
Electrical conductivity; 4iv011
Electrical impedance; 3ii112
Electrical properties; 4iv079
Electrical resistivity; 3v021
Energy; 2ii046
Environment; 1i003, 3ii093
Equilibria; 2ii057, 2ii058
Ettringite; 1i025, 2ii006, 2ii010, 2ii017, 2ii029, 2ii031 2ii056, 2ii070, 2ii074, 3iii022, 4iv012, 4iv018, 4iv031, 4iv060, 4iv062, 4iv065
Evaporable water; 3v019
Expansion; 2ii006, 2ii074, 3iii017, 3v022, 4iv057, 4iv060, 4iv062, 4iv064
Expansive cement; 1i001, 2ii010
Extraction methods; 3v020

F
False set; 3iii013
Ferrite phase; 1i008, 1i015, 1i060, 3iii005, 3v003
Ferroaluminate; 4iv029
Filler; 1i020, 2ii002, 2ii020, 3ii081, 4iv056
Fineness; 1i007, 2ii001, 2ii002, 2ii018, 2ii043, 2ii060, 3ii088, 3v008, 4iv060
Fingerprinting; 3v010, 3v011
Fire; 4iv073
Fire damage; 4iv067
Flow; 2ii017, 3v024
Flue gas desuphurisation product; 3ii090
Fluidity; 2ii001, 2ii002, 2ii012
Fluoride phases; 2ii043, 3v002
Fly ash; 3ii081, 3ii082, 3ii083, 3ii084, 3ii085, 3ii086, 3ii087, 3ii088, 3ii089, 3ii090, 3ii110, 3ii115, 3ii116, 3ii122, 3v006, 3v020, 3v021, 4iv004, 4iv009, 4iv012, 4iv019, 4iv020, 4iv023, 4iv058, 4iv077
Fracture mechanics; 2ii075
Free lime; 1i016, 1i045, 2ii049, 4iv036
Freeze-thaw damage; 2ii016, 3iii019, 4iv034, 4iv035
Freezing; 4iv033
Friedel's salt; 4iv027, 4iv080
Fuels for clinker making; 1i013, 1i019

G
Gel; 3ii105, 3iii007, 3iii022, 4iv074
Glass; 1i046, 1i051, 3ii088, 3ii119, 4iv030, 4iv055
Grinding aids; 2ii020, 3v014
Grinding technology; 1i009, 1i040

Ground silica; 3ii120
Grout; 2ii005
Gypsum; 2ii040, 2ii044, 2ii060, 3ii093, 3ii115, 3iii025, 3v008, 3v023, 4iv017

H
Hardening; 2ii008, 2ii034, 2ii039, 2ii047, 2ii052, 2ii054, 2ii076, 3ii112, 3v016, 4iv071
Heat capacity; 4iv033
Heat evolution; 2ii021, 2ii035, 2ii051, 2ii076, 2ii077, 3ii102, 3ii105, 3iii029, 3v016, 4iv042, 4iv072
Heavy metals; 1i043, 2ii014, 3v010, 3v013, 4iv041, 4iv043
High alumina cement; 2ii023, 2ii033, 3iii010, 3ii096, 4iv013, 4iv027, 4iv038
High performance; 2ii035, 2ii038, 3ii108, 3v006, 3v021
High strength; 2ii037, 3ii120
High sulphate clinker; 2ii011
High temperature; 3ii111, 3iii020, 4iv067
Humidity; 4iv011, 4iv079
Hydration; 1i022, 1i057, 1i059, 2ii004, 2ii006, 2ii008, 2ii007, 2ii012, 2ii013, 2ii015, 2ii019, 2ii021, 2ii022, 2ii023, 2ii024, 2ii025, 2ii026, 2ii028, 2ii029, 2ii030, 2ii031, 2ii033, 2ii035, 2ii036, 2ii039, 2ii040, 2ii041, 2ii042, 2ii043, 2ii044, 2ii046, 2ii047, 2ii050, 2ii052, 2ii055, 2ii057, 2ii058, 2ii061, 2ii067, 2ii069, 2ii070, 2ii078, 3ii089, 3ii094, 3ii097, 3ii099, 3ii100, 3ii101, 3ii102, 3ii107, 3ii116, 3ii118, 3ii119, 3iii008, 3iii014, 3iii015, 3iii019, 3iii025, 3v006, 3v016, 3v018, 4iv072, 4iv071
Hydrothermal synthesis; 1i017

I
Identification; 3v010
Image analysis; 4iv084
Immobilization; 2ii014, 2ii016, 2ii052, 4iv043, 4iv045
impact prediction; 1i003
Impact evaluation; 1i003
Induction period; 2ii019, 2ii055
Infra red absorption spectra; 3ii104
Inhibitor; 3iii033
Interfacial zone; 4iv050, 4iv051, 4iv053, 4iv056, 4iv084
Interground cements; 1i013, 3v026
Interstitials; 2ii007
Ion exchange resin; 4iv045
Ionic assocoiation, 4iv083
Ions; 2ii036, 2ii046, 2ii065, 3iii012, 3iii013, 4iv075, 4iv079
Iron mud; 1i021
Isomorphism; 1i059

K
Kinetics; 1i005, 1i035, 1i044, 1i052, 2ii019, 2ii023, 2ii028, 2ii043, 2ii055, 3ii098, 3iii008, 4iv076

L
Latex; 3iii008
Leaching; 2ii014, 4iv012, 4iv041, 4iv043, 4iv045
Light microscopy; 3iii031, 3v007
Lignosulphonates; 2ii004, 3iii013, 3iii021
Lime; 2ii049, 2ii074, 3ii084, 3iii005, 4iv010
Limestone; 1i047, 1i048, 2ii022, 4iv018
Long age; 2ii016, 4iv050
Low energy; 1i034, 2ii045
Low temperature; 1i018, 1i029, 1i037, 2ii009, 2ii013, 2ii038, 3iii014, 3v017
Lumos; 2ii079

M
Magnesium chloride; 4iv022
Magnesium sulphate; 4iv022
Magnesium oxide; 1i023, 2ii064, 3v012
Magnesium phases; 1i057
Mass spectroscopy; 3v014
Maturity; 3ii111
Macro Defect Free; 3iii010, 3iii011, 4iv013
Mechanical properties; 3v025
Mechanism; 1i046, 2ii025, 2ii026, 2ii035, 2ii050, 2ii057, 2ii058, 3ii100, 3iii003, 3iii006, 3iii012, 3iii025,, 3v014, 4iv074
Melt; 1i008, 1i011, 1i012, 1i014, 1i029, 1i046, 3v005
Mercury Intrusion Porosimetry; 3ii104
Metakaolin; 3ii113, 3ii114, 4iv011
Method; 2ii021, 3v011, 3v013, 3v016, 3v018, 3v022, 3v023, 4iv081
Microcrack; 4iv021
Microgravity; 2ii075
Microscopy; 1i029, 1i030, 1i039, 1i051, 1i052
Microstructure 1i038, 1i039, 1i047, 1i049, 1i052, 2ii008, 2ii014, 2ii018, 2ii037, 2ii064, 2ii075, 3ii091, 3ii095, 3ii096, 3ii099, 3iii014, 4iv005, 4iv015, 4iv025, 4iv037, 4iv047, 4iv050, 4iv051, 4iv053, 4iv055, 4iv068, 4iv084
Mineralisers in clinker making; 1i028, 1i030, 1i031, 1i033, 1i034, 1i037, 1i050, 3v002
Mineralogy; 1i046, 3ii087, 3ii105
Mineral phase; 1i015, 2ii009, 2ii015, 4iv028
Mixing procedure; 3ii120
Mobility; 2ii065, 4iv083
Modelling; 1i038, 1i044, 1i045, 2ii048, 2ii052, 2ii078, 3ii085, 3ii084, 3iii013, 3v004, 4iv005, 4iv070, 4iv071, 4iv073, 4iv078
Modified cement; 2ii004, 2ii020, 3ii085, 3ii097, 3ii104, 3iii021, 3iii023
Moisture; 2ii079, 3iii011,3v004, 4iv010, 4iv013, 4iv062
Molybdic compounds; 1i054, 1i055
Monosulphate; 2ii056
Mortar; 4iv033

N
Naphtalene Formaldehyde Sulphonate; 3iii003, 3iii009, 3iii030
Nitrate attack; 4iv002
Nodulization in clinker formation; 1i007
Non-equilibrium burning; 1i011
Nuclear Magnetic Resonance; 1i024, 2ii028, 2ii056, 2ii067, 2ii068, 3iii007, 3v001, 3v002, 3v003, 3v004, 3v005, 3v006

O
Oilwell cement; 2ii013, 3iii014
Organic; 3v015
Osmotic pressure; 4iv049

P
Packsetting; 2ii079
Particle size distribution; 1i009, 2ii018, 2ii053, 3ii110, 3v024
Pattern recognitin; 3v010
Penetration; 2ii005, 2ii038, 3ii109, 4iv080
Performance; 4iv073
Permeability; 4iv008, 4iv075
Petroleum coke; 3ii090
pH; 4iv065
Phase composition; 3ii091
Phase diagram; 1i050, 1i052, 2ii024, 2ii057, 2ii058, 4iv066, 4iv074,
Phase transition; 4iv033
Phase transformation; 4iv034
Phosphate; 4iv057
Physical properties; 3v025
Plasticizers; 2ii020
Polymer; 3iii008, 3iii009, 3iii010, 3iii027, 4iv013
Polymorphs; 1i053
Pore size distribution; 4iv077
Pore solution; 2ii036, 3iii003, 3iii013, 3iii022, 3ii091, 4iv040, 4iv069
Pore structure; 2ii037, 2ii066, 3ii111, 3iii009, 3iii018, 3v017, 4iv001, 4iv005, 4iv080
Porosity; 2ii036, 2ii048, 2ii066, 2ii072, 3ii085, 3ii119, 3iii023, 3v017, 4iv006, 4iv007, 4iv008, 4iv013, 4iv017, 4iv024, 4iv040, 4iv048, 4iv054, 4iv078
Portland cement; 3ii107, 3iii006, 3v025, 4iv012
Potentiometry; 4iv083
Powder; 2ii002
Pozzolana; 1i020, 2ii073, 2ii077, 3ii106, 3ii107, 3ii108, 3ii112, 3ii115, 3ii117, 3ii123, 3ii124, 3v001
Pozzolanic cement; 4iv036
Pozzolanic reaction; 3v006
Pozzolanic reactivity; 3ii088
Pre-calciners for clinker making; 1i028
Prehydration; 2ii079
Process parametres; 1i047

Q
Qualitative; 1i004, 3v010, 3v011, 3v015
Quantitative; 1i039, 1i056, 3v007, 3v012, 3v013, 3v015, 3v020
Quartz; 1i048

R
Rapid hardening cement; 2ii017
Rate equations; 1i044
Reaction products; 4iv049
Reactivity; 1i016, 1i018, 1i047, 1i060, 2ii049, 2ii050, 3ii082, 3ii109, 3ii110, 3v020, 4iv016, 4iv050
Refractory; 2ii027, 4iv053, 4iv057
Relative humidity; 2ii073
Residual silica; 4iv049
Retarders; 3iii007, 3iii020, 3iii032
Rheology; 2ii003, 2ii004, 2ii011, 3iii003, 3iii027
Rice husk; 1i019
Rice Husk Ash; 3ii108, 3ii109, 3ii110
Rietveld analysis; 1i039, 1i056, 3v007
Roller compaction; 3ii086
Rotary kiln; 1i007, 1i019

S
Salt scaling; 4iv001
Scanning Electron Microscopy; 1i002, 2ii078, 3ii083, 3ii120, 3iii008, 3v019, 4iv037, 4iv064
Sea water; 4iv025
Secondary ettringite formation; 4iv065
Self deccication; 2ii073
Setting; 1i038, 2ii019, 2ii039, 2ii053, 2ii063, 3ii101, 3ii112, 3iii006, 3iii012, 3iii023, 3iii026, 3v008
Sewage; 3ii123, 3ii124, 4iv038, 4iv039
Shotcreting; 3iii027
Shrinkage; 1i032, 3iii018, 4iv036, 4iv056
Silica; 3ii080
Silica colloid; 3ii106
Silica fume; 2ii037, 3ii105, 3ii106, 3ii110, 3ii116, 3ii120, 3v001, 4iv014, 4iv069
Silica modulus; 1i035
Silicate; 2ii060, 3iii027, 4iv065
Simulation; 2ii078, 3iii001
Sintering; 1i005, 1i007, 1i022, 1i032
Slag; 1i020, 3ii080, 3ii092, 3ii094, 3ii097, 3ii100, 4iv050, 4iv051, 4iv058
Slump loss; 3iii003, 3iii020
Sodium chloride; 4iv022
Solid solution; 1i014, 1i023, 1i057, 2ii059, 1i060, 3v009
Solid state reactions; 1i042
Solidification; 4iv042
soluble glass; 2ii033

Sorption isotherms; 4iv077
Specific surface; 3iii028
Spectrophotometry; 3v012
Stability; 4iv065
Stabilization; 1i016, 2ii045, 4iv041
Standards; 3v025
Steam curing; 3ii102, 4iv036, 4iv063
Steel; 4iv014, 4iv082
Steric repulsive force; 3iii001
Strain softening; 2ii075
Strength; 1i048, 1i058, 3ii109, 4iv057
Strength development; 1i029, 1i038, 1i041, 2ii007, 2ii017, 2ii018, 2ii033, 2ii051, 2ii053, 2ii054, 2ii060, 2ii063, 2ii072, 2ii076, 2ii077, 3ii085, 3ii089, 3ii097, 3ii111, 3ii117, 3ii119, 3ii121, 3iii004, 3iii026, 3iii028, 3iii029, 3v024, 4iv024, 4iv052, 4iv054, 4iv055, 4iv056, 4iv058, 4iv063
Strength retrogression; 4iv019
Stress; 4iv049
Structure; 1i005, 1i014, 1i056, 2ii054, 2ii066, 2ii067, 2ii068, 2ii069, 2ii076, 4iv007, 4iv025, 4iv042, 4iv043, 4iv075
Sucrose; 3iii006
Sulphate; 1i049, 2ii012
Sulphate attack; 4iv002, 4iv018, 4iv020, 4iv021, 4iv024, 4iv057, 4iv059
Sulphate resistance; 3iii004, 3iii015, 4iv017, 4iv019, 4iv023
Sulphoaluminate; 1i001, 1i025, 2ii029, 3iii026, 3v009, 4iv029, 4iv030, 4iv068
Sulphoaluminoferrite; 1i014
Superplasticizers; 2ii002, 2ii004, 3iii001, 3iii002, 3iii019, 3iii020, 3iii021, 3iii030, 4iv001
Support; 2ii015
Synthesis; 1i015, 1i024, 1i033, 2ii064, 3ii113

T
Temperature; 1i005, 1i007, 1i008, 1i012, 2ii021, 2ii023, 2ii026, 2ii043, 2ii066, 3iii002, 3iii029, 3v001, 4iv047, 4iv060, 4iv068, 4iv069
Terminology; 4iv046
Texture; 1i048
Thawing; 4iv033
Thermal stress; 4iv072
Thermal treatment; 1i027
Thermodynamics; 1i042, 2ii024, 2ii057, 2ii058, 2ii059, 2ii062, 2ii066, 4iv039, 4iv066
Thermogravimetry; 2ii049, 3ii105, 3iii011 4iv003, 4iv037
Thermoporosimetry; 3v017
Tobermorite; 2ii064, 2ii065, 3v003
Trace components; 1i021
Transmission Electron Microscopy; 2ii068
Tricalcium silicate; 1i049 2ii041, 2ii044

U
Unreacted core model; 2ii051

V
Vibration; 2ii017
Viscosity; 1i014, 1i032, 2ii001, 2ii003, 2ii005
Void spacing factor; 3v024
Volume change; 2ii009, 2ii039, 2ii071, 2ii072, 4iv031

W
Waste disposal; 4iv012
Waste material utilization; 1i010, 1i019, 1i022, 1i025, 1i026, 1i027, 1i033, 2ii052, 3ii081, 3ii093, 3ii101, 3ii116, 3ii118, 3ii119, 3ii121, 3ii123, 3ii124, 3v003, 3v013, 4iv014, 4iv024
Water; 4iv075
Water sorption; 4iv008
Water suction; 4iv008, 4iv011, 4iv078
Water-to-cement ratio; 2ii071
Waterglass; 3ii092
Wedge splitting; 2ii075
White Portland Cement; 3iii004
Workability; 2ii011, 3iii029

X
X-ray Diffraction Analysis; 1i051, 1i016, 2ii041, 3iii028, 3ii087, 3ii114, 3v008, 4iv003
X-ray Fluorescense Analysis; 3v011
X-ray Powder Diffraction; 1i002, 1i010, 1i056, 2ii065, 4iv018

Z
Zeolites; 1i020, 1i024, 4iv028, 4iv045, 4iv046
Zeta potential; 3iii001, 3iii002

S 424 -10.3-

Proceedings of the 10th International Congress on the Chemistry of Cement : Volume 3: Additives, admixtures, characterisation techniques
<Hrsg.>: Justnes, Harald
Göteborg (1997)

Inventarnr. 50206

Entleiher	Ausleihdatum
~~Dr. Hübner~~	~~05. SEP. 1997~~
~~Dr. Spanka~~	
~~Dr. Schneider~~	
~~Rickert~~	~~23.10.00~~
~~Figge~~	~~10.10.2006~~
~~Schmidt, Ms.~~	~~03.07.08~~
~~Runge~~	~~29.01.10~~

PROCEEDINGS OF THE 10TH INTERNATIONAL CONGRESS ON THE CHEMISTRY OF CEMENT
Gothenburg, Sweden, June 2-6, 1997

VOLUME 4

PERFORMANCE AND DURABILITY OF CEMENTITIOUS MATERIALS

10th
ICCC
Göteborg 1997

Edited by

Dr. Harald Justnes
SINTEF Civil and Environmental Engineering, Cement and Concrete
Trondheim, Norway

Published by Amarkai AB and Congrex Göteborg AB in 1997

Copyright © Amarkai AB and Congrex Göteborg AB

All rights reserved. No part of this publication may be reproduced, stored in a retrieval system, or transmitted in any form or by any means, electronic, mechanical, photocopying, recording or otherwise without prior permission of the publishers.

Inform Trycket AB, Göteborg 1997
ISBN 91-630-5498-1

List of contents for Volume 4

IV PERFORMANCE AND DURABILITY OF CONCRETE AND CEMENT BASED SYSTEMS

IV.A Pore structure, chemical interactions and their influence on permeability and diffusivity of gases (e.g. carbon dioxide), liquids (e.g. water) and dissolved ions (e.g. chlorides)

E. Lang, J. Geiseler: "Utilization of High Slag Blastfurnace Cement for High-Performance Concrete - Influence of Pore Structure and Permeability", 4iv001, 4 pp

G. Balázs, E. Csányi, F. Tamás: "Effect of Air Pollution on Portland Cement Concrete - Case Studies and Model Experiments", 4iv002, 8 pp

Mª T. Gaztañaga, S. Goñi, A.Mª Guerrero, Mª S. Hernandez: "Carbonation of Hydrated Calcium Aluminate Cement and Ordinary Portland Cements of Varying Alkali Content", 4iv003, 8 pp

S. Goñi, C. Alonso, E. Menendez, A. Hidalgo, C. Andrade: "Microstructural Characterization of the Carbonation of Mortar made with Fly Ashes", 4iv004, 8 pp

S. Matala: "Carbonation Mechanism in the Granulated Blast Furnace Slag Concrete", 4iv005, 10 pp

S. Pagliolico, L. Cussino, F. Curcio, R. Ferrari : "Effect of the Carbonation on a 54-Year Old Concrete Road Pavement", 4iv006, 6 pp

A. Beeldens, D. Van Gemert, E. De Winne, B. De Blaere, C. Caestecker, M. Van Messem: "Structure and Performance of Porous Concrete", 4iv007, 8 pp

D. Fairhurst, A.K. Platten: "The Unsaturated Mass Transfer through Hardened Cement Paste Modified by the Partial Replacement with Silica Fume: The Sorptivity and Vapour Phase Transport", 4iv008, 8 pp

D. Fairhurst, A.K. Platten: "Moisture Distributions and the Hydraulic Diffusivity of Hardened Cement Pastes Modified by Partial Replacement with PFA and GGBS", 4iv009, 4 pp

K. Van Balen, C. Van Den Brande, E.E. Toumbakari, D. Van Gemert: "Influence of Moisture Content on the Effective Diffusion Coefficient in Lime Mortars with Different Porosities", 4iv010, 9 pp

W.J. McCarter, D. Watson: "Desorption and Infiltration within the Surface Region of Exposed Concrete", 4iv011, 4 pp

H.P. Unsworth, J.S. Lota, F.H. Hubbard, R.K. Dhir: "Microstructural and Chemical Changes During Leaching of Cementitious Materials", 4iv012, 4 pp

S. Harsh, S.K. Handoo, S.C. Ahluwalia: "Investigations on Moisture Absorption and its Effect on the Performance of HAC Based MDF Cement", 4iv013, 4 pp

H.A. El-Sayed, A.H. Ali, B.A. El-Sabbagh: "Effect of Microsilica Incorporation in Concrete on the Corrosion Protection of Embedded Reinforcement", 4iv014, 8 pp

J. Deja: "Chloride Resistance of the Pastes and Mortars Containing Mineral Additives", 4iv015, 8 pp

U. Wiens, P. Schiessl: "Chloride Binding of Cement Paste Containing Fly Ash", 4iv016, 10 pp

IV.B Physio-chemical (e.g. sulphates), thermal (e.g. freeze-thaw) and biological degradation, including environmental and synergistic effects

R. Sersale, R. Cioffi, B. de Vito, G. Frigione, F. Zenone: "Sulphate Attack of Carbonated and Uncarbonated Portland and Blended Cement Mortars", 4iv017, 7 pp

W.G. Piasta, Z. Sawicz, G. Koprowski, Z. Owsiak: "Influence of Limestone Powder Filler on Microstructure and Mechanical Properties of Concrete under Sulphate Attack", 4iv018, 8 pp

Z. Giergiczny: "Sulphate Resistance of Cements with Mineral Admixtures", 4iv019, 4 pp

D. Križan, B. Živanović: "Resistance of Fly-Ash Blended Cement Mortars to Sulphate Attack", 4iv020, 4 pp

D. Nazarsky: "Deformation and Microcracking of Concrete Loaded in Sulphate Environment", 4iv021, 4 pp

D. Bonen: "The Microstructure of Concrete Subjected to High-Magnesium and High-Magnesium Sulphate Brine Attack", 4iv022, 8 pp

S.R. Miletić, M.R. Ilić: "Effect of Ammonium-Sulphate Corrosion on the Strength of Concrete", 4iv023, 8 pp

A. Mª Guerrero, MªS. Hernandez, S. Goñi: "Reaction between Simulated Sulphate Radioactive Liquid Waste and Cement Based Materials", 4iv024, 7 pp

K. Scrivener, M. Lewis, J. Houghton: "Microstructural Investigation of Calcium Aluminate Cement Concrete from Structures", 4iv025, 6 pp

A.M. Dunster, N.J. Crammond: "Alkaline Hydrolysis with Carbonation in High Alumina Cement Concrete Beams", 4iv026, 7 pp

W. Kurdowski, S. Duszak, B. Trybalska: "Behaviour of the Paste Rich in Hydrogarnet and Gibbsite in Chloride Solution", 4iv027, 8 pp

C. Lu, R. Li: "Resistance to Chemical Attack of High Performance FKJ Concrete", 4iv028, 8 pp

M. Su,Y. Wang, L. Zhang, D. Li, M. Deng: "Preliminary Study on the Durability of Sulfo/Ferro-Aluminate Cements", 4iv029, 12 pp

Y. Wang, S. Li, M. Su, J. Xu, F. Zhang: "Sulpho-Aluminate Cement with Low Alkalinity", 4iv030, 4 pp

J. Stark, S. Stürmer: "Investigation of Compatibility of Cements with Several Salts", 4iv031, 4 pp

Q. Yang, X. Wu, S. Huang: "Concrete Deterioration due to Physical Attack by Salt Crystallization", 4iv032, 5 pp

V. Penttala: "Dilation and Phase Transitions in Mortar During Cooling", 4iv033, 9 pp

J. Stark, H.M. Ludwig: "Influence of C_3A Content on Frost and Scaling Resistance", 4iv034, 8 pp

J. Stark, H.-M. Ludwig: "Freeze-Thaw and Freeze-Deicing Salt Resistance of Concretes Containing Cement Rich in Granulated Blast-Furnace Slag", 4iv035, 8 pp

S.A. Zoubekhine, B.E. Ioudovitch: "Non Shrinkage Frost Resistant Pozzolanic Cement", 4iv036, 4 pp

M. Ribas Silva, L. A. M. Garcia: "Microbiological Identification of Microorganisms Responsible for Degradation of Concrete", 4iv037, 4 pp

K. Hormann, F.J. Hofmann, M. Schmidt: "Stability of Concrete Against Biogenic Sulfuric Acid Corrosion - A new Method for Determination", 4iv038, 4 pp

V.I. Babushkin, A.A. Plugin, D.Yu. Zelensky, G.Ya. Drozd: "Concrete of Sewage Collectors and Their Protection: Corrosion Mechanism ", 4iv039, 4 pp

J. Madrid, J.M. Diez, S. Goñi, A. Macias: "Durability of Ordinary Portland Cement and Ground Granulated Blast Furnace Slag Cement in Acid Medium", 4iv040, 9 pp

F.M. Miller, W.A. Klemm: "Mechanistic Considerations for the Efficiency of Portland Cement in Waste Stabilization", 4iv041, 9 pp

C. Shi, J. Stegemann, R. Caldwell: "Use of Heat Signature in Solidification Treatability Studies", 4iv042, 4 pp

W. Nocuń-Wczelik, J. Małolepszy: "Study on the Immobilization of Heavy Metals in Cement Paste - C-S-H Leaching Behaviour", 4iv043, 8 pp

A. Risch, H. Pöllmann, M. Ecker: "Application of Portland Cement and High Alumina Cement for Immobilization/Solidification of a Waste Model Composition", 4iv044, 8 pp

S. Bagosi, L.J. Csetenyi: "Immobilisation of Cs-loaded ion Exchange Resins in Zeolite-Cement Blends", 4iv045, 8 pp

IV.C Cement aggregate compatibility (e.g. alkali-aggregate reactions) and structure↔performance relationships

P. V. Krivenko: "Alkaline Cements: Terminology, Classifications, Aspects of Durability", iv046, 6 pp

A.K. Mullick, G. Samuel, R.C. Wason, S.K. Sinha: "Thermal Activation of Alkali Silica Reaction in Concrete", 4iv047, 8 pp

Y. Kihara: "The Influence of Carbonation of the Akali-Aggregate Reaction Mechanism", 4iv048, 4 pp

V. Michaud, A. Nonat, D. Sorrentino: "Experimental Simulation of Mechanisms Involved in the Building of Stresses in Concrete Subjected to Alkali-Silica Reaction", 4iv049, 9 pp

B. Marchese, G. Frigione: "Interfacial Long Age Reactivity of Slag/Clinker Compacts", 4iv050, 8 pp

S.-i. Igarashi, M. Kawamura, N. Arano, S. Kawaguchi: "Alkali Reactivity of High-Carbon Ferrochromium Slag and its Applicability as an Aggregate for Concrete", 4iv051, 4 pp

K.K. Sideris, A.E. Savva, K.D. Baltzopoulou, C.M. Economou, K. Sideris: "Influence of Silica and Limestone Aggegates on the Final Compressive Strength of Blended Cement Concretes prepared with the Use of Three Different Pozzolanas", 4iv052, 6 pp

O.V. Rybakova, A.R. Krivoborodov: "Effect of Aluminous Clinker as Aggregate on Microstructure of Interfacial Zone in Refractory Concrete", 4iv053, 4 pp

T.S. Um, H.K. Oh, S.H. Choi: "The Synthesis and Behaviour of Calcium Silicates-Fibers Composites", 4iv054, 5 pp

M.-Y. Jeong, J.-T. Song: "The Mechanical Properties of Alkali Resistance Glass Fibre Reinforced Concrete under Different Curing Conditions", 4iv055, 4 pp

V. Glukhovskiy, Y. Biryukovich, N. Mikhailishina, T. Dashkova: "Peculiar Features of Contact Zone Formation between Cement Paste and Vitreous Silicate Filler", 4iv056, 4 pp

S.C. Sharma, S. Chaturvedi: "Effect of Addition of Phosphate Bearing Materials on Strength Development Characteristics of High Temperature Refractory Concrete", 4iv057, 4 pp

Y. Bazhenov, S. Pavlenko: "Physico-Mechanical and Deformation Properties of Cementless Fine-Grained Ash-Slag Concrete over a 5-Year Period", 4iv058, 6 pp

IV.D Influence of physico-chemical aspects during early material history on durability (e.g. high curing temperature → secondary ettringite formation)

W.A. Klemm, F.M. Miller: "Plausibility of Delayed Ettringite Formation as a Distress Mechanism - Considerations at Ambient and Elevated Temperatures", 4iv059, 10 pp

S. Kelham: "Effects of Cement Composition and Hydration Temperature on Volume Stability of Mortar", 4iv060, 8 pp

K. Scrivener, M. Lewis: "Microstructural and Microanalytical Study of Heat Cured Mortars and Delayed Ettringite Formation", 4iv061, 8 pp

J. Stark, K. Bollmann: "Ettringite Formation - A Durability Problem of Concrete Pavements", 4iv062, 8 pp

G. Camarini, M.A. Cincotto: "Delayed Ettringite Formation in Steam Cured OPC and Slag Cement Pastes and Its Effects on Mortar Compressive Strength", 4iv063, 4 pp

I. Meland, H. Justnes, J. Lindgård, S. Smeplass: "Durability Problems Related to Delayed Ettringite Formation and/or Alkali Aggregate Reactions", 4iv064, 8 pp

V. Michaud, A. Nonat, D. Sorrentino: "Experimental Simulation of the Stability of Ettringite in Alkali Silica Solutions, Produced by Alkali-Silica Reaction, in Concrete", 4iv065, 9 pp

D. Damidot, F.P. Glasser: "Thermodynamic Imvestigation of the CaO-Al_2O_3-$CaSO_4$-$CaCl_2$-H_2O System at 25°C and the Influence of Na_2O", 4iv066, 8 pp

S.K. Handoo, S. Argarwal, S.K. Argarwal, S.C. Ahluwalia: "Effect of Temperature on the Physico-Chemical and Mineralogical Characteristics of Hardened Concrete", 4iv067, 4 pp

C.-K. Park, B.-K. Kim, S.-Y. Hong, G.-Y. Shin, H.-K. Oh: "Microstructural Change of Calcium Sulphoaluminate Cement Paste due to Temperature", 4iv068, 6 pp

C.K. Larsen, J. Tritthart: "Effect of Temperature on Chloride Ingress and Chloride Binding in Hardened Cement Paste", 4iv069, 9 pp

IV.E Modelling and mechanisms of degradation processes

N. R. Buenfeld, N.M. Hassanein, G.K. Glass: "Neural Networks for Modelling the Influence of Cement Chemistry on Concrete Durability", 4iv070, 8 pp

V.L. Chernyavski, V.Y. Dubnitsky: "The Investigation of Cement Concrete Corrosion by an Imitation Model", 4iv071, 9 pp

F. Tomosawa, T. Noguchi, C. Hyeon: "Simulation Model for Temperature Rise and Evolution of Thermal Stress in Concrete Based on Kinetic Hydration Model of Cement", 4iv072, 4 pp

A.K. Platten, Z. Huang, J. Roberts: "Computer Modelling of Thermal Performance of Reinforced Concrete Subjected to Fire", 4iv073, 4 pp

R. Dron, F. Brivot, T. Chaussadent: "Mechanism of the Alkali-Silica Reaction", 4iv074, 8 pp

A.N. Plugin, I.G. Prokopova, S. Wild, A.A. Plugin: "The Mechanism of Water and Ionic Permeability of Concrete", 4iv075, 8 pp

C. R. Schweizer, A.C. Johnson, P. Baccini: "The Degradation of Calcium Silicate Hydrates (CSH): A Kinetic Study", 4iv076, 8 pp

A. Xu: "Adsorption Isotherm of Concrete", 4iv077, 8 pp

O. Francy, S. Bonnet, R. François, B. Perrin: "Modelling of Chloride Ingress into Cement-based Materials due to Capillary Suction", 4iv078, 8 pp

A.F. Bernatsky: "Electrical Properties of Cement", 4iv079, 3 pp

IV.F Life cycle analyses and input parametres

R.N. Swamy: "The Myths and Misconceptions of Chloride Penetration into Concrete", 4iv080, 7 pp

H. Justnes, E. Rodum: "Chloride Ion Diffusion Coefficients for Concrete - A Review of Experimental Methods", 4iv081, 10 pp

M^{a}C. Alonso, C. Andrade, M. Castellote: "The Influence of the Electrical Potential in the Chloride Threshold for Rebar Depassivation", 4iv082, 8 pp

A. Hidalgo, C. Andrade, S. Goñi, C. Alonso: "Single Ion Activities of Unassociated Chlorides in NaCl Solutions by Ion Selective Electrode Potentiometry", 4iv083, 9 pp

A.G. Constantinou, K.L. Scrivener: "Corrosion of Steel in Carbonated Concrete", 4iv084, 8 pp

TOPIC IV.A

Pore structure, chemical interactions and their influence on permeability and diffusivity of gases, liquids and dissolved ions

UTILIZATION OF HIGH SLAG BLASTFURNACE CEMENT FOR HIGH-PERFORMANCE CONCRETE - INFLUENCE OF PORE STRUCTURE AND PERMEABILITY

Eberhard LANG and Jürgen GEISELER, Forschungsgemeinschaft Eisenhüttenschlacken, Duisburg, Germany

Abstract Blastfurnace slag cement has been demonstrated to possess very good properties when utilized as binder for High Performance Concrete (HPC). The porosity of this concrete is very low and the impermeability against organic chemical liquids is very high. HPC is an excellent material for catchment tanks in the chemical industry. Due to its low porosity the freeze-thaw and deicing agent resistance is very high without artificial air voids.

Keywords: Blastfurnace slag, Pore structure, Salt scaling, Superplasticizers,

INTRODUCTION

Results of laboratory investigations as well as long experiences in practice indicate the special benefits of blastfurnace slag cements. This is because of their comparatively low capillary porosity, their high resistance against sulphate attack, against alkali-aggregate reaction and to the diffusion of chlorides into the concrete. Recent research has also shown a high binding capacity of chlorides in blastfurnace slag cement pastes. A further aspect of importance for the corrosion protection of reinforcecement is the comparatively low electrical conductivity of concrete made with blastfurnace slag cement. Due to their low heat of hydration, blastfurnace slag cements help to prevent cracks in concrete structures resulting from temperature stresses at early ages (Weber et al. (1991); Geiseler, Kollo, Lang (1995); Geiseler, Lang (1994)).

EXPERIMENTAL DETAILS

Materials

Blastfurnace slag cement CEM III/A 42,5 (slag content of 50%) and CEM III/B 32,5 (slag content of 77%) were used. Silica fume was used in form of a slurry with a water content of 50%. The coarse and fine aggregates consisted of natural gravel and sand from the Rhine area and crushed air-cooled blastfurnace slag with a particle size distribution of 2/8 mm and 8/16 mm. Different types of superplasticizers were used and this paper highlights the use of superplasticizer based on sulfonated melamine formaldehyde, naphthalene sulfonated polymer, lignosulfonates and poly-carboxylate.

Test Methods

The mortars were tested in accordance with the EN 196 and concrete in accordance with the German standard DIN 1048. The pore size distribution was measured by a Mercury pressure porosimeter series 4000 by Carlo Erba in the range 1.85 to 7500 nm radius. The freeze-thaw and deicing salt resistance of concrete was determined according to Rilem draft recommendation for test method for the freeze-thaw-resistance - tests with sodium chloride solution - CDF (Capillary suction of Deicing solution and Freeze thaw test), RILEM (1995).

The impermeability was tested by a method of the DAfStb (1992). The samples were drilled cores with a length of 150 mm and diameters of 80 mm. These were stored in water at 20°C for seven days and then stored until 56 days at 20 °C and 65% relative humidity. In order to achieve a one-dimensional transport process the cores were sealed at their circumferential surfaces. During the test the burette was filled rapidly with the test liquid to a level of 500 mm above the

sample, and the exact initial level recorded from the graduations. During the subsequent 72-hours test the quantity of liquid which had penetrated could be observed at time intervals which allowed the rate of absorption to be determined.. After 72 hours the cores were unwrapped and split parallel to the longitudinal axis, and the visible penetration front of the liquid was recorded.

RESULTS AND DISCUSSION

Selection of Superplasticizer

From mortar tests the optimal type of superplasticizer for CEM III were selected. Figure 1 shows the influence of the w/c-ratio of different superplasticizers. All these mortars had the same consistence than the normalized mixture with a w/c-ratio of 0.50. Some plasticizer reduced the w/c-ratio in combination with silica fume more than other. In combination with high slag blastfurnace cements superplasticizer based on naphthalene sulfonated polymers showed optimal results with reference to the workability, strength development and modulus of elasticity, for instance FM 1. The water-reducing ability of Ca-lignosulfonates was lower and the early strength was very low in comparison with all the other types of plasticizer. But generally the strength after 28 days is higher and especially the heat of hydration is reduced.

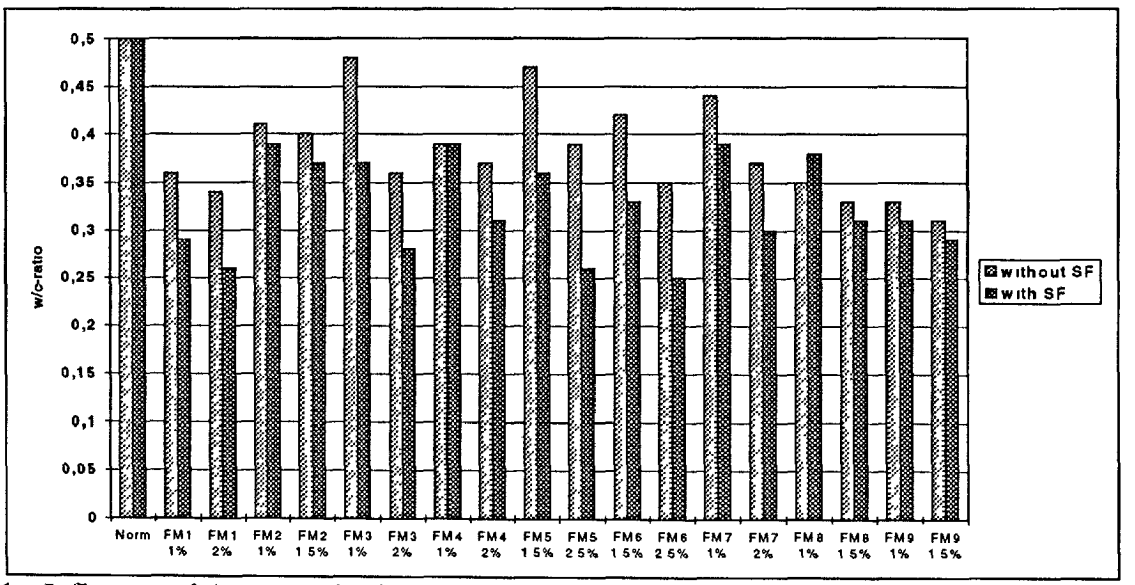

Fig 1 Influence of the superplasticizer of the w/c-ratio of CEM III/B 32,5 with and without silica fume

A statistical series of tests was used to find the optimal content of plasticizer and silica fume for different properties of the cement mortar. Figure 2 (for instance) shows the results of CEM III/A 42,5. Using these results it is possible to minimize the content of silica fume and plasticizer in relation to the desired properties. HPC with high slag blastfurnace cement can be produced without silica fume if the demand for the early strength after two days is lower than 35 MPa. Aptitude tests are necessary.

Porosity

Figure 3 shows the different pore size distribution of CEM IIII/A 42,5 with the superplasticizer FM 1 and two different contents of silica fume. The workability of these four mortars were the same. The capillary porosity > 30 nm was reduced with and without silica fume in the same range. The age of the samples was 28 days. The change of pore size distribution after 28 days is very low.

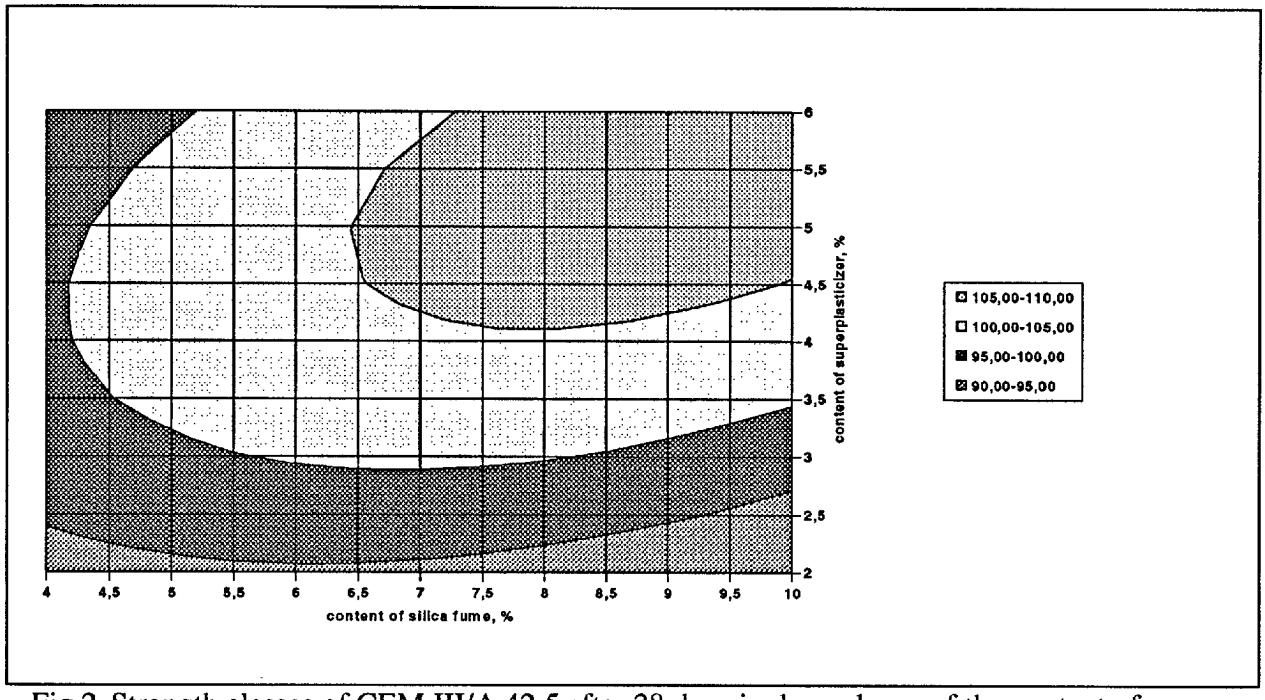

Fig 2 Strength classes of CEM III/A 42,5 after 28 days in dependence of the content of superplasticizer and silica fume

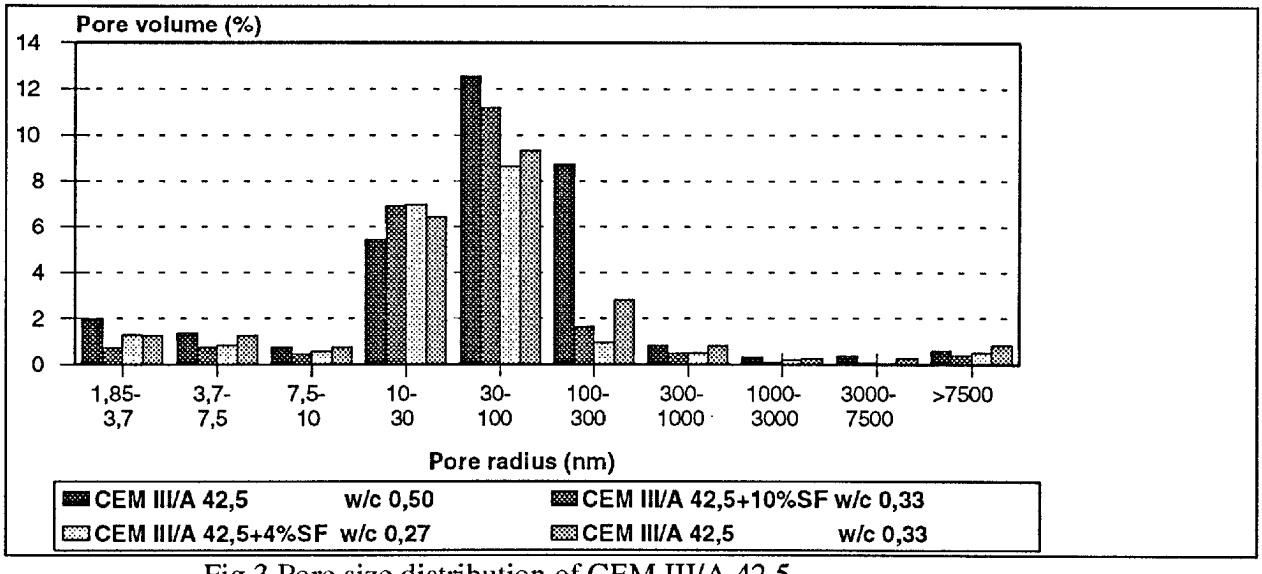

Fig 3 Pore size distribution of CEM III/A 42,5

Impermeability to organic liquids

The chemical industry catchment tanks made of uncoated concrete are secondary retaining barriers for limited periods of time (in general ≤ 72 hours) if the storage tank is damaged. The capillary porosity of concrete with blastfurnace slag cement is lower than of concrete with Portland cement and the chemical resistance in general is higher. Thus a lot of catchment tanks in Germany have been constructed with blastfurnace slag cement. It is for this application why the impermeability of HPC was tested. The research on this field is continuing. Figure 4 gives first results for the penetration depth of 4 different chemical liquids. The ordinary concrete has a cement content of 320 kg/m³ and a water/cement-ratio of 0.50.

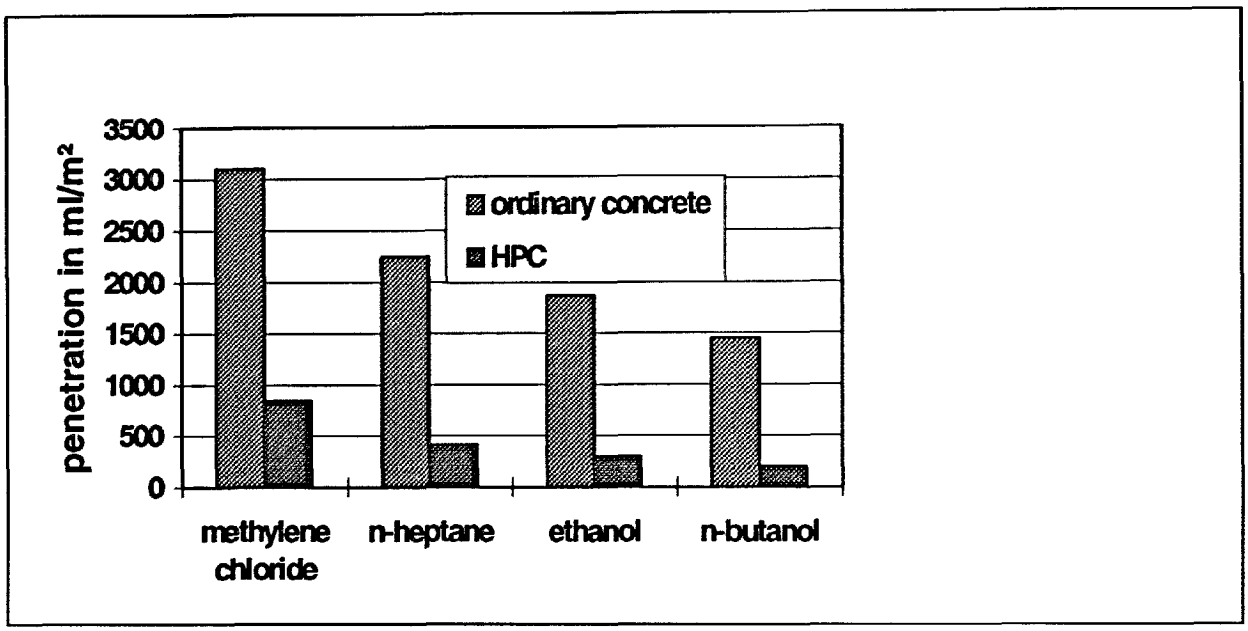

Fig 4: Impermeability of ordinary and high performance concrete

Freeze-Thaw-Resistance

The scaling of ordinary concrete with CEM III/A 42,5 tested by CDF with 3% NaCl-solution ranged between 1000 and 1500 g/m² and for CEM III/B 32,5 between 1500 and 2500 g/m². The scaling of HPC with CEM III/A 42,5 is lower than 300 g/m² and for CEM III/B 32,5 is lower than 1500 g/m². In practice, concretes with blastfurnace slag cements are known to have adequate freeze-thaw resistance having been observed in many sewage clarification plants and waterway constructions in marine environments.

CONCLUSION

All types of blastfurnace slag cements may be used for high performance concrete. The low capillary porosity of concrete made with blastfurnace slag cements is further decreased in HPC significantly but only marginally by the additional use of silica fume. This is the reason why the impermeability of concretes is improved in the same sequence. HPC made with blastfurnace slag cement has a high freeze-thaw-resistance even without air-entraining agents.

REFERENCES

DAfStb - Deutscher Ausschuß für Stahlbeton: „Richtlinie für Betonbau beim Umgang mit wassergefährdenden Stoffen" Deutsches Institut für Normung e.V. (1992) 9.

DIN EN 196 : 1990-03, Methods of testing cement.

DIN 1048 : 1991-06, Prüfverfahren für Beton, Part 1-5.

Geiseler, J.; Kollo, H. and Lang, E.: „Influence of Blastfurnace Cements on Durability of Concrete structures", ACI Materials Journal, Vol. 92, No. 3, May-June, 1995, pp. 252-257.

Geiseler, J. and Lang, E.: „Long-term durability of non-air-entrained concrete structures to marine environments and freezing and thawing cycles", Third CANMET/ACI International Conference on Durability of Concrete, Nice, 1994, Supplementary Papers, pp. 715-737.

RILEM: „Draft Recommendation for test method for the freeze-thaw resistance of concrete - Test with water (CF) or with sodiumchloride solution (CDF)", Materials and Structure, 1995, No. 28, pp. 175-182.

Weber, R. et al: „Hochofenzement - Eigenschaften und Anwendung im Beton", Beton-Verlag, 1991.

Effect of Air Pollution on Portland Cement Concrete — Case Studies and Model Experiments

György BALÁZS*, Erika CSÁNYI*
Ferenc TAMÁS**

*Technical University, Dept. of Building Materials, Budapest, Hungary
**University of Veszprém, Dept. of Silicate- and Materials Engineering, Veszprém, Hungary

ABSTRACT
The degree and the effect of the incorporation of air polluting agents (primarily SO_2 and NO_2) into concrete was investigated, partly by case studies (old concrete structures in chemical-industrial zones or on busy highways), and partly by laboratory tests, on paste and mortar specimens made of different cements and subjected to different atmospheres. Results indicate considerable increase of sulfates in the external layers of concrete structures. Highest sulfate uptake (and lowest pH) was observed in case of concrete incorporating blastfurnace slag.

Key-words: air pollution, acid attack, sulfate attack, nitrate attack, case studies

INTRODUCTION
Worldwide urbanisation and industrialisation cause an increase of some conventional components of the air (e.g. carbon dioxide), and of some polluting ingredients (e.g. sulfur and nitrogen oxides). These affect not only human health, but may have deteriorating effects even on materials considered durable, such as concrete. Several air pollution maps exist (in Hungary air pollution is monitored and mapped by the National Health Authority). According to these data, the most important pollutants - from the point of concrete - are the sulfur and nitrogen oxides, which acidify the air (rainwater of pH = 4 is by no means an exception), and these acid constituents can get into the concrete by dry or wet precipitation through capillaries. The effect of dusts and aerosols is indicrect.

Several researchers have dealt with the response of concrete to the increase of air-CO_2 (Junge, 1963; Levelook, 1971) and other pollutants (Scholl and Knöfel, 1991; Weawer, 1988), and even equations have been derived to predict the mechanism of deterioration (Hensel, 1985). The authors' first observation regarding this topic was when crumpling concrete cover of a concrete railway bridge was investigated and found its gypsum content to be the sevenfold of the original quantity, introduced by the raw materials. The bridge was in the vicinity of a sulfuric acid factory. After this first observation, phenomena has been investigated by case studies and model experiments.

CASE HISTORIES
Table 1. shows some data on old (older than 20 years) reinforced concrete structures being in the vicinity of industrial zones or mass traffic highways. (Percentages in the table refer to cement weight). Some general conclusion can be drawn from these results.

Sulfate (SO_4^{--}) content was the highest in the external layers (less than 1 cm) of the concrete. It was not rare that the quantity of SO_4^{--}-ions here was here three times the normal. In case of low-strength concrete structures, or those being within polluting chemical plants, sulfates were concentrated in the deeper zones (this could be partly attributed to the action of rainwater too).

It is hard to estimate the role of age/strength interrelationships, but it is a fact that the highest SO_4^{--}-concentration was measured in the external layer of the oldest structure.

The structure being most remote from sources of pollution (the Dömös column foundation) showed - in spite of its age - practically no increase of the sulfate content. The nitrate (NO_3^-)-concentration of the structures was considerable in the external layers only, with the exception of a column in a chemical factory, where it was quite high, even in the deeper layers.

Table 1.
Investigation of material drilled from various concrete structures

Structure	Depth of layer [mm]	Bulk density [kg/m^3]	Compr. strength [MPa]	Water uptake [mass %]	pH	SO_4^{--} [%]	NO_3^- [%]
Highway bridges							
Sajó bridge (Industrial zone, NE Hungary (age: 35 years)	0- 10				11.7	7.5	0.08
	10- 20				11.7	4.0	0.07
	20- 30				11.9	2.2	<0.01
	60-100			5.6			
	100-160	2200	29,0				
Nyíregyháza, Ér-patak bridge (age: 45 years)	0- 10				9.2	6.1	<0.01
	10- 20				9.3	5.3	<0.01
	20- 30				9.6	2.7	<0.01
	60-100			5.5			
	100-160	2150	18				
Győr (Highway No. 1. flyover (age: 24 years)	0- 10				11.0	4.5	0.05
	10- 20				11.9	6.2	<0.01
	20- 30				12.0	3.4	<0.01
	60-100			5.5			
	100-160	2320	34				
Fences, columns							
Budapest (Highway No. 2) Fence (age: 90 years)	0- 10				10.0	14.0	0.05
	10- 20				10.8	4.9	0.06
	20- 30				11.9	4.3	<0.01
	60-100			4.9			
	100-160	2280	36				
Tokodaltáró (Highway No. 10), transmission line column (age: 60 years)	0- 10				10.9	8.2	<0.01
	10- 20				11.5	3.9	<0.01
	20- 30				11.8	2.7	<0.01
	60-100			6.5			
	100-160	2200	15				
Dömös, transmission line column foundation (age: 60 years)	0- 10				10.8	3.8	<0.01
	10- 20				10.8	3.0	<0.01
	20- 30				11.3	3.1	<0.01
	60-100			7.5			
	100-160	2080	11.5				

Chemical industry plant

BORSODCHEM Ltd.	0-10				8.3	13.5	6.8
Industrial zone, NE-Hungary	10-20				8.3	9.9	6.6
(column in a workshop)	40-50				8.4	4.4	6.3
(age: 30 years)							

Comparing pH values in the various layers it can be concluded that pH is the lowest in the oldest and crumpled (i.e. low strength) layers. This decrease can be mostly attributed to carbonation, although, in heavily polluted areas other acid media can affect the concrete.

MODEL TESTS

Description of the tests

Starting from industrial raw materials, (ground to 350 m^2/kg Blaine) three sorts of cements were made by a thorough mixing and homogenisation:

- Ordinary Portland cement (OPC)
- Blastfurnace slag-cement, with 40% slag (BFSC)
- Fly-ash cement, with 20% fly ash (FAC)

Prismatic specimens (size 10 × 10 × 50 mm) were made of cement paste (W/C = 0.4) and of mortar (W/C = 0.5, sand fineness max 1 mm). Specimens were removed from the mould after 24 hours and stored in room temperature, 100% R.H. space for 28 days. After that four sides of the mortar prisms were coated with an epoxy paint and all specimens transferred to experimental chambers, containing the following atmospheres:

200 ppm SO_2
80 ppm NO_2
3 vol.% CO_2
air.

The gas mixtures were kept in motion by a fan.

Results with paste specimens

pH values of paste prisms change only slightly, even after 90 days of exposure. **Table 2** shows results. Although changes are slight, it still can be observed that CO_2 affects pH to the highest extent.

Table 2. pH of paste prisms after 90 days of exposure

Type of cement	Starting pH	Curing atmosphere			
		air	CO_2	SO_2	NO_2
OPC	13.05	12.71	12.48	12.65	12.55
BFSC	13.00	12.59	12.00	12.52	12.46
FAC	13.06	12.70	12.39	12.56	1257

The change of sulfate-ion quantity in function of time is shown in **Fig 1**. Independently on cement type, it slightly increases in the beginning; the rate of increase is higher between 90 and 180 days. This increase, at the end of the experiment, was approx. 2.5-, 3- and 6-fold, for FAC, OPC and BFSC, respectively. A yellowish-white salt efflorescence was observed after 90 days in OPC and BFSC pastes; in case of the latter, this salt scaled off after 180 days (**Fig. 2**).

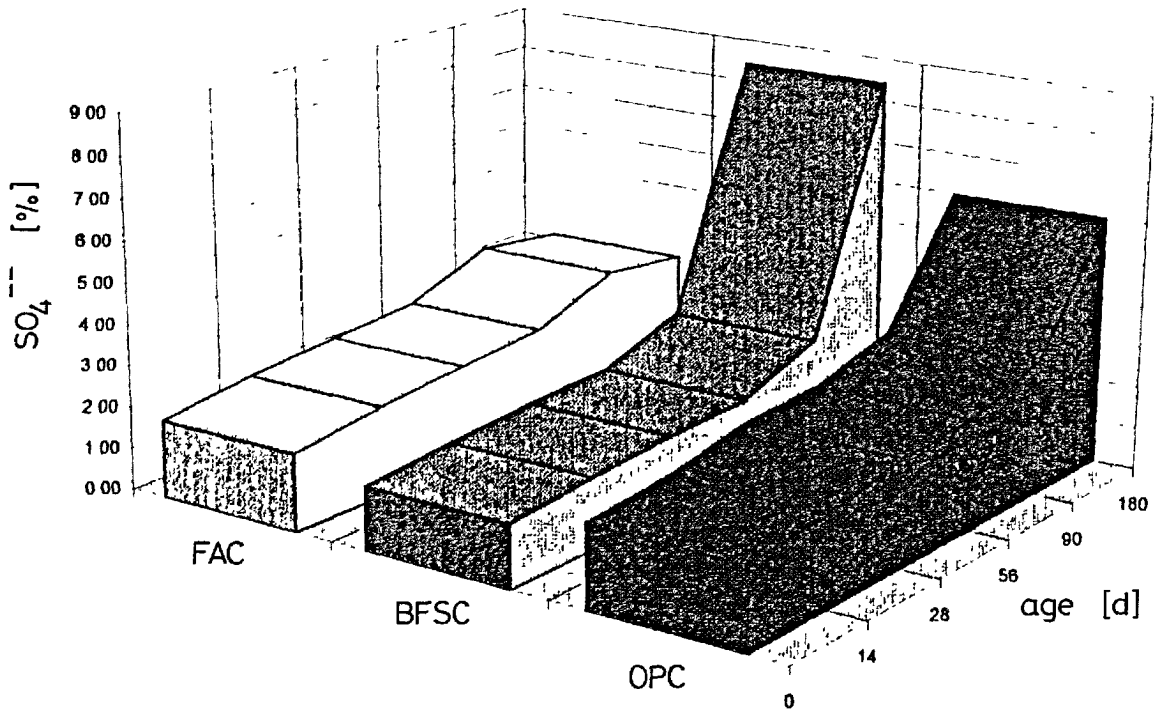

Fig. 1. Change of sulfate ion content, as a function of time, of pastes made of different cements

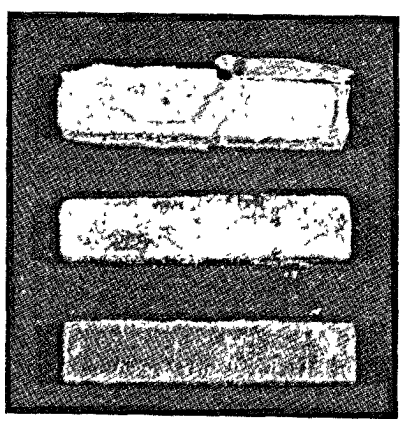

Fig. 2. Light layer on the surface of an OPC paste specimen

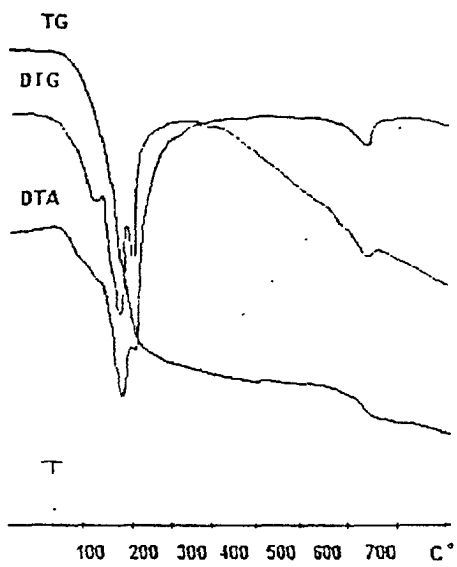

Fig. 3. Thermal curves of the layer

Approx. 80% of this layer consisted of gypsum, as shown by thermoanalytical tests (**Fig. 3**). The origin of this secondary gypsum can be studied with the aid of **Table 3**, which shows the $Ca(OH)_2$ and $CaCO_3$ content of the samples (again by TGA) before the experiment and after 90

days of SO_2-curing. It is evident, that the loss in $CaCO_3$ was - almost independently of cement type - somewhat less than 50%, while the loss of $Ca(OH)_2$ was definitely the highest in case of BFSC, and the lowest in OPC.

The change of nitrate ion quantity in function of time is shown in **Fig. 4.** It is evident that measurable amounts of nitrate could be observed already after 14 days, and by the end of the experiment this increased to 1.2 - 1.4, almost independently of cement quality.

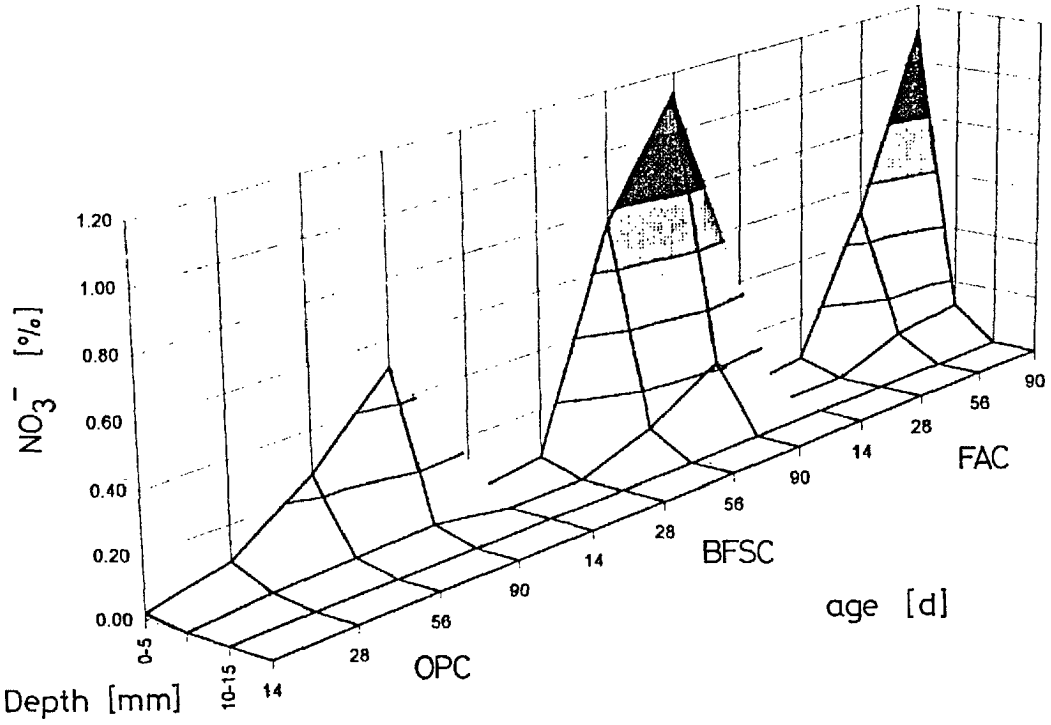

Fig. 4. Change of nitrate ion content, as a function of time, of pastes made of different cements

Table 3 Thermoanalytical results of SO_2-cured paste samples

	Time of curing	H_2O loss of $Ca(OH)_2$		CO_2 loss of $CaCO_3$	
Cement type	[days]	Quantity [%]	Change [%]	Quantity [%]	Change [%]
OPC	0	3.82	-	9.08	-
	90	3.50	-8	4.95	-45
BFSC	0	2.69	-	6.73	-
	90	1.79	-34	2.39	-44
FAC	0	2.95	-	8.87	-
	90	2.57	-13	4.36	-49

Results with mortar specimens

These specimens, being coated by an impermeable layer on their sides, give a possibility to study the depth of corrosive gases. pH values of 90-day old mortar specimens are shown in **Table. 4.**

Table 4. pH values of mortar specimens after 90 days of curing in SO_2 and NO_2.

Cement type	Layer depth	Starting value	Curing atmosphere	
			SO_2	NO_2
OPC	0 - 5	12.42	12.22	12.13
	5 - 10	12.48	12.15	12.26
	10 - 15	12.50	12.16	12.30
	15 - 25	12.51	12.17	12.28
BFSC	0 - 5	12.26	10.60	11.91
	5 - 10	12.26	10.75	11.95
	10 - 15	12.26	11.00	11.97
	15 - 25	12.27	11.20	11.98
FAC	0 - 5	12.35	11.75	11.92
	5 - 10	12.35	11.93	12.02
	10 - 15	12.35	12.00	12.05
	15 - 35	12.36	12.01	12.08

Most intensive reduction of pH can be observed in case of BFSC-mortars, in SO_2 atmosphere; here pH is reduced by one full degree (i.e. hydroxide ion concentration by one tenth), even in deeper layers. pH reduction was less, and least, in case of FAC- and OPC-mortars, respectively.

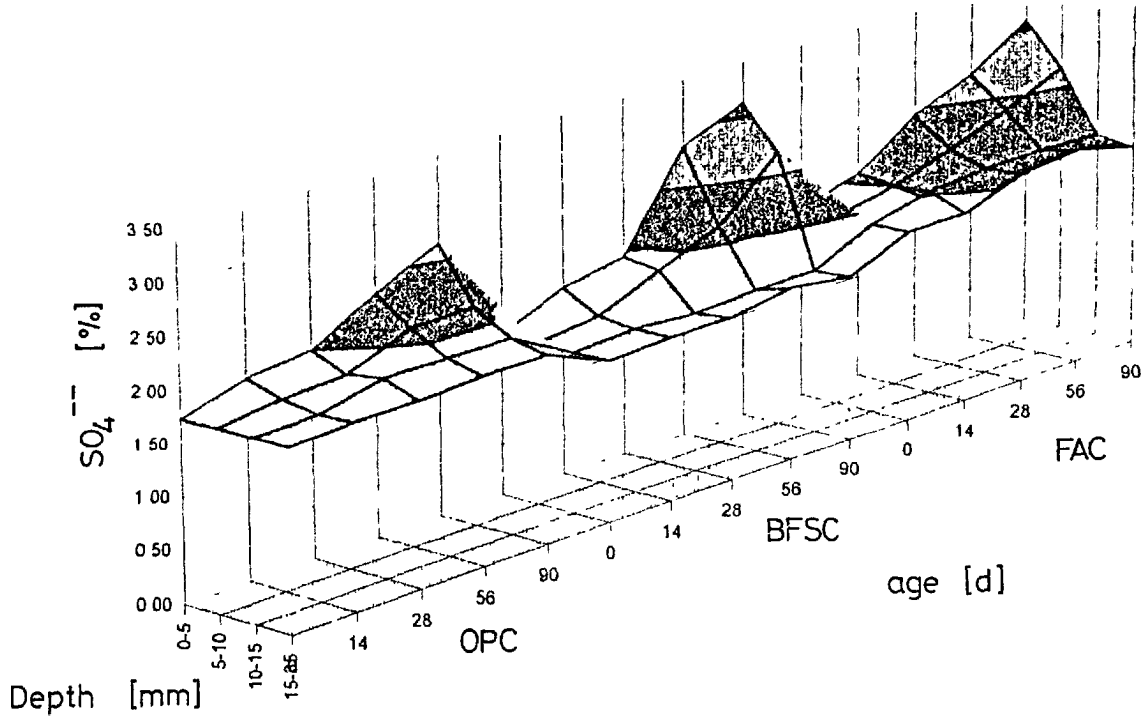

Fig. 5. Change of sulfate ion content, as a function of time, of mortars made of different cements

Increase of sulfate ions, as a function of time is shown in **Fig. 5.** Increase is evident in case of all cements, especially in the external layers, where this increase amounted 1.5-, 1.6- and 2-fold of the original SO_4^{--} content, in OPC, FAC and BFSC, respectively. **Fig. 6** shows a layer, formed on the end of a mortar specimen, subjected to SO_2 gas flow for several hours. 84% of this layer consisted of gypsum, as shown by the thermal tests.

Nitrate ion content in different depths of mortars is shown in **Fig. 7.** No nitrate was found, up to 90 days in layers deeper than 10 mm. In shallower layers nitrates were incorporated, but not to the same extent in case of different cements. Again OPC proved to be superior, where the highest NO_3^--content was only 0.5%, as contrasted to the two other cements, where the nitrate content was approx. the double of the above value.

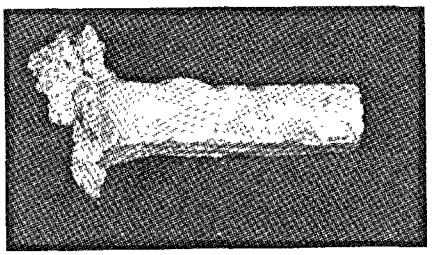

Fig. 6. Layer on a specimen subjected to SO_2 flow

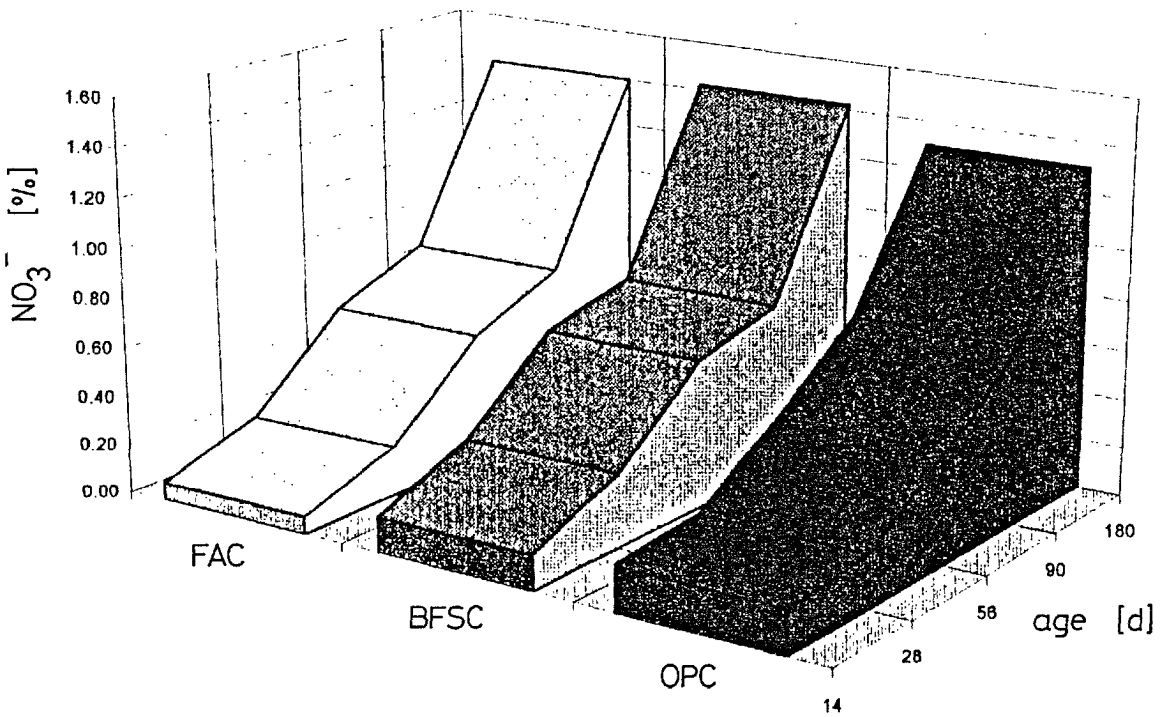

Fig. 7. Nitrate ion content in different depths of mortar specimens

SUMMARY

The degree and the effect of the incorporation of air polluting agents (primarily SO_2 and NO_2) into concrete was investigated, partly by case studies (old concrete structures in chemical-industrial zones or on busy highways), and partly by laboratory tests, on paste and mortar specimens made of different cements and subjected to different atmospheres. Results indicate considerable increase of sulfates in the external layers of concrete structures. Highest sulfate uptake (and lowest pH) was observed in case of blastfurnace slag containing cements. The effect of NO_2 is less intensive: nitrate incorporation amounted to 0.05 - 0.08%, even in case of intensive pollution (with the exception of a structure in a chemical factory, where nitrate content exceeded 6%.

In laboratory experiments OPC showed the least sulfate incorporation, while in case of BFSC, the original sulfate content was doubled after a 180-day exposition to an SO_2-enriched atmosphere. In some cases even a gypsum layer appeared on the surface, formed mainly of the $Ca(OH)_2$-content of the hydrated cement. No significant difference of various cement sorts exists in the response of samples to an atmosphere containing 80 ppm NO_2, although the presence of blastfurnace slag proved to be disadvantageous even in this case.

ACKNOWLEDGEMENT

The financial help of OTKA (National Scientific Research Fund) is gratefully acknowledged.

REFERENCES

Hensel, W. (1985): "Chemische Reaktionen von Atmosphärilien mit zementgebundenen Baustoffen" Betonwerk und Fertigteil Tech. **11** 714-21

Junge, C.E.(1963): "Atmospheric chemistry and radioactivity" Academic Press, New York - London

Levelook, J.E. (1971): "Air pollution and climatic change" Atmospheric Environment **5** 403-11

Scholl, E. and Knöfel, D. (1991): Der Einfluss von Luftschadstoffen auf Betonbauwerke". Beton [1] 17-21

Weawer, M.E. (1988): "Acid rain". The Construction Specifier [7] 54-59

CARBONATION OF HYDRATED CALCIUM ALUMINATE CEMENT AND ORDINARY PORTLAND CEMENTS OF VARYING ALKALI CONTENT

Mª Teresa GAZTAÑAGA, Sara GOÑI, Ana Mª GUERRERO and Mª Soledad HERNANDEZ, Institute of Construction Science Eduardo Torroja (CSIC), Madrid, Spain.

ABSTRACT Carbonation in laboratory atmosphere (40%-50% rh) of a Hydrated Calcium Aluminate Cement (HCAC) and two Hydrated Ordinary Portland Cements (HOPC) of varying alkali content (1.03% and 0.43% Na_2O equivalent) was studied during a period of 800 days from mixing. The kinetic of the process was followed from the $CaCO_3$ content by means of thermogravimetric analysis. The evolution of the new crystalline carbonated compounds was studied from X-ray diffraction (XRD).

Key-words: Carbonation, alkali, calcium aluminate cement, thermogravimetric, X-ray Diffraction Analysis.

INTRODUCTION

The known problems in structures fabricated in Spain with calcium aluminate cement, between 1950 and 1975, have induced the Spanish researches, in the last years, to intensify the investigation on degradation processes of this kind of cement. Specially, those related to the composition of expressed pore solution, due to the important role that pore solution plays either in the stability of its microstructure or corrosion of metallic reinforcements (Goñi et al. (1991), Gaztañaga et al, (1993), Goñi et al. (1994), Puertas et al. (1995), Goñi et al. (1996), Gaztañaga (1996) and Macias et al. (1996), among others). The present paper is part of an extensive investigation program related to the influence of both ambiental and accelerated 100% CO_2 carbonation on the microstructrue of hydrated calcium aluminate cement (HCAC) and two kinds of hydrated ordinary Portland cements (HOPC) of varying alkali, C_3A and C_3S contents (Gaztañaga, (1996)). The ambient carbonation process is presented in this work. It was studied by X-ray diffraction (XRD) and Themogravimetric analyses during a period of 800 days.

EXPERIMENTAL PROCEDURE

Pastes of two ordinary Portland cements called OPC-1 and OPC-2, of varying alkali and Al_2O_3 contents, and a Fondu Calcium Aluminate Cement (CAC) were prepared with deionized water at a water-to-solid ratio of 0.4. Table 1 and Fig 1 present the chemical composition and XRD analysis of the three cements. The mineralogical composition of both OPC-1 and OPC-2, calculated according to the Bogue equations, is shown in Table 2.

Table 1. Chemical composition of the cements.

(%)	IL	IR	SO_3	SiO_2	Al_2O_3	Fe_2O_3	CaO	MgO	Na_2O	K_2O
OPC-1	3.5	1.6	3.4	19.2	5.9	4.2	59.9	0.58	0.42	0.92
OPC-2	2.0	0.98	3.4	20.6	3.2	3.9	64.3	1.4	0.13	0.45
CAC				2.7	43.5	14.2	38.5	0.44	0.046	0.082

* I.L.= ignition loss
* I.R.= insoluble residue

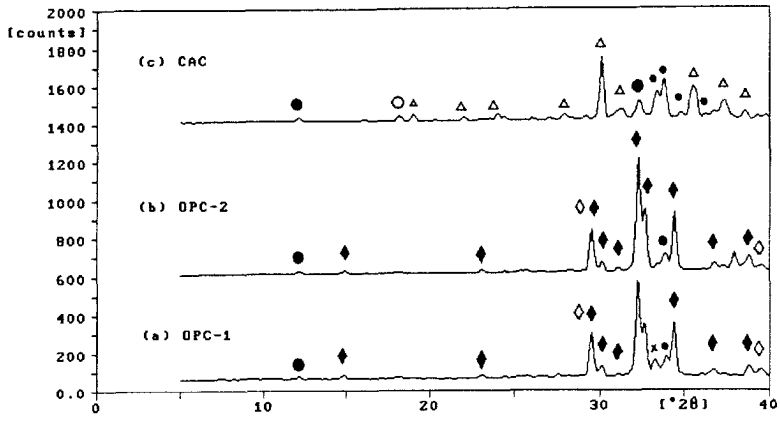

Figure 1 XRD analysis of the unhydrated cements: ● C_4AF; ♦ C_3S; × C_3A; ▲ CA; o $C_{12}A_7$.

Table 2 Mineralogical composition according to Bogue equations (%) by weight.

Cements	C_3S	C_2S	C_3A	C_4AF
OPC-1	43	23	8.5	12.8
OPC-2	68	7.5	1.9	11.9

The OPC-1 has the higher content of both alkali (1.03 Na_2O equivalent) and C_3A (8.5%) in comparison with that of OPC-2: 0.43% (Na_2O equivalent) and 1.9% for C_3A. There are also remarkable differences between the C_3S and C_2S contents for the two cements (Table 2). Series of 12 (1x1x6 cm) specimens were kept at 100% rh and 20±2°C for periods up to 800 days. After 28 days of curing at 100% rh, similar series of samples were stored at the laboratory atmosphere (40%-50% rh) (0.03% CO_2) for equivalent periods.

RESULTS AND DISCUSSION

X-Ray Diffraction Analysis

As shown in Fig. 2, when the three samples were stored during 800 days at 100% rh and 20±2°C, calcite is the only $CaCO_3$ variety formed (see curves (b) in Fig. 2). The intensity of the calcite-XRD-reflections are the highest, whereas those of portlandite ($Ca(OH)_2$) are the lowest, in the case of HOPC-1, what indicates its ability for carbonating even at 100% rh.

For the HCAC the carbonated crystalline compounds detected are the carboaluminate (C_4AcH_{11}) and calcite. The presence of both the cubic C_3AH_6 and hexagonal CAH_{10} shows that conversion has taken place.

In contrast, when the hydrated cements were stored during 800 days at laboratory ambient (40%-50% rh) (curves (a) in Fig 2) the three varieties of $CaCO_3$ (calcite, vaterite and aragonite) develop. Calcite is the predominant one for the HOPC-1 whereas vaterite is the predominant for the HOPC-2. The presence of vaterite could indicate the topochemical carbonation of CSH gel as Sauman (1971),(1972) and Berger (1979), among others, pointed out. The ettringite XRD-reflections disappear when the two HOPC samples are stored at the ambient, showing that ettringite could be carbonated. Accordingly the sulphate content in the extracted pore solution increases from 0.0006M to 0.01 for HOPC-1 samples stored at 100% rh and at laboratory ambient during 800 days, respectively, and from 0.0014M to 0.0022M in the case of equivalent HOPC-2 samples. These results suggest that the

mechanism of ettringite carbonation could be "via dissolution", although the pH of the pore solution (12.0) is considerably higher to that of ettringite dissolution (10.6) (Reardon, 1990).

Similar behaviour was observed and stated in a paper presented in this Symposium by Goñi et al (1997) on carbonation of OPC mortar with and without fly ash addition. The increase of sulphate content of the pore solution caused by carbonation of ettringite together with the decrease of pH are important factors to be considered from the point of view of the corrosion of metallic reinforcements. Kobayashi et al. (1989) also pointed out the release of SO_4^{2-} from ettringite and monosulphate carbonation, which could migrate to the external part of the concrete.

In the case of the HCAC the main carbonated crystalline compounds are the calcium carboaluminate C_4AcH_{11}, vaterite and aragonite. Calcite XRD-reflections appear less intense than those of the sample stored at 100% rh.

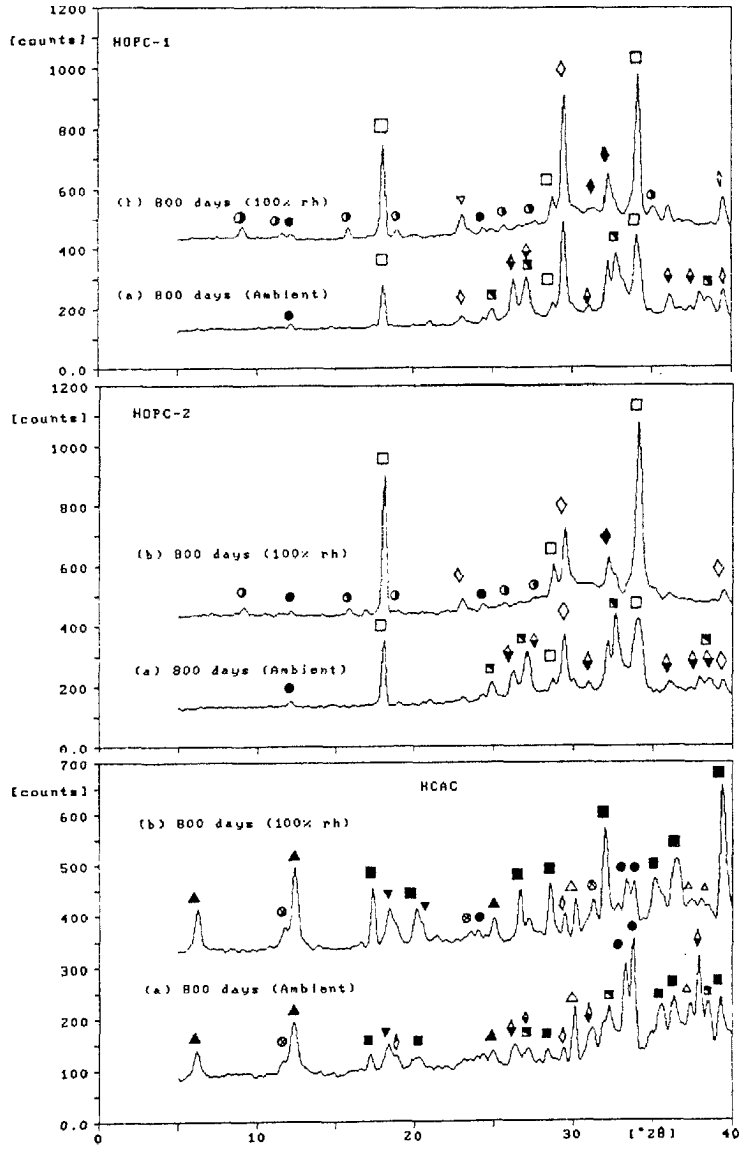

Figure 2. XRD patterns of carbonated samples: ● C_4AF; ♦ C_3S; × C_3A; Δ CA; ▲ CAH_{10}; ■ C_3AH_6; ▼ AH_3(gibbsite); ◊ AH_3(nordstrandite); ◊ Cc(calcite); ◆ Cc(aragonite); ◘ Cc(vaterite); □ CH; ◑ AF_t; ⊗ C_4AcH_{11}.

The XRD-reflections of hexagonal CAH_{10} and cubic C_3AH_6 are remarkably lower, specially those of cubic C_3AH_6, for the sample stored at the ambient. This fact would suggest that either conversion is inhibited, by carbonation of the hexagonal CAH_{10}, or both hexagonal and cubic are being carbonated. If the mechanism of carbonation is via dissolution, hexagonal CAH_{10} will dissolve firstly due to its high solubility product ($Ks = 10^{-7.6}$) in comparison with the cubic C_3AH_6 ($Ks = 10^{-22.3}$). In the former case the pH of dissolution of hexagonal will be 11.35 and in the later case 10.8. Due to this the dissolution of CAH_{10} caused by the neutralization of the pore solution will maintain the pH of the pore solution at a value of 11.35. In the case of carbonation of HOPC, the solubility of portlandite maintains the alkalinity levels of the pore solution at pH values of 12.5. For this reason, among others, ordinary Portland Cements are considered more resistant against carbonation than calcium aluminate cement.

Thermal Analysis

The decomposition of $CaCO_3$ produces a weight loss starting just after that of the portlandite, for the HOPC-2 (Fig. 3). The corresponding DTG curve shows a wide peak with several maxima centered at 620°C, 680°C and 770°C. The later intense peak is due to decomposition of the calcite variety of $CaCO_3$. The others maxima could be attributed to decomposition of either aragonite and vaterite, or to amorphous carbonate. The profile of TG and DTG curves of HOPC-1 are similar to those of HOPC-2. Portlandite is still present after 800 days of exposure to the ambient, as the XRD results also manifested.

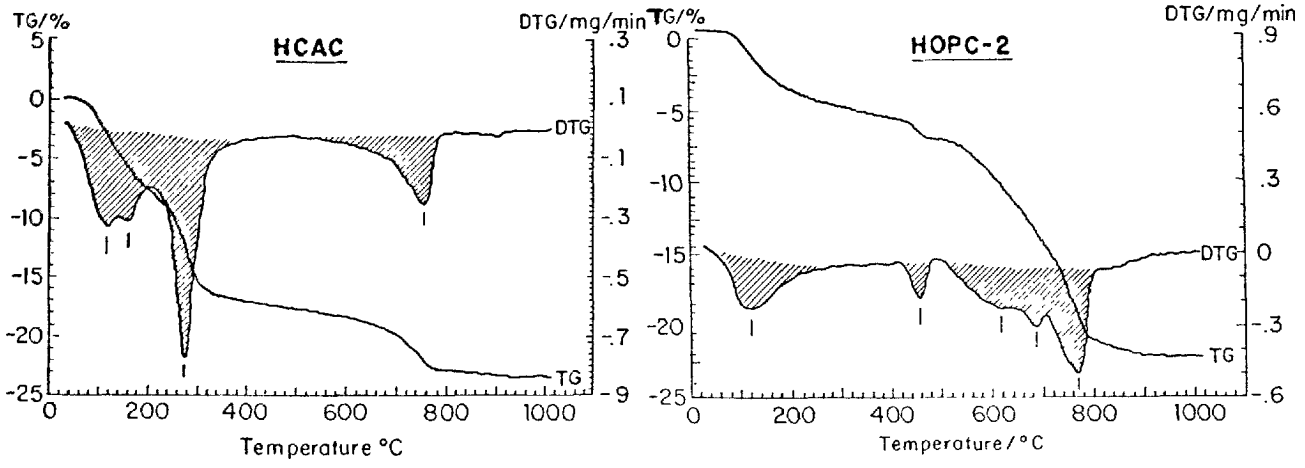

Figure 3. TG and DTG curves of HOPC and HCAC.

In the case of HCAC, the profile of TG and DTG curves is very different. The decomposition of carbonate from both the carboaluminate and $CaCO_3$ gives rise to a weight loss between 600°C and 800°C and a DTG peak centered at 780°C with a shoulder at 680°C.

According to Busnell-Watson and Sharp (1992), the water weight loss of AH_3 gel, hexagonal CAH_{10} and C_4AcH_{11} is produced between 60°C and 130°C; 100°C and 160°C and 180°C and 200°C respectively. The cubic C_3AH_6 decomposition takes place between 290°C and 350°C and that of crystalline gibsitte between 260°C and 330°C. These ranges of temperatures may vary upon different parameters such as; heating rate, amount of sample, dynamic atmosphere, etc.

As shown in Fig. 3 a double DTG peak is detected between 25°C and 200°C with the first maximum centered at 100°C which is due to the AH_3 gel decomposition and the second one centered at 150°C due to the CAH_{10} decomposition. The weight loss between 200°C and 350°C could be due to the water evaporation from both the crystalline gibsitte and cubic C_3AH_6 decomposition. The carboaluminate does not produce an valuable DTG peak.

The main parameters quantified from thermal analysis are presented in Table 3. The cumulative fraction carbonated (CFC) was calculated by dividing the corresponding carbonate contents (expressed as CaO) by the CaO content of unhydrated cements (see Table 1). The 0 days on the Table was the moment in which the samples were exposed to the ambient (after 28 days of curing at 100% rh).

Table 3. Cumulative fraction carbonated (CFC) and Global parameters quantified from thermogravimetric analysis

Cements	t	Comb.Water	$CaCO_3$	$Ca(OH)_2$	Unreac.CaO	CFC
	(days)	(mol % on residue)				
HOPC-1	0	0.82	0.024	0.27	1.05	0.022
	20	0.93	0.06	0.20	1.01	0.056
	164	0.65	0.21	0.18	0.86	0.20
	222	0.59	0.22	0.15	0.85	0.21
	320	0.53	0.28	0.15	0.79	0.26
	416	0.43	0.32	0.11	0.75	0.30
	773	0.44	0.42	0.074	0.65	0.39
HOPC-2	0	1.01	0.04	0.27	1.11	0.035
	20	0.99	0.06	0.23	1.09	0.052
	190	0.67	0.16	0.21	0.99	0.14
	262	0.62	0.18	0.21	0.97	0.16
	346	0.51	0.25	0.16	0.90	0.22
	441	0.52	0.28	0.14	0.87	0.24
	773	0.43	0.38	0.087	0.77	0.33
HCAC	0	1.6	0	-	0.69	0
	20	1.4	0	-	0.69	0
	90	1.72	0.017	-	0.67	0.025
	213	1.69	0.045	-	0.64	0.065
	272	1.09	0.066	-	0.62	0.096
	467	0.77	0.077	-	0.61	0.11
	773	1.21	0.13	-	0.56	0.19

As it can be seen in Fig 4, an inverse linear correlation, with a slope value = -0.47, is obtained between the $Ca(OH)_2$ content and the $CaCO_3$ content for both HOPC-1 and HOPC-2 materials. According to the (1:1) stoichiometry of the $Ca(OH)_2$ carbonation reaction, the value of the slope has to be 1. Therefore, other compounds than $Ca(OH)_2$ are being carbonated.

The same conclusion can be deduced from the higher value (-1.8) of the slope obtained when the combined water is plotted against the $CaCO_3$ content, which suggests that more water molecules are released than the needed for the $Ca(OH)_2$ carbonation reaction. The two last points, corresponding to the combined water of the more carbonated samples, are not considered for the correlation calculus because they probably content some water liberated during carbonation.

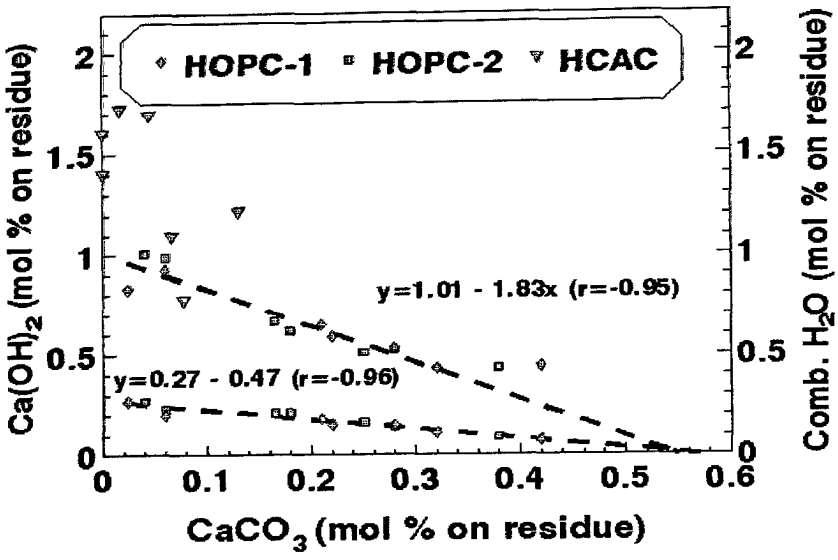

Figure 4. $Ca(OH)_2$ and combined water versus $CaCO_3$ content.

These results corroborated that CSH gel, and probably ettringite, are carbonated at the same time as $Ca(OH)_2$ as Parrot, (1991/92) and Dunster, (1989), among others authors, pointed out. Dunster (1989) stated that the carbonation of both $Ca(OH)_2$ and CSH occurs simultaneously, but a residue of $Ca(OH)_2$ reacts more slowly. This was considered to be consistent with a rate determining process controlled by the CO_2 diffusion through a $CaCO_3$ coating formed on the $Ca(OH)_2$ crystals.

In the case of HCAC, no correlation between the content of both combined water and $CaCO_3$ is obtained. The combined water values are considerably higher than those of HOPC, which indicate the lower porosity of these samples (Gaztañaga, 1996). As expected, when the cumulative fraction carbonated is plotted versus the square root of time (Fig. 5), a linear correlation is found suggesting that diffusion is the rate-controlling of $CaCO_3$ formation.

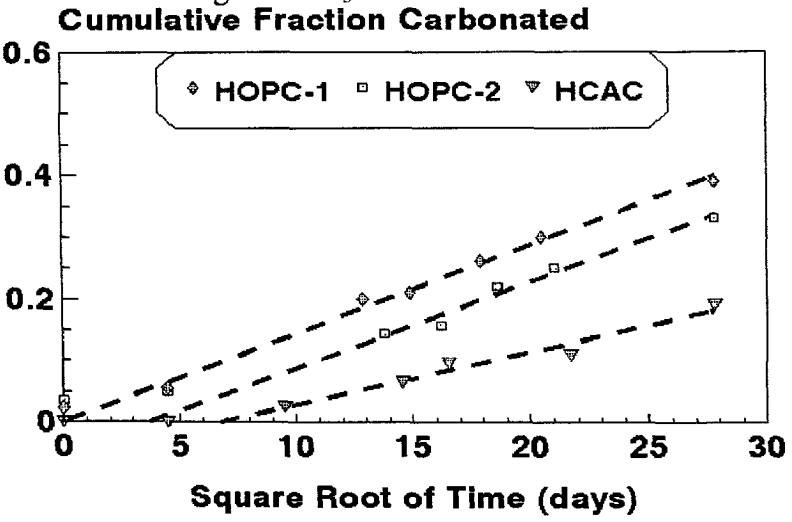

Figure 5. Cumulative fraction carbonated versus time.

HOPC-1 and HOPC-2 have the same slope values (Table 4) but the induction period is longer for the HOPC-2. In contrast, the slope value of HCAC is the lowest and its induction period is the longest.

Table 4 Parameters of the linear correlations of Fig. 5

Cements	r	a	Slope (CFC-day$^{0.5}$)	Induction time (days)
HOPC-1	0.996	0.002	0.014	0
HOPC-2	0.987	-0.05	0.014	13
HCAC	0.981	-0.058	0.0086	46

These results seem to show that the alkali content of the cements do not play any role from the point of view of ambient carbonation, which is in disagreement with the results of Kobayashi and Uno (1990), who found higher carbonation rates for cements with higher alkali content. An hypothetical explanation to this disagreement could be related to the different content of C_3S and C_2S (43% and 23% for OPC-1 and 68% and 7.5% for OPC-2). The minor amount of C_3S in the case of HOPC-1, of higher alkali content, could counteract the action of alkalies. For example, the porosity and pore mean diameter of the HOPC-1 at 28 days of curing (0 point on the graphs) are higher (11.5% and 0.041 μm) than those of HOPC-2 (9.4% and 0.024μm) favouring the initial CO_2 penetration. Accordingly, the absence of induction period can be also explained.

The lowest porosity of HCAC at 28 days of curing (4%) could be one of the microstructural reasons to explain its larger induction period and slower carbonation rate. Information on either porosity and strength changes will be published in a next work. Finally, it is important to take into account that although the HCAC seems to be more resistant against carbonation (during the period studied), its low carbonatable materia (CaO content) could, at longer carbonatable periods of exposure, be consumed before than that of HOPC.

CONCLUSIONS

HCAC presents the lowest carbonation rate during the period studied, that could be due to its lowest porosity. Nevertheless, the lowest amount of carbonatable material in the case of HCAC, could facilitate, at longer carbonation periods, the total carbonation of samples. The hexagonal CAH_{10} to cubic C_3AH_6 conversion is inhibited by the carbonation process. The amount of alkalies of HOPC does not influence the carbonation rate due to the different C_3S content of the two HOPC-1 and HOPC-2 materials. CSH gel and ettringite are carbonated at the same time than portlandite. Consequently SO_4^{2-} ions are released to the pore solution.

ACKNOWLEDGMENTS

The authors are grateful to C. Andrade for the fruitful discussions and the literature provided, and to the DGICYT for the financial support.

REFERENCES

Goñi, S., Andrade, C. and Page, C.L., "Corrosion Behaviour of Steel in High Alumina Cement Mortar Samples: Effect of Chloride". Cem. and Concr. Res., Vol. 21, 1991, pp. 635-646.

Gaztañaga, M.T., Goñi, S. and Sagrera, J.L., "Reactivity of High Alumina Cement in Water: Pore-Solution and Solid Phase Characterization". Solid State Ionics, Vol. 63-65, 1993, pp. 797-802.

Goñi, S., Gaztañaga, M.T., Sagrera, J.L. and Hernández, M.S., "The Influence of NaCl on the Reactivity of High Alumina Cement in Water: Pore-Solution and Solid Phase Characterization". Journal of Materials Research, Vol. 9, 1994, pp. 1533-1539.

Puertas, F., Fernández Carrasco, L., Blanco Varela, T., Vázquez, T., de la Fuente, A., "Carbonatación de Morteros de Cemento Aluminoso. Influencia de los Alcalis sobre la Formación de Fases". 1r. Congrés. El cas dels sostres. Experiències i perspectives. ADIGSA. Tema 26. Vol. Ciencia. Barcelona, 1995.

Goñi, S., Andrade, C., Sagrera, J.L., Hernández, M.S. and Alonso, C., "A New Insight on Alkaline Hydrolysis of Calcium Aluminate Cement Concrete: Part I. Fundamentals". J. Mater. Res., Vol. 11 (7), 1996.

Gaztañaga, M.T., "Effect of Carbonation on the Microstructure of Different Hydrated Cement Pastes". Ph. D. Thesis. University Complutense Madrid, Spain., 1996.

Macias, A., Kindness, A. and Glasser, F.P., "Corrosion Behaviour of Steel in High Alumina Cement Mortar Cured at 5, 25 and 55°C: Chemical and Physical Factors". Journal of Materials Science, Vol. 31, 1996, pp. 2279-2289.

Sauman, Z., "Carbonation of Porous Concrete and its Main Binding Components". Cem. and Concr., Vol. 16, 1971, pp 645-662.

Sauman, Z., "Effect of CO_2 on Porous Concrete". Cem. and Concr., Vol. 2(5), 1972, pp 541-549.

Sauman, Z. and Lach, V., "Long Term Carbonization of the Phases 3CaO.Al2O3.6H2O and $3CaO.Al_2O_3.4H_2O$". Cem. and Concr., Vol. 2(4), 1972, pp 435-446.

Berger, R.L., "Stabilization of Silicate Structures by Carbonation". Cem. and Concr. Res. Vol. 9, 1979, pp 649-651.

Reardon, E.J., "An Ion Interaction Model for the Determination of Chemical Equilibria in Cement/Water Systems". Cem. and Concr. Res., Vol. 20, 1990, pp. 175-192.

Goñi, S., Alonso, C., Menéndez, E., Hidalgo, A. and Andrade, C.,"Microstructural Characterization of the Carbonation of Mortar Made with Fly-Ashes". 10th International Congress on the Chemistry of Cement, 2.6th of June 1997. Göteborg, Sweden.

Kobayashi, K. Shirako, R., Kawai, K. and Hoshino, T."Migration and concentration of sulphate ion induced by carbonation of concrete". Seisan Kenkyu 41(12), 1989, pp. 940-943, Chem. Abst. 112, 184803.

Bushnell-Watson, S.M. and Sharp, J.H.,"La Aplicación de Análisis Térmico a las Reacciones de Hidratación y Conversión de Cementos Aluminosos". Materiales de Construcción, Vol. 42[228], Octubre/Noviembre/Diciembre, 1992, pp 13-32.

Parrot, L.J., "Carbonation , Moisture and Empty Pores". Advances in Cement Research, 4 (15), 1991/92, pp. 111-118.

Dunster, A.M., "An Investigation of the Carbonation of Cement Paste using Trimethylsilylation". Adv. Cem. Res., Vol. 2(7), 1989, pp. 99-106.

Kobayashi, K. and Uno, Y., "Influence of Alkali on Carbonation of Concrete, Part. 2. Influence of Alkali in Cement on Rate of Carbonation of Concrete". Cem. and Concr. Res. Vol. 20 (4), 1990, pp. 619-622

MICROSTRUCTURAL CHARACTERIZATION OF THE CARBONATION OF MORTAR MADE WITH FLY ASHES.

Sara GOÑI, Cruz ALONSO, Esperanza MENENDEZ, Ana HIDALGO and Carmen ANDRADE, Inst. EDUARDO TORROJA of Const. Sc., Madrid, Spain.

ABSTRACT Present paper study the microstructural changes produced by the carbonation when fly ashes (FA) are used replacing OPC partially. The resistance to carbonation is significantly reduced when replacement of OPC by FA is higher than 15%. High FA contents (50%) induced changes in the microstructural properties and compounds of carbonated mortar.

Key-words: admixtures, fly ash, carbonation, durability, blended cement

INTRODUCTION

The carbonation of concrete is a matter of increasing concern since many structures have their surface directly exposed to the action of the atmosphere and the standards allow relatively low depth of covers. Carbonation of concrete normally involves a chemical reaction between atmospheric carbon dioxide and that of cement hydration products if there is sufficient pore water. An important consequence is that the alkalinity of the pore fluid drops from a pH > 12.5 to a value of about 8. At this point the risk of corrosion increases significantly (Alonso,1986,1987).The chemical changes induced by carbonation create also variations of microstructure i.e. porosity (Verbeck,1958, Parrot,1987).

Among the factors influencing carbonation rate, the type of cement has an increasing importance due to the increasing use of blended cements (Litvan,1986, Bijen,1991, Parrot,1996). In the case of fly ashes most of the knowledge has been developed in the kinetic of carbonation process (Bijen,1991, Malami, 1994, Torii,1994). However few studies have been done on microstructure changes induced by carbonation in presence of fly ashes. Present paper deals with the microstructural changes provoked by carbonation of mortar made with 0, 15, 35 and 50% replacement of OPC with FA. The influence of the acceleration of the process has also been studied at 100%, 5%, and at atmospheric CO_2 content.

EXPERIMENTAL PROCEDURE

Preparation of specimens

Four identical sets of mortar specimens of 1x1x6cm size were casted with OPC and partial sustitutions of fly ashes ASTM type F (15, 35 and 50%), whose chemical analysis are shown in Table 1. The mortars were prepared at an aggregate to cement + fly ash ratio of 1:3 and deionized water to cement + fly ash ratio of 0.5. Cement and fly ashes were first dry mixed in a mixer. After mixing the specimens were kept sealed for 24 hours in the mould. At the end of this period the specimens were demoulded and cured for 28 days in a humidity saturated chamber.

Table 1 Chemical analysis of the portland cement and fly ash.

%	I.L.	I.R.	SO_3	SiO_2	Al_2O_3	Fe_2O_3	CaO	MgO	Na_2O	K_2O	Cl^-
Cement	1.53	1.92	3.89	19.9	3.05	4.12	63.7	1.55	0.13	0.45	0.02
Fly ash	5.77	0.19	0.00	46.9	17.3	18.1	5.83	1.65	0.54	2.30	0.00

Testing Methodology

After curing, one set of specimens (reference) were characterized by porosimetry, scanning electron microscopy, expressed pore solution analyses (Na^+, K^+, pH, $SO_4^=$, Ca^{+2}, $CO_3^=$ and HCO_3^-) and flexural strength. Similar set of specimens were exposed during one year to the laboratory atmosphere (40%-50%RH) for natural carbonation. Previously to start the accelerated carbonation, the other two sets of specimens were conditioned at 65% RH. Afterwards, the accelerated carbonation started at both 5%CO_2 or 100% CO_2 gas flow. The carbonation evolution was determined several times during the process, by spraying phenolphthalein (pH indicator solution) on a piece of fresh fractured specimen. At the end of the test, the specimens were characterized through the same techniques that those used for reference materials.

Porosimetry and pore size distribution were investigated by mercury porosimetry.The SEM observation was accompanied by simultaneous microanalysis. The pore solution was extracted by a high pressure device. The Na^+ and K^+ concentration were determined by atomic absorption spectroscopy, and sulphate concentration by ion chromatography. The pH was measured using a combined electrode for the range 0 to 14.

Table 2 summarizes the testing time for each condition. High FA contents significantly reduced the carbonation time.

Table 2 Duration of carbonation for the various fly ash additions and type of carbonation.

Test Cond.	Carbonation time (days)			
	0% FA	15% FA	35% FA	50% FA
Reference	0	0	0	0
Natural	365	365	365	365
5% CO_2	365	365	175	99
100% CO_2	365	365	35	24

RESULTS

Pore solution analyses

The composition of the expressed pore solution at the begining and at the end of the carbonation processes is represented in Fig 1. As shown the pH data are good indicators for the carbonation state. The higher the replacement of cement with fly ash is, the higher the pH drops for the three carbonation conditions. The total neutralization of the pore solution, according to the phenolphthalein indicator (pH<9), is only achieved for accelerated carbonation in the presence of high fly ash content. After 1 year of natural carbonation, the pH value of the pore solution is still high except in that of high FA content (50%), which seems to indicate that the total carbonation has not been reached, at least in the pore solution. This is probably due to the highest uncarbonated content of $Ca(OH)_2$ in plain OPC. As a consequence of carbonation, alkalies (Na^+ and K^+) are dramaticaly removed from the pore solution (Fig 1).

An opposite behaviour is observed with $SO_4^=$ ions as they dramaticaly increase with carbonation process (Fig 1). This behaviour is stronger for accelerated carbonation and for the high cement replacement with fly ash (50%).

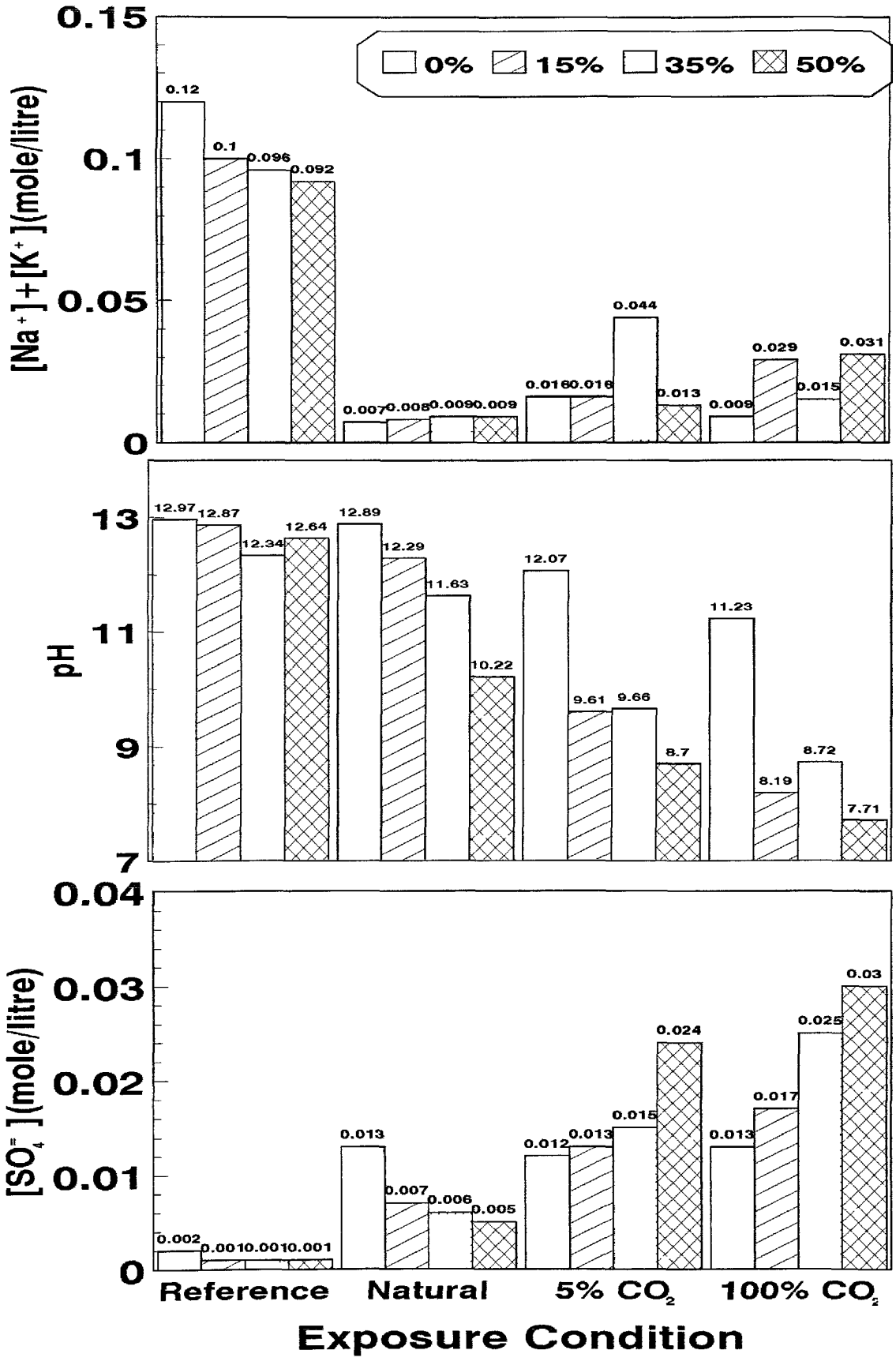

Figure 1 Pore solution analysis.

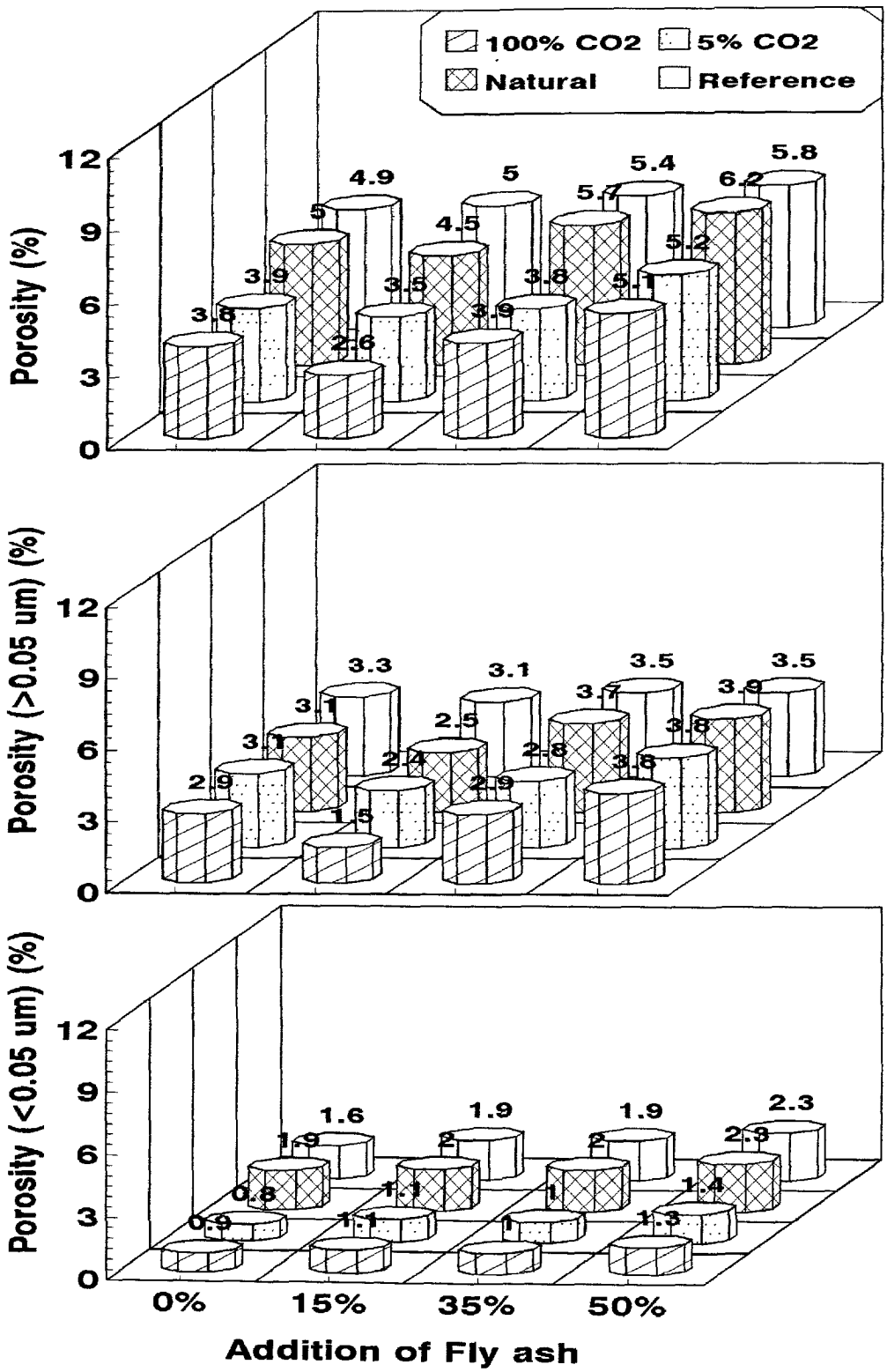

Figure 2 Porosity of the samples.

Microstructural and flexural studies

The changes of porosity caused by carbonation are represented in Fig 2. As expected, the decreasing total porosity is a funtion of the carbonation. In the case of the highest FA content (50% in present case), the changes in porosity have been less relevant than those of OPC (22% reduction in OPC respect to 12% with 50%FA). In general, both size pores (>0.05μm and <0.05μm), decreased as a result of the carbonation, being remarkable the decreasing percentage (45%) in the pores of lower size. The changes of mechanical flexural strength caused by the carbonation (Fig 3) are opposite to the porosity ones. So, an increase of the flexural strength is produced in all the samples.

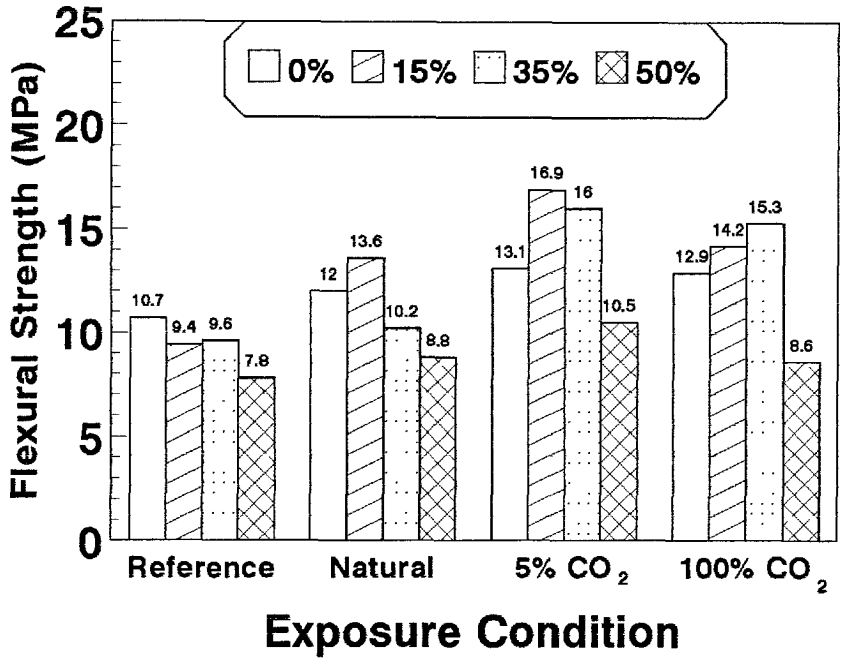

Figure 3 Flexural strength results.

DISCUSSION

In general, for plain OPC concretes, the carbonation process involves the transformation of both the solid phase and pore solution. These changes result in a densification of the microstructure of the paste as the carbonation products fill the pore system obstructing the continuity of the pores. Nevertheless, the reasons for these changes, are still unkown, being a subject of discussions and controversy in the case of concrete made with pozzolanic additions.

According to the porosity changes the more relevant aspect is the lower reduction in porosity with high fly ash replacement.Similar results were found by Distler (1994) and Malami (1994) when using cement with low clinker or high fly ash content.There are some differences in behaviour if the carbonation is natural or accelerated. In the natural carbonation, after one year exposure, the total porosity decreases slightly with low fly ash content (<15%), whereas for higher additions of FA (35% and 50% in present experimentation) the total porosity increases slightly.This means that the material is almost not affected from the point of view of its porous microstructure. Although full carbonation results are necessary to confirm this behaviour. The

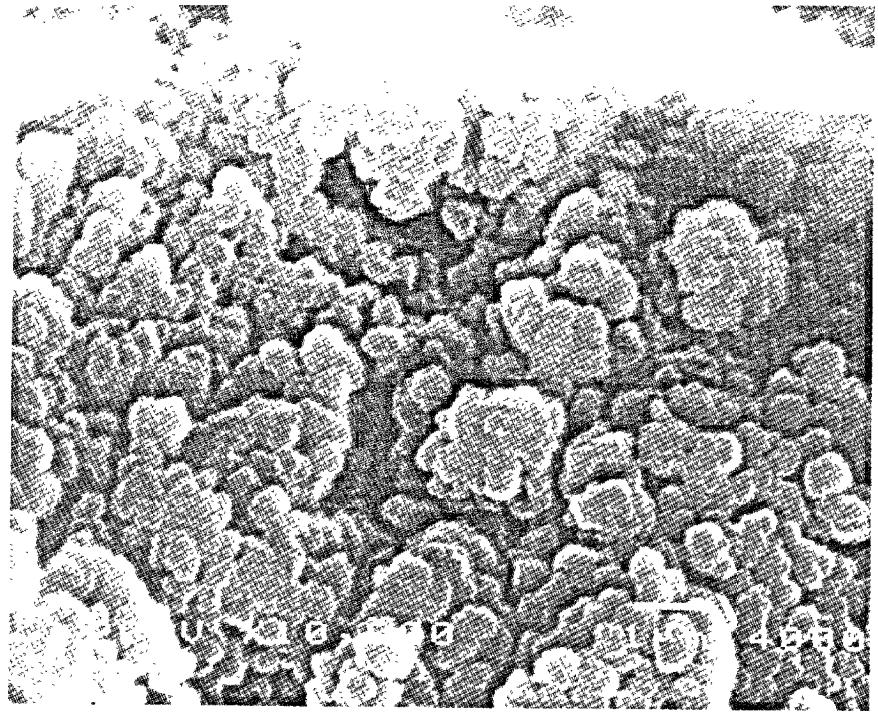

(a)

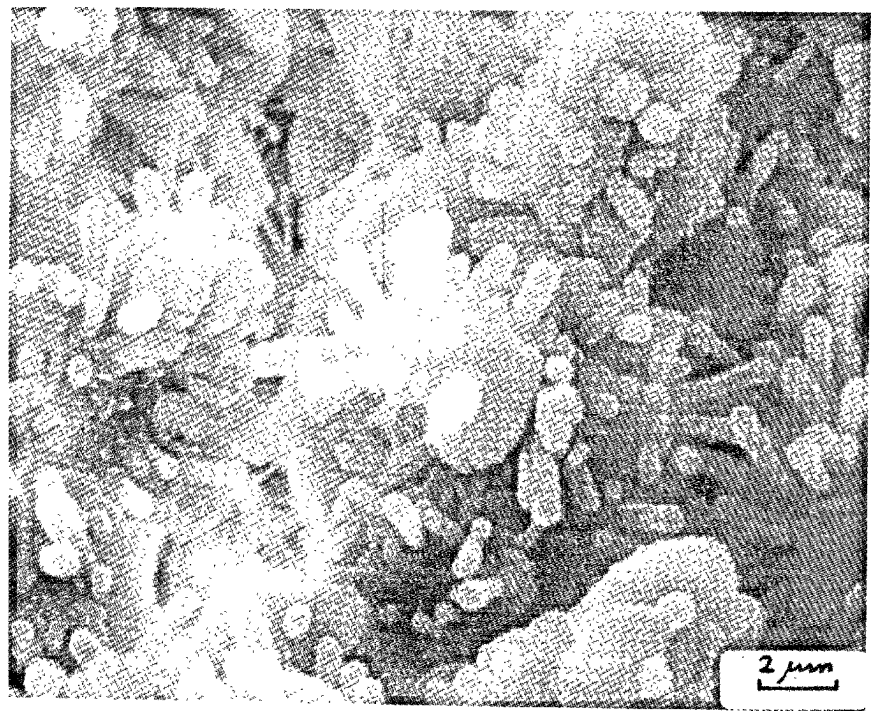

(b)

Figure 4. (a) SEM photograph of the mortar without fly ash addition, carbonated at 100% CO_2. (b) SEM photograph of a mortar with 50% fly ash addition, carbonated at 100% CO_2.

pore solution reveals that only in presence of FA the values of pH are below 12.5 where the dissolution of the portlandite has taken place. Nevertheless, these changes are not manifested in porosity, (see Fig 2).

When the carbonation is accelerated, the densification of the microstructure is clearly observed. The lower densification also occurs with high FA replacement. But in this case the samples are completely carbonated. SEM studies of mortar specimens (Figs 4(a) and 4(b)) confirmed that the OPC sample, carbonated with 100% CO_2 (a), has denser aspect than the one with 50% FA replacement (b).

On the other hand, the neutralization of the pore solution causes a dissolution of ettringite and CSH gel (Reardon (1990)), what justifies the dramatic increase of sulphate ions in the pore solution, as Kobayashi et al. (1989) and Gaztañaga et al. (1997) have also detected.

In Fig 5 the dissolution of ettringite needles is shown. The dramatic decrease of Na^+ and K^+ concentration could be due to their absorption by the solid hydrated phases in order to balance the decalcification of CSH gel, as other authors pointed out (Taylor (1990), Gaztañaga (1996). Page (1983), Sergi (1986). From X-ray diffraction data calcite and vaterite were the only crystalline carbonated phases detected irrespective of the carbonation rate, although the amount of vaterite increases with the percentage of fly ash sustitution. The natural exposure condition also promotes higher amounts of vaterite respect to 100% CO_2.

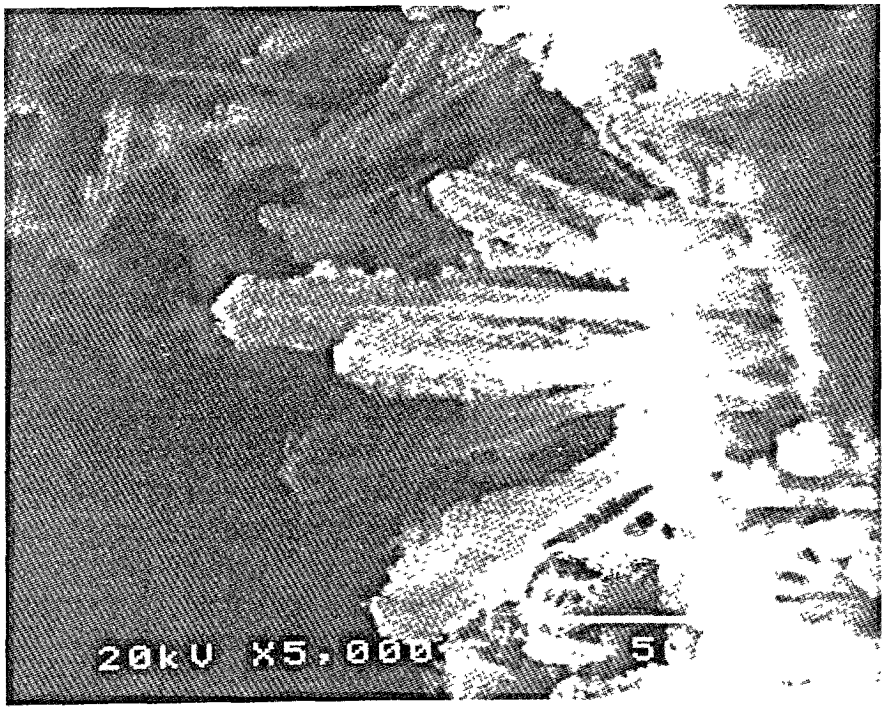

Figure 5 SEM photograph of a mortar with 50% fly ash addition, carbonated at natural condition.

CONCLUSIONS

The replacement of OPC by FA < 15% does not modify the carbonation process. On the contrary 50% replacement alters the microstructure of the carbonated compounds which result in a less dense system. Sulphates are released to the pore solution in higher concentration as FA replacement increases.

ACKNOWLEDGEMENTS

The authors are grateful to the spanish fly ash producers, specially to ASINEL, ENDESA, OCICARBON and OCIDE which have supported present experimentation.

REFERENCES

Alonso, C., Andrade, C., Santos, P., "Corrosion behaviour of steel during accelerated carbonation of solutions which simulate the pore concrete solution", 8th Int. Cong. on the Chemistry of Cement. Rio de Janeiro, (1986).

Alonso, C., and Andrade, C., "Effect of cement type and cement proportion in the corrosion rate of rebars embedded in carbonated mortar", Mater. de Const., vol. 37,N 205,(1987) pp 5-15.

Bijen, J., and Van Selst, "Fly ash as addition to concrete", Eds. CUR, Report 144, (1991).

Distler, P. and Kropp, J., "Effect of agging on pore structure and permeability of cementitious materials", The modelling and microstructure and its potential for studying transport properties and durability. Eds Jennings,H. et al, (1996) pp 339-350.

Gaztañaga, M. T., Goñi, S., Guerrero, A. and Hernández, M. S., "Carbonation of hydrated calcium aluminate cement and ordinary Portland cements of varying alkali content", Proceeding of the 10th International Congress on the Chemistry of Cement, June 1997. Goteborg, Sweden.

Kobayashi, K., Shirako, R., Kawai, K. and Hoshino, T., "Hydration and concentration of sulphate ion induced by carbonation of concrete", Seisan Kenhyn, 41, (12), 1989, pp.940-943, Chem. Abst., 112, 184803.

Litvan, G.and Meyer, A., "Carbonation of gbfs concrete during 20 years of field exposure", ACI, SP-91, Madrid Proc., Vol. 2 (1986) pp 1445-1462.

Malami, C. H., Batis, G.,Koulomb, N.,and Kalaidas, V., " Influence of pozzolanic and hydraulic cement additions on carbonation and corrosion of reinforced mortar specimens". Int. Cong. on corrosion and Protection of steel in concrete, Shefield, Vol. 2 (1994) pp 668-682.

Malami, C. H., Malami, Ch, Kaloidas, V., Batis, G., Kouloumbi. N., "Carbonation and porosity of mortar specimens with pozzolanic and hydraulic cement admixtures", Cement and Concrete Res., Vol. 24, no.8, pp.1444-1454, 1994.

Page, C. L. and Vennesland, Ø., "Pore solution composition and chloride binding capacity of silica fume cements pastes". Materiaux et Constructions, Vol. 16, n° 91 (1983).

Parrot, L. J., "A review of carbonation in reinforcement concrete", Report C/1 BRE/BCA, July (1987).

Parrot, L. J., "Some effects of cement and curing upon carbonation and reinforcement corrosion in concrete". Mat.and Structures, Vol. 29 (1996) pp 164-173.

Reardon, E. J., "An ion interaction model for the determination of Chemical Equilibria in Cement/Water systems". Cem. and Concr. Res., vol. 20, 1990, pp. 175-192.

Sergi, G., "Corrosion of Reinforcements" PHD Thesis, Aston University (1986).

Taylor, H. F. W., "Cement Chemistry", Publishers Academic Press Limited, London, 1990.

Torii, K., Sasatani and Kawamura, M., "Carbonation and steel corrosion in concretes containing mineral admixtures under different environments", Int. Cong. on Corrosion Protection of steel in concrete (Shefield) Vol. 2 (1994), pp 658-667.

Verbeck, G., "Carbonation of hydrated portland cement", ASTM, N 205 (1958) pp 17-38.

CARBONATION MECHANISM IN THE GRANULATED BLAST FURNACE SLAG CONCRETE

Seppo MATALA, Helsinki University of Technology, Concrete Laboratory, Finland

ABSTRACT Gel structure and the greater liability of GBFS concretes for carbonation of the CSH gel, and the lack of calcium hydroxide in hydrated GBFS mixes, were found to explain the powerful redistribution of porosity in GBFS concretes. GBFS compositions are more disposed to carbonation of the CSH gel, which transforms the initially relatively dense gel towards a more porous silica hydrate gel. On the basis of literature and the test results a carbonation model to explain the redistribution of porosity during carbonation of the GBFS concrete is proposed.

Key-words: Carbonation, Modelling, Pore structure, Microstructure, Blastfurnace slag

INTRODUCTION

Carbonation changes the chemical, mineralogical, microstructural and pore structural characteristics of the paste in concrete. Changes occurring in pore structure alter the durability charasteristics of concrete, especially carbonation rate and frost and frost-deicing resistance. For these reasons the knowledge about the mechanism by which the observed changes take place in the OPC and GBFS concretes during carbonation is of great importance. The following discusses the microstructural and pore structural differences in the OPC and GBFS concretes before and after carbonation and carbonation of different phases in concrete. Finally, a carbonation model to explain the redistribution of porosity during carbonation of the GBFS concrete is presented.

MICROSTRUCTURAL DIFFERENCES IN OPC AND GBFS CONCRETES

Similarities in the overall microstructure of OPC and GBFS concretes can be seen in the existence of three well-defined regions in the binder pastes, and the presence of CSH gel in these areas. There is wide consensus as to the separation of these regions as follows: 1) an area of inner hydration products formed within the original grain boundaries; 2) an area of outer or external hydration products formed between the grains; and 3) an area situated in the interface between the binder paste and aggregate particles. Hydration products and their proportions formed in these regions differ depending on the chemical composition of the slag and cement.

The first defined region can be thought to form within the binder grain boundaries, where the morphologies of OPC and GBFS gel structures differ significantly due to differences in hydration kinetics. In OPC pastes the formation of shells around the clinker grains is the first eventual feature in the development of cement paste microstructure with regard to its later age properties. This shell is composed of CSH products and CH, and inward or outward extensions of ettringite needles or thin calcium monosulfate plates. The inner hydrate consists of CSH gel, small quantities of CH, and AFm rather than AFt phases which are reported to exist outside the shell in the outer hydrate and in transition zones (Diamond 1987, Scrivener 1989).

In GBFS pastes the glassy slag hydrated in OPC forms first a layer of Portland cement hydrates on its surface, followed by the formation of a so-called inner hydrate layer due to the attack of Ca^{2+} ions and alkali metal ions from the supersaturated solution (Tanaka et al. 1983). The inner hydrate layer comprising well-crystallized hydrates becomes denser; the diffusion of Ca^{2+} ions from outside slows down, and the dissolution of Ca^{2+} and Al^{3+} ions from the unhydrated slag is accelerated. These ions are partially bound in the hydrated layer and also move to the outside

aqueous phase, taking part in the formation of the outer hydrate. The surface layer of the slag particle transforms gradually into the inner hydrate by the supply of Ca^{2+} ions, developing a crystallized and dense structure. The Ca/Si ratio has been observed to be higher in the outer than in the inner hydrate, and lowest in the surface layer where concentrations of Al^{3+} and Mg^{2+} ions are highest (Regourd 1987). Mg-rich phases at the border of the inner hydrate have also been reported by Feng et al. (1989). The space left by the original unhydrated slag particle is assumed to be occupied by the hydration products of the inner hydrate, the hydrates of the skeleton hydrate layer on the surface of the unhydrated slag, and the residual unhydrated slag grain. Once the slag grain is consumed totally, the innermost portion of the inner product forms a porous network consisting mainly of hydrotalcite (Glasser 1989).

The outer hydrate and the transition zones in OPC and GBFS pastes are obviously very similar. the differences can be found in the quantities of the AFt and CH phases and porosities which are higher with the OPC pastes.

Hydration products formed during the hydration of GBFS/OPC blends are CSH, AFt and AFm phases, and hydrogarnet and hydrotalcite-like phases. Mixed forms of calcium aluminate and calcium magnesium hydrates have also been reported. The CSH gel in hydrated GBFS blends activated by OPC possesses the typical Ca/Si ratio of roughly 1.2-1.5 to 1.7-2.2, the former belonging to the pastes of high slag contents and the latter being typical average values in pure OPC pastes and in the outer slag hydrate with moderate or low slag contents. The elemental distribution from the skeleton to outer hydrate shows increasing Ca/Si ratio, decreasing Al/Si ratio from the inner to the outer hydrate, and clear Mg enrichment in skeleton hydrate, strongly supporting the existence of a hydrotalcite-like phase in this gel space (e.g. Odler and Hinrichs 1989, Taylor 1990, Uchikawa et al. 1991, Richardson and Groves 1992b, Matala 1995).

In hydration the free lime in GBFS pastes is consumed faster than it is liberated from alite and belite phases. This means that the amount of free lime in slag cements increases as hydration progresses only for a certain period, and declines thereafter. The amount of CH for OPC pastes is typically from 20% to 28% depending on curing time and on water-binder ratio. The corresponding values for the GBFS pastes with high slag contents are 3-10 % showing a gradual decrease with curing time and water-binder ratio. Generally the non-evaporable water or the chemically bound water contents are clearly lower for GBFS pastes, being roughly 50-80% of those in OPC pastes depending on the mix composition.

According to the literature two main observations concerning the pore structural differences of the OPC and GBFS concretes can be drawn. First, GBFS seems to give a finer pore structure than OPC when the curing time exceeds 28 days but a coarser structure with shorter curing times. The results are in accordance with the differences in hydration kinetics and hydration products formed in OPC and GBFS pastes. Different results are obtained with regard to total porosity. In most cases this seems to be higher with GBFS replacement, but when long curing times are used it appears lower.

Feng et al. (1989) have studied the porosity of GBFS mixes separately in the skeleton and inner and outer hydrates. At fully hydrated slag grain, the inner product comprising the volume of the original slag boundaries had a porosity of 53-61% and the remaining hydration product a porosity of 20-22%. This was explained by a decrease in specific volume occurring during gel crystallization and by continuing outward migration of Ca, transforming the once dense inner

slag hydrate shell to a more porous microstructure. This results in an accumulation of residual porosity on the site of the former slag grain. Total porosity is changed only slightly, and the lowered permeability is a consequence of the pore size redistribution. The observation is well in line with the conclusion of the total porosity and permeability in GBFS blends drawn by Harrison et al. (1987). The distribution of macroscopic porosity into three well-defined parts in the GBFS gel structure is of great importance in its further behavior. If the gel structure remains in this state when hydration ends and the aging processes begins, the minor changes in the gel structure of the inner slag hydrate (ISH) layer may cause changes in overall permeability and in the ability of the binder matrix to become water saturated in a moist environment.

CARBONATION OF OPC AND GBFS CONCRETES

Carbonation mechanisms

Carbonation can be defined as an aging process whereby dissolved CO_2 in pore solution or free CO_2 in pores attacks the unhydrated or hydrated products of cement by a through-solution process or by a topochemical process, changing the chemical, mineralogical, microstructural and pore structural characteristics of the binding component of concrete. In cement based materials carbonation is able to change almost all components in paste comprising unhydrated, hydroxylated and hydrated phases. The volume fraction of the CH and CSH phases in fully hydrated OPC pastes is roughly 70 to 75 wt.-% of the hydrated phases. This means that also the carbonation products of these phases represent the majority of all carbonated products in OPC and GBFS concretes. However, there exists a variety of aluminate and sulphate phases able to carbonate. The most important of these are tri- and monosulfate phases and the cubic and hexagonal forms of aluminate hydrates. Carbonation of these phases have been discussed earlier (Matala, 1995).

From hydroxylated phases the role of the CH phase in the carbonation of OPC and GBFS concretes is evidently the most important. The CH content in OPC paste may reach 25 wt.-% and in GBFS paste half of that, while the percentage of carbonatable alkali oxides in OPC is only 2 to 3% and in GBFS cements even lower. Carbonated forms of alkalis are highly unstable. The MgO content in slag cements may rise to 12-14 wt.-%, and enrichment of Mg ions is observed at specified sites such as the inner and skeleton hydration products of slag binder. The exact forms of hydration or hydroxylated products at Mg rich cites are still unclear. In principle, the formation of $MgCO_3$ in low basicity solution may be possible with concretes of high slag contents.

Carbonation of the CH phase is obviously very similar in both OPC and GBFS concretes. The main difference naturally lies in the amount of carbonates precipitated from the CH phase, GBFS concretes showing the lower amounts. Carbonation of CH is generally assumed to take place, and even to finish, before the carbonation of other components in cement paste begins. However, this assumption has recently been proved to be incorrect. Simultaneous progression of carbonation of the two main carbonatable components in cement paste have been reported by e.g. by Bier (1988), Matsusato et al. (1992), Richardson et al. (1992) and Matala (1995). This is confirmed by the simultaneous existence of silica gel as a residue of carbonated CSH gel and CH in cement paste.

The differences in CSH compositions, in overall gel structures and in CH contents between GBFS and OPC pastes evidently affect the carbonation process. In principle, the carbonation

process is similar for CSH gel formed from either GBFS or OPC, although changes in the Ca/Si ratio may affect different kinetics in the carbonation process. Carbonation of CSH gel have been studied e.g. by Essing and Hilsdorf (1976), Suzuki et al. (1985), Bier (1988), Richardson et al. (1992), Ikeda et al. (1993), Atlassi (1993) and Matala (1995). Bier and Matala have studied the carbonation of the CSH gel in GBFS concretes.

The level by which the CSH gel carbonates depends on the degree of carbonation in the paste and on the initial amount of CH and on the moisture content of paste. It is obvious that the pore structure controls also the balance between the carbonation of the CH and CSH phases. The more open pore structure enables the mobility of water serving the carbonation of the CH phase. In the aforementioned studies on the carbonation of the CSH gel it is observed that different types of modified CSH and/or SH gel develops and calcium carbonate in a form of calcite, vaterite and aragonite precipitates. Richardson et al. (1992a) have reported the silica hydrate gel to be a three dimensional network of silicate units. Ikeda et al. (1992 and 1993) have observed that the double chain structure with Si-O-Si bridges of the silicate phase in non-carbonated tobermorite was destroyed and a silica gel with a three dimensional cross-linked framework structure being formed instead. Noticeable in the last study was the finding that the double chain structure still exists at relatively high degrees of carbonation from 60% to 80%. Suzuki et al. (1985), Bier (1988) and Atlassi (1993) have reported that during carbonation the so-called Ca-modified CSH gel being formed first, after which CSH loses its SiO_2 to form amorphous silica gel. In the process a new organization of SiO_4 tetrahedra takes place in the gel. The layered structure of CSH is bound by two of four corners in tetrahedra, but with the amorphous silica gel all corners may act as bridging components forming a three-dimensional and porous network of silicon chains. Carbonation products exist as microcrystallized material on the surface of the modified gel or as a part of it. The gel is only partly in its original form, being mostly an SH gel.

The morphologies of calcium carbonates depend on the sites where and on time when precipitation takes place. In the beginning, vaterite forms first transforming later to calcite. Further small pore sizes, as in the inner CSH, inhibit the crystallization of calcite and preferably vaterite, aragonite or modified CSH-$CaCO_3$ type product is formed. Richardson et al. (1992a) observed that calcite and vaterite precipitated in the outer product of CSH gel, with a microcrystal size of the order of 100 nm. At a later stage only very fine 10 nm poorly crystalline vaterite particles formed in the inner product gel. Obviously the inner product of CSH suffers from a net loss of calcium due to the fact that it does not contain pores large enough to allow for the nucleation of carbonates. In general, vaterite is the first product in the carbonation process, and is a poorly and small-crystallized form of $CaCO_3$ that converts easily to calcite if there is space enough for precipitation. Aragonite is also a small-crystallized form that is observed to be very soluble in chloride solution (Stark and Ludwig 1995).

Effects of carbonation on pore structure

The effect of carbonation on the pore structure of OPC blends has been widely studied. Pore size distribution becomes denser due to loss of coarse capillaries; continuity of pores decreases, resulting in lowered permeability. Some contradictory results of the effect of carbonation on the total porosity exist, but the general understanding is that overall porosity is diminished. Certain redistribution of the finest pores 1.5 to 20 nm caused by the carbonation of the CSH gel is reported by Essing and Hilsdorf (1976). Few studies exist on the pore structural changes in carbonated GBFS concretes, mortars or pastes. E.g. Litvan and Meyer (1986), Bier (1988), Distler et al. (1992), De Ceukelaire et al. (1992), Parrot (1992) and Matala (1995) have worked

in the field. Bier observed that carbonation in an atmospheric climate coarsens the pore structure of GBFS pastes but not of OPC pastes. They explained this phenomenon in terms of the formation of a porous silica gel resulting from the decomposition of CSH. An overall decrease in porosity was observed both in total porosity and especially in capillary porosity, the latter occurring especially in small capillaries where $CaCO_3$ precipitates from CH. In carbonated OPC pastes the decrease in total and capillary porosity was caused by a change in porosity in the range 2 to 20 nm. Slight coarsening was observed in the range 100 to 200 nm, which correspond to the coarsest pores of SH. The specific surface area determined by SAXS decreased due to carbonation in the outer CSH gel of OPC paste. Total porosity decreased in carbonated GBFS concrete, as in OPC concrete, but with no observable decrease in capillary porosity. The portion of small capillaries decreased clearly. The outer CSH gel disappeared and was replaced by porous SH gel, and the specific surface area decreased strongly due to carbonation.

Identical results on coarsening of the pore structure in GBFS blends was reported by Litvan and Meyer (1986), Distler et al. (1992), Parrot (1992) and De Ceukelaire et al. (1992) and Matala (1988 and 1995). In the last study a clear differences in the redistribution of porosity between the OPC and GBFS binders during carbonation took place. Coarsening of the pore structure, i.e. the increase in the macroporosity ($r>4$ nm) and the corresponding decrease in gel porosity, takes place with both binder types but at the expense of different gel pore ranges. The reduction in total porosity and increased capillarity due to carbonation takes place with OPC blends at the expense of micropores ($r<1.5$ nm) and with GBFS blends due to the reduction in microcapillaries ($1.5 \text{ nm} < r < 4$ nm). The ISH gel is the most probable site for the large amount of microcapillaries in GBFS blends. The outer slag hydrate in GBFS clearly resembles obviously the gel structure in OPC blends. The skeleton structure between the ISH and the unhydrated slag is the most porous part among the slag hydrates within the initial border of the slag particle. Now, coarsening of the ISH gel during carbonation opens the dense barrier between the closed skeleton porosity and the relatively open outer porosity. As a result, redistribution of the porosity in GBFS compositions causes a certain increase in permeability of the matrix, enabling the ingress of CO_2 through the ISH hydrate and the precipitation of carbonates also in the skeleton space and, to a certain extent, also in the coarsened ISH gel.

CARBONATION MODEL FOR GBFS CONCRETE

The model to be presented in the following is only a contribution toward explain the pore structural changes in carbonated OPC and GBFS concretes. It is based on the literature and on the test results of the project in which the effect of carbonation on the pore structure of OPC and GBFS concretes were studied mainly by low-temperature calorimeter, MIP, XRD, TG and IR methods (Matala 1995).

The main differences in the hydration kinetics of GBFS and OPC pastes lie in their *in-situ* products,but according to the literature the outer CSH formed is alike. Naturally OPC pastes comprise more portlandite and sulfate phases, which play an important role during carbonation in the most porous spaces of the cement matrix, in large capillaries and in porous transition zone areas. In GBFS pastes the dense inner slag hydrate layer (ISH) separates the two areas of the most porous hydrates, the outer slag hydrate (OSH) and the skeleton hydrate (SKH), as shown in Fig 1. In OPC pastes the inner hydration product is more porous but the connection of its homogeneous structure to the unhydrated material is more uninterrupted (Fig 2).

Carbonation begins with the attack of dissolved carbon dioxide in the OSH gel. In this phase available calcium hydroxide is consumed and tri- and monosulfates begin transforming to their carbonated forms. Carbonation resembles that of OPC, with the exception that more Ca^{2+}ions must be released from CSH to maintain the alkalinity in the pore solution. Carbonates precipitate as calcite or as vaterite in the open capillaries in the transition zones between the aggregate particles and binder paste and the OSH gel (stages 1 and 2, Figs 1 and 2). Due to the lower lime content in GBFS paste, simultaneous carbonation of the CH and CSH gel is more likely in GBFS. When the most easily available CaO is consumed, the CSH gel starts losing its Ca^{2+} and OH^- ions present in the interlayer regions of the tobermorite-like gel or mixed tobermorite-jennite like gel.

When more CO_2 penetrates the binder matrix and dissolves in the pore water, and when the availability of buffering Ca^{2+} ions from the OSH gel becomes insufficient, the ISH gel serves as a buffering reserve for the pore solution with increased CO_3^{2-} concentration in the OSH gel space. Interlayer water in the gel, adsorbed water on gel surfaces and on pore walls, and water released during carbonation guarantee the mobility of Ca^{2+} ions by diffusion to the species of the OSH gel large enough for precipitation of carbonates (stages 2 and 3, Fig 1). Overall porosity in the ISH increases as a consequence of the net loss of calcium and water from the gel matrix. It is possible that lost Ca^{2+} ions from the ISH framework may be partly replaced by Mg^{2+} ions enriched in the ISH gel. In any case, the net effect is increased porosity. Once the porosity in this pore space has increased enough, the penetration of CO_2 into the ISH and through it into the SKH gel is eventual (stage 4, Fig 1). More Ca^{2+} ions are released and carbonation may proceed as precipitation of the finest morphologies, i.e. vaterite in SKH gel and partly also in the most porous spaces of the ISH gel (stage 5, Fig 1).

In OPC pastes the dissolution of Ca^{2+} ions from the outer and inner CSH gel is slower than in GBFS pastes, since the lime from CH enables longer buffering of the pore solution. Consequently the transformations of the CSH gel structure take longer throughout the cement matrix, in the inner and outer hydrates, and also in the transition zones (stages 2 to 4, Fig 2).

The morphology of calcium carbonates inside the borders of the initial slag particle, i.e. in the spaces of ISH and SKH, is vaterite and its further crystallization into calcite is probably impossible or very slow. Two facts supports this polyform. First, there is insufficient space in these gels for the formation of well-crystallized calcite. Second, the enrichment of Mg^{2+} ions in the gel space inhibits vaterite from transforming into calcite. Calcium carbonates formed in the inner CSH of OPC blends clearly also have the metastable polyform of vaterite, but only due to lack of precipitation space rather than the incorporation of foreign ions. The more open structure of OPC compositions in this gel space may also enable precipitation of more crystallized polyforms. The morphologies of calcium carbonates in the outer hydrate gel are vaterite, aragonite and calcite for both binders. The metastable phases vaterite and aragonite are formed first, followed by transformation into calcite to an extent determined by the dimensions of the open porosity.

When modeling the carbonation process in GBFS concrete with high slag content, the role of MgO should not be neglected. Mg^{2+} ions in the ISH and SKH gels have deviating ionic radii that retard or totally inhibit crystallization of calcite in these gel areas. Evidently then, these ions form part of the mixed vaterite phase. There are, however, at least in principle, two ways in which carbonates involving MgO compounds can form. The first is the formation of magnesium

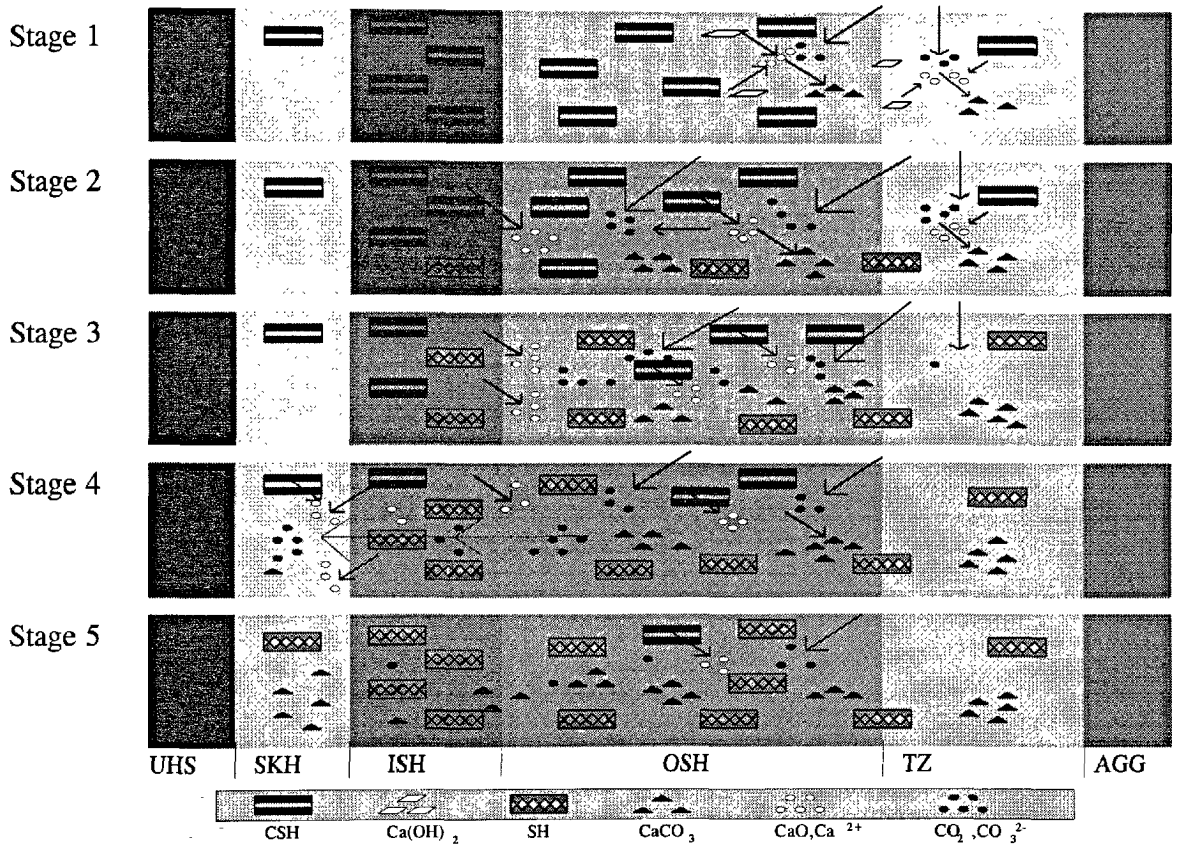

Figure 1. Schematic representation of the proposed carbonation model for GBFS concrete.

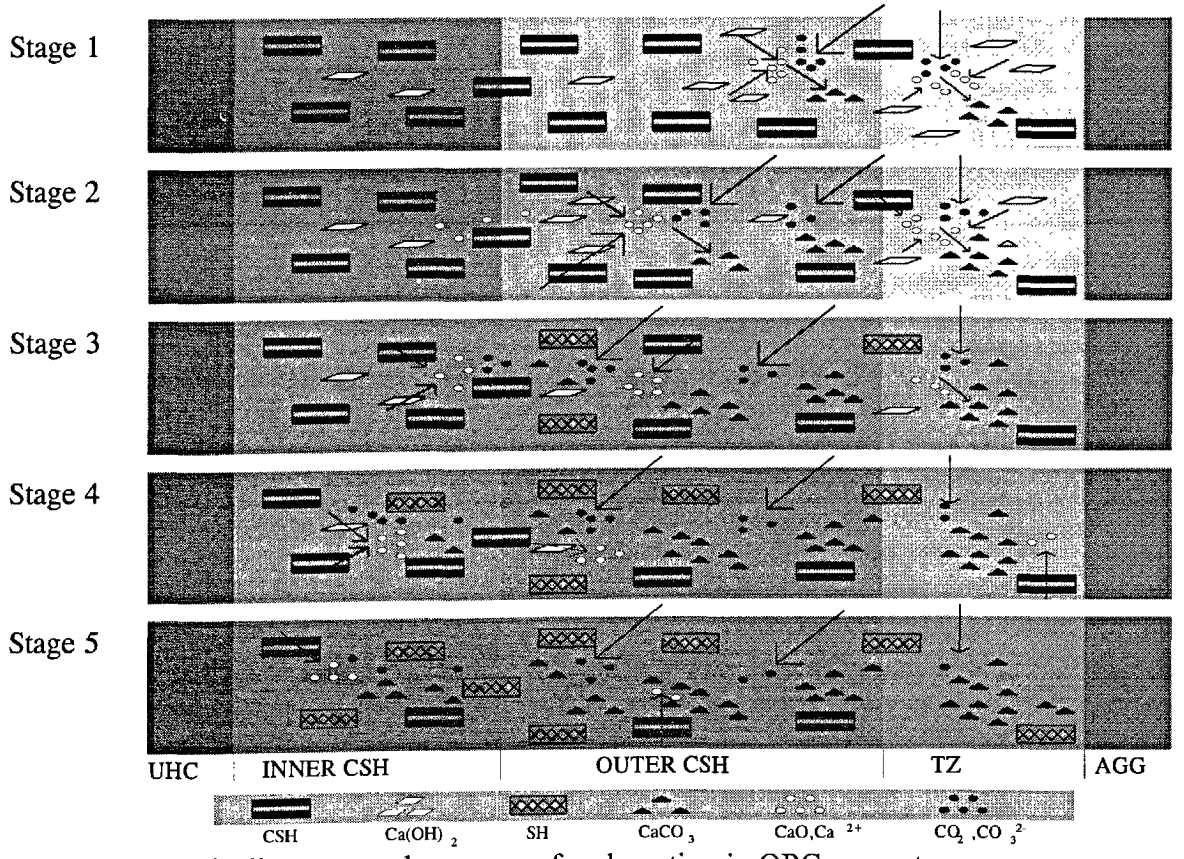

Figure 2. Schematically presented progress of carbonation in OPC concretes.

Figs 1 and 2 are also supplied as colour print for clarity at the end of proceedings.

carbonate from the brucite phase. Although the solubility of this phase in water is low, it is possible that at a low pH level of high CO_3^{2-} concentration in the pore solution it dissolves, and that subsequent formation of $MgCO_3$ is possible. Possibly this kind of direct carbonation seldom occurs in extreme conditions of well-saturated pastes with high CO_3^{2-} concentrations in the pore solution. The second is the existence of hydrotalcite $M_6A\bar{C}H_{12}$ by itself in GBFS concrete. What the chances are of this compound forming during carbonation is not clear. Perhaps its appearance is merely associated with the hydration process as a result of the direct reaction of cement containing carbonates with magnesium aluminate hydrates, being analogous to the direct formation of carboaluminates. Its separation from monosulfate and carboaluminate phases by XRD is obscure, and at least the results of XRD tests in this study do not support the formation of hydrotalcite during carbonation at relatively low RH.

Redistribution of pore sizes during carbonation is explained by the changes in interlayer regions of the tobermorite-like gel or of the mixed tobermorite-jennite-like gel, by the silicon polymerization that results, and by the loss of interlayer water of the gel. Calculations of C/S and H/S ratios showed that CSH gel in GBFS mixes loses roughly 75% of its CaO and about 40% of its H_2O during carbonation. The corresponding losses with OPC mixes were 70% and 50%. The rearrangement of silicon tetrahedra after the escape of Ca^{2+} and OH^- ions causes a certain volumetric decrease in the remaining gel. A rough estimate for the volumetric decrease due to the 75% loss of Ca^{2+} ions from the CSH network could be as high as 40%. One dimensional change is about 20%. Assuming that the CSH gel is composed of two of the three 14 Å tobermorite layers, with one adsorbed water layer between and along the sheets, one dimensional decrease of 20% in the thickness of the initial gel is enough to double an average gel pore radius of 1.5 nm. Negative pressure in the gel at low RH assists the rearrangement of silicon tetrahedra in the remaining SH gel into more ordered position. Of course, this contributes to the increase in gel pore space.

Carbonation at low RH accelerates modification of the pore structure in the ISH gel and, possibly due to the parallel effects of carbonation and drying, the changes are greatest at the lower level of intermediate humidities, i.e. 45% to 50% RH. When carbonation occurs at higher RH the coarsening process differs from the described one. Ingress of CO_2 into the pore system of the OSH gel and the transition zone is slower but the effect is the same as described in stages 1 and 2 above. Differences exist with regard to the transformation of the ISH gel and to the changes in the SKH gel. The higher degree of saturation in the pores enables the dissolution of Ca^{2+} ions from unhydrated slag, and Ca^{2+} ion diffusion occurs through the ISH gel to the OSH gels. This may take place by direct diffusion or by a restoring process in which lost Ca^{2+} ions from the tobermorite-jennite-like gel of the ISH needed to buffer the pore solution in the OSH gel are replaced by the Ca^{2+} ions dissolved in the SKH gel. This leads to a net increase in the porosity of the SKH gel, the porosity of the ISH gel remains unchanged, and the barrier between the more open gel structures of the SKH and OSH gels may densify even further. The open porosity of the SKH gel remains isolated from the rest of the paste as long as the ISH preserves its density. If carbonation proceeds at lower RH or drying-induced coarsening of the ISH gel begins, the density of the isolating barrier diminishes and the gel structure becomes more permeable. The porous SKH gel then comes within the field of activity of the penetrated substances.

As a consequence of both the above hypotheses, the gel structure coarsens. The more homogeneous structure of the inner hydrate in OPC compositions gives a relatively smaller redistribution in overall porosity of the binder matrix than is the case in GBFS mixes. At what

rate coarsening occurs depends naturally on the predominant RH. At high RH, carbonation is slow and carbonation-induced coarsening is at least partly compensated for by further hydration. However, as the results with samples cured by repeated wetting and drying treatment show, a certain amount of coarsening takes place anyway.

CONCLUSIONS

The proposed carbonation model explains the strong redistribution of the gel and capillary porosity found in the GBFS concretes. In that the role of the inner slag hydrate is of great importance. This initially very dense layer before carbonation becomes porous and permeable during the carbonation of the CSH gel affecting the decrease of gel porosity below 4 nm and the corresponding increase in coarser capillary porosity. Coarsening of the inner slag hydrate gel causes an overall increase in the porosity of the ISH gel space and in the continuity of pores in GBFS concrete, as the dense separative barrier is lost between the most porous parts of the GBFS matrix, the outer slag hydrate and the skeleton hydrate. The phenomenon was very observable in microcalorimetry tests in which the preparation of samples did not alter the pore structure. Due to the microstructural and pore structural differences the coarsening of pore structure of OPC concretes is much smaller.

The observed phenomenon declines the durability properties of carbonated GBFS concretes. Increased capillary porosity affects increased permeability and decreased frost and salt-frost resistance. Calcium carbonates in GBFS concretes were found to exist extensively in the polyforms of vaterite and aragonite. These polyforms have been reported to be very soluble in chlorine solution. Hence the frost-salt resistance is further diminished by chemical degradation.

REFERENCES

Atlassi, E.H., "A quantitative thermogravimetric study on the non-evaporable water in mature silica fume concrete", Chalmers University of Technology. Sweden. Publ. P-93:6, 1993, 169 p.

Bier, T.A., "Karbonatisierung und Realkalisierung von Zementstein und Beton", Massivbau, Baustofftechnologie, Karlsruhe. Heft 4, 1988, 170 p. +Anhang 48 p.

Diamond, M., "Cement paste microstructure in concrete", In: Microstructural Development During Hydration of Cement. Boston, MRS Symp. Proc. Vol 85, 1987, pp. 21-31.

De Ceukelaire, L. and Van Nieuwenburg, D.; "Accelerated carbonation of a blast-furnace cement concrete", Cement and Concrete Research. Vol. 23, 1992, pp. 442-452.

Distler, P., Kropp, J. and Hilsdorf, H.K.,, "Pore structure and transportation parameters of concretes containing blended cements". 9th Int. Cong. on the Chemistry of Cement, New Delhi, India, Vol. V, 1992, pp. 431-437.

Essing, K. and Hilsdorf, H.K. "Influence of Carbonation on Pore Structure of Hydrated Portland Cement Paste. In: Rilem Symposium on Carbonation of Concrete. Fulmer Grange 1976. 5 p.

Feng, Q.L., Lachowski, E.E. and Glasser, F.P., "Densification and Migration of Ions in Blast Furnace Slag-Portland Cement Pastes", In: Fly Ash and Coal Conversion By-Products, Eds. Hemmings et al., Boston, MRS Symp. Proc. Vol. 136, 1989, pp. 263-272.

Glasser, F.P., "Chemical, Mineralogical, and Microstructural Changes Occurring in Hydrated Slag-Cement Blends", In: Material Science of Concrete II, Eds. Skalny et al., 1989, pp. 41-82.

Harrison, A.M., Winter, N.B. and Taylor, H.F.W., "Microstructure and microchemistry of slag cement pastes" In: Microstructural Development During Hydration of Cement. Boston, MRS Symp. Proc. Vol. 85, 1987, pp. 213-233.

Ikeda, Y., Yasuike, Y., Kumagai, M., Takahashi, K., Yamamoto, M. and Takashima, Y., "A Study on Carbonation Reaction of Synthetic 11Å Tobermorite in Aqueous Solution", Journal of the Ceramic Society of Japan, Int. Ed., Vol. 101, 1993, pp. 140-143.

Litvan, G.G. and Meyer A., "Carbonation of Granulated Blast Furnace Slag Cement Concrete During Twenty Years of Field Exposure", ACI SP-91, Vol. II, 1986, pp. 1445-1462.

Matala, S., "Effects of carbonation on the pore structure of granulated blast furnace slag concrete", Helsinki University of Technology. Concrete Technology. Report 6. Dissertation. 1995. 161 p. + app. 49 p.

Matsusato, H., Ogawa, M., Funato, M. and Sato, T., "Studies on the carbonation of hydrated cement and its effect on microstructure and strength". 9th Int. Cong. on the Chemistry of Cement, New Delhi, India, Vol. V, 1992, pp. 363-369.

Odler, I. and Hinrichs, W., "Investigation of the hydration of Portland blast furnace slag cement: composition, structure and properties of the hydrated material", Advances in Cement Research, Vol. 2, 1989, pp. 15-20.

Parrot, L., "Carbonation, moisture and empty pores", Advances in Cement Research 1991/92, Vol. 4, No. 15, pp. 111-118.

Regourd, M., "Microstructure of cement blends containing fly ash, silica fume, slag and fillers", In: Microstructural Development during hydration of Cement. Boston, MRS Symp. Proc. Vol. 85, 1987, pp. 187-200.

Richardson, I.G., Groves, G.W., Brough, A., and Dobson, C.M., "Structural changes due to carbonation in hardened cement pastes", 9th Int. Cong. on the Chemistry of Cement, New Delhi, India, Vol. IV, 1992a, pp. 298-303.

Richardson, I.G. and Groves, G.W. "The composition and structure of C-S-H gels in cement pastes containing blast-furnace slags" 9th Int. Cong. on the Chemistry of Cement, New Delhi, India, Vol. IV, 1992b, pp. 350-356.

Scrivener, K.L., "The Microstructure of Concrete", In: Materials Science of Concrete. Ed. J.P. Skalny. The American Ceramic Society. Vol. I, 1989, pp. 127-161.

Suzuki, K., Nishikawa, T. and Ito, S., "Formation and carbonation of C-S-H in water", Cement and Concrete Research, Vol. 15, 1985, pp. 213-224.

Stark, J. and Ludwig, H.-M., "The influence of the type of cement on the freeze-thaw/freeze-deicing salt resistance of concrete", Proc. Int. Conf. on Concrete under Severe Conditions, Sapporo, Japan 2-4 August 1995, Ed. by K. Sakai et al., Publ. E & FN Spon, Vol.1., pp. 245-254.

Tanaka, H., Totani, Y. and Saito, Y., "Structure of hydrated slag in concrete", ACI Publ. SP-79. Vol. II, 1983, pp. 963-977.

Taylor, H.F.W., "Cement Chemistry", Academic Press, London, 1990, 473 p.

Uchikawa, H., Hanehara, S. and Sawaki, D.; "Influence of Water Cement Ratio on the Ionic Penetrability of Blended Cement Paste, Mortar and Concrete", Second CANMET/ACI Int. Conf. on Durability of Concrete. Supplementary Papers. Montreal, Canada, 1991, pp. 525-543.

EFFECT OF THE CARBONATION ON A 54-YEARS OLD CONCRETE ROAD PAVEMENT

Simonetta PAGLIOLICO (Politecnico di Torino, Italy)
Luciano CUSSINO, Francesco CURCIO, Roberto FERRARI (Centro Ricerche Unicem, Guidonia, Italy)

ABSTRACT Samples of concrete from the demolition of a non-reinforced road pavement built in 1938 have been studied, to evaluate the transformations occurred during its 54-years working life. The concrete slab thickness was 250 mm. By means of the phenophtalein method, the depth of carbonation has been measured: this showed that carbonation occurred from both sides of the slab (external and internal), a non-carbonated zone remaining in the middle. On carbonated and non-carbonated pieces, XRD, DTA, TGA, SEM and Porosimetry tests have been performed, with several physical and mechanical tests. Differences in the microstructure of the two phases have been recognized; these however have not influenced significantly the mechanical behaviour and the working life of the road. The slight decrease in compressive strengths due to the action of deicing salts (frequently used on this road, exposed to severe winter weathers) depends on the fact that carbonation has limited the deleterious effects of the calcium ossychloride formation.

Key Words : carbonation, cloride, de-icing salts, porosity

INTRODUCTION

Concrete samples taken during the demolition of non-reinforced slabs of a road pavement cast in 1938, have been studied to assess the changes that have occurred in the 54 years period.
It has been noticed that the 25cm thick slabs have undergone carbonation, as determined by the phenolphtalein method, to almost the same depth on the upper and the lower surface, while the central part is not carbonated.
Samples of both the carbonated and non-carbonated zones have been investigated by XRD, DTA and TGA, porosimetry, SEM, with the aim of studying the effects of carbonation.
Compressive strength and other physical properties have been measured on cubic samples sawed from both the carbonated and the non carbonated zones.
The differences in the microstructure caused by carbonation, as revealed by this investigation, did not bring about any sizeable effect on the mechanical behavior and on the useful life of the pavement.
The roads around Casale Monferrato before 1940 were mostly paved with concrete. Particularly a lenght of 5 km of Road 31 was paved in 1938 with 3.30 x 4 m, 25 cm thick slabs. These were separately placed by interposing wooden casing. The road had only one line 7 m wide lane.
Until recently Road 31 has been subjected to all the traffic going from Alessandria to Vercelli.
When the concrete surface was demolished and replaced by a bituminous concrete surface it was still in good service condition, even if some slabs showed cracks, probably caused by ground settling and the surface was very smooth.
This road perfomed satisfactorily for 54 years without any maintenance (except the filling of the joints with bitumen).
The good state of the slabs in 1992 is shown in Fig. 1.
Concrete was made up by Portland cement and river Po aggregates, mainly silicious, of the Casale Monferrato area. This town was at the time an important cement and hidraulic limes producing center, since natural marl was very abundant nearly.
The typical Casale Monferrato clinker had the follwing moduli:
Hydraulic modulus = 2.16, Silica modulus = 2.38, Alumina ratio = 2.15, LSF = 0.95.



Figure 1 : state of concrete slabs in 1992

The cement had the characteristics required by the 1925 italian standard (Table 1).

Table 1 : italian cement standard characteristics required by 1925

Max residue by sieve of 900 apertures	< 2 %
Max residue by sieve of 4900 apertures	< 20 %
Minimum density	> 3,00 g/cm^3
Setting time beginning	1 h
Setting time end	from 6 to 12 h
Flexural strength 7 days	≥ 18 kg/cm^2
Flexural strength 28 days	≥ 25 kg/cm^2
Compressive strength 7 days	≥ 180 kg/cm^2
Compressive strength 28 days	≥ 250 kg/cm^2
SO_3	< 1,50 %
MgO	< 3,00 %
$CaO / (SiO_2 + Al_2O_3 + Fe_2O_3)$	> 1,7

This type of cement, as far as compressive strength is concerned, can be compared to a 15N/mm^2 cement according to UNI-EN 196-1.

EXPERIMENTAL

During the demolition of the slabs several blocks were picked up and later used to obtain the samples.

Carbonation

A block of about 30 cm was sawed and the fresh surface treated with phenolphtalein. A non cabonated central zone was evident. The carbonation depth was about 7 cm from the top surface and about 5 cm from the bottom surface (Fig. 2).
As a result we have two types of concrete samples: carbonated and non-carbonated.

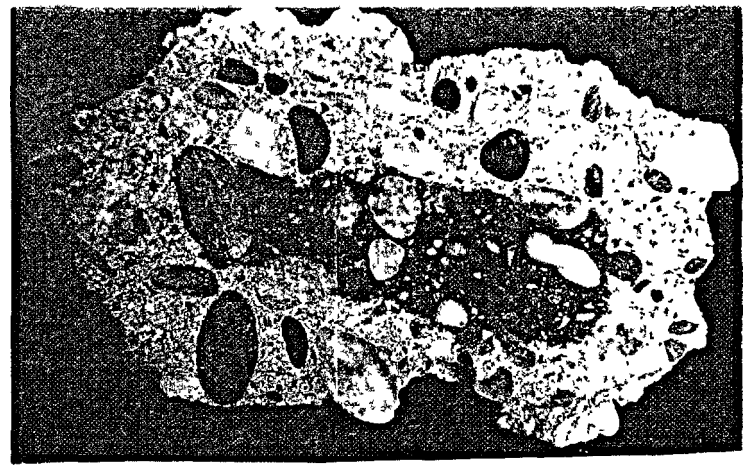

Figure 2 : carbonation depth

X-Ray Diffraction

In both types of samples we can see (Fig 3) hydrated calcium silicate (9.9 Å peak), quartz, calcite

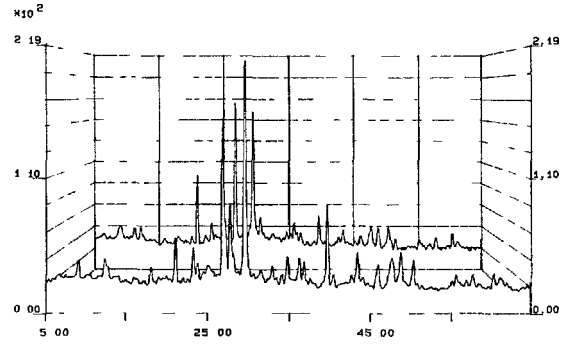

Figure 3 : X-Ray diffraction

Moreover, in the spectrum of non-carbonated concrete hydrated calcium chloroaluminate (3 CaO . Al_2O_3 . $CaCl_2$. $1OH_2O$) is present (7.92 Å, 2.93Å), while vaterite is present in the carbonated sample (3.57 Å, 2 93 Å)

Deicing salts did not react with aluminates since there is no evidence of damage. Particularly, on the carbonated surface the coumpound 3 CaO . $CaCl_2$. 15 H_2O, whose formation is thought to take place when chlorides attack concrete (Berntsson L , 1982, Monosi S., 1989; Monosi S.1990; Collepardi M ,1992), could not form since portlandite had been transformed into $CaCO_3$ by CO_2. One could have, instead, the formation of chloroaluminate, which in turn by reacting with CO_2 can originate hydroargillite, aragonite and vaterite (Rcharts W ,1969). The presence of vaterite in the carbonated sample and chloroaluminate in the non carbonated one seems to substantiate the above hypothesis.

DTA and TGA

The TGA curves up to 1100 °C (Fig. 4-5) show a total weight loss of 21% for carbonated concrete and 22% for the non carbonated one. The weigth loss at 420°C of the carbonated sample is about half that of the non carbonated sample and this is due to carbonation, while at 1030°C a larger loss is shown by the carbonated sample.

The DTA curve shows two endothermic peaks around 100°C, due to hydration products wich are almost absent in the carbonated sample and this is in agreement with the X-ray diffraction data.

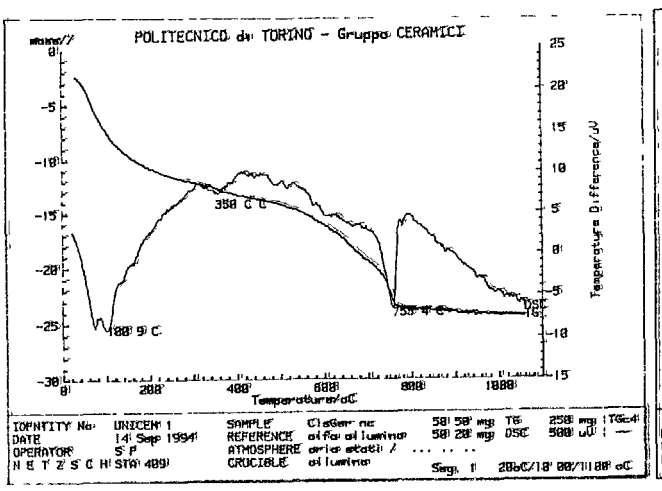

Figure 4 : DTA and TGA of not-carbonated

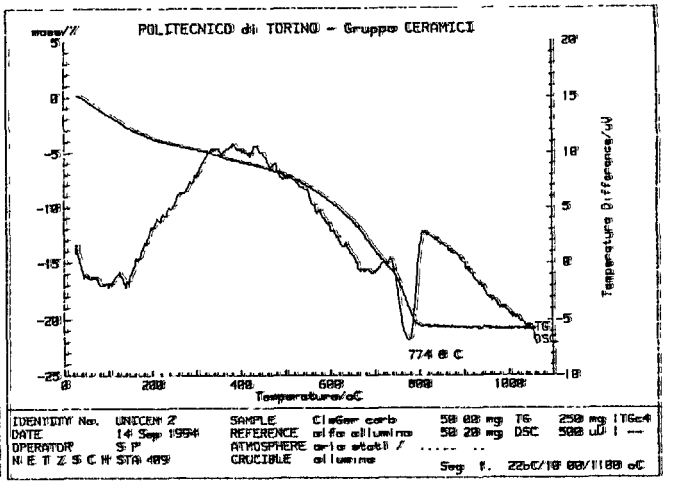

Figure 5 : DTA and TGA of carbonated

SEM

The SEM micrographs (Fig. 6-7) show a more compact and less porous carbonated sample. Also, the acicular crystal of carbonated concrete are covered by a large quantity of products of the carbonation process. Additional investigation are needed

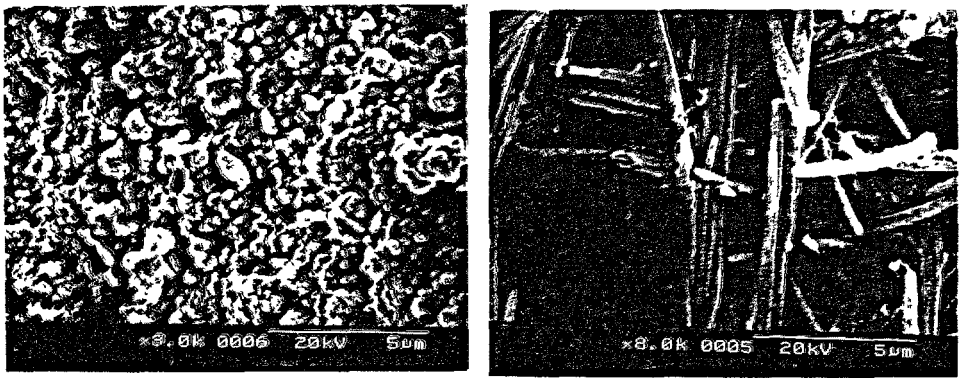

Figure 6 : SEM micrographs of not-carbonated

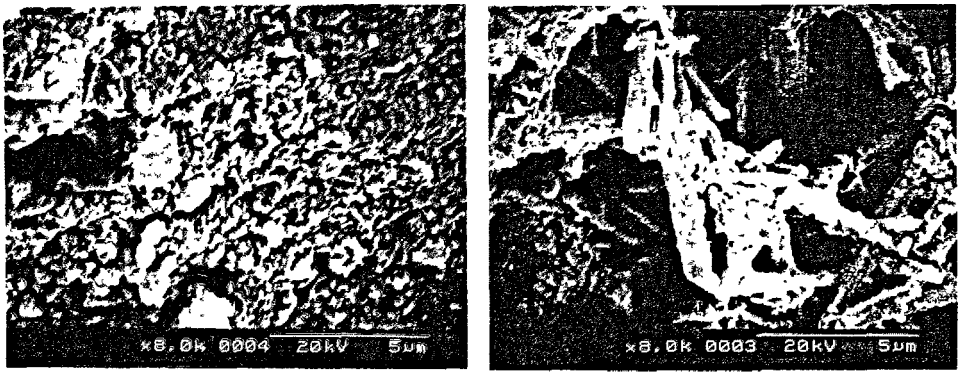

Figure 7 : SEM micrographs of carbonated

Porosimetry

It has been carried out by a mercury intrusion porosimeter on fragments of the two types of samples. The results are reported in Table 2, the figures are the average of the three most omogeneous data out of four mesurements. The carbonation did not modify the pore structure, as can be seen from the value of the mean radius, derived from the frequency curve.

Table 2 : porosimetry results

	Carbonated	Not carbonated
Total porosity (%)	25,6	19,7
Medium ray (μm)	0,05	0,05
Superficial specific area (m^2/g)	6,40	5,0

The specific surface area of the carbonated sample is, as expected, somewhat higher. The total porosity of carbonated concrete has increased. This is surprising and not in line with the SEM data that showed, at first sight, a less porous carbonated concrete as a consequence of the formation of carbonation products. The situation can be explained by considering that in the carbonated sample there is a chloride concentration, varying as a function of the depth, from 0.13 to 0.06% by weight.
The increased porosity may originate from the initial attack by the chloride, with the formation of calcium oxychlorides, because the frequent use of deicing salts. The development of the carbonation process seems to have slowed down and minimized the chloride attack. The use of deicing salts in Northern Italy during winter is very frequent and, also, the road under examination goes through the town. Anyway, we must remark that a porosity aroung 20% indicates a correctly made concrete, with a water/cement ratio near 0.50, certainly less than 0.55.

Physical and mechanical properties
Cubic samples of about 60 mm side were cut by using a diamond saw from one of the largest blocks, after determination of the carbonated area by the phenolphtalein method. Density and compressive strenght measurements were carried out (Table 3). Each reported value is the average of two samples. The data agree with the higher porosity of carbonated samples, wich gives a slight reduction of the mechanical properties. One could have expected, as a consequence of carbonation and the resulting increase in compactness, an increase in compressive strength. But the use of deicing salts changed the situation and the carbonation limited to a minimum the formation of oxychlorides (Collepardi M.; Monosi S., 1992; Collepardi M., 1994). The density value indicates that the concrete was accurately cast and had a low water/cement ratio.

Table 3 : physical and mechanical results

	Carbonated	Not carbonated
Compressive strength (N/mm2)	13,5	15,5
Density (g/cm3)	2,30	2,38

CONCLUSIONS

It can be said that this 54 year old pavement, even if deeply carbonated and with a relatively low compressive strength but in line with the performances required by the standards of the time, behaved remarkably well for a long time and with heavy traffic, without any maintenance, except the filling of the joints with bitumen. In this case the carbonation process played a positive role in limiting the effects of the frequently used deicing salts.

REFERENCES

Berntsson L., S.Chandra - Cement Concrete Research 12 pag.87-92 (1982)
Monosi S., I.Alvera, M.Collepardi ''L'attacco chimico del $CaCl_2$ sulla pasta di cemento portland'' - Il Cemento 2/1989

Monosi S., M.Collepardi ''Ricerca sul $3CaO*CaCl_2*15H_2O$ identificato nei calcestruzzi attaccati dal $CaCl_2$'' Il Cemento 1/1990

Collepardi M., S.Monosi Proc. of the 9° Congress on the Chemisty of Cements - Vol.5 pag.389-395, New Dehly (1992)

Rcharts W. Zement, Kalk, Gips, 10, pag.447-456 (1969)

Collepardi M., L.Coppola, S.Monosi ''Degrado del calcestruzzo provocato dal $CaCl_2$'' - Atti del Congresso "Omaggio scientifico a R.Turriziani"

Monosi S., M.Collepardi ''Influenza del contenuto di C3A sull'aggressione di paste cementizie da parte del $CaCl_2$ ''- Il Cemento 2/1992

Collepardi M., L.Coppola, C.Pistolesi ''Durability of concrete Structures exposed to $CaCl_2$ Base Deicing Salts'' - CANMET/ACI 1994 - Durability of Concrete p.107-120

STRUCTURE AND PERFORMANCE OF POROUS CONCRETE

Anne BEELDENS, Katholieke Universiteit Leuven, Belgium
Dionys VAN GEMERT, Katholieke Universiteit Leuven, Belgium
Etienne DE WINNE, Universiteit Gent, Belgium
Benny DE BLAERE, Universiteit Gent, Belgium
Chris CAESTECKER, Ministry of the Flemish Community, (LIN), Environment and Infrastructure Department, Flemish Brabant Road Division, Belgium
Marc VAN MESSEM, Ministry of the Flemish Community, (LIN), Environment and Infrastructure Department, Flemish Brabant Road Division, Belgium

ABSTRACT Porous concrete is a polymer modified cement concrete, designed to obtain high open porosity. The addition of polymer emulsion to the mixture provides the required workability and strength. The paper presents the results of the experimental study and discusses the structure of the porous polymer cement concrete and its performances.

Key-words: Composition, durability, porosity, structure.

INTRODUCTION

Porous concrete, also referred to as very open concrete (VOC) is a polymer modified concrete, designed to obtain high porosity (25% to 30% accessible porosity). This open structure makes the VOC well suited to be used as top layer on roads since it provides noise reducing capacities and good drainage properties. The durability and low maintenance, proper to concrete, allow to presume a long service life and little or no rutting under heavy traffic, which makes the open concrete preferable over open black topics.

The porosity is achieved by means of a gap-graded aggregate distribution in which there is a very low proportion of fine aggregates. In this research aggregates 4/7 mm are used, together with a small amount of fine sand 0/1 mm. Addition of polymer emulsion to the mixture gives the VOC the necessary tensile and compressive strength to withstand thermal stresses and traffic loads.

Laboratory tests concentrated on the physical and mechanical properties of the porous concrete, such as workability, porosity, strength, resistance against abrasion, freezing and thawing resistance and adhesion on a concrete sublayer. Three different kinds of polymer emulsions are tested. Besides the test results, the paper discusses the specific structure of the VOC and the influence of the cement-polymer paste on this structure and on the properties of the VOC.

MIXTURE PROPORTIONING

The basic mixture proportions are given in Table 1. The coarse aggregate size is chosen to be 4/7 mm and occupies 50 % of the volume of the fresh mixture. Larger aggregate sizes produce larger porosity but will diminish the workability of the VOC and the evenness of the surface, which is required for the noise reducing properties (Onstenck et al., 1994). A small amount of fine sand 0/1 mm is used. The cement used is CEMIII/A/42,5/LA. This cement is used because it is less subjected to shrinkage and it provides good resistance against environmental actions, primarily frost-thaw and thawing salts.

Four different types of polymer emulsions are used: two acrylic emulsions, one styrene-acrylic

emulsion and one styrene-butadiene emulsion. The polymer-cement ratio is equal to 0.10 (weight solid mass of the polymer emulsion/weight cement). The water-cement ratio is equal to 0.3 (water of the emulsion included).

Table 1 Mixture proportioning for the VOC

Coarse aggregate 4/7	1350 kg/m^3
Fine aggregate 0/1	90 kg/m^3
Cement CEM III/A/42.5	280 kg/m^3
Polymer emulsion (50% solids)	56 kg/m^3
Water (emulsion water not included)	56 kg/m^3

The mixing of the VOC is done as described by Ohama (Ohama Y., 1995): first the coarse aggregates, the sand and the cement are placed in the mixer. During mixing, first the water and consequently the polymer emulsion are added. Afterwards, mixing continues during 2 minutes. The curing conditions were taken similar to the outdoor conditions: the samples were covered by a polyethylene sheet during two days. After demoulding the samples were stored under laboratory conditions, sheltered from air current.

PROPERTIES OF THE FRESH MIXTURE

The workability of the fresh mixture is tested by means of the flow-test, according to NBN B15-233. The flow-index varies between 1.42 and 1.55 for the different mixtures, as indicated in Table 2.

Table 2 Results of the flow-test for the different mixtures

Acrylic emulsion 1	1.42
Acrylic emulsion 2	1.53
Styrene-Acrylic emulsion	1.55
Styrene-Butadiene emulsion	1.53

The first acrylic emulsion used gave a lower workability-index. This lower performance could be observed through all the tests. This can be explained by the type of polymer emulsion used: the first acrylic emulsion contains 50% solids, the second acrylic emulsion on the contrary only 30%. It seems that especially the larger amount of water, present in the second case improves the workability of the VOC. Also the type of polymer is important: the styrene-acrylic and the styrene-butadiene emulsion both contain 50% of water. Even though they show a good workability.
Another property of the fresh mixture is the behavior at compaction. This property is depending on the compaction method used (shocking, vibrating, with or without an extra weight placed on top of the sample), on the amount and the composition of the cement-polymer paste, on the sizes and the form of the aggregates and on the type of polymer modification. The possibility to compact is measured by means of the degree of compaction, equal to the density after compaction, divided by the calculated density at 27% porosity. The mixture proportioning is made to obtain approximately 27% of air volume into the sample at 100% vibration, with a (fresh) density equal to 1830 kg/m^3. Table 3 shows the results for the mixtures made with different types of polymers after shocking the samples and after vibration during 30 seconds. The third column shows the

density calculated on the fresh mixture, by means of a cylinder with a content equal to 8 liter, after compacting the fresh mixture by shocking the sample 8 times on the shock table, used for the ABRAMS flow-test according to the standard NBN B15-233 .

Table 3 Degree of compaction

	Vibrated		Shocked		Fresh mixture	
	density [kg/m^3]	degree of compaction [%]	density [kg/m^3]	degree of compaction [%]	density [kg/m^3]	degree of compaction [%]
Acrylic emulsion 1	1703	93%	1355	74%	-	-
Acrylic emulsion 2	-	-	1827	100%	1847	101%
Acrylic-Butadiene emulsion	1977	108%	1718	94%	1842	101%
Styrene-Butadiene emulsion	1981	108%	1699	93%	1821	99%

Similar results as in the flow test appear: the first acrylic emulsion reaches a much lower degree of compaction than the mixtures made with the other polymer emulsions, even though an identical compaction method is used. Differences between the other polymer emulsions are small, especially for the fresh mixture, where the degree of compaction is a reflection of the workability. Remarkable however is the good performance of the second acrylic emulsion: in spite of the low content of solids in the polymer emulsion, the mixture obtains a high degree of compaction and also produces good mechanical properties and a high durability.

The results show that the density obtained after compacting the sample depends not only on the compaction method, but also on the polymer emulsion used. To reach a degree of compaction of 100%, which corresponds to a porosity of 27%, it is necessary that the coarse aggregates are well positioned one towards the other to fit into each other. Shocking apparently does not produce enough energy to turn the aggregates into the right position. When the samples are vibrated, the coarse aggregates can more easily turn to form a compacter volume. To compact, the aggregates also have to overcome the frictional resistance between the aggregates. This is promoted by the polymer-cement paste. During mixing, the polymer-cement paste forms a fine layer around the aggregates. Polymer modification improves the compactibility of the concrete, due to the ball bearing action of the polymer particles and the dispersing effect of the surfactants, added to the emulsion (Ohama Y., 1995) and allows a good surrounding of the aggregates. The influence of the polymer in general is clearly visible: without polymer addition, the cement paste is not able to form a continuous layer around the aggregates. Therefore, the degree of compaction as well as the workability will be much lower in that case. The cement paste will not be continuously distributed over the material, which will also cause a decrease in strength.

The form of the aggregates is also important: gravel (round aggregates) will roll more easily over each other and will lead to a VOC with a smaller porosity, at the same compaction energy; VOC made with broken porphory aggregates on the other hand will be submitted to a much higher internal friction and will have a lower workability and a higher porosity. The form of the

aggregates will partly determine the final porosity of the VOC.

PROPERTIES OF THE HARDENED POROUS CONCRETE

The test program for the hardened porous concrete concentrated on the relationship compressive/tensile strength versus total/accessible porosity, related to the dry density of the samples. The test program included also performance and durability tests, such as freezing and thawing resistance, resistance against abrasion and against alkaline environment and the determination of the adhesion of the VOC on a concrete sublayer.

The relation total porosity-compressive strength is investigated by measuring the total porosity and the strength after 28 days on cubes of 150x150x150mm^3. Also the dry density of the cubes is measured. The relation total porosity-compressive strength and the relation total porosity-dry density are both linear (Fig 1 and Fig 2). A similar relation can be found between the tensile strength and the total porosity.

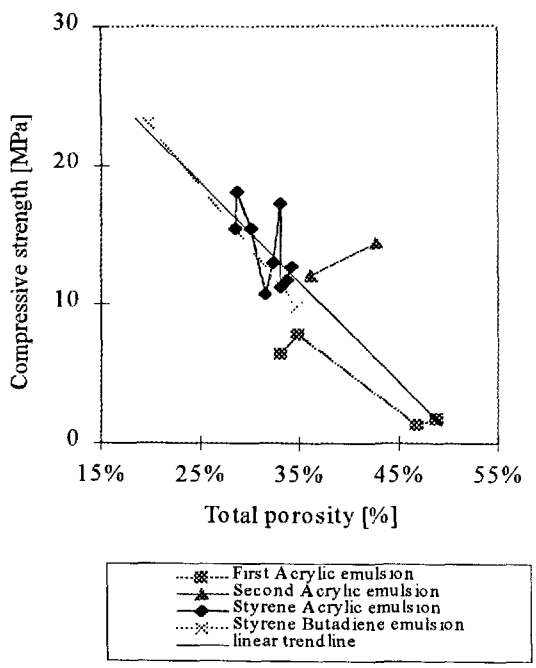

Figure 1 Total porosity-compressive strength

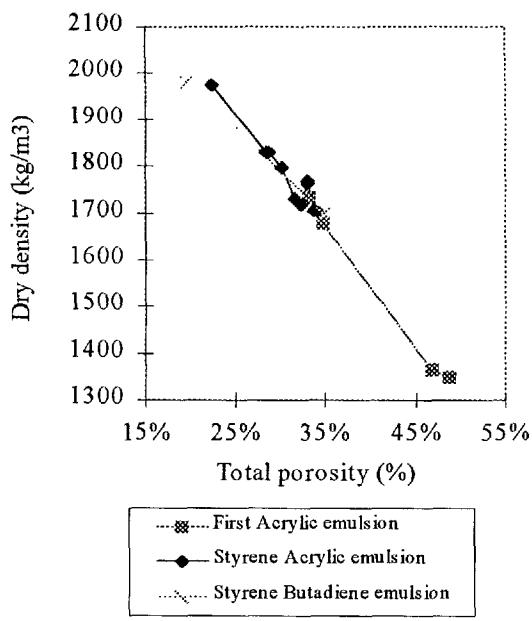

Figure 2 Total porosity-dry density

The influence of the kind of polymer is not directly visible in the relation strength-porosity. The kind of polymer plays a role in the compaction degree, obtained with the addition of a certain amount of energy, and consequently in the obtained porosity. Therefrom one observes the high porosity and the low strength for the samples made with the first acrylic polymer emulsion, since the possibility to compact was much lower for this mixture.

The durability of the VOC is tested on samples, which simulate the pavement conditions: VOC is laid on a concrete sublayer according to the wet-in-wet method. First the concrete sublayer (150 mm thick) is placed. After approximately three hours, the VOC layer (40 to 70 mm thick) is placed on top of the not completely hardened sublayer. Depending on the time between the placing of the two layers and depending on the compaction method of the VOC, the VOC and the concrete

sublayer will penetrate into each other. This will improve the adhesion of the VOC to the sublayer, but will gradually diminish the porosity over the height of the VOC layer.

The following performance and durability tests will be discussed briefly: abrasion test, road simulation test and resistance against freezing and thawing, with or without the addition of salts. The tests are carried out on samples made with the styrene-acrylic emulsion.

The abrasion test revealed promising results: no damage was visible and the abrasion was limited to 5% loss in thickness. The road simulation test showed similar results: after 100 000 cycles with a tire, which was inclined over 5° and submitted to a force equal to 5.5 kN, only a few aggregates came out of the VOC. These tests indicate that the VOC can withstand loads imposed by heavy traffic.

The freezing and thawing resistance is determined according to the European standard prEN 1340 (1993) on samples made with different polymer emulsions. Cores were taken from the two layer samples and were at the sides completely surrounded with an impermeable rubber cloth, in such a way that the VOC is completely submerged in water or ice during the whole test. 28 cycles are carried out, varying the temperature between -20°C and +20°C. To test the influence of a freezing medium, some of the samples were submerged with a 3% NaCl-solution. At the end of the test, the samples were unpacked, cut in two and visually inspected.

The samples made with the second acrylic emulsion and with the styrene-butadiene emulsion, tested without freezing medium were cracked at the transition of the VOC to the sublayer. For the samples, were the two layers flowed into each other, the crack was capricious, for the samples where the transition line was clearly visible, the crack formed also a straight line. The samples made with the styrene-acrylic emulsion showed no damage.

The samples tested with the 3% NaCl-solution were not damaged in the transition zone between the open concrete and the sublayer, but the upper surface of these samples was attacked by the salts. All the samples in this case showed similar damage: the aggregates from the upper surface were ripped of. Although the results were not completely satisfying it can be said that the VOC showed good durability, since the freezing-thawing test is very severe: in real circumstances, the water can flow out of the VOC due to the large porosity before freezing.

To ameliorate the freezing thawing resistance, a new mixture proportioning is introduced, where a part of the sand is replaced by cement. The polymer-cement ratio is not changed. Further study has to be made to reveal the influence of the amount of polymer emulsion added.

STRUCTURE

VOC is characterized by a specific structure with a large porosity. At 100% compaction it is composed of 50 volume-% coarse aggregate, 23 volume-% mortar (cement, polymer emulsion, water and sand), and 27 volume-% air. Macroscopically, three phases can be distinguished, which are homogeneously spread over the material (Fig 3). One phase consists of coarse aggregates and is discontinuously divided over the material. The second phase is continuously spread over the material and consists of the cement-polymer paste. This paste forms a matrix in which the coarse aggregates are embedded: the paste forms a fine layer (0.5 to 1 mm thick) around the aggregates and binds them together by means of 'bridges'. The third phase consists of the large pores, connected with each other through the material. These pores form a second matrix, twinned with

the cement-polymer comatrix.

Figure 3 shows an enlargement (50 X) of the mortar-film around an aggregate and of a 'bridge' connecting the aggregates, taken by means of a scanning electron microscope (SEM). Ideally the VOC is composed to contain just enough mortar to form a film around the aggregate and to connect the aggregates by means of "bridges", but not enough mortar to fill the open pores between the aggregates.

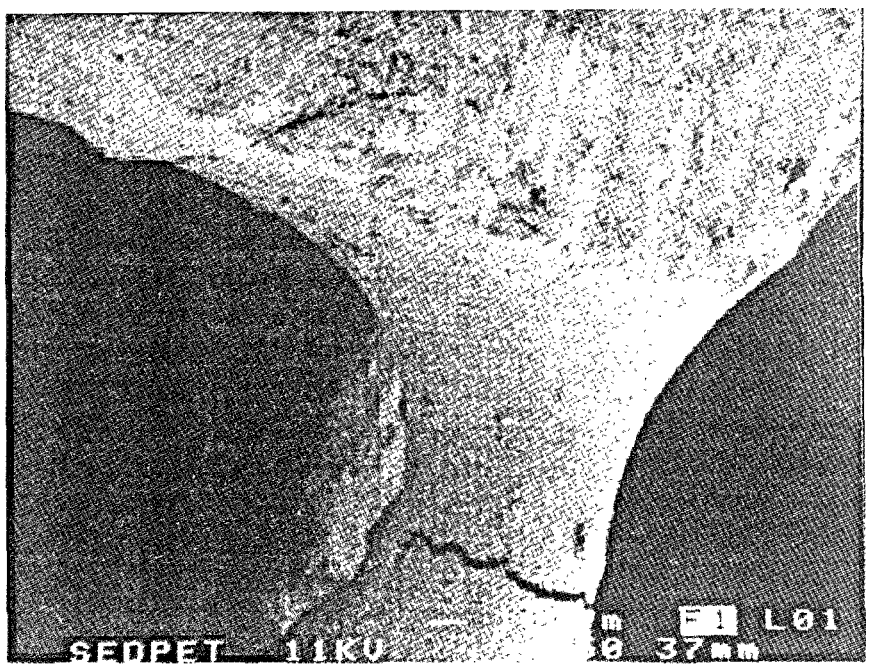

Figure 3 Cement-polymer comatrix around and in between aggregates (50 x)

Comparison between the samples made with and without polymer emulsion, indicates that the polymer facilitates the adhesion of the cement-polymer paste to the aggregate. A visual control of reference samples without polymer addition showed an incomplete covering of the aggregates by cement paste. With polymer addition (Fig 4), one observes a complete covering of the aggregate by the cement polymer paste. However the adhesion of the cement-polymer paste to the aggregate is present though not uniform. As shown in the central part of Fig 4 small pores and small cracks are present along the aggregate. This larger porosity decreases the strength of the transition zone. Ideally the VOC should contain a high amount of large pores, but a very low amount of small pores, which means that the difference between the total porosity and the accessible porosity should be as small as possible.

The task of the cement-polymer paste is dual: it provides the workability of the fresh mixture and enables a good compaction of the mixture; secondly after combined hydration and polymerization it produces a comatrix in which the aggregates are embedded. This comatrix provides the strength of the VOC. As seen in Fig 3, failure will occur in the weakest point: cracks occur at the bridges, where the cross-section is the smallest.

In general, failure occurs at three different places (Fig 5): in the bulk cement-polymer paste, in the transition zone between the aggregate and the paste and through the aggregate itself. In the second

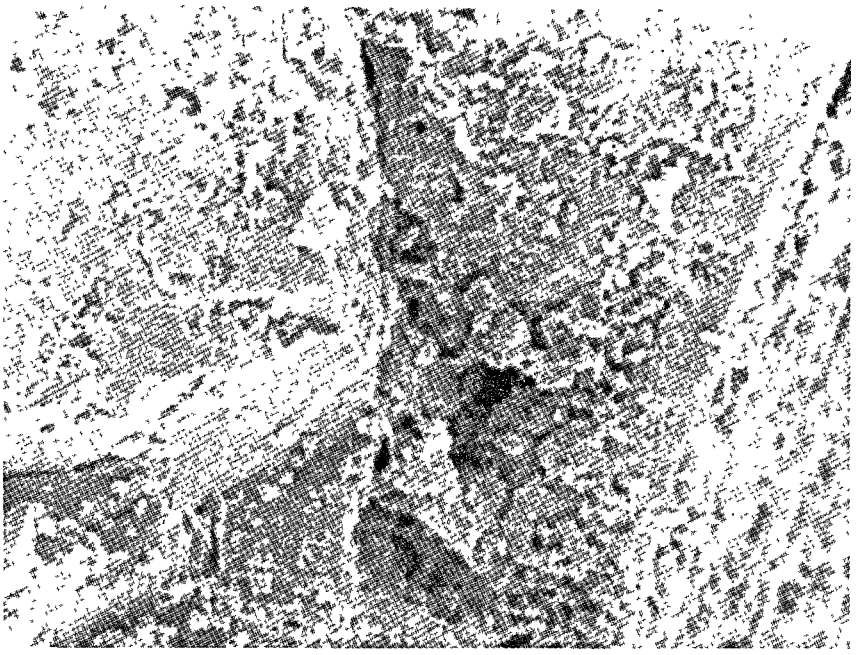

Figure 4 Transition zone between the polymer-cement and the aggregate (400 x)

case the cement-polymer paste is ripped off the aggregate. This is due to the larger porosity of the transition zone and to the non-uniform adhesion of the cement-polymer paste to the aggregate. The addition of the polymer emulsion will contribute to the stiffness and the tensile strength of the very open concrete: the formation of a continuous polymer film through the comatrix will increase the elasticity of the comatrix and will enlarge the resistance to tensile forces. However, care has to be taken to set bounds to the amount of polymer emulsion added. If a large amount of polymer

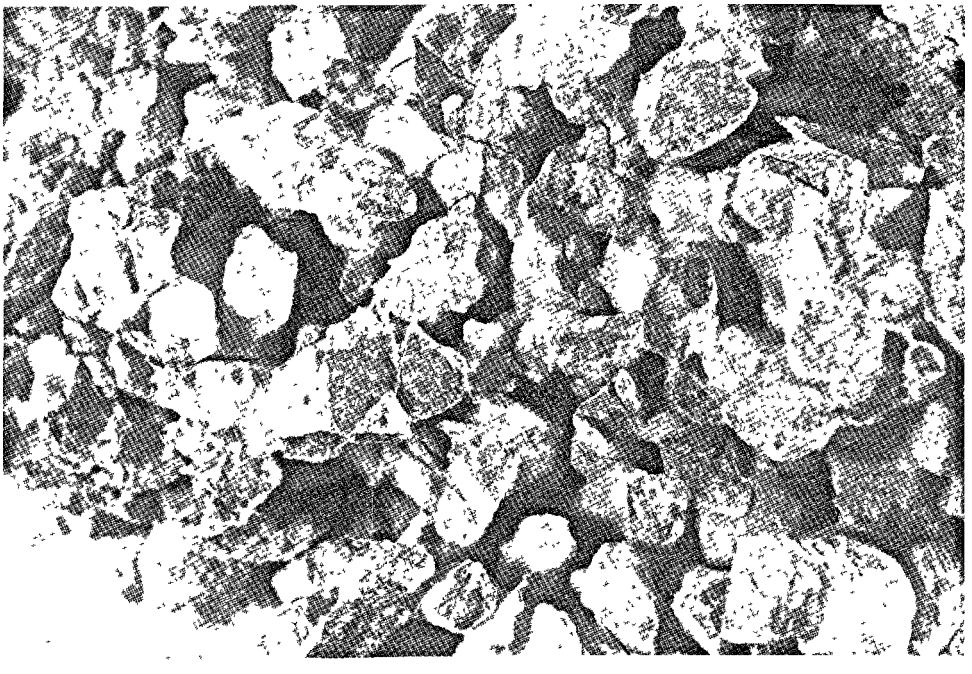

Figure 5 Fracture surface of VOC after compression test

emulsion is added, the cement particles can be completely surrounded by polymer emulsion and further hydration of the cement particles will be prohibited, and the formation of a continuous structure will not be possible anymore.

This kind of structure can also arise from a faulty mixing procedure: if the addition of the polymer emulsion to the mixture takes place before the water is added, the polymer emulsion will immediately enclose the cement particles and will prevent all contact with water to allow further hydration. The 'ideal' situation, where the cement hydration and the polymerization act together and where the cement hydrates are covered with polymer films will not be possible in such case. Besides an excessive amount of polymer will make porous concrete uneconomical.

CONCLUSIONS

Porous concrete is a polymer cement concrete, built up of three phases: the aggregates, the cement-polymer phase and the open pores. The open pores are connected with each other through the material and form a second matrix besides the matrix, consisting of cement hydrates and polymer films. The addition of the polymer emulsion improves the workability of the fresh mixture, enables a high degree of compaction and ameliorates the mechanical properties of the porous concrete. Care has to be taken at mixing: the addition of the polymer emulsion to the mixture before the addition of the water can hinder the continuous hydration of the cement particles.

REFERENCES

Ohama, Y., "Handbook of polymer-modified concrete and mortars, properties and process technology", Noyes Publications, 1995.

Onstenck, H.J.C.M. et al., "Concrete Pavements: safe and sound-proofing" (in Dutch), CUR-rapport 94-11, Centrum voor regelgeving en onderzoek in de grond-, water- en wegenbouw en de verkeerstechniek, Gouda, 1994.

Brite/Euram State of the art report, "Surface properties of concrete roads in accordance with traffic safety and reduction of noise", Brite/Euram project BE 3415, October 1994.

THE UNSATURATED MASS TRANSFER THROUGH HARDENED CEMENT PASTE MODIFIED BY THE PARTIAL REPLACEMENT WITH SILICA-FUME: THE SORPTIVITY AND VAPOUR PHASE TRANSPORT

Don FAIRHURST, University of Central Lancashire, Preston, England
Dr Andrew K PLATTEN, University of Central Lancashire, Preston, England

ABSTRACT In this paper the Sorptivity is reaffirmed from its introduction by Philip with a simplified mathematical method examined. Published values for the Sorptivity of hardened cement pastes are scarce for silica-fume blended pastes. This paper addresses the latter point, with values presented for pastes at 1, 3 and 7 days of age for 5 and 10% replacements. Further, values are presented for the vapour phase permeability obtained by diffusion cell technique, of 1, 3, and 7 day old hardened cement pastes, modified by partial replacement with silica-fume at 5% and 10% levels.

Key-words: Water sorption, Water suction, Porosity, Diffusivity, Permeability

INTRODUCTION

The fundamental transport mechanism underlying the unsaturated mass transfer through a porous body is the capillary diffusion. Under isothermal conditions, and disregarding osmotic effects, the hydraulic Diffusivity is a dominant function of the moisture content. For these defined conditions, the movement of moisture within the porous body is created by potentials arising from moisture gradients within the body and the subsequent attainment of equilibrium between these potentials. For practical purposes, the unsaturated state more readily reflects field conditions for building structures subject to wetting and drying cycles. This places an emphasis upon the study of unsaturated mass transfer and the need to develop models based on experimental data, that will allow predictive analysis of the serviceability of cementitious structures. To facilitate this, three transfer mechanisms have been studied for hardened cement pastes only.

In this paper, the Sorptivity (mathematically related to the hydraulic Diffusivity), is discussed with values presented for the Sorptivity of Condensed Silica-fume (csf) pastes. Unsaturated flow theory, however describes two phases of moisture movement within the porous body (liquid and vapour).

RELATED WORK

The effects on silica fume addition has been reported by many workers with respect to the mass transfer properties of concretes. In the context of concrete, the sensitivity of the Sorptivity to variations in the water/cement ratio and compaction, have been examined by Hall (Hall and Yau, 1987). Where, the Sorptivity was reported to reduce in magnitude with respect to increased compaction, but being relatively insensitive to the water/cement ratio. The presence of aggregate is known to reduce the Sorptivity (Marchese and D'Amore, 1990), both structurally in terms of tortuosity, and chemically at the paste/aggregate interface. Further, the quality and composition of concrete is variable within a very short distance from the cast surface (Emeritus, 1987), leading to anisotropic medium whose mass transfer properties are not constant. Such phenomena has been shown to influence the Sorptivity (McCarter, 1993). This paper considers the effects of silica fume inclusion, to the cement paste, with respect to the properties of

unsaturated mass transfer. Thus, dispersion and chemical effects associated with the presence of aggregates in concrete or mortars, require further study.

GENERAL CONCEPTS

Liquid Phase Unsaturated Flow

Derivation of the Sorptivity and General Unsaturated Flow Equation

It is common place to consider the parameter of Sorptivity as the rate of hydraulic absorption and infiltration of moisture into the porous matrix. The Sorptivity as a material property relates to the mass transfer of moisture into an initially dry porous body, where the driving force is predominantly derived from capillary tension.

Philip (1957), introduced the term Sorptivity (S), as a material property to describe the cumulative absorption (i), into a medium for elapsed time (t), with i being expressed so:

$$i = (\theta_1 - \theta_0)\int_0^1 x \, d\theta \qquad [1]$$

For the one dimensional flow of a liquid from a saturated surface into an initially dry semi-infinite porous solid, the distance (x), advanced of the wetting front, with respect to time, is given by:

$$x(\theta,t) = \lambda(\theta)\, t^{0.5} \qquad [2]$$

giving:

$$\lambda(x,t) = x\, t^{-0.5} \qquad [3]$$

In this instance the volumetric moisture content (θ), is taken as being a single function of λ, and substituting Eq 3 into Eq 1, gives the cumulative mass absorbed for elapsed time as:

$$i = \left[(\theta_1 - \theta_0)\int_0^1 \lambda \, d\theta\right] \cdot t^{0.5} \qquad [4]$$

with, the Sorptivity being defined by:

$$S = (\theta_1 - \theta_0)\int_0^1 \lambda \, d\theta \qquad [5]$$

Eq 3 states that the relationship for the distance advanced for the infiltrating moisture is linear with respect to the square root of time. Thus, not only can i be determined, but also the moisture content and its position in the porous body.

Experimentally, moisture gradients can be determined either destructively (Bruce and Klute, 1956), or by non-destructive means such as Gamma-spectrometry (Kumaran and Bomberg, 1985), and Electrical Resistivity (McCarter *et al*, 1996).

Simplified solutions exist (Kirkham and Powers, 1972), when the mass transfer properties are known, then prediction of the both the cumulative mass absorbed and distance advanced of the wetting front is possible. Though these solutions are an over simplification and more readily suited to soil hydrology, the basic relationship of porosity to both absorption and distance advanced are shown by:

$$i = \left(-2n_e\, k\, \Delta h_t\, A^2\right)^{0.5} \cdot t^{0.5} \qquad [6]$$

and,

$$x = \left(\frac{-2k\, \Delta h_t}{n_e}\right)^{0.5} \cdot t^{0.5} \qquad [7]$$

where,

k = the permeability (cm sec^{-1})
h_t = the hydraulic suction derived from the internal pore structure (cm)
n_e = the effective porosity

It is clear that i is proportional to the square root of the effective porosity, n_e with x being inversely proportional to the square root of n_e. The relationship of $i(t^{0.5})$, is considered in this paper. Eqs 6 and 7 introduce the components of the Darcy saturated flow equation (Darcy, 1856), expressed so:

$$i = -k\left(\frac{h}{x}\right) \qquad [8]$$

With, the second term RHS representing the hydraulic gradient, or pressure acting over distance. It must be remembered that Eq 8 is valid for flow through a saturated body and must be adapted for unsaturated flow, *viz.* k is a function of θ, possessing high values reaching saturation and decreasing to zero at dryness. The reduction in k with lowering θ is due primarily to reductions in the cross section available for flow and reduction in continuity of the liquid phase, thus flow must occur by other means than direct transfer (Rose, 1963); with h being a function of θ, whose magnitude is greater at low values, and zero at saturation. Thus, k and h must be qualified as being functions of the moisture content, $k(\theta)$ and $h(\theta)$, resulting in the extended Darcy flow equation, expressed as:

$$\frac{\partial \theta}{\partial t} = -\frac{\partial}{\partial x} k(\theta)\left(\frac{\partial h}{\partial x}\right) \qquad [9]$$

or, in the form of a moisture concentration difference, by:

$$\frac{\partial \theta}{\partial t} = \frac{\partial}{\partial x}\left(D(\theta)\frac{\partial \theta}{\partial x}\right) \qquad [10]$$

where,

D = hydraulic Diffusivity (cm^2 sec^{-1})

and is defined by:

$$D(\theta) = K(\theta)\frac{\partial \psi}{\partial \theta} \qquad [11]$$

where,

ψ = capillary force (cm) equivalent to h_t

Eqs 9 and 11 form the basis deriving solutions to the vapour phase flow now discussed.

Vapour Phase Unsaturated Flow

In the case of vapour transfer, ψ is the moisture potential in thermodynamic equilibrium with the water in a porous material with atmospheric pressure as datum, and is related to vapour pressure by:

$$rh = \exp\left(\frac{-Mg\psi}{RT}\right) \quad [12]$$

giving:

$$\left(\frac{RT}{Mg}\right) \ln rh = -\psi \quad [13]$$

$\left(\frac{RT}{Mg}\right)$ = 14279m for water at 30°C the working temperature used in this work, with the negative term indicating an expenditure of work associated with suction. Thus, where the vapour pressure potential determined by Eq 13, the vapour permeability is solved by:

$$i = -k_v \frac{\Delta\psi}{x} \quad [14]$$

with the vapour Diffusivity solved using Eq 11 by:

$$D_v(\theta) = k_v(\theta)\left(\frac{\partial\psi}{\partial\theta}\right) \quad [15]$$

The relationship of vapour phase transfer to that of hydraulic, can be observed at the tail of a moisture distribution plot. Though differentiating is difficult to determine from such plots, isolation of the vapour phase makes quantitative analysis possible, and therefore provides a full history of the moisture transfer process.

MATERIALS DETAILS

In this study, pastes used for the determination of the Sorptivity were modified by Elkem 500S "Microsilica", and for vapour phase analysis modified by "Micropoz". Samples used in the study of the Sorptivity were cast from 100mm diameter moulds, de-moulded after one day, and bath cured until the age of test. The samples were then cut to expose the structure of the paste and dried to a constant mass in a vacuum oven at 40°C. Samples used in the study of vapour phase flow were cast from 40mm diameter rings (≈2mm thickness), bath cured until the age of test and dried as before to a constant mass. A constant water/cement ratio of 0.5 was used throughout this study.

EXPERIMENTAL

The determination of the Sorptivity was undertaken using the method detailed by Hall (1989); where water from a free-water reservoir, is allowed to vertically infiltrate an isotropic sample of uniform initial moisture content. The cumulative mass absorbed was determined gravimetrically with respect to elapsed time.

Porosity was determined gravimetrically using water displacement. The samples were subjected to a vacuum pressure of 1 bar, for 10 minutes to remove entrapped air within the pore structure, which was displaced by infiltrating water. Samples were left to absorb water for 24 hours, whereupon their saturated mass was determined.

Vapour phase analysis was undertaken using a modified method of BS 3177 (1959); where the mass transfer through a sample, brought into an equilibrium moisture content, was determined gravimetrically with respect to elapsed time.

The samples were subjected to various relative humidities in a Vindon humidity cabinet. A vapour sink was supplied from silica-gel, maintaining zero moisture content in the diffusion cell. Thus, a potential difference in vapour pressure acted between the samples surface, inducing vapour flow.

RESULTS

The Sorptivity

The Sorptivity for the pastes studied in this work has been derived from the gradient of a straight line plot of $i(t^{0.5})$. For a straight line to be represented, four conditions must be satisfied: 1) the material must be homogeneous throughout the region of ingress, 2) the capillary absorption must be normal to the inflow face, neither converging nor diverging, 3) the water must be freely available at the suction surface, and 4) gravitational effects must not affect the absorption process. The pastes studied in this work satisfy the four conditions.

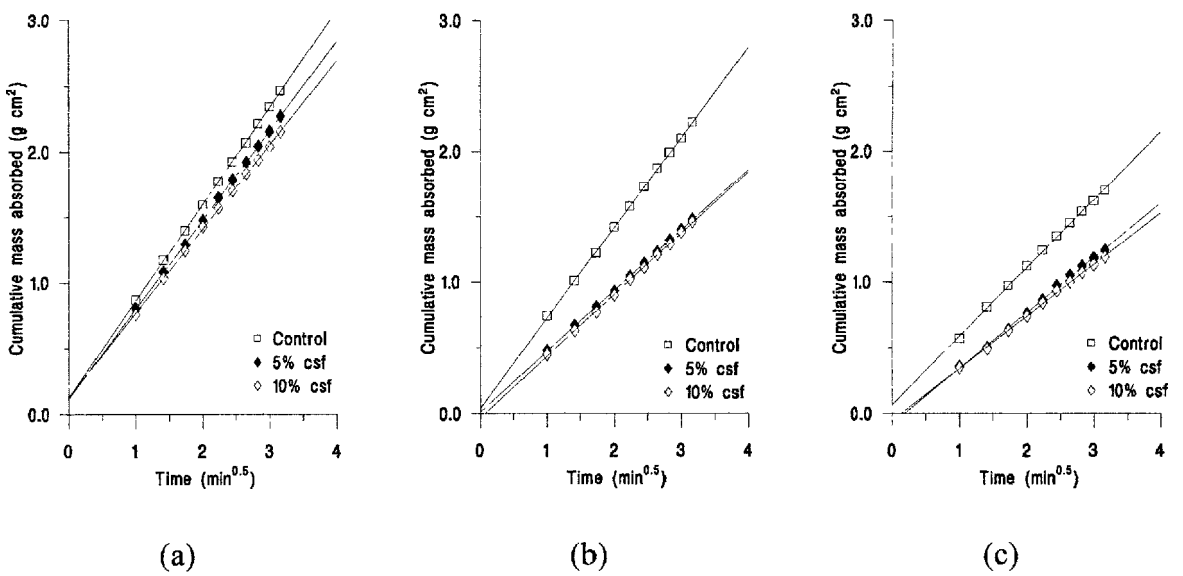

Figure 1 Cumulative mass absorbed for elapsed time for pastes at 1, 3 and 7 days of age (1a, 1b and 1c)

Qualification of the linear relationship of mass absorbed to the square root of time is illustrated in Fig 1, thus satisfying the four conditions of derivation from the gradient of $i(t^{0.5})$. Collectively, the data illustrate the effects of hydration on the water absorption properties of the

pastes. Individually, the data provides clear evidence of the effect of csf replacement, both for age of paste and percentage of replacement. Specific values for the Sorptivity of the pastes are presented in Table 1, with the results summarised as follows:

Table 1 Values for the Sorptivity

Age (days)	Replacement (%)	Sorptivity (mm $min^{0.5}$)
1	0	7.35
	5	6.82
	10	6.40
3	0	6.88
	5	4.62
	10	4.69
7	0	5.20
	5	4.20
	10	3.96

- 1 day pastes, Fig 1(a)- Though the water absorption of the pastes are comparable, both 5% and 10% csf replacement pastes exhibit reductions in the order of 7% and 12% respectively compared to the control paste.
- 3 day pastes, Fig 1(b)- At 3 days of age, the pastes exhibit reductions to 1 day values in the order of 6%, 32% and 27% for the control, 5% and 10% pastes respectively. Further, comparison with the control paste for the same age shows the 5% and 10% to have lower Sorptivity values in the order of 30% and 32% respectively, where a distinct banding is evident for csf pastes.
- 7 day pastes, Fig 1(c)- At 7 days of age, reductions in the Sorptivity are exhibited by all pastes, with values representing reductions in the order of 29%, 38% and 38% from day 1 values. Comparison with the control paste at the same age, shows the csf pastes again exhibiting lower values, in the order of 32% and 36%, for 5% and 10% replacement respectively.

For all ages of pastes, it is evident from the values presented, that whilst there is some reduction to the Sorptivity for increased csf replacement, this reduction is negligible.

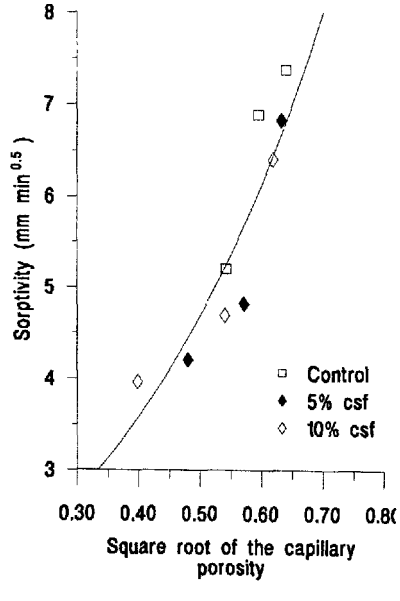

Figure 2 Relationship between the Sorptivity and square root of the porosity

Relationship between the Sorptivity and Porosity

A simplified method for deriving the cumulative mass absorbed has been discussed, Eq 6, where the Sorptivity was shown to be proportional to the square root of the porosity. Whilst it is reasonable to assume the Sorptivity to be proportional to the porosity mathematically, the linear relationship is not found to exist in the case of the cement pastes studied in this work. This is illustrated in Fig 2, where the plotted data follows a best fitted exponential curve (Sorptivity = $\exp^{(1.61x)}$), though the accuracy of the fit is only 0.82 which is not sufficient to derive a confident relationship. It seems probable that for the case of cement pastes, the relationship is not linear due to a wide pore size distribution and the effects of tortuosity, though this requires further investigation.

The porosities of the pastes studied in this work are presented in Table 2, where it is evident that at day 1, the porosities for all pastes are comparable and that it is at later ages that distinct reductions relative to csf replacement are apparent.

Table 2 Values for the porosity

Age (days)	Replacement (%)	Porosity (n_e)
1	0	40.94
	5	39.89
	10	38.27
3	0	35.36
	5	32.71
	10	29.20
7	0	29.46
	5	23.13
	10	15.85

The Vapour Permeability

The vapour permeabilities of the cement pastes studied in this work illustrate reductions for degree of hydration (age of paste at test), and for csf replacement. The latter is clearly shown in Fig 3a, where clear separation is evident between the control paste and the csf replacements. This trend is less pronounced at day 3 and 7, where all pastes exhibit comparable values.

All data illustrate that for increasing relative humidity: i.e. increasing moisture content; the vapour permeability increases in magnitude. This relationship supports the proportionality of the mass transfer to the permeability as a function of the moisture content of the paste, as reported by Rose (1963).

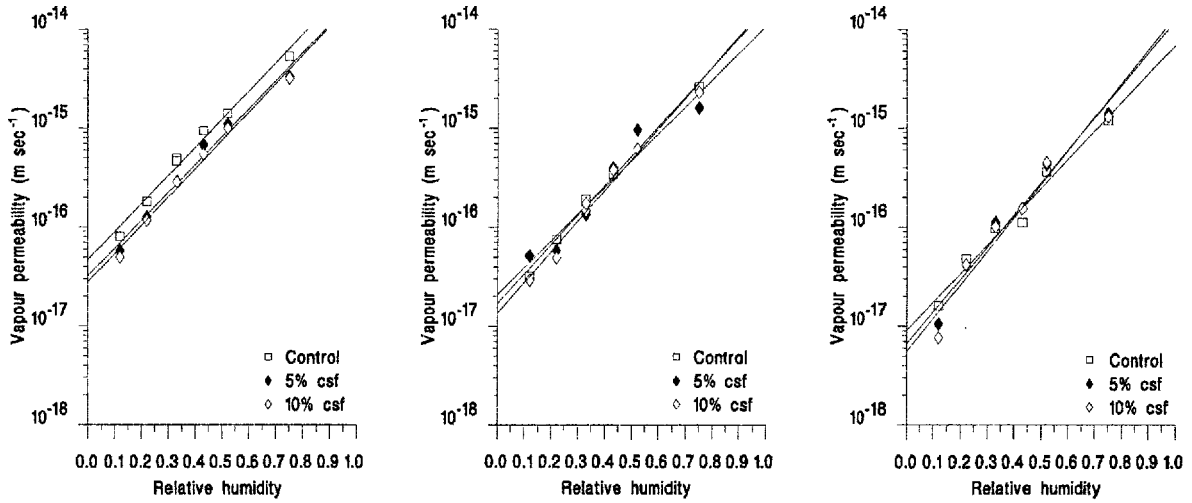

(a) (b) (c)

Figure 3 Vapour permeabilities with respect to relative humidity and age of pastes at 1, 3 and 7 days of age (3a, 3b, 3c)

CONCLUSIONS

- The Sorptivity is sensitive to changes in capillary porosity and reducing capillary pore radii, which are associated with hydration and csf replacement. The Sorptivity can therefore provide qualitative information on the durability of the paste.

- Results presented in this paper show that csf replacement reduces the mass absorption of cement pastes, both for increased percentage and for degree of hydration: i.e. age of paste.

- The proposition that the Sorptivity is proportional to the square root of the porosity has been shown to be invalid in this instance.

- A mathematical derivation of the unsaturated vapour transport mechanisms of the Permeability and Diffusivity, has been presented based on the liquid phase unsaturated flow equation.

- The vapour Permeability of csf replacement pastes has been shown to be reduced at day 1, but thereafter (upto 7 days of age), values are comparable to normal paste.

- The vapour Permeability has been shown to be a function of the moisture content, and to increase in magnitude with increasing relative humidity.

- Though values for two properties of unsaturated mass transfer have been reported, this study requires further investigation in relation to the inclusion of aggregates and their effects on the named properties.

ACKNOWLEDGEMENTS

Elkem Materials for supplying Elkem 500S and Phillip Jones for supplying the "Micropoz" csf. Stuart Pepper and Castle Cement for preparing the Micropoz into a slurrified form. Pam Curwen for her work in the experimental procedure.

REFERENCES

Bruce, R.R. and Klute, A., "The Measurement of Soil Moisture Diffusivity", Soil Science Society of America Proceedings, 1956, Vol. 20, pp. 458-462.

Darcy, H., "Les Fontaines Publiques de la Ville de Dijon", Dalmont, Paris, 1856.

Hall, C., "Water sorptivity of mortars and concretes: a review", Magazine of Concrete Research, Vol. 41, No. 147, June 1989, pp. 51-61.

Kirkham, D. and Powers W.L., "*Advanced soil physics*", Wiley Interscience, New York, 1972.

Kumaran, M.K. and Bomberg M., "A Gamma-spectrometer for determination of density distribution and moisture distribution in building materials", Proc. Int. Symp. Moisture and Humidity, 1985, pp. 485-490.

Marchese, B. and D'Amore, F., A contribution, Magazine of Concrete Research, 1990, 42, No. 151, Jun., pp. 105-109.

McCarter, W.J., "Influence of Surface Finish on Sorptivity on Concrete", *Journal of Materials in Civil Engineering*, Vol. 5, No. 1, February, 1993, pp. 130-136.

McCarter, W.J., Chrisp, T.M., Ezirim, H. and Basheer, P.A.M., "In-situ evaluation of properties of concrete in the cover zone", Proceedings of the International Congress "Concrete In The Service Of Mankind." University Of Dundee, June 1996, pp.113-123.

Philip, J.R. "The theory of infiltration: 4. Sorptivity and algebraic infiltration equations", Soil Science, 84, pp. 257-264, 1957.

Rose, D.A., "Water movement in porous materials: Part 2-The separation of the components of water movement", BRIT. J. APPL. PHYS., 1963, VOL. 14.

4iv009
4 pp

MOISTURE DISTRIBUTIONS AND THE HYDRAULIC DIFFUSIVITY OF HARDENED CEMENT PASTES MODIFIED BY PARTIAL REPLACEMENT WITH PFA AND GGBS

Don FAIRHURST, University of Central Lancashire, Preston, England
Dr Andrew K PLATTEN, University of Central Lancashire, Preston, England

ABSTRACT Cement replacements, such as pfa and ggbs, have been found to modify the microstructure of the cement matrix. Blended hardened cement pastes at the age of 28 days, with pfa and ggbs replacement levels of 10, 20 and 30%, were studied in the unsaturated condition. It is shown that 30% replacement enhances the performance of cement paste with respect to penetrating water. Further, values are presented for the hydraulic Diffusivity as a function of moisture content.

Key-words: Diffusivity, Blastfurnace slag, Pulverised fuel ash

INTRODUCTION

Durability issues for cementitious media are inherently related to the barrier qualities of the concrete. Aggressive compounds present in the environment, such as chloride ions and sulphates, may be carried in solution during the transport of moisture through the cement matrix. Further, the absorption of such compounds can lead to deterioration of the calcium hydroxide $Ca(OH)_2$ content of the hardened paste, leading to increased porosity and further infiltration of moisture (Sims, 1994). Predominantly, field concretes are not subjected to saturated conditions, and where such instances do arise, the diffusion of oxygen and not water is the primary concern. This observation places emphasis upon the study of unsaturated transfer processes, such as the hydraulic Diffusivity, where moisture gradients exist between the surface and inner mass. This paper is concerned with capillary phenomena in relation to pastes, and though such data obtained cannot be directly applied to predictive models for concrete, it does constitute an advancement in the study of the unsaturated mass transfer through cementitious media.

GENERAL CONCEPTS

Classical theory describes that for an initially dry porous body, the mass absorbed and depth of penetration obey a square root of time relationship (Kirkham and Powers, 1972). This relationship however, is subject to: a) the material properties such as porosity (Hall and Yau, 1987), and time (Emerson, 1990). It has been proposed (Hall, 1981), that the advance of the wetting front can be assumed to be sharp, where a steep moisture gradient exists over a relatively short distance lying behind the leading edge. Thus, enabling rudimentary prediction of the depth advanced, from data of the mass absorbed. Published results of the advancing wetting front for cement pastes are, however, uncommon. This paper addresses the latter point.

MATERIAL DETAILS

Following established mix design procedures and prescribed levels of cement replacement (BS 5328, 1991), the pastes replicated accepted practice. The cementitious factors (C_f) for pfa and ggbs were taken as being 0.3 and 0.7, respectively. The water/cement ratio was defined by $W / (C+C_fF)$, where, W is the water content, C is the cement content and F is the replacement content. A constant water/cement of 0.5 was used in this study, with all pastes being bath cured until test at 28 days of age.

THEORETICAL

Assuming the gravitational effects to be minimal, one-dimensional vertical flow in an homogeneous body can be written in a similar manner to the non-linear diffusion equation (Bruce and Klute, 1956).

$$\frac{\partial \theta}{\partial t} = \frac{\partial}{\partial x}\left(D(\theta)\frac{\partial \theta}{\partial x}\right) \quad [1]$$

where,

θ = volumetric moisture content (cm^3 water cm^{-3})
t = time (sec)
x = distance (cm)
D = hydraulic Diffusivity (cm^2 sec^{-1})

The initial and boundary conditions governing flow are:

$$\theta(x,t) = \theta_i \quad x>0 \quad t=0 \quad [2a]$$
$$\theta(x,t) = \theta_s \quad x=0 \quad t\geq 0 \quad [2b]$$

Assuming θ to be a function of a single variable $\lambda(x,t)$, the Boltzmann transformation:

$$\lambda = xt^{-\frac{1}{2}} \quad [3]$$

Thus, restating the relationship to the square root of time. Eq 1 now becomes the ordinary differential equation:

$$-\frac{\lambda}{2}\frac{d\theta}{d\lambda} = \frac{d}{d\lambda}\left(D\frac{d\theta}{d\lambda}\right) \quad [4]$$

Thus, Eq 1 can be integrated subject to the boundary conditions Eq 2a and 2b:

$$D(\theta) = \int_{\theta_i}^{\theta_i} \lambda d\theta \quad [5]$$

The Diffusivity being a function of the moisture content. The solution to $D(\theta)$ is the initial step in resolving the unsaturated flow equation, Eq 6:

$$D(\theta) = K(\theta)\left(\frac{\partial \psi}{\partial \theta}\right) \quad [6]$$

where,

K = hydraulic conductivity (cm sec^{-1})
ψ = capillary force (cm)

EXPERIMENTAL

Water was allowed to vertically infiltrate paste columns from a free-water reservoir for an initial moisture content, θ_i. At pre-determined times, the samples were removed, sectioned (at 5mm intervals), and weighed immediately to obtain the mass of each element. After drying to a

constant mass at 105°C, θ_0 ($\theta_i = \theta_0$), the elements were weighed, saturated, θ_s and re-weighed. Thus, the normalised moisture content, θ_r could be determined for each element and plotted with respect to distance. The effect of direct drying has been reported to have a significant effect upon the microstructure and transport properties of cement pastes (Parrott, 1983); such effects could not be determined at the time of this study and are therefore acknowledged, but not accounted for. As a check, the pastes were examined by Scanning Electron Microscopy to ascertain the presence of microcracks, none were evident in the pastes studied.

RESULTS

In this paper, results for the depth of penetration and values for the hydraulic Diffusivity, are presented where the linear relationship to the square root of elapsed time is preserved, thus satisfying Eq 3. The time for which this relationship exists is dependant on the physical properties of the specific paste. A typical moisture distribution plot, from which the hydraulic Diffusivity can be numerically derived, is illustrated in Fig 1.

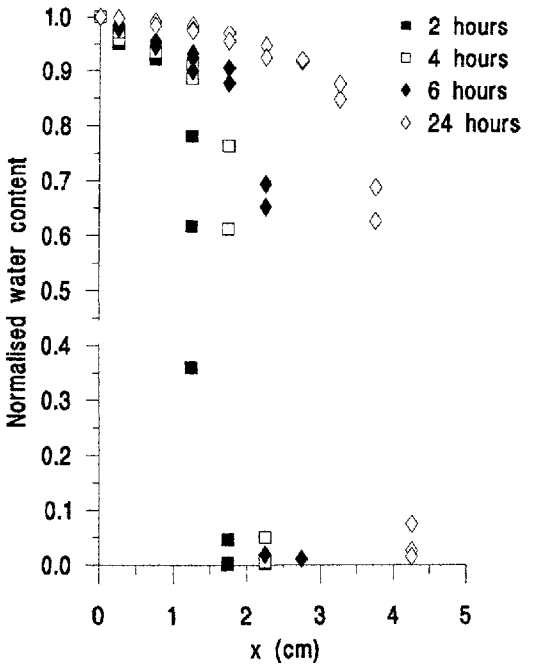

Figure 1 Moisture distributions for 20% replacement ggbs with respect to time (θ_r against x for different times)

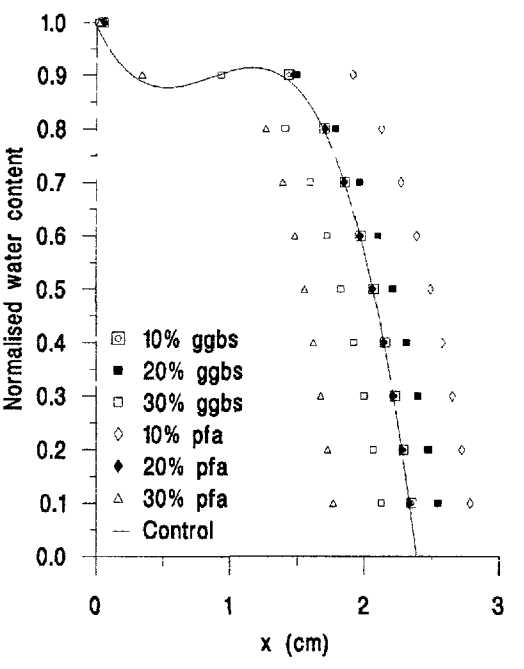

Figure 2 Moisture distributions after 6 hours infiltration for the pastes studied in this work

Moisture distributions for the pastes studied in this work are presented after six hours of infiltration, in Fig 2. The data points have been derived from a least squares polynomial fit determined from raw experimental data. It is noteworthy that the form of the wetting front suggests similarity of shape for the cement pastes tested in this work.

With respect to depth of penetrating moisture, the curves illustrate enhanced performance for increased cement replacement, subject to the following qualifications. For example, there is marked separation between 10% and 30% pfa replacement pastes, with the latter indicating enhanced performance characteristics. Conversely, for ggbs pastes there is little separation between 10% and 30% replacement.

Hydraulic Diffusivities for the pastes studied in this work are presented in Fig 3. There is little separation between the data points indicating that for porous systems such as cement pastes the hydraulic Diffusivity is approximately constant for a given moisture content.

The significance of the moisture content with respect to the hydraulic Diffusivity is also convincingly illustrated in the figure. For the pastes studied, the diffusion rate increases approximately by three magnitudes from dryness and saturation. This conforms to unsaturated theory, as Eq 5.

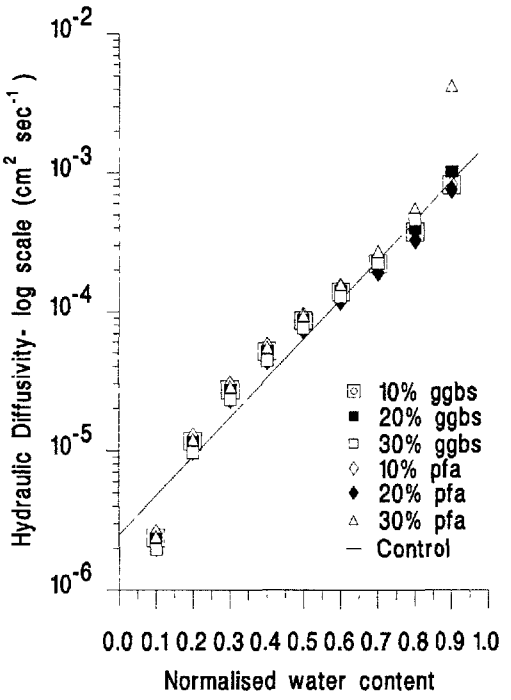

Figure 3 The Hydraulic Diffusivity $D(\theta)$, for pastes at 28 days of age (control paste is given as best fit line)

CONCLUSIONS

- Pfa and ggbs replacement levels of 30% enhance the performance of cement pastes to penetrating moisture. At lower levels of replacement, the performance is comparable to the control paste.
- The hydraulic Diffusivity is a strongly variant function of the moisture content. Indeed, the moisture state is the dominant factor in the Diffusion rate for unsaturated flow.
- Though the assumption of the sharp wetting front in this instance leads to the under estimation of the actual distance advanced, it is important to remember that certain degradation mechanisms require high moisture contents to be active. Thus, simplification can be justified for these purposes.

ACKNOWLEDGEMENTS

The authors are indebted to the Department of Built Environment, at the University of Central Lancashire, for funding this work, and to Michael Ward in preparing the samples.

REFERENCES

Bruce, R.R. and Klute, A., "The Measurement of Soil Moisture Diffusivity", Soil Science Society of America Proceedings, 1956, Vol. 20, pp. 458-462.

Emerson, M., "Mechanisms of water absorption by concrete", Proceedings of the International Conference on Protection of concrete, Dundee, Scotland Sept. 11-13 1990, pp. 689-700.

Hall, C., "Water Movement in Porous Building Materials-IV. The Initial Surface Absorption and the Sorptivity", *Building and Environment*. Vol. 16, No. 3, pp. 201-207, 1981.

Hall, C., and Yau, R.M.H. "Water movement in porous building materials- IX. The water absorption and Sorptivity on concretes", Building and Environment, Vol. 22, No. 1, 1987, pp. 77-82.

Kirkham, D. and Powers, W. L., "Advanced Soil Physics", Wiley Interscience, 1972.

Parrott, L.J., "Novel methods of processing cement gel to examine and control microstructure and properties", *Phil. Trans. R. Soc. Lond.* A, 310, pp. 155-166 (1983).

Sims, I. "The assessment of concrete for carbonation", CONCRETE, November/December 1994, pp. 33-38.

INFLUENCE OF MOISTURE CONTENT ON THE EFFECTIVE DIFFUSION COEFFICIENT OF CO_2 IN LIME MORTARS WITH DIFFERENT POROSITIES

Koenraad VAN BALEN, Prof., K.U.Leuven, Department of Civil Engineering, Belgium
Christophe VAN DEN BRANDE, civ.eng., K.U.Leuven
Eleni-Eva TOUMBAKARI, ass., K.U.Leuven, Department of Civil Engineering, Belgium
Dionys VAN GEMERT, Prof., K.U.Leuven, Department of Civil Engineering, Belgium

ABSTRACT The influence of the moisture content of hygroscopically moistened samples on the diffusion coefficient of CO_2 is important only for very high relative humidities. For water wetted samples, the diffusion coefficient decreases almost linearily with increasing water content, with an asymptotic smoothing in the capillar water content region. Diffusion becomes negligible, when the moisture content reaches the critical value below which only damp transport is possible. However, significant diffusion of CO_2 still takes place for moisture contents between the critical and capillar water content.

Key-words: carbon dioxide, carbonation, diffusion, lime, moisture.

INTRODUCTION

Lime mortars of various compositions have been widely used for centuries before being gradually replaced by cement mortars, both in new constructions and for restoration purposes. However, the last decades have seen an increase in examples of masonry deterioration due to mechanical and physicochemical incompatibilities between cement and stone, which brought about a renewed interest for the study of lime mortars. Due to the deformability and physical compatibility with masonry, the latter tend nowadays more and more to substitute pure cement mortars. However, the state of the art of lime performance and mechanical behaviour reveals a relatively small research history. Van Balen (1991) developed a mathematical model for lime mortar carbonation. This model has been limited to the study of CO_2 diffusivity up to the critical moisture content. In order to extend the mathematical model beyond this value, the influence of diffusivity has been further studied at water contents above the critical water content.

CARBONATION, HYGROSCOPIC BEHAVIOUR AND DIFFUSIVITY

Carbonation of lime mortars

The hardening of lime mortars is initiated by drying. After partial drying of the mortar, during which capillar forces provide the cohesion of the material, the carbonation reaction is allowed to take place, causing the further hardening of the lime mortar. The lime carbonation reaction can be described as follows:

$$Ca(OH)_2(s) + CO_2(g) \rightarrow CaCO_3(s) + H_2O \quad [1]$$

It can be divided in the following main stages:

Dissolution of $Ca(OH)_2$: $Ca(OH)_2$ (solid) $\rightleftharpoons Ca^{2+}$ (aq) + $2OH^-$ (aq) [2]
Carbon dioxide diffusion through the gaseous phase of the pores and reaction:

$$Ca^{2+}(aq) + 2OH^-(aq) + CO_2(g) \rightarrow CaCO_3(s) + H_2O \quad [3]$$

The role of water is fundamental for these reactions to occur. On the one hand, it occupies the volume of the pores, hindering the gas diffusion process. The diffusion coefficient of CO_2 in the air is 0.139 cm^2/sec and in water 10^4-10^5 times less (Richardson, 1988). On the other hand, it provides the medium, where reactions can take place. Carbonation is thus retarded when the material is saturated with water or, on the contrary, at low relative humidities when no water is present on the pore surface. The optimum water content for carbonation is the water content that corresponds to maximum adsorption on the surface of the pores before capillary condensation. The material's water content and the pore volume and geometry play therefore a key role in the diffusivity of carbon dioxide.

Hygroscopic behaviour of lime mortars

If a hygrothermal equilibrium between the pores and the environment is assumed, all pores with diameters smaller than the Kelvin diameter are completely filled with water, while the walls of the remaining pores will be covered with a continuous film of water molecules (Papadakis et al., 1991b). The Kelvin diameter can be computed by the Kelvin equation:

$$\ln\phi = - (4\sigma_w \cos\theta)/(\rho_w R t d_{eq}) \quad [4]$$

in which ϕ is R.H./100, σ_w is the surface tension (in N/m), θ is the contact angle (in°) and d_{eq} is the equivalent diameter (in m). During hygroscopical loading of the material, the water content remains too low to permit water transport through the sample. When the water content reaches values above the critical water content, e.g. due to rain, water transport through the material occurs. When the maximum water content (capillary moisture content) is reached, air is prohibited from flowing out of the material. Van Balen (1991) has shown that lime mortars are materials with a low hygroscopicity.

Effective gas diffusivity

In a binary gas mixture, the flux density is proportional to the concentration gradient in the direction of the diffusion and is described phenomenologically by Fick's first law:

$$N_A = -D_A \, dC_A/dx \quad [5]$$

in which N_A is the rate of transfer of a gas A (in moles of A per sec per m^2 of the medium normal to the direction of the flux), D_A is the diffusion coefficient of A (in m^2/sec) and dC_A/dx is the concentration gradient of A (in moles of A per m^3 per m). In porous materials, diffusion of gases occurs only through the gaseous phase of the open pores. In this case, the transport mechanism of gas is described by the following equation:

$$N_{eff} = -D_{eff} \, dC_A/dx \quad [6]$$

in which N_{eff}, D_{eff} are the "effective" rate of transfer and the "effective" diffusion coefficient respectively. The term "effective" is used to indicate that a transport coefficient applies to a porous material and not an homogeneous region. In a cylindrical pore, there exist different diffusion regimes, depending on the pore radius and the diffusing gas molecules. The influence of the latter is taken into account through the definition of the mean free path λ (in m)

$$\lambda = RT/NP\pi d^2 \quad [7]$$

in which R is the universal gas constant (8.314 J/mol K), P the pressure (in Pa), T the temperature (in K), N the number of Avogadro (6.023 10^{23} /mol) and d the molecular diameter (in m). If the radius r of the capillary and the gas pressure are such , that the mean free path is large compared to the pore diameters, Knudsen diffusion starts taking place. Knudsen diffusion appears for $r/\lambda < 0.1$ (Youngquist, 1970) . When $r/\lambda > 10$, ordinary molecular diffusion predominates. Finally, for r/λ between 0.1 and 10, combined diffusion occurs. Apart from the effective diffusion coefficient D_{eff}, the flow of gases within a porous solid can also be described by the diffusion resistance number. This number compares the diffusion resistance of a porous material to that of an air layer with the same volume in identical environmental conditions (p, T):

$$\mu = D_{AB}/ D_{eff} \qquad [8]$$

in which D_{AB} is the diffusion coefficient of a gas in air (in m^2/sec) and D_{eff} is the effective diffusion coefficient within the porous solid (in m^2/sec).

EXPERIMENTAL PROGRAM

Materials and specimens

A dry slaked hydrated lime has been used. In order to investigate the influence of the porosity upon diffusion, two different types of sand have been chosen. The norm sand fulfills the DIN 1164 and the finer sand of Zutendaal fulfills the specification n° 200 of the Flemish Ministry of Public Works (100 % passing throught the 0.5 mm sieve). Previous experiments have determined consistency values between 1.45 and 1.55 in order to achieve a good mortar workability. The compositions and physical properties of the samples are listed in Table 1. After being cured for two weeks in 20°C and 60 % R.H., the samples have been placed in a glass bulb containing 100 % CO_2 for six weeks in order to carbonate completely. Therefore, any carbon dioxide consumption during the diffusion measurements has been avoided. The grain-size distribution of the norm sand results in a higher density and, consequently, a lower porosity than the Zutendaal sand.

Table 1 Mix proportions and physical properties of the lime mortars

	Water (gr)	Sand (gr)	Lime (gr)	W/L	Mean bulk density (gr/cm^3)	Porosity	
						Water satur. %	Mercury Intrusion porosity %
Mortar 1 Zutendaal sand	425	1400	300	1.42	1.743	35.2	30.7
Mortar 2 norm sand	300	1350	256	1.17	1.909	28.2	28

Experiments

Previous studies concerning the hygroscopical behaviour of identical lime mortars showed that a significant moisture content occurs only for the highest levels of R.H. (Van Balen, 1991, Van Balen et al., 1994). Therefore, two values of R.H. have been chosen for the study of the hygroscopical

behaviour of lime mortars. After carbonation, the samples have been placed for a minimum of 6 weeks in two glass bulbs under (20°C, 86% R.H.) and (20°C, 98% R.H.) respectively before the measurement of their hygroscopic water content. The critical water content has been determined as follows: water saturated samples have been covered by wax except for one surface, placed for 20 days in a controlled environment (20°C, 60% R.H.) and allowed to dry. The cumulative humidity loss, the remaining water content and the dry flux have been measured in function of time. The critical water content corresponds to the change in the slope of the humidity loss versus time curve. This means that water vapore diffusion starts to govern the drying process. The capillar and saturation water contents have been measured according to NBN B 05-201. The pore size distribution of the samples has been determined with a mercury porosimeter. Effective diffusivity has been studied experimentally, using a Wicke and Kallenbach type of setup. It comprised a non-dispersive infrared adsorption analyser (UR AS 10E, Hartmann and Braun), manometer, flow regulating needle valves and diffusion cell. The analyser was linked to a PC, which recorded continuously the concentration of carbon dioxide. The setup is given in Fig 1.

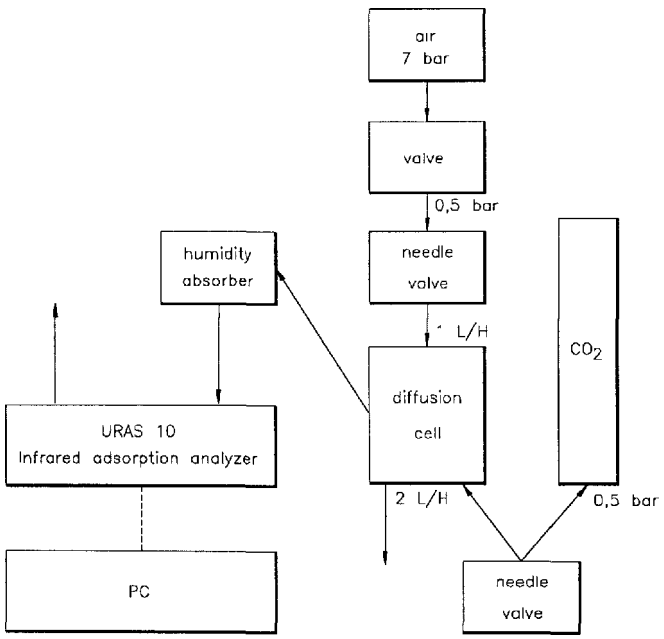

Figure 1 Experimental setup for effective diffusivity measurement of mortar

RESULTS

Microstructure

The pore size distribution of the fully carbonated samples is shown in Fig 2. The better grain size distribution of the norm sand results in a lime mortar with higher density and lower porosity than those of the Zutendaal sand mortars. However, both materials can be classified as "rough" porous materials (i.e. with pore volume peaks at around 1μm). Since the mean free path of carbon dioxide is λ= 0.045μm, bulk diffusion will dominate. The results concerning the various typical water contents of the samples are presented in Table 2. In the case of 86% R.H., the equivalent diameter is 0.014μm. Only 1.6% of the pore volume of the Zutendaal sand mortars and 1.5% of the norm sand mortars is below this value. The equivalent diameter for 98% R.H. is 0.11 μm and the

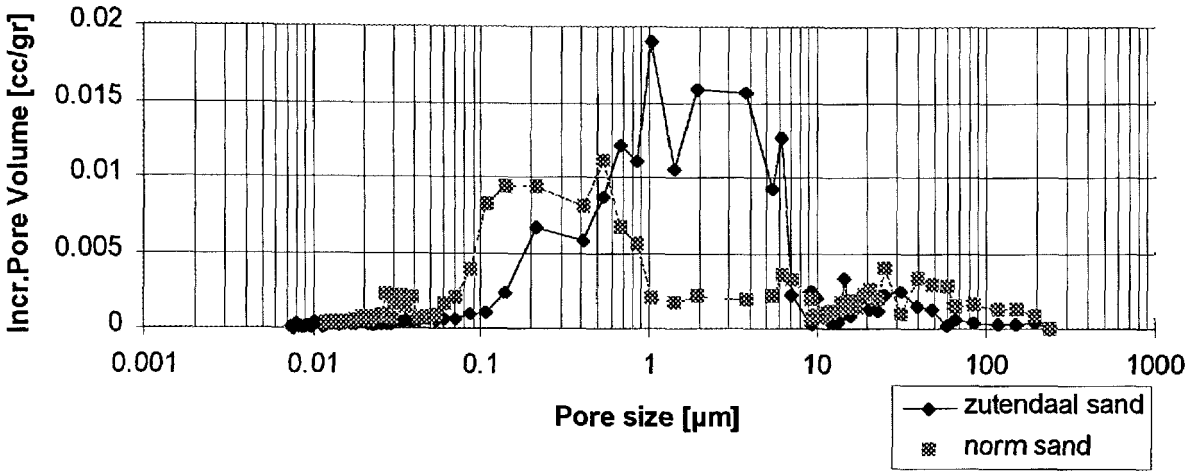

Figure 2 Pore size distribution of the mortars measured by mercury intrusion porosimetry

Table 2 Hygroscopical water contents (kg/m3)

	Mortar 1 Zutendaal sand	Mortar 2 norm sand
Moisture content at 86% R H	5 58	4 42
Moisture content at 98% R H	22.29	27.9
Critical water content	60 0	70 0
Capillar water content	215 9	208.7
Saturation water content	352.5	287.5

corresponding volumes become 6.33% and 9.72% for the Zutendaal sand and norm sand respectively. It was therefore confirmed that lime mortars cannot be significantly wetted through hygroscopic action.

CO_2 diffusion for hygroscopically moistured samples

The diffusion coefficient of the hygroscopically loaded samples is presented in Fig 3 The hygroscopic action, even for R H as high as 98%, does not have any significant impact on the diffusion coefficient. Application of linear regression analysis on these results gives the following equations

Zutendaal sand mortars: $D_{eff} = 4\ 52\ E\text{-}09\ w + 1.69\ E\text{-}06$ [9]

Norm sand mortars: $D_{eff} = 1.71\ E\text{-}09\ w + 1.36\ E\text{-}06$ [10]

CO_2 diffusion for water wetted samples

Measurements of at least ten different water contents have been carried out on different mortar samples, prepared either with Zutendaal or with norm sand. The results are presented in the Figs 3 till 7 below. These water contents have been achieved as follows: after diffusion testing of the

dry samples, water was added gradually from their upper surface, until the CO_2 concentration in the mixing chamber dropped below 1%. Then the samples were placed for about 1 week in a glass bulb in 98% R.H. and 20°C.

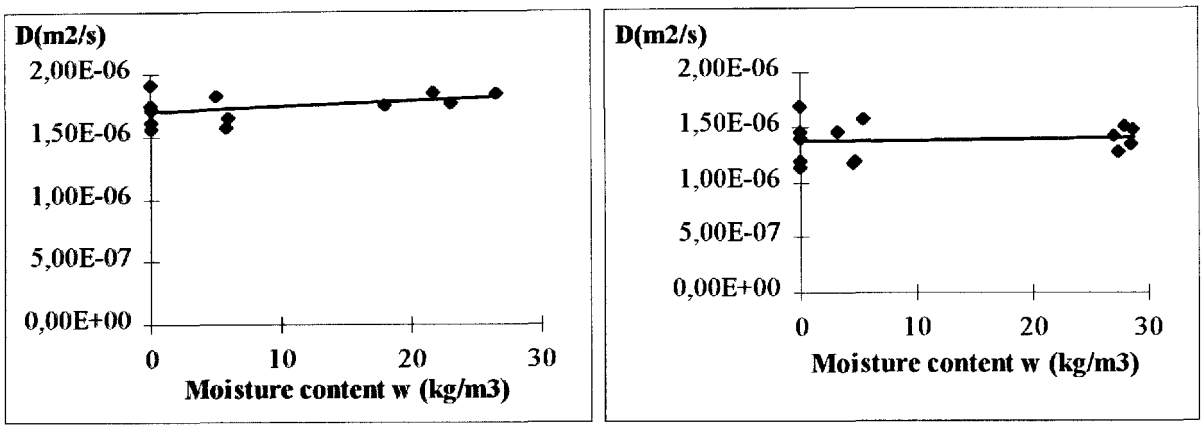

Figure 3 Diffusion coefficient of CO_2 for Zutendaal sand mortars (left) and norm sand mortars (right)

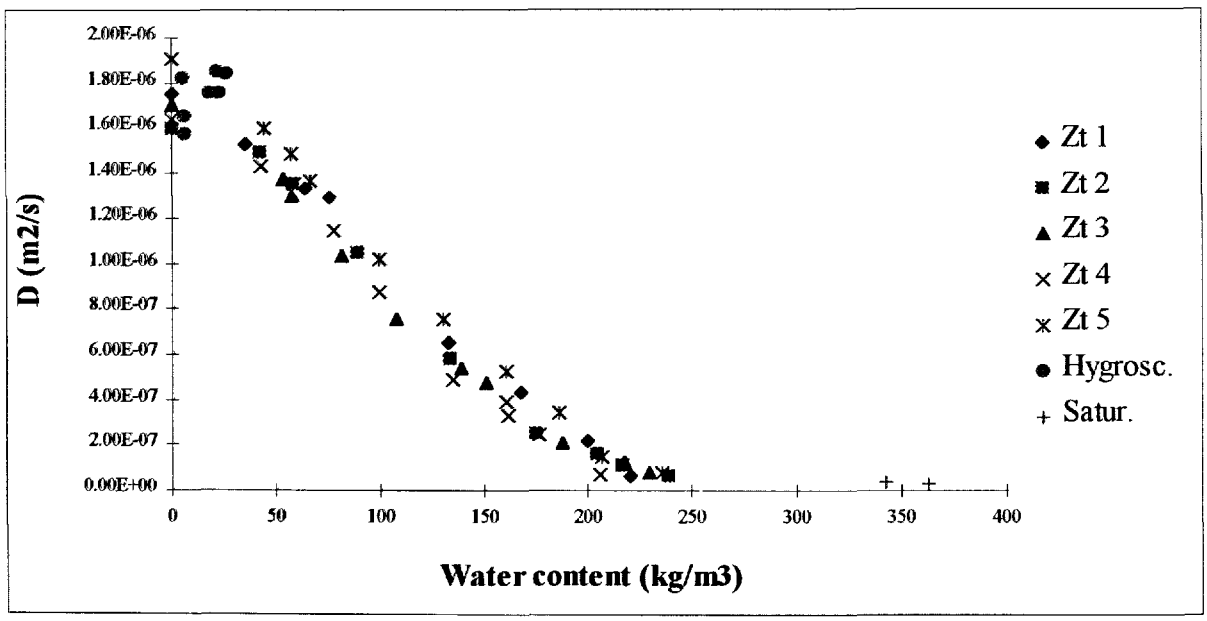

Figure 4 Diffusion coefficient for CO_2 of Zutendaal sand mortars

Concerning the Zutendaal mortars, for water contents below the critical water content, the slope of the diffusion coefficient curve is less pronounced than for water contents above this. This indicates that diffusivity is easier, since no continuous water paths are present in the specimen. Once the critical water content is reached, an almost linear decrease of the diffusion coefficient occurs. Finally, close to the capillar water content, the curve is flattened. The same tendency has been observed in the mortars made with norm sand: the diffusion coefficient decreases slowly below the critical water content, strongly between the critical and capillar water content till it reaches the capillar water content (Figs 4 and 5). Corresponding tendencies are observed relative to the diffusion resistance number, which does not significantly change up to the critical water content, then it starts increasing slowly and, above the capillar water content it increases almost exponentially (Figs 6 and 7).

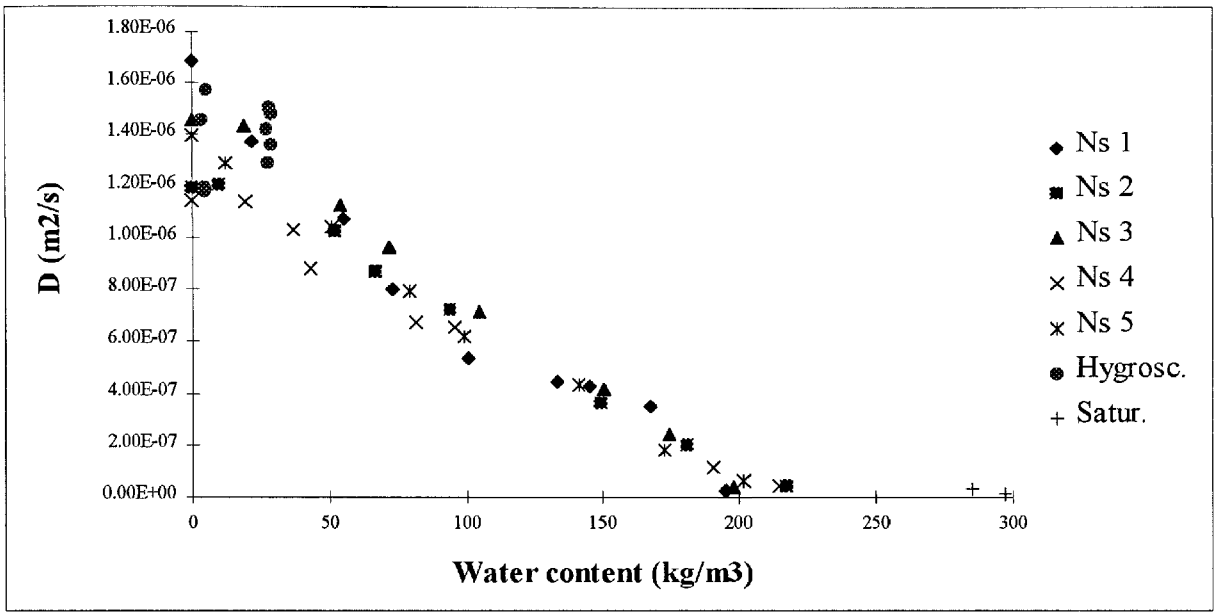

Figure 5 Diffusion coefficient for CO_2 of norm sand mortars

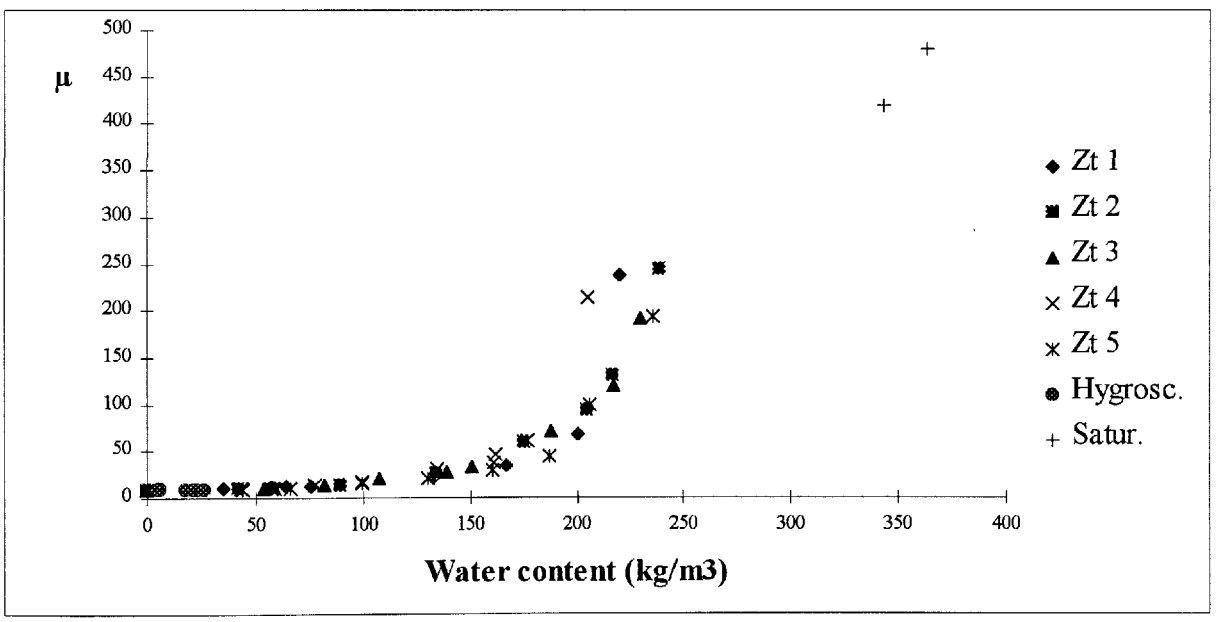

Figure 6 CO_2-Diffusion resistance number for Zutendaal sand mortars

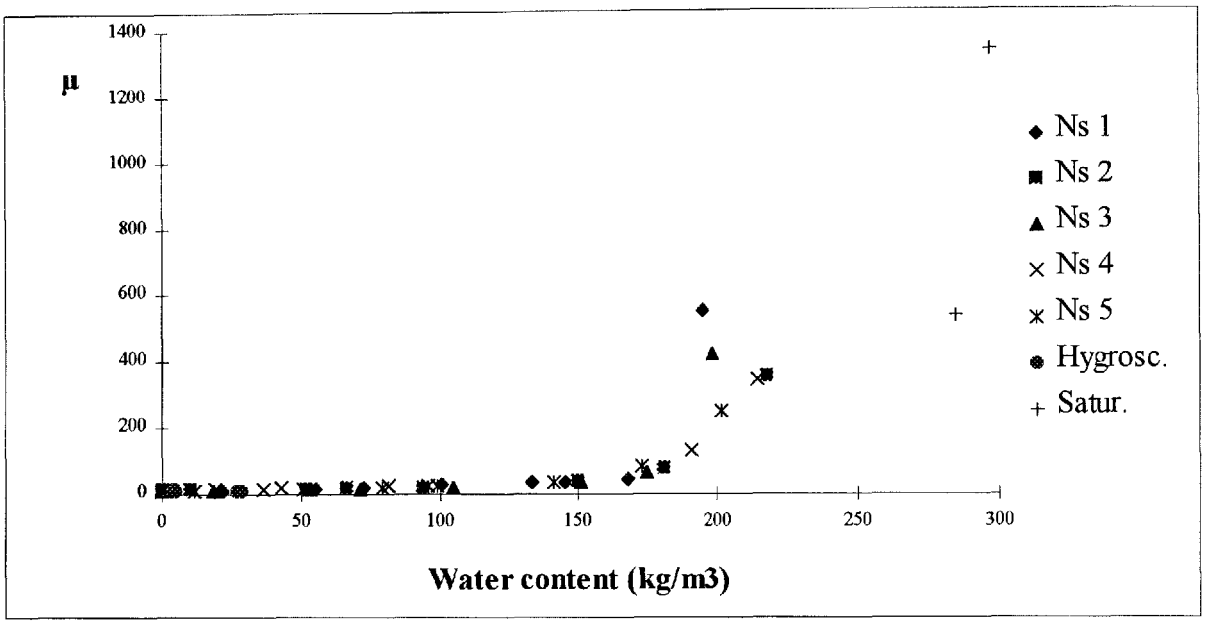

Figure 7 CO_2-Diffusion resistance number for norm sand mortars

CONCLUSIONS

Diffusivity measurements have been carried out, in order to describe the CO_2 transport within a carbonated lime mortar. It is assumed that there exists hygrothermal equilibrium between the pores and the environment. Under these conditions, the influence of the water content on CO_2-diffusivity is much less pronounced than e.g. in cement mortars. In practice, CO_2 diffusion still takes place at high water contents and is prohibited only above the capillar water content. The reason for this behaviour, which contrasts sharply to the behaviour of cement and concrete, must be attributed to the coarser pore size distribution of a lime mortar. The results of the research match with experimental findings that carbonation of lime mortars still occurs at high relative humidity. They also allow to extend the carbonation model developed for cases where the lime mortar has a water content higher than the critical water content. If the pore configuration permits to the lime mortars to carbonate even at very humid environments, it equally assures the water vapour transfer inside a masonry wall. This is obviously hindered when cement mortars are applied on masonry. Water is obliged to search an alternative path, namely through the more porous stones. This mechanism can be at the origin of the failure of many recent restorations of masonry buildings.

REFERENCES

Hens H., "Bouwfysica 1. Warmte en vocht: theoretische grondslagen", Leuven, 1981.

Houst Y.F., "The Role of Moisture in the Carbonation of Cementitious Materials", Int. Zeitschrift für Bauinstandsetzen, 2nd Year, No 1, 1996, pp.49-66.

Krischer O., "Die wissenschaftlichen Grundlagen der Trocknungstechniek", Springer-Verlag, Berlin, 1978, Chapter 5: "Die Stoffbewegung bei Strömung und Diffusion", pp.169-268.

Papadakis V.G., Vayenas C.G., Fardis M.N., "A reaction engineering approach to the problem of concrete carbonation", AIChE Journal, vol.35, No 10, October 1989, pp.1639-1650.

Papadakis V.G., Vayenas C.G., Fardis M.N., "Fundamental modelling and experimental investigation of concrete carbonation", ACI Materials Journal, vol.88, No4, July-August 1991, pp.363-373.

Papadakis V.G., Vayenas C.G., Fardis M.N., "Physical and chemical characteristics affecting the durability of concrete", ACI Materials Journal, vol.8, No2, March-April 1991, pp.186-196.

Richardson M., "Carbonation of reinforced concrete. Its causes and management", Dublin, 1988.
Van Balen K., "Carbonation of lime mortars and its influence on historical structures", Ph.D.Thesis, Faculty of Applied Sciences, KULeuven, 1991 (in Dutch).
Van Balen K., Van Gemert D., "Modelling lime mortar carbonation" , Materials and Structures, vol.27, 1994, pp.393-398.
Van den Brande C., "Influence of the moisture content on the carbonation of lime mortars", M.Sc.Thesis, Center for the Conservation of Historic Towns and Buildings, KULeuven, 1994.
Youngquist G.R., "Diffusion and flow of gases in porous solids", Industrial and Engineering Chemistry, vol. 62, No 8, August 1970, p.52-63.

DESORPTION AND INFILTRATION WITHIN THE SURFACE REGION OF EXPOSED CONCRETE

W John McCARTER, Heriot-Watt University, Edinburgh, Scotland.
David WATSON, Blyth and Blyth, Consulting Engineers, Edinburgh, Scotland.

ABSTRACT Water infiltration and subsequent moisture loss from the surface region of concrete samples were investigated. Data are presented on the moisture loss, volumetric gain, internal RH and electrical conductivity for plain OPC concrete and concrete containing metakaolin replacement. Monitoring electrical conductivity at discrete points within the surface 100mm allows an assessment of the convective zone, moisture distribution and on-going hydration / pozzolanic activity.
KEYWORDS Drying, Water suction, Humidity, Electrical Conductivity, Metakaolin.

INTRODUCTION

Absorption of water into the surface region of reinforced concrete, its distribution within this region and subsequent loss plays a important role in many of the processes that degrade concrete. Ingress of deleterious ionic species, corrosion, freeze-thaw damage, sulphate attack, ASR etc. are all dependent upon the presence of water. Cement microstructure, and therefore type and age of the concrete, has a role to play in this respect. Although it is relatively easy to measure the moisture flux through the surface, there is a dearth of information on the distribution of moisture within the surface zone and the influence of cementitious binder. This study presents some the results from a more extensive testing program in which concretes were subjected to cycles of drying and re-wetting extending over a period of 12 months. Electrical monitoring techniques and relative humidity (RH) measurements were employed to investigate the change in moisture state of the concrete within the surface 100mm. In parallel with these measurements, water gain and moisture loss were recorded.

EXPERIMENTAL

For the current work, concrete mix proportions and strengths (in MPa at 28 days and 360 days) are given in Table 1 with the water to cementitious binder ratio being 0.4 for both mixes. The binders comprised ordinary Portland cement (OPC) and OPC with metakaolin (MK) replacement. Crushed rock aggregate and matching fines were used throughout. Samples took the form of 150mm x 160mmϕ cylinders; pairs of stainless-steel pin-electrodes (1.5mmϕ) were cast into the samples at twelve discrete depths from the bottom (i.e. suction) surface. Four cavities were pre-formed (not drilled) in each sample during casting for internal RH measurements. After demoulding at 24-hours, the sides and top surfaces of the cylinders were sealed, the bottom (i.e. test) surface was then placed in water for 28 days.

Table 1: Mix proportions and strengths. (All materials in kg/m^3).

Mix	OPC	20mm	10mm	Fines	MK	F_{28}	F_{360}
OPC	525	775	390	530	-	72.1	81.4
OPC/MK	470	775	390	520	55	80.7	85.2

At 28 days all samples were then conditioned in cabinets under controlled temperature and humidity: 10%RH at 20°C for a period of 23 days followed by 60%RH for a further 5 days. The specimens were then subjected to a 24-hour water infiltration test during which volumetric gain measurements were taken at discrete time intervals. Samples were then allowed to dry for a

further period of 300 days in an atmosphere of 55-60%RH at 20°C before being subjected to a second 24-hour infiltration test, with volumetric gain being monitored as before.

Electrical conductance measurements were recorded using an impedance analyser operating at a frequency of 10kHz. The electrode array was calibrated in solutions of known conductivity thereby enabling conductance measurements to be converted to conductivity. Internal RH was measured using a Rotronic humidity probe inserted into the cavities. During infiltration testing, a perspex cap was secured to the suction surface of the sample with a head of approximately 850mm of water maintained on the surface; the volumetric gain was obtained from graduated burette on the cap. Mass loss was measured gravimetrically.

RESULTS AND DISCUSSION

The cumulative moisture loss per unit area of drying surface (in mm^3/mm^2) after the first and second drying periods outlined above are presented in Table 2 and denoted, respectively, i_{D1} and i_{D2} . During the two, 24-hour infiltration periods detailed above, data were plotted in the form (McCarter et al 1992; Dias, 1993),

$$i_W = A_W + S_W\sqrt{t} \qquad [1]$$

where i_W is the cumulative volume of water absorbed per unit area of inflow surface (mm^3/mm^2), t is the elapsed time (in hours) and S_W is the *sorptivity* of the material ($mm/h^{1/2}$); A_W is the intercept value on the t = 0 axis. The sorptivity is obtained from the slope of the i versus $\sqrt{t}$ curve. Sorptivity coefficients and intercept values obtained for the first and second infiltration tests are presented in Table 2 and denoted, respectively, S_{W1} and S_{W2} and A_{W1} and A_{W2}.

Table 2: Drying and Infiltration Results

Mix	i_{D1} mm^3/mm^2	A_{W1}	S_{W1} $mm/hr^{½}$	i_{D2} mm^3/mm^2	A_{W2}	S_{W2} $mm/hr^{½}$
OPC	1.025	0.244	0.039	2.809	0.292	0.122
OPC/MK	0.742	0.071	0.027	1.272	0.216	0.041

From Table 2, the sorptivity (S_W) values obtained after the short and long term drying regimes increase by a factor of ≈3 for the OPC mix but only ≈1.5 for the OPC/MK mix. These values reflect the moisture loss during the previous drying cycle which is quantified in terms of i_{D1} and i_{D2} . The drying loss (i_D) values gives an indirect, but simple, assessment of the water-vapour diffusion from the surface region which, itself, will be linked to microstructure. The differences in S_W values between the two mixes become more apparent with duration of drying. The OPC/MK concrete also displays a lower intercept (A_w) value. The intercept is as a result of rapid filling of open surface pores (Hall and Tse, 1986) on the face of the test specimens.

Figure 1 displays the variation of internal RH and electrical conductivity through the surface 100mm. Five profiles are presented for each mix:

(i) RH and conductivity immediately after curing period;
(ii) RH and conductivity just prior to the first absorption test and immediately after the 24-hour absorption test; and,
(iii) RH and conductivity just prior to the second absorption test and immediately after the 24-hour absorption test

As conductivity values can vary by over an order of magnitude between drying and subsequent rewetting, the conductivity axis has been placed on a logarithmic scale for both mixes. This also

allows all data points to be presented on the same axis without masking the general trends and also allows easier comparison of absolute values for the mixes. Rather than considering each conductivity and RH profile individually, it is more appropriate simply to highlight salient features from the responses. With reference to the conductivity profiles at the end of each drying period, conductivity values increases in the opposite direction to the direction of moisture loss. Values thus reflect the increasing degree of pore saturation with depth. When the conductivity drying profiles are taken in conjunction with the subsequent (respective) wetting cycle then the following should be noted:

(a) after the wetting cycle the zone of influence of the advancing water front can be detected as conductivity values have increased relative to the respective values before infiltration. There are points, however, were the conductivity values are unchanged. The point where the drying and wetting profiles become coincident is taken to represent that part of the surface zone most influenced by drying action - the so-called *convective zone* (van Brakel, 1980; Tutti, 1993). The depth of the convective zone (CZ) determined in this fashion is presented in Table 3 below for both mixes, where the subscripts 1 and 2 represent the first and second drying/wetting periods respectively.

(b) at depths greater than 60mm (i.e. those levels which could be assumed to be unaffected by drying action and water infiltration) there is a decrease in conductivity values with time relative to the respective values at 28-days cure. This can be attributed to on-going hydration and pozzolanic activity. This effect is more evident in the OPC/MK concrete due to the slower pozzolanic activity of the MK. Self desiccation of the binder could also contribute to reduction in conductivity and RH (Jensen and Hansen, 1995).

(c) generally, OPC/MK concrete has lower conductivity values than plain OPC concrete. This can, in the main, be explained by the increase in tortuosity and discontinuity of the pore network within the OPC/MK concrete;

Table 3: Depth of convective zone (CZ) estimated from conductivity profiles and RH profiles.

	CZ determined from conductivity profiles		CZ determined from from RH profiles	
Mix	CZ_1	CZ_2	CZ_1	CZ_2
OPC	25	30	30	30
OPC/MK	25	30	20	25

The internal RH measurements mimic the conductivity profiles (note that RH measurements were taken over the surface 45mm, whereas conductivity are presented over the surface 100mm). As vapour is lost from the surface region RH decreases and subsequently increases on rewetting increases, although not to its original level at 28-days cure. As with the conductivity profiles obtained before and after absorption, the RH profiles display a similar feature in that there is a *cross-over* point on the curves. This is taken to represent the depth of the convective zone discussed above and values obtained from the RH data are also presented in Table 3. These two sets of results agree well although conductivity profiles would appear to be more sensitive, particularly after short periods of drying and where replacement material is used in the binder.

CONCLUDING COMMENTS

Discretised conductivity measurements can provide a qualitative picture of how the moisture profile changes within the sample during drying and wetting. The testing methodology introduces a *third dimension* to the interpretation and understanding of water and moisture movement within the surface region of exposed concrete.

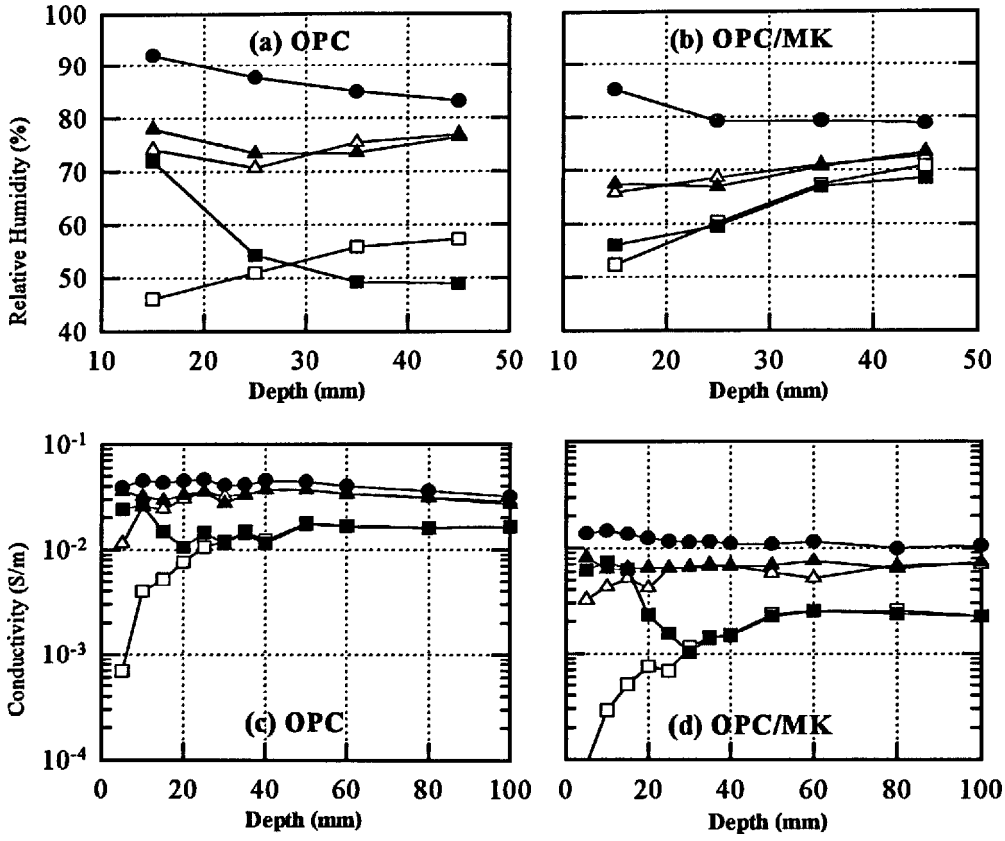

Figure 1: (a) and (b) internal RH and (c) and (d) conductivity profiles for OPC and OPC/MK concretes : (●) after 28-days curing; (Δ) after first drying period; (▲) after first infiltration; (□) after second drying period; (■) after second infiltration.

ACKNOWLEDGEMENTS

DW wishes to thank the EPSRC for financial support

REFERENCES

Dias W P S, 'Durability indicators of concretes subject to wick action', Mag. of Conc. Res., Vol. 45, No. 165, 1993, pp263-274.

Hall C and Tse T K, 'Water movement in porous building materials-VII. The sorptivity of mortars', Bldg. And Envir., 21, 2, pp113-118, 1986.

Jensen O M and Hansen P F, 'Autogenous relative humidity change in silica-fume modified cement paste', Adv. Cem. Res., 7, 25, Jan., pp 33-38, 1995.

McCarter W J, Ezirim H and Emerson M, 'Absorption of water and chloride into concrete', Mag. Conc. Res., 44, 158, Mar., pp 31-37, 1992.

Tutti K, 'Effect of cement type and different additions on service life', Proc Concrete 2000 Conference, Dundee, 7-9 Sept., (eds. R K Dhir and M R Jones), E & F N Spon, London, Vol. 2, pp 1285-1295, 1993.

van Brakel J, 'Mass transfer in convective drying', Advances in Drying, No. 1, 1980, pp217-267.

MICROSTRUCTURAL AND CHEMICAL CHANGES DURING LEACHING OF CEMENTITIOUS MATERIALS

Hugh P. UNSWORTH, Concrete Technology Unit, Department of Civil Engineering, University of Dundee, Dundee, Tayside, DD1 4HN, U.K.
Jasbir S. LOTA, Birchall Centre for Inorganic Chemistry and Materials Science, Department of Chemistry, Keele University, Keele, Staffordshire, ST5 5BG, U.K. (formerly at Dundee).
Fred H. HUBBARD and Ravindra K. DHIR, Concrete Technology Unit, Department of Civil Engineering, University of Dundee, Dundee, Tayside, DD1 4HN, U.K.

ABSTRACT
The leaching behavior of Portland cement and Portland cement/pulverized fuel ash mortars have been investigated by confined cell leach test. Marked differences in both the chemical and microstructural developments of the two mortar types have been identified. These features, which may be significant to the use of cementitious materials in waste containment, are explained in terms of the progress of leaching, as observed in the chemistries of the effluent solutions. The presence of PFA leads to a progressive development of a dense, low permeability, low pH product, while the PC mortar virtually maintains its original permeability and pH.

Key-words Portland cement, pulverized fuel ash, leaching, ettringite, waste disposal

INTRODUCTION
Assessment of the leaching performance of cementitious materials in a saturated environment is becoming more important with the increase in their use for waste disposal or containment purposes. Conventional wastes can be solidified and stored within cementitious lagoons, or cast into secondary containment drums, prior to disposal. This paper is concerned with the results from an accelerated confined Cell Leach Test (CCLT) (Unsworth 1997), in which samples have been subjected to a through flow by de-ionized filtered water. The work presented here shows the results for Portland cement (PC) and PC:pulverized fuel ash (PFA) barriers. The results are part of a wider research program (Unsworth, 1996) in which the CCLT was developed and tested using various toxic and aggressive solutions.

EXPERIMENTAL METHODS AND TECHNIQUES
The testing apparatus was of a similar design to a standard geotechnical triaxial cell (Michetis, 1985), with a confining pressure applied to the sample to stop external seepage and a hydraulic head applied to induce a through flow. The effluent was sequentially collected and its pH monitored. The elemental concentration of the effluent was measured using flame photometry for Ca, Na and K ions. Verification and trace element analysis (S, Mg, Al, Si) were undertaken by the developed copper disc evaporation test (Dhir *et al* 1995).

A Portland cement, complying with BS 12(1989) was used. The PFA complied with BS 3892:Part 1, and sieve analysis indicated a fineness of 0.9%. The methodology used for cell testing is described elsewhere (Unsworth 1997). Results shown are for a confining pressure of 400 psi and a pressure head of 300 psi.

RESULTS
Figures 1 and 2 show the results for PC and (50:50) PC:PFA mortars, tested under identical conditions. The results are representative of several similar test runs, and show the results from the longest test durations. The x-axis is a function of the effluent volume collected and the measured capillary porosity, this has been corrected for the changing porosity with test age. Testing was carried

out for all the elements present within cement. The Figures only include those elements found to be within detectable limits.

PC MORTAR

There is almost immediate Sodium (Na) leaching, with a rapid rise to a maximum concentration by two pore volumes (PV). Potassium (K) starts to leach from one PV rising to a maximum by three PV. This rise is accompanied by a slight release of sulfur (S). The region between the two dotted lines marks the area of most interest for the PC mortar. As the alkali metal concentrations start to decline, an increase in the Calcium (Ca) concentration is apparent. This rises steeply to a maximum concentration of 530 µg/l. Accompanying this there is a small temporary increase in the S concentration. Once the Ca has reached its maximum value Na and K leaching has effectively ceased, and there is maintenance of a steady Ca concentration. The pH of the effluent solution rises with an increase in alkali metal concentration, and is at its maximum value at the maximum alkali concentration, then drops to a consistent 12.5 during the Ca only leaching. Permeability shows a similar though less pronounced development to the pH.

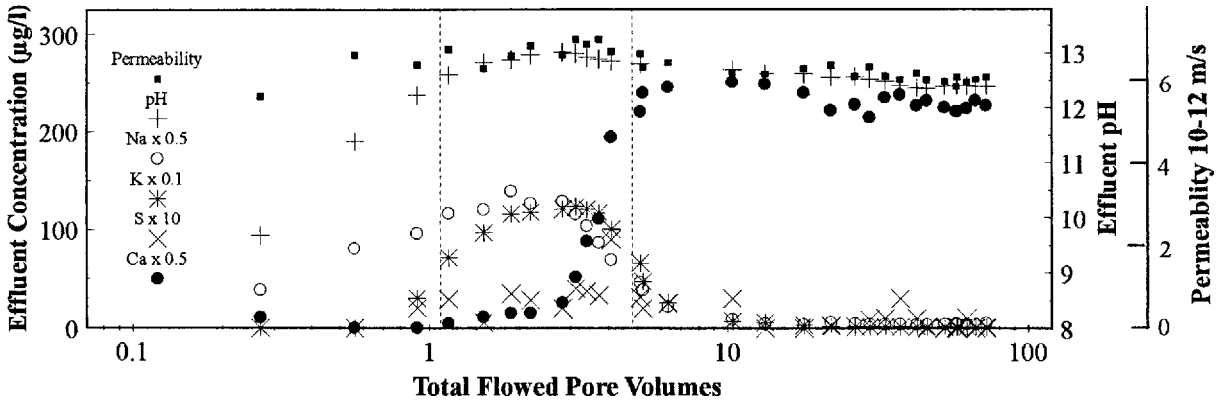

Figure 1. Effluent concentration, Permeability and pH data, for Portland cement mortar.

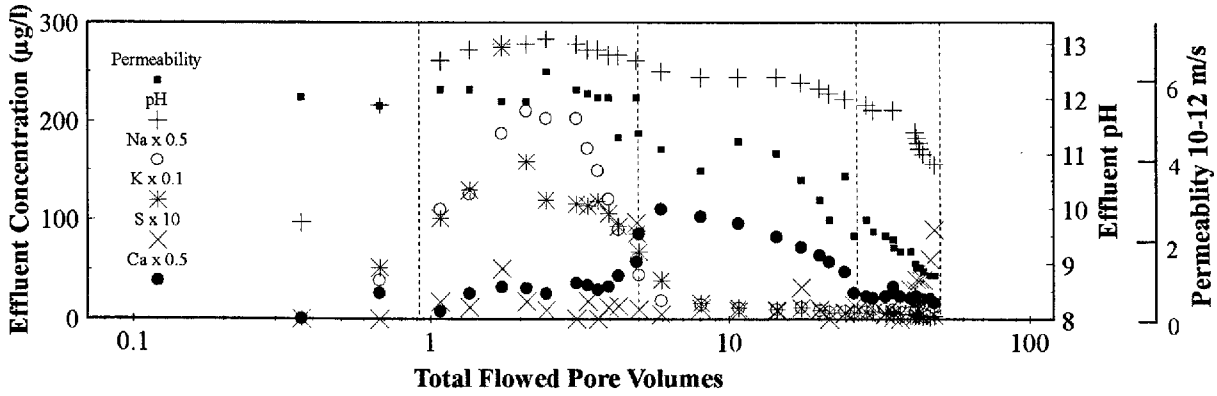

Figure 2 Effluent concentration, Permeability and pH data for Portland cement:PFA mortar.

PC:PFA

K and Na leaching commence simultaneously, in higher concentrations than with PC mortar. K in particular reaches a very high value of 2800 µg/l. Ca starts leaching out early, but at a low level of c.40 µg/l. This level is maintained until both the K and Na concentrations have begun to fall. There is a temporary leveling off in the K concentration, prior to its final fall. The Ca concentration increases at this point to c.220µg/l, and then progressively decreases to the base value of 40µg/l towards the end of

the test. Three main S peaks are observed, coinciding with the K peak, commencement of increase in Ca content and at the end of the test run. The sample permeability remains fairly constant to the point where the alkali concentration falls and the Ca concentration increases. From this point it progressively falls (to $1/8^{th}$ of its original value) in parallel with both the pH and Ca concentration. At the end of the test an increase in S is apparent, this corresponds to a sharper drop in pH, to its final value of 10.8. Upon removal physical examination revealed a highly friable sample.

SEM STUDIES

PC Mortar: X-ray and SEM studies at different test ages revealed an increase in ettringite concentration within the pore voids. Figure 3a shows a large pore void in the 160 day old PC control mortar, filled with $Ca(OH)_2$ crystals with dense CSH microstructure surrounding it. Figure 3b from the void/CSH boundary of a 160 day old cell test sample, shows the start of ettringite formation in a void. Ettringite was observed in the voids but not to any large extent in the interparticulate spaces or amongst CSH. From SEM micrographs it appears that the edge of the void acts as a permeable membrane, with ettringite only forming inside the pore. Figure 3c shows a large void with ettringite needles and CH blades.

PC:PFA Mortar: Figure 4a shows the dense microstructure of the PC:PFA mortar, with a cenosphere embedded in a 'slab' of CH. Figure 4b shows the remains of heavily leached CH particles within a pore, while Figure 4c shows calcium aluminate hydrate plates intermingled with CH.

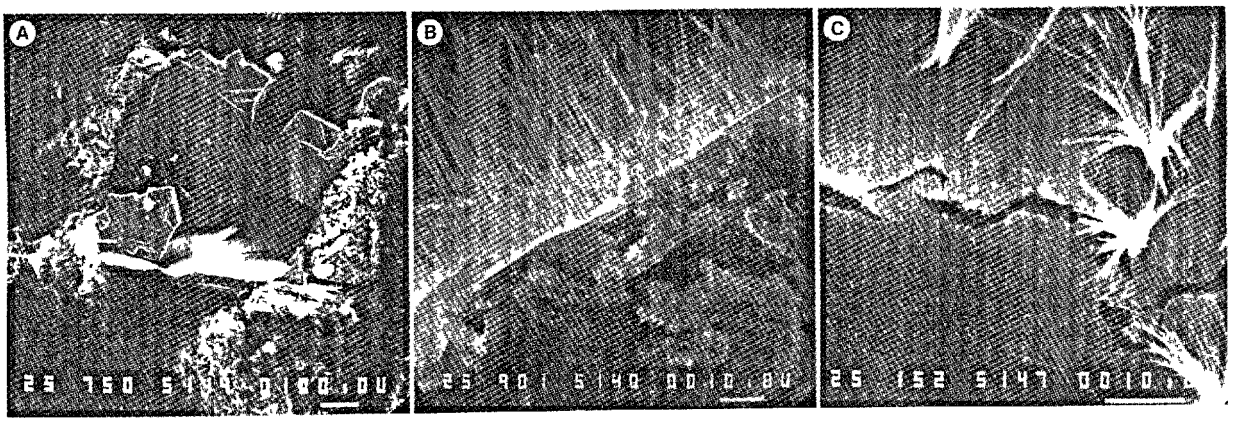

Figure 3 160 day old PC mortar; a - control, b, c - leached cell samples.

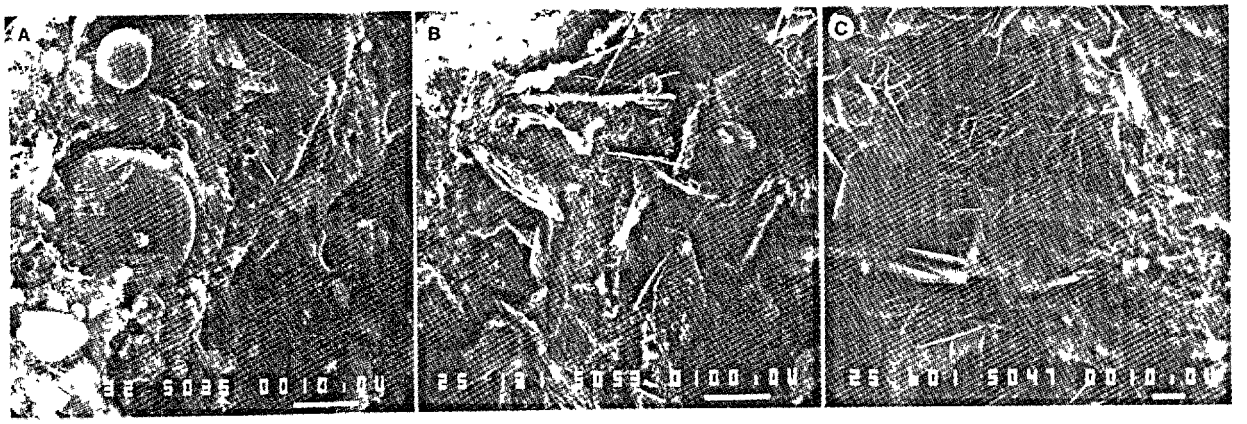

Figure 4 160 day old PC:PFA mortar; a - control, b, c - leached samples.

DISCUSSION

The leaching of the alkali metals follows known solubility data and the predictable test behavior is found for the PC mortar. The introduction of the PFA to the binder, however, profoundly influences both the chemical and physical development during testing. While the greater and more rapid rise and fall of the alkali content of the effluent in the early test stages may be attributed to the greater availability and accessibility of the alkalis from the PFA, the subsequent behavior of S, Ca, permeability and pH is due to the dynamic environment established by the CCLT in the test sample. Ca-bearing pore fluids flowing through the sample, readily react with the high quality fly ash, hydration continues, consuming CH from the solution thus causing a fall in the Ca effluent concentration thus causing a reduction in effluent pH. The continuing production of CSH from the PFA hydration densifies the microstructure, reducing porosity, pore connectivity and overall permeability. The final drop in pH below that expected from a CH solution is evidence that Ca leaching from CH has ceased. The small increase in S at the end of the test (bearing in mind the 10x scaling factor) may come from the solution of early formed ettringite within the sample. The source of calcium is therefore indicated to be CSH, and is reflected in the reduction in effluent pH.

Physical and microstructural evidence suggests that the PC mortar is more heavily affected by the through flow. Ettringite formation although only observed in the voids, could be disrupting the sample integrity. The friable nature is due to both the leaching of the CH, CSH and ettringite. The PC:PFA however was almost impermeable by the cessation of testing. The continuing production of CSH from hydration of the PFA causes a considerable change in sample porosity and connectivity. The formation of the CAH follows known patterns and is due to a the unavailibility of S within the binders.

CONCLUSIONS

The cell test results for the PC mortar show predictable trends, with maintenance of a constant Ca concentration and pH level after initial alkali leaching. The permeability remains constant throughout the test, despite the observed development of friability.

The high initial alkali leaching with the PC:PFA sample, indicates the availability and accessibility of the alkalis from the PFA. The Ca concentration falls from a low maximum, a consequence of continuing PFA hydration. This trend is paralleled by both pH and permeability.

These observations are of significance in selection of cementitious materials in the field of waste containment. Where permeability and pH are controlling factors.

REFERENCES

Dhir, R.K., Hubbard, F.H. and Unsworth, H.P., "XRF Thin Film Copper Disc Evaporation Test for the Elemental Analysis of Concrete Test Solutions", Cement and Concrete Research, Vol. 25, No. 8, 1995, pp. 1627-1632.

Michetis, P., "A True Triaxial Cell for Low and High Pressure Experiments", International Journal of Rock Mechanics, Vol. 22, No. 3, 1985, pp. 183-188.

Taylor, H.F.W., "Cement Chemistry", Academic Press, London, 1990, Chapter 5: "Hydration of Calcium Silicate Phases", pp. 127.

Unsworth, H.P., "Cementitious Materials In Waste Containment, Leach Studies", PhD thesis Department of Civil Engineering, University of Dundee, Scotland, (1996).

Unsworth, H.P., "The Influence of the Eluent Ions on the Properties of Leached Cementitious Materials," Invited paper, SCI Young Researchers Forum, London Feb. 20th 1997.

INVESTIGATIONS ON MOISTURE ABSORPTION AND ITS EFFECT ON THE PERFORMANCE OF HAC BASED MDF CEMENT

S HARSH, S K HANDOO AND S C AHLUWALIA*

National Council for Cement and Building Materials, New Delhi, India
*OCL India Ltd., New Delhi, India

ABSTRACT Moisture absorption by MDF cement at ambient relative humidity above 70 percent was 1.6 percent after 25 days of exposure and partially reversible at lowered humidity. MDF cement sheets stored at ambient humidity showed slight warpage. Immersion in water caused much higher weight gain and loss of flexural strength which was partially or completely recovered on drying. XRD studies revealed formation of C_3AH_6 in water immersed specimens.

Key-words: Macro Defect Free, Moisture, Polymer, Porosity, High alumina cement

INTRODUCTION

Moisture absorption leading to loss of strength and dimensional instability of MDF cement products has been reported (Poon et al, 1987; Young, 1991). The MDF cement has a high volume fraction (upto 30%) of water soluble polymer and a largely unhydrated cement fraction. Both are prone to attack by moisture. Attempts to improve the moisture resistance of MDF cement by using cross-linking/coupling agents have met with varying degree of success (Young, 1991).

The present paper reports additional data on moisture uptake by HAC based MDF cement which apart from substantiating the earlier findings suggests the need for further investigations on improving the water sensitivity of MDF cement products. The extent of moisture absorption at ambient humidity and on immersion in water is reported alongwith its consequent effect on the performance and mineralogy of MDF cement products.

EXPERIMENTAL

High alumina cement (HAC) having 32.95% CaO and 45.39% Al_2O_3 and 88 % hydrolysed polyvinyl alcohol (PVA) were used in the two compositions given in Table-1 to prepare MDF cement sheets of 30x30x0.3 cm following the method of Birchall et al (1981, 1982). Strips of 12x3 cm. were cut from large uncured sheets. Some of the cured specimens were soaked in hexamethylene diisocyanate (HMDI) for 1, 3, 18 and 24 hours followed by drying in oven at 80°C.

Moisture absorption was followed by recording the weight change of MDF cement specimens exposed to ambient humidity or immersed in water, upto a period of 50 days. After immersion in water for 1, 4 and 14 days, 3 strips were tested for flexural strength in wet state and three strips were tested after drying in oven. Water immersed MDF cement strips were dried at 80°C and powdered for XRD investigations.

Table 1 MDF Cement Compositions

Composition	HAC	PVA	Water
	(Parts by Weight)		
A	100	6	12
B	100	5	13

RESULTS AND DISCUSSION

Moisture absorption by MDF cement

Moisture absorption by MDF cement product, of composition A, at ambient relative humidity of 72-76 percent (Fig.-1), was relatively rapid initially resulting in 1.48 percent gain in weight after 22 days of exposure. Further moisture absorption took place at a slower rate, resulting in total weight gain of 1.6 percent after 43 days of exposure. A fall in humidity from 76 to 70 percent (on 32nd day) caused the sample to give off some of the absorbed moisutre. The fall in humidity from 76 to 58 percent, 43rd day onwards, resulted in 15.6 percent of absorbed moisture being given off,i.e., a residual moisture content of 1.36% on 53 rd day. These observations are in line with the earlier findings on the dependence of moisutre absorption on relative humidity (Young, 1991). Absorption of moisture by polymer phase and further hydration of cement grains are the factors causing moisture uptake by MDF cement. The loss of absorbed moisture at lower humidity indicates the partial reversibility of moisture absorption which is caused by drying up of the polymer phase.

Moisture absorption and resulting weight gain by MDF cement product was much higher on immersion in water. Specimens 1 and 2 of composition A and B absorbed moisutre rapidly at first and later at a progressively slower rate, gaining 14.7 and 11.1 percent weight respectively after immersion for 50 days in water (Fig.-2). Relatively lower weight gained by composition-B is on account of a lower percentage of polymer used as compared to composition A, suggesting a decrease in moisture sensitivity.

The factors leading to a change in the weight of water immersed specimens could be : (i) absorption of water by polymer phase and further hydration of cement leading to weight gain and, (ii) dissolution of polymer and leaching of cement hydration products in surrounding water leading to weight loss, as already reported (Young,1991). The sample weights reported here were recorded for wet specimens and thus included both the chemically combined and physically absorbed water. Oven drying of specimens at 80°C, after 50 days of

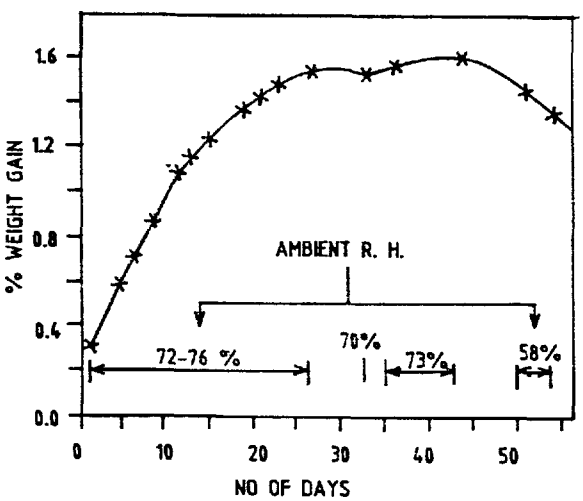

Fig. 1 Moisutre absorption by MDF cement at ambient humidity

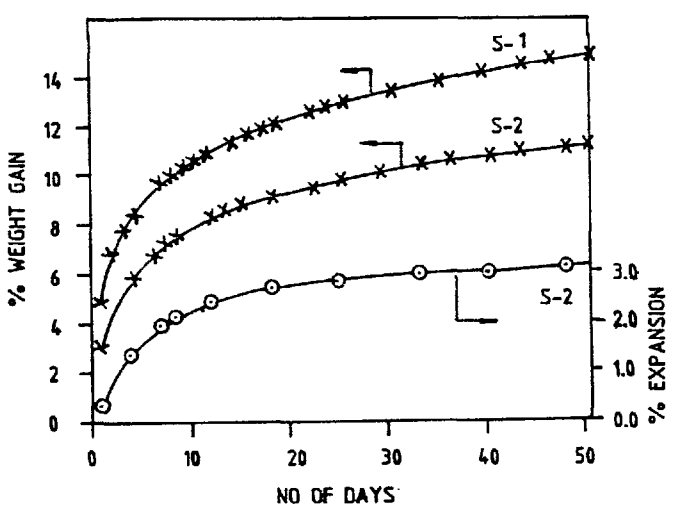

Fig. 2 Moisture absorption and expansion of MDF cement on immersion in water

immersion resulting in lowering of 25-39% of the weight gained, indicated evaporation of physically absorbed water. However, the samples still showed a net gain in weight, indicating that the weight loss on account of dissolution of polymer and leaching of cement was more than made up by further hydration of cement. However, after shorter immersion periods of 1-14 days, generally a net loss of 1-2.5% was observed in the weight of dried specimens.

Immersion of MDF cement in water also caused expansion leading to an increase of 3 percent in the length of specimen-2 (Fig.-2). At later ages, water immersed samples also underwent warpage. Small specimens exposed to ambient humidity did not show any apparent warpage, but larger specimens of 30x30x0.3 cm. showed slight warpage on being stored at ambient humidity.

Effect of Immersion in Water on Flexural Strength

Immersion in water for 1 day lowered the average flexural strength of wet specimens by 54.7 percent (Fig. 3). Drying at 80°C restored most of the lost strength. After longer immersion periods of 4 and 14 days the average drop in flexural strength was 68.7 and 73.02 percent respectively. However, on drying the specimens not only recovered the lost strength but showed a net gain over starting strength (Fig. 3).

Swelling and softening of polymer (Canon & Groves, 1986; Poon et al, 1987) and increase of porosity on account of dissolution of cement hydration products/ polymer (Young, 1991) could be the primary causes of the loss of strength in wet specimens. On drying MDF cement is reported to regain strength partially (Poon et al, 1987). The recovery of strength in dry specimens in our studies is seen to be partial after 1 day immersion, but complete after immersion for 4 days and 14 days. The probable reason for such a recovery is that the porosity created during early immersion periods could be getting filled up at later ages by cement hydration products. The unhydrated cement fraction present in MDF cement, would hydrate on immersion in water and the hydration products thus formed could get deposited in the pores created by earlier leaching of cement hydration products/dissolution of polymer. Filling up of pores, created in MDF cement on heating upto 500°C, by cement hydration products has also been reported (Young,1992).

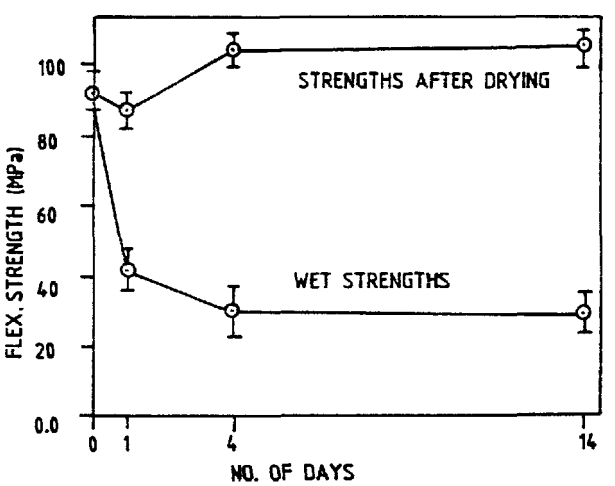

Fig. 3 Effect of immersion in water on flexural strength

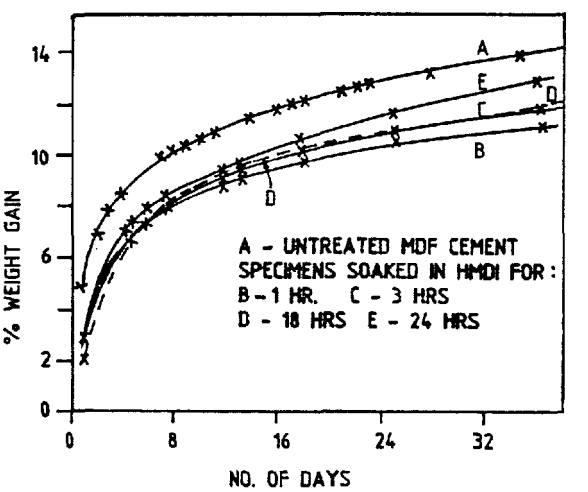

Fig. 4 Moisture absorption by HMDI soaked specimens on immersion in water

Effect of Soaking in HMDI on Moisture Absorption

Impregnation of MDF cement with hexamethylene diisocyanate (HMDI) causes cross-linking of PVA molecules and is reported to improve the moisture resistance of MDF cement (Kataoka, 1988). In our studies, improvement in the moisture resistance was attempted by soaking the cured MDF cement strips in HMDI for 1 to 24 hours. Moisture absorption by HMDI treated strips, on immersion in water for 1 day was lowered by 50-60 percent as compared to the moisture absorbed by untreated specimens (Fig.-4). However moisture absorption increased steadily on continued immersion in water. The time of soaking in HMDI did not influence the moisture absorption characteristics. Soaking of cured MDF cement in HMDI was not found effective in improving the moisture resistance, which could possibly be due to non-penetration of HMDI to any significant depth inside the specimen.

Mineralogical Investigations

Analysis of XRD patterns showed that the crystalline hydrated phase C_3AH_6, which was absent in unexposed MDF cement specimens was formed in water immersed specimens. The intensity of XRD peaks corresponding to C_3AH_6 was higher at longer immersion periods indicating growth of C_3AH_6 in specimens on continued immersion. On the other hand, the peaks corresponding to CA grew weaker. However, even after 14 days CA was present in the specimens, indicating scope for further hydration.

CONCLUSIONS

1. Moisture absorption by MDF cement at ambient humidity above 70 percent was significant and partially reversible at lowered humidities.
2. The moisture absorption on immersion in water was much higher leading to 10-14% gain in weight after 50 days,besides expansion and warpage.
3. Immersion in water initially causes a net loss in weight indicating increased porosity but a net weight gain at later ages indicated filling up of pores by cement hydration products.
4. Immersion in water for 1-14 days caused a lowering of flexural strength, which was partially or completely regained on drying.
5. Soaking the cured MDF cement in hexamethylene diisocyanate was not found to be effective in improving moisture resistance.

ACKNOWLEDGEMENT

The authors are grateful to Director General, NCB, New Delhi for granting permission to publish the work presented in this paper.

REFERENCES

Birchall, J.D. et al, Europ. Patents : 0021682 (1981); 0055035 (1982)

Canon, C.M. and **Groves**, G.W., "Time dependent mechanical properties of high strength cement", J.Mat.Sci., Vol. 21, 1986, 4009-4014.

Kataoka, N., "High strength cured cement article and process for manufacturing the same", Europ. Patent: 0280971 A1 (1988).

Poon, C.S.,**Wassell**,L.E. and **Groves**, G.W., "Stability of macro-defect-free cement", Mater. Sci, Tech., Vol 3, Dec. 1987, pp. 993-996.

Young, J.F., "Macro-defect-free cement : a review", Mat. Res. Soc. Symp. Proc., Vol. 179, 1991, pp. 101-121.

Young, J.F., "Macro-defect-free cement : a novel organo-ceramic composite", Mat. Res. Soc. Symp. Proc., Vol. 271, 1992, pp. 609-619.

EFFECT OF SILICA FUME INCORPORATION IN CONCRETE ON THE CORROSION PROTECTION OF EMBEDDED REINFORCEMENT.

Hamdy A.El-SAYED, Ali H.ALI and Basil A.El-SABBAGH
Building Research Institute, Cairo, Egypt.

ABSTRACT Silica fume (SF) has been demonstrated to assist retaining the reinforcement passivity and accentuate its resistance against the effect of harsh surrounding environments even after long-term curing. 10% silica fume in concrete continues to prove that it is the "optimum dosage". Incorporating a superplasticizer into the concrete mix is beneficial for up-grading steel passivity.

Key words : Corrosion - Steel - Silica fume - Waste material utilization

INTRODUCTION

The present work is the third part of a series of investigations devoted to determining silica fume effects on cement and concrete chemical, physical and mechanical characteristics as well as its role in counteracting salt attack on concrete (El-Sayed, Ali and El-Sabbagh, 1995 and 1996). It has been found that, 10% silica fume- to which a superplasticizer has been added-represents "the optimum dosage" to replace cement in order to achieve maximum strength improvement and maintain the alkaline nature of the concrete as well as increase its chemical resistance. The current third part of the work has endeavoured to study the effect of silica fume incorporation in concrete on the passivity retention of embedded reinforcement and hindrance of the corrosive attack due to invading aggressive agents from surrounding media.

EXPERIMENTAL

The ingredients of the concrete mix used were ordinary Portland cement, sand and gravel. The mix proportions were 1:2:4, respectively. The water cement ratio was 0.6, by mass. When using silica fume (SiO_2=96%, Particle size< 0.5μm and surface area=20m^2/g), the required amount was admixed to the cement before adding it to the dry concrete mix. Sulfonated naphthalene formaldehyde (SNF) superplasticizer was used as a high range water-reducer (HRWR). To keep the same workability (the same slump value) as that of the control concrete, the W/C ratio for the HRWR-incorporating concrete has been reduced to 0.47. The required amount-expressed as a percentage of cement by mass-was dissolved in the mixing water before adding it to the dry mix.

For pH measurements of concrete extract, plain or silica fume-incorporating concrete samples were cured in a humidity chamber for 28 days, then, a representative sample was powdered. 400g of the concrete powder were stirred in 1000ml of distilled water for 2hrs, then, the pH value of the concrete extract was measured.

The reinforcing steel used was mild steel, 6mm in diameter. Prepared reinforcing steel rods were centrally placed in cylindrical 5x10 cm steel moulds, then, the active-predetermined- areas were completely covered by the prepared concrete. The samples were cured for 24 hrs after casting, then, demoulded and continuously cured in the test media. The corrosion behavior of the steel-in-concrete electrodes was studied by means of the galvanostatic anodic polarization technique. The steel-in-concrete was made as an anode in a circuit using an auxiliary platinum electrode as cathode. A constant current density of 10μA/cm^2 was applied to the steel electrode and the corresponding potential was recorded as a function of time.

RESULTS AND DISCUSSION

It is expected that, when silica fume is used as a partial cement replacement, the pH of the concrete will decrease due to: a) the reduction in the cement content and the consequent reduction in the $Ca(OH)_2$ liberated upon cement hydration, b) the pozzolanic reaction of silica fume and the consumption of part of the liberated $Ca(OH)_2$ and 3) the reduction in the alkali-pore water concentration. Consequently, the reduction in pH associated with silica fume incorporation in concrete has been determined in order to assess the effect of silica fume on stabilizing (or destabilizing) the passive iron oxide film on the reinforcing steel surface. Thereafter, the work has been directed to investigate the effect of admixing concrete with silica fume on the corrosion behavior of embedded reinforcement upon exposure to different aggressive media,

Influence of silica fume on the pH of the water soluble concrete extracts

Water soluble extracts from concrete incorporating silica fume at the dosages 0,5,7.5,10 and 15% in absence and in presence of SNF superplasticizer were prepared for pH measurements. The results are given in Table 1. It can be seen that, the pH of the concrete extract of the control sample reaches 13.8. Replacement of cement by silica fume up to 15% reduces the pH to 13.2. It is to be noticed that, using a superplasticizer with silica fume in concrete does not alter the pH value relative to that of the control concrete except for the 15% silica fume concrete where the pH is reduced by only 0.1 unit, thus, being 13.7.

As the passivity of steel in concrete in maintained above pH 11.5 (Gouda, 1970), therefore, in case of silica fume at dosages up to 15%, the reduction in the pH value of the concrete will be far from sufficient to destabilize the passive iron oxide film on the steel surface with the consequent increase in vulnerability to corrosive attack. In addition, utilization of a superplasticizer with silica fume in concrete adds another benefit to the course of improving concrete characteristics which is maintaining the pH value of the concrete very close to that of the control sample. In other words, maintaining the highly alkaline nature of the concrete.

Table 1 pH values of water soluble extracts of silica fume concrete

Silica fume in concrete mix	**Silica fume %**				
	0.0	5	7.5	10	15
In absence of SNF	13.8	13.3	13.3	13.3	13.2
In presence of SNF	13.8	13.8	13.8	13.8	13.7

Corrosion behavior of reinforcing steel in silica fume concrete cured in different aggressive media

The overall property of concrete which controls its protective capabilities is its electrical resistivity. This is modified by factors such as porosity, chemistry of pore water, particularly pH, and aggressive ions content. High electrical resistivity of concrete will limit the corrosion of embedded reinforcement. As the corrosion of steel in concrete is associated with the formation of local electrolytic cells on the steel surface, thus, the quantity of electricity flowing through such local cells (overcoming the electrical resistivity of concrete) is equivalent to the amount of metallic corrosion in accordance to Faraday's law (Gouda, 1975):

The quantity of electricity Q(mC/cm^2)= Current density (mA/cm^2) X Time to reach passivation (s)

Consequently, the higher the quantity of electricity (or the longer the time to reach passivation) the lower is the corrosion resistance.

Therefore, in the present study the effect of silica fume in concrete upon modifying the concrete resistivity, hence, protecting the steel reinforcement against the corrosive effect of diffusing aggressive ions has been evaluated by determining the anodic polarization behavior of steel in concrete incorporating 5,7.5, 10 and 15% silica fume, as a cement replacement by mass, at a constant applied current density of $10\mu A/cm^2$ and recording the time to reach passivation potential (TTP). Such recorded time has been taken as a measure for the degree of steel passivation. If TTP is ≤ 7 , 7-15 and ≥ 15 minutes, the degree of passivation has been considered "high", "moderate" and "low", respectively (El-Sayed, 1994). The concrete curing media were selected simulating some of the affecting media in practice, namely, 2 , 3 , 4 and 5% NaCl solutions, 5 , 6 and 7% Na_2SO_4 solutions and sea water. The W/C+S ratio was 0.6. The curing ages tested were a relatively short-term age (28 days) and a long-term one (1year). For every curing medium, the performance of reinforcing steel in silica fume-free concrete has been determined as a reference (control) sample. The influence of incorporating SNF superplasticizer in the silica fume concrete on the corrosion behavior of the steel reinforcement has been determined as well.

Anodic polarization behavior of reinforcing steel in silica fume concrete cured in chloride media.

Chlorides may be either introduced into fresh concrete from chemical admixtures or from chloride contaminated concrete components or they may penetrate hardened concrete from external sources (such as deicing salts, sea water, underground water, etc.). In either case, some of the chloride ions will be available and presumably aggressive in the pore solution. The capacity of concrete to bind chlorides as well as the resistance it offers to their penetration are important factors in suppressing the corrosive effect of chloride ions. Therefore, the influence of silica fume inclusion in concrete on affecting the embedded steel passivity upon exposure to chloride media has been investigated. Firstly, the anodic polarization behavior of reinforcing steel in silica fume-free concrete cured in 2,3,4 and 5% NaCl solutions has been determined. Figure 1 presents the curves obtained after 28 days curing age compared to those obtained after 1 year age.

It is evident that, upon curing the steel-in-concrete for 28 days in NaCl solutions of concentrations varying from 2 to 5%, the steel passivity is not impaired and passivation potential could be reached after the elapse of 6 , 6 , 7 and 8 minutes for the steel in concrete cured in 2 , 3 , 4 and 5% NaCl, respectively. The fact that one should not rely on the apparent short-term behavior of reinforced concrete and should assure the behavior retention on the long-term is evidenced by the data obtained upon extending the curing age to 1 year. Figure 1 depicts that the observed steel passivity upon curing for 28 days in the different chloride media is a deceiving behavior where such passivity could not be maintained upon curing for 1 year and breakdown of steel passivity has occurred even at the lowest chloride concentration (2%).

A survey on investigations e.g. : (Biczok, 1964) , (Gouda, 1973), (Regourd; 1981) and (Buenfeld, 1986) concerning chloride attack on reinforced concrete indicated that, direct chemical damage of concrete by extraneous chlorides in unusual, but, chloride ions are capable of

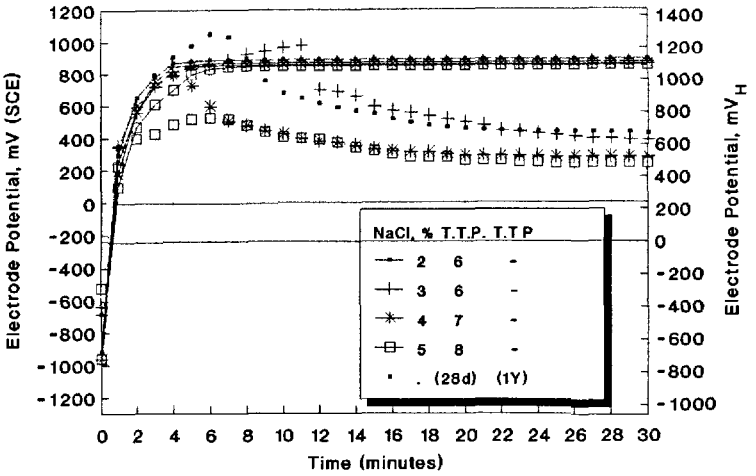

Figure 1 Anodic polarization of reinforcing steel in silica fume-free concrete cured in NaCl solution for 28 days (-) and 1 year (....) .

diffusing into concrete to exacerbate other deleterious reactions. The essence of these investigations is that, the individual actions of chlorides include: counteraction of the passivating effect of the hydroxyl ions derived from the cement hydration; depression of the pH of the pore fluid in the cement matrix; an increase in the conductivity of the cement paste, thus, facilitating the flow of the corrosion current; migration within the concrete to establish concentration corrosion cells; causing an increase in concrete shrinkage, and, therefore, a greater risk of cracking and oxygen access to embedded steel; reduction in the long-term polymerisation of the calcium silicates and, accordingly, an increase in the permeability of the concrete and exacerbation of sulfate attack and alkali-silica reaction in concrete. The real problem caused by chloride attack of concrete is the corrosion of the embedded steel reinforcement. It has been found (El-Sayed, 1993) that 2% NaCl, by mass of cement, incorporated in concrete represents the threshold concentration below which the steel passivity is being safe.

The effect of incorporating silica fume in concrete at the dosages used i.e. 0 , 5 , 7.5 , 10 and 15% on hindering the corrosion of steel reinforcement that could ensue upon curing in NaCl media of concentrations 2,3,4 and 5% for 28 days and 1 year has been investigated. Also, the effect of admixing silica fume concrete with SNF superplasticizer on the corrosion behavior of the embedded reinforcement has been evaluated.

Figure 2 (a and b) presents the anodic polarization behavior of reinforcing steel in silica fume concrete in absence and in presence of SNF superplasticizer after long-term curing for 1 year in the highest chloride concentration (5%) as an example of the results obtained. The curve pertaining to the admixture-free concrete is included in each figure for comparison.

These results show clearly that, using silica fume in concrete improves its ability to protect embedded reinforcement against the corrosive effect of diffusing chlorides. 10% silica fume, as a cement replacement by mass, in concrete represents the "optimum dosage" that offers the highest electrical resistivity i.e. the shortest time to reach steel passivation. Incorporating a

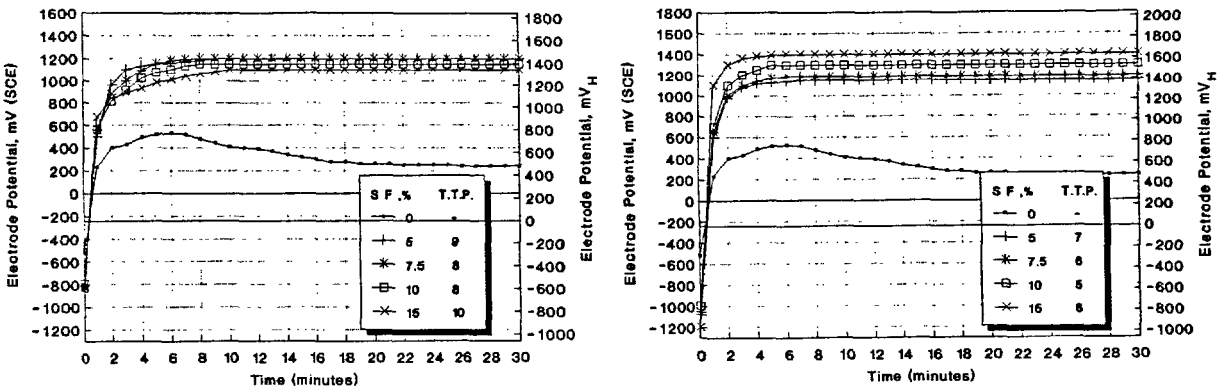

(a) (b)

Figure 2 Anodic polarization of reinforcing steel in concrete in absence (a) and in presence (b) of 0.5% SNF admixed to 5 , 7.5 , 10 and 15% Silica fume after curing in 5% NaCl solution for 1 year (C = SF, SNF - free concrete).

superplasticizer into the concrete mix is beneficial for up-grading the steel passivity. This is evidenced by shorter times to reach passivation relative to times elapsed in absence of the superplasticizer. Such high degree of corrosion protection afforded by silica fume-superplasticized concrete may be attributed to the gained low permeability, high electrical resistivity, limited mobility of chloride ions and reduced oxygen and chloride diffusion from outer media. It is worth mentioning that, the use of silica fume to obtain maximum cement savings in concrete may bring about adverse effects that may mitigate its beneficial role in improving the degree of steel passivation. Thus, an overdose of silica fume in concrete-exceeding 10%- could lead to- in addition to a certain extent of reduction of pore solution pH- an increase of the free chlorides, thereby, increasing the Cl^-/OH^- ratio and, hence, the risk of affecting the steel passivity. This is evident from Fig 2a where TTP has reached after 10 minutes for 15% silica fume dosage compared to 8 minutes for 10% silica fume as well as 6 minutes compared to 5 minutes, respectively, upon using SNF superplasticizer (Fig.2b).

Anodic polarization behavior of reinforcing steel in silica fume concrete cured in sulfate media

It is known that, $Ca(OH)_2$ and C_3A are the most vulnerable constituents of cement to sulfate attack. Hence, due to the reduction in the lime content-the phase mainly responsible for maintaining the steel passivity in concrete-depassivation of the steel could occur by invading sulfate ions from outer media. Therefore, reinforcing steel passivity as influenced by the incorporation of silica fume in the encasing concrete after curing in 5 , 6 and 7% Na_2SO_4 solutions for 28 days and 1 year has been investigated. Also, the effect of admixing the silica fume concrete with SNF superplasticizer on the reinforcement passivity has been assessed. Figure 3 introduces an example of the results obtained, thus, presenting the anodic polarization curves for the reinforcing steel in concrete incorporating 5 , 7.5 , 10 and 15% silica fume in presence of 0.5% SNF superplasticizer after curing for 1 year in the highest sulfate concentration (7%). The curve obtained for steel in admixtures-free concrete is included for comparison. It can be seen, while passivation of the steel in the silica fume-free concrete has reached after significantly long time interval (20 min.) reflecting a "low" grade of passivity, silica fume concrete revealed a significant suppression of the sulfate destructive attack as shown by the short time intervals elapsed to reach passivation. This effect could be attributed to the retardation in the ingress of the sulfate ions through the concrete due to its reduced permeability in addition to the adsorption of

part of the penetrating sulfate on the surface of the silica fume gel formed in the concrete. 10% silica fume still represents the optimum amount to be used as a cement replacement in concrete from the standpoint of maintaining a high degree of steel passivation resisting the sulfate attack. Also, addition of a superplasticizer to silica fume concrete has a distinct positive effect on retaining a high degree of steel passivity remarkably resistant to sulfate attack.

Anodic polarization behavior of reinforcing steel in silica fume concrete cured in sea water

Sea water, as a complex salt solution, is one of the most hostile media whether towards concrete or steel reinforcement. Therefore, it deemed of great interest to assess the prohibitive influence that silica fume in concrete could offer to the embedded reinforcement upon confronting such highly aggressive medium.

It is to be mentioned that, determination of the anodic polarization behavior of reinforcing steel in silica fume-free concrete after curing in sea water revealed that the steel passivity could sustain the sea water attack till a curing age of 28 days (TTP=12 min., a "moderate" grade of passivity), whereas steel passivity could not tolerate the sea water effect upon extending the curing age to 1 year and breakdown of steel passivity has occurred. Consequently, the anodic polarization behavior of reinforcing steel embedded in concrete incorporating 5 , 7.5 , 10 and 15% silica fume in absence and in presence of SNF superplasticizer after curing in sea water for 28 days and 1 year has been investigated. The results obtained for the latter curing age are graphically represented in Fig 4 (a and b) as an example of the data obtained. The curve pertaining to the steel in the admixtures-free concrete is included for comparison.

These results show clearly that, incorporation of silica fume in concrete has maintained the steel passivity even upon curing in sea water for 1 year. A noteworthy feature is that incorporation of 10% silica fume in concrete could retain a "high" degree of passivity to the steel reinforcement. Below 10% silica fume dosage, the steel passivity is "low" and above it the steel passivity is "moderate". In addition, utilization of SNF superplasticizer has enhanced the steel passivity and emphasized that 10% silica fume is the "optimum dosage" to be used where passivation has reached after very short time interval (3 minutes).

CONCLUSIONS

1. The reduction in pH of the concrete mix associated with the inclusion of silica fume at dosages up to 15%, as a cement replacement by mass, is far from sufficient to destroy the passivity of embedded steel reinforcement. In addition, utilization of a superplasticizer with silica fume concrete assists maintaining the pH value very close to that of the silica fume-free concrete.

2. Silica fume in concrete increases its electrical resistivity. This in addition to its role in reducing the penetration of aggressive ions are the main reasons for the better corrosion resistance of steel in silica fume concrete inspite of the shortage in the lime reservoir in the concrete.

3. 10% silica fume represents the "optimum dosage" to be used as a cement replacement in concrete on the basis of its role in retaining a high degree of steel passivity and combating the effects of highly aggressive salts migrating from surrounding media, an effect that is explicit even on the long-term. Incorporating a superplasticizer in the silica fume concrete mix is beneficial in this respect and is highy recommended.

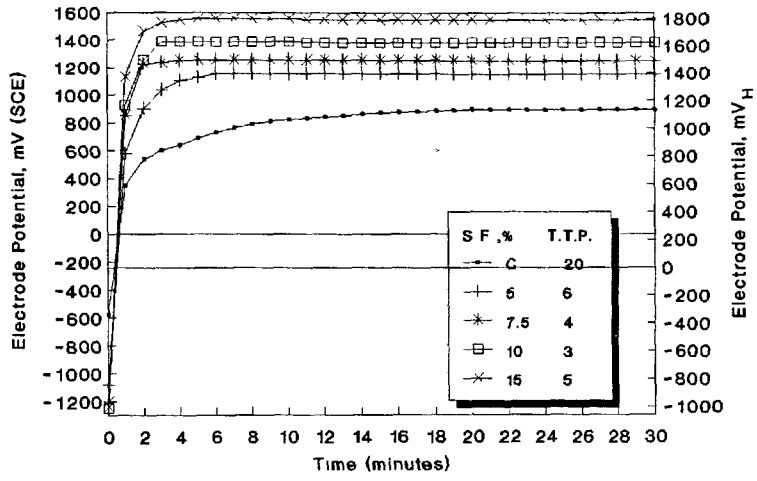

Figure 3 Anodic polarization of reinforcing steel in concrete incorporating 0.5% SNF admixed to 5 , 7.5 , 10 and 15% silica fume after curing in 7% $Na_2 SO_4$ solution for 1 year.

(a)

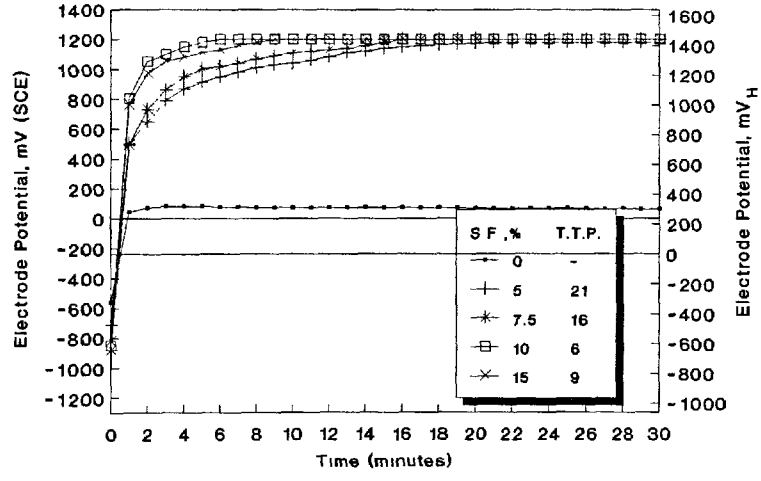

(b)

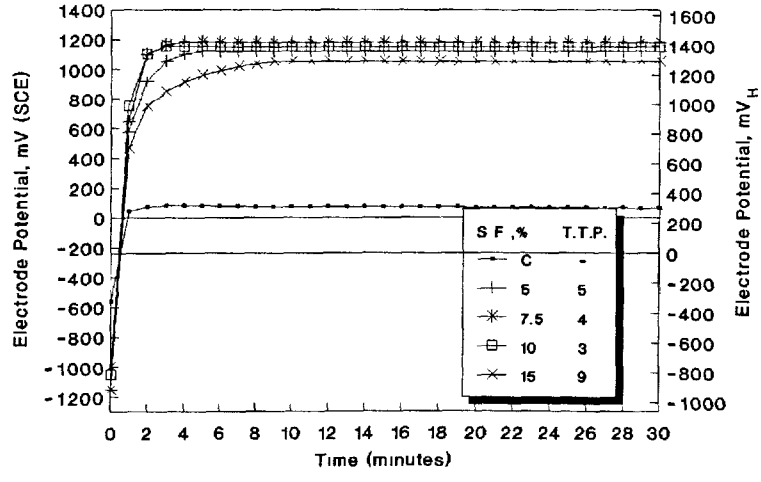

Figure 4 Anodic polarization of reinforcing steel in concrete in absence (a) and in presence (b) of SNF admixed to 5 , 7.5 , 10 and 15% silica fume after curing in sea water for 1 year.

REFERENCES

El-Sayed, H.A., Ali, A.H.and El-Sabbagh, B.A., "Some Aspects of Silica fume-Modified Cement and Concrete", Proc. ConChem Int. Confr. Nov. 28-30 1995, Brussels, PP.283-293.

El-Sayed, H.A., Ali, A.H.and El-Sabbagh, B.A., "Effect of Silica fume on Strength and Chemical Resistance of Portland Cement Concrete", Proc. 9 th Int. Tech. Confr. on Cem. and Build. Mater., Nov. 4-8 1996, Ras Al Khaima, United Arab Emirates, pp. 1-12.

Gouda, V.K., "Corrosion and Corrosion Inhibition of Reinforcing Steel: I Immersed in Alkaline Solutions", Br. Corros. J., Vol. 5, N0.3, 1970, P.P. 198-203.

Gouda, V.K., Shater, M.A. and Mikhail, R.Sh., "Hardened Portland Blast-Furnace Slag Cement Pastes: II The Corrosion Behavior of Steel Reinforcement", Cem.Concr.Res, Vol. 5, No. 1, 1975, pp. 1-13.

El-Sayed, H.A. and Ali, A. H., "Dual Effects of a Water-Reducing Concrete Admixture on Reinforcement Corrosion and Concrete Engineering Properties" Proc.
1 st Int. Confr. on Reinforced Concrete Materials in Hot Climates", April 24-27 1994, Alain, United Arab Emirates, PP. 587-597.

Biczok, I., "Concrete Corrosion and Concrete Protection", Publishing House of the Hungarian Academy of Sciences, Budapest, 1964, pp. 230.

Gouda, V.K., Mourad, W.E. and Mikhail, R.Sh. "Additives to Cement Pastes: Simultaneous Effects on Pore Structure and Corrosion of Steel Reinforcement', J.Colloid and Interface Sci., Vol. 43, No.2, 1973, P.P 294-302.

Regourd, M., Mourtureux, B. and Gautier, E., "Hydraulic Reactivity of Various Pozzolanas", Proc. 5 th Int. Symp. on Concrete Technol., Monterrey, 1981, pp. 1-8.

Buenfeld, N., "Chlorides in Concrete", Construction Repairs and Maintenance, Vol.2, No.4, 1986, PP. 7-10.

El-Sayed, H.A.and Ali, A.H., "Effects of Chloride-Based Accelerating Admixtures on Reinforcement Corrosion and Concrete Engineering Properties", Proc. Int. Confr. Concrete 2000, Dundee, Scotland, UK, 1993, PP.369-378.

CHLORIDE RESISTANCE OF THE PASTES AND MORTARS CONTAINING MINERAL ADDITIVES

Jan DEJA, University of Mining and Metallurgy, Kraków, Poland

ABSTRACT Partial replacement of portland clinker by mineral additions such as ground granulated blast furnace slag, silica fume strongly influenced the resistance of the pastes and mortars to the chloride solution. The diffusion coefficient of Cl ions in the pastes containing different binders have been studied. The mechanical and structural properties of the mortars stored in water as well as in chloride solution were measured. High chloride resistance of the samples containing mineral additives as well as nonclinker binders have been confirmed.

Key-words: blastfurnace slag, chemical attack, chloride, diffusion, microstructure

INTRODUCTION

One of the most aggresive agents affecting constructions of reinforced concrete are chloride ions. They are particularly dangerous because they lower pH of a pore filling solution adjacent to the reinforcement causing it's rapid corrosion. Chloride corrosion is a major problem in a field of an underground, marine and highway engineering. The decisive factor in a durability aspect of a concrete construction being exposed to the action of chlorides is the diffusion rate of these ions in a concrete structure and stability of hydration products in binding materials reacting with chloride solutions.

It is generally accepted that chloride ions diffusing through cement paste, substitute in it's structural constituent OH^- groups: Feldman (1986), Midgley at al (1984), Goto et al (1981), Page et al (1981), Midgley et al (1980). Following, these groups diffuse in the opposite direction into solution. Attention must be given to the fact that migration of ions in the hardened paste does not constitute a simple diffusion. In certain cases $C_3(A,F)\cdot CaCl_2\cdot 10H_2O$, and also basic chloride $Ca(OH)_2\cdot CaCl_2\cdot H_2O$ forms. Additionally, Goto at al (1981) found that cement paste behaves similarly to electropositive, semi-permeable membrane. As the effect of an absorption of Ca^{2+} ions, hydrates'surfaces are positively charged, which in turn leads to a creation of an electrical double layer that limits migration of cations. That's why, diffusion coefficients of chloride ions determined from Fick's equation are to be treated as "effective" only. As for the rate of diffusion of chlorides, structural constituent of cement and mineral additives to the concrete have essential significance. The smallest ratio of a diffusion flow resistance exist in portland cements with low content of C_3A - Efes et al (1985). Employment of slags or pozzolanas (fly-ash, silica fume) as additives to cement or concrete, lowers the effective rate of diffusion of Cl^- even 10^{-3} times - Efes et al (1985), Tomas et al (1990). Also, very good resistance properties to the destructive action of chloride ions have alkali activated slag binders: Deja et al (Montreal 1991, Nice 1994 and Sheffield 1994). The author conducted research of a diffusion rate of Cl^- ions through the partitions made from the pastes of portland cement, blast-furnace cement, alkali activated slag binders and cements modified by addition of granulated blast-furnace slag and active silica.. Beside diffusion coefficients, phase compositions, texture and resistance qualities of mortars based on a specific pastes were tested accordingly.

CHARACTERISTICS OF RAW MATERIALS

In the conducted research were employed: portland cement (CEM I 32.5R),blast-furnace cement (CEM III A 32.5), ground granulated blast-furnace slag and silica fume. Table 1 shows characteristics of these materials.

Additionally, as the activators for alkali activated slag mortars and pastes, sodium waterglass with silicate module MK=1.5 and sodium carbonate were used. Standard, silica sand was used in mortar preparations.

Table 1. Chemical composition and physical characteristics of raw materials.

	Ingredient content in %			
	Portland cement	Blast - furnace cement	Granulated blast furnace slag	Silica fume
CaO	65.08	53.56	41.20	0.66
SiO_2	22.28	30.62	38.20	93.15
Al_2O_3	5.70	5.28	9.60	1.12
Fe_2O_3	2.80	1.44	0.40	0.40
MgO	1.55	6.56	8.40	1.27
S_{tot}	2.83	1.56	1.00	-
Na_2O	0.13	0.22	0.30	0.31
K_2O	1.19	0.56	0.85	1.53
Loss of ignition	0.76	0.41	0.12	1.55
Specific surface [m^2/kg]	315	340	320 or 550	-
Glassy phase [%]	-	-	89	-

RESEARCH OF THE DIFFUSION RATE OF CHLORIDE IONS

Preparation of pastes

Altogether, seven different pastes were prepared out of the raw materials, and their composition is shown in Table 2.

Table 2. Composition of pastes

Paste notation	Ingredient content ,weight %							w/c ratio
	Portland cement	blast furn. cement	silica fume	slag [320m^2/kg]	slag [550m^2/kg]	Na_2CO_3	water glass	
PC-P	100.0	-	-	-	-	-	-	0.35
SC-P	-	100.0	-	-	-	-	-	0.35
PC/SF-P	92.5	-	7.5	-	-	-	-	0.41
PC/S3-P	80.0	-	-	20.0	-	-	-	0.35
PC/S5-P	80.0	-	-	-	20.0	-	-	0.35
AS/WG-P	-	-	-	-	85.0	-	15.0	0.35
AS/NC-P	-	-	-	-	95.0	5.0	-	0.35

Out of the pastes, tiles were made, 5 mm thick each and subsequently they underwent premilinary curing in standard conditions (temp.20±2 °C, relative humidity around 95%).

Exposure of samples

After initial period of premilinary curing tiles were placed in a specially prepared test cell (Fig.1). Each of the tiles worked as a divider between two solutions: NaCl solution of 196g/l concentration and saturated solution of $Ca(OH)_2$. Concentration of chloride ions inside of chambers filled with saturated solution of $Ca(OH)_2$ was measured in 30 days intervals. Measurements were conducted using amperometric titration method with $AgNO_3$ as a precipitation agent.

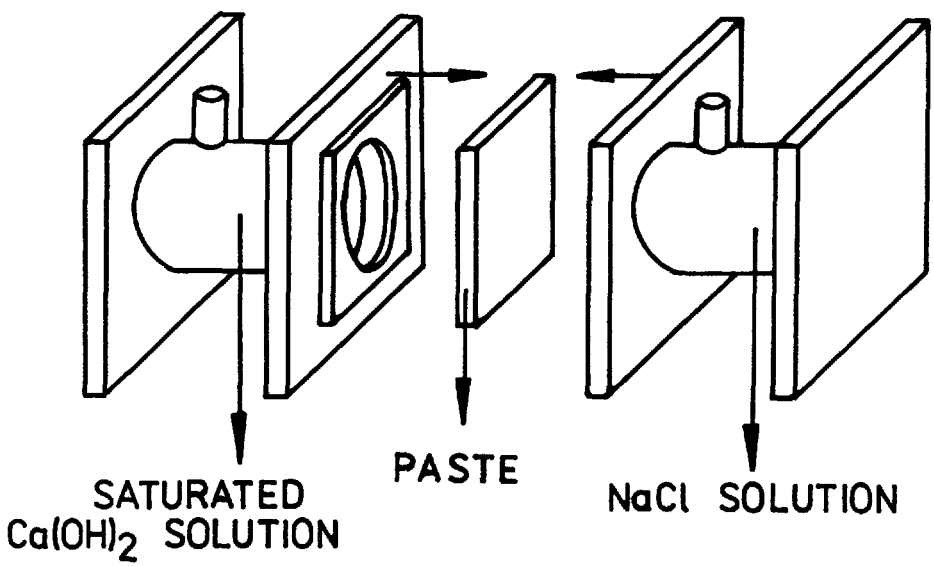

Figure 1. Diagram of a test cell for measuring of a diffusion rate of chloride ions.

Test results

Basing on a determinated contents of Cl^- in the solutions, and using Fick's Law, coefficients of diffusion were calculated. Following auxillary assumptions were taken into account during these calculations:

- during diffusion process, quantity of chlorides on the side of a high concentration is constant and equals initial concentration *Co*.
- within the timeframe from t_i to t_{i+1} diffusion takes place at mean concentration gradient equal to:

$$gradC = \frac{(Co - C_{(t_i)}) + (Co - C_{(t_i+1)})}{2d} \qquad [1]$$

- mean flow of diffusion "$\bar{J}$" within intervals of t_i to t_{i+1} can be expressed as:

$$\bar{J} = D \cdot gradC \qquad [2]$$

Calculated, mean "effective" diffusion coefficients for particular pastes are shown in Table 3.

Table 3. Diffusion coefficients of Cl^- in pastes:

Type of paste	Mean „effective" diffusion coefficients $\cdot 10^{-13}$ [m^2/s]				
	interval 0-30 days	interval 30-60 days	interval 60-90 days	interval 90-120 days	interval 0-120 days
PC-P	21.0	7.7	10.1	13.1	38.8
SC-P	4.9	0.1	1.3	1 4	8.4
PC/SF-P	1.3	0.9	1.6	2.6	6.4
PC/S3-P	2.7	2.9	5.6	2.9	14.2
PC/S5-P	1.3	3.8	8.6	13.8	13.5
AS/WG-P	0.8	0.3	0.8	0.1	1.9
AS/NC-P	14.4	1.3	0.7	4.6	19.6

To emphasize diferrences between diffusion coefficients, their mean values for a duration of a research period (0 - 120 days) are shown on Fig. 2.

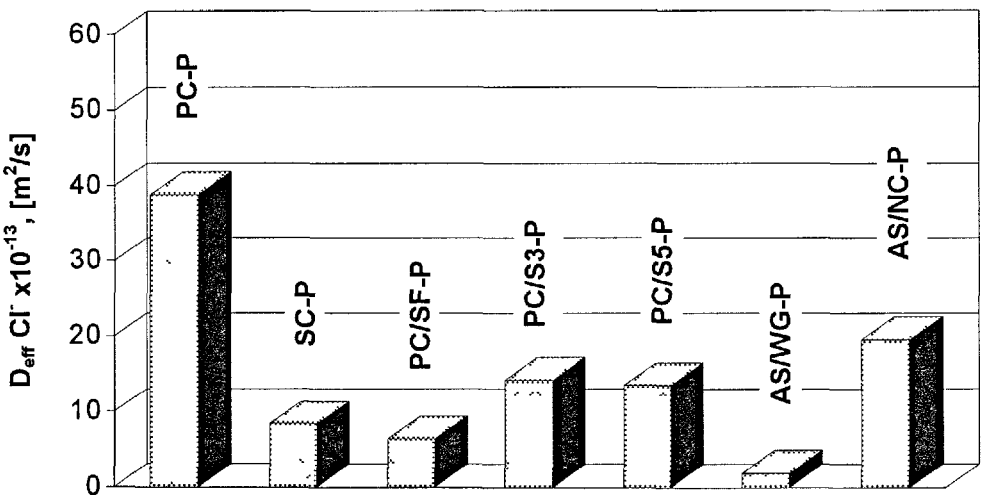

Figure 2. Mean "effective" diffusion coefficients of Cl^- in a 0 - 120 day interval.

The results shown in Table 3 and Fig 2 indicate significant influence of the mineral additives in a course of a diffusion process of chloride ions. If we are to analyze values of $D_{eff\,Cl}$ ratios during entire measurement process (120 days), we will see that they are the least advantageous for a "clean" portland cement. Then, noticeable high "tightness" against diffusing Cl^- shows in the cases of blast-furnace cement (SC-P), portland cement with an addition of a silica fume (PC/SF-P), and above all in an alkali activated slag paste activated with a water glass (AS/WG-P). Also, addition of a ground granulated blast furnace slag (20%) caused almost triple decrease in values of "effective" diffusion coefficient of Cl^-.

Analysis of the results leads to the conclusion that determining factor for this process lies within it's initial period (0-30 days). In most cases samples show the highest values of $D_{eff\,Cl}$. During the

next interval (30-60 days) these values are clearly lower (temporary sealing of a structure), and then again they increase (60-90 and 90-120 days). It seems that these fluctuations are caused by changes in characteristics of pastes as a result of a reaction between chlorides and hydrated phases of paste.
These changes in values of coefficients are the least visible in a case of a slag paste activated with a water glass; within whole time interval they are on a visibly lower level than in the case of other pastes.

Also, low values of $D_{eff\,Cl}$ have to be noticed when achieved in a case of a paste containing 7.5% of a silica fume (PC/SF-P). It has to be noted that in the case of this paste, to achieve consistency similiar to that of the other samples (very high specific surface of silica fume) w/c ratio of 0.41 had to be applied. Introduction of a superplasticizer and limiting w/c ratio to the level of 0.35 wold surely help achieve significantly lower values of $D_{eff\,Cl}$ than one of $6.4 \cdot 10^{-13}$ m^2/s .

RESISTANCE OF MORTARS TO THE CHLORIDE CORROSION

Standard mortars were prepared based on the pastes which contents were shown in Table 2. In all cases values of w/c ratio were equal to 0.5 except of an alkali activated slag mortar when w/c ratio of 0.45 was applied. (In this case, consistency identical to the other samples was achieved at w/s= 0.45, comparing to those of w/c =0.5).

After 28 days of a preliminary curing in a standard conditions, some of the samples were moved to the container filled with a NaCl solution of 196g/l concentration and other samples (as control samples) were placed in a container filled with tap water. Then, after 30, 90 and 180 days of curing, their resistance to bending and compression was tested accordingly. Based on a results, so called corrosion resistance ratio - Locher (1966) - values were calculated for bending and pressing (R_{Cl}/R_{water}). The results of a compressive strength tests are shown in Table 4, and calculated values of corrosion resistance ratios at bending and pressing are presented in Table 5.

Table 4. Compressive strength of the mortars.

Type of mortar	Compressive strength, MPa					
	30 days water	30 days NaCl	90 days water	90 days NaCl	180 days water	180 days NaCl
PC-M	40.6	43.2	43.2	53.7	52.2	40.7
SC-M	46.9	48.0	51.0	59.6	51.4	50.4
PC/SF-M	42.9	42.2	44.2	50.7	51.5	53.2
PC/S3-M	37.5	39.4	42.1	47.4	46.5	39.5
PC/S5-M	42.2	43.1	44.4	48.7	45.7	45.5
AS/WG-M	101.9	107.0	107.6	125.0	108.2	111.7
AS/NC-M	41.0	42.5	49.0	63.4	59.5	61.9

The results of a strenghth testing relate well to the observations of a diffusion coefficients of chloride ions. After 180 days under influence of an aquatic environment highly concentrated with chlorides, portland cement mortar shows the greatest loss of durability, it's compression resistance falls 22%.

In all cases, introduction of mineral additives caused improvement in a corrosion resistance factor. Very high strenghts of alkali activated slag mortars must be noted, both: those cured in

Table 5. Calculated ratios of corrosion resistance in mortars after 180 days of curing.

Type of mortar	Bending resistance $R_{180\ Cl} / R_{180\ water}$	Compression resistance $R_{180\ cl} / R_{180\ water}$
PC-M	1.03	0.78
SC-M	1.14	0.98
PC/SF-M	1.14	1.03
PC/S3-M	1.06	0.85
PC/S5-M	1.07	0.99
AS/WG-M	1.02	1.02
AS/NC-M	1.34	1.04

water and ones cured in a corrosive solution as well (AS/WG-M, AS/NC-M). Particularly high strenghts were noted (over 100 MPa) in the case of a slag mortar activated with water glass.

PHASE COMPOSITION AND MICROSTRUCTURE RESEARCH

After 180 days of curing samples of mortars in a NaCl solution, tests using diffraction method and microscopic observations with scanning microscope were conducted. These tests proved accomplished earlier results of a diffusion and strenght research.

In a standard portland mortar, the greatest quantities of Friedel's Salt ($C_3A \cdot CaCl_2 \cdot 10H_2O$) were found, also high numbers of portlandite and certain quantities of ettringite were registered. Presence of these phases were also observed in the remaining mortar samples based on cement, but their quantities were noticeable lower. The typical microstructure of portland cement mortar after 180 days of curing in NaCl solution is presented on Fig. 3.

Only in the case of alkali activated slag binders (non-clinker binders) their phase composition was diametrically different. Next to the typical of these binders significant quantities of CSH phase, there were none of the phases associated with products of corrosion as determined microscopically and by X-rays (alkali activated slag mortar microstructure is presented on Fig. 4).

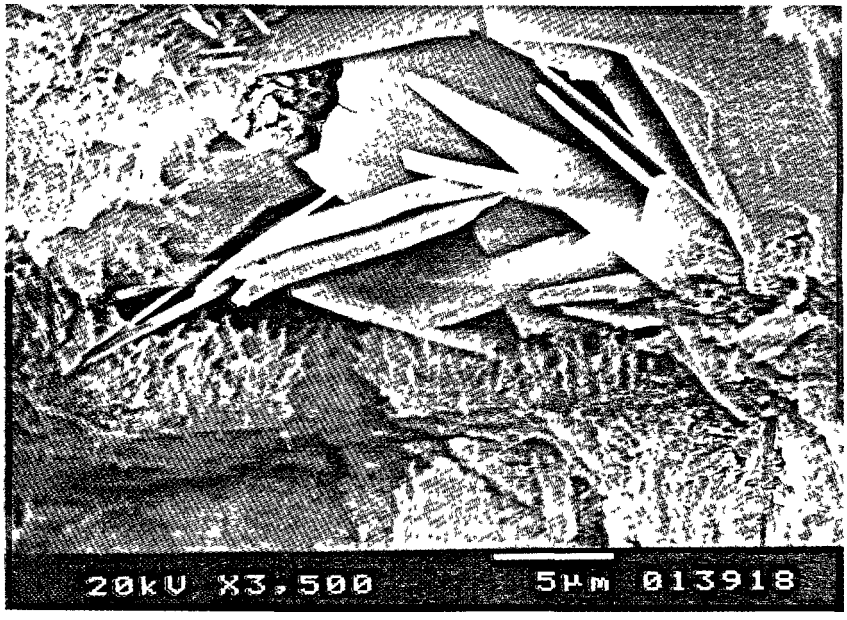

Figure 3. Microstructure of portland cement mortar after 180 days in chloride solution.

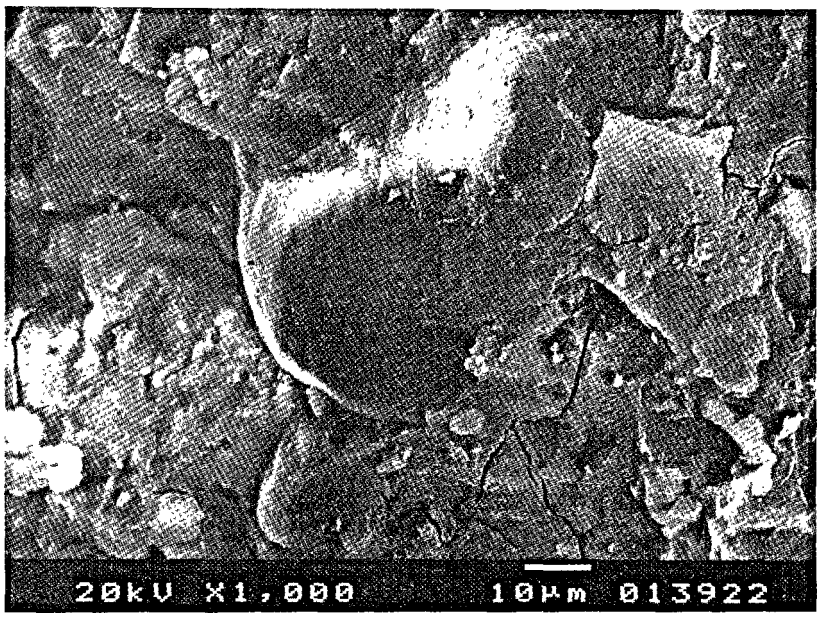

Figure 4. Microstructure of alkali activated slag mortar (AS/WG-M) after 180 days curing in NaCl solution.

CONCLUSIONS

Conducted research unequivocally confirmed a positive influence of mineral additives (granulated blast-furnace slag, silica fume) on the chloride ions diffusion process in a cement pastes and mortars. Also, earlier results indicating very high "tightness" of alkali activated slag mortars and pastes against chloride ions were confirmed - Deja et al (Nice 1994, Sheffield 1994).

If the quantity of chloride ions that diffused through the tile made of portland cement is given a value of 100%, in a case of a paste with addition of silica fume, only 16.5% of this value migrated, and regardingly only 5.1% in a case of a slag binder activated with water glass.

The results achieved during research of a diffusion rate of chloride ions relate well to the results of strength testing (corrosive resistance of mortars under influence of a water based NaCl solution).

Based on a positive relation between results accomplished by these two methods, it is allowed to assume that applied method of checking the rate of ions' diffusion could be used as a quick way to assess corrosion resistance properties of a wide variety of binders.

REFERENCES

Deja, J., Małolepszy, J. and Jaśkiewicz, G., Influence of Chloride Corrosion on the Durability of Reinforcement in the Concrete, 2nd Int. Conf. Durability of Concrete, vol. I, pp. 475 - 479, Montreal 1991.

Deja, J. and Małolepszy, J., Long-term Resistance of Alkali-Activated Sl;ag Mortars to Chloride Solution - Third CANMET/ACI Inter. Conf. on Durabilityof Concrete, p. 657 - 671, Nicea 1994.
Deja, J. and Małolepszy, L., Effekt of cementitious material on the corrrosion of steel development in the einvironment of high chloride content, Inter Conf. of Corosion and Corrosion of Steel in Concrete, Sheffield 1994.
Efes, Y., and Rankers, R., Zum Einfluβ der Zementart auf die Chlorid - Diffusion im Beton: Untersuchungen nach einer Chloridlagerungsdauer von 24 Monaten, Institut für Bauforschung der RWTH Aachen, Forschungsbericht No. F 176, Aachen 1985.
Feldman, R.F., 8 th ICCC Rio de Janeiro, t. I, p. 336, Rio de Janeiro 1986.
Goto, S. and Roy, D.M., Cement and Concrete Research, 11, 751, 1981.
Locher, F.W., Zement - Kalk - Gips, No. 9, p.395, 1966.
Midgley, H.G. and Illston, J.M., Cement and Concrete Research, 14, 546, 1984.
Midgley, H.G. and Illston, J.M., 7th ICCC t.III, p.VII - 101, Paris 1980.
Page, C.L., Skart, N.R., and El. Farras, F., Cement and Concrete Research, 11, 395, 1981.
Tomas, M., Matthews, J.D. and Haynes, C.A., Chloride diffusion and reinforcement corrosion in marine exposed concretes containing pulverisedfly ash, SCI Society of Chemical Industry pp. 198 - 212, Elsevier Applied Science, London 1990.

CHLORIDE BINDING OF CEMENT PASTE CONTAINING FLY ASH

Udo WIENS, Peter SCHIESSL, Institute for Building Materials Research (ibac),
University of Technology, Aachen, Germany

ABSTRACT The life time of reinforced concrete structures exposed to chlorides (see-water, deicing salts, etc.) strongly depends on the quality of the concrete cover. The rate of chloride ingress into concrete depends on the pore structure and the capacity of the hydration products to bind chlorides. It is well known that the use of fly ash improves the resistance of portland cement concretes against chloride attack. The main beneficial effect of fly ash or blast furnace slag is related to the refinement of the pore structure reducing diffusion rates. Limited studies exist about the influence of fly ash on the binding capacity of chlorides in concrete.

Key-words: Fly ash, Chloride binding, Diffusion resistance, CSH, Degree of hydration/reaction

INTRODUCTION

The densifying effect which fly ash has on the microstructure of materials is well known from numerous publications. In this context, the primary effect of fly ash is accountable to the sealing of pore openings and the narrowing of pore channels by the hydration products of the pozzolanic reaction („pore blocking effect"), as a result of which the permeability of concrete is reduced substantially (Marsh et al., 1985, Ngala et al., 1995, Schiessl and Haerdtl, 1994). The capillary pore volume is reduced only minimally if at all as a result of this effect, but certain parts of the pore volume are no longer accessible for the transport of media.

This phenomenon is confirmed by investigations on the resistance to chloride diffusion of mortars produced with the same raw materials as apply to the results presented in this publication regarding chloride binding in cement paste (Schiessl and Wiens, 1997). Schiessl and Wiens (1997) determined the resistance of mortars to chloride diffusion by the means of a so-called migration method (developed by Tang and Nilsson, 1992). In this rapid test the transport of chloride ions is accelerated by the induction of an electrical field, thus reducing the test period to < 7 days. From this rapid test, so-called migration coefficients for chloride can be caclulated, which are directly correlatable with pore structure parameters at a specific testing time. Compared to conventional diffusion tests the rapid test method has the advantage that the influences of time-dependent changes in pore structure are nearly eliminated. This is of particular interest with regard to additions, such as fly ash or blast-furnace slag, reacting over a long period. The pore structure of concrete and mortar with these materials changes over a period of years. It is thus often very difficult to specify the time at which a steady state prevails in conventional diffusion cells for determining intrinsic diffusion coefficients.

The pore parameter which should best reflect this „pore blocking effect" is the threshold radius. This parameter determined by the mercury intrusion porosimetry characterizes the pore radius below which a continous network of pores exists. The smaller this value, the lower will be the continuity of the pore network. Fig. 1 shows the interrelationship between the threshold radius and the migration coefficient $D_{Cl,M}$ that characterizes the resistance of mortar or concrete against chloride diffusion. The good correlation between the migration coefficient and the threshold radius confirms the model concept that permeability is reduced primarily through the reduction of this pore entry radius due to pozzolanic reaction of the fly ash (Fig. 1).

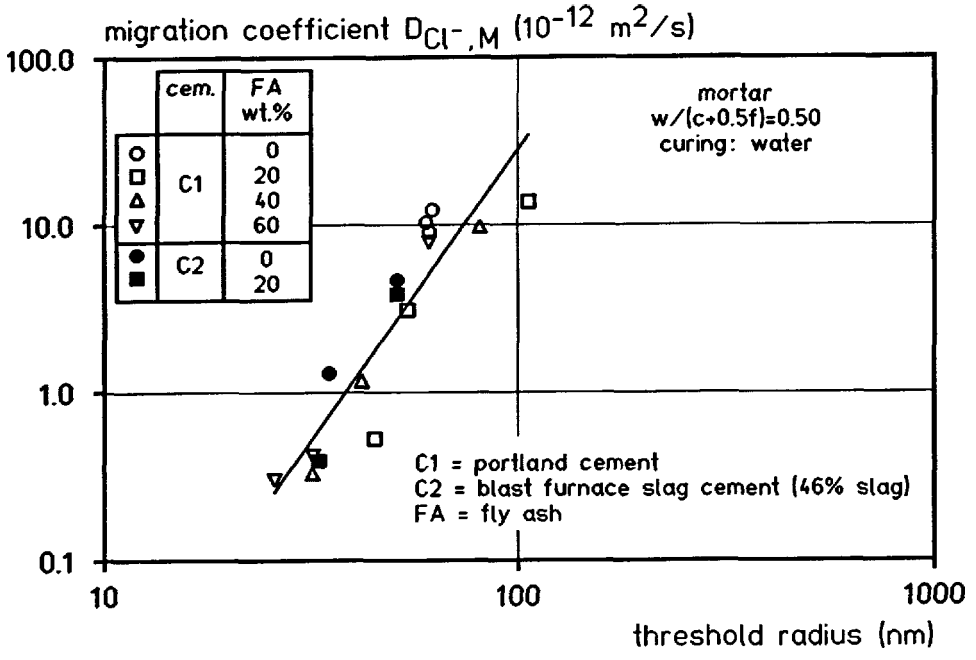

Figure 1: Relationship between the migration coefficient $D_{Cl,M}$ and the threshold radius (Schiessl and Wiens, 1997)

The pozzolanic reaction of the fly ash distinctly reduces the threshold radius as compared to the reference mix. The effect becomes more pronounced as fly ash content increases. This influence of fly ash occurs even with blast furnace slag cements, but it is less significant with these cements, since the reaction of the slag has already densified the pore structure.

In addition to microstructural changes, the binding capacity and the interactions of the ions with the surface of the CSH-gel are also of decisive importance to a realistic representation of chloride transport in concrete. The relationship between the migration coefficient and the threshold radius presented in Fig. 1 indicates that the reduction in ionic diffusion resulting from the use of fly ash is not accountable solely to the reduced continuity of the pore system due to the reaction of the fly ash. The mixes containing fly ash tend to reveal lower migration coefficients than those determined for the pure Portland cement mix at the same threshold radius. This indicates an increased chloride binding capacity or an intensification of the interactions between the gel surface of the CSH phases and the chloride ions in mixes containing fly ash, which has been confirmed by the studies carried out by different authors (Arya et al., 1990, Jensen and Pratt, 1989, Roy et al., 1986, Ngala et al., 1995).

The chloride binding capacity of cement paste is generally determined by establishing the difference between free and total chloride content. These parameters are relatively easy to determine, e.g. by pressing out pore solution or by acid decomposition. Another, more practical method of estimating the chloride binding capacity, which was applied in the course of the investigations presented here, involves determining sorption isotherms by immersing granulated cement paste into chloride solutions of varying concentrations (cf. Tang and Nilsson 1993, Tang and Nilsson 1991). The chloride sorption of the cement paste is then determined by the reduction of the chloride concentration in the storage solutions. Desorption tests which are performed after the chloride adsorption process enable the strength of the chloride binding to be deduced. This binding strength diminishes in the following order: chemically bound chloride (firm incorporation

into the crystal lattice of new reaction products) => chemisorptively bound chloride (e.g. covalent bond in the surface layer of the solid) => physiosorptively bound chloride (attachment due to van der Waal's forces). Thus, the chloride binding capacity of mixes containing fly ash has been studied on granulated cement paste immersed in 0.05, 0.1 and 0.5 molar NaCl-solutions (age: 365 days). Up to 40 wt.% of portland cement was replaced by the same amount of fly ash, respectively. From the interrelationship between the amount of free and bound chloride isotherms have been deduced to quantify the binding capacity. As sorptive binding processes cannot be considered separately from the available gel surface, the quantity of CSH-phases which is formed in the cement paste is determined on the basis of a hydration model which takes due account of the constituent of CSH resulting from the pozzolanic reaction of the fly ash (Haerdtl, 1995).

MATERIALS AND METHODS

Materials

A Portland cement, CEM I 32.5 R, and a fly ash of medium fineness from a dry bottom furnace approved as a concrete addition in accordance with German standard DIN 1045 (low calcium fly ash, class F according to ASTM C 618) were included in the test programme. The chemical compositions and selected physical properties of the raw materials are summarised in Table 1. The mineralogical composition of the Portland cement clinker was calculated according to Bogue from the results of the chemical analysis.

Table 1: Chemical and mineralogical composition and physical properties of the raw materials

Item	Unit	CEM I 32.5 R	Fly ash
Chemical Composition			
SiO_2		19.4	46.9
Al_2O_3		5.43	28.1
Fe_2O_3		3.07	9.24
CaO		63.4	3.54
MgO		1.03	2.02
K_2O		0.74	3.06
Na_2O		0.15	1.36
free CaO		1.57	0.43
SO_3	wt.%	2.56	1.62
C		0.35	0.76
Loss on ignition		2.04	2.07
Mineralogical Composition			
C_3S		62.6	-
C_2S		8.5	-
C_3A		10.0	-
C_4AFt		9.6	-
Fineness			
Density	kg/m^3	3140	2260
Surface area (Blaine)	m^2/kg	283	310
40 µm-residue (air jet sieve)	wt.%	27.4	23.6

n.d.: not determined

In order to produce the cement paste, the raw materials were mixed for 3 minutes and then poured into PE bottles without bubbles, up to the rims of the bottles. To prevent sedimentation

of the solids in the water, the specimens were rotated upside down for 24 hours, until hardening took place. The fly ash content of the produced cement pastes was 0, 20 and 40 wt.%, in relation to the total binding agent content (c+f). The water/cement ratio of the cement paste mixes without fly ash was 0.50. For the mixes containing fly ash, the w/(c+f) ratios were selected so as to enable roughly the same compressive strength to be attained after 28 days (see also Schiessl and Wiens, 1997). This was achieved via the uniform calculation of the fly ash with a cement equivalence value of k = 0.50 to the (w/(c+k·f)) value. According to the studies by Tang and Nilsson (Tang and Nilsson, 1993), the influence of the w/c on the sorptive binding of chloride in cement paste containing Portland cement is negligible.

Adsorption and desorption isotherms, $Ca(OH)_2$ and bound water content

In order to determine the chloride binding, adsorption tests were carried out on cement paste specimens according to the method described in (Tang and Nilsson, 1993). For this purpose, the cement paste (age: 365 days) was comminuted into grain size fractions of 0.5/1 mm and 0.063/0.125 mm, and the hydration process was stopped by placing the cement paste in methanol. 25 g of the granulated and dried cement paste respectively was then subjected to 50 ml of chloride solution of varying concentration (0.05, 0.10 and 0.50 molar NaCl solution in 0.2 molar KOH), and the chloride concentration in the solutions was subsequently determined after the cement paste had been in the solutions for a period of 1 and 5 days, via potentiometric titration. At the end of the adsorption test after 14 days' subjection to chloride, the residual chloride solution was filtered and the chloride concentration in the solution was determined. The specimen was then subjected once again to 50 ml of 0.2 molar KOH over a period of 14 days (desorption test) and the quantity of chloride released into the solution was determined via titrimetry. Prior to beginning the adsorption test and after completing the desorption test, thermogravimetric analyses were carried out on the specimens in the temperature range between 30 and 890 °C, in order to determine the bound water content and the calcium hydroxide content (for details see Meng and Schiessl, 1997). The calcium hydroxide bound by the fly ash was determined from the difference between the mix containing fly ash and the reference mix.

Determination of reacted fly ash content

As sorptive chloride binding takes place primarily on or in the surfaces of the hydration products, it is expedient to relate the chloride fraction which is bound in the cement paste to the total quantity of CSH phases which are formed in the course of cement hydration and the pozzolanic reaction. In the case of cements, it is common to determine the degree of hydration, e.g. from the quantity of chemically bound water, and thus to ascertain the quantity of CSH phases which are formed. In the case of fly ash, it is not possible to deduce the reacted fly ash content directly from the quantity of $Ca(OH)_2$ bound by the pozzolanic reaction. For this purpose, it must be known how much $Ca(OH)_2$ is converted when the complete fly ash content reacts. The reacted fraction of fly ash can only be determined via indirect experimental methods. Determination was carried out by applying the selective dissolving method in accordance with DIN V ENV 196 - 4; 1993, which is normally carried out to determine the content of pozzolanic material in non-hydrated cement, to cement paste specimens with 20, 40 and 60 % fly ash content by weight, in relation to (c+f). In contrast to the experiments to investigate chloride binding, the w/(c+f) value of the cement paste specimens was set at a uniform 0.50. The experiments relating to selective dissolution were carried out as part of a research project to explain the reaction processes in cement paste containing fly ash and silica fume with the aim of evolving thresholds for the application of these pozzolanic substances (Schiessl and Meng, 1996, Meng and Schiessl, 1997), and were not a direct part of the experiments to investigate chloride binding. The cement paste specimens were produced from the same raw materials, however. The dried cement paste is

treated in methanol with a solution of hydrochloric acid and salicylic acid. As a result, the clinker minerals and a proportion of the sulphate component are dissolved in the cement. Slowly, under constant stirring, 2.0 ± 0.1 g of the dried cement paste specimen which had been ground to a fineness of < 0.125 mm was placed in a 400 ml beaker containing 200 ml of the acid mix. This mix was then stirred for 30 minutes. After 24 hours, the solution was filtered through a weighed filter. The insoluble residue was washed approximately six times with 100 ml of methanol. The filter and insoluble residue were dried at 105°C until a constant mass was attained, cooled to room temperature in a desiccator and weighed.

After this treatment the unreacted fly ash content and a proportion of the sulphate component in the insoluble residue is left. After determination of the sulphate content in the insoluble residue and a corresponding correction, the reacted fly ash content can be calculated by subtraction.

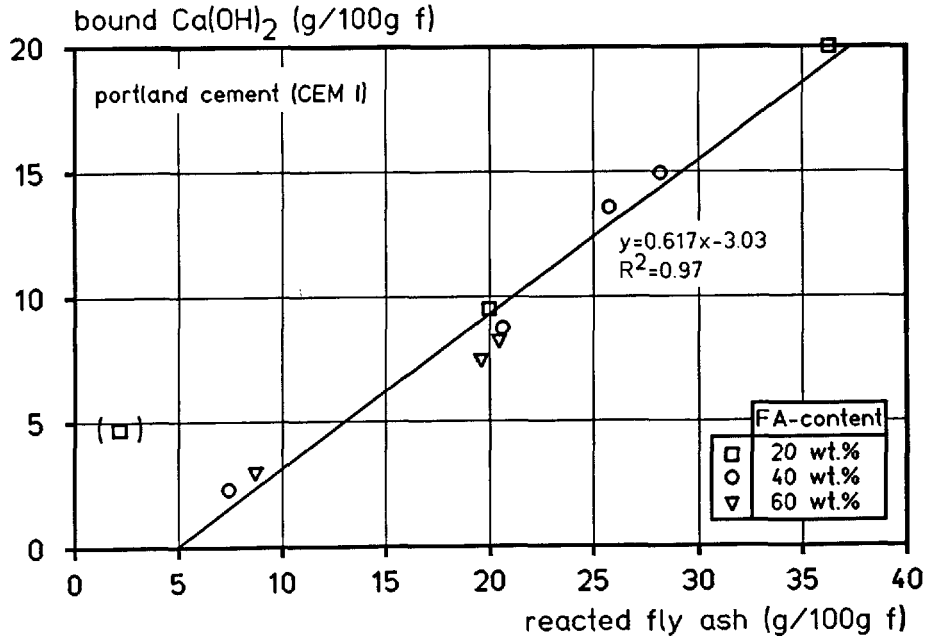

Figure 2: Relationship between the quantity of bound-$Ca(OH)_2$ and the reacted fly ash content; cement paste; w/(c+f) = 0.50; age: 7, 91, 365 and 640 days (Schiessl and Meng, 1996)

Fig. 2 shows that a relatively good correlation exists between the amount of reacted fly ash and the bound $Ca(OH)_2$ measured in dependence of the fly ash content. On the basis of this correlation, it is possible to determine the lime-binding capacity of the fly ash during the reaction in the cement paste. The slope of the line reveals a lime-binding capacity of 0.62 g of $Ca(OH)_2$ per g of reacted fly ash.

RESULTS AND DISCUSSION

When chloride enters into the concrete, chemical and physical (sorptive) binding processes take place. A number of findings have already been published with regard to the purely chemical binding of chloride in hydration phases (e.g. Friedel's salt) (Richartz, 1969, Smolczyk, 1984). These findings are frequently based on experiments in which chloride was added to the fresh concrete and mortar. Adsorption and desorption experiments provide a more effective method of assessing chloride binding under realistic practical conditions for the structural components, as these experiments primarily detect the quantity of chloride which is sorbed at the gel surface in

the course of the chloride transport process. Chloride sorption can have a substantial influence on the rate of transport. Fig. 3 and 4 show the time-dependent chloride sorption of the 0.5/1 and 0.063/0.125 mm cement paste fractions as a function of the fly ash content, by reference to the 0.1 molar NaCl solution (initial concentration).

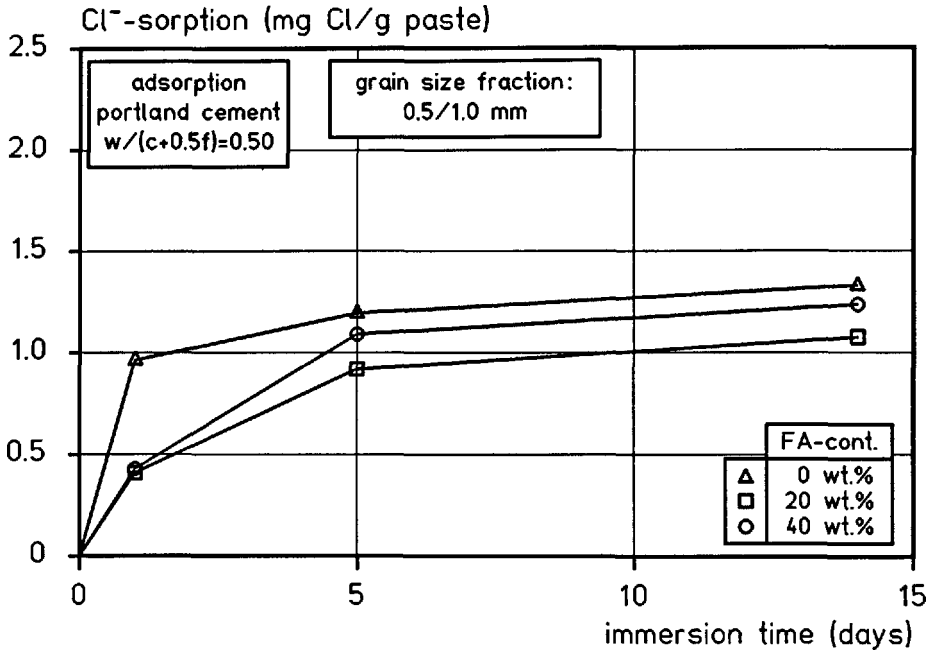

Figure 3: Time-dependent chloride sorption of the 0.5/1 mm fraction; w/(c+0.5·f) = 0.50; age of specimens at immersion in 0.1 molar NaCl solution: 365 days

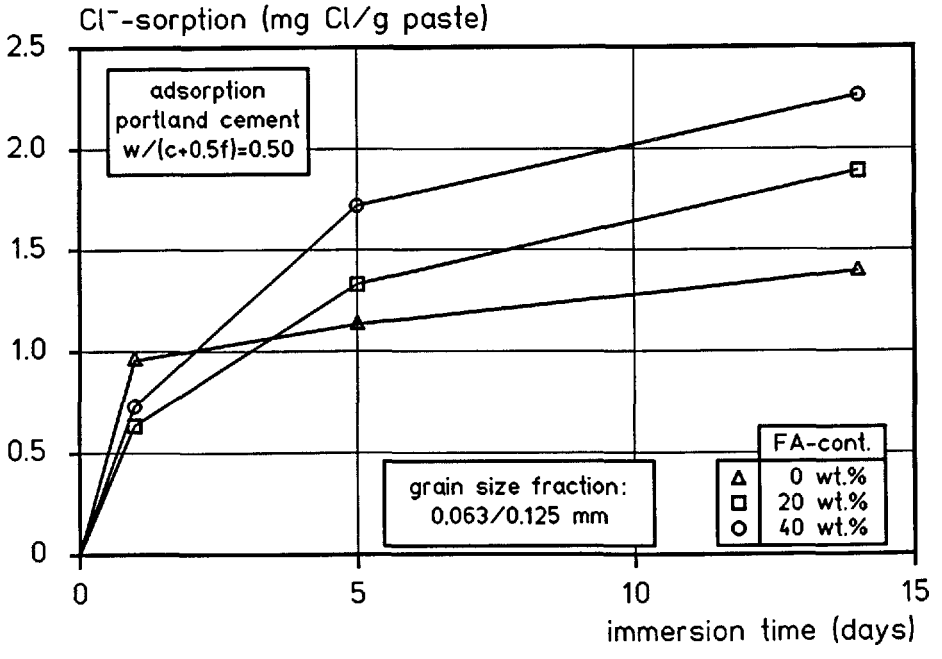

Figure 4: Time-dependent chloride sorption of the 0.063/0.125 mm fraction; w/(c+0.5·f) = 0.50; age of specimens at immersion in 0.1 molar NaCl solution: 365 days

The results obtained with the 0.5/1 mm grain-size fraction (Fig. 3) show that a state of equilibrium has apparently been attained between the storage solution and the pore solution, and that there is a tendency for smaller quantities of chloride to be bound in mixes containing fly ash. When the diffusion routes are further shortened by finer grinding of the cement paste specimens (0.063/0.125 mm fraction, Fig. 4), markedly higher quantities of chloride are bound in comparison to the reference specimen containing pure Portland cement, while the chloride-binding capacity of the pure Portland cement mix is virtually independent of the granulated material's grain size. As a result of the above-described microstructural densification (pore-blocking effect) in mixes containing fly ash, not all the pore spaces and pore walls are reached in the 0.5/1 mm grain-size fraction over a period of 14 days (cf. Fig. 1). As the sorption of chloride takes place primarily on and in the surfaces of the CSH phases, it is expedient to relate the results to the quantity of CSH phases. In this context, the term "CSH phases" refers to the totality of hydrate phases resulting from cement hydration and the pozzolanic reaction of the fly ash, with the exception of the $Ca(OH)_2$. In order to determine the CSH content, Haerdtl's formulation (Haerdtl, 1995) was selected, according to which the CSH content at the age of 365 days can be calculated as follows:

$$CSH_{(365)} = w_{n(365)} + \alpha_{(365)} - CH_{(365)} + \text{bound}\,CH_{(365)} / 0.62 \quad (g/100g\,c) \qquad [1]$$

whereby:

$w_{n(365)}$ non-evaporable water at 365 days,

$\alpha_{(365)} = \frac{w_{n(365)}}{w_{n(\infty)}}$ degree of hydration of the cement,

$$w_{n(\infty)} = 0.237 \cdot C_3S + 0.209 \cdot C_2S + 0.400 \cdot C_3A + 0.167 \cdot C_4AF = 22.2 \ (g/100g\,c) \qquad [2]$$

maximum of non-evaporable water, calculated from the mineralogical composition of the clinker (cf. table 1), (Haerdtl, 1995),

$CH_{(365)}$ calcium hydroxide content of cement paste at 365 days,

bound $CH_{(365)}/0.62$ quantity of CSH phases produced during pozzolanic reaction of the fly ash (1g of fly ash binds 0.62 g of $Ca(OH)_2$; corresponds to the slope of the straight line in Fig. 2).

It can be seen from Eq. [1] that in case of a low calcium fly ash as used in these test series no additional water is bound in the course of the pozzolanic reaction. Solely calcium hydroxide is the constituent in the pozzolanic reaction forming CSH-gel and the bound water content in the reaction products of the fly ash correspond to the bound water in the $Ca(OH)_2$. Table 2 summarizes the CSH content levels determined in accordance with Eq. [1] for the individual cement paste specimens at the age of 365 days.

Table 2: CSH content of the cement paste specimens at the age of 365 days; results of thermogravimetric analysis (CEM I 32.5 R)

Cement content	Fly ash content	$w_{n(365)}$	$\alpha_{(365)}$	$CH_{(365)}$	bound $CH_{(365)}$	$CSH_{(365)}$
wt.%		g/100 g c	%	g/100 g c		g/100 g (c+f)
100	0	17.3	78.1	21.6	-	73.8
80	20	18.3	82.5	15.8	5.8	75.5
60	40	18.8	84.4	10.7	10.9	66.0

At the age of 365 days, the CSH content as a percentage of the total binding agent content is higher in the mix containing 20 wt.% fly ash than in the reference mix, on account of the pozzolanic reaction of the fly ash. Smaller quantities of CSH phases are formed in the mix with 40 wt.% content, due to the reduced cement content. The contribution of the fly ash to the CSH content is not sufficient to compensate for the reduction in cement content. Fig. 5 shows the bound chloride content as a percentage of the CSH content in the cement paste specimens for all the examined storage solutions (0.05, 0.1 and 0.5 molar NaCl; 0.063/0.125 grain-size fraction), in the form of adsorption and desorption isotherms according to Freundlich. As the fly ash content increases, the bound chloride in relation to the CSH content rises. The increase in the level of bound chloride in the presence of fly ash may be accountable to the increase in the gel surface area due to the formation of additional CSH phases from the pozzolanic reaction, which promotes the sorption of chloride. Tang and Nilsson have found a larger gel surface area in cement paste containing 30 wt.% fly ash than in mixes containing pure Portland cement (Tang and Nilsson, 1991). The influence of the larger adsorbent surface on the physiosorptive binding of chloride can be largely factored out by relating the bound quantity of chloride to the gel surface area (Tang and Nilsson, 1991). Although the influence of an increased adsorbent surface area in mixes containing fly ash was compensated for by selecting the gel surface area as the reference basis for the quantity of bound chloride, the authors nevertheless discovered around twice as much bound chloride in the mix containing fly ash as in the cement paste containing pure Portland cement. This is assumed to be due to the higher content of aluminium oxide and iron oxide in the fly ash in comparison to the Portland cement, as a result of which the chemisorptive and/or chemical chloride binding of the cement paste is increased.

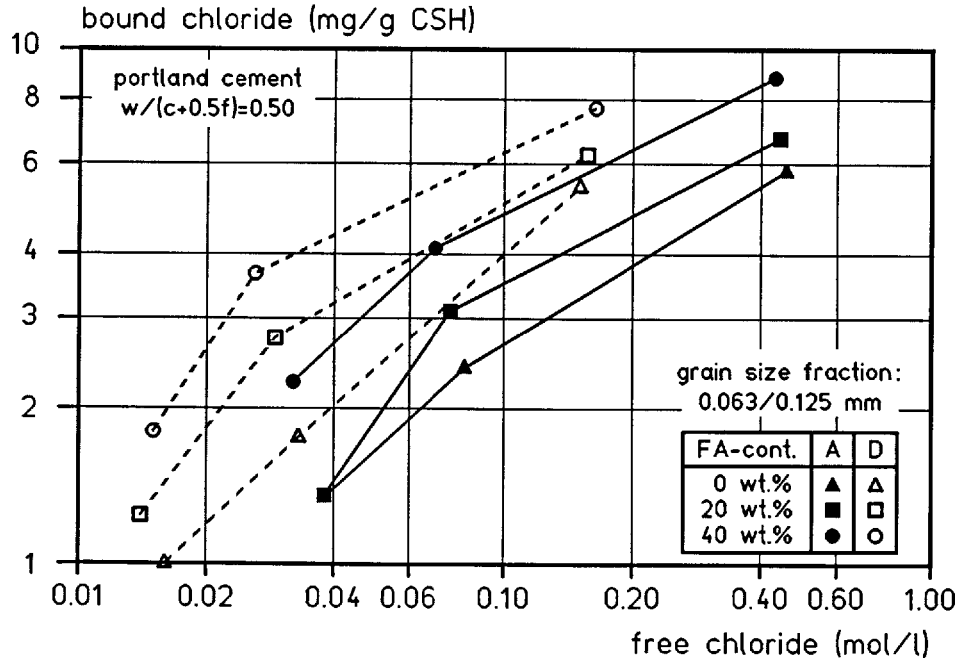

Figure 5: Ad- (A) und desorption isotherms (D) for chloride; cement paste with and without fly ash (fraction: 0.063/0.125 mm; w/(c+0.5·f) = 0.50)

This assumption is supported by X-ray diffraction analyses of the cement paste specimens containing 100 wt.% Portland cement and 40 wt.% fly ash, which were carried out after completion of the desorption experiments in this investigations. The mix containing 40 wt.% fly ash revealed more or better-crystallised Friedel's salt than the cement paste without fly ash. The results of the desorption experiments also indicated stronger chemisorptive and/or chemical

chloride binding in cement paste containing fly ash. In mixes containing 20 and 40 wt.% fly ash, an average level over all the examined concentrations of 91 and 85 % respectively of the chloride bound during adsorption remains in the cement paste after the end of the desorption process, while in the mix containing 100 % Portland cement by weight only around 80 % of the chloride from the adsorption process remains, i.e. around 20 % of the chloride is released again (desorbed).

CONCLUSIONS

On the basis of the completed experiments, it has been possible to derive models to explain the chloride binding of cement containing fly ash. The marked increase in the resistance of cement paste and mortar containing fly ash to penetration by chloride in comparison to the resistance of pure Portland cement is accountable primarily to the increase in physio- and chemisorptive binding capacity as a result of additional sorption surfaces (CSH phases) and the largely irreversible binding of chloride in and on hydrate phases. The high aluminium and iron oxide fractions in the fly ash, which are able to bind chloride in the form of the not readily soluble Friedel's salt, are assumed to be responsible for the increased chemisorptive and chemical binding capacity.

Beyond the increased chloride binding capacity, the transport rate of chloride is reduced as a result of the reduced permeability of the pore system in concretes containing fly ash. The reduced permeability of mixes containing fly ash results primarily from the effective interruption of the capillary pore system and the refinement of the pore structure by CSH phases, which occur as a result of the pozzolanic reaction („pore blocking effect").
The stated mechanisms result in a substantial prolongation of the period which elapses before a critical corrosion-inducing level of chloride content is attained on the reinforcing steel (so-called „incubation time"). It is possible to incorporate the results into an estimation of the lifetimes of concrete structures in environments containing chloride, taking due account of the employed binding agents. In the absence of appurtenant results, binding processes are often neglected in calculations to determine the time-dependent penetration of chloride. The established sorption isotherms can be employed to help render the calculation methods for chloride transport more precise.

Beyond the influence of fly ash on chloride binding in mixes containing Portland cement, it is also planned to include blast-furnace slag cement in combination with fly ash in the investigations into chloride binding. The appurtenant tests have largely been completed and are to be published in the near future.

REFERENCES

Arya, C., Buenfeld N.R.; Newman, J.B. „Factors influencing Chloride Binding in Concrete. In: Cement and Concrete Research 20 (1990), No. 2, 291-300

Haerdtl, R., „Veränderung des Betongefüges durch die Wirkung von Steinkohlenflugasche und ihr Einfluß auf die Betoneigenschaften". Berlin : Beuth. - In: Schriftenreihe des Deutschen Ausschusses für Stahlbeton (1995), Nr. 448 Dissertation (PhD-Thesis)

Jensen, H.U., Pratt, P.L., „The Binding of Chloride Ions by Pozzolanic Products in Fly Ash Cement Blends". In: Advances in Cement Research 2 (1989), No. 7, 121-129

Marsh, B.K., Day, R.L., Bonner, D.G., „Pore Structure Characteristics affecting the Permeability of Cement Pastes containing Fly-Ash". In: Cement and Concrete Research 15 (1985), No. 6, 1027-1038

Meng, B., Schiessl, P., „The Reaction of Silica Fume at Early Ages", 10th International Conference on Cement Chemistry, Gothenburg, 1997

Ngala, V.T., Page, C.L., Parrott, L.J., Yu, S.W., „Diffusion in Cementitious Materials: II: Further Investigations of Chloride and Oxygen Diffusion in Well-Cured OPC and OPC/30%PFA Pastes". In: Cement and Concrete Research 25 (1995), No. 4, 819-826

Richartz, W., „Die Bindung von Chlorid bei der Zementerhärtung". In: Zement Kalk Gips 58 (1969), No. 10, 447-456

Roy, D.M., Malek, R.I.A., Rattanussorn, M., Grutzeck, M.W., „Trapping of Chloride Ions in Cement Pastes containing Fly Ash". - Materials Research Society Symposium Proc. „Fly Ash and Conversion By-Products: Characterization, Utilization and Disposal II", 1986, Vol. 65, 219-226

Schiessl, P., Meng, B,. „Grenzen der Anwendbarkeit von Puzzolanen im Beton", Aachen: Institut für Bauforschung, (1994), Report No. F405

Schiessl, P., Haerdtl, R., „Relationship between Durability and Pore Structure Properties of Concretes Containing Fly Ash". Ottawa : CANMET, 1994. - In: P.K. Mehta Symposium on Durability of Concrete. Proceedings of a Symposium Honoring, Nice, France, May 22-28, 1994, (Khayat, K.H. ; Aitcin, P.C.(Ed.)), 99-118

Schiessl, P., Wiens, U., „Long-Term Influence of Fly Ash on Chloride-Induced Corrosion". To be published at Fourth CANMET/ACI International Conference on Durability of Concrete, Sydney, August 17-22, 1997

Smolczyk, H.-G., „Flüssigkeit in den Poren des Betons - Zusammensetzung und Transportvorgänge in der flüssigen Phase des Zementsteins". In: Beton-Informationen 24 (1984), No. 1, 3-11

Tang, L., Nilsson, L.-O., „Chloride Binding Capacity and Binding Isotherms of OPC Pastes and Mortars". In: Cement and Concrete Research 23 (1993), No. 2, 247-253

Tang, L., Nilsson, L.-O., „Rapid Determination of the Chloride Diffusivity in Concrete by Applying an Electrical Field". In: ACI Materials Journal 89 (1992), No. 1, 49-53

Tang, L., Nilsson, L.-O., „Chloride Binding Capacity, Penetration and Pore Structure of Blended Cement Pastes with Slag and Fly Ash". Int. Conf. on Blended Cements in Construction, (Swamy, R.N. (Ed)), Sheffield, 1991, 377-388

TOPIC IV.B

Physio-chemical, thermal and biological degradation, including environmental and synergistic effects

SULPHATE ATTACK OF CARBONATED AND UNCARBONATED PORTLAND AND BLENDED CEMENT MORTARS

Riccardo SERSALE, Raffaele CIOFFI, Benedetto de VITO, Dipartimento d'Ingegneria dei Materiali e della Produzione dell'Università degli Studi di Napoli (Italy)
Giuseppe FRIGIONE, Dipartimento di Chimica dell'Università degli Studi di Calabria, Arcavacata di Rende (Italy)
Fortunato ZENONE, Cementir Cementerie del Tirreno, Laboratorio Ricerche e Controlli, Spoleto (Italy)

ABSTRACT The influence of the binder's gypsum and C_3A content, both on carbonation and on resistance to sulphate attack, has been evaluated on a series of Iso standard mortars containing Portland,with 6% and 10% C_3A and blends of the same Portland cements with 70% blast furnace slag or with 35% true pozzolana, with gypsum addition varying from 1% to 5% as SO_3. The mortar carbonation process depends on type of cement and SO_3 content and improves response to sulphate attack.

Key-words: blended cement, carbonation, gypsum, porosity, sulphate resistance.

INTRODUCTION

It is well known that the carbonation of concrete can have both positive and negative effects (Taylor, 1990) The aim of the present paper is thus to evaluate the effects of the carbonation of Portland and blended cement mortars on the behaviour of sulphate attack, as part of a wider-ranging project to investigate the durability of cement structures. Permeability is predominantly affected by the presence of large pores and is thus typically the key factor in all durability problems; therefore, response to chemical attack was studied in conjunction with the determination of total porosity and pore size distribution in the carbonated and uncarbonated specimens, as there are some differences in the opinions to be found in literature (Mangat and Khatib, 1995).

These values were determined using mercury intrusion porosimetry which, although it has a number of limitations including over-estimation of the volume of the smaller pores as a result of the "ink-bottle" effect (Kjellsen et al., 1990), nevertheless measures a pore structure that can be reliably referred to the same factors that affect the penetration of fluids and ions (Roy, 1989).

This structure is essentially influenced by the following factors: fineness, water/cement ratio, chemical composition, product curing conditions and pozzolanic reaction. In general the addition of mineral additives to Portland cement reduces pore size or increases the porosity fraction for the smaller pores (Bakker, 1983).

For instance, the low permeability of blast furnace slag pastes has been attributed to differences in pore size distribution compared to Portland cement pastes (Feng et al., 1989) (Malek, et al., 1989). Furthermore, it must be taken into consideration that the smaller pores, which make up the main fraction of total porosity, tend to become unconnected, thus significantly reducing permeability.

Carbonation speed is also affected by the type of cement. In the experimental conditions adopted (Gebauer and Torrent, 1989) it can be seen that cement containing a high percentage of blast furnace slag (70%) shows a faster carbonation speed.

The strength of concrete prepared with ordinary Portland or blended cements is considerably affected by the curing conditions, and in particular by temperature and relative humidity (Mangat and Khatib, 1992) Moreover, the presence of a carbonate layer on the surface of the concrete has been shown to provide a greater resistance to sulphate attack, although numerous exceptions to this have been found. Whereas matrix pore structure and volume seem to have no direct influence on the concrete's resistance to sulphate attack.

This resistance increases when mineral additives are incorporated and after a carbonation process has been carried out. This increased resistance has been evaluated on the basis of the reduction of

calcium hydroxide in the surface layers and the resulting smaller volume of the products of reactions, which expand with sulphate ions.
These and other results found in the literature gave rise to the experimental research reported in this paper.

EXPERIMENTAL

Two samples of type I Portland cement were used with 6% and 10.8% C_3A. Their chemical and mineralogical composition according to Bogue are reported in **Table 1.**

These two samples were then used to prepare the corresponding blended cements by adding 70% granulated blast furnace slag (CEM III/B; CEN ENV 197-1) and 35% true pozzolana (CEM IV/B; CEN ENV 197-1), respectively. A quantity of natural gypsum (98% $CaSO_4 \cdot H_2O$ varying from 1% to 5% as SO_3 was then added to each of these cements in order to take into account its influence on the pore size distribution of the corresponding products, as already extensively verified in our previous investigations (Sersale et al., 1992).

Table1 Chemical and mineralogical composition of the clinkers, wt%.

	Chemical composition	
SiO_2	21.70	21.50
Fe_2O_3	3.13	2.80
Mn_3O_4	0.08	0.04
Al_2O_3	4.31	5.90
CaO	66.30	65.80
MgO	1.32	1.35
SO_3	1.25	0.80
Na_2O	0.23	0.31
K_2O	0.91	0.95
l.o.i.	0.40	0.30
	Mineralogical composition	
C_2S	8.4	21.5
C_3S	71.4	53.2
C_3A	6.0	10.8
C_4AF	9.8	8.6

The above cements were used to prepare prismatic samples (40x40x160 mm^3) of standard mortars (ISO-RILEM, 1968) which were moist-cured for one day and then cured in water for six days. At the end of this period the mortars were divided into three groups.
The first group was stored in water for six months, after which each specimen was immersed into equivalent strength sodium (0.35M) and magnesium (0.42M) sulphate solutions.
The second group was kept for six months (protected from rain) in air containing 400 ppm CO_2 at 70÷80% R.H. and 10÷30°C so as to facilitate the completion of the carbonation process in conditions similar to those actually encountered in the real world. At the end of the prescribed period the specimens were immersed into the same sulphate solutions.
Similarly, the third group was exposed for the same period of time to the same industrial atmosphere but without being subsequently immersed into the sulphate solutions in order to determine the carbonation depth reached.

RESULTS AND DISCUSSION

Table 2 reports the carbonation depth and mechanical strength values of the studied mortars reached after six months exposure to the above-mentioned industrial atmosphere. It can be seen

that the carbonation phenomenon affects the blended cements much more than Portland cement, and also that as the proportion of SO_3 in the blast furnace slag cement increases, the carbonation depth likewise increases, whereas the pozzolanic cement is affected to a much lesser extent by the SO_3 content.

Table 2 Compressive strength and carbonation depth of the mortars.

cement type	C_3A %	SO_3 %	Compressive strength (MPa)	Carbonation depth (mm)
Portland	6	2	49.4	<1
	"	3	51.9	<1
	"	4	63.8	<1
	"	5	63.8	<1
Portland	10	2	55.2	<1
	"	3	56.7	<1
	"	4	58.9	<1
	"	5	61.0	<1
Blast furnace slag	6	1	53.3	4.2
	"	2	44.1	4.3
	"	3	47.2	4.8
	"	4	40.2	5.7
	"	5	32.2	6.9
Blast furnace slag	10	1	44.8	4.4
	"	2	50.0	4.6
	"	3	42.9	5.1
	"	4	30.0	6.0
	"	5	28.8	7.2
Pozzolanic	6	1	45.7	4.8
	"	2	46.3	4.9
	"	3	47.5	5.1
	"	4	47.5	5.2
	"	5	41.4	5.4
Pozzolanic	10	1	39.9	4.9
	"	2	47.0	5.0
	"	3	45.6	5.0
	"	4	41.4	5.2
	"	5	39.2	5.5

The compressive strength values of the pozzolanic cement mortars considered are concentrated within a small range which makes it impossible to identify a predominant trend. However, there are significant differences in the carbonation depth values between the mortars made with Portland cement and those made with blended cements for the same compressive strength (50 MPa).

Table 3 reports the results of the chemical resistance tests conducted on the samples of mortars that were exposed for six months to an industrial atmosphere or were stored in water for the same period of time before both types were kept in the sulphate solutions for a total of twenty-one months.

With the cement samples used, the carbonation depth increases as the C_3A content increases both for blast furnace slag and pozzolanic cements. Furthermore, the carbonation depths of the Portland cement mortars after six months exposure to the industrial atmosphere turns out to be less than

one millimeter, which would make any differentiation relatively insignificant, nor does the trend of this phenomenon appear different after twenty-four months exposure to the same atmosphere. This suggested that it would be of no use to report the carbonation depths after twenty-four months, also because only the mortars carbonated for a six-month exposure have currently been subjected to sulphate attack.

Table 3 Chemical resistance of carbonated and uncarbonated mortars.

cement type	C_3A %	SO_3 %	Carbonatated Chemical resistance Na_2SO_4	Carbonatated Chemical resistance $MgSO_4$	Uncarbonatated Chemical resistance Na_2SO_4	Uncarbonatated Chemical resistance $MgSO_4$
Portland	6	2	***	*	**	**
	"	3	*	*	**	**
	"	4	*	*	**	**
	"	5	*	*	*	**
Portland	10	2	****	**	****	****
	"	3	****	**	****	***
	"	4	**	*	****	***
	"	5	**	*	****	**
Blust furnace slag	6	1	*	*	**	**
	"	2	*	*	*	**
	"	3	*	*	*	***
	"	4	*	*	*	**
	"	5	*	*	*	**
Blust furnace slag	10	1	*	*	**	***
	"	2	*	*	**	***
	"	3	*	*	*	***
	"	4	*	*	*	**
	"	5	*	*	*	**
Pozzolanic	6	1	*	**	*	****
	"	2	*	**	*	***
	"	3	*	**	*	***
	"	4	*	**	*	**
	"	5	*	**	*	**
Pozzolanic	10	1	****	*	**	****
	"	2	**	*	*	***
	"	3	*	**	*	***
	"	4	*	**	*	**
	"	5	*	**	*	**

**** Disgregated; *** Very demaged; ** Poorly demaged; * Not sensibly demaged.

Furthermore, it can also be seen that as the Portland cement mortars are not carbonated, they have higher compressive strength values, which are however determined partly by the cement's gypsum content (Sersale et al., 1992).

For the blast furnace slag cement considered, the carbonation depth values were concentrated in an interval that was fairly large according to the variation in the SO_3 content, and the compressive strength of the corresponding mortars is a function of the values of this depth.

Once this period of time had elapsed, the only specimens of uncarbonated mortars that were still intact after immersion in the sodium sulphate solution were the ones made with pozzolanic cement

containing 6% C_3A. The mortars that suffered the greatest attacks were, in order: those made with Portland cement containing 10.8% C_3A; those made with Portland cement containing 6% C_3A; those made with blast furnace slag cement containing 10.8% C_3A. The attack is initially manifested with low SO_3 contents and diminishes as this value increases, within the limits adopted.

As regards the behaviour of the mortar specimens carbonated through exposure to the industrial atmosphere and subsequently immersed for the same period of time in the sodium sulphate solution, at the end of the test the following specimens had not been attacked: the specimens of pozzolanic cement containing 6% C_3A; those made with blast furnace slag cement containing 6% and 10.8% C_3A. For low SO_3 values, the specimens were attacked in the following order: the specimens of pozzolanic cement mortar; those of Portland cement containing 6% C_3A; and, to a much higher degree, those of Portland cement containing 10.8% C_3A.

Therefore, the factors that most decisively regulate sulphate attack in the experimental conditions adopted seem to be as follows: the mineral additive, the content of C_3A and SO_3 in the binder, and the degree of carbonation.

Identical tests conducted using magnesium sulphate as the attacking solution showed that all the specimens of uncarbonated mortars made using the cements examined here had been attacked by the end of the test. The C_3A content of the cements seems to be main promoter of attack while the SO_3 content and the mineral additive do not seem to play a determining role.

Whereas, the carbonated mortar specimens that do not appear to be attacked by the end of the test are: those made with blast furnace slag cement containing 6% and 10.8% C_3A and those made with Portland cement containing 6% C_3A. The mortars made with Portland cement containing 10.8% C_3A turn out to be only slightly attacked while the specimens that suffered the greatest attack were those made with pozzolanic cement.

The SO_3 content in the binder does not seem to have a particular influence, while carbonation depth and content of C_3A, for Portland cement only, seem to be the main parameters involved.

Therefore, in the magnesium sulphate solution the mortars made with blast furnace slag cement seem consistently to resist well, whereas those made with pozzolanic cement are always attacked, although not to a great extent. The Portland cement mortars are only slightly attacked and varies according to the cement's C_3A content. For the two blended cements the C_3A and SO_3 content does not seem to have a determining influence. However, the magnesium sulphate solution turns out to be much more aggressive than the sodium sulphate for all the types of cement considered. This behaviour can be justified by considerations regarding the combination of a number of different factors: chemical, steric, electrical, and so forth.

Table 4 reports the pore size distribution values. It must first be pointed out that no comparison can be made between the carbonated and the uncarbonated Portland cement mortars as their carbonation depth at the end of the period of exposure to the industrial environment was consistently lower than 1 millimeter.

A comparison of the carbonated and the uncarbonated specimens of mortars made with blast furnace slag cement points out that the carbonation process causes a reduction in the percentage of pores smaller than 1000 Å, with a consequential increase in the larger ones, while the total porosity value on the whole remains unchanged. In the carbonated mortars the percentage of smaller pores increases as the content of SO_3 in the binder increases.

At the current stage of research, these results do not appear to be immediately correlatable with the results of the chemical strength tests and it must therefore be assumed that the carbonation process

and the SO_3 content of the cements considered here have different effects on pore size distribution. Future investigations will aim to shed more light on this issue.

TABLE 4 Pore size distribution of blast furnace slag-cement mortars.

Percentage of total cumulative of pores - Rp < 1000 Å			
% SO_3	2	3	4
BFS 6% C_3A			
Uncarbonated	70.28	78.88	89.67
Carbonated	67.37	76.79	84.73
BFS 10% C_3A			
Uncarbonated	76.10	88.79	89.21
Carbonated	71.38	77.69	82.10
Percentage of total cumulative of pores - 1000<Rp<10000 Å			
% SO_3	2	3	4
BFS 6% C_3A			
Uncarbonated	21.34	13.26	5.61
Carbonated	23.35	15.63	8.08
BFS 10% C_3A			
Uncarbonated	17.17	5.26	8.45
Carbonated	19.98	16.29	10.98
Percentage of total cumulative of pores - 10000<Rp<100000 Å			
% SO_3	2	3	4
BFS 6% C_3A			
Uncarbonated	8.38	7.86	4.72
Carbonated	9.13	7.59	7.19
BFS 10% C_3A			
Uncarbonated	6.73	5.95	3.35
Carbonated	8.64	6.02	6.92

CONCLUSIONS

The experimental results and the deductions that can be reasonably inferred from them indicate that:

- the mortar carbonation process improves response to sulphate attack both for the mortars prepared with Portland cement and those made with the blended cements used;
- the mortar carbonation process for all the cements examined is facilitated by their SO_3 content;
- the increase in the carbonation depth as the cement's SO_3 content increases is more evident for the blast furnace slag cement examined in this paper. This may partly explain the increase in resistance to sulphate attack as the SO_3 content increases, as can be seen with the blast furnace slag cement.

REFERENCES

Bakker, R.F.M., " Permeability of blended cement concrete", Fly ash, silica fume, slag and other mineral by-products in concrete", ACI, SP-79, 1983, Detroit, pp.589-605.

Feng, Q.L., Lachowski, E.E. and Glasser, F.P., "Densification and migration of ions in blast furnace slag-Portland cement pastes", Mat. Res. Soc. Symp. Proceedings, 137, 1989, Pittsburgh, pp.419-428.

Gebauer, J. and Torrent, R.J., "Effect of curing on some pore structure-dependent properties of concrete", Mat. Res. Soc. Symp. Proceedings, 137, 1989, Pittsburgh, pp.301-306.
ISO, "Methode d'essais méchaniques des ciments. Resistance à la compression et à la flexion du mortier plastique (Methode Rilem-Cembureau)", 1968, International Standard Organisation R.679, EN 196/1.
Kjellsen, K.O., Detwiler, R.I. and Gjorv, O.E., "Pore structure of plain cement pastes hydrated at different temperatures", Cement Concr. Res., 20, 1990, pp. 927-933.
Malek, R.I.A., Roy, D.M. and Fang, Y, "Pore structure, permeability and chloride diffusion in fly ash- and slag-containing pastes and mortars", Mat. Res. Soc. Symp. Proceedings, 137, 1989, Pittsburgh, pp.403-410.
Mangat, P.S. and Khatib, J.M., "Influence of initial curing on sulphate resistance of blended cement concrete", Cement Concr. Res., 22, 1992, pp. 1089-1100.
Mangat, P.S. and Khatib, J.M., "Influence of fly ash, silica fume and slag on sulfate resistance of concrete", ACI Material Journal, 92, 5, 1995, pp. 542-552
Roy, D.M., "Relationships between permeability, porosity, diffusion and microstructure of cement pastes, mortars and concrete at different temperatures", In:"Pore structure and permeability of cementitious materials", 1989, Pittsburgh, Eds. L.R. Roberts, J.P. Skalny. Mat. Res. Soc. Symp. Proceedings, 137, pp.179-189.
Sersale, R., Cioffi, R., Frigione, G. and Zenone, F., "SO_3 content of Portland and blended cements: porosity and behaviour of the resultant mortars", Proc. 9th Int. Congr. Chem. Cement, III, 1992, New Delhi, pp. 173-179.
Taylor, H.F.W., "Cement Chemistry", Academic Press, London,1990, pp. 366.

INFLUENCE OF LIMESTONE POWDER FILLER ON MICROSTRUCTURE AND MECHANICAL PROPERTIES OF CONCRETE UNDER SULPHATE ATTACK

Wojciech G. PIASTA, Zbigniew SAWICZ, Grzegorz KOPROWSKI, Zdzisława OWSIAK, Technical University of Kielce, Institute of Concrete Technology, Poland

ABSTRACT The paper deals with the effect of limestone and quartz powders on the changes in phase composition of cement paste and on their sulphate resistance. There was also studied the qualitative and quantitative dependence of concrete properties and its sulphate resistance on the three factors: amount of limestone powder, w/c-ratio and level of simultaneous sustained stress. The results confirmed much better sulphate resistance of all the OPC composites with limestone fillers mainly due to the formation of phase $C_3A.CaCO_3.H_{12}$.

Key-words: sulphate attack, creep, limestone powder, ettringite, X-ray powder diffraction

INTRODUCTION

Although the mechanism of ettringite expansion in concrete under sulphate attack is controversial, it is accepted that the formation of ettringite produces harmful swelling (Kurdowski, 1991, Roy, 1986). Susceptible phases of OPC paste to sulphate attack are CH, unhydrated C_3A, hydrates C_4AH_n, C_3AH_6, $C_3A.CaSO_4.H_{12}$ and their solid solutions $C_3A(CH,CaSO_4,CaCO_3)H_n$ (Kurdowski, 1991, Mehta et al., 1992). The resistance of the phases to sulphate solutions depends on their degree of crystallization, pore structure and pore size distribution in their internal microstructure (Piasta et al., 1989, Sawicz et al., 1996). The most resistant phase among aluminate hydrates is $C_3A.CaCO_3.H_{12}$. This phase is formed from limestone powder in the whole bulk paste and it is stable and strength-bearing (Kuzel et al., 1991, Polmann, 1992). Also when compared with other mineral fillers, the beneficial effect of coarse limestone aggregate is due to tighter and stronger transition zone (between grain and bulk paste) resulting from lower degree of orientation of portlandite and ettringite crystals (Mehta et al., 1992) and their smaller size, dissolution of calcium carbonate and its reaction on aluminates to carboaluminates (Maso, 1980).The positive influence of limestone aggregate on concrete properties was confirmed by its fine performance(Uchikawa et al., 1996) and resistance under hard and complex condition of sustained load and simultaneous sulphate attack (Piasta, 1992, Sawicz et al., 1996).

EXPERIMENTAL

The OPC with 12.1% C_3A content was used to make: 1) paste with 20% limestone powder, quartz powder and without addition; 2) concretes (with 350 kg/m^3 of OPC) and with different addition of limestone powder for a part of aggregate and different w/c-ratios. After 28 days of curing the cement pastes were immersed into 5% (35.1 mM) Na_2SO_4 solution The pastes were used to explain changes in phase composition under sulphate attack with the help of XRD. They were tested after 28 days. The concretes were previously loaded under sustained compressive stress of different levels (σ/R_{28}). Then the loaded concretes were also immersed into 5% Na_2SO_4 solution for one year. Concrete performance and resistance to sulphate attack was tested with respect to the three factors of following values: amount of limestone powder L (%) = 0, 7, 14, 21, 28; w/c = 0.50, 0.55, 0.60, 0.65, 0.70; compressive stress level σ/R_{28} = 0.25, 0.35, 0.45, 0.55, 0.65. The results were calculated as a quadratic response-surface at one factor of constant value and presented by contours of the surface.

RESULTS

Phase composition

Plain OPC paste

As it is shown in the X-ray diagram (Fig.. 1a) at d=4.91Å calcium hydroxide (CH) is a predominant well crystallized phase of the plain cement paste at the age of 28 days. There can also be detected large amounts of well crystallized ettringite (E) and it is represented by the X-ray reflection centered at d=9.75Å. The X-ray reflection R_1 at d=9.20Å is probably a metastable and disordered solid solution that is a constituent of the extended solid series between monosulphate (Ms) and hemisulphate (Hs).A broad X-ray reflection centered at d=8.50Å is probably caused by the fact that monosulphate is not stable in the presence of atmospheric CO_2 and a metastable compound or solid solution containing OH^-, CO_3^{-2} and SO_4^{-2} ions may be formed.(Kuzel et al., 1991).

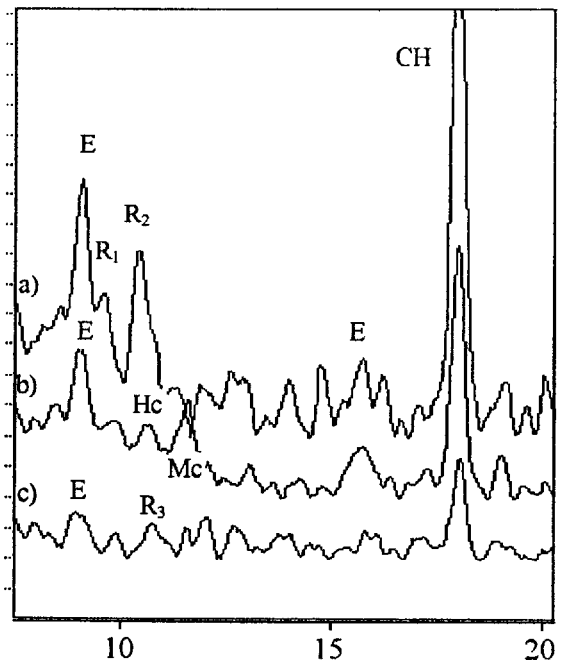

Figure 1 X-ray diffraction plots of pastes under standard condition after 28 days hydration

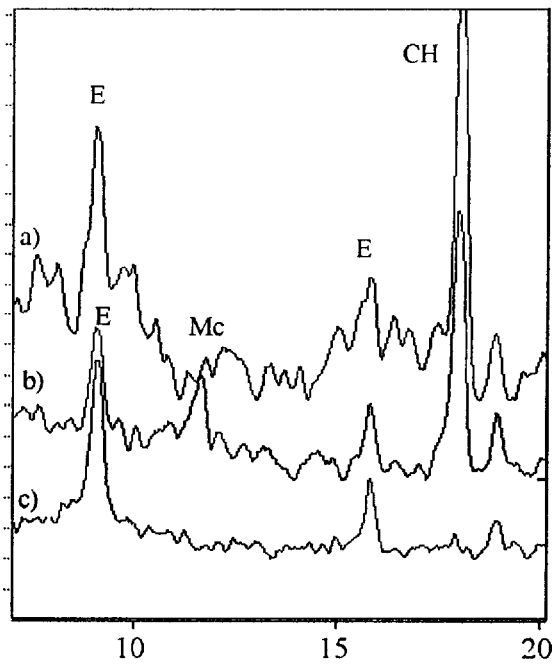

Figure 2 X-ray diffraction plots of pastes subjected to sulphate attack for 120 days.

a) without powder; b) with 20% limestone powder; c) with 20% quartz powder.

After 60 days of sulphate attack on plain paste, metastable phases R_1 and R_2, formed in time of curing under standard conditions, were transformed to hemisulphate (Hs) [d=8.70Å]. The amount of low-crystalline ettringite remained almost unchanged. After 120 days of the attack (Fig. 2a), the peak of the monosulphate (Ms) disappeared. The amount and degree of crystallization of ettringite increased in comparison with the paste after 60 days.

OPC paste with quartz powder

Well crystallized hydroxide phase and poor crystallized ettringite canbeseen in the cement paste with quartz powder at the age of 28 days (Fig. 1c). Some amount of monosulpate (Ms) and carboaluminate phases present were confirmed by the peaks at d=7.62Å and d=7.30Å. A broad reflection centered at d=8.20Å probably is a result of reflection interference (superposition) of peaks connected with hemicarbonate and poor ordered structure of solid solutions $C_3A.CaSO_4.H_{12} - C_3A.Ca(OH)_2.H_{12}$ and $C_3A.CaCO_3.H_{12} - C_3A.Ca(OH)_2.H_{12}$ (R_3).

An increase in crystallized ettringite and disappearance of solid solutions and carbonated phases resulted from the sulphate attack for 60 days. Their easy transformation in direction of secondary ettringite formation confirmed their low resistance to sulphate attack. All the metastable phases disappeared after 120 days in a Na_2SO_4 solution attack (Fig. 2c) and an increase in amount and crystallization degree of ettringite was observed. Thus, it was confirmed that the decrease in sulphate resistance of OPC paste was affected by the application of quartz powder.

OPC paste with limestone powder

Apart from calcium hydroxide (CH) and ettringite (E) the well crystallized monocarboaluminate (Mc) at d=7.60Å, small quantities of hemicarboaluminate (Hc) at d=8.20Å and trace of monosulphate (Ms) at d=8.92Å were found in the cement paste with limestone powder (Fig. 1b). After 60 and 120 (Fig. 2b) days of sulphate attack, the changes in phase composition of the paste with limestone powder are insignificant. Only small amounts of Hc and Ms, were slowly converted to ettringite (E). The monocarbonate phase stays at the same level as that formed in air conditions. Upto 120 days of sulphate attack, the monocarboaluminate phase (Mc) remained at the same level as that at the age of 28 days. The increase in amount of ettringite resulted from the chemical attack of SO_4^{-2} ions on the metastable solutions of monoaluminate phases. The quantitative and qualitative assessment of phase composition indicated much better durability of $C_3A.CaCO_3.H_{12}$ and in the same way it was confirmed that the paste with limestone addition is more stable and resistant to sulphate attack than the plain paste and the one with quartz powder.

Linear expansion of concretes

The investigation results of concrete swelling after one-year storage in 5% (35.1 mM) Na_2SO_4 solution are shown in the dependence on limestone powder amount L and w/c -ratio (Fig. 3). The influence of both independent variables on the expansion was significant even though the effect of any increase in the w/c-ratio, particularly in its interval from 0.60 to 0.70 , was much greater. The lowest expansion ($\varepsilon \cong 485 \cdot 10^{-6}$) of concrete was determined when the limestone addition was 14% and 21% and the minimum ($470 \cdot 10^{-6}$) of response-surface was calculated for the limestone addition of 16 percent.

Time-dependent deformations

The time-dependent free expansion and creep-related deformations results of concrete (w/c = 0.60) under the sustained compressive stress $\sigma = 0.45R_{28}$ indicated (Fig. 4) significant effects of limestone addition amount on the resistance to 5% Na_2SO_4 solution. The lowest magnitudes of deformations related to both simultaneous factors of sustained compression and sulphate attack were stated for concrete with 14% limestone addition. During the latest 3 months some decrease in creep-related deformations of all the concretes was noted. Normally no decrease in creep of concrete stored in water is observed. The lowering of all the creep curves confirmed an increasing effect of sulfate in time expansion. The free expansion of concrete with the 14% limestone addition was also the lowest in comparison with the others (Fig. 3). Thus, it was quantitatively assessed that the 14% amount of limestone powder addition affected the most stable performance of concrete under complex condition of sulphate attack.

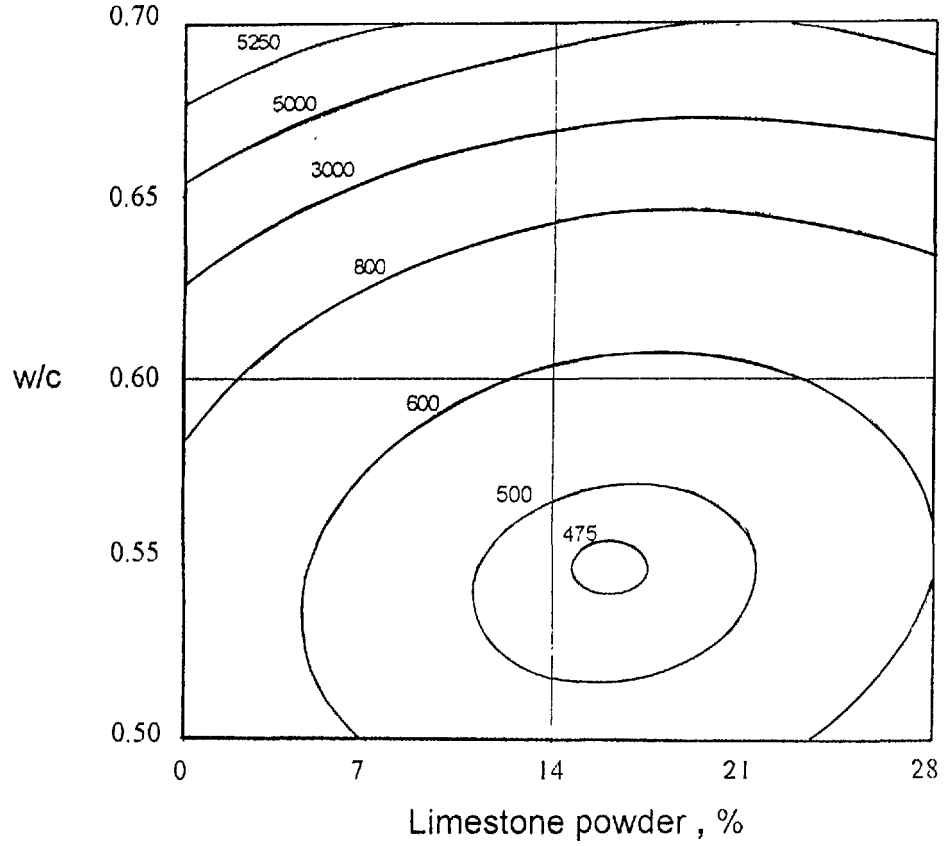

Figure 3 Expansion of concrete under 5% Na_2SO_4 attack as a function of w/c-ratio and limestone addition amount L.

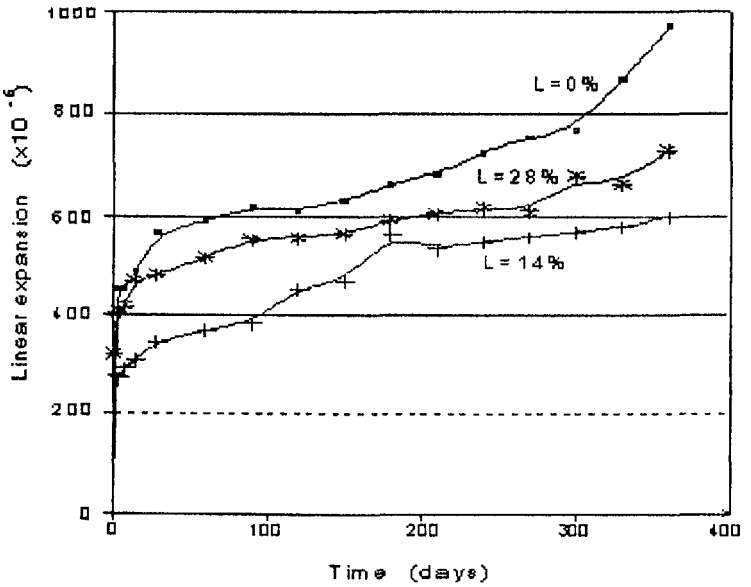

Figure 4 Effect of limestone addition amount L on time-dependent deformations of concrete under 5% Na_2SO_4 attack.

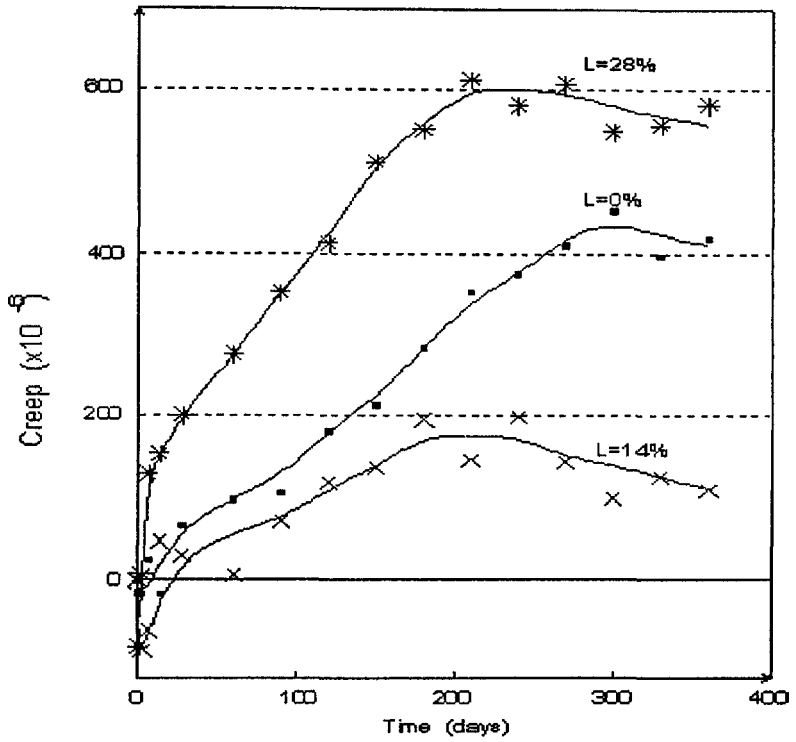

Figure 5 Effect of compressive stress level (σ/R_{28}) on the time-dependent deformation of concrete (w/c=0.60 ; L=14%).

Performance of concretes with limestone fillers was observed under combined condition of 5% Na_2SO_4 attack and simultaneous sustained compression of different levels. The creep- and sulphate attack-related deformations are shown for concrete with 14% limestone addition at the stress levels of 0.25, 0.45 and 0.65 in Fig. 5. The magnitude of deformation under the combined conditions was the highest at the stress level of 0.65 but it was the lowest at the level of 0.45 but not at the level of 0.25. Such a performance of concrete is not known under any conditions of moist air (RH = 100 per cent) or water. Also the decrease of deformation magnitudes found for the latest four months was directly connected with the sulphate swelling that is high in a later age contrary to creep.

Compressive strength of concretes

Compressive strength was determined for the concretes that had been previously loaded for one year under sustained compressive stress and immersed in 5% Na_2SO_4. The strength of the concretes is presented in the Figs 6a, 6b, 6c by the surface contours as values of strength function of w/c-ratio and σ/R_{28}-level for a constant amount L. The highest strength of concrete without addition (L=0%) was nearly 60 MPa (Fig. 6a) and it was found at w/c=0.56 and σ/R_{28}=0.35. Any higher w/c-ratio and σ/R_{28}-level decreased the strength of this concrete and caused even its failure at w/c≥0.65. When the amount of the addition was 14% (Fig. 6b) the strength properties of concrete under sulphate attack were much better and the highest strength (R ≅ 77MPa) was found at w/c=0.54 and σ/R_{28}=0.45, thus the optimum level of sustained stress was higher than that when L=0%. No failure of the concrete with 14% addition was noted at any w/c-ratio and σ/R_{28}-level. For the amount L=28% (Fig. 6c), the highest strength was only about 67 MPa but it was found at the higher level σ/R_{28}=0.55. In general, the lowest strength values were determined when the w/c-ratio was 0.70 and addition amount L was 0% or 28%.

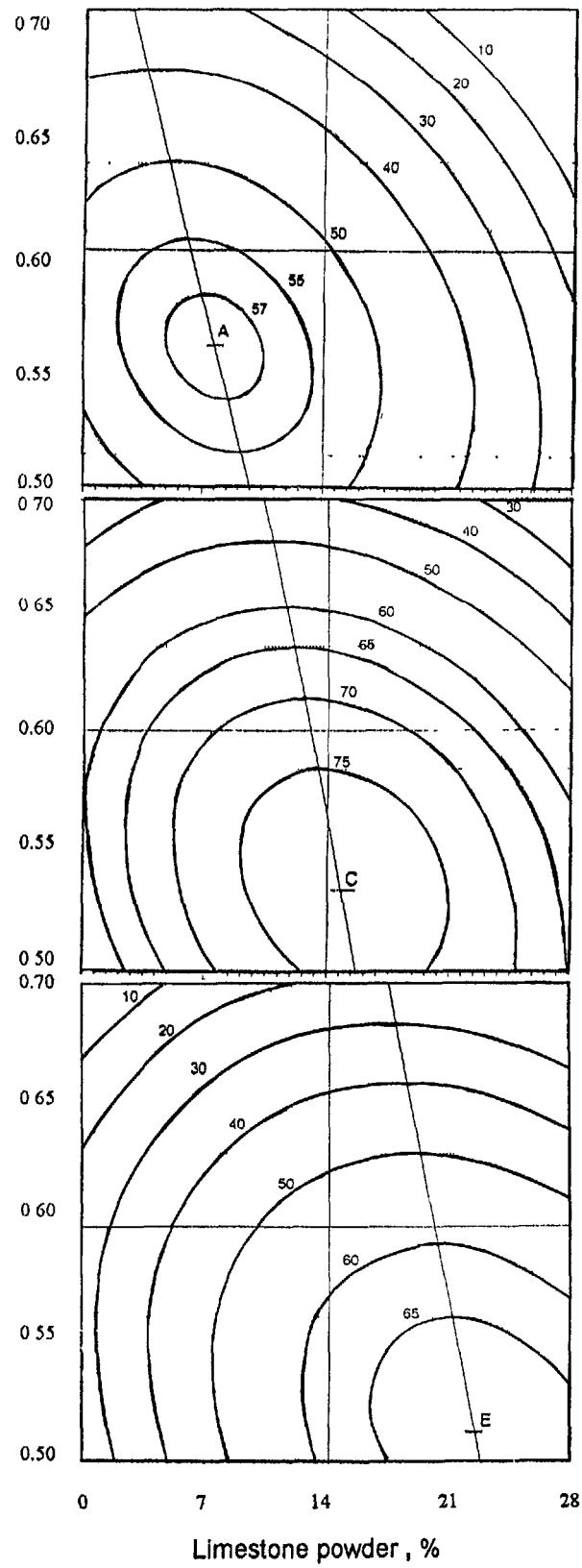

Figure 6 Effect of compressive stress level σ/R and w/c-ratio on compressive strength of concrete after one-year loading and immersion in 5% Na_2SO_4.
a) without limestone addition, b) with 14%, c) with 28%.

The highest values of compressive strength (Fig. 7) of concretes with all the amounts of lomestone powder stored under different complex conditions of one-year loading and sulphate attack are indicated by the points A, B, C, D and E. The points are related to the values of three independent factors L, σ/R and w/c.

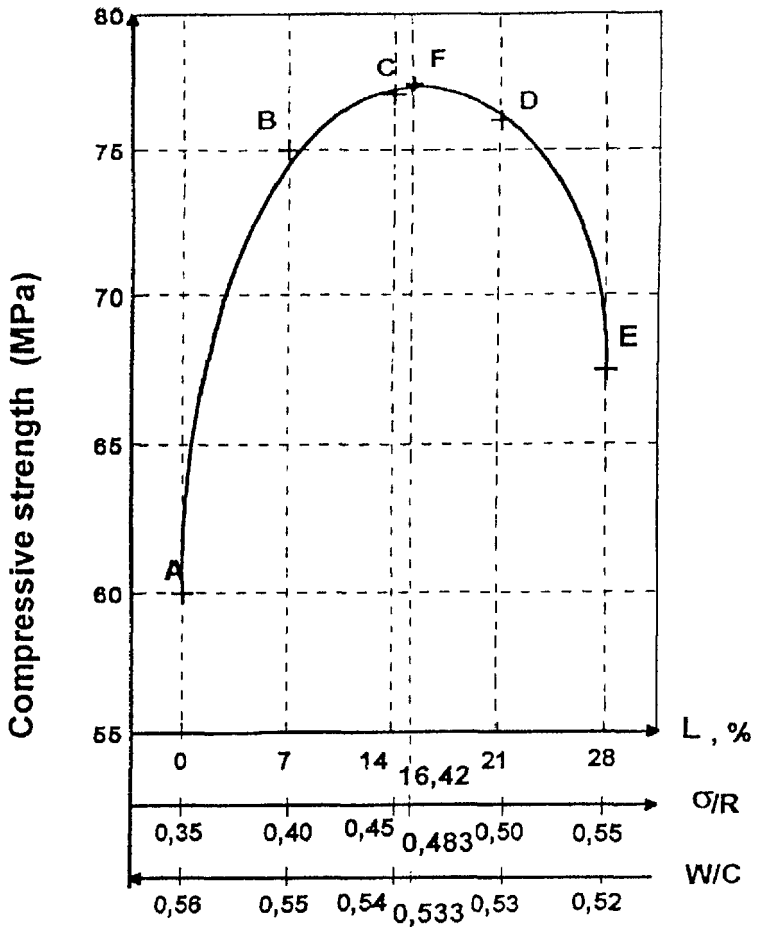

Figure 7 The maximum compressive stregth of concretes with different amounts of limestone addition L and optimum values of level σ/R and w/c-ration determined after one-year sustained loading and 5% Na_2SO_4 attack.

The maximum strength is equal to 78 MPa. It is indicated by point F for all the factors of their following optimum values L=16.4%, σ/R=0.48, w/c=0.53 that are pointed out on their axes. The intervals of the factors σ/R and w/c are indicated on the axes for the region of their optimum interaction (i.e. the best performance and the highest sulphate resistance) with the whole interval of limestone powder amount studied. It should be taken into consideration that higher stress level σ/R demands increase in the limestone powder amount in order to maintain the optimum strength of concrete. The optimum w/c-ratio was not the highest one among the investigated concretes.

CONCLUSIONS

1. The formation of ettringite under Na_2SO_4 attack is the main reason for any expansion, leading to the deterioration or failure of OPC composites.
2. Hydration of OPC with limestone powder addition results in formation of monocarboaluminate hydrate instead of monosulphoaluminate and aluminate hydrates. Ettringite remains unchanged. Formation of monocarboaluminates improves sulphate resistance and mechanical properties of hardened cement paste.
3. The influence of three independent factors (limestone powder amount, w/c-ratio, compressive stress level) on concrete performance and sulphate resistance is quantitatively assessed. The optimum values of the factors are following (as follows) L=16.4%; w/c=0.53; σ/R_{28}= 0.48.

REFERENCES

Kurdowski, W.,"Chemistry of Cement", PWN, Warszawa, 1991.

Kuzel, H.I.,Polmann,H.,"Hydration of C_3A in the presence of $Ca(OH)_2$, $CaSO_4.2H_2O$ and $CaCO_3$", Cem. Concr. Res., Vol.21, 1991, pp. 885-895.

Maso,J.C.,"The Bond between Aggregates and Hydrated Cement Paste",7th ICCC, Paris, Vol. VII-1, 1980.

Mehta, P.K.,Schiessel,P.,Raupach,M.,"Performance and Durability of Concrete Systems",9th ICCC, New Delhi, Vol. 1, 1992, pp. 571-662.

Piasta,W.G.,Sawicz,Z. Piasta, J.,"Sulphate durability of concretes under constant sustained Load", Cem. Concr. Res., Vol.19, 1989, pp. 216-227.

Piasta,W.G.,"Durability of Concrete with different Cements and Aggregate under sustained Load", 9th ICCC, New Delhi, Vol. 5, 1992, pp.136-142.

Pöllmann,H.I.,"Incorporation of SO_4^{-2}, CO_3^{-2} and OH^- in Hydration Products of Tricalciumaluminate," 9th ICCC, New Delhi, Vol.4, 1992, pp.363-369.

Roy,D.M.,"Mechanism of Cement Degradation due to Chemical and Physical Process", 8th ICCC. , Rio de Janeiro, Vol. 1, 1986, pp.359-376.

Sawicz,Z., Heng, S., „Durability of Concrete with Addition of Limestone Powder", Mag. Concr. Res., 48, No. 175, 1996, pp. 131-137.

Uchikawa, H.,Hanehara, S., Hirao, H.,"Influence of Microstructure on the Physical Properties of Concrete Prepared by Substituting Mineral Powder for Part of Fine Aggregate", Cem. Concr. Res., Vol. 26, 1996, pp.101-111.

SULPHATE RESISTANCE OF CEMENTS WITH MINERAL ADMIXTURES

Zbigniew GIERGICZNY, Institute of Mineral Building Materials, Opole, Poland

ABSTRACT The effect of aggressive sulphate containing environment on the compressive strength of cements with active mineral admixtures, such as low-calcium fly ashes, high calcium fly ashes, silica fume and ground, granulated blast furnace slag was studied. The corrosion resistance of standard mortars was evaluated basing on the compressive and flexural strength decrease within the 2 year observation period.

Key-words: characterization, fly ash, strength retrogression, sulphate resistance

INTRODUCTION

The mineral admixtures have been widely used in cement technology for many years. Their properties and dosage are the subject of standards in many countries; in some types of cements the blends of admixtures can be added [Peukert, Garbacik 1995]. These cements should ensure fairly good durability of concrete at later age. The mineral admixtures in cement cause the reduction of calcium hydroxide with the simultaneous C-S-H increase in hardened material. It is clearly visible particularly in the presence of silica fume [Giergiczny 1995]. The modification of phase composition is accompanied by the change of porosity. Owing to the modified pore structure the permeability of paste decreases and the strength of mortar increases. Only in the case of the low calcium fly ash the effects are observed at longer time of curing. In this work the strength of cements with mineral admixtures, stored in H_2SO_4 and $MgSO_4$ solutions is discussed. The tests were carried out within 2 years.

EXPERIMENTAL

Materials

Two portland cement clinkers of the following phase composition (in weight %) were used: clinker A: C_3S-49,5; C_2S-24,6; C_3A-8,8 and clinker B:C_3S-40,6; C_2S-30,1; C_3A-14,1 respectively. A low calcium fly ash from the black coal combustion, a high calcium fly ash from the brown coal combustion, silica fume and ground, granulated blast furnace slag were used as mineral admixtures. The chemical composition of admixtures is given in Table 1. The proportions between the particular components of cement blends are given in Table 2. The standard 40x40x160 mm mortar bars (cement/sand -1:3, water/cement - 0.5) were cured in water for 28 days and immersed in corrosive media. Some samples were stored in water for longer time as reference. The corrosive solutions were: sulphuric acid at SO_4^{2-} concentration 4800 mg/l and magnesium sulphate at Mg^{2+} concentration 3000 mg/l.

Strength tests of hardened mortars

The hardened mortars were subjected to the compressive strength tests after 90, 180, 360 and 720 days curing in corrosive media. The results are given in Table 3.

RESULTS AND DISCUSSION

The cements cured in the corrosive environment differ with the type and percentage of mineral admixtures. The corrosion resistance of cements was estimated basing on the compressive

strength decrease in relation to the values for reference samples within the 2 year observation period (see Table 3). The two different portland cement clinkers were used to produce cements with admixtures. The clinkers showed different C_3A contents: 8,8% for series of samples A and 14,1% for series of samples B respectively. The clinkers used were not sulphate resistant materials.

Table 1 Chemical composition of mineral additives.

Component	Percentage [wt.%] in admixtures			
	low calcium fly ash	high calcium fly ash	silica fume	granulated blast furnace slag
L.O.I.	2,9	1,9	2,1	0,1
SiO_2	52,2	44,8	90,4	39,8
Fe_2O_3	7,2	8,7	2,8	1,9
Al_2O_3	27,2	22,6	1,0	7,2
CaO	2,6	16,2	0,2	41,2
SO_3	1,6	2,1	---	---
MgO	1,6	1,9	---	7,0
Na_2O	0,3	0,1	0,6	---
K_2O	2,6	0,3	1,9	---
CaO_{free}	---	0,6	---	---

Table 2 Composition of cements.

Component	Percentage [wt.%] in particular cements							
	cement 1	cement 2	cement 3	cement 4	cement 5	cement 6	cement 7	cement 8
clinker	96	66	56	66	56	36	46	16
gypsum	4	4	4	4	4	4	4	4
low calcium FA	---	30	30	---	---	50	50	---
high calcium FA	---	---	---	30	30	---	---	---
silica fume	---	---	10	---	10	10	---	---
slag	---	---	---	---	---	---	---	80

One can notice that the progress of corrosion was more evident in the magnesium sulphate solution. The pastes from clinker B without admixtures totally collapsed between 6 and 12 months. The bars from clinker A showed only the surfacial fissures. The compressive strength after 2 years was relatively high - 37,6 MPa, though the 37% reduction as compared to the control samples stored in water was found (table 3). In the sulphuric acid environment the bars from cement B without mineral admixtures were totally destroyed between 12 and 24 months of curing. The bars from cement A showed a compressive strength 32,4% lower than the reference.

The mineral admixtures used in this work improved the resistance of cement mortar to the sulphate or magnesium sulphate aggressive environment. The silica fume was added together

with fly ash; the percentage of admixtures in cement was in the range from 30% to 80% (seeTable 2). One should underline that the same cements with admixtures attained higher strength at later age than the reference (see Table 3). The change of compressive strength in the corrosive media is discussed below.

Table 3 Compressive strength of mortars cured in aggresive solutions and in water.

Cured in	Sample No	Compressive strength in MPa at age							
		90 days		180 days		360 days		720 days	
		A*	B**	A	B	A	B	A	B
H_2O	cem. 1	53,6	34,6	55,9	38,6	60,3	42,1	60,1	45,7
	cem. 2	51,7	41,0	60,9	44,2	64,3	50,1	60,6	50,6
	cem.3	57,3	58,1	61,8	60,5	62,6	60,4	63,9	60,5
	cem. 4	57,5	43,4	60,3	49,5	60,8	49,6	68,2	55,8
	cem. 5	64,7	60,7	66,9	62,5	69,2	64,3	70,6	66,4
	cem. 6	45,6	44,8	47,2	49,8	48,0	54,0	47,0	52,5
	cem. 7	31,2	37,9	37,0	40,0	42,0	43,2	42,1	47,7
	cem. 8	32,7	42,5	36,7	45,9	42,2	48,7	43,0	52,0
H_2SO_4	cem. 1	53,6	32,6	49,3	40,4	42,7	36,2	40,6	collapsed
	cem. 2	54,4	38,9	59,7	45,4	62,9	51,7	58,8	48,9
	cem. 3	56,7	54,5	61,0	57,6	61,8	56,8	63,7	58,7
	cem. 4	56,7	44,3	62,5	49,0	58,3	49,3	66,7	50,3
	cem. 5	60,4	62,8	69,6	62,9	71,7	66,2	73,3	69,0
	cem. 6	45,5	45,9	47,9	47,8	48,4	50,3	45,6	49,0
	cem. 7	34,2	33,5	39,1	37,9	45,3	43,1	39,0	43,9
	cem. 8	32,7	44,5	35,1	45,3	40,1	47,5	42,2	50,5
$MgSO_4$	cem. 1	53,9	34,6	52,1	29,8	39,5	collapsed	37,6	---
	cem. 2	52,7	38,7	56,7	43,8	55,5	48,8	55,0	48,3
	cem. 3	53,6	55,6	57,0	57,6	51,6	53,7	51,0	57,5
	cem. 4	55,5	44,3	56,7	49,5	58,1	43,7	50,3	44,8
	cem. 5	63,4	56,8	66,2	57,9	63,5	55,3	62,9	47,9
	cem. 6	40,6	40,4	40,3	47,6	34,5	43,6	31,4	44,6
	cem. 7	31,2	35,2	40,7	38,9	43,4	40,3	38,5	39,2
	cem. 8	34,6	39,3	34,8	41,2	35,8	40,6	36,4	42,3

*- produced from clinker A, **- produced from clinker B

Sulphate resistance

The compressive strength decrease in the sulphuric acid environment is not too high, usually lower than 10% of reference value for cements containing 50% low calcium fly ash, stored 2 years in the corrosive solution. The highest strengths were observed for cement with 30% high

calcium fly ash and 10% silica fume (cement 5; Table 3). The beneficial effect of pozzolanic admixtures on the sulphate resistance results from the calcium hydroxide consumption in pozzolanic reaction and subsequently from the reduction of porosity due to the presence of calcium silicate hydrates and calcium aluminate hydrates, as well as from the delayed ettringite formation in the pores with no expansion. The calcium aluminate content decrease in cements with admixtures is also not without importance [Irassar, Batic 1989].

Magnesium sulphate resistance

This environment was more harmful for the mortars. The compressive strength decrease was in the range from 5% to almost 33% of reference value. Such a significant reduction took place after 1 year storage. The substantial strength lowering for cements with silica fume should be attributed to the decomposition of calcium silicate hydrates by magnesim sulphate [Kurdowski 1991]. The gypsum formed as a product in the reaction between magnesium sulphate and pozzolanic cement mortar is easily seen on the XRD pattern in Fig.1. $MgSO_4$ acts both as magnesium and sulphate corrosive medium.

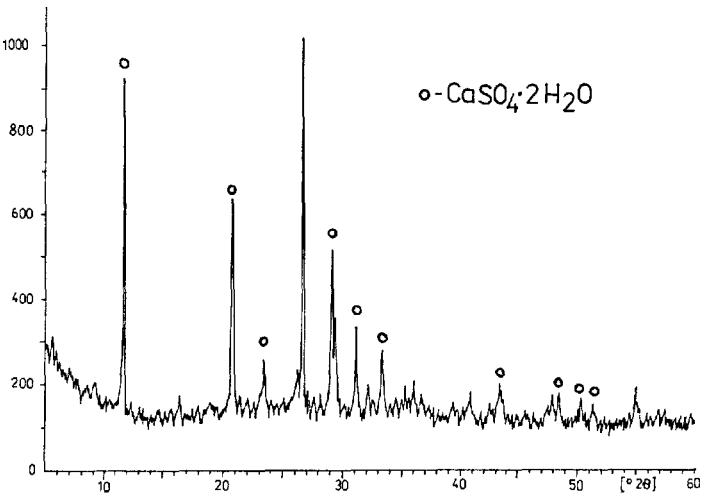

Figure 1 XRD pattern of "cement 6" mortar after 360 days in $MgSO_4$ solution.

CONCLUSIONS

1. Mineral admixtures improve the sulphate resistance of cements.
2. The samples stored in $MgSO_4$ solution show lower compressive strength than those cured in H_2SO_4.
3. The cements with mineral admixtures show higher compressive strength than reference samples without admixtures.

REFERENCES

Giergiczny, Z., "Fly ash cements with silica fume addition", Cement-Wapno-Gips, Vol.1, No1, 1995, pp.17-22. (in Polish)

Irassar, F., Batic, O., "Effect of low calcium fly ash on sulphate resistance of OPC cement ", Cement and Concrete Research, Vol. 19, No2, 1989, pp.194-202.

Kurdowski, W., "Chemistry of Cement", ed. PWN, Warszawa, 1991. (in Polish)

Peukert, S., Garbacik, A., "The properties of cements produced in Poland in the light of world-wide standards and as a material for concrete industry", Proc of XV Conference of Concrete Industry "Jadwisin 95", Rynia, 1991. (in Polish)

4iv020
4 pp

E. 12. C.. 2001 KNO DNR 33036

RESISTANCE OF FLY-ASH BLENDED CEMENT MORTARS TO SULPHATE ATTACK

Darko KRIŽAN, The IMS Institute, Belgrade, Yugoslavia
Branislav ŽIVANOVIĆ, Centre for Multidisciplinary Studies University of Belgrade, Yugoslavia

ABSTRACT This paper considers the influence of different aggressive environments (10% Na_2SO_4 and 10% $MgSO_4$ solutions) on ordinary Portland cements and blended cements. Ordinary Portland cement with middle content of $C_3A = 7.20\%$, and high content of $C_3A = 12.35\%$, are utilised. On the other side, blended cements of the above clinkers with 50 and 70% mechanical activated fly ash (specific surface $Sp \cong 700 m^2/kg$ and $1000 m^2/kg$), are prepared.
The measurements of flexural strengths were carried after 35, 49 and 77 days, and as a contribution of corrosion resistance we are followed the penetration of the aggressive ions using by energo-dispersive spectrometry (EDS).

Key-words: Fly-ash, Blended cement, Corrosion, Sulphate attack.

INTRODUCTION

In phenomenon of chemical corrosion of concrete the main part have a water, due to the fact that the solid and gas matters although aggressive, corrosion effect is present only if they are in water solution. Besides to content of C_3A in cement, resistance against water with sulphate ions, depends of cement content, W/C ratio and compact of hardened concrete. It is well-known that on the nature and rate of reaction, during sulphate attack, grate influence has cations, as the constituents of aggressive solutions. It was established, that all Portland cements are succumb to corrosion influence of $MgSO_4$, but in many cases, there is not an influence of sulphate ions, in reference to sulphoaluminate corrosion, that happened because of decomposition of binder caused by chemical effect of $MgSO_4$. This salt are react with hydrated silicates and formed $Mg(OH)_2$ and $CaSO_4$, but the free SiO_2 will precipitate. This kind of destruction's caused by chemical decomposition of cement constituents inside of dense hardened concrete and mortar are slow process if compared with pernicious influence of calcium sulphoaluminat hydrate ($C_6AS_3H_{32}$) or gypsum ($CaSO_4 \cdot 2H_2O$). As concentration Mg^{2+} ions in presence of SO_4^{2-} ions influence magnesium-gypsum or sulphoaluminate corrosion, in such a way concentration of SO_4^{2-} ions influence sulphoaluminate or only gypsum corrosion.
Reason for the work regarding with this problem, we are found, in long time ago established fact, that sulphate attack of concrete is one of the most dangerous corrosion, and also the running water in Yugoslavia are rich in aggressive sulphate ions. From the other side, amount of fly ash which are produced in combustion process of poor quality of coal with high amount of mineral admixtures is about cca 10 million tons per year.

EXPERIMENTAL

The programme for researching resistance of cement to the impact by sulphate attack envisaged characterisation of Portland cement clinker and fly ash. Corrosion resistant of homogeneous cements are obtained using by Steinegger-Koch method, as well energo-dispersive spectrometry (EDS).

Method for testing the influence of aggressive environments

Steinegger-Koch method for testing of cements in aggressive sulphate environments is used. According to this method, for resistance evaluation is made at the base of change on flexural strengths after 77 days (after 35, 49 and 77 days). This time is calculated from moment of the samples are prepared. As criteria for the resistance against sulphate attack on cement, coefficient Ks_{56} is used. This coefficient are obtained as rate of flexural strengths of samples

carried after 56 days in aggressive solutions, and same ages samples carried in the distilled water. The value of this coefficient above 0.7 gives a positive estimate of the constancy of cement in the given aggressive environment. Test samples, with the dimensions 1x1x6 cm, were made of a mixture of cement and quartz sand, in mass ratio 1:3 and with water/cement ratio 0.6. After preparing, the test samples were left to age for 24-40 hours in humid air, and then 21 days in distilled water. Flexural strength was tested. Other test pieces were left to age, in a certain number, in distilled water and in the specified solutions (10% $Na_2SO_4 \cdot 10H_2O$ and 10% $MgSO_4 \cdot 7H_2O$), until the end of periods 35, 49 and 77 days.

EDS method as qualitative estimate of corrosion resistance

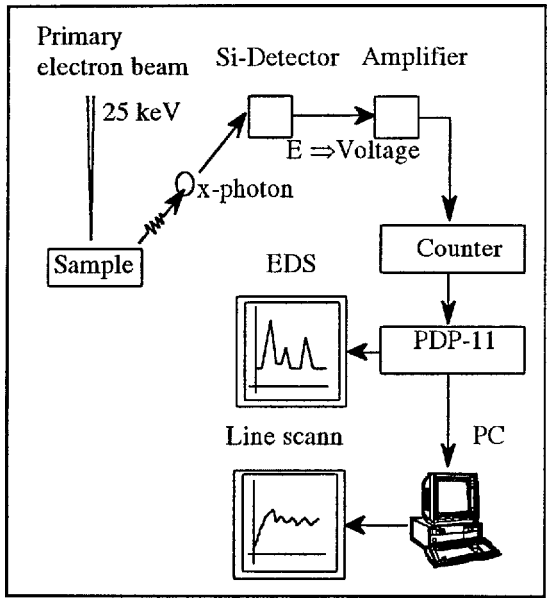

Energo-disperzive spectrometry was obtained using by scanning electron microscopy, SEM PHILIPS 515 and EDS device EDAX 9900 (Fig. 1). The test samples were evaporate by Pt/Au alloy, thickness 0.1μm. Evaporated layer was made with aim to provide a conductivity of the sample, without disrupting the morphology of the sample. The analysis was made as line scan. That is 1024 dotted analysis, on the half length of cross section of the prism (5mm). In each point, simultaneously was made 10 analysis, and medium value present one dot on the graph. Examination was made with 25 keV primary electron beam. With the increase of the energy of primary electron beam, we are reduce the measure resolution, and whole measuring range is covered.

Figure 1 Schematic survey of EDS method

RESULTS AND DISCUSSION

The potential mineralogical analysis of clinkers for ordinary and blended cements is given in Table 1.

Table 1 Mineralogical composition of clinkers

Material	Clinker for cement OPC 1	Clinker for cement OPC 2
C_3S	72.27	58.76
C_2S	6.95	12.35
C_3A	7.20	12.77
C_4AF	9.31	8.92

Results exhibit that two used kind of clinkers are with differ on percentage content of C_3A: clinker for OPC-1 contains 7.20%, and for OPC-2 contains 12.77%.

Chemical analysis of fly ash, obtain by combustion of soft brown coal-lignite, shows a rather large percentage of CaO and sulphates (CaO = 22.65%, SO_3 = 4.82%).This high percentage indicate on presence of the mineral ingredients (kaolinite type clays and schistose parts), which are overlap inside of coal. Pozzolanic activity with lime, of mechanical activated fly ash (Table 2) are very high. This is an agree with the fact that the mechanical activation is increased, not only free by surface of materials but also by increased surface reactivity. Tested chemical content of fly ash is: SiO_2 = 37.05%, Al_2O_3 = 21.02%, Fe_2O_3 = 5.83, MgO = 1.52%, Na_2O = 0.24%, K_2O = 1.20%, CO_2 = 0.72%, lost of ignition = 4.48% and insoluble residue = 20.49%.

The main physic-mechanical properties of fly ash is shown in Table 2.

Table 2 Physic-mechanical properties of fly ash

Pozzolanic activity with lime, MPa after 7 days	Activated fly ash Sp≅700m^2/kg	Activated fly ash Sp≅1000m^2/kg
a) Flexural strength	5.3	5.3
b) Compressive strength	20.1	21.1
Specific surface Sp [m^2/kg]	676	1021

Well known fact, that with increase amount of C_3A the corrosion resistant of ordinary Portland cement (OPC) decrease against aggressive sulphate solutions. This is on the Fig. 2 - 5.

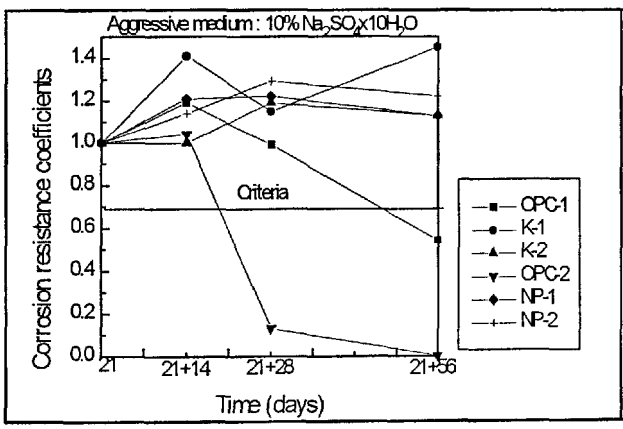

Figure 2 Corrosion resistance coefficients in 10% $Na_2SO_4 \cdot 10H_2O$ solution

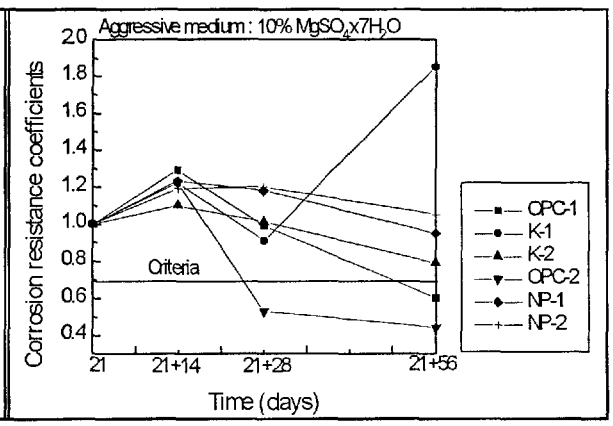

Figure 3 Corrosion resistance coefficients in 10% $MgSO_4 \cdot 7H_2O$ solution

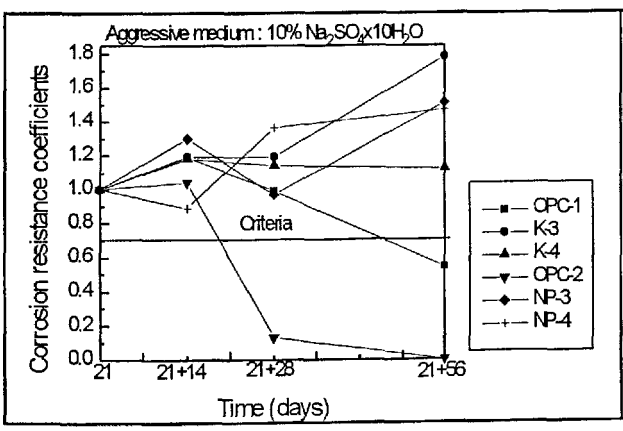

Figure 4 Corrosion resistance coefficients in 10% $Na_2SO_4 \cdot 10H_2O$ solution

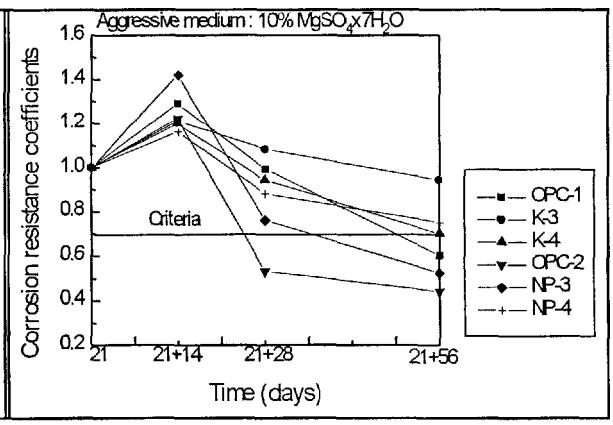

Figure 5 Corrosion resistance coefficients in 10% $MgSO_4 \cdot 7H_2O$ solution

Ordinary Portland cement (OPC-2, C_3A = 12.77%) became vulnerable after 56 days exposition in aggressive solution while samples after 77 days was completely destroyed. Ordinary Portland cement with decreased amount of this mineral (OPC-1, C_3A = 7.20%), also was a week, but this cement after 56 days was corrosion resistant. Explanation for this, we are found in fact that this cement has high amount of mineral C_3S, which increase high early strength and dense structure of microconcrete. Cements with lower content of C_3A, homogenised with 50% of fly ash (Sp≅ 700m^2/kg and

Sp ≅ 1000m^2/kg), K-1 and K-2 respectively, as cements with high amount of C_3A homogenised with same amount of fly ash, NP-1 and NP-2 respectively (Fig. 2 and 3), show a very good resistance to the aggressive sulphate ions as well as on the sulphates in presence of Mg^{2+} ions. Resistance coefficients for ordinary Portland cements and cements based on the same clinkers and 70% of fly ash are on , Fig. 4 and 5. K-3 and K-4 are the blended cements with lower content of C_3A, and NP-3, NP-4 are cements with higher content of C_3A. The better corrosion resistant of the blended cements is obvious.

From spectrogram (Fig. 6, OPC-1, sample of the ordinary Portland cement with lower content of C_3A after 56 carrying in to the 10% $Na_2SO_4 \cdot 10H_2O$), we can seen that the amount of Ca^{2+} ions from the plane of prism up to 2mm deep is decreased. That was result of the desolvation of $Ca(OH)_2$. The concentration of SO_4^{2-} ions are highest on the outside plane of prism and decreases into the bulk. Spectrogram of blended cement homogenised with same clinker and 50% of fly ash Sp ≅ 700m^2/kg (K-1), after 56 days caring in to the 10% $Na_2SO_4 \cdot 10H_2O$) is on Fig. 7. Solubility of main compounds decrease (relatively uniform amount of Ca^{2+} ions). But, concentration of sulphate ions are also low due to the fact that the prepared microconcrete with fly ash is very compact and penetration of aggressive ions into a bulk is minimised.

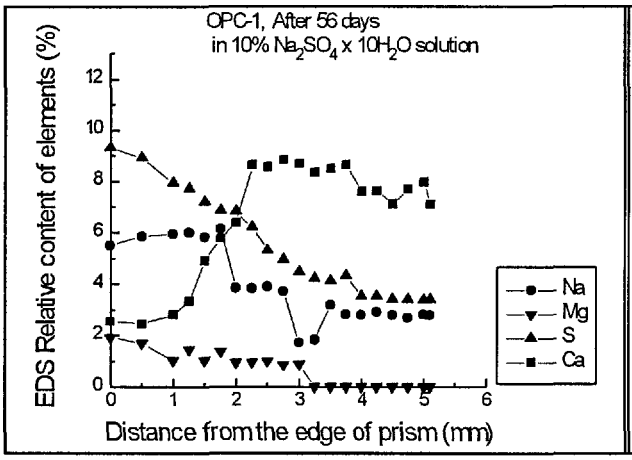

Figure 6 Spectrogram of sample OPC-1; Portland cement with middle content of C_3A

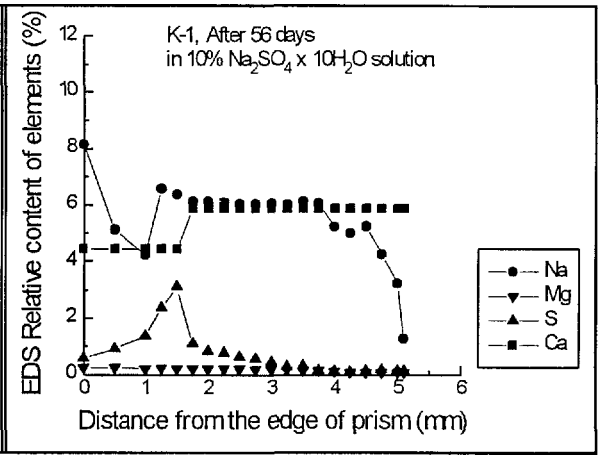

Figure 7 Spectrogram of sample K-1; Blended cement with middle content of C_3A and 50% of fly ash Sp ≅ 700m^2/kg

CONCLUSIONS

Corrosion resistance of cement against aggressive sulphate impact can be estimate only after researching on mortar or concrete in aggressive environments. The amount of aggressive ions in such case must be approximately equal to concentration of ions in real operating conditions. This kind of researching consider long-time tests, and cement estimating according to this methodology is without practical importance. According to this, quick method on small samples of microconcrete have a great significance.

With the sufficient amount of hydraulic admixture (good pozzolana activity) cement resistant against sulphate impact , no matter what amount of alumina in to the clinker or admixture, can be obtained.

REFERENCE

1. **Helmut**, R., Fly Ash in Cement and Concrete, Port. Cem. Assoc., Skokie, Illinois, 1987.
2. **Biczok**, I., Concrete Corrosion, Concrete Protection, Akad. Kiado, 8/e, Budapest,1972.
3. **Pandurović**, N., "Development of methodology for definition of sulphate resistant cements", Cement N°, Zagreb, 1969.

DEFORMATION AND MICROCRACKING OF CONCRETE LOADED IN SULPHATE ENVIRONMENT

Dimitre NAZARSKY, University of Architecture. Civil Engineering & Geodesy, Sofia, Bulgaria

ABSTRACT It has been found that the process of microcracking (lower boundary R_t^o) of concrete test samples in water starts at a stress of 0.45 R_b while for samples in an aggressive environment this boundary is about 0.35 R_b. The upper boundary of microcracking (R_t^v) of concrete test samples decreases from 0.70 R_b to 0.55 R_b in 1% ammonium sulphate solution. Finally, conclusions are made about the impact of an aggressive sulphate solution on the deformations and the boundaries of microcracking of concrete.

Key-words: Sulphate, Ammonium, Attack, Deformation, Microcrack

INTRODUCTION

A large part of the concrete and reinforced concrete structures in the industry, agriculture, hydraulic and transportation construction operate in aggressive environments, being liquid, aerosol or gaseous.

The state of stress with a parallel action of aggressive environment has an effect on the change of vvstrength and deformability properties of the concrete in the time, the extent of this effect being dependent first of all on the type and the magnitude of the stresses (Nazarsky, 1979). The mechanism of the combined effect of stresses and aggressive environment is related to the structural changes and the microcracking in the concrete, the latter being regarded as one of the most important processes in the deformation of the concrete under external loading.

Berg (1961) has found that in case of exerted pressure on the concrete, processes like compaction, decompaction and structural degradation occur. With the increase of stresses above certain boundary microdegradations appear that turn into microcracks and macrodegradations in case of further increase of the load. During the process of deformation two parametric points that characterise the transition from the one to the other state can be fixed: boundary of beginning of microdegradations R_t^o and upper boundary of microcracking R_t^v.

Absorption-active environments have an essential effect on the solids deforming in a certain environment as well as on their structure in case of loading. In the reduction of the strength due to absorption and the relief of deformations (Rebinder effect) the main role is played by the smallest hidden microcracks that are formed at certain value of the stresses. The surface-active substances, and also the solutions of acids, alkali and salts quickly penetrate into the microcracks formed whereby prevent their full closure after eliminating the load.

METHOD OF APPROACH

The specific nature of the durability of the concrete and reinforced concrete structures operating in liquid aggressive environments assumes investigation of the effect of similar environments on the boundaries of microcracking of the concrete R_t^o and R_t^v.

The investigated concrete was based on sulphate-resistant cement, produced by the cement plant "Devnia" with water-to-cement ratio w = 0.45. The selected component ratio was cement:sand:gravel = 1 : 1.9 : 3.3.

The test samples were prisms measuring 10/10/40 cm which, after the stripping were put under water for up to 7 days and afterwards exposed to air at normal temperature and humidity. The

prism strength of the concrete samples determined at the age of 90 days in an aerial dry condition was 275.10^5 Pa.

1% solution of ammonium sulphate $(NH_4)SO_4$ with sulphate ions content (SO_4^{II}) 7273 mg/dm^3 and ammonium ions - 2727 mg/dm^3. Besides, water from the water supply network was also chosen as a liquid environment that has to simulate molecular absorption or absorption of a non-electrolyte. Samples that have stayed in open air with relative humidity φ = 60 - 65% have been used as check series.

For measuring the longitudinal deformations of the samples deformers of indicator type with accuracy of 0.001 mm and 200 mm base have been used, and for transversal deformations - with 50 mm base. The deformations (longitudinal and transversal) have been measured at the two opposite sides of each sample.

Before the short-term compression load the samples stayed in the aggressive environment of 1% solution of ammonium sulphate and in water respectively. It was found that in the first 4 days their saturation with the solution or the water is most intensive whereby for the solution the amount of the absorbed liquid was 2.76% by mass, and for the water - 2.41%. The moisture of the samples of the check series that have stayed in open air during the tests was 1.84%.

For expression of the relation "stress - deformation" (σ - ε) one-side relation is usually made between the stresses, invoked by the external loading and the longitudinal deformation (ε_l). With the concrete as an elastic-plastic material the module of the elasticity E and the factor of Poisson μ are constants only in case of comparatively low levels of the state of stress. With the stress increase over a certain level the experimental data do not correspond any more to the law of elastic change of the volume.

According to Berg (1961) the properties of the concrete are clearly manifested through the investigation of its volumetric deformations at different load rates: change of sample volume - $\Theta = \varepsilon_l + 2\varepsilon_t$ and the differential coefficient of the transversal deformation - $\Delta\nu = \Delta\varepsilon_t / \Delta\varepsilon_l$.

In the course of investigations the volumetric deformations of the samples being in contact with the aggressive solution and the water as well as those of the check samples in open air were calculated by the experimentally received values of the longitudinal and the transversal deformations.

During the test of the samples saturated within the liquid environments (1% solution of ammonium sulphate and water) the levels of the state of stress were defined as part of the actual values of their prism strength R'_b which is smaller compared to that of the check samples because of the reduction of the strength due to absorption.

RESULTS

The changes of the volume Θ and of the differential coefficients of the transversal deformation $\Delta\nu$ of the concrete samples in the various environments depending on the magnitude of the stresses (σ/R_b) are shown on Fig 1 and Fig 2 respectively.

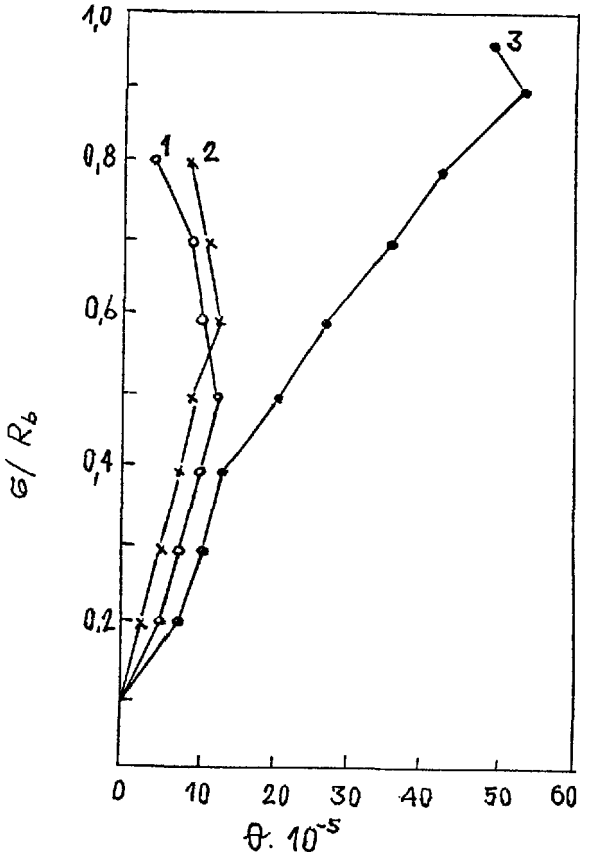

Figure 1 Volume Θ change depending on the magnitude of the pressure stresses
1 - in 1% solution of ammonium sulphate;
2 - in water; 3 - in open air

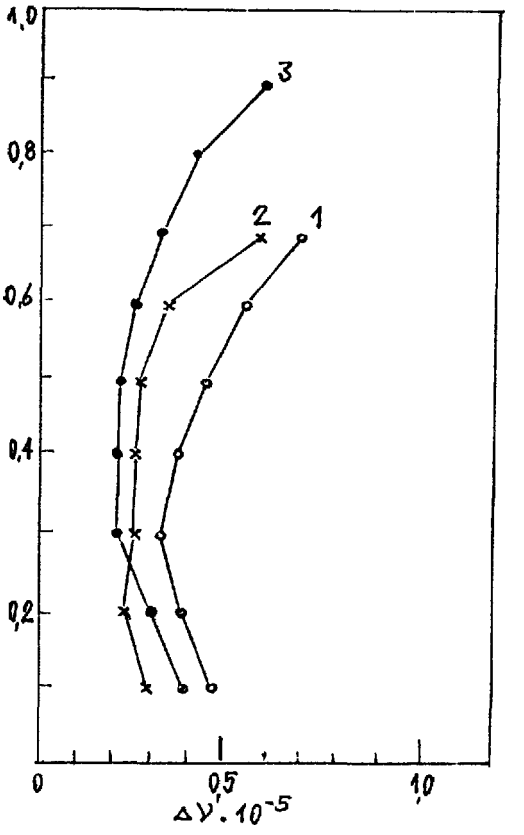

Figure 2 Change of differential coefficient of the transversal deformation Δν depending on the magnitude of the pressure stresses
1 - in 1% solution of ammonium sulphate;
2 - in water; 3 - in open air

The concrete deformations analysis under the combined action of compressed load and liquid aggressive environment shows the total longitudinal deformation of the check samples is considerably greater compared to the samples staying 4 days in 1% solution of ammonium sulphate and in water. The longitudinal deformations for loads closed to the degradation ones are around 120.10^{-5} for the samples exposed to air, and for the samples in the liquid environments the values do not differ essentially - they are around $55\text{-}60.10^{-5}$. The transversal deformations in contrast to the longitudinal ones are almost not influenced by the moist condition of the concrete and their values are within the range $51\text{-}56.10^{-5}$ but the nature of change of those deformations in the process of loading the concrete saturated in liquid environments is rather different. For stresses 0.45 - 0.5 R'_b the transversal deformations of the moist concrete significantly increase while for the check samples this process is observed for stresses above 0.7 R_b.

The reduction of the volume Θ (Fig 1) is most strongly manifested with the samples in open air (58.10^{-5}) and with the samples in aggressive environment it is in average 17.10^{-5}.

The changes in the differential coefficient values of the transversal deformations Δν (Fig 2) with the load increase show that the processes of structure decompaction of the concrete (R_t^o)

stayed in aggressive environment begin with stresses 0.3 - 0.4 R'_b , in water - with 0.40 - 0.45 R'_b , and for the check series in open air - with 0.5 = 0.55 R_b.

The action of the liquid aggressive environment reduces the magnitude of the upper boundary of the microcracks formation (R_t^v) at which the transition from decompaction to degradation of the structure occurs. For the check samples in open air R_t^v = 0.90 - 0.93 R_b , in aggressive environment R_t^v = 0.55 - 0.60 R'_b, and in water R_t^v = 0.65 - 0.70 R'_b.

CONCLUSIONS

1. There is a difference between dry and exposed to open air concrete, and such one immersed and saturated in liquid aggressive environment of 1% solution of ammonium sulphate which can be explained with the liquid filling the porous structure of the concrete takes part also in the deformation of the moist concrete. Under the compressed load impact a pressure of the liquid is created in the pores that obstructs the development of longitudinal deformations. Besides, this pressure causes an increase of the deformations in transverse direction of the acting pressure force whereby creating a possibility for increasing of the transversal deformation (ε_t). As a result the differential coefficient of the transverse deformation $\Delta\nu$ is greater for the concrete being in contact with the liquid aggressive environment.

2. The reasons for the influence of the liquid aggressive environments on the strength and deforming properties of the concrete under load are diverse and first of all related to the structural changes in the concrete. Corrosion-active environment is absorbed in the pores of the cement stone by the way of the surface diffusion through macro- and micro-capillaries. First of all the environment fills in the macro-capillaries without breaking the unity of the structure but relieves those points which are essential for the strength of the cement stone under the action of external load. Besides, the environment disrupts the unity of the concrete structure in the contact zone between the cement stone and the aggregates.

3. In the design of reinforced concrete structures operated in liquid aggressive environments it is necessary to take into account the reduced strength and the reduction of the values of the parametric points R_t^o and R_t^v of the concrete through introduction of a certain coefficient for work conditions by help of which the normative resistance of the concrete to be reduced.

REFERENCES

Berg, O. Ia., "Physical Foundations of Concrete and Reinforced Concrete Strength Theory", Gosstroyizdat, 1961.

Nazarsky, D., "Strength and Deformability of the Concrete Under Combined Action of Stresses and Aggressive Environments of Some Ammonium Salts", Dissertation, Sofia, 1979.

4iv022
8 pp

The Microstructure of Concrete Subjected to High-Magnesium and High-Magnesium Sulfate Brine Attack

David Bonen
USG Corporation, Research Center
700 North Highway 45, Libertyville, IL 60048, USA

Abstract

A microstructural study of three suites of concrete subjected to the attack of brines is reported. The first suite was exposed to the action of simulated magnesium sulfate brine for three years. The second category represents in-situ field concrete nine years in service that was recovered from the Waste Isolation Pilot Plant (WIPP) located in a formation. The third one represents an overcored grout that was placed in a borehole over than 20 years ago.

The specimens of the first category were markedly corroded due to magnesium sulfate attack. Massive deposits of gypsum were formed on the surface and within the paste. The C-S-H of the paste was altered to M-S-H at a rate ranging from 0.009 to 0.02 mm/day. In contrast, there was no sign that the field concrete specimens from the WIPP were chemically corroded by brines. Aside from near-surface deterioration, the specimens analyzed have been found to be compatible with the halite host rock. Along the contact with the host rock abundance of halite was deposited within the concrete as layers and as discrete crystals. Other near-surface degradation is related to carbonation, mainly associated with fractured zones.

Of interest is the uncommon mineralogy that has been observed in the grout. The alteration and secondary products include brucite, M-S-H, magnesium chloride hydrate, halite, sylvite, and Friedel's salt. The intact portion of the grout is characterised by the occurrence of large phenograins displaying a mosaic texture and abundance of portlandite. The grout, however, displayed a lower rate of deterioration than that of the first suite. This is attributed to the absence of sulfate in the sodium and potassium-rich brine.

Keywords: Durability, magnesium sulfate, magnesium chloride, and sodium chloride attacks on concrete.

1. Introduction

One of the on-going research efforts to secure safe disposal of radioactive waste considers burial and a lasting isolation of the waste in geological evaporite strata. Because of the aggressive environment and functional lifetime, the common usage of concrete as a solidification/stabilization agent does not necessary apply, rather its role lies in sealing man-made penetrations, such as shafts and boreholes that provide access to the repository. Under these conditions, aside from being structurally sound, the concrete has to be chemically compatible with the surrounding, durable, and possesses low permeability.

For almost two decades the US Army Engineer Waterways Experiment Station in cooperation with Sandia National Laboratories (SNL) has developed cement-based grouts and concrete for the WIPP (Waste Isolation Pilot Plant) repository facility. The WIPP is a research and development facility of the Department of Energy (DOE) established for demonstrating the safe disposal of defense-related transuranic waste generated by various facilities. The WIPP repository facility is located in a thick sequence of bedded evaporite rocks about 660 m below the ground surface, near Carlsbad, New Mexico. The evaporite rock in the WIPP repository horizon is mainly composed of halite (NaCl) with minor amount of anhydrite ($CaSO_4$), magnesite ($MgCO_3$), polyhalite ($K_2Ca_2Mg(SO_4)_4{\cdot}2H_2O$), quartz, and clay. The concrete at the WIPP is required to withstand attacks derived from brines and be compatible with surrounding salt beds. These brines display a wide compositional range(1) and contain magnesium-bearing solutions that are regarded as detrimental to concrete. A simulated high magnesium-bearing brine designated as H-1RSCM has a composition of 54.95 gram/liter (g/l) of sodium, 16.82 g/l potassium, 42.29 g/l magnesium, 209.88 g/l chlorine, and 18.24 g/l of sulfate as SO_4^{2-} (2). For comparison, the corresponding composition of sea water is about 10.5, 0.38, 1.28, 19, and 2.56 g/l, respectively. The concentration factors of Na, K, Mg, Cl, and $SO_4$2- in H-1RSCM brine over sea water are, therefore, 5, 44, 33, 11, and 7, respectively. It is evident that H-1RSCM brine is not a simple derivative of evaporation of sea water, and indeed considerable variations in K/Mg ratio were noted in the

natural brines(1).

Previous studies on the performance of companion specimens were conducted by the US Army Corps of Engineers at the Waterways Experiment Station(3-6). This paper summarizes the microstructural work that was carried out at ACBM, Northwestern University under contract to Sandia National Laboratories with the objectives of establishing the mechanism of the attack, characterizing alteration processes, and determining rates of deterioration, if any.

2. Materials, Exposure Conditions, and Examination Technique

Specimens representing three categories were examined. The first category comprises two specimens of concrete core 10 cm in diameter that were immersed in H-1RSCM brine for 3 years(7). The second category includes a number of field concrete specimens that were recovered from the Small-Scale Seal Performance Tests (SSSPT) after 9 years in service. Among these specimens one with the enclosing salt host rock was also included, thus permitting an examination of the contact between the concrete and the host rock. The other specimens were sampled from a fractured concrete zone some distance away from an old crack plane. The third category comprises 25 cm overcored halite host rock with an internal 9.8 cm grout plug that was placed over 20 years ago in a borehole next to a potash mine near the top of the Salado formation.

Formulation of concrete for underground disposal of defense-generated radioactive waste for the WIPP has been carried out for a number of years by the US Army Corps of Engineers, Waterways Experiment Station. The rational for this formulation and concrete properties are given elsewhere (e.g.,8). This concrete is made of ASTM Type H oil-well cement with a composition similar to ASTM Type V sulfate-resistant cement, Class C fly ash, a number of admixtures, and at water-to-solids ratio of about 0.33. Among the admixtures are Chem Comp III (a mixture of portland cement and calcium sulfoaluminate), and Cal-Seal anhydrite plaster. The latter two ingredients were incorporated to lend expansivity to the mixtures thus providing a good contact between the concrete and the salt rock. For a similar reason, granular NaCl salt constituting about 35% of the mixing water by mass was also introduced to the solid ingredients. This measure was taken in order to saturate the mixing water with respect to sodium chloride, thus eliminating a potential dissolution of the salt bed during placing and securing a good contact between the concrete and the host rock.

Unfortunately, there is no available information on the composition of the grout placed in the borehole. However, based on the appearance of large phenograins (distinct grains embedded in a finer groundmass in the paste, see nomenclature in ref(9)), it appears that the grout was also made of Type H cement, but in contrast to the other specimens it did not contain fly ash particles.

Aside from the specimens of the first category that were immersed in H-1RSCM solution, all the other specimens were exposed to the natural environmental condition of the surrounding salt beds with the possibility of being subjected to the action of brines.

Examinations were carried out in Hitachi S-570 Scanning Electron Microscope equipped with both G.W. backscatter detector and Tracor Northern EDXA (energy-dispersive X-ray analysis) system. Supplementary XRD analyses were carried out in a Philips X-Ray machine. Much of the SEM examination was conducted in a backscatter electron mode, although fractured surfaces were also viewed in secondary electron mode. Specimens analyzed in a backscattered electron mode were prepared by impregnating sliced specimens with an epoxy mix, reslicing and polishing with successively finer grades of diamond grit. The flat surfaces so produced were sputter coated with a thin layer of gold. In general, examination in a backscatter electron mode is preferred as it provides representative, unbiased surfaces, and permits a detailed appreciation of the spatial relationships and juxtapositions of the viewed features.

3. Features of Magnesium Sulfate Attack

It is well recognized that magnesium sulfate attack on concrete is associated with a severe degradation and ultimately may bring about complete disintegration. To date, a large body of literature documented various aspects of the attack. Microstructural studies have shown that at high magnesium sulfate concentration the main features that characterized the attack are secondary mineralization of brucite ($Mg(OH)_2$) and gypsum along with decalcification of the C-S-H and formation of M-S-H (e.g., 10-14).

The detailed microstructure may vary due to compositional changes, effects of mineral admixture, duration of the attack, etc. A "classical" microstructure, however, involves the formation of a double surface layer composed



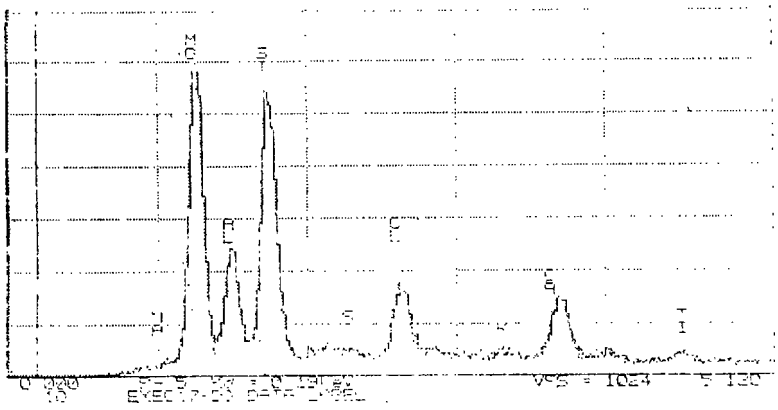

Figure 1(left): A backscatter electron image (BEI) micrograph of a number of gypsum layers (g) deposited in the paste at some 800 μm from the corroded surface. The low gray level of the previous C-S-H is due to strong decalcification and conversion to M-S-H. Ferrite is the only clinker phase that survived the attack.

2. Figure 2(right): X-ray pattern of the paste about 1 cm below the surface. The paste is mainly composed of M-S-H. The chlorine is either incorporated into the latter phase or chemisorbs on it.

of amorphous external brucite layer and an inner well-crystallized gypsum layer. Further inwards, the cement paste is intercepted by a few gypsum bands/layers that run parallel to the outer surface resembling Liesegang band formation involving rhythmic precipitation(10). This is accompanied by a distinct decalcification of the C-S-H from the intact core to the surface in which the Ca:Si of the former C-S-H continuously decreases as the surface is approached(11). The spatial distribution of this secondary mineralization is the result of the formation of two counter diffusion patterns in which hydroxide ions diffuse from the paste outward to produce insoluble brucite on the outer surface, and sulfate ions diffuse inward to form gypsum. The calcium needed for gypsum formation is first supplied by the decomposition of the CH ($Ca(OH)_2$), and subsequent to the consumption of local CH, additional Ca^{2+} is provided by the decalcification of the C-S-H.

It has been shown that the C-S-H is not readily transformed to M-S-H. First, the C-S-H undergoes a distinct decalcification and only at low Ca:Si this transformation takes place(15). Incorporation of aggregate and mineral admixture (e.g., silica fume and slag) modify to some extent the microstructure. Frequently, neither the outer surface double layer, nor the inner gypsum layers are continuous. Rather, gypsum forms discontinuous deposits, lines aggregate, fills voids, and the total amount of gypsum and brucite formed appears to be smaller(12,16). Gollop and Taylor(16) have suggested that the lower content of gypsum and brucite is due to the lower amount of portlandite formed in pozzolanic concrete. The latter microstructural changes appear to be related to a modification of the transport properties of the paste due to an increase of tortuosity and a refined pore microstructure. If so, it is expected that a decrease of the w:c would have similar effects. Nonetheless, it has been reported that the course of the attack is essentially the same even at a high mineral admixture dosage, and brucite, gypsum, decalcified C-S-H and M-S-H, all are formed(16).

4. Microstructure of SMC Stored in H-1RSCM Brine

Salado Mass Concrete (SMC) specimens were immersed in H-1RSCM solution for three years. The outer surfaces of the specimens are markedly corroded and extremely soft. The surface is characterized by a pitted corrosion in which loose-bonded quartz aggregates appear on the surface and are interbedded with well-crystallized, idiomorphic gypsum. Many quartz grains are barely cemented and a great part of their circumferences is exposed. Other phases viewed are small halite crystals and some amorphous materials. The depth of this highly corroded zone ranges from about 1 to 2 mm inward. XRD analyses yield similar results: the two main constituents are quartz and gypsum with minor amounts of halite. Other two unidentified phases appear as shoulders on the main peaks of gypsum and quartz at about d-spacing of 7.83 and 3.39Å, respectively.

It is worth mentioning that the pitted corrosion indicates disintegration and removal of materials. In agreement with a previous study(7), neither SEM nor XRD examinations recorded presence of brucite at the outer

corroded zone, nor at the subsurface. The absence of brucite might indicate that either brucite was not deposited, or it had been lost due to spalling or other reasons (handling and sample preparation). The latter interpretation cannot be overlooked. In fact, the exposed aggregate on the surface suggests that the outermost concrete surface, at least a few hundred microns thick was completely removed and lost because of expansion and spalling, thus destroying any evidences of brucite deposition.

Apart from the absence of the surface double layer, a characteristic microstructure of magnesium sulfate attack is viewed in Fig. 1. Several gypsum layers are deposited parallel to the outer surface and interbedded in highly decalcified C-S-H. The former C-S-H has lost its characteristic microstructure and possesses a typical low gray level (in a backscatter electron mode examination) due to the decalcification of the former C-S-H. Ferrite (C_4AF) is the only clinker phase that has survived the attack. Other typical features of sulfate attack are the formation of thick gypsum deposits around aggregate, within the paste, and in air voids. The depth of the interbedded gypsum layers extends some 800 μm from the present outer surface. Further inwards up to about 1 cm from the surface, the amount of gypsum precipitated decreases, and it appears as a partial lining of aggregates, in voids, and as disseminated grains all across the paste.

X-ray spot and area analyses (Fig. 2) show that the former C-S-H was converted to M-S-H. It may be argued that some of the chlorine is taken up to form Friedel's salt ($Ca_4Al_2Cl_2 \cdot 10H_2O$). However, as viewed in Fig. 2, a considerable amount of chlorine is either chemisorbed on the M-S-H or actually incorporated into its structure or is taken by other phases. In this respect, Burkes(7) reported the occurrence of magnesium chloride hydroxide hydrate ($Mg_2(OH)_3Cl \cdot 4H_20$) in the brine-affected zone of companion specimens. Wakeley et al.(3) also reported the formation of this phase at the interface of the halite host rock and a concrete plug. By contrast, Poole et al.(4) studied the effects of various brines on the paste composition. They noted that the affected pastes gained a small amount of magnesium, but no magnesium-bearing phase could be identified within the pastes.

X-ray spot analysis of a well-recognized feature is highly valuable as any change in the supposed chemical composition of the original feature may be directly related to alteration processes. This technique was employed in this study to identify the depth of alteration by spot-analyzing large phenograins. Several traverses normal to the outer surfaces have been made. In the first specimen, the diminishing effect of the aggressive solution is recognized at a depth of 1 cm below the corroded surface and it is manifested by the occurrence of partially reacted phenograins and limited amount of gypsum formation. Analyses at a greater disclose an unaltered paste with a common gray level, and a common Ca:Si of C-S-H. Area analysis conforms with the previous conclusion and the X-ray pattern fail to show high signals for sulfur and magnesium.

Examination of the second specimen yields similar results, but the paste is affected to a greater depth. Decalcification of the C-S-H and magnesium-bearing phases are identifiable as deep as 2 cm below the surface. At a depth of about 2.5 cm intact concrete is observed. The depth of alteration of the SMC varies, therefore, from about 1 to 2.2 cm. As the specimens were immersed for 3 years, the corresponding calculated linear rate of alteration ranges from 0.009 to 0.02 mm/day. This estimate conforms well with a previous one that is based on strength loss in which the rates of deterioration range from 0.015 to 0.03 mm/day(5). Despite the similar estimates, it is doubtful whether degradation advances inward linearly with respect to time.

Expansion and cracking are probably the main failure mechanisms associated with sulfate attack in which ettringite is formed. The above specimens, however, neither disclose ettringite formation nor any cracking pattern that can account for the measured strength loss(5). In fact, the total amount of gypsum precipitated is smaller than that of neat paste, probably due to the presence of pozzolans(16). It appears that degradation is not necessarily related to cracking associated with volume instability. Rather, as has been suggested(15), the decalcification of the C-S-H plays a major role in the degradation process. This is consistent with other studies pointing at this conclusion(17). SMC is made of cement with a composition similar to ASTM Type V sulfate-resistant cement and a high amount of Class C fly ash in part to grant a better resistance against $MgSO_4$ attack. These remedial measures may slow the attack but not prevent it. In the few studies documenting the degree of decalcification, it has been shown that mineral addition brings about extensive decalcification(11,12,16).

5. Microstructure of Field Concrete from the WIPP Site

Chloride attack on concrete has been extensively studied over the years, primarily because of its adverse effect on the depassivation and corrosion of reinforcing steel. However, there is little data relating to the effect of chloride on the paste performance.

The specimens of the second category exhibit a different microstructure. To the naked eye the contact between the halite host rock and the concrete is smooth and no specific spalling or physical deterioration is observed. Under SEM examination, however, some secondary mineralization did take place. Though the concrete was made with salt-saturated water, an abundance of NaCl crystals were deposited to a depth of 100-150 μm from the interface. A halite layer up to 50 μm thick was deposited in the interfacial transition zone along aggregates and across the paste. Figure 3 shows that the individual crystals are euhedral, and many of them have a distinct rhythmic zoning-a clear indication that they grew over time. Figure 4 exhibits X-ray maps for Cl (upper left), Na (upper right), Si (lower left) and the backscatter electron image of the analyzed area (lower right). The bar displayed at the top of the sodium map designates 60 μm. The image viewed extends from the salt host rock (white at the top) to about 350 μm below the interface. A distinct continuous layer of NaCl a few microns thick accompanies the interface at a depth of between 100 to 200 μm. This layer rims aggregate and runs across the paste. However, further away, except for the appearance of some sulfur-rich nodules, the X-ray maps fail to show any appreciable amount of secondary mineralization. A few disseminated signals for sodium and chlorine up to 300 μm from the surface correspond to relatively small halite grains within the paste. Similarly, a few signals of magnesium correspond to disseminated small dolomite particles and not to Mg-bearing alteration products.

In accord with the X-ray maps, the microscopical examination shows that apart from gypsum grains encountered within the paste there is no evidence for secondary mineralization either along aggregate boundaries or within the paste and cracks. The C-S-H has a typical gray level and Ca:Si. Large gypsum grains, some as large as 80 μm are embedded within the paste. Frequently, they lie along open cracks or are associated with open cracks. The crack widths range from 1 to 5 μm, but they are empty and clear from any deposits. The microstructure of the concrete 6 cm away from the interface is similar to that next to the interface. Apart from dispersed gypsum grains, no other mineralization is observed. Of interest is the occurrence of small gypsum that display sodium X-ray signals suggesting that such grains were precipitated from sodium-rich pore solutions. At this depth the concrete is cracked to about the same extent as described above.

That the gypsum grains are associated with cracks but none are deposited in cracks suggests that the cracking is post gypsum deposition, and cracks are more likely to propagate along gypsum boundaries rather than across the C-S-H. The origin of these gypsum grains is unclear. It might be related to an external sulfate ingress.



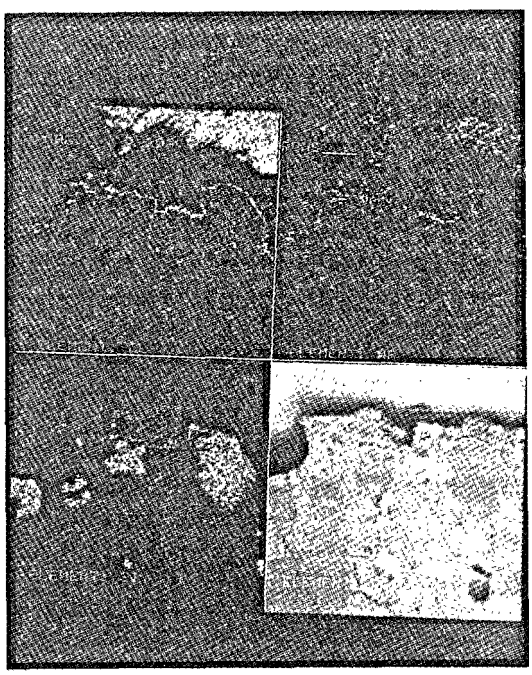

Figure 3(left): BEI micrograph of idiomorphic, cubic NaCl crystals deposited as a layer along aggregate (bottom) and within the paste (center). Note the distinct zoning of some of the NaCl crystals.

4. X-ray maps of Cl (upper right), Na (upper left), Si (lower left) and the BEI of the analyzed area that extends from the halite host rock at the top down to 350 μm below the interface. A distinct layer of NaCl a few microns thick was deposited along the aggregate as is delineated by the Si map and across the paste.

However, in view of the uniform distribution of gypsum irrespective to the distance from the host rock, and the absence of any other signs of brine ingress, it is more likely that the gypsum was deposited from the oversulfated pore solution of the original mixtures or, at least in part, the grains are residue of an incomplete reaction of the Cal-Seal anhydrite plaster.

Examination of a macro crack plane at the top shows abundance of surface deposition of NaCl embedded in corroded paste. Below the crack plane, the best part of the paste is carbonated to a depth of about 20-25 μm. Further inward, the paste retains a common microstructure and a common gray level. At the top, relatively wide open cracks run across aggregate and paste. Nonetheless, no secondary mineralization has been observed within the cracks. The same applies to the interior and except for the occurrence of large gypsum grains within the paste and voids, the paste had not experienced chemical alteration and deterioration. Similarly, there are no evidences that relate the cracking to chemical attack.

It appears that portland cement paste is chemically compatible with NaCl beds and the subsurface deposition of halite crystals observed has little effect. Lea(18) and recently Glasser(19) have made similar conclusions.

6. Microstructure of Grout Plug from the Borehole

Of much interest is the degree of alteration of the grout plug placed in an abundant borehole over 20 years ago. This grout has been clearly affected by brine and exhibits diversified mineralogy. Aside from the original main phases C-S-H and CH, it includes halite, sylvite (KCl), brucite, M-S-H, magnesium chloride hydroxide hydrate and/or magnesium chloride hydrate, and Friedel's salt. It is evident that the grout was influenced by Mg-bearing solution. The intimate association of halite and sylvite in the grout favours the suggestion that the aggressive solution derived from brine from a potash mine intersects the borehole.

Figure 5 exhibits the microstructure next to the contact with the halite host rock. At the interface brucite about 80 μm thick is formed and followed by numerous small halite and sylvite crystals in which the former is the preponderant phase. The brucite is distinguishable by a low gray level and its amorphic appearance. EDX analysis shows that it contains very little calcium and chlorine. Further inward, the C-S-H is converted to M-S-H that is associated with abundant salt crystals. However, the brucite layer is not continuous and in other areas M-S-H appears immediately at the interface. As previously noted, the M-S-H contains substantial amounts of chorine and calcium.

Two other magnesium-chloride-bearing phases are observed. Figure 6 presents a rare occurrence of a bundle of needle-like crystals with X-ray signals that correspond to $MgCl_2$ or $MgCl_2 \cdot nH_2O$. Of a greater importance is the occurrence of another amorphic, low-gray level phase that is associated with M-S-H. An interpretation of spot analyses as well as the low gray level suggests that this phase corresponds to magnesium chloride hydroxide or magnesium chloride hydroxide hydrate with Mg:Cl of 2:1 or 3:1.

Salt crystals appear in all the fields examined though their content is highly variable. Usually, halite is the predominant phase, followed in a decreasing order by sylvite, CH, and Friedel's salt. Sylvite is almost always associated with halite. They are idiomorphic and range in size from sub-micron to about 10 μm. Sylvite is distinguishable from halite by its somewhat higher gray level.

The depth of conversion of C-S-H to M-S-H in not uniform and extends up to about 1.8 mm from the interface. Further away, the unreacted paste has a mosaic texture in which large phenograins are accompanied with a notable amount of CH grains having amoebic appearance. Most of the phenograins are completely hydrated, but a few retain a sizable unhydrated C_3S core. Additional uncommon feature is the appearance of clusters of CH composed of large idiomorphic to sub-idiomorphic grains up to 50 μm across. The outlines of these CH grains display no corrosion despite that the grains are located in the altered paste zone.

As the halide crystals appear all across the grout to its interior, if the sodium and potassium originated from brine, the whole cross-sectional area of the plug was affected by external solutions. However, if the depth of alteration of the C-S-H is considered, the influence of the brine is markedly smaller. Nonetheless, despite the magnesium attack, the high amount of CH recorded indicates that the grout has retained its high alkalinity-the single most important factor for the chemical stability of the C-S-H.

The rate of alteration of the grout is not readily predictable as neither the actual exposure time to the action of the brine is known, nor the brine flux and composition. Provided the grout was exposed for a several years to brine, it displays a lower rate of deterioration than do the specimens immersed in H-1RSCM solution. One

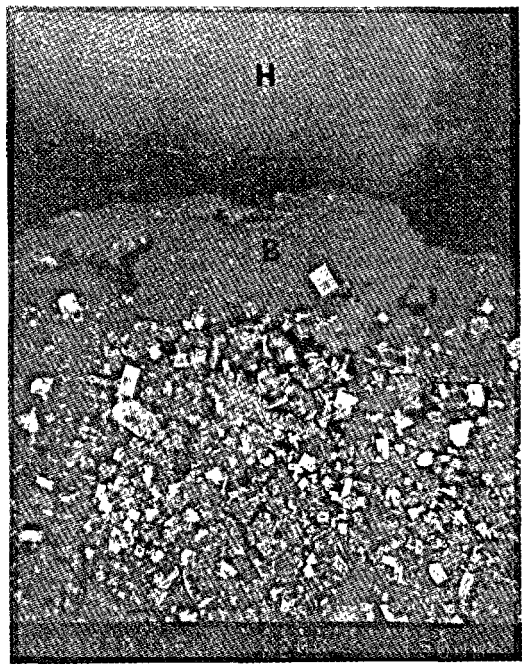



Figure 5(left): BEI micrograph showing the contact of the grout with the halite host rock (H). At the contact brucite (b) about 80 μm thick was formed. Further inwards the C-S-H was converted to M-S-H. Numerous small crystals (white)of halite and sylvite are embedded in the paste.

Figure 6(right): BEI micrograph of needle-like crystals with a composition of $MgCl_2$ or $MgCl_2 \cdot nH_2O$.

conspicuous feature is the absence of gypsum in the alteration products of the grout. This suggests that the sulfate content of the brine was low enough to permit any meaningful precipitation of gypsum. Thus, the grout was mainly exposed to the action of $MgCl_2$ rather than $MgSO_2$ solutions. In fact, it was long ago recognized that $MgCl_2$ corrosion is less destructive than $MgSO_4$ one(20). Lea(18) noted that solutions of 2% $MgCl_2$ and upwards gradually degrade the strength and concentrated solutions, e.g. 3M destroy portland cement concrete.

Unlike magnesium sulfate attack in which degradation is due to the combined action of magnesium and sulfate, in $MgCl_2$ attack the corrosion is because of a base exchange reaction in which:

$$MgCl_2 + Ca(OH)_2 \rightleftharpoons Mg(OH)_2\downarrow + CaCl_{2\,(sol)} \qquad (1)$$

Brucite is practically insoluble and deposits on the surface, whereas $CaCl_2$ is readily soluble and either leaches out or forms other compounds such as Friedel's salt:

$$C_3A + CaCl_2 + 10H_2O \rightarrow C_4A \cdot Cl_2 \cdot 10H_2O \qquad (2)$$

Biczok(20) attributed the higher resistance of portland cement to $MgCl_2$ attack to the formation of impermeable surface layer of brucite that suppresses the rate of ingress and subsequent degradation. However, since the brucite layer in the grout is not continuous it is doubted whether this explanation fully applies. Alternatively, the occurrence of M-S-H and magnesium chloride hydroxide hydrate may offer another explanation. Accordingly, the high concentration of Cl gives rise to:

$$Mg(OH)_2 + Cl^- \rightarrow Mg(OH)Cl + (OH)^- \quad \text{or} \quad 2Mg(OH)_2 + Cl^- \rightarrow Mg_2(OH)_3Cl + (OH)^- \qquad (3)$$

Suppose that the Ca:Si of C-S-H is 1.5, and the Mg:Si of M-S-H is close to 1(15), then a reaction that accounts for the formation of M-S-H and $Ca(OH)_2$ can schematically be described as:

$$C\text{-}S\text{-}H + MgCl_2 + (OH)^- \rightarrow M\text{-}S\text{-}H + CaCl_{2\,(sol)} + 0.5Ca(OH)_2\downarrow \qquad (4)$$

It should be mentioned, however, that an attempt to draw a stoichiometric reaction for eq. 4 is not readily attainable as the Ca:Si of C-S-H is usually greater than 1.5(21) and the M-S-H contains calcium. Nevertheless, eqs. 1-4 provide an explanation for the occurrence of the phases observed, and especially to the appearance of clusters of large CH grains in the altered C-S-H zone just 250 μm away from the surface.

7. Concluding Remarks

Analysis of the data shows that the Salado Mass Concrete is chemically compatible with evaporite beds. The halite rock or any other sodium chloride solutions originated from it exerted minor deleterious effects. This implies that sealing-off man made penetrations into evaporite rock with concrete is a viable solution. However,

satisfactory service life of the concrete is considerably shortened in the presence of $MgSO_4$ brine. Remedial actions in the forms of ASTM Type V sulfate resistance portland cement and addition of pozzolans do not prevent the attack. In the present study continuous exposure to the latter solution resulted in an alteration rate of 0.009 to 0.02 mm/year. Exposure to $MgCl_2$ solutions has been proven to be less detrimental.

8. Acknowledgement:
The author kindly acknowledge Dr. Frank D. Hansen, Sandia National Laboratories for his constructive comments on the manuscript. This paper is a contribution from the NSF Center for Advanced Cement-Based Materials at Northwestern University.

9. References

1. C.L. Stein and J.L. Krumhansl, "Chemistry of Brines in Salt from the Waste Isolation Pilot Plant (WIPP), Southeastern New Mexico: A Preliminary Investigation," SAN85-0897, Albuquerque, SNL, March 1986, p.37.
2. S. Lambert, " Recipes for Brines to be Used in Concrete Studies," SNL February 15,1991, p.5.
3. L.D. Wakeley, P.T. Harrington, and C.A. Weiss, Jr., "Properties of Salt-Saturated Concrete and Grout after Six Years In Situ at the Waste Isolation Pilot Plant," SAND93-7019, Albuquerque, SNL, June 1993, p. 36.
4. T.S. Poole, L.D. Wakeley and C.L. Young, "Individual and Combined Effects of Chloride, Sulfate, and Magnesium Ions on Hydrated Portland-Cement Paste," SAND93-7040, Albuquerque, SNL, March 1994, p. 50.
5. L.D. Wakeley, T.S. Poole, and J.P. Burkes, "Durability of Concrete Materials in High-Magnesium Brine," SAND93-7073, Albuquerque, SNL, March 1994, p. 52.
6. L.D. Wakeley, J.J. Ernzen, B.D. Neeley, and F.D. Hansen, "Salado Mass Concrete:Mixture Development and Preliminary Characterization," SAND93-7066, Albuquerque, SNL, June 1994, p. 50.
7. P. Burkes, scientific notebook, US Army Engineer Waterways Experiment Station, 1995.
8. L.D. Wakeley and D.M. Walley, "Development and Field Placement of an Expansive Salt-Saturated Concrete (ESC) for the Waste Isolation Pilot Plant (WIPP)," Technical Report SL-86-36, September 1986, p 31.
9. S. Diamond, and D. Bonen, "Microstructure of Hardened Cement Paste-A New Interpretation," J. Am. Ceram. Soc., Vol. 76[12] 2993-2999 (1993).
10. D. Bonen and M.D. Cohen, M. D., "Magnesium Sulfate Attack on Portland Cement Pastes- I. Microstructural Analysis," Cem. Concr. Res., Vol. 22[1] 169-180 (1992).
11. D. Bonen and M.D. Cohen, "Magnesium Sulfate Attack on Portland Cement Pastes- II. Chemical and Mineralogical Analyses," Cem. Concr. Res., Vol. 22[4] 707-718 (1992).
12. D. Bonen, A Microstructural Study of the Effects Produced by Magnesium Sulfate Attack on Plain and Silica Fume-Bearing Portland Cement Mortars," Cem. Concr. Res., Vol. 23[3] 541-553 (1993).
13. R.S. Gollop and H.F.W. Taylor, "Microstructural and Microanalytical Studies of Sulfate Attack. I. Ordinary Portland Cement Paste," Cem. Concr. Res., Vol. 22[6] 1027-1038 (1992).
14. R.S. Gollop and H.F.W. Taylor, "Microstructural and Microanalytical Studies of Sulfate Attack. II. Sulfate Resisting Portland Cement: Ferrite Composition and Hydration Chemistry," Cem. Concr. Res., Vol. 24[7] 1347-1358 (1994).
15. D. Bonen, "Composition and Appearance of Magnesium Silicate Hydrate and its Relation to Deterioration of Cement-Based Materials," J. Am. Ceram. Soc., Vol. 75[10]2904-2906 (1992).
16. R.S. Gollop and H.F.W. Taylor, "Microstructural and Microanalytical Studies of Sulfate Attack. IV. Reactions of Slag Cement Paste with Sodium and Magnesium Sulfate Solutions," Cem. Concr. Res., Vol. 26[7] 1013-1028 (1996).
17. O.S.B. Al-Amoudi, "A Discussion of the Paper A Microstructural Study of the Effect Produced by Magnesium Sulfate on Plain and Silica Fume-Bearing Portland Cement Mortars," Cem. Concr. Res. Vol. 24[2]371-372(1994).
18. F.M. Lea, The Chemistry of Cement and Concrete, p.727. Chemical Publishing Company, Inc. N.Y. third edition(1971).
19. F.M. Glasser, "Performance Testing of Cements," pp. 730 in Session HH2/II17, Cements in Radioactive Waste Management, MRS Abstracts, Fall Meeting, Boston(1996).
20. I. Biczok, Concrete Corrosion Concrete Protection, p.543. Chemical Publishing Company, Inc.N.Y.(1964).
21. D. Bonen and S. Diamond, "Interpretation of Compositional Patterns Found by Quantitative Energy Dispersive X-ray Analysis for Cement Paste Constituents," J. Am. Ceram. Soc., Vol.77[7] 1875-1882 (1994).

EFFECT OF AMMONIUM-SULPHATE CORROSION ON THE STRENGTH OF CONCRETE

Saša R. MILETIĆ and Marina R. ILIĆ
IMS Institute, Bul. vojv. Mišića 43, Belgrade
Yugoslavia

ABSTRACT This paper considers the sulphate corrosion of Portland cement with content of C_3A from 5.45% to 11.84% and the same Portland cement with 30% of fly ash. The test samples were prepared and then exposed to the influence of aggressive environment (solutions with SO_4^{2-} ions as well as NH_4^+ ions). The measurements of flexural strengths were carried out after 1, 2, 4 and 6 months. The results were analyzed and a correlation among the resistance factor was suggested.

Key-words: composition, corrosion, durability, fly ash, sulphate resistance

INTRODUCTION

Corrosion of concrete, as well as the related protection and ensuring of concrete structures against aggressive impacts by chemical agents, regardless whether this concerns liquid, gas or even solid phase under certain conditions, represents a complex problem of utmost importance for the economy in general, and especially for building construction and the construction industry.

This paper shows the influence by the composition of Portland cement clinker, that is, of Portland cement, on the resistance of cement stone to the impact by the aggressive environment. Solutions of sodium and ammonium sulphates with various concentrations were selected as the representatives of the aggressive environment, bearing in mind that in nature these ions are most frequently encountered in underground waters which come into contact with concrete.

The results show that there is a considerable influence by certain components of the mineral composition of Portland cement clinker, that is, of Portland cement, on the resistance to the impact by the aggressive sulphate and ammonium ions. This results in the need that in the course of designing concrete which will be exposed to the impact by aggressive ions, special attention be paid to the selection of cement according to Biczok (1972), Mehta (1983) and Mitrović, Dučić (1985).

Most of the exploited natural aggressive waters with which concrete comes into contact are sulphate waters, and thus the concept of chemical corrosion of concrete most often regards sulphate corrosion. This is certainly the reason why the problem of sulphate corrosion is dealt with by a large number of researchers from all over the world according to Moskvin et al (1980), Regourd (1980) and Taylor (1973).

Chemical corrosion of concrete is the consequence of reactions between the constituents of cement stone, i.e. calcium silicates, calcium aluminates and above all calcium hydroxide, as well as other constituents, with certain substances from water, solutions of soil, gases, vapours, etc. The most important aggressive agents are: SO_4^{2-}, Mg^{2+}, NH_4^+, Cl^-, H^-, HCO_3^-.

When we speak about sulphate corrosion, we primarily think of the impact by sulphate ions on cement stone. The sulphate ion is the cause of one of the most dangerous corrosions - the corrosion of expansion and swelling - because it causes the occurrence of expansive compounds, first of all ettringite- $C_3A{\cdot}3CaSO_4{\cdot}32H_2O$, in the shape of prismatic crystals.

For the process of concrete corrosion under the impact of sulphates, it is essential which cation is linked with the sulphate ion. Namely, cations linked with sulphate ions can be divided into three characteristic groups. The first group includes alkali metals Na^+ and K^+, which give extremely soluble hydroxides, while the second group comprises metals such as Mg^{2+} and Fe^{2+}, which give poorly soluble hydroxides, and the third group consists of cations such as NH_4^+ and H^+, which give volatile or neutral hydroxide. The third group of sulphates, that is $(NH_4)_2SO_4$ and H_2SO_4, covers the most aggressive compounds. In case of impact by these compounds on concrete, neither balancing nor creation of protective gel takes place. The destruction of concrete, in this case, occurs not only due to expansion, but also because of intensive dissolution of cement stone.

Bearing in mind all the above-mentioned, the basic idea and motivation for the work on this paper is to widen the knowledge about the overall effect of corrosion processes in microconcrete, and it is thus the continuation of several-year research in this field of Miletić, Ilić (1995) and (1996).

EXPERIMENTAL

The programme for researching resistance of cement to the impact by sulphate corrosion envisaged characterization of Portland cement and Portland cement with the addition of 30% of fly ash manufactured in Serbia:
- Portland cement (C11) and Portland cement with the addition of 30% of fly ash (C15)
- Portland cement (C21) and Portland cement with the addition of 30% of fly ash (C24)
- Portland cement (C31) and Portland cement with the addition of 30% of fly ash (C32)

Complete testings of the chemical composition of all materials were carried out, same as the testings of mechanical properties of cements, and the potential mineralogical analysis of clinker and Portland cement was given. In the second part, the testings of the influence by the selected aggressive solutions on cement products were carried out. On the basis of results of the implemented testings, the first estimate was given for the resistance of cements to sulphate corrosion, as well as their classification in this sense according to Ranogajec et al (1996) and Miletić et al (1996).

Description of aggressive environments

The solutions of sodium sulphate and ammonium sulphate were used as the aggressive environments, to which cement was exposed. Concentrations of sulphate solutions used are presented in **Table 1**:

Table 1 Concentrations of sulphate solutions

SO_4^{2-}, mg/l	Na_2SO_4,%	$(NH_4)_2SO_4$,%	NH_4^+,mg/l	Solution
1000	0.1478	-	-	I
2000	0.2956	-	-	II
1000	-	0.1375	320	III

The temperature of sulphate solutions was maintained at 20±1°C. In the course of the testings, the solutions were not changed. The concentration of the solution was kept constant. The solutions were renewed every 30 days.

Methods for testing the influence of aggressive environments

V.V. Kind's method, which is standardized (GOST 4798), was selected as the basic procedure in studying the influence of aggressive environment, that is, determining corrosion resistance of cements. The essence of the procedure in V.V. Kind's method is that it uses cement mortar prisms, with the dimensions 1x1x3 cm, prepared in a special way and then submerged parallelly into the solution whose influence is tested and into potable water. The ratio between values of flexural strengths of prisms in the aggressive solution and in potable water, gives the numerical value of resistance coefficients, which is used as the characteristic of corrosion resistance of cement to aggressive impacts. The value of the coefficient of corrosion resistance above 0.8 gives a positive estimate of the durability of cement in the given aggressive environment.

The adopted method for testing the resistance of cements to the impact by sulphates, according to previous researches, proved to be suitable especially when testing composite cements.

Test samples, with the dimensions 1x1x3 cm, were made of a mixture of cement and quartz sand with particle-size distribution of 0.4-0.5 mm, in mass ratio 1:3.5 and with water-cement ratio 0.4. After casting, the test samples were left to age for 24 hours in humid air, and then 14 days in potable water. Flexural strength was tested. Other test pieces were left to age, in a certain number, in potable water and in the specified solutions, until the end of periods of 1, 2, 4 and 6 months (without counting the above-mentioned 15 days).

Other testing methods used in this work

1. Determining the strength (EN 196-1)
2. Chemical analysis (EN 196-2)
3. Calculating the potential mineralogical analysis (ASTM C 150)

RESULTS AND DISCUSSION

The selected aggressive environments represent very strong aggressiveness which is most often present in underground waters in the territory of the Republic of Serbia (**Table 1**).

The potential mineralogical analysis, for all clinkers and Portland cements is given in **Table 2**. It can be seen that the cement used differ in C_3A content - C11 contains 11.84% of C_3A, C21 contains 9.74%, and C31 contains 5.45% of C_3A, which has its impact on sulphate resistance. The ordinary Portland cement is not resistant to the influence by sulphates because it has a considerable content of tricalciumaluminate - C_3A, whose hydrates react with sulphate ions, forming expansive compounds. Portland cement with increased resistance to sulphates must have a low content of C_3A.

Table 2 Mineralogical composition

Material	Clinker			Portland cement		
	K1	K2	K3	C11	C21	C31
C_3S	62.07	57.00	71.90	50.93	45.42	56.92
C_2S	14.79	17.63	6.77	18.77	22.90	17.70
C_3A	11.15	10.82	4.29	11.84	9.74	5.45
C_4AF	7.51	7.24	11.68	6.63	7.27	11.31
CaO free	0.00	0.48	0.03	1.18	3.47	1.19
$CaSO_4$	0.90	1.05	1.10	4.76	3.74	2.81
MgO	1.60	3.00	1.10	2.10	3.30	1.00

Table 3 Chemical analysis of mineral admixture

Composition	Fly Ash
SiO_2	44.12
Al_2O_3	14.55
Fe_2O_3	5.15
CaO	4.06
Insoluble residue	26.00
Moisture at 105°C	0.57
Loss on ignition	3.18
Na_2O	0.09
K_2O	0.55
S	0.00
SO_3	0.27
MgO	1.70
MnO	0.06

Table 3 presents the chemical composition of fly ash. Fly ash, by its chemical composition, shows traditional ash of lignite, which makes it relatively unsuitable for use in concrete (low content of the sum of oxides SiO_2, Al_2O_3 and Fe_2O_3, but the content of CaO is also low).

The chemical composition of cements is presented in **Table 4**. As regards the chemical composition, all the cements satisfy the conditions for quality of the Yugoslav standard JUS B.C1.011. The characteristic feature is an increased content of insoluble residue in cements with the addition of fly ash.

Table 4 Chemical composition of Portland cement and Portland cement with the addition of 30% of fly ash, (% mass)

Composition	Cement					
	C11	C15	C21	C24	C31	C32
SiO_2	19.95	17.46	19.94	18.89	21.15	19.18
Al_2O_3	5.86	7.25	5.20	8.37	4.43	6.84
Fe_2O_3	2.18	1.99	2.39	2.68	3.72	4.39
CaO	60.19	42.49	57.82	44.46	62.10	45.30
Insoluble residue	1.00	16.66	0.71	15.15	0.87	16.22
Moisture at 105°C	0.34	0.69	0.26	0.57	0.38	0.46
Loss on ignition	0.74	3.68	1.59	1.05	0.71	1.38
CO_2 in $CaCO_3$	0.16	0.37	0.10	0.42	0.23	0.28
CaO free	1.18	1.41	3.47	0.18	0.78	0.53
CaO in $CaCO_3$	0.20	0.47	0.13	0.54	0.29	0.36
CaO in $CaSO_4$	1.96	1.64	1.54	1.27	1.10	0.96
SO_3 in $CaSO_4$	2.80	2.35	2.20	1.82	1.57	1.38
CaS	0.09	0.20	0.13	0.00	0.00	0.00
MgO	2.10	1.70	3.30	1.70	1.10	1.41
Na_2O	1.10	0.73	1.00	1.15	1.19	1.06
MnO	0.07	0.09	0.05	0.08	0.18	0.12
FeO	0.03	0.70	0.14	0.38	0.12	0.17
P_2O_5	0.12	0.09	0.05	0.10	0.09	0.08

Table 5 Mechanical characteristics of Portland cement and Portland cement with the addition of 30% of fly ash

Cement	Flexural strengths, MPa				Compressive strengths, MPa			
	1day	3days	7days	28days	1day	3days	7days	28days
C11	5.1	6.6	7.8	8.7	20.6	36.5	43.1	55.5
C15	4.9	6.3	7.4	7.5	14.9	30.8	39.8	51.2
C21	3.2	5.7	7.2	8.0	11.8	24.3	33.0	42.6
C24	2.9	5.2	6.5	8.9	10.9	23.1	34.8	50.3
C31	2.8	5.0	6.2	8.3	11.1	22.6	33.9	50.8
C32	2.0	4.6	6.7	7.8	7.2	21.0	34.0	48.7

Table 5 gives values for flexural and compressive strengths of cements after 1, 3, 7 and 28 days. The addition of fly ash generally contributes to the increase in strengths, especially in the later phases of curing (above 28 days), which is its most important contribution. This can best be seen in cement C24.

In this way, complete characterization was implemented regarding all the cements used in this work. The results of testings of the impacts by aggressive solutions, that is, the resistance to sulphate corrosion of cements, carried out in line with V.V. Kind's method, are presented, by way of coefficients of corrosion resistance, in **Figs 1-3**.

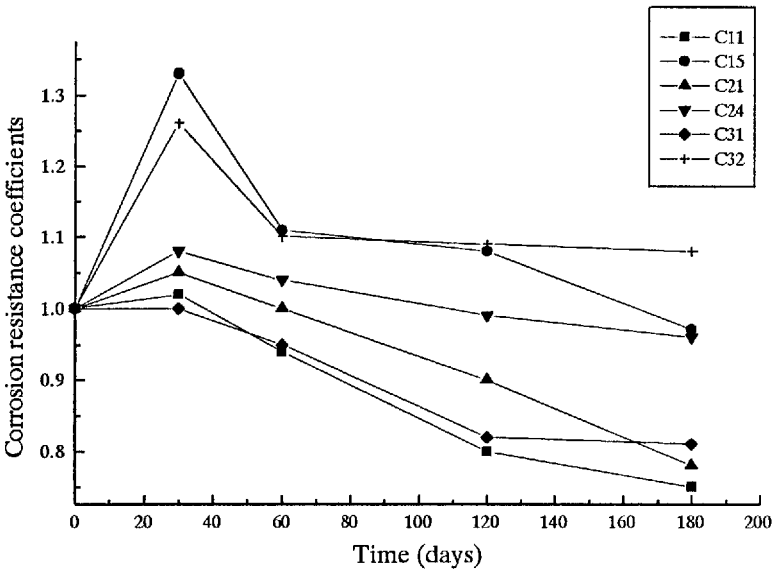

Figure 1. Corrosion resistance coefficients in solution I

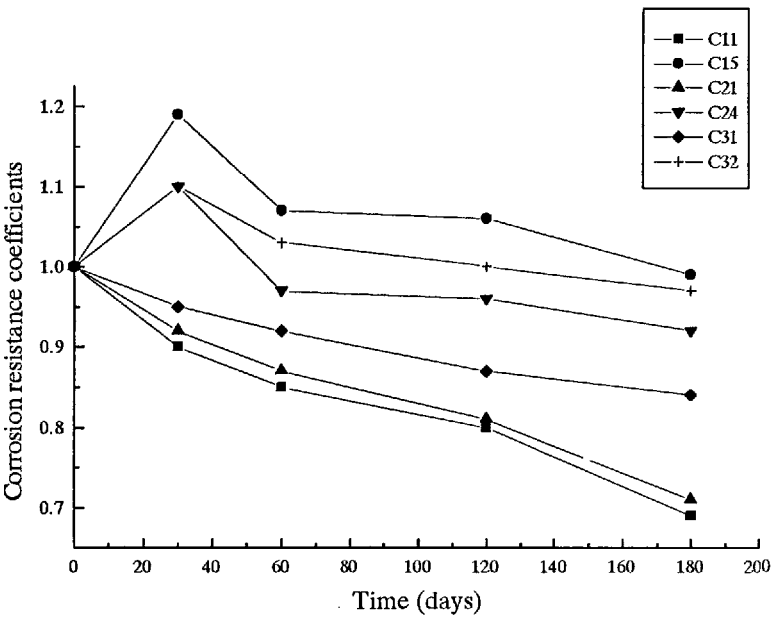

Figure 2. Corrosion resistance coefficients in solution II

Figs 1-3. presents coefficients of corrosion resistance of cements. From the diagrams, it can be clearly seen that cements with the addition of 30% of ash, show distinctly best characteristics in all the three aggressive solutions used. The increase of corrosion resistance in the very begining for all the cements is a normal phenomenon, because the formation of expansive compounds closes the pores and makes cement paste impervious to aggressive ions. However, further increase in the volume within the paste very quickly results in cracking.

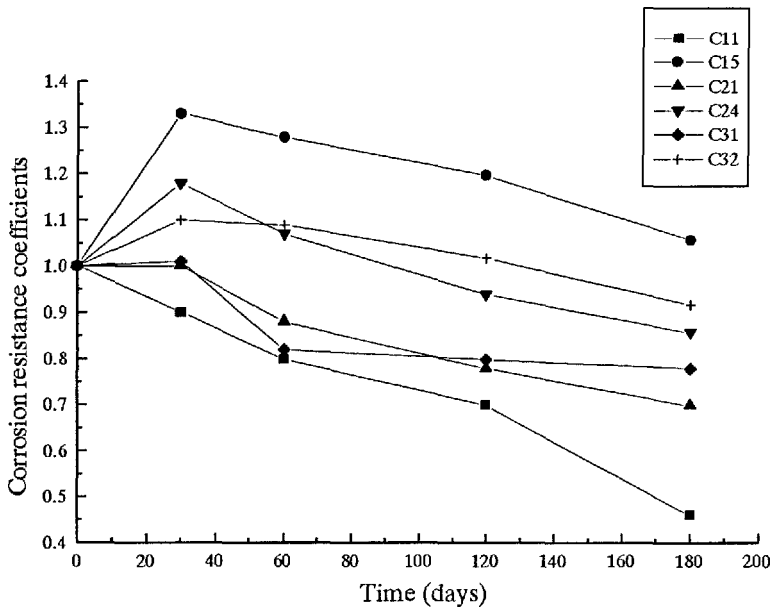

Figure 3. Corrosion resistance coefficients in solution III

The researches are evidently encouraging, because the addition of fly ash has pointed to realistic prospects for its positive effect. Therefore, cement C11 with the addition of ash (C15) shows very good resistance to the aggressive impact by sulphate solutions, although this cement is, due to its mineralogical composition, very unsuitable. When sulphate solutions of different cation compositions were compared, the ammonium sulphate solution showed considerably stronger effect than the corresponding sodium sulphate solution.

Adding fly ash to Portland cement C21, makes this cement become resistant to the sulphate aggressive environment. This is for both sodium sulphate and ammonium sulphate solutions. Adding fly ash to Portland cement C31, increases its durability in the solutions of sodium sulphate, used in this study, it also makes it resistant in the ammonium sulphate solution.

It is evident that the resistance of cement to sulphate aggression, regardless whether it concerns sodium sulphate solutions or ammonium sulphate solutions, is directly related to the content of C_3A in them.

CONCLUSION

On the basis of the tests done, following conclusions are drawn:

1. When comparing different sulphate solutions, it turns out that the aggressiveness of ammonium sulphate is of a higher degree than the solution of sodium sulphate.

2. The best resistance to sodium sulphate and ammonium sulphate solutions, was shown by cement with a lower content of tricalciumaluminate in clinker (C31), and especially by cements with the addition of fly ash, C15, C24 and C32.

3. The addition of fly ash to Portland cements was very efficient regarding their resistance to aggressive sulphate impact. The addition of ash in the quantity of 30% (replacement 30% of clinker with fly ash) improves to a considerable degree the durability of Portland cement to such influences.

4. Portland cements whose tricalciumaluminate content is high (C11 and C21), cannot be used even in the case of sulphate solutions with low concentration.

The above-cited testings of cements from the current production of the domestic cement industry, provided the basis for classification of these products regarding resistance to sulphate impact with various degrees of aggressiveness. This offers the possibility that in certain cases the ensuring of structures and their elements, which lie in contact with aggressive environment, be implemented by way of applying the selected cement with adequate composition and quality of concrete, thus avoiding special measures for protecting concrete by using expensive coatings, films and linings.

REFERENCES

Biczok, I.,"Concrete Corrosion, Concrete Protection", Eigth Edition, Budapest, 1972

Mehta, P.K., "Mechanism of Sulfate Attack on Portland Cement Concrete - Another Look", Cement and Concrete Research, Vol. 13, 1983, pp 39-51

Miletić, S., Ilić, M., "Sulphate corrosion of portland cement with various mineral compositions", Proc. of 15. Symposium Corrosion and Protection of Materials, Beograd, 1995, pp 255-262

Miletić, S., Ilić, M., "Cement stone corrosion in sulphate environment", NTP VJ, Vol 46, No. 3, 1996, pp 23-31

Miletić, S., Ilić, M., Ranogajec, J., Djurić, M., "Sulphate Corrosion of Portland Cement and Portland Cement Mixed With Fly Ash and Slag as a Function of its Composition", XVI Symposuim on Nordic Concrete Research, Helsinki, 1996

Mitrović, N., Dučić, V.,"Sulphate corrosion of concrete", Proc. of Yugoslav. Symposium, Split, 1985, pp 59-75

Moskvin, V.M., Ivanov, F.M., Alekseev, S.V., Guzeev, E.A., "Korozija betona i železobetona", Moskva, 1980

Ranogajec, J., Ilić, M., Miletić, S., Lazar, S., Milinković, Lj.,"Effect of sulphate and ammonium ions on the cement stone corrosion", Proc. of XX Congress JUDIMK, Cetinje, 1996, pp 97-102

Regourd, M., "Structure and Behaviour of Slag Portland Cement Hydrates", 7th Internacional Congress on the Chemistry of Cement, Vol. I ,1980, pp 278-291

Taylor, H.F.W., "Crystal Structure of Some Double Hydroxide Minerals", Mineralogical Mag., Vol. 39, 1973, pp 247-256

REACTION BETWEEN SIMULATED SULPHATE RADIOACTIVE LIQUID WASTE AND CEMENT BASED MATERIALS

Ana Mª GUERRERO, MªSoledad HERNANDEZ and Sara GOÑI. Institute of Construction Science Eduardo Torroja (CSIC). C/ Serrano Galvache, s/n 28033 Madrid, Spain.

ABSTRACT The durability of a specific backfilling pozzolanic cement mortar, which is employed in Spain, in concrete containers for the storage of low and medium level wastes (LLW) (MLW), has been studied by means of the Köch-Steinegger test at the temperature of 40°C during a period of 365 days. Mortar samples were immersed in a simulated radioactive liquid waste very rich in sulphate (0.68M), phosphate (0.89M) and chloride (0.51M) ions. The changes of the microstructure were followed by X-Ray Diffraction (XRD), Mercury Intrusion Porosimetry (MIP) and Scanning Electron Microscopy (SEM).

Key-words: Waste material utilization, sulphate attack, porosity, X-ray diffraction analysis, strength development.

INTRODUCTION

Studies on the durability of matrices made with the cement and the liquid radioactive wastes are numerous, specially those concerning leaching and diffusion of radioactive ions towards the biosphere (Rahman and Glasser, 1987, Komarneni and Roy, 1981, Macphee and Glasser, 1993, Hills et al., 1993, Glasser, 1992, Serne, 1989, Goñi et al., 1996, Hernández et al., Goñi et al., 1994, Guerrero et al., 1994, Hernández et al., 1996). But minor attention has been paid to the implications of the concentrated salts which accompanied the radioactive liquid wastes from the point of view of the durability of cement materials and concrete barriers employed in its storage (Li et al., 1996). Such concentrated solutions may contain a great amount of sulphate, phosphate, borate, chloride etc.. The aggressivity of sulphate to cement-based materials is well established, nevertheless, the degree of the attack depends to a great extension on the other accompanying ions. For example, the aggressivity of sulphate is lower in sea water, although its concentration is still sufficient to cause severe damage to concrete.

A very recent paper of Li et al. (Li et al., 1996) reported the formation of a new mineral designated "U" phase (a sodium substituted AFm phase, very aggressive), that only occurred in the simulated cemented low level wastes containing high amounts of Na_2SO_4 (10-15%). The authors pointed out that this phase can form only at very high alkali concentrations, not compatible with traditional cement paste. This phase transforms into ettringite when the alkalinity of the pore solution decreases for example by a water leaching process.

The present work deals with the durability of a pozzolanic backfill cement mortar (employed in Spain to assure the immobilization of the radioactive cemented matrices inside concrete containers), in a specific simulated radioactive liquid waste (SRLW), a mixture of sulphate (0.68M), phosphate (0.89M) and chloride (0.51M) ions. The study was carried out according to the Köch-Steinegger, (1960) test at the temperature of 40°C during a period of 365 days. The durability was evaluated from the changes of the flexural strength of the backfill mortar, immersed in the simulated solutions, which were compared with those obtained in similar samples immersed in deionized water. The changes of the microstructure were followed by X-Ray Diffraction (XRD), Mercury Intrusion Porosimetry (MIP) and Scanning Electron Microscopy (SEM).

EXPERIMENTAL

The backfill mortar was prepared at an aggregate to cement ratio of 1.75 and deionized water to cement ratio of 0.4. An organic additive was used at an additive to cement ratio of 0.012. The cement was pozzolanic (Spanish type IV) which is a mixture of Portland clinker (55%), pozzolanic fly ash (40%) and calcitic filler (5%). The chemical analyses of the cement components appear in Table 1.

Table 1 Chemical Analyses of the Pozzolanic Cement Components (% weight)

	I.L.	I.R.	SiO_2	Al_2O_3	Fe_2O_3	CaO	MgO	SO_3	Na_2O	K_2O
Clinker	0.20	-	21.6	2.64	4.2	66.8	1.68	2.05	0.13	0.50
Fly Ash	2.0	-	53.2	27.0	9.5	3.3	1.50	0.1	0.40	1.74
Filler	43.9	-	1.0	0.30	0.1	53.0	1.0	0.05	-	-

I.L. = ignition loss
I.R. = insoluble residue

In Fig. 1, the XRD analyses of both cement and aggregates are shown. The aggregates were a mixture of α-quartz and calcite. The percentage of calcite determined by thermogravimetric analyses, was 6%.

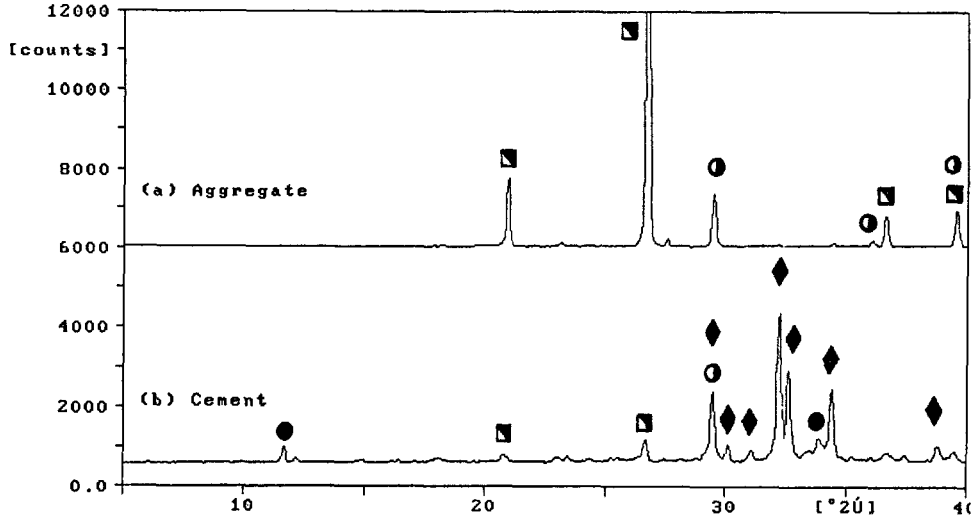

Figure 1 XRD patterns of cement and aggregate: ● C_4AF; ♦ C_3S; ◘ α-SiO_2; o Cc

After mixing, different portions were molded into 1 cm x 1 cm x 6 cm, specimens and compacted by vibration. After 1 day at 100% rh, the samples were demolded and cured in deionized water at 20°C ± 1 during 21 days. After this curing period, groups of 6 samples were immersed in the simulated radioactive liquid waste (SRLW) whose chemical composition is shown in Table 2. The samples were stored in sealed plastic bottles at the temperature of 40°C during a period of 365 days. The volume of SRLW was 800 ml per 6 samples. Similar groups of 6 samples were stored in deionized water as reference.

Table 2 Chemical composition of simulated radioactive liquid waste (g/l)

pH	Density (g/cc)	Na_2SO_4	NaH_2PO_4	Na_2HPO_4	$CaCl_2.6H_2O$	$FeCl_3.6H_2O$
5.5	1.2	96	30	60	8.8	39

X-ray diffraction patterns were recorded using a Philips PW-1730 diffractometer, graphite monochromator and Cu $K\alpha_1$ radiation. Porosity and pore-size distribution were investigated by mercury intrusion porosimetry carried out with a Micromeritics Pore Sizer 9310. SEM analysis was performed with a Jeol JSM 5400 microscope with an Oxford EDS microanalysis ISIS model. The samples were coated with C by sputtering.

RESULTS AND DISCUSSION

Flexural Strength Analysis

The flexural strength changes of the hydrated mortar immersed in deionized water and in the SRLW are shown in (Fig 2).

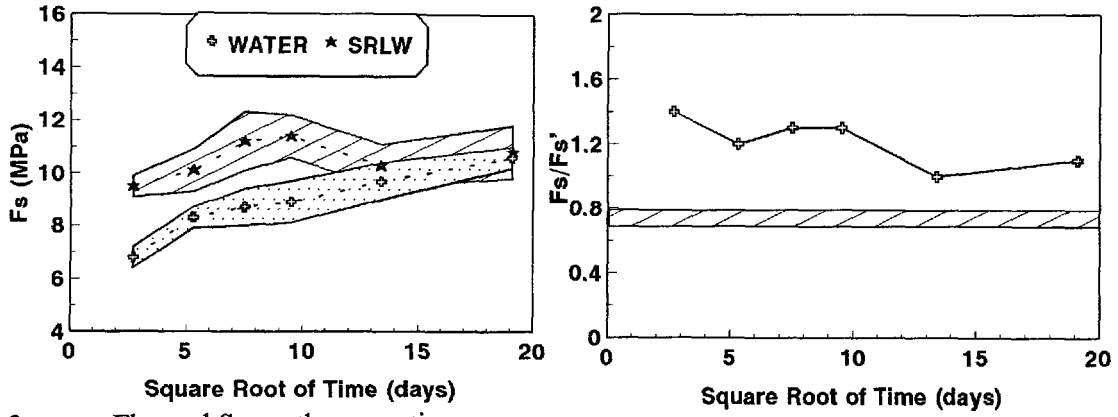

Figure 2 Flexural Strength versus time

Each value represents the average of 6 measurements; the dashed area is the standard deviation of the mean values. For the samples immersed in deionized water a remarkable increase of the flexural strength value is observed between 7 days and 28 days remaining afterward more or less constant. In contrast, the samples immersed in the SRLW during 7 days have a flexural strength value considerably higher than that of samples immersed in deionized water, progressively increasing during 90 days of immersion. The flexural strength starts decreasing thereafter up to the end of the experiment, when similar values independent of the medium are obtained.

The mechanical behaviour of the mortar immersed in deionized water could be related to the pozzolanic reaction of the flyash-cement which is activated at 40°C. Consequently, decreasing porosity of samples is associated with an increase of flexural strength.

The higher flexural strength values reached by the mortar samples, when immersed in the SRLW, could be due to the microstructural changes produced by the diffusion of ions and precipitation of new compounds, mainly of brushite type, within pores, as observed through XRD and SEM analyses. That precipitation process decreased the porosity causing a higher mechanical strength of the samples. According to the Köch-Steinegger test (Köch-Steinegger, 1960), the criterion to classify a material as durable in a specific aggressive medium is that the relative strength of aggressive-stored samples to water stored ones should be higher than 0.7-0.8. In all the cases, the relative strength is below the aforementioned threshold (Fig. 2).

X-Ray Diffraction Analysis

The main change detected for the samples immersed in deionized water is the decrease of the intensity of the portlandite ($Ca(OH)_2$) reflections, indicating the pozzolanic reaction of the fly ash-cement (Fig

3). In the case of samples immersed in the SRLW, new strong reflections appear after 7 days, which could be attributed to both brushite ($Ca(PO_3)(OH).\ 2H_2O$) and gypsum ($CaSO_4.\ 2H_2O$) (see Fig 3 (a)). The crystallographic similarities between gypsum and brushite, both compounds have a monoclinic structure with nearly identical cell dimensions, makes differentiation difficult (Beevers, 1958, Sakae et al., 1978).

The intensity of the reflections of those possible compounds strongly decreases after 90 days. Besides, the intensities of the portlandite reflections also strongly decrease. The ettringite reflections are very weak, but it seems that they slightly increase with time. These results indicate that phosphate and sulphate ions from the SRLW easily combine with Ca^{2+} ions. Nevertheless, brushite is not stable and dissolves over time as observed from SEM analysis, favouring the ingress of Na^+ and SO_4^{2-} ions, and increasing the porosity of the samples. This fact could explain the decrease of the flexural strength (see Fig 2). The intensity of the (001) reflection of portlandite at 18.0 2θ angular zone, is higher than the maximum intensity of the reflection at 34.1 2θ zone, which seems to show prefered orientation of the portlandite, as confirmed from SEM analyses.

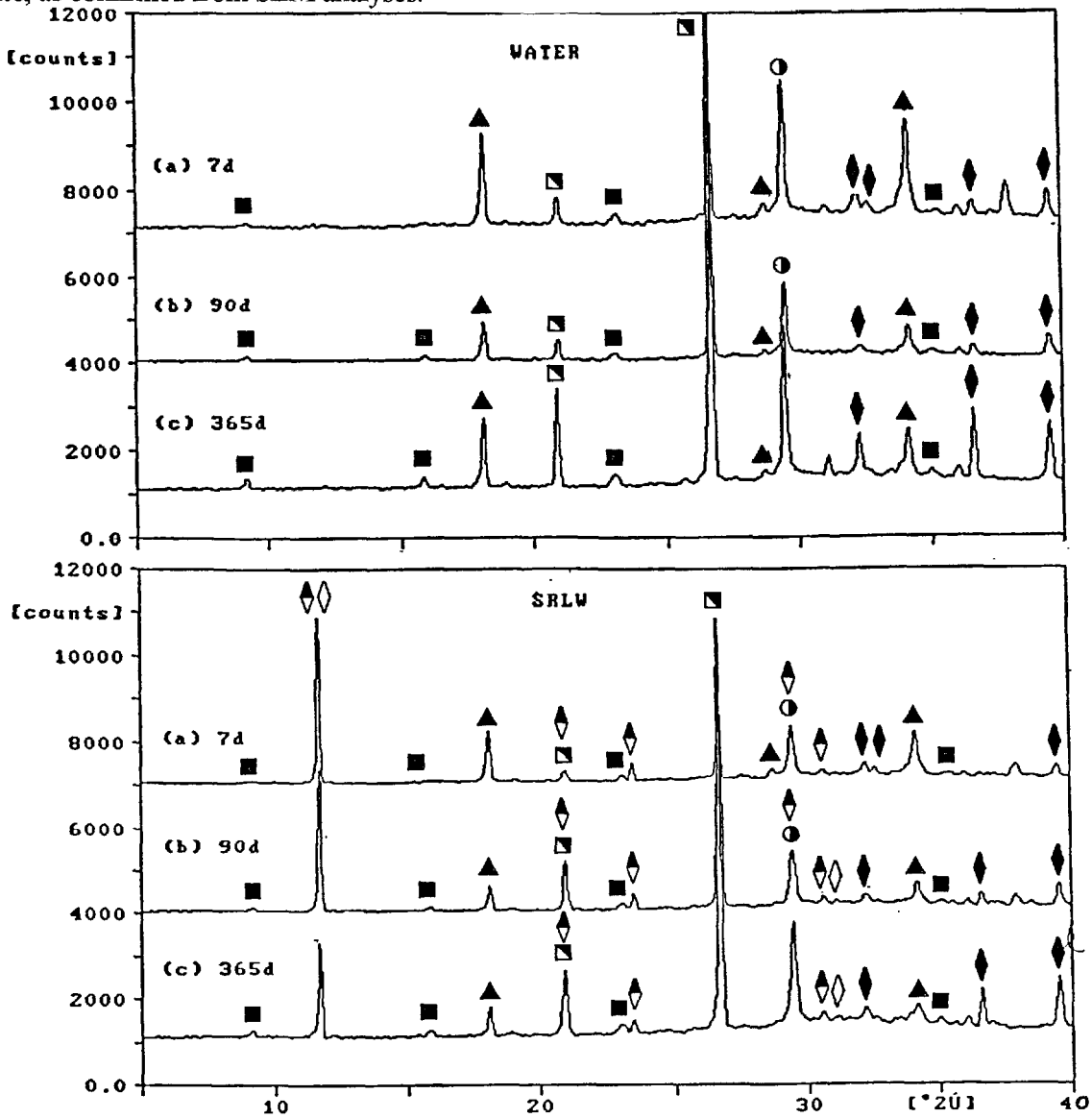

Figure 3 XRD results of the backfill mortar: ■ AF_t; ◪ SiO_2; ▲ CH; ♦ C_3S; ◊ $C\bar{S}H_2$; ○ $C\bar{C}$; ◈ $Ca(PO_3)(OH).2H_2O$

Porosity and Pore-Size Distribution Analysis

The pore-size distribution curves of mortar samples immersed in deionized water and in the SRLW are presented in (Fig 4). Cubes about 1 cm^3 were previously degasified under vacuum. As shown, the majority of pores have a diameter minor than 0.05 μm for samples immersed in deionized water. The total porosity decreased from 5.4% at 7 days to 3.0% after 365 days of immersion. For samples immersed in SRLW, the porosity decreased from 5.0% at 7 days to 4.4% at 365 days; nevertheless, the percentage of pores of diameter >0.05μm increased.

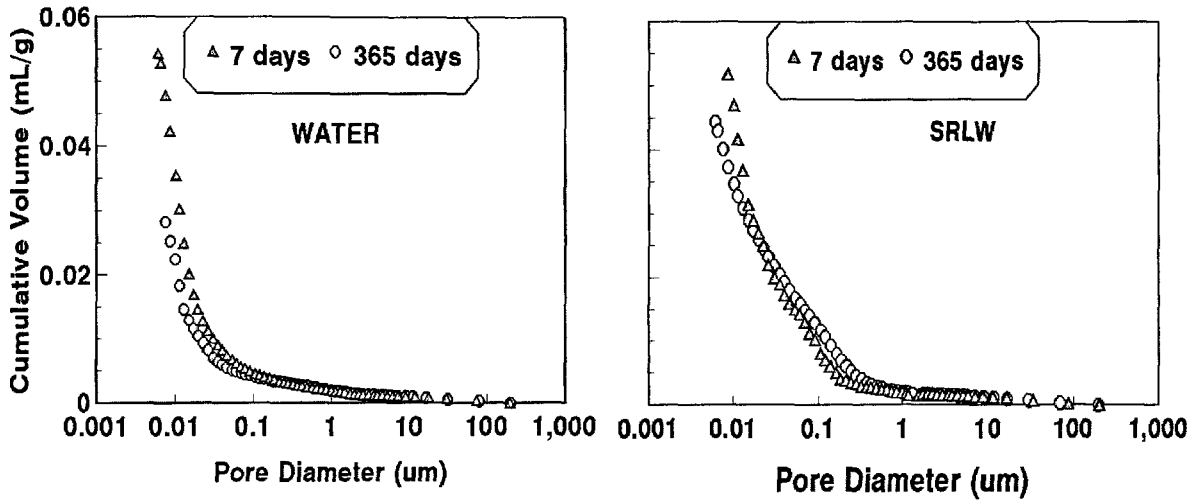

Figure 4 Pore size distribution curves of the backfill mortar

The main pore-size distribution changes for samples immersed in deionized water are produced in the range of pores of diameter < 0.05μm the volume of which strongly decrease between 7 days and 28 days (Fig 5).

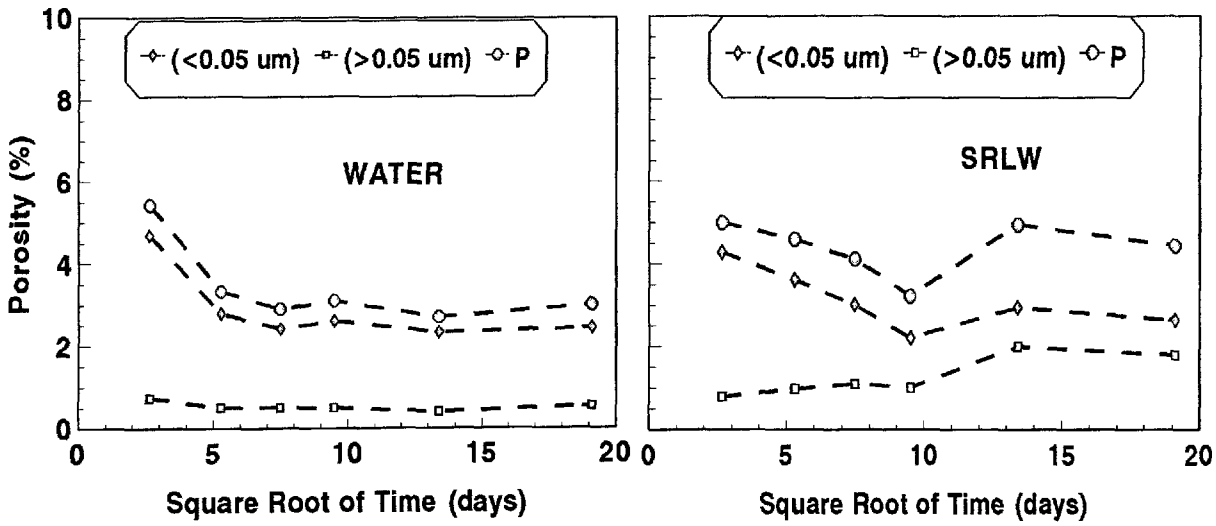

Figure 5 Percentage of pores of diameter > 0.05μm and < 0.05μm vs time

This is due to the pozzolanic reaction of the fly ash that generates hydrated calcium aluminate and silicate gels densifying the microstructure of the backfill mortar. When the mortar samples are immersed in SRLW, between 7 days and 90 days a progressive decrease is observed in the percentage of pores of diameter < 0.05μm. This could be related to the precipitation of brushite and gypsum within the pores. After 90 days an increase is observed, mainly in the percentage of pores of diameter

>0.05μm, which could be due to the dissolution of brushite and portlandite accompanying the decrease of the flexural strength (see Fig 2).

CONCLUSIONS

Despite of the high concentration of sulphate ion in the SRLW (0.68M), its potential aggressivity to the backfill mortar is avoided by the presence of phosphate ions. Phosphate ions easily combine with Ca^{2+} and OH^- from the pore solution forming brushite $Ca(PO_3)(OH).2H_2O$.

The external layer of brushite is very compact, impeding diffusion of sulphate and protecting the microstructure of the backfill mortar. Brushite is dissolved over time, increasing the porosity of the mortar, particularly pores of diameter >0.05μm. Consequently the diffusion of the ions; SO_4^{2-}, Na^+ and Cl^- was enhanced.

The flexural strength values of the backfill mortar are maintained below those of the samples immersed in deionized water throughout the experiment. Accordingly, the backfill mortar can be considered as a durable material in this specific simulated sulphated liquid waste.

In opinion of the authors, more extensive long term studies would be recommended, due to the partial dissolution of the protective brushite layer.

ACKNOWLEDGEMENTS

The authors gratefully acknowled the assistance of ENRESA (Empresa Nacional de Residuos, Sociedad Anónima) (Spain) for the financial support.

REFERENCES

Rahman, A.A. and Glasser, F.P., "Cements in Radioactive Waste Management, Characterization Requirements of Cement Products for Acceptance and Quality Assurance Purposes". Published by the Commission of the European Communities, Nuclear Science and Technology, EUR 10803 EN (1987).

Komarneni, S. and Roy, D.M., "Mechanisms of Immobilization of Nuclear Waste Elements by Cement Minerals, Cement and Mortar". Cem. and Concr. Res., Vol. 11, 1981, pp. 789-794.

Macphee, D.E. and Glasser, F.P., "Immobilization Science of Cement Systems". Mat. Res. Soc. Bull. XVIII; 1993, pp. 66-71.

Hills, C.D., Sollars, C.J. and Perry, R., "Ordinary Portland Cement Based Solidification of Toxic Wastes: The Role of OPC Reviewed". Cem. and Concr. Res., Vol. 23, 1993, pp. 196-212.

Glasser, F.P., "Progress in the Immobilization of Radioactive Wastes in Cement". Cem.and Concr. Res., Vol. 22, 1992, pp. 201-216.

Serne, R.J., "Grouted Waste Leach Tests: Pursuit of Mechanisms and Data for Long-Term Performance Assessment". Proceedings of Materials Research Society Symposium on Scientific Basis of Nuclear Waste Management XIII. Ed. V.M. Oversby and P.W. Brown: November 27-30, 1989, Boston, Vol. 176.

Goñi, S., Hernández, M.S., Guerrero, A. and Lorenzo, M.P., "Effect of Temperature on the Leaching Performance of Simulated Cement-Based Immobilization System. Calcium and Hydroxyl Behaviour". Construction and Building Materials, Vol.10, N°.3, 1996, pp. 171-177.

Hernández, M.S., Guerrero, A., Goñi, S. and Lorenzo, M.P., "Effect of the Temperature on the Leaching Performance of the Cement-Based Immobilization System. Sulfate and Chloride Behaviour" (to be published).

Goñi, S., Hernández, M.S. and Guerrero, A., "Effect of the Temperature on the Leaching of Cesium from Simulated Cement-Based Immobilization System". Proceedings of the III International Conference of ANQUE, Solid and Liquid Wastes: Their Best Destination (II), Puerto de la Cruz de Tenerife (Canary Island), Vol. 2, December 1994, pp. 455-464.

Guerrero, A., Goñi, S., Hernández, M.S. and Lorenzo, M.P., "Alkalinity of Cement-Based Materials and Their Confine Characteristics. Sodium and Potassium Leaching Behaviour". Proceedings of the III International Conference of ANQUE, Solid and Liquid Wastes: Their Best Destination (II), Puerto de la Cruz de Tenerife (Canary Island), Vol. 2, December 1994, pp. 465-474.

Hernández, M.S., Guerrero, A. and Goñi, S., " Pore Solution Composition of Simulated Borate Liquid Waste Cement Matrices. Changes Caused by Leaching at Different temperatures", Proceedings of Spectrum'96. Nuclear and Hazardous Waste Management International Topical. Washington, Vol. 1, August 1996, pp. 133-140 .

Li, G., Le Bescop, P. and Moranville, M., "The U Phase Formation in Cement-Based Systems Containing High Amounts of Na_2SO_4", Cem. Concr. Res., Vol. 26, N° 1, 1996, pp. 27-33.

Köch und H. Steinegger, A., "A Rapid Test for Cements for Their Behaviour Under Sulphate Attack", Zement-Kalk-Gips, 7, 1960, pp 317-324.

Beevers, C.A., "The Crystal Structure of Dicalcium Phosphate Dihydrate, $CaHPO_4.2H_2O$", Acta Crystallogr., 11, 1958, pp. 273-77.

Sakae, T, Nagata, H. and Sudo, T., "The Crystal Structure of Synthetic Calcium Phosphate.-Sulfate Hydrate, $Ca_2HPO_4SO_4.4H_2O$, and Its Relation to Brushite and Gypsum", Am, Mineral., 63, 1978, pp. 520-27.

MICROSTRUCTURAL INVESTIGATION OF CALCIUM ALUMINATE CEMENT CONCRETE FROM STRUCTURES

Karen L. SCRIVENER*, Matthew LEWIS, and Justine HOUGHTON
Imperial College, London, UK

ABSTRACT Three structures built from calcium aluminate cement were examined. Two of the structures were 60 years old, had w/c ratios around 0.6-0.7 and had been exposed to sea water. These exhibited a dense surface layer, containing a complex mixture of hydrates, extending some 5 cm into the concrete, then there was a gradual transition to a porous internal microstructure. The third structure, 25 years old, was made at w/c=0.4. This had a dense microstructure throughout, characterised by a fine distribution of C_3AH_6 and AH_3.

Key-words: Calcium aluminate cement, concrete, microstructure, structure, sea water

INTRODUCTION

Calcium aluminate cements (CACs) are made from limestone and bauxite and contain calcium mono aluminate, CA, as the principal reactive phase. These cements were originally developed at the beginning of the century in response to the need for cements which were durable under exposure to calcium sulfate solutions. The good performance of these cements in such conditions lead to their use in marine environments.

Calcium aluminate cements also came to be used for their rapid hardening qualities, the long term strength being achieved in as little as 6 to 8 hours. The long term strengths of CACs, due to the stable hydrates C_3AH_6 and AH_3, are similar, or somewhat lower, than those or Portland cement concretes at equivalent water/cement ratios. Transient high early strengths (>80 MPa) may be achieved in small sections cured at ambient temperatures, due to the formation of metastable hydrates (CAH_{10} & C_2AH_8). The inevitable transformation of these metastable hydrates to the stable ones with time is known as conversion. Design should be on the basis of converted strengths and current guidelines stress the importance of keeping the water/cement ratio below 0.4 and the cement content above 400 kg/m^3 to ensure adequate long term strength. In large sections the heat evolved during hydration will lead to self heating of the concrete to 70°C or higher, at such temperatures the stable hydrates are formed directly during hydration, so the material is converted from the beginning.

In the UK, in the early 1970s three catastrophic failures of prestressed roof beams made with calcium aluminate cement occurred. In only one of these cases was loss of strength due to conversion found to be a significant factors in the collapse, but consequently calcium aluminate cements have not been permitted for use in structural applications in many countries. Nevertheless, many structures of calcium aluminate cement concrete continue to exist and perform well, including around 50,000 prestressed structures in the UK.

The work presented here details a microstructural study of three structures from 25 to 60 years of age which have shown good durability. Two of these, built in the 1930s, Dagenham and Halifax, had water/cement ratios well in excess of the now recommended maximum and were exposed to sea-water, the other was built in 1969 to comply to the current guidelines. All of these structures are of such a size that significant self heating and immediate conversion would occurred during curing.

* present address, Lafarge, Laboratoire Central de Recherche, 95 rue du Montmurier 38291 St Quentin Fallavier, France.

STRUCTURES

Factory Piling's, Dagenham, UK

Calcium aluminate cement was chosen for this application due to sulfate contamination of the ground. Reinforced piles 0.4 m in diameter by 25 m in length were cast with mix proportions, cement:sand:aggregate of 1:2.5:4. The w/c ratio was not recorded, but to give an adequate slump for this mix is likely to have been around 0.6 and measurement from cores gave values of 0.65-0.8.

The rapid strength gain allowed the piles to be driven at an age of 24 hours. The piles originally supported a power station, this was recently demolished, but the piles are still in good condition. The cores were taken from a pile in contact with water from the adjacent Thames estuary.

Ocean pier, Halifax, Nova Scotia, Canada

This site is an ocean port, which experiences around 100 freeze/thaw cycles a year. CAC was chosen for the construction of hollow concrete cribs 32 × 16 × 16 m, which were then filled with gravel. The mix design was 1:2.28:3.35 (cement:sand:aggregate) and the w/c is estimated to have been 0.55-0.7.

The surfaces were sprayed with water during curing, but even so the surface temperatures were recorded as reaching 40°C, 8 hours after curing. The core examined in this study was taken from below the water line of the pier which is still in service today.

Bridge at cement factory, Frangey, France

Calcium aluminate cement was used for the construction of this bridge, which consists of a post tensioned deck (cement content of 500 kg/m3 and w/c = 0.32) and reinforced concrete piles with w/c of 0.4. The internal temperatures reached in trail blocks 2.6 × 1 × 1 m, cast in insulated form work were recorded at between 63 and 85°C. Cores were taken from both concrete types.

Further details of the mix design and construction of the field structures are given in George and Capmas (1994). Some results of the microstructural examination of the Dagenham sample are reported by Houghton and Scrivener (1994).

EXPERIMENTAL

For each structure sections were cut perpendicular to the surface, at the surface of the cores and near the end of the core furthest from the surface. The sections were resin impregnated and polished to ¼ μm with alumina grit and diamond paste. These polished sections were examined in a JEOL 35CF scanning electron microscope (SEM) in the backscattered electron (BSE) mode. The chemical composition of microstructural features was studied by energy dispersive spectroscopic (EDS) X-ray microanalyses. The porosity was measured by image analysis on 20 images at ×540 magnification.

RESULTS

Halifax and Dagenham

Due to the similarity between the microstructures of these samples they are presented together.

Examples of the interior microstructure of these samples are shown in Figure 1 and 2. Both have a very high porosity, which was measured as 14% and 15% for the Dagenham and Halifax samples respectively, nevertheless the cores were found to have a strengths of 17 - 22 MPa (Crammond 1992, Aitcin et al 1995). The relics of the original cement grains are still identifiable although most of the anhydrous phase have reacted. In some grains a reaction rim is visible surrounding still unreacted material (Fig. 1). Some remnants of iron containing phases

can be seen, identifiable by their bright appearance, but most of these phases have also reacted, which, by analogy with pastes hydrated at known temperatures, suggests a high temperature of hydration (Houghton and Scrivener 1994). The hydrates are very intermixed and difficult to analyse. However, three general types of hydrate could be identified: Dark isotropic areas, bright granular areas and regions of a platy phase. The dark isotropic areas were very high in alumina with varying lower amounts of other elements and are thus identified as AH_3 with other elements in solid solution or other phases intermixed. The analyses of the bright granular areas indicate hydrogarnet, C_3AH_6 although with indications of Si substitution. The compositions of the platy phases were very variable, with some analyses including chloride, in addition to calcium aluminium and silicon. The composition and morphology of these regions suggest they are intermixed AFm hydrates based on strättlingite (C_2ASH_8), Friedel's salt ($C_3A.CaCl.H_{12}$) and C_2AH_8.

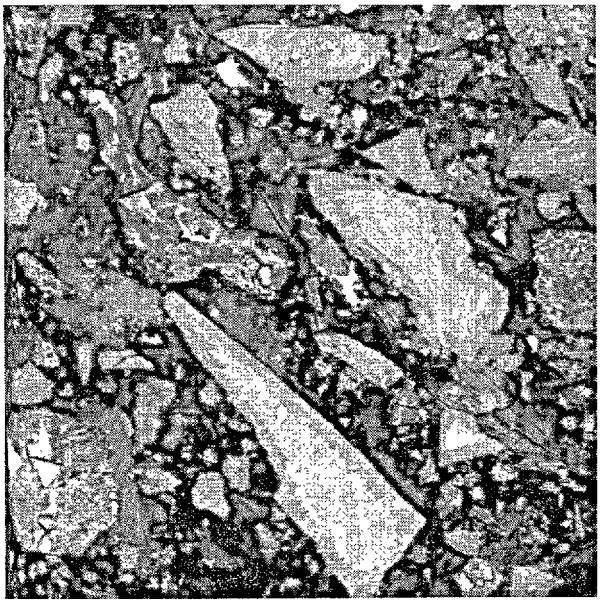

Fig. 1 Interior microstructure of core from Ford's Dagenham

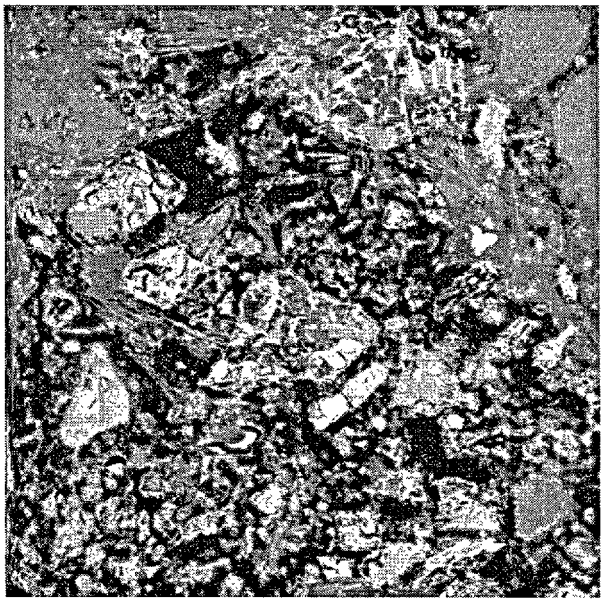

Fig 2. Interior microstructure of core from Halifax

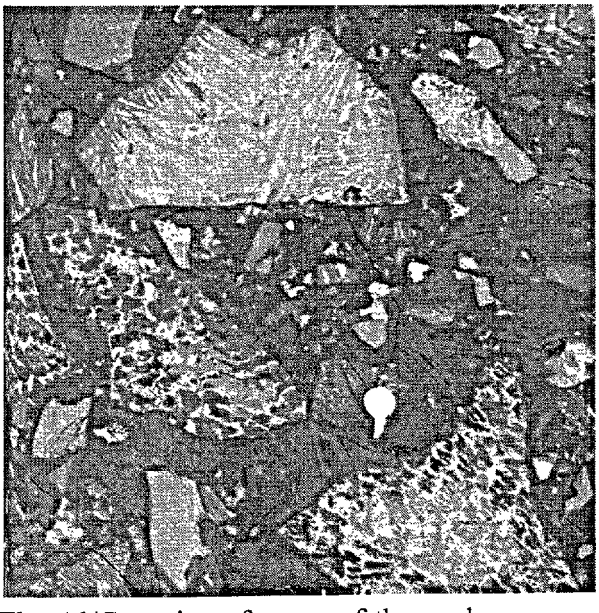

Fig. 3. Microstructure near surface of Dagenham sample

The microstructure near the surface of the sample from Dagenham is shown in Figure 3. It is immediately apparent that the level of porosity is much lower, this was measured as 1.7% by image analysis. The relics of the original cement grains are very clear and their appears to be little reaction of the iron containing phases. The matrix is filled with a darkish isotropic phases and a platy phase. As in the interior, the darker phases is very high in alumina, but here contains a significant concentration of chloride and some sulfate. The Al/Ca ratios of many of the analyses suggest the presence of CAH_{10} rather than AH_3. The

analyses of the platy phase again suggest intermixed AFm phases. The presence of metastable hydrates is unexpected, as significant heating, even at the surface would have been expected during the initial hydration. The metastable hydrates may have formed from the continuing reaction of the anhydrous phases at lower temperatures over time, or by reaction with ingressing ions, such as chloride, or sulfate, or a combination of the two processes.

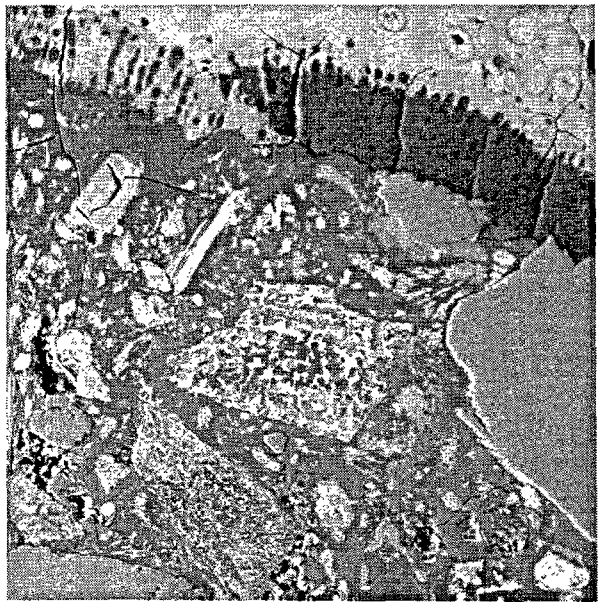

Fig. 4. Exterior microstructure of core from Halifax

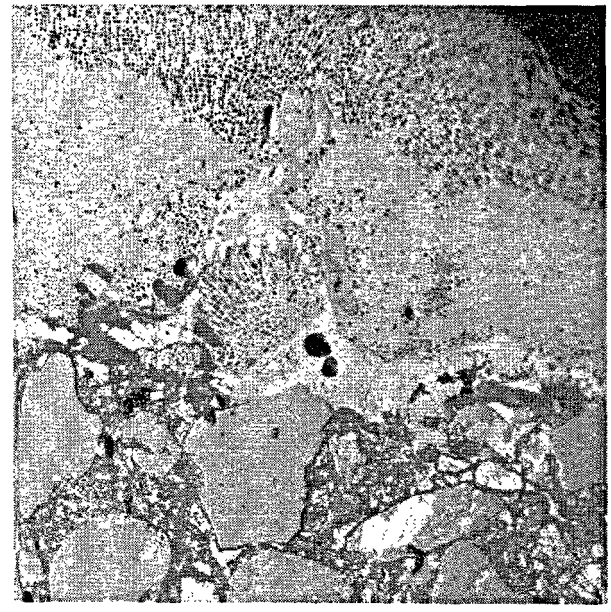

Fig 5. Exterior microstructure of core from Halifax

The microstructure at the surface of the Halifax core is shown in Figure 4 & 5. On the surface there are calcareous deposits from marine animals, directly below these, there is a layer of magnesium oxide, brucite, as has been found in Portland cement concretes exposed to seawater (Buenfeld 1986). Below the brucite layer the microstructure is similar to that of the Dagenham sample. There is a considerable amount of chloride in the analyses of the isotropic phase, which varies with depth as shown in figure 6.

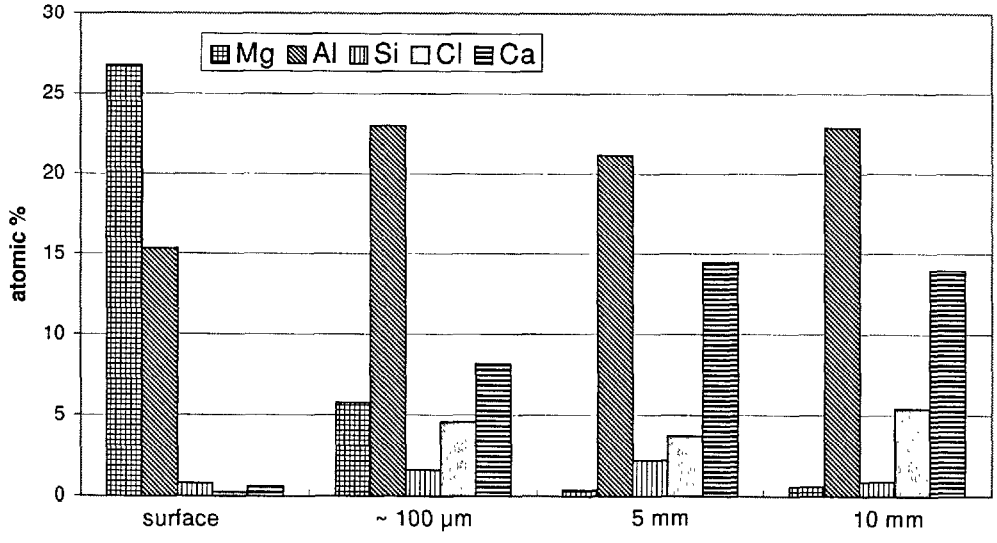

Figure 6. Average analyses of matrix isotropic phase at different depths for the Halifax sample.

The examination of both these samples shows a considerable variation of the microstructure with depth. In both a dense layer is present at the surface. The different properties of this surface region have been confirmed by measurements of O_2 permeability (Dunster 1995), which found the permeability of the surface 50 mm to be almost two orders of magnitude lower than that of the interior. The rapid decrease in chloride and sulfate concentrations reported in the same paper, suggest that this dense surface layer has played a significant role in the good durability of these structures.

Frangey Bridge

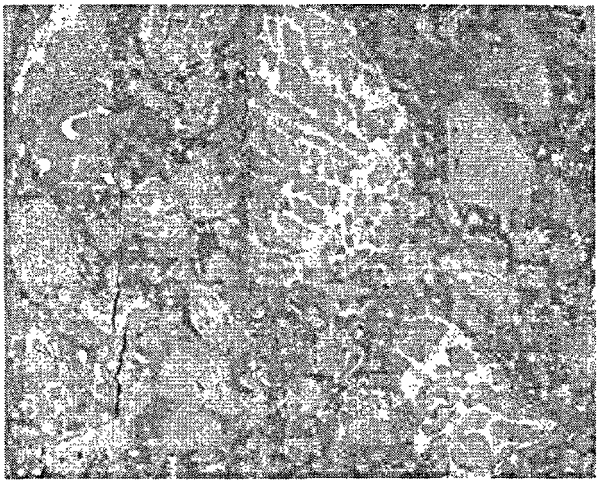

Fig. 7. Microstructure of near surface of Frangey core, column

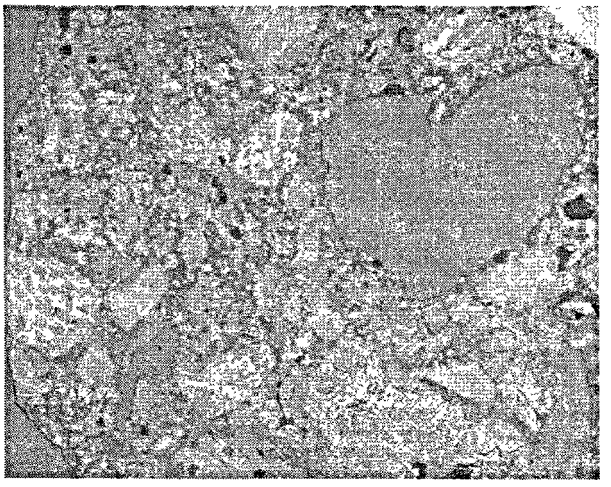

Fig 8. Microstructure 10 mm from surface

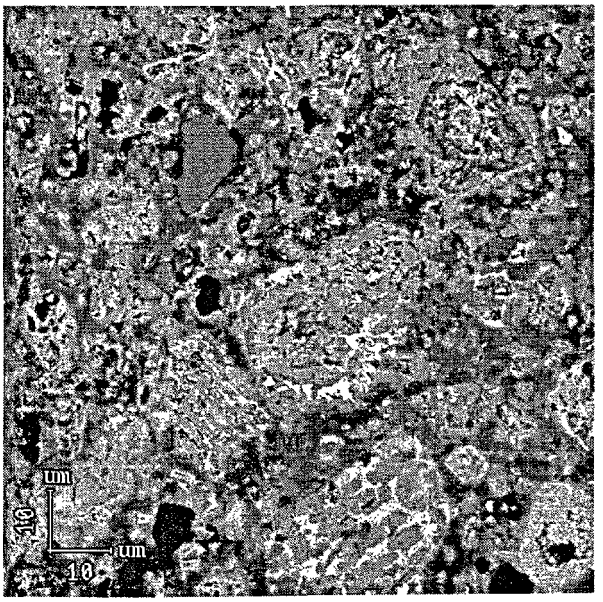

Fig. 9. Microstructure of interior of core from Frangey



Fig 10. Microstructure of interior at higher magnification

Figures 7 to 10 show the microstructure of the Frangey sample at various depths. The images shown are from the reinforced concrete column, although those from the prestressed bridge deck are very similar.

Unlike the two earlier samples with a relatively high w/c ratio, in these samples, with w/c<0.4, there was little noticeable difference between the surface and interior microstructures. All are very dense, the porosity level of the interior sample being measured at 2% by image analysis. The matrix consists of a finely divided mixture of a brighter, granular phase in a darker matrix (Figure 10). Microanalyses clearly indicated that these phases were C_3AH_6 and AH_3 respectively, although the scale of intermixing was too fine for accurate analyses to be obtained for either phase. Although the microstructures are very similar, the sequence of Figure 7-9 moving in from the surface, indicates that there is more reaction of the iron containing phases with greater depths, probably corresponding to greater maximum temperatures.

The O_2 permeabilities were measured at $0.1\text{-}0.7\times10^{-17}m^2$ (Dunster 1995) and the compressive strengths at 48-63 MPa (Marcdargent 1995). There was no clear difference between the two qualities of concrete for the bridge deck and the piles in terms of strength or permeability.

GENERAL DISCUSSION

The three structures examined in this study provide examples of good durability of CAC concrete. The two older samples were made at w/c well in excess of the current guidelines and the interior of these samples is very porous. However, the formation of a dense surface layer appears to be responsible for the relatively low penetration of chloride and sulfate ions over 60 years. This dense surface layer appear to contain 'unconverted' hydrates, which may be stabilised by the ingressing ions or by the low temperatures of exposure.

The third structure, made in accordance with present guidelines has a dense microstructure throughout, consisting of stable 'converted' hydrates. This converted microstructure almost certainly formed during the initial period of curing, due to the high degree of self heating.

As observed for pastes hydrated at different temperatures (Houghton and Scrivener 1994, Houghton 1996) the degree of reaction of the iron containing phases appears to increase at higher temperature, as experienced within concretes of large section.

REFERENCES

Aitcin, P. C., Blais, F. & George, C.M., "Durability of Calcium Aluminate Cement Concrete: Assessment of Concrete From Structure at Halifax, NS, Canada", Advances in Concrete Technology, Proceedings of 2nd CANMET/ACI Intl. Symp., Las Vegas, USA, June 11-14, SP-154-24, 1995.

Buenfeld, N.R., Newman, J.B., "The Development and Stability of surface layers on concretes exposed to sea water", Concrete and Cement Research, Vol 16, 5, pp 721-732, 1986.

Capmas, A., George, M., "Durability of Calcium Aluminate Cement Concretes", Advances in Cement and Concrete, ed M. Gruteck and S. Saker, Eng. Found, pp 377-405, 1994.

Crammond, N., Test Report, Building Research Establishment, UK, 1992.

Dunster, A., O_2 permeability test results, private communication, 1995.

Houghton, S.J., Scrivener, K.L., "A Microstructural Study of a 60 year old Calcium Aluminate Cement Concrete", Durability of Concrete CANMET/ACI Nice, France, June 1994.

Houghton, S.J., "Hydration and Durability of Calcium Aluminate Cements", PhD thesis, University of London, 1996.

Mardargent, S., Compressive strength results, Lafarge Aluminates, 1995.

ALKALINE HYDROLYSIS WITH CARBONATION IN HIGH ALUMINA CEMENT CONCRETE BEAMS

Andrew M DUNSTER and Norah J CRAMMOND
Building Research Establishment, Garston, Watford, WD2 7JR, UK.

ABSTRACT The authors have investigated a case of suspected alkaline hydrolysis with carbonation in a building constructed during the 1960's. Samples were analysed chemically and examined using optical and electron microscopy. The beams in locations with evidence of water penetration showed signs of deterioration at the lower (soffit) surfaces. The deteriorated samples contained granular carbonates and needle-like gibbsite in voids, giving a microstructure which was quite distinct from that normally associated with atmospheric carbonation.

Key words: Calcium aluminate cement, carbonation, chemical attack, durability

INTRODUCTION

Concrete made from High alumina cement (HAC), also known as calcium aluminate cement, was used extensively in the UK from the 1950's to the early 1970's in the manufacture of precast, prestressed concrete beams. Although the importance of carbonation in such concretes has been highlighted by BRE in recent years (Crammond and Currie, 1993), chemical attack under damp conditions, as reported in the present paper, is less common.

Alkaline hydrolysis with carbonation is a form of carbonation in which sodium and/or potassium salt solutions interact with atmospheric carbon dioxide (Taylor, 1990) to attack the hydrated calcium aluminates in the hydrated cement to form calcium carbonate and hydrated alumina. When alkaline hydrolysis with carbonation takes place there is a total lack of cohesion of the bonding cement paste, and the binder crumbles to a powder. This means that part of the concrete loses all strength. Although the interior of the concrete has not lost strength, there is still potential for it to do so as the depth of the cover concrete is progressively reduced. The usual representation of the reactions is given by the action of alkali carbonate on the hydrated calcium aluminates to give hydrated alumina and calcium carbonate. For C_3AH_6, the overall reaction may be represented as:

$$3CaO.Al_2O_3.6H_2O + 3CO_2 \xrightarrow{K_2CO_3 \text{ or } Na_2CO_3} 3\,CaCO_3 + Al_2O_3.\,3\,H_2O + 3\,H_2O \qquad (1)$$

It is important to realise that normal carbonation in HAC concrete in the absence of alkalis also produces $CaCO_3$ and $Al_2O_3.\,3\,H_2O$ (AH_3) as the final reaction products, although this is accompanied by an increase in strength (Raask, 1976). Alkaline hydrolysis with carbonation is relatively rare in practice and only a few cases have been identified by BRE.

The authors have investigated a case of alkaline hydrolysis with carbonation in the chemistry laboratories of a two-storey school building constructed during the 1960's. The building frame supports the flat roof of the building. There is also a suspended false ceiling. Together, the roof and false ceiling form the ceiling for the laboratories. The roof construction comprises precast HAC concrete 'T' beams, woodwool slabs and roof covering (Fig 1). There had been a history of water ingress due to roof leakage which had been remedied in the early 1990's. A routine visual inspection of the underside of the roof structure in early 1995 had revealed degradation of the

cement paste matrix on the underside (soffit) of one of the beams (Fig 1). This gave the building owners cause for concern and a detailed investigation involving BRE's Materials Diagnostic Unit was therefore initiated.

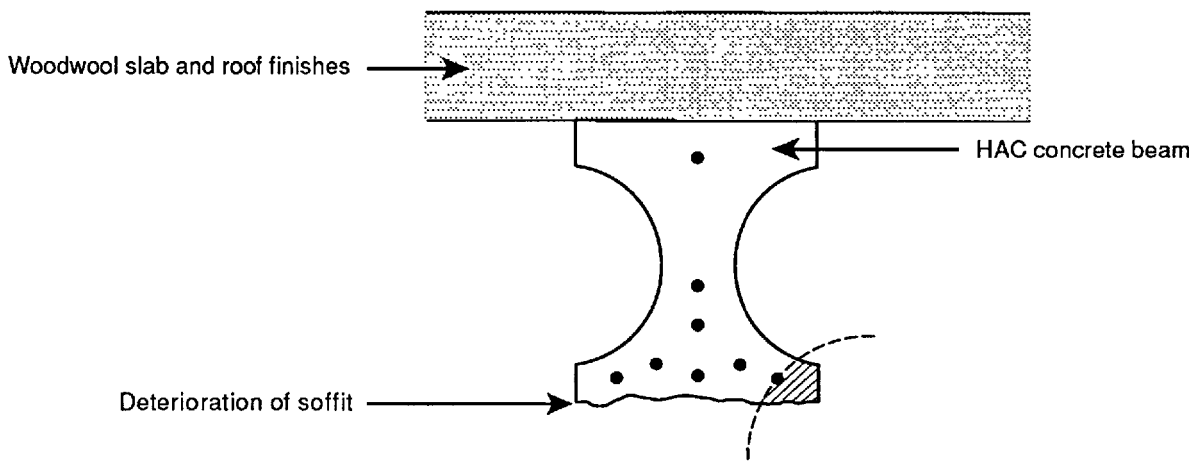

Figure 1: Diagram of roof construction. Shaded area indicates position of lump sample

Table 1: List of sampling locations

sample locations	type of sample collected*	Location
1	L and S	Laboratory A, beside rainwater pipe at location showing evidence of water penetration and deterioration of concrete surface.
2	L	Laboratory B, beside a rainwater pipe at location showing evidence of water penetration and deterioration of concrete surface.
3	L and S	Laboratory B, from a location showing evidence of water penetration and surface deterioration.
4	L and S	Laboratory A, adjacent to water pipe at location showing evidence of water penetration and surface deterioration. Mortar-like material was present adjacent to this sample.
5	L	Laboratory A. No evidence of deterioration or water leakage.
6	L	Corridor outside Laboratory A. No evidence of deterioration or water leakage.

* : concrete lump (L); scraping or mortar-like lump (S)

Table 2: Allocation of samples for materials analysis

sample location	Sample number			
	Optical microscopy	electron microscopy	chemical analysis	X-ray diffraction and thermal analysis
wet areas	1(L), 3(L), 4(L),	1(L), 3(L),	2(L), 3(L)	3(L)
			1(S), 3(S)	1(S), 3(S), 4(S)
dry areas (control)	5(L)	5(L), 6(L)	5(L), 6(L)	6(L)

SAMPLING AND MATERIALS ANALYSIS

Sampling

The more detailed phase of visual inspection was accompanied by the collection of lump samples from the HAC concrete for materials analysis (Table 2). Lump samples of concrete were collected from the soffits of four beams in areas of the roof where staining of the ceiling tiles and supporting frame provided evidence of water entry. Two "control" samples were collected from beams in one of the laboratories and in an adjacent corridor where there was no evidence of water penetration. Several additional lumps of mortar-like material and scrapings of soft material were also collected at some locations adjacent to the main concrete lump samples. The sampling locations are numbered from 1 to 6. Concrete lump samples have been designated by the suffix "L", mortar-like lumps or scrapings by "S". Visual signs of deterioration on the surface of the concrete were invariably restricted to those areas of the building showing evidence of water penetration. The erosion of material was limited to the soffit surfaces of the beams (approx. 1 mm to 2 mm depth) and in the majority of cases, the bulk was relatively hard and dense. On one of the beams, however, a soft sandy material (immediately adjacent to concrete lump sample 4) was present in a discrete narrow area surrounded by normal dense concrete. This observation, which is consistent with a mortar having been applied to the surface of the beam at some locations, was pursued in the subsequent laboratory investigations.

Materials Analysis

The samples were examined in BRE's laboratories using optical microscopy (to establish the extent of chemical attack) and chemical analysis (Table 1). Differential Scanning Calorimetry (DSC) and X-ray diffraction (XRD) were carried out on selected samples to check for the products of alkaline hydrolysis with carbonation. Several of the thin sections which were examined optically were polished, gold coated, and examined under the scanning electron microscope (SEM).

Samples were analysed chemically for total alkalis (sodium and potassium) by nitric acid extract and flame emission to check for alkaline hydrolysis with carbonation. Alumina was determined to establish cement content as well as total sulphate by LECO carbon sulphur analyser to check for sulphate attack. In these tests, a ratio of alumina to total equivalent alkalis of much less than 70, together with visual evidence of surface deterioration would indicate that a concrete has suffered alkaline hydrolysis with carbonation (BRE, 1994). Sulphate levels above the 0.2 % SO_3 normally present in HAC would imply ingress of sulphate from a source external to the cement.

RESULTS OF MICROSTRUCTURAL EXAMINATION AND CHEMICAL ANALYSIS

Undeteriorated beams

The samples 5(L) and 6(L), taken from nominally dry areas, showed the presence of dense calcium carbonate under the optical microscope. There were no signs of disruptive chemical attack or other forms of deterioration. There was, however, evidence from optical microscopy of a thin crust (< 200 microns thickness) of sulphate minerals on the soffit of both these beams and this was confirmed by electron microscopy.

The presence of sulphates in these nominally dry areas was surprising as migration of external sulphates from adjacent Portland cement materials in the absence of water would be unlikely. The presence of sulphates implies that some minor moisture movement and mobilisation of sulphates have occurred, possibly as a result of less severe dampness or water penetration than that which affected the deteriorated beams. There was no evidence for the use of repair mortar on these beams.

Deteriorated beams

In the deteriorated beams (sample locations 1 to 4, in areas of obvious roof leakage), the soffits of the beams had typically lost some of the cement paste matrix and were heavily eroded. Optical microscopy revealed granular calcium carbonate and needle-like crystals of AH_3 in voids (these were initially misidentified as gypsum which has a similar appearance optically). The open microstructure was thus distinctly different to the dense matrix associated with normal atmospheric carbonation . In addition, sulphate minerals (ettringite and gypsum) were present in cracks and voids or they formed a crust on the surface. The presence of needle-shaped crystals of secondary AH_3 was confirmed using SEM in combination with X-ray microanalysis. These needles were commonly associated with granular recrytallized calcite which had a "feathered" appearance (Fig 2). It is significant that the AH_3 in the apparently unaltered portion of the HAC

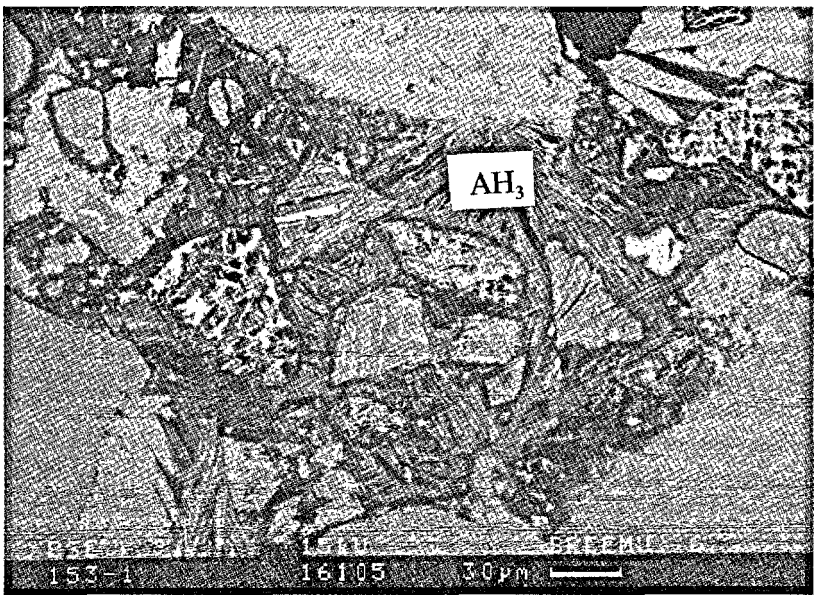

Figure 2 Electron micrograph showing needle like crystals of AH_3 (scale bar, 30 microns)

concrete was not needle-shaped. This implies that the needle-like AH_3 found in the deteriorated samples is a product of alkaline hydrolysis with carbonation.

In the deteriorated samples analysed chemically (samples 1 to 3), the ratios of alumina to total equivalent alkalis (Table 3) were well below the lower limit of 70 stipulated by BRE as an indicator of alkaline hydrolysis with carbonation (BRE 1994). This confirmed the presence of alkaline hydrolysis with carbonation. The high total sulphate values (in excess of 0.6% by weight of cement) in these samples implied that sulphates may also be involved in the deterioration. However, there was no evidence of disruption or cracking caused by sulphate attack and any sulphate minerals (ettringite and gypsum) were restricted to infilling voids or forming a crust on the surface.

RESULTS OF X-RAY DIFFRACTION AND THERMAL ANALYSIS

XRD (Table 4) showed that the unaffected beams contained two polymorphs of AH_3 (gibbsite with traces of bayerite) and that calcium carbonate was present predominantly as aragonite and vaterite with only traces of calcite. Similarly, the affected beams also contained AH_3 but as gibbsite with subordinate nordstrandite. Calcite as well as vaterite and aragonite were also present.

In all the samples examined (affected as well as unaffected), DSC clearly showed the presence of a strong AH_3 endotherm (approx. 250 to 270 °C). Smaller endotherms at approx. 110 °C and 150-170 °C were attributed to CAH_{10} and C_2AH_8 respectively. In all samples the absence of C_3AH_6 (which typically gives a distinct exotherm at approx. 300 to 310 °C) was confirmed by

Table 3: Results of chemical analysis (three concrete lump samples, two friable samples)

sample No.	sample type	location and environment (wet or dry)	Visual evidence of surface deterioration ?	Alumina/ equiv alkalis	SO_3 (% by wt of cement)
1(S)	sandy or loose material	laboratory (w)	yes	10	1.81
3(S)		laboratory (w)	yes	5	1.62
2(L)	concrete lump sample	laboratory (w)	yes	16	0.69
5(L)	concrete lump sample from unaffected beams (control)	laboratory (d)	no	53	0.28
6(L)		corridor (d)	no	64	1.09

Table 4 : Principal phases detected by DSC and XRD

Sample (and environment from Tables 2 and 3)	CAH_{10}	C_2AH_8	C_3AH_6	AH_3			$CaCO_3$		
				(G)*	(B)*	(N)*	(C)*	(V)*	(A)*
1(S) (mortar-like lump) (w)	✓	✓	x	✓			nd		
3(S) (at soffit surface) (w)	nd	✓ tr	x	x	x	x	✓	x	x
3(L) (at depth) (w)	✓	✓	x	✓	x	✓	✓	✓	✓
4(S) (suspected mortar) (w)	✓	✓	x	✓			nd		
6(L) (unaffected)(d)	✓	✓	x	✓	✓	x	tr	✓	✓

* G = Gibbsite, B = Bayerite, N = Nordstrandite, C = Calcite, V = Vaterite, A = Aragonite.
✓ = present, x = not detected, tr = trace, nd = not determined.

XRD. There were no significant differences between the DSC thermograms of the undeteriorated sub-sample (which was highly carbonated) and the thermograms of beams affected by alkaline hydrolysis with carbonation. The results imply that the stable hydrate C_3AH_6 in these samples has been degraded by normal atmospheric carbonation, alkaline hydrolysis with carbonation, or by a combination of the two, with a small residue of meta-stable CAH_{10} remaining uncarbonated. The presence of CAH_{10} also shows that even after some 30 years complete conversion of the hydrate phases had not been achieved.

The sample of mortar-like powder scraped from the soft area of the soffit (sample 4(S)) contained principally sand with a very low cement content and was shown to contain HAC using DSC. There was no evidence for the presence of sulphate minerals.

DISCUSSION

In the presence of alkalis and excessive and persistent penetrating water, progressive deterioration of HAC concrete is possible due to alkaline hydrolysis with carbonation. In this instance it appeared that there were three main ingredients involved in the deterioration: alkalis derived from Portland cement, possibly in the roof screed but more likely binding the woodwool slabs; sulphates (also derived from Portland cement); and finally leaks around roof outlet gullies providing the water. Erosion of the cement paste, and consequent loss of material from the soffits of beams in the deteriorated areas, made it difficult to diagnose the exact role of the alkalis and the part played by the sulphates (if any) in the deterioration process. However, visual and microscopic examinations together with chemical analysis proved that the beams in areas of obvious water penetration had been attacked locally at the surface by alkaline hydrolysis with carbonation. This attack was associated with deposition of sulphates in the voids which formed as a result of degradation of the cement paste. It is unclear, however, if the sulphates contributed

to the deterioration or if they were only deposited in the cracks and voids created by alkaline hydrolysis with carbonation.

Investigations of other buildings by BRE have shown that the presence of high alkali levels and moisture does not inevitably lead to alkaline hydrolysis with carbonation. Several cases have been identified where, in the presence of high alkalis and dampness or moisture, disruptive alkaline hydrolysis with carbonation of HAC concrete has not occurred. Laboratory studies currently in progress by the authors (unpublished) have shown that progressive erosion of HAC concrete surfaces can occur due to alkaline hydrolysis with carbonation if very wet alkaline conditions are allowed to persist over a period of several months. In good quality concretes, however, the rate of deterioration appears to be low. The presence of "mortar-like" material on one of the beams examined in the present study provides evidence that a relatively poor quality repair mortar may have been applied in the precasting factory to fill voids, etc. This would provide an explanation for the severity of attack at the soffits since mortar would be more porous, and thus more readily attacked, than the dense HAC concrete which appears to be in a good condition.

CONCLUSIONS

The HAC concrete beams, examined in locations which had been subjected to penetrating water, have shown evidence of deterioration at the soffit surfaces due to alkaline hydrolysis with carbonation. Alkalis for the reaction have probably been provided by prolonged roof leakage through the overlying woodwool slabs. Sulphates, which may also be involved, may have been derived by leaching from adjacent Portland cement-based materials or from a repair mortar applied at the surface. The presence of a mortar would provide an explanation for the severity of attack at the soffits since mortar would be more porous, and thus more readily attacked, than dense HAC concrete. Prolonged water leakage in combination with poor quality concrete appear to be prerequisites for damaging alkaline hydrolysis with carbonation and this may explain why cases are relatively rare in the UK.

Both alkaline hydrolysis with carbonation and normal atmospheric carbonation in HAC concrete produce AH_3 and $CaCO_3$ as the principal reaction products. However, each produces a distinctly different microstructure.

ACKNOWLEDGEMENTS

The authors wish to acknowledge Kelvin Pettifer, Simon Lane, David Rayment, Mike Bowley and Freda Halliwell of BRE for help with the microscopy and chemical analysis.

REFERENCES

Building Research Establishment Digest 392. "Assessment of existing high alumina cement concrete in the UK" March 1994.

Crammond, N.J, and Currie, R.J, "Survey of condition of precast HAC concrete components in 14 existing buildings". Mag.Concr. Res. Vol 45, No. 165, 1993. pp 275-279.

Raask, E. RILEM Int. Symp. Carbonation of concrete. Wexham. 1976.

Taylor, H.F.W, Cement Chemistry, Academic Press (London), 1990.

BEHAVIOUR OF THE PASTE RICH IN HYDROGARNET AND GIBBSITE IN CHLORIDE SOLUTION

Wiesław KURDOWSKI, Sylwester DUSZAK, Barbara TRYBALSKA
University of Mining and Metallurgy, Kraków, Poland

ABSTRACT

Paste composed mainly of gibbsite and C_3AH_6 was immersed in the solutions of $MgCl_2$ (150 g/l), $CaCl_2$ (175 g/l) and salt mine water (164 g/l $CaCl_2$ and 272 g/l $MgCl_2$). After several days of immersion the X-ray and SEM analysis showed the diminution of the hydrogarnet phase with the formation of Friedel salt and basic magnesium chloride in case of solutions containing $MgCl_2$. The presence of basic calcium chloride was also confirmed in salt mine water. In all solutions the samples revealed expansion which, however, was considerably lower in the $CaCl_2$ solution.

Key words: aluminate phase, chloride, corrosion, Friedel's salt, high alumina cements,

INTRODUCTION

The corrosion of the cement paste in chloride solution is not fully understood, and only few papers are devoted to the investigation of the phenomena connected with the reaction of chlorides with the cement paste (Smolczyk, 1968, Chatterji, 1978, Monosi et al., 1989, Conjeaud, 1982, Riedel, 1973 and Suzukawa, 1980). Nevertheless the problem is very important, not only with respect to concrete used in the underground salt mine but also for the durability of the containers for hazardous waste deposition and, finally, with the action of de-icing salts on concrete pavements.

For several years in our laboratory we have been investigating the corrosion of cement paste in strong chloride solutions (Kurdowski et al., 1989, 1990, 1994a and 1994b). Out of different types of cement examined, the best durability was presented by HAC and slag cement, activated with sodium salts (Kurdowski et al., 1990 and 1994b).

To obtain further information about the corrosion of calcium aluminate a special paste was prepared which contained mainly gibbsite and, in smaller quantities, hydrogarnet C_3AH_6. This paste was immersed in three different chloride solutions and the process of corrosion followed. The paper describes the results of these investigations.

MATERIAL AND METHODS

In order to obtain the paste rich in $Al(OH)_3$ a pure CA_2 phase were used. This phase was prepared by burning the mixture of suitable stechiometry of calcium carbonate and alumina hydroxide, both pure AR materials. CA_2 during reaction with water will give the paste rich in AH_3, namely:

$$3CA_2 + 21H_2O \longrightarrow C_3AH_6 + 10\,AH_3 \qquad [1]$$

The calcium aluminate CA_2 reacts very slowly with water and in order to accelerate this reaction and to obtain pure hydrogarnet (without admixtures of other calcium aluminate hydrates), the hydration was carried out in the saturated water vapour at the temperature of 80°C. The paste was made at w/c ratio of 0.54, from the ground powder of CA_2 of which small prism elements with dimensions 10×10×80 mm were prepared. These prism elements were then submitted to hydration in the saturated water vapour at 80°C during 72 hours and next stored in water at 20°±1°C during 7 days. The X-ray examination of the paste after this treatment showed that it was composed of gibbsite and hydrogarnet and contained also a very small amount of unhydrated

CA_2. The results of observation of this starting sample under SEM are presented on Figs 1 and 2, in which the crystals of hydrogarnet and the spherical agglomerates of platy crystals of gibbsite can be seen.

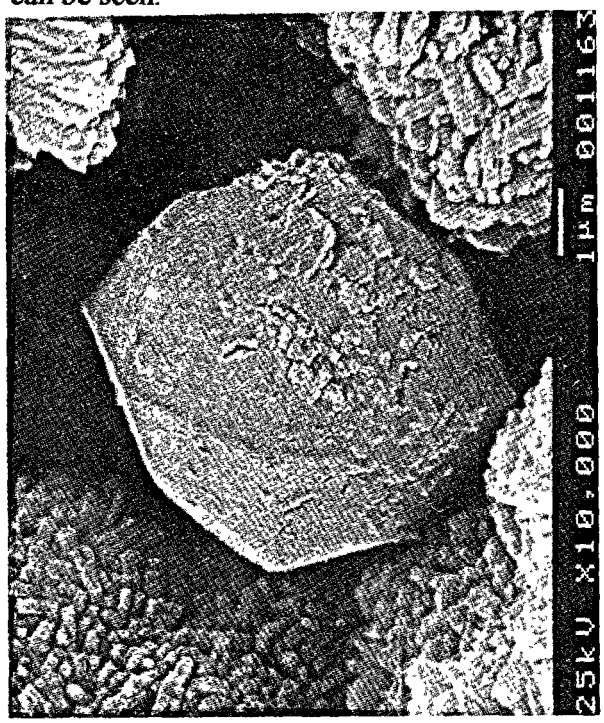

Figure 1 Starting paste. Crystal of hydrogarnet and agglomerates of platy crystals of gibbsite

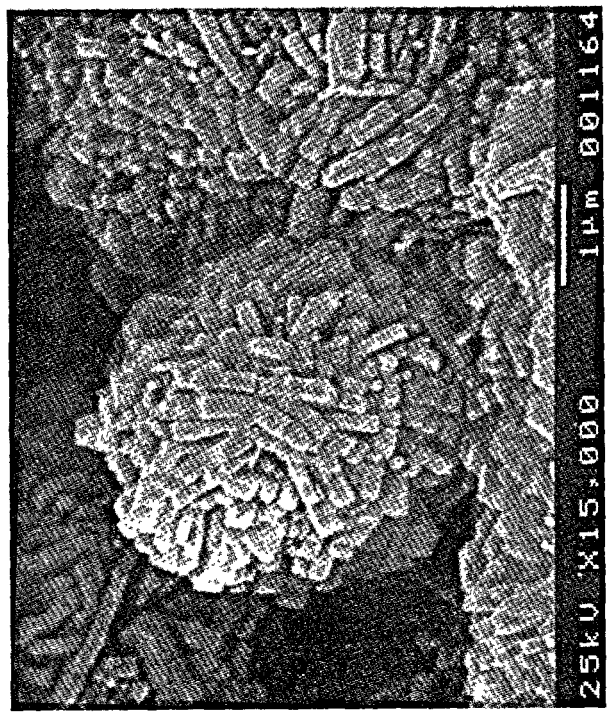

Figure 2 The agglomerates of gibbsite (the same as in Fig 1)

Table 1. Chemical composition of solutions

Solution	1	2	3
	Concentration in g/l		
$MgCl_2$	150	-	272
$CaCl_2$	-	175	164
NaCl	-	-	14
KCl	-	-	10
KBr	-	-	4

The elements of the paste of this composition were then immersed in three chloride solutions, namely: the solution of $MgCl_2$, the solution of $CaCl_2$ and, finally the solution imitating the salt mine water. The composition of these solutions are given in Table 1. For the sake of comparison one series of elements was stored in distilled water. After several days of immersion the change of phase composition of the samples was followed by X-ray, SEM and, for selected samples, also by DTA. In some cases the classical chemical analysis was also done.

EXAMINATION OF SAMPLES

The samples revealed expansion in all the solutions, which was the highest in the solution of $MgCl_2$ for 600 days. In this solution the expansion rises very quickly during the first 200 days, then quickly for 400 days. Then after 400 days a stabilisation of dimension of the samples is observed (Fig 3). In the salt mine water the change of dimension of the samples started with small shrinkage which was transformed into expansion after 30 days. The acceleration of expansion took place between 340 and 420 days. After this period the expansion became slow but took place till the last measurement after 762 days when it reached the highest value for all the

solutions. The expansion in the solution of $CaCl_2$ is relatively very small and reached about 2 mm/m after 762 days, and was about three times larger than in water.
The first examination of the phase composition of the samples took place after 200 days of immersion and then after 400 days and, finally, after 762 days. The X-ray examination of the samples immersed for 200 days in the salt mine water revealed the diminution of the intensity of lines of hydrogarnet and the appearance of the lines of Friedel salt. As another product of corrosion, the basic magnesium chloride $Mg_2(OH)_3Cl{\times}2H_2O$ gave strong peaks. The lines of gibbsite remained as strong as in the starting sample. The X-ray pattern of these samples after 400 days of immersion showed no substantial differences. All the time the peaks of hydrogarnet were present but evidently weaker, as well as strong lines of gibbsite. The lines of basic magnesium chlorides became stronger and new lines appeared, namely at 0.813, a diffuse band at 0.688÷0.641 and at 0.406. Also the increase of intensity of peaks of Friedel salt has to be noted. After 762 days of immersion the sample, according to the X-ray examination, was composed of gibbsite, Friedel salt and basic magnesium chloride. No lines of hydrogarnet could be found on the X-ray pattern.
The examination under SEM gave very similar results. A small quantity of basic calcium chloride was the only difference which can be found in the external layer of the sample (Fig 4). Also in the external part the platy crystals of basic magnesium chloride were abundant (Fig 5).
The phase composition of the samples immersed in the magnesium chloride solution was quite similar. In the function of time of immersion on the X-ray patterns the intensity of the lines of hydrogarnet decreased and these of gibbsite remained unchanged. As new formations, the peaks of Friedel salt and basic magnesium chloride appeared.

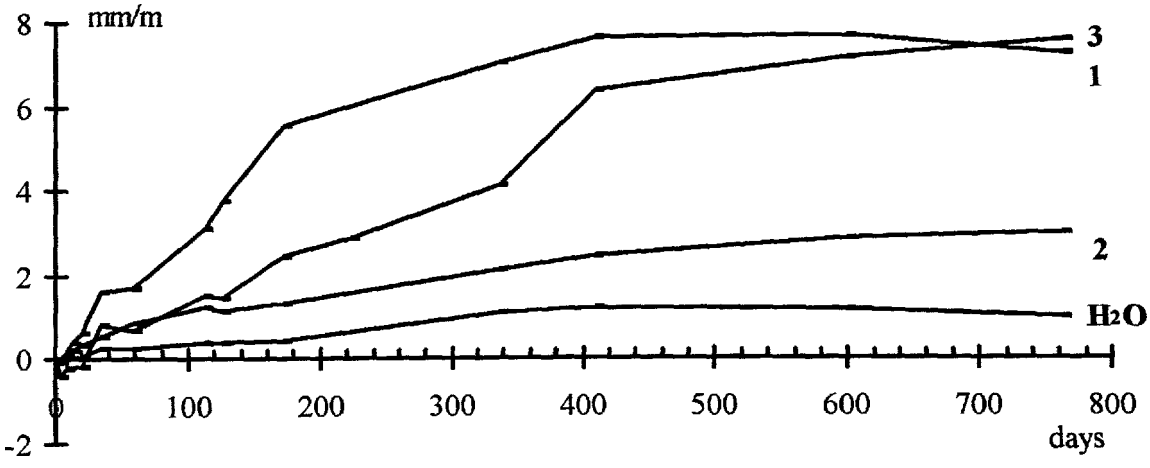

Figure 3 Expansion curves, the number of solutions as in Table 1

The smallest changes of phase composition were noted for the samples immersed in the solution of calcium chloride. Friedel salt is the only product of corrosion. It is preferentially formed in the outer layer of the sample, whereas the core remained unchanged. The porous region can be seen under the compact external layer (Fig 6) which is probably connected with the dissolution of hydrogarnet and the crystallisation of Friedel salt in the external layer. No basic calcium chloride could be found either by the X-ray examination or by the SEM observations.
The SEM examination after 762 days showed only very small quantity of hydrogarnet crystals with the corroded surface (Fig 7). Also the cracked crystal with the layer, probably of Friedel salt, was found (Fig 8). Very small hexagonal crystal of this phase can be seen under large magnification.



Figure 4 Crystals of basic calcium chloride, solution 3, 400 days of immersion



Figure 5 Crystals of basic magnes. chloride solution 3, 400 days of immersion

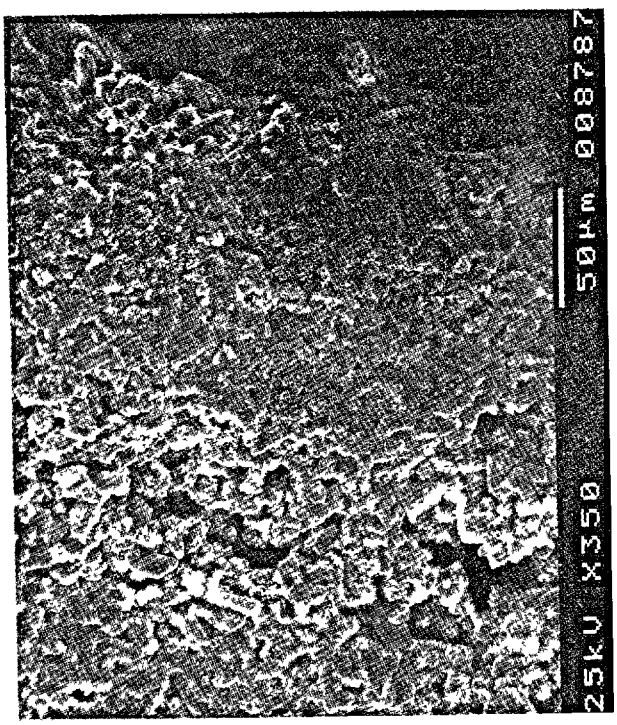

Figure 6 Three layers: external - compact, intermediate - porous and unchanged, solution 2, 400 days of immersion

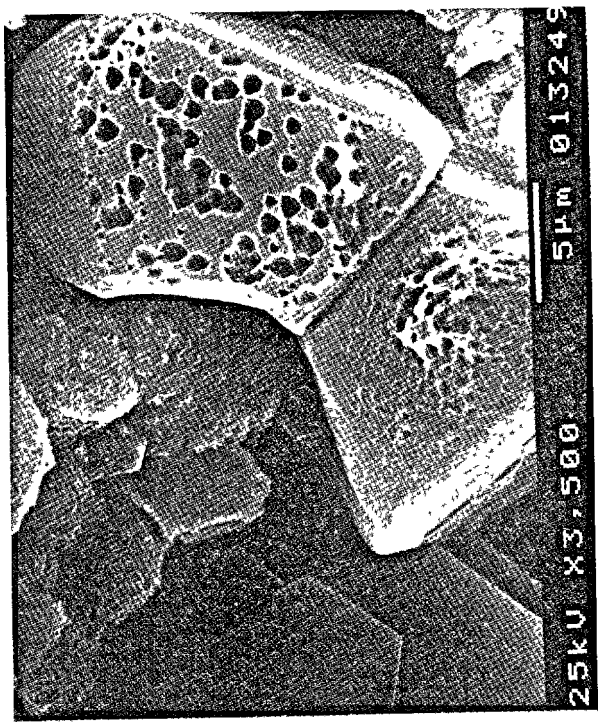

Figure 7 Corroded crystals of hydrogarnet, solution 2, 762 days of immersion

The chemical composition of the external layer of the sample (about 20% of total volume), obtained from the prism element by extracting the core, proves also the total decomposition of

hydrogarnet. This analysis is shown in Table 2 and when we compare with the calculated composition, according to the formula:

$$C_3AH_6 + CaCl_2 + 4H_2O \longrightarrow C_3A{\times}CaCl_2{\times}10H_2O \qquad [2]$$

we can see good conformity of both compositions. The only difference is in the lime content whose value found experimentally is too small. The excess of chlorine may depend on the adsorption of these ions by AH_3 gel.

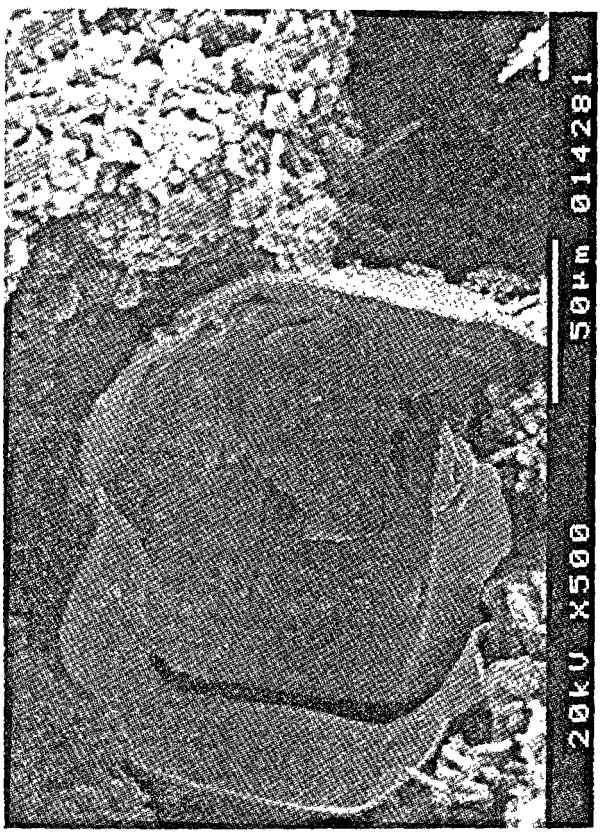

Figure 8 Cracked hydrogarnet crystal with of layer of Friedel salt on the surface, solution 2, 762 days of immersion

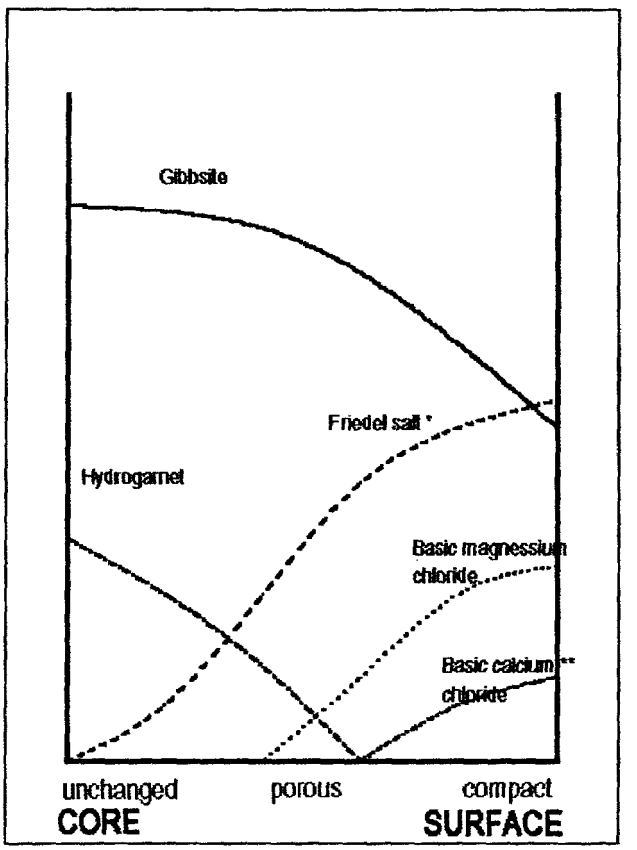

Figure 9 Model of phase composition of samples during corrosion
*) in case of solution 2 only Friedel salt
**) only in case of solution 3

The samples cured in water also show small changes in their phase composition. The intensity of hydrogarnet lines on the X-ray pattern became somewhat weaker and some lines of hexagonal hydrate C_4AH_{13} appeared. Doubtlessly, it is the product of the reaction of remaining CA_2 with water. This hydration process causes a small expansion of the elements cured in water.
The hydration process practically ended after 400 days which was expressed in the stabilisation of dimensions of the samples (Fig 3). Also under the influence on CO_2 from atmosphere the calcite crystals were formed which gave their peaks on X-ray diagram and which can be found with SEM and on the DTA curves (Fig 10).
As it can be seen on DTA curves (Figs 10 and 11), each sample contains some gel which may be principally AH_3 gel. This gel can be formed, among others, during the reaction of magnesium chloride with hydrogarnet:

$$4MgCl_2 + 1^2/_3\ C_3AH_6 \longrightarrow MgCl_2{\times}3Mg(OH)_2{\times}4H_2O + C_3A{\times}CaCl_2{\times}10H_2O + 1^1/_3\ AH_3 \qquad [3]$$

The presence of basic magnesium chloride gel in solutions containing magnesium chloride cannot be excluded, especially because in case of salt mine water this gel was found in the SEM observations.

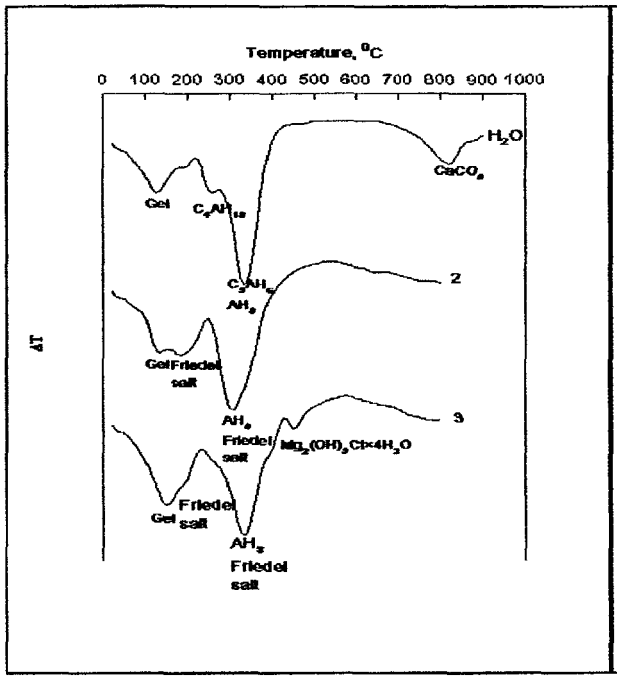

Figure 10 DTA curves, samples after 400 days of immersion, number of solutions as in Table 1

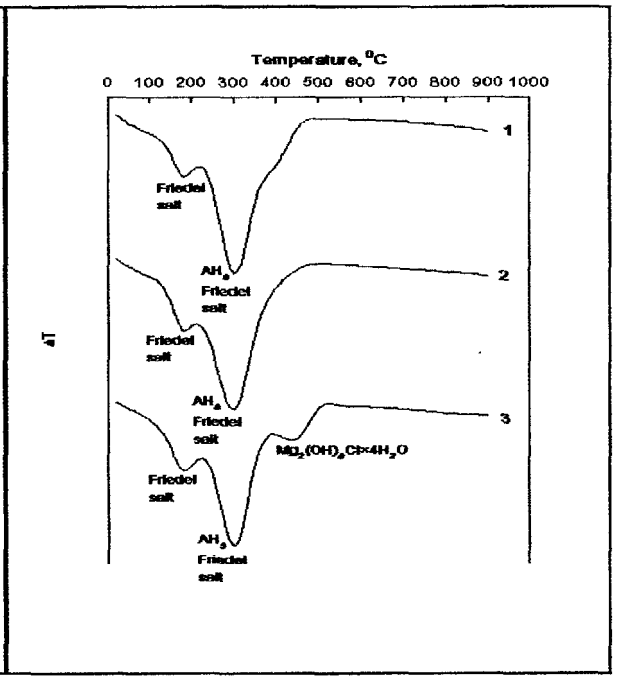

Figure 11 The same as in Fig 10 but after 762 days of immersion

Gibbsite and C_3AH_6 give the strongest peak at about 320°C and in case of samples immersed in chloride solutions this peak is also linked with the decomposition of Friedel salt.
Finally, for the sample cured in water, C_4AH_{13} gives a small peak at 240°C on the DTA curve and on the curve of the samples cured in solutions containing magnesium chloride basic magnesium chloride gives peak at about 440°C. The intensity of this peak is the highest for the sample cured in salt mine water after 762 days of immersion (Fig 11, curve 3) and much more weaker for the sample immersed in $MgCl_2$ solution (Fig 11, curve 1).

DISCUSSION OF THE RESULTS

In the paste gibbsite is stable in the chloride solution and hydrogarnet reacts with this solution giving new compounds which are: Friedel salt in all chloride solutions and basic magnesium chloride in salt mine water and $MgCl_2$ solution and, finally, basic calcium chloride in salt mine water. The formation of Friedel salt is accompanied by a very limited expansion so the paste will be rather stable in the $CaCl_2$ solution. The formation of basic magnesium chloride leads to a high expansion which must end with the destruction of the paste. The formation of basic calcium chloride was only found in salt mine water which contains a high concentration of both chlorides, i.e. of calcium and of magnesium.
Basing on the X-ray examinations and the SEM observation the model of phase composition and the microstructure of the samples can be presented (Fig 9). The external corroded layer is rather compact and contains all new phases, chiefly Friedel salt and basic magnesium chloride. Under the external layer comes a porous layer which is caused by dissolution of hydrogarnet.Gibbsite is the main phase in this region. Under the porous layer the microstructure is transformed gradually into an unchanged core, with small concentration of adsorbed chlorine. This higher content of

chlorine in the core as compared to magnesium is caused by much higher velocity of diffusion of Cl^- in comparison with magnesium (Ushiyama and Goto, 1974).

Table 2 Chemical analyses of external layer of samples after 762 days of immersion

Solution	Content in wt. %			
	CaO	MgO	Al_2O_3	Cl
1	9.2	6.4	45.9	7.6
2	13.6	-	45.9	7.9
2*	16.7	-	45.6	5.3
3	7.1	9.0	44.1	13.3

*) calculated according to Eq 2

Several conclusions can be drawn from the chemical analysis shown in Table 2. It can be well seen that aluminium is not leached and its quantity remains stable in the samples and the Friedel salt is crystallised in the pores of the samples. The confirmation of this hypothesis can be found in the porosity measurements, executed for all samples after 762 days of immersion (Fig 12). This porosity is the highest for the sample cured in water. The sample immersed in salt mine water has the smallest total porosity. The samples immersed in magnesium and calcium chloride solutions have the same total porosity, yet the content of the big pores, between 100 and 2000 nm is the largest in case of the sample immersed in the calcium chloride solution.
On the contrary, lime is leached from the samples and this process is the most intensive in case of salt mine water.

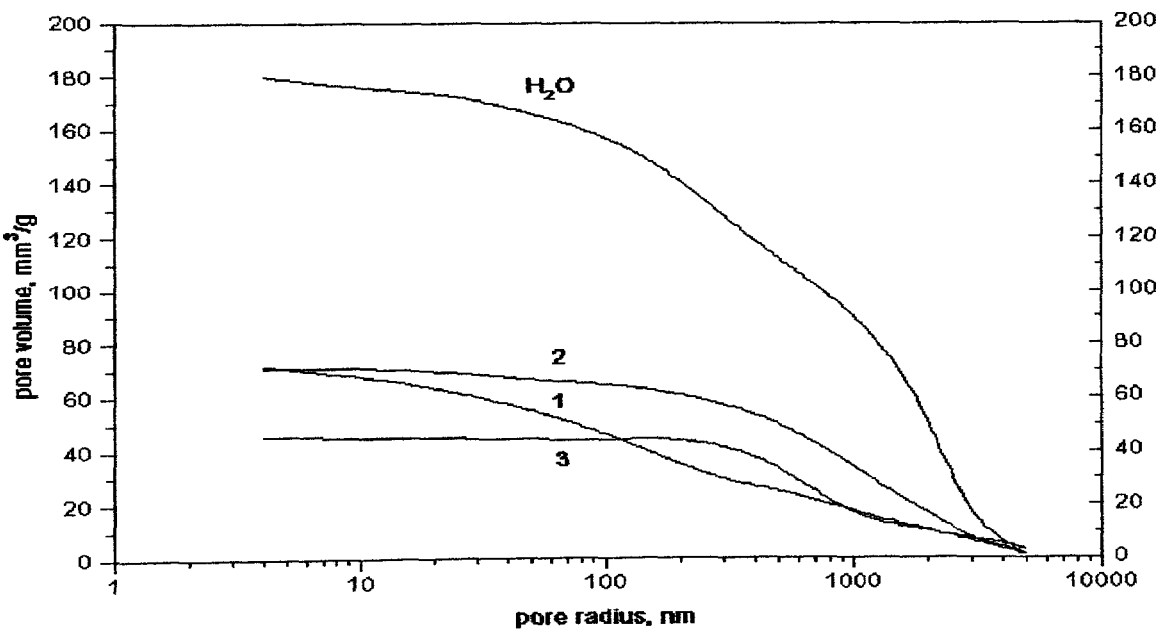

Figure 12 Porosity of samples immersed 762 days in chloride solutions, number of solutions as in Table 1.

The content of chlorine in the external layer of the samples depends strongly on the concentration of chlorine ions in the corrosive solution. In case of magnesium and calcium chloride solutions which are of equal ionic force the content of chlorine is practically the same.
In case of salt mine water whose ionic force is twice larger the content is also about twice the value for two other solutions.

When we compare the corrosion process of the HAC cement (Kurdowski et al., 1990) with the gibbsite/hydrogarnet paste, we can see substantial differences. In case of the HAC paste the skin is formed on the surface of the samples and this skin is composed of brucite and basic magnesium chloride. In case of gibbsite/hydrogarnet paste we did not observe the skin formation and we did not find brucite.
This behaviour is due to the differences of the microstructure of the paste. In case of the HAC paste we have a very dense microstructure with an amorphous AH_3 gel. The densification of the gel, accompanied by shrinkage, causes strong decrease of porosity of the external layer of the paste. Also the skin, when stable, can be regarded as a protecting barrier. In our samples, which are much more crystalline, the shrinkage is very limited and took place only in case of elements immersed in salt mine water (Fig. 3). The diffusion of chlorine and magnesium ions is much quicker in case of the gibbsite/hydrogarnet paste. However, because of the durability of gibbsite phase, the corrosion is limited and the destruction of the paste is slow. The skin is not formed because the simultaneous diffusion of magnesium and chlorine prevails over the countercurrent diffusion of Cl^- and OH^- ions.

CONCLUSIONS

1. Basic magnesium chloride is the main corrosion product in chloride solutions with magnesium ions and the largest expansion of the paste is connected with the formation of this phase.
2. The calcium chloride solution causes only the transformation of hydrogarnet into Friedel salt which is accompanied by a small expansion of the paste.
3. Gibbsite is stable in magnesium and calcium chloride solutions
4. In case of solution containing magnesium and calcium chlorides simultaneously, the basic calcium chloride is also formed
5.The investigation of paste rich in gibbsite proves that HAC will be not destroyed in calcium chloride solution

Acknowledgements
Financial support of this work was provided by the Polish Committee for Scientific Research (KBN) under Grant 7 7308 92 03.

REFERENCES

Chatterji S.(1978), Cem.Concr.Res.,8, p. 461
Conjeaud M. (1982), Int. Seminary on Calcium Aluminates, Ed. M. Murat, Torino
Kurdowski W., Taczuk L. and Trybalska B. (1989), "Durability of Concrete", 2nd Int. Seminar, June 1989, p. 85, Swedish Council for Building Research, Stockholm
Kurdowski W., Taczuk L. and Trybalska B. (1990) Behaviour of HAC in Chloride Solutions, in "Calcium Aluminate Cements", Ed. R.J.Mangabhai, E.& F.N. Spon, London, p. 222
Kurdowski W., Duszak S. and Trybalska B., (1994), Section of Building Materials of Polish Ceramic Society, Corrosion of Cement Paste, Ed. Kurdowski, Krakow, p. 85.
Kurdowski W., Duszak S. and Trybalska B., (1994), 1th Int. Conf. "Alkaline Cements and Concretes, Kiev, Ed. by V. Krivienko, vol. II, p. 961.
Monosi S., Alverf I. and Collepardi M. (1989), 2, p. 97
Riedel W. (1973), Zement-Kalk-Gips,26 p. 286
Smolczyk H.G. (1968), 5th Int. Symp. on the Chemistry of Cement, III, p. 274, Tokyo
Suzukawa Y. (1980), 7th Int. Congress on the Chemistry of Cement, III, p. VII-124, Paris
Ushiyama H. and Goto S. (1974) 6th Int. Congr. on the Chem of Cem. Moscow, vol II/1, p. 331.

RESISTANCE TO CHEMICAL ATTACK OF HIGH PERFORMANCE FKJ CONCRETE *

LU Changgao, LI Ruihua, Suzhou Concrete and Cement Products Research Instiute State Adiministration of Building Materials Industry, 215004, P. R. CHINA

ABSTRACT In this paper, the study of the resistance of high performance fly ash slag-alkali concrete (namely FKJ * * Concrete) to chemical attack and durability in the H_2SO_4, HCl, HNO_3, NaCl, $MgCl_2$, Na_2SO_4 solutions, seawater etc attack agents as well as in the atmosphere are highlighted respectively. Simultaneously, the mechanism of resistance of FKJ concrete to chemical attack and its suitable application scope are also advanced.

Key – Words: Alkali, Chemical Attack, Corrosion, Mineral phase, Zeolites.

INTRODUCTION

On the basis of the author's inventive pantent(Lu, 1988), the high performance of FKJ concrete is the scientific research achievements we have contributed to for many years. Nowadays, we have developed FKJ corrosion resistance sewer pipe which was used in sewer pipeline systems of Shanghai Municipal Engineering and Chemical plant. In order to fully understand the resistance ability of FKJ concrete to chemical corrosion, we have carried out the study of its resistance to the above acids, alkalis, salts, seawater as well as in the atmosphere in recent years. On the one hand, by means of macroscopic tests of corrosion resistance for FKJ concrete, We get the understanding of its corrosion resistance degree and work out the suitable application scope of FKJ concrete by combining safety and reliability of its application in an engineering project. On the other hand, by means of microscopic analysis (including X – Ray, SEM, EDAX and po ım
such as ıa-
nism o

THE STRENGTH DEVELOPMENT AND LONG – TERM STABILITY OF FKJ CONCRETE UNDER AMBIENT TEMPERATURE

The mortar specimens and concrete specimens are exposed to naturel curing(atmosphere in a room). The strength development and long-term stability are shown in Fig 1. It can be seen from the curves that the FKJ concrete is featured with early strength. Their R_{1d} strength of it under ambient temperature is more

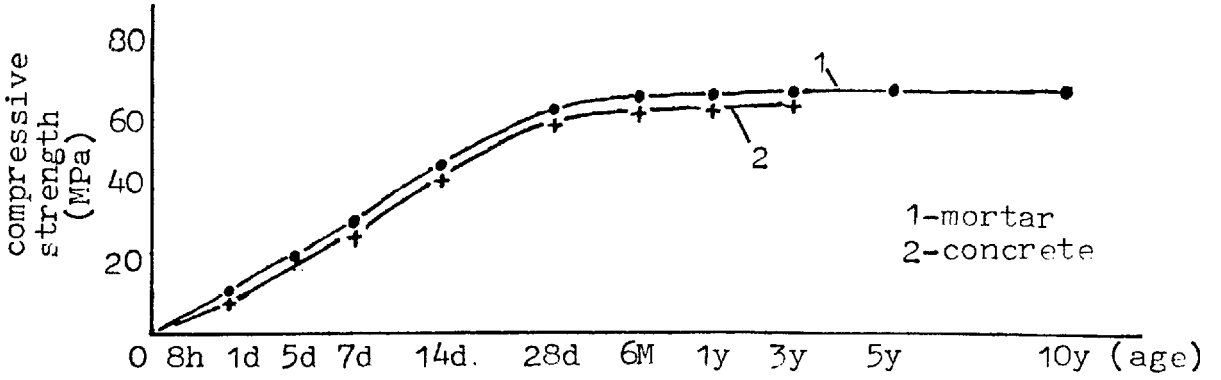

Fig 1 The strength development and long-term stability of FKJ concrete under conditions of ambient temperature.

* This is the aid financil project of national science foundation of China.

* * FKJ refers to the abbreviation of Chinese spelling.

than 10MPa, their R_{28d} strength is more than 55MPa. It is indicated from the data determined in 1, 3, 5, 10 years that the strength of FKJ concrete is slightly increased. which means that mineral phase formed is stable and has fine resistance to weathering(Lu, 1995).

THE RESISTANCE OF FKJ CONCRETE TO ACIDS

According to our analysis, the main mineral phase of FKJ binder is silicoaluminate of Zeolite type and we think the sodium silicoaluminate hydrate of analcite type is the main mineral phase in the system. The fine resistance to chemical corrosion of FKJ concrete is due to the existance of this mineral. viewing from the characteristic of natural zeolite, it is featured with strong acid resistance. After natural zeolite is treated with 2N, 4N, 6N HCl for 2 hours under 90℃, no corrosion failure phenomenon is shown in the crystal structure(Lu, 1994).

Futhermore, we carried out acceleration acid resistance testing for FKJ mortar specimens, that is, immersing and bathing the specimens into 6N HCl solution, heating them up to 90℃ and keeping this for 2 hours, no chemical reaction can be observed during testing. The strength of specimens after testing remained 50. 6MPa, without any decreasing. Whereas the ordinary blastfurnace slag cement mortar specimens(1:3 cement mortar) with oringinal strength of 30 MPa treated with the similar way was severely corroded and pulverized. measured remaining strength of specimens was less than 3 MPa.

In order to highlight the acid resistance degree of FKJ concrete, three strong acids commonly used (H_2SO_4, HCl, HNO_3) were selected as the attack medium and four different concentration were used, which the PH = 2 acidity was chosen in account of the application of a project. During the tests, their acidities were adjusted regularly. The testing results are shown in Table 1. It must be indicated that the ordinary concrete specimens were severely corroded in chemical reaction under the action of strong acid

Table 1 The testing results of acid resistance of FKJ concrete

type of medium name	corrosive acidity	age (day)	after corrosion strength (MPa)	apperance	strength of compara. (MPa)	coeffi. of corr. resista.
H_2SO_4	2%	365	39.3	microcrack	57.0	0.69
	1%	365	52.5	fine	57.0	0.92
	0.5%	365	57.1	fine	57.0	1.00
	PH=2	365	62.0	fine	64.3	0.96
HNO_3	10%	365	44.0	fine	57.0	0.77
	5%	365	54.7	fine	57.0	0.96
	1%	365	58.0	fine	57.0	1.02
	PH=2	365	67.0	fine	64.3	1.04
HCl	10%	365	30.7	fine	57.0	0.54
	5%	365	47.6	fine	57.0	0.84
	1%	365	57.3	fine	57.0	1.01
	PH=2	365	62.3	fine	64.3	0.97
H_2SO_4 + HNO_3 + HCl mixed acid	10%	365	32.3	microcrack	57.0	0.57
	5%	365	47.8	fine	57.0	0.84
	1%	365	56.5	fine	57.0	0.99
	PH=2	365	65.3	fine	64.3	1.02

with high concentration(>2%), those specimens were obviously destroyed after testing.

It can be seen from the testng results in Table 1 that the corrosion degrees of specimens to the different acids are dissimilar. The corrosion resistance of specimens to H_2SO_4 and mixed acid with high concentration is relatively poor. Nevertheless, we think if the corrosion resistance coefficient of the specimens to acids after tested for one year is bigger than 0.8, then their corrosion resistance to acid is up to standard. Therefore, the limit of resistance of FKJ concrete to acid is as follows: H_2SO_4—1%, HNO_3—5%, HCl—5%, mixed acid—5%.

In order to incorporate its application with an engineering project and compare it with ordinary concrete, we put FKJ concrete specimens and ordinary concrete (OPC) specimens into (H_2SO_4 + HCl + HNO_3) mixed acid solution of PH = 2. After 1 year the strength of OPC specimens decreased by 43% (from 59.0 MPa down to 34.0MPa) and it was severely corroded; while the strength of FKJ specimens did not decrease (from 64.3MPa up to 65.3MPa) and apperance is fine, as shown in Fig 2. Consequently, the test indicated that the resistance to acid of the FKJ concrete is fine and greatly exceeds that of the ordinary concrete, increased about 20 – 30 times.

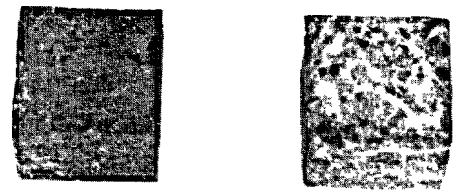

FKJ OPC

Fig 2 The Specimen apperance in mixed acid solution of the PH = 2 (H_2SO_4 + HCl + HNO_3) after 1 year.

THE RESISTANCE OF FKJ CONCRETE TO ALKALI

We put FKJ concrete specimens into 10%, 5%, 1% and NaOH with PH = 13 and $Ca(OH)_2$ dense solution respectively, the reason we selected PH = 13 alkality was in account of its application of a project. The testing results of specimens after 1 year are shown in Table 2. It can be seen from testing results

Table 2 the testing results of resistance to alkali of FKJ concrete

type of medium name	corrosive alkality	age (day)	after corrosion strength (MPa)	apperance	strength of compara. (MPa)	coeffi. of corr. resista.
NaOH solution	10%	365	33.5	microcrack	64.3	0.52
	5%	365	54.0	fine	64.3	0.84
	1%	365	65.0	fine	64.3	1.01
	PH = 13	365	65.2	fine	64.3	1.01
Lime solution	PH = 13	365	63.7	fine	64.3	0.99

that the corrosion resistance of specimens to NaOH solution with high concentration is relatively poor. we think that if the coefficient of corrosion resistance of the specimen to alkali is greater than 0.80 after 1 year, its corrosion resistance to alkali is up to standard. Therefore, the limit of resistance of FKJ concrete to alkali (NaOH) is 5%, its alkaline resistance is similar to that of the ordinary pordland cement concrete.

THE CORROSION RESISTANCE OF FKJ CONCRETE TO SALTS

We put the FKJ mortar specimens into seawater, $MgCl_2$ solution with 25 – 30° Be', NaCl solution with 26%, (NaCl + $MgCl_2$) mixed silution with 25% and pure chemical $Na_2SO_4 \cdot 10H_2O$(the concentration of sulfate ion in solution is 2500mg/1) respectively. The testing results are shown in Table 3. It can be seen from the testing results that the corrosion resistance of FKJ specimens is strong, no matter they were put into seawater, $MgCl_2$, NaCl, NaCl + $MgCl_2$ mixed solution or $Na_2SO_4 \cdot 10H_2O$ solution after

immersed for three years, their appearance remained fine and the strength were not decreased, but increasing a bit. Their coefficient of corrosion resistance are more than or equal to 1.

Table 3 The testing results of resistance to salts of FKJ mortar specimens.

type of medium name	corrosive concentra.	age (year)	after strength (MPa)	corrosion apperance	strength of compara. (MPa)	coeffi. of corr. resista.
seawater	manual preparation	1	54.0	fine	52.5	1.03
		3	57.9	fine	54.6	1.06
$MgCl_2$ solution	25 – 30° Be'	1	52.5	fine	52.5	1.00
		3	54.6	fine	54.6	1.00
Na_2SO_4 solution	2500mg/1	1	53.1	fine	52.5	1.00
		3	59.3	fine	54.6	1.00
NaCl solution	26%	1	53.6	fine	51.5	1.04
NaCl + $MgCl_2$ mix. solu.	25%	1	55.2	fine	51.5	1.07

THE REINFORCEMENT PROTECTION PROPERTY OF THE FKJ CONCRETE

In the corrosion tests of above acids, akalis, salts, ø6 × 20mm reinforcements were put in the FKJ specimens. After the specimens were cut apart, all cover of concrete protecting reinforcement was more than 5mm, the reinforcement surfaces were not rusted, so their reinforcement protection property is fine.

THE MECHANISM OF RESISTANCE OF FKJ CONCRETE TO CHEMICAL CORROSION

Microstructural aspects of the hardened FKJ binder paste

The FKJ binder is a new type of non-clinker cement which was worked out by author according to mineralization conditions of natural zeolite mineral. Based on our research and determination, in the FKJ binder the main hydrate products and mineral phases possibly produced are sodium silicoaluminate hydrate of analcite type; the secondary products are calcium silicoaluminate hydrate of scolecite type and sodium-calcium-silicoaluminate hydrate of thomsonite type, meanwhile a small amount of low-alkaline calcium silicate hydrate are also produced(Lu, 1992).

Author consider that the reason why the FKJ binder concrete has fine durability and resistance to chemical attack is due to its relation to the microstructure of its silicon(aluminium)-oxygen tetrahedron. For instance, the sodium-silicoaluminate hydrate of analcite type forms tetrogon-triakisoctahedron crystal, the pore passage in silicon(aluminium)-oxygen crystal lattice mainly consist of hexatomic ring. It forms one-dimensional tube pore pasage, pore diameter is about 2. 6Å and unifmly distributed. Its crystal lattice energy is higher (21214.4KJ/mol), while its solubleness is lower (about 0.02 Kg/m^3). Therefore, its this one mineral phase and microstructure that determines a series of fine characteristics, specially its stronger resistance to chemical corrosion.

Pore structure of the hardened FKJ binder paste

It's well known that many big or small pores are distributed in concrete. By means of changing pore-size distribution in the concrete (specially in the cement paste), some of characteristics of concrete can be improved (Ramachandran et al, 1981) The pore-size distribution of the hardened FKJ binder paste were determined by using mercury porosimetry, as shown in Table 4. It can be seen from the values in Table 4

Table 4 The pore-size distribution of the hardened FKJ binder paste

w/c	total pore (cc/g)	pore-size distribution (%)			
		$>14^4$Å	10^4-10^3Å	10^3-10^2Å	$<10^2$Å
0.4	0.1184	6.0	36.5	18.0	39.5

that there are many <100Å pore-size distribution(amount up to 39.5%), which more than the hardened OPC paste, usually its pore-size distribution of the <100Å is about 20% (w/c=0.4). These pores are not only non-harmful but also can increase the impermeability of concrete. So from the viewpoit of pore structure, the resistance to chemical attack of FKJ concrete is strengthened.

The mechanism of resistance of FKJ concrete to acids

It's well known that acid attack to ordinary concrete is the most serious corrosion among the different corrosion types. Normally, in the acidic environment (PH≤6.5), ordinary cement concrete is unstable

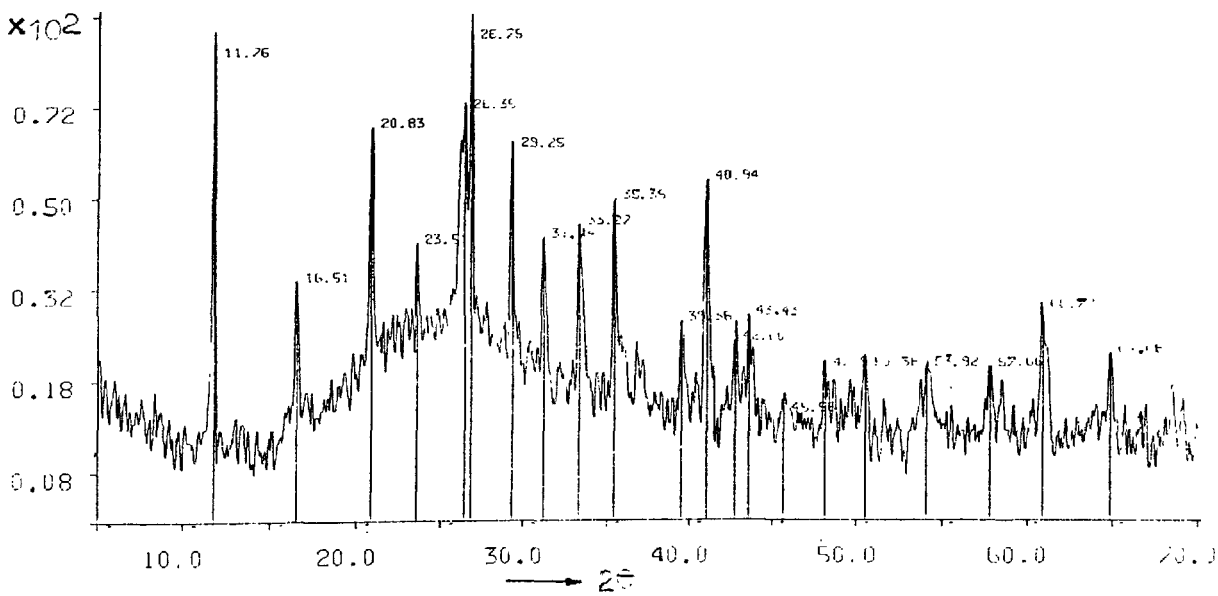

Fig 3 The X-Ray diffracto-spectrogram for FKJ binder specimen, after one year in the 5% (H_2SO_4 + HCl + HNO_3) mixed acid.

Table 5 The recorded data of diffraction for FKJ binder specimen

2θ	d (Å)	I/Imax(%)	2θ	d (Å)	I/Imax(%)	2θ	d (Å)	I/Imax(%)
11.76	7.52	100.00	31.14	2.87	21.30	45.56	1.99	9.47
16.51	5.36	22.20	33.27	2.69	26.96	47.99	1.89	9.47
20.83	4.26	50.63	35.35	2.54	30.04	50.38	1.81	9.47
23.51	3.78	18.72	39.38	2.29	13.35	53.92	1.70	9.47
26.35	3.38	44.02	40.94	2.20	40.27	57.67	1.60	9.47
26.76	3.33	68.38	42.61	2.12	11.98	60.72	1.52	14.79
29.25	3.05	41.50	43.43	2.08	14.79	64.69	1.44	9.47

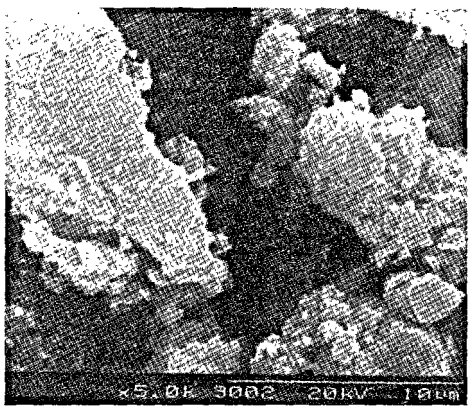

Fig 4 The crystal form of SEM for FKJ binder specimen.

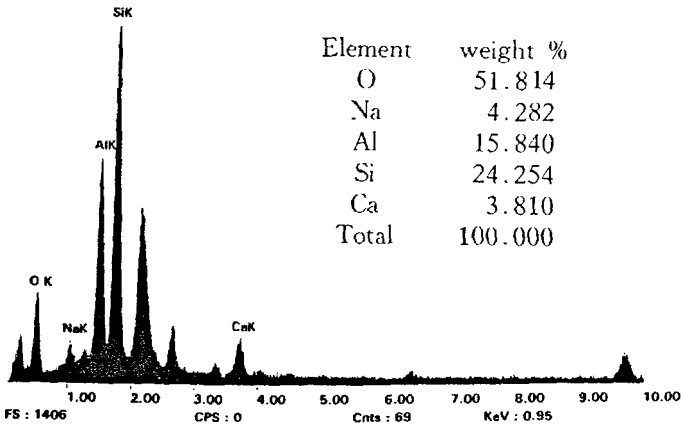

Element	weight %
O	51.814
Na	4.282
Al	15.840
Si	24.254
Ca	3.810
Total	100.000

Fig 5 The EDAX of FKJ binder specimen.

on the thermodynamics and may be corrosively damaged sooner o later (Knofel, 1978). However, the degree of resistance to acid of the FKJ concrete is stronger. We put FKJ binder paste specimen into 5% (H_2SO_4 + HCl + HNO_3) mixed acid solution after one year, we carried out X－Ray, SEM and EDAX examination respectively, as shown in Fig 3, 4, 5 and in Table 5. By comparing Fig 3 and Table 5, it can be seen that in FKJ system the sodium-silicoaluminate hydrate of analcite type remained existing without being corroded ($2\theta = 16.51, 26.35, 29.25$; correspondently $d = 5.36, 3.38, 3.05$Å). Its crystal form (Fig 4) is complete and the element quantity of EDAX is also correct (Fig 5).

But, the calcium silicate hydrate in the FKJ system was basically corroded. Its chemical corrosion reaction are as follows:

$$2CaO \cdot SiO_2 \cdot nH_2O + 4HCl \rightarrow 2CaCl_2 + SiO_2 + (n+2)H_2O;$$
$$2CaO \cdot SiO_2 \cdot nH_2O + 2H_2SO_4 \rightarrow 2CaSO_4 + SiO_2 + (n+2)H_2O,$$
$$CaSO_4 + 2H_2O \rightarrow CaSO_4 \cdot 2H_2O;$$
$$2CaO \cdot SiO_2 \cdot nH_2O + 4HNO_3 \rightarrow 2Ca(NO_3)_2 + SiO_2 + (n+2)H_2O;$$

Among which the $CaCl_2$ and $Ca(NO_3)_2$ products were dissolved, while the $CaSO_4 \cdot 2H_2O$ products were not dissolved and remaining in the body, as well as the silicon gel produced also remaining in the body. In the recorded diffracto-spectrogram (Fig 3, Table 5), $d = 7.52, 4.26, 3.33$Å, it belongs to gypsum; $d = 2.20, 1.99, 1.52$Å, it belongs to silicon gel.

Increasing acidity, means increasing H^+ ion concentration in the system, its damaging intensity to the FKJ binder is strengthened. It can be seen from testing results (Table 1) that when the concentration of acid was increased from 5% to 10%, after one year, the crystal lattice of the silicoaluminate hydrate of zeolite type begun to corrode.

It must be pointed out that in the 2% concentration of H_2SO_4 solution although the silicoaluminate hydrate of zeolite type was not corrosively damaged, but since the calcium silicate hydrate was corrosively damaged, producing more expansive salts (gypsum) and leading to the expansive corrosion of sulphate. Therefore, the resistance to sulfuric acid of FKJ concrete is lower, its limit only 1%.

The mechanism of resistance of FKJ concrete to alkalis

It can be seen from the data in Table 2 that the limit of resistance of FKJ concrete to alkali (NaOH) is 5%. Increasing from 5% to 10% , its resistance to alkali is not up to standard. Therefore, FKJ binder was attacked by the concentrated solution of alkali. Its attack mechanism is as follows:

As the FKJ specimens were corroded by high concentration of NaOH solution for a long time. part of sodium silicoaluminate hydrate of analcite type was corrosively changed into the sodium zeolite ($Na_2O \cdot Al_2O_3 \cdot 3SiO_2 \cdot 7H_2O$), and in the X-Ray diffracto-spectrogram (Fig 6 and Table 6): d = 14.36, 8.76, 5.71Å. It can be seen from the SEM crystal morphology in Fig 7 that it formed fibrous cluster crystal, and intergrowth with the sodium silicoaluminate hydrate of analcite type. Fig 8 shows the results of EDAX of this micro area. Its summary of element concentration (weight %) conforms to the actual situation. In

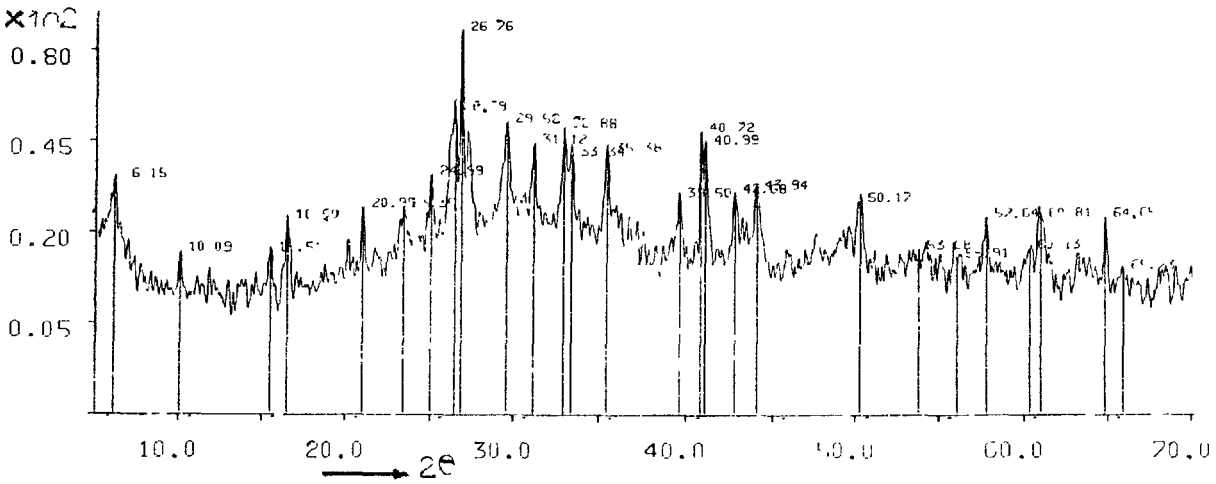

Fig 6 The X－Ray diffracto-spectrogram for FKJ binder specimen after one year in the 10% NaOH solution.

Table 6 The recorded data of diffraction for FKJ binder specimen

2θ	d (Å)	I/Imax(%)	2θ	d (Å)	I/Imax(%)	2θ	d (Å)	I/Imax(%)
6.15	14.36	17.97	24.99	3.56	17.06	33.34	2.69	25.00
10.09	8.76	12.10	26.38	3.38	51.47	35.37	2.54	30.73
15.51	5.71	12.10	26.76	3.33	100.00	39.50	2.28	16.17
16.50	5.37	20.84	29.52	3.02	35.74	40.72	2.21	71.38
20.99	4.23	18.90	31.12	2.87	20.84	40.99	2.20	38.39
23.35	3.81	13.66	32.88	2.72	30.73	42.68	2.12	17.06

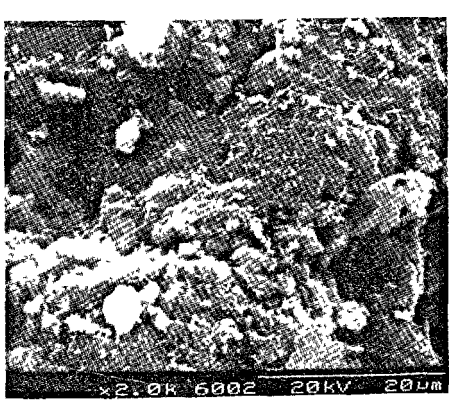

Fig 7 The crystal form of SEM of FKJ binder specimen

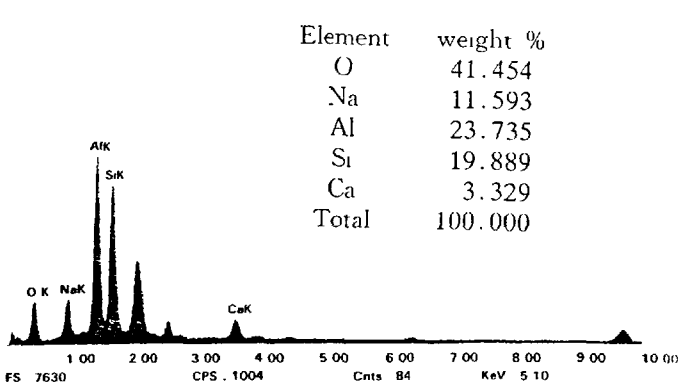

Element	weight %
O	41.454
Na	11.593
Al	23.735
Si	19.889
Ca	3.329
Total	100.000

Fig 8 The EDAX of FKJ binder specimen.

the process of corrosive change, the crystal lattice is rearranged, forming internal stress in the structure, Hence the whole strength of the system is weakened.

The alkaline solution can reacts with calcium silicate hydrate to form products which poor cementing power and easily separating out by alkaline solution:

$$2CaO \cdot SiO_2 \cdot nH_2O + 2NaOH \rightarrow 2Ca(OH)_2 + Na_2SiO_3 + mH_2O.$$

Similar to the ordinary concrete, when the alkaline solution permeates into the pores of FKJ concrete, it reacts with CO_2 in atmosphere to form $Na_2CO_3 \cdot 10H_2O$ crystal. Its volume is 2.5 times bigger than the original sodium hydroxide. Therefore, producing greater crystallization pressure and leads to the damage of cement stone structure.

The mechanism of resistance of FKJ concrete to salts.

It can be seen from Table 3 that the resistance of FKJ concrete to salts is fine. Its corrosion resistance mechanism is as follows:

The ordinary concrete contains more $Ca(OH)_2$, whereas the FKJ concrete almost does not contain $Ca(OH)_2$, which blocks the source of the corrosion.

The ordinary concrete contains a number of calcium aluminate hydrate which can corrosively reacts with sulphate. However , the FKJ concrete does not exist this hydrate products which blocks the source of the corrosion.

Part of calcium silicate hydrate is included in FKJ system, though magnisum sulphate in seawater can corrosively react with it:

$$2CaO \cdot SiO_2 \cdot nH_2O + MgSO_4 \cdot aq \rightarrow CaSO_4 \cdot 2H_2O + Mg(OH)_2 + SiO_2 \cdot aq.$$

As the amount of this product is quite less, so unfavorable effect to the system will not be occurred.

SUITABLE APPLICATION SCOPE OF FKJ CONCRETE

we think that the resistances of FKJ concrete to acids and alkalis are the two important aspects in the corrosion resistance and also the criterion to decide its application scope of FKJ concrete. According to our research results and practical conditions of engineering application in concerning the safety of its application in an engineering project, we think FKJ concrete is suitable to be used in the corrosion resistance constructional engineering project with PH = 2 – 13 (including the urban corrosion protection sewer pipeline, the concrete structures in saline-alkali zone and marine structure etc).

REFERENCES

LU Changgao, China inventive patent, "ZL88100181.3, [51]Int. Cl^5, CO4B 18/06"(the method activated fly ash) 1988.

LU Changgao, "The research of the reaction products and mineral phase for cementitious material", 9th International Congress on the Chemistry of Cement, Vol. 111. pp319 – 324, New Delhi, 1992.

LU Changgao, Li Ruihua, "High performance FKJ concrete", Fourth NCB International Seminar on Cement and Building Materials, New Delhi, 1994.

LU Changgao, Li Ruihua, "The research of the high performance FKJ concrete " Proceeding of International Symposium on New Development in Concrete Science and Technology, pp557 – 564, Nanjing China. 1995.

Knofel D., Corrosion of Building Material, Germany, 1978.

Ramachandran V. S., Feldman. R. F., Beaudoin. J. J., Concrete Science – Treatise on Current Research, Canada, 1981.

LU Changgao, "A new type of durable building material – FKJ concrete", Concrete and Cement Products, NO. 6. 1991. China.

PRELIMINARY STUDY ON THE DURABILITY OF SULFO/FERRO-ALUMINATE CEMENTS

Muzhen SU, Yanmou WANG, Liang ZHANG, Dedong LI, China Building Materials Academy, Beijing 100024, P.R.China
Min DENG, Nanjing University of Chemical Technology, Nanjing 210009, P.R.China

ABSTRACT The third cement series (TCS) comprises cement clinkers identified by their content of $C_4A_3\bar{S}$ and giving ettringite in hardened pastes. In this paper, we essentially discussed TCS' outstanding durability performances, such as the long-term strength, permeability, anti-freezing, thermostability and the resistance to chemicalattack, carbonation, rusting and alkali-aggregate reaction, etc., according to over 20 year of experience in China.

Key-words : durability, sulfoaluminate, ferroaluminate

INTRODUCTION

Sulpho-aluminate cements (SAC) and Ferro-aluminate cements (FAC) are two new cement series developed by China Building Materials Academy (CBMA). These two cement series were formally put into industrial-scale production in 1974 and 1983 respectively and the Chinese standards for SAC and FAC were issued in 1987 and 1991.

Due to the similarities in the principal minerals in clinkers, in the major hydrates and in the performances, SAC and FAC are called by a joint name -- the third cement series (TCS), to be distinguished from ordinary Portland cement (OPC) and calcium aluminate cement (CAC), which may be named as the first cement series and the second cement series, respectively.

TCS is a type of hydraulic cement made by heating mixtures of limestone, bauxite and calcium sulfate up to a temperature of about 1325℃with one more form of calcium sulfate added during grinding. TCS can be classified by performance into five main types as rapid-hardening cement, high-strength cement, expansive cement, self-stressing cement and low-alkalinity cement.

With major content of $C_4A_3\bar{S}$ and/or C_4AF in clinker, TCS was sharply distinguished from the other two main cement series, OPC and CAC. For the same reason, TCS was found to have low energy-consumption in cement manufacture. It was also found to have many other advantages, for example, high early strength, good impermeability, good freezing-resistance, outstanding chemical corrosion resistance, satisfactory strength development and low-temperature application, low dry-shrinkage and low alkalinity of its hydration solution, etc.

After more than 20 years of industrial production and development, annual output of TCS has reached 800,000 tones in 1995 and will be over 1.5 million tones at 2005 in China. TCS had been successfully used in a wide range of general and specialized applications, such as winter construction, underground structure, marine construction, corrosion-resisting application and in production of a wide range of building elements.

An increasing importance has been attaching to the durability of TCS along with the expansion of its application area, especially increasing concrete strengths (the strength of cast-in-place concrete has reached 80 MPa). As the durability of concrete is very complicated, each application has different

Table 1 Mineral compositions of the third cement series clinker

	$C_4A_3\bar{S}$	C_2S	C_6AF_2 (C_4AF)
SAC clinker	50-70%	10-25%	3-10%
FAC clinker	45-60%	10-20%	15-25%

requirements. To answer all the question about the durability of TCS, a relatively new cement series, a series of researches have been and will be done for each type of the in each application. This paper focuses on only two types of TCS, rapid-hardening and expansive cements. Some initial results are reported.

MANUFACTURE OF TCS RAPID-HARDENING AND EXPANSIVE CEMENTS

Rapid-hardening and expansive TCS cements are produced by pulverizing respectively by SAC and FAC clinker consisting essentially of $C_4A_3\bar{S}$, C_2S and C_6AF_2 (or C_4AF), usually containing gypsum and limestone as interground additions. The amount of gypsum added for rapid-hardening cement is about 10-15%, but for expansive cement it is about 20-25%. The typical mineral constituents of the two clinkers are shown in Table 1.

Comparing the two, there is a notable difference in the ratio of $C_4A_3\bar{S}$ to C_6AF_2 (or C_4AF). Since the hydraulic minerals in SAC and FAC clinkers are similar, the two cements have similar hydration products, mainly AFt, AFm, (mostly present in rapid-hardening cement), C-S-H gel, aluminum oxide gel and iron oxide gel (mainly present in FAC cement). TCS performance and its hardened paste structures differ considerably from those of OPC and CAC.

PRINCIPAL SPECIFICATIONS FOR TCS RAPID-HARDENING AND EXPANSIVE CEMENTS

Physical properties

Under the Chinese Standard (ZB Q11005-87, JC435-91), the standard strength of TCS rapid-hardening cement is the compressive strength determined according to GB177-85 (Standard Test Method for Strength of Hydraulic Cement Mortars) at 3 days. Three classes of standard strength for the commercial products are covered: Class 425, Class 525 and Class 625, shown in Table 1 and Table 2.

The commercial TCS expansive cements are categorized as mini-expansive and expansive cements according to unrestrained mortar expansivity under Chinese standard ZB Q11007-87 and JC436-91. Only one class of the expansive cement is commercially available at present, Class 525, which standard strength is determined at 28 days (Table 3). TCS expansive cements have a relatively high early strength, especially for mini-expansive types.

Minimum W/C ratio for complete hydration

Compared with OPC, TCS paste has a comparatively high minimum W/C ratio for complete hydration. The principal hydration products of hydrated TCS are $C_3A \cdot 3C\bar{S} \cdot 32H$ (AFt), $C_3A \cdot C\bar{S} \cdot 12H$ (AFm), AH_3 gel, and FH_3 gel; all have fairly high levels of chemically bound water. According to a theoretical calculation the non-evaporable water per unit mass of cement of a fully hydrated paste for TCS rapid-hardening and mini-expansive types is in the range of 0.40-0.45; the typical value for OPC is only about 0.23-0.24. Comparing TCS and OPC concretes if the amount of water is fixed to constant slump, quantity of chemically bound water for TCS is much higher than for OPC, whereas

Table 2 Physical and mechanical indexes of the rapid hardening cement

Clinker	Class	Setting time	Compressive strength (MPa)			Flexural strength (MPa)		
			12h	1d	3d	12h	1d	3d
SAC	425#	Initial ≤25min	29.4	34.4	41.7	5.9	6.4	6.9
	525#	Final ≥180min	36.8	44.1	51.5	6.4	6.9	7.4
	625#		39.2	51.5	61.3	6.9	7.4	7.8
			1d	3d	28d	1d	3d	28d
FAC	425#	Initial ≤25min	34.5	42.5	49.0	5.9	6.4	6.9
	525#	Final ≥180min	44.0	52.5	59.0	6.9	7.4	7.8

Table 3 Physical and mechanical indexes of the expansive cement (Strength: MPa)

Clinker	Class	Setting time	Comp. strength			Flex. strength			Free expansion ratio	
			1d	3d	28d	1d	3d	28d	1d	28d
SAC	Mini-expansive	Initial ≤30min	31.5	41.0	52.5	4.9	5.9	6.9	≤0.05%	≥0.5%
	Expansive	Final ≥180min	27.5	39.2	51.5	4.4	5.4	6.4	≤0.10%	≥1.00%
FAC	425#	Initial ≤30min	31.5	41.0	52.5	4.9	5.9	6.9	≤0.05%	≥.0.5%
	525#	Final ≥180min	27.5	39.2	51.5	4.4	5.4	6.4	≤0.10%	≥1.00%

the evaporable water for TCS was obviously less than for OPC. This is one of the main reason why TCS has relatively lower porosity than OPC and why TCS concrete has excellent impermeability, carbonation resistance, freeze-thaw resistance and high resistance to many forms of chemical attack.

Evolution of hydration heat

The total quantity of heat evolved by TCS rapid-hardening cement and expansive cement at 7days (when most of hydration is finished) is typically 190-210 kJ/kg, somewhat less than ordinary Portland cement (400-480 kJ/kg) and calcium aluminate cement (325-400 kJ/kg), but due to the speed of the reaction, nearly all this heat is produced within 24 hours, as shown in Figure1.

This special feature of heat evolution on hydration gives TCS rapid-hardening cement a very useful advantage — so call "self-steam curing". Therefore, the steam curing procedure sometimes used in concrete work may be omitted, with decreased energy consumption. On the other hand, TCS is suitable for low temperature. It can concreted as usual at subzero temperature (0℃ to -25℃) by adding an appropriate amount of anti-freezing agent and adopting some simple heat loss prevention measures, for its 3 days strength can reach 80% of its ultimate strength. In massive concrete construction, special attention should be attached to the absolute temperature rise inside the structure and the temperature gradient between the structure and ambient conditions. If the difference exceeds 20℃, thermal cracking may occur and if the absolute temperature exceeds 100℃, the expansion produced upon cooling by ettringite reformation causes the concrete to crack. Thus temperature effects could lead to serious deterioration of TCS concrete.

Pore structure of the hardened cement paste

The pore structures for rapid-hardening cement and expansive cement are quite different from those of

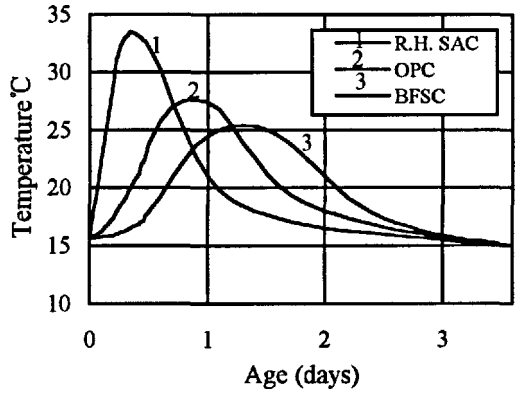

Fig. 1 The heat evolution on hydration for rapid-hardening SAC. (R.H SAC — Rapid-hardening Sulfo-aluminate cement; BFSC — Blast furnace slag cement. The results are tested according to the Chinese Standards concerned)

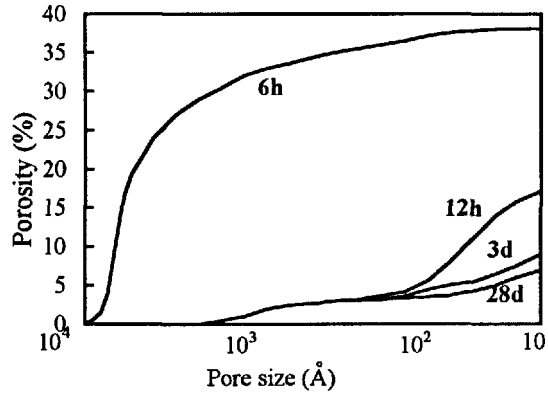

Fig. 2 The general porosity of TCS paste, w/c = 0.30, ambient temperature, the specimens were continuously evacuated to the constant weight at 100-160 mmHg.

Table 4 Pore size distribution of different cement mortar (C:S=1:1)

Cement / Pore size	OPC, Jiangnan plant		Type K expansive cement		Rapid-hardening SAC	
	Volume (ml/g)	%	Volume (ml/g)	%	Volume (ml/g)	%
55,000-10,000 Å	0.0023	5.52	0.0016	3.25	0.0012	4.07
10,000-1,000 Å	0.0044	10.55	0.0026	5.28	0.0046	15.59
1,000-500 Å	0.0047	11.27	0.0012	2.44	0.0012	4.07
500-250 Å	0.0138	33.09	0.0082	16.67	0.0012	4.07
250-100 Å	0.0084	20.14	0.0232	47.15	0.0032	10.85
100-50 Å	0.0045	10.79	0.0068	13.82	0.0072	24.41
50-25 Å	0.0036	8.64	0.0056	11.39	0.0101	36.95
Total porosity	0.0417		0.0492		0.0295	
Position of peak (Å)	458		246		<25	

OPC. Mercury intrusion porosimetry (MIP) results are shown in Table 4, for 1:1 mortar under uniaxial restraint. According to MIP results and other from helium pyknometry, pore structures of TCS rapid-hardening cement and expansive cement have the following features:

(1)The total pore volume for TCS is significantly lower than for OPC (see Table 4).

(2)The average pore radius is relatively small: most are less than 300 (see Figure 2) and the maximum-lickhood of pore radius less than 25Å (Table 4).

(3)The morphology of most pores had an ink-bottle sharp.

These features contributed to the performances of TCS concrete, notably to freezing resistance, impermeability, corrosion resistance, anti-carbonization and reduced dry-shrinkage, etc. All these advantages will be beneficial to durability.

Table 5 Strength development of the FAC and OPC concretes

Cement	Comp. strength(MPa)/Ratio to the 28 days' strengths				
	0.5d	1d	3d	28d	180d
525# rapid-hardening FAC	20.0/0.38	36.0/0.60	51.6/0.86	60.3/1	68.5/1.14
525# OPC, Jidong plant	5.8/0.1	19.2/0.38	37.8/0.65	58.5/1	62.5/1.07

Table 6 Properties of the concrete with the third cement series

Cement content (kg/m^3)	Admixture	W/C	Slump (cm)	Air content (%)	Bulk density (kg/m^3)	Setting time (h:m)	
						Initial	Final
480	Special admixture ZB-1	0.34	9.0	1.1	2474	2:35	3:03

Strength (MPa)	1d	3d	28d	6m	1y
Compressive strength	44.6	61.9	69.2	80.7	81.0
Splitting strength	2.85	4.24	5.38		5.74
Flexural strength		7.23	8.70		8.81

Note: ZB-1 is a kind of compounded superplasticiser specially used for adding in TSC concretes to reduce water and control their setting time and workable time. It is a proprietary product.

MAJOR PROPERTIES INVOLVED WITH TCS CONCRETE DURABILITY

Physical properties for TCS rapid-hardening cement and its concrete

The development of strength of Class 525 TCS rapid-hardening and Class 525 OPC are compared in Table 5, and splitting and bending strengths in Table 6. The early strengths of TCS were higher and the splitting and bending strengths for TCS concrete grew in pace with its curing time and compressive strength.

Impermeability of TCS concrete

As mentioned above, the evaporable water in TCS, rapid-hardening and expansive, are less than in OPC, so the former were more dense than OPC. Therefore, it was found that the former had better impermeability, especially the mild-expansive concrete; results are shown in Table 7 and 8. This advantage is believed to be of benefit to resist corrosion of embedded steel reinforcement in the concrete and to improve the durability.

Freezing-thaw resistance

TCS rapid-hardening and expansive concretes showed outstanding anti-freezing performance. Experimental results by China Building Materials Academy (CBMA) as well as from Ssangyong Group, South Korea, a common conclusion derived was that the strength decreases were slight after 270-300 cycles of freezing and thawing (Tables 9 and 10). There was few if any strength loss for TCS casting concrete under the ambient temperature changed alternatively normal and minus (see Figure 3).

Carbonation resistance

Table 11 shows that comparatively shallow penetration of CO_2 into TCS concrete at 28 days thus indicating that the concrete will protect reinforcement.

Table 7 Impermeability of the rapid-hardening cement concrete

28 days' comp. Strength (MPa)	Water pressure (kg)	Permeability	Osmotic height (mm)
40.7	30	impermeable	38
35.3	30	impermeable	75

Table 8 Impermeability of different concretes

Varieties of concrete	Time of keeping pressure (h)				Permeated height (mm)
	1.47 MPa	1.96 MPa	2.45 MPa	2.94 MPa	
OPC Water-proof	8	0	0	0	120~140
FAC	8	8	8	8	50~60
Type-U Shrinkage-compensated	8	8	8	8	60~80
Type-EA Shrinkage-compensated	8	8	8	8	60~80
Water-proof concrete with $FeCl_3$	8	8	8	8	150
Water-proof concrete with organ silicon	8	8	0	0	150

Table 9 Freeze-thaw resistance of FAC concrete

Admixture	W/C ratio	Slump (cm)	Compressive Strength after 300 cycles (MPa)	Compressive strength of control specimens (MPa)	Loss ratio of Strength (%)
Special admixture ZB-1	0.40	18	66.6	67.7	1.62

Table 10 Comparison of rapid freezing and thawing resistance of OPC, the rapid-hardening and mini-expansive SAC concrete

Cement type	Slump (cm)	Air con-tent (%)	Comp. Strength at 28 days(MPa)	Variation of comp. strengths after the following cycles (%)						
				0	30	60	90	150	210	270
R.H. SAC	16.0	3.0	56.1	100	99.7	100.7	99.6	99.6	99.7	97.0
M.E. SAC	14.5	2.5	28.0	100	98.7	99.0	98.7	99.9	99.4	95.1
OPC	15.6	2.4	53.1	100	93.7	84.7	88.7	72.3	59.9	/

Note: R.H.SAC—Rapid-hardening Sulfo-aluminate cement; M.E.SAC—Mini-expansive Sulfo-aluminate cement; Extreme temperatures of freeze-thaw cycle are -20℃and +20℃.

Chemical-attack resistance

TCS cements were found to have excellent resistance to sulfate attack and many other forms of chemical attack, especially to their combinations on site. Tables 12,13,14 and 15 give some results of the chemical resistance test completed by China National Lab for Railway Construction, which indicate that TCS has a relatively greater coefficients of corrosion resistance (corroded strength/control strength) compared with other types of cement. Most of the TCS specimens showed increased strength after a certain time in corrosive solution. It was also found that TCS has a very good resistance to recrystallization damage.

Table 11 Carbonation resistance of FAC concrete

Cement	Admixture	W/C	Slump (cm)	Carbonated depth (mm)
FAC from Tangshan plant	\	0.52	7	1.29
FAC from Tangshan plant	ZB-1	0.40	18	0.98
FAC from Lengshuitan plant	ZB-1	0.30	5	0.26

Note: The results in the Table were obtained from the specimens carbonated for 28 days under the standard condition (CO_2: 20±3%; T: 20±5℃; RH: 70±5%). Because different raw materials were adopted, the proportions of $C_4A_3\bar{S}$ and ferrite phase in clinker have some differences between the FAC's from Lengshuitan plant and Tangshan plant.

Table 12 Coefficients of corrosion resistance to salt water of high concentration

Corrosion solution / Cement	Luntai Water	Ruoqiang Water	5% Na_2SO_4	5% $MgSO_4$	5% NaCl	15%NaCl + 5%$MgSO_4$
425# Slag Cement	0.44	0.83	0.6	Destroyed	0.79	
525# OPC	0.16	0.34	0.67	Destroyed	0.82	
High Alumina Cement	0.79	1.02	Destroyed	1.22	0.95	
Sulfate-Resistant Portland Cement				0.71		0.16
Low Heat and Mini-expansive cement	0.21	0.91	1.13	Destroyed	0.98	0.54
Early-Strength SAC	1.3	1.33	1.13	1.14	1.11	1.17
Early-Strength SAC + 20%Slag	1.36	1.48	1.34	1.29	1.22	
Early-Strength SAC + 40%Slag	1.54	1.41	1.18	1.51	1.11	

Note: The characteristics of Luntai water: Na^+ and K^+=83,800mg/l, Mg^{2+}=8,400mg/l, Cl^- =143,000mg/l, SO_4^{2-}=14,600mg/l; The characteristics of Ruoqiang water: Na^+ and K^+=100,800mg/l, Mg^{2+}=12,566 mg/l, Cl^-=127,090mg/l, SO_4^{2-} = 71,040mg/l.

Resistance to alkali-aggregate reaction

Damage caused by alkali-aggregate reaction (AAR) has occurred in many concrete structures. Finding the best cementitious material to limit AAR is a goal of researchers and customers. We found that TCS can effectively restrain the expansion caused by the reactions of alkali with the silica in highly active quartz glass and especially with the carbonate in highly active dolomite.

10×10×40mm mortar specimens and 20×20×60mm concrete specimens were tested to determine expansion features of alkali-silica and alkali-carbonate reactions (ASR and ACR) respectively. A high alkali content OPC (1.0%) was employed as the control specimen and three curing temperatures (20 ℃, 60℃and 75℃) were used.

The result showed that the specimens of SAC, FAC and those with 30% fly ash added remained dimensionally stable with age but marked expansions and cracks occurred in the controls. According to the Arrherius formula and the activation energy (91.4 kJ/mol) of ACR, the age of the concrete cured for 80 days at 75℃and for 160 days at 60℃are equivalent to about 120 years cure at 20℃. Therefore, it can be concluded that TCS will be alternative to deal with the AAR problem, especially ACR.

Table 13 Corrosion resistance to complex solutions of magnesium sulfate

Concentration (mg/l)		Sulphate-resistant Cement	SAC
SO_4^{2-}	Mg^{2+}		
5,000	500	0.85	1.15
5,000	1,000	0.90	1.11
10,000	1,000	0.92	1.29
10,000	2,000	Damage	1.21
15,000	1,500	Damage	1.16

Table 14 Coefficient of crystallization-restruction resistance

Testing Method / Corrosive Solution / Cement	Crystallizing for 28 cycles by lowering the temperature	Crystallizing for 14 cycles by lowering the temperature	14 dry-wet cycles
	Luntai Water	$10\%Na_2SO_4$	$10\%Na_2SO_4$
425# Slag Cement	0.79	0.72	0.22
525# OPC	0.89	0.63	0.25
Low Heat and Mini-Expansive Cement	0.79	0.97	/
Early-Strength SAC	1.13	0.93	0.41
Early-Strength SAC + 20%Slag	1.52	1.16	1.36
Early-Strength SAC + 40%Slag	1.28	0.98	1.31

Table 15 Corrosion state of concretes buried for 3 years on-the-spot

Cement	Standard strength (MPa)	Luntai area			Ziniquan area		
		Strength (MPa)	Ratio (%)	Appearance	Strength (MPa)	Ratio (%)	Appearance
525# R.H. SAC	57.0	54.2	95	sand dropped slightly clear edges and angles	51.2	90	complete edges and angles
525# R.H. SAC + 20% Slag	50.0	46.5	93	sand dropped slightly clear edge and angle	48.0	97	complete edges and angles
525# R.H. SAC + 40% Slag	40.0	38.0	94	sand dropped slightly clear edges and angles	43.9	109	complete edges and angles
525# moderate heat OPC	63.8	26.0	41	stone showed, angles dropped seriously	17.3	27	stone showed, angles dropped seriously
525# sulfate-resistant cement	65.2	38.0	58	stone showed, angles dropped seriously	/	/	broken to pieces
425#slag cement	48.8	34.1	64	stone showed, angles dropped slightly	14.8	30	angles dropped seriously

Note: 1.W:C:S:A=0.5:1:1.90:2.90; 2.The size of the specimens was 40×40×40mm; 3.Medium size sand, 5-20mm broken stone were used. 4.The water in Luntai Area: Cl^- is up to as high as 180,000 mg/l, SO_4^{2-} up to 20,000mg/l and Mg^{2+} up to 3,000mg/l; The water in Ziniquan Area: Cl^- is up to as high as 150,000mg/l, SO_4^{2-} up to 110,000mg/l and Mg^{2+} up to 15,000mg/l.

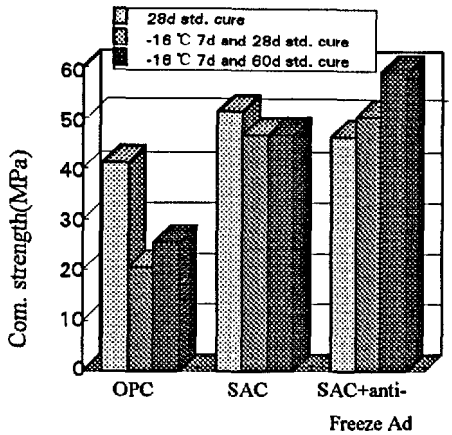

Fig. 3 Comparison of the freeze resistance at the early stage (The same mix proportion was used. The specimens were immediately put into refrigerator after casted.)

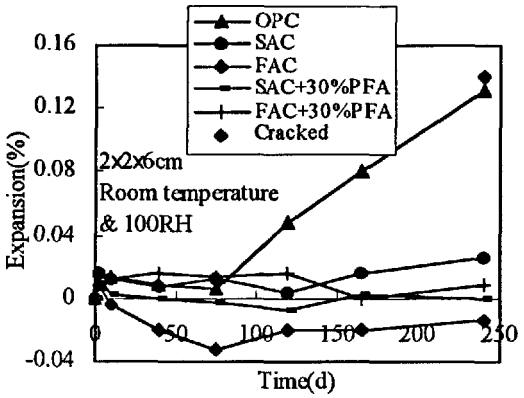

Fig. 4 The relationship between the expansion caused by alkali-aggregate reaction (ASR) and the ages, specimen size: 20×20×60 mm; active aggregate: Silex glass; ambient temperature; alkali content in the OPC = 1.0%.

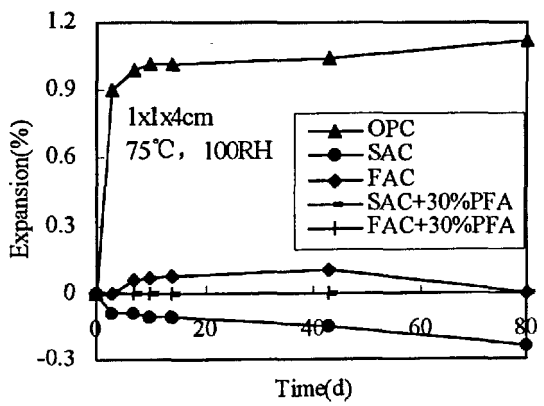

Fig. 5 Expansion caused by ASR. Specimen size: 10×10×160 mm; active aggregate: Silex glass; curing temperature: 75 ℃; alkali content in the OPC = 1.0%.

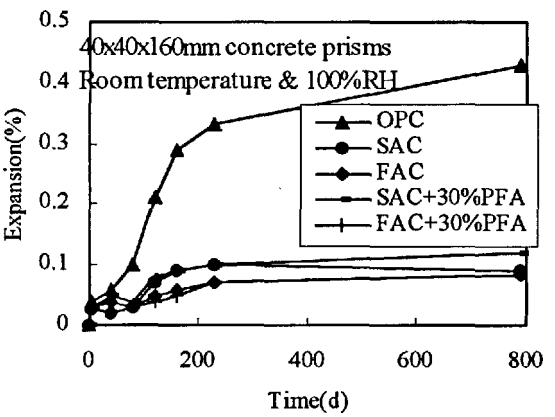

Fig. 6 The long-term development of the expansion caused by ASR, active aggregate: Silex glass; alkali content in the OPC = 1.0%.

Rusting resistance

A sufficient importance has been attached to the corrosion of steel reinforcement in SAC and FAC concretes. During the last 25 years, a series of examination have been done under the different environments in which the concretes have to serve and by different testing methods, for instance, accelerated tests, examining specimens buried in moist ground and those placed in tidelands. The conclusions from these examinations are consistent. Steel reinforcement in SAC concrete had some slight rust spots at early age (up to 3 days), but further attack was effectively inhibited. The alkalinity 11.5-12.0 in SAC is somewhat less than in OPC. A passive film, therefore, is established and stabilized with difficulty. This is considered to be the major reason why slight spots rusting occurs in early curing. However, as the hydration of SAC proceeds, the cathodic reaction of the rusting process will soon be

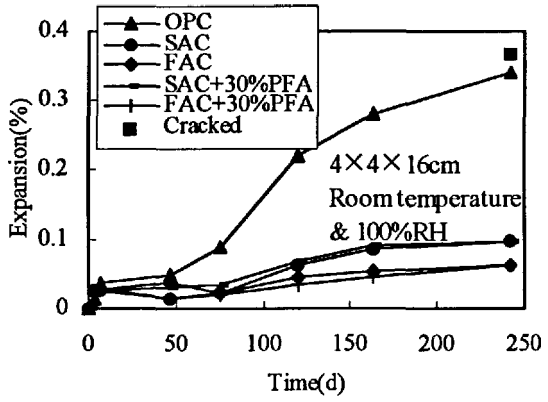

Fig. 7 The development of expansion caused by alkali-aggregate reaction (ACR), active aggregate: Dolomite; alkali content in the OPC = 1.0%.

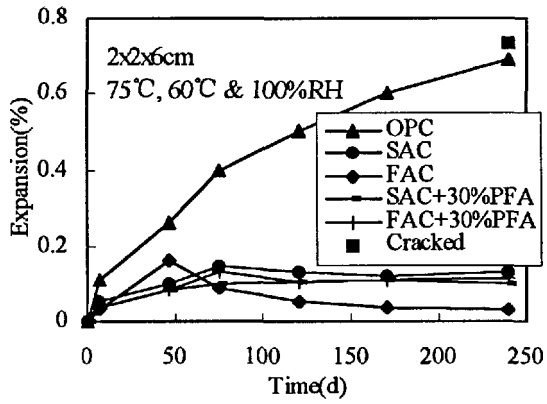

Fig. 8 The relationship between the expansion caused by ACR and the curing time, curing temperature: at 75℃for 80 days and consequently 60℃ for 160 days; active aggregate: Dolomite; alkali content in the OPC = 1.0%.

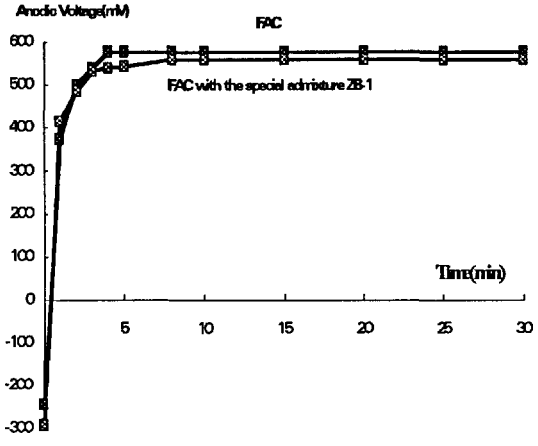

Fig. 9 The anodic polarization curve for the hardening paste of FAC

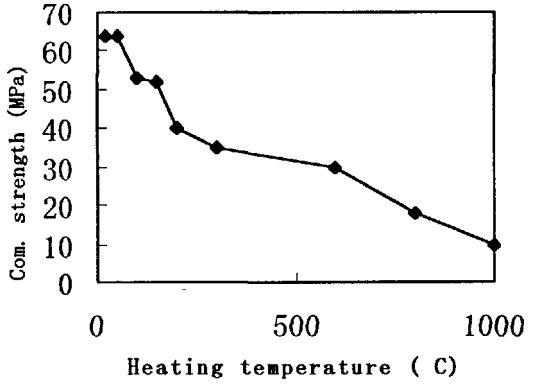

Fig. 10 The strength losses for TCS by heating at different temperatures

restrained because the pores do not contain the water necessary to promote the reaction and the extent of penetration by O_2 is small in dense SAC concrete. This conclusion is strongly supported by an examination on a 13-year-old SAC pipe placed in tidelands on the coast of East China Sea.

In addition to having a similar density to SAC, FAC presents a higher alkalinity (pH 12.5 -13.0) in its pore solution than SAC and is close to that of OPC, so a passive film can be stabilized on the surfaces of the steel bar in FAC concrete. FAC, therefore, will have a better rusting resistance than SAC or OPC.

Long-term strength development

The main hydrates in TCS system are AFt, AFm, C-S-H gel and alumina gel, which are all stable minerals under ordinary temperature. Unlike calcium aluminate cement, there is no so-called

Table 16 Long-term strengths of the rapid hardening cement

Concrete proportion	Compressive strength (MPa)					
	1m	3m	6m	1y	2y	6y
1:1.33:2.81:0.42	41.5	45.0	49.0	51.9	52.3	55.1
1:1.69:3.69:0.50	36.1	38.8	41.3	43.1	45.1	46.7
1:2.30:4.58:0.62	31.8	33.3	34.4	35.4	37.9	39.8

Table 17 Long-term strengths of high-strength FAC concrete with the special admixture

W/C ratio	Slump (cm)	Compressive strength (MPa)			
		3d	7d	28d	3.5y
0.25	4		82.9		122.6
0.28	6	72.2		80.5	111.9

conversion problem in TCS systems. Proved to the hilt by over 20 year's experience in China, its long-term strength is stable and a certain increase with time has been observed. During last 20 years, over 8 million tones of TCS have been produced and used in a variety of building constructions and concrete products. There is no any report on the structural accident caused by strength loss. Some laboratory results about the long-term strength of TCS concrete are shown in Tables 16 and 17.

Thermostability

TCS' thermostability had been being attached an increasing importance considering the principle hydration products is ettringite (around 40 to 60%). We have intensively investigated the strength loss of TCS paste. The conclusions may be initially derived as in the following:

(1)After heating for 24 hours, TCS' compressive strength will keep in a relatively steadfast value and does not change with the heating time.

(2)The strength falls off as the temperature increases. At 100℃-150℃, the strength loss was relatively small, about 15%; at 300℃, the strength loss would reach 45%. The strength loss curve is shown in Figure 10.

(3) XRD results shown that there is no decomposition product yielded by the dehydration was detected before 600℃. The decomposition productions above 600℃ are $C_4A_3\overline{S}$, $C_{12}A_7$, $CaSO_4$, $\beta - C_2S$ and $2C_2S \cdot CaSO_4$.

(4) As opposed to OPC, ettringite, C-S-H and alumina gel will be reformed on subsequent curing in water after the heating. TCS' strength is, therefore, restored and may even be somewhat higher than that before. It was also found that the higher is the heating temperature, the higher is the restored strength (see Figure 11).

CONCLUSIONS

The third cement series, consisting of Sulpho-aluminate and Ferro-aluminate cement, has been developed in China since 1972 and over 8 million tones of TCS produced in industrial-scale, which all

used in a great variety of building constructions and concrete products.

Its excellent performances were the main reasons to attract architects, concrete engineers and customers, such as rapid setting and hardening, impermeability, freezing resistance and alkali-aggregate resistance, etc.

The research on the durability for a relatively developed cement is a slow and complex task. We have done a lot of work and started joint researches with groups form the U. K., Japan, France, South Korea and Germany, but these are just initial steps to establish new cement binders.

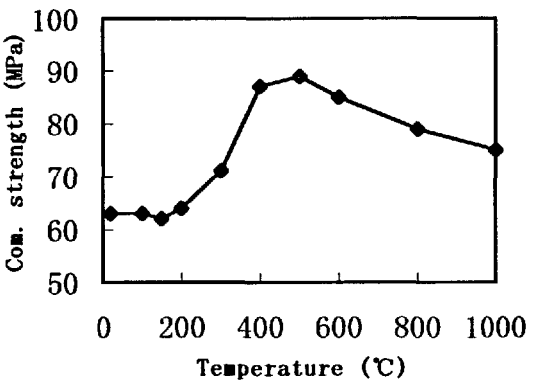

Fig. 11 The strength changes for the TCS paste cured in water for 14 days after being heated to different temperatures.

REFERENCES

Dedong, LI and Jun'an, DENG, "Research on the Thermostability of the Rapid-hardening Sulpho-aluminate Cement", Journal of the Chinese Ceramic Society, Vol. 11, No. 3, 1983, pp. 32-38.

He, LI and Boshan, XU, "Application of the Rapid-hardening Sulfo-aluminate Cement in Winter Construction", Technical report of China Capital Iron & Steel Co., 1992 .

Yaping, XU and Heyun, CHEN, "Study on the Chemical-attack Resistance of Ferro-aluminate Cement", Proceedings of the third annual meeting of China Building Materials Academy, 1986, pp. 116-130.

Zhongzi, XU, Min, DENG and Mingshu, TANG, "Study on the Alkali-aggregate Reaction of Sulfo- and Ferro-aluminate Cement", Technical report of Nanjing University of Chemical Engineering, 1994.

SULPHO-ALUMINATE CEMENT WITH LOW ALKALINITY

WANG Yanmou, LI Shaozheng, SU Muzhen, XU Jingjun, ZHANG Fengqin

ABSTRACT A new type of low alkalinity cement with pH value of 10.5 was described, which is composed of sulpho-aluminate clinker and some amount of additions. SIC method was adopted to study the strength reservation rate of glass fibre in this kind of low alkalinity cement and the corrosion of glass fibre was investigated by SEM. All the results show that this cement has a very slight corrosion to glass fibre and confirm that the service life of the GRC products with it will be over 100 years .

Key-words: Corrosion Durability Sulphoaluminate Glass

INTRODUCTION

The composite of glass-fibre and cement or concrete is known as glass fibre reinforced cement or concrete (GRC) . It is obviously that the strength and toughness of GRC, using concurrently alkali-resistant glass fibres and ordinary Portland cement, are reduced quickly with time. The reasons are mainly that alkali-resistant glass fibres are still attacked with very high alkalinity (pH=13 ~ 14) in hardened ordinary Portland cement paste. Since 1980s, in order to improve the durability of GRC a lot of works have been done by many researchers in china and abroad. Low alkalinity sulphoaluminate cement that will be introduced in this paper is a new type of low alkalinity cement developed specially for improving the durability of GRC. We own the invention patent.

EXPERIMENTAL AND RESULTS

Composition and property of low alkalinity sulphoaluminate cement (LSAC)

The major mineral components are $C_4A_3\bar{S}$ and C_2S in sulphoaluminate clinker, and based on it we have developed the low alkalinity cement by adding just right amount of some additives and anhydrite. The annual output will be up to 200,000 tons by 1997. The chemical composition and properties of the low alkalinity cement are presented in Table 1, 2 and 3.

Table 1 Chemical composition of LSAC

Composition	Si_2O_3	Al_2O_3	Fe_2O_3	CaO	SO_3
(%)	3 ~ 7	19 ~ 22	1 ~ 2	41 ~ 44	14 ~ 16

Table 2 Strength and setting time of LSAC (Curing in 20 ± 2 ℃ water)

Grading	W/C	C/S	Comp. (MPa)		Bend. (MPa)		Setting time (min)	
			1d	7d	1d	7d	Ini.	Fin.
425#	0.42	1:2.5	32.0	42.5	4.5	6.0	≮ 25	≯ 180
525#	0.42	1:2.5	39.0	52.5	5.0	6.5	≮ 25	≯ 180

Table 3 Drying shrinkage rate of cements

Type of cement	C/S	Drying shrinkage rate (%)							
		1d	3d	7d	14d	21d	28d	42d	56d
RSAC	1:2.5	0.03	0.04	0.06	0.06	0.06	0.06	0.06	0.07
LSAC	1:2.5	0.01	0.02	0.03	0.04	0.04	0.04	0.04	0.04
RSAC	1:0.5	0.04	0.06	0.07	0.07	0.08	0.08	0.09	0.10
LSAC	1:0.5	0.03	0.05	0.05	0.05	0.07	0.06	0.06	0.08

NOTE : RSAC — rapid-hardening sulphoaluminate cement ; C/S — cement sand ratio
Curing in 20 ± 3 ℃ water ; Relative humidity=60 ± 5%

Besides, the free expansion rate of LSAC at 28 days is 0.00 ~ 0.10%; and the pH value of its suspension (cement-water ratio is 1:10) at 1 hour is about 10.5.

Experiment of LSAC attack on glass fibre

The method of fibre remaining strength in cement mortar (SIC) was used in this experiment. The sample size of SIC is shown in Figure 1.

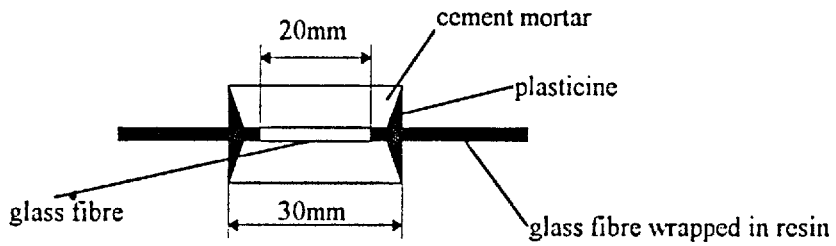

Figure 1 A SIC specimen

The results of accelerated ageing test were presented in Table 4, 5 and Figure 2, 3, in which specimens were immersed in 80 ℃ water.

Table 4 SIC results (immersed in 80 ℃ water)

Cement	Glass fibre	Tensile strength of fibre (KN)							
		Prim.	Demould	1d	3d	7d	14d	21d	28d
LSAC	Cem-fil I	4.28	4.16	3.68	3.73	3.01	3.24	2.70	2.38
OPC	Cem-fil I	4.28	3.28	2.29	1.71	1.33	1.08	1.31	0.91

NOTE : LSAC — Low Alkalinity Sulphoaluminate Cement ; OPC — Ordinary Portland Cement

Table 5 SIC results (immersed in 80 ℃ water)

Cement	Glass fibre	Retained tensile strength of fibre (%)							
		Prim.	Demould	1d	3d	7d	14d	21d	28d
LSAC	Cem-fil I	100	97.20	85.98	87.15	70.33	75.70	63.08	55.61
OPC	Cem-fil I	100	76.64	53.50	39.95	31.07	25.23	30.61	21.26

NOTE : LSAC — Low Alkalinity Sulphoaluminate Cement ; OPC — Ordinary Portland Cement

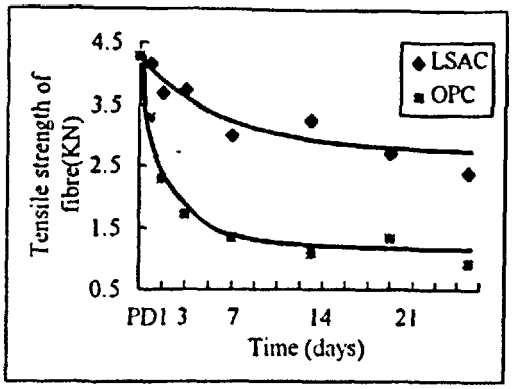

Figure 2 Variation of tensile strength of fibre with time

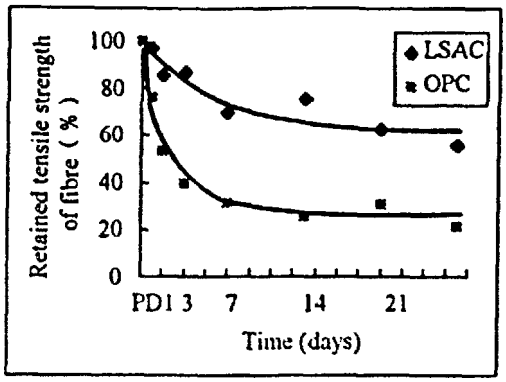

Figure 3 Variation of retained fibre's tensile strength with time

(P — initial ; D — after demoulding)

It may be seen from Table 5 that the glass fibre strength retention ratios at 1 day were 85.98% and 53.50% as using LSAC and OPC respectively; and they were 55.61% and 21.26% at the age of 28 days. Because there is a correlation between the accelerated ageing test with specimens curing in 80 ℃ water and the natural ageing test with specimens exposing to the air, and 1 day accelerated ageing corresponds to 4 ~ 5 years natural ageing. If the fibre strength retention ratio is suggested to be 50% the demarcation point for judging whether or not the durability of materials is satisfactory. Clearly the service life for Cem-fil I glass fibre reinforced LSAC will exceed 100 years, and that for OPC GRC will be only 4 ~ 5 years.

In the mean time, SEM results (Figure 4) confirm that LSAC has a very slight corrosion to glass fibres.

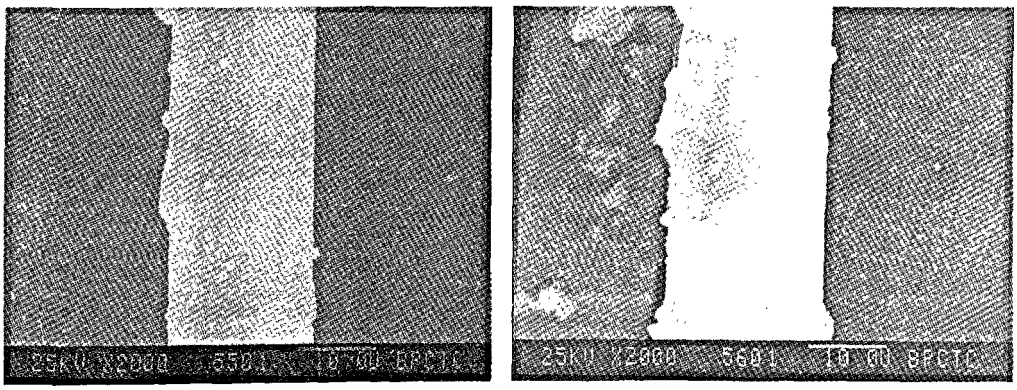

(a) Reinforced LSAC (b) Reinforced OPC

Figure 4 SEM photographs of glass fibres taken from SIC specimens(immersed in 80 ℃ water for 7 days)

DISCUSSION

The low alkalinity sulphoaluminate cement has very little corrosion to glass fibres, affecting mainly by the mineral compositions and hydration characteristics of LSAC. As to sulphoaluminate cement system, the major hydration reactions are as follows :

$$C_4A_3\overline{S} + 2CaSO_4 + 38H_2O \rightarrow C_3A \cdot 3CaSO_4 \cdot 32H_2O + 2AH_3 \quad [1]$$

$$C_2S + 2H_2O \rightarrow C-S-H + Ca(OH)_2 \quad [2]$$

$$3Ca(OH)_2 + 3CaSO_4 + AH_3 + 26H_2O \rightarrow C_3A \cdot 3CaSO_4 \cdot 32H_2O \quad [3]$$

It can be seen from Eqs1 — 3 that there is only temporarily $Ca(OH)_2$ present in the system. So sulphoaluminate cement is a kind of low alkalinity cement developed on the basis of sulphoaluminate cement by adding some additive. Thus the LSAC system possesses much low alkalinity and less corrosion to glass fibre. According to above results, we have achieved the goal of increasing greatly the durability of GRC. Heidelberger Zement AG in Germany researched the durability of GRC produced with Cem-fil II alkali resistance glass fibre and LSAC. The results were exciting as presented in Table 6.

Table 6 Results of accelerated ageing test

Conditions	Limit of proportionality		Modulus of rupture		Elongation (ε)	
	MPa	Relative value (%)	MPa	Relative value (%)	%	Relative value (%)
Before immersion in 80 ℃ water	9.96	100	35.2	100	10.2	100
Immersion in 80 ℃ water for 3 days	9.79	98.3	31.0	88.1	9.73	94.7
Immersion in 80 ℃ water for 7 days	8.33	83.6	29.4	83.5	9.52	92.7
Immersion in 80 ℃ water for 14 days	9.65	96.9	29.9	84.9	9.28	90.4

NOTE : Glass fibre — Cem-fil II ; Cement — Chinese low alkalinity sulphoaluminate cement

CONCLUSION

1. The low alkalinity sulphoaluminate cement is of low alkalinity, high strength (especially early strength), small free expansion and small dry shrinkage.
2. The service life of GRC made of LSAC and alkali-resistance glass fibres will exceed 100 years.
3. Due to possessing various excellent properties, the low alkalinity sulphoaluminate cement would be a more ideal cement for GRC.

INVESTIGATION OF COMPATIBILITY OF CEMENTS WITH SEVERAL SALTS

by J. STARK and S. STÜRMER, Bauhaus-University Weimar

ABSTRACT During their service life mortars are often exposed to salt solutions. Most methods described in literature determine the resistance of mortar immersed in salt solutions, that means only external attack. The described method determines the compatibility of cement mortars with salts. This way the cements are in contact with salts from the beginning of hydration. The point of this paper is not the damage by hygroscopicity of salts and their cristallization or hydration pressure, but the possibility of reactions of salts with certain compounds of the cements.

Key-words: Air entraining,Chemical attack,Differential thermal analysis,Ettringite,volume change

CHARACTERISTICS OF CEMENTS AND SALTS The binding materials used in the investigation are 3 commercially used cements according to German Standard DIN 1164-1, part 1: a low C_3A high-sulfate resistant Portland cement (PC) CEM I 42.5 R-HS, a high C_3A PC CEM I 42.5 R, a high sulfate resistant cement rich in granulated blastfurnace slag CEM III 32.5 - NW/HS and a binding material consisting of granulated blastfurnace slag, anhydrite and cement (SSC) similar to the former standardized sulfate slag cement.

Chemical, physical and phase-analytical investigations were carried out to characterize the binding materials used. The chemical analyses of the cements is given in Table 1.
Sulfates, nitrates and chlorides were used as salts which are detrimental to buildings. Two different sulfates and two different nitrates were included in the investigations, because the degree of danger to building materials caused by salts is not only dependent on the kind of anions but also on the kind of cations.

Calcium sulfate dihydrate can be found as a salt inherent in various building materials but it can also penetrate into the building material from outside: SO_2 in the air or sulfate attack from water, soils and gases. Magnesium sulfate will often be found in its hydrate stages where sulfates e.g. from plaster mortars attack dolomite-containing building materials in the presence of moisture. Sodium chloride in coastal regions, however, can only penetrate from outside. Possible sources are: atmospheric attack, splashing water containing de-icing salt solutions, ground water and mixing water containing chloride and acification agents based on hydrochloride acid. Nitrate attack in buildings is also due to outside factors. A possible source is the presence of nitrifying bacteria. Nitrates are also formed by chemical reaction of ammonium and NOx compounds with building materials containing lime and alkali in presence of oxygen from the air.

EXPERIMENTAL To test compatibility in periods which lend themselves to investigation it is important to bring the systems to be investigated in close contact and to avoid too high dilution of the reacting components. For this reason cement paste, usually employed for injections, were used instead of mortars containing aggregates. For storing the specimens you should find conditions which favour the formation of hydrous expansive minerals, i.e. low temperatures and high humidity. To investigate the influence of pore space on the compatibility of above mentioned systems air pores were entrained into the cement paste by means of a tenside. These mixtures are called foam pastes (fp). Production and properties of foam mortars have already been reported elsewhere [Stürmer et al. 1994]. For all experiments the water/binder ratio was 0,5. A cement paste/foam volume ratio of 2:1 was used in any case. The parameters of hardened cement paste (hcp) and foam paste are given in Table 2.
For the simulation of the internal attack the salts with contents of 10 % related to the weight of cement were dissolved in mortar mixing water. The simulated attacking mechanism occurs in restoration practice, e.g. if salts on the surface of building materials like natural stone surfaces are dissolved when getting into contact with fresh mortar in the case of injection.

Table 1: Analytical data of cements

Chemical Analysis (%)	CEM I 42.5R-HS PZ 45 F-HS	CEM I 42.5R PZ 45 F	SSC	CEM III/B 32.5 NW/HS
L.O.I.	1.30	3.20	+	+
CaO	64.20	64.00	42.90	47.30
SiO_2	21.50	20.70	32.10	28.00
Al_2O_3	4.00	5.50	10.30	11.00
Fe_2O_3	6.10	2.10	0.98	1.40
MgO	0.20	0.80	6.80	3.40
K_2O	0.52	0.96	0.73	0.95
Na_2O	0.11	0.12	0.34	0.39
SO_3	2.20	2.90	5.10	3.90
Cl^-	<0.01	<0.01	<0.01	0.03
CaO_{free}	0.40	1.50	-	-

Table 2: Some properties of hardened cement pastes (hcp) and foam pastes (fp)

	Hardened Cement Paste			Foam Paste		
Cement	Tensile Strength N/mm^2)	E-Modulus (N/mm^2)	Porosity (%)	Tensile Strength (N/mm^2)	E-Modulus (N/mm^2)	Porosity (%)
CEM I 42.5 R-HS	0.7	20400	37	0.60	8500	68
CEM I 42.5 R	0.8	21000	36	0.40	9000	73
CEM III/B 32.5 NW/HS	n.i.	n.i.	37	0.30	n.i.	73
SSC	1.2	15400	46	0.58	7600	75

n.i. ... not investigated

The change in length which took place when the systems came into contact and its progress during the test period were taken as a measure of compatibility [Stürmer et al. 1993]. In addition the change in weight was measured. If the change in length was high, a sample was taken and examined by X-ray diffraction and diffential thermoanalysis (DTA) in order to detect the cause.

The specimens were stored at 10°C and 85 % relative humidity (values that are relevant to historical buildings [Garrecht et al. 1991]) an at 10 °C under water. All cement/salt mixtures were stored separately, whereby all specimens were immersed in the same water volume. Immersion in water was to support the formation of hydrous expansive minerals so that changes in the microstructure of specimens can be observed as soon as possible. Storage in water can result in dissolution of salts in the surrounding water or in the alkaline environment which corresponds to a combined internal and external attack. The change of weight served as an indication of possible dissolution process.

Table 3 a- e: Changes of length as the difference between hcp and fm with an without salts
a) with KNO_3 b) with NH_4NO_3 c) with $CaSO_4$ d) with $MgSO_4$ e) with NaCl

KNO_3	Change in Length (mm/m)		Evaluation of Compatibility	
	Cement Paste	**Foam Paste**	**Cement Paste**	**Foam Paste**
CEM I 42.5 R-HS	0.56	0.88	*	*
CEM I 42.5 R	1.18	1.17	-	-
CEM III/B 32.5 NW/HS	0.63	0.38	*	+
SSC	0.59	0.27	*	+

NH_4NO_3	Change in Length (mm/m)		Evaluation of Compatibility	
CEM I 42.5 R-HS	1.95	1.27	-	-
CEM I 42.5 R	3.67	2.54	-	-
CEM III/B 32.5 NW/HS	0.76	0.32	*	+
SSC	n.m.	n.m.	-	-

$CaSO_4$	Change in Length (mm/m)		Evaluation of Compatibility	
CEM I 42.5 R-HS	1.20	1.10	*	*
CEM I 42.5 R	19.2*)	2.80**)	- C	- C
CEM III/B 32.5 NW/HS	6.88	3.64	- C	- C
SSC	0.22	0.20	+	+

$MgSO_4$	Change in Length (mm/m)		Evaluation of Compatibility	
CEM I 42.5 R-HS	3.15	2.95	-	-
CEM I 42.5 R	19.4	5.75***)	-	- C
CEM III/B 32.5 NW/HS	11.07	24.04	- C	- C
SSC	0. 24	0.32	+	+

NaCl	Change in Length (mm/m)		Evaluation of Compatibility	
CEM I 42.5 R-HS	1.20	0.64	*	*
CEM I 42.5 R	1.90	0.66	-	*
CEM III/B 32.5 NW/HS	2.05	0.53	-	+
SSC	1.82	0.40	-	+

*) ... could only be measured up to 270 days ***) ... could only be measured up to 56 days
**) ... could only be measured up to 90 days n.m. ... could not be measured

RESULTS AND CONCLUSIONS The results of length measurements as the difference between hcp and fp samples with salts and without salts (zero specimens) immersed in water are given in Table 3 a-e. To evaluate compatibility the progress of change in length after 2 years in contrast to the zero specimen and also the state of the specimens (cracks, scaling and bending) were checked. The results of this evaluation can be found in column 4 and 5 of Table 3 a-e.

- incompatibility + good compatibility
* moderate compatibility C formation of cracks

In contact with KNO_3 SSC and CEM III/B 32,5 NW/HS specimens with foam show a good compatibility. C_3A-rich CEM I 42,5 R was observed to be incompatible with KNO_3. Up to now new phase formation could not be detected.

In the presence of NH_4NO_3 higher changes in length were found, both with the specimen bars without and with foam. As soon as water was added ammonia was released from all binding materials with NH_4NO_3, which lasted for several days. In the case of SSC no length measurement was possible as there was a distinct hardening defect. X-ray diffraction did not show any crystalline changes compared to the sample without salts. By DTA, however, two dehydration peaks were detected which could be an indication of the formation of calcium nitrate. According to equation (1) the reaction between ammonium nitrate and the $Ca(OH)_2$ of hcp results in the formation of calcium nitrate and ammonia which escapes as a gas:

(1) $2\ NH_4NO_3 + Ca(OH)_2 + H_2O \rightarrow 2\ NH_3 + Ca(NO_3)_2 * 4\ H_2O$

As this reaction occurs in all of binding materials tested, it is impossible to elucidate, why it is only in SAC that the hardening defect takes place, only by relating the phenomenon to calcium nitrate formation. Both PC showed the same distinct incompatibility, whereby the presence of a larger pore space only slightly influenced the change in length. DTA also showed these two

dehydration peaks and a small increase of ettringite. According to [Hoffmann 1991] in the presence of binders containing calcium aluminate not only the reaction of the nitrate with the portlandite is possible, but also with the C_3A which may lead to the formation of Tricalciumaluminate mononitrate hydrate. This can be formed, only if there are still distinct quantities of reactive C_3A after the formation of ettringite taking place during hardening of cement paste.
The C_3A-rich PC and the CEM III/B 32.5 NW/HS show with and without foam in the presence of $CaSO_4$ strong changes in length due to higher ettringite formation. SSC shows very good compatibility with $CaSO_4$. Increased porosity of foam mortars limited the length increase of binders CEM I 42.5 R and CEM III/B 32.5 NW/HS in contact with $CaSO_4$, but not to an extent to speak of compatibility. The use of C_3A-poor PC in structures attacked by $CaSO_4$ is possible, if inert aggregates and/or mineral additives are used to „dilute" the cement content.

Only SSC could resist the internal attack of $MgSO_4$, although hardening was retarded when hydration started. In contact with $MgSO_4$ the highest expansions connected with crack formation were observed. Even foam pores could not prevent them. The increase of ettringite in C_3A-rich cement can be compared with that after contact to NH_4NO_3, though much lower expansions were registered. The negative effect of $MgSO_4$ is based both on the reaction of $CaSO_4 * 2\ H_2O$ with C_3A and on the possible reaction whith strength-forming C-S-H phases according to equation (2), which is connected with a weakening of microstructure and an increase in diffusion rate of sulfate:

(2) $MgSO_4 + Ca(OH)_2 + 2\ H_2O \rightarrow Mg(OH)_2 + CaSO_4*2\ H_2O$

$C_3A + 3\ CaSO_4*2\ H_2O + 26\ H_2O \rightarrow C_3A*3\ CaSO_4*32\ H_2O$

$3\ CaO*2\ SiO_2*n\ H_2O + MgSO_4 \rightarrow 3\ CaSO_4*2\ H_2O + 3\ Mg(OH)_2 + 2\ SiO_2*n\ H_2O$

Foam paste made with SSC was well compatible with NaCl. Foam pastes made with C_3A-rich PC and CEM III 32.5 NW/HS showed moderate compatibility, while the hcp of C_3A-rich PC and slag-rich CEM III/B 32.5 NW/HS could not resist the internal NaCl attack. Increased porosity resulted in a marked reduction of the change in length.

SUMMARY $MgSO_4$ showed the greatest damaging effect among all salts relevant to buildings. The highest changes in length were measured in this system leading in some cases to the complete destruction of the samples already after 56 days. Until now only SSC could resist this attack in our investigations. KNO_3 did the least harm to hcp and fm specimens. The increase in porosity of hcp by addition did not improve the compatibility in any case. This can be explained by the fact that even though the porous structure offers additional pore space for new phase formation, fp has a lower resistance to the high pressure that the thin borders of hcp between the air pores are subjected to. The reaction with $MgSO_4$ leads not only to ettringite formation but is also harmfull to strength-forming C-S-H phases which affects the less strong microstructure of the fp more severely. Best results in contact with salts were found with SSC and C_3A-poor PC.

REFERENCES **Garrecht**, H., Kropp, J., Hilsdorf, H.K., „Microclimate - an Important Criteron in Assessing Moisture Damage", Conservation of Historically Important Buildings (in German), SFB 315, Jahrbuch 1990, Verlag Ernst&Sohn, Berlin 1991, p. 41-61.
Hoffmann, D., „Corrosive Effect of Nitrate Solutions on PC Mortars" (in German), Silikattechnik 42 (1991) 7, p. 234-237.
Stürmer, S., Mielke, I., Stark, J. „Injection Foam Mortar for Restoration" (in German) Wiss. Z. Hochsch. Archit. Bauwes. - Weimar 40 (1994) 5/6/7, p. 15-21.
Stürmer,S., Mielke,I., „Compatibility Investigations, Part 1: Compatibility Investigations with Various Binders and Historical Material" (in German), Wiss. Z. Hochsch. Archit. Bauwes.-A/B-Weimar 39 (1993) 3, p. 99-105.

CONCRETE DETERIORATION DUE TO PHYSICAL ATTACK BY SALT CRYSTALLIZATION

YANG Quanbing WU Xueli HUANG Shiyuan
(Wu Dong Road Campus at Tongji University, 100 Wu Dong Road, Shanghai 200433, China)

ABSTRACT Under the various conditions, the length and strength changes caused by sodium sulfate crystallization were measured and compared with those by chemical attack of sodium sulfate. Results showed that: 1)for concrete exposed to the wetting-drying cycle with sodium sulfate solutions, the expansion and damage by salt crystallization were much larger than those by chemical attack of salt, especially for a high concentration of sodium sulfate; 2) the higher the air content of concrete was, the smaller the expansion and damage by salt crystallization were; 3)some improving methods were suggested according to the test results.

Key-words: Air-entraining Expansion Sulfate attack

INTRODUCTION

Geologists have long since studied the phenomena of salt damage in rocks, and have used various terms for them, such as salt weathering, salt crystallization damage and salt decay. ASTM C 88, Soundness of Aggregate by Sodium sulfate or magnesium sulfate, uses the physical attack mechanism of salt for evaluating the durability of aggregate. However, physical attack on concrete by crystallization has received little attention because it seems that the problem is often misidentified as other common damages, such as sulfate attack and deicer scaling due to frost.

Physical damage to concrete from salt crystallization manifests itself in the form of surface scaling and its mass loss is progressive, similar in appearance to freeze-thaw damage, and for poor quality concrete the distress can cause total disintegration.

Reading(1984) showed examples of structural elements from a dam that were damaged only by physical attack of sodium sulfate. Tests showed that chemical sulfate attack was not present. Stark(1989) observed that badly deteriorated specimens had the bottom portions of the beams in excellent condition, but the exposed upper portions of the beams where drying occurred were deteriorated. Controlled specimens in the laboratory, which were continuously immersed in sulfate solution, showed no evidence of deterioration.

Salt solution enters concrete due to capillary action, permeation and diffusion when exposed to the environment abounded with salt solution. However, salt concentration becomes enough high to cause crystallization when pore water evaporates from concrete surface due to changes in ambient temperature and relative humidity. Repeated cycles of dissolution and crystallization can cause deterioration of concrete if the salt crystalliztaion is accompanied by a volume expansion, but this concept needs further study and clarification.

EXPERIMENTAL PROCEDURE

Mix proportions

Concrte specimens with the size of 4 × 4 × 16cm were used. The proportion is W:C:S:G= 0.60:1:1.72:3.19. In order to investigate the effect of air-entraining agent on the salt crystallization, a mixture with the air content of about 3.2% was prepared. Slump was 20±2 cm for all mixes.

Ordinary portland cement with about 15% slag, quartz sand as fine aggregate, 5~12mm marble stone as coarse aggregates were used to make concrete. All specimens were cured in water (20±2 ℃) for 28 days.

Test method

In this paper, crystallization of sodium sulfate was accelerated by drying-wetting cycles. Specimens were dried at 105±5 ℃ for 4 hours and soaked in Na_2SO_4 solutions (0, 10, 20%Wt) at 25~30 ℃, which constitutes one cycle. Companion specimens were immersed in these solutions all the time, which were dried before immersed in order to accelerate concrete soaking the solution. Wet and dry specimen lengths were measured after every cycle, and the mass loss and strength were measured after several cycles.

RESULTS AND DISCUSSION

Expansion

Expansion results under various conditions are shown in Figs 1 and 2. From Fig 1 it can be seen that the effect of drying and wetting in water cycles on the length of specimens is little, and the wet length is always larger than that after drying. However, for the specimens under drying and wetting in Na_2SO_4 solutions cycles, the length of specimen increases continuously after every cycle, and the wet length before drying is always smaller than the dry length after drying. It means that the drying process also causes the expansion of specimen saturated with Na_2SO_4 solution, especially for a Na_2SO_4 solution of high concentration. The expansion by drying-wetting cycles increases with the increase in the concentration of Na_2SO_4. The expansion by 20% Na_2SO_4 is very high, about 0.4% and is 3.5 times as that by 10% Na_2SO_4 after 21 cycles.

For the specimens immersed in solutions all the time, the expansion by sodium sulfate crystallization can be ignored, and therefore is mainly caused by chemical attack of sulfate and moisture expansion. Fig 2 shows that the specimen expansion in solutions increases slowly. It is interest that the expansion in 10% Na_2SO_4 increases more quickly than that in 20% Na_2SO_4, but their final expansions are similar, about 0.04%. Due to low aluminate in cement, the amount of SO_4^{-2} in these solutions is much more than that needed for chemical reaction of sulfate, and therefore the final expansions by chemical attack of these solutions are similar. From Fig 3 it can be seen that the weight of specimens in water increases more quickly than that in Na_2SO_4 solutions, and the amount of water in specimens in 20% Na_2SO_4 is much lower than that in 10% Na_2SO_4 and in water, which may be a reason for these phenomena.

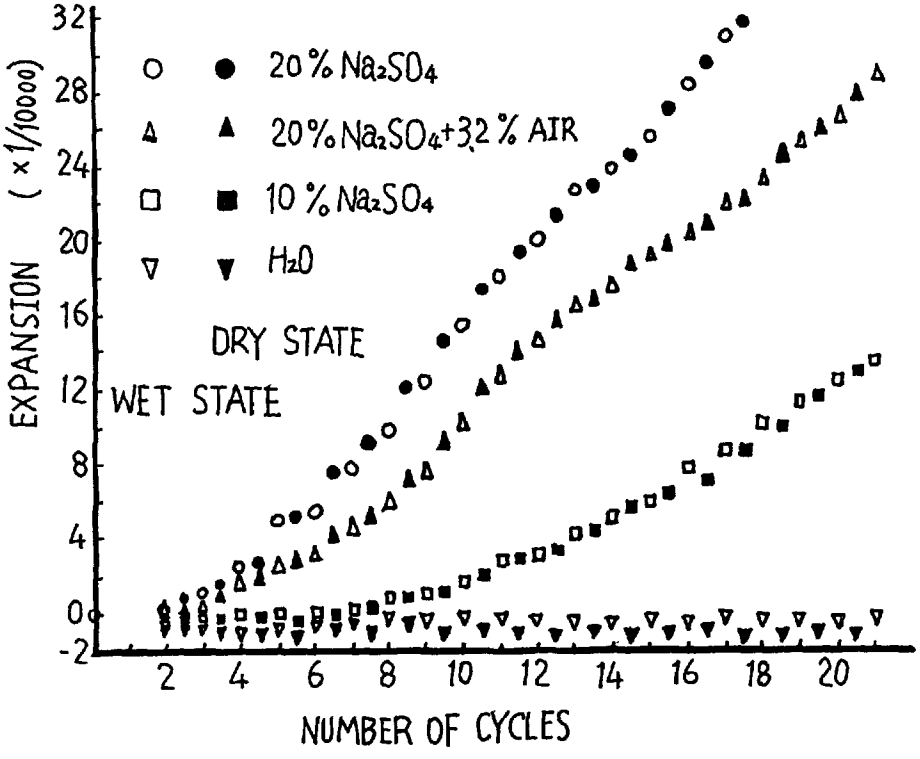

Fig 1 The expansion of specimens under drying-wettingcycles

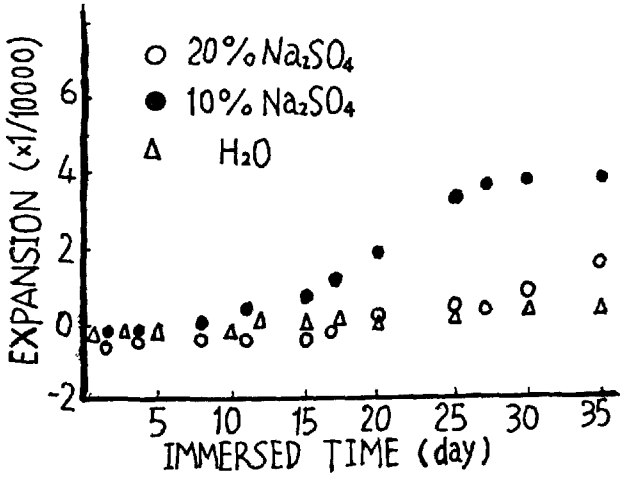

Fig 2 Expansion of specimens immersed in Na_2SO_4 solutions

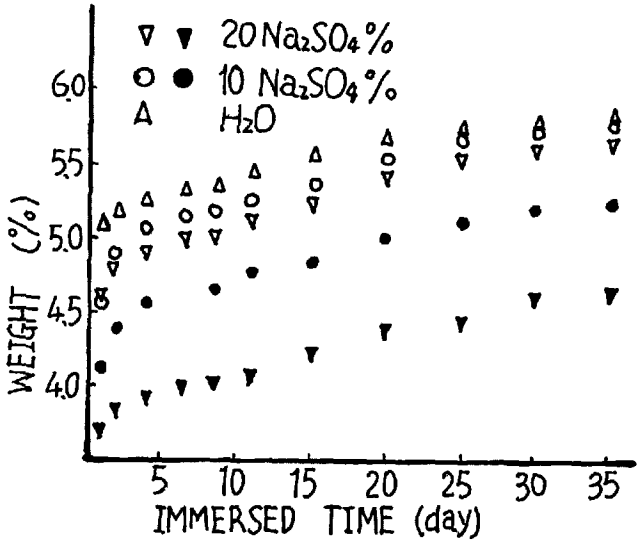

∇ and O — Amount of water in specimen

∇ and ● — Amount of solution in specimen

Fig 3 Weight changes of specimens immersed in Na_2SO_4 solutions

From above results it can be seen that the expansion (Esc) by salt crystallization (or drying-wetting cycles) is much larger than that by chemical attack of sulfate (Eca). Esc is about 10 times as Eca for 20% Na_2SO_4, and about 3.5 times as Eca for 10% Na_2SO_4. Therefore, for the environment where water in concrete evaporates easily, the deterioration of concrete is mainly caused by salt crystallization.

Scaling and strength

From Table 1 it can be seen that the strength of concrete immersed in Na_2SO_4 solutions decreases a little, and that after 21 drying-wetting cycles decreases a lot for 20% Na_2SO_4, but increases a lot for 10% Na_2SO_4. In fact, compressive strength is not a good index to evaluate the damage of concrete by salt crystallization, because a little of salt crystallization can make concrete denser and therefore enhance compressive strength. Compressive strength decreases of course when the expansion by salt crystallization is high enough. Tensile strength is sensitive to the damage, but measured values are very dispersive.

The scaling of concrete is a good index to evaluate the damage by salt crystallization. Table 1 shows that drying and wetting in water doesn't cause scaling, but in Na_2SO_4 solutions, it causes severe scaling. The scaling of concrete increases quickly with the increase in the concentration. It is observed that some aggregates scale off. The scaling by 20% Na_2SO_4 is 1240 g/m^2 after 21 cycles, about 9 times as that by 10% Na_2SO_4. However, for concrete immersed in solutions, the scaling is very small, only about 120 g/m^2 even in 20% Na_2SO_4.

These results confirm the conclusion obtained from the expansion test again, i.e., the deterioration of concrete by salt crystallization of Na_2SO_4 is severer than that by chemical attack of sulfate.

Effect of air content

The expansion from physical attack of Na_2SO_4 under drying-wetting cycles is caused by salt crystallization pressure of Na_2SO_4. Does air-entraining agent have the same effect on the damage by salt crystallization as on that by frost action ? From Fig 1 it can be seen that the air-entraining content of about 3.2% significantly reduces the expansion by salt crystallization. The expansion

Table 1 Scaling and strength of concrete under various conditions

Na_2SO_4	Air content	Immersed in solutions for 25 days		21 drying-wetting cycles	
%	%	Strength, MPa	Scaling, g/m^2	Strength, MPa	Scaling, g/m^2
0	0	45.4	0	42.4	0
	3.2	37.3	0	36.7	0
10	0	44.2	56	49.6	150
20	0	43.4	120	37.2	1240
	3.2	36.8	38	34.5	420

Note: The time immersed in solutions for 25 days is equal to that after 21 drying-wetting cycles

is 0.29%, about 70 percent of that of concrete without air-entraining after 21 cycles. Table 1 also shows that the application of the air-entraining agent lessens the scaling and strength loss of concrete by salt crystallization, and the scaling of concrete with the air-entraining agent is 420 g/m^2, only about one third of that without the air-entraining agent. However the air-entraining agent retards the expansion by salt crystallization, the expansion of concrete with air-entraining agent still increases quickly with the increase in the number of cycles. Therefore the application of air-entraining agent doesn't solve this problem completely.

The main reasons that air-entraining agent mitigates the damage by salt crystallization are that a lot of air bubbles entrained by air-entraining agent can receive more salt crystals and retard concrete soaking salt solutions.

SUMMARY

Under drying-wetting cycles, the expansion and scaling due to physical attack by salt crystallization of Na_2SO_4 are much larger than those by chemical attack of sulfate, and the deteriorated surface has an appearance similar to that of damage by freezing-thawing cycles. The air-entraining agent obviously mitigates the damage of concrete by salt crystallization.

Concrete of high permeability is most susceptible to this deterioration. The main methods in preventing the deterioration are to produce concrete of low water-cement ratio and with air-entraining agent.

ACKNOWLEDGMENT

The authors would like to thank National Foundation of Natural Science for the financial support.

REFERENCES

Reading, T.J., "Physical aspects of sodium sulfate attack on concrete", ACI, SP-77, 1982, pp75-81.
Stark, D., "Durability of concrete in sulfate-rich soils", Research Development Bulletin RD097, Portland Cement Association, Skokie, IL, 1989, pp14.

DILATION AND PHASE TRANSITIONS IN MORTAR DURING COOLING

Vesa PENTTALA, Helsinki University of Technology, Concrete Technology, Espoo, Finland

ABSTRACT Simultaneous dilation and heat evolution of mortar samples were measured from +20 to -70° C in a low temperature calorimeter. Both normal and air-entrained mortars were studied. In the mortar samples preserved in the highest relative humidity (94-96%) expansion was observed during the first freezing of the pore water while the mortars preserved in the lower relative humidity (89-90%) were detected to contract after the first freezing. All mortars expanded when the major portion of gel water freezes in the temperature range -40 to -45° C.

Key-words: Mortar, dilation, phase transition, freezing, thawing, heat capacity

INTRODUCTION

There are presented several theories of the freezing phenomena of wet pastes, mortars, and concrete but relatively few dilation tests of freezing-induced strains and simultaneous ice evolution in porous solids have been performed. In this presentation test results of small mortar prisms cooled in a low temperature calorimeter will be discussed. The compressive strengths of the mortars were 30.4 MPa and 34.6 MPa (air-entrained) measured by 100 mm cubes. The mortar prisms were cooled from +20 to -70° C and thereafter heated back to +20° C with a cooling rate of 3.0° C/h and a heating rate of 4.2° C/h. Mortar prisms were stored in different relative humidity (89-96%) and therefore possessed different pore water amounts filling their pore system.

A CONCISE LITERATURE REVIEW

Four different research groups or scientists have presented freezing theories of wet porous solids. The first important group to study concrete paste was T. C. Powers (Powers 1945,1949) together with his coworkers T. L. Brownyard and R. A. Helmuth (Powers et al. 1947, 1953). Powers started his deduction from the physical fact that during freezing water expands about 9% and if the pore structure was water filled over 91% freezing caused deterioration of the matrix. Later his theory of hydraulic pressure was refined to take into consideration the fact that during cooling the water in the largest pores freezes first and only after the smaller pores have been frozen would the expansion be hindered causing large hydraulic pressures and subsequent paste destruction.

Powers and his coworkers observed also another freezing mechanism: The growth of the bodies of ice in the capillary cavities or air voids by diffusion of water from the nanometer-sized gel pores. However, they assumed that also this mechanism always caused expansion in hardened Portland cement paste. Their experiments showed that empty air voids limit the hydraulic pressure and shorten the period during which ice in the cavities can increase. The closer these entrained air voids are to each other the more effective they are in controlling the two freezing mechanisms. They also noticed the effects of the freezing rates. At low freezing rate the diffusion of gel water is dominant feature causing drying shrinkage in the gel structure while at fast freezing rate diffusion of the gel water has not time to evolve and hydraulic pressure governs the freezing deterioration and induces cracks into the matrix. They were also able to show that osmotic pressures have a role in freezing of cement paste especially when considerable amounts of salts are present in the pore liquid.

Based on thermodynamics, generalized Gibbs-Thomson's equation, and Laplace's equation D. H. Everett and J. M. Hayes (Everett 1961; Everett et al. 1965) showed that ice in a larger pore could expand or grow to a smaller, water-filled pore only when the interface between ice and the water in the connecting tube between the large and smaller pore would be curved. Due to this curvature a lower pressure would be induced into the smaller, unfrozen pore water which would draw water from the smaller pores to the ice crystal until ice could not expand any more because of lack of space.

The third important theoretical impact on the freezing theories of porous solids was done by C. G. Litvan (Litvan 1971, 1973; Sidebottom et al. 1971). According to Litvan's model the surface forces of pores have an important effect during the freezing of the pore liquid. These surface forces hinder ice crystal formation and the water layer situating few molecular diameters from the surface remain structurally oriented during the freezing of the rest of the pore water. According to Litvan the vapor pressure of these meta-stable, undercooled structural water layers exceed the vapor pressure of the solid phases of ice and matrix causing a moisture transport from the pores to the outer surface of the test sample. Similarly, according to Litvan if the cooling rate of the sample is faster than the rate of the before mentioned transport process freezing damage occurs.

M. J. Setzer (Setzer 1977) criticizes Litvan's assumptions of constant surface stresses in the adsorbed interface between vapor and the capillary condensed liquid where Litvan assumes zero angle between liquid meniscus and pore surface. Due to Litvan's simplified assumptions for example gel water could not freeze. Setzer presented a revised thermodynamic model based on Litvan's basic assumptions but taking into consideration the changes in surface stresses in the adsorbed water layer on the pore surface during the thickness changes of this adsorbed, structurally oriented water layer. This structurally oriented, superficial water layer freezes only in very low temperature around -90...-100° C. In his presentation Setzer is the first one to derive an approximate equation for the pressures caused into a porous material during freezing. Setzer's linear relationship is of a very approximate nature because of the rather crude assumptions Setzer has had to do regarding the coefficients of surface tension which has been assumed constant while it really is a function of pore size.

Actual empirical freezing tests with porous solids were performed by T. C. Powers and T. L. Brownyard (Powers et al. 1947), Powers and R. A. Helmuth (Powers et al. 1953), A. A. Antoniou (Antoniou 1964), C. G. Litvan (Litvan 1971, Sidebottom et al. 1971), and B. V. Enüstün, H. S. Sentürk, and O. Yurdakul (Enüstün et al. 1978). Antoniou's tests and Enüstün's and his coworkers tests were done with porous glass specimens while the others used hardened Portland cement pastes.

The first tests of Powers and Brownyard with crushed cement paste samples were rather inaccurate due to the indirect measuring method of liquid solution but the second method done together with Helmuth using tubular, saturated paste specimens provided more accurate results. According to the test results they explained the freezing mechanisms to be a combination of the generation of hydraulic pressure as water freezes in the capillary cavities and the growth of the bodies of ice in the capillary cavities or air voids by diffusion of water from the gel pores. Litvan noticed in his tests two expansion freezing temperatures, around -8° C and another around -40° C which he considered as anomality. Antoniou was the first one to do calorimetric measurements together with simultaneous observations on length changes in saturated Vycor glass. During the tests temperature cooled from +20 to -40° C and he noticed two volume expansion temperature

ranges: One from -9 to -15° C and another from -20 to -26° C. The apparent heat capacity of the phase transformations could also be detected. Enüstün and his coworkers used a mercury dilatometer equipped with a capillary stem. Saturated Vycor rod expanded at -17° C . The lowest temperature measured was -25° C.

Table 1 Composition, consistency, and compressive strength results of the test mortars.

Test mortar	**M30**	**M35A**
Aggregates (kg/m^3) Total	1283	1266
- # 1-2 mm	295	291
- # 0.5-1.2 mm	295	291
- # 0.1-0.6 mm	385	380
- # < 0.125 mm	308	304
Cement (kg/m^3)	424	390
Water (kg/m^3)	340	232
Air-entraining admixture (kg/m^3)	-	1.95
Compressive strength (MPa) 100-mm cubes	30.4	34.6

Table 2 Chemical composition and physical properties of cement CEM52,5.

Chemical composition (w-%)	**CEM52,5**
CaO	62.3
SiO_2	20.3
Al_2O_3	4.5
Fe_2O_3	2.9
MgO	3.9
K_2O	0.84
Na_2O	0.92
SO_3	3.2
Loss of ignition (950° C)	0.8
Physical properties	
Compressive strength (MPa)	
1 d	31.2
7 d	48.8
28 d	56.9
Specific area (Blaine) (m^2/kg)	446

TEST SPECIMENS AND ARRANGEMENTS

Two mortar samples were produced for the cooling tests. The composition of the mortars was chosen to represent the ingredients of normal concrete where the aggregate fractions from 2 to 16 mm have been omitted. This explains the large binder amounts of the test mortars presented in Table 1. Test mortar M30 was a normal mortar where no air entraining admixtures were used while in test mortar M35A extra air was introduced into the mix with an air-entraining agent. The air content of mortar M30 was 0.7% and of mortar M35A 8.4%. The binder was rapid hardening

Portland cement CEM52,5 of local origin produced by Finnsementti Oy, Table 2. The aggregates were sieved into 4 fractions and their petrographic composition was mostly granite. The air-entraining admixture was a vinsol resin.

After mixing for 4 minutes the test mortars were poured into 2 dl polyethylene bottles which were rotated for 5 hours to prevent any segregation. At the age of 3 days the bottles were cut open and 10•10•55 mm^3 prisms were cut. Two strain gauges were glued on the opposite sides of the prisms and they were placed into vessels where the relative humidity was held constant by saturated salt solutions. Four relative humidity levels were studied, 89, 90, 94, and 96%. The humidity level was checked by special humidity meters produced by Vaisala Oy. A comparison prism was dried in oven at 105° C temperature for 5 days before the dilation test. At the age of 32 days two strain gauges were glued on the dry comparison sample, wires were soldered to the strain gauges and it was placed into the reference chamber of a low-temperature calorimeter. At the same time the wet sample was taken from the storage environment and wires were similarly soldered to the strain gauges and the sample was placed into the other measuring cell of the calorimeter. The wiring procedure of the wet sample lasted from 7 to 10 minutes and during this time considerable amount of water evaporated from the wet mortar prisms.

During the cooling test the strains of the wet and dry samples were measured every 40 seconds. The strain values of the strain gauges were calibrated by steel samples from which the coefficient of temperature expansion was known. The difference in the heat capacities of the wet and dry test samples was measured by the low-temperature calorimeter produced by Setaram. The cooling rate of the test was 3° C/hour and the following heating rate 4.2° C/hour. The test started from +20° C and the temperature dropped linearly to -70° C and again increased back to +20° C after a few hours waiting at -70° C.

TEST RESULTS

The dilation strain results of the test samples and ice evolution are presented in Figures 1-5. Heat capacities of the wet test mortars are presented in Figure 6. The relative water and ice amounts of the test prisms are presented in Table 3.

Table 3 The relative water and ice amounts compared to the wet weights of the test prisms.

Test mortar/relative humidity (%)	Weight of water / weight of the wet prism	Weight of ice at -70° C / weight of the wet prism
M30/RH96	0.0777	0.0284
M30/RH94	0.0761	0.0255
M30/RH90	0.0691	0.0176
M30/RH89	0.0627	0.0148
M35ARH96	0.0785	0.0228
M35ARH94	0.0734	0.0202
M35A/RH90	0.0694	0.0168
M35A/RH89	0.0652	0.0110

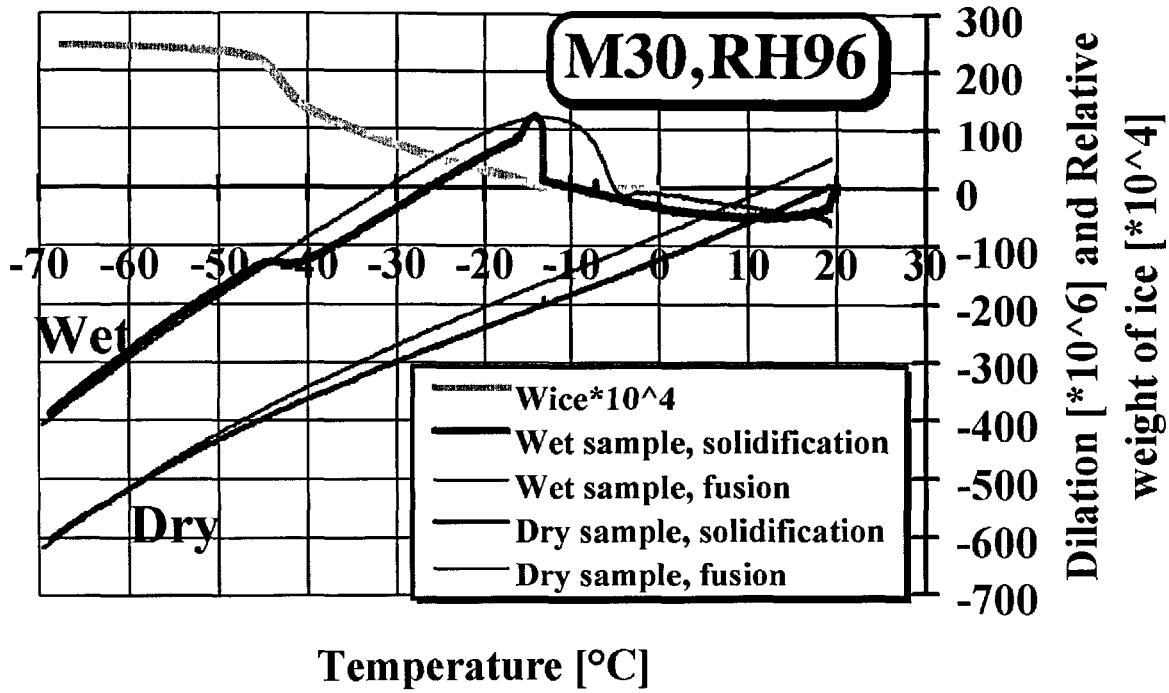

Figure 1 The curves of dilation and the relative weight of ice of wet and dry mortar prisms M30 stored at 96% relative humidity.

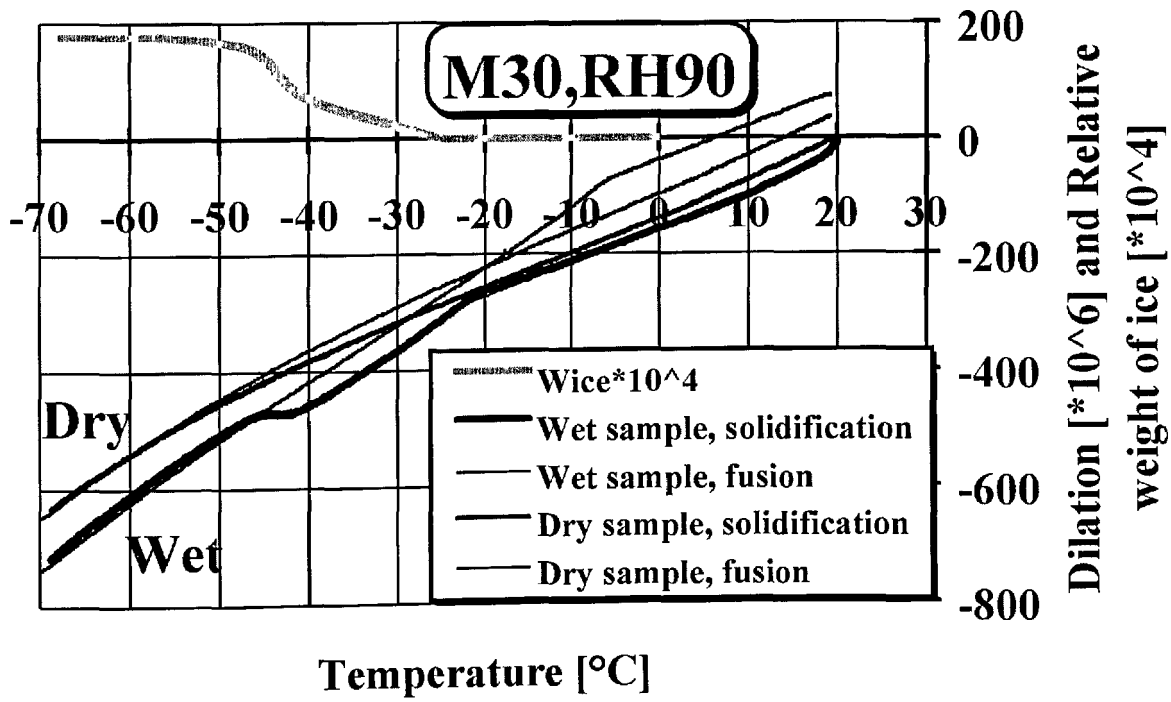

Figure 2 The curves of dilation and the relative weight of ice of wet and dry mortar prisms M30 stored at 90% relative humidity.

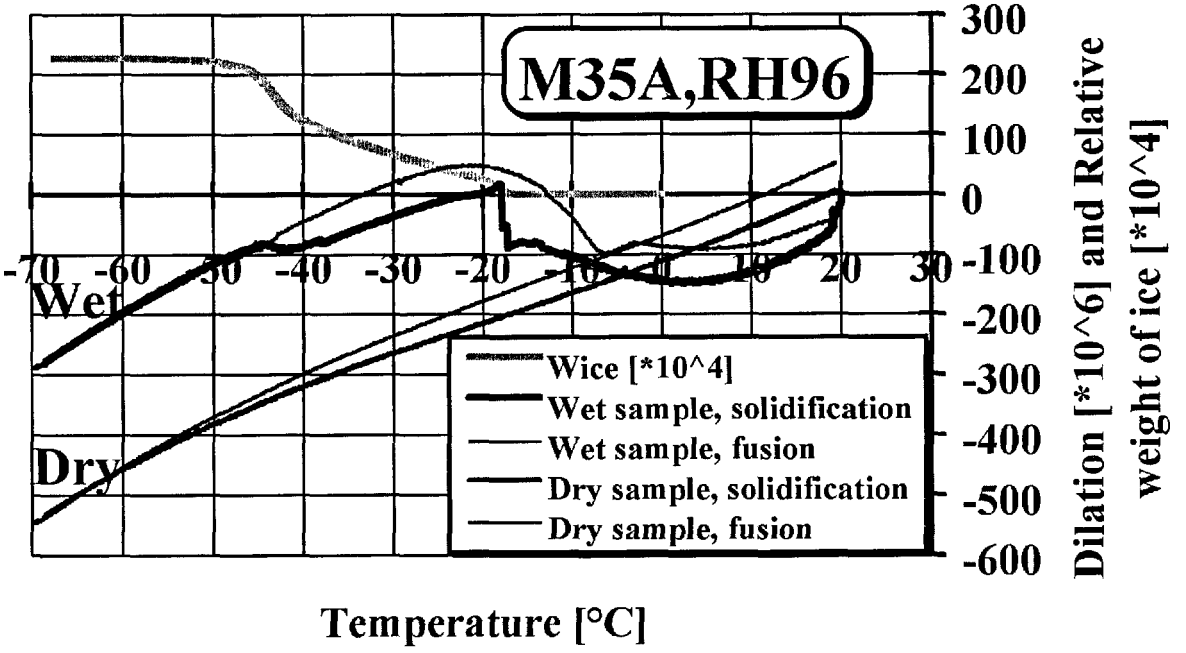

Figure 3 The curves of dilation and the relative weight of ice of wet and dry mortar prisms M35A (air-entrained) stored at 96% relative humidity.

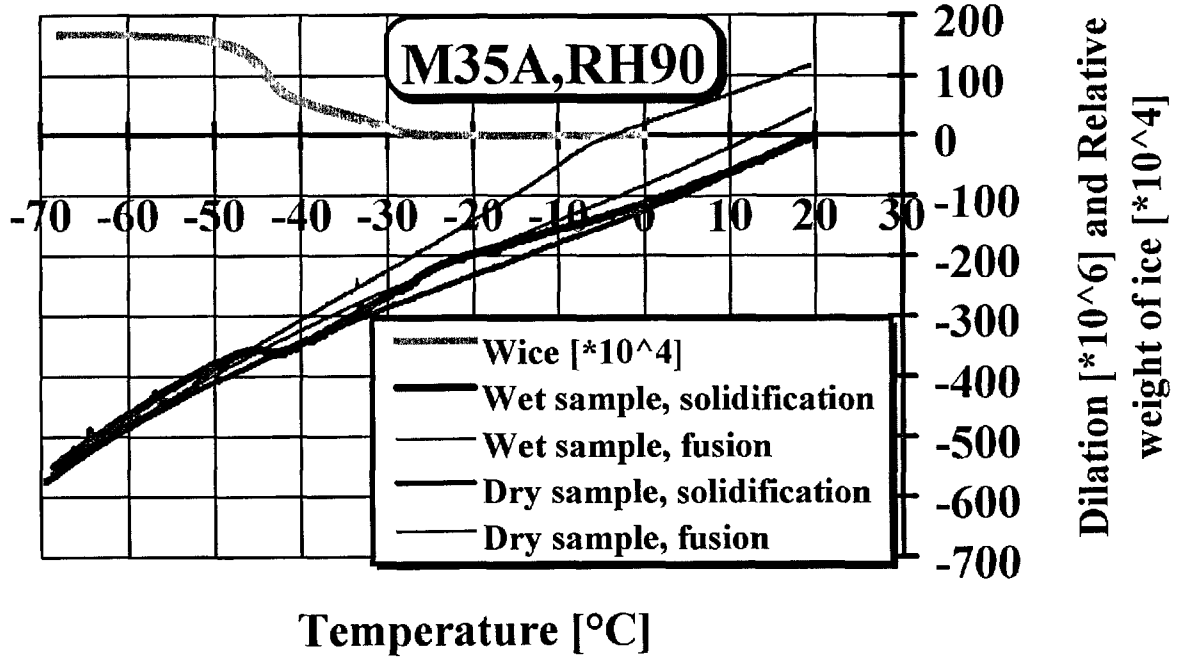

Figure 4 The curves of dilation and the relative weight of ice of wet and dry mortar prisms M35A (air-entrained) stored at 90% relative humidity.

DISCUSSION

As can be seen from Figures 1,3,5, and 6 when the test mortar has been stored in the environment of 96% relative humidity the first freezing of pore water causes a large, stepwise expansion in the mortars irrespectively of the air-entrainment. According to the fusion dilation in Figures 1 and 3 this expansion strain of $1.2 \bullet 10^{-5}$ does not seem to cause irreversible cracking in the test samples. This is quite understandable because this expansion causes in the mortar prisms a smaller than 0.4 MPa tensional stress which is well below the tensional strength of the mortars in question. The contraction and expansion of the test mortars stored in 96 and 94% relative humidity during the cooling from +20° C to the temperature of the first freezing expansion are caused by the evaporation of the water and subsequent shrinkage of the wet test samples during the sample preparation before they were transferred into the calorimeter chamber. During the temperature decrease part of the evaporated water amount is returned into the test mortars and part of the shrinkage is retained.

The dilation results of both mortar types M30 and M35A stored in the two lowest relative humidity environment behave quite differently compared to those stored in the relative humidity of 94 and 96%. When ice formation was first detected, thereafter the test prisms contracted until the temperature fell to -40° C when an expansion took place. The expansion of the test prisms stored in 96% relative humidity was surely caused by the generation of hydraulic pressure as water freezes in capillary cavities as Powers has predicted. The contraction after ice formation was detected from the heat capacity curves presented in Figure 6 in the specimens stored in the two lowest relative humidity percents has another physical explanation. When ice is first forming into the largest water filled pores there is enough space for the free expansion of the ice crystal without any restraints from the binder matrix. The chemical potential of the ice surface is smaller than the chemical potential of the unfrozen pore water in the smaller pores and this causes a lower pressure in pore system and a diffusion of pore water to the ice crystals. When gel water is expelled from the gel structure which has a large specific surface area remarkable shrinkage strains will be expected and this will also contribute to the contraction of the mortars. What part of the contraction is caused by the lower pressure and what portion by the shrinkage of the gel matrix cannot be evaluated by these test results but judging from the expansion strains after the test (Figures 2 and 4) the permanent dilations are larger compared to specimens stored in larger relative humidity. Therefore, severe cracking of the gel structure due to shrinkage seems to be at least partly responsible for the contraction. The dilation behavior of the mortars in this situation differs from the propositions of Powers and Litvan. Powers assumed that an expansion would result from the water diffusion and Litvan presented that pore water would diffuse on the outer surface of the specimen and freeze there.

It should be noticed that the dilation curves below -40° C of all test specimens seem to be almost identical. Studying the heat capacity curves of Figure 6 it can be seen that during the freezing of gel water between -40 and -50° C the heat capacities follow the order of the storage relative humidity. One cannot draw very far fetched conclusions from this neither to the gel water amount nor to the amount of how much gel water has diffused away from the gel structure because in these heat capacity values is summed up also the freezing of the superficial, unfrozen layer of adsorbed water between the ice and the pore wall in the larger pores.

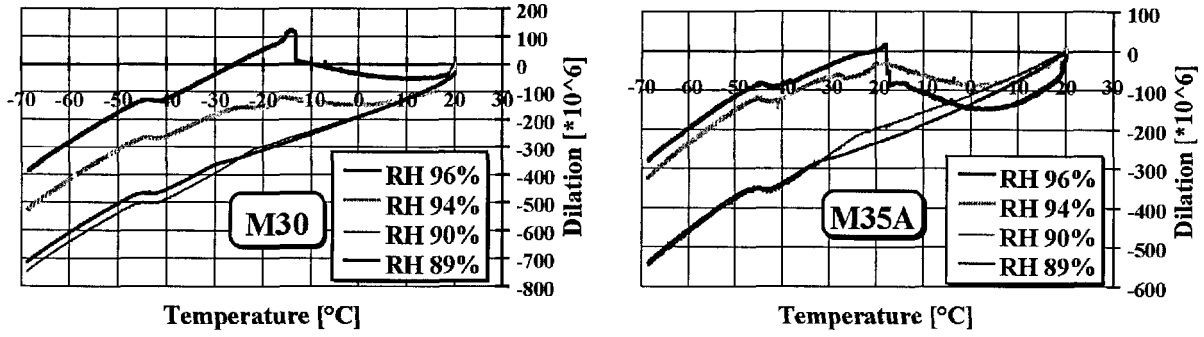

Figure 5 Dilations of the test prisms.

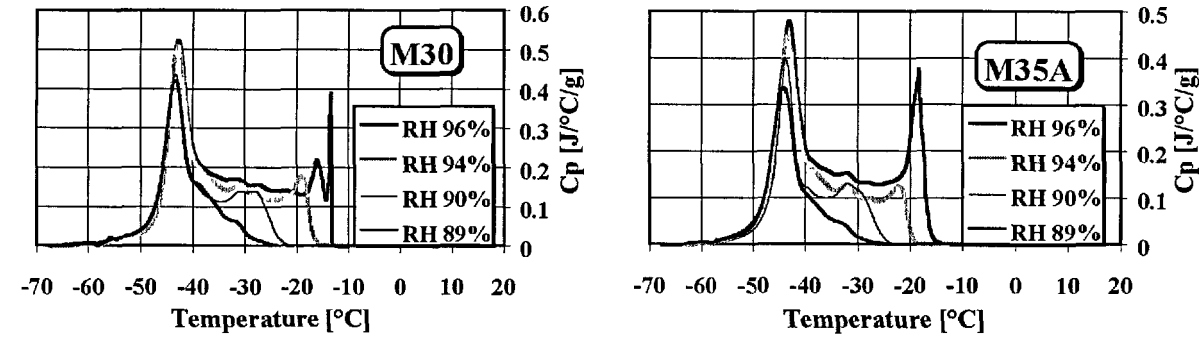

Figure 6 The heat capacities of the wet test specimens.

Comparing the first freezing temperatures to the storage relative humidity of the test prisms one can notice that in mortars M30 they were -13.3, -15, -22, and -24° C in the descending order of the storage relative humidity. For air-entrained mortars M35A the similar first freezing temperatures were -14.4, -18.5, -24, and -25.5° C. These rather small differences can be due to the larger cement amount and somewhat higher compressive strength of the air-entrained mortar M35A and not due to the larger protective pore amount caused by the use of the air-entraining admixture. Actually, in comparing the results of the air-entrained mortars to those of normal mortars very small differences can be noticed. It seems that in the environment below 96% relative humidity air-entrainment has a very small effect on the freezing durability of mortars.

CONCLUSIONS

1. The theory of hydraulic pressure where freezing pore water causes expansion in mortar is valid only if it has been stored in nearly hundred percent relative humidity. In mortars of 30-35 MPa compressive strength this expansion takes place only if storage environment humidity exceeds 95-96%.
2. When the storage environment humidity is below 90-92% the mortar specimens contract after pore water freezes. This is caused by the diffusion of pore water from the smaller, unfrozen pores onto the ice surfaces in larger pores. If there is enough pore space for the additional ice growth the gel structure shrinks due to gel water diffusion. The other reason for the contraction is the lowering of the pressure in the pore system caused by the thermodynamic water and moisture diffusion.

3. In the temperature range -40...-50° C a major portion of gel water freezes and this causes expansion in the mortars. From temperature -40° C downward the dilation of all the test mortars was nearly identical.
4. When 30-35 MPa mortars were stored in and under 96% relative humidity no differences in the dilation behavior could be noticed between air-entrained and normal mortars where no air-entraining admixtures were used.

REFERENCES

Antoniou, A.A., "Phase transformations of water in porous glass", The Journal of Physical chemistry, Vol. **68**, No. 10, 1964, pp. 2754-2764.

Enüstün, B.V., Sentürk, H.S. and Yardakul, O., "Capillary freezing and melting", Journal of Colloid and Interface Science, Vol. **65**, No. 3, 1978, pp. 509-516.

Everett, D.H., "The thermodynamics of frost damage to porous solids", Transactions of the Faraday Society, Vol. **57**, 1961, pp. 1541-1551.

Everett, D.H. and Haynes, J.M., RILEM Bulletin, New series, Vol. **27**, No.31, 1965.

Litvan, C.G., "Phase transition of adsorbates. III. Heat effects and dimensional changes in nonequilibrium temperature cycles", Journal of Colloid and Interface Science, Vol. **38**, No. 1, 1971, pp. 75-83.

Litvan, C.G., "Phase transition of adsorbates: IV, Mechanism of frost action in hardened cement paste", Journal of The American Ceramic Society, Vol. **55**, No. 1, 1971. pp. 38-42.

Litvan, C.G., "Phase transition of adsorbates. V. Aqueous sodium chloride solutions adsorbed on porous silica glass", Journal of Colloid and Interface Science, Vol. **45**, No. 1, 1973, pp. 154-169.

Powers, T.C., "A working hypothesis for further studies of frost resistance of concrete", Journal of the American Concrete Society, Vol. **16**, No. 4, 1945, pp. 245-271.

Powers, T.C., "The air requirement of frost-resistant concrete", Proceedings of the Highway Research Board, Vol. **29**, Portland Cement Association, Bulletin 33. 1949. 28 p.

Powers, T.C. and Brownyard, T.L., "Studies of the physical properties of hardened Portland cement paste, Part 4. The thermodynamics of adsorption of water on hardened paste", Journal of the American Concrete Institute, Vol. **18**, No.4, 1947, pp.549-602.

Powers, T.C. and Brownyard, T.L., "Studies of the physical properties of hardened Portland cement paste, Part 8. The freezing of water in hardened Portland cement paste", Journal of the American Concrete Institute, Vol. **18**, No. 8, 1947, pp. 933-969.

Powers, T.C. and Helmuth, R.A., "Theory of volume changes in hardened Portland-cement paste during freezing", Proceedings of the Highway Research Board, Vol. **32**, 1953, pp. 285-297.

Setzer, M.J., "Einfluß des Wassergehalts auf die Eigenschaften des erhärteten Betons", Deutscher Ausschuss für Stahlbeton, Heft 280, 1977, pp. 43-117.

Sidebottom, E.W. and Litvan, C.G., "Phase transitions of adsorbates. Part 2. Vapour pressure and extension isotherms of the porous-glass+water system below 0 °C", Transactions of the Faraday Society N:o 585, Vol. **67**, No. 9, 1971, pp. 2726-2736.

INFLUENCE OF C_3A CONTENT ON FROST AND SCALING RESISTANCE

Jochen STARK, Bauhaus-University Weimar, Germany
Horst-Michael LUDWIG, Bauhaus-University Weimar (today Schwenk Zementwerke KG, Karlstadt), Germany

ABSTRACT The effects of chemical transformation processes on the frost and frost-deicing salt resistance of concrete are by far not of the same order as the physical effects, but they are nevertheless significant. Our investigations showed that monosulphate (AFm phase) is particularly instable and will transform to ettringite (AFt phase) under frost and also under frost-deicing salt attack. This formation of secondary ettringite, which is supported by thermodynamic conditions at low temperatures, may reduce considerably the frost and frost-deicing salt resistance of concretes without air-entrainment.

Key-words: Aluminate phase, AFm, AFt, Phase transformation, Freeze-thaw damage.

INTRODUCTION

Practical experience of many years has shown that it is possible to produce Portland cement with a high frost and scaling resistance - independent of the types of phases of the cement -, if favourable air void parameters are created by air-entraining agents, if the water-cement ratio is kept low, and if frost and deicing-salt resistant aggregates are employed. On the other hand, however, it is well-known that Portland cement concretes and mortars without air-entrainment which differ only in the type of Portland cement used may vary considerably in their frost and scaling resistance. This is the reason why already for decades attempts have been made to discover a relationship between the types of phases in Portland cements and the frost and scaling resistance of the respective concretes. In the discussions on the influence of cement on frost and scaling resistance the evaluation of the clinker phases of Portland cements is of particular interest.

Most publications deal with the influence of the C_3A content on the frost and scaling resistance of concrete. Still there are completely different opinions held on this question.

Some authors hold the view that the C_3A content has a favourable influence on frost and scaling resistance (Joosting, 1968; Stark et al., 1991; Rasmussen, (1985). Other authors conclude from their test results that frost and scaling resistance is adversely affected by the C_3A content (Jackson, 1955; Rose et al., 1989; Peterson, 1993).

Schrämli (1978) compared the varying statements on the C_3A content and supposed that the differences had been caused by different test conditions. In his opinion the influence of the C_3A content on frost and scaling resistance can only be understood if the basic mechanisms are revealed. The C_3A content in itself cannot be a factor directly influencing frost and scaling resistance because there is hardly any non-hydrated C_3A left when the frost and/or freeze-deicing salt attack begins. It can only be of importance if there is a direct relationship between the C_3A content of the cement and the physical and/or chemical factors of influence (pore size distribution, degree of hydration etc.) Any correlation of C_3A content and frost and scaling resistance is only an attempt to predict the influence of the cement by means of the clinker phase composition without knowing the cause of a possible influence of the C_3A.

The aim of the investigations described in this paper was to find out whether hydrate phases are formed from C_3A that show a different stability under frost and/or freeze-deicing salt attack than hydrate phases from C_4AF. Basic studies were made to find out which phase transformations in calcium sulpho-aluminate and/or calcium sulpho-aluminate ferrite hydrates may occur under frost attack and what the differences between these hydrates are. In a second step the question was considered whether these phase transformations have an effect on the frost and scaling resistance of concrete and which role the C_3A content of the cements may play in this connection.

BASIC INVESTIGATIONS - FROST ATTACK

In the basic investigations into frost attack synthesised C_3A in a stoichiometric mixture with gypsum was hydrated to monosulphate and ettringite respectively, stored for 28 days and then subjected to 28 freeze-thaw cycles (+ 20°C / - 20°C). The comparison of these specimens with other non - frozen specimens showed the different stability of monosulphate and trisulphate under the specific humidity and temperature conditions of a freeze-thaw attack. Whereas ettringite proves very stable, part of the monosulphate is transformed to ettringite during freezing (Fig. 1).

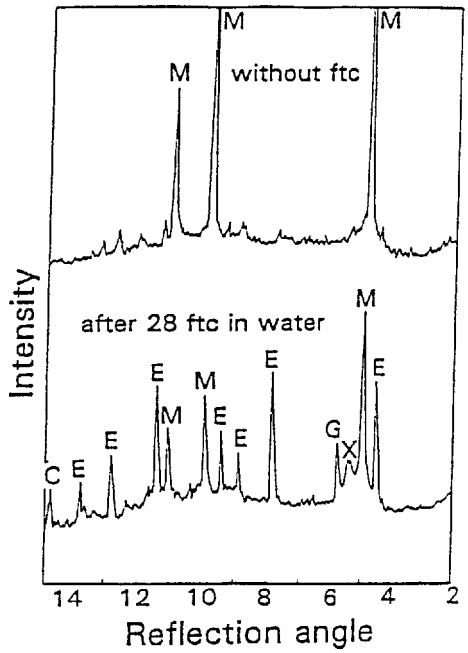

Figure 1 XRD patterns of monosulphate (frost) - M-monosulphate, E-ettringite, G-gypsum, X-monocarbonate.

The main cause of these transformation processes is the change in the thermodynamic stability conditions at low temperatures. Compared to monosulphate, there is an increasing probability that trisulphate - expressed as a negative free formation enthalpy - will form with a drop in temperature, so that at low temperatures the formation of trisulphate is supported by thermodynamic conditions.

The XRD-diagram of the non-frozen monosulphate shows that after pre-storage the added gypsum has almost completely been transformed. That means that, prior to freezing, there was no sulphate available for the transformation of monosulphate to ettringite, which is supported by thermodynamic conditions at low temperatures.

The results of the investigations lead to the conclusion that the sulphate required becomes available through the partial decomposition of the monosulphate due to carbonation. The gypsum formed in this process may then form ettringite with the non-carbonated mono-sulphate. An indication of this reaction mechanism is given by the phase analysis of the reaction products of the carbonation of monosulphate. Both gypsum and calcite (XRD, DTA) as well as aluminium hydroxide (DTA, SEM) could be detected as new formations in addition to ettringite. The reaction proceeds as follows:

$$3\ C_3A{\cdot}C\bar{S}{\cdot}12H + 6CO_2 + 2H_2O \rightarrow C_3A{\cdot}3C\bar{S}{\cdot}32H + 6CaCO_3 + 4Al(OH)_3$$

The results achieved in an examination of AFm phase made from C_4AF correspond to those of the monosulphate tests. The AFm phase also proved instable under frost attack and was partly transformed to AFt phase, gypsum, calcite and aluminium hydroxide.

The morphology of the secondarily formed trisulphate is similar for C_3A and C_4AF (REM). In both cases needle-shaped trisulphate of comparable size is formed. Taking into account the x-ray results and the thermoanalytical tests, the TG curves of the thermoanalysis allow the quantities of both phases to be estimated by means of the dehydration temperatures which are different for ettringite/AFt phase and monosulphate/AFm phase. The quantities determined by this method (Table 1) confirm the results of the x-ray tests. We see that the rate at which AFm phase is decomposed and AFt phase is secondarily formed is nearly identical to the decomposion of monosulphate and the secondary formation of ettringite in C_3A.

Table 1 Monosulphate (AFm) and ettringite (AFt) contents approximately determined by means of TG curves

	monosulphate from C_3A in % by weight		AFm-phase from C_4AF in % by weight	
	monosulphate	ettringite	AFm-phase	AFt-phase
initial sample	95.8	0.0	91.6	0.0
28 ftc/ H_2O/ 14 d	42.9	37.4	35.2	37.6

The formation of the possibly expansive secondary ettringite depends on how much SO_3 is produced by the decomposition of the monophases. If the rate of decomposition of the monophases is the same it should be possible by means of the amount of monosulphate before freezing to predict the new formation of ettringite (AFt phase) and also the potential of the cement for a later damage.

BASIC INVESTIGATIONS - FREEZE-DEICING SALT ATTACK

During the freeze-deicing salt test which consisted of 28 freeze-thaw cycles in a 3 % NaCl solution, the monosulphate was totally transformed into Friedel's salt and ettringite (Fig. 2). After 28 freeze-thaw cycles (ftc) no phase transformations were found in the ettringite examined.

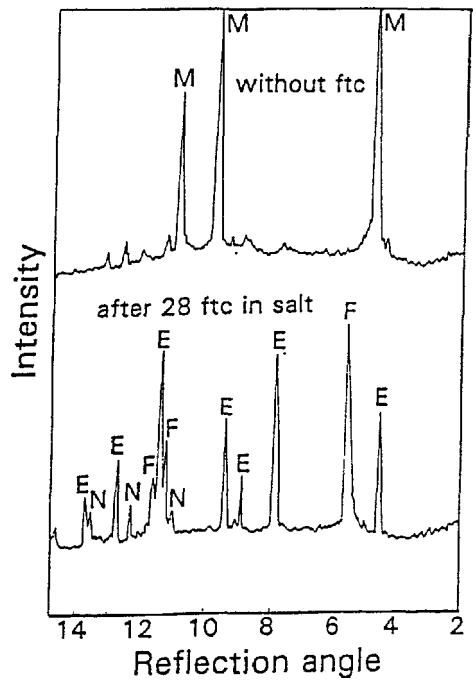

Figure 2 XRD patterns of monosulphate (frost + salt) - M-monosulphate, E-ettringite, F-Friedel's salt, N-sodium chloride.

Contrary to freezing in pure water the combined freeze-deicing salt attack gave no indication of a carbonation of the monosulphate. Obviously the lower solubility of CO_2 in the presence of chlorides leads to a slow-down of the carbonation reaction. It may be concluded that the SO_3 which is required for the formation of ettringite is set free by the partial transformation of monosulphate to monochloride. This hypothesis is supported by investigations by Dorner (1986) who found out that in the presence of NaCl solution a transformation of monosulphate to ettringite will take place even if the work is done in an atmosphere of nitrogen and with nitrogen-saturated water.

The transformation processes which occurred in the AFm phase under freeze-deicing salt attack are comparable in quality to those in the monosulphate from C_3A. Also here AFm phase was decomposed and AFt phase and Friedel's salt were formed. As under frost attack the secondarily formed trisulphate shows again a needle-shaped morphology. The size of the needles is again similar in both C_3A and C_4AF mixes. The decomposition of AFm phase proceeds, however, much more slowly than that of monosulphate. After 28 days only about half of the AFm phase has transformed to other phases (Table 2).

Another source of sulphate than that occurring under frost attack may be assumed to be the reason for the slower decomposition of AFm phase compared to monosulphate. The notoriously bad bonding of chlorides in ferritic phases (Neroth, 1985; Smolczyk, 1984; Lukas, 1983) does not only lead to a reduced formation of monochloride but also to the fact that in comparable periods of time less SO_3 may be provided for the secondary formation of trisulphate than in pure monosulphate from C_3A. The different rate of transformation of monophase under freeze-deicing salt attack indicates that by means of the monosulphate amount (AFm amount) before freezing statements on the potential of the cements for a later damage will not be possible without taking the Fe-content of these phases into consideration.

Table 2 Monosulphate (AFm), ettringite (AFt) and monochloride contents approximately determined by means of TG curves

	monosulphate from C_3A in % by weight			AFm-phase from C_4AF in % by weight		
	mono-sulphate	ettringite	mono-chloride	AFm-phase	AFt-phase	mono-chloride
initial sample	95.8	0.0	0.0	91.6	0.0	0.0
28 ftc/ NaCl/ 14 d	0	47.4	42.3	50.7	20.2	18.0

EFFECTS ON FREEZE-THAW AND FREEZE-DEICING SALT RESISTANCE OF CONCRETE

The phase transformations of synthetically produced aluminate-containing hydrate phases which had been observed in our basic investigations were found by some other authors also in mortars and concretes (Kukko, 1993; Illgner et al., 1991; Ghorab et al., 1981). However, the significance of these phenomena for the real damage by frost and/or freeze-deicing salts has hardly been evaluated as yet.

Within the context of technological investigations into cement and concrete at the Bauhaus-University Weimar it was studied to what extent the new formation of trisulphate may influence the freeze-thaw and freeze-deicing salt resistance of concrete. For this a total of 16 cements with C_3A contents ranging from 0.4 % to 13.7 % were used. With those cements concretes were produced (z = 350 kg/m^3 , w/c ratio = 0.50) with and without artificial air voids, which were then tested by CF test in pure water as well as by CDF test in 3-percent NaCl solution (RILEM, 1995) for their freeze-thaw and freeze-deicing salt resistance.

It was found that concretes without air voids showed big differences in the degree of damage in both tests which has to be attributed to the different cements because mixtures were kept identical and curing was the same for all concretes tested (Fig. 3). Differences in scaling were extreme; under freeze-deicing salt attack the amount of scaled material ranged from 770 g/m^2 up to 5212 g/m^2. Even under frost attack alone where normally only minor scaling can be observed different amounts of scaled material occurred (from 97 g/m^2 to 1079 g/m^2) depending on the cement used.
Damages of concretes with artificial air voids proved not to be dependent on the cements used. All of those concretes showed a high freeze-deicing salt resistance with very small amounts of scaled material.
Evaluating the results from tests with freeze-thaw and freeze-deicing salt attack no clear relationship exists between the composition of clinker phases in portland cements - in this case C_3A content - and their freeze-thaw and freeze-deicing salt resistance. Physical as well as physical-chemical parameters like the degree of hydration of cement or pore size distribution in the concrete also fail to explain the influence of the different cements in concretes without artificial air voids on their freeze-thaw and freeze-deicing salt resistance. Following hypothesis was formulated: the formation of secondary ettringite, which is supported by thermodynamic conditions at low temperatures, as found in basic investigations, influences damage of concrete.

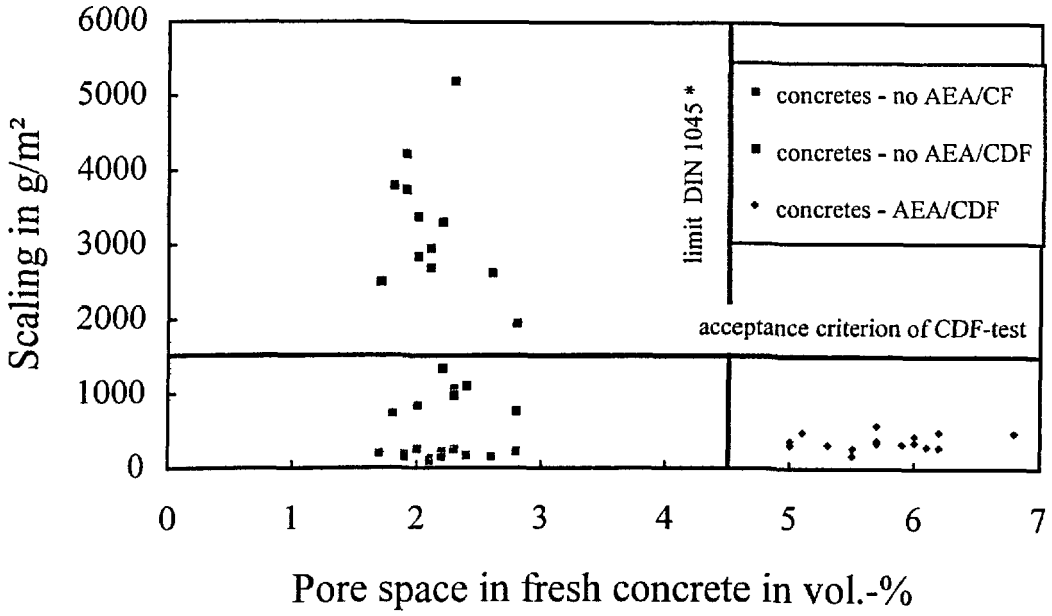

Figure 3 Amount of scaling of concretes with and without air-entrainment (AEA) in dependence on the pore space in fresh concrete in the frost test (CF) and the freeze-deicing salt test (CDF)

After the respective attacks a new formation of ettringite was observed in all concretes, mainly in cracks or at the interface of hydrated cement and aggregate. Obviously some aggregate was forced out of the texture due to the formation of secondary ettringite. A quantification of the newly formed ettringite was not possible because of the diluting effect of the aggregate.
Now it was investigated which aluminate and/or aluminate-ferritic hydrate phases are formed by the 16 cements after 28d hydration and to what extent these hydrate phases are transformed during the CF and/or CDF tests. For this purpose the aluminate-containing clinker phases, the sulphates and the alkalis of the cements were enriched by means of salicylic acid extraction and then hydrated in saturated calcium hydroxide solution. The procedure applied is described in

detail in the literature (Stark et al., 1994, 1992). After 28 d hydration the extractions were subjected to frost and/or freeze-deicing salt attack.
The formation of secondary ettringite (AFt formation), which occurred during freezing the hydrated extraction residues in CF and CDF test, was quantified by thermoanalysis and then correlated to the freeze-thaw and freeze-deicing salt resistance of the concretes tested. The results hint towards a close statistical relationship between the phase transformation as observed and the freeze-thaw and freeze-deicing salt resistance of concretes without artificial air voids (Fig. 4).

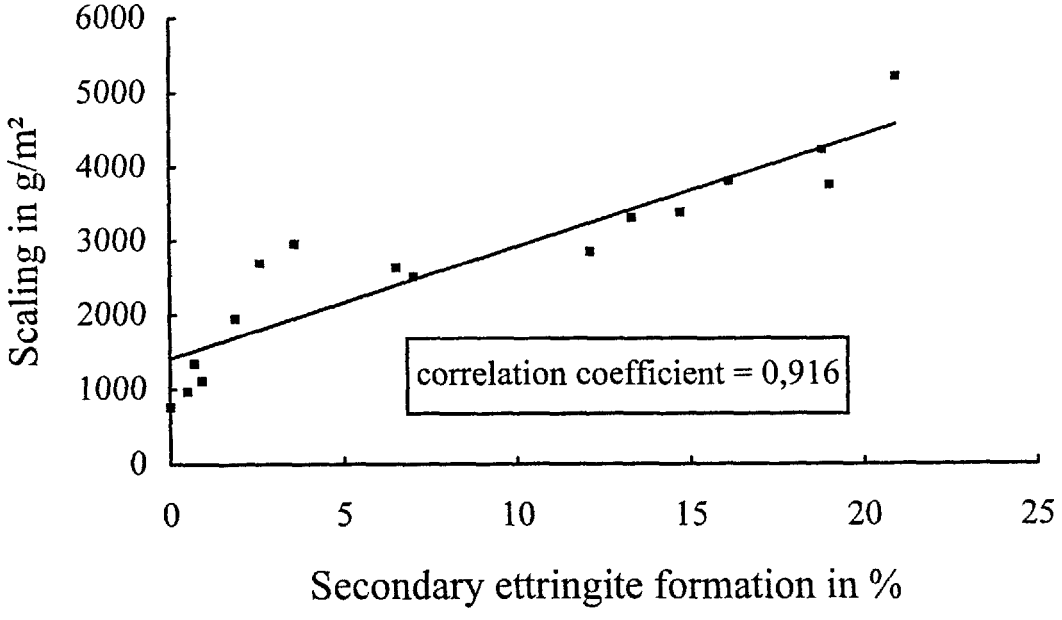

Figure 4 Amount of scaling of concretes in depence on the formation of secondary ettringite in the freeze-deicing salt test (CDF)

Between the formation of new ettringite (new AFt formation) and the amount of scaled concrete material a correlative factor was established of 0.886 under freeze attack and of 0.916 under freeze-deicing salt attack.
The potential of the cement for a later damage, i.e. the formation of new ettringite (new AFt formation), obviously depends on the amount of monosulphate (AFm phase) existing prior to freezing. In addition to that the Fe-content of the monosulphate and AFm phase is important under combined freeze-deicing salt attack. As it is not yet possible to say how the original cement composition influences the content of monosulphate (AFm-content) prior to freezing nothing can be predicted from the clinker phases concerning the potential of the cement for a later damage. A direct relation between the amount of monosulphate (AFm-amount) prior to freezing and the C_3A-content does not exist.
The aim of future investigations should be to determine the factors influencing the increase in the formation of monosulphate (AFm). Then specific measures may be taken to improve the freeze-thaw and freeze-deicing salt resistance by optimising the cement composition.

The importance of the influence of chemical transformation processes is shown in Fig. 5, where the concretes made of two different cements without air-entrainment are compared to air-entrained concrete. It may be seen that these phenomena play a minor role compared to the physical influencing factors such as air-entrainment.

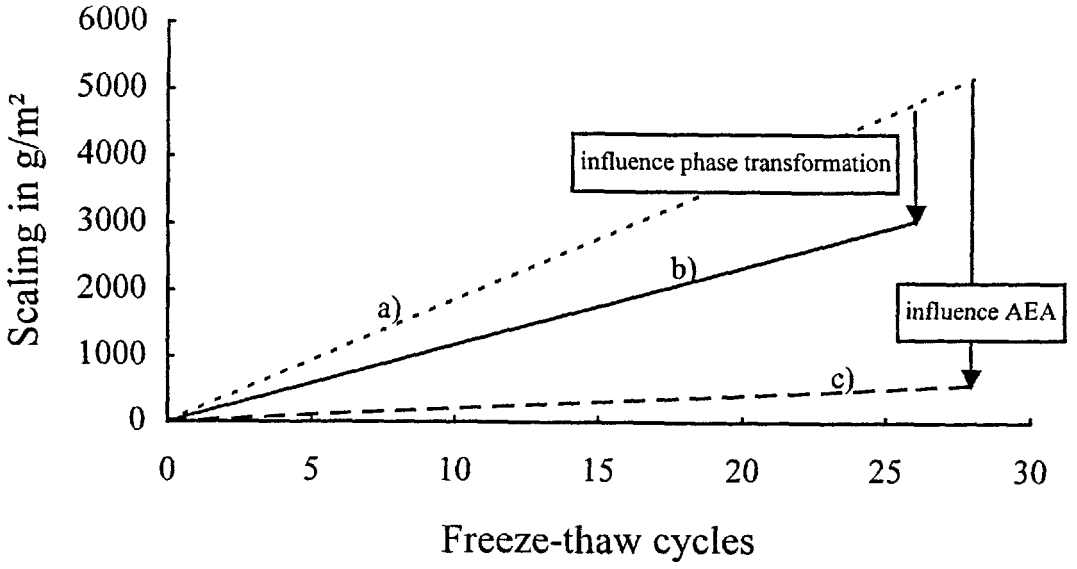

Figure 5 Effect of physical and chemical factors of influence on the freeze-deicing salt resistance (CDF test)
a) concrete with cement A (great amount of newly-formed ettringite)
b) concrete with cement B (small amount of newly-formed ettringite)
c) concrete with cement A and with air-entraining agent (AEA)

The results show that it is possible to produce concretes with a very high freeze-thaw and freeze-deicing salt resistance, independent of the clinker composition. The new findings may, however, be of importance for the future optimisation of concrete with regard to high requirements on its freeze-thaw or freeze-deicing salt resistance. Furthermore phase transformations, as observed in latest investigations, play an important part when the damage of high performance concrete without artificial air voids under freeze-thaw and freeze-deicing salt attack is concerned.

REFERENCES

Dorner, H., and Rippstain, D., "Einwirkung wäßriger Natriumchloridlösungen auf Monosulfat." Tonindustriezeitung, Vol. 110, No. 6, 1986, pp. 383-386.

Ghorab, H.Y., and Ludwig, U., "Modellversuche zur Klärung von Schadensursachen an wärmebehandelten Betonfertigteilen. Teil I: Zur Stabilität von Monophasen und Ettringiten." Tonindustriezeitung, Vol. 105, No. 9, 1981, pp. 634-640.

Illgner, R., and Bubig, M., "Alterung des Betons durch Veränderung physiko - chemischer Gleichgewichte unter Nutzungsbedingungen." Proceedings, 11. Internationale Baustoff- und Silikattagung, Weimar, 1991, Vol. I, pp. 220-231.

Jackson, F.H., "Long-Time Study of Cement Performance in Concrete. ACI - Journal, Vol. 27, 1955, pp. 159-193.

Joosting, R., "Über den Einfluss der Portlandzementmarke auf die Frostbeständigkeit des Betons und des Mörtels." Schweizerische Bauzeitung, Vol. 86, No. 49, 1968, pp. 881-883.

Kukko, H., "Frost Effects on the Microstructure of High Strength Concrete, and Methods for their Analysis. Diss., Helsinki University of Technology, 1993.

Lukas, W., "Zur Frage der Chloridbindung und -korrosion von Stahl bei nachträglicher Einwirkung von Chlorid auf Beton." Proceedings, International Kolloqium Werkstoff-wissenschaften und Bausanierung, Esslingen, 1983, pp. 171-173.

Neroth, G., "Zur Bindung von Chlorid in Zementstein." Baustoffe '85, Bauverlag, Wiesbaden/ Berlin, 1985, pp. 140-147.

Peterson, P.E., "Scaling Resistance Tests of Concrete. Experience from Practical Use in Sweden." Proceedings, International Workshop on Freeze-Thaw and Deicing Salt Scaling Resistance of Concrete, Quebec, 1993, pp. 249-259.

Rasmussen, T.H., "Long-Term Durability of Concrete." Nordic Concrete Research, Vol. 4, 1985, pp. 159-178.

RILEM TC 117-FDC, "Draft Recommendation for Test Method for the Freeze-Thaw Resistance of Concrete. Test with Water (CF) or with Sodium Chloride Solution (CDF). Materials and Structures, Vol. 28, 1995, pp. 175-182.

Rose, K.; Hope, B.B.; and Ip, A.K.C., "Statistical Analysis of Strength and Durability of Concrete made with different Cements. Cement and Concrete Research, Vol. 19, 1989, pp. 476-486.

Schrämli, W., "An Attempt to assess beneficial and detrimental Effects of Aluminate in the Cement on Concrete Performance. World Cement Technology, Vol. 9, No. 3, 1978, pp. 35-42 and No. 4, pp. 75-80.

Smolczyk, H.-G., "Flüssigkeit in den Poren des Betons - Zusammensetzung und Transport-vorgänge in der flüssigen Phase des Zementsteins." Beton - Information, Vol. 24, No. 1, 1984, pp. 3-11.

Stark, J., and Ludwig, H.-M., "Effects of Low Temperature and Freeze-Thaw Cycles on the Stability of Hydration Products." Proceedings, 9th International Congress of the Chemistry of Cement, New Dehli, 1992, Vol. IV, pp. 3-9.

Stark, J., and Stürmer, S., "The Influence of the C_3A-Content on the Durability at Freezing and Thawing. Report TVBM - 3048, RILEM TC 117, Lund, 1991, pp. 155-166.

Stark, J.; Müller, A.; and Stürmer, S., "Hydration of C_3A and $C_2(A,F)$ - separated from Sulphate-Resisting and White Portland Cement - under Conditions of Normal Hardening and Heat Treatment." Cement and Concrete Research, Vol. 24, 1994, pp.503-513.

FREEZE-THAW AND FREEZE-DEICING SALT RESISTANCE OF CONCRETES CONTAINING CEMENT RICH IN GRANULATED BLAST-FURNACE SLAG

Jochen STARK, Bauhaus-University Weimar, Germany
Horst-Michael LUDWIG, Bauhaus-University Weimar (today Schwenk Zementwerke KG, Karlstadt), Germany

ABSTRACT Whereas blast-furnace cement concretes have proved successful in structures subjected to freeze-thaw attack, their use in structures subjected to freeze-deicing salt attack is still a problem. It was found out that the freeze-deicing salt resistance of blast-furnace cement concretes is closely related to the carbonation of the surface area. The carbonation of blast-furnace cement concretes does not only lead to an increase in capillary porosity but also to metastable calcium carbonates soluble in NaCl. Based on the results of investigations ways of improving the freeze-deicing salt resistance of blast-furnace cement concretes are proposed.

Key-words: Blast furnace slag, Concrete, Carbonation, Freeze-thaw, De-icing salts

INTRODUCTION

This paper presents the results of several years research work in the field of freeze-thaw and freeze-deicing salt resistance. It should help to clarify the contradictions between the high frost resistance of concretes rich in granulated blast-furnace slag (content > 60%) on the one hand and their low freeze-deicing salt resistance in laboratory tests on the other.

FROST RESISTANCE OF BLAST-FURNACE CEMENT CONCRETE

The problem of frost attack is a problem of the volume, i.e. in addition to surface scaling the interior microstructure may also be destroyed. This fact is reflected in the frost resistance testing criteria of concretes, which consider not only the change in mass and/or the amount of scaling but also characteristics describing the state of the microstructure within the concrete (decrease of the dynamic modules of elasticity, of the ultrasonic speed, of the compressive strength etc.). Because density of the concrete microstructure plays a predominant role in frost resistance, the degree of hydration of the cement at the beginning of freezing is of great importance. Nearly all characteristics relevant to damage such as pore size distribution, total porosity, compressive and tensile strength will depend on the degree of hydration.

There was a test program carried out on how the different degrees of hydration of blast-furnace cements and portland cements at the beginning of freezing will influence pore size distribution and frost resistance. The freeze tests were made according to procedure A of TGL 33433/06. The degree of hydration of blast-furnace cement was determined by using the method of selective solution (by employing methyl-alcoholic salicylic acid, Stark et al. 1990). Comparing portland and blast-furnace cement studies show opposite tendencies. Blast-furnace cements form a considerably denser microstructure than portland cements at the same degree of hydration. For example, in contrast to portland cements blast-furnace cements show a high gel porosity and only a small content of capillary pores, at a degree of hydration of 60 %. On the other hand the rate of hydration of blast-furnace cement is slower than that of portland cement. Thus the portland cement achieved the degree of hydration mentioned above after only 3 days, whereas the blast-furnace cement took 28 days for the hydration of the same amount of cement.

For freeze-thaw resistance the degree of hydration and thus the state of the microstructure at the moment of freezing (test usually after 28 days standard storage) is a decisive factor. After 28 days standard storage (7 days in water and 21 days in the air at 20°C and 65 % relative humidity) the degree of hydration of the portland cements studied was between 85 and 90 %. Depending on the quality of the granulated blast-furnace slag (F2 = $[CaO + MgO + Al_2O_3]/SiO_2$ = 1.1 - 1.8) and

the fineness of cement (Ao = 2000 - 5000 cm^2/g) degrees of hydration from 30 to 65% were established in the blast-furnace cements (slag content c. 65 %) after the same storage time. Fig. 1 (pore classification acc. to Romberg, 1978) shows the effects that different degrees of hydration have on the microstructure.

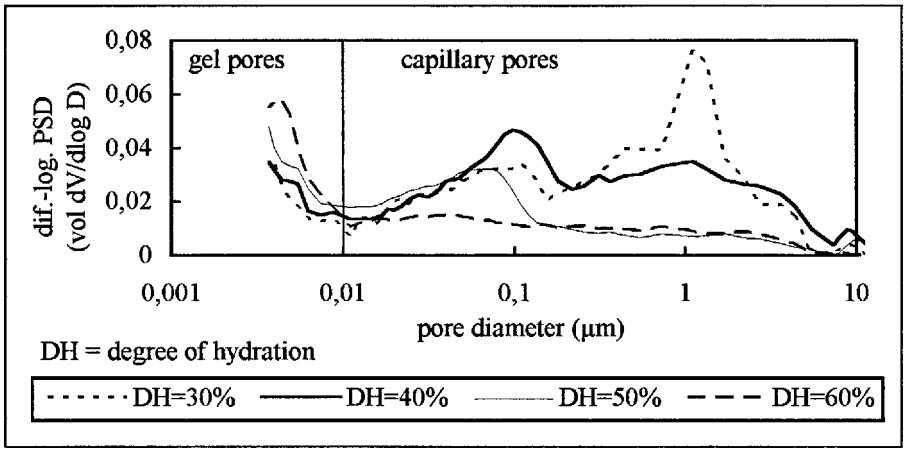

Figure 1 Pore size distribution (PSD) of blast-furnace cement mortar at different degree of hydration after 28 days hydration time

With increasing degree of hydration, the microstructure clearly becomes denser, which becomes apparent through an increase in gel porosity and a decrease in capillary porosity. The peak of capillary pores moves from larger to smaller pore diameters.
A comparison of the pore size distribution between portland (OPC) and blast-furnace cements (BFC) shows that the slower hydration of blast-furnace cement may be compensated for by the denser microstructure which occurs at a degree of hydration from 50 % on. Blast-furnace cement with a degree of hydration of 50 % has a pore size distribution similar to that of portland cement with a degree of hydration of 90 %. High-quality blast-furnace cements with a degree of hydration of more than 50 % develop a denser microstructure than portland cements, regardless of the much lower degree of hydration.
The degree of hydration had a strong influence on the frost resistance of mortars and concretes in laboratory tests. For determining the relationship between the degree of hydration and frost resistance we used the above mentioned cements for the production of concretes without air-entrainment, which were afterwards tested for their frost resistance (cement content = 350 kg/m^3, water-to-cement ratio = 0.5).

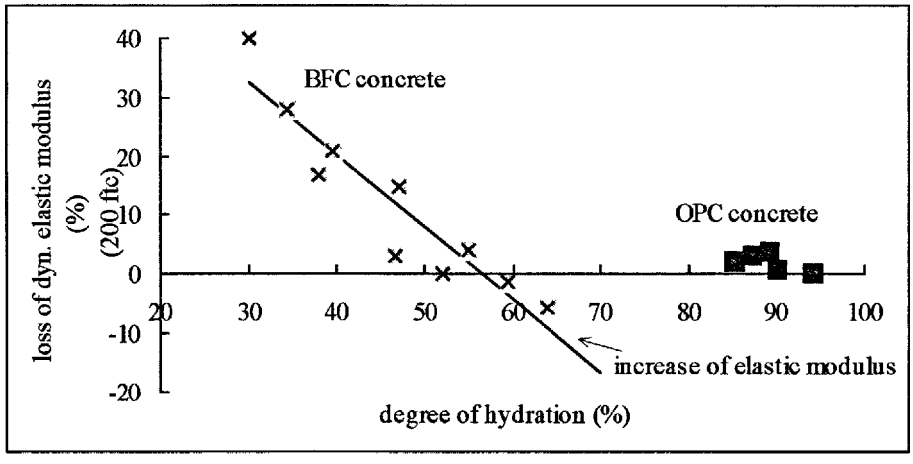

Figure 2 Dependence of frost resistance on the degree of hydration of the cements

As may be seen in Fig. 2, there is a linear relationship between frost resistance and degree of hydration of blast-furnace cement.
Compared to portland cement blast-furnace cements may be subdivided into three ranges, which depend on pore size distribution:

$\alpha_H < 50$ % - the lower degree of hydration leads to a highly capillary-porous microstructure; frost resistance is lower than that of portland cement mortars and concretes

$\alpha_H = 50$ % - the low degree of hydration may be compensated for by the denser microstructure, frost resistance corresponds to that of portland cement mortars and concretes

$\alpha_H > 50$ % - the formation of a very dense microstructure results in a frost resistance which is higher than that of portland cement mortars and concretes

The studies of frost resistance show that a general assessment of blast-furnace cement concrete is not possible. The frost resistance differs greatly, depending on the cement quality, particularly on the quality of the granulated blast-furnace slag, and the curing. In this context it has to be emphasised that all blast-furnace cements examined contained slag which was in accordance with the requirements of DIN 1164 (1990) for an F2 value of ≥ 1. However, an F2 value of at least 1.5 was required to achieve a high frost resistance.

FREEZE-DEICING SALT RESISTANCE OF BLAST-FURNACE CEMENT CONCRETE

As already stated, the freeze-deicing salt resistance of blast-furnace cement concretes is generally considered to be worse than that of comparable portland cement concretes.
Again there was reason to suppose that the degree of hydration is responsible for the different freeze-deicing salt resistance of blast-furnace and portland cement concretes. To verify this assumption the concretes without air-entrainment described in the passage above were not only tested for their freeze-thaw resistance, but also for their freeze-deicing salt resistance by means of the CDF procedure. The CDF procedure developed by Setzer and Hartmann is descripted in RILEM (1995).
In contrast to the pure freeze test the results of the freeze-deicing salt tests showed no relationship between the freeze-deicing salt resistance and the degree of hydration. This becomes apparent if it is taken into account that, unlike pure frost attack, freeze-deicing salt attack causes damage primarily to the surface of the concrete. Studies showed that, even with great surface scaling, no significant interior damage of the concrete could be observed, Siebel (1992). Therefore almost all procedures of determining the freeze-deicing salt resistance of concrete are confined to determining the loss in weight and/or the amount of scaled material. Freeze-deicing salt tests conducted using the CDF procedure at the Bauhaus-University resulted in amounts of scaling between 90 g/m^2 and 6000 g/m^2 after 28 cycles of freezing and thawing, depending on the quality of the concretes. If, assuming a bulk density of 2300 kg/m^3 various scalings are expressed in terms of an average depth of scaling the result will be a layer of 0.04 mm to 2.6 mm in depth.
The above considerations lead to the conclusions that the degree of hydration and the state of the microstructure of the concrete as a whole are of minor importance to whether a concrete exhibits sufficient freeze-deicing salt resistance or not. The properties of a thin concrete surface layer are decisive.
To understand the different freeze-deicing salt resistance of blast-furnace and portland cement concretes, it is important to know in which stage of freezing differences will occur. Whereas in tests for frost resistance under water the scaling of both blast-furnace and portland cement concrete is linear (Fig. 3), heavy initial scaling is observed in tests for the freeze-deicing salt resistance of concrete containing cements rich in granulated blast-furnace slag (content ≥ 60 %) in 3 % NaCl solution (Fig. 4).

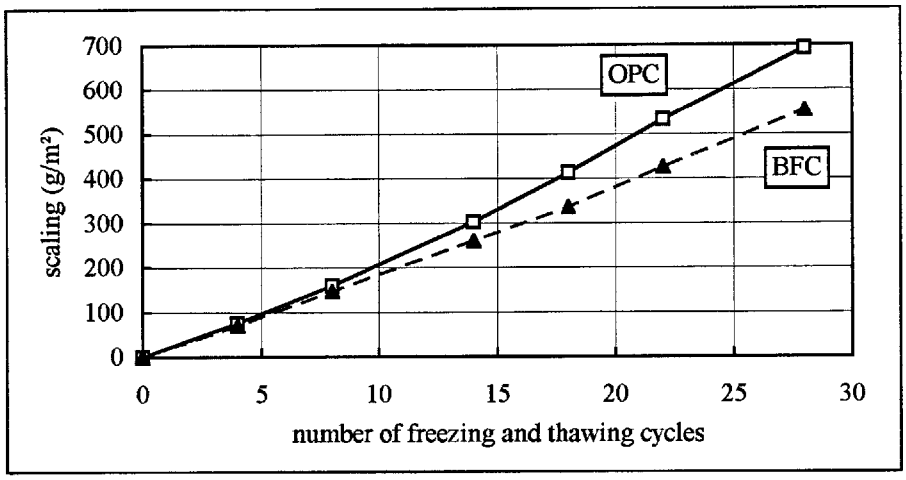

Figure 3 Typical courses of scaling of portland cement concrete and blast-furnace cement concrete (without air-entraining agents) under frost attack (CF test)

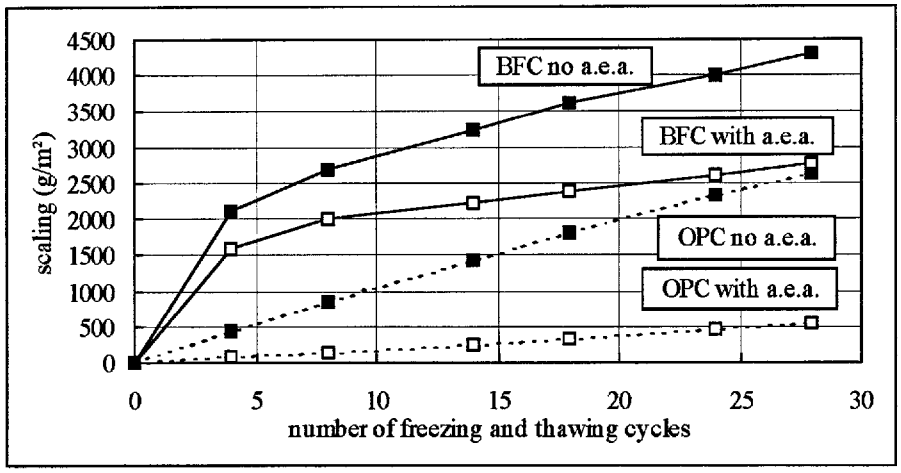

Figure 4 Typical courses of scaling of portland cement concrete and blast-furnace cement concrete with and without air-entraining agents (a.e.a.) under freeze deicing salt attack (CDF test)

This heavy initial scaling occurs both in concretes with and without air-entrainment and is responsible for the fact that in many cases blast-furnace cement concretes show a lower freeze-deicing salt resistance than comparable portland cement concretes and that air-entraining agents are less effective in cements rich in granulated blast-furnace slag. After the initial scaling in the first 4-8 cycles of freezing and thawing the curve changes appreciably and - as a rule - indicates in the second phase a similar or even lower intensity of damage compared to portland cement concretes. The reasons for the heavy initial scaling of blast-furnace cement concretes are not yet known. As the material scaled at the beginning of the damage is identical to the surface layer of the concretes it may be assumed that the initial scaling is influenced by the carbonation of the concrete.

TESTS FOR THE INFLUENCE OF CARBONATION

In order to find out whether the heavy initial scaling of blast-furnace cement concretes is related to the carbonation, the depth of carbonation of different blast-furnace cement concretes prior to freezing was compared to the calculated depth of scaling at the break point of the curve of scaling. The results of these studies (Fig. 5) show conclusively that the decrease in the intensity

of damage (break point of scaling curve) occurs precisely when the damage proceeds from the carbonated to the non-carbonated zone of the blast-furnace cement concretes.

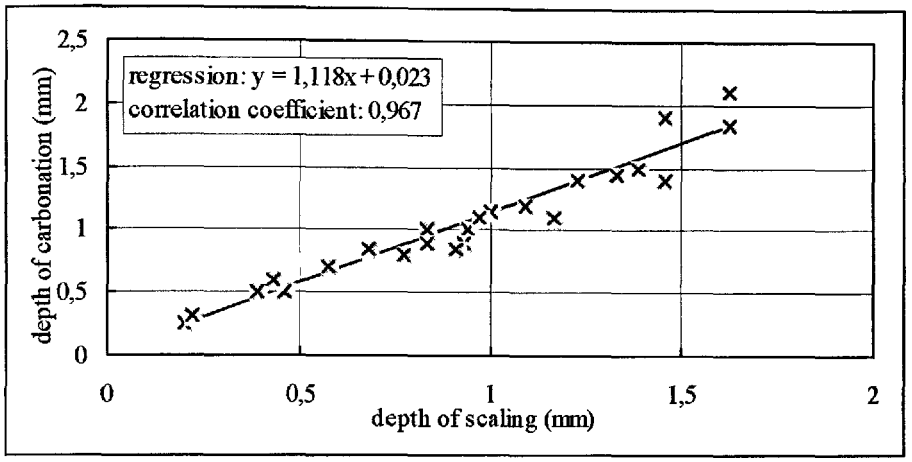

Figure 5 Relationship between depth of initial scaling and depth of carbonation of blast-furnace cement concrete with and without air-entraining agents

Furthermore, the scaled material was subjected to thermoanalysis and the amount of calcium carbonate in the material was determined by means of the DTA/TG curve for each phase of freezing. The comparison of the calculated amounts of calcium carbonate with the behaviour of the curves of scaling shows, in accordance with the studies into the depths of carbonation, that exactly at the break point of the curve of scaling the content of carbonate in the scaled material decreases considerably. That means that heavy scaling will occur only in the carbonated surface area, whereas the non-carbonated core shows sufficient resistance to freeze-deicing salt attack.
Investigations on blast-furnace cement concrete stored in different CO_2 concentration confirm the strong influence of carbonation. Specimens stored without CO_2 under nitrogen showed no progressive initial scaling and exhibited the best freeze-deicing salt resistance. The freeze-deicing salt resistance of the concrete stored in increased CO_2 concentration (3 % CO_2) was the worst of all concretes. The initial scaling covered a longer period of time and reached greater depths. In all cases the depth of carbonation corresponds to the depth of initial scaling.

RESEARCH INTO THE CAUSES OF INFLUENCE OF CARBONATION

In order to study the causes of the adverse effect of carbonation on the initial scaling of blast-furnace cement concretes, basic investigations into cement pastes (phase-analytical investigations) and concretes (investigations into the microstructure) were carried out.
Differences between blast-furnace and portland cement concrete became apparent through the effect of carbonation on the microstructure. While carbonation led to a slight densification of the microstructure in portland cement concrete, the microstructure of blast-furnace cement concrete became coarser. In fact, the total porosity decreased also in this case, at the same time the portion of capillary pores increased. Nevertheless, it occurred after an even smaller degree of carbonation than that of portland cement concrete. The coarser microstructure of blast-furnace cement concretes due to carbonation has already been stated by Manns and Zeus (1979), Bier (1987), Hilsdorf et al. (1984). The increase of capillary pores due to carbonation, however, cannot be the main reason for blast-furnace cement concretes behaviour under freeze-deicing salt attack, since in this case also under frost attack a higher intensity of damage in the carbonated surface area should have been expected. In contrast to the freeze-deicing salt attack, no break point is observed for the pure freeze-thaw attack under water when the damage proceeds from the carbonated to the non-carbonated zone of the concrete (Fig. 4).

The different course of scaling of blast-furnace cement concretes under frost attack in water and in NaCl solution indicates that there is a chemical cause.
Phase analyses of the carbonated surface area (by XRD) prior to freezing showed in blast-furnace cement that in addition to calcite two other $CaCO_3$ modifications, aragonite and vaterite, occur in considerable amounts (Fig. 6). In portland cement, however, only calcite could be detected. The causes of the occurrence of different calcium carbonate modifications in blast-furnace cement are to date not completely clear. Possibly the different carbonate phases found in portland cement and blast-furnace cement are due to the fact that $Ca(OH)_2$ carbonates to calcite whereas the C-S-H phases or AFm and AFt phases carbonate to aragonite and vaterite (Suzuki and Nishikawa 1992, Nishikawa et al. 1992).

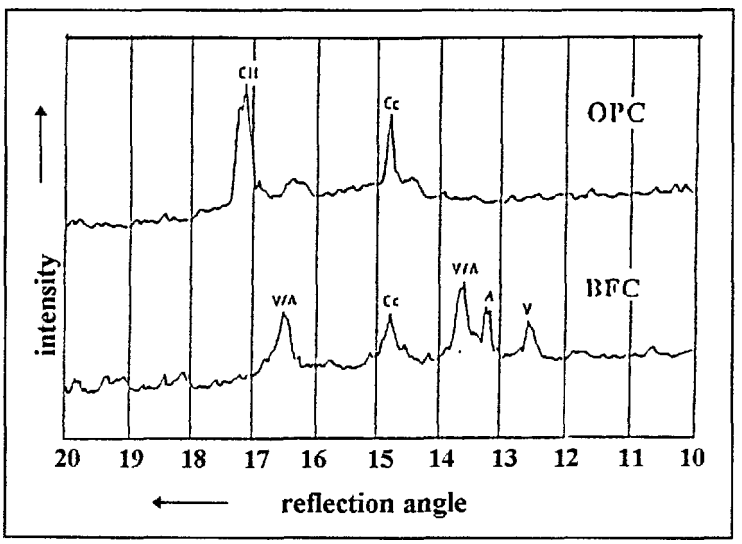

Figure 6 XRD of carbonated surface area of portland cement pastes and blast-furnace cement pastes; CH = portlandite, Cc = calcite, A = aragonite, V = vaterite

Thermoanalyses showed that in all cases the decarbonation temperature of the $CaCO_3$ was between 800-900°C. During the DTA test heating period the metastable $CaCO_3$ modifications are transformed to calcite at about 300-400°C. Examinations of the scaled material and the damaged surface area after the freeze-deicing salt attack showed that large amounts of $CaCO_3$ had already decomposed at about 650°C. It was proved by mass spectrometry that this reaction is indeed a decomposition of $CaCO_3$. According to Cole and Kroone (1960) a lower decomposition temperature indicates badly crystallized calcite. X-ray analysis showed that the new formation of this calcite is accompanied by an intense reduction of aragonite and vaterite. These observations coincide with the existing publications on stability and transformation of calcium carbonate modifications. According to them the solubility constants of the metastable modifications are larger than those of the calcite, and these differences increase considerably in chloride solutions (Schröder 1962, Richter 1993). From the order of solubilities CS (calcite) < CS (aragonite) < CS (vaterite) it follows that a solution which is saturated with respect to vaterite and aragonite is always over-saturated with respect to calcite. Under certain conditions the decomposition of vaterite and aragonite is followed by formation and growth of calcite nuclei.
Based on the test results the following hypothesis about the heavy initial scaling of concretes rich in granulated blast-furnace slag may be proposed: The metastable modifications of $CaCO_3$ - vaterite and aragonite - are dissolved by the combined attack of frost and chloride. This leads to an extensive erosion of the concrete surface. In the deeper carbonated layers the dissolution of vaterite/aragonite may lead to the new formation of calcite in the microstructure. The change in volume implied may further aggravate the damage initiated by the dissolution processes. After the

entire carbonated layer has been scaled in this way the speed of damage decreases appreciably - a clear break point is to be observed in the curve of scaling (Fig. 5).
Additional SEM and EPMA tests confirm the results of the phase analysis and support the above hypothesis about the mechanism of damage. Figure 7a and 7b show the microstructure of the cement paste before and after the freeze-deicing salt attack. In addition to rhombohedrally calcite, well-crystallised aragonite needles and vaterite spherolites can also be recognized before freezing. But after the cycles of freezing and thawing only calcite is still visible in a crystalline form. The metastable $CaCO_3$ modifications have been decomposed almost completely.

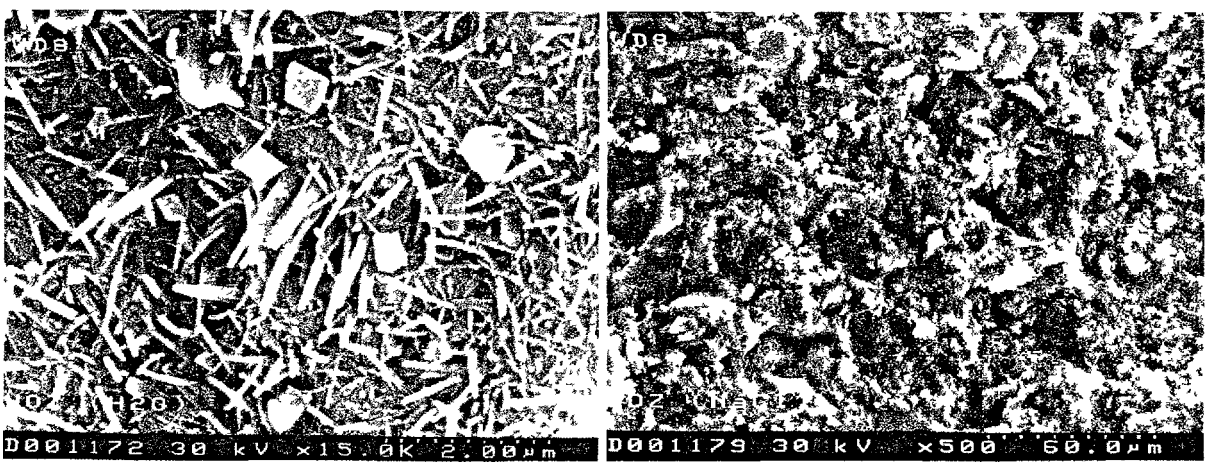

Figures 7a and 7b Surface layer of blast-furnace cement pastes prior to freeze-deicing salt attack (left side) and after freeze-deicing salt attack (right side)

WAYS OF REDUCING THE INITIAL SCALING OF BLAST-FURNACE CEMENT CONCRETES

There are two ways of improving the frost and freeze-deicing salt resistance. On the one hand, it would be desirable to reduce carbonation and/or the rate of carbonation by technical means. On the other hand, it should be explored whether the formation of the metastable calcium carbonate modifications may be minimized or even prevented by modifications concerning the materials used.
As a technical means the use of draining formwork material proved successful. In this way the surface area will be densified so that the carbonation of this thin surface area will be reduced considerably. Furthermore, the effect of curing agents as another way of improving the frost and freeze-deicing salt resistance is being investigated and seems to be promising. On the other hand the addition of small amounts of $Ca(OH)_2$ might stabilise the C-S-H phases of the blast-furnace cement (higher C/S ratio) and thus form an additional impediment to the carbonation. The effects of the use of draining formwork material and of an addition of $Ca(OH)_2$ on the initial scaling of blast-furnace cement concretes were at first tested by means of the CDF procedure on concretes without air-entrainment.
The results show (Fig. 8) that the use of the newly developed formwork material (Zemdrain) increases the freeze-deicing salt resistance of the blast-furnace cement concrete considerably. The extreme reduction in the depth of carbonation made the initial scaling disappear completely. Also the addition of 10 % $Ca(OH)_2$ to the concrete led to a reduction in initial scaling from 1500 to 1000 g/m², the prevention of initial scaling was by no means possible. Compared to the use of Zemdrain this method is considered as less effective.

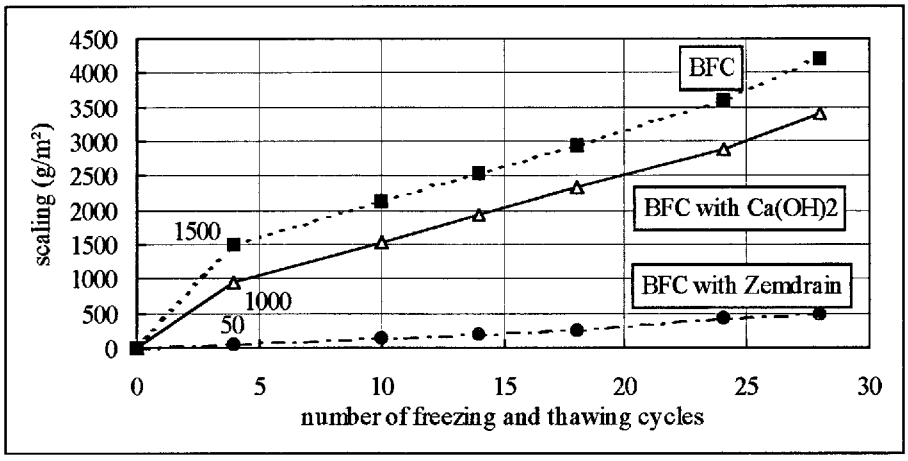

Figure 8 Initial scaling of blast-furnace cement concrete

CONCLUSIONS

The investigations show that the freeze-deicing salt resistance of concretes rich in granulated blast-furnace slag is strongly influenced by the carbonation of the surface layer. The coarser microstructure due to carbonation as well as the existence of metastable carbonates (vaterite, aragonite) lead to a freeze-deicing salt resistance of the carbonated layer which is lower than that of the concrete core. In order to achieve a high freeze-deicing salt resistance it is therefore necessary to minimize the carbonation of these concretes. Draining formwork material is particularly suitable.

REFERENCES

Bier, T.A., "Karbonatisierung und Realkalisierung von Zementstein und Beton." Diss., Universität Karlsruhe, 1987.

Cole, W.F., and Kroone, B., "Carbon Dioxide in Hydrated Portland Cement." Journal ACI, Vol. 31, No. 6, 1960, pp.1275-1295.

Hilsdorf, H.K., Kropp, J., and Günther, M., "Karbonatisierung und Dauerhaftigkeit von Beton." Fortschritte im konstruktiven Ingenieurbau, Berlin: Verlag Ernst&Sohn 1984, pp. 89-96.

Manns, W., and Zeus, K., "Zur Bedeutung von Zuschlag und Zement für den Frost-Taumittel-Widerstand von Beton." Straße und Autobahn, Vol. 30, No. 4, 1979, pp. 167-173.

Nishikawa, T., Suzuki, K., Ito, S., Sato, K., and Takebe, T., "Decomposition of Synthesized Ettringite by Carbonation." Cement and Concrete Research, Vol. 22, 1992, pp. 6-14.

Richter, A., " Ein Beitrag zur Fällung und Phasenumwandlung von Calciumcarbonat." Diss., Bergakademie Freiberg, 1993.

RILEM TC 117-FDC, "Draft Recommendation for Test Method for the Freeze-Thaw Resistance of Concrete. Test with Water (CF) or with Sodium Chloride Solution (CDF)." Materials and Structures, Vol. 28, 1995, pp. 175-182.

Romberg, H., "Zementsteinproben und Betoneigenschaften." Beton - Information, Vol. 18, No. 6, 1978, pp. 269-277.

Schröder, F., "Vaterit, das metastabile Calciumcarbonat, als sekundäres Zementsteinmineral." Tonindustriezeitung, Vol. 86, No. 10, 1962, pp. 254-260.

Siebel, E., "Frost- und Frost-Tausalz-Widerstand. Beurteilung mittels Würfelverfahren." Beton, Vol. 42, No. 9, 1992, pp. 496-501.

Stark, J., Ludwig, H.-M., and Müller, A., "Zur Bestimmung des Hydratationsgrades von Schlackenzementen." Zement-Kalk-Gips, Vol. 43, No. 11, 1990, pp. 557-560.

Suzuki, K., and Nishikawa, T., "Formation and Carbonation of C-S-H in Water." Cement and Concrete Research, Vol. 15, 1985, pp. 213-224.

NON SHRINKAGE FROST RESISTANT POZZOLANIC CEMENT

Serguei A. ZOUBEKHINE, Boris E. IOUDOVITCH
NIICement, Moscow, Russia

ABSTRACT Modified pozzolanic cement (MpC) with accelerated pozzolanic reaction has been designed and produced on the base of oversaturated-by-lime ferrous special Portland cement clinker (SPCC), natural sedimentary (ns-) pozzolana and gypsum.

Key-words: Clinker composition. Free lime. Pozzolanic cement. Shrinkage. Steam curing.

INTRODUCTION

Pozzolanic reaction degree (p.dg., % by weight) in water hardening (during 1 month) pozzolanic cement (pC) paste with ns-pozzolana is usually under 15. Shortcomings of pC properties are connected with low p.dg. and existence of contour pores around pozzolanic particles (Entine, 1993). Said pores can be filled in when p.dg. reachs 70 (from percolation theory by Chizmadjev et al.,1971). Attempts of p.dg. raising are known, e.g. by: 1) leaving C_{free} in PCC under 10% (Druzhinin, 1934); p.dg. raises by 10, but coarse C_{free} grains in clinker deteriorates pC properties; 2) raising of pC fineness; p.dg. grows by 10-15 (Rabilero, 1988); this is not enough for said pores filling; 3) adding of anhydrous lime to pC (10%, Volzhensky et al.,1991); p.dg. growth is abt 10; 4) two-clinker based pC, in which the 1-st clinker (40%) is alitic, the 2-nd clinker (20%) is belitic with free lime in it under 25% relating to 2-nd clinker weight, ns-pozzolana 35%, gypsum 5%. In this case p.dg. after 1 month is 30-40; this level is not enough for frost resistance (Zoubekhine, Ioudovitch et al.,1994). The results of next attempt of p.dg. raising are written down here.

EXPERIMENTAL AND METHODS

On the plant stage 3 wet process gas fired (3000 m^3/h) rotary kilns (3.6 x 70 m) were used for SPCC burning with throughput (Q.) about 11t/h as in ordinary PCC burning without changes of kiln conditions. Raw materials are chalk, Jurassic black clay and pyrite ores. Pozzolana is weathered kieselgur from Volsk (Russian name - opoka) with activity level 180 - 240 mg of lime absorbed by 1 g of opoka during 30 days (std. min.60 mg/g). SPCC(60%) + opoka(40%) + gips (5% over) were ground jointly in 3-chambered mill (2.6 x 13 m, open cirquit) with Q. for MpC 18 t/h versus(v.) 16 t/h for pC (based on PCC, other the same) upto the fineness: 2-3% of residue on sieve No. 008 (80 mkm), Blaine number under 800 m^2/kg, and v. Q. = 12 t/h for ordinary PC (OPC, type II/A-P) ground to Blaine number 550 m^2/kg. Chemical and phase compositions were analysed by ethyl-glycerate, X-ray fluorescence, diffraction (XRD) and selective chemical (SC) methods. SC analysis (Panina et al.,1992) based on 10% alcohol (alc.) maleic acid solution (calcium silicates solubility [s.,%] 98-99, aluminates and alumino-ferrites s.$\leq$ 1), 0,4% acetoacidic mannite alc. solution (aluminates s.> 99, aluminoferrites s.$\leq$ 0.5) and 3% orthonitrophenol alc. solution (alite s. $\geq$ 99, belite s.$\leq$1). Impurities are determined from solutions. DTA (with parallel wet analysis of CH in pastes) was used for p.dg. determination. Hydration and hardening of MpC and comparing pC were studied with microscopy, XRD, std. physical and mechanical methods.

RESULTS

Raw mix composition was projected with lime saturation factor [LSF=(C - 1,65A - 0,35F)/2,8S] 1.15÷1.45,silicate[S/(A+F)] and aluminate (A/F)moduli 1.7$\pm$0.2; 0.7$\pm$0.2. Chemical compositions of 1) raw mix, 2) SPCC, 3) opoka, by main oxides (%) are next: 1): L.O.I.33-40, S 12-14.5, A 0.5-2.5, F 2-5.5, C 44-50; 2): S 14-21, A 1-3.8, F 3.3-8.5, C 69-80, free C 5-11; 3): S 75-78, A

5-6.6, F 3.5-4.5, C 4.5-5. Powder XRD pattern of SPCC shows reflexes of alite, all in polyplicate form (e.g. profile of peak at d=1.76.10^{-10}m is quadriplicate), and of $C_2(A,F)$ mainly. Phase composition of SPCC sample by SC and limites of that by XRD methods are shown in Table 1.

Table 1. Phase composition of special Portland cement clinker (SPCC)

Minerals (working names are in invert commas)	Oxide content in weight % by SCm in oversaturated-by-lime ferrous SPCC					Integral formula	XRD content, weight %
	SiO_2	Al_2O_3	Fe_2O_3	CaO	Σ		
``Hyperalite`` (analog of alite)	15.96	1.20	0.08	53.36	**70.60**	3.6 CaO. SiO_2 . . $0.04Al_2O_3$	**60 ÷ 85**
Belite	0.25	0	0	0.50	**0.75**	2 CaO . SiO_2	traces÷15
``Calcium ferroaluminate``- analog[1]	2.00	2.84	4.51	7.06	**16.41**	4.5 CaO . Al_2O_3 . . Fe_2O_3 . 1.2 SiO_2	**10 ÷ 25**
``Calcium aluminate analog`` (glass)	0.64	0.48	0.48	1.50	**3.10**	5.8 CaO . Al_2O_3 . . 0.6 Fe_2O_3 . 2.3 SiO_2	traces÷3
Free lime solid solution	0	0	0.86	5.59	6.45	18.5 CaO . Fe_2O_3	-[2]
Impurities(alkalies et al)	-	-	-	-	2.69	-	2 ÷ 3
Sum	**18.85**	**4.52**	**5.93**	**68.01**	**100.00**	-	**85 ÷ 95**

Notes: [1] With C_2S inclusions probably; [2] Abt 5 ÷ 15 by slightly modified microchemical method

This results testifies that in SPCC: 1) there is *hyperalite* with C/S higher than 3.17 for max. dense alite lattice (Taylor, 1994). Hyperalite has also much higher hydration rate: in neat PC and MpC micropreparations with water/solid ratio 10 by Astreeva`s method (1959) hyperalite hydration degree (h.dg.,%) is estimated as 60 and 80 at 24-28h, 80 and 100 at 48h v. 10/15 and 15/20 for alite in OPC/pC micropreparations. In mortars cured in 100% R.H. air h.dg. of hyperalite in MpC is 20-30 at 1 d., in water 40-50 at 7 d., 70-90 at 28 d. v. 5-10, 25-30 and 50-60 for alite in pC. In water keeping neat PC paste samples 1,41[3] cm h.dg. for hyperalite is 30 and 80 - 100 at 1 and 7 d. v. 15 and 50 for alite. C/S ≥3.3 may be result of lime endotaxy along boundaries of mosaic alite blocks during burning; 2) there is much of S in calcium ferroaluminate and S+F in aluminate. It *does not mean* that any quaternary compounds present in system C-A-F-S, seems to be the result of C_2S-submicroresidues in interlayer spaces of *calcium ferroaluminate* and silicate inclusion in *aluminate glass. Slow hydration* of *both* (h.dg. is 5-10 by month) supports this point of view and *inverses the phases sequence* in hardening cements to the first CH/C-S-H formation and AFt-/AFm-phases much later on; SO_4^{2-} (not CO_3^{2-}) partly goes to C-S-H; 3) free C is amorphous as partly in PCC from marl mix. So the fineness of SPCC raw mix was lowered v. usual level for PCC in connection with raising solution rate and solubility of S in C-supersaturated ferrous melt. Said amorphous free lime under 15% *does not* cause the unsoundness of i)neat PC from SPCC and ii) MpC, and *does not* irritate personnel` mucous membranes. After 3 months SPCC nodules (5-15 mm) kept in the open air are fell to grains (0.5-2 mm in size without dust). Kept over 2 year without alterations grains have the same hydraulic activity as initial SPCC. Average CH content in MpC hardened paste is only slightly more than in pC one, because the essential increasing rate of pozzolanic reaction. So in 1,41[3] cm MpC samples p.dg. is 70-75 at 1 and 90-100 at 2 months v.15 and 25 in pC. Thus amorphous free C of SPCC and more reactive hydrolytic CH (than in pC and OPC pastes) accelerates the pozzolanic reaction in MpC paste and said contour pores around any pozzolana particles can be filled in with the reaction products.

PROPERTIES OF MODIFIED POZZOLANIC CEMENT

Cement strength (GOST 10178) *v. content of pozzolana* or std. blastfurnace *slag* is shown in Fig. 1. Designations: *black triangles*: neat PC and MpC based on SPCC+opoka+gyps; *empty squares*: the same based on alitic PCC+opoka+gyps; *empty rings*: alitic PCC+slag+gyps. Hardening conditions:**a**)in moist air 1 d.,further keeping in water); **b**) after std. steam curing (2 h - exposure, 3 h-raising of temperature,6 h-isothermal curing at 80°C,2 h-cooling;further keeping in moist air).

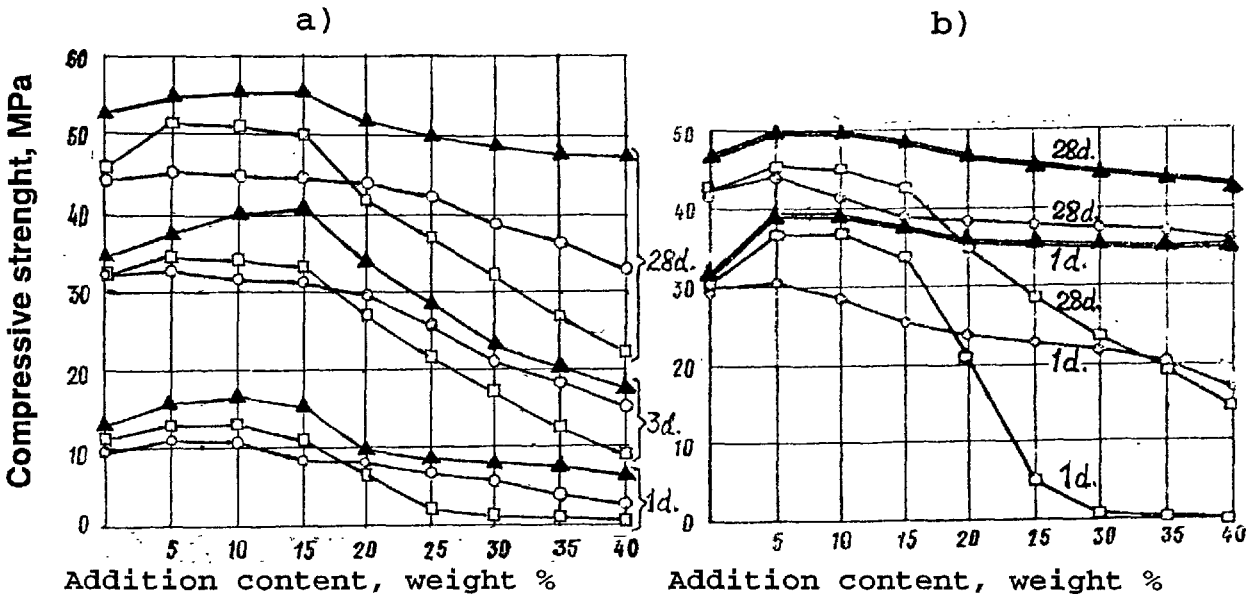

Figure 1. Cement strength versus active mineral additions content

It is evident that the strength of MpC is higher than pC and slag base cement at all hardening times. After steam curing this effect is larger and seen upto 40% addition; it connects with higher temperature stability of C-S-H/hydrogarnets v. AFm-/AFt-phases. The properties of concretes made with MpC and OPC (type IIA-P, opoka content 10%) are shown in Table 2.

Results have shown that the shrinkage of MpC is much smaller than that of OPC. Besides it is stable from 28 to 180 days (0.01 to 0.12 mm/m). In despite of equality of std. strength classes MpC is better than OPC responds to steam curing. So the products have the greater strength and resistance to different environmental conditions though the clinker part in MpC concrete is only 0.57 of OPC concrete. The adducing data testify that *MpC is practically non-shrinkage, frost- and sulphate resistant cement* owing preferentially to clinker composition and high p. dg. MpC is good to use in fine grained concretes with clay rich sands which shortcomings are decreased.

REFERENCES

Astreeva, O.M., ``Petrography of binding materials``. Gosstrojizdat, Moscow, 1959, pp. 158.

Chizmadjev, Yu.M., Markin, V.S., et al., (Levich, V.G. (Ed.)): ``Macrokinetics of liquid flow in porous media``, Nauka edition, Moscow, 1971, part II, pp.363.

Drushinine, S.A. Trudy (Proc.of) All-Union Cement Institute (VNITs),1934, No 9, pp. 30.

Entine, Z.B. Doct. Tech. Sci. Thesis. Mendeleev`s Chemistry-and-Technology University, Moscow, 1993, 49 pp. (in Russian as like preceding refs.).

Rabilero, A., ``Las puzolanas``. Editorial Oriente, Santiago de Cuba, 1988, p. 114.

Panina, N.S., et al. Trudy (Proc.of) NIICement,1992, No.106,pp.34 - 39 (in Russian)

Taylor, H.F.W. Private Communication: during visit of NIICement, Moscow, May 1994.
Volzhensky, A.V., Chistov, Yu.D., Karpova, T..A., Proc.VIII All-Union.Conf. on the Chemistry and Technology of Cements, Moscow, 1991, pp.159 -162 (in Russian, as like next ref.)
Zoubekhine, S.A., Ioudovitch B.E.,et al., Trudy (Proc.of) NIICement,1994, No.107,pp.149-184

Table 2 Properties of concretes based on MpC and OPC(strength class 32.5 of both)[1]

Characteristics (all methods are standartized in Russia - GOST 24452,24544 etc)	OPC	MpC
Consumption(projected)***and parameters of materials in concrete***:cement,kg/m^3	350	300
- including clinker part - `` -	300	171
- quartz sand, fraction 1-5 mm (with D. Abrams` fineness modulus 1.73) - `` -	600	620
- granite broken rock, fraction 5-20 mm (coarse aggregate) - `` -	1200	1230
- water (practically no influence of mineral addition content) - `` -	178	180
- water / cement (W / C) ratio versus(l) water,%, in paste of normal consistency	0.51|26	0.6|27
Properties of fresh concrete: target slump of D. Abrams` cone, cm	0.5	0.5
- viscosity by vibrating-chink-efflux viscosimeter: at 30 min. after mixing, sP	1520	1250
- entraining of air, volume %	2.6	2.0
- flowability time of fresh concrete, hours	2.0	3.5
-***Shrinkage*** in prisms 4x4x16 cm in mortar (cement:sand 1:1, W/C=0.35),mm/m^2	1.32	0.12
Cured concrete characteristics *(curing+keeping conditions are showed above):*		
- *Compressive strenght* in cubes,15^3 cm, after 2 and 3 days, MPa	27.8/29.4	36.1/44.3
- 28 days, - `` -	33.5	51.7
-*Compressive strength* in prisms,10x10x40 cm, after 28 days / 36 days, - `` -	24.8/26.5	39.9/39.3
- - after creep testing, kept after 36 d. on 60-70% R.H. air upto 150 days - `` -	23.4	39.3
- *Class of strength*, B	23.5	39.5
- *Modulus of elasticity in compression*: of cubes, x 10^4, MPa	33.8	31.6
- the same modulus in axial compression of prisms, x 10^4, MPa	34.1	32.5
- microcracking limit (ratio: limit of proportionality / ultimate stress [u.s.])	0.78	0.89
- specific complete axial deformation`s limit (at stress level = 0.95 [u.s.]), mm/m	1.3	1.7
- ***Watertightness class***, W	2	4
- std. water absorbtion, volume %	5.9	5.4
- swelling of mortar (1:3) samples 1x4x16 cm in water after 270 days, mm/m	2.85	1.75
-***Creep deformations*** (prism test beginning after 38 days, stress level=0.3[u.s.], 150 days (on 60-70% R.H. air), (Δi / I) x 10^{-5}	-10.6	+23.0[3]
-***Sulphate resistance*** by extension in Na_2SO_4 of mortar samples 1x4x16 cm,mm/m	14.63[4]	1.95
solution [SO_4^{2-} 34 g/dm^3] after 270 days of concrete samples 4x4x16 cm, -`` -	0.75	0.08
-***Frost resistance class***[5]in 5%NaCl sol., frost t° = -50°C; limit of strenght loss 5%	F75	F50[6]

Notes: [1] These data had obtained in NIIZhB, Moscow. [2]GOST 11052, after 6 months in 60-70% R.H. air. [3]After taking off the load extension is greater than creep. [4]Extension of neat sulphate resistant PC (GOST 22266, ASTM type V) is 9.36 mm/m, i.e. much larger than of MpC. [5]GOST 10050; F-decrease in compare with OPC is caused by smaller cement consumption in concrete.[6]Frost resistant class of blastfurnace cement (Eurotype IIIA) is F30 and of pC is F < 10.

MICROBIOLOGICAL IDENTIFICATION OF MICROORGANISMS RESPONSIBLE FOR DEGRADATION OF CONCRETE

Moema RIBAS SILVA, ENC-FT, University of Brasília, Brasília-DF, Brazil
Lenise Aparecida Martins GARCIA, BIOCEL, University of Brasília, Brasília-DF, Brazil

ABSTRACT Techniques to study the microstructure of building materials as well as microbiological methods have been used in order to try to identify microorganisms responsible for biodeterioration of cement and aggregates of concrete taken from structures of Brasília. The presence of Thiobacillus has not been detected but colonies of Bacteriae and Fungi have been counted. Some images observed at the scanning electronical microscope are presented.

Key-words: Microstructure, Durability, Scanning Electronic Microscopy, Thermogravimetry.

INTRODUCTION

Concrete structures are frequently deteriorated by several agents which act in different ways. Among these, biodeterioration of concrete have been studied recently but the researches did not yet lead to final results. The first phase of the research was related to the role of the environmental conditions on concrete biodeterioration. Next, a tentative was initiated, through microbiological techniques, in order to identify some of the several microorganisms observed by scanning electronical microscopy at the proximity of corroded crystals of concrete. In this phase, now in progress, the presence of Thiobacillus (absent) is searched and colonies of heterotrophic Bacteriae and Fungi have been counted. The aim of this paper is to present some of the results obtained through scanning electronical microscopy and microbiological techniques.

APPLIED TECHNIQUES

The scanning electronic microscopy (SEM) followed by energy dispersive analyser (EDS) applied on fractures are the best techniques to verify the presence of microorganisms in concrete (Ribas Silva, 1990). Besides the presence of microorganisms, the SEM has been used in order to detect deterioration products as well as the corrosion of compounds of concrete (cement and aggregates). The use of SEM allows also the identification of most of mineral compounds of concrete.

However, the SEM is not sufficient to study the biodegradation of the material (Ribas Silva, 1990). To complete the study, the following techniques must to be applied: complete chemical analysis (CA), differential thermal analysis (DTA), thermogravimetry (TG) and X-ray diffraction (XRD). In addition, a mineralogical calculation (MC) will be used to process the results of chemical analysis and thermogravimetry. The application of these techniques, now in progress, will help on identifying and studying biodeterioration mechanisms.

In order to verify the presence of microorganisms in concrete as well as to identify them, microbiological methods are required.

CETESB Standard L5.217 (1991) has been applied to detect the presence of *Thiobacillus* (Hutchinson et al., 1969; Milde at al., 1983); the heterotrophic Bacteriae and Fungi have been counted using Standards CETESB L5.201 (1986) and CETESB L5.204 (1988), respectively.

METHODOLOGY

In a previous study, it has been verified which environmental conditions could be responsible for the development of microorganisms. Concrete from structures submitted to three different climates (long periods of dryness and humidity, with a relatively stable temperature; high temperatures and high relative humidity; and low temperatures and high relative humidity) have been studied (Ribas Silva, 1995 and 1996).

The phase concerning this paper is related to samples taken from the same structures of the first part of the research (low humidity and high temperatures), but the microbiological analysis have been added to the applied techniques, in order to identify the microorganisms.

The verification of the presence of *Thiobcillus*, has used different medium of culture: Medium 9K modified, for *Thiobacillus Ferrooxidans* (simple and double concentration); Medium of Postgate modified for *Thiobacillus thioparus* (simple and double concentration); Medium Postgate modified with green of bromocresol for *Thiobacillus thiooxidans* (simple and double concentration).

Samples from the same concretes have been observed at the SEM in order to verify the presence of microorganisms, but the results of the complementary techniques, now in progress, are not yet completed.

OBTAINED RESULTS

The first phase of the study leads to conclude that climate is not so important on the development of microorganisms but it influences the kind of microorganisms present in concrete. However, the same components of cement and aggregates appear solubilized in the concrete submitted to the three studied climates (Ribas Silva, 1991 and 1995). In other words, the kinds of microorganisms were variable but the solubilization of concrete compounds were similar. This leads to think that many microorganisms can be responsible for the same kind of deterioration.

The deteriorated compounds most frequently observed at the SEM were: calcic products from cement, such as portlandite (Fig. 1) and calcium carbonates; siliceous products from aggregates, such as quartz, feldspars, micas (Fig. 2) and other unidentified crystals (Fig 3). But many other crystals appeared corroded.

Besides the deteriorated compounds of hydrated cement and aggregates, the microscopy showed also the presence of microorganisms such as Algae (Fig. 4), Fungi (Fig. 5), Bacteriae (Fig. 6) and Protozoa. Thermogravimetry and differential thermal analysis are able to confirm the presence of microorganisms. The deficiency of silica can be detected by the mineralogical calculation (Deloye, 1986) and the crystalized compounds are detected by DRX.

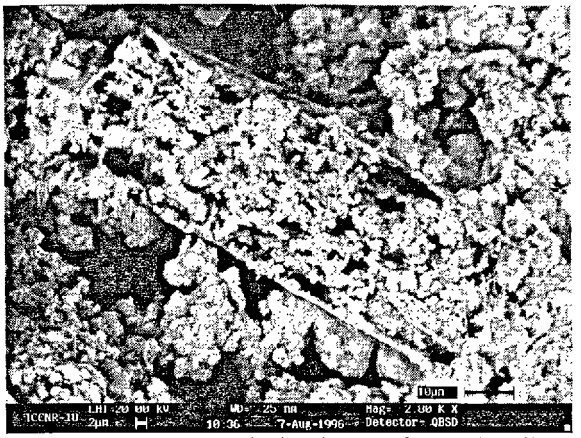

Figure 1 Corroded plate of portlandite seen in many concrete samples.

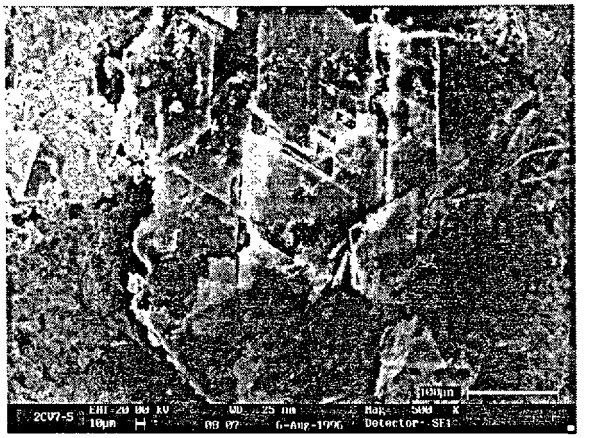

Figure 2 Deterioration of biotite (Fe) described by Estoule-Choux and Blanchet (1987).

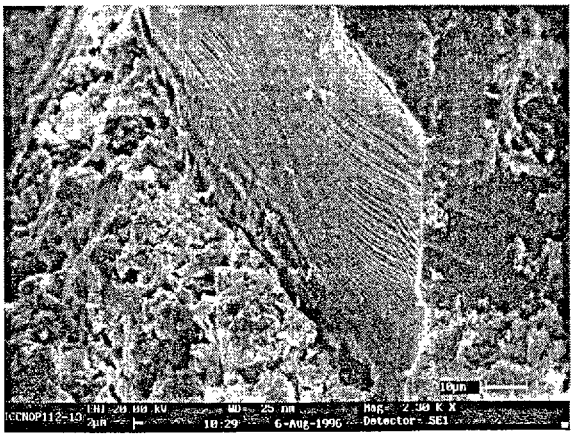

Figure 3 Solubilization of siliceous crystal compound of concrete.

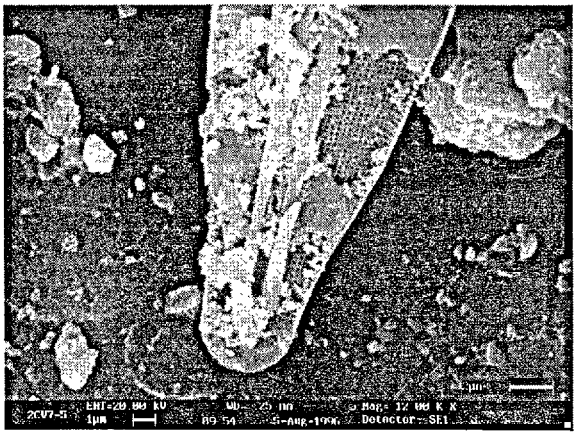

Figure 4 Diatom Algae which storages silica taken from concrete.

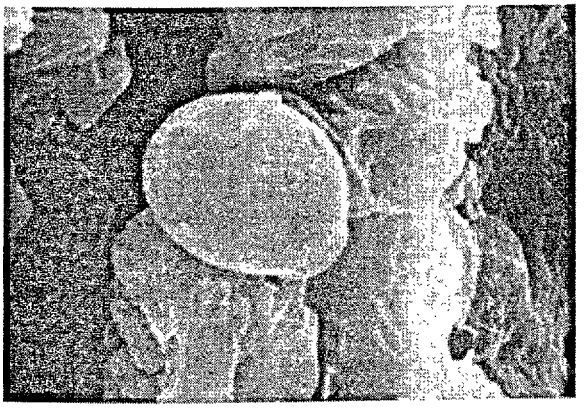

2CPAR 15j 20 kV 6.000 X 1

Figure 5 Unicel Fungi ($\phi \cong 4\mu m$) probably responsible for deterioration of mica and feldspars.

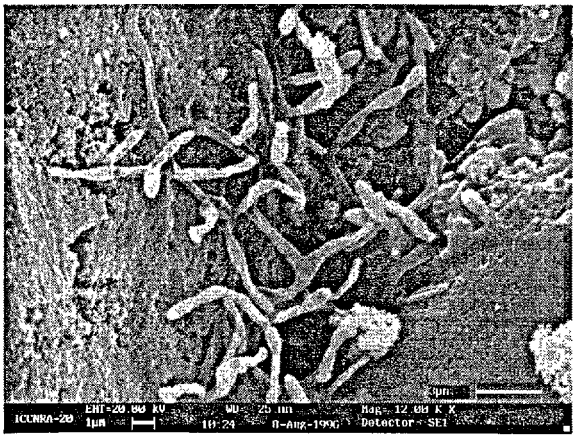

Figure 6 Morphology which seems to be Bacteria, observed in concrete.

CONCLUSION

The mechanisms of the biodeterioration of concrete are not well known but since the mineralogy of soil and natural stones of monuments are similar to concrete, the study of the two first materials, today much more developed, can be extended to concrete.

Taking in account this similarity, the solubilization of calcic products can be explained by the production of acid by microorganisms such as two kinds of Nitrificant Bacteriae which oxyde ammonium in azotic acid and this substance combines with calcium, resulting in a soluble calcium nitrate which is transported out of the concrete (Bock, 1986).

The solubilization of micas and feldspars could be due to the action of Thiobacillus, by the acidification of the medium and realeasing of K but, in this study, this kind of microorganism has not been detected by the applied techniques (Berthelin, 1988).

In this case, the K could be released as a result of the action of fungi, detected by microbiological techniques. Another way to have mica destroyed is through the production of acids (by Bacteriae), when pH can drop under 3, solubilizing the micas (Berthelin, 1988).

Next step will be to identify the Bacteriae and the Fungi which have been counted through microbiological techniques.

REFERENCES

Bock, E. "Corrosion biologique des pierres: forte attaque par des nitrifiants". In: Attaques Biologiques des Pierres, Lab. C. P. Et Ch., Paris, 1990 pp. 9-18. Trad. S. Proeschel.

Berthelin, J. "Microbial weathering process in natural environments", Ph.and Chemical Weathering in Geochemical Cycles, 1988, pp. 33-59. Eds. A. Lerman and M. Meybeck.

Deloye, F.X. "L'analyse des bétons durcis", Lab. C. des Ponts et Chaussées, Paris, 1986. 80p.

Estoule-Choux, J.; Blanchet, C. "L'altération directe de muscovites et de biotites en halloysite: mise en évidence par microscopie électronique à balayage", Clay Minerals, 22:11-20, 1987.

Hutchinson, M.; Johnstone, K.I.; White, D. "Taxonomy of the genus *Thiobacillus*: the outcome of numerical taxonomy applied to the groups as a whole". J. Gen. Microbiol., 57: 397-410, 1969.

Milde, K.; Sand, W.; Wloff, W. And Bock, E. "*Thiobacilli* of corroded concrete walls of the Hamburg Sewer System". J. Gen. Microbiol., 129: 1327-1333, 1983.

Ribas Silva, M. "Étude de la microstructure du béton sous l'influence de variations hygrométriques importantes", Lab. C. P. Ch., Paris, 1991. 220 p. Série Ouvrages d'Art OA10.

Ribas Silva, M. "The microscopic study of biodegradation of concrete submitted to cold and humid climate". Fifth Euroseminar on Microscopy Applied to Building Materials. Loeven, Bélgica, 1995. pp. 162-169.

Ribas Silva, M. "Climates and biodeterioration of concrete". 7th International Conference on Durability of Building Materials and Components. Stockholm, 1996. pp. 191-200.

ACKNOWLWDGEMENTS

The authors are gratefull to CNPq and FAPDF for the finnancial support to the research; to the Laboratory of Furnas and to the University of Santa Catarina for the use of the SEM.

STABILITY OF CONCRETE AGAINST BIOGENIC SULFURIC ACID CORROSION- A NEW METHOD FOR DETERMINATION

Dr. Klaus HORMANN; Dr. Fritz-J. HOFMANN; Dr. Michael SCHMIDT; Heidelberger Zement AG, Dept. of Research, Development and Consulting, Leimen, Germany

ABSTRACT Biogenic sulfuric acid corrosion (BSAC) is responsible for damages on cement based sewer systems all over the world. For an economic development of more resistent concrete mixtures, the Department of Biotechnology of Heidelberger Zement AG created a new test system to simulate this BSAC attack, which lasts normally 5- 10 years in the sewer system, within 3 to 5 months. Using the microorganism *Thiobacillus thiooxidans*, responsible for the sulfuric acid synthesis, a differentiation between various concrete mixtures was possible.

Key-words: Bacterial attack, corrosion, high alumina cements, sewage, acid attack

INTRODUCTION

Biogenic sulfuric acid corrosion (BSAC) is a serious problem in particular parts of sewer systems. After first reports from warmer regions like South Africa or Australia (Gilchrist, 1953; Thistlethwayte, 1972), in the last decades damages were found also in temperate zones like north or central Europe (Holmström and Hultman, 1978; Milde et al., 1983).

In anaerobic parts of the sewer system, e.g. in pressure pipes or in deeper zones of biofilms coating the surfaces of pipes and construction buildings, sulfate-reducing microorganisms degrade sulfur containing compounds to hydrogen sulfide (H_2S). These compounds like some amino acids from proteins or sulfate are found in public as well as industrial sewage in significant amounts.

Due to a decrease of the pH-value or by turbulences of the sewage H_2S is emitted into the atmosphere of the sewer pipes or buildings (Thistlethwayte, 1961). Oxygen oxidizes H_2S to elementar sulfur, which is deposited on the concrete surfaces above the sewage. This sulfur is a preferred substrate for microorganisms of the genus *Thiobacilli*. The biochemical activities of these organisms result in a permanent decrease of the surface pH of the concrete down to values below 1.0 (**Eq 1;** Kelly, 1989). At least only *Thiobacillus thiooxidans* previously called *T. concretivorus* (Parker, 1945) is able to live under these extreme conditions. Sulfuric acid, the end product destroys the cement stone and chalky aggregates (Wierig and Nelskamp, 1982).

$$S_8 + 8\,H_2O + 12\,O_2 \text{ -------> } 8\,H_2SO_4 \qquad [1]$$

BSAC in the sewer net work of Hamburg, Germany, with repair expenses of about DM 50 Mill. in the seventies (Flemming, 1994) led to extensive research activities by members of the University of Hamburg (Milde et al., 1983, Sand et al., 1983). The amount of *T. thiooxidans* cells on the surface of the concrete was correlated with the corrosion rate (Sand and Bock, 1984). A breeding chamber with a controlled H_2S atmosphere to simulate BSAC was established (Sand et al., 1983). Using optimized growth conditions for *Thiobacilli* the normal corrosion period of about 8 years, measured by test blocks inserted in the sewer system of Hamburg, was reduced to 1 year in the laboratory (Sand, 1987).

Nevertheless for an economic development of more resistent concrete mixtures against BSAC investigation cycles of 5 to 10 years in a sewer system as well as 1 year in a breeding chamber seems to be to long.

BIOGENIC SULFURIC ACID CORROSION - SIMULATION SYSTEM

The Research, Development, and Consulting Departement of Heidelberger Zement AG developed a BSAC-simulation system giving results within 3 to 5 months. *Thiobacillus thiooxidans* is grown under optimal growth conditions. Elemental sulfur serves as substrate in analogy to the sewer, where emitted H_2S is oxidized to sulfur prior to the utilization by *T. thiooxidans* (Milde et al., 1983). Although *T. thiooxidans* is able to decrease the pH on concrete surfaces below 1.0, pH for optimal growth is about 3.0 (Rao and Berger, 1971). Therefore our test system is separated into a growth and a reaction part. In a 25 l fermentor *T. thiooxidans* was cultivated to give maximal cell counts and biochemical activity. A separate testreactor contained various mortar specimens (1 x 1 x 6 cm) in stainless steel holders. Controlled by a programmable logic controller (PLC) these specimens were flooded periodically for 5 min by an aliquot of the fermentor content, including *T. thiooxidans* cells and sulfur, followed by an 1 hour break. This procedure simulates events in the sewer system, e.g. after a rainy day. Sulfur, which is normally very hydrophobic, is wetted by *T. thiooxidans* through secretion of surface active agents into the medium. These agents are nescessary for the cells to attach and oxidize the sulfur to sulfuric acid (Rao and Berger, 1971). After a few flooding cycles a biofilm was established on the surface of the specimens, built by cells of *T. thiooxidans* together with little amounts of wet sulfur. The principle of this test system is shown in Fig. 1.

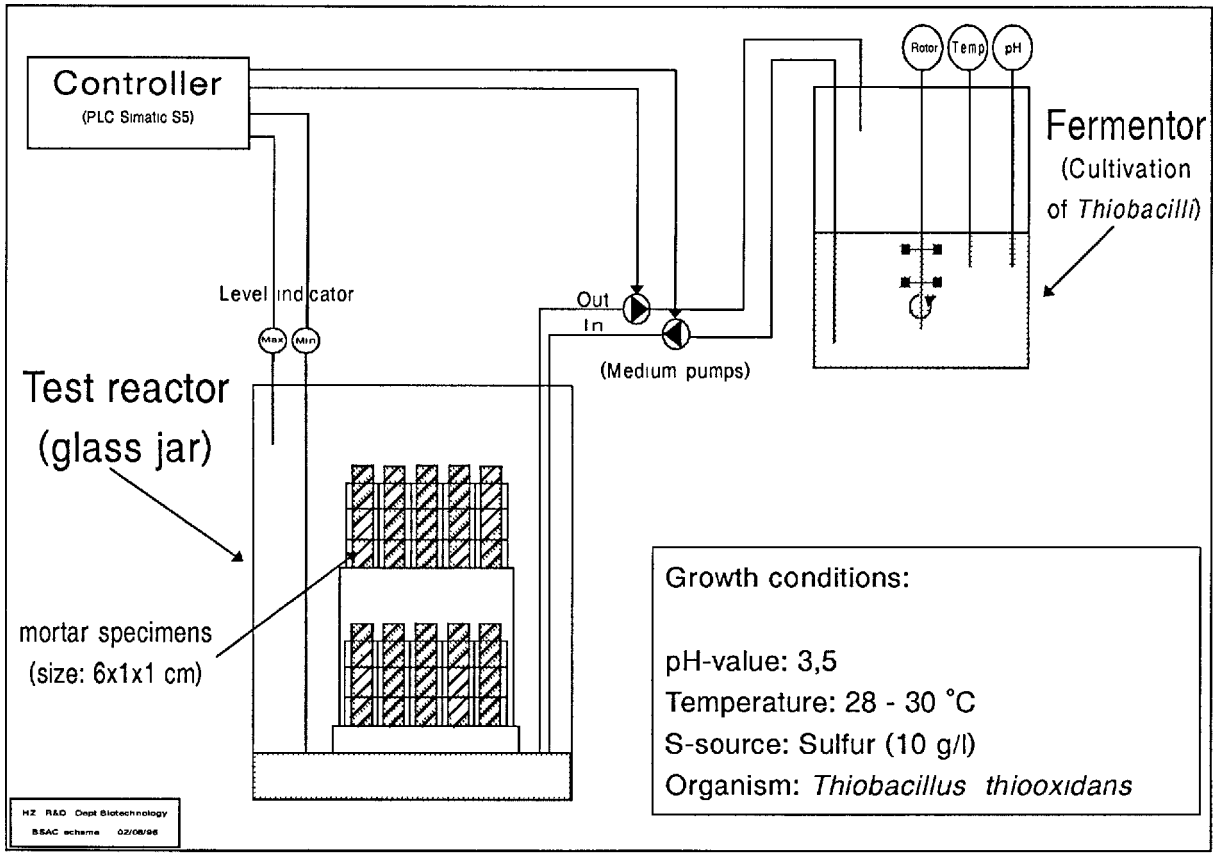

Figure 1: Test sytem for demonstration of biogenic sulfuric acid corrosion

MATERIALS AND METHODS

The test specimens were made of 40 g cement and 120 g aggregates. The water to cement ratio was 0.40. 70 % (w/w) of the aggregate particels were between 0.50 and 1.00 mm, the remaining 30 % (w/w) between 0.25 and 0.50 mm. German CEM I 32,5 R and US Type I-II were used as reference for ordinary Portland cement (OPC). Further specimens were made using high calcium aluminate cement (HAC) with different amounts of Al_2O_3. American traprock, HAC clinkers, limestone, and quartz were used as aggregates. All specimens were stored under water for 28 d and weighed prior to incubation in the test reactor. After 30, 60, 90, 120, and 150 d specimens of each mixture were removed from the reactor. Determination of cell counts on the surface were done according to Sand et al. (1994). To remove remaining loose material from the surface the specimens were treated in an ultra sonic water bath. After a final weighing the loss of weight could be calculated for each specimen.

RESULTS

The behaviour of different cement mixtures regarding their loss of weight is shown in Fig. 2. Whereas the HAC based specimens showed good resistance (3 to 4 % b.m. loss of weight) the OPC based specimens lost under the severe sulfur acid attack 18 and 31 % (b.m.), respectively, of their prior mass. A tendency could be shown already after 30 d, when most of the HAC based specimens showed no loss of weight in contrast to the OPC mixtures (Fig. 2). Regarding the different aggregates HAC-clinker (unmilled material) gave best results, although quartz and broken traprock had only litte higher values. The measurement of the cell counts on the surface of OPC as well as HAC based specimens gave values of about 10^8 cells/ cm^2.

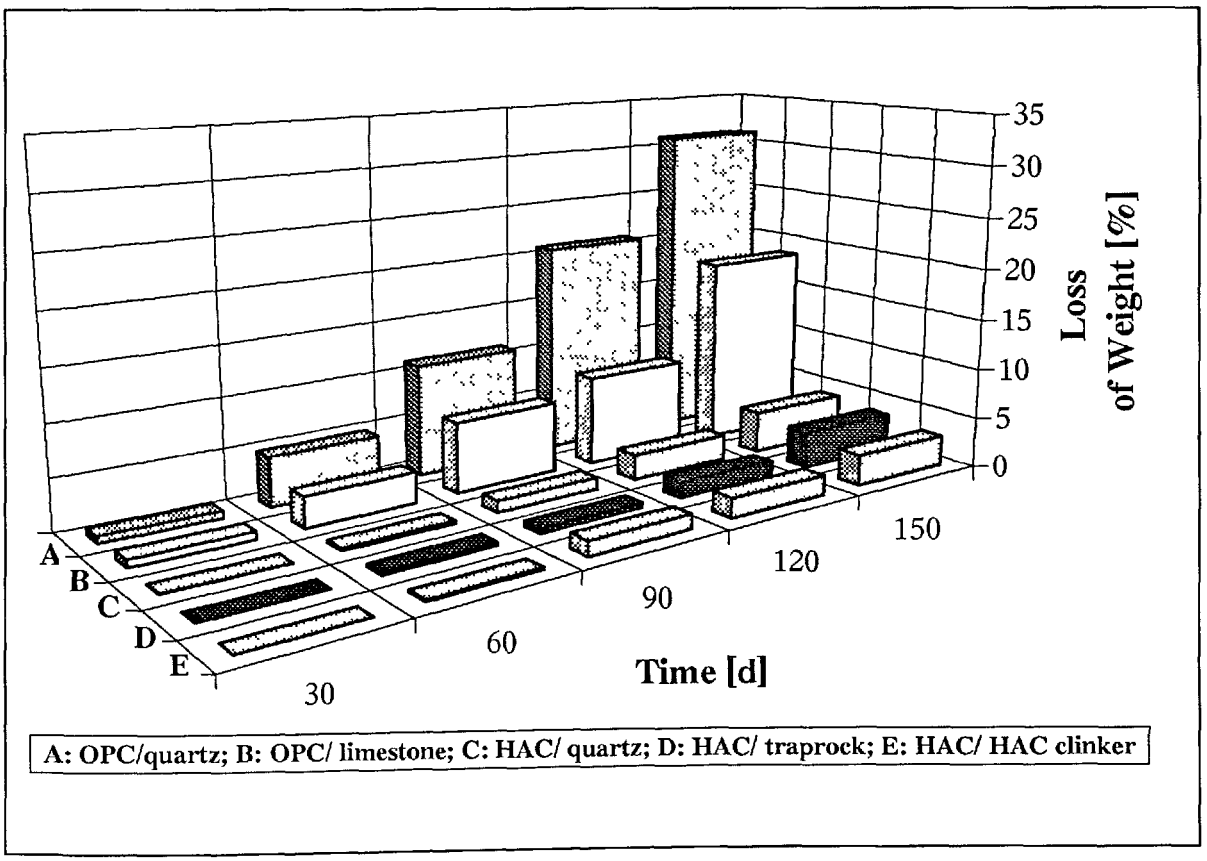

Figure 2: Loss of weight for different cement mixtures

CONCLUSIONS

Using this new test system for BSAC only very short investigation cycles to get information about the resistance of concrete mixtures against this attack are nescessary. In comparison the group in Hamburg reported corrosion rates for OPC from 1 to 4 % within 9 to 12 months (Sand et al, 1983; Sand and Bock, 1984; Sand et al. 1987) whereas with this new system loss of weight values of 18 to 31 % were measured after 5 months. 3 to 5 % loss were found already after 2 months for both the OPC mixtures, showing a further significant reduction of the nescessary investigation time for monitoring BSAC in laboratory. In comparison with OPC, HAC based concrete seems to have a several times higher resistence against BSAC, which correlates with previous data (Sand et al., 1994). Our results should taken into consideration planning or maintaining sewer pipes or buildings. Particular for parts of the system, where high amounts of H_2S are emitted into the sewer atmosphere the use of HAC may be a very good alternative to normal concretes.

REFERENCES

Flemming, H.-C., „Microbial Deterioration of Materials - Fundamentals: Economical and Technical Overview", Werkstoffe und Korrosion, Vol. 45, 1994, pp 5-9.

Gilchrist, F.M.C., „Microbiological Studies of the Corrosion of Concrete Sewers by Sulphuric Acid Producing Bacteria", South Afric. Industr. Chem., Vol. Nov., 1953, pp 214-215.

Holmström, H. and Hultman, B., „Practical Experiences of Hydrogen Sulfide Formation and Sulfuric Acid Corrosion in Sweden", Berichte zur Abwasser- und Abfalltechnik (Techn.-wiss. Schriftenreihe des ATV), Vol. 7, 1978, pp 85-91.

Kelly, D.P. (Schlegel, H.G. and Bowien, B.(Eds.)): „Physiology and Biochemistry of Unicellular Sulfur Bacteria", Autotrophic Bacteria, Springer Verlag, Berlin, 1989, pp 193-217.

Milde, K., Sand, W., Wolff, W. and Bock, E., „Thiobacilli of the Corroded Concrete Walls of the Hamburg Sewer System", J. Gen. Microbiol., Vol. 129, 1983, pp 1327-1333.

Parker, C.D., „The Function of *Thiobazillus concretivorus* (Nov. Spec.) in the Corrosion of Concrete Exposed to Atmospheres Containing Hydrogen Sulfide", J. Exp. Biol. Med. Sci., Vol. 23, 1945, pp 91-98.

Rao, G.S. and Berger, L.R., „The Requirement of Low pH for Growth of *Thiobacillus thiooxidans*", Arch. Microbiol., Vol. 79, 1971, pp 338-344.

Sand, W., „Importance of Hydrogen Sulfide, Thiosulfate, and Methylmercaptan for Growth of *Thiobacilli* during Simulation of Concrete Corrosion", Appl. Environ. Microbiol., Vol. 53, 1987, pp 1645-1648.

Sand, W. and Bock, E., „Concrete Corrosion in the Hamburg Sewer System", Environ. Technol. Lett., Vol. 5, 1984, pp 517-528.

Sand, W., Milde, K. and Bock, E., „Simulation of Concrete Corrosion in a Strictly Controlled H_2S - Breeding Chamber", Progr. Biohydrometallurgy- Cagliari, Vol. May, 1983, pp 667-677.

Sand, W., Bock, E and White, D.C., „Biotest System for Rapid Evaluation of Concrete Resistence to Sulfur Oxidizing Bacteria", Mat. Performance, Vol. March, 1987, pp 14-17.

Sand, W., Dumas, T. and Marcdargent, S., „Accelerated Biogenic Sulfuric-Acid Corrosion Test for Evaluation the Performance of Calcium-Aluminate Based Concrete in Sewage Applications", ASTM Spec. Tech. Publ., 1994, pp 234-249.

Thistlethwayte, D.K.B., „Control of Sulfides in Sewerage Systems", Butterworth, Melbourne, 1972.

Wierig, H.-J. and Nelskamp, H., „Betontechnologische Untersuchungen in Abwasseranlagen", EWPCA-Documentation - Corrosion in Sewage Plants, EWPCA-Sekretariat, St. Augustin, 1982, pp 41-59.

CONCRETE OF SEWAGE COLLECTORS AND THEIR PROTECTION: CORROSION MECHANISMS

Vladimir I. BABUSHKIN, Andrei A. PLUGIN, Dmitry Yu. ZELENSKY
Kharkov State Technical University of Construction and Architechture, Ukraine
Gennady Ya. DROZD, Donbass State Academy of Construction and Architecture, Makeevka, Ukraine

ABSTRACT The analysis of investigations aimed at the study of chemical and biochemical processes taking place in sewage collectors is performed. The mechanism of concrete corrosion in above-water part of the sewage collectors is explained. The measures of their protection and durability providing are developed.

Key-words: Sewage, Bacterial attack, Acid attack, Corrosion, Thermodynamics.

INTRODUCTION

The total length of city sewage networks in Ukraine is a few tens of thousands kilometers. The 40% of them are made with the use of reinforced concrete tubes. One failure per each 10 km of the collectors happens every year. Approximately 70% of the failures is caused by the corrosion decay of concrete in the above-water part of the collectors.

THE CORROSION STUDY

The authors investigated a few free-flow collectors made of reinforced concrete in Kharkov. The collectors were the most typical ones by the composition and types of the industrial and domestic wastes transported. When the investigation started, they have been in service more than 30 years. One could notice the multiple corrosion damages in the above-water vault part of the collectors. The damages became more noticeable after connection of the pressure pipelines from the industrial enterprises to the sewage network. Particularly, it was concerned with the drop (relief) wells and the legs with the flow rates more than 1-1.2 m/s. The damages were absent in the under-water flume parts of the collectors and in the vault part of them in the legs with high level of filling up and the flow rates not exceeding 0.6 m/s. The vault corroded across of whole width of the walls here and there, which caused repeated collapses of the vault and ground.

The results of investigations of the concrete and cement paste samples taken from the typical elements of collector are given in Table 1. The results of analysis of the sewage water composition and gas-air containment of sewage collectors as well as the results of calculations of concentrations of the components are shown in Table 2. Here, the data on concentration of substances and ions in sewage water and partial pressure of the gases and vapors in the gas environment were obtained with the use of both Yakovlev's (1975) and own data. The hydrogen pH index of sewage water was 6-9 and more (the mean value is 7.5). The pH in the moisture on the above-water surface of collector is considerably lower than the one in the effluent stream. It can fall to 1 and less values in the moisture. The data obtained by Drozd (1986) and our recent results on micro-biological analysis of sewage water samples and samples scraped off the concrete surface allowed to establish the species of bacteria which live in the effluent stream and on the above-water surfaces of the collector.

THE CHEMICAL REACTIONS ANALYSIS

The complex chemical and biological processes proceed in the sewage collectors. Mainly, they are caused by vital functions of various species of bacteria living in the effluent stream and on both the

Table 1 The results of investigation of the concrete cement stone of sewage collector

Place of sample taken	pH of water extract	Chemical composition ,%					Minerals
		SiO_2	CaO	Al_2O_3	Fe_2O_3	SO_3	
noncor-roded part	11.8	36.3	27.1	6.5	5.0	3.2	$2CaO{\cdot}SiO_2{\cdot}H_2O$, $4CaO{\cdot}Al_2O_3{\cdot}19H_2O$, $4CaO{\cdot}Al_2O_3{\cdot}13H_2O$, β-$2CaO{\cdot}SiO_2$ ets.
collector bottom	12.5	26.4	23.4	9.0	3.5	2.4	
collecttor vault	5.8	30.7	17.3	6.4	1.3	16.6	$4CaO{\cdot}Al_2O_3{\cdot}30H_2O$, $3CaO{\cdot}Al_2O_3{\cdot}CaCO_3{\cdot}12H_2O$, $CaSO_4{\cdot}2H_2O$, β-SiO_2, $SiO_2{\cdot}nH_2O$ ets

Table 2 The sewage water composition and gas-air containment of sewage collectors

Ingredient	Concentration in the sewage water		Partial pressure in the gas environment, atm
	C, mole/l	mg/l	
SO_4^{2-}	$(0\text{-}1.9){\cdot}10^{-3}$	0-181	-
S^{2-}	$(0\text{-}1.5){\cdot}10^{-5}$	0-0.5	-
Cl^-	$(0.5\text{-}4.3){\cdot}10^{-3}$	16-151	-
PO_4^{3-}	$(0\text{-}1.9){\cdot}10^{-4}$	0-12	-
NH_4^+	$(0\text{-}4.6){\cdot}10^{-3}$	0-82	-
O_2	$(0\text{-}3.1){\cdot}10^{-4}$	-	0-0.21
CO_2	$(6.1\text{-}9.2){\cdot}10^{-3}$	-	0.08-0.12
CH_4	$(1.2\text{-}1.3){\cdot}10^{-5}$	-	$(1.4\text{-}1.5){\cdot}10^{-2}$
NH_3	$(0\text{-}3.3){\cdot}10^{-3}$	-	$(0\text{-}7.9){\cdot}10^{-5}$
H_2S	$(0.9\text{-}1.3){\cdot}10^{-2}$	-	$(0.9\text{-}1.3){\cdot}10^{-3}$
petroleum products	-	0-23	0.11-0.12
proteins	-	6-154	-
fats	-	4-105	-
carbohydrates	-	1-63	-

above-water and under-water surfaces of the walls of the collector. Proceeding from the composition analysis of the effluent stream and the gas-air containment, the authors analyzed a lot of chemical reactions which could take place in the collectors with participation of the bacteria and without them. Besides, we studied balance equations of the reactions at pressure equal to 1 atm and temperature 25° C. The most important processes and reactions as well as the names of the bacteria which caused the ones are given in Tables 3 and 4. But in some cases we did not consider the intermediate reactions leading to the formation of intermediate products. In these cases the general reaction schemes of the end products formation are presented. For example, in principle, during a sulphate reduction, a sulfate ion may form not only hydrogen sulphide but elementary sulphur and sulphur oxides as well. But, anyway, the latter compounds oxidize into sulphuric acid later on.

In our opinion, the oxidizing-reducing reaction of the sulphate reduction and the reactions of sulphur

Table 3 Chemical and biochemical processes, taking place in sewage collectors

Processes	Reactions or schemes of reactions	Conditions	Bacteria
fermentation and decay of organic substance	proteins → aminoacids → → RCOOH + NH_3, H_2S, CO_2, H_2; fats → $C_3H_5(OH)_3$ + RCOOH, ROH, CO_2; carbohydrates → saccars → → RCOOH; ROH; CO_2 .	anaerobic - in sewage water and sludge	lacticacid, propionicacid, buturicacid, acetonicbutul, cellulose etc.
methane fermentation of fat acids and alcohols	RCOOH; ROH → CH_4, CO_2, H_2O: $CH_3COOH=CH_4+CO_2$, $4CH_3OH=3CH_4+CO_2+H_2O$ etc.	"	methane-forming
ammoni-fication of urea	$CO(NH_2)_2+H_2O=2NH_3+CO_2$, or $CO(NH_2)_2+2H_2O=2NH_3+H_2CO_3$.	"	ammonifying (urealytic)
nitrification	$(NH_4)_2CO_3 \rightarrow HNO_3, HNO_2 \rightarrow \rightarrow N_2, CO_2, H_2O$: $2(NH_4)_2CO_3+3O_2=2N_2+2CO_2+8H_2O$.	aerobic - in sewage water with dissolved oxygen	nitrifying
denitrifi-cation		anaerobic - in sewage water and sludge	denitrifying
sulphate-redusing	reaction No1 in Table 4	"	sulphate-redusing
oxidation of hydrogen sulphide	reaction No2 in Table 4	aerobic -in condensate moisture on wall surface subaqueous	tionic
formation of carbonic acid	reaction No3 in Table 4	"	-

Table 4 The results of balance calculation at pressure 1 atm and temperature 25°C

No	Reaction	Reaction energy ΔG, kkal/mole	Balancy constant K	Balancy equation
1	$SO_4^{2-}aq+8e^-+10H^+aq=H_2S\ g+4H_2O\ lq$	-57.06	$6.8\cdot10^{41}$	$lgP_{H2S}-lg[SO_4^{2-}]+10pH-$ $-135.1Eh-41.8=0$
2	$H_2S\ g+2O_2g=H_2SO_4\ aq$	-169.26	$1.2\cdot10^{124}$	$lg[H_2SO_4]-lgP_{H2S}-lgP_{O2}-124.1=0$
3	$CO_2\ g+H_2O\ lq=H_2CO_3\ aq$	1.94	$3.8\cdot10^{-2}$	$lg[H_2CO_3]-lgP_{CO2}+1.43=0$

and carbonic acids formation out of hydrogen sulphide and carbonic acid gas correspondingly, determine the corrosion risk of collector environment. An analysis of the balance equations of the reactions, given in Table 4 showed as follows:

1) the sulphatereduction reaction in sewage water will proceed at collector conditions in section with high concentration of SO_4^{2-} and low partial pressure of H_2S, in case decreasing pH and increasing oxidizing potential Eh this reaction become more active;

2) it is necessary to have so high concentration of sulphuric acid in moisture to provide equilibrium

of sulphuric acid and hydrogen sulphide that the reaction of the hydrogen sulphide oxidizing in collector is thermodynamically irreversible even at insignificant partial pressures of oxigen inherent to the containment;
3) the equilibrium of carbonic acid gas and carbonic acid in the moisture of collector establishes at the concentration values of the order of 10^{-2} mole/l.

THE MECHANISM OF THE CORROSION ENVIRONMENT FORMATION

An analysis of the above-stated shows that a sewage collector is a sort of a biochemical reactor where complex processes proceed. It is possible to distinguish three main steps in the processes. These steps determine the corrosion environment formation process. They are as follows:
1) the biochemical formation of hydrogen sulfide in the effluent stream given necessary concentration of sulphate-ions, decrease of pH, increase of Eh of the stream as well as the formation of carbonic acid gas, hydrogen sulphide, etc., as a result of organics fermentation;
2) the hydrogen sulphide, carbonic acid gas, etc., extraction out of the stream into the gas containment of collector in the places where the flow behavior and rate change sharply;
3) the biochemical formation of sulphuric acid out of hydrogen sulphide in moisture on the surface of vault and the chemical formation of the carbonic acid out of carbonic acid gas, that damages concrete of the vault.

Thus, the main causes of decay of the vault and other above-stream elements of the free-flow collectors (wells, shafts, etc.) made of concrete and reiforcd concrete are the biogenic sulphuric acid and carbonic acid corrosions. The mechanism of these kinds of corrosion is described in details by Babushkin (1989) and other authors.

THE CORROSION PROTECTION

The authors analysed the equilibriums of the components present in corrosion environment of collector and the mechanism of cement paste, concrete and reinforced concrete corrosion as a whole. As a result, the authors developed a number of construction and organizational measures on corrosion protection of both the newly built and currently operational sewage collectors. The measures are directed towards the decrease of sulphates content in the stream, the aerobic conditions in the effluent stream ensuring, the decrease of gas extraction out of the stream, the use of bactericidal construction, repair and protective materials, including the new ones, resisting attacks of sulphuric acid. The percularity of work of the materials in the collectors is the simultaneous action of neutral sewage water in the flume part and of highly concentrated acid in the vault part. The authors developed acid-proof binding compositions, mortars and concretes based on acid-proof filling agents, sodium liquid glass, sodium silicofluoride and some other special agents which increase waterproofness and provide bactericidal properties. The samples of the materials have been successfully tested in the sewage collectors during 2 years. The application of the measures offered allows to increase the durability of the sewage collectors, to decrease the running costs and to eliminate the negative effect of the failures on ecological situation.

REFERENCES

Babushkin, V.I., "Protection of Building Structures from Corrosion, Aging and Wear", 1989, Kharkov, Vishya Shkola, 168 pp., (in Russian).
Drozd, G.Ya., "Active Life of Microorganisms in the Pores of Concrete", Applied Biochemistry and Microbiology, 1986, Vol.6, XXII, pp.844-849, (in Russian).
Yakovlev, S.V. et al, "Canalization", 1975, Moskow, Stroyizdat, 632 pp., (in Russian).

DURABILITY OF ORDINARY PORTLAND CEMENT AND GROUND GRANULATED BLAST FURNACE SLAG CEMENT IN ACID MEDIUM

Julio MADRID, Jesús María DIEZ, Sara GOÑI and Angeles MACIAS, Institute of Construction Science Eduardo Torroja (CSIC), Madrid, Spain.

ABSTRACT The durability of an Ordinary Portland Cement (OPC) and a Blast Furnace Slag (BFS) blended cement in buffered acetic/acetate medium was studied by means of the Köch-Steinegger test. Changes on the solid phases were evaluated by X-ray diffraction, scanning electron microscopy, mercury intrussion porosimetry and measuring the flexural strength. Finally, Ca^{2+}, K^{+}, Na^{+}, $SO_4^{=}$, OH^{-} and Ac^{-} concentrations were measured in the extracted pore solutions. Results show that both materials undergo a corrosion attack, more severe for OPC/BFS blended cement, in the acid medium that is not correctly evaluated through flexural strength measurements.

Key-words: Acid attack, blastfurnace slag, durability, porosity, pore solution.

INTRODUCTION

The highest durability of portland cement with pozzolanic additions is well stated (Douglas, 1987, Feng and Glasser, 1990, Malek et al., 1989 and Malhotra, 1987). This superior durability is based on the decrease of porosity resulting from the active pozzolanic addition that lowers the permeability of the paste impeding the ingress of potential aggressive agents from the environment.Thus, blast furnace slag cements are regarded as superior to portland cement with respect to resistance against penetration of chloride ions and resistance to sulphate attack when the slag content of the cement exceeds 65% (Osborne, 1989 and Wiebenga, 1987). Nevertheless, due to the pozzolanic reaction of active additions, both the lower portlandite content (Hinrichs and Odler, 1989) and lower pH of pore solution (Canham et al., 1987 and Andersson et al., 1989) could negatively affect its behaviour in acid environment.

Sulphate resistance and sea water resistance of concrete are mostly discussed under chemical durability of concrete whereas acid attack has not traditionally attracted much attention, even when cement composites are severely attacked by acids. The acids completely decompose the hydrated and unhydrated cement paste components: calcium hydroxide is dissolved and the hydrated silicate and aluminate phases are decomposed, with removal of Ca^{2+}.

The lack of standard methods to assess the performance of cements in acid environments together with the different aggressiveness of the acid which depend on its pH and nature (those giving insoluble products tend to be less aggressive), make difficult to correlate the results of the few systematic chemical studies found in the literature (Kong and Orbison, 1987, Spirin et al., 1987, El Hakim, 1987 and Chandra, 1988). Pavlik (1994a,b and 1996) makes a remarkable work on acid attack of cement pastes in a series of papers in which he studied the rate of corrosion of hardened cement paste in solutions of nitric, hydrochloric, sulfuric, acetic and formic acid. He concluded that the rate of corrosion of cement paste in acids giving easily soluble Ca-salts depends, to a large extend, on the acid's dissociation constant. He also analysed the chemical composition of the layer of corrosion products covering the undamaged cement paste and found a mathematical relation to express the depth of hydrated cement paste corrosion as a function of the water/cement ratio, the concentration of the aggressive acid solution and the duration of attack.

The behaviour of slag blended cement in acid solution is still less studied than this of plain portland cement. Samarin and Roper (1987), based on the results of the weight loss test, suggested that the

short term HCl resistance of portland blast furnace slag cement containing 35% OPC was mainly influenced by the cement content. De Ceukelaire (1992) working also in hydrochloric acid attack of mortar came to the conclusion that a blast furnace cement mortar proves to be more resistant to acid attack than pure portland cement mortar, due to only part of the cementing skeleton in the outest layer is destroyed by the acid attack, although the depth of the affected area is rather larger.

The need of further studies of acid attack, specially for slag blended cements, and the influence of the degradation of cement in acid environment that takes place in the tests used to characterize the immobilization of toxic wastes in cement matrices (accelerated test involves acetic medium of different pH values) have encouraged the authors to analyse the durability of portland cement and blast furnace slag blended cement in buffered acetic/acetate medium (pH=4.5).

EXPERIMENTAL

Materials

The chemical composition of the Ordinary Portland Cement (OPC) and the ground granulated Blast Furnace Slag (BFS) used are shown in Table 1.

Procedure

Cement pastes with and without addition of 80% (by weight of mixture) were prepared at a W/C of 0.4. Specimens of 1x1x6 cm were molded and compacted by vibration. After 1 day at 100% r.h. the specimens were demolded, put in insulated bags and submitted to a curing period of 21 days at 100% r.h.. After curing, groups of six samples were immersed in an acid buffer solution of 0.87M AcH/AcNa (pH=4.5) and in distilled water. In all cases, the samples were stored in sealed bottles and kept at room temperature for different periods of time. The volume of liquid was 800 ml per 6 samples.

After removing the specimens from the solutions, they were submitted to pore extraction using a high pressure compression device (Barneyback and Diamond, 1981). The extracted pore solution was partly used for determination of OH^- concentration by titration. The Na^+, K^+ and Ca^{2+} concentrations of the remaining pore solution were determined by atomic absorption spectroscopy (using Model 1100B, Perkin Elmer Corp.), and those of sulphate and acetate by ion chromatography (using a Model 2000i/SP, Dionex Corp.). The pH was also measured with a combined electrode for the pH range 0 to 14.

X-ray diffraction patterns were recorded using a Philips PW-1730 diffractometer, graphite monochromator, Cu $K_{\alpha 1}$ radiation. Porosity and pore-size distribution were investigated by mercury intrusion porosimetry carried out with a Micromeritics Pore Sizer 9320. SEM anlysis were performed with a Jeol JSM 5400, equiped with an EDAX Oxford Link System ISIS model.

Table 1 Chemical composition of OPC and BFS (In Wt%).

Oxide	CaO	SiO_2	Al_2O_3	Fe_2O_3	SO_3	MgO	Na_2O	K_2O	S^{2-}	L.I.	I.R.
OPC	65.3	20.1	5.3	2.9	3.1	1.3	0.2	1.6	-	1.5	0.8
BFS	40.2	37.6	12.5	1.2	-	8.2	0.2	0.6	1.2	1.4	0.1

RESULTS AND DISCUSSION

Attack by buffered acetic-acetate (pH=4.5) solution

As it is well established, a soft and porous layer of corrosion products is developed on the surface of cement pastes as a consequence of the chemical attack of the acid solution. The thickness and colour of this layer are different in the two materials used, OPC and OPC/BFS.

For plain OPC samples after 1 day immersion in acetic/acetate buffered solution, an external white layer with perpendicular cracks, easily removable, could be seen in a cross section of the sample. Underneath this layer is also possible to observe another internal light grey layer of altered, more amorphous and porous cement. After seven days, the external layer has a yellowish colour attributable to the precipitation of iron products, as other authors have pointed out (Pavlik, 1994b and De Ceurkelaire, 1992) and in the interface between the internal layer and the undamaged core of the sample a white front of ettringite crystals appears, as analysed and detected by SEM and X-ray techniques. After 28 days, the massive precipitation of crystals in this white front causes the scaling off of the coat disclosing another internal degradation coat of altered material.

In the case of OPC/BFS samples, it is only possible to see an external degradation layer in the cross section observation. The surface of the sample has an orange-yellowish colour and the external corrosion layer is white changing to yellow in its center and then dark grey near the interface with the unaltered core. The white precipitation front seen in plain OPC samples is not present in OPC/BFS ones.

In Fig 1 the values of the corrosion depth are presented versus the square root of time. There is a linear relationship ($y = a + bt^{0.5}$) that confirms a diffusion controlled mechanism for the acid attack. The relationship found for the external layer is similar to that reported by Pavlik (1994) ($d=0.163 \cdot t^{0.525}$) for acetic acid solution of pH= 3.73.

In Fig 1 it is also shown that although the growing of external layer follows the same law with time its thickness is twice for OPC/BFS than for plain OPC samples.

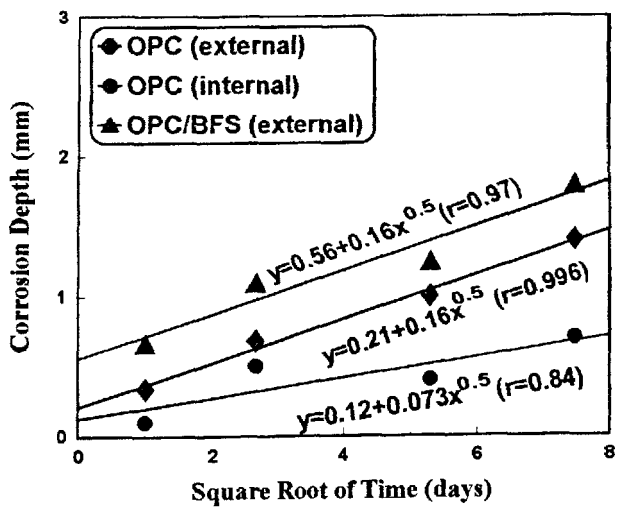

Figure 1 Depth of corrosion layers vs time.

The slope value in the equation expressing the time dependence for the internal layer thickness in plain OPC samples is less than a half for the external layer. This means a deceleration of the acid attack in this layer that can be explained on the basis of a protection of the material by the external coat (difficult to explain due to his high porosity and cracking), or by a change in the core microstructure of the paste that make them less permeable difficulting the entry of acid solution as it can be proved later.

Analysis of the pore solutions

The results of pore solution analysis from OPC and OPC/BFS samples are presented in Tables 2 and 3 respectively. The

columns Σz^+ and Σz^- are the calculated mass-charge balances of ions. The overall charge balances are in reasonable agreement.The 0 days on the table correspond to samples cured during 21 days at 100% r.h.

The pH value of OPC samples immersed in distilled water decreases from an initial value of 13.89 to a final value of 13.20 at 56 days of immersion. This decrease of pH is due to the leaching of alkalis (mainly K^+) from the cement paste. The quantity of $Ca(OH)_2$ detected by XRD stays the same at the different ages tested.

When the samples are immersed in acetic/acetate buffered solution of pH 4.5, the decrease of pH is more acute, being measured pH values about 11 at the end of the test. In this case, the decrease of pH is also due to the destruction of $Ca(OH)_2$ by attack of the acid medium. The quantity of portlandite diminishes with the time of immersion in acid medium as can be inferred from the X-ray diffractograms; nevertheless, at 56 days a significative amount is still present in the pastes. K^+ ion is leached out into the solution whereas Ac^- and Na^+ penetrate from the acid solution reaching already at seven days values that are almost in equilibrium with the concentrations of these ions in the acid medium ($[Ac^-]$ = 870 mM and $[Na^+]$ = 174 mM). Ca^{2+} concentration is always higher than that corresponding to the thermodynamic solubility product of calcium hydroxide at the pH values measured on the pore solutions. The Ca^{2+} concentration increases in order to balance the negative charges of Ac^- present in the pore solution.

The pH values of pore solutions for OPC/BFS samples immersed in distilled water do not vary with time of immersion (pH values stay around 13) and K^+ ion leaches only moderately from the pastes. This behaviour of OPC/BFS samples agrees with his lower permeability compared to plain OPC.

On the other hand, when OPC/BFS samples are immersed in acetic/acetate buffered solution, a high

Table 2 Pore solution analysis of OPC samples.

days	Λ	pH	OH^-	SO_4^{2-}	Ac^-	Na^+	K^+	Ca^{2+}	Σz^+	Σz^-	I
	(mS)		(mM)						(meq·L^{-1})		(M)
											Test in distilled water
0	71.9	13.89	666	12	0	81	664	1	746	690	1.46
1	87.6	13.70	578	8	0	71	515	1	587	594	1.20
7	-	13.73	410	1	0	62	349	2	415	412	0.83
28	47.7	13.35	290	0	0	49	261	1	311	290	0.60
56	27.4	13.20	190	1	0	42	186	2	231	191	0.43
											Test in acetic acid/sodium acetate buffer (pH=4.5)
1	-	13.11	118	2	460	140	339	16	510	582	1.13
7	26.5	11.98	12	5	637	170	100	140	550	659	1.50
28	23.9	10.89	1	3	827	141	46	346	879	834	2.41
56	19.9	11.61	8	4	1140	180	32	412	1036	1155	3.02

Table 3 Pore solution analysis of OPC/BFS samples.

days	Λ	pH	OH^-	SO_4^{2-}	Ac^-	Na^+	K^+	Ca^{2+}	Σz^+	Σz^-	I
	(mS)		(mM)						(meq·L^{-1})		(M)
											Test in distilled water
0	23.80	13.03	147	1	0	35	98	1	135	149	0.29
1	21.25	12.91	125	7	0	29	80	2	114	139	0.27
7	-	12.87	88	1	0	28	57	3	91	90	0.19
28	18.01	13.05	118	2	0	30	97	0	127	122	0.25
56	17.24	13.00	88	1	0	32	46	1	79	89	0.17
											Test in acetic acid/sodium acetate buffer (pH=4.5)
1	15.25	10.49	6	2	334	97	37	82	299	343	0.81
7	-	6.54	0	2	712	140	10	254	668	716	1.89
28	21.32	9.21	0	2	616	112	30	255	652	620	1.79
56	-	6.45	0	4	704	169	17	340	866	711	2.27

decrease in the pH value of pore solution occurs very quickly: at seven days pHs bellow 7 are measured, that are in equilibrium with this of the surrounding acid solution (see Table 4). Ac^-, K^+ and Ca^{2+} concentrations follow a similar pattern to that previously described for plain OPC samples. In this case, XRD analysis reveals $Ca(OH)_2$ depletion after seven days in the solid phase.

Porosity and pore size distribution analysis

The pore size distribution curves of plain OPC and OPC/BFS samples immersed in both distilled water and acid aggressive solution appear in Fig 2.

As shown, at 0 days OPC/BFS sample has a porosity value about 50% higher than the plain OPC one, nevertheless, the pore size distribution is shifted to a lower pore diameter value. The total porosity decreased over time from 17.8% at 0 days to 12.4% at 56 days of immersion in distilled water for the OPC/BFS samples, and from 10.1% to 9.1% for the plain OPC ones. The remarkable decrease of porosity in OPC/BFS samples suggests the pozzolanic activity of the addition which, as known, produces hydrated calcium silicate and aluminate gels which densify the microstructure.

As previously indicated, when the OPC samples were immersed in the acid aggressive solution, two different corrosion layers developed at the acid/sample interface: the so called external corrosion layer with almost no adherence, and the internal one. To make the porosity analysis, the external

Table 4 pH values of the surrounding media at different ages.

Immersing	1 day		7 days		28 days		56 days	
Media	OPC	OPC/BFS	OPC	OPC/BFS	OPC	OPC/BFS	OPC	OPC/BFS
Deionized Water	9.2	11.4	12.4	11.9	12.3	12.0	12.6	11.9
Acid Medium	4.5	4.6	5.3	4.7	6.5	4.6	5.7	5.7

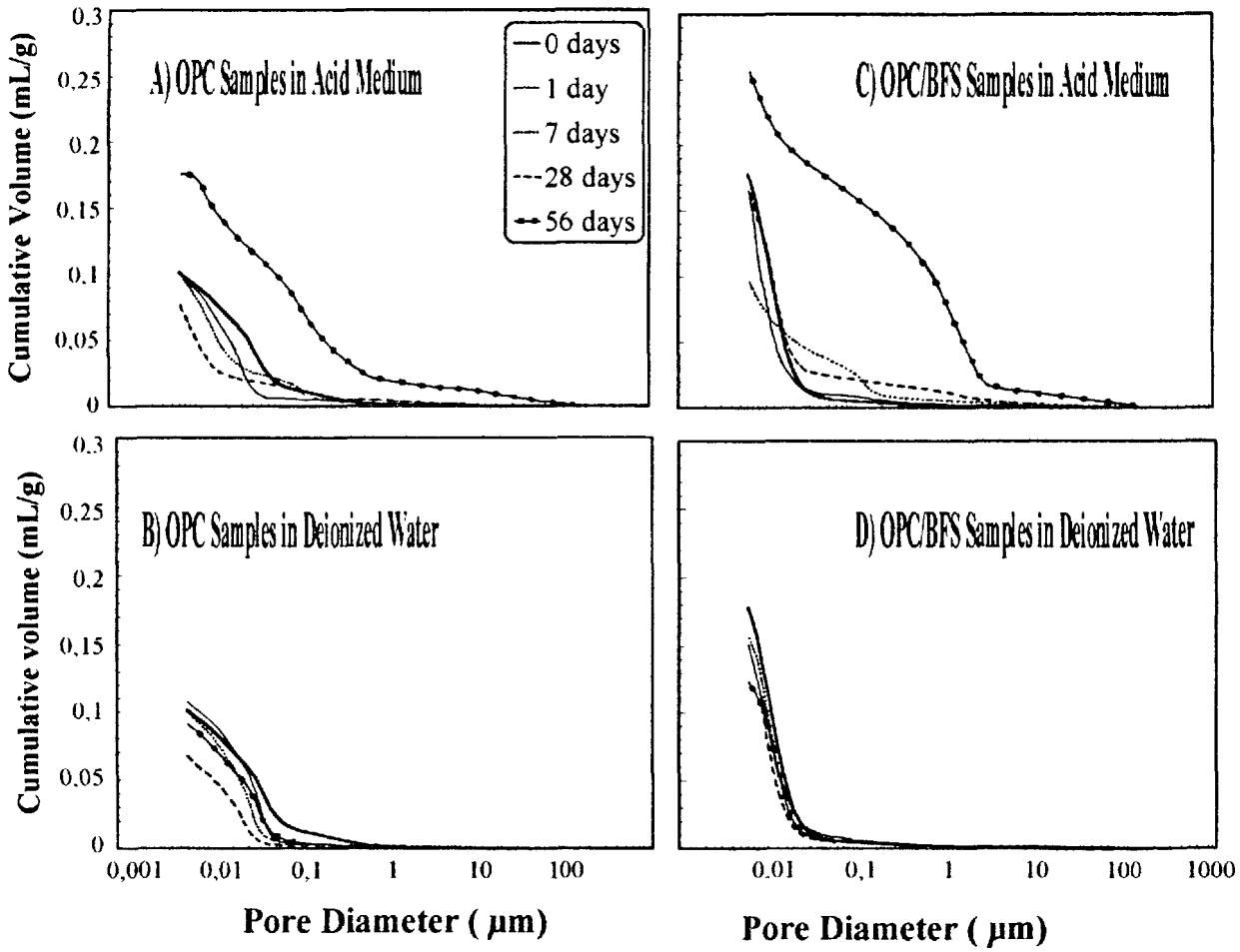

Figure 2 Pore size distribution curves for OPC and OPC/BFS samples.

corrosion layer was removed in all of the samples except those immersed during 56 days in the acid aggressive solution, due to the small dimensions of the core.

The evolution of OPC curves from 0 to 28 days shows a decrease of the porosity from 10.1% to 7.8% and a shift of the pore size distribution to lower pore diameter values. These results seem to suggest that the core of the samples is being densified. This densification was verified by SEM examination of the samples. In the samples stored in acid medium the C-S-H gel has a lower pore content, a lower Ca/Si ratio and higher content of Na than that of C-S-H gel formed in OPC samples immersed in distilled water. This densification of the gel was also found by Kurdowsky and Duszak (1995) in strong chloride solution. If so, consequently, the flexural strength will increase, as it will be seen later.

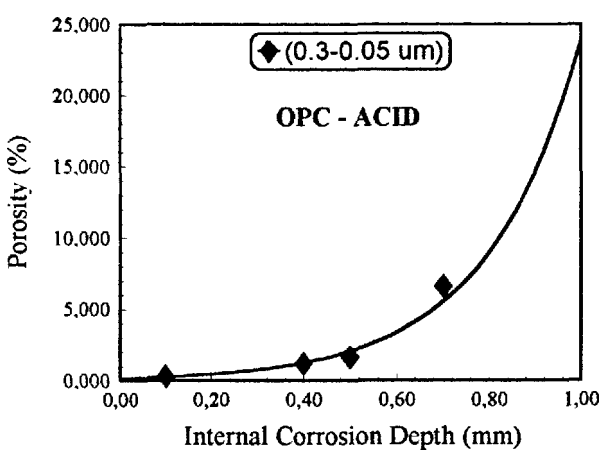

Figure 3 Volume of pores of diameter between 0.3-0.05 μm vs internal layer depth.

On the contrary, the percentage of pores with diameter ranging from 0.3 μm to 0.05 μm

increased. This increase is related to the internal corrosion layer of the samples, as shown in Fig 3 where an exponential correlation is obtained between both parameters.

The more relevant feature for the OPC/BFS samples is the increasing percentage of the pores with diameter >0.02 μm, that could be related to remaining zones of the external corrosion layer not easily removable, due to its better adherence.

The curve profiles of the samples immersed in the acid during 56 days are very different to the rest of the samples. The porosity increased remarkably as well as the percentage of pores with diameter higher than about 0.05 μm. These results are strongly related to the corrosion layers which, for the plain OPC samples, are denser than for those of OPC/BFS.

Finally, it is interesting to note that, the different porosity data obtained are a function of the kind of the corrosion layer. So, the external layer is very porous, as the porosity data after 56 days of immersion indicated, being the results in agreement with those previously reported by Bajza (1992) who used formic acid solutions instead of buffered acetic/acetate ones. Also it is interesting to note that the external corrosion layer is considerably denser in the case of OPC samples. This fact points out the difference of resistance degree to the acid attack between the two cement materials used.

Flexural strength analysis

The evolution of the flexural strength (F_s) versus the square root of time is given in Fig 4, each value representing the average of 6 measurements. The dashed zone is the standard deviation of the mean

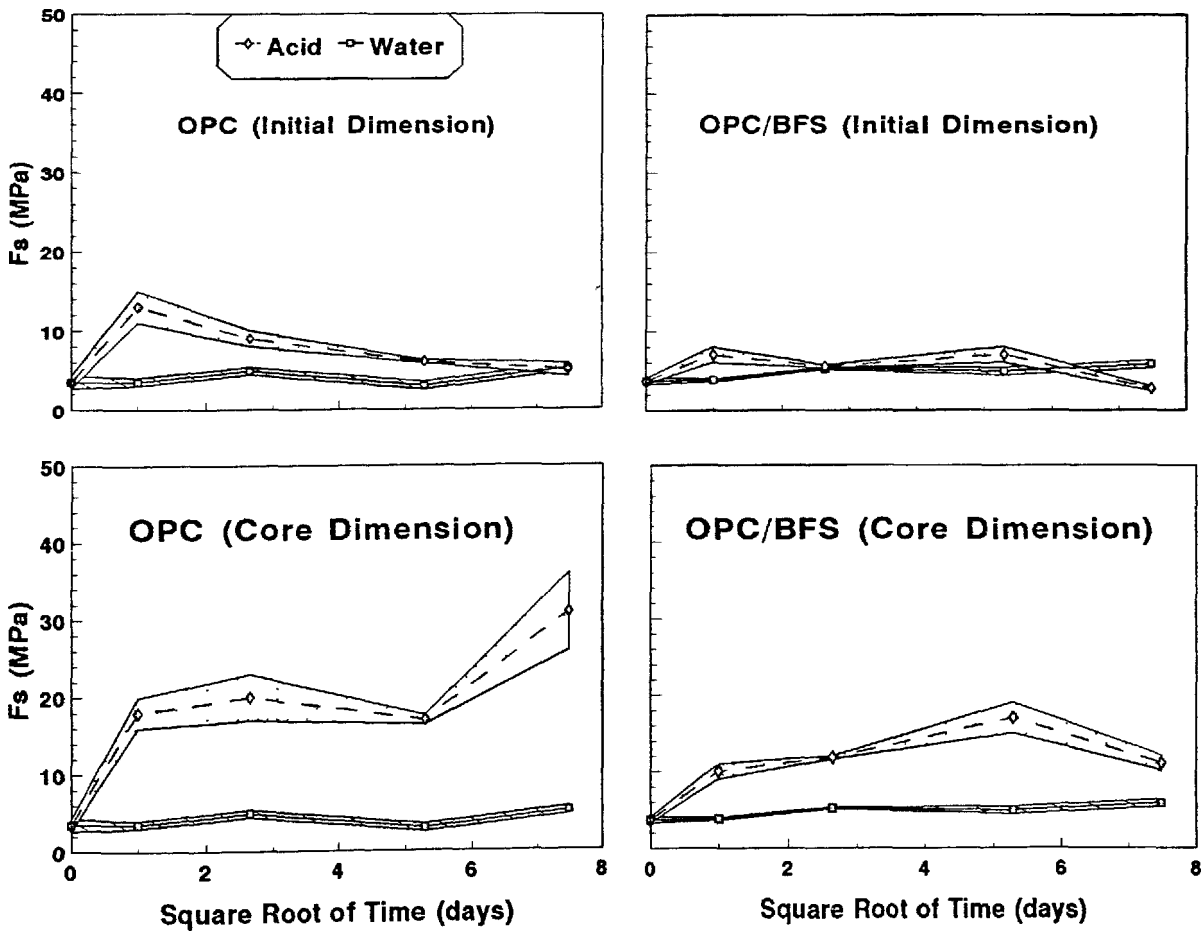

Figure 4 Evolution of flexural strength vs square root of time.

value. When both samples OPC and OPC/BFS were immersed in distilled water, the flexural strength values were very similar. In the case of the acid aggressive medium, the flexural strength strongly increased after 1 day for the plain OPC samples and in a minor extension for the OPC/BFS ones. Afterwards, the values started to decrease until reaching a plateau for the plain OPC. The behaviour for the OPC/BFS samples is more regular, as it can be seen data only have slight variations over time.

The aforementioned decrease of the flexural strength observed after 1 day for the OPC samples could be related to the corrosion layer (more porous than the core). If the flexural strength is measured on the core dimensions, the corresponding values increased with time, showing that the core is being densified (in agreement with the porosity data).

For the OPC/BFS samples and taking into account the core dimensions, the flexural strength values increased in a minor proportion than those of equivalent OPC, suggesting that the core is densified in a minor extension.

From these results and according to the test employed, both samples of plain OPC and OPC/BFS seem to be resistant to the buffered acid acetic/acetate, in the conditions here studied, and in a great measure for the plain OPC samples. But, as we previously proved, both materials are chemically attack by the acid medium been degradated and loosing sections. The simultaneous process of C-S-H gel densification that takes also place in acid medium compensates the loss of strength due to cement destruction in the corroded layers. These results are not in agreement with those reported by De Ceukelaire (1992), who concluded that blast furnace cement mortar was more resistant to hydrochloric acid attack than plain OPC one based on its superior mechanical behaviour.

CONCLUSIONS

The durability tests based on flexural strength measurements are not suitable to characterize the attack of the cement in acid medium. The densification of cement C-S-H gel that takes place in acid medium compensates the loss of strength produced by lost of section due to cement deterioration in the corrosion acid layers.

OPC/BFS pastes are less durable in acid medium than OPC plain samples: the decrease of pH in the pore solution, the consumption of $Ca(OH)_2$ and the depth of the degradation coat are higher for OPC/BFS samples than for OPC, being consequentely more severely attacked by the acid medium.

ACKNOWLEDGEMENTS

The authors are grateful for financial assistance from CICYT (project AMB 93-0022).

REFERENCES

Andersson, K., Allard, B., Bengtsson, M. and Magnusson, B., "Chemical Composition of Cement Pore Solutions", Cement and Concrete Research, Vol.19(3): 327-32 (1989).

Bajza, A., "Corrosion of Hardened Cement Pastes by Formic Acid Solutions", 9th ICCC congress, Vol.V Theme IV, New Delhi, India (1992).

Barneyback Jr,R.S. and Diamond,S., "Expression and Analysis of pore fluids from hardened cement pastes and mortars", Cement and Concrete Research, Vol. 4: p279-85, (1981) ,

Canham, I., Page, C.L. and Nixon, P.J., "Aspects of the Pore Solution Chemistry of Blended Cements Related to the Control of Alkali Silica Reaction", Cement and Concrete Research, Vol.17(5): p839-44 (1987).

Chandra, S., "Hydrochloric Acid Attack on Cement Mortar - An Analytical Study", Cement and Concrete Research, Vol.18: p193-203, (1988).
De Ceurkelaire, L., "The Effects of Hydrochloric Acid on Mortar", Cement and Concrete Research, Vol.22: p903-14, (1992).
Douglas, E., "Blast Furnace Slag Cement Mortar and Concrete: Durability Aspects", Suplementary Cementing Materials for Concrete, V.M. Malhotra ed., Canmet, Canada (1987).
El Hakim, F.A., "Rate of Chemical Degradation of Normal- Weight Concrete Subjected to HCl Solution", KFAS proceedings Series, Vol.2: p567-78 (1987).
Feng, Q.L. and Glasser, F.P. "Microstructure, Mass Transport and Densification of Slag Cement Paste", MRS Symposium Proceedings 178: p57-65 (1990).
Hinrichs, W. and Odler, I., "Investigation of the Hydration of Potland Blast Furnace Slag Cement: Hydration Kinetics", Advanced in Cement Research, Vol. 2(5): p9-13 (1989).
Kong, H.L. and Orbison, J.G., "Concrete Deterioration due to Acid Precipitation", ACI Materials Journal, Vol.84(2): p110-16 (1987).
Kurdowski, W. and Duszak, S., "Changes of C-S-H gel in strong chloride solution", Advances in Cement Research, Vol. 7(28): p143-49 (1995).
Malek, R.I.A., Roy, D.M. and Fang, Y., "Pore Structure, Permeability and Chloride Diffusion in Fly Ass and Slag Containing Pastes and Mortars", MRS Symposium Proceedings 137: p403 - 10 (1989).
Malhotra, V.M., "Properties of Fresh and Hardened Concrete Incorporating Ground Granulated Blast Furnace Slag",Suplementary Cementing Materials for Concrete, V.M. Malhotra ed., Canmet, Canada (1987).
Osborne, G.J. "Determination of Sulfate resistance of Blast Furnace Slag Cements using Small-Scale Accelerated Methods of Test", Advances in Cement Research, Vol.2(5): p21-7, (1989).
Pavlik, V., "Corrosion of Hardened Cement Paste by Acetic and Nitric Acids Part I: Calculation of Corrosion Depth", Cement and Concrete Research, Vol.24(3): p551-62 (1994).
Pavlik, V., "Corrosion of Hardened Cement Paste by Acetic and Nitric Acids Part II: Formation and Chemical Composition of the Corrosion Products Layer", Cement and Concrete Research, Vol.24(8): p1495-508 (1994).
Pavlik, V., "Corrosion of Hardened Cement Paste by Acetic and Nitric Acids Part III: Influence of Water/Cement Ratio", Cement and Concrete Research, Vol.26(3): p475-490 (1996).
Samarin, A. and Roper, H., "The Effect of High Replacement Areas of Portland Cement with Granulated Ground Blast Furnace Slag on Concrete Durability", Proceedings of International Seminar on Durability of Concrete - Asoects of Admixtures and Industrial By-Products, L. Nilsson ed., Gothemberg, Sweden (1987).
Spirin, P., Shcherbina, G., Alferova, F. and Pavlenko, L., "Optimization of the Composition of a Paste for Producing High-Strenght Acid-Resistant Concrete", Chemical Abstract, Vol.106 200807 (1987).
Wiebenga, J.G., "Blast Furnace Slag in the Netherlands", Proceedings of International Workshop on Granulated Blast Furnace Slag in Concrete, Canadian Center for Mineral and Energy Tecnology, Toronto, Canada (1987).

MECHANISTIC CONSIDERATIONS FOR THE EFFICIENCY OF PORTLAND CEMENT IN WASTE STABILIZATION

F. MacGregor MILLER, Construction Technology Laboratories, Inc., Skokie, IL, U.S.A.
Waldemar A. KLEMM, Construction Technology Laboratories, Inc., Skokie, IL, U.S.A.

ABSTRACT Portland cement has found increasing use in the solidification and stabilization of hazardous wastes containing regulated heavy metals such as Cd, Cr, Pb, and As. Multiple metals hydroxide sludge, with Cd, Cr(III), and Pb(II), were all well-stabilized both in cement pastes and in soil-cement matrices. Three different stabilization mechanisms were in effect, pH control, AFt formation, and C-S-H substitution. As(V) was stabilized better than As(III) in soil-cement mixes containing large additions of $FeSO_4 \cdot 7H_2O$. Iron-arsenic complexes appeared to be responsible.

Key-words: Stabilization; AFt phase; CSH; Heavy metals; Leaching

INTRODUCTION

The process of solidification/stabilization (S/S) is a widely accepted treatment/disposal process for a broad range of wastes, particularly those classified as toxic or hazardous which are not suited for normal methods of disposal and where special treatment is necessitated. Generally, for inorganic wastes, the hazard resides in the toxic and heavy metals content. Portland cement is the material found to be most useful for the purpose of S/S due to its ability for fixation and immobilization of a broad range of heavy metals. As categorized by Weitzman (1990), two of the major S/S processes which have the most value for conditioning inorganic hazardous wastes containing heavy metals include, a) cement-based binders, including portland cement and cement kiln dust (CKD), and b) lime-based binders, including lime, lime kiln dust, and lime-fly ash mixtures. Cements are uniquely suited to the task, as they not only provide the alkaline pH conditions for the precipitation of many heavy metals as insoluble hydroxides, but also provide a strong chemical bonding as well as physical encapsulation. The hydration process results in a high surface area C-S-H reaction product for immobilization of many hazardous constituents, matrix strength development, and formation of metals-substituted calcium aluminate hydrates such as AFt phases. During the solidification process, large quantities of water are incorporated into the hydration products. Regulations under the Resource Conservation and Recovery Act (RCRA) prohibit land disposal of wastes containing free liquid, and a minimum compressive strength of 0.345 MPa (50 psi) in treated waste is the usual guideline for industrial practice.

A number of investigations, relevant to the present work, on the stabilization of metals-containing waste using S/S techniques have been carried out previously. Conner et al (1992), Bishop (1988), and Zamorani and Serrini (1992) have investigated the mechanism of metal fixation in S/S systems using portland cement. Bishop (1988) also studied leaching characteristics of selected S/S systems. Glasser (1992, 1994) and Macphee and Glasser (1993) have analyzed the chemical aspects of portland cement interactions with hazardous wastes, including the effects of oxidizing and reducing agents in cement to modify its redox behavior and the incorporation of soluble oxyanions into the ettringite structure.

CADMIUM, CHROMIUM, AND LEAD — MULTIPLE METAL SLUDGES

Introduction

In previous work, Bhatty and West (1993) investigated the solidification/stabilization of cadmium (Cd), chromium (Cr), lead (Pb), and mercury (Hg) in both ASTM Type I and Type V portland cement matrices. The metals, as Cd(II), Cr(III), Pb(II), and Hg(II) were added individually as single insoluble oxides or as salt solutions, and in concentrations as high as 3% CdO, 3% Cr_2O_3, 5% PbO, and 0.05% HgO, by mass of cement. The addition of metals as oxides or metal salt solutions decreased the workability of Type I cement significantly more than Type V cement. The addition of chromium (III) salts accelerated both setting time and strength development, whereas both variables were retarded with lead(II) additions. Although these metals influenced early hydration reactions, ultimate cement hydration was as complete as the control samples. When added as either oxides or salt solutions, all four metals were well stabilized as determined by the

U.S. EPA's Toxicity Characteristic Leaching Procedure (TCLP). The stabilization of cadmium and chromium was particularly good, but some high pH leachability of lead was observed. Inasmuch as metals in wastes usually occur as hydroxide sludges, or are rapidly converted to that form by lime or portland cement, future work utilized multiple metal sludges prepared in that way.

Materials and Methods

A Type I portland cement was used for all experimental work, which had the composition of 55% C_3S, 19% C_2S, 9% C_3A, 7% C_4AF, 0.01% Na_2O, 0.62% K_2O, 3.10% SO_3, and 1.31% LOI.

Multiple metal hydroxide sludges were prepared using $CdCl_2 \cdot 2.5H_2O$, $Cr(NO_3)_3 \cdot 9H_2O$, and $Pb(NO_3)_2$. The salts were dissolved in about one litre deionized water, and $Ca(OH)_2$ powder was added until the pH reached 10.0 and remained at that value for at least 30 minutes. The precipitates were vacuum-filtered using a Büchner funnel. A small sample was removed and oven-dried at 110° C to determine the moisture content. The remaining sludge was retained in a sealed container over water until used in a cement paste mix within the next 36 hours. Cement pastes were prepared at a 0.6 water/cement ratio, which includes water from the sludge. Pastes were cast into 25.4 mm (1-in.) cube molds, and removed after three days. Compressive strength measurements were made at 3, 7, 28, and 90 days. Two series of mixes were prepared. The first mix contained Type I portland cement, with an added multiple-metal sludge containing cadmium, chromium, and lead, each at 1% (10,000 mg/kg) concentration in the total paste by mass on a metal basis. The second mix contained a similar multiple-metal sludge, each metal at a 0.1% (1,000 mg/kg) concentration by mass in the total paste.

Leaching solutions consisted of acetic acid leaching solution, and synthetic acid rain. The acetic acid leaching solution was prepared by diluting 114 mL glacial acetic acid with deionized water to a volume of 20 litres, giving a pH of 2.88. The synthetic acid rain was prepared by adding 6 mL concentrated sulfuric acid (18 M) and 4 mL concentrated nitric acid (12 M) to deionized water and diluting to 1 litre. A 100 mL aliquot was further diluted with deionized water to a final volume of 20 litres and a pH of 3.0. Paste cubes were prepared for leaching by curing for 90 days, followed by crushing to pass a 74 μm (No. 200 mesh) sieve and dried with acetone. They were subjected to sequential batch leaching of 28.01 g of high metals (1%) concentration paste and 26.39 g of low metals (0.1%) concentration paste, in 450 mL of the appropriate leaching solution. For each one-day leaching step, the 500 mL HDPE plastic leaching bottles were slowly rotated, overnight, for 16 to 20 hours. At the end of the leaching period, the bottles were removed and the contents filtered through a Büchner funnel containing a 0.7 μm pore size acid-washed glass filter. The resulting final leachate pH was measured, and the leachate was then acidified and submitted for analysis of the three multiple metals, as well as the concentrations of calcium, silicon, aluminum, and iron. The solid on the filter was subsequently returned to the original leaching bottle, which was then filled with a fresh 450 mL quantity of leaching solution for the next day of leaching.

Compressive Strength of Multiple Metals Pastes

Compressive strength measurements of two cement pastes, containing cadmium, chromium, and lead multiple hydroxide sludges, are shown in Table 1.

Table 1 Compressive strength measurements of multiple metal cement pastes.

	Compressive Strength, MPa (psi)			
Metals Addition Level	3 days	7 days	28 days	90 days
0.1% (1,000 mg/kg)	24.7 (3580)	35.2 (5100)	55.5 (8050)	61.0 (8850)
1% (10,000 mg/kg)	31.6 (4580)	36.9 (5350)	52.6 (7630)	56.4 (8180)

Acetic Acid Leaching of Multiple Metals Pastes

Sequential batch leaching, using the nominally 0.1 M acetic acid leachant for the first 7 steps and then 0.05 M acetic acid from the eighth step until the end of the sequential batch leaching, was carried out on mature pastes which had been cured for 90 days. Fig 1 shows the cumulative leach of the three metals as a function of decreasing pH for the 1% concentration mix. Each pH value plotted represents the final leachate pH after a specific leaching step. Cadmium does not begin to

leach until the pH is below about 9.5, but increases rapidly thereafter. At high multiple metals concentration, lead is leached to a slight degree at high pH, but then is well stabilized to below pH 6. Chromium has a low but finite solubility from high pH down to pH 6. It is increasingly leached below this pH value. Again, cadmium solubility seems to be nearly exclusively dictated by the pH. It is interesting to note that there appears to be a degree of suppression of leachability of all three metals apparently related to their combined presence. For the paste mix containing the 0.1% metals concentration, similar leaching behavior was observed. Compared to earlier studies of single metal leaching behavior, the solubility of the multiple metals system is somewhat lower. Lead, particularly, is less soluble at any given pH in the multiple metals leaching system. However, small but potentially significant levels of lead do leach out in the early batch leaching steps when the pH is high. In order to avoid the high pH conditions, ancillary experiments were conducted (Bhatty et al, 1996) in which silica fume was added to the multiple metal cement paste system in an amount stoichiometrically equivalent to all the $Ca(OH)_2$ to be formed by C_3S and C_2S hydration. Sequential batch leaching tests showed a reduction in the high pH leachability of lead, and no additional leachability down to pH 4.

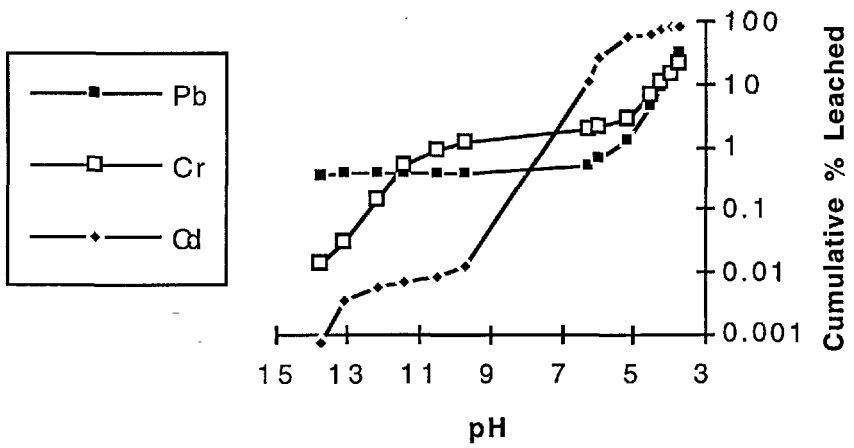

Figure 1 Summary of Pb-Cr-Cd multiple metals (1% each) leach with acetic acid.

As another means of comparing the effectiveness of portland cement stabilization of cadmium, chromium, and lead, their solubilities as a function of pH for the various leaching steps were compared to corresponding calculated solubilities from Conner et al (1992). The multiple metals in a cement matrix showed significantly lower solubilities than predicted by their theoretical hydroxide solubilities. The situation is most dramatic for lead, in that over a broad pH range, lead was found to be nearly three orders of magnitude less soluble than would be predicted by the solubility of $Pb(OH)_2$.

Cumulative % leach quantities of lead and aluminum from the 1% metals paste with acetic acid are depicted in Fig 2. The very close correspondence suggests that there is mutual synergy in the leaching of these two elements. It appears that a significant fraction of the lead may be associated with the alumina in ettringite or ferrite, since it only begins dissolving when the alumina also becomes solubilized. At pH values greater than about 11.5, lead shows some leachability due the formation of the plumbite ion, $Pb(OH)_3^-$. This oxyanion, however, has not been confirmed as forming a substituted ettringite, although the capacity of the ettringite structure to accommodate a wide variety of oxyanions is well known. In a situation similar to lead and aluminum, there is a strong correlation of leachability and pH between chromium and silica, as also seen in Fig 2. The correspondence is striking, and suggests that some of the chromium may be stabilized in the C-S-H system rather than ettringite. The ionic radii of $Cr(OH)_4^-$ and $Si(OH)_4$ are fairly closely comparable. Bensted and Prakash Varma (1971) showed that it was possible to replace Al in ettringite with trivalent Cr^{3+} and Pöllmann et al (1989, 1993) prepared chromate-substituted ettringites. However, Bensted and Prakash Varma (1972) found that the larger size of hexavalent CrO_4^{2-} oxyanions in ettringite channels appear to sterically hinder the replacement of $[Al(OH)_6]^{3-}$ octrahedra by trivalent metals such as Cr^{3+}. Only trivalent chromium was added in this Cd-Cr-Pb

system, although the possibility of limited oxidation does exist. Due to the close association of chromium leaching with silica in the multiple metal sludge mixes, it is more likely that Cr(III) substituted, in part, for Si in C-S-H as observed by Ivey et al (1990) and Lin et al (1996). It is also possible that a minor amount of Cr(III) has substituted into the aluminate phases.

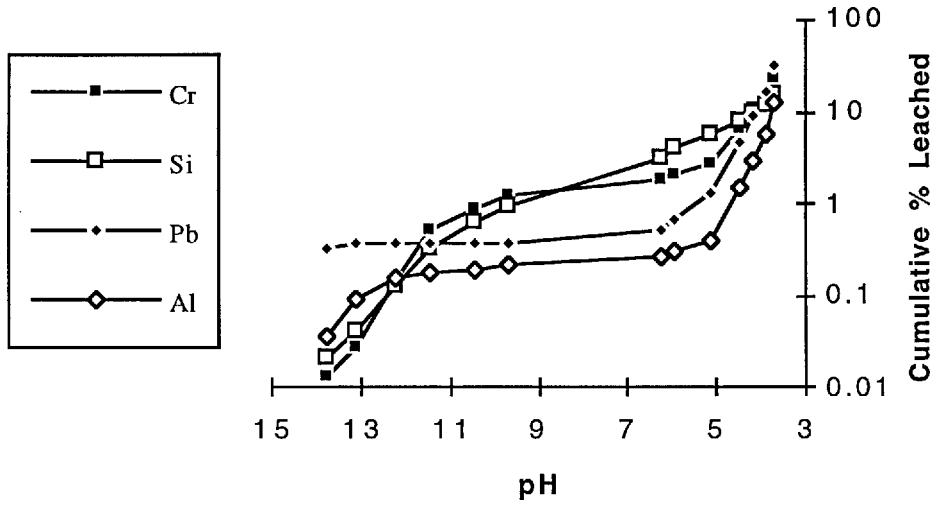

Figure 2 Lead-alumina (1% Pb) and chromium-silica (1% Cr) leaching with acetic acid.

Synthetic Acid Rain Leaching

Synthetic acid rain is a much less aggressive leaching solution than the acetic acid solution. This is not surprising when the actual number of moles of acid (hydrogen ion) available for leaching is calculated for the two systems. The acetic acid solution was 0.10 M, with a pH of 2.88, and the synthetic acid rain contained 0.00024 M nitric acid and 0.00054 M sulfuric acid for a total normality of 0.00132 N and a pH of 3.0. Thus, synthetic acid rain would require 76 leach cycles to furnish an amount of acid equivalent to that supplied by one acetic acid leach cycle. Therefore, with synthetic acid rain as a leachant, the pH never dropped below 13.0, and the degree of leaching experienced was far lower than that observed with the acetic acid leaching solutions. The initial high-pH leachability of chromium and lead was observed to continue for several cycles. The total amount leached, however, was very low for all metals, even after 16 sequential leaches.

LEACHABILITY OF CONTAMINATED SOILS AND OILY WASTE

Materials and Methods

In order to determine the behavior of cadmium, chromium, and lead in soil-cement matrices, with and without the contamination of oil, soil samples were prepared according to a procedure outlined by the U.S. EPA (1988). The soil composition is shown in Table 2. Two soil types were prepared, a) a dolomitic soil (37.14% SiO_2, 14.47% CaO, 9.63% MgO, 26.62% LOI) and b) a siliceous soil (75.27% SiO_2, 1.67% CaO, 0.88% MgO, 7.24% LOI). The silt required in the siliceous mix was prepared by grinding the silica sand to the appropriate fineness.

Table 2 Proportions of materials required for preparation of synthetic soil matrix.

Soil Ingredients	Proportion, mass %	Sources for Soil Types
Gravel (No. 9)	5.7	a) Dolomitic b) Siliceous
Sand	31.5	a) Dolomitic b) Siliceous
Silt	28.3	a) Dolomitic b) Siliceous
Bentonite	5.4	Mississippi
Kaolinite	9.4	Kraft clay
Topsoil	19.7	Local garden shop

Three soil samples were each prepared in 5 kg batches for compressive strength determinations and metals leachability, all containing 8% (400 g) of Type I portland cement and approximately 400 mL of water. The moisture content was estimated (from one experimental test with only soil and cement) to be that required for maximum density by ASTM D 558. All of the soil-cement mixes contained 7.0 g each of cadmium, chromium, and lead. The mixture of metals was added as a freshly prepared wet sludge, as described earlier. For each metal this is about 1% added to a paste of 640 g with a 0.6 w/c ratio.

A soil composition termed "Dry-Calcareous" was prepared as above and contained dolomitic soil constituents, cement, and multiple metals sludge. A second soil was termed "Oily," and was prepared with dolomitic soil, cement, metals sludge, and the further addition of 8% SAE 10-weight motor oil which had been previously aged in an oven at 100° C for 72 hours. This aging process helped to simulate the condition of contaminated oily soils usually found in the field. Additionally, to help emulsify the oil, a combination of two surfactants (31 g of Triton X-45 and 10 g of Triton X100, from Union Carbide Corporation) were added as a replacement for about 30 mL of mix water. The third soil, termed "Siliceous," was also prepared with cement, oil and metals sludge, but contained a siliceous soil composition.

Soil mixes were tamped into standard 50 mm (2-in.) cube molds. The soil specimens were cured at 23° C and 100% relative humidity prior to removal from the molds at 3-days. Cubes were tested to determine compressive strength and, after at least 28 days of curing, were crushed and dried. Soil samples containing oil were air dried and the non-oily soil was dried with acetone, prior to being subjected to the acetic acid leaching procedure described previously.

Compressive Strength of Multiple Metals Soils

Compressive strength determinations, at 7, 28, and 90 days, were subsequently made on the three soil compositions containing cadmium, chromium, and lead multiple hydroxide sludges and are shown in Table 3. Strengths exceed the industry guideline minimum of 0.345 MPa (50 psi).

Table 3 Compressive strength measurements of multiple metal soil-cement cubes.

	Compressive Strength, MPa (psi)		
Sample	7 days	28 days	90 days
Dry-Calcareous (no oil)	1.24 (180)	1.59 (230)	2.55 (370)
Oily (calcareous)	1.17 (170)	1.72 (250)	3.17 (460)
Siliceous (with oil)	1.24 (180)	1.79 (260)	2.34 (340)

Acetic Acid Leaching of Multiple Metals Soils

The three synthetic soil-cement compositions were leached with 0.012 M acetic acid as previously described. Solid leaching samples weighed between 24 and 32 g and were leached using 450 mL of leachant. The results of these sequential batch leaching steps are presented in Fig 3, which shows a comparison of the cumulative % leaching of Cd, Cr, and Pb, over a pH range of 13 to 5, for calcareous soil, oily calcareous soil, and oily siliceous soil. Each metal extracted from all three soil types showed similar leaching characteristics and tended to be grouped together by metal type.

As expected, due to its pH dependence, cadmium showed the greatest insolubility at pH values above 8, but was rapidly solubilized as the pH was lowered. Both chromium and lead were stabilized well over the range of pH 13 to 6, but lead was retained better than chromium. A comparison of leachability between the three soil types reveals some interesting trends. For the stabilization of chromium, the two calcareous soils appear to be significantly more effective in all pH ranges. For cadmium, the calcareous soils outperformed the siliceous soil at pH values above 8, but lagged at lower pH values. In the case of lead, above a pH of 9, both oil-containing soils provided better stabilization against leaching. However, below a pH of 9, the oily calcareous soil performed best. In regard to differences between the calcareous and siliceous soils, for a given amount of acetic acid used, the siliceous soil system attained a much lower pH than its dolomitic equivalent, because of the neutralizing capacity of the dolomite. At a pH of 5.0, there was a

significant amount of unreacted calcium left in samples at the end of 13 leach cycles, in spite of the acidic pH. The calcium was principally in the form of unreacted dolomite.

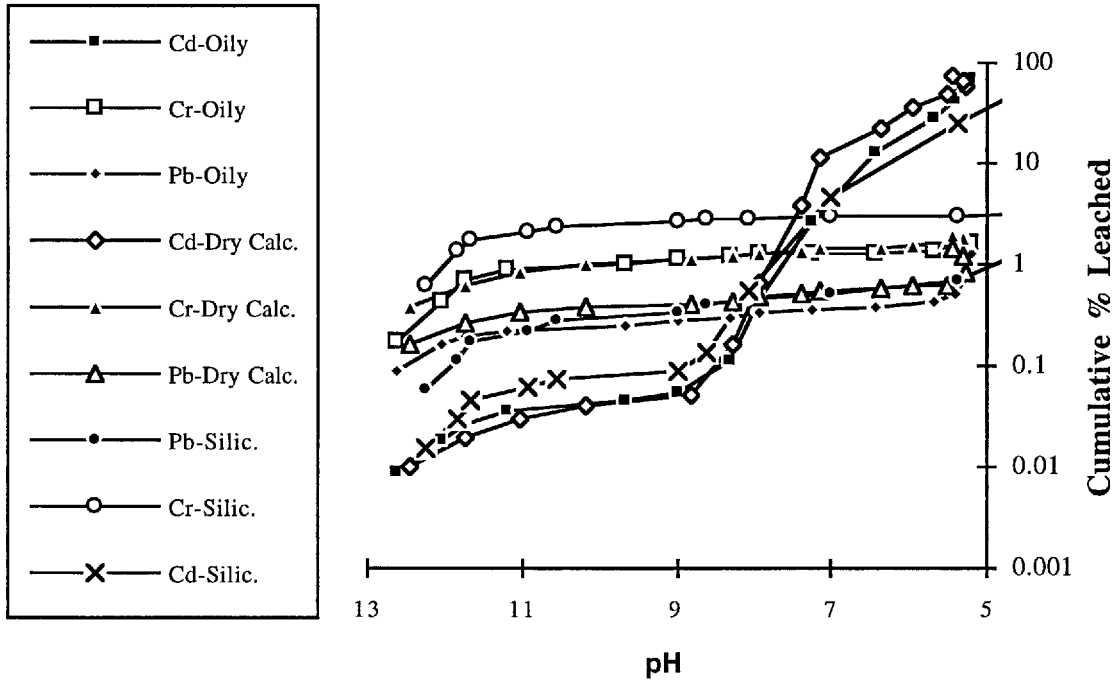

Figure 3 Comparison – cumulative % leach for oily waste, calcareous soil, and siliceous soil.

ARSENIC LEACHABILITY FROM SILICEOUS SOILS

Materials and Methods

Five soil samples were prepared in 4 kg batches for compressive strength determinations and arsenic leachability. The soil mixes, designated ASC1 through ASC5, each contained 15% (600 g) of portland cement in the synthetic siliceous soil composition described previously. Three mixes (ASC1-ASC3) contained As(V) as $Na_2AsO_4 \cdot 7H_2O$ (50 g) and two (ASC4-ASC5) contained As(III) as $NaAsO_2$ (21 g), which gives an arsenic concentration of 2% by mass of cement. Mixes ASC1, ASC4, and ASC5 also contained $FeSO_4 \cdot 7H_2O$ (267 g), which provides a six-fold molar excess of iron(II) over the arsenic. Robins (1988) reports that Fe(II) does not reduce As(V) to As(III), but that it does stabilize the arsenic in a hydrated cement matrix. These soils also required an increase in the amount of water required for proper mixing. Mix ASC2 contained EDTA (20 g), but no ferrous sulfate, in order to chelate lime and perhaps encourage the formation of substituted AFt phases. Mix ASC5 contained 20 mL of 30% H_2O_2 (6 g) in the mix water to oxidize all of the arsenite in the mix to arsenate. Additionally, a paste mix (ACP) was prepared containing cement, As(V), and Fe(II) in the same proportions as in the soil mixes.

The five soil mixes were tamped into 50 mm (2-in.) cube molds, cured, and treated as previously described. The paste sample (ACP) was cast into a 25.4 mm (1-in.) mold and cured. Cubes were tested for compressive strength and, subsequently, crushed, acetone-washed, and leached with 0.03 M acetic acid. Soil samples weighing 32 g were leached with 450 mL of leachant. The ACP sample (26 g) was leached with 0.1 M acetic acid for 7 days and then the leachant was changed to 0.05 M acetic acid for subsequent batch leaching. The change to a more dilute leachant solution at later leaching times served to expand the pH scale for lower pH values. All samples were batch leached for 11 days.

Composition and Compressive Strength of Arsenic Soils

Compressive strength determinations were made at 7 and 28 days on arsenic-containing siliceous soils. The paste sample (ACP) had a 4-day strength of 0.34 MPa (50 psi) and a 28-day strength of 6.34 MPa (920 psi). Mix compositions and soil strength data are given in Table 4.

Table 4 Composition and compressive strength of arsenic soil-cement cubes.

Mix	Additions	Compressive Strength, MPa (psi)	
		7 days	28 days
ASC1	arsenate + $FeSO_4$	0.34 (70)	3.10 (450)
ASC2	arsenate + EDTA	1.31 (190)	3.38 (490)
ASC3	arsenate	1.03 (150)	1.72 (250)
ASC4	arsenite + $FeSO_4$	0.69 (100)	6.00 (870)
ASC5	arsenite + $FeSO_4$ + H_2O_2	0.28 (40)	3.10 (450)

Acetic Acid Leaching of Arsenic Soils and Paste

The five arsenic soil cement mixes (ASC1-ASC5) and the arsenic cement paste mix (ACP) were all subjected to sequential batch acetic acid leaching. Over the 11-day period of leaching, the pH continuously decreased from approximately 13 to a final range between 3.3 and 3.6. A summary of test results showing cumulative % arsenic leached over the 11-day extraction period is given in Fig 4. All mixes had a maximum arsenic solubility at a pH of about 9.5, which corresponds, generally, to the fifth day of batch leaching. The two mixes without ferrous sulfate had excessive solubility at this pH, and eventually over 40% of the total arsenic was extracted.

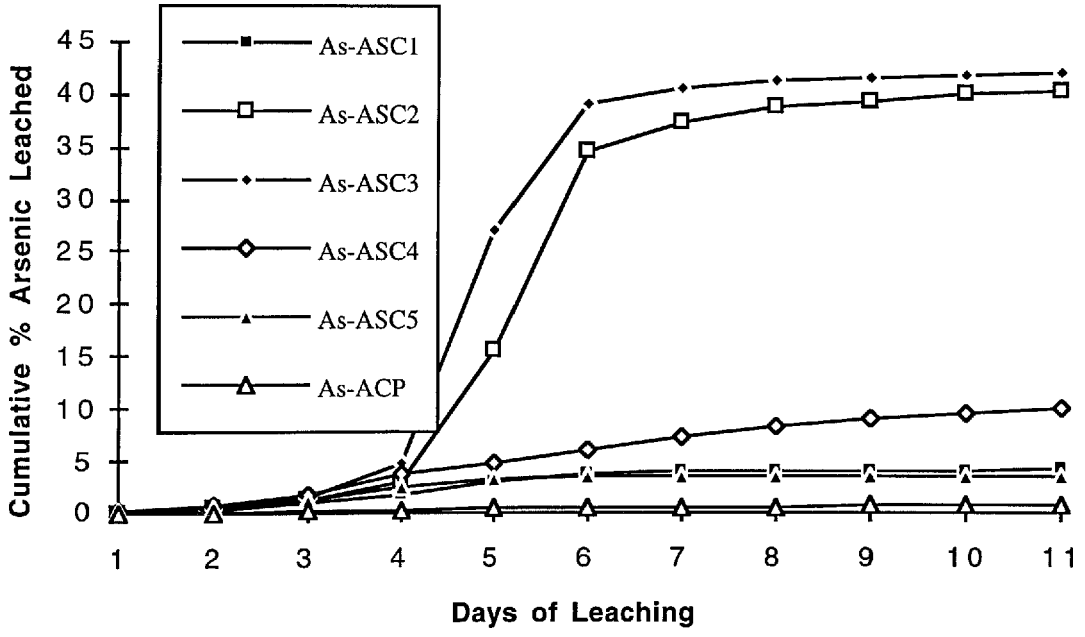

Figure 4 Summary of arsenic leach test results for synthetic soil cement and paste mixes.

The addition of EDTA (ASC2) had no real beneficial effect. At a pH below 4.0 (11th extraction), the soil containing arsenite and $FeSO_4$ (ASC4) had a cumulative loss of 10% As. The two mixes which contained arsenate with $FeSO_4$ (ASC1) and oxidized arsenite with $FeSO_4$ (ASC5) had cumulative losses of 4.1 and 3.5% As, respectively. The paste sample (ACP), containing both arsenate and $FeSO_4$, released only 0.7% of its available arsenic.

The formation of calcium arsenate was the procedure generally used in the past to stabilize arsenic. Recently, however, Taylor and Fuessle (1994) studied the interactions of iron salt precipitants with both As(III) and As(V), as stabilizing agents for arsenic. The validity of this approach was confirmed in the present study. A plausible stabilization mechanism for arsenic also involves the formation of arsenic-substituted ettringites, where the arsenate or arsenite oxyanions may replace sulfate and be incorporated into the channels between structural columns of the ettringite crystal structure. An arsenate-substituted ettringite, as well as ettringites containing B, Mo, Se, and V oxyanions, were synthesized and characterized by Hassett et al (1989) and Kumarathasan et al

(1990). However, in the arsenic cement soil experiments, an X-ray diffraction pattern taken after 28 days of curing (but, before leaching), showed the presence of a significant amount of AFt phase, probably iron-substituted ettringite. The arsenate oxyanion is probably unable to substitute into ettringite due to competition from the high excess sulfate concentration. Further evidence that arsenic is not stabilized to any significant degree in the AFt phases is provided by the low amount of arsenic leached at low pH values during sequential batch leaching when the AFt phases are being decomposed.

SUMMARY

This research was undertaken with the goal of establishing the mechanisms by which portland cement and portland cement-based stabilizing reagents immobilize certain regulated trace metals in inorganic form in S/S systems. The metals studied included Cd, Cr, Pb, and As, with addition levels of usually 1% by mass of cement. Inasmuch as metals usually occur in wastes in the form of hydroxide sludges, Cd, Cr, and Pb were added in that form to cement paste mixes and also to synthetic soil-cement matrices. In paste systems, sequential batch leaching with 0.1 M acetic acid and synthetic acid rain showed, with the exception of early high-pH leachability of lead, that very little of any of the metals were dissolved by increments of these two leachants. The effectiveness of stabilization was, in most cases, orders of magnitude better than would be projected from their respective hydroxide solubilities.

Lead showed the greatest improvement in stabilization, followed by chromium, and then by cadmium. Lead dissolution at low pH values corresponded closely with the loss of alumina, suggesting an ettringite or ferrite stabilization mechanism. In a similar fashion, the increased chromium loss at low pH values was correlated to a corresponding dissolution of silica, which indicates Cr(III) substitution for Si in C-S-H. The leachability of cadmium is continuous as the pH decreases from 9.5 to lower values during the batch leaching steps, and confirms a simple insoluble hydroxide stabilization mechanism and pH-controlled dissolution. Silica fume additions were also found to reduce high-pH lead leachability.

Stabilization in a soil matrix, both dry and oil-contaminated was also studied with additions of the Cd-Cr-Pb multiple hydroxide sludge. Cement (8%) was added to two soils, a dolomitic soil and a siliceous soil. Stabilization of the metals, especially chromium, in a soil matrix was at least as good as in cement paste. Generally, dolomitic soils stabilized the metals better than the siliceous soil. For the oily waste, appropriate emulsifiers avoided phase separation, and leaching results of oily soils were essentially comparable to those without oil. Arsenic (2%), in siliceous soil-cement matrices, was effectively stabilized through the use of ferrous sulfate additions and a Fe/As ratio of at least 6. Arsenate was found to be better stabilized, under these conditions, than arsenite. Stabilization was through formation of an iron-arsenic complex, and not by AFt phases.

ACKNOWLEDGEMENT

This work was supported by the Portland Cement Association, Skokie, IL, under PCA Project Index Nos. 90-08 and 94-16. The contents of this paper reflect the views of the authors, who are responsible for the facts and accuracy of the data presented. The contents do not necessarily reflect the views of the Portland Cement Association. The authors thank Presbury B. West, Javed I. Bhatty, Börje W. Öst, and JoAnne B. Delles for their valuable contributions to this work.

REFERENCES

Bensted, J. and Prakash Varma, S., "Studies of Ettringite and its Derivatives, Part 1," Cement Technology, Vol. 2, No. 3, pp. 73-76, 100, May/June 1971.
Bensted, J. and Prakash Varma, S., "Studies of Ettringite and its Derivatives, Part 2: Chromate Substitution," Silicates Industriels, Vol. 37, No. 12, pp. 315-318, 1972.
Bhatty, J.I. and West, P.B., "Interaction of Heavy Metals in Portland Cement Stabilized Waste Systems: Effects on Paste Hydration," Emerging Technologies Symposium on Cement and Concrete in the Global Environment, Portland Cement Association, Skokie, IL, March 1993.

Bhatty, J.I., Miller, F.M., West, P.B., and Öst, B.W., "Stabilization of Heavy Metals in Portland Cement, Silica Fume/Portland Cement, and Masonry Cement Matrices," PCA R & D Serial Number 2067, Portland Cement Association, Skokie, IL, 1996.
Bishop, L.P., "Leaching of Inorganic Hazardous Constituents for Stabilized/Solidified Hazardous Waste," Hazardous Waste and Hazardous Materials, Vol. 5, No.2, pp.129-143, 1995.
Conner, J.R., Cotton, S., and Lear, P.R., "Chemical Stabilization of Contaminated Soils and Sludges Using Cement and Cement By-Products," Proceedings, First International Symposium on Cement Industry Solutions to Waste Management, Canadian Portland Cement Association, Calgary, Alberta, Canada, pp. 73-97, October 1992.
Glasser, F.P., "Application of Cements to the Treatment and Conditioning of Toxic Wastes," Proceedings, 9th International Congress on the Chemistry of Cement, Vol. VI, New Delhi, pp. 114-117, 1992.
Glasser, F.P., "Environmental Uses of Cement in Waste Conditioning," Engineering Foundation Conference Proceedings, Advances in Cement and Concrete, Grutzeck, M.W. and Sarkar, S.L., Eds., American Society of Civil Engineers, New York, pp. 499-507, 1994.
Hassett, D.J., Pfughoeft-Hassett, D.F., Kumarathasan, P., and McCarthy, G.J., "Ettringite as an Agent for the Fixation of Hazardous Oxyanions," Proceedings, 12th Annual Madison Waste Conference on Municipal and Industrial Waste, University of Wisconsin, Madison, Wis., pp. 471-482, September 1989.
Ivey, D.G., Heimann, R.B., Neuwirth, M., Shumborski, S., Conrad, D., Mikula, R.J., Lam, W.W., "Electron Microscopy of Heavy Metal Waste in Cement Matrices," Journal of Materials Science, Vol. 25, No. 12, pp. 5055-5062, 1990.
Kumarathasan, P., McCarthy, G.J., Hassett, D.J., and Pflughoeft-Hassett, D.F., "Oxyanion Substituted Ettringites: Synthesis and Characterization; and their Potential Role in Immobilization of As, B, Cr, Se and V," Fly Ash and Coal Conversion By-Products: Characterization, Utilization and Disposal V, Day, R.L.and Glasser, F.P., Eds., Symposia Proceedings Vol. 178, Materials Research Society, Pittsburgh, PA, pp. 83-104, 1990.
Lin, C-K., Chen, J-N., and Lin, C-C., "An NMR and XRD Study of Solidification/Stabilization of Chromium with Portland Cement and β-C_2S," Journal of Hazardous Materials, Vol. 48, pp. 137-147, 1996.
Macphee, D.E. and Glasser, F.P., "Immobilization Science of Cement Systems," MRS Bulletin, Vol. 18, No. 3, pp. 66-71, 1993.
Pöllmann, H., Kuzel, H.-J., and Wenda, R., "Compounds with Ettringite Structure," Neues Jahrbuch für Mineralogie, Abhandlungen, Vol. 160, No. 2, pp. 133-158, 1989.
Pöllmann, H., Kuzel, H.-J., and Wenda, R., "Solid Solution of Ettringites. Part II: Incorporation of $B(OH)_4^-$ and CrO_4^{2-} in $3CaO{\cdot}Al_2O_3{\cdot}3CaSO_4{\cdot}32H_2O$," Cement and Concrete Research, Vol. 23, No. 2, pp. 422-430, 1993.
Robins, R.G., "The Stability of Arsenic Bearing Residues," Arsenic Metallurgy Fundamentals and Applications, Reddy, R.G., Hendrix, J.L., and Queneau, P.B., Eds., The Metallurgical Society, Warrendale, PA, pp. 469-488, 1988.
Taylor, M. and Fuessle, R.W., "Stabilization of Arsenic Nonwastewaters," Draft Final Report submitted to Illinois Department of Energy and Natural Resources, Hazardous Waste Research & Information Center, ENR Contract: HWR 92095, Bradley University, Peoria, IL, March 1994.
U.S. EPA, "Synthetic Soil Matrix (SSM-SARM) User's Manual," U.S. Environmental Protection Agency, Risk Reduction Engineering Laboratory, Edison, NJ, December 1988.
Weitzmann, L., "Factors for Selecting Appropriate Solidification/Stabilization Methods," Journal of Hazardous Materials, Vol. 24, pp. 157-168, 1990.
Zamorani, E., and Serrini, G., "Stabilization of Hazardous Inorganic Waste in Cement-Based Matrices," Proceedings, First International Symposium on Cement Industry Solutions to Waste Management, Canadian Portland Cement Association, Calgary, Alberta, Canada, pp. 373-382, October 1992.

USE OF HEAT SIGNATURE IN SOLIDIFICATION TREATABILITY STUDIES

Caijun **SHI**, Julia **STEGEMANN** and Robert **CALDWELL**, Water Technology International Corporation, Burlington, Ontario, Canada

ABSTRACT A computerized Quadrel™ system was used to monitor the setting and structure formation of cement solidified arc furnace dust through the measurement of the adiabatic heat evolution profiles. The setting and structure development of solidified waste could be described using several parameters: initial time of setting; final time of setting, maximum heat evolution rate and total heat evolution. Experimental results indicated that the system could be used for the selection of cementing materials and for the quality control of cement solidified wastes.

Key-words: Arc Furnace Dust, Calorimetry, Heat evolution, Solidification, Structure

INTRODUCTION

The hydration of cementitious materials is accompanied by heat evolution that has been widely used to monitor the hydration and structure formation process of cement concrete [Shi and Day, 1995]. The addition of a waste to cementitious materials usually interferes with the hydration and changes the heat evolution characteristics of cementing materials. Thus, the measurement of heat evolution can be used to monitor the setting and structure development characteristics of solidified wastes. In this study, a computerized Quadrel™ system was used to measure the adiabatic heat evolution of cement solidified arc furnace dust. The purpose of this study was to examine the potential application of this system as a screening test for the selection of cementing materials for the stabilization/solidification of wastes and the quality control of cement solidified wastes.

EXPERIMENTATION

Materials

Two cementitious materials were investigated - alkali-activated slag binder (ASC) and a regular typical Type I portland cement (PC). ASC consisted of 65.9% blast furnace slag, 26.4% hydrated dolomitic lime, 7.7% silica fume and 2% Na_2SiO_3 by mass. The blast furnace slag, hydrated dolomitic lime and silica fume were pre-blended before mixing with the waste. Na_2SiO_3 for the ASC was dissolved in mixing water. The waste was dry electric arc furnace dust (AFD) from a specialty steel production, which contained a high level of B, Cr, Hg, Pb, Ni and Zn. The characteristics of the waste have been described elsewhere [Stegemann, Caldwell and Shi, 1996]. The mixing proportions of different batches are shown in Table 1.

Preparation of Specimens

Solidification mixing was performed at a temperature of 23±2°C using a Hobart mixer. The cementing materials were first mixed with water (for PC) or Na_2SiO_3 solution (for ASC) for approximately 30 seconds first, then with arc furnace dust for approximately 5 minutes. The mixing water was adjusted to produce mixtures with a normal consistency. Once the mixing was finished, the mixtures were cast into plastic cylinder moulds with a diameter of 6 inches and a height of 12 inches, then weighed and placed into a QD0612 Qdrum™ Calorimeter to measure the adiabatic heat signature of the mixtures.

Table 1 Mixing Proportions of Solidified Arc Furnace Dust (by mass)

Batch Symbol	ASC (%)	PC (%)	Arc Furnace Dust (%)	Water to Solid Ratio	Water to Cementing Material Ratio
ASC0	100		0	0.43	0.43
ASC30	70		30	0.35	0.50
ASC60	40		60	0.30	0.75
PC0		100	0	0.28	0.28
PC30		70	30	0.26	0.37
PC60		40	60	0.25	0.63

Measurement and Analysis of Adiabatic Heat Signature (AHS)

The computerized Quadrel™ system, which consists of a Qdrum™ calorimeter, QuadLogger™ datalogger and Quadrel™ software, is described in detail in a published report [Radjy et al, 1995]. The datalogger and calorimeter were programmed before mixing and started recording signals once the specimen was placed into the calorimeter drum. Thus, the first recording started approximately 10 minutes after mixing water or Na_2SiO_3 solution was added to the mixtures. The recording was checked every day and stopped when no significant temperature change was observed. The Quadrel™ software analyzed the recorded results and converted the hydration time into equivalent time at 20°C using a maturity approach [Radjy et al, 1995]. Fig.1 illustrates the determination of some parameters, such as: equivalent initial time of setting (t_{ei}), equivalent final time of setting (t_{ef}) and maximum heat evolution rate (R_{max}) by the Quadrel™ software.

EXPERIMENTAL RESULTS AND DISCUSSIONS

Figure 2-a shows the adiabatic heat evolution of ASC0, ASC30 and ASC60. At early ages, the addition of AFD to ASC decreased the heat of hydration. The higher the AFD content was, the lower the total heat evolution was. The cementing materials in ASC0 released heat quickly before

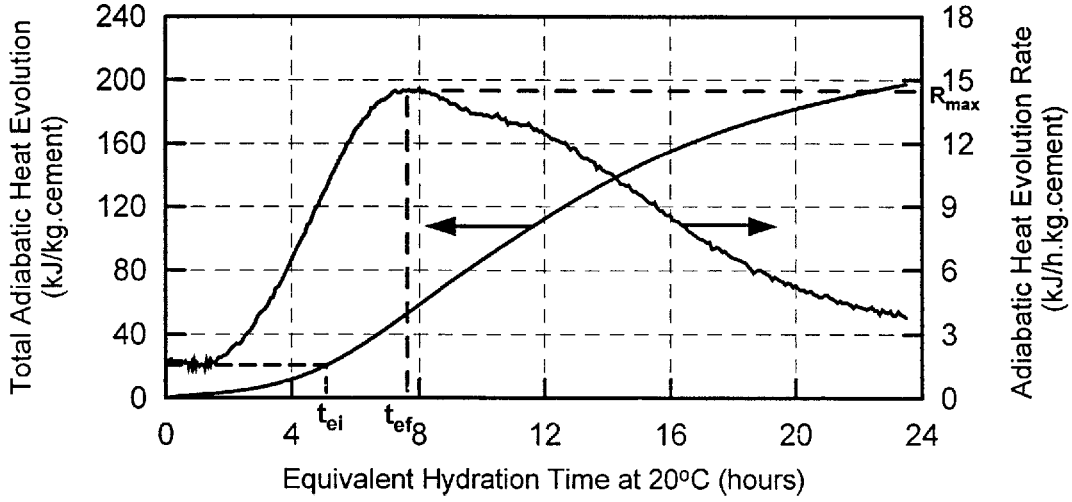

Figure 1 Determination of Setting Times and Maximum Heat Evolution Rate by Quadrel™

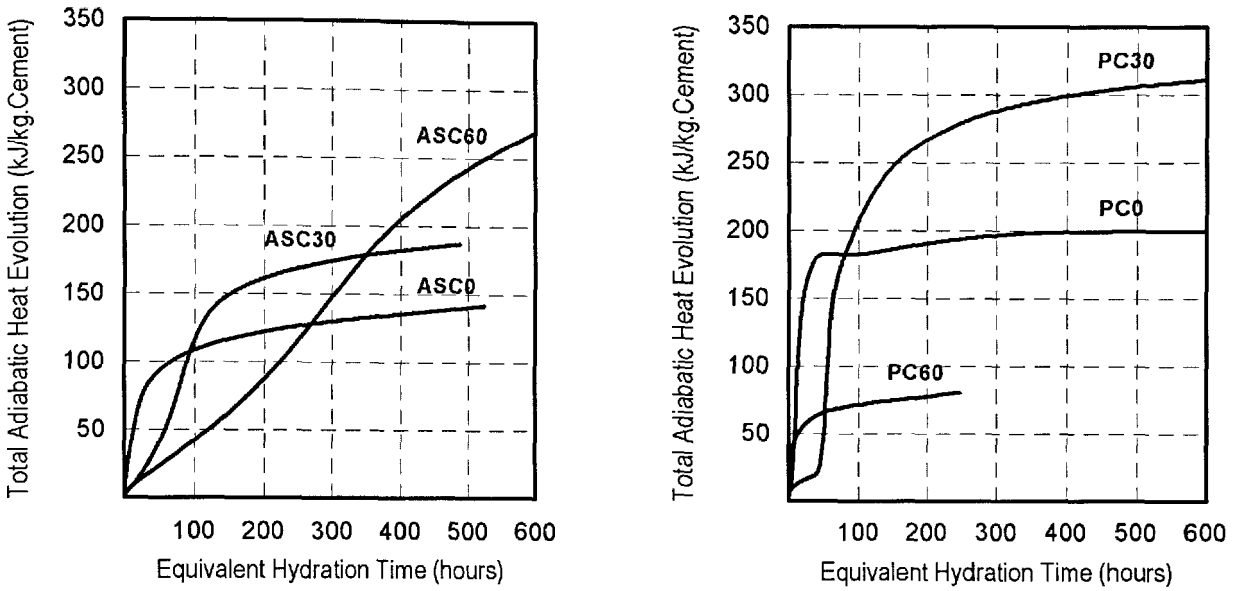

(a) ASC Solidified AFD (b) PC Solidified AFD

Figure 2 Effect of AFD Dosage on Adiabatic Heat Evolution of Solidified AFD

70 equivalent hours and very gradually thereafter. ASC30 and ASC60 released less heat than ASC0 before 70 equivalent hours and continuously released heat at a higher rate than ASC0 thereafter. At approximately 100 equivalent hours, ASC30 released more heat than ASC0. ASC60 released more heat than ASC0 after 260 equivalent hours, and. more heat than ASC30 after 350 equivalent hours. It appeared that the presence of arc furnace dust retarded the early hydration but was beneficial to the later hydration of the slag.

The adiabatic heat evolution curves of PC0, PC30 and PC60 are shown in Figure 2-b. PC0 exhibited a very short induction period at the beginning of hydration, then released heat very vigorously until approximately 40 equivalent hours and reached a plateau thereafter. The appearance of the plateau resulted from the shortage of water for further hydration. According to T. C. Powers' theory [Powers, 1958], the minimum water-to-cement ratio for the complete hydration of portland cement under sealed conditions is 0.42. The water-to-cement ratio in PC0 was only 0.28 and therefore sufficient for 67% cement to hydrate. The release of heat from PC30 was retarded for approximately 50 equivalent hours, and then behaved as PC0. However, PC30 released heat gradually at later ages. Although the water-to-cement ratio in PC30 was 0.35 which theoretically enabled 83% cement to hydrate, no plateau was observed in the heat evolution curve of PC30. PC60 did not exhibit any induction period at the beginning, but had a very brief vigorous release of heat and released much less heat than PC0 and PC30 at later ages. The total released heat is closely related to the degree of hydration and strength of hardened cementing materials [Radjy and Vunic, 1994]. It can be expected that PC60 will not have a dense and strong structure due to only a small portion of portland cement being hydrated.

The curves for heat evolution rates are not presented here due to space limitation. Equivalent times of setting and heat evolution characteristics of all batches are summarized in Table 2. The addition of AFD retarded the initial and final setting of the ASC based mixtures. The higher the AFD content was, the more retarded the setting. The addition of 30% AFD retarded initial and

Table 2 Times of Setting and Heat Evolution Characteristics of Solidified AFD

Batch	t_{ei} (hours)	t_{ef} (hours)	R_{max} (kJ/h.kg.cement)	Q_{28} (kJ/kg.cement)	Q_{90} (kJ/kg.cement)
ASC0	3.5	16.5	2.4	146.1	169.0
ASC30	45.3	83.7	1.8	192.8	206.1
ASC60	144.2	336.8	0.6	398.8	544.7
PC0	6.1	9.3	14.0	199.6	201.4
PC30	45.7	53.8	9.7	313.5	329.0
PC60	1.2	214.2	0.1	87.3	90.3

final setting of PC, while the addition of 60% AFD caused a rapid initial setting and a retarded final setting. As the AFD content increased, it reduced the heat evolution rate of PC much more significantly than that of ASC. The predicted heat evolution at 28 (Q_{28}) and 90 days (Q_{90}) was very consistent with above statement.

From the times of setting and heat evolution characteristics of solidified AFD, it could be seen that the increase in AFD content from 30 to 60% showed a much more significant effect on the hydration of PC than on that of ASC. The rapid initial setting of PC60 will affect the mixing and placing of solidified wastes. It could be concluded that ASC was better than the Type I portland cement for the stabilization/solidification of the AFD and was selected for a field solidification study [Stegemann, Caldwell and Shi, 1996]. Extensive experiments have confirmed that ASC60 shows a very dense and durable structure after 28 days of curing, while PC60 specimens are still very weak and porous after more than one year of curing at room temperatures.

CONCLUSIONS

The Quadrel™ system could monitor and determine the hydration and structure formation of cement solidified wastes using parameters, such as equivalent times of setting, maximum heat evolution rate and total heat evolution. Based on the adiabatic heat evolution measurement, it could be concluded that ASC was better than the commercial Type I portland cement for the stabilization/solidification of the AFD because the former was less sensitive to AFD content than the latter.

REFERENCES

Powers, T. C., Structure and Physical Properties of Hardened Cement Pastes, Journal of American Ceramic Society, Vol.41, No.1, 1958, pp.1-6.

Radjy, F. F. and Vunic, D. W., Heat Signature Testing of Concrete, Proceedings of Structural Materials Technology - An NDT Conference, Atlantic City, Technomic, February, 1994.

Radjy, F. F., Vunic, D. W., Hammons, M. I. and Harrington, P., Development of Automated Concrete Quality Control and Simulation Planning System, prepared for U.S. Army Corps of Engineers, Final Report CPAR-SL-95-1, March 1995.

Shi, C. and Day, R. L., Early Hydration Characteristics of Alkali-Slag Cements, Cement and Concrete Research, Vol.25, No.6, 1995, pp.1333-1346.

Stegemann, J. A., Caldwell, R. J. and Shi, C., (Gilliam, T. M. and Wiles C. C. (Eds)):"Field Validation of Test Methods for Solidified Waste Evaluation - A Status Report", Stabilization and Solidification of Hazardous, Radioactive, and Mixed Wastes, STP 1240, American Society for Testing and Materials, 1996, pp.467-476.

STUDIES ON IMMOBILIZATION OF HEAVY METALS IN CEMENT PASTE - - C-S-H LEACHING BEHAVIOUR

Wiesława NOCUŃ-WCZELIK, University of Mining and Metallurgy, Kraków, Poland
Jan MAŁOLEPSZY, University of Mining and Metallurgy, Kraków, Poland

ABSTRACT The effect of heavy metal containing compounds, such as $Zn(NO_3)_2$, $Pb(NO_3)_2$, $CdCl_2$ and Na_2CrO_4 on the phase composition, microstructure and leaching behaviour of calcium silicate hydrates cured at ambient temperature and in hydrothermal conditions was investigated. In the presence of heavy metal compounds the highly disordered C-S-H formation is accelerated and recrystallization is retarded. A high degree of Zn, Pb and Cd stabilization in C-S-H has been shown; Cr(VI) is immobilized with lower effectiveness.

Key-words: CSH, heavy metals, immobilization, leaching, structure

INTRODUCTION

Application of cementitious systems in heavy metals immobilization has been widely reported for a few years [Glasser 1992, 1994; Grutzeck 1992]. The Cr, Pb, Cd and Zn compounds are succesfully immobilized in normal portlan cement matrix [Reinhardt 1993; Tamas, Csetenyi, Tritthart 1992]. The C-S-H produced as a result of processes occurring in cement pastes plays a decisive role of "cut-off wall" (when cement concrete is used to surround the area of waste storage) or stabilizer (when waste sludge is mixed with cement and thus solidified), forming a physical barrier due to special physical and chemical properties (microstructure, high pH value of residual liquid, high specific surface etc.) [Glasser 1994].

EXPERIMENTAL

Materials

The mixtures of calcium hydroxide (analytically pure), silica-gel (pure) and water with CaO to SiO_2 molar ratio equal to 0.83 and 1.5 respectively were prepared. Apart from the reference samples without admixtures, the following heavy metal containing compounds of analytical purity, calculated as 2 wt.% of anhydrous $CaO+SiO_2$ substance, were introduced to the batches: $Zn(NO_3)_2$, $Pb(NO_3)_2$, $CdCl_2$ and Na_2CrO_4.
The samples, thorougly homogenized with w/c=1.5 were subsequently sealed in polyethylene bags and stored at ambient temperature for several months or subjected to 24 hours thermal treatment in a laboratory autoclave, at 200°C. After treatment the hardened samples were ground and washed with acetone before drying in a laboratory drier (60°C); pieces of fractured samples were kept in acetone for SEM observations.

Methods

The effect of heavy metal compounds on the phase composition of hydrating mixtures was studied by XRD, DTA and TG analysis (determination of bound water content and carbonates). The microstructure was characterized through the SEM observations and EDS measurements. The leaching behaviour of calcium silicate hydrates cured at ambient temperature as well as in hydrothermal conditions was investigated on the leachates obtained by the liquid phase separation from the suspensions prepared at water to solid ratio of 50 - the powdered samples were mixed with water and shaken for 1 hour period. Finally, the silicate anion structure before and after the lixiviation was evaluated by the molybdate complexing method [Thilo, Wieker, Stade 1965].

RESULTS - CaO/SiO_2=0.83

Results from the XRD and DTA-TG experiments, at ambient temperature, in the presence of heavy metal compounds show that a highly disordered C-S-H formation is accelerated, but the transformation of the structure or its recrystallization during hydrothermal treatment is retarded. The strong peaks corresponding to d=0.307nm (nearly amorphous C-S-H) and d=0.490; 0.2628nm ($Ca(OH)_2$)are visible on XRD patterns of the samples stored at room temperature. The patterns for the autoclaved samples show no $Ca(OH)_2$ peaks and some further small ones attributed to the calcium silicate hydrate C-S-H (see Fig.1). Only in two cases: the product without additive and that synthesized with $Pb(NO_3)_2$, the 1.1nm peaks corresponded to the more ordered, tobermorite-like structure: these two materials seem to be better crystallized.

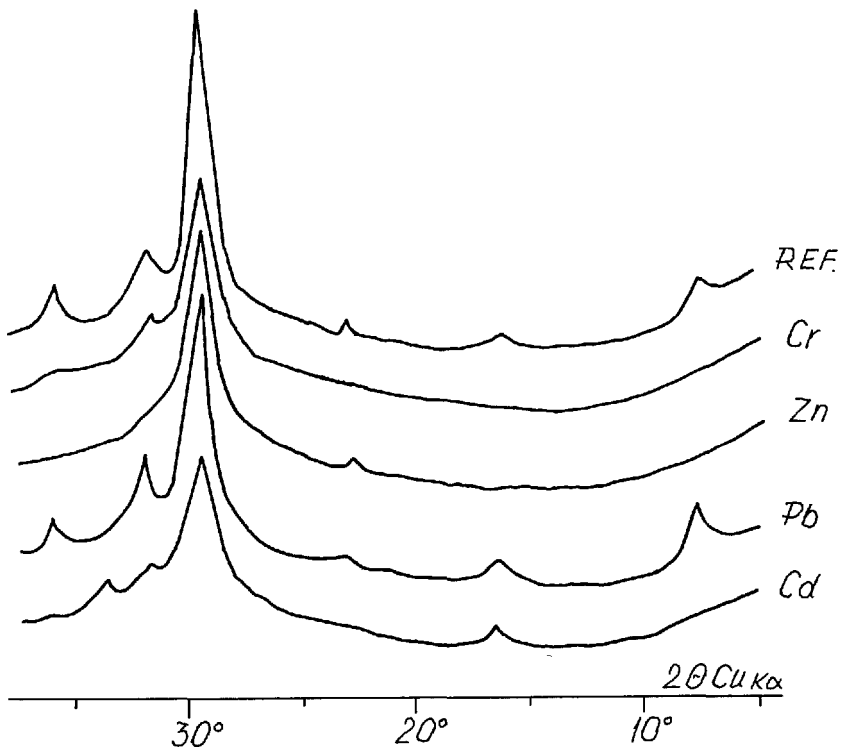

Figure 1 XRD patterns of the autoclaved samples (200°C/24h). CaO/SiO_2=0.83.

Results from the DTA-TG measurements given in Table 1, disclose thet samples synthesized at room temperature with heavy metal compounds have higher water release contents during C-S-H decomposition in the range 100-200°C and simultaneously lower $Ca(OH)_2$ contents.

Table 1 Results of DTA-TG studies. CaO/SiO_2=0.83.

Sample	Reference	Na_2CrO_4	$Zn(NO_3)_2$	$Pb(NO_3)_2$	$CdCl_2$
cured at room temperature for 6 months					
H_2O in C-S-H	8,9 %	13,6 %	13,6 %	12,6 %	13,9 %
$Ca(OH)_2$	13,5 %	10,0 %	2,0 %	5,2 %	3,0 %
$CaCO_3$	14,9 %	9,2 %	12,7 %	3,2 %	17,5 %
autoclaved 200°C/24 hours					
H_2O in C-S-H	8,3 %	14,9 %	10,0 %	10,3 %	11,0 %

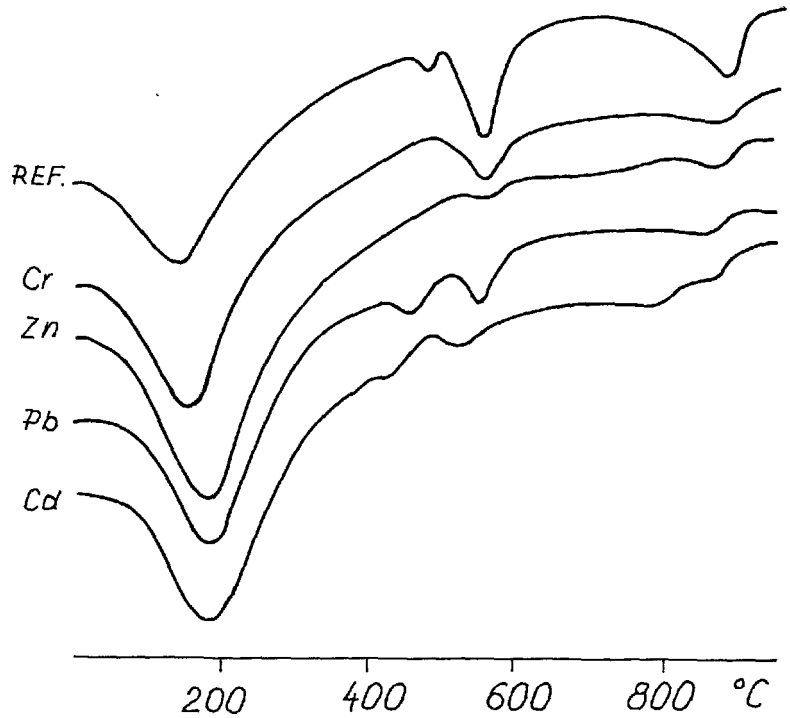

Figure 2 DTA curves for the samples cured at room temperature for 6 months. C/S=0.83.

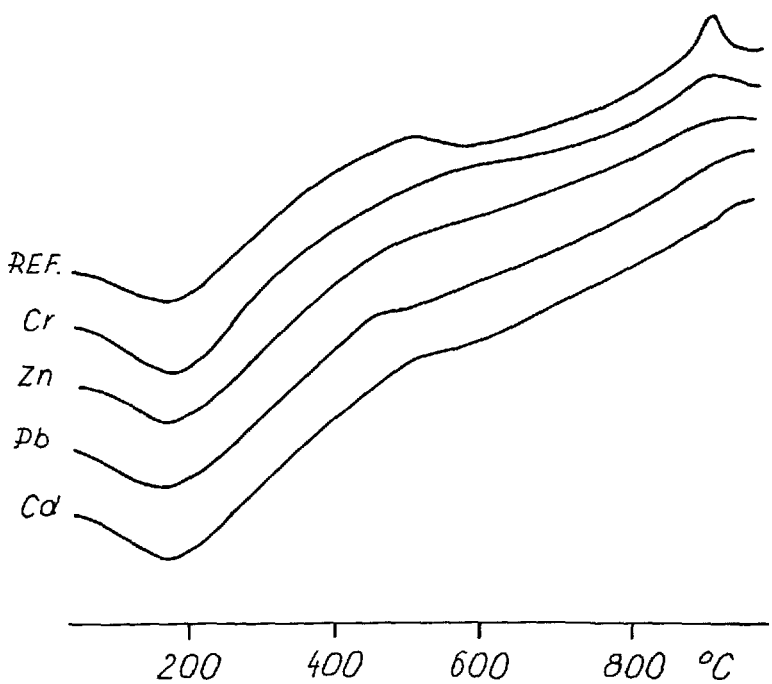

Figure 3 DTA curves for the samples autoclaved at 200°C/24h. C/S=0.83.

There are also some small effects which can be attributed to the decomposition of the heavy metal hydroxides and salts (see Fig.2), not detectable by XRD. The DTA curves for the autoclaved samples show only the dehydration effect at 100-200°C (see Fig.3). Up to about 800°C the curves exhibit no peaks - which would suggest that the calcium hydroxide and

additives have been totally consumed and incorporated to the structure of calcium silicate hydrates. Only in the cases of the sample with no admixture and that of Na_2CrO_4 the peak usually attributed to wollastonite synthesis is visible. This may mean that some amount of the chain silicate anions has been formed in in the precursor hydrates. The autoclaved calcium silicate hydrates doped with heavy metal compounds, as well as those cured at ambient temperature, show a significantly higher water content. This may be as a consequence of their highly disordered, more "open" structures. The samples stored for a long time at room temperature also show the presence of carbonates (DTA - TG results) but it is rather difficult to find a relationship between the admixture, calcium hydroxide and carbonate contents. The CO_2 content in the sample with $Pb(NO_3)_2$ is the lowest.

Results from the SEM observations, which were the subject of a more detailed report [Nocuń-Wczelik, Trybalska and Rakowska 1994], show that the C-S-H phase produced with heavy metal compounds is generally poorly crystallized, composed of small grains or flakes. The autoclaved material with no admixtures shows the presence of well developed plate-like and lath-like morphologies. A similar morphology is observed also in the autoclaved material with Pb compound. The examples of microstructures are presented in Figs 4 and 5.

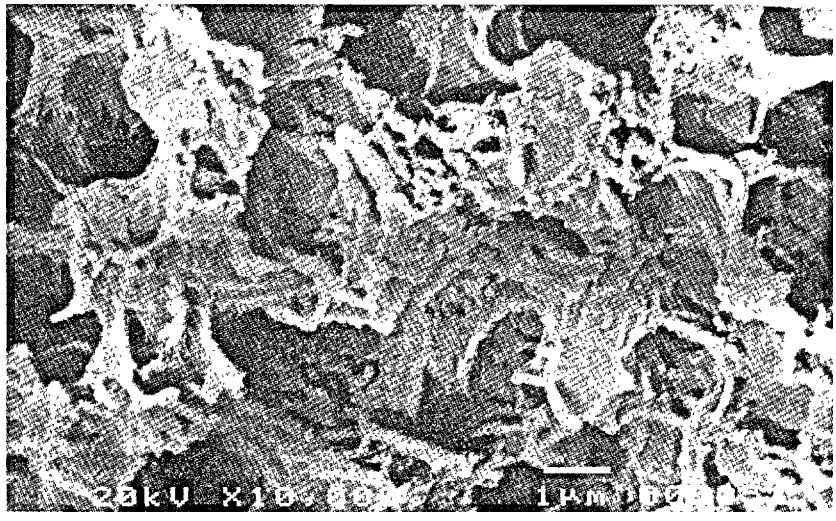

Figure 4 SEM. Microstructure of autoclaved (200°C/24h) sample. 2% $Zn(NO_3)_2$. C/S=0.83.

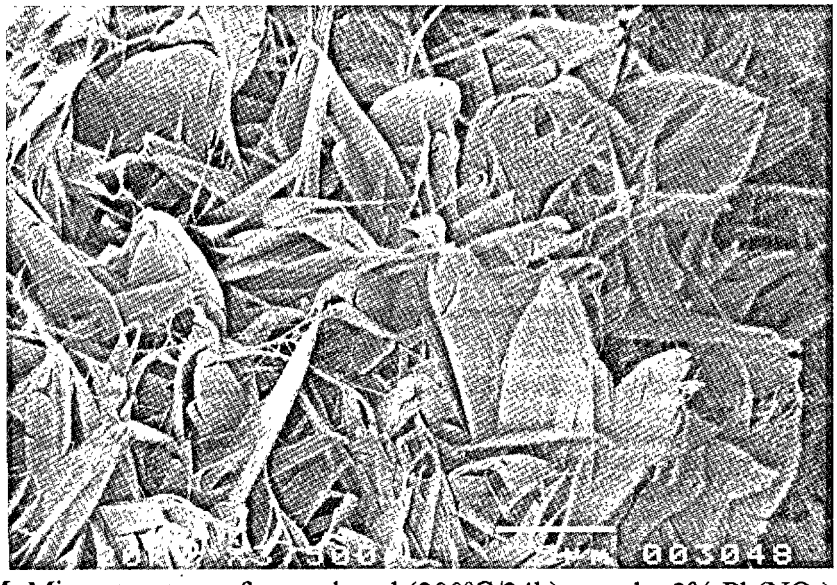

Figure 5 SEM. Microstructure of autoclaved (200°C/24h) sample. 2% $Pb(NO_3)_2$. C/S=0.83.

The EDS studies showed the homogenous distribution of the metallic elements introduced with admixtures.
The results of leaching tests are shown in Table.2. The high degree of Zn, Pb and Cd stabilization (exceeding 99.8%) in C-S-H formed both at room temperature and in hydrothermal conditions has been shown; Cr(VI) is immobilized with lower effectiveness.

Table 2 Results of leaching tests. Water to solid =50. CaO/SiO_2=0.83.

Sample curing	Cr [immobilized]	Zn [immobilized]	Pb [immobilized]	Cd [immobilized]
20°C/6 months	95,15% (498 ppm)	99,91% (48 ppm)	99,87% (138 ppm)	99,97% (18 ppm)
200°C/24h	95,85% (451 ppm)	99,96% (28 ppm)	99,97% (34 ppm)	99,96% (23ppm)

RESULTS - CaO/SiO_2=1.50

In all the samples cured at room temperature, irrespectively of the additive used, the strong d=0.307 nm peaks corresponding to the poorly crystallized C-S-H are observed, together with the strong d=0.490; 0.2628 nm peaks of unreacted calcium hydroxide. The XRD patterns are very similar. In the autoclaved samples (200°C/24h) the tobermorite occurring together with C-S-H (I) are found. This C-S-H shows a significantly ordered structure as it can be derived from the sharp peak d=1.25 nm. Only in the sample with Na_2CrO_4 can unreacted $Ca(OH)_2$ be detected by XRD. Analyzing the XRD data one also notes that the structural order slightly decreases from the sample without admixture and with $Zn(NO_3)_2$ through those with $CdCl_2$ and $Pb(NO_3)_2$ to the Na_2CrO_4 doped hydrating mixture respectively (see Fig.6). In both series of samples, neither the admixture nor the other phases formed with these admixture were detected by XRD. The presence of $CaCO_3$ cannot be totally excluded because of the coincidence of carbonate peaks with those of C-S-H and $Ca(OH)_2$.

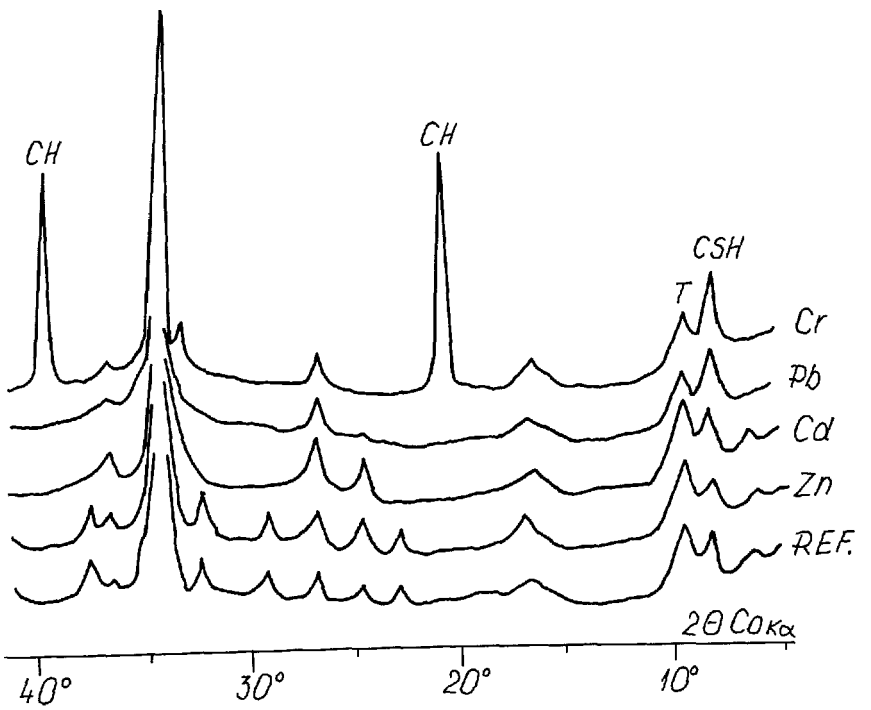

Figure 6 XRD patterns of the autoclaved samples (200°C/24h). CaO/SiO_2=1.50.

The DTA-TG measurements add some new information to the results. On the DTA curves the peaks of hydrate decomposition in the range up to over 200°C, as well as the peaks corresponding to the calcium hydroxide dehydration at 400-600°C and those relating to the $CaCO_3$ decarbonation are visible. On the basis of the TG results the bound water, calcium hydroxide and carbonate contents were calculated (Table 3).

Table 3 Results of DTA-TG studies. CaO/SiO_2=1.50.

Sample	Reference	Na_2CrO_4	$Zn(NO_3)_2$	$Pb(NO_3)_2$	$CdCl_2$
cured at room temperature for 9 months					
H_2O in C-S-H	3,8 %	3,6 %	5,2 %	5,3 %	4,7
$Ca(OH)_2$	10,5 %	8,2 %	3,3 %	6,2 %	7,8 %
$CaCO_3$	7,1 %	14,1 %	12,9 %	10,8 %	10,9 %
autoclaved 200°C/24 hours					
H_2O in C-S-H	1,0 %	0,9 %	0,9 %	4,2 %	2,3 %
$Ca(OH)_2$	-	1,8 %	-	-	-
$CaCO_3$	4,2 %	3,6 %	2,2 %	2,3 %	4,5 %

The sample without admixture, stored at room temperature has the highest $Ca(OH)_2$ content. In the admixtured samples the amounts of unreacted hydroxide are lower but the contents of carbonate increase, presumably in finely dispersed form, as one can conclude from the lowered decomposition temperature. The formation of carbonates with cations introduced to the mixtures cannot be excluded. Undoubtedly, the presence of accompanying acid anions promotes the carbonation of pastes [Fournier, Fournier, Bellaoui, Pit 1995]. The TG studies confirm that the calcium hydroxide is consumed in hydrothermal conditions; apart from the sample with Na_2CrO_4, the carbonation is low.

From the SEM observations, the C-S-H phase produced with heavy metal compounds at room temperature is poorly crystallized, composed of sponge-like aggregates and crumblyd flakes. The autoclaved material with and without admixtures shows more or less platelike and fibrous morphologies (C-S-H, tobermorite); an example of microstructure is given in Fig 7.

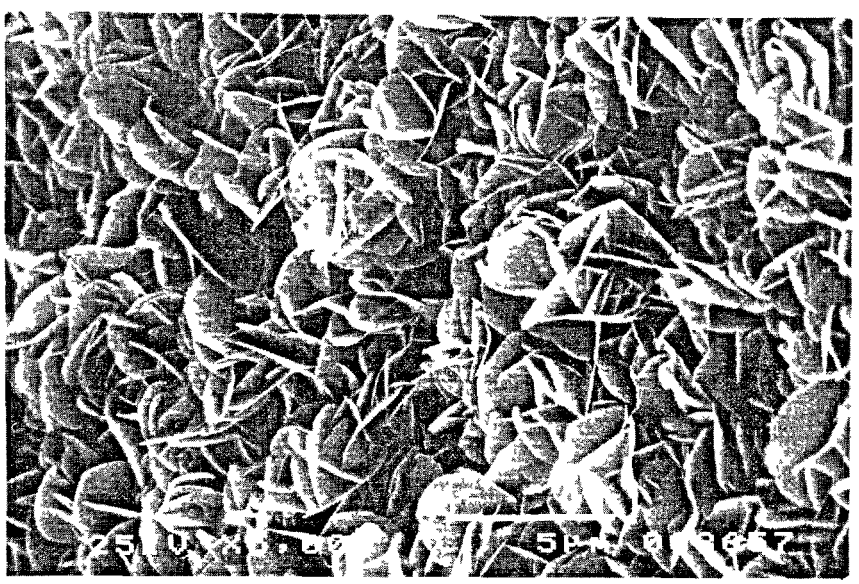

Figure 7 SEM. Microstructure of autoclaved (200°C/24h) sample. 2% $CdCl_2$. C/S=1.50.

The results of leaching tests are shown in Table.4. The high degree of Zn, Pb and Cd stabilization (exceeding 99.8%) in C-S-H formed both at room temperature and in hydrothermal conditions has been shown; as one could expect Cr(VI) is immobilized with lower effectiveness. These data are in good agreement with the earlier results and reports.

Table 4 Results of leaching tests. Water to solid=50. CaO/SiO_2=1.50.

Sample curing	Cr [immobilized]	Zn [immobilized]	Pb [immobilized]	Cd [immobilized]
20°C/9 months	83,28% (20 ppm)	99,99% (11 ppm)	99,96% (54 ppm)	99,99% (7 ppm)
200°C/24h	81,83% (22 ppm)	99,93% (89 ppm)	99,96% (44 ppm)	99,98% (138 ppm)

For the series of samples cured at room temperature the degree of silicate anion condensation before and after leaching was evaluated by the molybdate complexing method and plotted in Figs 8 and 9 as percentage of silica complexed vs. time.

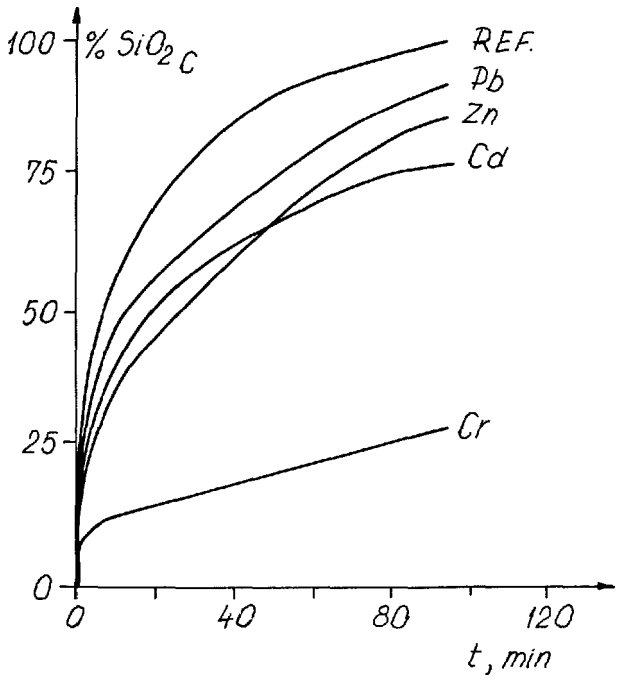

Figure 8 Molybdate complexing curves. CaO/SiO_2=1.50. 20°C/9 months. Before leaching.

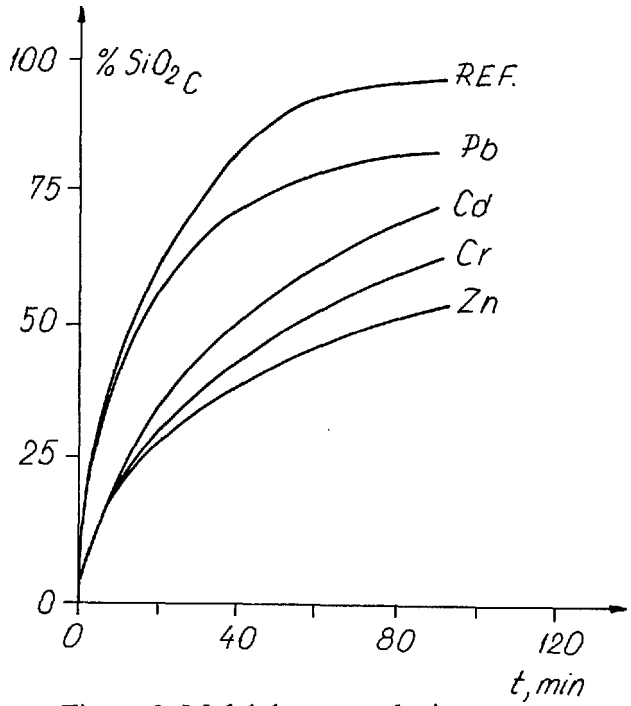

Figure 9 Molybdate complexing curves. CaO/SiO_2=1.50. 200°/24h. After leaching.

The results of the molybdate complexing studies can be summarized as follows:
- the admixtures introduced to the hydrating batch bring about an increase in the fraction with higher silicate anion condensation degree: this effect is particularly strong for the sample with Na_2CrO_4,
- the lixiviation by water destroys the structures formed on hydration, the changes observed for the reference sample with no admixture are not so evident as for the other samples,
- in the samples produced with $Zn(NO_3)_2$, $Pb(NO_3)_2$ and $CdCl_2$ the condensation of the silicate anion after leaching is generally observed; in turn, the silicate anion structure in the presence of Na_2CrO_4 decomposes on leaching.

The course of molybdate complexing curves depends on many factors. The admixtures introduced to the hydrating mixtures play a decisive role. The higher condensation degree in

the presence of admixtures results from the better dissolution of initial components and acceleration of calcium silicate hydrates formation; the carbonation of paste favourizes also this process. Subsequently, the mobile, acidic anions accompanying the cations immobilized as hydroxide or complex compounds in the matrix, are removed on leaching from the pore water or from the structure, thus promoting the condensation. The reverse situation in the presence of Na_2CrO_4 can be explained by the presence of sodium cations which strongly accelerate the dissolution of silicate component during the formation of hydrates and the simultaneous action of chromate components reinforcing the polymerized structure. This "competition" mechanism results in the condensation degree decrease on leaching.

CONCLUSIONS

1. Calcium silicate hydrates formed at room temperature in the presence of heavy metal compounds are poorly crystallized; admixtures accelerate the calcium hydroxide consumption and carbonation of pastes.
2. The silicate anion structure is significantly affected by the presence of heavy metal compounds - the fraction of high condensation degree increases.
3. In hydrothermal conditions the crystallization of hydrates is accelerated but generally the retarding action of heavy metal compounds on the structural transition to more ordered forms is observed.
4. Zn, Pd and Cd are immobilized in C-S-H with very high, exceeding 99.8% effectiveness, irrespectively of curing conditions and CaO/SiO_2 ratio in the matrix. Cr (VI) is immobilized with lower effectiveness. The degree of Cr immobilization becomes lower as CaO/SiO_2 ratio in C-S-H increases from 0.83 to 1.50.

REFERENCES

Fournier, P.G., Fournier, J., Bellaoui, B., Pit, R., "Effet du pH sur les resultats de lixiviation", C.R.Acad. Sci. Paris, Vol. 320, II, 1995, pp.43-50.

Glasser, F.P., "Progress in the Immobilization of Active Wastes in Cement", Cem.Concr.Res., Vol. 22, No2/3, 1992, pp.201-216.

Glasser, F.P., "Immobilisation Potential of Cementitious Materials", Environmental Aspects of Construction with Waste Materials", ed. J.J.J.M. Goumans, H.A. van der Sloot and Th.G.Aalbers, Elsevier Science Publishers, Amsterdam, 1994, pp.77-86.

Grutzeck, M.W., "Hazardous Waste (Organic, Heavy Metal): Cement Disposal", Proc. 9th Int.Congr.on the Chemistry of Cements, Vol.VI, New Delhi, 1992, pp.119-124.

Nocuń-Wczelik, W., Trybalska, B., Rakowska, A., "The Microstructure of C-S-H Formed in the Presence of Heavy Metal Compounds", Ceramics 46, 1994, Polish Ceramic Bulletin 8, ed. Polish Academy of Science - Kraków Division, Papers of the Commissions on Ceramic Science - Polish Ceramic Society, pp.289-291 (in Polish).

Reinhardt, H.W., "Entsorgung und Bindung von Schadstoffe mit Zement und Beton. Theoretisch Grundlagen und internationaler Stand des Wissens", Zement und Beton, 1993, pp.2-6.

Tamas, F.D., Csetenyi, L., Tritthart, J., "Effect of Adsorbents on the Leachability of Cement Bonded Electroplastic Wastes", Cem.Concr.Res., Vol. 22, No2/3, 1992, pp.399-405.

Thilo, E., Wieker, W., Stade, H., "Uber Beziehungen zwischen dem Polymerisationsgrad silicatischer Anionen und ihrem Reaktionsvermogen mit Molybdansaure", Zeitschrift fur anorg. und allg. Chemie, Vol.340, No 5/6, 1965, pp.261-276.

APPLICATION OF PORTLAND CEMENT AND HIGH ALUMINA CEMENT FOR IMMOBILIZATION/SOLIDIFICATION OF A WASTE MODEL COMPOSITION

RISCH, A., Department of Mineralogy, University of Erlangen, Germany
POELLMANN, H., Department of Mineralogy and Geochemistry, University of Halle, Germany
ECKER, M., Bilfinger&Berger Umweltverfahrenstechnik GmbH, Mannheim, Germany

ABSTRACT

Samples containing HAC, OPC, and different aggregates were mixed with a composition of different pollutants. The long term physico-chemical stability was investigated by a weathering cycle lasting five month. The development of strength, further phase crystallization, elution behavior, structural change and element distribution on the surface was evaluated. The results are giving a good stability for waste immobilizates in different solution when the mixtures are attuned for specific applications.

Key-Words: Immobilization; solidification; life cycle analysis; leaching; heavy metals;

INTRODUCTION

The accumulation of polluted, non-reusable industrial waste products (flue gas desulfurization products, fly-ashes (PFA), contaminated sludge etc.) requires environmentally acceptable disposals. Immobilization and solidification of these pollutants can be achieved by adding cement to the waste products or by mixing adequate proportions of different industrial waste products. The resulting stabilized product of this treatment is containing different reservoir minerals (AFm phases, AFt phases) intimately intergrown with non reactive material. The solidified waste containing the immobilized pollutants itself can be used as an „Inner Barrier System" of a waste dump. For this application the immobilizates have to be resistant against atmospheric conditions and also have to be stable under the geochemical conditions in the waste dump.

Object of this study was the investigation of two different cement mixtures with the same content of pollutants, which comply with the requirements of homogenizing, with the specifications of the pollutants and aggregates, specific gravity and strength, and to determine if further crystallization of phases occurs.

Both mixtures were classified according to the German environmental legislation „TA-Siedlungsabfall" with three different elution processes.

In the next step the physico-chemical long term stability of the solidified waste products was evaluated. Therefore the weathering conditions in a waste dump were simulated by a five month weathering cycle (Fig. 1).

In the course of weathering, phase changes and structural changes occur: strength, leaching and the distribution of environmentally relevant elements on the surface of the immobilizates was observed.

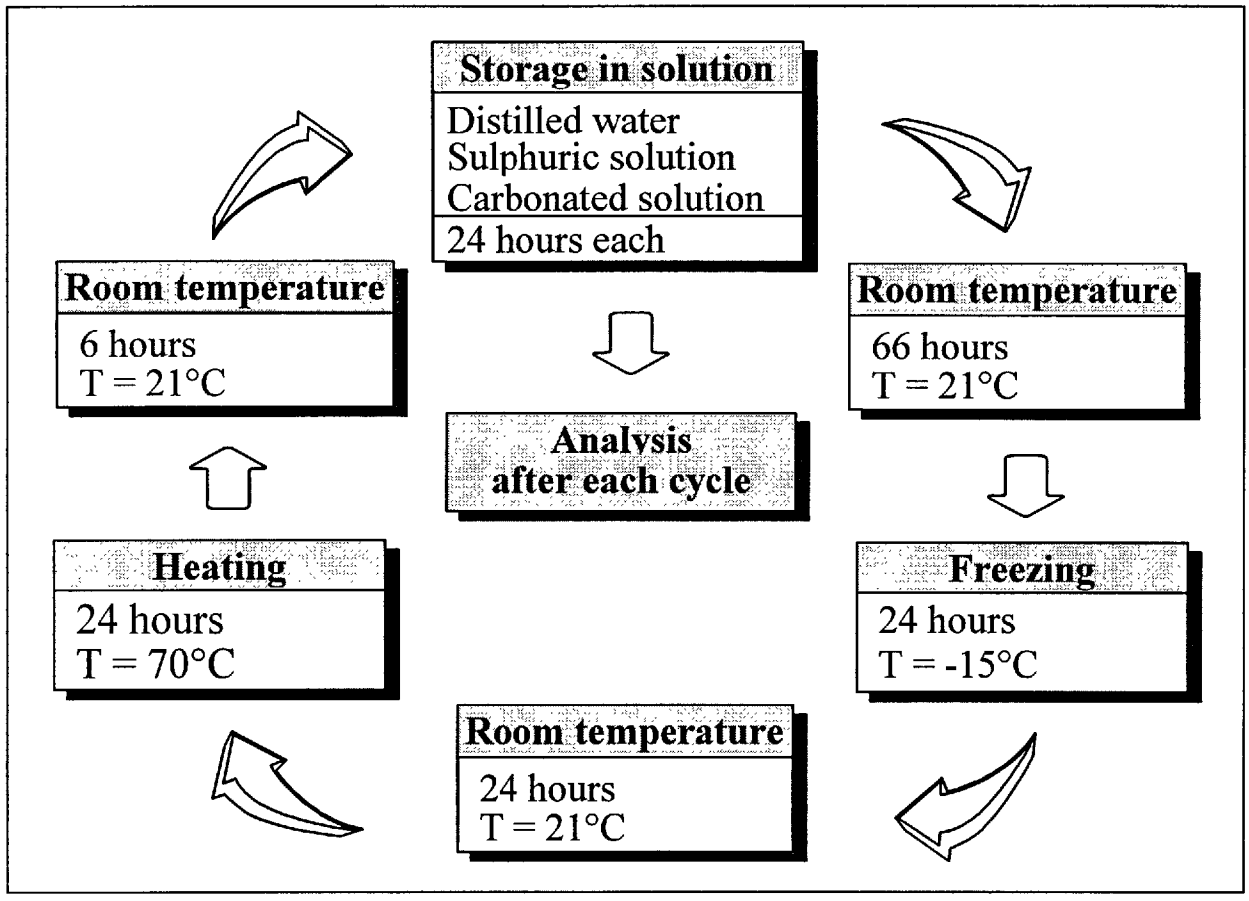

Figure 1: Weathering cycle

EXPERIMENTAL

After investigation of different mixtures in an accelerated weathering test, only two stabilized waste products (enough strength for further studies) could be formulated: one consisting a Portland cement - High alumina cement mixture with the ratio 1:1 (*HAC/OPC-mixture)* and the other using only High alumina cement (*HAC-mixture*). Quartz sand was used as filling material. In order to increase strength, part of cement was substituted by PFA. The pollutant content of 20% was achieved by adding a mixture of calcium chromate, cadmium sulfate, copper sulfate, lead sulfate (poorly soluble) and sodium hydrogen arsenate. The water/cement-ratio for each sample was 0.6 (Table 1).

The constituents were mixed in a concrete standard mixer with water for 10 minutes. The mass was filled into a standard mortar prism with 4*4*16 [cm]. The consolidation and degasing was done with a table vibrator. The prism was cut with a diamond saw cooled with isopropanol to get a 4*4*4 [cm] sized cube. The heating and freezing time during the five month weathering cycle was realized in a climatic cabinet under atmospheric conditions; storage in solution (sample weight/solution volume = 1/10) was investigated with three different solvents:

- distilled water
- saturated CO_2-solution (pH=4-4,5)
- H_2SO_4-solution (starting pH=4)

The solvents were renewed after each weathering cycle.

Table 1: Composition of the samples

Constituents	HAC-mixture weight- [%]	HAC/OPC-mixture weight- [%]	
High alumina cement	30	16,5	**Cement**
Portland cement		16,5	
PFA	20	20	**Aggregates**
Quartz sand	20	20	
CaO	10	7	
$CaCrO_4$	5	5	**Pollutants**
$CuSO_4 \cdot 5H_2O$	5	5	
$CdSO_4$	2,5	2,5	
$CdCl_2$	2,5	2,5	
$PbSO_4$	3	3	
Na_2HasO_4	2	2	
w/c-ratio	0,6	0,6	

RESULTS

XRD-Analysis

In both mixtures a similar phase formation was observed after seven days hydration time: AFt phases, AFm phases, and calcite could be determined beside the added quartz. Reflection lines of remaining alite occur in the *HAC/OPC-mixture*.

In course of weathering alite in the *HAC/OPC-mixture* reacts to give CSH-phases. The amount of AFt-phases increases inside the *HAC-sample*, when delayed crystallization of ettringite leads to cracking. Additionally the penetrated solution causes formation of calcite in the cracks.

In the *HAC/OPC-mixture*, cracking could not be observed; because of the lower amount of aluminate phases, less AFm and AFt phases formed, and alite persisted.

The XRD of the surface showed mainly calcite as the detectable product in all of the specimens examined (Figs. 2 and 3).

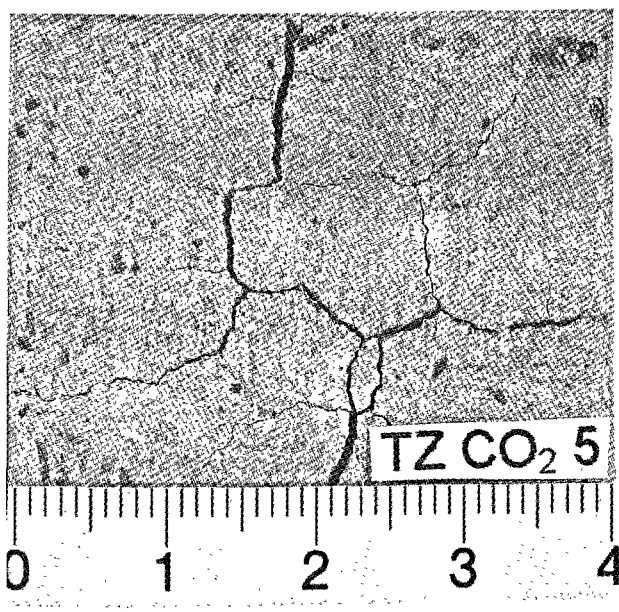

Figure 2: Cracking by the HAC-mixture after five month weathering with CO_2-solution

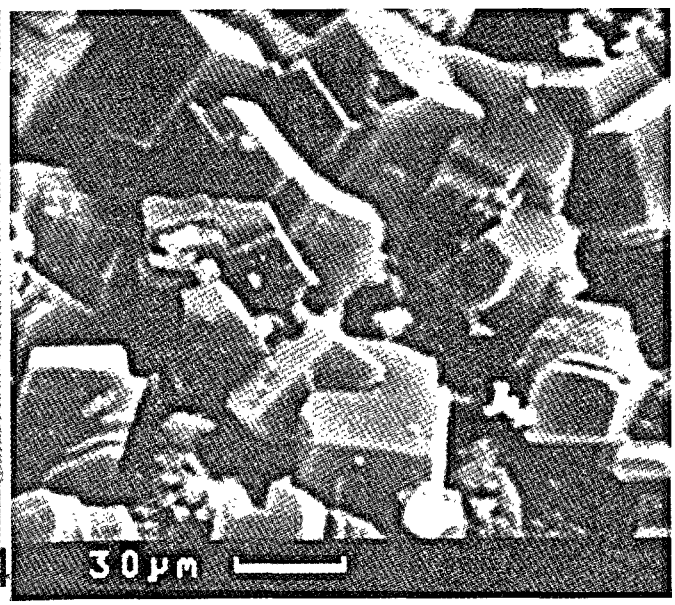

Figure 3: Calcite at the surface of the HAC-mixture

Transmitted-light microscopy, EDX-Detection

The microstructural analysis by transmitted-light microscopy showed the effects of weathering in the surface region (Fig. 4) of both different mixtures. The effects are nearly independent of the way the samples were stored in solution. On the surface, a covering layer (calcite) with the dimension of 0.5 [mm] was determined; beneath lies a leached zone (1 [mm]). In the deeper parts the matrix of both mixtures were not influenced by weathering.

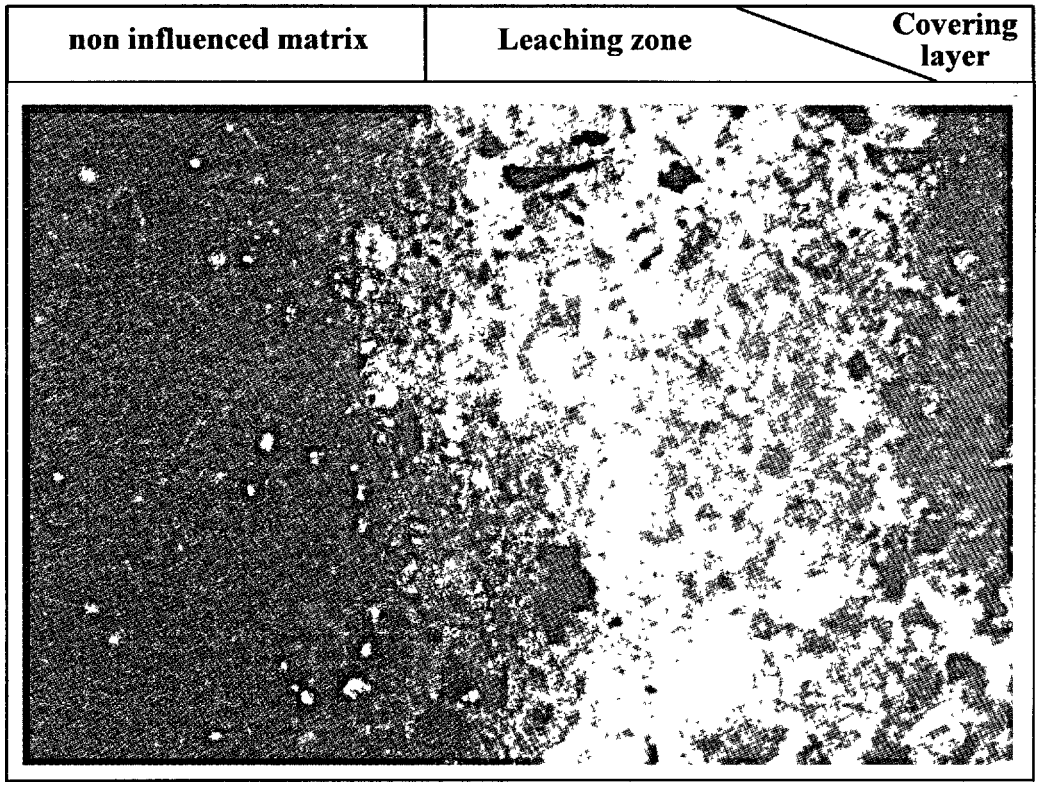

Figure 4: Transmitted-light microscopy of the HAC-mixture after five month weathering with saturated CO_2-solution; image width: 3 [mm]

The transmitted-light-microscopy-samples were also used to investigate the distribution of the environmentally-relevant elements in the surface by EDX-detection.

Sulfur and heavy metals are depleted in the covering layer. Calcium, carbon and oxygen are enriched in these region. In the transition between the covering layer and unaltered matrix the distribution of the elements is reversed: calcium, carbon and oxygen are depleted while sulfur and the heavy metals are enriched.

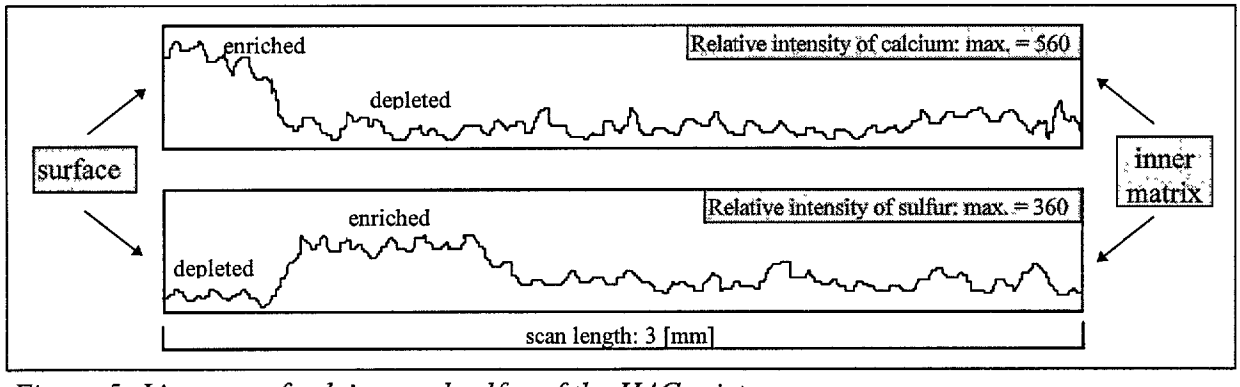

Figure 5: Linescan of calcium and sulfur of the HAC-mixture

Strength development

The compressive strength of the two specimen types depends on the composition of the mixtures and on the type of leachant solution. After five month the *HAC-mixtures* had lost about 25% of its 7 day strength during storage in sulfuric and in carbonated solution. No further reduction in strength was found by storing in distilled water. The decrease of strength results from cracking the *HAC-mixtures* by delayed crystallization of ettringite combined with thermal cycling: freezing and thawing.

The 7 day strength of the *HAC/OPC-mixtures* reached with 20 [N/mm^2] the same value as the *HAC-mixtures*. After five month weathering the cubes showed a corresponding high strength: between 24 and 29 [N/mm^2]. The reaction of remaining alite to CSH-phases during weathering could be responsible for the increased strength and for compensating the effects of thermal cycling (Table 2, Fig. 6).

Table 2: Development of compressive strength after five month weathering (5 measurements per specimen; maximum deviation from average value for each sample: 1.8 [N/mm^2])

HAC-mixture			
7 day strength	**sulfuric solution**	**carbonated solution**	**distilled water**
20 [N/mm^2]	16 [N/mm^2]	15 [N/mm^2]	19 [N/mm^2]
HAC/OPC-mixture			
7 day strength	**sulfuric solution**	**carbonated solution**	**distilled water**
20 [N/mm^2]	29 [N/mm^2]	25 [N/mm^2]	24 [N/mm^2]

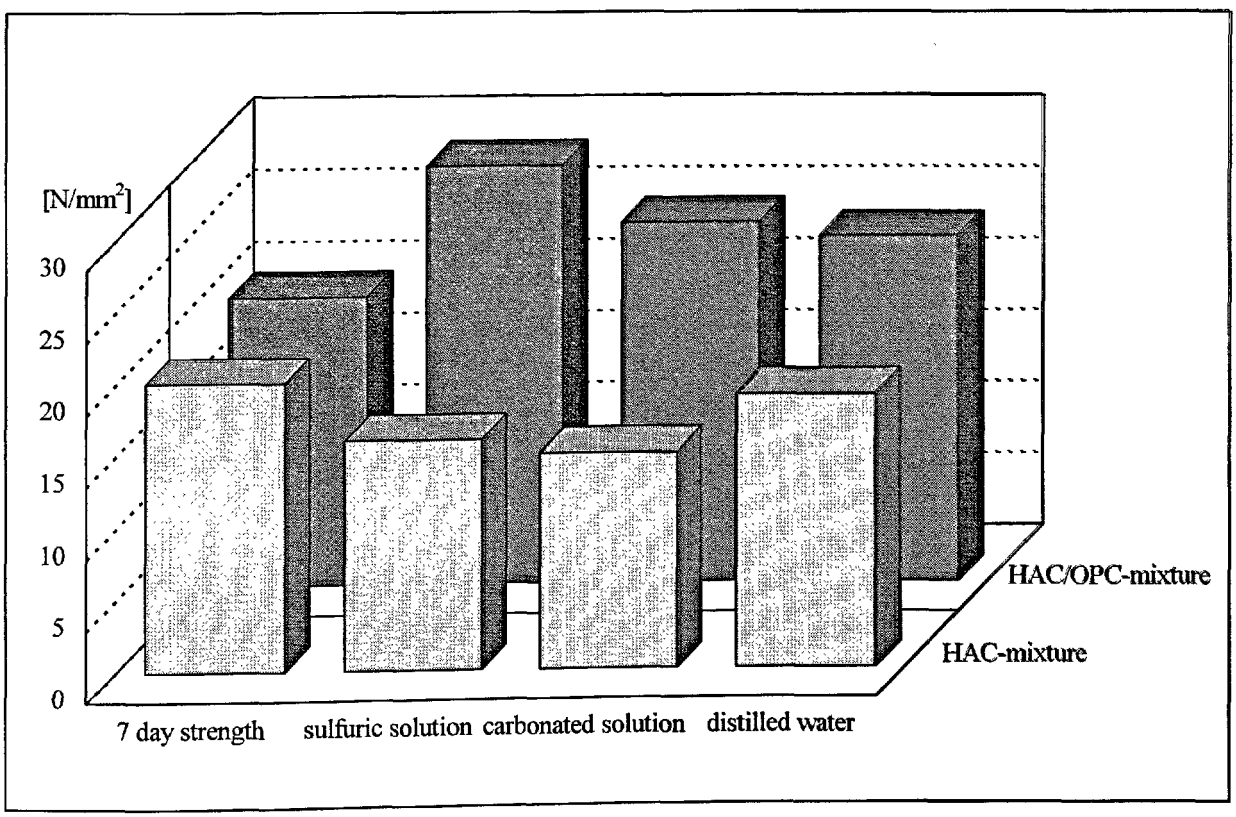

Figure 6: Compressive strength after five month weathering

Elution behavior

The measurement of pollutants in solution during the five month weathering cycle showed the maximum concentration of leached elements in this period of time. As well the elution behavior as a function of weathering time could be observed. The measured concentrations ([mg/l]) of the different elements after each storage in solution were compared to the limiting values of the German environmental legislation „TA-Siedlungsabfall". This legislation regulates the limit values of waste deposits to classify different „deposit classes".

In the course of weathering the determined concentrations of arsenic are in accordance with the requirements for „deposit class 1" for both mixtures stored in distilled water, sulfuric solution and carbonated solution (Table 3). By elution with sulfuric solution and distilled water the copper concentrations lie within the limits of „deposit class 1" and cadmium within the limits of „deposit class 2". Both elements could not fulfill the requirements for „deposit class 2" by storing in carbonated solution. Chromium(VI) was never below the limiting values of the legislation after storing in any solution. The immobilization of Chromium(VI) in AFm phases was hindered, caused by the insufficient homogenizing and the great agglomeration of added calcium chromate during mixing the specimens.

Table 3: Evaluation of the leached elements

Elements	German legislation [mg/l]		This study
	„deposit class 1"	„deposit class 2"	
Chromium(VI)	0.05	0.1	higher values
Cadmium	0.05	0.1	lower „deposit class 2" except carbonated solution
Copper	1	5	lower „deposit class 1" except carbonated solution
Arsenic	0.2	0.5	lower values

Generally the *HAC-mixture* showed higher leaching values than the *HAC/OPC-mixture*. During weathering, carbonation of the *HAC/OPC-sample* surfaces caused a conspicuous reduction of elution (Fig. 7). This reduction could not be observed for the *HAC-mixture*. The formation of cracks regards a higher soluble surface and therefore leaching values did not decrease.

A model calculation for a weathering depth of 2 [mm] (transmitted-light microscopy) demonstrated, that in the *HAC-mixture* only 0.15% and in the *HAC/OPC-mixture* 0.10% of the added pollutants were totally leached during weathering time.

The process of leaching Chromium(VI) with carbonated solution as a function of time is plotted for both mixtures in Fig. 7. The initial leaching values are equal for both samples. A decrease caused by carbonation can be observed in the first 5 weeks by weathering the *HAC/OPC-mixture* and after 10 weeks for the *HAC-mixture*. Increasing Chromium(VI) concentrations after 12 weeks are due to the formation of cracks in the *HAC-sample*. The Chromium(VI) leaching concentrations of the *HAC/OPC-mixture* after 6 weeks of weathering are nearly constant.

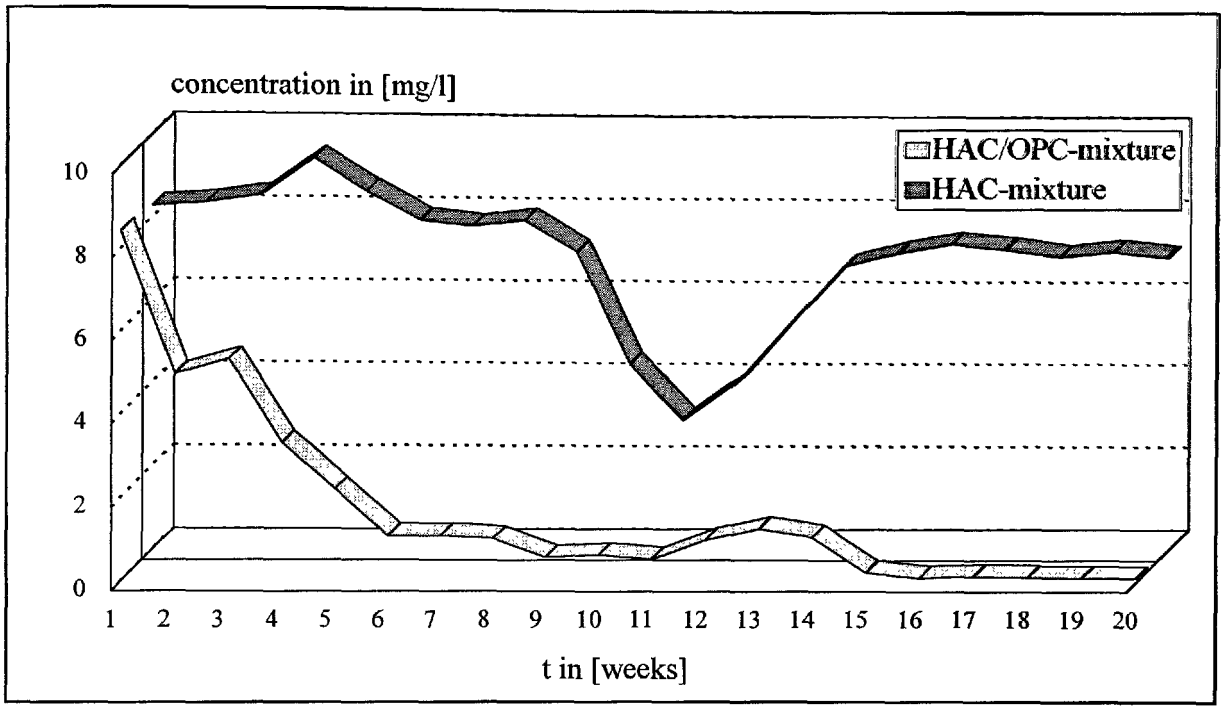

Figure 7: Elution behavior of Chromium(VI) stored in carbonated solution

DISCUSSION OF THE RESULTS

The influence of atmospheric and geochemical conditions in a waste dump on the stability of a immobilized waste model composition based on OPC and HAC has been investigated. The results give a good stability for waste immobilizates in various solutions, when the mixtures are attuned for the specific application.

The combination of calcium silicates with calcium aluminates for immobilization of waste materials is represented with the HAC/OPC-mixture. The slowly hydration of silicates during weathering leads to an „inner physical barrier" by compensating the effects of thermal cycling and possible delayed ettringite crystallization. The silicates are able to increase strength about a long time comparable with a self-heeling-process. The hydration of aluminates forms AFm and AFt phases, which are responsible for the „inner chemical barrier" (immobilization of pollutants in reservoir minerals). Particular high leaching values of added heavy metals are caused by an insufficient homogenizing of the mixtures and partly agglomeration of the pollutants. However carbonation of the surface leads to a decreasing elution by this physically stabilized immobilizates and to an accumulation of soluble elements in the transition of carbonated surface to unaltered cement matrix.

The very low content of silicates from added PFA in the HAC-mixture has a negative effect on the strength development and the leaching values. The high alumina content is responsible for cracking during the weathering time caused by continuously delayed ettringite formation and thermal cycling. This cracks are enlarging the leachable surface and decreasing the physical stability of the immobilizates. Carbonation of the surface and the cracks would reduce the leaching values, but more and more forming cracks are leading to higher elution of the heavy metals.

Fortunately the application of valuable cement should be substituted in further investigations by using industrial waste products with similar physical and chemical attributes. Also the quality of

the physical and chemical stability of immobilizates could be optimized by testing different ratios of aluminates/silicates. Additionally the leaching of the environmental relevant elements could be reduced by reducing the ratio of surface/volume.

ACKNOWLEDGEMENTS

The authors gratefully acknowledge the financial support of this work provided by the Bilfinger&Berger Umweltverfahrenstechnik GmbH, Mannheim. We also like to thank Dr. P. Czurratis, LEO GmbH, for examinations with a Leica Stereoscan 440 with EDX-Detector.

REFERENCES

Auer, S. (1992): "Bindung umweltrelevanter Ionen in Ettringit und in Schichtstrukturen vom Typus TCAH", PhD Thesis - Department for Mineralogy of the University Erlangen, pp. 240.

Bambauer, H. U., Gebhard, G., Holzapfel, T., Krause, C. und Willner, G. (1988): "Schadstoffimmobilisierung in Stabilisaten aus Braunkohleaschen und REA-Produkten, I. Mineralreaktionen und Gefügeentwicklung; Chlorid-Fixierung" - Fortschr. Miner. 66(2), pp. 253-279.

Bambauer, H. U., Gebhard, G., Holzapfel, T. und Krause, C. (1988): "Schadstoffimmobilisierung in Stabilisaten aus Braunkohleaschen und REA-Produkten, II. Schwermetallfixierung, Bilanzen" - Fortschr. Miner. 66(2), pp. 281-290.

Glasser, P. (1992): "Application of cements to the treatment and conditioning of toxic wastes" - 9th ICCC, New Delhi, Volume VI, pp. 114-119.

Gebhard, G und Pöllmann, H. (1993): "The practical usage of mineral reservoirs for safety-mechanism of waste disposal sites" - Int. Con. Appl. Min., Perth.

Helmer, R. (1973): "Ergebnisse aus Laboruntersuchungen zur Auslaugung von Abfallstoffdeponien." - ISWA-Informationsblatt Nr. 12.

Hills, C.D., Sollars, C.J. und Perry, R. (1993): "Ordinary Portland cement based solification of toxic wastes: The role of OPC reviewed" - Cement and Concrete Research, 23, pp. 196-212.

Pöllmann, H., Auer, S.,Wenda, R. und Kuzel, H.-J. (1990): "Fixierung von Sulfat, Chromat, Borat und Hydroxid an Verbindungen mit Ettringitstruktur" - Europ. J. Min., Beihefte.

Pöllmann, H., Auer, S., Neubauer, J. und Stemmermann, P. (1991): "Bildung eines Innere-Barriere Systems in Abfalldeponien. Immobile Bindung von Chlorid und Schwermetallen in Speichermineralen" - Buch der Umweltanalytik 3, pp. 82-83.

Pöllmann, H. (1991): "Die Bildung von Speichermineralen aus industriellen Reststoffen zur Ablagerung in Deponiekörpern" - Europ. J. Min., Beihefte, pp. 213.

Pöllmann, H. und Neubauer, J. (1993): "Anwendung des Konzeptes der „Inneren Barriere" auf industrielle Reststoffe" - Geotechnica, Köln.

Roy, D.M., (1992): "Cementitious materials in nuclear waste management" - 9th ICCC, New Delhi, Volume VI, pp. 88-119.

TA Siedlungsabfall (Entwurf vom 22.11.1991): "Technische Anleitung zur Vermeidung, Verwertung, Behandlung und sonstige Entsorgung von Siedlungsabfällen." - 6. allgemeine Verwaltungsvorschrift zum Abfallgesetz.

IMMOBILISATION OF Cs-LOADED ION EXCHANGE RESINS IN ZEOLITE-CEMENT BLENDS

Sandor BAGOSI, Laszlo J. CSETENYI
University of Veszprem, Department of Silicate and Materials Engineering
H-8200 Veszprem, P.O. Box: 158, Hungary (Phone/Fax: +36 88 423 091)

ABSTRACT Water leaching of caesium-loaded cemented ion exchange resin and the mechanism of Cs-immobilisation were studied in the cement-resin-zeolite system as a whole as well as, for simplification, in parts as all three constituents are porous structure complex materials interconnected by the pore fluid. Present work focuses on reduction of significant Cs leaching (in terms of the total Cs adsorbed on the resin) by blending natural and chemically treated zeolites to the cement. Addition of natural zeolites decreased the Cs-release by 70-75% the course of a three year leaching period.

Key-words: immobilization, leaching, zeolites, ion exchange resin

INTRODUCTION

In several countries radioactive waste immobilisation strategies are based on cementitious materials (Glasser, 1992). Exhausted ion exchange resins from the primary cooling circuit of pressurised water reactor systems are favourably cemented for disposal. Heavy metals readily precipitate in the high pH environment of cements, but alkali metals, such as ^{137}Cs, remain substantially soluble. Cementation of Cs-loaded resins is important from two main aspects: (i) Cs accumulates in the resin during operation of the reactor, (ii) Cs-loaded resins, when cemented, show one or two orders of magnitude higher leach rates than on their own.
Because of the high leaching of Cs from a preliminary set of cemented samples in comparison with that from uncemented cesium-loaded resins, development of a matrix material was targeted which can significantly reduce this leachability. To comply with this aim, admixing zeolite seemed to be an obvious solution since zeolites have large occurrences in Hungary. Thus, release of isotopes from specimens, prepared using zeolite in natural and in various chemically treated forms, was investigated. The optimum composition (cement/zeolite ratio) was worked out by strength measurements, capacity and selectivity studies of zeolites and ion exchange resins, the migration of ions in solid phase was assessed by diffusion experiments with cements and zeolite admixed cement samples.

MATERIALS AND THEIR PERFORMANCES

Solutions

In practice, final storage time of radioactive wastes is usually determined by the ^{137}Cs isotope ($t_{1/2}$=30 yr.). In present study the shorter half life isotope, ^{134}Cs was instead used ($t_{1/2}$=2.05 yr.). For the saturation of ion exchange resins, for the distribution and selectivity measurements as well as for the leaching tests, CsCl solutions in various (chemical and radiochemical) concentrations were employed, which contained the active isotope ^{134}Cs. All determinations of caesium were carried out by radioisotope tracing techniques except for the Cs-containing inactive solutions equilibrated with resins and zeolites, where flame emission spectroscopy was used. Activities of the liquids were detected by a scintillation detector equipped with a NaI(Tl) cluster crystal.

Cement

For preparation of specimens to be used in leaching experiments, 350-10 coded Ordinary Portland Cement (OPC) containing 10% PFA was used. Chemical composition of the cement is given in Table 1. The caesium adsorption potential of hardened cement paste and caesium distribution ratios between solid and solution phases, calculated with the help of Eq. 1, are demonstrated in Table 2: for test conditions, see the relevant Table footnote.

Table 1 Chemical and mineralogical composition of cement and zeolite used , in % (by weight)

Components	Chemical composition of cement* [%]	Chemical composition of zeolite [%]
SiO_2	24.19	72.69
Al_2O_3	4.87	12.67
K_2O	0.65	3.32
CaO	58.23	2.23
Fe_2O_3	5.19	1.28
MgO	2.64	0.89
Na_2O	0.44	0.28
TiO_2	0.26	0.07
SO_3	1.96	n/d
Ign. loss	1.31	6.14
Total	99.74	99.57

Mineralogical composition of zeolite [%]	
Clinoptilolite	50
K-feldspars	20
Quartz	10
Cristobalite	10
Volcanic glass	10

*Hungarian standard MSz 4702/2, produced at Beremend Cement Works

$$R_d = \frac{(Cs^+)}{[Cs^+]} \qquad [1]$$

( ): concentration of solid phase,
[ ]: concentration of liquid phase

Table 2 Caesium distribution ratios between hardened cement pastes and different caesium concentrations of the saturating solutions

Cs concentration of saturating solution [mg/dm^3]	Cs conc. of solution after contacting [mg/dm^3]	Cs conc. of cement paste after contacting [mg/g]	Distribution ratios (R_d) [cm^3/g]
1	0.671	0.0163	24.34
10	9.025	0.0483	5.34
1000	98.96	0.0511	0.52

hydration time: 28 days, W/C=0.35, hydration temp.: room temp., grain size of ground hydrated cement <200μm, mass of hydrated cement: 0.5 g, volume of saturating solution: 25 cm^3, time of contacting: 2 weeks

Zeolite

The zeolite used originates from the Tokaj Hills (Hungary) occurrence. For the mineralogical composition, assessed by XRD, XRFS and morphometric studies, as well as for the chemical composition of tuff see Table 1. The 0.5...1.0 mm fraction of the zeolite was used in the sample preparation. Since ion exchange properties alter on replacing the mobile ion in the zeolite (Bish, 1988), the ground mineral was pre-treated by various methods (Na^+-form(1): Szász (1977); NH_4^+ and H^+-form: Valyon et al (1979); Na^+-form(2): Hlavay et al. (1987)) to obtain different exchangeable cation contents. Characterisation of one natural and the above mentioned four modified zeolites was performed by a radioisotopic method, their break-through and saturation capacities were determined by a dynamic method (Table 3, Fig. 1). The caesium adsorption potential of untreated zeolite and caesium distribution ratios between solid and solution phases are demonstrated in Fig. 4, for test conditions see the Table footnote.

Table 3 Break-through and saturation capacities of zeolites

Form of zeolite	Break-through volume [cm^3]	Break-through capacity [mg/g]	Saturation volume [cm^3]	Saturation capacity [mg/g]
Natural	19	40.00	33	69.51
H^+	33	68.05	51	107.92
NH_4^+	48	101.14	66	139.15
$Na^+(2)$	67	145.53	72	151.91
$Na^+(1)$	78	164.54	90	189.79

column: Ø10x100 mm, mass of zeolite: 6.3 g, Cs conc. of saturating solution: 0.1 mol/dm^3, flow rate: 6 BV/h

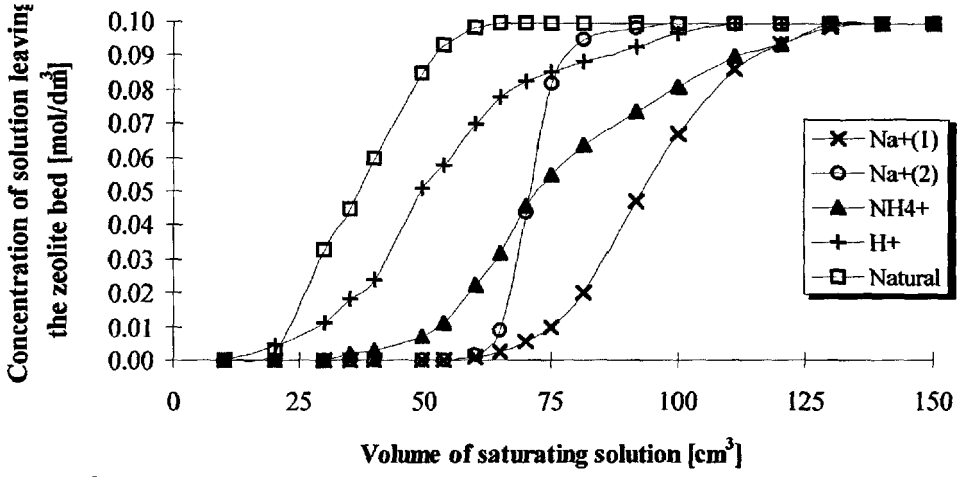

Figure 1 Break-through curves of zeolites

Table 4 Caesium distribution ratios between untreated zeolite and different caesium concentrations of the saturating solutions

Cs concentration of saturating solution [mg/dm^3]	Cs conc. of solution after phase-contaction [mg/dm^3]	Cs conc. of zeolite after phase-contaction [mg/g]	Distribution ratios (R_d) [cm^3/g]
10	0.78	0.917	1175.7
100	6.44	9.353	1450.9
1000	401	59.89	149.35
10000	9156	84.01	9.17

volume of saturating solution: 100 cm^3, mass of zeolite: 1 g, grain size 0.5-1.0 mm, contacting time: 2 weeks

Out of the four variously treated zeolites, the one in hydrogen form showed inferior ion exchange capacity and selectivity to the natural zeolite, therefore the H^+-form zeolite was excluded from subsequent cement addition experiments. A reason for the unsatisfactory behaviour may be that the zeolite looses part of its crystal water content and thus significant changes occur in its structure (Olaszi, 1982).

Ion Exchange Resin

In the course of leaching studies, for the preparation of specimens, a high purity ion exchange resin (VARION KS-N) was used.This resin, in combination with VARION AT-N resin, is also used for the water cleaning system of Nuclear Power Plant Paks (Hungary). Saturation of the pre-treated resins was done by a static method, whose essence is that a known quantity of the resin to be saturated is contacted for prolonged time (1 week) with a know concentration of

saturating solution (solution/resin volume ratio 2.08). The advantage of the method is that it results in resin beads of nearly similar saturation. In the course of the one week saturation period the caesium solution contacting the resin was shaken several times every day. The quantity of caesium ions bonded in the resin was determined from the difference of the signal frequencies (cps) of 1 ml samples taken before and after the saturation procedure. For saturation data of used ion exchange resins for leach sample preparation see Table 5. The caesium adsorption potential of ion exchange resin and caesium distribution ratios between solid and solution phases are demonstrated in Table 6; for test conditions, see the Table footnote.

Table 5 Caesium saturation of ion exchange resins used

Resin	Saturation of resin [mol/dm^3]	Resin	Saturation of resin [mol/dm^3]
A_u	0.612	A_c	0.350
B_u	0.725	B_c	0.378
C_u	0.807	C_c	0.629
D_u	0.949	D_c	0.708
E_u	1.164	E_c	0.807

u: uncemented c: cemented

Table 6 Caesium distribution ratios between ion exchange resins and different caesium concentration saturating solutions

Cs concentration of saturating solution [mg/dm^3]	Cs conc. of solution after phase-contaction [mg/dm^3]	Cs conc. of ion exchange resin after phase-contaction [mg/dm^3]	Distribution ratios (R_d)
1	0.5	3167	$6.33 \cdot 10^4$
10	7.51	30830	$4.11 \cdot 10^4$
1000	586.2	137933	$2.35 \cdot 10^3$
10000	9584.4	138520	$1.45 \cdot 10^2$

volume of saturating solution: 100 cm^3, volume of ion exchange resin: 0.3 cm^3, time of contacting: 2 weeks

Selectivity measurement of ion exchange resin for Cs^+ - Ca^{++}

Selectivity ratios of ion exchange resins for Cs^+ - Ca^{++} were determinated by following a static method. 10-10 cm^3 quantities of E_c, termed saturated resin, were weighed into airtight polythene vessels and contacted with 100 cm^3 $Ca(OH)_2$ solutions of different Ca^{++} concentrations. Equilibration was accelerated by shaking the sealed vessels for 2 weeks. After this, 1 cm^3 sample each were taken from both the standard CsCl solution and the calcium hydroxide solutions. Signal frequencies of these samples were determined. By knowing the saturation degree of ion exchange resin samples, the signal frequency of a 1 cm^3 sample of known concentration CsCl standard solution, from which solution samples for resin saturation purposes were previously taken, the differences between signal frequencies (cps) and the quantity of caesium washed off by the $Ca(OH)_2$ solutions one can calculate selectivity ratios with the help of Eq. 2. Calcium concentrations were determined by titrimetry before and after $[Ca^{2+}]$ phase contaction, by the difference of which one could calculate the concentration of Ca on the resin (Ca^{2+}). (Values of R_s (selectivity ratio) are to be found in Table 7. The given equation (see Table 7 for symbol definitions) refers to the exchange of Cs^+ and Ca^{++} ions and gives selectivity ratios for Ca^{++}: the more Ca^{++} is bonded in the resin, the higher the value of R_s.

$$R_s = \frac{[Cs^+] \cdot (Ca^{++})}{[Ca^{++}] \cdot (Cs^+)} \qquad [2]$$

Table 7 Results of the Cs^+ - Ca^{++} selectivity determinations for the ion exchange resin

Sign of sample	Ca^{++} concentration in solutions before contacting [mol/dm^3]	[Cs^+]	[Ca^{++}]	(Cs^+)	(Ca^{++})	Cs^+ - Ca^{++} Selectivity ratios R_s
		[mol/dm^3]		[mol/dm^3 resin]		
R1	$1.51 \cdot 10^{-3}$	$1.53 \cdot 10^{-3}$	-	$7.92 \cdot 10^{-1}$	$1.51 \cdot 10^{-2}$	-
R2	$1.76 \cdot 10^{-3}$	$1.13 \cdot 10^{-2}$	-	$6.95 \cdot 10^{-1}$	$1.76 \cdot 10^{-2}$	-
R3	$2.14 \cdot 10^{-3}$	$3.00 \cdot 10^{-2}$	$8.70 \cdot 10^{-5}$	$5.07 \cdot 10^{-1}$	$2.05 \cdot 10^{-2}$	13.96
R4	$2.39 \cdot 10^{-3}$	$4.38 \cdot 10^{-2}$	$9.30 \cdot 10^{-5}$	$3.70 \cdot 10^{-1}$	$2.30 \cdot 10^{-2}$	29.24
R5	$6.05 \cdot 10^{-3}$	$6.08 \cdot 10^{-2}$	$1.26 \cdot 10^{-4}$	$1.99 \cdot 10^{-1}$	$5.92 \cdot 10^{-2}$	143.65

( ): concentration of resin phase, [ ]: concentration of liquid phase

Preparation of leach test samples

There were three series of leaching tests performed in this study. The first series comprised uncemented resin samples, the second investigated cemented samples, whereas the third series determined behaviour of resins in zeolite admixed cements.

In order to assess the leaching character of uncemented resins, resin samples, previously saturated to various degrees (A_u...E_u), were placed in 45 mm diameter 4.4 mm high (70 cm^3 volume) perforated polythene walled vessels also equipped with a lid (Goór, 1989). For the second series of leach tests resin samples were first saturated to the required degrees (A_c...E_c) and then cemented by mixing 24 cm^3 resin, 93.2 g cement and ion free water to achieve a paste of W/C = 0.3. For the third series, the suitable cement/zeolite ratio was selected by also considering the results of strength tests (Bagosi, 1992), *i.e.* the highest zeolite content still ensuring sufficient strength was chosen. From compressive and tensile strength tests, as well as the water/solid ratios, a zeolite/cement ratio of 40/60 (by weight) was found to be the optimum. The zeolite containing samples (either with Natural B, Na^+(1)B, NH_4^+B or Na^+(2)B) were prepared by mixing 24 cm^3 resin (A_c), 55.9 g cement, 37.3 g zeolite and ion free water to achieve a paste of W/C = 0.3. These were prepared as reference samples (B) similar in composition to the samples of the second test series.

Leach tests

In the course of the leach tests, specimens were stored in 1 liter volume airtight PVC vessels filled with 750 cm^3 ion free water and covered with a lid. The perforated ring on the bottom of the specimens and the size of the vessels ensured that the samples were surrounded with at least 20 mm of water on each side. The leach tests were done without renewal of leachant, that is, the sampled leachants were returned to the vessel after measurement. The equipment used is illustrated in Fig. 2. During the first week of investigation, samples were taken daily, for the next month weekly, then at longer periods. The activites of the sample solutions (500 cm^3 each time) were measured in a Marinelli vessel which, due to its unusual shape, enabled the detector to be surrounded by the

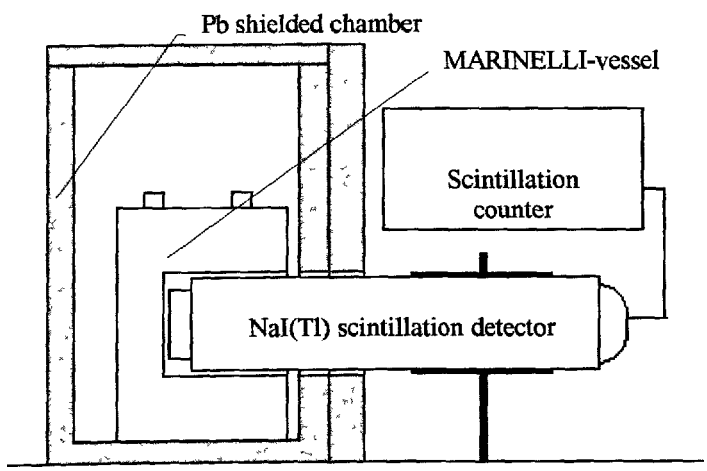

Figure 2 Measuring system to detect activities of leachates

solution. The effect of background radiation was reduced by a 50 mm thick lead jacket around the measurement assembly.
From the CsCl stock solution, previously used for making solutions to saturate the resins, a standard solution of 10^{-3} mol/dm^3 concentration was prepared by dilution. Signal frequency (activity) of this solution was determined before and after each series of measurements. This was done for two reasons, first, to compensate for probable instabilities of the measuring system, and second, to determine the absolute Cs concentrations of the leachates by taking the actual activity of a standard solution as reference.

RESULTS AND DISCUSSION

On comparing leaching of Cs from uncemented and cemented ion exchange resins (1st and 2nd series), it can be seen that Cs-concentrations of leachates are more than one order of magnitude higher for the 2nd series samples. Considering the effect of increasing saturation degrees of the resins, the amount of leached Cs decreases for the uncemented resin. In a cementitious environment, however, on increasing the resin saturation the amount of leached Cs increases (Fig. 6). Removal of Cs from the uncemented resin is low, not exceeding 0.06 - 0.88 % of the initially bonded ions. As a consequence of cementation, these values change between 6.4 - 41.6 % depending on the saturation degree of the resin (Table 8.).
Due to Ca^{2+} ions liberated during hydration reactions as well as readily soluble alkali, Cs^+ ions bonded on the resin are washed out at a significant degree (Table 7, R_1...R_5 1.9, 14.0, 37.2, 54.3 and 75.3 %, resp., of the initially bonded quantities depending on the concentration within the resin). Cs retaining capacity of the cement/resin system on its own is rather low, as is that of the pure OPC used (Table 2.). In order to suppress leaching, *i.e.* to lower the relatively high Cs concentration within the pore fluid of the cement when cementing resins, the 3rd series of samples were prepared by mixing cement, resin and zeolite in selected compositions. The connection between the three constituents, each being porous also on their own, is established by the pore fluid interconnecting elements of the system. Therefore, the overall behaviour of the matrix is dependent on several equilibration processes (ion exchange, sorption, hydration etc.). Zeolites, especially those containing clinoptilolite, show excellent Cs-retention (Table 4.), which can be further improved by simple chemical treatments.

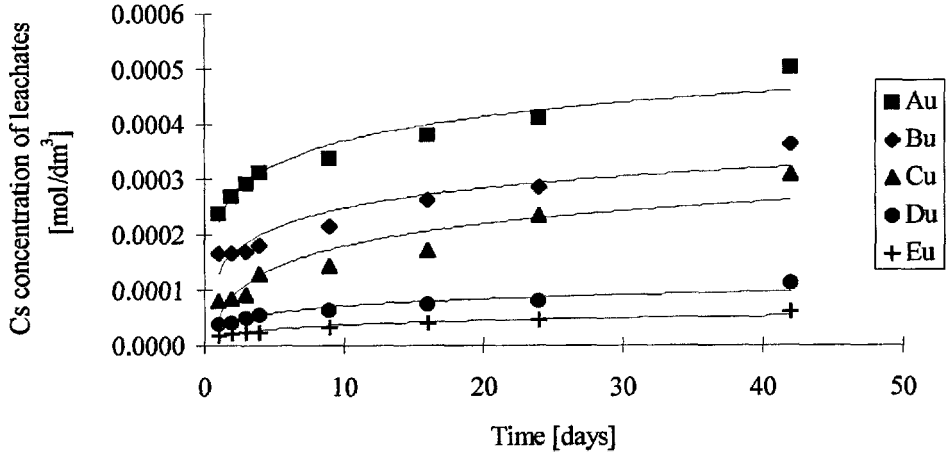

Figure 3 Caesium concentration of leachates in time for uncemented ion exchange resin samples (1st series)

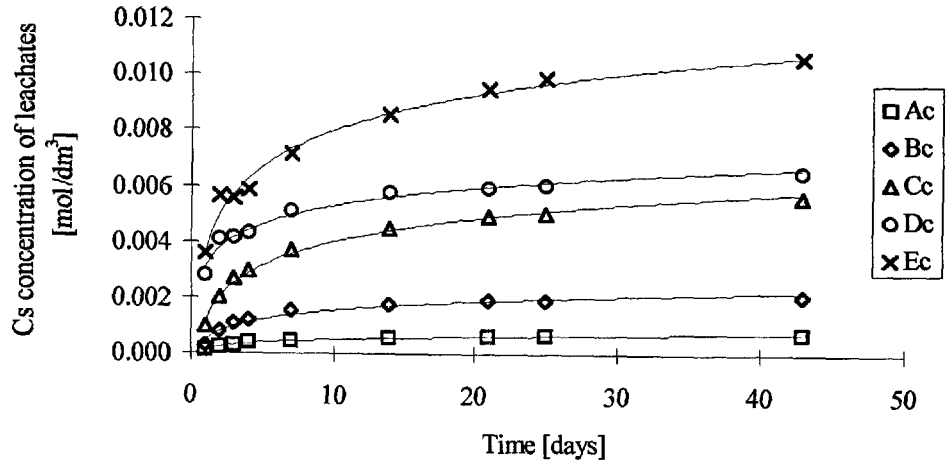

Figure 4 Caesium concentration of leachates in time for cemented ion exchange resin samples (2nd series)

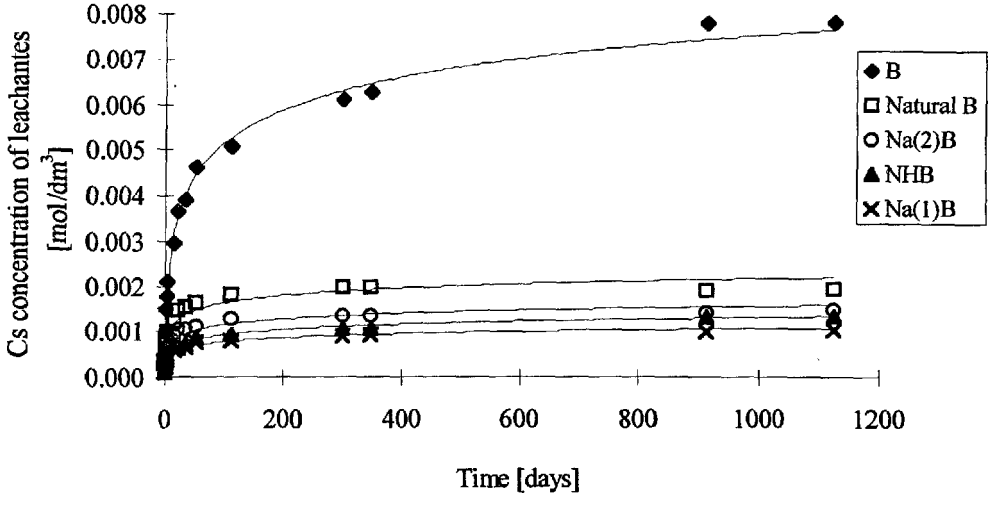

Figure 5 Caesium concentration of leachates in time for zeolite admixed cemented ion exchange resin samples (3rd series)

Table 8 Distribution ratios (R_d) of caesium between resin and liquid phases as well as exclusion of caesium from ion exchange resins in percentage [%] of the original amount

1st series			2nd series			3rd series		
Sign of samples	R_d	[%]	Sign of samples	R_d	[%]	Sign of samples	R_d	[%]
A_u	1207	0.88	A_c	454.9	6.4	B	1.3	70.4
B_u	1986	0.54	B_c	147.9	17.4	Natural B	14.9	17.3
C_u	2610	0.41	C_c	79.5	28.2	Na^+(1)B	20.4	13.3
D_u	8478	0.13	D_c	75.9	29.2	NH_4^+B	22.5	12.2
E_u	18947	0.06	E_c	43.8	41.6	Na^+(2)B	30.4	9.3

In the 3rd series the saturation degree of the resin was set to a relatively low value to simulate conditions in nuclear power plants, where, due to operation safety reasons, ion exchange columns of the water treatment system are allowed to saturate to a moderate degree only.

On examining leaching for more than three years, one may conclude that the cemented resin containing no zeolite has lost 70.4 % of its originally bonded Cs content (Table 8.), nevertheless the major part of the caesium was removed within the first 100 days of leaching. With the presence of natural zeolite in the matrix, the amounts leached fell to one quarter. With previous treatment of the zeolite to obtain Na^+ or NH_4^+ forms, further decreases in Cs leachability can be achieved. In the last two years of leaching, increase of Cs concentration of the leachates is lower for the zeolite containing samples.

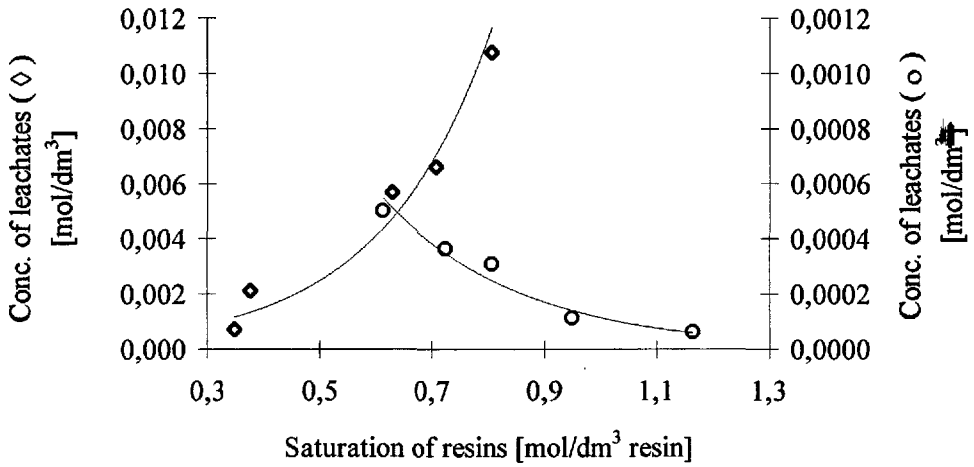

Figure 6 Comparison of leach behaviour of cemented (◊) and uncemented (o) resin samples. Change of caesium concentration of leachates as a funcion of resin saturation after 40 days.

CONCLUSIONS

The oldest and most often used technique for stabilisation/solidification of radioactive wastes, *i.e.* cementation is not satisfactory for immobilisation of Cs-containing spent resins.
For suppressing the leaching from the repository after the unlikely event of soil water intrusion, the cement/zeolite matrix gives better performance.
Admixing zeolites to the backfill between the solidified waste packages could further increase the safety of disposal.

ACKNOWLEDGEMENT

Authors are indebted to the Commission of the European Communities for their financial support (COST-PECO project ERBCIPDCT 930447) and LJC for the SOROS Foundation (247/6676).

REFERENCES

Bagosi S. "Leaching Study of Cs Ions from Zeolite Admixed Cement", M.Sc. Thesis, Univ. of Veszprem, 1992.
Bish, D.L. "Effects of Composition on the Dehydration Behavior of Clinoptilolite and Heulandite", Eds.: D. Kalló and H.S. Sherry, Academy Press, Budapest, 1988, pp. 565-577.
Glasser, F.P. "Progress in the Immobilization of Radioactive Wastes in Cement", Cem. Conc. Res., **22** 1992 pp. 201.
Goór, Á. "Leaching Study of Cs Ions from Ion Exchange Resins", M.Sc. Thesis, Univ. of Veszprem, 1989.
Olaszi, V., Csikós, Cs., Jánossy, A., "Acid treatment of Clinoptilolite and Mordenite" Investigation and Employment of Hungarian Natural Zeolites (I.) Hung. Academy of Sciences, Hungary, 1982, pp. 155-166.
Polyák, K., Hlavay, J. "Selectivity of Clinoptilolite for Some Heavy Metals", Investigation and Employment of Hungarian Natural Zeolites (II.) Hung. Academy of Sciences, Hungary, 1987, pp. 73-89.
Szász, Á. "Investigation of sorption of divalent metal ions on clinoptilolite", Ph.D. Thesis, Univ. of Veszprem, 1977.
Valyon, J., Papp, J., Kalló D. "Investigation of gas adsorption characteristics of Hungarian Natural Clinoptilolite" Magyar Kémiai Folyóirat, Hungary, Vol. 85, No. 2, 1979, pp. 55-61.

TOPIC IV.C

Cement aggregate compatibility and structure↔performance relationships

ALKALINE CEMENTS: TERMINOLOGY, CLASSIFICATION, ASPECTS OF DURABILITY

Pavel KRIVENKO, Scientific Research Institute on Binders and Materials, Kiev, Ukraine

ABSTRACT The questionable problems arising from inadequate views on role the alkalis perform in producing hydraulic properties by mineral binder systems and terminology in the field of alkaline cements are dealt with and discussed. A classification of alkaline cements based on theoretical regularities of these cements synthesis has been suggested. Taken as a main distinguishing feature was a phase composition of hydration products of cement stone since it was found to be a determining factor affecting service properties, first of all, durability.

Key-words: alkaline cement, aluminosilicate, classification, durability, terminology, zeolites

INTRODUCTION

The investigations of Professor V.D.Glukhovsky and associates demonstrated and proved that alkalis and alkali metal salts, under condition of required concentration and ability to create high values of pH in a disperse medium, interact with glassy and crystalline aluminosilicate compounds of natural and artificial origin (Glukhovsky, 1959: 1965; Glukhovsky et al, 1979; Glukhovsky et al, 1979; 1983; Krivenko, 1986). Water- resistant alkaline and alkaline-alkali-earth alumino- and ferrosilicate compounds, analogous to naturally occurring minerals of zeolite and mica type, are found to be the interaction products (Glukhovsky et al, 1983). Some researchers restrict the role of alkaline compounds only to activators but not as constructive elements of the cement stone phases. That's why these systems are called "alkali-activated cementitious systems", what seems to be somewhat incorrect and does not reflect the true role of the alkalis in producing hydraulic properties (Feret, 1939; Purdon, 1940; Kuhl, 1958; Roy et al, 1993; Jolicoeur, 1993; Shi, 1993; Wang et al, 1995).

TERMINOLOGY

Theoretical fundamentals of possibility to produce and use of alkaline cements in construction have been laid supported by geological data on conditions of occurrence of sedimentary and metamorphous silicate rocks and constitutional composition of main rock-forming minerals (Glukhovsky, 1959; 1965). Due to the fact that at the initial stage of development of the alkaline cements, substances of natural origin were involved as raw materials, these cements were called "soil cements" (Glukhovsky, 1959; 1965), and materials based on them- "soil silicates". In 1976 Professor Davidovits was granted first patents for analogous alkaline cements in which sintering products of kaolinite and limestone or dolomite were used as aluminosilicate constituent (Davidovich, 1976: Davidovits and Sawyer, 1986; Davidovits, 1988). These cements were called "geopolymers" and have been put into practice under trademarks Pyrament, Geopolymite, Trolit, Geopolymere, Geopolyceram, etc. The cements of this type were called "SKJ-binder" in China (Changgo, 1991), "F-cement" in Finland (Forss, 1991) and "geocements" in Ukraine (Krivenko et al, 1991) to underline the presence within the hydration products of analogues to natural minerals. The interest to alkaline aluminate(Krivenko et al., 1984), portland (Glukhovsky et al., 1990) cements and their varieties (Krivenko et al., 1991) in which alkalis act as activators and structure-forming elements has grown steadily for the last 10-15 years.

CLASSIFICATION

The classification of alkaline cements, depending upon the phase composition of hydration products, which, in its turn, is caused by both the type of aluminosilicate constituents used and quantity of the alkali introduced, was developed (Fig 1). As it follows from Fig 1, the alkaline cements may be divided into two groups. The main hydration products of the cements belonging to the first group are the alkaline and alkaline- alkali-earth zeolite-like hydroalumino- and ferrosilicates, and low basic calcium, magnesium, strontium hydrosilicates serve as auxiliary hydration products, and vice versa: the main hydration products of the cements of the second group are the low basic calcium, magnesium, strontium hydrosilicates, and the alkaline and alkaline- alkali-earth zeolite-like hydroalumino- and ferrosilicates serve as auxiliary hydration products. The zeolite-like hydration products resulting from their more slower crystallization, are detected in cement stone at later stages. Being formed, predominantly, in pores they fill them and promote the formation of strong crystallization bonds between primary phases of hydrosilicates and hydroaluminosilicates of calcium.

ASPECTS OF DURABILITY

Durability is associated in many aspects with the structure and properties of cement stone and concrete, the phase composition of hydration products being the determining factor. The hydration products of conventional cements are known to be presented by calcium hydrosilicates and hydroaluminates which possess increased basicity at initial stages lowering with time, leading to destructive processes occurring in the cement stone. Free and bound calcium as well as aluminates are capable to come into cation-exchanging processes with atmospheric reagents easily promoting corrosion of cement stone. Such formations are not found in nature proving their instability.

A characteristic feature of the alkaline cements is that free lime and calcium hydroaluminates are not found in them, the basicity of calcium hydrosilicates is lower, and their hydration products contain within them more stable and less soluble zeolite-like new formations analogous to naturally occurring ones (Glukhovsky, 1959; 1965; Glukhovsky et al, 1979; Krivenko, 1986).

Professor Davidovits concluded that extremely high durability of ancient structure (pyramids, etc.) may be attributed to zeolite-like new formations of analcime type which had been detected in the concrete of ancient structures (Davidovits and Sawyer, 1985; Davidovits, 1986). The comparative testing of ancient and modern concrete structures demonstrate that under similar weather conditions the specimens made from conventional portland cement failed earlier the period specified by the standards for shelf life (50 years), while the ancient concretes remained undamaged over thousands of years. Extremely high durability of the ancient structures as well as similarity of their compositional build-up to alkaline cements suggested to draw a conclusion that the latter should also possess the same high durability as compared with that of known cementitious systems.

PRACTICAL EXPERIENCE

The geocements are widely used in composite materials to replace organic polymers. They possess high fire-, heat- and acid resistance and may be effectively used as a matrix in the immobilization of hazardous wastes such as heavy metals, radioactive nuclides, etc., as glues and adhesives for concrete, glass, ceramic, metal, wood, etc., hydro-insulating mastics, as binder in the production of mineral wool articles, heat-, sound-insulating, decorative, constructive materials, including those with organic aggregates.

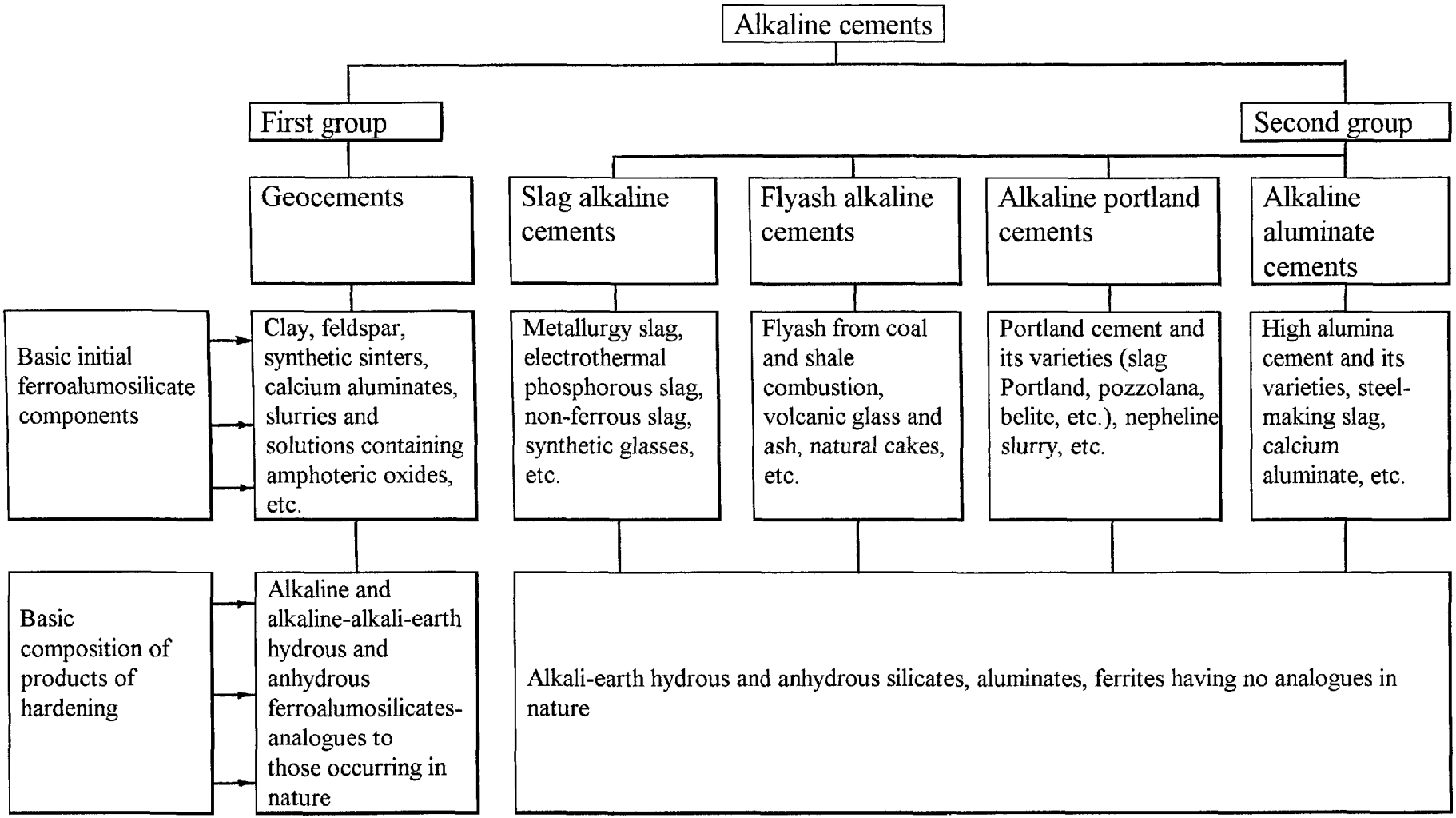

Figure 1 Classification

1995							
					High-rise building from precast- and cast-in-situ concrete		Compounds for radioactive waste immobilization
1990				Articles and structures from acid resistant concretes			
				Floors, landings from cast-in-situ concrete	Blocks for buildings, garages, storage houses, etc.		Bodies of precise machine tools
1985		Heavy-duty road pavements Access roads and storage sites of chemical plants					
				Articles and structures from heat resistant concretes	Floor slabs, foundation wall blocks, foundation blocks, piles	Oilwell mortars and grouts	Dies, moulds
1980							Linings of MD-pumps for aluminium melts
1975		Road bases from strengthened soils					
1970	Tubbings of anti-slipping systems	Pavements from cast-in-situ concrete and precast reinforced concretes slabs Pedestrian way slabs, edges of pavement, landing field slabs	Pasture sites, storage sites for fertilizers, silo pits from cast-in-situ and precast concrete	Foundation blocks, floor slabs,columns, beams, foundation wall blocks, elements of cleaning-up systems		Reinforced pit props, sleepers	
1965	Sea breakwaters Irrigation systems from cast-in-situ and precast prestressed concrete						
1960							
	Hydraulic	Road	Agricultural	Industrial	Residential	Mining	
	Constructional Engineering						Non-constructional engineeringengineering

Figure 2 Practical Experience

The slag and flyash alkaline cements in their properties are superior to conventional portland and high alumina cements. Of great advantage is a set of special properties they have allowing their use not only in construction, but in machine-manufacturing, foundry, etc.

The alkaline portland and high alumina cements surpass considerably the conventional cements in strength gain, including of at subzero temperatures, the greater activity, higher density, fire- and corrosion resistance, wear resistance, etc. resulting in great energy saving due to possibility to introduce a larger quantities of fillers without loss in quality as well as to involve industrial wastes.

High durability of the alkaline cements is proved by the vast experience gained by the scientific school of Professor Glukhovsky from manufacture, and use of the alkaline cements in constructional and non- constructional special and common fields of application (Fig 2)(Krivenko, 1986; 1992). Although this experience is not as large as that gained from ancient concretes, it may be of special interest, especially when these concretes were in service under severe conditions.

REFERENCES

Blaakmeer, J.,"Diabind: an Alkali- Activated Slag Fly Ash Binder for Acid Resistant Concrete", Proceed. Ist Int. Conf. on Alkaline Cements and Concretes, Vipol Publish., Kiev, Ukraine, 1994, Vol.1, pp.345- 360.

Changgo, L., "A New Type of Durable Building Materials-FKJ Concrete, Concrete and Cement Products", China, No 6, 1991.

Davidovits, J.,"Geopolymer Chemistry and Properties", Proceed.First European Conference on Soft Mineralurgy "Geopolymer'88" ,1-3 June 1988, Compiegne, France, Vol.1, pp. 25-48.

Davidovits, J. and Sawyer, J.L., U.S.Patent No 4,509,985, 1985; EP No 0153097, 1985.

Davidovits, J., "X-ray Analysis and X-ray Diffraction of Casing Stones from the Pyramids of Egypt and the Limestone of the Associated Quarries, Science in Egyptology, Manchester University Press, 1986, pp.511- 520.

Feret, R., Slags for the Manufacture of Cement, Rev.Mater.Constr.Trav.Publish, July, 1939.

Forss, P.,"F-Cement: A New Low Porosity Slag Cement", Silic.Ind.Journal, 1983, 48, No 3.

Glukhovsky,V.D., Soil Silicates, Gosstroi Publish., Kiev, Ukraine, 1959, 154 pp.

Glukhovsky,V.D.,"Soil Silicates: Properties, Manufacturing Technology and Application", Doct.Tech.Sc.Degree Thesis, Civil Engineering Institute, Kiev, Ukraine, 1965, pp.320.

Glukhovsky,V.D., Soil Silicate-Based Articles and Structures (Gruntosilikatny Viroby I Konstruktsii), Budivelnik Publish.,Kiev, Ukraine, 1967, 155 pp.

Glukhovsky,V.D. et al., Alkaline and Alkaline-Alkali-Earth Hydraulic Binders and Concretes, Vyscha Shkola Publish., Kiev, Ukraine, 1979, 232 pp.

Glukhovsky,V.D., Skurchinskaya, Ja.V. and Petrenko,I.Yu.,"On Interaction of Clay Minerals with Sodium Hydroxide, Collection of Works, Kiev, Ukraine, Part 24, 1983.

Glukhovsky,V.D., Gelevera, A.G. and Blazhis A.R., "Alkaline Portland Cements", Tsement Journal, No 11, Leningrad, USSR, 1990, pp.22-23.

Jolicoeur, C., Simard, M.A., Sharman,T.J., Zamojska,R., Dupuis,M., Spiratos,N., Douglas,E., and Malhotra,V.M.,"Chemical Activation of Blast Furnace Slag:: An Overview and Systematic Experimental Investigations", Advances in Concrete Technology, CANMET, 1993, pp.483-514.

Krivenko, P.V.,"Synthesis of Binders with Required Properties in the System "R_20-RO-R_20_3-$Si0_2$-H_20" Doct.Tech.Sc.Degree Thesis, Polytechnic Institute, Kiev, Ukraine, 1986, 380 pp.
Krivenko, P.V. and Ryabova, A.G., "Flyash Alkaline Binders", Tsement Journal, Leningrad, USSR, No 11, 1990, pp.14-16.
Krivenko, P.V. et al., "Investigation of the Processes of Hydration of Calcium Aluminate in the Presence of Alkali Metal Compounds", Izvestiia VUZov Journal, Chemistry and Chemical Engineering Moscow, USSR, Series, Vol. 27, No 10, 1984, pp.1204- 1208.
Krivenko, P.V., Chirkova, V.V., and Tarasova, T.V. "Alkaline Portland Cements Based on Feldspar Rocks", Tsement Journal, Leningrad, USSR, Nos 11-12, 1991, pp.29-33.
Krivenko, P.V., "Special Slag Alkaline Cements", Budivel'nik Publish.,Kiev, Ukraine, 1992.
Kuhl, H., Zement-Chemie, Verlag technik, Berlin, Germany, Band III, 1958, 19, 1930, 262 pp.
Purdon, A.O., "The Action of Alkalis on Blast Furnace Slag", Journal of the Society of Chemical Industry, Vol.59, 1940, pp.191-202.
Roy, D.M. and Malek, R.I.A., "Hydration of Slag Cement" , Mineral Admixtures in Cement and Concrete, ABI Books Pvt Ltd., 1993, Vol.4, pp.84-117.
Shi, C.,Wu, X. and Tang, M."Research on Alkali-Activated Cementitious Systems in China: A Review", Advances in Cement Technology, 1993, 5, No 17, pp.1-7.
Wang, S.-D., Pu, X.-C., Scrivener, K.L. and Pratt,P.L. "Alkali-Activated Slag Cement and Concrete: A Review of Properties and Problems", Advances in Cement Research, 1995, 7, No 27, pp.93-102.

4iv047
8 pp

THERMAL ACTIVATION OF ALKALI SILICA REACTION IN CONCRETE

Ajoy K MULLICK, George SAMUEL, Ramesh C WASON, Surendra K SINHA
National Council for Cement and Building Materials, New Delhi, India

ABSTRACT Linear expansion tests on mortar bar or concrete prism specimens made with slow/late expanding aggregates showed strong dependence on test temperature upto 80°C. Continuous exposure of aggregate pieces to KOH with or without $Ca(OH)_2$ solution at 80°C comprised a severe test, leading to cracking and fracture of samples.

Key-words: Activation, Alkali Silica Reaction, Microstructure, Temperature

INTRODUCTION

Deleterious chemical reactions between certain types of 'reactive' silica in concrete aggregates and alkalies from the cement have been reported for the last fifty years. The reactivity of silica could be due to its amorphous metastable state as in Chert, Chalcedony, Opal etc., or due to defects in the crystal lattice of quartz (Brown, 1955, Mielenz, 1958, Mullick, 1987). In practice, the reaction takes long time to manifest and still longer to come to completion (Tuthill, 1982). Accelerated tests are, therefore, resorted to in assessing the potential reactivity of concrete aggregates so that meaningful guidance can be obtained in days (ASTM C-289), or within a period upto 6 months (ASTM C-227). The acceleration is achieved by either increasing the amount of reactant i.e. exposing the aggregate to abundant presence of alkali solution (Oberholster and Davies, 1986) or increasing the temperature of reaction (Mullick, Wason and Sinha, 1992) or both.

In order that the short-term accelerated tests are useful in predicting long-term behaviour, the dependence on the accelerating medium as well as the resultant mechanism of attack should be understood (Mullick, 1984). This paper investigates the role of temperature in accelerating alkali-silica reaction in concrete with aggregates, whose reactivity is due to the presence of strained quartz and not any metastable silica mineral. Such aggregates are commonly referred to as 'slow' or 'late' expanding type (Mullick, 1994). The findings of the investigation are relevant to concrete constructions in tropical countries where the temperature inside mass concrete could be quite high. The results also allow a critical evaluation of various accelerated tests employing storage temperature upto 80°C.

SCOPE OF EXPERIMENTAL PROGRAMME

In all, 25 naturally occurring aggregate samples were evaluated. The description of the aggregates including modal composition are reported elsewhere (Mullick, 1994). The aggregates did not contain conventionally known reactive silica minerals like Chert, Chalcedony, Opal, Tridymite etc. On the other hand, quartz grains showed strain effect indicative of disorder in crystal lattice. The undulose extinction angle, measured as per the procedure of Dolar-Mantuani (1983) ranged from 11° to 40° and the percentage of quartz showing strain effect 15 in Dolerite to 90 in Quartzites.

The evaluation of aggregates was carried out in mortar bars or concrete prism specimens as well as singly in rapid chemical test, and continuous immersion in KOH, with or

without $Ca(OH)_2$ solution. In the latter case, observations were made using Scanning Electron Microscopy and Optical Microscopy techniques.

MORTAR BAR TESTS

One of the most widely used methods of assessment of concrete aggregates for potential alkali-silica reactivity is measurement of linear expansion in mortar bar specimens. The size of the specimens, mix proportions and test procedures are described in ASTM C-227. These tests, either at 38°C or 60°C, take upto six months to give meaningful results. In order to cut down the time of observation further, procedure evolved at National Building Research Institute of South Africa (NBRI test) envisage storage of mortar bar specimens in 1N NaOH solution at 80°C and expansion after 14 days form the criteria (Oberholster and Davies, 1986). In order to assess the effect of test temperature, mortar bar tests were carried out at 27°C, 38°C, 60°C and 80°C. The results are presented in **Fig 1.**

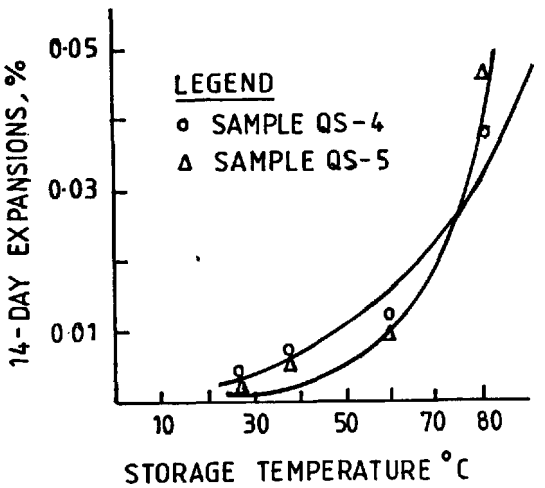

Figure 1 Effect of Temperature on Mortar Bar Expansion

It is observed that linear expansion of mortar bars increased exponentially with test temperature. In the authors' opinion, the accelerating effect of temperature on the slow/late expanding aggregate containing strained quartz was greater than in 'classical' reactive aggregates. To substantiate this, the mortar bar expansions at 38°C and 60°C using high alkali cement in case of aggregate samples containing strained quartz obtained in this investigation and those in case of classical reactive aggregate, as reported in the literature are compared in **Fig 2**. Although the results are only indicative, the regression equations imply that ratio of expansions at 60°C and at 38°C are greater in case of strained quartz type aggregate.

Mortar bar expansions at 80°C, both in 1N NaOH solution (NBRI test) and over water (as in ASTM C-227 test) were compared (Mullick and Wason, 1996). Results in **Table 1** indicate that presence of external alkali solution accelerates the expansion in addition to

that of temperature. Accordingly, combination of presence of external alkalies and increased temperature comprise a severe tests regime for aggregate containing strained

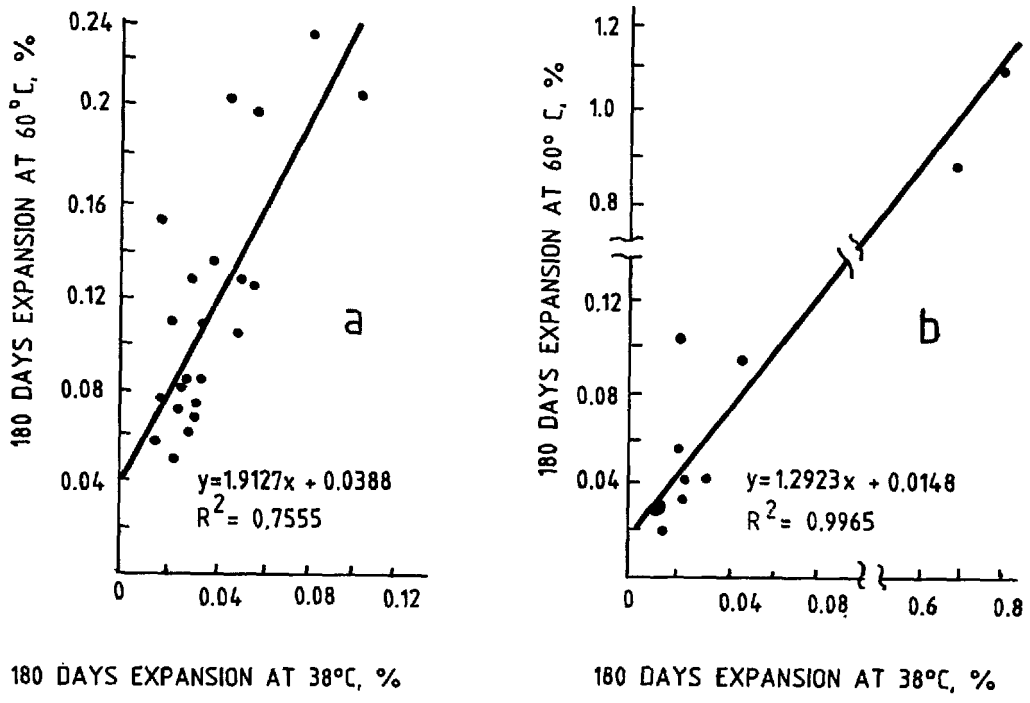

Figure 2 Correlation between Mortar Bar Expansion for (a) Aggregates Containing Strained Quartz and (b) Classical Reactive Aggregates

quartz, which may make NBRI test not discerning enough (Mullick and Wason, 1996). This aspect is examined further in exposure tests of aggregates reported later.

CONCRETE PRISM TEST

Candian Standard CAN 3-A23.2-14A prescribes a method for determination of potential expansion of cement-aggregate combination in concrete specimens of size 75x75x350 mm. With slight modification of the CSA method, storage temperatures of 38°C and 60°C were used in the present investigation. Cement contents (having alkali content of 1.0 percent as Na_2O equivalent) in the concrete mixes were varied so as to result in total alkalies to be 5, 6 and 8 kg per m^3 of the mix.

Table 1 Comparison of Expansions in NBRI and ASTM C-227 Tests at Same Temperature

Sl No	Aggregate Sample	14-day Expansion, %	
		NBRI Test+	ASTM C-227 Test+
1	QS-4	0.1524	0.0380
2	QS-5	0.1884	0.0464

+Test Temperature 80°C in both cases.

Results of linear expansion upto 400 days are shown in **Fig 3**. The ratio of expansions at 60°C and at 38°C generally varied between 2.04 to 1.35, with one value as high as 5.61. For any particular aggregate, the ratio was greater, when the total alkali in the concrete mix was the lowest i.e. 5 kg/m^3.

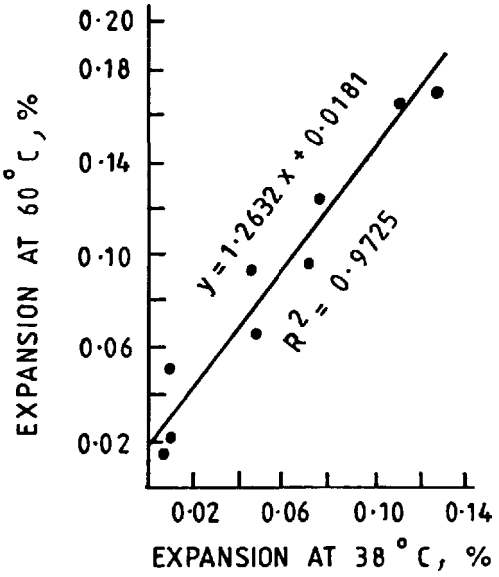

Figure 3 Correlation between Concrete Prism Expansions (Strained Quartz Aggregates)

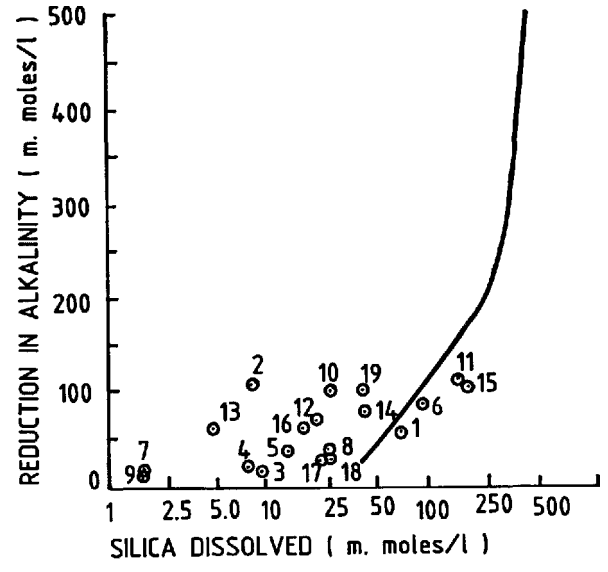

Figure 4 Results of Rapid Chemical Tests for Aggregates Containg Strained Quartz (1 day data)

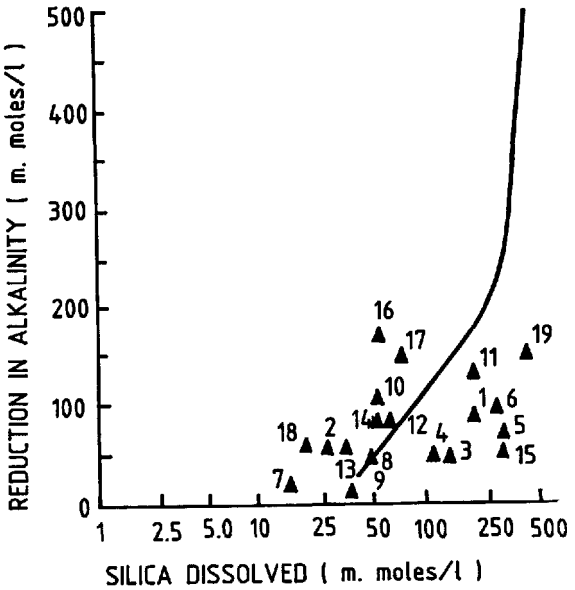

Figure 5 Results of Rapid Chemical Tests for Aggregates Containing Strained Quartz (3 days data)

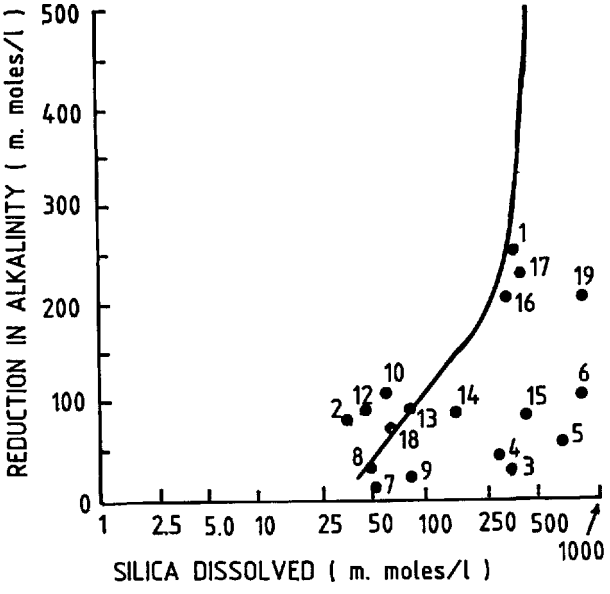

Figure 6 Results of Rapid Chemical Tests for Aggregates containing Strained Quartz (7 days data)

EXPOSURE TESTS ON AGGREGATES

Apart from testing in mortars and concrete mixes, aggregates are also assessed by immersion in alkali solution. Rapid chemical method as per ASTM C-289 is one such method in which the aggregate samples ground to sand fineness are immersed in 1N NaOH solution at 80°C. The dissolution of silica and reduction in alkalinity of the solution after 24 hours form the basis of assessment. The method is not regarded to be reliable for aggregates such as Graywacke, Quartzite, Granite etc. (Oberholster, 1994).

Assessment of the aggregate samples used in this investigation by ASTM C-289 Chemical method has been reported earlier (Mullick, Wason and Sinha, 1992, Mullick, 1994). After 24 hours' exposure, the aggregates were found to be 'innocuous' (**Fig 4**); however, more and more aggregates fell in the 'potentially deleterious' category, as the period of exposure increased to 3 days (**Fig 5**) and 7 days (**Fig 6**). This pattern is consistent with what is expected of slow or late expanding aggregates, where the kinetics of reaction could be different from that of 'classical' reactive aggregates (Mullick, 1994).

To assess the behaviour under exposure to alkali solution for longer time, three aggregate samples containing strained quartz were chosen. The rock types were Quartzite, Graywacke and Diorite. A small chip of each aggregate sample was cut with a diamond saw and stored in a container in 1N KOH solution. In view of the importance of the presence of $Ca(OH)_2$ for occurrence of expansive alkali silica reaction (Diamond, 1989), samples were also stored in solutions of KOH and $Ca(OH)_2$. The containers were kept in oven at 80°C. After continuous exposure of 55 days, the samples were washed and examined under Scanning Electron Microscope and Optical Microscope. The salient results are described below.

SEM + EDAX Study

SEM and EDAX studies were conducted on a Philips SEM 515 with EDAX PV 9900. A typical example of a Quartzite grain after treatment in KOH solution is in **Fig 7(a),** which shows typical cracks associated with disintegration of grains. After treatment with KOH and $Ca(OH)_2$ (50:50) the crumbling of grains and cracking were observed as shown in **Figs 7(b)** and **7(c)** respectively. **Fig 7(d)** shows typical features of reaction products. **Fig 7(e)** shows a representative EDAX spectrum of the reaction products. The elemental analysis of reaction products was quite similar to those reported in case of ASR occurring in concrete structures in service (Samuel, Mullick, Ghosh and Wason, 1984; Mullick and Samuel, 1986) and can be described as lime-alkali-silica gel; so aptly identified and described by Regourd et al (1978) and Thaulow and Knudsen (1975). These tests showed exposure to KOH solution at 80°C led to severe distress to these aggregates, which was further aggravated in presence of $Ca(OH)_2$.

Optical Microscopy

Aggregate samples after prolonged exposure to KOH and $Ca(OH)_2$ solution at 80°C were examined under a Zeiss Polarising Microscope. Thin sections of treated and untreated rock samples were prepared using Canada Balsam for fixing on the glass slide. The grain sizes were determined using occular micrometer. For samples exposed to KOH solution, development of cracks on quartz grains and crumbling and deposition of foreign materials were noticed **[Fig 8(a)]**. For samples exposed to both KOH and $Ca(OH)_2$, severe crumbling of quartz grains and deposition of foreign materials in voids, with some

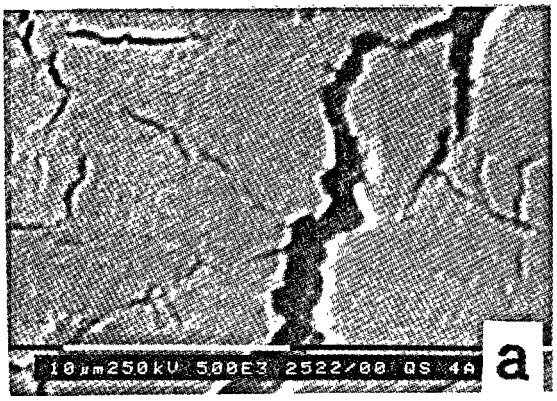

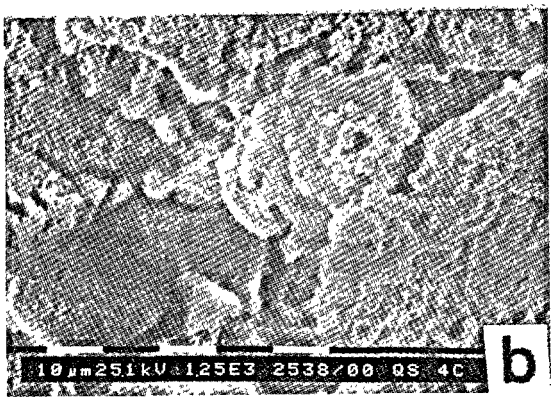

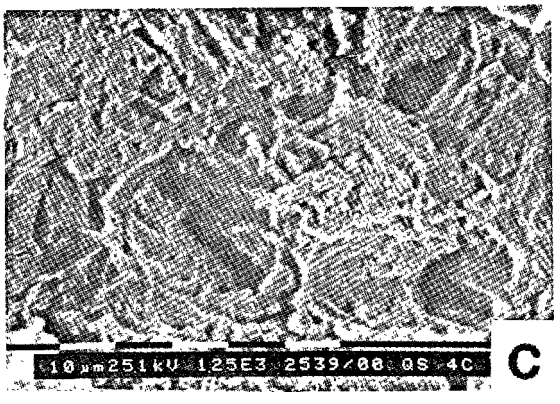

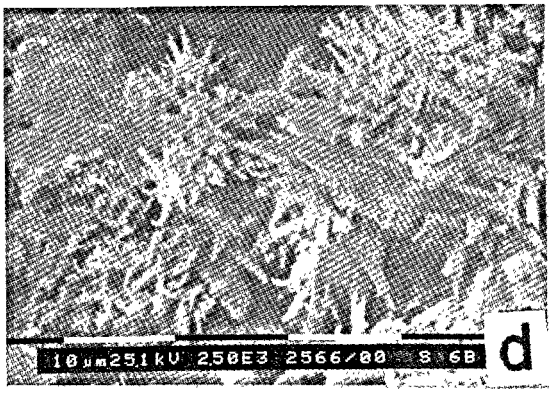

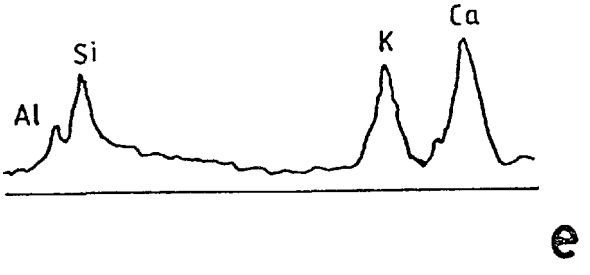

Figure 7 Scanning Electron Micrographs & EDAX of aggregates treated in salt solution at 80°C for 55 days.

(a) Quartzite, KOH
(b) Quartzite, KOH+$Ca(OH)_2$
(c) Quartzite, KOH+$Ca(OH)_2$
(d) Typical Reaction Product
(e) EDAX of Reaction Products

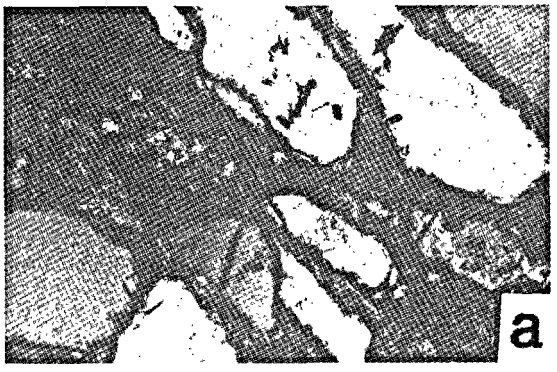



Figure 8 Photomicrographs, x 400
(a) Graywacke, KOH ; (b) Graywacke KOH + $Ca(OH)_2$

faint fractures were visible **[Fig 8(b)]**. However, in no case any change in the percentage of quartz grains showing strain effect and undulatory extinction, as compared to untreated samples, were noticed.

CONCLUSION

Like many other chemical reactions, alkali-silica reaction can be thermally activated. In mass concrete construction in tropical countries, where the temperature inside concrete pour could be of the order of $60^{o}C$ due to heat of hydration, the incidence of ASR could be higher. This fact, and the need of quick results in accelerated tests justify adoption of higher temperatures upto say $60^{o}C$ in testing. However, in presence of abundant alkali solution and storage temperature of $80^{o}C$, the attack on aggregates could be severe and such testing regimes may give unreliable results.

ACKNOWLEDGEMENT

This paper is published with the permission of Director General, National Council for Cement and Building Materials, New Delhi.

REFERENCES

Brown. L.S., "Some Observations on the Mechanics of Alikali-Aggregate Reaction", ASTM Bulletin No 205, 1955, pp 1-9.

Diamond, S., "ASR - Another Look at Mechanisms", Keynote Lecture, Proceedings of the 8th International Conference on 'Alkali-Aggregate Reaction', July 17-20, 1989, Eds. Okada, K., Nishibayashi, S. and Kawamura, M., Kyoto, Japan, pp 83-94.

Dolar-Mantuani, L., "Handbook of Concrete Aggregates, A Petrographic and Technological Evaluation", Noyes Publication, Far Ridge, NJ, USA, 1983, 345 pp.

George Samuel, Mullick, A.K., Ghosh, S.P., and Wason, R.C., "Alkali Silica Reaction in Concrete - SEM and EDAX Analyses", Proc.of the Sixth Int. Conf. on 'Cement Microscopy', March 26-29, 1984, Albuquerque, New Mexico, USA, pp 276-291.

Mielenz, R.C., "Petrographic Examination of Concrete Aggregate to Determine Potential Alkali Reactivity", Highway Research Board, Report 18-C, 1958, pp 29-35.

Mullick, A.K., "Accelerated Tests for Prediction of Service Life of Concrete Structures", Proc. of the Third Int. Conf. on 'Durability of Building Materials and Components', VTT Symposium, August 1984, Espoo, Finland, Vol. 1, pp 123-134.

Mullick, A.K., and George Samuel, "Reaction Products of Alkali Silica Reaction - A Microstructural Study", Proceedings of the 7th International Conference on 'Alkali-Aggregate Raction', August 18-22, 1986, Concrete Alkali Aggregate Reactions, Ed. Grattan-Bellew, P.,E., Ottawa, Canada, pp 381-385.

Mullick, A.K., "Evaluation of ASR Potential of Concrete Aggregate containing Strained Quartz", NCB Quest 1(1), 1987, pp 35-46.

Mullick, A.K., Wason, R.C. and Sinha, S.K., "Potential Reactivity of Quartzite Aggregates containing Strained Quartz", Proc. of 9th Int. Conf. on 'Alkali Aggregate Reaction' July 27-31, 1992, The Concrete Society, London, Vol. 2, pp 673-682

Mullick, A.K., "Alkali-Silica Reaction due to Slowly Reactive Aggregates : Indian Experience", P.K. Mehta Symposium on 'Durability of Concrete', May 23, 1994, Eds. K.H. Khayat and Pierre-Claude Aitcin, Nice, France, pp 175-206.

Mullick, A.K., and Wason, R.C., "NBRI Tets on Aggregate Containing Strained Quartz", 10th International Conference on 'Alkali-Aggregate Reaction in Concrete', August 19-23, 1996, Ed. A. Shyan, Melbourne, Australia, pp 340-347.
Oberholster, R.E., and Davies, G., "An Accelerated method for Testing the Potential Alkali Reactivity of Siliceous Aggregates", C. & C.R 16(2), 1986, pp 181-189.
Oberholster, R.E., "Alkali-Silica Reaction", Fulton's Concrete Technology, Chapter 11, 1994, Ed. B.J. Addis, Portland Cement Institute, Midrand, South Africa, pp 181-207.
Regourd, M. et al, "Microstructure of Concrete in Aggressive Environments", Proc. of the First Int. Conf., August 21-23, 1978, 'Durability of Building Materials and Components', Eds. P.J. Sereda and G.G. Litvan, Ottawa, Canada, pp 253-268.
Thaulow, N. and Knudsen, T., "Quantitative Microanalyses of the Reaction Zone between Cement Paste and Opal", Proc. of the Symposium on 'Alkali-Aggregate Reaction, Preventive Measures', August 1975, Reykjavik, Iceland, pp 189-203.
Tuthill, L.H., "Alkali Silica Reaction - 40 years Later", Concrete International, Design and Construction, ACI, 4, 1982, pp 32-36.

THE INFLUENCE OF CARBONATION ON THE ALKALI-AGGREGATE REACTION MECHANISM

Yushiro KIHARA, Brazilian Association of Portland Cement and São Paulo University, São Paulo, Brazil

ABSTRACT Experimental studies on reactive aggregates (pyrex glass, chalcedony and mylonitic granite) with different reaction rates on NBRI accelerated test allowed us to investigate the influence of carbonation on reducing cement mortar expansion due to alkali-aggregate reaction. The intensity of reaction regulated the quantity of expansive gels in the following order: pyrex glass>chalcedony>mylonitic granite. Carbonation reduced $Ca(OH)_2$ availability to form expansive gels. Porosity was greatly reduced in samples with low expansion rates but little changes occurred in those with high expansion rates.

Key-words: carbonation, durability, alkali-aggregate reaction, porosity

INTRODUCTION

The increasing occurrence of alkali-aggregate reaction affecting concrete structures has motivated interest on studying the reaction kinetics and factors which could minimize expansion effects.

GASKIN (1947) on investigating the effect of CO_2 on the expansion of mortar bars using an alkali-react
minimized
the Moxot
(CAVALCANTI et al., 1989) showed, after regular measurements over a period of 180 days, that injection of CO_2 in a $1m^3$-concrete block decreases expansion rate significantly.

The influence of carbonation on the alkali-aggregate reaction mechanism and on mortar microstructure makes up the subject of this paper.

EXPERIMENTAL PROCEDURES AND RESULTS

Starting Materials

For the experiments, mortar bars were made using ASTM Type I portland cement (with 4% gypsum, 1.37%-Na_2O equivalent) and three potentially alkali-reactive aggregates: pyrex glass, chalcedony gravel and deformed quartz-bearing mylonitic granite.

Experimental Techniques and Results

NBRI South African Accelerated *Alkali-Aggregate Reaction Test and Carbonation Test*.

After demoulding the mortar bars, two bars were cured in water for 28 days and two others were cured for the same period in a carbonation chamber with 10% CO_2. Later on all the bars were immersed in a 1N NaOH solution at 80°C and daily measurements of the bars'length were made. Results are given in Figure 1 and Table 1.

Mercury-Intrusion Porosimetry

Mercury-intrusion porosimetry was conducted with a MICROMERITCS Autopore II-9215 model. Results are listed in Table 1.

Ultraviolet Fluorescence Analysis

The insitu identification of alkali-aggregate reaction was made using the technique described by NATESAIYER & HOVER (1988). The samples were soaked in a uranyl acetate solution and then placed under a short wave ultraviolet lamp and the presence of gels was indicated by the characteristic greenish yellow fluorescence of the uranyl ion selectively adsorbed onto the gel surface. Results observed are showed in Table 1.

Table 1 Results of mortar bar accelerated test, porosimetry and *insitu* fluorescence test.

Mortar bar nr.	Materials	Mortar bar expansion NBRI Test 28 days (%)	Porosimetry (%)	Observation of alkali-aggregate reaction products by fluorescence test
1	Pyrex glass	0,511	23,50	Fluorescence spots disperse and frequent in all samples
2*	Pyrex glass	0,012	23,20	Fluorescence spots distributed preferentially at the borders and rare at the core of the sample
3	Chalcedony	0,200	23,46	Fluorescence spots disperse and common in all samples but less frequent than in nr. 1
4*	Chalcedony	0,019	20,86	Fluorescence spots limited to the borders of the bar, preferentially at the apex
5	Granite	0,056	20,24	Rare fluorescence spots
6*	Granite	0,018	14,06	Fluorescence spots not observed

(*) Carbonated

X-Ray Diffraction Analyses (XRD)

XRD analyses were carrried out using a RIGAKU, DMAX 1.100 with CuKα radiation. XRD-peak patterns emphasizing the carbonation rate are presented in Figure 2.

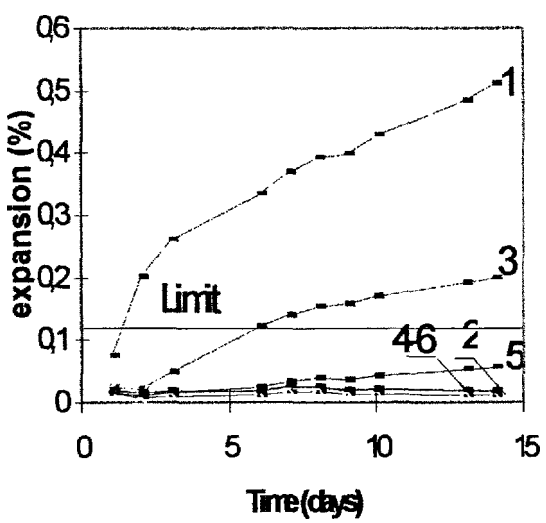

Fig. 1: Expansions of mortar bars.

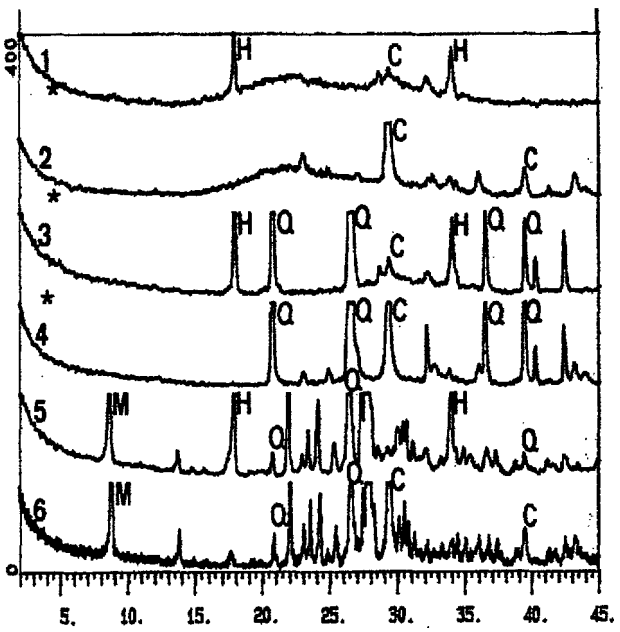

Fig. 2: XRD pattern of mortar bar (H=portlandite, C=calcite,Q=quartz, M=mica).

Scanning Electron Microscopy with Energy-Dispersive X-Ray (EDX)

The scanning electron microscopy (SEM) studies of the microstructure and gel phases found in reaction product were made with a JEOL T300 model SEM photographs are presented in Figures 3, 4, 5 and 6.

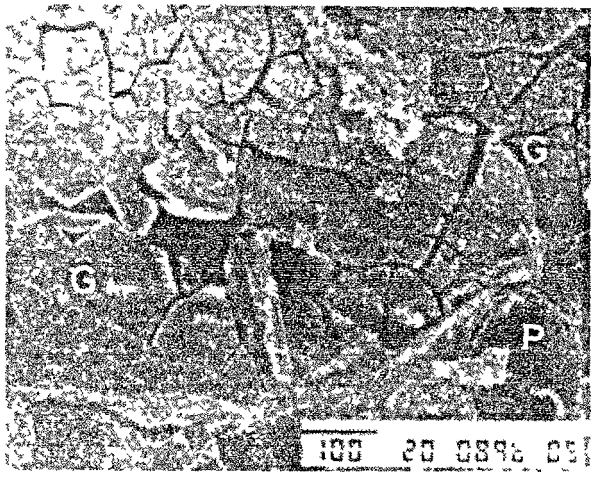

Fig.3: Microcraked pyrex glass (G) with abundant grated gel (sample 1).

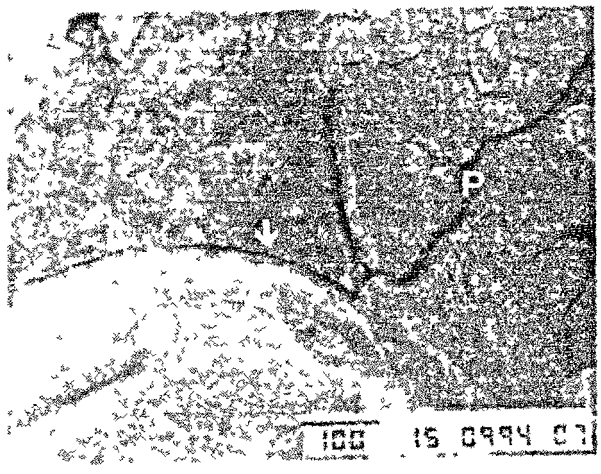

Fig.4: Chalcedony (Q) (sample 3) with reaction border and pore (P) filled with expansive gel

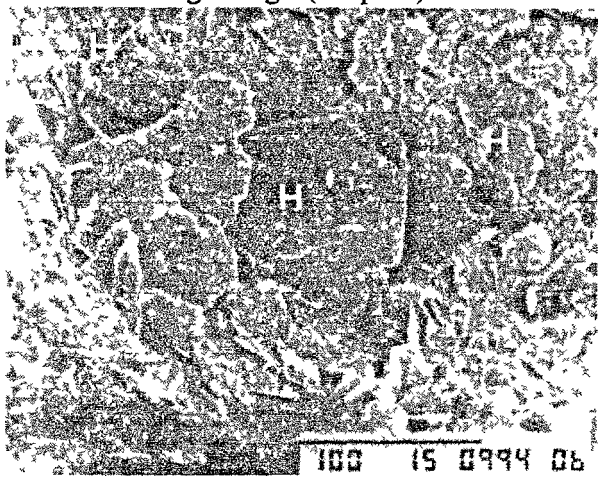

Fig.5: $Ca(OH)_2$, crystals (H) filling void (sample 5, pyrex glass).

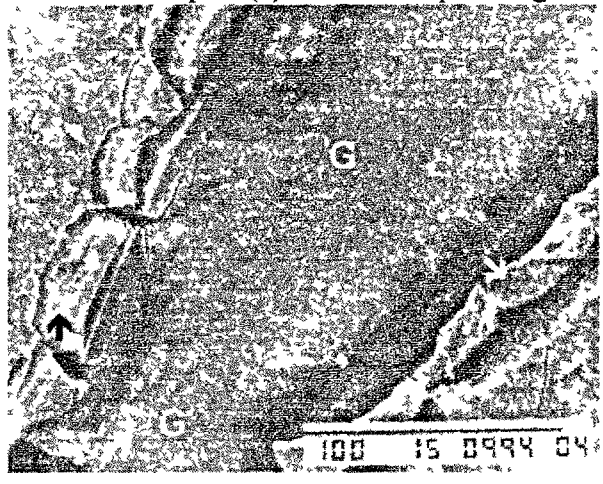

Fig.6: Reaction border with little developed expansive gel (carbonated sample 2, pyrex glass).

DISCUSSION AND CONCLUSIONS

The potentially alkali-reactive aggregates developed distinct expansions in the mortar bars. The pyrex glass showed to be the most reactive on the NBRI accelerated test with mortar bar expansion of 0 511% at 14 days. The mylonitic granite mortar bar presented the lowest expansion (0.019%) and chalcedony mortar bar gave intermediate values (0.20%). Carbonation reduced the expansion of mortar bars made with pyrex glass, chalcedony and mylonitic granite 96%, 86%, and 44% in average, respectively.

Quantity and distribution of expansive gels (Table 1) is regulated by the intensity of reaction which in turn depends on the different kinetics of reaction of silica in the aggregate crystal structure (in this case lower for the strained quartz structure in mylonitic granite, higher for the amorphous silica in pyrex glass and microcrystalline silica in chalcedony). Sample 1, with the

highest expansion rate, presented highly fractured pyrex glass and abundant expansive gel distributed on the grain interface with the paste (transition zone), filling voids and fractured surfaces. Gels were less frequent in sample 3 although reaction borders in some chalcedony grains were observed (Fig. 4). In sample 5 the occurrence of gels was rare and restricted to the mortar pores.

The products of the alkali-aggregate reaction were massive gels, alkali-chalcosilicate in composition with the presence of very small amounts of K and Na, as observed from the EDX spectra. Typical reaction products (DAVIES et al. 1988) were not found and botrioidal gels were rare. $Ca(OH)_2$ hexagonal plaques were encountered on transition zones and in a few pores in the mortar (Fig. 4), their occurrence being more frequent the lower the gels contents, in the following order: pyrex glass < chalcedony < mylonitic granite. Carbonation reduced $Ca(OH)_2$ availability to form gels (Fig. 6) and therefore strongly curbed cement mortar expansions due to alkali-aggregate reaction. Reaction products were limited to the outward regions with a higher concentration at the apex of the mortar bars made with chalcedony and pyrex glass and apparently did not form in the mortar bars with the less reactive mylonitic granite. The abscence of $Ca(OH)_2$ XRD peaks and low expansions in samples 2, 4 and 6 (Table 1) testify for the efficiency of carbonation.

The effect of carbonation on porosity of mortar bars varied according to the intensity of expansion reaction. The mylonitic granite mortar bars with lower expansion, less intense microcracking and higher $Ca(OH)_2$ availability, had porosity 44% reduced while mortar bars made with chalcedony and pyrex glass, with higher expansions, more intense microcracking and lower $Ca(OH)_2$ availability had porosity reduced 12,5% and 1%, respectively. The present measures to minimize the effects of alkali-aggregate reactions on concrete structures are costly and of limited efficacy. Although a controvert issue, studies on the use of carbonation to curb expansion provoked by these reactions are justified in view of the limitations of existent methods and the results obtained in this work.

ACKNOWLEDGMENT

The author would like to express gratitude to ABCP for permission to publish this study and acknowledge A.F. Battagin and E. H. Nakakura for technical support.

REFERENCES

Cavalcanti, A.J.C.T.I. & Silveira, J.F.A., 'Investigations on the Moxotó Power House Concrete Affected by Alkali-Silica Reaction", Proceedings of 8th International Conference on Alkali-Aggregate Reaction, 1989, Kyoto, pp. 797-802.

Davies, G. & Oberholster, R.E., 'Alkali-Silica Reaction Products and their Development', Cement and Concrete Research, v.18, 1988, pp. 621-635.

Gaskin, A.J., 'The Effect of Carbon Dioxide, Studies in Cement-Aggregate Reaction', Bull. 229, Council for Scientific and Industrial Research, Melbourne, Australia, 1947.

Natesaiyer, K.C. & Hover, K., 'Some Field Studies of the New Insitu Method for Identification of Alkali-Silica Reaction Products', Proceedings of 8th International Conference on Alkali-Aggregate Reaction, 1989, Kyoto, pp. 555-558.

Natesaiyer, K.C. & Hover, K., 'Insitu Identification of Alkali-Silica Reation Products in Concrete', Cement and Concrete Research, v.18, 1988, pp. 455-463.

EXPERIMENTAL SIMULATION OF MECHANISMS INVOLVED IN THE BUILDING OF STRESSES IN CONCRETES SUBJECTED TO ALKALI-SILICA REACTION

V. MICHAUD, LAFARGE CANADA INC., C.T.S., Montreal, Quebec, Canada
A. NONAT, C.N.R.S., Laboratoire de Recherches sur la Réactivité des Solides, Dijon, France
D. SORRENTINO, LAFARGE, Laboratoire Central de Recherche, Saint Quentin Fallavier, France

ABSTRACT Alkali silica reaction leads to cracking of concrete. It results from an interaction between reactive silica included in the aggregate particles and the hydroxide ions of the pore solution. Following are the consequences :

- the partial dissolution of the silica and to the ionization of the residual silica,
- the formation of hydrated calcium silicate alkali products by reaction,
- the creation of sufficient stress to generate the cracking of concrete.

The aim of this paper is to improve the understanding of the chemical and physical phenomena involved in the stress creation. It has been demonstrated from a simple model system simulating concrete that the presence of calcium, reactive silica, alkali and hydroxide ions are sufficient to generate cracking of concrete. Silicate solution, residual silica and the product precipitated may be involved. The cracking appears to result essentially from the product reaction formation. The residual silica contribution is not excluded.

KEY-WORDS : Alkali silica reaction, stress, reaction products, residual silica, alkali silicate solutions, osmotic pressure, crystallization pressure.

INTRODUCTION

Alkali silica reaction leads to cracking of concrete and to the formation of a reaction product localized in the cracks and at the aggregate / paste interface. It results from an interaction between reactive silica included in the aggregate particles and the hydroxide ions of the pore solution. As three of the direct consequences of this interaction:

- the reactive silica and the hydroxide ions react together. This leads to the partial dissolution of the silica, thus to the presence of alkali silicate entities in solution, and to the ionization of the residual silica,
- a hydrated calcium, silicate, alkali products is formed by reaction between the alkali-silicate entities in solution and the calcium ions provided by the calcium phases of the cement paste,
- sufficient stress to generate the cracking of concrete are created.

The first two consequences are quite well known. However, the third consequence requires further study. Concerning the latter, some people claim that the residual silica is the major source of the stress creation, whereas some others holds the reaction product is responsible for this. Following are the hypothesis proposed :

- The residual silica would swell by solution absorption (Struble, 1987; Wang and Gillott, 1991; Poole 1992).
- The reaction products would swell by absorbing solution (Wen, 1989). If the products are in confined spaces, stress will be generated.

- The formation of reaction products, by reaction between the calcium ions provided by the cement paste and the alkali silicate entities in the solution resulting from the silica dissolution, and their growths in a confined space would generate stresses. It has been demonstrated by thermodynamics that the formation of a product can create pressure (Ping and Beaudoin, 1992). This pressure known as crystallization pressure would be generated by the better crystallized hydrates calcium alkali silicate reaction products (C-N-S-H and C-K-S-H) (Dron and Brivot, 1993).

These propositions have not been evaluated. In the first two cases, the expansion is commonly associated to osmotic phenomena (Hansen, 1944; Powers and Streinour, 1955; Krogh, 1975; Dent Glasser, 1979; Dent Glasser and Kataoka, 1981; Diamond, 1989). However no real scientific arguments have been brought forward to define the origin of the process and the pressures have never been quantified. Only one experimental work initiated by Krogh (1975) and followed up by Struble and Diamond (1981) has been conducted. The aim was to measure the pressures exerted by water absorption by either reaction products or residual silica; it was not precisely specified. The solid was simulated by synthetic silico-alkali and calco-silico-alkali solids. Nevertheless, although the measured pressures reached in some cases 10 MPa, no conclusion can be drawn from these experiments because :

- the measured pressures were not reproducible,
- the experimental conditions were far from the real ones. The solution absorbed by the solid was pure water and the products had been synthesized by exchange of sodium silicate solution on a resin to obtain a silicilic acid to which hydroxide ions have been added.

The purpose of this paper is to shed some light on the chemical and physical phenomena involved in the stress creation during alkali silica reaction by :

- determining the constituents responsible for generating sufficient stresses leading to concrete cracking.
- making an inventory of the different possible stress sources.
- making an attempt to determine the stress associated to each of these sources.

To reach these objectives, model systems were elaborated.

WHAT ARE THE CONSTITUENTS WHICH ARE SUFFICIENT TO MAKE CONCRETE CRACK BY ALKALI SILICA REACTION ?

The simplest model system representative of a concrete portion, i.e. silica aggregates coated by cementious materials submerged in the pore solution, has been reconstituted and is shown in Fig 1. The components have been chosen to promote alkali silica reaction. The system under study consists of a pellet composed of reactive silica coated with porous cementious matrix composed only of C-S-H and portlandite, submerged in a rather high sodium hydroxide solution concentration (1 mol/kg). The composition of this solution corresponds to that of the pore solution in a cement paste prepared from cement with about 1 % Na_2O eq.

The silica pellet was made by compacting powder silicagel. The porous C-S-H and portlandite matrix were obtained by hydrating C_3S in saturated calcium hydroxide solutions for more than 28 days to hydrate most of it; following is the C_3S hydration reaction :

$C_3S + H_2O \rightarrow C_{(\approx 1.8)}\text{-S-H} + 1.2\ Ca(OH)_2$.

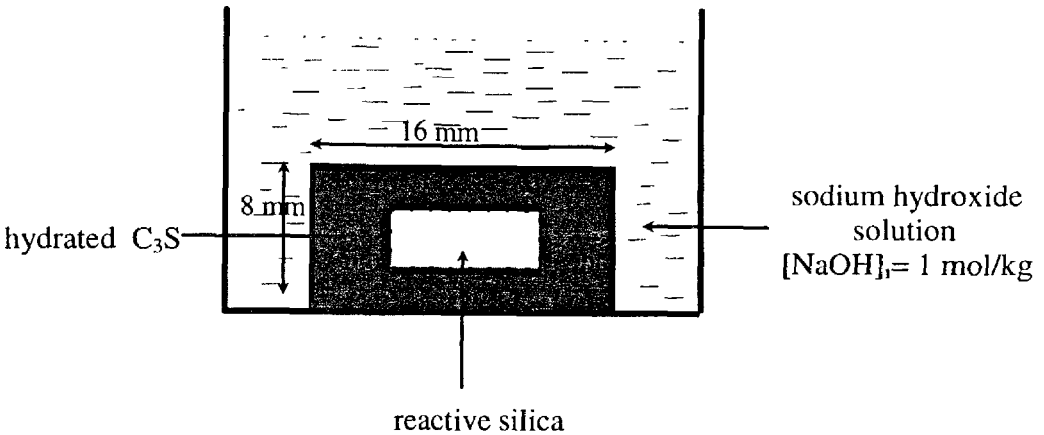

Figure 1 Transverse section of the experimental model which permits the simulation of concrete susceptible to alkali silica reaction.

The state evolution of the "sandwich" was followed up. After 3 or 4 weeks, the "sandwich" was cracked in the silicagel pellet plane (Fig 2).

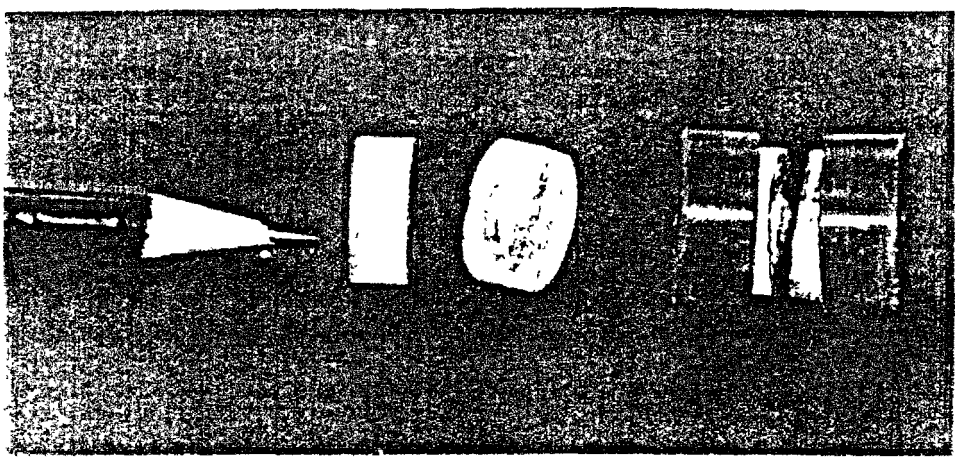

Figure 2 Photograph of the sample composed of a pellet of reactive silica coated with porous cementious matrix (hydrated C_3S) after being submerged in a sodium hydroxide solution with a concentration 1 mol/kg.

Therefore, the sole presence of calcium, reactive silica, alkali and hydroxide ions is sufficient to generate concrete cracking.

WHAT ARE THE DIFFERENT POSSIBLE STRESS SOURCES IN THIS "SANDWICH" AND THE STRESS ASSOCIATED TO EACH OF THEM ?

The system simulating the concrete portion is composed of an alkali solution and silica separated by a porous cement paste. The hydroxide and alkali ions of the alkali solution can therefore diffuse through the cement paste. The hydroxide ions will react with the silica which will lead to the dissolution of part of the silica, therefore to the formation of alkali silica solution in contact with the silica. Consequence of this reaction is the ionization of the residual silica as well.

The reaction between the alkali silicate entities in the solution and the calcium ions provided by the portlandite in the cement paste will lead to the formation of a hydrated calcium, alkali, silicate reaction product.

Consequently, alkali silicate solution, residual silica and reaction product may be involved in stress creation.

It was examined if each of these possible expansion source could generate stresses and if so by what mechanisms. An attempt has been made to quantify the pressure exerted by each of them.

Can stresses be generated by the alkali silicate solution ?

It is well known that alkali silicate solutions are composed of alkali silicate entities with different sizes, varying from monomer to polymer ions when the silicates concentration is quite high, even colloidal particles if it is very high.

Referring to the previously mentioned system, two solutions with different compositions, a sodium hydroxide solution and a sodium silicate solution, are separated by a porous barrier (the cement paste). These two solutions can not be completely mixed together because polysilicate entities can not migrate through the barrier. For reaching equilibrium state, the chemical potential of the solvent (water) have to be equal on both side of the barrier. The chemical potential of the solvent is a function of the activity of the solute which composes this solution and of the pressure exerted on the solution at a given temperature. Since the biggest polyions can not migrate, if the initial activities of the constituents of the alkali-silicate solution is higher than the initial activities of the constituents of the sodium hydroxide solution, in order to equalize the water chemical potential on each part of the barrier, water will diffuse from the sodium hydroxide solution towards the alkali silicate solution to dilute it, until the pressure exerting on the alkali silicate solution compensates the difference of activity of the constituents which compose the solution on each side of the barrier. The resulting pressure will be as high as the difference of activity is high.

Therefore, in this way, the alkali silica solution can generate pressure.

The existence of this pressure has been confirmed with a classic dialysis experiment. The experimental conditions were chosen such that the measured osmotic pressure was maximum. The experimental device is shown in Fig 3.

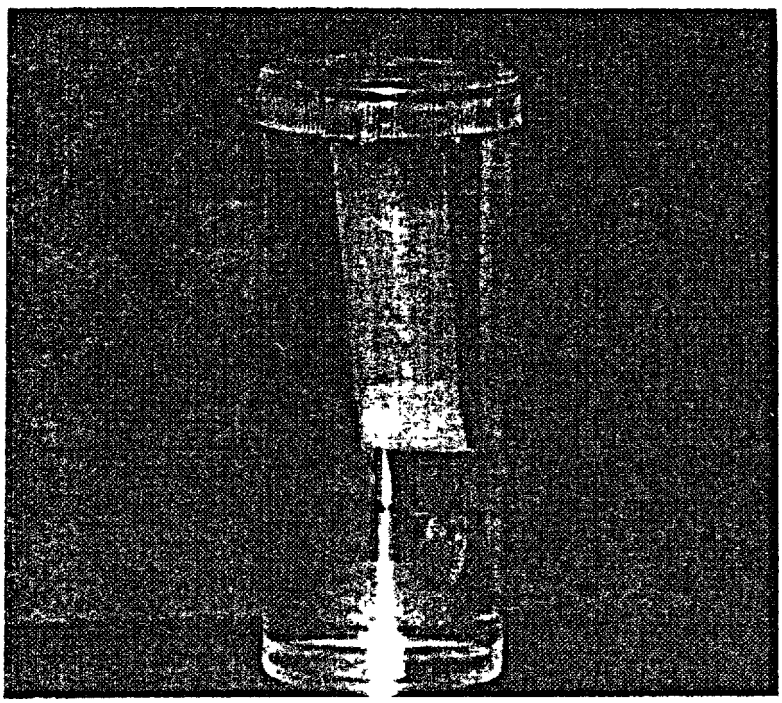

Figure 3 Experimental model used to determine if the alkali silicate sols may generate stresses

A dialysis membrane was filled with an alkali silicate solution composed of large size particles (a colloidal solution) in order to avoid most of the silicate particles going through the membrane. Therefore, a very concentrated alkali silicate solution ($[Na^+]$=0.84 mol/l and $[SiO_2]$ = 1.8 mol/l) was used here. This membrane was submerged in water in order to maximize the difference of solvent chemical potential in the solution inside and outside of the membrane. After 2 hours, the membrane had swollen.
The swelling results from the equalization of the chemical potential of the solvent in the solutions on each side of the membrane by diffusion of water towards the inside of the membrane. The diffusion is also accompanied by a diffusion of a low proportion of the sodium and silicate ions (small-size ions) towards the outside of the membrane. The diffusion stops as the pressure exerted by the membrane on the solution compensates for the difference between the activity of the solute in the solution inside and outside the membrane.

The pressure exerted by the system initially composed of alkali silicate solution and water separated by an osmotic membrane, has been measured by comparison with that exerted by polymers. For the latter, the pressure can be calculated and the relation between the pressure and the concentration is effectively known. The pressure is very low, about 1 kPa.

Can stresses be generated by the residual silica ?
If residual silica is the cause of stress creation, the process involved is osmotic as well. Contrary to the previous case, the presence of a membrane is not necessary to generate osmotic potential.
It is well known that the negative charges of the residual silica are compensated by the positive charges of the alkali ions, and that a part of these latter ions is not condensed.
Therefore, very schematically, if two silica surfaces are facing each other (two surfaces which belong either to the same particle or to two different particles), some alkali ions are not condensed and behave as ions in solution between the two surfaces. Nevertheless, they remain necessary localized between the two surfaces in order to compensate the negative charges of the ionized silica. The alkali ions, which are not condensed on the silica, participate therefore to the activity of the localized solution between the two silica surfaces. This solution is in equilibrium with the one which has a different composition outside the two surfaces. Therefore, if the activity of the solute in the solution between the two surfaces is higher than the activity of the solute in the solution outside of two surfaces, the system will evolve to dilute the solution between the two surfaces until the pressure exerted on the two surfaces compensate for the difference of activity of the solute in the solutions when the system is at the thermodynamic equilibrium.
This pressure has not been measured. No model system has been successfully conceived to isolate the pressure which would be exerted by the residual silica from that exerted by the alkali-silicate solution and the reaction product formation.

Can stresses be generated by the formation of the calcium, alkali, silicate reaction product?
As it has been proposed previously, it can be postulated that the formation of a reaction product from calcium ions and sodium silicate entities, which result from the silica dissolution, and their growth in a confined environment can generate stress.
A model system which permits the formation of a reaction product in a confined environment by avoiding the presence of residual silica was conceived. It was composed of a source of calcium ions and an alkali silicate solution and is presented in Fig 4. Two cementious paste pellets (hydrated C_3S) were in contact to each other and submerged in an alkali silicate solution with a

high silicate concentration ([SiO_2] = 3 mol/l and [Na^+ or K^+]=0.84 mol/l). In this condition, the portlandite resulting from the C_3S hydration constitutes the source of calcium ions.

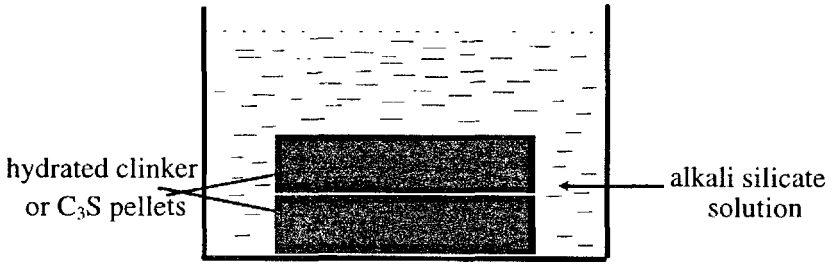

Figure 4 Experimental model which permits the formation of the hydrated calcium alkali silicate reaction product in a confined environment.

The formation of a white reaction product has been observed at the interface between the two pellets. As shown in the Fig 5, its morphology is very similar to that of the of the alkali silica reaction products observed in damaged constructions.

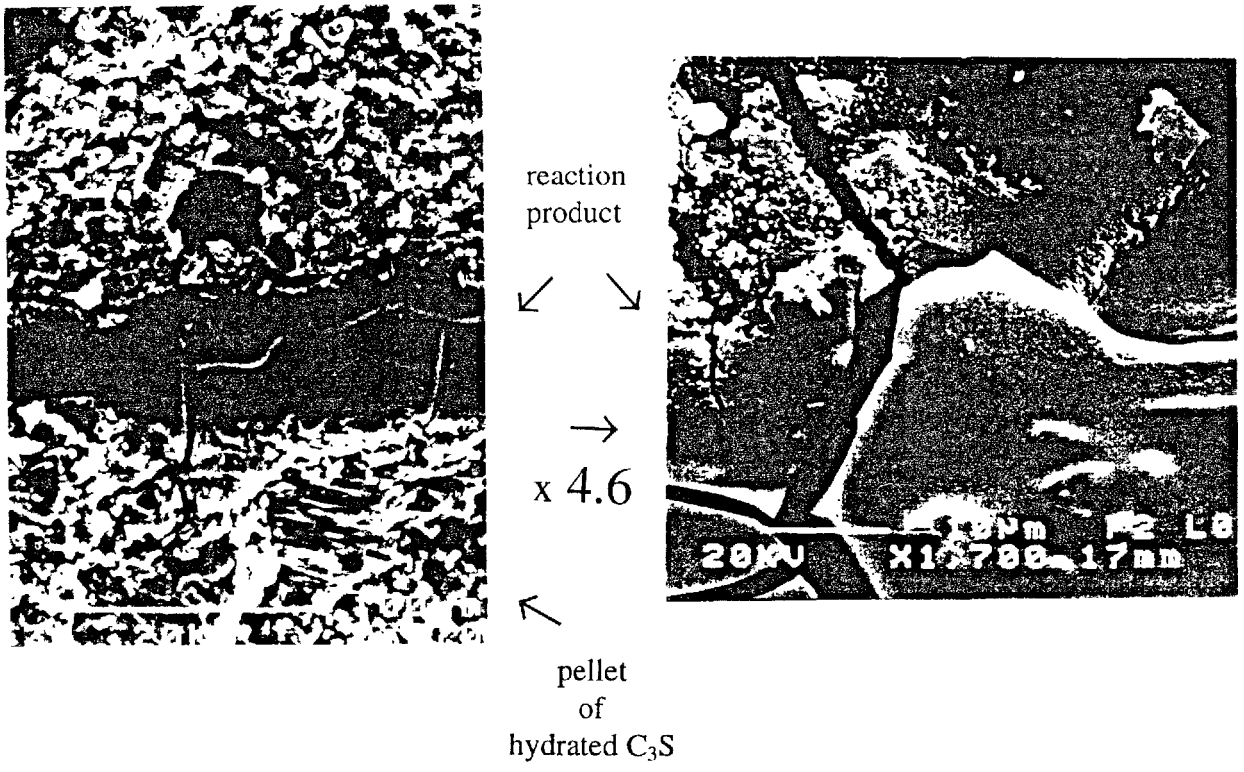

Figure 5 S.E.M. Photographs of the reaction product at the interface of two hydrated clinker paste pellets.
The two pellets initially were in contact to each other and submerged in a sodium silicate solution with alkali and silicate concentrations of 1 and 3 mol/kg respectively.

The changes in pressure exerted by the formation of this product with time was followed with a specially conceived experimental equipment and described below.

Experimental equipment designed to follow the pressure evolution with time generated by the formation of the calcium, alkali, silicate reaction product.

To quantify the pressure exerted by the formation of the calcium, alkali, silicate reaction products, it was necessary to keep the two pellets in contact to each other in a confined environment by preventing any displacement of the pellets and to measure the exerted pressure with time. In this way, the measured pressure would refer to that of the reaction product.

The experimental equipment which was conceived is shown in Figs 6 and 7.

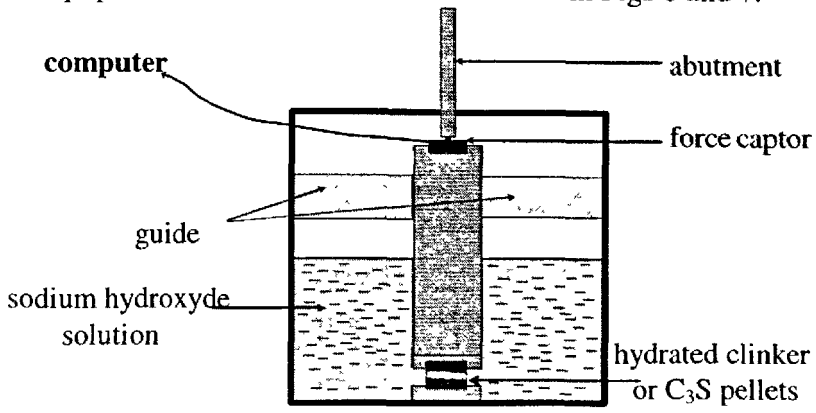

Figure 6 Transverse section of the experimental equipment designed to follow the pressure evolution with time generated by the formation of the calcium, alkali, silicate reaction product.

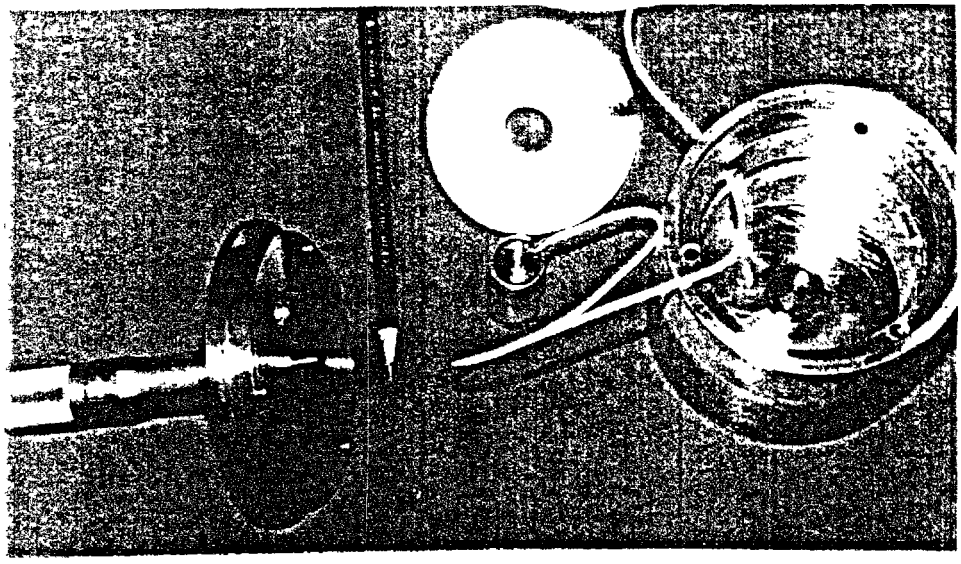

Figure 7 Photograph of the experimental equipment designed to measure the pressure exerted by the system simulating a portion of concrete composed of calcium - silica - alkali and hydroxide ions.

It consists of a stainless steel tank. Each pellet is placed in a support in P.V.C. By attaching one of the supports to the bottom of the tank and the other to a stainless steel shank, the two pellets are in contact to each other. To prevent any movement of these pellets, an abutment is attached to the cover, which is tied to the tank by screws. The pressure exerted by the sample is measured by a pressure captor consisting of a stress guage placed between the top of the shank and the bottom of the abutment [Entran ELM-16A-50].

Actually, the design of the stress guage does not permit to quantity the pressure exerted by the reaction product for two reasons :

- deformation is not totally prevented. The stress guage is effectively composed of a membrane which has a low deformation when effort is exerted on it. Therefore, this equipment permit only to provide an evolution profile of the pressure with time.
- the geometry of the system does not prevent any flow of the reaction product out of the two pellets interface. Therefore, the measured pressure would probably be underestimated.

Evolution profile of the pressure generated by the reaction products

The changes in pressure with time are shown in Fig 8.

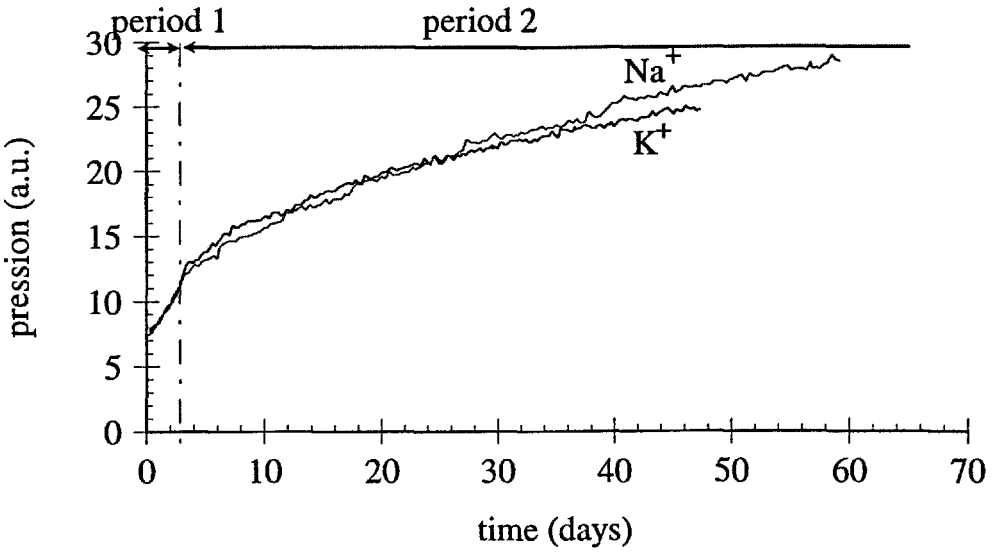

Figure 8 Evolution profile with time of the pressure exerted by the experimental model composed initially of two pellets in contact to each other and submerged in a alkali (sodium or potassium) silicate solution with alkali and silicate concentrations of 1 and 3 mol/kg respectively.
The initial pressure corresponds to the one exerted to maintain the pellets in contact to each other.

The profile of the pressure in time is reproducible and similar whatever the alkali ions nature (K^+ or Na^+) in the alkali silicate solutions. Two periods are distinguished; an initial one characterized by a sigmoidal increase, following by a second one during which the pressure increases slower.
Conductimetry experiments showed that for the first period the increase of the pressure is mainly due to the formation of the reaction products.

CONCLUSIONS

The present study shows that the sole presence of calcium, reactive silica, alkali and hydroxide ions generate a sufficient pressure to make concrete cracking.
Alkali silicate solution can generate pressure but its value is too low to contribute to the disruption of concrete.
Residual silica and reaction product can generate pressure as well. For the former, osmotic phenomena would be the cause. The ability of the reaction product to generate pressure has been confirmed by following pressure with time.

The pressure exerted by the last two sources has nevertheless not been quantified, thus their respective contributions has not been determined.
It is important to keep in mind that the pressure which is necessary to make the concrete cracking can be very lower than the resistance of the concrete. Defects are always present in concrete; therefore, to make the concrete cracking it is not necessary to initiate defects what requires high pressure, but only to propagate the cracks, what requires a very lower pressure.

REFERENCES

Dent Glasser, L.S., "Osmotic pressure and the swelling of gels", Cement and Concrete Research, 9, 515-517 (1979)

Dent Glasser, L.S., and Kataoka, N., "The chemistry of alkali-aggregate reactions", Proc. 5th Int. Conf. on Alkali-aggregate Reaction in Concrete, Cape Town, Paper S252/23, 1-7 (1981)

Diamond, S., "ASR, another look at mechanisms", Proc. 8th Int. Conf. on Alkali- Aggregate Reaction in Concrete, Kyoto, 83-94 (1989)

Dron, R., and Brivot, F., "Thermodynamic and kinetic approach to the alkali-silica reaction. Part 2 : experiment", Cement and Concrete Research, 23, 93-103 (1993)

Hansen, W.C., "Studies relating to the mechanism by which the alkali-aggregate reaction produces expansion in concrete", Journal of the American Concrete Institute, 40, 213-227 (1944)

Krogh, H., "Examination of synthetic alkali-silica gels", in Symposium on Alkali- Aggregate Reaction, Preventives Mesures, Reykjavik, 131-163 (1975)

Maggion, R., "Etude de l'évolution microtexturale de pâtes de silicate tricalcique hydraté", Thèse de doctorat, Université d'Orléans (1992)

Ping, X., and Beaudoin, J.J., "Mechanism of sulphate expansion. I. Thermodynamic principle of crystallization pressure", Cement and Concrete Research, 22, 631-640 (1992)

Poole, A.B. "Alkali silica reactivity mechanisms of gel formation and expansion", Proc. 9th Int. Conf. on Alkali-aggregate reaction in Concrete, London, 1, 782-789 (1992)

Powers, T.C., and Steinour, H.H., "An interpretation of some published researches on the alkali-aggregate reaction, Part 1 : the chemical reaction and mechanism of expansion", Journal of the American Concrete Institute, 26, 497-516 (1955)

Powers, T.C., and Steinour, H.H., "An interpretation of some published researches on the alkali-aggregate reaction, Part 2 : a hypothesis concerning safe and unsafe reactions with reactive silica in concrete", Journal of the American Concrete Institute, 26, 785-811 (1955)

Struble, L.J., and Diamond, S., "Unstable swelling behavior of alkali silica gels", Cement and Concrete Research, 11, 611-617 (1981)

Struble, L.J., and Diamond, S., "Swelling properties of synthetic alkali silica gels", Journal of American Ceramic Society, 64, 6526-655 (1981)

Struble, L.J, " The influence of cement pore solution on alkali-silica reaction", Thesis Ph.D. Purdue University (1987).

Wang, H., and Gillott,J.E., "Mechanism of alkali-silica reaction and the significance of calcium hydroxide", Cement and Concrete Research, 21, 647-654 (1991)

Wen, Z., " Formation et caractérisation de sols alcalins de silice. Conditions de leur transformation en gel au contact de sels et d'hydroxydes, notamment de ceux qui sont présents dans le béton. Etude particulière du rôle de la portlandite", Thèse de doctorat, Université de Bourgogne (1989)

4iv05(
8 pp

INTERFACIAL LONG AGE REACTIVITY OF SLAG/CLINKER COMPACTS

Bernardo MARCHESE, Dipartimento Ingegneria Materiali e Produzione, Facolta' Ingegneria Universita' di Napoli, Italy
Giuseppe FRIGIONE, Dipartimento di Ingegneria Chimica e dei Materiali, Facolta' di Ingegneria, Universita' della Calabria, Italy

ABSTRACT Reactivities of blast furnace slag, ground to 370 m^2/kg, in contact with different aqueous solutions are reported. Disks of slag, clinker and slag+clinker (50+50), five centimeters in diameter, were obtained by cold compaction. Pairs of discs: slag/slag, slag/clinker and (slag+clinker)/(slag+clinker), were separated with filter paper hanging saturated lime solution or distilled water. Each pair was stored in a closed box at room temperature for ten years.
Composition and microstructure modifications of the matching layers of compacts were determined by Scanning Electron Microscopy (SEM), X-ray Diffraction (XRD), Differential Thermal Analysis (DTA) and Thermogravimetry (TG).
A low reactivity resulted in slag in contact with lime solution, while medium reactivity in contact with the alkaline solution from hydrating clinker. Highest reactivity was shown by slag in touch with hydrated phases from clinker. A special reactivity of the slag grain, when activated topochemically by the unique pore solution of hydrating clinker, can be hypothesized.

Key-words: Slag, Reactivity, Interfacial zone, Microstructure, Long age.

INTRODUCTION

The hydration of blast furnace slag is activated by lime of different origins. According to Nurse, Nurse (1964), there is a substantial difference between the activation promoted by $Ca(OH)_2$ saturated solution or by the portlandite liberated by the hydration of Portland clinker silicates. In contrast, Krüger has suggested that the slag hydration reaction is the same whatever is the origin of lime, Krüger (1976).

In slag cements, the slag hydration occurs very slowly in the first stage and with a higher speed then, Hooton (1987). This behaviour has been explained by a mechanism involving the development of a semi-protective layer of hydrates that quickly envelopes the surface of slag grains, decreasing hydration rate of the slag. At the same time, the hydration of clinker grains proceeds increasing in turn the CH content. Then, the CH accumulated outside the slag grains develops a chemical potential between the cores of the unhydrated slag grains and the hydrated cement matrix. "The membrane of hydrated products enveloping the slag grain acts as an ion pump : water diffuses inward to maintain the hydration reaction, while mobile hydrophilic ions (Ca, Si, etc.) migrate in the opposite direction into the more hydrous outer regions", Fig. 10 Glasser (1990).

As the hydration progresses, on the other hand, the clinker grains transform in a cellular matrix of interconnected pores and small particles. In the matrix there are immersed larger grains - phenograins - composed of: CSH, with different crystallinity; calcium hydroxide; and residual unhydrated clinker constituents, Diamond and Bonen (1993).
In the present work the effect on the slag activation due to different source of CH is described.

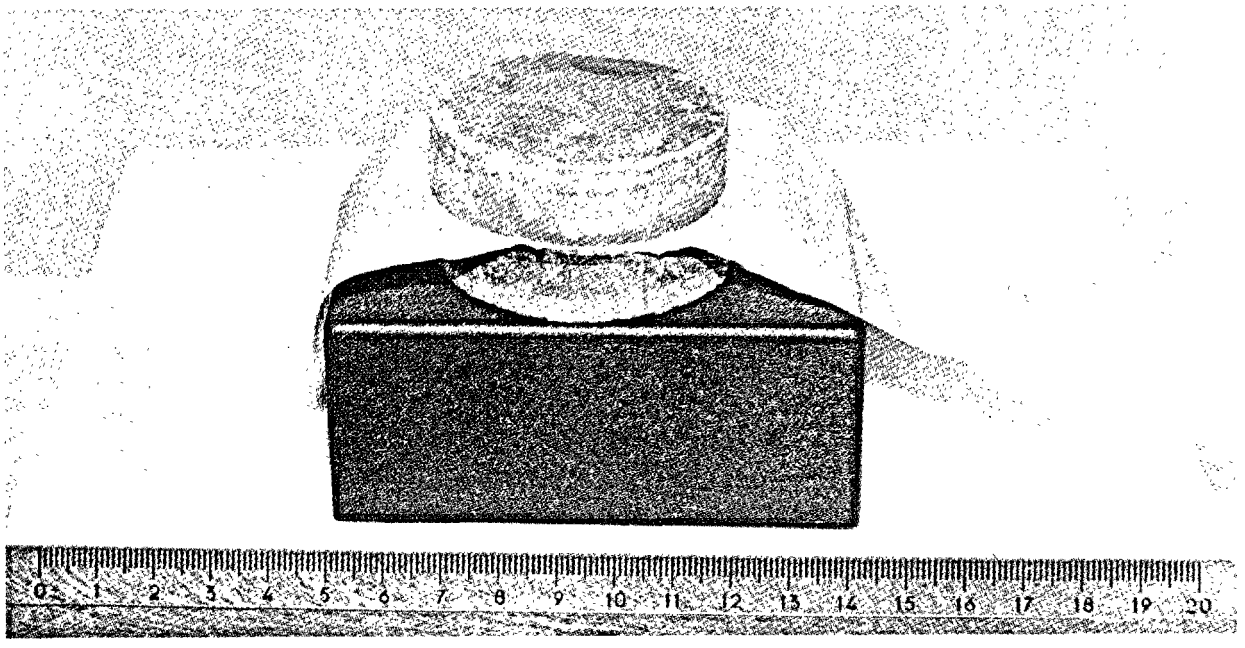

Figure 1 Surfaces of a pair of specimens hydrated by solution permeating through interposed filter paper.

EXPERIMENTAL

Cylindrical specimens, 50 mm in diameter and 15 mm in height, of ground slag, clinker and a mixture of 50slag+50clinker were obtained by cold compaction. Compositions were reported previously, Frigione and Marchese (1996).In different laboratory containers three pairs of discs: slag/slag (L/L), slag/clinker (1L/1K) and (50slag+50clinker)/(50slag+50clinker) (L+K)/(L+K) were kept in contact for ten years through an intermediate filter paper. The filter paper of the first couple was immersed in an oversaturated solution of calcium hydroxide and the one of the others two couples in distilled water. By capillarity the solutions were able to reach the surfaces of specimens.

For the examinations by SEM thin transversal slices of samples were fractured and the two halves were put on the same specimen holder and coated with Au. A Stereoscan Cambridge 240 SEM was used.

XRD patterns were obtained from both the external surface and the internal one obtained by lapping after remotion of a layer of about 200 μm of thickness, for each sample. A Philips PW1710 Series automatic diffractometer was used with a X-ray source of $CuK_{\alpha 1}$ radiation (λ = 1,5406 Å).

The powdered samples obtained by grinding were kept in oven at 60 °C for 24 hr to remove the most of the evaporable water, and submitted to thermal analysis using a Stanton Redcroft STA-780 series simultaneous analyser with an N_2 fluent atmosphere and heating of 10 °C/min.

Actually carbonation does not occur because of the rapid lack of water during the oven-drying, Bakker (1988).

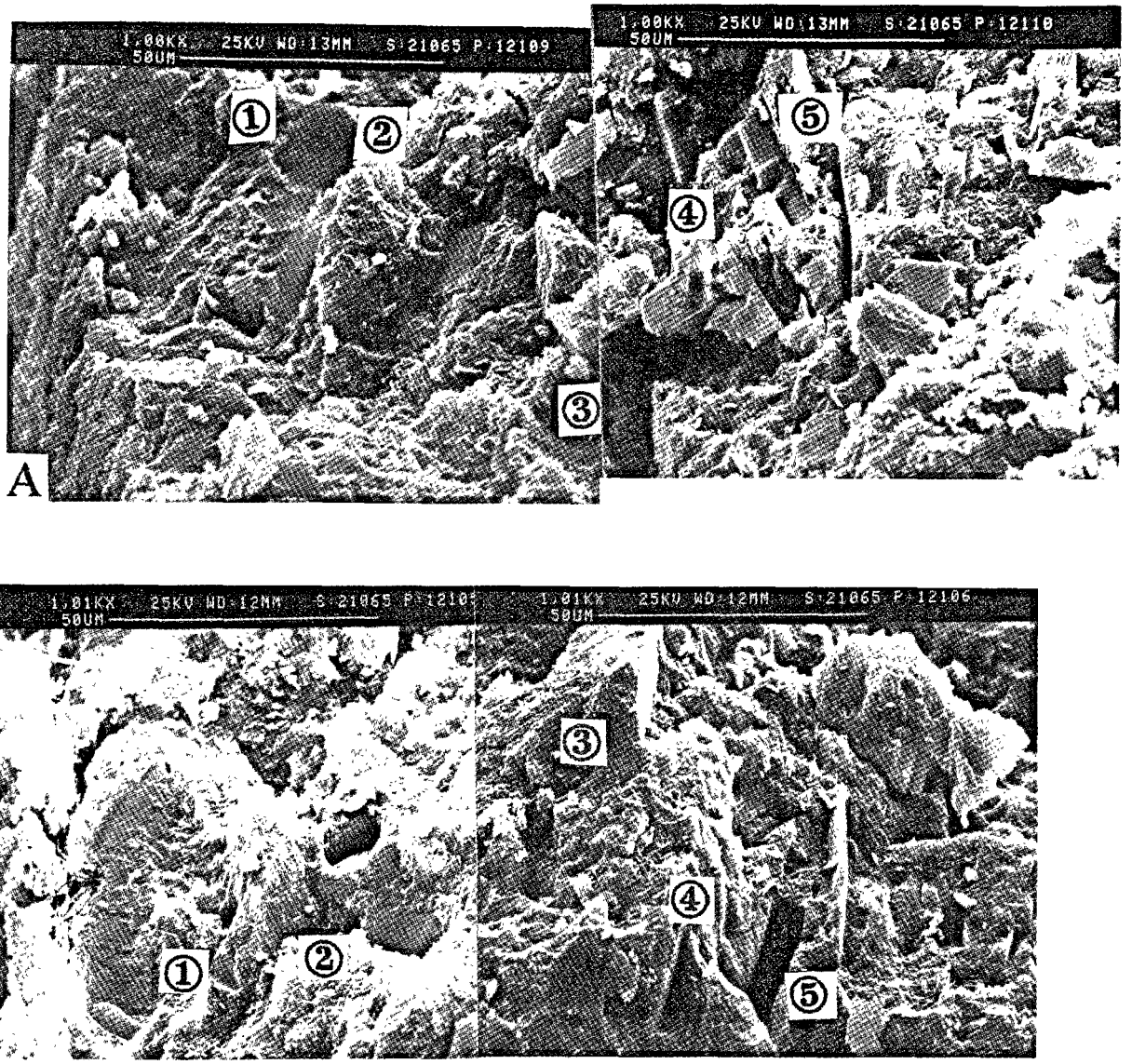

Figure 2 SEM of matching fracture surfaces, A and A', of the slag compact, L. The CH solution was penetrating from the left. Magnification 700x.

RESULTS AND DISCUSSION

SEM Observations

Micrographs in Figs 2, 3 and 4 show selected images of fracture surfaces normal to the external surface in contact with aqueous solution.

In Fig 2 the matching or "twin" surfaces of a slag compact L, show the high porosity of the whole mass. At left in micrographs, large masses, as those marked with 1, were originated by slag grains permeated by the CH solution. However, hydrated products were not able to occupy all the intergranular volume. Isolated grains, like 4 and 5, remain visible with evident smooth surfaces. Areas like 3 are voids left by the slag grains, signed also as 3, visible in the other matching micrograph.

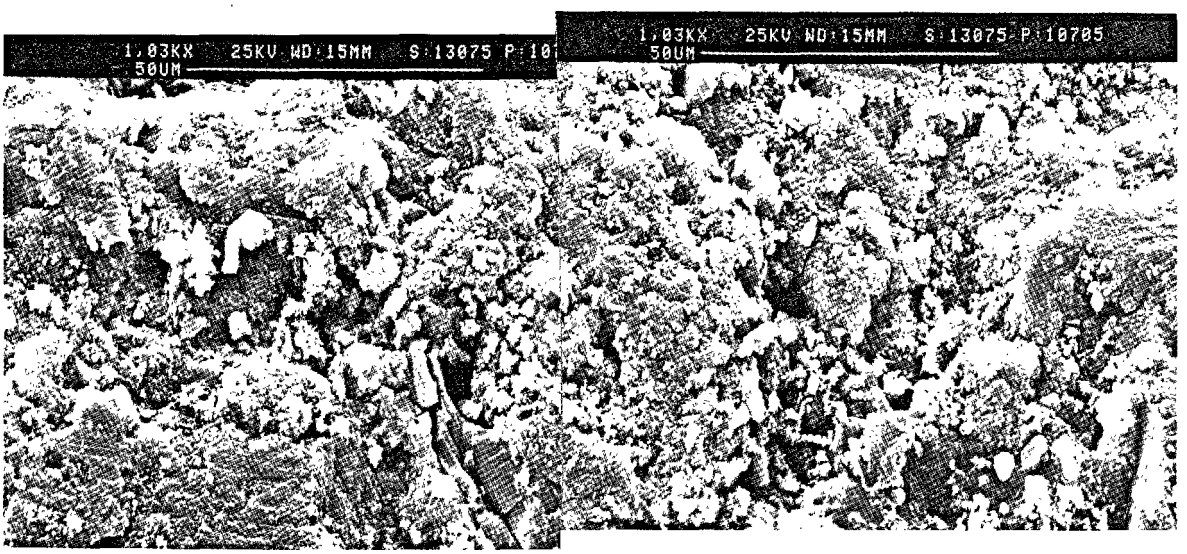

Figure 3 SEM of fracture surface of the slag compact, 1L. The solution from hydrating clinker was penetrating from the right. Magnification 700x.

In Fig 3 the internal mass of the slag compact, 1L, appears composed of slag grains covered by the hydrated products originated by the highly alkaline solution originating from the opposite clinker specimen, 1K. The resulting mass seems less porous than the mass in Fig 2.

Micrographs of matching surfaces reveal instead the very dense mass of the (L+K) compact, Fig 4. Aqueous solution hydrates quickly the clinker grains producing voluminous C-S-H gel which has a tendency to fill the interstitial space and to adhere to the surface of surrounding slag grains. On the other hand a layer of hydrates, just formed on slag surface, operates as a membrane which permits diffusion of OH ions into grain core and diffusion of Ca, Si, Mg, and other mobile ions, in opposite direction, Glasser (1990).

The very high specific surface of C-S-H along with the permeating solution rich in OH^- and other ions make the attack of slag very active controlling at the same time the oversaturation and the precipitation of solid phases.
The hydrated products from both clinker and slag grains are now interconnected and the solution moves freely through their porosities, Bourdette et al (1995). However in some zones, presented by number 3, lamellar CH was evident. Conchoidal smooth surfaces and their impressions, marked 4 and 5, reveal slag grains. The final mass may be described as pseudomorph phenograins surrounded by hydrated products, Diamond and Bonen (1993).

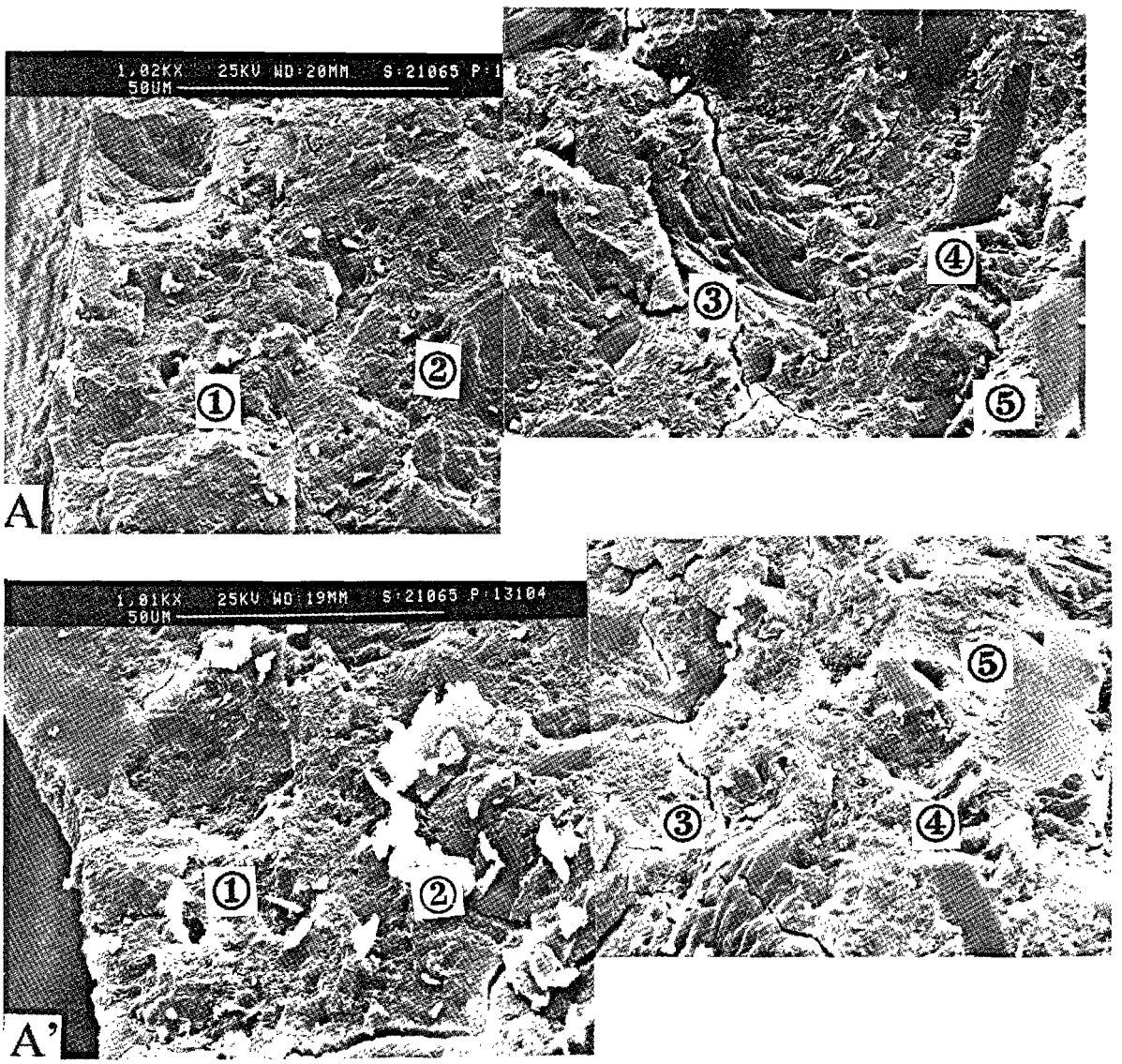

Figure 4 SEM of matching fracture surfaces, A and A', of the 50slag+50clinker compact, L. Aqueous solution was penetrating from the left. Magnification 700x.

X-ray Diffraction

In Fig 5A the broad peak around 28-32 °2θ denotes the vitreous structure of slag. The permeating CH solution originates calcium carbonate and calcite peaks appear in XRD traces of the surface layer. Hydrotalcite-type phases are not well observed due to their low amount, Wang and Scrivener (1995). C-S-H reflexes near the very strong calcite peak confirm the alkaline activation of slag. The XRD trace for underlying surface, at about -180 μm, shows less intense peaks of crystalline phases whereas remains the broad peak of slag for the reduced presence of CH solution.

In Fig 5B the XRD trace of surface of slag (1L) presents intense peaks of calcite due to contact with solution originating by the opposite clinker specimen. They disappear on the intermediate internal surface at -80 μm because the calcite layer was very thin and impermeable.

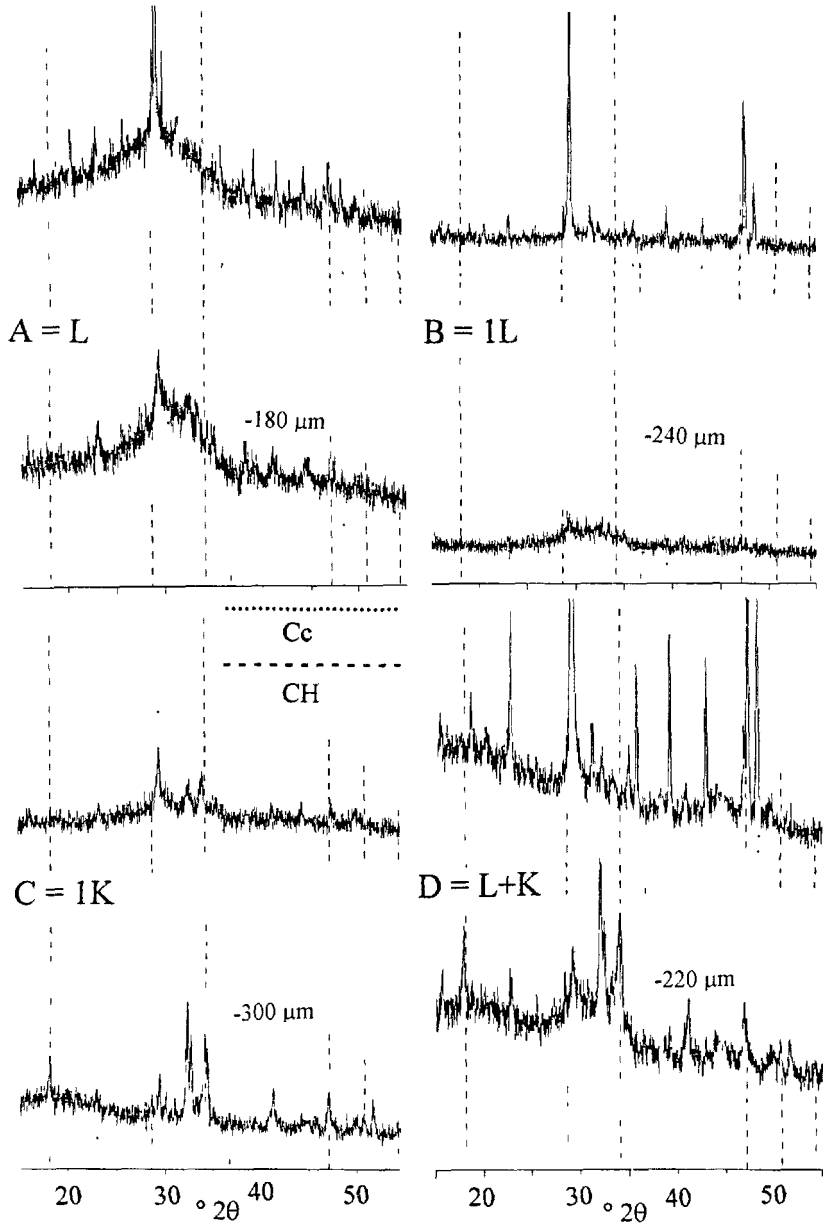

Figure 5 XRD patterns for external surfaces of the specimens and internal ones resulting after remotion of the external layer. A = slag (L), B = slag (1L) at contact with C = clinker (1K), D = 50slag+50clinker (L+K). Calcite (Cc) and calcium hydroxide (CH) lines with intensities from JCPDS index are overimpressed.

In Fig 5C the XRD pattern of the 1K clinker surface reveals peaks of calcite (Cc) with intensities different by the corresponding JCPDS card. They disappear on the internal surface meanwhile the CH, 32 -33 °2θ of C-S-H and also the anhydrous clinker reflexes are visible.

The highest reactivity of 50slag+50clinker sample is evidenced from diffractogram in Fig 5D. On the external surface numerous peaks of the crystalline phases are observed. On the internal surface the carbonation is less evident and the CH peaks with the clinker ones are now emerging.

Thermal Analysis

Aqueous solutions furnished by intermediate filter paper were able to penetrate in the two facing specimens for capillary absorption controlled initially by nature, particle-size distribution and porosity of compact and then by hydrated products of the superficial layers.
From the surfaces previously in contact, two samples of each specimen were removed by lapping and collected. Their hydrated and carbonated phases were detected by simultaneous thermal analysis.
DTA profiles and TG data were used to measure the effects of three endothermal decompositions: (a) C-S-H decomposition and water loss in the 20 - 170 °C range; (b) CH dehydroxilation and water loss in the 400 and 500 °C interval; (c) Calcite (Cc) decarbonation and CO_2 loss in the 550 and 740 °C range, Frigione and Marchese (1996).

Table 1 Weight losses and ratios between weight losses and residues at 900 °C, at two temperature ranges. In (CH) there is added the stoichiometric amount from Cc. Initial mass = 20 mg.

sample	thickness μm	20-400° (C-S-H)	400-740° (CH)	$R_{900°}$	20-400° (C-S-H)/ $R_{900°}$	400-740° (CH)/ $R_{900°}$
L	0 - 90	1,16	0,89	17,73	6,5	5,0
	90 - 180	1,13	0,68	18,06	6,3	3,8
1L	0-80	1,30	1,08	17,32	7,5	6,2
	80-240	1,05	0,41	18,35	5,7	2,2
1K	0-110	1,45	1,60	16,40	8,8	9,8
	110-300	1,38	0,74	17,70	7,8	4,2
L + K	0 - 150	2,92	0,78	13,94	20,9	5,6
	150 - 220	1,75	0,64	17,43	10,0	3,7

Residues at 900 °C are to be considered inversely proportional to the total content of thermolable phases. In fact it is evident that external layers have a hydrated products amount higher than of the internal layers of each specimen. The higher figure was shown by the (L + K) specimen.

Two approximations can be made. The first one was to attribute the weight loss up to 400 °C, indicated as (CSH), to the water of hydrated products, namely CSH, monosulphate and ettringite, Rahman and Glasser (1989). The second one concerns the weight loss between 400 °C and 740 °C, indicated as (CH), which has been considered as due to decomposition of free CH and the CH stoichiometrically equivalent to the Cc content. This latter represents the amount of $CaCO_3$ formed by carbonation of only CH. As a matter of fact the carbonation affects both CH and CSH, Rahman and Glasser (1989).
The first ratio, (C-S-H)/$R_{900°}$, show the highest values for (L + K) samples that is the highest content of hydrated phases. That means that the slag fraction present as 50% in initial mixture, contributed actively to hydrated product. The figure appears even higher than the corresponding of the plain clinker, 1K.
Compared to Portland cements pozzolanic cements have lower portlandite content and higher CSH content (Massazza, 1991).

Also the ratios (CH)/ $R_{900}°$ may indicate the reactivity of mixtures. For the L and 1L slag specimens their values indicate that some solution was penetrating and originating some of CH and/or Cc solid phases.
For the (L + K) sample the low figure for the inner layer means that part of the CH produced by clinker fraction was consuming by the slag fraction resembling the pozzolanic reaction.

CONCLUSIONS

Different hydration degrees have been shown by the cold compacted slag grains after ten years. A low reactivity was shown at contact with the oversaturated CH solution and a medium one with the solution produced by the clinker grains hydration. Highest reactivity was reached in the 50:50 by mass slag:clinker mixture with formation of a well compacted hydrated mass.
Highest reactivity appears to be attributed to the slow transformation of the clinker grains into phenograins which allows the development of chemical potential and increase the hydration of surface layers around the slag grain.
A topochemical attack of the slag grains by cooperation both of the special solid phase formed by the cellular matrix of cement paste and the permeating CH-rich solution could be hypothesized.

Authors would like to thank Mrs A. Annetta and G. Mocci for valid technical assistance.

REFERENCES

Bakker R.F.M., "Initiation Period" Chapter 3 in "Corrosion of Steel in Concrete. Report of the Technical Committee 60-CSC RILEM" Ed. Schiessl P. ,Chapman and Hall, 1988, pp. 22-54.
Bourdette B., Ringot E. and Ollivier J.P., "Modelling of the Transition Zone Porosity", Vol. 25, No. 4, May, 1995, pp. 741-751.
Diamond S. and Bonen D., "Microstructure of Hardened Cement Paste. A New Interpretation", J. Am. Ceram. Soc. Vol. 76, No. 12, 1993, pp. 2993-2999.
Frigione G. and Marchese B., "Reattivita' e microstruttura alla interfaccia clinker/loppa dopo lunga stagionatura", Proc. III AIMAT, September 25-27 1966, Napoli, Ed. De Frede, Napoli, Italy, 1996, pp. 298-306.
Glasser F.P., "Cements from Micro to Macrostructures", Br. Ceram. Trans. J., 1990, Vol. 89, No. 6, pp. 195-202.
Hooton R. D., "The Reactivity and Hydration Products of Blast-furnace Slag", in "Supplementary Cementing Materials for Concrete, Ed. V.M. Malhotra, Canmet Canada, 1987, pp. 245-288.
Krüger J. E., "Contributions to Knowledge of Vitreous Blast-furnace Slag with a High Magnesia Content", D.Sc. Thesis, University of Pretoria, R.S.A., 1976, 175 pp.
Massazza F., "Microstructure of Hydrated Pozzolanic Cements", Proceedings of the International RILEM Workshop "Hydration and Setting of Cements", July 3-5 1991, Dijon, Ed. A. Nonat and J.C. Mutin, E & FN Spon, pp. 393-412.
Nurse R.W., in "Chemistry of Cements", H.F.W. Taylor Ed., Academic Press, London 1964, Vol. 2, pp. 37-67.
Rahman A.A. and Glasser F.P., "Comparative Studies of the Carbonation of Hydrated Cements", Advances in Cement Research, 1989, Vol. 2, No. 6, pp. 49-54.

ALKALI REACTIVITY OF HIGH-CARBON FERROCHROMIUM SLAG AND ITS APPLICABILITY AS AN AGGREGATE FOR CONCRETE

Shin-ichi IGARASHI, Dept. of Civil Engineering, Kanazawa University, Kanazawa, Japan
Mitsunori KAWAMURA, Dept. of Civil Engineering, Kanazawa University, Kanazawa, Japan
Noriyuki ARANO, Denki Kagaku Kogyo Co. Ltd., Omi, Japan
Sotoaki KAWAGUCHI, NKK Corporation, Shin-minato, Japan

ABSTRACT Mechanical properties of high carbon ferrochromium (FCr) slag mortar were investigated. Strength of FCr slag mortar was greater than the mortar with natural river sand, especially in later ages Fluorescence microscopy and SEM examination revealed that failure occurred in the matrix at a distance away from the real interface. Rough surfaces of the slag particles were found to be filled with cement paste matrix. Better performance of FCr slag mortar can be attributed to the greater bond strength due to the reaction of glassy phase with cement paste matrix and the improved mechanical interlocking due to rough surfaces of the grains.

Key-words: Interfacial zone, Microstructure, Slag

INTRODUCTION

Utilization of various industrial by-products as construction materials has been of great interest from the standpoint of saving of energy in the world. By-products such as blast furnace slag and silica fume have already been quite important materials to provide concrete with improved properties. Recently, the ferronickel slag of by-products in the electric furnace has been standardized as aggregate for concrete in Japanese Industrial Standard (JIS) since the quality of ferronickel slag was confirmed to be comparable to that of blast furnace slag. High carbon ferrochromium slag (FCr slag) is also a by-product at the production of ferroalloy. This FCr slag is expected to be used as aggregate for concrete since its mechanical strength is high enough for concrete aggregate. Furthermore, the slag may have additional effects to improve mechanical properties of concretes if the quenching process of the slag leads to the formation of a glass phase. The purpose of this study is to reveal mineralogical compositions of FCr slag in relation to the alkali reactivity with a cementitious matrix. Effects of their reactivity on mechanical properties of the mortar with FCr slag are also discussed in terms of the crack path and microscopic failures around FCr slag grains.

EXPERIMENTAL

Materials and Mix Proportions

The cement used was ordinary Portland cement. Alkali reactivity of FCr slag was determined by chemical method of ASTM C 289. Its Rc and Sc are 37mmol/l and of 73mmol/l, respectively. Physical properties of FCr slag and the natural river sand used as aggregate are shown in Table 1. Water:cement ratios of mortars for compressive strength and wedge-loading compact tension tests were 0.35 and 0.55. The mortar for expansion tests was prepared at a water:cement ratio of 0.50 and a cement : aggregate ratio of 2. In the mortar for expansion

Table 1 Physical Properties of Aggregates

	Specific Gravity	F.M.
Coarse FCr Slag	2.90	6.85
Fine FCr Slag	3.09	3.36
River Sand	2.64	2.49

Table 2 Mix Proportions of Concrete for Expansion Test

Unit Content (kg/m^3)					
C	W	Fine Slag	Coarse Slag	Super-prasticizer	NaOH
400	86	1079	973	4	77.4
500	127	962	868	5	77.4
600	167	847	764	6	77.4

tests, the replacement level of FCr slag varied. Mix proportions of concrete prisms for expansion tests are given in Table 2.

Characterization of FCr Slag

Chemical and mineral compositions of the FCr slag were determined by X-ray diffraction, chemical analysis (JIS A-5011, JIS M-8209～8266, JIS R-5202), polarizing microscopy and SEM-EDXA examinations for the polished surface of the slag grains.

Expansion Test

The mortar bars of 40×40×160mm and concrete bars of 75×75×400mm prisms were stored in a fog box maintained at 40±2℃. The length changes of the bars were measured according to JIS A 5308.

Compressive Strength and Wedge Loading Compact Tension Tests

40 × 40 × 160mm prisms and compact tension specimens (Fig.1) were produced. FCr slag aggregate of which grading was adjusted to have the same grading curve as the river sand, was used in the specimens for the wedge loading compact tension test. All specimens were stored in water at 20℃ for prescribed time. Compressive strength tests for the mortars were carried out according to JIS R 5201.

A crack from a notch was forced to extend by wedge loading. Fracture toughness of the mortars was calculated using Eq.(1). Experimental procedure was described in detail elsewhere (Igarashi and Kawamura, 1995).

$$K_{eff} = \frac{P}{B\sqrt{W}} Y\left(\frac{a}{W}\right) \qquad [1]$$

Fluorescence Microscope and SEM Examination

Cracked specimens after compact tension test were impregnated with the epoxy resin containing a fluorescence die. After the resin hardened, the surface of specimens was polished for fluorescence microscopy (Igarashi and Kawamura, 1995) and SEM examinations.

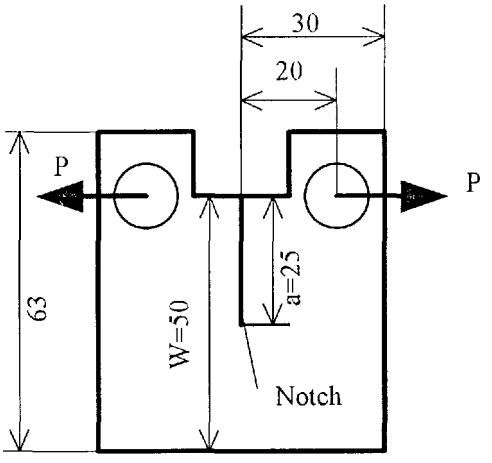

Thickness B=10mm

Fig.1 Wedge-loading compact tension specimen.

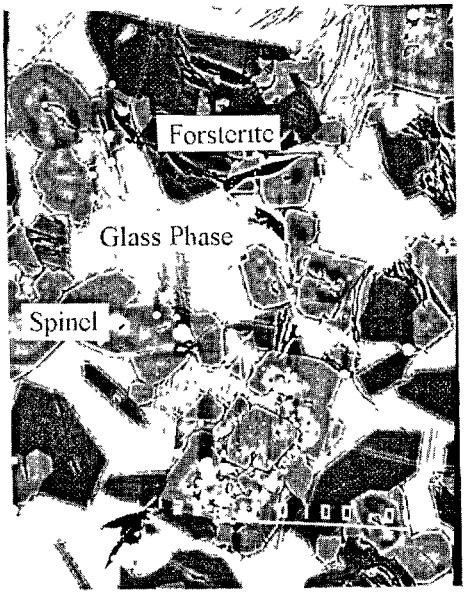

Fig.2 Backscatter electron image of the polished surface of slag particles.

RESULTS AND DISCUSSION

Mineral Compositions of FCr Slag

XRD patterns and polarizing microscopic examination showed that FCr slag had two crystalline phases in a glass matrix. Those crystalline phases were identified

Table 3 Chemical and mineral compositions of FCr slag

Constituent Phases	Chemical Content(wt%)					Mineral Content
	SiO_2	MgO	Al_2O_3	Cr_2O_3	others	(wt%)
Spinel		3.9	11.4	1.4		16 7
Forsterite	11.8	17 2		0.8	4 3	34.1
Glass Phase	22 9	5 5	13.3	2 3	5 2	49.2
Total	34.7	26.6	24.7	4.5	9.5	100.0

as spinel and forsterite. The constitution of the slag was clearly seen in the BEI micrograph (Fig.2). The compositions of the FCr slag determined by chemical analysis are given in Table 3. It is found that the slag mainly consists of SiO_2, MgO and Al_2O_3, and contain other minor components such as Cr_2O_3. EDXA analysis showed that the glass phase was similar to the cordierite of which the formula is $2MgO \cdot 2Al_2O_3 \cdot 5SiO_2$. Analytical results of the mineral compositions given in Table 3 were compared with the phase diagram of SiO_2-MgO-Al_2O_3 system. As expected, the composition of the slag falls in a triangle of spinel-forsterite-cordierite. The mineral contents calculated from EDXA analysis were consistent with those in the phase diagram. Furthermore, it was confirmed that the glass phase was preferably formed since it was hard to crystallize under the condition of the constitution of FCr slag. Consequently, it seems that the constitution of mineral compositions of the FCr slag was controlled by the chemical composition of SiO_2-MgO-Al_2O_3. The characteristics of the slag as an aggregate for concrete was related to the formation of glass phase and its composition.

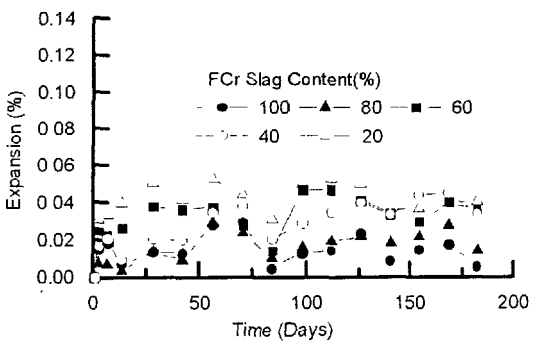

Fig. 3 Expansion of mortars with FCr slag.

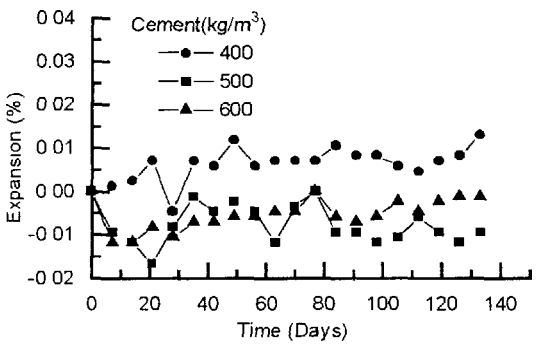

Fig.4 Expansion of concretes with FCr slag.

Alkali Reactivity of FCr Slag

The plot of the value of Rc and Sc for the FCr slag falls in the region of "Deleterious". However, the expansion of the mortar bars with the FCr slag was far lower than the critical value of 0.1% at 6 months (Fig.3). Expansion of the concrete prisms with much added NaOH was also small (Fig.4). Therefore, the use of the FCr slag as an aggregate for concrete is considered not to give rise to the deterioration of concrete due to the alkali silica reaction.

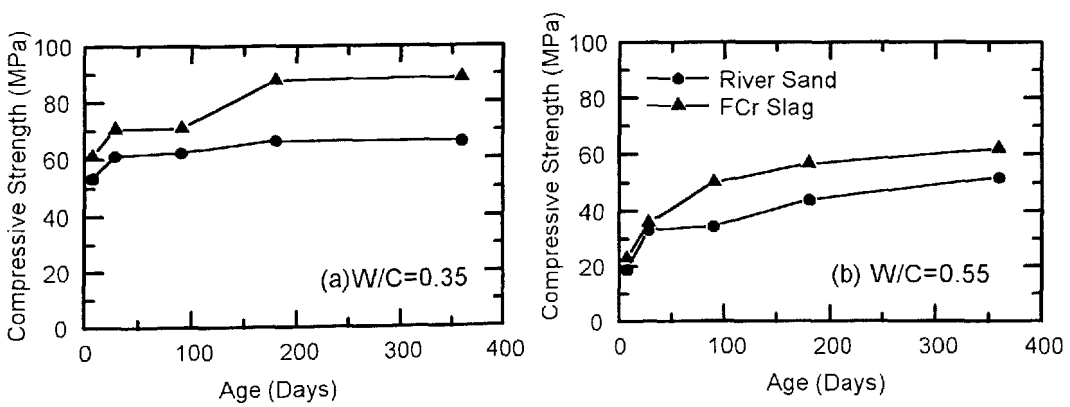

Fig. 5 Comparison in compressive strength between the FCr slag mortar and the control.

Mechanical Properties of FCr Slag Mortar

Fig.5 shows the comparison in compressive strength between the FCr slag mortar and the control. The compressive strength of the FCr slag mortar was greater than the control. The compressive strength of the FCr slag mortar steadily increased with time even after 28 days, while the gain of

strength in the control at later ages was relatively small.

Fracture toughness of FCr slag mortar and the control is shown in Fig.6 At the age of 28 days there was little difference in the values of K_{eff} between both mortars. However, a considerable difference in fracture toughness between both was found at the age of 180 days.

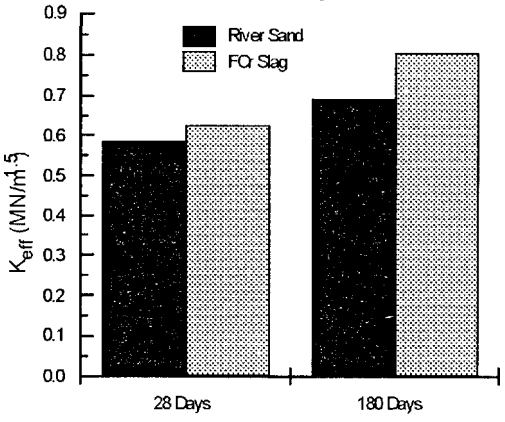

Fig. 6 Fracture toughness of mortars.

Fig.7 shows the crack path of a main crack around the slag particles. A crack propagating toward the slag grain deflected at the interfacial zone. The path of the crack after deflection was apart from the real interface between the slag particle and the cement paste. A bright rim, which is a portion of the matrix seems to be attached to the surface of the slag. Namely, debonding has not occurred in the real interface, but in the weak interfacial transition zone formed apart from the real interface. As mentioned earlier, the FCr slag is reactive to some extent. It seems that chemical interaction took place to form a stronger bond across the real interface, and a crack shifted into porous areas (Bentur, 1990).

Fig.8 also shows the crack propagating in the vicinity of FCr slag particles. A crack appears as a dark gray area at the center of the micrograph, because cracks were filled with the epoxy resin. The main crack appears to have passed about 50 μm away from the aggregate surface. The FCr slag particles have irregular shape and uneven surface. However, cement paste fully penetrated into the concavities of the surface of the slag particle. These geometrical effects also lead to the greater bond by mechanical interlocking. It is suggested from Figs. 7 and 8 that greater strength and toughness of the mortar with the FCr slag can be attributed to the increase in bond strength due to those chemical and mechanical functions between the slag particles and the cement paste matrix.

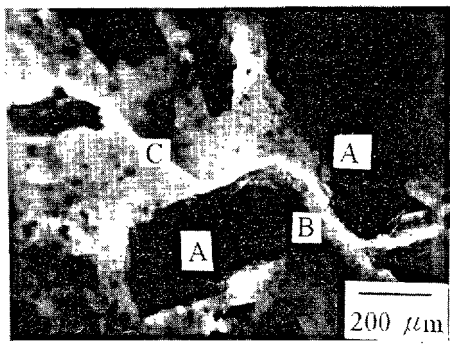

Fig. 7 Crack path around FCr slag particles. (A:aggregate B:original surface C:crack)

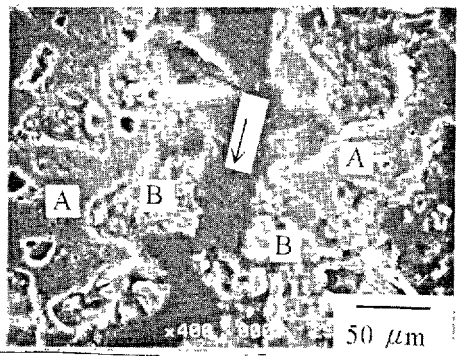

Fig.8 Mechanical interlocking by rough surfaces of the FCr slag particles. (A:aggregate B:cement paste ↓ :crack path)

CONCLUSIONS

The FCr slag has the potential reactivity with cement paste matrix. However, the reaction does not result in the deterioration of concrete due to the alkali silica reaction. On the contrary, the reactivity of the FCr slag contributed to the increase in bond between aggregate and cement paste. Irregular geometry of the slag particles also contributed to the increase in bond strength and crack growth resistance. Those interactions can enhance the function of aggregates as reinforcement and crack arresters.

REFERENCES

Bentur, A., Ceramic Transactions (ed. S. Mindess), Am. Ceram Soc., Vol.16, pp.523-549, 1990.

Igarashi, S. and Kawamura, M., J. of Am. Ceram Soc., Vol.78, No.7, pp.1715-18,1995.

INFLUENCE OF SILICA AND LIMESTONE AGGREGATES ON THE FINAL COMPRESSIVE STRENGTH OF BLENDED CEMENT CONCRETES PREPARED WITH THE USE OF THREE DIFFERENT POZZOLANAS

Kosmas K. SIDERIS. Reinforced Concrete, Democritus University of Thrace, Xanthi, Greece
Athena E. SAVVA. Building Materials, Democritus University of Thrace, Xanthi, Greece
Katerina D.BALTZOPOULOU Buil. Materials, Democritus University of Thrace, Xanthi,Greece
Christos M. ECONOMOU Reinf. Concrete, Democritus University of Thrace, Xanthi, Greece
Konstantin SIDERIS Building Materials, Democritus University of Thrace, Xanthi, Greece

ABSTRACT. The cement hydration equation is applied to determine the equation of the compressive strength of concrete. The equations of the compressive strength of fourteen concrete mixtures, prepared with different blended cements and silica and limestone aggregates, were defined. Based on these equations the influence of the pozzolana content and of the aggregate's type on the compressive strength is examined.

Key-words: Cement hydration equation, concrete strength development, blended cements.

INTRODUCTION

Concrete's compressive strength is one of the material's properties affecting the safety of the structures. During the last decates several reasons forced the Cement Industry at the production of pozzolanic cements. In most cases these cements develop the major part of their compressive strength after the age of 28 days (Figs 1 and 2) , due to their different mineralogical composition.

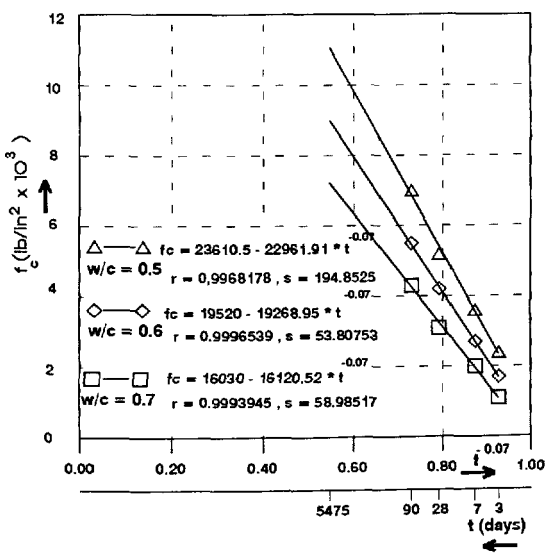

Figure 1: Compressive strength of concrete versus modified time scale. [measured values taken from Lea (1970)].

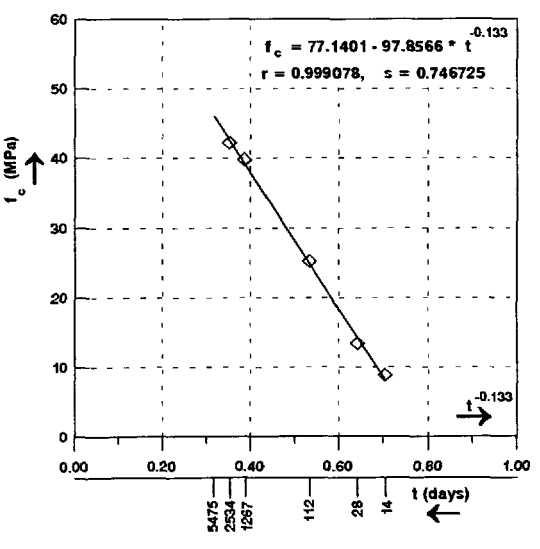

Figure 2: Compressive strength of concrete versus modified time scale. [measured values taken from Hansen (1990)].

This observation led several investigators to perform long-term laboratory tests in order to compare the performance of blended cement concretes with this of Portland cement concrete (OPC concrete). Most of these tests stopped at the age of 2 or 3 years, mainly because of the difficulties of the long-term studies.

In this work the final compressive strength of fourteen concrete mixtures, made with silica and limestone aggregates, is experimentally investigated. The calculation of the concretes' compressive strength at older ages was obtained with the use of the cement hydration equation $K= K_{\infty} \pm b*t^{-p}$ according to Sideris (1993). When the hydration criterion K of the concrete's compressive strength is examined, this equation takes the form:

$$\mathbf{f_c = f_{c\infty} - b*t^{-p}},$$

where: f_c: the concrete compressive strength at any age t (days)

$f_{c\infty}$: a constant, determined with the aid of linear regression

b : is the slope of the straigth line determined with the aid of the linear regression

t: is the age of hydration (days, t>>0)

p: is the hydration number depending only on the chemical composition of the cement type used.

The cement hydration equation was applied to the compressive strength of concrete which determined for a hydration time up to 90 [Karayannis (1994), Sideris K.K. et al (1994), Sideris K.K. et al (1995)], 365 [Sideris K.K. et al (1994)], 730 [Sideris K.K. et al (1994), Sideris K.K. et al (1995), Sideris K.K. et al (1996)], 840 [Sideris (1993)], 1095 [Sideris et al (1994)] and 2534 days [Hansen (1990)]. For the above examples (Figs 1, 2) the measured values of the concrete compressive strength were taken from Lea (1972) and Hansen (1990). In the second case long term laboratory tests were performed up to 2534 days (7 years).

EXPERIMENTS

The blended cements used in this research were prepared by the replacement (wt%) of OPC by three different pozzolanas: one natural pozzolana (Santorini earth - SE) and two lignite fly ashes, a high-calcium fly ash (Ptolemaida fly ash - PFA) and a low-calcium fly ash (Megalopoli fly ash - MFA) (Table 1).

Evaluation of the hydration number p

In order to determine the hydration number of the seven cements used, cement paste specimens were prepared. These specimens were prisms 4X4X16 (cm) which were prepared and cured according to DIN 1164. The water to binder ratio was 0.45 and the specimens were crashed and tested at the ages of 3, 7, 14, 28, 60 and 90 days. Using linear regression for the pairs (β_{Dmeas} - t^{-p}), the hydration number p was estimated for each case, according to the procedure described by Sideris (1993) and Sideris K.K. (1996). The estimated p values are shown in Table 2.

Compressive strength of concrete

Fourteen concrete mixes -twelve blended cement concretes and two OPC concretes- were prepared as it is shown in Table 1. A binder (cement + pozzolana) content of 300Kg/cm^3 and a water to binder ratio (w/(cement + pozzolana)) = 0.60 was used in each case. Broken silica stone and limestone aggregates of the area of northern Greece were used. The aggregates' grading curve was equal to the curve B32 of the standard DIN 1045.

The concrete specimens were cubes 15X15X15 (cm) which were cured at 20±2° C in a room with a relative humidity of 95-98° C. Crash tests were performed at the ages of 3, 5, 7, 14, 28, 60 and 90 days. The compressive strength for each age was calculated as the mean strength of the experimentally measured values of three cubes. Results are shown in Table 1.

Defining the concrete compressive strength equations

Based on the measured concrete compressive strength for each age and the hydration number p estimated above, linear regression was performed for the pairs ($f_{c,meas(t)}$ - t^{-p}), for each mixture. The method of drawing up the compressive strength equations is explained in Table 3 with the aid of the measured values of concrete mixture 1. Using the results of the linear regression, the equations of the compressive strength for each mixture were deduced (Table 2). With the use of these equations, the accurate estimation of the concrete compressive strength at the ages of 7, 28, 60, 365 and 5475 days (final hydration time) was possible. The so calculated values are shown in figures 3-8. The end of the hydration was estimated to be at the age of 15 years (5475 days), according to Sideris (1993).

Table 1 Concrete mixtures prepared and compressive strength's values measured (MPa).

Concrete Mixture		Hydration time (days)						
		3	5	7	14	28	60	90
1	OPC - Limestone Aggregates	28.14	31.40	33.42	37.77	40.90	42.77	43.50
2	OPC - Silicate Aggregates	20.88	26.00	27.28	32.06	35.15	37.51	39.10
3	90% OPC+10%SE - Limestone Aggregates	23.26	28.65	33.04	36.75	37.93	44.45	45.97
4	90% OPC+10%SE - Silicate Aggregates	16.84	21.15	24.20	28.98	32.90	40.71	41.40
5	70% OPC+30%SE - Limestone Aggregates	18.13	20.85	22.81	25.82	29.91	33.69	35.22
6	70% OPC+30%SE - Silicate Aggregates	11.79	15.20	17.91	21.94	26.24	33.26	34.43
7	90% OPC+10%PFA - Limestone Aggregates	28.71	32.20	35.53	39.42	44.00	48.00	50.00
8	90% OPC+10%PFA - Silicate Aggregates	22.50	27.10	30.30	35.47	41.06	43.40	45.78
9	70% OPC+30%PFA - Limestone Aggregates	21.76	26.64	29.45	35.19	39.42	41.55	45.74
10	70% OPC+30%PFA - Silicate Aggregates	17.82	23.12	25.92	33.02	39.12	42.27	46.67
11	90% OPC+10%MFA - Limestone Aggregates	26.62	30.90	34.12	37.20	42.42	46.06	47.71
12	90% OPC+10%MFA - Silicate Aggregates	17.61	23.13	27.08	30.95	37.96	41.64	44.10
13	70% OPC+30%MFA - Limestone Aggregates	21.40	24.50	27.20	33.44	37.47	40.53	43.20
14	70% OPC+30%MFA - Silicate Aggregates	15.00	19.30	21.94	27.55	34.55	41.55	42.98

Table 2 Compressive strength equations of the concrete mixtures prepared.

Concrete Mixture		Compressive strength equations
1	OPC - Limestone Aggregates	$f_c = 50.9832 - 33.7012 * t^{-0.346}$, r=0.998113, s=0.401586
2	OPC - Silicate Aggregates	$f_c = 46.9574 - 36.6971 * t^{-0.346}$, r=0.998374, s=0.416906
3	90% OPC+10%SE - Limestone Aggregates	$f_c = 71.1413 - 56.9061 * t^{-0.181}$, r=0.986766, s=1.449846
4	90% OPC+10%SE - Silicate Aggregates	$f_c = 70.8497 - 66.5083 * t^{-0.181}$, r=0.994844, s=1.051241
5	70% OPC+30%SE - Limestone Aggregates	$f_c = 81.1808 - 70.1802 * t^{-0.094}$, r=0.999020, s=0.316322
6	70% OPC+30%SE - Silicate Aggregates	$f_c = 95.8980 - 93.8254 * t^{-0.094}$, r=0.996292, s=0.825159
7	90% OPC+10%PFA - Limestone Aggregates	$f_c = 99.3779 - 79.2191 * t^{-0.106}$, r=0.999141, s=0.364983
8	90% OPC+10%PFA - Silicate Aggregates	$f_c = 100.100 - 86.2912 * t^{-0.106}$, r=0.994683, s=0.992583
9	70% OPC+30%PFA - Limestone Aggregates	$f_c = 150.189 - 135.631 * t^{-0.058}$, r=0.991830, s=1.210064
10	70% OPC+30%PFA - Silicate Aggregates	$f_c = 176.435 - 168.309 * t^{-0.058}$, r=0.995917, s=1.058176
11	90% OPC+10%MFA - Limestone Aggregates	$f_c = 67.7441 - 51.7148 * t^{-0.211}$, r=0.998145, s=0.526741
12	90% OPC+10%MFA - Silicate Aggregates	$f_c = 69.1457 - 64.6596 * t^{-0.211}$, r=0.997613, s=0.747309
13	70% OPC+30%MFA - Limestone Aggregates	$f_c = 72.9184 - 62.1755 * t^{-0.164}$, r=0.997251, s=0.679036
14	70% OPC+30%MFA - Silicate Aggregates	$f_c = 82.0091 - 81.6413 * t^{-0.164}$, r=0.996015, s=1.074466

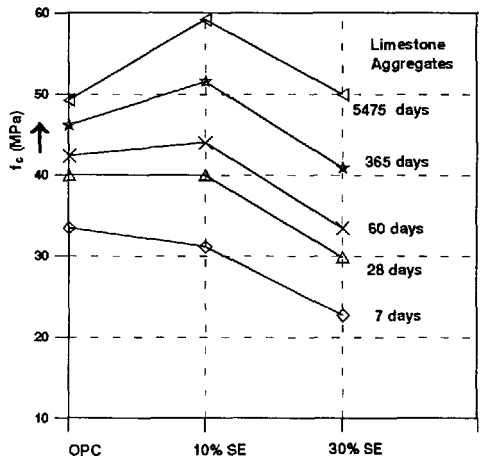

Figure 3: Compressive strength of different SE concretes for various hydration age.

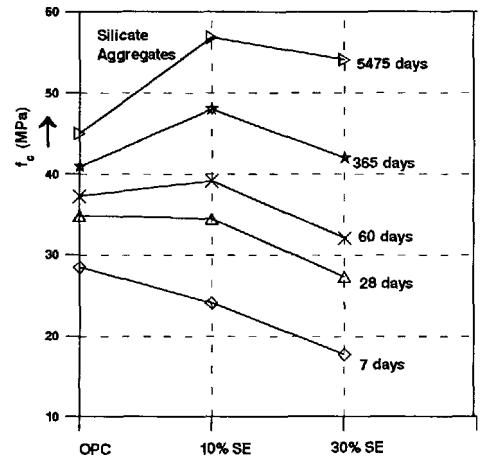

Figure 4: Compressive strength of different SE concretes for various hydration ages.

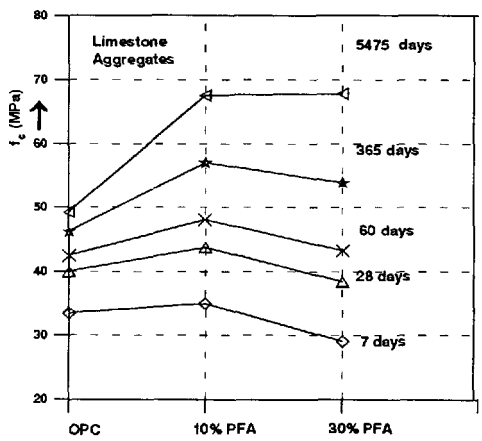

Figure 5: Compressive strength of different PFA concretes for various hydration ages.

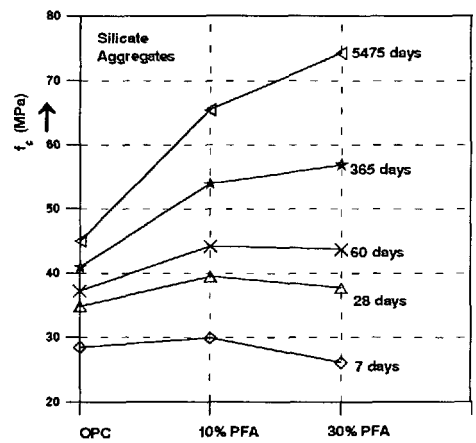

Figure 6: Compressive strength of different PFA concretes for various hydration ages.

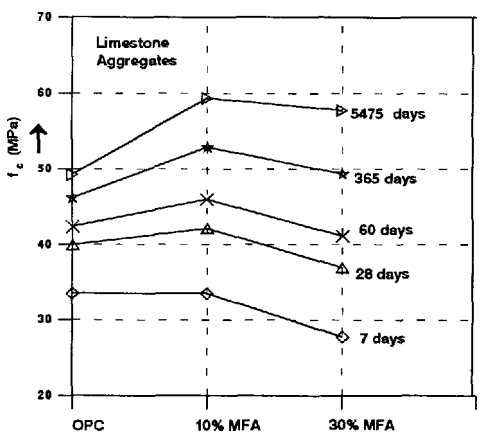

Figure 7: Compressive strength of different MFA concretes for various hydration ages.

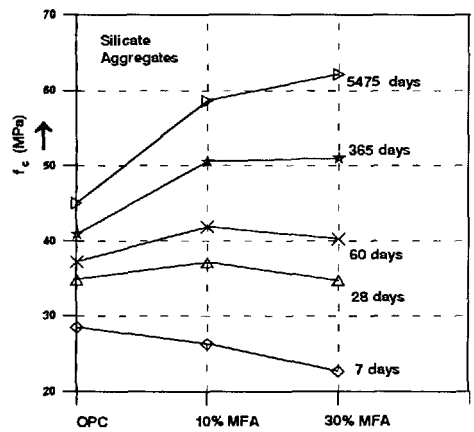

Figure 8: Compressive strength of different MFA concretes for various hydration ages.

The influence of aggregates' type and of the pozzolana content on the compressive strength is shown in figures 3-8. In the case of OPC concrete the ratio $f_{c,5475}/f_{c,28}$ is greater for the concretes prepared with silicate aggregates (1.285, Table 4) than to the concretes with limestone aggregates (1.221, Table 4). This greater development of strength from 28 to 5475 days is the proportion of the bond strength (cement-aggregate bond), which is higher in the case of concrete prepared with silicate aggregates (Schwiete, 1968/69).

Table 3 Determination of the hydration equation for concrete compressive strength and of degree of hydration for the concrete mixture 1.

Hydraton age (days)	3	5	7	14	28	60	90	365	5475
fc_{meas} (MPa)	**28.14**	**31.40**	**33.42**	**37.77**	**40.90**	**42.77**	**43.50**	----	----
$(1/t)^{0.346}$	0.6838	0.573	0.5100	0.4013	0.3157	0.2425	0.2108	0.1299	0.0509
Linear regression	28.14	31.40	25.50	32.06	34.73	37.33	38.30		
for the pairs	0.6838	0.573	0.5100	0.4013	0.3157	0.2425	0.2108	----	----
fc_{meas} - $(1/t)^{0.346}$	correlation coefficient **r = 0.998113** standard deviation s = 0.401586 (MPa) hydration equation: **$f_c = 50.9832 - 33.7012 * (1/t)^{0.346}$ (MPa), $t \geq 3$**								
fc_{calc} (MPa)	27.94	31.67	33.80	37.46	40.34	42.81	43.84	47.54	49.27
Degree of hydration fc_{calc}/fc_{5475}	**0.567**	**0.643**	**0.686**	**0.760**	**0.819**	**0.869**	**0.890**	**0.965**	**1.000**

Table 4 Degree of hydration for the concrete mixtures prepared.

	Concrete Mixture	Degree of hydration ($f_{c,calc}/f_{c,5475}$)					$\frac{f_{c,5475}}{f_{c,28,calc}}$
		7	28	60	365	5475	
1	OPC - Limestone Aggregates	0.686	0.819	0.869	0.965	1.000	1.2211
2	OPC - Silicate Aggregates	0.616	0.778	0.840	0.934	1.000	1.2848
3	90% OPC+10%SE - Limestone Aggregates	0.526	0.676	0.744	0.872	1.000	1.4777
4	90% OPC+10%SE - Silicate Aggregates	0.372	0.606	0.689	0.844	1.000	1.6496
5	70% OPC+30%SE - Limestone Aggregates	0.455	0.598	0.669	0.819	1.000	1.6714
6	70% OPC+30%SE - Silicate Aggregates	0.328	0.504	0.592	0.776	1.000	1.9821
7	90% OPC+10%PFA - Limestone Aggregates	0.517	0.647	0.711	0.843	1.000	1.5451
8	90% OPC+10%PFA - Silicate Aggregates	0.457	0.603	0.675	0.824	1.000	1.6575
9	70% OPC+30%PFA - Limestone Aggregates	0.428	0.566	0.637	0.794	1.000	1.7674
10	70% OPC+30%PFA - Silicate Aggregates	0.351	0.508	0.588	0.766	1.000	1.9700
11	90% OPC+10%MFA - Limestone Aggregates	0.564	0.710	0.774	0.891	1.000	1.4080
12	90% OPC+10%MFA - Silicate Aggregates	0.448	0.633	0.714	0.862	1.000	1.5790
13	70% OPC+30%MFA - Limestone Aggregates	0.480	0.639	0.712	0.853	1.000	1.5647
14	70% OPC+30%MFA - Silicate Aggregates	0.365	0.559	0.649	0.821	1.000	1.7879

CONCLUSIONS

The equation which correlate the compressive strength of concrete mixtures with time, can be formulated by the application of the cement hydration equation. Using this equation, the compressive strength of concrete can be reliably estimated at any age, up to the end of the hydration, without performing long-term laboratory tests. The formulation of the compressive strength equation can easily be obtained using values of the concrete compressive strength, measured at the early ages of the hydration (up to 28 days for OPC concrete and 28-365 days for blended cement concrete depending on the pozzolana content).

The influence of pozzolana's content and of aggregates' type on the compressive strength of concrete can be examined by the determination of the degree of hydration and the ratio $f_{c,5475}/f_{c,28,calc}$ (Table 4). These results indicate that blended cements, due to the pozzolanic reactions, develop a greater part of their strength after the age of 28 days, than to portland cements.

In spite the fact that the condensation of the mixtures was better for the concretes prepared with limestone aggregates, the final compressive strength of blended cement concretes is higher when silica broken aggregates were used (Figs 3-8).

REFERENCES

Hansen, T.C.: "Long-Term Strength of High Fly Ash Concretes", Cement and Concrete Research, vol. 20, 1990, pp. 193-196.

Karayannis, C.G.: "Determination of the influence of W/C ratio on the final compressive strength of concrete, according to the cement hydration equation", Proc. of 11th Greek Concrete Conference, Corfu May 1994, Vol. I, pp 54-63 (in Greek).

Lea, F.M.: "The Chemistry of Cement and Concrete", Third Edition, Arnold, London (1970) Table 59, pp 392.

Schwiete, H-E., Ludwig, U., Albeck, J.: "Die Bindung von Zuschlagstoffen an Zementstein", Veröffentlichungen aus dem Institut fÜr GesteinshÜttenkunde, TH Aachen, Band 14, 1968/69, pp. 143-146.

Sideris, K.: "The cement hydration equation", Zement-Kalk- Gips,12/1993, Edition B, pp E337-E344 .

Sideris, K.K, Baltzopoulou, K.D., Karayannis, C.G.: "A proposal for the evaluation of concrete strength using ultrasonics". Proc. of the First Joint Belgian - Hellenic Conference on Non Destructive Testing, Patras, Greece, May 22-23, 1995, pp 259-265.

Sideris, K.K., Konsta, M.S.: "Influence of the water to cement ratio on the compressive strength of concrete - An application of the cement hydration equation to concrete", Proc. of the 4th Greek National Congress on Mechanics, Xanthi, Greece, June 26-29, 1995, Vol. I, pp. 167-174.

Sideris, K.K., Konsta, M.S., Karayannis, C.G.: "Application of the Cement Hydration Equation to Concrete", Proc. of the Int. Conf. Concrete in the Service of Mankind, Dundee, June 1996, Volume Appropriate Concrete Technology, pp. 343-349.

Sideris, K.K., Konsta, M.S., Karayannis, C.G.: "Determination of the influence of aggregate's grading curve on the final compressive strength of concrete, according to the cement hydration equation", Proc. of 11th Greek Concrete Conf., Corfu May 1994, Vol. I, pp 29-37 (in Greek).

Sideris, K.K., Sideris, K.: "Application of the hydration equation of concrete on the concrete compressive strength according to the measured values taken from the literature" as below:

a.**Sivasundaram,** V., Carette, G.G., Malhotra, V.M.: "Mechanical Properties, Creep and Resistance to Diffusion of Cloride of Concretes Incorporating High Volumes of ASTM Class F Fly Ashes from Seven Different Sources", ACI Materials Journal, vol. 88, July-August 1991, pp. 407-416,

b.**Papayianni,** I.: "Research for the use of Ptolemaida Fly Ash on Concrete Production", PhD Thesis, Thessaloniki 1981, Greece,

c.**Langley,** W.S., Carette, G.G., Malhotra, V.M.: "Strength Development and Temperature Rise in Large Concrete Blocks Containing High Volumes of Low-Calcium (ASTM Class F) Fly Ash", ACI Marerials Journal, vol. 89, July-August 1992, pp. 362-368,

d.**Malhotra,** V.M., Carette, G.G., Bilodeau, A.: "Mechanical Properties and Durability of Polupropylene Fiber Reinforced High-Volume Fly Ash Concrete for Shotcrete Applications", ACI Materials Journal, vol. 91, September-October 1994, pp. 478-486, and other authors.

Report of Laboratory of Building Materials, Xanthi, 1994 (in Greek).

EFFECT OF ALUMINOUS CLINKER AS AGGREGATE ON MICROSTRUCTURE OF INTERFACIAL ZONE IN REFRACTORY CONCRETE.

Olga RYBAKOVA, Alecsander KRIVOBORODOV, JSC "Concern Cement", Moscow, Russia

ABSTRACT The effectiveness of refractory concrete depends on the properties of cement and aggregate. This paper presents a study of formation of interfacial zone between hydrates and initial compounds. The usage of hydraulic aggregate permits to obtain concrete with high refractory performance.

KEY-WORDS: Aggregate, interfacial zone, microstructure,refractory

INTRODUCTION

There are numerous studies of the contact zone between aggregates and cement paste in concrete (Butt, et.al., 1985; Dhir and Sangha, 1974; Kouznetsova, 1986;). According to most of them, the bond between aggregates and cement paste has dramatic impact on mechanical performance of concrete.Maso (1980) shows that the bond plays a major role in the crack propagation process and the failure of concrete. Then bond strength is higher, the strength in traction is higher. Scrivener and Gartner(1988), Zilbermann (1985) showed that the main constituent of the contact zone is calcium hydroxide which is also mainly responsible for the cement-aggregate bond. The bonding region is the result of the adhesion between cement paste and aggregates due to epitaxial growth of calcium hydroxide on the aggregate surface. The microstructure of the contact zone is characterized by porosity, composed of relatively large pores and large crystals of calcium hydroxide. Monteiro and Mehta (1986) used expansive cement with the aim to reduce porosity of the interfacial zone . In this case the modified interfacial zone contains a higher amount of ettringite and discontinuous calcium hydroxide crystals. This zone in expansive concrete resists crack propagation and therefore is stronger than typical interfacial zone in portland cement concrete. However, the interfacial zone in refractory concrete is caused both by hydration process and dehydration under high temperature, therefore a great attention is to be attributed to the interaction between aggregate and cement matrix. This paper presents the investigation of contact zone between aluminate cement hydrate products and initial compounds.

EXPERIMENTAL

Materials and techniques

For the investigation the samples on the basis of aluminate cement with corundum and hydraulic active aggregate were prepared. Cement-to-aggregate ratio was 1:3 and water-to-cement ratio (W/C) was 0.38.

The samples cures at standard conditions and at the air conditions under heating to 100-800°C, because refractory concrete is characterized by strength after drying at 100°C and after heating at 800°C. All samples were examined by optical and electron microscopy, X-ray diffraction and infrared spectroscopy.

Results and discussion

The samples up to 28 days old were examined. Optical microscopy of the samples shows that corundum grains are surrounded by hydrate products of aluminate cement. The thickness of contact zone is about 10-15 μm. Probably contact zone is formed due to epitaxial growth of crystals of calcium hydroaluminate on the surface of corund grains without chemical reaction.

Contact zone between hydraulic active aggregate (technical calcium aluminates - TCA) and cement paste is hardly observed. There is a layer of hydrates on TCA grain surface which is an evidence of its by their various structure because aluminate cement as well as TCA are presented by calcium monoaluminate (CA) and dialuminate (CA_2) phases having different crystal growth rate.

The investigation of the samples containing corundum as the aggregate shows that microcracks appear along the aggregate grains, i.e. by surface of contact zone. In case of aluminate cement with TCA very densety interface zone developed both along initial unhydrate crystals, gel phase and TCA grains. SEM analyses shows that interaction between TCA aggregate and cement matrix leads to appearance of dense contact zone, thus provide a high strength of the samples. It is also promoted by the rise of hydration degree of cement and aggregate leading to reduction of the structure porosity.

The experimental data shows that contact zone between cement paste and TCA aggregate is 30-40 μm and represented by aluminium hydroxide and calcium hydroaluminate crystals of which growth from both cement paste side and from TCA aggregate grains. In case of corund use as aggregate the adhesion of cement paste to the aggregate is essentially due to physical forces. These results explain the different behavior of concrete contained the various aggregates.

Table 1 shows the compressive and bending strength of the samples cured at standard conditions for 28 days. According to the given data the strength of the samples with TCA aggregates much greater than with corund ones.

Tadle 1. Strength of cement stone with different aggregates

Cement	Aggregate	Strength, MPa	
		bending	compressive
High alumina cement	Corundum	6.7	53.6
High alumina cement	TCA aggregate	11.2	78.8

Investigation of hydration of the above mentioned mixes shows that the liquid phase becomes supersaturated during the first minutes of hydration and crystallization of hydrate products is occured on the surface of aggregates. Nuclear on active centres during further growth promote the appearance of intergrowth with the starting sheet. Intergrowth with other surface zones is restricted by the decrease of migration activity of crystal nuclears, leading to the unability of their growth. During further hydration cement grains are covered by the layer of the reaction products which lead to decrease of ion migration into the liquid phase the degree of supersaturation.

On of the main properties of refractory concrete is the compressive strength after heating up to 800°C. In Table 2 the strength of concrete obtained by the use the different aggregates is given. Table 2 data shows that compressive strength of refractory concrete with TCA aggregate is higher than one of concrete with corundum aggregate at the various temperature. These values are equal to 63.3-71% of the strength after the drying by 100°C while the similar value of corundum concrete is only 35-47%.

Table 2. Compressive strength of refractory concrete

Concrete number (Aggregate type)	Compressive strength, MPa, %					
	standard curing, days			after heating, t°C		
	1	2	3	100	800	1200
1.TCA aggregate	27	36	50	40/100	28/71	26/63
2.Corund	15	20	36	34/100	16/47	12/35

Heat resistance is very important for refractory concrete.It provides the stability of concrete under influence of high temperature. The results show that this value is in the range of 40 cycles of heating and cooling.

Temperature deformation under loading of 0.2 MPa promotes the ability of concrete to withstand against high temperature and loading simultaneously. Table 3 presents the data of these properties of concrete.

Table 3. Heat resistance and deformation of concrete

Heating-cooling,	Temperature deformation, °C		
	beginning of softening	4%	40%
40	1350	1520	1610
35	1400	1600	1650

CONCLUSION

The contact zone in refractory concrete depends on the type of aggregate. In case of corund aggregate the contact zone is formed due to adhesive cement paste to the aggregate. Compared to the contact zone in TCA aggregate concrete, it is obvious that contact zone is formed due to chemical reaction and crystal growth. This leads to crack propagation and good performance of refractory concrete.

REFERENCES

Butt, J.M.,Timashev, V.V.,Bakshutov, V.S.,"Hydroaluminate crystall growth in hardened cement stone", Journal "Cement",No 5, 1972, pp.10-11.

Dhir, R.K.,Sangha, C.M."Development and propagation of microcracks in plain concrete", Materiaux et Constructions,No 37, 1974, pp.17-23.

Kuznetsova, T.V., "Aluminate and sulfoaluminate Cements", Moscow, 1986, Stroiizdat, 206 p.

Maso, J.C."The bond between aggregates and hydrated cement paste", Proceedings of 7th International Congress on Cement Chemistry, v.1, 1980, pp.YII-1/4-1/14.

Scrivener, K.L.,Gartner, E.M. "Microstructural Gradients in Cement Paste Around Aggregate Particles", Proceedings of the Materials Research Society Symp. Proc.,v.114,1988, pp.77-85.

Zilbermann, R. "A contribution to the problem of cement-aggregate bond", Cement and Concrete Research,v.15, 1985, pp.801-808.

Monteiro, P.J.M. and Mehta, P.K. "The transition zone between aggregate and type K expansive cement",Cement and Concrete Research", v.16, 1986. pp.111-114.

THE SYNTHESIS AND BEHAVIOR OF CALCIUM SILICATES-FIBERS COMPOSITES

*Tai Sun UM, *Hee Kap OH,**Sang Heul CHOI
*Ssang Yong Cement Industrial Co. LTD., Taejon, Korea.
**Inorganic Materials Eng. Hanyang Univ. Seoul, Korea.

ABSTRACT The microstructure of calcium silicates-fibers composites were studied. The reactivity of the silicates was important for lighting the weight and increasing the performance of composites. The C/S molar ratio, reactivity of silicates, pressure and fibers were main factors determining physical properties because these conditions affect the porosity, crystal shapes and bending strength of hydrates-fibers composites. The higher the reactivity of silicates increases, the higher the properties of performance, lightness, the crystal size of crystalline and physical properties increased.

Key-words : Calcium silicate, Autoclavation, Porosity, Strength development

INTRODUTION

Calcium silicates-fibers composites are mainly produced by applying pressure in an autoclave after gel synthesis using various materials. The performance and physical properties of the composites are affected by the reactivities of silicates, the shapes of the hydrates and the contents of fibers because different shapes of hydrates have different point of contact, and optimum fiber volume is determined according to the properties of both matrix and fibers(Okada, 1994 ; Talor, 1965 ; Mitsuda, 1989). This report was studied how to change the the microstructure of hydrates with various silicates and conditions of manufacture, and how to control physical properties under these conditions.

EXPERIMENTAL PROCEDURE

Starting Materials ; The raw materials used were shown in Table 1.

Table.1. Chemical compositions of the starting materials

No	Materials	Chemical composion (%)								Remark
		SiO_2	Al_2O_3	Fe_2O_3	CaO	MgO	Na_2O	K_2O	L.O.I	(m^2/kg)
I	Fly ash(A)	60.5	23.9	4.7	3.0	0.9	0.25	0.89	4.9	88μ:5%
II	Slag(B)	35.1	15.2	0.4	42.4	5.8	0.32	0.57	-	450
III	Diatom earth(E)	78.5	9.3	2.4	0.1	0.3	0.21	1.23	7.5	320
IV	Sand(F)	92.8	3.5	1.0	0.3	0.1	0.08	1.42	0.7	88μ:8%
V	Calcium hydroxide	0.1	0.4	0.1	74.7	0.4	0.01	0.02	24.3	88μ:10%
VI	Type I Cement	20.6	6.7	3.3	61.6	3.1	0.13	0.76	-	320
VII	ARG	50.7	16.7	0.8	21.6	0.3	0.25	0.16	0.9	L:13mm
VIII	Pulp	Solid / Water : 5 %								L:4mm

※ ARG : Alkali Resistance Glass Fiber(Density : 2.7g/㎤)

Mix Designs ; The mix designs were (I + II + III + VI)/IV=1, VI/(I + II + III)=0.11 using raw materials as shown in Table 1, CaO/SiO_2 mole=0.67, 0.77, 0.87, 0.97 Water/Solid=3.0 Fibers (pulp, ARG) were added into the composites about 2.0, 3.5, 5.0%.

Process ; Gel synthesis was first initiated at 90-100℃, for 2-4hrs in a water bath and compressed at 10, 25, 40kg/㎠. Subsequently, it was autoclaved at 180℃ for 8hrs. It was cut into 2x2x4cm pieces for compressive strength tests, and into 2x2x5cm pieces for bending strength tests. These samples were analyzed by XRD, DT-TGA, SEM and porosimeter.

RESULTS AND DISCUSSION

Gel Synthesis and Hydrates The gel reaction was very slow for A mix (fly ash) but for B mix(slag) or E mix(diatom earth) the reaction rate was fast, and C-S-H, ettringite and monosulfate were detected. Especially, for E mix (diatom earth), gel synthesis was almost over in about 4hrs and the hydrates were mainly C-S-H gel with spongiform structures. In DT-TGA, the rates and contents of reactions were in sequence, E mix>B mix>A mix (Fig 1 and Fig 2).

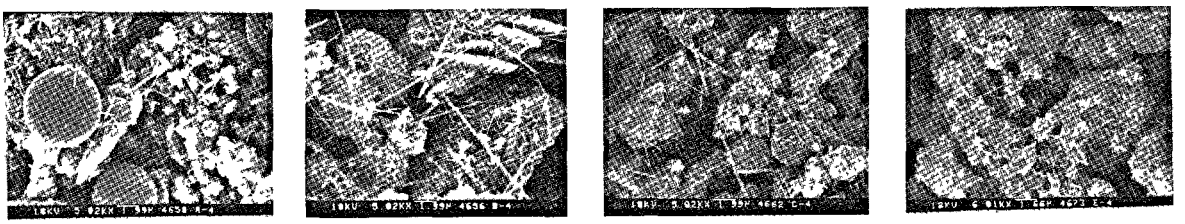

<Fly ash> <Slag> <Fly ash+Slag> <Diatom earth>

Fig.1. SEM micrographs of hydrates after gel synthesis(4hrs) used the various silicates

Casting and Gravity The higher the content of gels were increased, the higher the castability was improved. The castability of mix designs were, in sequence : E mix>B mix>A mix. Average gravity of composites were, in descending order : E mix(0.73) <B mix(0.78) <A mix(1.05). The lower C/S mole became, the lower the gravity because of the increasing content of gel.

Porosity and Physical property C/S mole and casting pressure of hydrate non-adding fibers were decreased to increase the porosity to the 1-0.02㎛ range, and increase the size of crystals. When size of crystals and porosity were decreased, bending strength/gravity increased because of the increasing number of contacts. Compressive strength/gravity was more affected by porosity than by the size of crystal(Fig 3). Here, diatom earth was superior to the other silicates in gel reaction, performance, lightness and physical property.

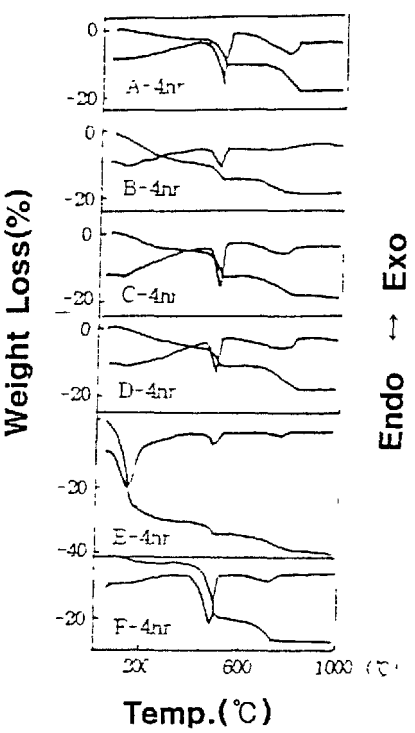

Fig.2. DT-TGA results of hydrates after gel reaction(4hrs)

Physical property and Microstructure of Calcium Silicate Hydrates-Fibers Compositions These changes in the shape of crystals and physical properties for adding fibers can result in a reduction of compressive strength, but also in reduced weight and greater bending strength(Table 2, 3 and 4).

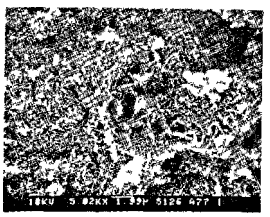

<Fly ash- I >

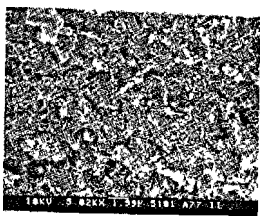

<Fly ash- II >

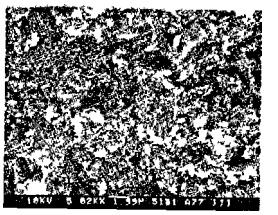

<Fly ash-III>

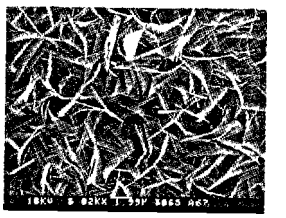

<Fly ash-67>

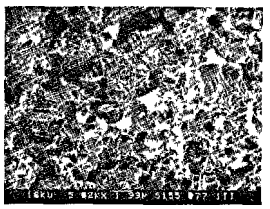

<Slag-III>

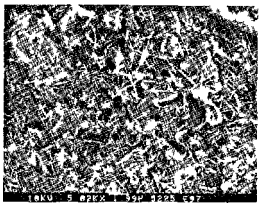

<Diatom earth- I >

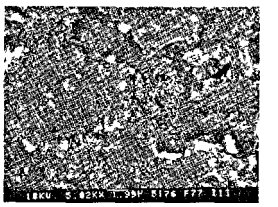

<Sand- I >

Condition	Fly ash- I	Fly ash- II	Fly ash-III	Fly ash-67	Slag-III	Diatom earth- I	Sand- I
C/S	0.77	0.77	0.77	0.67	0.77	0.77	0.77
Press(kg/cm)	10kg/cm	25kg/cm²	40kg/cm²	10kg/cm²	40kg/cm²	10kg/cm²	10kg/cm²
Bend.str./gra.	43.8kg/cm²	54.5kg/cm²	78.8kg/cm²	28.3kg/cm²	35.8kg/cm²	36.0kg/cm²	56.1kg/cm²
Comp.str./gra.	153kg/cm²	222kg/cm²	334kg/cm	207kg/cm²	188kg/cm²	202kg/cm²	361kg/cm²
Gravity	1.02	1.18	1.22	0.84	0.98	0.7	1.19

Fig.3. Physical properties and microstructures of hydrates made with the various silicates

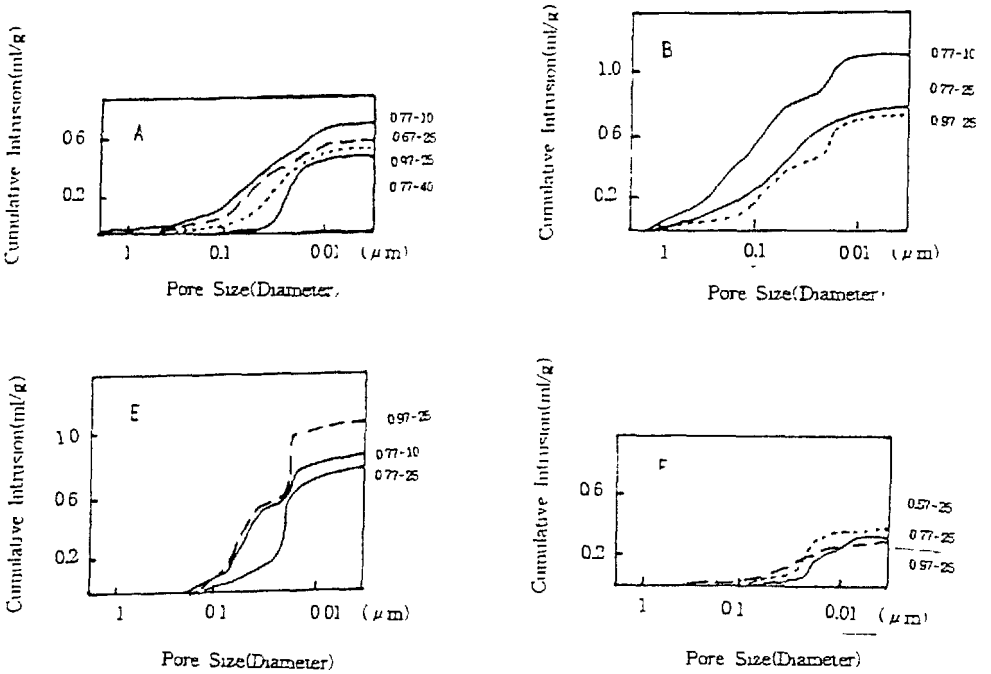

Fig.4. Porosities of hydrates applied with the various manufacturing conditions

On the other hand, decreased C/S mole in mix design and pressure leads to increasing strength due to decreasing the shape of crystals, increasing the point of contact and decreasing the corrosion of ARG (Fig 5 and 6). Increased activity of silicates led to the composites being lightened and increased strengths and performance, but strength was least for B mix because it developed cracks after autoclaving. For these reasons, we determined the optimum conditions of the composites using diatom earth as : C/S 0.67, pulp 5%, glass fiber 2%, pressure 10kg/㎠.

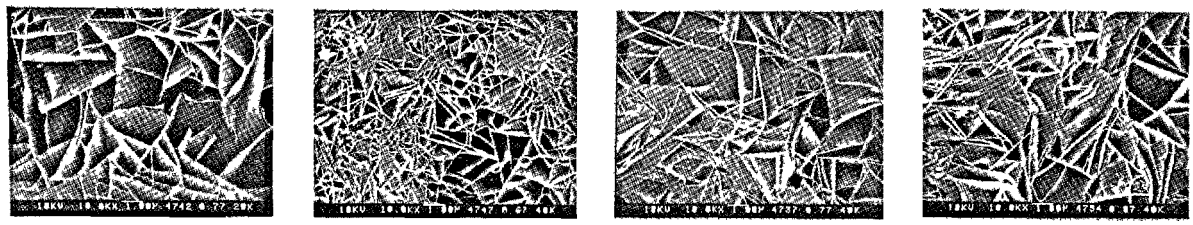

<C/S 0.77-20kg/㎠> <0.67-40kg/㎠> <0.77-40kg/㎠> <0.87-40kg/㎠>

Fig.5. SEM micrographs of tobermorite in hydrates according the change of C/S mole and pressure

Table.2. Average physical properties of composites adding fibers about 2.0-5.0%

Materials	Diatom earth				Slag		Fly ash+Slag		Fly ash	
Press(kg/㎠)	10	25	10	25	10	25	10	25	10	25
C/S	0.67	0.67	0.77	0.77	0.77	0.77	0.77	0.77	0.77	0.77
Bend.str.(kg/㎠)	167.0	139.4	84.4	65.3	53.7	28.9	46.1	38.9	91.8	83.0
Gravity	0.64	0.72	0.63	0.74	0.69	0.84	0.74	0.83	0.87	0.93

Table.3. Change of physical properties according to the contents of fibers

Condition	A.R. Glass fiber			Pulp		
	2.0%	3.5%	5.0%	2.0%	3.5%	5.0%
Bend.str.(kg/㎠)	96	84.6	83.0	62.8	88.5	112.3
Gravity	0.75	0.76	0.78	0.74	0.79	0.74

Table.4. Change of physical properties by the condition of manufacture

Condition	C/S			A.R.Glass fiber.			Pulp		
	0.67	0.77	0.87	3%	4%	5%	3%	4%	5%
Comp.str.(kg/㎠)	48.1	21.5	22.0	36.8	29.5	28.5	39.7	31.6	23.5
Gravity	0.55	0.56	0.58	0.55	0.58	0.57	0.59	0.55	0.56

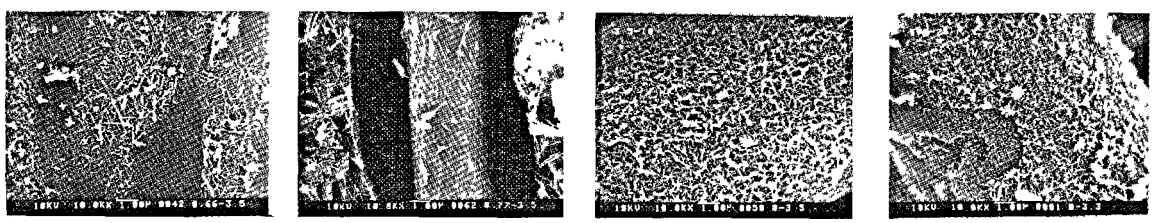

<C/S 0.67> <C/S 0.77> <Press 10kg/㎠> <Press 25kg/㎠>

Fig.6. SEM micrographs of the corrosion of ARG by the condition of manufacture

CONCLUSIONS

The influence of the shapes of hydrates and fibers in composites using various silicates was investigated. The conclusion are :

(1) The activity of silicate is important for lightness, high performance and the strength of the composite. Diatom earth is the best of all materials for these purposes, and this gel reation was over in 4hrs.

(2) Decreased C/S molar ratio and increased pressure promotes reductions in crystal size and matrix porosity, which leads to increased bending strength. Compressive strength is mainly affected by porosity, rather than by crystal size.

(3) ARG has little effect on strengths improvement because of the corrosion of glass fibers in the autoclave. Increasing the C/S molar ratio and casting pressure of composites increases the corrosion of ARG and decreases the strength of composites. The optimum condition are C/S 0.67, press 10kg/㎠, ARG 2% and pulp 5%.

REFERENCES

Okada Y, "Influence of Starting Materials on the Formation of 1.1㎚ tobermorite" J. Ceram. Soc. Japan 102(12), 1994, pp1148-1153.

Talor. H.F.W, "Review of Autoclaved Calcium Silicates" Symp. on school of phamacy(university of London), May 18-21, 1965, pp195-205.

Mitsuda T, "Synthesis of tobermorite" J. Am. Ceram. Soc. 5. 1989, pp206-213.

THE MECHANICAL PROPERTIES OF ALKALI RESISTANCE GLASS FIBER REINFORCED CONCRETE UNDER DIFFERENT CURING CONDITIONS

Moon-Young JEONG and Jong-Taek SONG
Dept. of Materials Science & Engineering, Dankook University, Cheonan, Korea

ABSTRACT The mechanical properties of alkali resistance(AR) glass fiber reinforced concrete(GFRC) under different curing conditions are investigated in this study. The specimens were formed by extrusion process, and then steam cured and autoclaved. An autoclaved specimen showed the elastic-brittle behavior up to 4% of fiber volume fraction. But it was found that the fracture behavior for steam cured specimen was changed to the elastic-plastic with crack branches fracture from 3 vol% of fiber.

KEY WORDS Alkali, Glass, Curing, Strength development, Microstructure

INTRODUCTION

Cement-based materials have a good compressive strength, durability and cost competition for building materials. But they have a poor flexural strength and ductility. Especially thin products(e.g., board and panel), flexural property is more important than other mechanical ones. In order to improve flexural performance, fiber reinforcement is employed in various concrete structure(Shah, 1991). Reinforcement effects depend on the individual materials constituent(fiber, matrix, and interface), fiber geometry(aspect ratio) and fiber orientation(Toutanji and Katz, 1993).

As for GFRC, it has been known that the mechanical property degraded(Bijen, 1983, Kosa et al, 1991) after long-term exposure to weathering because glass fibers were damaged by the reaction with the highly alkaline cement matrix(Yilmaz and Glasser, 1991). But most of previous reports the results when the samples were moist cured between 20-65℃. In this paper, test was conducted at a relatively high temperature.

EXPERIMENTAL PROCEDURE

The proportion of the matrix and fibers is shown in Table 1. All of mixing is represented by weight. AR-glass fiber was mixed with cement using Omni mixer, followed by mixing with other ingredient for 2 minutes. Then dry mixed composite was thoroughly mixed with water by kneader for 3~5 minutes. At that time, small amounts of water and kneading time were varied with fiber content.

Table 1 Batch Proportions (by wt.%)

Fiber volume fraction (%)	Cement [1]	Silica powder[2]	ARG [3]	HPMC [4]	Water(%) [5]
	Controlled CaO/SiO_2 mole ratio is 0.86				
0	99.35		0.00	0.65	25.8
1	98.12		1.20	0.68	27.2
2	96.89		2.39	0.72	28.6
3	95.62		3.62	0.76	29.8
4	94.36		4.83	0.81	31.3

(1)Ordinary portland cement (type I) (2)About 93% of SiO_2 in composition and blaine value is 2,750cm^2/g (3)Length is 6 and 12mm, diameter is 14㎛ (4)Hydroxy Propyl Methyl Cellulose =viscosity 30,000 cps. at 20℃ of 2% aqueous solution(RV type 20 r.p.m. with No.6 spindle) (5)Proportions of water is based on the total amounts of dry raw material.

The board-shape specimen having the size of $450\times80\times10mm^3$ were made by vacuum extruder. All specimens were steam-cured at 60℃ for 8 hours and half of them were autoclaved at 180℃ for 8 hours. And then all samples were aged for about 1 week before testing. The mechanical property was tested with a three-point loading employing the computer controlled testing machine(Autograph AG-10TE) with a span of 300mm and a cross head speed of 5mm/min.

RESULTS and DISCUSSION

Fracture Behavior

The plain matrix(i.e, without fiber) cured by steam or autoclave are very brittle but their flexural strength were different(Mobasher and Shah, 1989). The flexural strength increased with fiber volume fraction used both for an autoclaved specimens(ACS) and steam-cured specimens(SCS) (Fig 1). The load-deflection curve shown in Fig 2 depicted the sudden loss of strength after crack formation at the peak load(Ho and Woodham, 1982). ACS also showed the elastic-brittle behavior up to 4% of fiber volume fraction. While the fracture behavior for SCS was changed to the elastic-plastic with crack branches from 3 vol.%. It was thought that the adhesion strength between fiber and matrix was not sufficient, so the fracture behavior of SCS was not affected by ultimate strength of fiber(Bentur and Diamond, 1984). AR-glass fiber had a brittle character because it had a very short elongation at rupture. This implied that the post-cracking zone for SCS was caused by fiber pullout. The critical pullout of glass fiber for this matrix was found for fiber of 12㎜ length.

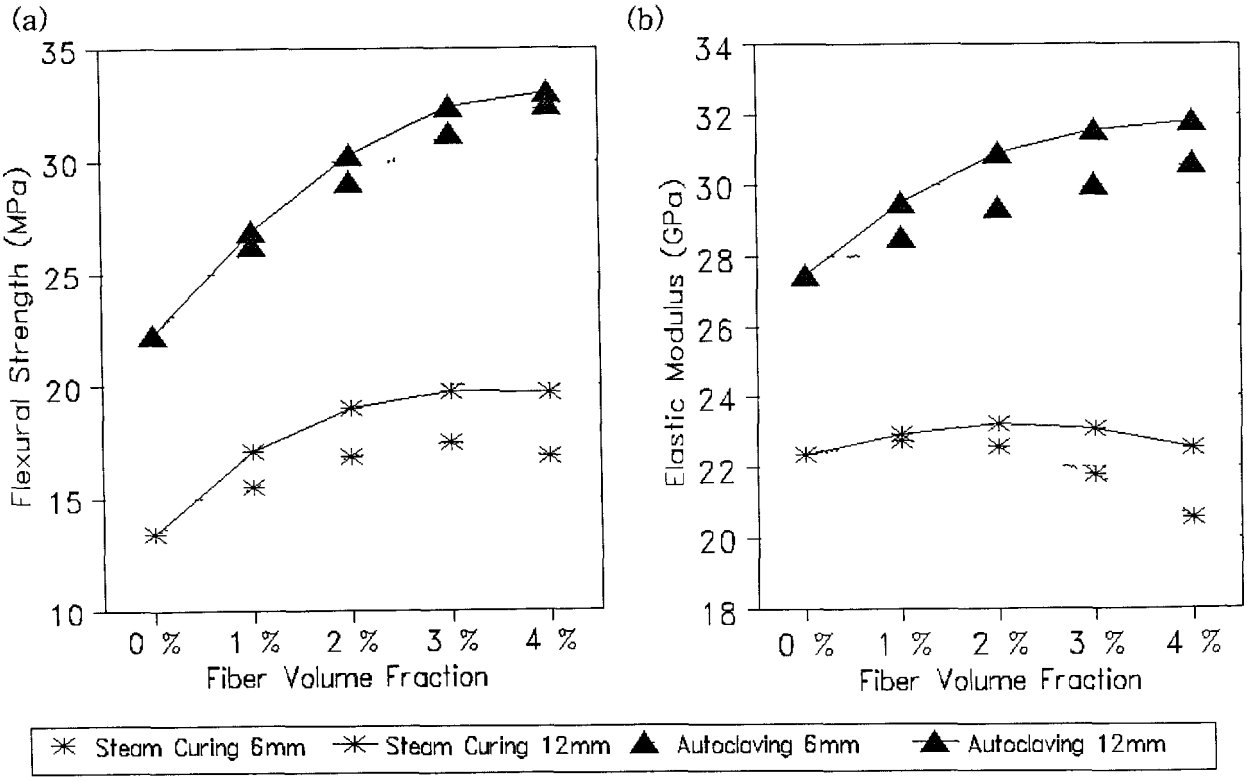

Figure 1 Effect of fiber volume fraction on flexural strength(a) and elastic modulus(b) of steam cured and autoclaved GFRC.

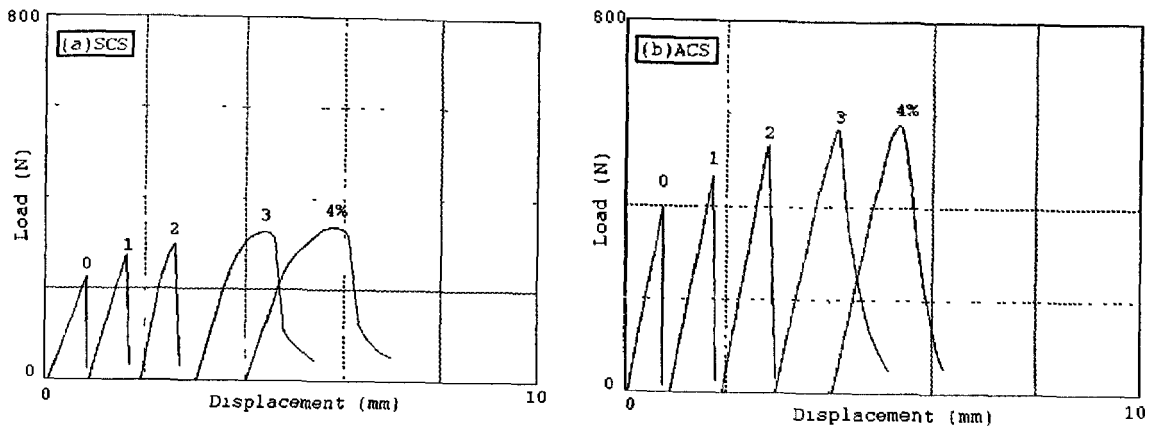

Figure 2 Load-deflection curve of SCS(a) and ACS(b) with varing fiber content

Fiber Orientation

The flexural strengths of line direction are increased with fiber content. However those for the cross direction are slightly decreased with fiber content (Fig 3). These showed that the fiber was arranged with 2-dimensional orientation. The 3-dimensional oriented fibers were rearranged into extrusion direction because this direction received relatively small shear stress of fluidity during extrusion.

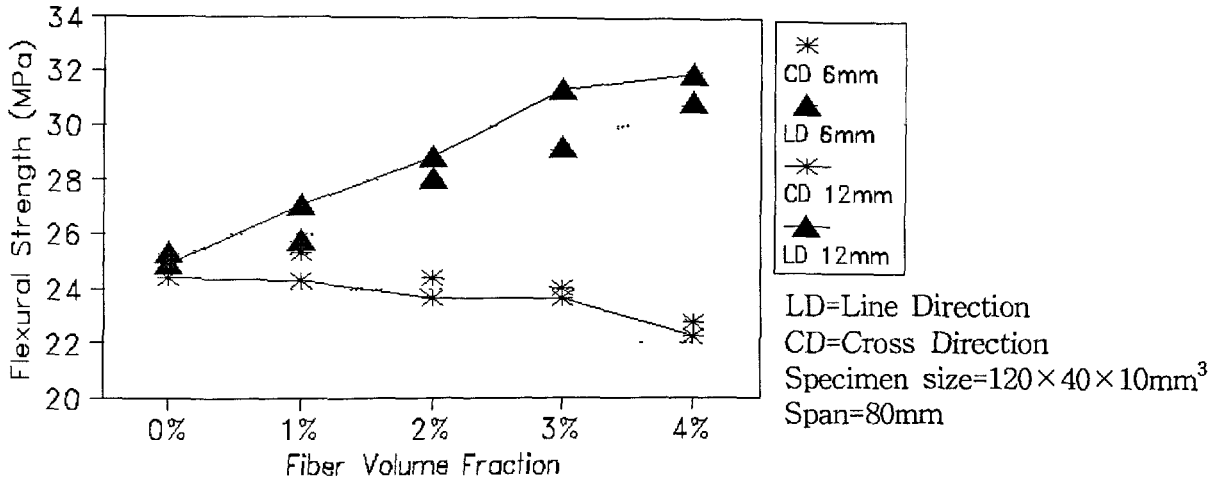

Figure 3 Flexural strength of LD and CD in various fiber content

Corrosion of Fiber

Fig 4 is the SEM photographs of surface of glass fibers. It showed that no visible corrosion of glass fiber occurred at the interface for SCS. But there were small amount of cement hydrate formed at the interface between fiber and matrix. On the other hand, the fibers in the ACS clearly show the corrosion of the surface. It might be thought that the cement hydrates formed were tenaciously bonded to the glass fiber at the interface. As a consequence of surface corrosion, glass fibers became weaker with the curing temperature. The chemical stability of the interfacial zone was important, but the improved properties of ACS are to be retained.

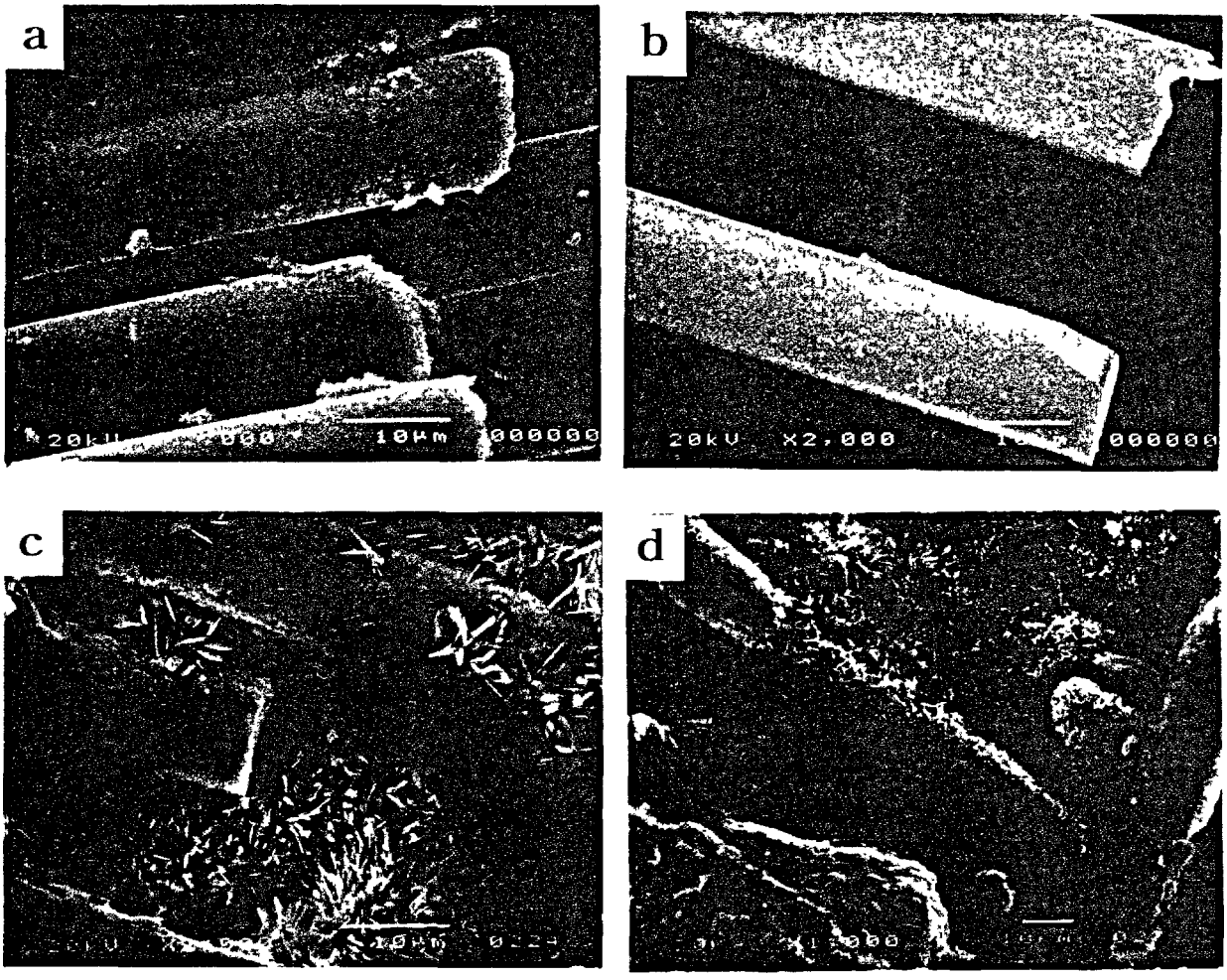

Figure 4 SEM of AR-glass fibers of SCS and ACS. virgin fiber(a), SCS(b), ACS(c) and E-glass fiber as reference(d).

REFERENCES

Benture, A., Diamond, S., "Fracture of glass fiber reinforced cement" Cem. Concr. Res., Vol.14., 1984, pp.31-42

Bijen, J., "Durability of Some Glass Fiber Reinforced Cement Composites" ACI Mat. Jour., Jul-Aug, 1983, pp.305-311.

Ho, J. L. K., Woodhams, R.T., "Fracture Toughness of Fiber Reinforced Sulfur Concrete" ACI Mat. Jour., 1982, pp.288-295.

Kosa, K., Naaman, A.E., Hansen, W., "Durability of Fiber Reinforced Mortar" ACI Mat. Jour., Vol.88, No.3, 1991, pp.310-319.

Mobasher, B., Shah, S. P., "Test Parameters for Evaluating Toughness of Glass-Fiber Reinforced Concrete Panels" ACI Mat. Jour., Vol.86, No.5, 1989, pp.448-458.

Shah, S, P., "Do Fibers Increase the Tensile Strength of Cement-Based matrixes" ACI Mat. Jour., Vol.88, 1991, pp.595-602.

Toutanji, H.A., El-Korchi, T., Katz, R.N., Leather, G.L., "Behavior of Carbon Fiber Reinforced Cement Composites in Direct Tension" Cem. Concr. Res. Vol.23, 1993, pp.618-626.

Yilmaz, V. T., Glasser. F. P., "Reaction of alkali-resistance glass fibres with cement. Part2. Durability in cement matrices Conditioned with Silica Fume" Glass Technology, Vol.32., No.4., 1991, pp.138-147.

PECULIAR FEATURES OF CONTACT ZONE FORMATION BETWEEN CEMENT PASTE AND VITREOUS SILICATE FILLER

Vladislav GLUKHOVSKIY, Yury BIRYUKOVICH, Nina MIKHAILISHINA, Tatyana DASHKOVA, Technical University of Ukraina"Kyiv Polytechnical Institute", Kyiv, Ukraine

ABSTRACT The results of investigations of the processes occurring in a contact zone between the hardening cement and the vitreous silicate filler, carried out with taking matrix shrinkage induced stresses arising inside such contact zone into account, are presented.

Key-words: Diffusion, Filler, Interfacial zone, Shrinkage, Strength development.

RESULT

The investigations of peculiar features of contact zone formation between the products of the cement hydration and the silicate filler revealed occurrence of chemical processes in a contact zone. Thus, in particular case, the strength decrease of composites on the base of portland cement (or other binders) and reinforcing component in the form of glass fibers with different compositions (see Table 1) may result from such chemical interactions.

It is known that if glass fibers are used as a component, the film of newly formed compounds resulting from the chemical interactions between the filler and the matrix may precipitate on the surface of glass fibers (Pashchenko et al, 1988, Pashchenko et al, 1979, Budnikov et al, 1966, Majumdar et al, 1977, Stucke et al, 1976). Still, the authors observe no changes of the optic properties of fiber cores providing the prolonged period of their interaction with the binder (Budnikov, Slobodianik et al, 1966), same the value of Young's modulus remains constant (Majumdar et al, 1977).

The investigations of such new compounds layers formed on the fiber surface, which have low-basic calcium hydrosilicates prevailing in their composition, have shown that the microhardness of these layers with a thickness of 0.1 - 0.6 μm amounts to 350 - 4100 MPa, the microbrittleness reaches 200 - 1780 pJ, the minimal load on microhardness tester penetrator resulting in cracking of a layer of newly formed compounds (P_t) makes 1.1 - 9.9 cH. These characteristics are lower then such of initial fibers: in 1.4 - 8.0 times for microhardness values, in 1.4 - 8.0 times for microbrittleness values, in 3.2 - 45.0 times for values of a minimal load on microhardness tester penetrator resulting in a layer cracking. Besides, it was found, that stabilization of the major properties of new compounds layer continues for 150 hours of mix's hardening, whereas the deformation of the shrinkage matrices may be observed within 300 - 360 days.

It was found in the course of kinetics study of the strength changes in mixes that the mostly explicit dependence exists between the rate of strength drop on a proper stage of mix's hardening and the mean size value of the opened capillary pores (λ) (Brusser, 1971, Turkestanov, 1964) estimated at the beginning of this period (see Figure 1), which is the evidence that such processes occur in a diffusion-controlled area. The existence of the new compounds layer completely formed after 150 hours of its hardening and the process of intensive decrease of mix's strength continuing during more then 360 days in diffusion-controlled area, allows to assume the possibility of processes, resulting in destruction of a new compounds layer, inside the contact zone. The process of matrix shrinkage, the maximal intensity of whereof takes place within the first 300 ... 360 days of hardening, may be one of the possible causes of such destruction.

Table 1. Kinetics of the strength changes in mixes on the base of portland and alumina cements.

Type of reinforcing component	The limit bending strength (MPa) after mix's hardening during a period of (in months)					
	1	3	6	12	60	180
			Gypsum-alumina cement			
alkali-free fiber	29.0	29.2	29.3	25.4	20.5	20.1
same with protective coating	29.0	31.5	33.4	31.7	33.0	33.0
			Portland cement			
alkali-free fiber	38.0	26.5	20.3	13.7	11.2	11.1
same with protective coating	33.5	28.5	26.2	23.3	21.0	20.0
			Simulated terms of service (in months)*			
	12		24	60		120
alkali-free fiber	17.5		14.2	12.2		11.4
same with protective coating	25.1		22.5	18.0		16.7

* Pashchenko A.A.(1988)

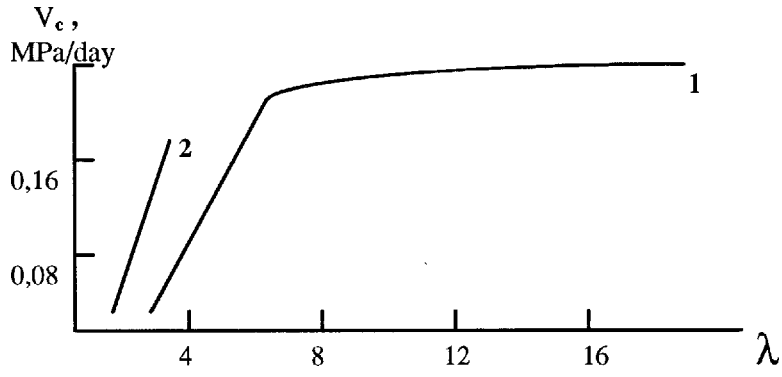

Figure 1. Dependence of the rate of bending strength decrease (U_c) from the pore mean size value (λ) for the mixes of portland cement and glass fibers with (1) and without (2) the protective coating.

The calculations of the values of stresses (P_y) arising due to the matrix shrinkage, which were carried out for the purposes of these values comparison with the values of minimal load resulting in the cracking of a layer of new compounds (P_t), were based on the following data:

· It was found by the electronic microscopy study that the cement paste and the layer of new compounds on the glass fiber surface do contact through the sites with diameter of 1 - 10 μm, separated by the distances of 10 - 100 μm (Pashchenko et al, 1988).

· The value of a pressure bearing upon a layer of new compounds due to the matrix shrinkage was estimated on the base of a known solution of Lamé-Gadolin task (Bezukhov, 1953), in assumption of hexagonal arrangement of fibers in a mix:

$$q = \frac{0{,}952\varepsilon_m E_f}{\sqrt{V_f}\left[(1-\nu_f)+\frac{E_f}{E_m}\left[\frac{0{,}906+V_f}{0{,}906-V_f}-\nu_m\right]\right]} \qquad [1]$$

Here, ε_m is the relative deformation of matrix shrinkage; V_f is the volume ratio of fibers in a composite; E_f, E_m, ν_f and ν_m are the values of elasticity modulus and Poisson's ratio for fibers and matrix, respectively.

In this case, in assumption that within the i- length of a fiber it contacts with a matrix, at least, in two points symmetric about the fiber axis, the value of a matrix shrinkage stress in the contact zone will be: $P_y=\pi qiD_f/4$. Here, q is defined in accordance with Eq.1, D_f is the fiber diameter.

The calculated values of matrix shrinkage stresses (P_y) are presented in Fig. 2 versus the age of a mix with taking the experimentally defined inherent deformation of portland cement matrix into account.

As it is known, the anomalistically high strength level of glass fibers, which was put into foundation of the idea of mixes, depends on the state of fiber surface. Just this factor determines the dependence of mix's durability from the state of surface of reinforcing component, which may undergo changes during a long enough period due to the physico-chemical and physico-mechanical processes taking place in a contact zone. One of the methods to prevent the unwanted influence of such contact zone processes at the final strength of mixes is to use the silicate glass fibers as the reinforcing components, as far as the strength of such fibers doesn't depend on the state of their surface. The physico-chemical characteristics of such mixes are presented in Table 2.

It was found in the course of complex physico-chemical investigations of the contact zones of such mixes, carried out using derivatography, X-ray, IR - spectroscopy and electronic microscopy methods of analysis, that the process of interaction of new compounds produced by the binder with the surface of reinforcing component is accompanied by the decrease of calcium hydroxide content

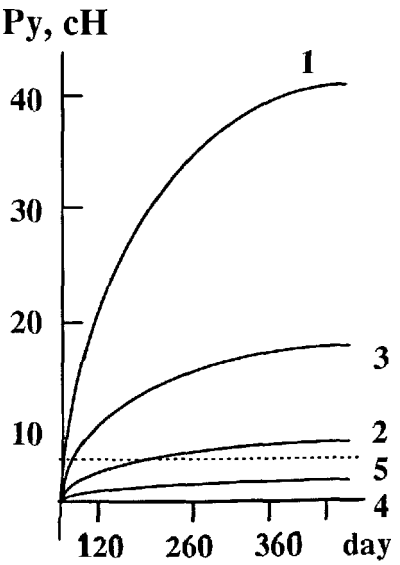

Figure 2. Kinetics of the strength changes in a new compounds layer versus the shrinkage of cement (1,2) and sand cement (3,4) matrices, calculated for the i = 100μm (1,3) and i = 10μm (2,4) length of fiber in comparison to P_t (5).

Table 2. Kinetics of the strength changes in mixes on the base of portland cement.

Ratio of reinf., in %	The limit bending strength (MPa) after mix's hardening during a period of (in months)					
	1	6	12	24	60	90
	Natural hardening in a water					
10	20	32.3	36.8	38.4	41.2	48.2
20	26.5	46.4	52.7	53.8	55.9	58.1
30	29.2	53.8	54.2	58.1	58.6	65.3
	After wet thermal treatment					
10	---	32.7	33.1	40.3	---	---
20	---	41.0	47.2	56.2	---	---
30	---	55.3	56.4	60.7	---	---

inside the contact zone. The fiber surface layer of new compounds similar in its composition and physico-mechanical properties to such of the mixes studied earlier was shown to exist in these mixes as well. Yet, in this case a growth of intensity of interaction processes inside the contact zone results in a growth of mix's strength.

CONCLUSIONS

Formation of a new compounds layer at the vitreous silicate filler inside the hardening portland cement is a result of chemical interactions of filler surface with reactive components of hydrating binder (mainly of calcium hydroxide).

The shrinkage deformations of a matrix cause stresses in a zone of contact between the new compounds layer and the matrix. Mostly it is accompanied by microcracking providing the possibility of reactive components diffusion to the "fresh" surfaces of a filler. These processes are just a reason, why mix doesn't undergo stabilization within the first 150 hours of its hardening after formation of a new compounds layer.

One of the possible ways of obtaining mixes with a long term of service on the base of portland cement is to use the glass fibers as reinforcing component, as far as the physico-chemical charcteristics of such component doesn't depend on the state of its surface.

REFERENCES

Bezukhov, N.I.: "Theory of resiliency and plasticity", Moscow : Gostekhteorizdat, 1953, p.568 (in Russian).

Brusser, M. I. Transactions of a conference of hydraulic engineering, Vol. 68, 1971.

Budnikov, P.P., Pashchenko, A.A., Serbin, V.P.: "Investigations of structure of cement stone reinforced with mineral fibre". Izv. AN SSSR. Inorganic materials, 1966, V2(4), pp.741-744 (in Russian).

Budnikov, P.P., Slobodyanik, I.Ya., Pashcenko, A.A., Serbin, V.P.: "Cement stone reinforced with glass fibre". Stroitelni materialy, 1966, 4, p.17, (in Russian).

Majumdar, A., West, J., Larner, L.: "Properties of glass fibres in cement environment". J. ater. Sci., 1977, 5, pp. 927-936.

Pashchenko, A.A., Serbin, V.P., Glukhovskiy, V.V. et al.: Reinforcement of inorganic binding agents with mineral fibres. Moscow, Stroyizdat, 1988, 200 pp. (in Russian).

Pashchenko, A.A., Serbin, V.P.: Reinforcement of cement stone with mineral fibre. Kyiv, Vishcha skola, 1979, 222 pp. (in Russian).

Stucke, M., Majumdar, A.: "Microstructure of glass fibre-reinforced cement composites". J. Mater. Sci., 1976, pp.1019-1030.

Turkestanov, G.A.: "Porosity of cement stone and quality of concrete ". Concretes and ferro-concretes, 1964, N11.

EFFECT OF ADDITION OF PHOSPHATE BEARING MATERIALS ON STRENGTH DEVELOPMENT CHARACTERISTICS OF HIGH TEMPERATURE REFRACTORY CONCRETE

S C SHARMA and S CHATURVEDI

National Council for Cement and Building Materials
New Delhi, India

ABSTRACT In the present study, an attempt has been made to investigate the effect of addition of phosphate bearing materials to various aggregates & also to optimise the type of aggregate, their particle size distribution & dosage,etc on strength development characteristics of high temperature refractory concrete. The refractory concrete so made had the bulk density 3.150 g/cm^3, thermal expansion , CCS and MOR : + 0.62 %, 450 kg/cm^{2}and 115 kg/cm^2 respectively at 1300°C .

KEY WORDS : Refractory, Aggregate, Phosphate, Binder, Strength .

INTRODUCTION

Phosphate bonded refractory concretes are characterised by excellent abrasion and spalling resistance, high modulus of rupture and high crushing strength at elevated temperatures. The main constituents of these types of refractory concretes are refractory aggregates and phosphate binders. The auxiliary constituent used is setter /inhibitor required to control setting behaviour. Two types of refractory concretes are normally available based on their setting characteristics i.e. air setting and heat setting types. In case of air setting type of refractory concretes, setting takes place at room temperature and in case of heat setting type the setting takes place at elevated temperatures only. Orthophosphoric acid and Mono aluminum phosphates (MAP) are the normally used phosphate binders.

Dry binders are preferred over wet ones owing to their distinct advantage of easy mixing and longer shelf life. The quality of a phosphate binder, to be used in refractory concrete, is determined by its P_2O_5 content, which determines the ultimate binding propeties. It has been reported that with the increase in P_2O_5 content, both Hot MOR and Hot crushing strength increase and porosity is reduced but simultaneously unstability is introduced at high temperature. On the other hand, reduction of P_2O_5 leads to insufficient strength development.

MECHANISM OF PHOSPHATE BONDING

It has been reported that the end products of all the reactions, in case of phosphate bonding are generally $AlPO_4$, $CrPO_4$, $Mg_3(PO_4)_2$ or Na_3PO_4. Their composition depends largely on the nature and type of aggregates, binders and setters used. The mechanism of formation of tertiary phosphates is based on physico-chemical transformation followed by neutralization process. In case of orthophosphoric acid as binder with high alumina aggregate, the probable sequence of reactions, which has been reported (Petzold & Rohrs, 1970) without incorporating any setter, are as follows :

i) At room terperature $Al(H_2PO_4)_3$ is formed;
ii) Around 250°C, polymerization of $Al(H_2PO_4)_3$ takes place along with the formation of aluminium pyrophosphate;
iii) At 500°C, pyrophosphate melts and aluminium metaphosphate is formed ;
iv) At higher temperatures, formation of crystalline $AlPO_4$ bonding phases take place resulting in lower strength;

EXPERIMENTAL WORK

Raw Materials Evaluation

Two types of aggregates viz. fireclay and fused alumina were selected initially. The chemical and mineralogical characteristics of these are as given in **table 1.**

Table 1 Chemical and Mineralogical Characteristics of Aggregates

Characteristics	Fireclay	Fused Alumina
Chemical Comp.(%)		
Al_2O_3	48.59	93.51
Fe_2O_3	5.52	0.38
SiO_2	42.11	-
Mineralogical Comp. %		
Corundum	Moderate	Most predominent
quartz	Predominent	Traces
Mullite	Predominent	-
Crystobalite	Most predominent	-

Orthophosphoric acid (H_3PO_4) and mono-aluminium phosphate (MAP) were initially selected as binders. The P_2O_5 content of orthophosphoric acid was 48.90% and that of mono-aluminium phosphate was 55.57%. Mag-chrome powder (60:40) was used as a setter.

Sample Preparation

The dry aggregate and setter were blended in the required proportion. The binders were added slowly to the dry materials and mixed for 5 minutes. The mix was than cast into (50x50x50) mm molds with 100 nos. of fixed strokes. After demolding, the specimens were dried at 110°C. For determination of strengths at 600°C, the specimens were heated first at 400°C for 5 hrs and then at 600°C for another 5 hrs. The heating rate was kept 2°c /min. (approx.) in both the cases.

Choice of Aggregates

Fire clay and fused alumina were mixed separately with orthophosphoric acid (10% by wt.). Strength of specimens made was determined at 400°C and 1050°C. While the specimens made from

fire clay showed very low strength development at 400oC which further droped at 1050°C. The specimen of fused alumina showed remarkably high strength development and was selected for further investigation. The results are given in **table 2.**

Table 2 Effect of type of aggregate on strength development

Temperature (°c)	Average strength (kg/cm^2)	
	Fireclay	Fused Alumina
400	112	220
1050	69	533

Optimisation of grain size distribution of aggregate

The specimens were prepared by mixing varying proportions of fine and coarse fractions of fused alumina and the strength were determined after firing at 600°C. For this experiment, 12% orthophosphoric acid and mag-chrome powder (25% by wt. of aggregate) were added to the aggregate. The results are as shown **Table 3.**

Table 3: Effect of grain size distribution of fused alumina

Mix Proportioning (%)		Avg. Strength at
Coarse (-14+325 mesh)	Fine (-325 mesh)	600°C (kg/cm^2)
75	25	940
50	50	1235
35	65	1240
25	75	1240

It is obvious that with increase of fine fraction of fused alumina from 25% onward, strength increases but beyond 50% it did not gain strength considerably. Therefore fused alumina with 50% coarse fraction and 50% fine fraction were optimised for further studies.

Choice of Binders

Orthophosphoric acid and MAP were mixed seperately with fused alumina of the optimised grain size as shown above. The dose of binders were varied from 6% to 20% (by wt.). Mag-chrome powder was used as setter and the specimens were fired at 600°C. It was observed that development of strength with H_3PO_4 as binder is much higher when compared with that of MAP. The strength development in case of H_3PO_4 increased progressively on increasing its dose. Hence use of MAP was discarded and orthophosphoric acid was used for further investigations. From the above investigations. The following observations were made.

1. Fused alumina was preferable over fire clay aggregates.
2. Orthophosphoric acid was preferable over MAP as binder.
3. Mag-chrome powder was an effective setter

Optimisation of Binder Percentage

Taking the aggregate with optimised grain size distribution and setter, the % of addition of H_3PO_4 as binder was optimised on the basis of higher modulus of rupture.It was observed that the optimum value of binder was 8 % by vol. or 13.68 % by wt.

HIGH TEMPERATURE PROPERTIES OF OPTIMISED REFRACTORY CONCRETE

The specimen with the optimised proportions of various constituents were prepared and were evaluated for various properties such as chemical composition, Bulk density, CCS, MOR, PCE, etc. The properties are as given in **Table 5.**

Table 5 Properties of Phosphate Bonded Refractory Concrete

Characteristics		
Al2O3 (%)		78.86
SiO2 (%)		1.95
Fe2O3 (%)		0.88
Service temperature (Max.)		1600°C
Pyrometric Cone Equivalent (°C) PCE		1804°C
Bulk Density (110°C) kg/m^3		3150
Thermal expansion (% at 1300°C)		(+) 0.62
MOR (kg/cm^2) at	110°C	173
	600°C	230
	1300°C	115
CCS (kg/cm^2) at	600°C	600
	1300°C	450

CONCLUSIONS The investigations carried out revealed that the fused alumina is preferred as an aggregate on account of its improved chemico-mineralogical characteristics as compared to fireclay and the addition of orthophosphoric acid as binder has a positive effect on strength development of refractory concrete. The refractory concrete so developed has exhibited the improved values of physical and thermal properties viz. Bulk density, thermal expansion, cold crushing strength and MOR.

Acknowledgement
This paper is being published with the permission of Director General, National Council for Cement and Building Materials, New Delhi, India.

REFERENCES :

1. Petzold, A. and Rohrs, M., "Concrete for high temperatures ", Applied Science London, 1970.

PHYSICO-MECHANICAL AND DEFORMATION PROPERTIES OF CEMENTLESS FINE-GRAINED ASH-SLAG CONCRETE OVER A 5-YEAR PERIOD

Yury BAZHENOV, Building University of Moscow, Russia
Stanislav PAVLENKO, SSAMM, Novokuznetsk, Russia

ABSTRACT Physico-mechanical and deformation properties of a cementless fine-grained ash-slag concrete (patent of 21.01.93) developed by the SSAMM have been studied for 5 years in order to predict its future performance. The compressive strength of the concrete was 5 to 20 MPa which is suitable for the construction of cast in-situ low-rise building and the production of silica brick. Over the 5-year period, the concrete improved its characteristics: compressive strength, modulus of the elasticity, compressibility, extensibility, prism-to-cube strength ratio of the concrete increased by 1.53 (from 15.2 to 23.3 MPa), 1.58 (from 12.1 to 18.64 MPa), 1.22 (from 0.87 to 1.07 mm/m), 1.5 times (from 0.12 to 0.18 mm/m), and 1.54 (from 12 to 19 MPa), respectively.

INTRODUCTION

In this work, the main physico-mechanical and deformation properties of the concrete developed were studied over 5-year period. The concrete was entirely made of waste products from thermal power plants (ash and slag) and ferroalloy plant (silica fume). High-calcium ash from burning brown coals of Kansko-Achinsky Power Complex and silica fume were binding materials. Two-stage heat treatment was applied to the concrete: the use of hot water (60-80 °C) for mixing and then curing concrete in stream-curing chambers (for concrete articles) or heating concrete in formworks (for cast in-situ structures).

MATERIALS

High-Calcium Fly Ash

The ash from Abakanskaya thermal power plants, burning brown coals of the Irsha-Borodinsky deposit, was used. Physical properties and chemical analysis of the ash are given in Table 1 and 2, respectively.

Table 1 Physical Properties of Fly Ash, Slag Sand and Silica Fume

Properties	Fly Ash	Slag Sand 0...5 mm	Silica Fume
Fineness-passing 45 mm, %	92.50	0.25	100
Blaine, m^2/kg	240	-	2900
Specific Gravity	2.76	2.68	2.25
Bulk Density, kg/m^3	1120	1580	245
Setting Time, h : mm			
-Initial	0.56	-	-
-Final	5.48	-	-
-Colour	grey	black, green	light grey

As shown by the investigations of the Siberian branch of the Russian Academy of Sciences (Savinkina and Logvinenko, 1979), SibZNIIEP (Ignatova, 1990) and by our study (Pavlenko, 1995), binding properties of high-calcium ash can be determined by the so-called coefficient of quality (C_q) according to the formula:

Table 2 Chemical Analysis of Fly Ash, Slag Sand and Silica Fume

Oxides, %	Fly Ash	Slag Sand 0...5 mm	Silica Fume
SiO_2 total	39.45	51.47	90.11
including free SiO_2	14.20	14.57	82.00
CaO total	31.20	29.92	0.71
including free CaO	8.96	-	-
MgO	6.31	3.50	0.97
Al_2O_3	7.11	8.16	1.93
FeO	0.87	8.20	1.82
Fe_2O_3	9.92	1.43	-
MnO	0.18	0.17	0.20
P_2O_5	0.06	0.05	1.18
SO_3	0.86	0.01	0.89
TiO_2	0.90	-	0.02
Na_2O	0.40	-	0.87
K_2O	0.70	-	1.16
Loss on Ignition	1.85	-	2.05

$C_q = (CaO + Al_2O_3 + MgO) / SiO_2 = (31.20 + 7.11 + 6.31) / 39.45 = 1.13$

If the coefficient is more than 1, then the ash has good binding properties. In our investigation, the coefficient was 1.13. However, C_q of this ash is considerably lower then that from Novosibirskaya thermal power plant, and has to be ground in a ball mill to the fineness of 400 to 450 m^2/kg. The grinding activates strength of the ash, makes it possible to use free silica of fly ash (14.2%) and silica fume (82%) for binding free calcium oxide (8.96%) as well as activates minerals containing magnesium.

Granulated Slag

Slag sand from Abakanskaya thermal power plant was studied in accordance with the requirements of State Standard 26644-85 (1991). The date are given in Table 1 and 2. Testing for oxides contents was carried out according to State Standard 5382-91 (1994) and 25583-83 (1983). A system of slag removal at the thermal power plant is based on the principle of granulation (removal of the fiery liquid slag with hydrocooling) (Panteleyev et al, 1985). Granulated slag is then ground to sand with a particle size of 0 to 5 mm (Pavlenko, 1989). Testing of the slag for silicate and ferruginous decomposition and frost resistance was done according to State Standard 9758-86 (Pavlenko, 1991). Losses of weight of the slag during the testing for silicate and ferruginous decomposition were up to 6.7 and below 4%, respectively, as compared with 8 and 5% according to State Standards. Frost resistance of the slag was 235 cycles versus 200 cycles according to State Standard.

Silica Fume

Silica fume from Kuznetsk Ferroalloy plant was a super dispersed powder (5-6 times finer than cement) of a light grey colour with a fineness of 2200 to 3000 m^2/kg. The data on test results are given in Table 1 and 2. X-ray diffraction and DTA showed the presence of silicon mostly in the amorphous form which increased the hydraulic of the silica fume while reacting with lime and binding free lime of high-calcium ash. The hydraulic activity was evaluated by determining the

amount of lime absorbed by silica fume from a saturated solution at 85 °C. It was 102 mg CaO/g.

OPTIMUM MIXTURE PROPORTIONS OF CEMENTLESS CONCRETE

As a result of previous investigation of the process of structure formation and strength characteristics of cementless concrete using the method of experimental planning and a computing technique (Pavlenko, 1991 b, Pavlenko, 1992, Pavlenko and Oreshkin, 1992, Pavlenko and Chayka, 1993), optimum mixture proportions of the fine-grained ash-slag concrete were developed which are given in Table 3. Main physical and deformation properties of the concrete developed were studied for the period of 5 years (1990 to 1995).

Table 3 Mixture Proportions of Cementless Concrete

Quantities, kg/m^3				Mix	Mix	Compressive
Fly Ash	Silica Fume	Slag Sand	Water	Slump, cm	Density, kg/m^3	Strength at 28 days, MPa
650	70	720	480	8-10	1920	15

EXPERIMENTAL PROCEDURE

Test cubes, 100*100*100 mm in size, and prisms, 100*100*400 mm in size, were cast for studying physico-mechanical and deformation properties of the fine-grained cementless ash-slag concrete. Mixture were made in a laboratory positive mixer using hot water (70-80 °C), vibrated, cured for 4 hours at room temperature steam-curing chamber at 85-95 °C using 3+10+3h cycle.

Strength Characteristics

Compressive strength was determined on 100-mm cubes and prism strength on 100*100*400 mm prisms in accordance with the methods of NIIZHB (1976, a) at the following ages: 24h, 28, 365, 730, 1095, 1460 and 1825 days. The data are given in Table 4. It is evident from the data that the cementless fine-grained ash-slag concrete increased its compressive and prism strength by 53 and 58%, respectively, over a 5-year period. The highest strength gain was at 28 to 365 days (18 to 26%), beyond this period the strength development was slow (5% and lower). Ordinary concrete showed increase in strength by 10% during the first year, and by 15 to 18% at the age of 5 years. The modulus of elasticity was also determined in accordance with the NIIZhB methods (1976, b). It increased by 54% over the 5-year period which exceeded the requirements of the Building Code for fine-grained concretes (Gosstroy USSR, 1985 a) by 15 to 20% (Table 4).

Table 4 Main Physico-Mechanical Characteristics of Cementless Concrete

Concrete Characteristics	Period of testing, days						
	1	28	365	730	1095	1460	1825
Compressive strength, MPa	10.80	15.20	18.00	19.80	20.96	22.08	23.30
Prism strength, MPa	8.10	11.96	15.07	16.63	17.61	18.55	18.96
Prism-to-Cube strength Ratio	0.75	0.78	0.83	0.84	0.84	0.84	0.85
Initial Modulus of Elasticity, MPa	9.50	12.10	17.60	17.72	17.96	18.03	18.64
Compressibility, mm/m	0.85	0.87	1.04	1.05	1.06	1.07	1.07
Extensibility, mm/m	0.09	0.12	0.16	0.17	0.17	0.18	0.18

Shrinkage and Creep Deformation

Drying shrinkage and creep tests were performed using the methods of NIIZhB (1976, c). Prism specimens, 100*100*400 mm in size, were cured at 18 to 22 °C and 50 to 75% relative humidity. Shrinkage strains were determined by a dial type indicator with 0.001 mm scale. The measurements were made in the following periods: immediately after cooling of the specimens; at 30 min, 2, 4, 12 and 24 h; once a day between 2 and 6 days ; once a 2-day period between 7 and 14 days and once a week beyond this period until the complete stabilization of the shrinkage. The shrinkage strains were 0.3 mm/m and 0.6 mm/m at 24 h and 28 days, respectively. Between 28 and 180 days, they increased up to 0.65 mm/m and stopped beyond this period. At 5 years, the shrinkage strain was 0.66 mm/m which exceeded the requirements of the Building Code (Gosstroy USSR, 1985 b) for fine-grained concretes (up to 0.75 mm/m). The drying shrinkage of the ash-slag concrete developed smoother than that of a sand concrete (Fig. 1) which was attributable a lower bleeding of the first. Due to the lower bleeding and higher strength gain as compared to the cement sand concrete, the ash-slag concrete attained a higher crack resistance.

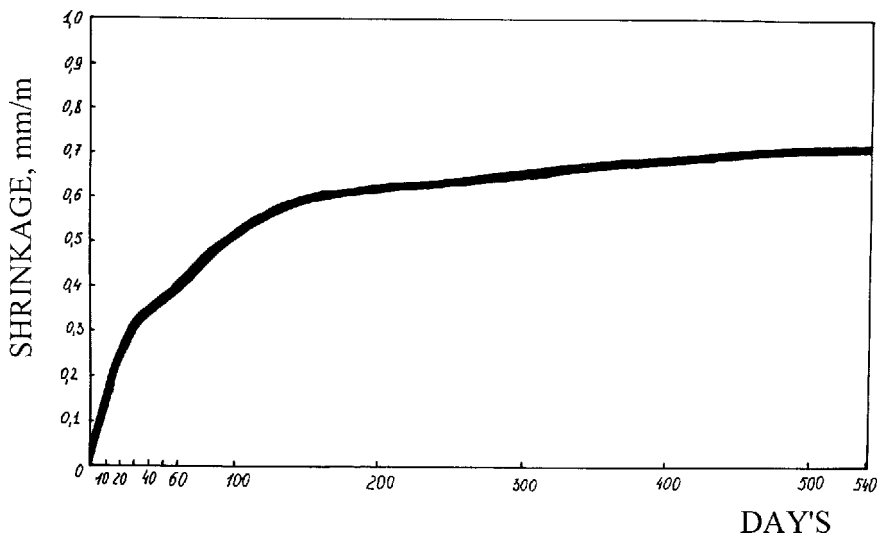

Figure 1 Relative shrinkage of fine-grained concrete

Creep tests were started at 28 days. Prisms were subjected to a long-term loading at the applied stresses constituting 50% of the prism strength (0.5R prism). The measurements were taken in the following peroids: at 30 min, 1, 3, 6 and 12 h, once a day between 2 and 6 days, once a 2-day period between 7 and 15 days, twice a week beyond this period and once a month after the stabilization. It can be seen that the creep strain of the cementless ash-slag concrete achieved 0.8 mm/m at 20 days, and the magnitude of the creep increased insignificantly between 20 and 180 days (up to 0.94 mm/m) stopping beyond this period (Fig. 2). The concrete showed 12 to 15% less creep than data reported for a fine-grained sand concrete (1985 c).

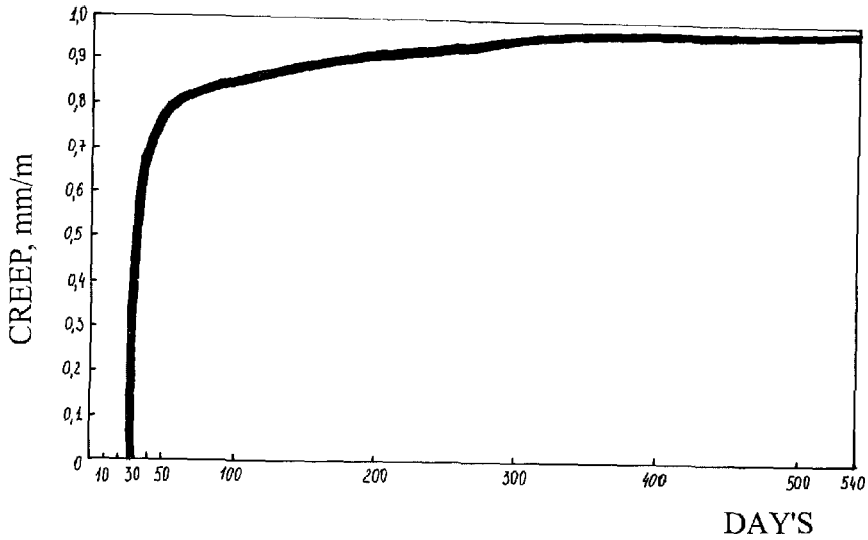

Figure 2 Relative creep of fine-grained concrete

CONCLUSIONS

The conclusions arrived at from this work may be stated as follows:

1) Cementless ash-slag concrete produced from waste products of the thermal power plant and ferroalloy plant based on high-calcium ash may be used as a replacement for ordinary cement sand concretes of B10-15 classes (15 to 20 MPa).

2) The main physico-mechanical and deformation properties of the concrete meet the requirements of State Standard and Building Code of Russia for concretes of this strength and, in some respect, exceed them.

3) The concrete developed seems to be a promising material for the twenty first century. Excluding the use of both natural and artificial energy consuming materials permits to solve economic, ecological and social (housing construction) problems.

ACKNOWLEDGEMENTS

The author would like to thank the Heavy Concrete Laboratory, NIIZhB, headed by M.I. Brusser, Concrete Laboratory, SibZNIIEP (A.A. Bezverhy, O.A. Ignatova), V.F. Jakushenko, the Head of the Materials Testing Laboratory, Sibstrinvest, for the participation in the work and consultations.

REFERENCES

Gosstroy USSR. Concrete and reinforced concrete structures, SNIP 2.03.01-84, Moscow, 1985, pp. 12-20.

Ignatova, O.A. "Study of the Homogeneity of HIgh-Calcium Ashes from Kansko-Achinsky Coal and Development of Standard Requirements for use in Concretes", Proceedings of the All-Union Conference on Concrete Containing Ash and Slag Sand from TPP and their Use in Construction, Edited by S.I. Pavlenko, Vol. 1, 1990, pp. 146-149.

NIIZhB "Guide for determination of strength and structure characteristics of concretes under shot-and-long duration loading", Moscow, 1976, pp. 10-76.

NIIZhB "Guide for investigation of shrinkage and creep of concrete", Moscow, 1976, pp. 10-76.

Panteleyev, V.G., Larina, E.A., and Melentjev, V.A., "Composition and Properties of Ash and Slag from Thermal Power Plants", Reference Bvok Edited-by V.A. Melentjev, Leningrad, Energoatomizdat, 1985, pp.7-12.

Pavlenko, S.I., and Chayka, E.A. "Development of High-Calcium Fly Ash and Slag Sand Concrete", Concrete 2000, Economic and Durable Construction through Exelance, Proceedings of the International Conference held at the University of Dundee, Scotland, UK, September 1993, Edited by R.K. Dhir and M. Radeck Toms, New Application E & FN Spoon, London, 1993, Vol. 2, pp. 1297-1303.

Pavlenko, S.I., and Oreshkin, A.B. "Structure Formation of Cementless Concrete made with Slag Sand and High-Calcium Ash From Thermal Power Plants", 9th International Congress on the Chemistry of Cement 1992. The Collection of Proceedings, November 23-28, New Delhi, India, 1992, pp. 647-653.

Pavlenko, S.I. "Concrete on the Basis of the Steam Electric Station Ash and Crushed Slag", Third CANMET/ACI International Conference on the Fly Ash, Silica Fume, Slag and Natural Pozzolans in Concrete, Supplementary Papers, Trondheim, Norway, 1989, pp. 738-755.

Pavlenko, S.I. "Fine-Grained Cementless Concrete made with High-Calcium Fly Ash and Slag Sand from Thermal Power Plants", Fourth CANMET/ACI International Conference on Fly Ash, Silica Fume, Slag and Natural Pozzolans in Concrete, Supplementary Papers, Istanbul, 1992, pp. 749-763.

Pavlenko, S.I. "Heat Treatment of Fine-Grained Cementless Concrete Based on High-Calcium Fly Ash and Slag from Thermal Power Plants", Proceedings, Fifth CANMET/ACI International Conference on Fly Ash, Silica Fume, Slag and Natural Pozzolans in Concrete, Editor V.M. Malhotra, Vol. 1, SP-153, 1995, pp. 497-512.

Pavlenko, S.I. "Lightweight Cementless Concrete on the Base of High-Calcium Fly Ash and Slag Sand from TPP", Proceedings of the International Conference on Blended Cements in Construction, held ot the University of Sheffield, UK, 9-12 September, 1991, Edited by R.N. Swamy, Elsiver Applied Science, London and New York, 1991, pp. 95-106.

Savinkina, M.A. and Logvinenko, A.T. "Ashes Produced from the Kansko-Achinsky Brown Coal", Novosibirsk, "Nauka", 1979, p.83.

State Standard 5382-91 "Cements and Cement Products. Methods of Chemical Analysis", Gosstroy USSR, Moscow, Izdatelstvo Standartov, 1994.

State Standard 26644-85. "Rubble and Sand from Slag of Thermal Power Plants Used for Concrete", Gosstroy, USSR, Moscow, Izdatelstvo Standartov, 1991.

State Standard 25589-83 "Rubble, Gravel and Sand for Construction. Methods for Determining the Contents of Sulphate and sulphurous Compounds", Gosstroy USSR, Moscow, Izdatelstvo Standartof, 1983.

TOPIC IV.D

Influence of physico-chemical aspects during early material history on durability

PLAUSIBILITY OF DELAYED ETTRINGITE FORMATION AS A DISTRESS MECHANISM - CONSIDERATIONS AT AMBIENT AND ELEVATED TEMPERATURES

Waldemar A. KLEMM, Construction Technology Laboratories, Inc., Skokie, IL, U.S.A.
F. MacGregor MILLER, Construction Technology Laboratories, Inc., Skokie, IL, U.S.A.

ABSTRACT Recent debate on delayed ettringite formation (DEF) as a distress mechanism for ambient- and steam-cured concrete has inspired this paper, which examines relevant data from the literature and from the authors' laboratory. DEF can be associated with distress in high temperature concrete, but not for ambient-curing in the absence of external SO_3 sources, or an aggregate sulfate source. The two internal SO_3 sources cited as potentially responsible—anhydrite in clinker and high SO_3 concentrations in the silicate phases—are shown to be absent or fundamentally innocuous.

Key-words: Anhydrite; Delayed ettringite formation; AFt phase; Sulphate attack; Curing

DELAYED ETTRINGITE FORMATION

Introduction

Delayed ettringite formation is one form of what will here be termed Internal Sulfate Attack (ISA). ISA in concrete may occur through the presence of sulfate in aggregate, or from the deliberate or inadvertent inclusion of high levels of gypsum in the system. These varieties of ISA will not be dealt with here.

The two forms of concrete distress to be treated here will be those in which the sulfate and aluminate are furnished by the cementitious materials. These are expansion and cracking in concrete that has been cured at high temperature (>70°C), caused by formation of ettringite in mature concrete. Also considered are expansion and cracking reported in concretes that have been cured under ambient conditions. The high-temperature effect is usually termed delayed ettringite formation, while the ambient temperature hypothesis has been given the title "late" ettringite formation. Taylor (1996) has given a very good description of the process of ettringite formation under various conditions.

Taylor (1996), Scrivener (1996), Kelham (1996), Fu and Beaudoin (1996) and others have established that when concrete is cured at temperatures over 70°-80°C, ettringite which may have been produced in the initial pre-curing period is decomposed, and the formation of new ettringite is impeded. Early thinking seemed to favor the stability of monosulfoaluminate ($C_3A{\cdot}CaSO_4{\cdot}12H_2O$) under these conditions, but it now appears that a more likely explanation involves adsorption of the sulfate by the C-S-H gel phase. The alumina is also adsorbed, and it is believed (Fu and Beaudoin, 1996) that the sulfate and alumina are held more tightly if curing temperatures are high. Subsequently, when the concrete is cooled, it is postulated that the sulfate and alumina desorb from the C-S-H and can potentially reform ettringite. The slow desorption of sulfate from the C-S-H occurs well after the strength of the concrete has developed.

However, the desorption of sulfate from the C-S-H does not necessarily lead to concrete distress. Scrivener's work (1996) has established that the tendency toward expansion of the system depends upon the sulfur-to-alumina ratio of the C-S-H. If the molar ratio is close to three, there is expansive stress, but if it is near unity, no such expansion is observed. Kelham (1996) has stated that there must be juxtaposition of several factors for steam curing to lead to distress:

- sulfate-resisting cements (with low C_3A) are not susceptible to DEF
- there is a pessimum in the SO_3 level for any given clinker
- increases in cement fineness, alkali level, and MgO level all appear correlated to increased expansion

Johansen and co-workers (1995) have explained that the effect of alkalies seems to relate to the temperature of instability of ettringite. The higher is the alkali content, the lower this temperature limit becomes.

Another issue with respect to internal sulfate attack is the issue of temperature and service conditions of concrete cured at ambient conditions. Stark and co-workers (1992) concluded that in addition to the temperature of heat treatment, the temperature attained during the utilization of hardened concrete has great influence on the durability of the concrete, especially in concretes with a dense structure (low w/c ratio), a cement SO_3 content of >3.3%, and exposure conditions consisting of drying temperatures of ≥60°C combined with longer wetting periods. Under these conditions structural deterioration may result . They also note that deterioration first becomes apparent in small specimens.

The test of Grabowski and co-workers (1992) probably measures both delayed ettringite formation and ISA from this kind of thermal cycling. Their conditions (very short pre-cure, very high temperature with fast ramp, short time at temperature, slow cooling) would largely maximize the probability of problems, if any could occur, and exacerbate their severity. The Duggan test itself "...involves measuring length changes in concrete cores, 22 mm in diameter, 50 ± 5 mm long. After soaking in water for 3 days, the cores are subjected to 3 cycles of heating and cooling over a period of 7 days. The cores are then placed in distilled water and length change measurements are taken for 20 days. Trials indicate that cores which expand by 0.05% or more after the 30 days are from concretes with a potential for deleterious expansion."

Fu and Beaudoin (1996) distinguish between DEF and the exposure-induced distress, terming the latter "secondary ettringite formation" (SEF). In the case of SEF, severe drying decomposes the sulfoaluminate hydrates. When re-wetting occurs, the calcium sulfate dissolves and reacts rapidly with aluminates to form ettringite. They indicate that the Duggan test, which is designed to assess the potential for DEF, may be showing SEF potential instead. It appears to the present authors that the Duggan test measures both mechanisms.

The third mechanism, that of sulfate becoming available only after the concrete has developed strength, in samples cured under ambient conditions, has been discussed by Hime (1996a, 1996b, 1996c) and Mielenz et al. (1995). Hime (1996a) states that,

"If the precast concrete is not air-entrained, and exposure to water will be frequent, then DEF may occur if either: a) the concrete temperature during curing or in service reaches a temperature high enough to decompose ettringite. Depending on cement composition, this temperature may be as low as 140°F (60°C); or b) the clinker contains a substantial amount of slowly soluble sulfate. Clinker sulfate levels may be as low as 1.5% to cause DEF. For high-alkali cements, the lower SO_3 limit may be 2% or more."

In another paper, Hime [1996b] indicates that ambient DEF can be avoided by keeping *clinker sulfate below 1%.* The position is that if the belite crystals contain very high levels of sulfate, this sulfate will not become available until the belite hydrates, which is well after the development of rigidity in the concrete. Furthermore, according to this hypothesis, there is the possibility that high-sulfur fuels will cause large accumulations of anhydrite in the clinker, which will not be exposed by grinding, and which will become available only slowly, after the development of concrete rigidity. The results obtained in the present studies are not consistent with this hypothesis, and the balance of this paper will address this issue.

"Slowly Soluble Sulfate"

As mentioned above, recent literature references hypothesize that sulfate which is "slowly soluble" in ambient curing scenarios can cause distress. One of the goals of the present work was to try to discover what sulfated clinker phases might be slowly soluble, and what their effect might be on volume stability due to late ettringite formation. One of the chief difficulties in trying to measure this elusive parameter is that the measurement techniques themselves may alter the form of the sulfate.

As an example, one may consider the adaptation, for determination of water-soluble sulfate in cements, of the ASTM procedure for determination of water-soluble alkalies (C 114). This method uses a high ratio of water-to-cement and a relatively short duration of exposure of the cement to the water. Irrespective of the short exposure period, there is a good possibility that rapidly soluble sulfate, such as hemihydrate, soluble anhydrite (γ-calcium sulfate), or alkali sulfate, will go into solution and immediately be taken out of solution again by reaction with the aluminates. This sulfate will therefore be measured as slowly soluble or insoluble, when in fact it is highly soluble. Furthermore, using ASTM Method C 265 for determination of unreacted calcium sulfate is also unrepresentative of field conditions, because it uses a low ratio of water to mortar, a coarse specimen to be leached, and a very short duration of exposure (2 minutes), followed by filtration. As such, it is unlikely to result in the dissolution of any "slowly soluble" sulfate.

Recently, Jøns (1996) published a method for determination of soluble and insoluble sulfate in clinker and cement, based on the use of a dilute solution of sodium carbonate. His work shows that the results of the water extraction method indicate high levels of insoluble sulfate even when there is no clinker sulfate, (i.e., when all sulfate is furnished by gypsum or hemihydrate). The soda extraction method measures insoluble sulfates which correlate well with the level of sulfate in the silicate phases determined in the residue of extraction of clinker or cement using KOH-sucrose extraction solution (Gutteridge, 1979). Jøns' method seems applicable to the determination of soluble and insoluble sulfate during early hydration. It seems to be inapplicable to the determination of slowly soluble sulfate in hydrated samples, because it may partially decompose ettringite and monosulfate.

EXPERIMENTAL PART

Distribution of Sulfur in Modern North American Clinkers

The present research has been focused on the determination of how sulfur is distributed in present-day clinkers. For this study, 33 clinkers with SO_3 contents ranging from 0.03-3.00% were received from participating cement plants. These samples were subjected to chemical analysis by X-ray fluorescence (XRF) with results organized in order of increasing SO_3/alkali ratio, as shown in Table 1.

Table 1 Selected Chemical Analytical Results, 33 Industrial Clinkers.

Plant No.	Process	%C_3S	%C_3A	Silica Ratio	% SO_3	% Na_2O	% K_2O	Molar SO_3/Na_2Oeq
2	Long Wet	63.1	6.0	3.36	0.03	0.09	0.45	0.06
7	Long Wet	55.7	6.6	2.63	0.14	0.35	0.39	0.18
3	Long Wet	74.8	7.1	2.34	0.07	0.11	0.18	0.24
15	Long Wet	64.8	11.4	2.70	0.19	0.14	0.53	0.30
1	Long Wet	44.3	10.2	2.65	0.38	0.36	0.93	0.30
25	Long Dry	71.3	8.7	2.34	0.12	0.14	0.22	0.33
13	Long Wet	68.2	6.3	2.34	0.19	0.13	0.41	0.37
5	Long Wet	65.0	10.6	2.54	0.34	0.26	0.43	0.48
6	Long Dry	74.3	7.8	2.55	0.46	0.15	0.71	0.58
24	Precalciner	61.7	11.3	2.76	0.95	0.27	1.08	0.75
27	Preheater	50.7	8.6	3.75	0.79	0.27	0.61	0.91
18	Long Wet	64.5	10.0	2.91	0.64	0.09	0.65	0.96
16	Long Wet	72.9	9.5	2.58	0.34	0.15	0.18	0.98
17	Long Wet	64.5	9.6	2.88	1.29	0.15	1.23	1.04
11	Preheater	66.0	0.0	3.38	0.74	0.14	0.61	1.06
22	Preheater	62.3	9.4	2.93	1.58	0.32	1.11	1.16
19	Preheater	66.5	13.1	2.27	1.86	0.32	1.27	1.25
12	Preheater	63.8	9.8	2.57	1.58	0.20	1.17	1.26
14	Long Wet	65.4	6.4	2.58	1.01	0.14	0.71	1.29
28	Precalciner	62.7	8.8	2.74	1.18	0.08	0.93	1.32
33	Long Dry	71.7	6.8	2.61	1.33	0.06	1.09	1.32
32	Preheater	67.5	6.6	2.59	1.77	0.06	1.26	1.54
10	Precalciner	62.9	10.5	2.92	1.84	0.33	0.88	1.57
8	Precalciner	62.1	9.8	2.59	3.00	0.32	1.75	1.58
4	Precalciner	67.2	9.1	2.47	1.46	0.15	0.78	1.70
31	Long Dry	68.2	5.7	3.00	1.14	0.22	0.45	1.71
30	Preheater	56.6	6.6	2.91	1.54	0.13	0.86	1.71
9	Long Dry	55.7	11.3	2.51	2.27	0.38	0.96	1.74
29	Long Dry	58.8	12.1	2.60	2.12	0.09	1.20	1.87
20	Precalciner	71.9	5.3	2.67	1.24	0.13	0.54	1.98
21	Precalciner	51.5	7.2	2.77	2.48	0.29	0.92	2.14
26	Precalciner	76.1	9.0	2.38	1.95	0.28	0.56	2.33
23	Precalciner	71.9	5.3	2.67	1.63	0.20	0.45	2.54

The mineralogy of the sulfur-containing phases in clinker was determined using powder X-ray diffraction (XRD) spectrometry combined with selective extraction techniques. Methanolic salicylic acid (Takashima, 1958) was used to extract the free lime and calcium silicates from the aluminates, ferrites, and the sulfate salts. The residues were analyzed by XRF and subjected to XRD examination. This selective dissolution technique concentrated these salts by about a factor of 5, and facilitated interpretation of the XRD spectra. Potassium hydroxide/sucrose solution (Gutteridge, 1979) was used to extract the aluminates, ferrites, and sulfates from the calcium silicates, free lime, and periclase in the parent clinkers. These residues were also studied using XRF and XRD.

The sulfate phases were readily observed on the salicylic acid/methanol extraction (SAMX) residues by XRD. Results of the analysis for alkalies and sulfur, and the XRD findings, are given in Table 2, in order of increasing molar SO_3/alkali ratio:

Table 2 Salicylic Acid/Methanol Residues-Chemical & XRD Analyses.

Plant No.	Process	% SO_3	% Na_2O	% K_2O	SO_3/Na_2Oeq	Phases Found*
2	Long Wet	0.08	0.44	1.17	0.05	None
25	Long Dry	0.09	0.43	0.52	0.09	None
7	Long Wet	0.37	1.01	0.95	0.18	Arc(tr)
3	Long Wet	0.15	0.36	0.44	0.18	None
15	Long Wet	0.51	0.66	1.48	0.24	Arc(tr)
1	Long Wet	1.09	1.20	2.65	0.29	Arc
13	Long Wet	0.51	0.50	1.06	0.33	Arc
5	Long Wet	0.95	0.75	1.19	0.48	Arc, Aph
16	Long Wet	0.58	0.52	0.57	0.50	None
6	Long Dry	1.33	0.45	2.33	0.52	Arc
24	Precalciner	3.78	0.93	4.36	0.77	Arc, Aph
18	Long Wet	2.14	0.37	2.40	0.85	Arc, Aph
27	Preheater	3.28	1.05	2.91	0.86	Arc, Aph
17	Long Wet	4.84	0.67	5.51	0.87	Arc, Aph, CL
11	Preheater	3.19	0.45	2.86	1.06	Arc, Aph, CL
22	Preheater	5.82	1.00	4.76	1.09	Arc, Aph(+)
14	Long Wet	3.53	0.54	2.96	1.10	Arc, Aph, CL
19	Preheater	6.03	1.11	4.77	1.10	Arc, Aph, CL
33	Long Dry	5.01	0.23	4.59	1.19	Arc, Aph, CL
28	Precalciner	4.49	0.28	3.99	1.20	Arc, Aph, CL
12	Preheater	5.92	0.66	4.68	1.23	Arc, Aph
32	Preheater	6.98	0.25	5.09	1.50	Arc, Aph, CL
8	Precalciner	10.89	1.19	6.70	1.51	Arc, Aph
4	Precalciner	5.80	0.57	3.37	1.61	CL, Aph, Arc, SA
10	Precalciner	7.77	1.09	3.84	1.66	Aph
9	Long Dry	8.33	1.29	3.73	1.72	CL,Aph,SA
30	Preheater	6.71	0.47	3.81	1.75	Arc, Aph, CL
31	Long Dry	5.43	0.80	2.32	1.81	Aph, CL
29	Long Dry	8.85	0.33	5.18	1.83	Arc, Aph, CL
21	Precalciner	10.65	1.16	4.32	2.06	CL, Aph, Arc, SA
20	Precalciner	5.24	0.48	2.15	2.14	CL, SA
26	Precalciner	8.79	1.04	2.77	2.38	CL, Aph, SA
23	Precalciner	7.48	0.73	2.14	2.71	CL, Aph, SA

*- Arc=arcanite, Aph=aphthitalite,CL=calcium langbeinite, SA=soluble anhydrite (γ-$CaSO_4$)
tr=trace, (+)= large amount

The chemical analysis of the KOH/sugar residues permits determination of their sulfur content, and thus the potential for slowly soluble sulfate from belite. The results were in line with expectation, and indicate that the sulfate in modern North American clinkers is distributed in the following mineralogical forms:

- Arcanite (K_2SO_4)
- Aphthitalite (a solid solution series, nominally $3K_2SO_4 \cdot Na_2SO_4$)
- Calcium langbeinite (usually designated $2CaSO_4 \cdot K_2SO_4$)
- Sulfate substituted in silicates (probably chiefly in belite)

The arcanite, aphthitalite, and calcium langbeinite are readily identified using XRD. The sulfate incorporated in belite (and alite) appears in the analysis of the KOH/sugar solution residues, from material balance calculations subtracting the sulfate in the SAMX residues from the total clinker sulfate, and from the appearance of "soluble anhydrite" (γ-$CaSO_4$) in the SAMX residues. In no case does this represent more than 0.85% SO_3 in the silicates, or 0.68% for the clinker as a whole. No natural β-anhydrite was found in any clinkers, either in the whole clinkers or in the SAMX residues. (Detection limits for the

presence of anhydrite are estimated at 0.5% in whole clinker and 0.1% in the SAMX residue on a whole clinker basis.) (It should be pointed out that γ-$CaSO_4$ has an XRD pattern very similar to that of hemihydrate, and completely different from that of β-$CaSO_4$. There can be no mistaking what the phase identified is, and that its formation can only be understood on the basis of small quantities of water present in the methanolic salicylic acid. Our experience indicates that only trace quantities of water are required to form this phase.)

The Gutteridge method for KOH/sugar extraction makes no mention of the efficiency in extraction of sulfur- containing phases other than silicate-lattice sulfate. For this reason, an experiment was performed to establish whether any other sulfur-containing phases might be present in the extraction residue, leading to inaccuracies in the determination of the silicate sulfur. Two such residues, from high sulfur clinkers (Nos. 9 and 21) were subjected to DSC examination for the presence of ettringite and/or syngenite (the clinkers had contained substantial quantities of calcium langbeinite). The derivative of the heat curves (rate of change of endotherm or exotherm) was also plotted. Evidence for small amounts of C-S-H phase were found, but no endotherm for ettringite or syngenite was found. The evidence of the derivative curve was particularly convincing; the addition of 1% ettringite to the sample gave a strong inflection at 100-110°C.

As further confirmation of the efficiency of extraction, a one-gram sample of pure synthetic ettringite was subjected to extraction with KOH/sugar. The sample was extracted and filtered, and the filtrate was subjected to chemical analysis for sulfate ion. 98.6% of the sulfate content of the original ettringite was found in the filtrate. In view of the very low solubility product for ettringite (of the order of 1×10^{-40}), it is clear that the sugar is very effectively chelating the calcium ion and ensuring the solubility of sulfate sources other than those incorporated within the calcium silicate phases.

Correlation of SO_3 Insoluble in the "Soda Method" and SO_3 in the Silicates

The sulfate contents in the silicate phases would be expected to be similar to the SO_3 content in the clinker that might be "slowly available"; the rest of the sulfate might be anticipated to dissolve in the dilute sodium carbonate solution utilized by Jøns (1996). To check this hypothesis, seven of the clinker samples (samples 1, 3, 9, 11, 19, 21, and 26) were extracted with Jøns' solution at two finenesses: passing 147 μm (100 mesh), and passing 45 μm (325 mesh). Figure 1 illustrates the correlation for the finer clinker; the correlation is quite good, with an R^2 value of 0.87. Figure 2 gives the same information for the coarser sample, with a correlation coefficient of 0.88.

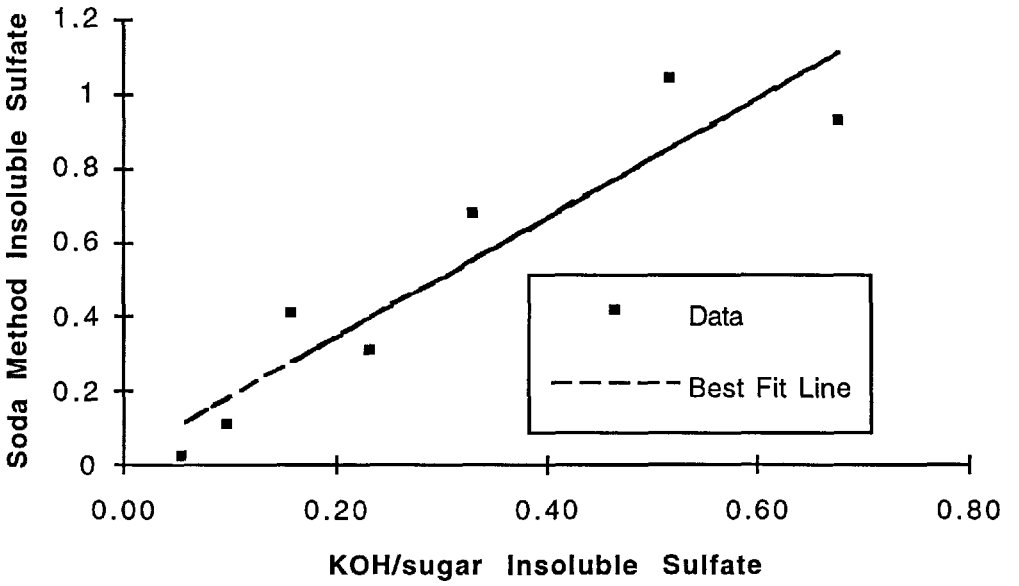

Figure 1 KOH/Sugar Insoluble SO_3 vs Soda Method Insoluble SO_3 - 45 μm Clinker.

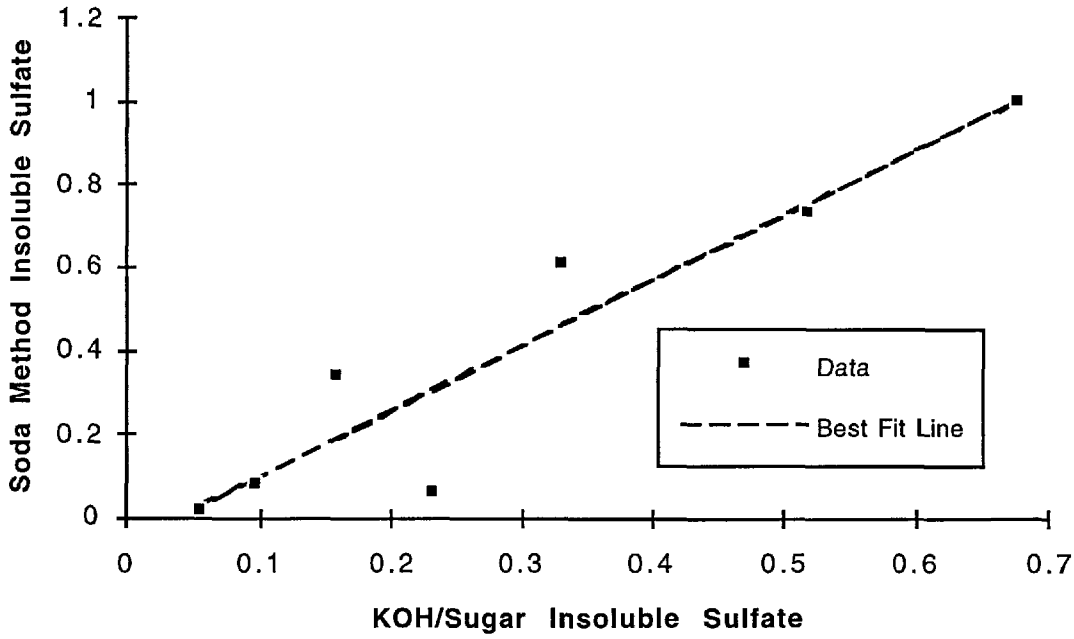

Figure 2 KOH/Sugar Insoluble SO_3 vs Soda Method Insoluble SO_3 - 147 μm clinker.

It will be noted that, although there is a good correlation, the sulfate content of the residue from the soda method extraction is generally higher than that of the residue from the KOH/sugar extraction. It seems likely that there may be a small amount of ettringite, or perhaps syngenite, formed during the process of extraction with soda; further work would be needed to verify this hypothesis.

Rate of Release of Sulfate from High Sulfate Clinker

It was considered of interest to determine the fate of the sulfur compounds in a cement made from a clinker with high sulfate level. The XRD pattern for clinker no. 9 had shown the presence of relatively large amounts of calcium langbeinite, together with aphthitalite and some γ-$CaSO_4$. The formation and disappearance of phases was followed using differential scanning calorimetry (DSC). There was particular interest to determine whether calcium langbeinite hydrated to syngenite, how fast the endotherm corresponding to the decomposition of syngenite disappeared from the DSC trace, the rate of formation and disappearance of peaks attributable to gypsum or hemihydrate, and the rate of formation of ettringite. The authors' laboratory has recently developed a useful, reproducible semiquantitative method for separating the endotherms attributable to ettringite, monosulfoaluminate, gypsum, hemihydrate, syngenite, and calcium silicate hydrate, so that the abundance of these phases can be at least approximated.

Table 3 shows the rate of appearance and disappearance of the phases of interest, and the % of each as a function of time.

Table 3 DSC Results, Cement Made from High Sulfur Clinker (Clinker #9)

Sample ID	Ettring.,J/g	Gypsum, J/g	Syngnte,J/g	% Ettringite	% Gypsum	% Syngenite
Cement	-	8.21	-	-	1.8	-
2 min paste	34.37	12.31	2.62	5.3	2.7	1.6
5 min paste	37.88	13.46	2.87	5.9	3.0	1.7
10 min paste	38.71	11.99	4.11	6.0	2.6	2.5
30 min paste	41.96	13.01	3.17	6.5	2.9	1.9
1 hr paste	45.80	13.85	1.60	7.1	3.0	1.0
2 hrs paste	49.12	13.92	1.41	7.6	3.1	0.8
3 hrs paste	57.62	13.24	0.48	8.9	2.9	0.3
24 hrs paste	213.59	-	-	33.1	-	-

Immediately after mixing with water, syngenite began to form. It was measured at 2 minutes, 5 minutes, and reached a maximum at 10 minutes. Thereafter, the endotherm at 270°C began to decline, and three hours after mixing the cement and water, the syngenite was almost completely gone. Gypsum increased also for a period of 2 hours, but declined thereafter, and was gone after 24 hours. The most important change noted was in the ettringite peak, which increased steadily, until after 24 hours, the peak corresponded to 33.1% ettringite. This ettringite quantity is equivalent to an amount of SO_3 greater than the total sulfate content of the cement. Not only did all sulfur incorporated within the calcium langbeinite, gypsum, and aphthitalite become converted to ettringite, but by 24 hours, even the sulfur associated with the silicate phases, 0.52% as SO_3 in the clinker, had hydrated. This finding provides strong evidence that even for clinkers with high sulfur levels, and with high sulfur/alkali molar ratios, all the sulfur is rapidly available to form ettringite while the paste is still plastic.

Discussion of Silicate SO_3 and Anhydrite

It should not be surprising that β-anhydrite was not found in any of the clinkers. Anhydrite is unstable at cement kiln burning zone temperatures. It has been found in mineralized clinker made with additions of calcium sulfate and calcium fluoride (Borgholm et al, 1995), but these are burned at temperatures of approximately 1350°C. Even here, however, the SO_3/alkali ratios necessary for anhydrite to form result in unstable kiln operation. The SO_3/alkali ratios which are maintained in production of the mineralized clinker are such that anhydrite does not occur in the commercially available cement. Pollitt and Brown (1968) provide microscopical evidence of clinker anhydrite; however, the photomicrograph of an anhydrite-containing clinker sample they show was almost certainly a laboratory clinker with a very high sulfur/alkali ratio, burned at low temperature. They provide a table of "works clinkers", in which almost all the sulfate content is shown to be water-soluble. Furthermore, they make no mention of sulfur incorporation into the clinker phases, and provide complete sulfur balances without allowance for this possibility. The anhydrite they generated proved to be very water-soluble, and some of it may have been γ-$CaSO_4$. Dreizler et al (1985) were unable to find evidence for anhydrite even in clinkers rich in sulfate but of low alkali content. Hanic et al (1985) have provided useful information on its decomposition in the range of 1170-1450°C, which shows that the calcium oxide generated by decomposition can form an eutectic melt with calcium sulfate. This effect inhibits the ability of lime to deter the decomposition; hence anhydrite normally decomposes very readily at cement kiln clinkering temperatures. The removal of CaO by reaction with C_2S or by dissolution in the clinker melt would tend to further accelerate the decomposition. Pliego-Cuervo and Glasser (1979) show a decomposition pressure at about 7.6 mm Hg at 1200°C, and indicate further that anhydrite is not stable in the presence of C_3A, but only in the presence of $C_4A_3\bar{S}$. Further insight into this issue is provided by Demoulian et al (1980). The authors refer to two different kinds of alite--one with smooth borders, and the other with corroded edges. They interpret the former, for clinkers with excess or equivalent alkali, as resulting from the slow vaporization of K_2SO_4, and condensation of the same. The vaporization is slow and does not disturb the cohesion, which in fact is aided when it condenses again. By contrast, in high sulfur environments, the compounds present are the Klein ternary, $C_4A_3\bar{S}$, and anhydrite ($CaSO_4$). Both of these compounds normally decompose rapidly at temperatures above 1350°C, and rapidly perturb the internal structure and the surface of the grains of clinker. Therefore, although anhydrite may be present in clinker manufactured with mineralizers that permit alite formation at reduced temperatures, one would not normally anticipate finding anhydrite in clinker samples produced in kilns operated at temperatures above 1400°-1450°C. An exception to this rule applies when the alkali content of high-sulfur clinker is very low; in such a case, small amounts of anhydrite may occasionally be found in clinker burned at normal temperatures.

As a practical matter, the amount of sulfate dissolved in the calcium silicate phase is self-limiting. This fact results from the inhibiting effect of calcium sulfate on the reaction of belite and lime to form alite. Work done by Gutt and Smith (1968), Odler and Abdul-Maula (1982), and Christensen and Johansen (1980) indicates that calcium sulfate (especially in the presence of alumina) strongly inhibits the conversion of belite to alite. In practice, high free lime values cause the kiln operator to increase the temperature; this would tend even more to volatilize the stoichiometric excess of sulfur over alkali. The solubility of calcium sulfate in belite is cited by Gutt and Smith (1968) as 1.1 mole % at 1200°C and 1.7 mole % at 1000°C. Taylor (1996) cites the work of several authors who report that real or "works" clinkers may have SO_3 levels as high as 2.5-3.4%; alite SO_3 levels are lower, but less than 0.9%. In production, however, he claims that silicate sulfur will probably never exceed 1% as SO_3, and that half of this will be in the alite phase. Gartner and Tang (1987) also point out that magnesia reduces the solubility of SO_3 in the belite. These findings are in agreement with the earlier work by Gutt and Smith (1968). Since magnesia reduces the incorporation of sulfate into belite, it will counteract the inhibition of belite's conversion to alite.

CONCLUSIONS

The intent of this paper has been to investigate internal sulfate attack, in systems that contain no aggregate sulfate. The mechanisms may include delayed ettringite formation, when the concrete has been cured at high temperature, or subjected to severe temperature or moisture cycles. However, ambient internal sulfate attack in the absence of aggregate sulfate appears inconsistent with the results obtained in these studies, as only very minor amounts of clinker sulfate appear to be insoluble in the first day of hydration, and when such more slowly soluble clinker sulfates do dissolve, they do so in the presence of stoichiometric excess of alumina. To ensure reasonable, accurate, and defensible explanations of expansion and cracking of mortars or concretes in service, hypotheses should be supported by appropriate analytical data, not simply microscopical pictures showing the presence of a phase or phases without confirming supporting data from other measurement techniques.

ACKNOWLEDGEMENT

The research reported in this paper (PCA R&D Serial No. 2079) was conducted by Construction Technology Laboratories, Inc., with the sponsorship of the Portland Cement Association (PCA Project Index No. 95-10). The contents of this paper reflect the views of the authors, who are responsible for the facts and accuracy of the data presented. The contents do not necessarily reflect the views of the Portland Cement Association.

REFERENCES

Borgholm, H.E., Herfort, D., and Rasmussen, S., "A New Blended Cement Based on Mineralised Clinker,", *World Cement*, Research and Development Section, August, 1995, pp. 27-33

Christensen, N.H. and Johansen, V., "Mineralizers and Fluxes in the Clinkering Process, Part II. Kinetic Effects on Alite Formation," *Proceedings of the 7th International Congress on the Chemistry of Cement*, Vol. II, Paris, France, 1980, pp. I-1–I-5, also in "Alkaliers og Sulfaters Indflydelse på Dannelseshastighed af Alit (The Influence of Alkalies and Sulfates on the Rate of Formation of Alite)," F.L. Smidth &Co. A/S, Internal Report, May 15, 1979; also in *FLS Review*, No. 38, 1980, pp. 9-12

Demoulian, E., Gourdin, P., Hawthorn, F. and Vernet, C., "Anomalies de cuisson-Structures microscopiques, Propriétés des clinker et ciments (Burning anomalies-Microscopic Structures-Properties of Clinkers and Cements)", *Proceedings of the 7th International Symposium on the Chemistry of Cement*, Vol. II, Paris, France, 1980, pp. I-212–I-217

Dreizler, I.E., Strunge, J., and Knöfel, D.F.E., "Effect of Alkalies and Sulfur on the Formation of Clinker Phases and on the Cement Properties," *Proceedings of the 7th International Conference on Cement Microscopy*, Fort Worth, TX, 1985, pp. 100-126

Fu, Y. and Beaudoin, J. J., "On the Distinction between Delayed and Secondary Ettringite Formation in Concrete," *Cement and Concrete Research*, Vol., 26, No. 6, 1996, pp. 979-980

Gartner, E. M. and Tang, F. J., "Formation and Properties of High Sulfur Portland Cement Clinkers," *Il Cemento*, Vol. 84, April-June, 1987, pp. 141-164

Grabowski, E., Czarnecki, B., Gillott, J.E., Duggan, C.R., and Scott, J.F.,"Rapid Test of Concrete Expansivity Due to Internal Sulfate Attack", *ACI Materials Journal*, September-October, 1992, pp. 469-480

Gutt, W., and Smith, M. A., "Studies of the Role of Calcium Sulphate in the Manufacture of Portland Cement Clinker," *Transactions of the British Ceramic Society* , Vol. 67, No. 10, October, 1968, pp. 487-509.

Gutteridge, W.,"On the Dissolution of Interstitial Phase in Portland Cement," *Cement and Concrete Research*, Vol. 9, No. 3, 1979, pp. 319-324

Hanic, F., Galikova, L., Havlica, J., Kapralik, I., and Ambruz, V., "Kinetics of the Thermal Decomposition of $CaSO_4$ in Air,"*Transactions of the British Ceramic Society*., Vol. 84, 1985, pp. 22-25

Hime, W.G., "Delayed Ettringite Formation—A Concern for Precast Concrete?," *PCI Journal*, July-August, 1996a, pp. 26-30

Hime, W.G., "Clinker Sulfate: A Cause for Distress and a Need for Specification", *Concrete for Environment Enhancement and Protection,* Edited by R.K. Dhir and T.D. Dyer, 1996b, Published by E & FN Spon, London, U.K., pp. 387-395

Hime, W.G., Connolly, J., Marusin, S., "Delayed Ettringite Formation", *Proceedings of the Eighteenth International Conference on Cement Microscopy*, 1996c, Houston, TX, pp. 378

Johansen, V., Thaulow, N., Skalny, J., "Chemical Degradation of Concrete", Transportation Research Board. 74th Annual Meeting, January 22-28, 1995, Washington, D.C.

Jøns, E., "Measuring the Solubility of Sulphate in Cement," World Cement Research and Development Section, June 1996, pp. 65-68

Kelham, S., "The Effect of Cement Composition and Fineness on Expansion Associated with Delayed Ettringite Formation", *Cement and Concrete Composites*, Volume 18, No. 3, 1996, pp. 171-179

Mielenz, R.C., Marusin, S.L., Hime, W. G. and Zugovic, Z.T., "Prestressed Concrete Railway Tie Distress: Alkali-Silica Reaction or Delayed Ettringite Formation, *Concrete International,* Vol. 17, No. 12, December 1995, pp. 62-68

Odler, I., and Abdul-Maula, S., "Intensivierung des Brennprozesses bei der Herstellung von Portlandzementklinker durch Verwendung von Mineralisatoren (Intensification of the Burning Process in the Manufacture of Portland Cement Clinker through the Use of Mineralizers)," *Research Report T 82-040*, 1982, Bundesministerium für Forschung und Technologie

Pliego-Cuervo, Y.B., and Glasser, F.P., "The Role of Sulphates in Cement Clinkering Reactions: Phase formation in the System CaO-Al_2O_3-SiO_2-$CaSO_4$-K_2SO_4," *Cement and Concrete Research*, Vol. 9, No. 5, 1979, pp. 573-581

Pollitt, H.W.W., and Brown, A.W. , "The Distribution of Alkalis in Portland Cement Clinker," Supplemental Paper I-126, *Proceedings of the Fifth International Symposium on the Chemistry of Cement*, 1968, Tokyo, Japan, pp. 322-333

Scrivener, K.L., "Delayed Ettringite Formation and Concrete Railroad Ties", *Proceedings of the Eighteenth International Conference on Cement Microscopy*, 1996, Houston, TX, pp. 375-377

Stark, J., Bollmann, K., and Seyfarth, K., "Investigation into Delayed Ettringite Formation in Concrete," *9th International Symposium on the Chemistry of Cement*, Vol. 5, 1992, New Delhi, India, pp. 348-354

Takashima, S., "Systematic Dissolution of Calcium Silicate in Commercial Portland Cement by Organic Acid Solution" *Review of the 12th General Meeting*, 1958, Cement Association of Japan, Tokyo, pp. 12-13

Taylor, H.F.W., "Ettringite in Cement Paste and Concrete,", *Conference 'Béton du Matériaux á la Structure'* in honor of M. Moranville Regourd, 1996, Arles, France

EFFECTS OF CEMENT COMPOSITION AND HYDRATION TEMPERATURE ON VOLUME STABILITY OF MORTAR

Steve KELHAM, Blue Circle Technical Centre, Greenhithe, Kent DA9 9JQ, UK

ABSTRACT Mortar prisms were cast from >70 laboratory ground cements prepared from 7 production clinkers with a range of chemistries. After initial curing at various temperatures up to 90°C the prisms were stored in water at 20°C. Expansions of 20°C control prisms were <0.1%, decreased with cement surface area and increased with cement SO_3. Expansions after 90°C curing increased with surface area and were greatest at SO_3 contents of ~4%. Addition of KOH or K_2SO_4 accelerated and increased expansions after 90°C curing and led to expansion after 80°C curing.

Key-words: Expansion, Ettringite, Composition, Fineness, Temperature

INTRODUCTION

The volume stability of heat treated mortars and concretes has been studied widely in recent years. Expansion during subsequent moist storage is often observed, associated with delayed (or secondary) ettringite formation (DEF). The ettringite is found filling voids and cracks, particularly around aggregate particles. The paste/aggregate interface appears to be important, since the nature of the aggregate affects expansions, but expansions have also been reported in paste samples. A full explanation of the expansion process is not yet available.

The published data indicate a critical early age temperature of ~70°C below which no expansions are observed. Higher temperatures may lead to subsequent expansion but some cements do not expand even after prolonged initial curing at 100°C. It has recently been suggested that certain clinkers may lead to expansion through a similar process in the absence of high temperatures during or after hydration. The present study is an attempt to clarify the influences of temperature and cement composition and fineness on expansions associated with DEF. A set of laboratory prepared cements has been used to allow controlled variations of the factors believed to be important. Knowledge of the factors which determine the relative susceptibility of cements will assist in the development of models of the expansion process.

MATERIALS

Seven clinkers were used to produce the cements tested. The chemical analyses of the clinkers are given in Table 1 together with phase compositions from Bogue calculations. Clinker A is high in C_3A, clinker B high in K_2O, clinker C high in MgO and low in Na_2O eq. and clinker D low in SO_3. Clinker E is low in C_3A and suitable for producing sulfate resisting cement to BS 4027 or ASTM C 150 Type V. Clinker F has moderate levels of all parameters and clinker G is a mineralised active clinker produced at the same works as clinker F. The Bogue analysis for clinker G assumes that all the sulphate is present as $CaSO_4$. Three sources of added SO_3 were used:- a natural gypsum, a natural anhydrite and a flue gas desulfurisation (FGD) gypsum. The natural anhydrite was used blended with a small proportion of natural gypsum, giving 20% of the SO_3 present as the dihydrate. Limestone was used in some grinds. The limestone meets the requirements in ENV 197-1 for the production of Portland Limestone Cements. The cements prepared with clinkers A to E were ground in a 450 mm diameter laboratory mill. The grinding was carried out cold and the cements then heat treated at 105°C for four hours to produce a similar degree of gypsum dehydration to that found in production cements. The grinds carried out are summarised in Table 2. The limestone was used at 5% and 15% levels in grinds with clinker A and natural gypsum. The target specific surface areas

Table 1. Clinker analyses [% w/w]

Clinker	A	B	C	D	E	F	G
SiO_2	20.7	21.6	19.8	22.4	21.4	21.9	22.6
Al_2O_3	6.0	5.2	5.2	5.1	3.5	4.9	2.2
Fe_2O_3	2.4	3.2	3.0	2.4	5.1	3.2	0.8
CaO	66.8	66.3	66.2	67.5	66.0	67.0	70.0
MgO	0.7	1.0	2.5	0.6	2.0	0.7	0.6
SO_3	1.5	1.0	1.6	0.3	0.4	0.5	2.6
Loss on ignition	0.4	0.2	0.2	0.3	0.3	0.5	0.3
K_2O	0.59	0.83	0.48	0.48	0.51	0.49	0.31
Na_2O	0.22	0.17	0.06	0.26	0.14	0.25	0.22
Na_2O eq	0.61	0.72	0.38	0.58	0.48	0.57	0.42
Free Lime	1.5	0.4	1.8	0.4	2.0	1.0	1.2
C_3S	64.8	64.6	72.5	65.2	67.1	64.8	85.0
C_2S	10.5	13.2	2.1	15	10.8	14.0	0.7
C_3A	11.8	8.4	8.7	9.5	0.6	7.6	4.5
C_4AF	7.3	9.7	9.1	7.3	15.5	9.7	2.4

(SSA) are given as 350 and 450 m^2/kg but the grinds were actually designed to give a similar clinker fineness to that in the equivalent grind without limestone, as indicated by the 45μm residue. The actual SSAs were therefore higher, particularly for the 15 % limestone grinds. The cements prepared from clinkers F and G were ground in a pilot scale closed circuit ball mill equipped with a high efficiency separator (REMA). Target SO_3 contents were 3.5% and target SSAs 400 and 550 m^2/kg.

METHODS

Mortars (3:1:0.5 sand:cement:water) were prepared as described in EN 196-1. The standard silica sand used was German 'Normensand' supplied in pre-weighed bags. 16 x 16 x 160 mm prisms were cast with stainless steel studs in their end faces. Up to four moulds, each containing three prisms, were used for each mortar mix. The prisms were cast in a single layer and compacted with 60 jolts. After striking off excess mortar a top-plate in each prism compartment provided essentially sealed curing conditions. Each mould was further sealed in a polyethylene bag together with a water soaked cloth to ensure 100% rh during curing. Samples were either maintained at 20°C or subjected to a heat treatment regime. 70° and 80°C cures were carried out in environmental cabinets. After a 20°C pre-cure for 4 hours the temperature was increased by 20°C/hour up to the required maximum temperature, which was maintained for 12 hours. Cooling was also at 20°C/hour. 90°C curing was carried out in an accelerated curing tank. The moulds were held ~50 mm above the surface of the water. After the 4 hour pre-cure at 20°C the water was heated to 95°C in 1 hour and maintained at this temperature for 12 hours. Calibration with sand filled moulds showed that this gave a sample

Table 2. Grinds prepared and tests performed

			Clinker						
Sulfate	SSA [m^2/kg]	SO_3 [%]	A	B	C	D	E	A+5% limestone	A+15% limestone
Gypsum	250	4	O	-	-	-	-	-	-
		5	O	-	-	-	-	-	-
	350	4	O	O	O	●	●	O	O
		5	O	O	O	●	●	O	O
	450	4	●	●	●	●	●	●	●
		5	O	O	O	●	●	O	●
Anhydrite	250	4	●	-	-	-	-	-	-
		5	O	-	-	-	-	-	-
	350	4	●	O	O	●	●	-	-
		5	O	O	O	●*	●	-	-
	450	3	●	●	●	●	-	-	-
		4	●K	●K	●KH	●	●	-	-
		5	●H	●	●H	●*	●	-	-
FGD	350	4	●	●	-	-	-	-	-
		5	●	●	-	-	-	-	-
	450	4	●	●	-	-	-	-	-
		5	●	●	-	-	-	-	-

* Clinker D, anhydrite 5% grinds replaced by 4.6% AND 5.6%.

\- No cement ground.

O Tested at 20°, 70°, 80°C.

● Tested at 20°, 70°, 80°, 90°C.

K Also tested with added K_2SO_4.

H Also tested with added KOH.

temperature of 90°C. Unforced cooling to 20°C took ~6 hours. All prisms were demoulded at 24 hours and subsequently stored in water at 20°C. Lengths and weights were measured at regular intervals. Data for up to 5 years of water storage are available. All cements were tested with 20°, 70° and 80°C curing. Those also tested at 90°C are indicated in Table 2. Some additional mortars were prepared with K_2SO_4 or KOH dissolved in the mixing water to raise the SO_3 and/or Na_2O eq. levels. The cements used are also indicated in Table 2.

RESULTS

Control prisms

Length changes of prisms maintained at 20°C were always <0.1%. The data for cements based on clinker D are plotted in Fig 1. The data for the other cements are similar. Any expansion takes place during the first 28 days and the prisms are then stable within the accuracy of the present tests. The expansions of prisms cured at 20°C are plotted against cement SO_3 content in Fig 2. The plotted values are the means of the data for times greater than 600 days in order to reduce the scatter. The lines in the plot connect data points for cements which were ground from the

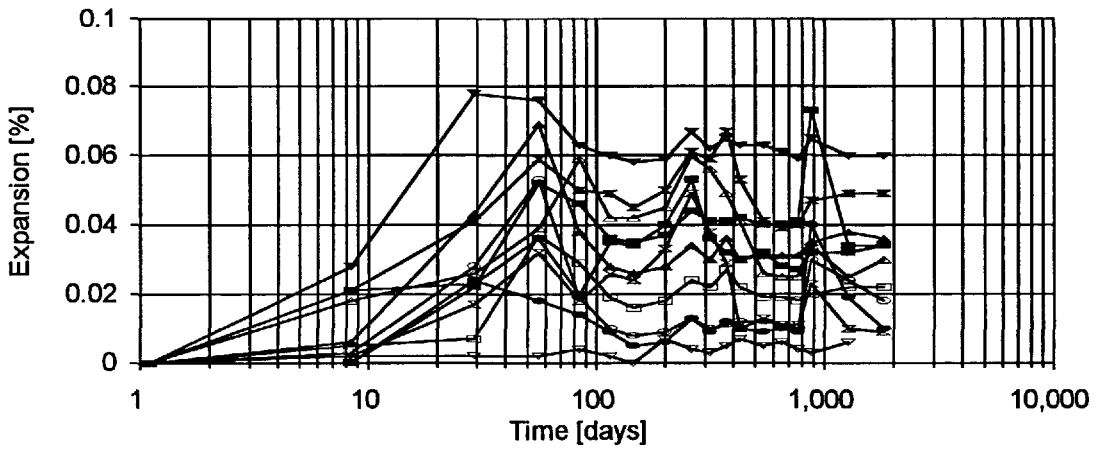

Figure 1. Expansion of mortars cured at 20°C (Clinker D cements).

same clinker and sulfate source to the same target SSA and thus differ only in SO_3 content. It can be seen that generally the expansion increases as the sulfate content increases. Cements based on clinker C appear to expand more than the others at the same sulfate content which may be due to the high MgO content. Fig 3 shows the same data plotted against cement surface area. The lines connect data points for cements with the same clinker, sulfate source and target sulfate content. There is a clear decrease in expansion as the surface area increases. In both plots vertical lines connect results for repeated measurements and indicate the reproducibility of the method.

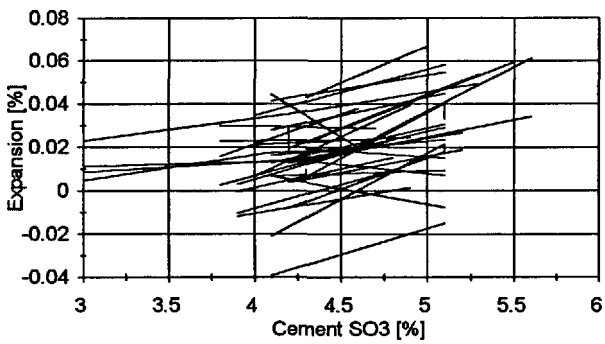

Figure 2. Dependence of expansion of mortars cured at 20°C on cement SO_3 content.

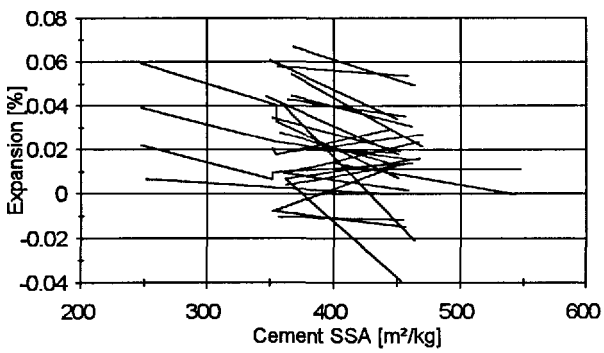

Figure 3. Dependence of expansion of 20°C cured mortars on cement surface area.

Heat treated mortars

The mortars cured at 70° and 80°C normally gave no significant expansion while most 90°C cured mortar expanded by ~1% between 56 and 200 days. A typical set of curves is shown in Fig 4. The only mortars to expand after curing at 80°C were those containing added K_2SO_4 or KOH. No expansions were observed with cements containing the sulfate resisting clinker (E). Where initial rapid expansion took place continued water storage gave further slow expansion but, in order to analyse the effect of various parameters on the expansion, plots such as Fig 4 have been used to estimate a value for the ultimate long term expansion for each set of prisms. Expansions were associated with increases in weight, 1% expansion corresponding to ~1.5% weight increase.

Fig 5 shows the dependence of the ultimate expansion on the cement surface area for mortars cured at 90°C in the same format as Figs 2 and 3. It can be seen that in all cases where expansion takes place an increase in surface area gives an increase in expansion. The results for cements based on clinker E are not included. The cements with low expansions at ~450 m^2/kg are based on clinkers B and D and have SO_3 contents >5%.

In Fig 6 the dependence on cement sulfate content is plotted. The expansions pass through a maximum at sulfate contents near 4%. Only clinker C gives expansion at 3% SO_3. The results for cements based on clinker E are not included. The cements giving low expansions at ~4% SO_3 are ~350 m^2/kg grinds based on clinker D. The vertical lines on the plot again indicate results from repeated tests.

The grinds containing 5% or 15% limestone gave similar ultimate expansions to the equivalent grinds without limestone, although the expansion occurred earlier.

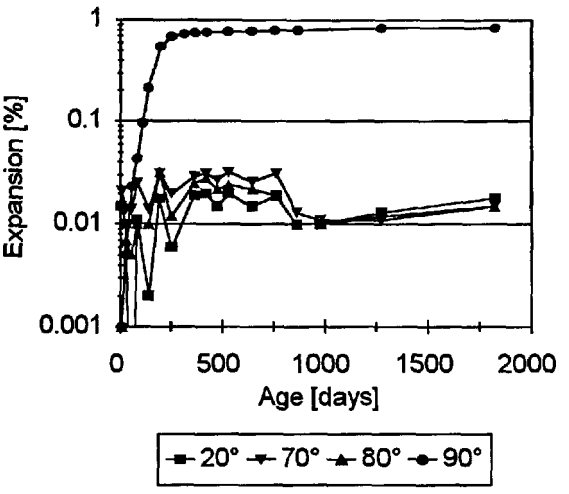

Figure 4 Typical expansion data for mortars cured at different temperatures.

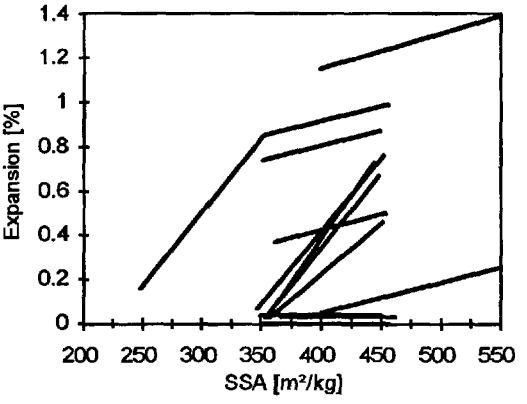

Figure 5. Effect of cement SSA on expansion after curing at 90°C.

Effect of added alkali

The tests with added K_2SO_4 were carried out on cements prepared from clinkers A, B and C with target SO_3 contents of 4% as indicated in Table 2. The quantity of K_2SO_4 used was calculated to give the same sulfate content in the mortar as in that containing the equivalent cement with a target sulfate content of 5%. Control and 70°C prisms were cast only for the cement prepared from clinker A. The added alkali had no effect on the expansion of these prisms. After curing at 80°C all the mortars with added K_2SO_4 gave significant expansions of ~0.5% while after curing at 90°C the expansions were very large, ~2%. Adding sulfate in the form of $CaSO_4$ during grinding thus leads to a lower expansion after curing at 90°C while adding the same quantity of sulfate as K_2SO_4 dissolved in the mixing water leads to much higher expansions. The expansion data are given in Table 3.

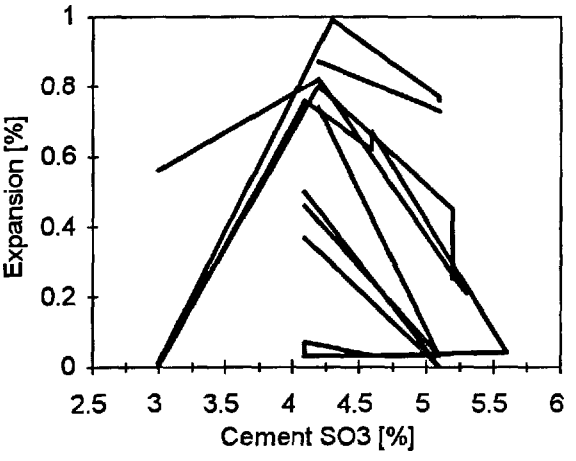

Figure 6. Effect of cement SO_3 content on expansion after curing at 90°C.

KOH was added to mortars prepared with a clinker C grind with a target sulfate content of 4%

Table 3. Expansions [%] of mortars with added K_2SO_4.

		Curing temperature [°C]			
Clinker	Sulfate [%]	20°	70°	80°	90°
A	4.3	0.015	-0.011	0.008	1.00
	5.1	0.013	0.014	0.020	0.82
	4.3+0.8 as K_2SO_4	0.022	0.019	0.550	2.20
B	4.2	0.018	0.015	0.015	0.84
	5.2	0.028	0.030	0.015	0.29
	4.2+1.0 as K_2SO_4	-	-	0.41	1.74
C	4.2	0.040	0.026	0.032	0.78
	5.3	0.059	0.032	0.026	0.22
	4.2+1.1 as K_2SO_4	-	-	0.375	1.80

(see Table 2) at various levels to increase the effective Na_2O eq. from ~0.4% to 0.6%, 0.8% and 1.2%. As with the K_2SO_4, the KOH was dissolved in the mixing water. The expansion data are plotted in Fig 7. The alkali level has no effect on the expansion after curing at 20°C or 70°C but the high alkali mortar expands after curing at 80°C. Curing at 90°C gives large expansions with all the mortars and the expansion increases as the alkali content increases.

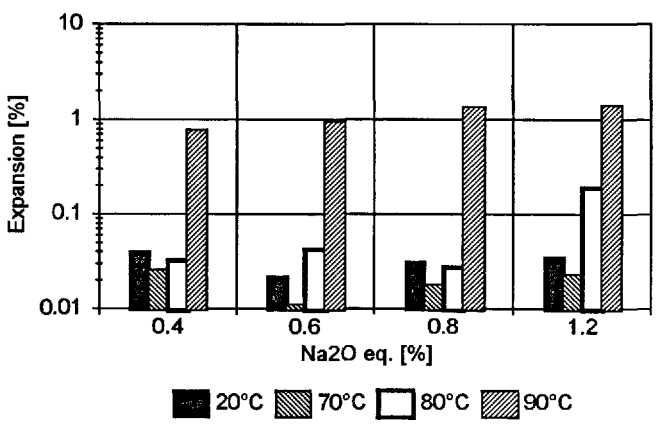

Figure 7. Effect of alkali content on expansions after curing at various temperatures.

DISCUSSION

The short term expansion data of the mortars cured at 20°C are similar to data obtained by Hobbs (1978) who also observed increasing expansion with increasing cement SO_3 content and decreasing fineness. The precision of the present data is not sufficient to make a detailed analysis worthwhile but expansions appear to increase with clinker C_3A and MgO contents.

It has recently been suggested that cements with high clinker sulfate contents, particularly when linked with low alkali contents, may give long term expansions due to 'late' ettringite formation (Diamond, 1996; Hime, 1996). It is proposed that the clinker sulfate may be unavailable during early hydration, either because it is in an insoluble form or is incorporated in the clinker minerals. Clinker sulfate is normally present as alkali sulfates and calcium langbeinite ($K_2SO_4.2CaSO_4$) and is readily soluble. As the sulfate content increases the proportion of potassium present as calcium langbeinite increases. An estimate of the 'excess' SO_3 in a clinker can be calculated by assuming that all sodium

in the clinker is present as Na_2SO_4 and all potassium as calcium langbeinite. Such 'excess' sulfate would be expected to occur as $CaSO_4$ or in solid solution in the C_2S (Taylor, 1990). Applying this method to the clinker analyses in Table 1 gives excess SO_3 contents of 0.4% in clinker C and 1.6% in clinker G. Only alkali sulfates and calcium langbeinite would be expected in the other clinkers. Despite this excess SO_3 the cements based on these clinkers behaved in the same way as all the other cements, with no signs of continuing or late expansions.

The curing temperature is clearly the dominant factor in determining whether large mortar expansions are observed. Expansions after curing at 70°C are the same as those obtained with no heat treatment. Curing at 80°C, for high alkali mortars only, or 90°C for most of the mortars leads to large expansions. These results are in agreement with other published data (e.g. Day, 1992; Lawrence, 1995). No large expansions are observed with curing temperatures below some critical value, typically ~80°C, unless other expansion mechanisms are also present such as alkali silica reaction (Shayan and Ivanusec, 1996; Diamond et al., 1994). Long delays have been observed before significant expansion takes place in the case of heat treated pastes (Lawrence, 1995) but no such delayed expansions have been reported with heat treatments below the critical temperature giving expansions in the usual time scale.

The evidence from laboratory investigations thus indicates that a temperature above ~70°C is necessary for subsequent expansion due to DEF. The reports of expansions not associated with high temperatures during curing have all involved investigations of field concretes. Analysis of crack patterns and the distribution and form of ettringite may be argued to be consistent with cracks having developed through the late formation of ettringite but the large number of unknown factors makes definite identification of the cause of damage very difficult. It is generally accepted that ettringite will be deposited in cracks caused through some other mechanism but the extent to which the growth of such crystals can contribute to crack growth and damage to the concrete is still not clear.

The expansion data for mortars cured at 90°C have been analysed previously (Kelham, 1996). The expression

$$\text{Exp}(90°C) = 0.00474*SSA + 0.0768*MgO + 0.217*C_3A + 0.0942*C_3S + 1.267*Na_2O \text{ eq.} - 0.737*ABS[SO_3 - 3.7 - 1.02*Na_2O \text{ eq.}] - 10.1$$

was found to give good agreement with the data, as shown in Fig 8. The factors involving SSA, SO_3 and Na_2O eq. are consistent with the data presented in Figs 5, 6 and 7 and Table 3. The model is generally consistent with the published data (Heinz et al., 1989; Day, 1992; Lawrence, 1995; Odler and Chen, 1995). The factors SSA, C_3S and Na_2O eq. suggest that the rate of early silicate hydration is important. Kelham (1996) noted a correlation between early strength and expansion.

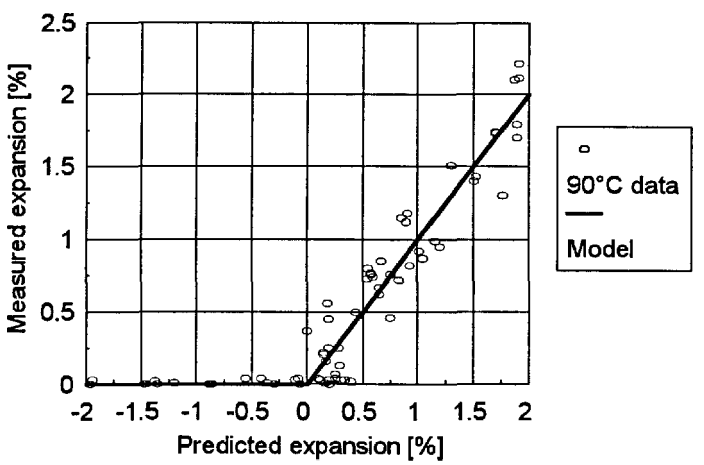

Figure 8. Comparison of predicted and measured expansions.

CONCLUSIONS

The dominant factor in determining expansions is the curing temperature. Curing at temperatures below 70°C would seem to be safe for current UK cements.

The small expansions observed in mortars maintained at 20°C increased with cement SO_3 content and decreased with cement surface area.

Cements prepared from clinkers containing 'excess' sulfate showed no abnormal expansions.

For mortars cured at 90°C expansions :-

increase with

- Cement fineness (SSA)
- Alkali (Na_2O eq.) content
- C_3A (Bogue) content
- C_3S (Bogue) content
- MgO content.

show a maximum at a cement SO_3 of ~4%, increasing with cement alkali content.

REFERENCES

Day, R. L., "The Effect of Secondary Ettringite Formation on the Durability of Concrete: a Literature Review", Research and Development Bulletin RD108T, Portland Cement Assoc., Skokie, Illinois, 1992.

Diamond, S. and Ong, S., "Combined Effects of Alkali Silica Reaction and Secondary Ettringite Deposition in Steam Cured Mortars", In Cement Technology, edited by E.M. Gartner and H. Uchikawa, Ceramic Transactions, Vol. 40, Amer. Ceram. Soc., Westerville, OH., 1994, pp. 79-90.

Diamond, S., "Delayed Ettringite Formation - Processes and Problems", Cem. Conc. Comp., Vol. 18, No. 3, 1996, pp. 205-215.

Heinz, D., Ludwig, U. and Rüdiger, I., "Delayed Ettringite Formation in Heat Treated Mortars and Concretes", Conc. Precasting Plant and Technology, Vol. 55, No. 11, 1989, pp. 56-61.

Hime, W.G., "Clinker Sulfate: A Cause of Distress and a Need for Specification", Proc. Int. Conf. Concrete in the Service of Mankind, Concrete for Environmental Enhancement and Protection, Dundee, UK, 24-26 June, 1996, pp. 387-395.

Hobbs, D.W., "Expansion and Shrinkage of Oversulphated Portland Cements", Cem. Conc. Res., Vol. 8, No. 2, 1978, pp. 211-222.

Kelham, S., "The Effect of Cement Composition and Fineness on Expansion Associated with Delayed Ettringite Formation", Cem. Conc. Comp., Vol. 18, No. 3, 1996, pp. 171-179.

Lawrence, C. D., "Mortar Expansions due to Delayed Ettringite Formation. Effects of curing period and temperature", Cem. Conc. Res., Vol. 25, No. 4, 1995, pp. 903-914.

Odler, I. and Chen, Y., "Effect of Cement Composition on the Expansion of Heat-cured Cement Pastes", Cem. Conc. Res., Vol 25, No. 4, 1995, pp.853-862.

Shayan, A. and Ivanusec, I., "An Experimental Clarification of the Association of Delayed Ettringite Formation with Alkali-Aggregate Reaction", Cem. Conc. Comp., Vol. 18, No. 3, 1996, pp. 161-170.

Taylor, H.F.W., "Cement Chemistry", 1990, Academic Press Ltd., London.

A MICROSTRUCTURAL AND MICROANALYTICAL STUDY OF HEAT CURED MORTARS AND DELAYED ETTRINGITE FORMATION

Karen SCRIVENER* and Matthew LEWIS, IMPERIAL COLLEGE, London, England

ABSTRACT Cements with various sulfate levels were prepared from a production clinker. Mortars from these cements were cured at 20, 80 and 90°C. The dimensional variation of the mortars was followed along with their microstructure and microchemistry. It was found that the evolution of X-ray microanalyses made in the C-S-H gel around anhydrous grains, was characteristic of the expansion behaviour of the mortars. This finding supports the view that expansion in heat cured mortars occurs due to ettringite formation within the C-S-H gel matrix.

Key-words: AFm phase, C-S-H, Delayed ettringite formation, Backscattered electron image.

INTRODUCTION

The phenomenon of expansion of concretes and mortars cured at elevated temperatures and subsequently exposed in wet or humid conditions has achieved much attention in recent years. The most characteristic feature of this type of expansion is the formation of gaps around aggregate particles, usually, but not always, filled with massive deposits of ettringite. In addition, it is generally agreed that the amount of ettringite formed during hydration decreases with temperature of curing, such that above a temperature of 70-90°C (depending on the characteristics of the cement) no ettringite is present in the paste after curing at elevated temperature. Subsequently, in moist conditions at lower temperatures (around 20°C), ettringite reforms over time in pastes, mortars and concretes which expand and also in those which do not. These observations have led to the use of the term 'delayed ettringite formation', DEF, even though the relationship between ettringite formation and expansion is still the subject of considerable controversy.

Field and laboratory studies of this phenomenon and possible mechanisms of expansion have been reviewed elsewhere (Lawrence, 1995 and Taylor, 1996). This paper summarises the results of an extensive laboratory programme to study the effect of various parameters on the expansion of mortars (Lewis, 1996). These parameters included sulfate level of the cement, temperature of curing, alkali content and additions of blast furnace slag. Throughout the expansion process the mortars were subject to detailed microstructural and microanalytical study. Preliminary findings of this study have been published previously (Lewis et al, 1994; Lewis and Scrivener 1995).

EXPERIMENTAL

The cements were prepared from a production clinker whose composition is given in Table 1.

Table 1 Chemical composition of clinker used.

SiO_2	Al_2O_3	Fe_2O_3	Mn_2O_3	P_2O_5	TiO_2	CaO	MgO	SO_3	LOI	K_2O	Na_2O
20.7	6.0	2.4	0.07	0.08	0.24	66.8	0.7	1.5	0.4	0.59	0.22

The clinker was ground in the laboratory with a natural anhydrite to give cements with total sulfate contents of 3, 4 and 5 wt% at specific surface areas of 450m^2/kg, and a cement with 4% sulfate at a specific surface area of 350m^2/kg. These cements were used to produce mortars at w/c = 0.5 and sand/cement=3. Eleven heat cured mortars were produced as detailed in Table 2; for each of these a control mortar cured at 20°C was also produced. The mortars were cast as

* Present address, Lafarge, Laboratoire Central de Recherche, France

25mm cubes and 16×16×160mm prisms. After a 4 hour precure they were brought to the relevant temperature (90, 80 or 20°C) over 1 hour, maintained at this curing temperature for 12 hours and then allowed to cool to room temperature. The samples were then demoulded and placed in water.

In the majority of cases expansion data was already available (Kelham, 1996), therefore characterisation times were chosen at equivalent points during expansion, i.e.:

1) one day after heat treatment
2) just before the start of expansion
3) midway through the expansion
4) at the end of expansion
5) extended period after the end of expansion, ~ 500 days.

Mortars which did not expand, including the control samples cured at 20°C, were characterised at the same time as the most closely analogous samples which did expand.

Table 2 Details of mortar composition, curing and expansion.

	cement sulfate wt%	mix water addition	slag subst. wt%	overall sulfate wt%	overall alkali $\%Na_2O_{eq}$	agg. type	curing temp °C	ultimate expansion mm/m
1	3	-		3	0.6	siliceous	90	0
2	4	-		4	0.6	"	90	9.8
3	4	-		4	0.6	"	80	0
4	4*	-		4	0.6	"	90	8.4
5	4	-		4	0.6	limestone	90	1.3#
6	4	1% K_2SO_4		5	1.4	siliceous	90	22
7	5	-		5	0.6	"	90	7.6
8	5	KOH		5	1.4	"	90	20.6
9	5	KOH		5	1.4	"	80	3.5
10	4		50	2	0.54	"	90	0
11	4		50 + sulf	4	0.54	"	90	0

* surface area 350 m^2/kg

expansion started after about 500 days and is still continuing at 1050 days

The main characterisation techniques used were X-ray diffraction (XRD), observation of baskscattered electron (BSE) images of polished surfaces in the SEM and X-ray energy dispersive spectroscopy (EDS) microanalyses in the SEM.

RESULTS

Expansion

The ultimate expansions of the heat cured mortars are given in Table 2. None of the mortars cured at 20°C expanded measurably, even at the high sulfate content of 5%. Amongst the heat cured mortars, the degree of expansion is not a linear function of sulfate content; at 3% SO_3 there was no expansion, at 4% a considerable expansion of 9.8mm/m and at 5% a slightly lower expansion of 7.6 mm/m. The addition of alkali appears to increase the ultimate expansion, while it is reduced for a lower surface area of the cement. The mortars with additions of blast furnace slag, even when the overall sulfate content was increased to 4%, did not expand.

The mortar made with a limestone aggregate did not start to expand until after 500 days, but at 1050 days has expanded 1.3mm/m and shows no signs of levelling off.

X-ray diffraction

Fig 1(a) and (b) show the typical development of the x-ray diffraction curves with time for a room temperature cured and a heat cured mortar respectively. In the room temperature cured mortar significant ettringite can be seen in the paste immediately after the heat cure (period 1) and remains throughout the period of study. Significant quantities of monosulfate are only detected at later ages alongside hemi-carbonate.

In the heat cured pastes there is virtually no evidence of ettringite at period 1. Over the subsequent periods the formation of ettringite can be clearly observed, this pattern of delayed ettringite formation was similar both in mortars which did and in those which did not expand.

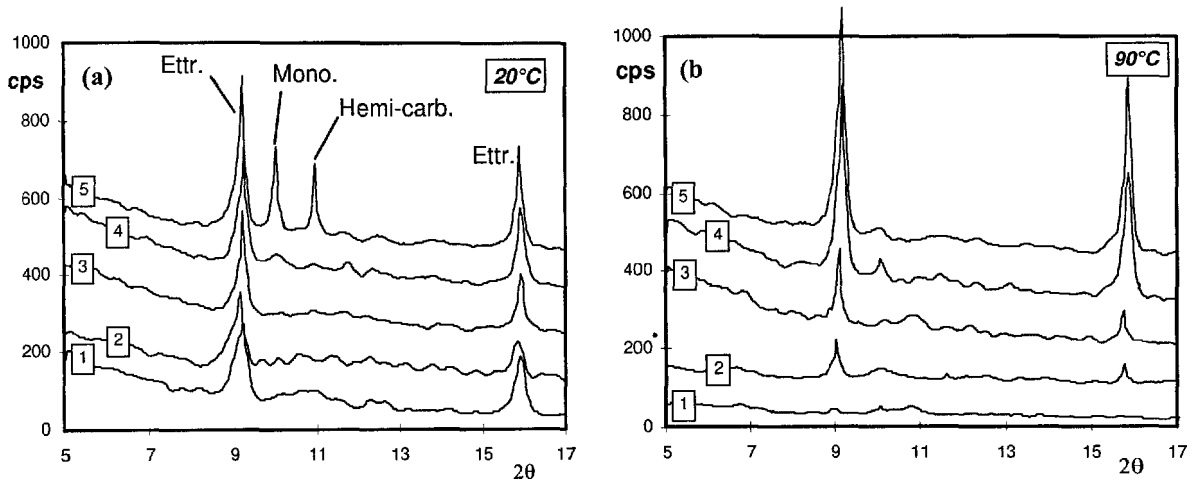

Figure 1 XRD pattern development over the five periods for, (a) room temperature cured, and (b) 90°C cured mortar, mortar 2.

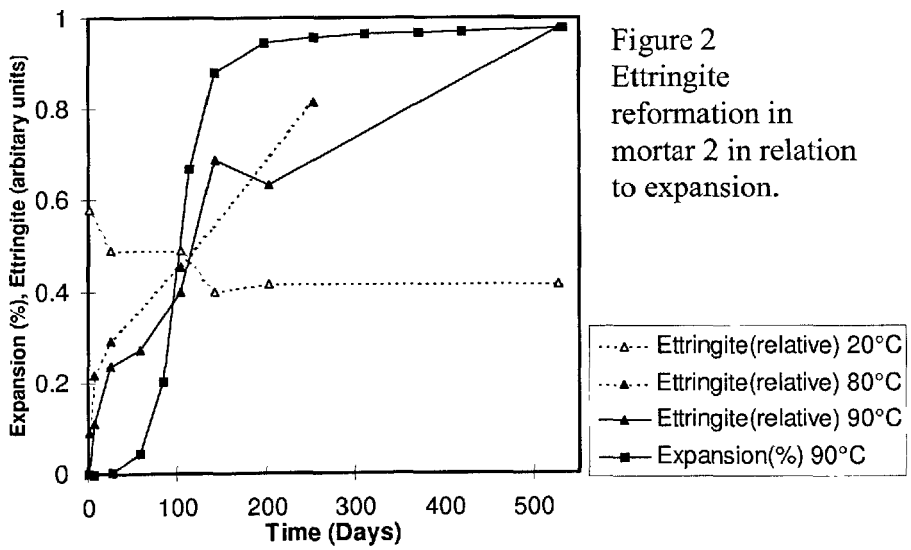

Figure 2 Ettringite reformation in mortar 2 in relation to expansion.

Figure 2 shows the development of ettringite measured semi-quantitatively by XRD and the expansion curves for the mortars made with the 4% sulfate cement cured at the three temperatures, 90, 80 and 20°C. The formation of ettringite is virtually identical in the specimens cured at 80 and 90°C, despite the fact that one expands and the other does not. There is also a considerable increase in the amount of ettringite detected in the samples cured at 90°C between period 4 and 5, despite the fact that no further expansion occurs between these two times. These observations indicate that the ettringite detectable by XRD is not directly responsible for the

expansion of the mortars. The continued increase in the amount of detected ettringite after the end of expansion suggests that ettringite continues to recrystallise, by a process of Ostwald ripening, in the space made available by the expansion of the paste.

Scanning Electron Microscopy (SEM)

The microstructural development of the mortars has been more fully described elsewhere (Lewis, 1996; Lewis and Scrivener, 1995). In the expanded mortars, bands filled, completely or partially with ettringite and, in some cases, calcium carbonate were observed around the sand particles. The relics of the original cement grains exhibited C-S-H with two grey tones (Scrivener, 1992) corresponding to C-S-H formed during the heat curing and that formed later at room temperature; Fig 3 shows a typical example of this. In those pastes which expanded an additional feature was observed at later ages shown in Fig 4. Here the outer, originally lighter product appears to have expanded away from the originally darker cores, leaving a gap between the two and the C-S-H now appears to be of uniform grey level. This feature has also been reported by (Patel et al, 1996), although they provided a different explanation of their formation.

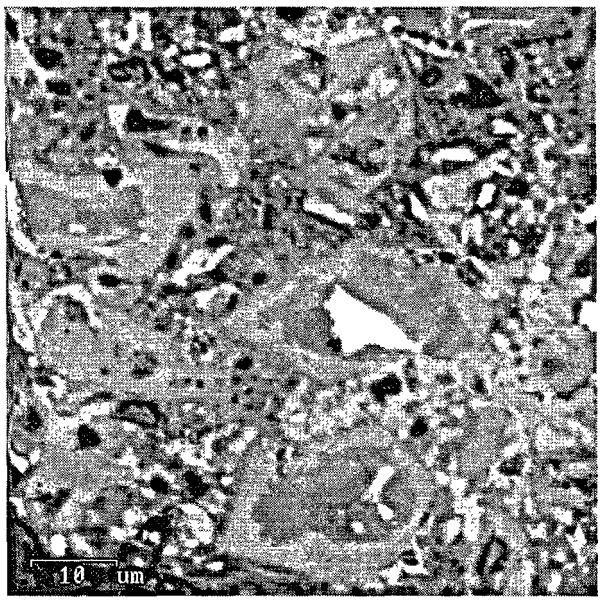

Figure 3 Relic of original cement grain showing two toning of the C-S-H.

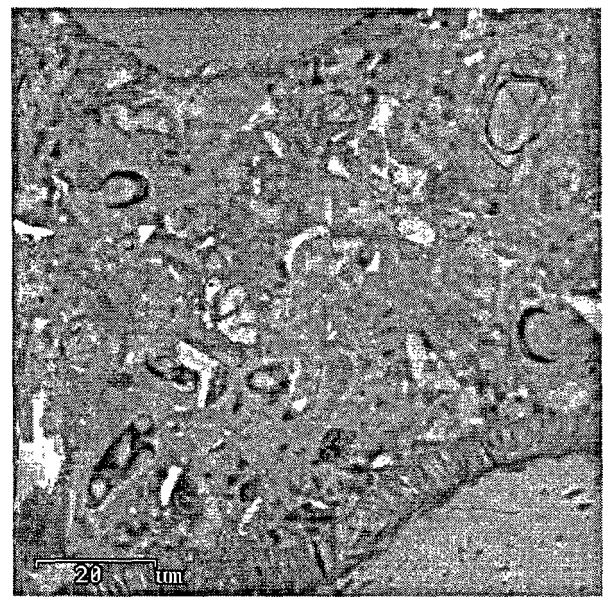

Figure 4 Localised C-S-H expansion away from inner cores.

X-ray microanalysis, EDS

In cement paste microstructures, phases are generally very finely intermixed on the submicron scale. As each microanalysis samples a region approximately one micron in volume, microanalyses taken at random will vary widely one from another. Therefore to study differences between the different mortars at the different time periods it was decided to carry-out the analyses on the C-S-H of homogeneous appearance around the partially hydrated clinker grains, often referred to as 'inner product'. In cases where two tones of C-S-H were present, the brighter outermost region was the area analysed in this study. In each sample some twenty or more analyses were made on different grains widely dispersed throughout the specimen in order to obtain a representative group of analyses. The most useful way of depicting the microanalyses was found to be on plots of S/Ca versus Al/Ca. On these plots tie lines are drawn between AFt (ettringite) and the origin and between AFm (monosulfate) and the origin. Mixtures of 'C-S-H' and AFt and of 'C-S-H' and AFm would be expected to fall along these lines, but definite identification of the mineralogy of the phases present cannot be made in the SEM.

The development of the C-S-H microanalyses followed a pattern corresponding to the expansive behaviour of the samples. These can be classified into groups described below:

1) Heat cured mortars which do not expand.
2) Heat cured mortars which do expand.
3) Heat cured mortar containing limestone aggregate.
4) Room temperature cured mortars.

1) Heat cured mortars which do not expand

These were the mortars 1 (3% sulfate); 3 (4% sulfate, cured 80°C); 10 & 11 (with slag substitution). Figure 5 shows the typical evolution of microanalyses for this groups of samples. In these mortars the microanalyses at period 1 fall between the two tie lines for C-S-H-AFt and for C-S-H-AFm. The lack of any definite ratio between the sulfate and aluminate ions suggests that they are not combined in a crystalline phase but sorbed in the C-S-H gel. Over time the sulfate and, to a lesser extent, aluminate content in the C-S-H gel fall until the analyses lie around the C-S-H-AFm tie line. At the same time ettringite is seen to form in pores and voids in the mortar, but there is no expansion.

2) Heat cured mortars which do expand

These were the mortars 2, 4, 6, 7, 8 and 9. The typical evolution of the microanalyses for this group of samples is shown in Figures 6 and 7. At period 1 the microanalyses fall around the C-S-H-AFt tie line, or, as in the case of the example shown in Figure 6 slightly below. However, the form of the sulfate and aluminate ions is unlikely to be as ettringite due to the heat curing and as with the other samples the ions are probably sorbed in the C-S-H gel. At period 2 (just before expansion) there is a marked shift of the analyses up to the C-S-H-AFt tie line which indicates that a phase with a definite stoichiometry, i.e. ettringite, has formed within the C-S-H gel. At subsequent periods the analyses points drop down towards the C-S-H-AFm tie line as with the none expanding samples. This may indicate that mixtures of C-S-H and microcrystalline AFm are quasi-stable. The plot of Al/Ca versus Si/Ca indicates that calcium also leaves the C-S-H gel during the expansion process.

Figure 8 shows the analyses of all the mortars at period 1 on the same plot, indentified as coming from expanding or non-expanding mortars. This graph shows a clear difference between the two sets of analyses, which has been indicated by an arbitrary threshold level. This threshold may indicate the level above which the potential for the formation of microcrystalline ettringite within the C-S-H exists.

3) Heat cured mortar containing limestone aggregate

The analyses for the mortar containing limestone aggregate are shown in Figure 9. This mortar had not expanded at the end of the original study, 400 days, but at that time the analyses were in the same position as at period 1, immediately after the heat cure. Thus, if the interpretation of Figure 8 is correct, this mortar should still have a potential for expansion. At the age of 860 days this mortar had started to expand and the analyses had dropped towards the C-S-H-AFm tie line.

4) Room temperature cured mortars

At period 1 at 20°C the degree of hydration is very low and clear rims of 'inner product' do not exist. Analyses made at this period inevitably include normal ettringite intermixed in the outer product and thus are very variable with some points lying on the C-S-H-AFt tie line, but at much higher sulfate and aluminate levels, Figure 10. At later ages when clearly defined rims exist the analyses fall below the threshold line.

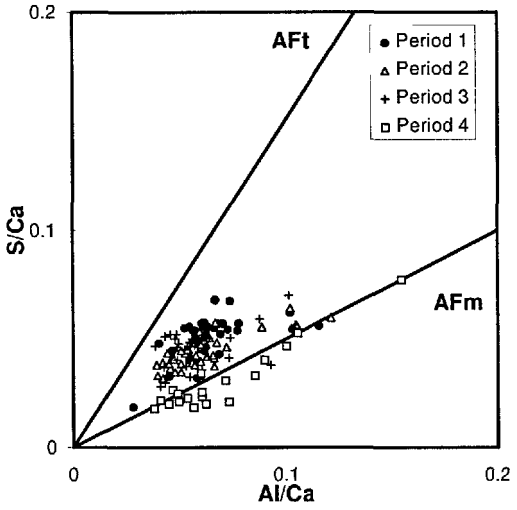

Figure 5 Mortar 1 microanalyses at periods 1-4.

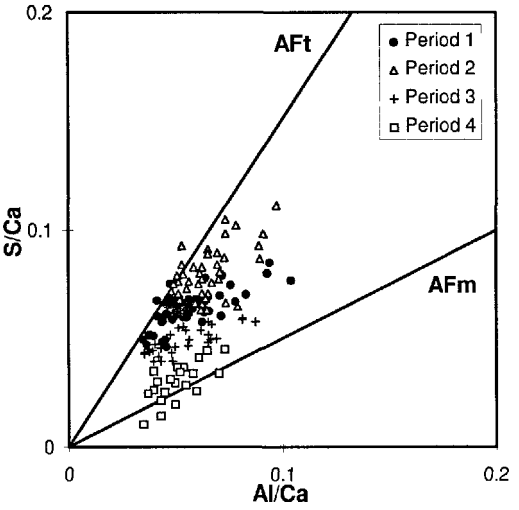

Figure 6 Mortar 2 microanalyses at periods 1-4.

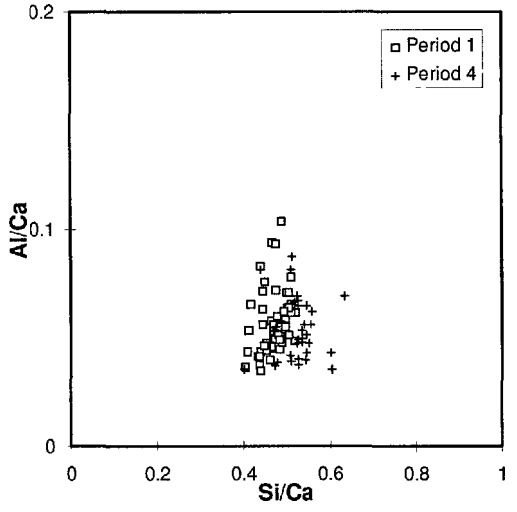

Figure 7 Mortar 2 microanalyses at periods 1 and 4.

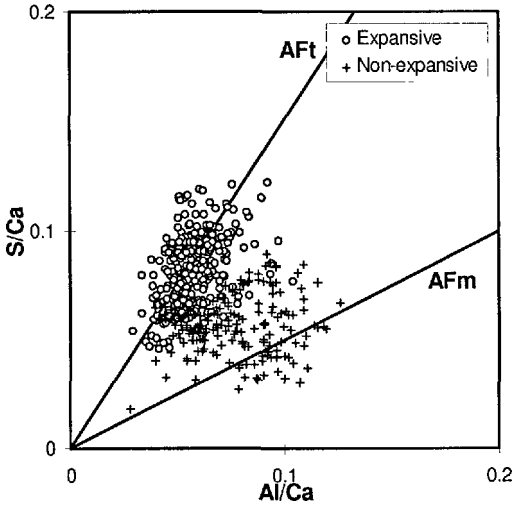

Figure 8 Period 1 microanalyses of all the mortars studied.

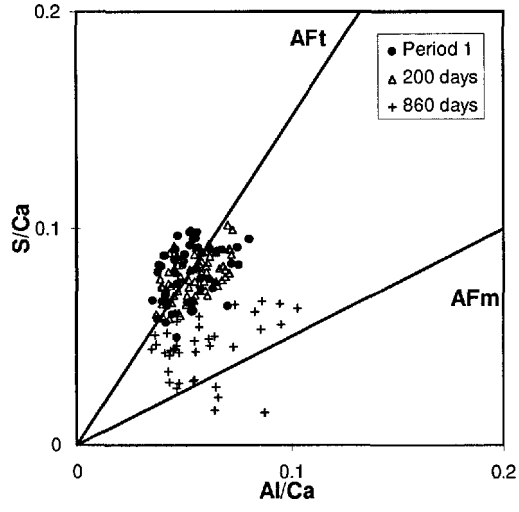

Figure 9 Mortar 5 microanalyses at 3 extended periods.

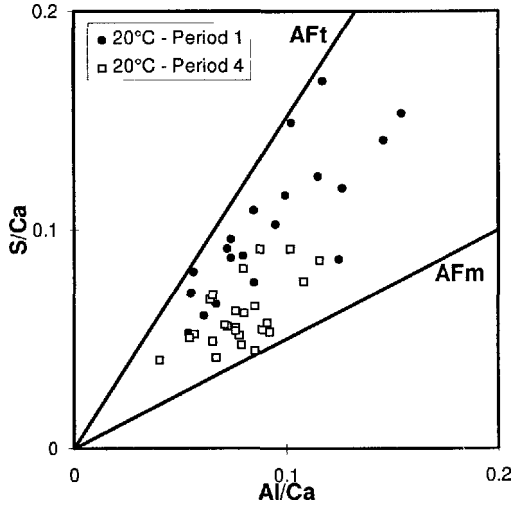

Figure 10 20°C cured mortar 2 microanalyses at periods 1 and 4.

DISCUSSION

In a previous publication (Scrivener and Taylor, 1993) it was proposed that, after curing at elevated temperatures, the delayed formation of ettringite takes place within the C-S-H gel matrix and that this ettringite subsequently recrystallises to give the large deposits seen in pores and voids and in gaps around aggregate particles. The formation of even and sometimes empty or partially filled gaps around aggregate particles, whose width is proportional to the size of the aggregate (Johansen et al, 1993) indicates that the expansion occurs relatively evenly throughout the cement paste component and that ettringite subsequently recrystallises 'opportunistically' in these gaps. Several features of the present work support these views and further indicate that the expansive processes is localised in the C-S-H gel.

First, the change in microanalyses between period 1 and 2 (Fig 6) for the expanding mortars indicates the formation of ettringite within the regions of C-S-H gel. If this is the case, this initial formation of ettringite could well be microcrystalline, perhaps poorly ordered and possibly with a low or variable water content. In such circumstances this ettringite would not be detected by X-ray diffraction.

Secondly, the difference between the microanalyses at period 1 for the expansive and non expansive mortars (Fig 8) strongly suggests that this potential for formation of ettringite within the C-S-H gel matrix determines the expansive behaviour of the mortar.

Thirdly, the appearance of the cement grain relics in the microstructure of the specimens after expansion (Fig 4) indicates that the C-S-H formed during heat curing expands relative to that formed at ambient temperatures.

Fourthly, the increase in ettringite measured semi-quantitatively by XRD (i.e. that which is seen in pores, voids and gaps) between periods 4 and 5, when no further expansion occurs, supports the view that the recrystallisation of ettringite by a process of 'Ostwald ripening' occurs after the gaps have been formed by expansion occurring throughout the paste.

Several aspects of this proposed mechanism remain to be clarified. The exact state of the aluminate and sulfate ions in the C-S-H gel after the heat curing are not known. Also there is no direct evidence for the formation of microcrystalline ettringite within the C-S-H gel. However, it is not unreasonable to suggest that such a reformation of ettringite in the C-S-H gel matrix leads to the imbition of water and so a volume increase and hence expansion. The imbition of water may be directly by uptake from the pore solution to form ettringite or indirectly as ettringite takes water locally from the surrounding C-S-H which in turn imbibes water from the pore solution (as suggested by Taylor).

If assumptions are made as to the probable composition and density of C-S-H, it can be calculated that if all the sulfate present in the C-S-H at period 1 were transformed locally to ettringite with the imbition of the requisite amount of water a volume increase of the C-S-H gel of roughly 10% would occur. In the present work linear expansions of ~1% (equivalent to ~3% volume) were observed. Considering that somewhat over 50% on the volume of cement paste is C-S-H gel and that not all of this potential increase would be realisable, the calculated figure is consistent with the experimental observations.

A major finding of the present work is the clear difference between microanalyses of mortars which subsequently expand and those which do not. One must be cautious in extrapolating this finding to other clinkers without further experimental work, but nonetheless this method of characterisation could have practical implications for providing information in a very short time period on the expansive potential of a system. Furthermore the finding that at the end of expansion all the C-S-H in all the mortars tends toward the same composition might prove diagnostic of a dimensionally stable situation in a mortar or concrete. The aforegoing relate to mortars which have been heat cured; the generalisation of these conclusions to mortars cured at ambient temperatures is difficult due to problems in applying the analysis techniques.

While the above may provide an explanation of whether or not expansion occurs, further work is necessary to explain the magnitude of expansion and the relationship of the process parameters (including cement composition) to the composition of the C-S-H gel formed during heat curing.

CONCLUSIONS

1. The present work support the hypothesis of delayed ettringite formation within C-S-H gel.
2. Evidence was found for expansion of the C-S-H which would lead to the relatively uniform expansion of the cement phase and so to the formation of even gaps around aggregate particles with a width proportional the to aggregate size.
3. The microanalyses (and so potential for ettringite formation) within the C-S-H gel after heat treatment differentiate between expansive and non-expansive mortars for the series studied.

Johansen, N. Thauwlow, N. and Skalny, J. "Simultaneous Presence of Alkali-Silica Gel and Ettringite in Concrete.", Advances in Cement Research Vol. 5, pp. 23-29, 1993.
Kelham, S. "The effect of cement composition and finess on expansion associated with DEF." Cement and Concrete Composites, Vol. 18, no. 3, pp. 171-179, 1996.
Lawrence, C.D. "Delayed Ettringite Formation: An Issue?", Materials Science of Concrete IV, The American Ceramic Society, Westerville Ohio, 1995.
Lewis, M.C. Scrivener, K.L. and Kelham, S. "Heat Curing and Delayed Ettringite Formation", Materials Research Society Symposium Proceedings, Vol. 370, pp. 67-76, 1994.
Lewis, M.C. and Scrivener, K.L. "Microchemical Effects of Elevated Temperature Curing and Delayed Ettringite Formation" Materials Research Society Symposium Proceedings, 1995.
Lewis, M.C. "Heat Curing and Delayed Ettringite Formation in Concretes", PhD thesis, University of London, 1996.
Patel, H.H. Bland, C. Poole, A.B. "Microstructure and Sulphate Levels Within Hydrated Matrix of Steam Cured Concrete", Proceeding 18th International Conference on Cement Microscopy, pp. 112-124, 1996.
Scrivener, K.L. "The effect of Heat Treatment on Inner Product CSH." Cement and Concrete Research, Vol. 22, pp. 1224-1226, 1992.
Taylor, H.F.W. "Ettringite in Cement Paste and Concrete", Proceedings CANMET/ACI Symposium , "Beton - Du Materiau a la structure", Arles, France,1996.

ETTRINGITE FORMATION - A DURABILITY PROBLEM OF CONCRETE PAVEMENTS

Jochen STARK, Bauhaus University Weimar, Germany
Katrin BOLLMANN, Bauhaus University Weimar, Germany

ABSTRACT The formation of ettringite in hardened concrete is not only a problem of heat treatment. It also occurs in not heat-treated concrete, which is exposed only to normal varying climatic conditions. In some cases the mechanism of damage in concrete pavements correlates with this ettringite formation in the hardened concrete. The ettringite formation itself as well as the combined action of frost and de-icing salt after filling the artificially entrained air voids with ettringite crystals may cause damages.

Key-words: Delayed ettringite formation, Durability, Ettringite, Expansion, Moisture

INTRODUCTION

The durability of concrete pavements is still an unsolved problem. Sometimes crack formation with different appearances occurs even after a short time of utilization. Cracks with a network pattern on the surface have to be caused by internal stresses for instance as consequence of physical processes like differences in temperature and moisture or by chemical reactions like the alkali-silica reaction (ASR) as well as the recrystallization of ettringite. The recrystallization of ettringite in a hardened concrete in form of the so-called "delayed ettringite formation" (DEF) during moist storage as a result of heat treatment is known to be followed by expansion and possible cracking of the concrete (Ghorab, 1981, Heinz and Ludwig, 1982, Heinz, 1986, Sylla, 1988, Neck, 1988, Ludwig, 1991, Seyfarth, 1991, Johansen, 1993, Stark, 1995, Glasser, 1996, Diamond 1996). This mechanism occurs because of the primary ettringite being unstable above a temperature of approximately 60-70°C due to the amount of alkalis in the pore liquid. Thus, if the concrete is exposed to such temperatures, primary ettringite will not be formed and that which was formed prior to such heat treatment will decompose. But also in many of the samples taken from damaged aged concrete pavements, which are in general not heat treated, a conspicuous ettringite formation was found in the interface between cement paste and aggregate and in cracks and voids, which were originally empty (Bollmann, 1991, Stark, 1992 , 1995, Springenschmid, 1993). An additional external supply of sulfate is excluded. This leads to the conclusion that another mechanism has to take place. Also the primary cause of damage and the chronological development of the destructive mechanism have not been completely determined. It has not been proved whether the ettringite formation in the hardened concrete itself is the cause of crack formation or whether the cracks in microstructure as a result of stress due to other influences like temperature, moisture, frost and de-icing salt are enlarged by the crystallization pressure of ettringite crystals. This paper deals with the ettringite formation in normal hardened concrete which was exposed to normal environmental and climatic conditions.

LABORATORY EXAMINATIONS

To find out what the reason is for accumulation of ettringite in larger spaces a laboratory program of alternating temperature and moisture conditions was developed to simulate the climatic conditions during utilization like sun-radiation, varying temperatures, rain and frost. Three levels of stress differing in the temperature of drying were investigated. The samples exposed to the 1st level of stress (drying at 20°C) are used for comparison. The 2nd and 3rd levels of stress include a higher drying temperature up to 60°C and freeze-thaw cycles. The temperature of 60°C in the surface of concrete panels was found to be realistic under intensive sun-radiation by measuring the temperature in open air stored concrete panels in the upper concrete layer. A minimum of 3 cycles at each level was necessary to create clear results (Table 1).

Table 1 Program of alternating temperature and moisture conditions.
(only 1 cycle is described for each level)

level of stress	time		temperature	humidity
1st level of stress (1 cycle)	2 weeks	permanent	**20°C**	65 %
	8 weeks	permanent	20°C	water
2nd level of stress (1 cycle)	2 weeks	24 hours	**60°C**	→ 0 %
		24 hours	**20°C**	<40 %
	8 weeks	permanent	20°C	water
	24 hours	4 hours	20°C → -20°C	water saturated
		3 hours	-20°C	
		4 hours	-20°C → 20°C	
		1 hour	20°C	
3rd level of stress (1 cycle)	2 weeks	permanent	**60°C**	→ 0 %
	8 weeks	permanent	20°C	water
	24 hours	4 hours	20°C → -20°C	water saturated
		3 hours	-20°C	
		4 hours	-20°C → 20°C	
		1 hour	20°C	

drying storage in water freezing

To investigate changes in microstructure due to varying temperature and moisture conditions different measurement methods were applied to get suitable characteristic values. During the laboratory treatment bulk density, porosity, compressive strength, expansion, variation in mass, in ultrasonic pulse velocity, and in the modulus of elasticity were determined and microscopical as well as phase-analytical investigations were carried out. In addition to this the change of frost/ de-icing salt resistance due to laboratory treatment was determined by the CDF test.
In concrete samples exposed to the described alternating climatic conditions, a conspicuous ettringite formation in the hardened concrete and damages in the microstructure became evident in some cases depending on the concrete composition (Fig 1).

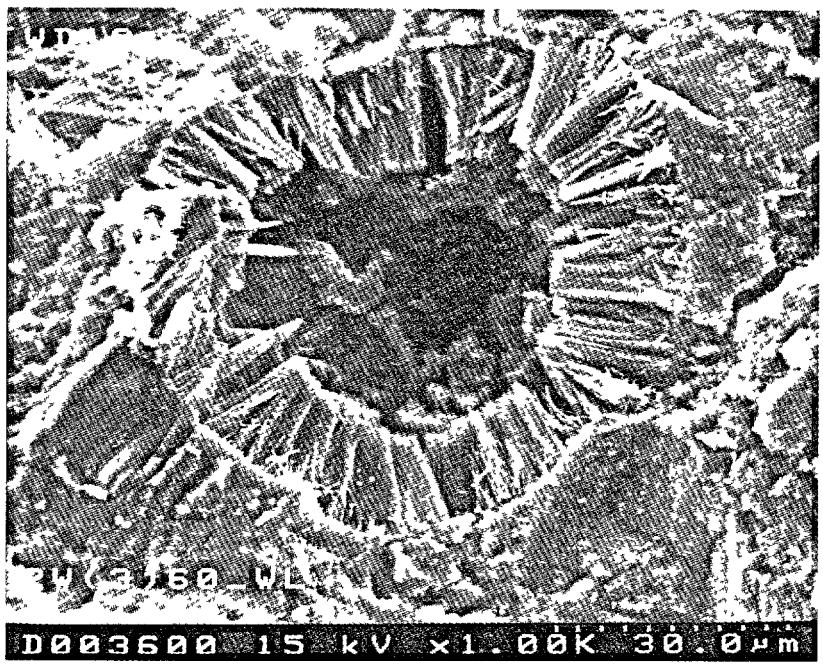

Figure 1 SEM micrograph of a concrete with entrained air: Ettringite formation in an air void after 2 cycles of laboratory treatment at the **3rd level of stress.**

That means it is possible to create the same processes in concrete in the laboratory in a relatively short time under conditions relevant to practice as under natural climatic conditions (Fig 2).

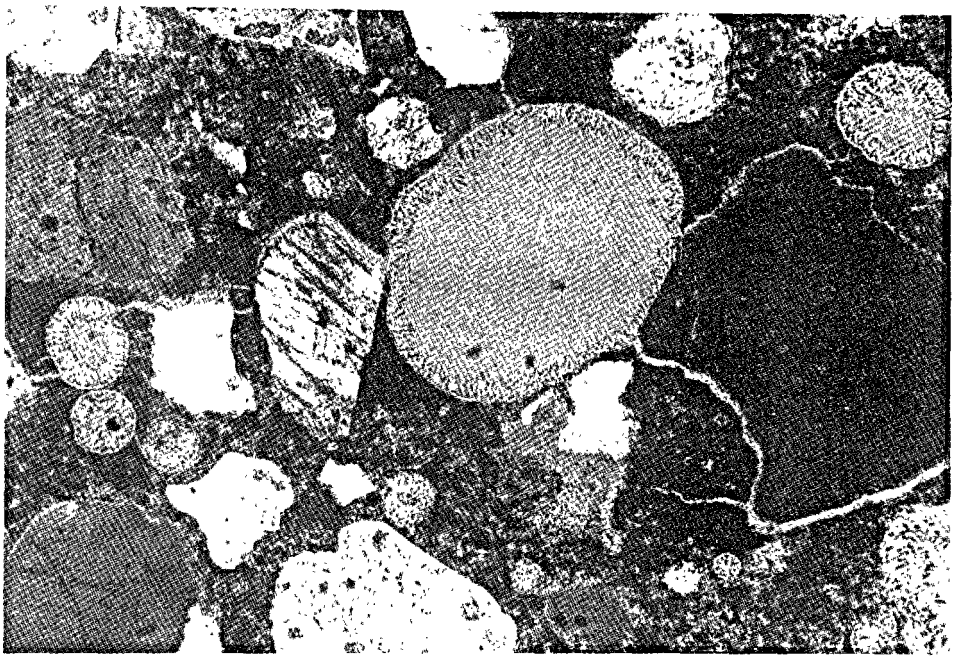

Figure 2 Polished thin section micrograph of a "naturally" aged concrete pavement: Ettringite formation in air voids.

The following results were received from a concrete pavement with a minimum compressive strength of 35 N/mm² and 340 kg/m³ of cement CEM I 32.5 R (SO_3 content = 3.2 %, Na_2O-äquiv. = 0.79%), w/c < 0.45 as well as an air void content of 5.5 %. Beams of 100mm x 100mm x 400mm were taken from a hardened concrete pavement within 2 weeks after placing. These samples were treated in the laboratory according to the described program of alternating cycles. The results of the different stress levels were compared. Furthermore the data which were received from comparable concrete samples produced in the laboratory (same water/cement ratio) without air-entraining agent were taken into account.

RESULTS

The changes of concrete microstructure, such as accumulation of ettringite and cracks caused by the laboratory treatment, became visible by optical microscopy, scanning electron microscopy (SEM) and microanalysis on fractured surfaces and polished sections and were reflected by expansion of the samples, decrease in ultrasonic pulse velocity and deterioration of the microstructure transmission behaviour.

The higher the level of stress the higher the increase of expansion during the laboratory treatment. The total expansion of samples during the alternating temperature and moisture conditions is among other things attributed to changes in microstructure and fractures. Expansion of more than 0,5 mm/m are generally expected to be associated with possible defects. But it should be taken into consideration, that the total expansion consists of the expansion due to microstructural change as well as the expansion due to change in moisture content, which is reversible to a large extent and exists independent of defects in microstructure. The expansion taken place at the 1st level of stress can be attributed to changed moisture contents and is reversible to a large extent.

The 2nd and 3rd level of stress leads to an increase of expansion in tendency. The difference in expansion between the 1st and 2nd level of stress and the 1st and 3rd level of stress reflects the change in microstructure caused by different treatment in the laboratory (Fig 3).

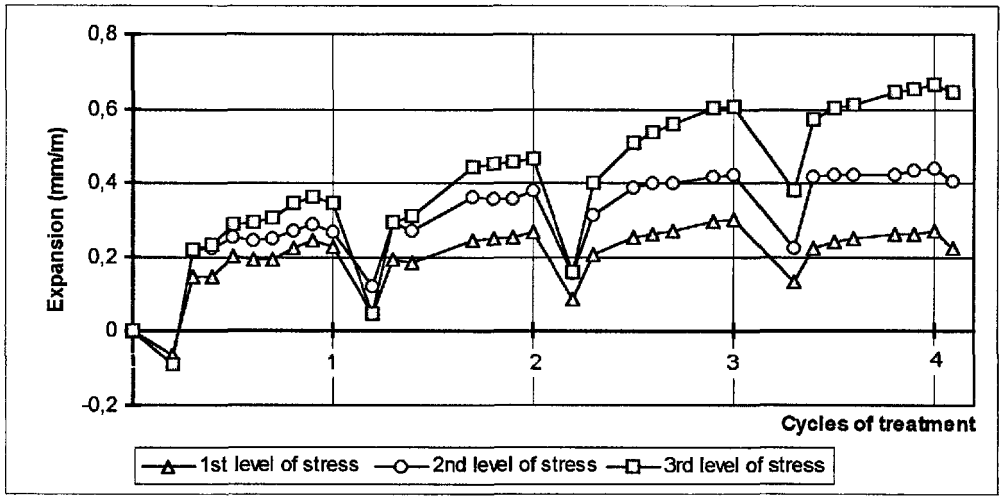

Figure 3 Expansion of samples from pavement concrete (100mm x 100mm x 400mm; same composition) during the laboratory treatment at 3 different levels of stress.

The change in microstructure induced by the different levels of stress becomes obvious by SEM. In each case at the end of the storage in water the formation of new compounds on the inside of air voids is observed (Fig 1, 4).

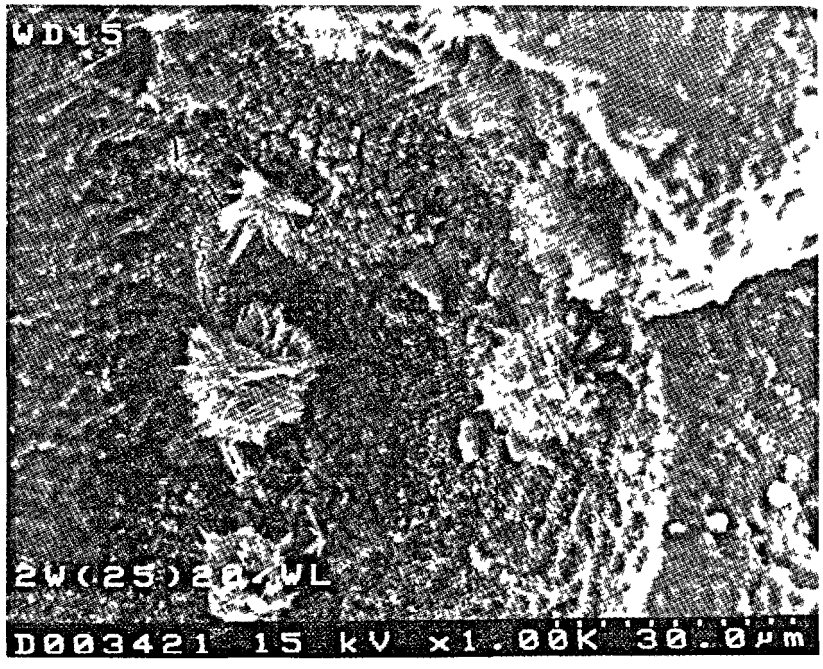

Figure 4 SEM micrograph of a concrete with entrained air: Bundles of ettringite crystal formations on the inside of an air void after 2 cycles of the laboratory treatment **(1st level of stress)**

In samples treated at the **1st level of stress** sporadically placed small bundles of ettringite crystal formations detected on the inside of air voids probably close to capillary voids (Fig 4) become

larger at each cycle of treatment. They arise probably by mobilization of phase forming components in the pore liquid and their local accumulation in weak areas and defects of the microstructure like the interface between paste and aggregate, voids or cracks where the capillary transportation is interrupted. Because the concrete remains moist during drying periods (20°C), the moisture movement and the resulting amount of transported reactants is small and only some new ettringite formations arise.

In samples treated at the **3rd level of stress** the insides of air voids are predominantly evenly covered with greater amounts of needle-shaped or compact ettringite crystals (Fig 1). With the number of alternating cycles in laboratory treatment the degree of filling of voids with new phase formations increases up to the complete filling. Due to the intensive drying (60°C) during the cycles of the 3rd level of stress the movement of moisture and thus the amount of transported reactants in the microstructure is considerably larger in comparison with the 1st level of stress. Therefore it is possible that an essentially larger amount of typically shaped ettringite in air voids can be formed.

Johansen (1993) also agrees that the ettringite formation in microstructure defects is obviously promoted by frequent drying and repeated wetting. The higher the amount of water passing the capillary system and the possible resulting transport of reactants during the changing moisture conditions, the higher the apparent amount of ettringite in pores detected by SEM and micro-analysis. Because of the lower stability of small crystals compared to larger crystals, it is possible that the small ettringite crystals within the paste may dissolve in the pore liquid and recrystallize as larger crystals in available larger spaces, such as pores and cracks (Johansen, 1993). This occurs mainly in microstructure defects like voids and microcracks caused by environmental effects. The mechanism of this ettringite formation is promoted and accelerated by the temperature effect up to 60°C, which may occur under using conditions in the upper concrete layer. The temperature of 60°C itself is not the only reason for the mechanism of damage. It has been detected by SEM that ettringite crystals arising in the voids are stable up to 60°C. It was also found that the SO_3 content of the cement (alkali content < 1%) is not of great importance for the formation of ettringite in the hardened concrete, because it also occurs in concrete made with a cement of a SO_3-content of 2.3 % (Stark and Bollmann, 1992, 1995).

In all represented samples of pavement concrete after 4 cycles no obvious damages were found in spite of the different behaviour in expansion due to laboratory treatment. The compressive strength and the ultrasonic pulse velocity show in each case the same level or an increasing tendency. During the first moisture cycles the air voids in concrete, which contains artificially entrained air voids but has a dense mortar matrix, offer expansion space for ettringite to accumulate without impediment. Therefore in these concretes with entrained air also at the highest level of stress by the laboratory treatment no essential decrease in the typical properties of hardened concrete was discovered. On the contrary comparable concretes with the same water/cement ratio without artificial entrained air voids show at the same level of stress considerable defects in microstructure like cracks, reflected by considerable expansion up to 10 mm/m and more. However, the laboratory treatment at the 1st level of stress causes for both concretes, with and without air voids, a change in length of the same level (0.3 mm/m) exclusively caused by moisture (Stark and Bollmann, 1995).
What is the correlation between the conspicuous ettringite formation in air voids of pavement concrete and the observed damages in concrete pavements?

The frequent drying and wetting in addition to higher temperatures up to 60°C may cause a complete filling of the air voids (Fig 5) whereby a frost/ de-icing salt resistance can no longer be guaranteed.

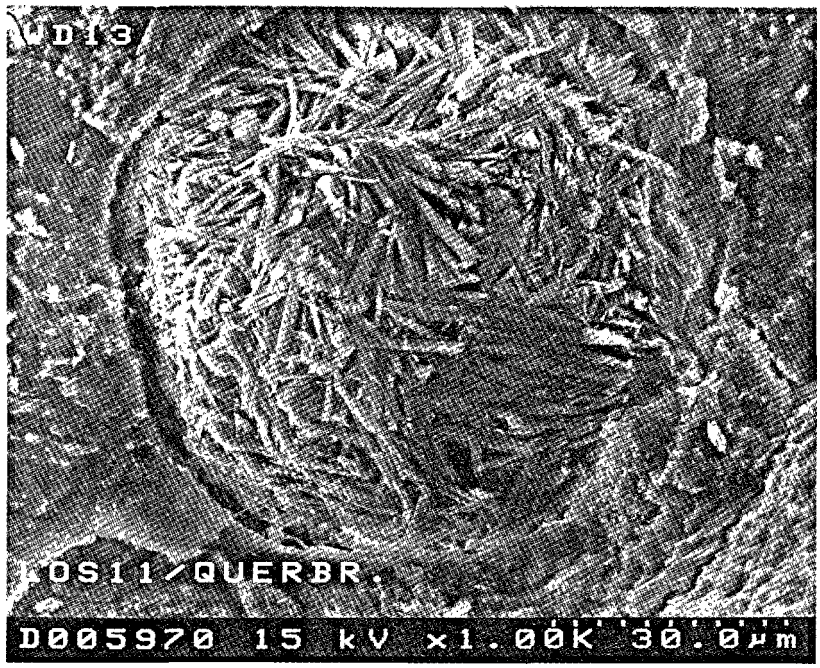

Figure 5 SEM micrograph of a "naturally" aged pavement concrete: Air void completely filled with ettringite crystals.

The frost/de-icing salt resistance test (CDF) of pavement concrete, exposed to 4 cycles of the laboratory treatment, shows the influence of microstructural changes on the frost/de-icing salt resistance. Already the increased capillary suction of NaCl solution of the samples treated at the 3rd level of stress points to detrimental changes in microstructure before CDF test (Fig 6). The influence of 28 cycles of freezing and thawing induces an exponential increase of scaling development (Fig 7). The considerable structural defects after 28 cycles of freezing and thawing were reflected by the poor transmission behaviour of the microstructure. The ultrasonic frequency spectrum analysis indicates the destruction of microstructure in concrete treated at the 3rd level of stress (Fig 8). A pavement concrete resistant to frost and de-icing salt at the age of 28 days looses its resistance as a result of microstructural changes as a consequence of the alternating temperature and moisture conditions. It decomposes during the frost/de-icing salt resistance test (CDF).

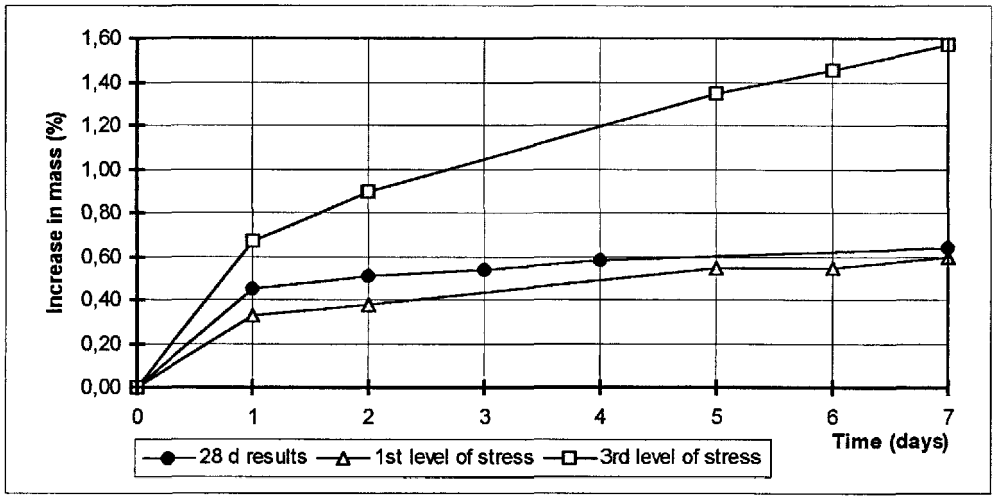

Figure 6 Capillary suction of NaCl solution: Pavement concrete after 28 days and after 4 cycles at the 1st and 3rd level of stress.

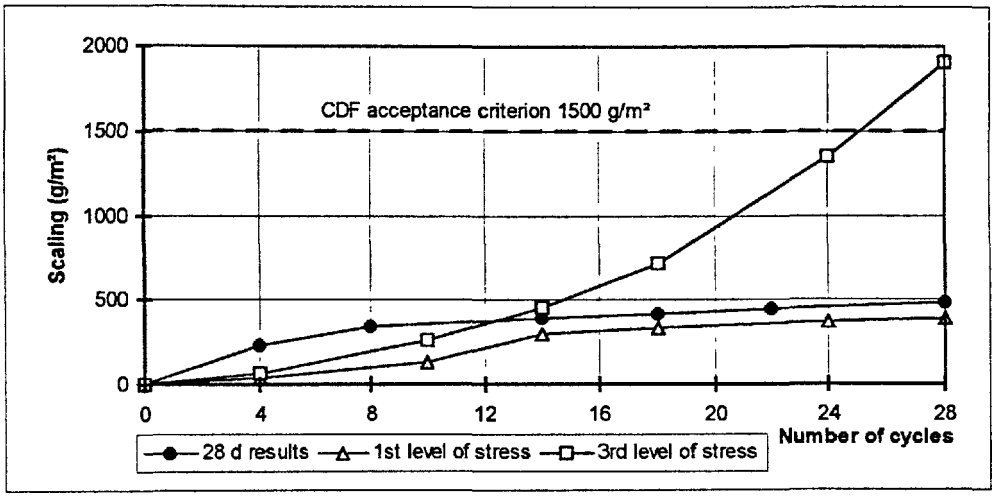

Figure 7 Scaling curves of pavement concrete after 28 days and after 4 cycles at the 1st and 3rd level of stress according to CDF test

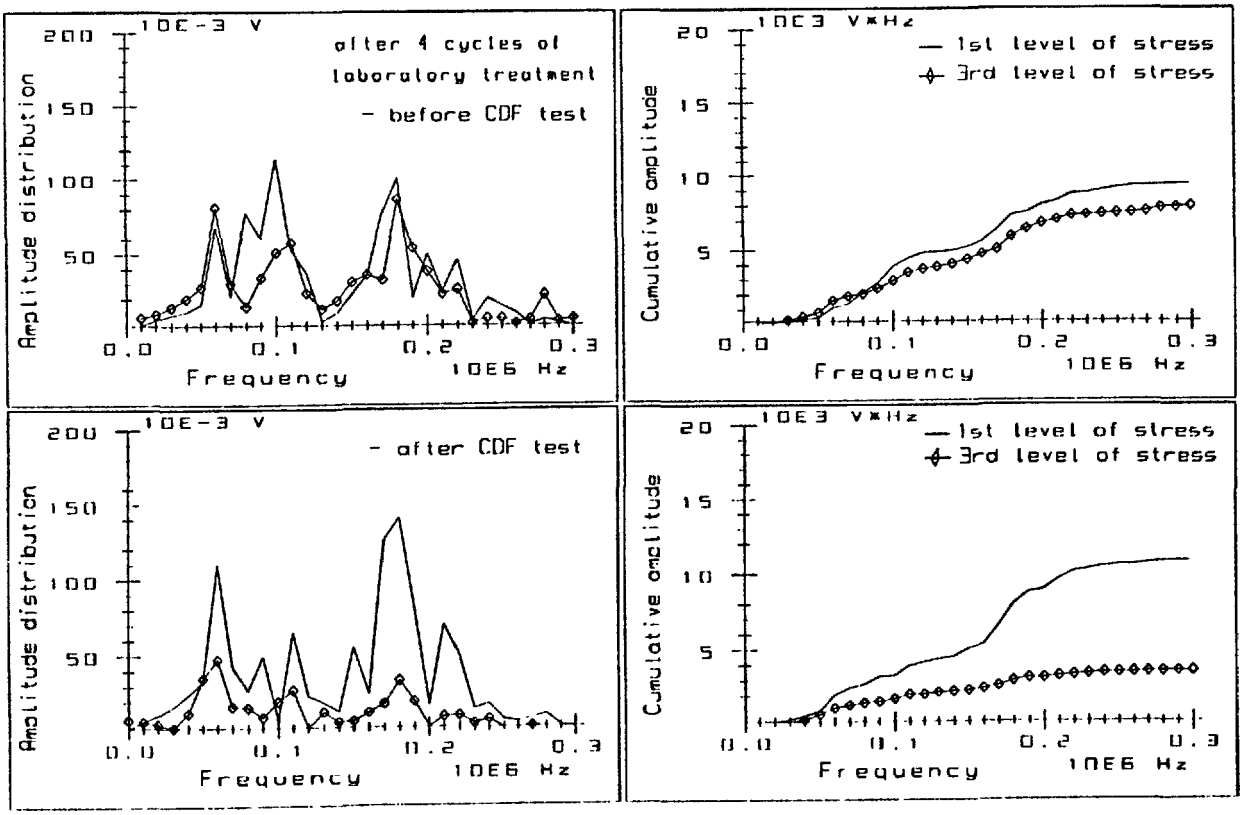

Figure 8 Ultrasonic frequency spectrum *(left)* and integral curve *(right)* of a pavement concrete after 4 cycles at the 1st and 3rd level of stress before *(upper)* and after *(below)* 28 cycles of freezing and thawing

CONCLUSIONS

Structural changes due to ettringite formation are caused above all by varying moisture conditions and by resulting transportation of moisture and substances within the concrete structure. That means that primary ettringite from the cement paste may dissolve in the pore liquid and recrystallize in larger available spaces like pores and cracks. The mechanism of this ettringite formation is just promoted and

accelerated by the temperature effect up to 60°C because of the intensive drying. However, microstructural defects like microcracks may also be created at this temperature and later on filled and widened by ettringite crystals. The expansion of the concrete is reduced by the entrained artificial air voids, because of the larger available space for ettringite formation. In concrete pavement samples no well defined indications were found for ettringite to be the primary cause of crack formation. The cracks can be caused by stresses as a result of ettringite formation itself, but also another mechanism of failure may occur: Artificial entrained air voids can be completely filled by ettringite crystals and are subsequently not available to guarantee the frost/de-icing salt resistance. Consequently damages by frost and de-icing salt such as cracks cannot be excluded, and these cracks may also be filled and widened by ettringite crystals.

REFERENCES

Bollmann, K., Stark, J.," Ein Beitrag zur Dehnung von Beton unter Einwirkung von Feuchte und erhöhten Temperaturen", 11. ibausil (1991), vol. 1, pp. 103-114

Diamond, S.,"Delayed Ettringite Formation - Prozesses and Problems", Cement & Concrete Composites, vol. 18, No. 3, 1996, pp. 205-215

Ghorab, H.Y., Ludwig, U.,"Modellversuche zur Klärung von Schadensursachen an wärmebehandelten Betonfertigteilen", part I , TIZ No.9, 1981, pp. 634-640

Glasser, F. P.,"The Role of Sulfate Mineralogy and Cure Temperature in Delayed Ettringite Formation", Cement & Concrete Composites, vol. 18, No. 3, 1996, pp. 187-193

Heinz, D., Ludwig, U., Nasr, R.,"Modellversuche zur Klärung von Schadensursachen an wärmebehandelten Betonfertigteilen", part II ,TIZ No. 3, 1982, pp. 178-183

Heinz, D.,"Schädigende Bildung ettringitähnlicher Phasen in wärmebehandelten Mörteln und Betonen", diss. 1986, RWTH Aachen

Johansen, V., Thaulow, N., Idorn, G.M., Skalny, J.,"Chemical degradation of concrete", RH&H Bulletin, No. 56, 1995

Johansen, V., Thaulow, N., Idorn, G. M.,"Dehnungsreaktionen in Mörtel und Beton", Zement-Kalk-Gips (1984) 3, pp. 150-155

Johansen, V., Thaulow, N., Skalny, J., "Simultaneous presence of alkali-silica gel and ettringite in concrete", RH&H Bulletin, No.40, 1993

Johansen, V., Thaulow, N., Jakobsen, U. H., Palbol, L.,"Heat cured induced expansion ", RH&H Bulletin, No. 47, 1993

Ludwig, U., "Probleme der Ettringitrückbildung bei wärmebehandelten Mörteln und Betonen", 11. ibausil (1991), vol. 1, pp. 164-177

Neck, U.,"Auswirkungen der Wärmebehandlung auf Festigkeit und Dauerhaftigkeit von Beton"; beton (1988) 12, pp. 488-493

Seyfarth, K., Stark, J." Zur Dauerhaftigkeit wärmebehandelter Betone", 11. ibausil (1991), vol. 1, pp. 179-189

Springenschmid, R., Fleischer, W.,"Untersuchung der Ursache von Oberflächenrissen (Netzrissen) in Betondecken", Forschung Straßenbau und Straßenverkehrstechnik, No.651, Bonn 1993

Stark, J., Bollmann, K., Seyfarth, K.," Investigation into delayed ettringite formation in concrete", 9th International Congress on the Chemistry of Cement, Dehli 1992

Stark, J., Bollmann, K., "Untersuchungen zur Bildung von Oberflächenrissen in Betonfahrbahndecken", Wissenschaftliche Zeitschrift der Hochschule für Architektur und Bauwesen Weimar- Universität-, 41 (1995), No. 6/7, pp. 65-74.

Stark, J., Seyfahrt, K., "Schädigende Ettringitbildung im erhärteten Beton ", Wissenschaftliche Zeitschrift der Hochschule für Architektur und Bauwesen Weimar - Universität-; 41 (1995), No. 6/7, pp. 37-64.

Sylla, H.-M.,"Reaktionen im Zementstein durch Wärmebehandlung", beton (1988)11, pp. 449-454

DELAYED ETTRINGITE FORMATION IN STEAM CURED OPC AND SLAG CEMENT PASTES AND ITS EFFECTS ON MORTAR COMPRESSIVE STRENGTH

Gladis CAMARINI, State University of Campinas - UNICAMP, Campinas - SP, Brazil
Maria Alba CINCOTTO, University of São Paulo - USP, São Paulo - SP, Brazil

ABSTRACT Steam curing at 60°C, 80°C and 95°C were applied to ordinary Portland cement and slag cements (35%, 50% and 70% of slag) totalizing 60 complete curing cycles. After the heat treatment their mortar presented a compressive strength loss from 28 to 90-days. XRD and SEM techniques showed delayed ettingite formation at these ages, which can contribute for the strength loss.

Key-words: blastfurnace slag, delayed ettringite formation, steam curing, strength development.

INTRODUCTION

Steam curing is a suitable technique for precast mortar and concrete products in order to accelerate early strength development. This procedure follows curing cycles with various periods. As slag hydration is slower than that of clinker it could be advantageous to employ thermal activation in precast industry with slag cements. The aim of an experimental work was to observe the performance under steam curing of ordinary Portland cement (OPC) and slag cements (35%, 50 and 70% of slag), according to the Brazilian Standards. The specimens (pastes and mortars) were steam cured at 60°C, 80°C and 95°C, in five different curing periods, resulting 60 complete curing cycles (Camarini and Cincotto, 1996a). The results already available are about the effects of curing temperature on compressive strength (Camarini and Cincotto, 1996a), selection criterion of best steam curing condition (Camarini and Cincotto,1996b) and characteristics of early hydration of slag cements (Battagin et al., 1996c). In this paper are presented the results of delayed ettringite formation and its probable effect on compressive strength decrease after 28 days.

EXPERIMENTAL PROCEDURE

Materials

Cements

Four cements from the same clinker were employed in this study, one OPC and three slag cements. Their clinker and slag proportions are presented on Table 1, and their chemical compositions and physical properties are reported on Table 2.

Table 1 Weight Proportions of Clinker and Slag on Cements

Cement	OPC	AF-1	AF-2	AF-3
Clinker+Gypsum (%)	100	65	50	30
Slag (%)	0	35	50	70

Pastes and Mortars

Paste specimens were cylinder (ϕ 100 mm, h = 10 mm) and cast with cement;water proportions equal to 1;0,40. Mortar specimens were cylinder (ϕ 50 mm, h = 100 mm) and cast according to

the Brazilian Standards, that is cement:sand:water proportions equal to 1:3:0,4. Pastes were analysed by X ray diffraction (XRD) and secondary electrons image (SEI) in SEM. Mortar specimens were tested under compressive strength.

Table 2 Chemical Composition and Physical Properties of Cements and Slag

Oxides	Cement Types				
	OPC (%)	Slag (%)	AF-1 (%)	AF-2 (%)	AF-3 (%)
SiO_2	18.51	33.25	23.67	25.89	28.83
Al_2O_3	4.32	11.29	6.76	7.81	9.20
Fe_2O_3	4.08	0.53	2.84	2.31	1.59
P_2O_5	0.94	0.01	0.65	0.47	0.286
TiO_2	0.35	0.53	0.42	0.45	0.48
CaO	60.14	44.93	54.82	52.54	49.49
MgO	5.98	6.28	6.09	6.13	6.19
Na_2O	0.12	0.19	0.15	0.16	0.17
K_2O	0.56	0.36	0.49	0.46	0.42
SO_3	3.15	1.60	2.61	2.38	2.07
Mn_2O_3	-	-	-	-	-
Fe	-	1.00	0.35	0.50	0.70
CaO free	0.75	-	0.49	0.38	0.23
L.O.I.	1.32	-	0.86	0.66	0.40
Insoluble Residues	0.19	-	0.12	0.10	0.08

Potential Composition*				
Cement Types				
	OPC (%)	AF-1 (%)	AF-2 (%)	AF-3 (%)
C_3S	60.27	39.17	30.14	18.08
C_2S	7.61	2.66	3.81	2.28
C_3A	4.55	2.96	2.28	1.37
C_4AF	12.42	8.07	6.21	3.73

Physical Properties				
Spec. Surf. m^2/kg	324	380	395	400
Initial Set h:min	2:30	4:00	5:00	5:15
Slag Specific Surface = 500 m^2/kg				

* Potential Composition by clinker contribuition on the cement:slag mix

Curing Conditions

The control specimens were cured in standard conditions, that is, they were kept in their molds for 24 hours at room temperature (20°C); after demolding they were maintained in a water bath at 20°C for different periods of time: 2, 28 and 90-days, until the date of testing. In steam curing, each cement followed a complete curing cycle with a presteaming period equal to the initial set of cement, temperature rise and cooling periods of 20°C/hour and steaming periods of 3:00, 4:30, 6:00, 7:30 and 9:00 hours. The maxima temperatures employed were 60°C, 80°C and 95°C. After steam curing, some of the specimens were tested immediately after the steam cycle (RIC), and others maintained in water bath at 20°C until the dates of testing, that is, at 2, 28 and 90-days.

RESULTS AND DISCUSSION

Compressive Strength

Statistical analysis of compressive strength showed that during the studied periods, the highest strength was attained at 28-days. At 90-days, the compressive strength were equal to or lower than that, and the results did not indicate a relationship with the steaming period and its maximum temperature. Table 3 presents the compressive strength losses occured in OPC and slag cements and indicates the correspondingly steaming periods. It is observed that each cement

has its own performance after steam curing and all of them can lose compressive strength, being the higher values those with 50% of slag (AF-2). This performance can be explained by its chemical composition after steam curing, obtained by XRD and SEM analysis.

Table 3 28 and 90-days Strength (MPa) (and Strength Loss, Percent) in Steam Cured Mortar (in Different Steaming Periods)

T (°C)	CEMENTS			
	OPC	AF-1	AF-2	AF-3
60	45,2 - 43,5 (3,8) 40,2 - 38,2 (4,5) 39,9 - 34,5 (13,5)	52,9 - 48,7 (7,9)	57,4 - 47,6 (17,1) 52,1 - 48,2 (7,5) 54,7 - 40,1 (26,7)	58,6 - 47,2 (19,5) 52,2 - 47,6 (10,5) 53,6 - 48,7 (9,1) 48,0 - 42,7 (11,0)
80	-	48,8- 45,7 (6,4)	57,6 - 48,8 (13,9) 51,1 - 46,0 (10,0) 53,3 - 45,7 (14,3) 49,3 - 36,6 (25,8)	56,0 - 44,4 (20,7) 46,3 - 41,3 (10,8)
95	17,3 (3:00)	44,6 - 40,0 (10,3)	53,3 - 43,6 (18,2) 49,1 - 47,8 (2,60) 44,8 - 37,7 (15,8)	-

X Ray Diffraction

In anhydrous slag cements, as the clinker phase diminished, the peaks corresponding to its anhydrous phases also diminished, corresponding to its proportion present in these cements. And as slag content increased a diffuse band appeared from about 28° to about 32° 2θ. In standard curing, by 2-days, the slag cement AF-1 hydrates the same way of OPC, with lower peaks due to clinker substitution by slag. AF-2 and AF-3 presented few peaks showing that the hydrated compounds were not well crystallized. By 28-days and 90-days, the anhydrous peaks disappeared and the calcium hydroxide peaks in OPC were the highest and in slag cements they diminished, indicating their consumption by slag reaction. It is interesting to observe that the slag cements showed few peaks of both anhydrous and hydrated phases, but their compressive strength were higher than OPC.

After the heat treatment, OPC specimens presented several peaks of hydrated compounds and as curing temperature increased, their quantity and intensity also increased. In slag cements as slag content increased the peaks of hydrated compounds diminished and even with temperature increase they did not became more intense. The Portlandite peak at 0,490 nm for all slag cements presented an intensity decrease with the increase of slag content and curing temperatures. Peak of C-A-H phase at 0,820 nm was clear for all cements cured at 60°C in all ages, but at 80°C and 95°C it was found only in advanced ages. Gypsum peaks appeared in OPC at 0,756 nm and were not present in slag cements; for these cements it was identified at 0,427 nm only at 95°C. With the presence of gypsum and aluminate phases after steam curing, its is possible the formation of delayed ettringite at advanced ages. Etringite peaks at 28 and 90-days were clear slag cements steam cured at 95°C.

It is known that elevated temperature enhances the rate of gypsum consumption by C-S-H (Fu et al., 1995) (Scrivener and Wieker, 1992), which is liberated with age, which was identified in XRD for all ages and temperatures in this study. Moreover, EDS analysis of paste specimens showed considerable sulphate present in C-S-H gel of all cements steam cured specimens. This

phenomenon occuring between 28 and 90-days can be the reason for the mortar compressive strength loss. For this reason, as shown in Fig 1, delayed ettringite was observed at 28-days, in steam cured OPC paste at 60°C for 4:30 hours, which were standard cured after the heat treatment.

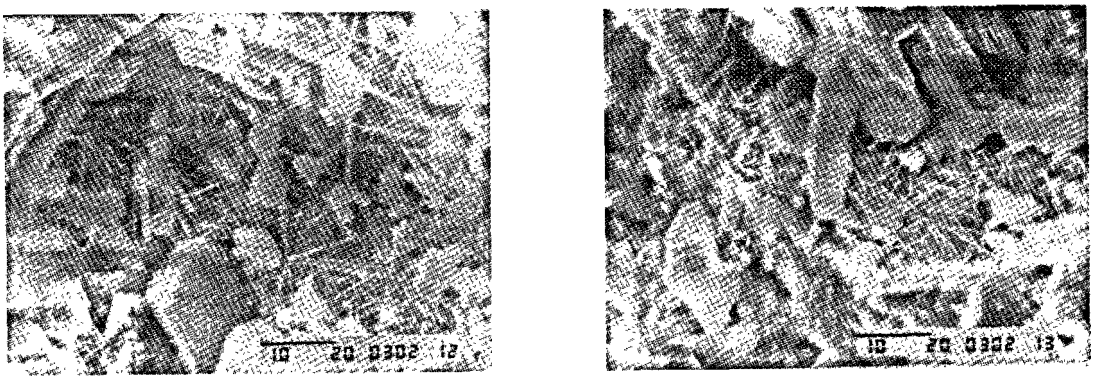

Figure 1 SEI in SEM of delayed ettringite formation in OPC pastes steam curing at 60°C, plus standard curing, at 28-days.

CONCLUSIONS

The present results permit to conclude that, in fact, thermal activation is more advantageous to slag cements than to OPC. In spite of XRD does not present many peaks, compressive strength of slag cements improves. In most cases, for longer curing cycles and higher temperatures the compressive strength decreases with age. After steam curing, free gypsum and aluminate phases are ready to react to form delayed ettringite, observed by XRD and SEM, which may be the reason for mortar compressive strength loss. Its formation was favored by standard curing after the heat treatment.

REFERENCES

Camarini, G. and Cincotto, M.A., "Different Steam Curing Conditions Effects on Compressive Strength of Slag Cement", Proceedings of International Congress on High Strength Concrete and Performance and Quality of Concrete Structures, Florianópolis, Santa Catarina, Brazil, 1996a, pp.542-553.

Camarini, G. and Cincotto, M.A., "Selection Criterion of Steam Curing Condition", 4th Brazilian Congress of Cement, São Paulo, São Paulo, Brazil, 1996b. (to be published, in portuguese).

Battagin, A.F., Camarini, G. and Cincotto, M.A., "A Study of Early Hydration of Slag Cement Pastes Subjected to Thermal Curing", 1996c (this Congress).

Fu, Y., Gu, P., Xie, P. and Beaudoin, J.J., "A Kinectic Study of Delayed Ettringite Formation in Hydrated Portland Cement Paste", Cement and Concrete Research, Vol. 25, N. 1, 1995, pp. 63-70.

Scrivener, K.L. and Wieker, "Advances in Hydration at Low, Ambient and Elevated Temperatures", ICCC, 9th, Vol. 1, New Delhi, India, 1992, pp. 449-484.

DURABILITY PROBLEMS RELATED TO DELAYED ETTRINGITE FORMATION AND /OR ALKALI AGGREGATE REACTIONS

Inger MELAND, Harald JUSTNES, Jan LINDGÅRD, SINTEF Civil and Environmental Engineering, Cement and Concrete and Sverre SMEPLASS, Dept. of Structural Engineering, Norwegian University of Science and Technology, Trondheim, Norway

ABSTRACT SEM- examination of concrete - and mortar prisms cured at elevated temperatures and stored in water for 1 - 2 years indicates that their volume expansions and loss of compressive strength may be caused by delayed ettringite formation. Delayed ettringite formation may also be the reason why abundance of ettringite has been observed by thin section analyses of concrete cores taken from dam structures and investigated for alkali aggregate reations, which indicates that the hydration temperature in the structure may have reached about 70° C or more.

Key - words: Expansion, Delayed ettringite formation, Scanning Electron Microscopy

INTRODUCTION

Expansion and degradation of mortars and concretes hydrated at elevated temperatures (≥ 70° C) and subcequently stored under moist conditions have been studied by quite many researchers (Heinz and Ludwig, 1986), (Scrivener and Taylor, 1993), (Hammer et al., 1995), (Beaudoin et al, 1995), (Glasser et al., 1995). It has been shown that the reason for this kind of expansion / degradation is delayed ettringite formation (DEF). Ettringite is voluminous crystals normally formed during the early hydration period between sulphates and calcium aluminate (C_3A) or ferrite (C_4AF) and causes no problem. Contrary, delayed ettringite formation takes place in hardened concrete and is associated with voids and cracks filled with ettringite, particularly around aggregate particles. In recent years the simultanous occurance of alkali aggregate reactions and delayed ettringite formation has been observed and studied (Pettifer and Nixon, 1980), (Shayan and Quick, 1992), (Johansen et al., 1993).

This paper presents data on compressive strength, volume and linear expansions of laboratory concrete cured at elevated temperature and stored under water at 20°C for 2 years. Microstructural appearance and characteristics of secondary ettringite have been studied, using Scanning Electron Microscope (SEM) and Wave Dispersive Analysis of X-rays (WDAX) . It is also shown that addition of silica fume prevents the formation of secondary ettringite (DEF). The possibility of delayed ettringite formation in dam structures showing alkali aggregate reactions is discussed as well.

EXPERIMENTAL.

Materials and Methods

Concretes of normal density were made using Ordinary Portland Cement (OPC) with - and without addition of slilica fume. Chemical analysis and mineral composition of the cement are given in Table 1. Compositions and handling of the mixes investigated are given in Table 2.

Table 1 Chemical composition of OPC (% of cement)

Oxides							Minerals			
SiO_2	CaO	Fe_2O_3	Al_2O_3	SO_3	MgO	Alk*	C_3S	C_2S	C_4AF	C_3A
20,9	63,4	3,5	4,6	3,1	1,8	0,9	55	19	10,8	6,2

* Na_2O-ekv.

Table 2 Composition and handling of concrete mixes

Mix no.	w/s	Silica fume % of cem.	$D_{max.}$ (mm)	Cement type	Resting time (h)	Max. temp. (C°)	Test / analysis
1	0,45	0	16	OPC	1,5	20 / 85	Compress. strenght, Linear expansion, Microscope
2	0,40	0	16	OPC	6	20 / 70 / 85	Volume change, Microscope
3	0,40	8	16	OPC	6	85	Volume change, Microscope

From mix no. 1 10 x 10 x 10 cm^3 cubes were cast for compressive strength measurements. From the same mix prisms of 40 x 40 x 160 mm with partly embedded knobs were cast for linear expansion detections. Cylinders with Ø = 100 mm, h = 300 mm were cast from mixes 2 and 3 for measuring volume expansion. Volume expansion was determined according to Archimedes law by weighing the cylinders in air and water. The casting of specimens was performed within 20 - 60 minutes after addition of water. The specimens were placed in temperature controlled water baths within 1 - 2 hours after mixing and precaution were taken against leaching of materials. After a hydration time of 1.5 hour for the specimens of mix 1, and 6 hours for those of mixes 2 and 3, the specimens were cured at elevated temperatures (see Table 2). Temperature was raised 10° C / hour for the specimens of mix 1, and 12° C / hour for the specimens of mixes 2 and 3. At the end of curing period (72 hours) at elevated temperatures the specimens were stored in water of 20° C until testing.

For examination of alkali aggregate reactions in a 50 years old dam, concrete cores were drilled from the dam crest. The samples were investigated by thin section analyses at 3 levels, at both sides and in the middle of the cores.

Microscopical examinations

After being cured at different temperatures and stored in water of 20° C for 1 year, laboratory samples were prepared for microscopical examinations. Slices for macro examination were cut from mix 2 and 3, impregnated with flourescent epoxy, plane polished and studied in ultra-violet light (UV-light). Further, samples from all 3 mixes were impregnated with epoxy, plane polished to a micro level before subjected to investigation by Scanning Electron Microscope (SEM) in Back Scattered Electron - (BSE) and/or Secondary Electron mode (SE) and Wave Dispersive Analysis of X-rays (WDAX).

Test Procedures, SEM / WDAX and thin section analysis

Using Secondary Electron modus (SE) in Scanning Electron Microscope (SEM) gives the opportunity to study the surface topography of a preparation, and in this case to observe cracks on the mortar surfaces. Using Back Scattered Electron modus (BSE) for examination of mortar gives the possibility to distinguish between different phases and their distribution. It is important that the sample is properly plane polished. The backscatter process depends strongly on the average atom number of the sample, sample density and the energy of the primary electrons. Phases with high average atom number and / or samples with a dense structure will have bright colours on a BSE image. On the other hand, phases with low average atom number and samples with porous structures will appear dark.

Together with a SEM-investigation, WDAX diagrams may be recorded. WDAX gives semiquantitative compositions of solids. The principle for the method is based upon the exitement of the electrons of each atom in the sample. When the electrons return to their stable energy level, the atoms in the sample will emit X-rays of a certain energy specific for each chemical element. The results will appear as peaks in a diagram with variation of energy as X-axis. The position (X) determines the element, while the height (Y) of the peaks gives the amount of the spesific elements in the sample. By use of WDAX small volumes ($\approx$ 1 μm^3) of a sample are analysed with respect to chemical composition.

For thin section analysis of the concrete from the dam, samples were cut from the cores, impregnated with flourescent epoxy, ground to a thickness of 20 - 25 μm and examined in polarizing Optical microscope. Alkali reactions and growth of crystals like ettringite can easily be observed by thin section anlysis.

RESULTS AND DISCUSSION

Compressive strength and linear expansion, Mix 1

The compressive strength development and linear expansion of mix 1 cured at 20° C and 85° C are shown on Figures 1 and 2, respectively. The compressive strength has been followed for 1 year, and the result shows a considerable strength reduction between 90 days and 1 year for the concrete exposed to curing temperature 85° C compared to that exposed to a curing temperature of 20° C, which coincides with a pronounced length expansion in the prisms cured at 85° C (Fig. 2). Both linear expansion and loss in strength of mix 1 are assumed to be caused by the elevated curing temperature.

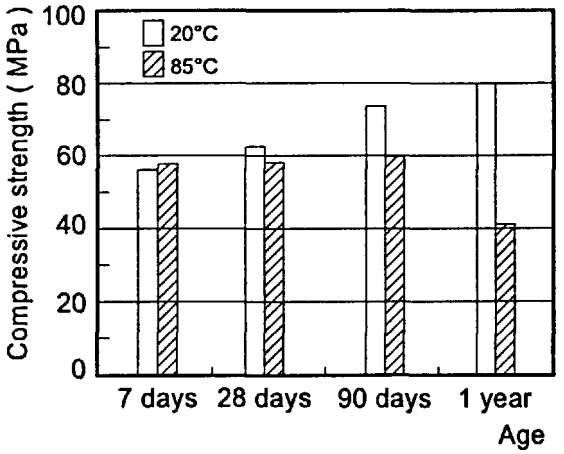

Figure 1 *Compressive strength development, mix no 1, w/s = 0.45, curing temperature 20°C and 85°C*

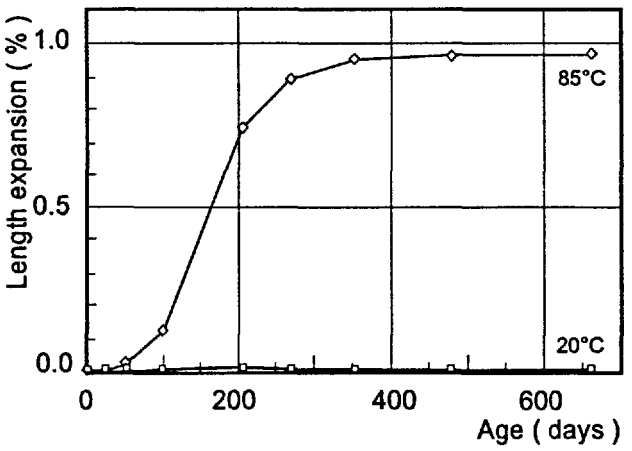

Figure 2 *Length Expansion for mix no 1, w/b = 0.45, P30 cement*

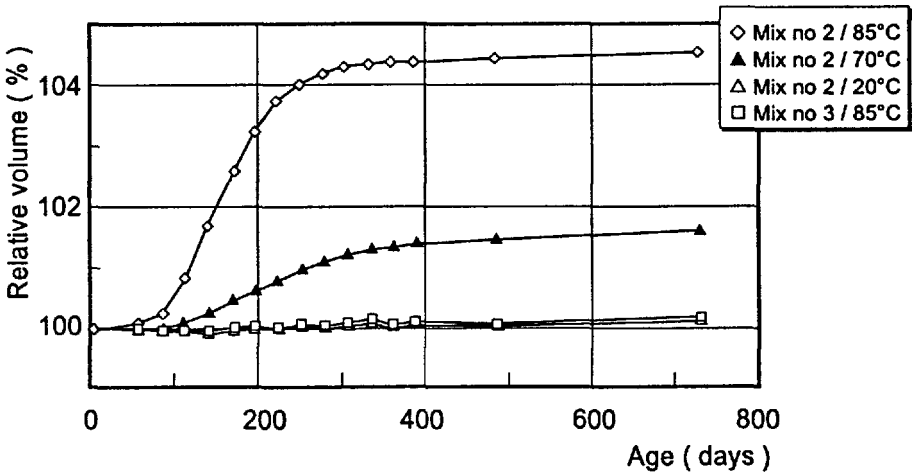

Figure 3 *Relative volume expansion for mixes no 2 and no 3 w/s = 0.4*

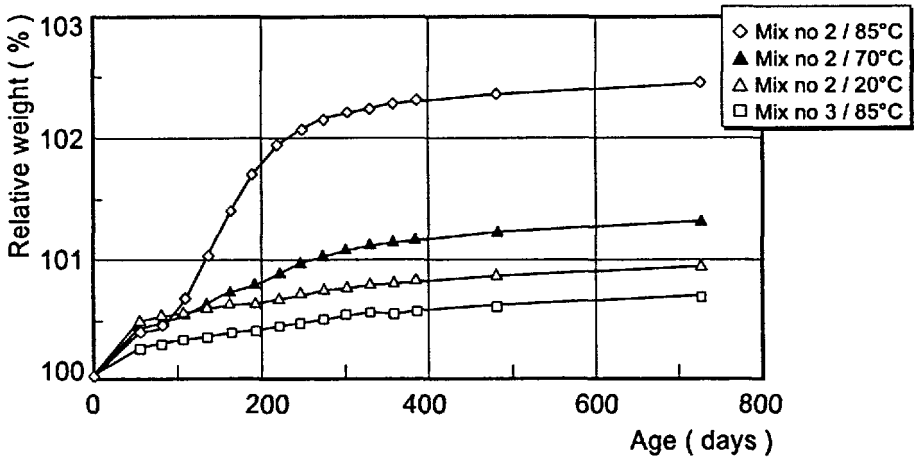

Figure 4 *Relative weight increases for mixes no 2 and no 3*

Volume expansion, Mixes 2 and 3

Volume expansions for samples of mix 2 cured at 20, 70 and 85° C respectively, and for mix 3 with 8 % silica cured at 85° C have been followed for about 2 years. The results as relative changes in volume are shown on Figure 3. When measuring changes in volume, the corresponding changes in weight of the samples were observed, calculated as relative changes in weight as shown on Figure 4. Figure 3 shows an extensive volume increase taking place from 50 days till 1 year for samples of mix 2 cured at 85° C. Also the specimens cured at 70° C showed a significant volume expansion in the same period compared to the samples cured at 20° C. In his experiments Kelham (1996) found 70° C to be a safe curing temperature for the current UK cements. As can be seen from figure 3, our experiments indicate a critical curing temperature < 70° C to avoid DEF. As a matter of fact the Norwegian Standard, NS 3420 claims a curing temperatur ≤ 65° C.

The increase of weight is due to penetration of water (ρ = 1.0 kg/l) and weight increase / unit volume may therefore be compared with the measured volume expansions and give informations as the fraction of cracks are filled with water or water-bearing products. The increases in weight for the samples of mix 2, after 2 years storage in water of 20° C, have been calculated as % of concrete volume and set up in Table 3 together with the results from the measured volume expansion. The results indicate that all cracks may be filled with water / water-bearing products. In addition the samples contain some absorped water due to the porosity of the concrete.

Table 3 Mix no. 2 - weight increase and volume expansion

Curing temperature	85 ° C	70° C	20° C
Weight increase (W / V) %	5.7	2.8	2.2
Volume expansion (V / V) %	4.5	1.2	0.05

Microstructural examinations

The macro examination of fluorescent impregnated cores revealed a normal shrinkage crack pattern for all specimens cured at 20° C. Specimens containing silica fume also showed this micro crack pattern, notwithstanding curing temperature. These cracks, which are due to self desiccation shrinkage, radiating from the aggregates into the matrix could not be observed in samples without silica fume with curing temperatures of 70° C respectively 85° C. Typical for the last mentioned specimens were cracks in the transition zone between aggregate and matrix (i.e. typical for expanding matrix), and the extent of cracks clearly increased by increasing curing temperature. The results from these macro structure examinations were further confirmed by micro structure analyses. On studying the micro structure of the surface of specimen from mix 1 cured at 85°C, using SEM (SE-mode), numerous cracks could be observed in the transition zones. This is shown on Figure 5. SEM (BSE-mode) and microanalyser indicated that these cracks to a large degree were filled with calcium sulpho-aluminate hydrates of the AFt-modification (SO_3 / Al_2O_3 ≈ 2.04), shown on Figure 6. Crystals of the AFt-modification were also observed in the matrix of these samples. Also in samples cured at 70° C the AFt-modification of the sulpho-aluminates could be observed in some cracks. But analyses of sulpho-aluminate crystals found in the matrix of these specimens as well as in the specimens cured at 20° C, and in samples containing silica fume, the ratio SO_3 / Al_2O_3 indicated sulpho-aluminate crystals more like the AFm-modification (SO_3 / Al_2O_3 = 0.75).

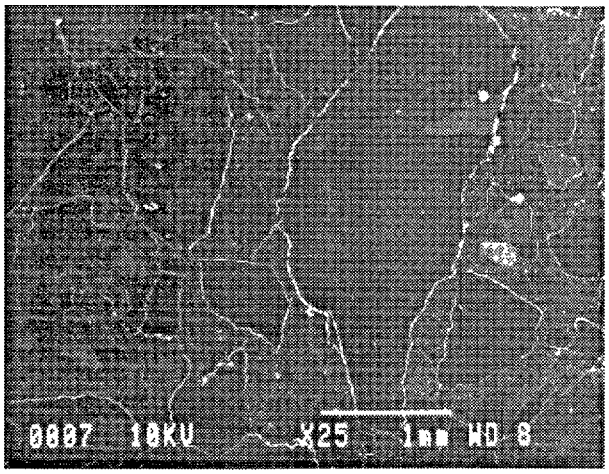

Fig. 5 Cracks in transition zone (aggregate / matrix).
Mix no. 1. Curing temp.: 85° C.
SEM (SE), 25 x

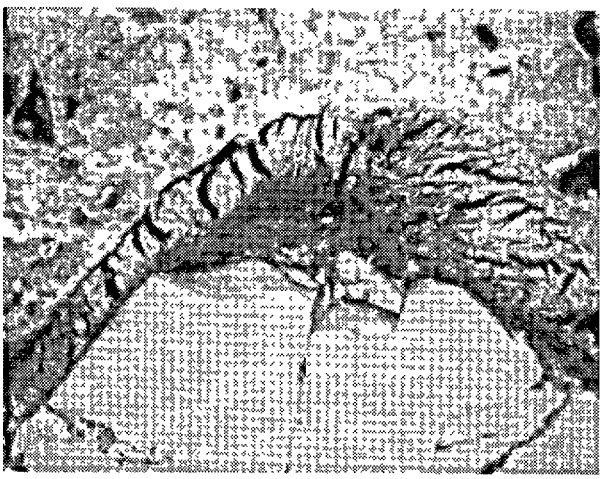

Fig. 6 Ettringite filled crack in transition zone.
Mix no. 2. Curing temp.: 85° C.
SEM (BSE), 2000 x

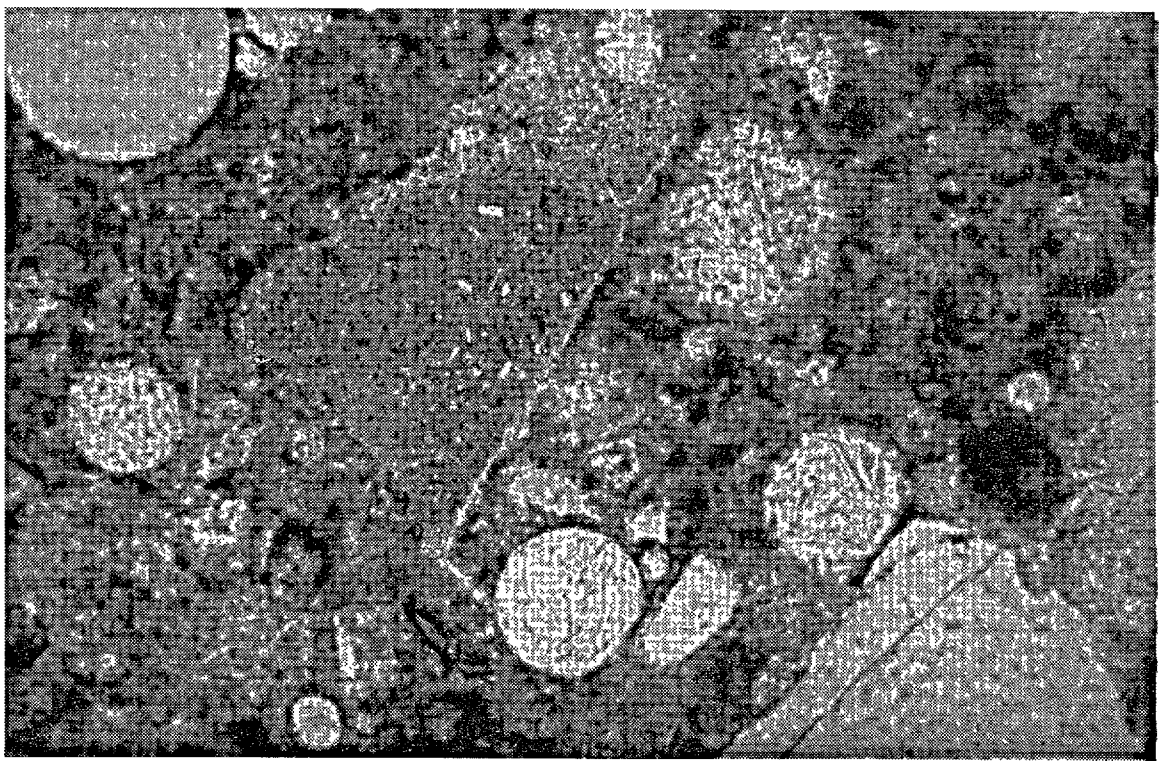

Fig. 7 Alkali-gel and ettringite filled pores in concrete.

The reason why silica fume seems to prevent or postpone DEF is not quite understood. According to Barnes (1983) addition of active silica might accelerate the formation of ettringite and increase the conversion to monosulphate in sulphate-poor systems. This may be the reason why the AFm-modification was observed in the specimen containing silica fume. Glasser et al. (1995) and Kelham (1996) found that increasing of alkali content in the clinker, or alkalis added with the mixing water affected DEF leading to increased expansion of mortar prisms. In addition to a reduced alkali content in silica-substituted cement, the alkalis also react with silica fume, and a reduced alkali content in the pore fluid of silica-blended paste may also be a reason why DEF seems to be overcome by use of silica fume. Whilst Hammer, T. A. et al. (1995) suggested that the lack of DEF in concrete containing silica fume, most likely is due to chemical reactions between aluminate phases and the active silica forming more stable silicon rich aluminate phases (C_3AH_6-C_3AS_3).

Delayed ettringite formation and alkali-aggregate reaction

Many petrographic examinations [Pettifer and Nixon (1980), Shayan and Quick (1992), Johansen et al. (1993)] of thin sections of concrete in which alkali-aggregate reaction is to be expected, also reveal large quantities of ettringite. Simultaneous existence of these two chemical reactions has first and foremost been observed in precast concrete cured at elevated temperatures. In a condition survey of Norwegian dams, concrete cores from several dams were examined for alkali aggregate reactions. The cores refered to in this paper were taken from the crest of the dam. Thin sections analyses of these concrete cores showed alkali-silica gel in specimens taken from the interior of the cores and very often pores in the vicinity of alkali reactive aggregates were quite filled with ettringite crystals as shown on Figure 7. Neither alkali-aggregate reactions nor an abnormal content of ettringite crystals could be observed in samples taken from layers near the exterior sides of the cores. Thus it may be supposed that the abundance of ettringite observed in pores and cracks of these cores, is due to delayed ettringite formation caused by the hydration temperature in the middle of the dam structure. There were no indications that delayed ettringite formation, in this case, had lead to any formation of cracks or similar degradation of the concrete. However, if delayed ettringite formation is observed in concrete damaged by alkali reactive aggregates, it has to be taken into consideration when evaluating the damages.

CONCLUSIONS

* Initial curing temperature at elevated temperatures causes delayed ettringite formation.
* Critical curing temperature in order to avoid DEF is below 70° C.
* High initial curing temperatures give an extensive formation of cracks in the transition zone between aggregate and matrix.
* Addition of silica fume prevents or postpone delayed ettringite formation.
* Sulpho-aluminates observed in concrete cured at elevated temperatures, were of the AFt-modification. Sulpho-aluminates in concrete cured at 20° C and in concrete containing silica fume and cured at any temperatures were of the AFm-modification.
* Delayed ettringite formation may cause linear - and volume expansion and loss in strength.

REFERENCES

Barnes, P.: "Structures and Performance of Cements"

Beaudoin J. J. et al: "A Kinetic Study of Delayed Ettringite Formation in Hydrated Portland Cement Paste", Cement and Concrete Research, Vol. 25, No. 1, pp. 63 - 70, 1995.

Glasser, F. P., Damidot, D. and Atkins M.: "Phase Development in Cement in Relation to the Secondary Ettringite Problem", Advances in Cement Research, 1995, 7,No. 26, Apr. 57 - 68.

Hammer, T.A. Rønne, M., Justnes, H.: "Chemical Stability of LWAC Exposed to High Hydration Generated Temperatures". Proceedings. International Symposium on Structural Ligthweight Aggregate Concrete, Norway, 1995.

Heinz, D. and Ludwig, U.: "Mechanism of Subsequent Ettringite Formation in Mortar and Concrete after Heat Treatment", Proc, VIII Intl. Congr. Chem. Cement, Rio de Janeiro, Vol.5, pp. 189-194, 1986.

Johansen, V., Thaulow, N. and Skalny, J.: "Simultaneous Presence of Alkali-Silica Gel and Ettringite in Concrete." Advances in Cement Research, 1993, 5. No. 17, Jan. pp 23 -29.

Kelham, S.,: "The Effect of Cement Composition and Fineness on Expansion Associated with Delayed Ettringite Formation". To be published 1996.

Pettifer, K. and Nixon, P. J.: "Alkali Metal Sulphate - a Factor common to both Alkali Aggregate Reaction and Sulphate Attack on Concrete", Cement and Concrete Research, Vol. 10, pp 173 - 181, 1980.

Scrivener, K. and Taylor, H. F. W.: "Delayed Ettringite Formation: A Microstructural and Microanalytical Study". Advances in Cement Research, 1993, 5. No 20, pp 139 -146.

Shayan, A. and Quick, G. W. : "Sequence of Formation of Deleterious AAR Products and Secondary Ettringite in the same Mortar and Concrete Specimens". Proc. Int. Conf. Cem. Microsc. 14th, 1992, pp 11 - 21.

41V065
9 pp

EXPERIMENTAL SIMULATION OF THE STABILITY OF ETTRINGITE IN ALKALI SILICA SOLUTIONS, PRODUCED BY ALKALI-SILICA REACTION, IN CONCRETE.

V. MICHAUD , LAFARGE CANADA INC., C.T.S., Montreal, Quebec, Canada
A. NONAT, C.N.R.S., Laboratoire de Recherches sur la Reactivité des Solides, Dijon, France
D. SORRENTINO, LAFARGE, Laboratoire Central de Recherche, Saint Quentin Fallavier, France

ABSTRACT Ettringite formation after the setting period of cement is often blamed for generating cracking of concrete. The objective of this study is to determine if the crystallization of secondary ettringite in an hardened paste is promoted while subjected to alkali-silica reaction. Experimentally, the pore solution surrounding the aggregates was simulated by synthetic solutions with various silica and sodium hydroxide concentrations. Ettringite or various proportions of C_3A and gypsum were mixed with these solutions until the system reached the thermodynamic equilibrium state.
The experiments show that hydrated calcium sulphoaluminate phases are not stable in silicate solutions. They all evolve towards the formation of amorphous or semicrystalline phases, depending on the initial composition of the mixtures, including calcium, silicate, aluminate and alkali ions. Their characteristics are similar to A.S.R. products. Sulphate ions are not incorporated in the solid phases. They are available in the pore solution and can migrate towards areas where the silica concentration is low enough to react with calcium and aluminate, and subsequently ettringite crystallizes.

KEY-WORDS : Alkali-silica reaction, secondary ettringite formation, ettringite stability, alkali silicate solution, durability, pH, silicate concentration.

INTRODUCTION

Ettringite and alkali aggregate reaction gel are often simultaneously observed in damaged concrete. The frequent simultaneous occurrence of sulfate and alkali reaction attacks raises the questions : are these two attacks interconnected and can they promote each other.

So far this state is neither known nor wholly understood. The several studies conducted to verify this aspect only provide hypothesis rather than certitudes. Some of them are based on empirical arguments only.
Now, several authors (Brown and Bothe Jr, 1993; Ebied, El-Didamory, Amin and Mosalamy, 1993; French, 1986; Mehta, 1978; Pettifer and Nixon, 1980; Shayan and Quick, 1991/92, 1992) agree and support the suggestion that "sulfate attack" and alkali aggregate may be interconnected. Brown and Bothe Jr (1993), French (1986), Jones and Poole (1987), Shayan and Quick (1991/92) suggested the proposal that ASR creates conditions favouring ettringite formation. Following are the prevailing arguments :

1. According to Jones and Poole (1987), the ettringite nucleation would occur preferentially in the ASR gel and that latter would offer an advantageous growth medium
2. The formation of ASR gel consumes locally alkali and hydroxide ions of the pore solution. This will lower the pH of the solution and subsequently will promote ettringite formation (Brown and Bothe Jr, 1993).
3. The extensive microcracking due to ASR increases the access of moisture to the interior of the concrete promoting ettringite precipitation.

Whereas Pettifer and Nixon (1980), Regourd, Hornain and Poitevin (1981) and Shayan and Quick (1992) have blamed ettringite formation for promoting ASR because it would liberate hydroxide ions in the pore solution.

The aim of this study is to shed some light on this state by examining if alkali reaction may promote secondary ettringite formation.

It is well known that the alkali reaction results from an interaction between reactive silica phases of aggregate particles and the hydroxides ions of the pore solution. That leads to the partial dissolution of the silica. Therefore, the pore solution around an aggregate including reactive silica can be very concentrated in silicate ions. If the hydrated paste is prepared from a cement containing 1% eq. Na_2O, the alkali concentration in the pore solution will be about of 0.7 mol/kg and the silicate concentration may reach locally around the aggregate a value as high as 1.5 mol/kg (Dent Glasser and Kataoka, 1981).
So far, the behaviour of ettringite which would be locally in contact with the pore solution is unknown. The influence of the presence of silicates ions in the pore solution on the stability of ettringite and more generally of the hydrated calcium sulphoaluminate phases has not been examined. This is the purpose of this paper.
The thermodynamic stability of hydrated calcium sulpho-aluminate phases in the system CaO-Al_2O_3-Na_2O-SO_3-SiO_2-H_2O has been experimentally determined.

EXPERIMENTAL CONDITIONS AND METHODS

This study has been conducted using pure phase materials. Either gypsum and C_3A (S.S.B. equal to 330 m^2/g) or ettringite were mixed at 25°C in diluted suspension with sodium silicate solutions. The compositions of the sodium silicate solutions are representative of those of the pore solution in contact with aggregate containing reactive silica when the cement has an equivalent Na_2O level of about 1%. Once the system had reached its thermodynamic equilibrium (4 weeks), the solid and liquid phases were separated by filtering. The solid phases, after being washed with acetone and ether, were analyzed by X.R.D. The calcium, silicates, sodium, aluminate concentrations in the filtrate were measured by atomic absorption spectroscopy, the sulfate ions by turbidimetry with a Hach 300 colorimeter and the hydroxide activity by pH-measurement with a high alkalinity electrode.

The compositions of the alkali silicate solutions used for this study are : $[Na^+]$ = 0.7 mol/kg, $[SiO_2]$ = 0.035, 0.525 and 1.05 mol/kg. They have been chosen using the results of Dent Glasser and Kataoka (1981). In this study and as shown in Fig 1, it was demonstrated that the composition of the pore solution around an aggregate containing reactive silica depends on the quantity of the reactive silica.
The compositions of the solutions used here are similar to those for the mixtures shown with black dots in Fig 1 upon reaching thermodynamic equilibrium.

Different initial gypsum and C_3A quantities and gypsum / C_3A ratios were used. Different ettringite amounts were used as well.

Firstly, we will discuss the evolution of gypsum and C_3A in sodium silicate solution with the average initial silicate concentration (0.525 mol/kg), and later with the low (0.035 mol/kg) and the high (1.05 mol/kg) silicate concentrations. Then the evolution of ettringite in the same solutions will be examined.

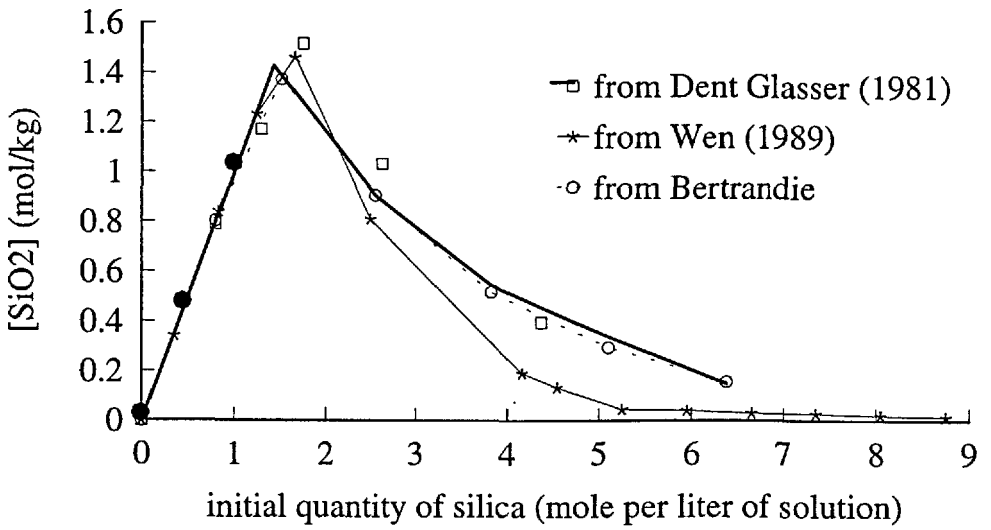

Figure 1 Evolution of the silicate concentration of the solution with the initial quantity of silica per liter of solution once the mixture composed initially of various quantities of silicagel (reactive silica) and a sodium hydroxide solution at 1 mol/kg is at the thermodynamic equilibrium,.
The test solutions have the same composition than the residual solutions of mixtures marked with a black dot.

RESULTS AND INTERPRETATION

Evolution of gypsum and C_3A in sodium silicate solutions

Alkali silicate solution with initially an average silicate concentration (0.525 mol/kg)
The silicate solution was mixed with 0.01 mole per liter of C_3A and different quantities of gypsum varying from 0 to 0.4 mole per liter, also with 0.05 mole per liter of C_3A and 0.30 mole per liter of gypsum.

Ettringite or other hydrated calcium sulphoaluminate phases do not precipitate when the initial quantities of calcium phases are low. It has been confirmed by analyzing the residual solids by X-Ray diffraction and ^{27}Al N.M.R. spectroscopy.
From the X-Ray patterns, presented in Fig 2, only the hydrated calcium sulphoaluminate phase has been detected and in very little amount when 0.01 mole per liter of C_3A was mixed with at least 0.33 mole per liter of gypsum, and when 0.05 mole per liter of C_3A has been mixed with 0.30 mole per liter of gypsum. In this last case, ettringite was detected.
The ^{27}Al N.M.R spectra showed that the aluminate sites are different in ettringite and in the synthesized compounds. In ettringite, and more generally in all of the hydrated calcium sulfoaluminate phases, the aluminium core structure is octahedral and it is mainly tetrahedral in the residual solids.

Independent upon the initial mixture, amorphous or semicristalline phases are being precipitated from gypsum, C_3A and the alkali silicate solution.

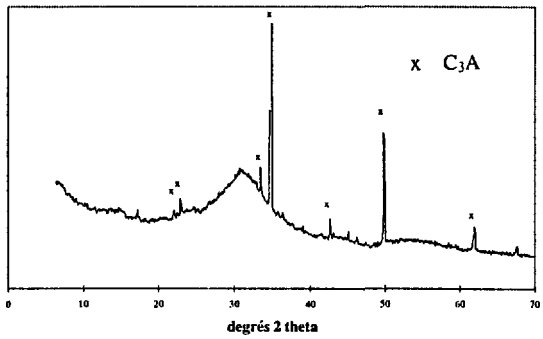

C_3Ai = 0.01 mole + $CaSO_4i$ = 0.03 mole per liter of solution

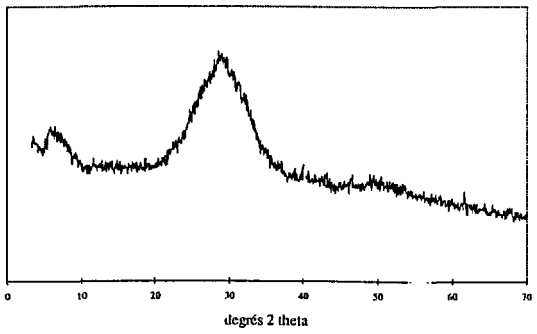

C_3Ai = 0.01 mole + $CaSO_4i$ = 0.06 mole per liter of solution

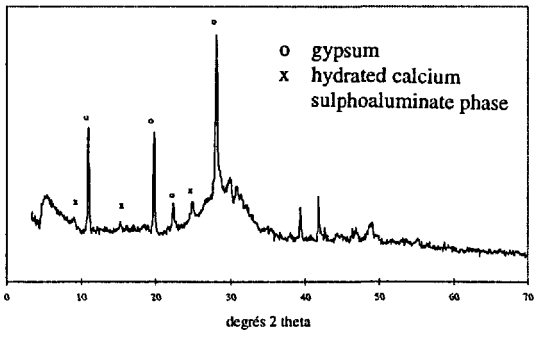

C_3Ai = 0.01 mole + $CaSO_4i$ = 0.33 mole per liter of solution

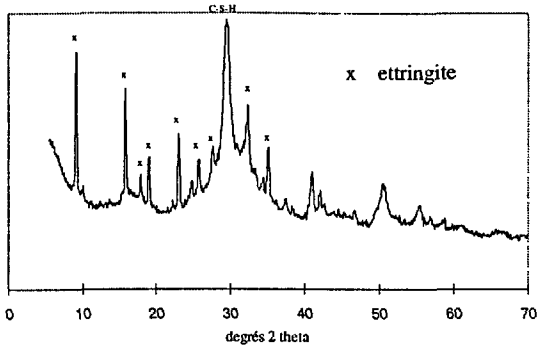

C_3Ai = 0.05 mole + $CaSO_4i$ = 0.30 mole per liter of solution

Figure 2 X-ray patterns of the solids formed from various quantities of C_3A and gypsum and a sodium silicate solution ($[SiO_2]$=0.525 mol/kg, $[Na^+]$=0.7 mol/kg).

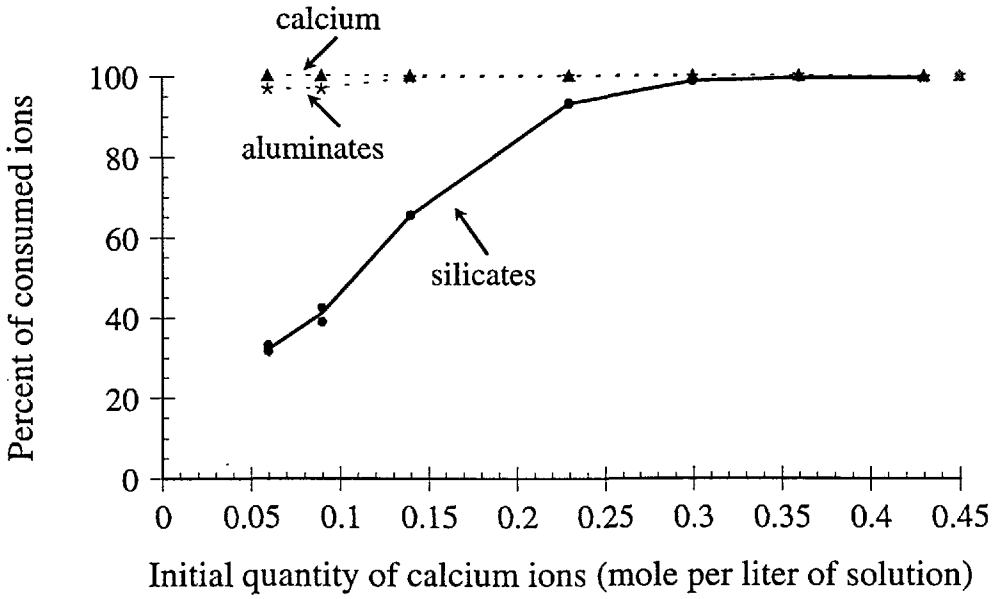

gypsum + C_3A 0.01mole per liter of solution

gypsum 0.30 mole + C_3A 0.05 mole per liter of solution

Figure 3 Proportion of calcium, aluminate and silicate ions present in the initial mixtures incorporated in the final solids. The final solids have been precipitated from various quantities of C_3A and gypsum and a sodium silicate solution ($[SiO_2]$=0.525 mol/kg, $[Na^+]$=0.7 mol/kg).

Analysis of the residual solution shows that the precipitates are composed of calcium, sodium, silicates and aluminate ions, and do not contain any sulphate ion. According to the Fig 3, they incorporate the total calcium and aluminate ions of the initial mixture, and the totality of the silicate ions when the initial quantities of calcium phases are high as well. As long as the initial quantity of calcium ions is below 0.23 mole per liter of solution, the silicates ions are shared between the solid and the liquid phases.

Fig 4 shows a decrease in pH value of the residual solution with the increase in the initial quantities of calcium phases.

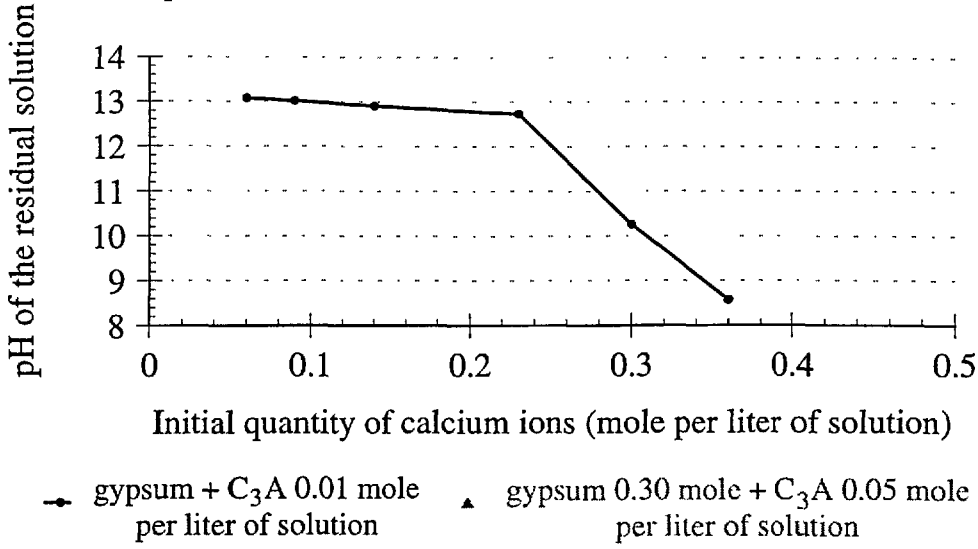

Figure 4 pH in the residual solutions of the mixtures composed initally of various quantities of C_3A and gypsum and a sodium silicate solution ($[SiO_2]$=0.525 mol/kg, $[Na^+]$=0.7 mol/kg), versus the initial quantity of calcium ions.

Residual gypsum is also present only when the initial quantity of gypsum was equal or higher to 0.33 mole per liter.

This shows that gypsum and C_3A are not stable in a sodium silicate solution. Calcium and aluminate ions in solution react preferentially with the silicate ions of the solution to precipitate an amorphous hydrated calcium, silicate, aluminate, sodium reaction compounds which has a structure and a stoechiometry close to those of alkali-reaction products, rather than along with the sulfate ions to form an hydrated calcium sulphoaluminate phase. The sulfate ions do not take part in the formation of the amorphous solid phases. They remain in solution.
Hydrated calcium sulphoaluminates were observed only for mixtures with a high initial amount of calcium phases, that is for the mixtures whose final solution has both a very low final silicate concentration (around 1 mmol/kg) and a low pH value. Mixtures with a low silicate concentration are those for which all of the silicate ions initially present were consumed by the calcium and the aluminate ions to form the amorphous hydrated calcium, sodium, silicate, aluminate reaction compounds.

Therefore, the hydrated calcium sulphoaluminate phases appear to be stable only in solutions with a very low silicate concentration and low pH value. The previous experiments do not permit to determine if rather the silicate concentration or the pH value has the greater influence on the stability of hydrated calcium sulphoaluminate phases. This is the purpose of the next parts.

Alkali silicate solution with initially a high pH (13.7) and a low silicate concentration (0.035 mol/kg)

The silicate solution was mixed with 0.01 mole per liter of C_3A and different quantities of gypsum varying from 0 to 0.2 mole per liter.

The nature of the precipitated phases for the different test mixtures are given in Fig 5.

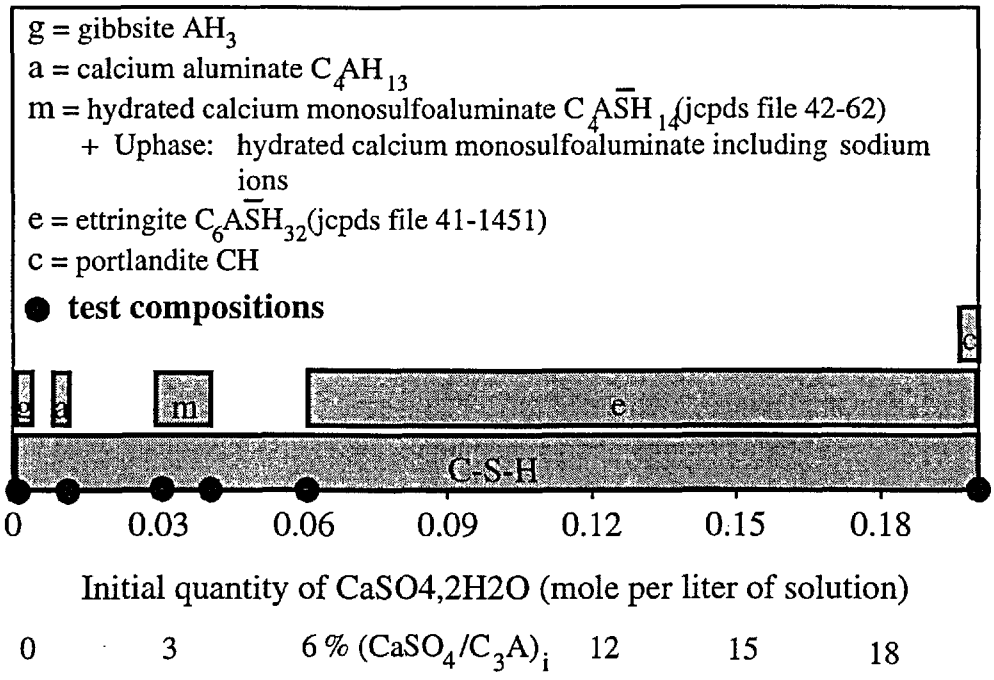

Figure 5 Phases precipitated from the mixtures initially composed of 0.01 mole per liter of C_3A, various quantities of gypsum and a sodium silicate solution ($[SiO_2]$=0.035 mol/kg, $[Na^+]$=0.7 mol/kg), versus the initial quantity of gypsum.

The proportions of silicates, aluminate and calcium ions precipitated from the initial mixtures are shown in Fig 6 and the pH values of the residual solutions in Fig 7.

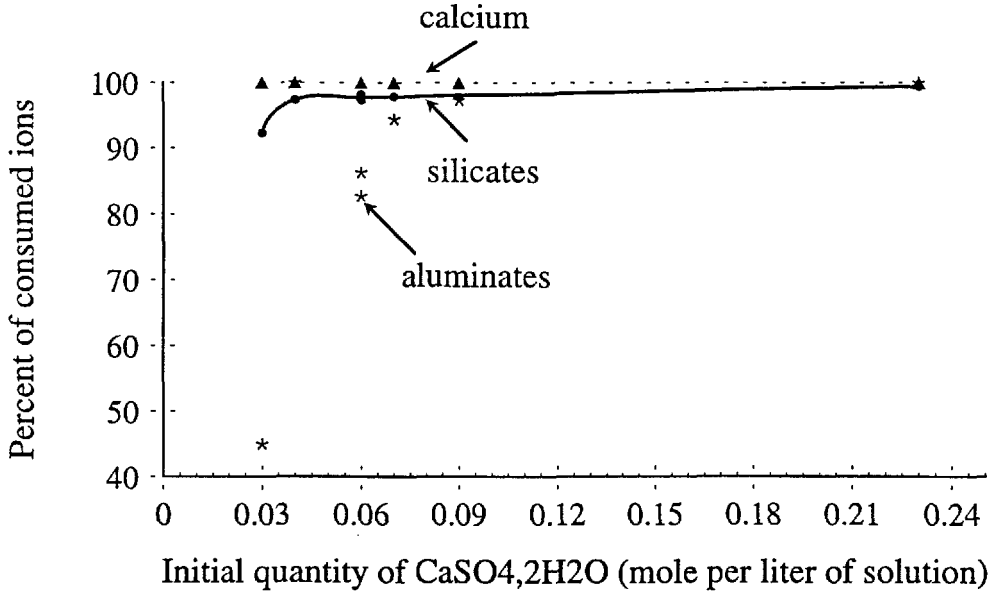

Figure 6 Proportion of calcium, aluminate and silicates ions present in the initial mixtures incorporated in the final solids. The final solids have been precipitated from 0.01 mole per liter of C_3A, various quantities of gypsum and a sodium silicate solution ($[SiO_2]$=0.035 mol/kg, $[Na^+]$=0.7 mol/kg).

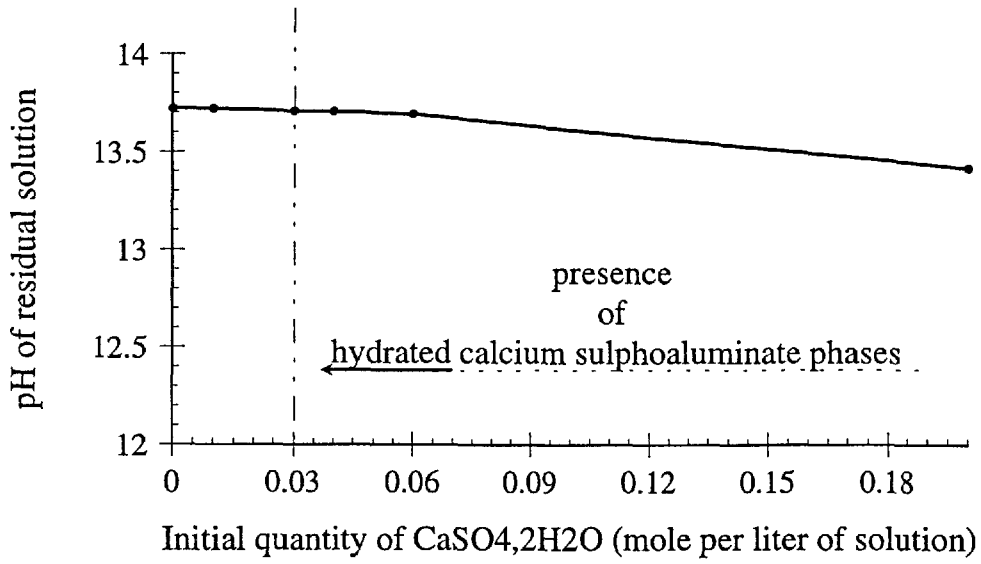

Figure 7 pH evolution in the residual solutions of the mixtures initally composed of 0.01 mole per liter of C_3A, various quantities of gypsum and a sodium silicate solution ($[SiO_2]$=0.035 mol/kg, $[Na^+]$=0.7 mol/kg), versus the initial quantity of gypsum.

As seen before, gypsum and C_3A react preferentially with the sodium silicate solution to precipitate hydrated calcium, silicate, sodium reaction compounds (C-S-H phase in the present case) rather than to form hydrated calcium sulphoaluminate phases. These phases were observed only when all of the silicate ions initially present in the solution were consumed to form C-S-H phase, whereas the pH value of the final solution was equal to 13.7.

Alkali silicate solution with initially a low pH (11.4) and a high silicate concentration (1.05 mol/kg)

The silicate solution was mixed with 0.03 mole per liter of gypsum and 0.01 mole per liter of C_3A. After 4 weeks all C_3A and gypsum have reacted to form only amorphous phases. As before, all the calcium and aluminate ions are incorporated in the final solid. The silicate concentration and pH value of the final solution are equal to 0.74 mol/kg and 11.4 respectively.

These results show that the stability of the hydrated calcium sulphoaluminate phases is governed rather by the silicate concentration of the solution in thermodynamic equilibrium with the solid than by its pH value. Hydrated calcium sulphoaluminate phases are not stable in silicate solution, even when the solution pH value is quite low. Nevertheless, they may be stable at high pH values if the silicate concentration is low.

Evolution of ettringite in sodium silicate solutions

The evolution of ettringite in sodium silicate solutions was studied for two silicate concentrations of 0.035 and 1.05 mol/kg.

Ratio of 0.016 mole and 0.010 mole per liter of ettringite were mixed with these sodium silicate solutions.

For the sodium silicate solution with the lower initial silicate concentration, 97% of the silicate ions initially present in the solution reacted to form a C-S-H phase after 4 months, and residual ettringite was observed. In the second case, all the ettringite had reacted after 7 weeks and the final compositions of both the solid and the solution were similar to those of the mixture with a similar initial composition composed of gypsum and C_3A.

CONCLUSIONS

This study clearly shows that ettringite and more generally hydrated calcium sulphoaluminate phases are not stable in contact with alkali silicate solutions with a silicate concentration higher than very few mmol/l. Therefore, in a concrete with aggregates containing reactive silica, and cement with a high proportion of alkali ions (at least 1% eq. Na_2O), locally, around aggregates which include reactive silica, the solution will be concentrated in silicates ions. If hydrated calcium sulfate, aluminate or sulfoaluminate are in contact with the pore solution concentrated in silicate ions, these phases will be destabilized. The calcium, aluminate and silicates ions will react together to form an amorphous or semicrystalline hydrated calcium, silicate, sodium, eventually aluminate reaction compounds, depending on the initial composition of the mixtures. Their structures and compositions will be similar to those of alkali-reaction products.

These products do not include any sulfate ions. These ions remains available in solution and can diffuse through the pore solution. If locally the silicate ions concentration is low enough and calcium and aluminate ions are available, the ions may react together to form ettringite.

In this way, alkali-silica reaction may promote secondary ettringite formation.

This study also provides indications on ettringite stability in alkaline solution. It shows that ettringite may be stable at high pH values contrary to what is sometimes suggested. Therefore, ettringite formation is not likely to be promoted by alkali silica reaction due to the decrease of the hydroxide ions of the pore solution as suggested by Brown and Bothe Jr. (1993) but the decrease of silicate concentration.

REFERENCES

Bertrandie, D., private communication

Brown, P.W. and Bothe Jr,J. V., "The stability of ettringite", Advances in Cement Research, Vol. 5, No. 18, April, 1993, pp. 47 - 63.

Dent Glasser, L.S. and Kataoka, N, "The chemistry of alkali-aggregate reactions", Proc. 5th int. Conf. on Alkali-aggregate Reaction in Concrete, Cape town, 1981, paper S252/23, pp.1-7.

Ebied, E, El-Didamory, H., Amin, A.M., Mosalamy, F.H., "Influence of sulfates on the hardening of calcium-silicate products", Il Cemento, Vol. 2, 1993, pp.101-111.

French, W. J., "A Rewiew of Some Reactive Aggregates from the United Kingdom with Reference to the Mechanism of Reaction and Deterioration", Proc. 7th Int. Conf. on Alkali-aggregate Reaction in Concrete, Ottawa, 1986, pp. 446 - 450.

Jones, T.N. and Poole, A.B., "Alkali Silica Reaction in Several U.K.Concretes : The Effect of Temperature and Humidity on Expansion, and the Significance of Ettringite Development", Concrete Alkali-Aggregate Reaction, P.E. Gratten Bellew, Noyes Publications, N.Y., 1987, pp. 446-450.

Mehta, P.K.,"Effect ofchemical additions on the alkali silica expansion", Proc. 4th Int. Conf on Alkali-aggregate Reaction in Concrete, 1978.

Pettifer, K. and Nixon, P.J., "Alkali metal sulphate - a factor common to both alkali aggregate reaction and sulphate attack on concrete", Cement and Concrete Research, Vol. 10, 1980, pp. 173 - 181

Regourd, M, Hornain, H. and Poitevin, P., "Alkali Reaction - Concrete Microstructural Evolutions", Proc. 5th Int. Conf. on Alkali-aggregate Reaction in Concrete, Capetown, 1981, paper S252/35.

Shayan, A. and Quick, G.W., "Relative importance of deleterious reactions in concrete: formation of AAR products and secondary ettringite", Advances in Cement Research, Vol. 4, No. 16, 1991/92, pp. 149-157.

Shayan, A. and Quick, G.W., "Microscopic Features of Cracked and Uncracked Concrete Railway Sleepers", ACI Materials Journal, Vol. 89, No. 4, July - August 1992, pp. 348 - 361

Taylor, H.F.W., "Cement Chemistry", Academic Press, 1990
Wen, Z., "Formation et caractérisation de sols alcalins de silice. Conditions de leur transformation en gel au contact de sels et d'hydroxydes, notamment de ceux qui sont présents dans le béton. Etude particulière du rôle de la portlandite", Thèse de doctorat, Université de Bourgogne (1989)

THERMODYNAMIC INVESTIGATION OF THE $CaO-Al_2O_3-CaSO_4-CaCl_2-H_2O$ SYSTEM AT 25°C AND THE INFLUENCE OF Na_2O

Denis DAMIDOT, Department of Chemistry, University of Aberdeen, Scotland.
Frederik P. GLASSER, Department of Chemistry, University of Aberdeen, Scotland

ABSTRACT Phase equilibria in the $CaO-Al_2O_3-CaSO_4-CaCl_2-H_2O$ system at 25°C have been calculated: sixty seven stable solid assemblages coexist with the aqueous phase, nine of which define invariant points. Ettringite and calcium monochloroaluminate hydrate coexist stably and the range of aqueous solution compositions over which they coexist at equilibrium has been defined. Conditions under which calcium monochloroaluminate hydrate transforms into ettringite and vice-versa have been defined. Preliminary calculations of the influence of alkalis on equilibria in the system are presented.

Thermodynamics, Aluminate phase, Phase diagram: $CaO-Al_2O_3-CaSO_4-CaCl_2-H_2O$, Alkalis.

INTRODUCTION

Cement paste is unstable in contact with saline waters. Many phenomenological investigations report the rate of ingress of chloride and of the mineralogical zonation which results. These studies are valuable qualitative indicators but to progress further, it is desirable to develop and apply thermodynamic methodologies for the study of complex equilibria. These are described and applied in the course of this paper.

Ettringite, $3CaO.Al_2O_3.3CaSO_4.32H_2O$, is a commonly-occurring constituent of cement paste: Its stability domain has been refined by thermodynamic investigation of the $CaO-Al_2O_3-CaSO_4-H_2O$ system with and without alkalis: Damidot and Glasser (1993, a, b). Changes to the stability of ettringite are also expected to occur as a consequence of adding additional soluble constituents to the $CaO-Al_2O_3-CaSO_4-H_2O$ system: for example, chloride. However the behaviour of chloride is more complex than that of alkali. Study of the $CaO-Al_2O_3-CaCl_2-H_2O$ system at 25°C indicates that the calcium monochloroaluminate hydrate, $3CaO.Al_2O_3.CaCl_2.10H_2O$, is a stable phase: Damidot et al (1994). Thus the relative amounts of sulphate and chloride in solution should determine whether ettringite and/or calcium monochloroaluminate hydrate are stable in contact with a permeating solution. Experimental results seem to indicate that three cases can occur: ettringite and monochloroaluminate occur together: Ftikos et al, (1980), monochloroaluminate transforms to ettringite: Zhang et al, (1980) and ettringite is converted to monochloroaluminate: Zhang et al, (1980).

The aim of this study is to define more precisely the boundary conditions in terms of aqueous solution compositions corresponding to these three cases. This is achieved by calculating the equilibrium diagram of the $CaO-Al_2O_3-CaSO_4-CaCl_2-H_2O$ system. This system includes three main sub-systems: $CaO-Al_2O_3-CaSO_4-H_2O$, $CaO-Al_2O_3-CaCl_2-H_2O$ and $CaO-CaSO_4-CaCl_2-H_2O$. The first two have already been reported: Damidot and Glasser (1983), Damidot et al (1994); the third is calculated for this paper. Finally, the modifying role of Na_2O on phase stability is examined.

METHOD OF CALCULATION

The method used is based on the calculation of the stable invariant points of a given chemical system by minimisation of the free energy. For calculations, we use solubilities previously

determined for the $CaO-Al_2O_3-CaSO_4-H_2O$ and $CaO-Al_2O_3-CaCl_2-H_2O$ systems (Table I). For the $CaO-Al_2O_3-CaSO_4-CaCl_2-H_2O$ system, no solid phases exist containing all five components:

Table 1 Calculated composition of the solution in equilibrium with selected solids dissolved in water at 25°C

solids	[Ca] mmol/kg	[Al] mmol/kg	[SO_4] mmol/kg	[Cl] mmol/kg
C_3AH_6	3.711	2.474		
CH	21.95			
AH_3 (gibbsite)		3.25e-6		
ettringite	1.651	0.550	0.826	
gypsum	15.20		15.20	
FS*	6.575	3.287		3.287
3-1-15*	146.10			73.08
1-1-2*	1997.1			2997.1
$CaCl_2.6H_2O$	4000.5			8001.0

*3-1-15=$3CaO.CaCl_2.15H_2O$: 1-1-2=$CaO.CaCl_2.2H_2O$
FS = calcium monochloroaluminate hydrate, or Friedel's salt.

thus no additional phases have to be considered. Each potentially stable phase assemblage is then defined by linear combinations of the solids contained in the system and the composition of the aqueous phase in equilibrium is calculated using a program derived from PHREEQE: Parkhurst et al (1980). Activity coefficients are calculated using Pitzer's relations: Pitzer (1973), Pitzer and Mayorga (1973). The coefficient used in Pitzer's relation for alumina have been taken from Reardon (1990). This program also enables calculation of the saturation index of the solids (the saturation index of phases at equilibrium is equal to 0). If calculation discloses that no solids occur having a positive saturation index, (i.e., the solution is supersaturated with respect to these solids), the phase assemblage thus defined is stable. Once all the stable invariant assemblages have been defined, phase assemblages with $F \neq O$ but having fewer solid phases than the maximum, are determined by a simple linear combination of the solids defining each invariant point. If the dimension of the system is less than 5, it is practicable to represent the results graphically: a schematic phase diagram can be drawn simply by linking the related invariant points by straight lines. The position of the boundaries thus sketched is not precise, but this simplified phase diagram contains much of the same information as one which has been completely calculated.
The pH of a cement paste is unlikely to be less than 7, so, to simplify the presentation, we have not considered low pH regions. As a consequence, the phase diagram relevant to cement can be shown diagramatically.

RESULT OF CALCULATIONS

The $CaO-CaSO_4-CaCl_2-H_2O$ system at 25°C

The $CaO-CaSO_4-CaCl_2-H_2O$ system has five solids stable at 25°C: $Ca(OH)_2$ (CH), $3CaO.CaCl_2.15H_2O$ (3-1-15), $CaO.CaCl_2.2H_2O$ (1-1-2), $CaCl_2.6H_2O$ and gypsum ($CaSO_4.2H_2O$). The phase diagram (Fig 1), contains three invariant points at 25°C:

- CH + $3CaO.CaCl_2.15H_2O$ + gypsum + aqueous phase
- $3CaO.CaCl_2.15H_2O$ + $CaO.CaCl_2.2H_2O$ + gypsum + aqueous phase

- $CaO.CaCl_2.2H_2O + CaCl_2.6H_2O$ + gypsum + aqueous phase

Solution compositions at these invariant points are given in Table 2. Phases containing essential chloride appear at high aqueous chloride concentrations; note that $3CaO.CaCl_2.15H_2O$ appears only at [Cl] > 3.25 mol/kg. On the other hand, the sulphate concentration in equilibrium with gypsum is considerably reduced by the presence of chloride, typically by more than one order of magnitude, i.e., gypsum solubility decreases as [Cl] increases

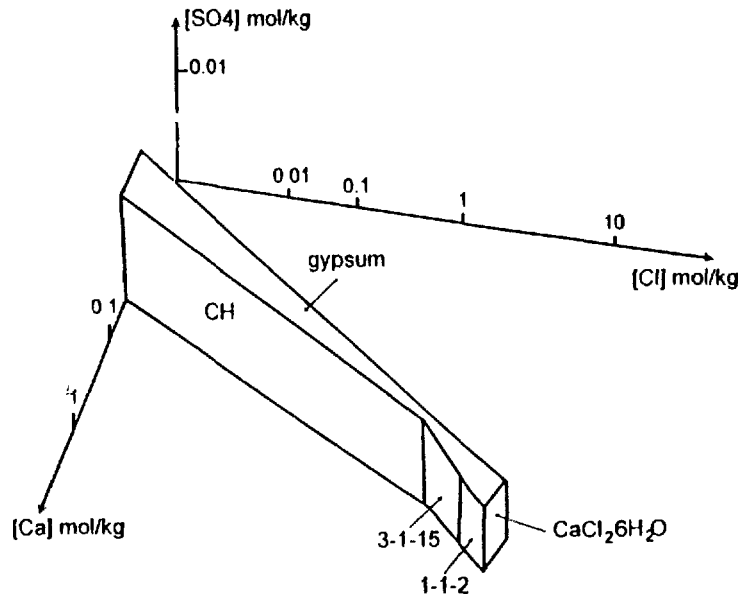

Figure.1.Three dimensional representation of the $CaO-CaSO_4-CaCl_2-H_2O$ system at 25°C. A non-linear graduation, fifth root of the concentration, is used for this and following figures.

Table 2. Calculated compositions or invariant points in the $CaO-CaSO_4-CaCl_2-H_2O$ system at 25°C

Solids in equilibrium with aqueous phase	[Ca] mol/kg	[SO_4] mol/kg	[Cl] mol/kg
CH + 3-1-15	1.641	-	3.220
3-1-15 + 1-1-2	3.248	-	6.424
1-1-2 + $CaCl_2.6H_2O$	4.025	-	8.0158
CH	0.0219	-	-
CH + gypsum	0.0338	0.0124	-
gypsum	0.0152	0.0152	-
CH + 3-1-15 + gypsum	1.658	4.03E-3	3.247
3-1-15 + 1-1-2 + gypsum	3.250	1.25E-3	6.426
1-1-2 + $CaCl_2.6H_2O$ + gypsum	4.025	7.14E-4	8.015

$CaO-Al_2O_3-CaSO_4-CaCl_2-H_2O$ system at 25°C

From a knowledge of the sub-systems $CaO-Al_2O_3-CaSO_4-H_2O$, $CaO-Al_2O_3-CaCl_2-H_2O$ and $CaO-CaSO_4-CaCl_2-H_2O$ and the experimentally-determined absence of additional solid phases, the number of stable solids can be determined as nine: CH, AH_3 (crystalline, gibbsite), C_3AH_6,

gypsum, ettringite, $3CaO.CaCl_2.15H_2O$ (3-1-15), $CaO.CaCl_2.2H_2O$ (1-1-2), $CaCl_2.6H_2O$ and calcium monochloroaluminate hydrate (or Friedel's salt, abbreviated FS). As explained previously during investigation of the $CaO-Al_2O_3-CaCl_2-H_2O$ system, chlorine-ettringite is not stable at 25°C (3). Quaternary hydrates containing all the constituents of the system have been reported (10): solid solutions between calcium monochloroaluminate hydrate and calcium monosulfoaluminate ($3CaO.Al_2O_3.CaSO_4.14H_2O$) exist. The maximum substitution is equal to ~50%: $3CaO.Al_2O_3.0.5CaSO_4.0.5CaCl_2.yH_2O$. The evolution of the value of the solubility product of calcium monochloroaluminate hydrate as a function of chloride: sulphate ratio can be assessed using the approach developed by Tardy and Fritz (11) in which the end members of the solid solution are used, in which case the expression of its solubility product,
for $X\ SO_4$ ($X \leq 0.5$), is:
$\log K_{FS+X\,SO4} = (1-X) \log K_{FS} + X \log K_{monoS} + X \log X + (1-X) \log (1-X)$
where "monoS" is monosulfoaluminate.
At X=0.5, the variation of the value of log K for calcium monochloroaluminate is equal to -0.82. As a consequence, calcium monochloroaluminate partially substituted by sulphate is slightly more stable than FS itself. The modification of the log K value when calculating the phase diagram is, however, within limits of error and solid solutions have not been taken into account in calculations reported in this paper.

The results of the calculation indicate the presence of nine stable invariant points (Table 3). From the solids coexisting at the invariant points, it is possible to determine all the stable phase assemblages of lower dimensionality; 25 stable assemblages of 3 solids and 24 stable assemblages of 2 solids coexist in equilibrium with an aqueous phase:

♦ the assemblages of two solids in equilibrium with an aqueous phase are:

- AH_3, C_3AH_6
- AH_3, ettringite
- AH_3, FS.
- C_3AH_6, ettringite
- C_3AH_6, FS.
- ettringite, FS.
- AH_3, gypsum
- ettringite + gypsum
- gypsum, FS.
- AH_3, $CaCl_2.6H$
- gypsum, $CaCl_2.6H$
- FS, $CaCl_2.6H$
- CH, C_3AH_6
- CH, ettringite
- CH, FS
- CH, 3:1:15
- ettringite, 3:1:15
- FS, 3:1:15
- CH, gypsum
- gypsum.3:1:15
- gypsum, 1:1:2
- FS, 1:1:2
- 1:1:2, $CaCl_2.H_6$
- 3:1:15, 1:1:2

♦ the assemblages of three solids in equilibrium with an aqueous phase are:

- AH_3, C_3AH_6, ett
- AH_3,C_3AH_6, FS
- AH_3, ett, FS
- C_3AH_6, ett, FS
- AH_3, ett, gyps
- AH_3, gyps, FS
- ett, gyps, FS
- AH_3, gyps, $CaCl_2.H_6$
- AH_3, FS, $CaCl_2.H_6$
- Gyps. FS, $CaCl_2H_6$
- CH, C_3AH_6, ett
- CH, C_3AH_6, FS
- CH, ett, FS
- CH, ett, 3:115
- CH, FS, 3:1:15
- Ett, FS, 3:1:15
- CH, ett, gyps
- CH, gyps, 3:1:15
- Ett, gyps, 3:1:15
- Gyps, FS, 3:1:15
- Gyps, FS, 21:1:2
- Gyps, 1:1:2, $CaCl_2H_6$
- FS, 1:1:2, $CaCl_2H_6$
- Gyps, 3:1:15, 1:1:2
- FS, 3:1:15. 1:1:2

ett., gyps.: ettringite & gypsum

A geometric representation of the system is difficult if water is in excess due to its dimensionality of four. It is however possible to decrease the dimensionality of the system by fixing the concentration of one or more constituents. If, for example, the chloride concentration

is kept constant, the dimensionality of the system at constant temperature is reduced to three and projections can be drawn of selected isopleths. Fig. 2 shows the isopleth at 0.2mol/kg at which AH_3, CH, gypsum, ettringite and calcium monochloroaluminate hydrate are stable in contact with solution. Ettringite and calcium monochloroaluminate are in equilibrium along a range of aqueous compositions corresponding to the boundary curve defining their equilibrium surface. Compared to the $CaO-Al_2O_3-CaSO_4-H_2O$ system, crystallisation of C_3AH_6 is suppressed; it reacts at the invariant point: CH + C_3AH_6 + FS + ettringite + aq, for which [Cl]= 9.58E-3 mol/kg.

Table 3. 25°C invariant solution compositions for in the $CaO-Al_2O_3-CaSO_4-CaCl_2-H_2O$ system.

Solids in equilibrium with aqueous phase	[Ca] mol/kg	[Al] mol/kg	[SO_4] mol/kg	[Cl] mol/kg	pH
CH , C_3AH_6 , FS , ettringite	2.59E-2	7.18E-6	7.29E-6	9.58E-3	12.50
AH_3 , C_3AH_6 , FS , ettringite	1.05E-2	2.79E-4	8.21E-6	1.18E-2	11.86
CH , 3-1-15 , gypsum , ettringite	1.659	2.8E-11	4.03E-3	3.247	11.82
CH , 3-1-15 , FS , ettringite	1.656	3.8E-10	7.03E-4	3.248	11.82
AH_3 , gypsum , FS , ettringite	2.826	4.32E-7	1.60E-3	5.648	9.47
3-1-15 , gypsum , FS , ettringite	2.864	5.3E-11	1.65E-3	5.658	11.44
3-1-15 , 1-1-2 , gypsum , FS	3.250	2.7E-11	1.25E-3	6.426	11.34
AH_3 , gypsum , $CaCl_2.6H_2O$, FS	4.001	9.56E-8	7.04E-4	8.001	9.07
1-1-2 , gypsum , $CaCl_2.6H_2O$, FS	4.025	4.7E-11	7.14E-4	8.015	10.73

Ettringite is stable over a wider range of sulphate concentrations compared to calcium monochloroaluminate hydrate. However, higher chloride concentrations increase the stability domain of calcium monochloroaluminate relative to ettringite, as shown in Fig. 3, for the isopleth at [Cl]=4.5mol/kg. In this case, CH is no longer stable in contact with an aqueous phase and is replaced by $3CaO.CaCl_2.15H_2O$. Relative to the previous isopleth, the saturation surfaces are progressively shifted towards higher calcium concentrations as the chloride concentration increases: this is necessary to maintain electroneutrality of the solution, with its high solubility for both OH^- and chloride. This chloride concentration - 4.5mol/kg - is close to the invariant point: 3-1-15, gypsum, FS, ettringite, aq and is the highest chloride concentration at which ettringite is stable. Experimentally, the chloride content of ettringite at this point is negligible.

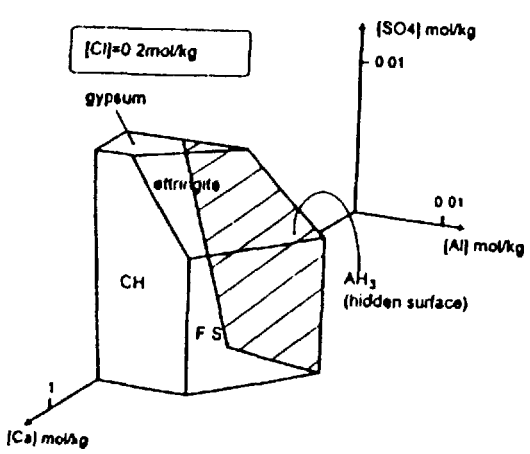

FIG.2 Three dimensional representation of the $CaO-Al_2O_3CaSO_4-CaSO_4-H_2O$ system at 25°C: [Cl] = 0.2mol/kg.

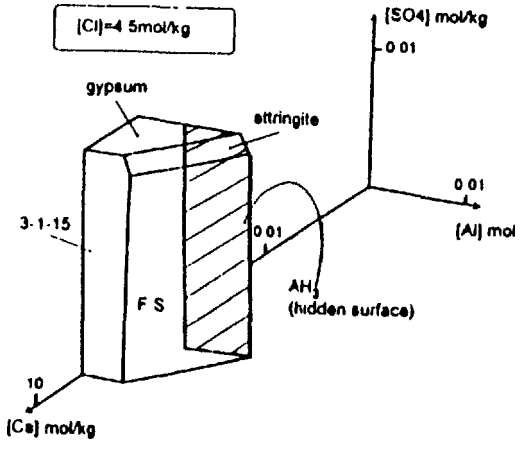

FIG.3 Three dimensional representation of the $CaO-Al_2O_3CaSO_4-CaSO_4-H_2O$ system at 25°C with Cl fixed at 4.5mol/kg.

DISCUSSION OF THE RESULTS

Ettringite and calcium monochloroaluminate domains of stability

The system of nine solids contains 67 stable assemblage coexisting with an aqueous phase: 24 assemblages of 2 solids, 25 assemblages of 3 solids and 9 assemblages of 4 solids (invariant points). This complex pattern of stable coexistence may explain the scatter of the experimental results and apparently contradictory conclusions reached in the literature: most previous studies describe only portions of the system. Contrariwise, phase assemblages that are not included here must be unstable; the calculations confirm the results of experiments cited in the introduction: ettringite and calcium monochloroaluminate hydrate can form a stable pair of solids and, depending on the relative sulphate to chloride ratio in the aqueous phase, either ettringite can be transformed into calcium monochloroaluminate or vice-versa. The region of coexistence of these two hydrates depends on the chloride and sulphate concentrations in solution. Geometrically, the region is a surface that is defined by two boundaries: the first starts from the invariant point: CH, C_3AH_6, FS, ettringite, aq, follows the boundary curve: CH, ettringite, FS, aq, passes through the invariant point: CH, 3-1-15, FS, ettringite, aq, thereafter following the boundary curve: 3-1-15, ettringite, FS, aq and terminates at the invariant point: 3-1-15, gypsum, FS, ettringite, aq. The second boundary also starts from the invariant point: CH, C_3AH_6, FS, ettringite, aq and follows the boundary curve: C_3AH_6, ettringite, FS, aq, passing: AH_3, C_3AH_6, FS, ettringite, aq, follows the boundary curve: AH_3, ettringite, FS, aq, passes through: AH_3, gypsum, FS, ettringite, aq, follows the boundary curve: gypsum, ettringite, FS, aq, eventually terminating at the same invariant point as the first boundary. The two boundaries appear to be close in projection on the sulphate-chloride plane (Fig.4) but a phase transformation requires uptake or release of anions, so the system is buffered with respect to change and the boundaries, although closely spaced on a $\sqrt[5]{}$ scale, have real physical significance.

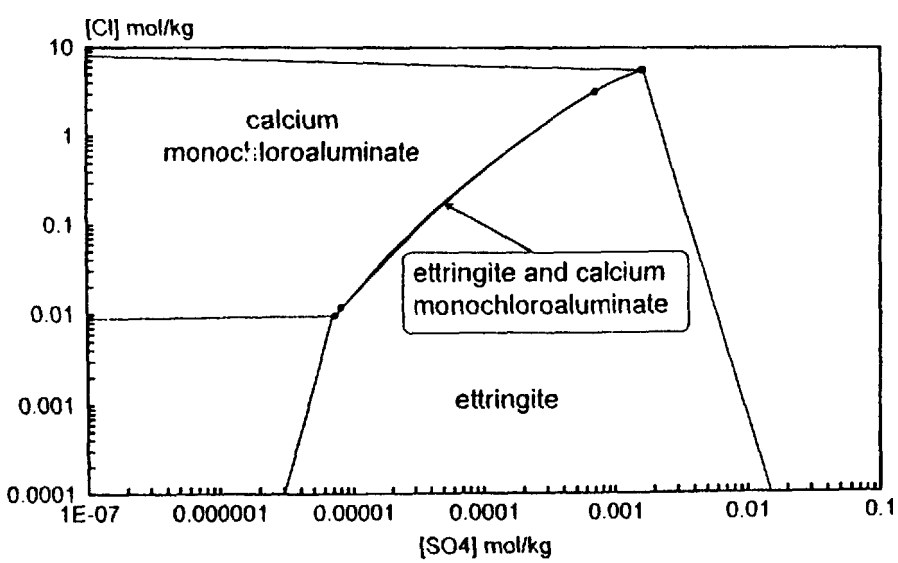

FIG.4 Stability fields of ettringite and monochloroaluminate projected onto the sulfate-chloride plane: temperature = 25°C.

Compared to the $CaO-Al_2O_3-CaSO_4-H_2O$ system, high aqueous chloride concentrations stabilise ettringite to lower pH: as low as pH=9.5, compared with a minimum of 10.5 in the system $CaO-Al_2O_3-CaSO_4-H_2O$.

Evolution of the System with Added Na_2O: The $CaO-Al_2O_3-CaSO_4-CaCl_2-Na_2O-H_2O$ System

Readily soluble constituents added to the system modify the equilibrium domains but, at low concentrations, do not generate additional stable solids. Since sodium is commonly encountered as the charge balancing soluble cation for chloride and sulphate, parts of the $CaO-Al_2O_3-CaSO_4-CaCl_2-Na_2O-H_2O$ system have been calculated. Although NaCl is formally the component added, i.e., [Na] = [Cl], the two components react differently with cement substance: Na is weakly removed while Cl reacts more strongly with aluminates, forming Friedel's salt. As a consequence, and to help predict mineral zonation, Na and Cl contents have to be treated as independent variables. With increasing sodium concentration, NaCl is the first sodium-containing solid to become stable at the invariant point: gypsum, NaCl, FS, $CaCl_2.6H_2O$ 1:1:2: aq. Aqueous concentrations at this point, are [Na] = 1.014mol/kg, [Cl] = 8.4mol/kg, $[SO_4]$=7.7E-4 mol/kg, [Ca]=3.704mol/lkg and [Al]=5E-11mol/kg. With increasing sodium concentrations, the region of NaCl crystallisation expands and NaCl precipitates at progressively lower chloride concentrations. The other sodium-containing phases, $Na_2SO_4.10H_2O$ (mirabilite), Na_2SO_4 and NaOH, are calculated to be stable only at high sodium concentrations, beyond the limits of our confidence in ionic strength corrections.

As a consequence, at sodium concentrations lower than 1mol/kg, solid phase formation in the $CaO-Al_2O_3-CaSO_4-CaCl_2-Na_2O-H_2O$ system is comparable with the $CaO-Al_2O_3-CaSO_4-CaCl_2-H_2O$ system previously described: phases containing essential sodium are not stable. But the addition of sodium modifies the location of the phase regions; a decrease in calcium concentration occurs but aluminate, chloride and sulphate concentrations increase: the evolution of chloride and sulfate concentrations of the assemblage: CH, C_3AH_6, ettringite, FS., aq. is shown in Fig. 5 as a function of added sodium. As sodium increases, saline solutions have to be progressively more concentrated in sulfate and chloride in order to stabilise ettringite or/and calcium monochloroaluminate hydrate.

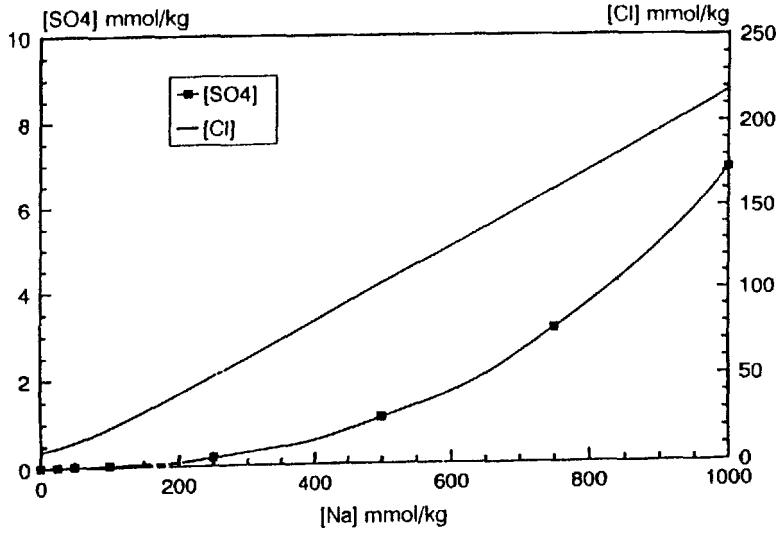

Figure.5.Evolution of the sulfate and chloride concentration at the invariant point CH, C_3AH_6,, ettringite, calcium monchloroaluminate hydrate (Friedel's salt), aq. as a function of the concentration of added Na^+: temperature = 25°C.

CONCLUSION

The calculation of the $CaO-Al_2O_3-CaSO_4-CaCl_2-H_2O$ system at 25°C has demonstrated the ability and power of computational thermodynamics applied to aqueous cement systems . The stability domains of ettringite and calcium monochloroaluminate hydrate have been defined. Ettringite and calcium monochloroaluminate hydrate are in equilibrium with solutions having compositions starting at the invariant point: CH, C_3AH_6, ettringite, calcium monochloroaluminate hydrate, aq. and extending to the invariant point: $3CaO.CaCl_2.15H_2O$, gypsum, ettringite, calcium monochloroaluminate hydrate, aq. In the presence of sodium, more chloride and sulphate must dissolve in order to stabilise calcium monochloroaluminate hydrate and ettringite. The phase equilibria thus determined can be applied flexibly to a wide range of problems of mineral stability and cement deterioration in aggressive chemical environments. The data tables and diagrams presented are often sufficient for qualitative calculations but recourse to the computer-based routines may be necessary for more quantitative approaches.

ACKNOWLEDGEMENT

This work has been supported by the Commission of the European Communities as part of its radioactive waste management program, contract number F12W-CT90-0035.

REFERENCES

Damidot, D. and Glasser, F.P., "Thermodynamic investigation of the $CaO-Al_2O_3-CaSO_4-H_2O$ system at 25°C and the influence of Na_2O", Cem. Conc. Res., 23, 221-38 (1993)

Damidot, D. and Glasser, F.P., "Thermodynamic investigation of the $CaO-Al_2O_3-CaSO_4-K_2O-H_2O$ system at 25°C", Cem. Conc. Res., 23, 1195-1204 (1993)

Damidot, D., Birnin-Yauri, U. and Glasser, F.P., "Thermodynamic investigation of the $CaO-Al_2O_3-CaCl_2-H_2O$ system at 25°C and the influence of Na_2O", Il Cemento, 91, 243-54 (1994)

Ftikos, C., Kasselouris, V., Tsimas, S. and Parissakis, G.,"A study on the action of sea water on hydrated cement pastes" 7th Int. Symp. on the Chemistry of Cement, Paris, 4, 357-62 (1980)

Kuzel, H.J., "Rontenuntersuchung im system $3CaO.Al_2O_3.CaSO_4.nH_2O$ - $3CaO.Al_2O_3.CaCl_2.nH_2O$ - H_2O", N. Jahr. f. Mineralogie Monat.,13,193-200 (1966)

Parkhurst, D.L., Thorstenson, D.C., Plummer, L.N." PHREEQE - A computer program for geochemical calculations" U.S. Geological Survey, USGS-WRI-80-96 (1980)

Pitzer, K.S., "Thermodynamics of electrolytes. I. theoretical basis and general equations" J. Phys. Chem, 77, 268-77 (1973)

Pitzer, K.S. and Mayorga, G., "Thermodynamics of electrolytes. II. activity and osmotic coefficients for strong electrolytes with one or both ions univalent", J. Phys. Chem. , 77, 2300-08 (1973)

Reardon, E.J., "An ion interaction model for the determination of chemical equilibria in cement water systems", Cem Conc Res., 20(2), 175-192 (1990)

Tardy, Y. and Fritz, B., "An ideal solid solution model for calculating solubility of clay minerals" Clay Minerals ,16, 361-73 (1981)

Zhang, F., Zhou, Z. and Lou, Z., "Solubility product and stability of ettringite", 7th Int. Symp. on the Chemistry of Cement,Paris,2,88-93 (1980)

EFFECT OF TEMPERATURE ON THE PHYSICO-CHEMICAL AND MINERALOGICAL CHARACTERISTICS OF HARDENED CONCRETE

Surrinder K HANDOO, Sanjeev AGARWAL, Satish K AGARWAL and Subhash C AHLUWALIA *

National Council for Cement and Building Materials,
New Delhi,India.
* OCL India Limited,New Delhi,India.

ABSTRACT A parametric study on concrete cubes prepared from the cement of known chemical,mineralogical and physical characteristics and fired to various temperature regimes has been carried out using DTA/TGA and XRD, to correlate the effect of temperature on changes occurring in the mineralogical composition of cement hydration products and the compressive strength.Such a correlation can be used to determine fire conditions and the consequent expected deterioration in compressive strength of the damaged concrete.

Key-words: Calcium hydroxide,Fire damage,High temperature,Curing

INTRODUCTION

Harmathy (1968) demonstrated the use of differential thermogravimatric technique for gauging the temperature to which concrete could have been exposed during the fire.Raina et al (1978) and Handoo and Agarwal (1993) reported the application of DTA/TGA technique for assessing fire damaged concretes.A number of specific case studies on rehabilitation of fire damaged concrete buildings have been carried out by National Council for Cement and Building Materials (NCB) (1987 ,1993). However , no systematic study has so far been reported to simulate the conditions of temperatures generally experienced in concrete structures exposed to high temperatures such as an accidental fire and to correlate with the physico-chemical and mineralogical characteristics of the damaged concrete with the extent of damages.

EXPERIMENTATION

Concrete grade M-20,with cube compressive strength of 20 N/mm^2 at 28 days was designed as per Indian standard IS:10262-1982 using standard aggregates and OPC having performance characterictics as listed in Table 1.The concrete cubes of 100 mm size were prepared and cured under water at ambient conditions for 28 days.Each set of three cured cubes was dried in air and exposed to temperature regimes upto 1000°C in the steps of 100°C in a hot air

Table 1 PHYSICAL CHARACTERITICS OF ORDINARY PORTLAND CEMENT

Compressive Strength* N/mm^2			Setting Time (Minutes)		Soundness autoclave	Blaine's
3day	7days	28days	IST	FST	(%)	m^2/kg
30	34	47	50	160	0.01	295

* Measured on 1:3 mortar cubes as per IS:4031-1988.

Table 2 Compressive strength of concrete cubes fired upto 1000oC

Temp. (^oC)	ambient	100	200	300	400	500	600	700	800	900	1000
Comp.stregth (N/mm^2)	36	37	36	36	35	32	16	15	13	10	nil

oven/muffle furnace for a constant retention period of 5 hours.The fired cubes after cooling to ambient temperature were immerersed in water for 48 hours before testing for compressive strength.The change in average compressive strength of three cubes with temperature is given in Table 2. The DTA/TGA and XRD studies were carried out on the mortar part of the cubes drawn at areas representing the exposed surface and the core at the depth of 50mm,using simultaneous Mettler Thermo analyser TA 1 and Rigaku's X-ray diffractometer with $CoK\alpha$ radiation.

RESULTS AND DISCUSSIONS

The average compressive strength of concrete cubes after curing in water for 28 days was found to be 36 N/mm^2.The concrete cubes exposed to a temperature regime for a constant period of 5 hours have negligible effect on their compresssive strength upto 400^oC. The concrete suffered a significant loss of strength,nearly 45 percent in the temperature range of 400° to 600^oC due to the loss of crystal water resulting in decrease in $Ca(OH)_2$ content besides due to the changes in the morphology and microcracks formations.The concrete cubes showed distinct distress beyond 800^oC. Similar pattern of reduction in strength of concrete specimens has also been reported by Orchard (1979) and Neville (1995).

DTA/TGA study on the mortar samples drawn depthwise representing the surface and the core indicated that concrete at surface suffered more damage compared to the core at all temperatures (Fig 1a).The change in $Ca(OH)_2$ content determined by corresponding TG loss in mortar samples of the fired concrete cubes reveals that at 700^oC it is reduced to 80 percent of its content at ambient temperature.Beyond 700^oC,$Ca(OH)_2$ was not detected by DTA in the exposed surface samples of the concrete.The rate of dehydration in the core at the depth 50 mm of the cubes was rather slow due to a temperature gradient from the surface. Consequently the residual $Ca(OH)_2$ in the core samples of the cubes fired upto 900^oC was still found to be 13.2 percent of its content at ambient temperature.

XRD studies on the matured concrete cubes have shown the presence of normal hydrated phases such as ettringite,calcium silicate hydrates, $Ca(OH)_2$, $Mg(OH)_2$ in few cases and $CaCO_3$. The diffractograms of exposed surface and core of the fired cubes (Fig 1b) confirm the change in mineralogy and gradual reduction in $Ca(OH)_2$ content with increase in temperature as evaluated by DTA/TGA as well.

The decrease in the $Ca(OH)_2$ content in the core as well as the exposed surface of the concrete cubes with the increase in temperature has been correlated with the decrease in the compressive strength. This correlation (Fig 2) can possibly be

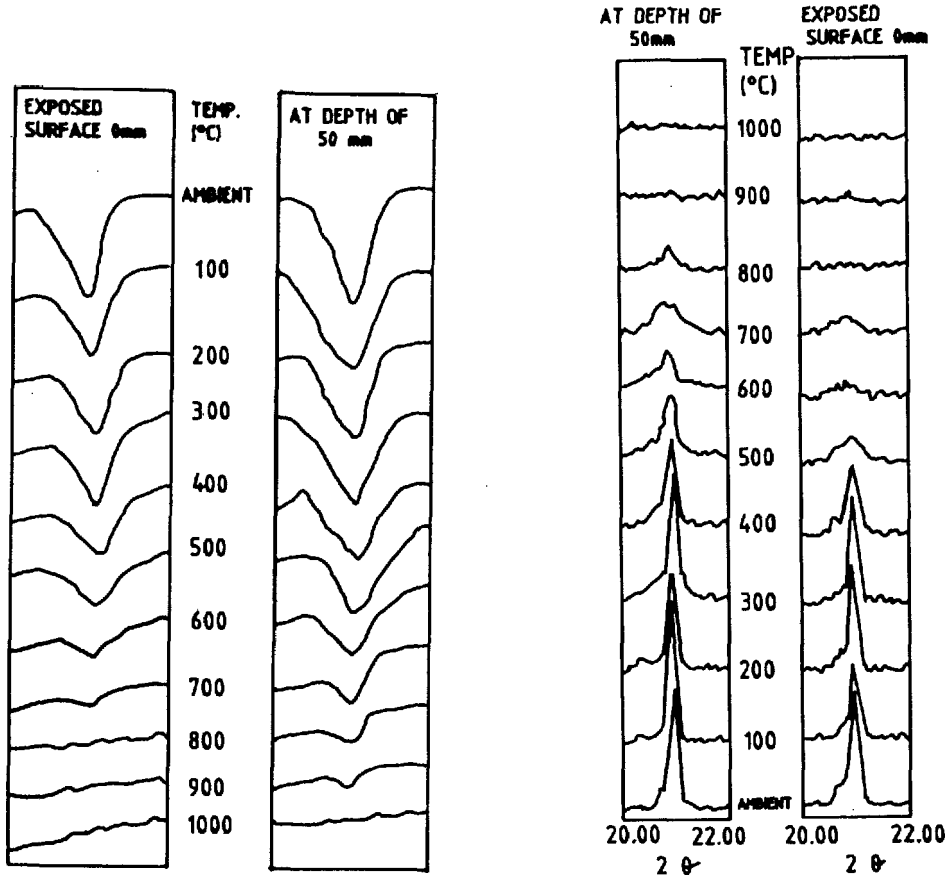

Figure 1 : (a) DTA Curves showing the dehydration of $Ca(OH)_2$ and corresponding XRD patterns (b)

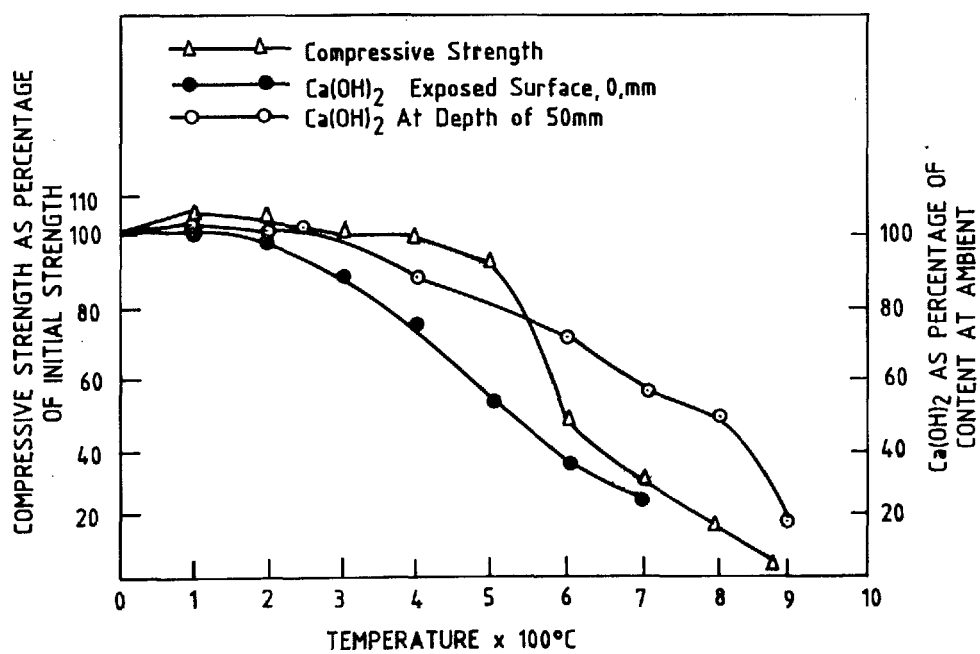

Figure 2 : Variation of change in compressive strength and $Ca(OH)_2$ content in concrete cubes with temperature

used for determining the temperature to which a concrete has got exposed to and consequent reduction in its compressive strength during the exposure to temperatures like in accidental fire. This data can provide information for making the recommendations for possible rehabilitation of the damaged concrete structure.Further studies are being carried out to establish the reliability of the correlation vis-a-vis the actual deterioration in concrete.A large number of investigations on the extent of fire damage in the structures have been carried out at NCB and the application of these techniques for assessing the extent of damage have proved useful.

CONCLUSIONS

1. The effect of temperature on the compressive strength of concrete cubes is negligible upto 400°C.Subseqnently there is a rapid fall in the strength of the cubes fired upto 600°C after which the rate of loss of strength becomes lower.

2. The content of $Ca(OH)_2$ in the concrete is reduced in a definite pattern with the increase in temperature.At 700°C, it is reduced to 80 percent of its content at ambient temperature under the conditions of the experiment.

3. The correlation derived between simultaneous reduction in compressive strength and content of $Ca(OH)_2$ in the concrete with increasing temperature can be used to predict qualitatively the temperature to which a concrete has got exposed during the fire.

ACKNOWLEDGEMENT

The authors have freely drawn the information/data from the published/unpublished literature and reports of NCB.This paper is being published with the permission of Director General,National Council for cement and Building Materials.

REFERENCES

Harmathy T.Z.,"Determining the temperature history of concrete constructions following fire exposure", Journal of the American Concrete Institute, No. 11, November 1968, pp. 959 - 964.

Handoo S.K.,Agarwal S.,and Maiti S.C," Application of DTA/TGA for the assessment of fire damaged concrete structures", Proceedings of 8th National Seminar on Thermal Analysis, 1991, Bhubneshwar, India.

NCB projectreport,"Investigation on the fire damage to a factory building", June, 1987, (unpublished)

NCB project report,"Investigation on fire damage to a auditorium building", May, 1993. (unpublished)

Neville A.M.,"Properties of Concrete,4th Ed.,1995,The English Language Book Society and Pitman,pp.385-390.

Orchard D.F.,"The properties of cement and concrete", Concrete Technology,Vol.1,1979 Applied Science Publishers Ltd.,London, pp. 317 -328.

Raina S.J.,Vishwanathan V.N. and Ghosh S.N, "Instrumental techniques for investigation of damaged concrete",Indian Concrete Journal, Vol. 52, 1978, pp. 147-149.

MICROSTRUCTURAL CHANGE OF CALCIUM SULPHOALUMINATE CEMENT PASTE DUE TO TEMPERATURE

Choon-Keun PARK, Byung-Kwon KIM, Sung-Yoon HONG, Gyoo-Youn SHIN and Hee-Kap OH
Research Center of Ssangyong Cement Ind. Co., Taejon 305-345, Republic of Korea

ABSTRACT

Ettringite formed from C_4A_3S and/or calcium sulphoaluminate cement loses water in its structure when heat was applied. The ettringite changes to amorphous phase at greater than 120°C, even though the framework of ettringite texture still remains at above 400°C. The amorphous calcium sulphoaluminate phase decomposes above 600°C, forming C_4A_3S, $CaSO_4$ and CaO. The dehydration causes changes in microstructure and specific surface area of ettringite.

INTRODUCTION

Calcium sulphoaluminate cement (hereafter CSA cement), comprising calcium sulphoaluminate, calcium silicate and calcium sulphate, has many desirable properties, such as high early strength development, less drying shrinkage, good durability etc. Calcium sulphoaluminate mineral, C_4A_3S ($4CaO \cdot 3Al_2O_3 \cdot SO_3$), reacts with water and forms ettringite at an early hydration stage. The ettringite, $3CaO \cdot Al_2O_3 \cdot 3CaSO_4 \cdot 31\text{-}32H_2O$, causes high early strength development and expansion of hardened structure.

Many researches have been conducted to produce the C_4A_3S and explore its properties.

Teoreanu and Georgescu (1988) studied the C_4A_3S - $CaSO_4$ - CaO - H_2O system and suggested that the hydration rate of C_4A_3S would depend on concentrations of Ca^{++}, SO_4^{--} and chemically bonded water in the calcium sulpoaluminate hydrate also would vary with these ion concentrations. The ettringite structure has also been reported that combined water molecules are dependent on environmental conditions, such as $Ca(OH)_2$, $CaSO_4$ atmosphere by Bannai and Nakakawa(1968). They suggested that the ettringite would be similar to zeolitic structure. The ettringite contains zeolitic water in the channel of column of its structure and the zeolitic water is evaporable(Moore and Taylor, 1970). The status of water plays an important role to develop physicomechanical properties and durability of the hardened cement structure.

In this paper, calcium sulphoaluminate mineral and calcium sulpho-aluminate cement containing calcium sulphoaluminate, calcium silicate, calcium aluminoferrite and calcium sulphate were hydrated, and status of water and microstructural change of hydrates due to temperature up to 1000 °C were investigated.

EXPERIMENTAL

Materials

The calcium sulphoaluminate mineral was prepared with molar mixes corresponding to C_4A_3S using pure grade chemicals, $CaCO_3$, Al_2O_3 and $CaSO_4$. The mixes were sintered at 1280 °C for 3 hours and the sintered specimens were ascertained to be composed of C_4A_3S by using the XRD method. The CSA cement comprising 60% C_4A_3S, 18% C_2S, 6% C_4AF and 16% $CaSO_4$, was synthesized at 1300 °C for 3 hours.

Specimen preparation and experiment

Pure ettringite was prepared with molar mixes corresponding to $3CaO \cdot Al_2O_3 \cdot 3CaSO_4 \cdot 32H_2O$ using synthesized C_4A_3S, pure grade CaO, $CaSO_4$ and water as shown equation (1) in the later Ettringite part. Specimens were prepared at W/C=0.4 and cured at 20°C in a constant humidity cabinet with R.H 90% for characterizing properties. The status of water in specimens was analyzed using a weight loss by heat treatment method and DT-TGA. Hydrates and heat treated specimens were examined by means of XRD, BET, and SEM for investigating structural change.

RESULTS AND DISCUSSION

Hydration

Figure 1 shows the XRD patterns of hydrated specimens made with CSA cement as a function of curing time. The main reactant, C_4A_3S, decreases with the curing time and remains as an unhydrated form until 28 days even though the intensity of the XRD peak as much decreased, compared with the early hydration time. At an early hydration time C_4A_3S would be reacted with Ca^{++}, SO_4^{--} in aqueous solution, resulting in forming ettringite (AFt), since Ca^{++} and SO_4^{--} are abundant around C_4A_3S particles, and monosulphate (AFm) is identified after 3 days.

Figure 2 presents results of DT-TGA of specimens hydrated for 7 days. Ettringite which was prepared with C_4A_3S, $CaSO_4$, CaO and water shows one big endothermic peak around 130 °C and another very broad endothermic peak around 270 °C. But CSA cement hydrate specimen give three distinguished endothermic peaks, around 130 °C, 200 °C and 270 °C. The first endothermic peak is attributed to decomposition of ettringite, and the second endothermic peak is associated with decomposition of ettringite and calcium monosulphate hydrate, and the last endothermic peak is due to the decomposition of OH^- group from the framework of ettringite and monosulphate hydrate (Bannai et al., 1968; El-Didamony, 1980).

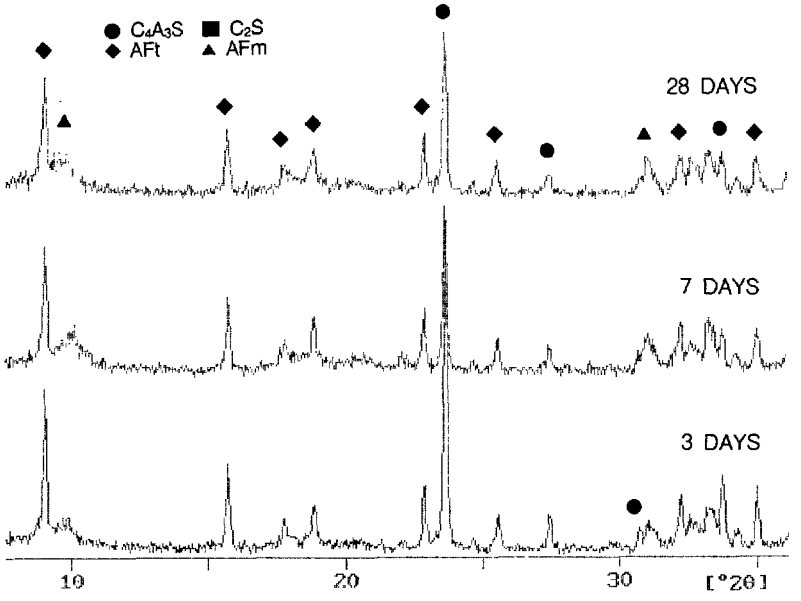

Figure 1. XRD patterns of CSA cement hydrates as a function of curing time. AFt : Ettringite, AFm : Monosulphate

Ettringite

When calcium ion and sulfur ion present in solution, the C_4A_3S reacts with these ions to form ettringite. In the study, the C4A3S was hydrated as follows.

$$4CaO{\cdot}3Al_2O_3{\cdot}SO_3+8CaSO_4+6CaO+96H_2O \text{ in aq. } \longrightarrow 3[3CaO{\cdot}Al_2O_3{\cdot}3CaSO_4{\cdot}32H_2O] \quad \text{--- (1)}$$

Moore and Taylor (1970) suggested the structure of ettringite as shown in Figure 3. Ettringite has the formula $\{Ca_6[Al(OH)_6]_2{\cdot}24H_2O\}{\cdot}3(SO_4){\cdot}2H_2O$, the columns $\{Ca_6[Al(OH)_6]_2{\cdot}24H_2O\}^{6+}$ are based on $[Al(OH)_6]^{3-}$ octahedral running along c axis, each $[Al(OH)_6]^{3-}$ linked to each of its neighbors through three Ca ions which are eight-coordinated by four H_2O molecules and four OH^- groups. There are two H_2O molecules and three SO_4 in the channels of the $[Al(OH)_6]^{3-}$ columns (Wang et al., 1986). Table 2 shows the weight loss and d value for (10·0) plane of hexagonal ettringite due to dehydration. The ettringite loses its combined H_2O molecules rapidly until 100 °C, and then gradually until 270 °C. The combined H_2O molecules were almost decomposed at about 600 °C.

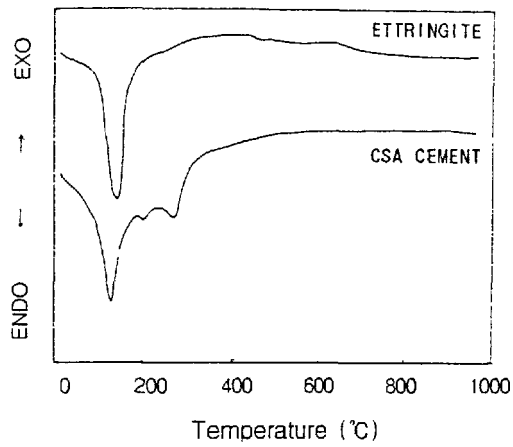

Figure 2. DTA results of ettringite and CSA cement hydrate.
(hydrated at 20 °C for 7 days.)

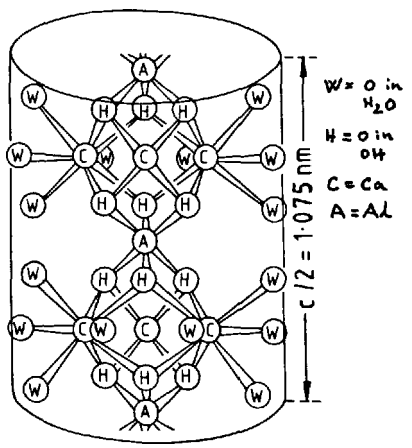

Figure 3. Part of single column of ettringite gite crystal structure. (Moore and Taylor)

Table 1. Weight loss and change of d value of ettringite as a function of temperature applied to heat.

Items	Trapped water	Temperature (°C) 20	40	60	80	100	110
Wt. loss	4.1	-	3.1	10.6	14.7	26.7	31.1
Combined H_2O mole		31.7	28.6	20.3	16.9	8.7	6.3
Ettringite d value* (A°)		9.7102	9.7131	9.7313	9.7488	9.7588	9.7708

Items	Temperature (°C) 120	190	230	270	400	600	800	1000
Wt. loss	35.0	37.9	39.9	41.9	43.5	44.1	45.0	45.1
Combined H_2O mole	4.3	3.0	2.1	1.3	0.6	0.4	-	-

* hkil = (10·0)

Decomposition of combined H_2O molecules causes the structural change of ettringite texture. The d value of hexagonal structure of ettringite increases until 110 °C. The parameter a of hexagonal crystal increases from 9.71 A° to 9.77 A° as the combined H_2O molecules decompose from 31.7 to 6.3. At temperature greater than 120 °C the ettringite crystal changes to an amorphous phase. The change of ettringite structure which had been characterized by XRD method was given in Figure 4. The dehydration of ettringite causes characteristic XRD peak position shift to low angle (refer to the change of d value in Table 2). This result is accounted that the framework of ettringite changes with dehydration. At 120 °C or higher temperature the characteristic peak of ettringite completely disappeared even though calcium sulphoaluminate hydrate still contain little amount of water in the structure. The remained water seems to be water of octahedral $[Al(OH)_6]^{3-}$ differently from the decomposed water below 120 °C. As the temperature increases greater than 600 °C no portlandite is identified and the amorphous calcium sulphoaluminate start decomposing, and begins to form $CaSO_4$. At temperature greater than 800 °C the amorphous phase of dehydrated calcium sulphoaluminate vigorously decomposes, so that $CaSO_4$, CaO and C_4A_3S, which are start materials in this system, increase quantitatively.

When the combined H_2O molecules decomposes, change of specific surface area of ettringite accompanied. The change of specific surface area in ettringite as a function of temperature

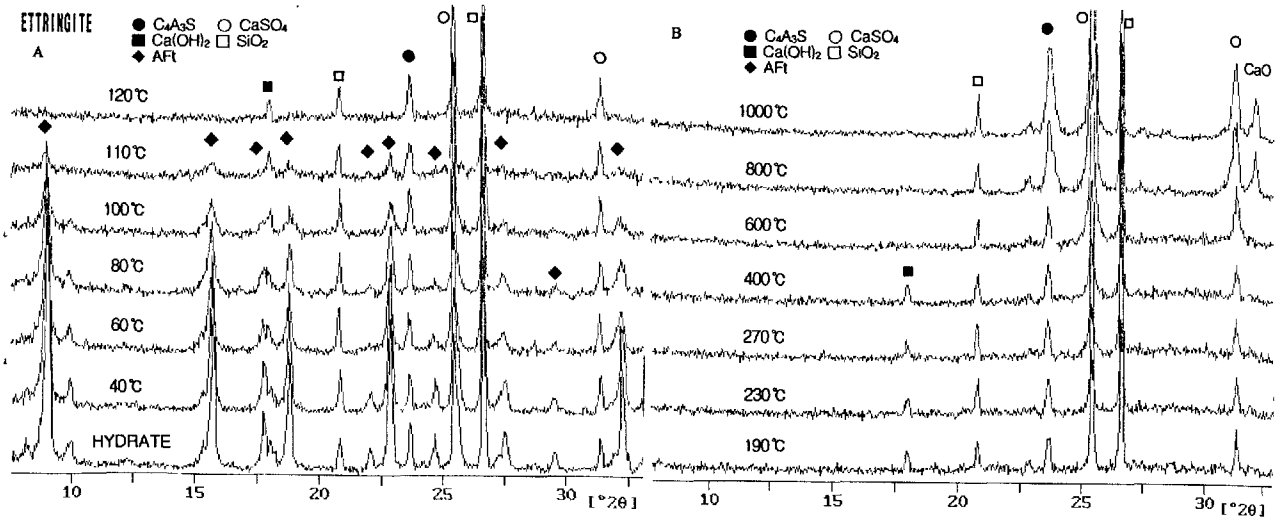

Figure 4. X-ray diffraction patterns of ettringite as a function of temperature applied to heat. A : XRD patterns from room temperature to 120 °C, B : XRD patterns from 190 °C to 1000 °C. AFt = Ettringite

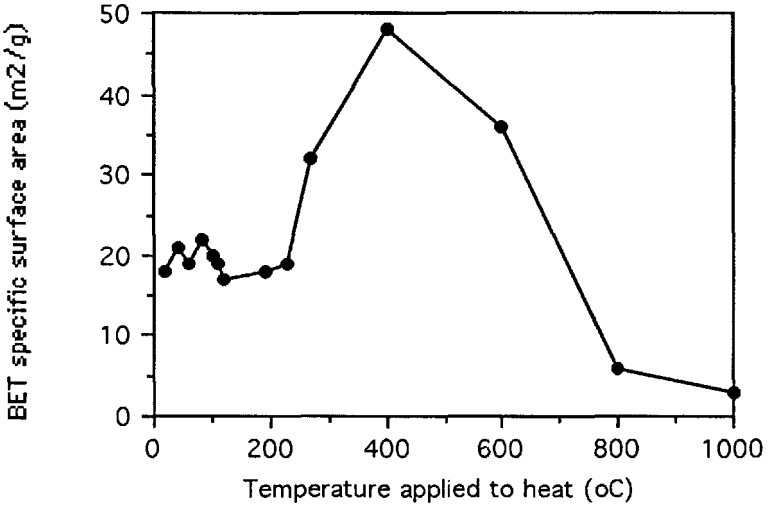

Figure 5. Specific surface area of ettringite as a function of temperature applied to heat measured BET method using N_2 gas.

measured by BET using N_2 gas is given Figure 5. BET specific surface area slightly increases until 100 °C and then decreases about 18 m^2/g until about 200 °C. At greater than 200 °C the BET specific surface area abruptly increases and presents maximum value at 400 °C. And then, the BET specific surface area value decreases steeply to 1000 °C which shows minimum BET specific surface value. The result agrees well with the result of weight loss in ettringite structure. That is, when combined water in the channels and columns between octahedral $[Al(OH)_6]^{3-}$ decompose no big structural change occurred [$2H_2O$ and $24H_2O$, respectively in the ettringite formula $\{Ca_6[Al(OH)_6]_2 \cdot 24H_2O\} \cdot 3(SO_4) \cdot 2H_2O]$, but decomposition of the OH^- group of the base framework $[Al(OH)_6]^{3-}$ causes microstructure change.

Figure 6 shows the microstructure change of ettringite due to dehydration observed by scanning electron microscope. The pure ettringite is a long needlelike crystal at room temperature, but the long axis become short as the temperature increased to 80 °C. No big shape change of dehydrates occur until 190 °C, but the radius and length are more shorten at about 400 °C. Therefore, it seems that the number of short needlelike particle and the amount of micropore to be maximized at

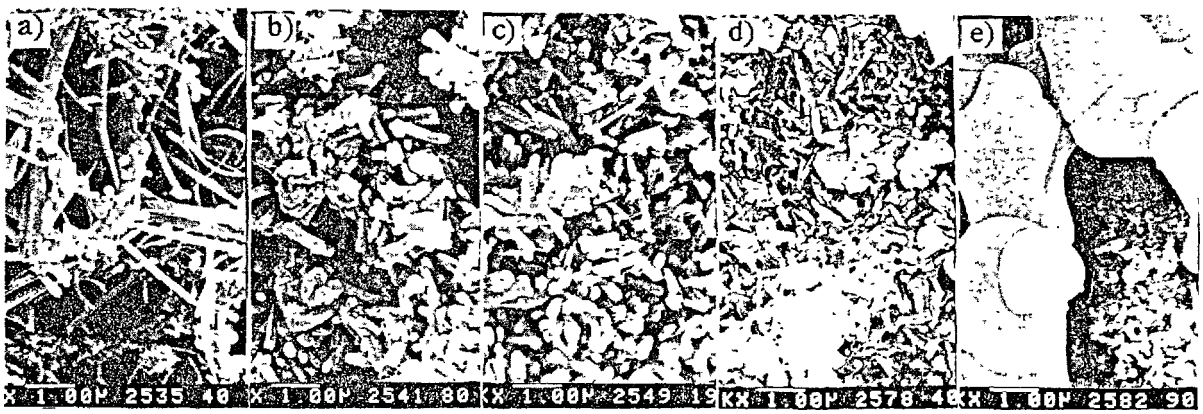

Figure 6. SEM photographs of ettringite paste as a function of temperature applied to heat
a) 40 °C b) 80 °C c) 190 °C d) 400 °C e) 900 °C

about 400 °C. As the temperature increases needlelike texture collapse. At 900°C, sintered grains observed,which are grown to few micrometers. These results related to the trend of BET specific surface area changes.

Cement hydrate

Figure 7 shows the weight loss and BET specific surface area as a function of temperature for the calcium sulphoaluminate cement paste. The trend is similar to that of ettringite. The water decomposes abruptly until 270 °C and then gradually to 1000 °C.
The decomposition of water in the cement paste causes microstructure change, resulting in showing different BET specific surface area as shown in Figure 7(B).

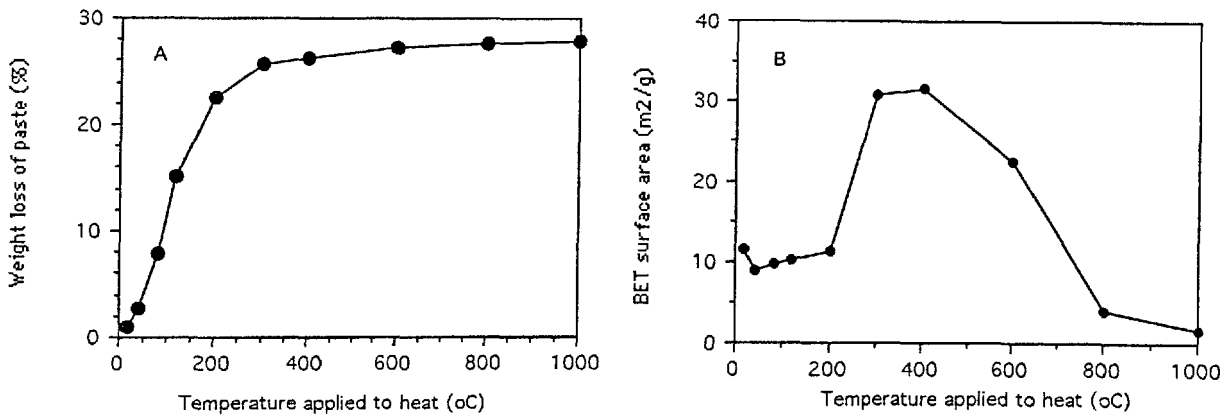

Figure 7. Weight loss and BET specific area of CSA cement paste cured for 7 days as a function of temperature. (A: Weight loss, B: BET specific surface area)

Figure 8 shows the XRD patterns of cement pastes hydrated for 7 days as a function of temperature. The trend of decomposition of cement paste is similar to that of ettringite. The ettringite formed in this system is considered as a solid solution of ettringite since the d value of XRD characteristic peak (10·0) is 9.748 A°, compared with d = 9.710 A° of pure ettringite as shown in Table 2. The ettringite decomposes H_2O molecule with increasing temperature, resulting in changing its structure from hexagonal crystal to amorphous phase. The ettringite, main hydrate of cement paste, appears at less than 120 °C. At greater than 120 °C no crystalline ettringite is noted even though calcium sulphoaluminate hydrate still contains little amount of water in the structure. When the remained water decomposes at high temperature, the BET specific surface area increases because the decomposition of water offer more spaces which small size N_2

gas can enter into. In this system, monosulphate hydrate is identified, and unidentified phase is noted at around d=8.0 A° in the specimens heated at 80 °C and 120 °C. This unidentified phase, which seems to be modified calcium sulphoaluminate hydrate with 7~10 mole H_2O formed from monosulphate (Turriziani, 1964), appears and increases its intensity of XRD peak as ettringite and monosulphate hydrate decrease. As the temperature increases greater than 600 °C the calcium sulphate forms due to the decomposition of calcium sulphoaluminate hydrate. At greater than 800°C the increases in quantity. This sintering process decreases BET specific surface area.

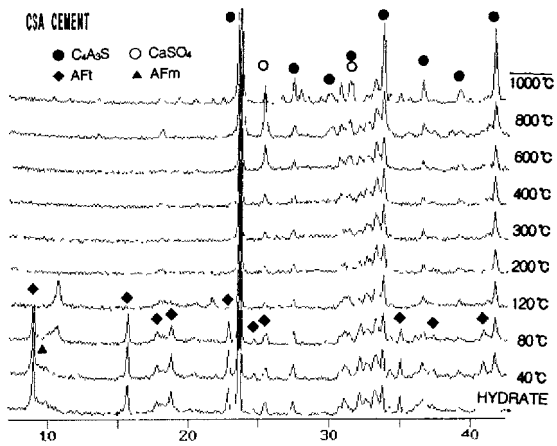

Figure 8. XRD patterns of CSA cement hydrates as a function of temperature applied to heat.

SUMMARY AND CONCLUSIONS

1. The ettringite formed from the C_4A_3S-CaO-$CaSO_4$-H_2O system contains 31.7 combined H_2O moles. The combined H_2O moles are decomposed from the structure of ettringite with increasing temperature.

2. When decomposition occurs, the water bound in the channel and column between octahedral $[Al(OH)_6]^{3-}$ dehydrates first, and then the OH- group of the base $[Al(OH)_6]^{3-}$ framework dehydrates. Furthermore, the ettringite changes its structure from crystal to amorphous phase at greater than 120 °C.

3. The amorphous phase of calcium sulphoaluminate hydrate decomposes at greater than 600 °C, resulting in forming CaO and $CaSO_4$. At 800 °C C_4A_3S forms from ingredients which were decomposed of calcium sulphoaluminate hydrates.

4. The dehydration causes change the specific surface area of ettringite. The BET specific surface area slightly changes until 200 °C, and then abruptly increases to 400 °C. At greater than 400 °C the BET specific surface area decreases.

REFERENCES

Bannai, H. and Nakakawa, K. , "Thermal Properties of Ettringite", Gypsum and Lime, No. 97, pp. 253-259, 1968

El-Didamony, H.,"Application of Differential Thermogravimetry to The Hydration of Expansive Cement Pastes", Thermochimica, Vol. 35, pp. 201-209, 1980

Moore, A. E. and Taylor, H. F. W. , "Crystal Structure of Ettringite", ACTA. Cryst., B266, pp.386, 1970.

Teoreanu, I. and Georgescu, M., "Processes in The System C_4A_3S-CaO-$CaSO_4 \cdot 2H_2O$-H_2O", Il Cemento, No. 4, pp. 267-276, 1988

Turriziani, R. and Taylor, H. F. W, " The Calcium Aluminate Hydrates and Related Compounds", The Chemistry of Cements, Academic press, 1964, Vol. I, Chapter 6, pp. 260-263.

Wang, S. B., Ji, S. X., Liu, Y. J. and Hu K. Y., "Effect of Alkali on The Expansive Properties of Sulphate Cement Pastes", 8th ICCC, Vol. IV, pp. 301-305, 1986.

EFFECT OF TEMPERATURE ON CHLORIDE INGRESS AND CHLORIDE BINDING IN HARDENED CEMENT PASTE

Claus K. LARSEN, Norwegian Road Research Laboratory, Oslo, Norway
Josef TRITTHART, TVFA, University of Technology, Graz, Austria

ABSTRACT: Pure and blended cement pastes were stored in chloride solutions at 5, 20 and 40°C for up to 100 days. Chloride ingress and chloride binding decreased as the temperature increased from 5 to 20°C. The effects were reversed from 20 to 40°C. The observed effects were most likely complex interactions between temperature, degree of hydration and microstructure. Silica fume decreased chloride ingress and binding.

Key-words: Chloride Binding, Pore solution, Temperature, Silica fume

INTRODUCTION

Chloride initiated reinforcement corrosion is the predominant form of concrete deterioration in most highway bridges. Chloride sources are usually sea spray or de-icing salt. In cold climates where de-icing salts are used, concrete is in many cases exposed to chlorides only at low temperatures. This is the case, for instance, in Central Europe. In coastal areas, concrete can be exposed to chlorides at relatively high temperatures during summer. In the Scandinavian countries, with both cold winters and warm summers, concrete along the coast is exposed to chlorides at both low and high temperatures. Due to solar radiation temperatures on the concrete surface can be relatively high. Most of the research work on chloride ingress and binding is, however, done at room temperature.

The present work is a collaboration between the Norwegian Road Research Laboratory in Oslo and TVFA at TU-Graz in Austria. The reason for this collaboration is partly based on different opinions regarding the effect of silica fume upon chloride binding in blended cements (Byfors, Hansson and Tritthart, 1986; Page and Vennesland, 1983).

EXPERIMENTAL

Cement

Two types of cement were used, one Austrian and one Norwegian. The Austrian cement EZ375 is a normal OPC while the Norwegian HS65 is a high strength low alkali OPC. They are both commonly used in their respective countries. Cement composition is shown in Table 1.

Table 1 Cement composition, in %

	SiO_2	Al_2O_3	Fe_2O_3	TiO_2	CaO	MgO	K_2O	Na_2O	SO_3	$L.o.i.$
EZ375	19.41	4.93	2.86	0.32	61.55	1.85	1.79	0.32	3.0	3.09
HS65	21.41	5.57	3.34	0.35	63.27	1.40	0.79	0.33	2.8	0.98
"Bouge" composition	C_3S	C_2S	C_3A	C_4AF						
EZ375	57.2	12.5	8.2	8.7	Calculated values					
HS65	44.6	27.7	9.1	10.2	Calculated values					

Silica fume

Silica fume (SF) from Elkem AS in Norway was used. The chemical composition of the SF is not exactly known, but on average it contains 95% SiO_2 and 2% C. Surface area as measured by N_2-sorption was 16.3 m^2/g.

Sample preparation

The cement pastes were prepared using a high-speed mixer (8000 rps), to ensure a complete dispersion of cement and SF. Codes for the pastes used are listed in Table 2. SF dosage, when used, was 10% of binder weight as cement replacement. All pastes had a water binder ratio (w/b) of 0.60. After mixing for four minutes, small plastic bottles (100 ml, Ø50 mm) were filled and rotated at room temperature for 24 hours to prevent segregation. Half of the samples were then wet-cut in 5 mm thin discs and without drying immersed in the storing solutions. The second half were stored at 21°C for 27 more days prior to cutting and immersion.

Table 2 Paste codes

Paste	Cement	SF
PN-	Norw.	-
PNN	Norw.	Norw.
PA-	Austr.	-
PAN	Austr.	Norw.

At each exposure temperature; 5±0.2, 20±1 and 40±2 °C; two different chloride solutions were used. Soft chloride-free tap water and NaCl were used to make the solutions that had chloride concentrations of 18 and 54 g/l. The discs were placed on racks with a spacing of 10 mm, to ensure that each disc was surrounded with an adequate amount of chloride solution. The volume of solution in each container was about seven times greater than the paste volume. All storing solutions were stirred from time to time to ensure an even chloride concentration within the container. Chloride concentrations in the solutions were checked regularly and found to be sufficiently constant.

Sets of two discs made up the test samples. One disc was used for pore solution expression, the other one for total chloride determination. All discs were removed from the storing solution just before testing. They were kept wet in a plastic bag and, immediately before testing, all excess solution was wiped off using a clean wet cloth.

Pore solution expression

To determine chloride concentrations in the pore solution of the pastes, the pore solution was expressed. The technique described by Tritthart (1991) was used. The disc to be tested was broken in about 1 cm big pieces and put into the test cylinder, with as little contact with the air as possible. Each disc "produced" about 1.5 ml pore solution, which was collected in small glass or plastic containers, and sealed with a cap. Chloride concentrations were determined using automatic potentiometric titration with 0.01M $AgNO_3$. This was done the same day the pore solution was expressed.

Total chloride determination

The discs were dried at 105°C for one day. They were then ground to a fine powder, passing 9μm sieve, to ensure a total decomposition in the heated concentrated acetic acid. Chloride concentration was determined using the procedure mentioned in the section above. Parallel control tests were made using nitric acid to check that the acetic acid was able to decompose the paste powder completely. All tests showed that there were practically no differences. Acetic acid was preferred because nitric acid sometimes caused difficulties in the titration. The reasons for this are not known.

XRD and electron microprobe analysis

The discs investigated with XRD and electron microprobe were taken from their respective solutions after 37 days of storage. After drying over Silica-gel ("blue gel") in vacuum for two days, the XRD samples were ground and sieved (9 μm).

The samples for EDXA were cut to ensure a plain clean surface for the investigation. To prevent the chlorides from being washed out during cutting, no cooling water was used. All samples were then dried over P_2O_5 in vacuum at room temperature for two more days before investigation. XRD scans were performed using the Cu-anode, a count time of 2.0 seconds per step, a step size of 0.02° and scanning from 5 to 42° (2θ). A Philips SEM 505 electron microscope and the EDAX-DX4 (ultrathin window) X-ray spectrometer was used for the electron microprobe analysis. The samples were coated with a thin layer of carbon and count-time was 100 seconds.

Chloride profiles through the discs were determined by scanning along lines, four mm long and one μm wide, parallel to one of the exposed surfaces, as shown in Fig 1. The outer scan was approximately 0.05 mm from the one exposed surface, with the following scans in 0.5 mm steps into the center of the disc. It was assumed that the chloride profile would be symmetrical around the center line, leaving half the profile unexamined. In three cases the whole profile was examined, with the conclusion that this assumption was correct.

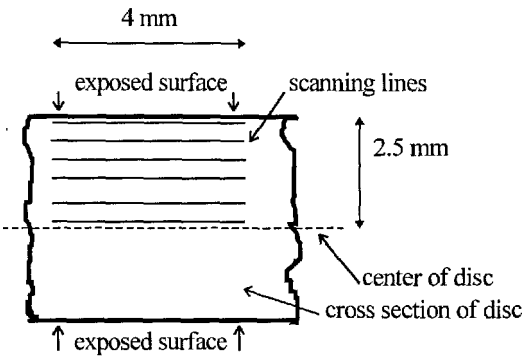

Figure 1 Setup for chloride profile

RESULTS AND DISCUSSION

"State of equilibrium"

When considering the inaccuracy of the microprobe analysis, four of the seven investigated discs had gentle chloride profiles (Fig 2). This indicates that the chloride ingress was more or less homogeneous through these discs. The two PA- pastes and one of the PN- pastes (20°C, 1d), however, had a steeper gradient. The "state of equilibrium," that is the difference between chloride content at the surface and in the center of the disc, is therefore questionable in these three discs. It must be pointed out that these investigations were done on samples exposed for 37 days. It is therefore likely that the pastes after exposure for 100 days, even for the PA- samples, will be close to equilibrium, in the sense of practically no chloride gradient through the disc.

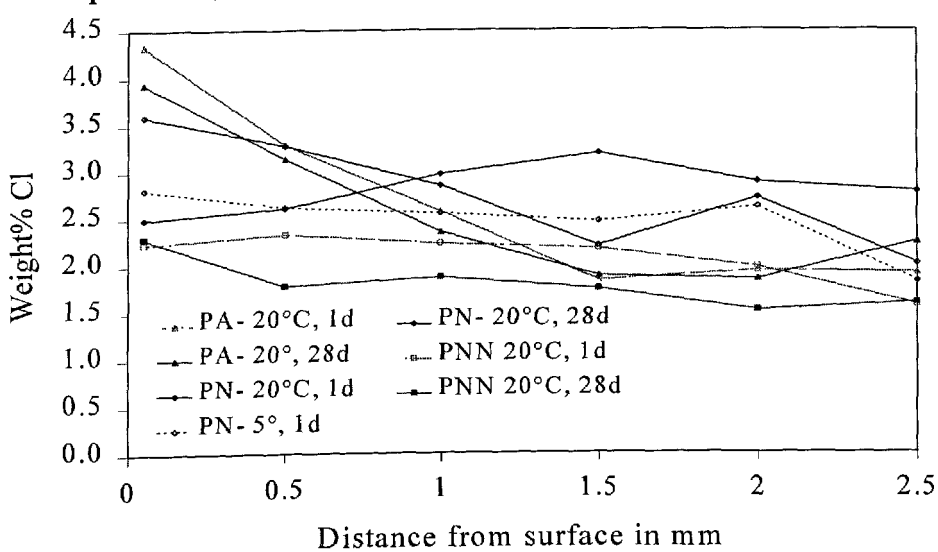

Figure 2 Chloride profile through the disc. Pastes cured for one and 28 days before exposed in a 18 g/l chloride solution for 37 days.

Total chloride content

All individual results from the total chloride determination are given in Table 3. Generally, the chloride ingress was highest in the pure cement pastes and lowest in the pastes containing SF. With decreasing chloride content the general ranking was: PA-, PN-, PAN and PNN.

Table 3 Total chloride content in % of dry sample mass.

Sample	Curing	Exposure time	Exposure solution					
			18 g/l			54 g/l		
			5°C	20°C	40°C	5°C	20°C	40°C
PN-	1 day	37 d	2.50	2.20	2.18	3.61	3.43	3.85
		100 d	2.80	2.86	2.87	4.25	3.48	4.11
	28 days	37 d	1.94	1.91	2.04	3.19	3.02	3.61
		100 d	1.97	1.92	2.38	3.64	3.27	3.84
PNN	1 day	37 d	2.48	1.86	1.98	3.55	3.09	3.23
		100 d	2.56	2.68	1.99	4.10	3.19	3.30
	28 days	37 d	1.53	1.50	1.66	2.66	2.65	2.98
		100 d	1.65	1.58	1.95	3.61	2.84	3.31
PA-	1 day	37 d	2.48	2.39	2.62	3.66	3.62	4.00
		100 d	3.02	2.87	2.56	4.92	3.83	5.22
	28 days	37 d	1.82	2.13	2.31	3.34	3.56	4.18
		100 d	2.09	2.10	2.64	3.81	3.80	4.90
PAN	1 day	37 d	2.49	1.91	1.98	3.54	3.31	3.56
		100 d	2.53	2.84	2.26	4.28	3.60	3.74
	28 days	37 d	1.71	1.56	1.83	3.31	3.13	3.05
		100 d	1.94	1.79	2.34	4.07	3.31	3.73

Statistically one can calculate the effect of each experimental parameter on the chloride ingress. Using the method described for a two-level factorial design (Box, Hunter and Hunter, 1978) the results are summarised in Table 4. The listed effect is an average response for the indicated parameter changing from one level to the other over all conditions of the other experimental parameters.

Table 4 Effect of the experimental parameters on total chloride content. % of dry sample mass

Sample combinations			Parameter changed					
		From:	5°C	20°C	HS65	0% SF	18 g/l	37 days exp.
		To:	20°C	40°C	EZ375	10% SF	54 g/l	100 days exp.
Curing time	Temperature °C	Grand average*)						
1 day	5 and 20	3.12	-0.35		0.34	-0.24	1.19	0.48
1 day	20 and 40	3.02		0.14	0.43	-0.47	1.28	0.39
28 days	5 and 20	2.57	-0.14		0.41	-0.29	1.50	0.28
28 days	20 and 40	2.71		0.42	0.52	-0.52	1.47	0.29

*) Average of total chloride content for all parameters for the indicated sample combinations.

As an example, pastes cured for 28 days and exposed at 5 and 20°C have an average chloride content of 2.57% of dry sample mass. For this combination of samples the effect of replacing 10% of the binder content with SF was that the chloride content decreased on average 0.29% of dry sample mass (minus means a decreased chloride content in the pastes).

It is interesting to notice that for paste cured one day and exposed 37 days, as presented in Fig 3, all samples at 5°C, independent of type of binder and exposed to the same concentration, had about the same chloride content. The reason for this is most likely the slow cement hydration at low temperature, so that the various binders approximately hydrated equally. At the higher temperatures, the hydration was accelerated. The binders therefore hydrated differently and caused the distinct chloride content between each paste. This is seen by the scattered curves.

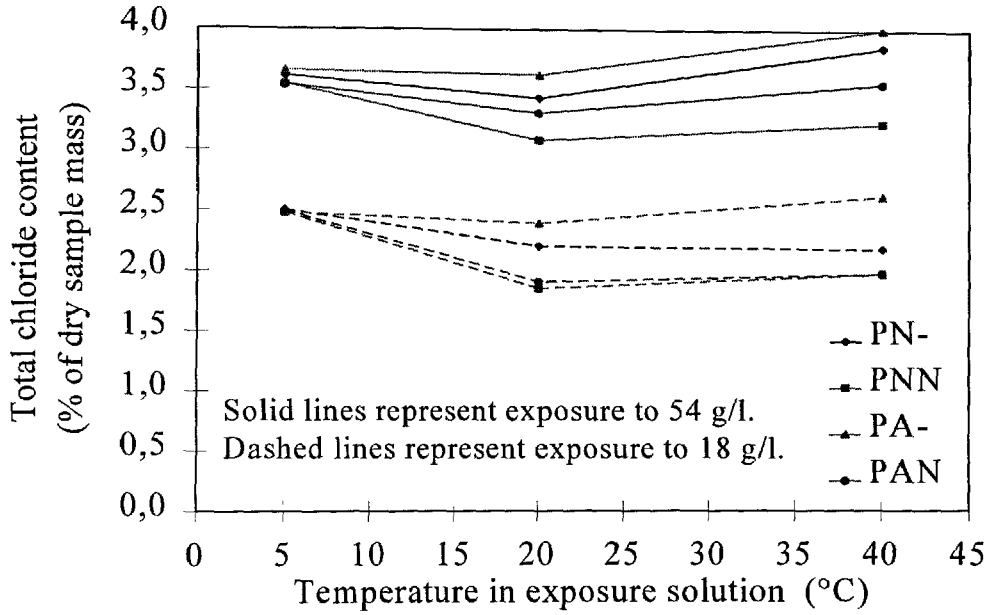

Figure 3 Total chloride content versus exposure temperature.
Paste cured for one day and exposed for 37 days.

When looking at the effect of temperature on chloride content, the picture seems a bit confusing. It is, however, obvious from Table 4 that an increase from 5 to 20°C decreased the chloride ingress. This can be seen as negative effects for both one day (-0.35) and 28 days curing (-0.14). The effect for samples cured one day was 2.5 times greater than for samples cured 28 days. One reason for this is probably that the pastes cured for one day at 20°C developed a denser microstructure faster than at 5°C. This caused, in spite of the increased temperature itself, less chloride diffusion. Another reason might be a shift in the adsorption/desorption equilibrium as the temperature increased. Besides a shift of the equilibrium towards desorption caused by the increased kinetic ion energy, a shift in the same direction is accompanied by the decreased (positive) ζ-potential of the hydrated cement (Ludwig and Singh, 1986) as temperature is increased. Less chloride ions are therefore adsorbed on the surface of the hydrated cement as the temperature increases. On the other hand the surface area of the samples cured for one day, must be much higher at 20 than at 5°C, due to the higher degree of hydration. It is therefore hard to believe that the observed differences are caused by adsorption effects only. Another factor of greater influence on the chloride uptake is the chloride concentration of the pore solution. This will be discussed later. For the only disc exposed at 5°C investigated with EDXA, the observed chloride content at the surface was lower than that of the corresponding disc exposed at 20°C, although the total chloride content of the 5°C sample was higher (Tab 3). In the centre of the disc the increased temperature had little effect.

From Table 4 it is also clear that an increased temperature from 20 to 40°C led to an increased chloride ingress. The average responses for the samples cured for one and 28 days, were 0.14 and 0.42, respectively. The increased chloride content was 3 times greater for the samples cured for 28 days. A possible reason might be that hydration at 40°C, after one day pre-curing, densified the microstructure even more than at 20°C. At 40°C the densified microstructure in the samples one day counteracted the effect of the increased ion mobility and thereby the diffusion rate of chlorides in the pastes. This is in agreement with Dhir et al. (1993). The pastes cured for 28 days were already well hydrated and had a highly developed microstructure when exposed in the chloride solutions. The increased temperature affected the microstructure insignificantly in these samples, so that the increased diffusivity was not counteracted. All this shows the strong influence of the microstructure of cement based materials upon chloride ingress, and it clearly points out that curing prior to exposure has a major influence on chloride uptake.

As expected, the use of SF decreased the chloride ingress. An increase in both exposure concentration and time, also as expected, increased the content of chlorides in the samples.

Chloride binding

The free chloride content was calculated using measured values of evaporable water (from the disc used for total chloride determination) and chloride concentration in the pore solution. The chloride binding was then found by subtracting the free content from the total content of chlorides. As for chloride ingress, the statistical effects on binding were calculated (Table 5).

Table 5 Effect of the experimental parameters on chloride binding. % of dry sample mass

Sample combinations			Parameter changed					
		From:	5°C	20°C	HS65	0% SF	18 g/l	37 days exp.
		To:	20°C	40°C	EZ375	10% SF	54 g/l	100 days exp.
Curing time	Temperature °C	Grand average*)						
1 day	5 and 20	1.57	-0.50		0.06	-0.28	0.05	0.11
1 day	20 and 40	1.38		0.11	0.28	-0.51	0.07	0.19
28 days	5 and 20	1.08	-0.01		0.30	-0.43	0.15	0.14
28 days	20 and 40	1.18		0.22	0.43	-0.53	0.16	0.14

*) Average of bound chloride content for <u>all</u> parameters for the indicated sample combinations.

A discussion of the chloride binding results is difficult as neither the chloride concentration of the pore solution nor the total chloride content was constant and thereby not directly comparable. The inaccuracy of the calculated binding values depend strongly on the chloride concentration of the pore solution as well as the amount of pore solution itself. However, as can be seen from Table 5, the chloride binding decreased on average from 5 to 20°C for the samples cured for one day and was practically unchanged for the samples cured for 28 days. From 20 to 40°C the binding increased. One would expect, in equally hydrated pastes, a decreased binding as the temperature is increased. The reasons for this are the decreased ζ-potential, as discussed before, and the decomposition of Friedels salt (Maslehuddin et al., 1996). Why the present results are in contradiction to this is possibly explained by the likely interactive effects as the degree of hydration, and thereby surface area and microstructure, is changed. These combined effects will probably affect the various binder types differently, and thereby causing an even more complex situation. Dhir et al. (1993) have also pointed out that "the effects of temperature on different binder types is not consistent."

Further, the chloride binding was higher in the EZ375-containing pastes, in the samples exposed to the highest chloride concentration and in samples exposed for 100 days. The use of SF decreased the chloride binding. The latter is in agreement with the findings of Page and Vennesland (1983), but in contradiction to Byfors et al. (1986). The reason Byfors et al. found an increased chloride binding in SF-containing pastes, might be in connection with the particular cement used (a Swedish OPC). Pure cement pastes made of this cement, had a much higher chloride concentration in the pore solution than pastes made of the other two OPCs investigated (an Austrian and a Danish). The actual concentration was in the range normally obtained in pastes made of sulphate resistant cement (Tritthart, 1989).

Chloride concentration of the pore solution

All individual chloride concentrations are given in Table 6.

Table 6 Chloride concentration in pore solution. Concentrations in ppm

Sample	Curing	Exposure time	Exposure solution					
			18 g/l			54 g/l		
			5°C	20°C	40°C	5°C	20°C	40°C
PN-	1 day	37 d	26200	19100	20300	57450	53200	53100
		100 d	22950	31300	23100	63200	50100	55050
	28 day	37 d	18900	18900	20200	50700	50700	52300
		100 d	20900	18900	22250	54650	52800	57450
PNN	1 day	37 d	25000	18200	20400	53900	48800	53700
		100 d	23450	30100	22450	65250	54400	59000
	28 day	37 d	18200	17000	19500	50000	46800	51100
		100 d	21900	18400	23500	59200	53150	57600
PA-	1 day	37 d	24350	20450	20550	53300	50800	53600
		100 d	21900	30000	20900	-	53250	56450
	28 day	37 d	18600	18800	20400	50300	48500	50100
		100 d	20000	18350	23850	58550	50600	59100
PAN	1 day	37 d	23700	18600	21350	53500	52000	54700
		100 d	20850	29200	23500	63250	53700	57850
	28 day	37 d	18200	18600	19900	53200	50800	49800
		100 d	20950	19150	23050	61550	53350	58850

Surprisingly, the chloride concentration in the pore solution was found to be higher at 5°C than at both 20 and 40°C, in the samples cured for one day and exposed for 37 days in the 18 g/l solution (solid lines in Fig 4). A possible explanation of this observation is that equilibrium had not yet been reached in 37 days. Another reason might be that weakly bound chlorides at 5°C were pressed out during pore expression. The picture seems more complex when considering the same samples after 100 days of exposure (dashed lines in Fig 4). Now, the concentrations at 5 and 40°C were approximately equal, but there had been a major increase in the 20°C-concentration. The reason cannot be explained at the moment, but the above discussed interactive effects might be important in this matter. However, it must be pointed out that the chloride concentrations of the exposure solutions were checked regularly, and used-up chlorides replaced.

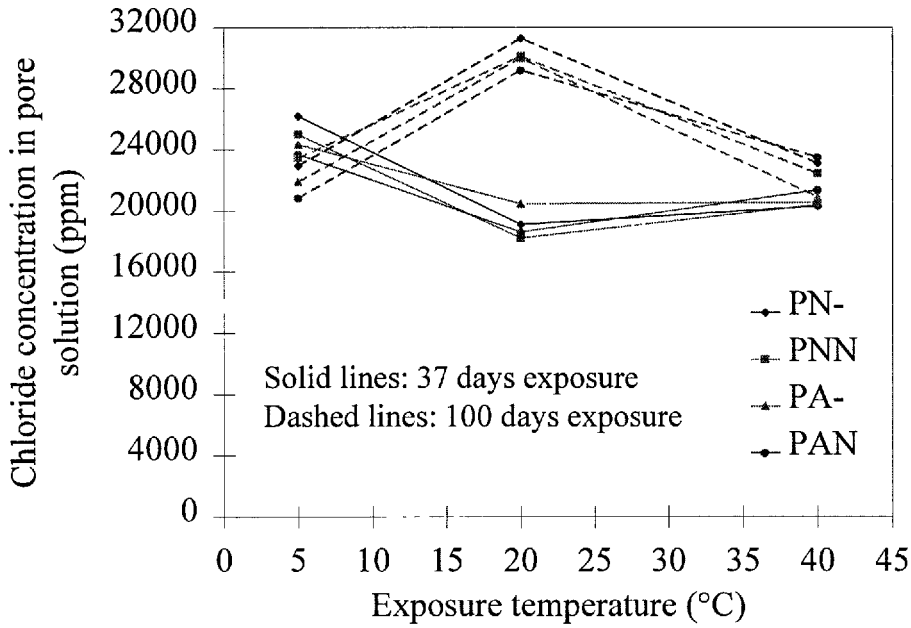

Figure 4 Chloride concentration in pore solution versus exposure temperature. Paste cured for one day and exposed in a 18 g/l solution.

XRD

The pastes made of Austrian cement contain more Friedel's salt than the pastes made of Norwegian cement. This can be seen in Figs 5 and 6. Friedel's salt can be identified as peaks at 11.2°, 22.8°, 30.9° and about 39° (2θ). This was not expected because the Norwegian cement contained a bit more C_3A than the Austrian. A possible reason for this might be that the amount of sample investigated was not completely the same. Other investigations not discussed in detail here, gave no indication that SF affects the formation of Friedel's salt. They showed further that longer curing before exposure to chlorides and higher chloride concentration, will tend to decrease the formation of Friedel's salt. These results were not significant, but there was a clear trend for curing time and a weak trend for concentration.

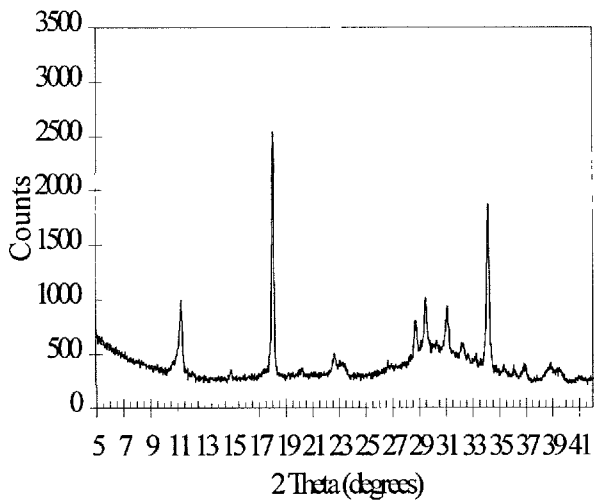

Figure 5 XRD-spectra from PA-. Exposed 37 days in 18 g/l at 20°C. Cured 28 days.

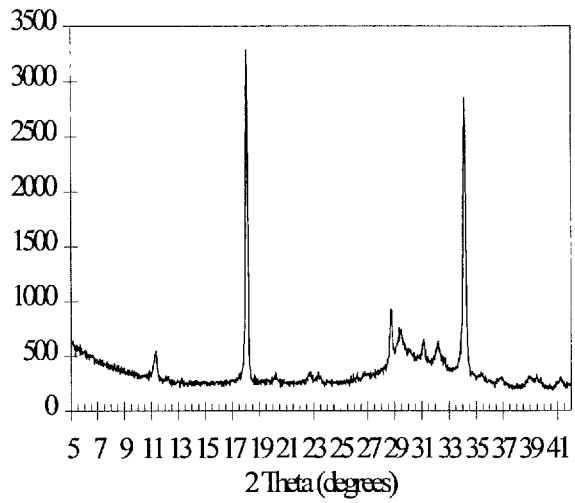

Figure 6 XRD-spectra from PN-. Exposed 37 days in 18 g/l at 20°C. Cured 28 days

SUMMARY AND CONCLUSIONS

In this investigation, the influence of temperature on chloride ingress and binding in pure and blended cement pastes was evaluated. The results showed that some of the 5 mm thin discs investigated with EDXA after 37 days exposure were not at equilibrium, in the sense of no chloride gradient through the disc. Both total chloride content and chloride binding decreased from 5 to 20°C and increased from 20 to 40°C. The observed effects were most likely complex interactions between temperature, degree of hydration and microstructure. Silica fume decreased chloride ingress and binding.

The results show the strong influence of microstructure on chloride ingress, and they clearly point out that curing, age and temperature have a major influence on the speed and degree of chloride uptake. It follows from the results that young concrete exposed to chlorides at low temperatures might experience not only a greater chloride uptake, but also a greater penetration depth. Further research is needed to clarify this.

ACKNOWLEDGEMENT

The present paper is part of the "OFU Bridge Repair Project" financed by the Norwegian Public Roads Administration (NPRA), Rescon AS and The Norwegian Industrial and Regional Development Fund (SND). The project is managed by NPRA.
The electron microprobe analysis was performed by energy-dispersive X-ray spectrometry (EDAX-DX4) at the Institute for Electron Microscopy at TU-Graz. This device was sponsored by the "Jubiläumsfonds der Österreichichen Nationalbank."

REFERENCES

Box, G.E.P., Hunter, W.G., Hunter, J.S., "Statistics for Experimenters," John Wiley & Sons, Inc., USA, 653 p., 1978.
Byfors, K., Hansson, C.M., Tritthart, J., "Pore Solution Expression as a Method to Determine the Influence of Mineral Additives on Chloride Binding," Cement and Concrete Research, V.16, 1986, pp. 760-770.
Dhir, R.K., Jones, M.R., Elghaly, A.E., "PFA Concrete: Exposure Temperature Effects on Chloride Diffusion," Cement and Concrete Research, V.23, No. 5, 1993, pp. 1105-1114.
Ludwig, U., Singh, N.B., "Kinetics and mechanism of alite hydration," Zement-Kalk-Gips, V.39, No. 12, 1986, pp. 688-692.
Maslehuddin, M., Page, C.L., Rasheeduzzafar, Al-Mana, A.I., "Effect of Temperature on Pore Solution Chemistry and Reinforcement Corrosion in Contaminated Concrete," Proc. of the 4th Int. Symposium on Corrosion of Reinforcement in Concrete Construction, Cambridge, 1996, pp. 67-75.
Page, C.L., Vennesland, Ø., "Pore Solution Composition and Chloride Binding Capacity of Silica Fume Cement Pastes," Materials and Construction, V.16, No. 19, 1983, pp. 19-25.
Tritthart, J., "Chloridinduzierte Betonstahlkorrosion," Schriftenreihe Straßenforschung, Heft 346, Wien, 1989, 117 p. (In German)
Tritthart, J., "Auspressen der Porenlösung aus kleinen Betonproben.", Zement und Beton, No. 2, 1991, pp. 42-43. (In German)

TOPIC IV.E

Modelling and mechanisms of degradation processes

NEURAL NETWORKS FOR MODELLING THE INFLUENCE OF CEMENT CHEMISTRY ON CONCRETE DURABILITY

Nick R. BUENFELD,)
Nadir M. HASSANEIN, } Department of Civil Engineering,
Gareth K. GLASS,) Imperial College,
London, UK

ABSTRACT Neural networks (NNs) are introduced as a method of analyzing cement/concrete performance data to quantify the effects of individual cement components on concrete deterioration mechanisms. NNs developed to predict chloride binding and carbonation depth are presented as examples.

Keywords: carbonation, chloride binding, durability, modelling

INTRODUCTION

Cement chemistry is expected to influence most concrete deterioration mechanisms. There are numerous papers in the literature describing the performance under particular test/exposure conditions of concretes of specified mix proportions and binder composition. However, such studies have rarely allowed the effects of any but the most dominant chemical constituents to be quantified because a large number of variables are required to characterize cement and it is very unusual to find cements of almost identical composition with the quantity of only one or two constituents varying to allow a direct comparison. Consequently, despite large amounts of apparently relevant data, it is rarely possible to accurately predict the performance of a cement of known composition, necessitating the expense and time commitment of further testing.

This paper shows how neural network (NN) analysis of cement/concrete performance data can be used to isolate and quantify effects to provide insights not possible with conventional methods. A brief introduction to NNs is presented. This is followed by two examples of NN analysis of durability data; these relate to chloride binding and carbonation. The wider applicability of NNs in this field is then discussed.

NEURAL NETWORKS

A NN consists of a number of processing units (neurons) grouped together in layers and connected to form a complex net-like structure (e.g. Fig 1). An input layer consists of neurons describing the influencing factors, ideally with each variable that is thought to possibly influence the output represented by an input neuron. An output layer gives the response to the set of inputs. In addition, there are usually 1 to 3 *hidden* layers. Neurons receive the output signal from many other neurons. A neuron calculates its own output by determining the weighted sum of its inputs, generating an activation level and passing it through a *transfer function*. Two neurons communicate via a *connection* and the strength of the connection between two neurons is its *weight*.

NNs are trained by presenting a series of inputs and the desired output. The most popular learning method is by example and repetition; the NN is presented with a set of facts and each time an input is presented the NN sends back an answer of what it thinks the output should be. This is compared with the correct output. If the output is incorrect, the NN makes corrections to the weights. This training process is repeated until the discrepancy is minimised. The NN is then tested to determine its accuracy by presenting it with sets of input data (not previously seen by the NN) and comparing the outputs with the known correct outputs. Finally, the NN

is used, i.e. it is presented with input combinations of interest data and predicts unknown output values. The NNs described in this paper were developed using the back propagation algorithm, delta learning rule and sigmoid ($(1+e^{-x})^{-1}$) transfer functions with NeuralWorks Professional II/PLUS (NeuralWare, 1993).

CHLORIDE BINDING

All cements bind a proportion of any chloride present. This reduces the depth of chloride penetration from an external source, but results in higher chloride levels nearer the exposed surface than if binding did not occur. Chloride binding may also influence the threshold level required for corrosion. Numerous experimental studies of chloride binding have been reported, with some of the findings being contradictory. No individual study has encompassed all of the influencing variables. A major attraction of NN analysis was to assimilate data from a number of independent studies to allow the most accurate possible prediction of chloride binding.

The output was chosen as free chloride concentration, avoiding errors associated with estimating pore solution volume to convert published data to percentage bound. A total of 18 input variables (listed in Table 1) were used, including total chloride content, the phase composition of the cement, Na_2O equivalent and SO_3 contents, pore solution OH^- concentration, replacement levels of PFA, GGBS and silica fume (SF), free water/cement ratio (w/c), sand/cement ratio (s/c), chloride ion source (internal or external) and cation (Na or Ca). Two different methods have been used to determine free chloride content: extraction of pore solution from a chloride contaminated sample (*pore pressing*) and equilibration of the pore solution with an external solution (*equilibrium method*). Method was included as an input variable to allow any discrepancy to be isolated. Only room temperature data from pastes and mortars (not concretes) were included.

Approximately 500 datapoints drawn from 21 papers (listed in Glass et al, 1996) were used to develop the NN. An indication of the distribution of variable values in this data is provided by the typical ranges given in Table 1; although more extreme values were present, predictions outside of the typical ranges are likely to be less accurate.

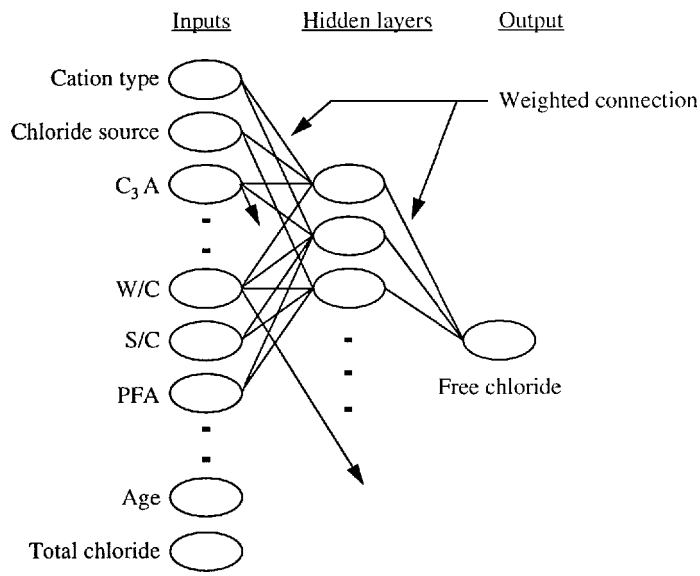

Figure 1 Schematic diagram of chloride binding neural network.

Table 1 Chloride binding NN input variables and their individual effects on free chloride concentration (typically 0.313M) at a total chloride content of 1%.

Variable			Free chloride	
Type	Typical range	Typical value	Concentration (M)	Change
Total Cl^- (%)	0 → 2.5	1		
C_3A (%)	2 → 14	8	0.495 → 0.192	97%
C_3S (%)	42 → 68	55	0.415 → 0.241	56%
SF (%)	0 → 20	0	0.313 → 0.474	52%
w/c	0.4 → 0.7	0.55	0.398 → 0.243	50%
GGBS (%)	0 → 65	0	0.313 → 0.160	49%
OH^- (M)	0.03 → 0.77	0.4	0.251 → 0.390	45%
Cation	$Na^+ \rightarrow Ca^{2+}$	Na^+	0.313 → 0.193	38%
C/S	2.9 → 3.3	3.12	0.260 → 0.375	37%
Na_{eq} (%)	0.3 → 1.2	0.75	0.289 → 0.343	17%
s/c	0 → 2	0	0.313 → 0.265	15%
Method	pp → eqbm	pp	0.313 → 0.270	14%
Cl^- source	int → ext	int	0.313 → 0.348	11%
PFA (%)	0 → 35	0	0.313 → 0.284	9%
SO_3 (%)	2 → 4	3	0.299 → 0.327	9%
Age (days)	10 → 250	130	0.323 → 0.303	6%
C_4AF (%)	7 → 14	10.5	0.317 → 0.310	2%
Conditioning	wet → sealed	sealed	0.309 → 0.313	1%

There is no widely applicable systematic means of determining the optimal number of hidden layers, number of hidden neurons and other NN parameters. This was achieved largely by educated trial and error involving the development and testing of over 100 NNs. NN accuracy was assessed according to the average percentage error for chloride concentrations above 0.05M This was a compromise between assessing absolute error which would have attributed too much importance to the larger values and percentage error applied to the entire data set which would have given undue weight to the unresolvable differences at low values and presents difficulties at the origin. In addition, the relations generated by each NN were compared with well-established relations in the literature. It was encouraging to observe that the same relations were predicted for nearly all of the NNs assessed in the process of optimization.

The optimised NN had 8 neurons in the first hidden layer and 3 in a second. It predicted the training set with an error of 19.4%, the test set (drawn from the training set papers, but not used in training) with a error of 19.0% and a validation set (4 independent data sets not used in training) with an error of 20.2%. Significant variations (up to 50%) have been reported in the determination of both free and total chloride contents by different laboratories (Byfors et al, 1986 and Grantham and van Es, 1995). The closeness of the error in the prediction of these data sets implies that the *noise* (variations uncorrelated with either inputs or output) in the training data did not significantly affect the NN predictions. The relative importance of each variable was assessed by predicting the change in free chloride concentration (expressed as a percentage of the typical concentration) when the variable was assigned the minimum and maximum values in its typical range, all other variables being held at their typical values. The variables are listed in Table 1 in order of importance at the 1% total chloride level; it should be recognised that the relative importance assigned to variables depends on the range of the variable which in practice

may differ from that in this study. The NN was able to separate the effects of factors that are otherwise difficult to assess individually in a laboratory environment. For example, the strong effect previously attributed to PFA was shown to be largely due to accompanying changes in OH^-. Including test method as a variable indicated that there is negligible difference in binding between internal and external chlorides, the effect attributed to chloride source in the literature probably being due to errors in the determination of the total chloride content originating from an external source. The somewhat surprising effects attributed to C_4AF, C_3S and C/S largely result from the assumption in the above analysis that all the variables are independent. However, variables which depend on the oxide composition of the cement are partially dependent due to both the requirement that the sum of these compositions cannot exceed 100% and other interactions. The influence of phase composition was investigated further by varying pairs of variables, constrained by the Bogue equations. In practice an increase in C_3A content is generally accompanied by a decrease in the C_4AF content. The predicted effect of C_3A did not change significantly when combined with variations in C_4AF. However, the combined effects of C_3S and C/S partially cancelled with a marginal increase in binding occurring when both C_3S and C/S increased.

The NN provides a method of estimating chloride binding data in a manner which reduces the effect of unexplained variations present in individual measurements. The NN is now used to predict binding isotherms for use in numerical models of chloride transport (Buenfeld, 1996a). See Glass et al (1997) for a detailed description of the development and application of this NN.

CARBONATION

A literature search located over 100 papers containing carbonation depth data. These were reviewed to identify the variables believed to affect carbonation. Papers with many key variable values missing were discarded. The vast majority of the studies measured carbonation depth using phenolphthalein; data based on other methods were discarded. This left around 7000 carbonation depth measurements from 88 papers (listed in Buenfeld et al, 1996b). NNs were then formulated, based on training with data from 68 of the papers and testing with data from the other 20. The final stage of development involved assessing the performance of 30 NNs, involving different NN parameters.

The optimum NN, described here, used 39 inputs (indicated by • in Table 2). Cements were defined according to type and Bogue composition, plus alkali content. If cement composition was not provided in a paper, information in the paper concerning the source of the cement was used to estimate the composition; accuracy trials showed that this approach was preferable to allowing the mean or mid-range value to be adopted and was effective for other variables too. To ensure that the NN had every opportunity of learning the effect of free water content, cement content and w/c, all three were included as neurons, even though any two of these factors effectively define the third. Curing was characterized by temperature, moisture state at the surface of the concrete and duration. Moisture state was described on a scale of 0 to 10, defining water immersion as 10, >95% RH (e.g. sealed curing) as 8, 90-95% RH as 6, <90% RH as 4 and no curing as 0. Curing duration was entered as a logarithmic value to assist the NN in identifying the diminishing effect of prolonged curing. Such transformation of important variables allows expert knowledge to be used to advantage in developing NNs. A major complication of modelling carbonation in relation to the chloride binding study was the number of variables required to describe the exposure environment. Ideally exposure environment would be specified entirely in terms of well-defined environmental parameters. The difficulty is that in most natural exposure environments, these vary with time in an unpredictable fashion.

Average temperature, average ambient RH and annual rainfall were included as *quantitative neurons*. *Qualitative neurons* were used to identify whether exposure was internal, external and sheltered or external and unsheltered and to indicate from which of five world-wide regions the data originated. Data from elevated CO_2 laboratory studies were included in the NN to allow correlation between natural and accelerated carbonation.

Table 2 Carbonation NN input variables.

	Defaults		Defaults
CEMENT		**CONDITIONING**	
• Rapid hardening portland (Y/N)	No	**(only applies to accelerated**	
• Sulphate resisting portland (Y/N)	No	**tests)**	
• C_3S (%)	63%	• Cond. RH (RH-40%)	
• C_2S (%)	20%	• Cond. period (log(days))	
• C_3A (%)	8%		
• Na_2O equiv. (%)	0.6%		
ADDITIONS		**EXPOSURE**	
• PFA (% replacement)	0%	**(applies to all cases)**	
• PFA *CaO content (%)*	0%	• Temperature (°C)	9°C
• PFA passing 45μm (%)	0%	• Relative humidity (RH-50%)	78% RH
• GGBS (% replacement)	0%		
• SF (% replacement)	0%		
MIX PROPORTIONS		**NATURAL EXPOSURE**	
• Water content (kg/m^3)	180	Region: • UK (Y/N)	Yes
• Cement content (kg/m^3)	325	• Scandinavia (Y/N)	No
• Water/cement (ratio)	0.55	• Japan (Y/N)	No
• Maximum aggregate (mm)	20	• Germany (Y/N)	No
• Coarse/fine aggregate (ratio)	2	• Gulf (Y/N)	No
• Air content (%)	1%	• External (Y/N)	Yes
		• Sheltered from rain (Y/N)	Yes
		• Rainfall (mm/year)	60mm
		Exposure period: • (years)	Stated
		• (√years)	
CURING		**ACCELERATED EXPOSURE**	
• Moisture state (0-10)	8	CO_2 concn: • (%)	0
• Curing/conditioning temp. (°C)	20°C	• (log(%))	
• Duration (log(days))	3 days	Exposure period: • (weeks)	Stated
• Maturity after curing (log(°Chr))		• (√weeks)	

The optimum NN had 39 neurons in the first hidden layer and 19 in a second. Different methods of monitoring training and assessing NN accuracy were investigated. The least root mean square (RMS) absolute error achieved in training was 0.0245, but this NN was overtrained in that it learned some of the noise in the data. The optimum NN was trained up to an RMS of 0.029. The average error (absolute error/measured value) over the entire testing file was 27.5% and the error was smaller for the more critical cases where carbonation depth was large. Predictions for real structures were as accurate as for naturally exposed specimens (see Fig 2). The error can be partially attributed to factors that influence carbonation that are rarely reported

in papers, such as mould oil application and micro-environmental factors such as wind direction. Error is also due to the variability of concrete, with samples tested not being truly representative.

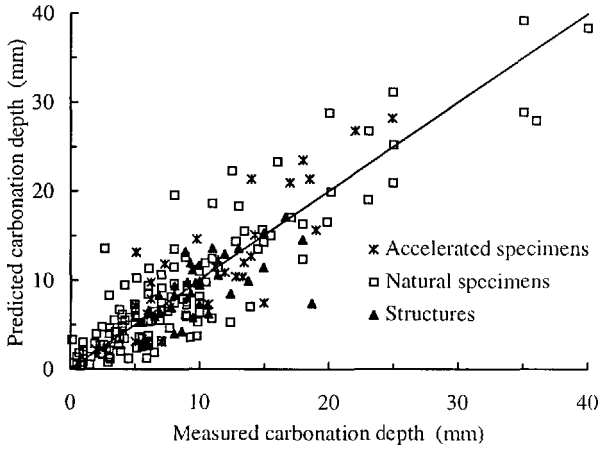

Figure 2 Predicted vs. measured carbonation depths.

The NN was used to predict the effects of concrete and environmental variables on carbonation. In the following examples, unless indicated to the contrary, the input neurons were set to the values listed in the righthand column of Table 2. Relatively well-established relationships were replicated; for example, Fig 3 shows the effects of w/c, cement content and exposure type. Fig 4a shows the time dependence of carbonation for typical levels of cement replacement; it should be recognised that these mixes are compared on the basis of similar mix proportions and that the strengths would be different. The NN allows the effect of factors that are not normally varied in a single study to be investigated. Fig 4b shows the effect of world location and involved selection of appropriate values of average temperature, RH and annual rainfall, as well as region neuron; this may be useful when considering the applicability of particular national codes in other parts of the world. When varied independently, both C_3S and C_2S were found to reduce carbonation depth. When varied dependently, according to the Bogue equation $C_2S = 2.87S - 0.754C_3S$, the predicted influence of C_2S is reversed (Fig 5).

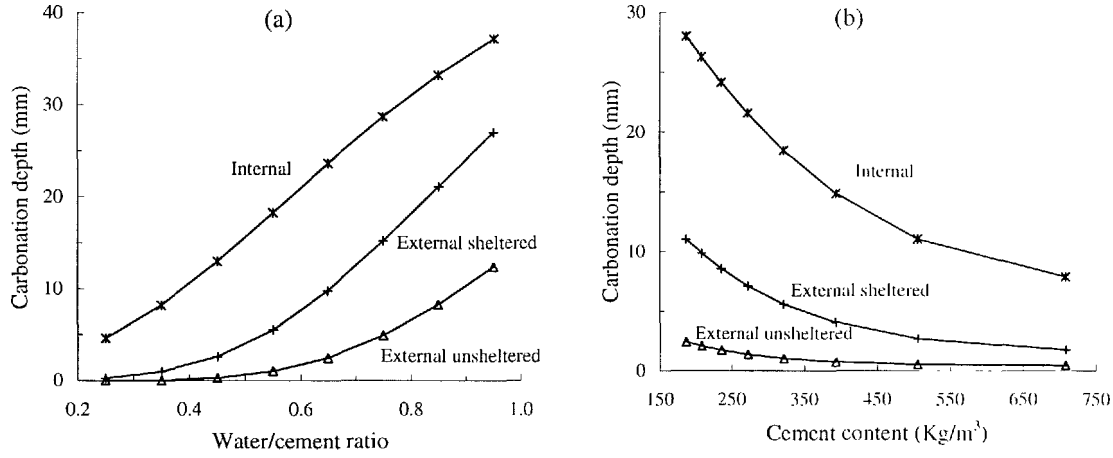

Figure 3 Carbonation depth vs. (a) w/c at constant cement content and (b) cement content at constant w/c, for 3 exposure conditions.

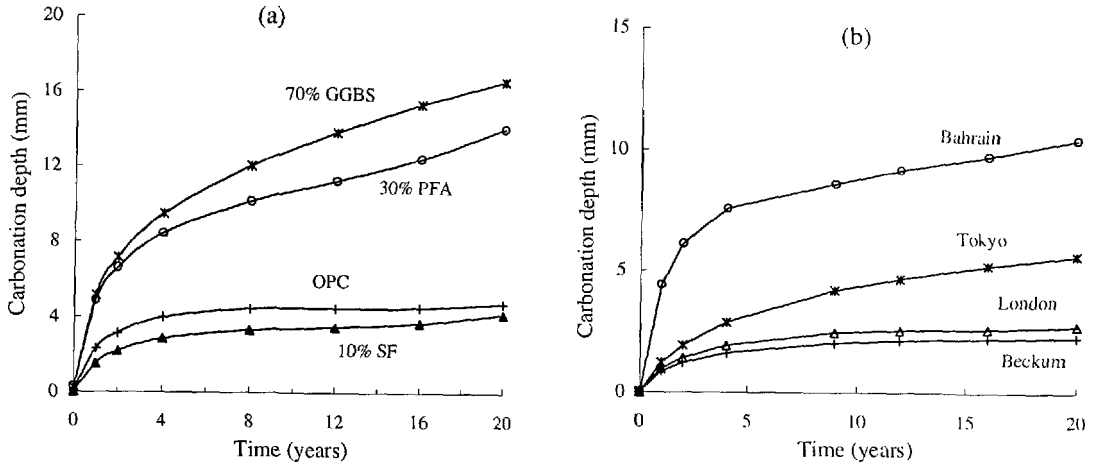

Figure 4 Carbonation depth vs. time for (a) cement replacements and (b) world location.

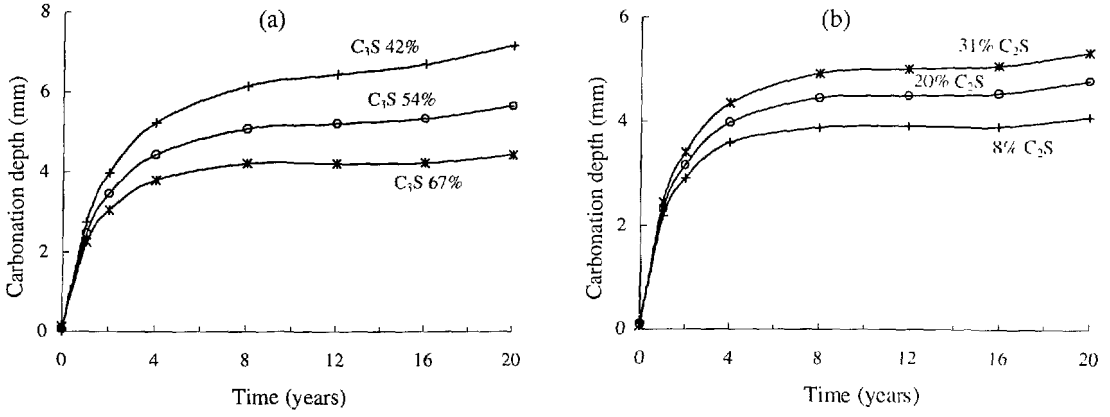

Figure 5 Carbonation depth vs. time for different levels of (a) C_3S and (b) C_2S.

There was very little carbonation depth training data for exposure periods beyond 20 years and it would therefore have been unwise to use the NN directly to predict to longer times. Long-term predictions are best achieved by using the NN to determine the time dependence of carbonation depth within the time range of the training facts then fitting a function (e.g. $A + Bt^n$) to allow extrapolation to longer times. See Buenfeld et al (1996b) for a more detailed description of the development and application of this NN.

CONCLUSIONS REGARDING APPLICABILITY OF NNs TO DURABILITY MODELLING

Deterioration processes affecting concrete structures are influenced by many variables including those relating to cement composition, concrete mix proportions and environmental exposure. NNs can cope with the large numbers of variables involved and do not require the effects of secondary variables to be overlooked when considering the effects of the main variables. NNs are able to generalise, i.e. to draw conclusions about something that has not been observed before, by learning of the effects of the input variables in other situations. This is essential when dealing with a topic involving so many variables. However, a NN is only as good as the data on which it is trained. A moderate amount of training data spread across the whole domain of interest is more valuable than a vast amount of data limited to only a subset of all of the

variables of interest. Incomplete input sets can be accommodated and in some cases where data are missing for an influential input, a separate NN can be developed to predict the missing values (e.g. Hills et al, 1995).

The NN approach requires knowledge of the variables that may be important, but does not require prior understanding of the relationships between each variable and the output of interest; for example, a NN has been developed to predict chloride profiles without the assumption of Fick's Law compliance (Hassanein, 1996). Once trained, the NN can be used to quantify these relationships. Non-linear relationships are common in the concrete durability field; for example, the effect of curing regime on carbonation depth is dependent upon binder type. It is difficult to identify and quantify such interactions with conventional analytical methods; NNs are well-suited to this kind of problem, but care should be taken when assessing the effect of cement chemistry inputs to ensure that dependent inputs are also varied appropriately. This is an argument against using concrete properties (e.g. strength) as well as concrete constituents and proportions as inputs.

Individual laboratory studies and natural exposure trials necessarily only investigate subsets of the influencing variables. NNs can be used to combine and analyze such data; this approach tends to average out noise and is recommended as a means of synthesizing previous research, identifying what remains uncertain, prior to undertaking a new study. A NN may also be a practical method of encompassing results from a large number of different studies to validate or modify design code durability recommendations.

ACKNOWLEDGEMENTS
This research was supported by the Engineering and Physical Sciences Research Council.

REFERENCES

Buenfeld, N.R. and Hassanein, N.M., "Neural networks for Predicting the Deterioration of Concrete Structures", NATO/RILEM Workshop on the Modelling of Microstructure and its Potential for Studying Transport Properties and Durability, St Remy-les-Chevreuse, France, 10-13 July 1994, Kluwer Academic Publishers, 1995, pp. 415-432.

Buenfeld, N.R., "Measuring and Modelling Transport Phenomena in Concrete for Life Prediction of Structures", STATS Conference, 16 November 1995, Chapman and Hall, 1996a.

Buenfeld, N.R., Hassanein, N.M. and Jones, A.J., "An Artificial Neural Network for Predicting Carbonation Depth in Concrete Structures", 2nd ASCE Monograph on Artificial Neural Networks in Civil Engineering, American Society of Civil Engineers, 1996b.

Byfors, K., Hansson, C.M. and Tritthart, J., "Pore Solution Expression as a Method to Determine the Influence of Mineral Additives on Chloride Binding", Cement and Concrete Research, Vol. 16, No. 5, 1986, pp. 760-770.

Grantham, M. and van Es, R., "Admitting that Chlorides are Variable", Construction Repair, Vol. 9, No. 6, 1995, pp. 7-10.

Glass, G.K., Hassanein, N.M. and Buenfeld, N.R., "Neural Network Modelling of Chloride Binding, accepted for publication in, Magazine of Concrete Research, 1997.

Hassanein, N.M., "The Application of Neural Networks to Service Life Prediction of Concrete Structures", University of London PhD thesis, 1996.

Hills, C.D., Hassanein, N.M. and Buenfeld, N.R., "An Examination of Factors Affecting Solidified Hazardous Waste Forms by Neural Network Analysis", International Congress on Waste Solidification/Stabilization Processes, Nancy, France, November 1995.

Neural Ware, NeuralWorks Professional II/PLUS, 1993.

THE INVESTIGATION OF CEMENT CONCRETE CORROSION BY AN IMITATION MODEL.

V.L.CHERNYAVSKY, V.Y.DUBNITSKY.
Kharkiv State Technical University of Building and Architecture

ABSTRACT A structural functional model of cement concrete is proposed to be used in numerical simulation of processes taking place in it at all stages of its life cycle, including corrosion actions. The model consists of a system of Kolmogorov-type linear differentional equations for Markov's processes with a discrete condition and continuous time. The model identification has been made.

Key words: Corrosion, Design life, Hardening, Hydration, Modelling

INTRODUCTION.

In corrosion of cement materials (hardened paste, concrete) taking place under interaction of their structural components therebetween and strongly influenced by environment some complicated processes are involved hardly describable in an analytical form for a number of reasons (presence of clinker, slag, ash and other relicts, polymineral composition of hydration and corrosion products, time-changing role of creative and destructive processes in structure formation) defines a non-monotorous nature of cement hardened paste property alteration and makes impossible a formal extrapolation of the concrete properties as a whole.

To study cement structure formation under the action of environment we proposed an imitative model of cement hardened paste (the most corrosion-sensitive part of concrete) structure based on grouping its structural components by common functional properties. The basic principles of grouping cement hardened paste structure components into model elements were described by Mchedlov-Petrossyan et al. (1970).

OBJECT OF WORK.

The object of this work is to create an imitative model for quantitative study of alteration with time of structural and functional characteristics of cement materials (hardened paste, concrete) acted upon by environment of any type and aggressiveness, taking into consideration creative and destructive process emerging in those materials in the course of long-term operation of building constructions.

Hypotheses taken in model building.

For simulation a concept has been received about the structure of cement hardened paste in concrete based on grouping its component into blocks (model components V_i, **i=1,4**) by common functional properties.

Relative content of non-hydrated cement particles is designated as V_1; relative content of hydrate formations as V_2; relative content of voids ($r > 10^{-5}$ m) as V_3; relative content of corrosion products as V_4. In constructing connections between model elements the following assumptions were made:

-in every unit volume all model components Vi are present and disposed uniformly along all coordinate axes, their ratios corresponding in average to the ratios of structural components in the actual material;

-the condition

$$\sum_{i}^{4} Vi = 1 \qquad [1]$$

is met along the whole time interval of model functioning;
-all components V_i within a unit volume for which the condition [1] is met are equally accessible to the rest of model elements, a connection of each element V_i to any element $V_j(\alpha_{ij})$ being a continuous one;
-only such processes can proceed in the model: hydration of component V_i, "extraction" of components V_1, V_2, V_4 "accumulation" of components V_3, V_4 or linear combinations of these processes;
-alteration intensity of components V_1, V_2, V_4 for a given medium is independent from mineral composition of their actual prototypes;
-the liquid phase in cement hardened paste is represented by chemically bound, crystallisation, adsorption, capillary and gravity forms and is taken into consideration during construction and evaluation of each of the model components. The relations between model components are presented in the from of an oriented weighted graph

$$G=g(V_i,\alpha_{ij}),\ i=\overline{1,4},\ j=\overline{1,4}. \qquad [2]$$

Apices Vi correspond to model components having the same subindices, arcs show transition directions, arc weight α_{ij} corresponds to intensity of transition $V_i \rightarrow V_j$, i.e. to the part of element V_i that passed into element $V_i\left(i=\overline{1,4}\right) V_j$ for unit time Δt. Then, according to the sense of model , transitions $V_1 \rightarrow V_2$; $V_3 \rightarrow V_2$ would describe creative processes, whereas transitions $V_1 \rightarrow V_4$; $V_2 \rightarrow V_3$; $V_1 \rightarrow V_4$; $V_2 \rightarrow V_4$; $V_3 \rightarrow V_4$ refer to destructive ones.
The graphs corresponding to each of the models considered are shown in *Fig.1.*

EXPERIMENTAL RESEARCH

The object of our study were cement hardened paste specimens from concrete's mode using 13 cements in which the content of basic clinker mineral were (in %): $C_3S-41\ldots67$; $C_2S-15\ldots33$; $C_3A-4\ldots9$; $C_xA_yF_z-10\ldots15$. The following external actions were assumed: normal storage in a moist air medium, filtration of mild water with pH≈5, action of a sulphate - containing aqueous solution with pH≈7.5, cyclic action of sulphate - containing aqueous solution and heating at 60°C. The duration of laboratory studies was 10...12 years. Numerical values of model components Vi were obtained at an optical microscope by quantitative petrographic analysis of flat parallel sections (Mchedlov-Petrossyan et al., 1974). It has been distribution of model component Vi is normal by monofactorial dispersion analysis it is shown that the time alteration of cement hardened paste model component content is statistically connected to the change in the concrete strength properties which may be considered as a confirmation of the model adequacy.

REASONING OF MODEL EQUATION

For each apex of any graph shown in Fig.1 an equation is composed of the type:

$$\frac{dV_i}{dt} = -\sum_{i=1}^{P}\alpha_{ij}V_i + \sum_{j=1}^{P}\alpha_{ji}V_j, i=\overline{1,P} \qquad [3]$$

$$j=1,2,\ldots,i-1,i+1,\ldots,P$$

For cement hardened paste with hydration processes taking place in it the system of differential equations has the form

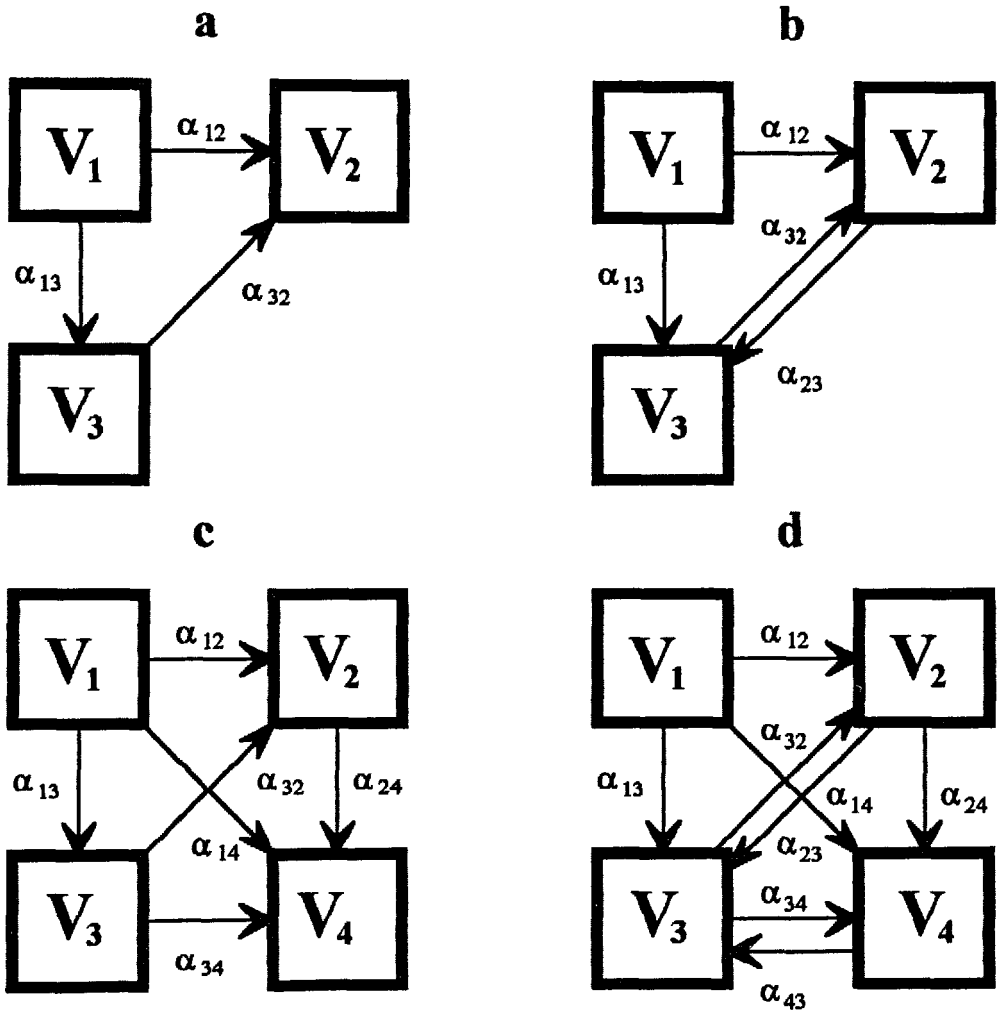

Figure 1 Model graphs
1a) cement hardened paste corrosion absent
1b) extraction of cement hardened paste components
1c) accumulation of corrosion products in cement hardened paste
1d) joint development of processes 1b, 1c in cement hardened paste

$$\begin{cases} \frac{dV_1}{dt} = -\alpha_{12}(t)V_1 - \alpha_{13}(t)V_1 \\ \frac{dV_2}{dt} = \alpha_{12}(t)V_1 + \alpha_{32}(t)V_3 \\ \frac{dV_3}{dt} = \alpha_{13}(t)V_1 - \alpha_{32}(t)V_3 \end{cases} \quad [4]$$

a graph corresponding to this system being shown in Fig.1a.

A system of equations for cement hardened paste with processes of hydration and extratplace in it has the form

$$\begin{cases} \dfrac{dV_1}{dt} = -\alpha_{12}(t)V_1 - \alpha_{13}(t)V_1 \\ \dfrac{dV}{dt} = \alpha_{12}(t)V_1 - \alpha_{23}(t)V_2 + \alpha_{32}(t)V_3 \\ \dfrac{dV}{dt} = \alpha_{13}(t)V_1 + \alpha_{23}(t)V_2 - \alpha_{32}(t)V_3 \end{cases} \quad [5]$$

its graph being shown in Fig.1b.

A system of equation for cement hardened paste with processes of hydration and accumulation of corrosion products taking place in it has form

$$\begin{cases} \dfrac{dV}{dt} = -\alpha_{12}(t)V_1 - \alpha_{13}(t)V_1 - \alpha_{14}V_1 \\ \dfrac{dV}{dt} = \alpha_{12}(t)V_1 - \alpha_{24}(t)V_2 + \alpha_{32}(t)V_3 \\ \dfrac{dV}{dt} = \alpha_{13}(t)V_1 - \left(\alpha_{32}(t) + \alpha_{34}(t)\right)V_3 \\ \dfrac{dV}{dt} = \alpha_{14}(t)V_1 + \alpha_{24}(t)V_2 + \alpha_{34}(t)V_3 \end{cases} \quad [6]$$

its graph being shown in Fig.1c.

A system of equation for cement hardened paste with processes of hydration, extraction of structural components and accumulation of corrosion products taking place in it has form

$$\begin{cases} \dfrac{dV_1}{dt} = -\alpha_{12}(t)V_1 - \alpha_{13}(t)V_1 - \alpha_{14}(t)V_1 \\ \dfrac{dV_2}{dt} = \alpha_{12}(t)V_1 - \alpha_{23}(t)V_2 - \alpha_{24}(t)V_2 + \alpha_{32}(t)V_3 \\ \dfrac{dV_3}{dt} = \alpha_{13}(t)V_1 + \alpha_{23}(t)V_2 - \alpha_{32}(t)V_3 - \alpha_{34}(t)V_3 + \alpha_{43}(t)V_4 \\ \dfrac{dV_4}{dt} = \alpha_{14}(t)V_1 + \alpha_{24}(t)V_2 + \alpha_{34}(t)V_3 - \alpha_{43}(t)V_4 \end{cases} \quad [7]$$

its graph being shown in Fig.1d.

IDENTIFICATION OF MODEL.

In Eqs 4...7 the value of αij(t) is to be defined using the data of numeric values of elements V_i ($i = \overline{1.4}$) found experimentally. Let us consider the identification of model elements at an example of the most complicated system, Eq.7

By transition from infinitely small values to finite increments, assuming that $\Delta t = 1$ we obtain a system like Eq. 8

$$\begin{cases} \Delta V_1^{(m)} = -\left(\alpha_{12}^{(m-1)} + \alpha_{13}^{(m-1)} + \alpha_{14}^{(m-1)}\right)V_1^{(m-1)} \\ \Delta V_2^{(m)} = \alpha_{12}^{(m-1)}V_1^{(m-1)} - \left(\alpha_{23}^{(m-1)} + \alpha_{24}^{(m-1)}\right)V_2^{(m-1)} + \alpha_{32}^{(m-1)}V_3^{(m-1)} \\ \Delta V_3^{(m)} = \alpha_{13}^{(m-1)}V_1^{(m-1)} + \alpha_{23}^{(m-1)}V_2^{(m-1)} - \left(\alpha_{32}^{(m-1)} + \alpha_{34}^{(m-1)}\right)V_3^{(m-1)} + \alpha_{43}^{(m-1)}V_4^{(m-1)} \\ \Delta V_4^{(m)} = \alpha_{14}^{(m-1)}V_1^{(m-1)} + \alpha_{24}^{(m-1)}V_2^{(m-1)} + \alpha_{34}^{(m-1)}V_3^{(m-1)} - \alpha_{43}^{(m-1)}V_4^{(m-1)} \end{cases} \quad [8]$$

In construction of system Eq. 7 and similar ones the following assumptions have been made. The whole type of process development T is divided into M unit length intervals. Within each interval, i.e. at $t^{(m-1)} < t \le t^{(m)}$, $m = \overline{1.4}$, the value of V_j ($j = \overline{1.4}$) and αij $\left(j = \overline{1.4}\right)$ are constantly changing spasmodically in response to changing index **m** which confirm the hypothesis of a first continuous approximation of the elements forming Eqs. 4 -7.

Using condition in Eq. 1 let us exclude one of the variables, say V_j, and the **j**-th equation corresponding to it. The variables may be always renumbered so that the first variable and its respective equation be never taken into consideration.

Then instead of variable V_1, using Eq. 8 we introduce

$$V_1^{*(m)} = 1 - \sum_{j=2}^{p} V_j^{(m)},\ j = 2,3,\ldots P;\ m = \overline{1, m} \quad [9]$$

Hereafter we shall commit the symbol [*] in order to simplify the record unless it causes ambiguities. The system of model equation has some peculiarities caused by its structure:

- each **j**-th line contains $p'_j < p$ variables;
- coefficients at the variables are either monoials (αij) or their linear combinations $C_l\left(\alpha_{jk_1}, \alpha_{jk_2}\ldots\alpha_{jk_u}\right),\ l = 1,2,\ldots, z.$
- all coefficients forming a **l**-th linear combination separately come into other lines of the system different from the **j**-th line.

Then a **j**-th line may be presented in the form

$$\Delta V_j^{(m)} = \sum_{k\neq 1}^{p_j} d_{jk}^{(m-1)}\tilde{V}_j^{(m-1)} + \sum_{l=1}^{z} C_l^{(m-1)}\left(\alpha_{jk_1}, \alpha_{jk_2}, \ldots, \alpha_{jk_u}\right)\tilde{V}_j^{(m-1)},\ m = 1,2,\ldots, M \quad [10]$$

Let $\Delta\tilde{V}_{ji}^{(m-1)}, \tilde{V}_{ji}^{(m-1)}$ mean respective values obtained in i-th (i=1,2,...,N) experiment.
Then using a standard least square procedure and solving a problem like

$$\left(L_j^{(m)}\right)^2 = \sum_{i=1}^{N}\left(\tilde{\Delta}V_{ji}^{(m)} - \Delta V_{ji}^{(m)}\right)^2 \rightarrow \mathbf{min} \qquad [11]$$

at **j=2,3,...,(p-1),p; m=1,2,...,M**

we obtain estimated $\hat{\alpha}_{jk}^{(m-1)}$ and $\hat{G}_l^{(m-1)}$ of values $\alpha_{jk}^{(m-1)}$ and $G_l^{(m-1)}$.

As these estimates are obtained for each **j**-th line independently at a fixed **m**, some additional limitations cuoght to be introduced.
Let $\hat{\alpha}_{jkh}^{(m-1)}$ mean the least one and $\hat{\alpha}_{jkb}^{(m-1)}$ the largest one of estimates of $\alpha_{jk}^{(m-1)}$ obtained at **m**-th step and belonging to different lines of system Eqs. 7 of equations. To estimates $\hat{G}_l^{(m-1)}$ of linear combinations it is required that

$$\hat{G}_l^{(m-1)}\left(\alpha_{jk_1}, \alpha_{jk_2}, \ldots, \alpha_{jk_u}\right) = \sum_{S=1}^{u}\alpha_{jk_S} \qquad [12]$$

Finally, the problem of identification of the model system of equations is formulated as:

$$\sum_{j=2}^{P}(L_j^{(m)})^2 + \sum_{l=1}^{Z}\left(\hat{G}_l^{(m-1)} - \sum_{S=1}^{k}\alpha_{jk_S}\right)^2 \rightarrow \mathbf{min}$$

[13]

at limitations

$$\hat{\alpha}_{jkh}^{(m-1)} \le \hat{\alpha}_{jk}^{(m-1)} \le \hat{\alpha}_{jkb}^{(m-1)};\ j \ne k = 2,\ldots p;\ m = \overline{1, m} \qquad [14]$$

In Connotation Eq. 11 symbol $\hat{\Delta V}_{ji}^{(m)}$ means a calculated value of $\Delta V_j^{(m)}$ obtained by substitution into the system equations of optimal estimates $\alpha_{jk}^{(m-1)}$ defined by solution of problem Eq. 6, where ΔV_{ji} exp is an experimentally found value.

To evaluate the quality of results of identification of models proposed a special two-stage procedure is used. All specimens that served as a source of numerical values of components V_i were divided into two equal groups. Using sources forming the first group of models in Eqs. 4 - 7 that were identified according to algorithms in Eqs. 10 - 14 and then the adequacy of equations obtained was evaluated at every step of discretization by **F** criterion, the number of degrees of freedom in the numerator being diminished by so many units how many common elements α_{ij} there were in all lines of corresponding systems in Eqs. 4 - 7.
The specimens forming the second group were used to evaluate predictability of the models obtained.
To this end the value

$$\xi = \|\hat{V}\| / \|\tilde{V}\| = \left[\sum \hat{V}_i^2\right]^{1/2} / \left[\sum \tilde{V}_i^2\right]^{1/2} \qquad [15]$$

was calculated where $i = 1, 3$ for model in Eq. 4, $i = 1,3,4$ for models in Eqs. 5 - 7. Index (^) means that a corresponding value of V_i was obtained by calculation whereas index (~) means that the corresponding value of V_i was obtained using experimental data. Index $i = 2$ was committed by the condition Eq. 1.

The mean relative error of the norm of vector $\|\hat{V}\|$ relative to vector $\|\tilde{V}\|$ was 14.7% for system in Eq. 4, 15.1% for system in Eq. 5, 12.8% for system in Eq. 6, 11.6% for system in Eq. 7.

Actually all aggressive actions of inorganic media, especially heat and moisture actions of constant and cyclic nature, create emergence of constructive and destructive processes in cement concrete. Basing on the model proposed it became possible to describe the endowment of constructive component

$A^{(m)} = \alpha_{12}^{(m)} V_1^{(m)} + \alpha_{32}^{(m)} V_3^{(m)}$ and destructive component $B^{(m)} = \alpha^{(m)}{}_{13} V^{(m)}{}_1 + \alpha^{(m)}{}_{23} V^{(m)}{}_2 + \alpha^{(m)}{}_{14} V^{(m)}{}_1 + \alpha^{(m)}{}_{24} V^{(m)}{}_2 + \alpha^{(m)}{}_{34} V^{(m)}{}_3$ as well as to define the resulting characteristic $C^{(m)} = A^{(m)} - B^{(m)}$

In this connection a stagewise character of $G^{(m)}$ was obviously fixed as well as actual independence of intensities of $A^{(m)}$ and $B^{(m)}$ from mineral composition of the binder at the final stage of concrete interaction to the active medium.

The first stage is predominantly constructive when $A^{(m)} \geq B^{(m)}$, whereas the second stage is predominantly destructive, $A^{(m)} < B^{(m)}$.

By this modelling the transitions $V_1 \rightarrow V_2$ and $V_1 \rightarrow V_4$ were quantitatively separated for the first time, i.e. the percentage of cement relicts transiting into products of hydration and products of corrosion were defined. Up to this time nobody managed to do it experimentally. It has been found that at the beginning of such common maintenance actions at steel works as a cyclic action of sulphate-containing aqueous solutions of industrial origin under elevated (up to 100°C) temperatures, the values of α_{12} are two-three times larger than those of the sum $(\alpha_{13} + \alpha_{14})$. Later on the dependence is gradually altered and the values of said intensities become roughly equal until the number of cement relicts reaches $V_1^{(m)} \leq 0.15...0.3$ relative units.

The validity of choice of model components as characteristics that sufficiently completely describe the cement hardened paste and the processes taking place in it (transitions $V_i \rightarrow V_j$) has been proved by an obvious statistical connection between the model components and certain properties of cement concrete. Particularly, there exists a sufficiently stable correlation between critical levels of the percentage of faulty areas $V_3 + V_4 > 0.25$ and the ratio $R^{(m)} / R^{(0)} < 0.7$. It is also found that the structures of cement hardened paste made of portland cements having different mineral compositions become statistically indistinguishable at the moment of destruction as to components V_1 and $V_3 + V_4$ in spite of different duration of test time (Mchedlov-Petrossyan et al., 1972).

To define the area of values of initial parameters of cement hardened paste structure (components $V_i^{(0)}$) that provide for continuation of maintenance properties of concrete (strength, deformation resistance,

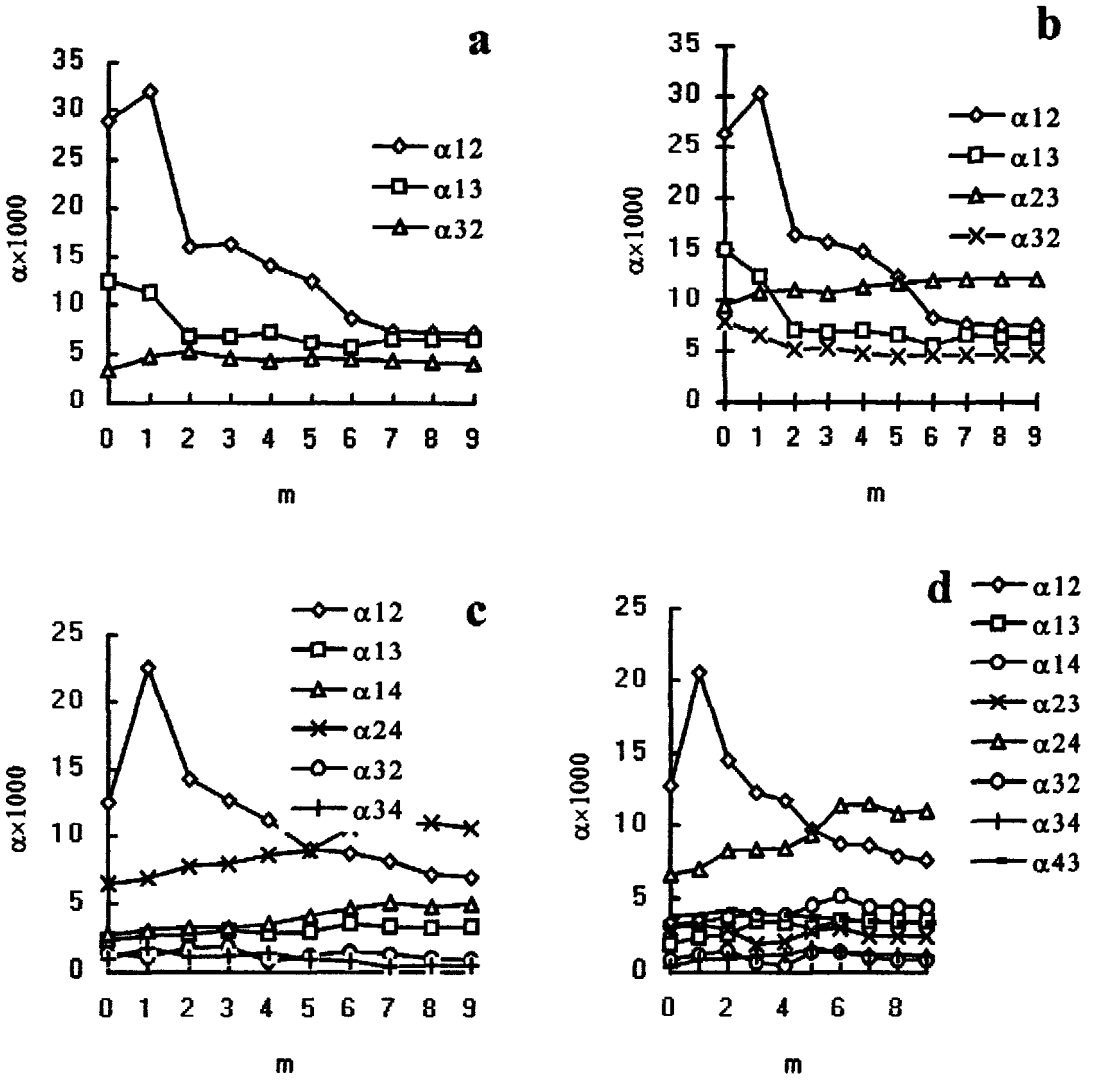

Figure 2 Results of model identification
2a) for system in Eq. 4, graph shown in Fig. 1a)
2b) for system in Eq. 5, graph shown in Fig. 1b)
2c) for system in Eq. 6, graph shown in Fig. 1c)
2d) for system in Eq. 7, graph shown in Fig. 1d)

protection) at an efficient level a problem of optimisation of initial condition of cement hardened paste has been solved for a necessary degree of binder hydration (in terms of the model $r_f = V_1^{(0)} / V_2^{(0)}$). It has been shown that the longest period of concrete resistance has a corresponding value of $r_f = 1$

Thus, all speculations relating to acceleration of the degree of cement hydration in concrete at the stage of construction manufacture by way of increased fineness of cement grinding may be annulled.

CONCLUSION

A structural and functional model of cement concrete under prolonged action of an aggressive medium is described. Numerical values of the model parameters have been defined. Optimisation tasks of structural change imitation in cement hardened paste under four types of corrosive actions have been solved. A substantial role of constructive processes connected to hydration of clinker relicts in cement hardened paste is shown which explains a temporary improvement of concrete properties at early stages of corrosive destruction.

The data obtained allow to regulate the properties of cement hardened paste by stimulation of its adaptability.

REFERENCES

Mchedlov-PetrossyanO.P., Dubnitsky V.Y., Fridgan L.B. and Chernyavsky V.L., "On Formulation of Cement Concrete Structure Model Regarding its Aging", Izvestiya Vuzov, Stroitel'stvo i Arkhitectura, № 12, 1970, pp 67-71

Mchedlov-PetrossyanO.P., Dubnitsky V.Y., Olginsky A.L. and Chernyavsky V.L., "Application of Multidimentional Statistical Analysis to Study of Cement Concrete Service Life", Izvestiya Vuzov, Stroitel'stvo i Arkhitectura, № 6, 1974, pp 62-65

Mchedlov-PetrossyanO.P., Dubnitsky V.Y., Chernyavsky V.L., "An Imitation Model Study of Cement Hydration Advanced Stages", Doklady AN SSSR, vol. 256, №2, 1984, pp 583-585

SIMULATION MODEL FOR TEMPERATURE RISE AND EVOLUTION OF THERMAL STRESS IN CONCRETE BASED ON KINETIC HYDRATION MODEL OF CEMENT

Fuminori TOMOSAWA, The University of Tokyo, Tokyo, Japan
Takafumi NOGUCHI, The University of Tokyo, Tokyo, Japan
Cheol HYEON, Dea Dong Corporation, Seoul, Korea

ABSTRACT As an application of a newly proposed hydration model of cement, a simulation for heat liberation, temperature rise and thermal stress of concrete was made. These characteristics were calculated on the every finite element, where the rate of hydration and the development of strength and elastic modulus were affected by its own temperature, and hence the differences of these time -dependent changes in each element were calculated and the distribution of thermal stress could be predicted.

Key-words: Hydration, Heat evolution, Adiabatic temperature rise, Thermal stress

INTRODUCTION

Hydration-induced temperature rise of concrete and subsequent thermal cracking cause serious problems for high strength or mass concretes. To cope with these problems, it is necessary to estimate accurately the temperature in members and assess the risk of thermal cracking before the start of construction. However, most conventional techniques of estimating temperature have the irrationality of expressing the test results of adiabatic temperature rise in the form of an equation and applying it to portions which are not in adiabatic conditions. It has therefore been difficult to adapt the histories of temperature distribution in members to actual situations. Tomosawa developed a hydration model of cement (1974, 1997) modifying the unhydrated core model. This paper reports on the application of this model to the estimation of heat liberation rate of cement hydration and adiabatic temperature rise of concrete, as well as temperature distribution and thermal stress in members. The comparison between the estimation and the measurements is reported as well.

OUTLINE OF HYDRATION MODEL

The hydration model of cement, **Eq1**, expresses the rate of hydration as a function of the degree of hydration. It was derived by assuming that as the hydration proceeds the initial protective layer is formed and destructed around spherical cement particles, and that the hydration rate of cement is determined by the rate of the inward diffusion of external water equivalent to the outward diffusion of reaction products and the chemical reaction rate on the core surfaces.

$$-\frac{d\alpha}{dt}=\frac{3C_w}{\nu\rho r_0^{\,2}}\cdot\frac{1}{\dfrac{1}{k_d r_0 \alpha^{2/3}}+\dfrac{\alpha^{-1/3}-(2-\alpha)^{-1/3}}{D_e}+\dfrac{1}{k_r r_0 \alpha^{2/3}}} \qquad [1]$$

where α = unhydrated percentage of cement, ρ = density of cement
ν = stoichiometric ratio of water to cement (by mass)
r_0 = radius of unhydrated cement particles at the beginning of hydration
k_d = mass transfer coefficient within initial protective layer ($k_d=B/\alpha^{1.5}+C\cdot\alpha^3$)
D_e = effective diffusion coefficient of water in hydration products
k_r = coefficient of hydration rate per unit area of cement
C_w = water concentration outside hydration products
If $1-\alpha \leqq m$, then $C_w = 1$
If $1-\alpha > m$, then $C_w = \exp\{-n(1-\alpha-m)\}$
where $m = p\cdot(W/C)^{1/3}$, n and p = constants, W/C = water-cement ratio

As the hydration of cement proceeds, D_e decreases due to the decreasing pore diameter in the gel as follows:

$$D_e = D_E[\ln\{1/(1-\alpha)\}]^2 \quad [2]$$

B, C, D_E, and k_r are affected by temperature, following the Arrhenius's law as follows:

$$\begin{aligned} B &= B_{20} \cdot \exp[-\beta_1(1/T-1/293)] \\ C &= C_{20} \cdot \exp[-\beta_2(1/T-1/293)] \\ D_E &= D_{E20} \cdot \exp[-\beta_3(1/T-1/293)] \\ k_r &= k_{r20} \cdot \exp[-E/R(1/T-1/293)] \end{aligned} \quad [3]$$

where B_{20}, C_{20}, D_{E20}, and k_{r20} = values of B, C, D_E, and k_r at 20℃
T = absolute temperature (K)
β_1, β_2, β_3, and E/R = coefficients determined for each cement type and W/C

HEAT LIBERATION RATE OF CEMENT

To ensure that the above model expresses the changes in the heat liberation rate of any cement independently of the temperature of the hydration environment, the heat liberation curve of each cement given in **Table1** was actually measured with a conduction calorimeter and each coefficient was calculated by means of repetitive calculation, so that the model coincides with the measured curve. Four levels of temperature were selected: 10, 20, 40, and 60℃. The water-cement ratio was fixed at 50%. In the case of ordinary portland cement (OP), the use of a high-range water-reducing agent was also investigated with a water-cement ratio of 35%.

Table2 gives the calculated coefficients, and **Fig1** shows the comparison between the heat liberation rates actually measured and those calculated from the model. This figure shows that the calculation appropriately expresses not only the peak values of heat liberation rate but also the extended induction periods due to the addition of a high-range water-reducing agent. In other words, the model was found to be capable of adequately describing actual hydration of cement.

ADIABATIC TEMPERATURE RISE OF CONCRETE

In order to confirm the applicability of the model to the estimation of adiabatic temperature rise of concrete, the adiabatic temperature rise of four types of concrete was actually measured, and the measurements were compared with the calculation by the model as shown in **Fig2**. The specific heat of concrete, Θ_c, was assumed to change in the course of hydration as expressed by **Eq4**. The calculations and the measurements are found to agree well with each other. Accordingly, the model is considered to be capable of estimating adiabatic temperature rise of concrete by using the coefficients given in **Table2** with an accuracy sufficient for practical use.

$$\Theta_c = \frac{1}{W + C_e + S + G}(W + 0.904C_e + 0.796S + 0.771G)\alpha + 1.17(1-\alpha) \quad [4]$$

where W,C_e,S and G=unit mass of water, cement, fine aggregate and coarse aggregate (kg/m^3)

THERMAL STRESS OF CONCRETE MEMBERS

To confirm the applicability of the model to the estimation of temperature distribution and thermal stress in real concrete structures, the authors examined the changes in the temperature and thermal

Table 1 Cements used in the experiments

Type	ig.loss	CaO	SiO_2	Al_2O_3	Fe_2O_4	SO_3	C_3S	C_2S	C_3A	C_4AF
OP	1.6	64.2	21.1	5.2	2.8	1.9	56.6	17.9	9.0	8.5
HP	1.5	66.1	20.5	5.0	2.5	3.0	67.5	7.9	9.0	7.6
BP	1.1	62.7	26.6	3.0	3.3	1.8	23.0	59.0	3.9	2.2

Table 2 Values of coefficients of the hydration model

Cement (W/C)	B_{20}	C_{20}	D_{E20}	k_{r20}	β_1	β_2	β_3	E/R	n	p
OP (50%)	1.0E-8	8.5E-3	2.9E-10	6.5E-6	-1973	4026	7456	4893	15	0.6
OP (35%)	1.0E-8	1.7E-3	2.9E-10	6.5E-6	-1973	6234	7456	4893	15	0.6
HP (50%)	7.0E-9	7.2E-3	1.2E-9	6.8E-6	160	1935	6917	4990	25	0.75
BP (50%)	5.1E-10	5.4E-2	1.8E-10	3.4E-6	6343	-1696	3726	5850	6	0.25

strain over time of reinforced concrete columns shown in **Fig3** with water cement ratios of 0.395 and 0.33 at the points shown in **Fig3**. The measurements were compared with the calculations using the model. Ordinary portland cement was used and the temperature of concrete at the time of placing was 26℃. The temperature and thermal stress were analyzed using difference calculus and FEM, respectively, regarding a quarter of the section. The heat transfer coefficient of the concrete surfaces, heat conductivity of concrete, and specific heat of concrete were assumed to be 33.5kJ/m²h℃, 7.12kJ/mh℃, and 1.17kJ/kg℃, respectively. The external restraint was

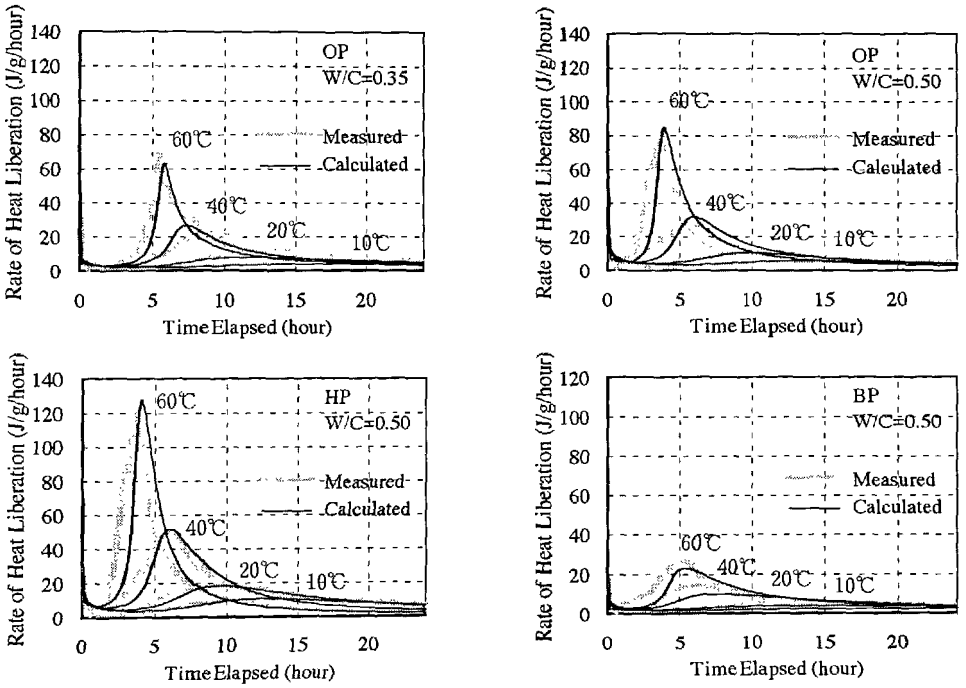

Figure 1 Heat Liberation Rate of Various Cements

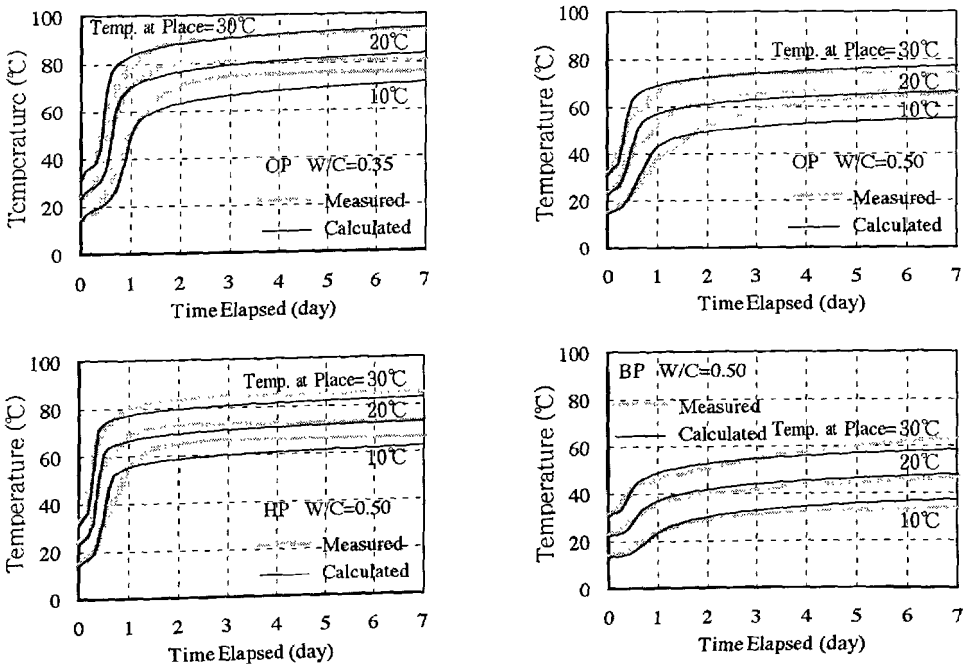

Figure 2 Adiabatic Temperature Rise of Concrete with Various Cements

disregarded and only the internal restraint was taken into account for the thermal stress analysis.

Figure4 shows the comparison between the measured temperature histories and those calculated using the model. The calculations by the model are found to be capable of estimating the peak temperature, time of peak, and ascending and descending temperature slope with an accuracy sufficient for practical use both deep in the concrete and near the surfaces. **Figure5** shows the comparison between the thermal stress histories calculated on the basis of the measured strain and those calculated on the basis of the model. The tensile strength curves in the figure are those near the surfaces. In this study, tensile strength is assumed to be 1/13 of compressive strength calculated by Powers's method (1958) based on the degree of hydration determined from **Eq1**. The estimation of thermal stress based on the model agrees well with the measured values, suggesting the effectiveness of the model for the estimation of thermal stress of members.

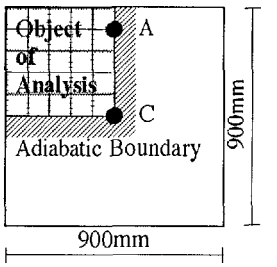

Figure 3 Dim. of Column

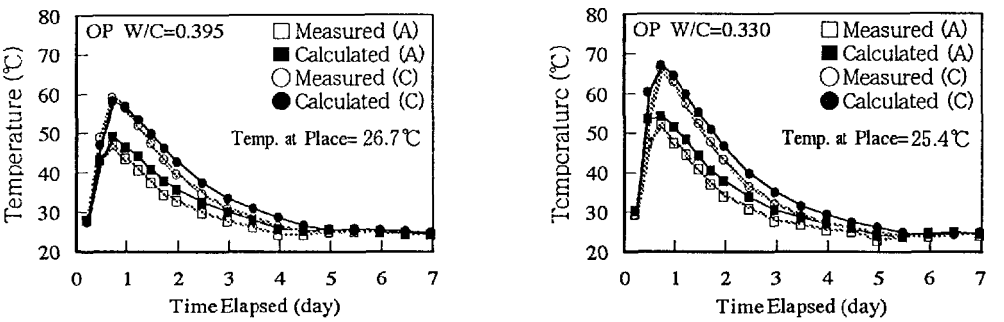

Figure 4 Temperature History in Reinforced Concrete Column

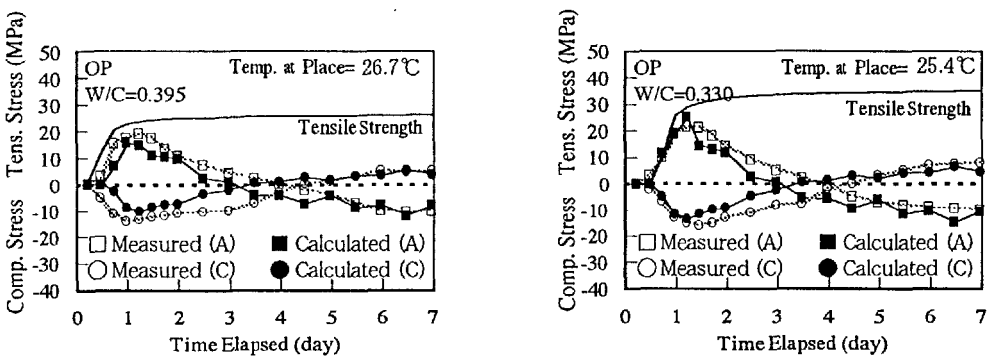

Figure 5 Thermal Stress in Reinforced Concrete Column

CONCLUSION

The coefficients for the cement hydration model were calculated from the measured data of heat liberation rate curves of cement. The model was found to be applicable to the estimation of the adiabatic temperature rise of concrete as well as temperature distribution and thermal stress of real structures under any environmental conditions with an accuracy sufficient for practical use.

REFERENCES

Tomosawa, F., "A Hydration model of cement", Proc. of Annual Meeting on Cement Technology, Cement Association of Japan, Vol.28, 1974, pp.53-57

Tomosawa, F., "Development of a Kinetic Model for Hydration of Cement", Proc. of 10th ICCC, June 2-6 1997, Gothenburg, Sweden

Powers, T.C., "Structure and Physical Properties of Hardened Portland Cement Paste", Journal of American Ceramic Society, Vol.41, No.1, 1958, pp.1-6

COMPUTER MODELLING OF THERMAL PERFORMANCE OF REINFORCED CONCRETE SUBJECTED TO FIRE

Andrew PLATTEN, Zhaohui HUANG, and John ROBERTS
Department of Built Environment, University of Central Lancashire, Preston, PR1 2HE, U. K.

ABSTRACT A theoretical analysis of heat and moisture transfer in concrete was made which incorporated the simplifications that energy transfer by convection and diffusion in concrete could be neglected. Based on this analysis a non-linear finite element procedure was proposed to predict the temperature distribution history in the cross section of structural members in fire conditions.

KEYWORDS: Concrete, Fire, Performance, Modelling

INTRODUCTION

There has been a number of studies on using non-linear finite element procedure to predict the temperature distribution history in reinforced concrete subjected to fire conditions Bizri (1973), Becker et al (1974). The objective of this study is to develop a computer model which, based on the theoretical heat and mass transfer in concrete, predicts the temperature distribution history in reinforced concrete subjected to fire conditions.

THE THEORETICAL BACKGROUND OF THE MODEL

Since concrete is a capillary-porous material, the thermal analysis of reinforced concrete in fire conditions is complicated by the presence of moisture. Sahota (1976) proposed a theoretical model which takes into account mass diffusion, convection, evaporation, and condensation. No dry-wet interface was postulated. Based on the literature review the theoretical model developed by Sahota [1976] was adopted as the theoretical foundation in this research.

One-dimensional energy equation

In one dimensional form the energy equation can be expressed as, Sahota (1976),

$$\frac{\partial T}{\partial t}=\alpha\frac{\partial^2 T}{\partial x^2}+\left\{\frac{1}{\rho C_p}\frac{\partial k}{\partial x}-C_r\left[u_m+\frac{D(C_{p,v}-C_{p,a})}{C_{p,m}}\frac{\partial w_a}{\partial x}\right]\right\}\frac{\partial T}{\partial x}-\frac{1}{\rho C_p}\left[h_{fg}\Gamma_m-\frac{\partial}{\partial t}(\rho_m R_m T)\right] \quad [1]$$

Sahota (1976) carried out an order of magnitude analysis for the various terms in the governing equation. Sahota's analysis provides guidelines to determine the range of parameters required to describe the general result and the following simplifications may be made in the Eq 1: the orders of magnitude of terms $C_r u_m$ and $C_r[D(C_{p,v}-C_{p,a})/C_{p,m}](\partial w_a/\partial x)$, which respectively represent energy transfer by convection and mass diffusion, are <<1. For the term $\partial(\rho_m R_m T)/\partial t$, which is the result of the difference between the enthalpy and internal energy of air-vapour mixture, the order of magnitude is also << 1. Compared to the conduction terms for which the orders of magnitude are unity, the three terms noted above may be neglected. Thus the simplified energy equation can be written as:

$$\frac{\partial T}{\partial t}=\alpha\frac{\partial^2 T}{\partial x^2}+\frac{1}{\rho C_p}\frac{\partial k}{\partial x}\frac{\partial T}{\partial x}-\frac{1}{\rho C_p}h_{fg}\Gamma_m \quad [2]$$

Which is the ordinary conduction equation with a heat sink term due to evaporation of water. If one is interested only in the temperature field, Eq 2 can be solved for T with initial and boundary conditions if Γ_m is known. The following assumptions are made to evaluate Γ_m: (1) The energy transfer due to mass diffusion is negligible compared to that by conduction. This implies that the contribution due to evaporation of water is unimportant as long as liquid water does not start to boil. (2) The boiling point of water in concrete is seen to be in range from 100 to 140 ^0C, Haksever and Anderberg (1981/82). In this study it is assumed that water boils at 120^0C; for the purpose of calculating the temperature field the average pressure is taken as two atmospheres. (3) Movement of the liquid water is neglected. As a result of assumption (1), Γ_m in Eq 2 is put equal to zero at each point in the wet region in the interior of the concrete elements where temperature is less than 120^0C. Γ_m is also zero in the dry region. As the temperature at a wet node approaches 120^0C, it cannot increase further according to assumption (2) until all the liquid water at that node is evaporated. Therefore, Eq 2 can be used to calculate the value of Γ_m:

$$\Gamma_m = \frac{1}{h_{fg}}\left[k\frac{\partial^2 T}{\partial x^2} + \frac{\partial k}{\partial x}\frac{\partial T}{\partial x}\right] \qquad [3]$$

As $\partial T/\partial t = 0$. Once Γ_m is known, a new liquid density is calculated at that node using continuity equation for the liquid. That is, $\partial \rho_l/\partial t = -\Gamma_m$.Once the liquid density becomes zero, the temperature increases again with $\Gamma_m = 0$.

Two-dimensional energy equation

From Eq 2, the two-dimensional energy equation can be expressed as follows:

$$\rho C_p \frac{\partial T}{\partial t} = \frac{\partial}{\partial x}\left(k\frac{\partial T}{\partial x}\right) + \frac{\partial}{\partial y}\left(k\frac{\partial T}{\partial y}\right) + H \qquad [4]$$

where, H is internal heat generation, for concrete: $H = -h_{fg}\Gamma_m$, for steel: $H = 0$. Eq 3 can be used for calculation of Γ_m in the two-dimensional analysis, that is

$$\Gamma_m = \frac{1}{h_{fg}}\left[\frac{\partial}{\partial x}\left(k\frac{\partial T}{\partial x}\right) + \frac{\partial}{\partial y}\left(k\frac{\partial T}{\partial y}\right)\right] \qquad [5]$$

MATERIAL PROPERTIES AND NUMERICAL PROCEDURE

In this study the thermal properties of concrete have been considered as temperature and moisture dependent and the properties of steel is temperature dependent. The details of the models used can be found in Huang (1995). The finite element method has been used as the solution technique. A non-linear fire boundary condition was used to model the heat transfer between fire and concrete surface. The temperature of a pseudo-fire is represented by a standard fire curve. The detail numerical procedure used in this paper can be found in Huang (1995).

PROVING TESTS

In this study, there are a actual test data sets, Haksever and Anderber (1981/82), with which the predictions of the analytical method are compared. The schematic diagram of cross-section of the column (2 m in length) is shown in Fig 1. The concrete used for the column specimens had a cube

strength of about 46 MPa with a testing age of 110 days. The moisture content of the concrete was measured on cubes $(0.15\times0.15\times0.15)\ m^3$ and was about 6%. The other values of parameters of normal weight concrete used in this calculation are listed in Table 1.

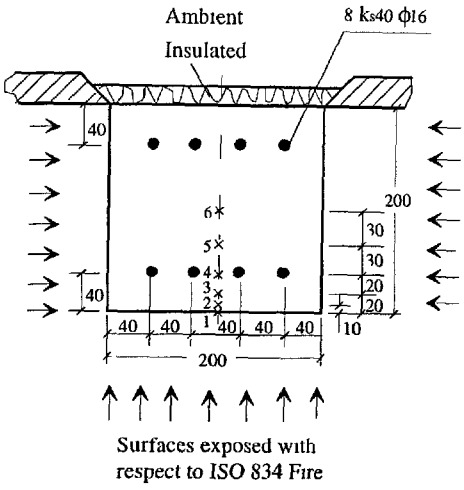

Figure 1. Schematic diagram of cross-section of column for proving tests (dimensions in mm)

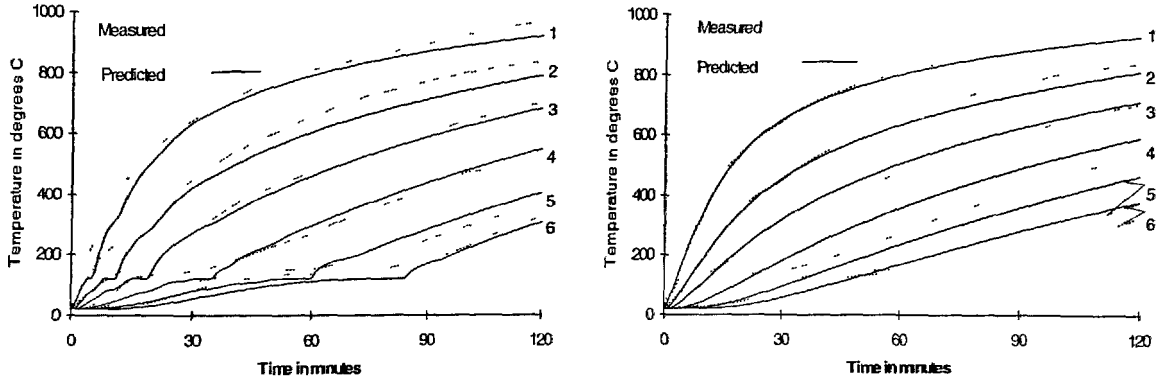

(a) (b)

Figure 2. Comparison of predicted and measured temperatures at mid-section of the column exposed to ISO 834 Fire (flame emissivity of fire = 0.75), (a) $w=6\%$, (b) $w=0$.

Results and discussion

The results of the tests are shown in Fig 2. It can be seen from both the sets of measured points and the prediction curves that the presence of moisture has a significant effect on the temperature histories in concrete during fire conditions. It is seen that, overall, the model proporsed produces a fairly good agreement with test data. To improve the accuracy of prediction the thermal properties of material at elevated temperature are required further investigation. Conclusions derived from the work include the following: (1) The model proposed in this study is capable of predicting the temperature distribution histories of cross-section of reinforced concrete structural members subjected to fires with a reasonable good accuracy, the total deviation observed over the range of parameters examined was found to be 6% to 13%. (2) The effect of moisture is significant on the temperature distribution histories in concrete during fire conditions, especially for higher initial moisture content which should be taken into account in the thermal analysis of reinforced concrete. (3) The temperature distribution histories in reinforced concrete are sensitive to the value of the flame emissivity of fire, ε_f, used. It appears reasonable to use values in the range of 0.75 ~ 0.85 for the ε_f.

Table 1 Values of the parameters used in Figure 2

$\varepsilon = 0.21$	$\rho_l^* = 985.0$	$C_{p,l} = 4187.0$	$k_m = 0.026$	$k_{d,\infty} = 1.75$	$\varepsilon_s = 0.9$
$\rho_d = 2400.0$	$h_{fg} = 2.1991 \times 10^6$	$k_{s'} = 3.31$	$v_2 = 0.5$	$v_1 = 1.0$	$C_{p,d,\infty} = 850.0$
$N = 1.25$	$A = 2.5$	$a = 0.9$	$k_l = 0.651$	$\sigma = 5.67 \times 10^{-8}$	

NOMENCLATURE

a, absorption of surface

A, convection coefficient of fire $[W\ ^0C^{-N}\ m^{-2}]$

C_p, specific heat at constant pressure $[J\ ^0C^{-1}kg^{-1}]$

C_r, $\rho_m C_{p,m} / (\rho C_p)$, heat capacity ratio, moist air/concrete

D, diffusion coefficients for Fick's law for air-vapour mixture $[m^2 s^{-1}]$

h_{fg}, heat of evaporation of water $[J kg^{-1}]$

k, thermal conductivity $[J\ ^0C^{-1}s^{-1}m^{-1}]$

$k_{s'}$, thermal conductivity of the solid phase of concrete without pores $[J\ ^0C^{-1}s^{-1}m^{-1}]$

N, convection power factor

R, gas constant per unit mass $[J\ ^0C^{-1}kg^{-1}]$

t, time $[s]$

T, temperature $[^0C]$

u, velocity $[m s^{-1}]$

v, radiation view factor (v_1 for horizontal surfaces and v_2 for vertical surfaces)

w, moisture content by weight [%]

w_i, ρ_i / ρ_m, mass fraction of specie i with respect to the density of air-vapour mixture

x, y, Cartesian co-ordinates $[m]$

α, thermal diffusivity $[m^2 s^{-1}]$

Γ_m, production rate of moisture vapour per unit total volume $[kg\ m^{-3} s^{-1}]$

ε, porosity of concrete

ε_f, flame emissivity of fire

ε_s, surface emissivity

ρ, density $[kg m^{-3}]$

ρ_l^* mass of liquid water per unit volume of liquid water $[kg\ m^{-3}]$

Subscripts:

a, air

d dry concrete

i, specie i

l, liquid

m, moist air

p, constant pressure

v, vapour

∞, ambient.

REFERENCES

Becker, J. et al, "FIRES-T: a Computer Program for the Fire Response of Structures-Thermal", Report No. UCB FRG 74 - 1, University of California, Berkely, 1974.

Bizri, H., "Structural Capacity of Reinforced Concrete Columns Subjected to Fire Induced Thermal Gradients", Structural Engineering Laboratory, Report No. 73 - 1, University of California, Berkeley, 1973.

Haksever, A. and Anderberg, Y., "Comparison Between Measured and Computed Structural Response of Some Reinforced Concrete Columns in Fire", Fire Safety Journal, Vol. 4, 1981/82, pp. 293-297.

Huang, Z., "The Analysis of Thermal and Fire Performance of Cementitious Building Components", PhD Thesis, University of Central Lancashire, 1995.

Sahota, M. S., "Heat and Mass Transfer in Porous Concrete Structures Subject to Fire", Ph.D. Thesis, University of California, Berkeley, 1976.

MECHANISM OF THE ALKALI-SILICA REACTION

Roger DRON, Françoise BRIVOT and Thierry CHAUSSADENT
Laboratoire Central des Ponts et Chaussées
58 Bd Lefebvre - 75732 Paris Cedex 15 - France

ABSTRACT The Le Chatelier principle of through-solution processes suffices to completely explain the ASR mechanism. The essential steps (dissolution of reactive silica in the alkaline pore solution and formation of reaction products from silicate solutions and solid calcium hydroxide) were studied separately *in vitro*. The properties of the system K_2O-CaO-SiO_2-H_2O are represented in a two-dimensional projection of the chemical potential diagram μ_{KOH}-μ_{SiO2}-μ_{CaO}. The formation conditions for two kinds of products (precipitates and gels) are examined.

Key-words: Alkali silica reaction, CSH, Gel, Mechanism, Phase diagram

INTRODUCTION

Most authors attribute the degradation known under the name of alkali-silica reaction (ASR) to the belated formation, within concrete made with sensitive aggregates, of masses of hydrated compounds visible under the scanning electron microscope and containing silicon, calcium and alkalis in poorly defined proportions (Dent Glasser and Kataoka, 1981, Davies and Oberholster, 1988).

Research aimed at determining the mechanism of this reaction has a practical purpose. The objective is less to describe than to provide a key for understanding what takes place in order to suggest ideas capable of preventing disorders or remedying them. If such means are effective, the proposed mechanism will stand some chance of corresponding to reality.

The experimental study of the mechanism can rarely be accomplished on the real or simulated system. The difficulty is due to the fact that, *in vivo*, the stages are not separated in time so that, at a given instant, it is possible to find simultaneously products formed at different stages and not reveal those that have only a transient or brief existence. Therefore it is necessary to begin with a hypothetical scheme based on a guiding principle and to try to obtain separately, *in vitro*, the assumed main stages, removing the reagents which intervene only in the next stages or using, as reagent, products supposed to have formed during the preceding stages. In this way, it can be shown that such stages are plausible.

THE LE CHATELIER PRINCIPLE

Based on the new vision introduced by the Gibbsian revolution, the great French scientist Henry Le Chatelier considered that cement also obeyed the essential laws of chemistry, as they were established in the early 1900. He had perfectly assimilated the subtle concepts of phase and chemical potential and knew that, at ordinary temperature, transfer of matter is practically nonexistent in the solid state. Thus he drew the conclusion that the aqueous solution, that filled the pores of cement paste, was the surface dissolution agent of the anhydrous phases, as well as the vehicle of the resulting ions and the mother liquor of the hydrates.

In connection with this aspect of Le Chatelier's work, one should not speak of theory. What was involved was simply a scientific attitude, let us say a principle, more general than the crystalloid theory that he deduced therefrom. We shall use this unique guiding idea as our support.

SOURCES AND RESERVOIRS OF REAGENTS

Alkalis come mainly from the cement itself. Initially present in the diffuse state in the anhydrous phases, during hydration they go to the liquid phase under the form of K^+OH^- and Na^+OH^- and, as they do not take part in the formation of normal cement hydration products, they accumulate in the interstitial solution until a concentration of about 1 $mol.l^{-1}$. The quantity present in solution is thus, approximately proportional to the degree of advancement of the hydration reaction but the concentration grows slightly faster, owing to the partial consumption of water. As both asymptotic behaviours are approached simultaneously, it may be said, roughly, that the first condition of the alkali-reaction is met only when hydration comes to an end. The alkali reserve is then totally in a dissolved form.

Reactive silica of interest to us is, by definition, that of the aggregates. Every variety of silica is practically insoluble in pure water but, because of the acid nature of SiO_2 , some may dissolve in anionic form in aqueous solutions of strong bases. The action of such a dissolution process in the alkali reaction is altogether plausible since, in hardened concrete, the requisite conditions are met by the accumulation of alkalis. The equilibrium to which it leads depends on both the final pH and the reacting solid variety. To this component of the reactivity, of a thermodynamic nature, should be added the kinetic component which, in practice, may turn out to be more important.

The most accessible source of the CaO constituent is portlandite present in the hardened paste under the form of microcrystals dispersed in a rather uniform manner. However, its dissolution is problematical because the law of the solubility product, $K_s = [Ca^{2+}].[OH^-]^2$, applies to the equilibrium of dissolution. In the very basic medium resulting from the accumulation of alkalis, the Ca^{2+} ions have an extremely low concentration level. They can initiate a reaction but they do not enable it to be maintained considering that their available amount in solution is very weak. However, even partial, their consumption in any reaction is sufficient to make the solution undersaturated, thus leading to a dynamic shifting of the dissolution equilibrium. Due to this coupling, the solution can take, as it requires, the calcium hydroxide from the solid reserve.

In the absence of any diffusion, the silica and calcium hydroxide dissolution process would be located in the vicinity of the liquid-reagents solid interface. Diffusion alone can ensure the transfer of matter beyond, and only in dissolved form, in this case ions. Indeed it is by diffusion that the Ca^{2+} and OH^- ions coming from the dissolution of the portlandite as well as the silicate ions resulting from the attack of the silica can move away from the interface. Diffusion also allows, in the opposite direction, the supply of OH^- ions necessary for this attack and the movement that brings these ions into contact with each other.
It is thus possible to find, within the solution, under certain conditions and in varied forms, at certain locations and at certain moments, in addition to water, which is omnipresent, the ingredients necessary for the formation of hydrated compounds including lime, silica and alkalis if two fundamental acts take place *in vivo*:
- changeover to solution in the form of anions of reactive silica by hydroxyl attack.
- reaction of these anions with the cation Ca^{2+}, coupled with the dissolution of the portlandite.

EXPERIMENTAL PART

The research consisted in reproducing separately *in vitro* the two acts considered above. Silica attack by alkaline solutions was investigated in the absence of calcium hydroxide and, in the study

of the reaction between calcium hydroxide and the dissolved silicates, we used synthetic solutions similar to those resulting from the attack of the silica.
The basis of this research and the results were published in several articles to which it may be useful to refer (Dron *et al.* 1992, 1993, 1994, 1996). In the present general article, we shall explain the approach, summarise the essential findings, develop the interpretation and draw the consequences.

Dissolution of silica in alkaline solutions

The principle and the operating conditions were those of the ASTM C 289-71 test. Three parameters (contact time, temperature and sodium concentration) were varied in relation to the standard version. In the present study, 50 ml of sodium solution was allowed to act on 25 g (160-315 μm grains) of the tested aggregate. An original apparatus makes it possible to maintain the suspension.
The measurement is based on the analytical determination of the amount of silica going into solution for a given time. We worked on different varieties of silica, in particular an opal from central France. Its high reactivity enabled us to complete the entire process in 24 hours, the composition of the solution did not show any further change after that time.
The existence of an induction period of about one hour is noted. A steady state is then established, with the rate decreasing gradually towards zero as the silica concentration approaches the sodium concentration (0.5 $M.l^{-1}$ or 1 $M.l^{-1}$).
The dissolution rate, measured at the inflexion point, is approximately proportional to the OH^- concentration (kinetic order near 1). It is divided by 2.8 when the temperature drops from 67 to 57°C, which corresponds to an activation energy, taken from the law of Arrhenius, of 96 $kJ.M^{-1}$.
It is deduced that the standard ASTM test, conducted at 80°C, is accelerated by a factor of the order of 400 in relation to what it would be at 25°C.
This rate depends essentially on the variety of silica. For the solution at 1 $M.l^{-1}$, the rate, expressed in moles per litre and per hour and referred to 25°C, was found to be equal to 7.10^{-7} for quartz, 9.10^{-5} for silex and 5.10^{-3} for opal, representing a progression by a factor of about 100.

The gradual slowing of the attack is explained quite easily by the conventional calculation of species in solution. When the solution becomes richer in silica, the Na^+ ion concentration remains constant while the pH and the anion charge decrease in a related manner.

Difficulties related to the presence of polymer forms are avoided by considering the species S^0, S^1 and S^2, defined by a silicon site linked to zero, one or two charged oxygen carriers, or HO-Si-OH for S^0, HO-Si-O^- for S^1 and $^-$O-Si-O^- for S^2. For the couples S^0/S^1 and S^1/S^2, the values of pK_a are taken equal, namely 9.8 and 12.6, to the corresponding monomer couples ($H_3SiO_4^-$ for S^1 and $H_2SiO_4^{2-}$ for S^2).

Fig 1 summarises the results of these calculations. It shows that the form S^1 becomes exclusive (average anionic charge per atom of silicon tending towards -1) as the pH tends towards 11.2.
At the maximum amount of S^1, the pH has fallen to the theoretical value of 11.2 so that, for kinetic as well as thermodynamic reasons, the attack can no longer continue further.
It is in fact the electroneutrality of the solution that fixes the final concentration of silica at a level near that of the alkaline ions, which remains constant throughout the attack.
In our experiments, such a limit was reached only in the case of opal. The time required for this saturation in an agitated medium depends only on the liquid/solid ratio.

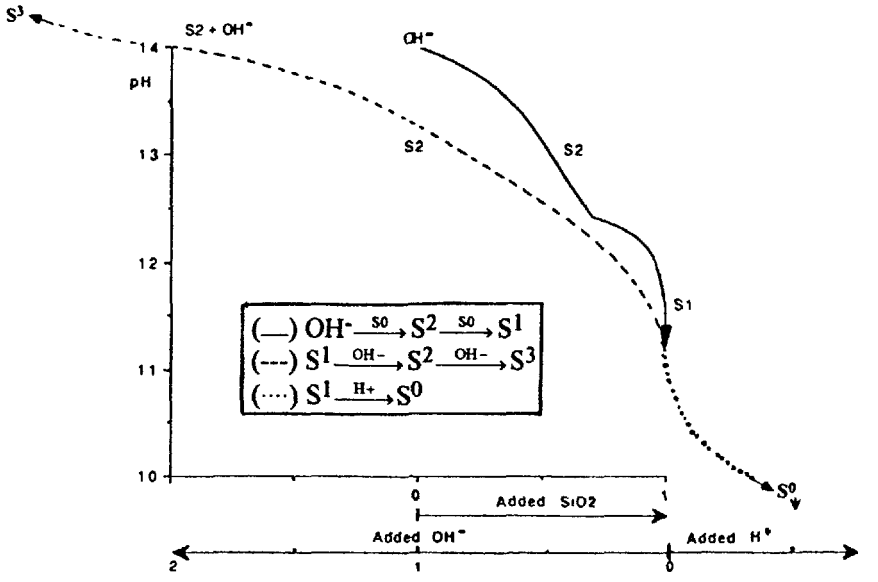

Figure 1 Acid-base reactions with silica entities in solution

In the real system, diffusion occurs, and the saturation time depends in particular on the thickness of the film in which the produced solution is confined. Considering the liquid-volume/reactive-surface ratio allows this thickness to be estimated. In the ASTM test, it is of the order of one millimetre and would be about ten times smaller for concrete containing 1,250 kg of a reactive aggregate exhibiting an area of 0.5 $m^2.kg^{-1}$.
The orders of magnitude found in the case of silex would allow the approach of saturation with time of the scale of a year, and even less if the attack liquor remained confined in the vicinity of the reactive surface.

Interpretation in light of NMR spectroscopy of ^{29}Si

This research technique provides precise information on the distribution of the many siloxane bonds, from 0 to 4, around silicon atoms (sites Q^0, Q^1, Q^2, Q^3 and Q^4) and thus enables the interpretation of experimental facts on the scale of atomic arrangements.
Differences in reactivity between the various varieties of silica are thus explained to a great extent by differences in structure: practically inert forms such as quartz are made up only of Q^4 entities, i.e. each silicon atom is bound to four others by siloxane bridges. They are partially replaced in the reactive forms by Q^3s, the fourth bond being occupied by a hydroxyl (silanol group). The induction period may be related to the breaking of the Q^3s prior to the Q^2s one which would then take place during the actual attack phase. This would also explain the loss of alkalinity observed during the attack of large specific surface materials, such as silica gel, by chemisorption of the K^+OH^- couple at the breaking place of the Q^3.
Also very instructive are the studies of NMR of ^{29}Si relative to alkaline silicate solutions. Engelhardt and Michel (1987) investigated the distribution of Q^n entities on solutions of various silica concentrations, on the one hand, and various $R_m = [SiO_2]/[M_2O]$ on the other.
We adjusted these data on semi-empirical expressions, i.e. forms such that, upon approaching the limit values, they are rigorous for theoretical reasons (Dron, 1994). Thus we were able to

calculate the relative abundance of each Q^ns for any composition and, especially for the fixed concentration $[Na^+] = 1$, the percentage of each form as a function of the concentration $[SiO_2]$.
Monomers, which correspond to the Q^0s, represent the majority in low concentrations of silica and become a very small minority upon the approach of $[SiO_2] = 1$ mol.l^{-1}, whereas Q^3s begin to appear. Neglecting the contribution of Q^3s, it is possible to deduce the average length of the linear polymers.
Monomers are predominant as long as the SiO_2 concentration does not exceed 0.4 mol.l^{-1}. Above this concentration, linear-chain polymerisation becomes dominant. Then, branched-chains appear, revealed by the presence of Q^3 sites. We shall consider that, at the start of the attack, the only silicate anions compatible with the high alkalinity are monomers, essentially the $H_2SiO_4^{2-}$ species, whereas, as we approach saturation, the linear-chains having about five patterns become the predominant form. The branched-chains, revealed by the Q^3s, become significant only upon approaching the limit concentration level at 1 mol.l^{-1}.

Reactions between calcium hydroxide and alkaline silicate solutions

We used an extensive experimental framework bringing together, under agitation, a fixed amount (1 g) of finely dispersed calcium hydroxide and a fixed volume of potassium silicate solutions (100 ml).
These synthetic solutions were prepared by mixing commercial silicate (ratio $K_2O/SiO_2 = 3.8$), potash 4 M.l^{-1} and water. thus it was possible to vary, as desired and independently (in steps of 0.25 M.l^{-1}), the silica and potassium concentrations. Work based on very similar principles had been undertaken independently by Way and Shayan (1992) who, reaching the same conclusions as we did, published the results before us. We have noted their priority (Dron and Brivot, 1993) and stressed the points of agreement which appear to be essential, and which we are repeating below, namely:
"The existence of two fields in the space x = [K], y = $[SiO_2]$ at equilibrium when a fixed amount of calcium hydroxide has been added to solutions of KOH and SiO_2 in various proportions. The lower field corresponds to precipitates + mother liquor. The upper field corresponds to macroscopically homogeneous gels impregnated by a serum. The precipitates are characterised by XRD as similar to C-S-H(I) and the gels are amorphous systems with a broad band centred at 0.305 nm. There exists a definite relation between the composition of each washed solid and the composition of the corresponding mother liquor or serum."
We pointed out in the same discussion the most important of our observations:
"The system, obtained by mixing up to 1.85 g of calcium hydroxide and 100 ml of potassium silicate solution [K] = 2 M.l^{-1}, $[SiO_2]$ = 1.5 M.l^{-1}, exhibits the surprising behaviour of complete dissolution of the particles and leads to a clear and fluid solution, as if Ca^{2+} were complexed, as it is by EDTA in high pH media."
Our NMR studies of ^{43}Ca (Nieto *et al*, 1995) have demonstrated a very close kinship of the Ca's present in the complex and the gel, very different from the Ca^{2+}s. The coagulation could result from a rearrangement of the Si-O···Ca···O-Si intra-ionic bridges into inter-ionic bridges.

Diagram of chemical potentials governing equilibria

On the occasion of the International Congress on Cement Chemistry which was held in Moscow in 1974, we pointed out the great interest for cement chemistry of the representation of ternary and quaternary systems in equilibrium by chemical potential diagrams in bidimensional projection (Dron, 1974). Then we then applied this to the $CaO-Al_2O_2-SiO_2-H_2O$ system and stressed its advantages over former representations. Those findings apparently did not come to the attention of Gartner and Jennings (1987) who later developed the same idea.

In our opinion, the value of these diagrams is not of a descriptive nature but rather of an explanatory, and even pedagogical nature. They contain all the thermodynamic information available and their remarkable simplicity results from the use of variables which are linear by construction. The relative arrangement of the phase domains and the slope of the straight lines which generally separate them are of greater importance than their exact position. Thermodynamic tables have, in the best of cases, only data relative to the compounds with fixed and integer stoechiometric coefficients, which is almost the exception in cement chemistry. For the others, the only data available are those of the chemical analysis of the solid phases and of the solutions. They can be translated by means of conventional formulae into solubility products and, more generally, into ionic products whose logarithm is an affine magnitude of the chemical potential. Taking into account the activity coefficients changes nothing in the general configuration and very little in the position of boundaries. They may be omitted without detriment and only what is essential may be considered. What is essential, in the present problem, is relative to the variance.

The K_2O-CaO-SiO_2-H_2O system has four independent constituents. The aqueous phase is always present. At constant pressure (1 atm) and temperature (298°K), the variance is $V = 4 - \Phi$. Let $\Phi' = \Phi - 1$ be the number of solid phases. Then we have $V = 3 - \Phi'$.

The number of solid phases in equilibrium, always at least equal to one, is thus at most equal to three ($V = 0$). A first version of the chemical potential diagram based on this conventional vision is represented in Fig. 2a.

The calculations were carried out on the basis of usual rules of the chemistry of solutions: conservation of matter, electroneutrality, action mass law applied to concentrations. They include an important innovation: they make use, not of silicate ion concentrations, which is not possible given the polymerisation, but those of S^0, S^1 and S^2 entities as we defined them earlier.

The chemical potentials are calculated by means of the following relations:

$$\mu_{K2O} = 2.R.T.\ln[K^+].[OH^-] \quad \mu_{SiO2} = R.T.\ln[S^1]/[OH^-] \quad \mu_{CaO} = R.T.\ln[Ca^{2+}].[OH^-]^2$$

Within a given domain, the orientation of the level lines of the chemical potential of CaO is obtained by applying the Gibbs-Duhem relation (taking $d\mu_{CaO} = 0$) for the local stoechiometry. The slope of the frontier between two contiguous domains is obtained by elimination of μ_{CaO} between the equations of the two corresponding plans.

Determined by establishing the coherence of all our analytical results, this version is true only as a first approximation. The difference with reality is not so much the result of simplifications which were made during the calculation, but is due rather to the fact that no account is taken of two basic characteristics resulting from our experimentation:

a) Monovariant lines (phase domain boundaries) and the supposed invariant points are formally contradicted by the absence, at the expected locations, of any link between the two composition variables [Si] and [K] of the liquid phase.

b) The composition of solid matter, which is expressed by the couple (K_2O%, SiO_2%), varies in a strictly continuous manner within a given domain.

In the μ_{K2O}-μ_{SiO2}-μ_{CaO} space, the diagram 2a would be represented by a polyhedral whose sides intersect two by two on straight edges, converging at the invariant points. For most of them, these edges have no existence. They are rounded off and we go strictly in a continuous manner from one domain to another, to the extent that one can still speak of domains.

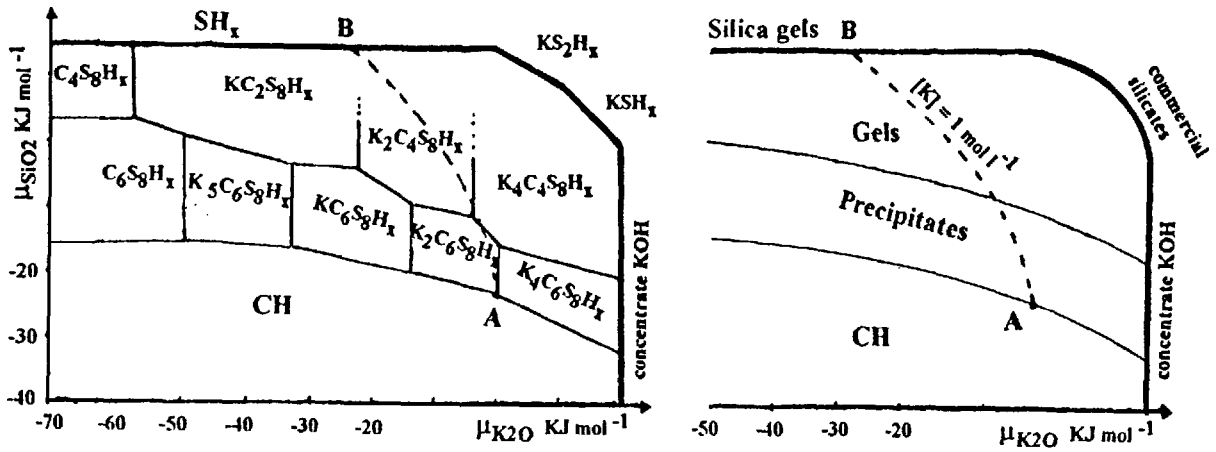

a: Idealized diagram

b: General features of the true diagram

Figure 2 Chemical potential diagram

The correct orientation (Fig 2b) of the level lines μ_{CaO} = cte was determined, for each of the experimental points, by using, in the application of the Gibbs-Duhem relation, the effective composition of the solid phase.

CONCLUSION

Chemical potential is a local, instantaneous and evolutive magnitude. It is thus possible to characterise an element of active volume, in local equilibrium, by a point on the diagram. For this, we shall initially use the approximate version of Fig 2a, more pedagogical and easy to transpose later mentally on the more correct version of Fig 2b.

At the "zero" instant of the ASR, which we take towards the end of the hydration of cement, the interstitial liquor is roughly the same throughout. It contains about 1 mol.l^{-1} of OH^- and is saturated in $Ca(OH)_2$, which places it at point A.

The interstitial liquor in strict contact with the portlandite has no reason to evolve, but the one in contact with the reactive silica tends to equalise its potential with that of the solid phase so that evolution takes place in the direction of point B.

This situation would remain in the absence of any diffusion, but its occurrence will upset this precarious equilibrium, the course of events being determined by the choice of the limiting stage.

a) <u>If the limiting stage is the attack of the silica:</u> The diffusion assures the evacuation of the rare silicate ions formed, first in the surrounding alkaline liquor, where they depolymerise into $H_2SiO_2^{2-}$ monomers and co-precipitate with the rare Ca^{2+} ions, renewed immediately after being consumed, in the presence of many K^+ ions. The figurative point will separate from point A only what is necessary for adjusting the dissolution flux of the portlandite. The neo-formed product will be a precipitate, and in any case a crystalloid, because it is made up of ions which are sufficiently small so as not to be arranged randomly. This product does not have two phases as diagram 2a would suggest, but a single phase (continuous solid solution) of intermediate composition in conformity with diagram 2b. This calm precipitation in quasi-equilibrium does not involve a high energy level and hence is of no great danger for the structure.

b) <u>If the limiting stage is diffusion:</u> The process described in (a) is restricted to the immediate vicinity of the solution-reactive aggregate interface and takes place until the depletion of the immediately accessible portlandite. The figurative point moves in the direction of point B following the line [K] = 1 mol.l^{-1}. A radical dissymmetry is established in the concrete:
- in contact with the aggregate, we find a solution saturated in silica represented by point B. The silicate ions forming it are mostly polymers.
- throughout the rest of the paste, including portlandite, the solution is represented by point A.
It is at the interface between the two antagonist domains that the destructive reaction occurs. This means the complexation of the Ca^{2+} ion by the silicate polyanions which take it from the surface of the portlandite crystals, inexorably gnawing at them. The representative point of the solution of the complex, as long as a solid phase does not form, is free to escape over the surface (flat or curved) which will be assigned to it *in fine* by the return to equilibrium. The level of μ_{CaO} can rise up to that of the portlandite. The break of this metastable equilibrium takes place in the form of a coagulation, in which the disorder increases as the difference increases between the present system, at a very high lime potential, and the biphase stable system (matrix + serum, gel in the sense of colloid chemistry) to which it is transformed. The free energy made available by this sudden break can cause irreversible mechanical damage, especially as it occurs in a sector made fragile by voids resulting from the dissolution of the portlandite. It can be understood why the solid which forms under such conditions and from very disparate and partially branched polyanions is completely amorphous. This gel moreover has properties liable to attract pure water by an osmosis phenomenon.

REFERENCES

Davies, G. and Oberholster, R.E.,"Alkali-silica reaction products and their development", Cem. Concr. Res., Vol. 18, No. 166, Sept., 1988, pp. 621-635.

Dent-Glasser, L. and Kataoka, F., "The chemistry of alkali-aggregate reactions", Proc. 5th Int. Conf. on Alkali-aggregate Reaction in Concrete, Cape Town, 1981, S252/23.

Dron, R. and Brivot, F., "Thermodynamic and kinetic approach to the alkali-silica reaction", Cem. Concr. Res., Vol. 22, No. 5, 1992, pp. 941-948, and Vol. 23, No. 1, 1993, pp. 93-103.

Dron, R. and Brivot, F., "A discussion on the paper of S.J. Way and A. Shayan", Cem. Concr. Res., Vol. 23, No. 4, July 1993, pp. 1001-1002.

Dron, R. "Experimental and theoretical study of the CaO, Al_2O_3, SiO_2, H_2O system" , The VIth Int. Congr. on the Chemistry of Cements, suppl. paper, Section II, Moscow, 1974, pp. 3-16.

Dron, R. and Brivot, F., "Solid-liquid equilibria in K-C-S-H/H_2O systems", 10th Int. Conf. on Alkali-aggregate Reaction in Concrete, Melbourne, 1996.

Dron, R., "Polymerization of silicate ions in aqueous solutions", Workshop on Applications of NMR spectroscopy to cement science, held in Guerville, France, 25-26 March 1992, edited by P. Colombet and A.-R. Grimmer, Gordon and Breach Science Publishers, 1994, pp. 403-412.

Engelhardt, G. and Michel, D., High resolution solid state NMR of silicates and zeolites, John Wiley & sons, Chichester, 1987.

Gartner, E.M. and Jennings H.M., "Thermodynamics of calcium silicate hydrates and their solutions" J. Am. Ceram. Soc., 70[10], 1987, pp. 743-749.

Nieto, P. Dron, R., Thouvenot, R., Zanni, H. and Brivot, F., "Etude de la transformation sol-gel du complexe calcium-polysilicate par RMN du ^{43}Ca", C. R. Acad. Sci. Paris, t. 320, Série II b, 1995, pp. 485-488.

Way, S. J. and Shayan, A. ,"Study of some synthetically prepared hydrous alkali-calcium silicates", Cem. Concr. Res., Vol. 22, No. 5, Sept., 1992, pp. 915-926.

THE MECHANISM OF WATER AND IONIC PERMEABILITY OF CONCRETE

Arkady N. PLUGIN, Irina G. PROKOPOVA, Kharkov State Academy of Railway Transport, Ukraine
Stan WILD, University of Glamorgan, United Kingdom
Andrei A. PLUGIN, Kharkov State Technical University of Construction and Architecture, Ukraine

ABSTRACT The durability and serviceability of concrete structures are resulting from deformation and filtration properties of concrete and construction. Mechanism of these properties and tensile strength are described by fundamental aspects of Colloid Chemistry and Physico-Chemical Mechanics and corresponding equations are given. New methods of concrete composition calculation, new methods of concrete water permeability measurements, new methods and materials for concrete protection are developed with help of the new theoretical concept.

Key-words: structure, durability, permeability, water, ions.

INTRODUCTION

Insufficient durability and serviceability of concrete structures are resulting from imperfection of theoretical concepts about concrete structure, concrete deformation and filtration properties and imperfection of assessment and diagnostic methods too. Our theoretical concepts on these aspects are based on fundamental aspects of Colloid Chemistry and Physico-Chemical Mechanics of dispersed systems and materials developed by us with allowance for electrosurface properties, phenomena and interactions in cement-water systems (Plugin, 1989; Plugin and Plugin, 1995; Plugin et al, 1995).

When heavy concrete is compressed the stress is transferred in a form of two components - the uniformly distributed one between broken stone and mortar and the concentrated (contact) stress in the interphases between them. It is considered that the stone grains are incompressible in comparison to the mortar component of concrete. At this condition, the relative deformations and stresses in the interlayers between the grains are much higher than in the space between the stone grains. The analogous situation on the distribution of relative deformations and stresses takes place between the grains and particles (structure forming elements SE) in the mortar component and the cement paste of concrete. Accordingly, the destruction of concrete, mortar and cement paste begins with the deformations in the compressed contacts and the subsequent destruction of the stretched contacts between the SE at different structure levels. Depending on the concrete structure, redistribution of stress between matrix and structure forming elements in all the levels takes place under the influence of gel water filtering from the matrix into the pore space.

The above-stated predetermines that the structure, strength and deformations of the interlayers and the filtration properties of cement paste play leading role in demonstration of strength and deformation properties by cement paste and concrete as a whole.

THE STRENGTH THEORY. THE WATER FILTERING FROM GEL

Concrete is a polydispersed system, in which different levels - macro-, mezo-, micro-, submicro- and supermolecular of structures are combined. These levels are characterized by medium sizes of the structure forming elements (SE), accordingly large aggregate - 10-15mm, sand - 0.2-0.5mm, unreacted cement particles - 10-50μm, microcrystalline hydration new formations - 250-500nm, hydrosilicate gel particles - <50nm. Since the structure is a multi-level one, matrix is disperse and

consists of its structure forming elements - matrix particles (PM) (sand particles in concrete, cement particles in mortar, new formation particles in cement paste). The experiments and calculations show that the width of matrix layer in each level is comparable to the sizes of the structure forming particles of the matrix (PM). It allows to represent a generalized model of the matrix in interlayer in a form of three possible patterns of the matrix particles packing between the SE, Fig.1. The packing optimal by the average number of the contacts, density, tensile strength and deformability is the one shown in the Fig.1b,c. The coefficient of the structure forming elements (particles) extension (removing) is the generalized characteristic of the particles packing in the structure:

$$K_r = V_m / V_{pse}, \qquad [1]$$

where V_m - matrice volume, m^3; V_{pse} - volume of a pore in the skeleton, produced by structure forming elements, m^3.

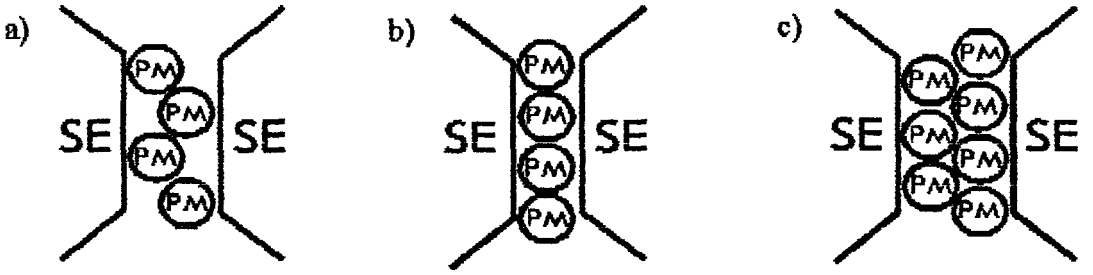

Figure 1 The generalized model of matrix in interlayer.

Among the hydration products microcrytalline hydration products have positively charged surfaces (positive electrosurface potential). The rest - negatively charged (except carbonate aggregates) (Plugin,1989; Babushkin and Novikova,1973). The electrosurface potentials ψ of some minerals are shown in Table 1.

Table 1 The electrosurface properties of some materials

Materials	ψ_0, v	ψ_{pH12}, v	n_c, $1/m^2$	n_e, $1/m^2$	a, nm	z_{pdi}	d, nm
quartz SiO_2	-0.55	-	$4 \cdot 10^{15}$	$4 \cdot 10^{15}$	6.0	4	0.152
portlandite $Ca(OH)_2$	-	+0.54	$9.8 \cdot 10^{15}$	-	10.2	2	0.240
tobermorite-like hydrosilicates $C_5S_6H_n$	-	-0.44- -0.56	$7.6 \cdot 10^{15}$- $-9.6 \cdot 10^{15}$	-	11.7- -10.4	2	0.405

According to our concepts about electroheterogeneous hardening of the cement paste, mortar and concrete structure is resulting from electroheterogeneous contacts EHC (between opposite charged surfaces of the structure forming elements). EHC determine strength, water resistance and hydraulic properties of portland cement concretes. An equivalent scheme of the EHC is presented in Fig.2 where a positively charged crystallohydrate block forms contact with a negatively charged surface of crushed stone or sand surface or with particles of hydrosilicate gel. The latter ones can be spherical, scaly or fibrous. The equivalent scheme of EHC type presented allows to apply the Physico-Chemical theory of dispersed systems strength by Rehbinder-Schukin (Rehbinder et al, 1964) and the formula of tensile strength of such systems modified by us (Plugin et al, 1995) to qualitative analysis of tensile strength of concrete, mortar and cement stone:

$$R_t = P \cdot n \cdot \gamma, \qquad [2]$$

where P- strength of bonding between the active centers (potential determining ions PDI); n - surface

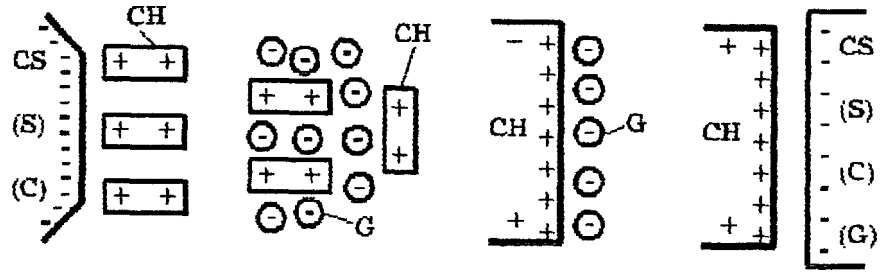

Figure 2 The equivalent scheme of the electroheterogeneous contacts (EHC): CS, S, C, CH, G - particles of crushed stone, sand, crystallohydrates, gel. CS-S-CS - macro-level; S-C-S - meso-level; C-CH,G-C - micro-level; CH-G-CH - submicro-level.

concentration of the active centers; γ -share of surface occupied by structure forming elements SE in tension cross-section.

Surface charge q, Kl/m^2, surface concentration of the charges (PDIs) n, 1/m^2 and electrosurface potential ψ, v are connected by equation for flat double electrical layer DEL:

$$n = \frac{q}{ze} = \frac{\varepsilon\varepsilon_o\psi}{4\pi dze}, 1/m^2, \qquad [3]$$

where ε, ε_0 - relative dielectric permeability and absolute dielectric constant (ε_0=8.85×10^{-12}); d - distance between potential determining ion PDI and anti-ion AI (counter ion) in dense DEL (between cation and anion), m; z - valence of ion; e - electron charge, 1.6×10^{-12} Kl. Quantity d is determined with the help of the crystallographic characteristics, i.e. the length and ionic bond direction. The calculated quantities of the surface concentration of the potential determining ions n_c and experimental n_e - of the active centers for the quartz SiO_2, for the portlandite and calcium hydrosilicate $C_5S_6H_n$ (tobermorite-like) are shown in Table 1.

The bonds between structure forming elements in different levels are determined by interactions between surface active centers, t. i. between potential determining ions and the total strength of solids in addition to it is determined by their concentration. The attractive force in this bond is determined by equation:

$$P = \frac{z_1 z_2 e^2}{8\pi\varepsilon\varepsilon_o h^2} + \frac{2z_{1(2)}\psi_{1(2)}\mu_d}{4\pi\varepsilon\varepsilon_o h_\mu^3}, N, \qquad [4]$$

where h - distance between the interacting ions (centers), m; μ_d - dipole moment of water molecule, (6.1×10^{-12} Kl·m). The tensile strength of such bond R_t=P/S_{ion} (S_{ion} - area of ion) is equal to 10^4-10^5 MPa. It is in accordance to theoretical tensile strength of solids. Real tensile strength of solids may be determined by the next formula:

$$R_t = \left(\frac{z_2 e\psi_1}{32\pi^2 d_1 h^2} + \frac{z_2\mu_d\psi_1}{8\pi^2 z_1 d_1 h_\mu^3}\right)\cdot\gamma = \left(\frac{508 z_2\psi_1}{d_1 h^2} + \frac{773 z_2\mu\psi_1}{z_1 d_1 h_\mu^3}\right)\cdot\gamma, Pa, \qquad [5]$$

where 1, 2 - correspond to the opposite charged ions.

The main structure forming elements in portland cement are the positively charged portlandite and hydrosulphoaluminate microcrystals, but the gel-like products are represented mainly by hydrosilicates. The submicrocrystalline hydrosilicate particles of xonotlite and tobermorite compounds of $C_5S_6H_n$ type, where n = 0,5-2,4 for 9-14 A° tobermorites, are the most imposing ones accordingly to (Ilukhin, 1979). Lets assume 14 A° tobermorite to be basic one. Its electrosurface potential ψ = -0,44 V. The parameters of bonding in active center are: d=2.4A°, h=5.2A°, h_μ=2.8A°, z_i=2. According to Eq.5 strength of cement stone (at γ=1) R_t=13.3MPa. Having assumed that compres-

sion strength exceeds tensile strength 10 times ($R_c \approx 10R_t$), which is inherent to concretes and other stone materials, we obtained $R_c^c \approx 133$MPa , which corresponds with experimental data $R_c \approx 140$MPa.

The γ value which determines concentration of the electroheterogeneous contacts in a unit of stretched cross-section, is calculated as a product of concentration of crystallohydrates γ_{ch} in cement paste and concentration of gel γ_g in water.:

$$\gamma = \frac{2CA\alpha_h \cdot 1.5}{\rho_{ch}\left[(C/\rho_c) + W - W_{cc}\right]} \times \frac{CB\alpha_h \cdot 1.5}{\rho_g W} = k\frac{(C/W)^2}{C/W + \rho_c\left[1-(W_{cc}/C)/(W/C)\right]}, \quad [6]$$

where $k=6.6\alpha_h^2AB$; A and B - stoichiometric mass correlation of crystallohydrate and gel products of cement hydration; α_h - hydration pitch. The coefficient 2 is to take into account that the electro-heterogeneous contacts form in both surface of break of cement stone. The coefficient 1.5 is surface concentration-to-volum concentration ratio. At A=0.57, B=0.67, α_h=0.5, W_{cc}/C=0.25 quantity k=0.26. The results of calculations γ^c and R_c^c and the corresponding experimental data received by Sitnikov and Vandone (Italy) independently and presented in (Kireyenko,1961) are given in Table 2.

Table 2. The calculated and experimental data on γ and R, MPa.

W/C	C/W	Experimental data		Calculated data		
		R_c^e	γ^e	γ^c	R_c^c	$\gamma^{sp}=\gamma^c R/138.7$
0.1	10	42	0.3	0.35	46.7	0.34
0.2	5	105	0.75	0.74	98.7	0.71
0.25	4	140	1	1.04	138.7	1
0.3	3.33	100	0.71	0.75	100	0.72
0.4	2.5	60	0.43	0.44	58.7	0.42
0.5	2	40	0.29	0.29	38.7	0.28
0.6	1.67	26	0.19	0.21	28.0	0.2
0.7	1.43	17	0.12	0.15	20.0	0.15
0.8	1.25	12	0.09	0.09	12.0	0.09
0.9	1.11	9	0.07	0.08	10.7	0.08
1.0	1	7	0.05	0.07	9.3	0.07

The calculated values of strength R_c^c and specific coefficient $\gamma^{sp}=\gamma^c R/138.7$ are very close to the experimental data. Therefore it is very difficult to evaluate the difference between the calculated and experimental data in graph (Fig.3). This fact demonstrates the correctness of the theory and the cement paste strength formula offered, which allows to explain nature of strength of cement stone, mortar and concrete on this basis.

Strength of cement paste, mortar and concrete is determined by the number of electroheterogeneous contacts EHCs in the stretched cross-section. The influence of W/C on strength is connected with decrease of crystallohydrates concentration. The compression strength exceeds the tensile strength because the compression force is taken not only by stretched EHC but by the compressed EHC and electrohomogeneous (with the same charged surfaces between gel particles) ones as well. The latter one favors uniform distribution of load all over the volume of cement paste and concrete, because hydrosilicate gel is the finest dispersed component of hydrate new formations. The gel specific surface ($S_g \approx 200 m^2/g$) is considerably higher the one of crystallohydrates ($\approx 2\text{-}5 m^2/g$). Therefore, it is possible to obtain that whole physico-chemical combined water ($W_{pcc} = W - W_{cc}$, where W - initial water, W_{cc} - chemical combined water) belongs to hydrosilicate gel. The electron microscope

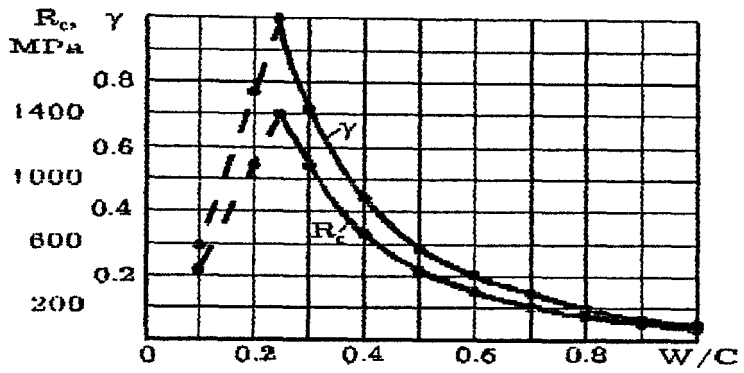

Figure 3 Depending calculated and experimental quantities strength R_c and coefficient γ^{ep} from W/C

photos made by Wild et al (1990) are the convincing demonstrations of moisture capacity of hydrosilicate gel.

Submicrostructure and microstructure of the cement paste will be optimum if $(W/C)_{opt}=0.25$. In this case hydrosilicate gel particles of different forms are connecting crystalline particles by electroheterogeneous mechanism in optimum dence crystallohydrate skeleton. There is forming of openwork skeleton filled with floaded gel and there are conditions for the extrusion of water from gel and for the concrete deformations in case $W/C>(W/C)_{opt}=0.25$. The skeleton is porous if $W/C<(W/C)_{opt}$.

Hydrosilicate gel under load at W/C>0.25 compresses at the expence of water filtering out of it but into pore space. As it is compressed the load is taken by crystallohydrate frame by means of its compressing EHCs, and as these contacts are compressed the load is transferred to the stretched EHCs. In the limiting state, which corresponds to strength of cement paste and concrete, water molecule is removed out of the elementary contacts and the contacts move together till the Ca-O chemical bonding formed between potential determining ions in active centers. In this case, the d and h distances become equal to the length of chemical bonding d=h=2,4A° and the contact in each active center of portlandyte is realised. In case of absence of water in the contact, its electrosurface potential becomes equal to ψ_0=+1.25v.The pressure needed for such contact formation is equal to R_{cc} = 91.9MPa.

The structure of crystallohydrate frame with the EHC compressed till the chemical bonding formed correponds to the structure of cement paste with limiting strength and W/C=0.25. The width of water layer in hydrosilicate gel h_g and gel resistance R_g, Pa in this case are equal:

$$h_g = \frac{W_{pcc}}{S_g} = \frac{W - W_{cc}}{BC\alpha_h S_g / \rho_g} = 4.23nm, \qquad R_g = \frac{q\psi}{2h_g} = \frac{\varepsilon\varepsilon_o\psi^2}{8\pi d h_g}, \qquad [7]$$

For ε=40 and ψ=+1.25v R_g=22MP and the resulting compression strength $R_c = R_{cc} + R_g + R_t = 91.9 + 22.0 + 13.3 = 127.2$ MPa. Accordingly $n=R_c/R_t=127.2/13.3=9.5\approx10$, which corresponds with real values.

The γ value in the strength equation and, therefore, the number of electroheterogeneous contacts and, correspondingly, strength and durability of cement paste and concrete depend not only on W/C but on composition of products of cement hydration. Here, the maximum strength will be reached if the optimum ratio between the number of positively charged particles of crystallohydrates and all other negatively charged particles will take place. The curves in Fig.4 confirm this statement. They are the

curves for two-component silicate systems and aluminate binders. One can see sharp extremums at the points of the optimum ratio beween mass of crystallohydrate products of hydration and mass of gel hydration products.

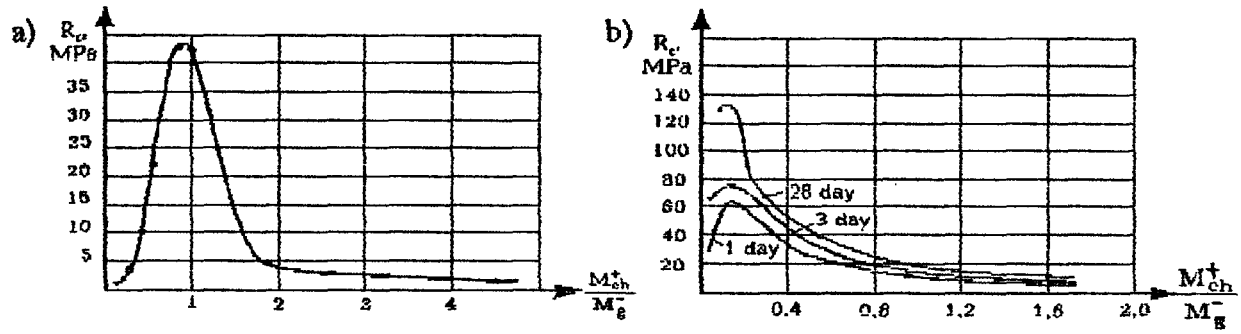

Figure 4 Depending R_c from ratio between the mass of positively charged crystallohydrate products M_{ch}^+ and the mass of negatively charged gel products M_g^- for silicate (a) and aluminate (b) binders.

THE GEL WATER FILTERING UNDER LOAD AND DURABILITY OF CONSTRUCTIONS

Lets consider the quantitative aspect of the process of water filtering caused by compression stresses. In principle, this process is close to the process of filtering caused by pressure. However, this mechanism is considered here taking into account electrosurface phenomena (Plugin, Wild et al, 1995). The extrusion of water from the gel, induced by the concrete compression of its own weight or because of the concrete prestress, may be described by an equation for filtration coefficient K_f:

$$K_f = \frac{\Delta V_w L}{S \Delta\tau \Delta P}, \qquad [8]$$

where ΔV_w - water volume filtered throught the concrete, m^3; $\Delta\tau$ - duration of filtration, s; ΔP - pressure of filtration, N/m^2; L - length of the filtration way, m.

From here:

$$\Delta\tau = \frac{\Delta V_w L}{S \Delta P K_f}. \qquad [9]$$

The extrusion of water from gel is the major reason of the concrete creep. In this case the duration of filtration of water $\Delta\tau$ throught the concrete and the filtration coefficient are the major characteristics of the concrete creep and of the concrete durability, when sagging of the construction, induced by the creep f, is more of tolerate f_{tol}. The quantity of the construction creep f are defined from the water volume extruded from the concrete:

$$\Delta V_{ex} = C(W/C - 0.25)\left(1 - \mu_{opt}/\mu\right)\left(1 - \alpha_{opt}/\alpha\right), \qquad [10]$$

where μ, α - coefficients of the sand and large aggregate removing, which may be determined by Eq.1; μ_{opt}, α_{opt} - optimum coefficients of removing, which may be determined $(K_r)_{opt} = 2.1\,(1+D_{pm}/D_{se})^3 - 1.1$ with accordance the particles sizes (Plugin et al, 1995).

The quantity of tension N causes by its own weight for the beam construction is determined by:

$$N = \frac{3\rho L^2}{4H}, \qquad [11]$$

where ρ - concrete density with the accounting of the static load, t/m^3; H, L - height and length of the construction, m.

With regard to Eq.9:

$$\Delta\tau = \frac{2C(W/C - 0.25)}{3\rho K_f}\left(\frac{H}{L}\right)^2\left(1 - \mu_{opt}/\mu\right)\left(1 - \alpha_{opt}/\alpha\right). \qquad [12]$$

The example: $C = 0.45 t/m^3$; $W/C = 0.5$; $K_f = 10^{-11} m/s$ (not high water resistance); H=1m; L=10m; $\mu = 1.97$, $\alpha = 1.35$ for S(sand)$= 600 kg/m^3$; LA(large aggregate)$= 1200 kg/m^3$; $\mu_{opt} = 1.28$; $\alpha_{opt} = 1.1$; $\rho = 2500 kg/m^3$

(of reinforsed concrete). For this data by Eq.9 $\Delta\tau=1.4\cdot10^6$s=3.2years. For $K_f=10^{-13}$m/s (water resistant concrete) $\Delta\tau$=320years. The quantity of the specific sagging h^s may be calculated by $h^s=0.125\Delta V_{cr}/H$. For H=1m by this formula and Eq.10 $h^s=1/208$. This quantity limits of the tolerate sagging quantities h_t^s=1/200-1/1000. The latter shows that the above mentioned aspects are principally correct.

THE ELEMENTS OF CONCRETE FILTERING THEORY

As it is known, in case of water filtering through concrete takes place leach of the less stable in water environment crystallohydrate products, particularly, portlandite $Ca(OH)_2$. As a result, accordingly to the curves in Fig.4 , the ratio between masses of crystallohydrate and gel products will deviate from the optimum. Besides, it will cause the decrease of the number of the electro-heterogeneous contacts and, correspondingly, strength and durability of concrete will degrade. The other kinds of chemical instability of concretes are connected with water filtering together with either aggressive salts and acids or agressive gases from air solved in water. However, filtration characteristics of concrete determined in the standard way by pressing water through a sample do not reflect real filtration properties of concrete in real constructions, where pressure is absent, but concrete is leaking. Water goes through concrete not only because of outer pressure ΔP but mainly because of internal pressure. The internal pressures are the ones connected with the well known in colloid chemistry fenomena: capillar rise pressure P_{cr}, osmotic pressure P_{os}, electro-capillar pressure P_{ec}, capillar-osmotic pressure P_{co} (Fig.5) and flow potential pressure P_{fp} (for ΔP) (Plugin et al, 1995; Plugin, Babushkin, 1996). The equality of all the forces causes stationary mode of flow: $F+P_{fp}=\Delta P+P_{cr}+P_{ec}+P_{os}+P_{co}$, or:

$$\frac{2l\eta V}{r\delta_{dl}}+\frac{\varepsilon^2\varepsilon_o^2\psi\zeta\Delta P}{4\pi^2 dr\eta k}=\Delta P+\frac{2\sigma}{r}+\frac{\varepsilon\varepsilon_o\psi^2\delta_p}{\delta_{dl}\pi r^2}+RT\frac{\varepsilon\varepsilon_o\psi}{2\pi drF}+\frac{4\varepsilon\varepsilon_o\zeta\psi\delta_p}{\pi r^3(1-h_o/r)^2}, \quad [13]$$

where r-capillar radius; δ_p-size of particles in capillar wall; δ_{dl}-width of double electric layer inside capillar; σ-water surface tension; l - capillar length; η – water viscosity; V - water flow rate in capillar. The DEL width should be assumed to be the distance along which the rate drops to zero.

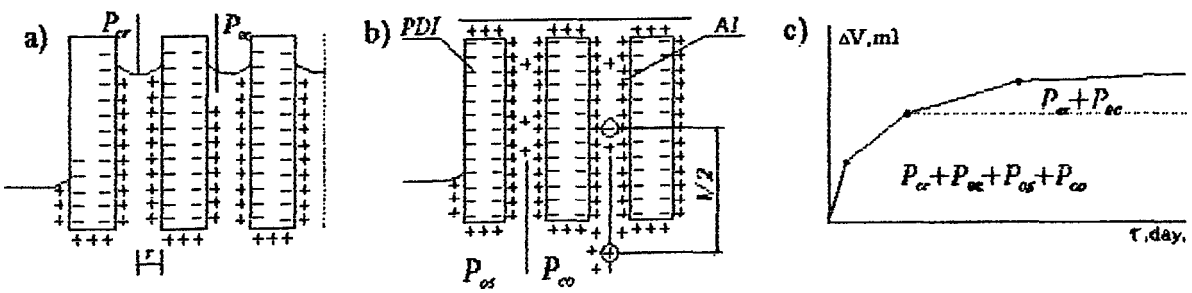

Figure 5 The filtration characteristics of concrete and water filtering at free-flow conditions (without ΔP).

The capillar and electro-capillar pressures predominate in case of water saturation when condensate or rain moisture accumulates on concrete surface. The osmotic pressure is caused by difference of concentrations ΔC of electrolyte outside and inside capillars of concrete.The flow rate V is constant if the flow is stationary. It allows to derive V and coefficient filtration K_f:

$$K_f=\frac{Vl}{\eta\Delta P}=\frac{r\delta_{dl}}{2\eta^2}+RT\frac{\varepsilon\varepsilon_o\psi\delta_{dl}}{4\pi dF\eta^2\Delta P}+\frac{2\varepsilon\varepsilon_o\zeta\psi\delta_p\delta_{dl}}{\pi\eta^2r^2(1-h_o/r)^2\Delta P}-\frac{\varepsilon^2\varepsilon_o^2\psi\zeta\delta_{dl}}{8\pi^2 d\eta^2 k}, \quad [14]$$

Calculations show that the internal pressure in capillars with radius up to 1000A° (the capillars in hydration products of cement) is higher than the outer one used in standard methods of filtration properties of concrete evaluation. The internal pressure can reach up to tens and hundreds of MPa.

As one can see, filtering properties, particularly, filtration coefficient of cement stone and concrete, depend on radius of capillar and its electrosurface properties. It allows to efficiently control the filtering properties and ensure durability of concrete in constructions.The easiest way to do it is to optimise concrete structure (when manufacturing constructions) at micro- (W/C), meso- (μ) and macro- (α) levels with the use optimum structure of concrete (Fig.1) with maximum strength, water-resistance and minimum deformability by (Plugin, 1989; Plugin et al, 1995).

CONCLUSION

Thus, concrete destruction, particularly, in the protective layer of the stretched zone, is caused by creep in compressed zone. The creep is caused by the filtration desplacement of physico-chemically combined water of hydrosilicate gel in concrete with in optimal structure. It is followed by subsequent loss of density of cement paste and concrete in the stretched zone. It favors gradual destruction of the electoheterogeneous contacts and subsequent complete destruction of concrete. It appears especially active in the stretched zone of concrete because the electroheterogeneous contacts break down in tension only. In the conditions of flooded constructions or in case of their hydroisolation break this process is aggravated by leach of concrete. It leads to decrease of the number of the electroheterogeneous contacts, strength degradation and porosity rise. Based on the above-stated views, successful research works and practical recommendations development on durability providing to reinforced concrete constructions, including the measures on protection, repair and rebuilding of the currently operational and destructing constructions, are carried out.

REFERENCES

Babushkin,V.I.and Novikova,S.P.,"On the Role of Colloid Chemistry Phenomena in Volume Changes of Cement Stone and Concrete", Proc. of Ukrniivodgeo, 1973, Moscow, pp.133-144, (in Russian).

Ilukhin,V.V., Kuznetsov,V.A., Lobachova,A.N.and Backmutov, V.S.,"Calcium Hydrosilicates. Syntesis of Mono-Crystals and Crystallography", 1979, Moscow, Science, 184 pp., (in Russian).

Kireenko,I.A. ,"Calculation of Composition of Higly Strong and Ordinary Concretes and Mortars",1961, Kiev, Gosstroyizdat UkrSSR, 79pp. (in Russian).

Plugin,A.N.,Vdovenko,N.V., Birukov,A.I and Ovcharenko, F.D.," On Mechanism of Rise of Electrosurface Potential of Different Substances in Water Solutions", RAS (Reports of Academy of Sciences) USSR, 1988, V.298, No3, pp.656-661., (in Russian).

Plugin,A.N.," Electroheterogeneous Interactions at the Process of Cement Binders Hardening", The DSc(Chem) degree thesis, 1989, Kiev, ICCCW, 282 pp. (in Russian).

Plugin,A.N., Wild,S., Prokopova, I.G. and Plugin, A.A., "Kinetic Laws of Water Filtering through Concrete", Proc. of Intern. Sc.-Tech. Conf. "The Development of Technical Chemistry in Ukraine",Vol.1, 1995, Kharkov, pp. 168-170, (in Russian).

Plugin,A.N. and Plugin, A.A. "Colloid-Chemical Aspects of Strength and Waterproofness of Various Binders and Composite Materials", Proc. of 4th Intern. Conf. "Modern Building Materials, Structures and Techniques", Vol. 1, 1995, Vilnius, pp. 206-211.

Plugin, A.N., Kalinin, O.A. and Plugin, A.A. "Strength of Concrete and Main Technological Strength-Determining Parameters", In the same place, pp.43-48.

Plugin, A.N.and Babushkin,V.I., "Colloid Chemical Problems of Building Materials", Chemical Industry of Ukraine, 1996, No1, pp.40-46, (in Ukrain).

Sheikin, A.E., Chekhovsky,Yu.V. and Brusser, M.I.,"Structure and Properties of Cement Concretes", 1979, Moscow, Stroyizdat, 344pp., (in Russian).

Wild, S., Haadi, M. and Leng Ward, G., "Expansion Mechanism and Cementation in Cured PFA-Lime Composite", Advanses in Cement Research, 1990, 3, No10, pp.55-74.

THE DEGRADATION OF CALCIUM SILICATE HYDRATES (CSH): A KINETIC STUDY

Christa R. SCHWEIZER, Annette C. JOHNSON, and Peter BACCINI
Swiss Federal Institute for Environmental Science andTechnology (EAWAG), 8600 Duebendorf Switzerland

ABSTRACT

For the assessment of the long-term behavior of cement stabilized and municipal solid waste incinerator products, an understanding of the degradation of calcium silicate hydrates is needed. The series CSH- tobermorite- xonotlite were chosen to determine the relationship between ageing crystallinity and stability. Initial dissolution experiments were conducted with xonotlite in a through-flow reactor. The dissolution rates were calculated and interpreted in terms of surface complex theory. The dissolution rates of xonotlite in the pH range 9-11 were found to range 25 $\mu mol.g^{-1}.h^{-1}$ - 3.5 $\mu mol.g^{-1}.h^{-1}$. The rates were compared to those of naturally occurring minerals. They appear to be faster than those of aluminosilicates but slower than calcite. Supporting evidence from field studies suggest that CSH dissolution could be controlled either by kinetic or thermodynamic factors in a field situation depending on the hydrology of the system.

Key-words: CSH, Kinetics

INTRODUCTION

The use of cement to stabilize wastes containing heavy metals or radioisotopes has been widely considered or applied because of the propensity of cement to immobilize inorganic constituents such as heavy metals. The mobility of heavy metals via leaching is influenced by two factors, the geochemistry of the waste material and the hydrology of the deposit. The composition and the pH of the leachate are controlled by the interaction of the solid material with the leachate water. Minerals which are sufficiently soluble can buffer the solution pH, as is known for CSH or $CaCO_3$. The pH in turn controls the mobility of heavy metals retained by various mechanisms such as adsorption, precipitation and ion exchange. Though ideally cement stabilized products should be virtually impermeable to water, investigations in deposits filled with cement stabilized filter ash from municipal solid waste incinerator (MSWI) show that water can enter such systems (IMRA, 1991).The leachate water contains low concentrations of heavy metals (in the range of µmol/l) at present but over long time periods when buffering minerals are no longer present, the chemical environment can change causing lower pH values. In such a situation the metals cations will become more mobile (Johnson et al., 1995). For the assessment of the long-term behavior of cement stabilized products, an understanding of the important mineral water interactions is needed.

Thermodynamic studies provide evidence on reactions at equilibrium conditions. However, in field situations equilibrium is often not achieved, especially in systems with high permeabilities such as landfills of MSWI bottom ash. In such cases, kinetic studies of dissolution rates permit the estimation of the composition of a

leachate. The understanding of the dissolution reaction mechanism can give additional information on the long-term behavior. The dissolution rates of mineral-water interactions depend on the presence, amount and residence time of water. Recent studies of weathering processes in geological systems have clearly demonstrated that the rates of these reactions are strongly dependent of the surface structure of the mineral and that the kinetic mechanism is mainly controlled by formation of the surface complexes (e.g. Aagaard and Helgeson, 1982; Casey et al., 1988).
From synthesis studies it is known that amorphous CSH exposed to hydrothermal conditions forms tobermorite and then xonotlite (El-Hemaly et al, 1977; Glasser, 1995). We have decided in an initial step to investigate dissolution kinetics of on xonotlite in order to set up the methodology. In a second step the dissolution rates of tobermorite and CSH, which are presumably faster, will be investigated. In this paper we present results of dissolution experiments carried out on the crystalline CSH mineral xonotlite in a flow-through reactor. These are interpreted in terms of surface complexation theory and the rates compared with other minerals and with field results.

MATERIALS AND METHODS

Starting Material Xonotlite

The minerals used in the experiments were synthesized according to the method of Glasser (1995). $CaCO_3$ (Merck) was calcined at a temperature of 1000°C for 2 hours. A quantity of the resulting product (3.73g) and SiO2 (4.00g, Aerosil 300, Degussa) was mixed with ~100ml bidistilled water boiled under argon. This mixture was shaken (125rpm) for 24h. The reactants were then autoclaved at 200°C for 1 week and subsequently freeze dried. XRD analysis showed the product to be pure. The xonotlite was crushed in an agate mortar and sieved. The size fraction between 100-200μm was separated and used for the experiments. The total external surface area (BET method, N_2) was found to be $24.4 m^2 g^{-1}$. Raster electron microscopy photograph of the product showed nearly spherical particles.

Dissolution Experiments

Experiments were conducted in a continuously stirred polycarbonate flow-through reactors (250ml, Fig 1). The reactor was placed on a balance (Mettler PM6000) connected via an interface to a peristaltic pump. Another pump was used to remove reactor solution at a rate of approximately 20ml/h. The weight of the reactor was kept constant by a feed solution which was pumped from a 2 liter polyethylene reservoir via the peristaltic pump into the reactor. The outlet solution passed through a 0.45μm filter as it exited the reactor. In order to maintain a constant solution pH value, a computer-controlled Dosimat (Metrohm 665) was used to add acid or base. In order to minimize the influences of CO_2 from air all experiments were carried out under argon atmosphere. The argon was passed through a NaOH (Merck) solution and presaturated with the eluent. Unless otherwise stated, the temperature was kept constant at 298K and the ionic strength was fixed at 0.1 with NaCl (Merck) solution. The pH values during the experiment were measured with a Ross Sure-Flow Electrode (81-72BN) and automatically

registered every three minutes. The pH electrode was calibrated by titration before and after every dissolution experiment.

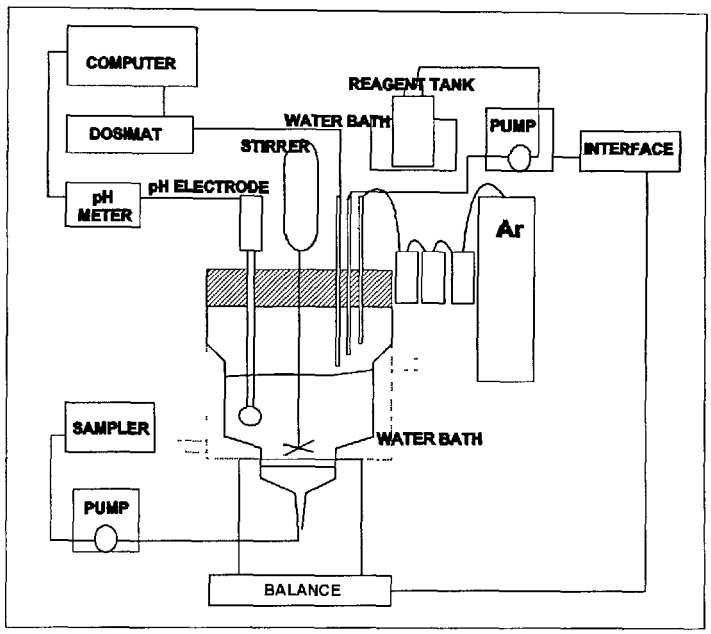

Figure1 Schematic representation of the flow-through reactor.

The experiments were conducted with xonotlite under variable pH conditions to investigate the pH dependence of dissolution rate and reaction stoichiometry.
A 100-200μm fraction of xonotlite powder was suspended in the 0.1M NaCl solution (0.5g/50ml) added to the reactor and was stirred with a hanging stirrer (Metrohm 722). At pH 9 the computer controlled Dosimat (Metrohm 665) added 1M HNO_3 at pH 10.5 0.1M NaOH, at pH 11 1M NaOH, at pH 10.18 no acid or base were added. HNO_3 and NaOH solutions were prepared from Titrisol (Merck) from bidistilled water boiled under argon. These solutions were also stored under argon. The dissolution experiments required ~300 hours.
Outlet solutions were continuously collected and were examined for silicon and calcium. Calcium was analyzed by atomic absorption spectroscopy (Varian SpectrAA) and silicon was analyzed by the molybdate blue colorimetric procedure (ASIA, Ismatec). Analytical detection limits for silicon were 0.02ppm and for calcium 0.2ppm.

Calculation of Dissolution Rates

The dissolution rates R were calculated according to the method proposed by FURRER et al. (1993) with Eqn. 1

$$R = c/(\tau^* c_s) \qquad [1]$$

The average of the steady-state concentrations c ($mol.l^{-1}$) were divided by the mean residence time τ (h) of the solution in the flow-through reactor and by the particle concentration c_s ($g.l^{-1}$). The residence time τ (h) is the quotient of the reactor volume V (ml) and the flow rate of the effluent r ($ml.h^{-1}$) (Eqn. 2).

$$\tau = V/r \qquad [2]$$

This method is based on the assumption that all particles are of the same size and remain spherical throughout the dissolution experiment.

RESULTS AND DISCUSSION

Concentrations versus Time

Fig.2 shows the calcium and silicon concentrations in function of time in the pH range 9-11.

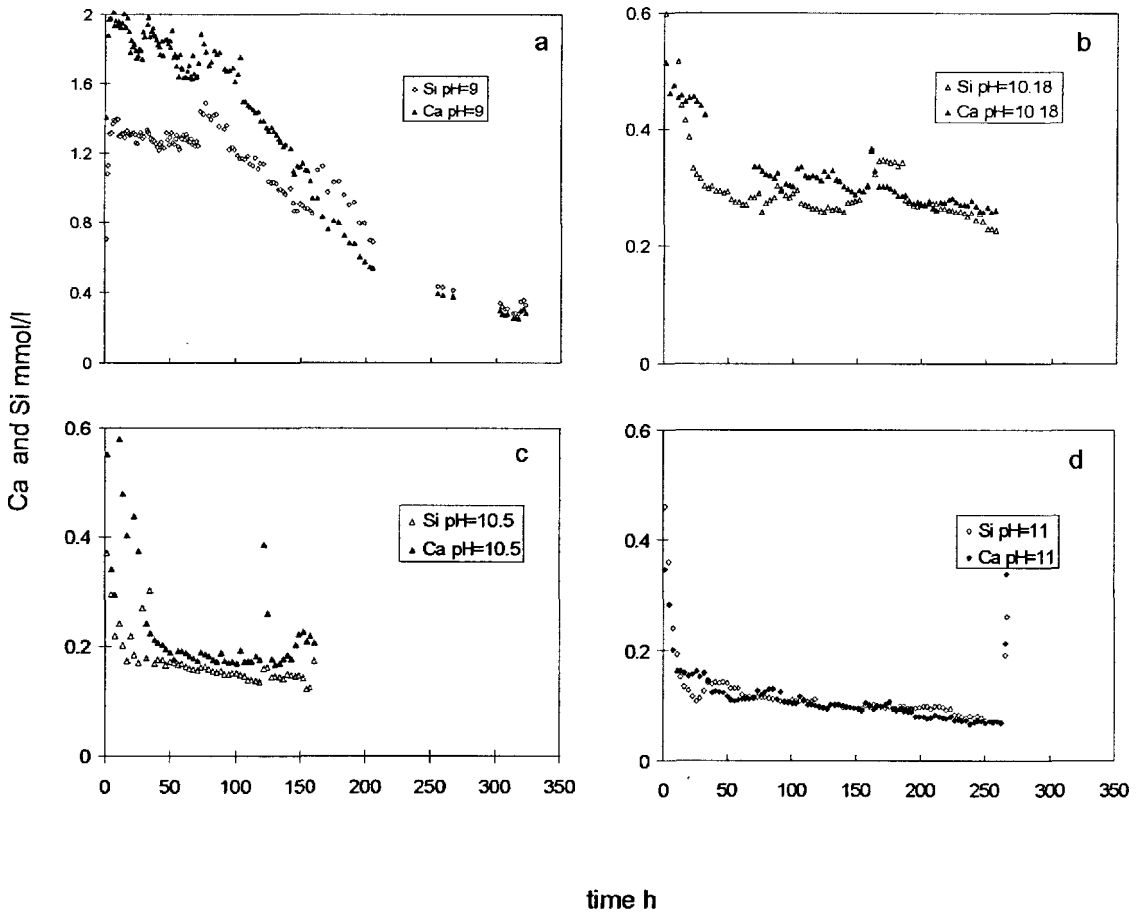

Figure 2 Silicon and calcium concentrations of xonotlite (mmol.l^{-1}) in 0.1 M NaCl at 25°C and at different pH a.) pH 9, b.) pH 10.18, c.) pH 10.5 and d.) pH 11.

In all experiments outlet solution chemistry follows the trend noted by other flow-through reactor studies (e.g. Chou and Wollast, 1984; Mast and Drever, 1987, Stilling and Brantley, 1995): an initial, rapid increase in solute concentration which gradually decreases with time to a nearly constant value (steady state). The steady-state silicon concentrations are more rapidly reached at lower pH, namely after 10 hours at pH 9, 50 hours at pH 10.5 and after 60 hours at pH 11. The

calcium and silicon concentrations increase with decreasing pH. After 10 hours at pH 9, the silicon concentrations attain a value of 1.3 mmol.l^{-1} . At pH 10.18 the steady-state concentrations are 0.28 mmol.l^{-1} at pH 10.5 0.18 mmol.l^{-1} and at pH 11 0.1 mmol.l^{-1}. The stoichiometric ration Ca/Si varies from 1.4 to 1. Dissolution tends to be stoichiometric at more basic pH values. In more acidic conditions calcium concentrations are initially greatly enhanced but stoichiometry is attained at steady state.

Preferential release of calcium cations or ionic exchange with protons during the initial stage of dissolution with acid suggests the early development of a calcium-depleted surface layer. This phenomenon is well documented and has been illustrated in a conceptional model by Schnoor (1990). Adopting this model, initial dissolution is characterized by rapid, outward diffusion of calcium from within the mineral through a calcium-depleted surface layer. As the thickness of the surface layer increases, diffusion of calcium slows until at steady state, the transport rate of calcium through the surface layer equals the dissolution rate silicon. After this point, dissolution will proceed congruently where the detachment of the surface complex silicon is the rate-determining step.

Dissolution Rates vs. pH

The dissolution rates of these experiments are evaluated according to Eqns. 1 and 2 and have been calculated from the silicon steady-state part (see Fig 3). At pH 9 the first plateau concentration has been used.

The pH dependence of the xonotlite dissolution is shown in Fig 3. The silicon dissolution rate decreases with increasing pH values. The measured points in the curve suggest a linear dependence of the dissolution rate in the pH range 9 to 11. Although for an accurate verification more measurements are needed. We estimate the error in the flow rate of the eluent to be ±2% - ±5% and the error in c to be ±5 - ±10%. Therefore the estimated error in R can range from ±7% to 15%. In these calculations the decrease of surface area was not considered.

Various conceptional models have been proposed in order to interpret the pH dependent dissolution of soluble minerals (Lasaga, 1981; Stumm and Furrer, 1987). The models are based on experimental observations that the dissolution of most oxides and silicates at low temperature is controlled by surface chemical processes. Transition state theory (TST) has been used as a theoretical framework to establish kinetic rate laws for surface controlled dissolution reactions. Far from equilibrium, the elementary step in such a dissolution is the detachment of an activated complex. Furrer and Stumm (1986) and Wieland et al. (1988) propose the coordinative chemical model of mineral dissolution and combine the TST and the surface coordination model. The dissolution rate of most oxides increases both with increasing surface protonation and with decreasing deprotonation (or hydroxylation). The overall rate of the dissolution can be calculated using

$$R = k'_H (C^s_H)^j + k_{OH}'(C^s_{OH})^i + k'_L (C^s_L) + k'_{H2O} \qquad [3]$$

with R the sum of the individual reaction rates, assuming that dissolution occurs in parallel at different metal centers. k'_H and k_{OH}' denote the experimental rate constant for proton and hydroxide-promoted and k'_L the experimental rate constant for ligand-promoted dissolution. C^s_H or C^s_{OH} the surface concentration of protons or

hydroxides and C^{s}_{L} the surface concentration of ligands (Stumm et al, 1990). The values of the exponents j and i represent the order of the overall reaction with

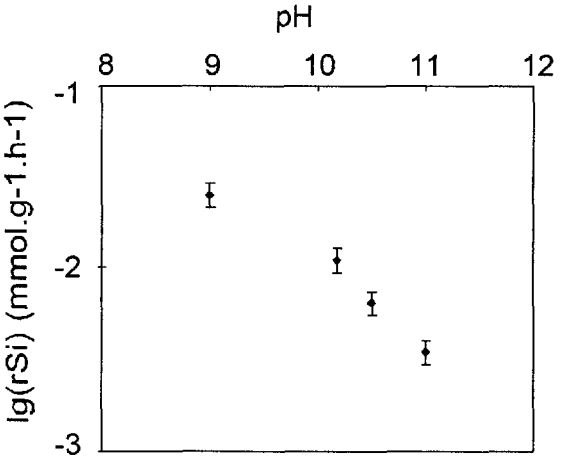

Figure 3 Silicon dissolution rates of xonotlite in $mmol.g^{-1}.h^{-1}$ as a function of pH at 25°C.

respect to surface charge and are the key parameter used to interpret the stoichiometry of proposed activated complex. This model shows that the protonation or deprotonation of detachable surface sites could explain the pH dependence of dissolution rates for simple oxides. Rates are compared in terms of surface concentrations of protons and hydroxides and not solution chemistry. The pH of zero point of charge is approximately 10.1. The surface of xonotlite in acidic conditions has a predominately positive charge below pH 10 and according to the dissolution model described above, the rate is a function of the first term $k'_{H}\ (C^{s}_{H})^{j}$ and corresponds according to the leached layer model (see before) with regard to the release of silicon. Reactions in solutions above pH 10 are controlled by the term $k'(C^{s}_{OH})^{i}$. The discrepancy between surface charge and the dependency of dissolution rate on pH had yet be clarified with further experiments.

The dissolution rates of xonotlite are compared to naturally occurring minerals (Fig 4). It should be noted, that with the exception of wollastonite ($CaSiO_3$), quartz and calcite the minerals are all aluminosilcates. All these minerals with the exception of quartz can engage in acid/base buffering reactions in field conditions. Dissolution rates limit the efficiency of these processes. The dissolution rates of xonotlite is between the two extremes calcite and quartz followed by the dissolution rates of aluminosilcates. There could be a relationship between aluminosilicates structure and dissolution rate. The dissolution rate of the chain silicate enstasite is approximately one order of magnitude higher than the framework silicates anorthite, albite and bytownite. These in turn are around one order of magnitude higher than that of the sheet mineral muscovite. In parallel fashion the sheet mineral tobermorite might also have a slower dissolution rate than that of xonotlite. The least crystalline CSH can be expected to have the most highest rates comparing with tobermorite and xonotlite.

The dissolution rates of the minerals depend on the presence, the residence time and the composition of the percolating water. Equilibrium could be achieved if conditions are favorable. In the lysimeter study with cement stabilized municipal solid waste incinerator filter ash (IMRA, 1991), in which 20% of rainwater infiltrates

the waste material, thermodynamicaly calculations (Schweizer, 1996) show that the leachate is saturated with respect to CSH or tobermorite and gypsum.

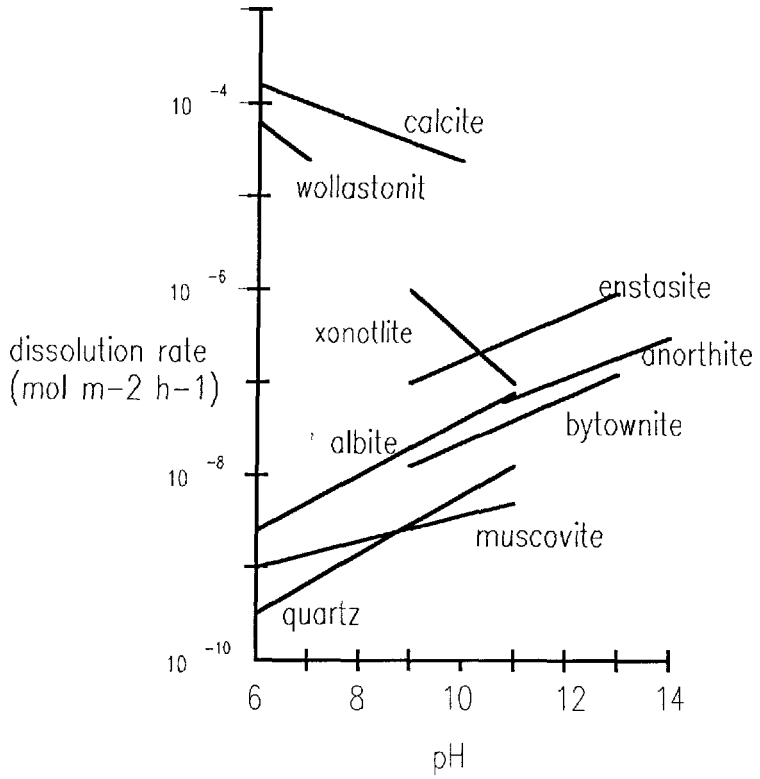

Figure 4 *Dissolution rates in mol.m^{-2}.h^{-1}of different minerals as a function of pH* at 25°C. (**Quartz:** Wollast, R. and Chou, L.; **muscovite:** Kalinowski, B.E. and Schweda, P.; **bytownite, anorthite and enstasite** Brady, P.V and Walther, J.V.; **albite:** Chou, L. and Wollast, R.; **calcite:** Chou, L. and Wollast, R.; **wollastonite:** Rimstitdt, J.D. and Dove, P.M.)

In contrast leachate concentrations of calcium and silicon of a MSWI bottom ash landfill are undersaturated (Schweizer and Johnson, 1996). Since water residence times are approximately ten time greater in the example, hydrological factors could play an important role.

CONCLUSIONS

The dissolution rates of xonotlite lie within the large range of naturally occurring minerals. They appear to be faster than these of aluminosilicates but slower than calcite. The dissolution kinetics can be described by the surface complex model. Evidence from field studies indicate, that depending on water residence time either thermodynamic equilibrium or kinetically controlled dissolution calculations must be applied to describe CSH dissolution. It is therefore necessary to obtain a depth

understanding of the least crystalline CSH minerals to be able to more accurately model these reactions in field systems. We are presently working on the dissolution behavior of tobermorite and CSH.

ACKNOWLEDGMENT

We would like to thank Christian Ludwig and Felix Ziegler for their encouragement and discussions. In addition, we would like to thank Madeleine Langmeier, Hermann Mönch and Sandro Brandenberger for their technical advice and assistance.

REFERENCES

Aagaard, P. and Helgeson, H.C., " Thermodynamic and kinetic constraints on reaction rates among minerals an aqueous solutions. 1. Theoretical consideration", Amer. J. Sci., *282*, 1982, pp. 237-285.
Brady, P.V and Walther, J.V, Geochim. Cosmochim. Acta, *53*, 1989, pp. 2823-2830
Casey, W.H., "Entropy production and the Ostwald Step Rule", J. phys. Chem., *92*, 1988, pp. 226-227.
Chou, L. and Wollast,R., "Study of Weathering of Albite at Room Temperature and Pressure with a Fluidized Bed Reactor", Geochim. Cosmochim. Acta, *48*, 1984, pp. 2205-2217.
Chou, L. and Wollast, R., Amer. J. Science, 1985, *285*, 963
Chou, L. and Wollast, Chem. Geol. 1989, *78*, 269
El-Hemaly, S.A.S., Mitsuda, T. and Taylor, H.F.W, "Synthesis of Normal and Anomalous Tobermorites", *Cem. Conc. Res., 7*, 1977, *pp.* 429-438.
Furrer, G. and Stumm, W., " The coordination chemistry of weathering: I. Dissolution kinetics of δ-Al_2O_3 and BeO" Geochim. Cosmochim. Acta, *50*, 1986, pp. 1847-1860
Furrer, G., Zysset, M. and Schindler, P.W., in "Geochemistry of Clay-Pore Fluid interactions", ed. by Manning, D.A.C., Hall, P.L. and Hughes, C.R., London, Chapman and Hall, 1993.
Glasser, F.P. (1995), oral information.
IMRA, Bundesamt für Umwelt, Wald und Landschaft, "Immobilisierung von Rauchgasreinigungsrückständen aus Kehrichtverbrennungsanlagen" ("Immobility of municipal solid waste incinerator filter ash"), (1991).
Johnson, A.C, Brandenberger, S. and Baccini, P., " Acid Neutralizing Capacity of Municipal Waste Incinerator Bottom Ash", Env. Sci. Tech., *28*, 1995, pp. 142-147.
Kalinowski, B.E. and Schweda, P., Geochim. Cosmochim. Acta, *60*, 1996, pp. 367-385.
Lasaga, A.C. in "Kinetics of Geochemical Processes", (ed. Lasage); Rev. Mineral, *8*, 1981, pp.1-68.
Mast, M.A. and Drever, J.I., "The effect of oxalate on the dissolution rates of oligoclase and tremolite", Geochim. Cosmochim. Acta, *51*, 1987, pp. 2559-2568.
Rimstidt, J.D. and Dove, P.M., Geochim. Cosmochim. Acta, *50*, 1986, pp. 2509-2516
Schnoor, J.L. in "Aquatic Chemical Kinetics", (ed. Stumm, W.), 1990, pp. 475-504, Wiley.
Schweizer, Ch.R., PhD-Study, Swiss Federal Institute of Technology (ETH) Zuerich, Department XB, in preparation, 1996.
Schweizer, Ch.R. and Johnson, A.C., "Zementchemie in Verbrennungsrückständen", EAWAG Jahresbericht 1995, 1996
Stilling, L.L. and Brantley, S.L., Geochim. Cosmochim. Acta, *59*, 1995, pp. 2559-2568
Stumm, W. and Furrer, G., in "Aquatic Surface Chemistry", (ed. Stumm, W.), 1987, Wiley.
Stumm, W. and Wieland, E., in "Aquatic Chemical Kinetics", (ed. Stumm, W.), 1990, pp.367-400, Wiley.
Wieland, E., Wehrli, B. and Stumm, W., " The coordination chemistry of weathering: III. A generalization on the dissolution rates of minerals", Geochim. Cosmochim. Acta, *52*, 1988, pp. 1969-1981
Wollast, R. and Chou, L. in "Chemistry of Weathering"(J.E. Drever,Ed., Reidel Dordrecht,1985).

41V077
8 pp

ADSORPTION ISOTHERM OF CONCRETE

Aimin XU, STK Inter Test AB, S-254 67 Helsingborg, Sweden

ABSTRACT The multi-layer adsorption theory, BET equation is discussed in this paper. On the evidence of more energy level change occurring between the adsorbed layers than that originally assumed by BET isotherm which empirically valid only in a small relative pressure range, a new isotherm equation is obtained which can be applied in a much greater range. The analysis of the moisture adsorption character of concrete containing fly ash, using this isotherm, has shown that the indices provided by the new function are closely related to the concrete parameters.

Key-words: Adsorption, Drying, Fly ash, Pore size distribution, Sorption isotherms

INTRODUCTION

Adsorption of molecules on a solid material is a phenomenon occurs in various situations. The most common cases in building materials include the moisture and ions adsorption/desorption, which affect the building environment and the gaseous/ionic transport process related durability of concrete structures.

In a comprehensive exposition of adsorption methods for the assessment of the surface area of the solids, Gregg and Sing (1982) showed that the adsorbed amount is governed by the energies of solid surface and the molecules, the size of surface area and presence of pores in the solid. The multi-layer adsorption isotherm by Brunauer-Emmett-Teller (BET) (1938, 1943), and the relation between meniscus and pore size by Kelvin equation, are the fundamentals for the most widely applied methods, in spite of that earlier experimental data only confirmed BET isotherm in the low relative pressure (of gaseous adsorbed molecules) range, e.g. $x = p/p^\circ < 0.35$.

The dependence of moisture / length change on the relative vapor pressure (or relative humidity, $RH = 100p/p^\circ$) is a primary interest to concrete scientists. Numerous investigations have been carried out since the1940s as summarized by Powers (1960). The fact that concrete or cement paste is a porous material containing capillaries of micro-meter size (excluding the entrapped air voids) down to micro-pores of inter-lattice distance, has led to several complicated phenomena in desorption-adsorption (or sorption, in general) isotherms, e.g. difference in surface area measured by N_2 compared to that by water, and the hysteresis between the desorption and adsorption, especially that at low p/p° range attributable to some inter-lattice water loss and reenter as addressed by Feldman (1968) who thus questioned the reversibility of the water isotherms. Considerable effort has been made by researchers to estimate the pore size distribution of porous solid, which in concrete science is represented by work of Mikhall *et al* (1968), Radjy and Sellevold (1972) on relationships between micro-pore filling and adsorbed layer thickness.

However, the calculation of thickness of the adsorbed layer by BET equation still presents a problem, as mentioned earlier that BET equation predicts a too high uptake value even at moderate dry conditions. Therefore in practice, other equations, such as Halsey equation (1948) was used for the calculation. From the view point of both theory and practice, it is important to re-examine the basic assumptions, the validity and applicable range of the BET theory.

The weakness of BET equation in fitting the experimental data, and some of its theoretical assumptions, have led to debates and several refinements (Hill, 1952). Halsey (1948) pointed out that the hypothesis: $E_2 = E_L$ (the heat of adsorption at the second and higher layers is equal to the heat of liquefaction) leads to erroneous indications for the theory itself, however no modifications have been followed in this line.

The modifications of BET equation did extend the application range, best represented by that made Brunauer himself and co-authors (1969), that the volume of the adsorbed molecules V relates to the relative pressure x by:

$$V = \frac{V_m ckx}{(1-kx)(1-kx+ckx)} \qquad [1]$$

where V_m is the monolayer capacity, c is a coefficient depending upon energy and temperature. Compared to the original form, this equation introduces a factor $k < 1$, on the hypotheses that the number of adsorbed layer is infinite at a pressure exceeds the saturation pressure, which determines the isotherm shape at $x > 0.4$. $k = 0.57$ to 0.79 was reported for nitrogen adsorption isotherm of various adsorbents. Several earlier and later research works on sorption theory, e.g. Anderson (1946) and Hillerborg (1985), presented forms essentially identical to Eq.1.

It is reasoned by Brunauer *et al* on the thickness of the adsorbed layer built up at the saturation vapor pressure, that k is a measure of the attractive force field of the adsorbent. However, this is only a speculation. It will be shown here that the discarding the hypothesis $E_2 = Q_L$ leads to a new form of multi-layer adsorption isotherm. Its application in analyzing water sorption isotherms of concrete samples is demonstrated with a discussion about influences of pore size, change or aging of hydrates on the sorption.

A MODIFIED MULTILAYER ADSORPTION ISOTHERM

Although the theory can be applied to both the adsorption of ions (solid in solution) and gas molecules, it is convenient to take the latter case for discussion. On a solid surface, gas molecules that collide with it will stay for a moment then leave. When the rates of the coming and going (i.e. *adsorption* and *desorption*) become equal, an equilibrium occurs. The rate of adsorption is proportional to the concentration of the molecules, and to the surface area which has not yet been covered by adsorbed molecules, assuming the surface has uniformly distributed adsorption sites. Furthermore, molecules can stack upon one another at an adsorption site, resulting in the multi-layer adsorption. The total number of the adsorbed molecules is

$$Z = Z_m(A_1 + A_2 + ... + A_n) \qquad [2]$$

where A_1, ..., A_n are the fractions of the surface covered by 1 to n layers of molecules respectively. It is defined that $A_0 + A_1 + ... + A_n = 1$. Z_m is the total number of adsorption sites, which is unchanged during the process. This assumption, in drying of cement paste, is only conditionally satisfied, thus it is important to clarify this before proceeding further.

Surface area and dry state

Formed by cement hydrates of various shapes, such as foils (e.g. C-S-H), needles (e.g. ettringite) and plates (e.g. $Ca(OH)_2$), the surface of cement paste is far from flat. With drying, water between layers of hydrates, e.g. C-S-H gel, may exit at low relative pressures, resulting in close-down of this part of area. In terms of sorption isotherm, it shows a hysteresis between the desorption and adsorption, such as that demonstrated by Feldman (1968) on moisture and length change isotherms of cement paste degassed at 80°C. He thus questioned the validity of using

water adsorption data to measure the surface area of cement paste, since a part of the area is only available to water but not to other molecules, e.g. N_2.

Powers (1960) showed that a substantial reduction in surface area of cement paste with drying (to 0.00002 p/p°) and re-wetting cycles, i.e. more than 30% reduction occurred after 8 cycles. Powers speculated that gel particles are brought together by shrinkage forces, though he also doubted on extent of this effect. To clarify this, it may help mentioning that the specific surface can be expressed as (Gregg and Sing, 1982)

$$S = \frac{f}{L} \qquad [3]$$

where L is a characteristic length, and f is a coefficient approaching to 6, 4, and 2 for uniform size particles of sphere (or cube), rod, and plate respectively. This implies that it is possible to have a significant surface area reduction by partial fusion of gel particles, e.g. joining spheres to plates may lead to a 1/3 surface area reduction.

Nevertheless, during one drying process, surface area change is not significant. In experiments of drying cement mortar samples at 20°C, it was observed that the hysteresis between desorption and adsorption in small range (at about 10% intervals) is so small that it can be accounted for by the evaporation of capillary water; and the desorption and adsorption between 11% and 33% RH was practically reversible (Xu, 1992). The large hysteresis shown by Feldman (1968) can be due to the severe drying condition used, i.e. > 80°C. Cong and Kirkpatrick (1995), by using ^{29}Si and ^{1}H MAS NMR technique, showed that C-S-H dried at 9% RH had somewhat higher local structure disorder and lost some water in C-S-H, compared to the samples dried at 51 or 71% RH; whereas drying at 110°C resulted in a significant change in the NMR signals indicating that heating removes both inter-layer water and gel water, the loss of C-S-H water is evidenced by a stronger ^{1}H-^{29}Si coupling for Q^1 peak. In fact, it is well known that many hydrates are unstable during prolonged drying at 80°C, e.g. ettringite, gypsum, etc.

Therefore, the sorption isotherms determined at moderate temperatures, e.g. 20°C, and the drying to about 10% RH can be considered to be thermal dynamically reversible. And the sorption site is so assumed to be constant.

Equilibrium

With the on-going desorption and adsorption, the equilibrium on a solid surface for the first layer of adsorbed gaseous molecules established when:

$$a_1 v p A_0 = Z_m A_1 \nu_1 e^{-E_1/RT} \qquad [4]$$

where a_1 is the fraction of the collisions resulting in adsorption, v and p are the speed and pressure of the gas, ν_1 the oscillation frequency of molecules at the first layer, and E_1 is the difference in energy between the molecules at the 1st layer and the 'hard' adsorbed state, i.e. *the heat of adsorption.*

The equilibrium at the higher adsorption layers can be similarly written by changing subscripts (Eq.4) i to $i+1$. The heat of adsorption approaches that of liquefaction with more stacked layers. The original hypothesis of BET equation is: $E_1 \neq E_2 = E_3 = \ldots = E_n = Q_L$. However, this is not true in many cases, such as that shown by Harkins and Jura (1944) that for water adsorption on anatase the heat of adsorption between the 2nd and 3rd layers was still quite significant.

We can go a little further by letting $E_1 \neq E_2 \neq E_3 = ... = E_n = Q_L$,, thus make a slight modification for BET equation. Introducing parameters $\alpha = A_1/A_0$, $\beta = A_2/A_1$, $c = \beta/\alpha$, and $k\beta = A_{i+1}/A_i$ for i = 2, 3, ... n, one obtains $A_i = cA_0k^{i-1}\beta^i$. Substituting these into Eq.2 (when n is large, or assuming that $n = \infty$ for simplicity) and rearranging yield:

$$\frac{Z}{Z_m} = \frac{c\beta\left[1-(1-K)(1-K\beta)^2\right]}{K(1-K\beta)\left[1-K\beta+c\beta(1-K\beta+\beta)\right]} \qquad [5]$$

At saturation pressure $p°$ when condensation occurs, the coverage of the second layer is equal to that at the first layer, that is $A_1 = A_2$, which results in $\beta = p/p°$. Note that $A_1 = A_2$ is not a necessary condition, it can be a certain ratio due to the configuration influenced by the geometry (e.g. a curved surface) and the nature of the adsorbed molecules / ions. This clearly indicates that the adsorbed layer may be limited even at $\beta = 1$. Considering $V/V_m = Z/Z_m$, (though configuration of adsorbed molecules may involve lateral distribution as well as stacking which will lead to a slightly higher V/V_m ratio,) and writing $\beta = x$, one obtains the relative adsorbed thickness:

$$\Theta = \frac{V}{V_m} = \frac{cx\left[1-(1-k)(1-kx)^2\right]}{k(1-kx)\left[1-kx+cx(1-kx+x)\right]} \qquad [5a]$$

where V_m is the monolayer capacity, c and k are parameters depending on temperature and the difference in adsorption heat of molecules at different layers: $c \propto exp[\,(E_{ad} - E_2)/RT]$, and $k \propto exp[-\,(E_2 - Q_L)/RT]$. At k=1, Eq.5a reduces back to the original BET equation. The form of Eq.5a with limited n (max. adsorbed layer) is provided in Appendix. I showed previously (1992) that Eq.5a is numerically similar to Eq.1, thus the definitions of c and k given here can also be applied to BET equation, (Eq.1). Figure 1 illustrates this isotherm function at various parameters.

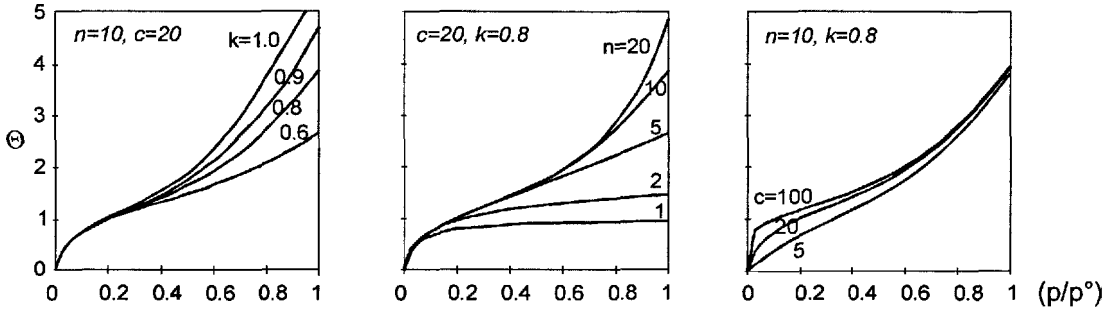

Figure 1. Modified BET isotherm varying with parameters n, k and c.

Some comments

Although Eq.5a has a singular point at (1- kx) = 0 which apparently indicates that when $p/p° = 1/k$ the adsorbed layer is infinite, one should *not* take it so, since this is simply because of the assumption n=∞. (It can be proven that $V/V_m \,|_{1-kx\to 0} = (n+1)/2$, for $n >> 1$. c.f. Appendix) Unfortunately, this singular point was used by previous researchers as one of major arguments in deriving their adsorption equations, which led to confusions.

To obtain V_m, c and k from experimental data, Eq.5a can be written to a $y = b_0+b_1x+b_2x^2$ form:

$$\frac{x}{1-kx}\cdot\frac{1+2(1-k)x-k(1-k)x^2}{V} = \frac{1}{cV_m}(1+(c-k)x+c(1-k)x^2) \qquad [5b]$$

try k values for the left hand side of Eq.5b, and calculate the coefficients by: V_m=1/(c b_0), $k = (1 - b_1/b_0 + \sqrt{(b_1/b_0 - 1)^2 + 4(b_1 - b_2)/b_0}\,)/2$, $c = b_1/b_0 + k$, until the k value converges. It may be noted that Eq.5b is very sensitive to the small change in k value, and a great care is needed in the trial calculation.

The extent of drying, as discussed before, though for the validity of application in cement / concrete study should not include very low RH condition, however, it is convenient to use traditional drying methods, i.e. D-drying and 105°C oven drying, to obtain the total evaporable moisture content for desorption, or a defined "dry" condition for adsorption. For the former, the error induced due to the gel water loss would not be large (the mass fraction of this part of water in the gel or crystals is very small); for the latter, the surface area alteration renders the specific surface under study only a comparative value, be it determined by H_2O or by N_2 adsorption.

MOISTURE SORPTION ISOTHERMS OF CONCRETE

Concrete contains large capillaries and micropores. The adsorption of moisture on walls of pores contributes a part of its total moisture content during drying, and a major part of moisture uptake during wetting to approximately 75-85% RH (at which capillary condensation occurs for my experimental results). Since that hydrated cement which has a great specific surface dominates the adsorption, and the majority of pores are formed in cement paste, the sorption isotherms are better expressed as the moisture per mass of cement (or cement + pozzolanic admixtures).

As an example, sorption isotherms of a concrete containing 30% fly ash replacing cement, with water to binder (cement + fly ash) 0.465 are shown in Figure 2. The adsorption was measured on samples dried at 105°C. Apparently the adsorption branch is much lower than the desorption, attributable to a number of differences, such as capillary meniscus curvatures and large pores connected with smaller pores for the high RH range; and the surface area for the low RH part.

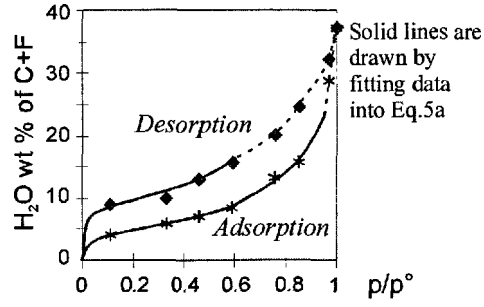

Figure.2. Desorption and adsorption isotherms of concrete, average of six specimens.

Desorption isotherm influenced by pore size distribution

The analysis of pore size distribution by desorption isotherm is based on the fact that, the moisture in pores (radius r) starts to evaporate when the curvature of the meniscus meets the criterion expressed by the *Laplace-Kelvin equation*:

$$\frac{2\gamma}{r} = \frac{RT}{M_V}\ln(x) \tag{6}$$

where γ is the surface tension (note: in micropores, it is a function of curvature, Gregg and Sing, 1982) and M_V the molecular volume for water. The adsorbed film on the wall (thickness $t_f = \Theta d$, d is the diameter of adsorbed molecules) in the mean time, will make the meniscus curvature slightly smaller and new equilibrium will then be established for the pores whose radius of the *core* satisfies Eq.6, that is, $r = r_{pore} - t_f$. The moisture loss is mainly due to the core water and thinning of the adsorbed film. Strictly speaking, the pore solution contains various ions thus has a lower chemical potential than the pure water, and its saturation vapor pressure is lower as well. But this effect is practically intermingled with the experimental error, and rarely observable.

The relation between volume of water in pore (V_p) and water in the core (V_c) is $V_c=V_pQ$, where $Q= 1- t_f / r_{pore}$ for the parallel slit-like pores, and $Q= (1- t_f / r_{pore})^2$ for the cylindrical pores. By setting a model of pore shape, the pore size distribution can be estimated (Xu, 1992). During calculation, it is necessary to adjust the parameters of the adsorption isotherm, i.e. c and k in Eq.5a. Figure 3 demonstrates pore size distribution of concrete, obtained by the moisture desorption, analyzed on the assumption of slit-like pore shape. No attempts were made in further evaluating the micro-pores, so the pore volume corresponding to the smallest pore size in Figure 3, is a sum of all smaller pores. It can be seen that the pure cement mortar has a higher micro-pore fraction than its fly ash containing counterparts. And mortars with higher $w/(c+f)$ ratios contain higher volume of large pores (r > ca. 80 Å).

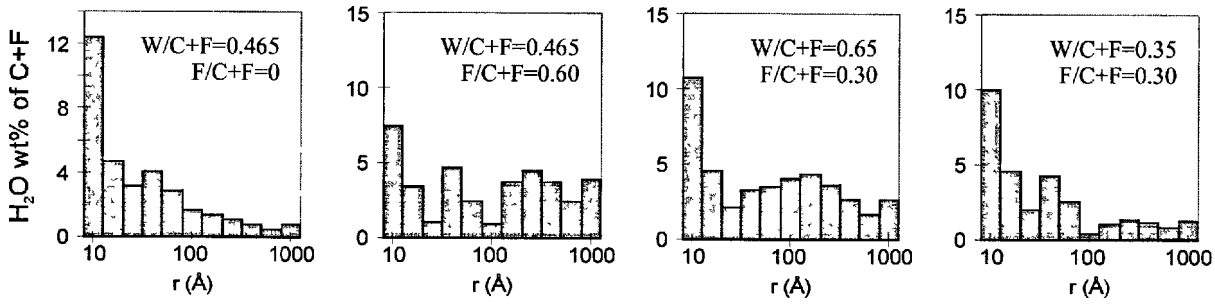

Figure 3. Pore size distribution of concrete determined by moisture desorption.

Surface area and sorption characteristics

Analysis of the isotherms in Figure 2 by Eq.5a results in V_m= 152 m^2/g of binder (4.3 g H_2O /g of binder), c= 38 and k=0.85 for adsorption (dried at 105°C before re-wetting); and V_m= 284 (8.0 g H_2O/g), c=145 and k=0.80 for desorption. The adsorption isotherm is lower than that of desorption, largely because of the drying induced surface area change for the low p/p° part as discussed before and indicated by the values of V_m; and in a given pore size the mean meniscus curvature may be smaller at adsorption; other reasons including the difference in liquid-solid contact angels for drying and wetting, presence of "ink-bottle-like pores", etc. are discussed elsewhere (Gregg and Sing, 1982).

In particular, the presence of "ink bottle" pores, pores having a narrower entrance than the body, may be responsible for a quite abrupt moisture loss between about 42% and 33% RH sometimes observed (Fig.4). Powers (1968) showed, at p/p°=0.40 the tension caused by lowering in p/p° is about 1200 atm (111 MPa), the limit of cohesion strength between water molecules. Thus there would be no meniscus exist at lower RH, and water formerly enclosed in the "bottles" is released.

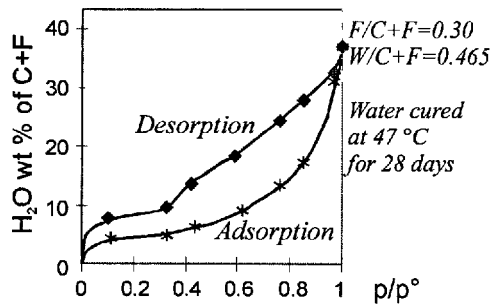

Fig. 4. Desorption at about 40% RH leads to an abrupt drop, Xu (1992).

It is observed that the coefficient c is lower for the adsorption compared with desorption, whereas k is slightly higher. By definition, as derived here, these imply a reduction in adsorption heat between molecules at the first and second or higher adsorption layer. It can be speculated that the apparent reduction in V_m is due to that the surface energy of the cement hydrates changes with drying, and number of adsorption sites reduces.

Concrete parameters, such as *w/c*, partial replacement of cement by pozzolanic material, and the factors that affect concrete properties, such as carbonation, aging etc., significantly influence the sorption isotherms. For example, large replacement of cement by fly ash (Class F) results in a decrease in V_m and lower c and k values. The latter was also seen for the effect of *w/c*, which however does not influence V_m (thus the specific surface) determined at adsorption.

CONCLUDING REMARKS

The adsorption function presented in this paper describes the adsorption isotherm of cement paste / concrete over the range about 10% to 80% (restricted to the stability of cement paste and presence of pores). The modification of BET equation, by assuming that $E_2 \neq E_3$ based on experimental evidences, introduces a parameter k which allows the application of this equation to 100% RH for non-porous material. It clearly shows, the relative thickness of adsorbed molecules at 100% RH (or rather, at $1 - kx = 0$) is about half of the probable highest layer.

Pores in cement paste influence the desorption isotherm, which in turn can be used for estimating the pore size distribution. Empirically, the desorption curve can also be expressed by the equation presented here, provided that the curve is smooth.

It should be pointed out, that the derivation of the adsorption equation in this paper is not restricted to the type of adsorbed substances. The adsorption isotherm function, i.e. Eq.5, can be applied to the ion sorption on solid in solution.

REFERENCES

Gregg, S.J. and Sing, K.S.W., *Adsorption, Surface Area and Porosity*. 2nd Edition, Academic Press, London, 1982.

Brunauer, S., Emmett, P.H., and Teller, E., *J. Amer. Chem. Soc.* Vol.60, (1938), p.309.

Brunauer, S., *The Adsorption of Gases and Vapors*, Princeton University Press, New Jersey, 1943.

Halsey, G., "Physical Adsorption on Non-Uniform Surfaces", *J. Chemical Physics*, Vol.16, No.10 (1948), pp.931-937.

Hill, T.L., "Theory of Physical Adsorption", *Advances in Catalysis and Related Subjects*, Vol.IV (1952), pp.211-258.

Brunauer, S., Skalny, J. and Bodor, E.E., "Adsorption on Nonporous Solids", *J. Colloid and Interface Science*, Vol.30, No.4 (1969), pp.546-552.

Hillerborg, A., "A Modified Absorption Theory", *Cem. Conc. Res.*, Vol.15, No.5 (1985), pp.809-816.

Harkins, W. and Jura, G., "Surface of Solids. Part X: Extension of the Attractive Energy of a Solid, an Adjacent Liquid or Film, the Decrease of Energy with Distance, and the Thickness of Films", *J. Amer. Chem. Soc.*, Vol.66 (1944), pp.919-927.

Xu, A., *Structure of Hardened Cement-Fly Ash Systems and Their Related Properties*, Publ. P-92:7 Dept. of Building Materials, Chalmers University of Technology, Göteborg, Sweden.

Powers, T.C., "Physical Properties of Cement Paste", *Proc. 4th International Symposium on Chemistry of Cement*, Washington D.C., 1960. pp.577-609.

Feldman, R.F.,"Sorption and Length-Change Scanning Isotherms of Methanol and Wter on Hydrated Portland Cement", *Proc. 5th Internationa Symposium on Chemistry of Cement*, Tokyo, 1968. Vol.III pp.53-66.

Mikhail, R.Sh., Brunauer, S. and Bodor, E.E., "Investigations of a Complete Pore Structure Analysis. I. Analysis of Micropores; II. Analysis of Four Silica Gels", *J. of Colloid and Interface Science*, Vol.26, 1968. pp.45-53; pp.54-61.

Radjy, F. and Sellevold, E.J., "A Phenomenological Theory for the *t*-Method of Pore Structure Analysis. I. Slit-Shaped Pores; II. Circularly Cylindrical Pores", *ditto.* Vol.39, 1972. pp.367-378; pp.367-378.

Cong, X. and Kirkpatrick, R.J., "Effects of the Temperature and Relative Humidity on the Structure of C-S-H Gel", *Cem. Conc. Res.*, Vol.25, No.6, 1995. pp.1237-1245.

APPENDIX: Adsorption isotherm for the case when n is limited:

$$\frac{Z}{Z_m} = \frac{c\beta\left[1-(n+1)(K\beta)n+n(K\beta)^{n+1}-(1-K)(1-K\beta)^2\right]}{(1-K\beta)\left\{(1-K\beta)K+c\beta\left[(1-K\beta)K+K\beta-(K\beta)^n\right]\right\}}$$

At $1\text{-}k\beta=0$:

$$lim\frac{Z}{Z_m} = \frac{c((n+1)n-2(1-K))}{2(c(n+k-1)+K^2)}$$

MODELLING OF CHLORIDE INGRESS INTO CEMENT-BASED MATERIALS DUE TO CAPILLARY SUCTION

Olivier FRANCY[1], Stéphanie BONNET[2], Raoul FRANÇOIS[1], Bernard PERRIN[2]

[1] Laboratoire de Matériaux et Durabilité des Constructions, INSA-UPS Toulouse
[2] Laboratoire d'Etudes THErmiques et Mécaniques, INSA-UPS Toulouse

ABSTRACT
To forecast the ingress of chloride ions by capillary suction of salt solutions, we simulate the pore structure of mortars by a monodimensional porous network with randomly distributed radius sizes. This model associated with a simplified suction theory and the knowledge of chloride binding isotherms shows good correlation with experimental data, provided that binding kinetics is quite slow. However, experimental binding is almost instantaneous. We must then assume that suction induces a delay in chloride binding.

Key-words: chloride, chloride binding, water suction, porosity, modelling.

MAIN NOTATIONS

r :	pore radius	g :	gravity
t :	time	C :	volume concentrations
ρ :	mortar density	C_s :	surface concentrations
K :	maximum suction height	N :	number of pore families

INTRODUCTION
Salt transport in unsteady state porous media is complex because of the coupling between transport phenomena. On the one hand, salt ingress is linked to moisture flows inside the material and on the other hand, salt influences water phase changes.

In order to study such transports, we performed suction tests on mortars with sodium chloride solutions. These tests led to the building of a network porosity model which can be used to predict profiles of both water and chloride content.

After presentation of the model and its performances, we deal with the required parameters and above all with the kinetics of chloride binding.

MATERIAL MODEL

Geometrical description
Following-up of water content in mortar during capillary suction shows that there is no real water front and that the material can be in an unsteady state, even when imbibition is ended (Perrin, 1995).

We consider N families of pores, with different radii and as a result different suction kinetics. Pores of various sizes are thus distributed randomly in the model in order to respect porosity, porometric distribution and specific area. We finally obtain a porous network constituted of vertical cylinders whose radii are varying along the suction direction (Fig 1).

With such a method, we are able not only to correlate very well with experimental results but also, which was our initial aim, to have unsteady state in the upper layers of the specimen.

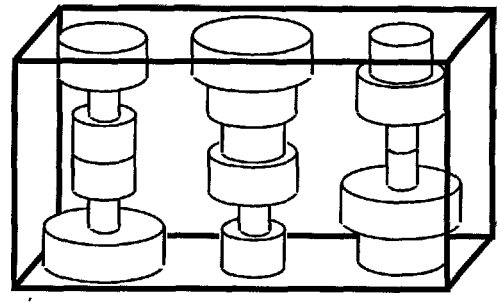

Figure 1: schematics of porous network

Model inputs

Our model requires two main parameters:

- Porosity and porometric distribution of the material provided by Mercury porometry. The experimental porometric distribution is discretized in a finite number of representative families.

- Chloride binding isotherm.
  It was measured and calibrated by a Freundlich expression (Bigas, 1994):

$C_{s\infty} = a\, C^{\gamma}$ $C_{s\infty}$: bound chloride at equilibrium (weight% of cement paste)
C : equilibrium chloride concentration of porewater (kg/m^3)
In our case, $a = 2.32\times10^{-3}$ and $\gamma = 0.36$.

Moreover, we make some hypotheses concerning:

- Kinetics of capillary suction.
  In one of the model's pore i, the final height K_i is given by balancing the weight of the water column and the vertical capillary force:

$$\lambda \frac{2\pi}{r(K_i)} = \int_0^{K_i} \rho g \pi r(h)^2 \, dh \qquad [1]$$

λ depending on: surface tension of water,
porosity,
tortuosity of medium.

Suction height in pore N° i is then given by:

$$h_i(t) = K_i \frac{\sqrt{t}}{\sqrt{t + z_i}} \qquad [2]$$

According to the first results, z_i can be taken equal to 1, whatever the pore radius and its variation. Otherwise, the kinetics should vary with the suction height. This simple

kind of kinetics shows good correlation with both experience and suction theory in cylindrical pores (Volkwein, 1993) and facilitates the numerical part.

- Kinetics of chloride binding.
  For a first approach, we choose a simple kinetics based on first-order chemical reactions (Fripiat, 1971):

$$C_s(t) = C_{s\infty} (1 - e^{-\eta t}) \qquad [3]$$

η depending on the material.

Such an evolution proves quite close to experimental measures (Tang, 1993).

Mathematical resolution

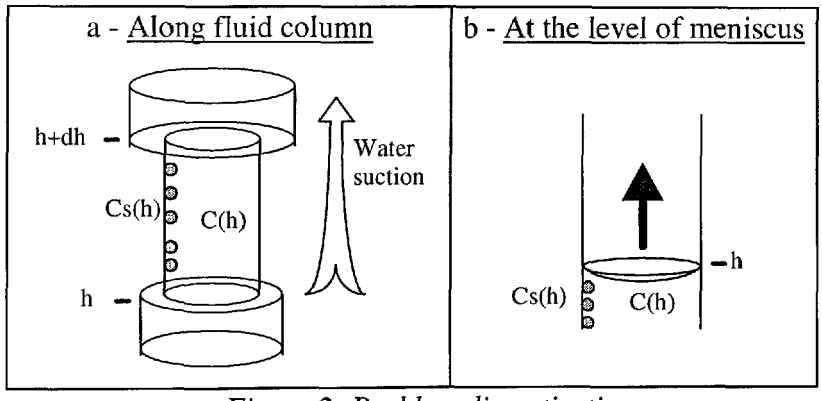

C(h): Cl vol. concentration of porewater at h

Cs(h): bound Cl surface concentration at h

Figure 2: Problem discretization

We can write the mass balance equations along the fluid column and at the level of the meniscus during capillary suction.

Along the column between t and t+dt (Fig 2a):

$$\pi\, r(h)^2\, dh\, C(h) = \pi\, r(h)^2\, dh\, dC(h) + \pi\, r(h+dh)^2\, dh\, C(h+dh) + 2\,\pi\, r(h)\, dh\, dCs(h)$$

$$r^2C(h+dh) - r^2C(h) = - r^2\, dC(h) - 2\, r\, dCs(h)$$

$$\frac{\partial\, r^2C}{\partial\, h}\, dh = - r^2\, \frac{\partial\, C}{\partial\, t}\, dt - 2\, r\, \frac{\partial\, Cs}{\partial\, t}\, dt \qquad [4]$$

$$\frac{\partial\, Cs}{\partial\, t}(h,t) = a\,\gamma\,(1 - e^{-\eta(t-th)})\, \frac{\partial\, C}{\partial\, t}\, C^{\gamma-1} + a\,\lambda\, C^{\gamma}\, e^{-\eta(t-th)}$$

th: time when water reaches h

and $$dh = \frac{K}{2}\left[\frac{1}{\sqrt{t}\,\sqrt{t+z}} - \frac{\sqrt{t}}{\left(\sqrt{t+z}\right)^3}\right] dt \qquad [5]$$

At the level of the meniscus between h et h+dh (Fig 2b):

$$\pi\, r(h)^2\, dh\, C(h) = \pi\, r(h+dh)^2\, dh\, C(h+dh) + 2\,\pi\, r(h)\, dh\, dCs(h+dh)$$

$$r^2C(h) - r^2C(h+dh) = -2r\frac{\partial Cs}{\partial t}(h+dh)\,dt$$

Keeping first order terms: $$\frac{\partial r^2C}{\partial h}dh = -2r\frac{\partial Cs}{\partial t}dt \quad [6]$$

and $$dt = 2zK^2\frac{h}{(h^2-K^2)^2}dh \quad [7]$$

MODEL VALIDATION

Experiments

Vertical suction tests were made on two kinds of mortar: cement CEM I 42,5 , W/C=0.38, sand volume content resp-. 19% (M1) and 57% (M2). Specimens were 70 mm-high prisms initially dried at 50°C with only a few percent of RH kept by silica-gel. Then, they were put in contact with salt solutions of various concentrations ([NaCl] = 0, 20 and 80 g/l). Their lateral faces were made watertight by a polymer resin in order to keep a monodimensional moisture flow. Water concentration profiles were recorded thanks to the gammaray attenuation technique (Perrin, 1995).

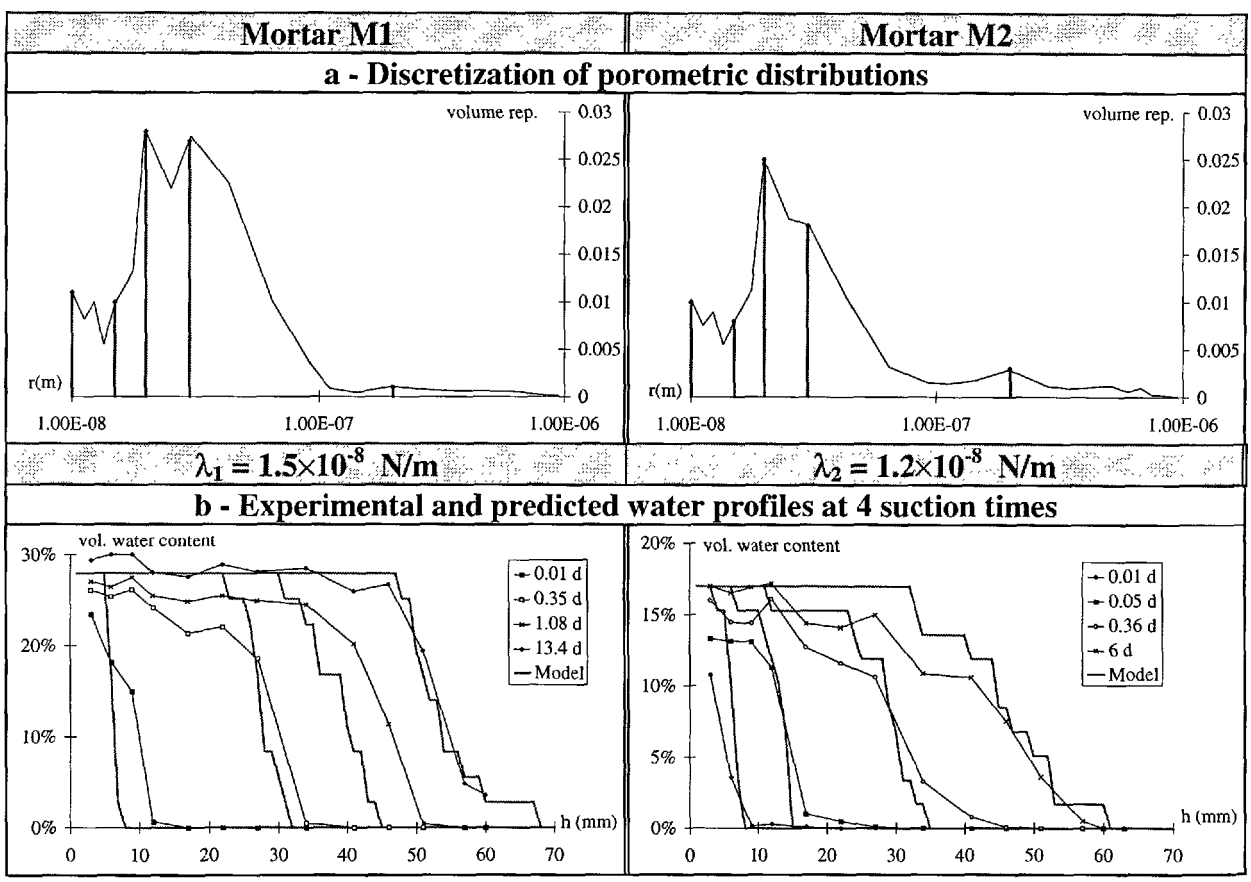

Figure 3: discretization of porometry results and compared water profiles for mortars 1 and 2

Salt concentration showed poor influence on height and kinetics of capillary suction which greatly simplifies our work. But, as expected, binding of chloride ions (essentially on C-S-H) induces a decrease of chloride content along the suction direction.

Water profiles prediction

First of all, we have to build the porous network. Experimental porometric distribution (Bigas, 1994) is discretized into N pore families (Fig 3a). The radii of those families are equal for the two mortars and only their distributions vary from one mortar to the other.

As we can notice, simulations provide good results (Fig 3b). Let us outline that, in these simulations, porous networks are only constituted of ten vertical major pores, which makes the calculation faster but resulting profiles not very smooth.

Chloride binding kinetics

Chloride binding kinetics was investigated by immersing 20 g of mortar powder (particles size inferior to 2 mm) into 50 ml of basic chloride solution (NaOH: 1 g/l, KOH: 4.65 g/l, NaCl: 32.96 g/l) and recording the solution concentration from the earliest times. Powder was previously vacuum-dried at 20°C for 3 days in a desiccator filled with silica gel and then kept in a decarbonized air at 11% RH imposed by a saturated LiCl solution for 7 days (Tang, 1993). Solutions were agitated and concentration measured by a chloride-selective probe.

Chloride binding seems to end after 4 hours and solutions show no change for 15 days (Fig 4). Between 15 and 30 days, the amount of bound chloride seems to increase but on the one hand, dispersion of measures prevents us from making such an assumption and on the other hand, all our imbibition tests last less than 15 days.

If we keep a first-order chemical kinetics to describe the phenomenon (Fig 4), such an evolution can be modelled by the following equation: $C_s(t) = C_{s\infty} (1 - e^{-40\,t})$

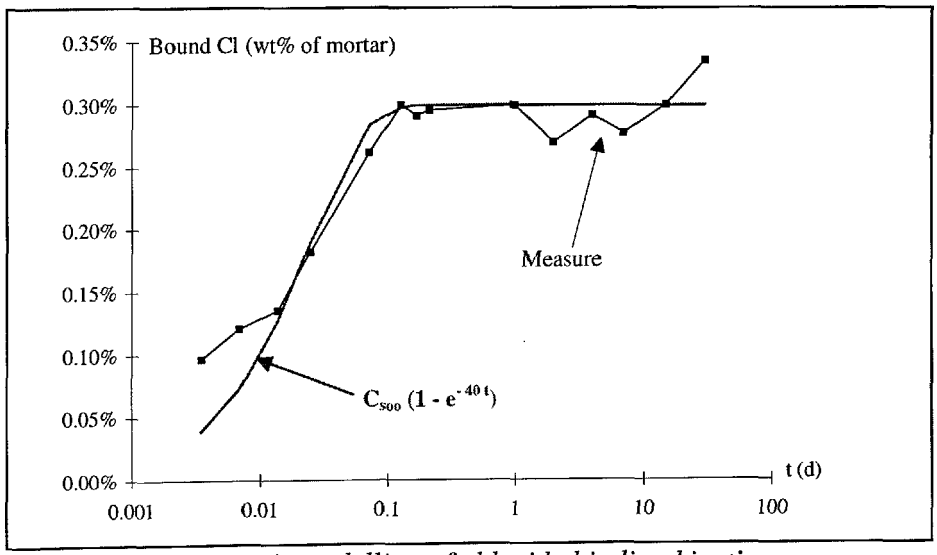

Figure 4: modelling of chloride binding kinetics

We could suppose that binding kinetics is linked to solution concentration. But binding isotherms measured (at present time in the LCPC Paris) on synthetic C-S-H demonstrated the poor influence of chloride concentration upon binding kinetics. However, kinetics is too fast and dispersion too important to quantify this influence.

Chloride profiles simulations

If we simulate the chloride profiles obtained by salt solutions suction with our experimental

chloride binding kinetics, the predicted profiles appear to be very far from reality. To correlate quite well with experience results, the value of η has to be decreased from 40 to 0.4 (Fig 5). Moreover, as pore radii are randomly distributed, the porous network does not remain exactly the same for every simulation. As a result, we studied the model dispersion which never exceeds 0.0012 g Cl / g mortar (Fig 6).

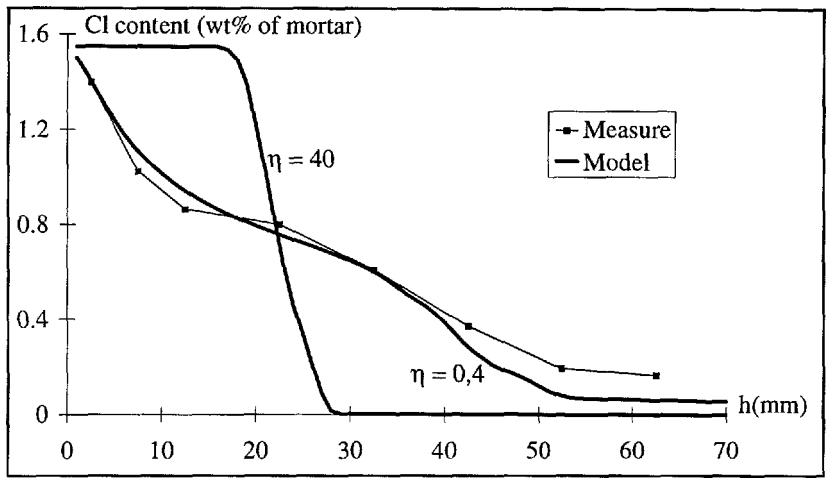

Figure 5: Influence of parameter η upon chloride profiles for M1 - 80 g/l

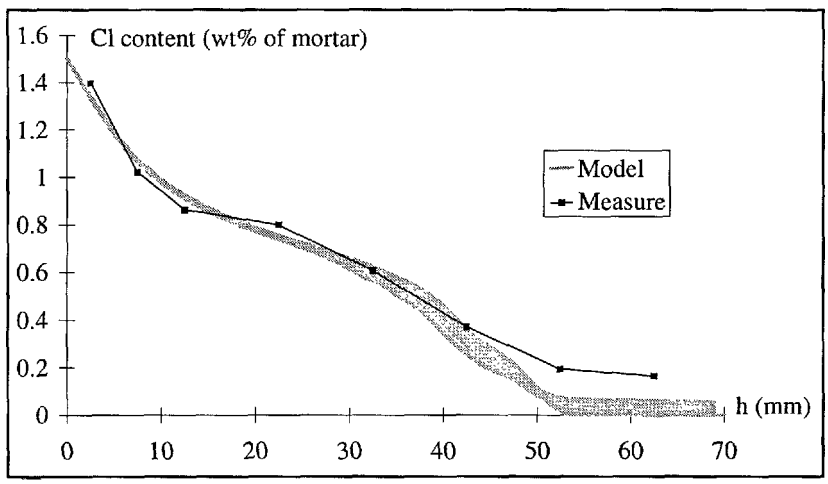

Figure 6: Model dispersion for M1 - 80 g/l and η = 0.4 (10 simulations)

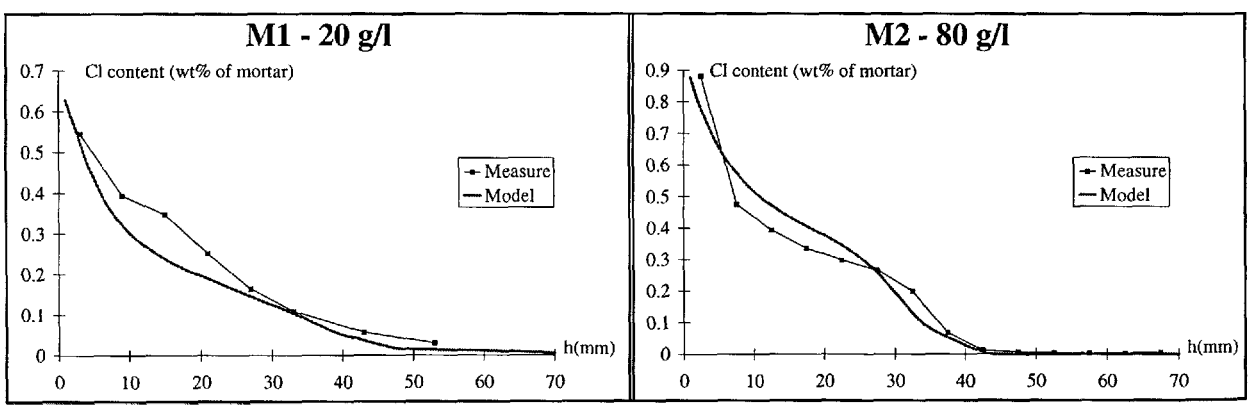

Figure 7: Compared experimental and predicted chloride profiles for 2 other tests

Besides, the value of 0.4 provides a good correlation between measured and predicted profiles

for all other tests (Fig 7).

Discussion about chloride binding

As a result, why should chloride binding be delayed during capillary suction? We can find many explanations to this problem but each one is very difficult to quantify. The only thing we can positively state is that the liquid flow is dragging ions and preventing them from binding as quickly as usual.

Even if pores are very thin, liquid flow in the porous media remains faster than the binding equilibrium. Consequently, some of the chloride ions initially likely to bind (according to the porewater concentration) are dragged away before equilibrium is reached. In fact, the flow prevents them from accessing some minor pores or from finding instantly a free site on the pore walls (Fig 8).

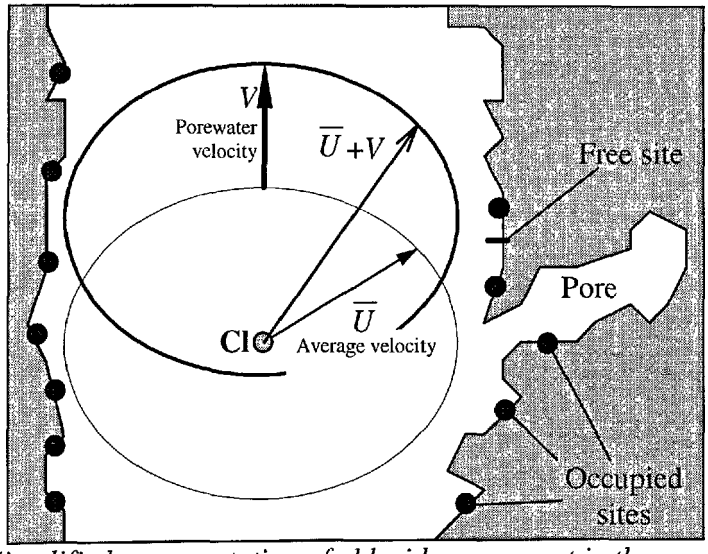

Figure 8: Simplified representation of chloride movement in the porous medium

We can try to quantify those effects with simple numerical considerations.

Let dM_∞ be the total weight of Cl that might be bound (for a given concentration) over one discretization step dh.

$dM_\infty = C_{s\infty} (\rho\ S\ dh)$

For a 20 g/l concentration, $dM_\infty = 0.0141$ dh and $dM_\infty = 1.41\times10^{-2}$ g for dh = 1 mm

The evolution of occupied sites is then: $dM = dM_\infty (1 - e^{-\eta t})$

Because of porewater flow, each chloride ion spends $\tau = \frac{dh}{V(h)}$ within the distance dh and for instance: $\tau\ (\frac{K}{100}) \approx \frac{2\ z}{100\ K}$ dh (Eq 5)

For a maximum suction height of 60 mm and dh = 1 mm, $\tau\ (\frac{K}{100}) = 0.33\times10^{-3}$ s

Such a time is required to occupy the first 1.3% of the total number of sites which represents less than 2×10^{-4} g and correlates well with our need to decrease η by a hundred times.

CONCLUSION

With a simple geometrical model, we were able to predict quite perfectly the combined transport of water and chloride ions during capillary suction tests. We have also highlighted the abnormal binding kinetics of chloride ions during such a test since the velocity of liquid flow prevents some part of the ions from binding instantly on pore walls.

Of course, we could hesitate about using mercury porometry results to build such a model as such an experiment does not provide true information on the internal structure of the material. But, as we only consider intrusion phenomena (Winslow, 1988) and since the model has shown its efficiency in predicting water profiles, we can be quite trustful.

REFERENCES

Bigas, J.P., "La Diffusion des Ions Chlore dans les Mortiers, Ph.D. INSA Toulouse, 1994.

Fripiat, J, Chaussidon, J., Jelli A., "Chimie-Physique des Phénomènes de Surface", Publ. Masson et Cie, Paris, 1971.

Perrin, B., Bonnet S., "Experimental Results Concerning Combined Transport of Humidity and Chloride in Non Steady State", Intl RILEM Workshop Chloride Penetration into Concrete, Saint-Rémy-les-Chevreuses, October 1995.

Tang, L., Nilsson, L.O., "Chloride Binding Capacity and Binding Isotherms of OPC Pastes and Mortars", Cement and Concrete Research,Vol. 23, N° 2, pp. 247-253, 1993.

Volkwein, A., "The Capillary Suction of Water into Concrete and the Abnormal Viscosity of the Porewater, Cement and Concrete Research, Vol. 23, N° 4, pp. 843-852, 1993.

Winslow, D., "Some Experimental Possibilities with Mercury Intrusion Porosimetry", Proceedings Materials Research Society Symposium, Pore Stucture and Permeability of Cementitous Materials, Boston, November 1988.

ELECTRICAL PROPERTIES OF CEMENTS

Anatoly F. BERNATSKY, Siberian Research Institute of Energetics.
Novosibirsk, Russia

ABSTRACT Electrical properties of main portland cement clinker minerals, products of hydration of portland cement (hydrosilicates, hydroaluninates, hydroalumoferrites of calcium) and solidified cement in dry and water saturated states were investigated. Power analysis of main products of clinker minerals hydration on calculation of electrical strength was carried out.

Key-words: Electrical, Properties, Drying, Humidity, Ions.

INTRODUCTION

Investigations of electrical properties of cements and concretes based on cement have been carring out at the Siberian Research Institute of Energetics for thirty years, and constructions for power building have been developing too. Thus, knowledge of electrical properties of solidified cement is of practical importance.

Cement stone is a total combination of hydratic new formation with clinker minerals which haven' t reacted with water. Portland cement clinker minerals have extremely irregular crystal lattices with vacancies in points of lattice and varied ions in sites between points. The bonds of these ions are weaker than those in regular crystals, that affects physical and chemical properties of clinker minerals and their electrical conductivity too. Joint action of thermal motion and electrical field can lead to a situation when this or that ion can become a carrier under certain conditions. Thus, electrical conductivity of clinker minerals can be classified as ionic type. The importance of electrical conductivity in many respects depends on ordering of ions in a crystal lattice.

DISCUSSION

The introductionary remarks are confirmed by researches of electrical conductivity of main clinker minerals in temperature ranges from 20 to 1150 °C (Mackenzie,1978). It was found that temperature coefficients of β- C_2S , C_3S and CaO are proportional among themselves. It makes possible to come to a conclusion that electrical conductivity of above mentioned minerals is caused by diffusion of ions Ca^{2+}. Conductivity of C_3A is close to conductivity of pure Al_2O_3, but can be changed to a great extent in the presence of ions Ca^{2+}. Conductivity of C_4AF and pure Fe_2O_3 are close. It means that carrying of electrical charge in C_4AF is realized by ions Fe^{2+} and Fe^{3+}.

Electrical conductivity of hydrated compound of cement stone in many respects depends on quantity of percentage of water in it and on forms of bonds of liquid phase with a solid body. The part of water used for mixing concrete ingredients with water is used directly for formation new compounds of crystalline hydrates, the remaining part is adsorbed or is kept in pores of cement stone, firstly in pores of cement gel. Electrical conductivity of cement gel as a colloid system is connected with existence of water in it, the full removal of which leads to destruction of crystalline hydrates at high temperature. Crystalline hydrates of cement stone contain molecules of water in chemically connected state which were included in the crystal lattice. The part of electrical conductivity related to gel is to a great extent more than the part related to crystalline hydrates. This is confirmed by data given in Table 1.

Table 1 Specific volume electrical resistance of crystalline hydrates of cement stone.

Compound	Resistance, Ω · m
(0.8-1.5) $CaO \cdot SiO_2 \cdot$ (0.5-2.0) H_2O	$9 \cdot 10^4$ - $5 \cdot 10^7$
$3CaO \cdot Al_2O_3 \cdot 6H_2O$	$8 \cdot 10^6$ - $2 \cdot 10^7$
$4CaO \cdot Al_2O_3 \cdot 12H_2O \cdot 3CaCl_2 \cdot 12H_2O$	$8 \cdot 10^6$ - $2 \cdot 10^7$
$4CaO \cdot Al_2O_3 \cdot nH_2O$	$1 \cdot 10^6$ - $3 \cdot 10^6$
Hydrated C_4AF	$1 \cdot 10^6$
$3CaO \cdot Al_2O_3 \cdot 3CaSO_4 \cdot 32H_2O$	$6 \cdot 10^4$
(1.7 - 2.0) $CaO \cdot SiO_2 \cdot nH_2O$	$1.2 \cdot 10^4$ - $6.7 \cdot 10^4$

High-based hydrosilicates and hydrosulphoaluminates of calcium have minimal resistance but one-based hydrosilicates, tricalcium hydroaluminate - maximal. Specific electrical resistance of cement stone is not reduced lower than 10^4 Ω·m in air-dry state and can reach values of 10^9-10^{10} Ω·m.

Electrical conductivity of water saturated cement stone is increasing. Electrical resistance of wet cement stone and its humidity are connected together by a following relationship (Bernatsky, 1980):

$$\rho = \frac{K}{W^{2.6}},$$

where ρ - specific volume electrical resistance of cement stone (Ω·m);
K - coefficient of proportionality, depending on structure of cement stone;
W - absolute humidity of cement stone (%).

The removal of free and partially adsorbed moisture on inner surface of cement stone is the result of its drying. It affects an increase of electrical resistance of cement stone to values equal to 10^9-10^{12} Ω·m. The degree of cement stone dehydration is determinated to a considerable extent by temperature at which the drying is carried out. The higher the temperature of drying the lower balanced humiduty of cement stone can be achieved. Free moisture from capillary-porous body can be removed as a resullt of drying at 105 °C. The temperature of drying must be higher for removal of adsorbed moisture. Thus, electrical conductivity of dried concrete and other electrical characteristics connected with conductivity must be determined to a considerable extent by temperature of drying . This is corroborated completely by the results of experimental investigations given in Table 2.

Table 2. The influence of temperature of drying on electrical characteristics of cement stone.

Type of cement, the conditions of hardening	Temperature of drying, °C	ρ , Ω·m	tgδ
Portland cement, steaming	105	10^7	more 1.0
Sand portland cement, autoclave	140	$2.7 \cdot 10^{10}$	0.16
The same	150	$5.0 \cdot 10^{10}$	0.15
The same	200	10^{11}	0.07

Considerable quantity of new formation in sement stone, its structural and crystal chemical variety, difficulties in their synthesis and identification are the main reason of that electrical properties of these components are little known nowadays. It is related in particular to its electrical strength. The method of power analysis (Bernatsky,1980) was developed for definition of electrical strength of cement crystal hydrates. The results of calculations of electric strength of cement stone components are given in Table 3.

Table 3 Power characteristics of crystalline hydrates of cement stone.

The name of compound	Crystal chemical formula	Calculated values of impulse dielectric strength, kV/sm
	Hydrosilicates of calcium	
Hyrolite	$Ca_2[Si_4O_9(OH)_2] \cdot 3H_2O$	76.5
Tobermorite	$Ca_5[Si_6O_{18}H_2] \cdot 4H_2O$	145
Hillerbrandite	$Ca_{12}[Si_6O_{17}] \cdot (OH)_4 \cdot 12Ca(OH)_2$	148
C_3SH_2	$Ca_4[Si_2O_7] \cdot (OH)_2 \cdot 2Ca(OH)_2$	149
Xonotlite	$Ca_6[Si_6O_{17}] \cdot (OH)_2$	154
Hydrate α -C_2S	$Ca_2[SiO_3 \cdot (OH)] \cdot (OH)$	167
Phasa Y	$Ca_6[SiO_4] \cdot [Si_2O_7] \cdot (OH)_2$	173
	Hydroaluminates of calcium	
C_2AH_8	$2[Ca(OH)_2] \cdot 2[Al(OH)_3] \cdot 3H_2O$	76.5
C_3AH_6	$3[Ca(OH)_2] \cdot 2[Al(OH)_3]$	119.5
C_4AH_{13}	$[Ca_2Al(OH)_7] \cdot 6H_2O$	80
C_4AH_{19}	$2\{Ca_2[Al(OH)_7] \cdot 6H_2O\}$	41
	Hydrosulphoaluminates of calcium	
$C_3A \cdot Cs \cdot H_{32}$	$Ca_6Al_2[(SO_4)(OH)_4]_3 \cdot 26H_2O$	66
$C_3A \cdot Cs \cdot H_{12}$	$Ca_4[Al(OH)_6]_2 \cdot (SO_4) \cdot 6H_2O$	85
	The other compounds	
β-C_2S	Ca_2SiO_4	199
C_3S	$Ca_2[(SiO_4)(CaO)]$	181
C_3A	$3CaO \cdot Al_2O_3$	190

CONCLUSION

Analysing the data received we can stress that electrical strength of starting clinker minerals is higher than that of the products of its hydration. Hydrosilicates of calcium have higher electrical characteristics than hydroaluminates and hydrosulphoaluminates of calcium.

REFERENCES

Bernatsky, A.F., Tselebrovsky , Yu. V. and Chunchin, V.A., "Electrical properties of concrete ", Power, Moscow, 1980 , 270 pp.

Mackenzie, K. J. D. , "Electrical properties of some portland cement clincer minerals", Trans. and J. Brit. Ceram. Soc., Vol. 77, No 1, 1978, pp. 13-17.

TOPIC IV.F

Life cycle analyses and input parametres

THE MYTHS AND MISCONCEPTIONS OF CHLORIDE PENETRATION INTO CONCRETE

Narayan SWAMY, University of Sheffield, Sheffield, England

ABSTRACT This paper examines the conventional tests used to determine the amount and process of chloride penetration into concrete. It is shown that chloride penetration into concrete is a time-dependent process involving physical processes and chemical interactions, and that chlorides penetrate not only in the direction of gravity i.e., depth, but also in a direction lateral to the depth. One dimensional models of chloride diffusion are thus inapplicable to concrete. A two-dimensional model for chloride diffusion is proposed.

Key-words: chloride, penetration, Friedel's salt, pore structure, diffusion

INTRODUCTION

Conventional tests to determine the penetration of chloride into concrete are fundamentally of limited value in terms of the amount of chlorides penetrating the concrete, and the process of chloride ion intrusion into concrete. The standard diffusion cell test, for example, which involves the flow of ions due to a difference in ion concentration to measure the chloride diffusion coefficient, although well established, assumes that chloride penetration is a one-dimensional process, and the unique coefficient of diffusion derived from the test does not represent what happens in practice (Swamy et al 1994).

Accelerated chloride diffusion tests, on the other hand, rely either on increasing the concentration of the chloride solutions, or testing at elevated temperatures in order to accelerate the chloride intrusion. The most widely used accelerated test is the application of an electric field to a test specimen to drive chloride ions through the concrete towards an anode. A potential difference across the test specimen is applied, and the chloride diffusivity is expressed in terms of the total charge in coulombs passed over a period of six hours. Many variations of this test are reported in literature, with the electrical field ranging from a potential difference of 2 volt dc to 60 volt dc. A number of factors influence the results of these tests, such as, the temperature rise during the test, migration of all of the ions present and not just the chloride ions, and the application of Fick's first law of diffusion, which ignores the effects of the electrical field. The value of the results of these tests is thus highly dubious; at best, the test gives a comparative chloride diffusion index, and at worst, the test alters the physical processes of chloride penetration through changes in the chemical structure and porosity of the medium, such that the mechanism of chloride intrusion is totally different to what happens in real life.

The aim of this paper is to establish a better understanding of the amount and chlorides that diffuse through concrete, and to obtain data based on processes and mechanisms that are realistic and relevant to real life situations.

EXPERIMENTAL BACKGROUND

To achieve these objectives, the test specimens chosen for this study were reinforced concrete slabs, 1000 x 1000 x 150mm, or 1000 x 500 x 150mm, with fairly large exposed surface areas, simulating pavements and bridge decks. The slabs were subjected to chloride penetration by cyclic ponding with 4% sodium chloride solution for 7 days, and drying in ambient air for 3 days. At intervals, the concrete slabs were exposed to a drying environment, similar to what occurs in

practice, to enable carbonation processes to occur. The acid-soluble chloride contents, and chloride profiles, were determined indirectly by Volhard's method described in BS 1881, 1988.

To establish the direction of chloride penetration, some of the slabs were partially coated with an acrylic-based surface coating system with extensive test evidence of very high resistance to chloride penetration (Swamy and Tanikawa, 1990, 1991a, 1991b, 1995). Cores were taken from the uncoated and coated parts of the slabs to determine the chloride concentration profiles using Volhard's method.

TEST RESULTS AND DISCUSSION

A large amount of data has been collected from these tests on chloride penetration into concrete slabs. The main variables investigated are water-binder (w/b) ratio, amount and type of mineral admixtures, time of exposure to the chloride penetration regime, and duration of test. Currently, the tests have been in progress for about 9 years, and typical selected data are presented here to highlight the main theme of this paper.

Time-dependency of chloride penetration

The results of chloride concentration profiles for two sets of slabs with a water-binder ratio of 0.60, and containing cement replacements of 30% fly ash, or 65% ground granulated blastfurnace slag after 10, 20 and 50 cycles of exposure to chlorides are shown in Figs 1 and 2 respectively. These results are typical of other data obtained in this study with concretes containing portland cement only, or, those containing other mineral admixtures or combinations of mineral admixtures. These results show conclusively the following:

1. The amount of chlorides penetrating concrete, and the depths of their penetration are dependent on the structure of the concrete mix i.e. the type of concrete mix.
2. The process of chloride penetration is a time-dependent phenomenon, implying that short-term tests do not represent what happens in practice.
3. The surface concentration of chlorides in a concrete element is not constant, but varies with the duration of exposure, and inevitably, with the severity of exposure i.e. chloride concentration in the environment.

Directions of chloride penetration

To obtain conclusive proof of the direction of penetration of chlorides, one-half of 1000 x 1000 x 150mm slabs was coated with an acrylic-based coating system, and the other half left uncoated, and then, the entire slabs were subjected to the cyclic chloride penetration regime described earlier. However, the ability of the coating part to resist chloride penetration needs to be completely reliable to validate the directions of chloride transportation. To confirm this, 1000 x 500 x 150mm slabs, made of portland cement only, but with three different water-cement ratios, and fully coated with the acrylic system, were then exposed to cyclic chloride penetration regimes. In both cases, three water-cement ratios of 0.45, 0.60 and 0.75 were used, and only normal portland cement was used in these slabs.

The chloride penetration profiles in the three fully coated slabs 1000 x 500 x 150mm, after 70 cycles of exposure, are shown in Table 1. The data in this table give conclusive proof that no chlorides have penetrated the acrylic surface coating, even after long-term exposure to a salt-laden environment, justifying the test methodology adopted in using the partially coated slabs.

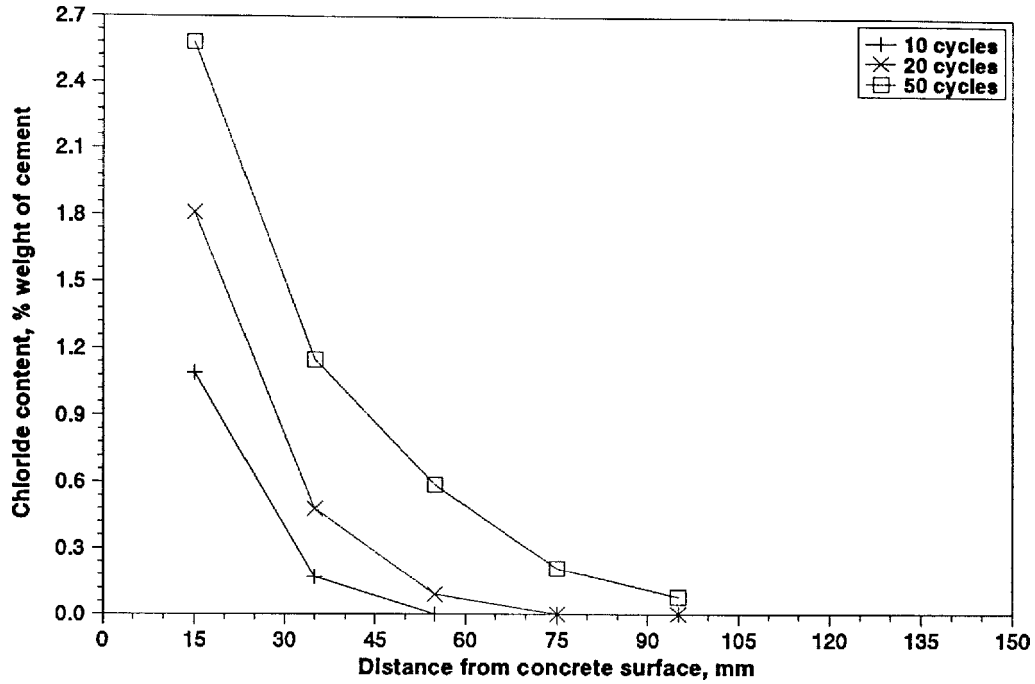

FIG 1 Chloride profiles in slag concrete after different cycles of exposure (w/b = 0.60)

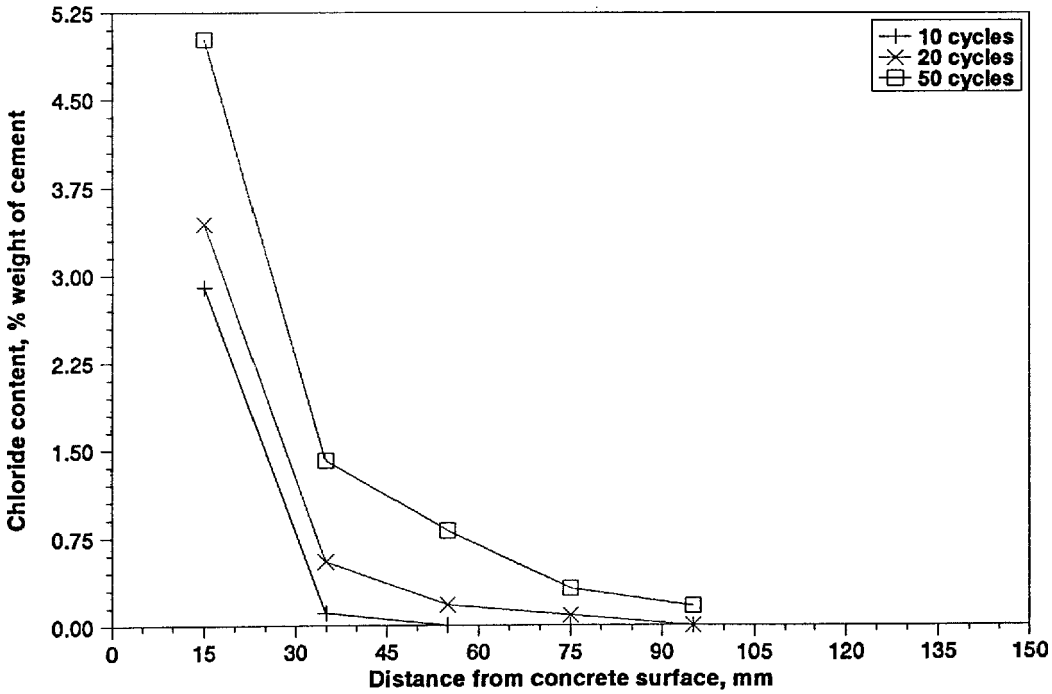

FIG 2 Chloride profiles in fly ash concrete after different cycles of exposure (w/b = 0.60)

Table 1 Acid soluble chlorides by percentage weight of cement

Slab number	w/c ratio	Depth intervals (mm)					
		0-5	5-25	25-45	45-65	65-85	85-105
S4, S5and S6	0.45, 0.60 and 0.75	0.00	0.00	0.00	0.00	0.00	0.00

The results of the chloride concentration profiles of the partially coated slabs 1000 x 1000 x 150mm are shown in Figs 3, 4 and 5. In these slabs and figures, the chloride concentration was determined in the uncoated parts, and at three locations in the coated parts - along lines X1, X2 and X3 at distances of 70, 210 and 350mm from the junction between the coated and uncoated parts as shown in Fig 6. The data in Figs 3 to 5, bearing in mind the results shown in Table 1, prove conclusively the following:

1. Chlorides diffuse both in the direction of depth, i.e. gravity, and in a direction lateral to the depth of the concrete. The amount of chlorides that diffuse in the lateral direction, and the depth they diffuse to laterally, are a function of the w/b ratio, duration of exposure, and obviously, the severity of exposure concentration of chlorides.
2. In practice, the lateral transportation of chlorides will take place in all concretes, irrespective of their w/b ratio, because of continuing duration of exposure, and cracking, arising from various processes, such as, wetting/drying cycles, freezing and thawing, thermal movements, and of course, external loads.
3. The surface concentration of chlorides on a concrete element is again shown to be not a unique constant, but a highly variable parameter which has implications to the diffusion model applicable to concrete.

Other implications

The data shown in Figs 1 to 5 give rise to many implications, which, lack of space will not permit full discussion here. However, these are briefly referred to below:

1. The time-dependency of chloride transportation into concrete implies changes with time, of the physical processes and chemical interactions involved in the chloride transportation process.
2. The stability of Friedel's salt formed due to the interactions between the penetrating chlorides and the C_3A phase in the cement is a function of the alkalinity changes of the concrete arising from atmospheric carbonation. The dissolution of Friedel's salt will increase the free-chloride ion concentration in the concrete (Swamy and Suryavanshi, 1996).
3. The presence of mineral admixtures will have an influence on the dissolution of Friedel's salt present at the concrete external surface.
4. Ettringite will also become unstable in severely carbonated concrete.
5. Prolonged exposure to a carbonating environment after chloride penetration can enable the formation of well-crystallised and amorphous calcite below the exposed surfaces, and the presence of acid-soluble chloride appear to have no influence on the mechanism leading to their formation (Suryavanshi and Swamy, 1997).
6. Penetrating chlorides will change the pore structure of the cover concrete. Extensive microstructural studies show that voluminous chloride-bearing compounds such as Friedel's salt, and calcium chloride, preferentially precipitate in the coarser pores, which results in a significant reduction in the number of coarser pores (> about 30nm in diameter) with reductions in both total accessible pore volume, and porosity of the chloride contaminated concrete (Swamy and Suryavanshi, 1996). Chloride contamination of the outer surface layers of exposed concrete can thus lead to reduced permeability of the cover concrete to further ingress of chlorides.

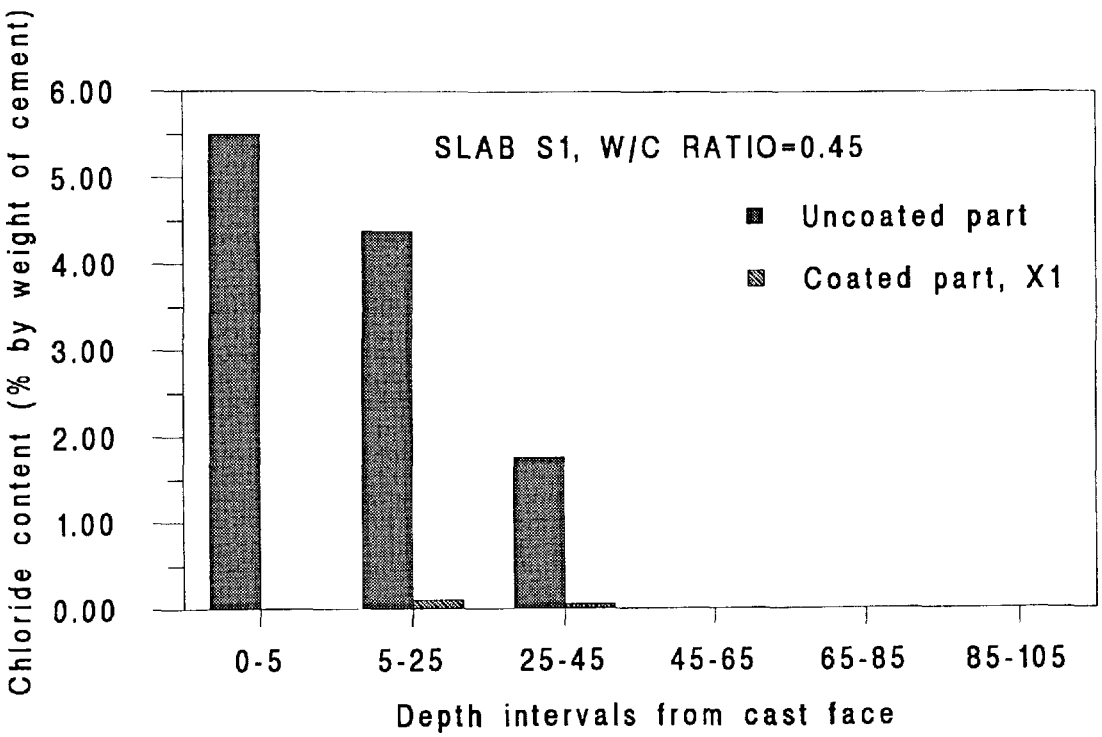

FIG 3 Chloride profiles in uncoated and coated parts of slab with w/b = 0.45.

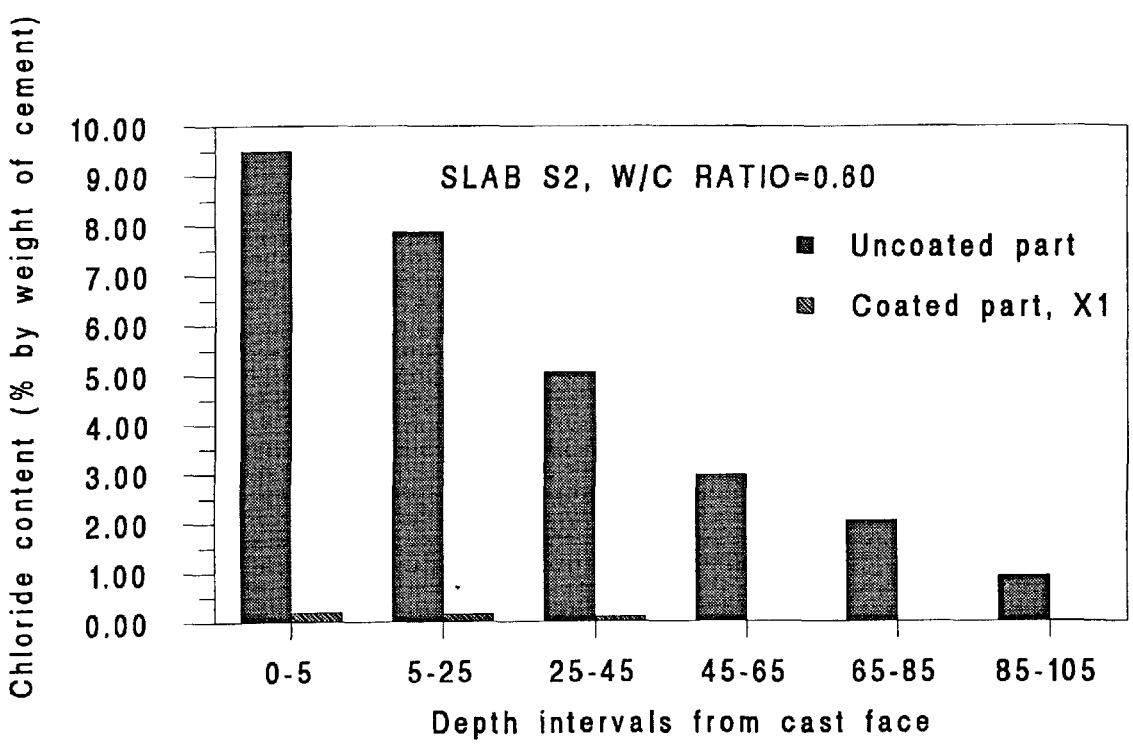

FIG 4 Chloride profiles in uncoated and coated parts of slab with w/b = 0.60.

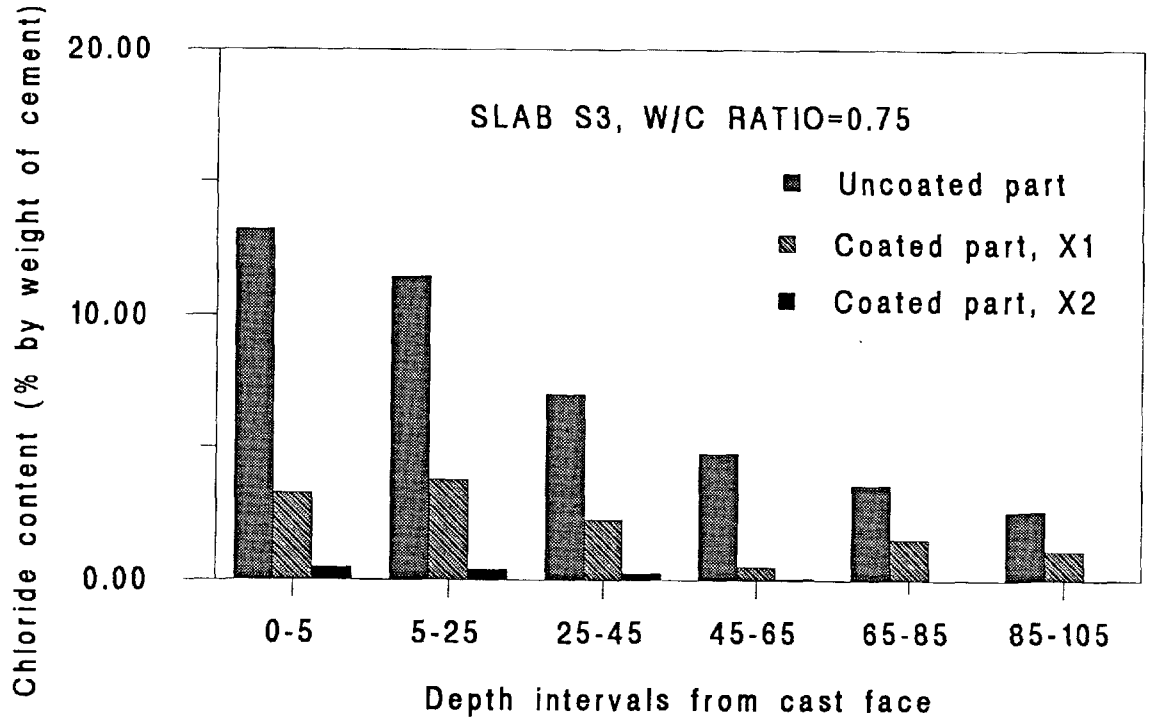

FIG 5 Chloride profiles in uncoated and coated parts of slab with w/b = 0.75.

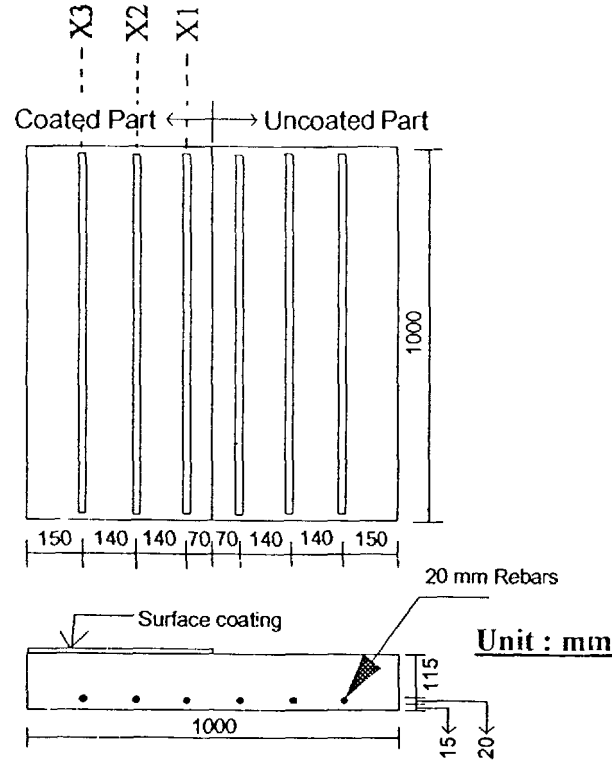

FIG 6 Locations X1, X2 and X3 for chloride profiles in coated part of slab.

Chloride diffusion models

The data presented in Figs 1 to 5 question the validity of one-dimensional chloride diffusion models, and in particular, of the diffusion coefficients calculated on the basis of Fick's second law of diffusion for one-dimensional non-steady state, namely,

$$\frac{dc}{dt} = D\left\{\frac{d^2c}{dx^2}\right\} \tag{1}$$

A more realistic model representing the two-dimensional diffusion process is given by

$$\frac{dc}{dt} = D\left\{\frac{d^2c}{dx^2} + \frac{d^2c}{dy^2}\right\} \tag{2}$$

Research is currently in progress to analyse the data presented here on the basis of the above two-dimensional model, and the results will be reported when this work is completed .

CONCLUSIONS

This paper critically examines the current conventional tests to determine the chloride concentration profiles when concrete is exposed to a salt-laden environment. Test results derived from concrete slabs subjected to a cyclic chloride solution ponding and drying regime are then presented to show that chloride intrusion into concrete is a time-dependent phenomenon, involving both physical processes and chemical interactions, and that, the chloride diffusion process involves chloride transportation both in the vertical and lateral directions. A two-dimensional diffusion model is proposed to represent chloride intrusion into concrete.

REFERENCES

Suryavanshi, A. K., and Swamy, R. N., "Well-crystallised and Amorphous Calcite in Concrete Slabs Exposed to Long-Term Atmospheric Carbonation", To be published in Advances in Cement Research, 1997.

Swamy, R. N., Hamada, H., and Laiw, J. C., "A Critical Evaluation of Chloride Penetration into Concrete in Marine Environment", Proceedings, International Conference on Corrosion and Corrosion Protection of Steel in Concrete, Ed. R. N. Swamy, Sheffield Academic Press, Vol. 1, 1994, pp. 404-419.

Swamy, R. N., and Tanikawa, S., "Surface Coatings to Preserve Concrete Durability", Proceedings. International Conference on Protection of Concrete, Ed. R. K. Dhir and J. W. E. Green, E & F N Spon, London, 1990, pp. 149-165.

Swamy, R. N., and Tanikawa, S., "Control of Steel Corrosion in Chloride Contaminated Concrete Through Aron Wall Surface Coating", Proceedings, International Conference on Durability of Concrete, Montreal, ACI Publ., SP-126, Ed. V. M. Malhotra, 1991a, pp. 371-391.

Swamy, R. N., and Tanikawa, S., "A Highly Elastic Surface Coating to Protect Structures Exposed to Coastal/Marine Environments", Proceedings, International Conference on Evaluation and Rehabilitation of Concrete Structures and Innovation in Design", ACI Publ. SP-128, Vol. 1, Ed. V M Malhotra, 1991b, pp. 1-18.

Swamy, R. N., and Tanikawa, S., "An External Surface Coating to Protect Concrete and Steel from Aggressive Environment", Materials and Structures, Vol. 26, Oct 1995, pp. 465-478.

Swamy, R. N., and Suryavanshi, A. K., "Durability of Blended Cement Concrete Structural Elements of Higher Water-Binder Ratio Against Chloride and Carbonation Attack", To be published, 1996.

CHLORIDE ION DIFFUSION COEFFICIENTS FOR CONCRETE - A REVIEW OF EXPERIMENTAL METHODS

Harald JUSTNES and Eva RODUM, SINTEF Civil and Environmental Engineering, Dept. Cement and Concrete, N-7034 Trondheim, Norway.

ABSTRACT The mathematical theories for determining diffusion coefficients from experiments based on pure diffusion or migration in an impressed electrical field, both under steady state and non-steady state conditions, have been reviewed. Literature data from comparative studies of the relation between theory and experimental results support the validity of the calculation of pure diffusion coefficients from migration experiments. Diffusion coefficients obtained by steady and non-steady state methods can not be interchanged, due to the dependence on chloride binding of the latter. Thus, diffusion coefficients to be used in for instance service life analyses should be obtained by non-steady state methods since this is the diffusion mode in practice, although in some cases suction may dominate over diffusion as transport mechanism.

Key-words: Chloride, diffusion, methods.

INTRODUCTION

There is a number of accelerated methods for determination of chloride diffusion coefficients in concrete in the literature, and there is still a great confusion with respect to the fundamentals of the applied equations and the validity of the methods, although some recent papers have clarified some of the matter. The present paper is a review of the different available methods and the theories they are based on. In order to ease the comparison, uniform symbols have been used throughout, although they may deviate from the symbols used by the original authors.

MATHEMATICAL THEORIES

Laboratory methods for determining the rate of chloride ion penetration into concrete may be classified into four categories: Steady state diffusion, non-steady state diffusion, steady state electrical migration and non-steady state electrical migration.

Steady State Conditions

The calculation of diffusion coefficients from laboratory experiments has to be based on the fundamentals of transport processes in solutions. The general equation for transport processes in a solution is named Nernst-Planck equation, which can be written as (Andrade, 1993 and Bockris and Reddy, 1970):

$$-J_j(x) = D_j \frac{dC_j(x)}{dx} + \frac{z_j F}{RT} D_j C_j \frac{dE(x)}{dx} + C_j v(x) \qquad [1]$$

where:

$J_j(x)$ = unidirectional flux of species j [kg/m^2·s]
D_j = diffusion coefficient of species j [m^2/s]
dC_j = variation of concentration (e.g. in compartment 2, Fig 1) [kg/m^3]
dx = variation of distance [m]
z_j = electrical charge of species j (z_{Cl} = - 1) [equivalent/mol]
F = Faraday number = 96,500 [C/equivalent]
R = gas constant = 8.314 [J/mol· K]
T = absolute temperature [K]

C_j = bulk concentration of species j (e.g. in compartment 1, Fig 1) [kg/m^3]
dE = variation of voltage across specimen [V]
v = artificial or forced velocity of ion [m/s]

which means that the unidirectional (x) flux of a particular ion (J_j) is governed by the sum of its diffusion, migration and convection components. Convection does not operate inside the concrete, so the last term of Eq 1 is to be omitted when chloride ion transport in concrete is considered.

Diffusion

The classic steady-state diffusion experiment can be carried out with an equipment as sketched in Fig 1, but without electrodes.

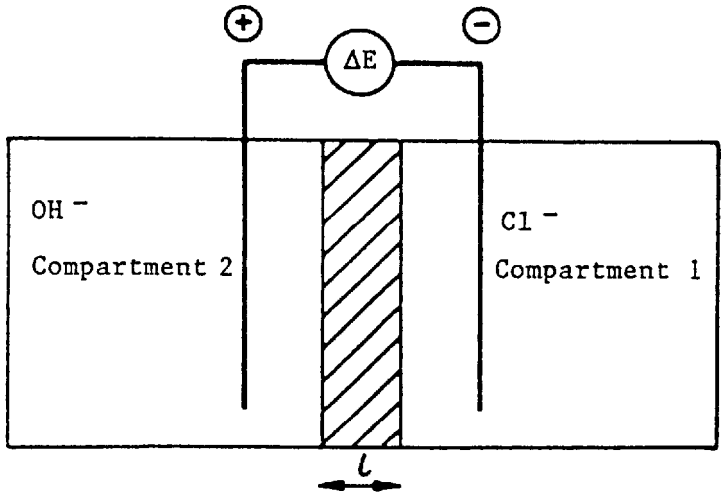

Figure 1 Sketch of cell for testing of chloride flux through porous materials.

The results from the steady-state experiments may be expressed graphically as increasing chloride concentration in compartment 2 (C_2) with increasing time (t), as shown schematically in Fig 2.

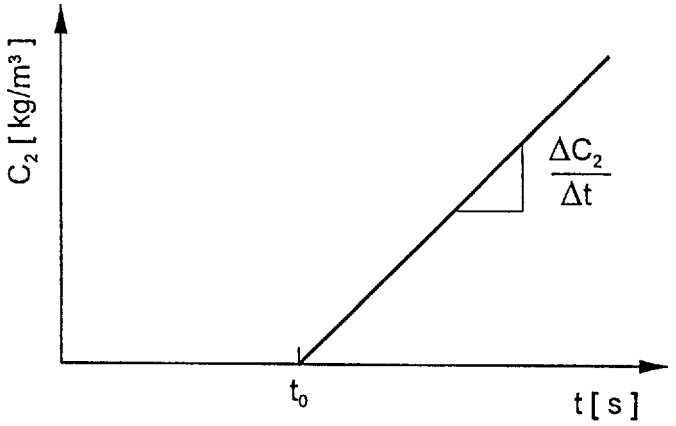

Figure 2 Schematical plot of chloride concentration in compartment 2 versus time.

The rectilinear plot of C_2 versus t, $\Delta C_2/\Delta t$, may be extrapolated to $C_2 = 0$ which corresponds to the initiation time, t_0, for penetration of chlorides. The diffusion coefficient, D [m^2/s], can then be expressed according to Eq 2 (Fick's 1. law, e.g. Page et al, 1981) since the flux $J = \Delta C_2 \cdot V_2/\Delta t \cdot A$:

$$D = \frac{l}{C_1} \cdot \frac{V_2}{A} \cdot \frac{\Delta C_2}{\Delta t} \qquad [2]$$

where:

C_1 = chloride concentration in compartment 1 [kg/m^3] or [mol/ℓ]
l = concrete disk thickness [m]
V_2 = volume of compartment 2 [m^3]
A = cell cross-sectional area [m^2]
$\Delta C_2/\Delta t$ = increase in chloride concentration in compartment 2 with time (slope of the plot on Fig 2) [kg/m^3·s] or [mol/ ℓ· s]

Migration in electrical field

Andrade (1993) has proposed a procedure to calculate the diffusion coefficient, D [m^2/s], from the total chloride flux recorded according to Eq 1 utilizing electrical field experiments (e.g. with set up as sketched in Fig 1). Andrade (1993) measures the reduction of chlorides in compartment 1, but for a steady state this flux should be equal to the increase in chlorides in compartment 2, since $C_1 \cdot V_1 = C_2 \cdot V_2$. Assuming that the contribution of diffusion is negligible compared with migration when an electrical field high enough (> 10 V) is applied to the concrete specimen, and since convection does not operate inside the concrete, Eq 1 can be reduced to (Andrade, 1993, Andrade et al, 1994), remembering that the flux $J = \Delta C_2 \cdot V_2/\Delta t \cdot A$:

$$D = \frac{RTlV_2}{z_{Cl}F\Delta E\gamma_{Cl}C_1A} \cdot \frac{\Delta C_2}{\Delta t} \qquad [3]$$

where:

γ_{Cl} = activity coefficient of chloride
ΔE = voltage drop across specimen [V]

It should be noted that the voltage drop across specimen, ΔE, is less than the applied voltage, ΔU, given by:

$$\Delta U = \Delta E + E^{rev}_{H_2O} + \eta \qquad [4]$$

where:

E^{rev}_{H20} = reversible dissociation potential of water [V] (= 0.463 V at 25 °C and pH=13).
η = polarization effects [V]

McGrath and Hooton (1996) described recently a method of setting the potential ΔE over the sample length by using reference electrodes and Luggin capillaries. They measured the difference ΔU-ΔE to vary from 1.91 to 2.36 V for an impressed potential, ΔU, ranging from 6 to 30 V. Or in other words, the "driving force" ΔE ranged from 68 to 92 % of the nominal voltage. Thus, a higher impressed voltage is preferred if the potential drop over the specimen can not be measured, as long as the temperature rise in the specimen is taken into account.

The NORDTEST method (1989) utilized Eq 2 to obtain a "chloride permeability factor" until 1996 in spite of being a steady state experiment accelerated by an electrical field, but is recently revised to give a chloride diffusion coefficient in accordance with Eq 3.

Zhang and Gjørv (1994) deduced an equation equivalent to Eq 5 based on a theoretical evaluation of steady state migration in an electrical field. β_0 is a correction factor for ionic interaction, ranging from 1.22 for 0.1 N NaCl to 1.70 for 0.5 N NaCl, while the other symbols are defined in the preceding text. Appart from the ion interaction correction factor, it is worth noting that Eq 5 is simply the solution of the Nernst-Planck equation for diffusion (Eq 2) multiplied with the term RT/zFΔE. Thus, it is not in accordance with the solution of the Nernst-Planck equation (Eq 1) for migration of ions in an electrical field when the diffusion term is neglected (Eq 3).

$$D = \beta_0 \cdot \frac{RT}{zF\Delta E} \cdot \frac{lV_2}{C_1 A} \cdot \frac{\Delta C_2}{\Delta t} \qquad [5]$$

Non-Steady State Conditions

Gau and Cornet (1985) formulated the following equation, based on Nernst-Planck (Eq 1), for non-steady state transport processes when D is concentration independent, where the time dependent concentration flux can be expressed as the sum of diffusion and migration terms (convection is omitted):

$$\frac{dC}{dt} = -\frac{dJ}{dx} = D\left(\frac{d^2C}{dx^2} + \frac{zF}{RT}\cdot\frac{dE}{dx}\cdot\frac{dC}{dx} + \frac{zFC}{RT}\cdot\frac{d^2E}{dx^2}\right) \qquad [6]$$

Diffusion

The classic non-steady state diffusion experiment is carried out by immersing a concrete specimen, sealed on all sides except the surface to be exposed, into a NaCl-solution (e.g. the APM302 method developed at the AEC Laboratory in Denmark). Uni-directional transport of chloride ions by pure diffusion (non-steady state) is expressed by Fick's second law (first term in Eq 6 when D is assumed to be concentration independent):

$$\frac{dC}{dt} = \frac{d}{dx}\left(D\frac{dC}{dx}\right) \qquad [7]$$

The solution of Fick's second law for a concentration independent diffusion coefficient gives the chloride content as a function of exposure time, t, and the distance from exposure surface (AEClaboratory, 1991):

$$C_x = C_0 - (C_0 - C_i)\ erf\left(\frac{x}{2\sqrt{D\cdot t}}\right) \qquad [8]$$

where:

C_x = chloride concentration, measured at the depth x at the exposure time t [mass %]
C_0 = boundary condition at the exposed surface (calculated surface concentration, x=0) [mass %]
C_i = the initial chloride concentration in the sample [mass %]
x = depth below the exposed surface [m]
t = exposure time [s]
erf = the error function

Migration in electrical field

Luping and Nilsson (1992, 1993) utilized Eq 6, assuming linear electric field over the specimen with $dE/dx = \Delta E/l$ and $d^2E/dx^2 = 0$ (may be doubtful in the case of non-steady state);

$$\frac{dC}{dt} = D\left(\frac{d^2C}{dx^2} - \frac{zF\Delta E}{RTl}\cdot\frac{dC}{dx}\right) \qquad [9]$$

in the development of their rapid penetration method. For the actual boundary conditions, and neglecting the pure diffusion term, the exact analytical solution of Eq 9 can be found as:

$$C = \frac{C_0}{2}\left[e^{ax}\, erfc\left(\frac{x + aDt}{2\sqrt{Dt}}\right) + erfc\left(\frac{x - aDt}{2\sqrt{Dt}}\right)\right] \qquad [10]$$

where $a = zF\Delta E/RTl$ and other symbols as defined earlier.

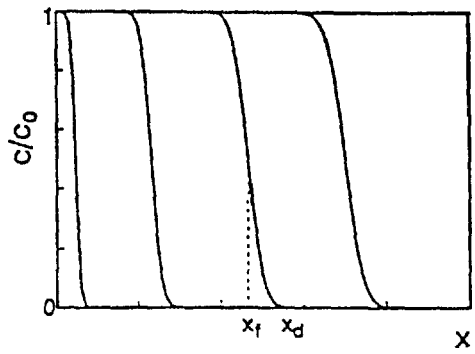

Figure 3 Theoretical concentration profiles according to Eq 10 (Luping and Nilsson, 1992).

Fig 3 illustrates the concentration profiles of Eq 10, and shows that there is an apparent concentration front in each profile. This implies the possibility of calculating diffusivity from the penetration depth. In fact, it can be found from Eq 10 that the profile has an inflection point at x_f:

$$x_f = \frac{zF\Delta E}{RT\,l}\,Dt \qquad [11]$$

Although it is difficult to determine x_f, the penetration depth x_d can be measured by using a colorimetric method based on chlorid precipitation by silver nitrate. The relationship between x_f and x_d can be obtained by using a numerical solution;

$$x_f = x_d - \alpha \cdot x_d^{\beta} \qquad [12]$$

where α and β are regression coefficients depending on the experimental conditions. The diffusion coefficient, D, can then be found by combining Eq 11 and Eq 12:

$$D = \frac{RTl}{zF\Delta E}\left(\frac{x_d - \alpha x_d^{\beta}}{t}\right) \qquad [13]$$

where t is testing time in hours.

Sha'at et al (1994) presented a solution to Eq 9 which can derive the diffusion coefficient, D [m^2/s], from a migration experiment with impressed voltage, ΔU, with a set-up as sketched in Fig 2 by measuring the chloride concentration in chamber 2, C_t, at a given time, t:

$$C_t / Co = erfc \{ [l - (D \cdot z \cdot F \cdot \Delta U \cdot t / R \cdot T \cdot l)] / 2\sqrt{D} \cdot t \} \quad [14]$$

where: erfc = (1 - erf), the complement of the error function
C_t = the outflow concentration in chamber 2 at time, t.
C_0 = inflow concentration in chamber 1 at t = 0
and the other symbols as explained for previous equations

Sha'at et al (1994) showed that calculations by Eq 14 gave diffusion coefficients of chlorides comparable to those obtained by pure diffusion tests. They applied voltages of 10, 30 and 60 V. The obtained D decreased only slightly with increasing ΔU, and was in fact closer to the pure diffusion coefficient for the highest ΔU when the temperature rise in the sample was taken into account. This might be due to the relative difference between ΔE (should replace ΔU in Eq 14) and ΔU (see Eq 4) being less for higher ΔU.

Andrade et al (1994) deduced using an analogy with natural diffusion experiments, when the pure diffusion is neglible compared with migration in an electrical field, that the equation for a non-steady state migration can be formulated as

$$\frac{dC}{dt} = \frac{zF\Delta E}{RT} \cdot D \cdot \frac{d^2C}{dx^2} \quad [15]$$

where $zF\Delta E/RT$ is simply the accelerating factor. The solution of Eq 15 can be achieved analogously to pure diffusion under non-steady state conditions to:

$$C = C_0 \, erfc \left(\frac{x}{2\sqrt{\frac{zF\Delta E}{RT} \cdot D \cdot t}} \right) \quad [16]$$

which is similar to Eq 8 for pure diffusion (since erfc = 1 - erf). Eq 16 is a much simpler solution than Eq 10. Their comparison between acceleration in electrical field with pure diffusion placed the diffusion coefficients of the two concretes in the same order, but the magnitudes were 2-3 times higher for the pure diffusion (lowest Cl^- concentration in concrete).

Crank (1975) showed that the non-steady state diffusion coefficient, D, independent of concentration can be calculated from the intersection of the steady state line with the abscissa in Fig 2, t_0, for porous materials:

$$D = \frac{l^2}{6\tau_0} \quad [17]$$

The factor 6 in Eq 17 is called the "time lag" and may depend on the material characteristic, which make the formula too uncertain for practical use in concrete technology.

DISCUSSION

It is important to notice that diffusion coefficients deviated from steady state (D_{ss}) and non-steady state (D_{ns}) conditions can not be compared directly, since the ratio between them depend both on the porosity and the chloride binding capacity of the material. In a recent model for chloride penetration, Tang and Nilsson (1996) used the following expression;

$$\frac{D_{ss}}{D_{ns}} = \epsilon + K_b \cdot W_{gel} \qquad [18]$$

where:

ε = porosity of the concrete,
K_b = chloride binding constant [m^3 solution/kg gel]
W_{gel} = hydrated gel content [kg gel/m^3 concrete]

Apparently Tang and Nilsson (1996) assumed in Eq 18 that chloride binding is dominated by adsorption on the CSH-gel, which may not be true for systems with high contents of calcium aluminate hydrates (e.g. HAC, fly ash blends and slag blends). In the calculations of D_{ns} it has until recently been assumed that the ratio between free and bound chlorides are independent of the chloride concentration, which is not correct neither for chemical binding (e.g. Friedel salt formation) nor adsorption. Tang and Nilsson (1996) used a Freundlich isoterm and terms correcting for OH^- concentration and temperature variations when calculating the bound (i.e. adsorbed) chloride content in their numerical model (chemical binding neglected). A high chloride binding capacity will lead to a steeper profile of total chlorides and thereby a smaller D_{ns} than in reality (i.e. when binding is saturated or reversed by sulphates or carbonation), which may create significant errors in service life predictions. In spite of the fundamental difference between D_{ss} and D_{ns}, many obtain diffusion coefficients by steady-state experiments and use them in life cycle calculations for structures where chloride diffuses in a non-steady manner, but other uncertainties are larger.

McGrath and Hooton (1996) compared D_{ss} and D_{ns} for the same concrete in the same experiment similar to the set-up sketched in Fig 1. D_{ss} was calculated from Eq 3 after obtaining steady state flow, while D_{ns} was calculated directly from Eq 10 utilizing a "break through" time, t, defined as $C/C_0 = 0.03$, after the methodology of Halamickova et al (1995) who used $c/c_0 = 0.005$. McGrath and Hooton (1996) realized that the D_{ns} is related to pore solution concentrations and porous area fractions, and they divided D_{ss} by a simple approximated area fraction prior to comparison with D_{ns}. Furthermore, chemical binding will slow down the "break through" time thus reducing D_{ns} relative to D_{ss}. The D_{ns} was quite constant at all voltages (ΔU = 6, 12, 20 and 30 V), and the D_{ss} quite comparable at the two lower voltages, but increased substantially for the two highest voltages. The latter might be due to temperature effects that did not seem to be taken into account in the study.

To complicate the matter further, suction may dominate over diffusion as the transport mechanism in tidal and splash zones in marine environment as pointed out by for instance Volkvein (1993). He also claimed that the suction due to underpressure created by the contraction of the continued hydration also plays a role in the transport process of fluids in young concrete. Roelstra et al (1996) also modelled chloride penetration taking into account important effects of moisture migration and cement hydration. Jones et al (1996) discussed chloride ingress into unsaturated concrete in terms of sorptivity and capillary diffusivity. Note that the preceding methods of obtaining diffusion coefficients rely on the assumption of

saturated pores.

A third matter that must be taken into account when diffusion coefficients are going to be applied in calculations, is their time dependence. This aspect has been discussed thoroughly the later years by Poulsen (1993, 1996), while Mejlbro (1996) recently presented the mathematical solution of Fick's second law of diffusion with time-dependent diffusion coefficient and surface concentration. The particular importance of this aspect for slow reacting binders like fly ash has been pointed out by Thomas and Jones (1996). However, if a diffusion coefficient obtained for say a 60 days old concrete is treated as constant in modelling, the resulting service life will be underestimated, which leaves one at the safe side of the uncertainty. Nevertheless, if not the time dependence of the diffusion coefficient for the particular concrete mix is determined, a single determination on a mature concrete (e.g. 1 yr moist curing) is recommended.

A fourth important matter, the concentration dependence of the diffusion coefficient, seems to have been neglected. All methods for determination of non-steady state diffusion coefficients rely on that it is independent of the concentration. This topic should be focused on in future studies.

The preceding electrical migration methods rely on that the potential drop over the concrete specimen is linear ($dE/dx = \Delta E/l$ and $d^2E/dx^2 = 0$) which may not be true in particular for non-steady state experiments. In addition, the applied theory of electro-migration is developed for dilute electrolytes. The latter has been tried to be counteracted by the activity coefficient, γ_{Cl}, in Eq 3 or the ion interaction factor, β_0, in Eq 5. The concept of an activity coefficient is the deviation from ideal behaviour, which in the case of an electrolyte of ionic strength, $I = \frac{1}{2}\sum c \cdot z^2$ (mol/ℓ), mainly is due to the ionic interaction, but also ion-solvent (water) interaction. The average ion activity coefficient for an electrolyte may be estimated by advanced Debye-Hückel limiting law modified by a linear correction term;

$$\log \gamma_{\pm} = -\frac{A \cdot z_+ \cdot z_- \cdot \sqrt{I}}{1 + B \cdot a \cdot \sqrt{I}} + b \cdot I \qquad [19]$$

where in the case of NaCl ($z_+ = z_- = 1$), the experimental coefficients a = 0.4 nm and b = 0.055 ℓ/mol, while the temperature dependent constants A = 0.50925 $\ell^{1/2}/mol^{1/2}$ ($\propto T^{-3/2}$) and B = 3.2864 $\ell^{1/2}/mol^{1/2}\cdot nm$ ($\propto T^{-1/2}$) for water at 25°C. Thus, in the case of NaCl, $0.68 < \gamma_{\pm} < 1.00$ with a minimum at a concentration of ≈1 M. Note that in the actual diffusion or migration process, iteraction between the moving ions and the solids of the concrete, and/or the additional ions of the pore water, may lead to a different "activity coefficient". However, choosing a correct activity coefficient may be a minor adjustment compared to the preceding discussed fundamentals.

CONCLUSIONS

From the evaluation of the different methods for determining chloride diffusion coeffisients, the present authors recommend the following;

1) The determination of *steady state chloride diffusion coefficients* should be performed by an experiment utilizing acceleration by electrical field and relying on Eq 3. The activity coefficient for chlorides could be calculated according to Eq 19. If the imposed potential exceeds 10 V, the temperature rise in the specimen should be determined and applied in Eq 3 instead of the ambient temperature. The true potential drop over the

specimen should be used instead of the impressed potential in Eq 3. This method will be a revised NORDTEST NT Build 355 method in 1997.

This method is mostly useful for determining material parametres when the chloride binding is saturated in order to compare different concrete qualities or recipes. The steady state chloride diffusion coefficient can not be used directly in service life calculations for structures where chlorides in practice is transported in a non-steady state manner.

2) The determination of *non-steady state chloride diffusion coefficients* should be performed by the diffusion method describe by AEClaboratory (1991), relying on Eq 8, and accelerated by concentration (16.5 % NaCl). The method has lately (November 1995) been accepted as NORDTEST NT Build 443 method. The method could easily be further accelerated by an electrical field requiring a set-up as in Fig 1, but this needs to be documented.

   This method is most relevant for submersed concrete structures (e.g. lower part of bridge pillars). Due to the influence of sulphates on chloride binding, and the dependency of D_{ns} on chloride binding, the exposure liquid should be enriched, artificial sea water rather than the prescribed NaCl.

3) The determination of an *apparent non-steady state chloride diffusion coefficient* should rely on Eq 8, but the eposure to the chloride source should be cyclic in terms of ponding or salt-spray in order to simulate tidal zones or splashing of sea water at the coast. Such an experiment should give apparent (since the transport is a mix of diffusion and suction) diffusion coefficients more relevant to practice and better suited for service life predictions.

In all three situations, the concrete should be mature (>90 days water cured) prior to testing, unless the time-dependency of the obtained diffusion coefficients are determined.

REFERENCES

Andrade, C.: "Calculation of Chloride Diffusion Coefficients in Concrete from Ionic Migration Measurements". Cement and Concrete Research, Vol 23, No 3, 1993, pp 724-742.

Andrade, C., Sanjuán, M.A., Recuero, A. and Río, O.: "Calculation of Chloride Diffusivity in Concrete from Migration Experiments, in Non Steady State Conditions". Cement and Concrete Research, Vol 24, No 7, 1994, pp 1214-1228.

Andrade, C., Alonso, C. and Acha, M.: "Chloride Diffusion Coefficient of Concrete Containing Fly Ash Calculated from Migrations Tests". Corrosion and Corrosion Protection of Steel in Concrete. Proceedings of International Conference held at the University of Sheffield, UK, 24-28 July 1994, pp 783-793 (Ed. R. Narayan Swamy).

AEClaboratory: "Concrete Testing. Hardened Concrete. Chloride Penetration". APM 302 2nd ed., AEC laboratory, Vedbæk, Denmark, May 1991.

Bockris, J. O'M. and Reddy, A.K.N.: "Modern Electrochemistry". Plenum Press, New York, 1970.

Crank, J.: "The Mathematics of Diffusion", 2nd Ed., Clarendon Press, Oxford, 1975, pp. 49-53.

Gau, Y and Cornet, I: "Penetration of Hardened Concrete by Seawater Chlorides With and Without Impressed Current", Corrosion (NACE), 41, pp 93-100, 1985.

Halamickova, P., Detwiler, R.J., Bentz, D.P. and Garboczi, E.J.: "Water Permeability and Chloride Ion Diffusion in Portland Cement Mortars: Relationship to Sand Content and Critical Pore Diameter", Cem. Concr. Res., Vol. 25, No. 4, 1995, pp. 790-802.

Jones, M.R., Thomas, M.D.A., Dhir, R.K. and Ng, S.L.D.: "Review of Estimating of Chloride Ingress into Concrete", Proceedings of the 7th International Conference of Building Materials and Components, Stochholm, Sweden, 19-23 May, 1996, Vol. 1, pp.107-116.

Luping T. and Nilsson L.-O.: "Rapid Determination of the Chloride Diffusivity in Concrete by Applying an Electrical Field." Chloride Penetration into Concrete Structures - Nordic Miniseminar Jan 1993. Publication P-93:1, pp 26-35.

Luping, T. and Nilsson, L.-O.: "Rapid Determination of the Chloride Diffusivity in Concrete by Applying an Electric Field". ACI Materials Journal, Vol 89, No. 1, 1992, pp 49-53.

Luping, T.: "Methods for Determining Chloride Diffusivity in Concrete". Chalmers University of Technology, Division of Building Materials, Publication P-93:8, Göteborg, 1993, 84pp.

McGrath, P.F. and Hooton, R.D.: "Influences of Voltage on Chloride Diffusion Coefficients from Chloride Migration Tests", Cem. Concr. Res., Vol. 26, No. 8, 1996, pp. 1239-1244.

Mejlbro, L.: "The Complete Solution of Fick's Second Law of Diffusion with Time-dependent Diffusion Coefficient and Surface Concentration", The publication "Durability of Concrete in Saline Environment", May 1996, Cementa AB Box 144 S-182 12 Danderyd, Sweden, pp. 127-158.

NORDTEST method NT BUILD 355; "Concrete, Repairing Materials and Protective Coating: Diffusion Cell Method, Chloride Permeability", approved 1989-11.

Page, C.L., Short, N.R. and Tarras, A.: "Diffusion of Chloride Ions in Hardened Cement Pastes". Cement and Concrete Research, Vol 11, 1981, pp 395-406.

Poulsen, E.: "On a model of Chloride Ingess into Concrete having Time-dependent Diffusion Coefficient", Proceedings of the Nordic Miniseminar "Chloride Penetration into Concrete Structures", Gothenburg, Sweden, January 1993, pp. 298-309. Publication P-93:1, work no 535, Chalmers Technical University, Dept. Building Materials, Edited by L.-O-. Nilsson.

Poulsen, E.: "Estimation of Chloride Ingress into Concrete and Prediction of Service Lifetime with Reference to Marine RC Structures", The publication "Durability of Concrete in Saline Environment", May 1996, Cementa AB Box 144 S-182 12 Danderyd, Sweden, pp. 113-126.

Roelstra, P.E., Bijen, J.M.J.M., Salet, T.A.M.: "Modelling Chloride Penetration into Ageing Concrete", Proceedings of the International Conference Concrete Repair, Rehabilitation and Protection, Dundee, Scotland, 27-28 June, 1996, pp. 245-255.

Sha'at, A. A-H., Basheer, P.A.M., Long, A.E. & Montgomery, F.R.: "Reliability of the Accelerated Chloride Migration Test as a Measure of Chloride Diffusivity in Concrete." Corrosion and Corrosion Protection of Steel in Concrete. Proceedings of International Conference held at the University of Sheffield, UK, 24-28 July 1994, pp 446-460 (Ed. R. Narayan Swamy).

Tang, L. and Nilsson, L.-O.: "Service Life Prediction for Concrete Structures under Sea Water by a Numerical Approach", Proceedings of the 7th International Conference of Building Materials and Components, Stochholm, Sweden, 19-23 May, 1996, Vol. 1, pp. 97-106

Thomas, M.D.A. and Jones, M.R.: "A Critical Review of Service Life Modelling of Concretes Exposed to Chlorides", Proceedings of the International Conference Radical Concrete Technology, Dundee, Scotland, 27-28 June, 1996, pp.723-736

Volkwein, A.: "Convection of Chlorides into Concrete due to Hydration Suction and Capillary Suction", Proceedings of the 6th International Conference of Building Materials and Components, Omiya, Japan, 26-29 October, 1993, Vol. 1, pp. 279-288.

Zhang, T. and Gjørv, O.E.: "An Electrochemical Method for Accelerated Testing of Chloride Diffusivity in Concrete", Cement and Concrete Research, Vol 24 (1994) No 8, pp. 1534-1548.

THE INFLUENCE OF THE ELECTRICAL POTENTIAL IN THE CHLORIDE THRESHOLD FOR REBAR DEPASSIVATION

Cruz ALONSO, Carmen ANDRADE and Marta CASTELLOTE, Institute of Construction Science "Eduardo Torroja", Madrid, Spain.

ABSTRACT Chloride/hydroxide threshold is considered as the most representative parameter to determine rebar depassivation. The influence of the electrical potential exhibited by the rebar when chlorides arrive has been studied by a statistical treatment. A mean value of Cl^-/OH^-=0.82 and % Cl free= 0.56 was found, although a big scatter appears which has been related to the nature of the passivating layer.

Key-words: chloride, corrosion, durability, steel

INTRODUCTION

Chlorides are known to be the most dangerous aggressive towards the steel passivity. When they reach the rebar in a certain proportion, a localized attack is developed. Chloride threshold to produce reinforcing steel corrosion varies according to several parameters and it is expresed in terms of free or total chloride as well as Cl^-/OH^- ratio.

Although Kaesche (1959) and Baumel (1959) were the first to try to determine a chloride limit for rebar corrosion in alkaline solutions, Lewis (1961) was the first to give a value (3000 ppm Cl^-) for corrosion initiation. Later on, Haussman (1967) and Gouda (1970) established that the threshold is related to the amount of hydroxides. They gave a mean value for Cl^-/OH^- of 0.63 and 0.4 respectively. Further studies from Goñi (1990) in solutions simulating pore solution indicated a Cl^-/OH^- threshold between 0.25-0.8 and found a correlation between rebar corrosion rate and Cl^-/OH^- values.

Less agreement between authors is found in the case of mortar and concrete, thus Gouda (1970) gave values from 0.15 to 0.75%of NaCl by weight of cement depending on the type of cement and surface of the rebar, Hope (1987) 0.2 to 0.4 and Page (1991) found a value of 1.5% Cl^- and also a Cl^-/OH^- = 3. Recently, Petterson (1994,1996) has obtained variations from 2-8 when testing under different conditions.

All these research have pointed out that the disagreement between authors on a single value for Cl^-/OH^- is due to the numerous variables that influence the threshold: Type of cement, w/c, porosity, temperature, chloride addition or penetration, quality of passivation layer and the electrical potential of the rebar. Among those variables, that less studied is the potential exhibited by the rebar when chloride arrive (Ishikawa,1969, Tuutti, 1982, Bertolini, 1996). In present paper results of Cl^-/OH^- are given in the region of potentials from -250 to +250mV SCE. The study has been made in a numerous set of mortar specimens in order to obtain statistically relevant results.

EXPERIMENTAL METHODOLOGY

Specimens Preparation

200 mortar specimens of 2x2x8 were fabricated with w/c=0.5 and c/s=1/3. Each had embedded a corrugated rebar with a exposed area of approx. 60 mm^2. The electrical contact was made in the emerging part of the rebar. The cover was of 5 mm. The specimens were kept in a chamber at 95%RH and 20°C until testing. Six types of cement were used:

1. OPC-I, with low C_3A (1.1%) and low alkali content (0.43% Na_2O eq.).
2. OPC-I, with high C_3A (9.7%) and high alkali content (0.84% Na_2O eq.).
3. OPC-I, low C_3A + 35% fly ash class F.
4. OPC-I, high C_3A + 35% fly ash class F.
5. Aluminous cement.
6. Portland-II with filler addition.

Testing Procedure

The surface in which the rebar is protuding, was covered with epoxy resin to avoid preferential entrance of chloride by the steel concrete interface. A set of identical specimens made of the same batch were immersed in 0.5M NaCl solution.

The passivation state of the rebar was tested before the penetration of chloride. Thus the measurements of corrosion potential indicated values more positive of -250mV (Vs.SCE) and corrosion rates <0.2 $\mu A/cm^2$ in all cases.

A mesh of stainless steel or titanium were employed as counter electrodes. As reference electrode a Mn/MnO_2 was used. The rebars of each specimen, were all connected in parallel as working electrode. A constant potential was then applied (potentiostatic test) and maintained in each specimen along the test. The potential tested were: +100,0,-100,-200,-300 and -400mV (Mn/MnO_2) or +250, +150, +50, -50, -150 and -250 mV (SCE).

The current flow was monitored at each rebar.When a sharp increase was observed,the specimen was taken out off the testing arrangement, and the Ecorr and Icorr was measured to check the rebar depassivation. Free and total chloride and hydroxide concentration at the rebar level were determined after depassivation.

RESULTS

When the steel depassivates under potentiostatic conditions a sharp increase of current is noticed. Fig 1 shows an example for the case of OPC-I high C_3A content and +150 mV (SCE).

The chloride content at the moment of rebar depassivation is represented in Fig 2 for the case of +50 mV (SCE) and the various cement tested. A scatter in the results is noticed for each cement type. The type II OPC is that showing higher Cl^- contents. The scatter widens when the plot is based on the Cl^-/OH^- ratio as Fig 3 depicts for -150 mV (SCE) test.

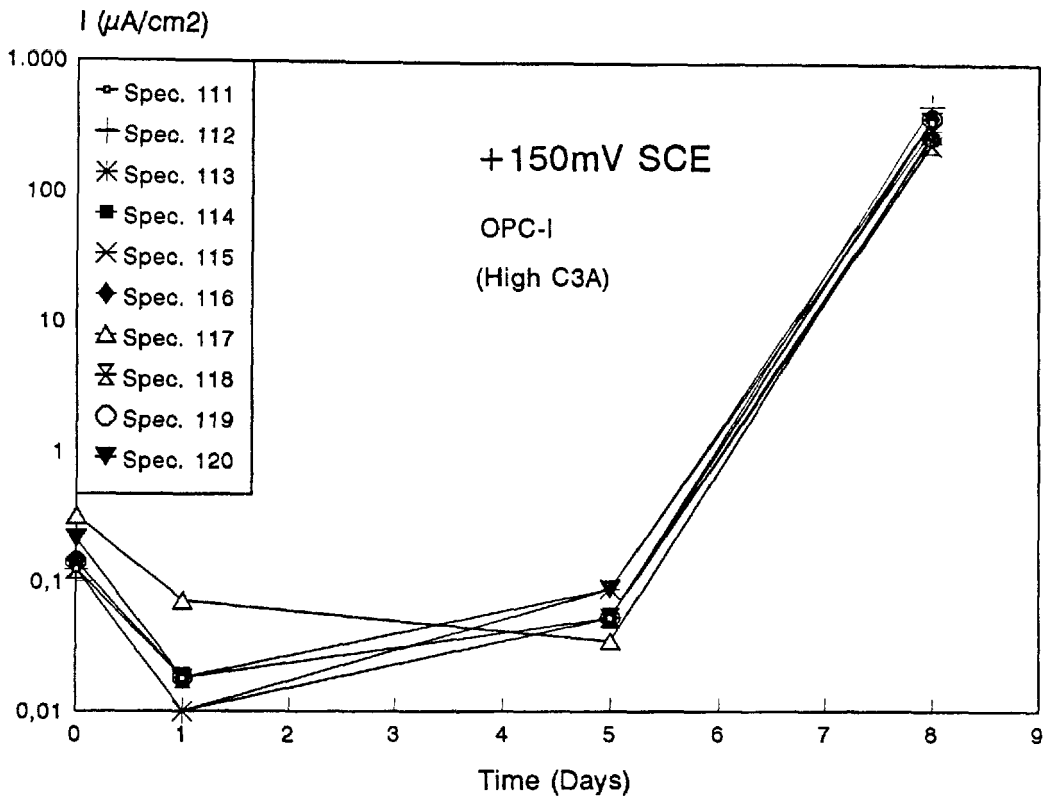

Figure 1 Current flow (in $\mu A/cm^2$) measured during rebar depassivation test at +150 mV (SCE).

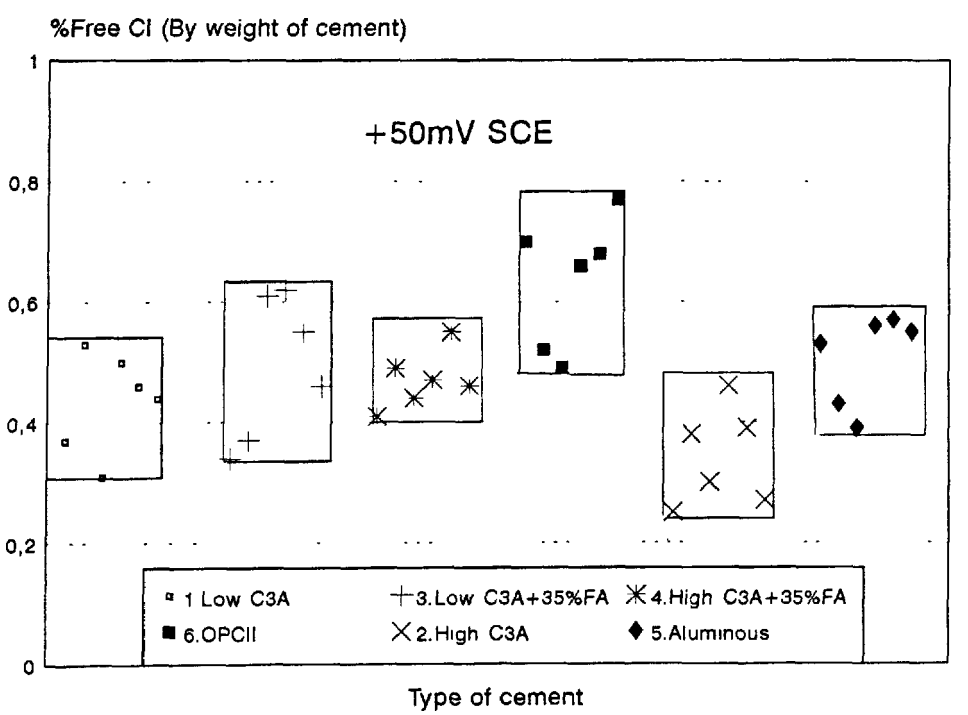

Figure 2 Percentage of free chlorides by weight of cement for rebar depassivation embedded in various cement types and polarized at +50 mV (SCE).

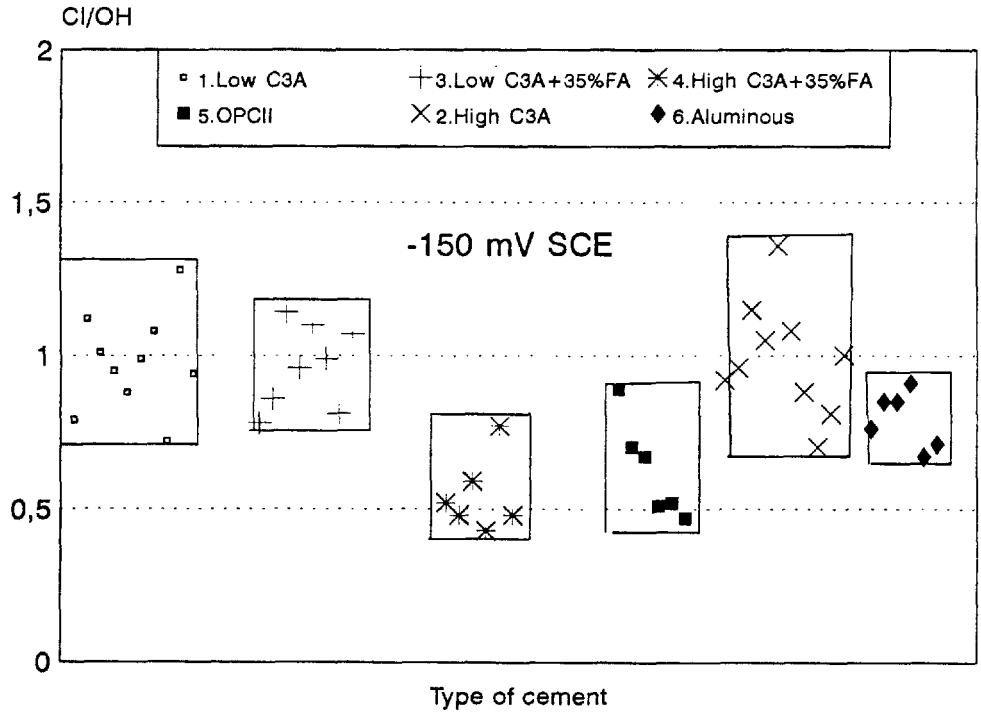

Figure 3 Cl^-/OH^- threshold for varios cement types. Polarization at -150 mV (SCE).

Statistical Study

The scatter found led to the need of an statistical treatment. As first approach a normal distribution law was considered. Thus, the determination of the mean and the standard deviation of the chloride and Cl^-/OH^- ratio at each potential was made. Fig 4 represents the mean for the %Cl free. A relationship with the C_3A content was not defined. This was attributed to the fact that the cover is too thin (5mm) to allow differences. Similar results were found for Cl^-/OH^- ratio.

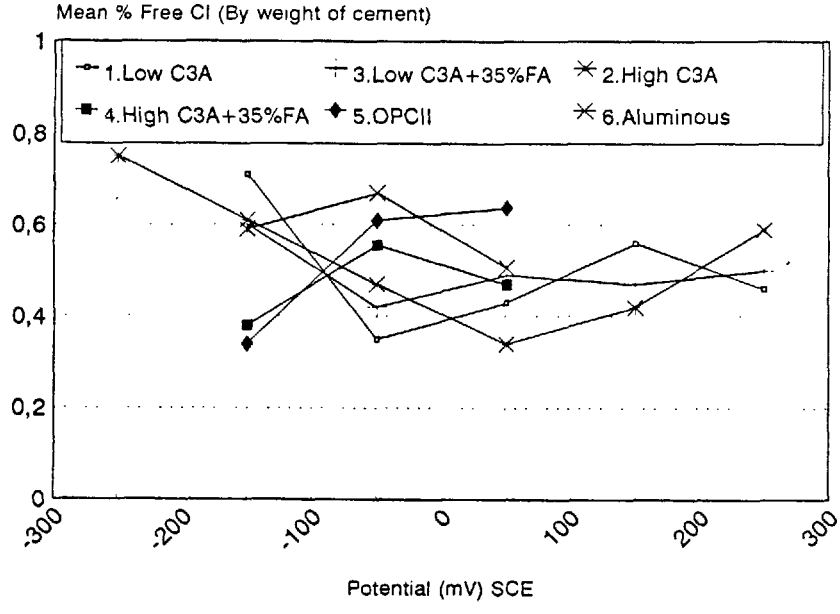

Figure 4 Mean critical chloride for the six types of cement in the range of potentials: +25 to -250mV (SCE).

As the type of cement was not a determinant parameter in present research, another treatment was made in funtion of the electrical potential. Fig 5 and Table 1 show the mean and the standard deviation. The mean of the mean at each potential resulted: 0.56 ± 0.17% Cl free and 0.73 ± 0.02 Cl total by weigth of cement and Cl^-/OH^- = 0.82 ± 0.018. These are the thresholds for rebar corrosion initiation found in present work.

Table 1 Results of the mean threshold for total chlorides and Cl^-/OH^- ratio.

Pol.Potent. (SCE)	Total chlorides %		Free chlorides %		Cl^-/OH^-	
	Mean	Stand.Dev.	Mean	Stand.Dev.	Mean	Stand.Dev.
+250 mV	0.73	0.06	0.516	0.054	0.78	0.075
+150 mV	0.76	0.05	0.483	0.058	0.77	0.04
+50 mV	0.70	0.12	0.480	0.09	0.74	0.15
-50 mV	0.741	0.16	0.513	0.11	0.79	0.16
-150 mV	0.743	0.17	0.54	0.13	0.83	0.19
-250 mV	-	-	0.70	0.11	1.026	0.176

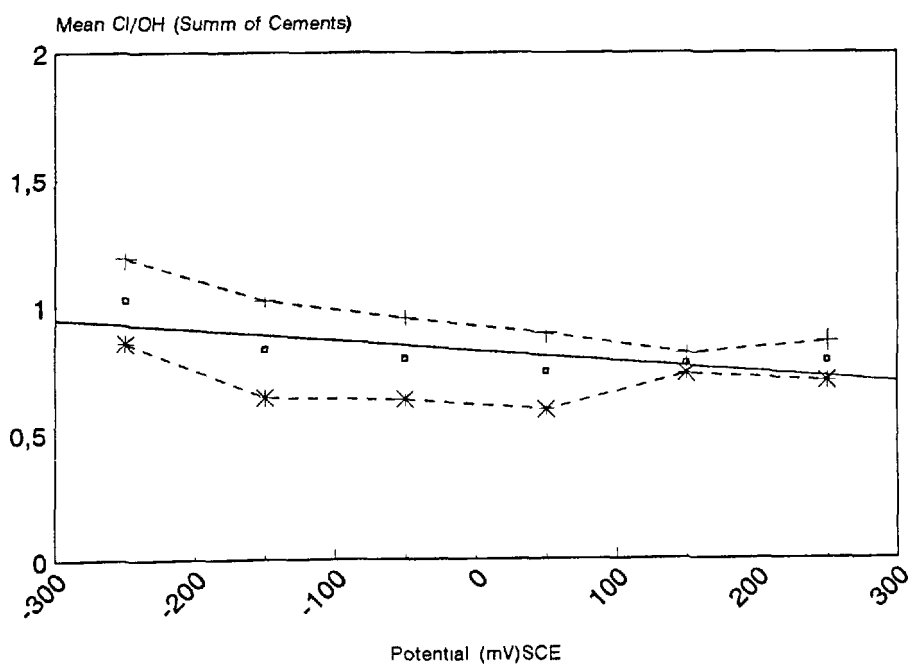

Figure 5 Mean and standard deviation of Cl^-/OH^- threshold in the range of potential: +250 to -250mV (SCE).

DISCUSSION

Type of cement in Cl^-/OH^-

The type of cement is considered a factor that influences rebar corrosion. It is well known that chloride combines with aluminates of cement forming a solid phase named Friedel salt. This ability of aluminates to remove free chlorides from the pore solution decreases the risk of corrosion for the rebars. The final effect is a delay in the time for depassivation. The reactivity of aluminates depends on: pH of pore solution, changes of temperature, origing of

the aluminates (e.i. from OPC, fly ash or aluminous cement) and also varies whether chlorides are present during setting or penetrate from outside.

In present experimentation no influence of the type of cement was found. Chloride and OH^- in the pore solution resulted very similar in all cements with a wide scatter. No particular reason has been found to explain this circumstance, as the values of the potentials applied were in the natural range of the rebars, and therefore any artificial acceleration in the penetration has been induced, except that of the cover too thin to allow the C_3A to efectively combine chloride before reaching the rebar surface.

On the other hand it is worth to point out that, the value in terms of free chlorides per weight of cement resulted slightly higher than that given in the standards (0.4% of cement weigth). Similarly the Cl^-/OH^- value is higher than that found in solution simulating the pore solution (0.6). Higher values were also found by other authors as Fig 6 shows (Hansson,1990, Page,1991, Petterson,1994,1996).

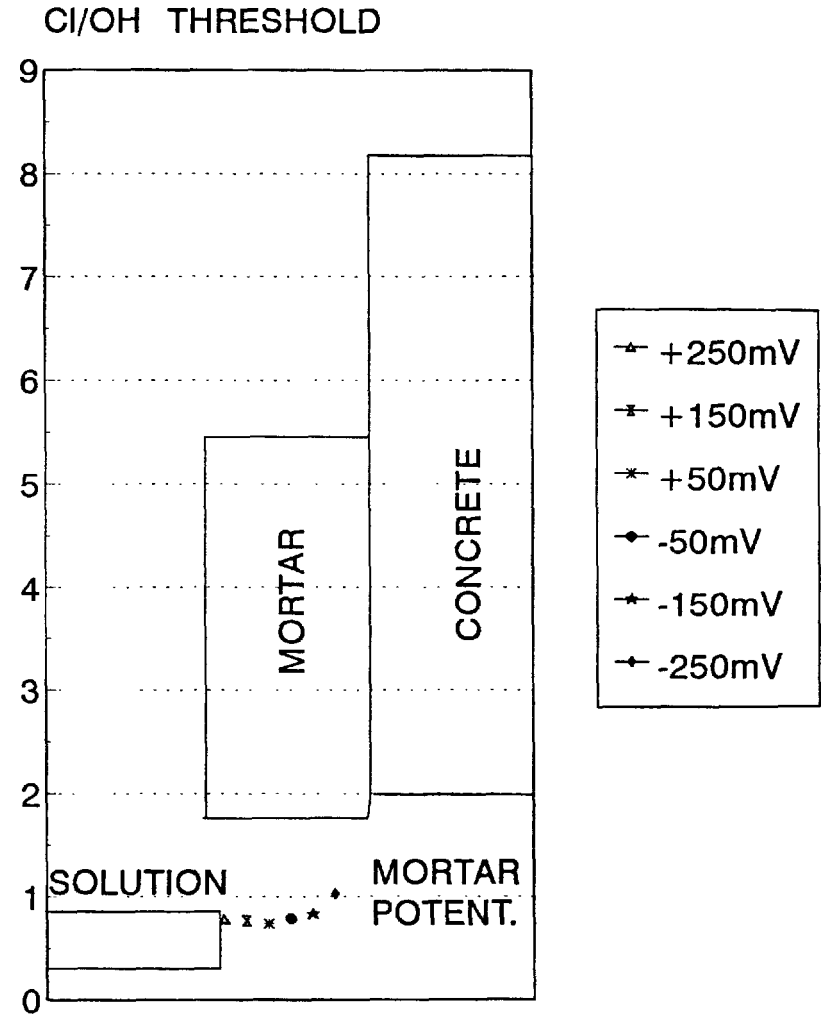

Figure 6 Cl^-/OH^- threshold at different potentials (+250 to -250mV SCE). Comparison with other authors (Hansson, Page, Petterson).

Electrical potential of the rebar in Cl^-/OH^-

As no systematic trend with the potential has been found present results indicate that, in the natural range of potential exhibited by passive rebars, the variations in the Cl^-/OH^- threshold is due to the normal scatter of the breakdown process of the passive layer. In consequence, cathodic prevention which is claimed (Bertolini, 1996) to increase the chloride threshold do not seem to make its influence at least in the range of potential values tested here >-250mV SCE.

CONCLUSIONS

Statistical determination of Cl^-/OH^- values (free chlorides) for rebar depassivation has given a threshold of 0.82 ± 0.018. This threshold ha not been found to vary in the range of values of potential between +250mV to -250mV (SCE). A mean value of 0.73% Cl total by weight of cement for rebar depassivation has also been found.

ACKNOWLEDGMENTS

The authors are grateful to the DG-XII-BRITE/EURAM Program for funding the work and also are grateful to Hosselet Didier and Antoine Pascal for their participation in the experimental part.

REFERENCES

Baumel, A., "The effect of additives on the corrosion behaviour of steel in concrete", Zement-Kalk-Gips,12,N7 (1959) pp 294-305.

Bertolini, L., Bolzoni, F., Pastore, T. and Pedeferri, P., "New experiences on cathodic prevention of reinforced concrete", Corrosion of steel in concrete, Eds. Page C.L., Bamforth, P.B. and Figgs, J.W. Edt. SCI.(1996) pp 389-398.

Goñi, S. and Andrade, C., "Sinthetic concrete pore solution chemistry and rebar corrosion rate in presence of chlorides", Cemt. Conc. Resch.,Vol20 (1990) pp 525-534.

Gouda, V. K., "Corrosion and corrosion inhibition of reinforcing immersed in alkaline solutions", Br. Corros. J., Vol5 (1970) pp 198-203.

Gouda, V. K. and Halaka, W. Y., "Corrosion and corrosion inhibition of reinforcing steel, I- Embedded in concrete",Br. Corros. J., Vol 5 (1970) pp 204-208.

Haussman, D. A., "Steel corrosion in concrete. How does it works?", Materials protection, Nov (1967) pp19-23.

Hansson, C. M. and Sorensen, B., "The threshold concentration of chloride in concrete for the initiation of reinforcement corrosion". Corrosion rates of steel in concrete, ASTM, STP, 1065, Eds Berke N.S., Chaker, V. and Whiting, D. (1990) pp 3-16.

Hope, B. B. and Alan, K. C., "Chloride corrosion threshold in concrete", ACI Mater. J., July-August (1987) pp 360-394.

Ishikawa, T., Cornet, I. and Bresler, B., "Electrochemical study of the corrosion behaviour of galvanized steel in concrete", 4th Int. Cong. on Metallic Corrosion. Amsterdam, Sept. (1969) pp 136-138.

Kaesche, H., "Testing corrosion danger to steel reinforcement due to admixtures in concrete", Zement-Kalk-Gips,12, N7 (1959)pp 289-294.

Lewis, D. A., "Some aspects of the corrosion of steel in concrete", First Int. Congr. On metal corrosion. London,April (1961).

Page, C. L., Lambert, P. and Vassie, P. R. W., "Investigations of reinforcement corrosion. I The pore electrolite phase in chloride contaminated concrete". Materials and Structures,Vol24 (1991)pp 243-252.

Petterson, K., "Chloride threshold value and corrosion rate in reinforced concrete". Corrosion and protection of steel in concrete. Eds. Swamy, R.N., Vol I (1994) pp 461-471.

Petterson, K., "Factors influencing chloride induced corrosion of reinforcement in concrete". Durability of building materials and components, Eds. Jostrom, S.J., vol I (1996) pp 334-341.

Tuutti, K., "Corrosion of steel in concrete", Doctoral thesis, Stockholm, (1982).

SINGLE ION ACTIVITIES OF UNASSOCIATED CHLORIDES IN NaCl SOLUTIONS BY ION SELECTIVE ELECTRODE POTENTIOMETRY

Ana HIDALGO, Carmen ANDRADE, Sara GOÑI and Cruz ALONSO, Institute of Construction Science Eduardo Torroja (CSIC), Madrid, Spain

ABSTRACT Ion-selective electrode (ISE) potentiometry is a useful technique for the determination of free ion activities. One of the causes of the break down of the steel reinforcement passivity is the attack by free chloride ions; so solution speciation in concrete aqueous phase is very important to determine the equilibrium state of such solutions. In this paper, activity coefficients of chloride ions are measured and compared with the calculated by different theoretical models. Finally a discussion about structural effects of ions in aqueous solutions and their influence on thermodynamic properties, is made.

Key-words: activity coefficients, chloride, ionic association, mobility, potentiometry.

INTRODUCTION

Solution speciation or the knowledge of aqueous species that are produced when water comes in contact with grouts, concrete or cement, is very important to determine the equilibrium state of such solutions. The use of mathematical models to calculate activity coefficients of these aqueous species (hydroyisis products, ion pairs or complexes) can thus considerably simplify the solution speciation, and consequently the calculation of chemical equilibrium states. Nevertheless experimental methods that involve the introduction of electrodes into natural media without contamination, are most appealing. Ion selective electrode (ISE) potentiometry has proved to be a useful technique for the determination of stability constants, because the potential of these electrodes depends mainly on the ion activity in the surrounding electrolyte and therefore it should be possible to use them as a non-destructive method of obtaining ion activities in cement and concrete structures. For instance, in-situ measurements of chloride activities in concrete can help to the early detection of risk of corrosion in existing structures allowing to follow the variation of the different aqueous species with time.

In this work, chloride activities in NaCl solutions up to 5 molal (m) using a chloride ISE, were made. Experimental results of chloride activity coefficients (γ_{Cl^-}) were compared with calculated values, trying to explain briefly the structural effects and the different types of interactions in aqueous electrolyte solutions, and how they can affect to the charge and mobility of the different species, and their influence on thermodynamic properties.

EXPERIMENTAL

Solutions were made up with NaCl Merck of analytical grade in deionized water; they were maintained at 25±0.1°C and stirred by magnetic stirrer. The following electrodes were used: Orion Research Inc., Cl^- selective (94-17) with a double-junction reference electrode (90-02-00) wich contained a 10% (w/v) KNO_3 outer filling solution. Measurements were made with an Orion 920 pH meter with a precision of ±0.1 mV.

RESULTS

Stable values of emf were attained within 1 minute (drift less than 0.1 mV/15 min).The measured potential corresponding to the level of chloride ion in solution is described by the Nernst equation:

$$E=E_{AgCl;Ag}-E_{ref}-\frac{RT}{F}\ln(m_{Cl^-}\gamma_{Cl^-})+E_a+E_j=E^{o'}-k\ln(m_{Cl^-}\gamma_{Cl^-}) \quad [1]$$

where $E^{o'}$ is the algebraic sum of the potentials of the internal Ag/AgCl electrode, $E_{AgCl;Ag}$, the reference electrode potential E_{ref}, the liquid junction potential, E_j, and the potential established at internal membrane surface, E_a.

In theory, the algebraic sum of these terms: $E_{AgCl;Ag}$, E_{ref}, E_j and E_a should be relatively constant with time and relatively independent of the test solution composition; so $E^{o'}$ would be a constant determined in a solution of unit chloride ion activity at 25°C. However, in relatively concentrated solutions, the magnitude of the liquid-junction potential is affected by the ionic strength of the test solution in addition to the pH, the structure of the liquid-liquid boundary and the temperature; so for rigorous measurements, a cell without liquid junction, where the other electrode is reversible to a cation in the test solution, must be used (Butler, 1969). Orion model 90-02 double junction reference electrode, use equitransferent filling solution; that is, the speed with which the positive and negative ions in the filling solution diffuse into the sample should be as nearly equal as possible. When the rate at which positive and negative charge is carried into the sample solution is equal, then no junction potential must result.

In practice the magnitude of the liquid junction potential changes and $E^{o'}$ must be measured from the results of an accurate electrode calibration, or using the method of known addition. Known addition is a convenient technique for measuring $E^{o'}$ and the slope of the Nernst equation, k, by adding known amounts of the same species to the sample solution, and recording the change in potential of the ion-selective electrode pair (Bruton, 1971).The observed emf values are listed in Table 1; also a comparison with literature values is shown.

Table 1 Comparison of the observed emf with some literature values.

m_{NaCl}	$E_{obsd}(1)$, mV	$E_{obsd}(2)$, mV	E_{obsd}, mV
0.001	160.5	160.9	-
0.01	106.3	106.7	104.7
0.05	-	-	64.6
0.1	52.3	53.4	48.7
0.2	37.3	38.6	32.2
0.4	-	-	17.1
0.5	16.9	17.3	12.7
1.0	1.3	1.3	-2.1
2.0	-14.2	-12.5	-17.3
3.0	-24.2	-	-28.2
4.0	-30.0	-30.1	-35.3
5.0	-40.0	-40.4	-43.1

(1) Shatkay and Lerman (1969).
(2) Bagg and Rechnitz (1973).

Experimental values of chloride activity coefficients, in molality scale, versus NaCl molality, are showed in Figure 1. In the same figure, chloride activity coefficients calculated by hydration theory (Robinson-Stokes, 1948), are drawn.

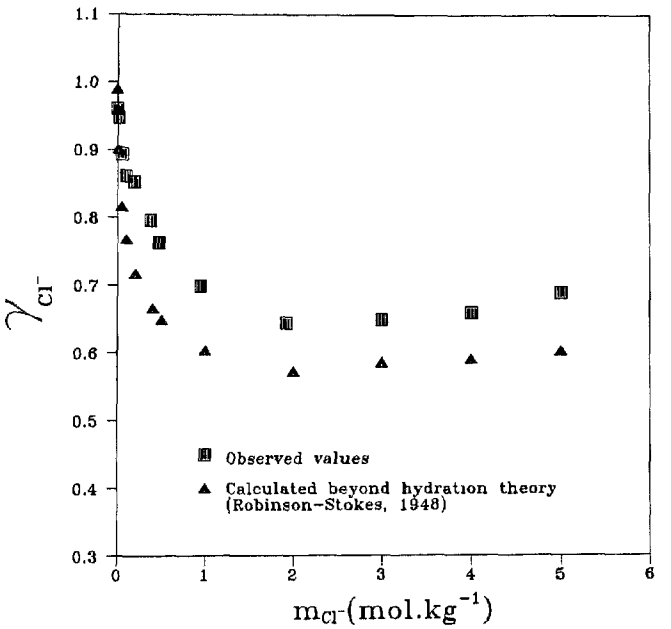

Figure 1. Experimental and calculated chloride activity coefficients

Mean activity coefficients in NaCl solutions from theoretical models

In Figure 2 experimental and calculated mean activity coefficients of NaCl versus molality, are drawn. Activity coefficients were calculated with MathCAD 4.0 program, and beyond: a extension of the Debye-Hückel equation (Davies, 1938), the hydration theory equations (Robinson-Stokes, 1948, 1959), and the specific ionic interaction equations (Pitzer, 1973, 1974, 1977, 1978).

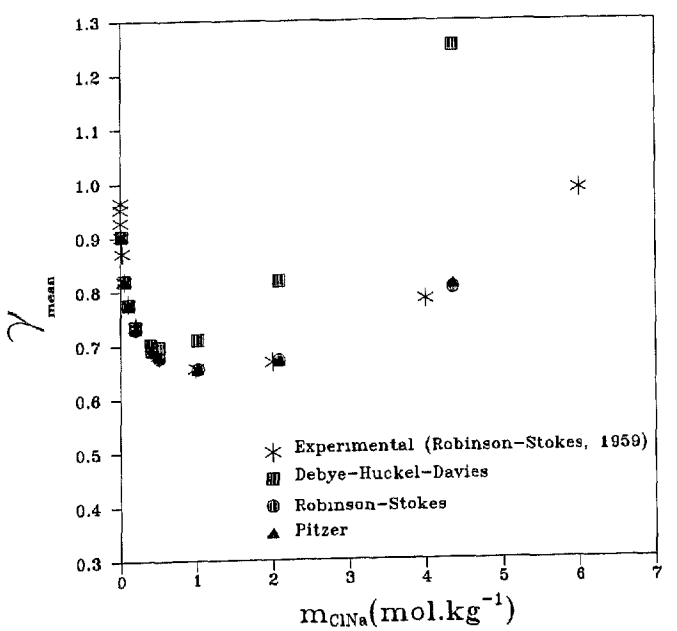

Figure 2. Mean activity coefficients in NaCl solutions

Debye-Hückel-Davies equation

The Debye-Hückel equation is a limiting law, correct in the limit at zero ionic strength, which predicts that the activity coefficient of an ion depends only on its charge and the ionic strength of the environment; that the identity of the other ions in the solution is unimportant beyond the specification of their charge; and that γ will decrease uniformly as I increases. All these predictions are true at extremely low ionic strength (Debye-Hückel, 1923).

At ordinary concentrations, for example at 0.1 m, the behaviour of real electrolytes deviates from the relatively simple predictions of the Debye-Hückel limiting law. Several more or less empirical extensions have been proposed; they fit the data with varying success at moderate values of the ionic strength, I. It is always possible to fit any set of empirical data with an equation which contains a large number of adjustable empirical parameters; such equations are not generally satisfactory, since they require the measurement and tabulation of otherwise meaningless constants for each ion studied. Davies (1938) propose the empirical equation:

$$\log\gamma\pm = -0.50|z_+z_-|\left(\frac{\sqrt{I}}{1+\sqrt{I}} - 0.2I\right) \qquad [2]$$

where I is the ionic force in molalities, and z_+, z_- are the cation and anion charges.

Experimentally a minimum in the activity coefficient occurs, followed by a more or less rapid rise of it at high concentrations. Davies's equation usually fails to give a reasonably accurate representation of observed activity coefficients at ionic strengths much greater than unity. To overcome this, further arbitrary terms in higher powers are sometimes introduced, but such equations are of no theoretical value.

The hydration theory

This theory (Stokes-Robinson, 1948) introduces the effect of ion-solvent interaction in terms of "hydration". There are spectroscopic evidences (Gmelin Handbuch, 1976) that the kinetic unit of the solute in many electrolyte solutions is an ion with several relatively firmly attached water molecules. One of the equations that this model proposes to calculate mean activity coefficients is:

$$\log\gamma\pm = -\frac{0.5092|z_+z_-|\sqrt{\mu}}{1+0.3286a\sqrt{\mu}} - \frac{n}{\nu}\log a_w - \log(1-0.018(n-\nu)m) \qquad [3]$$

where μ is the ionic strength in volume units (molarities), a_w is the water activity, m is the solute molality, υ is the number of ions that a mol of solute gives in solution, and the three terms on the right are: the Debye-Hückel term (D-H), the solvent term and the scale term. The D-H term is refered to the coulombic forces between solvated ions, and the solvent term to the ion-solvent forces.

This model certainly comes closer to the physical reality and it takes into account the observed lowering of the bulk dielectric constant by ionic solutes which arises from effects in the first layer of water molecules around the ion. Eq.3 is the simplest treatment of the effect of ionic solvation on the activity coefficient. This expression contains only two parameters: n or the number of moles of

"bound" water per mole of solute, and a or the dimensions of solvated ions. It has been extensively tested for aqueous solutions (Robinson-Stokes, 1959), and it is remarkably succesful with poorly associated electrolytes as NaCl or in general, electrolytes 1:1.

In this form, Eq.3, is capable of representing observed activity coefficients with accuracy in a wide range of concentration, extended in many cases to an ionic strength of 5. In very concentrated electrolyte solutions, there is a transition from a freely flowing solution to semi-solid gels and these phenomena suggest the possibility that the system could be treated as an adsorbent (solute) and an adsorbate (water).

The specific ionic-interaction: ionic association

As it have been seen, the effect of long-range electrostatic and the ion-solvent interactions, is not enough to predict accurate activity coefficients for most electrolytes. The Pitzer approach (Pitzer, 1973, 1974, 1977, 1978) initially developed by Guggenheim (1935) take into account long-range (attractive and repulsive) and short-range electrostatic forces, the net effect of solvation, London's dispersion forces, and any other effects of similar range; for instance, permanent dipoles or multipoles. General equations are derived from statistical mechanics for electrolyte theory, that yields thermodynamic functions from knowledge of the interionic potentials of mean force and the radial distribution functions; so activity coefficients are expressed in virial expansion.

In a solution of a single electrolyte MX, the simplest Pitzer's equations are reduce to (Pitzer and Mayorga, 1973):

$$\ln\gamma_{MX} = |z_M z_X| f^{\gamma} + m\left[\frac{2\nu_M\nu_X}{\nu}\right]B^{\gamma}_{MX} + m^2\left[\frac{2(\nu_M\nu_X)^{\frac{3}{2}}}{\nu}\right]C^{\gamma}_{MX} \qquad [4]$$

where υ_M and υ_X are the numbers of M and X ions in the formula ($\upsilon = \upsilon_M + \upsilon_X$), z_M and z_X give their respective charges in electronic units, and m is the conventional molality. B^{γ}_{MX} define the second virial coefficient, that represent the short range interaction between a pair of ions; C^{γ}_{MX} define the third virial coefficient, that represent the short range interaction between triplets of ions; and f^{γ} is a Debye-Hückel funtion that represent the electrostatic interactions. These quantities have the form:

$$f^{\gamma} = -A_{\Phi}\left[\frac{\sqrt{I}}{1+b\sqrt{I}} + \frac{2}{b}\ln(1+b\sqrt{I})\right.$$

$$B^{\gamma}_{MX} = 2\beta^{(0)}_{MX} + \beta^{(1)}_{MX} \times g_1(\alpha_1\sqrt{I}) + \beta^{(2)}_{MX} \times g_1(\alpha_2\sqrt{I})$$

$$C^{\gamma}_{MX} = \frac{3}{2}C^{\phi}_{MX}$$

Aϕ: Debye-Hückel coefficient for the osmotic function. It is related with the constant A from the Debye-Hückel expression by: $A_{\phi} = A/3 = 0.392$ at 25°C.

b: a constant, having a given value of 1.2 for all electrolytes.

α_1 and α_2: constant values that depends only from the electrolyte type 1:1, 1:2, 2:2, etc. (Pitzer and Mayorga 1973, Pitzer and Mayorga 1974, Pitzer and Silvester 1978).

$g_1(x)=2[1-(1+x-(1/2)x^2)e^{-x}]/x^2$.
$\beta_{MX}^{(0)}$, $\beta_{MX}^{(1)}$ y $\beta_{MX}^{(2)}$ are specific coefficients for every studied salt, they describe the second virial coefficient and C_{MX}^{ϕ} describe the third virial coefficient. $\beta_{MX}^{(0)}$, $\beta_{MX}^{(1)}$ y $\beta_{MX}^{(2)}$ and C_{MX}^{ϕ} can be calculated from osmotic coefficient data (Pitzer and Mayorga 1973).

One advantage of the ion association theory is that it can be applied to solutions of different salinities; for instance, brines or seawaters, for the speciation of constituents and the calculation of stability constants (Pabalan and Pitzer, 1988).

DISCUSSION

The measurement of single-ion activity coefficients is very convenient for complex mixtures, because these values can then be combined easily to obtain the mean activity coefficient for any of the numerous neutral species represented in the mixture.

From Figure 1 it can be seen that experimental activity coefficients of Cl^- are higher than the calculated from the hydration theory; maybe because in these calculations authors assume that chloride ions are not hydrated; but if the electrochemical process at an ion-selective electrode is characterized by n=1 in the Nernst equation, an uncertainty of 1 in the hydration number corresponds to an error of aproximately 0.5×m mV in the electrode potential (Bates et al. 1950). In Figure 2 we can see that mean activity coefficients of NaCl calculated by hydration theory and Pitzer equations, are in good agreement with experimental values from Robinson-Stokes, 1959. On the other hand, if we compare ionic activity coefficients of chloride ions with mean activity coefficients of NaCl (see Figure 2), and we assume that $\gamma\pm = \gamma_{Na+}$ (Hyman, 1962), we can say that in a non associated electrolyte as NaCl, the differences between γ_{Cl-} and γ_{Na+} are due to ion-solvent interactions. Nevertheless, it is important to make a difference between ionic association: stable ionic pairs, complexes or poli-ionic species, charged or uncharged, and electrostatic ionic interactions. In NaCl solutions, there are ion-solvent and ionic interactions, and the minimum in the curves can be explained in terms of changes in the "real" ionic strength resulting from the removal from the bulk solvent of water bound to the ions, and also in terms of an increasing of ionic interactions.

In the immediate vicinity of the ion, there is a primary solvation shell of water molecules that are essentially immobilized by the ionic charge and move only as a single unit with the ion.This region, sometimes termed *electrostrictive* because the water is compressed by the field of the ion, is more highly structured than bulk water (Bates and Pinching, 1950). There is an intermediate disordered or structure-broken region, in wich water is less structured than bulk water (Bell, 1958). In the outer region, the normal structure of bulk water exist. An interesting ion classification (Samoilov 1965, 1972) is based on the relative residence times of a water molecule in the vicinity of an ion. If on the average, the exchange of water molecules in the vicinity of an ion, is less frequent than the exchange of nearest-neighbor molecules in pure water, the phenomenon is termed positive hydration (structure-maker ions). If the reverse is true, that is, exchange more frequently than in pure water, the ion is said to undergo negative hydration. Positive and negative hydration correspond to hydrophilic structure making and to structure breaking, respectively (structure-breaker ions).

Na^+ ion is a typical structure maker and Cl^- ion is a structure breaking ion. This large monovalent ion is surrounded by a relatively weak electric field which may be comparable with the competing forces of normal dipole-dipole interactions between water molecules. These competing influences tend to cancel, so the hydration picture is one of little structural order. Around ions like Cl^- ion, water may be immobilized and electrostricted at most only in the first hydration shell; then a disordered structure

broken region predominates. Hydrophilic structure-making ions, like Na^+, undergo electrostrictive hydration; that is, the water molecules in the primary hydration shell, wich are oriented by the ionic field, are packed more tightly than in bulk water. Thus water in the vicinity of the ions becomes compressed owing the electric fields of the ions. Electrostrictive hydration produces three basic effects, all of which tend to reduce the mobility of an ion:

- The permanent tightly bound hydration shell, which moves as a single kinetic unit with the ion, increases the effective size of the ion in solution. Thus the Stokes radii of structure-making ions are greater than the corresponding crystallographic radii.
- The local viscosity of water in the vicinity of these ions increases.
- An additional retarding force acts on the moving ion owing to the relaxation effect of the water dipoles. This relaxation force arises because water dipoles that were originally oriented in the field of the ion require a finite time to return to their random orientation once the ion has passed.

These are the reasons why the limiting equivalent conductances of the electrostrictive ions are relatively low (λ°_{Na+}, 25°C = 50.20).

Very interesting is the mobility behavior of the structure breakers, such as the halide ions which have relatively high mobilities (λ°_{Cl-}, 25°C = 76.39) and for which the solvated radii calculated from the Stokes equation (Stokes 1948, 1957) turn out to be smaller than the corresponding crystallographic radii. The current explanation for this phenomenon is that structure breakers decrease the local viscosity of the solvent, thus increasing their mobility.

According to a rough calculation (Robinson and Stokes, 1959), the average separation between ions in a solution of a 1:1 electrolyte is 20Å at 0.1 M and 9.4 Å at 1.0 M concentration. At the same time, electrical fields due to ionic charges may perturb water up to distances of 7 Å or more from the center of an ion. Thus, when dealing with the concentration dependence of thermodynamic properties beyond the concentration of about 0.1M, it becomes necessary to consider ion-ion interactions resulting from the overlap of two such zones of water perturbed by the ionic fields (Robinson-Stokes 1948, 1959, Guggenheim, 1935, Frank and Robinson, 1940). According to Gurney (Gurney, 1953) the behavior of the activity coefficients of the alkali metal salts until 1.0m concentration can be explained in term of the overlap of their cospheres, which generates additional forces of either attraction or repulsion that are superimposed on the usual coulombic forces. Additional forces of attraction arise between ions like Na^+ and Cl^- whose structural influences are mutually compatible, leading to a decrease in the free energy.

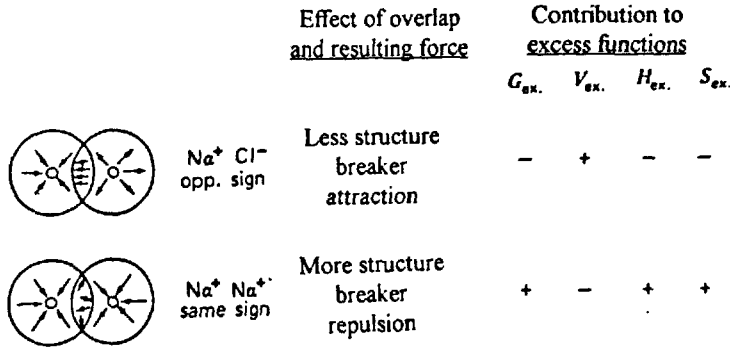

Figure 3.Structural hydration interaction model (Desnoyers et al., 1969)

Vaslow (1963) postulated that small structure-making ions, such Na^+, can fit into the holes of water structure without disrupting it and with the formation of a relatively stable uncharged ion pair and a lowering of the activity coefficients. From the concentration at which the minimum occurs, the activity coefficient increases, and this fact can indicates that there is a transition from the water structure in solution, to the crystal structure where the water molecules can be considered as adsorbed; that is to say, at high concentrations charged poly-ionic species are formed and an incresing of activity coefficients is observed.

CONCLUSIONS

Structure breaker ions such as Cl^- ions, have relatively high mobilities. This phenomenon can be explained with the hydration theory: around the Cl^- ion a disordered structure broken region of water molecules predominates (around Cl^- ions water may be immobilized at most in the first hydration shell) and the local viscosity of the solvent decreases. When the concentration increases ionic-interactions appear and the mobility results to be lower.

Around small structure-maker ions like Na^+, the water molecules are compressed and a ordered structure region predominates; thus the local viscosity of water in the vicinity of these ions increases.The ion moves with the bound hydration shell as a single kinetic unit and its mobility is reduced. When the concentration increases the ionic-interactions disturb the ordered structure, and the mobility results higher.

In NaCl solutions the minimum in the mean activity coefficient curves can be explained in terms of an increasing of the concentration of uncharged [Na^+Cl^-] ion pairs. From the concentration at which the minimum occurs, charged poly-ionic species are formed and activity coefficients increase.

REFERENCES

Bagg, J., Rechnitz, G.A., *Analytical Chemistry*, Vol. 45, No. 2, February, 1973, pp. 271-276.

Bates, R.G., Pinching, G.D., *J. Am. Chem. Soc.*, Vol. 72, 1950, p.1393.

Bates, R.G., Staples, B.R., Robinson, R.A., *Analytical Chemistry*, Vol. 42, No. 8, July, 1970, pp. 867-871.

Bell, R.P., *Endeavour*, Vol.17, 1958, p.31.

Butler, J.N., "Thermodynamic studies", *Proceedings of the Symposium "Ion-selective electrodes"*, January 30-31 1969, Gaithersburg, Ed. R. A. Durst, National Bureau of Standards, Chapter 5, pp. 143-189.

Bruton, L. G., *Analitycal Chemistry,* Vol. 43, No. 4, 1971, p. 579.

Debye, P., Hückel, E., *Phys. Z. (Leipzig)*, Vol. 24, 1923, p.185 and 305.

Desnoyers, J. E., Arel, M., Perron, G., Jolicoeur, C., *Journal of Physical Chemistry*, Vol. 73, 1969, p.3346.

Frank, H. S., Robinson, A. L., *J. Chem. Phys.*, Vol. 8, 1940, p. 933.

Gmelin Handbuch der Anorganischen Chemie, Ed. Hartmut Katscher, Springer-Verlag, Berlin, 1976.

Guggenheim, E. A., *Phil. Mag.*, Vol.19, 1935, pp.588-643.

Gurney, R. W., *"Ionic processes in solution"*, Mcgraw-Hill Book Company, New York, 1953.

Hyman, E. S., *Analitycal Chemistry*, Vol.34, 1962, p.365.

Pabalan, R. T., Pitzer, K. S., *"Chemical modeling of aqueous systems. II"*, Eds. R. L. Basset and D. C. Melchior, American Chemical Society, Washington, 1990.

Pitzer, K. S., *J. Phys. Chem.*,Vol. 77,No. 2, 1973, pp.268-277.

Pitzer, K. S., *"Activity coefficients in electrolyte solutions"*, Vol.1, Ed. Pytkowicz, CRC Press, Florida, 1979, Chapter 14: "Theory: ion interaction approach" pp.157-208.

Pitzer, K. S., Mayorga, G., *J. Phys. Chem.* Vol. 77, No.19, 1973, pp.268-277.
Pitzer, K. S., Mayorga, G., *J. Sol. Chem.* Vol. 3, No. 7, 1974, pp.539-546.
Pitzer, K. S., Peterson, J. R., Silvester, L. F., *J. Sol. Chem.*, Vol.7, No.1, 1977, pp.45-56.
Pitzer, K. S., Silvester, L. F., *J. Phys. Chem.*, Vol. 82, 1978, pp.1239-1242.
Robinson, R. A., Stokes, R. H., *"Electrolyte Solutions"*, Butterworths, London, 1959.
Samoilov, O. Ya., *"Structure of aqueous electrolyte solutions and the hydration of ions"*, Consultants Bureau, New York, 1965.
Samoilov, O. Ya., *"Water and Aqueous Solutions"*, Ed. R. A. Horne, Wiley Interscience, New York, 1972, Chapter 14: "Residence Times of Ionic Hydration".
Shatkay, A., Lerman, A., *Analytical Chemistry*, Vol. 41, No. 3, March, 1969, pp. 514-517.
Stokes, R. H., *Trans. Faraday Soc.*, Vol.44, 1948, p.295.
Stokes, R. H., Robinson, R. A., *J. Am Chem. Soc.*, Vol. 70, 1948, pp.1870-1878.
Stokes, R. H., Robinson, R. A., *Trans. Faraday Soc.*, Vol. 53, 1957, p.301.
Vaslow, F., *J. Phys. Chem.*, Vol. 67, 1963, p.2773.

CORROSION OF STEEL IN CARBONATED CONCRETE

Anastasia G. CONSTANTINOU* and Karen L. SCRIVENER†, Imperial College, London, UK.

ABSTRACT The behaviour of steel in carbonated concrete was investigated. The initial microstructure of the concrete around the steel was studied by the use of a scanning electron microscope (SEM) in the backscattered electron (BSE) mode and by image analysis. This technique was also used to study the microstructural development during corrosion. The corrosion of the steel was monitored by the linear polarisation resistance technique.

Key-words: Interfacial zone, Image analysis, Microstructure, Carbonation, Corrosion.

INTRODUCTION

In earlier work, image analysis of backscattered electron (BSE) images was used to characterise the microstructure of cement paste around aggregate particles in concrete (Scrivener et al, 1988, Crumbie 1994). The aim of the current work was to extend these techniques to the study of the interfacial zone around reinforcing steel in concrete and to the study of the active corrosion process in carbonated concrete.

The results presented here relate to three fairly independent aspects of the study:

- characterisation of the interfacial transition zone (ITZ) before carbonation;
- carbonation of the specimens and discussion of the similarities between the accelerated method used and natural carbonation;
- study of the ITZ after a period of active corrosion.

After a general section on the preparation of the samples these aspects are presented separately.

EXPERIMENTAL

Concretes were produced at three different w/c ratios, varying the cement content to achieve approximately constant slump:

1. w/c = 0.47, cement content 373 kg/m^3;
2. w/c = 0.56, cement content 315 kg/m^3 and
3. w/c = 0.65, cement content 275 kg/m^3.

These were cast into cylindrical moulds 100 mm in diameter by 200 mm in length, with steel reinforcement bars (8 mm diameter) at cover depths of 11 mm and 20 mm. The samples were demoulded after one day and then half were air dried and half were cured for a further 7 days under damp sacks. A set of samples was then sectioned at 28 days to study the ITZ. The remaining samples were carbonated and then placed in different humidity regimes.

CHARACTERISATION OF STEEL ITZ

Little work has been done to characterise the microstructure of the interfacial transition zone (ITZ) around reinforcing steel in concrete. Qualitative studies based on the examination of fracture surfaces (Page 1975, Monteiro 1985, Sagoe-Crensil and Glasser, 1990), discuss the

* current address RBB R&D, Horsham, RH12 4QG, U.K.
† current address Lafarge, Laboratoire Central de Recherche, France.

predominance of a layer of calcium hydroxide adjacent to the steel surface. Some work on image analysis of the ITZ around reinforcing steel in concrete was also reported by Zayed and Slater-Haase (1992).

Sections of the reinforced samples were cut using a slow speed precision saw. The sections were then resin impregnated, lapped with 9 μm alumina powder, polished with diamond pastes, to ¼ μm and then carbon coated. A JEOL-35CF scanning electron microscope (in the backscattered electron, BSE, mode) was used to examine the samples. Forty images were collected around the steel interface at a magnification of ×480 (1650 × 1650 μm) for each of two sections. The relative areas of aggregate, anhydrous material, calcium hydroxide and porosity were measured in bands about 5 μm in thickness radiating out from the steel interface. The values were averaged for each band for the eighty images and the percentage area against distance plotted for each phase. A typical image used for image analysis is shown in Fig 1. At the depth of the reinforcement, there was no effect of the different curing regimes used.



Figure 1: The steel / concrete interfacial zone for a sample with w/c = 0.65

Packing of Aggregate Particles

The maximum size of the aggregate used was 10 mm, approximately the same as the steel cross-section, and much larger than the size of the individual images used for analysis. Thus the results obtained for the aggregate distribution are not statistically representative of the overall aggregate distribution. The variability of the results for nominally identical samples and for the different w/c ratios can be seen in Fig 2. Despite the variability, the general trend of increasing aggregate area fraction with distance from the steel is clear. The lack of aggregate particles close to the steel interface is a result of the 'wall effect', whereby large particles cannot pack efficiently against a relatively flat surface.

To compensate for the variability of the aggregate distribution the relative proportions of the other components were calculated relative to the paste volume.

Distribution of Anhydrous Particles

During mixing and placing of the concrete, the anhydrous cement grains pack between the aggregate particles with varying degrees of efficiency. Therefore, even when the volume of anhydrous is normalised relative to the paste fraction, the distribution of aggregate still has an influence. The variation of remaining anhydrous material with distance from the steel is shown in Fig 3 for the three concretes. As with the studies of the ITZ around aggregate particles (Crumbie, 1994), the wall effect results in a depletion of cement grains adjacent to the steel interface. In these mature samples, the amount of unreacted anhydrous material is relatively low. Close to the steel the packing effect dominates and the values for all three concretes are similar, increasing steeply in the first 20 μm and more slowly thereafter to give values in the 'bulk' which increase with decreasing w/c as expected. The effective width of the ITZ relative to the anhydrous distribution of some 50 μm is similar to that found around aggregate particles by Crumbie (1994).

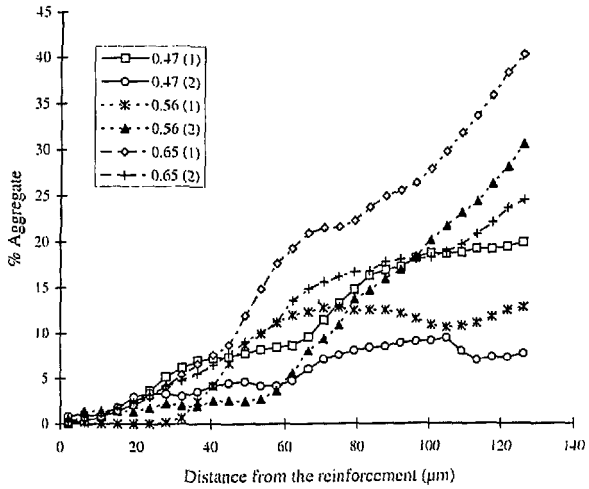

Figure 2: The distribution of aggregates around the steel / concrete interfacial zone.

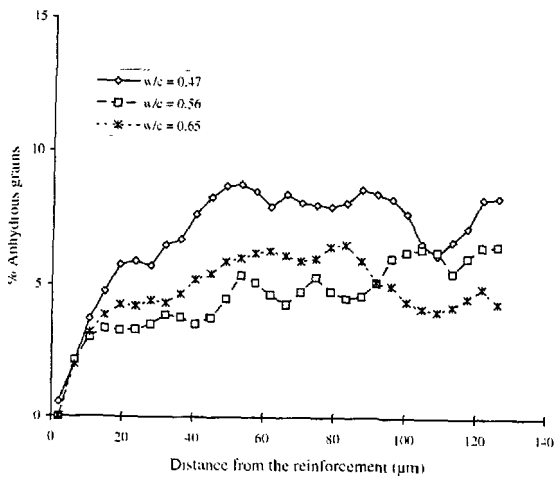

Figure 3: The distribution of anhydrous cement grains at the steel / concrete interface.

Distribution of Porosity

Due to the wall effect on the packing of the cement grains, and as with the ITZ around aggregate particles, the porosity increases in the ITZ around the steel as the interface is approached, Fig 4. The porosity at the interface increases significantly with the w/c ratio from 25% to 35%, and these figures are very similar to those measured around aggregate particles (Crumbie 1994). The porosity drops with distance from the steel over about 45-50 μm to a 'bulk' level which increases with w/c.

Distribution of Calcium Hydroxide

The distribution of calcium hydroxide in the steel ITZ is shown in Fig 5. The most notable feature is the lack of calcium hydroxide at the steel interface in contrast to the elevated level found in the ITZ around aggregate particles and to the expectation that growth of calcium hydroxide should be favoured by the increased porosity.

This result is also different from that reported by Zayed and Slater-Haase (1992), who found a constant value of 14% for the ITZ around steel in a concrete at w/c 0.45. The possibility of some calcium hydroxide removal during specimen preparation cannot be ruled out, although values in the bulk of the concrete are similar to other observations. Nevertheless it is clear that there is no continuous 'layer' of calcium hydroxide around the steel as has been suggested by some workers.

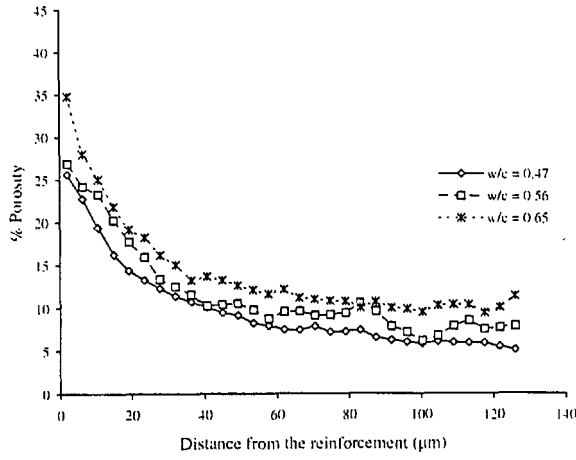

Figure 4: The distribution of porosity around the steel / concrete interfacial zone.

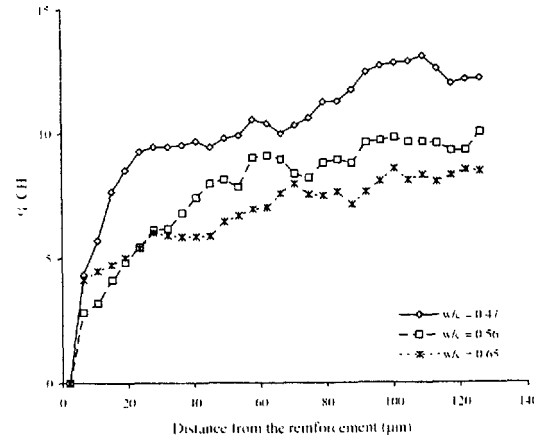

Figure 5: The distribution of calcium hydroxide at the steel / concrete interface.

MICROSTRUCTURE AFTER ACCELERATED CARBONATION

To accelerate the carbonation process in order to induce active corrosion in the reinforcing steel the specimens were placed in an environment of 100% CO_2 and 65% RH at 20° C. The progress of carbonation was checked regularly by spraying phenolphthalein indicator on parallel control samples cast without reinforcement. After carbonation samples were prepared as before.

It was found that the w/c ratio and the curing regime affected the rate of carbonation, but the effects on the microstructure were very similar.

The carbonation regime clearly differs significantly form natural carbonation of a CO_2 concentration of 0.03%. Therefore, the microstructure after carbonation was compared with a naturally carbonated field sample 40 years old.

Fig 6 shows the microstructure of a concrete (w/c = 0.56 and 1 day curing) subject to accelerated carbonation. Comparing this microstructure with the initial microstructure in Fig 1, the most obvious differences are the reduced porosity, due to the deposition of the carbonation products, i.e. $CaCO_3$ in the pores of the concrete and the absence of calcium hydroxide. Another feature of the fully carbonated microstructure is the attack of the anhydrous cement grains by CO_2. The attacked grains are easily distinguishable with the original grains of alite (faceted) and belite (round) parts turning dark grey and the interstitial parts remaining unaffected (white). These dark areas were found by EDS x-ray microanalysis to have high Si/Ca ratios due to depletion of calcium.

Comparison of the microstructure of the concretes subject to accelerated carbonation with that of a naturally carbonated microstructure indicated that they were very similar. Attacked, dark relics of anhydrous grains were observed in both samples although these were more prevalent in the accelerated sample, due to the younger age at carbonation. Overall it was judged that the accelerated carbonation process did not result in differences likely to affect the subsequent corrosion process significantly.

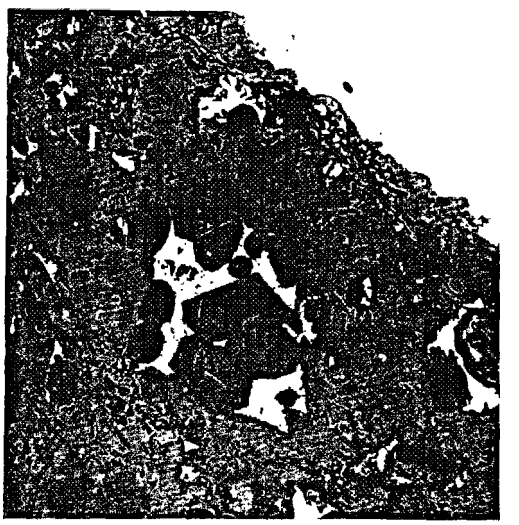

Figure 6: Steel / concrete interface of a fully carbonated sample with w/c = 0.56 and 1 day cure.

STUDY OF THE CORROSION PROCESS

After full carbonation, the samples were placed in two humidity regimes at 90% and 70% RH. The corrosion rate of the steel reinforcement was followed by the linear polarisation technique using a potentiostat. Fig 7 shows the measurements of corrosion rate with time for the w/c = 0.56 sample. The rate was slightly higher at 90% RH than at 70%, when one of the 90% samples was subsequently placed in 43% RH the corrosion stopped, as shown in the figure. The rate of corrosion was slightly higher in the w/c = 0.65 samples.

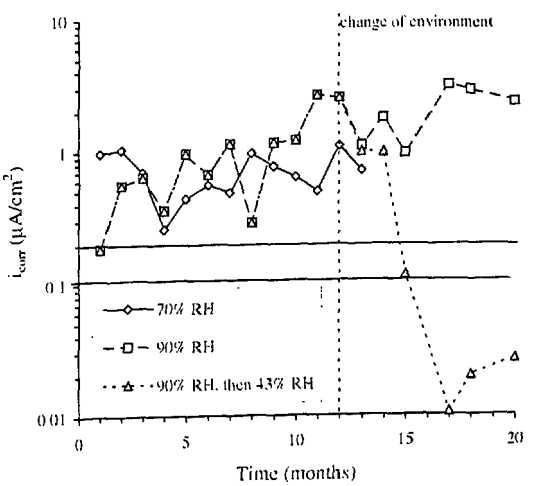

Figure 7: The effect of the various RHs on the corrosion rate of a sample with w/c = 0.56.

One sample from each of the batches at 70 and 90% RH was removed from the tank for microscopical examination after six, twelve and eighteen months. Adjacent images were collected around the interface (between 50-60) to make up a montage of the whole interface at a magnification of x200. The interfaces were examined, the amount of corrosion products traced onto paper and the relative corroding area measured using a planometer. The maximum thickness of the corrosion layer was also measured.

Fig 8 shows the steel / concrete interface of a sample with w/c = 0.56, after 1 year in 90% RH after corrosion has taken place. The layer of cement paste which has been affected by the deposition of the corrosion products is clearly visible. The presence of cement grain relics indicates that the corrosion products have diffused into and deposited in the cement paste. Two discrete layers are apparent. The first layer, closest to the steel interface, is dense and by its high grey level contains a high proportion of iron oxide. In the second layer further out the iron oxide is more diffusely mixed with the cement paste.

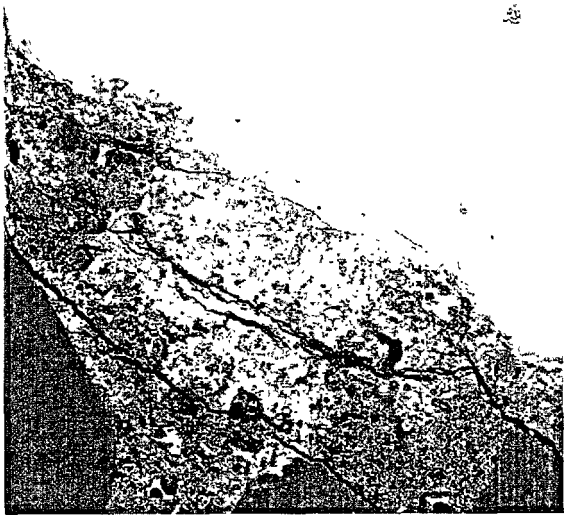

Figure 8: The steel / concrete interface of a sample with w/c = 0.56 after 1 year in 90% RH.

A montage of the entire interface of the sample with w/c = 0.56, after 1 year at 90% RH is shown in Fig 9. The top of the figure represents the side of the steel which is closest to the surface of the steel. It can be seen that the heaviest corrosion is on this side closest to the surface whereas the other side is just starting to corrode. This effect is probably due to the availability of oxygen.

The corrosion processes in carbonated concrete is usually considered to be homogeneous and generalised. At a microscopic level it is clear that the distribution of corrosion products is in fact very heterogeneous, although the scale of heterogeneity is much finer that that found in chloride induced pitting corrosion.

Some cracks are observed in the region most heavily corroded. There may be due to the build-up of corrosion products but could also be caused by the specimen preparation.

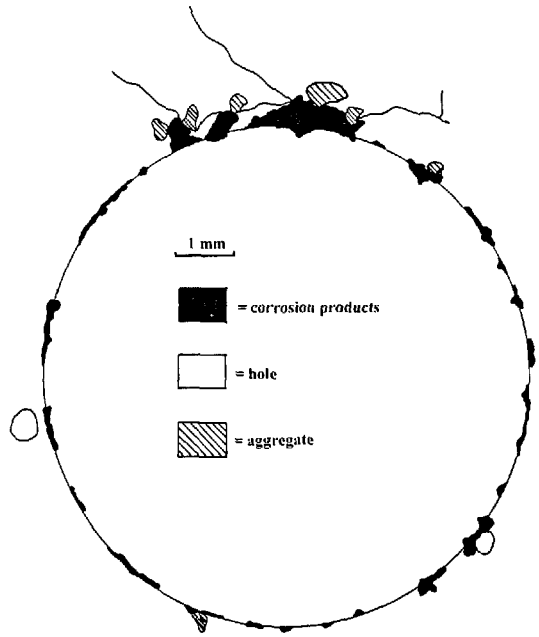

Figure 9: The schematic diagram for the steel / concrete interface of a sample with w/c = 0.56, after 1 year in 90% RH.

CONCLUSIONS

1. The distribution of the various phases around the reinforcement is dominated by the packing of the aggregate particles and to a lesser extent by the packing of the anhydrous particles. The w/c ratio has a slight effect.
2. A region of high porosity in the paste adjacent to the steel was observed in all the samples. The lower the water / cement ratio of the mix, the lower the amount of the porosity.
3. Carbonation led to a more compact microstructure of the concrete paste due to the deposition of $CaCO_3$ into the pores with no visible CH.
4. The humidity regime appears to have little effect on the corrosion rate of steel in carbonated concrete. However, when the sample was placed in 43% RH after 90% RH the corrosion rate dropped to very low values.
5. Corrosion products form two distinct layers. The corrosion was heaviest in the region closest to the surface of the concrete. The corrosion was localised with small "pits" distributed fairly evenly around the steel.

ACKNOWLEDGEMENTS

The authors would like to thank Dr. N.N Dioh for help with the planometer readings. NGC would like to thank the Building Research Establishment (BRE) and W.R. Grace for financing this work.

REFERENCES

Andrade, C., C. Alonso, P. Santos and A. Macias, "Corrosion behaviour of steel during accelerated carbonation of solution which simulate the pore concrete solution", in "8th Congress on the Chemistry of cement", Brazil 1986, V5, pp. 256-262.

Constantinou, A. G., "Laboratory and field investigation of the corrosion of steel in concrete", M.Sc. Thesis, University of London, 1991.

Constantinou, A. G. and K. L. Scrivener, "Study of the Corrosion of Steel in Concrete by Backscattered Electron Imaging in the Scanning Electron Microscope", Proceeding of the. 2nd Interernational Conference "Microscopy of oxidation", Ed. S.B. Newcomb and M.J. Bennett, Institute of Materials, 1993, pp.59-66.

Crumbie, A.K., Ph.D. thesis, The University of London, 1994.

Dunster, A.M., "The microstructure of concrete exposed to natural and accelerated carbonation regimes", in "Cement and concrete science", Oxford, September 1992 (oral presentation).

Monteiro, P.J.M., Gjorv, O.E. and Mehta, P.K. "Microstructure of the steel-cement paste interface in the presence of chlorides", Cement and concrete research Vol. 15, No. 5, 1985.

Page, C. L., "Mechanism of corrosion protection in reinforced concrete marine structures", Nature, Vol. 258, Dec. 1975, pp.514-515.

Sagoe-Crentsil, K.K. and Glasser, F.P., "Analysis of the steel: concrete interface" in 3rd symposium on "Corrosion of reinforcement in concrete", Ed. C.Page, K.W.J. Treadaway and P.B. Bamforth, Elsevier applied science,1990, pp. 74-86.

Scrivener, K.L., Crumbie, A.K. and Pratt, P.L., "A study of the interfacial region between cement paste and aggregate in concrete", Proceedings of the MRS meeting "Bonding in cementitious composites", December 2-4 1987, Boston, Ed. S. Mindess and S.P. Shah, Materials Research society, Vol.114, pp.77-86.

Zayed, A.M.and A. Slater-Haase, "The nature of the concrete/steel rebar interface and its effect on corrosion initiation", 47th Annual conference and exposition of the National association of corrosion engineers, "Corrosion 1992", National Association of Corrosion Engineers (NACE), USA.

Richardson, I.G., Groves, G.W., Brough, A.R. and Dobson, C.M., "The carbonation of OPC and OPC/silica fume hardened cement pastes in air under conditions of fixed humidity", Advances in cement research, Vol.5, No.18, pp.81-86, 1993.

AUTHOR INDEX

A
M.S. Abdel-Aziz; 3v012
A.A. Abdel-Kader; 2ii027
A. H. Abedel-Reheem; 3ii124
A. Achmetov; 2ii013
F. Adenot; 3v003
A. D. Agnihotri; 1i003
S.C. Ahluwalia; 1i019, 1i031, 1i044, 1i045, 1i053, 2ii006, 3ii094, 4iv013, 4iv067
H. Ai; 3iii018
V.G. Akimov; 1i006
I. G. Al-Alm Rashed; 3ii124
B.S. Albats; 1i015, 1i007
A.H. Ali; 4iv014
M.M. Ali; 2ii006
M[a]C. Alonso; 4iv004, 4iv082, 4iv083
V. Alunno Rossetti; 3v026
Ö. Andaç; 1i050
T. Ando; 2ii017
C. Andrade; 4iv004, 4iv082, 4iv083
M.V. Anufriev; 1i032
H. Anzai; 3v013
N. Arano; 4iv051
S. Argarwal; 4iv067
S.K. Argarwal; 4iv067
P. Arjunan; 3v020
V.K. Arora; 1i019
K. Asaga; 3ii107, 3iii022
E. Asakura; 2ii005
M.A. Aviles; 3v019

B
O. Baumanis; 3v025
Sh.T. Babaev; 3iii021
V. Babkov; 2ii048
V.I. Babushkin; 4iv039
P. Baccini; 4iv076
S. Bagosi; 4iv045
G. Balázs; 2ii060, 4iv002
K.D. Baltzopoulou; 4iv052
J.R. Baragaño; 3iii004
V.D. Barbanyagre; 1i011, 1i059
P. Barret; 2ii024
N.F. Bashlykov; 3iii021
A.F. Battagin; 3ii102, 3ii103
Y. Bazhenov; 4iv058
A. Beeldens; 4iv007
V. Belyaeva; 1i004
M. Benkaddour; 2ii041
J. Bensted; 3iii014
D.P. Bentz; 2ii078
J. Berekta; 2ii029
H. Bergqvist; 3ii106
A.F. Bernatsky; 4iv079
C. Bessada; 3v002
R. Bhargava; 1i031, 2ii006
K.N. Bhattacharjee; 3ii115
Y. Biryukovich; 4iv056
M[a]T. Blanco-Varela; 1i034, 3ii096, 3ii113, 3iii004, 3iii015
A.I. Boikova; 1i057, 1i058
K. Bollmann; 4iv062
L. Bonafous; 3v002
D. Bonen; 4iv022
S. Bonnet; 4iv078
M. Boros; 2ii060
S. Bouraoui; 2ii012
P. Bowen; 3iii002
S. Boyko; 3v004, 3v022
M. Braiman; 3v022
K.D. Breneman; 2ii057, 2ii058
F. Brivot; 4iv074
A.R. Brough; 3v001
H.J.H. Brouwers; 2ii052
L. Brower; 3iii031
W. Brylicki; 3ii095
N. R. Buenfeld; 4iv070
T.A. Bürge; 3iii002

C
R. Cabrillac; 3v003
C. Caestecker; 4iv007
R. Caldwell; 4iv042
G. Camarini; 3ii102, 4iv063
L. Cassar; 1i027
P. Cassat; 3v014
M. Castellote; 4iv082
S.L. Centurione; 2ii079
W.-H. Chae; 1i036
J. Champa; 3iii027
S. Chanda; 3ii092
S. Chandra; 3ii106
P.K. Chang; 3v006
I. Chartschenko; 2ii010
A.K. Chatterjee; 1i008, 1i033, 2ii039

S. Chaturvedi; 4iv057
T. Chaussadent; 4iv074
M. Chen; 3iii016
Y. Chen; 1i010, 2ii031
H. M. Cheong; 1i049, 2ii037
V.L. Chernyavski; 4iv071
Y. Chi; 1i054, 1i055
V. Chistyakov; 2ii019, 2ii023
D.W. Cho; 2ii037
H. Choi; 3iii009
S.H. Choi; 1i036, 1i049, 4iv054
B.J. Christensen; 2ii057
M.A. Cincotto; 3ii102, 4iv063
R. Cioffi; 4iv017
P. Colombet; 3iii003, 3v002, 3v014
D. Constantiner; 3iii013
A.G. Constantinou; 4iv084
F. Corazza; 3iii003
U. Costa; 3iii003
J.-P. Coutures; 3v002, 3v005
T. Coverdale; 3iii027
N.J. Crammond; 4iv026
E. Csányi; 4iv002
L.J. Csetenyi; 4iv045
F. Curcio; 3v026, 4iv006
L. Cussino; 4iv006

D
M. Daimon; 2ii002, 2ii017, 2ii022, 3ii088, 3ii107, 3iii022
D. Damidot; 2ii024, 2ii025, 2ii026, 3iii007, 4iv066
T. Dashkova; 4iv056
B. De Blaere; 4iv007
B. De Vito; 4iv017
E. De Winne; 4iv007
M. Degenkolb; 2ii074
A.E. Degtyaryev; 2ii019
J. Deja; 4iv015
K. Demura; 3iii033
M. Deng; 4iv029
S.P. Dennington; 3iii008
R.K. Dhir; 4iv012
G. Diaz; 3v023
S. Dietz; 3ii087
J.M. Diez; 4iv040
S. Dimitrova; 3ii101
A.M. Dmitriev; 3iii021
C.M. Dobson; 3v001
A. Douy; 3v005
A. Dozono; 2ii001
M. Drabik; 3iii011
R. Dron; 4iv074
G.Ya. Drozd; 4iv039
V.Y. Dubnitsky; 4iv071
G. Dumitru; 3iii015
A.M. Dunster; 4iv026
S. Duszak; 4iv027

E
C.M. Economou; 4iv052
M. Ecker; 2ii032, 4iv044
L. Eckert; 3iii027
A.N. El-Afify; 3ii124
E.B. El Aouni; 2ii041
B.A. El-Sabbagh; 4iv014
H.A. El-Sayed; 4iv014
A. Emanuelson; 1i060
Z.B. Entine; 1i020, 1i046, 3v024
H. Ezirim; 3ii112

F
D. Fairhurst; 4iv008, 4iv009
V.R. Falikman; 3iii021
Y. Fang; 1i010
S.A. Farrington; 3iii013
P. Faucon; 3v003
X. Feng; 2ii043
A. Fernandez-Jimenez; 3ii098
V. Fernon; 3iii003
R. Ferrari; 4iv006
R.C. First; 2ii075
R. Flatt; 3iii002
O.I. Fomicheva; 1i057, 1i058
E. Forssberg; 3ii104
L.S. Fraiman; 3ii081
R. François; 4iv078
O. Francy; 4iv078
G. Frigione; 4iv017, 4iv050
X. Fu; 1i054, 1i055
H. Fujisawa; 2ii005
H. Fujiwara; 2ii001
K. Fukuda; 1i025, 1i052

G
L. Galikova; 3iii011
S.P. Gandhe; 1i033
A. Garbacik; 1i018

M.C. Garci; 2ii058
L. A. M. Garcia; 4iv037
S. Gauffinet; 2ii055
M. Gawlicki; 3ii089
M^{a}T. Gaztañaga; 4iv003
J. Geiseler; 4iv001
S. George; 1i003
W. Gessner; 3iii007, 3v018
D. Ghosh; 1i008, 1i033, 1i047
S.N. Ghosh; 3ii092
S.P. Ghosh; 1i030, 2ii018
G. M. Giaccio; 2ii036
Z. Giergiczny; 4iv019
C. Gilioli; 1i027
P. Gill; 3iii024
N. Giuliani; 1i051
G.K. Glass; 4iv070
F.P. Glasser; 1i050, 3ii091, 4iv066
V. Glukhovskiy; 4iv056
F. Goetz-Neunhoeffer; 1i056
L. Ya. Goldstein; 1i013
E. Gomez; 3v019
S. Goñi; 4iv003, 4iv004, 4iv024, 4iv040, 4iv083
J.W. Goodwin; 3iii008
V.K. Gore; 1i047
G. Goswami; 3v008
R.K. Goswami; 1i044, 1i045
S. Goto; 2ii070
A.M. Grabiec; 3iii019
M.L. Granizo; 3ii113
L.V. Grishchenko; 1i058
I. Grosvalds; 2ii009
G.W. Groves; 3v001
M. Grutzeck; 2ii067
G. Gu; 3iii016
A. Mª Guerrero; 4iv003, 4iv024
G.L. Guerrini; 1i027
R.S. Gupta; 1i053

H
H. Hagiwara; 3iii017
J. Han; 3ii122
K. S. Han; 1i049
M. Handa; 2ii017
S.K. Handoo; 3v019, 4iv013, 4iv067
S. Hanehara; 2ii014, 3iii001
F. Hanic; 3iii011
S. Hansen; 1i060
N. Hara; 2ii065
S. Harsh; 1i044, 1i045, 4iv013
M. Hasegawa; 3iii010
N.M. Hassanein; 4iv070
M. Hatano; 3iii009
A.S. Heble; 2ii039
H. Hedlund; 2ii077
D. Heidemann; Plen2
E. Henderson; 1i060
M^{a}S. Hernandez; 4iv003, 4iv024
A. Hidalgo; 4iv004, 4iv083
T. Higaki; 3iii022
M. Hilger; 1i009
H. Hirao; 2ii014
S. Hirose; 3iii022
F.J. Hofmann; 4iv038
H. Hofmann; 3iii002
S.-Y. Hong; 4iv068
K. Hormann; 4iv038
S. Hoshino; 2ii002
J. Houghton; 4iv025
Y.F. Houst; 3iii002
G. Hu; 1i023
S. Huang; 4iv032
Z. Huang; 4iv073
F.H. Hubbard; 4iv012
C.L. Hwang; 2ii035; 3ii108, 3v006, 3v021
C. Hübert; Plen2
C. Hyeon; 4iv072
R. Härdtl; 3ii082

I
M. Ichikawa; 3iii005
K.A. Idriss; 3v012
S.-i. Igarashi; 4iv051
T. Iisaka; 2ii003
T. Ikabata; 2ii007
K. Ikeda; 1i025
M.R. Ilić; 4iv023
N. Inoue; 2ii065
Y. Inoue, 2ii040
B.E. Ioudovitch; 1i020, 1i046, 3iii021, 4iv036
G. C. Isaia; 3ii110
A. Ishida; 3iii017
Y. Ishikawa; 2ii003
Y. Isojima; 3ii109, 3ii119
S. Ito; 1i052, 3ii121
J. Iwanciw; 1i022

H. Iwasaki; 3iii033

J
J.F. Jacquinot; 3v003
H.J. Jakobsen; 2ii056
S. Jalali; 3ii084
I. Y. Jann; 3v021
I. Jedda; 2ii020
H.M. Jennings; 2ii057, 2ii058
O.M. Jensen; 2ii056
M.-Y. Jeong; 4iv055
L. Ji; 2ii030
S.P. Jiang; 2ii053
W. Jiang; 3ii100, 3iii030
A.C. Johnson; 4iv076
J.-E. Jonasson; 2ii077
M. Jorda; 3v003
D.M. Joshi; 3ii092
H. Justnes; 1i038, 2ii069, 3iii012, 4iv064, 4iv081

K
K. V. Kalyani; 1i003
M. Kanaya; 3iii005
I. Karimov; 2ii048
A. Katz; 3ii083
S. Kawaguchi; 4iv051
M. Kawamura; 4iv051
T. Kawano; 3iii010
S. Kelham; 4iv060
M. Kersten; 2ii059
S.A. Khadilkar; 1i008, 1i047
Y. Kihara; 3ii085, 4iv048
H. Kikukawa; 2ii003
B.-K. Kim; 4iv068
N.-H. Kim; 2ii044
A. Kindness; 3ii091
P. Kittl; 3v023
V. Klassen; 1i004
J. Kļaviņš; 3v025
W.A. Klemm; 4iv041, 4iv059
A. Klusov; 2ii013
D. Knöfel; 2ii074
T. Kobayashi; 3iii010
M.M. Komljenović; 1i017
P.G. Komokhov; 2ii016
J. Komonen; 3iii029
N. Kondo; 2ii017
V.I. Kondrashchenko; 2ii066
Z. Konik; 1i022
G. Koprowski; 4iv018
H. R. Kota; 3ii104
M.V. Kougiya; 1i043, 3ii081
T.V. Kouznetsova; 1i001, 2ii027, 2ii028
J. Krištín; 3v009
É. Kristóf-Makó; 3v010
P.V. Krivenko; 2ii033, 4iv046
A.R. Krivoborodov; 4iv053
Y.R. Krivoborodov; 1i014, 1i040, 2ii013
D. Križan; 3ii085, 4iv020
R. Krzywobłocka-Laurów; 3iii019
A.B. Kudryavtsev; 2ii028
H. Kuga; 3ii107
W. Kurdowski; 4iv027
S. Kwan; 2ii067
L. J. Kyu; 2ii022
B. Ködderitzsch; 3v018
U. König; 1i039

L
E. E. Lachowski; 3ii091
A. Łagosz; 3ii089
S. Lagzdina; 1i035, 2ii009
A. Landa-Cánovas; 1i060
E. Lang; 4iv001
J. LaRosa-Thompson; 2ii067, 3iii024
C.K. Larsen; 4iv069
X. Lecoq; 2ii055
H.-S. Lee; 2ii044
I.S. Lee; 2ii044
S. H. Lee; 3ii088
Y.-J. Lee; 2ii044
P.G. Lele; 1i008, 1i047
M. Lewis; 4iv025, 4iv061
D. Li; 4iv029
P. Li; 1i028
R. Li; 4iv028
S. Li; 4iv030
V. Lilkov; 3ii116
J.R. Lim, 2ii037
L.K. Lin; 3ii108
J. Lindgård; 4iv064
C. Liu; 1i028
J.N. Liu; 3ii114
J.S. Lota; 3iii014, 4iv012
C. Lu; 1i012, 4iv028
H.M. Ludwig; 4iv034, 4iv035
I.G. Luginina; 1i029, 1i057

M. Lukach; 3v022
K. Luke; 3ii091
T. Lyashenko; 3v004

M
A. Macias; 4iv040
J. Madrid; 4iv040
N. Maeda; 3iii010
Y. Maejima; 2ii005
S. C. Maiti; 3iii020
J. Majling; 3v009
I. Maki; 1i052
R.I.A. Malek; 1i024
J. Małolepszy; 2ii064, 3ii089, 4iv043
S. Manjit; 3ii093
B. Marchese; 4iv050
E. Marciano Jr.; 2ii079, 3ii103
V. Maringolo; 2ii079
M. Marroccoli; 2ii029
V. Martinez; 3v023
D. Massiot; 3v002, 3v005
S. Matala; 3v017, 4iv005
V.K. Mathur; 1i053
V.A. Matviyenko; 2ii076
W.J. McCarter; 3ii112, 4iv011
O.P. Mchedlov-Petrossyan; 1i042, 2ii021
S.N. Mehrotra; 1i002
I. Meland; 4iv064
V.S. Melentyeva; 3ii117
E. Menendez; 4iv004
B. Meng; 3ii105
H.W. Meyer; 3v007
V. Michaud; 2ii011, 4iv049, 4iv065
A. Miezis; 3v025
T. Mihara; 3iii017
N. Mikhailishina; 4iv056
S.R. Miletić; 4iv023
F.M. Miller; 4iv041, 4iv059
K. Miskiewicz; 3ii087
S. Miyazawa; 2ii071
K. Mohan; 1i030, 2ii018
B.N. Mohapatra; 3v008
G.K. Moir; 1i041
G. Morales; 3ii123
M. Morioka; 3iii017
H. Motzet; 1i039
J.F. Muller; 3v014
A.K. Mullick; Plen1, 1i031, 3v019, 4iv047
D. V. Mundshtukov; 2ii020
J.C. Mutin; 2ii053
D. Müller; 3iii007
U. Mäder; 3iii002
S. Möhmel; 3v018

N
M. Nadu; 3v022
S. Nagataki; 2ii001
A. Nakamura; 2ii022
H. Nakata; 2ii070
S. Nakaya; 2ii017
D. Nazarsky; 4iv021
B. Nedumaran; 1i002
L.S. Nefyodova; 3v024
H. Nemoto; 3v013
C. M. Neubauer; 2ii057, 2ii058
J. Neubauer; 1i039, 1i056, 3v007
Y. Nikaido; 2ii017
T. Nishikawa; 3ii121
J. Nissenbaum; 3v022
W. Nocuń-Wczelik; 4iv043
T. Noguchi; 4iv072
H. Noma; 2ii065
A. Nonat; 2ii053, 2ii055, 4iv049, 4iv065
E.C. Nygaard; 3iii012

O
I. Odler; 1i026, 2ii063
H. Ogata; 2ii005
H.-K. Oh; 1i036, 4iv054, 4iv068
Y. Ohama; 3iii033
Y. Ohba; 2ii002, 2ii022
A. Ohno; 3v015
A. Olginsky; 2ii015
G.B. Olson; 2ii058
L. Opoczky; 1i009, 2ii004
A.P. Osokin; 1i005, 1i006, 1i014
Z. Owsiak; 4iv018

P
S. Pagliolico; 4iv006
A. Palomo; 1i034, 3ii096, 3ii113, 3iii004
J.G. Palomo; 1i034
M. T. Palou; 3v009
Y. Pan; 1i021, 1i054, 1i055
J.D. Panda; 3v008
P.K. Panigrahy; 3v008
I. Papayianni; 3ii086
A. Papo; 2ii004

C.-K. Park; 4iv068
P. Parmentier,; 3ii120
M. Pátkai-Horváth; 3v010
P. Paulini; 2ii072
S. Pavlenko; 3ii080, 4iv058
V. Penttala; 3iii029, 4iv033
J.L. Perez-Rodriguez; 3v019
B. Perrin; 4iv078
B. Persson; 2ii073
O.E. Petrov; 3ii116
S. Peukert; 2ii034, 3iii023
W.G. Piasta; 4iv018
A.K. Platten; 4iv008, 4iv009, 4iv073
A.A. Plugin; 4iv039, 4iv075
A.N. Plugin; 2ii054, 4iv075
A. Poltavtsev; 2ii019
A. Pompo; 2ii029
E.N. Potapova; 1i005, 1i006
J.H. Potgieter; 2ii049, 3v011
P.L. Pratt; 3iii014
I.G. Prokopova; 4iv075
J.R. Prusinski; 3ii090
F. Puertas; 1i034, 3ii096, 3ii098, 3ii113, 3iii004, 3iii015
E.K. Pushkaryeva; 2ii033
G.K.D. Pushpalal; 3iii010
R. Pyare; 1i016
Z. Pytel; 2ii064
H. Pöllmann; 1i039, 2ii032, 3iii032, 3v007, 4iv044

Q
V.A. Quarcioni; 3ii085

R
M. Radenkova-Yaneva; 2ii047, 3ii101
K. Raina; 1i002
K. Rajczyk; 2ii045
Sh. M. Rakhimbaev; 2ii046
X. Ren; 2ii030
A. Rettel; 2ii026, 3iii007
M. Ribas Silva; 4iv037
I.G. Richardson; 2ii068, 3v001
A. Risch; 4iv044
J. Roberts; 4iv073
E. Rodum; 4iv081
Mª.L. Romero; 3ii096
V. Ronin; 3ii104, 2ii077
G. Rosenthal; 3iii031
A. Rosić; 1i017
W. Roszczynialski; 3ii097
D.M. Roy; 1i010, 3ii100, 3ii114, 3iii030, 3v020
R. Roy; 1i010
R.F. Runova; 2ii054, 3ii117
O.V. Rybakova; 4iv053
P.F. Rymyantsev; 1i037

S
S. Sahu; 3v009
A. Saini; 1i051
E. Sakai; 2ii002, 2ii017, 2ii022, 3ii088, 3ii107
S.V. Samchenko; 1i014
G. Samuel, 4iv047
M.A. Sanitsky; 3iii025
R. Sanjaasuren; 1i037
S. Sano; 3iii005
S.L. Sarkar; 3ii090
L. Sas; 1i048
A.E. Savva; 4iv052
D. Sawaki; 3iii001
Z. Sawicz; 4iv018
B.E. Scheetz; 3ii111, 3iii024
M. Schieber; 3v022
P. Schiessl; 3ii105, 4iv016
M. Schmidt; 3ii087, 4iv038
C. R. Schweizer; 4iv076
K.L. Scrivener; 2ii026, 4iv025, 4iv061, 4iv084
H. Sedaira; 3v012
U. Sedmalis; 1i035, 2ii009
Y.P. Sehti; 1i019
K. Seki; 3iii009
Ž. Sekulić; 3iii028
M.M. Seleim; 3v012
E.J. Sellevold; 2ii069
V. Serbin; 2ii023
V.N. Serdyuk; 3iii021
R. Sersale; 4iv017
N.N. Shangina; 2ii016
S.V. Shapet'ko; 2ii033
K.M. Sharma; 1i053, 3ii094
P.S. Sharma; 3ii094
S.C. Sharma; 4iv057
M.A. Shater; 3ii124
Y.N. Sheen; 2ii035
A.L. Shein; 1i015

N. Sherman; 2ii029
V. Shevchenko; 2ii019
C. Shi; 3ii099, 4iv042
H. Shi; 1i012
L. Shi; 2ii031
Y. Shigetomi; 2ii040
H. Shima; 1i025
G.-Y. Shin; 4iv068
S.M. Shingote; 1i003
M. Shmelkov; 3ii080
M. Shoya; 3ii109, 3ii119
D. Shtakelberg; 3v004, 3v022
A.K. Shukla; 3ii115
K. Sideris; 2ii061, 4iv052
K.K. Sideris; 2ii061, 4iv052
M.R. Silsbee; 1i010, 3ii100, 3ii114, 3iii024, 3v020
N.B. Singh; 3ii115
Vinaya K. Singh; 1i016
Vipin K. Singh; 1i016
S.K. Sinha; 4iv047
A.G. Sinyakin; 2ii021
S.P. Sivkov; 2ii020
E. Sjöstedt; 1i060
J. Skibsted; 2ii056
R.C.T. Slade; 3iii011
S. Smeplass; 4iv064
K.A. Snyder; 2ii078
J.-T. Song; 4iv055
V.P. Sopov; 2ii066
D. Sorrentino; 4iv049, 4iv065
F. Sorrentino; 2ii025
J. D. Sota; 2ii036
J. Stark; 1i005, 2ii010, 4iv031, 4iv034, 4iv035, 4iv062
M. Stefanović; 3iii028
J. Stegemann; 4iv042
E.T. Stepkowska; 3v019
A. Stok; 1i022
J. Strigáč; 3v009
C.A. Strydom; 2ii049
P.E. Stutzman; 2ii078
S. Stürmer; 4iv031
St. Stöber; 3iii032
M. Su; 2ii030, 3iii026, 4iv029, 4iv030
L.G. Sudakas; 2ii008
R. Suderman; 2ii011
S. Sugita; 2ii043, 3ii109, 3ii119
L.M. Sulimenko; 1i007, 1i040
U. Sulser; 3iii002
T. Suzuki; 2ii005
L.B. Svatovskaya; 2ii062
K. Svinning; 1i038
R.N. Swamy; 4iv080
L.I. Sychova; 1i032
J. Szczerba; 3iii023

T

A. Tagnit-Hamou; 2ii012
S. Takahashi; 3ii107, 3v013
T. Takahashi; 2ii070
H. Takemura; 2ii007
Y. Takuma; 3ii118
F. Tamás; 2ii060, 3v010, 4iv002
C.E.S. Tango; 3ii085
E. Tazawa; 2ii071
J.J. Thomas; 2ii058
D.W. Thompson; 3iii008
F. Tomosawa; 2ii051, 4iv072
E.E. Toumbakari; 4iv010
B. Touzo; 3v005
R. Trettin; 2ii050
J. Tritthart; 3v010, 4iv069
D. Trumeau; 3v005
B. Trybalska; 4iv027
Y. Tsuchida; 3ii118
Y. Tsukinaga; 3ii109, 3ii119
N. Tsuyuki; 3iii009

U

S. Uchida; 3ii118
H. Uchikawa; 2ii014, 3iii001
T.S. Um; 4iv054
W.S. Um,; 2ii044
H.P. Unsworth; 4iv012
A. V. Usherov-Marshak; 2ii021, 2ii066, 3v016
H. Ushiyama; 2ii040
J.I. Ustimenko; 3ii117

V

H. Vaishnav; 3ii092
G.L. Valenti; 2ii029
K. Van Balen; 4iv010
C. Van Den Brande; 4iv010
R.J. van Eijk; 2ii052
A. Van Gemert; 2ii069
D. Van Gemert; 2ii069, 3ii120, 4iv007,

4iv010
M. Van Messem; 4iv007
F. Van Rickstal; 3ii120
K. Vanbelle; 3ii120
P. Vanis; 2ii063
L.B. Vasiliyeva; 2ii008
T. Vázquez; 1i034, 3ii096, 3iii004, 3iii015
F. Verboven; 2ii069
A. Vichet; 3iii003, 3v014
J. Virlet; 3v003
K. Viswanathan; 2ii039
V. Voznesensky; 3v004

W
A. Walliser; 2ii075
J.F. Wang; 2ii038
P. Wang; 3iii006, 3iii016
X. Wang: 3iii016
Y. Wang; 4iv029, 4iv030
R.C. Wason; 4iv047
D. Watson; 4iv011
J. Widmer; 3iii002
W. Wieker; Plen2
U. Wiens; 4iv016
S. Wild, 4iv075
J. Wu; 3iii006
K. Wu; 3ii122
X. Wu; 4iv032

X
Y. Xi; 3ii111
A. Xu; 4iv077
J. Xu; 4iv030

Y
D. Yadav; 3ii094
S. B. Yadav; 1i003
T. Yamamoto; 3v015
Q. Yang; 4iv032
Q. Ye; 2ii042
K. Yoshida; 2ii070
J.F. Young; 3iii018
Q. Yu; 2ii043, 3ii109, 3ii119
G.-C. Yum; 1i036

Z
N.M. Zaitchenko; 2ii076
M. Zdaniewicz; 3iii023
D.Yu. Zelensky; 4iv039
F. Zenone; 4iv017
R. L. Zerbino; 2ii036
F. Zhang; 4iv030
H. Zhang; 1i026
L. Zhang; 3iii026, 4iv029
X. Zhang; 3ii122
H. Zhuo; 1i028
B. Živanović; 3iii028, 4iv020
B.M. Živanović; 1i017
S.A. Zoubekhine; 3iii021, 4iv036

KEY-WORD INDEX

A

Accelerated test; 3iii033
Accelerators; 3ii103, 3iii005, 3iii012, 3iii014, 3iii022, 3iii027, 3iii032,
Acid attack; 3ii109, 4iv002, 4iv021, 4iv038, 4iv039, 4iv040
Activation; 1i006, 2ii016, 2ii045, 2ii062, 2ii076, 3ii083, 3ii092, 3ii094, 3ii098, 3ii099, 3ii100, 3ii103, 3ii104, 3ii113, 3ii114, 3iii028, 4iv047
Activation energy; 1i053
Activity coefficient; 4iv083
Additives; 1i009, 1i020, 1i035, 2ii003, 2ii009, 2ii045, 2ii074, 3ii116, 3iii017, 3iii032
Adiabatic temperature rise; 4iv072
Admixtures; 2ii012, 2ii034, 2ii036, 2ii047, 3ii087, 3ii095, 3ii097, 3iii001, 3iii002, 3iii004, 3iii009, 3iii018, 3iii019, 3iii023, 3iii024, 3iii025, 3iii026, 3iii029, 3iii030, 3iii031, 3v015, 4iv004
Adsorption; 2ii001, 3iii002, 4iv077
AFm phase; 2ii032, 3iii032, 3ii089, 4iv034, 4iv061
AFt phase; 1i060, 4iv034, 4iv041, 4iv059
Aggregate; 2ii015, 3v024, 4iv053, 4iv057
Air entraining; 4iv031, 4iv057
Air pollution; 4iv002
Alinite; 2ii030, 3ii118
Alite; 1i006, 1i015, 1i041, 1i050, 2ii040, 2ii042, 2ii056, 3ii107, 3ii117, 3iii005, 3iii031
Alkali; 1i002, 1i012, 1i028, 1i035, 1i049, 2ii012, 2ii065, 3ii083, 3ii098, 3ii100, 3ii103, 3ii113, 3ii114, 3ii117, 3iii025, 4iv003, 4iv028, 4iv055, 4iv066
Alkali aggregate reaction; 3iii033, 3v022, 4iv048
Alkali silica reaction; 4iv047, 4iv049, 4iv065, 4iv074
Alkali silicate solutions; 4iv049, 4iv065
Alkaline cement; 4iv046
Alumina; 2ii027, 2ii026, 3iii010
Aluminate phase; 1i001, 1i022, 1i051, 1i056, 2ii041, 2ii060, 3iii010, 3iii015, 4iv027, 4iv034, 4iv066
Aluminoferrite; 1i004, 1i005, 1i055, 2ii031
Aluminosilicate; 1i024, 4iv046
Anhydrite; 1i032, 2ii011, 2ii022, 2ii029, 3ii092, 4iv059
Aragonite; 1i042
Arc furnace dust; 4iv042
Asbestos; 1i027
Ash; 3ii080
Autoclavation; 3ii120, 4iv054
Autoclave soundness; 1i023
Autogeneous shrinkage; 2ii069, 2ii070, 2ii071, 2ii073

B

Backscattered electron image; 2ii014, 4iv061
Bacterial attack; 4iv038, 4iv039
Bamboo dust; 1i019

Barite; 1i036
Barium phases; 1i058
Belite; 1i006, 1i015, 1i018, 1i041, 1i052, 2ii007, 2ii040, 2ii045, 2ii056, 3v009
Belite cement; 1i036
Binder; 1i059, 2ii047, 2ii054, 3ii080, 3ii101, 3iii021, 4iv057
Blastfurnace slag; 2ii068, 2ii074, 3ii082, 3ii093, 3ii095, 3ii096, 3ii098, 3ii099, 3ii101, 3ii102, 3ii103, 3ii104, 3ii115, 3ii122, 3iii009, 3iii017, 4iv001, 4iv005, 4iv009, 4iv015, 4iv035, 4iv040, 4iv063
Blended cement; 1i020, 3ii089, 3ii091, 3ii111, 3ii114, 3ii115, 3ii121, 3v026, 4iv004, 4iv017, 4iv020, 4iv052,
Bogue calculation; 1i039, 3v007, 3v009
Borax; 1i036
Bottom ash; 3ii090
Bound water; 2ii072, 3iii019, 3v019
Brick; 3ii080
Brownmillerite; 1i022, 2ii029, 2ii032,
Burnability of raw mixes; 1i021, 1i030, 1i031, 1i034, 1i040, 1i041, 1i045, 1i048, 1i054
Burning conditions of clinker; 1i018, 1i023

C
Calcium carbonate; 1i042
Calcium aluminate; 2ii022, 2ii025, 2ii050, 3iii022, 3v005
Calcium aluminate cement; 2ii024, 2ii026, 2ii027, 2ii028, 3iii007, 3v018, 4iv003, 4iv025, 4iv026
Calcium aluminate sulphate; 2ii010, 4iv068
Calcium aluminozincates, 1i059
Calcium hydroxide; 2ii049, 2ii059, 3ii082, 3ii106, 3ii107, 3ii108, 3ii112, 3iii031, 3v019, 4iv067
Calcium fluoride; 1i032, 2ii042
Calcium langbeinite; 2ii011
Calcium nitrate; 3iii012
Calcium phosphate; 1i036
Calcium phosphate cement; 2ii063
Calcium silicate; 1i035, 1i055, 2ii055, 2ii050, 2ii062, 4iv054
Calcium sulphate; 1i012
Calorimetry; 2ii021, 2ii025, 2ii041, 2ii066, 3iii032, 3v016, 3v017, 4iv042
Capillary; 2ii048
Carbon dioxide; 1i024, 2ii032, 4iv010
Carbonation; 2ii073, 4iv003, 4iv004, 4iv005, 4iv006, 4iv010, 4iv017, 4iv026, 4iv035, 4iv048, 4iv070, 4iv084
Case studies; 4iv002
Cement; 3ii092
Cement hydration equation; 2ii061, 4iv052
Characterization; 1i008, 2ii062, 3ii088, 3v011, 3v020 3v023, 3v026, 4iv019
Chemical analyis; 3v012
Chemical attack; 4iv015, 4iv026, 4iv028, 4iv031
Chemical prestressing; 3iii016

Chemical shrinkage; 2ii069, 2ii070, 2ii072
Chloride; 1i002, 1i012, 2ii030, 3ii118, 4iv006, 4iv015, 4iv027, 4iv078, 4iv080, 4iv081, 4iv082, 4iv083
Chloride Binding; 4iv016, 4iv069, 4iv070, 4iv078
Classification; 4iv046
Clay; 2ii020
Clinker; 1i048, 1i058
Clinker composition; 1i028, 4iv036
Clinker formation; 1i004, 1i006, 1i008, 1i010, 1i011, 1i026, 1i031, 1i037, 1i043, 1i044, 1i046, 1i049, 1i054, 2ii006, 3ii118
Cluster; 1i003
Coal; 1i047, 3ii090
Composite cements; 1i009, 2ii016, 2ii034, 3ii122
Composition; 2ii007, 2ii071, 3v004, 3v011, 3v026, 4iv007, 4iv023, 4iv060
Concrete; 2ii035, 3ii108, 3iii024, 3iii029, 3v021, 3v022, 4iv025, 4iv035, 4iv073
Cooling of clinker; 3v005
Corrosion; 2ii006, 4iv014, 4iv020, 4iv023, 4iv027, 4iv028, 4iv030, 4iv038, 4iv039, 4iv071, 4iv082, 4iv084
Creep; 4iv018
Cross-linking; 3iii011
Crystal; 2ii015
Crystal size; 1i051, 3iii031
Crystal structure; 1i055, 2ii048
Crystallisation pressure; 4iv049
Crystallography; 2ii054
CSH; 2ii044, 2ii047, 2ii053, 2ii055, 2ii059, 2ii064, 2ii067, 2ii068, 3ii082, 3ii093, 3ii121, 3v001, 3v003, 4iv016, 4iv041, 4iv043, 4iv061, 4iv074, 4iv076
Curing; 2ii037, 2ii078, 3ii091, 4iv055, 4iv059, 4iv067

D

Deformation; 4iv021, 4iv058
Degree of hydration; 2ii051, 2ii053, 2ii062, 2ii077, 3v019, 4iv016
De-icing salts; 4iv006, 4iv035
Delayed ettringite formation; 4iv059, 4iv061, 4iv062, 4iv063, 4iv064
Delayed expansion; 3iii016
Design life; 4iv071
Dicalcium silicate; 1i017, 1i053
Differential thermal analysis; 2ii041, 4iv031
Diffusion; 2ii046, 3ii084, 3ii098, 4iv010, 4iv015, 4iv016, 4iv056, 4iv080, 4iv081
Diffusivity; 4iv008, 4iv009
Dilation; 4iv033
Dispersion; 2ii005
Disposal; 1i027
Dopant; 1i053
Drying; 3iii018, 3v018, 4iv011, 4iv077, 4iv079
Durability; 2ii011, 3ii095, 3iii024, 3v022, 4iv004, 4iv007, 4iv022, 4iv023, 4iv026, 4iv029, 4iv030, 4iv037, 4iv040, 4iv046, 4iv048, 4iv062, 4iv065, 4iv070, 4iv075, 4iv082

E
Economy; 1i036, 3ii114
Ecology; 1i043
Electron microscopy; 1i060
Electron spectroscopy for chemical analyses (ESCA); 2ii044
Electrical conductivity; 4iv011
Electrical impedance; 3ii112
Electrical properties; 4iv079
Electrical resistivity; 3v021
Energy; 2ii046
Environment; 1i003, 3ii093
Equilibria; 2ii057, 2ii058
Ettringite; 1i025, 2ii006, 2ii010, 2ii017, 2ii029, 2ii031 2ii056, 2ii070, 2ii074, 3iii022, 4iv012, 4iv018, 4iv031, 4iv060, 4iv062, 4iv065
Evaporable water; 3v019
Expansion; 2ii006, 2ii074, 3iii017, 3v022, 4iv057, 4iv060, 4iv062, 4iv064
Expansive cement; 1i001, 2ii010
Extraction methods; 3v020

F
False set; 3iii013
Ferrite phase; 1i008, 1i015, 1i060, 3iii005, 3v003
Ferroaluminate; 4iv029
Filler; 1i020, 2ii002, 2ii020, 3ii081, 4iv056
Fineness; 1i007, 2ii001, 2ii002, 2ii018, 2ii043, 2ii060, 3ii088, 3v008, 4iv060
Fingerprinting; 3v010, 3v011
Fire; 4iv073
Fire damage; 4iv067
Flow; 2ii017, 3v024
Flue gas desuphurisation product; 3ii090
Fluidity; 2ii001, 2ii002, 2ii012
Fluoride phases; 2ii043, 3v002
Fly ash; 3ii081, 3ii082, 3ii083, 3ii084, 3ii085, 3ii086, 3ii087, 3ii088, 3ii089, 3ii090, 3ii110, 3ii115, 3ii116, 3ii122, 3v006, 3v020, 3v021, 4iv004, 4iv009, 4iv012, 4iv019, 4iv020, 4iv023, 4iv058, 4iv077
Fracture mechanics; 2ii075
Free lime; 1i016, 1i045, 2ii049, 4iv036
Freeze-thaw damage; 2ii016, 3iii019, 4iv034, 4iv035
Freezing; 4iv033
Friedel's salt; 4iv027, 4iv080
Fuels for clinker making; 1i013, 1i019

G
Gel; 3ii105, 3iii007, 3iii022, 4iv074
Glass; 1i046, 1i051, 3ii088, 3ii119, 4iv030, 4iv055
Grinding aids; 2ii020, 3v014
Grinding technology; 1i009, 1i040

Ground silica; 3ii120
Grout; 2ii005
Gypsum; 2ii040, 2ii044, 2ii060, 3ii093, 3ii115, 3iii025, 3v008, 3v023, 4iv017

H
Hardening; 2ii008, 2ii034, 2ii039, 2ii047, 2ii052, 2ii054, 2ii076, 3ii112, 3v016, 4iv071
Heat capacity; 4iv033
Heat evolution; 2ii021, 2ii035, 2ii051, 2ii076, 2ii077, 3ii102, 3ii105, 3iii029, 3v016, 4iv042, 4iv072
Heavy metals; 1i043, 2ii014, 3v010, 3v013, 4iv041, 4iv043
High alumina cement; 2ii023, 2ii033, 3iii010, 3ii096, 4iv013, 4iv027, 4iv038
High performance; 2ii035, 2ii038, 3ii108, 3v006, 3v021
High strength; 2ii037, 3ii120
High sulphate clinker; 2ii011
High temperature; 3ii111, 3iii020, 4iv067
Humidity; 4iv011, 4iv079
Hydration; 1i022, 1i057, 1i059, 2ii004, 2ii006, 2ii008, 2ii007, 2ii012, 2ii013, 2ii015, 2ii019, 2ii021, 2ii022, 2ii023, 2ii024, 2ii025, 2ii026, 2ii028, 2ii029, 2ii030, 2ii031, 2ii033, 2ii035, 2ii036, 2ii039, 2ii040, 2ii041, 2ii042, 2ii043, 2ii044, 2ii046, 2ii047, 2ii050, 2ii052, 2ii055, 2ii057, 2ii058, 2ii061, 2ii067, 2ii069, 2ii070, 2ii078, 3ii089, 3ii094, 3ii097, 3ii099, 3ii100, 3ii101, 3ii102, 3ii107, 3ii116, 3ii118, 3ii119, 3iii008, 3iii014, 3iii015, 3iii019, 3iii025, 3v006, 3v016, 3v018, 4iv072, 4iv071
Hydrothermal synthesis; 1i017

I
Identification; 3v010
Image analysis; 4iv084
Immobilization; 2ii014, 2ii016, 2ii052, 4iv043, 4iv045
impact prediction; 1i003
Impact evaluation; 1i003
Induction period; 2ii019, 2ii055
Infra red absorption spectra; 3ii104
Inhibitor; 3iii033
Interfacial zone; 4iv050, 4iv051, 4iv053, 4iv056, 4iv084
Interground cements; 1i013, 3v026
Interstitials; 2ii007
Ion exchange resin; 4iv045
Ionic assocoiation, 4iv083
Ions; 2ii036, 2ii046, 2ii065, 3iii012, 3iii013, 4iv075, 4iv079
Iron mud; 1i021
Isomorphism; 1i059

K
Kinetics; 1i005, 1i035, 1i044, 1i052, 2ii019, 2ii023, 2ii028, 2ii043, 2ii055, 3ii098, 3iii008, 4iv076

L
Latex; 3iii008
Leaching; 2ii014, 4iv012, 4iv041, 4iv043, 4iv045
Light microscopy; 3iii031, 3v007
Lignosulphonates; 2ii004, 3iii013, 3iii021
Lime; 2ii049, 2ii074, 3ii084, 3iii005, 4iv010
Limestone; 1i047, 1i048, 2ii022, 4iv018
Long age; 2ii016, 4iv050
Low energy; 1i034, 2ii045
Low temperature; 1i018, 1i029, 1i037, 2ii009, 2ii013, 2ii038, 3iii014, 3v017
Lumos; 2ii079

M
Magnesium chloride; 4iv022
Magnesium sulphate; 4iv022
Magnesium oxide; 1i023, 2ii064, 3v012
Magnesium phases; 1i057
Mass spectroscopy; 3v014
Maturity; 3ii111
Macro Defect Free; 3iii010, 3iii011, 4iv013
Mechanical properties; 3v025
Mechanism; 1i046, 2ii025, 2ii026, 2ii035, 2ii050, 2ii057, 2ii058, 3ii100, 3iii003, 3iii006, 3iii012, 3iii025,, 3v014, 4iv074
Melt; 1i008, 1i011, 1i012, 1i014, 1i029, 1i046, 3v005
Mercury Intrusion Porosimetry; 3ii104
Metakaolin; 3ii113, 3ii114, 4iv011
Method; 2ii021, 3v011, 3v013, 3v016, 3v018, 3v022, 3v023, 4iv081
Microcrack; 4iv021
Microgravity; 2ii075
Microscopy; 1i029, 1i030, 1i039, 1i051, 1i052
Microstructure 1i038, 1i039, 1i047, 1i049, 1i052, 2ii008, 2ii014, 2ii018, 2ii037, 2ii064, 2ii075, 3ii091, 3ii095, 3ii096, 3ii099, 3iii014, 4iv005, 4iv015, 4iv025, 4iv037, 4iv047, 4iv050, 4iv051, 4iv053, 4iv055, 4iv068, 4iv084
Mineralisers in clinker making; 1i028, 1i030, 1i031, 1i033, 1i034, 1i037, 1i050, 3v002
Mineralogy; 1i046, 3ii087, 3ii105
Mineral phase; 1i015, 2ii009, 2ii015, 4iv028
Mixing procedure; 3ii120
Mobility; 2ii065, 4iv083
Modelling; 1i038, 1i044, 1i045, 2ii048, 2ii052, 2ii078, 3ii085, 3ii084, 3iii013, 3v004, 4iv005, 4iv070, 4iv071, 4iv073, 4iv078
Modified cement; 2ii004, 2ii020, 3ii085, 3ii097, 3ii104, 3iii021, 3iii023
Moisture; 2ii079, 3iii011,3v004, 4iv010, 4iv013, 4iv062
Molybdic compounds; 1i054, 1i055
Monosulphate; 2ii056
Mortar; 4iv033

N
Naphtalene Formaldehyde Sulphonate; 3iii003, 3iii009, 3iii030
Nitrate attack; 4iv002
Nodulization in clinker formation; 1i007
Non-equilibrium burning; 1i011
Nuclear Magnetic Resonance; 1i024, 2ii028, 2ii056, 2ii067, 2ii068, 3iii007, 3v001, 3v002, 3v003, 3v004, 3v005, 3v006

O
Oilwell cement; 2ii013, 3iii014
Organic; 3v015
Osmotic pressure; 4iv049

P
Packsetting; 2ii079
Particle size distribution; 1i009, 2ii018, 2ii053, 3ii110, 3v024
Pattern recognitin; 3v010
Penetration; 2ii005, 2ii038, 3ii109, 4iv080
Performance; 4iv073
Permeability; 4iv008, 4iv075
Petroleum coke; 3ii090
pH; 4iv065
Phase composition; 3ii091
Phase diagram; 1i050, 1i052, 2ii024, 2ii057, 2ii058, 4iv066, 4iv074,
Phase transition; 4iv033
Phase transformation; 4iv034
Phosphate; 4iv057
Physical properties; 3v025
Plasticizers; 2ii020
Polymer; 3iii008, 3iii009, 3iii010, 3iii027, 4iv013
Polymorphs; 1i053
Pore size distribution; 4iv077
Pore solution; 2ii036, 3iii003, 3iii013, 3iii022, 3ii091, 4iv040, 4iv069
Pore structure; 2ii037, 2ii066, 3ii111, 3iii009, 3iii018, 3v017, 4iv001, 4iv005, 4iv080
Porosity; 2ii036, 2ii048, 2ii066, 2ii072, 3ii085, 3ii119, 3iii023, 3v017, 4iv006, 4iv007, 4iv008, 4iv013, 4iv017, 4iv024, 4iv040, 4iv048, 4iv054, 4iv078
Portland cement; 3ii107, 3iii006, 3v025, 4iv012
Potentiometry; 4iv083
Powder; 2ii002
Pozzolana; 1i020, 2ii073, 2ii077, 3ii106, 3ii107, 3ii108, 3ii112, 3ii115, 3ii117, 3ii123, 3ii124, 3v001
Pozzolanic cement; 4iv036
Pozzolanic reaction; 3v006
Pozzolanic reactivity; 3ii088
Pre-calciners for clinker making; 1i028
Prehydration; 2ii079
Process parametres; 1i047

Q
Qualitative; 1i004, 3v010, 3v011, 3v015
Quantitative; 1i039, 1i056, 3v007, 3v012, 3v013, 3v015, 3v020
Quartz; 1i048

R
Rapid hardening cement; 2ii017
Rate equations; 1i044
Reaction products; 4iv049
Reactivity; 1i016, 1i018, 1i047, 1i060, 2ii049, 2ii050, 3ii082, 3ii109, 3ii110, 3v020, 4iv016, 4iv050
Refractory; 2ii027, 4iv053, 4iv057
Relative humidity; 2ii073
Residual silica; 4iv049
Retarders; 3iii007, 3iii020, 3iii032
Rheology; 2ii003, 2ii004, 2ii011, 3iii003, 3iii027
Rice husk; 1i019
Rice Husk Ash; 3ii108, 3ii109, 3ii110
Rietveld analysis; 1i039, 1i056, 3v007
Roller compaction; 3ii086
Rotary kiln; 1i007, 1i019

S
Salt scaling; 4iv001
Scanning Electron Microscopy; 1i002, 2ii078, 3ii083, 3ii120, 3iii008, 3v019, 4iv037, 4iv064
Sea water; 4iv025
Secondary ettringite formation; 4iv065
Self deccication; 2ii073
Setting; 1i038, 2ii019, 2ii039, 2ii053, 2ii063, 3ii101, 3ii112, 3iii006, 3iii012, 3iii023, 3iii026, 3v008
Sewage; 3ii123, 3ii124, 4iv038, 4iv039
Shotcreting; 3iii027
Shrinkage; 1i032, 3iii018, 4iv036, 4iv056
Silica; 3ii080
Silica colloid; 3ii106
Silica fume; 2ii037, 3ii105, 3ii106, 3ii110, 3ii116, 3ii120, 3v001, 4iv014, 4iv069
Silica modulus; 1i035
Silicate; 2ii060, 3iii027, 4iv065
Simulation; 2ii078, 3iii001
Sintering; 1i005, 1i007, 1i022, 1i032
Slag; 1i020, 3ii080, 3ii092, 3ii094, 3ii097, 3ii100, 4iv050, 4iv051, 4iv058
Slump loss; 3iii003, 3iii020
Sodium chloride; 4iv022
Solid solution; 1i014, 1i023, 1i057, 2ii059, 1i060, 3v009
Solid state reactions; 1i042
Solidification; 4iv042
soluble glass; 2ii033

Sorption isotherms; 4iv077
Specific surface; 3iii028
Spectrophotometry; 3v012
Stability; 4iv065
Stabilization; 1i016, 2ii045, 4iv041
Standards; 3v025
Steam curing; 3ii102, 4iv036, 4iv063
Steel; 4iv014, 4iv082
Steric repulsive force; 3iii001
Strain softening; 2ii075
Strength; 1i048, 1i058, 3ii109, 4iv057
Strength development; 1i029, 1i038, 1i041, 2ii007, 2ii017, 2ii018, 2ii033, 2ii051, 2ii053, 2ii054, 2ii060, 2ii063, 2ii072, 2ii076, 2ii077, 3ii085, 3ii089, 3ii097, 3ii111, 3ii117, 3ii119, 3ii121, 3iii004, 3iii026, 3iii028, 3iii029, 3v024, 4iv024, 4iv052, 4iv054, 4iv055, 4iv056, 4iv058, 4iv063
Strength retrogression; 4iv019
Stress; 4iv049
Structure; 1i005, 1i014, 1i056, 2ii054, 2ii066, 2ii067, 2ii068, 2ii069, 2ii076, 4iv007, 4iv025, 4iv042, 4iv043, 4iv075
Sucrose; 3iii006
Sulphate; 1i049, 2ii012
Sulphate attack; 4iv002, 4iv018, 4iv020, 4iv021, 4iv024, 4iv057, 4iv059
Sulphate resistance; 3iii004, 3iii015, 4iv017, 4iv019, 4iv023
Sulphoaluminate; 1i001, 1i025, 2ii029, 3iii026, 3v009, 4iv029, 4iv030, 4iv068
Sulphoaluminoferrite; 1i014
Superplasticizers; 2ii002, 2ii004, 3iii001, 3iii002, 3iii019, 3iii020, 3iii021, 3iii030, 4iv001
Support; 2ii015
Synthesis; 1i015, 1i024, 1i033, 2ii064, 3ii113

T
Temperature; 1i005, 1i007, 1i008, 1i012, 2ii021, 2ii023, 2ii026, 2ii043, 2ii066, 3iii002, 3iii029, 3v001, 4iv047, 4iv060, 4iv068, 4iv069
Terminology; 4iv046
Texture; 1i048
Thawing; 4iv033
Thermal stress; 4iv072
Thermal treatment; 1i027
Thermodynamics; 1i042, 2ii024, 2ii057, 2ii058, 2ii059, 2ii062, 2ii066, 4iv039, 4iv066
Thermogravimetry; 2ii049, 3ii105, 3iii011 4iv003, 4iv037
Thermoporosimetry; 3v017
Tobermorite; 2ii064, 2ii065, 3v003
Trace components; 1i021
Transmission Electron Microscopy; 2ii068
Tricalcium silicate; 1i049 2ii041, 2ii044

U
Unreacted core model; 2ii051

V
Vibration; 2ii017
Viscosity; 1i014, 1i032, 2ii001, 2ii003, 2ii005
Void spacing factor; 3v024
Volume change; 2ii009, 2ii039, 2ii071, 2ii072, 4iv031

W
Waste disposal; 4iv012
Waste material utilization; 1i010, 1i019, 1i022, 1i025, 1i026, 1i027, 1i033, 2ii052, 3ii081, 3ii093, 3ii101, 3ii116, 3ii118, 3ii119, 3ii121, 3ii123, 3ii124, 3v003, 3v013, 4iv014, 4iv024
Water; 4iv075
Water sorption; 4iv008
Water suction; 4iv008, 4iv011, 4iv078
Water-to-cement ratio; 2ii071
Waterglass; 3ii092
Wedge splitting; 2ii075
White Portland Cement; 3iii004
Workability; 2ii011, 3iii029

X
X-ray Diffraction Analysis; 1i051, 1i016, 2ii041, 3iii028, 3ii087, 3ii114, 3v008, 4iv003
X-ray Fluorescense Analysis; 3v011
X-ray Powder Diffraction; 1i002, 1i010, 1i056, 2ii065, 4iv018

Z
Zeolites; 1i020, 1i024, 4iv028, 4iv045, 4iv046
Zeta potential; 3iii001, 3iii002

COLOUR FIGURES

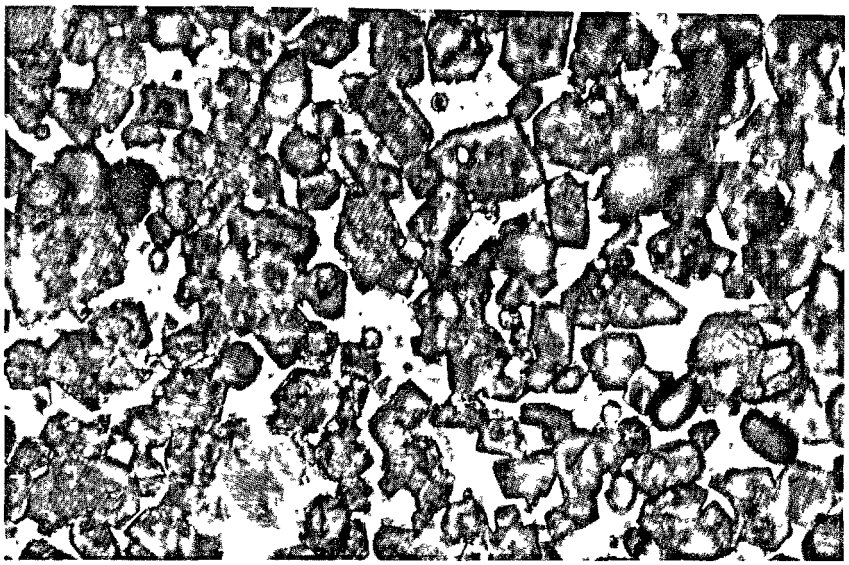

Fig. 4:
Idiomorphic Alite within grey aluminate rich ground mass
(Sample 11, LSF=102.9)
------ 20 µm

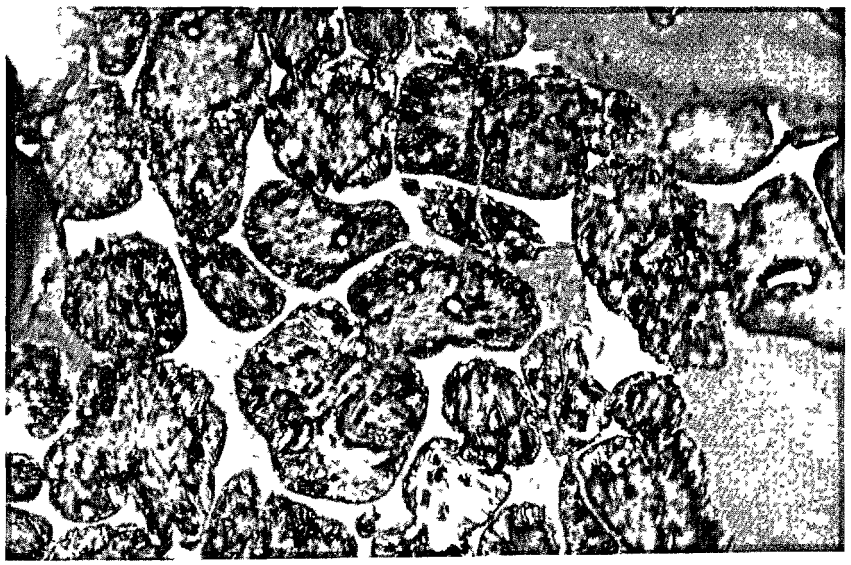

Fig. 5:
Rounded Belite in cluster
(Sample 11, LSF=102.9)
------- 10 µm

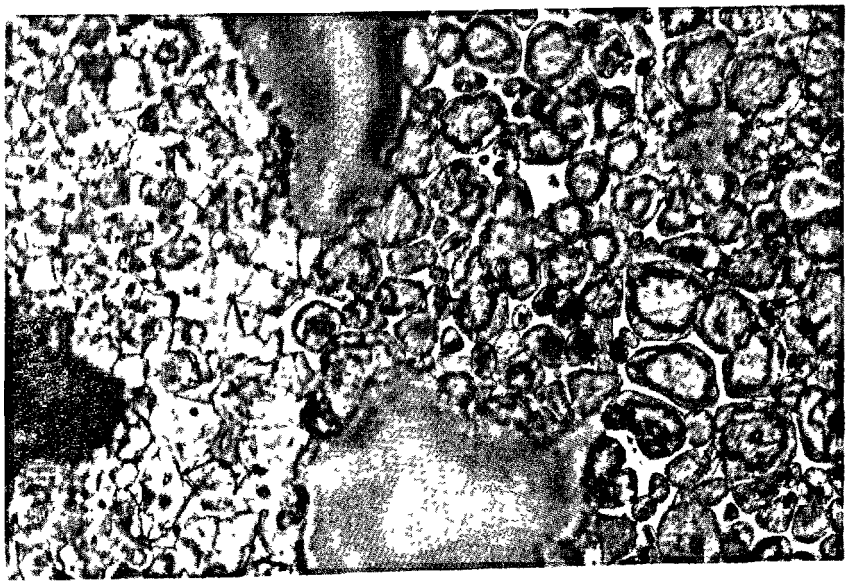

Fig 6:
Belite cluster (right part) and Alite (left part)
(Sample 10, LSF 101.9)
------ 20 µm

Figure 4

Back scattered electron image and distribution of element in hardened cement paste by adding various elements (W/C=0.5, 20°C, 14days)

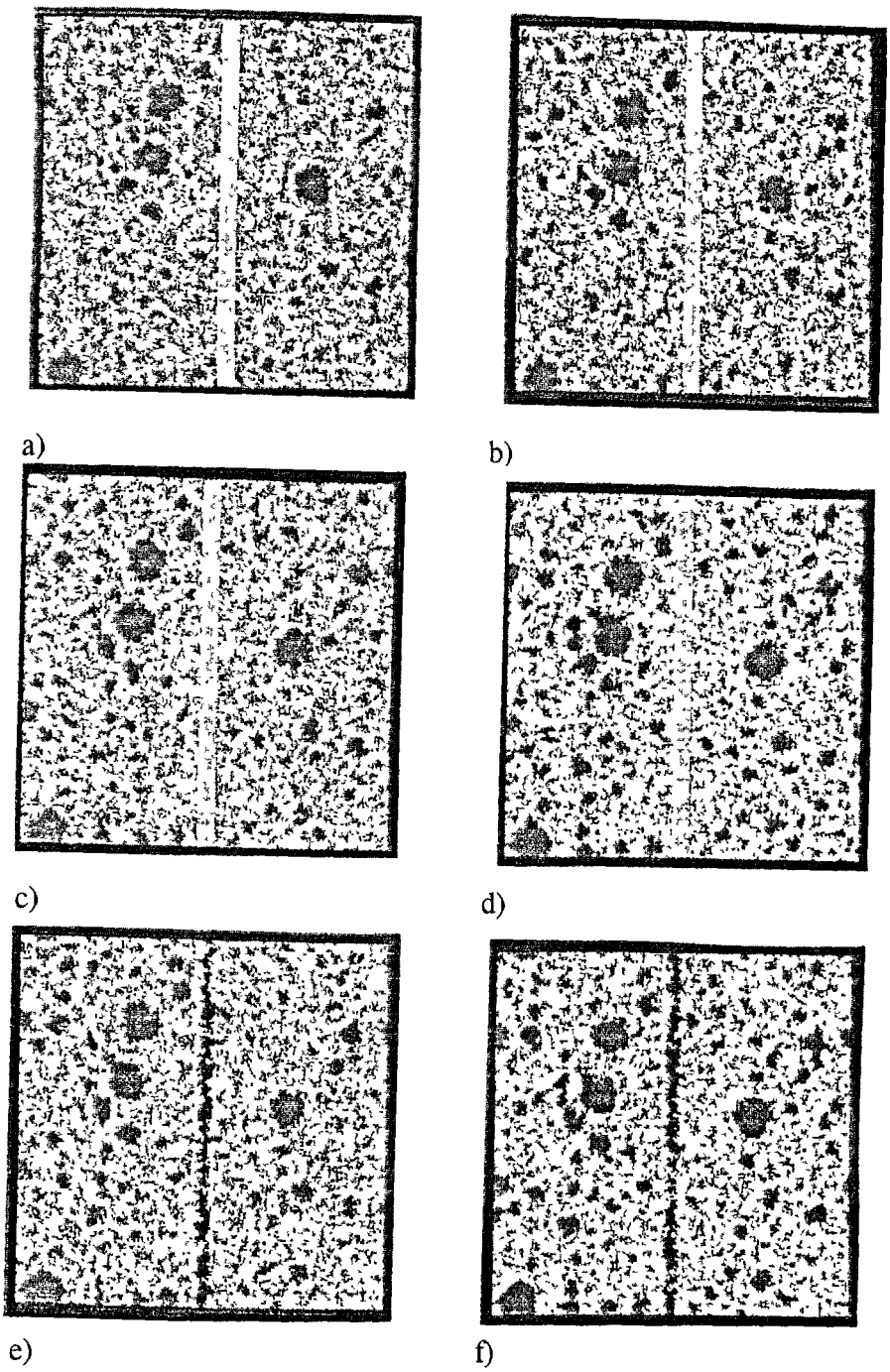

Figure 1 Final simulated microstructures (15 cycles) : (a) 0 % carbon, (b) 1 % carbon, (c) 3 % carbon, d) 7 % carbon, (e) carbon aggregate + 0% carbon, (f) carbon aggregate + 3 % carbon.
Black=Porosity, red=C_3S, yellow=CSH, cyan=CH, grey=Inert, blue= Carbon, white=Carbon Water.

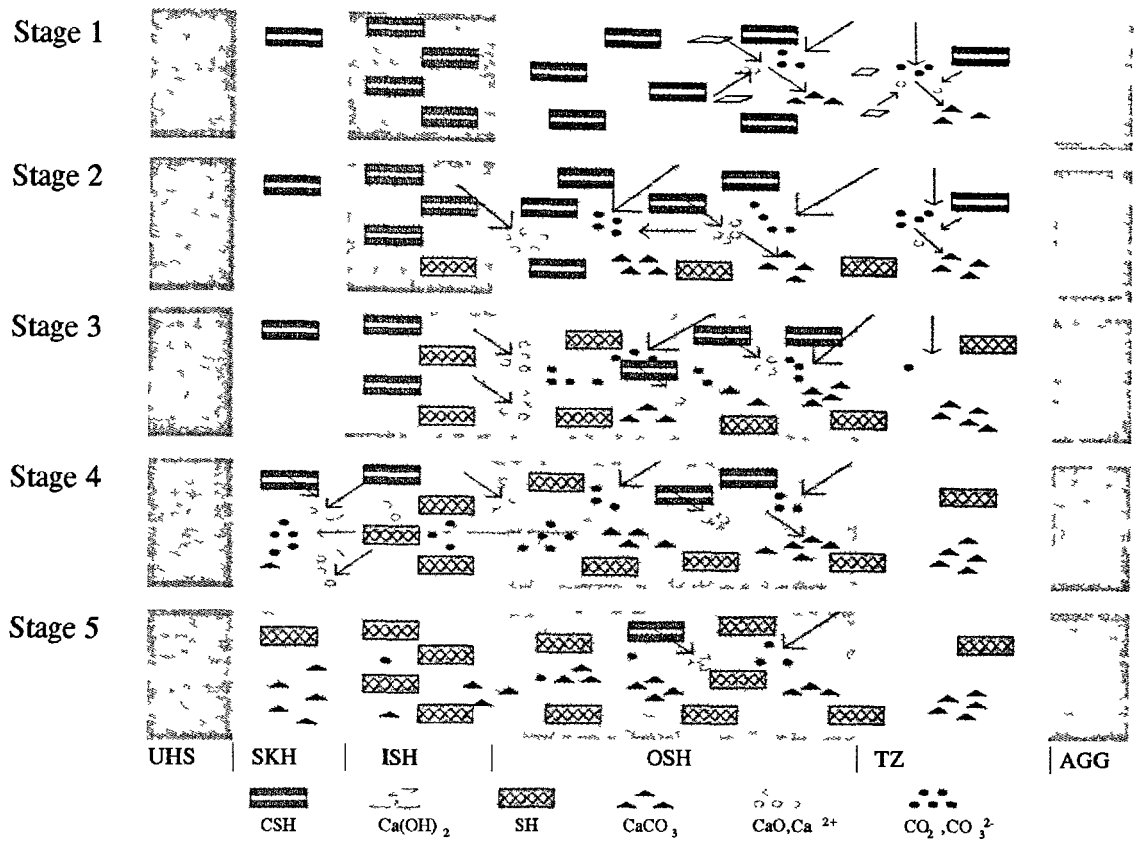

Figure 1 Schematic representation of the proposed carbonation model for GBFS concrete

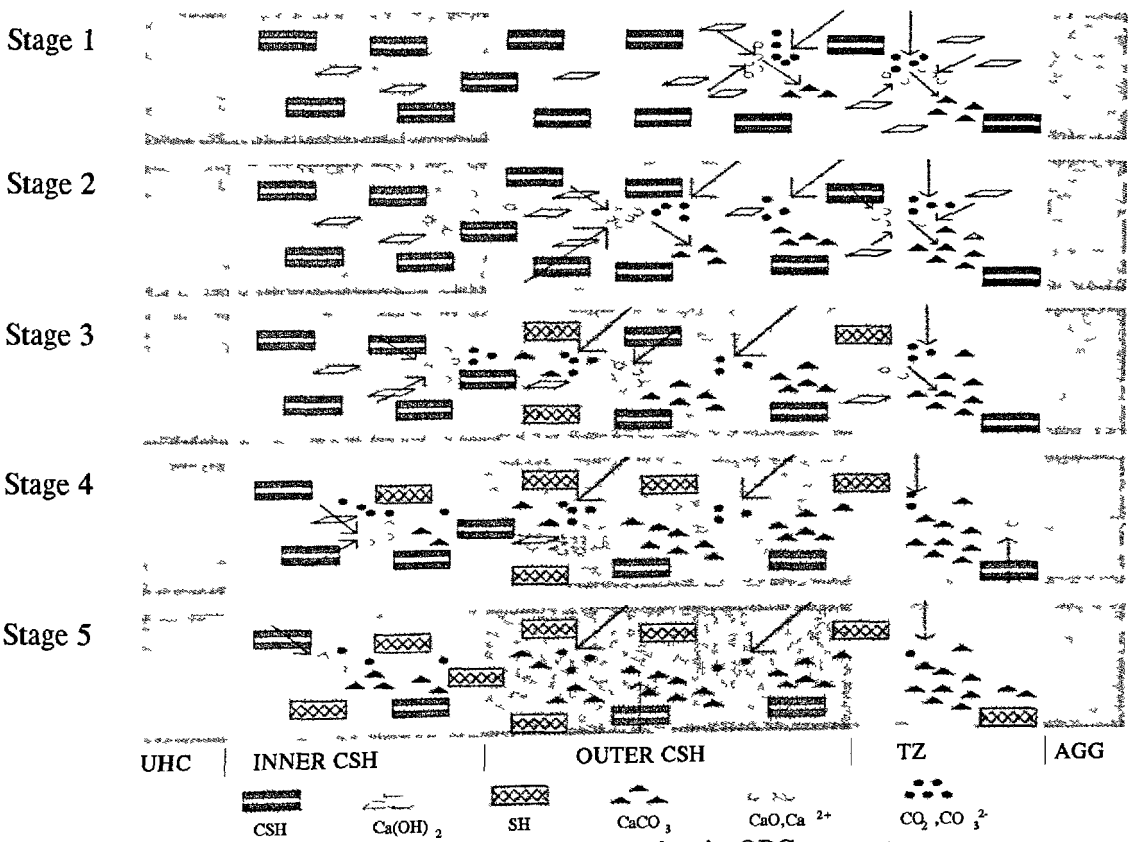

Figure 2 Schematically presented progress of carbonation in OPC concretes

S 424 -10.4-
Proceedings of the 10th International Congress on the Chemistry of Cement : Volume 4: Performance and durability of cementitious materials
<Hrsg.>: Justnes, Harald
Göteborg (1997)
Inventarnr. 50207

Entleiher	Ausleihdatum
~~Dr. Lichtmann~~	05. SEP. 1997
~~Dr. Spanka~~	
~~Dr. Schneider~~	
~~Pickett~~	~~23.10.00~~
~~Runge~~	~~29.01.10~~

Papers to be Presented,
but not Included in Proceedings

MICROSCOPY METHODS IN CEMENT AND CONCRETE SCIENCE

Karen L. SCRIVENER,
Lafarge, Laboratoire Central de Recherche, France

1. Why microscopy?

A rather simple answer to this question might be that cement is a microscopic material — a grey powder whose grains range from around 100μm down to less than 1μm in size. However, its end uses, in concrete, are anything but microscopic and include some of the largest manmade structures. The challenge is to link the microscopic to the macroscopic and here microscopy has a role to play.

The question of what we can hope to achieve by microscopic study has three broad responses :

1. Understanding reaction mechanisms
2. Diagnosis of damage processes
3. Microstructure—Property relationships

In all of these cases microscopy can only supply partial answers, which must be integrated with results from other techniques into a coherent conceptual or theoretical framework. In the first two cases, qualitative examination of the microstructure, perhaps combined with local chemical analysis, may be sufficient to indicate or confirm a mechanism.

The last of these three goals is perhaps the most difficult, as here, some kind of quantitative measure of the microstructure is necessary (Scrivener 1989a). Yet understanding the links between microstructure and properties is the essential precept of materials science, necessary if the development of cementitious materials is to be anything other than empirical. Obtaining numbers from images is the goal of image analysis.

1.1 Why this paper?

The international cement chemistry conferences bring together a wide range of people concerned with the manufacture and use of cement, not all of whom are directly involved in research, and an even fewer who are involved with microscopy on a day to day basis. Therefore I was asked to write something along the lines of a tutorial overview of the current use of microscopy for the study of cementitious materials. It does not aim to be a comprehensive account of the published literature, but rather a personal view of the state of the art. The emphasis is on the use of microscopical techniques, rather than the details of microstructural development (for this see for example Scrivener 1989b). I have tried as far as possible to make it comprehensible to the non-specialist. To put microscopic techniques in context, I felt it useful to bring together many things which are often considered to be 'old hat' and known by 'everyone'. To those of my colleagues who say there is nothing new here, I apologise, but hope that others will find it useful as an introduction to the subject. I have also tried to present some of the difficulties and drawbacks in microscopic study as well as the strengths.

1.2 Microscopy — usage and abusage

Most of us are familiar with the expression, *"the camera never lies"* and fully appreciate the simultaneous truth and irony behind those words. The position for microscopy is analogous — a micrograph is a truthful representation of one particular area of the sample under a particular set of preparation and observation conditions — whether it tells us anything of general value to understanding the original sample is another matter.. Many people have tried to estimate the *total* volume of material (cement and concrete), which have been looked at through a microscope. It is probably something less than 1 mm^3 by TEM, 10,000 mm^3 by SEM and several m^3 by optical microscopy, but none of these are very large in comparison with the amount of cement and concrete produced *annually* (around 2 billion m^3). Microscopy has to be selective and the extent to which it is representative depends on the skill (and luck) of the microscopist. The process of selection is made much more difficult by the highly heterogeneous nature of concrete, with features ranging over some ten orders of magnitude, from several hundreds of millimetres for aggregates to a few nanometers for the smallest pores.

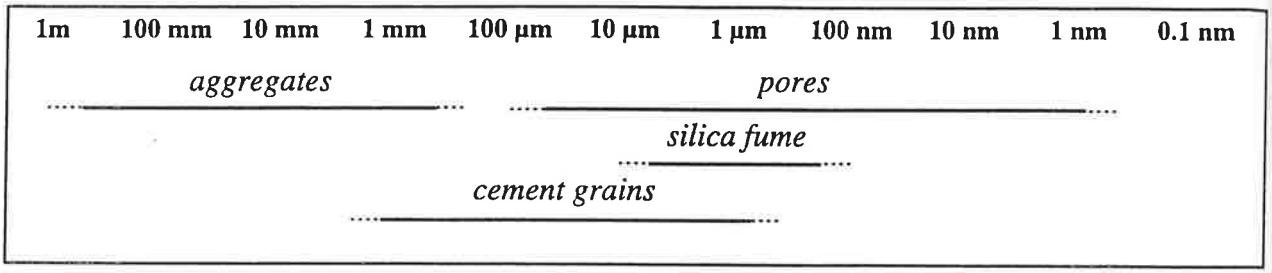

2. Types of microscopy

Figure 1 summarises the different microscopical techniques applied to the study of cement and concrete, before and after hydration.

2.1 Optical

Optical microscopy in both the transmission and reflection modes is widely used for the study of cementitious materials. A principal advantage of this technique is the wide spread availability of equipment, there are probably several hundred optical microscopes used for every electron microscope.

For the study of cement clinker the refection mode is the most common, with the use of suitable etchants (e.g. HF vapour) on polished sections, Figure 2. Generally the silicate phases, alite (impure C_3S) and belite (impure C_2S) are easily identifiable. The ferrite and aluminate phases may be individually identified in more coarsely crystalline interstitial material, found in slowly cooled clinkers, but at rapid cooling rates, these phases may be so finely divided that they are difficult to distinguish. The sulfates present in the clinker may also be seen, although these may be removed during the polishing or etching processes.

The spatial distribution of the phases can reveal much about the clinkering process, but further details are outside the scope of this overview, the interested reader is referred to Campbell (1986). Optical microscopy is very effective for the assessment of clinker and it is used for this purpose in many cement plants.

The relative proportions of the various phases within clinkers may be determined by point counting. A comparative study of optical microscopy, backscattered electron image analysis and x-ray diffraction, indicated that optical microscopy is still probably the most efficient method for this purpose, being more accurate and less time consuming than SEM image analysis

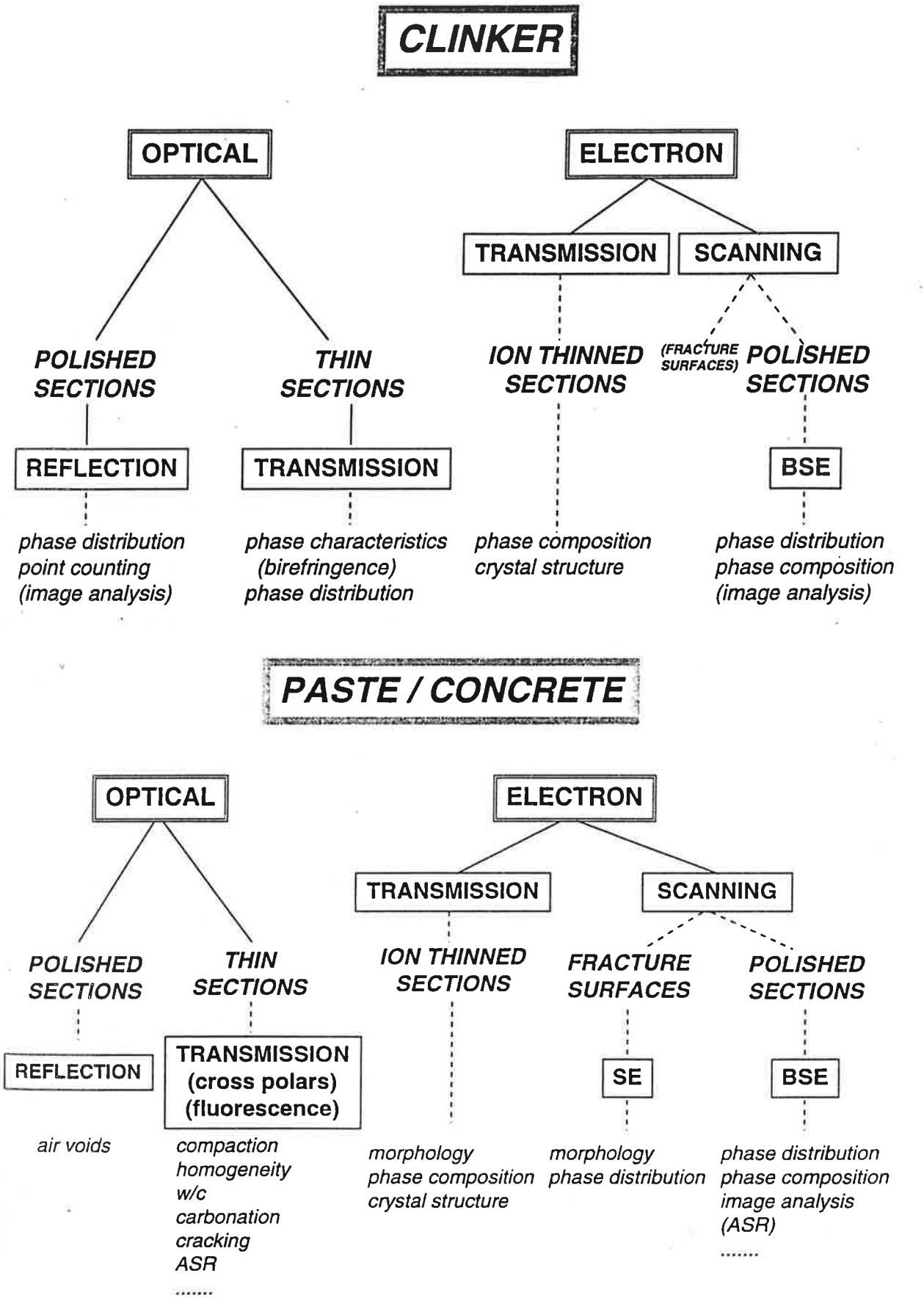

Figure 1. Summary of microscopical techniques and their application to cement before and after hydration

(Stutzman et al. 1989). The variability of the etching process makes this measurement difficult to automate, although progress is being made (e.g. Theisen 1997).

Transmission optical microscopy is also used for the study of anhydrous materials, although less extensively than reflection. The preparation and observation of thin sections permits other features, such as the birefingence of the phases to be determined. Such features can be related to kiln operating conditions according to the Ono method (Ono 1980)

Thin sections are more widely used for the study of hardened concrete, where this is the primary technique for quality assessment and diagnosis of deterioration (e.g. Thaulow and Jackobsen, 1997, Jackobsen et al. 1997). Here the main advantage of optical microscopy is the ability to study large areas. Nevertheless the preparation of thin sections covering a large area is a specialised technique. Sections 100 mm square or larger can be prepared, but a more usual size, would be around 35×45 mm. Even with larger specimen sizes, careful selection of the sections from the macroscopic sample is necessary, to account for possible heterogeneity. Another strength of the technique is that specimens do not need to be pre-dried, so that with careful preparation the crack pattern existing in the original concrete may be studied.

Two important techniques used in conjunction with transmission optical microscopy are cross polars and fluorescence. The use of cross polars, above and below the specimen, is a classic petrographic technique. Highly symmetric (cubic) crystals or amorphous phases are isotropic (have the same properties in all direction) and therefore do not change the direction of polarisation of light, and so appear dark. Other crystals in which the speed of light varies according to direction, may rotate the plane of polarisation and so transmit light through cross-polars. This phenomenon permits different phases to be identified. Examples of the use of this technique are : determination of the depth of carbonation, by the depletion of calcium hydroxide and/or presence of calcite ; identification of alkali-silica gel, formed by reaction of susceptible aggregates, which is non-crystalline and therefore isotropic.

A sample may also be impregnated with resin containing a fluorescent dye, which fluoresces, when viewed under a suitable light source. This technique can enable an estimation of the original water to cement ratio (w/c) of the paste or concrete to be made (e.g. Romer and Dobrolubov 1974, Thaulow et al. 1982, Mayfield 1990). Accurate results depend on the comparison of the unknown, with well prepared standards at known w/c ratios. As the fluorescent dye fades over time, these standards must be remade regularly, but an experienced user can obtain results to within 0.05 or less. This technique is widely used as a quality control measure in Denmark. For important structures, such as the bridge-tunnel links between islands the concrete may be cored at seven days, to ensure correct mixing and placing. This is particularly important in mixes using high quantities of superplasicizer, where there is an increased possibility of segregation.

Figure 3, gives some examples of images obtained by optical microscopy of thin sections (G.M.Idorn Consult 1997)

The main limitation of optical thin section microscopy is the resolution. This is limited more by the thickness of the section, some tens of microns, than the resolution of the microscope itself which is less than 1 μm. The other disadvantage of optical microscopy is that it is not possible to obtain information on the chemical composition of phases. However, it is important to reiterate the primary role of optical microscopy, especially for the diagnosis of deterioration, where damage must be assessed in a wider context. In general the use of electron microscopy should be as a adjunct to and not a replacement for optical microscopy.

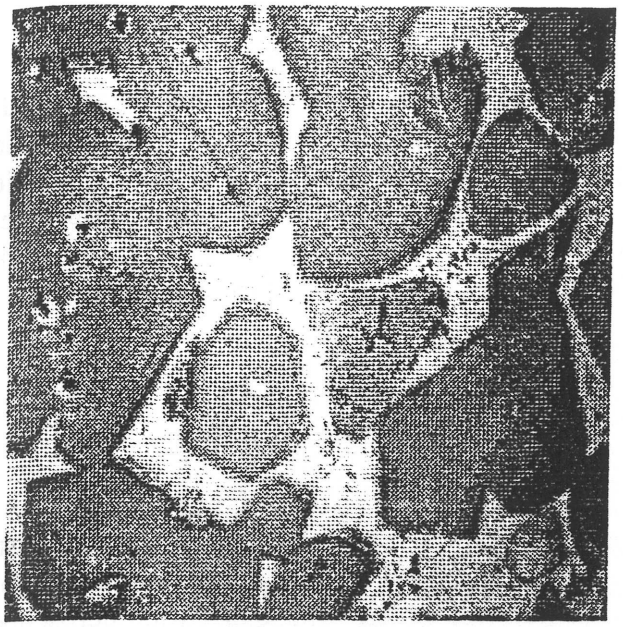

Clinker

Figure 2. (left), Polished section of clinker, etched with HF, alite brown, belite blue and interstitial phases white.

Figure 3. (below), Thin sections viewed by optical microscopy: fluorescence of low w/c paste; carbonated paste viewed through cross polars; aggregate craked due to ASR reaction; paste showing uniform expansion associated with delayed ettringite formation

(all images from GM.Idorn Consult web site)

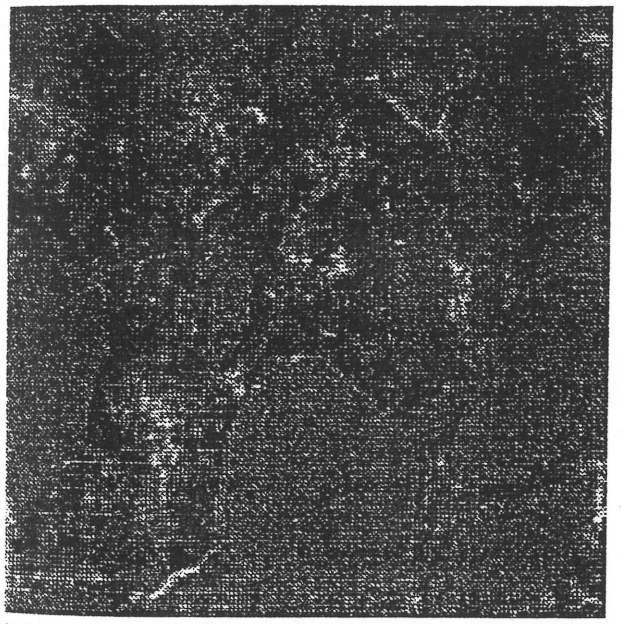

low W/C

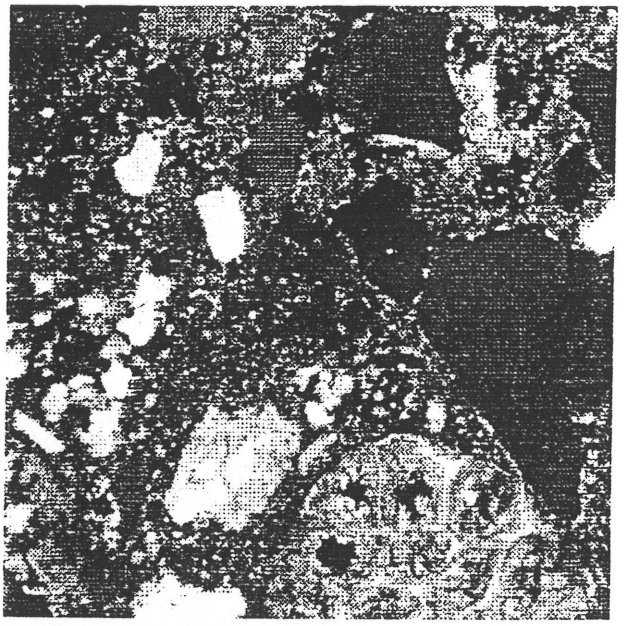

Carbonated

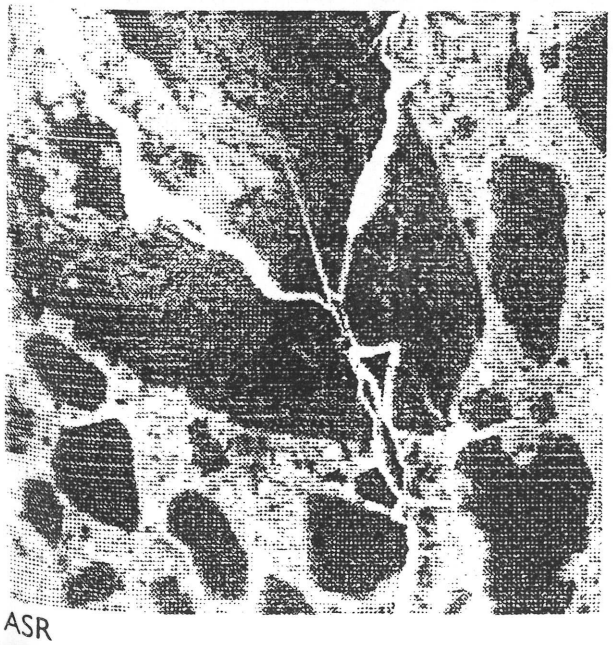

ASR

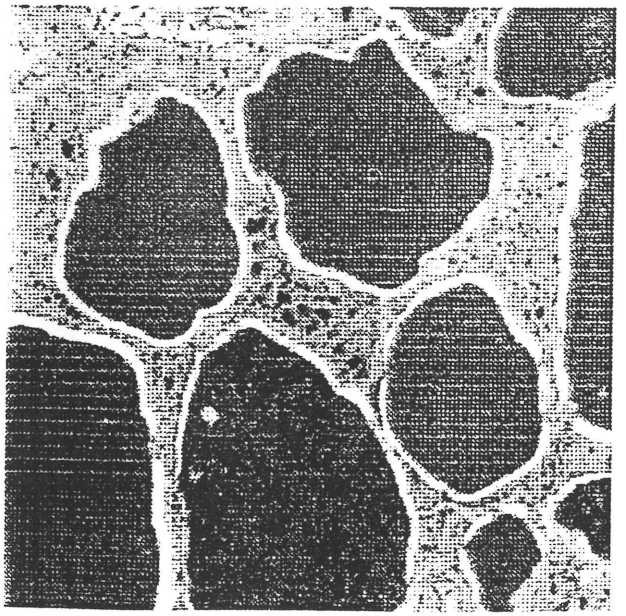

DEF

2.2 Transmission Electron Microscopy (TEM)

With TEM, in terms of resolution we move, from one extreme to the other, but regarding the principals of image formation the TEM is analogous to the optical microscope, with the use of electrons rather than light to image the specimen. In theory, the considerably smaller wavelength of electrons (~ 2 Å) should enable individual atoms to be resolved easily. However, electromagnetic lenses used to focus electrons are far less effective than those for visible light, so near atomic resolution is only realisable under ideal conditions of specimen and instrument.

The TEM can provide a unique combination of information about a specimen :

- imaging,
- crystallographic information and
- local chemical analysis.

The type of imaging relevant to cementitious materials, is called mass thickness contrast. Electrons are absorbed more strongly, by areas of the specimen of higher relative mass or of greater thickness. An example is shown in Figure 4, taken in a high voltage electron microscope with environmental cell, without prior drying of the sample. Here a partially hydrated cement grain can be seen surrounded by hydration products, the unhydrated cement absorbs more electrons and so appears darker. In such images the typical resolution is around 10 nm.

In the TEM it is also possible to observe electron diffraction patterns from local areas. Electron diffraction is analogous to the better known X-ray diffraction, but, in the TEM, can be carried out on features of less than a micron in size. This enables known crystal structures to be *identified*, but the difficulty of obtaining accurate intensity information, means that the technique is of limited value in *determining* unknown crystal structures..

The third type of information is the determination of local chemical composition, from analysis of characteristic X-rays (see 2.3.3). Due to microscope geometry, difficulty of comparison with standards and of determining specimen thickness accurately the chemical accuracy of the analyses are somewhat less than in the SEM, however, the spatial resolution is much higher, around 10 nm in comparison to 1 μm in the SEM. Chemical information can also be obtained by analysis of the electron energies in the transmitted beam (EELS, electron energy loss spectroscopy). As the electrons pass through the specimen some may interact with the atoms of the specimen and some of the energies lost as a result are characteristic of the elements in the specimen. This technique can give chemical information on an even finer scale and can also give information on the local environment of particular atoms. For example, Richardson et al (1994) have used this technique on slag/cement pastes to confirm the presence of aluminium in bridging sites of silcate polymers in C-S-H.

Two factors limit the widespread use of transmission electron microscopy for the study of cementitious materials : availability of equipment and difficulty of specimen preparation. There are perhaps 10 or more scanning electron microscopes (SEMs) to every one TEM.

There are basically three methods of specimen preparation for TEM:

- dispersed particles,
- surface replicas and
- thin sections.

For all these techniques, representativity is a major problem. The sample size for TEM is 3 mm, but the observable area is much smaller than this, as a specimen must be very thin to transmit electrons (~100 nm).

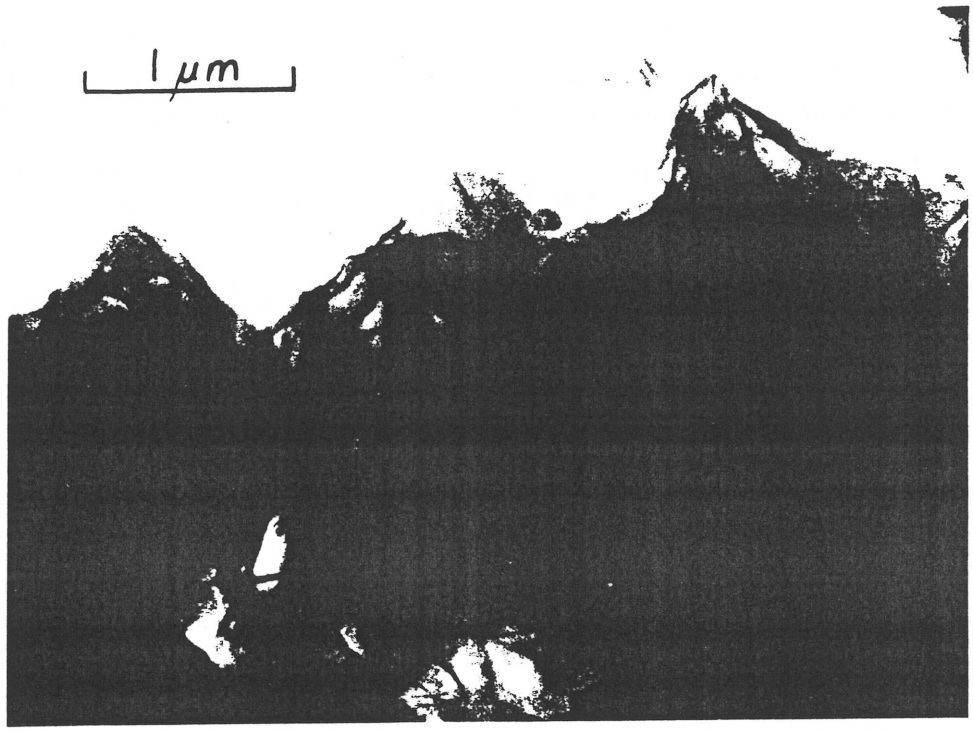

Figure 4. C_3S hydrated for 1day, observed without prior drying in the HVEM. The foil like structure of the C-S-H can be seen.

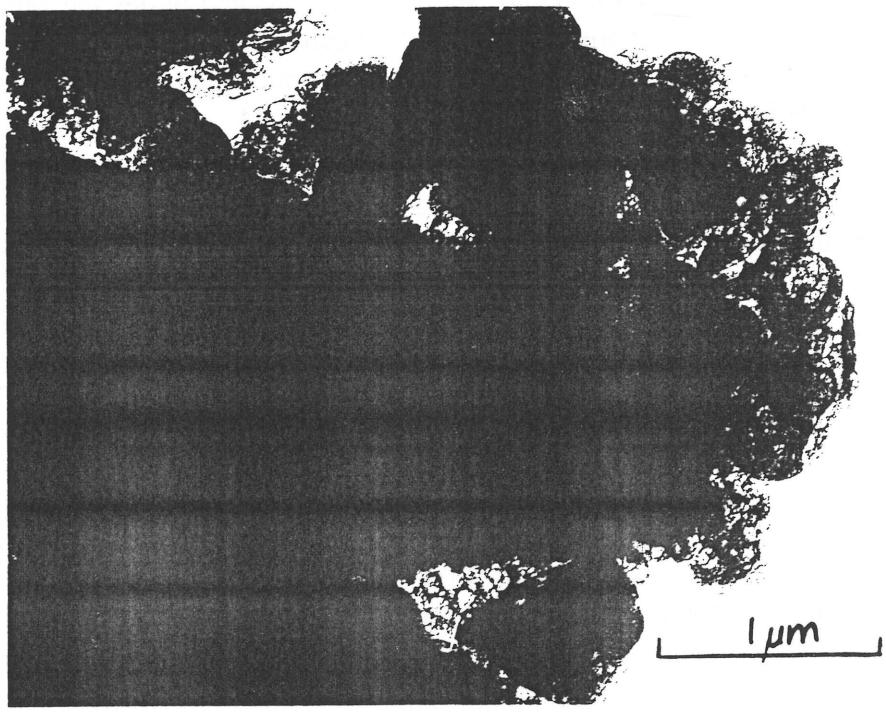

Figure 5. C_3S hydrated for 1 hour. After exposure to the electron beam in the HVEM for a few seconds the product 'bubbles' up.

The simplest technique is to grind a sample to give particles less than a few microns in size. These are then dispersed on a supporting carbon film. This technique was used in early studies of cement (e.g. Grudemo 1960, 1964) and has been used more recently to analyse the chemical composition of hydrates (e.g. Lachowski et al 1980). The main drawback to this technique is that spatial information about the arrangement of phases in the microstructure is lost.

The replica technique, for fracture surfaces was used fairly extensively before the availability of SEMs (e.g. Cottin 1971), but has now being effectively replaced by the direct observation of fracture surfaces in the SEM.

The best technique for observation of microstructure in the TEM is the preparation of thin sections. For cementitious materials these are usually prepared by ion beam milling.. Electron transparent regions are generally obtained by thinning a specimen until a hole appears. There will then be a region around the hole, thin enough to be studied in the TEM. With brittle and fragile cementitious materials this process can be quite difficult and it is almost impossible to control the position of the observable region, further adding to the problem of possible unrepresentativeness.

Another major problem in TEM is the sensitivity of cement hydrates to the electron beam. If the beam is focused on an area for only a few seconds, the products dehydrate and may bubble up. Figures 5 shows an image after beam damage. The electron beam may also lead to preferential volatilisation of some elements, with implications for the accuracy of chemical analyses.

Despite the difficulties, TEM studies have made an important contribution to the understanding of cementitious materials in recent years. The work of Groves and Richardson is particularly notable in this area (e.g. Groves 1986, Richardson and Groves 1990,). The morphology of 'inner' and 'outer' types of C-S-H can be distinguished, as can phases finely intermixed with C-S-H such as hydrotalcite in rims around slag grains. In carbonated pastes the fine intermixing of calcium carbonate and silica gel formed from C-S-H can be resolved (Richardson et al. 1992). More recently lattice images of C-S-H gel, have been published by Viehland et al. (1996). These have a resolution of less than a nanometre and indicate that C-S-H contains nanocrystalline regions.

Probably more than other microscopic techniques, it is important not to use TEM in isolation. However, when the general arrangement of features is well known from the SEM or optical studies, it is of great value.

2.3 Scanning Electron Microscopy (SEM)

The scanning electron microscope is more recent in development than the TEM, the first commercial instruments arrived in the early 1960s. The principal for image formation is radically different from either the TEM or the optical microscope. Essentially images are formed via coupled scanning of the electron beam over the specimen and of the output signal from the specimen on a TV screen, or similar viewing device. The magnification results from the difference in size of the two scans : thus if the scan on the specimen is 400 μm in dimension, and that on the screen is 200 mm the magnification will be ×500. The main advantage of the SEM is its flexibility, a magnification range of more than three orders of magnitude is possible (~×20 to >×50,000), and a range of signals can be used to form the image. The three kinds of signal most commonly used for the study of cementitious materials are:

- secondary electrons,
- backscattered electrons and
- characteristic X-rays.

These signals are generated by the interaction of the incident electron beam with the atoms of the sample, which occurs in a tear drop shaped region, known as the interaction volume, Figure 6. The size of the interaction volume increases with the energy of the incident electrons, which is dependent on the accelerating voltage used. Thus lower accelerating voltages should give better resolution than high ones, but this must be traded against the strength of the signal which decreases with accelerating voltage. For backscattered images a threshold voltage is needed to obtain contrast between phases, for light elements and oxides (as in cements) this threshold is higher than for heavier elements. Also for chemical analysis the energy of the incident electrons must be sufficient to excite the atoms present in the sample. For most SEMs an accelerating voltage of 15 kV is a good compromise, but with more modern instruments it is possible to obtain good images at lower voltages.

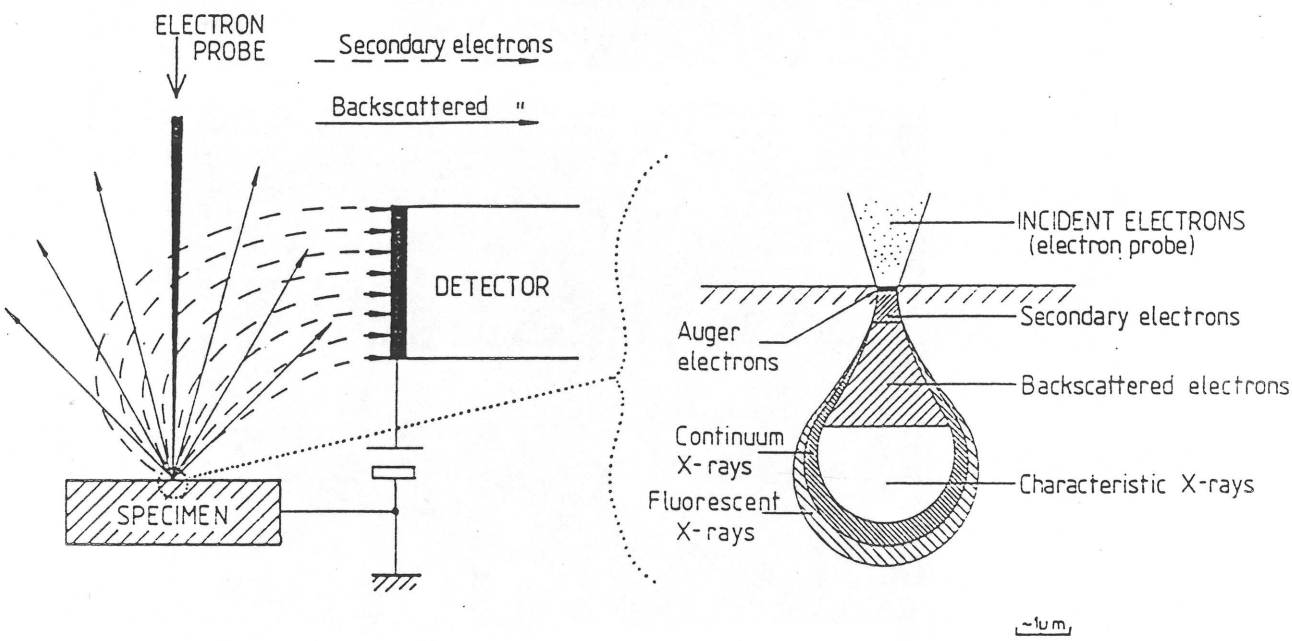

Figure 6. Generation of signals in the SEM

2.3.1 Secondary Electron Imaging of Fracture Surfaces

Secondary electrons result from inelastic scattering processes within the specimen, they have much lower energy than the incident electrons and so only escape from within a few angstroms of the specimen surface. This means that the potential resolution of secondary electron images is higher than that of other signals. The intensity of secondary electrons is influenced to some extent by the local atomic number of the sample, but the major effect on contrast is the inclination of the specimen surface to the horizontal (topography), this makes them ideal for imaging rough surfaces, such as produced by fracture. Secondary electron are collected by a detector with a small positive bias, which enables them to be separated from the more energetic incident and backscattered electrons.

Fracture surfaces are easily produced by smashing a hardened sample with a hammer or chisel. For cement pastes the specimen must first be dried before placing in the high vacuum of conventional electron microscope and coated with of a conducting material such as gold or carbon, to prevent charge build-up from the incident electron being unable to escape from the specimen. In SEMs with a low vacuum facility prior drying may be avoided.

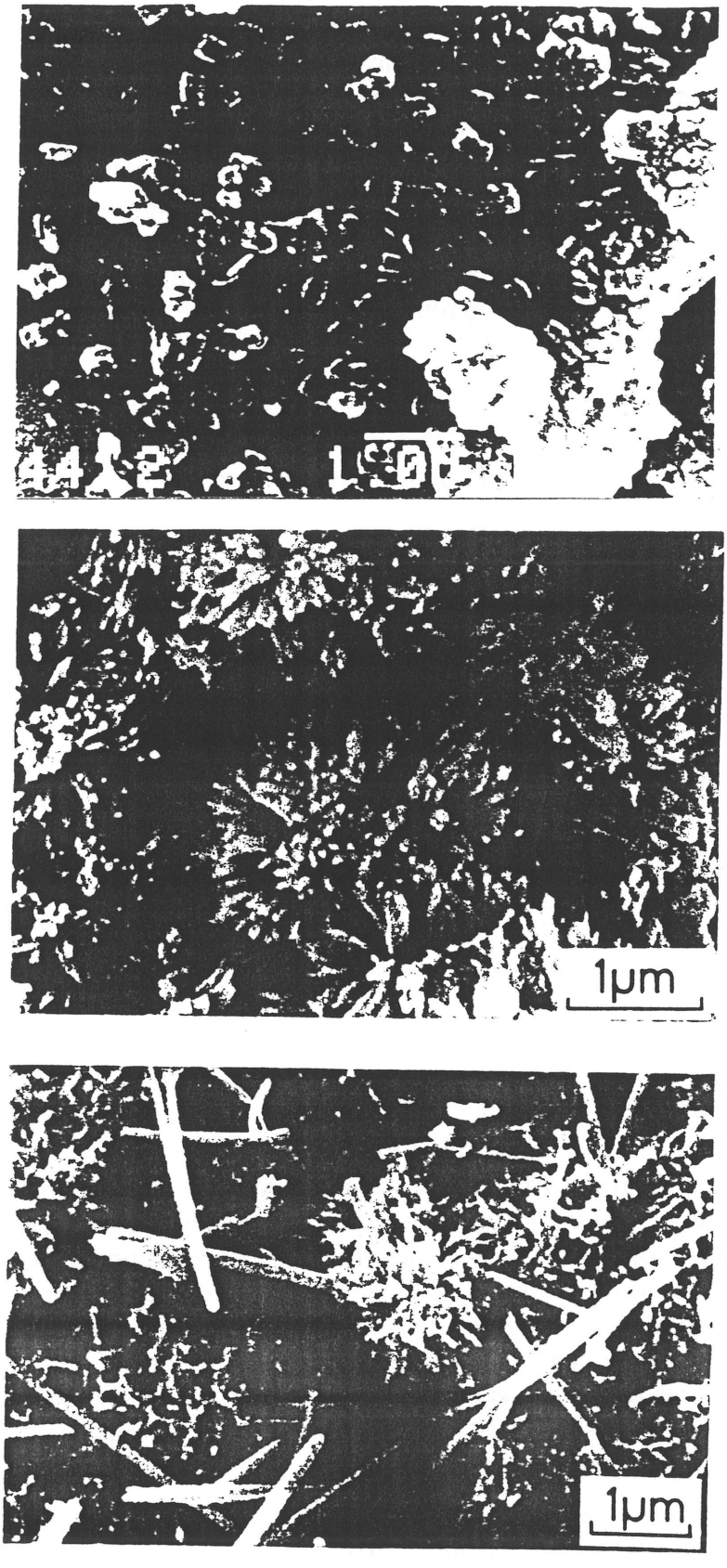

Figure 7. Fracture surfaces of cement paste after 1hr, 10hrs and 24hrs hydration.

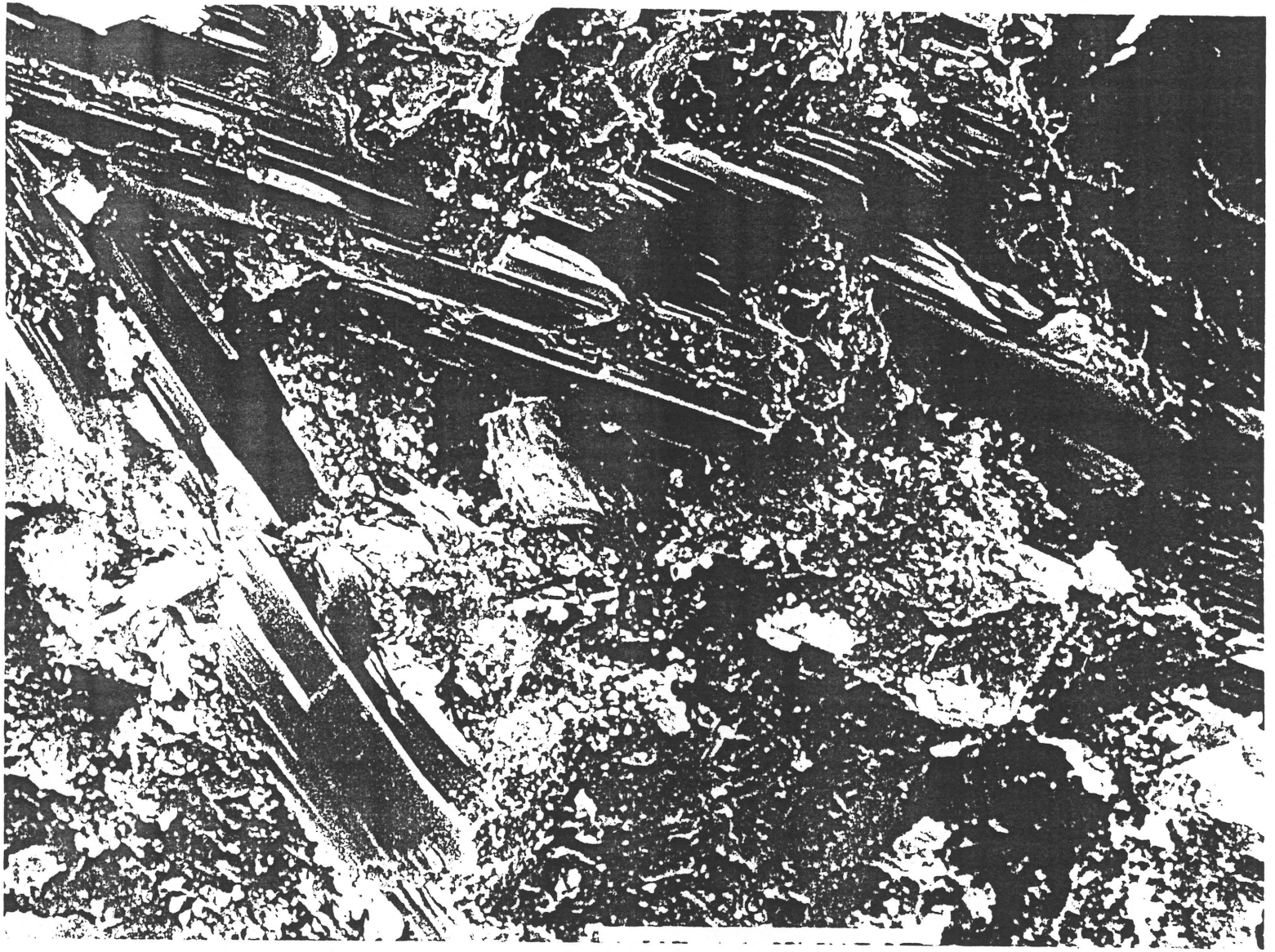

Figure 8. Fracture surface of 28 day old cement paste

As with all microscopical techniques the examination of fracture surfaces has advantages and limitations. The principal advantages are the good resolution and ability to observe the morphology of hydration products. This makes the technique well suited to the study of the early period of hydration. For example, Figures 7 shows fractures surface of a cement paste after 1, 10 and 24 hours of hydration. At 1 hour, small grains of ettringite can be seen on the surface of the cement grains, at 10 hour there has been a significant growth of C-S-H around the grains and at 24 hours both C-S-H and further ettringite are visible. However, these microstructures also illustrate some of the cautions which must be observed when studying fracture surfaces. In the 1 hour microstructure, the presence of the small ettringite crystals on the grain surface is frequently interpreted as their formation close to the grain surface, even as topochemical formation. Such interpretations misleading as other techniques show that the ettringite crystals form in the solution phase away from the grain (Scrivener 1984, 1989b). During the drying process the crystals will fall back onto the underlying grain. Similarly the spiky morphology of the C-S-H in Figure 7b is also accentuated by the drying process. In the undried state, this phase has a less defined, more foil-like morphology, Figure 4.

After about 1day of reaction , the microstructure becomes more dense. The fracture path will run through the weakest areas, which are thus the areas observed. With increasing densification at later ages, it becomes increasingly difficult to interpret the microstructure as a whole (Figure 8) which is dominated, by dense areas of C-S-H and calcium hydroxide. In addition, only relatively small regions of the rough surface will be in focus at any one time. Consequently, the microscopist is drawn to the study of 'interesting', but perhaps unrepresentative features.

2.3.2 Backscattered Electron imaging of Polished surfaces

Polished sections can be prepared to give a representative cross-section of the microstructure. However, these cannot be imaged satisfactorily with secondary electrons, due to the lack to topography. In this case backscattered electrons (BSE) are used for imaging, these are incident electrons which have been scattered through large angles so that they re-emerge from the sample. Their intensity is mainly dependent on atomic number (larger atoms are more likely to cause scattering and produce a high backscattered electron intensity). The resolution of BSE images, a few hundred nanometers, is somewhat less than that of secondary electron images, but this drawback is vastly outweighed by their flexibility. This imaging mode was used on early electron microprobes, but the image quality was poor. The advent of solid state backscattered detectors in the 1980s, enabled high quality backscattered electron images to be obtained and this technique has become more and more widely used for the study of cementitious materials.

In a sample, the intensity is proportional to the local BSE coefficient (C_{BSE}), which is the average of the BSE coefficients of the elements present weighted according to their relative mass:

$$C_{BSE} = \sum C_i m_i \qquad (C_i, \text{ BSE coeff. of } i^{th} \text{ element. } m_i, \text{ mass fraction of } i^{th} \text{ element})$$

Figure 9. shows the relative BSE coefficients of some of the phases found in cementitious materials. Generally the anhydrous phases appear brighter than the hydrates and pores appear dark. A typical image of an hydrated Portland cement is shown in Figure 10. The contrast is complicated by the presence of microporosity, particularly in C-S-H gel, this lowers the BSE coefficient, but the precise relation with the level of porosity is not known.

By and large the images of clinker are very comparable to those obtained by optical microscopy, Figure 11, except the higher resolution and good contrast between the ferrite and aluminate phases, makes the fine detail of the interstitial material clearer. The reproducible contrast between the phases makes BSE images well suited for automated image analysis, however, the

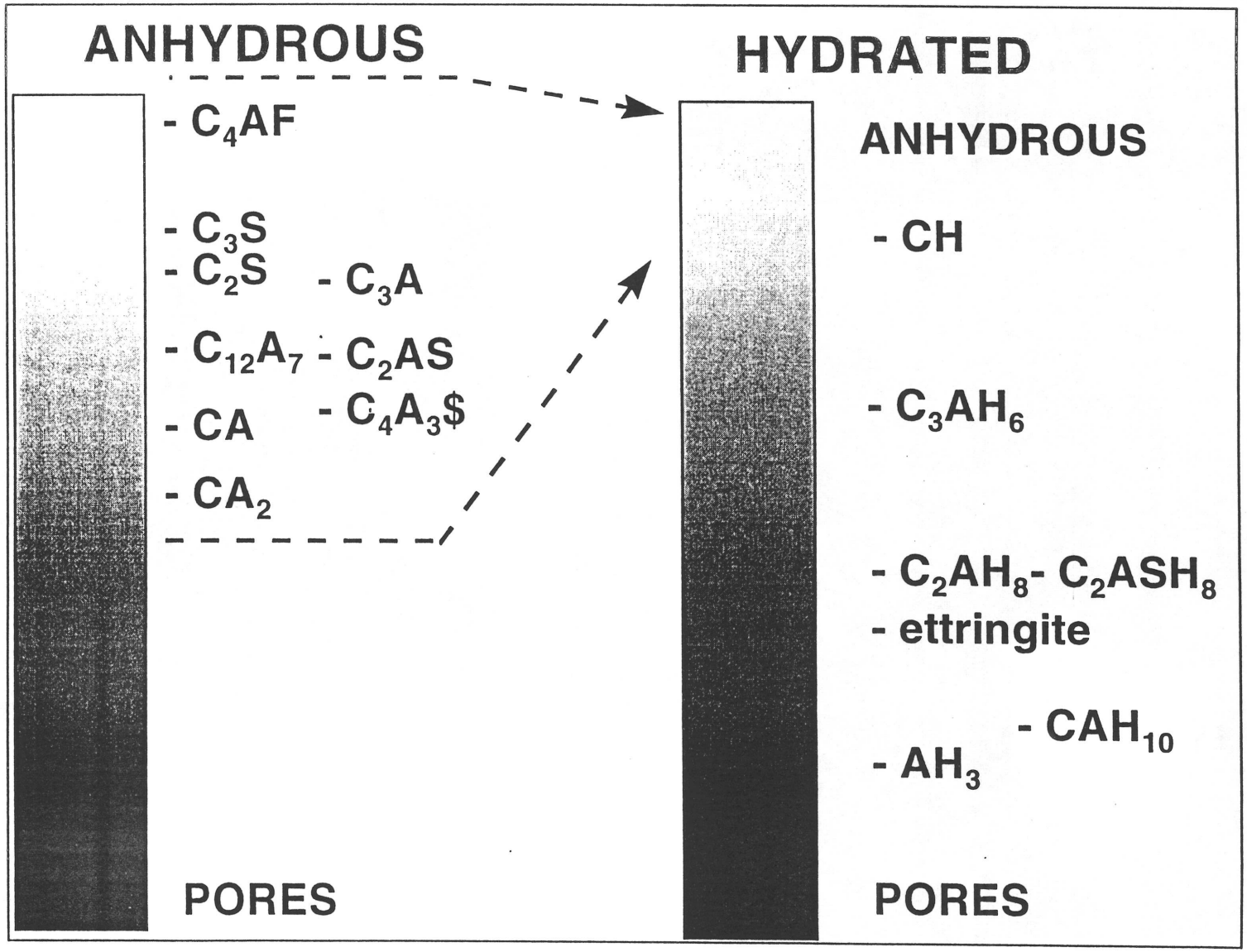

Figure 9. Relative backscattered electron coefficients for cementitious phases

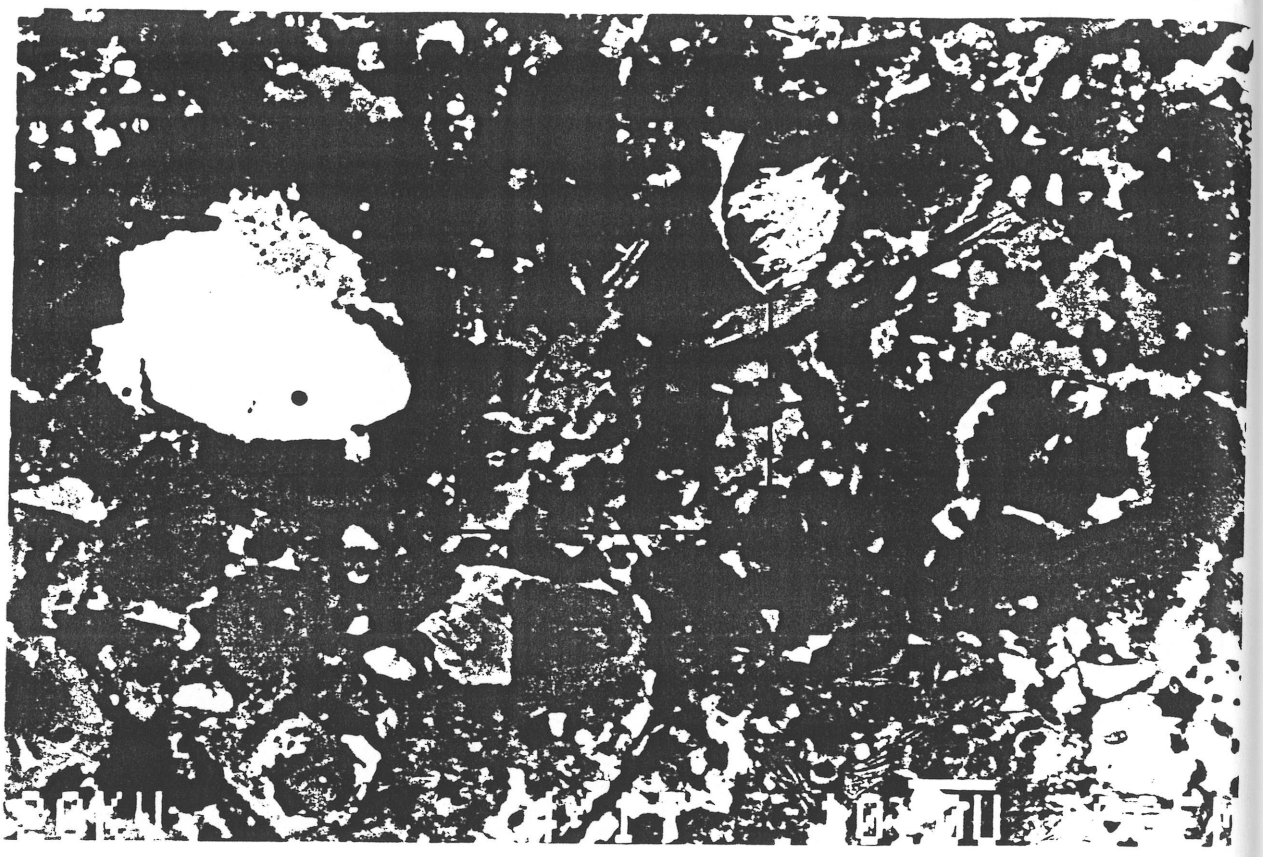

Figure 10. BSE image of polished section of Portland cement paste hydrated for 28 days. N.B. black box indicates similar area to whole image in of fracture surface in Figure 8.



Figure 11. BSE image of polished section of cement clinker.

very similar BSE coefficients of the belite and aluminate phases poses a problem in practice. Several methods have been developed, usually in combination with chemical information from X-ray signals (see 2.3.3), (e.g. Scrivener 1987, Stutzman 1991, Sutter et al, 1997). The technique may equally well be applied to a ground cement, dispersed in resin and polished. Here the improved resolution over optical microscopy is more important, although, quantitative measures cannot be realistically used for grains less than a few microns in size.

For the study of cement pastes, and concretes, the effective resolution of SEM/BSE is considerably greater than for optical thin sections. The major advantages of the technique are the ability to obtain quantitative information by image analysis and the possibility to use the X-ray signal to make local chemical analyses. Both these techniques are described in more detail below.

2.3.3 Characteristic X-rays for chemical analysis.

Some of the scattering events which occur as the incident electron beam penetrates the sample will result in the emission of X-rays, these consist of characteristic X-rays, specific to individual elements, superimposed on a continuous background, Figure 12.

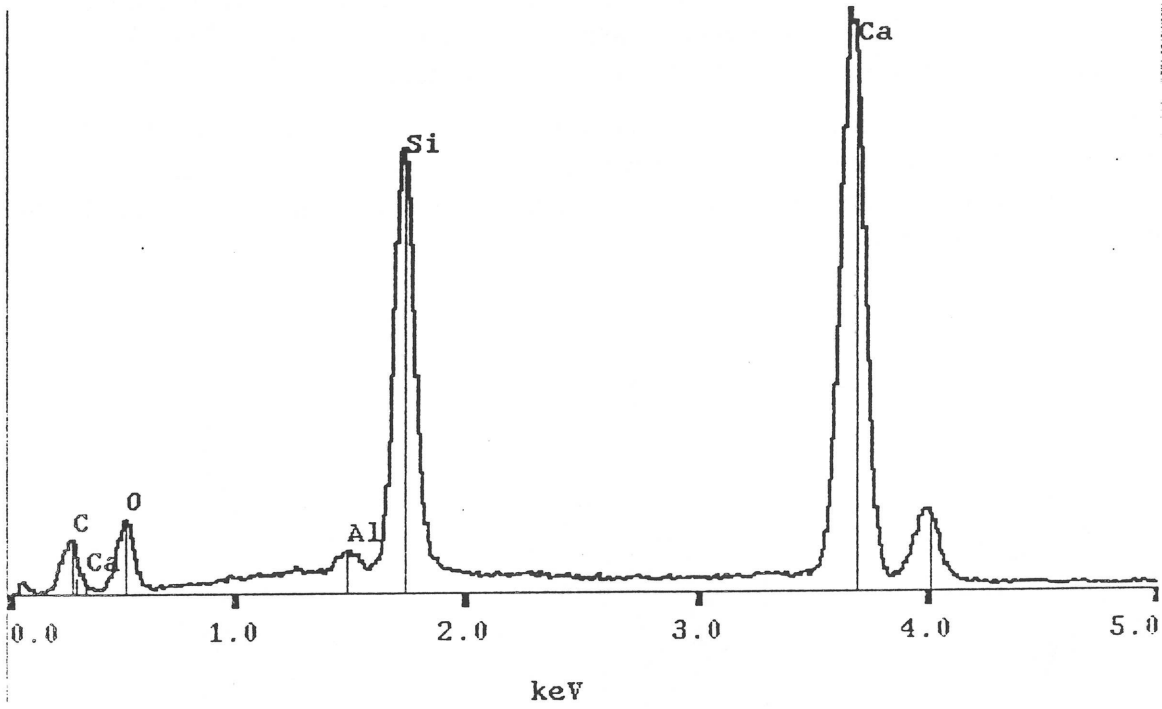

Figure 12. X-ray spectrum emitted from belite grain sample in the SEM.

The characteristic energies correspond to differences between electron energy levels in the atoms. The emitted X-ray may be analysed, either according to their energy (energy dispersive spectroscopy, EDS) or wavelength (wavelength dispersive spectroscopy, WDS).

EDS analysis is by far the most widely available, the whole energy range can be analysed at the same time so that a spectrum can be obtained for qualitative purposes in several seconds, and a spectrum for quantitative analysis in 50-100s. The disadvantage of EDS is the relatively low signal to noise ratio, this means that the detection limit is at best 0.1 wt % absolute and the accuracy between ±0.2 and ±2%, depending on the absolute amount and the analysis procedure. The EDS detector is usually protected by a window, which does not allow elements lighter than sodium to be detected. Thin, ultra thin window and windowless detectors are becoming increasingly common, these allow light elements to be detected down to Boron, but the accuracy in this range is much lower.

WDS is the technique used on specialised microprobes and occasionally on conventional SEMs. The spectrum is acquired by scanning through the range of wavelengths. To obtain a complete spectrum takes considerably longer than EDS, but the technique is usually used to scan a narrow, predefined range to detect a specific element. For quantitative analyses a good signal can be acquired in a few microseconds for each element, a microprobe will usually have at least three detectors to analyse several elements simultaneously. The detection limits and accuracy are about an order of magnitude better than for EDS analysis.

In both cases, accurate quantitative analyses, depend on comparison with spectra obtained from standards of known composition, obtained under identical conditions — accelerating voltage, beam current, specimen height, specimen tilt, etc.. In compounds containing several elements, the signal form one element, will be affected by the presence of the other elements, due to absorption and secondary fluorescence. Commercial analysis software, makes corrections for these effects automatically, 'ZAF' and 'phi-rho-Z' being the mathematical models most commonly used (the phi-rho-Z correction is best adapted to the light elements found in cementitious materials.). Commercial software is designed to give good results across the complete range of materials, e.g. metals and oxides, which are not necessarily optimal for any one class of materials, e.g. cements. Therefore, the analyses from a system dedicated to cements, may be optimised by using cement phases as standards.

Accurate X-ray microanalysis depends on having a flat specimen. The type of artifacts which can be produced by rough surfaces are shown in Figure 13. Therefore X-ray analysis should not be used on fracture surfaces, for anything other than to get a very rough idea of the chemistry of the area being examined.

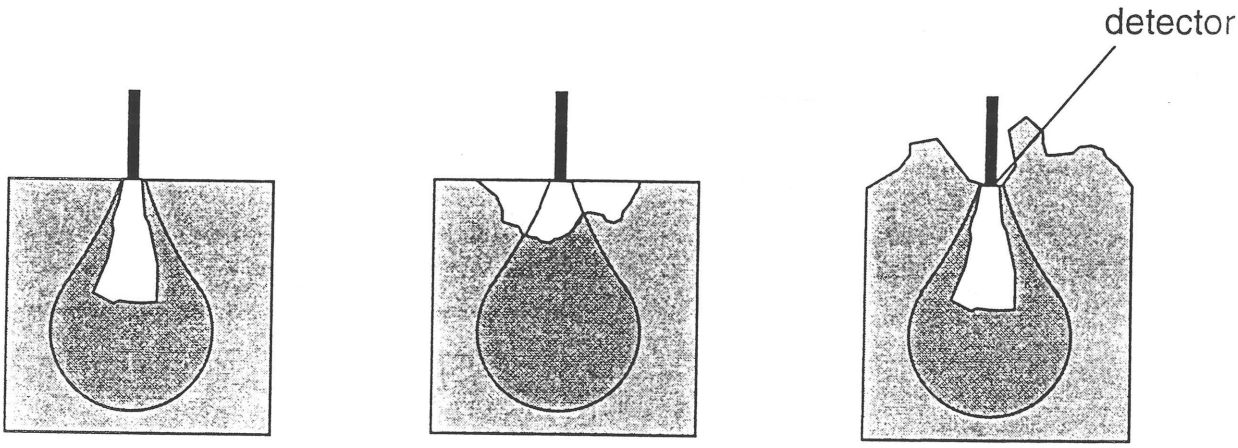

Figure 13. Possible artifacts in chemical analysis

The main limitation to X-microanalysis in the SEM is the size of the interaction volume from which X-rays are collected, this is of the order of 1-2 μm in cementitious materials (Figure 6). In many cases, particularly for hydrated materials, phases are intermixed on a scale finer than this and cannot be analysed separately. In these situation graphical representations of sets of individual analysis points can assist interpretation. This technique was first used by Harrison et al. 1986 to study the composition of hydrates in slag/cement blends.

An example of the use of atom/ratio plots is shown in Figures 14 and 15. This shows analysis of hydrates in a paste of an alkali activated slag (Wang & Scrivener 1995). On the fracture surface (Fig. 13a)) some thin plates can be seen amongst a fairly featureless 'gel', but no sensible analyses can be made by this technique. In the BSE image of a polished surface (Fig.13b)), the plates are difficult to identify and individual analyses cannot be made. When the results of

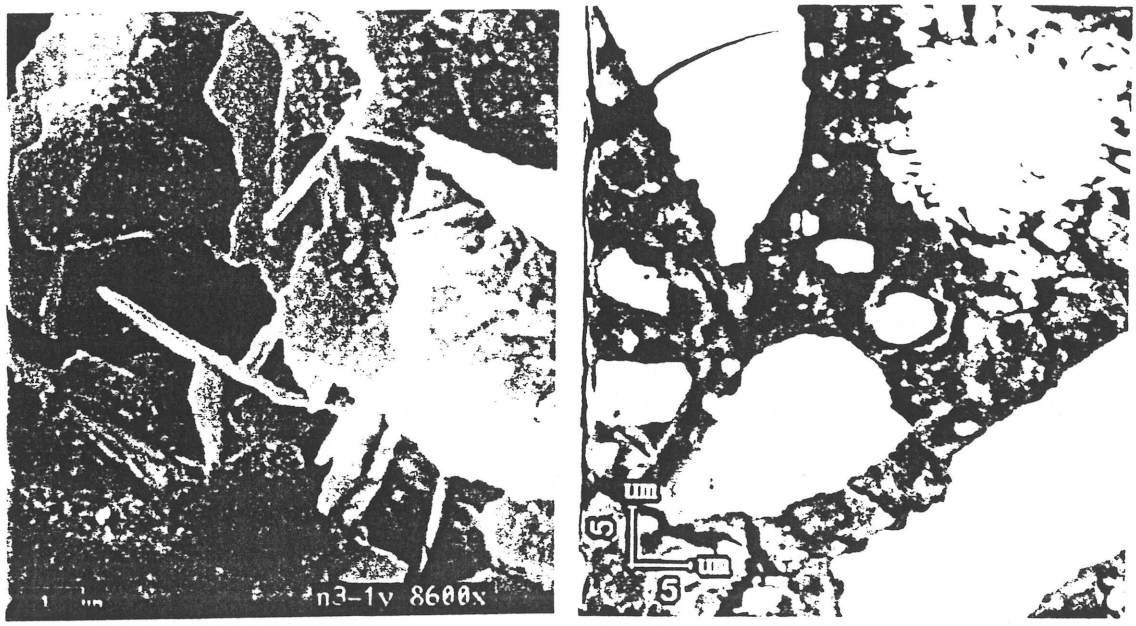

Figure 14. Fracture surface and polished surface of slag activated with NaOH solution hydrated for 1 year

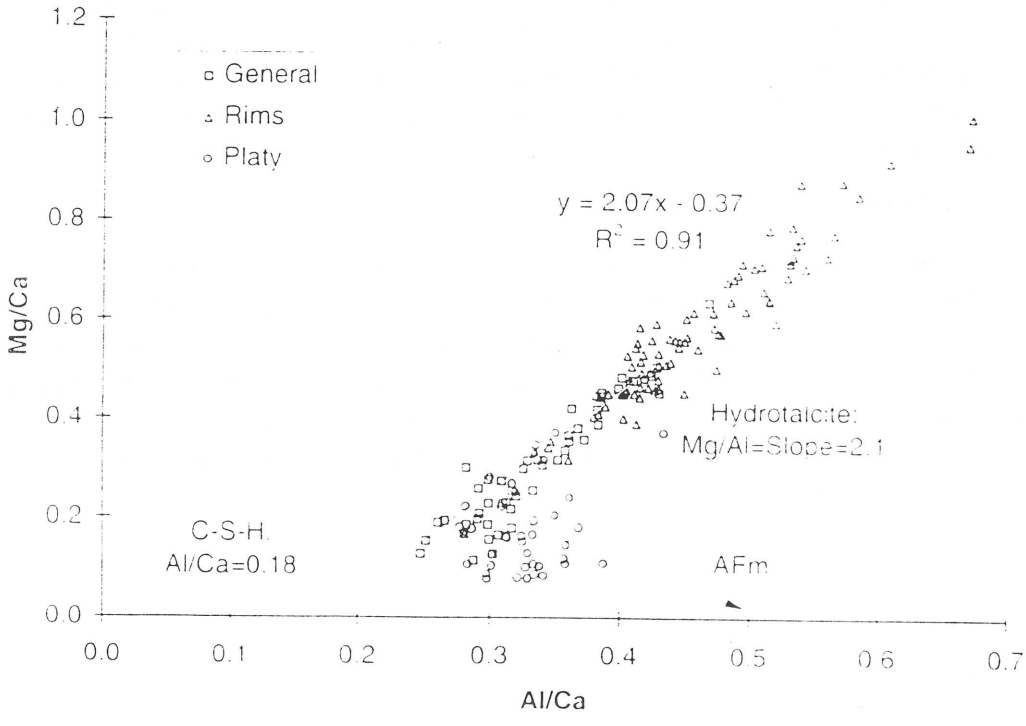

Figure 15. Microanalyses of slag activated with NaOH plotted Mg/Ca against Al/Ca

many point analyses are plotted on a graph of Mg/Ca to Al/Ca, the intermixed phases can be identified. The larger plates visible on the fracture surface are an AFm phase and the analyses centred on these plates fall around a line between a C-S-H and AFm. The featureless 'gel' is a C-S-H, but the distribution of the analyses indicated that there is finely dispersed hydrotalcite within this, which could not be seen in the microscope images. It is also evident that the amount of hydrotalcite in the C-S-H is higher in the 'rims' around the slag grains. These deductions were supported by the results of X-ray diffraction and thermal analysis. Other examples of this type of analysis, for the study of delayed ettringite formation in heat cured pastes can be found in Scrivener and Lewis (1997)

In addition to point analyses, X-ray signals may be used for mapping. Here the intensity of the signal associated with one elemental peak is collected as the beam scans the specimen. Such maps can be very useful in visualising the distribution of an element, but they are time consuming to acquire and the resolution is limited, not only due to the interaction volume, but also by the signal to noise ratio of the x-ray signal.

3. Sample preparation

Before considering the theme of image analysis, it is worth considering the question of sample preparation. The importance of this is often underestimated, but good sample preparation may be far more critical to obtaining good images than skill at operating a microscope, and certainly more important to meaningful image analysis than sophisticated mathematical routines. As electron microscopes operate under vacuum, free water must be removed from samples before examination. Then the sample must be polished (for optical microscopy or BSE in the SEM).

Finally for the electron microscope, measures must be taken to avoid charge build up, as cementitious materials are non-conducting. For fracture surfaces a layer of gold (or other metal) is vapourised onto the surface. The vapourisation process is good for giving a continuous film on rough surfaces and the good electrical conduction of gold means that only a very thin layer is necessary. The disadvantage of gold is that it gives a characteristic X-ray peak in the same position as sulfur, so for polished samples on which chemical analysis is to be carried out, carbon is usually used.

3.1 Drying Techniques

There has been considerable controversy as to the best technique for removing free water from cementitious specimens; inevitably, any technique induces some change in the specimen. The choice of the most suitable technique will depend to some extent on the age of the specimen, the equipment available and the principal features to be observed. In the SEM for example the maximum practical resolution is well above 10 nm, therefore techniques which undoubtedly damage the fine gel pores of C-S-H (~ 2 nm) will not have a visible effect on the specimen. The techniques most commonly proposed are :

- oven drying
- vacuum drying
- freeze drying
- solvent exchange

Oven drying has a very destructive effect on the microstructure, 'blurring' the fine morphology of the hydrate phases and inducing microcracking. Therefore, this is a technique which should be avoided. Otherwise, at least for samples more than a few days in age, there is little discernible difference between the remaining techniques at the microscopic level.

The main advantages of freeze drying are its speed and the minimal damage during water removal. Specimens are dropped into a mixture of solid CO_2 (cardice) and methanol at −80°C (the thermal shock of liquid N_2 can shatter specimens). For small specimens of a few centimetres in size the freezing is almost instant so that early age samples hydrated for as little as a few minutes may be examined. After freezing the specimens are transferred to a cooled chamber under vacuum, where the water sublimes directly from solid to gas so avoiding the destructive effect of a retreating liquid interface. In addition any solutes present in the pore solution, will be simply deposited on the hydrate surface without crystallisation, they are thus 'invisible' at the microscopic level.. The main drawback of freeze-drying is the need for specialist equipment, also for specimens of any size the drying process may be very slow.

Drying under vacuum is a relatively slow process, which will take several days, even for very small samples. It is only suitable for mature specimens (older than about 28 days), which have a fairly low free water content anyway.

Solvents may partially dehydrate phases such as C-S-H and ettringite. However, such dehydration probably has little effect on the outward morphology of the crystals, so is more important from the point of view of X-ray diffraction and thermal analysis than microscopy. The problem with solvent exchange is that it is also a relatively slow process and for samples of a few millimetres the exchange process will take several days. Therefore, it is only suitable for older samples. For younger samples, the hydration may be stopped more rapidly by grinding the sample, but in this case valuable spatial information about the microstructure is lost.

3.2 Polishing

A good polish, without relief, is essential to the examination of samples by BSE. With many materials i.e metals, this is comparatively easy. The preparation of cementitious materials, especially concretes, is somewhat more complex and difficult to achieve. Traditionally clinkers and concretes have been studied by optical microscopy where the use of water and heating during sample preparation is generally acceptable. The impregnation of the pore structure of the material with resin is also less critical for these techniques as the resloution is lower.

Cements and concretes are multiphase materials with complex microstructures. They materials have variable moisture states, and different hardnesses of constituents and within the microstructure. The most important constituents within a concrete are usually the cementitious phases. These are generally softer and more porous than aggregates and need attention for successful preparation.

The basic procedure for the preparation of polished sections involves: initial cutting of the bulk section to a manageable size; impregnation of the pore structure, precision cutting or grinding to expose the material surface, lapping of the surface with abrasive compounds to so it is flat prior to the polishing stages, and finally polishing to a size of 0.5μm or less. The choice of appropriate techniques and equipment for preparation depends on the particular type of sample and on the analyses intended; i.e porosity, surface regions, chemistry.

For impregnation there are many resins commercially available today with different in viscosities and chemical compositions; a lower viscosity resin generally enables better penetration and impregnation of the material but these resins tend to contain significant amounts of chlorine.

The next step is to expose a surface of the material which still has resin within the pore structure. Grinding with diamond discs and silicon carbides, and/or precision cuts are generally employed for this task. The exposed resin impregnated surface is subsequently *lapped* with free abrasives,

corundum (Al_2O_3) or silicon carbide (SiC), and then *polished* with diamond grits on pellon cloths. Generally corundum powders are less aggressive than SiC grits and are more successful with softer materials. If the use of water is undesirable alcohol and/ or oil based lubricants need to be used.

Between each grit size the surface condition should be assessed with optical microscopy to ensure successful completion of one stage before starting the next, and the samples should be ultrasonic cleaned in appropriate solvents. Careful attention to each preparation stage is important for successful results.

It is important to understand the type of material and the sample preparation process in order to avoid and identify artifacts, which hamper or prevent proper microstructural examination. Perhaps the most common artifact is "relief", where one component (e.g, aggregate) is polished and stands 'proud' of the others (e.g. paste) which remains poorly or unpolished. In the worse case this can prohibit polishing of the cementitious phases and therefore BSE microstructural imaging in concrete. On a smaller scale relief can result in both topographical and atomic number contrast which complicates the grey scale/atomic number relationship so that subsequent feature discrimination for image analysis is inaccurate. Relief can also result in the local charging, which affects both imaging and chemical analysis.

Another common artifact is "plucking", whereby softer phases are removed (i.e. calcium hydroxide) to leave pores. Plucking can also significantly distort the pore network, size, shape and total porosity. This problem can be minimised or avoided all together if the pore structure of the material is adequately supported by impregnation with epoxy resin.

Microcracking is also a fairly common artifact which results from the initial stages of sample preparation; either from the removal of the "free" water, or during the coarse cutting and grinding processes. Microcracking can be minimised by removing the water in the least aggressive way possible i.e solvent exchange, and by precision cutting of the surface followed by lapping with corundum powders.

Despite the difficulties it is possible to polish concretes successfully. Each stage must be carefully considered and the time must be taken to do the work necessary, since as for many other techniques there are no easy answers or short cuts.

4. Image analysis

Image analysis is essentially the process of obtaining quantitative information from images. Simplistically the number of different quantities which can be derived from an image is effectively infinite, therefore the problem is to produce quantities which have some use. The process of image analysis can be considered in two stages :

- discrimination of the features of interest from the microstructure;
- measurement of the discriminated features.

4.1 Feature discrimination

The main criterion used to discriminate microscopical features is grey level in BSE images or colour in optical images. [The reproducibility of grey level (determined by average atomic number) in BSE images, as opposed to colours (determined by etching) in optical images makes them better adapted to image analysis.] For a typical Portland cement paste, a histogram of the grey level distribution is shown in Figure 16. From bright to dark, peaks can be identified for

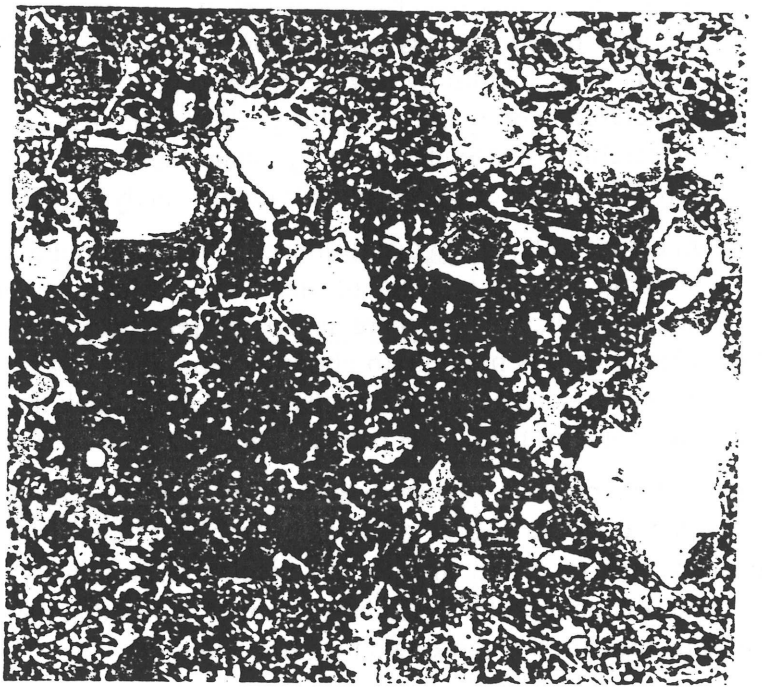

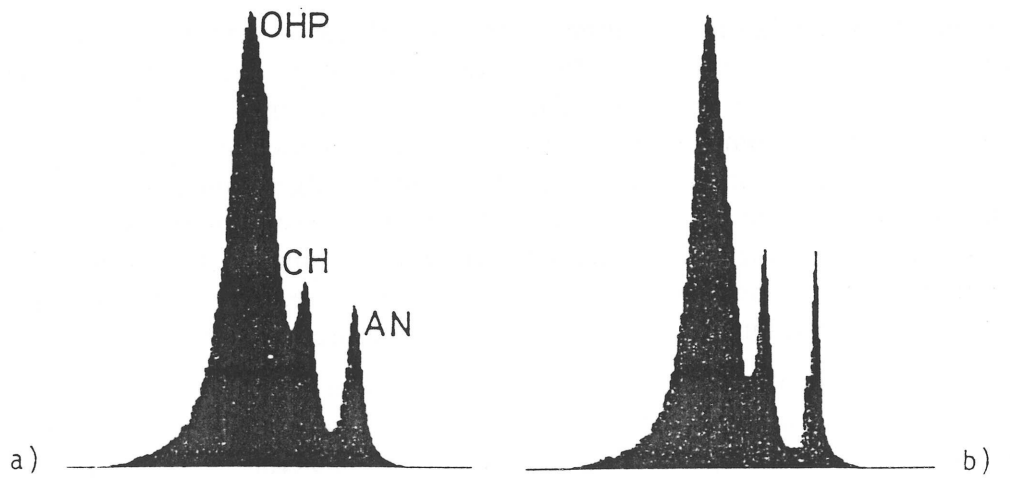

Figure 16. BSE image of 28 day old cement paste for image analysis and associated grey level histogram, a) before and b)after smoothing

the anhydrous cement phases, calcium hydroxide and for the other hydrates (mainly C-S-H). The separation of the peaks can be improved somewhat by smoothing the image.

From this histogram threshold values may be chosen to extracted the anhydrous cement. Comparisons of the anhydrous material measured by image analysis for this phase, compare well with calculations based on loss on ignition measurements (Patel 1987, Scrivener et al. 1987) (Figure 17a)). The calcium hydroxide can also be discriminated, although it can be seen that there is considerable overlap between this peak and that from C-S-H. Generally it is found that measures of calcium hydroxide made by image analysis tend to be slightly higher than measures by X-ray diffraction or by thermogravimetric analysis (Figure 17b)).

The real problem comes in trying to discriminate the pores from the C-S-H. Part of the problem comes from the range of grey levels of the C-S-H and inherent microporosity, but high magnification images indicate that there is no discrete boundary between these two phase. Despite these difficulties it is possible to choose a reproducible grey level threshold, which can be used to make comparisons between samples [Patel 1987, took the point of intersection of the tangents to the lower side of the C-S-H peak and the rising curve of the pores].

The question is often posed — what is the minimum pore size detected by image analysis? Clearly pores integral to the C-S-H gel are not resolved, but what about the 'capillary' pores. The simple answer is to relate this to the pixel size, which is typically 0.3 μm at ×320 magnification and 0.1 μm at ×1000. However, table I shows that there is no significant increase in the pore volume measured at these two magnifications.

Table I, Porosity measured at three different magnifications of cement paste (w/c=0.5) at two ages (Scrivener 1989), area % (std. error)

	× **110** (4 fields)	× **320** (9 fields)	× **1000** (9 fields)
1 day	17.8 (0.7)	23.2 (0.3)	24.5 (1.2)
28 days	6.8 (1.3)	12.7 (0.3)	14.6 (1.2)

The reason for this lies in the nature of the thresholding — the pixels which are discriminated as 'pores' are in fact those in which the average level of porosity is greater than a certain value, close to, but not equal to 100%. Thus the porosity 'over estimated' in a pixel with an actual porosity of 95% is compensated for by the porosity 'missed' in a pixel containing 5% of pores, which is not included in the measurement of porosity. This compensating effect mean that there is no simple pore size cut off, and in fact the total measure of porosity is very similar to that measured by other methods, which can access much smaller pore sizes. This can be seen in Figure 17c) shows the comparison of porosity measured by image analysis (nominal cut-off 5000Å), with the volume of pores above 368 Å measured by solvent replacement.

In terms of available software a large range of other criteria are available for discriminating features — circularity, aspect ratio, size, etc.. In general, it has been very difficult to find routines which work reproducibly in cementitious materials. For example, it is possible to identify fly ash particles on the basis of circularity in young pastes, but in older pastes the boundary of the particles cannot be reliably discriminated. In addition many fly ash particles are not spherical, and the overall error in measurement is not acceptable.

A particular problem is posed by the discrimination of aggregate particles in concrete. The mineralogy, even of primarily siliceous aggregates, is too variable for them to be reliably discriminated by grey level thresholding, even in combination with other selection criteria. In

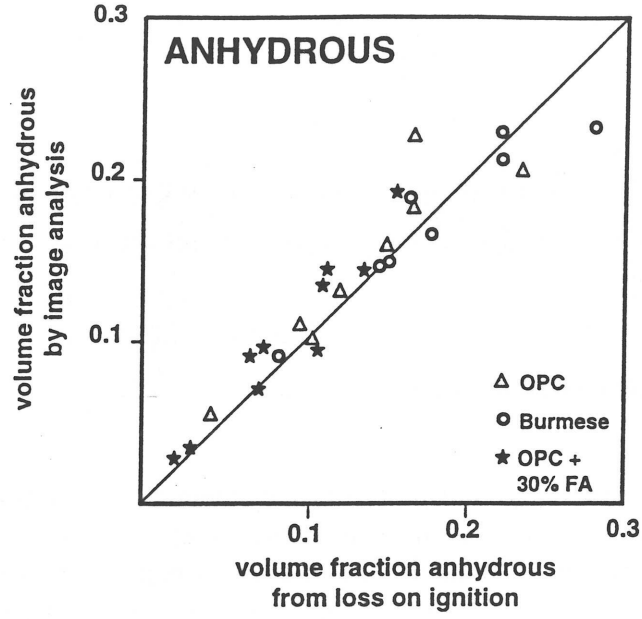

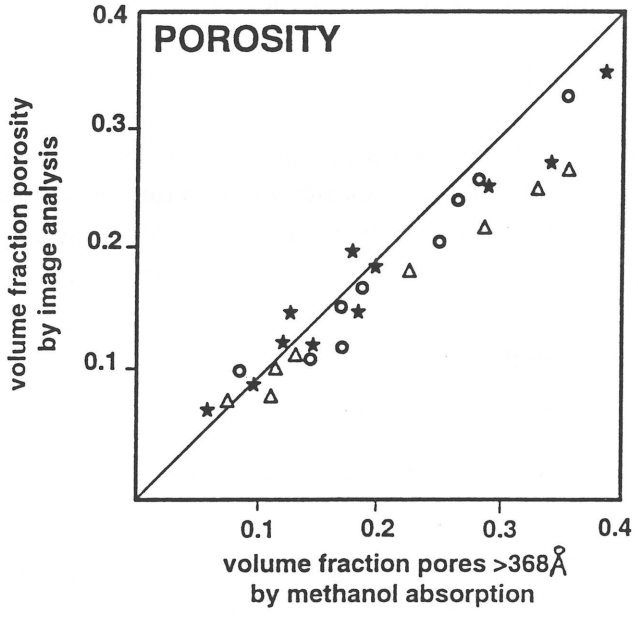

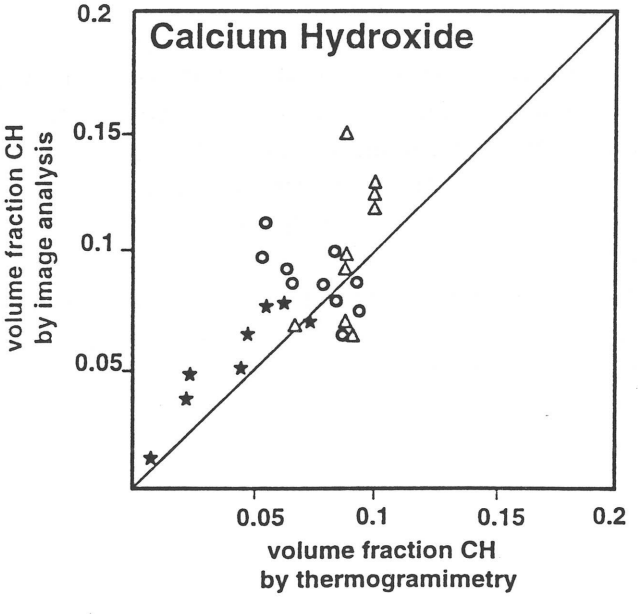

Figure 17
Comparison of anhydrous cement, porosity and calcium hydroxide measured by image analysis of BSE images with measurements by classical techniques, from Patel 1987

general it has been found necessary to draw round the particles by hand, which is somewhat, though not very, time consuming.

4.2 Quantification

The utility of any quantity measured by image analysis is governed by two major concerns:

1. How can a measure made on a two dimensional section be related to a three dimensional microstructure? (Stereological aspect)
2. Is the measure representative of the sample from which it comes? (Statistical aspect)

These two aspects are not independent of each other.

4.2.1 Stereological aspects

A first class of measures are those for which there exist mathematically simple relationships between three dimensional quantities and their measurements in two dimensional sections. There are very few such measures, but fortunately one of these is perhaps the most useful, that of the volume fraction of a phase. The relationship between the volume fraction (V_V), area fraction (A_A), line fraction (L_L) and point fraction (P_P) was found in the 19th century to be:

$$V_V \equiv A_A \equiv L_L \equiv P_P$$

This means that, within the limits of statistical considerations the volume fraction of a phase, can be estimated from the area fraction of that phase on random two dimension sections, or from the intercept fraction of that phase on random lines, or from the fraction of random points falling within that phase (point counting). There are a few important prerequisites for the validity of this identity:

- the phases must be randomly distributed
- the sampling areas, lines or points must be at random
- the measures must be made globally - i.e. the identity does not apply to a subset of area fractions classified by size.

Other quantities which can be uniquely estimated from measures on two dimensional sections are the surface area of a phase per unit volume and the line length (of cracks for example) per unit volume.

A second class of measures are those which can be estimated from two dimensional measures, if some assumptions are made, into this category fall measures of particle size distribution. Exact expressions exist only for very simple geometrical shapes and distributions such as monosized spheres. The problem here is one common to many 'inverse' problems. Given a known three dimensional distribution, the expected two dimensional distribution can be calculated, but from a given two dimensional distribution there is not unique solution for the parent three dimensional distribution — for example a circular section of given size may be the equatorial section, for a sphere of equal size, or the non-equatorial section of larger size, Figure 18. The accuracy of the solution then becomes basically statistical in nature.

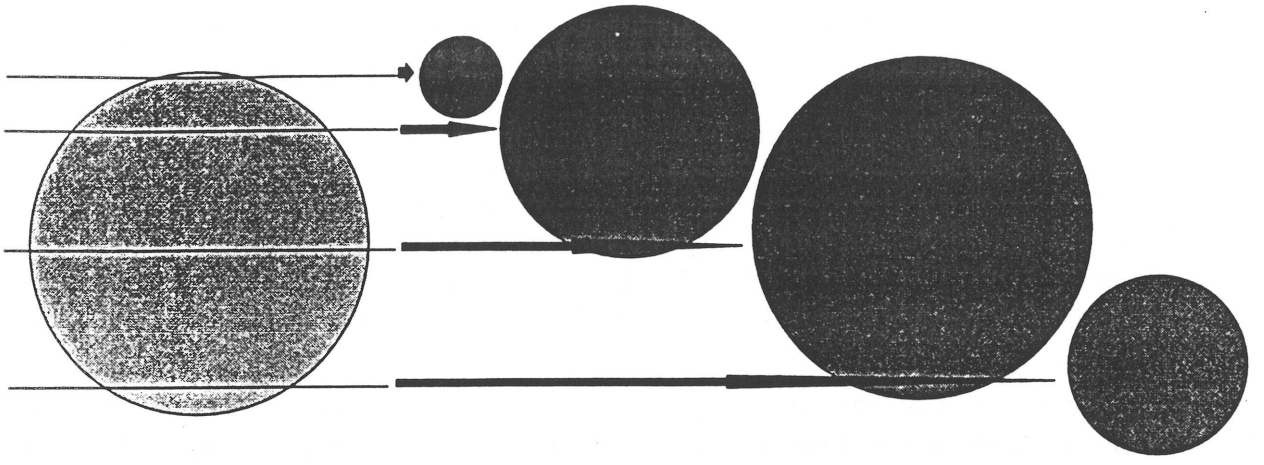

Figure 18. A given *particle* size may give rise to different sized *sections* in a 2D image, also the *sections* in a 2D image may originate from *particles* of different sizes.

Despite the problems, fairly reasonable routines exist for calculating size distributions for discrete, reasonably rounded particles. However, many microstructural features of interested features in cementitious materials do not fall into this category — the prime example being pores. The first question in this context is the meaning of a pore size. Although other measures, such as mercury intrusion porosimetry, also suffer from the problem of what exactly is the 'pore size' measured.

The third class are parameters which cannot be estimated directly from measures on two dimensional sections, the classic example being connectivity, which again concerns the characterisation of pore structure.

4.2.2 Statistical aspects

As in all measurements which can be made to characterise materials, errors arise from bias in the technique or finite precision in the method which have to be analysed by statistical procedures. However in stereological measures by image analysis we are forced by the very nature of measurement process to *sample* the true 3-D structure, the extent to which this sampling reveals the *'truth'* about what is there is fundamentally a statistical problem (Russ 1986)

In microscopic image analysis the area of sample actually measured is very small in relation to a macroscopic sample of concrete or paste. It is also much smaller than the volume sampled in 'bulk' measures such as X-ray diffraction or mercury intrusion porosity. In image analysis it is usual to speak of a measured value as an *estimate* of the actual value for the whole sample. The reliability of this *estimate* depend on the number of measures made and on the heterogeneity of the sample. If the goal of image analysis is to quantify differences between samples

Typically if the measures from N fields are averaged an idea of the variation of this average (compared to that for a different N fields) is given by the *standard error* (=standard deviation/$\sqrt{N}$). Clearly increasing the magnification of an image facilitates the discrimination of the microscopical features, however this reduces area measured in a given field. For example at a magnification of ×1000, four times as many images are needed to cover the same area as at a magnification of ×500. Generally the benefits of analysing a larger area outweigh the advantages of improving feature discrimination, this is encapsulated in the phrase:

Do more less well

The effect in cement paste can be seen in the measures in Table I, where the standard error of the porosity measured from nine fields at ×320 is four times that of the measurement for nine fields at ×1000.

The *error* of a given set of measurements will also depend on the way in which the fields to be measured are chosen. The most efficient sampling strategy (i.e. that giving the lowest error for a given number of measurements) is *uniform random*, in which the first field is chosen at random and then the other fields are chosen in a uniform spacing from this field. Within reason it is also best to space the fields as far apart as possible to have measurements from throughout the specimen.

In cement pastes 10 images at a magnification of ×400, gives an error of around 7% for the estimate of the volume fraction of anhydrous cement, around 4% for the estimate of porosity and around 15% for the measurement of calcium hydroxide (Scrivener et al. 1987). The cement paste fraction in concrete is more variable and it is necessary to measure more than 20 images to get similar levels of accuracy at the same magnification. In the case of concrete it is necessary to 'edit out' the aggregate particles to obtain measurements relative to the cement paste fraction. To give some idea of the meaning of these kind of accuracy levels, the calculated volume fraction of anhydrous materials in a cement paste at w/c=0.4, before any reaction is 45.2% and for w/c=0.45, 42.3%, i.e. a difference of about 7%.

For more complex measures it becomes more difficult to assess the statistical reliability. For example, the distribution of phases in the interfacial transition zone between aggregate and cement paste in concrete varies considerably from place to place. Measurement of the microstructural gradient around one aggregate may be very different from that measured around a second. In order to assess, the average microstructural gradient, many images on different aggregate particles need to be measured. Crumbie (1994, Scrivener et.al. 1988) measured 50 images, but even this was insufficient to confirm that some of the differences between samples were *statistically* significant.

4.3 Progress in image analysis of cementitious materials

With image analysis one moves beyond, 'pretty pictures' with the aim of obtaining 'useful' numbers. It is an area of tremendous potential, but unfortunately one can easily end up with 'pretty', but not very useful numbers'.

In general one can say that the simplest measures are the best — i.e. volume fraction. Despite their simplicity such measurements can be very useful. For example the volume fraction of anhydrous material can be used to calculate the degree of reaction if the original w/c ratio is known. Measurement of the microstructural gradients around aggregate particles at different ages also enables the pattern of deposition of the hydration products to be deduced (Crumbie 1994, Scrivener & Pratt 1996).

The time necessary to make the requisite number of measurements is a major impediment to the further use of image analysis. However, given the time investment necessary it is even more important that the measures made should be those relevant for relating microstructure to properties. Here collaboration is necessary between researchers in different areas.

The big challenge for image analysis is the characterisation of the pores structure, due to the importance of the porosity in the durability of concrete. Here it is possible that progress can be made by linking 3 dimensional computer models of microstructure with real microstructures through measurements on 2D sections (Kunzel et al. 1997).

5. Environmental Microscopy

A major problem with classical electron microscopes is the need to remove free water from a sample before it can be exposed to the high vacuum. Therefore, there is considerable interest in the use of 'environmental' microscopes , in which samples can be kept 'wet', for the study of cement and concrete. The first environmental microscopes were transmission electron microscopes (HVEM) operating at a very high accelerating voltage of 1 million volts, which produced electrons with high enough energy to penetrate thick samples. Two types of 'environmental' cell were produced. In the first 'window' type the cement, and water, were contained completely between two thin windows and could be examined periodically during hydration (Double et al 1978). The disadvantages of this arrangement, was the relatively low resolution, due to the presence of the windows and the high w/c ratios needed for electron transmission. The morphology of hydrates in cement pastes is highly dependent on water cement ratio above about 1. C-S-H can form long thin needle like growths and long ettringite crystals are also favoured.

The second type of cell used was the differentially pumped apertures cell. Here there are two apertures above and two below the specimen, with an independent pumping system between them. The area around the specimen can be maintained at up to 300τ. This arrangement was used by Jennings and Pratt (1980) and by Scrivener (1984) — the micrograph shown in Figure 4 was taken in such a microscope. Here, cements pastes at realistic water cement ratios were used. Carbon coated grids were placed in the pastes and removed specified time intervals. Samples could be studied from very early times, limited only by the time to mix the samples and place the grid in the microscope. As drying is not totally prevented, the samples could only be studied for 10 minutes or so, before the hydrates became damaged by drying. Unfortunately these type of high voltage microscope were very expensive to maintain and the performance deteriorated with age, so they have now been dismantled.

In the late 80s, a totally different type of environmental *scanning* microscope (ESEM) was developed. The area around the specimen is separated from the rest of the microscope by a differentially pumped aperture and fairly high pressures can be maintained in the vicinity of the sample. The microscope uses the ionisation of the gas in the specimen chamber to amplify the emission of electrons from the sample so contribute to the image formation. The specimen stage can be cooled, such that it is possible to condense liquid water on the sample. However, it is misleading to expect that this enables the hydration of cement to be followed 'in-situ'. Firstly, unlike the HVEM, the incident electrons have similar energy to a conventional SEM (~15-25 kV) and so cannot penetrate far through water. Therefore if liquid water is present, one sees the surface of the water and not the cement underneath. Secondly, as discussed for high w/c ratios the microstructural development of cement is a function of the *system* of cement plus water, thus repeated wetting and drying of the sample is not representative of the conditions existing is a normal paste (this phenomenon has been studied by Damidot & Sorrentino 1996).

The main advantage of the ESEM is that samples can be examined without prior drying or coating as for the HVEM with environmental cell. Neubauer & Jennings (1996) have discussed the use of the ESEM for the study of cement paste and concrete. A major area they have developed is the study of shrinkage as a paste is dried in the microscope.

The design of the electron optics in the ESEM are not optimal for the detection of X-rays, so the sensitivity and precision of chemical microanalysis is lower than in an conventional SEM.

6. New techniques

6.1 X-ray microscopy

The refractive index of X-rays in solids is very close to unity. This means that X-rays cannot be focused by conventional lenses and it used to be thought that X-ray microscopy was impossible. However, monochromatic X-rays can be focused by diffraction through Fresnel zone plates. These are circular diffraction gratings comprised of concentric opaque and transparent zones, Figure 19. X-ray microscopy requires an intense source of soft X-rays, which can be produced by a synchrotron. The development of synchrotrons and the increasing precision with which zone plates can be made has led to rapid advances of this technique, which has been widely applied to biological materials. The principal advantage of X-ray microscopy over electron microscopy is that specimens do not need to by dried (can even be immersed in water) and there is much less beam damage. In addition, the X-ray wavelength can be 'tuned', to maximise or minimise the absorption by different elements (e.g; O, N, Fe, Mg, Co, Ni, Ca, F), so permitting a kind of chemical imaging. The best resolution achievable today by X-ray microscopy is about 50 nm (very similar to the resolution of BSE images for cement).

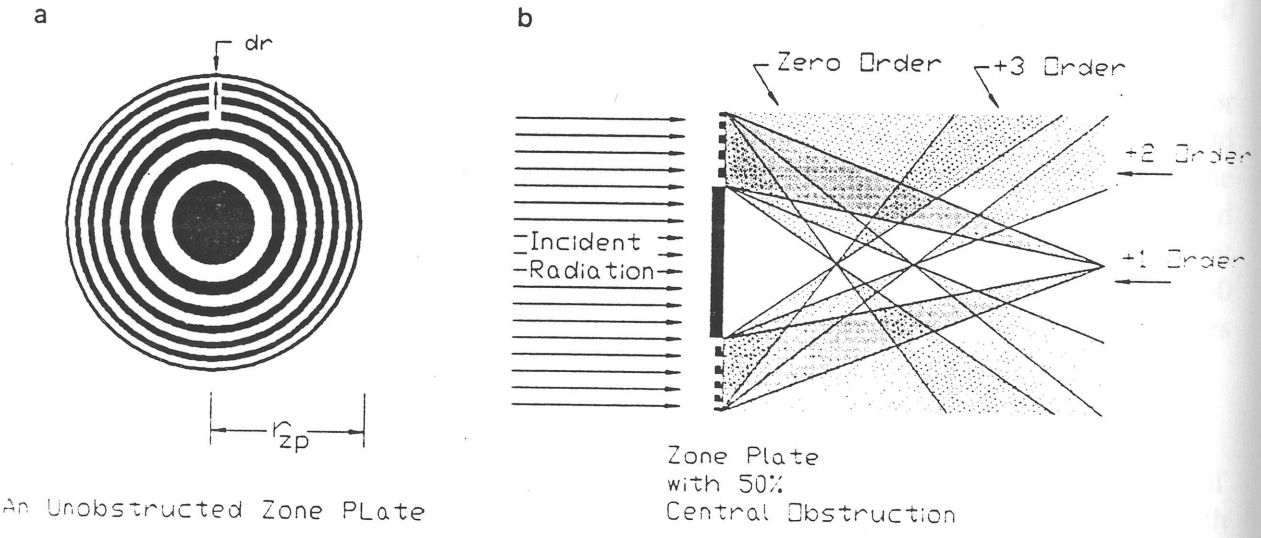

Figure 19. A Fresnel Zone plate and the principal of X-ray focusing with this device.

Soft X-ray transmission microscopy is being used to study cementitious materials by Kurtis et al. 1997, using the ALS (advanced light source) at the Lawrence Berkeley Laboratory in California. Figure 20 shows one of their images of an alkali silica gel in sodium hydroxide solution. The sample is immersed in the solution and the dissolution and repolymerisation can be followed 'in-situ'. This is clearly a technique with considerable potential.

6.2 Atomic force microscopy

In the atomic force microscope (AFM) a sharp tip is scanned over a specimen surface, with a separation between tip and specimen of about 10 Å. A force is generated between the specimen and the tip due to electron tunnelling, which is measured by the deflection of a cantilever on which the tip is mounted. The variation of the force across the specimen surface can be used to produce images of the surface relief, with atomic resolution (~2 Å) for suitable materials. This technique does not need to be operated under vacuum and images of solid surfaces can even be formed under water. Hall (1995) has used this technique, to study the dissolution and growth of gypsum and to image cement clinker under water. Mitchell et al (1996) have also studied the

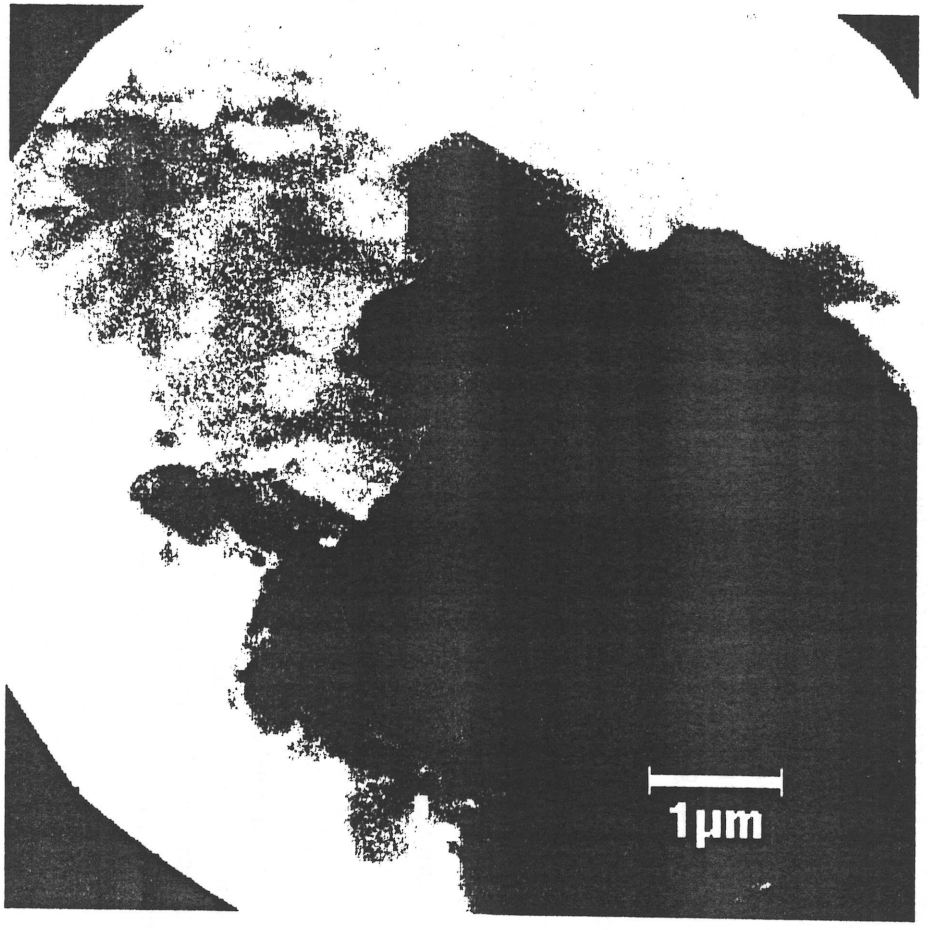

Figure 20. soft X-raytransmission microscope image of alkali silica gel
(courtesy of K.Kurtis and P.J.M. Monteiro, University of California, Berkeley)

surface of cement clinker, hydrated under various conditions. In the case of clinker, where, unlike gypsum atomic resolution, is not yet possible, the interpretation of the images is rather difficult, as there is no means of identifying the phases on the surface, only the overall relief of the surface is seen. Nevertheless this is a very new technique, which is developing rapidly and clearly or interest for the study of cementitious materials.

6.3 Imaging spectroscopies

Rapidly improving imaging capacities are being developed for many spectroscopic techniques — infra-red, Raman, NMR (nuclear magnetic resonance), SIMS (secondary ion mass spectroscopy), etc. As resolution develops these are becoming, in effect, microscopic techniques. The main benefit of this microscopic ability is the possibility to obtain spectra from local regions. At present most of these techniques have a fairly low resolution, typically 5 μm at best, which means that individual phases cannot be distinguished in hydrated cement and much of the advantage is lost. In some cases (e.g. infra-red, Raman) the resolution will be ultimately limited by the wavelength of the probe (as is light microscopy). Nevertheless this is a rapidly evolving field, in which it is clear that much progress will be made. The application of these techniques to cementitious materials is as much hampered by their complexity and lack of knowledge regarding crystal structures, as by the availability of the techniques themselves.

7. Concluding Remarks

The wide range of microscopical techniques available have much to contribute to the study of cementitious materials. Looking back only fifteen years, it is clear that our understanding of hydration and microstructure have advanced considerably in this time, due to improvements in imaging techniques and the wider availability of electron microscopes. However, it is important to remember that looking too closely, one may not be able to see the wood for the trees and that optical microscopy has an important role to play, not only for its convenience, but because larger areas can be studied, without undue drying of damage to the sample microstructure.

In the field of quantification of microstructure, through image analysis, there is tremendous potential, but progress is relatively slow. This is mainly because these techniques are inherently time consuming and the statistical aspects have not yet been extensively studied. Here I think progress must come from co-ordinated collaborative studies.

I have tried to give an idea of the limitations of techniques as well as their advantages, because I believe such knowledge is essential to the proper interpretation of the results. Microscopy is only one tool among a range of characterisation techniques, which can, and should, be used to advance or understanding of these complex materials. Hopefully so as to contribute to improving their performance and durability and to materials development.

8. References

Campbell, D.H., 1986, "Microscopical Examination and interpretation of Portland cement and clinker", Portland Cement Association.

Cottin, B., 1971, "Etude microscope electronique de pâtes de ciment alumineux hydratées en C_2AH_8 et en CAH_{10}", Cem.Concr.Res. **1**(2), 177-186.

Crumbie, A.K., 1994, "Microstructure of Concrete", PhD thesis, University of London

Damidot, D. & Sorrentino, F., 1996, "Observation of the hydration of cement paste by ESEM: care needed to study the early hydration" pp342-355, Proc. 18th Int.Conf.Cem.Microsc., Houston, Int.Cem.Microsc.Assn.

Double, D.D., Hellawell, A. and Perry, S.J., 1978, "The hydration of Portland cement", Proc. Roy. Soc. Lond. **A359**, 435-451

G.M.Idorn Consult, 1997, internet site: http://www.ramboll.dk/gmic/gmic.2.htm

Groves, G.W., 1987, "TEM studies of cement hydration", pp3-12 in Microstructural Development During Hydration of Cement", ed. L.J. Struble and P.W. Brown, MRS Symp.Proc. **85**, Materials Research Society.

Grudemo, 1960, "The microstructure of hardened cement paste", Proc.4thInt.Symp.Chem.Cem., Washington, paper V-2, **I**, 615-647.

Grudemo 1964, "Electron microscopy of Portland cement pastes", pp371-389 in Vol. I, The Chemistry of Cements, ed. H.F.W. Taylor, Academic Press, London

Hall, C. 1995, SPE International Symposium on Oilfield Chemistry, 533

Harrison, A.M., Winter, N.B. & Taylor, H.F.W., 1986, "An examination of some pure and composite Portland cement pastes using scanning electron microscopy with X-ray analytical capacity", 8th Int.Cong.Chem.Cem., Rio, Vol. 4, 170-175

Jennings, H.M. & Pratt, P.L., 1980, "The use of a high -voltage electron microscope and gas reaction cell for the microstructural investigation of wet Portland cement", J.Mat.Sci., **15**, 250-253.

Jackobsen, U.H., Johansen, V., Thaulow, N., 1997, "Optical microscopy - a primary tool in concrete examination", pp275-294 in Proc.19thInt.Conf.Cem.Microsc., Cinncinati, Int.Cem.-Microsc.Assn.

Kunzel, H., Quenard, D., Xu, K, Bentz, D.P., Martys, N.C., 1997, "Microstructure and transport properties of porous building materials", to be published, Materials and Structures.

Kurtis, K.E., Monteiro, P.J.M., Brown, J.T., Meyer-Ilse, W., 1997, submitted for publication

Lachowski, E.E., Mohan, K., Taylor, H.F.W. & Moore, A.E., 1980, "Analytical electron microscopy of cement pastes, Pt II Pastes of Portland cements and clinkers", J.Am.Ceram.Soc., **63**, 447-452.

Mayfield, B., 1990, "the quantitative evaluation of the water/cement ratio using fluorescence microscopy", Mag. Concr. Res. **150**, 45-49

Neubauer, C.M. & Jennings, H.M., 1996, "The role of the ESEM in the investigation of cement-based materials", Scanning, **18**, 515-521.

Ono, Y., 1980, "Microscopical estimation of burning condition and quality of clinker", Proc.7th Int.Cong.Chem.Cem., Paris V.2, pp206-211

Patel, H.H., 1987, "Porosity, microstructure and properties of cement paste", PhD, University of London.

Richardson, I.G. & Groves, G.W.,1990, "The microstructure of blastfurnace slag/high alumina cement pastes", pp282-293 in Calcium Aluminate cements, ed. R.J. Mangabhai, E&FN Spon, London.

Richardson, I.G., Groves, G.W., Dobson, C.M., 1991,"Structural changes due to carbonation in hardened cement pastes", Proc. 9thInt.Cong.Chem.Cem., New Delhi, Vol.IV, 298-304.

Richardson, I.G., Brough, A.R., Brydson, R., Groves, G.W., Dobson, C.M., 1993,"Location of aluminium in substituted C-S-H gels as determined by 29Si, 27Al NMR and EELS", J.Am.Ceram.Soc, **76**(9), 2285-2288.

Romer, B. & Dobrolubov, G., 1974, "Angewandte mikroskopie bei der baustoffprüfung", beispiel beton-mörtel-zement-kalk-gips-keramik, Mitt. Wissenschaft und Technik, Leitz, bd. VI, 4, pp.34-44.

Russ, J.C., 1986, Practical Stereology, Plenum Press, New York.

Scrivener, K.L., 1984,"The development of microstructure during the hydration of Portland cement", PhD thesis, University of London.

Scrivener, K.L. 1987, "The microstructure of anhydrous cement and its effect on hydration", pp39-46 in Microstructural develoment during hydration of cement, ed. L.J. Struble and P.W. Brown, MRS Symp. Proc. **85**, Materials Research Society.

Scrivener, K.L, Patel, H.H., Pratt, P.L. & Parrott, L.J., 1987, "Analysis of phases in cement paste using backscattered electron images, methanol absorption and thermogravimetric analysis" pp67-76, in Microstructural develoment during hydration of cement, ed. L.J. Struble and P.W. Brown, MRS Symp. Proc. **85**, Materials Research Society.

Scrivener, K.L., Crumbie, A.K. & Pratt, P.L. 1988, "A study of the interfacial regionbetween cement paste and aggregate in concrete", pp87-88 in Bonding in Cementitious Composites, eds. S. Mindess, S.P. Shah, MRS Symp.Proc. **114**, Materials Research Society

Scrivener, K.L., 1989a, "Quantification of microstructure", pp3-13, in Advances in Cement Manufacture and Use, ed. E. Gartner, Engineering Foundation, New York.

Scrivener, K.L., 1989b, "The microstructure of Concrete" pp127-161, in Materials Science of Concrete, ed. J.P. Skalny, American Ceramic Society.

Scrivener, K.L., 1989c, "The use of backscattered electron microscopy and image analysis to study the porosity of cement paste", pp129-140, in Pore structure and permeability of cementitious materials, ed. L.R. Roberts and J.P. Skalny, MRS Symp. Proc. **137**, Materials Research Society.

Scrivener, K.L. & Pratt, P.L., 1996, "Characterisation of interfacial microstructure", pp3-17 in Interfacial Transition Zone in Concrete, RILEM Rep. 11, ed. J.C. Maso, E&FN Spon, London.

Scrivener, K.L. & Lewis, M.C., 1997, "Microstructural and Microanalytiacal study of cement moratr subject to heacuring", this proceeidngs.

Stutzman, P., Lenker, S., Struble, S., Kanare, H., Tang, F., Campbell, D., 1989, pp154-16? "Standard cement clinkers for phase analysis", Proc.11th Int.Conf.Cem.Microsc., New Orleans, Int.Cem.Microsc.Assn.

Stutzman, P.E., Lenker, S., Kanare, H., Tang, F., 1991, "Quantitative phase abundance analysis of three cement clinker reference materials by scanning electron microscopy", Ceramic Transactions **16**, 199-210.

Sutter, L.L., Lehoux, P., Dewey, G.R., 1997, "Composition based phase distribution analysis of Portland cement clinker", pp14-29, in Proc. 19th Int. Conf. Cem. Microsc., Cinncinati, Int.Cem.Microsc.Assn.

Thaulow, N., Jensen, A.D., Chatterji, S., Christensen, P. & Gudmondson, H., 1982, "Estimation of the compressive strength of concrete samples by means of fluorescence microscopy" Nordisk Beton no. 2-4, pp.1-2.

Thaulow, N., Jackobsen, U.H., 1997, "The diagnosis of chemical deterioration of concrete by optical microscopy", pp3-13, in Mechanisms of chemical degradation of cement-based systems, ed. K.L.Scrivener and J.F.Young, E&FN Spon, London.

Theisen, K., 1997, "Quantitative determination of clinker phases and pore structure using image analysis", pp 30-44 in Proc. 19th Int.Conf.Cem.Microsc., Cinncinati, Int.Cem.Microsc.Assn.

Viehland, D., Li, J-F, Yuan L-J, Xu, Z, 1996, "Mesostructure of C-S-H gels in Portland cement pastes: short range ordering, nanocrystallinity and local compositional order", J.Am.Ceram.Soc, **79**(7) 1731-44.

Wang, S-D & Scrivener, K.L., 1995, "Hydration products of alkali activated slag cement", Cem.Concr.Res., **25**, 561-571

DEVELOPMENT OF HIGH SLAG BLAST FURNACE SLAG CEMENT WITH AN IMPROVED EARLY STRENGTH

Andreas EHRENBERG, Eberhard LANG and Jürgen GEISELER
Forschungsgemeinschaft Eisenhüttenschlacken, Duisburg, Germany

ABSTRACT The aim of this investigation was the variation of parameters having influence on the early strength of blast furnace slag cements while the characteristic positive properties of slag cement should be ensured. The separately ground laboratory cements contained granulated slag among 45 and 75 wt.-%. The early strength has been increased by 70% with positive consequences for the early strength of the concrete, too. The relative compressive strength of concrete cubes after 2 days (β_2/β_{28}), which usually is about 20-30%, has been increased to 50%.

INTRODUCTION

Having the same 28-days compressive strength the blast furnace slag cements show, depending on their slag content, lower early strength after 2 days and higher final strength after 91 days (Smolczyk, 1980). This characteristic strength development is desirable and often necessary due to the low heat of hydration. On the other hand an improved early strength is required for some fields of application, for example to reduce the time needed for removing shutterings or prestressing.

AIM OF THE INVESTIGATIONS

In the past a lot of researchs has been carried out to clarify the mechanisms having influence on strength development of blast furnace slag cements and to improve their early strength. During the first half of this century many scientists developed the fundamental knowledge on the hardening behaviour of slag cements (Passow, 1908, Grün, 1924+1928, Lea, 1935, Keil, 1949, Kühl, 1950, Taylor, 1964). On the basis of these results during the second half of the century the knowledge has been further developed. Summarizing the results of these investigations it can be stated that following factors can improve the early strength of blast furnace slag cements:

- increasing lime saturation factor and sulfate content, decreasing alkali content of the clinker (Frigione and Sersale, 1985, Smolczyk, 1981)
- high C_3S, low C_2S content of the clinker (Kollo, 1991)
- increasing contents of CaO, MgO, Na_2O, Al_2O_3 and decreasing contents of SiO_2, FeO, TiO_2, MnO, MnS of the slag (Kollo and Geiseler, 1987, Kollo, 1991)
- high glass content of the slag (Keil, 1963, Erntroy, 1992)
- optimal SO_3 content and initiation conditions for the latent hydraulic granulated blast furnace slag (Ludwig, 1968, Frigione, 1984, Sersale, 1992, Dahlhoff, 1994)
- mixtures of Sulfatetypes (Schwiete, 1963, Ludwig, 1968)
- reactive or inert fine minor additional constituents (Payá, 1995)
- increasing fineness (Dahlhoff, 1994)

Each of these parameters presents a different potential of optimization, but not each of them can be realized within a technical scale. With respect to given raw materials for clinker and iron production changes of the chemical composition are not possible in most cases. Both the material and transport costs and the availability of the materials play an additional important role. Within the frame of the investigations discussed below possibilities should be developed to improve the early strength of blast furnace slag cements *without* decreasing the proportion of granulated slag

and *without* changing the chemical composition of the cement constituents. The proportion of slag has essential importance for a lot of special positive slag cement and concrete properties (Geiseler and Lang, 1994). These properties, like low heat of hydration, high resistance against chemical and sea water attack, high sulfate resistance and resistance against alkali-aggregate-reaction and low conductivity, should be insured. In the same way the transferability of optimized mortar characteristics to the concrete is of high importance. Therefore some concretes using optimized blast furnace slag cements and trade cements should be produced and tested.

EXPERIMENTATION

More than 160 laboratory cements with slag proportions among 45 and 75 wt.-% using 3 clinkers, 7 different slags, 5 sulfatetypes and 2 fine minor constituents have been characterized. The influences of the specific surface of the ground granulated slag and the clinker, of the grain size distribution, of SO_3-content and the types of sulfate have been investigated (Ehrenberg and Lang, 1996). The materials resulted from current industrial production. As reference cements 4 trade cements (1 Portland cement, 3 blast furnace slag cements with different contents of slag) have been chosen. The chemical composition of the slags used in laboratory cements represents the average of German granulated blast furnace slags. The investigations have been performed according to DIN EN 196. Using slag cements with an increased early strength additionally 12 concretes have been investigated. **Table 1** shows the test program.

Table 1: Test program

Parameter	Quantity	Variation
Constituents:		
blast furnace slag	7	Al_2O_3: 11,4 - 14,6 wt.-%, C/S: 1,07 - 1,34
Portland cement clinker	3	C_3S: 56,2 - 69,4, C_2S: 7,3 - 18,4, C_3A: 7,6 - 11,2 wt.-%
type of sulfate	5	anhydrite II (AH), natural anhydrite/dihydrate-mixture, natural gypsum, desulfogypsum (by-product), β-hemihydrate (HH)
Cements:		
ratio slag / clinker	4	0/100, 45/55, 60/40, 75/25 (wt.-%)
sulfate content	3	2, 3, 4 wt.-%
specific surface (slag)	6	2100 - 8000 cm²/g (Blaine)
specific surface (clinker)	5	1700 - 6200 cm²/g (Blaine)
grain size distribution (slag)	6	d' = 42,1 - 8,7 µm, n = 0,92 - 0,85 (RRSB-grid)
grain size distribution (clinker)	5	d' = 48,2 - 8,8 µm, n = 0,89 - 0,80 (RRSB-grid)

Cement characterization:	**Mortar characterization:**	**Concrete characterization:**
water demand	spread	spread and raw density
setting time	compressive strength (prisms)	air pore volume
volume stability	flexural strength	compressive strength (cubes)
	dyn. E-modulus	porosity/pore size distribution
	bound water	carbonation depth

A detailed discussion of all results is beyond the scope of this paper, therefore only some aspects of the investigations carried out will be discussed.

RESULTS AND DISCUSSION

Proportion and composition of granulated blast furnace slag

Independent of the chemical composition of the slags the early strength clearly decreased with increasing proportions of slag. In consideration of constant parameters cements including granulated blast furnace slags with higher contents of Al_2O_3 and higher CaO/SiO_2 (C/S) ratios showed higher early strength. For example, slag cements with a slag/clinker ratio of 75/25, specific surfaces of 4900 cm^2/g (slag) and 4200 cm^2/g (clinker), anhydrite II and a SO_3-content of 4 wt.-% had the lowest 2-days strength using a slag with 11,9 wt.-% Al_2O_3 and a CaO/SiO_2 ratio of 1,07 but the highest 2-days strength using slag with 14,6 wt.-% Al_2O_3 and a basicity C/S of 1,34. However it has to be stated, that the influence of the chemical composition within the investigated frame is lower than the influence of other parameters like the specific surface or the sulfate content.

Proportion of minor additional constituents

As additional constituents Microsilica (slurry) and white lime hydrate (powder) have been used in the range of 1-5 wt.-%. The mean diameter d' (RRSB-grid) of these materials was 1,7 µm (Microsilica) and 9,1 µm (lime hydrate) and the slope of the grain size distribution was 1,12 (Microsilica) and 1,03 (lime hydrate). The use of these materials in slag cements with slag/clinker ratios of 60/40 and 75/25 in all cases led to an improved strength development. Especially the early compressive strength has been increased by about 50-80% (60/40) and 20-60% (75/25) respectively; the relative compressive strength of mortar bars after 2 days (β_2/β_{28}) increased from 0,22 to 0,30-0,34 (60/40) and from 0,30 to 0,34-0,42 (75/25) respectively. Using 5 wt.-% Microsilica the capillary porosity (pores > 30 nm) in the age of 2 days has been decreased from 24 to 17 vol.-%; the matrix of the cement stone showed a higher density. However the use of the fine additions impaired the processing characteristics. For example the spread of mortars including Microsilica decreased from 15,5 to 13,6 cm (60/40) and from 15,6 to 13,2 cm (75/25) respectively; the water demand increased from 26,5 to 29,5 wt.-% (60/40) and from 27,5 to 29,5 wt.-% (75/25). These problems occur in general in the case of mixing cement constituents with additions having very high specific surfaces without a control and modification of the grain size distribution. **Fig. 1** shows the results for mortars using slag cement with a slag/clinker ratio of 75/25 and 5 wt.-% additional constituents.

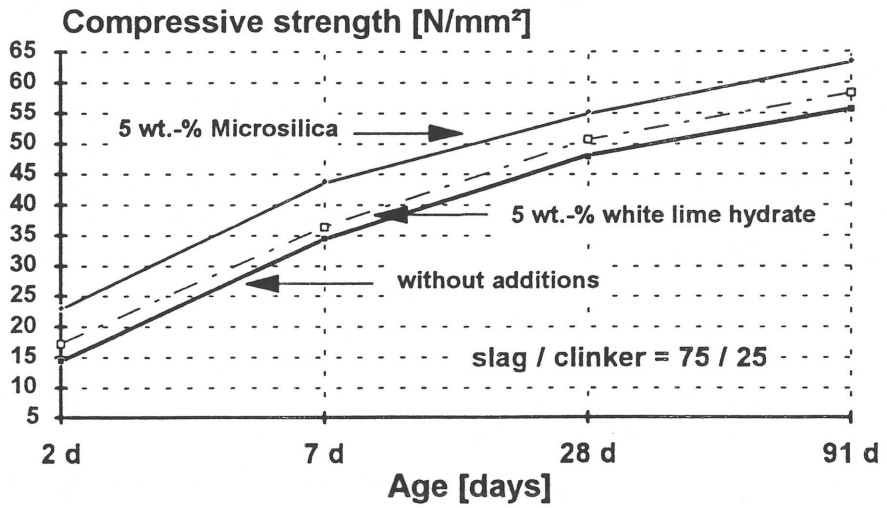

Figure 1: Influence of Microsilica and white lime hydrate on the strength development of blast furnace slag cement

Specific surface of the main constituents

Fig. 2 shows the 2-days compressive strength for different slag/clinker ratios. While the specific surface of the granulated blast furnace slag has been increased from 2100 to 6300 cm²/g other parameters have been left unchanged (4 wt.-% SO_3, anhydrite II, specific clinker surface 4200 cm²/g). Increasing the slag fineness from 2100 to 3500 cm²/g increased the 2-days compressive strength by 11 N/mm² or 20% per 100 cm²/g. But increasing the slag fineness by the same amount of 1400 cm²/g from 4900 to 6300 cm²/g raised the 2-days strength only by 1,6 N/mm² or 1% per 100 cm²/g. These examples make evident, that the possibility to compensate a lower early strength by a higher specific surface is limited mainly to lower and medium surface values. The investigations led to the result, that the aim of a higher early strength of slag cements requires a minimum fineness of the ground granulated slag which should be about 3500 cm²/g. But on the other hand increasing the slag fineness above a upper limit leads to only a small raise of the early strength which often does not justify the higher energy input to grind the slag finer.

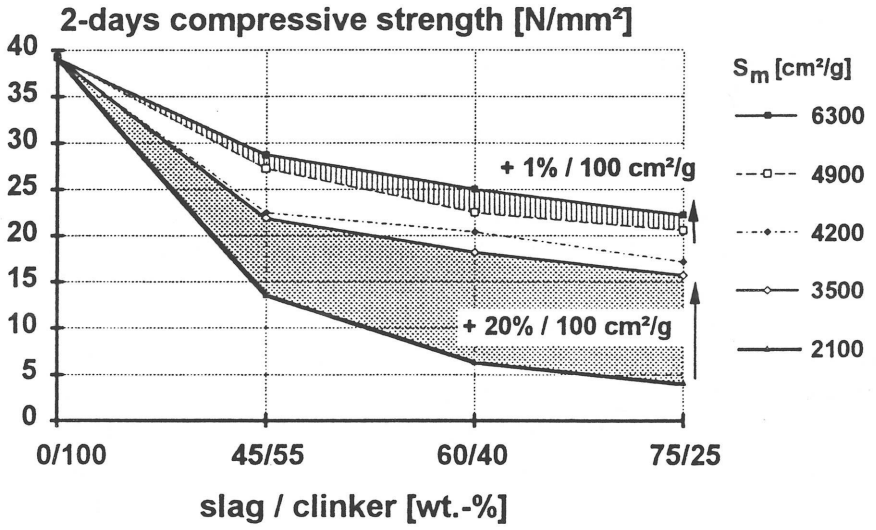

Figure 2: Increase of the compressive strength by increasing the specific surface (S_m)of the granulated blast furnace slag

Grain size distribution of the main constituents

To describe the fineness of a material there are used two methods: Measuring the specific surface (Blaine, BET) and the grain size distribution (laser granulometry, sedimentation analysis). But it is well known, that with a constant specific surface different grain size distributions can be connected. The mean diameter d' and the slope of the grain size distribution n (RRSB-grid) have a big influence on the behaviour of powder materials like cement. Therefore these parameters deliver more informations with respect to the water demand and other properties. The slope of the grain size distribution depends on the individual milling aggregate, the milling conditions like feed material or grinding media filling ratio and the characteristic of the material being ground. The investigations showed, that using one laboratory ball mill for different kinds of material (slag, clinker, sulfates) led to nearly constant values of n in the range of 0,80-0,95. Considering only *one* milling aggregate ($n \approx$ constant) the mean diameter d' and the specific surface are corresponding in an almost linear way. Therefore an increasing early strength as a result of increasing specific surfaces was connected with lower mean diameters. Additionally therefore the grain size distribution has been modified by mixing ground slags from different mills: The mixed slag cements show wider grain size distributions (n = 0,65-0,72) and mean diameters in the range

of 13-25 µm. Using these mixed slag cements it is possible to raise the early strength without any disadvantageous influence on water demand or spread. Summarized it can be stated that a lower mean diameter and a wider particle size distribution of the ground slag and of the cement have a positive influence on the strength development, especially at early age. **Fig. 3** shows one example of the results obtained by these investigations, which shall be continued.

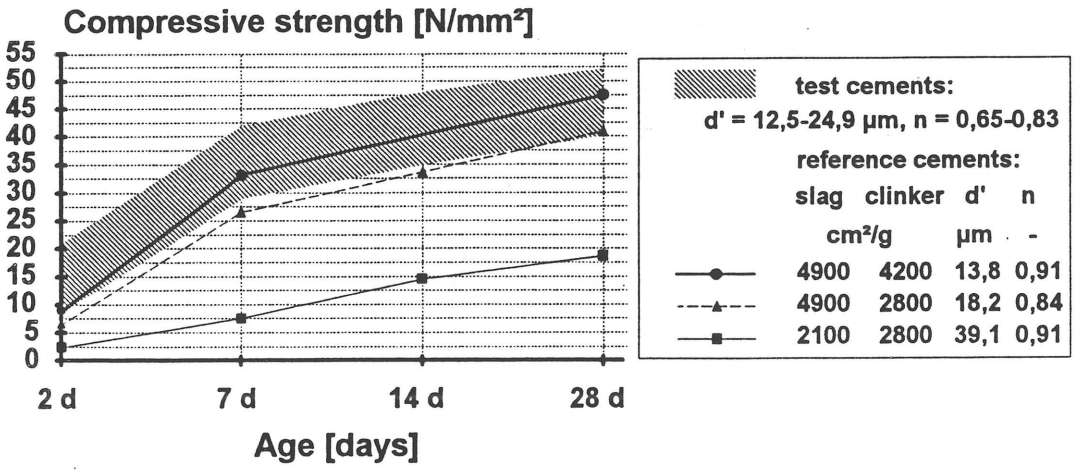

Figure 3: Increase of the compressive strength by variation of the grain size distribution (slag / clinker = 75 / 25, 4 wt.-% SO_3, HH / AH = 15 / 85)

Sulfate content of the cement

The sulfate content is important for regulating the setting and hydration characteristic of cements. Among others the optimal value depends on C_3A-content of the used clinker and the slag/clinker ratio; usually slag cements need a lower sulfate content to delay the setting. But especially for slag cements the early strength development is strongly influenced by the sulfate content, too. So the variation of the SO_3 content in slag cements with different slag/clinker relatios among 2-4 wt.-% showed, that in most cases a sulfate content of 4 wt.-% led to the highest early strength; 2 wt.-% sulfate led in more than 160 laboratory cements to the lowest 2-days strength. In some but not all cases a small decrease of the 28-days compressive strength was connected with the increase of the early strength. The results verify those of Frigione (1984) and Soroka (1986). In **Fig. 4** the change of the 2-days compressive strength by variation of the sulfate content is presented, resulting from 45 different blast furnace slag cements with 5 slags, 2 clinkers and anhydrite II. Only the limit lines of all test results are plotted. The positive effect of increasing SO_3-contents for cements with lower slag contents is evident; with higher slag/clinker ratios the test results deviate more from another. Therefore this effect is not ascertainable in the same extent. This seems to be an indicator for the dominant interaction of sulfate content and clinkerphases like C_3A and C_4AF forming ettringite, monosulfatehydrate and tetracalcium hydroaluminoferrite. With respect to the decrease of the early strength with increasing slag contents (see shifting the strength level of the grey fields within **Fig. 4**) it is possible to partly compensate the strength loss by optimization of the SO_3-content.

Type of sulfate

The solubility and the solution velocity of the sulfates are important for the setting and the early strength. Both are depending on the type of sulfate, the fineness and the distribution in the cement (Soroka, 1984). For example the solubility of sulfate variates, depending on the temperature, between 0,18 g/100 cm³ (dihydrate), 0,38 g/100 cm³ (anhydrite II) and 0,83-1,01 g/100 cm³ (α-, β-hemihydrate). The reactive specific "inner" surface of different types of

sulfate is different, too. Having the same surface according to Blaine the BET surface of hemihydrate is 4times higher than that of anhydrite. The investigations showed, that substituting anhydrite II totally by other types of sulfate led to lower 2-days-strength by up to 30%. But small additions of β-hemihydrate (HH/AH = 15/85 - 35/65 corresponding to 0,5-1,4 wt.-% SO_3 from HH) in cements with higher slag contents led to a raise of the 2-days strength in the range of 3 N/mm². This experience is verified in industrial scale by partly dehydration of natural gypsum during the milling process. Elder investigations have shown, that SO_3 contents more than 2-3 wt.-% resulting from hemihydrate response "false setting". The initial set has been prolonged from 250 min (AH) to 305 min (HH/AH = 15/85), the setting time of 40-45 minutes was not influenced significantly. **Fig. 5** shows an example with results for slag cements with a slag/clinker ratio of 75/25 and a total sulfate content of 3 wt.-% (clinker: 4200 cm²/g, slag: 4900 cm²/g).

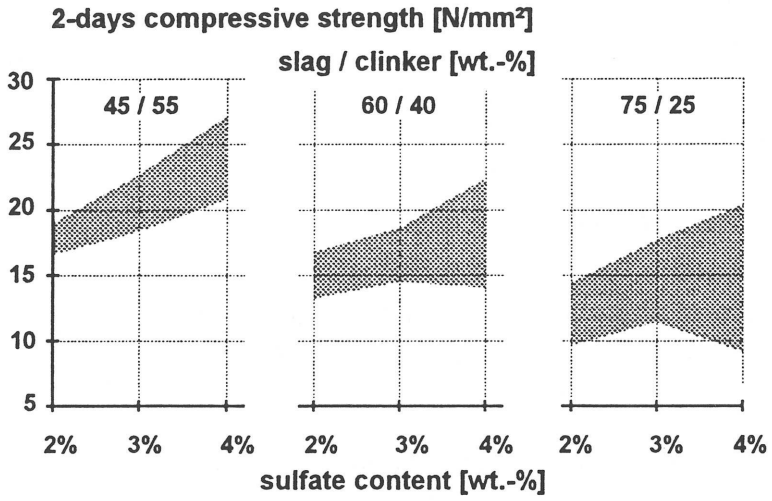

Figure 4: Change of the compressive strength by variation of the sulfate content (results from 5 slags, 2 clinkers and 45 blast furnace slag cements)

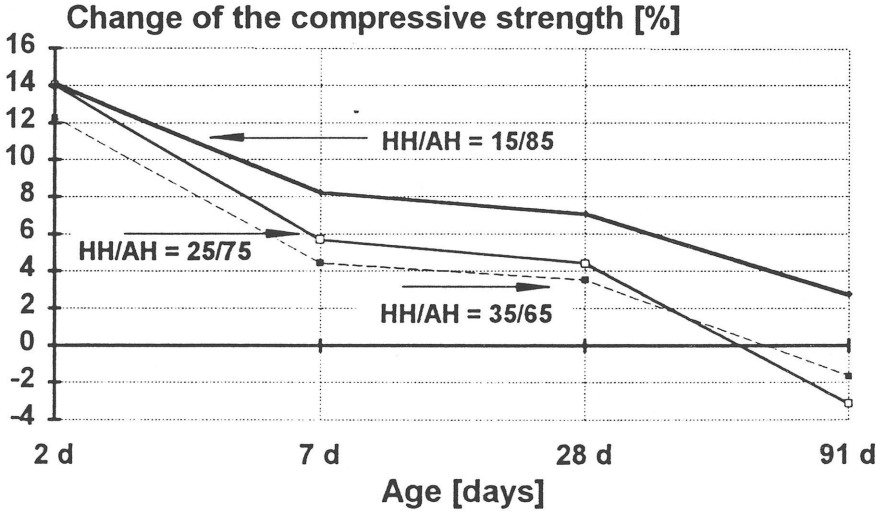

Figure 5: Influence of β-hemihydrate (HH) on strength development (slag / clinker = 75/25, 3 wt.-% SO_3)

Concrete investigations

With 6 slag cements, optimized with respect to their sulfate content and specific surface, 1 Portland cement and 3 trade slag cements using the same clinker and slag like in the laboratory investigations 10 concrete mixtures have been tested in laboratory scale. For the concretes 350 kg/m³ cement, 1850 kg/m³ aggregate (Rhine gravel and sand) and a water/cement ratio of 0,50 have been used. **Fig. 6** shows a good linear correlation of the compressive strength of mortars and concretes (coefficient of correlation = 0,96, standard deviation s = 4,6 N/mm²). This strong correlation is partly based on the constant laboratory conditions. But it is cognizable, that the strength potential of optimized slag cements determined on mortars can be transferred to concretes, too.

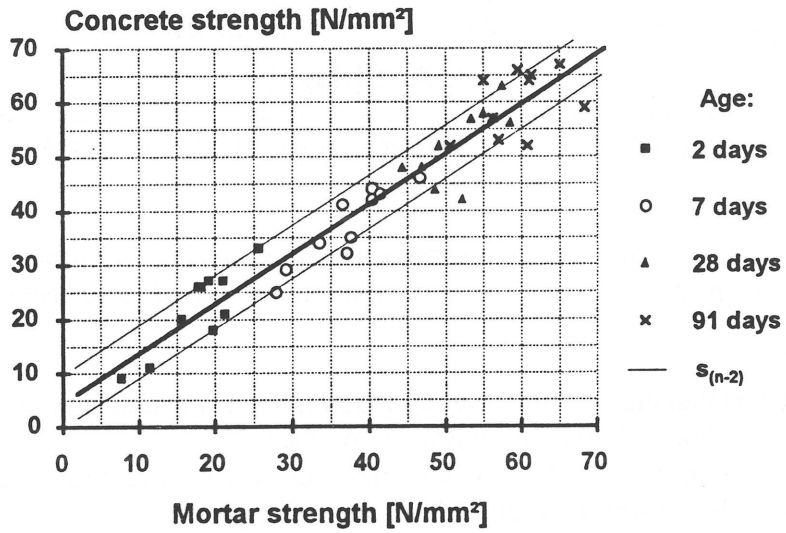

Figure 6: Compressive strength of laboratory mortars and concretes

Compared with trade cements the optimization of slag cements led to an increase of the early strength of mortars in the range of 20-70%. This increase had positive consequences for the early strength of the concrete, too. The relative compressive strength of concrete after 2 days (β_2/β_{28}), which usually is about 0,2-0,3, has been raised to 0,4-0,5, as illustrated in **Fig. 7**. The laboratory slag cements Z 8 and Z 9 have slag/clinker ratios of 75/25, the corresponding trade slag cement of 78/22. The specific surface of the slag and the clinker within both laboratory cements was 4900 cm²/g and 4200 cm²/g respectively; the sulfate content of Z 8 was 2 wt.-% and of Z 9 4 wt.-%. For the production of the trade slag cement CEM III/B 32,5 NW HS (NW: low heat of hydration, HS: high sulfate resistance) and of the laboratory cements the same clinker and slag have been used. The specific surface of the trade cement was 3900 cm²/g, the mean diameter d' was 15,9 µm and the slope n was 1,09; the sulfate content was 1,2 wt.-%. Using higher SO_3-contents, higher specific surfaces, lower mean diameters (Z 8: 13,1 µm, Z 9: 12,8 µm) and a wider grain size distribution (Z 8: 0,94, Z 9: 0,92) a higher early strength of the concrete between 122 and 189% has been realized. The relative 2 days strength (β_2/β_{28}) increased from 0,21 to 0,42 (Z 8) and 0,50 (Z 9). Therefore it can be stated, that the increased early strength of optimized slag cements was transferred to the concrete, too. The investigations will be continued by further optimization of the grain size distribution of slag cements.

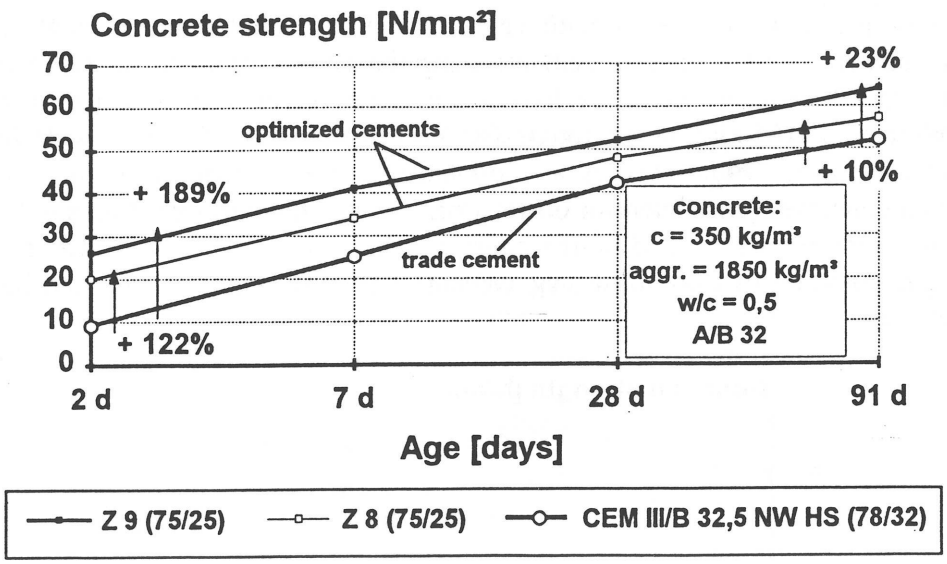

Figure 7: Increase of concrete compressive strength by using optimized slag cements in comparison with concrete using trade slag cement (slag/clinker)

REFERENCES

Dahlhoff, U., Untersuchungen an Mörtel und Beton zur Entwicklung von Hochofenzement mit erhöhter Anfangsfestigkeit, Dissertation RWTH Aachen, 1994

Ehrenberg, A., Lang, E., "Weiterentwicklung von Hochofenzementen im Hinblick auf ihre Anfangsfestigkeit", Beton-Informationen, Vol. 36, 1996, pp. 12-18

Erntroy, H. C., "The effect on compressive strength of the glass content of blastfurnace slag when used as a cementitious constituent", Zement-Kalk-Gips, Vol. 45, 1992, pp. 533-535

Frigione, G., Sersale, R., "The influence of the chemical composition of the clinker on the strength properties of blast furnace slag cement", Cement and Concrete Research, Vol. 15, 1985, pp. 159-166

Frigione, G., "Gypsum in cement", Advances in cement technology, ed. by S. N. Gosh, pp. 485-535, Oxford and New York, 1984

Geiseler, J., Lang, E., "Long-term durability of non-entrained concrete structures exposed to marine environments and freezing and thawing cycles", 3rd CANMET/ACI International Conference on Durability of Concrete, Nice, 1994

Grün, R., "Über die Mahlfeinheit von Hochofenzement", Tonindustrie-Zeitung, Vol. 48, 1924, pp. 18-24

Grün, R., "Der Hochofenzement", 4th ed., Berlin, 1928

Keil, F., "Hochofenschlacke", Düsseldorf, 1949 (1st ed.), 1963 (2nd ed.)

Kollo, H., Geiseler, J., "Beurteilung der Qualität von Hüttensand anhand von Kennwerten", Beton-Informationen, Vol. 21, 1987, pp. 48-51

Kollo, H., "Einfluß der chemischen Zusammensetzung von Hüttensand auf dessen Hydraulizität", Beton-Informationen, Vol. 31, 1991, pp. 22-23

Kühl, H., "Zement-Chemie", 1st ed., Berlin, 1950

Lea, F. M., "The chemistry of cement and concrete", 1st ed., London, 1935

Ludwig, U., "Über die Einflußnahme verschiedener Sulfate auf das Erstarren und Erhärten von Zementen", Zement-Kalk-Gips, Vol. 21 ,1968, pp. 81-90, pp. 109-119, pp. 175-180

Passow, H., Die Hochofenschlacke in der Zementindustrie, Würzburg, 1908

Payá, J., et al., "Early strength development of Portland cement mortars containing air classified fly ashes", Cement and Concrete Research, Vol. 25, 1995, pp. 449-456
Schwiete, H.-E., Dölbor, F.-C., "Einfluß der Abkühlungsbedingungen und der chemischen Zusammensetzung auf die hydraulischen Eigenschaften von Hämatitschlacken", Forschungsberichte des Landes NRW, Nr. 1186, Köln, 1963
Sersale, R., et al., "SO_3 content of Portland and blended cements: Porosity and behaviour of the resultant mortars", Proc. 9th Int. Congress on the Chemistry of Cement, New Delhi, 1992
Smolczyk, H.-G., "Slag structure and identification of slags", Proc. 7th Int. Congress on the Chemistry of Cement, Paris, 1980
Smolczyk, H.-G., "Zum Einfluß des Klinkers auf die Festigkeitsentwicklung von Hochofenzement", Beton-Informationen, Vol. 21, 1981, pp. 43-49
Soroka, I., Abayneh, M., "Effect of gypsum on properties and internal structure of PC paste", Cement and Concrete Research, Vol. 16, 1986, pp. 495-504
Taylor, H. F. W. (ed.), "The chemistry of cements", London, 1964